Assessment of erosion, sedimentation, and water quality impacts of the Mountain Valley Pipeline and Equitrans Expansion Project's proposed crossing of the Jefferson National Forest as it pertains to the U.S. Forest Service's Draft Supplemental Environmental Impact Statement dated December 2022

Prepared by Jonathan A. Czuba, Ph.D., Licensed Professional Engineer - February 9, 2023

REFERENCES
1

February 21, 2023

DRAFT

USER'S REFERENCE GUIDE

Revised Universal Soil Loss Equation Version 2

(RUSLE2)

Prepared for
USDA-Agricultural Research Service
Washington, D.C.

May 15, 2008

Acknowledgements

RUSLE2 was developed cooperatively by the USDA-Agricultural Research Service (ARS), the USDA-Natural Resources Conservation Service (NRCS), and the Biosystems Engineering and Environmental Science Department of the University of Tennessee. Each project participant maintains a RUSLE2 Internet site directed toward their specific interests. Consult these sites for a list of the employees of these organizations who contributed to the development of RUSLE2. Contributors from several other organizations also participated in the development of RUSLE2.

The USDA-ARS was responsible for providing the erosion science on which RUSLE2 is based including the mathematical equations used in RUSLE2, core data values used to calibrate RUSLE2, scientific documentation, and a user's reference guide for RUSLE2.

The USDA-NRCS was the principal client for RUSLE2. The NRCS provided information to ensure that RUSLE2 could be easily used in their local field (district) offices. The NRCS also developed an extensive RUSLE2 operational (working) database, primarily for cropland. The NRCS has developed RUSLE2 templates and user guides specifically for their purposes.

The interests and needs of a wide variety of other users were considered during RUSLE2's development. RUSLE2 was developed to be land-use independent to give RUSLE2 the wide applicability range possible and to accommodate the needs of these users.

The University of Tennessee participated in the development of the mathematical equations used in RUSLE2, developed the computer science used in RUSLE2, and developed the RUSLE2 computer program. They also developed user guides and other RUSLE2 information for their clients.

This RUSLE2 User's Reference Guide was reviewed by USDA-Natural Resources Conservation Service technical specialists from several disciplines; Kenneth G. Renard (retired), USDA-Agricultural Research Service, Tucson, Arizona, and Seth Dabney, USDA-Agricultural Research Service, Oxford, Mississippi.

Preface

This RUSLE2 User's Reference Guide describes RUSLE2 in detail in semi-technical language. This Guide describes how RUSLE2 works, how to select input values, how to apply RUSLE2 to make erosion estimates for the wide range of conditions represented by RUSLE2, how to interpret values computed by RUSLE2, how to evaluate RUSLE2's adequacy for conservation and erosion control planning, RUSLE2's accuracy, and how to conduct sensitivity analysis with RUSLE2. This Guide also describes similarities and differences between RUSLE2 and the USLE and RUSLE1, widely used predecessor technologies, and how to select input values and make interpretations when comparing erosion values estimated by these technologies.

RUSLE2 is land use independent and applies to all land uses where soil erosion occurs by erosive forces applied to exposed mineral soil by raindrop impact and surface runoff produced by Hortonian overland flow. This User's Reference Guide is targeted to technical specialists, who in turn, can use the information in this Guide to develop application-specific RUSLE2 user guides.

This User Reference Guide provides information on contact agencies that can provide additional information on RUSLE2.

A companion RUSLE2 Science Documentation describes the mathematical procedures used in RUSLE2.

Disclaimer

The purpose of RUSLE2 is to guide and assist erosion-control planning. Erosion-control planners should consider information generated by RUSLE2 to be only one set of information used to make an erosion-control decision. RUSLE2 has been verified and validated, and every reasonable effort has been made to ensure that RUSLE2 works as described in RUSLE2 documentation available from the USDA-Agricultural Research Service. However, RUSLE2 users should be aware that errors may exist in RUSLE2 and exercise due caution in using RUSLE2.

Similarly, this RUSLE2 User's Reference Guide has been reviewed by erosion scientists and RUSLE2 users. These reviewers' comments have been faithfully considered in the revision of this document.

Every reasonable effort has been made to ensure that this document is accurate. The USDA-Agricultural Research Service alone is responsible for this document's accuracy and how faithfully the RUSLE2 computer program represents the information in this document.

Table of Contents

Glossary of Terms

Term	Description
10 yr EI	Storm EI with a 10-year return period
10 yr-24 hr EI	Storm EI for the 10 yr-24 hr precipitation amount
10 yr-24 hr precipitation	24 hour precipitation amount having a 10-year return period
Antecedent soil moisture subfactor	See cover-management subfactors.
Average annual, monthly, period, and daily erosion	RUSLE2 computes average daily erosion for each day of the year, which represents the average erosion that would be observed if erosion was measured on that day for a sufficiently long period. Average period, monthly, and annual erosion are sums of the average daily values.
Average erosion	Average erosion is the sediment load at a given location on the overland flow path divided by the distance from the origin of overland flow path to the location.
b value, also b_f value	Coefficient in equation for effect of ground cover on erosion; values vary daily with rill-interrill erosion ratio and residue type
Birth of biomass	Refers to the addition of live aboveground and root biomass simultaneous with the death during growth periods when canopy cover and root biomass is increasing
Buffer strips	Dense vegetation strips uniformly spaced along overland flow path; can cause much deposition
Burial ratio	Portion of existing surface (flat) cover mass that is buried by a soil *disturbing* operation; dry mass basis-not area covered basis
Calibration	Procedure of fitting an equation to data to determine numerical values for equation's coefficients
Canopy cover	Cover above soil surface; does not contact runoff; usually provided by vegetation
Canopy shape	Standard shapes used to assist selection of effective fall height values for waterdrops falling from canopy
Canopy subfactor	See cover-management subfactors.
Channel order	Relative position of a channel in a concentrated flow network
Climate description	Input values for variables used to represent climate (primarily temperature, precipitation, and erosivity density); stored in RUSLE2 climate database component under a location name
Concentrated flow area	Area on landscape where channel flow occurs; ends overland flow path
Conservation planning soil loss	A conservation planning erosion value that gives partial credit to deposition as soil saved; credit is function of location on overland flow path where deposition occurs
Contouring	Support erosion-control practice involving ridges-furrows that

	reduces erosion by redirecting runoff around hillslope
Contouring failure	Contouring effectiveness is lost where runoff shear stress exceeds a critical value
Contouring description	Row grade (steepness) used to describe contouring; stored in RUSLE2 contouring component database under name for contouring practice; ridge height in *operation* description used in cover-*management* description also key input in addition to row grade
Core database	RUSLE2 database that includes values for base conditions used to validate RUSLE2; input values for a new condition must be consistent with values in core database for similar conditions
Cover-*management* description	Values for variables that describe cover-management; includes dates, *operation* descriptions, *vegetation* descriptions, yields (vegetation production level), applied external residue (*residue* description) and amount applied; named and saved in RUSLE2 management component database
Cover-management subfactors (subfactors used in RUSLE2 listed below in italics)	Cover-management subfactor values used to compute detachment (sediment production) by multiplying subfactor values, subfactor values vary through temporally
Canopy	Represents how canopy affects erosion, function of canopy cover and effective fall height
Ground cover	Represents how ground cover affects erosion; primarily function of portion of soil surface covered
Surface roughness	Represents how soil surface roughness and its interaction with soil biomass affect erosion
Soil biomass	Represents how live and dead roots in upper 10 inches of soil and buried residue in upper 3 inches and less of soil affects erosion
Soil consolidation	Represents how a mechanical disturbance and it interaction with soil biomass affect erosion, erosion decreases over time after last disturbance as the soil consolidates (a soil bonding effect that occurs with wetting and drying of the soil-not a mechanical effect)
Ridging	Represents how ridges increase detachment (sediment production)
Ponding	Represents how a water layer on soil surface reduces erosion
Antecedent soil moisture	Represents how previous vegetation affects erosion by reducing soil moisture, used only in Req zone
Critical slope length	Location along a uniform overland flow path where contouring fails
Cultural practice	Erosion control practice, such as no-till cropping, where cover-management is used to reduce erosion
Curve number	An index used in NRCS curve number method to compute runoff; RUSLE2 computes curve number value as function of hydrologic

	soil group and cover-management conditions
Database	RUSLE2 database stores both input and output information in named descriptions
Dead biomass	Represents live above ground and root biomass that has been converted to dead biomass by *kill vegetation* process in an *operation* description; dead biomass decomposes
Dead root biomass	A *kill vegetation* process in an *operation* description converts live root biomass to dead root biomass, dead roots decompose at the same rate as surface and buried residue
Dead standing biomass	Represents live aboveground biomass converted to dead standing biomass by a *kill vegetation* process in an *operation* description; dead standing biomass does not contact soil surface; dead standing biomass decomposes more slowly than surface and subsurface dead biomass
Dead surface biomass	Represents surface biomass that resulted from live aboveground biomass being killed and flattened to become surface biomass, buried residue that has been brought to the soil surface by a soil disturbing process in an operation description, and material that has been applied as external residue; in contact with soil surface
Death of biomass	Refers to the loss of live aboveground and root biomass simultaneous with birth of live biomass during growth periods when canopy cover and root biomass is increasing; daily death of live aboveground biomass adds to surface residue pool and daily death of root biomass adds to dead root biomass pool
Decomposition	Loss of dead biomass as a function of material properties, precipitation, and temperature; decomposition rates for all plant parts and buried and surface biomass are equal; decomposition rate for standing residue is significantly decreased because of no soil contact
Deposition	Transfers sediment from sediment load being transported by runoff to soil surface; net deposition causes sediment load to decrease with distance along overland flow path; depends on sediment characteristics and degree that sediment load exceeds sediment transport capacity; enriches sediment load in fines; computed as a function of sediment particle class fall velocity, runoff rate, and difference between sediment load and transport capacity
Deposition portion	Portion of overland flow path where net deposition occurs
Detachment	Process that separates soil particles from soil mass by raindrops, waterdrops falling from vegetation, and surface runoff; net detachment causes sediment load to increase along overland flow path; detachment is non-selective with respect to sediment characteristics; computed as function of erosivity, soil erodibility, distance along overland flow path, steepness of overland flow path, cover-management condition, and contouring

Disaggregation	Mathematical procedure used to covert monthly precipitation and temperature values to daily values assuming that values vary linearly; daily precipitation values sum to monthly values; average of disaggregated daily temperature equal average monthly value
Diversion/terrace/ sediment basin	A set of support practices that intercept overland flow to end overland flow path length.
Diversions	Intercepts overland flow and directs it around hillslope in channelized flow; grade is sufficiently steep that deposition does not occur but not so steep that erosion occurs in the diversion
EI_{30}	Storm (rainfall) erosivity; product of storm energy and maximum 30-minute intensity; storm energy closely related to rain storm amount and partly to rainfall intensity
Enrichment	Deposition is selective, removing the coarse and dense particles, which leaves the sediment load with an increased portion of fine and less dense particles
Enrichment ratio	Ratio of specific surface area of sediment after deposition to specific surface area of soil subject to erosion
Ephemeral gully erosion	Erosion that occurs in concentrated flow areas
Eroding portion	Portion of overland flow path where net detachment (erosion) occurs
Erosivity	Index of rainfall erosivity at a location; closely related to rainfall amount and intensity; monthly erosivity is average annual sum of individual storm erosivity values in month; annual erosivity is average sum of values in year; storm rainfall amount must be ½ inch (12 mm) or more to be included in computation of erosivity
Erosivity density	Ratio of monthly erosivity to monthly precipitation amount
External residue	Material, usually biomass, added to soil surface or placed in the soil; affects erosion same as surface residue and buried residue from vegetation
Fabric (silt) fence	Porous fabric about 18 inches wide placed against upright posts on the contour; these barriers pond runoff and cause deposition; widely used on construction sites
Fall height (effective)	Effective fall height is the effective height from which waterdrops fall from canopy; depends on canopy shape, canopy density height gradient, and top and bottom canopy heights
Filter strip	A single strip of dense vegetation located at the end of an overland flow path; can induce high amounts of deposition
Final roughness	Soil surface roughness after roughness has decayed to unit plot conditions, primarily represents roughness provided by soil resistant clods
Flattening ratio	Describes how much standing residue that an operation flattens; ratio of standing residue mass before operation to standing residue mass after operation; depends on operation and residue; dry mass

	basis
Flow interceptors	Topographic features (ridges, channel) on an overflow path that collect overland flow and direct the runoff around hillslope; end overland flow path; diversions, terraces, and sediment basins are flow interceptors
Form roughness	Represents the hydraulic roughness provided by soil surface roughness, vegetation, and residue; reduces detachment and sediment transport capacity of runoff
Gradient terraces	Terraces on a uniform grade (steepness)
Grain roughness	Represents the hydraulic roughness provided by the soil; responsible for detachment and sediment transport by flow
Ground cover	Represents the portion of the soil surface covered by material in direct contact with soil; includes plant litter, crop residue, rocks, algae, mulch, and other material that reduces both raindrop impact and runoff (surface flow) erosivity
Ground cover subfactor	See cover-management subfactors
Growth chart	The collection of values that describe the temporal vegetation variables of live root biomass in upper 4 inches (100mm), canopy cover, fall height, and live ground cover; values are in a vegetation description
Hortonian overland flow	Overland flow generated by rainfall intensity being greater than infiltration rate; although flow may be concentrated in micro-channels (rills), runoff is uniformly distributed around hillslope
Hydraulic (roughness) resistance	Degree that ground cover, surface roughness, and vegetation slow runoff; varies daily as cover-management conditions change
Hydraulic element	RUSLE2 hydraulic elements are a channel and a small impoundment
Hydraulic element flow path description	Describes the flow path through a sequence of hydraulic elements, named and saved in RUSLE2 hydraulic element component database
Hydraulic element system description	Describes a set of hydraulic element paths that are uniformly spaced along the overland flow path described without the hydraulic element system being present; named and saved in RUSLE2 hydraulic path component database
Hydrologic soil group	Index of runoff potential of a soil profile at a given geographic location, at a particular position on the landscape, and with the presence or absence of subsurface drainage
Impoundment	A flow interceptor; impounds runoff; results in sediment deposition, represents typical impoundment terraces on cropland and small sediment basins on construction sites
Impoundment parallel terrace	Parallel terraces-impoundments (PTO) where terraces cross concentrated flow areas; impoundment drains through a riser into

	underground pipe
Incorporated biomass	Biomass incorporated (buried) in the soil by a *soil disturbing* operation; also biomass added to the soil from decomposition of surface biomass; amount added by decomposition of surface material is function of soil consolidation subfactor
Inherent organic matter	Soil organic matter content in unit-plot condition
Inherent soil erodibility	Soil erodibility determined by inherent soil properties; measured under unit-plot conditions (see soil erodibility)
Initial conditions	Cover-management conditions at the beginning of a no-rotation cover-management description
Initial input roughness	Soil surface roughness index value assigned to *soil disturbing* operation that occurs on the base condition of a silt loam soil with a large amount of biomass on and in the soil; actual initial roughness value used in computations is a function of soil texture, soil biomass, existing roughness at time of soil disturbance, and tillage intensity
Injected biomass	Biomass placed in the soil using an *add other residue/cover* process in a *soil disturbing* operation description (see *operation* processes); biomass is placed in lower half of disturbance depth
Interrill erosion	Erosion caused by water drop impact; not function of distance along overland flow path unless soil, steepness, and cover-management conditions vary; interrill areas are the spaces between rills where very thin flow occurs
Irrigation	Water artificially added to the soil to enhance seed germination and vegetation production
Land use independent	RUSLE2 applies to all situations where Hortonian overland flow occurs and where raindrop impact and surface runoff cause rill and interrill erosion of exposed mineral soil; the same RUSLE2 equations are used to compute erosion regardless of land use
Live aboveground biomass	Live aboveground biomass (dry matter basis); converted to standing residue (dead biomass) by a *kill vegetation* process in an *operation* description.
Live ground (surface) cover	Parts of live aboveground biomass that touches the soil surface to reduce erosion.
Live root biomass	RUSLE2 distributes input values for live root biomass in upper four inches of soil profile over a constant rooting depth of 10 inches for all vegetation types and growth stages. A *kill vegetation* process in an *operation* description converts live root biomass to dead root biomass. Primarily refers to fine roots that are produced annually; RUSLE2 uses live and dead root biomass in the upper 10 inches of soil profile to compute a value for the soil biomass subfactor
Local deposition	Deposition that occurs very near, within a few inches, from the point of detachment in surface roughness depressions and in

	furrows between ridges; given full credit for soil saved
Long term roughness	Soil surface roughness that naturally develops over time; specified as input in cover-*management* description; depends on vegetation characteristics (e.g., bunch versus sod forming grasses, root pattern near soil surface) and local erosion and deposition, especially by wind erosion; RUSLE2 computes roughness over time; develops fully by time to soil consolidation
Long term vegetation	Permanent vegetation like that on pasture, range, reclaimed mined land, and landfills; vegetation description can include temporal values starting on seeding date through maturity, any arbitrary date after seeding date, or only for the vegetation at maturity
Management alignment offset	Used to sequence cover-*management* descriptions along an overland flow path to create alternating strips
Mass-cover relationship	Equation used to compute portion of soil surface covered by a particular residue mass (dry basis)
Mass-yield relationship	Equation used to compute standing biomass (dry basis) of vegetation as a function of production (yield) level
Maximum 30-minute intensity	Average rainfall intensity over the continuous 30 minutes that contains the greatest amount in a rain storm
Non-erodible cover	Cover such as plastic, standing water, snow, and other material that completely eliminates erosion, material can be porous and disappear over time
Non-uniform overland flow path	Soil, steepness, and/or cover-management vary along an overland flow path; path is divided into segments where selections are made for each segment
NRCS curve number method	Mathematical procedure used in RUSLE2 to compute runoff using precipitation amount; a daily runoff value is computed using the 10 yr-24 hr precipitation amount. Daily runoff amount varies as daily curve number varies based on temporally varying cover-management conditions
NWWR	Northwest Wheat and Range Region; a region in the Northwestern US covering eastern Washington and Oregon, northern Idaho; see Req zone
Operation	An operation changes soil, vegetation, or residue; typically represents common farm and construction activities such as plowing, blading, vehicular or animal traffic, and mowing; also represents burning and natural processes like killing frost and germination of volunteer vegetation
Operation disturbance depth	Surface residue buried by a soil disturbing operation is a function of depth of soil disturbed by operation (operation disturbance depth)
Operation description	Information used to describe an operation; named and stored in the operation component of the RUSLE2 database
Operation processes	Processes used to describe an operation; describes how an operation changes cover-managements and soil conditions that affect erosion,

(processes used in RUSLE2 listed below in italics)	net result of an operation depends on sequence of processes used to describe a particular operation
No effect	Has no effect on computations; commonly used to reference dates in a cover-*management* description and to cause RUSLE2 to display information for a particular set of dates
Begin growth	Tells RUSLE2 when to begin using data from a particular *vegetation* description
Kill vegetation	Converts live aboveground biomass to standing residue and to convert live root biomass to dead root biomass
Flatten standing residue	Converts a portion of the standing residue to surface residue
Disturb (soil) surface	Mechanically disturbs soil (removes consolidation effect for portion of soil surface disturbed); required to bury surface residue; resurfaces buried residue; creates soil surface roughness and ridges; required to inject external residue directly into the soil
Add other cover	Adds external residue to the soil surface and/or places it in the soil
Remove live above ground biomass	Removes a portion of the live aboveground biomass, leaves a portion of the affected biomass as standing and surface (flat) residue
Remove residue/cover	Removes a portion of standing and surface (flat) residue
Add nonerodible cover	Adds nonerodible cover such as plastic, standing water, snow, or other material that allows no erosion for portion of soil surface covered; nonerodible cover disappears over time, cover can be porous; nonerodible cover has no residual effect, not used to represent erosion control blankets and similar material.
Remove nonerodible cover	Removes nonerodible cover, nonerodibile cover has no residual effect
Operation speed	Surface residue buried by a *soil disturbing* operation is a function of operation speed.
Overland flow path	Path taken by overland flow on a smooth soil surface from its point of origin to the concentrated flow area that ends the overland flow path; runoff is perpendicular to hillslope contours
Overland flow path description	Described by steepness values, *soil* descriptions, and cover-*management* descriptions for segments along an overland flow path; a uniform profile (overland flow path) is where steepness, soil, and cover-management do not vary with distance along overland flow path, a convex profile is where steepness increases with distance along the overland flow path; a concave profile is where steepness decreases with distance along the overland flow

	path; a complex profile is a combination of convex, concave, and/or uniform sub-profiles; description involves segment lengths and segment steepness; Soil and cover-management can vary along overland flow paths
Overland flow path length	Distance along the overland flow path from the origin of overland flow to the concentrated flow area (channel) that intercepts runoff to terminate overland flow; does not end where deposition begins (see USLE slope length and steepness)
Overland flow path segments	Overland flow path is divided into segments to represent spatial variability along an overland flow path; conditions are considered uniform within each segment
Overland flow path steepness	Steepness along the overland flow path; not hillslope steepness (see USLE slope steepness)
Permeability index	Index for the runoff potential of the unit-plot soil condition; used in RUSLE2's soil erodibility nomographs; inversely related to hydrologic soil group
Plan description	Collection of RUSLE2 *profile* (overland flow path) descriptions; used to computed weighted averages for a complex area based on the portion of the area that each profile represents; description named and saved in plan component of RUSLE2 database
Ponding subfactor	See cover-management subfactors
Porous barriers	Runoff flows through a porous barrier; does not affect overland flow path length; typically slows runoff to cause deposition; examples are stiff grass hedges, grass filter strips, fabric (silt) fences, gravel dams, and straw bales
Precipitation amount	Includes all forms of precipitation; RUSLE2 disaggregates input monthly values into daily values to compute residue decomposition and temporal soil erodibility
Production (yield) level	A measure of average annual vegetation live aboveground biomass production; user defines yield measure and preferred units on any moisture content basis; input value used to adjust values in a *vegetation* description at a base yield; maximum canopy cover in *base vegetation* description must be less than 100 percent
Profile (overland flow path) description	Information used to describe profile (overland flow path); includes names for location, topography, soil, cover-management, and support practices used to make a particular RUSLE2 computation; *profile* descriptions are named and stored in the profile component of the RUSLE2 database
Profile shape	See overland flow path description
Rainfall (storm) energy	Computed as sum of products of unit energy and rainfall amount in storm intervals where rainfall intensity is assumed uniform; storm energy is closely related to rain storm amount
Rainfall intensity	Rainfall rate express as depth (volume of rainfall/per unit area) per unit time

Relative row grade	Ratio of row grade to average steepness of overland flow path
Remote deposition	Deposition that occurs a significant distance (tens of feet) from the point where the sediment was detached; examples include deposition by dense vegetation strips, terraces, impoundments, and toe of concave overland flow paths; only partial credit is given to remote deposition as soil saved; credit depends on location of deposition along overland flow path; very little credit is given for deposition near end of overland flow path
Req	Equivalent erosivity for the winter months in the Req zone, used to partially represent Req effect
Req effect	Refers to Req equivalent erosivity; erosion per unit rainfall erosivity in the winter period in the Req zone is much greater than in summer period; increased Req winter effect is mainly because of a greatly increased soil erodibility; effect partially results from an elevated soil water content, increased runoff, and soil thawing
Req zone	Region where erosion is elevated in the winter months because of the Req effect, region is primarily in eastern WA and OR, portions of ID, CA, UT, CO, and limited area in other western US states
Residue	Has multiple meanings in RUSLE2; generally refers to dead biomass, such as crop residue, created when vegetation is killed; plant litter from senescence; and applied mulch material such as straw, wood fiber, rock, and erosion control blankets used on construction sites; material is assumed to be biomass that decomposes; also used to represent material like rock that does not decompose by setting a very low decomposition coefficient value
Residue description	Values used to describe residue; named and stored in the residue component of the RUSLE2 database
Residue type	Refers to fragility and geometric residue characteristics; affects residue amount buried and resurfaced by of an operation; affects degree that residue conforms to surface roughness; affects erosion control on very steep slopes
Resurfacing ratio	Portion (dry mass basin) of the buried residue in the soil disturbance depth that a *soil disturbing* operation brings to the soil surface; function of residue and operation's *soil disturbing* properties
Retardance	Degree that vegetation (live aboveground biomass) and standing residue slows runoff; varies with canopy cover; function of production (yield) level; part of vegetation description
Ridge height	Height of ridges created by a *soil disturbing* operation; major variable, along with row grade, that determines contouring effectiveness; decays as a function of precipitation amount and interrill erosion
Ridge subfactor	See cover-management subfactors
Rill erosion	Caused by overland flow runoff; increases with distance along the

	overland flow path
Rill to interrill erosion ratio	Function of slope steepness, rill to interrill soil erodibility, and how cover-management conditions affect rill erosion different from interrill erosion
Rock cover entered in *soil* description	Rock cover entered in the soil description; represents naturally occurring rock on soil surface; operations do not affect this rock cover, rock cover created by an operation that *adds other cover* (rock residue) is treated as external residue; *soil disturbing* operations bury and resurface rock added as external residue
Root biomass	See dead and live root biomass
Root sloughing	Annual decrease in root biomass; RUSLE2 adds the decrease in live root biomass to dead residue biomass pool
Rotation	Refers to whether a list of *operation* descriptions in a cover-*management* description is repeated in a cycle; length of cycle is rotation duration; list of *operation* descriptions are repeated until average annual erosion value stabilizes; eliminates need to specify initial conditions for rotations; operation descriptions in a no-rotation cover-management descriptions are sequentially processed a single time; first operation descriptions in cover-*management* description establish initial conditions in a no-rotation cover-*management* description
Rotation duration	Time (cycle duration) before the list of operation descriptions in a rotation type cover-*management* description repeats; rotation duration is time period over which RUSLE2 makes its computations in a no-rotation cover-*management* description
Rotational strip cropping	A rotation type cover-*management* description that involves periods of dense vegetation that are sequenced along the overland flow path to create strips of alternating dense vegetation that cause deposition
Row grade	Grade along furrows separated by ridges; usually expressed as relative row grade
Runoff	Computed using NRCS curve number method and the 10 yr-24 hour precipitation amount; used to compute contouring effect, contouring failure (critical slope length), and deposition by porous barriers, flow interceptors, and concave overland flow paths
Sediment basin	Small impoundment typical of those used on cropland and construction sites; discharge is usually through a perforated riser that completely drains basin in about 24 hours
Sediment characteristics	Deposition computed as a function of sediment characteristics, which are particle class diameter and density and the distribution of sediment among particle classes
Sediment particle classes	RUSLE2 uses sediment particle classes of primary clay, silt, and sand and small and large aggregate; diameter of aggregate classes and the distribution of sediment among particle classes at point of detachment are computed as function of soil texture; RUSLE2

	computes how deposition changes the distribution of sediment particle classes
Sediment load	Mass of sediment transported by runoff per unit hillslope width
Sediment transport capacity	Runoff's capacity for transporting sediment, depends on runoff rate, overland flow path steepness, and hydraulic roughness; deposition occurs when sediment load is greater than transport capacity
Sediment yield	Sediment load at the end of the flow path represented in a RUSLE2 computation; flow path ends at overland flow path unless hydraulic elements (channel or impoundment) are represented in RUSLE2 computation; sediment yield for site only if RUSLE2 flow path ends at site boundary
Segments	The overland flow path divided into segments to represent spatial variation of steepness, soil, and cover-management
Senescence	Decrease in vegetation canopy cover; senescence adds biomass to surface (flat) residue unless RUSLE2 is instructed that a decrease in canopy cover, such as leaves drooping, does not add to surface residue
Shear stress applied by overland flow	Function of runoff rate and steepness of overland flow path; total runoff shear stress is divided into two parts of shear stress acting on the soil (grain roughness) and shear stress acting on surface residue, surface roughness, live vegetation, and standing residue (form roughness); shear stress acting on the soil is used to compute sediment transport capacity, total shear stress is used to compute contouring failure
Short term roughness	Roughness created by a soil disturbing operation; decays over time as a function of precipitation amount and interrill erosion
Slope length exponent	Exponent in equation used to compute rill-interrill erosion as a function of distance along overland flow path; function of rill to interrill erosion ratio.
Soil biomass subfactor	See cover-management subfactors
Soil consolidation effect	Represents how wetting/drying and other processes cause soil erodibility to decrease over time following a mechanical soil disturbance; increase in soil bulk density (mechanical compaction) not the major cause; affects accumulation of biomass in upper 2 inch (50 mm) soil layer and effect of soil biomass on runoff and erosion
Soil consolidation subfactor	See cover-management subfactors
Soil description	Describes inherent soil properties that affect erosion, runoff, and sediment characteristics at point of detachment; named and saved in soil component of RUSLE2 database
Soil disturbance width	Portion of the soil surface disturbed; weighted effects of disturbance computed as a function of erosion on disturbed and

	undisturbed area used to compute effective values for time since last disturbance, effective surface roughness, and effective ground cover
Soil disturbing operation	*Operation* description that contains *disturb soil* process
Soil erodibility	RUSLE2 considers two soil erodibility effects, one based on inherent soil properties and one based on cover-management; inherent soil erodibility effect represented by K factor value empirically determined from erosion on unit plot; part related to cover-management is represented in cover-management subfactors
Soil erodibility nomograph	Mathematical procedure used to compute a K factor value, i.e., inherent soil erodibility
Soil loss	Proper definition is the sediment yield from a uniform overland flow path divided by the overland flow path length; loosely used as the net removal of sediment from an overland flow path segment
Soil loss from eroding portion	Net removal of sediment from the eroding portion of the overland flow path
Soil loss tolerance (T)	Erosion control criteria; conservation planning objective is that "soil loss" be less than soil loss tolerance T value; special considerations must be given to non-uniform overland flow paths to avoid significantly flawed conservation and erosion control plans
Soil mechanical disturbance	Mechanical soil disturbance resets soil consolidation effects; *disturb soil* process must be included in an operation description to create surface roughness and ridges and to place biomass into the soil
Soil saved	Portion of deposited sediment that is credited as soil saved; computed erosion is reduced by soil saved to determine a conservation planning soil loss value; credit depends on location of deposition along overland flow path
Soil structure	Refers to the arrangement of soil particles in soil mass; used to compute soil erodibility (K) factor values
Soil texture	Refers to the distribution of primary particles of sand, silt, and clay in soil mass subject to erosion
Standing residue	Created when live vegetation is killed; decomposes at a reduced rate; falls over at a rate proportional to decomposition of surface residue
Strip/barrier description	Support practice; describes porous barriers; named and stored in the strip/barrier component of the RUSLE2 database
Subfactor method	See cover-management subfactors
Subsurface drainage description	Support practice that lowers water table to reduce soil water content, runoff, and erosion; RUSLE2 uses difference between hydrologic soil groups for drained and undrained conditions to compute erosion as affected by subsurface drainage
Support practices	Erosion control practice used in addition to cultural erosion control

	practices, hence a support practice; includes contouring, filter and buffer strips, rotational strip cropping, silt (fabric) fences, stiff grass hedges, diversions/terraces, gravel dams, and sediment basins
Surface (flat) residue	Material in direct contact with the soil surface, main source is plant litter, crop residue, and applied mulch (external residue).
Surface roughness	Random roughness; combination of soil peaks and depressions that pond runoff; created by a *soil disturbing* operation, decays as a function of precipitation amount and interrill erosion
Surface roughness index	A measure of soil surface roughness; standard deviation of surface elevations measured on a 1 inch grid about mean elevation; effect of ridges and land steepness removed from measurements
Surface roughness subfactor	See cover-management subfactors
Temperature	Input as average monthly temperature; disaggregated into daily values; used to compute biomass decomposition and temporal soil erodibility
Template	Determines the computer screen configuration of RUSLE2 and inputs and outputs; determines the complexity of field situations that can be described with RUSLE2
Terraces	Flow interceptors (channels) on a sufficiently flat grade to cause significant deposition
Three layer profile schematic	Some RUSLE2 templates include a overland flow path schematic having individual layers to represent cover-management, soil, and topography; used to graphically divide the overland flow path into segments to represent complex conditions
Tillage intensity	Degree that existing soil surface roughness affects roughness left by a *soil disturbing* operation
Tillage type	Identifies the relative position within soil profile where a soil disturbing operation initially places buried residue, also relates to how operation redistributes buried residue and dead roots
Time to soil consolidation	Time required for 95 percent of the soil consolidation effect to be regained after a soil disturbing operation
Topography	Refers to steepness along the overland flow path and the length of the overland flow path
Uniform slope	Refers to an overland flow path where soil, steepness, and cover-management do not vary along the overland flow path
Unit rainfall energy	Energy content of rainfall per unit of rainfall; function of rainfall intensity
Unit plot	Base condition used to determine soil erodibility; reference for effects of overland flow path steepness and length; cover-management, and support practices; continuous tilled fallow (no vegetation; tilled up and downhill, maintained in seedbed conditions; topographic, cover-management, support practice factor values equal 1 for unit plot condition; land use independent, i.e.,

	applies to all land uses including undisturbed land such as pasture, range, and forest lands
USLE slope length and steepness	Distance from origin of overland flow to a concentrated flow area (e.g., terrace or natural waterway) or to the location where deposition occurs; USLE soil loss is sediment yield from this length divided by length (mass/area); USLE steepness is steepness of the slope length; uniform actual overland flow path is often represented with uniform steepness
Validation	Process of ensuring that RUSLE2 serves its intended purpose as a guide to conservation and erosion control planning.
Vegetation description	Information used by RUSLE2 to represent the effect of vegetation on erosion; includes temporal values in growth chart, retardance, and biomass-yield information; named and stored in vegetation component of RUSLE2 database
Verification	Process of ensuring RUSLE2 correctly solves the mathematical procedures in RUSLE2
Worksheet description	Form in RUSLE2 program; used to compare conservation and erosion control practices for a given site; used to compare *profile* descriptions; named and saved in the worksheet component of the RUSLE2 database

1. WELCOME TO RUSLE2

Version 2 of the Revised Universal Soil Loss Equation (**RUSLE2**) estimates soil loss, sediment yield, and sediment characteristics from rill and interrill (sheet and rill) erosion caused by rainfall and its associated overland flow. **RUSLE2** uses factors that represent the effects of climate (erosivity, precipitation, and temperature), soil erodibility, topography, cover-management, and support practices to compute erosion. RUSLE2 is a mathematical model that uses a system of equations implemented in a computer program to estimate erosion rates. The other major component of RUSLE2 is a database containing an extensive array of values that are used by the RUSLE2 user to describe a site-specific condition so RUSLE2 can compute erosion values that directly reflect conditions at a particular site.

RUSLE2 is used to evaluate potential erosion rates at specific sites, guide conservation and erosion control planning, inventory erosion rates over large geographic areas, and estimate sediment production on upland areas that might become sediment yield in watersheds. **RUSLE2 is land use independent. It can be used on cropland, pastureland, rangeland, disturbed forestland, construction sites, mined land, reclaimed land, landfills, military lands, and other areas where mineral soil is exposed to raindrop impact and surface overland flow produced by rainfall intensity exceeding infiltration rate (i.e., Hortonian overland flow)**.

The RUSLE2 computer program, a sample database, user instructions, a slide set that provides an overview of RUSLE2, and other supporting information are available for download from the USDA-Agricultural Research Service (ARS) Official RUSLE2 Internet Site at http://www.ars.usda.gov/Research/docs.htm?docid=6010. The University of Tennessee also maintains a RUSLE2 Internet site where older versions of the RUSLE2 can be downloaded and where additional RUSLE2 information is available. The address is www.rusle2.org. The USDA-Natural Resources Conservation Service (NRCS) also provides and distributes information on RUSLE2 including databases and other materials that it uses to apply RUSLE2 in each of its county level offices across the US. Contact the NRCS Internet site at http://fargo.nserl.purdue.edu/rusle2_dataweb/RUSLE2_Index.htm or contact the NRCS state agronomist in your state to obtain NRCS information on RUSLE2. The NRCS Internet site contains an extensive RUSLE2 database that must be used in NRCS-related applications involving RUSLE2. Information in this database can also be downloaded for other RUSLE2 applications as well. Other organizations that use RUSLE2 may also have RUSLE2 Internet sites that contain databases for their specific RUSLE2 applications.

2. WHY UPGRADE FROM RUSLE1 TO RUSLE2?

RUSLE2 is a second generation of RUSLE1, but it is not simply an enhancement of RUSLE1. **RUSLE2** is a new model with new features and capabilities. If you are using any version of RUSLE1, you should upgrade to **RUSLE2. RUSLE2** uses a modern, powerful graphical user interface instead of the text-based interface of RUSLE1. ***RUSLE2*** *can be used in either US customary units or SI units.* **RUSLE2** can globally switch between the two systems of units or the units on individual variables can be changed to one of several units. Those who work with metric units will find **RUSLE2** much easier to use than RUSLE1. **RUSLE2** can also manipulate attributes of variables, which includes graphing, changing units, and setting number of significant digits. **RUSLE2** is much more powerful than RUSLE1, has improved computational procedures, and provides much more output useful for conservation planning than does RUSLE1.

Even though **RUSLE2** appears quite different on the computer screen from RUSLE1, it has many similarities with RUSLE1. The general approach is the same and many of the values in the database are the same for **RUSLE2** and RUSLE1. Thus, conversion from RUSLE1 to **RUSLE2** should be relatively easy.

3. ABOUT RUSLE2 USER'S GUIDES AND DATABASES

3.1. RUSLE2 User Instructions

RUSLE2 is a straight forward, easily used computer program that is best learned by using it. A set of user instructions is available on the **USDA-Agricultural Research Service (ARS)** RUSLE2 Internet site http://www.ars.usda.gov/Research/docs.htm?docid=6010 to help you get started with RUSLE2. A self-guided tutorial is available on the **University of Tennessee** http://bioengr.ag.utk.edu/rusle2/tutorial.htm to help you learn the mechanics and operation of the **RUSLE2** computer program. The **USDA-Natural Resources Conservation Service (NRCS)** Internet site http://fargo.nserl.purdue.edu/rusle2_dataweb/RUSLE2_Index.htm provides instructional material and database information that helpful for any RUSLE2 user, but is required for NRCS-related **RUSLE2** applications. Also, other organizations provide training and instructional materials targeted to a specific land use such as construction sites that you can also use to learn RUSLE2.

3.2. RUSLE2 Database

The **RUSLE2** download on the USDA-ARS RUSLE2 Internet site includes a sample database. This sample database should only be used to help you become acquainted with **RUSLE2** and how it works. This database is not intended for use in actual **RUSLE2** applications. You can obtain that database information by downloading from the USDA-Natural Resources Conservation Service (NRCS) national **RUSLE2** database or from another database having values that have been properly established for your purpose. You can download information from the NRCS national **RUSLE2** database by contacting the Internet site http://fargo.nserl.purdue.edu/rusle2_dataweb/RUSLE2_Index.htm. Additional information can be obtained by contacting the State Agronomist in each NRCS State Office.

Values in your **RUSLE2** operational database must be based on the **RUSLE2 core database** (see **Section 16**). Values in your operational database must be consistent with those in the core database to ensure that **RUSLE2** give expected results and to ensure consistency in **RUSLE2** applications among clients, locations, and other situations where similar erosion estimates are expected. This consistency is very important when **RUSLE2** is used by a national agency where adequacy of the erosion prediction technology is partly judged on consistency of estimates. The NRCS national **RUSLE2** database has been extensively reviewed to ensure consistency, minimal error, and expected erosion values computed with **RUSLE2**. Make sure that the same quality control has been used in the preparation of other **RUSLE2** databases that you might use for the source of data in your **RUSLE2** operational database.

Some values in the RUSLE1 database can be used in **RUSLE2** and directly transferred to the **RUSLE2** database using procedures included in **RUSLE2.** However, the best approach is download values from a quality-controlled **RUSLE2** database, such as the NRCS national **RUSLE2** database, rather than transfer values from a RUSLE1 database. Values for several input variables are different in **RUSLE2** from those in RUSLE1. Also, new input variables have been added to **RUSLE2** that are not in RUSLE1. Furthermore, core values, including those for rainfall erosivity, in the **RUSLE2** database have updated based on new analysis.

3.3. RUSLE2 HELP

The **RUSLE2** computer program contains an extensive set of **HELP** information. Most of the **HELP** information is arranged by variable within **RUSLE2**. Information on a particular variable can be obtained at the location within **RUSLE2** where the variable occurs.

3.4. RUSLE2 Slide Set

A **slide set** is available with the **RUSLE2** download at the ARS RUSLE2 Internet site. This **slide set** provides an extensive overview of **RUSLE2**. The speaker notes that accompany many of the slides provide additional background. Also, slides can be used for **RUSLE2** training and for making presentations on **RUSLE2**.

3.5. RUSLE2 User Reference Guide

This **User's Reference Guide** describes **RUSLE2**, its factors, selection of input values, and application of **RUSLE2**. The **Table of Contents** lists the topics covered by the **User's Guide.** Rather than reading the entire **User's Guide**, specific topics can be selected from the **Table of Contents** and individually reviewed. Also, the **Glossary of Terms** provides information on specific topics.

This **User's Reference Guide** is intended to serve as a **reference** for RUSLE2 technical specialists rather than a guide for the routine RUSLE2 user. User guides and manuals for these users should be developed for specific applications based on information in this **Guide**.

3.6. Getting Started

Like all other hydrologic models, **RUSLE2** requires a proper approach for selecting input values, running the model, and interpreting its output values. **RUSLE2** has particular limitations that must be considered. Before applying **RUSLE2,** you should become well acquainted with **RUSLE2** and its factors by reviewing the **RUSLE2 Slide Set**. After installing **RUSLE2**, run the sample database that can be downloaded with **RUSLE2** that

includes several example overland flow path profiles. Change selected variables including location, soil, overland flow path length and steepness, and cover-management and support practices in these examples to help learn the mechanics of the **RUSLE2** computer program and to help learn how main inputs affect computed erosion and other output variables. Start out with the uniform slope templates rather than the complex slope templates.

3.7. Scientific and Technical Documentation

The **RUSLE2** Scientific Documentation describes the equations and mathematical procedures used in RUSLE2. It is available from the USDA-Agricultural Research Service http://www.ars.usda.gov/SP2UserFiles/Place/64080530/RUSLE/RUSLE2_Science_Doc.pdf.

4. CUSTOMER SUPPORT

If needed information is not available in **RUSLE2** documentation, contact one of the **RUSLE2** experts. The USDA-Agricultural Research Service (ARS) is the lead research agency, in cooperation with the University of Tennessee, that developed **RUSLE2**. The USDA-Natural Resources Conservation Service (NRCS), the major user of **RUSLE2,** has much experience in RUSLE2 applications and developed extensive database information for many different types of applications of **RUSLE2** across the US and other locations. Contact your NRCS State Agronomist to obtain additional databases, information, and direct assistance on **RUSLE2** applications.

RUSLE2 Contacts

Topic: Science and new applications

Seth M. Dabney, Research Agronomist
USDA-Agricultural Research Service
National Sedimentation Laboratory
P.O. Box 1157
Oxford, Mississippi, 38655, USA
Telephone: 662-232-2975
Email: seth.dabney@ars.usda.gov

Topic: Computer program, interface, and linking to RUSLE by other programs

Daniel C Yoder, Professor
Department of Biosystems and Environmental Science
P.O. Box 1071
Knoxville, TN, 37901, USA
Telephone: 865-974-7116
Email: dyoder@utk.edu

Topic: NRCS databases and applications

Dave Lightle, Conservation Agronomist
USDA-Natural Resources Conservation Service
National Soil Survey Center
100 Centennial Mall North, Room 152
Lincoln, NE 68508-3866, USA
Telephone: 402-437-4008
Email: dave.lightle@lin.usda.gov

5. ABOUT RUSLE2

5.1. Fundamental Definitions

RUSLE2 uses several important terms to describe erosion (see **Glossary of Terms**). In the mid-1940's, W. D. Ellison defined erosion as, "... a process of detachment and transport of soil particles."[1] **Detachment** is the separation of soil particles from the soil mass and is expressed in units of mass/area. Soil particles separated from the soil mass are referred to as **sediment**. Sediment movement downslope is sediment transport, described as **sediment load** expressed in units of mass/width of slope. The sediment load at the end of the **RUSLE2** hillslope profile is defined as sediment yield or sediment delivery. **Deposition**, expressed as mass/area, is the accumulation of sediment on the soil surface.

Detachment transfers sediment from the soil mass to the sediment load so that sediment load increases along the hillslope where detachment occurs. Conversely, deposition transfers sediment from the sediment load to the soil mass with a corresponding accumulation of sediment on the soil surface. Deposition is a selective process that **sorts** sediment. This process **enriches** the sediment load in fines in comparison to the soil where detachment originally produced the sediment.

RUSLE2 considers two types of deposition, local and remote. **Local deposition** is sediment deposited very near, within a few inches of where it was detached. Deposition in micro-depressions (**surface roughness**) and in low gradient furrows is an example of local deposition. The difference between local detachment and local deposition is called **net detachment** (or **net deposition**). **Remote deposition** is sediment deposited some distance, 10's of feet (several meters) from the origin of the sediment. Deposition on the toe of a concave slope, at the upper side of vegetative strips, and in terrace channels is an example of remote deposition. **Full credit for soil saved** is taken in **RUSLE2** for local deposition. Only **partial credit** that depends on the location of the deposition is given to remote deposition for soil saved. Sediment deposited at the end of an overland flow path is given very little credit as soil saved.

5.2. Hillslope Overland Flow Path (Hillslope Profile) as the Base Computational Unit in RUSLE2

The base **RUSLE2** computational unit is a single overland flow path along a hillslope profile as illustrated in Figure 5.1. An **overland flow path** is defined as the path that runoff flows from the origin of overland flow to where it enters a major flow concentration. **Major flow concentrations** are locations on the landscape where sides of a hillslope intersect to collect overland flow in defined channels. **Ephemeral or**

[1] Ellison, W.D. 1947. Soil erosion studies. Agricultural Engineering. 28:145-146.

classical gully erosion occurs in these channels. These defined channels are distinguished from **rills** in two ways. Rills tend to be parallel and are sufficiently shallow that they can be obliterated by typical farm tillage and grading operations as a part of construction activities. When the rills are reformed, they occur in new locations determined by **microtopograpy** left by soil disturbing operations like tillage. In contrast, concentrated flow areas occur in the same locations, even after these channels are filled by tillage. Location of these channels is determined by **macrotopography** of the landscape.

An infinite number of overland flow paths exist on any landscape. A particular overland flow path (**hillslope profile**), such as the one labeled **A** in Figure 5.1, is chosen for the one on which the conservation plan is to be based. The overland flow path (profile) that represents the 1/4 to 1/3 most erodible part of the area is often the profile selected for

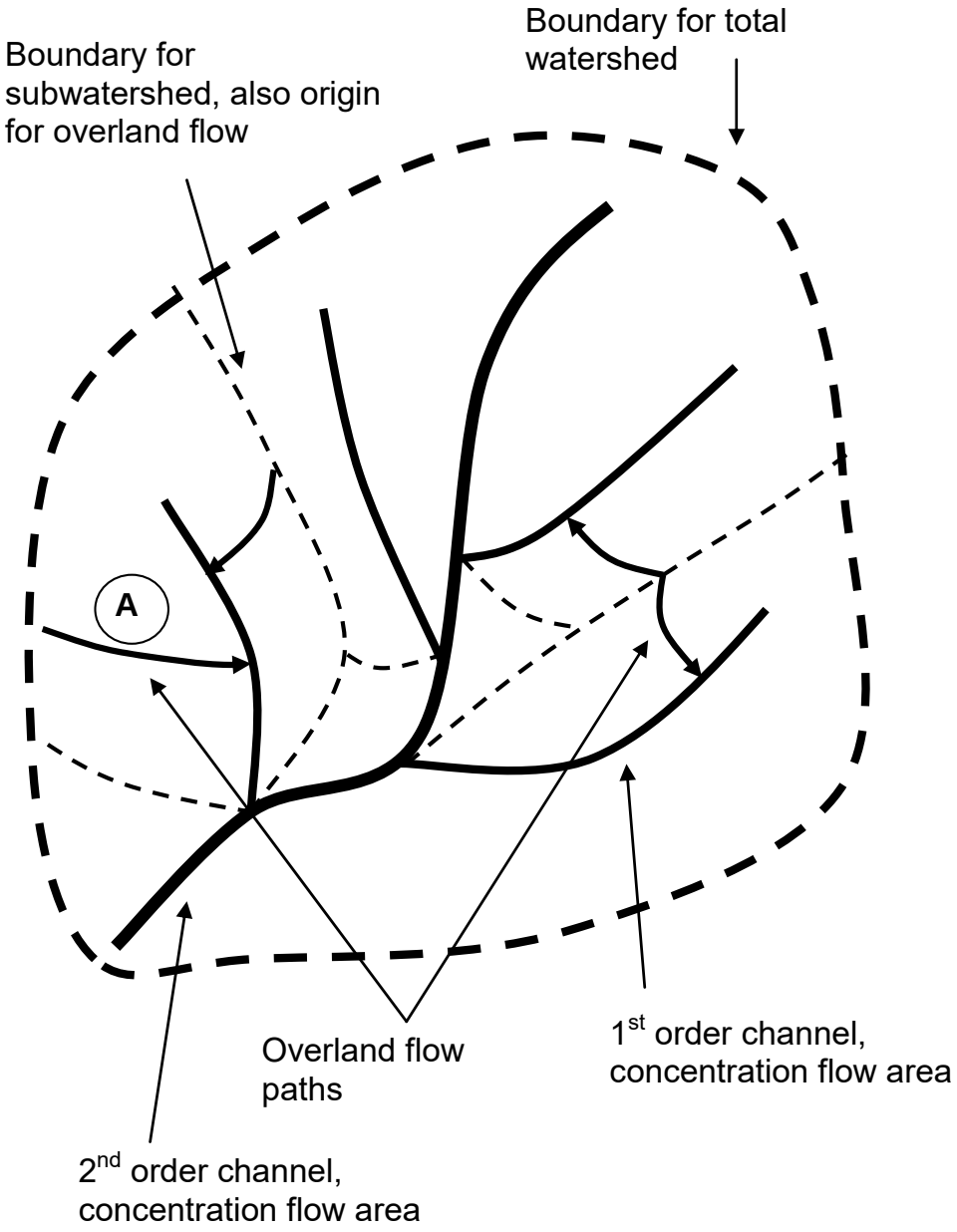

Figure. 5.1. Overland flow paths in a typical application of RUSLE2

applying RUSLE2 when the **conservation planning** objective is to protect the soil resource from degradation by excessive erosion. **RUSLE2** is used to estimate erosion for this profile for each of several alternative land use practices that might be used at the site. Those practices that give a RUSLE2 estimated soil loss that meets the **conservation planning** criteria are considered to provide acceptable erosion control. Organizations such as the NRCS have specific guidelines on how **RUSLE2** is to be used in their programs.

The first step in describing the selected profile is to identify a base point on the hillslope through which the overland flow path is passes. The overland flow path through that point, such as profile **A** in Figure 5.1, is described by dividing the slope into segments and specifying distance and steepness for each segment. The overland path is traced from the origin of overland flow through the base point to where the overland flow is terminated by a concentrated flow channel as illustrated in Figure 5.1.

Figure 5.2 shows the shape of a typical overland flow path on a common natural landscape. This **complex** hillslope profile has an upper **convex** section and a **concave** lower section. This profile has two important parts. The upper part is the **eroding portion** where **net erosion** occurs, and the lower part is the **depositional portion** where **net deposition** occurs. The average erosion rate on the eroding portion of the hillslope is defined as **soil loss** (mass/area). Soil loss on the eroding portion of the landscape degrades the soil on that portion of the landscape and the landscape itself. A typical conservation planning objective is to reduce soil loss to a rate less than **soil loss tolerance (T)** or another quantitative planning criterion. Keeping soil loss to less than T protects the soil so that its productive capacity is maintained and the landscape as a whole is protected from excessive erosion.

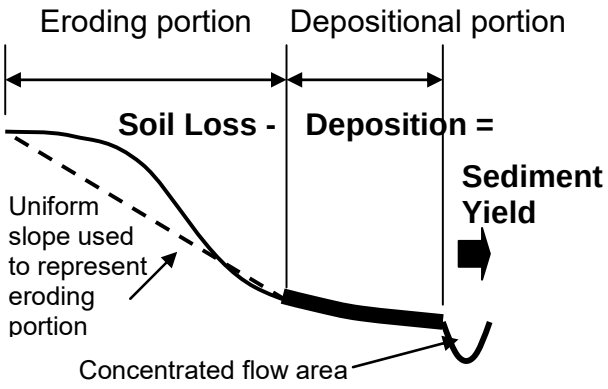

Figure 5.2. Complex hillslope, convex-concave profile

Sediment yield from the hillslope profile and the site is also an important conservation planning consideration. Excessive sediment leaving a site can cause downstream sedimentation and water quality problems. Sediment yield is less than soil loss by the amount of deposition. The sediment yield computed by **RUSLE2** is

the sediment leaving the overland flow path represented in **RUSLE2**. This sediment yield will be the sediment yield for the site only if the **RUSLE2** flow path ends at the boundary of the site.

Many conservation-planning applications involve only the eroding portion of the hillslope, which can be approximated by a **uniform slope** as illustrated in Figure 5.2. The **slope length (overland flow path length)** in this application is the distance from the origin of overland flow to where deposition begins, which is the traditional definition of **slope length** in the USLE and RUSLE1. However, soil loss estimated using a uniform slope of the same average steepness and slope length as a non-uniform shaped profile will differ from the average erosion rate for the non-uniform profile, sometimes by as much as 15%. The difference is especially important on convex shaped hillslopes where the erosion rate near the end of the overland flow path can be much larger than the erosion rate at the end of a uniform profile. Deposition like that in Figure 5.2 for concave hillslope sections does not occur on the **uniform** and **convex** shaped hillslopes illustrated in Figure 5.3. Sediment yield equals soil loss on those profiles.

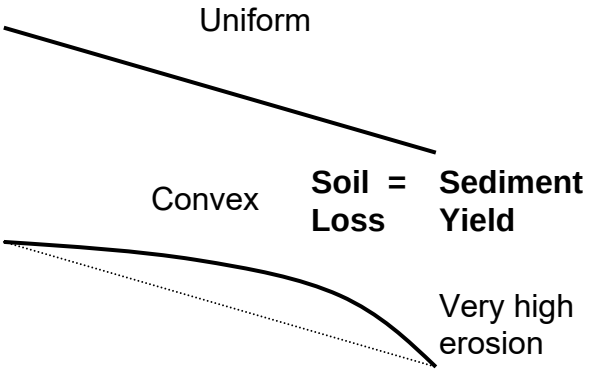

Figure 5.3. Sediment yield equals soil loss on uniform and convex slopes

Another important **complex** hillslope shape is shown in Figure 5.4 where a **concave** section occurs in the middle of the hillslope. A field example is a cut slope-road-fill slope that is common in hilly terrain being logged. **Deposition** can occur on the mid-section of the hillslope where the roadway is located if steepness of the roadway is sufficiently flat. Soil loss occurs on the cut slope and downslope on the fill slope in situations where overland flow from the cut slope continues across the roadway onto the fill slope. Although the steepness and length of the fill slope is the same as that for the upper cut slope, erosion rate is much greater on the fill slope than on the cut slope because of increased overland flow. Although the USLE and RUSLE1 cannot easily describe this hillslope, **RUSLE2** easily determines appropriate **overland flow path lengths**, and computes **erosion** on the two **eroding portions** of the overland flow path, **deposition** on the **depositional portion** of the overland flow path, and **sediment yield** from the overland flow path. Note that the **overland flow path** used in RUSLE2 does not end where deposition begins for this overland flow path.

In addition to computing how slope shape affects erosion, RUSLE2 can also compute how variations in soil and management along a hillslope profile affect erosion.

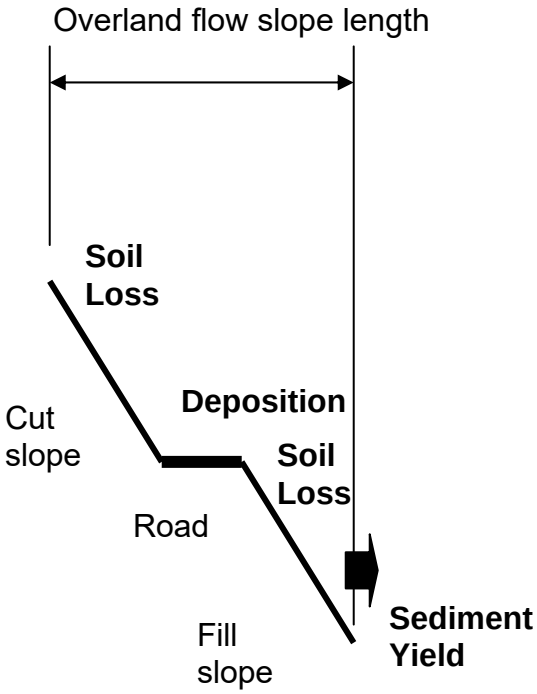

Figure 5.4. Soil loss, deposition, and sediment yield from a complex slope, concave-convex shape.

5.3. Does RUSLE2 Not Apply to Certain Conditions?

5.3.1. Rill erosion or concentrated flow erosion?

RUSLE2 does not apply to concentrated flow areas where ephemeral gully erosion occurs. **Whether or not RUSLE2 applies to particular eroded channels is not determined by size or depth of the channels.** The determination depends on whether the channels in the field situation would be included if RUSLE2 plots were to be placed on that landscape. The core part of **RUSLE2** that computes **net detachment** (**sediment production**) is empirically derived from data collected from plots like those illustrated in Figures 5.5 and 5.6. The length of these plots typically was about 75 ft (25 m) and width ranged from 6 ft (2 m) to about 40 ft (13 m) wide with plots as wide as 150 ft (50 m) at one location. These plots were always placed on the sides of the hillslope where overland flow occurred, not in the swales where concentrated flow occurs. Thus, RUSLE2 can estimate soil loss for rills 15 inches (375 mm) deep on sides of hillslopes because these rill would be in plots placed on this part of the landscape but not erosion from a 4 inch (100 mm) deep ephemeral gully or 10 ft (3 m) deep classical gully in a concentrated flow area because plots were not be placed in these locations.

5.3.2. Can RUSLE2 be Used to Estimate Sediment Yield from Large Watersheds?

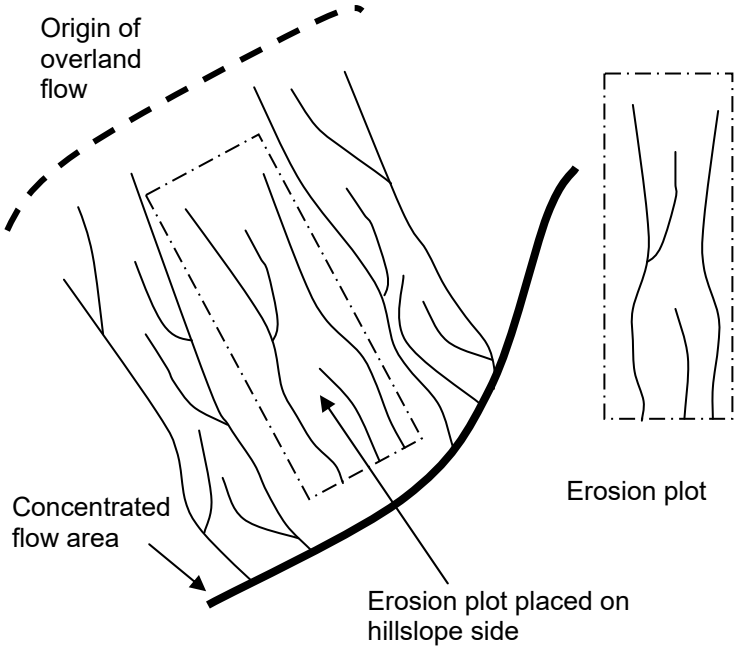

Figure 5.5. Relation of erosion plots to landscape

Sediment yield from most large watersheds is often less than sediment production within the watershed. Thus, much sediment is deposited within a typical watershed. **RUSLE2**, in contrast to the USLE and RUSLE1, can estimate the deposition that occurs on the overland flow portion of the landscape. This deposition, up to 75 percent of the sediment produced on the eroding portion of the hillslope, can be substantial on many hillslopes. **If RUSLE2 is used to estimate sediment yield in watersheds, it should be applied only to the eroding portion of the landscape to compute a soil loss comparable to that computed by the USLE. Otherwise, a different set of sediment delivery ratio values from those used by the USLE would have to be used with RUSLE2 to take into account deposition on overland flow areas.**

Figure 5.6. Erosion plots 12 ft wide (3.65 m) and 72.6 ft (22.1 m) long near Columbia, MO.

In addition to the sediment produced by interrill and rill erosion on upland areas (estimated by **RUSLE2)**, erosion in concentrated flow areas (ephemeral gullies), classical gullies, stream channels, and mass movement of material into channels are other major sources of sediment that

contribute to sediment yield, which are not estimated by **RUSLE2**.

5.3.3. Estimating Soil Loss with RUSLE2 for Large Areas

RUSLE2 can be used to estimate soil loss for large areas. The approach is to select sample points over the inventory area where RUSLE2 will be applied to compute soil loss. These sample points should be selected according to the requirements of the inventory, giving special attention to required accuracy and how soil loss estimates will be aggregated according to soil, topography, land use, and conservation practice. RUSLE2 can be applied in several ways. One way is to estimate a "point" soil loss at the sample point. A slope length[2] to the point and values for steepness, soil, and cover and management at each sample point are determined. A slope segment 1 ft (0.3 m) long at the end of the slope length along with the other RUSLE2 input values for the segment are used in RUSLE2 to compute soil loss at the point.

Another approach is to determine a slope length through the point that extends to the location that deposition begins or to a concentrated flow area if deposition does not occur. Values for conditions along the slope length are used in RUSLE2 to compute a soil loss for the slope length. A limitation of this approach is that soil loss values cannot be aggregated based on conditions that vary along a slope length, such as multiple soil types.
A third approach, which was used by USDA-NRCS for the National Resources Inventory (NRI), uses the slope length through the point to either deposition or a concentrated flow area and conditions at the point to compute soil loss. This approach does not provide an estimate of soil loss at the point. Soil loss values cannot be aggregated for variables that are related to position on the slope. For example, the same soil loss is computed at the top of slope as at the bottom of slopes when slope steepness is the same for both locations.[3] A major advantage of computing soil loss for the entire slope length is that the number of sample points needed to obtain an accurate estimate of average soil loss for the area is significantly reduced. However, this procedure can not be used where the main variables, such soil erodibility or steepness, depend on landscape position.

An approach that absolutely should not be used is to determine spatially averaged values for slope length and steepness, soil, and cover-management conditions for the inventory area and use these values in RUSLE2 to compute a single soil loss value for the area. Soil loss estimates by this method are inaccurate because of nonlinearities in the RUSLE2 equations. No simple, universally applicable method can be developed to select the proper input values for this method. The issue is directly related to the proper

---

2 Slope length refers to the traditional USLE definition of slope length, which applies to the eroding portion of the RUSLE2 overland flow path length.

3 For discussion of the mathematics related to this approach, see Foster, G.R. 1985. Understanding ephemeral gully erosion (concentrated flow erosion). In: Soil Conservation, Assessing the National Resources Inventory. National Academy Press. Washington, D.C. pp. 90-125.

mathematical procedures for spatial integration, which is exactly the reason why RUSLE2 is much superior mathematically to the USLE or RUSLE1 as discussed below.

5.4. Equation Structure of RUSLE2

RUSLE2 uses an equation structure similar to the Universal Soil Loss Equation (USLE) and RUSLE1. RUSLE2 computes long-term average soil loss on each *ith* day as:

$$a_i = r_i k_i l_i S c_i p_i \qquad \textbf{[5.1]}$$

where: a_i = long-term average soil loss for the *ith* day, r_i = erosivity factor, k_i = soil erodibility factor, l_i = soil length factor, S = slope steepness factor, c_i = cover-management factor, p_i = supporting practices factor, all on the *ith* day.[4] The slope steepness factor S is the same for every day and thus does not have a subscript. To emphasize, values for these factors are long–term averages for a particular day—not for the year, which is the reason that lower case symbols are used rather than upper case as in RUSLE1 and USLE. Equation 5.1 is exactly like the USLE except that it computes soil for a given day rather than an annual soil loss.

RUSLE2 computes deposition when sediment load exceeds transport capacity on overland flow profiles like the one illustrated in Figure 5.2 using:

$$D_p = (V_f / q)(T_c - g) \qquad \textbf{[5.2]}$$

where: D_p = deposition, V_f = fall velocity of the sediment in still water, q = overland flow (runoff) rate per unit width of flow, T_c = sediment transport capacity, and g = sediment load. **RUSLE2** computes runoff rate using the 10-yr, 24 hr storm amount, the NRCS curve number method, and a runoff index (curve number) computed from cover-management variables. **RUSLE2** computes sediment transport capacity using:

$$T_c = K_T q s \qquad \textbf{[5.3]}$$

where: s = sine of the slope angle and K_T = a transport coefficient computed as a function of cover-management variables. The steady state conservation of mass equation is to compute sediment load as:

$$g_{out} = g_{in} + \Delta x D \qquad \textbf{[5.4]}$$

where: g_{out} = sediment load leaving the lower end of a segment on the slope, g_{in} =

4 Lower case letters are used to denote daily variables in comparison to the upper case letters used in the USLE and RUSLE1 that denote average annual values.

sediment load entering the upper end of the segment, Δx = length of segment, and D = net detachment or deposition within the segment. The sign convention is "+" for detachment because detachment adds to the sediment load, and "-" for deposition because it reduces the sediment load. Equation 5.4 is graphically illustrated in Figure 5.7.

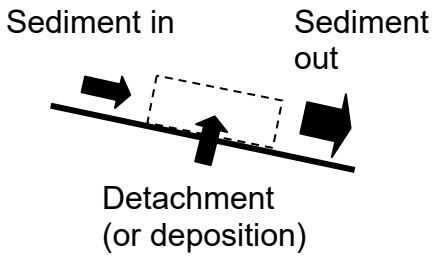

Figure 5.7. Schematic of conservation of mass equation for computing sediment load along the slope

Equations 5.2-5.4 are solved for each of the five particle classes of primary clay, primary silt, small aggregate, large aggregate, and primary sand. The distribution among these classes at the point of detachment is computed by RUSLE2 as a function of soil texture. The wide range in fall velocity for sediment particle classes allows equation 5.2 to compute the sorting of sediment where coarse and dense sediment are deposited first, which enriches the sediment load in fines and less dense particles.

Average annual soil loss is computed as:

$$A = \left(\sum_{i=a}^{365m} a_i \right) \Big/ m \qquad \textbf{[5.5]}$$

where: A = average annual soil loss, m = number of years in the analysis period, and 365m = the number of days per year. The value for m is 1 for continuous vegetation on range, pasture, and other lands where conditions are the same year after year, while m = the number of years of cropping-management rotations on cropland and the number of years following a disturbance such as construction, logging, grading of a reclaimed surface mine, or closing of a land fill where conditions are changing year to year.

For comparison, RUSLE1 is:

$$A = RLSP\left\{ \left[\sum_{k=1}^{24m} \left(f_k k_k \right) \right] \Big/ m \right\} \left[\sum_{k=1}^{24m} \left(f_k c_k \right) \right] \Big/ m \qquad \textbf{[5.6]}$$

where: R = average annual erosivity, f_k = distribution of erosivity by half month period, L = slope length factor, P = supporting practices factor, and k = index for the half month period. The 24 in equation 5.6 is the number of half month periods in a year. Values for the terms K and C are computed from:

$$K = \left[\sum_{k=1}^{24m}\left(f_k k_k\right)\right] \Big/ m \qquad \textbf{[5.7]}$$

and:

$$C = \left[\sum_{k=1}^{24m}\left(f_k c_k\right)\right] \Big/ m \qquad \textbf{[5.8]}$$

Values for K and C were computed and placed in tables so that RUSLE1 could be used in a "paper version" as A=RKLSCP. A computer program for RUSLE1 is also available to compute K, C, and P factor values from basic subfactor variables along with a procedure for computing soil loss for non-uniform shaped overland flow paths.

The USLE is:

$$A = RKLSP\left[\sum_{j=1}^{N}\left(f_j c_j\right)\right] \Big/ m \qquad \textbf{[5.9]}$$

where: j = the index for crop stage periods and N = the number of crop stages over the analysis period. A crop stage period is one where the cover-management factor c can be assumed to be constant. Values for C were computed from:

$$C = \left[\sum_{j=1}^{N}\left(f_j c_j\right)\right] \Big/ m \qquad \textbf{[5.10]}$$

Values for C were placed in tables so that the USLE could be used easily in a "paper version" as A=RKLSCP.

The numerical integration used in RUSLE2 to solve equations 5.1 and 5.5 is much superior to the approximations used in RUSLE1 and the USLE. The difference in soil loss estimates between RUSLE2 and the other equations can be as much as 15 percent because of differences in the mathematical integration procedures. Modern computers are readily available to solve complex equations to eliminate the need for a "paper version" of RUSLE2. The equations and procedures in RUSLE2 are too complex for a "paper version." Although RUSLE2 can compute C factor values, RUSLE2 does not use the standard RKLSCP factor values to compute erosion.

The USLE, introduced in the early 1960's and revised in 1978,[5] was totally empirical, having been derived from more than 10,000 plot years of data from natural runoff plots and an estimated equivalent of 2,000 plot-years of data from rainfall simulator plots. The strength of the USLE is its empiricism, which is also its weakness. The USLE cannot be applied to situations where empirical data are not available for a specific field condition to derive appropriate factor values. Also, the USLE subfactor procedure for non-cropland (Table 10, AH537) is missing important variables including soil surface roughness and biomass production level.

Federal legislation in the 1980's required erosion prediction technology applicable to almost every cropland use, a requirement that the USLE could not meet. A "subfactor" method that estimates values for the cover-management factor C allows RUSLE1 to be applied to any land use. Process-based equations were also added to estimate the values for the support practice factor P so that soil loss could be estimated for modern strip cropping systems that could be estimated with the USLE. Data needed to derive USLE P factor values were not available for these systems. This hybrid approach of starting with an empirical structure and then adding process-based equations where empirical data were limited greatly increased the power of RUSLE1 over the USLE.

RUSLE2 significantly expands on this hybrid approach by combining the best of empirical-based and process-based erosion prediction technologies. Modern theory on erosion processes of detachment, transport, and deposition of soil particles by raindrop impact and surface runoff was used to derive **RUSLE2** relationships where the required equations could not be derived from empirical data. **RUSLE2** is well-validated erosion prediction technology that builds on the success of the USLE and RUSLE1. **RUSLE2** validation is described in **Section 17**.

5.5. Major Factors Affecting Erosion

The four major factors affecting interrill and rill erosion are: (1) climate, (2) soil, (3) topography, and (4) land use.

5.5.1. Climate

Rainfall drives interrill and rill erosion. The most important characteristics of rainfall are rainfall intensity (how hard it rains) and rainfall amount (how much it rains). Soil loss is high in Mississippi where much intense rainfall occurs, whereas soil loss is low in the deserts of Nevada where very little rainfall occurs. Thus, rainfall erosivity varies by location. Specifying the location of a site identifies the erosivity at the site.

---

5 Wischmeier, W.H. and D.D. Smith. 1978. Predicting rainfall-erosion losses: A guide to conservation planning. U.S. Dept. of Agriculture, Agriculture Handbook # 537.

5.5.2. Soil

Some soils are naturally more erodible than are other soils. Erosion by raindrop impact is not easily seen, but varying degrees of rilling indicate differing erodibility among soils. Knowledge of basic soil properties such as texture provides an indication of erodibility. For example, soils high in clay and sand have low erodibilities while soils high in silt have high erodibilities. Soils are mapped and named as map units and components that make up map units. Soil properties, including erodibility, are assigned by soil component and map unit. These properties are, in effect, specified when the name of a soil mapping unit is selected. Soils on highly disturbed lands like reclaimed mine sites can not be mapped and require special considerations to determine erodibility.

5.5.3. Topography

Topography, especially steepness, affects soil loss. Intense rilling is evidence that steep slopes like road cuts and fills experience intense erosion when bare. Runoff that accumulates on long slopes (overland flow path lengths) is also highly erodible, especially when it flows onto steep slopes. Thus, slope steepness and overland flow path length, to a lesser extent, are major indicators of how topography affects erosion. Slope shape (steepness along the overland flow path), illustrated in Figure 5.2, 5.3, and 5.4, also affects erosion and deposition as evidenced by both erosion and deposition on concave slopes.

5.5.4. Land Use

Erosion occurs when soil is left bare and exposed to raindrop impact and surface runoff. Vegetative cover greatly reduces soil loss. Two types of practices are used to control soil loss. One type is cultural practices like vegetative cover, crop rotations, conservation tillage, and applied mulch. The other type is supporting practices like contouring, strip cropping, and terraces that “support” cultural management practices. Of the factors of climate, soil, topography, and land use, land use is most important. It has the greatest range of effect on soil erosion, and it is the one that can be changed most readily to control soil loss and sediment yield.

A powerful feature of RUSLE2 is that it is land use independent. By using fundamental variables to represent cover-management effects, RUSLE2 can be applied to any land use. These variables include percent canopy cover; fall height; ground cover provided by live vegetation, plant litter, crop residue, and applied materials; surface roughness; soil biomass; degree of soil consolidation, and ridge height. RUSLE2 applies to cropland, rangeland, disturbed forestland, construction sites, reclaimed mined land, landfills, military training sites, and other areas where “mineral” soil is exposed to the forces of raindrop impact and overland flow produced by rainfall in excess of infiltration.

5.6. Computing Soil Loss with RUSLE2

RUSLE2 computes soil loss and other erosion values using inputs for climate, soil, topography, and use practices and conditions. These values stored in the RUSLE2 database under names for locations, which identify climatic variables; soil; cover-management conditions and practices; and supporting practices. The user selects a name from a menu list for each of these factors to compute erosion. RUSLE2 "pulls" the values associated with each input name from the RUSLE2 database. The user changes values of particular variables from those stored in the database as needed to represent site-specific conditions related to topography, yield (production level), rock cover, and type and amount of applied materials like manure and mulch.

In many ways, RUSLE2 is a set of database components that operate like a spreadsheet. Values are stored in each database component for the variables that RUSLE2 uses in its computations. When the user changes a particular value to represent a site-specific condition, RUSLE2 immediately updates its computations, much like a spreadsheet updates its computations when a change is made in a cell.

RUSLE2 is never started from a "blank sheet." It always starts with information already stored in a database component. The user changes the values for particular variables if the values stored in the database are not appropriate for the field conditions where RUSLE2 is being applied.

5.6.1. Computational Database Components

All RUSLE2 database components accept input and make computations. However, three RUSLE2 database components are the primary computational components. These components are the (hillslope) **profile**, **worksheet**, and **plan view** components.

The overland flow path along a hillslope **profile** is the basic computational unit of RUSLE2. Information on the location (climate), soil, cover-management, supporting practices, and topography of a specific overland flow path describes a particular hillslope **profile**. Once this information has been entered in RUSLE2 to describe a particular hillslope profile, the profile can be named and saved in the **profile** component of the RUSLE2 database.

The RUSLE2 **worksheet** component is used to facilitate conservation planning by computing erosion for a set of alternate conservation practices for a **uniform** hillslope profile for a particular location, soil, and topography. The worksheet provides a convenient way to compare alternatives. Another RUSLE2 worksheet is available that can be used to compare hillslope profiles where conditions including location, soil,

topography, cover-management, and supporting practice can vary along hillslope profiles and among the profiles.

The RUSLE2 **plan view** component can be used to compute average soil loss and other erosion variables for a spatial area like a field or watershed where profiles vary over the area.

Individual profile, worksheets, and plan views can be named and saved.

5.6.2. RUSLE2 Database Components

The major components of the RUSLE2 database are listed in Table 5.1. With the exception of a few site-specific inputs, RUSLE2 uses values stored in its database to make its computations. Later sections discuss the major variables in each RUSLE2 database component. Information on each variable and how it is used along with information on how to select input values is provided.

Table 5.1. RUSLE2 database components

Components	Comment
Plan view	Computes average erosion for a spatial area like a field or watershed
Worksheet	Computes erosion for alternative management practices and alternative hillslope profiles (overland flow paths)
Profile	Computes soil loss for a single hillslope profile (overland flow path), the basic computational unit in RUSLE2
Climate	Contains data on erosivity, precipitation amount, and temperature
Storm erosivity	Contains data on the distribution of erosivity during the year
Soil	Contains soil data including erodibility, texture, hydrologic soil group, time to consolidation, sediment characteristics, soil erodibility nomographs
Management	Contains descriptions of cover-management systems; includes dates, operations, vegetation, type and amount of applied materials
Operation	Contains data on operations, which are events that affect soil, vegetation, and residue; includes the sequence of processes used to describe each operation; whether an operation places residue in the soil; includes values for flattening, burial, and resurfacing ratios; ridge heights; and initial soil roughness
Vegetation	Contains data on vegetation; includes residue types associated with particular vegetations, yield, amount of aboveground biomass at maximum canopy, senescence, flow retardance, root biomass, canopy cover, fall height, live ground cover
Residue	Contains data that describe the residue description assigned to each vegetation description; includes values for decomposition, mass-cover

	relationship, how residue responds to tillage
Contouring	Contains values for row grade used to describe degree of contouring
Strips/barriers	Contains data that describes filter strips, buffer strips, and rotational strip cropping; includes cover-management in strips, width of strips, number of strips across slope length, whether or not a strip is at the end of the slope; and offset of rotation by strip; includes information on barriers used on construction sites.
Hydraulic system	Identifies the hydraulic elements and their sequence used to describe hydraulic systems of diversions, terraces, and impoundments; includes number across overland flow path length and whether or not a system is at the end of the slope; includes specific locations of practice on the overland flow path length
Hydraulic element	Contains data on grade of named channel for terraces and diversions
Subsurface drainage system	Contains data on the percent of the area covered by optimum drainage

5.6.3. Templates

RUSLE2 uses **control files** known as **templates** and **access/permission files** that control the RUSLE2 computer screen and the variables accessible to the user. **Templates** determine the appearance of the computer screen and the complexity of the problems that can be analyzed. **Templates** can be customized by the user to change the appearance of the screen. Two standard templates, **uniform slope** and **complex slope**, are available for download from the **USDA RUSLE2 Internet site** at http://www.ars.usda.gov/Research/docs.htm?docid=6038. The **uniform slope** template is for application of RUSLE2 to uniform slopes where all conditions are the same along the slope except for regularly spaced strips such as buffer strips and strip cropping. The **uniform slope** template should be used to learn RUSLE2. It is also the template that makes RUSLE2 most comparable to the USLE and RUSLE1 for estimating soil loss. The **complex slope** template can be used to analyze slopes where conditions such as soil, steepness, cover-management conditions, and certain support practices vary along the slope.

RUSLE2 can display information on many more variables than is displayed on the **uniform slope** and **complex slope** templates. Contact your RUSLE2 administrator for information on how to obtain templates that display additional output. Also, you can edit templates yourself to add a display of certain variables to your current templates. The revised template can be saved under an existing name or saved with a new name. **Of course, saving a template under an existing name means that the template as it existed before the change is lost.** Templates can be transferred among users.

5.6.4. Access/Permission Files

RUSLE2 uses **access/permissions** files that can be named and saved. These files determine the variables that are seen and the variables that are seen but cannot be edited. A main benefit of **access/permissions** files is to protect users from making unauthorized changes in a database. Contact your RUSLE2 administrator for information on changing RUSLE2 access control especially if you find that you cannot manipulate key variables because you are apparently locked out of them. In some cases, you can change values and store the information under a new name. Also, don't be surprised to learn that RUSLE2 has many other variables of interest that someone "upstream" has chosen to keep hidden from you.

5.6.5. Computer Program Mechanics

Information on RUSLE2 computer interface mechanics is summarized in documents available on the USDA-ARS (http://www.ars.usda.gov/Research/docs.htm?docid=6010), University of Tennessee (www.rusle2.org), and USDA-NRCS (http://fargo.nserl.purdue.edu/rusle2_dataweb/RUSLE2_Index.htm) Internet sites.

When the RUSLE2 program is first started, the opening screen provides two choices. Select either a **profile** or **worksheet** to perform erosion computations or select one of the other **database components** to work on stored input values such as those for cover-management and support practices, vegetation, operation, residue, and soil properties, and climate inputs. The second choice is to select a **template**. Templates control the appearance of the RUSLE2 interface and determine the complexity of the field problems that can be analyzed. RUSLE2 is easiest to use for a simple uniform slope, which is the **uniform slope** template. As you become familiar with RUSLE2, move to the **complex slope** and other templates to analyze complex slopes. Also, once you learn the program, you can change the program so that the program starts with alternative screens and **default profiles, worksheets, and plan views**.

Input values in the database can be changed during a particular RUSLE2 analysis. However, you may be locked out of certain database elements because of settings in the RUSLE2 **access control file**.

6. CLIMATE DATABASE COMPONENT

This section describes the variables in the **climate database component**, the role of each variable, and how to determine values for key variables. Values on erosivity, precipitation amount, and temperature are the principal information in the climate database component.

Three types of erosivity inputs can be used in RUSLE2. The preferred method is to enter values for **erosivity density**, which is the ratio of monthly erosivity to monthly precipitation. Erosivity density values were recently determined from analysis of modern weather data as a part of the RUSLE2 development. The second method is to enter monthly erosivity values. The third method is to enter an average annual erosivity value along with an erosivity distribution curve for the EI zone containing the site where RUSLE2 is being applied. The third method is the same as that described in AH703 for RUSLE1. However, do not use values from AH703 because those values are based on old data from the 1930's to 1950's period. **Erosivity values determined from the modern data are about 10 percent larger on average than values based on the older data.**[6]

RUSLE2 uses a storm with a 10 year recurrence interval in its runoff computations. **Two types of inputs for this storm can be used in RUSLE2 (see Section 6.5.2).** One option, which is recommended, is to enter a value for the 10 year-24 hour precipitation amount. RUSLE2 computes a corresponding 10 yr EI. The other option is to enter a 10 yr EI value. RUSLE2 computes a corresponding 10 yr-24 hr precipitation amount. Although the two options yield similar results in the eastern US, entering the 10 yr-24 hr precipitation amount yields significantly improved results in the western US.

6.1. Major Climate Variables

Table 6.1 lists the variables in the RUSLE2 **climate database component** for the **preferred erosivity density** approach, which should be used when applying RUSLE2 to locations within the continental US. Table 6.2 lists the erosivity variables for the annual

6 This overall 10 percent increase in average annual erosivity should not be attributed necessarily to climate change. The increase could be related to differences in measurement techniques and equipment and analytical procedures used to determine erosivity values from the measured data. Data limitations including temporal and spatial variability, missing data, and errors in weather data do not allow conclusions contribute to the difference. In general, the monthly distributions of erosivity changed less than the overall increase in erosivity. The erosivity values produced by this analysis are superior to previous erosivity values, especially for the Western US, for conservation and erosion control planning using RUSLE2. This 10 percent difference in erosivity values must be interpreted along with RUSLE2's accuracy in the context of the particular RUSLE2 application (see **Section 17**).

R and EI distribution zone approach, which may be convenient when applying RUSLE2 outside of the US.

Table 6.1. Variables in climate database component for **erosivity density** procedure

Variable	**Symbol**	**Comment**
Monthly erosivity density	α_m	Ratio of monthly erosivity to monthly precipitation; RUSLE2 uses these values and monthly precipitation to compute monthly erosivity
Annual erosivity	R	RUSLE2 sums monthly erosivity values to determine an annual erosivity value (not an input)
Monthly erosivity	R_m	RUSLE2 computes monthly erosivity using monthly values for erosivity density and precipitation (not an input)
Daily erosivity	r_i	RUSLE2 "disaggregates" monthly erosivity values into daily values (not an input)
Monthly precipitation	P_m	Average annual monthly precipitation (rainfall plus snow), used to compute monthly erosivity, the temporal variation of soil erodibility, and decomposition of dead plant materials (litter, residue, roots)
Daily precipitation	p_i	RUSLE2 "disaggregates" monthly precipitation values into daily values (not an input)
Annual precipitation	P_t	RUSLE2 computes annual precipitation from the monthly precipitation values; used to compute time to soil consolidation (not an input)
10 yr 24 hr precipitation	$P_{10y,24h}$	This precipitation, representative of a moderately infrequent erosive rain, is used to compute a storm erosivity and runoff; these variables, in turn, are used to compute transport capacity and deposition for concave slopes, vegetative strips, and channels; reduction of erosion by ponding; effectiveness of contouring; and critical slope length for contouring
EI for 10 yr 24 hr precipitation	$EI_{10y,24h}$	RUSLE2 determines this values from 10 yr 24 hr precipitation and maximum monthly erosivity density value (not an input)
Monthly temperature	T_m	Average annual monthly temperature, used to compute the temporal variation of soil erodibility and decomposition of dead plant materials (litter, residue, roots)
Daily temperature	T_i	RUSLE2 "disaggregates" monthly temperature values into daily temperature values (not an input)
In Req Area?	Yes or no	The Req area is a region in the Northwestern part of the US where the erodibility of certain cropland and other highly disturbed soils is greatly increased during winter months; answer **Yes** to use Req relationships for these land uses

Use Req distribution?	Yes or no	Wintertime adjustment for increased erodibility does not apply to land uses like pasture and rangeland; if answered no, Req relationships will not be used
R equivalent	R_{eq}	The effect of the greatly increased erodibility is accounted for in the Req region by using an equivalent erosivity value based on annual precipitation (not an input)
EI distribution for Req	-	An erosivity distribution that describes the greatly increased erodibility during the winter
Adjust for soil moisture	Yes or no	An adjustment is made for soil moisture when the Req relationship is selected for cropland and other situations of highly disturbed soil, only applies to Req zone
Vary soil erodibility with climate	Yes or no	With the exception of when the Req relationships are used, select **Yes** to vary soil erodibility values through time as a function of monthly precipitation and temperature (may not be available on most templates)
Note: Not all of these Req-type variables are available on some templates. For example, if **No** is the input for **In Req area?,** then RUSLE2 automatically varies soil erodibility with climate.		

Table 6.2. Variables in climate database component for monthly or annual R and EI distribution procedure. Note: Refer to AH703 for information on these variables.

Variable	**Symbol**	**Comment**
Average annual erosivity	R	An erosivity index that indicates how the erosivity of rainfall varies by location
Erosivity distribution	EI zone identifier	Describes how erosivity varies during the year by half-month periods. Not an input when monthly erosivity values are entered.
Monthly erosivity	R_m	RUSLE2 computes monthly erosivity using annual erosivity value and erosivity (EI) distribution by half month period when method of entering annual erosivity is used.
Daily erosivity	r_i	RUSLE2 "disaggregates" half month erosivity values into daily values (not an input)
10 year storm erosivity	EI_{10yr}	This storm represents a moderately infrequent erosive rain; EI_{10yr} value is used to compute runoff, which along with the storm erosivity, is used to compute transport capacity and deposition for concave slopes, vegetative strips, and channels; reduction of erosion by ponding; effectiveness of contouring; critical slope length for contouring

6.2. Basic Principles

RUSLE2 is based on the assumption that net **detachment** caused by a single storm is directly proportional to the product of a storm's **energy E** and its **maximum 30-minute intensity I_{30}**. **The relationship between detachment and storm erosivity EI is linear**, which means that individual **storm EI** values can be summed to determine monthly and annual erosivity values. This linear relationship also means that average annual erosion can be mathematically computed for each day as represented by Equation 5.1 even though erosion does not occur on every day during a year.

The **average annual erosivity value R** is an index of erosivity at a location. For example, R-values in central Mississippi are about 10 times those in Western North Dakota. If all things are equal, erosion in central Mississippi is 10 times that in Western North Dakota. Erosivity reflects the effects of both rainfall amount and rainfall intensity on erosion. Thus, erosivity values can vary significantly among locations having nearly equal rainfall amounts because of difference in rainfall intensity among locations.

6.2.1. Computing Erosivity for Individual Storms

Storm erosivity EI is the product of a storm's total **energy E** and its **maximum 30-minute intensity I_{30}**. A storm's total energy is most related to the total amount of rainfall in a storm. It is also partially related to intensity because the energy content per unit rainfall (**unit energy**) is related to rainfall intensity. Rainfall intensity also has a direct affect on erosion besides its effect on storm energy. The **maximum 30-minute intensity** is a better measure of the intensity effect than either **average intensity** or **peak intensity**. The 30-minute time period over which to average intensity was determined from analysis of empirical erosion data for the continental US. Other time periods such as 15 minutes are better in other places of the world where rainfall characteristics differ from those in the continental US. **The EI product for storm erosivity captures the effects of the two most important rainfall variables that determine erosivity; how much it rains (rainfall amount) and how hard it rains (rainfall intensity).**

Total energy for a storm is computed from:

$$E = \sum_{k=1}^{m} e_k \Delta V_k \qquad \textbf{[6.1]}$$

where: e = unit energy (energy per unit of rainfall), ΔV = rainfall amount for the *kth* period, k = an index for periods during a rain storm where intensity can be considered to be constant, and m = number of periods. Unit energy is computed from:

$$e = 0.29\left[1 - 0.72\exp\left(-0.082i\right)\right] \quad \textbf{[6.2]}$$

where: unit energy e has units of MJ/(ha·mm) and i = rainfall intensity (mm/h).[7] Table 6.3 illustrates computation of total energy for a storm. The total energy for the example storm is 8.90 MJ/ha.

The next step is to determine the maximum 30-minute intensity I_{30}. Maximum 30-minute intensity is the average intensity for the continuous 30 minutes with the maximum rainfall. (Also, I_{30} = 2·amt of rain in the 30 minutes having the maximum rainfall amt) Plotting cumulative rainfall for the storm as illustrated in Figure 6.1 is helpful for determining maximum 30-minute rainfall. This storm is unimodal (single peak), which means that the 30 minutes with the most rainfall contains the time that the peak intensity occurs. The amount of rainfall is 27.4 mm for the 30 minutes with the most rainfall, which gives an intensity of 57.4 mm/h for I_{30}.

Table 6.3. Sample computation of erosivity EI for an individual storm

Time (hrs:min)	Duration of interval (minutes)	Cumulative rain depth (mm)	Rainfall in interval (mm)	Intensity (mm/h)	Unit energy (MJ/ha* mm)	Energy in interval (MJ/ha)
4:00		0.0				
4:20	20	1.3	1.3	3.8	0.137	0.17
4:27	7	3.0	1.8	15.2	0.230	0.41
4:36	9	8.9	5.8	38.9	0.281	1.64
4:50	14	26.7	17.8	76.2	0.290	5.15
4:53	3	30.5	3.8	76.2	0.290	1.10
5:05	12	31.8	1.3	6.4	0.166	0.21
5:15	10	31.8	0.0	0.0	0.081	0.00
5:30	15	33.0	1.3	5.1	0.152	0.19
Total	90		33			8.88

The erosivity for the storm is the product of 8.90 MJ/ha (storm energy) and 57.4 mm/h (maximum 30-minute intensity) = 512 MJ·mm/(ha·h). **The computation of storm erosivity in US customary units is similar, except that storm erosivity values are divided by 100 to provide convenient working numbers.**

7 Equation 6.2 differs from the corresponding equation used in RUSLE1 (AH703). The 0.082 coefficient in equation 6.2 was 0.05 in AH703. For additional discussion, see McGregor, K.C., R.L. Bingner, A.J. Bowie, and G.R. Foster. 1995. Erosivity index values for northern Mississippi. Transactions of the American Society of Agricultural Engineers. 38(4):1039-1047.

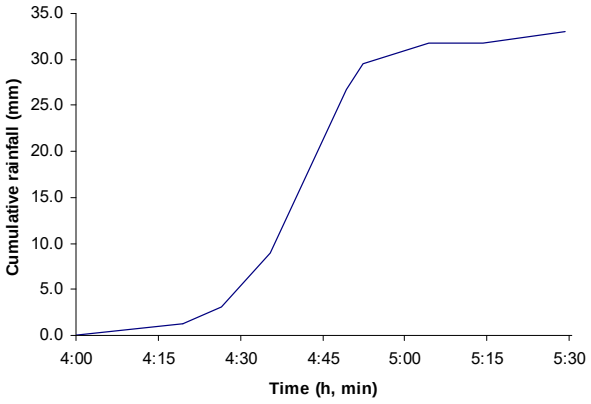

Figure 6.1. Cumulative rainfall for a storm.

Rains less than 0.5 inch (12.5 mm) and separated from other rains by more than 6 hours are not included in the computations unless the maximum 15-minute intensity exceeds 0.5 inch/hour (12.5 mm/h). When erosivity values were first computed in the late 1950's, these small storms were omitted to significantly reduce the amount of rainfall data that must be processed in an era before data could be processed with computers. These storms add little to the total annual erosivity. However, storms less than 0.5 inch (12.5 mm) were also deleted in computing erosivity for RUSLE2 to give some effect of computing reduced erosion at low rainfall amounts and intensities because of little or no runoff.

Average annual erosivity is the sum of the storm erosivities over M number of year as:

$$R = \left[\sum_{m=1}^{M} \sum_{j=1}^{J(m)} (EI_{30})_j \right] \Big/ M \qquad \textbf{[6.3]}$$

where: R = average annual erosivity, EI_{30} = the erosivity of an individual storm, j = an index for each storm, J(m) = number of storms in the *mth* year, and m = an index for year.[8]

6.2.2. Why New Erosivity Values were Computed from Modern Data

A concern has existed for sometime that erosivity values for the eastern US needed to be recomputed based on modern precipitation data. Average annual erosivity values in AH703 for the Eastern US, as well as erosivity values in AH282 and AH537, were based on data collected in the approximate period of 1935 to 1957. This period included two major droughts in large regions of the US. Also, a possible climate change over the last 70 years may have increased rainfall amounts and intensities and caused a corresponding increase in erosivity. To address these concerns, precipitation data from the 1960's through 1999 were analyzed to develop a modern set of erosivity values.[9] **Based on this**

[8] The R factor has units. In this guide, the US customary units for R are hundreds of (ft tons in)/(ac yr hr). Metric units in the SI system are (MJ mm)/(ha*h) for erosivity and (t h)/(MJ mm). See AH703 for additional information.

[9] Precipitation data from 15-minute stations across the US were assembled by the Illinois State Water Survey (ISWS), who computed storm energy and maximum 30-minute intensity for the qualifying

analysis, modern average annual erosivity is about 10% greater over much of the eastern US than that for the1935-1957 period.

Differences in erosivity values derived from the 1930's-1950's data and those derived from the 1960's-1990's data should not be interpreted as having been caused by climate change. Differences in record length, analysis procedures, and interpretation at different points in time and by different people prevent such a direct comparison of values.

Erosivity values described in this RUSLE2 User Reference Guide determined from the modern data should be accepted as representing the best erosivity values currently available for applying RUSLE2 at the local field office level for conservation and erosion control planning—nothing more, nothing less.

6.2.3. Erosivity Density Values

The erosivity density method used to derive erosivity values was developed to maximize the precipitation data that could be used to compute erosivity values and to provide a consistent set of erosivity value for conservation and erosion control planning. **Erosivity density** is the ratio of the monthly erosivity to monthly precipitation. Erosivity density values were computed across the US at about 1610 stations. Statistical analysis showed that erosivity density is independent of elevation, which means that the erosivity density could be smoothed and mapped using GIS techniques for the entire continental US as a spatial unit (See the RUSLE2 Scientific Documentation for additional information). Precipitation data with intensity values needed to compute erosivity are very limited

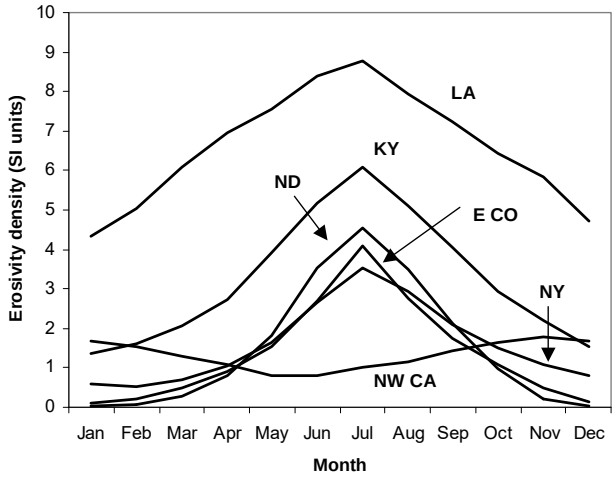

Figure 6.2. Erosivity density at selected locations. LA-Louisiana, KY-Kentucky, ND-North Dakota, E CO-Eastern Colorado, NY-New York, NW CA-Northwestern California

rainstorms. The ISWS and the USDA-NRCS National Water and Climate Center (NWCC) analyzed the data to remove storms with greater than a 50-yr return period, snow events, and invalid data because of equipment failure, a short record length, or other reasons. University of Tennessee personnel performed the spatial analysis of the data.

at higher elevations. The applicability of erosivity density values is limited at elevations higher than about 3,000 m (10,000 ft), especially in the winter months.[10]

Erosivity density is a measure of erosivity content per unit of precipitation. Erosivity density is low during the winter months and high during the summer months with the exception of the western most portion of the US. Erosivity density is greater in the southern part of the US than in the northern part. Erosivity density is more uniform over the year in the southern part of the US than in other parts of the US.

Unsmoothed erosivity density values directly computed from the weather data at individual stations are both spatially and temporally irregular. Trends are sometimes difficult to discern when comparing data among individual weather stations. However, patterns like those in Figure 6.2 emerge when data from several stations are averaged over areas like the quadrants of Indiana.[11] The erosivity density values were spatially smoothed using GIS techniques to provide spatial and temporal consistency required by conservation and erosion control planning applications of RUSLE2. The objective in RUSLE2 is to represent the main geographic trends in the historical data and not the details in historical weather data. Preferably the probability of weather events, both dry and wet, would be the same at all locations in the climate data used by RUSLE2.

Erosivity density values for the continental US are shown in Figure 6.3-6.14. RUSLE2 users can read values from these figures to create entries in their RUSLE2 operational database. However, RUSLE2 users are advised to download values for their RUSLE2 application from the NRCS RUSLE2 National Database rather than to create their own RUSLE2 entries by reading values from these Figures. However, some users may wish to create an entry in their database for a specific site rather than use the NRCS database values. Values for erosivity density can be read from these figures with sufficient accuracy to apply RUSLE2.

The principal application of RUSLE2 is for conservation and erosion control planning. The objective is to capture main effects and consistency so that farmers, contractors, and others impacted by RUSLE2 are treated fairly, especially where costs, benefits, and regulatory impacts are involved. No one should be penalized or rewarded based on unusual events occurring at a location.

[10] Erosivity density values are highly variable in the western US. Also, the number of locations is very limited. Because of these data limitations, statistical tests that show that the hypothesis that erosivity density values are not a function of elevation are not robust. Obviously erosivity density values decrease with elevation in the winter because of increasing amounts of snow at higher elevations. Also, erosivity density values probably decrease slightly with elevation in the summer.

11 See RUSLE2 Science Documentation, USDA-Agricultural Research Service.

6.2.4. Monthly Erosivity Values

RUSLE2 computes a monthly erosivity by multiplying monthly erosivity density by monthly precipitation as:

$$R_m = \alpha_m P_m \quad \textbf{[6.4]}$$

where: R_m = monthly erosivity, α_m = monthly erosivity density, and P_m = monthly precipitation. Annual erosivity is computed as the sum of the monthly erosivity values. Figures 6.15 and 6.16 illustrate average annual R-values for the continental US. The values in these figures are for illustration only. Actual values used in RUSLE2 should be downloaded from the NRCS national RUSLE2 database. Average annual erosivity values for the western US and the mountainous regions of the eastern US are much more variable than indicated in these figures. Nevertheless, these figures can be compared to similar figures in AH282, AH537, and AH703.

6.3. Input Values for Monthly Erosivity Density, Precipitation, and Temperature

6.3.1. Selecting Climate Input Values for Continental US

RUSLE2 requires monthly values for erosivity density, precipitation, and temperature appropriate for the site where RUSLE2 is being applied. A sample set of these values are included with the download of RUSLE2. A complete set of these values can be obtained from the NRCS national RUSLE2 database or by contacting the NRCS state agronomist in your particular state of interest.

The climate values in the NRCS national RUSLE2 database have been assigned by county for those counties in the US where the values can be considered to be uniform over the county. In mountainous areas, the RUSLE2 weather inputs vary over space because of elevation effects. In those regions, NRCS has organized the data by precipitation depth zones that vary with elevation. The precipitation and temperature values in the NRCS national RUSLE2 database are based on 1961-1990 data.

RUSLE2 users in the US should generally use RUSLE2 climate input values from the NRCS national RUSLE2 database. However, in some cases, climate values may be needed for a specific location rather than for the precipitation depth zones used in the NRCS national RUSLE2 database. Erosivity density values at a particular location can be read from Figure 6.3-6.14. Precipitation and temperature values at a specific location can be obtained from the PRISM database available from the USDA-NRCS. PRISM

monthly and precipitation values are on a 4 km by 4 km grid throughout the continental US.[12]

Current PRISM values are based on historical data from 1961-1990. The data were not processed to remove unusually dry or wet events. That is, the return periods (probability) of events vary significantly by location, resulting in spatial variability that is inappropriate for conservation and erosion control planning. The PRISM model, considered state-of-the-art, produces precipitation values that can vary greatly over a relatively short distance, which can result in a corresponding wide variation in erosion estimates.

6.3.2. Climate Input Values Outside of Continental US

When RUSLE2 is applied outside of the continental US, input climate data should be assembled using procedures outlined above if possible.[13] However, RUSLE2 is frequently applied where detailed weather data are not available.

Several points should be considered in developing input values for RUSLE2 where weather data are limited. RUSLE2 is a conservation and erosion control planning tool that captures main effects of the variables that affect rill and interrill erosion and general spatial trends. Weather data can be very irregular between locations, especially if the period of record is short. While short records may have to be used out of necessity, the values should be carefully inspected and smoothed based on technical judgment by those knowledgeable of local and regional weather and climate conditions.

Estimating erosivity as outlined above requires precipitation data that include rainfall intensity values. However, these intensity data may not be available. Erosivity can be estimated from monthly and daily precipitation data, provided sufficient data are available to calibrate the procedures.

---

[12] These PRISM-based values were developed by the NRCS, Oregon State University, and other cooperators using the PRISM model that takes measured precipitation and temperature station (point) data and spatially distributes these values taking into account effects of elevation, proximity to a major water body, atmospheric inversions, and other factors (see Daly, C., G. Taylor, and W. Gibson. 1997. The PRISM approach to mapping precipitation and temperature, 10th Conf. on Applied Climatology, American. Meteorological Society.)

[13] The NRCS National RUSLE2 Database contains values for Alaska, Hawaii, Puerto Rico and US Territories in the Pacific Basin and Virgin Islands.

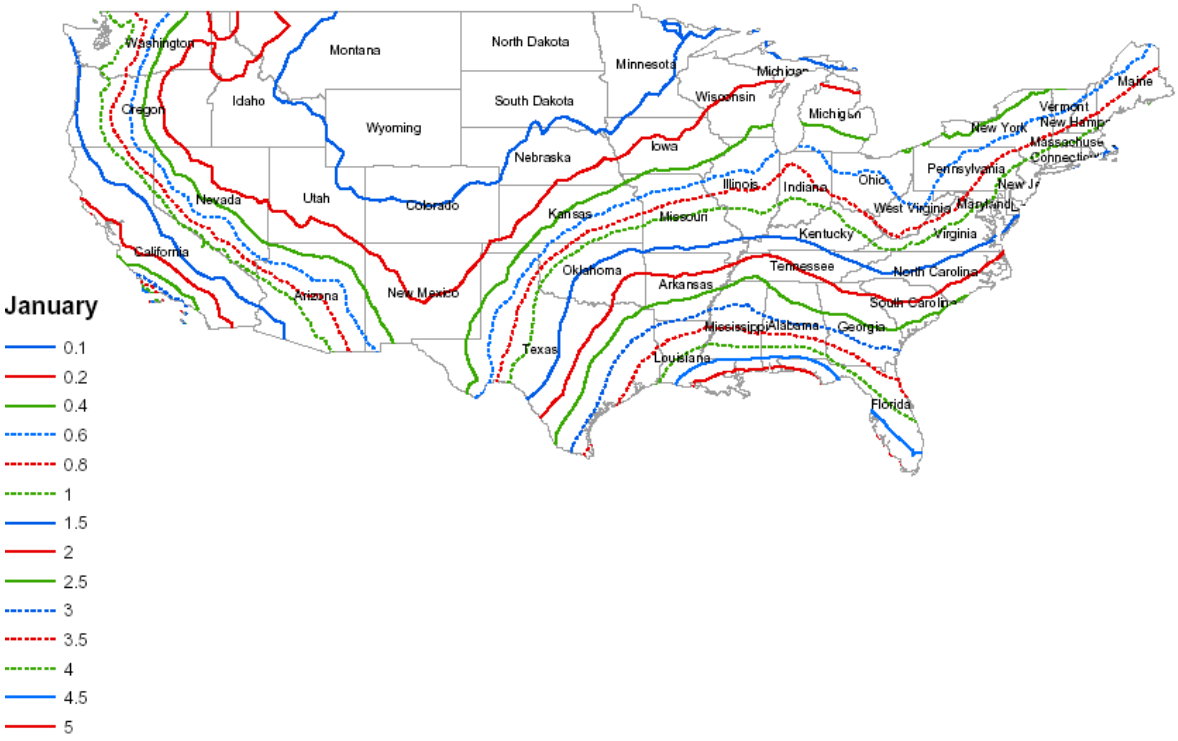

Figure 6.3. Monthly erosivity density [monthly erosivity (SI units)/monthly precip (mm)] for January.

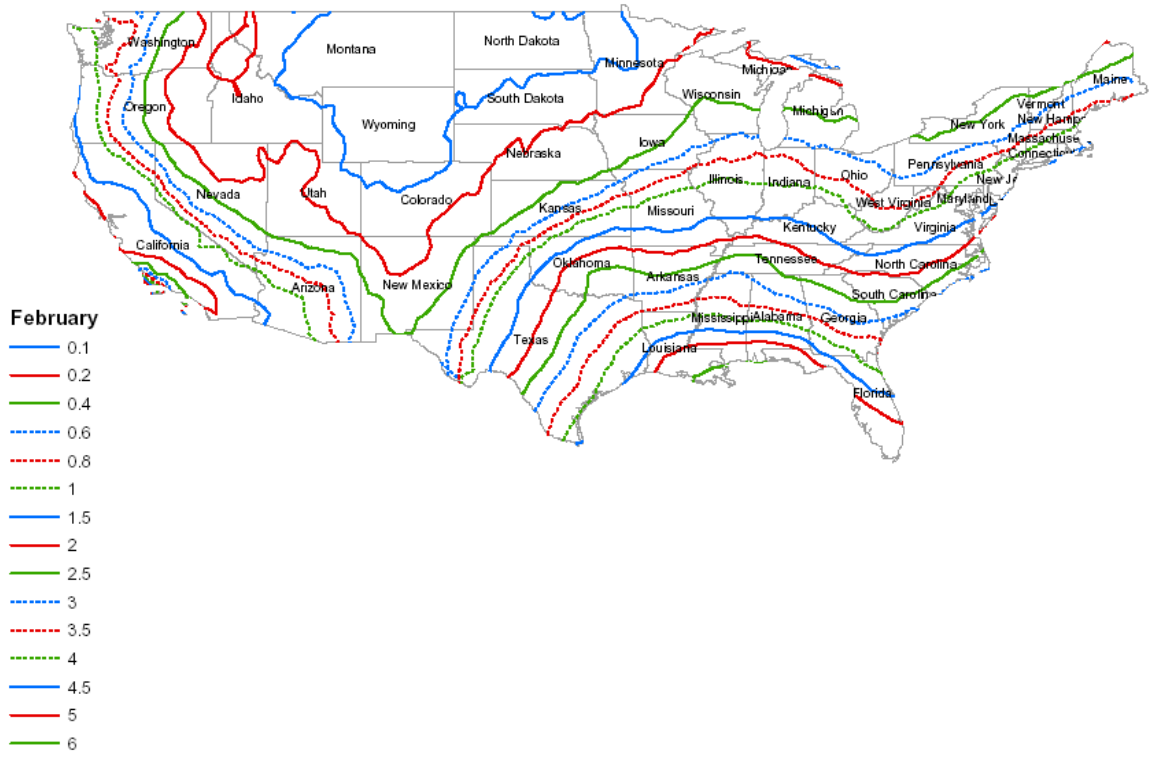

Figure 6.4. Monthly erosivity density [monthly erosivity (SI units)/monthly precip (mm)] for February.

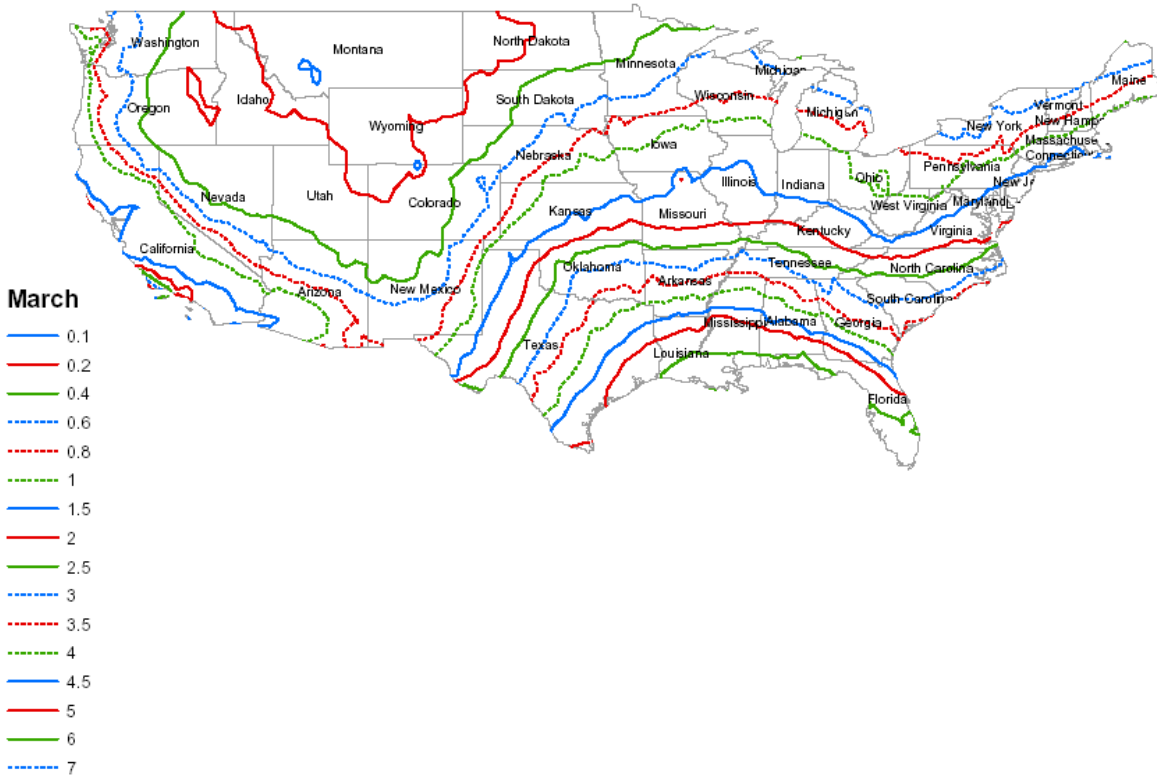

Figure 6.5. Monthly erosivity density [monthly erosivity (SI units)/monthly precip (mm)] for March.

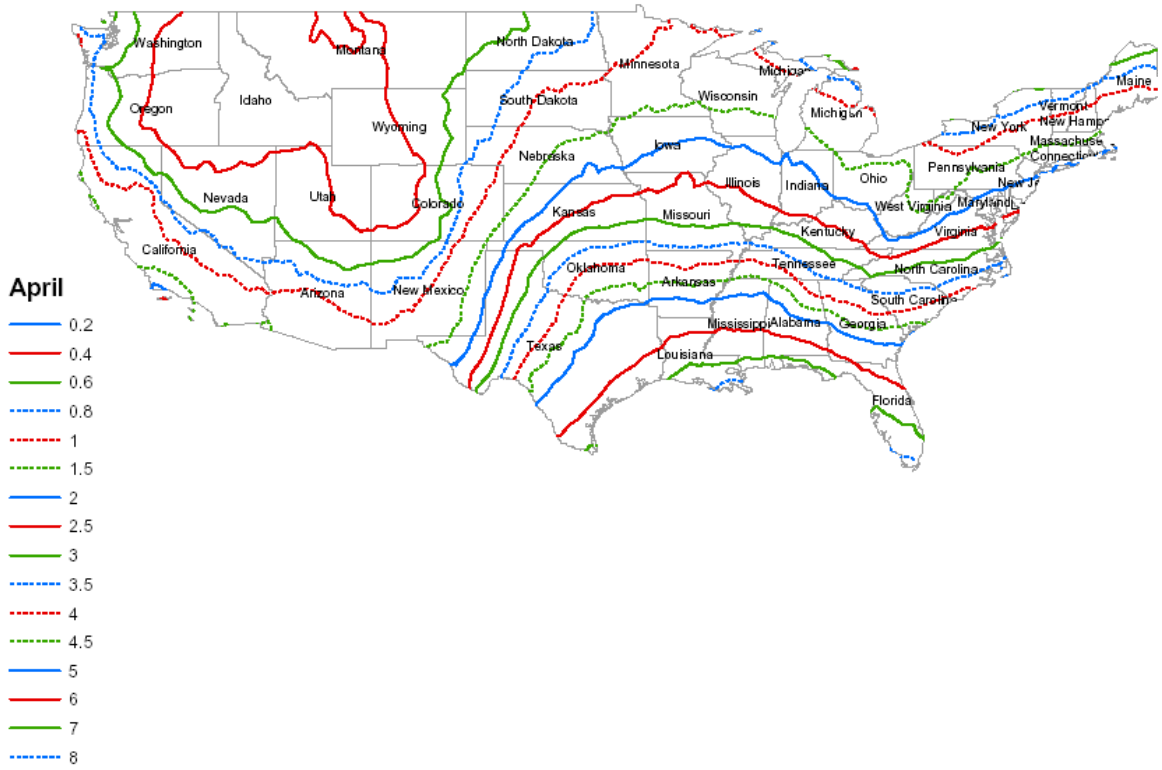

Figure 6.6. Monthly erosivity density [monthly erosivity (SI units)/monthly precip (mm)] for April.

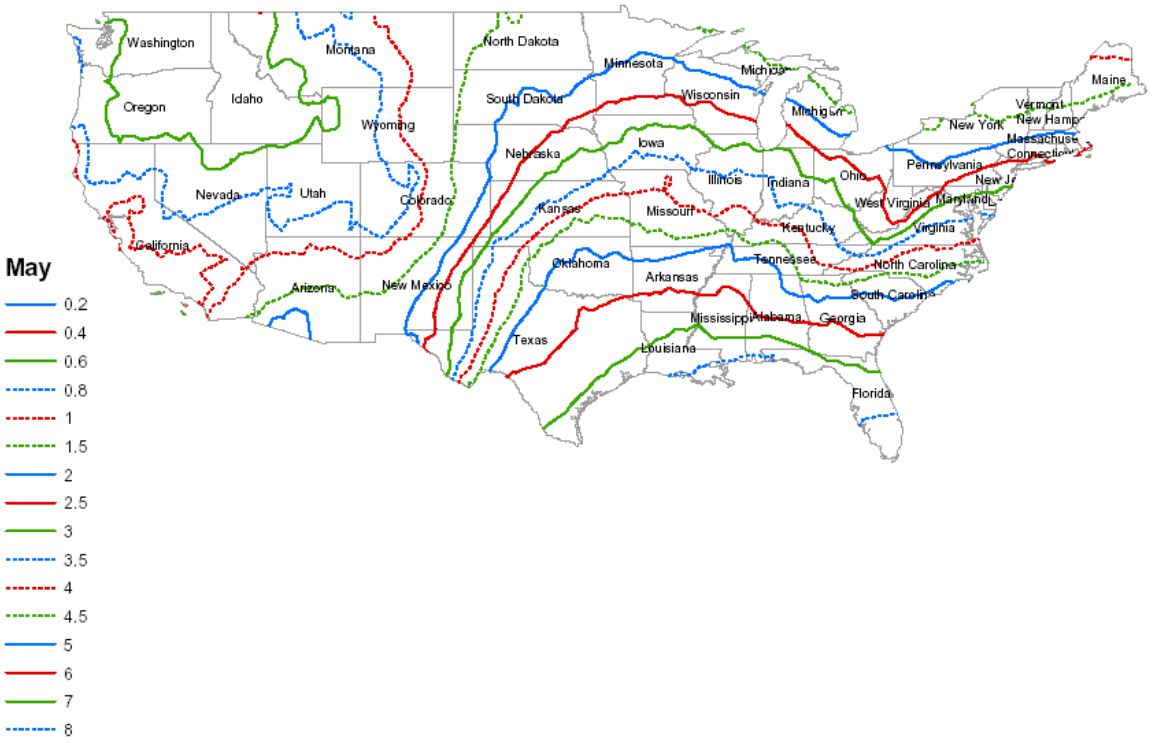

Figure 6.7. Monthly erosivity density [monthly erosivity (SI units)/monthly precip (mm)] for May.

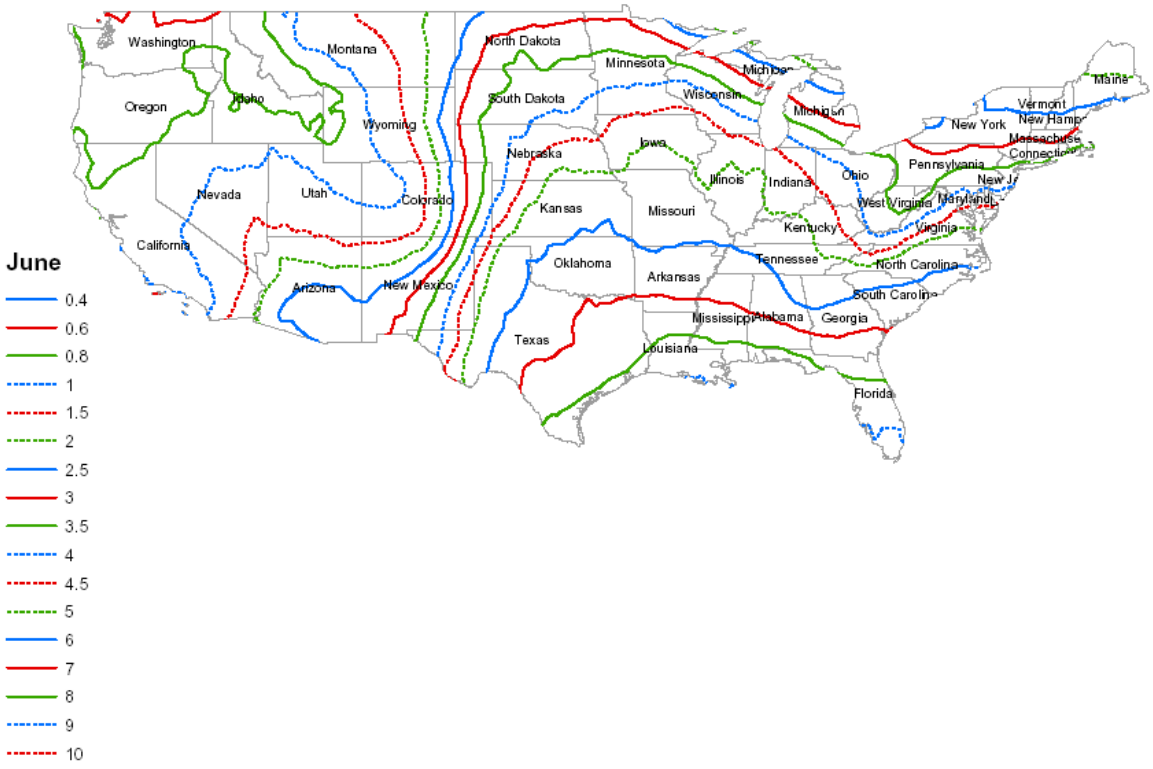

Figure 6.8. Monthly erosivity density [monthly erosivity (SI units)/monthly precip (mm)] for June.

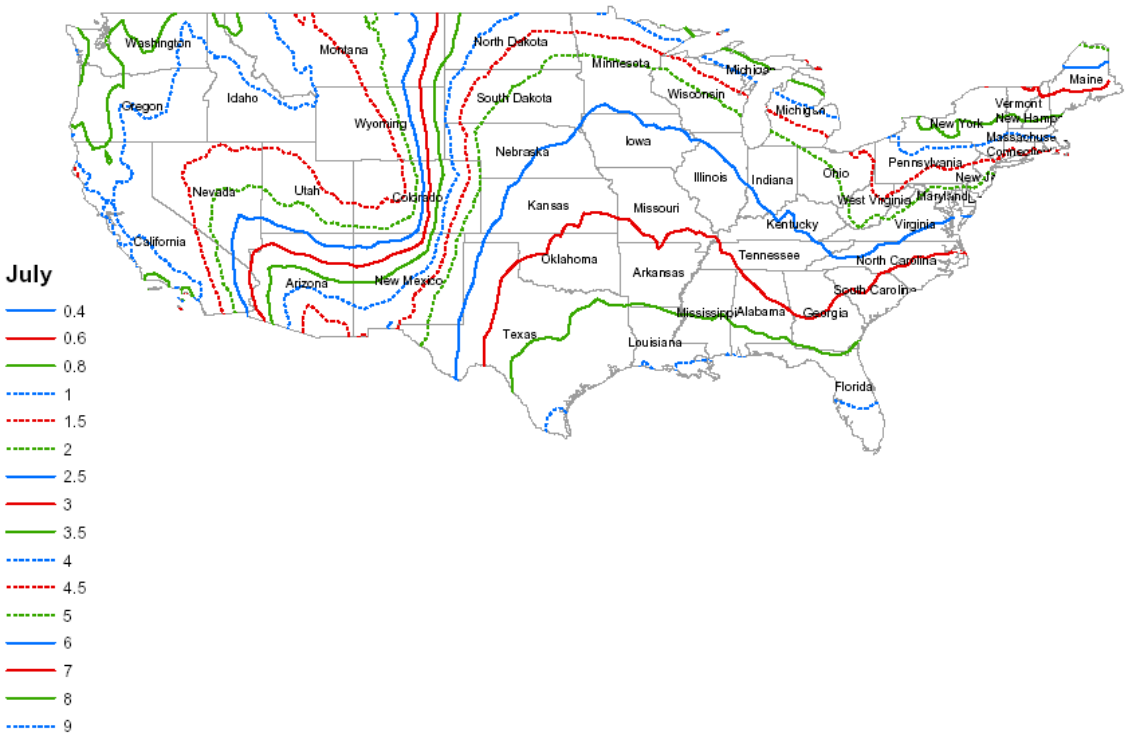

Figure 6.9. Monthly erosivity density [monthly erosivity (SI units)/monthly precip (mm)] for July.

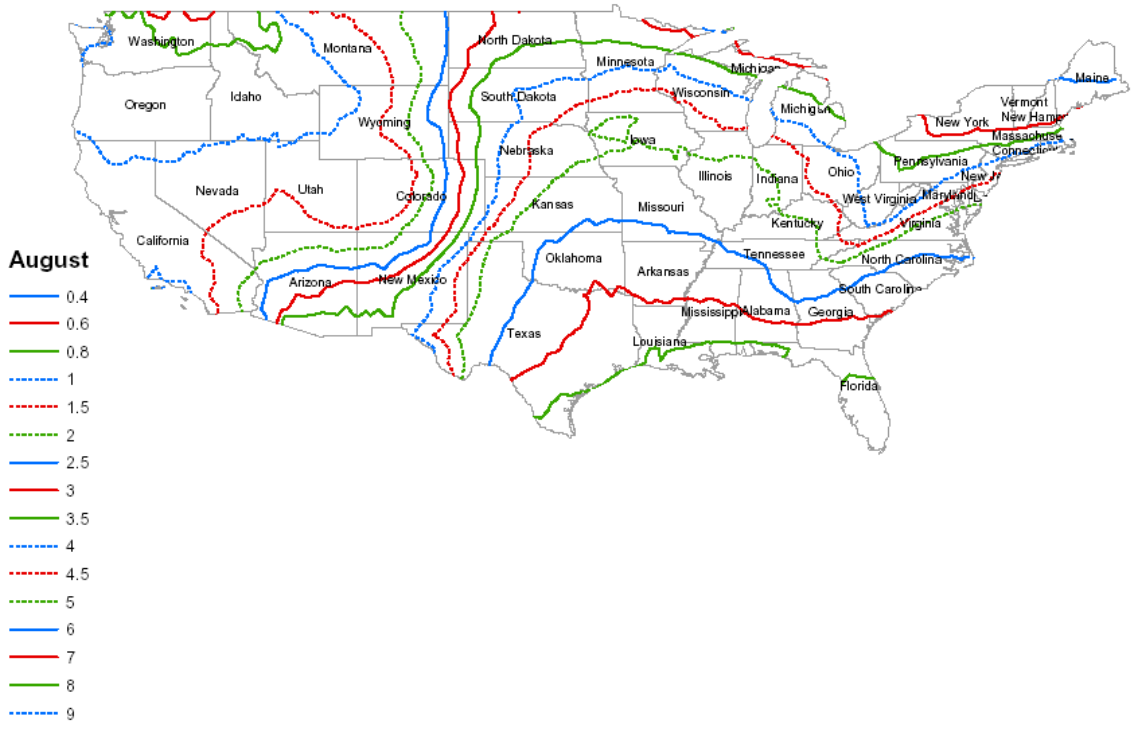

Figure 6.10. Monthly erosivity density [monthly erosivity (SI units)/monthly precip (mm)] for August.

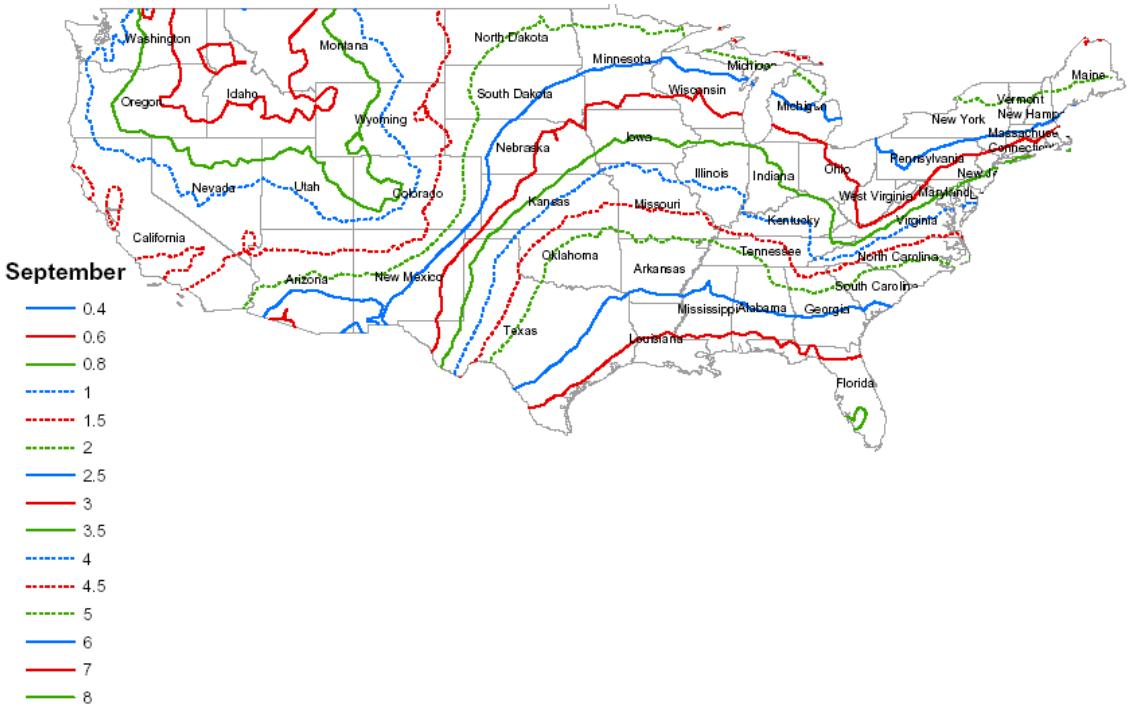

Figure 6.11. Monthly erosivity density [monthly erosivity (SI units)/monthly precip (mm)] September.

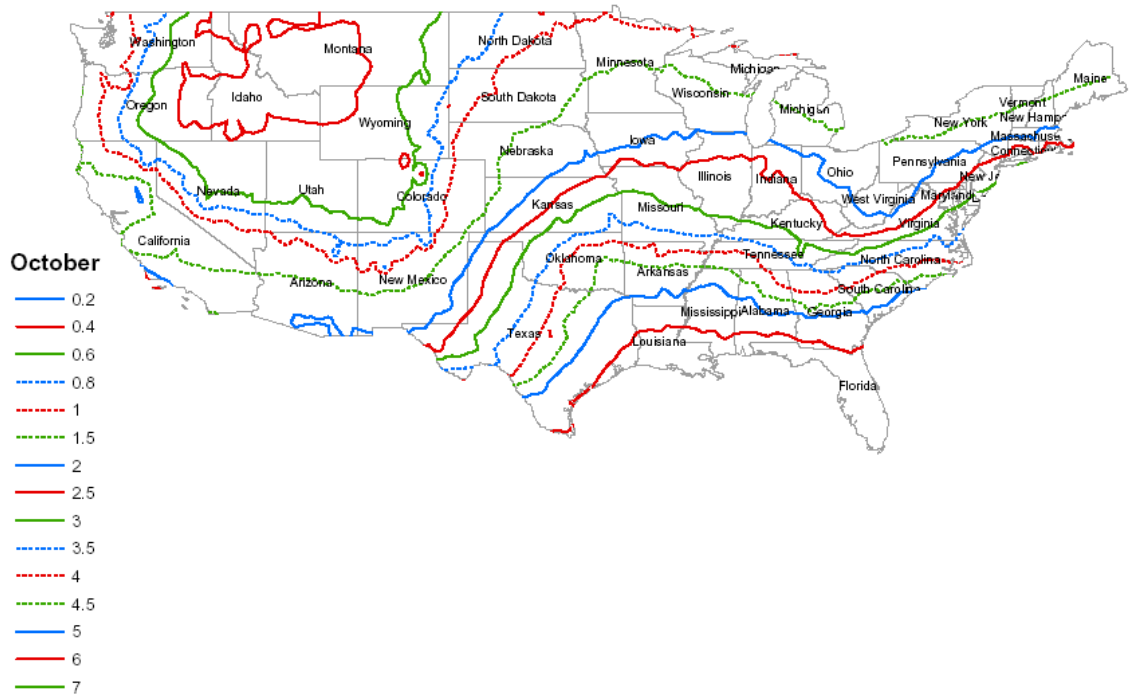

Figure 6.12. Monthly erosivity density [monthly erosivity (SI units)/monthly precip (mm)] October.

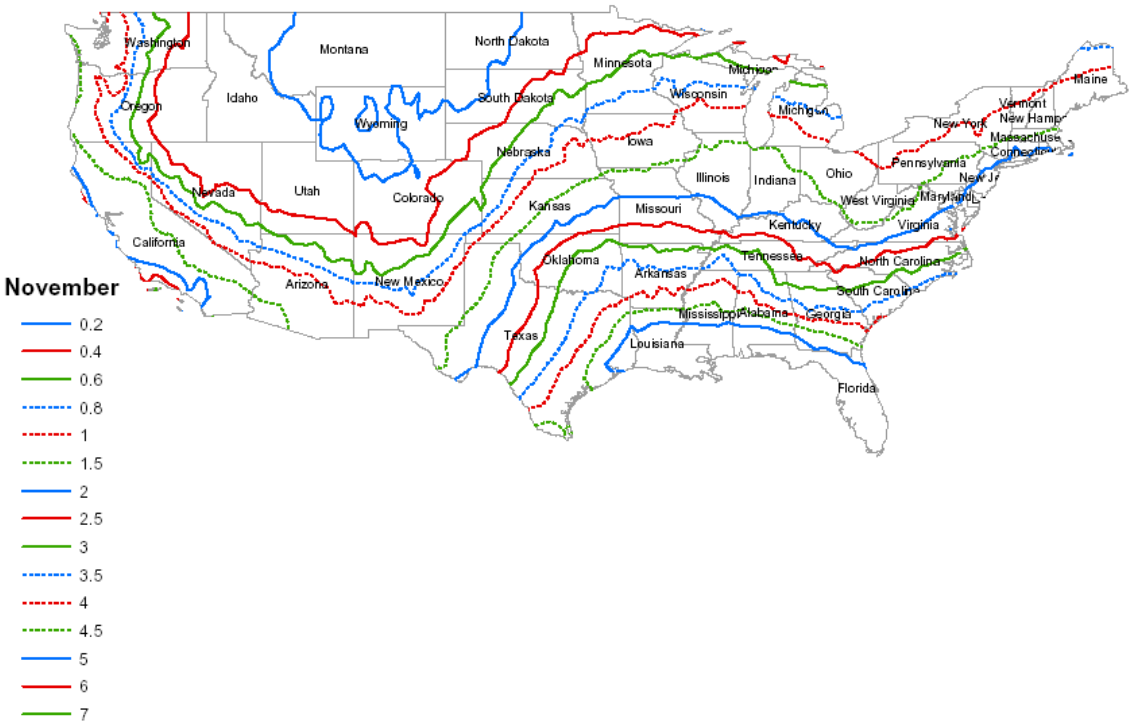

Figure 6.13. Monthly erosivity density [monthly erosivity (SI units)/monthly precip (mm)] November.

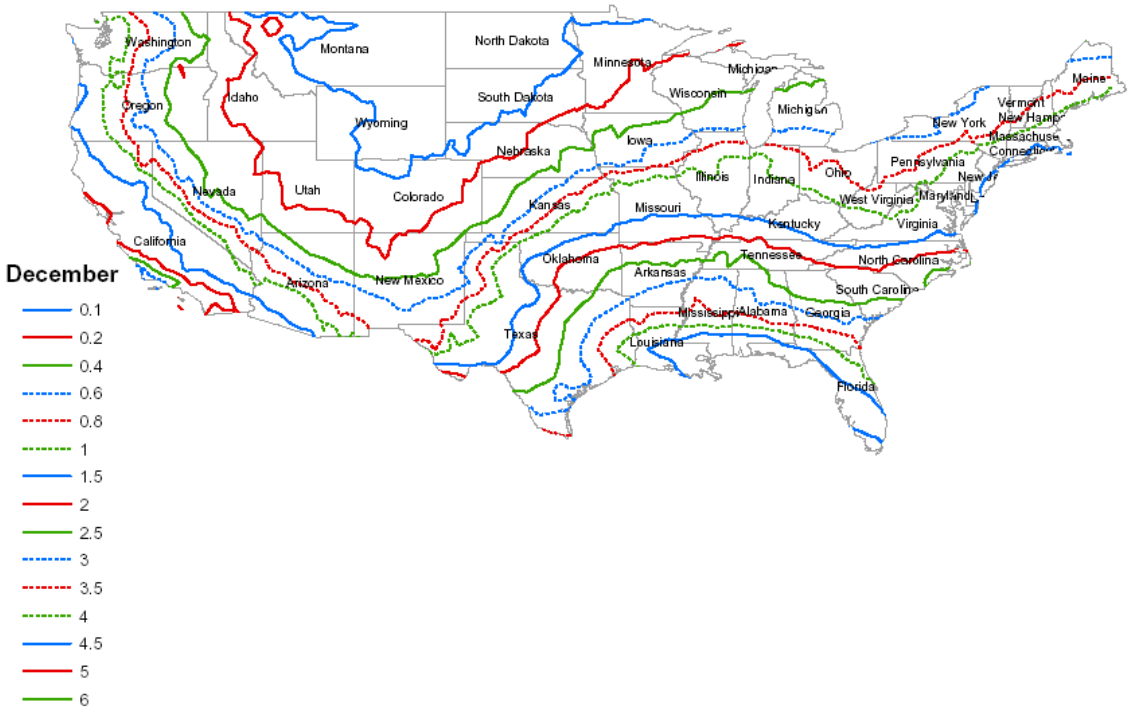

Figure 6.14. Monthly erosivity density [monthly erosivity (SI units)/monthly precip (mm)] December.

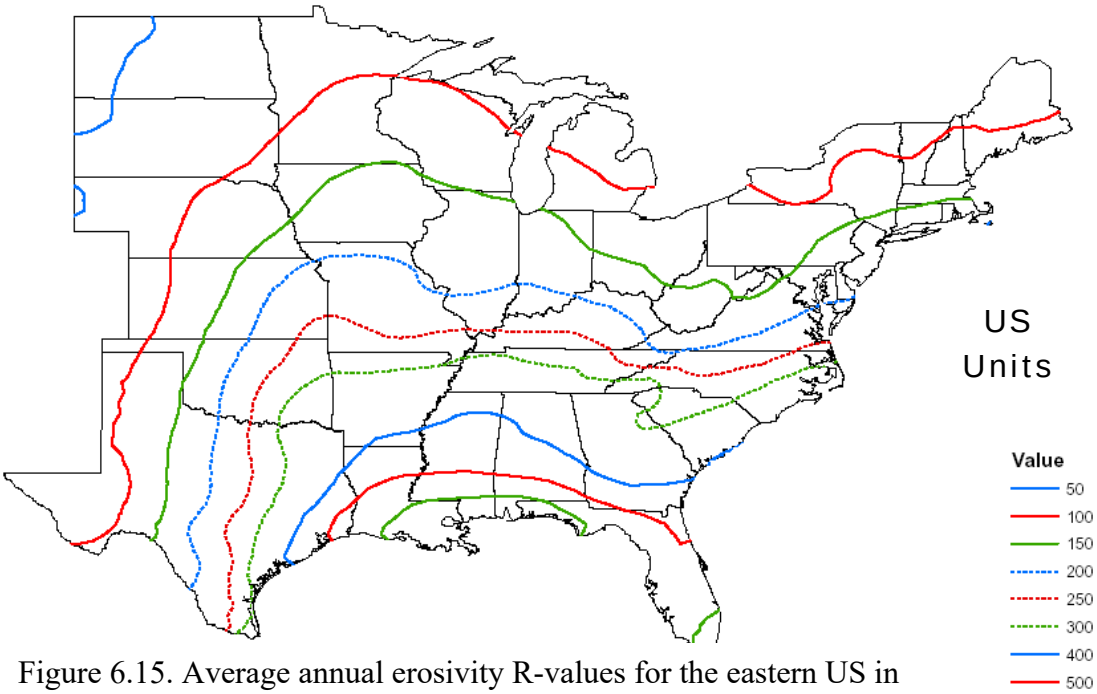

Figure 6.15. Average annual erosivity R-values for the eastern US in customary US units (See Foster, G.R., D.K. McCool, K.G. Renard, and W.C. Moldenhauer. 1981. Conversion of the universal soil loss equation to SI metric units. Journal of Soil and Water Conservation 36(6):355-359.

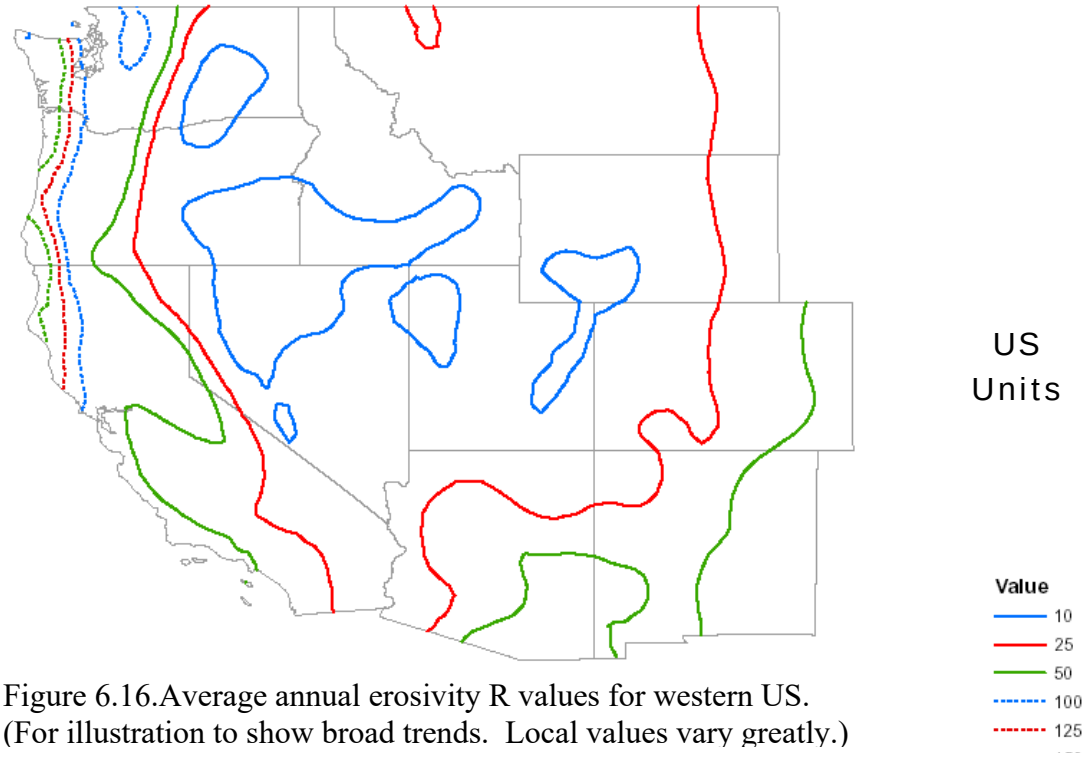

Figure 6.16.Average annual erosivity R values for western US. (For illustration to show broad trends. Local values vary greatly.)

When storm data are used to estimate erosivity, storm erosivity can be computed from storm rainfall amount using the non-linear equations:

$$R_s = aP_s^b \quad \textbf{[6.5]}$$

where: R_s = storm erosivity, P_s = storm precipitation amount, and values for coefficients **a** and **b** are determined by **nonlinear** analysis of empirical data. A logarithmic transform and linear regression does not return the proper values for the **a** and **b** coefficients in equation 6.5. The coefficient **a** and exponent **b** varies by season of the year and by location as represented by the different shaped curves in Figure 6.2.

Monthly precipitation can also be used to estimate monthly erosivity from empirically derived equations. Equation 6.4 implies a linear relationship between monthly precipitation and monthly erosivity. However, the relationship between monthly erosivity and monthly precipitation is actually non-linear. A linear equation can only be used to estimate monthly erosivity using monthly precipitation when the year is divided into months and having erosivity density values that vary by location and by month in sufficient spatial resolution to stepwise approximate non-linear temporal and spatial variations in erosivity. That is, linear equations can be used in a stepwise fashion to approximate non-linear equations if the temporal and spatial steps have sufficient resolution.

6.3.3. Erosivity Values for High Elevation, Snow Cover, Snow Melt, and Req Zone

Applying RUSLE2 to high elevations, periods when a snow cover is present, and snow melt are discussed below in **Section 6.9** related to applying RUSLE2 in the special **Req** zone.

6.3.4. Erosivity Values for Irrigation

The major types of irrigation are surface applied and sprinkler applied water. RUSLE2 can not be used to estimate erosion from surface irrigation systems because runoff and erosion decrease along the flow path for surface irrigation, whereas RUSLE2 assumes an increase.

Most sprinkler irrigation systems apply water at a sufficiently low intensity that erosion does not occur. Thus, the applied water has little or no erosivity. However, irrigation does affect rill-interrill erosion by increasing soil moisture, and increasing vegetation production (yield) level, which decreases erosion. The increased soil moisture increases runoff and erosion when rainfall occurs during irrigation periods, and the added water

increases decomposition of biomass on and in the soil. **Section 14.5** describes how to use RUSLE2 to estimate how irrigation affects rill-interrill erosion caused by rainfall.

6.3.5. Erosivity Values for Subsurface Drainage

Subsurface drainage reduces both soil moisture, which reduces runoff and erosion. RUSLE2 uses a soil erodibility factor value for the drained situation that differs from the soil erodibility value for the undrained condition to compute how subsurface drainage affects erosion. Subsurface drainage also increases vegetation production (yield) level, which reduces erosion. **Section 14.4** describes how to use RUSLE2 to estimate how subsurface drainage affects erosion.

6.4. Disaggregation of Monthly Values into Daily Values

As indicated by Equation 5.1, RUSLE2 uses long term average daily values in its computations. RUSLE2 uses a disaggregation procedure to compute long term average daily weather values from long term daily monthly values. This procedure uses linear equations that interpolate between the monthly values. The RUSLE2 disaggregation equations compute daily values that preserve monthly averages in the input data. The resulting daily values are sometimes not smooth, especially for rainfall values that vary up and down from month to month in comparison to the smooth trends in temperature. Preserving average monthly values was considered to be more important than having a smooth curve. Disaggregation of the monthly erosivity and temperature values for Birmingham, AL is shown in Figure 6.17.

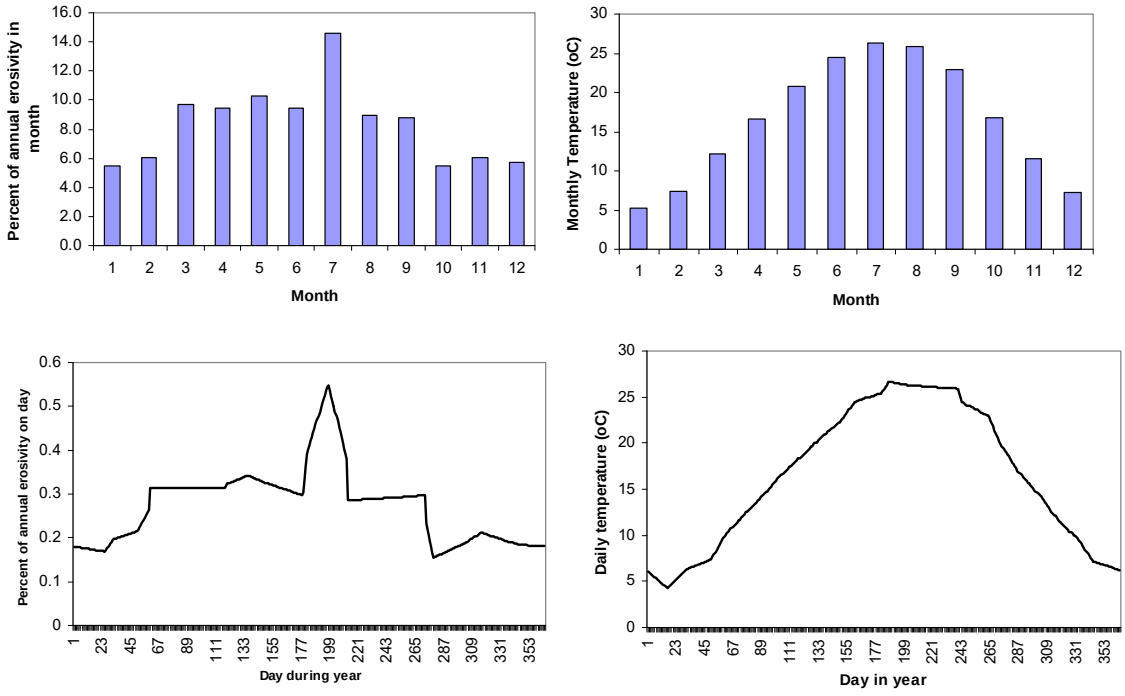

Figure 6.17. Disaggregation of monthly erosivity and temperature into daily values for Birmingham, AL.

6.5. Ten Year Storm

RUSLE2 uses a storm having a 10 year recurrence interval in its runoff computations. Two ways are provided in RUSLE2 for obtaining values for this storm. The strongly recommended way, especially for the eastern US, is to enter values for the 10-year-24 hour precipitation amount. The second way is to enter values for the 10 year EI event like that used in RUSLE1. The 10 year EI event is the storm erosivity that a 10 year recurrence interval.

6.5.1. 10 Year-24 Hour Storm

RUSLE2 uses the 10 year-24 hour (P_{10y24h}) storm to compute storm erosivity and runoff values that are used to compute factor values for contouring, critical slope length for contouring, sediment transport capacity, and the effect of ponding on reducing erosivity. Sediment transport capacity is used to compute deposition by runoff entering slope segments with a concave shape, dense vegetation, high ground cover, or rough soil surface. The 10 year-24 hour precipitation value is the storm amount that occurs in a 24 hour period that has the probability of occurring once every 10 years (a 10-year return period). Values for the 10 year-24 hour precipitation amounts in the NRCS national RUSLE2 database are by county in the eastern US and by precipitation depth zone in the

eastern US. Those values were taken from the most recent National Weather Service published values. Values for the 10 yr-24 hour precipitation are illustrated in Figure 6.18 for the eastern US and for New Mexico in Figure 6.19 as an example of the values available for the western US. These figures are taken from older publications (national maps have not been updated) and are for illustration purposes only. More recent data are available that should be used. The modern data are available at http://hdsc.nws.noaa.gov/hdsc/pfds/.

Figure 6.18. (Full illustration only) 10 yr-24 hour precipitation for the US

The P_{10y24h} value is used to compute an erosivity value associated with this precipitation. The procedure used by RUSLE2 computes an EI_{10y24h} value as:

$$EI_{10y24h} = 2\alpha_m P_{10y24h} \quad \textbf{[6.6]}$$

where: m = the month with the largest erosivity density value.

6.5.2. 10-Year EI Storm

Although use of the 10 year-24 hour storm is the preferred storm input in RUSLE2, the 10-year EI storm has been retained in RUSLE2 as an option. The 10-year EI method gives good results in the eastern US but not in the western US. The 10-year EI value is used to estimate a precipitation amount that is used in the same way that the 10 year-24 hour precipitation amount is used in RUSLE2. The reason that this method does not work well in the western US is that the precipitation amount for this storm is underestimated because the erosivity density (erosivity content per unit precipitation) is much less in the western US than in the eastern US.

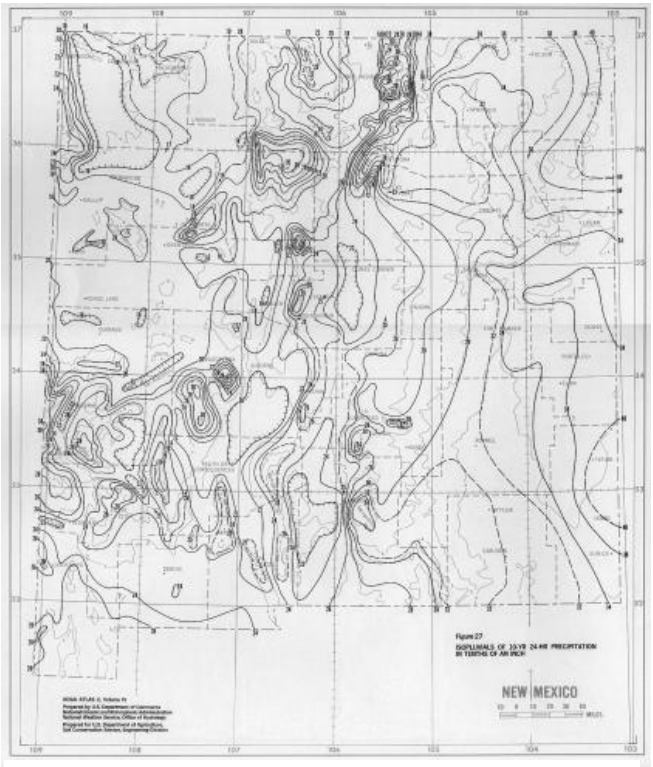

Figure 6.19. (For illustration only) 10 yr 24 hr precipitation for New Mexico.

The map of 10-year EI values has been revised from that in AH703 to greatly smooth the lines to only capture the major trends across the eastern US rather than local variations that reflect unexplained variability in the data rather than "real" differences. The 10-year EI values shown in Figure 6.20 should be used in RUSLE2 and in RUSLE1 rather than the values given in AH703.

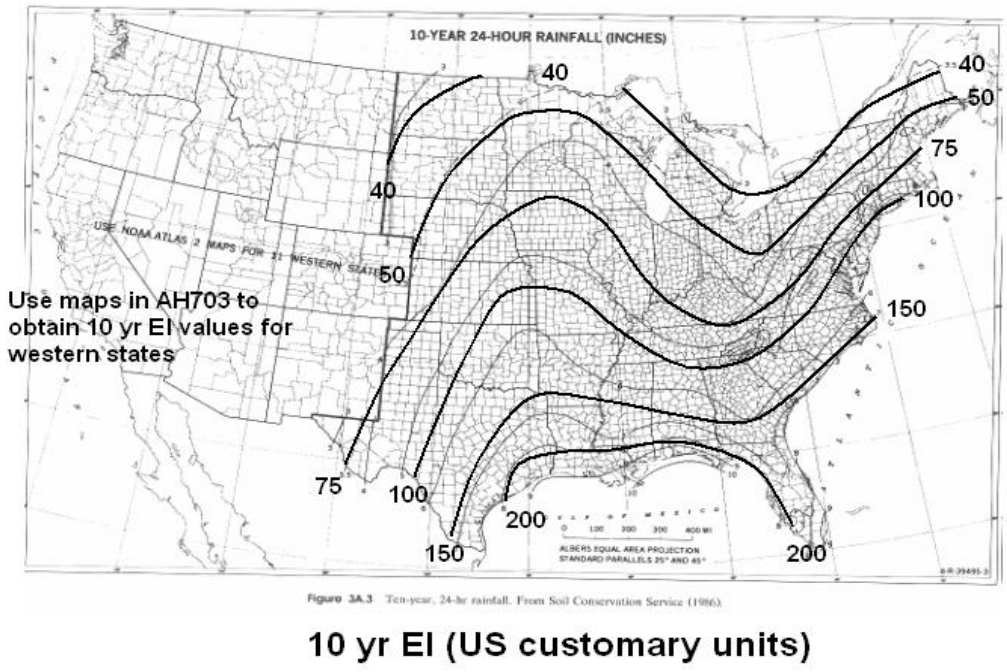

Figure 6.20. 10-year EI values.

6.6. Distribution of Erosivity During the Year

Figure 6.2 illustrates how erosivity density varies temporally by location. Monthly erosivity is computed as the product of erosivity density and precipitation values. Daily erosivity values are computed from the monthly values using the disaggregation procedure discussed in **Section 6.4**. Figure 6.21 illustrates how daily erosivity varies by locations. In central Louisiana, erosivity is nearly the same throughout the year. In contrast, erosivity is very peaked in North Dakota and in eastern Colorado, but the peak occurs at different times of the year. The erosivity density in central Kentucky and New York is similar, but the erosivity tends to be concentrated later in the year in New York than in Kentucky. The climate in northwest California, and other parts of the western continental US, is quite different from that for the eastern US. In this western region of the US, erosivity is highest in the winter months and lowest in the summer months.

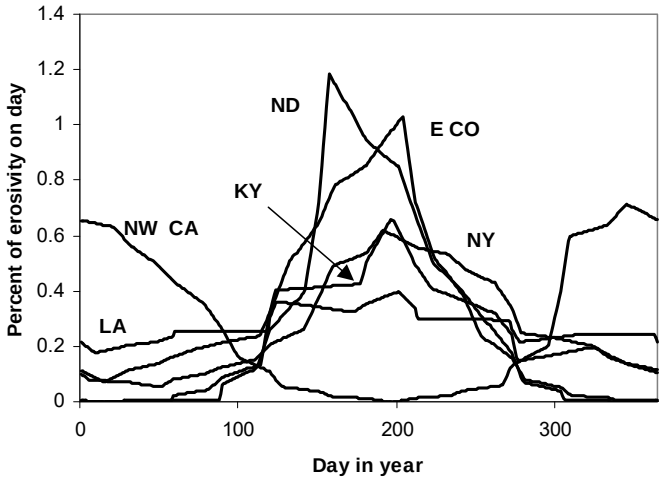

Figure 6.21. Temporal erosivity distribution for several US locations.

The temporal distribution of erosivity significantly affects soil erosion if the soil is exposed during the peak erosivity periods. For example, almost 60% of the annual erosivity in North Dakota occurs in June and July, a period when clean tilled row crops are especially susceptible to erosion because little cover is present. Therefore, on a relative basis, greater erosion occurs with clean tilled crops like corn per unit **annual erosivity R** in North Dakota than in New York because much of the erosivity in New York occurs after a significant canopy cover has developed, leaving the soil less susceptible to erosion. Growing a crop like wheat, rather than corn, that provides the greatest protection during peak erosivity can significantly reduce erosion. Thus, an erosion control practice is to change crops to ones that provide maximum protection during the most erosive period. Similarly, one way to reduce erosion on construction sites is to perform operations that expose the soil at times other than periods of peak erosivity.

6.7. Varying Soil Erodibility with Climate

RUSLE2 varies soil erodibility as a function of monthly precipitation and temperature. This capability is used for all locations and conditions where the standard erosivity relationships are used. However, RUSLE2 does not vary the soil erodibility with climate for the Req zone described in **Section 6.9**. This variation is taken into account in the temporal erosivity distribution used in the Req zone.

6.8. RUSLE2 Reduces Erosivity for Ponding

Intense rainfall on slopes less than about 1 percent steepness causes ponded water that reduces the erosivity of raindrop impact, an effect very important in the Mississippi Delta Region where both precipitation amount and intensity are high. RUSLE2 automatically computes the effect of ponding on erosivity using a cover-management sub-factor (See **Sections 9.1 and 9.2.7**). The reduction is computed as a function of slope steepness and the 10 yr-24 precipitation amount. The 10 yr-24 hr storm captures the effect of a

moderately intense and moderately infrequent storm where ponding is most likely to have its greatest effect. In contrast to RUSLE1, RUSLE2 assumes that ponding reduces erosivity on both flat and ridged surfaces. The adjustment for ponding in RUSLE2 cannot be "turned off" as it could in RUSLE1.

6.9. Req Erosivity Relationships

6.9.1. Req Definition, Zones, and Values

The erosion processes in the Northwestern Wheat and Range Region (NWRR),[14] adjacent areas with similar climate, and certain other areas of the western US differ from those in other regions. Erosion from rainfall and/or snowmelt on thawing cropland, construction sites, and other sites of highly disturbed soils in this region is much greater than expected based on standard **R**-values computed according to Equations 6.1 and 6.2. Therefore, equivalent **R**-values, $\mathbf{R_{eq}}$ values, are used to apply **RUSLE2** to these special conditions. In addition, a modified erosivity distribution and special equations for the topographic and cover-managements factors are also used. The Req erosivity distribution is described in this section and the topographic and cover-management relationships are described in **Sections 8 and 9.**

These conditions occur in the Req zones illustrated in Figures 6.22 and 6.23. Northwestern Colorado, southwestern Colorado, southeastern Utah, and northern California are special transitional areas that use different relationships from those in the Req zone. Values for R_{eq} are used instead of standard R-values in the Req zones. Values for Req are computed from annual precipitation as:

$$R_{eq} = 7.86P_a - 50.5 \qquad \textbf{[6.7]}$$

[14]The Northwest Wheat and Range Region (NWRR) includes about 10 million acres of non-irrigated cropland in parts of eastern Washington, north central Oregon, northern Idaho, southeastern Idaho, southwestern Montana, western Wyoming, northwestern Utah, northern California, and other western US regions. Runoff and erosion processes in this area are dominated by winter events. Many of these events involve rainfall and/or snowmelt on thawing soils. The thawing soils remain quite wet above the frost layer and are highly erodible until the frost layer thaws allowing drainage and soil consolidation. The transient frost layer near the surface limits infiltration and creates a super-saturated moisture condition such that almost all rainfall and snowmelt runs off. This condition occurs most intensively on cropland where the soil has been finely tilled and a well defined interface exists between the tilled soil and the untilled soil. In addition, mechanical soil disturbance (tillage in most cases) has mechanically broken the soil matrix into small soil aggregates. This mechanical soil disturbance breaks bond within the soil and greatly reducing its strength under super-saturated thawing conditions. The effect seems less under cropping management systems like no-till and pasture where little mechanical disturbance has occurred or if mechanical disturbance has not occurred for three or more years. Also, the Req region is characterized by frequent periodic, wide swings in temperature above and below freezing during the winter months. Another important feature is the probability of having rainfall during a thaw of the soil surface when the soil has low strength and is highly vulnerable to erosion.

where: R_{eq} = the equivalent erosivity (US units) and P_a = average annual precipitation (in). Equation 6.7 is an empirical equation developed primarily for the Req zone illustrated in Figure 6.22 across eastern Washington into Idaho. Equation 6.7 should not be applied to situations that give an R_{eq} value greater than 200 US erosivity units. Similarly, an R_{eq} value greater than 200 US erosivity units should not be used in RUSLE2. See **Section 6.10** for guidance on applying RUSLE2 to high elevations where Req > 200 US units.

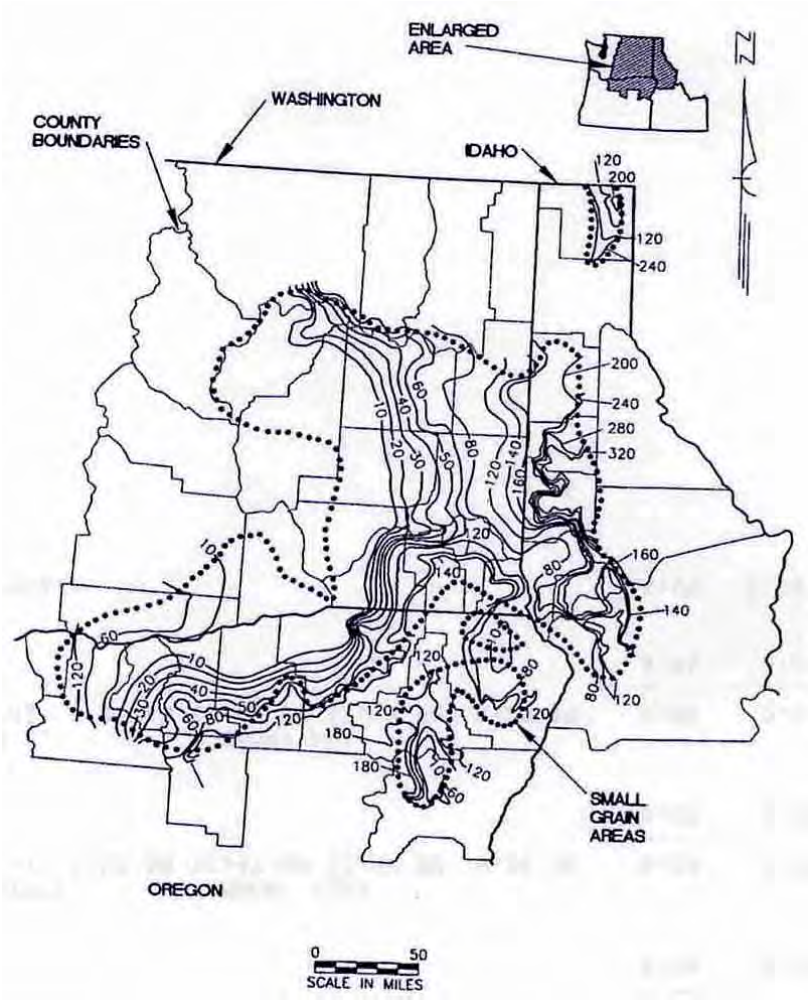

Figure 6.22. Outline of Req zone in Washington, Oregon, and northern Idaho. Only the boundary of area is important. Disregard contour lines.

The Req procedure using equation 6.7 in RUSLE2 can probably be applied to the Req zone illustrated in Figure 6.23. However, the temporal erosivity distribution has to be adjusted to account for differences in temporal precipitation patterns between the Req zones illustrated in Figures 6.22 and 6.23. Also, the Req procedure using equation 6.7 can not be used in the transitional zones in Colorado, Utah, and other areas.

Another consideration in applying the Req approach in the transitional zones is the topographic and cover-management equations. The RUSLE2 equations for the effect of topography and cover-management for the "standard" erosivity regions

differs from those for the Req zones.[15] RUSLE2 uses a single set of these equations for the year. That is, RUSLE2 does not apply one set to the winter months when the Req effect occurs and another set to the summer months when the "standard" erosivity effect occurs. This selection of equation is made when the Req choice is made.

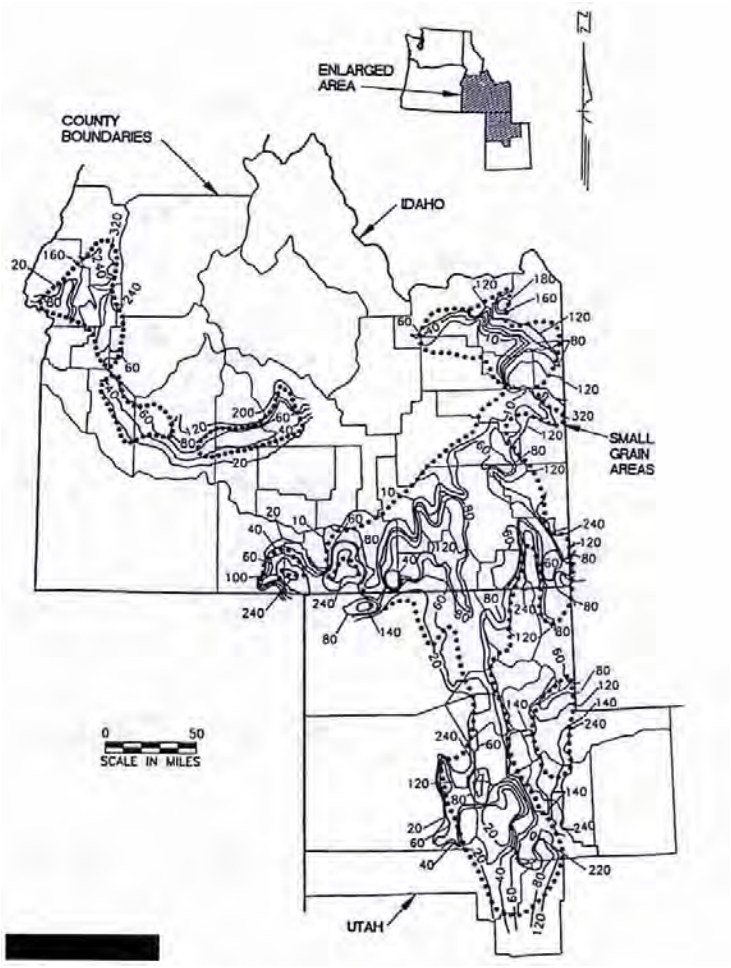

Figure 6.23. Req zone in southern Idaho and northern Utah. Only the boundary of the area is important. Disregard contour lines.

A value for R_{eq} can be entered directly into the RUSLE2 climate database for a particular location, or RUSLE2 can compute it from average annual precipitation using equation 6.7.

At first, the **R_{eq}** effect may appear to apply to areas beyond the Req zones illustrated in Figures 6.22 and 6.23 where frozen soils and runoff from snowmelt occurs, such as the northern tier of states in the U.S. However, that region does not experience the repeated freezing and thawing that is characteristic of the Req zone. Instead, the freezing, thawing, and runoff on thawing soils in those areas is limited to about one month instead of occurring repeatedly throughout the winter months as occurs in the Req zones. Research at Morris, Minnesota showed that only about seven percent of the annual erosion at that location is associated with erosion during the spring thaw. The soil is much more susceptible to erosion during the thawing period. That effect is partially considered in the

[15] Req-type effects occur in many locations of the western US. Also, these effects vary greatly within a local region. The Req procedures in RUSLE2 should be used very carefully when used in regions outside of the Req zone illustrated in Figure 6.22. Consult with ARS or NRCS RUSLE2 support personnel for advice on a recent RUSLE2 version to represent Req-type effect.

temporally varying soil erodibility factor **K** for all areas of the US except for the Req region. The Req value and the Req erosivity distribution account for the temporal variation of soil erodibility.

Rainfall and runoff on thawing soil is common to the upper Mid-South, lower Midwest regions, and similar regions of the US that experience repeated freezing and thawing events and where rainfall routinely occurs during the winter. Even though repeated freezing and thawing is experienced, the soil is not super-saturated by a restricting frost layer several millimeters (a few inches) below the soil surface as in the Req zone. The temporally varying soil erodibility factor **K** partially takes into account the increased erosion during freezing and thawing in the non-Req regions. In contrast to the western US, the increased erosion in late winter and early spring is small relative to the total annual erosion. As mentioned above, erosion during this period at Morris, Minnesota, where annual erosivity is low relative to other parts of the eastern US, is only seven percent of the annual soil loss.

6.9.2. Req distribution

A special erosivity distribution is needed for the Req zone to account for the greatly increased erosion that occurs during the winter months. The Req erosivity distribution is shown in figure 6.24 along with the erosivity distribution based on standard erosivity computations. The distribution shown in Figure 6.24 is for the Pullman, WA area where about 87% of the erosion on the unit plot[16] condition occurs during the winter months. This Req distribution is referred to as an 87-13 Req distribution. This distribution can be used throughout the Req zone illustrated in Figure 6.22. A different distribution should be used in the Req zone illustrated in Figure 6.23 and in the transitional Req zones like north and southwestern Colorado, northern

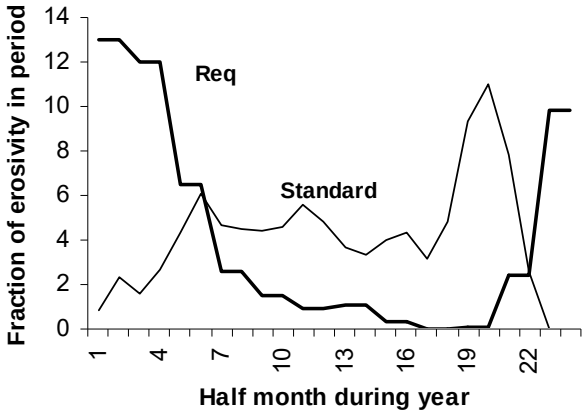

Figure 6.24. 87-13 Req erosivity distribution compared to distribution for standard erosivity at Pullman, WA.

[16] See **Section 7.2** for a definition of unit plot.

California, southeastern Utah, northern Arizona, and northern New Mexico. Less erosivity is concentrated in the winter in these areas. Contact ARS or NRCS personnel for information on Req values and Req erosivity distribution values for these regions.

6.9.3. Should Req Zone be Selected? Yes or No?

Several considerations are necessary in applying RUSLE2 in the Req zone. The first consideration is whether or not to use the Req relationships. Definitely the Req relationships are used for cropland where annual tillage disturbs 100 percent of the soil surface. The Req relationships also apply to certain recently disturbed areas where a well defined soil interface exists just below the soil surface and the upper soil layer is much like a finely tilled cropped soil. However, if the last disturbance occurred more than three years ago, the Req relationships should not be used. Thus, the Req relationships do not apply to undisturbed lands like pasture and rangelands.

Special consideration is required for hay and similar lands where mechanical soil disturbance (cultivation) occurs infrequently. Also, special consideration is required as time elapses after landfill closure or final grading of a reclaimed mine site. Erosion is computed assuming both the Req relationships and the standard erosivity relationships. A soil loss is interpolated between these two values depending on how frequently a mechanical soil disturbance occurs or how much time has elapsed since a disturbance. These same interpolations can be used in the transitional Req zones. RUSLE2 does not make smooth transitions in its computations between Req and standard zones or conditions, which requires professional judgment in applying RUSLE2. These considerations in applying RUSLE2 emphasizes that RUSLE2 is a guide to conservation and erosion control planning.

If the Req relationships, including those for topography and cover, are to be used, answer **Yes** to the question **In Req area?** and **Yes** to the question **Use Req EI distribution**. The standard Req erosivity distribution that is in the RUSLE2 sample database should be used throughout the Req zone illustrated in Figure 6.22. Contact ARS and NRCS personnel regarding Req values and Req distributions for locations outside of the zone illustrated in Figure 6.22.

Answer **Yes** to the question **adjust for soil moisture** when the Req relationships are used in RUSLE2. The amount of moisture in the soil profile during the winter months greatly affects erosion in the Req zone. Certain management practices and crops grown ahead of the winter greatly reduce soil moisture, runoff, and erosion. Answering **Yes** instructs RUSLE to take these effects into account. Answer **No** to the question **Vary soil erodibility with climate** when the Req relationships are used. Answer **Yes** for **varying soil erodibility with climate** when the standard erosivity is used, including all other

The soil moisture relationships are unique to the Req zone and should not be used outside of the Req zone.

areas of the US, including the Western US.

6.10. Applying RUSLE2 at High Elevations in Western US

Special considerations are required when applying RUSLE2 at high elevations in the western continental US. A major consideration involves snow. **If snow is continuously present on the soil surface, RUSLE2 does not apply to those months that the snow cover is present.** RUSLE2 can be applied to the non-winter months by using the standard erosivity relationships and by **turning RUSLE2 off** during the winter period. The way to **turn erosion off** is to use an operation that **adds a non-erodible cover** on the date that the winter period begins and an operation that **removes the non-erodible cover** on the date that the winter period ends. The choice of dates can be based on local observations or long term weather data for snow cover. An alternate approach is to use the date that RUSLE2 computes that the average daily temperature decreases to 1.7 ^{o}C (35 ^{o}F) temperature in late fall or early winter as the beginning date for the non-erdoble winter period. The ending date of the non-erodible winter period date in late winter or early spring is the date that RUSLE2 computes that average daily temperature increases to 7.2 ^{o}C (45 ^{o}F).

Special consideration is required where annual precipitation gives Req values greater than 200 US units. The first factor to consider is whether the Req relationships should be applied to the particular land use. Unless the land use is cropland or a particular type of highly disturbed land condition, the Req relationships probably do not apply. Also, if the precipitation is sufficiently high that a snow cover is present much of the winter and rarely disappears during the winter, the Req relationships do not apply. Even if all of the conditions are met for using the Req relationships but the Req value exceeds 200 US units, RUSLE2 should not be used during the winter months at that location. RUSLE2 is not considered sufficiently accurate to extrapolate it to Req values greater than 200 US units.

A statistical analysis of the erosivity density values showed that erosivity is not a function of elevation. **This statistical result is valid based on the data.** Unexplained variability in the data and the lack of precipitation data at elevations much above 3000 m (10,000 ft) prevent a rigorous testing of the hypothesis that erosivity density does not vary with elevation. This assumption of no elevation effect on erosivity density values is sufficient in the eastern US, but not in the western US during the winter for elevations higher than 3000 m (10,000 ft). The assumption is accepted as valid during the summer months at all locations in the continental US, with the understanding that erosivity is probably being slightly over estimated at elevations above 3000 m (10,000 ft) in the western US.

6.11. Snowmelt Erosivity

RUSLE2 is not designed to estimate erosion caused by snowmelt. The Req relationships do not apply to conditions where snow covers the soil for most of the winter months nor does it estimate the erosion that occurs when the snow melts. RUSLE2 can be **turned off** during the winter period by applying a non-erodible cover at the start of the snow cover and **turned on** after the snowmelt has ended by removing the non-erodible cover using operation descriptions described in **Sections 13.1.9 and 13.1.10.**

However, empirical values that account for snowmelt erosivity can be added to the standard monthly erosivity values to obtain effective monthly erosivity values. These effective monthly erosivity values can be entered in RUSLE2 using the monthly erosivity procedure when the standard topographic and cover-management relationships are being used. An Req value and an appropriate temporal Req erosivity distribution is developed if the Req topographic and cover-management relationships are used. Consult ARS or NRCS personnel for guidance.

7. SOIL DATABASE COMPONENT

This section describes the variables in the **soil database component**, the role of each variable, and how to determine values for key variables. Values for soil erodibility, soil texture, hydrologic soil group, rock cover, and time to soil consolidation are the principal information in the soil database component. These values are available from the local NRCS office in their soil survey database for cropland and similar land uses. These values are also included in the NRCS national RUSLE2 database. Values for most highly disturbed lands like construction sites and reclaimed mined lands must be obtained from on-site determinations.

7.1. Major Soil Variables

The values included in the RUSLE2 **soil database component** are listed in Table 7.1.

Table 7.1. Variables in soil component of RUSLE2 database

Variable	Symbol	Comment
Soil erodibility factor	K	Obtain from NRCS soil survey for cropland and similar lands; must be determined from on-site measurements for highly disturbed lands; **includes no effect of rock surface cover, but includes effect of rock in soil profile**
Soil texture		USDA soil texture class. If sand, silt, and clay content entered, RUSLE2 assigns appropriate textural class
Sand, silt, clay content		Based on USDA classification; if texture entered, RUSLE2 selects values for sand, silt, and clay % in mid-point of textural class
Hydrologic soil group (undrained)		Index for potential of undrained soil to produce runoff under unit plot conditions; a (lowest runoff potential), B, C, D (highest runoff potential)
Hydrologic soil group (drained)		Index for potential of soil to produce runoff under unit plot conditions with a high performing subsurface drainage system; **hydrologic soil group not automatically an A for drained conditions because soil properties may limit drainage**
Rock cover		Portion of soil surface covered by rock fragments sufficiently large not to be moved by runoff; rock diameter generally must be larger than 10 mm (3/8 inch) to qualify as cover
Calculate time to soil consolidation		Answer **Yes** for RUSLE2 to compute time to soil consolidation
Time to soil		Time for soil erodibility to decrease and level out after a soil

consolidation		mechanical disturbance. Enter a value or have **RUSLE2** compute based on average annual precipitation.
T value	T	Value used as criteria in conservation or erosion control planning; NRCS soil loss tolerance T value is typically used for protecting soil; another value besides T may be used for highly disturbed lands based on local regulatory or other requirements; criteria for sediment yield control depend on off-site conditions affected by sediment delivery

7.2. Basic Principles

Soils vary in their inherent susceptibility to erosion. The soil erodibility **K** factor is a measure of erodibility for the **unit plot** condition. The unit plot is 72.6 ft (22.1 m) long on a 9 percent slope, maintained in continuous fallow, tilled up and down hill periodically to control weeds and break crusts that form on the soil surface. Unit plots are plowed, disked, and harrowed, much like for a clean tilled row crop of corn or soybeans except no crop is grown. The first two to three years of erosion data after a unit plot is established are not used to determine a K value. Time is required for residual effects from previous cover-management to disappear, especially following high production sod, forest conditions with lots of roots and litter, or any condition with high levels of soil biomass. About 10 years of soil loss data are required to obtain an accurate estimate of K. The data record should be sufficiently long to include moderate and large storms.

The K value for a soil is the slope of a straight line passing through the origin for measured erosion data plotted versus storm erosivity as illustrated in Figure 7.1. The equation for this line is:

$$A_u = EI_{30}K \qquad \textbf{[7.1]}$$

where: A_u = the soil loss from the unit plot measured for an individual storm and EI_{30} = the erosivity of the storm that produced the storm soil loss. Data from storms less than 12.5 mm (0.5 inch) are not included in the analysis.

The unit plot procedure determines empirical K values for specific soils where the effect of cover-management on soil erodibility has been removed. Not all soils occur where erosion can be measured under unit plot conditions. The equations used by RUSLE2 for topographic and cover-management can be used to adjust measured erosion data to unit plot conditions. These equations are discussed in later sections.

The soil erodibility factor **K** represents the combined effect of susceptibility of soil to detachment, transportability of the sediment, and the amount and rate of runoff per unit

rainfall erosivity for unit plot conditions. Fine textured soils high in clay have low **K** values, about 0.05 to 0.15 tons per US erosivity unit, because they are resistant to detachment.[17] Coarse textured soils, such as sandy soils, have low **K** values, about 0.05 to 0.2 tons per US erosivity unit, because of low runoff even though these soils are easily detached. Medium textured soils, such as silt loam soils, have moderate **K** values, about 0.25 to 0.45 tons per US erosivity unit, because they are moderately susceptible to detachment and they produce moderate runoff. Soils having very high silt content are especially susceptible to erosion and have high **K** values. Sediment is easily detached from these soils, which also tend to crust, produce large amounts and rates of runoff, and produce fine sediment that is easily transported. Values of **K** for these soils typically exceed 0.45 tons/acre per US erosivity unit and can be as large as 0.65 tons per US erosivity unit.

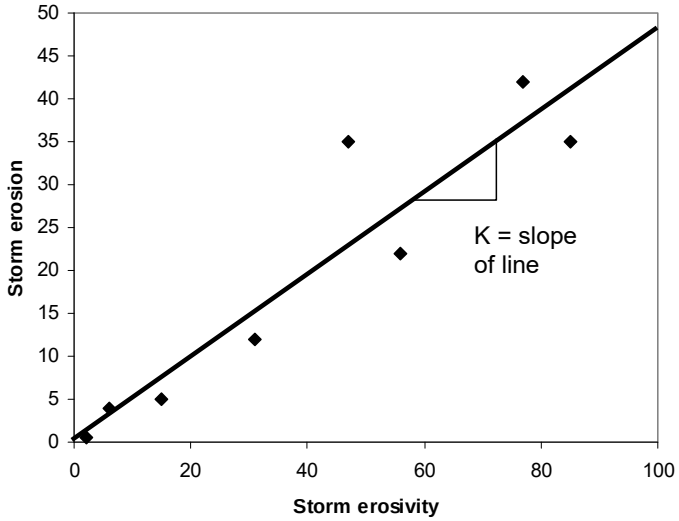

Figure 7.1. Determining a value for the soil erodibility K factor from measured erosion data for unit plot conditions.

The RUSLE2 soil erodibility factor is an **empirical measure** defined by the erosivity variable EI_{30} (product of storm energy and maximum 30 minute intensity) used in RUSLE2. It is not directly related to specific erosion processes, and it is not a soil property like texture. RUSLE2 K values are unique to this definition, and erodibility values based on other erosivity measures, such as runoff, must not be used for K. Values for K are not proportional to erodibility factor values for other erosivity measures. Also, K values may not increase or decrease in the same sequence as other definitions of soil erodibility. For example, the RUSLE2 K value for a sandy soil is low whereas an erodibility factor value based on runoff is high for sand.

[17] The R and K factors have units. In this guide, the US customary units for R are hundreds of (ft tons in)/(ac yr hr). The corresponding US customary units on K are tons /[(hundreds of ft tons in)/(ac hr)]. Metric units in the SI system are (MJ mm)/(ha∗h) for erosivity and (t h)/(MJ mm) for erodibility. See AH703 for additional information.

Soil organic matter reduces the K factor value because it produces compounds that bind soil particles and reduce their susceptibility to detachment by raindrop impact and surface runoff. Also, organic matter increases soil aggregation, which increases infiltration and reduces runoff and erosion. Permeability of the soil profile affects **K** because it affects runoff. Soil structure affects **K** because it affects detachment and infiltration. Soil structure refers to the arrangement of soil particles, including primary particles and aggregates, in the soil. Soil mineralogy has a significant effect on **K** for some soils, including subsoils, soils located in the upper Midwest of the US, and volcanic soils in the Tropics.

Many factors affect soil erodibility. Values for the RUSLE2 soil erodibility K factor, which is a measure on inherent soil erodibility, are for unit plot conditions where the effects of management have been removed. These RUSLE2 definitions were also used in the USLE and RUSLE1.

Values for **K** for several "benchmark" soils have been determined from experimental erosion data. Values for **K** can be estimated for other soils by comparing their properties with those of the benchmark soils and assigning K values based on similarities and differences in properties that affect K values. As a part of its soil survey program, the USDA-NRCS has determined K values for cropland and other similar lands where the soil profile has not been disturbed or the soil mixed.[18] RUSLE2 includes two soil erodibility nomographs, discussed in **Section 7.3.2.,** that can be used to estimate K values. See AH703 for additional information on the soil erodibility factor K.[19]

7.3. Selection of Soil Erodibility K Values

7.3.1 From NRCS soil survey

Values for **K** should be selected from the USDA-Natural Resources Conservation Service (NRCS) soil survey for RUSLE2 applications where the soil profile has not been disturbed and mixed. Values for K for both topsoil and subsoil layers are available for most US soils. The greatest detail is for cropland soils and less for rangeland and forestland soils. Values for K are not available for soils on construction sites, landfills, and reclaimed surface mines because of soil mixing and soil-like materials associated

[18] The USDA-NRCS has mapped most US soils on cropland and other land uses where the soil profile has not been disturbed. Soils were mapped as soil map units (names). Descriptions and properties of each soil map unit are published in soil surveys by US county or other survey area. Soils information is available in a computer database and paper form at local USDA-NRCS offices. The soils data required by RUSLE2 have been extracted from the NRCS soil survey database and included in the NRCS national RUSLE2 database.

[19] Renard, K.G., G.R. Foster, G.A. Weesies, D.K. McCool, and D.C. Yoder. 1997. Predicting soil erosion by water: A guide to conservation planning with the Revised Universal Soil Loss Equation (RUSLE). U.S. Dept. of Agriculture, Agriculture Handbook 703, 404 pp. Much of the information in AH703 on soil erodibility applies to RUSLE2, except for the part on temporal variability of K.

with surface mining. The RUSLE2 modified soil erodibility nomograph can be used to estimate K values for these soils.

Make sure that K values extracted from the NRCS soil survey are the ones where no adjustment has been made for rock on the soil surface and where the effect of rock in the soil profile has been considered.

Multiple K values for a given soil mapping unit are given in the NRCS soil survey database. Select the K value where no adjustment has been made for rock fragments on the soil surface. Using a K value that has been adjusted for surface rock fragments can cause a major error in RUSLE2 erosion estimates. RUSLE2 uses a single composite ground cover that takes into account overlap of rock by crop residue and plant litter. The RUSLE2 mathematical relationships used to compute the effect of ground cover on erosion are nonlinear. Treating each ground cover individually causes errors because of this nonlinearity.

7.3.2. Estimating K values with the RUSLE2 soil erodibility nomographs

7.3.2.1. Background on nomographs.

RUSLE2 includes two soil erodibility nomographs that can be used to estimate soil erodibility K factor values. One nomograph is the **standard nomograph** described in AH703.[20] This nomograph is used to estimate soil erodibility values for cropland and similar soils where the soil profile has not been disturbed. The other nomograph is the **RUSLE2 modified nomograph**. This nomograph is used to estimate soil erodibility K factor values for highly disturbed lands where the soil profile has been disturbed and the soil mixed.

The difference between the standard and the modified soil erodibility nomographs is in the structure effect. The standard nomograph gives K values that decrease as structure changes from a blocky, platy structure to a granular structure. This trend is inconsistent with accepted science on how erosion varies with soil structure. The standard nomograph was derived from about 55 soils, primarily in Indiana, that were mostly medium textured soils without a wide, uniform sample of soil textures and soil structures. The result is that K values from the standard erodibility nomograph are too high for very high clay soils and too low for very high silt soils. The **standard nomograph** is satisfactory for most cropland soils.

[20] For background information, see Wischmeier, W.H., C.B. Johnson, and B.V. Cross. 1971. A soil erodibility monograph for farmland and construction sites. J. Soil Water Conservation. 26:189-193. However, information provided in this RUSLE2 User Guide determines the RUSLE2 application of the nomograph rather than information from other sources.

The **RUSLE2 modified soil erodibility nomograph** should be used to estimate K factor values for highly disturbed lands like constructions sites, landfills, military training sites, and reclaimed mined land. The RUSLE2 modified nomograph gives more credit to the effect of soil structure than does the standard nomograph. The RUSLE2 modified soil erodibility nomograph is exactly the same as the standard nomograph except that the equation for soil structure has been reversed. The two nomographs give the same K values for a moderate to coarse granular soil structure.

AH703 lists equations for estimating K factor values for special cases. Those equations were not included in RUSLE2 because some input values can not be obtained easily or K values computed by some of the equations seemed questionable. Carefully examine those equations and review original source materials before using values from those equations in RUSLE2.

7.3.2.2. Nomograph inputs.

The inputs for both the **RUSLE2 modified** and the **standard** soil erodibility nomographs are the same. Therefore, the single set of inputs listed in Table 7.2 applies to both nomographs. The definitions and variable descriptions used in the nomograph must be carefully followed.[21]

Table 7.2. Variables used in RUSLE2 soil erodibility nomographs

Variable	Symbol	Comment
Sand content		Based on mass (weight), proportion of the total for the clay, silt, and sand, 0.050 mm < sand dia ≤ 2.0 mm
Silt+very fine sand content		Based on mass (weight), proportion of the total for the clay, silt, and sand, 0.002 mm < silt dia ≤ 0.050 mm, 0.050 mm < very fine sand dia ≤ 0.10 mm; RUSLE2 can estimate very fine sand content.
Inherent organic matter content		Based on mass (weight), proportion of the total clay, silt, sand, and organic matter; **organic matter content is for unit plot conditions; do not use organic matter content in nomograph to reflect management different from the unit plot conditions.**
Structure class		Arrangement of primary particles and aggregates in soil
Permeability class		Used to indicate runoff potential under unit plot conditions. Represents the entire soil profile, not just soil surface layer. Should not be determined from a pereameter measurement.
Is		Select **Yes** and RUSLE2 assumes that the permeability class

[21] See the USDA-NRCS soil survey manual for a description of the terms used in the soil erodibility nomograph and procedures for determining values for the nomograph variables. This manual is available on the NRCS Internet site www.nrcs.usda.gov.

permeability with coarse fragments present		has been chosen giving consideration to rock in the soil profile. **Strongly recommend selecting permeability based on professional judgment rather than allowing RUSLE2 to adjust for rocks in soil profile.** Select **No** and RUSLE2 will adjust the permeability class for rock in the soil profile. This adjustment does not apply to soils with large rock fragments like mined land.
Coarse fragment content		Based on mass (weight) proportion of total soil made up of rock fragments > 3 in (75 mm) diameter

7.3.2.3. Special nomograph considerations.

Organic matter content is a major variable in the soil erodibility nomographs. **The input value for this variable is the organic matter content of the soil in the unit plot condition after previous land use effects have disappeared.** RUSLE2 has an upper limit of 4% for this organic matter content input. Applying animal manure, plowing under "green" manure, improving residue management, and other management practices that add biomass significantly reduce erosion. **RUSLE2 considers this important effect using equations for cover-management effects rather than the soil erodibility factor.** The soil erodibility factor is for a base condition where the effects of management have been removed.[22]

Adjusting K to account for organic matter as influenced by land use is double accounting and is a misuse of RUSLE2. Similarly, the permeability class in the soil erodibility nomographs is not adjusted to represent how cover-management and support practices affect runoff.

The permeability effect in the nomographs is based on how the **entire soil profile** affects runoff for unit plot conditions. The input permeability code **should not** be based only on the upper 4 inches (100 mm) to 6 inches (150 mm) of soil. Permeability tests on soil samples from this layer should not be the sole basis for determining the permeability input to the nomographs. The input permeability code entered in the nomograph should take into account how restricting layers, such as a rock, fragipan, caliche, or clay layer, below the soil surface affect runoff. The input permeability code should also reflect how

[22] Considering how land use affects organic matter and soil erosion by adjusting the organic matter input in the soil erodibility nomographs to compute K values seems possible because the nomographs include an organic matter variable. However, the erodibility nomographs must not be used for this purpose. RUSLE2 is an empirical equation based on certain definitions that must be carefully followed. Adjusting K to account for the effect of cover and management on organic matter and runoff is inconsistent with RUSLE2 definitions, structure, and equations.

restricting layers, such as a plow pan or a dense compacted layer created by construction traffic, if these layers that are not routinely broken up by ordinary tillage or other soil distributing operations. RUSLE2 takes into account how subsoiling affects erosion by breaking up these layers.

Values computed with the RUSLE2 soil erodibility nomographs apply to a central, base location, which is Columbia, Missouri.[23] Soil erodibility K factor values vary by location even when soil properties are exactly the same between locations. The K factor values are higher (or lower) at those locations where rainfall amount and frequency and other factors caused increased (or decreased) runoff per unit rainfall in relation to climatic conditions at Columbia, Missouri. This effect is taken in account by computing temporal soil erodibility factor values that are referenced to the climate at Columbia, Missouri (see **Section 7.4**)

The K factor values computed by the RUSLE2 nomographs are solely a function of soil properties. Theoretically, these K values should be increased or decreased as the ratio of runoff to rainfall varies by location. Although, this adjustment is seldom made, RUSLE2 takes the effect into account in its computation of temporal soil erodibility values.

The soil erodibility nomograph does not apply to soils of volcanic origin, organic soils such as peat, Oxisols, low activity clay soils, calcareous soils, and soils high in mica. Also, the nomograph is less accurate for subsoils than for topsoils. Professional judgment is used to assign K values for those soils. Contact the NRCS State Soil Scientist in your state for assistance.

7.4. Temporal Variability in K

Soil erodibility K factor values vary during the year. The values tend to be high during and immediately following thawing and other periods when the soil is wet. The values tend to be low when soil moisture and runoff is low because of increased soil evaporation caused by high temperatures. The input K value is a base value that is assumed to represent an average value during the "frost free" period, which is defined as the time that the temperature is above 4.4 ^{o}C (40 ^{o}F). Temporal soil erodibility values computed by RUSLE2 are shown in Figure 7.2 for Columbia, Missouri; St. Paul, Minnesota; Birmingham, Alabama; and Tombstone, Arizona.

[23] Columbia, Missouri is used as a base location in both RUSLE1 and RUSLE2. USLE values for slope length and steepness effect, soil loss ratio, and support practice factors are assumed to apply at Columbia, MO. RUSLE2 adjusts its values for these factors about the Columbia, MO base values. The weather at Columbia, Missouri is near the "middle" of the data for the Eastern US.

RUSLE2 computes the ratio of daily **K** values to the base K value as a function of the ratio of daily temperature to the base average frost free temperature at Columbia, Missouri and the ratio of daily precipitation to the base average frost free precipitation at Columbia, Missouri. The ratio of daily K to base K increases as the ratio of daily precipitation to base average frost free precipitation increases. This effect represents the increased runoff per unit precipitation caused by increased soil moisture during high precipitation periods. The ratio of daily K to base K decreases as the ratio of daily temperature to base average frost free temperature increases. This effect represents decreased runoff per unit precipitation because of decreased soil moisture on the unit plot conditions during periods when soil evaporation is high. The relative effect of precipitation is greater than that of temperature in these computations. The effect of cover-management on soil erodibility is computed using equations described in **Sections 7 and 9** for cover-management effects.

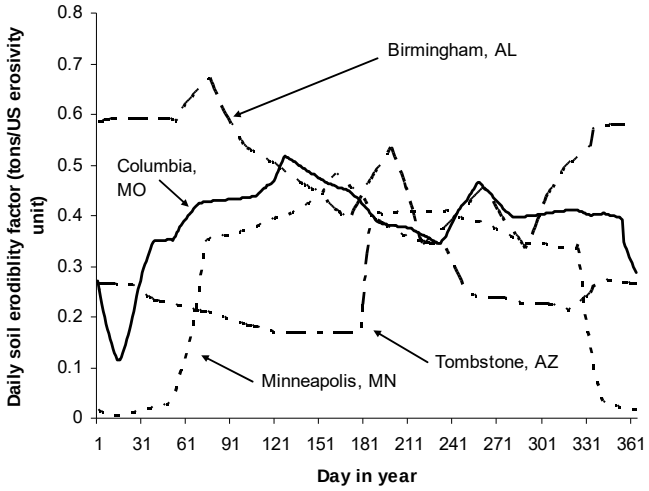

Figure 7.2. Temporal soil erodibility factor values. Base K is 0.42 US units.

When temperature decreases below -1.1 ^{o}C (30 ^{o}F), RUSLE2 reduces K values exponentially as a function of temperature until the K factor value becomes very close to zero at a temperature of -9.4 ^{o}C (15 ^{o}F). The very low K values for Minneapolis, Minnesota during the winter months represent frozen soil that is nonerodible. The same effect is seen for Columbia, Missouri where K values are partially reduced during the winter.

RUSLE2 does not represent increased erodibility during and immediately after the thawing period. The observed data are too few to empirically determine a relationship for this period. Also, the increased erosion during this period is small relative to the total annual erosion for the eastern US. For example, research measurements at Morris, Minnesota showed that erosion during this period was less than 7% of the total annual erosion. This percentage decreases for locations further south. However, the increased erodibility during this period is important in southwestern Colorado, Southeastern Utah, and similar locations in the western US where annual erosivity is low. The relative contribution of the erosion during and immediately after the thawing period is much greater in the western US than in the eastern US. Adjustments can be made in the

monthly erosivity values to account for the increased erosion during this period. See **Sections 6.9 and 6.10**.

The peak in erodibility values for Birmingham, AL in March results from increased rainfall, not from the thawing effect. The main influence of temperature on temporally varying K values is in late summer when increased temperature increases soil evaporation and reduces runoff and erosion. The peak erodibility occurs during the summer for Tombstone, AZ because most of the annual rainfall at this location occurs during this period.

As described in Section 7.3.2.3, the RUSLE2 soil erodibility nomographs computes soil erodibility values solely as a function of soil properties. These nomographs do not take into account how soil erodibility factor values are increased in wet locations such as Birmingham, Alabama and are decreased in dry locations such as Tombstone, Arizona. The temporal soil erodibility equations used in RUSLE2 take this effect into account. For example, Figure 7.2 illustrates how the annual average soil erodibility value is much lower at Tombstone than at Birmingham even though the base soil erodibility factor value computed with a RUSLE2 soil erodibility nomograph is the same at both locations.

A constant erodibility value that does not vary during the year can be used in RUSLE2 by answering **No** to the question **Vary erodibility with climate** in the Climate database component. Assuming that soil erodibility varies temporally is recommended for all areas except the Req zones because the Req procedure captures the increased erodibility during the winter in these regions (See **Section 6.9**). The fit of the equation that computes temporal soil erodibility K factor values is weak, and statistically the hypothesis that soil erodibility does not vary with time can not be rejected.[24]

In contrast to RUSLE1 where the time varying soil erodibility relationships were not used in the Western US, the temporally varying erodibility relationships should be used in the Western US for RUSLE2, except in Req applications.

7.5. Soil Texture

Soil texture is the distribution of the primary particles of sand, silt, and clay in the soil. RUSLE2 uses values for sand, silt, and clay fractions to compute soil erodibility, the

[24] A major difference between RUSLE2 and RUSLE1 is in the temporal soil erodibility computations. The differences in erosion between the models can be as large as 25% in the central Midwest and in the New England regions because of the difference in erodibility computations. The RUSLE1 equations (See AH703) were heavily influenced by data from the Morris, MN and Holly Springs, MS locations. While the relationship for temporal erodibility was well defined at these locations, it was not well defined at eight other locations. Given the overall data, a new temporal erodibility relationship was developed for RUSLE2. The current recommendation is that a constant K value be used in RUSLE1.

distribution of the sediment particle classes at the point of detachment, and the diameter of the small and large aggregate particle classes. See **Section 7.5** for a description of the RUSLE2 sediment classes used.

The fractions for soil texture are based on mass (weight) of the total of these three primary particle classes. The sizes of these classes, which are based on the USDA classification, are given in Table 7.3. Refer to the USDA-NRCS soil survey manual for procedures to determine soil texture from soil samples.[25] These procedures involve dispersing a soil sample to breakup soil aggregates into their constituent primary particles. Sieves are typically used to determine the size distribution of the sand classes and the total sand content. Sieves are screens having various sized openings that sort particles by size. A hydrometer or pipette is typically used to determine clay content. This technique is based on fall velocity. Strongly aggregated soils, including some Tropic soils of volcanic origin, may be difficult to disperse and require special procedures. Silt content is 1.0 minus the clay and sand contents.

Table 7.3. Diameter of primary particle classes. Based on USDA classification.

Primary particle class	**Diameter (mm)**
Clay	dia ≤ 0.002
Silt	0.002 < dia ≤ 0.05
Sand	0.05 < dia ≤ 2
Very fine sand	0.05 < dia <0.1
Fine sand	0.1 ≤ dia < 0.5
Coarse sand	0.5 < dia < 1
Very coarse sand	1 ≤ dia < 2

Primary particles are the smallest, discrete mineral soil particles. Obviously, aggregates are larger than the primary particles that form them. The density of aggregates is less than the density of primary particles because of open space within aggregates. This open space can be partially filled with water, and the rate that pore space becomes filled (rate of soil wetting) greatly affects aggregate stability, soil erodibility, and sediment aggregate size. Rapid wetting significantly reduces aggregate stability and increases soil erodibility. Difference in rate of soil wetting is partially why erosion varies greatly between similar storms.

RUSLE2 input values for sand, silt, and clay content (soil texture) are for the upper soil layer susceptible to erosion. This layer is usually assumed to be 4 inches (100 mm) thick depending on the degree and depth of rill erosion. Soil texture values in the NRCS soil survey database can be used as input in RUSLE2 without processing soil samples from the site **provided the soil profile has not been disturbed and soil mixing has not occurred.** The site is located on a soil survey map to identify the soil map unit at the site. Texture values for that soil map unit are given in the NRCS soil survey database.

If the soil profile has been disturbed and the soils mixed, such as at a construction site or reclaimed mine, soil samples from the site must be processed to determine RUSLE2 soil input values.

[25] Soil Survey Manual available on the Internet site www.ftw.nrcs.usda.gov/tech_ref.

RUSLE2 assigns the appropriate textural class when values are entered for sand, silt, and clay content.

If the sand, silt, and clay content is not known, select the soil textural class as the RUSLE2 input if it is known or can be determined by professional judgment such as from feel of the soil. RUSLE2 assigns central values for sand, silt, and clay content for the input textural class based on the textural triangle. The values assigned by RUSLE2 are shown in Table 7.4.

Sometimes the sand, silt, and clay of a soil are known, but the very fine sand content is not known. RUSLE2 can estimate the very fine sand content using the equation:

$$f_{vfsandt} = 0.74\, f_{sand} - 0.62\, f_{sand}^{2} \qquad [7.2]$$

where: $f_{vfsandt}$ = the fraction of the total primary particles (sand+silt+sand) that is composed of very fine sand and f_{sand} = the fraction of the primary particles that is sand. This equation was derived by regression analysis using data in the NRCS soil survey database for Lancaster County in southeastern Nebraska.

7.6. Sediment Characteristics at the Point of Detachment

RUSLE2 uses values for sediment characteristics to compute deposition. Values used to describe sediment can be computed by RUSLE2, which is the recommended approach, or values can be user entered to create a custom sediment distribution.

.

7.6.1. RUSLE2 computes sediment characteristics

Rill and interrill erosion produces sediment that is a mixture of primary particles and aggregates. RUSLE2 uses the five particle classes of primary clay, primary silt, small aggregate, large aggregate, and primary sand to represent sediment. The sediment distribution for many soils has two peaks, one in the silt size range and one in the sand size range. Comparison of sediment size distributions before and after dispersion shows that much of the sediment in these peaks is aggregates. The two aggregate classes represent this sediment. The primary clay, silt, and sand classes represent the sediment that is eroded as primary particles.

RUSLE2 computes the distribution of these five particle classes and the diameters of the small and large aggregate classes at the point of detachment as a function of soil texture.[26]

[26] The equations used by RUSLE2 are described by Foster, G.R., R.A. Young, and W.H. Neibling. 1985. Sediment composition for nonpoint source pollution analyses. Trans. ASAE 28(1):133-139, 146.

Cover-management also affects sediment characteristics. Increased soil biomass increases the fraction of the sediment composed of aggregates and the size of the aggregates. However, sufficient experimental data are not available to derive equations to describe how cover-management affects sediment characteristics.

In general, the fractions and diameters for the aggregate classes increase as the soil's clay content increases. Clay is assumed to be a binding agent that increases aggregation. .

Table 7.4. Sand, silt, and clay contents assigned for a textural class. Based on USDA classification.

Textural class	Sand (%)	Silt (%)	Clay (%)
Clay	20	20	60
Clay loam	33	33	34
Loam	41	41	18
Loamy sand	82	12	6
Sand	90	6	4
Sandy clay	51	5	44
Sandy clay loam	60	13	27
Sandy loam	65	25	10
Silt	8	87	5
Silt loam	20	65	15
Silty clay	6	47	47
Silty clay loam	10	56	34

Table 7.5. Characteristics of sediment classes assume

Sediment class	Density (specific gravity)	Diameter (mm)	
Primary clay	2.6	0.002	Fraction = 0.2
Primary silt	2.65	0.01	Fraction strong
Small aggregate	1.8	0.03 to 0.1	Fraction and d
Large aggregate	1.6	0.3 to 2	Fraction and d
Primary sand	2.65	0.2	Fraction strong

Values assumed by RUSLE2 for each sediment class are listed in Table 7.5. Fall velocity V_f of each sediment class is used in equation 5.2 to represent sediment "depositability." Fall velocity is a function of diameter and density of the sediment particles. RUSLE2 computes fall velocity using Stokes law for the small particle classes and standard drag relationships for the large particle classes assuming that the sediment particles are spheres.

Table 7.6. Sediment characteristics for a silt loam soil (20% sand, 60% silt, 20% clay) at detachment and (0% sand, 56% silt, 44% clay) after deposition by a dense grass strip on the lower 10% of slope length.

Sediment class	Diameter (mm)	% at detachment	% after deposition
Primary clay	0.002	5	43
Primary silt	0.01	24	54
Small aggregate	0.03	36	3
Large aggregate	0.4	28	0
Primary sand	0.2	7	0

Deposition enriches the sediment load in fines, which RUSLE2 computes as illustrated in Table 7.6. Deposition changes the distribution of the sediment classes from that at the point of detachment. RUSLE2 also computes the sand, silt, and clay content in the sediment leaving the RUSLE2 hillslope profile. RUSLE2 computed that the fraction of primary clay sediment class leaving the grass filter strip after deposition is 43% in comparison to 5% at the point of detachment in the example illustrated in Table 7.6. Also, the total clay content in the sediment was 44% versus 20% in soil surface layer.

RUSLE2 assumes that small aggregates are composed of clay and silt primary particles and that large aggregates are composed of clay, silt, and sand primary particles. RUSLE2 computes the distribution of these particles in each aggregate class as a function of soil texture. RUSLE2 also computes an enrichment ratio as specific surface area of the sediment at the lower end of the last RUSLE2 element divided by the specific surface area of the sediment at the point of detachment. The enrichment ratio for the Table 7.6 example is 1.9, which means that the specific surface area of the sediment is almost twice that of the soil. The specific surface areas assumed in RUSLE2 for primary particles are 20 m^2/g for clay, 4 m^2/g for silt, and 0.05 m^2/g for sand. Specific surface area indicates the relative importance of each primary particle class as a binding agent and for transporting soil-absorbed chemicals. The specific surface area of each aggregate class depends on the composition of primary particles.

7.6.2. User entered values.

Although the RUSLE2 names assigned the five sediment classes are arbitrary, the names of the classes and the number of classes can not be changed. However, values for fraction, diameter, and density assigned to each class can be user overwritten to create a

custom sediment description. RUSLE2 does not properly compute enrichment if these values are manually overwritten.

7.7. Rock Cover

Rock cover on the soil surface acts as ground cover and reduces erosion much like plant litter, crop residue, and applied mulch, except that rock does not decompose and add biomass to the soil. RUSLE2 combines rock cover with other ground cover to obtain a single composite ground cover value, taking into account the overlap of plant and applied materials on the rock cover. This single ground cover value is used in the equations that compute cover-management effects on erosion (See **Section 9.2.2**.). This overlap of cover is the reason that values for rock cover and other ground cover cannot be added to obtain the total cover. Also, the effects of rock and other ground cover cannot be computed separately and then combined to determine the total ground cover effect because of the nonlinearity in the equation used to compute the ground cover effect on erosion.

The nonlinearity in the equations used to compute the ground cover effect is the reason that a K factor value cannot be used in RUSLE2 where an adjustment has already been made for rock cover.

RUSLE2 handles "rock cover" entered as a soil input differently than ground cover added through a cover-management input. The soil input rock cover remains constant through time, is not buried, and does not decompose. The rock cover variable can also be used to represent mosses, which provide substantial ground cover on rangelands, and other types of ground cover that can be assumed remain constant through time.

See Section 12 for special considerations needed when a mechanical soil disturbance is used to bury rock or other material that does not decompose.

The soil rock cover input is a site-specific entry based on field measurements. The same technique used to measure other ground cover like plant litter and crop residue can be used to measure rock cover.[27] To be counted as ground cover, rock must be sufficiently large not be moved by raindrop impact or surface runoff. The minimum rock size that is measured is site specific, but as a guideline, the minimum rock size is 10 mm (3/8 inch) diameter except on coarse texture rangeland soils where the minimum size is 5 mm (3/16 inch).

[27] A typical procedure used to measure ground cover is to lay a line transect, such as a knotted string or measuring tape, across the soil surface diagonal to any cover orientation. An estimate of ground cover is the percentage of knots or markings on a tape that contact ground cover. Another approach is to photograph the surface, lay a grid over the photograph, and count the intersection points that touch ground cover.

Do not use rock cover values or rock content in the soil profile from the NRCS soil survey database to determine rock cover. The definitions of rock cover in that database do not correspond with RUSLE2 definitions.

The appropriate time to measure rock cover is during the 1/4 to 1/3 period of the year or crop rotation when the hillslope is most susceptible to erosion. Measure rock cover on cultivated land after rainfall has exposed the rock so that the rock and its influence can be readily seen.

7.8. Hydrologic Soil Group

Hydrologic soil group is an index of the runoff potential of the soil under unit plot conditions. These designations are A (lowest potential), B, C, and D (highest potential). **RUSLE2** uses the hydrologic soil designation in the NRCS curve number method to compute runoff. Hydrologic soil group designations are available by map unit and component in the NRCS soil survey database. The USDA-NRCS hydrology manual provides information on assigning hydrologic soil group designations for those soils not included in the NRCS soil survey.[28] The soils with the lowest runoff potential, such as deep sandy soils, are assigned an A hydrologic soil group. The soils where almost all of the rainfall becomes runoff are assigned a D hydrologic soil group. Examples of hydrologic group D soils include high clay soils and silt soils that readily crust causing significantly reduced infiltration. Soils having a restrictive layer like a fragipan, rock, plow pan, or traffic pan near the soil surface also are assigned a D hydrologic soil group.

RUSLE2 uses the hydrologic soil group designations for drained and undrained conditions to compute the soil loss reduction caused by tile and other drainage practices. The equation used in the soil erodibility nomographs for the effect of permeability on soil erodibility are used to compute the effect of drainage on erosion. The four hydrologic soil groups are scaled over the six permeability classes so that a hydrologic soil group designation can be converted to a permeability class to use the erodibility nomograph equation.[29]

Two hydrologic soil group designations are entered for a soil. One is for the **undrained** condition and one for the **drained** conditions. Runoff potential can be high because of a perched water table or the soil occupying a low-lying position on the hillslope even though soil properties would indicate a low runoff potential. Artificially draining these

[28] Contact the NRCS Internet site at www.nrcs.usda.gov for additional information

[29] Although hydrologic soil group and the permeability class are directly related, RUSLE2 requires separate inputs for these two variables. Therefore, the user needs to ensure that the inputs for these variables are consistent when one of the nomograph is used to compute a K value.

soil with deep parallel ditches or buried tile lines can greatly increase internal drainage and reduce surface runoff and erosion.

The hydrologic soil group assigned for the drained condition represents runoff potential under drained conditions based on soil properties and assuming a high performance drainage system. A drained soil does not imply that an A hydrologic soil group should be assigned. For example, a drained sandy soil might be assigned an A hydrologic soil group whereas a drained clay soil might be assigned a C hydrologic soil group because the clay limits internal drainage and infiltration.

7.9. Time to Soil Consolidation

RUSLE2 assumes that the soil is 2.2 times as erodible immediately after a mechanical disturbance than after the soil has become "fully consolidated."[30] Erosion decreases with time and "levels out" as illustrated in Figure 7.3. A double exponential decay curve is used to describe this decrease in erodibility. The equation used in RUSLE2 for this curve was derived from erosion data at Zanesville, OH that were collected over time after tillage stopped on a fallow plot. The time required for the erosion rate to "level out" after a mechanical disturbance is the **time to soil consolidation**. Erodibility of a fully "consolidated" soil is 45 percent of that immediately after mechanical disturbance. The time to consolidation is at the time when 95 percent of the decrease in erodibility has occurred.[31]

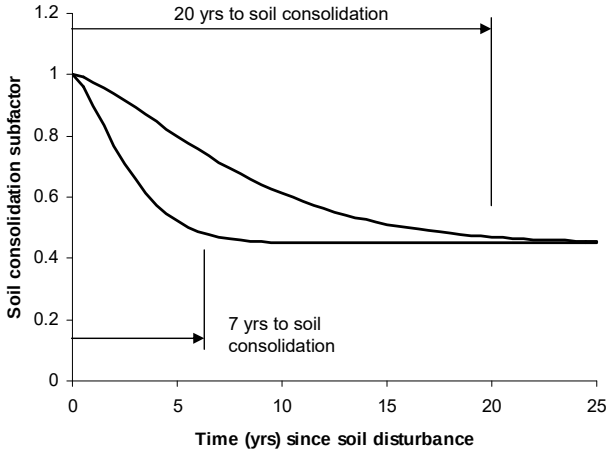

Figure 7.3.Effect of time on decrease in soil erodibility following a mechanical disturbance.

This decrease in erodibility occurs because of soil wetting and drying and biological soil activity. RUSLE2 assumes seven years for the **time to soil consolidation,** but another value can be entered. Also, RUSLE2 can compute the time to soil consolidation based on average annual precipitation as describe below.

[30] Soil consolidation does not refer to the physical process of the bulk density of the soil increasing over time. Instead, it refers to a change in erodibility over time.

31 The 95 percent is used rather than 100 percent because the equation from is such that an infinitely long time is required for the computed values to actually reach the fully consolidated condition.

Time to soil consolidation is a function of soil properties. However, insufficient data are available to derive a relationship between soil properties and time to soil consolidation and soil properties and the degree of soil consolidation. The degree of soil consolidation (i.e., the increase in erodibility because of a mechanical disturbance, is less for a high sand soil than for a high clay soil. Also, the relative effect of mechanical disturbance seems to be greater for rill erosion than for interrill erosion.

Answering **Yes** to the question, **Calculate time to consolidation from precipitation**, causes RUSLE2 to compute a **time to soil consolidation** that is a function of average annual precipitation. RUSLE2 assumes seven years for the **time to soil consolidation** where average precipitation exceeds 30 inches (760 mm) and computes a **time to soil consolidation** that increases to 20 years in the driest areas of the Western US, as illustrated in Figure 7.3. The time to soil consolidation increases linearly from 7 years to 20 years between as average annual precipitation decreases from 30 inches (760 mm) to 10 inches (250 mm). A value of 20 years for time to soil consolidation is assumed for average annual precipitation less than 10 inches (250 mm). This increased time to soil consolidation reflects how the effects of a mechanical soil disturbance persist longer in low precipitation areas where reduced water is available and less frequent wetting and drying cycles occurs.

7.10. Soil Loss Tolerance (T)

The objective in conservation and erosion control planning is to control average annual erosion to an acceptable level.

7.10.1. Purpose of "T-value" input

The "T-value" in the RUSLE2 soil database component is the acceptable average annual rill-interrill erosion rate for a particular situation. RUSLE2 is used to identify erosion control practices that give estimated rill-interrill erosion equal to or less than the "T-value" assumed in the particular conservation planning application. In many cases, the T-value used in conservation planning will the NRCS-assigned soil loss tolerance value.

The "T-value" varies with the situation. For example, the "T-value" can be increased from the standard soil loss tolerance T-value for construction sites where the soil is exposed to erosion for a relatively short time. The standard soil loss tolerance T-value is used for cropland where long term productivity must be maintained or landfills where the buried waste must be protected from exposure by erosion over hundreds of years. An especially low "T-value" may be required to control off-site sediment delivery to protect a sensitive downstream resource such as a fish habitat. In many RUSLE2 applications, the "T-value" is determined by applicable government program or regulations.

The "T-value" entered in the RUSLE2 soil database component should be appropriate for the particular application.

Rather than reducing erosion to an absolute "T-value," the erosion control objective in some applications is to reduce erosion by a certain percentage relative to a base condition. Although a "T-value" is not needed in those applications, a nonzero "T-value" must be entered so that RUSLE2 can compute the ratio of segment erosion to the "T-value" adjusted for slope position, as discussed below.

7.10.2. NRCS-assigned soil loss tolerance values

Soil loss tolerance values assigned to each soil map unit by NRCS as a part of its soil survey program are often entered in RUSLE2 as the "T-value." Soil loss tolerance values range from 1 tons/acre (2 t/ha) per year to 5 tons/acre (11 t/ha) per year based primarily on how erosion is judged to harm the soil and to cause other damage. Shallow and fragile soils that can not be easily reclaimed after serious erosion are assigned low soil loss tolerances values. Limiting erosion rate to soil loss tolerance protects the soil as a natural resource and maintains the soil's long term productive capacity. Soil loss tolerance values consider the damages caused by erosion and the benefits of soil conservation. Also, soil loss tolerance values include a socio-economic element by considering the availability of reasonable and profitable erosion control technology.[32]

Although soil loss tolerance values were principally developed for cropland soils, soil loss tolerance values are also used for erosion control planning for reclaimed surface mines, landfills, and military training sites. Applying mulch controls erosion and promotes seed germination and early growth of vegetation. Erosion control facilitates establishing and maintaining vegetation, which is essential to long term site protection and similar to cropland requirements. Reclaimed land regulations require that excessive rill erosion be prevented. A rule of thumb is that rill erosion begins when soil loss for the eroding portion of the overland flow path exceeds about 7 tons/acre (15 t/ha) per year. A major concern on waste disposal sites is that buried waste not be exposed by rill erosion. Controlling soil loss to less than 5 tons/acre (11 t/ha) per year significantly reduces the likelihood of rill erosion. A well designed surface runoff collection system in addition to the rill and interrill erosion control practice is also required to prevent incised gully erosion.

Soil loss tolerance values are primarily for protecting the soil as a natural resource and not for protecting offsite resources from excessive sedimentation or water quality degradation. The criteria for controlling sediment yield from a site should be based on potential off-site sediment damages.

---

[32] The factors considered in assigning soil loss tolerance values are discussed by Toy, T.J., G.R. Foster, and K.G. Renard. 2002. Soil Erosion: Processes, Prediction, Measurement, and Control. John Wiley and Son, New York, NY. The definition for soil loss tolerance given in AH537 implies that erosion can occur indefinitely at soil loss tolerance even though soil loss tolerance values exceed soil formation rates by about a factor of ten.

7.10.3. Taking hillslope position into account

A uniform slope for the **eroding portion** of the overland flow path is usually assumed in analyses where soil loss tolerance values are used in erosion control planning. See **Section 5.2** and Figures 5.2 and 5.3 for illustrations of overland flow paths and the eroding portion of an overland flow path. **Soil loss** is computed for this uniform profile and compared to the soil loss tolerance value. A satisfactory erosion control practice is one that reduces soil loss to the "T-value" or less.

However, special considerations should be given to applying soil loss tolerance values where steepness varies along the overland flow path. Average erosion for the profile is underestimated when a uniform profile is assumed for convex shaped profiles and overestimated for concave profiles. This difference is illustrated in Table 7.7 were average erosion is computed for uniform and convex profiles of the same length and average steepness. The average erosion for the convex profile is about 25% greater than the average erosion for the uniform profile. The difference in the erosion between the profiles increases as the degree of curvature of the convex profile increases. The ratio of steepness at the end of the convex slope to average steepness is a measure of curvature. In this example, the steepness at the end of the convex slope is about 1.7 times the average steepness of the profile.

An erosion control approach is to reduce the average erosion for the convex profile to the "T-value," which is illustrated in the two right hand columns of Table 7.7. Average erosion rate does not adequately account for the high erosion rate at the end of convex profiles. The erosion rate on the last segment at the end of the convex profile illustrated in Table 7.7 is more than twice the average erosion rate for the profile. The erosion rate at the very end of the convex profile is higher yet. Therefore, average erosion for the entire profile is not a satisfactory erosion control measure for a convex profile, especially one with significant curvature. Extra protection is needed on the lower end of the convex profile to provide comparable erosion control to that on the uniform profile.

Table 7.7. Soil loss along uniform and convex profiles of same length and average steepness. A = average erosion for entire profile and Adj T = T-value adjusted for position on profile. Assume "T-value" = 5.0.

	Uniform			Convex				
				Same practice as uniform profile			Practice changed to give same A as for uniform profile	
Segment	Steepness (%)	Segment erosion	Erosion/ Adj T	Steepness (%)	Segment erosion	Erosion/ Adj T	Segment erosion	Erosion/ Adj T
1	6	2.50	0.99	2	1.09	0.32	0.88	0.26
2	6	4.22	1.00	4	2.85	0.65	2.29	0.52
3	6	5.29	1.00	6	5.29	1.00	4.26	0.81
4	6	6.12	1.00	8	8.44	1.40	6.81	1.10
5	6	6.84	1.00	10	13.10	1.80	10.50	1.50
		A = 5.0			A = 6.2		A = 5.0	

An erosion control approach for convex profiles could be to reduce erosion rate on the last segment to the "T-value." However, erosion rate for each segment is a function of the segment length. Basing erosion control on segment erosion would make erosion control a function of segment length, which is improper. An alternative approach is to reduce "point" erosion rate to be less than the "T-value," but this approach provides greater protection for the convex profile than is considered necessary for the uniform profile having the same average steepness as the convex profile. Thus, the two profiles are not being compared on an equal basis.

Erosion rate increases along a uniform profile so that the erosion rate at the end of the uniform profile is substantially higher than the "T-value" when average erosion for the profile equals the "T-value." The erosion rate on the last segment on the uniform profile illustrated in Table 7.7 is 6.8, which is about 35% greater than the "T-value." Therefore, a procedure is needed that puts non-uniform profiles on the same basis as uniform profiles when comparing segment erosion to "T-values."

RUSLE2 computes the ratio of segment erosion to T adjusted for position to put erosion on an equal basis when comparing non-uniform shaped profiles.

RUSLE2 computes a **ratio of segment erosion to a "T-value" adjusted for position along the profile** so that erosion on non-uniform shaped profiles can be compared on an equal basis to erosion on uniform profiles when selecting erosion control practices.[33] The reason for having the comparison on an equal basis is that the soil loss tolerance concept is based on a uniform profile. The erosion control objective is that the ratio of segment erosion to "T-value" adjusted for position should be one or less. Note that this ratio is 1

[33] See AH703 for a discussion of this adjustment, including the mathematics used to make the adjustment.

everywhere along the uniform profile illustrated in Table 7.7, which shows that the ratio takes out the position effect along the profile in comparing segment erosion values to "T-values."

The analysis involving the ratio of segment erosion to "T-values" adjusted for position along the profile should be for the eroding portion of the profile and not include depositional portions of concave profiles.

The same level of erosion control is achieved on the convex profile as on the uniform profile when the ratio of segment erosion to "T-value" adjusted for slope position is one or less for all segments. In the example in Table 7.7, the convex profile requires increased erosion control on the last two segments than is required on the uniform profile of the same average steepness as the convex profile because the convex profile accelerates erosion near its end. Similarly, less erosion control is needed on the upper three segments than on the uniform profile because the ratio of segment erosion to "T-value" adjusted for position is less than 1. In this example, the average erosion for the convex profile must be reduced to 3.3 tons/acre to provide the same level of erosion control on the last segment of the convex profile as provided on the last segment of the uniform profile.

8. TOPOGRAPHY

Topographic information is stored in the profile and worksheet components of the RUSLE2 database. Topography is a part the overall description of an **overland flow path** that includes information on cover-management, soil, and steepness along the flow path. This description involves three layers of information, illustrated in Figure 8.1. An overland flow path is also referred to as a RUSLE2 **hillslope profile**.

Segments are created for each layer by specifying the locations where cover-management, soil, or steepness changes along the flow path. Inputs are selected from the RUSLE2 database for each management and soil segment, and values for segment break locations and steepness are user entered. Thus, RUSLE2 computes how change in cover-management, soil, and steepness along the overland flow path affect erosion and deposition. Segment break locations need not coincide among the layers as illustrated in Figure 8.1.

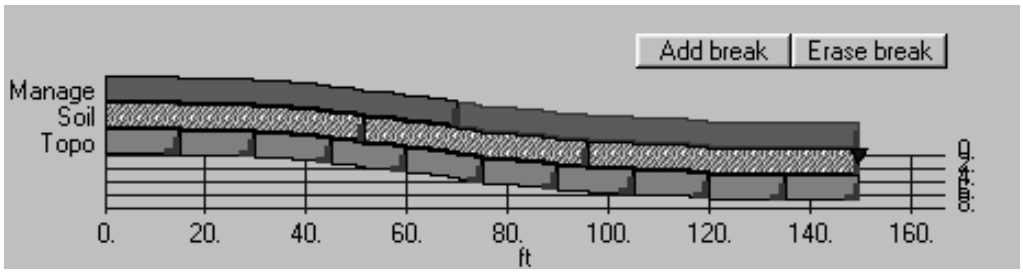

Figure 8.1. Schematic of the three layers that represent an overland flow path (a RUSLE2 hillslope profile).

8.1. Basic Principles

RUSLE2 uses equation 5.4 to compute erosion along an overland flow path. For generality, assume that all RUSLE2 profiles are composed of multiple segments, like Figure 8.1. Each layer (management, soil, topography) has its own segments. RUSLE2 assembles the segments for each layer into a composite set of segments. A composite segment end is located at a change in any one of the three layers.

8.1.1. Detachment

The computations that solve equation 5.4 start at the upper end of the overland flow path and step down slope segment by segment, which "routes" the water and sediment down slope. The sediment load g_{in} entering a particular segment is known from the computation of the sediment load g_{out} leaving the adjacent upslope segment. No sediment enters the first segment because it is at the origin of the overland flow.

The amount, expressed as mass per unit area, of net detached sediment (sediment produced) within the *ith* segment is computed with:

$$D_i = rkScp_c(x_i^{m+1} - x_{i-1}^{m+1}) / \lambda_u^m (x_i - x_{i-1}) \quad \textbf{[8.1]}$$

where: D_i = net detachment (mass/area), r = erosivity factor, k = soil erodibility factor, S = slope steepness factor, c = cover-management factor, p_c = contouring factor, x_i = distance to lower end of the segment, x_{i-1} = distance to the upper end of the segment, λ_u = length of the unit plot (either 72.6 ft or 22.1 m), and m = slope length exponent. All variables are for a particular day and for the *ith* segment.34 Equation 8.1 is equation 5.1 applied to a segment.

The slope length exponent **m** for the *ith* segment is computed from:

$$m = \beta/(1+\beta) \quad \textbf{[8.2]}$$

where: β = ratio of rill to interrill erosion for the *ith* segment, which in turn is given by:

$$\beta = \left[\frac{k_r}{k_i}\right]\left[\frac{c_{pr}}{c_{pi}}\right]\left[\frac{\exp(-0.05 f_g)}{\exp(-0.025 f_g)}\right]\left[\frac{(s/0.0896)}{3s^{0.8}+0.56}\right] \quad \textbf{[8.3]}$$

where: k_r/k_i = the ratio of rill erodibility to interrill erodibility; c_{pr}/c_{pi} = the ratio for below ground effects for rill and interrill erosion, respectively, which is a prior land use type effect; $\exp(-0.05f_g)/\exp(-0.025\ f_g)$ = the ratio of the ground cover effect on rill and interrill erosion, respectively; $(s/0.0896)/(3s^{0.8}+0.56)$ = the ratio of slope effects for rill and interrill erosion, respectively; s = sine of the overland flow path slope angle; and f_g = percent ground cover.[35] All variables in equation 8.3 are for the *ith* segment. The ratio k_r/k_i is computed as a function of soil texture where the ratio decreases as clay increases because clay makes the soil resistant to rill erosion. The ratio increases as silt increases because silt decreases the resistance of soil to rill erosion. The ratio c_{pr}/c_{pi} represents how rill erosion decreases relative to interrill erosion as both soil consolidation and soil biomass increase. The term $\exp(-0.05f_g)/\exp(-0.025f_g)$ represents how ground cover has a greater effect on rill erosion than on interrill erosion. The term $(s/0.0896)/(3s^{0.8}+0.56)$ represents how slope steepness has a greater effect on rill erosion than on interrill erosion.

---

[34] See the RUSLE Science Documentation for a complete description of the equations used in RUSLE2. The equations in this RUSLE2 User's Reference Guide are for illustration only and are not the complete equations.

[35] Equation 8.3 replaces the selection of an LS "Table" in RUSLE1.05 and earlier RUSLE1 versions and replaces having to select a land use in RUSLE1.06. RUSLE2, in effect, selects the proper LS relationship based on cover-management conditions.

A constant value of 0.5 is used for m in the Req zone.

The RUSLE2 slope length effect from equation 8.1 is:

$$L_i = (x_i^{m+1} - x_{i-1}^{m+1}) / \lambda_u^m (x_i - x_{i-1}) \quad \textbf{[8.4]}$$

where: L_i = the slope length factor for the *ith* segment. The slope length effect in RUSLE2 adjusts soil loss from the unit plot up or down depending on whether the ith segment position is located less or greater than the unit-plot length λ_u of 72.6 ft (22.1 m) from the upper end of the overland flow path. Values for the slope length effect are less than 1 when location of the segment is less than the unit plot length and greater than 1 when the location is greater than the unit plot length.

The slope length effect in RUSLE2 is a function of rill erosion relative to interrill erosion except in the Req zone. Interrill erosion is assumed to be caused by raindrop impact and therefore independent of location along the overland flow path, assuming that the variables that affect interrill erosion are constant along the overland flow path. Rill erosion is assumed be caused by surface runoff and to vary linearly along the overland flow path because of runoff accumulation. The slope length exponent **m** in equation 8.2 varies between 0 and 1 and reflects the relative contribution of rill and interrill erosion. The exponent m is near 0 when almost all of the erosion is by interrill erosion, such as on a flat slope, and m is near 1 when almost all of the erosion is from rill erosion, such as on a bare, steep slope. Slope steepness, cover-management, and soil affect RUSLE2's slope length effect because of their different effect on rill erosion relative to interrill erosion. The RUSLE2 slope length effect varies daily as cover-management conditions change. The USLE slope length factor is independent of the other USLE factors, except for slope steepness. The RUSLE1 slope length factor only partially varies with the other RUSLE1 factors.

RUSLE2 spatially integrates equation 5.4 in its computations. A spatial integration of the USLE and RUSLE1 is possible for a limited set of conditions, but the integration must be done manually and is laborious. Few users perform the integration. RUSLE2 performs the integration internally without extra steps required of the user other than to divide the overland flow path into segments and specify the inputs for each segment. Just as RUSLE2 differs from RUSLE1 and the USLE in temporal integration, RUSLE2 also differs from them in spatial integration and interaction among factors. Although RUSLE2 uses fundamentals from the USLE and RUSLE1, RUSLE2 is essentially a new model. These mathematical differences give RUSLE2 much more power than the other equations.[36]

[36] The difference in temporal integration can result in as much as 20% differences in erosion estimates between RUSLE2 and the USLE and RUSLE1. The difference in spatial integration between RUSLE2 and RUSLE1 is generally not great provided the proper selections are made in RUSLE1. However, few users

The RUSLE2 slope steepness factor is computed with:

$$S = 10.8s + 0.03 \qquad \text{slope} < 9\% \qquad \textbf{[8.5]}$$

$$S = 16.8s - 0.50 \qquad \text{slope} \geq 9\% \qquad \textbf{[8.6]}$$

for all areas except the Req zone, where equation 8.7 is used.

$$S = (s / 0.0896)^{0.6} \qquad \text{slope} \geq 9\% \qquad \textbf{[8.7]}$$

where: slope = slope steepness in percent.[37] The slope steepness factor S has a value of 1 for a 9% slope. Values for the S factor are less than 1 for slope steepness less than 9 percent and greater than 1 for slope steepness greater than 9 percent. The slope steepness factor in RUSLE2 adjusts the soil loss values from the unit plot up or down depending on whether the field slope is steeper or flatter than the 9 percent steepness of the unit plot.

The slope steepness S factor should be a function of the soil and cover-management similar to equation 8.3. However, neither the empirical data nor theory is sufficient for incorporating those effects into RUSLE2.

8.1.2. Runoff

RUSLE2 uses discharge (flow) values for runoff to compute sediment transport capacity, contouring effectiveness, and critical slope length for contouring. Discharge rate at a location is computed from:

$$q = q_{i-1} + \sigma_i (x - x_{i-1}) \qquad \textbf{[8.8]}$$

where: q = discharge rate (volume/width·time) at the location x between the segment ends x_{i-1} and x_i, q_{i-1} = discharge rate at x_{i-1}, and σ_i = excess rainfall rate (rainfall rate - infiltration rate) on the *ith* segment. Excess rainfall rate is computed using the NRCS runoff curve number method that computes runoff depth. RUSLE2 assumes that runoff rate is directly proportional to runoff depth. RUSLE2 computes curve number values, the major parameter in the NRCS curve number method, as a function of hydrologic soil group, soil surface roughness, ground cover, soil biomass, and soil consolidation to represent the effect of cover-management on runoff. In general, RUSLE2 computes reduced runoff as these variables increase, except for soil consolidation that interacts with soil biomass. If soil biomass is very low, soil consolidation increases runoff, typical of a bare construction site. If soil biomass is high, typical of high production pasture, soil

---

properly select inputs for RUSLE1 to achieve this similarity in results.

[37] The slope factor equations are the same in RUSLE2 and RUSLE1.

consolidation decreases runoff.[38] The curve number method is configured within RUSLE2 to compute negative values for rainfall excess (σ) so that RUSLE2 can compute decreasing discharge along a segment having very high infiltration that receives run-on from upslope.

Discharge in RUSLE2 is typically used as a ratio of discharge computed for a given condition to a base runoff computed for moldboard plowed, clean tilled, low yielding corn grown on a silt loam soil in Columbia, MO. RUSLE2 starts with empirical erosion factor values taken from AH537, which is a summary of data collected over a wide range of conditions at many locations. RUSLE2 uses ratios, such as the one involving discharge, in process-based equations to adjust the empirical erosion factor values up or down from a base value. RUSLE2 often computes a departure from a base value rather than an absolute value. Computing departures is more stable and robust than computing absolute values. This approach combines the best of empirically based and process based variables and equations.

Columbia, MO is used as a base because it is centrally located in the US and represents "typical" weather values in the eastern US. The moldboard plowed, clean-tilled, row cultivated corn best represents the condition for contouring and critical slope length values in AH537. These AH537 values are directly related to runoff and serve as calibration data.

8.1.3. Sediment transport capacity

Sediment transport capacity ($T_{c,up}$ and $T_{c,low}$) is computed at both the upper (x_{i-1}) and lower (x_i) ends of each segment using equation 5.3 and the discharge rates and slope steepness of the segment. This approach results in a step change in sediment transport capacity at segment ends, even when steepness varies smoothly in continuous fashion. Slope steepness values for adjacent segments could have been averaged to obtain a smoothly varing transport capacity along the slope. However, such an approach would have increased the difficulty for users to represent sharp changes in steepness, such as the flat top and steep sideslope of a landfill. Transport capacity is also a step function where cover-management conditions, such as at the upper end of a grass strip change as a step function, or slope steepness changes as a step function, such as the change in steepness from the top of a landfill to the sideslope. RUSLE2 computes transport capacity at the lower end of a segment based on conditions for that segment and at the upper end of the adjacent segment using the conditions for that segment to capture step changes. These step changes in transport capacity are illustrated in Figure 8.2.

The product qs in Equation 5.3 represents runoff erosivity. It is proportional to runoff's total shear raised to the 3/2 power. Total shear stress is divided between that acting on the soil (skin friction) and that acting on form roughness elements (form friction). The

[38] Soil consolidation is used as an indicator variable, not as a cause and effect variable.

shear stress acting on the soil is assumed to be responsible for runoff transporting sediment. The coefficient K_T is a measure of the fraction of the flow's total shear stress that acts on the soil to transport sediment. Values for K_T and transport capacity decrease as form hydraulic roughness increases even though total hydraulic roughness increases..

Manning's n is a measure of form and grain (skin) roughness combined. RUSLE2 uses Manning's n values to compute K_T values. In turn, RUSLE2 computes values of Manning's n as a function of standing live and dead vegetation, ground cover, and surface roughness, which are form roughness elements.

The variable K_T is also a calibration coefficient that represents transportability of the sediment. RUSLE2 does not vary K_T as a function of sediment properties, which means that sediment transport capacity is not a function of sediment characteristics. A base value for K_T was determined by calibrating RUSLE2 to a field plot experiment of deposition on a concave slope. The steepness of this concave slope decreased from 18% at the its upper end to 0% at its lower end. Deposition began at the location where steepness was 6%. This condition was assumed to represent moldboard plowed, clean tilled, low yield corn on a silt loam soil at Columbia, MO. The calibration was checked against general field observations and data from laboratory experiments on sediment transport and deposition.

8.1.4. Sediment routing

Several cases must be considered in routing the sediment down slope (i.e., solving equation 5.4 sequentially by segment starting at the upper end of the overland flow path).

8.1.4.1. Case 1: Detachment over the entire segment

Detachment occurs over the entire segment when the transport capacity $T_{c,up}$ at the upper end of the segment is greater than the incoming sediment load g_{in} and the transport capacity $T_{c,low}$ at the lower end of the segment is greater than the maximum possible sediment load at the lower end of the segment. The maximum possible sediment load is the incoming sediment load plus the sediment produced within the segment by detachment. This case occurs on uniform and convex shaped slopes and the upper portion of a concave slope.

Sediment load at the lower end of the segment is given by:

$$g_{out} = g_{in} + D_i(x_i - x_{i-1}) \qquad \textbf{[8.9]}$$

where: D_i = net detachment (sediment production) computed with equation 8.1 for the *ith* segment.

Another possibility is that the potential sediment load computed with equation 8.9 exceeds transport capacity at the lower end of the sediment while the potential sediment load based on interrill erosion is less than transport capacity. If this condition exists, RUSLE2 computes a reduced rill erosion so that the sediment load at the end of the segment just fills transport capacity without overfilling it.

RUSLE2 assumes that interrill erosion always occurs at a "capacity" rate. Interrill erosion is computed like net detachment (equation 8.1) except for an interrill erosion slope steepness factor, the slope length factor being 1 (i.e., interrill erosion does not vary by location along the overland flow path), and multiplying by 0.5 based on the assumption that interrill erosion equals rill erosion for unit-plot conditions. The RUSLE2 equation for interrill erosion rate is:

$$D_{ir,i} = 0.5rk(3s^{0.8} + 0.56)cp_c \qquad \textbf{[8.10]}$$

No local deposition occurs for **Case 1** conditions when slope steepness is sufficiently steep.[39] However, at low steepness, interrill erosion can be greater than sediment transport capacity, which causes local deposition. Local deposition occurs where interrill erosion rate exceeds the increase in transport capacity with distance (i.e, $D_{ir} > dT_c/dx$). Equation 8.1 empirically includes local deposition in its computation of net detachment. Local deposition is selective causing coarse particles to be deposited and the sediment load to be enriched in fine particles. RUSLE2 uses the procedure that computes deposition in **Case 2** to compute sediment characteristics and the enrichment ratio for this local deposition (See **Section 7.5**).

The distribution of the sediment added to the sediment load by detachment is the sediment distribution at the point of detachment described in **Section 7.5**. The particle class distribution in the sediment load is the same as that at the point of detachment unless local deposition or remote deposition is computed.

8.1.4.2. Case 2: Deposition over the entire segment

Deposition occurs along an entire segment when the sediment load exceeds transport capacity at both the upper and lower ends of the segment. An example of this case is deposition in a narrow grass strip illustrated in Figure 8.2. Table 7.6 shows values computed by RUSLE2 for an example like this case.

---

[39] **Local deposition** is deposition very close (few inches, tens of millimeters) to the detachment point. Deposition in the depressions on a rough soil surface is an example of local deposition. **Remote deposition** is deposition a considerable distance (tens of feet, several meters) from the detachment point.

Equation 5.2, which computes deposition, is applied to each particle class. Sediment characteristics used in these computations are described in **Section 7.5.** The transport capacity for each particle class is computed by dividing the total sediment transport capacity computed with equation 5.3 among the particles in proportion to the mass distribution of the sediment classes in the total sediment load. The distribution of sediment transport capacity among the particle classes changes as deposition occurs along the overland flow path because each particle class is deposited at a different rate based on fall velocity

Equation 5.2 has two unknowns, deposition rate and sediment load. Equation 5.2 is combined with the continuity equation to solve for deposition rate and sediment load. The continuity equation for **Case 2** is:[40]

$$\Delta g / \Delta x = D_{ir} + D_p \qquad \textbf{[8.11]}$$

where: $\Delta g/\Delta x$ is the change in sediment load Δg over the distance Δx, D_{ir} = interrill erosion and D_p = deposition rate.

An important assumption involves interrill erosion in equation 8.11. **Does interrill erosion occur simultaneously with deposition?** CREAMS assumes that rill erosion **does not** occur simultaneously with deposition, while RUSLE2 assumes that interrill erosion **does** occur simultaneously with deposition. This assumption is valid for interrill erosion on ridges where deposition occurs in the furrows between the ridges. However, the assumption is not clear-cut where deposition occurs on flat soil surfaces, such as the toe of a concave slope. Deposition is dynamic and spatially varied. Flow depth and transport capacity vary considerably across the slope leaving "exposed" areas where interrill erosion occurs. Deposition and flow patterns change during deposition.[41]

While not a perfect assumption, RUSLE2 assumes that interrill erosion occurs simultaneously with deposition. A consequence of this assumption is that less enrichment of sediment in fines is computed than when no interrill erosion is assumed.

Equations 5.2 and 8.11 and transport capacity being distributed among particles classes based on their distribution in the sediment load creates a very complex and interactive set of equations to be solved. The equations are solved numerically in RUSLE2 because simple, closed form solutions were not found. The RUSLE2 numerical solution divides the portion of the overland flow path where deposition occurs into small sub segments. Decreasing sub segment length increases computational accuracy but noticeably

[40] The sign convention is that detachment is positive (increases the sediment load) and deposition is negative (decreases the sediment load).
[41] See Toy et al. (2002) for additional discussion.

increases computational time, which required a compromise between the two. The procedure was carefully designed to minimize differences related to how a user segments the overland flow path. The user will seldom see much effect of segment division on RUSLE2 results. The accuracy of the deposition computation with respect to the numerical solution matching the "true" mathematical solution is well within the overall accuracy of RUSLE2.

RUSLE2 computes deposition rate, total sediment load, and the sediment load of each particle class along each segment. The sediment load g_{out} leaving the segment is the sediment load computed at the end of the segment, which is the sediment load g_{in} entering the next downslope segment. The distribution of the particle classes in the sediment load indicates how deposition enriches the sediment in fines. RUSLE2 computes an enrichment ratio based on specific surface area of the sediment at the end of the last segment on the overland flow path (See **Section 7.5**). The value computed for enrichment ratio is related to the fraction of the sediment load that is deposited. The enrichment ratio increases as the deposition fraction increases.

8.1.4.3. Case 3: Deposition ends within the segment

Deposition ends within a segment when deposition occurs at the upper end of the segment and transport capacity increases within the segment at a rate greater than interrill erosion rate if the segment is sufficiently long as illustrated in Figure 8.3. Sediment load exceeds transport capacity at the upper end of the segment and decreases within the segment while transport capacity increases within the segment. The two become equal within the segment, which is the location x_e that deposition ends. RUSLE2 computes deposition and the sediment load on the upper portion of the segment using the deposition procedure described for **Case 2.**

The same conditions described for **Case 1** exist for the lower portion of the segment beyond the location x_e where deposition ends. Net detachment is computed using equation 8.1 where x_e is substituted for x_{i-1}. Rill erosion is reduced, if necessary, to avoid the sediment load "overfilling" transport capacity. Sediment load at the end of the segment is computed from:

$$g_{out} = g_{xe} + D_{>xe}(x_i - x_e) \qquad \textbf{[8.12]}$$

where: g_{xe} = sediment load at the point where deposition ends and $D_{>xe}$ = net detachment on the lower portion of the segment beyond the location where deposition ends.

8.1.4.4. Case 4: Deposition begins within the segment

Deposition begins within a segment when the transport capacity at the upper end of a segment is greater than sediment load, and transport capacity decreases within the

segment to become less than sediment load. This case occurs on a segment where cover-management and/or soil change so that infiltration rate is so high that runoff and transport capacity decrease within the segment. This case is illustrated in Figure 8.4.

Deposition begins at the location where sediment load and transport capacity become equal. RUSLE2 computes the deposition on the lower portion of the segment using the procedure described for **Case 2.**

8.1.5. Computing sediment yield, soil loss from eroding portion, total detachment, conservation planning soil loss, and erosion by segment

RUSLE2 displays several values produced by these computations. These output values are used in conservation and erosion control planning to select erosion control measures appropriate for the site conditions.

8.1.5.1. Sediment yield

Sediment yield is the amount of sediment leaving the overland flow path.[42] It is used in erosion control planning where the objective is to reduce the amount of sediment leaving the site. RUSLE2 computes sediment yield as sediment load at the end of the overland flow path divided by the overland flow path length. That is:

$$SY = g_{out,I} \big/ \lambda_{ofpl} \qquad \textbf{[8.13]}$$

where: SY = sediment yield from the overland flow path length (mass/area), $g_{out,I}$ = the sediment load at the end of the last segment on the overland flow path, I = the index of the last segment, and λ_{ofpl} = the overland flow path length.

8.1.5.2. Soil loss from eroding portion

The eroding portions of an overland flow path are where no deposition occurs, except for local deposition. Figure 5.2 illustrates the eroding portion of a complex shaped profile for an overland flow path. The **soil loss from eroding portion** is used in conservation planning where the objective is to protect eroding areas from excessive erosion to maintain soil productivity, prevent rilling, and reduce sediment yield.

The soil loss for the eroding portion of the overland flow path is computed from:

$$A_{ep} = \sum (g_{out,k} - g_{in,k}) \big/ \sum (x_{out,k} - x_{in,k}) \qquad \textbf{[8.14]}$$

[42] This sediment yield is the sediment yield for the site only if the overland flow path ends at the site boundary.

where: A_{ep} = soil loss (mass/area) for the eroding portions of the overland flow path and the index k refers to each portion of the overland flow path that is an eroding rather than a depositional area. Soil loss for the eroding portions of the overland flow path is the total sediment produced on the eroding portions divided by the total length of the eroding portions.

8.1.5.3. Total Detachment

Total detachment represents the sediment produced for the entire overland flow path, including depositional areas. In contrast, soil loss for the eroding portion of the overland flow path excludes depositional areas.

Total detachment for the overland flow path is the sum of the detachment amount (sediment production) for each segment divided by the overland flow path length. That is:

$$D_T = \sum D_{f,i}(x_i - x_{i-1}) \big/ \lambda_{ofpl} \qquad \textbf{[8.15]}$$

where: D_T = the total detachment (mass/area) for the overland flow path length and D_f = the sediment production for each segment. Sediment production for a segment is the value computed by equation 8.1 if rill erosion is not limited as described in **Section 8.1.4.1** or remote deposition does not occur as described in **Sections 8.1.4.2-8.1.4.4.** If rill erosion is limited, the sediment production is the sum of the interrill erosion and the rill erosion required to just fill transport capacity. If remote deposition occurs, sediment production equals interrill erosion.

8.1.5.4. Conservation planning soil loss

Neither **soil loss for the eroding portion** or **total detachment** take any **credit** for **remote deposition** as "**soil saved**," although RUSLE2 gives full credit to **local deposition** as "soil saved" because local deposition is empirically considered in equation 8.1 that computes net detachment. **Giving credit to remote deposition is a matter of judgment.** In the USLE (AH282, AH537), half credit was given to deposition by gradient terraces and full credit was given to deposition by rotational strip cropping.[43] No credit was given to deposition on the toe of concave slopes because this deposition ended the USLE slope length. RUSLE1 gave credit to deposition by terraces based on

[43] Gradient terraces are terraces on a uniform grade less than about 1% and may be level for moisture conservation. These terraces reduce overland flow path length and "save" soil by causing deposition uniformly along their length. The deposited sediment is spread by periodic mechanical operations required to maintain flow capacity. Rotational strip cropping is a system of alternating uniform width strips of dense vegetation that deposit sediment and strips where erosion is significantly higher than with the dense vegetative strips. The strips are systematically rotated by position on the hillslope over the crop rotation cycle.

terrace spacing. If the terraces were close together, about half credit was taken, and the credit was reduced to none as terrace spacing increased to 300 ft (100 m). Credit for deposition with narrow permanent vegetative strips (e.g., buffer and filter strips) was not discussed in AH282 or 537. In RUSLE1, the amount of credit given to deposition depended on the location of the deposition. Deposition near the end of the overland flow path was given very little credit. The credit increased to more than 60% for deposition near the origin of the overland flow path.

The **conservation planning soil loss** computed by RUSLE2 gives full credit for deposition with rotational strip cropping, i.e., the **conservation planning soil loss equals sediment yield**. RUSLE2 gives partial credit to deposition that occurs with permanent vegetative strips based on the location of the deposition. Very little credit is given to deposition at the end of the overland flow path, and the credit increases to about 60% for deposition located close to the overland flow origin. The same credit is given to deposition on concave portions of an overland flow path. Very little credit is given for the deposition if it is near the end of the overland flow path like that illustrated in Figure 5.4 and increased credit is given to deposition near the origin of the overland flow path.

The justification of the conservation planning soil loss in RUSLE2 is based on the following principles.

1. Deposition is beneficial. The quality of the soil, hillslope, and landscape is better with the deposition than without it. That is, deposition has a **soil saved** benefit.
2. Deposition that occurs and remains on very small areas relative to the entire hillslope area provides much less benefit that deposition that occurs on and is spread over a significant sized area by mechanical operations such as tillage and terrace maintenance.
3. Deposition that occurs near the end of the overland flow path has almost no value for maintaining the quality of the overall hillslope. Deposition in these locations is essentially "lost" from the hillslope with little chance for recovery.
4. Deposition upslope on the hillslope represents soil that is captured and not "lost" from the hillslope. A benefit can be gained by spreading the deposited sediment using common mechanical operations without having to physically transport the sediment upslope.

In general, the **conservation planning soil loss** is greater than **sediment yield**, except for rotational strip cropping where the conservation planning soil loss equals sediment yield. The conservation planning soil loss is less than the **total detachment** for the slope. The difference between total detachment and the conservation planning soil loss represents the **credit taken for deposition**. **Soil loss on the eroding portion** of the slope is the highest value of the set.

8.1.5.5. Erosion by segment

RUSLE2 computes erosion along the overland flow path. The user can obtain these erosion values by dividing the overland flow path into segments. The average **erosion for a segment** depends on segment length because point erosion varies with distance within the segment.

Point erosion at a can be computed with RUSLE2 using a very short segment such as 1 ft (0.3 m) at the location where the point erosion is desired.

Net erosion for a segment is computed as:

$$a_i = (g_{out,i} - g_{in,i})/(x_i - x_{i-1}) \qquad \textbf{[8.16]}$$

where: a_i = erosion for the *ith* segment (mass/area). A positive value means that the segment experiences a net loss of sediment (detachment) and a negative value means that the segment experiences a net gain of sediment (deposition). Even though either net detachment or net deposition occurs overall for a segment, a part of the segment can

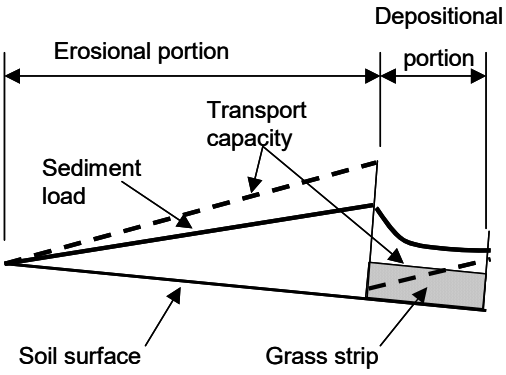

Figure 8.2. Narrow grass where deposition occurs over entire segment

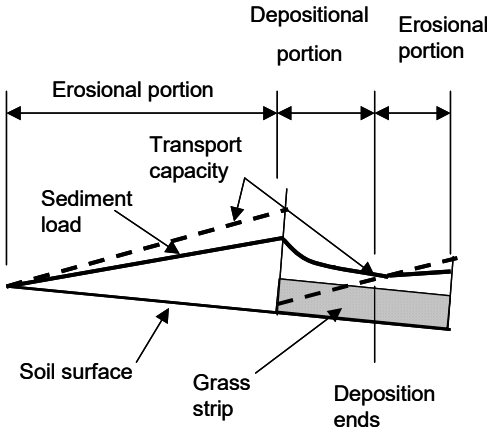

Figure 8.3. Grass strip sufficiently wide that deposition ends within segment and erosion occurs on lower portion of segment

experience net detachment while another part experiences net deposition, such as illustrated in Figures 8.3 and 8.4.

The segment erosion values must be carefully interpreted with respect to the erosion control planning criteria. **Is the erosion control criterion for point erosion or for average erosion for a uniform shaped slope, such as the soil loss tolerance value?**

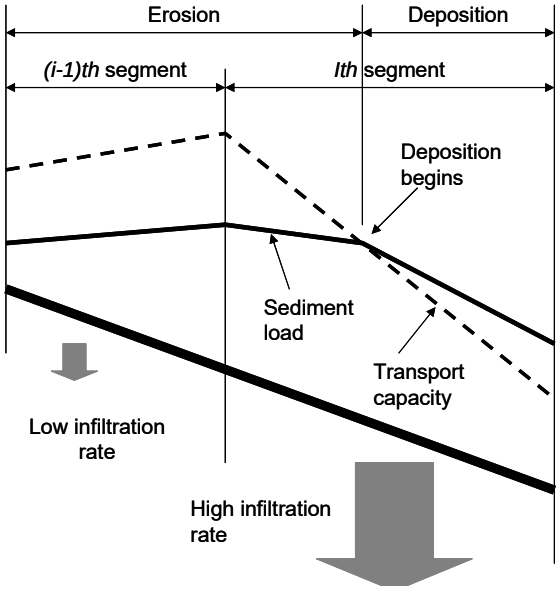

Figure 8.4. Deposition begins within a segment on a segment with a very high infiltration rate

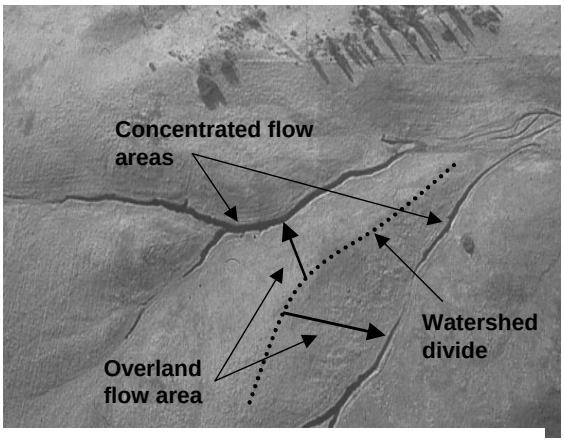

Figure 8.5. A natural landscape with concentrated flow areas and divides where overland flow originates

Comparing a point erosion value computed by RUSLE2 with an erosion control criteria based on average erosion for a uniform slope can produce misleading results and under designed erosion control practices that do not provide sufficient protection or over designed erosion control practices that are too costly. See **Section 7.9** for information on how to interpret RUSLE2 segment erosion values with respect to erosion control criteria based on average erosion for a uniform slope.

8.1.5.6. General comments

RUSLE2 displays a variety of erosion values that can be used in conservation and erosion control planning. Also, RUSLE2 can be applied in variety of ways to a field site. For example, RUSLE2 can be applied in the traditional USLE way by assuming a uniform slope and that deposition ends slope length. The erosion values computed by RUSLE2 can be compared with soil loss tolerance values or other erosion control criteria just as USLE soil loss values were used.

The other option is to apply RUSLE2 to an overland flow path that passes through depositional areas and is terminated by a concentrated flow area. The effect of variability in soil, steepness, and cover-management on erosion along the overland flow path can be analyzed. The RUSLE2 sediment yield estimates are greatly superior to the USLE soil

loss estimates for estimating the sediment amount leaving a site. RUSLE2 provides detailed information about how erosion varies along the overland flow path so that a cost effective erosion control practice can be tailored to the specific site conditions better than could be done with the USLE.

Users must understand how to apply RUSLE2 and interpret its computed values. The user must be aware of differences between the USLE, RUSLE1, and RUSLE2 when comparing these models and values from by them. The user must not assume that USLE and RUSLE1 procedures apply automatically to RUSLE2.

8.2. Representing Overland Flow Path Profiles

8.2.1. General considerations

Applying RUSLE2 requires selecting and describing an overland flow path. A hillslope involves an infinite number of overland flow paths. **Section 5.2** describes how to choose overland flow paths for applying RUSLE2 in conservation and erosion control planning.[44]

A point on the hillslope is selected through which the overland flow path passes. The overland flow path is traced from its origin through the point to the concentrated flow area that ends that particular overland flow path as illustrated in Figures 5.1 and 8.5. This flow path is traced perpendicular to the contour lines assuming that the soil surface is flat and ignoring how ridges or micro topographic features affect flow direction.

Overland flow paths are best determined by visiting the site, pacing flow paths, and making measurements directly on the ground. Contour map intervals greater than 2-ft (1-m) should be used cautiously, if at all, to determine overland flow paths. Contour map intervals of 10-ft (3-m) should not be used because concentrated flow areas that end overland flow paths cannot be adequately delineated. Also, these maps do not provide the detail needed to identify depositional areas and the slope steepness with sufficient precision to accurately compute deposition (See **Section 8.2.5**). Overland flow paths are generally much too long when contour intervals greater than 10 ft (3 m) are used to determine them.

Overland flow path lengths on many landscapes generally are less that 250 ft (75 m), and usually do not exceed 400 ft (125 m). Path lengths longer than 1000 ft (300 m) can not be used in **RUSLE2** because the applicability of **RUSLE2** at these long path lengths is questionable. Overland flow often becomes concentrated flow on most landscapes before

[44] See AH703 for additional discussion on identifying, selecting, and describing overland flow paths.

such lengths are reached. The maximum of 1000 ft (300 m) is an extrapolation from the longest plot of about 650 ft (200 m).

RUSLE2 applies to overland flow path lengths as short as zero, which means that RUSLE2 can be applied to ridges and beds like those used in vegetable production as discussed in **Section 8.3.6.2**.

RUSLE2 applies to steepness between flat (0%) and a 100% (1:1) maximum. This maximum of 100% is an extrapolation from 30%, the maximum steepness of the plots used to derive RUSLE2.

Length values like overland flow path segment lengths, distance from the origin of overland flow to lower segment end, overland flow path length, and land area are based on a horizontal measure for internal computations in **RUSLE2**. However, such length values can be input into RUSLE2 based on measuring along the hypotenuse (i.e., parallel to the soil surface). Field measurement parallel to the land surface is easier than measuring horizontally. The difference between horizontal and hypotenuse measurements is insignificant for slope steepness less than 20 percent. Distance and areas measured from maps is a horizontal measure. All references to land areas in RUSLE2 are horizontally based, even if the overland flow path length values were entered on a hypotenuse basis.

Overland flow profiles are segmented to represent differences in steepness, soil, and cover-management along the overland flow path. Topographic segments can be entered in RUSLE2 by distance from the origin of the overland flow path to the lower end of the segment or by segment length. The choice of entry method is based on user preference.

8.2.2. Profile shapes

The profiles for overland flow paths have various shapes as illustrated in Figure 8.6.[45] Simple shapes are uniform, concave, and convex. A uniform shaped profile is one where steepness is the same everywhere along the overland flow path. A convex profile is one where steepness increases everywhere along the overland flow path. RUSLE2 computes net detachment everywhere along uniform and **convex** profiles such that the entire profile is an **eroding portion** (See **Section 5.2**). A **concave** profile is one where steepness decreases everywhere along the overland flow path. If the lower part of a concave profile is sufficiently flat, transport capacity is less than sediment load and deposition occurs. These profiles have an upper **eroding portion** and a lower **depositional portion,** as

[45] Although the terms **hillslope profile** and **overland flow path profile** are often used interchangeably, the two terms are different. A RUSLE2 overland flow path profile does not start at the top of a hill and run to the bottom of the hill. Instead, a RUSLE2 overland flow path profile starts at the origin of overland flow, which is a runoff divide, and perpendicularly crosses contour lines. A RUSLE2 overland flow path is ended by a concentrated flow area.

illustrated in Figure 5.2. However, if the profile does not flatten sufficiently, deposition will not occur and the entire profile is an **eroding portion**.

Deposition does not occur on all concave shaped profiles. A decrease in steepness is not enough by itself to cause deposition.

Simple profile shapes are combined to form complex shaped overland flow profiles. A complex:convex-concave profile is one where the upper part is convex and the lower part is concave. Deposition occurs on the concave portion if steepness flattens sufficiently for transport capacity to become less than sediment load. If deposition occurs, the upper part of the profile is an eroding portion and the depositional area is the depositional portion as illustrated in Figure 5.2. Another complex shaped profile is complex:concave-convex. Deposition occurs on the concave portion if it flattens sufficiently. Runoff can continue as overland flow across the depositional area onto the lower convex portion. If deposition occurs, this profile has both an upper and lower eroding portion separated by the depositional portion. Erosion on the lower eroding portion is directly related to runoff that originates on the upper portion of the overland flow path. Therefore, the path length used to compute erosion on the lower eroding portion of the profile must include the entire path that generates runoff that flows onto the lower eroding portion.

Deposition does not end an overland flow path in RUSLE2.

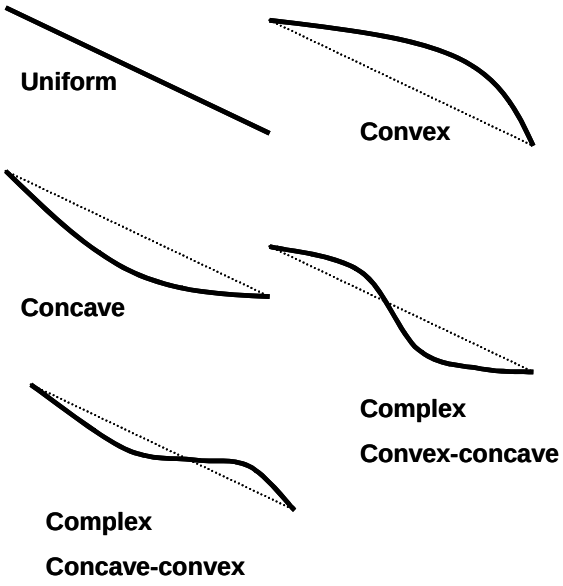

Figure 8.6. Overland flow path profiles

8.2.3. Importance of representing non-uniform profile shapes in RUSLE2

Many conservation and erosion control planners using USLE and RUSLE1 assumed uniform profiles even though procedures were available for applying these models to irregular slopes. This section discusses how profile shape affects RUSLE2 erosion estimates.

The overland flow path profile is a complex:convex-concave shape for many natural landscapes. This profile is illustrated in Table 8.1 along with RUSLE2 computed erosion values. The length of this profile is 250 ft (76 m) and has an average steepness of 4.1%. RUSLE2 computed erosion values are also shown for uniform and convex profiles having the same length and average steepness as the complex profile.

Table 8.1. Computed erosion by segment for three profle shapes, all having the same length and average steepness

			Convex-Concave			Uniform			Convex		
Segment Number	Distance to lower end of segment (ft)	Segment length (ft)	Steepness (%)	Erosion (tons/acre)	Sediment load (lbs/ft width)	Steepness (%)	Erosion (tons/acre)	Sediment load (lbs/ft width)	Steepness (%)	Erosion (tons/acre)	Sediment load (lbs/ft width)
1	28	28	2	4	5	4.1	7	8	0.5	1	2
2	64	36	4	10	22	4.1	11	26	1.5	4.2	9
3	107	43	8	28	78	4.1	14	53	2.8	9	27
4	149	42	6	25	125	4.1	16	84	4.2	16	58
5	181	32	4	-1	125	4.1	17	109	5.4	24	94
6	218	37	2	-28	77	4.1	19	141	6.6	34	151
7	250	32	1	-21	46	4.1	20	170	7.7	44	216
Average			4.1	4		4.1	15		4.1	19	

The computed erosion values differ greatly for the three profile shapes. The average erosion on the complex profile is 4 tons/acre (8.8 t/ha) while the average erosion on the uniform profile is 15 tons/acre (33 t/ha). Negative segment erosion values indicate net deposition for the segment. The reason for the large difference is deposition on the complex profile. Although the average erosion for the complex profile is much lower than average erosion for the uniform profile, the maximum segment erosion of 28 tons/acre (62 t/ha) for the complex profile is significantly larger than the maximum segment erosion of 20 tons/acre (44 t/ha) for the uniform profile. Figures 8.7 and 8.8 illustrate the variation in segment erosion and sediment load along the complex profile.

Another comparison is between the convex profile and the uniform profile. As expected, deposition is not computed for either the uniform or the convex profile. However, the average erosion of 19 tons/acre (42 t/ha) for the convex profile is significantly higher than the average erosion of 15 tons/acre (33 t/ha) for the uniform profile. This difference illustrates that uniform profiles underestimate average profile erosion when a uniform profile is assumed to represent a convex profile. The maximum segment erosion on the convex profile is 44 tons/acre (97 t/ha) while the maximum segment erosion is 20 tons/acre (44 t/ha) for the uniform profile. The uniform profile seriously underestimated maximum segment erosion for the convex profile.

Another comparison involves the average erosion for the eroding portion of the profile. The eroding portion of the profile represented in Table 8.1 is between the origin of overland flow and 165 ft (50 m), where deposition begins. The eroding portion of the slope can be approximated with a uniform profile with a length of 165 ft (50 m) on a steepness of 5.2%, which is the average steepness of the eroding portion. The average erosion for the uniform profile is 16 tons/acre (35 t/ha), while the erosion computed with

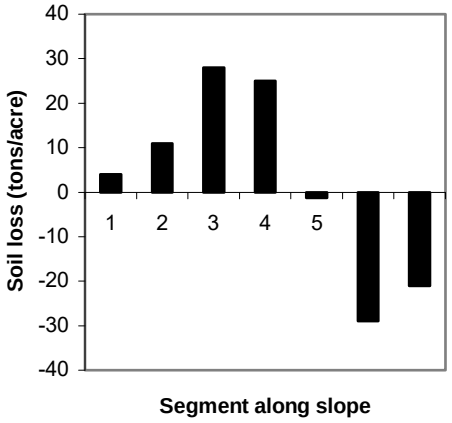

Figure 8.7. Segment erosion along a complex convex-concave hillslope profile

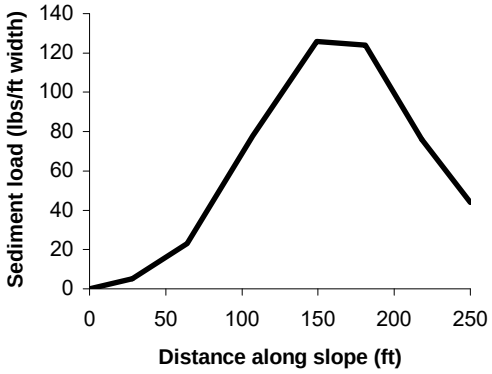

Figure 8.8. Sediment load along a complex convex-concave hillslope profile

the actual non-uniform profile is 18 tons/acre (40 t/ha) for the eroding portion. The average erosion for the eroding portion is about the same with these two methods. However, the maximum segment erosion computed with the non-uniform profile is 28 tons/acre (62 t/ha) while it is 23 tons/acre (51 t/ha) computed with the uniform profile approximation. The uniform profile approximation significantly underestimates the potential for rill erosion on the convex portion of the overland flow path

8.2.4. Implications of using uniform profiles to represent non-uniform profiles for conservation and erosion control planning

Assuming a uniform profile is common when the USLE and RUSLE1 were used in conservation and erosion control planning. A uniform profile is easy to describe, requiring only a length and steepness. The computational procedure for applying the USLE to non-uniform profiles is cumbersome and laborious. The non-uniform slope procedure in RUSLE1 is easy to use, but it only considers the effect of non-uniform steepness. It does not consider variation of soil erodibility or cover-management along the overland flow path.

Interpreting segment erosion values along non-uniform profiles (overland flow paths) is complex where using an erosion control criteria based on average erosion for a uniform profile. RUSLE2 is much more powerful than either the USLE or RUSLE1. RUSLE2 considers the interactive effects of spatial variation in soil and cover-management relative to position along non-uniform profiles. The RUSLE2 inputs are easy to enter, and RUSLE2 provides aids for interpreting segment erosion values (See **Section 7.9)**.

Based on the discussion in **Section 8.2.3**, the implications of using uniform profiles of the same length and average steepness to represent non-uniform profiles are:

1. Uniform profiles underestimate profile (average erosion over the profile length) for convex profiles depending on degree of curvature of the convex profile. The difference can easily be as large as 20%.
2. Uniform profiles seriously underestimate local (segment) erosion for convex profiles and results in inadequate erosion control for rill erosion on the lower end of the convex profile. The difference can easily be as high as a factor of two or more.
3. Uniform profiles overestimate profile erosion for concave profiles. The error can be very large if most of the eroded sediment is deposited on the concave profile. The difference can be large as a factor of five or more.
4. Uniform profiles applied to the eroding portion of concave profiles overestimate profile erosion. The difference can be as large as 20%.
5. Uniform profiles applied to the eroding portion of a concave profile give maximum erosion that is comparable to maximum erosion on the concave profile.
6. Uniform profiles applied to complex:convex-concave profiles overestimate average profile erosion if deposition occurs on the concave portion.
7. Uniform profiles applied to the eroding portion of a complex:convex-concave profile can give about the same average erosion for the eroding portion as representing the non-uniform profile.
8. Uniform profiles applied to the eroding portion of a complex:convex-concave profile can significantly underestimate maximum erosion on the eroding portion of the profile.
9. Deposition does not end the overland flow part on complex:concave-convex profile.
10. Dividing a complex:concave-convex into two separate uniform profiles seriously underestimates erosion on the lower convex portion of the profile.

The strong recommendation is that non-uniform overland flow profiles be represented in RUSLE2, especially convex shaped profiles. Users should recognize that representing a convex profile with a uniform profile will result in erosion control being less than needed (under-designed). Using a uniform profile to represent the eroding portion of a concave profile will result in erosion control being greater than needed (over-designed).

8.2.5. Implications for using RUSLE2 for estimating sediment yield for watersheds

RUSLE2 computes deposition on overland flow areas and the sediment leaving the overland flow path represented in the RUSLE2 computations. For example, RUSLE2 computes a sediment delivery of 4 tons/acre (8.4 t/ha) from the overland flow path as Table 8.1 illustrates. That sediment delivery is the sediment yield for the site only if the overland flow path ends at the site boundary. RUSLE2 overland flow profiles end in concentrated flow areas illustrated in Figures 5.1 and 8.5. These concentrated flow areas are typically within the site boundary. Both erosion (ephemeral gully) and deposition can occur in the concentrated flow areas so that the sediment delivered from site can differ significantly from the RUSLE2 computed sediment delivered from the end of the overland flow profile. That is, sediment leaving the overland flow portion of the site may only be a portion of the site sediment yield because of erosion and/or deposition that occurs in concentrated flow areas.

The USLE is widely used to estimate sediment yield from watersheds by multiplying USLE soil loss estimates by a sediment delivery ratio (SDR).[46] Sediment delivery ratios are typically less than one to account for the deposition that occurs in many watersheds. The sediment mass leaving the watershed is typically less than the sediment produced by rill and interrill erosion. Much of this deposition occurs on the overland flow areas of the watersheds.[47] Although RUSLE2 can compute the deposition on overland flow areas, RUSLE2 should be used to compute erosion on the eroding portion of the overland flow profile because the sediment delivery ratio values already reflect the deposition on overland flow areas as well as deposition by concentrated and channel flow areas.

[46] The USLE soil loss has a particular meaning. It is sediment mass delivered to the end of the uniform slope assumed to represent the eroding portion of the overland flow path. The USLE soil loss is expressed as mass delivered to the end of the ULSE slope length per unit width divided by the USLE slope length.
[47] See Toy et al. (2002) for a discussion of this deposition.

Thus, the proper way to use sediment delivery ratio values with USLE soil loss estimates is to use RUSLE2 to compute erosion on the eroding portion of the overland flow profile. That erosion value, which is comparable to the USLE soil loss value, is multiplied by the sediment delivery ratio to obtain a sediment yield for the watershed. For example, assume that the sediment delivery ratio is 0.15 for a particular watershed that contains the representative profile described in Table 8.1. Sediment yield is computed by multiplying the 18 tons/acre (39.6 t/ha) erosion value for the eroding portion of the overland flow path by the sediment delivery ratio of 0.15 to give a sediment yield of 2.7 tons/acre (5.9 t/ha). Multiplying the RUSLE2 computed sediment yield value of 4 tons/acre (8.8 t/ha) for the overland flow path by sediment the delivery ratio value based on a USLE type soil loss value gives a sediment yield that is much too low.

8.2.6. Importance of properly representing steepness at end of concave profiles where deposition occurs

The deposition computed by RUSLE2 is directly related to sediment transport capacity. Accurately computing deposition is very difficult because slight variability in the flow hydraulics on a depositional surface can greatly affect sediment transport capacity. The error in deposition computations is much greater than error in detachment computations.

Even if the computations could be made perfectly, an accurate description of the steepness along the flow path where deposition is needed. For example, the sediment yield from the complex profile illustrated in Table 8.1 is 4.0 tons/acre (8.8 t/ha ac). If the steepness for the last segment, which covers a relatively small portion of the profile, had been estimated at 2%, the estimated sediment yield would have been 7.8 tons/acre (17.2 t/ha). If the steepness had been estimated at 0.5%, the estimated sediment yield would have been 2.6 tons/acre (5.7 t/ha). These differences illustrate the importance of carefully determining the steepness at the end of the overland flow path on concave profiles where deposition occurs.

Deposition estimates are much less accurate than detachment estimates. Also, obtaining accurate deposition estimates requires a more carefully measured steepness than does detachment, especially where deposition occurs at the end of an overland flow profile.

8.3. Applying RUSLE2 to particular profile shapes

This section describes how to apply RUSLE2 to particular overland flow profile shapes commonly encountered in conservation and erosion control planning.

8.3.1. Uniform profile

Uniform profiles (slopes) are often assumed because only a slope steepness and slope length are required to topographically describe them.[48] Uniform slopes are used to represent the eroding portion of overland flow paths, not the entire path (See **Section 5.2**). The **slope steepness** of the uniform slope is set to the average steepness of the eroding portion of the overland flow path.

Slope length, as used in the USLE, is the distance from the origin of overland flow to the upper edge of deposition for concave profiles, illustrated in Figure 5.2, or to concentrated flow areas for convex profiles, illustrated in Figure 5.3. See AH703 for additional illustrations.

The best approach for determining slope length and steepness is to make measurements during a site inspection.

Determining the upper edge of deposition is easy on cropland, construction sites, and other land areas that readily erode. However, deposition may not be apparent where rill erosion does not occur and deposition is low, where heavy vegetative cover obscures the soil surface, or where recent mechanical soil disturbance has mixed deposited sediment with underlying soil.

A rule of thumb is that deposition begins where steepness is one half of the average steepness of the concave portion of the profile.

Two examples illustrate the procedure. The first example is a concave profile that decreases from 18 percent steepness at the upper end to 2 percent steepness at the lower end. The average steepness is 10 percent and one half of the average steepness is 5 percent. Deposition begins at the location where the flow path has flattened to 5 percent steepness as shown in Figure 8.7.

The second example is a concave profile that decreases from 4 percent at the upper end to 2 percent at the lower end. The average steepness is 3 percent and one half of the average steepness is 1.5 percent. Deposition does not occur because the steepness at the lower end of this profile is greater than the steepness where deposition would be expected to occur.

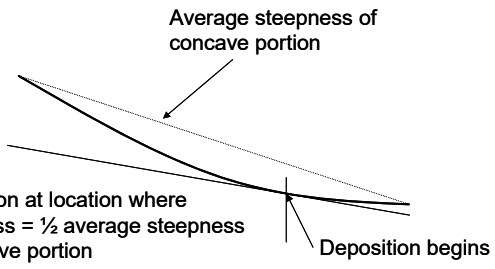

Figure 8.7. Rule of thumb for location of upper edge of deposition on a concave profile

This procedure only captures how degree of profile curvature affects deposition. Other factors also affect deposition. Deposition occurs when

4
u
s

Reference Guide. It is the length of the overland flow path. Slope steepness

sediment load produced by upslope erosion exceeds transport capacity of the runoff. If the sediment load produced by upslope erosion is low relative to transport capacity, deposition begins further downslope than when sediment load is high relative to transport capacity.

RUSLE2 can estimate the location of deposition by segmenting the overland flow profile and entering steepness values for each segment. Negative segment erosion values indicate deposition. RUSLE2 computes erosion for the eroding portion of the overland flow path that can be used in conservation and erosion control planning (See **Section 8.1.5.2**).

Terraces, diversions, grassed waterways, ephemeral gullies, and similar concentrated flow areas are easily identified as ending slope length. Slope length can often be easily determined on cut and fill slopes involved in construction, landfills, and surface mine reclamation. Many landscapes include converging areas where overland flow is collected in defined channels, which are areas where ephemeral gully erosion occurs. These channels are illustrated in Figures 5.1 and 8.5. Slope length ending concentrated flow areas on natural landscapes, such as western rangelands, may not be obvious because the concentrated flow areas are not eroding channels.

The fact that experts can look at the same landscape and choose different slope lengths may seem troubling. Determining slope length involves judgment, and the variability in slope length among RUSLE2 users is a part of the uncertainty in RUSLE2 erosion estimates (See **Section 17.4**). One element in the judgment is how well plots used to derive RUSLE2 represent the specific field site where RUSLE2 is being applied. The data used to determine RUSLE2 were collected from plots that ranged in width from about 6 ft (2 m) to 12 ft (4 m), with some as wide as 75 ft (25 m). Plots lengths were as long as 350 ft (100 m) in two cases, but most plots were about 75 ft (25 m). These plots are illustrated in Figures 5.5 and 5.6. Slope length should not extend beyond the hillslope location where plots of these dimensions and flow conditions would represent erosion.

The depth of an eroded channel on a hillslope does not determine whether RUSLE2 applies. Is this channel parallel to other channels and of comparable size to neighboring channels as illustrated in Figure 5.6? Or is the channel much larger than neighboring channels because runoff has been collected rather than being spread uniformly across the hillslope?

Fortunately RUSLE2 erosion estimates are not sensitive to slope length for slope steepness less than 2 percent. For example, slope length being off by a factor of two for a 0.5 percent steepness has almost no effect on estimated erosion. Estimated erosion is less sensitive to slope length than to slope steepness for steepness between 2 and 20 percent. Above 20 percent steepness, estimated erosion is almost as sensitive to slope length as to slope steepness. Therefore, the uncertainty in estimating slope length does not have a

major effect on estimated erosion for steepness less than 10 percent. Much more careful attention should be given to estimating slope steepness than to slope length.

Slope length and steepness values should be determined from field measurements, but site inspections may not be feasible. Problems associated with using contour maps and digital elevation data are discussed in **Section 8.2.1**. In general, those data are seldom satisfactory for determining slope lengths and often are not satisfactory for determining slope steepness because the data do not have sufficient resolution.

Slope length and steepness values have been assigned to soil map units in some cases.[49] These values may be acceptable for large scale regional analyses, but they should not be used for site-specific conservation and erosion control planning. The range in slope steepness across soil map units can give widely different estimated erosion values. For example, the land steepness of a soil map unit can range from 1 percent to 5 percent. The average steepness is 3 percent, which might give an estimated erosion rate of 12 tons/acre (26 t/ha). The estimated erosion values for the extremes of the slope steepness for the soil map unit are 4 tons/acre (9 t/ha) and 22 tons/acre (48 t/ha) for the 1 percent and 5 percent steepness, respectively. The importance of profile shape, especially if the profile is convex, should not be overlooked.

A principle in applying RUSLE2 is that a similar level of precision be used for all inputs for a specific site. Therefore, if a uniform slope is assumed, then a single soil and a single cover-management should be assumed for the slope. Uniform width and uniform spaced cover-management strips can be placed on the uniform slope to represent filter and buffer strip and rotational strip cropping support practices. However, soil and cover-management (e.g., to represent the variation of yield along the slope) should not be varied along a uniform slope that is being used to represent a non-uniform profile, especially a convex profile shape. For example, high soil erodibility at the end of a convex profile can give far higher erosion rates than will be computed assuming a uniform slope.

Not using the same level of precision for all inputs can result in very seriously flawed conservation plans when the planning criteria is to an absolute standard such as soil loss tolerance.[50] This problem is reduced but not eliminated for conservation planning to a relative standard, such as an 80 percent erosion reduction. Profile (overland flow path) averages can be very misleading for both concave and convex profiles because of non-linearity in the RUSLE2 equations. Soil map units sometimes involve multiple soil components where soil erodibility differs significantly among the components.

---

[49] Griffin, M.L., D.B. Beasley, J.J. Fletcher, and G.R. Foster. 1988. Estimating soil loss for topographically nonuniform field and farm units. J. Soil and Water Conservation 43:326-331.

[50] An analogy is using a micrometer to measure the sand grain roughness in a concrete pipe while guessing at the diameter of the pipe and expecting an estimate of discharge rate to be of comparable precision to the sand grain measurements.

Sometimes one of the components is chosen as the dominant component if it occupies more than 50 percent of the soil map unit. An alternative is to take averages. However, a soil component that occupies about 25 percent of the overland flow path with a very high soil erodibility located at the lower end of a convex shaped profile is the dominant soil in terms of the erosion on the profile. The soil component that occupies most of the profile is not necessarily the dominant soil in terms of erosion, although it may be the dominant soil for other processes such as crop production.

If the spatial variation in soil and/or cover-management is sufficient to warrant dividing the overland flow profile into segments, then the variation in steepness along the overland flow path should be entered as well.

The problem is not limited to convex profiles. A uniform profile computes maximum erosion at the end of the profile whereas maximum erosion occurs on a concave profile in the upper part of the profile, not at the end. The positioning of soil components along the profile strongly interacts with profile shape. The result is that erosion computed with uniform slopes and assuming a spatially average soil erodibility or a dominant soil component based on occupying the highest fraction of the profile can produce erosion estimates that greatly differ from those computed using a non-uniform profile shape and the proper placement of the soil and cover-management conditions along the profile.

RUSLE2 users must be aware of the importance of precision in the inputs and the importance of spatial interaction among variables. The same level of precision should be applied to all RUSLE2 inputs. Even though uniform slopes have long been standard practice in conservation planning, most conservation planners have little awareness of the impact of that assumption on the adequacy of the resulting plans.

8.3.2. Complex:convex-concave profile

The profile for overland flow paths on many natural landscapes is complex:convex-concave (See **Section 8.2.2**). The potential for deposition always exists on concave shaped profile sections. The segments used to represent the profile must be carefully chosen to ensure that RUSLE2 correctly make its computations, especially where deposition occurs. The critical choices are number of segments and steepness of the last segment experiencing deposition.

Segments can be long where steepness changes slowly. Segments should be shorter where steepness changes most rapidly. The deposition computations are more sensitive to changes in steepness than are the detachment computations. Therefore, shorter segments are needed in depositional areas than in the detachment areas. The rule of thumb given in **Section 8.3.1** can be used as a first approximation where deposition begins to help in initially choosing segments for the depositional portion of the profile.

A minimum of three, preferably four, segments should be used in the depositional area. If segments are too long in the depositional area, RUSLE2 will incorrectly show no or much too little deposition. A minimum of three segments, preferably four, should be used to describe the eroding portion of the profile. However, each non-uniform profile behaves differently depending on degree of curvature of the convex and concave sections of the profile.

As discussed in **Section 8.2.6,** steepness of the last segment experiencing deposition has a major impact of estimated sediment yield. Make sure that this segment is not too long to help avoid entering a steepness at the end of the profile that is too steep resulting in computed sediment yield being too high. The difference between 1 percent steepness and 2 percent steepness can affect sediment yield by a factor of two.

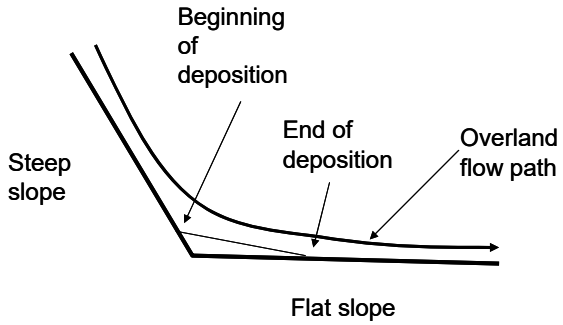

Figure 8.10. Flat uniform slope at toe of uniform steep slope.

Varying segment length is more efficient than using uniform segment lengths for the entire profile. Profile sections of uniform steepness do not need to be divided into segments. A relatively flat slope at the toe of a steep slope is a special case of a concave slope that illustrates that profiles sections of uniform steepness do not need to be divided into segment. This profile is illustrated in Figure 8.10. This profile can be described with two segments, one for the steep slope and one for the flat slope. RUSLE2 computes deposition over a short distance on the upper portion of the flat slope and erosion over the lower portion of the flat slope. RUSLE2 correctly makes these computations without dividing the flat slope into segments.

The most important factor in selecting segments to represent profiles where steepness varies along the profile is that shorter segments are needed where steepness changes most rapidly. Also, shorter segments are needed in depositional than in detachment areas.

8.3.3. Complex:concave-convex profile

Deposition potentially occurs on the lower end of the concave part of the profile provided steepness is sufficiently flat. The guidelines in **Section 8.3.1** can be used to initially estimate whether deposition will occur on the profile and where the depositional area might be as a guide to choosing segments to represent the profile. The same guidelines

above for the complex:convex-concave profile (See **Section 8.3.2**) apply for choosing segments to represent a complex:concave-concave profile. An increased number of segments is needed in the depositional area and where steepness is changing most rapidly. An easily made mistake on this profile is to choose segments that are too long in the depositional area. If the segment are too long, RUSLE2 will incorrectly show no deposition when deposition should have been computed.

Deposition on the concave portion of the profile does not end the overland flow path assuming that the flow continues across the depositional area onto the lower part of the slope as overland flow.

The cut-roadway-fill profile illustrated in Figure 8.10 is a special case of a complex: concave-convex profile. Runoff from the cut slope is assumed to flow across the roadway onto the fill slope. If the roadway slopes outward at a sufficient steepness, erosion rather than deposition occurs on an earthen roadway. The overland flow path begins at the top of the cut and extends across the roadway to the bottom of the fill slope assuming that the flow remains as overland flow.

The roadway can be on a sufficiently flat steepness that deposition occurs on the roadway. If the runoff continues across the roadway as overland flow onto the fill slope, the overland flow path begins at the upper end of the cut slope, continues across the roadway, and ends at the bottom of the fill slope. The flow on the fill slope is composed of runoff generated from the cut slope above the roadway so far as runoff produced on the fill slope. The overland flow path length reflects the amount and rate of runoff, which is the reason that it includes the fill slope in this case even though deposition may occur on the roadway. Deposition on the roadway does not end slope length so far as computing soil loss from the fill slope provided the runoff flows across the roadway onto the fill slope as overflow and does not become concentrated flow, perhaps because of a ridge left by a road grader on the outer edge of the road.

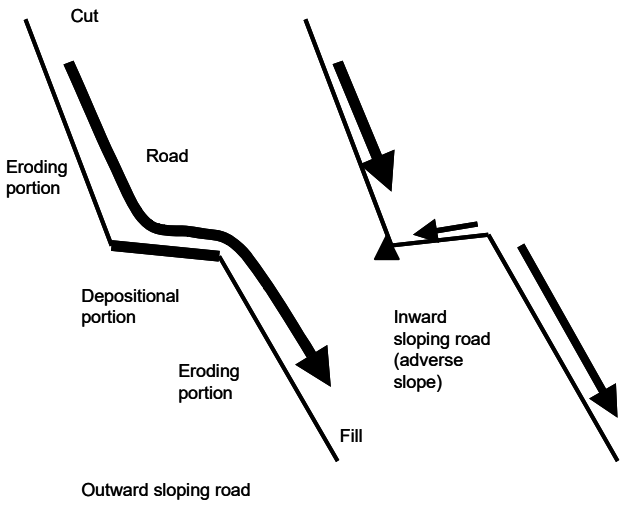

Figure 8.10. Cut-road-fill hillslope illustrating how an inward and outward sloping road section affects overland flow path lengths and that deposition on the outward sloping road does not end overland flow path length

Erosion on the cut slope can be significantly reduced by intercepting and diverting runoff so that the runoff from the cut slope and the roadway do not flow onto the fill slope. A diversion could be placed at the top of the fill slope to intercept the runoff, which is illustrated in **Section 8.3.5**. Placing the diversion at the top of the fill slope reduces erosion on the fill slope, but deposition still occurs on the roadway, which is objectionable.[51]

A better solution is to slope the roadway inward on an adverse steepness back toward the cut slope, as illustrated in Figure 8.10. This profile configuration can be represented very simply in RUSLE2 by entering a negative value for steepness on the roadway to represent an adverse slope. This profile configuration can be described in RUSLE2, as illustrated in Table 8.2, by entering a negative steepness value for the roadway segment. Sloping the road inward creates three overland flow path lengths, one each for the fill slope, roadway, and cut slope segments. RUSLE2 analyzes both profiles illustrated in Figure 8.10 without having to break the analysis into parts. Segments that describe each portion of the profile are entered into RUSLE2, and RUSLE2 automatically determines and handles the overland flow path lengths.

[51] Diversions are considered to be support practices in RUSLE2. Support practices include contouring (ridging), diversions, terraces, vegetative strips, porous barriers, and small sediment basins. See **Section 14** that discusses diversions.

Entering an adverse slope for the roadway causes RUSLE2 to create a channel at the intersection of the cut slope and the roadway. This channel intercepts runoff from the cut slope and collects runoff from the roadway. The sediment yield computed by RUSLE2 is the total sediment yield for the entire profile.

RUSLE2 automatically places a channel where a profile segment with a positive steepness intersects with a profile segment with a negative steepness (an adverse slope). This channel can be described with a grade to compute deposition if the grade is sufficiently flat. RUSLE2 does not compute erosion in channels. This channel ends the overland flow path.

Table 8.2. Erosion on a cut-road-fill slope

Segment #	Distance to lower end of segment (ft)	Segment length (ft)	Segment type	Steep-ness (%)	Soil loss (tons/acre)	Segment type	Steep-ness (%)	Soil loss (tons/acre)
1	75	75	fill outward	33	162	fill inward	33	162
2	95	20	sloping	2	-493	sloping	-2	5.8
3	170	75	cut	33	353	cut	33	162
					Sediment yield = 169 tons/acre			Sediment yield = 143 tons/acre

8.3.4. Overland flow path with porous barriers (e.g., vegetative strips, fabric fences) and flow interceptors (e.g., diversions, terraces)

RUSLE2 represents two major types of flow barriers. One type is porous barriers where the overland flow is assumed to continue through the barrier onto the portion of the profile downslope of the barrier. Examples of porous barriers include vegetative strips (filter, buffer, stiff grass), fabric fence, gravel bags, and straw bales. The other type of barrier is flow interceptors that cut off the runoff and redirect it around the slope in defined channels. Examples of flow interceptors are diversions and terraces. Diversions and terraces function exactly the same way in terms of intercepting runoff. The difference is that diversions are defined in RUSLE2 as channels that are placed on a sufficiently steep grade that no deposition occurs in them but the grade is not so steep that erosion occurs in the channel. Conversely, terraces are intentionally placed on a sufficiently flat grade that deposition does occur in them. Diversions are placed at critical places on the overland flow profile to intercept runoff and prevent it from flowing onto a steep part of the profile, such as on the landfill example illustrated in Figure 8.12. In contrast, terraces are typically installed as system of uniform spaced channels.

Both diversions and terraces required a runoff disposal system to move the collected runoff down the slope without causing channel erosion. RUSLE2 does not consider the water disposal channel system.

The purpose of porous barriers is to cause substantial deposition. Even though these barriers induce deposition, the overland flow path length does not end at the deposition because the runoff continues through the strip as overland flow. A profile with multiple grass strips that induce deposition has only one overland flow path length as illustrated in figure 8.11b.

Deposition at a grass strip does not end the path length with a new one beginning below the strip. Cover-management segments do not end the overland flow path.

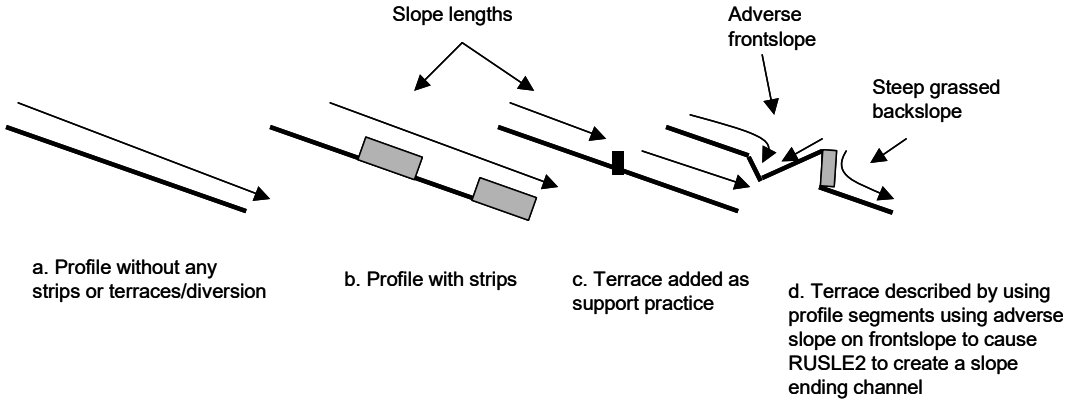

Figure 8.11. How vegetative strips and terraces are described in RUSLE2 and how these practices affect slope lengths assumed by RUSLE2

In contrast, terrace and diversion channels intercept runoff in concentrated flow areas that end the overland flow path. A new overland flow path begins at the terrace/diversion ridge because that is where overland flow originates that flows across the next portion of the profile.

Terraces and diversions can be described in one of two ways in RUSLE2. One approach is used in most conservation planning. RUSLE2 assumes that the terrace/diversion channel and ridge are infinitely thin as illustrated in Figure 8.11c. This approach is used in RUSLE2 where terraces/diversions are represented as a support practice. The other approach is to describe the actual hillslope profile configuration, including the cover-management on each segment such as the grass on a steep backslope of a terrace/diversion.

The overland flow path that is entered in RUSLE2 is the path without the terraces/diversions. The segments are added to create the profile illustrated in Figure 8.11d. RUSLE2 automatically creates a channel where segments with a positive and a negative (adverse) steepness intersect. Such channels end the overland flow path. RUSLE2 determines the appropriate overland flow path lengths without the analysis having to be broken into parts.

8.3.5. Overland flow path for diversions that intercept runoff above steep slopes

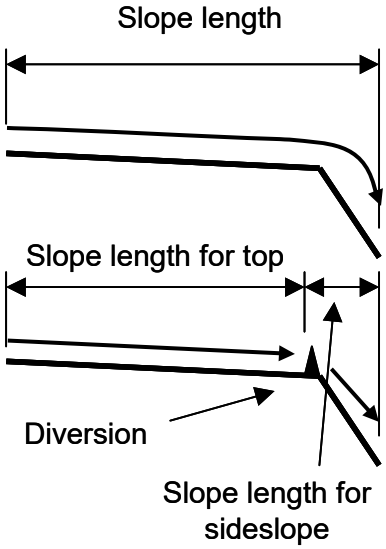

Figure 8.12. Landfill with relatively flat top and steep side slope, with and without a diversion

Table 8.3. Soil loss on a landfill with and without a dversion at the top of the steep sideslope

			Soil loss(tons/acre)	
Segment	Distance to end of segment (ft)	Steep-ness (%)	Without diversion	With diversion
1	250	2	9	9
2	300	33	538	130

Erosion is high at the end of convex shaped hillslope profiles and where runoff from a long slope flows onto a steep slope like the sideslope of a landfill. Placing a diversion at the top of the sideslope as illustrated in Figure 8.12 is an effective practice for reducing erosion on the steep sideslope as shown in Table 8.3. The entire profile description is entered into RUSLE2 and then a diversion is applied at the top of the steep sideslope. RUSLE2 automatically ends the overland flow path for the relatively flat top slope and begins a new overland flow path at the top of the steep sideslope. As expected, the diversion did not reduce erosion on the top of the landfill but significantly reduced erosion on the sideslope.

8.3.6. Overland flow path for contouring (ridging)

The effect of contouring, ridging, and bedding on erosion can be represented in three ways in RUSLE2.[52] The **first method** is that the surface can be represented using a ridge (bed)-furrow description where the overland flow path length is from the top of the ridge (bed) to the furrow that separates the ridges or beds **provided** the ridges and beds are so well defined, so high, and on a sufficiently uniform grade that the runoff flows in the furrows separating the ridges or beds that the flow flows in the furrows along their total length until reaching the end of the furrow or a defined concentrated flow area. The **second method** to describe an overland flow path along the ridges-furrows when the ridges are well defined and flow stays within the ridges as just described.

[52] The effect of contouring on erosion is highly variable and is very difficult to accurately predict. Slight variations can result in wide variations in erosion. For example, under certain conditions, contouring can actually increase erosion, while in other similar conditions, the same contouring can be highly effective. The high variability in effectiveness is partly related to storm severity. The contouring relationships in RUSLE2 represent the main effects that supported by the data. See **Section 14.1** for additional discussion.

The **third method** is to describe an overland flow path assuming a flat soil surface without the ridges and without considering how the ridges affect the flow pattern. This method is used in ordinary cases of ridges like those left in farm fields by tillage equipment such as tandem disks, chisel plows, and field cultivators or those left by ridgers on highly disturbed lands such as reclaimed mine sites.

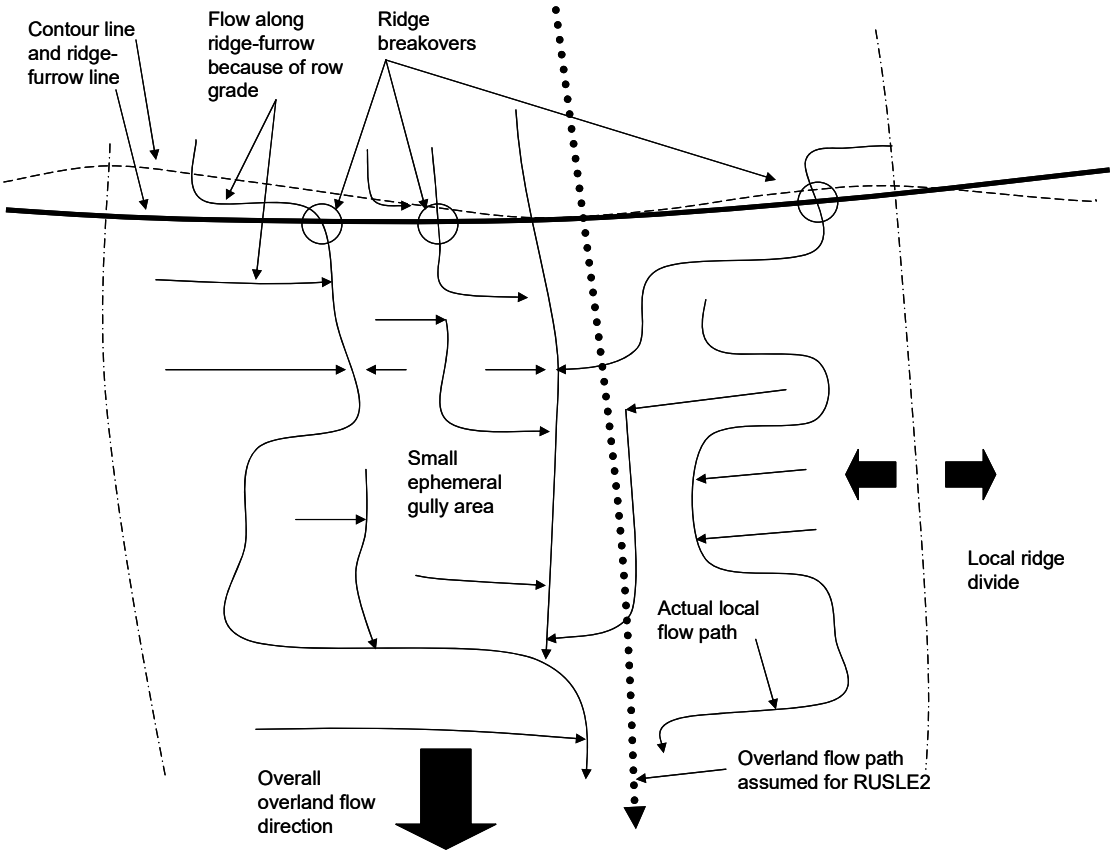

Figure 8.13. Overland flow patterns in a typical field where local runoff flows along ridge-furrows because of a row grade, breaks over in local areas, and accumulates in small local ephemeral gully areas.

These field situations are illustrated in Figure 8.13. Runoff flows along the furrows a distance [a few to several ft (m)] before breaking over one or more ridges before the runoff is intercepted by a sufficiently large ridge to direct runoff along a furrow. The breakovers are located randomly between the major concentrated flow areas. Breakover locations are random and can not be determined after the ridge forming operation in advance of the erosion event because of non-uniform ridge height and non-uniform grade along the furrows. **The first two methods should not be used for the conditions illustrated in Figure 8.13**.

These three methods can give significantly different results, which partially reflects the great difficulty of accurately estimating the effect of contouring (ridging). Use RUSLE2 as a guide to conservation and erosion control planning rather than considering it to provide absolute erosion estimates for any particular site.

8.3.6.1. Overland flow path for ordinary contouring, ridging, and bedding

Contouring, including ridging and bedding, is normally treated as a support practice in RUSLE2. See **Section 14.1** for a description of contouring as a support practice. To treat contouring, ridging, and bedding as a support practice, enter the overland path description in RUSLE2 as the path that the overland flow would follow as if the soil surface is flat and no ridges are present to influence the flow pattern.

8.3.6.2. Overland flow path for a ridge (bed)-furrow description

RUSLE2 can directly compute erosion on ridges and beds and the deposition in the furrows that separate them. RUSLE2 can accommodate overland flow path lengths as short as a zero length. Thus, RUSLE2 can be applied to ridge-furrow and bed systems, like those illustrated in Figure 8.14 for vegetable production.[53] RUSLE2 can also be applied where plastic is added and removed on the beds (See **Section 13.1.9** for a description on how to use RUSLE2 to describe the effect on erosion of adding and removing plastic to beds).

[53] Actually a finite, small number like 0.001 ft (0.5 mm) must be entered, which gives the same result as entering a zero. The erosion rate at a zero overland flow path length is entirely interrill erosion. An erosion rate exists for a zero overland flow path length but the amount of erosion is zero because erosion amount for a uniform profile is the product of average erosion rate for the overland flow path and the overland flow path length.

Representing ridges and beds as the overland flow path and "hillslope profile" is used when the ridges and beds are so high that flow is unquestionably contained in the furrows between the ridges and beds until it reaches a well defined concentrated flow area. RUSLE2 can also compute deposition that occurs in the furrows but not erosion by flow in them.

The overland flow path length is one half of the spacing of the ridges and beds. In this example, 20% is assumed for the steepness of the bed sideslope, and 1% is assumed for the steepness of the top of the beds and 50% is assumed for the steepness of the bed sideslope. An adverse steepness (negative values), illustrated in Table 6.14 is used for the segments on either side of the beds. The positive steepness of one sideslope intersecting with the negative (adverse) steepness on the adjacent ridge or bed causes RUSLE2 to create a channel that ends the overland flow path length. The grade that RUSLE2 automatically assumes for the default channel is so steep that no deposition occurs. However, the actual grade can be entered so that RUSLE2 can compute deposition that occurs in the furrows between the ridges or beds.

Table 6.14. Soil loss for ridges and beds

Ridges				Beds			
Segment #	Segment length (ft)	Steepness (%)	Soil loss (tons/acre)	Segment #	Segment length (ft)	Steepness (%)	Soil loss (tons/acre)
1	1.5	20	20	1	0.9	1	3
2	1.5	-20	20	2	0.6	50	27
				3	0.6	-50	3
				4	0.9	-1	27
Soil loss = 20 tons/acre				Soil loss = 13 tons/acre			

8.3.6.3. Summary comments

RUSLE2 does not give the same results for all these three approaches for representing ridges-furrows. The approach of explicitly describing the configuration of the ridges and beds works when the ridges contain the flow until a major well-defined concentrated flow area is reached. Although RUSLE2 can estimate deposition in furrows on a relatively flat grade, RUSLE2 can not estimate erosion in the furrows, which RUSLE2 has represented as channels.

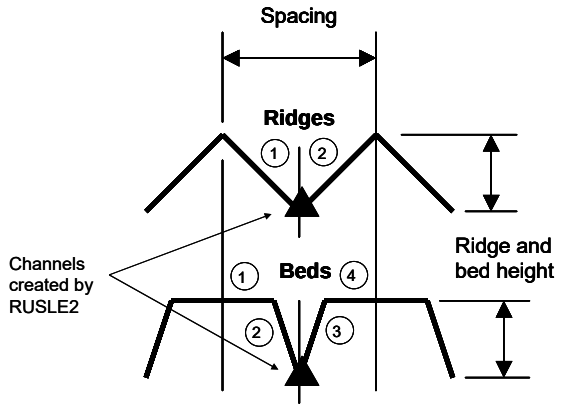

Figure 8.14. Ridge and bed systems.

The approach of representing the overland flow path as if the ridges-furrows are not present works best when the flow pattern is irregular as illustrated in Figure 8.13.

8.4. Influence of Upslope Areas on Overland Flow Path

RUSLE2 is sometimes applied to a field site that is downslope from an area that contributes runoff to the site. The recommended approach is to represent the entire overland flow path even though the upslope area is not a part of the analysis area. The soil loss computed for the downslope area should not be compared to soil loss tolerance, but the procedure described in **Section 7.9.3** where a ratio of soil loss to T value adjusted for position on the slope is computed. A conservation practice should be chosen that reduces this ratio to 1.

RUSLE2 takes into account cover-management conditions on an upslope area for computing transport capacity on downslope segments where cover-management is quite different from the upslope area. However, RUSLE2 does not fully take into account how reduced runoff from the upslope area reduces detachment on the downslope segment. In some applications, **RUSLE2** is applied to a field downslope from an upslope area that is very different from the field. The following approach can be used to take into account how reduced runoff from the upslope segment affects detachment on the downslope segment. If runoff production on the upslope segment is less than that on the downslope segment, the overland flow path length to the upper edge of the downslope segment should be shortened. An example is an undisturbed forest on the upslope area where the overland flow path length begins at the upper edge of the site because no surface runoff is assumed to occur from the undisturbed forest. If the upslope area is pasture and only produces half the runoff that a downslope field produces, the overland flow path length at the upper edge of the field should be one half the distance of the slope length across the pasture area.

Conversely, if the upslope area produces more runoff than does the field, the overland flow path length at the upper edge of the field should be greater than the actual distance in proportion to the differences in runoff potential for the two areas.

9. COVER-MANAGEMENT SUBFACTORS

Cover-management refers to how vegetation, soil condition, and material on and in the soil affect erosion. RUSLE2 describes the effects of cover-management using basic variables applicable to any cover-management system. The basic cover-management variables used in RUSLE2 are canopy (vegetative material not in contact with soil surface), ground (surface) cover (material in contact with soil surface), soil surface roughness, soil ridge height, below ground biomass (live and dead roots and incorporated material), and soil consolidation and antecedent soil moisture in the Req zone (see **Section 6.9**).

RUSLE2 is land use independent, which means that it can be applied to any land use where mineral soil is exposed to raindrop impact and Hortonian overland flow. RUSLE2 can be applied to crop, pasture, hay, range, disturbed forest, mined, reclaimed, construction, landfill, waste disposal, military training, park, wild, and other lands. RUSLE2 does not apply to undisturbed forestlands and lands where no mineral soil is exposed and surface runoff is produced by a mechanism other than rainfall intensity exceeding infiltration rate.

Because RUSLE2 is land use independent, it applies to transitions between land uses. For example, a lightly disturbed military training site may behave much like a pasture or rangeland, a moderately disturbed site may behave like a cropped field, and a highly disturbed site may behave like a very rough construction site. A "fresh" landfill and a recently reclaimed mine site not yet vegetated may behave like a freshly graded construction site but behave like pasture or range land over time. Pasture and rangeland may be periodically converted to and from cropland.

Erosion models based on specific land uses typically do not produce the same erosion values at a common point between land uses resulting in uncertainty between erosion estimates. RUSLE2 does not have this problem.

9.1. Basic Principles

Equation 7.1 estimates soil loss for the unit plot, which is a fallow (no vegetation) condition periodically tilled up and down slope to break the crust and to control weeds. This special condition is used to define and determine soil erodibility factor values (see **Section 7.2**). The daily cover-management factor **c** in equations 5.1 and 8.1 "adjusts" the unit-plot erosion to site-specific field conditions as affected by cover-management.

The cover-management factor c describes how cover-management affects both erosivity and erodibility. For example, vegetation and ground cover affect erosivity by reducing the erosive forces applied to the soil by raindrop impact and surface runoff. Both live

and dead roots and organic material in the soil increase infiltration, which reduces erosivity by reducing runoff. These materials reduce erodibility by decomposing in the soil to produce chemical bonding agents that increase the soil's resistance to detachment. Soil mechanical disturbance, which creates a very rough soil surface that ponds water, reduces the erosivity of both raindrop impact and surface runoff. Large soil clods that form the roughness peaks reduce erodibility by being resistant to detachment in comparison to a mechanical disturbance that finely pulverizes the soil. Thus, the effects of both erosivity and erodibility are included in other RUSLE2 factors besides just the erosivity and erodibility factors in equation 8.1.

RUSLE2 uses an index-based method to estimate soil loss without mimicking (explicitly modeling) erosion processes. RUSLE2 involves specific definitions and rules that must be followed, even when logic suggests something different.

A subfactor method used in RUSLE2 to compute values for the cover-management factor c gives RUSLE2 its land use independence.[54] This method uses subfactors that are universally important in how any cover-management system affects rill and interrill erosion. The RUSLE2 subfactors, listed in Table 9.1, are canopy, ground cover, soil roughness, ridge height, soil biomass, soil consolidation,[55] and antecedent soil moisture used in the Req zone. RUSLE2 computes a value for each subfactors for each day and uses equation 9.1 to compute a daily c factor value in equation 8.1.

$$c = c_c g_c s_r r_h s_b s_c p_p a_m \qquad [9.1]$$

where: c_c = canopy subfactor, g_c = ground cover subfactor, s_r = soil surface roughness subfactor, r_h = ridge height subfactor, s_b = soil biomass subfactor, s_c = soil consolidation subfactor, p_p ponding effect subfactor, and a_m = antecedent soil moisture subfactor.

Cover-management variables also affect the RUSLE2 topographic and support practice factors. Thus, the topographic, cover-management, and support practice factors must be examined to see the entire effect of land use and management on RUSLE2 erosion estimates.

[54] The RUSLE2 daily cover-management factor c is comparable to the soil loss ratio used in the USLE and RUSLE1. Soil loss ratios in the USLE applied to a crop stage period and to a 15-day period in RUSLE1. The C factor in the USLE and RUSLE1 is an average soil loss ratio value weighted by the temporal distribution of erosivity (EI distribution). Although RUSLE2 can compute a C factor value, RUSLE2 does not use a C factor value and a C factor value from another source can not be entered into RUSLE2 to compute erosion. The RUSLE2 subfactor method involves more variables and a different set of equations than used in the USLE or RUSLE1.

[55] Soil consolidation refers to how erosion decreases with time after a mechanical soil disturbance. Soil consolidation includes how the increase in soil bulk density after a mechanical soil disturbance affects erosion, but the major effect is how wetting and drying and other processes cement soil particles.

Table 9.1. Cover-management subfactors used in RUSLE2.		
Subfactor	Symbol	Comment
Canopy cover	c_c	Influence of above-ground vegetative material not in contact with soil surface; includes both live and dead vegetation
Ground cover	g_c	Material in contact with soil surface; includes both live and dead plant material and other material like manure, mulch, and "roll" erosion control materials applied to the soil surface
Soil (surface) roughness	s_r	Random roughness created by a mechanical soil disturbance; includes peaks and depressions that are randomly shaped and located without an orientation to runoff direction
Ridge height	r_h	Ridges formed by a mechanical soil disturbance; ridges and furrows between ridges redirect flow if not oriented up and down hill
Soil biomass	s_b	Includes plant and other organic material in the soil that has been incorporated by a mechanical soil disturbance, grown there as live roots that become dead roots, or moved into the soil by worms or other organisms
Soil consolidation	s_c	Refers to how a mechanical soil disturbance loosens the soil to increase erosion and the degree to which erosion has decreased following a mechanical soil disturbance
Antecedent soil moisture	a_m	Used in the Req zone; refers to how previous vegetation reduces soil moisture so that subsequent runoff and erosion is decreased

9.2. Cover-Management Subfactors

This section describes each cover-management subfactor and how RUSLE2 computes a value for each subfactor.

9.2.1. Canopy

Canopy is live and dead vegetative cover above the soil surface that **intercepts raindrops** but does not contact the **surface runoff**. The portion of the **above ground plant biomass** touching the soil surface is treated as **live ground cover**.

9.2.1.1. Canopy effects

Canopy intercepts raindrops. Some of the intercepted rainfall reforms as waterdrops that fall from the canopy. The erosivity of these drops is directly related to their impact energy. The impact energy of a waterdrop is one half of the product of mass (determined by drop diameter) and the square of impact velocity (determined by fall height). In

contrast to raindrops that vary over a wide size range, all water drops falling from canopy are nearly of an equal size (about 3 mm) that is significantly larger than the median raindrop size (about 1.5 mm). Even though the mass of each waterdrop falling from canopy is greater than the mass of most raindrops, the impact velocity of waterdrops falling from canopy is generally much lower than the impact velocity of raindrops because of the low fall heights from plant canopy. However, if the bottom of the canopy is greater than about 30 ft (10 m), the erosivity of waterdrops falling from canopy is greater than that of raindrops because of the increased mass of the drops falling from canopy.

Some of the rainwater intercepted by canopy flows along plant stems to the soil surface. While this water has no erosivity to detach soil particles by waterdrop impact, it provides water for runoff, but the delay caused by the water flowing along the stems to the soil surface reduces peak runoff rate, which in turn reduces runoff erosivity. Dense canopies retain a significant amount of water that never reaches the ground because it is evaporated after the storm. While this water is not significant for large storms, it can significantly reduce runoff for small storms.

The equation used to compute a value for the canopy subfactor is:

$$c_c = 1 - f_c \exp(-0.1 h_f) \qquad [9.2]$$

where: f_c = canopy cover (fraction) and h_f = effective fall height (ft). The two canopy variables of **canopy cover** and effective **fall height** are used to describe the effect of canopy on erosion.

9.2.1.2. Canopy cover (f_c)

Canopy cover is the portion of the soil surface covered by canopy in a horizontal plan view. The fraction of the soil surface covered by canopy is 1 minus the fraction of open space, which is the space through which a raindrop can fall to the soil surface without being intercepted by the plant canopy. Open space can be seen by looking down on the canopy from above and identifying the open space between the outer perimeter of the individual plant canopies and the open space within the outer perimeter of individual plant canopies. The

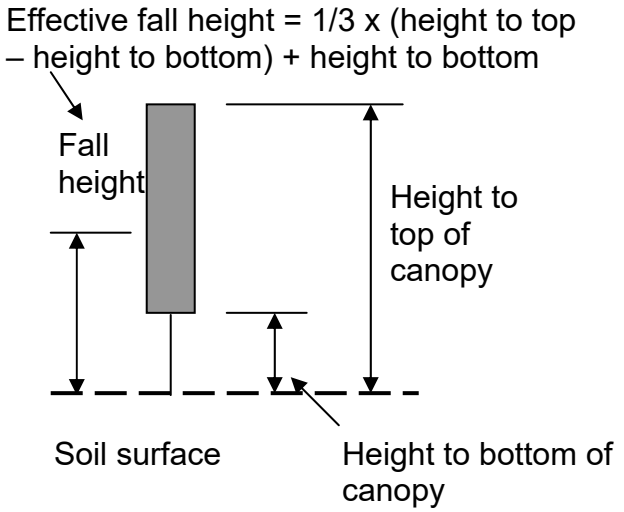

Figure 9.1. Effective fall height for a cylindrical shaped canopy of uniform density

effect on wind on the erosivity of raindrops or on how canopy intercepts raindrops is not considered in RUSLE2.

9.2.1.3. Effective fall height (h_f)

Waterdrops fall from various heights within the plant canopy, and some of the drops are intercepted by lower canopy. The total impact energy of these waterdrops is the sum of the impact energy of each drop on the soil surface. Effective fall height is the single fall height that gives the total energy if all drops fell from a single height. Effective fall height varies with plant maturity and shape, density gradient within the canopy, and heights to the top and bottom of the canopy. If the canopy shape is cylindrical and canopy density is uniform with height, the fall height is assumed to be one third of the way up from the bottom of the canopy as illustrated in Figure 9.1. The lower than average height reflects the likelihood that waterdrops falling from higher in the canopy are intercepted by lower canopy.

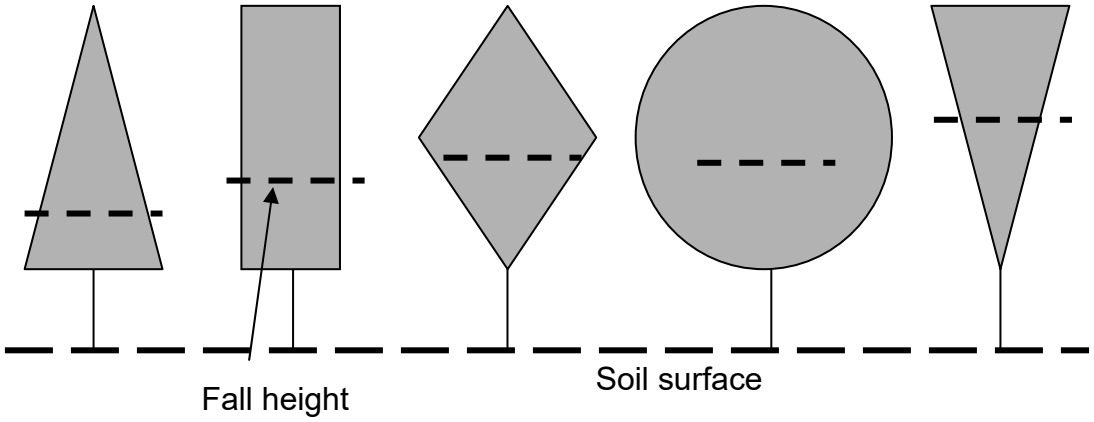

Figure 9.2. Effect of canopy shape on fall height

Canopy shape and density gradient of the canopy material with height influence effective fall height because lower canopy can intercept waterdrops that fall from higher in the canopy. Effective fall height is low when the canopy material is concentrated low in the canopy because of shape and density gradient as illustrated in Figures 9.2 and 9.3. If most of the leaves and branches of the plant are concentrated in the upper portion of the canopy, the effective fall height is one half to two thirds of the distance from the bottom to the top of the canopy. RUSLE2 includes a procedure that uses graphical shapes of these figures to assist in assigning effective fall height values for any particular vegetation throughout its growth.

Fall height assigned to a vegetation (plant community) should be assigned based on how the canopy of the particular plant community affects erosion relative to other plant

communities. Fall height must be consistent among vegetations in the RUSLE2 database and consistent with fall heights in the Core Database.

Because the effect of fall height in equation 9.2 is nonlinear, the heights cannot be averaged to determine an effective fall height.

Fall height can be measured at regular intervals along a transect where a rod is lowered through the canopy to the ground. The height to the lowest part of the canopy touching the rod is measured. Rather than averaging these values, the proper approach is to compute a canopy subfactor value by using equation 9.2 for each height and assuming that $f_c = 1$. These subfactor values are averaged and the effective fall height is computed from:

$$h_{fe} = -\ln(1 - c_{ca}) / 0.1 \qquad [9.3]$$

where: h_{fe} = effective fall height (ft) and C_{ca} = average canopy subfactor.

9.2.1.4. Understory

RUSLE2 uses a single vegetation description at any point in time. The values in this description are for the composite of the plant community that exists at the given point in time. RUSLE2 cannot take components of a plant community and aggregate values for each component into a composite value. The user directly assigns and enters a composite value for each RUSLE2 variable used to describe a particular vegetation.

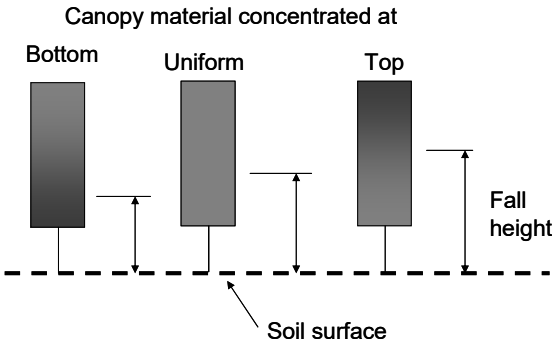

Figure 9.3. Effect of canopy density distribution on fall height

Some plant communities have distinct canopy components of over and understories. Examples include grass under shrubs on a rangeland, grass under vines on a vineyard, a legume interseeded in a small grain, a rye cover crop interseeded in corn, and volunteer weeds that begin to grow as crops approach maturity. Consideration must be given to overlapping canopies in determining an effective fall height. **The understory is often dominant in determining fall height especially if the understory is dense.**

9.2.1.5. Interaction with ground cover

Canopy that is directly above ground cover is assumed not to affect erosion. Thus, the effective canopy cover is computed from:

$$f_{ce} = f_c(1 - f_g) \qquad [9.4]$$

where: f_{ce} = effective canopy cover (fraction) and f_g = portion of soil surface cover by ground cover (fraction).[56] Also, RUSLE2 compares the canopy subfactor value with the ground cover subfactor value computed with the canopy cover value. RUSLE2 does not allow the canopy subfactor value to be less than this ground cover subfactor value. The effect of this comparison is that canopy cover behaves as ground cover as fall height approaches zero.

9.2.1.6. Effect of production level (yield)

RUSLE2 does not "grow" vegetation like a plant model "grows" vegetation. The user describes vegetative growth by entering values for retardance and above-ground biomass at maximum canopy, and values for root biomass, canopy cover, fall height, and live ground cover that vary through time. These values are entered in the vegetation component of the RUSLE2 database to describe a particular vegetation.

Variables used in RUSLE2 to describe vegetation are a function of production level (yield). **RUSLE2** can vary these values for these variables as a function of yield so that a vegetation description does not have to be created for each production (yield) level. A single vegetation description is created for a base yield, which RUSLE2 adjusts to the site specific yield.[57]

The purpose of entering a site-specific production (level) yield is so that RUSLE2 can determine values for biomass on and in the soil. Sources of biomass are **above-ground biomass** and **root biomass** from the vegetation grown on site and from **external residue**

[56]The RUSLE2 interaction between canopy and ground cover is similar to the one assumed in the USLE (AH537). No interaction between canopy cover and ground cover was assumed in RUSLE1 (AH703). As a result, the effect of canopy at low fall heights was too great in RUSLE1. In fact, RUSLE1erroneously computed a zero erosion for a 100% percent canopy cover when fall height was zero, rather than erosion for 100% ground cover. The RUSLE1 technique of using a zero fall height to shut off erosion for special purposes such as plastic mulch can not be used in RUSLE2. The **add** and **remove nonerodible cover processes** used to describe **operations** serves this purpose in RUSLE2.

[57] RUSLE2 differs from RUSLE1 in this regard. Different yields could only be accommodated In RUSLE1 by creating a vegetation description for each yield. A single base vegetation description is created In RUSLE2 for a base yield. RUSLE2 adjusts the base vegetation description to fit the specific site yield entered. However, a vegetation description for specific yields can be used in RUSLE2 just as in RUSLE1.

applied to the soil surface and/or incorporated into the soil. External residue includes straw, wood fiber, wood chips, organic-based roll erosion control materials, compost, leaves and forest debris, manure, and other similar materials that are typically applied to control erosion.[58]

Biomass values must be on a dry weight basis. The dry weight of external residue is known at the time of application from the user input value. The dry weight values for the above-ground and root biomass is determined from the production (yield) level entered by the user to represent a particular field site. RUSLE2 adjusts the aboveground biomass value at maximum canopy as a function of yield according to:

$$M_a = M_0 + b_a Y \qquad [9.5]$$

where: M_a = dry weight aboveground biomass at maximum canopy for the site specific yield, M_0 = the aboveground biomass at maximum canopy for a zero yield, and Y = yield in units chosen by the user. RUSLE2 determines values for M_0 and the slope term b_a from values entered by the user for two different yields. RUSLE2 uses a similar relationship to vary retardance with yield (see **Section 11.1.4**).

Dry weight values for root biomass are entered in RUSLE2 for a vegetation description at the base yield. RUSLE2 assumes that dry weight root biomass varies directly with yield, that canopy and live ground cover vary with the square root of yield, and that effective fall height varies with yield to the 0.2 power.

The base vegetation used to create vegetation descriptions at a new yield should be for a base yield where maximum canopy cover is less than 100 percent. The base maximum canopy cover must be less than 100 percent for the RUSLE2 yield adjust function to fully work. If the maximum canopy cover is 100 percent, RUSLE2 can adjust only for yield values greater than the base yield. RUSLE2 does not directly adjust vegetation values as a function of seeding rate, population, or row spacing. RUSLE2 can indirectly adjust for seeding rate and population by assuming a relationship between yield and these variables. Row spacing can only be considered in RUSLE2 by having a vegetation description for each row spacing. If canopy characteristics vary significantly between crop varieties, plant communities, or management practices, a vegetation description must be constructed to reflect each significant difference.

RUSLE2 computes the variation of above-ground biomass through time by assuming that above-ground biomass varies with the 1.5 power (see **Section 11.1.3.1**) of canopy cover.[59] RUSLE2 calibrates this relationship using the user entered values for above-

[58] External residue also includes inorganic materials such as rock and roll erosion control materials applied to the soil surface. These materials require special consideration. See **Section 12**.

[59] RUSLE2 tracks aboveground biomass through time, which is different from RUSLE1. A biomass value entered in RUSLE1 had to correspond to the date of an operation that affected aboveground biomass.

ground biomass at maximum canopy and the amount of above-ground biomass remaining after full senescence has occurred. This approach allows an operation to be entered at any date during a cover-management system without the user having to explicitly enter the biomass at that point in time. In some cases, the assumed relationship between canopy and aboveground biomass may not give the proper value for the aboveground biomass when an operation with a **kill** vegetation process occurs before the vegetation reaches maturity.[60] A vegetation description can be created where the above-ground biomass at maximum canopy is the aboveground biomass at the time that the vegetation is killed rather than the above-ground biomass at maximum canopy as the vegetation approaches maturity.

The yield entered in RUSLE2 for the vegetation at a particular field site must be consistent with the site climatic, soil, and management conditions. **RUSLE2 assumes that the user has selected a vegetation description and yield appropriate for the site.** Because RUSLE2 does not model vegetation growth, it can not determine the appropriateness of a vegetation description for a particular site nor does RUSLE make adjustments based on climatic, soil, or management conditions. For example, an operation description must be used to tell RUSLE2 to represent frost killing vegetation.

In RUSLE2, the users define production (yield) level in any terms that they choose, although customary usage is recommended. For example, yield can be expressed in terms of a "fresh" weight or a "dry" weight. Equation 9.5 converts the specified yield, which might be in fresh weight units, to the dry weight values that RUSLE2 needs for biomass.

Accounting for all of the biomass involved in a particular cover-management system is not necessary. **The amount of biomass left in the field to affect erosion is the critical variable.** The amount of biomass that leaves a field is unimportant.

RUSLE2 does not have this requirement. The biomass values are entered at maximum canopy and RUSLE2 tracks biomass through time. An operation can be entered in RUSLE2 at any time in a cover-management system without having to specify (enter) a biomass value in the vegetation description on the date of the operation.

[60] **Kill vegetation** has a particular definition in RUSLE2. Kill vegetation is one of several processes used to describe an operation. Killing vegetation converts live vegetation to dead vegetation. See **Section 13** for the RUSLE2 rules regarding manipulation of vegetation. A **kill vegetation process** must be used in an operation description to tell RUSLE2 that vegetation has died by maturity or has been killed by frost.

RUSLE2 uses a description of site specific conditions to compute erosion. The user carefully follows the RUSLE2 definitions and procedures to create this description. Multiple approaches can often be used to create a description. In general, RUSLE2 was designed so that vegetation descriptions can be created independently of the operations used to manipulate vegetation. For example, this approach allows RUSLE2 to use a single description for corn grown for grain and corn grown for silage. However, some cases may occur where a vegetation description is created to reflect the manipulations of an operation that can not be conveniently created using an operation. The important consideration is that RUSLE2 gets the values that it needs for its computations.

9.2.1.7. Senescence and other canopy losses

Canopy cover increases during the growth period when plants accumulate aboveground biomass. As plants become maturity, some vegetation, such as soybeans and perennial grasses, lose canopy cover by senescence. Other plants, such as cotton, lose canopy cover by being defoliated with chemicals. This loss of canopy cover transfers biomass from standing vegetation to plant litter (residue) on the soil surface. Once canopy material falls to the soil surface, RUSLE2 begins to compute its decomposition. Some plants, like corn, lose canopy cover by leaves drooping without falling to the soil surface, which RUSLE2 also considers (see **Section 11.2.4**).

Plants such as hay and pasture crops and permanent vegetation on rangeland, closed landfills, and other undisturbed areas experience a simultaneous birth and death of aboveground biomass during the growth period while cover is increasing. The death of live aboveground biomass adds a substantial amount of biomass to the surface litter (residue) pool. The daily death of live aboveground biomass is approximately one percent of the live aboveground biomass on that day.

The other way that canopy is lost is by **operations** that **remove live biomass**. Harvest, shredding, mowing, grazing, and burning are typical operations that reduce canopy cover (see **Section 13.1**).

9.2.1.8. Assigning values for canopy

Canopy values assigned to represent a particular vegetation must be consistent with those in the **RUSLE2 Core Database** and with values for other plant communities in the **vegetation component** of the RUSLE2 database. Core values are used to guide assigning values to new vegetation descriptions entered in the RUSLE2 vegetation database. Using consistent values with those in the Core Database helps ensure that RUSLE2 gives the expected erosion estimate and that erosion estimates are consistent between plant communities.

9.2.2. Ground Cover

Ground cover, which is material in contact with the soil surface, slows surface runoff and intercepts raindrops and waterdrops falling from canopy. Ground cover includes all material that touches the soil surface. Examples are rock fragments, portions of live vegetation including basal area and plant leaves that touch the soil, cryptogams (mosses), crop residue, plant litter, and applied materials including manure, mulch, and roll erosion control materials. Ground cover is probably the single most important variable in RUSLE2 because it has more effect on erosion than almost any other variable, and applying ground cover is the simplest, easiest, and most universal way of controlling erosion.

To be counted as ground cover, the material must remain in place and not be moved downslope by surface runoff during a rainstorm. Also, the material must contact the soil surface so that runoff does not flow between the material and the soil to cause erosion.

Operations in RUSLE2 do not affect rock cover entered in the soil component of the RUSLE2 database. Rock fragments added as an external residue are manipulated just like any other "residue" by operations in RUSLE2. See *Section 12* for special consideration regarding treating rock as an external residue

Rock fragments on the soil surface require special consideration. Generally rock fragments must be larger than 5 mm on coarse textured soils in arid and semi-arid regions where runoff is low and larger than 10 mm in other regions to be counted as ground cover. Rock fragments on the soil surface can be treated in one of two ways. They can be considered to be a part of the soil where a rock cover value is entered in the **soil component** of the RUSLE2 database (see Section 7.6). Rock fragments can also be "applied" as an **external residue**.[61]

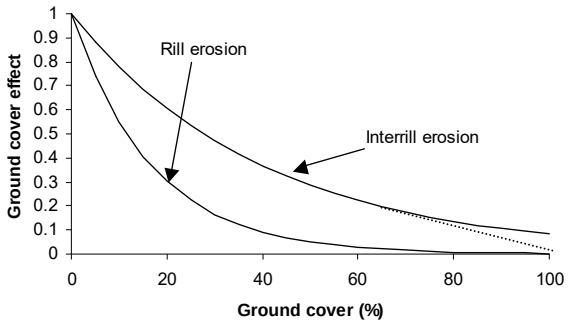

Figure 9.4. Effect of ground cover on rill and interrill erosion

9.2.2.1. Ground cover effect

Ground cover reduces erosion by protecting the soil surface from direct raindrop impact, which reduces **interrill erosion**. Ground cover also slows surface runoff and reduces its detachment and transport capacity, which reduces **rill erosion**. If

[61] **External residue** is RUSLE2 nomenclature that refers to any material added to the soil surface or placed in the soil from a source other than vegetation grown on site.

ground cover is low (less than about 15%) and ground cover pieces are long and oriented across slope, ground cover reduces soil loss by causing deposition in small ponds above ground cover pieces. As ground cover increases, deposition ends and ground cover reduces runoff detachment capacity, which reduces rill erosion. The ground cover effect for both interrill and rill erosion is illustrated in Figure 9.4.

Ground cover reduces rill erosion more than interrill erosion. That is, the ground cover subfactor is less for rill erosion than for interrill erosion for a given ground cover percent as illustrated in Figure 9.4. The net or overall effectiveness of ground cover depends on the relative contributions of rill and interrill erosion. The ground cover subfactor value is less when rill erosion makes the greater contribution to total erosion than when interrill erosion makes the greater contribution.

Factors that affect the relative contributions of rill and interrill erosion affect the ground cover subfactor. These variables include ratio of soil erodibility for rill erosion to soil erodibility for interrill erosion, soil biomass, soil consolidation, ground cover type, and the anchoring and bonding of ground cover to the soil. Obviously ground cover provides the greatest erosion control when it is well anchored and bonded to the soil. Conversely, ground cover is least effective where mulch pieces bridge across soil roughness so that runoff flows under the ground cover and where runoff moves poorly anchored ground cover. RUSLE2 partially represents these effects by reducing erosion for a given amount of ground cover when increased soil biomass is present.

These mechanical effects reduce the forces applied to the soil by waterdrop impact and surface runoff. An indirect effect is ground cover's effect on infiltration and runoff. Infiltration rate can be very high and runoff low on a freshly tilled soil without a surface seal.[62] If ground cover is placed on the soil before a crust is formed, the ground cover will reduce seal formation and help maintain high infiltration and low runoff. Therefore, ground cover has a lesser effect on reducing erosion when placed on a soil after it becomes crusted or placed on a soil where internal soil properties, such as a high clay content or high bulk density, reduce infiltration. A given amount of ground cover reduces erosion more for cover-management systems, such as no-till cropping, that maintain high soil biomass, improve soil quality, and reduce crusting because of increased infiltration. An interaction between soil biomass and soil consolidation is a major variable used by RUSLE2 to compute values for the ground cover subfactor.

Size and shape of ground cover material vary widely. Sizes and shapes include round rock fragments; thin, flat leaves; long slender pieces of unchopped wheat reside; long and increased diameter unchopped corn stalks; large pieces of woody debris left by logging operations; and continuous roll erosion control blankets. The portion of the soil surface

[62] A surface seal is a thin, dense layer of soil particles at the soil surface caused by soil particle dispersion associated with raindrop impact and other processes. This thin layer, which reduces infiltration, is known as a surface **seal** when wet and a **crust** when dry.

covered is used as a single variable to describe the effect of ground cover on erosion. Even though the geometry of individual ground cover pieces can vary greatly, even for the same type of ground cover, the portion of the soil surface covered integrates the effects of varying geometry of ground cover pieces on erosion, as illustrated in Figure 9.4. Ground cover (crop residue) provided by above-ground biomass from a typical agricultural crop includes leaves, pods, hulls, cobs, stems, and stalks and fine and coarse roots for below-ground biomass. Ground cover (slash) on a disturbed forest ranges from leaves and needles to broken tree limbs. Furthermore, certain operations, especially harvest operations, frequently reduce size of biomass pieces that becomes ground cover. Even though size and shape of residue pieces vary over a wide range for a particular residue, a single **residue type** is selected to represent the residue. **Residue type** is an entry in the **residue component** of the RUSLE2 database that is selected based on size and toughness of the residue.

Several types of ground cover may occur at a specific site and overlap each other. Examples include rock fragments, live ground cover (basal area and plant leaves), and plant litter. RUSLE2 assumes that ground cover produced by vegetative biomass and ground cover from external residue overlap rock cover represented in the soil description. RUSLE2 also assumes that live ground cover overlaps all other types of ground cover. RUSLE2 assumes that the last ground cover that arrives on the soil surface overlaps existing ground cover, except for live ground cover. RUSLE2 accounts for the overlap of individual ground cover pieces instead of adding the cover provided by each ground cover type.

The important consideration is the net effect of the composite ground cover, not how the individual ground cover materials affect erosion. RUSLE2 uses the net ground cover to compute a value for the ground cover subfactor. The best way to visualize the net ground cover is to determine the fraction of bare, exposed soil and subtract that value from one.

RUSLE2 accounts for ground cover on a mass per unit area basis (e.g., tons/acre, t/ha). RUSLE2 converts mass (weight) values to a percent (fraction) of the soil surface covered (see **Section 12**), accounts for overlap, and uses a net (effective) ground cover value to compute a value for the ground cover subfactor.

Although RUSLE2 tracks ground cover by mass, RUSLE2 displays ground cover in percent (fraction) to aid conservation planning that if often based on maintaining a certain ground cover percent.

9.2.2.2. Equation for ground cover subfactor

The main equation used in RUSLE2 to compute a value for the ground cover subfactor is:

$$g_c = \exp(-bf_g) \qquad [9.6]$$

where: **b** = a coefficient that describes the relative effectiveness of ground cover and f_g = ground cover (percent). The effectiveness of ground cover varies with the site-specific condition. For example, a 50% ground cover can reduce soil loss by 95% under some conditions while only reducing soil loss by 65% under other conditions. Values for **b** in RUSLE2 range from about 0.025 for the interrill erosion ground cover effect to 0.06 for the rill erosion ground cover effect, illustrated in Figure 9.4, to represent this variation in ground cover effectiveness.

Therefore, the net **b** value depends how interrill erosion varies relative to rill erosion. Consequently, the **b** value used by RUSLE2 in equation 9.6 varies daily with the ratio of rill to interrill erosion. RUSLE2 computes a net **b** value using equations based on rill and interrill erosion as:

$$a_t = a_r \exp(-0.06 f_g) + a_i \exp(-0.025 f_g) \qquad [9.7]$$

$$b = -\ln[(a_t /(a_i + a_r)]/ f_g \qquad [9.8]$$

where: a_t = total relative erosion with ground cover, a_r =relative rill erosion on the same bare soil with all other conditions the same as when ground cover is present, and a_i = relative interrill erosion on a bare soil with all other conditions the same as when cover is present. Values for relative interrill and rill erosion in equations 9.7 and 9.8 are computed using the variables in equation 8.3. These equations compute daily **b** values daily that capture the main effects of how the net effectiveness of ground cover on rill-interrill erosion is affected by soil, cover-management, and by slope steepness. These effects are described in **Section 9.2.2.1**.[63]

In Req applications, a constant **b** value of 0.046 is used because the majority of the erosion is assumed to occur from rill erosion. The 0.046 value is based on analysis of plot data.

[63] RUSLE2 eliminates the need to choose a **b** value for the effectiveness of ground cover required in RUSLE1.05 or the choice of a land use required in RUSLE1.06. RUSLE2 automates a manual selection of **b** required in RUSLE1. RUSLE2 computes **b** values as cover-management conditions vary through time that RUSLE1 did not compute.

RUSLE2 does not compute a composite ground cover subfactor value by computing a subfactor value for each ground cover type and then multiplying those values. That procedure would be an improper mathematical operation. Therefore, rock fragment cover must be combined with other ground cover considering overlap rather than using a soil erodibility factor value already adjusted for rock cover.

RUSLE2 reduces the effect of ground cover on steep slopes with little soil biomass. This feature represents how mulch is less effective on steep construction sites than crop residue and plant litter on crop, range, pasture, and disturbed forestland. RUSLE2 takes into account how small ground cover pieces that conform closely to the soil surface reduce erosion more than long pieces of ground cover that bridge across roughness elements like soil clods. This effect is greatest on steep, construction-like soil and slope conditions.

RUSLE2 assumes an interaction between soil surface roughness and ground cover such that the effectiveness of ground cover is reduced as surface roughness increases. For example, ground cover in the bottom of a depression filled with ponded water does not reduce erosion as much as does the same ground cover on a flat soil surface. RUSLE2 computes a low **b** value for flat slopes where interrill erosion dominates, a high **b** value on steep slopes where rill erosion dominates, and an increased **b** value on no-till and other soils conditions where ground cover increases infiltration. The interaction of soil consolidation and soil biomass is used to indicate conditions where ground cover increases infiltration. RUSLE2 also compute increased **b** values for soils susceptible to rill erosion based on soil texture and decreased **b** values for increased soil consolidation that is assumed to reduce rill erosion more than interrill erosion.

RUSLE2 b values are not always comparable to b values reported in scientific literature. In many cases, literature b values are based on plotting soil loss versus percent ground cover without considering other variables such as soil surface roughness, soil biomass, and soil consolidation. Values determined on that basis cannot be compared with RUSLE2 b values because RUSLE2 represents those effects in other variables. Also, reported b values are as large as 0.1, which are larger than can be obtained by RUSLE2. These high b values represent extremes rather than the typical condition represented by RUSLE2.

RUSLE2 biomass residue pools:
1. Standing (canopy cover)
2. Flat (ground cover)
3. Buried

9.2.2.3. How ground cover is added to and removed from the soil surface

Ground cover is added to the soil surface by live vegetation (live ground cover), senescence causing canopy material to fall to the soil surface, natural

processes causing standing residue to fall over, an operation (e.g., harvest)[64] flattening standing residue, an operation (e.g., tillage) resurfacing previously buried residue, or an operation applying **external residue** (e.g., mulch, manure, roll erosion control product) to the soil surface. Ground cover is removed when plant growth reduces leaves or other live plant parts from touching the soil surface, an operation (e.g., tillage) buries ground cover, or an operation (e.g., straw baling, burning) removes ground cover.

Live ground cover values are entered in the **vegetation descriptions** in the **vegetation component** of the RUSLE2 database (see **Section 11**). Live ground cover is controlled entirely by these values, and live ground cover does not decompose. **The mass of live ground cover is accounted for in the above-ground biomass of the live vegetation.** Senescence transfers material from the live above-ground biomass (canopy) to the soil surface where it is treated as ground cover (flat residue). Once on the soil surface, this residue decomposes as a function of daily rainfall, daily temperature, and decomposition half life (coefficient) assigned in the **residue description** entered in the **residue component** of the RUSLE2 database (see **Section 12**).

.

When live vegetation is **killed**, it becomes **standing residue**. Over time this residue falls over because of natural processes and becomes ground cover (i.e., becomes surface residue). The rate that standing residue "falls" (i.e., mass is converted from standing residue to surface residue) is proportional to the decomposition rate at the base of the dead standing residue. The base of the standing residue is assumed to decompose at the same rate as the **flat (surface) residue**.

Standing residue, which is not in contact with the soil surface, decomposes at a much slower rate than flat or buried residue because of no soil contact to provide moisture to accelerate decomposition.[65] Standing residue can also be converted to ground cover (flat residue) by an **operation** that includes a **flattening process**. **Flat residue** is lost by decomposition and burial by operations. **Buried residue** is also reduced by decomposition at the same rate as flat residue, and buried residue can be resurfaced by an operation that includes a **(mechanically) disturb soil process**, which adds material to ground cover. **External residue** can also be added to the soil surface by an operation that includes an **add other cover process**. External residue decomposes at the rate determined by the decomposition half life (coefficient) entered for the **residue description** in the **reside component** of the RUSLE2 database**.** See **Section 13** for a description of how operations manipulate ground cover.

---

[64] An operation is an event that mechanically disturbs the soil, changes the vegetation, or changes the residue.

[65] RUSLE2 assumes that flat residue, buried residue, and dead roots all decompose at the same rate. Standing residue is assumed to decompose at a much slower rate than residue in the other pools. Decomposition rate at the base of standing residue, which determines the rate that standing residue falls, is the same as the decomposition rate for flat residue.

The information in each RUSLE2 database component and the rules for manipulating RUSLE2 variables are a "language" and procedure used to describe field conditions through time. The objective in RUSLE2 is to describe field conditions as they exist, not to model processes as a way to describe field conditions. A check should always be made before making a RUSLE2 computation to verify that the user created description matches the actual field situation. RUSLE2 uses your field description to estimate erosion.

Nonerodible cover can be added to the soil surface to represent adding a plastic mulch used in vegetable production, a water layer used in rice production, a snow cover in winter months, and to shut off erosion for particular computational reasons. Nonerodible cover acts like other kinds of ground cover except that it completely shuts off erosion for the portion of the soil surface that it occupies. Half life and permeability are parameters used to describe nonerodible cover (see **Section 13.1.9**).

Most types of ground cover can be removed from the soil surface. Live ground cover is removed controlled by the values assigned through time in the **vegetation description**. Rock cover assigned in the **soil description** can not be removed. Other forms of ground cover can be removed by using an **operation** that has a **remove residue/cover process.** Buried residue biomass in the soil can be removed by using an operation to **resurface** the residue to become ground cover and then using another operation that removes this ground cover. Neither live nor dead roots can be removed from the soil. **RUSLE2**

RUSLE2 rules for transfer of residue among pools:
1. Residue is added to the soil surface by senescence, standing residue falls over by natural processes, standing residue that is flattened by an operation, or application of external residue
2. Senescence transfers biomass from live canopy to the soil surface, adding ground cover (flat residue)
3. Live vegetation cannot be flattened or buried
4. Killing live vegetation creates standing residue (dead plant material)
5. Standing residue becomes flat residue by falling over from natural processes or by being flattened by an operation
6. Only flat residue can be buried (standing residue must first be flattened by natural processes or by an operation before it can be buried)
7. Flat residue can only be buried by an operation that mechanically disturbs the soil
8. Twenty five percent of the daily decomposed flat (ground cover) residue becomes buried residue in the upper 2 inch (50 mm) soil layer where it decomposes again
9. Only buried residue can be resurfaced; roots can not be resurfaced
10. Buried residue can only be resurfaced by an operation mechanically disturbs the soil

assumes that a decrease in the live root biomass in the vegetation description represents root sloughing that becomes a part of the dead root biomass pool (see **Section 11.2.6.3**). **Also, RUSLE2 can represent daily additions to the dead root pool by root death during growth periods (i.e., when live root biomass is increasing).**

9.2.2.4. Conversion of residue mass to portion of soil surface that is covered

RUSLE2 uses the following equation to convert ground cover (residue) mass to portion of the soil surface that is covered:

$$f_g = 1 - \exp(-\alpha M_g) \qquad [9.9]$$

where: α = a coefficient that is a function of residue characteristics (units depend on the units of M_g) and M_g = residue mass per unit area (e.g., lbs/acre, kg/ha) expressed on a dry matter (weight) basis. Figure 9.5 shows a plot of equation 9.9 for four residue types.

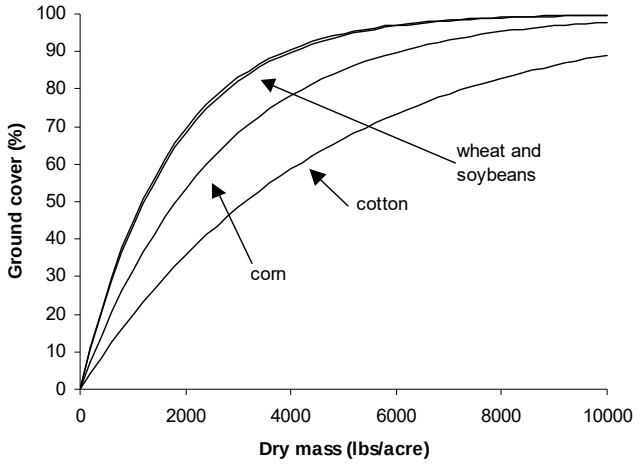

Figure 9.5. Relationship of ground cover to dry mass for four types of residue.

RUSLE2 uses data points entered in the **residue description** in the **residue component** of the RUSLE2 database to determine a value for α in equation 9.9 for each residue description in the residue component of the RUSLE2 database (see **Section 12.3**).

Figure 9.5 illustrates differences in residue types. Cotton residue is mainly composed of very coarse, woody stems, which requires a large mass of these residue pieces to produce a given ground cover. The other extreme is soybean residue, which is a mixture of several plant components including leaves, stems, and seed pods. The curve for wheat residue is similar to the one for soybean residue, but in this case, not a particularly large mass of hollow wheat stems is required to provide significant ground cover. Also, a significant amount of wheat residue is composed of leaves. Corn residue is intermediate. Much of the corn residue is large stalks that are solid but less dense than cotton stems. Also, much of the corn residue is composed of leaves.

The portion of the soil surfaced covered by residue does not change greatly as residue mass (weight per unit area) changes at high amounts of ground cover. For example, reducing the mass of the ground cover material by 50% has little effect on ground cover if mass of material on the soil surface is very large. In contrast, a slight change in mass per unit area at low mass values can significantly change ground cover. The small change in ground cover at large mass values is a major reason that RUSLE2 computes burial and resurfacing of material based on mass rather than on percent cover.

The best approach for selecting values for a residue description in the RUSLE2 database is to choose values based on information in the **core database** rather than making site specific field measurements. Field data are highly variable and should be avoided unless a large mass of data collected under research conditions are available (see **Section 9.2.2.6**).

Be cautious in developing residue descriptions for different crop varieties. Differences reported in scientific literature often represent unexplained variability rather than real differences.

RUSLE2 uses a single composite residue description for a particular residue although crop residue and plant litter are composed of a wide variety of plant components of different sizes. This approach is a compromise. A small mass of leaves gives a much greater percent ground cover than does the same mass of stems. Therefore, the relationship between cover and mass depends on the relative proportion of leaves and stems, or other plant components. This relationship changes through time because the residue components decompose at different rates. For example, leaves decompose much more rapidly than do stems. Consequently the mass-cover relationship is very different immediately after harvest when many leaves are present than later after the leaves have decomposed with only stems remaining. Also, the mass-cover relationship for a residue type can appear to differ by location for a particular plant community, when in reality the mass-cover relationship is reflecting how the proportion of leaves to stems varies by time and location.

The mass-cover values for the residue descriptions in the RUSLE2 core database were primarily chosen so that RUSLE2 computes erosion estimates that compare well with measured erosion values in research studies.[66] Also, the core database residue descriptions were chosen to represent the overall mass-ground cover relationship for the first year after harvest rather than fitting ground cover values at a specific point in time, such as one year after harvest. The result is that RUSLE2 may underestimate cover

[66] The major reason for having and using a RUSLE2 **core database** is to help ensure consistency in RUSLE2 estimates, especially by cover-management system and by location. Consistency is a major requirement when RUSLE2 is used to implement cost sharing and regulatory type programs so that all clients are treated fairly.

beyond about 12 months. The core database values were chosen to compute average annual erosion as a function of main effects rather than secondary effects associated with residue components decomposing at different rates. Fitting secondary effects, especially with limited data, is often fitting unexplained variability. The core database values represent several data sets rather than focusing on a single data set.

9.2.2.5. Spatially non-uniform ground cover

This section describes how to apply RUSLE2 where ground cover is concentrated in strips and patches. Examples of non-uniform ground cover are narrow strips mechanically disturbed by tillage and planting equipment, residue strips left by harvest operations, natural processes that cause residue to collect in strips, "patches" of highly disturbed soil left by logging and military training operations, and grass/shrub "clumps" on rangeland.

RUSLE2 uses different **cover-management descriptions** along the overland flow path to compute erosion for these conditions. Segments are created in the **management layer** illustrated in Figure 8.1. Cover-management descriptions are assigned to segments to represent non-uniform ground cover and disturbed soil along the flow path.

RUSLE2 assumes that ground cover is uniformly distributed for a particular cover-management description. RUSLE2 values for flattening, burial, and resurfacing ratios used to describe the manipulation of residue by operations are based on the entire area, not the local area where the residue is manipulated, such as in a tilled strip where seeds are planted.

The first example is the patchiness common to disturbed forest lands and military training sites where ground cover and soil disturbance vary randomly. The boundaries between the patches are the location of segment breaks. Cover-management descriptions are applied to each segment to represent each cover-management condition along the flow path.

A second example is landfills where vegetation and ground cover vary along the flow path because of soil differences. Segments are created in both the soil layer and the management layer in Figure 8.1. Appropriate soil and cover-management descriptions are assigned to each segment.

A third example is residue strips left by a combine without a straw spreader. Two cover-management descriptions are used to represent this condition. One description is for the strip that has standing residue with no flat residue from the vegetation just harvested. An operation with a **remove residue/cover process** is used to remove the flat residue that RUSLE2 assumes to be uniformly distributed. The cover-management description for

the other strip is the same except it **applies external residue** to add the residue removed in the first cover-management description. The management layer in Figure 8.1 is divided into segments based on the width of each cover-management strip and the appropriate cover-management description is applied to each strip.

A fourth example is for mechanically disturbed strips, such as in vineyard or orchard where clean tilled strips are maintained within a relatively undisturbed area. A cover-management description is created for each strip and the management layer in Figure 8.1 is divided into segments to represent each of these strips along the overland flow path. If the strips are uniform along the flow path, the **strip/barrier descriptions** can be used to facilitate dividing the flow path into segments (see **Section 8**). Dividing the profile illustrated in Figure 8.1 into many segments can be tedious and laborious. The important variable is the ratio of the sum of the segment lengths of one strip type to the entire overland flow path length. This variable is more important than the actual number of strips along the flow path provided the number of strips exceeds a total of about 20 for the combination of strips (10 of one strip type and 10 of the other strip type). The inputs for number of strips and width of strips must be coordinated to ensure that the relative portion of the flow path occupied by each strip type is maintained.

A RUSLE2 template that includes the profile schematic illustrated in Figure 8.1 must be used to apply this procedure. This template allows non-uniform segment lengths. Also, strips are not constrained to be on the contour.

HOWEVER, CARE SHOULD BE TAKEN IN APPLYING RUSLE2 TO STRIPS. THE POSSIBILITY OF RUNOFF RUNNING ALONG THE UPPER EDGE OF HIGH RETARDANCE STRIPS BELOW ERODIBLE AREAS MUST BE CONSIDERED.

9.2.2.6. What to do when RUSLE2 computes a ground cover value that is not the expected value

Ground cover is a key variable used in conservation and erosion control planning and in determining whether a conservation or erosion control plan has been properly implemented. Residue ground cover immediately after planting is often the key value for conservation planning on cropland. RUSLE2 is expected to provide a good estimate of this ground cover value. The acceptability of RUSLE2 is sometimes judged on the basis of this value. Comparisons are made between the RUSLE2 estimated residue cover values with research data, site-specific field measurements, and professional judgment. This section provides guidance on making these comparisons and how to adjust RUSLE2 inputs if ground cover estimates do not meet expectations.

Several factors must be considered in comparing RUSLE2 residue ground cover values with field observations. RUSLE2 computes “typical,” average annual daily residue cover

values rather than residue cover at any specific time. Residue cover values measured at a particular site vary greatly from year to year, requiring at least three years of data where a range of production (yield) levels and weather conditions occurred to obtain measured values comparable to RUSLE2 estimates. Also, residue cover varies greatly from location to location within a field site requiring numerous measurements at a site depending on the measurement procedure (e.g., a beaded string versus photographs of a meter (yard) square area).

Great care must be taken in measuring residue cover when the cover is spatially non-uniform in strips and patches to ensure that the sample density is sufficient when measuring residue cover using the bead-string or similar method, especially if the strips are narrow and residue cover is heavy in one strip type. In fact, the best way to measure residue cover for this condition is to use transects within each strip type rather than diagonally across strips and weight the values based on area represented by each strip type.

The RUSLE2 mass-cover and erosion equations are highly nonlinear. As a consequence, using residue cover averaged over the entire area to estimate erosion with RUSLE2 likely will not give the same result as that obtained when the spatially non-uniform cover is analyzed using segments as described in **Section 9.2.2.5**. Remember, the purpose of RUSLE2 is to serve as a tool to guide conservation and erosion control planning rather than being a scientific tool.

The error in residue cover measurements can be large for residue cover less than about 20 percent. Sometimes residue mass is estimated based on field measurements of residue cover percent converted to a mass using curves like those in Figure 9.5. The error in mass can be large, sometimes by as much as a factor of two, for residue cover values greater than 75 percent. The residue mass can change by a large amount with only a small change in ground cover because of the flatness of the mass-cover curve at high cover values. Also, the data used to develop curves like those in Figure 9.5 are highly variable based on the relative portion of leaves to stems and other factors.

Very carefully compare the values determined from site-specific field measurements with values in the **core database** and values reported in the literature. Ask the question, “Are the field measured values consistent with commonly accepted values and reasonable when the data as a whole are considered? If the measured values differ significantly from other values, can the differences be reasonably explained?”

Getting a good comparison between the RUSLE2 residue cover estimate and a measured value at a particular point in time, such as immediately before harvest, does not ensure a good average annual erosion estimate. The best average annual erosion is obtained from a good estimate of residue cover over the two to three month period during the most erodible part of the year. The most erodible period is determined by a combination of

peak erosivity and peak susceptibility of the field condition to erosion. RUSLE2 templates that display erosion through time can be used to identify the most erodible period.

RUSLE2 was constructed and calibrated, and values in the core database were carefully chosen to ensure that RUSLE2 produces average annual erosion estimates consistent with commonly accepted erosion scientific knowledge and the uncertainty in the research erosion measurements (see **Section 17** for a discussion of the uncertainty in erosion data and RUSLE2 erosion estimates). RUSLE2 was developed to capture main effects rather than secondary variability, which often reflects statistically unexplained viability. Thus, fitting RUSLE2 to data from a specific research study or measurements made at a specific field site often does not improve RUSLE2 estimates and in fact may degrade the quality of estimates. Residue cover can vary greatly from year to year as yield and weather vary.

Don't make changes just to get a better fit to local conditions. Always compare against a broad data set. Look at RUSLE2 estimates as representing main effects and typical conditions in a conservation planning context, not in a research context. Make sure that data being fitted are high quality, and collect as much supplemental data as possible, including yield, residue mass, and how residue cover varies during the year.

ALWAYS CHECK RUSLE2'S ESTIMATED EROSION. CHANGING INPUTS THAT AFFECT RESIDUE COVER ALSO AFECTS OTHER RUSLE2 COMPUTATIONS. DO NOT AUTOMATICALLY ASSUME THAT A RESIDUE COVER VALUE AT A PARTICULARLY TIME, SUCH AS IMMEDIATELY AFTER PLANTING OR BEFORE HARVEST, CORRECTLY COMPUTED BY RUSLE2 ENSURES A CORRECT AVERAGE ANNUAL EROSION ESTIMATE.

If one concludes that RUSLE2 is not computing the desired residue cover values, how does one change input values to obtain the desired residue cover values? The main factors that affect residue cover must be considered in a systematic, stepwise manner. The factors that affect residue cover affect many other RUSLE2 computations. Adjusting a particular RUSLE2 input may give the expected residue cover but adversely affect the RUSLE2 erosion estimate because other RUSLE2 computations were affected. The main variables to consider and the order to consider them are: (1) the amount of residue at harvest, (2) the distribution between standing and flat residue at harvest, (3) the mass-ground cover relationship, (4) values for the burial and resurfacing ratios of the operations, and (5) the decomposition half life (coefficient) value. Estimated residue cover and erosion values should be checked at each step. Sometimes changing a particular variable gives unexpected results. For example, changing the value for the

decomposition half life affects not only ground cover, but standing residue, buried residue, and dead roots as well.

9.2.3. Soil (Surface) Roughness

Soil (surface) roughness, illustrated in Figure 9.6, refers to the random peaks and depressions left by soil disturbing operations. This random roughness does not affect general overland flow direction in contrast to oriented roughness (ridges and furrows) that redirects runoff. Roughness characteristics at the time that the roughness is created depend on soil disturbing operation that creates the roughness, soil properties including texture and soil moisture, live vegetation, standing and flat residue, and soil biomass. Different types of soil disturbing operations produce widely differing distributions of aggregates and clod sizes depending on soil conditions, which affect roughness. Surface roughness decays over time to a smooth surface, except for a few persistent clods on some soils.

Figure 9.6. Soil surface with a 1.0 inch roughness just created by a mechanical disturbance.

9.2.3.1. Soil (surface) roughness effect

Soil surface roughness affects erosion in several ways. The depressions formed by surface roughness pond water and slow runoff, which reduce the erosivity of raindrops, waterdrops falling from vegetation, and surface runoff. Runoff's transport capacity through the depressions is very low, which causes local deposition. Soil surface roughness decays over time as deposition fills the depressions with sediment, interrill erosion wears away the roughness peaks, and the presence of water and weathering cause the soil to subside.

Soil clods resistant to detachment primarily form the roughness illustrated in Figure 9.6. Surface roughness is a partial measure of clodiness left by a soil disturbance. Large clods also produce deep depressions. Fine soil particles produced during the creation of the roughness are often left in the depressions where they are protected from erosion. Thus, erodibility of a rough soil surface is less than that of a smooth, finely pulverized soil surface. The degree that a soil forms clods depends on soil texture and soil moisture at the time of the soil disturbance. RUSLE2 does not consider the effect of soil moisture on soil roughness, mainly because RUSLE2 is an average annual model. Clods are smaller and less stable for coarse textured soils than for fine textured soils (see **Section 7.4**).

Soil surface roughness increases infiltration, which reduces runoff. Also, cloddy, rough soils resist sealing and crusting in comparison to finely pulverized soils that readily seal and crust, especially if soil biomass is low. Thus, rough soils reduce erosion because of decreased runoff.

RUSLE2 considers a **short term roughness** and a **long term roughness**. Short term roughness is created by tillage equipment, earth moving machines, and similar operations that mechanically disturb the soil. Long term roughness evolves over time after the last mechanical soil disturbance on pasture, range, landfills, and reclaimed land. Long term roughness is related to vegetation type (bunch versus sod forming), plant roots near the soil surface, local erosion and deposition by both water and wind, and animal traffic. RUSLE2 simultaneously keeps track of the decay of short term roughness and the natural development of long term roughness over the **time to soil consolidation** (see **Section 7.8**). Daily short term roughness decay is computed as a function of daily precipitation and daily interrill erosion. The effect of soil conditions at any point in time is captured by the effect of soil conditions on the initial roughness discussed in Section 9.2.3.3. Long term roughness is computed as a function of time and the final roughness roughness value that is a user input.

9.2.3.2. Roughness measure

RUSLE2 uses a roughness index that is the standard deviation of the micro-surface elevations about the mean elevation as a measure of soil surface roughness. Machines like scarifiers, moldboard plows, and heavy offset disks create rough soil surfaces [e.g., R_m > 1.5 inch (35 mm), R_m = field measured roughness value] while machines like rotary tillers pulverize the soil and leave a smooth soil surface [e.g., R_m < 0.2 in (5 mm)]. Machines, like bulldozers and road graders having blades that cut the soil also leave a smooth surface with a low roughness value.

The method of laying a roller chain on the soil surface and estimating roughness by how much the horizontal measurement between the ends of the chain is shorter than the chain length should not be used to measure roughness for RUSLE2. This procedure does not capture all roughness features important in RUSLE2.

Micro-relief meters are used in research to measure surface roughness. These meters measure micro-surface elevations over a grid by lowering pins to the soil surface or by using a laser system.[67] Because roughness index values depend on grid spacing, a standard spacing of 1 inch (25 mm) should be used to determine roughness index values for RUSLE2. Also, a plane should be fitted to the elevation data, and deviations taken

[67] Toy, T.J., G.R. Foster, and K.G. Renard. 2002. Soil Erosion: Processes, Prediction, Measurement, and Control. John Wiley and Son, New York, NY.

with respect to the plane to remove the effects of land slope. Also, the effect of ridges (oriented roughness) should be avoided or taken out of the data by analysis as well.

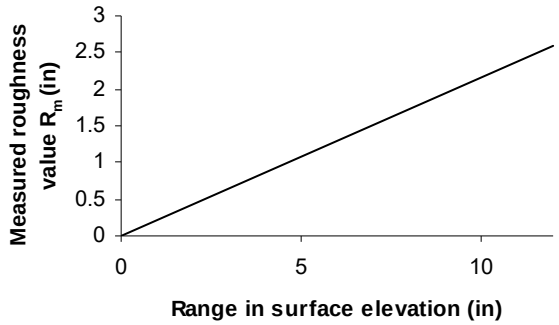

Figure 9.7. Relation of measured surface roughness value to range in elevation from highest roughness peak to deepest depression

Figure 9.7 provides an approximate estimate of surface roughness if a micro-relief meter is not available. The range in surface elevation from the highest roughness peak to the bottom of the deepest depression is measured by laying a 6 ft (2 m) straight edge across the roughness peaks.[68] A third approach for estimating surface roughness is to compare the appearance of the soil surface with photographs for soil surfaces having measured roughness values.[69]

Roughness values used in *operation descriptions* in the *operation component* of the RUSLE2 database are selected from the core database, not from field measurements at the site where RUSLE2 is being applied.

9.2.3.3. Soil surface roughness subfactor

Values for the RUSLE2 soil surface roughness subfactor are computed from:

$$s_r = \exp[-0.66(R_a - 0.24)] \qquad [9.10]$$

where: R_a = adjusted roughness value (inches) and 0.24 inches (6 mm) = the adjusted roughness value assigned to unit plot conditions (see **Section 7.2** for a description of unit plot conditions). The value for the roughness subfactor for the unit plot conditions is 1 by definition. Roughness subfactor values are less than 1 when the surface roughness effect of the site-specific condition is greater than on the unit plot and greater than 1 when the site-specific surface roughness effect is less than on the unit plot. An example of a soil surface that is smoother than the unit plot is a soil finely tilled with a rotary tiller for vegetable seeding. A soil surface with an adjusted roughness greater than the 0.24 in (6 mm) of the unit has roughness subfactor values less than 1. Roughness subfactor

[68] See Figure C-10, AH703 for details.
[69] See AH703.

values can range from almost 1.2 for a perfectly smooth surface to lower than 0.3 for an exceptionally rough surface as illustrated in Figure 9.8.

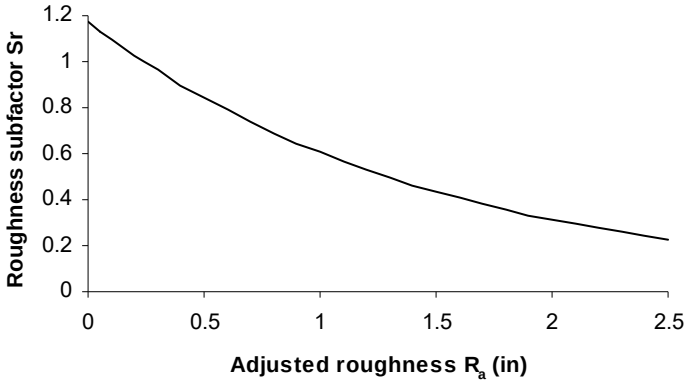

Figure 9.8. Relation of roughness subfactor to adjusted roughness

Computation of the adjusted roughness R_a starts with the initial base R_{ib} roughness assigned to **operation descriptions** having a **disturb soil process** in the **operations component** of the RUSLE2 database. The **initial base roughness** is assigned according to the roughness that the operation would produce for a smooth silt loam soil having a high soil biomass similar to a soil with a dense sod grass cover.

The input roughness value assigned to an operation is the roughness that the operation would create on a silt loam soil where the soil biomass is very high.

The first step in computing an adjusted roughness value to use in equation 9.10 is to adjust the initial roughness value R_{ib} for the effect of soil texture by multiplying by a soil texture adjustment factor. Soil texture adjustment factor values computed with the RUSLE2 equations for the midpoint of the soil texture classes are shown in Table 9.2.

The roughness adjustment factor is greater for high clay soils than for high sand soils. Consequently, RUSLE2 uses a higher roughness value for high clay soils than for high sand soils for a given initial (input) base roughness values, which means that soil surface roughness reduces erosion more on high clay soils than on high sand soils for a given operation. The adjustment factor for a silt loam soil is 1.0 because it is the base condition.[70]

The next adjustment is for soil biomass computed with:

$$R_a = 0.24 + (R_{it} - 0.24)\{0.8[1 - \exp(-0.0015 B_{ta})] + 0.2\} \quad [9.11]$$

70 The difference between 1.0 and the 1.02 value in Table 9.1 results from rounding and not being able to fit the equation to exactly 1.0 for the mid-point of the silt loam texture.

where: R_{it} (inches) = the initial (input) roughness adjusted for soil texture and B_{ta} = the total mass (dry weight basis) of buried residue and dead roots averaged over the soil disturbance depth after the operation (lbs/acre per inch depth). Figure 9.9 illustrates how the input roughness value is adjusted for soil biomass for a range of input roughness values.

Table 9.2. Factor to adjust input roughness as a function of soil texture

Soil texture class	Adjustment factor
clay	1.39
clay loam	1.22
loam	1.05
loamy sand	0.78
sand	0.69
sandy clay	1.25
sandy clay loam	1.13
sandy loam	0.90
silt	0.81
silt loam	1.02
silty clay	1.33
silty clay loam	1.23

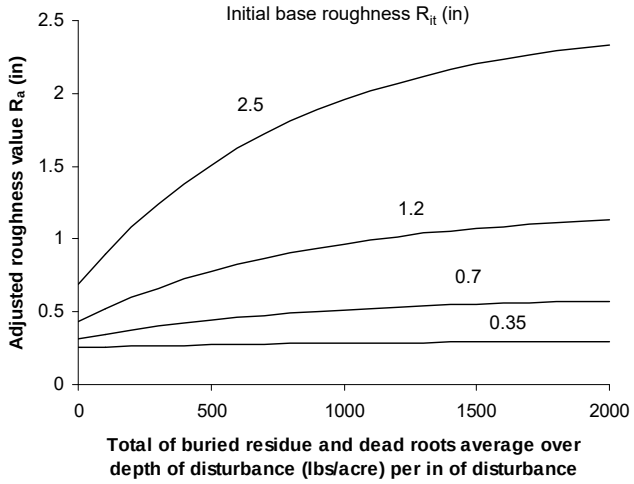

Figure 9.9. Roughness value adjusted from input value for soil biomass effect.

The effect of soil biomass on roughness can be observed in the field by comparing roughness after sod field is plowed with the roughness after a field in continuous low residue vegetable cropping is plowed. The difference in roughness can also be observed when a permanent grass strip beside a continuously cropped field is plowed. Soil surface roughness is much larger on the sod field and grass strip than on the continuously cropped fields having much lower biomass than the sod and grass conditions. The soil plowed out of sod turns up in "chunks" as if it is held together by roots. A similar effect occurs in chisel plowed wheat stubble fields.

The effect of roughness in a sod, meadow, and hay fields on erosion is very significant. According to Table 5-D, AH537[71] erosion immediately after moldboard plowing a high biomass condition is one fourth of that immediately after moldboard plowing a continuous row cropped field where biomass is reduced. The biomass effect on erosion depends on the sod, meadow, or hay production (yield) level, which determines the biomass of roots and buried residue. The roughness effect for moldboard plowing in a continuous cropped corn is also a function of yield as illustrated in Table 5, AH537. For example, the roughness subfactor value is about 0.55 for a 110 bu/ac yield and about 0.75 for a 50 bu/ac yield. A roughness related to biomass effect is also illustrated in Table 5,

[71] Wischmeier, W.H. and D.D. Smith. 1978. Predicting rainfall-erosion losses: A guide to conservation planning. U.S. Dept. of Agriculture, Agriculture Handbook # 537.

AH537 where the residue is removed, which reduces soil biomass. For example, the soil surface roughness subfactor is about 0.90 where the residue is removed for a 110 bu/acre corn yield while it is about 0.55 where the residue is not removed. The values in Tables 5 and 5-D, AH537 are based on measured soil loss data. Another illustration of how soil biomass affects the soil surface roughness is that a soil surface is noticeably smoother after tillage following soybeans than tillage following corn.

When roughness data from field research are analyzed to develop input roughness values for RUSLE2, field measured roughness R_m values must be adjusted for soil texture using Table 9.2 and for soil biomass using Figure 9.10. The best approach is to make roughness measurements under high soil biomass conditions to minimize the amount of adjustment required for biomass. As illustrated in Figure 9.10, biomass does not have much effect on the soil surface roughness value for soil biomass values (buried residue plus dead roots) greater than about 1000 lbs/acre per inch depth of disturbance.

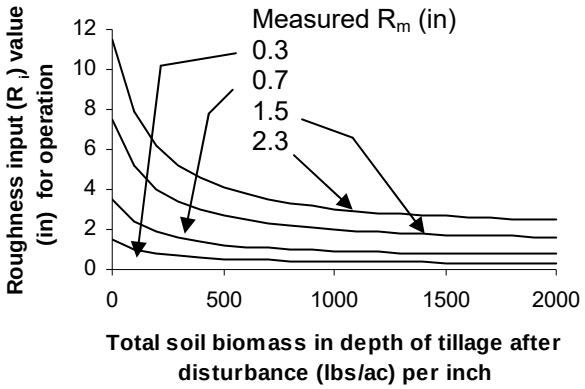

Figure 9.10. Conversion of a measured roughness value (R_m) to a roughness input value (R_i) (silt loam soil)

Roughness measurements made with yields of 200 bu/acre corn, 70 bu/acre wheat, and 4 tons/acre on hay or pasture land are conditions where measured roughness values need little if any adjustment for soil biomass.

The following example illustrates how to use Figure 9.10 to adjust a measured roughness value for biomass. Assume that the measured roughness is 1.5 inches (40 mm) and the average soil biomass is 500 lb/ac per inch depth of disturbance after the operation. A value of about 3.2 in (80 mm) is read from Figure 9.10, which would be the input roughness value for the operation that produced this roughness on a silt loam soil.

The input roughness values in the **operation descriptions** in the **operation component** of the RUSLE2 database are greater than are typically measured in the field because of the biomass effect. Roughness values computed by RUSLE2, rather than input values, should be compared to measured roughness values. Even then, field measured roughness values may not match those computed by RUSLE2. As described in **Section 9.2.3.1,** the RUSLE2 soil surface roughness subfactor captures more than just the physical effect of roughness geometry on soil loss. It also captures the effect of soil management as

represented by soil biomass on aggregate size distribution and stability and their effect on infiltration and erodibility. The roughness input value and the roughness subfactor have been developed together to reflect these effects. Priority is given to capturing these effects rather than reproducing roughness values that can be measured in the field.

Perhaps more than any other RUSLE2 variable, roughness values from the *core database* should be used rather than using roughness values measured at the specific site specific for input into RUSLE2.

9.2.3.4. Effect of existing roughness (tillage intensity effect)

The input roughness values represent the roughness that a particular operation creates when used on a smooth soil surface of silt loam texture and having high soil biomass as discussed in **Section 9.2.3.3.** The field roughness left by an operation depends on the roughness existing at the time of the operation. For example, the roughness left by a spike tooth harrow following a moldboard plow is much greater than the roughness left by the spike tooth harrow following a tandem disk. The spike tooth harrow has relatively little effect on roughness such that the roughness left by the harrow strongly depends on the existing roughness at the time of the operation. The roughness is only slightly greater when a tandem disk follows a moldboard plow than when it follows another tandem disk. The roughness following a moldboard plow is independent of existing roughness.

The influence of existing roughness is represented by the **tillage intensity** variable in RUSLE2. A soil disturbing operation where existing roughness has no effect on the roughness created by the operation is assigned a tillage intensity of 1. That is, the operation "wipes" out all effects of the existing roughness. Operations are assigned a tillage intensity less than 1 based on the degree that the roughness left by an operation is influenced by existing roughness at the time of the operation. For example, tillage intensity values of 0.4, 0.75, and 1 are assigned to spike harrows, tandem disks, and moldboard plows, respectively.[72]

A tillage intensity of 0.4 means that the operation converts 40 percent of the existing roughness to the operation's assigned roughness and leaves 60 percent of the existing roughness. A tillage intensity of 1 means that that 100 percent of the existing roughness

[72] RUSLE1 does not use a tillage intensity effect. RUSLE1 uses an absolute concept where an operation is assumed to create a particular roughness regardless of the existing roughness. That is, the roughness following a spike tooth harrow in RUSLE1 is the same regardless of whether the harrow follows a moldboard plow or a tandem disk. Input roughness values are the same for RUSLE1 and RUSLE2 for operations where the tillage intensity is 1. However, input roughness values for operations where tillage intensity is less than 1 are smaller in RUSLE2 than in RUSLE1 to achieve comparable roughness values in both models. However, the two models can not compute the same roughness values for all situations because of the tillage intensity factor effect.

is “wiped out,” and the resulting roughness is 100 percent of the operation’s assigned roughness.

Tillage intensity does not indicate the roughness left by an operation performed on a smooth surface. Soil disturbing operations like moldboard plows and heavy offset disks are assigned 1 for tillage intensity and leave a very rough surface. In contrast, a rotary tiller is also assigned 1 for tillage intensity value but leaves a very smooth surface. The key factor in both cases is that existing roughness has no effect on the resulting roughness, which is the basis for assigning a tillage intensity value of 1, not the roughness left by the operation.

If existing roughness is less than that created by an operation on a smooth soil surface, the surface roughness computed by RUSLE2 is not affected by the tillage intensity factor.

9.2.3.5. How RUSLE2 handles roughness when soil disturbance is in strips

Some operations like strip tillage, manure injection, and planting only disturb a portion of the soil surface. **The input roughness base value for these operations applies only to the portion of the soil surface that is disturbed.** RUSLE2 does not average the roughness values for the disturbed and undisturbed portions to determine an average roughness value because of non-linearity in equation 9.10 used to compute the roughness subfactor value. Instead RUSLE2 computes a roughness subfactor value using equation 9.10 for each strip (disturbed and undisturbed) and computes a composite roughness subfactor value based on the portion of the surface disturbed by the operation. This composite roughness subfactor value is used in a rearrangement of equation 9.10 to compute an effective roughness value for the entire surface. This effective roughness is then decayed based on rainfall amount and interrill erosion as described in **Section 9.2.3.7.**

The approach used to handle roughness with strips differs from the way that ground cover in strips is handled. Input roughness values only apply to the portion disturbed whereas input values for flattening, burial, and resurfacing ratios apply to the entire area.

9.2.3.6. Assigning roughness values

Input roughness base values for soil disturbing operations are assigned by selecting a value from the RUSLE2 “core database” by comparing characteristics of an operation with characteristics of operations in the “core database.” Basing input values on the “core database” values helps ensure consistency between RUSLE2 applications. Consult the research literature if no operations are in the “core database” that are sufficiently

close to your operation,. Use the largest possible database to estimate input roughness values and apply the adjustment procedures described in **Section 9.2.3.3.** Make sure that field measurements were carefully made and that sufficient measurements were taken to deal with spatial and temporal variability.

Field measurements should not be made at the specific site where RUSLE2 is being applied to determine an input roughness value for RUSLE2. Rather, values based on the RUSLE2 core database should be used.

9.2.3.7. Roughness decay

RUSLE2 decays the adjusted roughness, R_a in equation 9.10, each day based on daily precipitation and interrill erosion. About 40 percent of the roughness decay is by rapid subsidence and the remainder is by interrill erosion. Precipitation amount is used to compute the rapid subsidence of roughness that is assumed to be caused by soil wetting. Roughness decay by interrill erosion represents impacting waterdrops wearing away soil peaks and filling depressions with sediment. Interrill erosion is computed using the terms in the denominator of equation 8.3. The result is that roughness persists longer in dry climates than in wet climates and longer when the soil is protected from interrill erosion than when the soil is exposed to raindrop impact.

Roughness decays over time to a "final" roughness that is entered as an input for each **operation description** having a **disturb soil process** (see **Section 13.1.5**). A value of 0.24 inches (6 mm) is typically used for **final roughness** to represent the long term persistence of a few exceptionally stable soil clods. Although the final roughness value would seem to be a function of soil texture, a value of 0.24 inches (6 mm) is used for all soils. The reason for applying the 0.24 in (6 mm) value to all soils is to compute a surface roughness subfactor value of 1 for the unit plot condition for all soils when all roughness has decayed.

The expectation is that the final roughness value should be higher for high clay soils where clods persist than for sand soils that have no clods. However, such an adjustment should not be made because that effect is empirically considered in the K factor value.

However, an input final roughness other than 0.24 inches (6 mm) is used in RUSLE2 to represent conditions where an operation leaves the soil smoother than the unit plot condition. For example, rotary tiller and blading operations leave a smoother soil surface

than exists for unit plot conditions. When a **final roughness** value less than 0.24 in (6 mm) is entered, an **initial roughness** value equal to the **final roughness** value must be entered. RUSLE2 does not compute a change in roughness when the final roughness value is less than 0.24 inches (6 mm). Also, if the input initial roughness is greater than 0.24 inches (6 mm) and the input final roughness is less than 0.24 inches (6 mm), RUSLE2 will not decay the roughness to less than 0.24 inches (6 mm).

The rate of roughness decay is not a function of soil conditions in RUSLE2. RUSLE2 captures the effect of soil conditions on roughness at any time by making the initial roughness a function of soil conditions.

9.2.3.8. Long term roughness

As described in **Section 9.2.3.1**, RUSLE2 computes a long term development of soil roughness to an input natural roughness value. The development of long term roughness is assumed to be directly proportional to the soil consolidation subfactor value. The starting point for the development of long term roughness is 0.24 inches (6 mm). Long term roughness is reset to this value each time a soil disturbing operation occurs. If only a portion of the soil surface is disturbed, a weighted value for the long term roughness is computed as described in **Section 9.2.3.5.**

9.2.3.9. Overriding RUSLE2 roughness values

Sometimes the way that RUSLE2 computes roughness needs to be overridden for research purposes. Set the initial and final input roughness values to the same value and RUSLE2 will use this roughness value in equation 9.10 to compute roughness subfactor values. This procedure can be used in RUSLE2 so that RUSLE2 can use measured roughness values directly in its computations. However, RUSLE2 does not compute roughness decay when this procedure is used.

The adjustments that RUSLE2 makes for soil texture and soil biomass can not be easily overridden while retaining the RUSLE2 procedure for computing roughness decay. The only approach that can be used is to adjust RUSLE2 input values until RUSLE2 computes adjusted roughness values that correspond to the measured field values. A special template must be obtained to display the adjusted roughness values.

The proper approach for applying RUSLE2 in conservation and erosion control planning is to use roughness values from the core database and allow RUSLE2 to make its adjustments for soil texture and soil biomass rather than attempt to use field measured roughness values.

9.2.4. Ridges

Ridges affect soil erosion in two ways. One effect is on sediment production, which is discussed in this section, and the other effect is runoff flow direction, which is discussed in **Section 14.1**. Ridges, and the furrows that separate them, are referred to as oriented roughness because they redirect runoff from a direct, downslope direction (perpendicular to the contour) when the ridges are oriented in direction besides directly up and down slope. Orienting ridges parallel with the contour is an important conservation (support) practice known as contouring that can significantly reduce soil loss if the ridges are sufficiently high.

9.2.4.1. Ridge subfactor effect

The ridge subfactor describes how ridges affect sediment production by increased interrill erosion on steep ridge sideslopes. Erosion can be as much as twice that from a level soil surface for land slopes up to 6 percent.[73] The increase in soil loss caused by ridges is related to ridge sideslope steepness where interrill erosion increases according to $3s^{0.8}+0.56$ where s_i = sine of the ridge sideslope angle. This equation computes interrill erosion from a 30 percent steep ridge sideslope that is about three times the interrill erosion from a flat, level soil surface. Even when land slope is flat, the local ridge sideslope can be very steep, such as 30 percent so that interrill erosion is very high on the ridge sideslope.[74]

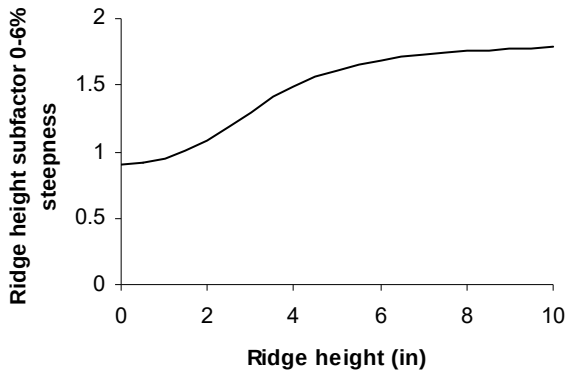

Figure 9.11. Ridge subfactor values as a function of ridge height for land slopes less

Figure 9.11 shows RUSLE2 ridge subfactor values as a function of ridge height when the land slope is less than 6 percent and the ridges are oriented up and down hill. Ridge height is used to represent ridge sideslope steepness because ridge height values can be easily visualized and measured for ridge forming operations. Using ridge sideslope steepness in RUSLE2 would require that a value for ridge spacing be entered, which is not always available, in addition to a ridge height value. Also, more ridges are often present than is often recognized. For example, the ridge spacing assumed for row crops is often the spacing of the rows. However, the planter may leave several small, but very important ridges besides the ridges directly associated with the

[73] Young, R.A. and C. K. Mutchler. 1969. Soil and water movement in small tillage channels. Trans. ASAE. 12(4):543-545. Also, personal communication with K.C. McGregor and C.K. Mutchler, USDA-Agricultural Research Service, National Sedimentation Laboratory, Oxford, MS.

[74] RUSLE1 does not include a ridge sufactor. RUSLE2 can compute up to twice the erosion for high ridges on slope less than six percent than that computed by RUSLE1.

plants. Determining ridge height is much easier for construction machines like scarifiers and bulldozer treads than determining ridge spacing.

A value of 1 corresponds to the ridge subfactor value for a unit plot. The unit plot condition based on being tilled up and down slope with a harrow is assumed to have a 1 inch (25 mm) ridge height. Thus, values for the ridge height subfactor as less than 1 for ridge heights less than 1 inch (25 mm) because of the unit plot condition being the reference in RUSLE2 and the unit plot having a 1 inch (25 mm) ridge.

The effect of ridges on sediment production diminishes in RUSLE2 as land slope steepness increases above 6 percent because the local steepness of the ridges becomes almost equal to the land slope at steepness above 30 percent. For example, the local steepness of the ridge sideslopes is 42 percent when the ridge sideslope is 30 percent and the land slope is 30 percent. Figure 9.12 shows ridge subfactor values as landslope increases above six percent. As illustrated, ridge subfactor values converge to 1 at steep land slopes. The values in Figure 9.11 were derived from experimental data while the values in Figure 9.12 were derived from a simple rill-interrill erosion model where rill erosion varies linearly with land slope steepness and interrill erosion with $3s^{0.8}+0.56$.

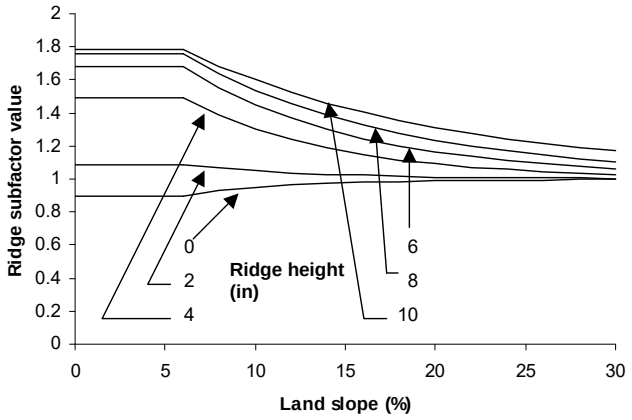

Figure 9.12. Ridge subfactor values as a function of ridge height and land slope steepness

9.2.4.2. Effect of ridge orientation on ridge subfactor

The ridge subfactor values in Figures 9.11 and 9.12 apply when ridges are oriented up and down slope. When the ridges are oriented on a direction different from up and down slope, ridge subfactor values decrease to 1 as ridge orientation approaches the contour. The relationship used to adjust ridge subfactor values as a function of ridge orientation (row grade) is shown in Figure 9.13. This relationship is a mirror image of Figure 14.3, the one used to adjust contouring factor values for ridge orientation, which is discussed in **Section 14.1**. The net effect of ridges is a composite of Figure 9.13 and Figure 14.3.

The need for Figure 9.13 seems questionable. Why does ridge orientation with respect the land slope affect sediment production? It doesn't. The reason for these adjustments is related to the empirical structure of RUSLE2 and constructing RUSLE2 so that it gives the expected erosion values with contouring.

9.2.4.3. Ridge formation and decay

Ridges are described in RUSLE2 by using a **soil disturbing operation**. An input ridge height value is entered in the **operation** component of the **RUSLE2 database** for each soil disturbing operation. This input value is the "typical" (representative) ridge height created by the operation. A "typical" ridge height is used because ridge height can vary with soil and cover-management condition, factors not considered in RUSLE2 in contrast to random roughness that RUSLE2 computes as a function of soil texture and soil biomass. The assumption is that ridge height is far more controlled by the physical mechanics of the operation than by soil conditions. Operations having different ridge heights for different soil conditions can be created for RUSLE2 to compute how ridge height affected by soil condition affects erosion.

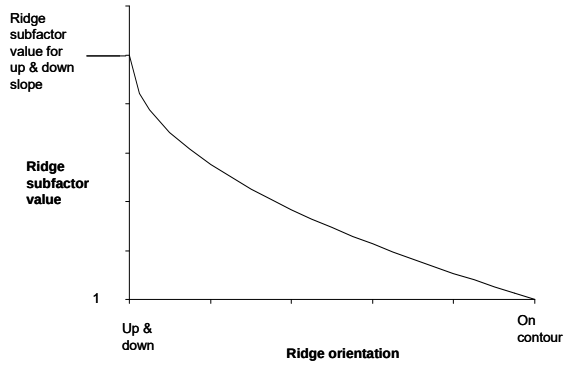

Figure 9.13. Effect of ridge orientation (row grade) on ridge subfactor

RUSLE2 computes a daily decay of ridge height as a function of daily precipitation and interrill erosion. The decay in ridge height by precipitation is independent of soil and cover-management conditions. The decay of ridge height by interrill erosion depends on rainfall erosivity, canopy cover, and ground cover. About 40 percent of the ridge height decay is from precipitation, which represents how the presence of water causes soil settlement. The remainder is from interrill erosion, which represents the wearing away of the ridge by raindrop impact.

The only way that ridges exist in RUSLE2 is to create them with a soil disturbing operation.

9.2.4.4 Assignment of input ridge height values

RUSLE2 input values for ridge height for an operation should be selected by comparing the characteristic of the operation with operations having ridge height values assigned in the RUSLE2 "core database." Ridge heights should not be selected based on field measurements. Ridge heights should be assigned very carefully to ensure consistency. Keep in mind that ridge heights affect both sediment production and contouring on erosion. Ridge height values in the RUSLE2 **core database** were selected very carefully to ensure that RUSLE2 computes the proper contouring effect. The tendency is to assign ridge height values that are too low and then be surprised that RUSLE2 computes too little contouring effect. Although RUSLE2 has been constructed to use easily measured field values, ridge heights is a situation where assigning values based on the **core database** gives far better results than can be obtained by entering field measurements of ridge height.

The effectiveness of contouring in RUSLE2 depends on ridge height: no ridge height, no contouring effect. To have a contouring effect, ridges must be present.

9.2.5. Soil biomass

Soil biomass in RUSLE2 includes live and dead roots, buried plant litter and crop residue from vegetation "grown" on-site, and added materials (external residue) that were buried or directly placed in the soil. These materials, including rock added as an "external residue," are assumed to be organic materials that decompose and reduce soil erodibility.

Buried inorganic materials including rock require special consideration. An extremely low value is entered for the decomposition coefficient for materials, such as rock, that do not decompose so that essentially no mass is lost by decomposition. RUSLE2 assumes buried inorganic material has the same effect as buried organic material, which may be too much effect.[75] For example, non-organic materials do not produce compounds that reduce soil erodibility. This problem can be accounted for in RUSLE2 by reducing the amount of inorganic material that is entered as having been added to an amount that has the expected effect on erosion. However, if this adjustment is made, the mass-cover relationships for the inorganic material must be adjusted so that RUSLE2 uses the proper ground cover percent in computing how a surface application of this material would affect erosion.

9.2.5.1. Soil biomass effect

[75] Rock cover entered in the **soil descriptions** in the **soil component** of the RUSLE2 database remains constant and is not subject to burial or decomposition. This rock cover is unaffected by operations in contrast to rock added as an external residue that is manipulated by operations.

Live roots affect soil loss by mechanically holding the soil in place, resisting erosive forces if the roots are exposed, and producing exudates that reduce soil erodibility. Also, live roots are a measure of plant transpiration that reduces soil moisture, which in turn increases infiltration and reduces runoff and soil loss.

When vegetation is "killed" in RUSLE2 by an operation that has a **kill process**, live roots becomes **dead roots** and begin to decompose. The physical presence of dead roots reduces erosion by reducing runoff erosivity if the dead roots are exposed, and dead roots also seem to hold the soil in "clumps" when the soil is mechanically disturbed.[76] Also, dead roots decompose to produce organic compounds that reduce soil erodibility and increase infiltration and reduce runoff.

Exposed **buried residue**[77] acts similar to exposed dead roots by physically reducing runoff's erosive forces applied to the soil, but buried residue does not mechanically hold the soil like roots hold the soil. Residue decomposes and produces organic compounds that reduce soil erodibility and increase infiltration and decrease runoff and erosion. Overall, buried residue is less effective than roots on reducing erosion because buried residue does not mechanically hold the soil in place, and buried residue is not associated with plant transpiration like roots.

Although buried residue occurs in a wide range of sizes and types of vegetative and organic material, the effect of all buried residue is treated the same based on experimental research that compared how crop residue, "green" manure, compost, animal manure, hardwood litter, and pine needles affected erosion.[78] However, preference is given to fine roots instead of coarse roots when root biomass values are entered in a **vegetation description** in the **vegetation component** of the **RUSLE2 database**. Fine roots have greater surface area per unit mass than coarse roots and often are very close to the soil surface where they have a greater effect on runoff and erosion than coarse roots. Fine roots readily slough and become a part of the soil organic matter pool. Not much of

---

[76] Some of the effect may well be roots mechanically holding the soil together. Another effect is that roots produce compounds that have caused a local increased in soil strength. Another effect is that the soil fractures along lines that expose the roots as if they are holding the soil in place. The fact is clearly obvious that soil roughness is increased with high levels of soil biomass when soil is disturbed.

[77] Buried residue is RUSLE2 nomenclature for organic material in the soil that affects soil loss that has been buried or placed in the soil by an operation. Buried residue also includes non-organic material in the soil, but this material requires special considerations.

[78] Browning, F.M., R.A. Norton, A.G. McCall, and F.G. Bell. 1948. Investigations in erosion control and reclamation of eroded land at the Missouri Valley Loess Conservation Experiment Station, Clarinda, Iowa, 1931-42. USDA Technical Bulletin 959.

Copley, T.L., L.A. Forrest, A.G. McCall, and F.G. Bell. 1944. Investigations in erosion control and reclamation of eroded land at the Central Piedmont Conservation Experiment Station, Statesville, North Carolina, 1930-40. USDA Technical Bulletin 873.

Hays, O.E., A.G. McCall, and F.G. Bell. 1949. Investigations in erosion control and reclamation of eroded land at the Upper Mississippi Valley Conservation Experiment Station near LaCrosse, Wisconsin, 1933-43. USDA-Technical Bulletin 973.

the mass of coarse roots is entered for root biomass because coarse roots are assumed to have relatively little effect on erosion.

9.2.5.2. Soil biomass subfactor

Equation 9.12 is used in RUSLE2 to compute values for the soil biomass subfactor.

$$s_b = c_b \exp(-0.0026 B_{rt} - 0.00066 B_{rs} / s_c^{0.5}) \qquad [9.12]$$

where: s_b = soil biomass subfactor, c_b = 0.951,[79] B_{rt} = the sum of the live and dead root biomass averaged over a 10 inch (250 mm) depth (lbs/acre per inch of depth), B_{rs} = the amount of buried residue averaged over a depth that linearly ranges from 3 inches (75 mm) if the soil is not consolidated (i.e., c_s = 1) to 1 inch (25 mm) if the soil is fully consolidated (i.e., s_c = 0.45), and s_c = the soil consolidation subfactor (see **Sections 7.8 and 9.2.6** for discussion of the soil consolidation subfactor). The coefficients 0.0026 for root biomass B_{rt} and 0.00066 for buried residue B_{rs} are multiplied by 1.65 for Req applications. Most of the erosion in Req situations is assumed to be caused by rill erosion. Soil biomass has a much greater effect on rill erosion than on interrill erosion.

All soil biomass variables are on a dry weight basis.

Equation 9.12 was empirically derived by fitting it to soil loss ratio values for the seedbed crop stage period[80] in Table 5 and accompanying tables in AH537.[81] These soil loss ratio values were for a wide range of soil biomass and soil consolidation conditions, including pasture and hay lands; no-till and reduced-till forms of conservation tillage for corn grain; and conventional clean-till corn grain, corn silage, soybean, and wheat cropping over a range of yields. Also, soil loss data on the effect of incorporation of green manure, animal manure, compost, hardwood litter, and pine needles into the soil were analyzed. Erosion data from rainfall simulator studies were used to determine values for effective root biomass for rangeland (see **Section 17.4.1.4**).

---

[79] Equation 9.12 also has a second part for very low soil biomass where c_b increases from 0.95 to 1 so that the soil biomass subfactor equals 1 when no soil biomass is present.

[80] Soil loss ratio values in AH537 are the ratio of soil loss with a given cover-management system at a particular crop stage period to soil loss from the unit plot for the same crop stage. The seedbed crop stage period is when the soil has been tilled to prepare a relatively smooth surface for seeding a crop so that the major effect is from soil biomass.

[81] The soil loss ratio values in AH537, except for conservation tillage and "undisturbed" land, are a summary of field measured soil loss for more than 10,000 plot-years of data. Erosion data are quite variable for unexplained reasons. Also, the length of record often varied between studies and locations, and the number of treatments and replications and other variables differed between locations, which prevents the data from being analyzed by common statistical procedures. Instead, the data must be analyzed and interpreted for main effects, which was expertly done by W.H. Wischmeier and D.D. Smith in AH537. The soil loss ratio values in AH537 are the most comprehensive available by far for calibrating RUSLE2 and are much better for calibrating and validating RUSLE2 than the original soil loss data.

The 10-inch (250 mm) depth over which root biomass is averaged was the best of several depths analyzed. A 3-inch (75 mm) depth over which buried residue is averaged also was the best of several depths analyzed. This 3 inches (75 mm) depth is linearly reduced in RUSLE2 to 1 inch (25 mm) as the soil consolidation subfactor c_s decreases from 1 to 0.45 to give increased credit to buried residue B_{rs} in the upper soil layer with no-till cropping and other cover-management systems that leave residue at the soil surface and

Soil consolidation refers to lack of soil disturbance and the soil becoming less erodible over time after a soil disturbance rather than the soil necessarily becoming dense.

do not disturb the entire soil surface. A similar feature is the division of the variable buried residue B_{rs} by the square root of the soil consolidation subfactor c_s, which also gives increased credit to buried residue as the soil consolidates. A major advantage of no-till cropping is the accumulation of organic matter in the upper two inches (50 mm) of soil. This layer promotes earthworm burrowing and other processes that decrease runoff and soil erodibility. Tillage and other mechanical soil disturbances disrupt this layer and cause an immediate increase in soil erosion. This zone requires about 5 years to develop in the eastern US, which is consistent with using 7 years for the time to soil consolidation to represent this time.

Table 9.3. Effect of corn yield and tillage system on the soil biomass subfactor at Columbia, MO

	Soil biomass subfactor		
	Type tillage system		
Yield (bu/acre)	Clean till	Reduced till	No till
50	0.78	0.74	0.57
100	0.66	0.60	0.38
200	0.48	0.40	0.16

Table 9.4. Effect of production level of a grass on the soil biomass subfactor

	Soil biomass subfactor		
Yield (lbs/acre)	St. Paul, MN	Columbia, MO	Baton Rouge, LA
1000	0.47	0.51	0.56
2000	0.22	0.27	0.33
4000	0.05	0.08	0.11

Tables 9.3 and 9.4 illustrate values for the soil biomass subfactor for the three corn tillage systems at different yield levels and grass at three production levels. The values for the soil biomass subfactor computed by equation 9.12 decrease as yield increases as illustrated in Table 9.3 because of increased buried residue and live and dead roots. The difference between the clean-till and reduced-till systems is that the reduced-till system leaves additional residue near the soil surface where it has greater effect than residue buried more deeply by the moldboard plow in the clean-till system. The major difference in the no-till system from the other systems is from additional residue near the soil surface and the additional credit given in equation 9.12 for buried residue B_{rs} because of a reduced soil consolidation subfactor c_s. The reduced soil consolidation subfactor has even greater effect in the grass system that has no soil disturbance than in the no-till system where narrow strips are disturbed to plant the seeds. Another factor that reduces the soil

biomass subfactor s_b in the grass system is greater live and dead root biomass at the high grass production level than for the high corn yield. More dead root biomass is produced by root sloughing (death) with the grass than is left after the corn harvest.

The soil biomass subfactor is a function of location as illustrated in Table 9.4 because decomposition of buried residue and dead roots is related to monthly precipitation and temperature, which vary by location. For example, the soil biomass subfactor for the 2000 lbs/acre grass production level is 0.22, 0.27, and 0.33 at St. Paul, MN; Columbia, MO; and Baton Rouge, LA, respectively. Decomposition is much higher at Baton Rouge, LA than at St. Paul, MN because of increased temperature and precipitation, especially during winter at Baton Rouge, LA where temperatures are sufficiently high for significant decomposition to occur. The relative effect of location increases as production level (i.e., biomass level) increases.

Values for the soil biomass subfactor are significant and comparable in magnitude to values for other subfactors. Although ground cover is frequently considered to be the single most important variable in RUSLE2, the soil biomass subfactor can be equally important. Perhaps most important is the total amount of biomass in a cover-management system and how that biomass is distributed between the biomass pools.

All features of cover-management systems should be considered rather than focusing on a single variable such as ground cover as a measure of erosion control effectiveness.

9.2.5.3. How biomass is added to and removed from the soil

9.2.5.3.1. Live root biomass. RUSLE2 obtains values for live root biomass from the **vegetation description** in the **vegetation component** of the RUSLE2 database for the **current vegetation**. A name for a vegetation description is entered for each operation with a **begin growth process** in each **cover-management description** in the RUSLE2 database. RUSLE2 begins to use values for this vegetation description on the date of the operation that contains the begin growth process.

The live root biomass values in a vegetation description are for the upper 4 inches (100 mm), whereas equation 9.12 uses live root biomass values for the upper 10 inches (250 mm). RUSLE2 uses the live root distribution illustrated in Figure 9.14 to compute live root biomass in the upper 10-inch (200 mm) depth from the input values for the 4 in (100 mm) depth.[82] The distribution in Figure 9.14 is used for all vegetations[83] and all time.

[82] RUSLE2 divides the soil into 1-inch (25 mm) layers to account for soil biomass. Depths of disturbance are rounded to the nearest 1-inch (25 mm) so that the depth of disturbance corresponds with the bottom of a soil layer. The number of layers considered in an operation depends on the number of 1-inch (25 mm) in the depth of disturbance. Thus, an operation with a 2-inch disturbance depth only involves two layers. The

Figure 9.14 shows that most of the live root biomass is in the upper 4 inches (100 mm) of soil, which is a major reason for the 4-inch (100 mm) depth used for the root biomass input values in the RUSLE2 database.[84]

An input for rooting depth is not required by RUSLE2, which does not consider how rooting depth varies with vegetation or plant maturity.

9.2.5.3.2. Dead root biomass. Live roots become dead roots in one of three ways. One way is by including an operation in the **cover-management description** that has a **kill process**. The live root biomass for the **current vegetation** on the date of this operation is added to the dead root biomass pool and the live root biomass becomes zero.

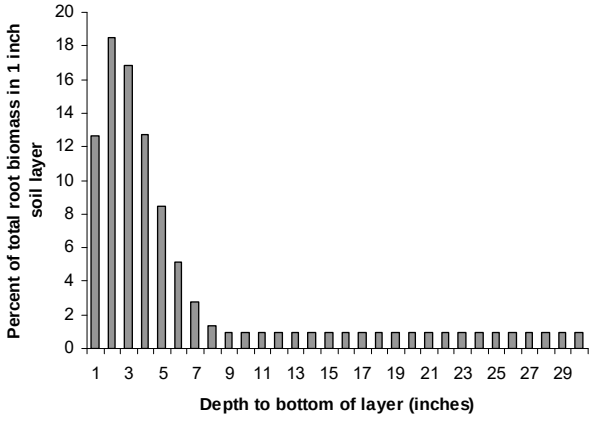

Figure 9.14. Distribution of live root biomass assumed for RUSLE2.

The second way that live root biomass becomes dead root biomass is by root sloughing and root death during growth periods, similar to canopy senescence (and live aboveground death during growth periods). Root death and sloughing is an important source of dead root biomass for perennial and similar types of vegetation to create a soil organic pool. The amount of root sloughing in a year ranges from about 25 to 40 percent of the root biomass.[85]

---

minimum depth that RUSLE2 recognizes is 1 inch (25 mm).

[83] Data from several literature sources for major agricultural crops of corn, soybeans, wheat, and cotton, several hay and pasture crops, and for selected vegetable crops were reviewed to determine the distribution in Figure 9.14 at plant maturity. The relative shape of the root distribution was very nearly the same for all crops. The rooting depth for the fine roots judged to have the most effect on soil loss did not vary among crops, except that the rooting depths for field and pasture crops was about twice that for vegetable crops. Even though rooting depth differs among plant types and with plant development, RUSLE2 empirically captures the main effect of roots on soil loss.

[84] The root distribution in RUSLE2 differs between from the one used in RUSLE1. RUSLE1 assumes that the root biomass in the second 4 inch (100 mm) soil layer is 75 percent of that in the top 4 inch (100 mm) layer and that no roots occur below 8 inches (200 mm). Based on Figure 9.14, RUSLE1 assumed significantly too much root biomass below the 4 inch (100 mm) soil layer below the upper 4 inches (100 mm) of soil.

[85] For additional information, see Reeder, J.D., C.D. Franks, and D.G. Michunas. 2001. Root biomass and microbial processes. In: The Potential of U.S. Grazing Lands to Sequester Carbon and Mitigate the Greenhouse Effect. R.K. Follett, J.M. Kimble, and R. Lal (eds). Lewis Publisher, Boca Raton, FL.

RUSLE2 represents daily root death during growth periods by multiplying daily live root biomass by a fraction. RUSLE2 represents root sloughing by a decrease in the root biomass during the year, much like RUSLE2 determines senescence by a reduction in canopy. Input values for root biomass increase when growth occurs and decrease after plant maturity when live root biomass is being lost by root sloughing.[86] Roots develop more rapidly than does canopy and reach maturity while the canopy is still adding biomass. Root sloughing can be assumed to either precede or parallel canopy senescence. Values for the temporal distribution of root biomass can be manually developed and entered for vegetations in the RUSLE2 database. Also, RUSLE2 includes an easy-to-use procedure that can be used to construct temporally varying root biomass values based on dates of maximum and minimum root biomass and root biomass values at those dates. RUSLE2 also has a procedure that estimates root biomass using built-in values for the ratio of root biomass to aboveground biomass production for selected plant communities. See **Section 11** that describes the vegetation component of the RUSLE2 database for additional information.

RUSLE2 determines the amount of root sloughing on each day by comparing the live root biomass values on a given day with the live root biomass on the previous day. RUSLE2 assumes that a decrease in live root biomass from one day to the next is caused by root sloughing and adds the decrease to the dead root biomass pool. RUSLE2 computes daily root biomass death by multiply daily root live biomass by a fraction. Daily root death biomass is added to the dead root biomass pool.

Using a single root biomass for the entire year for perennial type plants, including pasture and hay crops grown for several years, causes RUSLE2 to over estimate erosion because the dead root biomass pool that accumulates from root sloughing is not represented.

The third way that live root biomass becomes dead root biomass is when the live root biomass on the first day of a new **vegetation description** is less than the live root biomass on the last day when the current vegetation is used. The difference in live root biomass is added to the dead root biomass. This procedure is used when only a portion of the live root biomass is to be transferred to the dead root biomass pool because the **kill process** in an operation transfers the entire live root biomass to dead root biomass.

[86] The time invariant C factor in RUSLE1 uses a single representative value for root biomass for the entire year and does not consider root sloughing and the accumulation of a dead root biomass pool that can significantly reduce soil loss. Also, the time invariant C factor in RUSLE1 does not consider the accumulation of a buried residue biomass pool that can significantly reduce soil loss. Although the time invariant C factor in RUSLE1 was easy to use, it could seriously over estimate soil loss by not considering these important soil biomass pools. Thus, RUSLE2 does not include a time invariant cover-management computation, but it does include many of the easy to use features of the RUSLE1 time invariant C factor so that root sloughing can be easily considered using simple inputs that mimic RUSLE1 inputs. RUSLE1 can consider these soil biomass pools by using its time variant C factor with temporally varying canopy and root biomass values.

This procedure is used to apply RUSLE2 to intercropping type situations. Intercropping involves growing multiple crops at the same time where they typically have different seeding and harvest dates. Examples include planting a cover crop before silage harvest, planting a legume in small grain where the legume is harvest for hay after the grain is harvested, and weeds that develop before a crop is harvested. The procedure is illustrated where a cover crop is seeded before a silage corn crop is harvested. The cover crop provides vegetative cover to control erosion after the silage crop is removed by harvest. Values for live root biomass for this cover-management description are given in Table 9.5.

This **cover-management description** involves three **vegetation descriptions**. The first one is for the silage corn. The second one is for the composite of the rye, which is seeded on June 8, and the silage corn growing together. The third vegetation description is for the rye after the silage corn is harvested on August 8.

RUSLE2 detects that the live root biomass for the new vegetation, which is the rye after the silage has been harvested on August 8, is less than the live root biomass of the current vegetation, which is the composite of the corn and rye, on August 8. The difference of 950 lbs/acre in the upper 4 inches between the 1380 lbs/acre on August 8 for the current vegetation and the 430 lbs/acre for the new vegetation is the amount of live root biomass that is put in the dead root biomass. This 950 value represents the live root biomass of the silage corn on the date that it was harvested and killed. The live root biomass value

Root biomass and other values used in the vegetation description can start at any time as required to describe the vegetative conditions for a cover-management system. The values for day zero and beyond describe conditions on the day that RUSLE2 is to begin using that vegetation description.

for the rye vegetation immediately after the silage harvest represents conditions on the first day that this particular **vegetation description** is used, not the date that the vegetation was seeded.

The **silage harvest operation** does not include a **kill process** to kill the corn. If a kill process had been included in the operation, the entire live root biomass would have been transferred to the dead root biomass. Only the corn live root biomass is to be transferred to the dead root biomass. The difference of 950 lbs/acre in the upper 4 inches represents the change in live root biomass from "killing" the corn and allowing the rye to continue "growing." RUSLE2 adds this difference to the dead root biomass pool.

Dead root biomass is lost by decomposition, which is a function of daily precipitation and temperature, and the decomposition half life for the roots. RUSLE2 uses the same decomposition half life for the dead roots as for aboveground biomass. RUSLE2 maintains a biomass pool for dead roots, much like a litter layer on the soil surface. The

amount of biomass that RUSLE2 computes is a function of location. The biomass in these pools is greater at locations where decomposition is less because of reduced temperature and rainfall, such as the Northern US in comparison to the Southern US. The accumulation of biomass in the dead root biomass pool can significantly reduce erosion as computed by equation 9.12.

Although operations that include a disturb soil process resurface buried residue, these operations do not resurface dead roots. The dead roots that are most important for influencing rill and interrill erosion are fine roots that are assumed to be tightly bound to the soil so that they are not resurfaced.

Table 9.5. Values for two vegetations: silage corn interseeded with rye to provide cover after the silage is harvested

Calendar date	Days since begin growth	Root biomass (lbs/acre in top 4 inches)	Comment
			Operation with begin growth process that uses silage corn vegetation description
10-Mar	0	0	
25-Mar	15	40	
9-Apr	30	160	
24-Apr	45	320	
9-May	60	480	
24-May	75	760	
			Operation with begin growth process that uses a vegetation description for the composite of the silage and rye; rye seeded on this day
8-Jun	0	950	
23-Jun	15	980	
8-Jul	30	1080	
23-Jul	45	1280	
8-Aug	60	1380	Silage harest operation, silage corn harvested which removes the corn vegetative cover, kills corn roots, rye continues to grow
8-Aug	0	430	Silage harvest operation contains a begin growth process as last process in list of processes used to describe that operation. This begin growth process begins to use the rye vegettion description having values on day 0 appropriate for the date of the silage harvest
22-Aug	15	530	
7-Sep	30	610	

actual vegetation description includes additional dates to complete growth of the rye

9.2.5.3.3. Buried residue. Buried residue is added to the soil in three ways: (1) a fraction of the decomposed ground cover biomass is added, (2) a fraction of the ground cover biomass is buried by certain operations, and (3) biomass is placed directly into the soil with certain operations.

Each day, RUSLE2 arbitrarily adds a fraction of the surface (flat) layer of biomass (i.e., crop residue, plant litter) that decomposes on that day to the upper 2 inch (50 mm) soil layer. The fraction varies from zero if the soil has been recently mechanically disturbed to 0.25 if the soil is fully consolidated as a function of the soil consolidation subfactor s_c. RUSLE2 uses this procedure to accumulate organic matter at the soil surface on pastureland, rangeland, no-till cropland, and other lands not regularly tilled or mechanically disturbed.

Operations with a **disturb soil process** transfer (bury) a portion of the surface (flat) layer of biomass to the buried residue pool. The amount of residue that is buried is the product of the surface residue mass and a **burial ratio**. Values for the burial ratio are entered for each **operation description** having a disturb soil process in the **operation component** of the RUSLE2 database. RUSLE2 distributes the residue that it buries according to one of **three mixing distributions** illustrated in Figure 9.15. A distribution is selected when a **tillage type** is selected to describe an operation having a disturb soil process. The distributions **inversion with some mixing** is for operations like a moldboard plow that invert the soil. Most of the buried residue is placed in the lower half of the depth of disturbance. The distribution **mixing with some inversion** is for operations like a tandem disk, chisel plow, and field cultivator that place most of the residue in the upper half of the depth of disturbance. These operations bury residue primarily by mixing but involve some burial by inversion. The distribution **mixing only** applies where almost all of the burial is by mixing with very little burial by inversion for operations like rotary tillers, subsoilers, and manure and fertilizer injectors that place most of the residue in the upper one third of the depth of disturbance. One of these three mixing distributions is assigned to each operation with a **disturb soil** process when data for the operation are entered into the RUSLE2 database. The placement distribution for the **lifting and fracturing** and **compression** tillage types place the buried residue using the **mixing only** distribution.

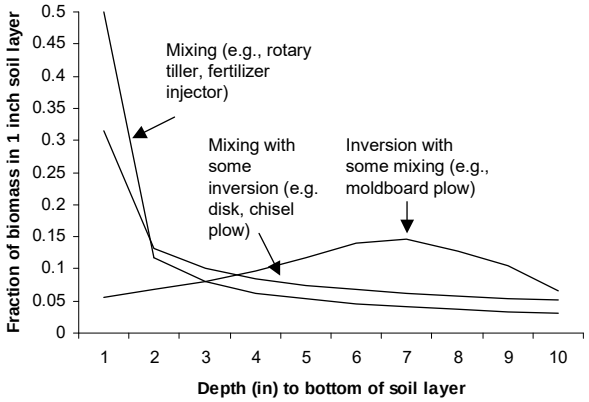

Figure 9.15. The initial distribution when residue is buried by an operation.

Buried residue can also be added to the soil in RUSLE2 by placing **external residue** in the soil with an operation that includes an **add residue process**. A disturb soil process must be included in the operation description to place external residue in the soil because the assumption is that the soil must be disturbed to place material in it. External residue is placed in the lower half of the disturbance depth as illustrated in Figure 9.16.

Buried residue is lost from the soil by being resurfaced by an operation that includes a **disturb soil process** and by decomposition. Buried residue is removed from the soil by being resurfaced and transferred to the surface (flat residue) pool by soil disturbing operations. The amount of **resurfaced residue** is the product of the amount of buried residue in the depth of disturbance at the time of the operation and a **resurfacing ratio** value assigned to the operation description in the RUSLE2 database. The resurfaced residue is extracted layer by layer by first taking out the entire buried residue in the layer, if necessary, from the top soil layer and then moving to the next and succeeding layers until the total mass of resurfaced residue is obtained. In many cases, only a portion of the buried residue in the top 1-inch (25 mm) layer is extracted. Extraction seldom extends beyond the second layer. RUSLE2 does not resurface dead roots as discussed in **Section 9.2.5.3.2.**

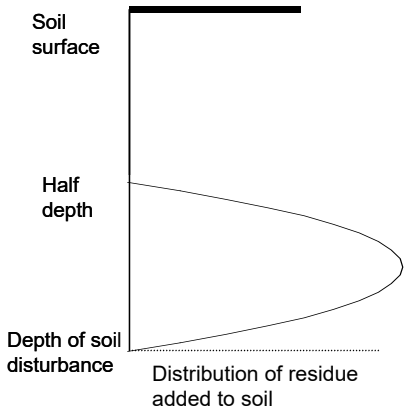

Figure 9.16. Distribution of residue placed in by an operation that has an "add residue" process.

Buried residue lost by decomposition as function of daily precipitation and temperature and the decomposition half life of the buried residue. RUSLE2 assumes that the decomposition half life is the same for buried residue as for the surface, flat residue. RUSLE2 maintains biomass pools for buried residue like it does for dead roots and a litter layer on the soil surface that is a function of location. The biomass in these pools is greater at locations where decomposition is less because of reduced temperature and rainfall, such as the Northern US in comparison to the Southern US. The accumulation of biomass in the buried residue pool can significantly reduce erosion as computed by equation 9.12.

Table 9.6. Retention coefficient values for redistributing residue among soil layers

	Mixing distribution		
Layer	Inversion w/mixing	Mixing w/inversion	Mixing
1 (top)	0.40	0.32	0.50
2	0.40	0.39	0.56
3	0.40	0.47	0.61
4	0.40	0.54	0.67
5	0.40	0.62	0.72
6	0.40	0.69	0.78
7	0.40	0.77	0.83
8	0.40	0.84	0.89
9	0.50	0.92	0.94
10	1.00	1.00	1.00

9.2.5.4. Redistribution of dead roots and buried residue in soil by soil disturbing operations

Operations with a **disturb soil process** redistribute buried residue and dead roots according to the **mixing distribution** assigned to that operation. When a soil disturbing operation occurs, RUSLE2 first redistributes the buried residue and dead roots and then buries the residue. Two steps are involved for an operation that has

an **inversion with some mixing** distribution. The first step is to invert the soil layers with their buried residue and dead roots by layer so that the biomass in the bottom layer becomes the biomass in the top layer, the biomass in the next to bottom layer becomes the biomass in the next to the top layer, and so forth. The second step transfers biomass between soil layers. A **filtering** concept is used in RUSLE2 where each soil layer is **sifted** so that some of the biomass in each layer is retained in the layer and the remainder of the biomass moves down to the next layer. The amount retained is the product of the biomass in the layer and a retention coefficient having values shown in Table 9.6.[87] The retention values for the **inversion with some mixing** distribution are all equal except for the values for the bottom two layers. The value for the bottom layer must be 1 so that no biomass passes through the bottom layer and the slightly higher value for the next to bottom layer was empirically determined to give a good fit between experimental data and computed values. The equal retention values imply that the biomass is equally likely to move downward in the lower part of the disturbance depth as in the upper part. In effect, the soil is uniformly "stirred, mixed, and sifted" over the disturbance depth.

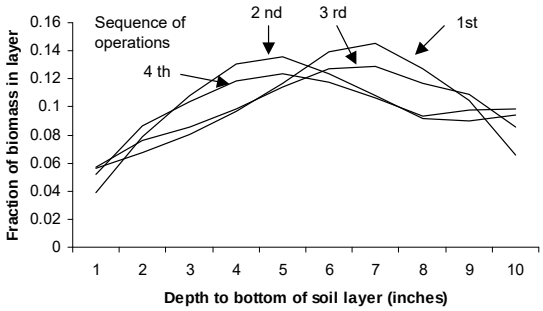

Figure 9.17. Initial burial and redistribution of residue by repeated operations with an inversion mixing distribution (e.g., moldboard plow)

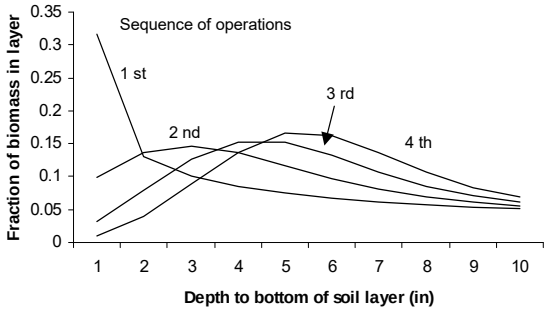

Figure 9.18. Initial burial and redistribution of residue by repeated operations with a mixing and some inversion mixing distribution (e.g., tandem disk)

Only one step is involved in redistributing biomass with the two mixing distributions that minimally involve inversion. The retention coefficient for the top layer is assumed to be same as the fraction of residue placed in the top layer by burial. The values for the retention coefficients for the remaining layers are linearly increased with depth to a value of 1 as shown in Table 9.6. The value of 1 for the last layer prevents biomass from passing through the bottom layer. The increase in retention values with depth means that biomass is more likely to move down in the upper part of the disturbance depth than in the bottom part and that stirring and mixing decrease with depth.

Figure 9.17 shows the buried residue distributions after each of four repeated

lure used to distribute buried residue in the soil
ts is described in **Section 13**. The RUSLE2
here material becomes uniformly distributed in
RUSLE1 assumes that the material is uniformly

operations for a moldboard plow that has an **inversion with some mixing** distribution where no additional residue is buried after the first operation. The buried residue distribution gradually becomes more uniform with each operation. Figure 9.18 shows buried residue distribution with repeated operations with a tandem disk where residue burial is mainly by mixing. After repeated operations, a bulge of biomass develops that moves downward in the soil. The bulge becomes increasingly concentrated with each operation and moves downward less with each operation. Thus rather than the distribution becoming increasingly uniform as assumed in some models, RUSLE2 computes an increasingly non-uniform distribution for the mixing type distributions. Implements like tandem disks and rotary tillers are assumed to bury residue uniformly in the soil, but in fact they only bury residue uniformly under certain conditions, which occurs with about two passes as can be seen from Figure 9.18.

9.2.5.5. Spatial non-uniformity of soil biomass

The soil biomass for live and dead roots and buried residue is spatially non-uniform for row crops, widely disperse plants like clumps of shrubs and grass on rangelands, and tree seedlings in a forest. However, RUSLE2 assumes that all soil biomass is uniformly distributed, even when the operation only disturbs a portion of the soil surface.

9.2.5.6. Assigning input values that determine soil biomass

The amount of soil biomass is a critical variable in determining how a cover-management system affects erosion. The three principal sources of soil biomass are from live root biomass, plant litter and crop residue, and externally added residue. The mass of external residue is based on dry matter basis and is known. Root biomass values for a **vegetation description** should be selected by comparing the vegetation's characteristics with those of vegetation descriptions in the RUSLE2 **core database**. When selecting root biomass values for a particular vegetation description, the role of fine roots versus coarse roots must be considered. For example, even though carrots and potatoes make up root biomass, their mass is not considered in assigning root biomass values because those "coarse roots" have little effect on erosion. In cases where some credit is to be taken for coarse roots, some, but not all, of their biomass is entered along with the biomass of the fine roots.

A key factor in selecting input root biomass values is to account for the temporal variation in root biomass so that the effect of root sloughing is captured by RUSLE2.

Do not make field measurements of root biomass values to determine input values for RUSLE2. Measuring root biomass is very difficult, tedious, and tiresome and should only be done in a research setting. Large errors are common unless extreme care is taken and even then the results may show much variability. The ratio values in the RUSLE2

core database used to determine root biomass values for rangeland plant communities have been chosen based on measured soil loss values obtained during rainfall simulator experiments.[88] Other root biomass values in the RUSLE2 **core database** have been selected from the scientific literature and these values were used when equation 9.12 was fitted to erosion data.

Use of root biomass values that have not been checked for consistency with values in the RUSLE2 *core database* can cause serious errors in RUSLE2.

The other major source of soil biomass is from decomposition of plant litter and crop residue on the soil surface and from the incorporation of crop residue into the soil. The amount of plant litter is determined by senescence of the plant canopy and the amount of biomass associated with that loss of canopy. The amount of residue produced by a crop is determined by the residue to yield relationships defined for the crop and is entered in the vegetation component of the RUSLE2 database. The other important factor that determines the amount of buried residue is the flattening, burial, and resurfacing ratios used to describe operations in the operation component of the RUSLE2 database.

Even though a plant community may be a mixture of species, RUSLE2 represents the plant community as a single vegetation description where input values are selected to describe the composite effects of the vegetation. RUSLE2 "grows" only one vegetation at a time. RUSLE2 cannot take data from two vegetation descriptions, such as corn and rye, and combine them into a single composite vegetation.

9.2.5.7. Comments

RUSLE2 does not consider how soil texture or other soil properties affect the distribution of residue and roots in the soil. Although RUSLE2 adjusts amount of biomass buried by a soil disturbing operations as a function of speed and depth, RUSLE2 does not adjust the distribution of the residue as a function of operation speed or depth.

9.2.6. Soil consolidation[89]

A mechanical disturbance loosens soil and increases its erodibility, which in turn increases erosion. After a mechanical soil disturbance, soil erodibility decreases as soil

[88] The data used to calibrate RUSLE2 to rangelands were collected as a part of the Water Erosion Prediction Project (WEPP) by R. Simantion and others, USDA-ARS, Tucson, AZ. See Table 5-4 in AH703.

[89] A prior land use (PLU) subfactor was used in RUSLE1. This subfactor was the product of the soil consolidation subfactor and the soil biomass subfactor. This same product is used to display RUSLE2 subfactor values in some of the templates.

primary particles and aggregates become cemented together by wetting and drying and other soil processes, which is the main soil consolidation effect. A mechanical soil disturbance decreases the bulk density of soil. Increases in soil bulk density do not greatly reduce soil erodibility, except when compaction is extreme.

Soil consolidation in RUSLE2 refers to the decrease in soil erodibility following a mechanical soil disturbance rather than an increase in bulk density.

9.2.6.1. Soil consolidation effect

Figure 7.3 is a plot of the soil consolidation subfactor s_c as it decreases with time after a mechanical soil disturbance. The soil is assumed to be 0.45 times as erodible at full consolidation as it is immediately after a disturbance. A soil disturbance resets the soil consolidation subfactor to 1 and it begins to decrease again with time. Seven (7) years is normally assumed for the time for the soil to become fully consolidated after a mechanical disturbance in the Eastern US where rainfall events are sufficiently frequent for the soil to experience repeated wetting and drying cycles required for the cementing process (See **Section 7.8**). RUSLE2 computes an increased **time to soil consolidation** up to 20 years as annual precipitation decreases from 30 inches (760 mm) to 10 inches (250 mm). A constant 20 years for time to soil consolidation is used where annual precipitation is less than 10 inches (250 mm). This increased time to soil consolidation reflects how the effects of a mechanical soil disturbance persist longer in low precipitation areas where reduced water is available and less frequent wetting and drying cycles occur.

The soil consolidation effect is greatest for those soils that have the greatest and most active cementing agents. These agents are most closely related to clay and organic matter particles because of their high specific surface area. Thus, the soil consolidation effect is greatest for soils having a high organic matter content, characteristic of cover-management systems involving a high level of soil biomass. The effect of organic matter content as affected by cover-management system is captured in the soil biomass subfactor s_b computed with equation 9.12.

The soil consolidation effect is also a function of soil texture because of the role of clay in cementing soil particles. The soil consolidation effect is greatest for fine textured soils with a high clay content and least for coarse textured soils with a low clay content. However, RUSLE2 does not consider the effect of soil texture on the soil consolidation subfactor.[90]

[90] The soil consolidation subfactor in RUSLE2 is one of the variables least well defined by scientific research. Its effect varies with many factors, but the research data are not sufficient to derive an empirical equation for the effect of soil conditions on the time to soil consolidation. Although, the soil consolidation

9.2.6.2. Importance of soil consolidation subfactor to other variables

The soil consolidation subfactor has indirect effects in RUSLE2 by being a variable in equations used to compute values for other cover-management subfactors. For example, the consolidation subfactor s_c is used in equation 9.12 to compute values for the soil biomass subfactor s_b. The soil consolidation subfactor is used to compute the rill-to-interrill erosion ratio in equation 8.3 where soil consolidation is assumed to reduce rill erosion much more than interrill erosion. The ratio of rill-to-interrill erosion affects the slope length effect and the ground cover subfactor g_c. Mulch is assumed to have reduced effectiveness on steep, cut construction slopes, which are detected in RUSLE2 by a low soil consolidation subfactor and low soil biomass values.

The soil consolidation subfactor is also a variable in RUSLE2 equations used to compute runoff index values (curve numbers) and runoff, which is used to compute how support practices affect soil loss (see **Section 14**). For example, when the soil is consolidated (i.e., s_c values near 0.45), infiltration is assumed to be low and runoff high if no soil biomass is present. A construction site where a surface soil layer was cut away without disturbing the underlying soil represents this condition. However, if the soil is undisturbed, which is indicated by a low s_c value, and contains a high level of soil biomass, infiltration is assumed to be high and runoff low. A high production permanent pasture represents this condition.

An undisturbed soil is required for a layer of high organic matter to develop at the soil surface on range, pasture, and no-till cropland. The soil consolidation subfactor is used as an indicator of the potential for this layer to develop. This effect is captured in equation 9.12 for the soil biomass subfactor s_b.

The portion of the soil surface that is mechanically disturbed during a cover-management system determines the overall effect of soil consolidation. The effects of the portion of the soil surface disturbed and the soil consolidation subfactor are illustrated in Figure 9.19 for a no-till corn cropping system at Columbia, MO.[91] One of the curves in Figure 9.19 is where the only soil disturbance is by a no-till planter that disturbs the soil in strips for a place to plant the seeds. The portion of the soil surface disturbed by the planter was varied from none to full width disturbance. No other variable such as burial ratio that would normally vary with the portion of the soil surface disturbed was changed. Thus the only effect represented is the effect of soil consolidation as reflected by portion of the soil surface disturbed. The other curve is where a fertilizer injector that disturbs 50

---

subfactor equation was primarily derived from soil loss measured at the single location Zanesville, OH, limited data from other locations indicate that the equation is valid in general.

[91] The effects computed for the soil consolidation subfactor differ between the non-Req and Req applications. The Req applications give increased credit for soil biomass, which is affected by the soil consolidation subfactor, but the Req applications do not adjust the slope length factor and the ground cover subfactor values as a function of the rill-to-interrill ratio that are used in non-Req applications.

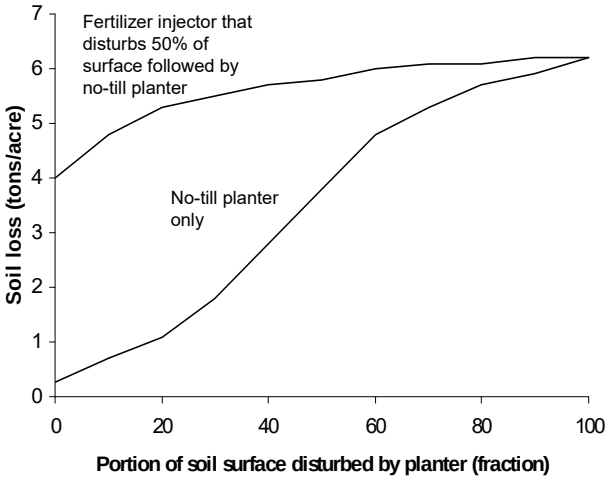

Figure 9.19. Effect of portion of soil disturbed on soil loss at Columbia, MO for no-till corn at 110 bu/acre. Fertilizer injector does not bury or resurface residue.

percent of the soil surface precedes the planter. Portions of the soil surface disturbed by the planter were varied while the 50 percent portion disturbed by the fertilizer injector was fixed.

The ratio of soil loss for the no-till planter with no disturbance and without the fertilizer injector to soil loss with full disturbance in Figure 9.19 is 0.04, which is much more effect than the 0.45 value for the full soil consolidation subfactor for no disturbance. Several variables cause additional effects beyond the 0.45 value directly associated with the soil consolidation subfactor. The soil consolidation affects the soil biomass subfactor as computed with equation 9.12. Another variable is the soil depth over which buried residue mass is averaged for equation 9.12 is reduced as the soil consolidation subfactor decreases. Another variable is the reduced slope length effect that is computed as a function of the rill to interrill erosion ratio that RUSLE2 computes as the soil consolidation subfactor decreases (see **Section 8.1.1**). Another variable is a decreased ground cover subfactor that is computed as a function of the rill-interrill erosion ratio that is a function of the soil consolidation subfactor (see **Section 9.2.2**).

The second curve in Figure 9.19 where a fertilizer injector precedes the no-till planter illustrates the importance of considering all soil disturbing operations in a cover-management system instead of giving attention solely to a single operation like a planter or drill. Varying the portion of the soil surface disturbed by the planter when it follows the fertilizer injection that disturbs a relative large portion of the soil surface had relatively little effect on erosion. The fertilizer injector is the dominant operation in terms of the soil consolidation subfactor effect. Most of the benefits of no-till cropping are lost by the fertilizer injector. The fertilizer injector disturbs the soil more than the no-till planter that follows the fertilizer injector. Consequently, adjusting the portion of the soil surface disturbed by the planter had little effect on the RUSLE2-computed soil loss..

9.2.6.3. Definition of mechanical soil disturbance

Soil disturbance, as used in RUSLE2, occurs when an operation fractures and loosens the soil, displaces soil, mixes soil and surface residue so that the interface between the residue and the surface soil is no longer distinct, and disrupts a high organic matter layer at the soil surface.

Operations that seed crops like corn, soybeans, and wheat in rows and that inject fertilizer and manure with thin shanks disturb only strips of soil and not the entire soil surface. An important input value, as illustrated in Figure 9.19, is the portion of the soil surface disturbed by each operation. A definition of mechanical soil disturbance is required to assign values for the portion of the soil surface that is disturbed by an operation.

A lower limit of 15% for portion of the soil surface disturbed should be used for no-till implements. This limit is related to the computational accuracy of RUSLE2; it is not related to definitions of no-till as used by NRCS or others.

When an operation displaces soil, the source area of the soil is included in the soil surface disturbed and the receiving area is included under certain conditions. The receiving area **is not** included in the area disturbed if the resulting soil depth from the displaced soil is so thin, less than 0.5 inch (10 mm) as a guide, that it has little effect on detachment by raindrop impact (interrill erosion) or detachment by runoff (rill erosion). The soil surface

New input values for portion of soil disturbed by an operation should be carefully examined for consistency and guidelines established so that input values are consistently assigned for other new operations.

should be essentially level after an operation to assign a low value to the portion of the soil surface disturbed. The receiving area **is** included in the disturbed area if the surface residue and soil were mixed by the operation or any high organic matter soil layer at the soil surface was disrupted. The receiving area **is** included in the area disturbed, even though the surface residue has not been mixed with soil or high organic matter layer at the soil surface has not been disrupted, if displaced soil is deeper than about 0.5 inches (10 mm) such that significant amounts of interrill and rill erosion occurs because of exposed bare soil. Ridges and furrows are an indication of a high portion of the soil surface disturbed, especially where soil thrown from either side meets to form the ridge. Machines and implements, like scarifiers and hoe drills that involve shanks and shovels typically disturb a greater portion of the soil surface than implements that involve straight coulters. However, concave coulters and disks can throw large amounts of soil, resulting in almost the entire surface being disturbed.

9.2.6.4. How RUSLE2 handles strips

RUSLE2 does not keep track of individual strips of disturbed areas through time. RUSLE2 computes only a single composite soil consolidation subfactor value at any

time. When an operation occurs that disturbs only a portion of the soil surface, RUSLE2 computes a composite soil consolidation subfactor value based on the portion of the soil surface that is disturbed by using a subfactor value of one (1) for the portion of the soil surface disturbed and the subfactor value at the time for the undisturbed portion at the time of the operation. This composite soil consolidation subfactor value is used in the RUSLE2 soil consolidation subfactor equation, represented by Figure 7.3, to compute an effective time after last soil disturbance. RUSLE2 accounts for time after a soil disturbance by starting with this effective time after last disturbance and proceeds.

9.2.6.5. Assigning values for portion of soil disturbed

A value of one (1) is assigned to the portion of the soil surface disturbed for most full width operations like scarifiers, moldboard plows, offset disks, tandem disks, chisel plows, and field cultivators. The portion of the soil surface disturbed by implements like row cultivators, planter, drills, and fertilizer and manure injectors that disturb strips of soil may be, but are not necessarily, less than one (1). Values for the portion of the soil surface disturbed selected for these operations should be consistent with values assigned to comparable operations in the RUSLE2 **core database**, which should be consulted first before values are assigned to new operations being put in the operation component of the RUSLE2 database. However, the portion disturbed can depend on local conditions, specific machines, and individual operators. Thus, input values may need to be adjusted from the **core values** based on the guidelines in **Section 9.2.6.3.**

Blading and grading used in construction operations must be carefully considered when a value for the portion of the soil disturbed is assigned to these operations. A grading operation for fill material should include a **disturb soil** process that uses a value of one (1) for the portion of the soil surface disturbed, even if the soil has been compacted with a roller or other compaction device. Compaction of the soil does not greatly reduce soil erodibility. Repeated wetting and drying and related soil processes must occur to cement the soil particles for the soil to be **consolidated**. A zero (0) is assigned to portion of the soil surface disturbed for a grading operation that cuts and removes a soil layer and leaves the underlying soil undisturbed. Thus, RUSLE2 assigns a value of one (1) for the soil consolidation subfactor for a fill slope and a value of 0.45 to a cut slope. However, if the cut slope has been ripped with a scarifier, disked for a seedbed, or mulch crimped in, a value is assigned to the portion of the soil disturbed according to the guidelines in **Section 9.2.6.3.**

Important RUSLE2 rules:
Surface material cannot be buried without using an operation with a *disturb soil* process
Material cannot be placed in the soil (e.g., manure injection) without an operation with a *disturb soil* process
Roughness cannot be created without an operation with a *disturb soil* process
Select values for portion of soil surface disturbed based on guidelines in section 9.2.6.3.

9.2.7. Ponding effect

Water ponds on flat lands during intense rainfall. The ponded water depth reduces rainfall erosivity. The effect is greatest along the Gulf Coast and the lower Atlantic Coast of the US. For example, RUSLE2 computes that the ponding effect reduces erosion by 46 percent at New Orleans, Louisiana on a 0.5 percent slope.

RUSLE2 computes values for the ponding sub-factor as a function of the 10 yr-24 hr precipitation amount and land steepness. The ponding effect sub-factor decreases as the 10 yr-24 hr precipitation amount increases, which is indicative of increased rainfall intensity. The ponding effect sub-factor increases as land steepness increases. For example, RUSLE2 computes only a 6 percent reduction in erosion because of the ponding effect for a 5-percent land steepness at New Orleans.

The RUSLE2 assumption is that the ponding effect is not affected by soil-surface roughness or soil ridges.

9.2.8. Antecedent soil moisture

The level of soil moisture affects infiltration and runoff to some degree at all locations. However, the effect is least where large amounts of rainfall frequently occur such as in the humid Southeastern US. The effect is more pronounced in the Western portion of the Great Plains in the US. Soil moisture is removed by growing crops depending on the type of crop and its production level. Soil loss is less following a crop that extracted much of the soil moisture in a low rainfall area. This effect is especially pronounced in the NWRR where rainfall is relatively low and environmental conditions associated with timing of rainfall and the freezing and thawing of soil under either high or low soil moisture content. A soil moisture subfactor is needed in the NWRR for Req applications to account for these special effects.

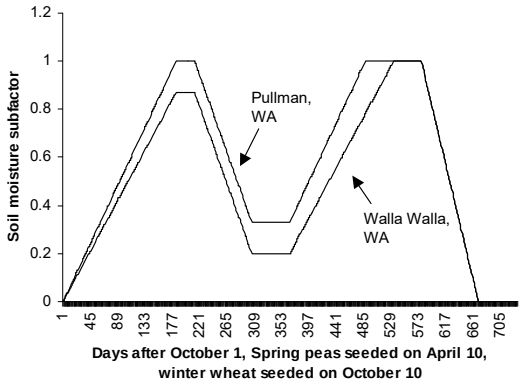

Figure 9.20. Antecedent soil moisture subfactor values for two locations in Washington for a winter wheat-spring pea rotation. The first peak is the effect of the winter wheat and the second one is the effect of spring peas.

9.2.8.1. Antecedent soil moisture subfactor effect

Values for the antecedent soil moisture subfactor s_m are illustrated in Figure 9.20. Subfactor values are 1 when the soil profile is "filled" relative to the unit plot and less than 1 when the soil profile is depleted of moisture relative to the unit plot.

As Figure 9.20 illustrates, the effect is a function of both location and type of crop. Antecedent soil moisture subfactor values are lower at Walla Walla, WA than at Pullman, WA because of less precipitation. Also, the values are lower following wheat than following spring peas because of the water usage difference between the two crops. As always, the values for the antecedent soil moisture subfactor are one (1) for unit plot conditions.

9.2.8.2. Assigning input values

An input value is assigned to each **vegetation description** in the **vegetation component** of the RUSLE2 database. Values are listed in **Section 11.1.6** and in the RUSLE2 **core database** that can be used as a guide for assigning input values used in the antecedent soil moisture subfactor.

The antecedent soil moisture subfactor must only be used in the NWRR for Req applications.

10. COVER-MANAGEMENT DATABASE COMPONENT

The **cover-management component** of the RUSLE2 database contains the **cover-management descriptions** that RUSLE2 uses to compute how cultural practices such as tillage systems for cropped fields, temporary erosion control practices for construction sites, and long term vegetation on a reclaimed mine sites affect erosion.

A **RUSLE2** cover-management description is primarily a list of operations and the dates on which each operation occurs. An **operation** is an event that changes the vegetation, residue, and/or soil in some way. Examples of operations are given in Table 10.1.

Table 10.1. Examples of operations

Operation	Effects	Comment
Moldboard plow	Kills vegetation, disturbs soil, buries residues, redistributions biomass in soil	Primary tillage, first step in growing a crop
Planting	Disturbs a strip of soil, seeds a crop	Includes a **begin growth** process. The name for the appropriate vegetation description is entered to represent the crop being grown
Broadcast seeding	Seeds a particular vegetation. This seeding operation does not disturb the soil.	Includes a **begin growth** process. The name for the appropriate vegetation description is entered to represent the vegetation that is seeded.
Volunteer weeds	Starts growth of volunteer weeds	Includes a **begin growth** process. The name for the appropriate vegetation description is entered to represent the volunteer weeds
Harvest	Kills vegetation and flattens some of the standing residue	Typical operation for crops like corn, soybeans, and wheat
Baling straw	Removes residue, flattens standing residue	Removes residue and flattens remaining standing residue
Silage harvest	Removes live biomass, kills vegetation	Leaves a portion of the live biomass in the field to represent harvest losses
Mowing	Removes live biomass, add cut material back as external residue, regrow vegetation	Cuts the live biomass but leaves it in the field. Does not kill vegetation. **Begin growth** process calls vegetation description that regrows vegetation after mowing
Baling hay	Remove live biomass,	**Begin growth** process calls vegetation

	regrows hay	description for vegetation that regrows after the hay harvest
Frost kills vegetation	Uses a **kill vegetation** process	RUSLE2 does not model plant growth. Must tell RUSLE2 when vegetation is killed, even if it occurs naturally
Fire	Remove residue/cover	RUSLE2 can not remove dead roots from the soil
Apply mulch	Add other residue/cover	Use to apply mulch to represent construction sites
Apply plastic mulch in a vegetable field, water in a rice field, or deep snow at a construction site in mountains	Apply non-erodible cover	Shuts off erosion for period that non-erodible cover is present. Use a **remove non-erodible cover** process to remove cover and to restart erosion.

The cover-management description includes the names of vegetation and residue descriptions needed by certain operations. An operation that includes a **begin growth** process requires that a vegetation description be specified for that operation. The **begin growth** process signals RUSLE2 to begin using information from the specified vegetation description on the operation's date. Similarly, operations with an **add other residue/cover** process require specifying a residue description and the amount of the material being added for the operation. RUSLE2 adds the cover at the specified amount on the date of the operation.

Additional non-event based information is also entered as a part of the cover-management description. For example, the user specifies whether the list of operations is repeated in a cycle (rotation) with a particular frequency or whether RUSLE2 is to compute erosion based on a single occurrence of each operation.

The variables in a cover-management description associated with the list of operations are listed in Table 10.2. The non-event variables that apply to a cover-management description are listed in Table 10.3.

Table 10.2. Variables in a cover-management description	
Variable	Comment
List of dates	List of dates for the operations used to describe the cover-management condition (practice)
List of operations	Name of operation description in operation component of the RUSLE2 database containing values that RUSLE2 uses to

	describe the effect of the operation on erosion. Operations are events that change vegetation, residue, and/or soil. The list of operations is the main part of a cover-management description, which represent how cultural practices affect erosion.
List of vegetation descriptions	Name of vegetation description in the vegetation component of the RUSLE2 database containing values used by RUSLE2 to represent the effect of vegetation on erosion. Only one vegetation description is used at a time by RUSLE2. That is, RUSLE2 can not combine multiple vegetation descriptions into a single description.
Yield	Identifies production (yield) level in user defined units
Operation depth	Specifies the disturbance depth of operations that disturbs the soil. Default value is "recommended" value in operation description in operation component of RUSLE2 database. RUSLE2 will adjust for a depth value different from the default value.
Operation speed	Specifies the speed of operations that disturbs the soil. Default value is "recommended" value in operation description in operation component of RUSLE2 database. RUSLE2 will adjust for a speed value different from the default value.
External residue	Name of material (residue description in residue component of RUSLE2 database) added to soil surface and/or placed in soil. RUSLE2 uses values in residue description to compute how material affects erosion. Vegetation produces plant litter and crop residue. That material is considered by operations that manipulate vegetation and its biomass. External residue is material other than that associated with the vegetation descriptions in the cover-management description. Typical external residue includes manure and mulch (applied erosion control materials),
Residue added/removed	User entered mass value (dry weight basis) for material added when external residue is applied. Value shown is for the amount of plant material added from the "current" vegetation is computed by RUSLE2.
Cover from residue addition	Portion of soil surface covered by the added external or vegetation material. Value is computed by RUSLE2. This value is only for the added material and does not include existing surface (flat) cover.
Vegetative retardance	Refers to the degree that the vegetation slows surface runoff. RUSLE2 computes value based on user enter information in the vegetation description.

Table 10.3. Non-event variables used in a cover-management description

Rotation and duration	Is RUSLE2 to process the list operations multiple times in a cycle (rotation) with a certain frequency to represent steady state conditions for the cycle? Duration is the time for the cycle to be repeated. Crops are frequently grown in a crop rotation. The same crop grown each year (e.g., continuous corn) has a one-year rotation. Constructions sites are typically analyzed as a no-rotation. That is, the list of operations in the cover-management description are processed as a single pass through them.
Long term roughness	The soil surface roughness index value that evolves over time after the last soil disturbance.
Build new rotation with this management	Use this procedure to combine existing cover-management descriptions to create a new cover-management description.
Relative row grade	Can be used to specify cover-management description used as a part of a contouring system
Management alignment offset	Specifies the timing of operations when the same cover-management description is used on multiple segments along the overland flow profile.

10.1 Creating a cover-management description

The cover-management description provides information that RUSLE2 uses to compute values for the cover-management subfactors described in **Section 9**.[92] Table 10.4 illustrates a cover-management description for a corn-soybean-wheat rotation while Table 10.5 illustrates a cover-management description for a construction site where mulch is applied, a temporary cover crop is seeded, and permanent vegetation is seeded.

Table 10.4. List of operations for a corn-soybean-wheat 3-yr rotation

Date	Operation	Vegetation	Yield
4/15/1	Twisted shovel chisel plow		
5/1/1	Tandem disk		
5/5/1	Field cultivator		
5/10/1	Planter	Corn 112 bu/ac base yield	150 bu/ac
6/10/1	Row cultivator		
10/15/1	Harvest		
4/15/2	Moldboard plow		
5/1/2	Tandem disk		
5/5/2	Field cultivator		

[92] See Section 17.4.1.4 for information on creating a cover-management description for range, pasture, idle, undisturbed, and similar lands using a time invariant approach.

5/10/2	Planter	Soybeans 25 bu/acre base yield	35 bu/ac
9/10/2	Harvest		
9/15/2	Tandem disk		
9/20/2	Double disk drill	Wheat 35 bu/acre base yield	50 bu/ac
7/1/3	Harvest		
Non-event variable	Long term roughness	0.24 inches (6 mm)	
Non-event variable	Rotation	Yes	
Non-event variable	Duration	3 years	
Non-event variable	Management alignment	Not applicable	
Non-event variable	Relative row grade	10 percent	

Table 10.5. Cover-management description for applying straw mulch, seeding spring barley as temporary vegetation, and seeding a local native grass for permanent cover at a construction site

Date	Operation	Vegetation	Yield	External residue	Amount external residue added/removed
4/1/1	Blade fill material				
4/2/1	Broadcast seed	Spring barley 35 bu/ac base yield	25 bu/ac		
4/3/1	Apply mulch			Wheat straw	4000 lbs/ac
9/15/1	Killing frost				
9/16/1	Shred standing vegetation				
9/17/1	Double disk drill	Local native grass	1000 lbs/ac		
Non-event variable	Long term roughness	0.6 inches (15 mm)			

Non-event variable	Rotation	No			
Non-event variable	Duration	10 years			
Non-event variable	Management alignment	Not applicable			
Non-event variable	Relative row grade	Not applicable			

The first step in creating a RUSLE2 **cover-management description** is to list the dates and events that affect the soil, vegetation, and/or residue. A RUSLE2 **operation description** is selected from the **operation component** (see **Section 13**) of the RUSLE2 database to describe each of these events, even if the event is a natural occurrence such as frost killing vegetation. In general, the list of operations mimics actual events. However, only events that affect erosion are included in the list. For example, an aerial pesticide application would not be included. Be careful not to overlook an important natural event, such as a killing frost. The second step is to add supporting information such as the names for required **vegetation and external residue descriptions** and **application rates** for external residue. RUSLE2 procedures and definitions must be followed in creating a cover-management description to describe a field situation, keeping mind that RUSLE2 is not a simulation model. The input is a description for the field conditions that affect erosion.

A cover-management description can involve as many operations and vegetation descriptions as required. A field description can often be created in multiple ways. An example is the development of permanent, perennial vegetation from seeding to maturity after erosion has stabilized. The **duration** of the cover-management description is longer than the time for the vegetation to reach maturity to allow time for a stable litter layer and soil biomass pool to develop. Assume that three years is required for the vegetation to reach maturity and that an additional three years is needed for the litter layer and soil biomass pool to fully develop. The additional time for the litter layer and soil biomass pool to fully develop depends on temperature and precipitation at the location. The duration of the cover-management description is six years to include time for RUSLE2 to compute the effect on erosion of a fully developed litter layer and soil biomass pools.

The vegetation for this condition can be described with a single vegetation description that covers the entire six year period where the last four years involve duplicate values. A second way to apply RUSLE2 is to create three vegetation descriptions, one for the first year, one for the second year, and one for the third and subsequence year. Each of the six years represented in the cover-management description includes an operation description with a **begin growth** process where the appropriate vegetation description is assigned to the particular year.

RUSLE2 is often used to evaluate erosion for the maturity period alone without concern for erosion during establishment of the permanent vegetation. Examples include estimating erosion on pasture, range, reclamined mine, and waste disposal lands. In this case, a vegetation description of one year is created to represent the vegetation at maturity. Values at the end of the year equal those at the beginning of the year to represent a complete annual cycle. The cover-management description is a 1-year rotation. RUSLE2 cycles through the annual vegetation description a sufficient number of times so that RUSLE2 computes a stable litter layer and soil biomass pool and thus computes a stable erosion rate representative of condition where the permanent vegetation is fully established.

The same agricultural crop such as corn, soybeans, or wheat can be grown year after year (continuous cropping). The same crops can also be grown in a rotation such as a corn-soybean rotation. A cover-management description can be created for each possible combination, although the number of cover-management descriptions becomes large and difficult to manage.

An alternative is to use the **rotation builder** in RUSLE2. The rotation builder is used to combine multiple cover-management descriptions into a single cover-management description. The rotation builder most often is used to combine annual cover-management descriptions to create multiple year cover-management descriptions. The rotation builder can also be used to combine partial year cover-management descriptions for a single crop to create a single year cover-management description such as for vegetable cropping. Another example is using the rotation builder to combine a one-year wheat cover-management description with a two-year corn-soybean cover-management description to create a three-year corn-soybean-wheat cover-management description. In general, the rotation builder can also be used to combine cover-management descriptions of any duration.

The RUSLE2 rules must be carefully followed.

10.2. Discussion of variables used in a RUSLE2 cover-management description[93]

10.2.1. Dates

10.2.1.1. Operations as discrete events and representing continuous activity

Operations are discrete events that occur on a particular day. More than one operation can occur on a given day. Having each operation occur on individual days in RUSLE2

[93] The variables displayed in RUSLE2 depend on the template used to configure the RUSLE2 computer screen. Variables are discussed that you may not see displayed in RUSLE2 depending on the template you are using.

rather than on the same day is sometimes useful for seeing the effect of individual operations and for locating errors in cover-management descriptions. **However, this procedure can cause very serious errors in certain situations.** An example is creating ridges and applying mulch on a construction site. These two operations should be on the same day to avoid erroneous critical slope length values (see **Section 14.1.2.5**).

Representing continuous activity like grazing requires applying an operation multiple times over the period that the activity occurs. For example, a grazing operation description might be used once a week for each week that the grazing occurs. A sensitivity analysis should be conducted to determine how best to represent a continuous activity with a set of discrete events. In many cases, such as grazing, the best way to represent a continuous activity is to create vegetation descriptions that include the effect of the activity rather than using multiple operations.

Keep in mind that RUSLE2 uses descriptions to compute erosion. In many cases, the desired description can be created in multiple ways.

10.2.1.2. Representing the year in dates

The year of the operation can be any integer provided the years are in sequential order (e.g., 1, 2, 3, …; 2004, 2005, 2006, …; 75, 76, 77). The years 1, 2, 3 were used in Tables 10.4 and 10.5 to represent the calendar year of the rotation.

10.2.1.3. Tracking time in RUSLE2

RUSLE2 begins tracking time on the date of the first operation in the cover-management description. RUSLE2 computes average annual erosion based on the date of the first operation. Sometimes annual erosion estimates are needed on a calendar year basis or time needs to start at the same point when erosion estimates from alternative cover-management descriptions are being compared. A **no operation** operation description, which is described with a single **no effect process**, is used as the first operation in each cover-management description. A no operation only marks time and has no effect on the RUSLE2 computations. The date of a no operation is set to **January 1, 1** so that RUSLE2 will display erosion estimate on an actual calendar year basis. The no operation can also be placed on another date such as September 1 as the starting point for annual erosion accounting.

10.2.1.5. Allowing RUSLE2 to set duration

RUSLE2 scans the dates in the list of operations to determine the **duration** of the cover-management description. Using a no operation in the last year of the duration ensures

that RUSLE2 makes the correct determination of duration. See **Section 10.2.8** for a discussion of rotation and duration.

A value for the duration can be entered in the cover-management description. RUSLE2 may over ride this duration based on the dates in the list of operations. An inadvertent error can occur that will not be noticed. To avoid this error, include a *no operation* in the list of operations to ensure that RUSLE2 determines the proper duration from the dates for the list of operations.

10.2.1.6. Initial conditions

The operations must always be in the proper sequence. The starting operation is unimportant for a rotation because RUSLE2 loops through the list of operations until the erosion computations become stable. Because of this computational feature, values for initial conditions for RUSLE2 are not required for rotations.

However, initial conditions are needed where the cover-management description is a **no rotation** such as applying RUSLE2 to a construction site. In this case, initial conditions must be set in RUSLE2. The first set of operations in the cover-management description are selected to create the desired initial condition. The default initial condition assumed by RUSLE2 is that the soil is bare, fully consolidated, and has no soil biomass. This condition is like that created by a blade and cutting away the surface layer of soil below the root zone without disturbing the underlying soil. If this situation is applicable to the actual field situation, no operations are needed to set initial conditions. Start with the first operation, which might be an application of mulch on a construction site. A common condition on construction sites is placing mulch on a freshly graded fill. An operation description named **blade fill material** can be used as the first operation description in the list of operations. This operation includes a **disturb soil** process with the result that the soil is not consolidated in contrast to the cut, default condition. Erosion on the fill slope will be twice that on the cut slope because of the soil consolidation effect. An initial condition of a rough soil can be created by using an operation description to create a rough surface keeping in mind that a disturb soil process is required in the operation to create the roughness that also eliminates soil consolidation at the time of the operation.

The initial condition may also involve soil biomass, a litter cover, and growing vegetation. The appropriate initial conditions are created by using an initial set of operations that create the desired description. A **no operation** can be used before and after the initial set of operations used to create the initial conditions to mark time so that RUSLE2 displays erosion on the desired date. Be sure to set up operations so that RUSLE2 displays average annual erosion starting on the desired date. Keep in mind that the average annual erosion displayed by RUSLE2 is for the entire cover-management description including the operation descriptions used to establish initial conditions.

RUSLE2 displays average annual erosion for each year that provides the erosion values that can be used to compute average annual erosion for any period during the entire duration of the cover-management description.

10.2.2. Operations

Operations are events that affect soil, vegetation, and/or residue. RUSLE2 uses the information in **operation descriptions** to compute how operations effect erosion.

Many RUSLE2 operations are created and named to represent actual events such as tilling, seeding, harvesting, burning, frost, grading, and applying mulch. A single operation description can often be created to represent an event such as tillage. However, cases arise where multiple RUSLE2 operations are used to represent a single actual field event. An example is a harrow drawn behind a tandem disk through the field as a single unit. A more accurate representation of how the composite implement buries residue can be obtained in RUSLE2 by representing the effects of tandem disk separate from the effects of the harrow. Thus, two operation descriptions are used on the same day, one to represent the tandem disk and one to represent the harrow, to represent a single actual field event. The operation descriptions can be put on two consecutive dates so that the effects of the tandem disk can be seen separate from the effects of the harrow in a test computation, but the two operations should be on the same day for the erosion control planning computation..

Having the operations in the proper sequence is an absolute necessity.

Operations represent discrete events. Representing a continuous activity like grazing is discussed in **Section 10.2.1.1**.

See **Section 13** for a complete discussion of operation descriptions.

10.2.3. Vegetation

RUSLE2 uses the information in a **vegetation description** in the **vegetation component** of the RUSLE2 database to compute erosion when vegetation is present. **Operation descriptions** with a **begin growth** process in a **cover-management description** instruct RUSLE2 to begin using data from a particular vegetation description in its computations. Thus, the name of a vegetation description must be entered for each operation that includes a **begin growth** process. RUSLE2 begins using data from the selected vegetation description on the date of the operation and references the first date, day zero, in the vegetation description to this date.

Various approaches are used in RUSLE2 to create cover-management descriptions involving vegetation. In the case of annual crops, a vegetation description for each crop

is used, which requires an operation description with a **begin growth** process to call a vegetation description for the appropriate crop in a **rotation** like a corn-soybeans-wheat rotation. The vegetation descriptions for annual crops like corn, soybeans, and wheat represent a year or less.

Multiple vegetation descriptions can also be used during a year. An example is using multiple vegetation descriptions to represent sequential planting and harvesting of two or more vegetable crops during the year.

A particular plant community can be divided into multiple vegetation descriptions. For example, the following sequence of vegetation descriptions can be used to represent a hay crop. The first vegetation description is for the period from fall seeding of alfalfa and through early growth, senescence, dormancy through the winter, and spring growth to the first harvest in the first harvest year. The second vegetation description describes the regrowth following the first and second harvests in the first harvest year. The third vegetation description describes the regrowth after the last harvest in the first harvest year, senescence, winter dormancy, and spring regrowth to first harvest in the second harvest year. The fourth vegetation description describes regrowth after the first and second harvests in the second harvest year. Additional vegetation descriptions are used as required to complete the rotation. Each vegetation description should represent the progression of growth in terms of **yield**, **canopy**, **live ground cover**, and **live root biomass**. For example, yield typically increases in the early years of a hay rotation while it may decrease in latter years.

Another example of using multiple vegetation descriptions is when RUSLE2 is applied to **intercropping**. Intercropping is when two crops grow together at the same time. An example is planting a legume crop in late winter in a small grain crop. The small grain is harvested in early summer. The legume crop continues to grow after the small grain is harvested until the legume is harvested for hay in late summer. Another example is planting a rye cover crop in corn before it is harvested for silage so that vegetative cover will be present after the vegetative cover is removed when the corn is harvested for silage. Another example of intercropping is ally-way cropping in commercial tree production and grass growing in the alley ways in vineyards and orchards. Another example is volunteer weeds that grow in crops like corn, soybeans, or cotton, especially in the southern US, as the canopy cover decreases after the crop matures. The weeds continue to grow after the crop is harvested.

The small grain-legume cropping system illustrates use of multiple vegetation descriptions. The cover-management description starts in the fall with primary tillage followed by secondary tillage and seeding of the small grain. The first vegetation description is for the period between the time that the small grain is seeded and the time that the legume is seeded. The second vegetation description is for the period between the time that the legume is seeded and the small grain is harvested when the combined

growth of both the small grain and legume is represented. The values for canopy, live ground cover, and live root biomass on day zero in this vegetation description should be the same as the same as the corresponding values on the last day that the previous vegetation description is used. The third vegetation description used in this 1-year rotation is for the period between the small grain harvest and the harvest of the legume. The values for canopy, live ground cover, and live root biomass on day zero in this vegetation description are less than corresponding values on the last day that the previous vegetation description was used to reflect the dead above ground and root biomass that was created with the harvest of the small grain.

RUSLE2 is often used to estimate erosion for a perennial plant community like that on a range, pasture, landfill, or reclaimed mine lands. The cover-management description to represent this condition is a 1-year rotation involving a single vegetation description. The **vegetation description** describes the vegetation over an entire year.

Another important application of RUSLE2 is to estimate erosion during the period immediately following grading of a construction site, landfill, or reclaimed mine to when the permanent vegetation becomes fully established. Temporary vegetation is seeded in the spring followed by seeding of the permanent vegetation in the fall. The vegetation description for this **no-rotation** cover-management description can be represented in two ways.

The first approach uses two **vegetation descriptions**. The first **vegetation description** represents the period between when the temporary vegetation is seeded and the permanent vegetation is seeded. The second vegetation description is for the period after the permanent vegetation is seeded until a stable litter layer and soil biomass pool has developed. The values for each year over the last few years of the description are repeats where the vegetation has matured and become stable on an annual cycle. The **long-term vegetation tool** discussed in **Section 11.2.6** can be used to create these vegetation descriptions.

The second approach uses multiple **vegetation descriptions** of the permanent vegetation. The first **vegetation description** is for the temporary vegetation. The second **vegetation description** is for the first year of the permanent vegetation. The third **vegetation description** is for the second year of the permanent vegetation. The fourth **vegetation description** is for the third year of the permanent vegetation, which represents maturity for this particular vegetation. The third year **vegetation description** is used as many years as necessary for the litter layer and soil biomass to become stable.

The RUSLE2 rules related to **vegetation descriptions** must be carefully observed. In particular RUSLE2 only uses a single **vegetation description** at a time, which is referred to as the **current** vegetation description. An **operation description** with a **begin growth** process is required to tell RUSLE2 when to begin using data from a particular vegetation

description. A vegetation description can start at anytime during the growth cycle of the vegetation. A vegetation description is simply that, a description of the vegetation at a given time. The first date in the vegetation description is day zero, which is referenced to the date that an operation calls that vegetation description. Decreases in **live root biomass** are assumed to become dead biomass that are put in the **dead root biomass** pools, respectively. Thus, the ending values of one vegetation description must properly match those of the next vegetation description used in a cover-management description. For example, the **canopy**, **live ground cover**, and **live root biomass** values at the end of a vegetation description used to represent a mature perennial plant community should be the same as corresponding values at the beginning (day zero) of that vegetation description.

Important RUSLE2 rules related to vegetation

1. **RUSLE2 uses only one vegetation description at a time. This vegetation description is referred to as the *current* vegetation.**
2. **A vegetation description describes the *composite* of plants present at a given time.**
3. **The length of time in a vegetation description should be as long as that vegetation description is used in a cover-management description. If the length of the vegetation description is too short, RUSLE2 uses the values on the last date in the vegetation description until a new current vegetation description is established.**
4. **A new, current vegetation is established by using an operation having a *begin growth* process.**
5. **A *decrease* in *live root biomass* between the first day (day zero in the vegetation description) of the new current vegetation description and the last day that the previous vegetation was used is considered to be dead roots and is added to the *dead root biomass* pool.**

The vegetation descriptions selected in a cover-management description must be consistent with site conditions. RUSLE2 does not check appropriateness of a vegetation description based on environmental conditions or other factors. RUSLE2 simply uses the values in the selected vegetation description. For example, RUSLE2 uses the same values for non-irrigated corn grown in a humid area as in a desert area.

Must be sure that the selected vegetation description is appropriate for the cover-management description and for the site specific environmental conditions.

See **Section 11** for a complete discussion of vegetation descriptions.

10.2.4. Yield

Each **vegetation description** is created for a particular **yield**. Multiple vegetation descriptions can be created for various yield values. A vegetation description having the desired yield can be selected when creating a **cover-management description**. RUSLE2 does not adjust yield based on environmental, management, or other factors. The input yield value must be consistent with site specific conditions, including precipitation, irrigation, temperature, soil, fertility, pest control, plant variety, and management, where RUSLE2 is being applied,.

Instead of selecting a vegetation description created for the desired yield, a vegetation description at a base yield can be selected. RUSLE2 assumes the base yield as the default yield, which the user can change to a value appropriate for the specific RUSLE2 application. RUSLE2 will adjust values in the base vegetation description to the input yield value. The base vegetation should be chosen so that maximum yield is less than 100 percent cover. The RUSLE2 yield adjusting equations, described in **Section 11.2.1**, can not adjust to yield values less than the base yield if maximum canopy of the base vegetation description is 100 percent. However, RUSLE2 can adjust to yield values greater than the base yield when maximum canopy is 100 percent.

The input yield value is in the user defined units for that particular vegetation description. Vegetation descriptions are typically created to use customary units. However, units vary among users applying RUSLE2 to various land uses. Open the vegetation description to determine how yield is defined for a particular vegetation description. If the units defined for that particular vegetation description are not the preferred units, create a new yield unit definition. The input yield units can be wet weight, dry volume, or number of items per unit area, for example. Also, the units can be non-customary and even original units created specifically for a particular RUSLE2 application. When defining units, the user enters values that RUSLE2 uses to convert input units values to dry mass values needed to compute subfactor values in equation 9.1 and related equations.

The input yield value must match site specific conditions.

10.2.5. Operation depth and speed

Operation **depth** refers to the **depth of disturbance** for those **operation descriptions** that include a **disturb soil** process. The default depth of disturbance is the recommended depth entered in the operation description. Similarly, operation **speed** refers to the speed of operation descriptions that include a disturb soil process. The default speed is the recommended speed entered in the operation description.

The amount of surface (flat) cover, crop residue in cropping-management systems, that is buried depends on machine depth of disturbance and speed. In general, **recommended** depth and speed values should be accepted and used in RUSLE2 computations. However, varying input values for depth and speed provides an indication of how residue cover can be affected by depth and speed of soil disturbing implements. Input values must fall within **limits** entered in the operation description.

A common assumption is that residue cover, especially in conservation tillage systems, can be easily manipulated by how tillage implements are operated. The two variables easiest to vary are depth and speed. The RUSLE2 relationships for the effect of these variables on residue burial are based on a very careful study of the research data. If RUSLE2 does not produce the desired residue ground cover value over the range of depths and speeds that are possible in the RUSLE2 inputs, then a particular ground cover can not be reasonably achieved by changing depth and/or speed.

The adjustments that RUSLE2 makes for operation depth and speed are discussed in **Section 13.1.5.3**.

Be very careful in assuming that practically any residue cover can be achieved with any implement based on changes in depth and speed. The RUSLE2 values are based on sound research. Assumptions for varying residue cover by adjusting implement depth and speed that are inconsistent with RUSLE2 computations should be rejected.

10.2.6. External residue and amount added

External residue refers to material added to the soil surface or placed in the soil. This material is usually organic material such as straw mulch, certain erosion control roll products, manure, and compost. In general, RUSLE2 assumes that external residue is organic material that produces organic compounds that reduce soil erodibility when the external residue decomposes. Some materials like rock such as gravel mulch do not decompose. Other materials, such as some roll erosion control products, deteriorate by a different process than the one assumed in RUSLE2. See **Section 12** for a discussion on how to handle these situations.

External residue can be placed entirely on the soil surface, entirely in the soil, or divided between the two. An **operation description** that includes an **add other cover** process tells RUSLE2 that external residue is being added. When an operation description having this process is in the list of operation descriptions in a **cover-management description**, a **residue description** from the **residue component** (see **Section 12**) of the RUSLE2 database is selected to identify the external residue being added. RUSLE2 uses the information in the selected residue description to compute how that external residue affects erosion. Important residue variables include residue type that affects how soil

disturbing operations bury the residue and the degree that the residue conforms to the micro-topography of the soil surface, the portion of the soil surface covered by a given residue mass, and a decomposition coefficient that determines how rapidly that the material decomposes as a function of daily precipitation and temperature at the location.

When external residue is placed in the soil, a **disturb soil** process must follow the **add other cover** process in the operation description used to apply the external residue. The information for this process determines the depth in the soil that the external residue is placed. RUSLE2 assumes that external residue placed in the soil is placed in the lower half of the disturbance depth with most of the residue concentrated near the three fourths disturbance depth as illustrated in Figure 9.16.

The value entered for amount of external residue added must be a mass value based on dry weight. Also, the value must be consistent with the mass values used in the residue description to describe the relationship for portion of the soil surface covered by a given residue mass.

Residue, including residue from vegetative growth and applied external residue, can be removed from the soil surface by using an operation description that includes a **remove residue/cove**r process. This process removes standing and flat residue but not buried residue. Operation descriptions use this process to represent burning and straw baling for example. **Buried residue** in the soil can be removed, by burning for example, by using an operation description that includes two steps. The first step is to resurface the desired amount of buried residue with a **disturb soil** process and then remove the resurfaced residue from the soil surface with a **remove residue/cover** process. The **resurfacing coefficient** in the disturb soil process is set so that the desired amount of buried residue is resurfaced. The value for the **portion of the soil surface disturbed** for this soil disturb process is usually set to 100 percent, which sets the **soil consolidation** subfactor to 1 (a fully disturbed soil) because RUSLE2 assumes that buried residue can not be removed from the soil without disturbing the soil. However, resetting the soil consolidation effect can be eliminated by setting the portion of the soil surface disturbed in the disturb soil process disturbed to 1 percent.

RUSLE2 does not resurface dead roots in the soil because the fine roots, which are the most important roots in affecting erosion, are assumed to be so tightly bound to the soil that a mechanical disturbance can not resurface them.

See **Section 12** for a detailed discussion of residue descriptions.

10.2.7. Long term soil surface roughness

Long term soil surface roughness is the roughness that develops over time by natural processes such as local erosion and deposition by both wind and water erosion (See

Section 9.2.3.1.) Long term soil surface roughness is also a function of vegetation characteristics such as grasses being bunch or sod forming grasses and the density of the vegetation.

Long term soil surface roughness begins to develop after the last soil disturbing operation. The time over which this roughness is assumed to develop is the **time to soil consolidation** (See **Section 7.8**.).

Entering an appropriate value for long term soil surface roughness is most important for range, pasture, reclaimed mine, and landfills lands where permanent vegetation exists. Recommended values for long term soil surface roughness are given in Table 10.6. Long term soil surface roughness is generally set to 0.24 inch (6 mm) for cropping-management systems.

Table 10.6. Long term roughness values for range and similar lands. (Source: AH703)

Condition	Long term soil surface roughness	
	(inches)	(mm)
California annual grassland	0.25	6
Tallgrass prairie	0.30	8
Shortgrass, desert	0.80	20
Mixed grass, prairie	1.00	25
Natural shrub	0.80	20
Pinyon/Juniper interspace	0.60	15
Sagebrush	1.10	28
Bare with rock fragments	0.6	15
Moderate pitted	1.10	28
Deep pitted	2.00	50
Root plowed	1.30	32

10.2.8. Rotation and duration

Rotation in RUSLE2 refers to whether or not the list of operations in the **cover-management description** is to be repeated as a cycle (rotation). The length of the cycle is the **duration** of the rotation.

Designating a cover-management description as a rotation causes RUSLE2 to cycle through the list of operations until average annual erosion for the cycle (rotation) becomes stable. Most RUSLE2 cropland applications involve cover-management descriptions that are rotations. The value entered for duration for a rotation-type cover-management description is the number of years from the first operation in the list of operation descriptions until that operation is repeated in the next cycle. Continuous cropping, such as for corn, has a 1-year duration. Also, a rotation-type cover-

management description for three vegetable crops grown in the same year has a 1-year duration. A 1-year duration is used to apply RUSLE2 to permanent vegetation on range, pasture, reclaimed mine, landfill, and similar lands. A 2-year rotation applies to corn and soybeans grown in subsequent years. A corn-soybean-wheat rotation is an example of a 3-year rotation. Three years elapses from the date of the first operation in the rotation until that operation is repeated in the next cycle.

Duration is not the same as the number of calendar years over which the operations occur. For example, operations for the corn-soybean-wheat rotation occur in four calendar years while 3 years is the duration for the rotation.

An actual field event need not occur in each year of a rotation. For example, corn could be grown in a 2-year corn-fallow rotation where no operations occur in the fallow year. This rotation is a 2-year duration because two years elapses between an occurrence of the first operation in the list of operations until its occurrence when the cycle is next repeated.

The listing of operation descriptions in a rotation can begin with any operation in the list. RUSLE2 cycles through the list until the average annual erosion rate becomes stable. Specifying initial conditions for rotations is not required because of this feature.

A **no-rotation** designation for a cover-management description instructs RUSLE2 to start its computations with the first operation in the list of operation descriptions and proceed through the list. The time period over which RUSLE2 computes erosion begins on the date of the first operation and continues through the number of years specified for duration. Cover-management descriptions for construction sites, establishment periods for vegetation on reclaimed mine and landfills, and recovery from disturbances on range, pasture and disturbed forest land are typically designated as no-rotations. RUSLE2 computes an average annual erosion for the duration, as well as average annual erosion for each year of the duration. See **Section 10.2.1.3** for guidance on how to use an operation description with a **no effect** process to set RUSLE2's starting point in its computations and to display output at desired times.

In a no-rotation cover-management description, the first few operations are used to establish initial conditions, which is discussed in **Section 10.2.1.6.**

RUSLE2 scan the dates in the list of operation descriptions to determine the duration of the cover-management description. In several cases, this computation needs to be over ridden by the user entering a different value for duration. An example is the corn-fallow rotation mentioned above where operations only occur in the first year of the rotation but the actual duration is two years. Another example is a construction site where mulch is applied and the site is temporarily seeded. An average annual erosion estimate is needed

over the next two years before the final grading and seeding occur. In these examples, RUSLE2 sets the duration to 1 year when the proper value is 2 years.

Even when proper values are entered for duration, RUSLE2 can unexpectedly change the duration, which causes serious errors. To prevent such errors, enter a *no-operation* operation description (an operation using a single *no effect* process) in each year (*not each calendar year*) of the duration for the cover-management description.

10.2.9. Build new rotation with this management

The **rotation builder** is a RUSLE2 tool that can be used to combine individual cover-management descriptions, including both rotation and no-rotation type cover-management descriptions, into a single cover-management description. The combined cover-management description can be named, saved, and used later in a RUSLE2 erosion computation. Also, the combined cover-management description can be used directly in a RUSLE2 erosion computation without naming and saving it. This tool is most often used in RUSLE2 cropland applications where the combination of single year cover-management descriptions into multi-year rotations is almost limitless. Having a cover-management description for each combination results in a large and cumbersome set of cover-management descriptions in the RUSLE2 database.

RUSLE2 has editing capability for copying and pasting between cover-management descriptions, which can be used to combine cover-management descriptions. The disadvantage of this approach is that the year in the dates must be changed for each individual cover-management description except for the first one. The rotation builder greatly facilitates the manipulation of these dates.

Refer to the RUSLE2 Summary User Manual at http://www.ars.usda.gov/SP2UserFiles/Place/64080530/RUSLE/RUSLE2_User_Manual.exe for information on the mechanics of using the rotation builder.

10.2.10. Relative row grade

Contouring is a support practice used in conjunction with cover-management practices to reduce erosion, especially on cropland. **Ridging** is a comparable practice used on reclaimed mined land and similar lands. The effectiveness of contouring (ridging) depends on ridge height and row grade, two major variables directly related to the cover-management practice. Ridge height is determined by values entered in **operation descriptions** that include a **disturb soil** process (soil disturbing operations). See **Section 13.1.5.4** for information on specifying ridge heights. Thus, one of the most important variables that determines effectiveness of contouring is actually specified in the **cover-management descriptions** rather than in a **support practice description**.

Row grade is the grade along the ridge-furrows created by soil disturbing operations. Contouring is most effective when row grade is perfectly level, but level row grades are seldom obtained in actual field contouring. The effectiveness of contouring decreases as row grade increases.

The recommended row grade input in RUSLE2 is **relative row grade**, which is the ratio of row grade to land steepness along the overland flow path assuming that the soil surface is flat (no ridges to redirect flow) so that runoff flows perpendicular to the topographic contours. Inputting relative row grade according to the guidelines in **Section 14.1.5** provides a more accurate RUSLE2 estimate of how contouring affects erosion than inputting absolute row grade. A major advantage of inputting relative row grade in a cover-management description is that the contouring effectiveness of a cover-management practice can be represented within a cover-management description. A cover-management description using relative row grade can be applied to any overland flow path without considering site-specific topography. This capability is advantageous for applying RUSLE2 in erosion inventories.

See **Section 14.1.5** for information on how to specify relative row grade to represent various conditions.

10.2.11. Management alignment offset

Rotational contour strip cropping is a support practice that uses a rotation cover-management practice having a combination of erodible and dense vegetation conditions. The hillslope is divided into a series of contour strips where the same rotation cover-management practice is applied to each strip. However, the rotation is sequenced differently among the strips along the overland flow path so that dense vegetation strips are alternated with erodible strips. The dense vegetation strips induce deposition to reduce net erosion.

The **management alignment offset** is the years that the rotation cover-management description is offset (delayed) relative the starting date in the cover-management description on the base strip, which is typically the uppermost strip but can be any of the strips. RUSLE2 applies the offset assigned to each strip to achieve the alternating pattern of erodible-dense vegetation strips along the overland flow path.

See **Section 14.2** for detail discussion of rotational contour strip cropping.

11. VEGETATION DATABASE COMPONENT

The **vegetation descriptions** in the **vegetation component** of the RUSLE2 database provide RUSLE2 with the information that it uses to compute how vegetation affects rill-interrill erosion. The RUSLE2 descriptions do not contain all of the information commonly used to describe vegetation. For example, RUSLE2 assumes the same rooting depth for all growth stages, plant types, and soil profiles. Even though rooting depth may affect erosion, the empirical erosion data used to develop RUSLE2 are not adequate for determining how rooting depth affects erosion. The main rooting effect captured in the data is the effect of root biomass.

RUSLE2 does not model vegetation growth. Instead, the RUSLE2 user explicitly describes the vegetation at the site where RUSLE2 is being applied. RUSLE2 does not compute how climate, soil, or management affects production (yield) level, canopy cover, height, or any other vegetative property that affect erosion.

When RUSLE2 users create vegetation, residue, operation, and cover-management descriptions, they should choose input values that ensure that RUSLE2 is using expected values for the variables that affect rill-interrill erosion. These variables include canopy cover, effective fall height, live ground cover, live root biomass, surface residue added by litter fall, standing and surface residue created at harvest, and dead roots created by root sloughing (death) and harvest.

Accounting for all of the biomass produced by the vegetation is not important in RUSLE2. The important biomass is the biomass that affects erosion. For example, the biomass left in the field after a hay harvest is a critical variable, not how much biomass left the field. Yield is only important as it is used to determine values for the biomass variables used in its computations.

RUSLE2 users create vegetation descriptions using RUSLE2 rules and procedures. These descriptions contain values for the variables that RUSLE2 uses to compute erosion. RUSLE2 vegetation descriptions are created with the focus on the information needed by RUSLE2 to compute erosion. The focus is not on accounting for biomass that leaves the site and has economic value.

Thee variables in a RUSLE2 vegetation description are listed in Table 11.1. The RUSLE2 vegetation descriptions also include **tools** listed in Table 11.2 used to develop input values for some of the variables listed in Table 11.2.

Table 11.1. Variables in a RUSLE2 vegetation description

Variable	Comment
Base production (yield) level	Production (yield) level for which a particular vegetation description applies. Value units defined by user.

Production (yield) level definition	User provided information that defines units for production (yield) level.
Amount of biomass at maximum canopy	RUSLE2 uses this information to determine amount of aboveground biomass based on canopy percent over the time represented in the growth chart. Value important in determining the amount of crop residue available at harvest and the amount of senescence (litter) fall. Values are on a dry weight basis.
Retardance	Indicates degree that vegetation retards (slows) runoff to affect critical slope length and transport capacity.
Residue	Name for residue description that applies to this vegetation description.
Relative moisture depletion rate	**Used only for Req applications.** Describes the degree that the vegetation extracts moistures during growth that affects erosion after the vegetation.
Growth chart involves the following variables	
Age (days)	Points through time used to describe temporal variation of vegetation. Starts at zero. RUSLE2 references day zero to the calendar date of the operation containing the begin growth process that tells RUSLE2 to begin using this vegetation description.
Root biomass	Mass (dry weight basis) of roots in upper 4 inch (100 mm) of soil.
Canopy cover	Portion of soil surface covered by canopy that intercept raindrops falling vertically.
Fall height	Effective height from which water drops fall where canopy has intercepted rainfall.
Live surface cover	Portion of the soil surface covered by live plant parts that touch the soil surface and affect erosion.

Table 11.2. Tools used to input values in vegetation description.

Tool	Comment
Develop growth chart for a production (yield) level other than base level	Used to create a growth chart for a new production (yield) level that can be used in a vegetation description.
Estimate fall height	A graphical tool that estimates fall height values based on heights to the top and bottom of canopy and a graphical description of canopy.
Develops the relationship between aboveground biomass and production (yield) level	User inputs aboveground biomass values at two yield values so that RUSLE2 can develop a relationship between aboveground biomass and production (yield) level.
Develops the relationship for senescence	User inputs canopy values that RUSLE2 uses to develop a relationship between canopy cover and aboveground biomass that is used to compute the mass of plant material

	that falls to the soil during senescence.
Develops a relationship between retardance and production (yield) level	User inputs retardance values at two production (yield) levels that RUSLE2 uses to determine a relationship for retardance as a function of production (yield) level.
Develops a growth chart for long term vegetation	Used to develop temporal values for perennial and permanent vegetation on range, pasture, reclaimed mine, wastes disposal, and similar lands.

11.1. Variables in a RUSLE2 vegetation description

11.1.1. Base production (yield) level

The RUSLE2 vegetation variables are a function of production (yield) level. Therefore, each **vegetation description** in the **vegetation component** of the RUSLE2 database is for a particular **production (yield) level**. When RUSLE2 is applied to a particular site, the vegetation's production (yield) level must match site-specific conditions. The vegetation and its production (yield) level must be consistent with the location's climate, irrigation, soil, fertility, pest control, and other management conditions. Because RUSLE2 is not a plant growth model, it does not adjust vegetation variables to match site-specific conditions. Production (yield) level is a user site-specific input that reflects long-term production levels rather than production in any specific year. Although RUSLE2 can indicate how erosion varies between dry and wet years, it is not intended for such applications.

The RUSLE2 production (yield) level input can be handled in one of two ways. One way is to create a vegetation description for a set of production (yield) levels where the user selects a vegetation description for the production (yield) level that is appropriate for the site. The second way is for the user to select a vegetation description at a base production (yield) level and input the site production (yield) level value. RUSLE2 will then adjust values in the base vegetation description to ones appropriate for the input production (yield) level value.

RUSLE2 can adjust to a production (yield) level value that is higher than the production (yield) level of the base vegetation description. However, the maximum canopy cover in the base vegetation must be less than 100 percent for RUSLE2 to adjust to a production (yield) level lower than the base production (yield) level. This restriction is related to the RUSLE2 equations used to adjust for production (yield) level. The user can alternately create a new vegetation description for a new production (yield) level if the RUSLE2 adjustments are not satisfactory.

The units for the production (yield) level are user defined (see **Section 11.1.2)** and can be almost any units that a user prefers.

Yield is important in RUSLE2 only to indicate the yield to which a particular vegetation description applies or as a variable that can be used to adjust values in a given vegetation description to the desired yield. The biomass associated with a harvestable part of vegetation and its yield are important only if that biomass in the harvestable part directly affects erosion and is represented by a RUSLE2 vegetation variables. For example, accounting for the biomass in the harvestable corn grain is not important. Accounting for the biomass in a harvestable hay crop is only important until the hay is harvested. The biomass in watermelons before harvest is not important, but the ground cover provided by watermelons may be important. The biomass left behind in the field after harvest is important, not the biomass taken from the field. RUSLE2 procedures are used to create a field description of the variables that affect erosion, not to account for vegetation in its entirety.

11.1.2. User definition of production (yield) level units

Almost any user preferred units can be created for inputting values for **production (yield) level** in RUSLE2. These units can be on any basis including dry or wet, mass (weight), volume, standard moisture such as 14 percent for corn grain, number such as bales of hay or straw, or even an original user created basis. The production (yield) level input must be on a per unit area basis. These units should be common usage for intended RUSLE2 users, convenient, and a reliable indicator of how values for RUSLE2 vegetation variables change with production (yield) level.

Two inputs are used to define the production (yield) level units. The first input is the displayed yield unit, typically a common unit such as bushels per acre (liters/ha), lbs per acre (kg/ha), tons per acre, or hundred weight per acre.

The second input is a **conversion factor.** RUSLE2 multiplies the user production (yield) level input value by this conversion factor to convert the input value, which may be a mass, volume, or number per unit area value, to a mass value. Converting the production (yield) level input to a mass value facilitates using rules of thumb for estimating crop residue at harvest. The production (yield) level value expressed as a mass is multiplied by a residue:yield ratio to estimate residue at harvest.

To illustrate, the conversion factor for corn is 56 lbs/bushel at the standard 14 percent moisture content. Multiplying a 100 bu/acre corn yield by this conversion factor gives a corn grain yield of 5600 lbs/acre in terms of mass. Multiplying this mass value by the 1:1 to the residue:yield rule of thumb gives an estimate of 5600 lbs/acre of corn residue at harvest. A linear equation, discussed in **Section 9.2.1.6** is used in RUSLE2 to estimate residue at harvest rather than a simple residue:yield ratio because the residue:yield ratio varies with yield. The input data needed for this equation are discussed in **Section**

11.2.1.

The conversion factor value for converting production (yield) level inputs to a mass value is plant specific. The conversion factor for corn is 56 lbs/bushel while it is 32 lbs/bushel for oats. The input units for some plants, such as hay, are already a mass value. The conversion factor for those plants can be one (1) or it may be different from 1 if a conversion from a wet to dry basis is involved. A conversion of dry basis can either be made in this conversion factor on in the computation of aboveground biomass as a function of production (yield) level.

RUSLE2 uses the production (yield) level input to compute aboveground biomass values. This computation involves two steps. One is to multiply the input production (yield) level value by a conversion factor to obtain a mass value and the second is to convert the production (yield) level value to aboveground plant biomass values on a dry basis. The user arranges these two steps as desired to end up with the appropriate aboveground biomass values. For example, a wet to dry basis conversion can be made in the first step or the second step. The input and conversion values must be consistent so that the final result is a mass on a dry basis.

11.1.3. Live Aboveground biomass at maximum canopy cover

RUSLE2 computes daily values for live aboveground biomass as a function of daily canopy cover. Coefficient values in the equation for this computation value are determined from user input values for **live aboveground biomass at maximum canopy cover** and the value for **live above ground biomass at minimum canopy cover.**

11.1.3.1. Basic principles

The input values entered in a **vegetation description** are selected to provide RUSLE2 with the values that it needs to compute erosion. Consequently, not all of a plant's aboveground biomass is necessarily included in the input for **aboveground biomass at maximum canopy cover**. Only that plant material that becomes litter fall or that will become standing, surface, or incorporated residue is included in the input. For example, harvestable grain is not included in this input because the grain is removed from the field without affecting erosion. If a harvestable product is left in the field to provide standing or surface (flat) residue or is incorporated into the soil to provide soil biomass, it should be included in the aboveground biomass input.

RUSLE2 uses the input for aboveground biomass at maximum canopy cover to estimate daily live aboveground biomass during the time period represented by a vegetation description. Three stages of vegetation growth are represented in RUSLE2. These stages are: (1) new growth, (2) senescence/regrowth, and (3) stem growth, which are illustrated

in Figure 11.1.

The general equation for all three stages is:

$$B = B_0 + \alpha(C - C_0)^{1.5} \quad [11.1]$$

where: B = live aboveground biomass (mass/area), B_0 = live aboveground biomass at the canopy cover C_0, C = canopy cover (percent), and α = a coefficient. Figure 11.1 represents these growth stages for a plant community that reaches is already or reaches maturity in a single growth cycle. RUSLE2 determines values for B_0, C_0, and α from user input values.

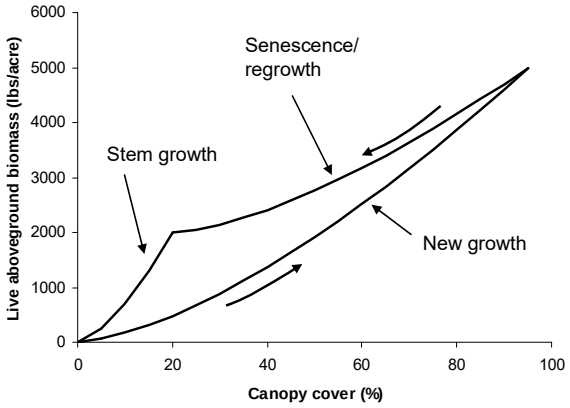

Figure 11.1. Canopy cover-live aboveground biomass relationship for a plant community that reaches maturity in a single growth cycle.

Equation 11.1 works best where maximum canopy cover is less than 100 percent. It works less well for conditions where aboveground biomass increases significantly after canopy cover reaches 100 percent. Equation 11.1 was chosen for its simplicity, robustness, and ability to be calibrated with minimal user inputs after an evaluation of alternate equation forms, including exponential forms.

A plant community well represented by Figure 11.1 is soybeans. The new growth period represents the relation between canopy cover and live aboveground biomass from plant emergence after seeding until full maturity and senescence begins. Equation 11.1 for the new growth period is:

$$B_n = \alpha_n C_n^{1.5} \quad [11.2]$$

where: B_n = live aboveground biomass and C_n = canopy cover during the new growth stage. RUSLE2 computes a value for α_n using:

$$\alpha_n = B_{mx} / C_{mx}^{1.5} \quad [11.3]$$

where: B_{mx} = the user entered value for live aboveground biomass at maximum canopy cover C_{mx}.

Senescence occurs during the period of decreasing canopy after the plant community has reached maturity. Equation 11.1 during the senescence stage is:

$$B_r = B_{mn} + \alpha_r (C_r - C_{mn})^{1.5} \quad [11.4]$$

where: B_r = live aboveground biomass and C_r = canopy cover during the senescence period and B_{mn} = the user entered value for live aboveground biomass at minimum canopy cover C_{mn}.

RUSLE2 computes a value for α_r using:

$$\alpha_r = (B_{mx} - B_{mn}) / (C_{mx} - C_{mn})^{1.5} \quad [11.5]$$

In general, RUSLE2 assumes that any decrease in canopy cover within a vegetation description represents senescence, except for special plants like corn. Leaves droop on those plants that reduce canopy cover but do not fall to the soil surface. A user input tells RUSLE2 to not apply equation 11.4 to those plant communities.

The stem growth stage represents conditions when canopy cover is less than the minimum canopy cover that results after senescence is completed. This growth stage is important, for example, when a plant community is mowed or hay is harvested, which leaves a canopy cover that is less than the minimum canopy cover after full senescence. Equation 11.1 for the stem growth stage is:

$$B_s = \alpha_s C_s^{1.5} \quad [11.6]$$

where: B_s = the live aboveground biomass and C_s = the canopy cover during the stem growth stage. RUSLE2 computes a value for the coefficient α_s using:

$$\alpha_s = B_{mn} / C_{mn}^{1.5} \quad [11.7]$$

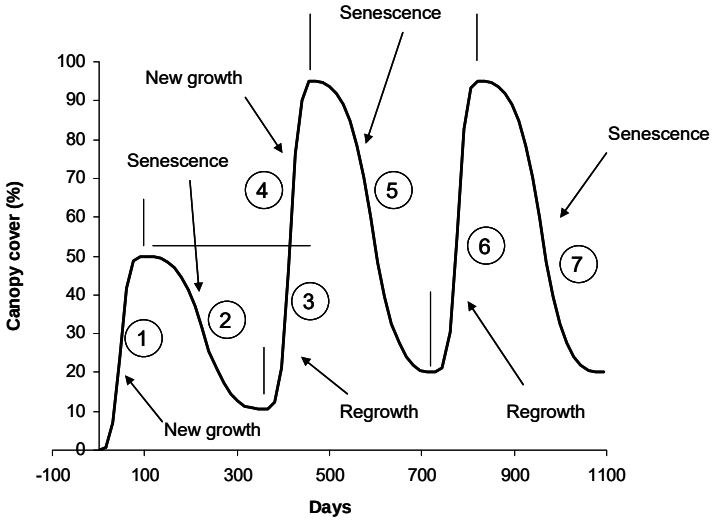

Figure 11.2. Canopy cover for a plant community that requires two cycles to reach maturity

Figure 11.2 illustrates canopy cover for a plant community that takes two growth cycles to reach maturity. The third growth cycle in Figure 11.2 represents full maturity. The plant community can be described in RUSLE2 by

using the **long-term vegetation tool** or by creating a vegetation description for each growth cycle. The principles that are used in the long-term vegetation tool should be used in creating individual vegetation descriptions for plant communities like those represented in Figure 11.2.

Period 1 is new growth that begins on day zero and continues to the date of the maximum canopy cover in the first growth cycle. Period 2 is senescence that begins at maximum canopy cover in the first growth cycle and continues until minimum canopy cover at the end of the first growth cycle. Period 3 is regrowth that begins at the minimum canopy cover at the beginning of the second growth cycle and ends on the date that the canopy cover in the second growth cycle reaches the maximum canopy cover in the first growth cycle. Period 4 is new growth that begins at the date that canopy cover in the second growth cycle reaches maximum canopy cover in the first growth cycle and continues until maximum canopy cover in the second growth cycle. Period 5 is senescence that begins at maximum canopy cover in the second growth cycle and continues until minimum canopy cover at the end of the second growth cycle. Period 6 is regrowth that begins at minimum canopy cover at the beginning of the third growth cycle, which is the first full mature growth cycle. The regrowth period 6 continue until the maximum canopy cover of the third growth cycle. Period 7 is senescence that begins at maximum canopy cover in the third growth cycle and continues until the minimum canopy cover at the end of the third growth cycle. A growth cycle that represents full maturity does not contain any new growth periods.

Figure 11.3 shows the canopy cover-live aboveground biomass relationships for the plant community illustrated in Figure 11.2. Period 1 represents the new growth period in the first growth cycle. Period 2 represents senescence in the first growth cycle. Period 3 represents regrowth in the second growth cycle. Plant regrowth stage is assumed to retrace canopy loss during the previous senescence. Consequently, the same equation is used for the regrowth stage that follows the immediately previous senescence stage. That is, the same equation is used to describe both periods 2 and 3. Another equation is used to describe both periods 5 and 6.

Once canopy cover reaches the maximum canopy cover in the previous growth cycle, plant growth shifts from regrowth to new growth. Plant growth “rejoins” the previous new growth. The same equation is used for new growth in all growth cycles. Plant communities that have three or more growth cycles to reach maturity are represented using these same principles. These principles are repeatedly applied to each growth cycle until maturity is reached. New growth stages are not involved in the growth cycle that represents plant maturity.

The user inputs in the RUSLE2 **long-term vegetation tool** are **live above ground biomass for maximum canopy cover at maturity** and **live above ground biomass at minimum canopy cover at maturity**. RUSLE2 uses these inputs and the canopy cover

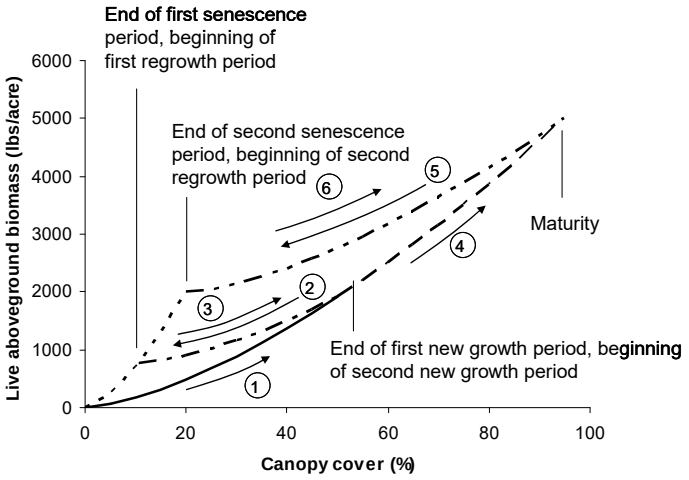

Figure 11.3. Canopy cover-live aboveground biomass relationship for a plant community that reaches maturity in two growth cycles.

values entered by the user to determine similar values for local maxima and minima canopy covers for growth cycles before plant maturity. A RUSLE2 assumption is that canopy cover for the local minimum canopy cover at the end of a growth cycle equals the product of minimum canopy cover at maturity and the ratio of local maximum canopy cover for the growth cycle to the maximum canopy cover at maturity. Another RUSLE2 assumption is that the live aboveground biomass, minimum canopy cover data point for each growth cycle must lay on the stem growth curve given by equations 11.6 and 11.7.

The other RUSLE2 option for describing plant communities having multiple growth cycles is to create a vegetation description for each growth cycle. The assumptions used in the RUSLE2 **long-term vegetation tool** should be used in creating these vegetation descriptions to ensure continuity between the individual vegetation descriptions.

Maintaining continuity between vegetation descriptions in a cover-management description is very important.

Equation 11.1 allows RUSLE2 to use the same **vegetation description** in different **cover-management descriptions** where the vegetation is killed on different dates.[94] For example, a wheat cover crop used to provide winter erosion control is killed on different spring dates depending on the main crop (e.g., corn versus cotton) and early or late planting. RUSLE2 needs an aboveground biomass estimate on the date that the wheat crop is killed and the main crop is planted. RUSLE2 estimates a value for that biomass by substituting the canopy cover value in the vegetation description on the date that the

[94] RUSLE1 differs from RUSLE2 regarding the input value for biomass when the vegetation is killed. The RUSLE1 vegetation descriptions contain the values for residue mass at the time that the vegetation is killed. Separate RUSLE1 vegetation descriptions are required for each date that the vegetation is killed. Also, two separate RUSLE1 vegetation descriptions are required for silage corn and grain corn. In RUSLE2, the same vegetation description can be used for both silage and grain corn, and the same vegetation description can be used when the vegetation is killed on different dates.

wheat is killed into equation 11.1. Without equation 11.1, RUSLE2 would require a vegetation description for each date that the wheat is killed in alternative cover-management descriptions.

RUSLE2 can also use vegetation descriptions that end on the date that the vegetation is killed where the input for aboveground biomass is for the maximum canopy cover on that day. This input technique can be used to ensure that RUSLE2 uses a particular value for aboveground biomass on the date that the vegetation is killed rather than the one computed with equation 11.1. This procedure can be used when equation 11.1 is considered to be a poor representation of the canopy cover-live aboveground biomass.

Perennial vegetation including hay and pasture crops and plant communities on rangelands, closed landfills, and other undisturbed areas exhibit a simultaneous birth and death of live aboveground biomass during new and regrowth periods. RUSLE2 computes a daily death amount of aboveground biomass as a fraction, approximately 0.01, of the live aboveground biomass on that day (see **Section 11.2.6**). This daily biomass amount is added to the surface litter (residue) biomass on that day.

RUSLE2 also considers a daily "mechanical" loss of live aboveground biomass that is added to surface litter. This daily addition is a fraction of the daily live aboveground biomass. This computation represents the loss of live aboveground biomass by mechanical processes such as animal traffic or by vehicular traffic (see **Section 11.2.6**).

11.1.3.2. Consistency between inputs for aboveground biomass at maximum canopy cover with processes in operation descriptions

RUSLE2 inputs for cover-management, vegetation, residue, and operation are descriptions based specifically on RUSLE2 rules and procedures. A particular field condition can often be described in multiple ways. However, the individual vegetation, residue, and operation descriptions used to create a cover-management description must be consistent with each other. A key element in this consistency is ensuring that the input value for aboveground biomass at maximum canopy cover in the vegetation description is consistent with the operation descriptions.

The value entered in a *vegetation description* for *aboveground biomass at maximum canopy cover* must be consistent with the *processes* in the *operation descriptions* in the *cover-management description* to ensure that RUSLE2 has the proper biomass values for standing residue, flat residue, and soil biomass for its computations.

Four examples are used to illustrate selecting values for aboveground biomass that are consistent with operation descriptions.

Example 1. Corn

Corn is grown for grain or silage. When corn is grown for harvestable grain, all of the aboveground biomass, except for the grain, is left in the field as standing and flat residue. When corn is grown for silage, almost all of the aboveground biomass is removed from the field as a harvestable product. Only a small amount of plant material is left in the field as standing and flat residue.

Table 11.3 lists **processes** that would be used in a **harvest operation description** for alternative input values for aboveground biomass at maximum canopy cover. Alternative 1 for corn grain is where the input value for aboveground biomass at maximum canopy cover is the amount of biomass that will be left in the field after the actual harvest removes the harvestable grain from the field. Alternative 2 is where the input value for aboveground biomass includes the entire aboveground plant material (i.e., fodder and grain). The harvest operation description for this vegetation description must include either a **remove live biomass process** before the **kill process** or a **remover residue/cover process** after the **kill process** to remove the grain. These processes are not required in Alternative 1 because the biomass for the grain is not included in the accounting. If the grain is not removed in Alternative 2, the amount of residue assumed by RUSLE2 after the harvest will be too high. Alternative 1 is the recommended procedure for corn grain.

The RUSLE2 objective is not to fully account for all of the biomass, but to describe only the biomass that affects erosion.

The alternatives for corn silage are similar to those for corn grain. Alternative 1 is where the aboveground biomass includes only the fodder without the grain, which is the same vegetation description as Alternative 1 for the corn grain. The harvest operation for this alternative includes a remove live biomass process before the kill process. Just as in Alternative 2 for the corn grain, a remove residue/cover process can be used after a kill process. In any case, plant material must be removed so that RUSLE2 has the proper value for the residue left in the field after the actual field operation. Alternative 2 for the corn silage is where the input value for aboveground biomass value at maximum canopy cover is the amount of residue that exists in the field after the actual field harvest operation.

Table 11.3. Harvest operation descriptions for corn grain and corn silage production			
Grain		Silage	
Alternative 1		Alternative 1	
Process	Comment	Process	Comment
Alternative 1 Aboveground biomass at max canopy does not include grain		Alternative 1 Aboveground biomass at max canopy includes all of the aboveground plant material except the grain	
Kill vegetation	Converts live aboveground biomass to standing residue, amount of standing residue directly related to input for aboveground biomass at maximum canopy	Remove live biomass	Removes most of live aboveground biomass from RUSLE2's accounting of aboveground biomass but leaves behind a small portion as flat residue
Flatten standing residue	Converts a portion of the standing residue to flat residue	Kill vegetation	Converts the remaining live aboveground biomass to standing residue
		Flatten standing residue	Converts a portion of the standing residue to flat residue
Alternative 2 Aboveground biomass at max canopy includes grain		Alternative 2 Aboveground biomass at max canopy is only the residue that will be left after the harvest operation	
Remove live biomass	This process removes the grain and leave the remaining as material that will become residue	Kill vegetation	Converts live aboveground biomass to standing residue
Kill vegetation	Converts live aboveground biomass to standing residue	Flatten standing residue	Flatten the portion of the standing residue that is to be left as flat residue
Flatten standing residue	Flatten the portion of the standing residue that is to be left as flat residue		

Example 2. Harvesting hay and mowing permanent vegetation.
Forage crops such as alfalfa regrow after each hay harvest. Similarly, permanent vegetation such as that on a landfill regrows after it is mowed. The objective is to provide RUSLE2 with inputs so that it can determine the amount of surface residue added by a hay harvest or mowing operation. Two alternatives, illustrated in Table 11.4, can be used for the hay harvest/mowing operation descriptions. In Alternative 1, the input value for the aboveground biomass at maximum canopy cover includes all of the aboveground plant material. RUSLE2 uses equation 11.1 to compute the aboveground biomass on each day, including the date of the hay harvest/mowing. Given a particular aboveground biomass on the date of the hay harvest or mowing, what is the amount of

this biomass that is added to the surface residue? The two processes of **remove live biomass process** and a **begin growth process** are used in both the hay harvest and mowing operation descriptions. The begin growth process identifies the vegetation description that RUSLE2 is to use immediately after the hay harvest/mowing operation. In addition to the input for aboveground biomass at maximum canopy cover, the other key inputs are the **portion of the aboveground biomass that is affected** and the **portion of the affect biomass that is left as surface residue** for the remove live biomass process.

To illustrate, assume that the aboveground biomass on the date of the hay harvest is 3600 lbs/acre. The input for the portion affected in the remove live biomass process in the hay harvest operation is 98 percent, which means that 3528 lbs/acre of biomass is affected. The input for the portion of the affected biomass that is left is 5 percent, which means that 176 lbs/acre is added to surface residue as a result of the hay harvest operation.

The inputs used to describe mowing a short grass permanent vegetation are similar to those used to describe the hay harvest. Assume that the amount of aboveground biomass on the date of the mowing is also 3600 lbs/acre. The input value is assumed to be 50 percent for the portion of the aboveground biomass affected by the mowing, which is 1800 lbs/acre. The input value for the portion of the affected biomass that is left as added surface residue is 100 percent, which means that 1800 lbs/acre is added to the surface residue as a result of the mowing.

The input values for these operation descriptions are both machine and vegetation specific. For example, assume that the permanent vegetation is a tall grass at the same production 3600 lbs/acre level as the short grass. Assume that 75 percent of the aboveground biomass is affected by the mowing with the tall grass in comparison with the short grass because of differences in vegetation characteristics even though the mower is operated at the same height with both vegetations. The amount of affected aboveground biomass is 2700 lbs/acre. The portion of the affected biomass that is added to the surface residue is still 100 percent, which means that 2700 lbs/acre of biomass is added to the surface residue for the tall grass mowed at the same height as the short grass where aboveground biomass was the same for both grasses. The portion of the aboveground biomass that is affected depends on the vegetation, the machine, and its cutting height.

These inputs, which can be cumbersome and confusing, must be handled very carefully according the RUSLE2 rules and procedures to avoid errors. The intent in RUSLE2 is not to mimic machines, their operations, and settings, but to provide a way to enter information that RUSLE2 needs to determine the surface residue cover and the vegetation conditions after the operation. The operation and vegetation descriptions must be consistent and considered together to ensure that RUSLE2 has the desired values for

its computations.[95]

Alternative 2 applies when RUSLE2 is to use a user-entered value for the surface residue added by a hay harvest or mowing operation. The input value for aboveground biomass at maximum canopy is only important in determining the litter fall and the aboveground biomass on the date that the vegetation is killed. In contrast to Alternative 1, it plays no role in determining the surface residue added by the hay harvest/mowing operation. The **processes** in the hay harvest/mowing operation descriptions are **remove live biomass**, **add external residue/cover**, and **begin growth**. The input values for the **remove live biomass process** are 100 percent for the portion of the aboveground biomass affected and 0 percent for the portion of the affected biomass that is left behind as added surface residue. This process removes all of the aboveground biomass on the date of the hay harvest/mowing operation. The **add external residue/cover process** is used to add a specific user entered value for the biomass added to the surface residue by the hay harvest/mowing operation. The inputs for the **add external residue process** are a residue description for the material that is to be added to the soil surface by the operation and the amount of the material that is added. In the mowing example, the value entered for amount of external residue added might be 2000 lbs/acre.

An advantage of this approach is that the effect of cutting height can be quickly and easily evaluated by changing the input value for amount of external residue added. A disadvantage of Alternative 2 is that RUSLE2 does not automatically change this input value as production (yield) level changes because the effect of yield can only be accommodated by manually entering different values for the amount of external residue added. The value for surface residue added that RUSLE2 computes in Alternative 1 does vary with yield as expected.

Table 11.4. Alternative descriptions for hay harvest/mowing operations.

Alternative 1. Operation description uses aboveground biomass to estimate surface residue added by operation		Alternative 2. Operation description assigns surface residue added by a direct input	
Process	Comment	Process	Comment
Remove live biomass	Removes a portion of the live aboveground biomass at the time of harvest and leaves a part of it in the field as surface residue added	Remove live biomass	Removes all of the live aboveground biomass from the system

[95] RUSLE2 was not designed to use absolute cutting height for hay harvest and mowing operations so that user-entered information is not required on the vertical biomass distribution for each vegetation description and how that changes through time. Such inputs for describing vegetation are not readily available. A major advantage of the RUSLE2 approach, which may seem crude, is that practically any situation can be represented with simple, easy-to-understand inputs.

Begin growth	Identifies the vegetation description that RUSLE2 to use after the hay harvest/mowing operation	Add other cover	Adds external residue in a user entered amount to represent the surface residue added by the operation
		Begin growth	Identifies the vegetation description that RUSLE2 is to use after the hay harvest/mowing operation
Note: A kill vegetation process was not used. A kill vegetation process transfers the live root biomass into the dead root biomass pool, which does not occur in a hay harvest or mowing operation for vegetation that regrows following the operation.			

Example 3. Cover crop.
Vegetation such as rye can be used as a cover crop to reduce erosion over the winter after harvest of the main crop until it is replanted in the spring. A **vegetation description** for a cover crop can be created in either of two ways.

The preferred approach is to develop a vegetation description that extends beyond the last possible date when the cover crop would be killed. The input value for above-ground biomass at maximum canopy cover is for the day in the vegetation description having the maximum canopy cover. This vegetation description can be used in **cover-management descriptions** where the date of the **operation description** that kills the cover crop can vary from day zero until the last day in the vegetation description. RUSLE2 uses equation 11.1 to estimate aboveground biomass on the date on the cover crop killing operation description.

Another approach is to describe the cover crop from its seeding date to the date that the cover crop is killed. The input value for the aboveground biomass at maximum canopy is the amount of aboveground biomass on the date that the cover crop is killed, assuming that the cover crop has not reached maturity and canopy cover is still increasing. The ending date of this vegetation description should coincide with or be within a few days of the date for the cover crop killing operation description. A disadvantage of this approach is that getting these dates to coincide is cumbersome and inconvenient. Another disadvantage is that a separate vegetation description is needed for each date that the cover crop might be killed, which varies according to main vegetation (e.g., cotton is planted later than corn) and early or late planting. The advantage of this approach is that the user can control the amount of biomass at the time that the vegetation is killed instead of letting RUSLE2 use equation 11.1 to estimate aboveground biomass at the date that the cover crop is killed. If the cover crop killing date occurs before the last date in the vegetation description, RUSLE2 will still use equation 11. 1 or 11.2 to estimate aboveground biomass on the date that the cover crop is killed. A few days difference in the killing date and the last date in the vegetation description has only a minimal effect on the results. If the date of the cover crop killing operation occurs after the last day in

the vegetation description, RUSLE2 assumes the value on the last day of the vegetation description for all later days. Make a careful check to avoid this condition.

Example 4. Green beans.
Green beans can be cropped in several ways. Mechanically harvested green beans often involve a single harvest that kills the green beans. A vegetation description for green beans can be developed specifically for this cover-management description where the last date in the vegetation description corresponds with the mechanical harvest date. The input value for the above-ground biomass at maximum canopy cover would be for the harvest date, assuming that plant maturity and maximum canopy cover are not reached before the harvest.

A second way of cropping green beans is to hand pick them multiple times before the green beans are mechanically killed by tillage or chemically killed to plant the vegetable crop that follows the green beans. A vegetation description for the green beans is constructed that ends on the date of the operation description that kills the green beans. The input for above-ground biomass at maximum canopy cover would differ in this vegetation description from corresponding input in the vegetation description for the mechanically harvest green beans because the green beans would be killed later than with the single mechanical harvest green beans.

A third way that green beans can be grown is to hand pick the green beans multiple times and let the green beans grow until they die naturally. A vegetation description for this cropping method describes the green beans from seeding until the date that the green beans are assumed to die naturally. An operation description with a kill vegetation process must be included in the cover-management description on the date that the green beans are assumed to die naturally. This operation is needed to convert the live aboveground biomass and live roots to standing residue and dead root biomass.

The input for aboveground biomass at the natural maximum canopy cover is the aboveground biomass amount just before senescence begins. This vegetation description can also be used for the other two types of green bean production methods. This vegetation description has the advantage of not requiring a vegetation description for each production method and also has the advantage of not requiring the cumbersome process of matching the last date in the vegetation description with the date in the cover-management description for the operation description that kills the green beans. The advantage of ending the vegetation description on the date that the green beans are killed is that the user can control the value that RUSLE2 uses for aboveground biomass on the date that the green beans are killed rather than relying on RUSLE2 to use equation 11.1 to estimate the live aboveground biomass value on that date.

11.1.3.3. Residue:yield ratio

The value for aboveground biomass at maximum canopy cover can be entered in one of two ways. The recommended way is to directly enter a value for biomass in terms of dry biomass per unit area. The alternative is to enter a value for residue:yield ratio. RUSLE2 multiplies the value for this ratio by the input yield value and the conversion factor that computes a yield mass (see **Section 11.1.2**) to compute a value for aboveground biomass at maximum canopy cover. See Section **11.2.1** for a discussion on how RUSLE2 adjusts aboveground biomass as a function of production (yield) level.

Make sure that when the residue:yield ratio, yield, and conversion factor are all combined, the resulting aboveground biomass value is on a dry basis.

Residue:yield ratios are primarily rules of thumb, which are useful if values for aboveground biomass are not available. Residue:yield ratio values are a function of yield. Assuming a constant residue:yield ratio value over a working range is acceptable for several crops, but residue yield ratio values can be significantly larger at low yield than at high yields.

The residue:yield ratio values can vary by crop variety. Some of the common rule of thumb residue:yield ratio values were developed 40 or more years ago. Make sure that those values, although widely used, apply in your situation.

Be slow in having different residue:yield ratios in an attempt to compute how crop variety affects erosion. RUSLE2 is not sufficiently accurate for basing conservation planning on such differences. The main intent of RUSLE2 is to represent how main plant types, such as wheat, affect erosion in relation to another crop type, such as corn. The same is true for capturing the differences between plant community types for permanent vegetation on pasture, range, reclaimed mine, and landfills.

11.1.3.4. Selecting input value for aboveground biomass at maximum canopy cover

The input for aboveground biomass at maximum canopy is one of the most important inputs in RUSLE2 because this value determines the amount of litter fall and crop residue that ends up on the soil surface as ground cover to affect erosion. In most situations involving disturbed land, ground cover has more effect on erosion than any other variable. The input value for this aboveground biomass should be chosen very carefully and must be consistent with the values in the **RUSLE2 core database**. The values shown in the RUSLE2 core database were used to calibrate RUSLE2. If a user assumes different values for the RUSLE2 core database conditions than were used by the RUSLE2 developers in their calibration of RUSLE2, then RUSLE2 will give erroneous results.

Consistency between inputs and the RUSLE2 core database must be followed.

Scientific literature is a source of data for values for aboveground biomass at maximum canopy cover. These data can be quite variable. Assemble as much data as possible and review the data as a whole. Select input values that represent the data as a whole rather than trying to capture the effects of individual studies. Some or even most of the differences between individual studies can be unexplained by variability that occurs between particular years and locations.

11.1.4. Vegetative retardance

Vegetative retardance refers to the degree that vegetation slows runoff to reduce its erosivity and transport capacity. Vegetative retardance depends on type, growth stage, and density of the vegetation. For example, the retardance of dense, sod forming grasses is much greater than that of vines in a vineyard. The retardance of sod forming grasses is greater than that for bunch grasses. The retardance of a sod forming grass is very low if its production (yield) level is very low. Retardance increases during the growing season as plant material develops. Plant material must be in contact with the soil surface and slow the runoff to affect vegetation retardance. Additional factors such as soil surface roughness, surface residue cover, and live ground cover are considered by RUSLE2 to determine the overall retardance as it varies through time in a RUSLE2 computation.

Eight retardance classes ranging from none to the greatest, which is for a dense sod forming grass, are used to represent the vegetation retardance at maximum canopy cover at the base yield. RUSLE2 adjusts the class selected to represent the vegetation description as canopy cover changes during the time and as yield varies from the base yield represented by the vegetation description.

The input for retardance class for a **vegetation description** is discussed in **Section 11.2.5**. The retardance class that RUSLE2 assigns to the vegetation description at the input yield value is displayed in the **cover-management description** window of the RUSLE2 computer program for certain **user template** RUSLE2 program configurations. The purpose for giving the user access to vegetation retardance class during a RUSLE2 computation is to allow the user to manually override RUSLE2's selection of the retardance class for the input yield, if desired.

11.1.5. Residue

As described in **Section 11.1.3,** aboveground plant material can reach the soil surface as litter fall or by mechanical operations such as mowing and harvesting. RUSLE2 uses data on plant material properties to compute how this material, referred to as **residue** in RUSLE2 terminology, affects erosion. These properties include how well the material

conforms to the soil surface, resists breaking into smaller pieces when the soil surface is mechanically disturbed (fragility), the portion of the soil surface cover by a given mass of material, and the rate that the material decomposes under a standard environmental condition.

Data for these properties are input for **residue descriptions** contained in the **residue component** in the RUSLE2 database. A residue description is selected and assigned to each **vegetation description** depending on how a vegetation description is used in a **cover-management description**. Plant litter (residue) is typically composed of several plant components including leaves, seed pods, chaff, and fine and coarse stems that vary greatly in their properties. A residue description represents a composite of all plant components present in the residue at the time that residue description is being used in RUSLE2. Assigning a residue description to a vegetation description is almost always a compromise. For example, immediately after harvest, the leaves in soybean residue provide a high degree of soil cover, but these leaves decompose very rapidly so that the residue becomes composed primarily of stems. The stems cover a far smaller area than do the leaves for a given mass, and the stems decompose far more slowly than do the leaves. Thus, the net properties of the soybean residue change greatly through time as the relative mass of the residue components change through time.

RUSLE2 does not consider how the properties of a residue description change through time.

Select a residue description to obtain the best overall results, which is usually an estimate of average erosion rather than erosion for a particular period. Values for residue and other variables in the RUSLE2 core database were chosen to give good estimates for average annual erosion.

However, cases arise where a different residue description should be selected for a particular plant community, such as wheat, depending on how the vegetation description is used in a cover-management description. Mature wheat straw decomposes much more slowly than does wheat residue when the wheat is killed in its early growth stage. Thus, two wheat residue descriptions should be developed, one for wheat grown to maturity where the grain is harvested and wheat straw remains and one for wheat grown as a cover crop that is killed before the wheat reaches maturity. Thus, the residue assigned to wheat depends on whether the wheat vegetation description is used in a cover-management description for grain or in a cover-management description where the wheat is used as a cover crop that is killed before reaching maturity.

The same residue description can be used for multiple vegetation descriptions. For example, several vegetation descriptions can be developed for corn based on days to maturity. The same residue description can be used for all of these corn descriptions.

11.1.6. Relative moisture depletion

A value for the variable **relative moisture depletion** is entered in vegetative descriptions used when RUSLE2 is applied to Req zones (see **Section 6.9**). This variable describes how a previous crops depletes soil moisture, which reduces runoff and erosion in subsequent periods in a crop rotation.[96] Recommended values for relative moisture depletion are given in Table 11.5.

A value of 0.00 for relative moisture depletion means that the vegetation (crop) does not remove sufficient water to significantly affect erosion. In comparison, a crop such as winter wheat is assigned the maximum value of 1.00. See **Section 9.2.7** for discussion on how this variable affects erosion computed by RUSLE2.

Table 11.5. Recommended value for relative moisture depletion for vegetation description used in applying RUSLE2 to Req zones. (Source: AH703)

Crop	Relative moisture depletion input value
Winter wheat and other deep rooted crops	1.00
Spring wheat and barley	0.75
Spring peas and lentils	0.67
Shallow-rooted crops	0.50
Summer fallow	0.00

11.1.7. Growth chart variables

A **vegetation description** includes arrays of input values for the **temporal variables** of age (time), live root biomass, canopy cover, effective fall height, and live surface (ground) cover. The collection of these values is referred to as the **growth chart** for a vegetation description. A value for each variable is entered for each **time** in the growth chart. Each entered value is the value for a variable on that day, not an average or representative value over a time interval.

RUSLE2 uses a descriptive procedure to input values for vegetation variables that affect erosion rather than using a plant model to compute values for those variables. The focus in creating and using vegetation descriptions is to describe, not to model. This RUSLE2 feature gives RUSLE2 great power and flexibility.

A vegetation description is just that, a description of the vegetation condition over the time represented in the growth chart. This description is for the composite field condition on each day. RUSLE2 can not combine vegetation descriptions from multiple

[96] Contact Donald K. McCool, USDA-Agricultural Research Service, Pullman, WA for additional information.

plant communities into a new vegetation description for a plant community composed of multiple components. That is, a single set of vegetation values are used to describe intercropping, where two or more plant types are growing at the same time, rather than combine values for the component parts. For example, the input values for canopy cover and fall height are the values that you want RUSLE2 to use to represent the composite field condition on each day. See **Section 10.2.3.**

11.1.7.1. Age

Age in days is the time variable used in the growth chart. The first entry in a growth chart is always for **day zero (0),** which represents conditions on the date that this **vegetation description** begins to apply. RUSLE2 references day 0 to the date in the **cover-management description** for the **operation description** with a **begin growth process** that instructs RUSLE2 to begin using this particular vegetation description. A set of time (age) values are chosen to describe the temporal variables in the vegetation description. RUSLE2 assumes that variables are linear between each time value. Only a time at the beginning and a time at the end of a period are entered if values for all of the temporal variables do not change over the time period. Similarly, only times at the beginning and end of a period are entered if the temporal variables vary linearly over the time period. Additionally, closely spaced times are used to represent periods when one or more of the temporal variables change non-linearly. A sensitivity analysis (see **Section 17.3**) may be needed to determine the spacing of the times in these non-linear periods.

The growth chart for a RUSLE2 vegetation description often uses days on a 10-day or 15-day internal for convenience. [97]

The days in the growth chart for a vegetation description need not be on a fixed interval.

Day zero in a vegetation description is not necessarily the date that the vegetation is seeded. The values on day 0 describe conditions that exist on the day that RUSLE2 begins to use this vegetation description. Value for day 0 should be entered very carefully. RUSLE2 compares the root biomass and canopy cover values on day 0 with corresponding values for the last day that the previous vegetation description is used. RUSLE2 assumes that a decrease in live root biomass between two vegetation descriptions represents an event where the decrease in live root biomass should be added to the dead root biomass pool. An example is the wheat-legume intercropping cover-management description discussed in **Section 10.2.3.** The live root biomass on day 0 for

[97] Vegetation descriptions in RUSLE1 must be on a 15-day time interval. Although that 15-day time interval is often retained where RUSLE1 data files are imported into RUSLE2, day values in RUSLE2 can be on any interval and the interval can vary throughout a RUSLE2 vegetation description.

the legume vegetation description that represents conditions after the wheat harvest is less than the live root biomass of the combined wheat-legume vegetation on the day of wheat harvest. The effect represented by this decrease is that the wheat harvest killed the wheat and transferred the wheat's live root biomass to the dead root biomass pool. A harvest operation with a **kill vegetation process** is not used in this cover-management description because that process would have transferred the entire live root biomass, not just the wheat live root biomass, to the dead root biomass pool.

The last day in the vegetation description should be carefully selected as discussed in **Section 11.1.3.2.** The last day in the vegetation description should be later than the date in the cover-management description for the operation description that kills the vegetation. In special cases, the last day in the vegetation description and date of the kill vegetation operation should be the same or nearly the same to ensure that RUSLE2 uses a particular value for aboveground biomass at maximum canopy cover. However, if the last day in the vegetation description is less than the date of the kill vegetation operation, RUSLE2 uses values for the last day in the vegetation description until RUSLE2 begins to use the next vegetation description.

No time limit exists for the last day in a vegetation description. Many vegetation descriptions are for a year or less.[98] For example, the duration of vegetation descriptions vary from 60 days for spring broccoli, 120 days for corn grain, 255 days for winter wheat, and 365 days for a mature pasture. In RUSLE2, the time can be as long as desired to represent the full duration of the vegetation, which can be multiple years. For example, the vegetation description for seeding and establishment of permanent vegetation on a landfill or reclaimed mine may be 10 years that includes the initial three-year establishment period and an addition seven years required for a stable litter and soil biomass pool to develop. The RUSLE2 long term vegetation tool described in **Section 11.2.6** can be used to construct these multi-year vegetation descriptions. A set of three vegetation descriptions can be used in this example rather than using one long 10-year vegetation description. Three 1-year vegetation descriptions would be used, one for the first year starting at seeding, one for development during the second year, and one for the third year and every year thereafter, which represents maturity. An operation with a begin growth process is used each year to tell RUSLE2 which vegetation description to use for that year.

Another example where multiple vegetation descriptions are used is to represent mowing permanent vegetation and hay harvests (see **Section 11.1. 3.2**). The main use of the multiple vegetation description is to represent regrowth of the vegetation following mowing or hay harvest. Simultaneous with the representation of mowing and harvest, multiple vegetation descriptions can be used to represent both the increase and decrease of vegetative production between renovations of the vegetation. See **Section 10.2.3** for a

[98] The duration of a vegetation description in RUSLE1 is limited to 1 year. Vegetation descriptions in RUSLE2 can be of any duration.

discussion of an alfalfa cover-management description where multiple vegetation descriptions are used.

11.1.7.2. Live root biomass

Live roots reduce erosion by mechanically protecting and holding soil in place, producing exudates that reduce soil erodibility, becoming a part of the soil dead root biomass by root sloughing (death) or the vegetation being killed, and indirectly representing increased infiltration, reduced runoff, and reduced erosion (see **Section 9.2.5**). The most important roots are the fine ones very near the soil surface. Coarse roots, especially tap roots, have much less effect on erosion than the fine roots. A value for **live root biomass per unit area in the upper four inches (100 mm) of soil** is entered for each time in the **growth chart**. RUSLE2 uses each value in the array to estimate live root biomass values for the entire rooting depth according to the distribution illustrated in Figure 9.14.

Live root biomass values for annually seeded plants, such as the corn and winter wheat illustrated in Figure 11.4, start from zero on day zero (0) in the growth chart and increase through time to a maximum value. In the case of spring planted corn, the values increase as an S-shaped curve and level off at a maximum. The pattern for fall planted winter wheat differs from that for the spring planted corn. The winter wheat experiences early growth during the fall and dormancy during the winter, reflected by the plateau from about day 50 to day 170 in Figure 11.4. The degree of fall growth for the winter wheat and the length of dormancy is climate dependent. RUSLE2 does not adjust vegetation descriptions to account for those climatic differences. Instead, users create multiple vegetations by climatic regions, such as cropping zones. Figure 11.4 illustrates vegetation descriptions for annually seeded crops. Figure 11.5 illustrates vegetation descriptions for permanent vegetation. Two types of erosion analysis are made for permanent vegetation. One analysis is to compute erosion from the date of seeding until the vegetation becomes mature, fully established along with a fully developed litter layer and soil biomass pool. The other analysis is to estimate erosion for a fully established permanent vegetation (see **Section 10.2.8**).

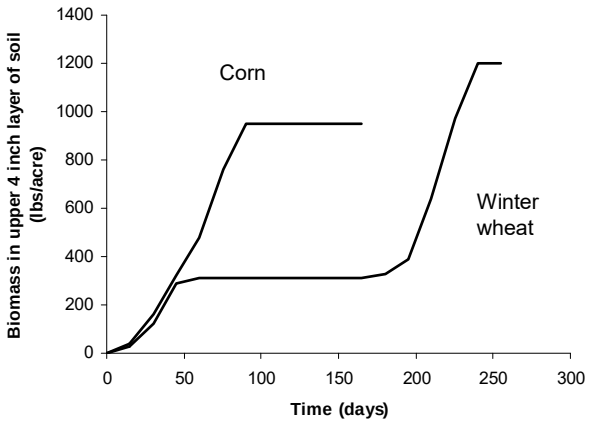

Figure 11.4. Live root biomass values for corn and winter wheat.

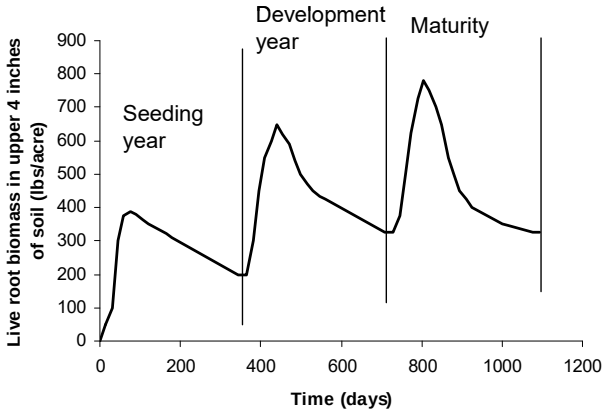

Figure 11.5. Live root biomass for three vegetation descriptions used in series to represent the establishment of permanent vegetation

A single **vegetation description** can be created to describe the vegetation from seeding through complete establishment. The vegetation can also be described with a set of three vegetation descriptions as illustrated in Figure 11.5. The time period for each vegetation description is an entire year. The ending live root biomass for one vegetation description matches the live root biomass at the beginning of the next vegetation description. In the mature year, the beginning live root biomass matches the ending live root biomass. The vegetation description for the mature year is repeated for as many years as necessary for RUSLE2 to compute a stable litter layer and soil biomass pool. This **cover-management description** is a **no-rotation** with a **duration** sufficiently long for fully established conditions to be represented.

Only the vegetation description for the mature year is used to compute erosion for a vegetation completely established. This cover-management description is a **rotation** with a 1-year **duration**. RUSLE2 automatically repeats the computations for as many years as necessary to compute the development of a stable litter layer and soil biomass pool.

The value for live root biomass on day 0 begins at zero for plants started from seed. However, live root biomass on day 0 begins at a value greater than zero when describing vegetable transplants, for example, to reflect the presence of live root biomass is when RUSLE2 begins to use this vegetation description.

Live root biomass is the source of the dead root biomass pool represented by RUSLE2. An **operation description** with a **kill vegetation process** transfers the entire live root biomass that exists on the date of the kill vegetation operation description to the dead root biomass pool. Live root biomass becomes zero on that day and the dead root biomass pool is increased by this amount of live root biomass.

A kill vegetation process in an operation description transfers the entire live root biomass to the dead root biomass pool. Sequential vegetation descriptions without a kill vegetation operation description are used to transfer only a portion of an existing live root biomass pool to the dead root biomass pool.

Root sloughing (death) is also a major source of dead root biomass for permanent vegetation on range, pasture, landfills, and reclaimed mine lands. Up to 40 percent of the annual root biomass can be sloughed (see **Sections 9.2.5.1 and 9.2.5.3.2**). RUSLE2 assumes that a decrease in live root biomass, as illustrated in Figure 11.5, during the time represented by a vegetation description is root sloughing. RUSLE2 can also compute death of root biomass during growth periods by assuming that daily root biomass death is a fraction of the daily live root biomass. The decrease in live root biomass between days is added each day to the dead root biomass pool. Using a constant live root biomass in a permanent vegetation description prevents RUSLE2 from computing an accumulation of dead root biomass, which can result in a serious overestimate of erosion.[99]

Time varying root biomass values should be used in vegetation descriptions for permanent, multiple year forage crops, and similar vegetation.

Situations, such as intercropping, exist where only a portion of an existing live root biomass pool should be transferred to the dead root biomass pool. An example is the small grain-legume **cover-management description** discussed in **Section 10.2.3.** A similar situation is winter weed growth in southern US regions. The canopy of crops like corn, soybeans, and cotton decrease before harvest so that volunteer weeds begin to grow and continue to grow after crop harvest. These weeds provide vegetative cover during the winter to significantly reduce erosion, which is especially important because of the high erosivity during winter months in this region.

Sequential vegetation descriptions are used in RUSLE2, such in these cover-management descriptions, when only a portion of an existing live root biomass pool is to be transferred to the dead root pool. Three vegetation descriptions are used: (1) the wheat only period from seeding until the legume is seeded (corn only), (2) the period when the wheat and legume grow together until wheat harvest (corn and weeds together), and (3) the period after wheat harvest where the legume continues to grow (also, weeds after corn harvest). RUSLE2 makes no change to the dead root biomass pool between periods 1 and 2 because the live biomass values at the end of period 1 equals the live root biomass at the beginning of periods. RUSLE2 adds to the dead root biomass pool between periods 2 and 3 because the live root biomass decreases from that at the end of period 2 to the live biomass at the beginning of period 3. The addition to be dead root biomass pool is the amount of the decrease in the live root biomass. This procedure represents harvest

[99] The time-invariant C-factor procedure in RUSLE1 does not directly account for the effect of dead root biomass on erosion.

killing one vegetation while allowing growth of another vegetation to continue.

Figure 11.5 illustrates a situation where no live root biomass should be transferred to the dead root biomass when RUSLE2 switches vegetation descriptions in the cover-management description. The vegetation descriptions for Figure 11.5 were constructed with the biomass value at the end of one vegetation description matching the live root biomass value at the beginning of the next vegetation description in the sequence so that a smooth continuous condition in live root biomass is represent between vegetation descriptions.

Hay harvest of forage crops that regrow after harvest and permanent vegetation that regrows after mowing are cover-management descriptions where an event causes a major change to occur in the aboveground biomass but no change in the live root or dead root biomass pools. Principally two vegetation descriptions are used, one to represent conditions through the day of the hay harvest/mowing and one to represent regrowth conditions after hay harvest/mowing. The live root biomass value at the end of the first vegetation description matches the live root biomass value at the beginning of the second vegetation description. The two live root biomass values should be equal on the day of harvest and the day after harvest so that no change in the dead root biomass occurs. Multiple vegetation descriptions can be created to shows a progression of live root biomass over time where a hay (pasture) crop reaches maximum production and then declines until the hay (pasture) crop is renovated.

RUSLE2 makes no change in the dead root biomass when the live root biomass increases either within a vegetation description or between vegetation descriptions.

Inspect the vegetation descriptions used in a cover-management description to avoid an unintended decrease in live root biomass and addition to dead root biomass between vegetation descriptions.

The recommended approach for selecting input values for live root biomass is to use the values listed in the **RUSLE2 core database** as a guide. Start by selecting a vegetation description in the RUSLE2 core database that is similar to the plant community for which you are selecting input live root biomass values. Modify the live root biomass values for the selected core database plant community based on how you think differences between the two plant communities would affect live root biomass. This approach for selecting live root biomass values is far better than making field measurements of live root biomass values. Measuring root biomass is very difficult and time consuming, which is evident by the huge range of values given in the literature for wildland type plant communities (see **AH703**). The variability is much less for agricultural and pasture land crops, but is still significant. If input values for live root biomass are to be selected based on field measurements, make many measurements, being careful to measure the fine roots, which have the greatest effect on erosion.

The research literature is a source of live root biomass values that are reliable for vegetable and field crops but not for wildland plant communities. Be very careful in selecting live root biomass values based on literature sources. Many data sources should to be reviewed to determine overall main effects. The best way to select live root biomass values for wildland plant communities is to use the ratio of effective root biomass to average annual aboveground biomass production listed in **Section 17.4.1.4**. These values were obtained by using measured erosion data to back calculate effective live root biomass values using the subfactor equations described in **Section 9**.

A major problem with using measured root biomass values for wildland type plant communities is knowing the credit to give to fine roots versus the credit to give to coarse roots. The input values for live root biomass should be based primarily on the annual production of fine roots. However, erosion and root research has not provided definitive information on how to measure root biomass for use in RUSLE2, which was overcome in the RUSLE2 approach that back calculates effective live root biomass values from measured erosion data.

A major requirement is that input values for live root biomass values are consistent with values in the RUSLE2 core database to ensure that RUSLE2 computes the expected erosion values. RUSLE2 was calibrated with the values given in the RUSLE2 core database to give expected average annual erosion estimates. If input values are not consistent with the core values used to calibrate RUSLE2, then RUSLE2 may give erroneous results. Do not use live root biomass values without checking them for consistency with RUSLE2 core values.

11.1.7.3. Canopy cover

Canopy cover is the portion of the soil surface covered by plant material that is above the soil surface. Canopy cover intercepts raindrops but has no effect on surface runoff, (see **Section 9.2.1**). Canopy cover is a major variable in the canopy subfactor, and it is also used by RUSLE2 to estimate live aboveground biomass during the time represented by a **vegetation description** (see **Section 11.1.3.1**).

Canopy cover values are entered for each time value in the **growth chart**. RUSLE2 interprets an increase in canopy cover as plant growth adding aboveground biomass. Conversely, RUSLE2 interprets a decrease in canopy cover as a transfer of live aboveground biomass to the soil surface. Senescence and litter fall are natural processes where leaves fall from mature plants to the soil surface and become surface (flat) cover. Most permanent vegetation and some agricultural crops like soybeans experience senescence. Also, a senescence type process is chemically induced in cotton just before harvest. Not all decreases in canopy cover represent a transfer of biomass from the live aboveground biomass to surface residue. For example, mature corn leaves droop without

falling to the soil surface. RUSLE2 uses data are entered in the **senescence tool** in the vegetation description to calibrate equation 11.2 that computes values for live aboveground biomass as a function of canopy cover.

A decrease in canopy cover between the last day of the previous vegetation description and the canopy cover on day zero of the next vegetation description has no significance to RUSLE2. RUSLE2 makes no changes in residue cover when canopy cover changes between vegetation descriptions. In contrast, RUSLE2 assumes that a decrease in live root biomass between vegetation descriptions is dead root biomass that is added to the dead root biomass pool. **Operation processes**, such as **kill vegetation**, in **operation descriptions** to explicitly describe changes in standing and surface residue between vegetation descriptions.

A **kill vegetation process** in an **operation description** converts the entire live aboveground biomass to standing reside rather than just a part. **Understanding this feature is important** for describing intercropping represented in the wheat-legume cover-management description discussed in **Section 10.2.3**. The wheat harvest creates a large pool of standing and flat wheat straw residue. However, the live aboveground biomass for the legume should remain unchanged after the wheat harvest.

A similar situation is hay crops that regrow after hay harvest and permanent vegetation that regrows after mowing. These **cover-management descriptions** typically involve a harvest operation description that includes a **remove live biomass process** to manipulate the live aboveground biomass amounts to add the desired amount of surface (flat) residue and a **begin growth process** to identify the vegetation description that RUSLE2 is to use immediately after harvest. **The value that RUSLE2 uses for standing residue needs to be checked to ensure that RUSLE2 is leaving the proper amount of standing residue. This check is critically important in cover-management descriptions like wheat-legume intercropping because of the large mass of residue left by the wheat harvest.**

Input values for canopy cover should be selected by comparing your vegetation description with vegetation descriptions contained in the **RUSLE2 core database**. Select canopy cover values by adjusting core database values based on differences in characteristics between your vegetation and the core database description being used as a guide.

The literature is a source of canopy cover values. However, make especially sure that the canopy cover values reported in the literature are consistent with **RUSLE2 definitions**. For example, literature values often includes leaves touching the ground as **canopy cover** that the RUSLE2 definitions require counting as **live ground cover** (see **Sections 9.2.2.1 and 11.1.7.5**). Review as many data sources as possible because of data variability. The data should be reviewed to determine overall main effects rather than focusing on the

data for a single location.

In some cases, field measurements may be necessary. One way to estimate canopy cover is to sum the open space between plants and open space within the perimeter of the plant canopy and subtract this sum expressed as a percent of the total area from 100. Canopy cover can be estimated from plan view photographs for certain plant communities like corn where live vegetation does not touch the soil surface. A better approach for measuring canopy cover of permanent vegetation on range, pasture, landfills, and reclaimed mine land where some of the live vegetation touches the ground is to lay a transect across the field slope, lower a pointed rod vertically to the soil surface, and count the number of hits for canopy cover, surface (flat) residue (litter), and live parts of the vegetation touching the soil surface (live ground cover). Make sure that a large number of measurements are taken to properly deal with spatial and temporal variability, such as that associated with hillslope position.

11.1.7.4. Canopy Fall Height

Canopy fall height is the effective height from which intercepted rainwater forms drops that fall from the plant canopy (see **Section 9.2.1.1**). **Effective fall height** is less than the canopy height but greater than the height to the canopy bottom. Effective fall height is also a function of canopy shape and the vertical density distribution within the canopy. Some plant communities like grass growing under shrubs on rangelands have two distinct canopies. The understory is the main determinant of effective fall height if the understory is dense. Enter an effective fall height value for each time in the **growth chart**.

Several procedures are available for selecting effective fall height values. One approach is to compare characteristics of your vegetation with **vegetation descriptions** in the **RUSLE2 core database** and assign effective fall height values based on that comparison. Another approach is to inspect plants in the field or in photographs and assign effective fall height values. Another approach is to measure the height to the lowest part of the canopy at locations along a transect. Effective fall height is the average of those values. A fourth approach is to use the **fall height tool** in a RUSLE2 vegetation description to estimate effective fall height. This procedure uses height values to the top and bottom of the canopy, canopy shape, and the density gradient within the plant canopy to estimate effective fall height (see **Section 9.2.1.3**).

Review effective fall height values to ensure consistency among vegetation descriptions so that RUSLE2 computes expected differences in erosion among plant communities.

11.1.7.5. Live ground cover

Live ground cover is live vegetation that touches the soil surface to affect raindrop impact and surface runoff as does other ground cover (see **Section 9.2.2.1**). Live ground cover is one form of ground cover along with crop residue, plant litter, and rock fragments. The portion of the soil surface covered by live ground cover can be very high in early plant growth when the vegetation is composed almost entirely of very low leaves. As the vegetation grows and stems develop, live ground cover can decrease, even to the point that no part of the plant, other than the stems, touches the soil surface to provide live ground cover. Live ground cover inputs also include basal area of the vegetation. A value for live ground cover is entered for each time value in the **growth chart**.

The best way to select live ground cover input values for a vegetation description is to make comparisons with **vegetation descriptions** in the **RUSLE2 core database**. Field measurements can also be made. Many measurements are needed to deal with both temporal and spatial variability. Field measurements can be made using points along a transect. Live ground cover is measured even if it lies on top of plant litter, crop residue, rock, or other types of ground cover. RUSLE2 accounts for overlap of ground cover from different sources. Input values for live ground cover should be reviewed for consistency among the vegetation descriptions in the RUSLE2 database. Also, field inspections of plant communities are helpful, especially if field measurements of live ground cover are not made.

The mass in live ground cover is included in the live aboveground biomass inputs. RUSLE2 does use a relationship between cover and mass for live ground cover as it does for crop residue, plant litter, or applied residue.

11.2. Tools used to develop input values for vegetation descriptions

11.2.1. Develop growth chart for a new production (yield) level

Each **vegetation description** in the RUSLE2 database is for a particular **production (yield) level**. Adjustments are required in a vegetation description to apply RUSLE2 to other production (yield) levels (see **Section 9.2.1.6**). Two options are available to make the adjustments.

One option is to enter the desired production (yield) level value in the **cover-management description** where the vegetation descriptions are selected. RUSLE2 can adjust any vegetation description to a production (yield) level greater than the assigned value for the selected vegetation description. However, the maximum canopy cover must be less than 100 percent in the selected vegetation description for RUSLE2 to adjust to a production (yield) level less than the assigned value for the selected vegetation description. RUSLE2 adjusts values for aboveground biomass at maximum canopy; live root biomass, canopy cover, effective fall height, and live ground cover in the growth

chart; and retardance index values to represent the new value entered for production (yield) level. Live aboveground biomass at maximum canopy is assumed to vary with yield according to equation 9.5. RUSLE2 assumes that live root biomass varies linearly with aboveground biomass at maximum canopy cover; canopy and live ground cover vary with the square root of live aboveground biomass at maximum canopy cover; and effective fall height varies with the 0.2 power of live aboveground biomass at maximum canopy. RUSLE2 varies the retardance index as a linear function (retardance index = a + b·yield) (see **Section 11.2.5**).

The second option is to use the RUSLE2 tool **develop growth chart for new production (yield) level** to create a new vegetation description for the desired production (yield) level. This RUSLE2 tool starts with the selection of a base vegetation description at its assigned production (yield) level. A value is entered for the new production (yield) level and RUSLE2 creates a new vegetation description for the new production (yield) level. This new vegetation can be saved in the RUSLE2 database and used in other RUSLE2 computations. The same requirements and equations discussed above for entering a new production (yield) level in a cover-management description apply in the **develop new growth chart tool**. The advantage of using the develop new growth chart tool is that the adjustments do have to be made by hand and manually entered in a new vegetation description in the RUSLE2 database.

11.2.2. Estimate effective fall height based on canopy characteristics

As discussed in **Section 9.2.1.2, effective fall height** varies with heights to the top and bottom of the canopy, canopy shape, and the vertical density gradient of plant material within the canopy that affects fall height. The RUSLE2 tool that estimates **effective fall heights as a function based on canopy characteristics** can be useful in assigning effective fall height values and improves consistency among users assigning effective fall height values.

Effective fall height varies temporally during plant growth and senescence. Input values for canopy characteristics are entered into the fall height tool at selected times during the period represented by a **vegetation description**. These inputs include values for heights to the top and bottom of the canopy, selection of a canopy shape from those illustrated in Figure 9.2, and selection of a canopy density gradient. The canopy density gradient refers to whether canopy material affecting fall height is uniformly distributed with height in the canopy, concentrated near the bottom of the canopy, or concentrated near the top of the canopy. The base condition is for a uniform canopy density gradient where effective fall height is one third of the difference in heights between the top and bottom of the canopy plus the height to the bottom of the canopy as illustrated in Figure 9.1. The effective fall height is adjusted up or down with respect to canopy shape as illustrated in Figure 9.1 and adjusted up if the plant material affecting fall height is concentrated near the top of the canopy or down if the material is concentrated near the

bottom of the canopy.

RUSLE2 computes an effective fall height at each of the times where values are entered for canopy characteristics. RUSLE2 then linearly interpolates between these effective fall height values to assign effective fall height values for each time value in the **growth chart**.

11.2.3. Live aboveground biomass at maximum canopy as a function of production (yield) level

The input for **live aboveground biomass at maximum canopy cover** determines the mass of vegetative material that becomes standing and surface (flat) residue, both of which have a major effect on erosion (see **Sections 9.2.2, 9.2.5, and 11.1.3**). The amount of live aboveground biomass varies with production (yield) level as illustrated in Figure 11.6. RUSLE2 uses equation 9.5, represented by the fitted line in Figure 11.6, to estimate live aboveground biomass at maximum canopy cover as a function of **production (yield) level** (see **Section 9.2.1.6**).

The **biomass-yield tool** [live aboveground biomass at maximum canopy as a function of production (yield) level] is used to input values that define the fitted line illustrated in Figure 11.6 for a particular vegetation description. The procedure is to plot observed data for live aboveground biomass at maximum canopy as a function of production (yield) level and fit a straight line to the data. The production (yield) level units in this relationship are the ones created for this particular **vegetation description** (see **Section 11.1.2**).

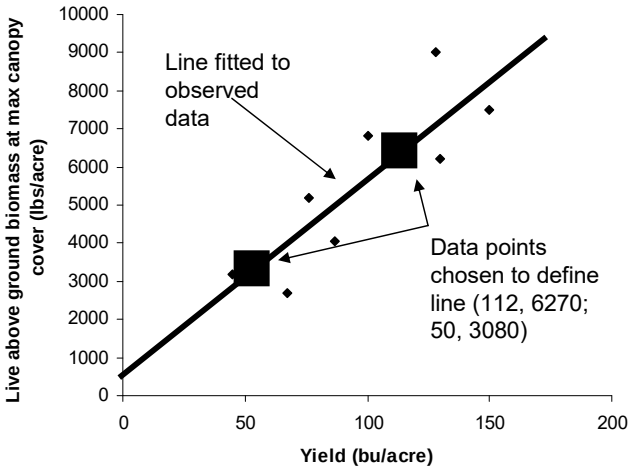

Figure 11.6. Fitting line to aboveground biomass data as a function of yield.

Values for two data points on the line are chosen and entered in the biomass-yield tool. RUSLE2 uses these two data points to compute values for the coefficients M_0 and b_a in equation 9.5. The data point for the higher production (yield) level is the production (yield) level for which the vegetation description applies and the second data point is at a lower production (yield) level. If the same values are entered for both data points, RUSLE2 assumes that the value for the intercept M_0 is zero (0) and that the slope b_a equals the value entered for

live aboveground biomass live divided by the production (yield) level. This procedure can be used to describe forage crops and permanent vegetation. Otherwise, this procedure should only be used within a limited production (yield) range. See the discussion later in this section related to the variation of the ratio of live aboveground biomass to production (yield) level.

The value for the intercept (coefficient M_0) represents the live aboveground biomass at maximum canopy at zero production (yield) level. The intercept value is greater than zero for grain and vegetable crops like corn, soybeans, wheat, green beans, and cucumbers, while the intercept value is zero for the typical production (yield) level definitions used for forage crops and permanent vegetation. The value for the coefficient b_a is the slope of the line fitted to the data illustrated in Figure 11.6. It represents the increase in the live aboveground biomass at maximum canopy for a unit increase in production (yield) level.

The input values for live aboveground biomass at maximum canopy must be on a dry basis. The input values are for the live aboveground biomass at maximum canopy cover, not the live aboveground biomass at harvest. RUSLE2 accounts for loss of live aboveground biomass by senescence using the live aboveground biomass at maximum canopy cover as its starting point. Input values used by RUSLE2 to calibrate equation 11.4 to compute loss of live aboveground biomass by litter fall and senescence tool are entered in the senescence tool (see **Section 11.2.4**).

The two input values for live aboveground biomass provide RUSLE2 with the information it uses to compute the mass of above ground plant material that influences erosion. The objective is not to account for all of the biomass in the system but only that biomass that affects erosion. For example, harvested soybean grain does not end up on the soil surface to affect erosion, but pods around the grain do and should be counted in the live aboveground biomass input. Another example is woody-type vegetation such as shrubs on rangelands. The amount of aboveground biomass that becomes litter fall is the only important biomass under most permanent vegetation conditions. However, if the woody-type material becomes surface residue, perhaps as a part of rangeland renovation, then the woody-type biomass must be accounted for in the vegetation description and in the **residue description** selected for the vegetation description.

The values entered for live aboveground biomass at maximum canopy must be consistent with values entered in the senescence tool in a vegetation description.

Input values for the biomass-yield tool can be obtained in several ways. One way is to compare your vegetation with vegetation descriptions in the **RUSLE2 core database** and select input values based on this comparison. A data source is residue-yield research data published by agricultural experiment stations to which you can use to fit equation 9.5. Ensure that yield definitions used in these data are consistent with the RUSLE2 yield

definition used in the vegetation description. Also, adjustments may be needed in crop residue data measured at harvest where senescence has occurred. The input values used by RUSLE2 are for the live aboveground biomass at maximum canopy, which is different from the aboveground biomass at harvest after senescence has occurred and surface residue has been lost by decomposition.

Research data vary greatly from study to study. Assemble as much data as possible and choose values that best represent the data as a whole rather than focusing on data from a single location or localized region. Also, be careful about attempting to represent differences between crop varieties. RUSLE2 was calibrated to represent main effect differences between plant communities such as between corn and wheat and not differences between crop varieties.

Rule of thumb values for residue:yield ratios can be used to estimate values for the two input data points in the RUSLE2 biomass-yield tool (see **Section 11.1.3.3**). Values for residue:yield ratios are given in Appendix D of Agriculture Handbook (AH) 703 for particular crops for a range of yields. Assume that the residue:yield ratio value applies to the middle of the yield range. Enter the yield value for the midpoint of the yield range and the residue:yield ratio for the first residue-yield data point. For the second data point, enter the yield for the lower end of the yield range in AH703 and the residue:yield ratio times 1.1. For example, the value for the residue:yield ratio value for corn in AH703 is 1.0. The residue to yield ratio value that would be entered for a 50 bu/ac yield, the lower end of the yield range in AH703, would be 1.0·1.1=1.1.

The assumption of a constant residue:yield ratio only applies over an upper range of yield values for vegetation descriptions where the intercept M_0 value is greater than zero. The equation for residue:yield ratio derived from equation 9.5 is:

$$M_a / Y = M_0 / Y + b_a \qquad [11.8]$$

where: M_a/Y = the ratio of live aboveground biomass at maximum canopy to production (yield) level, which is equivalent to residue:yield ratio after proper consideration for senescence. Residue:yield ratio values for the data illustrated in Figure 11.6 are shown in Figure 11.7. Note that residue:yield ratio values approach infinity at a zero yield and decrease to almost a constant value for yield greater than 50 bu/acre. The change in residue:yield ratio for these data is sufficiently small that a constant residue:yield ratio value could be assumed for yields greater than 50 bu/acre. A constant residue:yield ratio can be used in vegetation descriptions provided the production (yield) level does not vary too widely. However, the best approach is to enter values for live aboveground biomass at maximum canopy at two production (yield) levels rather than residue:yield ratio values. If the intercept M_0 for equation 9.5 is zero, the ratio of live aboveground biomass at maximum canopy to production (yield) level is constant and equal to the b_a coefficient in equation 9.5, which is appropriate for forage crops and permanent vegetation.

Crop residue cover immediately after planting is used as an indicator of the level of erosion control provided by conservation tillage systems. If RUSLE2 does not compute expected residue cover values, users can make changes in RUSLE2 inputs so that RUSLE2 computes the expected cover values. These changes should be made very carefully to avoid unexpected consequences. For example, change the live aboveground biomass at maximum canopy cover does affect the residue cover after planting computed by RUSLE2. Changing this value also affects the amount of belowground biomass computed by RUSLE2, which can have a significant effect on RUSLE2's erosion computations. Consider the following variables, their interactive effects, and their effects on other variables that affect erosion estimates in making changes to RUSLE2 inputs related residue cover after planting:

1. **Amount of live aboveground biomass at maximum canopy cover**
2. **Relationship between portion of soil surface covered for a given residue mass (mass-cover relationship in residue description)**
3. **Decomposition coefficient (half life) value in the residue description selected for the vegetation description**
4. **Flattening, burial, and resurfacing ratio values entered for the operation descriptions used in the cover-management description**

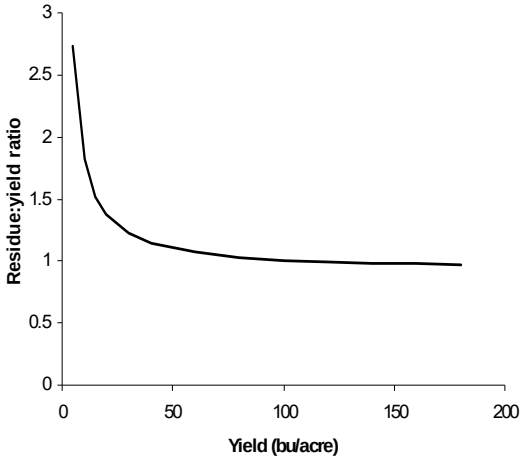

Figure 11.7. Residue:yield ratio for data illustrated in Figure 11.6.

11.2.4. Senescence

Values are entered in the **senescence tool** that RUSLE2 uses to calibrate equation 11.4 to represent senescence and litter fall as a transfer of live aboveground biomass to the surface (flat) residue pool. RUSLE2 computes senescence and litter fall as a function of a decrease in canopy cover (see **Section 11.1.3.1**). The two inputs entered in the senescence tool are portion of the live aboveground biomass at maximum canopy that is subject to senescence (litter fall) and canopy cover after complete senescence has occurred.

As permanent vegetation and agricultural crops like soybeans approach maturity, leaves fall from the plant canopy to the ground, which is senescence and litter fall. The decrease in live aboveground biomass results in a corresponding increase in biomass in the surface

(flat) residue pool. In most cases, the entire live aboveground biomass is not subject to senescence. The value entered for portion of the live aboveground biomass subject to senescence is greater than the actual amount that falls to account for the fact that most of this plant material is leaves. A value of 0.6 for the ratio of biomass that falls during senescence to the aboveground biomass at maximum canopy seems to work well for crops like soybeans and cotton. A high value, perhaps up to 0.9, is appropriate for some grass-type vegetation. RUSLE2 multiplies this fraction by the live aboveground biomass at maximum canopy cover to estimate the potential biomass that will be transferred to the soil surface. RUSLE2 distributes the transfer over time using equation 11.2 and the decrease in canopy cover values entered in the **growth chart** of the **vegetation description**. The input in the senescence tool for canopy cover after complete senescence should be less than the minimum canopy cover that occurs after maximum canopy cover in the growth chart.

The standard assumption in RUSLE2 is that senescence occurs during the period of decreasing canopy cover. However, litter fall can also occur during growth periods when canopy cover is increasing, especially for perennial vegetation. RUSLE2 computes the daily litter fall by death during growth periods by multiply the live aboveground biomass on each day by a fraction that is typically 0.01, unless more specific information is available. If RUSLE2 is not to compute litter fall during growth periods, a zero (0) is entered for the death coefficient. Similarly RUSLE2 can compute death of the live root biomass during growth periods entering a non-zero (0) value for the death coefficient for live roots. Generally the same value (0.01) should be used for both live aboveground and root biomass.

Some plants lose canopy cover without aboveground biomass falling to the soil surface. An example is corn where the leaves droop as the plant approaches maturity. For this and similar types of vegetation that lose canopy cover without losing canopy mass, enter a zero for the portion of the aboveground biomass that experiences senescence. This entry prevents RUSLE2 from computing a decrease in aboveground biomass along with an increase in surface (flat) residue when canopy cover decreases.[100]

The objective is to account for the dead biomass that reaches the soil surface in association with a decrease in canopy cover rather than perfectly model senescence as a process.

The reason that a high value is entered for the portion of the live aboveground biomass subject to senescence is related to RUSLE2 using a single **residue description** to represent a composite of plant components that vary greatly in their properties. Above ground plant material is composed of leaves, stems, seed pods, chaff, and other

[100] This input in RUSLE2 is comparable to the input in RUSLE1 for no senescence in the table where operations are entered for each vegetation in the time variant C factor.

components. Leaves cover a much greater portion of the soil surface per unit mass than do stems. Leaves decompose much more rapidly than do stems. The value for a property in a residue description depends on the relative mass of the plant components in the residue. This distribution changes through time because the components decompose at greatly different rates, which means that residue properties change through time even though RUSLE2 assumes constant residue properties.

Consequently, the input for the portion of the live aboveground biomass subject to senescence is a compromise. The values entered in the residue description for the mass-cover relationship often gives priority to stems because the stems remain long after the leaves have disappeared. Entering a value for the actual amount of fallen plant material significantly underestimates the ground cover provided by senescence and litter fall because most of this material is leaves that provides high ground cover for their mass. To offset the underestimation in ground cover, an artificially high value is entered for the portion of live aboveground biomass subject to senescence to give ground cover values that more closely match actual field ground cover values during the senescence period. This approach works satisfactorily for agricultural and vegetable crops like soybeans, cotton, and green beans because of the importance in the portion of the soil surface covered in the erosion computations and the relatively short time between the beginning of senescence and harvest that converts live aboveground biomass to standing and flat residue.

Both the portion of the soil covered by plant material transferred by senescence and litter fall and the biomass amount must be considered when selecting inputs for permanent vegetation. The residue description for permanent vegetation should represent the composite of plant material that reaches the soil surface during an annual growth cycle. Similarly, the input values for live aboveground biomass at maximum canopy and the portion of this biomass that reaches the soil by senescence and litter fall should represent the actual biomass transfer rather than the artificially high values used for agricultural and vegetable crops discussed above. The residue description for permanent vegetation that is never mowed can be different from the residue description for permanent vegetation that is periodically mowed. The decomposition rate for biomass reaching the soil surface by mowing could be greater than the biomass from the same vegetation that reaches the soil surface by litter fall after plant maturity because of differences in decomposition properties of plant material at different growth stages. These residue descriptions are similar to having a residue description for wheat grown a cover crop that is killed well before maturity and different from the residue description for wheat grown to maturity and harvested for grain.

An approach that sometimes can be used to better represent differences among residue properties at certain times is to use multiple vegetation and residue descriptions for the same vegetation. For example, the residue description assigned in the vegetation description that applies to the senescence period reflects residue being mostly composed

of the leaves that fall during senescence. The residue description assigned to the vegetation description for the period that begins immediately after the end of senescence reflects a high proportion of coarse plant parts like stems.

The best guidance for selecting input values to describe senescence and litter fall is to compare your vegetation with the vegetation descriptions in the **RUSLE2 core database**. Consistency between your values for a particular vegetation description and values in the RUSLE2 core database and values for other vegetation descriptions in your database is very important to ensure that RUSLE2 computes expected erosion values. Assigning these input values involves judgments that may seem counter intuitive.

11.2.5. Retardance

Retardance describes the degree that vegetation slows overland flow. RUSLE2 uses information on vegetation retardance, along with information on ground cover and soil surface roughness, to compute values for Manning's n, a hydraulic roughness index. The retardance index and Manning's n are used to compute the contouring effectiveness of rows of closely spaced vegetation, transport capacity used to compute deposition caused by dense vegetation strips, and critical slope length associated with contouring (see **Section 14**). Retardance depends primarily on the type, stiffness, and density of vegetation parts that touch the soil surface to slow surface runoff. Retardance is two dimensional, having a value for vegetation grown in strips on the contour perpendicular to the overland flow and a value for the same vegetation grown in rows up and down slope parallel to the overland flow direction.

Retardance for vegetation in contour strips is specified using one of eight classes listed in Table 11.6. These eight retardance classes represent the entire range in retardance from no retardance where the vegetation hardly slows the runoff to maximum retardance produced by a dense, sod forming grass. **The eighth class, retardance index 7, is a special case used to represent exceptionally dense, erect, stiff grass strips, fabric (silt) fences, gravel dams, straw bales, and similar erosion control measured used on overland flow areas.**

A retardance class is selected for a vegetation description along this scale based on the degree that the vegetation is judged to slow runoff considering vegetation type, stiffness, and density. Crops at typical yields are listed with each retardance class to guide the selection of a retardance class.

Table 11.6. RUSLE2 retardance classes for overland flow through vegetation in strips on the contour.

Retardance class at maximum canopy cover	Class index value	Comment

No retardance	0	Vegetation has no appreciable effect on slowing runoff
Low retardance	1	Slightly slows runoff, much like corn at 125 bu/acre
Moderate low retardance	2	Slows runoff somewhat, much like soybeans at 35 bu/acre, cotton at 1 ½ bales/ac, corn at 200 bu/acre
Moderate retardance	3	Slows runoff moderately, much like wheat at 45 bu/acre
Moderately high retardance	4	Slows runoff significantly, much like a moderate yield (3 tons/acre) legume hay before mowing
High retardance	5	Slows runoff very significantly, much like moderate yield (3 tons/acre) legume-grass hay before mowing, dense bunch grass
Very high retardance	6	Slows runoff almost to the maximum degree, like a dense, sod forming grass
Extreme retardance	7	Used as a special class to represent the retardance of stiff, erect, very dense grass strips (hedges), fabric (silt) fences, gravel dams, and straws bales used on overland flow areas

Retardance is also a function of plant growth stage and production (yield) level. The **retardance tool** is used to enter retardance classes at two production (yield) levels for a vegetation description at maximum canopy cover. RUSLE2 uses these inputs to calibrate a linear equation that computes retardance as a function of production (yield) level as illustrated in Figure 11.8. RUSLE2 internally treats the retardance as a continuous variable rather than an integer that changes stepwise. Thus, computed erosion values affected by retardance vary in a continuous fashion rather than in a stepwise fashion between retardance classes. RUSLE2 computes a base hydraulic roughness index value as a function of retardance at maximum canopy cover. RUSLE2 uses this base values to compute a daily hydraulic roughness index that varies with the 0.3 power of daily effective fall height.

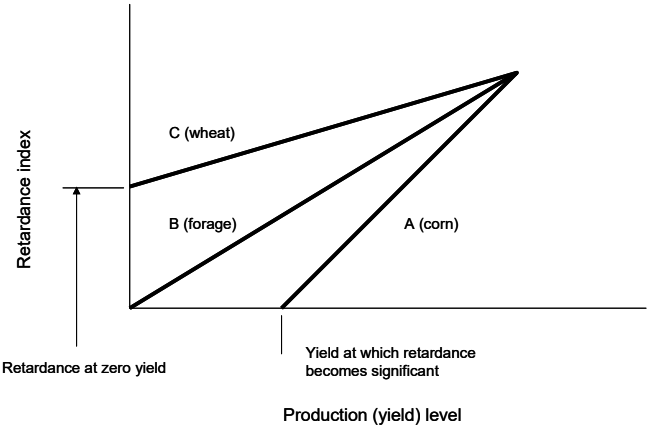

Figure 11.8. Retardance index relationships for different vegetation types

Figure 11.8 shows retardance index-yield relationships for three types of vegetation. Type A vegetation is where plant population must increase to a significant level before retardance becomes significant. For example, corn yield must exceed 100 bu/acre before retardance becomes significant. The entry for this condition in the retardance tool is **Yes**

for **Does no retardance apply for a yield greater than zero?** and the second entry is the **Maximum yield at which no retardance applies**, which is 100 bu/acre in this example. RUSLE2 assumes that corn provides no retardance for yields less than 100 bu/acre and that retardance increases linearly for yields greater than 100 bu/acre as illustrated in Figure 11.8

The question **Does no retardance apply to a yield greater than zero?** is answered **No** for vegetation types B and C. RUSLE2 then asks that a retardance class be selected for a zero yield. Type B vegetation is forage-type vegetation grown on hay, pasture, landfills, and reclaimed mine lands. This vegetation is sufficiently dense and stiff to provided retardance that begins to develop at a zero yield. The **no retardance** class is selected for a zero yield, even for a dense sod forming grass that provides maximum retardance at a high yield. Type C vegetation is vegetation like wheat that provides significant retardance at zero yield. The retardance selection for Type C vegetation at zero yield depends on the stiffness and density of the vegetation at zero yield. The type of vegetation and the retardance entries at zero yield are related to the yield definition used in the vegetation description.

Information on retardance at a high yield is entered in the retardance tool for a second data point. The input for this data point along with the entry for the first data point discussed above are used by RUSLE2 to determine values for the coefficients that define the linear equations depicted in Figure 11.8. This second yield point need not correspond with the yield for which the vegetation description applies. In fact, the best yield for the second data point is the highest yield for which this vegetation description might possibly be applied.

Vegetation type in relation to retardance and the entries used to describe the retardance-yield relationship depend on the yield definition used in the vegetation description. For example, a woody-type vegetation could have a significance retardance index for a zero yield where the yield definition is based on annual production rather than the accumulation of biomass over several years.

The second major input in the retardance tool is used by RUSLE2 to define retardance when the vegetation is grown in rows parallel with the assumed flow direction (up and down slope). Row spacing is used as an indicator of this retardance. The retardance for up and down hill rows ranges from no retardance for widely spaced rows and for vegetation grown on ridges where the vegetation does not contact the down slope overland flow to maximum retardance when the vegetation is in a random pattern. The retardance for the random pattern (i.e., no orientation effect) is assumed to be the same as the retardance for the vegetation grown in a contour strip perpendicular to the overland flow. A retardance class for a particular vegetation description is selected from the six classes listed in Table 11.7 between these extremes using row spacing as an indicator.

Although row spacing is used as an indicator, the selection is actually the degree that the vegetation affects retardance at maximum canopy when rows of the vegetation are oriented in an up and down hill direction.

Table 11.7. Row spacing classes used to indicate retardance for vegetation at maximum canopy cover in rows oriented up and down slope.

Row spacing class	Comment
Wide row	Vegetation provides no retardance to overland flow. Row spacing for typical agricultural crops would be 30 inches or wider.
Vegetation on ridges	Vegetation is on ridges sufficiently high that vegetation does not come in contact with overland flow and provides no retardance to the flow. Actual spacing is unimportant.
Moderate	Rows of vegetation and vegetation characteristics such that the vegetation provides a slight but significant retardance relative to the same vegetation in a random pattern. Row spacing for typical agricultural crops would be 15 inches.
Narrow	Rows of vegetation and vegetation characteristics provide moderate retardance relative to the same vegetation in a random pattern. Row spacing for typical agricultural crops would be 7 inches.
Very narrow	Rows of vegetation and vegetation characteristics provide major retardance so that retardance in the down slope direction is almost as great as retardance when the vegetation is in a random pattern. Row spacing for typical agricultural crops would be 3 inches.
No rows, random, broadcast	Characteristics of the vegetation are such that orientation has no effect on retardance because the vegetation is grown in a random pattern.

RUSLE2 adjusts retardance between the value for vegetation grown in rows up and down slope and retardance for contour vegetation strips based on relative row grade to take into account row orientation of the vegetation. For example, if row grade is up and down slope and the vegetation has been assigned a wide row spacing, RUSLE2 will compute no retardance for the vegetation and no deposition will be computed if the vegetation in grown in strips with an up and down hill row orientation.

The best approach for selecting input values for retardance is to use values in the **RUSLE2 core database** as a guide. Maintaining consistency with the RUSLE2 core database is critically important because RUSLE2 was calibrated and validated against values in the RUSLE2 core database.

11.2.6. Long-term vegetation

The **long-term vegetation tool** is useful for creating multiple year duration **vegetation**

descriptions for permanent vegetation. In many cases, the long term vegetation tool can create a vegetation description that can be used without manual adjustments. Even when manual adjustments are required, the long term vegetation tool greatly facilitates the creation of long duration vegetation descriptions. A graph of canopy cover in a vegetation description created with the long term vegetation tool is illustrated in Figure 11.9. This 10-year vegetation description covers the time from seeding, through development, and into full maturity. The long term vegetation tool is most useful for creating vegetation descriptions for permanent vegetation like that on pasture, range, landfills, reclaimed mine, and similar lands.

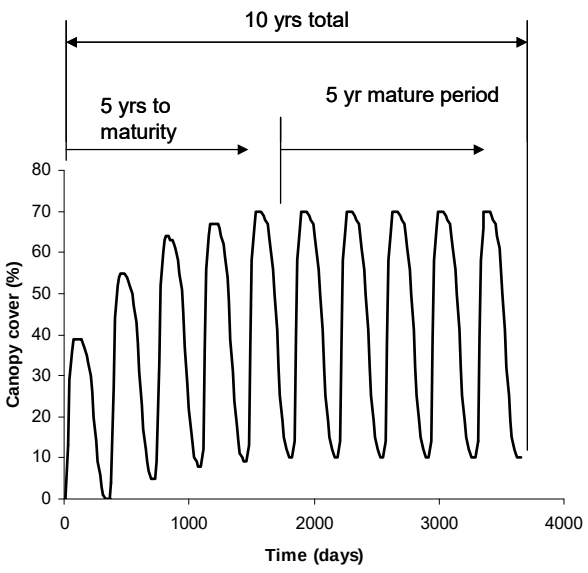

Figure 11.9. 10-year long term vegetation description created with long term vegetation tool.

The inputs entered in the long term vegetation tool are listed in Table 11.8. RUSLE2 uses spline-type equations to temporally distribute values between those entered for the minima and maxima of the variables in the **growth chart** of a vegetation description based on duration and annual timing inputs.

11.2.6.1. Duration inputs

The first set of inputs in the long term vegetation tool is related to **duration** of the vegetation description. The duration of a vegetation description is one year when RUSLE2 is used to estimate erosion for mature vegetation (see **Section 10.2.8**). The **yes-no** input for **rotation** in the **cover-management description** is set to **Yes** with a **1-year duration**. A value of **0** is entered for the **number of years to maturity** and a value of **1 year** is entered for the duration of the vegetation description **(# of years to include in growth pattern**) in the long term vegetation tool to create a vegetation description for mature vegetation.

The long term vegetation tool can also be used to create a vegetation description that starts on the seeding date and continues through the development phase and into the completely mature phase, like the vegetation description illustrated in Figure 11.9. This vegetation description can be used in RUSLE2 to analyze erosion during the establishment period for permanent vegetation on landfills, construction sites, and reclaimed mine lands. The duration of this vegetation description includes a mature period sufficiently long for RUSLE2 to compute a stable litter layer and soil biomass

pool.[101] In the example illustrated in Figure 11.9, the development period is five years (time to maturity), and the mature period is five years. A value of **5 years** is entered for the time required for the vegetation to reach maturity (the development phase) and a value of **10 years** is entered for the entire duration.

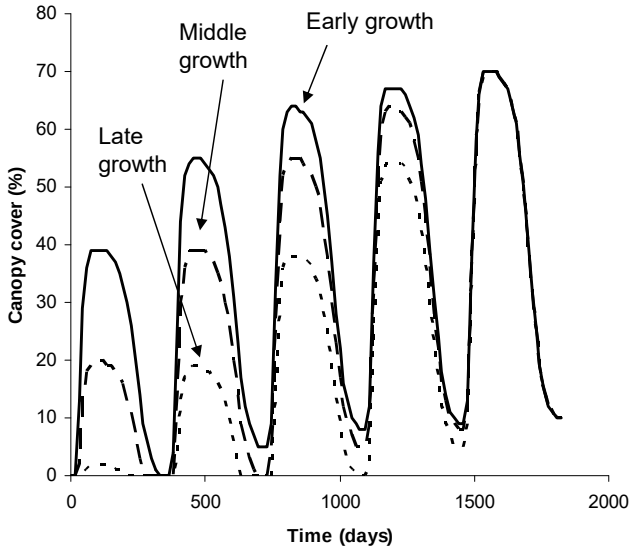

Figure 11.10. Fast growth in the early, middle, or late part of development stage.

The next input is a selection for the period when overall growth is most rapid during the development phase. The choices of **early**, **middle**, and **late** are illustrated in Figure 11.10. Values for all three choices converge in the mature year. Choose the entry appropriate for your vegetation considering seeding date and environmental conditions related to climate, soil, and management at the location where RUSLE2 is being applied. An input of **early** was selected for the vegetation description illustrated in Figure 11.9.

11.2.6.2. Annual timing inputs

The next set of inputs are the **annual timing inputs** related to dates of annual maximum and minimum live aboveground biomass and when most rapid growth and decline occur during the year.

The first timing input is the date of the annual maximum live aboveground biomass, which is also the date when all other temporal variables, including live ground cover, are at a maximum. This date for the example illustrated in Figure 11.9 is July 1. The maximum values occur on this date for every year in the vegetation description created with the long term vegetation tool.

The second timing input is the date that live annual aboveground biomass is minimal, which is also the date that the values for all temporal variables are minimal. RUSLE2 assumes this date for day zero for the vegetation description. The values for all temporal variables are zero on day zero unless the vegetation description has been created for

[101] Stability is defined in terms of litter and soil biomass daily values repeating each year.

mature vegetation.[102] In the example illustrated in Figure 11.9, the date of annual minimum live aboveground biomass is April 1. The date of the **operation description** in the **cover-management description** that uses this vegetation description should be April 1.

Inspect the main vegetation description, including all of the support tools discussed in Section 11.2, to ensure that the proper values are entered and displayed. The long-term vegetation does not transfer all required information into the main vegetation description and the supporting tools.

The time between the dates for maximum and minimum biomass can be any value. Six months between these dates gives a symmetrical distribution during the year. The long term vegetation tool creates non-symmetrical distributions when dates are more or less than six months apart as illustrated in Figure 11.9.

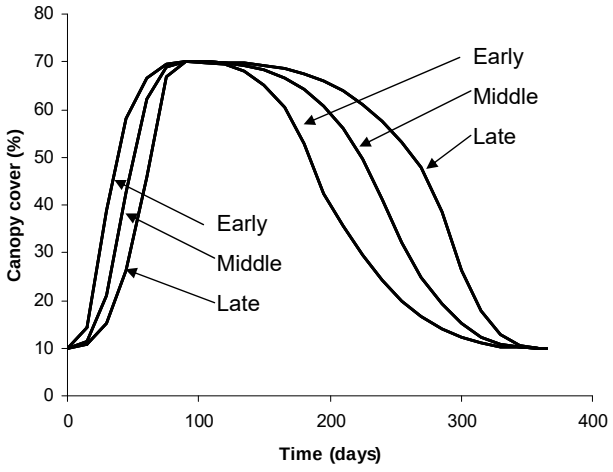

Figure 11.11. Timing of rapid growth and senescence during year.

An important consideration is whether the date of minimum live aboveground biomass corresponds with the seeding date. In the example illustrated in Figure 11.9, the seeding date and date of minimum biomass are the same. However, that assumption is not true for fall seeding when the annual minimum live aboveground biomass occurs in the spring. The long term vegetation tool has no provision for dealing with situations where seeding date and date of minimum live above ground do not correspond. However, the long term vegetation tool is still useful for developing a vegetation description even though manual adjustments are required for these situations. For example, assume that the seeding date is September 1 rather than April 1. The same input values would be used as in the example illustrated in Figure 11.9, but with a change in the selection for the **time that most rapid growth occurs during the development period** and **the time to maturity**. Rather than entering **early,** as in the example, a **middle** selection is made. The time to maturity would be six rather than five years. The

102 This statement applies to vegetation descriptions created with the **long-term vegetation tool**. RUSLE2 can also use multiple annual vegetation descriptions. The temporal values would not be zero on day zero for these vegetation descriptions. However, such annual vegetation descriptions can not be created with the **long-term vegetation tool**.

user manually make changes to values in the vegetation description **growth chart** to correspond to a September 1 seeding date. The manually adjusted values are blended into the values created by the long term vegetation tool. Manual entry of the entire vegetation description is not required.

The third and fourth timing inputs are the times during the year when most rapid growth (gain in live aboveground biomass) and senescence (litter fall, decline in live aboveground biomass) occur. The choices are **early**, **middle**, and **late**. These choices are illustrated in Figure 11.11. One selection can be made for the growth period, such as **early** in the example illustrated in Figure 11.9, and another selection can be made for the senescence period, such as **middle** for the example illustrated in Figure 11.9.

11.2.6.3. Biomass inputs

The **biomass inputs**, which must be on a dry basis, in the **long term vegetation tool** are the same as those in the main part of the **vegetation description** and the **growth chart** discussed in **Section 11.1**. However, a few of the inputs are in a different form. The values entered for **maximum annual live ground biomass** and the corresponding **canopy cover** are for the date of annual maximum canopy cover after the vegetation has reached maturity, which is the date entered in the **annual timing inputs** for maximum biomass. The values entered for **minimum annual live ground biomass** and the corresponding **canopy cover** are for the date of annual minimum canopy cover after the vegetation has reached maturity, which is the date entered in the **annual timing inputs** for minimum biomass.

The input value for annual minimum live aboveground biomass is similar to, but different from, the inputs entered in the senescence tool (see **Section 11.2.4**). The input entered in the long term vegetation tool for annual minimum live aboveground biomass is the ratio f_{mx} of annual minimum live aboveground biomass to annual maximum live aboveground biomass after the vegetation has reached maturity. The value for annual minimum live aboveground biomass is given by:

$$B_{amn} = f_{mx} B_{amx} \qquad [11.9]$$

where: B_{amn} = annual minimum live aboveground biomass at maturity, B_{amx} = annual maximum live aboveground biomass at maturity, and f_{mx} = the ratio of the annual minimum live aboveground biomass at maturity to annual maximum live aboveground biomass at maturity. Essentially the same information must be entered in the **senescence tool**, and it must correspond to the information entered in the long term vegetation tool. The entry in the senescence tool related to biomass is the portion f_s of the annual maximum live aboveground biomass that is available for senescence. The annual minimum live aboveground biomass computed with f_s is given by:

$$B_{amn} = B_{amx} - f_s B_{amx} \quad [11.10]$$

$$B_{amn} = B_{amx}(1 - f_s) \quad [11.11]$$

Combining equations 11.9 and 11.11 shows that the fraction of maximum live aboveground biomass available for senescence that is entered in the senescence tool is related to the ratio of annual minimum live aboveground biomass to annual maximum live aboveground biomass as:

$$f_s = 1 - f_{mx} \quad [11.12]$$

That is, the value entered in the senescence tool equals one minus the ratio of annual minimum live aboveground biomass to annual maximum live aboveground biomass, which is the value entered in the long term vegetation tool for minimum annual live aboveground biomass.

The value entered for canopy cover after full senescence in the senescence tool should be the same as the canopy cover value entered in the long-term vegetation tool for canopy cover for annual minimum live aboveground biomass at maturity.

A value of zero (0) for the **death rate coefficient** for the death of live aboveground is entered biomass when the process of litter fall during the growth period is not be represented. Enter a value of approximately 0.01 when this process is to be represented. A value of 0.01 seems appropriate for a wide range of plant communities.103

The production (yield) level definition, value for production (yield) level and the biomass-yield relationship inputs should be entered in the vegetation description. These values should be carefully checked to ensure that the live aboveground biomass value displayed in the vegetation description is the maximum live aboveground biomass intended from the inputs made in the long term vegetation tool.

.

[103] Dubeux, Jr., J. C. B.; L. E. Sollenberger, J. M. B. Vendramini, R. L. Stewart, Jr. and S. M. Interrante. (2006). Litter Mass, Deposition Rate, and Chemical Composition in Bahiagrass Pastures Managed at Different Intensities. 46:1299-1304.

Thomas, R.J. and N.M. Asakawa. 1993. Decomposition of leaf litter from tropical forage grasses and legumes. Soil Biology and Biochemistry. 25:1351-1361.

Enter the value for **effective fall height** for the annual maximum live aboveground biomass at maturity. See **Sections 9.2.2.2 and 11.1.7.4** for guidelines for selecting effective fall height values as a function of heights to top and bottom of the canopy, canopy shape, and density gradient within the canopy. Also, the **effective fall height tool** discussed in **Section 11.2.2** can be used to adjust the temporal effective fall height values created by the long term vegetation tool.

Values for **live ground cover** should be entered for most permanent vegetation on range, pasture, landfills, reclaimed mine and similar lands. Enter values to represent live (green) leaves, the basal area, and other live vegetative parts that slow runoff during a rainfall event. The temporal pattern of the live ground cover values created by the long term vegetation tool is exactly the same as the temporal pattern for canopy cover values. This pattern may not be appropriate for live ground cover. For example, live ground cover may develop early in the annual growth period ahead of canopy cover and then decrease while canopy cover is still developing. The values created by the long term vegetation tool can be manually adjusted in the vegetation description as desired.

The long-term vegetation tool multiples the input value for the **ratio of live root biomass to live aboveground biomass** by the value for live aboveground biomass to create values for live root biomass. This ratio is for the biomass (dry basis) of predominantly fine roots in the upper 4 inches (100 mm) of soil to the average annual production of aboveground biomass. RUSLE2 assumes that the ratio of live root biomass to live aboveground biomass is constant over time, which means that live root biomass values follow exactly the same pattern as the live aboveground biomass values. In the field, annual live root development usually precedes development of the live aboveground biomass and root sloughing usually precede senescence and litter fall. The RUSLE2 assumption that the two are the same is considered adequate for erosion estimates used in conservation and erosion control planning. RUSLE2 is designed to be an easy-to-use tool for conservation and erosion control planning rather than a model of actual processes. However, RUSLE2 is quite flexible. The live root biomass values can be manually adjusted in the growth chart to represent any desired pattern.

Obtaining reliable information on live root biomass values is very difficult as discussed in **Section 11.1.7.2**. The recommendation is that the ratio values previously stored in RUSLE2 by plant community be used rather than selecting values from the literature or making field measurements. Selecting a plant community in the long term vegetation tool selects the ratio value stored in RUSLE2 for that plant community. A RUSLE2 previously stored plant community ratio value can be overridden by entering another value. The values for ratio of live root biomass to live aboveground biomass stored in RUSLE2 by plant community types are based on field simulated rainfall erosion experiments where values for these ratios were back calculated using RUSLE2 subfactor equations and measured erosion values. Values for these ratios are given in **Section**

17.4.1.4.[104]

RUSLE2 assumes that a daily decrease in live root biomass represents root sloughing where this decrease represents live roots that become dead roots that is added to the dead root pool. RUSLE2 can also compute root death during the growth period when live root biomass is increasing. If this root death process is not to be represented enter a zero (0) for the daily fraction of live root biomass that becomes dead roots during the growth period. If this process is to be represented, enter a value of 0.01, which is the daily fraction of the live root biomass that becomes dead roots during the growth period. In general, the value selected for this fraction should the same as the value for the comparable fraction of daily live aboveground biomass that becomes surface litter.

Table 11.8. Inputs in the long-term vegetation tool used to create vegetation descriptions for permanent vegetation on pasture, range, landfills, reclaimed mine, and similar lands.

Input	Comment
Duration inputs	
Number of years to maturity (development phase)	If a vegetation description for mature vegetation is being created, enter 0; otherwise, enter the number of years required for the vegetation to reach a stable annual pattern (5 yrs for example in Figure 11.9)
Total number of years in the vegetation description (duration)	Enter total number of years in the vegetation description; should include enough years after maturity for a stable litter layer and soil biomass pool to develop at the location where vegetation description is being used; (10 yrs for example in Figure 11.9)
Fastest growth in development period occurs when? (early, middle, late)	Select the time period during the development phase when most rapid development occurs; (Early for example in Figure 11.9); see Figure 11.10 for illustrations of each period.)
Annual timing inputs	
Annual day of maximum live aboveground biomass at maturity (month/day)	Select date of annual maximum canopy cover, which is also the date of annual maximum live aboveground biomass; maximum of all temporal variables is assumed to occur same date; same date assumed for all years in vegetation description; (7/1 for example in Figure 11.9)

[104] The time invariant C factor procedure in RUSLE1 is frequently used to estimate erosion for permanent vegetation. Single values that represent temporal conditions over the year are used as input rather than the temporal values used in RUSLE2. Also, this RUSLE1 procedure does not include the accumulation of a soil biomass pool or the effect of decomposition of the litter layer at the soil surface. Both RUSLE1 and RUSLE2 can give comparable results if the recommended procedures for each model are carefully followed.

Annual day of minimum annual biomass (month/day)	Select date of annual minimum canopy cover, which is also the date of annual minimum live aboveground biomass; minimum of all temporal variables is assumed to occur on same date; same date assumed for all years in vegetation description; (4/1 for example in Figure 11.9)
Fastest growth occurs when during year? (early, middle, late)	Select early to describe vegetation where most rapid growth occurs early in annual cycle; select late to describe vegetation where early development is slow and most rapid development occurs just before maximum live aboveground biomass is reached; (early for example in Figure 11.9); see Figure 11.11 for illustration.
Fastest decline in growth occurs when during year? (early, middle, late)	Select early to describe vegetation where most canopy is lost immediately after senescence (litter fall) begins in annual cycle; select late to describe vegetation where loss of canopy mass is very slow after maximum aboveground biomass is reached and is very high just before the end of senescence; (middle for example in Figure 11.9); see Figure 11.11 for illustration.
Biomass inputs	
Maximum annual live aboveground biomass at maturity (dry basis)	Enter the live aboveground biomass at maximum canopy for the vegetation when it is mature; in general, annual biomass production rather than long term accumulation of biomass is used for this input; the yield value in main vegetation description where yield is defined must correspond with this value; (1000 lbs/acre for example in Figure 11.9)
Canopy cover at maximum biomass (maximum canopy) at maturity	Enter the canopy cover at annual maximum live aboveground biomass at maturity; (70% for example in Figure 11.9)
Effective fall height at maximum canopy cover at maturity	Enter the effective fall height value at annual maximum canopy cover at maturity; (0.3 ft for example in Figure 11.9)
Live ground cover at annual maximum live aboveground biomass at maturity	Enter the live ground cover at annual maximum live ground cover; check live ground cover computed by tool; values may need adjustment so that live ground cover develops earlier than canopy cover; (15% for example in Figure 11.9)
Ratio of annual minimum live aboveground biomass at maturity to annual maximum live aboveground biomass at maturity (dry basis)	The amount for the annual minimum live aboveground biomass is the product of the ratio entered and the annual maximum live aboveground biomass; this value must correspond to the value entered in the senescence tool for amount of annual live aboveground biomass that is available for senescence; (20 % for example in Figure 11.9)
Canopy cover at minim live	Enter the minimum canopy cover provided the annual

aboveground biomass	minimum live aboveground biomass; value must correspond with value entered in senescence tool; (10% for example in Figure 11.9)
Death fraction for live above ground biomass	Enter the fraction of live aboveground biomass that becomes daily surface litter by death during the growth period when canopy cover is increasing (use 0.01 unless other information is available)
Mechanical loss coefficient	Fraction of live aboveground that is added daily to the surface litter biomass; represents mechanical processes such as animal trampling and vehicular traffic
Plant community	Select the plant community that this vegetation description represents; selection of a plant community causes RUSLE2 to select a ratio of live root biomass to live aboveground biomass; select **Enter root mass/live aboveground biomass** if your plant community is not in the list so that you can enter your own value for this ratio; (southern grasses selected for example in Figure 11.9)
Ratio for live root biomass in upper 4 inches (100 mm) of soil/live aboveground biomass ratio (dry basis)	Selection of a plant community causes RUSLE2 to use the ratio value assigned and stored in RUSLE2 for this plant community; user can override value by entering a new value; (4.5 is stored in RUSLE2 for plant community in the example in Figure 11.9)
Death fraction for live root biomass	Enter the fraction of live root biomass that becomes daily dead root biomass by death during the growth period when live root biomass is increasing (use 0.01 unless other information is available, value should generally be the same as that used for comparable fraction for live aboveground biomass)
Grazing/haying/mowing inputs	
Dates	Enter dates that operations begin
Duration	Enter duration (days) of operation
Regrowth period	Enter days in regrowth period
Fraction live aboveground biomass remaining after operation	Enter the fraction of the live aboveground biomass that remains at the end of the operation; fraction is based on live aboveground biomass that exists on day that operation begins

12. RESIDUE DATABASE COMPONENT

Residue descriptions in the **residue component** of the RUSLE2 database contain values that RUSLE2 uses to compute how residue affects erosion. A residue description is assigned to each **vegetation description** and to **external residue**. A residue description assigned to a vegetation description describes the material that remains after the vegetation is killed with an **operation description** having a **kill vegetation process**. A residue description represents a composite of all plant components including leaves, stems, seed pod, and roots present in a sufficient amount to affect erosion. Thus, the values in a residue description for vegetation depend on the relative mass of each plant component in the residue.

The **residue description** selected for an **operation description** that adds **external residue** is used to describe materials added to the soil surface or placed in the soil that affect erosion. External residue includes applied mulch (e.g., straw), manure, gravel, compost, papermill waste, pine needles, roll erosion control products, and other similar materials. The materials represented by residue descriptions are assumed to be organic and decompose much like natural plant materials. Non-organic materials require special considerations that are described in this section.

The variables used to describe residue are listed in Table 12.1.

Table 12.1. Variables used to describe residue

Variable	Comment
How residue responds to mechanical disturbance (residue type)	Describes fragility (how easily material fractures into smaller pieces) to mechanical disturbance and the size and stiffness of the residue pieces in relation to how well the residue conforms to the soil surface to affect erosion
Decomposition coefficient	A variables that determines the rate that residue decomposes under the standard condition of non-limiting moisture and a temperature of 90 ^{o}F (32.2 ^{o}C)
Decomposition half life (days)	Time required for one half of the residue mass to decompose under the standard conditions of non-limiting moisture and a temperature of 90 ^{o}F (32.2 ^{o}C)
Mass-cover relationship	Portion of the soil surface covered by a given mass on a dry weight basis

12.1. How residue responds to mechanical soil disturbance (residue type)

RUSLE2 includes five predefined residue types listed in Table 12.2. Residue type

represents two important residue properties that are related. One is the fragility and size of residue pieces that determine how much residue is flattened, buried, and resurfaced by an operation and the size and stiffness of residue pieces that determine how closely the residue conforms to the soil surface. Assigning a residue type to a residue description requires consideration of both properties.

Table 12.2. RUSLE2 predefined residue types.

Residue type	Comment
Fragile-very small	Small pieces (about 1 inch, 25 mm), easily broken into smaller pieces, moderate conformity to soil surface, similar to soybean residue
Moderately tough-short	Short to moderate pieces (1 to 5 inch, 25-125 mm), moderately tough (resistant) to being broken into smaller pieces, moderate conformity to soil surface, similar to wheat residue run through a straw chopper
Non fragile-medium	Moderate length pieces (3 to 10 inch, 75- 250 mm), non fragile, not easily broken into smaller pieces, low conformity to soil surface, similar to corn residue run through a combine
Woody-large	Long pieces (> 10 inch, 250 mm), very tough, only breaks into smaller pieces with a very aggressive machine, low conformity to soil surface, similar to woody debris left on disturbed forest land by logging, debris left by aggressive mechanical renovation of shrub dominated rangelands
Gravel	Small to moderate sized pieces with gradation of sizes to fill voids, pieces are not reduced in size by mechanical operations, high conformity to soil surface, similar to gravel and crushed stone about ¾ inch (20 mm) used on driveways.
Note: Woven and netting type erosion control products like erosion control blankets are assigned a residue type based primarily on their conformity to the soil surface micro-topography.	

Mechanical soil disturbance by tillage, construction, logging, and similar equipment break residue into smaller pieces. The susceptibility to residue being broken into smaller pieces is referred to as residue fragility. Conversely, the resistance of residue to size reduction is referred to as residue toughness. The size, length, and fragility of residue pieces affect residue flattening, burial, and resurfacing by operations. Consequently, the ratio values for these processes assigned in operation descriptions (see **Section 13.1**) vary with residue properties represented by the five residue types. Fragile residue like soybeans is more easily buried and conforms more to the soil surface than tough residue like woody debris. Long, stiff, and tough residue is not easily buried and does not conform to the soil surface. Gravel and rock fragments conform very closely to the soil surface.

The residue type assigned to roll erosion control products like blankets that are woven or bound together with netting is determined by their conformity to the soil surface. Similarly, a residue type is assigned to spray products used to control erosion on construction sites. The mechanical fragility of these erosion control products is not important unless mechanical operations are performed on the soil after these materials are placed that affects their coverage of the soil surface. The size and nature of residue pieces is not important in assigning a residue type to these products. For example, a gravel residue type can be assigned to these products where the material conforms very closely to the soil surface and perfect contact with the soil exists.

The degree that residue conforms to the soil surface is the other factor considered in selecting a residue type for a residue description. Small, flexible, stable residue pieces that closely conform to the soil surface provide greater erosion control than do long, stiff residue pieces that bridge soil clods. Runoff can partially or completely flow under the residue pieces with greater erosivity than when residue fully contacts the soil surface.

Selection of a residue type assigns one of three conformity index classes to the residue description to describe how the residue conforms to and is in contact with the soil surface. The three residue conformity index classes are low, moderate, and high. The **gravel** residue type listed in Table 12.2 are assumed to provide high conformity (contact with the soil surface), **fragile-very small** (e.g, chopped soybean residue) and **moderately tough-short** (e.g., chopped wheat straw) residue types are assumed to provide moderate conformity, and **non fragile-medium** (e.g., not-chopped corn stalks) and **woody** (e.g., slash on a logged site) residue type is assume to provide low conformity. The conformity class associated with each residue type is internal in RUSLE2 and can not be changed by the user.

The residue conformity index is most important when applying RUSLE2 to steep (greater than 33%), bare construction-type slopes. For example, the residue conformity index makes only about 14 percent difference in RUSLE2 erosion estimates between the low and high residue conformity class for corn residue in a no-till **cover-management description** applied to a 6 percent steep slope. The effect of residue conformity decreases as soil biomass increases. In contrast, the residue conformity makes about 110 percent difference in RUSLE2 estimated erosion between a residue type with low conformity and one with high conformity for a fully consolidated, cut slope with no soil biomass on 33 percent steepness. The difference in RUSLE2 estimated erosion between residue types with low and high conformity class is 40 percent for recently graded fill material on a 33 percent steep slope. RUSLE2 assumes better contact between soil and residue on recently graded fill material than on hard, fully consolidated soil.

The relative effectiveness of residue for controlling erosion decreases as slope steepness increases above about 33%. The loss of erosion control effectiveness is greater for residue types that provide low conformity than for those residue types that provide high

conformity.

Residue types in terms of fragility (toughness) are defined only by the values entered for flattening, burial, and resurfacing ratios in the operation descriptions. However, conformity classes for each residue type are internally assigned in RUSLE2 and can not be changed by the user.

12.2. Decomposition coefficient (decomposition half life)

The decomposition rate of organic residue depends on the organic properties of the material, area and thickness of residue pieces, mechanical fracturing (e.g., fine chopping) of residue pieces to expose easily decomposed material inside a decomposition-resistant outer shell (e.g., corn stalks), and the relative composition of plant parts including leaves, seed pods, chaff, stems, and coarse and fine roots. Residue decomposition rate changes through time as these characteristics change through time. For example, leaves decompose at a much faster rate than stems, which leaves residue main composed of stems that slowly decompose.

The decomposition coefficient value assigned to each residue description is used by RUSLE2 to compute residue loss as a function of daily precipitation and temperature at the location where RUSLE2 is being applied. The decomposition coefficient ϕ value for a residue description is determined by fitting the RUSLE2 decomposition equations to empirical field data. A residue with a large decomposition coefficient ϕ value decomposes more rapidly than does a residue with a low decomposition ϕ value for particular environmental conditions.

Decomposition half-life is another way to express the decomposition coefficient ϕ. Half-life is the time required for half of the residue to be lost under the standard condition of 90 ^{o}F (32.2 ^{o}C) temperature with plentiful, non-limiting moisture. A residue with a long half-life is lost more slowly than residue with a short half-life. The relationship between half-life and the decomposition coefficient is an inverse one where half-life values increase as the decomposition coefficient values decrease. The mathematical relationship between the two is give by:

$$d_{1/2} = 0.693 / \phi \qquad [12.1]$$

where: $d_{1/2}$ = residue decomposition half-life (days) and ϕ = residue decomposition coefficient (days^{-1}).

Decomposition computations are based on residue mass. Residue cover is computed using the mass-cover relationship assigned to the residue description. Half-life refers to residue decomposition under the standard condition of 90 ^{o}F (32.2 ^{o}C) and plentiful moisture, which differs from residue decomposition under actual field conditions.

Figure 12.1 illustrates how RUSLE2 computes residue decomposition as a function of location and residue half-life. Decomposition occurs more rapidly in central Mississippi than in central Missouri because of increased precipitation and temperature, especially in the fall and winter. The 43 day half-life residue decomposes much more rapidly than does the 86 day half life residue. Field decomposition rates are slower than the optimum decomposition conditions used to express half-life values.

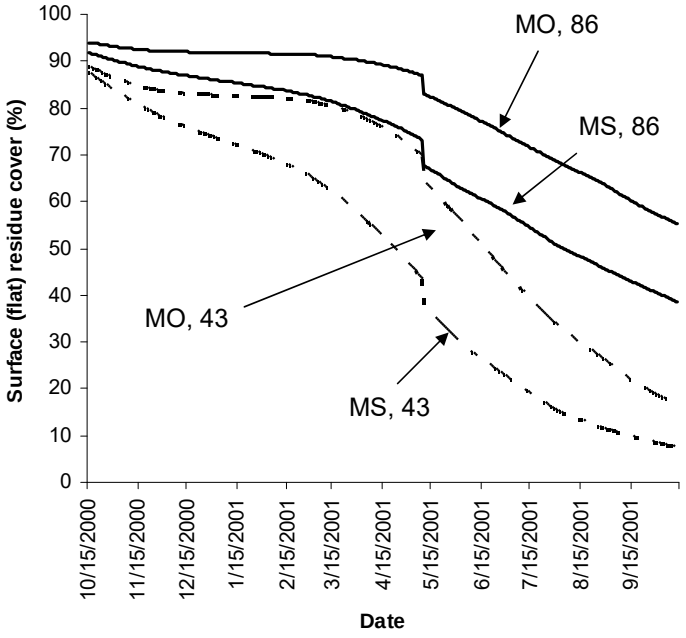

Figure 12.1. Effect of location (Columbia, MO, Jackson, MS) and decomposition half life (43, 86 days) on decomposition of corn residue in a no-till cover-management description.

The intent in RUSLE2 as an erosion control and conservation planning tool is to reflect the main effects of the material (as represented by the decomposition coefficient) and location (represented by precipitation amount and temperature that varies with location) on decomposition. By intent, RUSLE2 does not capture everything that affects decomposition. The following comments discuss particular areas where RUSLE2 represents a compromise and adjustments that users might make to partially overcome the RUSLE2 limitations while retaining RUSLE2's utility.

12.2.1. Soil Moisture

RUSLE2 does not directly consider the effect of soil moisture on decomposition other than how soil moisture is empirically related to precipitation in the decomposition data used to determine RUSLE2 decomposition coefficient ϕ values. Soil moisture is influenced by both cover-management and soil texture. Decomposition coefficient ϕ values can be increased for soil and cover-management conditions that retain water because soil moisture increases decomposition when moisture, rather than temperature, limits decomposition. Thus, the effect of soil texture and cover-management on soil moisture affecting residue decomposition can be partially captured in RUSLE2 by adjusting decomposition coefficient ϕ values. Decomposition coefficient ϕ values are

assigned to residue descriptions based on how soil texture and soil moisture are assumed to affect decomposition at that location. A residue description having a decomposition coefficient ϕ value that reflects site-specific field conditions is chosen. However, based on comparisons with the WEPS and WEPP models, the effect of soil moisture as influenced by soil texture and cover-management is so small that the effect is best ignored in RUSLE2. Therefore, the same decomposition coefficient ϕ value is used for soil, cover-management, and climatic conditions except in the Northwestern US (Req region).

12.2.2. Above ground and below ground biomass decomposition

Buried residue is expected to decompose more rapidly than flat residue on the soil surface. However, research data used to derive decomposition coefficient ϕ values for RUSLE2 were inconclusive regarding this expected difference, especially when adjustments are taken into account for how residue confined in mesh bags used in decomposition measurements decomposes at a different rate than unconfined residue typical of field conditions. Therefore, RUSLE2 uses the same decomposition coefficient ϕ value for residue lying flat on the soil surface and residue buried in the soil. Most error, if any) that exists because RUSLE2 uses the same decomposition coefficient ϕ value for buried residue as surface residue is minimized because the RUSLE2 equation for the soil biomass subfactor (equation 9.12) is calibrated using RUSLE2 computed soil biomass values, not measured values (see the **RUSLE Science Documentation**).

RUSLE2 computes decomposition at the base of standing residue at the same rate as residue lying on the soil surface. RUSLE2 uses decomposition rate at the base of standing residue to compute the rate that standing residue is flattened by natural processes (see **Section 9.2.2.3**). However, RUSLE2 assumes that the decomposition coefficient value for standing residue is three tenth of the decomposition coefficient value for surface (flat) residue. Standing residue is assumed to decompose much more slowly than surface residue because of the lack of moisture that soil contact provides to surface residue.

The RUSLE2 user can not change decomposition coefficient values to reflect decomposition differences between surface and buried residue or between above ground plant components and roots. Also, the user can not change the ratio of the decomposition coefficient for standing residue to the decomposition coefficient for surface residue. Decomposition coefficient values can not be entered for individual plant components.

12.2.3. Differences in decomposition among plant components

Individual plant components of leaves, pods, stems, stalks, coarse roots, and fine roots decompose at different rates. For example, leaves decompose much more rapidly than

stems, and finely chopped stems decompose more rapidly than intact stems. RUSLE2 uses a single residue description with a single decomposition coefficient ϕ value to represent a composite of plant components. The single, constant decomposition coefficient ϕ value for a residue description causes RUSLE2 to compute decomposition rates that are too low immediately after harvest before the leaves decompose and too high after most of the residue has decomposed. Residue decomposition slows over time as the residue becomes increasingly composed of decomposition-resistant plant parts, which RUSLE2 does not take into account with its constant decomposition coefficient value. Differences between computed and observed residue mass are illustrated in Figure 12.2.[105]

The RUSLE2 composite residue structure and its equations for computing decomposition are a compromise. Separately tracking individual plant components such as leaves and stems with their own decomposition coefficient value would be better scientifically than the RUSLE2 composite approach. However, the RUSLE2 developers' judged that data were not available to derive the decomposition coefficient values for individual plant components for the wide range of residue descriptions needed by RUSLE2 when used as a conservation and erosion control planning tool.

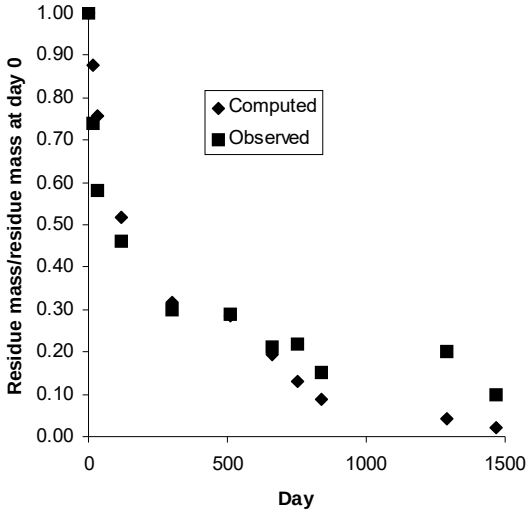

Figure 12.2. Comparison of computed residue mass with observed residue mass for corn in Missouri. (Parker, 1962)

The RUSLE2 composite residue structure must be considered when evaluating residue cover values computed by RUSLE2. Decomposition coefficient values were determined by empirically fitting the RUSLE2 decomposition equations to field residue data to give the best overall fit during the first year after harvest. In many agricultural cropping systems, the annual harvest residue input is much larger than the residue mass immediately before harvest. Errors in residue mass immediately before harvest has little effect on the overall residue mass. Also, errors in residue cover immediately before harvest are often not significant because of low erosion rates at that time. Residue cover should be accurately estimated during the most erosive period,

---

105 Parker, D.T. 1962. Decomposition in the field of buried and surface-applied cornstalk residue. Soil Science Society of America Proceedings. 26:559-562.

which is the late spring and early summer before complete canopy develops for most US row crops. The most important RUSLE2 residue cover estimates at a point in time are those immediately after planting. The RUSLE2 residue decomposition may be too high for times longer than a year for agricultural crops where harvest does not provide a large residue mass input. Overall decomposition coefficient values are chosen to give good residue cover estimates during the most erosive period rather than residue cover values at particular points in time, especially if residue cover errors at those times have little effect on estimated erosion.

These concerns with estimating residue mass over time are much less significant for construction sites where mulch and erosion control products are much more uniform than the residue pieces associated with agricultural crops. However, the problem can be very significant on disturbed forest land where residue ranges from leaves to fine branches to coarse limbs.

Decomposition coefficient ϕ values for a particular residue are preferably location independent, but that objective is not always achieved. For example, the decomposition half-life is 28 days for soybeans grown in the Midwestern US while it is 53 days for soybeans grown in the Southern US. Differences in the vegetative properties of soybeans grown in the two regions partly contribute to the difference in decomposition half-life. The other contributor is climatic differences. The climate in the Southern US is warm and wet during the winter so that the leaves decompose very rapidly after harvest leaving residue in the spring that is primarily composed of stems that decay much more slowly than leaves. In contrast, the climate in the Midwestern US is cold so that little decomposition occurs after harvest during the winter, as illustrated in Figure 12.1. Thus, soybean residue has a higher ratio of leaves to stems in the spring in the Midwestern US than in the Southern US, which gives an apparent higher decomposition coefficient.

Another example where decomposition coefficient ϕ values differ between regions is for wheat residue. The decomposition half-life for wheat grown in the Northwest Wheat and Range Region (NWRR) is 40 days while it is 87 days for wheat grown in other parts of the US. Wheat residue seems to decompose much more rapidly in the NWRR than in other regions.[106] A contributing factor is the difference in climate between the NWRR where precipitation is very low immediately after harvest in comparison to the central Midwestern US. Although the reasons for this difference are not fully understood, the empirical data are more than sufficient to substantiate the difference.

The objective is to obtain the best average annual erosion estimate for conservation and erosion control planning.

[106] The NWWR is a major portion of the region where the Req RUSLE2 relationships are used. **See Section 6.9.**

12.2.4. Decomposition coefficient ϕ values based on stage of growth

The organic properties that affect decomposition of plant materials vary with stage of growth. For example, the residue from a wheat cover crop killed well before maturity decomposes at a much faster rate than does the residue from a wheat crop harvested for grain. The decomposition half-life for wheat cover crop residue is 41 days while it is 87 days for residue from wheat harvested for grain. Therefore, two residue descriptions are created for wheat, one for wheat used as a cover crop that is killed well before maturity and one for wheat harvested for grain. The data inputs into RUSLE2 are always to create a description rather than to model a process. The residue description that best fits the situation is assigned to the vegetation description or selected for external residue.

12.2.5. Decomposition coefficient ϕ values for manure

Manure ranges widely from being almost entirely composed of straw used for bedding to liquid slurry. The important properties of manure include its dry matter biomass content and its decomposition properties. The residue descriptions for manure represent a composite of straw, wood shavings, manure, and other materials that may be present. The decomposition half-life assigned to a particular manure depends on the relative mass of individual components and the decomposition properties of each component, including the type of manure. Four classes of manure are recommended for use in RUSLE2. These classes are listed in Table 12.3.

Table 12.3. Recommended classes for residue descriptions for manure.

Class	Decomposition half-life (days)	Comment
Slow decomposition	87	Manure with high content of straw bedding
Moderately slow decomposition	41	Manure from open lots
Moderately rapid decomposition	23	Manure stored in settling basins
Rapid decomposition	14	Poultry litter

12.2.6. Decomposition coefficient ϕ values for erosion control products used on construction sites

Straw mulch is widely used on construction sites to control erosion. A decomposition half-life of 87 days is recommended for straw mulch. The decomposition half life for other erosion control materials used on construction sites can be determined by comparing their longevity with the longevity of wheat straw and adjusting the decomposition half life accordingly. For example, the decomposition half-life for native

hay would be shorter than for wheat because of the greater proportion of leaves and fines in the native hay than in the wheat straw. Manufacturers' literature for roll products often includes information that can be used to estimate a decomposition half-life relative to that for wheat straw.

12.3. Mass-cover relationship

Although RUSLE2 tracks residue by mass, RUSLE2 computes the effect of surface (flat) residue on erosion using portion of the soil surface that the residue covers (see equation 9.6). RUSLE2 uses equation 9.9 to convert surface (flat) residue mass to portion of the soil surface cover by residue. User entered values in the residue description for data points (residue mass, cover) are used by RUSLE2 to determine values for the coefficient α in equation 9.9. These data points are the mass of residue that provides 30, 60, and 90 percent ground cover, respectively. RUSLE2 will use a single data point or an average of multiple data points to compute a value for α based on the data points for which values have been entered. Enter a mass value for 60 percent cover if only a single value is entered. The next best choice is a mass value for 30 percent cover. A single data point for 90 percent should be avoided because the mass-cover curve is very flat at high cover for many residue types, as Figure 9.5 illustrates. The best combination of two data points is 30 and 60 percent cover, and the poorest combination is one that involves a data point for 90 percent ground cover. Cover is very insensitive to a change in mass at high cover values where the curve is nearly flat. A value at this high cover is very poor for computing a value for α in equation 9.9 because residue mass value can vary over a wide range without affecting cover, which can result in great error when extrapolated to small cover values.

A RUSLE2 residue description is a composite that represents the net cover provided by the combined mass of the individual plant components of stems, leaves, pods and other plant parts. Leaves cover much more of the soil surface for a given mass per unit area than do stems, as illustrated in Figure 12.3. Thus, the mass-cover relationship for the composite residue depends on the relative mass of each plant component in the residue**.** A given residue mass covers much more of the soil surface immediately after harvest before the leaves decompose than later after the leaves have decomposed and only stems remain. For example, leaves decompose very rapidly and only stems are left soon after harvest for soybeans in the Southeastern US where fall and winter temperature and precipitation are high. In contrast, soybean leaves persist longer in the upper Midwestern US, and thus the leaves should be given greater consideration in selecting input values for the residue mass-cover relationship in the upper Midwestern US than in the Southeastern US.

RUSLE2 underestimates percent cover for a given mass per unit area immediately after harvest and overestimates percent cover late in the first year and beyond, as illustrated in

Figure 12.2. Refer to **Section 12.2.3** for information on how to best represent cover-mass for time periods that extend beyond one year after residue is added to the soil surface.

.

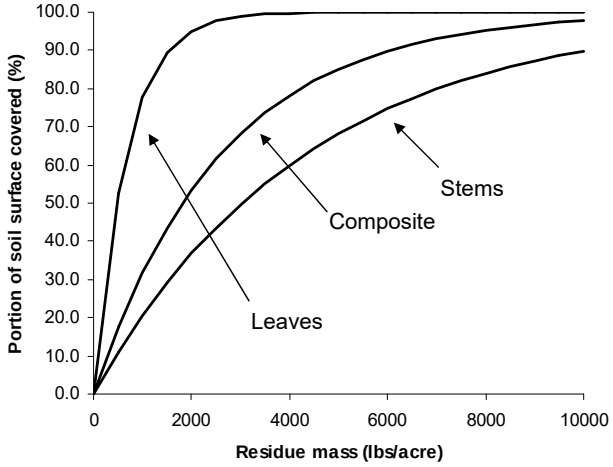

Figure 12.3. The relationship of cover to mass for leaves, stems, and the composite.

12.4. Non-organic residue

Non-organic materials, including stone, are used as mulch applied to the soil or incorporated into the soil. These materials are treated as **external residue** in RUSLE2. Input values in the residue descriptions for these materials must be carefully selected, especially if the materials are manipulated by operations.

12.4.1. Stones (rock fragments, gravel)

Stone, rock fragments, and gravel on the soil surface act as ground cover to reduce erosion (see **Sections 7.6, 9.2.2.1**). Values for rock cover can be entered in the **soil descriptions** in the **soil component** of the RUSLE2 database. RUSLE2 treats the rock cover value entered in a soil description as a constant that is not changed by operations.

Rock cover can also be added to the soil surface as an **external residue** by using an **operation description** that includes an **add other cover process** in a **cover-management description.** Rock cover added as an external residue is affected by soil disturbing operations (operation descriptions that include a **disturb soil process**). RUSLE2 treats rock added as an external residue as biomass that has the same effect on erosion as soil biomass described in **Section 9.2.2.1**. Adjustments should be made in the residue descriptions for rock added as external residue to prevent RUSLE2 from computing a soil biomass effect for rock.

Two special considerations are required to represent rock as external residue. The first step is to assign zero (0) for the decomposition coefficient value.[107] If the rock is not incorporated (buried) in the soil by a soil disturbing operation, no further adjustments are needed.

A second step is required if the rock is incorporated into the soil with a soil disturbing

[107] A very small value like 0.00001 should be entered rather than 0 to avoid a mathematical error in RUSLE2.

operation so that RUSLE2 does not treat rock as soil biomass. An index that has values less than 1 is used to represent the mass of the applied rock. For example, an index value of 0.2 could be used to represent 200,000 lbs/acre of applied rock cover. Values entered in the residue description to define the mass-cover relationship would be based on this index. The biomass subfactor equation (equation 9.12) in **Section 9.2.5.2** will use the index value as if the rock is biomass, but the equation will compute essentially no effect because the index indicates a very small biomass. Should you wish for RUSLE2 to compute an erosion reduction caused by rock incorporated into the soil, adjust the rock mass index until RUSLE2 computes the desired effect.

Be very careful in making these adjustments. See *Section 7.6.* The effect of rock in the soil on erosion is not well understood.

12.4.2. Non-organic erosion control materials that decay

Non-organic materials that decay by ultra-violet radiation are sometimes used at construction sites to control erosion. This decay process differs from the decomposition process assumed for **external residue**. Several special steps are required to develop **residue descriptions** for these materials.

Step 1 involves determining a decomposition coefficient value. RUSLE2 computes decomposition as a function of temperature and precipitation, whereas the decay of these materials is related to ultra-violent (u-v) radiation. Decomposition coefficient values must be determined by location or climatic region because the decomposition of these materials varies by location as u-v radiation, temperature and precipitation conditions that vary by location but are not internally represented in RUSLE2. Decomposition coefficient values are selected by running RUSLE2 and changing decomposition coefficient values until a value is determined that gives the desired loss of erosion control material over time.

Step 2 involves making adjustments for the fact that RUSLE2 adds a portion of the computed decomposed mass to the upper two inches of the soil (see **Section 9.2.5.3**). The decay products of these materials are assumed to have no effect on erosion. The adjustment for these non-organic materials that decay is like the one used for rock. An index is chosen for the erosion control product mass that numerically has values less than 1. The value entered in the **cover-management description** for the mass of the applied materials must be based on this index, and the values entered in the **residue description** for the cover-mass relationship must be consistent with the index definition.

Some erosion control materials are a combination of organic material and non-organic materials, such as compressed straw mulch between a plastic netting. The input values in the residue description should represent a composite of the material, much like residue with multiple plant components is represented as a composite. For example, the mass of

the netting could be entirely ignored.

12.5. Selecting input values

The recommended approach for selecting input values for **residue descriptions** is to compare characteristics of the given residue with those in the residue descriptions in the RUSLE2 **core database.** The values in the core database are based on research data and have been evaluated to ensure that RUSLE2 computes erosion estimates appropriate for conservation and erosion control planning.

If the input values can not be selected based on a comparison with residue descriptions in the RUSLE2 core database, research literature may be a data source that can be used to derive RUSLE2 input values for residue descriptions. Otherwise field measurements may be required. Data used to determine RUSLE2 input values should meet certain conditions regardless of source. Data from multiple data sets, sources, locations, and measurements at a location are needed to deal with both spatial and temporal variability. Residue data, especially mass-cover values, are highly variable. The measurements should be made over at least a three year period at various times during the year. The objective is to capture main effects and trends rather than the details or differences between individual measurements. Differences often represent unexplained variability rather than characteristics of a particular residue.

The best measurements are from actual field conditions rather than from laboratory or specialized field experiments. This empirical approach also captures residue loss by other means besides decomposition such as by wind and worms. The purpose of RUSLE2 is not to be an accurate representation of processes but to be an easy-to-use conservation planning tool. Input values determined from measured data for residue descriptions should be compared among themselves and with those in the RUSLE2 core database for consistency. Such consistency is especially important for agencies implementing RUSLE2 on a national basis where fairness is an important requirement for those impacted by RUSLE2 estimates.

The input values in residue descriptions should reflect the most erosive period for the conditions where RUSLE2 is being applied. The values listed in the RUSLE2 core database were chosen to best fit the first year of the data, which is most important for agricultural cropping systems where annual harvest provides a relatively large biomass input. RUSLE2 tends to overestimate residue cover immediately after harvest and underestimate residue cover for periods longer than a year. Fitting the first year of data overall was considered more important than fitting the residue cover at end of the first year or fitting residue cover values beyond the first year. However, certain conditions exist where fitting over a longer period is important. Non-uniformity in the residue such as plant components that range from leaves to stems contributes significantly to RUSLE2 not fitting residue values beyond one year as well as during the first year. RUSLE2 fits residue data much better when residue pieces are uniform.

Surface residue cover values estimated by RUSLE2 are frequently used to judge the adequacy of RUSLE2. The first requirement in making these judgments is to ensure that the residue cover values being used to evaluate RUSLE2 values meet the requirements discussed above.

If RUSLE2 computed surface residue cover values do not match field measurements sufficiently well, do not immediately conclude that the residue decomposition coefficient value (half-life) should be modified. Numerous factors affect the surface residue cover values computed by RUSLE2. Changing the value for a single variable like the decomposition coefficient ϕ can have unexpected consequences that result in seriously erroneous erosion estimates even if the expected surface residue cover values are computed. That is, numerous other factors besides residue (ground) cover affect erosion. For example, changing the decomposition coefficient ϕ value, which affects residue cover, also affects buried residue and dead roots, which can significant affect computed erosion, especially for high yield, no-till corn cropping systems.

Several factors in addition to decomposition affect surface residue cover. These factors include the residue mass at harvest, the distribution between standing residue at harvest and surface (flat) residue, the rate that standing stubble falls, the relationship between residue cover to mass, and flattening, burial, and resurfacing of residue by operations. All of these factors should be systematically considered in correcting a surface residue cover problem.

13. OPERATION DATABASE COMPONENT

The **operation descriptions** in the **operation component** of the RUSLE2 database contain the information that RUSLE2 uses to compute how operations affect erosion. An **operation** is an event that affects the **soil**, **vegetation**, and/or **residue**. Operations play a major role in determining the values for variables used in the subfactor equations described in **Section 9**.

The variables used to describe an operation are given in Table 13.1. Speed of the operation is one of the variables used to describe an operation. Speed affects residue burial, much like disturbance depth. These two variables are discussed together in **Section 13.1.5.3**.

Table 13.1. Variables used to describe an operation

Variable	Comment
Recommended speed	The speed for which values in the operation description apply. The usual input value is the speed recommended by the manufacturer if the operation represents a machine
Minimum speed	RUSLE2 can adjust values in the operation description if the operation occurs at a speed that differs from the recommended speed. The minimum speed is the slowest speed that RUSLE2 will allow for the adjustment
Maximum speed	RUSLE2 can adjust values in the operation description if the operation occurs at a speed that differs from the recommended speed. The maximum speed is the fastest speed that RUSLE2 will allow for the adjustment
Sequence of processes	A set of processes is used to describe the operation. The processes must be listed in the proper order to have the desired effect. The variables used to describe processes are listed in Table 13.2.
List of processes that can be used to describe an operation	
No effect	Process has no effect. Typically used to cause RUSLE2 to display information on particular dates
Begin growth	Identifies the vegetation description that RUSLE2 is to begin using on the date of the operation description in the cover-management description. RUSLE2 references day zero in the vegetation description to the date of the operation
Kill vegetation	Converts live aboveground biomass and live root biomass to dead biomass that decomposes
Flatten standing residue	Transfer biomass from the standing residue pool to the surface (flat) residue pool. Does not affect live biomass
Disturb soil	Represents a mechanical disturbance of the soil. Creates roughness and ridges. Buries and resurfaces buried residue. Redistributes buried

	residue and dead roots in the soil. Does not affect live roots.
Live biomass removed	Takes a portion of above ground live biomass from the site. The removed biomass is no longer involved in RUSLE2's biomass accounting
Remove residue/cover	Removes residue (dead biomass) and other material from the soil surface.
Add other (external) cover	Adds external residue (e.g., mulch, manure, rolled erosion control materials) to soil surface. Also used to place materials like manure in the soil, which must be accompanied by a disturbed soil process in the operation description
Add non-erodible cover	Adds non-erodible cover including plastic used in vegetation production, water used to flood rice fields, and snow cover. RUSLE2 computes no erosion for portion of soil surface covered by non-erodible cover
Remove non-erodible cover	Removes non-erodible cover.

Some processes like **disturb soil** use additional variables to describe them. Those processes and variables and the variables used to describe them are listed in Tables 13.2.

Table 13.2. Variables used to describe particular operation processes

Process	Variables	Comment
Flatten standing residue	Flattening ratio	Portion of the standing residue mass (dry basis) that is flattened by the operation. Value entered for each residue type
Disturb soil	Tillage type	Describes where operation places buried material in soil and how it redistributes buried residue and dead roots in the soil
	Tillage intensity	Describes the degree that operation obliterates existing roughness
	Recommended depth	Typical depth of disturbance. Use value recommended by manufacturer if operation represents a machine
	Minimum disturbance depth	RUSLE2 adjusts values in operation description if disturbance depth differs from recommended depth. Minimum depth is the shallowest depth that RUSLE2 will use to make an adjustment.
	Maximum disturbance depth	RUSLE2 adjusts values in operation description if disturbance depth differs from recommended depth. Maximum depth is the deepest depth that RUSLE2 will make an adjustment.
	Ridge height	Height of ridges created by operation

	Initial roughness	Roughness left by operation when used on a smooth, silt loam soil when surface and soil biomass are very great
	Final roughness	Roughness after roughness has fully decayed
	Portion of surface area disturbed	Portion of the surface disturbed when disturbance occurs in strips.
	Burial ratios	Portion of surface (flat) residue (dry basis) that is buried. Value entered for each residue type
	Resurfacing ratios	Portion of buried residue in the disturbance depth brought to the soil surface and added to surface (flat) residue pool. Value entered for each residue type
Live biomass removed	Biomass affected	Portion of live aboveground biomass (dry basis) affected by operation
	Amount left on surface	Portion of the affected live biomass (dry basis) added to the surface (flat) residue pool by operation
	Amount left as standing residue	Portion of the affected live biomass (dry basis) added to the standing residue pool by operation
Remove residue/cover	All residue affected	Determines whether operation applies to all residue that is present or to the last residue added
	Flat residue removed	Portion of surface (flat) residue (dry basis) removed by operation
	Standing residue removed	Portion of standing residue (dry basis) that is removed by operation
Add other cover	Portion of external residue added to soil surface	Distributes added external residue between soil surface and placement in the soil over lower half of soil disturbance depth
Add non-erodible cover	Cover added	Portion of soil surface receiving non-erodible cover. Erosion is zero on the portion of the soil surface covered by the non-erodible cover
	Cover half life (days)	Time in days that half of the cover disappears by any process. Value entered must be appropriate for location because RUSLE2 does not consider environmental variables in computing loss of non-erodible cover.
	Cover permeability	Determines the degree that the non-erodible cover affects infiltration and runoff. 100% permeability means that the cover has no effect on infiltration. 0% permeability means that all precipitation on the non-

		erodible cover portion runs off
Remove non-erodible cover	Portion of non-erodible cover removed	Portion of current non-erodible cover removed by the operation.

13.1. Processes Used to Describe Operations

Operations are **discrete events** that change properties of **vegetation**, **residue**, and/or the **soil** that affect erosion. Examples of operations include tilling, planting, harvesting, grazing, burning, frost, ripping, blading, and applying mulch. Operations are described using a **sequence of processes**. Both the processes themselves and their sequence determine an operation's effect. Additional variables are used to describe some processes.

13.1.1. No Effect

The **no effect process** has no effect on RUSLE2 computations. It's main use is in a ***no operation* operation-description** to cause RUSLE2 to display output information on certain dates and for certain periods. **Section 10.2.1.3** discusses how to use a *no operation* operation-description to set the starting point for RUSLE2's tracking of time in an erosion computation. Also, users will sometimes place *no operation* operation-descriptions in a **cover-management description** where other users will later substitute other operation descriptions.

13.1.2. Begin growth

The **begin growth process** is used in an **operation description** to identify the **vegetation description** that RUSLE2 is to begin using on the date of the operation description in a **cover-management description**. RUSLE2 references day zero in the vegetation description to the date of the operation description containing the **begin growth process**. **Section 10.2.3** describes how a **begin growth process** is used in RUSLE2.

RUSLE2 uses only a single vegetation description at any time during its computations (i.e., only one vegetation description is **current** and being used at any time). RUSLE2 begins using a new vegetation description at each occurrence of an operation description with a **begin growth** process in a cover-management description. RUSLE2 does not combine information from multiple vegetation descriptions.

RUSLE2 uses certain rules regarding the **begin growth process** when an operation description with a begin growth process occurs where the previous vegetation description was not ended with a **kill vegetation process**. RUSLE2 adds the decrease between live

root biomass on the last day the previous vegetation description was used and the live root biomass on day zero of the new vegetation description to the dead root biomass pool. RUSLE2 makes no change in the dead root biomass pool if live root biomass increases between vegetation descriptions.

RUSLE2 does not adjust residue pools as a result of differences in canopy cover or live aboveground biomass between vegetation descriptions. Any changes to these biomass pools must be explicitly represented using processes in operation descriptions. However, RUSLE2 DOES adjust the dead root biomass pool between vegetation descriptions. RUSLE2 assumes that a decrease in live root biomass between two vegetation descriptions is dead root biomass that is added to the dead root biomass pool on the date that the change in vegetation description occurs.

13.1.3. Kill vegetation

The **kill vegetation process** converts live aboveground biomass to standing residue and live roots to dead roots and sets values for live root biomass and live ground cover to zero. This process is used in most tillage and harvest **operation descriptions** that end vegetative growth. It is also used in frost killing operation descriptions and in burning operation descriptions if burning entirely kills the vegetation. If an operation such as burning or harvest kills only a portion of the vegetation, the procedure described below is used (see **Section 11.1.3.2**).

Because RUSLE2 uses a descriptive approach and is not a process model, an *operation description* using the *kill vegetation process* must be used to end vegetation growth.

The **kill vegetation process** "kills" all vegetation represented by the current vegetation description. A **kill vegetation process** also ends RUSLE2's use of information from the current vegetation description. If RUSLE2 computations extend beyond the last date represented in a vegetation description, RUSLE2 uses the values on the last date in the vegetation description until an operation description with either a **kill vegetation process** or a **begin growth process** occurs in the **cover-management description**.

Two processes are used in an operation description to represent a partial kill of vegetation. These processes transfer only a portion of the live aboveground biomass to the standing and surface (flat) residue pools and a portion of the live root biomass to the dead root biomass pool. The **first process** is **remove live biomass**, which determines how much of the live aboveground biomass that is affected by the operation and the portion of the affected biomass that is transferred to the standing and surface (flat) residue pools. The **next process** in this operation description is a **begin growth process**

that identifies the vegetation description that follows the current vegetation description. RUSLE2 compares the live root biomass on day zero in the new vegetation description with the live root biomass in the current vegetation description on the transfer date. RUSLE2 transfers a **decrease** in live root biomass between the vegetation descriptions to the dead root biomass pool. An increase does not change the dead root biomass pool.

A *kill vegetation process* transfers all live aboveground biomass for the current vegetation to the standing residue pool and all live root biomass to the dead root biomass pool. Use *remove live biomass* and *begin growth processes* to transfer only a portion of live biomass to dead biomass.

13.1.4. Flatten standing residue

Biomass is transferred from the standing residue pool to the surface (flat) residue pool by natural and mechanical processes that flatten the standing residue (see **Section 9.2.2.3**).[108] Flattening of standing residue by natural processes is represented internally in RUSLE2 based on decomposition at the standing residue base. The **flatten standing residue process** is used in **operation descriptions** to represent mechanical flattening of standing residue. For example, this process is used in operation descriptions that describe flattening of standing residue by foot or vehicular traffic. Also, this process is used in operation descriptions for tillage operations that bury crop residue because standing residue must first be flattened before it can be buried according to RUSLE2 rules. This process is also used in harvest operation descriptions to describe the distribution between standing and flat residue after harvest. For example, about 50 percent of wheat residue is left standing after harvest, while only 5 percent of soybean residue is left standing. The difference is primarily related to combine cutter bar height. The amount of residue left standing for corn harvest can range from about 15 to 85 percent depending on combine snapper height or whether the corn was harvested by combine, picker, grazing, or hand. This process can be used in operation descriptions to represent wind flattening standing residue where the RUSLE2 internal procedures for natural processes do not compute sufficient fattening. To flatten live vegetation, a **begin growth process** is used to call a new vegetation description to describe characteristics of the live vegetation after flattening. **A flatten standing residue process** can not be used to descrbe flattening of live vegetation because a RUSLE2 rule is that only standing residue can be flattened..

Two rules apply in using the **flatten standing residue process** in an operation description. The **first rule** is only standing residue can be flattened. Live vegetation must first be converted to standing residue using a **kill vegetation process** or a **remove live biomass process** in an operation description. The **flatten standing residue process** has no effect on live vegetation. Live vegetation can be flattened and continue to live

[108] The companion values for burial and resurfacing ratios are entered in the **disturb soil process**.

(e.g., wheat blown over by wind before maturity). An operation description that includes a **begin growth process** and associated vegetation description that represents flattened live vegetation is used to describe this condition. The **second rule** is that standing residue can not be buried by an operation until the standing residue has been converted from standing residue to surface (flat) residue. Therefore, a tillage operation description that buries standing residue must include a **flatten standing residue process** before a **disturb soil process**. Sequence of processes is important.

Flattening ratio is the input used to describe the **flatten standing residue process**. This ratio is defined as the portion of mass (dry basis) of standing residue that is flattened to the mass (dry basis) of standing residue before flattening. A flattening ratio of 0 means that no standing residue was flattened, and a value of 1 means that the entire standing residue was flattened. The portion of standing residue flattened by a mechanical process depends on both residue type (e.g., the standing residue of some vegetation types resists flattening), type of mechanical process (e.g., vehicular traffic versus harvest, corn combine versus corn picker), and properties of the process (e.g., cutter bar height). A value for the flattening ratio in an operation description is entered for each residue type (see **Section 12.1**). The values must also represent the particular process (e.g., type of machine) and the properties of the process (e.g., how the machine is operated). Multiple operations are required for a particular machine operated in different ways (e.g., cutter bar set at different heights). Values for the flattening ratio are largest for residue types most easily flattened by mechanical action and cutter bar height close to the ground, such as for soybeans.

Values entered for flattening ratio in an operation description should be based on a comparison with operation descriptions in the RUSLE2 **core database**. If a selection can not be made on that basis, research literature may provide data that can be used to determine flattening ratio values. The third possibility is to make field measurements. Data used to determine flattening ratio values should be sufficient to deal with variability, and the emphasis should be on capturing main effects rather than details that may well be unexplained variability. Values determined from the literature or from actual measurements should be checked for consistency with values in the RUSLE2 core database.

13.1.5. Disturb Surface (Soil)

The **disturb surface (soil) process** represents a mechanical disturbance of the soil that, with one exception, resets the soil consolidation subfactor to 1 for the portion of the soil surface that is disturbed (see **Section 9.2.6**). RUSLE2 assumes that the soil must be disturbed to bury surface (flat) residue, to create soil surface roughness and ridges, to mechanically smooth the soil, and to place material in the soil. The exception is the compression tillage type that buries residue without loosening the soil (see **Table 13.3**).

Also, RUSLE2 assumes that a infinitely thin surface layer of soil can be cut away without disturbing the underlying soil. The **operation description** that describes this action would **not** include a **disturb soil process** but would include a **Remove residue/cover process** that removes all above ground and surface vegetation and cover. This operation description does not affect any soil biomass.

Input values for the variables listed in Table 13.2 are required to described the **disturb soil process** for a particular **operation description**.

13.1.5.1. Tillage type

Assigning a **tillage type** from the list in Table 13.3 for an **operation description** provides information to RUSLE2 how a **soil disturbing** operation vertically distributes surface residue when it is buried. This input also provides information on how the operation vertically redistributes existing buried residue and dead roots. The **disturb soil process** has no effect on the distributions of live roots. Live root biomass must be transferred to the dead root biomass pool before root biomass can be redistributed in the soil by a soil disturbing operation. The distribution and redistribution functions represented by the tillage types are described in **Sections 9.2.5.3.3 and 9.2.5.3.4.**

The **inversion+some mixing** tillage type is used to describe machines like moldboard plows and manual operations that bury residue by inverting the soil. These operations bury most of the residue in the lower one half of the disturbance depth as illustrated in Figure 9.15. One way to represent how a soil disturbing operation redistributes buried residue and dead roots is to describe the pattern that results after the operation is applied repeatedly. Repeated applications of the inversion+some mixing tillage type operation results in buried residue and dead roots being nearly uniformly distributed as illustrated in Figure 9.17.

The **mixing with some inversion** tillage type is used to describe machines like heavy offset disks, tandem disks, chisel plows, and field cultivators and manual operations that primarily bury residue by mixing but also bury some residue by soil inversion. These operations bury most of the residue in the upper one half of the disturbance depth as illustrated in Figure 9.15. The second application of an operation of this tillage type mixes the residue fairly uniformly in the upper one half of the disturbance depth as illustrated in Figure 9.18. Subsequence applications result in a moderate bulge of material that moves downward in the soil.

The **mixing only** tillage type is used to describe machines like rotary powered tillers and manual operations that incorporate residue by mixing with hardly any soil inversion. These operations tend to bury residue in the upper one third of the soil depth as illustrated in Figure 9.15 rather than uniformly over the disturbance depth as commonly assumed. Repeated applications of this tillage types results in a well defined bulge of

material that moves downward in the soil.

The **lifting, fracturing** tillage type is used to describe machines like fertilizer and manure injectors, subsoilers, and sacrifiers and manual operations that have a similar effect on the soil and residue. This tillage type assumes almost no mixing or inversion, and an operation of this tillage type buries residue in the upper one third of the disturbance depth. The residue distribution and redistribution relationships for **mixing only** are used to describe this tillage type.

An **add other residue/cover process** is used to place external residue in the soil. This process must be followed by a **disturb soil process** in the **operation description**. The lifting, fracturing tillage type is selected for the operation. RUSLE2 places the inserted material in the lower one half of the disturbance depth as illustrated in Figure 9.16. This procedure assumes that the material is placed in the soil by injection. Material can be also placed in the soil by applying it to the soil surface and incorporating it using machines like disks, chisel plows, field cultivators, or rotary powered tillers or manual implements. The operation description for this method of incorporation includes an **add other residue/cover process** followed by a **disturb soil process**.

Table 13.3. Tillage types used in RUSLE2			
Tillage type	Burial pattern	Redistribution characteristics with repeated applications	Comment
Inversion + some mixing	Most of material is placed in lower 1/2 of disturbance depth	Material is nearly uniformly distributed	Used to represent soil disturbing machines like moldboard plows that invert soil
Mixing with some inversion	Most of material is placed in upper 1/2 of disturbance depth	2nd application results in a fairly uniform pattern in the upper ½ of soil disturbance depth after which a moderate bulge develops that moves downward in soil	Used to represent soil disturbing machines like chisel plows, field cultivators, and disks
Mixing only	Most of material placed in upper 1/3 of disturbance depth	A well defined bulge rapidly develops that moves downward in soil	Used to represent powered rotary tillers
Lifting, fracturing	Most of material placed in upper 1/3 of disturbance depth	A well defined bulge rapidly develops that moves downward in soil	Used to represent fertilizer injectors, manure injectors, subsoilers, and sacrifiers
Compression	Most of material placed in upper 1/3 of disturbance depth	No redistribution	Used to represent sheep's foot roller and animal traffic that presses residue into the soil. The soil consolidation subfactor is not reset to 1
Note: When external residue is placed in the soil, the **add other residue/cover process** must be followed with a **disturb soil process** in the operation description, which places the inserted material in the lower one half of the disturbance depth			

The **compression** tillage type is used to describe cattle trampling, a sheep foot's roller, and similar operations pressing residue into the soil without loosening the soil. The **mixing only** distribution relationship is used to vertically distribute the buried residue. Operations of this tillage type are assumed to not redistribute buried residue or dead roots. **An important difference between this tillage type and the other tillage types is that the soil consolidation subfactor is not reset to 1.**

The best way by far for assigning tillage types to soil disturbing operations is to base the selection on Table 13.3 in conjunction with comparisons with tillage types assigned in

the RUSLE2 **core database**. Consistency between the assigned tillage type and those in the core database is essential.

A very important feature of the soil mixing relationships used in RUSLE2 is that material does not become uniformly mixed in the soil with repeated applications of the operation except for the *inversion+some mixing* tillage type. The distribution becomes more non-uniform with repeated applications of operations described with the other tillage types.

13.1.5.2. Tillage intensity

Tillage intensity refers to the degree that a soil disturbing operation obliterates existing roughness. Tillage intensity relates to the aggressiveness of the soil disturbance. A tillage intensity value of 1 means that existing soil roughness has no effect on the roughness created by the operation. A tillage intensity value of 0 means that roughness after the operation is the same as before the operation, unless the existing roughness is smoother than the roughness created by the operation on a smooth soil.

A moldboard plow and a rotary powered tiller are both assigned tillage intensity values of 1 because these aggressive machines totally eliminate any signs of existing roughness. In contrast, a spike tooth harrow, which is non-aggressive, is assigned a tillage intensity of 0.4 because the harrow hardly changes existing roughness. For example, soil surface roughness is greater when the harrow follows a moldboard plow than when it follows a tandem disk because of differences in existing roughness and the minimal effect that the harrow has on roughness. The harrow does some smoothing but does not totally work the soil to eliminate all existing soil surface roughness to create a totally new soil surface roughness. Tillage intensity values range from 0.5 to 0.9 machines like field cultivators, tandem disks, and chisel plows depending on the machine's "aggressiveness."

When the roughness immediately before an operation is smoother than the roughness created by the operation on a smooth soil, the tillage intensity variable has no effect on the roughness value estimated by RUSLE2. The roughness value for the operation is set to the **input (initial) roughness value** for the operation, adjusted for soil texture and soil biomass (see **Section 9.2.3**).

Tillage intensity is not necessarily related to the initial roughness created by an operation. For example, both a moldboard plow and a rotary powered tiller are assigned 1 for tillage intensity but the soil surface roughness left by the two machines is very different. The moldboard plow leaves a very rough surface and the powered rotary tiller leaves a very smooth surface. Both machines are very aggressive and completely disturb the soil. Machines that have low tillage intensity values also tend to leave a relatively smooth surface when used on a smooth soil.

Tillage intensity values should be assigned using values in the RUSLE2 **core database** as a guide. The selection is the operation's aggressiveness for obliterating signs of existing soil surface roughness, not the soil surface roughness left by the operation. The RUSLE2 assumption is that tillage intensity is not a function of soil properties. However, different intensity values can be assigned based on soil properties. The RUSLE2 user then chooses the operation description having the tillage intensity values most appropriate for the site-specific condition.

13.1.5.3. Recommended, minimum, and maximum speed and disturbance (tillage) depths

The portion of the surface (flat) residue mass buried by a **soil disturbing operation** (e.g., tillage) increases as disturbance depth and speed increase as illustrated in Figures 13.1 and 13.2. These relationships were derived from analysis of research data. The manufacturer of tillage implements and soil disturbing machines often specify a recommended disturbance depth and speed along with working ranges where the machine operates satisfactorily. The input burial ratio values are for the **recommended disturbance depth and speed**.[109] No other variable, including residue resurfacing, is affected by disturbance depth and speed in RUSLE2.

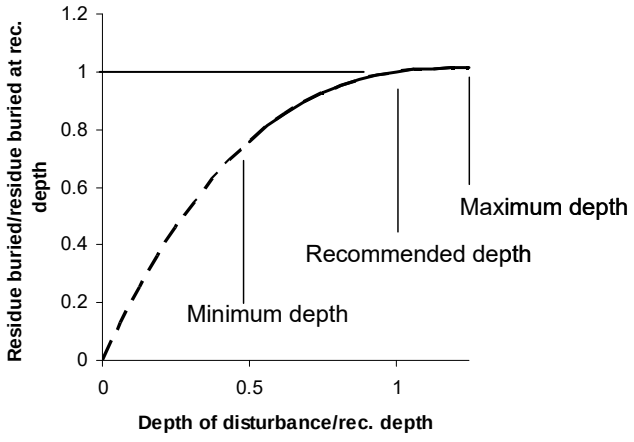

Figure 13.1. Effect of disturbance depth on residue burial (mass basis).

Increasing disturbance depth at shallow depths significantly increases residue burial, but increasing disturbance depth to depths deeper than the recommended depth does not greatly increase residue burial. Increasing speed does not significantly increase residue burial. The effect of speed on residue burial is generally less than the effect of disturbance depth.

[109] Disturbance depth in RUSLE2 is for the entire disturbance (tillage) depth, which differs from the incorporation depth used in RUSLE1. The RUSLE1 incorporation depth is the effective depth of residue burial assuming that residue is buried uniformly with depth. The RUSLE1 incorporation depth is shallower than the RUSLE2 disturbance depth.

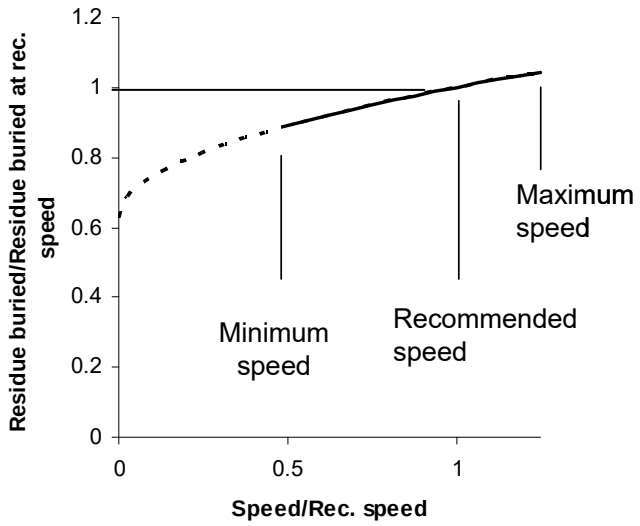

Figure 13.2. Effect of speed on residue burial (mass basis)

In most RUSLE2 applications, the recommended disturbance (tillage) depth and speed are accepted as default values.[110] Input values for disturbance depth and speed entered in **cover-management descriptions** must be within the minimum and maximum values entered in each **operation description.**

The common belief is that practically any surface residue cover can be achieved by varying how a machine is operated. Disturbance depth and speed are the two machine variables that can be changed easily. The assumption that a particular residue cover can be achieved by varying machine operation should be checked. The range in residue cover that can be achieved by varying disturbance depth and speed is determined by making RUSLE2 computations at the minimum and maximum disturbance depth and speed values. If RUSLE2 shows that the desired residue cover is not obtained by varying disturbance depth or speed, another change in the machine such as changing shovel type is required.

Input values for disturbance depth and speed can often be obtained from manufacturer's literature. Also, values given in the RUSLE2 **core database** can be used as a guide to selecting input values. The preferred approach is to select a tillage depth based on the implement type rather than selecting value specific to an individual machine or operator. The disturbance depth and speed values shown in the RUSLE2 core database were chosen to give the desired differentiation between implement types. Input values should be reviewed for consistency among themselves and with values in the RUSLE2 core database.

Input values for disturbance depth and speed should not deviate significantly from those in the RUSLE2 core database for a particular type of machine.

[110] Depth and speed of operations in a **cover-management description** may not be displayed by the RUSLE2 template used to configure your RUSLE2 screen. Choose an alternate RUSLE2 template that displays additional variables so that disturbance depth and speed can be entered for each operation in a **cover-management description**.

13.1.5.4. Ridge height

Ridge height has two effects in RUSLE2. One effect is that increased ridge height increases erosion when the ridges are oriented up and down hill perpendicular to the contour. This ridge effect is considered in the subfactors used to compute **cover-management** effects (see **Section 9.2.4**). The other effect is that increased ridge height decreases erosion when the ridges are on the contour (parallel to the contour). This ridge effect is considered in **support practice** relationships used to compute the **contouring** effect (see **Section 14.1**). The overall ridge height effect, which is the net between these effects, also varies with row grade (grade along the furrows between the ridges).

Operation descriptions that include a **disturb soil process** must be used in a **cover-management description** to create ridges for RUSLE2 to compute a contouring support practice effect. RUSLE2 assumes that ridges can not be created without disturbing the soil, which resets the soil consolidation subfactor to 1 for the portion of the soil surface that is disturbed by the operation that creates the ridges.

Input values for initial ridge height are entered in operation descriptions that include a **disturb soil process**. Ridge height created by an operation is not affected by ridge height that existed before the operation. In effect, an operation obliterates any ridge height that existed prior to the operation even when the operation minimally disturbs the soil. The ridge height entered for an operation should reflect the ridge height that exists when the operation is used in combination with other operations. RUSLE2 computes loss of ridge height over time as a function of precipitation amount and interrill erosion.

The best way, by far, to assign ridge height values is to use the values in the RUSLE2 **core database** as a guide. RUSLE2's estimate of the contouring effect on erosion is RUSLE2's most uncertain estimate. Too frequently, initial ridge height values are entered that are too low, which results in RUSLE2 not computing the expected contouring effect (see **Section 14.1**). Field measured ridge height values may be lower than the corresponding values in the RUSLE2 core database. Also, important ridges are also overlooked when field measurements are made.

If RUSLE2 is not computing as much contouring effect as expected, initial ridge height values in key operation descriptions may need to be increased.

13.1.5.5. Initial roughness

As described in **Section 9.2.3**, RUSLE2 computes decreased sediment production (i.e., detachment, see equations 5.4, 8.1, 9.1, 9.10) as soil surface roughness increases. RUSLE2 also computes decreased runoff rates as soil surface roughness increases (see **Section 5.4**). RUSLE2 uses runoff rate to compute how contouring affects erosion (see **Section 14.1**) and to compute sediment transport capacity (see equation 5.3). RUSLE2

uses sediment transport capacity to compute deposition, sediment yield, and enrichment of the sediment in fines on rough surfaces; on concave shaped slopes; upslope of strips of dense vegetation, rough soil surfaces, and heavy ground cover; and in low grade terrace/diversion channels (see **Section 14**).

RUSLE2 assumes that the soil must be disturbed to create roughness, which resets the soil consolidation subfactor to 1 for the disturbed portion of the soil surface, with one exception. The exception is a **compression tillage type** that creates soil surface roughness but does not reset the soil consolidation subfactor to 1 (see **Section 13.1.5.1**). Therefore, **operation descriptions** that include a **disturb (soil) surface process** must be included in **cover-management descriptions** to describe surface roughness. The input value for **initial roughness** in the disturb soil process in an operation description is an index for the roughness that the operation creates for a standard condition. **This standard condition is a smooth, silt loam soil, where the amount of soil biomass from buried residue and dead roots is very high in the soil disturbance depth after the operation** (see **Section 9.2.3.3**). RUSLE2 adjusts the input initial roughness value to obtain an **adjusted roughness** value for its erosion computations.

These adjustments are for:
soil texture (increased roughness for fine textured soils, decreased for coarse textured soils),

soil biomass in disturbance depth after operation (decreased roughness with decreased soil biomass), and

tillage intensity if the existing roughness is greater than the roughness created by operation on a smooth soil (resulting roughness is least affected by existing roughness as tillage intensity increases).

The initial roughness input value applies only to the **portion of the soil surface disturbed** and not to the entire soil surface. **The input value is not a net for the entire surface.**[111] RUSLE2 does not arithmetically average the roughness values for the disturbed and undisturbed portions of the soil surface. Instead, RUSLE2 computes a roughness subfactor value (see equation 9.10) for both the disturbed and undisturbed portions. These subfactor values are averaged based on the portion of the soil surface disturbed. This average roughness subfactor value is used to compute an **equivalent roughness** value for the entire surface that gives the proper net erosion for the entire surface.[112] This equivalent roughness value is decayed over time by precipitation amount and interrill erosion.

---

[111] The roughness input is different from the inputs for residue burial and resurfacing in the **disturb (soil) surface process** description. Burial and resurfacing input values are net for the entire soil surface.
112 Proper erosion is the net erosion that is computed to occur based on the undisturbed and disturbed surfaces. An equivalent roughness is determined that gives this net erosion.

The best approach for selecting input values for initial roughness is to base them on values in the RUSLE2 **core database**. Like other variables, the values in the RUSLE2 core database were selected to represent operation classes and types to ensure that RUSLE2 computes main effect erosion differences among operations based on research data and professional judgment. User selected initial roughness input values should be reviewed for consistency among implements, machines, and manual types of soil disturbance and for consistency with RUSLE2 core database values. The requirement is that RUSLE2 estimate expected erosion rather than exactly reproducing a field roughness measurement.

The scientific literature is a source of initial roughness input values, but literature values require modification using equations in **Section 9.2.3.3** before using them in RUSLE2. For example, the RUSLE2 initial roughness input values are often higher than comparable values used in other erosion models because of the standard condition used to define RUSLE2 initial roughness. The internal RUSLE2 adjusted roughness values are often similar to input values used in other models.

The RUSLE2 standard condition used to define initial roughness is the same as the one used in RUSLE1 (AH703). However, the RUSLE2 initial roughness input values differ from the RUSLE1 values because of the RUSLE2 tillage intensity effect that is not used in RUSLE1. RUSLE2 initial roughness values are less than comparable RUSLE1 values where tillage intensity is less than 1.

RUSLE1 initial roughness values can not be used directly in RUSLE2 without adjusting for the tillage intensity effect

Field measurements can be made to determine RUSLE2 input initial roughness subfactor values (see **Section 9.2.3.2**). The measurements are on a 1 inch (25 mm) grid using pins lowered to the soil surface or elevations determined using a non-contact method. The chain method should not be used to determine roughness values for RUSLE2. Elevations related to ridges should be removed, and a plane should be fitted to the data to remove land slope effects. The roughness measure used in RUSLE2 is the standard deviation of elevations about this plane. Equations described in **Section 9.2.3.3** must be used to adjust measured values for a particular field condition to the RUSLE2 standard condition for initial roughness. Sufficient measurements are made to account for both temporal and spatial variability. The intent is to characterize main effects of roughness using a diverse data set rather than representing a single, specific site condition.

13.1.5.6. Final roughness

The RUSLE2 subfactors described in **Section 9**, including the roughness discussed in **Section 9.2.3**, are relative to the unit plot conditions used to determine soil erodibility

factor values (see **Section 7.2**). The value for each subfactor is 1 for unit plot conditions. A roughness value of 0.24 inches (6 mm) is assumed to represent unit plot roughness. This roughness is similar to the roughness at harvest of a row crop where a moldboard plow, tandem disk, field cultivator, and row cultivator were used to till the soil. A 0.24-inch (6 mm) roughness is nearly but not completely smooth. A perfectly smooth soil surface has a roughness value of 0 inches (0 mm).

The 0.24-inch (6 mm) roughness represents the effect of a few erosion resistance clods on erosion. Even though **final roughness** represents the effect of a few erosion resistant clods, the input value for final roughness is not a function of soil texture. The effect of soil texture on final roughness is empirically represented in the soil erodibility factor values derived from unit plot conditions.

This empirical effect of soil texture on final roughness being included in the soil erodibility factor is but one reason why RUSLE2 definitions must be understood and followed.

A final roughness value of 0.24 inches (6 mm) is typically used in RUSLE2 for operation descriptions that create a roughness greater than 0.24 inches (6 mm) on a smooth soil. However, some operations leave a smoother surface than 0.24 inches (6 mm). A rotary powered tiller used to prepare a very fine seedbed is an example. This tiller creates almost uniform, small-sized soil aggregates (clods) and leaves almost no large clods in comparison to a moldboard plow, heavy offset disk, or chisel plow. Another example is a bulldozer or a road grader that cuts away soil leaving a very smooth surface. A 0.15-inch value is used for final roughness for these operations.

If the input value for final roughness is greater than or equal to 0.24 inches (6 mm), RUSLE2 decays roughness from a starting value to the final roughness value based on daily precipitation and daily erosion. If the input value for final roughness is less than 0.24 inches (6 mm), the input value for initial roughness should be the same as the input value for final roughness. RUSLE2 does not decay this roughness value.

Similarly, RUSLE2 does not decay roughness when the input values for both initial and final roughness are the same, even when the input value for final roughness is greater than 0.24 inches (6 mm). These inputs cause RUSLE2 to use a specific roughness value. An example of this application is representing roughness created by animal traffic, which also involves selecting compression for tillage type (see **Section 13.1.5.1**).

***Long term natural roughness*, discussed in *Section 10.2.7*, is the soil surface roughness that develops over time to soil consolidation after a soil disturbance. Final roughness and long term roughness are not the same, and the values entered for the two variables are not the same.**

13.1.5.7. Surface area disturbed

Some operations like planters disturb only a portion of the soil surface. The variable **portion of soil surface disturbed** directly affects the soil consolidation and soil surface roughness subfactors and indirectly affects the soil biomass subfactor, the effect of distance along an overland flow path on erosion, the effect of surface cover on erosion, and runoff (see **Section 9.2.6**).

Selecting proper values for the portion of the soil disturbed requires an understanding of the definition of soil disturbance, knowing the effect of soil disturbance on erosion, and recognizing indicators of soil disturbance. The definition of soil disturbance is given in **Section 9.2.6.3.**

Soil disturbance, as used in RUSLE2, occurs when an operation fractures and loosens the soil, displaces soil, mixes soil and surface residue so that the interface between the residue and the surface soil is no longer distinct, and disrupts a high organic matter layer at the soil surface.

The portion of the soil surface disturbed includes a **soil source area** and the **soil receiving area** that collects soil displaced from the soil source area. The soil source area is mechanically disturbed (disrupted) where the soil disturbing tool (e.g., disk blade, shank, or shovel) fractures, loosens, and displaces soil. This area is considered disturbed if the tool action penetrates below the residue (litter)-soil interface to mix underlying soil and residue (litter) and expose and displace mineral soil. The area disrupted by the tool should be considered to be disturbed if the disturbance depth exceeds an inch (25 mm) or two (50 mm).

Some tools run beneath the residue (litter)-soil interface and do little more than fracture and loosen the soil. This action is also soil disturbing even though mineral soil may not be exposed. However, the input value for the portion of the soil surface disturbed may be less that the actual field width of disturbance for conditions where the residue (litter)-soil interface remains largely intact and undisturbed. Selecting an input value for portion of the soil surface disturbed by undercutting involves comparing the surface high organic soil layer left after undercutting with this layer where no disturbance occurs.

The soil receiving area receives mineral soil displaced from the soil source area. The soil receiving area is considered disturbed if the residue (litter)-soil interface is disturbed and

Assigning input values for portion of the soil surface disturbed requires judgment. The effect being represented in RUSLE2 needs to be understood. A set of rules is highly useful to ensure that consistency is achieved in assigning input values among types of soil disturbances.

soil and residue (litter) are mixed. If the displaced soil is sufficiently deep that rill erosion does not penetrate the displaced soil layer, the buried residue (litter) has little direct effect on erosion and the entire receiving area should be considered disturbed. In this case, the portion of the soil surface disturbed includes the soil source area and all of the soil receiving area. A displaced soil depth of ½ inch (12 mm) or more is used as a guide in making this determination. The input value for the portion of the soil surface disturbed is reduced where rill erosion erodes through the displaced soil layer to the underlying intact reside (litter). The residue (litter) reduces erosion only after it becomes exposed.

Ridges are evidence of soil disturbance. Ridge creation requires a soil source area, and the receiving (ridge) area is soil of sufficient depth that erosion is unaffected by the underlying residue (litter). Ridges higher than ½ to 1 inch (12 to 50 mm) are considered to be disturbed areas.

The degree of soil disturbance is highly important considerations in determining the effectiveness of no-till cropping systems for controlling erosion. The two characteristics of these systems most responsible for their high erosion control effectiveness are the continuous presence of surface residue and a surface soil layer of high organic matter content, both of which are reduced by soil disturbance. **Both conditions must be present; high residue cover alone is not sufficient for the full no-till effect.** RUSLE2 uses **portion of the soil surface disturbed** along with the **soil consolidation subfactor** and **soil biomass** in the upper 2-inch (50 mm) soil layer to compute the effect of the upper high organic matter soil layer on erosion (see **Section 9.2.6**).

Portion of the soil surface disturbed by an operation and the **time since the last mechanical disturbance** are key variables. According to RUSLE2, surface residue cover is restored quickly in three years or less for much of the Eastern US after a single major disturbance such as moldboard plowing that buries almost the entire surface residue. About three to five years are required in much of the Eastern US to restore soil biomass in the upper 2-inch layer based on decomposition. This determination can be made by setting the **time to soil consolidation** to 1 year, which eliminates the effect of soil consolidation on the accumulation of soil biomass.

The accumulation of soil biomass in the upper 2-inch (50 mm) layer and the effect of this soil biomass on erosion are functions of the soil consolidation subfactor. Consequently, the total time for the no-till effect to be fully regained after a soil disturbance is about the same as the time entered in the **soil description** for the **time to soil consolidation**. The standard assumption for **time to soil consolidation** is seven years in most of the Eastern

US. RUSLE2 computes that most of the no-till effect is regained in about five years, as Table 13.4 illustrates for no-till 112 bu/ac corn **cover-management description** for Columbia, MO. This RUSLE2 estimate is consistent with the rule of thumb that five years is required for the full effect a no-till cropping system to be realized.

RUSLE2 computes a loss of the no-till effect that is almost as great with undercutting blade, chisel plow, field cultivator, and disk-type implements that disturb 100 percent of the soil as with soil inversion implements like moldboard plows. About one half of the no-till effect is lost directly through changes in the soil consolidation subfactor and the other half is lost through the effect of the soil consolidation subfactor being used as a variable in the soil biomass subfactor (see Figure 7.3 and equation 9.12).

Table 13.4. No-till effect after long term no-till is moldboard plowed in one year

Time (years) in no-till after moldboard year	Annual no-till effect (soil consolidation subfactor·soil biomass subfactor) weighted by erosivity distribution
1	0.61
2	0.49
3	0.39
4	0.32
5	0.28
6	0.25
7	0.24
8	0.23

All operations in a **cover-management description** are important in determining the degree of the no-till (lack of soil disturbance) effect. A single operation, such as a fertilizer/manure injector that disturbs as much as 50 percent of the soil surface causes RUSLE2 to compute a significantly reduced no-till effect (i.e., values closer to 1 for the product of the soil consolidation and soil biomass subfactors means a reduced no-till effect). The no-till effect is 0.54 where an injector that disturbs 50 percent of the surface is used with a planter that disturbs 15 percent of the surface for no-till 112 bu/acre corn at Columbia, MO. The no-till effect is 0.22 if the injector is not used for.

Multiple occurrences of an operation that minimally disturbs the soil surface in a cover-management description reduce the no-till effect. For example, the no-till effect is 0.22, 0.32, and 0.40 for one, two, and three occurrences, respectively, of a no-till planter on the same day in the Columbia, MO no-till corn example. **Section 9.2.6.4** describes the mathematical procedure that RUSLE2 uses where only a portion of the soil surface is disturbed by an operation. The net effect is similar to RUSLE2 assuming that most, but not all, of the soil disturbance is in an undisturbed area. RUSLE2 does not assume that a planter runs in the same place each year. However, the overlap effect was empirically considered by fitting RUSLE2 to no-till field data so that the expected erosion estimate is computed.

The large effect of the portion of the soil surface disturbed on estimated erosion is illustrated in Figure 9.19. This difference is significant when using RUSLE2 to estimate erosion for wide row (e.g., 30-inch width) no-till planters and narrow row no-till drills

(e.g., 7-inch width). The no-till effect is 0.22, 0.30, 0.57, and 0.62 for 15, 25, 65, and 85 percent for portion of the soil surface disturbed, respectively, for a no-till 112/bu/acre corn cropping system at Columbia, MO. These values illustrated that a small change in portion of the soil surface disturbed has a greater effect on estimated erosion when little of the soil surface is disturbed in comparison to when most of the soil surface is disturbed. The soil disturbance characteristics for both wide row and narrow row seeding implements should be very carefully considered in assigning values for **portion of the soil surface disturbed**. The tendency is to assign values that are too low for wide row implements and values that are too high for narrow row implements.

The effect of no-till cropping on soil erosion was analyzed in depth during the development of RUSLE2. To achieve maximum benefits from no-till cropping, the portion of the soil surface disturbed must be minimized.

13.1.5.8. Burial and resurfacing ratios

RUSLE2 assumes that an **operation description** with a **disturb soil process** buries **surface residue** and resurfaces **buried residue** as described in **Sections 9.2.5.3.3 - 9.2.5.5**. RUSLE2 only buries surface residue because standing residue must be flattened before it can be buried. Therefore, if an operation is being used to bury **standing residue**, the operation description must include a **flatten standing residue process** followed by a **disturb soil process**. RUSLE2 only resurfaces buried residue; it does not resurface **live** or **dead roots**.

The processes in an operation description must be entered in the proper sequence. To bury standing residue, proper sequence is flatten standing residue and disturb soil. A reverse order of these processes in an operation description will give a very different result.

The residue mass left on the soil surface after a soil disturbing operation is the **net** between the residue that is buried and the residue that is resurfaced. Having both residue burial and resurfacing components allows RUSLE2 to compute an increase in surface residue after an operation in certain conditions. An example is a field cultivator following a tandem disk and a moldboard plow in a high yield corn **cover-management description**.[113]

Input values for burial and flattening ratios are on a **mass basis** rather than on the

[113] RUSLE1 does not include a resurfacing component in its residue equations. Consequently, RUSLE1 can not compute an increase in residue cover following an operation like a field cultivator. RUSLE1 can not duplicate the residue burial values computed by RUSLE2. The residue burial ratio values used in RUSLE2 differ from those used in RUSLE1 because of the resurfacing component in RUSLE2.

portion of the soil surface covered even though RUSLE2 uses portion of soil surface covered to estimate erosion. RUSLE2 displays values for portion of the soil surface covered (e.g., percent cover) that are useful in conservation and erosion control planning.

The best information for selecting input values for burial and resurfacing ratios is the RUSLE2 **core database**. The values in the RUSLE2 core database have been carefully selected based on research data and the validation of RUSLE2 to ensure that it computes good estimates of surface residue cover immediately after planting and that it computes good estimates of average annual erosion.

Values for net residue burial ratio are widely available in the technical literature. Unfortunately, much of this literature fails to specify whether the values are based on residue mass or portion of the soil surface covered by residue. In many cases, a mixture of the two was unknowingly included because original sources failed to describe the basis for the values. Consequently, many of the widely available and accepted burial ratio values are not appropriate for RUSLE2 use.

Residue burial values based on mass are very different from those based on percent cover because of the strong non-linear relationship between residue mass and the portion of the soil surface covered by a given residue mass.

Residue burial ratio values in the technical literature almost always represent net burial (net effect of burial and resurfacing combined) rather than burial alone as required by RUSLE2. Consequently, RUSLE2 residue burial ratio values are higher than the common values in technical literature.

The net residue burial ratio computed by RUSLE2 for an operation depends on the operations and their sequence in the cover-management description and the soil biomass in the operation's disturbance depth. For example, RUSLE2 computes 17 percent for the net burial ratio for a tandem disk for a 150 bu/acre corn cover-management description where the tandem disk follows a moldboard plow. In contrast, RUSLE2 computes 53 percent for the net burial ratio for the same tandem disk following a chisel plow with straight points. This illustrates a reason for variability in field observed residue net burial ratio values.

Residue burial and resurfacing ratio values must be assigned to operation descriptions not in the RUSLE2 core database. Sometimes adjustments to the values in the RUSLE2 core database may be desired. The value RUSLE2 computes for surface residue mass after a soil disturbing operation is very sensitive to the resurfacing ratio value. Unfortunately, very little research data are available for determining values for the resurfacing ratio. **The best approach is to accept the resurfacing ratio values in the RUSLE2 core database without adjustments.** Residue burial ratio values are adjusted until RUSLE2 computes the desired residue cover following a particular operation.

The proper field data required to determine RUSLE2 residue burial and resurfacing ratio values are where as operation has been repeated three or more times in the same area.[114] A value for the resurfacing ratio can not be determined from a single occurrence of an operation. Repeated occurrences of an operation establish the equilibrium surface residue mass as illustrated in Figure 13.3. The first occurrence of the operation can be used to estimate a residue burial ratio value provided soil biomass is insignificantly low in the operation's disturbance depth.

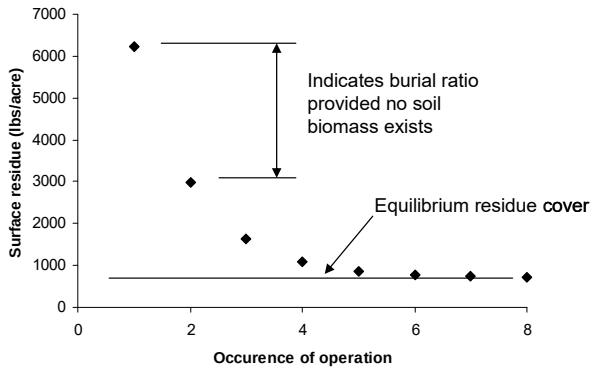

Figure 13.3. Residue burial by repeated occurrences of a field cultivator.

This residue burial ratio value along with the equilibrium surface residue mass can be used to estimate a resurfacing ratio value. The proper procedure for determining values for residue burial and resurfacing ratios is to fit RUSLE2's complete set of residue equations to field data.

Both residue burial and resurfacing ratios are a function of residue type discussed in **Section 12.1**. In general, residue burial ratio values are larger for residue that is in small, fragile pieces that break easily from the forces of a soil disturbing operation. Conversely, resurfacing ratio values are typically larger for residue composed of long, tough pieces. Therefore, size, shape, and fragility (inverse of toughness) all must be considered in selecting both burial and resurfacing ratio values. Rock/gravel is a special case where size and shape is a major factor.

The values in the RUSLE2 core database have been selected to represent the main classes of implements and machines that bury and resurface residue rather than describing specific machines operated in a specific way. The intent with RUSLE2 is to capture main effects within the overall accuracy of RUSLE2. The assigned burial and resurfacing ratio values, regardless of how they were obtained, should be consistent with values in the RUSLE2 core database and with values in the user's working database so that RUSLE2 computes the expected relative effects of the operation on erosion.

---

[114] Two excellent examples of the type of data needed to determine burial and resurfacing ratio values are:
Brown, L.C., R.K. Wood, and J.M. Smith. 1992. Residue management, demonstration, and evaluation. Applied Engineering in Agriculture. 8:333-339.
Wagner, L.E. and R.G. Nelson. 1995. Mass reduction of standing and flat crop residues by selected tillage implements. Transactions of the ASAE. 38:419-427.

The common assumption is that machines can be adjusted to produce almost any desired residue cover. This assumption is often erroneous. RUSLE2 includes relationships discussed in **Section 13.1.5.3** that describe how speed and disturbance depth affect residue burial based on research data. **Input residue burial ratio values outside of the range computed by RUSLE2 on the basis of varying disturbance depth or speed are highly questionable.**

13.1.6. Live biomass removed

The **remove live biomass process** removes live aboveground biomass without **killing** the current vegetation. This process is used in **operation descriptions** used to represent such operations as silage harvest, hay harvest, and mowing permanent vegetation. It's most important use is where a portion, but not all, of the live aboveground biomass is converted to standing and/or surface (flat) residue without killing the current vegetation. Examples include intercropping where one crop is harvested and a second crop continues to grow, volunteer weeds and cover crops that continue to grow after a main crop is harvested, and vegetation that regrows after a mowing or hay harvest. In these cases, some or all of the live root biomass remains, and some or all of the live aboveground biomass remains. The **kill vegetation process** can not be used in **cover-management descriptions** for these vegetation systems because this process converts **all** live aboveground biomass to standing residue and **all** live roots to dead roots, rather than portions of these biomass pools.

RUSLE2 assumes that live aboveground biomass can not be removed without substantially affecting the vegetation. Therefore, RUSLE2 requires that a **begin growth process** or a **kill vegetation process** follow the **remove live biomass process** in an **operation description**. The **begin growth process** identifies the **vegetation description** that RUSLE2 is to use immediately after the operation. If the live root biomass on day zero of the new vegetation description is less than the live root biomass on the last day that the previous vegetation description was used, **the difference is added to the dead root biomass pool because the operation is assumed to have killed a portion, but not all, of the current vegetation.**

Changes in aboveground biomass caused by the operation are described using the input values for the variables that describe the remove live biomass process. These variables are portion of live aboveground biomass **affected** by the operation, portion of the affected biomass left as **surface (flat) residue**, and portion of the affected biomass left as **standing residue**. Although the biomass removed from the local area (field, site) is not important to RUSLE2, this variable is used for user input convenience. RUSLE2 needs a description of the biomass at the site at any particular time to compute erosion. Thus, the biomass left behind either as remaining live biomass and residue after the operation are key variables. The values in the vegetation description identified by the **begin growth process** in the operation description describe the vegetation variables that

affect erosion after the operation. Therefore, the remove live biomass process tells RUSLE2 how much residue is left behind for an operation that affects the current vegetation but does not kill it.

Table 13.5 illustrates the input values for three typical operation descriptions where the **remove live aboveground biomass process** is used. The first example is mowing permanent vegetation where the biomass above the cutting height is left as surface residue and the vegetation regrows after the mowing. The amount of live biomass affected is the biomass above the cutting height. The affected biomass is assumed to be 50 percent of the total live aboveground biomass at the time of the mowing. All of the cut (affected) biomass is assumed to become surface residue. Thus, the input for portion of the affected biomass that becomes surface residue is 100 percent. The input is zero for the portion of affected biomass that is left as standing residue because the operation creates no standing residue. A **begin growth process** follows the **remove live biomass process** in the operation description to identify the vegetation description that RUSLE2 uses immediately after mowing. The canopy cover is reduced to reflect the mowing but the live root biomass remains the same between the current vegetation description and the new one.

Table 13.5. Input values for three operation descriptions that use the remove live aboveground biomass process (values on a dry matter basis)

Operation	Live aboveground biomass at time of operation (lbs/ac)	Live aboveground biomass affected (%)		Surface residue left by operation		Standing residue left by operation	
		Portion (%)	Mass (lbs/ac)	Portion (%)	Mass (lbs/ac)	Portion (%)	Mass (lbs/ac)
Mowing permanent vegetation that regrows	3,000	50	1,500	100	1,500	0	0
Legume hay harvest, hay regrows	2,000	95	1,900	5	95	0	0
Harvest small grain in a small grain-legume hay intercropping system	5,000	80	4,000	50	2,000	50	2,000

Note: Values for Portion are user entered input values. Mass values are computed by RUSLE2.

The second example is a legume hay harvest that removes live aboveground biomass and where the legume hay crop regrows after the hay harvest. In this example, 95 percent of the live aboveground biomass on the day of the operation is assumed to be affected. Only a small amount of stubble is left unaffected. The amount of the live aboveground biomass that is affected is 1,900 lbs/acre (= 2,000·95/100). All of the affected biomass is removed from the field except for five percent, which is 95 lbs/acre (= 1,900·5/100), that remains as surface residue. None of the affected biomass is left as standing residue. The surface residue left in the field is from leaf shatter and inefficiencies of the harvesting machines. The operation description includes a **begin growth process** immediately after the **remove live biomass process**. The **begin growth process** identifies the vegetation description that RUSLE2 is to use after the hay harvest. The canopy cover on day zero will be very low because the harvest left nothing but very short stubble. The root biomass does not change between the two vegetation descriptions because the hay harvest has no effect on live root biomass.

The third example is for an intercrop of small grain and legume hay. The small grain is seeded in the fall and the legume hay is seeded in late winter. The small grain is harvested in late spring, which kills that portion of the vegetation. The legume continues to grow after the small grain harvest to be killed by a hay harvest in late summer. The small grain harvest is represented with an operation description that includes a remove live biomass process followed by a **begin growth process**. The total live aboveground biomass at the time of the small grain harvest is 5,000 lbs/acre. Eighty percent (= 5,000·80/100 lbs/acre) of the total live aboveground biomass is affected by the small grain harvest. Half (50 percent) of the affected biomass is left as surface residue, which represents the straw discharged by the combine that harvested the small grain. The other half (50 percent) of the affected biomass is left as standing residue, which represents the standing small grain stubble left by the harvest. The **begin growth process** identifies the vegetation description that applies after the small grain harvest. Both the canopy cover and effective fall height values on day zero in the new vegetation description are reduced slightly from the values on the last day that the previous vegetation description was used. The legume already has a sufficient understory by the time of the small grain harvest that the legume is the major determinant of canopy cover and effective fall height (see **Section 9.2.1**). The live root biomass on day zero in the new vegetation description is significantly reduced from that on the last day for the previous vegetation description, which represents the combined small grain-legume hay vegetation. RUSLE2 assumes this difference to be dead root biomass created by the small grain harvest.

Relative (fractions, percents) rather than absolute variables are used to describe the remove live biomass process. Using an absolute variable like height above which the biomass is removed (e.g., cutting height) could be used for common machine operations

like mowing and hay harvest. However, using an absolute height as an input variable also requires user entered values for vegetation height and user entered values or user selected relationships that describe the distribution of the vegetation's biomass within the plant height. The judgment of the RUSLE2 developers was that users could more easily estimate the portion of total plant biomass involved in a remove live aboveground biomass process than users could determine the distribution of biomass within the plant height. Furthermore, relative variables generalize RUSLE2, which gives RUSLE2 additional power and broadens its applicability. For example, RUSLE2 can be used to evaluate operations like hand picking of leaves over the entire canopy, which can not be described using an absolute height approach where all biomass above a given height is affected. Also, this approach gives the user direct control of aboveground biomass values that RUSLE2 uses in its computations.

Unfortunately the relative variable approach means that input values that describe the remove live biomass process are functions of the height above which the biomass is removed, vegetation type, and stage of growth. For example, a particular mower is operated at the same height regardless of the vegetation and its stage of growth. The portion of the biomass affected might be 90 percent for mature, tall weeds but less than 50 percent for early growth weeds and some grasses. Users should develop typical operations that use the remove live biomass process for several vegetation types and conditions.

Values in the RUSLE2 **core database** can be used as a guide for selecting input values for the remove live biomass process. Input values should be checked by making RUSLE2 computations to ensure that the values give expected standing and surface residue amounts. Input values should also be checked for consistency with values in the RUSLE2 core database and values in the user's working database.

Input values for the remove live biomass process are selected considering that the RUSLE2 objective is to describe a field condition rather than to model (simulate) the condition.

13.1.7. Remove residue/cover

The **remove residue/cover process** removes standing and surface (flat) residue. This process is used in **operation descriptions** such as burning and baling straw where a preceding operation description has created standing and/or surface (flat) residue. This process is also used in operation descriptions to represent silage and hay harvests where the current vegetation is live at the time of the operation. A **kill vegetation process** must precede the **remove residue/cover process** in a silage or hay harvest operation description to convert the live aboveground biomass to standing residue and/or surface (flat) residue. **The remove residue/cover process only removes standing and surface (flat) residue**; it does not remove live aboveground biomass. See **Section 13.1.6** for

information on how to remove live aboveground biomass.

The three variables used to describe the remove residue cover process are: (1) are all residues affected, (2) portion of surface (flat) residue removed, and (3) portion of standing residue removed.

The first variable is related to how many residue applications on the surface that are to be removed. A **cover-management description** may involve several **residue descriptions** when multiple vegetation descriptions are involved. (e.g., corn, soybean, wheat). Multiple residue descriptions may also be involved when residue is added with the **add other cover process** (see **Section 13.1.8**). Added residues include manure spread on the soil surface and surface applied mulch, such as wheat straw, woodchips, erosion control blankets, and rock.

The input **yes** for the variable **are all residues affected** tells RUSLE2 to remove the same portion of all residues regardless of source, age, or how the residue was placed on the soil surface. An example operation description for this **yes** input is a burning operation that removes some of all residues that are present at the time of the operation.

An example of a **no** input is for a baling straw operation description in a cover-management description for a corn-soybean-wheat crop rotation. The baling straw operation description follows a wheat harvest operation description that kills the wheat to create standing and surface (flat) residue.[115] The **no** input tells RUSLE2 to only remove a portion of the wheat residue, which is the **last** residue description considered by RUSLE2 before the baling straw operation. Residue from previous crops of corn, soybeans, and wheat would not be removed. That is, the **no** input causes only the most recent residue application to be affected.

Inputs for the second and third variables are for the portions of the surface (flat) and standing residue that are removed by the remove residue/cover process. **These variables are on a dry mass basis**. In the baling straw operation description, a zero (0) is entered for the portion of the standing stubble removed because the baling operation has no effect on the standing straw stubble left after the wheat harvest other than to flatten it. If the **flatten standing residue process** occurs in the operation description before the remove residue/cover process, RUSLE2 will remove a portion of the surface (flat) residue created by the **flatten standing residue process** along with the same portion of the other surface (flat) residue.

In the burning operation description, a value of 90 percent is entered for the portion of the standing stubble removed by burning and 25 percent is entered for the portion of the

[115] The processes that describe the wheat harvest and the baling straw operations could be combined into a single operation description provided the harvest and straw baling operations occurred within a few days of each other before residue biomass decreases significantly by decomposition.

surface (flat) residue removed. The reason for the different input values is that the standing residue is assumed to be dry and to burn much more completely than the surface residue that is in contact with soil.

RUSLE2 can remove **buried residue**, but the residue must first be resurfaced with an operation description that includes a **disturb soil process** (see **Section 10.26**). Once the buried residue has been resurfaced as surface (flat) residue, it can be removed with an operation description that includes a remove residue/cover process. Dead roots can not be removed because RUSLE2 has no direct way to remove dead roots and dead roots can not be brought to the surface with a disturb soil process.

Values in the RUSLE2 **core database** can be used to guide the selection of input values for the remove residue/cover process. RUSLE2 computations should be made with the selected input values to ensure that RUSLE2 computes the expected residue cover left by the operation with a remove residue/cover process. Also, input values for the process should be checked for consistency with comparable values in the RUSLE2 core database and the user's working database.

13.1.8. Add other cover

The **add other cover process** is used in **operation descriptions** to place material that affects erosion on the soil surface and in the soil.[116] Typical operations descriptions using this process describe applying mulch on construction sites and in strawberry fields and manure and organic municipal and industrial waste (e.g., papermill waste) to crop and other lands.

The **add other cover process** involves three variables. Two variables are the description of the material added and the amount (dry mass basis) of the material added. These inputs are entered in the **cover-management description** that contains the operation description that uses the add other cover process (see **Section 10.6**). The entry for the type of material added, referred to as **external residue**, is selected from the list of **residue descriptions** in the **residue component** in the RUSLE2 database (see **Section 12**). The material added by this process has sufficient size to reduce the erosive forces of raindrop impact and runoff. Also, the material is generally assumed to be organic (biomass) that decomposes and affects erosion similarly to the decomposition of crop residue and plant litter. The procedure for handling non-organic material such as rock and synthetic erosion control blankets applied to the soil surface to control erosion is described in **Section 12.4**.

The third input, which describes the **add other cover process** itself, is the portion (dry

[116] This process is **not** used to add irrigation water (e.g., see **Sections 6.3.4, 10.2.4**). Also, this process is **not** used to represent the addition of chemical compounds that affect soil erodibility. That effect must be represented by adjusting soil erodibility factor values (see **Section 7.3**)

mass basis) of the material that is added to the soil surface. RUSLE2 places the remainder of the added material in the soil. A 100 percent value is used to represent applying straw mulch at a construction site, for example, where none of the material is incorporated into the soil. A value less than 100 percent instructs RUSLE2 to place some of the material in the soil. A zero (0) value places all of the added material in the soil.

If the **add other cover process** places some of the added material within the soil, a companion **disturb soil process** must immediately follow the **add other cover process** in the operation description. RUSLE2 assumes that the soil must be disturbed for material to be placed in the soil, which resets the soil consolidation subfactor to 1 for the portion of the soil surface disturbed except when a **compression tillage type** is assumed.[117] Material placed in the soil using the **add other cover process** is placed in the lower one half of the disturbance depth as illustrated in Figure 9.16. The value for disturbance depth is entered in the **disturb soil process** that follows the **add other cover process** in the operation description.

13.1.9. Add non-erodible cover

RUSLE2 describes the effect of both erodible cover and non-erodible cover. **Erodible cover** is surface cover provided by residue and live ground cover. Residue includes material left by vegetation growth, applied mulch, erosion control blankets, and rock. These materials are referred to as erodible covers because RUSLE2 computes erosion even when these materials completely cover (100 percent cover) the soil surface.

The *add non-erodible cover process* can not be used to represent the application of erosion control blankets and similar materials. That effect is represented using the *add other cover process*.

In contrast, RUSLE2 computes no erosion for **non-erodible cover** for the portion of the soil surface covered by these materials. Consequently, RUSLE2 computes no erosion when these materials completely cover the soil surface. Examples of non-erodible cover include plastic sheeting used in vegetable production, a water depth produced by flooding rice fields, and deep snow.

RUSLE2 assumes a linear relationship between erosion and non-erodible cover, in contrast to the non-linear relationship illustrated in Figure 9.4 for surface residue. Therefore, erosion varies linearly with non-erodible cover as it disappears over time.

---

[117] An exception is that a **compression tillage type** can be selected in the **disturb soil process** to place material in the soil without resetting the soil consolidation subfactor value to 1. However, this tillage type is specifically meant to describe the effects of animal traffic, sheep's foot soil compaction machines, and similar operations and not meant to describe injection of manure and fertilizer by typical machines used in these operations.

A non-erodible cover is also used to "shut off" RUSLE2's erosion computations for certain periods. An example is turning off erosion computations during winter periods during frozen soils and/or snow cover. Another example is turning off erosion computations for periods when the RUSLE2 annual computational period does not correspond with the erosion control planning period. Some erosion control regulations for constructions sites require a certain level of erosion control between the date of final grading and the date that vegetation reaches a particular canopy cover. The assumption is that erosion control is adequate once the vegetation reaches a certain canopy cover. Thus, erosion computations are turned off for dates beyond the end date based on canopy cover.

13.1.9.1. Applications of add non-erodible cover process

The **add non-erodible cover process** is used in **operation descriptions** to cause RUSLE2 to compute no (zero) erosion for the portion of the soil surface covered by the non-erodible cover. Example applications include applying strips of plastic mulch in vegetable production, applying ponded water in rice production, representing no erosion during snow cover, and setting computed erosion to zero for computational purposes.[118] An operation description with a **remove non-erodible process** is used to remove non-erodible cover when the period of no erosion ends.

An example of using the **add non-erodible cover process** for computational purposes is a construction site where the overland flow path changes during construction and reclamation. The first analysis period represents the exposed hillslope from clearing and scalping until the topography is reshaped. The second analysis period represents the time after the hillslope is reshaped and erosion control practices are applied before permanent vegetation becomes established. The third analysis period is for mature, fully established vegetation.

Reshaping the hillslope creates a new overland flow path, which requires multiple sets of RUSLE2 computations because RUSLE2 can not change overland flow paths during a **cover-management description**. In this example, a cover-management description is created for each analysis period, and a RUSLE2 computation is made for each overland flow path using the corresponding **soil**, **cover-management**, and **support practice descriptions**. Table 13.6 outlines the three RUSLE2 computations for this example.

The date that RUSLE2 starts its computations must be set first. RUSLE2 operates and accounts for erosion on an annual basis. In this example, the 9/1/0 start date is set one year before the day that the hillslope is reshaped that creates a new overland flow path. The date that the hillslope is reshaped is the reference date in this example. **Section**

[118] This procedure is used in RUSLE2 to set erosion to zero. The comparable procedure used in RUSLE1 to set erosion to zero was to enter a 100 percent canopy cover at a zero fall height. This RUSLE1 technique can not be used in RUSLE2 (see **Section 9.2.1**).

10.2.1.3 describes procedures that can be used to cause RUSLE2 to start tracking time on a particular date.

The first RUSLE2 computation must end on the day before the new overland flow path is created. The erosion that RUSLE2 computes between 9/1/0 and 4/15/1 must be excluded from RUSLE2's accounting of erosion. This erosion is excluded by using an operation description that adds non-erodible cover on 9/1/0 and an operation description that removes the non-erodible cover on 4/15/1. The non-erodible cover causes RUSLE2 to set erosion to zero during this preliminary period. This approach starts RUSLE2's erosion accounting on 4/15/1 with the clearing and scalping of the hillslope.

Table 13.6. RUSLE2 computations for a construction site example where the overland flow path changes during construction and reclamation

RUSLE2 computation	Date	Event	Overland flow path	Cover-management description	Soil description
1	9/1/0	RUSLE2 starts tracking time	Natural topography	Non-erodible cover	Natural soil profile
	4/15/1	Cleared and scalped		Bare soil, freshly disturbed	
2	9/1/1	Reshaped, temporary erosion control, permanent vegetation seeded	Reshaped topography	Graded, temporary erosion control applied, permanent vegetation seeded	Highly disturbed
3	9/1/4	Permanent vegetation becomes established		Mature vegetation conditions	

Notes:

1. The first date is set so that RUSLE2's annual erosion accounting for the first period ends on the last day before the topography is reshaped that creates a new overland flow path.
2. NRCS soil survey data applies to the natural topography. Soil conditions after reshaping are highly disturbed, which requires use of the RUSLE2 modified soil erodibility nomograph.
3. Cover-management conditions after reshaping could be described with a single cover-management description rather than two as illustrated.

The second analysis period begins on the date (9/1/1) that the hillslope is reshaped and a new overland flow path is established. The third analysis period begins when the

vegetation has become mature and fully established (see **Section 11.2.6**). The last two analysis periods can also be combined into a single period using a single cover-management description.

An alternative approach is to start RUSLE2's tracking time on the clearing and scalping date (4/15/1). However, because of RUSLE2's annual accounting, it will include erosion computed from 4/15/1 through 4/14/2 using the first overland flow path. The computed erosion from 9/1/1 through 4/14/2 must be excluded in RUSLE2's erosion accounting to obtain an erosion estimate for just the 4/15 to 9/1 period. This erosion can be excluded by using an operation description that adds non-erodible cover on 9/1/1.

The accounting date in RUSLE2 computations for the second analysis period can start on 9/1 by having the first date in the cover-management description be on 9/1 or it can start on 4/15 if an erosion estimate is needed for each year starting on 4/15. To start RUSLE2's accounting on 4/15/1 for the second analysis period, use an operation description that adds non-erodible cover on 4/15/1 and an operation description that removes the non-erodible cover on 9/1/1. RUSLE2 will set erosion to zero during this period when non-erodible cover is present. The estimated erosion for the period 4/15/1 to 4/14/2 can be obtained by adding the annual erosion from these two RUSLE2 computations.

13.1.9.2. Variables used to describe add non-erodible process

The variables used to describe the **add non-erodible cover process** are the portion of the soil surface covered by the non-erodible cover, half-life of the cover, and permeability of the cover. The value entered for the **portion of the soil surface covered** is the portion of the total area having zero erosion because of the non-erodible cover. This value is 100 percent for applying ponded water on rice fields or for the computational purpose described above where erosion is to set to zero for the entire area. Erosion is set to zero on the entire area. The value is less than 100 percent when strips of plastic are applied in a vegetable field resulting erosion being set to zero for only a portion of the total area.

Half-life is the time required for half of the non-erodible cover to disappear based on a simple exponential relationship involving time. RUSLE2 does not compute the loss of non-erodible material as a function of environmental conditions as it does for residue. The value entered for half-life must represent how local site conditions, such as ultraviolet radiation, temperature, or precipitation, affect loss of the non-erodible cover. Thus, input values for half-life for non-erodible cover can vary with location.

The loss of non-erodible cover is computed solely on an area basis, although mass per unit should be considered in assigning half-life input values. RUSLE2 does not use a mass-cover relationship for non-erodible cover like it does in residue descriptions.

A very large value, such as 1,000,000 days is input for half-life where non-erodible cover does not disappear over time. Refer to manufacture's literature for selecting input values for plastic and similar products. A half-life value can be used to approximate the loss of snow cover, but using RUSLE2 to compute erosion by snowmelt is questionable (see **Sections 6.9.1 and 6.11**). Selected input half-life values should be checked by making RUSLE2 computations to ensure that RUSLE2 computes the expected non-erodible cover over time for the conditions where RUSLE2 will be applied.

Although RUSLE2 computes no erosion for the portion of the soil surface covered by the non-erodible cover, RUSLE2 needs information on how non-erodible cover affects runoff. Deposition computed by RUSLE2 on concave-shaped overland flow paths, behind dense strips of vegetation, and in terrace channels is a function of runoff. If non-erodible cover significantly increases runoff, the computed deposition amount may be significantly reduced. RUSLE2 uses the value entered for non-erodible cover permeability and portion of the soil surface covered by the non-erodible cover to compute runoff.

The input value entered for **non-erodible cover permeability** is the portion of the precipitation that passes through the cover. Many non-erodible covers, such as plastic used in vegetable production and ponded water in rice fields, are impermeable. A value of zero (0) is entered for those materials. If all of the precipitation passes through the cover, 100 percent is entered. An input value less than 100 percent is entered when some but not all of the precipitation passes through the non-erodible cover. For example, 50 percent is entered if half of the precipitation passes through the non-erodible cover and the other half runs off the cover onto the soil surface.

Non-erodible cover such as plastic on the top of beds in vegetable fields completely eliminates both interrill and rill erosion. However, significant rill erosion can occur where runoff accumulates and flows onto the portion of the soil surface not covered. Also, runoff can accumulate under non-erodible cover to cause erosion. Therefore, the presence of non-erodible is not sufficient *alone* to completely eliminate erosion in all situations.

13.1.10. Remove non-erodible cover

The **remove non-erodible cover process** is used in **operation descriptions** to remove part or all existing non-erodible cover. The single variable used to describe this process is the portion of the non-erodible cover that is removed by the process. An input value of 100 percent completely removes non-erodible cover. An input value less than 100 percent removes that portion of the non-erodible cover. For example, assume that non-erodible cover is 62 percent and 50 percent is the input value for portion removed. The non-erodible cover after the removal operation will be 62% ·50%/100 = 31%. The non-erodible cover may have covered 100 percent of the soil surface when it was initially

applied, but it only covers 62 percent of the soil surface on the removal date because of loss by ultraviolet radiation or other processes.

14. SUPPORT PRACTICES DATABASE COMPONENTS

Support practices include contouring (ridges around the hillslope), filter and buffer strips (strips of dense vegetation on the contour), rotational strip cropping (a system of equal width cropping strips that are annually rotated with position along the overland flow path), terraces and diversions (ridges and channels that divide the overland flow path, collect runoff, and redirect it around the hillslope), and small impoundments (impoundment terraces and sediment traps). These practices are referred to as support practices because they are used to support primary cultural erosion control practices based on vegetation, crop residue, plant litter, and applied mulch. The effect of cultural erosion practices on erosion is described with the cover-management variables (see **Section 10**). Most support practices affect rill and interrill erosion and sediment delivery by reducing runoff's erosivity and transport capacity by redirecting the runoff around the hillslope; dividing the overland flow path that reduces the accumulation of runoff; slowing the runoff with strips of rough soil surface, heavy surface residue, or dense vegetation; and capturing and ponding runoff.

RUSLE2 computes how support practices affect **interrill** and **rill erosion** and **sediment yield** at the end of the flow path represented in a RUSLE2 computation (see **Sections 5.1, 5.3.1, 8.2.5**). Most properly designed, installed, and maintained support practices also reduce ephemeral gully erosion. However, RUSLE2 is not a conservation or erosion control planning tool for ephemeral gully erosion because RUSLE2 does not estimate ephemeral gully erosion.[119] RUSLE2 gives partial, indirect credit for reduction of ephemeral gully erosion by contouring and rotational strip cropping. Some of the data used to empirically derive RUSLE2's contouring relationships were measured on small watersheds, less than about 5 ac in size, where ephemeral gully erosion occurred on the non-contoured experimental watershed.

The benefits of support practices for controlling ephemeral gully can only be considered using a procedure other than RUSLE2.

Each support practice affects erosion and sediment delivery in a unique way. Therefore, each major support practice is discussed individually.

14.1. Contouring (ridge orientation relative to overland flow path)

14.1.1. Description of practice

[119] Conservation planners sometimes assume that the USLE and RUSLE1 describe all erosion that occurs within farm fields, which is not the case with these prediction technologies or with RUSLE2. Ephemeral gully erosion is not estimated with any of these technologies and can amount to one half or more of the total sediment production that occurs within field sized areas.

Contouring is the creation of ridges and furrows by tillage equipment, earth moving machines, and other soil disturbing operations to redirect runoff from a path directly downslope to a path around the hillslope.[120] Grade along the furrows is zero when contouring is "perfectly on the contour," which results in runoff spilling uniformly over the ridges along their length. If furrow grade is not level, runoff flows along the furrows until it reaches low ridge heights or local low areas on the hillslope. The runoff break over ridges in these locations as illustrated in Figure 8.13.

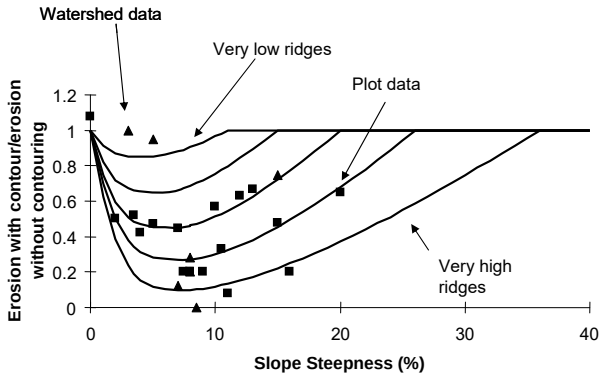

Figure 14.1. Experimental data on how contouring affects erosion.

Section 8.3.6 describes the three RUSLE2 methods that can be used to estimate how contouring affect erosion. The first two methods apply where the ridges are so high, well defined, and on a sufficiently uniform grade that runoff flows to major concentrated flow areas on a hillslope before overtopping the ridges. Application of these two methods is based on a detailed overland flow path description. The **third method** is for typical ridges left in farm fields by tillage equipment like tandem disks, chisel plows, and field cultivators and on reclaimed mined land and other highly disturbed lands by ridgers. This method uses the RUSLE2 relationships that describe contouring (ridging) as a support practice and a overland flow path description based on a flat soil surface.

14.1.2. Basic principles

RUSLE2 uses a daily value for the contouring factor p_c in equation 8.1 to compute the effect of contouring. This subfactor is the ratio of erosion with contouring to erosion without contouring. A value of 1 means that contouring has no effect on erosion. The value for the contouring subfactor is lowest when contouring has its greatest effect on erosion.

The effect of contouring on erosion that was measured on research plots and watersheds is illustrated in Figure 14.1. The effect of contouring varied greatly among the studies.

[120] Contouring in RUSLE2 refers to how orientation of ridges with respect to the overland flow path affects erosion. Standards for erosion control practices published by organizations like the USDA-Natural Resources Conservation Service require that ridging meet certain specifications to be considered the specific erosion control practice of contouring.

For example, contouring reduced erosion as much as 90 percent in one study but did not reduce erosion in another study also conducted on a 6 percent slope steepness.

Information from the research studies represented in Figure 14.1 and from other research studies was not sufficient to empirically derive RUSLE2 contouring relationships. The data were sufficient, however, to identify the main variables that determine how contouring affects erosion. That basic information, along with accepted erosion scientific knowledge and scientific and technical judgment were used to develop the mathematical relationships used in RUSLE2 to compute how contouring affects rill and interrill erosion.

14.1.2.1. Steepness

The first variable considered in developing the equations used to describe the contouring effect illustrated in Figure 14.1 was slope steepness. Contouring does not affect erosion at a flat slope because no preferred runoff path exists. Contouring also has no effect at very steep slopes because the ridge top is at a lower elevation than the ridge base (furrow) on the upper side of the ridge as illustrated in Figure 14.2. The ridge top elevation relative to the elevation of the upslope furrow is a function of both slope steepness and ridge height, which determine the slope steepness that contouring loses its effectiveness.

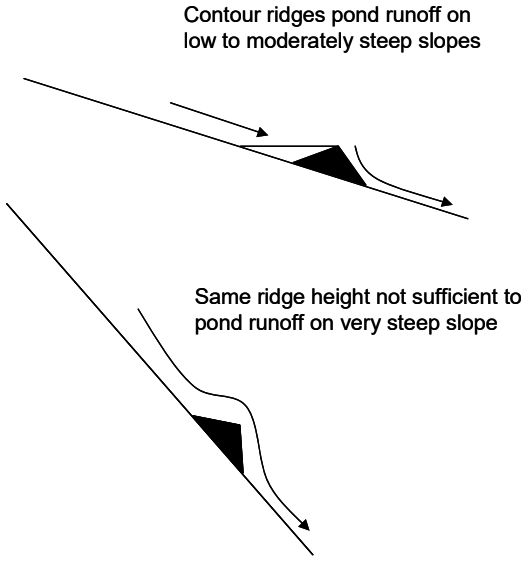

Figure 14.2.Effect of slope steepness and ridge height on contour ridges ponding runoff.

The general shape of the RUSLE2 relationship for contouring's effect on erosion is illustrated in Figure 14.1. The curve decreases from a value of 1, which means that contouring has no effect on erosion, for a flat slope (zero steepness) to a minimum value at a moderate slope steepness, which is the slope steepness that contouring has its greatest reduction on erosion. The curve increases from the minimum value to 1 (no effect) at a steep slope based on the concept that the steepness is so great that no runoff is ponded as illustrated in Figure 14.2 (see AH537, AH703). [121]

14.1.2.2. Ridge height

[121] The relative effect of slope steepness on contouring in RUSLE2 is the same as that in the USLE. The middle curve in Figure 14.1 is very similar to the contouring-slope steepness effect in the USLE (AH537).

The second variable considered was ridge height. The basic concept is that contouring's effect on runoff and erosion is a function of ridge height. Figure 14.2 illustrates the concept for steep slopes. Field data from research plots also showed that erosion decreased as ridge height increased. The ridges on these plots were perfectly on the contour on a moderate slope steepness. The overall variability illustrated in Figure 14.1 for the effect of contouring on erosion was interpreted as being caused by a variation in ridge height.

Contouring is assumed to lose its effectiveness over time as ridge height decays. In RUSLE2, ridge height decays after it is created because water from precipitation causes the soil to subside and as interrill erosion erodes the ridges (see **Section 9.2.4.3**).

Experimental data involving wheat and soybeans showed that closely spaced stems in rows on the contour affect erosion much like soil ridges on the contour. Therefore, RUSLE2 adds an effective vegetative ridge height to the soil ridge height to give an overall ridge height that is used by RUSLE2 to compute the effect of contouring on erosion. The effective vegetative ridge height increases as vegetative retardance increases, which is a function of the retardance class assigned in the vegetation description (see **Section 11.1.4**), yield (production) level, and growth stage.

14.1.2.3. Storm severity and runoff

Experimental plot data showed that contouring's effectiveness (p_c) is greater for small storms than for large storms (i.e., p_c values are less for small storms than for large storms). One reason for this difference in effectiveness is that a higher percentage of the excess rainfall (rainfall in excess of infiltration) is stored in ponded runoff behind the ridges for small storms than for large storms. Similarly, contouring reduces erosion more for low runoff amounts than for high runoff amounts. Therefore, RUSLE2 computes values for the contouring subfactor p_c that decrease as runoff depth decreases.

The minimum contouring factor value at the low point of each curve illustrated in Figure 14.1 is reduced linearly with runoff depth. Also, the slope steepness above which contouring has no effect on erosion is computed as a function of runoff depth raised to the 0.857 power. This power is based on the assumption that the maximum slope steepness at which contouring is effective for a given ridge height is a function of the shear stress that the runoff applies to the soil. The runoff variable used by RUSLE2 to compute contouring subfactor values is the ratio of runoff computed for the site specific condition to runoff computed for the base condition of a moldboard plowed, clean tilled, low yielding corn grown on a silt loam soil in Columbia, MO (see **Section 8.1.2**).

Field data from contouring on small watersheds (less than five acres) in the south central US showed that the effectiveness of contouring is related to storm severity. The data showed that erosion with contouring can be greater for very intense storms than for a

comparable non-contoured situation. The intense storms caused much ridge breakovers, concentration of overland flow in a few rills which causes increased rill erosion, and a cascading effect similar to dam failures releasing water. These effects partially accounts for contouring subfactor values being greater than 1 in Figure 14.1. Also, moderate and large storms cause most of the erosion. The 24-hour precipitation amount with a 10-year return period rather than a precipitation amount based on an average annual return period is used in RUSLE2 to compute runoff depth. The 10-year return period captures how a more severe than average annual storm has a dominant effect on how much contouring reduces erosion.

The RUSLE2 computed contouring subfactor values vary daily as cover-management conditions change. The runoff curve number is a key variable in the NRCS runoff curve number method. RUSLE2 computes values for the curve number as a function of surface roughness, ground cover, soil biomass, and soil consolidation, which in turn means that runoff and contouring subfactor values vary daily in RUSLE2.

14.1.2.4. Relative row grade (ridge-furrow orientation relative to overland flow path)

In this RUSLE2 procedure for computing how contouring affects erosion, the overland flow path is determined assuming a flat soil surface without ridges. The contouring subfactor p_c value is 1 by definition for a ridge-furrow orientation directly **up and down hill** (parallel to the overland flow path). Contouring subfactor values are less than 1 when the ridge-furrow orientation is **perfectly on the contour** (perpendicular to the overland flow path).[122] **Relative row grade**, which is the ratio of absolute row (furrow) grade to the overland flow path steepness, is RUSLE2's measure of ridge-furrow orientation to the overland flow path.[123] A relative row grade of 1 means that the ridge-furrow orientation is up and down hill parallel to the overland flow path, and a relative row grade of zero (0) means that the ridge-furrow orientation is perfectly on the contour and perpendicular to the overland flow path. A 0.1 relative row grade means that the ridge-furrow orientation is slightly off contour, and a 0.5 relative row grade means that the ridge-furrow orientation is half way between being perfectly on the contour and up and down hill.

[122] The **cover-management description** must include a **soil disturbing operation description** that creates ridges with a greater than zero height for RUSLE2 to compute a contouring subfactor value less than 1. That is, ridges with a height greater than zero must be present for RUSLE2 to compute a contouring effect.
[123] Even though absolute row grade can be entered into RUSLE2, RUSLE2 uses relative row grade to compute how ridge-furrow orientation to the overland flow path affects erosion.

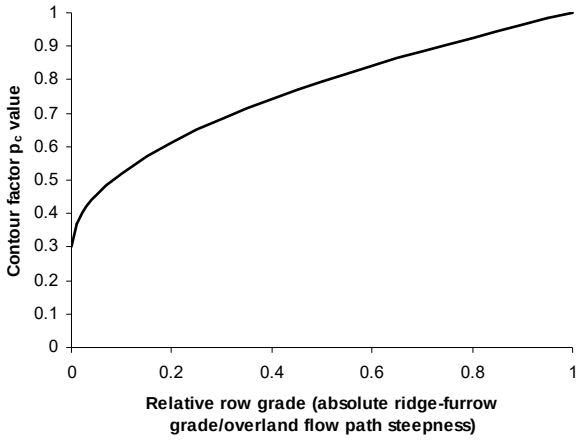

Figure 14.3. Effect of relative row grade on the contouring subfactor p_c.

RUSLE uses the empirical relationship illustrated in Figure 14.3 to compute contouring subfactor p_c values for ridge-furrow orientations between these two extremes. The assumption implicit in Figure 14.3 is that contouring rapidly loses effectiveness as ridge-furrow orientation deviates from being perfectly on the contour (i.e., as relative row grade increases from zero). This assumption is supported by the limited research data available for validation.

14.1.2.5. Contouring failure (critical slope length)

Contouring fails and totally loses its effectiveness when the combination of runoff rate and steepness along the overland flow path becomes too great for the given cover-management condition. The high contouring subfactor values in Figure 14.1 represent such failure based on the description of the field conditions in the research report. On simple uniform overland flow paths where soil, steepness, and cover-management do not vary spatially, a **critical slope length** is defined as the location along the path where contouring fails from that location through the end of the overland flow path. The contouring subfactor value for the upper portion of the overland flow path from its origin to the critical slope length location is the RUSLE2 computed values for contouring (i.e., contouring is fully effective). The contouring factor value is set to 1 for the portion of the overland flow path from the critical slope length location to the end of the path (i.e., contouring has completely failed). The contouring subfactor makes a step increase, rather than a gradual increase, at the critical slope length location as illustrated in Figure 14.4. Contouring subfactor values do not vary with distance along the overland flow path because RUSLE2 contouring subfactor values are based on runoff depth, not runoff rate.

RUSLE2 does not compute contouring failure and a critical slope length if the overland flow path length is sufficiently short. ***Also, contouring failure and critical slope length are not a function of ridge height or soil erodibility properties.***

RUSLE2 assumes contouring failure when the runoff applies a shear stress to the soil in the ridges that exceeds a critical shear stress related to ridge stability.[124] The shear stress

[124] Shear stress applied to the soil is a frictional type force per unit area much like the frictional force felt

applied to the soil by runoff **increases** as runoff rate and steepness of the overland flow path increase and **decreases** as total hydraulic roughness provided by cover-management increases.[125] Runoff rate is a function of both runoff depth and location along the overland flow path (see **Section 8.1.2**). Shear stress applied to the soil decreases as cover-management intensity increases because of the effect of cover-management on both runoff depth (hence, runoff rate) and the total hydraulic roughness (see **Section 14.2.3**).[126] Contouring failure increases and critical slope length decreases for a given cover-management condition as steepness of the overland flow path increases. Contouring failure increases with a change in location where storm erosivity represented by the 10-year, 24 hour precipitation amount increases. Conversely, contouring failure is reduced by increased soil surface cover, soil-surface roughness, and vegetation retardance and cover-management practices that reduce runoff, all of which reduce runoff's shear stress that causes contouring failure. Contouring failure on long overland flow paths is reduced by changing cover-management conditions that reduce runoff's shear stress and/or by dividing the overland flow path with terraces/diversions.

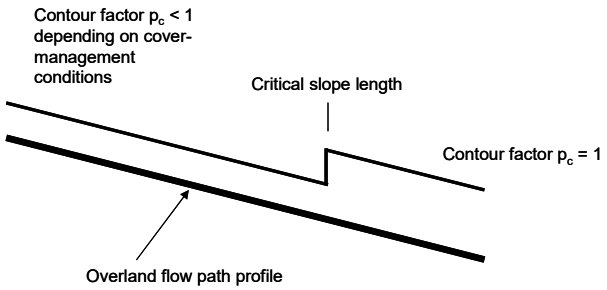

Figure 14.4. Illustration of critical slope length and contouring subfactor values for a uniform overland flow path.

Depending on conditions, RUSLE2 computes zones of contour failure along complex overland flow paths, like that illustrated in Figure14.5. Contouring failed in the mid-portion of the overland flow path because of the combination of runoff rate (represented by distance from the path origin) and steepness. Runoff's shear stress acting on the soil exceeds the soil's critical shear stress in this zone. Contouring does not fail on the upper portion of the overland flow path. The combination of runoff rate and steepness is low because distance is short even though steepness becomes large. Contouring failure ends on the lower portion of the overland flow path because the combination of runoff rate and steepness decrease so that the runoff's shear stress acting on the soil decreases below the soil's critical shear stress even though distance is large.

---

when your hand is rubbed by sandpaper.

[125] Total hydraulic roughness is composed of two parts, the part related to the shear stress that the flow exerts on the soil particles (referred in channel hydraulics as grain roughness) that causes erosion and sediment transport and the part related to the shear stress applied to hydraulic elements (referred to as form roughness) including soil surface roughness (e.g., clods), ground cover (e.g., surface residue and live ground cover), and plant stems.

[126] An increase in cover-management intensity refers to an overall increase in soil surface roughness, surface residue cover, aboveground biomass, soil biomass, vegetative retardance, and soil consolidation.

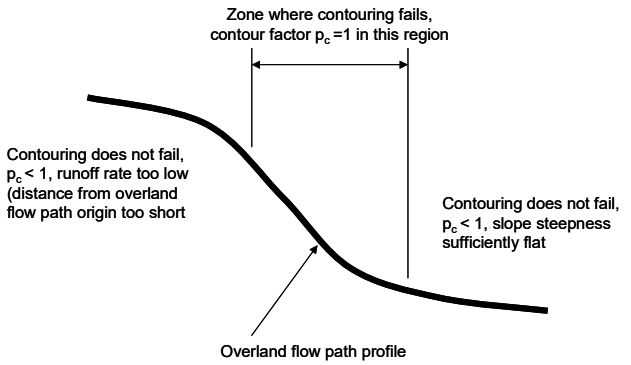

Figure 14.5. Zone on a complex shaped overland flow path where contouring fails because the combination of distance and steepness.

Figure 14.6 illustrates how RUSLE2 handles an overland flow path with an intense cover-management strip upslope from the end of the overland flow path. Several zones are identified in Figure 14.6. Contouring does not fail and the contouring subfactor value is less than 1 in Zone 1 because the combination of runoff rate (represented by distance from the path origin) and steepness is not sufficient for runoff's shear stress applied to the soil to exceed the soil's critical shear stress for the given cover-management condition. The applied shear stress equals the critical shear stress at the boundary between Zones 1 and 2 and exceeds the critical shear stress in Zone 2. Contouring fails and the contouring subfactor value equals 1 in Zone 2. The intense cover-management in Zone 3 greatly reduces the runoff's shear stress applied to the soil to less than the soil's critical shear stress. Contouring does not fail and contouring subfactor values are less than 1 in Zone 3.

Zone 4 is a special situation. The cover-management condition in Zone 4 is the same as in Zones 1, 2, and 5. Because contouring failed in Zone 2, the expectation is that contouring also fails in Zone 4 based on runoff rate, steepness, and cover-management condition. However, the difference is that the intense cover-management strip in Zone 3 is assumed to spread the runoff so that it leaves the strip in a very thin flow. The flow's shear stress applied to the soil is less than soil's critical shear stress in Zone 4. RUSLE2 assumes that the shear stress applied to the soil at the upper end of Zone 4 equals the shear stress applied to the soil at the lower end of Zone 3. The runoff's shear stress increases over Zone 4 and becomes equal to the soil's critical shear stress at the boundary between Zones 4 and 5. Contouring does not fail and the contouring subfactor value is less than 1 in Zone 4.

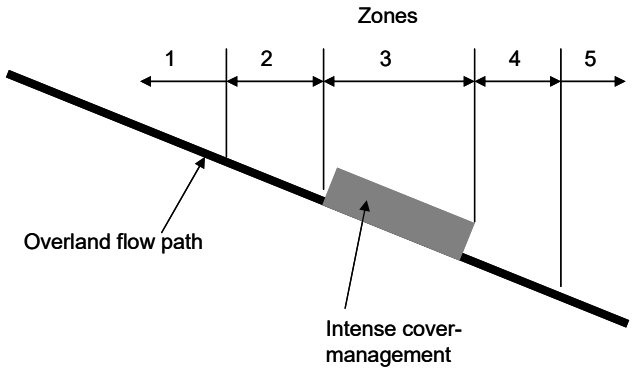

Figure 14.6. Zones along an overland flow part with an intense cover-management strip.

Runoff leaves the intense cover-management strip spread in a thin flow across the slope. The runoff becomes concentrated again in rill flow with distance in Zone 4.

This flow concentration increases the shear stress that the runoff applies to the soil and equals the soil's critical shear stress at the boundary between Zones 4 and 5. Contouring fails in Zone 5 because the runoff's shear stress applied to the soil exceeds the soil's critical shear stress and the contouring subfactor value equals 1 in Zone 5.[127]

14.1.2.6. Temporal changes in contouring subfactor values and contouring failure

RUSLE2 computes a daily value for the contouring subfactor p_c. The value changes daily because the soil ridge height decays daily and the effective vegetation ridge height changes as vegetative retardance changes daily. Cover-management conditions change daily to influence runoff depth that RUSLE2 uses to compute daily contouring subfactor p_c values. The daily contouring subfactor p_c value also changes on days that soil disturbing operations occur that creates ridges with a new height.

Runoff rate and shear stress applied to the soil by runoff change daily as cover-management conditions change. Runoff rate also changes as daily erosivity changes, which captures the likelihood of an intense storm occurring when the cover-management condition is vulnerable to contouring failure. The daily erosive precipitation amount used to compute runoff rate is the product of the 10 year, 24 hour precipitation amount and the ratio of daily erosivity to the maximum daily erosivity.[128]

This effect of combining a vulnerable cover-management condition for contouring failure with the likelihood of an intense storm is illustrated in Figure 14.7 for a conventionally tilled corn **cover-management description** at Lincoln, NE. This example is for a uniform overland flow path where the contouring fails beyond the critical slope length on the lower portion of the overland flow path. The most vulnerable period to contouring failure is from the first secondary tillage operation (tandem disk) on May 1 until harvest on October 15 because the soil surface is smooth with very little surface residue and the vegetation provides little retardance, even at maturity.

---

[127] Equation 8.1 is used to compute detachment in each zone in Figure 14.6. The contouring subfactor p_c value for Zone 4 is computed based on runoff depth, steepness, cover-management condition, and relative row grade assuming no contouring failure. Even though runoff is spread in a thin sheet flow that has reduced erosivity, the values of no other factor are changed in equation 8.1 because the intense cover-management strip spreads runoff. That is, the only erosion reduction computed by RUSLE2 for Zone 4 is from the contouring subfactor value being less than 1 for Zone 4 because the intense cover-management strip spreads the runoff. The contouring subfactor value would equal 1 because of contouring failure if the intense cover-management was not on Zone 3.

[128] The daily erosive precipitation amount used to compute runoff rate is not the same as the daily precipitation amount determined by disaggreagtion of the monthly precipitation amounts in a location's **climate description**.

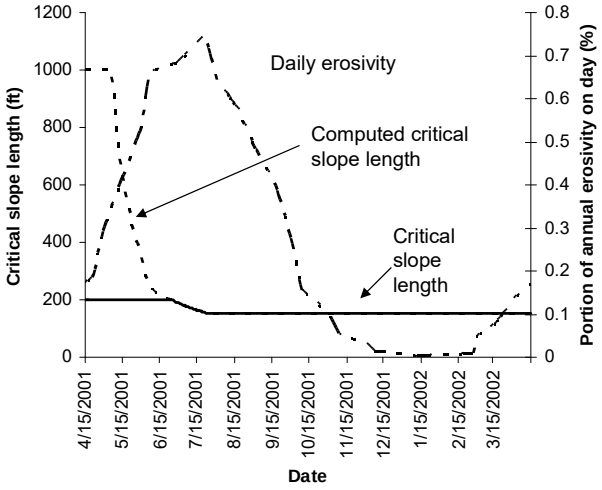

Figure 14.7. Daily critical slope length.

The critical slope length shown in Figure 14.7 is 200 ft, which is the overland flow path length, from April 15 to June 25.[129] A RUSLE2 displayed critical slope length that equals the overland flow path length means that the computed critical slope length is longer than the overland flow path length. A computed critical slope length longer than the overland path length has no consequence because contouring does not fail within the actual overland flow path length. The RUSLE2 computed critical slope length starts at 1000 ft, which is the longest overland flow path that RUSLE2 considers. The computed critical slope length becomes less than 1000 ft on May 7 and steadily decreases to 200 ft on June 25. The reason for the decrease is the increase in the daily erosive precipitation amount used to compute shear stress, which is indicated by the increase in the daily erosivity to July 22 in Figure 14.7. The vulnerability of the cover-management condition to contouring failure in this example does not change significantly during this period. However, in other cases, vulnerability to contouring failure can increase significantly over time as roughness and surface residue decay.

After June 25, the computed critical slope length decreases to a value less than 200 ft, which means that RUSLE2 has computed contouring failure and has set the contouring subfactor p_c value to 1 on the lower portion of the overland flow path. The critical slope length ultimately decreases to a minimum of 154 ft on July 22, the date of peak erosivity. Even though the site condition was slightly more vulnerable to contouring failure earlier, the shortest critical slope length did not occur until later when the combination of cover-management vulnerability and daily erosive precipitation was maximal.

The potential for contouring failure decreased significantly after July 22 because the daily erosivity decreased as illustrated in Figure 14.7. However, the critical slope length did not increase. Similarly, harvest on October 15 added a very heavy surface residue cover that greatly reduced the vulnerability for contouring failure, but the critical slope length did not increase at harvest. Once contouring fails, contouring effectiveness is not

[129] The actual critical slope length before June 25 is longer than 200 ft, but RUSLE2 does not display critical slope length value longer than the overland flow path length. The computed critical slope length can be seen by entering 1000 ft for the overland flow path length, which is the longest value that can be entered in RUSLE2.

restored until the next **operation description** that includes a **disturb soil process** to create new ridges. In RUSLE2, contouring failure is assumed to occur by runoff breaking through ridges; consequently ridges must be recreated to restore contouring effectiveness. Critical slope length is reset when new ridges are created. See **Section 14.1.2.5** for discussion on the importance of critical slope length in conservation planning.

In this example, the first soil disturbing operation after the critical slope length reached its minimum on July 22 is a moldboard plowing operation on April 15. This operation resets computed critical slope length, which is the reason for the increase in critical slope from 154 ft on April 14 to 1000 ft on April 15. The contouring subfactor p_c value remains at 1 for the portion of the slope beyond the critical slope length until new ridges are created to restore contouring effectiveness.

This example is for a uniform overland flow path. The same concepts apply to a non-uniform overland path. Contouring fails on portions of the overland flow path where runoff's shear stress applied to the soil exceeds the soil's critical shear stress for contour failure. That area expands as the combination of vulnerable cover-management and erosive conditions increase. Once contouring fails on an area, RUSLE2 sets the contouring subfactor value to 1, and contouring effectiveness is not restored until a soil disturbing operation occurs that creates new ridges.

***Dates* for *operation descriptions* must be carefully selected for *no rotation cover-management descriptions* where critical slope length is important. Operations that occur together to create a particular field condition should be combined into a single operation, or the same date should be used for the operation descriptions. An example is creating ridging and applying mulch that occur together on a construction site. These two operation descriptions should either be combined into a single operation description or occur on the same date to prevent RUSLE2 from computing erroneous contouring failure (critical slope length) values.**

14.1.2.7. Use of critical slope length information in conservation planning

The usual conservation and erosion control planning objective is to avoid contouring failure anywhere along the overland flow path. In the case of uniform overland flow paths, this objective corresponds to the critical slope length not being less than the overland flow path length.

If contouring failure occurs, the two frequently used corrective measures are to change the cover-management practice or add terraces/diversions along the overland flow path. Reducing land steepness is a possible alternative on landfills, construction sites, reclaimed mine, and other similar highly disturbed lands where topography can be modified. An average erosion rate for the erodible portion of the overland flow path less

than the planning criteria, such as soil loss tolerance, is usually not sufficient for adequate erosion control when contouring fails. Local erosion can be too high where contouring fails on an overland flow path even though the average erosion for the erodible portion of the overland flow path is sufficiently low.

14.1.3. Calibration

RUSLE2's contouring equations, which capture these contouring principles, were calibrated to the experimental field data illustrated in Figure 14.1.[130] The middle curve in Figure 14.1 was assumed to represent the overall, main effect of contouring on erosion. This curve is comparable to the contouring subfactor values in AH537. The calibration procedure required assuming a base condition to represent this overall, main effect curve in Figure 14.1.

Most of the experimental data illustrated in Figure 14.1, which includes the data that were the basis for the AH537 contouring subfactor values, are from research studies conducted from the early 1930's to the mid 1950's.[131] The base condition used in the RUSLE2 contouring calibration represented those conditions rather than modern conditions.[132] The assumed base condition was a conventionally tilled, low yield (60 bu/ac) corn cover-management description at Columbia, MO (see **Footnote 23**). The operations in this cover-management description included a moldboard plow in the spring for primary tillage, two secondary tillage operations to prepare the seedbed, row planter to seed the crop, row cultivation to control weeds, and harvest .

A second cover-management description used in the calibration was conventionally tilled soybeans and wheat added to the base corn cover-management description. This cover-

---

[130] The data sources are listed in Tables 6-1 and 6-2, AH703.

[131] Using modern data to calibrate RUSLE2 contouring computations was preferred, but unfortunately adequate modern data do not exist. The important output from RUSLE2 for most conservation and erosion control planning is average annual erosion rather than erosion for individual storms. Also, erosion is highly variable and data over several years are needed to obtain good average annual erosion estimates. This requirement is especially important for calibrating RUSLE2 for contouring because the effectiveness of contouring is strongly related to major storms that occur at vulnerable times. The best data for calibrating RUSLE2 are from natural runoff events on small watersheds (less than 5 ac). Natural runoff plot data supplement these data. Rainfall simulator plot data are not especially useful for calibrating RUSLE2, although these data are extremely important for developing principles, concepts, and basic equations.

The calibration data should be from a wide range of climatic, soil, topographic, and cover-management conditions to capture main effects and to deal with the extreme variability in contouring data. Unfortunately, by the end of the 1970's, many studies involving natural runoff plots were discontinued and the emphasis shifted to rainfall simulator studies. Similarly the number of small watershed studies decreased and remaining studies did not have common study conditions needed to calibrate RUSLE2.

[132] The common assumption is that AH537 contouring subfactor values from the 1930's to 1950's data apply to modern cropping practices. That assumption is highly questionable, if not invalid, because of differences in cropping practices in the two eras. For example, row cultivation is used much less in modern practices than in older practices and yields for most crops have increased significantly since the 1930's.

management description was used to calibrate RUSLE2's effective vegetative ridge height. Research data from a location in Illinois and a location in Oklahoma were used in the calibration. Another important study in the RUSLE2 contouring calibration was a 1960's field study in Northern Mississippi on the effect of relative row grade.

Two very important calibration inputs were ridge height and relative row grade (ratio of row grade along furrows to average steepness of overland flow path). The calibration input values for these variables must be followed when RUSLE2 input values are selected for conservation and erosion control planning. A 3 inches (75 mm) ridge height was input for the row cultivation operation, which had the greatest contouring effect among the operation in the base cover-management description. The second important input was the 10 percent relative row grade used to represent contouring on the small research watersheds and farm fields, which is in contrast to a zero (0) relative row grade used to represent contouring on research plots.

Ridge heights assigned to operation descriptions must be consistent with the 3-inch (75 mm) ridge height assigned to the row cultivation used in the RUSLE2 contouring calibration.

The second major calibration of the RUSLE2 contouring computations was for critical slope length on uniform overland flow paths and contouring failure in general on complex overland flow paths. RUSLE2 was calibrated to AH537 critical slope length values for contouring alone without strip cropping using the base condition described above.[133] AH537 critical slope lengths values for strip cropping were doubled from those for contouring alone. Instead, RUSLE2 computes contouring failure as a function of cover-management conditions along the overland flow path rather than using a multiple of critical slope length values for contouring alone.[134] A cover-management description involving a conventionally tilled corn, alfalfa-timothy hay rotational strip cropping system was used to calibrate RUSLE2's computation of contouring failure, especially as it relates to a hydraulically rough strip spreading runoff. Research strip cropping data from the 1930's to mid 1950's for LaCrosse, Wisconsin were used to partially validate these RUSLE2 computations. The validation was based on the ratio of average sediment yield from the strip cropping system to sediment yield from the same rotational cropping system not in strips. Measured values for this ratio were compared to RUSLE2 computed values.

---

[133] No explicit research data exist for critical slope length. Contouring failure has been observed and described in research reports, especially at locations in Arkansas and Texas, where severe runoff events occurred. Critical slope length values given in AH282 and AH537 were based on these and other visual field evidence of contouring failure from the early 1930's to mid 1950's. The critical slope length concept and the assigned values based on scientific and technical judgments continue to be accepted by conservation and erosion control planners and were, therefore, used in the RUSLE2 calibration.

[134] RUSLE1 assumes that strip cropping and buffer strips have critical slope lengths that are 1 ½ times those for contouring alone.

14.1.4. Interpretation of RUSLE2 contouring relationships

Of all the variables that affect erosion, contouring is easily the most difficult one to accurately represent, especially at a specific site. Slight, non-obvious differences seem to greatly affect how contouring affects erosion. Consequently, RUSLE2 erosion estimates affected by contouring are more uncertain than erosion estimates influenced by any other RUSLE2 factor. **Therefore, special care should be exercised in interpreting RUSLE2 erosion estimates in relation to contouring.**

RUSLE2 describes the established main effects of contouring in relation to major variables. These effects are valid in general, but an effect at a specific site may be quite different from the general effect. For example, the statement that contouring reduces erosion by 50 percent for a given condition is true in general, but the reduction may be 10 percent at one site and 90 percent at another site. Contouring is a good conservation practice but its effectiveness at a specific site is more uncertain than for other erosion control practices. RUSLE2 is designed to capture broad trends related to contouring. For example, use of the 10 -year, 24-hour precipitation amount is intended to capture differences in general contouring effectiveness by geographic region. Similarly, the relationship of contouring to runoff is meant to capture general trends of how cover-management conditions affect runoff that in turn affect how contouring affects erosion. These RUSLE2 estimates are not meant to explicitly describe how cover-management affect runoff and contouring's effectiveness at a specific site. RUSLE2 is a tool to assist conservation and erosion control planning.

Although, research data are sufficient to identify the main variables that affect contouring, the amount and quality of the data are insufficient to empirically derive and calibrate mathematical relationships for the effect of contouring on erosion except in the general sense. In addition, the contouring data used to develop RUSLE2 do not represent modern agronomic conditions. The RUSLE2 developers significantly extended contouring relationships beyond the main effect of slope steepness normally represented in contouring subfactor values (see AH537). Because research data are not available to validate these extensions, RUSLE2 computations were very carefully examined to ensure that computed values reflect the current scientific knowledge, are acceptable based on modern scientific and technical judgment, and are reasonable for use in conservation and erosion control planning.

14.1.5. Contouring inputs

The **contour systems description** in the RUSLE2 database involves the two inputs of **how row grade is specified** and the **input value for row grade**. The other important input for contouring is the **ridge heights** for the **operation descriptions** in the **cover-management description.**

14.1.5.1. Method of specifying row grade

Row grade can be entered in a **contour system description** using the methods listed in Table 14.1. When a contour system description is used to represent to represent contouring, the assumption is that the overland flow path input represents the flow path perpendicular to contour lines, not a flow path along the ridges and furrows.

The first method of **up and down slope** represents a no-contouring effect. RUSLE2 gives the same result obtained with the other three methods by inputting an **absolute row grade** that equals the overland flow path steepness or inputting 1 for **relative row grade**. This selection tells RUSLE2 to compute erosion without considering any contouring effect.

The method **set absolute row grade** is where a value for the actual furrow (row) grade at the site is entered. This method should be used only where ridges and furrows are well defined and runoff flows to major concentrated flow areas before breaking over the ridges.

Using the *set absolute row grade* input method for ordinary contouring provided by most typical agricultural implements is a *misuse* of RUSLE2.

Table 14.1. Ways to specify row grade.

Row grade specification method	Comment
Up and down slope	Specifically sets relative row grade to 1, i.e., absolute row grade equals overland flow path steepness
Set absolute row grade	Value entered for absolute row grade as measured in the field. **Should only be used in special cases**.
Set relative row grade	Relative row grade is the ratio of the absolute row grade to steepness of overland flow path. Should be used to represent most ordinary contouring situations.
Use management relative row grade	RUSLE2 uses relative row grade input in the cover-management description used in the particular RUSLE2 application.

The **set relative row grade** is the appropriate way to enter row grade for ordinary contouring that affects runoff as illustrated in Figure 8.13 (see **Section 8.3.6**). Relative row grade is the ratio of absolute row grade to overland flow path steepness. As discussed in **Section 14.1.4**, RUSLE2's estimates of how contouring affect erosion are more uncertain than for any other variable. **Contouring system descriptions** based on relative row grade can be developed, stored in the RUSLE2 database, and used so that

RUSLE2 computes the proper relative differences in erosion in relation to contouring. The proper relative difference related to contouring between field situations is not achieved when the absolute row grade entry method is used. Contouring effectiveness is related to how closely the ridge forming operation follows the actual field contours. Equal values for relative row grade imply the same contouring quality in relation to following field contours regardless of land steepness.[135]

The following example illustrates how inputting absolute row grade gives too much credit for contouring on steep land. Assume that an absolute row grade of 1 percent is entered for both a 6% and a 30% overland flow path (land) steepness. The relative row grade is 1/6 = 0.17 for the 6% slope, which gives a contouring subfactor value of 0.70 if the contouring subfactor value is 0.50 for perfect contouring. The relative row grade is 0.033 for the 30% slope, which gives a contouring subfactor value of 0.59 if the contouring subfactor value for perfect contouring is also 0.50. Assuming the same row grade regardless of land steepness computes a much greater relative benefit for contouring on steep slopes than on moderately steep slopes. Achieving this increased contouring benefit requires extra care, which is unlikely, with the ridge forming operation to maintain the 1 percent row grade on steep slopes. Furthermore, such precision implied by varying absolute row grade on steep slopes is unwarranted given RUSLE2's accuracy and quality of the contouring data used to calibrate RUSLE2.

The entry method **use management relative row grade** requires the same inputs as the set relative row grade selection. When this selection is made, RUSLE2 uses the relative row grade entered in the **cover-management description** (see **Section 10.2.10**). The advantage of this method is that contouring and cultural erosion control can be combined into a single erosion control practice described by a cover-management description, which is useful in erosion inventory analysis. The relative row grade should be set to 10% in the cover-management description for ordinary contouring.

14.1.5.2. Row grade

The **set absolute row grade** entry method requires that the **absolute row grade** along the ridges-furrows be entered. As discussed in **Section 14.1.5.1**, this entry method should only be used where the ridges-furrows are so well defined that runoff travels in the furrows to major concentrated flow areas before breaking over the ridges. An alternative method for applying RUSLE2 to this condition is discussed in **Section 8.3.6.**

Absolute row grade is the value that is determined by measuring a decrease in elevation over distance along the furrows (rise/run). In many cases row grade varies along the ridges-furrows, particular on either side of concentrated flow areas to reduce sharp bends in the ridges and to facilitate the ridge forming operation. A representative row grade

[135] Regardless of input method, RUSLE2 uses relative row in its computations.

must be selected because non-uniform row grades along the ridges-furrows can not be entered into RUSLE2.

Relative row grade is the ratio of row grade to overland flow path steepness. However, a more appropriate way to consider relative row grade is that values for relative row grade represent contouring classes, which are actually classes for ridge-furrow orientation with respect to the overland flow path. Five classes are listed in Table 14.2.[136] Additional classes are not warranted given RUSLE2's accuracy. The classes in Table 14.2 are **contour system descriptions** that have been created and placed in a RUSLE2 database.

Perfect contouring is where the ridges-furrows are oriented parallel to the contour. The row grade is perfectly flat and the ridge tops are level so that runoff spills over the ridge uniformly along the ridge. This condition is obtained in the field when a surveying instrument is used to lay out contour lines. This contouring class is used with high quality rotational strip cropping where row grade is level across concentrated flow areas. Strip cropping in the LaCrosse, Wisconsin area with its smooth sweeping curves with no evidence of ephemeral gully erosion is an example of perfect contouring.

Sometimes row grade associated with rotational strip cropping and buffer strips (see **Section 14.2**) is increased in the vicinity of concentrated flow areas to avoid sharp bends that hinder farming operations.[137] **Contouring with strips** (5% relative row grade) or **standard contouring** (10% relative row grade) should be selected for this situation. If the contouring subfactor value is 0.50 with perfect contouring, a 5% relative row grade gives a contouring subfactor value of 0.61.

Standard contouring (10% relative row grade) should be selected for contouring where no vegetative strips are present to guide ridge forming operations. Unless the topography is quite uniform, creating ridges and furrows perfectly on the contour is practically impossible. Also, row grade is often increased on either side of concentrated flow areas to facilitate ridge forming operations. If the contouring subfactor value is 0.5 with perfect contouring, a 10% relative row grade gives a contouring subfactor value of 0.66.

---

[136] The classes listed in Table 14.2 are names used for **contour system descriptions** in the RUSLE2 database that is downloaded from the RUSLE2 Internet site at the USDA-Agricultural Research Service-National Sedimentation Laboratory, Oxford, MS (http://msa.ars.usda.gov/ms/oxford/nsl/rusle/index.html) ARS reviewer, check this). The values for relative row grades in Table 14.2 are the important information. Users may change the names of the contour system descriptions to other names for convenience.

[137] Row grade should remain level across concentrated flow areas. Increasing row grade from level on either side of concentrated flow areas ensures that concentrated areas will persist and may require a grassed waterway to control ephemeral gully erosion. Contour strip cropping that does not have level row grades across concentrated flow areas will not eliminate concentrated flow areas and ephemeral areas as occurred so effectively with level grade contour strip cropping in the LaCrosse, WI area.

RUSLE2 has two contouring (ridge-furrow orientation) classes to represent "cross slope" ridging. The two classes are **moderately off contour**, which is a relatively row grade of 25%, and **half off contour**, which is a relative row grade of 50%. If the contouring subfactor value is 0.50 for perfect contouring, the contouring subfactor values are 0.75 and 0.93, respectively, for these two ridge-furrow orientations.

The last class is **up and down slope** (hill) where the ridge-furrow orientation is parallel to the land slope. The relative row grade is 100% and the contouring subfactor value is 1 for this class.

Table 14.2. Classes of relative row grades to represent contouring (ridge-furrow orientation to land slope)

Contouring (ridge-furrow orientation) class	Relative row grade	Comment
Perfect contouring	0	Ridges-furrows are exactly on the contour (orientation is parallel to contour), use with strips that exactly follow the contour laid out with surveying instruments
Contouring with strips	5%	Use with strips laid out on the contour with survey instruments but with row grade adjustments when approaching concentrated flow areas
Standard contouring	10%	Typical contouring that was initially laid out with survey instruments. Row grade adjustments are made when approaching concentrated flow areas
Cross slope-moderately off contour	25%	Ridge-furrow orientation ¼ off contour. Sufficiently close to the contour to merit significant credit for reducing rill-interrill erosion
Cross slope-half off contour	50%	Ridge-furrow orientation is ½ off contour (half way between on-the-contour and up and down slope). Merits some but not much credit for reducing rill-interrill erosion
Up and down slope	100%	Ridge-furrow orientation is parallel to land steepness. Merits no credit for reducing rill-interrill erosion

Note: The effect of ridge-furrow orientation on ephemeral gully erosion, which RUSLE2 does not estimate, should be considered in developing a complete erosion control plan.

Being able to enter a non-zero row grade in RUSLE2 does not imply that use of such row grades is encouraged or even acceptable. It is recognition that contouring can not be perfect in most field situations and that some credit should be given for rill-interrill erosion reduction for ridge-furrow orientations that are not directly up and down hill. Ridge-furrow grades greater than flat (zero) should be avoided so runoff does not flow along the furrows to concentrated flow areas on the landscape, which promotes ephemeral gully erosion. In fact, a slight row grade may cause more ephemeral gully erosion because the ridges and furrows discharge runoff in a concentrated flow area much further upslope than with a steep relative row grade. RUSLE2 does not consider ephemeral gully erosion; RUSLE2 only deals with rill-interrill erosion.

Conversely, effective erosion control is to place ridges-furrows on a continuous grade with a sufficiently high ridge to ensure that runoff flows to a concentrated flow area protected by a grassed waterway.

A complete erosion control plan includes consideration of both rill-interrill and ephemeral gully erosion.

14.1.5.3. Input ridge heights in relation to contouring

At least one **operation description** that includes a **disturb soil process** to create ridges must be in the **cover-management** description for RUSLE2 to compute a contouring effect (see **Section 9.2.4**). The RUSLE2 assumption is that ridges oriented at an angle to the overland flow path must be present for a contouring effect on erosion. The degree that contouring (ridging) reduces rill-interrill erosion depends on ridge height and row grade.[138] Input ridge height values are entered in the operation descriptions (see **Section 13.1.5.4**).

Ridge height (along with row grade) is the single most important variable that determines the effectiveness of contouring (ridge-furrow orientation to the overland flow path) in RUSLE2. If RUSLE2 computes less contouring effect than expected, ridge heights may be too low.

Ridge height after an operation is totally determined by the operation description, and the ridge height that existed before the operation has no effect on ridge height left by an operation, even when the operation minimally disturbs the soil. The ridge height input in a particular operation description should reflect the ridge height that exists when that operation is used in combination with other operations.

[138] The total effect of ridges on rill-interrill involves two parts. One part is the contouring effect which is related to the orientation of the ridge-furrows with respect to the overland flow path and the other part is the increased detachment caused by increased ridge height as described in **Section 9.2.4**.

After an operation description creates a ridge, ridge heights decay with precipitation amount and interrill erosion. RUSLE2 does not consider the loss of ridge height caused by deposition in the furrows. Daily ridge height used by RUSLE2 to compute the contouring effect can be much less than the input ridge height value.[139]

Ridge height values input in an operation description must be referenced to the initial 3-inch (75 mm) ridge height assigned to row cultivation used to calibrate the RUSLE2 contouring relationships for Columbia, MO (see **Section 14.1.3**). In assigning a ridge height to an operation description, ask the question of how the operation affects contouring in relation to row cultivation used for corn from the early 1930's to the mid 1950's? Measured ridge heights are a guide because RUSLE2 has been calibrated as much as possible to use ridge heights that are measured in the field. However, measured ridge heights may not always capture how RUSLE2 should compute contouring effectiveness for a particular operation description or for a cover-management description overall. Input ridge height values must be consistent with the ridge height values in the RUSLE2 **core database** because those values were selected to ensure that RUSLE2 computes the desired contouring effect.

Consequently, the best approach by far is to use ridge height values in the RUSLE2 **core database** as a guide in selecting an input value for an operation description. Consistency of ridge height values among operation descriptions is critically important so that RUSLE2 computes the expected relative erosion differences among contouring conditions. This requirement is especially important given the high variability and uncertainty in the research data used to develop RUSLE2 and the high variability in site specific contouring performance.

14.2. Porous Barriers

14.2.1. Description of practices

Porous barriers are support practices that do not terminate the overland flow path because runoff flows through these barriers. These practices must be placed on the contour or else their effectiveness is greatly reduced because runoff flows along them rather than through them. Examples include filter strips (dense vegetation strips at the end of overland flow paths), buffer strips (multiple narrow strips of dense permanent vegetation along the overland flow path), rotational strip cropping (equal width strips including some dense vegetation strips grown in a rotating and alternating fashion in time and space along the overland flow path), and fabric fences, gravel dams, and straw bales used on construction sites and similar lands.

[139] The ridge height values used in RUSLE2's contouring computations do not correspond with those in RUSLE1 because ridge heights change daily in RUSLE2. The RUSLE2 input values for ridge height are similar to the ridge height values used in RUSLE1 computations.

14.2.2. Basic principles

The high flow retardance of the most effective porous barriers slows runoff and ponds water on the upper side of the barrier. Runoff leaves the barrier spread across the slope in a uniform thin depth, which significantly reduces the potential for contouring failure immediately downslope of the barrier (see **Section14.1.2.5**).

14.2.2.1. Description of actual processes

Ponding (**backwater**) immediately upslope of a barrier reduces runoff's transport capacity, which can cause deposition. As much as 90 percent of the incoming sediment load can be deposited in the backwater until deposited sediment accumulates so much that the lower edge of the sediment wedge reaches the upper edge of the barrier as illustrated in Figure 14.8. Narrow width, dense, high retardance barriers less than 18 inches (500 mm) wide produce wide backwater that causes much deposition. **However, vegetation type barriers must be sufficiently wide to protect against localized failure and short circuiting of the runoff through the barrier that are caused by poor non-uniform plant stands, for example.**

As deposited sediment accumulates during runoff events, the upper edge of the backwater and deposited sediment combined advance upslope as illustrated in Figure 14.8. The upslope advancement of the deposited sediment increases transport capacity in the backwater and fills the ponded area with sediment. Sediment is transported into the barrier itself where sediment is deposited because the barrier's high flow retardance greatly reduces runoff's sediment transport capacity. Eventually both the backwater and barrier, such as a grass strip, become filled with sediment. The barrier becomes almost ineffective because it no longer causes deposition and does little to reduce sediment load. Vegetation strips regain flow retardance during reduced erosion periods if vegetation growth is not overly hindered by sediment.

14.2.2.2. RUSLE2 description

RUSLE2's representation of these very complex processes is simplified as illustrated in Figure 14.9. **RUSLE2 bases its computations solely on the hydraulics within the effective width of the barrier itself.** RUSLE2 does not compute backwater hydraulics and deposition in the backwater. Instead RUSLE2 represents the backwater by computing an additional width that is added to the actual width to create a total effective width for the strip/barrier. **Temporal changes in the backwater effect are not considered. Section 8.1.4** describes the RUSLE2 computational procedures for porous barriers.

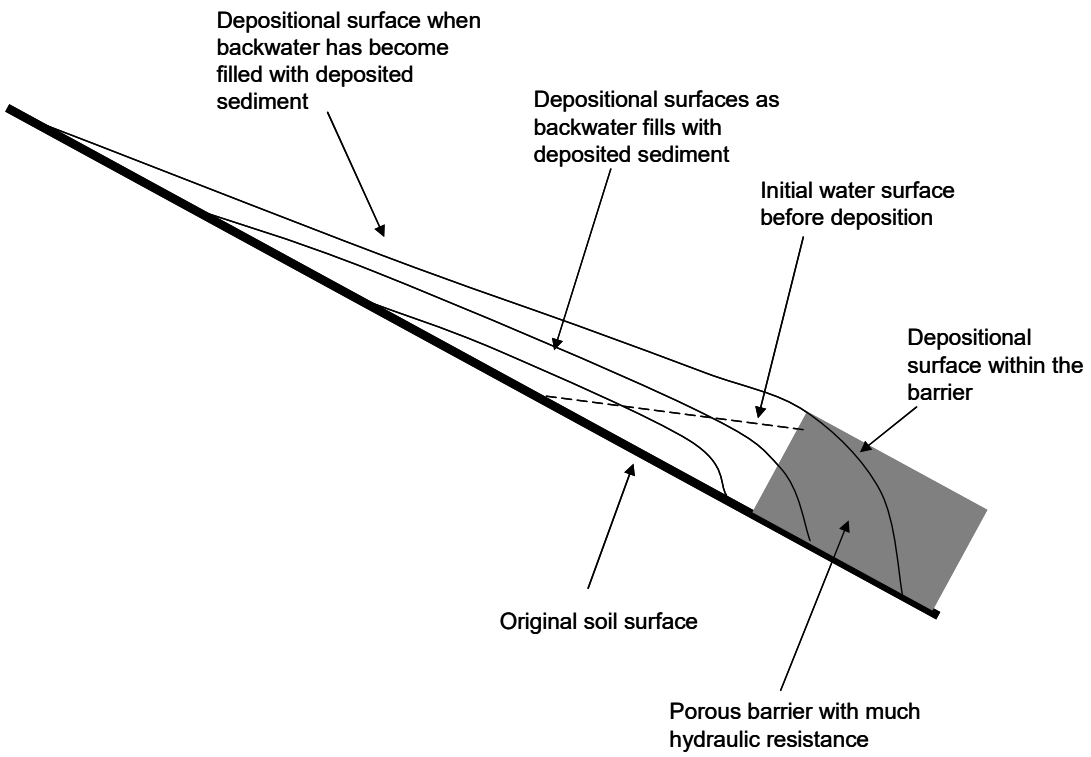

Figure 14.8. Deposition in backwater upslope of a porous barrier as deposition develops over time.

Neglecting deposition in the backwater and temporal changes is insignificant in most cases where barrier are wide such as with most grass buffer and filter strips.

The porous barrier's flow retardance must reduce runoff's sediment transport capacity to less than the incoming sediment load for RUSLE2 to compute deposition. If a barrier's retardance is low, the barrier will hardly slow runoff and transport capacity will not be sufficiently reduced at the barrier's upper edge for RUSLE2 to compute deposition. Also, RUSLE2 will not compute deposition by a barrier if the incoming sediment load is less than the transport capacity at the barrier's upper edge.

Deposition caused by a barrier reduces sediment load along the overland flow path, especially if a high retardance barrier is located at the end of the overland flow path. Detachment (sediment production) is typically low within high retardance barriers, but sediment production will not be greatly reduced if barriers are narrow with respect to the overland flow path length.

RUSLE2 computes deposition ending within a barrier as illustrated in Figure 14.9 where runoff's sediment transport capacity increases within the barrier, which is the usual case, and the barrier (e.g., grass buffer strip) is sufficiently wide. Increasing barrier width

when RUSLE2 computes that deposition ends within a barrier does not significantly increase the fraction of the incoming sediment load that is trapped by the barrier. The decrease in sediment yield from the overland flow path that occurs as barrier width is increased results from the barrier occupying an increased portion of the overland flow path. Increasing barrier width reduces sediment yield more because of very low detachment (sediment production) within the barrier than sediment yield is reduced by increased sediment trapping.

However, increasing barrier width increases sediment trapping if RUSLE2 computes deposition over the entire barrier width (i.e., deposition does not end within the barrier). RUSLE2 computes reduced sediment yield because of both increased deposition and reduced sediment production in this case.

Figure 14.9 illustrates the usual case where transport capacity increases within the barrier after a step decrease at the upper edge of a barrier. This increase in transport capacity occurs where runoff rate increases within the barrier because rainfall rate exceeds infiltration rate (see **Sections 8.12 and 8.1.3**). Runoff rate and transport capacity decrease within a barrier where infiltration rate is greater than rainfall rate. RUSLE2 does not compute deposition ending within a barrier when transport capacity decreases within the barrier. Runoff ends within a barrier when infiltration rate exceeds rainfall rate if the barrier is sufficiently wide.

The width required for runoff to end within a barrier depends on discharge rate of the upslope runoff where it enters the barrier as well as rainfall rate and infiltration rate within the barrier. If runoff ends within a barrier, runoff begins at the next location on the overland flow path where infiltration rate is less than rainfall rate, which is often at the upper edge of the strip immediately downslope of the barrier as illustrated in Figure 14.10. An example of runoff ending within a barrier is a high residue strip, left rough by a moldboard plow throwing soil upslope in the Northwest Wheat and Range Region (NWRR, see **Section 6.9.1**). The rainfall rate and flow rate of upslope runoff entering the strip is very low, about 0.25 in/hr (6 mm/h) and infiltration rate in the strip is relatively high.

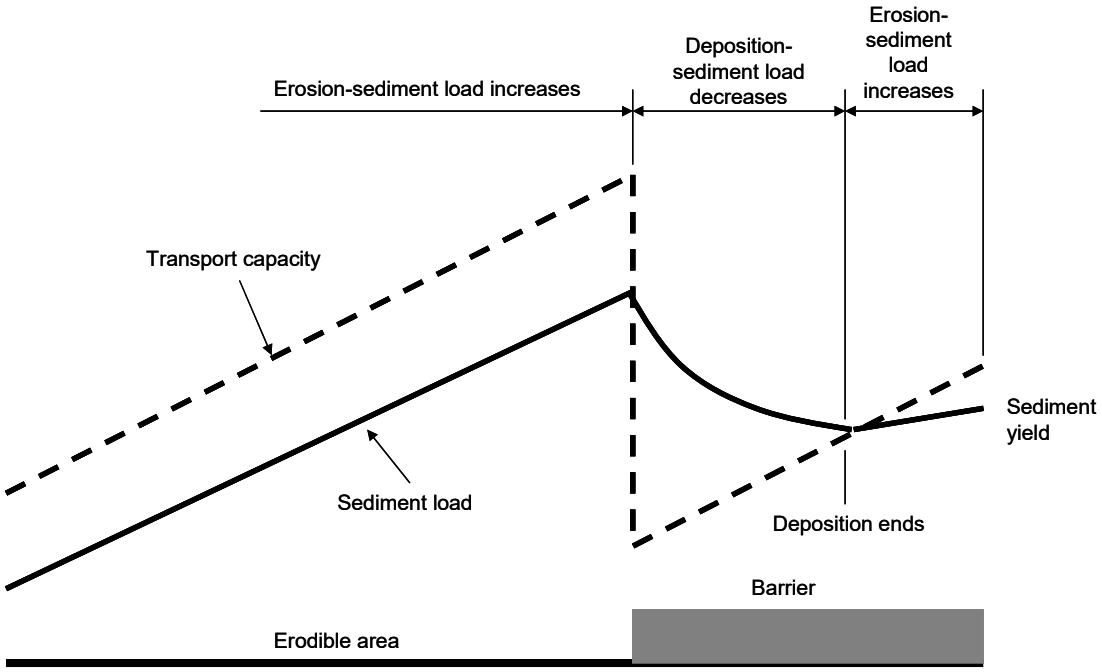

Figure 14.9. RUSLE2 hydraulic representation of a porous barrier.

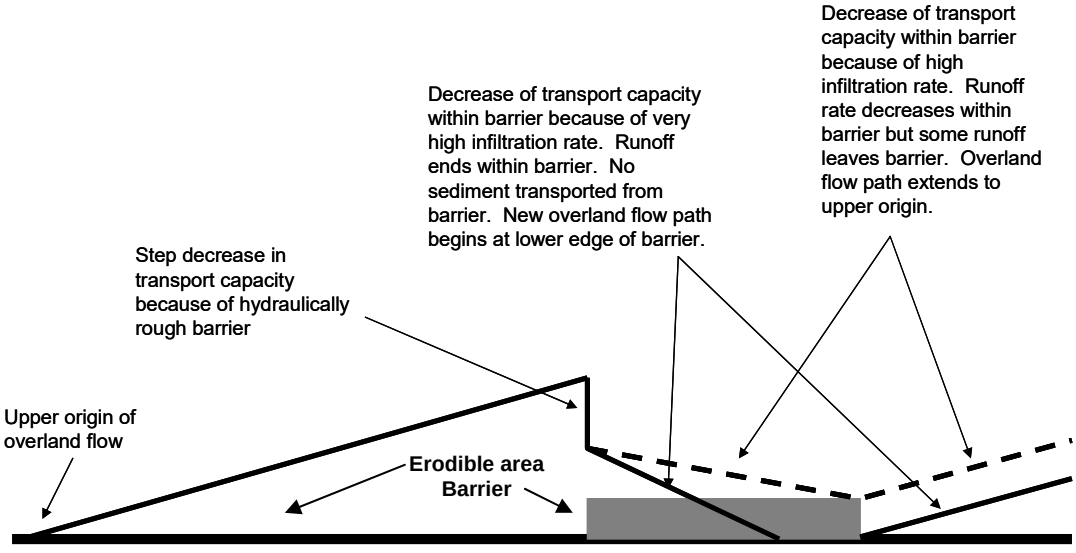

Figure 14.10. Effect of high infiltration rate within barrier that causes runoff date to decrease within barrier.

Most of the deposition caused by a porous barrier occurs in the backwater on the upper side of a strip/barrier. The length of this depositional area must be included with the actual physical width of the strip. Otherwise, RUSLE2 will overestimate sediment yield, especially if the strip is very narrow like a silt fence. RUSLE2 estimates a backwater

width based on runoff rate and flow retardance of the strip. RUSLE2 computes the backwater/depositional length along the overland flow path and add this length to the input value for actual strip/barrier width. To simplify the computations, RUSLE2 adds the backwater/depositional width to the lower edge of the barrier/strip, which increases the overland flow path length by the same amount. RUSLE2 computes the backwater/depositional length by first computing flow depth at the upper edge of the strip/barrier using the total Manning's n for the barrier, discharge rate at the upper edge of the barrier, and steepness of the barrier segment. This computation was calibrated based on erosion plot studies involving 1.5 ft wide (0.46 m) stiff grass hedges at Holly Springs, Mississippi. The backwater/depositional length is computed from this flow depth and the steepness of the segment immediately upslope of the barrier assuming a level water surface.

RUSLE2 uses the retardance classes assigned to **vegetation descriptions** to compute the flow depth at the upper edge of the strip/barrier.[140] The maximum width that RUSLE2 adds for any retardance and hydraulic resistance is 15 ft (5.0 m). RUSLE2 only sets a minimum for the retardance class 7 condition, where the minimum backwater/deposition width that is added is 3 ft (1.0 m). Retardance class 7 represents stiff grass hedge, silt fence, or similar porous barrier that have an especially high retardance (see **Section 11.2.5**). If the retardance of these barriers is similar to the retardance of vegetation, an appropriate vegetation retardance class is assigned. The width added for the other retardance classes is computed value, except that it can not exceed 15 ft (5.0 m).

The backwater/depositional length increases as the hydraulic resistance (retardance, ground cover, surface roughness) of the strip/barrier increases. Also, the backwater/depositional length increases as discharge rate increases. RUSLE2 uses the same temporally varied discharge rate to compute backwater/depositional length that it uses to compute contouring failure (critical slope length). The backwater/depositional width decreases as steepness upslope of the strip/barrier and slope steepness of the segment that contains the barrier increases.

The RUSLE2 overland flow path begins at the origin of overland flow assuming that rainfall rate exceeds infiltration rate everywhere along the possible overland flow path based on topography. This choice of an overland flow path includes situations where discharge rate decreases within a barrier placed along the overland flow path, including situations where runoff ends within the barrier. RUSLE2 properly takes into account variations in infiltration and runoff along the overland flow path because of barriers and other changes in cover-management along the overland flow path. However, if the cover-management upslope of an erodible area is known not to produce runoff, the overland flow path can be started at the upper edge of the erodible area where runoff

[140] A **vegetation description** is used to describe the retardance of mechanical porous barriers. The canopy cover should be 100 percent and the effective fall height should be set to 0 to minimize the detachment computed over the effective width for the strip/barrier. See **Section 14.2.5.1**.

begins. **Section 8.3.4** describes selecting RUSLE2 overland flow paths for porous barriers.

Barriers most effectively induce deposition and reduce sediment load when perfectly on the contour. Runoff may flow along but not through a barrier when the barrier's upper edge is on a grade. Runoff flows along the barrier until the runoff reaches a concentrated flow area where the runoff flows through and over the barrier. Porous barriers designed for overland flow generally perform very poorly in concentrated flow areas. The sediment trapping capacity of a barrier such as a grass strip is rapidly lost by becoming inundated with deposited sediment, or a barrier such as a fabric fence loses its sediment trapping capacity by structural failure. A ridge of soil can develop on the upper side of a barrier because of the combination of high rates of deposition and vegetation re-growing on top of the deposited sediment. Also, tillage in cropped fields and other soil disturbing operations can leave a ridge of soil at the upper edge of a barrier that causes runoff to flow along the barrier rather than entering it. Runoff may not reach a barrier when row grade is steep and ridges high on the inter-barrier area. The runoff flows along the ridges and furrows to concentrated flow area, where the concentrated flow causes the barriers to rapidly fail. [141]

Porous barriers should be analyzed as flow interceptors (e.g., terraces or diversions) when runoff flows along the upper edge of the barrier without entering the barrier.

When porous barriers are selected from the *strips-barriers component* of the *RUSLE2 database*, RUSLE2 requires that relative row grade (see *Section 14.1.5.2*) be 10 percent or less.

Sediment delivery ratio, which is the ratio of sediment leaving the overland path having porous barriers to sediment leaving the overland flow path without barriers is a measure of the degree that the barriers cause deposition. Values for the sediment delivery ratio determined from the RUSLE2 computed sediment yield values depend on the sediment load reaching a porous barrier relative to runoff's transport capacity within the barrier. That is, the sediment delivery ratio is near one, which means little deposition, when the incoming sediment load is only slightly greater than the transport capacity within the porous barrier. In contrast, deposition is much greater and the sediment delivery is much less than 1 when the incoming sediment load is much greater than the transport capacity

[141] RUSLE2 requires that a relative row grade of 10 percent or less be used when porous barriers are selected from the **strips-barriers RUSLE2 database component**. However, this restriction can be bypassed by selecting a **RUSLE2 template** that displays the three layer profile schematic (see **Section 8**), dividing the cover-management layer of the overland flow into segments, and selecting appropriate **cover-management descriptions** for each segment.

within the barrier. Therefore, the RUSLE2 sediment delivery ratio for a particular porous barrier depends on the erosion environment in which the porous barrier is placed as well as characteristics of the barrier itself.

The sediment delivery ratio based on RUSLE2 computations is not constant in general. For example, the sediment delivery ratio for a vegetation strip of moderate retardance is larger for no-till than for clean-till cropping on the inter-barrier area. The vegetation strip traps a smaller portion of the incoming sediment load from the no-till area than from the clean-till area because the incoming sediment load from the no-till area is only slightly higher than the transport capacity within the strip. Detachment and sediment production, which determine the incoming sediment load, is low with no-till cropping in comparison with clean-till cropping. Even though the sediment delivery ratio is higher for the clean-till cropping, overall erosion is less with the no-till cropping.

The RUSLE2 computed sediment delivery ratio for a porous barrier depends on the characteristics of the sediment that reaches the barrier. Sediment characteristics are determined by the properties of soil from which the sediment is eroded (see **Section 7.5**) and upslope deposition. For example, a high portion of sediment eroded from sandy soils is large, easily deposited particles. The RUSLE2 sediment delivery ratio for this sediment is much lower than for sediment eroded from high silt soils that produce a high portion of small, not easily deposited particles. A high portion of the sediment eroded from high clay soils is large, easily deposited aggregates. Clay is a bonding agent that contributes to sediment being eroded as aggregates. The RUSLE2 computed sediment delivery ratio is lower than is commonly assumed for sediment eroded from clay soils because of the high portion of large aggregates in the sediment eroded from these soils.

The RUSLE2 computed sediment delivery ratio for a porous barrier is high where much upslope deposition occurs. An example is a grass strip at the end of a concave-shaped overland flow path where much deposition occurred because of reduced steepness. This deposition removes a high portion of the coarse, easily deposited particles from the sediment load so that the sediment reaching the barrier is largely composed of fine, not easily deposited particles.

Sediment delivery ratio values for porous barriers do not depend very much on the erosion environment, except for sediment characteristics, where runoff's sediment transport capacity is near zero within the barriers. Dense grass strips are an example of this porous barrier.

Deposition is a selective process that enriches the sediment in fines because coarse, dense sediment like sand and large aggregates are more easily deposited than is fine sediment like clay, silt, and small aggregates (see **Sections 5.4 and 7.5**). RUSLE2 computes an **enrichment ratio** that is a measure of the degree that deposition enriches the sediment in fines. The enrichment ratio is the ratio of the specific surface area of the sediment

leaving the RUSLE2 overland flow path to the specific surface area of the soil subject to erosion. The enrichment ratio for a porous barrier increases as portion of the incoming sediment load that is deposited increases. That is, enrichment ratio values increase as values for the sediment delivery ratio decrease.

A major question is the credit given to sediment deposited by porous barriers as **soil saved**. This deposition is referred to as **remote deposition** where the deposition is localized in contrast to **local deposition** that occurs over most of the overland flow area. As discussed in **Section 8.1.5.4**, the credit given to remote deposition as soil saved is a matter of scientific and technical judgment. Keeping the sediment on the overland flow path is clearly preferred to the sediment leaving the overland flow path. Furthermore, sediment deposited upslope is preferred to the sediment deposited near the end of the overland flow path. Also, sediment deposited in localized, semi-permanent locations, such as above grass buffer strips, is less desirable than sediment deposited where soil disturbing operations, such as tillage operations associated with rotational strip cropping, routinely spread the deposited sediment. An increased portion of the overland flow path (i.e., hillslope) benefits when the deposited sediment is spread.

The **conservation planning soil loss** discussed in **Section 8.1.5** gives partial credit for the deposition that occurs with porous barriers as soil saved that benefits the landscape. The credit taken for deposition reduces the soil loss used in conservation planning. The credit taken for this deposition depends on both the location and amount of deposition. For example, RUSLE2 takes little credit for deposition that occurs near the end of the overland flow path, but can take more than 80 percent credit for deposition that occurs on the upper one third of the overland flow path. Rotation strip cropping (see **Section 14.2**) is a special case where full credit is taken for deposition.[142]

Erosion on the inter-barrier area is not greatly affected by the barrier, except for the immediate area downslope of the barrier where erosion may be reduced. Even though the infiltration rate within a porous barrier may be substantially higher than on the inter-barrier area, RUSLE2 does not consider how erosion below a barrier is affected by reduced runoff exiting the barrier. RUSLE2 does compute how reduced runoff affects contouring failure and sediment transport capacity downslope of a porous barrer. High retardance porous barriers spread the exiting runoff so that rill erosion is reduced for a distance downslope before the runoff becomes concentrated once again in rills. This distance has not been defined in research studies. Based on field observations, rill erosion and runoff concentrated in rills occurs immediately downslope of the barrier if the soil is highly susceptible to rill erosion. In other cases, rill erosion and runoff

[142] A rotational strip cropping support practice must be selected through the **strips/barriers component** of the RUSLE2 database in order for RUSLE2 to give full credit (i.e., set **conservation planning soil loss** value to the **sediment yield** value) for deposition associated with rotational strip cropping. Rotational strip cropping can be represented in RUSLE2 by dividing the **management layer** of the **overland flow path schematic** (see **Section 8**), but this procedure takes only partial credit for deposition.

concentrated in rills has been observed not to occur until beyond 3 ft (1 m) on soils moderately resistant to rill erosion. A 10 ft (3m) and greater distance is required for visible evidence of rill erosion downslope of porous barriers on soils highly resistant to rill erosion. Runoff exiting a porous barrier has a very low sediment load and, therefore, has increased erosivity, which increases rill erosion. The RUSLE2 assumption is that these effects offset each other. Consequently, RUSLE2 computes the same erosion rate below a barrier regardless of the presence or absent of the barrier, except for conditions where RUSLE2 computes no contouring failure immediately downslope of a barrier as discussed in **Section 14.1.2.5**.

14.2.3. Calibration

Calibrating RUSLE2 for porous barriers required determining mathematical relationships and numerical values for the K_T coefficient in equation 5.3, which is RUSLE2's equation for runoff's sediment transport capacity (see **Section 8.1.3**). . Equation 5.3 is based on the concept that total overland flow shear stress is divided into the two components of shear stress applied to soil and sediment particles (grain roughness) and shear stress applied to ground cover, soil surface roughness, and standing vegetation (form roughness) (see **Section 14.1.2.5**). The shear stress applied to the soil and sediment particles is used to compute runoff's sediment transport capacity. The shear stress applied to the soil and sediment particles is related to the ratio of the hydraulic resistance of a smooth soil to total hydraulic resistance.

The K_T coefficient involves two parts. One part represents the combined effects of sediment transportability with the hydraulic resistance (grain roughness) of a smooth soil surface and the second part represents the effect of total hydraulic roughness (resistance). Although sediment transportability is related to diameter and density of sediment particles, RUSLE2 uses the same transportability value for all soils even though sediment characteristics vary. **However, RUSLE2 captures the main effects of sediment characteristics on deposition by using equation 5.2, which involves sediment fall velocity that is a function of sediment particle diameter and density (see Section 7.5).** A single Manning's n value is used for all smooth soil; it does not vary as a function of soil particle diameter.

The RUSLE2 developers judged that using constant representative values for sediment transportability and grain resistance improved RUSLE2's robustness as a conservation and erosion planning tool.

A combined base value for grain roughness (resistance) of a smooth soil and sediment's transportability was determined by calibrating RUSLE2 to measured sediment load on a concave overland flow path profile. The RUSLE2 assumption is that sediment transport capacity equals sediment load at the location where deposition begins on a concave profile. The calibration data were from a simulated rainfall field study on a concave plot

35 ft (10.7 m) long where slope steepness decreased continuously from 18 percent at the upper end to 0 percent at the lower end. The bare silt loam soil was smooth so that the only hydraulic resistance was grain roughness. The slope profile was cut from a deep soil profile so that soil characteristics were uniform along the overland flow path. Deposition began at the location where steepness equaled 6 percent. A base value for the K_T coefficient for grain roughness only was determined by adjusting its value until RUSLE2's sediment transport capacity equaled measured sediment load at the 6 percent steepness location. Additional evaluations of the calibrated K_T value were made by comparing RUSLE2 estimates with measured values in laboratory deposition studies, visual field evidence of deposition, and scientific and technical judgments.[143]

The second part of the K_T variable involves the mathematical equation that computes K_T values as a function of the ratio of grain hydraulic resistance to total hydraulic resistance. This equation was derived from sediment transport theory. The Manning's n, which is widely used in hydraulic analyses, is used in RUSLE2 as the measure of total hydraulic resistance. A RUSLE2 total Manning's n value is the sum of the Manning's n values for ground cover, soil surface roughness, and standing vegetation. Values for Manning's n for ground cover and surface roughness were developed from field overland flow velocity measurements.[144]

Manning's n for standing vegetation is based on a retardance concept where seven retardance classes are used to describe the hydraulic resistance provided by standing vegetation (see **Section 11.1.4**). RUSLE2 uses an equation that converts retardance values to Manning's n values. The retardance classes and the empirical equation that computes Manning's n as a function of retardance class were based on both field velocity measurements and scientific judgment of how standing vegetation affects overland flow velocity and hydraulic resistance.

---

[143] Foster, G.R., W.H. Neibling, S.S. Davis, and E.E. Alberts. 1980. Modeling particle segregation during deposition by overland flow. *In:* Proceedings of Hydrologic Transport Modeling Symposium. American Society of Agricultural Engineers. St. Joseph, MI. pp. 184-195.

[144] e.g.,

Foster, G.R. and L.D. Meyer. 1975. Mathematical simulation of upland erosion by fundamental erosion mechanics. *In:* Present and Prospective Technology for Predicting Sediment Yields and Sources. ARS-S-40 USDA-Science and Education Administration. pp. 190-204.

Foster, G.R., L.J. Lane, and J.D. Nowlin. 1980. A model to estimate sediment yield from field sized areas: Selection of parameter values. *In:* CREAMS - a field scale model for Chemicals, Runoff, and Erosion from Agricultural Management Systems. Vol. II: User Manual. USDA-Conservation Research Report No. 26. USDA-Science and Education Administration. pp. 193-281.

Foster, G.R. 1982. Modeling the erosion process. Chapter 8. *In:* Hydrologic Modeling of Small Watersheds. C.T. Haan, H.P. Johnson, D.L. Brakensiek, eds. American Society of Agricultural Engineers. St. Joseph, MI. pp. 297-382.

The next step was to calibrate the equations used to compute sediment characteristics as a function of deposition. The coefficient value involved in these equations was calibrated by comparing RUSLE2 computation of sediment yield and sediment class distributions for very dense grass strips of 3, 6, and 9 feet (0.9, 1.8, and 2.6 m) widths where sediment transport capacity within the grass strips can be considered to be zero (0).

The final step in the calibration was to validate the equations as a complete set. These equations involve complex interactions, which prevents calibration of coefficient values except for very special conditions. The equations and coefficient values, therefore, had to be validated as a set over the conditions where RUSLE2 would likely be applied in conservation and erosion control planning. RUSLE2 computed values for sediment load and sediment particle distributions along and at the end of concave shaped overland flow paths were compared to measured values for both field and laboratory studies. Similar comparisons were made for sediment yield from the end of slopes involving mulch strips of different hydraulic resistance and placement along the overland flow path and contour strip cropping at several locations.[145] In all cases, evaluations were made to ensure that RUSLE2 computed values for sediment load and sediment class distribution are reasonable and consistent with accepted scientific knowledge and available data.

14.2.4. Interpretation

RUSLE2's erosion, deposition, and sediment load computations for porous barriers are for conservation and erosion control planning purposes. Numerous assumptions were made in that context to derive simple, robust RUSLE2 equations that give reasonable values consistent with research data and accepted scientific and erosion control principles. With the possible exception of contouring, porous barrier erosion control varies more with site-specific condition than any other factor. For example, a barrier not perfectly on the contour can result in runoff flowing along the barrier, collecting in a concentrated flow area, breaking over the barrier, and causing the barrier to fail and trap almost no sediment. The effectiveness of vegetative strips depends on a ridge of soil not accumulating along the barrier's upper edge that prevents runoff from entering the barrier. Also, vegetation uniformity and a high quality and dense plant stand must be maintained for vegetative barriers to be fully effective. Installation and maintenance of fabric fences is more important than any other factor in determining their effectiveness.

---

[145] e.g,
Foster, G.R., W.H. Neibling, S.S. Davis, and E.E. Alberts. 1980. Modeling particle segregation during deposition by overland flow. *In:* Proceedings of Hydrologic Transport Modeling Symposium. American Society of Agricultural Engineers. St. Joseph, MI. pp. 184-195.

Neibling, W.H. and G.R. Foster. 1983. Transport and deposition of soil particles by shallow flow. *In:* Proceedings of the D.G. Simons Symposium on Erosion and Sedimentation. Colorado State University, Ft. Collins. pp. 9.43-9.64.

Having and enforcing a good set of installation and maintenance specifications and standards is essential.

RUSLE2 **core database** values for porous barriers represent values that should be used in RUSLE2 applications in the judgment of RUSLE2 developers. RUSLE2 represents the general, overall main effects of these practices as they are judged to be commonly installed in the field. The effectiveness of porous barriers under ideal laboratory conditions is almost always much better than under typical field conditions. RUSLE2 input values for porous barriers values should reflect local conditions and the judgment of designers and regulatory officials for fabric fences, gravel dams, straw bales, and similar porous barriers typical of those used on construction sites.

14.2.5. Inputs

The inputs used to represent porous barriers in RUSLE2 include overland flow path description, a contouring description, and the specific inputs for the strip/barrier system. Porous barriers do not affect the overland flow path description because overland flow is assumed to pass through porous barriers. RUSLE2 accounts for infiltration variations along the overland flow path, including strips where infiltration is so high that runoff ends within the strip, to compute sediment transport capacity and contouring failure (critical slope length). The overland flow path length is selected as if runoff is produced along the entire overland flow path.

The upper edge of a strip/barrier system should be as close as possible to perfectly on the contour (zero row grade) for maximum effectiveness. Figures 14.11 and 14.12 illustrate the importance of a strip/barrier's upper edge being on the contour. If the upper edge is placed parallel to the site boundary as illustrated in Figure 14.11, a grade exists along the upper edge. This grade results in overland flow collecting and running along the upper edge of the strip/barrier to a concentrated flow area, where the flow can overwhelm the barrier. A much better layout is where the upper edge is on the contour as illustrated in Figure 14.12. Runoff enters the barrier uniformly along its length, and the barrier is much less likely to fail in concentrated flow areas. An advantage of having the upper edge of strips/barriers on the contour on cropland is that concentrated flow and ephemeral gully erosion can be greatly reduced.

Selecting a **strip/barrier description** from the RUSLE2 **strip/barrier database component** requires that relative row grade be 10 percent or less except for up and down slope (100 percent relative row grade) where runoff flows perpendicular into the strip/barrier. This restriction can be circumvented by using a RUSLE2 screen **template** that displays the three-layer profile schematic (see **Section 8**). In both input approaches, RUSLE2 assumes that the runoff flows into the porous barrier and that the only effect of the barrier being off grade is in the contouring effect described in **Section**

14.1. See **Section 14.1.5** for additional guidance on selecting contouring inputs for porous barriers.

Inputs specific to a strip/barrier system can be entered in one of two ways. Selecting a **strip/barrier description** from the RUSLE2 database is the intended approach for routine conservation planning. These descriptions involve simplifying assumptions such as uniform strip/barrier widths for convenience and consistency with RUSLE2's accuracy. However, the **three layer profile schematic** can be used to circumvent the 10 percent relative row grade rule when flexibility is needed to represent a complex field situation. The **management layer** in the profile schematic is divided into segments and **cover-management descriptions** are selected for each segment to represent the strips and barriers along the overland flow path.

The inputs for strip/barrier descriptions in the strip/barrier component of the RUSLE2 database are listed in Table 14.3.

Table 14.3. Input variables for strip/barrier descriptions

Input variable	Comment
Strip barrier type	Type refers to filter strip/barrier, buffer strip/barrier, or rotation strip cropping. A filter strip/barrier is permanent at end of overland flow path. Buffer strip/barrier type involves multiple permanent barriers along overland flow path. Rotational strip cropping involves multiple, equal width strips that alternate in time along the overland flow path
Number of strips/barriers crossing overland flow path	Assumption is that strips/barriers are equally spaced along overland flow path
How strip/barrier width is specified	Width can be specified in absolute units or as the portion of the overland flow path length
Absolute strip width	Strip/barrier width if input for width is specified in absolute units
Strip/barrier width relative to overland flow path length	Strip/barrier width if input for width is specified as the portion of the overland flow path length
Strip/barrier cover-management description	Select the cover-management description for the filter and buffer strip/barrier system. Cover-management description selected for profile is cover-management input for non-strip portion of the overland flow path. The cover-management description selected for the profile is the cover-management description that RUSLE2 uses for rotational strip cropping.
Strip/barrier at bottom of overland flow path	Selecting **yes** places a strip/barrier at the end of the overland flow path. Remaining strips are uniformly spaced along the overland flow path. Selecting **no** places the last strip/barrier

	the same distance above the end of the overland flow path that strips/barriers are spaced along the overland flow path.
Is strip/barrier used for water quality	For USDA-NRCS conservation planning. NRCS specifies require that last strip width be twice as wide as the other strips when explicit purpose is to improve water quality.

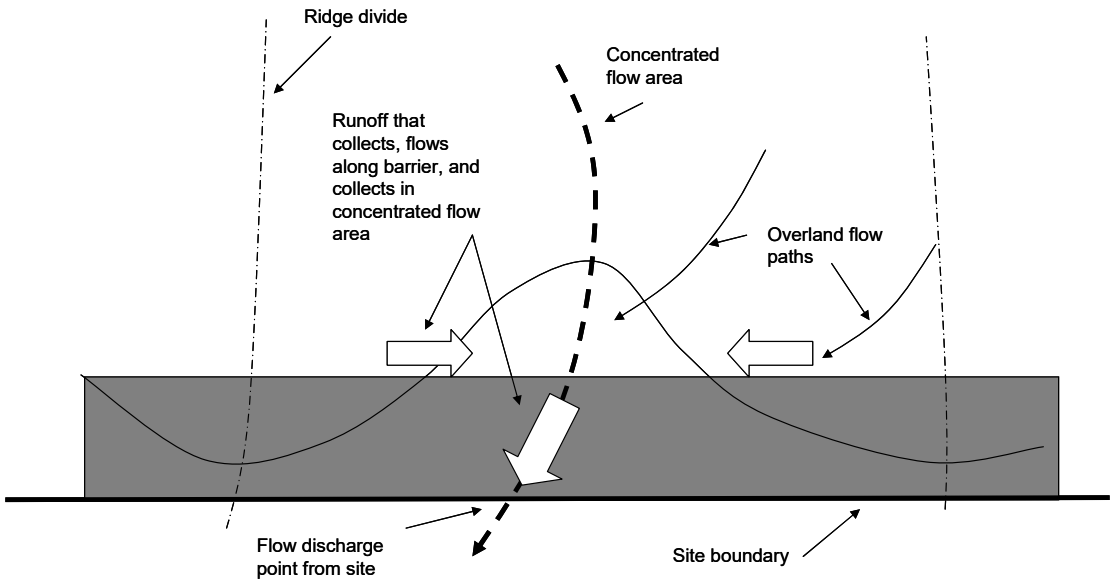

Figure 14.11. A strip where upper edge is parallel to site boundary.

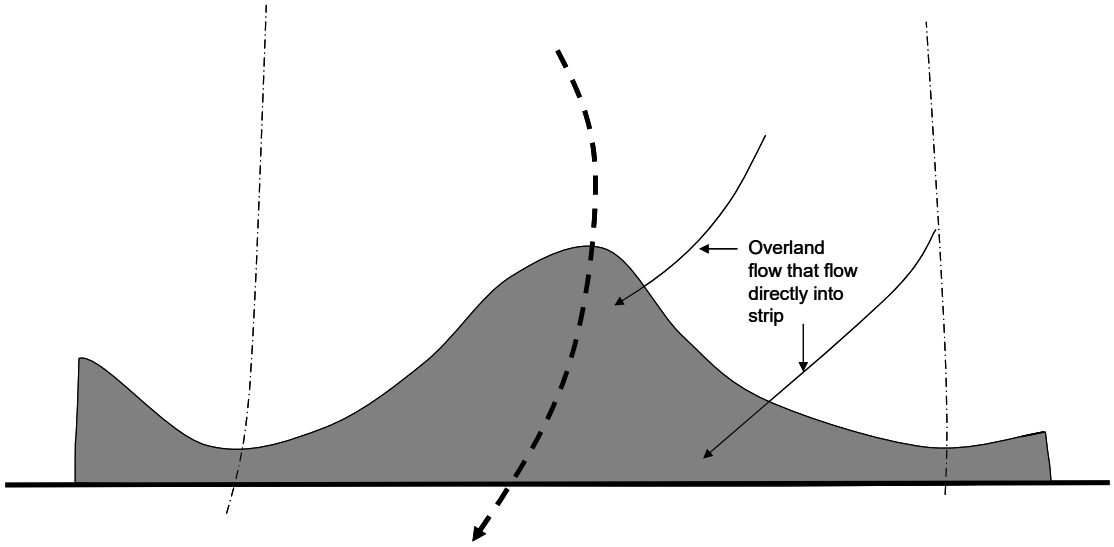

Figure 14.12. A strip where upper edge is perfectly on the contour.

14.2.5.1. Inputs for filter strip/barrier

A filter strip porous barrier is a single barrier at the end of the overland flow path. Four examples of a filter strip porous barrier are a wide strip of dense vegetation (e.g., grass strip) on cropland, a narrow strip of erect, stiff, dense grass (stiff grass hedge) on cropland, an undisturbed strip left along concentrated flow areas on disturbed forestland, and a fabric (silt) fence on a construction site. The specific inputs for a filter strip-type

porous barrier are: strip/barrier type (select **filter strip**), how strip/barrier width is specified, strip/barrier width, and cover-management description for strip/barrier.

The general recommendation for conservation and erosion planning is to specify **strip/barrier width** as the portion of the overland flow path length. A strip width of 10 percent of the overland flow path length is commonly assumed for general conservation and erosion control planning. An alternate is to specify the actual widths in absolute units instead of a portion of the overland flow path length.

Figure 14.12 illustrates that the portion of the overland flow path occupied by a filter strip/barrier of a fixed width varies by overland flow path. This variation means that the relative filter strip/barrier width depends on the overland flow path assumed in applying RUSLE2 to a particular site. The recommended approach is to choose an overland flow path and a representative filter strip/barrier width that are consistent with the conservation and erosion control planning objectives for the site. For example, a typical RUSLE2 application is to protect the eroding portion of the hillslope from excessive erosion so that the soil resource is protected. The one third portion of the hillslope having the highest erosion potential is typically selected as the area where RUSLE2 will be applied when conservation planning objective is to protect the soil resource. An overland flow path is assumed through this hillslope area, and the filter strip/barrier width for that overland flow path is used as the input width. However, if this width is not representative of the filter strip/barrier as a whole, use a representative filter strip width even if it does not match the actual width for the selected overland flow path.[146]

Filter strips/barriers are often used to reduce sediment yield from a site. RUSLE2 computes sediment yield from the area represented in a RUSLE2 computation. This area can include the entire overland flow area, diversions/terrace channels having deposition, and small impoundments, but it does not include concentrated flow areas where additional deposition and ephemeral gully erosion can occur (see **Sections 5.1 and 5.2**).

RUSLE2 computations should be made for a collection of overland flow paths when computing sediment yield where conditions vary over the area of interest. The sediment yield value for each overland flow path is weighted by the area represented by that path to obtain a sediment yield estimate for the entire area represented by the RUSLE2 computations. The **plan component** of the **RUSLE2 database** can assist in this computation where the sediment yield values are weighted by the sub-area that each overland flow path represents relative to the total area.

---

[146] RUSLE2 computes erosion and deposition values for porous barriers that are consistent with erosion science and research data. RUSLE2 is not meant to displace erosion control practice standards and specifications issued by agencies like the USDA-Natural Resources Conservation Service. However, such standards sometimes compromise erosion control performance for convenience of certain farming operations. RUSLE2 does not consider all factors important in conservation and erosion control planning. Use RUSLE2 values to guide developing an appropriate site-specific plan.

RUSLE2 only computes sediment yield from the overland flow area, diversion/terrace channels where deposition occurs, and small impoundments. RUSLE2 does not compute sediment yield from the site unless the flow paths represented by RUSLE2 end at the site boundary (see *Sections 5.1 and 5.2*).

RUSLE2 computes a backwater/deposition width and adds that value to the input width for the strip/barrier. This approach takes into account type and porosity of the barrier based on the retardance value assigned in the **vegetation description** used to represent the barrier (see **Sections 11.1.4 and 11.2.5**). This approach also takes into account how location, soil, and cover-management affect runoff and backwater/deposition width.

A **cover-management description** is selected to describe the filter strip/barrier, even for mechanical barriers like silt fences. The cover-management description for permanent vegetation strips should be a **no-rotation** type cover-management description (see **Section 10.2.8**). If the cover-management description on the upslope portion of the overland flow path is also a no-rotation type cover-management description, then consistency of the dates between the cover-management descriptions is not required. Similarly, consistency of dates between the cover-management descriptions is not important when cover-management description is a rotation type for the strip/barrier even though the upslope cover-management description is a no-rotation type. **However, if the cover-management descriptions are a no-rotation type for both the upslope area and the strip/barrier, then the dates in the two cover-management descriptions must be consistent.**

Strips/barriers can be added and removed at particular times over the computational period using operations in the cover-management description for the strip/barrier.[147] This RUSLE2 capability allows the use of a single cover-management description to describe a strip/barrier to compute erosion over the pre-construction, construction, and post construction phases.

A **vegetation description** is used to describe mechanical barriers such as fabric fences, gravel dams, straw bales, berms, and similar erosion control porous barriers used on construction sites. A selection is made from the **retardance classes** defined for vegetation plus the additional retardance class for silt fences and stiff grass hedges to describe the porosity of the barrier (see **Section 11.2.5**). Retardance class 7 for stiff grass hedges and silt fences is selected if the material provides extremely high retardance. Another retardance classes is used for more porous barriers. Also, the **production**

[147] A **begin growth process** in an **operation description** is used to install (put in place) a mechanical barrier (e.g., silt fence) because a vegetation description is used to represent the barrier. A **kill vegetation** and a **remove residue processes** are used in an operation description to remove a mechanical barrier.

(yield) level can be changed to alter the retardance (porosity) of the strip/barrier unless the **extremely high retardance class** is selected for the strip/barrier.

The canopy cover should be set to 100 percent and the effective fall height should be set to zero in the vegetation description used to describe a mechanical barrier to minimize detachment that RUSLE2 computes for the portion of the overland flow path occupied by the barrier.

High quality filter strips/barriers can greatly reduce sediment yield, but they do not significantly reduce the conservation planning soil loss (see **Section 8.1.5.4**). The deposition caused by the strip/barrier is near the end of the overland flow path unless the strip is very wide such as a strip that occupyies more than 40 percent of the overland flow path.

Porous barriers must be perfectly on the contour for effective performance. RUSLE2 assumes well designed, installed, and maintained barriers.

14.2.5.2. Inputs for buffer strips/barriers

A **buffer strip/barrier** type porous barrier is a set of equal width strips/barriers spaced uniformly along the overland flow path and having the same cover-management description and width. The same base **cover-management description** applies to all of the inter-strip/barrier areas. Examples include permanent grass strips on cropland and silt fences on a construction site.

The specific inputs for a buffer strip type porous barrier are:

barrier type (select **buffer strip**),
number of strips/barriers crossing the overland flow path,
how strip/barrier width is specified,
strip/barrier width,
cover-management description for strip/barrier,
whether a strip/barrier is at the end of the overland flow path, and
is the buffer strip system for water quality.

The **buffer strip/barrier description** in the **strip/barrier component** of the RUSLE2 database is for routine conservation and erosion control planning. A RUSLE2 template (see **Section 8**) that displays the three layer profile schematic can be used to apply RUSLE2 to complex, non-uniform conditions.

Several inputs for a buffer strip/barrier system are the same as for a filter strip barrier description. See **Section 14.2.5.1** for a description of the common inputs. Only the

additional inputs required to describe a buffer strip/barrier system are discussed in this section.

The number of strips/barriers is not the number of strips/barriers on the hillslope or in the field, but the number of strips/barriers that cross the overland flow path used in the RUSLE2 computation.

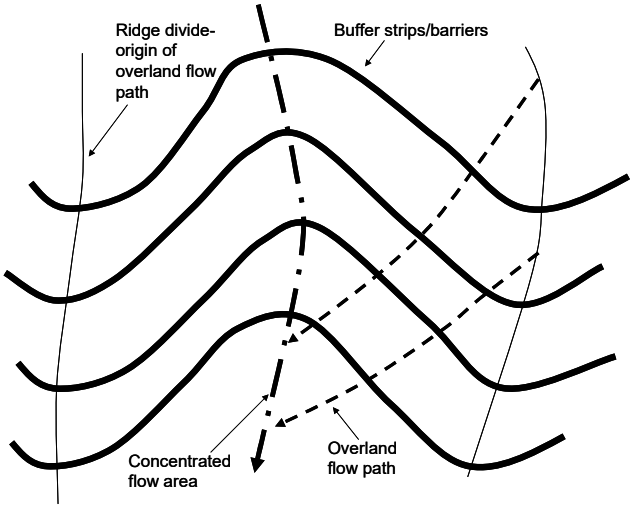

Figure 14.13. A buffer strip/barrier system on a typical hillslope illustrating various overland flow paths.

Enter a representative value for the number of strips/barriers that cross the overland flow path. The number will vary depending on the overland flow path that is chosen for the RUSLE2 computation as illustrated in Figure 14.13. Apply the guidelines described in **Section 14.2.5.1** regarding filter strip width for selecting a value for the number of strips/barriers that cross the overland flow path.

If a strip/barrier is placed at the end of the overland flow path, select **yes** for the input of **strip/barrier at the end of the overland flow path**. RUSLE2 divides the overland flow path into a number of barrier-interbarrier intervals equal to the number of strips/barriers crossing the overland flow path. This arrangement is illustrated in Figure 14.14.

The strip/barrier arrangement where a strip/barrier is not at the end of the overland flow path is also illustrated in Figure 14.14. In this case, the number of inter-strip/barrier intervals along the overland flow path is one greater than the number of strips/barriers. Consequently, the strips/barriers are more closely spaced than when a strip/barrier is at the end of the overland flow path. Sediment yield is increased when a strip/barrier is not at the end of the overland flow path to trap the sediment eroded on the last inter-strip/barrier area. Although sediment yield is reduced when a strip/barrier is at the end of the overland flow path, the conservation planning soil loss (see **Section 8.1.5.4**) may not differ greatly with strip/barrier placements.

As Figure 14.13 illustrates, the relationship of the last strip/barrier to the end of the overland flow path varies. Either chose the input that best represents the overall field situation or make RUSLE2 computations for both strip/barrier placements. The conservation or erosion control plan could be based on an average of the two computations or on the one where the erosion and sediment yield potential is greater.

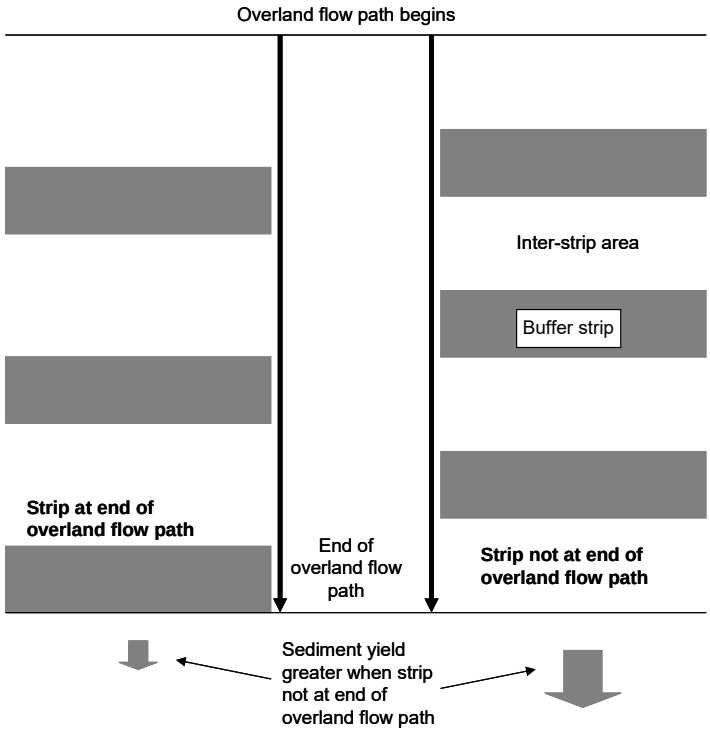

Figure 14.14. Illustration of a buffer strip systems where strip is at end of overland flow path and one where strip is not at end of overland flow path.

Select **yes** for the input **used for water quality** if the buffer strip/barrier description is being used for water quality purposes according to USDA-NRCS standards. Also, select **yes** for the input **to place a strip/barrier at the end of the overland flow path**. These selections cause the width of the strip at the end of the overland flow path to be twice the width of the other strips.

14.2.5.3. Inputs for rotational strip cropping

A rotational strip cropping system is a set of equal width strips that are annually rotated on the overland flow path in a sequence determined by a **cover-management description**. The cover-management description includes erodible periods and dense vegetations periods. Rotational strip cropping's effectiveness is from the deposition caused by the dense vegetation strips. The specific inputs for a rotational strip cropping type porous barrier are barrier type (select **rotational strip cropping**), number of strips/barriers crossing the overland flow path, the cover-management description, and the sequencing of the strips along the overland flow path.

Select a representative value for the number of strips that cross the overland flow path. The number of strips that cross the overland flow path varies with the overland flow path as described in **Section 14.2.5.2** for buffer strip systems. Also, the field overland flow path does not always begin and end on a strip boundary as assumed by RUSLE2. The idea is to a chose a number that best represents the overall field situation where RUSLE2 is being used as a conservation and erosion control planning tool. A RUSLE2 **template** that displays the three layer profile schematic can be used to estimate erosion on more complex situations that can be represented with the **rotation strip cropping description** in the **strip/barrier component** of the RUSLE2 database.[148] For example, this template

[148] If a RUSLE2 template with the three layer profile schematic is used to represent rotational strip cropping

is required to compute erosion for a rotational strip cropping system combined with a filter strip system because a filter strip description and a rotational strip cropping description from the RUSLE2 strip/barrier database component can not be combined.

The number of strips is not the number of strips on the hillslope or in the field, but the number of strips that cross the overland flow path used in the RUSLE2 computation.

Select a cover-management description that includes periods of dense vegetation that provide substantial flow retardance to cause deposition. The cover-management description, which is applied to all strips along the overland flow path, must include dense vegetation or other high hydraulic resistance conditions to cause deposition. The effectiveness of rotational strip cropping is achieved by having alternating strips of dense vegetation that cause deposition.

These alternating strips of dense vegetation are described by sequencing the cover-management description among the strips. The sequencing procedure used in RUSLE2 is to **offset** the starting date of the cover-management description by a particular number of years for each strip.

The following examples illustrate how to offset a cover-management description, which must be a rotation, to describe a rotational strip cropping system in RUSLE2. Assume a simple cover-management description of two years of corn followed by three years of hay represented by corn 1 - corn 2 - hay 1 – hay 2 – hay 3. Multiple years of each crop are grown together for convenience. Assume four strips along the overland flow path. The number of strips along an overland flow path need not match the years in the rotation as illustrated in this example. The number of strips will often be less than the number of years in the rotation.

Table 14.4 illustrates a rotation strip cropping description where the cover-management description is not offset for any strip. The result is that the same cover-management condition exists on all strips in any year. This system only reduces the conservation planning soil loss by reducing erosion that results from the three years of hay being much less erodible than is the corn. No deposition occurs among the strips because the hydraulic resistance does not increase between any two adjacent strips. This system is not rotational strip cropping because the dense vegetation (i.e., hay) are not alternated among the erodible (i.e., corn) strips.

Table 14.4. Example of no offset for a corn-corn-hay-hay-hay cropping rotation.

Strip	Years of	Year 1	Year 2	Year 3	Year 4	Year 5

and similar strip conditions where the strips must be sequenced along the overland flow path, the inputs to describe strip sequencing are entered in the **cover-management tab**.

Number	Offset					
1 (upper end of overland flow path	0	corn 1	corn 2	hay 1	hay 2	hay 3
2	0	corn 1	corn 2	hay 1	hay 2	hay 3
3	0	corn 1	corn 2	hay 1	hay 2	hay 3
4	0	corn 1	corn 2	hay 1	hay 2	hay 3

To achieve strip cropping, the cover-management description on some of the strips needs to be offset as illustrated in Table 14.5. The 2-year offset on strips 2 and 4 shifted the cover-management description by two years so that runoff from at least one corn strip runs through at least one hay strip. Sediment yield is reduced in the first two years because of a hay strip at the end of the overland flow path. However, sediment yield is increased in years 4 and 5 because the erodible corn strip is the last strip on the overland flow path. Both erosion and sediment yield are low in year 3 because the entire overland flow path is in the low erodible hay condition and only slight deposition occurs in this year.

Table 14.5. Example of a rotational strip cropping system where cover-management conditions are alternated by strip along the overland flow path.

Strip Number	Years of Offset	Year 1	Year 2	Year 3	Year 4	Year 5
1	0	corn 1	corn 2	hay 1	hay 2	hay 3
2	2	hay 1	hay 2	hay 3	corn 1	corn 2
3	0	corn 1	corn 2	hay 1	hay 2	hay 3
4	2	hay 1	hay 2	hay 3	corn 1	corn 2

Table 14.6 illustrates another possible strip cropping system described with a different set of offset years from the set illustrated in Table 14.5. The system illustrated in Table 14.6 is not as effective as the one illustrated in Table 14.5. In an example computation for Columbia, MO, the conservation planning soil loss for the system illustrated in Table 14.4 is 5.8 tons/acre. The conservation planning soil loss for the system illustrated in Table 14.5 is 2.6 ton/acre while it is 3.9 tons/acre for the system illustrated in Table 14.6. The major deficiency of the system illustrated in Table 14.6 is that it has fewer alternating strips of hay among corn strips than in the system illustrated in Table 14.5.

Table 14.6. Example of a rotational strip cropping system where the rotation is delayed a year on each subsequent strip.

Strip Number	Years of Offset	Year 1	Year 2	Year 3	Year 4	Year 5
1	0	corn 1	corn 2	hay 1	hay 2	hay 3
2	1	hay 3	corn 1	corn 2	hay 1	hay 2

3	2	hay 2	hay 3	corn 1	corn 2	hay 1
4	3	corn 2	hay 1	hay 2	hay 3	corn 1

RUSLE2 gives full credit to all deposition in the conservation planning soil loss for rotational strip cropping in contrast to the partial credit given for deposition caused by filter and buffer strip/barrier systems.

14.3. Flow Interceptors (diversions/terraces, sediment basins)

The conservation planning soil loss for rotational strip cropping is the same as the sediment yield when the *rotation strip cropping description* in the *strip/barrier component* of the RUSLE2 database is used. The two are not equal when the three layer profile schematic is used to represent rotational strip cropping by directing the overland flow path into segments.

14.3.1. Description of practices

Flow interceptors are topographic features that end the overland flow path (see **Sections 8.2 and 8.3**). Flow interceptors include diversions, terraces, and sediment basins. Diversions and terraces are constructed specifically to intercept overland flow and redirect the runoff around the hillslope in a low gradient channel. Terraces are constructed on a sufficiently low grade to cause deposition and even on a level grade with a closed outlet to conserve soil moisture in dry climates. Diversions are constructed on a sufficiently steep grade so that deposition does not occur but on a sufficiently flat grade so that erosion does not occur. Constructed terraces and diversions typically involve ridges and accompanying channels that convey the runoff to a protected open channel or an underground pipe that conveys the runoff downslope to a safe outlet. Disposal channels must be lined with vegetation, stone, or other material to prevent erosion because flow erosivity can be quite high in these channels.

The two major terrace types used on cropland are gradient and parallel tile outlet (PTO). Grade along a gradient terrace is nearly uniform, which requires plan curvature to fit the hillslope as illustrated in Figure 14.15. This curvature and the resulting non-uniform spacing between terraces along their length inconvenience farming operations. Gradient terraces generally divide the overland flow path length in shorter nearly uniform length overland flow paths between the terraces.

Parallel tile outlet terraces are relatively straight and are nearly uniformly spaced along their length. The terraces create small impoundments where they cross concentrated flow areas as illustrated in Figure 14.15. Impounded runoff drains through a vertical riser connected to an underground tile line (pipe). Grade along parallel terraces is typically non-uniform requiring that the grade be limited to prevent erosion. A variety of overland

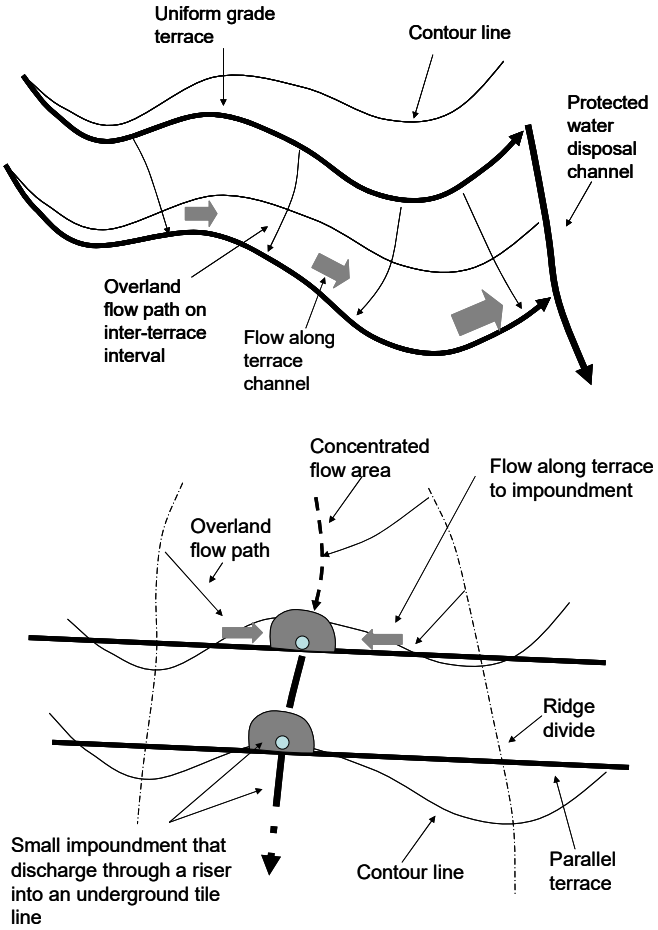

Figure 14.15. Illustration of a gradient terrace (top sketch) and parallel tile outlet (PTO) terrace systems (bottom sketch) and associated flow paths.

flow path lengths exist between parallel terraces. In contrast, to gradient terraces that almost always divide the overland flow path length, the longest overland flow path between parallel terraces may not be affected if the terraces are widely spaced. Sediment yield is low because of deposition in the small impoundment (sediment basin) in the concentrated flow areas.

Diversions, terraces, and sediment basins are also used on construction sites, reclaimed mine land, landfills, and other highly disturbed lands to shorten the overland flow path as illustrated in Figure 8.12 and reduce sediment yield, especially during periods when cover-management erosion control methods can not be used during soil disturbing operations.

Other features, including windrowed forest debris on disturbed forest land following site preparation for reseeding, act as diversion/terraces. Another example is a ridge of soil left by grading operations at the top of a cut or embankment on a construction site (see **Section 8.3.3**). Another example is an off-contour stiff grass hedge where tillage leaves a ridge of soil along the hedge that diverts the runoff rather than allowing it to flow through the hedge. A similar example is an off-contour silt fence on a construction site.

14.3.2. Basic principles

Flow interceptors involve two basic **hydraulic elements**, which are a **channel** and an **impoundment**. Diversions/terraces reduce rill and interrill erosion by shortening the overland flow path length, which is considered in the **topographic description** of the overland flow path (see **Section 8**).

Terraces also reduce sediment yield by causing deposition in the terrace channel. The basic principles described in **Section 5.4** for computing deposition on overland flow areas are used to compute deposition in diversion/terrace channels. The basic concept is that deposition occurs when the sediment load delivered to the diversion/terrace channel by overland flow on the inter-terrace interval exceeds transport capacity in the terrace channel. Deposition is computed with:

$$D = [\phi/(1+\phi)](dT_c/dx - D_o) \quad [14.1]$$

where: D = deposition rate (mass/time·unit channel width), T_c = transport capacity in the diversion/terrace channel (mass/time), x = distance along the channel, dT_c/dx = change of transport capacity along the channel (mass/time·distance), and D_o = sediment delivered to the channel from the overland flow area (mass/time·unit distance along channel). The variable φ is given by:

$$\phi = aV_f/q_c \quad [14.2]$$

where: α = a coefficient to be determined by calibration, V_f = fall velocity of the sediment particles, and q_c = discharge rate in channel per unit channel width, which is the discharge rate from the overland flow path that ends at the diversion/terrace channel. Transport capacity in the channel is computed by:

$$T_c = K_{Tc}Q_c s \quad [14.3]$$

where: K_{Tc} = a coefficient to be determined by calibration, $Q_c = q_c x$ = discharge rate in the channel, and s = sine of the grade angle of the channel.

Simplifying assumptions consistent with RUSLE2's purpose to serve as a guide for conservation and erosion control planning were made in solving these equations. The equations are applied to each sediment particle class assuming no interaction among the particle classes. Grade along the channel is assumed to be uniform, which gives the mathematical result that deposition is uniform along the channel. Consequently, channel length is not a factor in the computations and, therefore, is not an input.

Transport capacity for a sediment particle class is assumed to be proportional to its portion in the sediment load that reaches the channel. Deposition among the particle classes varies according to the particle class's fall velocity. RUSLE2 computes the particle class distribution and the sediment load leaving the channel. RUSLE2 computes an enrichment ratio that is a measure of how deposition enriches the sediment load in fines (see **Section 7.5.1**). The enrichment ratio increases as deposition increases (i.e., as the sediment delivery ratio decreases).

RUSLE2 also assumes a smooth, bare soil surface in a diversion/terrace channel. Deposition in these channels is highly localized, typically along the channel edge where overland flow enters the channel flow. Deposition covers most soil surface roughness and crop residue to leave a bare, smooth soil surface. RUSLE2 does not accurately compute deposition where vegetation in the channel retards the flow to cause deposition. This limitation is not especially important because most erosion and deposition occur during the cropping season before vegetation develops.

RUSLE2 does not consider channel cross section shape in its computations.

Sediment delivery ratio is a measure of deposition. In RUSLE2, the sediment delivery ratio for a given diversion/terrace channel varies with several factors including channel grade and runoff, sediment load, and sediment characteristics entering the channel from the inter-diversion/terrace area. For example, very little or no deposition occurs when the channel grade is steep because transport capacity is high. Very little deposition occurs when sediment delivery is low and runoff is high from the overland flow area. Deposition is reduced when incoming sediment is mostly fine particles caused by the source soil properties or deposition on the overland flow path, particularly near its end (e.g., deposition by a grass strip or a flat concave overland flow path segment at the channel edge). Consequently, the sediment delivery ratio computed by RUSLE2 for a diversion/terrace is not constant for a particular channel grade, but depends on the conditions on the inter-diversion/terrace area as well.[149]

RUSLE2 computes deposition in a small impoundment (sediment basin) using:

$$g_{out} = g_{in} \exp(-\beta V_f) \qquad [14.4]$$

where: g_{in} = sediment load coming into the sediment basin, g_{out} = sediment load leaving the sediment basin, and α = a coefficient determined by calibration. This equation is fundamentally for a simple settling tank where transport capacity is assumed to be zero and the effective length is determined by calibration. RUSLE2 computed deposition depends only on the characteristics of the incoming sediment. RUSLE2 typically computes large deposition amounts and fine sediment leaving the basin. RUSLE2 computes reduced deposition if the incoming sediment is fine, which is why RUSLE2 computes significantly less deposition by a second sediment basin than by the first basin in a series. RUSLE2 computes an enrichment ratio, which is a measure of deposition enriching the sediment in fines, for the outgoing sediment (see **Section 7.5.1)**.

[149] The RUSLE1.06 computes deposition by diversions/terraces similar to RUSLE2. However, RUSLE1.05 computes sediment delivery ratio solely as a function of diversion/terrace grade.

RUSLE2 computed deposition is not a function of basin geometry, hydraulics, or remaining basin capacity. That is, RUSLE2 does not consider design or maintenance in its impoundment (sediment basin) computations.

RUSLE2 takes partial credit for the deposition caused by terraces and impoundments as soil saved in protecting the soil resource. The amount of deposition credited as soil saved in computing the conservation planning soil loss depends on diversion/terrace spacing and location of the diversion/terrace along the overland flow path. Deposition in a terrace located near the end of the overland flow path gets very little credit as soil saved. Deposition in a terrace located about half way along the overland flow path gets approximately half credit as soil saved when diversion/terrace spacing is less than 90 ft (30 m). The credit decreases as spacing increases beyond 90 ft (30 m) to essentially no credit for spacing greater than 300 ft (100 m).

RUSLE2 is a conservation and erosion control planning tool. It is not a hydraulic design tool. See *Haan et al. 1994. Design Hydrology and Sedimentology for Small Catchments. Academic Press* for a description of procedures that can be used to design channels and impoundments. Also, RUSLE2 is not meant to displace standards used by agencies such as the USDA-NRCS, although those standards sometime compromise practice performance for farming convenience and other reasons not considered by RUSLE2.

14.3.3. Calibration

Calibrating RUSLE2 for flow interceptors involves two sets of calibration, one for deposition in terrace channels and one for deposition in small impoundments (sediment basins). The erosion component of the CREAMS and the RUSLE1.05 equation that computes sediment delivery as a function of terrace grade were major tools used in this RUSLE2 calibration.[150] The CREAMS erosion component represents experimental field data involving gradient terraces on a range of grades at numerous locations, which were also used to derive the RUSLE1.05 equation. Another data set used in the RUSLE2 calibration was from a study of deposition in a ridge-furrow system.[151] The first step in

---

[150] See:
AH703

Foster, G. R., L. J. Lane, J. D. Nowlin, J. M. Laflen, and R. A. Young. 1980. A model to estimate sediment yield from field sized areas: Development of model. *In:* CREAMS - a field scale model for Chemicals, Runoff, and Erosion from Agricultural Management Systems. Vol. I: Model Documentation. Conservation Research Report No. 26. USDA-Science and Education Administration. pp. 36-64.

Foster, G. R. and R. E. Highfill. 1983. Effect of terraces on soil loss: USLE P factor values for terraces. Journal of Soil and Water Conservation 38:48-51.

[151] Meyer, L.D. and W. C. Harmon. 1985. Sediment losses from cropland furrows of different gradients. Trans. ASAE. 28: 448-453, 461.

the calibration was to determine a value for the $\mathbf{K_{TC}}$ coefficient in the sediment transport capacity equation, equation 14.3, for a terrace channel. The value for this coefficient was adjusted until sediment transport capacity matched sediment load at the point that deposition was judged to begin based on field data as channel grade was reduced. Sediment transport capacity equals sediment load at the point that deposition begins according to RUSLE2 theory. The next step in the calibration was to determine a value for the coefficient **β** in equation 14.2. This equation determines the RUSLE2 computed particle class distribution in the sediment leaving the channel and determines deposition amount to a much lesser extent. Both the experimental field data and computed values from the CREAMS erosion component were used in this calibration.

The second set of calibrations was to determine a value for the coefficient **a** in equation 14.4 that RUSLE2 uses to compute deposition by particle class for a small impoundment. Once again, the CREAMS erosion component was used in the calibration because it had been calibrated using data from several field studies of impoundment, tile outlet terraces in Iowa. The primary calibration was to adjust values for the coefficient **β** until the RUSLE2 computed sediment delivery ratio matched experimental values. Also, the RUSLE2 computed values were evaluated against experimental values determined from sediment basins used on construction sites and mined land. The RUSLE2 computed sediment delivery ratio values matched the experimental values for sediment basins on highly disturbed land where the basins were well designed and constructed and were clear of sediment, i.e., functioning at optimum performance.[152]

14.3.4. Interpretation

RUSLE2 computations for **hydraulic elements** are for conservation and erosion control planning, **not for design**. RUSLE2 computes deposition in channels typical of diversions, terraces, and similar channels that intercept overland flow. RUSLE2 does not consider channel shape or hydraulic resistance in its computations. Although RUSLE2 computes average annual deposition, the computations represent an approximate 10 year return period. The channels are assumed to be in an environment, typically cropland and construction sites, where failure does not cause major damage and routine maintenance and repair are readily available.

---

[152] See:

Foster, G. R., L. J. Lane, J. D. Nowlin, J. M. Laflen, and R. A. Young. 1980. A model to estimate sediment yield from field sized areas: Development of model. *In:* CREAMS - a field scale model for Chemicals, Runoff, and Erosion from Agricultural Management Systems. Vol. I: Model Documentation. Conservation Research Report No. 26. USDA-Science and Education Administration. pp. 36-64.

Toy, T.J. and G.R. Foster (coeditors). 1998. Guidelines for the use of the Revised Universal Soil Loss equation (RUSLE1.06) on mined lands, construction sites, and reclaimed lands. USDI-Office of Surface Mining. Denver, CO.

However, a different environment exists in other RUSLE2 applications where a diversion failure causes major problems. Diversions are sometimes used on the steep side slopes of landfills and hazardous waste sites to reduce rill erosion. Deposition in the diversions should be avoided because it reduces flow capacity, which can cause overtopping, very serious gully erosion, and major failure of the diversion. Maintaining a uniform grade and avoiding adverse grades along these diversions is especially important to prevent overtopping. Also, differential settling on the overland flow area between diversions can cause overland flow to become concentrated flow that causes serious gully erosion and overwhelms downslope diversions. RUSLE2 provides no information on such localized failures.

Similarly, RUSLE2 computes average annual deposition by small impoundments (sediment basins) assuming optimum performance without considering basin geometry, hydraulics, or water and sediment chemistry. RUSLE2 computed values apply to small sediment basins similar in size and hydraulic performance to the impoundments created by parallel tile outlet terraces where impounded water is drained by a perforated riser pipe that discharges into an underground pipe. Retention time in these basins is about 24 hours and the maximum water depth is about 4 to 6 ft (1 to 2 m).

These sediment basins often have a life expectancy less than five years, which means that the probability of an extreme event occurring while they are in place is low. Therefore, RUSLE2's estimate of average annual deposition is reasonable for conservation and erosion control planning. Damages are likely to be minor if failure occurs. Construction cost is low and maintenance and repair are readily available. Cleaning the basin after major storms may be more cost effective than building a large basin based on an extreme event.

All hydraulic structures including channels and impoundments should be based on proper engineering design. *RUSLE2 IS NOT AN ENGINEERING DESIGN TOOL*. Good professional judgment should always be used in making final decisions rather than relying solely on RUSLE2. RUSLE2 is to be used as a guide to supplement other information.

14.3.5. Inputs

The **hydraulic element (open channel-impoundment) systems component** of the RUSLE2 database is used in routine conservation and erosion control planning to evaluate the effect of diversions/terraces and small impoundments (sediment basins) on erosion and sediment yield from the flow path represented in the RUSLE2 computation. The hydraulic element systems database component contains **diversions/terraces and sediment basin systems descriptions** that are applied to the overland flow path without the hydraulic elements in place. Each hydraulic element system description involves a **hydraulic element (channel/impoundment) flow path description** that is applied at

one or more equally spaced intervals along the overland flow path. A channel/impoundment flow path description lists the **hydraulic elements** (i.e., channels, impoundments) in the channel/impoundment flow path. Each diversion/terrace and sediment basin is assumed to be thin and to take up no space on the hillslope. This approach does not take into account how back and front slope characteristics of a diversion/terrace or sediment basin affect erosion.

A RUSLE2 **template** having the **three layer profile schematic** should be used (1) for complex conditions where the channel/impoundment flow paths are not equally spaced along the overland flow path, (2) where the individual channel/impoundment flow path differ, (3) where the soil, topography, and cover-management conditions of the embankment/channel should be described because of their effect on erosion, and (4) where soil, steepness, or cover-management vary along the overland flow path.

An example where the hydraulic element flow paths are non-uniformly spaced along the overland flow path is illustrated in Figure 8.12 where a diversion is placed at the top of a landfill sideslope. Figure 8.11 illustrates a detailed description of embankment/channel topography. Grass is often used on steep backslope terraces to prevent excessive erosion. The detailed soil, topography, and cover-management of such embankment/channels can be represented as described in **Sections 8.3.3 and 8.3.4**.

14.3.5.1. Inputs for a hydraulic element (channel/impoundment) system description

The inputs for a **hydraulic element (channel/impoundment) system description** are (1) number of hydraulic element (channel/impoundment) flow paths that cross the overland flow path, (2) whether a channel/impoundment flow path is located at the end of the overland flow path, and (3) the **hydraulic element (channel/impoundment) flow path description**.

When a hydraulic element (channel/impoundment) system description is used in RUSLE2, the overland flow path length is described without the hydraulic elements present. RUSLE2 uses the input for number of channel/impoundment flow paths that cross the overland flow path to determine the overland flow path length between the hydraulic element flow paths. This overland flow path length is the overall overland flow path length divided by number of channel/impoundment flow paths (diversion/terraces) if a channel/impoundment path is located at the end of the overland flow path. If a channel impoundment path is not located at the end of the overland flow path, the overland flow path length between channel/impoundment paths is computed as the overall overland flow path length divided by the number of channel/impoundment paths plus one.

The number of channel/impoundment flow paths that cross the overall overland flow path varies with the overland flow path chosen for the RUSLE2 computation. A

representative number should be chosen based on the conservation and erosion control planning objective, which is similar to choosing the number of porous barriers that cross the overland flow path (see **Sections 14.2.5.1 and 14.2.5.2**).

Extra consideration should be given to selecting the number of channel/impoundment flow paths that cross the overall overland flow path when representing parallel impoundment terraces. The overland flow path length between parallel impoundment terraces varies greatly as illustrated in Figure 14.15. The RUSLE2 computed overland flow path length should be checked to determine if this overland flow path length is appropriate. The RUSLE2 computed overland flow path length can sometimes be too short. An improvement in the erosion computation can be made by decreasing the number of channel/impoundment flow paths that cross the overall overland flow path. Also, the overall overland flow path can be lengthened for the hydraulic element computation but not for the computation when the hydraulic elements are not present. Another alternative is to apply RUSLE2 to a single inter-terrace interval.

The number of channel/impoundment paths is not the total number on the hillslope but the number that cross the selected overland flow path used in the RUSLE2 computation.

The input of whether a channel/impoundment (diversion/terrace) flow path is at the end of the overland flow path significantly affects computed sediment yield. A diversion/terrace at the end of the overland flow path is unnecessary when the sole purpose of the diversion/terrace system is to control rill-interrill erosion. In that case, a **no** input is selected for whether a channel/impoundment flow path is located at the end of the overland flow path. When **no** is selected, the sediment eroded on the last overland flow path interval leaves the RUSLE2 overall overland flow path without passing through the selected channel/impoundment flow path. If a channel/impoundment flow path is placed at the end of the overland flow path to trap sediment and control sediment yield from the site, select **yes** for whether a channel/impoundment flow path is located at the end of the overland flow path. This selection causes RUSLE2 to compute that sediment eroded on all overland flow path intervals passes through the selected channel/impoundment flow path.

The last input is to select a **hydraulic element (channel/impoundment) flow path description** from previously created entries in the RUSLE2 database.

14.3.5.2. Inputs for a hydraulic element (channel/impoundment) flow path description

A **hydraulic element (channel/impoundment) flow path description** gives the sequence of hydraulic elements (i.e., channel and impoundment) along the flow path.

Table 14.7 lists the possible sequences that can be used in RUSLE2.[153]

DO NOT ENTER SEQUENCES OTHER THAN THOSE LISTED IN TABLE 14.8.

Table 14.7. Possible sequences of channel and impoundment hydraulic elements used to represent hydraulic element (channel/impoundment) flow paths.

Sequence	Comment
Impoundment	Overland flow drains directly into impoundment. Typical application is a sediment basin on a construction site.
Impoundment-impoundment	Overland flow drains directly into the first impoundment, which in turn drains directly into the second impoundment. Typical application is two sediment basins in series on a construction site where sediment yield leaving the site must be very low.
Channel	Overland flow drains uniformly into channel along its length. No inflow at upper end of the channel can occur. Typical application are gradient terraces on an agricultural field or a diversion on a construction site or landfill.
Channel-impoundment	Overland flow area drains uniformly into channel along its length. No inflow at upper end of the channel can occur. Discharge from channel flows directly into impoundment. Typical applications are impoundment parallel terraces on an agricultural field and a diversion used to divert overland flow into a sediment basin on a construction site.
Channel-impoundment-impoundment	Same as a channel-impoundment sequence except that discharge from the first impoundment flows directly into the second impoundment. An example application is a diversion channel discharging overland flow into a series of two sediment basins on a construction site.
Note: When a segment on the overland flow path is adjacent to a segment with an adverse (negative) steepness, RUSLE2 assumes a channel hydraulic element at the intersection of the segments (see **Section 8.3.3**). The default channel assumed by RUSLE2 is steep so that no deposition occurs. A hydraulic element (channel/impoundment) flow path description from the RUSLE2 database can be substituted for the default channel, which allows RUSLE2 to compute deposition in channels at the intersection of the backslope and frontslope of a bench terrace system (see Figure 14.16) and in furrows separating ridges (see Figure 8.14), for example.	

An impoundment element can be the single element in the sequence, which represents overland flow discharging directly into an impoundment without first flowing through a channel. This sequence represents a sediment basin on a construction site.

[153] Other sequences besides those listed in Table 14.8 can be entered, but RUSLE2 does not properly compute deposition for other sequences.

Outflow from an impoundment is assumed to be a point discharge that can only flow into another impoundment. It can not discharge into a channel because a channel can not accept inflow at its upper end. Two or more impoundments can be placed in series to represent sediment basins in series.

A RUSLE2 channel hydraulic element is a channel of uniform grade that receives runoff uniformly along its length from the adjacent overland flow area. No inflow occurs at the upper end of the channel (i.e., discharge is zero at the upper end of the channel). **Only a single channel can be in the sequence of hydraulic elements used to describe a hydraulic element (channel/impoundment) flow path. If a channel is in the sequence, it must be the first hydraulic element in the sequence.**

RUSLE2 does not compute erosion in a channel. Ensure that the channel's lining is sufficient to prevent erosion for the channel's field grade.

A single channel is used to represent gradient terraces, illustrated in Figure 14.15, on an agricultural field, a diversion on a construction site, and a diversion at the top of the landfill sideslope illustrated in Figure 8.12. The discharge from a channel is a point discharge that can only flow into an impoundment element because of the no inflow requirement for a channel. A channel-impoundment sequence is used to represent parallel impoundment terraces illustrated in Figure 14.15.

The no inflow requirement for channels means that a sequence of channels can not be used to describe a variable grade diversion or terrace system, for example. A single grade must be entered to represent a variable grade channel. If the profile along the channel is concave, enter the grade over the last one fourth to one third of the channel. If the profile along the channel is convex, enter the grade over the first one third to one half of the channel.

Notes:
Grade along a RUSLE2 channel is uniform.
No inflow can occur at the upper end of a RUSLE2 channel, i.e., channels can not be in series to represent non-uniform grade channels.
RUSLE2 does not compute erosion in channels.
RUSLE2 is not a hydraulic design procedure. Proper hydraulic procedures should be used to design channels and impoundments.
The impoundments considered by RUSLE2 are small impoundments like sediment basins and impoundments associated with parallel tile outlet terraces.
RUSLE2 does not consider the disposal channel system associated with diversions and gradient terraces.

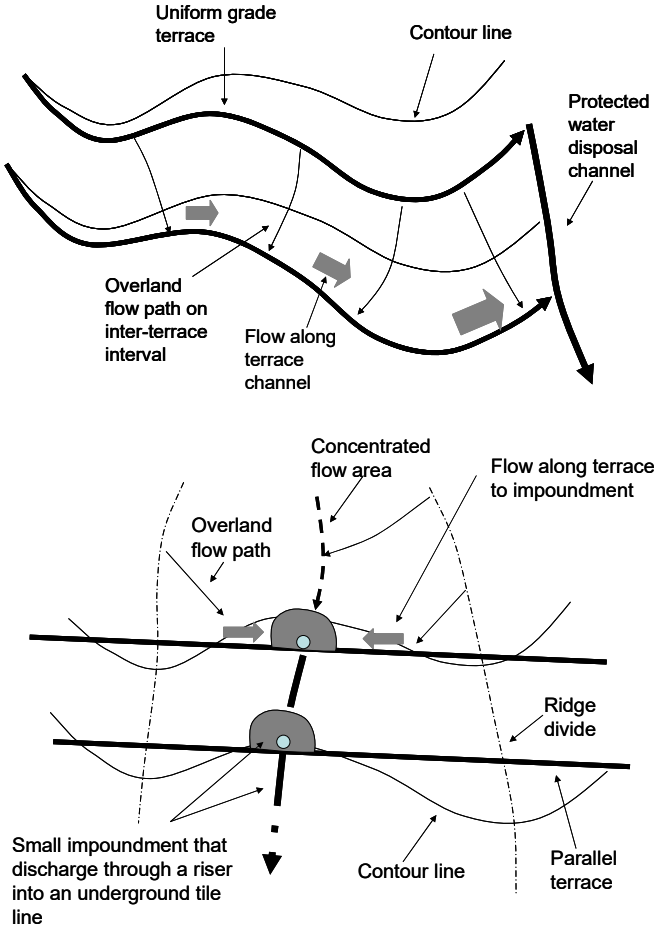

Figure 14.15. Illustration of a gradient terrace (top sketch) and parallel tile outlet (PTO) terrace systems (bottom sketch) and associated flow paths.

No inputs are required to describe an impoundment hydraulic element. Grade is the single input used to describe a channel hydraulic element. A typical RUSLE2 database contains channel descriptions over a range of grades from which selections can be made in describing channel/impoundment flow path systems.

RUSLE2 makes no distinction between a diversion or a terrace channel. Both are represented by the same channel hydraulic element. If a channel is intended to behave as a diversion where no deposition is expected, the RUSLE2 output should be reviewed for deposition. If deposition is computed in the diversion channel, a channel with an increased grade should be selected.

14.3.5.3. Inputs for the RUSLE2 default channel description

RUSLE2 automatically inserts a **default channel** when an overland flow path segment intersects with an overland flow path segment having an adverse (negative) steepness (see **Section 8.3.3**). Also, RUSLE2 may automatically assign a default channel at the end of the overland flow path. The grade of this default channel is already entered in the RUSLE2 database, and it can be changed. The grade is usually set at a very high steepness (e.g., 100 percent) so that RUSLE2 does not compute deposition in the default channel. Another channel that represents the field condition can be selected to replace the default channel in a particular RUSLE2 computation by selecting a channel/impoundment flow path description from the RUSLE2 database. By making this substitution, RUSLE2 can compute deposition in the channels that RUSLE2 assigns for

inward sloping bench terraces illustrated in Figure 14.16, in the furrows between ridges illustrated in Figure 8.14, and in a concentrated flow areas that separates two overland flow areas, which are created by dividing an overland flow path into two segments and entering a negative steepness for the second segment.

14.3.5.4. Inputs for bench terraces

Figure 14.16 illustrates bench terraces that can be represented by RUSLE2. The hydraulic element system component of the RUSLE2 database is not used in this RUSLE2 application. A RUSLE2 template having the three layer profile schematic is used to describe bench terraces.

The first bench terrace system is an outward sloping bench terrace where the benches slope outward away from the hillslope. The overland flow path is divided into segments where steepness values are entered into appropriate segments to represent the steep backslope and the relative flat bench. Runoff as overland flow is assumed from the top of the benches across each bench through the last bench. Different cover-management descriptions are selected for the backslope and bench segments.

The same procedure is used to describe inward sloping bench terraces where the benches slope inward to the hillslope. A negative steepness is entered for the inward sloping bench segments. Using this information, RUSLE2 determines the overland flow path lengths for each segment. RUSLE2 treats each backslope-bench combination as a separate catchment. RUSLE2 also assigns a default channel at the intersection of the backslope and bench. A channel on a low grade can be selected from the RUSLE2 database to replace the default channel so that RUSLE2 can compute deposition in the runoff that flows around the hillslope at the base of each backslope. Appropriate cover-management descriptions are selected for the backslope and bench segments.

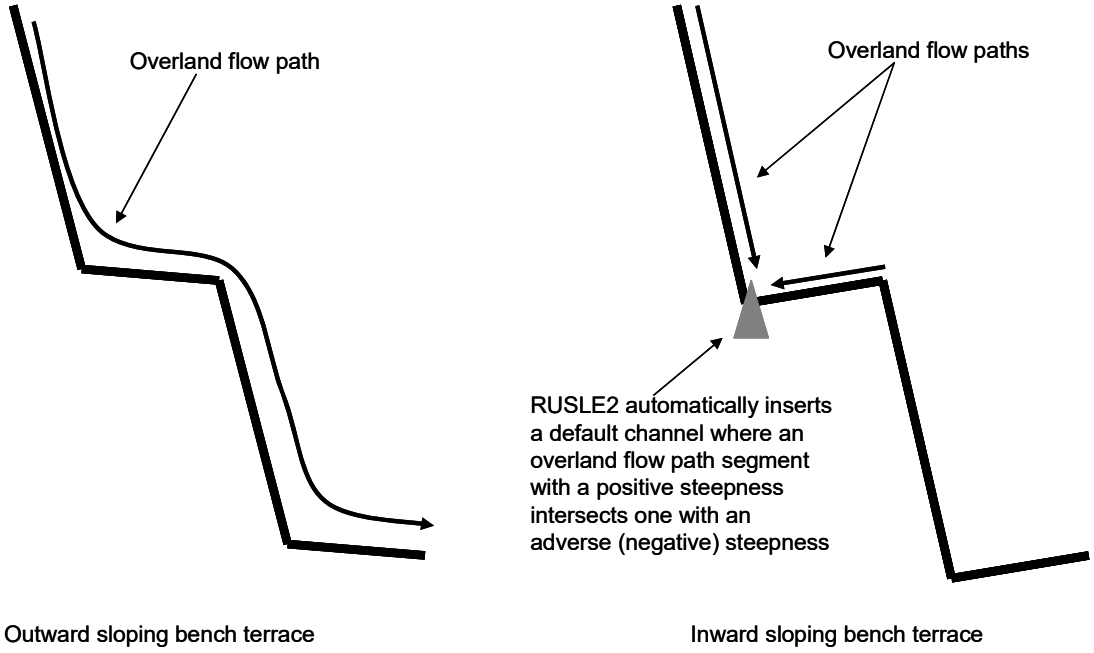

Figure 14.16. Overland flow paths for outward and inward sloping bench terraces.

14.4. Subsurface Drainage

14.4.1. Description of practice

Subsurface drainage is where lateral ditches or perforated pipe (tile line) placed about 2 to 3 ft (0.5 to 1 m) below the soil surface are used to reduce soil wetness to facilitate farming operations and improve crop yield. Subsurface drainage is most often used on relative flat slopes, less than 3 percent steepness, where the water table is near the soil surface over most of the site. Subsurface drainage lowers the water table and reduces soil water content, which in turn reduces runoff and erosion. Localized areas can also be subsurface drained. Examples include where a restricting layer causes a perched water table or in swales where the water table is high at the toe of hillslopes.

Installing tile drainage can be expensive, and therefore, a tile drainage system should be well designed based on site-specific conditions. The two major variables in a subsurface drainage system are depth and spacing of the tile lines and drainage ditches. Increasing depth and decreasing spacing improves subsurface drainage performance but also increases costs. Therefore, most subsurface drainage systems represent a balance between benefits and costs.

14.4.2. Basic principles

Subsurface drainage reduces rill-interrill erosion because it reduces surface runoff and increases vegetation production (crop yield) level. RUSLE2 uses the permeability subfactor equation in its soil erodibility nomographs to estimate how runoff potential reduced by subsurface drainage affects soil erodibility. The effect of increased production (yield) level is considered by inputting a production (yield) level value appropriate for the drained condition.

The two RUSLE2 soil erodibility nomographs include a permeability subfactor that adjusts soil erodibility based on the soil's runoff potential. The six permeability classes used in the nomographs describe runoff potential. Choice of a soil erodibility nomograph permeability class is based on texture and other surface soil properties, soil profile characteristics, presence of a naturally occurring restrictive layer, landscape position, location, and other factors that affect runoff potential under the unit plot condition (see **Sections 7.2 and 7.3.2**). Soil erodibility factor values increases as runoff potential increases.

Each **soil description** in the RUSLE2 database includes a hydrologic soil group designation, which is an index of runoff potential, for the undrained and drained conditions (see **Section 7.7**). RUSLE2 uses this index in the NRCS curve number

method to estimate runoff (see **Section 8.1.2**).[154] A **D** hydrologic soil group represents the highest runoff potential while an **A** hydrologic soil group represents the lowest runoff potential. The same factors that determine a permeability class in a RUSLE2 soil erodibility nomograph also determine a hydrologic soil group.

The degree that subsurface drainage changes the hydrologic soil group depends on site specific conditions. A very fine texture undrained soil may be assigned a **D** hydrologic soil group. Subsurface drainage will decrease the soil's runoff potential, but not greatly, resulting in a change of hydrologic soil group from **D** to **C** or **B**. Soil texture is a limiting factor in being able to economically drain this soil.

A coarse texture soil may be assigned a **D** hydrologic soil group because of a restrictive subsoil layer or being in a low position on the landscape. Subsurface drainage can greatly improve internal drainage of this soil resulting in the hydrologic soil group changing from a **D** to an **A**. A coarse soil texture does not limit internal drainage nearly as much as does a fine texture.

Subsurface drainage does not always change the hydrologic soil group designation to an A hydrologic soil group. Internal soil properties, especially texture, also affect the assigned hydrologic soil group for the drained condition.

RUSLE2 uses the permeability subfactor in its soil erodibility nomographs to compute how subsurface drainage affects erosion. RUSLE2 computes permeability subfactor values for the soil erodibility factor based on the hydrologic soil group assigned for the undrained and the drained conditions. RUSLE2 uses the permeability subfactor values and the soil erodibility factor for the undrained condition to compute an **effective soil erodibility factor** value for the drained condition. The four hydrologic soil group classes are scaled to match the six permeability classes used in the permeability subfactor so that a hydrologic soil group can be converted to a soil erodibility nomograph permeability class. RUSLE2 computed values for the effect of subsurface drainage on rill-interrill erosion are illustrated in Table 14.8.

RUSLE2 computes the greatest effect of subsurface drainage when soil erodibility factor (K) values are low. For example, RUSLE2 computes a 60 percent reduction in erosion for subsurface drainage that reduces runoff potential from a **D** to **A** hydrologic soil group for a silty clay soil with a 0.20 US units soil erodibility factor (**K**) value. This runoff potential reduction is too high for a fine textured soil. A more likely runoff reduction potential would be either from a **D** to **C** or **B** hydrologic soil group. RUSLE2 computes

[154] The permeability classes used in the RUSLE2 soil erodibility nomographs are essentially a runoff potential index in much way that the hydrologic soil group is a potential runoff index. The permeability class index is used in RUSLE2's soil erodibility nomograph to compute soil erodibility values and the hydrologic soil group index is used in RUSLE2 in the NRCS curve number runoff estimation method to estimate runoff in RUSLE2.

about a 20 percent reduction in erosion for this silty clay soil when runoff potential decreased from a **D** to **C** hydrologic soil group. RUSLE2 computes about a 25 percent reduction in erosion when the runoff potential decreases from **D** to **A** hydrologic soil group for a silt soil having a **K** value of 0.55 US units. These computations are based on the same crop yield for all cases.

The additive, rather than multiplicity, mathematical structure of the soil erodibility nomograph accounts for the much greater relative reduction in erosion by subsurface drainage at low soil erodibility factor values than at high soil erodibility factor values.

A lower limit of 0.2 is set in RUSLE2 for the ratio of erosion with subsurface drainage to erosion without subsurface drainage to prevent RUSLE2 from computing unreasonably low erosion estimates with subsurface drainage.

The RUSLE2 computed values for the effect of subsurface drainage on erosion is essentially not a function of location as illustrated in Table 14.8. Subsurface drainage should affect erosion more at a low precipitation location that at a high precipitation location, especially for coarse texture soils. Values for the hydrologic soil group for the drained condition entered in the **soil descriptions** in the RUSLE2 database can be selected to take this effect into account (see **Section 14.4.5**).

The runoff reduction provided by subsurface drainage depends on drain depth and spacing. This effect can be considered by the values entered in the soil descriptions for the drained condition (see **Section 14.4.5**).

Cover-management condition interacts with surface drainage to affect runoff. That effect is considered by the production (yield) level value for the drained condition entered in the **cover-management descriptions** in the RUSLE2 database (see **Section 10.2.4**). The production (yield) value in a RUSLE2 computation should be appropriate for the subsurface drainage condition.

The other effect of subsurface drainage that RUSLE2 considers is how reduced runoff affect contouring, contouring failure (critical slope length), and sediment transport capacity and deposition. A reduced runoff, which is used in these computations, is computed because of the reduced hydrologic soil group for subsurface drainage. Therefore, because of this reduced runoff, RUSLE2 computes less erosion and sediment yield for situations where contouring and deposition is involved.

If a subsurface drainage support practice is selected, the production (yield) level value should be changed accordingly from the undrained condition.

14.4.3. Calibration/validation

A rule of thumb is that tile drainage reduces rill-interrill erosion by about 40 percent.[155] RUSLE2 computations based on the principles described in **Section 14.2** were made for a wide range of soil textures and drainage intensities to ensure that RUSLE2 gives this result overall. Based on a review of the values listed in Table 14.8 and other values, RUSLE2 was judged to adequately capture the main effects of subsurface drainage on rill-interrill erosion for conservation and erosion control planning. The values shown in Table 14.8 do not consider how subsurface drainage affects yield and its consequent effect on erosion, which is an additional subsurface drainage effect.

14.4.4. Interpretation

Just as for other support practices, RUSLE2 erosion estimates for subsurface drainage represent broad, general effects more than site specific effects. RUSLE2 captures how factors related to site location, vegetation production (yield) level, soil properties, soil position on the landscape, and characteristics of the drainage system affect erosion. RUSLE2 results are much better than the rule of thumb that subsurface drainage reduces erosion by 40 percent. The accuracy of RUSLE2 erosion estimates for subsurface drainage is similar to that for other support practices, including contouring.

Sometimes subsurface drainage is given little consideration as an erosion control practice. It is seldom installed solely for erosion control because of its expense. However, research clearly shows that subsurface drainage significantly reduces erosion in certain conditions, and, therefore, erosion reduction should be recognized as an important benefit of subsurface drainage. Sometimes subsurface drainage is considered to be environmentally detrimental because it is used to drain wetlands, for example.

---

[155] See:
AH703

Bengston, R.I. and G. Sabbage. 1988. USLE P-factor for subsurface drainage in a hot, humid climate. ASAE Paper 88-2122. American Society of Agricultural Engineers. St. Joseph, MI.

Formanek, G.E, E. Ross, and J. Istok. 1987. Subsurface drainage for erosion reduction on croplands of northwestern Oregon. In: Irrigation Systems of the 21st Century. Proceeding Irrigation and Drainage Division Specialty Conference. American Society of Civil Engineers. New York, NY. pp. 25-31.

Schwab, G.O. 1976. Tile or surface drainage for Ohio's heavy soils? Ohio Report. March-April. Ohio Agricultural Experiment Station. Columbus, OH.

Schwab, G.O. and J.L. Fouss. 1967. Tile flow and surface runoff from drainage systems with corn and grass cover. Transactions ASAE 10:492-493, 496.

Skaggs, R.W., A Nassehzadeh-Tabrizi, and G.R. Foster. 1982. Subsurface drainage effects on erosion. Journal of Soil and Water Conservation 37:167-172.

Table 14.8. RUSLE2 computed effect of subsurface drainage on erosion as a function of soil erodibility factor value (K) ad hydrologic soil group at three locations (does not consider any change in yield)

	Erosion drained/erosion undrained
silty clay soil (K = 0.20 US units), change in hydrologic soil group from D to A	
Ft Wayne, IN	0.38
Raleigh, NC	0.38
Jackson, MS	0.38
silty clay soil (K=0.20), hydrologic soil group D to C	
Ft Wayne, IN	0.83
Raleigh, NC	0.78
Jackson, MS	0.75
sandy loam soil (K = 0.30), hydrologic soil group D to A	
Ft Wayne, IN	0.58
Raleigh, NC	0.57
Jackson, MS	0.60
silt soil (K = 0.55), hydrologic soil group from D to A	
Ft Wayne, IN	0.77
Raleigh, NC	0.76
Jackson, MS	0.77

However, subsurface drainage should be recognized for its merits in appropriate situations.

Perhaps more than any other practice, the subsurface drainage component in RUSLE2 is subject to misuse. For example, subsurface drainage is most effective on relatively flat hillslope areas less than 3 percent steep and in localized areas of wet soils. RUSLE2 does not identify where subsurface drainage should not be used. Technical standards should be consulted for information on subsurface drainage applications.

14.4.5. Input

The **deep (subsurface) soil drainage system descriptions** in the RUSLE2 database have a single input of **portion of the hillslope that is well drained.** The other RUSLE2 inputs to represent subsurface drainage are the hydrologic soil groups in the **soil description** for the undrained and drained conditions (see **Section 7.7**) and the production (yield) level input in the **cover-management description**s used for the drained and undrained conditions (see **Section 10.2.4**).

The hydrologic soil group input represents the degree that subsurface drainage reduces runoff potential of the soil under the unit plot condition given the site location, the soil's position on the landscape, soil profile properties, naturally occurring soil restrictive layers, and subsurface drain depth and spacing. Multiple **soil descriptions** for the same soil profile can be created for various drain depths and spacings. The input for the hydrologic soil group for the drained condition should reflect the site's location. For example, subsurface drainage may have a greater effect on the reduction of runoff potential on a coarse texture soil at a low precipitation location when compared to a high precipitation location. The input for hydrologic soil group for the undrained and drained conditions reflects soil profile properties, especially texture. As discussed in **Section 14.2**, subsurface drainage does not automatically reduce the hydrologic soil group to **A** for all soils, especially fine textured soils.

The NRCS soil survey database and the NRCS RUSLE2 database may have a hydrologic soil group assigned for drained conditions. Check the criteria that NRCS used to select hydrologic soil groups to ensure consistency with RUSLE2 criteria.

Vegetation production (yield) level is usually increased by subsurface drainage because increasing crop production is the major reason for subsurface drainage. Use appropriate yield values for both the undrained and drained conditions.

Subsurface drainage was installed decades ago in many farm fields. When applying RUSLE2 to these fields, the easiest approach is to ignore subsurface drainage if no assessment is being made on how subsurface drainage affects erosion. Make sure that the hydrologic soil group input for the undrained condition and the input for vegetation production (yield) level represents the current field condition. RUSLE2 computes a subsurface drainage effect only if the hydrologic soil group input for the drained condition differs from the corresponding input for the undrained condition, and different vegetation production (yield) level inputs are not entered for the drained and undrained conditions.

The input for **portion of the hillslope that is well drained** is used to compute erosion for an overland flow path where only a portion of it is subsurface drained. An overland flow path having a complex:convex-concave profile is an example. The lower concave portion of this profile can have high soil wetness because of a low landscape position. Localized subsurface drainage is used to eliminate this soil wetness. Soil wetness is not a problem on the upper part of the overland flow path. An input value less than 100 percent for **portion of the hillslope that is well drained** represents this situation. RUSLE2 uses this input to weight its detachment (sediment production) computations and the curve numbers it uses to computes runoff for the undrained and drained conditions.

Also, this input can be used to reduce the effect that RUSLE2 computes for subsurface drainage. For example, if RUSLE2 is judged to compute too much erosion reduction, a value less than 100 percent can be input to reduce the subsurface drainage effect computed by RUSLE2. If the trivial input of zero (0) is entered, RUSLE2 computes no subsurface drainage effect on erosion, unless different yield values are used for the undrained and drained conditions.

RUSLE2 does not notify the user when it computes questionable erosion estimates for subsurface drainage. The RUSLE2 user must know where and how subsurface drainage is used and must make the proper inputs.

14.5. Irrigation

14.5.1. Description of practice

Irrigation adds water to the soil to increase vegetation (crop) production or to dispose of waste. The principal irrigation types are surface, sprinkler, and subsurface applied water. Surface irrigation discharges water in a line source at an upslope field edge and water infiltrates along the flow path, which results in discharge rate decreasing with downslope distance.[156] Although surface irrigation can cause high erosion, RUSLE2 does not estimate this erosion because RUSLE2 assumes an increasing discharge rate along its flow path.

RUSLE2 can not be used to estimate erosion directly caused by irrigation.

Sprinkler irrigation applies water through a system of pipes and overhead spray nozzles. Water is applied to only a portion of the area at a time. The water application is moved through time to cover the entire area. A two week cycle might be used, for example, to cover the entire area with multiple applications over a crop production season. Water is applied at a sufficiently low rate so that no runoff, and thus no erosion, occurs.

Subsurface (drip) irrigation applies water through a system of underground pipes and emitters. This type of irrigation does not cause rill-interrill erosion.

Although RUSLE2 is not used to estimate rill-interrill erosion caused by any type of irrigation, it can be used to estimate erosion caused by rainfall to reflect how irrigation changes the field conditions that affect rill-interrill erosion.

14.5.2. Basic principles

A main effect of irrigation captured by RUSLE2 is increased soil moisture that increases soil erodibility, increases biomass decomposition, and decreases soil surface roughness and soil ridge height. The main inputs to represent irrigation in RUSLE2 are the vegetation production (yield) level appropriate for the irrigation management, amount of water added by irrigation, and amount of biomass added in the irrigation water.

[156] The erosion mechanics of surface irrigation are described by Toy, T.J., G.R. Foster, and K.G. Renard. 2002. Soil Erosion: Processes, Prediction, Measurement, and Control. John Wiley and Son, New York, NY.
.

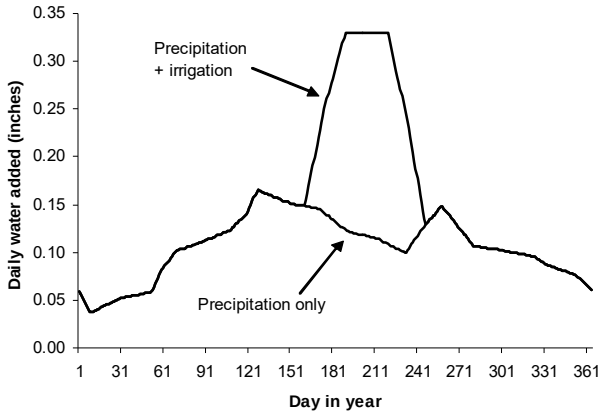

Figure 4.17. Precipitation and water added by irrigation for a 112 bu/ac corn crop at Columbia, Missouri.

RUSLE2 computations for the effect of irrigation were made for a 112 bu/ac conventionally tilled and a 112 bu/ac no-till corn crop at Columbia, Missouri. The results are summarized in Figure 14.17-14.20. In this example, irrigation water was added at the rate to just meet daily consumptive use, which is illustrated in Figure 14.17. The daily water added by irrigation is summed with daily precipitation, which is used to compute daily soil erodibility, daily decomposition, and daily loss of soil surface roughness and ridge height.

A major effect of irrigation computed by RUSLE2 is the increased soil erodibility during the irrigation period, which is illustrated in Figure 14.18. An upper limit is placed on how much added irrigation water can increase soil erodibility. No daily soil erodibility value can be greater than twice the soil erodibility value computed by a RUSLE2 nomograph.

The other major effect of irrigation is that it increases residue decomposition. Figure 10.19 shows the increase in decomposition computed by RUSLE2 for the 112 bu/ac no-till corn at Columbia, Missouri. The increase in decomposition was not great. The relative increase will be significantly greater in dry regions, such as Scotts Bluff, Nebraska. Very little of the decomposition effect continues beyond harvest because of the large amount of residue added by harvest.

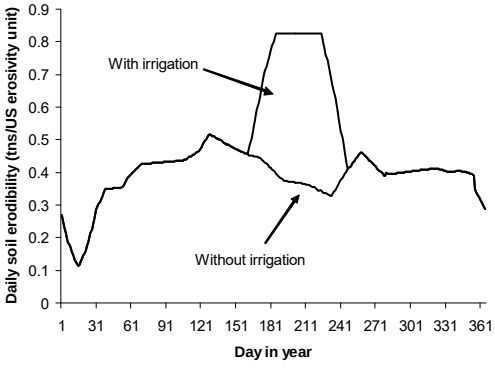

Figure 14.18. Effect of irrigation on daily soil erodibility at Columbia, Missouri.

Most of the effect of irrigation on erosion is during the irrigated period, as shown in Figure 10.20 by daily erosion rates computed for the 112 bu/ac conventionally tilled corn. The computed annual increase in erosion was from 24 to 30 tons/acre·year and 1.5 to 2.4 tons/acre·year, for the conventionally tilled and no-till crops, respectively. This difference in erosion

is for the same yield. These computations illustrate how irrigation affects RUSLE2 computed erosion if nothing changes other than adding irrigation. The proper calculation would have been to input a yield value appropriate for the irrigated conditions. The RUSLE2 computed erosion is 26 tons/acre·year if the irrigation is assumed to increase yield from 112 bu/ac to 150 bu/ac. Further erosion reduction would have occurred if the applied irrigation had a significant content of bio-solids.

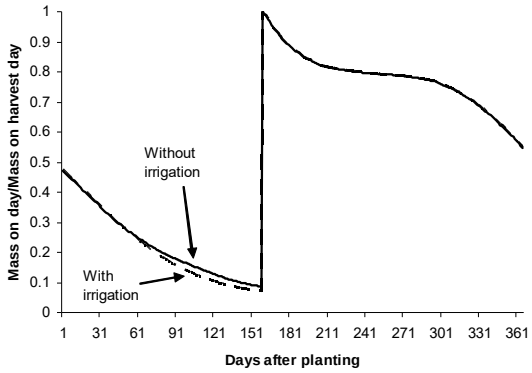

Figure 14.19. RUSLE2 computed decomposition for no-till corn at Columbia, Missouri.

14.5.3. Calibration

The RUSLE2 procedure that describes how irrigation affects erosion caused by natural precipitation (rainfall) and its associated runoff was not calibrated. Computed erosion values were not compared to measured values. However, erosion values were computed for a range of conditions and reviewed to ensure that RUSLE2 gives values acceptable for conservation planning.

14.5.5. Inputs

The input yield values should be appropriate for the irrigated management system (see **Section 10.2.4**). The effect of the increased yield that reduces erosion is just as important as the increased soil moisture that increases erosion. The best way to input yield values for irrigation is to create vegetation descriptions specifically for irrigated conditions. These vegetation descriptions include consumptive use values. A vegetation description is selected that is appropriate for the region, soil, and irrigation management system. Yield values in the cover-management descriptions using these vegetation descriptions can be varied to accommodate site-specific conditions. The RUSLE2 yield adjustment procedure for vegetation descriptions adjusts consumptive use values along with the other values.

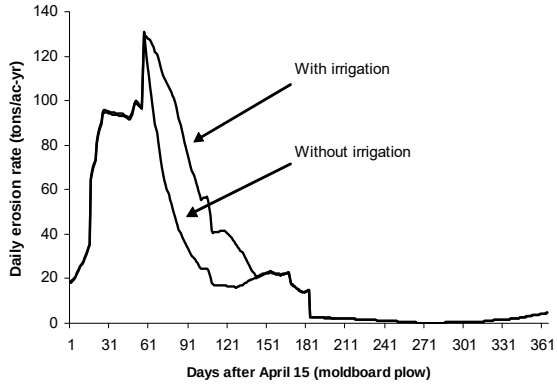

Figure 14.20. RUSLE2 computed effect of irrigation on daily erosion rate for 112 bu/ac conventionally corn at Columbia, Missouri.

The amount of water added by irrigation can be input using either of: (1) consumptive use through time, (2) dates and application rates on those dates, and (3) and period application depths. Irrigation systems are typically designed to supply water at the daily consumptive use of the crop being grown. Therefore, the consumptive use input method is preferred for inputting irrigation amount values in RUSLE2. Daily consumptive use values are entered in the vegetation description for the irrigated system, soil, and region. Consumptive use values depend on the crop and its yield, location, soil, and perhaps other factors.[157] If consumptive use is less than natural precipitation, such as for supplemental irrigation in the southeastern US, one of the other two input methods can be used to input irrigation amounts.

The other two input methods for irrigation amount are to enter application rates on particular days or to enter irrigation amounts (depths) by period. These periods are at the user's choice, which can be monthly, biweekly, or arbitrary non-uniform periods. Consideration should be given to reducing added water amounts for irrigation systems, such as drip irrigation, that do wet the surface soil.

The effect of added biomass that is applied by irrigation (e.g., for example waste disposal of bio-solids) is represented by including an **operation** that **adds external residue** in cover-management descriptions (see **Section 10.2.6**). Biomass added by irrigation is represented in a cover-management description having an **operation description** that applies **external residue** (see **Section 10.2.6**). This cover-management description involves the date of the operation that applies the biomass, biomass amount (dry matter basis) added by the operation (not the average annual mass applied), and the selection of a **residue description** that represents the applied biomass (see **Section 12**). RUSLE2 applies external residue by event rather than on a continuous daily rate. If biomass is applied by an irrigation system that operates on a cycle, the dates of the **add biomass** operation should be on the same frequency as the irrigation cycle. If the biomass is applied daily, the application can be approximated by applying a two week biomass amount once every two weeks. A sensitivity analysis (see **Section 17.3**) can be conducted to determine if the biomass can be applied in monthly intervals rather than in biweekly or other intervals. Decomposition characteristics of the biomass mainly determine the frequency of the biomass applications when approximating daily applications.

14.5.4. Interpretation

[157] Values for consumptive use and other information related to irrigation application rates can be obtained from local offices of the USDA-NRCS and Extension Service affiliated with Land Grant Universities in each state.

The RUSLE2 intent is to capture broad, main effects of increased soil moisture caused by the addition of water by irrigation. RUSLE2 does not capture hydrologic and hydraulic detail. The purpose of RSULE2 is to provide information useful for conservation and erosion control planning, not for irrigation system design. RUSLE2 estimated erosion for the effect of irrigation is comparable in accuracy to RUSLE2 computed values for other support practices, including contouring. Using RUSLE2 to evaluate the effect of irrigation on rill-interrill erosion by rainfall is much better than disregarding the effect.

15. APPLICATION OF RUSLE2 TO PARTICULAR LAND USES

RUSLE2 is **land use independent**, which means that RUSLE2 estimates rill-interrill erosion caused by rainfall and its associated Hortonian-type overland flow any where mineral soil is exposed (see **Section 5**). This capability is a major advantage when applying RUSLE2 to reclaimed mined land, waste disposal sites, disturbed forest land and mechanically disturbed military lands, and other lands where climate, soil, topography, and cover-management variables that affect erosion traverse the spectrum of conditions on common land use classifications such as cropland, rangelands, grazing lands, pasture lands, and disturbed forest lands. Erosion conditions on a common land use like cropland vary from a bare, highly erodible soil to a highly erosion resistant, well maintained pasture. Similarly, erosion conditions on rangeland vary from a highly erodible, recent mechanically disturbed pipeline construction site to a site never mechanically disturbed other than by wild animal presence. Well designed erosion prediction technology like RUSLE2 is based on a description of the fundamental variables that are land use independent. Erosion is a mechanical process where soil particles are detached and transported when the forces on them from raindrop impact and surface runoff become sufficiently strong.

Erosion prediction technologies designed for specific land uses like rangelands are much more limited than is RUSLE2, even when applied to that land use. RUSLE2's land-use independence allows it to be applied anywhere mineral soil is exposed to the erosive forces of raindrop impact and surface runoff produced by Hortonian overland flow.

However, many RUSLE2 users' applications will be limited to specific land uses such as construction sites. Easy-to-use RUSLE2 user guides targeted to specific land uses are needed. This RUSLE2 User's Reference Guide provides reference information on which to base user guides for specific land uses. Such RUSLE2 user guides will include input data and other land use specific information not available in this RUSLE2 User's Reference Guide. Also, user guides are needed that describe RUSLE2 computer program mechanics and operations for specific land uses.

An example of user guides for a specific land use includes a workbook and a user manual for construction sites and other highly disturbed lands. These documents are available from the International Erosion Control Association.

A primary source of RUSLE2 information is the USDA-ARS RUSLE2 Internet site http://www.ars.usda.gov/Research/docs.htm?docid=6010. The University of Tennessee and the USDA-Natural Resources Conservation Service, both of whom participated in the RUSLE2 development, also maintain RUSLE2 Internet sites.

Several RUSLE2 related documents are helpful for developing land use specific RUSLE2 user guides. Not all information in these and other RUSLE2 related documents applies to RUSLE2. Always check information from other sources to ensure that it is consistent with the RUSLE2 User's Reference Guide before using it in RUSLE2 applications.

15.1. Additional RUSLE2 Related Documents[158]

Dissmeyer, G.E. and G.R. Foster. 1980. A guide for predicting sheet and rill erosion on forest land. Technical Publication SA-TP-11. USDA-Forest Service-State and Private Forestry-Southeastern Area. 40 pp.

Renard, K.G., G.R. Foster, G.A. Weesies, D.K. McCool, and D.C. Yoder. 1997. Predicting soil erosion by water: A guide to conservation planning with the Revised Universal Soil Loss Equation (RUSLE). U.S. Dept. of Agriculture, Agricultural Handbook 703, U.S. Govt Printing Office, Washington, D.C.

Toy, T.J. and G.R. Foster (coeditors). 1998. Guidelines for the use of the Revised Universal Soil Loss equation (RUSLE1.06) on mined lands, construction sites, and reclaimed lands. USDI-Office of Surface Mining. Denver. CO.

Wischmeier, W.H. and D.D. Smith. 1965. Predicting Rainfall-Erosion Losses from Cropland East of the Rocky Mountains: A guide to conservation planning. U.S. Dept. of Agriculture, Agriculture Handbook No. 282. U.S. Govt Printing Office, Washington, D.C.

Wischmeier, W.H. and D.D. Smith. 1978. Predicting Rainfall-Erosion Losses: A guide to conservation planning. U.S. Dept. of Agriculture, Agriculture Handbook No. 537. U.S. Govt Printing Office, Washington, D.C.

[158] See the USDA-ARS RUSLE2 Internet Site at http://msa.ars.usda.gov/ms/oxford/nsl/rusle/index.html (ARS reveiwer, check this) for information on how to obtain copies of these and other RUSLE2 related documents.

16. CORE DATABASE

A core database was used to develop, verify, and validate RUSLE2 for a base set of conditions. Values selected for new entries in a user's RUSLE2 working database should be selected based on information in this **RUSLE2 User's Reference Guide** and values in the **RUSLE2 core database**. Values for new entries must follow RUSLE2 definitions and be consistent with RUSLE2 core database values. Also, the **RUSLE2 core database** values must be used when RUSLE2 is being evaluated against the USLE, RUSLE1, and other erosion prediction technologies, against research data, and other analyses.

The **RUSLE2 core database** can be obtained from the official USDA-Agricultural Research Service Internet site http://www.ars.usda.gov/Research/docs.htm?docid=6010 maintained at the National Sedimentation Laboratory in Oxford, Mississippi. The **RUSLE2 core database** is named **RUSLE2 core data**.

17. EVALUATION OF RUSLE2

17.1. Verification/Validation

Verification is the process of ensuring that RUSLE2 makes its calculations as intended. Verification ensures that the equations, parameter values, and logic that links the equations have been programmed as designed and give the expected results. Verification involves running the model for the range of: research data used to derive the model, the RUSLE2 core database, and field conditions for which RUSLE2 might be used. Also, verification involves running the model for special conditions to make sure that every equation and every logic step in the model is exercised. The objective is to test every element of the model to find and fix all errors.[159] This verification process was extensively and fully followed in developing RUSLE2.

No guarantee is made that RUSLE2 contains no computational errors, only that an aggressive effort was made to find and fix errors.

Validation is the process of ensuring that RUSLE2 serves its intended purpose as described…"[160]

The stated purpose of RUSLE2 is to guide conservation and erosion control planning by users at the field office level, such as the field offices of the USDA-Natural Resources Conservation Service (NRCS). RUSLE2 was designed to be land use independent and is to apply to all conditions where rainfall and its associated Hortonian overland flow cause rill-interrill erosion of exposed mineral soil (see **Section 5**). RUSLE2 does not apply to erosion caused by runoff during irrigation (see **Section 14.5**) or snow melt (see **Section 6.3.3**). RUSLE2 is not a process representation of erosion, and RUSLE2 is not a tool for discovering new, original scientific knowledge about erosion. RUSLE2 represents its developers' interpretation of research data, accepted scientific and technical information, and judgments about use of erosion prediction technology in conservation and erosion control planning (see **Section 17.2**).

The most important part of RUSLE2's validation is whether RUSLE2 leads to the desired erosion control decision, not how well RUSLE2 estimates compare to measured data. Validation certainly involves evaluating RUSLE2's accuracy, but many other considerations are also important in judging how well RUSLE2 serves its stated purpose. For example, a model could perfectly compute erosion, but if the resources required to use the model exceed available resources, the model is invalid, (i.e., it does not serve its intended purpose).

---

[159] Essentially a quote from Toy, T.J., G.R. Foster, and K.G. Renard. 2002. Soil Erosion: Processes, Prediction, Measurement, and Control. John Wiley and Son, New York, NY. p. 146.

[160] Essentially a quote from Toy et al., 2002. p. 146. Also, see pp. 146-149 regarding model validation.

RUSLE2 should be easy and convenient to use, including when it is used infrequently. RUSLE2 must not require excessive resources including: time required to learn the model; time to actually run the model in developing a conservation or erosion control plan; acquisition, assembly, and entry of input data; computer skills; and technical expertise required to run RUSLE2. Support documents, training, and assistance when problems arise must be available.

Are the benefits gained from using RUSLE2 worth its costs, especially in comparison to using alternative methods to develop conservation and erosion control plans? How does the quality of conservation and erosion control plans developed with RUSLE2 compare with those developed from use of other erosion prediction technologies? If two erosion prediction technologies result in the same conservation and erosion control plan, each technology performs equally well. The choice of a specific erosion prediction technology is, therefore, determined by preferences and resources required to use each technology.

RUSLE2 must accurately represents scientifically accepted trends of how major variables such as precipitation amount and intensity, soil texture, overland flow path length and steepness, ground cover, soil biomass, and contouring affect erosion. Research data available to develop erosion prediction technology are unavoidably incomplete and biased. The data do not represent all of the conditions where RUSLE2 will be applied, and consequently, numerous RUSLE2 applications will be extrapolations beyond the data used to derive RUSLE2. Therefore, whether RUSLE2 accurately represents scientifically accepted trends is a key factor in how well RUSLE2 performs when extrapolated. RUSLE2 was also developed to be robust so that extrapolations are conservative and conform to obvious, defined limits, (i.e., if RUSLE2 estimates are erroneous, the estimates will not be unreasonable).

Erosion data have a high degree of explained variability and bias. For example, regression fitting of an equation to a particular experimental data set gives the nonsensical results that the fitted equation computes increased erosion with increased ground cover. The data are obviously flawed or biased by incompleteness, measurements not based on RUSLE2 definitions, or measurement error. RUSLE2 describes accepted scientific trends even though the fit to particular observed data may be compromised.

RUSLE2 developers envisioned themselves in the position of land users impacted by RUSLE2. Given their knowledge of both erosion science and RUSLE2's representation of that science, RUSLE2 developers asked themselves the question, do they have sufficient confidence in RUSLE2 erosion estimates in particular situations to be willing to implement RUSLE2 based erosion control practices?

Users should assure for themselves the validity of RUSLE2. This RUSLE2 User's Reference Guide describes in detail how RUSLE2 was derived, what it represents, and how RUSLE2 represents accepted scientific and technical information.

17.2. Interpretations in the context of conservation and erosion control planning

The RUSLE2 developers followed several fundamental principles to interpret research data used to empirically derive and calibrate RUSLE2 equations and to validate RUSLE2. Whether or not RUSLE2 is considered valid depends on the acceptance of these principles.

17.2.1. Principle 1: Fit main effects

The first step in applying the **main effects principle** is to assemble the largest possible dataset for the erosion control practice or other condition being analyzed. These datasets are seldom ideal because of incomplete, non-uniform, and biased coverage, and much unexplained variability.[161] The second step is to identify the variables and equation form based on erosion theory and fundamental erosion process studies that will be used to describe the main effects. Analyzing erosion data for no-till cropping provides a case study for illustrating the main effects principle.

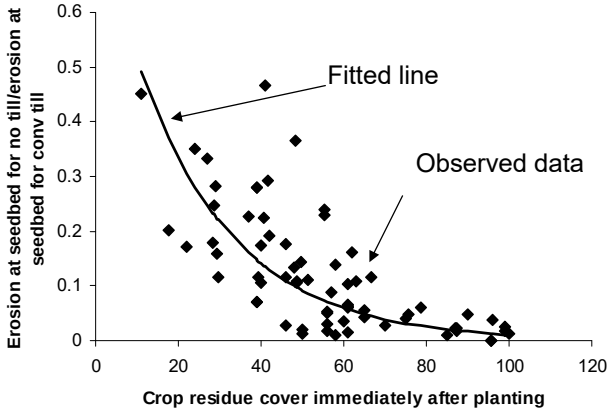

Figure 17.1. Relation of erosion with no-till cropping to erosion with conventional tillage for seedbed period.

Conservation tillage, including no-till, is widely used to control erosion on cropland. Experimental erosion data for no-till cropping are plotted in Figure 17.1 where the dependent variable is ratio of erosion with no-till to erosion with conventional till for the seedbed period. Results from many fundamental erosion studies involving applied mulch show that erosion decreases rapidly as ground cover increases as represented by Equation 9.6.[162]

[161] Nearing, M.A., G. Govers and L.D. Norton. 1999. Variability in soil erosion data from replicated plots. Soil Sci. Soc. Amer. J. 63: 1829-1835.

[162] See, for example,
Manering, J.V. and L.D. Meyer. 1963. Effects of various rates of surface mulches on infiltration and erosion. Soil Science Society of America Proceedings 27:84-86.

Therefore, ground cover is assumed to be a main effect variable for no-till's effect on erosion.

The deviation in erosion from the main effect is large in Figure 17.1. For example, the fitted value at 50 percent ground cover (crop residue cover) is 0.1 while the experimental values ranged from about 0.02 to 0.4. Other variables have a significant effect, which is captured in RUSLE2 by varying the coefficient **b** in equation 9.6.

Erosion theory and fundamental experimental erosion studies show that the coefficient **b** varies with the rill to interrill erosion ratio because of difference between rill erosion and interrill erosion mechanics. Ground cover reduces rill erosion more than it reduces interrill erosion.[163] Values for **b** are larger where rill erosion is dominant on bare soils, such as on relatively steep overland flow paths (greater than 12 %), than where interrill erosion is dominant, such as on relatively flat overland flow paths (less than 3%).

Fundamental erosion studies show that **b** values are increased when added ground cover increases infiltration, which in turn reduces runoff and rill erosion. Increased biomass in the upper soil layer accompanies increased ground cover in long term no-till cropping but not in short term no-till cropping or in mulch applied to freshly graded construction sites. Consequently, **b** values are a function of land use. Rather than making **b** values a function of land use classification, RUSLE2 computes **b** values as a function of cover-management variables.[164] For example, RUSLE2 detects the difference between a construction site and a no-till cropped field using the soil consolidation factor and the amount of soil biomass in the upper soil layer.

This approach of using equations to represent main effects of major universal climate, soil, topographic, and cover-management variables rather associating equations and coefficient values with a land use classification gives RUSLE2 its land use independence.

The concept in RUSLE2 is to describe the main effect that major variables have on erosion and then compute deviations about the main effect using secondary variables. RUSLE2 properly represents trends apparent from an overall analysis of the experimental data and erosion science even though RUSLE2 may not faithfully reproduce individual

---

Meyer, L.D., W.H. Wischmeier, and G.R. Foster. 1970. Mulch rates required for erosion control on steep slopes. Soil Science Society of American Proceedings 34:928-931.

[163] Foster, G.R. and L.D. Meyer. 1975. Mathematical simulation of upland erosion by fundamental erosion mechanics. *In:* Present and Prospective Technology for Predicting Sediment Yields and Sources. ARS-S-40 USDA-Science and Education Administration. pp. 190-204.

[164] RUSLE1.06 assigns **b** values as a function of land use classification. RUSLE1.05 assigns b_g values according to a user selected classification for rill to interrill erosion ratio.

data values in an experimental dataset. The RUSLE2 approach increases robustness, which means that RUSLE2 can be more confidently extrapolated beyond the data used to derive it than can regression equations involving a large set of variables fitted to the data.

Selecting equations and coefficient values based on best statistical fits to experimental field data can produce very flawed results for conservation and erosion control planning. The results can be especially flawed if the experimental data have a high degree of unexplained variability and are non-uniform in coverage, incomplete, and biased, problems impossible to avoid in erosion data. For example, the regression approach can result in nonsensical results where erosion is computed to increase as ground cover increases. RUSLE2 faithfully reproduces trends proven by erosion science rather than simply providing the best fit to experimental data that are almost always flawed.

17.2.2. Principle 2: Don't custom fit to local data or to specific data

Some users adjust RUSLE2 parameter and input values to fit a particular data point because that data point is considered more valid that other data points. Increased value is placed on that data point because the data came from a particular locale or because of familiarity with the investigator who collected the data. RUSLE2 adjustments and evaluations based on how well RUSLE2 fits a single data point are generally improper.

RUSLE2 is designed to fit main effects as described in **Section 17.2.1**. Erosion data are highly variable and have a high degree of uncertainty for unknown reasons, especially if the measured erosion rates are low (less than 1 ton/acre per year). The validity of any single data point is, therefore, highly questionable. The validity of a single data point must be judged against the dataset as a whole.

If a particular data point is judged to be valid, fitting RUSLE2 to the single data point should still be avoided. Calibrating RUSLE2 to a data point could well result in RUSLE2 estimates that are seriously erroneous because RUSLE2 no longer will fit the main effect. Either RUSLE2's fit of this single data point should be considered in a particular RUSLE2 application, or another erosion prediction procedure should be used instead of RUSLE2.

17.2.3. Principle 3: Follow RUSLE2 definitions, rules, procedures, guidelines, and core database values

RUSLE2 uses specific definitions, rules, procedures, and core database values that must be followed. RUSLE2 definitions, rules, and procedures were chosen for specific reasons that are sometimes not obvious. For example, adjusting RUSLE2 soil erodibility K factor values to account for increased organic matter resulting from organic farming or applying manure is improper and gives erroneous results. Similarly, soil erodibility factor values adjusted for surface rock fragments should not be used. RUSLE2 considers

the effect of rock cover and increased soil biomass in its cover-management computations. The soil erodibility factor applies specifically and only to unit plot conditions.

Similarly, RUSLE2 core database values must be followed because RUSLE2 was calibrated based on those values. The core database values were selected to represent main effects adequately supported by research data and erosion science. The values were selected to be consistent with accuracy of RUSLE2 and the data used to derive RUSLE2. Input values for database entries not represented in the RUSLE2 core database must be consistent with core database values for similar conditions.

While you as a user may not agree with the RUSLE2 definitions, rules, procedures, and core database values, they must be observed. Do not assume that USLE and RUSLE1 definitions, rules, procedures, and input values apply to RUSLE2, because many do not.

17.2.4. Principle 4: Don't evaluate RUSLE2 based on how well it fits secondary variables

RUSLE2 was developed, calibrated, and validated to ensure that it gives good average annual erosion estimates, even if the fit of RUSLE2 computed values for secondary variables (e.g., crop residue) is less than expected. For example, RUSLE2 typically under estimates residue cover for periods longer than about 1 year, but this underestimate does not mean that the average annual erosion estimate is erroneous, especially in rotation-type cover-management descriptions where a large amount of residue is added annually. The adequacy of RUSLE2 computed values for secondary variables is based on RUSLE2 computing the expected erosion estimate, not on how RUSLE2 computed values for secondary variables are used for non-RUSLE2 purposes.

RUSLE2 estimates of crop residue cover immediately after planting can be used in routine conservation planning and compliance activities.

However, situations arise where the RUSLE2 accuracy of a secondary variable is insufficient in a particular RUSLE2 application. An example is applying RUSLE2 to a construction site two or more years after only a single mulch application. Separate RUSLE2 computations using different input residue values for each year may be required to accurately compute erosion in particular years.

Users should use this RUSLE2 User's Reference Guide to determine where RUSLE2 erosion estimates may need special interpretations or RUSLE2 inputs may need adjustment.

17.2.5. Principle 5: Avoid fine tuning parameter and input values

If you must adjust parameter and input values, be sure that you understand the variable being adjusted and how it is used in RUSLE2. Carefully read and follow this RUSLE2 User's Reference Guide to avoid unintended consequences.

Adjusting input values so that RUSLE2 computes an expected residue cover is an example where adjustments are sometimes made. Because RUSLE2 has many interacting variables, changing the value for a single variable may affect several computations. For example, changing the value for the residue decomposition coefficient affects surface residue cover and soil biomass as well. Soil biomass affects computed values for the soil biomass subfactor, surface roughness, and runoff. If the change is only to affect surface residue cover, the residue decomposition coefficient value is not the input variable that should be changed.

Another example where changing the value of a single variable can have unexpected results is the width of soil disturbance. Changing the value for this variable affects more than the soil consolidation subfactor value because several RUSLE2 computations are a function of the soil consolidation subfactor.

Section 12.5 describes a procedure for adjusting input values to obtain an expected residue cover. This procedure is a guide for changing input values for other variables to achieve a particular result.

Make sure that the proper variables are being changed to achieve the desired result.

17.2.6. Principle 6: Make sufficient temporal and spatial field measurements according to RUSLE2 requirements

Canopy, surface cover, surface roughness, and yield are variables that are sometimes field measured as a part of evaluating RUSLE2 and collecting field data for RUSLE2 input. Measuring root biomass should not be attempted except in a very carefully managed research environment, and even then the results are questionable. Soil biomass as used in RUSLE2 should be back calculated from other variables because it is almost impossible to measure.

Field measured values vary randomly and systematically (e.g., a combine leaving residue in strips) in both space and time. Field measurements must be proper and in sufficient number to account for variability keeping in mind that RUSLE2 is designed to represent main effects. Canopy cover, surface cover, fall height, and other RUSLE2 variables must be measured based on RUSLE2 definitions, rules, and procedures to accurately evaluate

RUSLE2 and properly selected input values. Also, many RUSLE2 relationships are nonlinear, which affects how field measurements are made, analyzed, and interpreted. Follow this RUSLE2 User's Reference Guide closely in making field measurements.

Field measurements of residue surface cover are often made and used in the conservation planning and compliance determination on cropland. Given the importance of residue surface cover, special precautions should be observed in making residue cover measurements.

Field measurements must be made in accordance with RUSLE2 definitions, rules, and procedures.

Both high residue and low residue cover is difficult to measure and convert to residue mass values, partly because of the non-linear residue mass-cover relationship (see **Section 12.3**). Residue samples must be carefully collected and processed (e.g., soil particles carefully removed). The residue mass to cover relationship varies within the field and during the year as the relative composition of plant parts (leaves, stems, and other components) vary in the residue. The relationship also varies from year to year as weather, yield, and field operations vary. Residue measurements should be made over a minimum of three years to obtain values that can be compared to RUSLE2 estimates. Experience also shows that when residue surface cover is accurately measured, cover is often less than assumed based on visual observations.

Soil surface roughness values used in RUSLE2 computations are not the input values because RUSLE2 adjusts the input values for soil texture and soil biomass (see **Section 9.2.3.2**). Also, field measured values for soil surface roughness only match input values when roughness is measured for the base condition used to define RUSLE2 soil surface roughness input values.

The terminology and definitions of plant cover used in vegetation surveys may be quite different from the very specific definitions of canopy cover, ground cover, live ground cover, and fall height used in RUSLE2. Also, the definitions of vegetation production (yield) level may be quite difference from RUSLE2 definitions and input values in the RUSLE2 core database.

Before using information from vegetation surveys, ensure that the values taken from these survey are proper when using them for RUSLE2 input.

17.2.7. Principle 7. Avoid too much detail

Difference between RUSLE2 computed erosion estimates may not be significant. Significance in this context is not the same as statistical significance discussed in **Section 17.4**. In this context, significance refers to a sufficient difference resulting in a conservation planning or compliance decision being altered.

The general guideline is that difference in estimated erosion values should exceed 10 percent because the difference is considered practically significant.

RUSLE2 is not designed to capture the difference between machine adjustments on particular tillage machines, unless the effect of the adjustment is sufficiently great. RUSLE2 is designed to distinguish between machine classes such as straight, sweep, and twisted shovel type chisel plows. Some of the differences in residue burial that are often claimed to be achievable by machine adjustment are questionable (see **Section 13.1.5.3**). Input values should be for machine classes and not varied to reflect individual machine configuration or operation.

Similarly, RUSLE2 is not designed to capture differences between crop varieties other than major differences such as between popcorn and field corn, for example. When differences between crop varieties grown in different regions are sufficiently great to give erosion estimates that differ by more that 10 percent (i.e., the 10 percent rule), differences in crop varieties should be represented. Likewise, dates in cover-management descriptions should be selected to represent major differences such as early, mid, and late season planting and/or harvest, not to represent operations on particular dates. Also, RUSLE2 is not intended to capture how annual variation in operation dates within a cover-management description affects erosion.

RUSLE2 users, especially those who prepare RUSLE2 databases, have the responsibility of determining when difference are sufficiently great to warrant creating new entries in the RUSLE2 database with different input values. Differences in erosion estimates because of difference in inputs values for similar conditions are a partial measure of uncertainty and precision in RUSLE2 erosion estimates.

17.2.8. Principle 8. Computing erosion with RUSLE2 for historical events and individual storm events is an advanced application

RUSLE2 is a conservation planning tool, not a model that reproduces historical erosion events. RUSLE2 is not designed to be evaluated or calibrated by inputting historical data to compute erosion values that are compared to values measured at a particular site. Also, RUSLE2 is not designed to evaluate how historical events such as an unusually dry or wet season or year affected erosion. The uncertainty in RUSLE2 erosion estimates for these applications is much greater than in average annual erosion estimates.

RUSLE2 is not structured to readily accommodate input of historical data, especially weather data for multiple years. Also, RUSLE2 does not represent temporal variations in soil moisture that can greatly affect runoff from individual storm events. RUSLE2 does not conveniently represent residual effects from a previous year, although expert RUSLE2 users can capture much of the effects of these initial conditions. RUSLE2 does not model how vegetation responds to environmental conditions, but values that represent the vegetation and operations for a specific historical period can be input into RUSLE2.

The adequacy of the historical experimental data against which RUSLE2 is being evaluated must be considered. Are the historical, experimental data comparable to the data used to develop RUSLE2 parameter and input values? If not, RUSLE2 computed erosion may not compare well with the measured erosion. A poor fit does not necessarily indicate that RUSLE2 performs poorly, but that the historical experimental data are not representative of the main effects represented by RUSLE2.

A short record, such as three years, often produces data that differ significantly from average annual erosion values measured over an extended period or estimated by RUSLE2. The cover-management data used to develop RUSLE2 were analyzed to compute ratios of erosion values for a given cover-management condition to erosion values for a base condition. The advantage of the RUSLE2 approach is that these ratio values varied much less year to year than did absolute erosion values. RUSLE2 does not reflect how year to year variation in soil moisture, runoff, plant yield, and other variables affects erosion.

RUSLE2 has similar limitations when used to estimate how an especially dry or wet season or year affects erosion. In these extremes, the ratio of runoff to precipitation usually differs significantly from average annual values. Extreme storm events sometimes occur in dry years. Although annual rainfall may be quite low in a dry year, a few very intense rainfall events can cause exceedingly high erosion per unit precipitation. Conversely, a wet year can involve many relatively low intensity storms that cause reduced erosion per unit precipitation. Although RUSLE2 captures some but not all of these effects, RUSLE2 is limited because it does not compute runoff by individual storm event.

Input data for the climate, operation, vegetation, residue, and cover-management descriptions can be entered to represent a particular year. RUSLE2 computes erosion estimates that partially reflect how departure of these input values from average annual conditions affects erosion. Also, expert users can set up RUSLE2 to capture most residual effects from a previous year where conditions differed greatly from those for the year being analyzed. The RUSLE2 computed erosion is likely to be less than it should be for a wet year and greater than it should be for a dry year.

RUSLE2 can be configured to estimate erosion for a single storm by inputting values to represent conditions on the day of the storm. However, RUSLE2 does not estimate soil moisture and how runoff is affected by soil moisture on the day of the rainfall event. Thus, RUSLE2 erosion estimates will be low or high depending on how soil moisture departs from its average annual value for the particular event. Although RUSLE2 is not intended to estimate erosion from individual storms, its accuracy for individual storm event erosion estimates may be comparable to estimates from complex, process-based models.[165] **RUSLE2 is better for estimating individual event erosion than is commonly assumed.**

These RUSLE2 applications are quite advanced. Proper procedures must be followed. For example, no-rotation type cover-management descriptions should be used in most cases rather than using standard rotation-type cover-management descriptions, even when representing crop rotations. This RUSLE2 User's Reference Guide should be carefully studied and followed in applying RUSLE2 in these special applications.

If users understand how RUSLE2 works regarding individual storms and representing historical events and they have the expertise and other resources to apply RUSLE2, then RUSLE2 is valid in these applications if these RUSLE2 users consider RUSLE2 estimates to be useful.

17.2.9. Principle 9. Always evaluate the adequacy of the data

17.2.9.1. An ideal dataset

All measured erosion data available for developing and evaluating RUSLE2 are questionable in some way.[166] An ideal dataset represents modern climatic and land use conditions, soils and topography as they occur on actual hillslopes, and the full range of conditions where RUSLE2 is applied. Record length is sufficient to provide accurate average annual estimates and probability distributions. The dataset is complete, un-biased, and without measurement error. Replications and treatments are sufficient to define RUSLE2 relationships with a high degree of statistical accuracy. Measurements must be made according to RUSLE2 definitions, rules, and procedures.

17.2.9.2. Natural rainfall versus simulated rainfall

---

[165] Although RUSLE2 is not intended for estimating erosion for specific storm events, RUSLE2 is fundamentally an event-based procedure. The linearity between storm erosivity and storm erosion simplifies the RUSLE2 mathematical integration for estimating average annual erosion. See **Sections 5.4 and 7.2**.

[166] Toy, T.J., G.R. Foster, and K.G. Renard. 2002. Soil Erosion: Processes, Prediction, Measurement, and Control. John Wiley and Son, New York, NY.

Data from natural rainfall events are much preferred over data from simulated rainfall because simulated rainfall does not perfectly match natural rainfall. Most erosion data collected with rainfall simulators are for standard, uniform intensity storms in comparison with natural rainstorms having greatly varying intensities and amounts. Measured infiltration, runoff, and erosion are functions of temporal rainfall intensity pattern and its interaction with spatially varied soil conditions.[167] Energy for some rainfall simulators is much less than that of natural rainfall. **Data were not used in the development of RUSLE2 that were collected using simulated rainfall where energy was less than about 75 percent of that in natural rainfall.** Rainfall simulators having energies approaching natural rainfall typically apply water intermittently on a cycle ranging from about 5 seconds to 30 seconds, which affects infiltration, runoff, erosion, sediment transport, deposition, and sediment characteristics.

The standard storm set is typically applied only at a few times during the year, usually when the study condition is most vulnerable to erosion condition. In some erosion studies on rangelands involving rainfall simulators, the applied erosivity was much greater than typical annual rainfall erosivity at some locations.[168]

These differences between natural and simulated rainfall raise questions about the advisability of using simulated rainfall erosion data to develop and evaluate RUSLE2. The RUSLE2 developers judged that these data were useful in the context of RUSLE2 being a conservation and erosion control planning tool. Erosion data from simulated rainfall would be interpreted against erosion data from natural rainfall. Erosion data from simulated rainfall were primarily analyzed, except for the soil erodibility nomographs, by forming ratios of erosion for a given condition to erosion for a base condition, realizing that these ratios vary with storm characteristics and other factors (see Figure 17.1).

17.2.9.3. Measurement area size

Erosion plots that are either 35 ft long or 72.6 ft long and 6, 10, or 12 ft wide were widely used to measure the effect of climate, soil, land steepness, and cover-management on erosion. Plots of about 36, 72.6, and 150 ft long (plots as long as 370 ft were used in one study and 650 ft in another study) were used in multiple studies to determine the effect of overland flow path length on erosion. Small watersheds ranging in size from about 2 ac to 5 ac were used to measure the effect of contouring, rotational strip cropping, and terracing on erosion.

---

[167] Flanagan, D.C., G.R. Foster, and W.C. Moldenhauer. 1988. Storm pattern effect on infiltration, runoff, and erosion. Trans. ASAE 31:414-420.

[168] See:
Simanton, J.R., L.T. West, M.A. Weltz, and G.D. Wingate. 1987. Rangeland experiments for Water Erosion Prediction Project. Paper No. 87-2545. American Society of Agricultural Engineers. St. Joseph, MI.
Spaeth, Jr., K.E., F.B. Pierson, M.A. Weltz, and W.H. Blackburn. 2003. Evaluation of USLE and RUSLE estimated soil loss on rangelands. J. Range Management 56:234-246.

Do these erosion plots tilled manually or with small equipment adequately represent typical land use practices and non-uniform overland flow paths having lengths that range from 1 ft to 1,000 ft.? Do these small watersheds with their spatial variability of soil, topography, and cover-management conditions provide data suitable for developing RUSLE2?

Even though these and other questions can be raised about these measurement areas, the RUSLE2 developers judged that these measurement areas were appropriate for developing RUSLE2 as a conservation and erosion control planning tool. RUSLE2 users must interpret RUSLE2 erosion estimates in terms of how well these plots and small watersheds represent erosion on the field area where RUSLE2 is being applied (see **Sections 5.1, 5.2, and 5.3**). RUSLE2 developers judged that erosion data from small measurement areas about 3 ft by 3 ft (1 m by 1m) where essentially only interrill erosion occurs are not suitable for developing RUSLE2 or evaluating its estimates of rill and interrill erosion combined for typical overland flow paths.[169] This small measurement area is not suitable for determining RUSLE2 soil erodibility factor values or making relative comparisons of soil erodibility and erosion control practices. Erosion data from plots shorter than 35 ft were not used in the development of RUSLE2 where both interrill and rill erosion were being considered. However, data from interrill erosion type areas were used to develop RUSLE2 interrill erosion relationships.

Finding a suitable area on a natural hillslope for a set of erosion plots having uniform soil and steepness is difficult. A minimum of three replications along with a base treatment, and three treatments are needed, for example, in a simple study to evaluate mulch application rate for a particular mulch type. A set of 12 rainfall simulator plots are needed for this study, which requires a total width of about 220 ft. Finding a uniform area that wide is difficult on natural landscapes. The problem is especially acute on rangelands where erosion rates are low and spatial variability is great. The scale of the variability is on the order of the plot width and length. A slight shift in the placement of a plot can result in significantly different measured erosion rates.

17.2.9.4. Modern data

Modern data representative of current land use practices and climate conditions should be used to develop and evaluate RUSLE2. Modern climate data were used to develop RUSLE2 input erosivity, precipitation, and temperature values. However, the underlying natural rainfall erosion data used to calibrate the soil biomass subfactor equation (equation 9.12) were from the mid 1930's to the mid 1950's. Few natural rainfall erosion

[169] Foster, G.R., J.R. Simanton, K.G. Renard, L.J. Lane, and H.B. Osborn. 1981. Discussion of "Application of the Universal Soil Loss Equation to Rangelands on a Pre-Storm Basis." Journal of Range Management 34:161-165.

plot data were collected after the 1970's. Most modern erosion data were collected using simulated rainfall.

Therefore, a question is how well does RUSLE2 estimate erosion for modern conditions? Applying RUSLE2 to modern conditions represents an extrapolation from conditions quite different from current ones. RUSLE2 developers addressed this question and judged that RUSLE2 performs satisfactorily for modern conditions. They also judged that the cover-management subfactor procedure allows RUSLE2 to be extrapolated to conditions significantly beyond those represented in the underlying data.

17.2.9.5. Data record length

About 10 years are usually required to obtain representative average annual values for erosion data measured from natural rainfall for one- and two-year crop rotations. Erosion data for cropped conditions are available from only two locations where the record length exceeded a decade. However, interpretation of a long term data is difficult because of temporal weather variability and changes in farming practices over time. None of the data available for analyzing rotational strip cropping involving five-year and longer crop rotations are fully adequate because of short record length even though record length is about 10 years. A five-year rotation requires 20 or more years to obtain reasonable average annual data and even longer when the crop rotation is used in strip cropping. Collecting such data is often not feasible, which is the reason that these data do not exist.

Data having record lengths as short as three years for natural rainfall events were used in the development of RUSLE2. These data were primarily analyzed to determine ratios, which vary less temporally than do absolute values (see Figure 17.1). Data having a short record length are more susceptible to interpretation problems caused by extreme events occurring during the measurement period and to measurement equipment failure than data having a long record length.

Missing data can be a serious problem. An example is the high erosion rates that can occur during late winter and early spring thaws when soil erodibility is significantly increased. Too few events were measured to adequately represent them in the temporal erodibility equation (see **Section 7.3**). Few locations were adequately equipped to measure runoff and erosion in these environmental conditions, and the need to make those measurements was probably not recognized at the time.

17.2.9.6. Dividing the data into development and evaluation parts

Developers of models sometimes divide data into two parts, one part is used to develop the model and the other part is used to evaluate the model. The entire dataset was used to develop RUSLE2 rather than dividing the data. The best approach is to use the largest

dataset possible to develop erosion models given the variability, incompleteness, bias, and other shortcomings in erosion data.

Reports are sometimes published where measured data at a single location for a small, specific set of conditions are compared with RUSLE2 estimates. Such data should first be evaluated to determine how they fit with the RUSLE2 dataset as a whole to ensure that the specific study data are not outliers. Given the unexplained variability in erosion data (e.g., see Figure 17.1), either a good or poor fit of RUSLE2 to a single data point is by chance. Evaluations involving essentially a single data point usually provide very little information about RUSLE2's adequacy.

A main criterion in developing RUSLE2 is that it describes well established main effects. Fitting an erosion prediction equation to incomplete and biased data can produce nonsensical results such as erosion increasing as ground cover increases. The fit of RUSLE2 to experimental data as determined by statistical goodness of fit measures was sometimes compromised so that RUSLE2 accurately represents established main effects. Getting the best statistical fit to reduced quality data may not produce the best result for conservation and erosion control planning.

17.2.9.7. Users must make their own judgments

All developers of erosion prediction technology make judgments about erosion data used to derive equations, parameter values, and input values. Different people reach different conclusions when evaluating a particular dataset and in evaluating RUSLE2's adequacy relative to the dataset. The RUSLE2 developers' judgments are described in this RUSLE2 User's Reference Guide.

Users must make their own judgments about RUSLE2. Users should only use RUSLE2 when they are satisfied that RUSLE2 is suitable for their purposes.

17.2.10. Principle 10. Make sure that the inputs are proper

When RUSLE2 users obtain poor results, they often suspect a problem with RUSLE2, while RUSLE2 developers often suspect improper inputs. Always double check input values when evaluating and applying RUSLE2, and especially ensure that input values are consistent with the core database values. Do not use input values from other erosion models. RUSLE2 input values sometimes differ from values used for similar variables in other erosion prediction technologies, including the USLE and RUSLE1.

Ensure that RUSLE2 rules and procedures are followed. Errors in the sequence of processes used in an **operation description** can easily occur, for example. If a **flatten standing residue process** is used in a soil disturbing operation description, the results will differ significantly depending on whether the flattening process is placed in the

operation description before or after the **disturb soil process**. Another example of an input error is where the live root biomass value on day zero in a **vegetation description** is much less than the live root biomass on the last day in this vegetation description when it is used to represent mature vegetation. RUSLE2 adds the difference in the live root biomass between the ending and beginning dates to the dead root biomass pool when none should be added in this situation.

RUSLE2 results can be no better than the inputs.

17.2.11. Principle 11. Be alert for RUSLE2 users who believe RUSLE2

RUSLE2 estimates contain error and uncertainty. All RUSLE2 estimates should be examined, interpreted, and carefully considered before using them. Conservation and erosion control planners should always make planning decisions using RUSLE2 estimates as a guide.

17.2.12. Principle 12. RUSLE2 is only in error when it leads to a poor conservation or erosion control plan

RUSLE2's accuracy (see **Section 17.4**) should be evaluated in the context of conservation and erosion control planning.[170] Does RUSLE2 result in the desired conservation and erosion control planning decision? For example, RUSLE2 could compute annual erosion estimates of 50, 200, and 400 tons/acre for a particular highly erodible site given the uncertainty in RUSLE2 estimates. The range in these values represents significant numerical error. However, RUSLE2 leads to the correct conservation decision with each estimate; that is; erosion is excessive and needs to be significantly reduced. In fact, RUSLE2 probably is not needed in this situation because the erosion hazard is easily recognized from general erosion knowledge.

Similarly, RUSLE2 could compute an annual erosion estimate between 0.001 and 0.1 tons/acre for a rangeland site given the uncertainty in RUSLE2 estimates. Nevertheless, RUSLE2 leads to the desired conservation planning decision; erosion is low. Making erosion measures using plots that are 35 ft long and 12 ft wide to determine the "correct" value is difficult for low erosion rates, especially on rangelands. The 0.001 tons/acre value could have been 0.05 tons/acre if a gopher hole had been near the plot end or the soil had been slightly disturbed and exposed when placing a plot border or installing a plot end. The 0.1 tons/acre value could have been 0.01 tons/acre had the plot had been located differently because of non-uniform spatial variability within the plot and on the hillslope.

---

[170] For additional discussion, see Toy, T.J., G.R. Foster, and K.G. Renard. 2002. Soil Erosion: Processes, Prediction, Measurement, and Control. John Wiley and Son, New York, NY.

RUSLE2's accuracy is most important when erosion estimates are sufficiently close to the erosion control criteria such that errors result in substantial expense to apply unnecessary erosion control. RUSLE2 is typically used in conservation planning to compute a soil loss value that is compared against a soil loss tolerance value **T** or another erosion control criteria value. If the computed soil loss value is less than the erosion control criteria, erosion control is assumed to be adequate.

Assume that the erosion control criterion is an annual 5 tons/acre. If the RUSLE2 annual erosion estimate is 10 tons/acre, the RUSLE2 based conservation planning decision is that erosion is excessive and additional erosion control is needed. However, if the "correct" erosion estimate is an annual 5 tons/acre, the proper conservation planning decision is that erosion control is acceptable and no further erosion reduction is needed. The significance of the error is determined by the expense of additional erosion control when none was needed.

Fortunately RUSLE2 is most accurate in the critical range of annual estimates between about 2 to 20 tons/acre. Annual erosion greater than 20 tons/acre is usually considered excessive and annual erosion less than 1 ton/acre is generally considered to be acceptable. If RUSLE2 computes an annual erosion of 10 tons/acre with one practice and 20 tons/acre with a second practice, the erosion control planner can be confident that erosion with the first practice will be substantially less than with the second practice. However, if RUSLE2 computes 1 and 2 tons/acre annual erosion estimates for two practices, especially on pasture land, the difference between the two practices is not great, and the most that can be said is that erosion will likely be less with one practice than with the other practice and that erosion will be low with both practices.

RUSLE2 erosion estimates for support erosion control practices, especially contouring, are much more uncertain than those for cultural erosion control practices based on cover-management variables. RUSLE2 accurately represents the global effects of support practices but not their performance on specific sites. The uncertainty in the estimated erosion reduction by support practices on a specific site is much greater than the uncertainty in estimated erosion reduction by cultural erosion control practices.

17.3. Sensitivity analysis

A RUSLE2 sensitivity analysis is very helpful in understanding how RUSLE2 computes erosion, determining how a particular practice or condition affects erosion, determining the effect of a particular variable on erosion, and detecting input errors. The general procedure for conducting a sensitivity analysis is to change a single input while holding other inputs constant. For example, a sensitivity analysis can be conducted on how location affects erosion by making RUSLE2 computations for a set of locations using a single set of inputs for soil, topography, cover-management, and support practices. Likewise, a sensitivity analysis can be conducted on cover-management practices by

making erosion computations for a set of practices for a given location, soil, topography, and support practices.

A sensitivity analysis can also be conducted on a single variable such as overland flow path length. Changing input values from 10 to 1000 ft for the overland flow path length has little effect on RUSLE2 computed erosion where steepness is 1 percent or less. Therefore, carefully selecting a precise input value for overland flow path length on very flat slopes is not critical.

A sensitivity analysis for the single variable overland flow path length can be easily conducted by changing input values on the main RUSLE2 **profile** screen. Sensitivity analyses conducted on other individual variables usually requires changing values in the **RUSLE2 database description** that contains the values for that variable. For example, conducting a sensitivity analysis on canopy cover requires changing values in a **vegetation description**.

The effect of a single variable or a set of variables, such as those in cover-management descriptions, on erosion varies with the situation. For example, overland flow path length has little effect on erosion on very flat slopes. However, it has a moderate effect on steep slopes. Therefore, more care is needed in selecting input values for overland flow path lengths on moderate and steep slopes than on very flat slopes. Furthermore, the effect of overland flow path length also depends on soil and cover-management conditions. Similarly, the effect of a particular cover-management practice depends on location, soil, and topography.

Some variables are used in multiple RUSLE2 equations, which results in complex interactions that complicate sensitivity analyses. Surface biomass, soil biomass and the soil consolidation subfactor are examples of such variables. Each variable has a primary effect and several secondary effects. Surface (flat) cover is often assumed to be the most important RUSLE2 variable, which is true for many but not all conditions. Soil biomass can have a much greater effect on erosion than surface biomass in certain conditions. Surface biomass, soil biomass, and soil consolidation strongly interact so that the combined effect is more than expected based on the primary effect of each variable. Special inputs must be used in sensitivity analyses to isolate the primary effect of individual variables separate from their interactive effects.

Be very careful about generalizing results from a sensitivity analysis. Sensitivity analyses should be conducted over a wide range of conditions before drawing conclusions about the effect of a particular variable on erosion.

Inputs must be changed carefully to conduct sensitivity analyses on surface (flat) cover, which is an important variable in conservation planning on cropland. An input must be selected to change surface cover to conduct a sensitivity analysis on surface cover. An

obvious input is vegetation production (yield) level. Changing yield does change surface biomass, but it also changes soil biomass and canopy values. Changing yield is an important sensitivity analysis but not for conducting a sensitivity analysis on surface cover. Is the surface cover analysis to study the effect of surface biomass or is it to study the effect of the portion of the soil surface covered? If the purpose of the sensitivity analysis is to study the effect of surface biomass, inputs for the relationship of aboveground biomass to yield in a vegetation description can be changed. If the sensitivity analysis is to study the effect of how the portion of the soil covered affects erosion, inputs in a **residue description** that relate portion of the soil surface covered to the surface biomass can be changed.

An important sensitivity analysis is the effect of soil disturbance width on erosion (see **Section 9.2.6**). The soil disturbance width effect of a particular soil disturbing operation depends greatly on whether the operation is the only soil disturbing operation in the **cover-management description**. The soil disturbance width effect can be great if only one **soil disturbing operation** is in a cover-management description. The soil disturbance width effect for a particular operation is much less if other soil disturbing operations, especially ones that disturb the full soil width, are included in the cover-management description.

Although soil disturbance width has a minor effect on surface roughness, its major effect is on the soil consolidation subfactor and its secondary effects. The soil consolidation primary effect is illustrated in Figure 7.3. Its secondary effects are from being a variable in several other computations including the soil biomass subfactor, decomposition's transfer of surface biomass to soil biomass, runoff, and the rill-interrill erosion ratio that affects the slope length exponent in equation 8.1 and **b** value in equation 9.6 used to compute ground cover effect. A sensitivity analysis on soil disturbance width and on the soil consolidation effect requires sorting through an array of complex, interacting variables.

Care must also be taken in sensitivity analyses to ensure that the effect of a variable being studied is not being masked by another variable. An example is disturbance depth of secondary tillage. A primary tillage operation with a deep disturbance depth typically precedes secondary tillage operations in many cropland cover-management descriptions. Disturbance depth of secondary tillage operations has very little effect on erosion because primary tillage buries most of the residue below the disturbance depth of the secondary tillage operation. The effect of disturbance depth of the same secondary tillage operation can be significant when no primary tillage operations are in the cover-management description.

RUSLE2 uses a description of field conditions to compute erosion. Most variables in a RUSLE2 description are not automatically changed when input values for key variables are changed. For example, RUSLE2 does not change vegetation production (yield) level

when a new location (which changes precipitation and temperature), soil, or management is selected that affects yield. Therefore, a sensitivity analysis that involves changes in variables that affect yield requires changing the yield input value in the cover-management descriptions used in the analysis.

The value entered for yield must be consistent with the selected location's climatic, soil, and management.

17.4. RUSLE2 Accuracy

The assumption in developing RUSLE2 was that the widely accepted and used USLE and RUSLE1 were valid models for conservation and erosion control planning. RUSLE2 was developed to improve these technologies by significantly extending their applicability to practically every field situation where rill and interrill erosion occurs, increasing their power, and improving their underlying supporting science. Therefore, one assessment of RUSLE2's accuracy is to compare RUSLE2 and USLE computed erosion values. A second assessment is the fit of the USLE, and thus RUSLE2, to the research data from which the USLE was derived. A third assessment is identifying where RUSLE2 is most, (and least) accurate.

17.4.1. Comparison of RUSLE2 erosion estimates with USLE erosion estimates

Determining the accuracy of RUSLE2 for estimating how cover-management affects erosion is perhaps the most important assessment of RUSLE2 because of the major role of cover-management in conservation and erosion control planning. The soil loss ratio values in Table 5, AH537 represent measured values.[171] These values are a summary of a large mass of research data, 10,000 plot-years, as analyzed and interpreted by Wischmeier and Smith (AH537). The fully empirical USLE directly uses measured values to compute cover-management's effect on erosion. In contrast, RUSLE2 uses a set of equations that were fitted to the soil loss ratio values in Table 5, AH537 and other data (see **Section 9**). Therefore, one part of the assessment is how well the RUSLE2 subfactor equations fit measured soil loss ratio values.

17.4.1.1. Average annual erosion values for cropland

Table 17.1 shows erosion values computed with the USLE and RUSLE2 for a wide range of cover-management practices for Columbia, MO and for two cotton cover-management practices for Holly Springs, MS.[172] The values in AH537 represent a summary of

[171] Soil loss ratio values in AH537 are the ratio of soil loss with a given cover-management condition at a particular crop stage period to soil loss from the unit plot for the same crop stage.

[172] Columbia, MO is used as a base location in RUSLE2. AH537 values for slope length and steepness, soil loss ratio, and support practice factors are assumed to apply at Columbia, MO. RUSLE2 adjusts its values for these factors about the Columbia, MO base values. The weather at Columbia, MO is near the "middle"

measured values for the eastern US. Measured soil loss ratio values varied greatly among

Table 17.1. Estimated average annual erosion values (tons/acre) for the USLE and RUSLE2 (overland flow path length = 150 ft, steepness = 6%)

Management	USLE	RUSLE2
conv. cont corn, 112 bu/ac spring plow	16	17
conv. cont corn, 112 bu/ac fall plow	19	19
conv. cont. corn 50 bu/ac spring plow	23	28
conv. cont. corn 50 bu/ac fall plow	27	31
conv cont corn silage 112 bu/ac spring plow	28	28
conv cont corn silage 112 bu/ac fall plow	31	29
conv cont corn silage 50 bu/ac spring plow	34	37
conv cont corn silage 50 bu/ac fall plow	37	38
conv 112 bu/ac corn-25 bu/ac soybeans	20	22
conv 112 bu/ac **corn**-25 bu/ac soybeans	21	23
conv 112 bu/ac corn-25 bu/ac **soybeans**	18	21
conv 112 bu/ac corn-25 bu/ac soybeans fall plow	22	25
conv 112 bu/ac **corn**-25 bu/ac soybeans fall plow	23	25
conv 112 bu/ac corn-25 bu/ac **soybeans** fall plow	22	27
conv cont soybeans 25 bu/ac		27
conv cont winter wheat 30 bu/ac	9.4	13
conv 112 bu/ac corn - 25 bu/ac soybeans-30 bu/ac winter wheat	14	19
no till 112 bu/ac corn		1
mulch till 112 bu/ac corn		10
ridge till 112 bu/ac corn		10
conv. cont corn, 112 bu/ac spring plow manure 8000 lbs/ac (dry basis)		9
corn-corn-meadow-meadow-meadow (high production)	7	6
corn-**corn**-meadow-meadow-meadow (high production)	14	17
established meadow, 4 tons/acre	0.2	0.2
established alfalfa	1.1	0.9
conv cotton "flat" planted	32	37
cotton hipped	44	47

Notes:
1. conv - conventional
2. cont - continuous
3. erosion value is erosion in year for crop in bold
4. erosion values computed for Columbia, MO except for two cotton management where values are for Holly Springs, MS
5. meadow refers to hay production
6. Same R value and K value used in USLE and RUSLE2 comptuations
7. LS = 0.824 for USLE while "net" LS value for RUSLE2 varied from 0.73 for no-till corn to 1.01 for conv cont 50 bu/ac silage corn

locations. For example, the soil loss ratio value for the seedbed crop stage for conventionally tilled corn varied from about 0.2 to 0.8 in data collected in the 1970's at several locations.[173] The reasons for this variation could not be empirically determined

---

of the data for the Eastern US. Holly Springs, MS was used in RUSLE2 as the base location for cotton cover-management because research at that location and other nearby locations provided most of the data used to derive AH537soil loss ratio values for cotton.

[173] The seedbed crop stage is when the soil is finely tilled in preparation for crop seeding. No vegetation

because of unexplained variability in the data. However, fundamental research conclusively shows that erosion decreases as soil biomass increases. Therefore, the seedbed soil loss ratio value for conventionally tilled continuous corn at a particular yield should be higher in the southern US than in the northern US because increased precipitation and temperature significantly increase decomposition, which reduces soil biomass. RUSLE2 captures this and other effects in its cover-management subfactor equations that are not captured by the USLE.

The soil loss ratio values computed by RUSLE2 vary by location, soil, and topography in contrast to the USLE soil loss ratio values that do not vary with these factors. Therefore, a comparison between RUSLE2 and USLE estimated erosion values must be for a representative condition. Columbia, MO (a central location), a silt loam soil, and a uniform overland flow path 150 ft (50 m) long, 6 percent steep were chosen to compute the estimates shown in Table 17.1. Differences in RUSLE2 and USLE erosion estimates vary with location, generally becoming greater with distance from Columbia, MO as climatic conditions differ from those at Columbia, MO.

Even at Columbia, MO, RUSLE2 and the USLE do not compute the same erosion estimates because of differences in equation structure. The daily topographic length factor in RUSLE2 varies with cover-management, while the corresponding USLE L factor does not vary. RUSLE2 computes a "net" LS value that is a temporal integration of daily values weighted by the temporal distribution of erosivity. Values for the RUSLE2 "net" LS factor vary from a low of 0.73 for the 112 bu/ac no-till corn to 1.01 for the 50 bu/ac corn silage whereas the USLE LS value is 0.82 for all conditions in Table 17.1.

Even when the RUSLE2 "net" LS value is the same as the USLE LS factor value, RUSLE2 and the USLE likely will not compute the same erosion values because of differences in temporal integration. RUSLE2 multiplies its daily factors values to determine a daily erosion estimate and sums these values for an annual erosion estimate. The only temporal integration in the USLE is by crop stage period where the soil loss ratio values are weighted by the temporal erosivity distribution to compute a cover-management factor value, which is multiplied by the other factor values to determine an annual erosion estimate.

RUSLE2 does not use "net" factor values to compute annual erosion. These values are only for comparison with USLE factor values and for use in the USLE for conditions where empirical erosion data are not available to determine USLE factor values. **Multiplication of the RUSLE2 computed "net" factor values according to the USLE equation structure does not compute the same erosion estimate as that computed by RUSLE2 (see *Section 5.4*)**.

---

and very little surface residue cover are present in conventional moldboard plowed cropping systems that bury almost the entire residue from the previous year's crop.

An assessment of RUSLE2 based on a comparison of estimated erosion values with USLE estimates must consider differences in equation structure and the additional effects represented by RUSLE2 (see *Section 17.2*).

As illustrated in Table 17.1, RUSLE2 computed erosion values compare well with USLE values. Biomass is the principal factor that affects erosion for the conditions listed in Table 17.1. Biomass differences primarily account for the difference in erosion values from the high biomass meadow (hay) to the low biomass in 50 bu/ac corn silage. Biomass differences also principally account for the differences in erosion between the 50 and 112 bu/ac corn practices. A land use residual effect results from soil biomass loss over time after large amounts of biomass are buried in the soil and a large amount of roots are killed. Erosion increases over two years of corn following a high production meadow (hay) as soil biomass is lost.

Vegetation characteristics and vegetation management affect erosion (e.g., corn, wheat, and hay and hay versus grain production). As the values in Table 17.1 show, RUSLE2 captures the effect of these variables on erosion.

Other factors besides cover-management must be considered when evaluating the RUSLE2 values in Table 17.1. The topographic length factor discussed above is one of those factors. RUSLE2 does not vary the topographic steepness factor; it is constant just as in the USLE. However, the RUSLE2 topographic steepness factor differs from the USLE one. The RUSLE2 steepness factor value for a 6 percent steepness is 18 percent greater than the corresponding USLE value. Consequently, all RUSLE2 erosion estimates in Table 17.1 are systematically increased by 18 percent larger relative to the corresponding USLE values. The difference between the RUSLE2 and USLE steepness factors decreases for steepness less than 6 percent except for very flat steepness where the RUSLE2 values are greater than the USLE values. The RUSLE2 and USLE steepness factor values are equal at 9 percent steepness. Above 9 percent, the USLE values become progressively greater than the RUSLE2 values.[174]

Even when the RUSLE2 "net" soil erodibility value equals the USLE soil erodibility factor value and all other factors are the same, the erosion estimates computed by RUSLE2 and the USLE can differ. The daily RUSLE2 soil erodibility values temporally vary, which affects estimated erosion, especially when comparisons are made for

---

[174] See:
AH703

McCool, D.K., L.C. Brown, G.R. Foster, C.K. Mutchler, and L.D. Meyer. 1987. Revised slope steepness factor for the Universal Soil Loss Equation. Transactions of American Society of Agricultural Engineers 30:1387-1396.

multiple locations and soils. Also, the rill erodibility to interrill soil erodibility ratio

Therefore, differences in RUSLE2 and USLE erosion estimates can not be generalized on the basis of computations for a single location, soil, or topography.

varies among soils, which also affects results.

Conservation tillage, including no-till, mulch till, and ridge till, is a major erosion control practice used on cropland. However, no USLE erosion estimates are given in Table 17.1 for conservation tillage because AH537 soil loss ratio values for conservation tillage are considered unreliable. The AH537 values were based on research conducted early when conservation tillage was beginning to be adopted and do not represent modern conservation tillage. Other data on conservation tillage besides the AH537 values were used to develop the RUSLE2 cover-management subfactor equations. Data from a large number of references were reviewed and analyzed to give special attention to no-till because the USLE and RUSLE1 were highly criticized for not accurately computing erosion for no-till. As Figure 17.1 shows, the effectiveness of no-till varies greatly, even more than erosion with conventional tillage. A very detailed analysis of the empirical data did not provide the information required to describe the variability in the no-till data. RUSLE2 captures the main effect illustrated in Figure 17.1 and computes values about this line as a function of location, slope steepness, soil, crop, and yield.

The cover-management subfactor approach used in RUSLE2 computes erosion values that compare well with values computed by the USLE and, therefore, with the experimental data on which the USLE is based.

17.4.1.2. Soil loss values by crop stage for cropland

An additional assessment of RUSLE2's accuracy is how well it reproduces the soil loss ratio values in Table 5, AH537 for crop stage periods.[175] Tables 17.2, 17.3, and 17.4 show RUSLE2 computed soil loss ratio values for corn and cotton. The soil loss ratio values for the fallow crop stage period shows that RUSLE2 captures the effects of surface roughness and the values for crop stages 1, 2, and 3 shows that RUSLE2 captures the effect of a developing and mature crop. Differences between values in Tables 17.3 and 17.4 confirm that RUSLE2 captures the effect of ridges where repeated tillage operations bury almost the entire residue for a low residue cotton crop.

Comparisons for soil loss ratios were made for the other cover-management conditions listed in Table 17.1. The values in Tables 17.2, 17.3, and 17.4 and from the other comparison between RUSLE2 soil loss ratio estimates and the AH537 values indicate that RUSLE2 accurately computes the temporal variation in soil loss ratio values.

RUSLE2 is judged to accurately compute temporal cover-management effects during the year.

Table 17.2. Soil loss ratios for 112 bu/ac conv cont corn from AH537 and values computed with RUSLE2

Crop stage (defined in AH537)	AH537 Soil loss ratio	RUSLE2 Soil loss ratio
Fallow	31	28
Seedbed	55	54
1 -- 10% < canopy < 50%	48	52
2 – 50% < canopy < 75%	38	30
3 – to maturity	23	18
4 after harvest (stalks spread)	6	6

Table 17.3. Soil loss ratio values for 750 lbs/acre cotton flat planted at Holly Springs, MS. Values from AH537 and computed by RUSLE2

Crop stage (defined in AH537)	AH537 Soil loss ratio	RUSLE2 Soil loss ratio
Fallow	0.39	0.54
Seedbed	0.64	0.74
1--10% canopy < 35%	0.59	0.74
2--35% < canopy < 60%	0.46	0.49
3--to maturity	0.32	0.23
Defoliation to Dec 31	0.26	0.24
Jan 1 to Feb. tillage	0.32	0.32

Table 17.4. Soil loss ratio values for 750 lbs/acre cotton hipped (ridged) at Holly Springs, MS. Values from AH537 and computed by RUSLE2

Crop stage (defined in AH537)	AH537 Soil loss ratio	RUSLE2 Soil loss ratio
1st hip, no prior tillage	84	88
Split ridges with a “do-all”	54	52
Hip after 2 prior tillages	108	101
Split ridges with a “do all”	62	58
Hip after 3 or more tillages	110	112
Split ridges with a “do all”	64	64
Seedbed	64	64
1--10% canopy < 35%	59	64
2--35% < canopy < 60%	46	45
3--to maturity	32	21
Defoliation to Dec 31	22	23
Jan 1 to Feb. tillage	32	27

17.4.1.3. Crop residue cover immediately after planting

Crop residue cover immediately after planting is an important variable used in conservation planning and compliance determination on cropland. RUSLE2 is expected to accurately estimate this cover, which it does as illustrated in Table 17.5 for a wide range of conservation tillage systems and the major crops of corn and soybeans.

RUSLE2 accurately estimates crop residue cover immediately after planting for a wide range of tillage systems.

17.4.1.4. Erosion values for range, pasture, and similar lands

Both RUSLE1 and RUSLE2 apply to range and similar lands, although the USLE poorly estimates erosion for these lands.[176] The major problem is with Table 10, AH537, entitled "Factor C for permanent pasture, range, and idle land" used to apply the USLE to these lands. This table does not include a soil surface roughness effect, and it improperly links below ground biomass to ground cover. Table 10, AH537 does not allow rock cover to be considered separately from biomass ground cover, it does not properly account for production (yield) level, and the **b** value in equation 9.6 for the ground cover effect is about 0.026 rather than a much more preferred value of 0.035. Also, values for the USLE slope steepness are too large for steepness greater than 25 percent.

Differences between the RUSLE2 and RUSLE1.06 soil biomass subfactor equations required that new RUSLE2 values for the ratio of effective root biomass to annual above ground production be developed. Two major datasets known as the WEPP rangeland data[177] and the USDA Rangeland Study Team data[178] are available for determining these RUSLE2 ratio values and evaluating RUSLE2 for rangelands.

Only the WEPP data set was used because of problems with the USDA Range Study Team data. The USDA Range Study Team dataset was carefully analyzed to compute effective root biomass values or to evaluate RUSLE2. When the data were divided into plant type categories of sagebrush, bunch, sod, and tall grass, the relationship between surface cover and erosion empirically derived from the data showed that erosion increased as surface cover increased for some of the

[176] Spaeth, Jr., K.E., F.B. Pierson, M.A. Weltz, and W.H. Blackburn. 2003. Evaluation of USLE and RUSLE estimated soil loss on rangelands. J. Range Management 56:234-246.
[177] Simanton, J.R., L.T. West, M.A. Weltz, and G.D. Wingate. 1987. Rangeland experiments for Water Erosion Prediction Project. Paper No. 87-2545. American Society of Agricultural Engineers. St. Joseph, MI.
[178] Spaeth, Jr., K.E., F.B. Pierson, M.A. Weltz, and W.H. Blackburn. 2003. Evaluation of USLE and RUSLE estimated soil loss on rangelands. J. Range Management 56:234-246.

Table 17.5. Measured and RUSLE2 estimated residue cover (percent) immediately after planting

Crop	Tillage system	Observed cover	Estimated cover	Reference
corn	spring disk	15	21	1
corn	fall chisel, spring disk	13	12	1
corn	spring disk, spring disk	27	18	2
corn	spring chisel, spring disk	22	11	2
corn	spring disk	15	21	2
corn	fall chisel, spring disk	13	12	2
soybeans	spring disk, spring disk	27	18	2
soybeans	spring chisel, spring disk	22	11	2
corn	spring disk	8	20	2
corn	spring disk, spring disk	5	7	2
corn	spring chisel, spring disk	7	3	2
corn	field cultivator	24	20	2
soybeans	spring disk, spring disk	11	8	2
soybeans	spring disk	15	22	2
soybeans	spring chisel, spring disk	11	4	2
corn	fall chisel, spring disk	33	26	3
corn	spring chisel, spring disk	19	19	4
corn	spring disk, spring disk	30	27	4
corn	fall chisel, spring disk, spring field cultivator	9	14	5
soybeans	fall chisel, spring field cultivator, spring field cultivator	9	5	5
corn	fall chisel, spring disk, spring field cultivator	16	14	6
soybeans	fall chisel, spring field cultivator, spring field cultivator	3	5	6
soybeans	spring disk, spring disk	9	7	7
soybeans	spring disk, spring disk	9	7	8
soybeans	spring disk	13	18	8

Table 17.5 (continued). Measured and RUSLE2 estimated residue cover (percent) immediately after planting

References:			
1. Siemens, J. C., W. R. Oschwald.1976. Erosion from corn tillage systems. Trans. ASAE 19:69-72.			
2. Dickey, E. C., D. P. Shelton, P. J. Jasa, T. R. Peterson. 1985. Soil erosion from tillage systems used in soybeans and corn resides. Trans. ASAE 28:1124-1129, 1140.			
3. Lindstrom, M. J. and C. A. Onstad. 1984. Influence of tillage systems on soil physical parameters and infiltration after planting. J. of Soil and Water Cons. 39:149-152.			
4. Laflen, J. M., J. L. Baker, R. O. Hartwig, W. F. Buchele, and H. P. Johnson. 1978. Soil and water losses from conservation tillage systems. Trans. ASAE 21:881-885.			
5. McIsacc, G. F., J. K. Mitchell, and M. C. Hirschi. 1990. Contour and conservation tillage for corn and soybeans in the Tama Silt Loam Soil:hydraulics and sediment concentration.Trans. ASAE 33:1541-1550.			
6. McIsaac, G. F., J. K. Mitchell, M. C. Hirschi, and L. K. Ewing. 1991. Conservation and contour tillage for corn and soybeans in the Tama silt loam soil:the hydrologic response. Soil and Tillage Research 19:29-46.			
7. Shelton, D. P., P. J. Jasa, and E. C. Dickey. 1986. Soil erosion from tillage and planting systems used in soybean residue:Part I-influences of row spacing. Trans. ASAE 29:756-760.			
8. Jasa, P. J., E. C. Dickey, and D. P. Shelton. 1986. Soil erosion from tillage and planting systems used in soybean residue:Part II-influences of row direction. Trans. ASAE 29:761-766.			

plant types, which is unacceptable based on well accepted fundamental research. Measurements were taken at too few sites for the number of variables affecting erosion, and perhaps measurements of input variables were not made according to RUSLE definitions. In several cases, the plant litter cover was inconsistent with the production level (e.g., far too much litter cover for the annual production). Also, in the few cases when experimental sites for the WEPP and Range Study Team studies coincided or were close together much of the data for the basic cover-management variables from these common sites values did not agree. Some of these differences may have been caused by temporal differences because the experiments were conducted in different years.

The first step in determining these ratio values was to classify the WEPP data by plant community. The standard RUSLE2 soil erodibility, topographic, canopy, ground cover, surface roughness, and soil consolidation factor values were assumed to apply to these data, which reflects RUSLE2 land use independence. Measured erosion values were divided by the product of these factor values to compute a soil biomass subfactor value for each experimental site. A value for effective root biomass was next obtained by substituting the soil biomass subfactor value computed from the experimental data in

equation 9.12, where a zero buried residue biomass was assumed. The effective root biomass value computed by solving equation 9.12 was divided by the annual aboveground biomass production (yield) level to determine a value for the ratio of effective root biomass in the upper 4 inch (100 mm) soil depth to annual aboveground production. A non-linear procedure that fitted predicted erosion to measured (observed) erosion was used to determine ratio values for plant communities that occurred at multiple sites. The resulting values are shown in Table 17.6.

Table 17.6. Values for ratio of effective root biomass to annual above ground biomass production for vegetation typical of range, pasture, and similar lands.

Plant community	ratio effective root biomass in upper 4 inches (100 mm)/annual above ground production
N mixgrass	2.5
S mixgrass	3.1
tallgrass prairie	1.0
shortgrass prairie	3.0
desert grassland	6.1
southern grasses	6.4
CA annual grass	2.6
cold desert shrub	5.9
southern desert shrub	6.6
shinnery oak w/herb interspace	2.6
chaparral	1.3
pasture, sod grasses	6.0
pasture, bunchgrasses	3.7
pasture, weeds	2.3

The values shown in Table 17.6 may not be consistent with known rooting and other characteristics of these plant communities. One reason for the lack of expected trends is variability in the measured data, too few measurement sites for each plant community, and too few replications. A sufficient number of sites to obtain a reasonably accurate overall effective root biomass ratio value for a plant community were available for only the southern desert shrub and southern mixed grass prairie plant communities. With these two exceptions, the Table 17.6 values for each plant community were derived from data for a single site. The Table 17.6 value for a plant community could differ from the expected value by a factor of two based on data for the two plant communities that occurred at multiple sites.

The Table 17.6 values are also affected by applying the standard RUSLE2 soil erodibility factor and the soil consolidation factor values to rangeland conditions. Tilling coarse texture rangeland soils in the southwestern US to create unit plot conditions greatly increases infiltration and reduces runoff and erosion (see **Section 7.2**). The low erosion immediately after tillage is related to land use residual effects (see **Section 9.2.5**). For example, soil plowed out of high production meadow is only one fourth as erodible immediately after tillage as it is after two years of tillage for row crop production (AH537). This land use residual effect disappears over time as a soil is continuously maintained in a unit plot condition. Research on these southwestern US rangeland soils showed that erosion increased over about three years after an initial tillage but no

subsequent tillage, which indicates a strong land use residual effect in these soils.[179] The RUSLE2 assumption that standard erodibility values apply to rangeland conditions seem reasonable.

The soil consolidation effect assumes that tillage increases erosion by about 55 percent (see **Section 7.8**). This effect seems to have been masked in the land use residual effect in the research described above. The soil consolidation effect surely varies with soil properties and climate. However, research has not defined the relationship between the soil consolidation effect with these variables, even for cropland conditions and certainly not for rangeland conditions. The RUSLE2 soil consolidation relationship was empirically derived from data collected on a single soil at Zanesville, Ohio.

In any case, discrepancies between RUSLE2 soil erodibility and soil consolidation relationships and those for rangeland conditions were empirically incorporated in the Table 17.6 values. These soil and climate effects, along with data variability, account for any inconsistency in Table 17.6 values with vegetation characteristics.

Until research provides improved information, the values in Table 17.6 should be used even if they do not seem consistent with vegetation characteristics.

The Table 17.6 values were derived assuming the time invariant cover-management (C factor) procedure (AH703). Therefore, these values represent buried residue and dead roots as well as live roots. Vegetation, residue, and cover-management descriptions can be created so that RUSLE2 computes erosion using a time invariant C factor procedure similar to that in RUSLE1.06c. The **vegetation description** has a single entry in the **growth chart** on day zero. The entered value for live root biomass is the product of the site average annual production level and the ratio value in Table 17.6 for the plant community. Entered values for canopy cover, effective fall height, and live ground cover are representative values chosen to compute average annual erosion. The **cover-management description** includes an **operation description** having a **begin growth process** that tells RUSLE2 to use the single entry vegetation description and an **add other residue/cover process** that applies an **external residue** to give the desire ground cover. The **residue description** uses a zero value for the **decomposition coefficient** so

---

[179] See:

Simanton, J.R. and K.G. Renard. 1982. Seasonal change in infiltration and erosion from USLE plots in southeastern. Hydrol. Water Resources in Arizona and Southwest 12:p. 37-46.

Simanton, J.R., Johnson, C W., Nyhan, J.W., Romney, E.M. 1986. Rainfall simulation on rangeland erosion plots. Proc. Rainfall Simulator Workshop, Jan. 1985, Tucson, AZ, pp. 11-17.

Simanton, J.R., Renard, K.G. 1986. Time related changes in rangeland erosion. Proc. Rainfall Simulator Workshop, Jan. 1985, Tucson, AZ, pp. 18-22.

that the residue does not decompose to properly represent the time invariant approach. The cover-management description is a **no-rotation**
type with one year **duration**.

Rather than use this time invariant approach, the recommended procedure is to use RUSLE2's full temporal capability when applying it to range and similar lands. Two options are available for determining input values for live root biomass in the vegetation descriptions. One option is to use literature values or to make field measurements. The literature values are highly variable. For example, the reported ratio for root biomass to aboveground biomass ranged from 0.6 to 120 for the northern mixed grass prairie plant community (AH537). A problem with literature values and with field measuring roots, which are very difficult to measure, is knowing the root size above which to discard roots because large roots have little effect on erosion. The most important roots are the fine ones near the soil surface. Even if roots are accurately measured, research has not established the relationship of erosion to root characteristics.

The best option for determining live root biomass input values is to use the RUSLE2 **long-term vegetation tool** to construct vegetation descriptions (see **Section 11.2.6**). This tool uses Table 17.6 values to estimate live root biomass values. A major advantage of using Table 17.6 values is that they have been empirically determined directly from measured erosion data using RUSLE2 definitions and equations.

Although the Table 17.6 values include a buried residue and dead root effect when used in the time invariant C factor procedure, these values give good results when they are used to estimate live root biomass values for temporal vegetation descriptions. The RUSLE2 full temporal method using live root biomass developed from Table 17.6 values gave comparable erosion estimates to those from the RUSLE1.06c time invariant C factor procedure.

The RUSLE2's temporal procedures should be used when applying RUSLE2 to range, pasture, and similar lands rather than the time invariant C factor method.

WEPP data collected for plant communities that occurred at multiple sites provided a limited indication of the uncertainty in RUSLE2 erosion estimates. The south desert shrub plant community occurred at six sites and the southern mixed grass prairie plant community occurred at five sites.[180] Estimated (predicted) and measured (observed) erosion values are shown in Figures 17.2 and 17.3. RUSLE2 estimated erosion values compare reasonably well with measured erosion values for the south desert shrub plant community except for one data point in Figure 17.2 where the predicted erosion was

[180] Data from two additional sites for the south desert shrub plant community and from an additional site for the southern mixed grass prairie plant community were not used in the analysis because these data points were judged to be outliers.

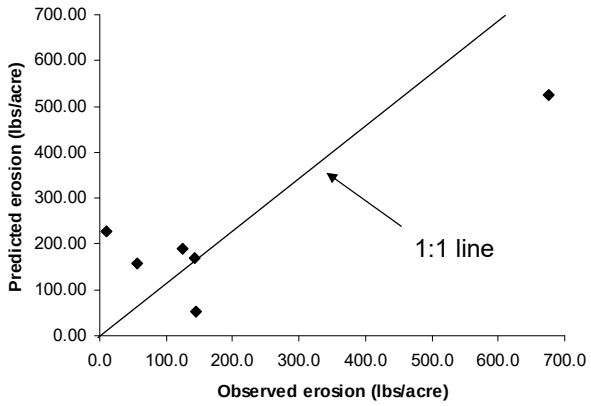

Figure 17.2. Predicted and observed erosion for south desert shrub plant community.

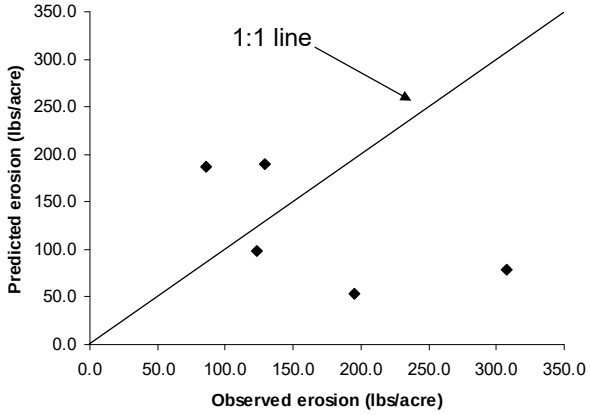

Figure 17.3. Predicted and observed erosion for southern mixed grass plant community.

about 220 lbs/acre while observed erosion was about 10 lbs/acre. However, other than this data point, the data are comparable to scatter in erosion data for cropland at such low erosion rates. Data for the southern mixed grass prairie plant community are shown in Figure 17.3. The error is large for two data points. Based on these results, a RUSLE2 erosion estimate for a particular rangeland site could be in error by a factor of five.

Even a modest evaluation of RUSLE2's accuracy for range and similar lands is essentially impossible because of limited research data (See **Section 17.2)**. The WEPP and Range Study Team datasets are the best available, but these data were produced using rainfall simulators and involved rainfall application at a single point in time rather than at several times during the year and over several years. The WEPP and Range Study Team data do not account for average annual seasonal changes or year to year changes. Even though above and surface ground cover can be measured, below ground measurements can not be easily made to determine the land use residue effect at the time of the experiments. Weather, vegetation, and soil conditions over several years preceding the experiments can greatly affect erosion measured at a single point in time.

The similarity of erosion generated by simulated rainfall and that produced by natural rainfall on western US rangelands is highly questionable. For example, the erosivity of single simulated storm in both the WEPP and Range Study Team experiments was about 50 US erosivity units whereas the average annual erosivity in much of the western US, where most rangeland occurs, is less than 20 US erosivity units. The data used to determine the Table 17.6 values were from a single simulated storm applied to dry soil conditions. These experiments also involved a second simulated storm applied to moist

conditions. Table 17.6 values and results of RUSLE2 evaluations depend greatly on whether one or two storms are used in the analysis. Also, the simulated rainfall was applied in a uniform intensity that can give significantly different erosion when infiltration rates are high and spatially varied than erosion from temporally varied intensity.[181] Applying multiple simulated rainfall multiple times during the year affects the conditions being studied because of the additional rainfall. This effect is very important in the dry climates where most rangeland occurs where the simulated rainfall is a significant portion of the annual rainfall.

Table 17.7. Erosion values from two side by side replicates for WEPP study

Erosion (lbs/ac)		
Low rep	High rep	ratio
8	20	0.42
55	85	0.64
0	56	0.00
34	91	0.37
4	100	0.04
14	27	0.54
0	3	0.00
0	0	-
0	330	0.00
0	0	0.00
26	68	0.38
213	375	0.57
145	194	0.75
0	10	0.00
0	0	-
0	0	-
22	79	0.28
0	20	0.00
350	464	0.75
244	300	0.81
50	203	0.24
0	23	0.00
302	581	0.52
3	48	0.06
7	44	0.16
0	0	-
0	0	-
5	69	0.07
15	43	0.36
0	4	0.00

Accurately measuring the low erosion rates typical of rangeland conditions (e.g., 50 lbs/ac in Figure 17.3) and having small differences, especially on a percentage basis, between replications is almost impossible. Table 17.7 shows a range of the ratio of measured erosion for the two replications in the WEPP study. These ratio values are not particularly meaningful given the low erosion rates. A slight soil disturbance near the end of a plot or a slight shift in the placement of plots could have easily produced significantly different measured erosion values. Expecting RUSLE2 or any other model to precisely fit data for individual sites is unrealistic and unreasonable because of the low erosion rates, spatial and temporal variability, and the difficulty of measuring low erosion rates. These data issues must be considered when evaluating RUSLE2 for its applicability to range and similar lands. RUSLE2 may perform better than the experimental data used to evaluate it.

Is RUSLE2 adequate for conservation and erosion control planning for range, pasture, idle, and similar lands? VERY DEFINITIVELY. RUSLE2 describes the main effects of how the major physical, biological, and ecological variables, affect erosion as conclusively proven by fundamental erosion research. RUSLE2 computes the low erosion rates that have been measured on range, pasture, idle, and similar lands. RUSLE2 accurately represents how changing major variables such as plant community, production level, removal of biomass, and mechanical soil disturbance affects erosion.

[181] Flanagan, D.C., G.R. Foster, and W.C. Moldenhauer. 1988. Storm pattern effect on infiltration, runoff, and erosion. Transactions of American Society of Agricultural Engineers 31(2):414-420.

RUSLE2 can be used as a conservation and erosion control planning tool for rangelands, pasturelands, idle, and other similar lands.

17.4.1.5. Erosion values for construction sites

Published data related to erosion control on construction sites using straw and other mulch types were extensively reviewed during the development of RUSLE1.06.[182] New RUSLE1.06 relationships were developed to describe the reduced effectiveness of mulch on construction sites relative to cropland. These new relationships also describe how mulch conformance to soil surface roughness affects erosion control on construction sites. Also, the effectiveness of simple sediment basins, surface roughness, ridging, and porous barriers on reducing erosion and trapping sediment was also extensively reviewed during the RUSLE1.06 development. Equations, input values, and other information developed for RUSLE1.06, along with information developed since the RUSLE1.06 release were used in the development and evaluation of RUSLE2 for its applicability to construction sites and similar conditions. RUSLE2 works significantly better for construction site conditions than does RUSLE1.06.

17.4.1.6. Erosion values for disturbed forestland

The Dissmeyer-Foster subfactor method used to estimate erosion on disturbed forestland is widely recognized and accepted.[183] The basic subfactor relationships used in that method are used in the RUSLE2. Therefore, RUSLE2 estimates erosion with comparable accuracy as does the Dissmeyer-Foster method. RUSLE2 is substantially better than the USLE with the Dissmeyer-Foster method because of RUSLE2's increased power and capability, such as applying to non-uniform overland flow profiles and improved relationships for computing revegetation of disturbed forestland following mechanical disturbance. RUSLE2 can also be applied to road construction in forested areas and can estimate erosion on logging roads where the runoff occurs as overland flow. RUSLE2 can also be used to evaluate how alternative burning treatments and forest fire affects erosion. Burning removes surface biomass and some buried biomass and roots. RUSLE2 represents burning removing surface and buried biomass, but it does not represent the removal of either live or dead root biomass by burning.

17.4.2. Accuracy of RUSLE2 by statistical measures

---

[182] Toy, T.J. and G.R. Foster (coeditors). 1998. Guidelines for the use of the Revised Universal Soil Loss equation (RUSLE1.06) on mined lands, construction sites, and reclaimed lands. USDI-Office of Surface Mining. Denver. CO.

[183] Dissmeyer, G.E. and G.R. Foster. 1980. A guide for predicting sheet and rill erosion on forest land. Technical Publication SA-TP-11. USDA-Forest Service-State and Private Forestry-Southeastern Area. 40 pp.

An analysis of the statistical fit of the USLE to the experimental natural runoff plot data used to develop the USLE showed that the USLE computes average annual erosion within 25 percent for average annual erosion between 4 and 30 tons/acre and within 50 percent for average annual erosion between about 0.5 and 4 tons/acre.[184] The uncertainty increases rapidly for average annual erosion less than 1 ton/acre and can exceed 500 percent for average annual soil loss less than 0.1 tons/acre (see **Section 17.4.1.4**). The uncertainty also increases, but not greatly, for average annual erosion greater than 30 tons/acre. The uncertainty in RUSLE2's estimates erosion are slightly greater than that for the USLE based on an evaluation of RUSLE1 using the same data and the similarities between RUSLE1 and RUSLE2.[185]

RUSLE2 (and RUSLE1) not fitting the data as well as the USLE is expected. The AH537 soil loss ratio values used in the USLE are essentially direct summaries of the experimental data whereas the soil loss ratio values used by RUSLE2 (and RUSLE) are computed with equations fitted to the AH537 values. As expected, the fitted equations do not exactly fit the data (see **Section 17.4.1.1)**.

Even though the fit of RUSLE2 to the experimental data is slightly less than the USLE fit, RUSLE2 is superior to the USLE because of RUSLE2's increased power and capability. In contrast to the USLE, RUSLE2 can be applied to conditions where experimental data have not been collected to empirically determine soil loss ratio values. Although the USLE has a cover-management subfactor procedure for "undisturbed, pasture, and idle lands," the procedure is deficient and should not be used. The RUSLE2 subfactor procedure is much better than the USLE procedure.

A statistical analysis of the fit of the USLE to the experimental data is not particularly robust because the natural runoff plot data have a high degree of unexplained variability.[186] A difference of 30 percent in measured erosion between adjacent plots is common for conditions where little difference would be expected. The difference in measured erosion between replicate plots can not be explained by measured differences in soil, topography plot preparation, or plot condition. Data quality must often be compromised in finding a hillslope where an adequate number of replications can be installed without excessive variation in soil or topographic properties that affect erosion

---

[184] Risse, L.M., M.A. Nearing, A.D. Nicks, and J.M. Laflen. 1993. Error assessment in the Universal Soil Loss Equation. Soil Sci. Soc. Am. J. 57: 825-833.

[185] See:

Rapp, J.F. 1994. Error assessment of the Revised Universal Soil Loss Equation using natural runoff plot data. M.S. Thesis. University of Arizona, Tucson.

Tiwari, A.K., L.M. Risse, and M.A. 2000. Evaluation of Wepp and its comparison with USLE and RUSLE. Trans. ASAE 43:1129-11135. (Based on this paper, RUSLE is slightly better than the process-based model WEPP.)

[186] Nearing, M.A., G. Govers. and L.D. Norton. 1999. Variability in soil erosion data from replicated plots. Soil Sci. Soc. Amer. J. 63: 1829-1835.

(see **Section 17.2**). Too few replications at individual locations, non-uniform coverage of the major variables that affect erosion and differences in statistical designs between locations in numerous studies prevent the use of common statistical methods to evaluate RUSLE2's statistical accuracy. The number of variables affecting erosion is very large, which in turn requires a large and high quality database to statistically evaluate RUSLE2. If the database is too small and does not uniformly cover the range of variables affecting erosion, erroneous conclusions are drawn. For example, Risse et al.[187] concluded that contouring does not affect erosion. However, when a proper dataset on contouring is assembled and analyzed, the analysis shows that contouring has a major effect on erosion although its effect is highly variable (see **Section 14.1**).[188]

Because RUSLE2 is, for the most part, empirically derived, RUSLE2's adequacy is determined by the data used to derive it. Therefore, RUSLE2's adequacy for a particular application is largely determined by how well the plots and small watersheds (<5 acres) used to derive RUSLE2 represent actual field conditions.

RUSLE2 provides an accurate representation of how major variables affect erosion as measured by plots and small watersheds (<5 acres).

17.4.3. Qualitative assessments of RUSLE2's accuracy

Qualitative assessments of RUSLE2's accuracy are useful in guiding conservation planning decisions. The following sections provide qualitative assessments of where RUSLE2 works best and where it is less well suited.

17.4.3.1 Temporal values

RUSLE2 is designed to estimate average annual erosion. It is not designed to estimate erosion from individual storms, specific time periods, probability distributions of erosion by storm, season, or year. Also, it is not designed to estimate erosion for a storm with a given recurrence interval. Information in AH537 can be used to construct probability

---

[187] Risse, L.M., M.A. Nearing, A.D. Nicks, and J.M. Laflen. 1993. Error assessment in the Universal Soil Loss Equation. Soil Sci. Soc. Am. J. 57: 825-833.

[188] The Risse et al. and Tiwari et al. papers are considered definitive papers on statistical evaluations of the USLE and RUSLE. However, these papers' shortcomings affect interpretation of their results. The evaluations described in both papers used only a portion of the available data (e.g., Tiwari et al. used only 1600 plot-years of data for 20 locations while Risse et al. used only 1700 plot-years of data at 23 locations out of more than 10,000 plot-years of data at 43 locations used to develop the USLE and RUSLE). The natural runoff plot data used to develop the USLE are not uniformly distributed for the main variables that affect rill-interrill erosion. Choosing an unbiased 20 percent sample from the entire dataset is difficult. For example, the evaluation dataset chosen by Risse et al. was biased. The dataset included 2 plots from Morris, MN, 13 plots at Guthrie, OK, and 18 plots from LaCrosse, WI. Neither paper provides information to show that the evaluation results were unbiased. Such statistical evaluations are not robust and their validity is questionable.

distributions for annual erosivity at individual locations that can be used in RUSLE2 to compute probability distributions of annual erosion for average soil and cover-management conditions. **RUSLE2** can not consider deviations in cover-management conditions by day, season, or year from the average condition.

An advanced user can compute erosion with RUSLE2 for a single storm. The erosion computed for this storm represents the average erosion produced by the storm occurring in many years on the storm's date.[189] Although RUSLE2 is not recommended for estimating erosion for individual storms, RUSLE2's accuracy for individual storms is comparable to that for process-based models like WEPP.[190] Other research has also shown that simple empirical models fitted to observed data perform as well as or better than process-based hydrologic models.

The USLE equation structure, which is used in RUSLE2, is said to underestimate erosion when average annual erosion and erosion from individual storms is large.[191] However, this statement does not accurately represent this equation structure. The USLE equation structure is fitted to estimate average annual erosion values. Consequently, it is self evident that this equation structure, when properly fitted to the data, both underestimates and overestimates large erosion. This equation structure underestimates erosion when a large storm produces an unusually high runoff relative to storm amount because the storm occurred on very moist soil. RUSLE2 has no explicit runoff term to represent increased runoff for a given rainstorm. Conversely, the equation structure overestimates erosion when the same storm occurs on very dry soil that produces low runoff. Estimating runoff is more difficult than estimating erosion based on W.H. Wischmeier's experience.[192] Process-based models' equation structure should give them an inherent advantage over RUSLE2 for estimating erosion for single storms, but that capability is barely realized in practical applications. The advantage of process-based models is lost because of

---

[189] The RUSLE2 is designed for conservation and erosion control planning where average annual erosion is used in the planning process. As a consequence, the RUSLE2 computer program is not designed to accept inputs for specific storms and, therefore, is inconvenient for computing erosion for individual storms.

[190] See:

Tiwari, A.K., L.M. Risse, and M.A. Nearing. 2000. Evaluation of Wepp and its comparison with USLE and RUSLE. Trans. ASAE 43:1129-11135.

Nearing, M.A. 1998. Personal communication.

[191] Risse, L.M., M.A. Nearing, A.D. Nicks, and J.M. Laflen. 1993. Error assessment in the Universal Soil Loss Equation. Soil Sci. Soc. Am. J. 57: 825-833. (In fact, Figure 1 in this paper shows that the USLE does not underestimate erosion for measured high erosion relative to moderate erosion. Figure 1 does show that the USLE overestimates erosion for low measured erosion. The overestimation occurs for annual erosion less than 1 ton/acre.)

[192] **Wischmeier**, W.H. 1966. Relation of field plot runoff to management and physical factors. Soil Sci. Amer. Proc. 30:272-277.

Wischmeier, W.H. mid 1970's. personal communication.

estimation errors in runoff and the many variables that are functions of environmental variables in these models.[193] The cumulative effect of having many more variables to calibrate in process-based models than in the USLE equation structure diminishes process-based model performance. Too often calibration of process-based models results in fitting unexplained variability rather than main effects.

17.4.3.2. Soils

Difficulty in estimating runoff from input climate data is the major reason why an explicit runoff term is not used in RUSLE2 except for computing the effect of support practices on erosion where an index-based approach is used to capture main effects.

RUSLE2 is most applicable to medium textured soils. It works moderately well for fine textured soils and acceptably for coarse textured soils and least well for high sand soils. Errors can be large when applied to rangeland coarse textured soils in the Southwestern US and to soils on reclaimed mined land having a very high content of large rock fragments. Technical judgment can be used in assigning soil erodibility factor values to overcome some of these difficulties (see **Section 7**).

RUSLE2 should not be applied to organic soils, such as peat.

17.4.3.3. Topography

RUSLE2 works best for overland flow path lengths between 50 (15 m) and 300 ft (100 m) long. It works moderately well for overland flow path lengths less than 20 ft long, including overland flow path lengths as short as 1 inch (25 mm), and for overland flow path lengths between 300 and 600 ft (100 and 200 m). It works acceptably for overland flow path lengths between 600 and 1000 ft long (200 and 300 m).

RUSLE2 should not be applied to overland flow path lengths greater than 1000 ft (300 m). The RUSLE2 program will not accept input values greater than 1000 ft (305 m).

RUSLE2 works best for overland flow path steepness between 3 and 20 percent. It works moderately well for steepness less than 3 percent and between 20 and 35 percent. It works acceptably for steepness between 35 and 100 percent. It should not be applied to steepness greater than 100 percent.

---

[193]Tiwari, A.K., L.M. Risse, and M.A. Nearing. 2000. Evaluation of Wepp and its comparison with USLE and RUSLE. Trans. ASAE 43:1129-11135.

RUSLE2 should not be used for overland flow path steepness greater than 100 percent. The RUSLE2 program does not accept input values greater than 100 percent

RUSLE2 can be applied to all overland flow path profile shapes, including those where deposition occurs (see **Section 5.2**). Its erosion estimates for the eroding portions of overland flow paths are significantly more accurate than deposition estimates for the depositional portions. Accurately estimating deposition by overland flow is very difficult because a slight change in overland flow hydraulics can greatly affect deposition. RUSLE2 estimates are most accurate for uniform cover-management along an overland flow path. RUSLE2 is less accurate where cover-management varies enough along the overland flow path to significantly affect runoff because RUSLE2 does not explicitly consider runoff in its detachment computations. Overland flow path segment lengths can be adjusted to partially to account for this RUSLE2 limitation (see **Section 8.4**).

17.4.3.4. Geographic Region

RUSLE2 works best where rainfall occurs regularly, rainfall is the dominant precipitation, and average annual rainfall exceeds 20 inches. **RUSLE2** works acceptably in low rainfall regions like the western US. In these areas, RUSLE2 results should be interpreted as representing average erosion for sites having conditions like the field site rather than representing erosion on the actual field site. RUSLE2 erosion estimates are more accurate for actual field sites in high than in low rainfall regions. RUSLE2's accuracy is significantly reduced in low rainfall regions where annual erosion is low, especially if it is less than 1 ton/acre. **RUSLE2** can be used to estimate erosion in the special winter condition represented by the Northwest Wheat and Range Region. Special adjustments are needed for other regions where Req-type effects occur (see **Section 6.3.3**).

RUSLE2 does not explicitly estimate erosion caused by snowmelt.

17.4.3.5. Land Use

RUSLE2 is land use independent. It applies to all land uses where mineral soil is exposed to the erosive forces of raindrop impact and Hortonian overland flow. RUSLE2 works best for all land uses where annual erosion exceeds 1 ton/acre. **RUSLE2** works best for cropland, construction sites, land fills, and moderate to highly disturbed military training sites. It works moderately well on pastureland, mine spoil and disturbed forestland. It works acceptably on rangeland, abandoned crop and pastureland, and similar wildlife lands with few trees.

RUSLE2 should not be used for undisturbed forestland.

17.4.3.6. Irrigation

RUSLE2 can be used to estimate erosion by rainfall on lands where irrigation is used.

RUSLE2 cannot estimate erosion by furrow, flood, or similar types of surface irrigation.

17.4.3.7. Processes

RUSLE2 estimates rill and interrill erosion from rainfall and its associated runoff produced as Hortonian overland flow. It estimates sediment yield from overland flow paths, from diversion/terrace type channels where deposition occurs, and from impoundments like small sediment basins and impoundment terraces (see **Section 5.2**).

RUSLE2 does not estimate erosion or deposition in concentrated flow areas like within-field ephemeral gullies, incised gullies, and stream channels. RUSLE2 does not estimate erosion by mass wasting or by piping (i.e., water flowing through "pipes" in the soil).

17.5. Relation of RUSLE2 to other USLE/RUSLE erosion prediction technologies

The USLE was first used for local field office conservation planning by the USDA-Soil Conservation Service in the early 1960's. AH282, published in 1965, documented this USLE version. The next version of the USLE was documented in AH537, and it remains the standard USLE version. RUSLE1 was first released in 1992. The NRCS officially adopted RUSLE1.05 for local field office conservation planning in the mid 1990's. RUSLE1.05 is documented in AH703. RUSLE1.06, intended to replace RUSLE1.05, was released in 1998 and documented in the OSM manual for applying RUSLE1.06 to construction, mine, and reclaimed lands.[194] An erroneous impression is that RUSLE1.05 should be applied to cropland and RUSLE1.06 to disturbed lands. All versions of RUSLE1.06 apply to all lands. RUSLE1.06c was released in 2003. Changes were made so that RUSLE1.06c erosion estimates more closely correspond with RUSLE2's estimates than those from previous RUSLE1.06 versions.

[194] Toy, T.J. and G.R. Foster (coeditors). 1998. Guidelines for the use of the Revised Universal Soil Loss equation (RUSLE1.06) on mined lands, construction sites, and reclaimed lands. USDI-Office of Surface Mining. Denver. CO.

Foster et al. describe major differences in these technologies.[195]

17.5.1. Erosivity

The erosivity values given in AH282, AH537, and AH703 were determined from precipitation data collected from the mid 1930's to mid 1950's for the eastern US. The RUSLE2 erosivity values were determined from precipitation data collected from 1960 through 1999 for the entire continental US (see **Section 6.2**). Overall, the erosivity values from the recent data are about 10 percent higher in the Eastern US than erosivity values from the early data. The RUSLE2 erosivity values for the western US are much better than the erosivity values in AH537 or AH703.

RUSLE2 erosivity values should be used in all USLE/RUSLE versions.

Erosivity values in AH537 were reduced along the US Gulf Coast to account for high intensity rainfall ponding water that creates a water depth and reduces raindrop impact erosivity. Erosivity values in AH703 were not reduced to account for this effect. Instead, a ponding subfactor that is a function of the 10 year EI value and slope steepness was used in all RUSLE1 versions, but the ponding subfactor was used only with ridges. RUSLE2 uses a similar ponding subfactor (see **Section 9.2.7**) that is applied regardless of the presence of ridges.

The AH703 10 yr EI values were also based on the 1930's to 1950's precipitation data. The 10 yr EI values were contoured in great detail, which resulted in a 10 yr EI map with long narrow ridges-valleys in the equal value lines. A 10 yr EI map was developed for RUSLE1.06c that eliminated these ridges-valleys to represents main trends across the US appropriate for computing how support practices affect erosion.

The new RUSLE1.06c 10 yr EI map should be used in all RUSLE1 versions.

RUSLE2 uses 10 yr-24 hr precipitation values, which are based on data collected from before the 1960's, rather than 10 yr EI values. Smoothed 10 yr-24 hr precipitation values used in RUSLE2 are shown in Figure 6.18. These values capture the main trends across the Eastern US, much like the new 10 yr EI map developed for RUSLE1.06c.

RUSLE2 uses modern precipitation and temperature data that should also be used in all RUSLE1versions.

---

[195] Foster, G.R., T.J. Toy, and K.G. Renard. 2003. Comparison of the USLE, RUSLE1.06c, and RUSLE2, for application to highly disturbed land. In: First Interagency Conference on Research on Research in the Watersheds. USDA-Agricultural Research Service. Washington, D.C. pp. 154-160.

Use the smoothed 10 year EI map developed for RUSLE1.06c for all RUSLE1 versions.

17.5.2. Soil erodibility

All USLE/RUSLE versions use the same base soil erodibility factor value. RUSLE1.05 and RUSLE1.06b temporally vary the soil erodibility factor value while RUSLE1.06c does not. The resulting erosion difference can be 20 percent in some Midwestern US and Northeastern US location. RUSLE2 uses a new procedure to temporally vary soil erodibility factor values that is much better than the old RUSLE1 procedure, especially in the western US outside of Req type regions. The net soil erodibility factor value computed by RUSLE2 can also differ from RUSLE1.05 and RUSLE1.06 net erodibility factor value by 20 percent. The net soil erodibility value computed by RUSLE2 is close to the base soil erodibility value used by RUSLE1.06c for most of the Eastern US.

The RSULE2 temporal soil erodibility equation also computes average annual soil erodibility values that vary with location, even when soil properties are the same between locations. This effect is greatest in the Western US where soil erodibility values can vary as much as 50 percent from base soil erodibility values.

Do not temporally vary soil erodibility factor values in any RUSLE1 version.

RUSLE2 includes the standard USLE soil erodibility nomograph (AH537, AH703) widely used to estimate soil erodibility values. RUSLE2 also includes a modified version of the USLE soil erodibility nomograph that computes a greater effect of soil structure on soil erodibility than does the standard USLE nomograph (see **Section 7.3.2**). The trend of soil erodibility with soil structure in the standard USLE nomograph is not consistent with the trend identified by fundamental research.

The RUSLE2 modified soil erodibility nomograph should be used in all USLE/RUSLE versions when applied to highly disturbed lands. The standard USLE soil erodibility nomograph can be used on cropland.

The USLE does not consider sediment characteristics. RUSLE1.05 uses a single value deposition coefficient that does not vary with soil properties or upslope deposition. RUSLE1.06b and c use a deposition coefficient that is computed as a function of soil texture, but it does not change with upslope deposition. RUSLE2 computes sediment characteristics values for five sediment classes at the point of detachment as a function of soil texture. RUSLE2 computes how deposition changes the distribution among the sediment classes as deposition occurs. RUSLE2 computed deposition depends on how

much upslope deposition has enriched the sediment in fines. RUSLE2 computes an enrichment ratio based on specific surface area, which is a function of soil texture and the portion of the detached sediment that is deposited.

17.5.3. Topography

The USLE slope length exponent varies only with slope steepness for steepness less than 5 percent. The RUSLE1.05 slope length exponent varies with slope steepness over the full range of steepness from zero to 100 percent. Also, the RUSLE1.05 slope length exponent is a function of the rill to interrill erosion ratio where the user selects from one three classes. In RUSLE1.06b and c, the slope length exponent is computed from the rill to interrill erosion ratio where the user selects from land use classes. Also, the RUSLE1.06 slope length exponent is a function of the rill soil erodibility to interrill soil erodibility ratio computed from soil texture. RUSLE2 computes the slope length exponent as a function of soil, steepness, and cover-management variables that affect the rill to interrill erosion ratio (see **Section 8.1.1**).

The slope length exponent used in the USLE and all RUSLE1 versions is constant over the computational period (i.e., duration in cover-management description). In contrast, RUSLE2 computes a slope length exponent value that varies daily as cover-management conditions change daily.

As a minimum, the RUSLE1.05 slope length relationship (AH703) should be used in the USLE.

The slope steepness relationship in the USLE has a quadratic form empirically derived from data collected at La Crosse, WI. This equation does not apply well to slope steepness less than about 2 percent or to slope steepness greater than about 25 percent. The RUSLE1 and RUSLE2 slope steepness relationship is based on a wide ranging dataset and is much more linear than the USLE quadratic relationship. No USLE, RUSLE, or RUSLE2 version varies the slope steepness relationship with any variable including time, soil, or cover-management.

The RUSLE slope steepness relationship (AH703) should be used in the USLE.

The USLE irregular slope procedure works well for determining how overland flow path profile shape affects erosion on the eroding portion of the flow path. It is not easily used where cover-management varies along the flow path. **The USLE does not compute deposition on concave flow path profiles.** RUSLE1.05, 1.06b, and 1.06c compute deposition on concave overland flow path profiles but do not vary the deposition coefficient along the overland flow path as deposition changes sediment characteristics. These models are not easily used where cover-management varies along the overland

flow path except for rotational strip cropping. RUSLE2 computes how deposition changes sediment properties along the overland flow path that in turn affect downslope deposition. RUSLE2 is easily applied where cover-management varies along the overland flow path in any pattern (see **Section 17.4.3.3**)

17.5.4. Cover-management

RUSLE2 computes soil loss ratio values that can be compared to AH537 values. Also, RUSLE2 can be used to compute soil loss ratio values to use where experimental research has not determined values for the USLE. However, a much better approach is to use RUSLE1.06c rather than the USLE. The cover-management relationships in RUSLE1.06c are comparable to those in RUSLE2 and an error in the RUSLE1.05 and RUSLE1.06b computer programs in the soil biomass subfactor was corrected in RUSLE1.06c. The erosion reduction computed for no-till was reduced between RUSLE1.06b and RUSLE1.06c to be consistent with analysis conducted during the RUSLE2 development. Also, the interaction between canopy cover and ground cover used in the USLE and RUSLE2 is used in RUSLE1.06c but not in other RUSLE1 versions.

The AH537 soil loss ratio values for "conventional tillage" were used to calibrate **RUSLE2** so that the soil loss ratio values computed by **RUSLE2** match, as closely as possible, AH537 values.[196] The AH537 values for conservation tillage were not used in the **RUSLE** calibration because the AH537 values were based on research data collected in the late 1960's and early 1970's that do not represent modern conservation tillage. An extensive set of data from a literature survey was assembled and used to validate **RUSLE2** for no-till and other conservation tillage types.

Several considerations are important to ensure proper comparisons of RUSLE2 computed soil loss ratio values with AH537 and other soil loss ratio values.

RUSLE2 uses a ridge subfactor that is not used by RUSLE1. The effect of ridges is not represented in the AH537 soil loss ratio values except in Table 5-A. for cotton. Daily values of the RUSLE2 C and the ridge subfactors must be multiplied and integrated using the temporal erosivity distribution to compute a RUSLE2 soil loss ratio that can be compared to AH537 soil loss ratios.

The AH537 soil loss ratio values for crop stage four, the period following harvest, were not used to calibrate RUSLE2. Most of the data used to develop AH537 soil loss ratio

[196] Soil loss ratio is the ratio of erosion in a given period, like a crop stage, to erosion from the "unit plot" for the same period where all other conditions are the same. A crop stage is a period where cover-management conditions can be assumed to be constant. Equation 5.9 shows how soil loss ratios and crop stage periods are used to compute a cover-management factor value in the USLE.

values for cropland, except for conservation tillage and cotton, were from about 1935 to 1955. Farming practices in this period left corn stalks standing more erect after harvest than do modern combines that shred and spread the stalks. Also, AH537 soil loss ratio values for flat residue are based on a surface cover effect (mulch subfactor) having a b_f value of 0.026 (see equation 9.6), much lower than the now accepted value of 0.035. The data used to determine and evaluate **b** values in **RUSLE2** included the data used to develop the AH537 mulch subfactor curve plus additional data.

Many of the AH537 soil loss ratio values are for yields lower than modern yields, especially for corn. For example, the AH537 yield for high production corn is 112 bu/ac, whereas a modern corn yield is easily 150 bu/ac or more.

Soil loss ratios in AH537 are independent of location, whereas **RUSLE2** computed soil loss ratio values vary with location. For example, **RUSLE2** soil loss ratio values for corn are significantly lower in the upper Midwestern US than in the lower part of the Mid-South US because of the low soil biomass in the Mid-South where a humid, warm climate greatly increases biomass decomposition in comparison with the climate of the upper Midwest. Climate data at Columbia, Missouri were used to calibrate **RUSLE** and to represent typical conditions that would produce soil loss ratio values to compare with AH537 values, except for cotton where climate data from Holly Springs, MS were used.

To make comparisons between RUSLE2 soil loss ratio values and AH537 values, use Columbia, MO climate to compute RUSLE2 soil loss values for all AH537 conditions, except for cotton where the Holly Springs, MS location should be used. Climate data from Pullman, WA or Pendleton, OR should be used to compute RUSLE2 soil loss ratio values and other values to compare with research determined values in the Northwest Wheat and Range Region.

RUSLE2 was calibrated with the RUSLE2 core database. RUSLE2 soil loss ratio values should be computed using the RUSLE2 core database when making comparisons with AH537 values. Also, the RUSLE2 production (yield) level adjustment procedure should be used when comparing RUSLE2 computed soil loss ratio values with AH537 values for different production levels.

Table 10, AH537 is widely used in the USLE to compute erosion on range, pasture, idle, and undisturbed lands. **This procedure should not be used because it has major shortcomings (see Section *17.4.1.4*).** RUSLE2 and RUSLE1.06c provide much better estimates than the USLE for these conditions.[197] Also, RUSLE1.06c is much improved over RUSLE1.05 and earlier RUSLE1.06 versions for these conditions.

[197] Spaeth, Jr., K.E., F.B. Pierson, M.A. Weltz, and W.H. Blackburn. 2003. Evaluation of USLE and RUSLE estimated soil loss on rangelands. J. Range Management 56:234-246.

A major advantage of RUSLE2 and RUSLE1.06c is their land use independence that allows them to be applied to conditions that vary from highly disturbed to undisturbed over the period of interest. Examples include construction sites, reclaimed mine land, disturbed forestland, and landfills from the time of the last disturbance through recovery and stabilization. Also, RUSLE2 and RUSLE1.06c work well for military training sites and similar areas where conditions at the site range from highly disturbed to undisturbed and for rangeland sites that move back and forth with cropland depending on farming economics. If different models are applied to different time periods or to different land use conditions, the likelihood is almost 100 percent that erosion estimates from the different models will differ significantly at common point in time when common estimates are expected. These erosion estimate differences complicate interpretation of the values and raise questions about the validity of one or more of the models. Users may not know the correct erosion estimate, but they can easily recognize that differences are being computed where values should not be different.

RUSLE2 can be used to compute soil loss ratio values for any land use where RUSLE2 applies. These values can be used in the USLE for conditions where experimentally derived soil loss ratio values are not available. *RUSLE1.06c should be used rather than the USLE.*

17.5.5. Support practices

17.5.5.1. Contouring

The AH537 contouring subfactor values typically used in the USLE vary only with steepness of the overland flow path. All RUSLE1 versions compute contouring subfactor values that vary with the major variables that affect the relation between erosion and contouring. RUSLE1 uses input values for cover-management condition and ridge height that represent the entire computational period. These inputs are selected to compute average annual erosion. RUSLE2 uses equations similar to those in RUSLE1 to compute daily contouring subfactor values (**see Section 14.1**). A relative row grade of 10 percent and climate data for Columbia, MO should be used when comparing RUSLE2 and RUSLE1 contouring subfactor values with AH537 values. Also, cover-management conditions, including yield, used in RUSLE2 and RUSLE1 should be chosen to represent farming practices in the 1930’ to mid 1950’s to compute contouring subfactor values to compare with AH537 values.

RUSLE2 computes a net contouring subfactor value by integrating daily contouring factor values with the temporal erosivity distribution values. However, RUSLE2 net contour values are not the proper values to compare with AH537 values. The proper RUSLE2 contouring subfactor value to compare with an AH537 value is the ratio of RUSLE2 computed average annual erosion for a 10 percent relative row grade to average

annual erosion for an up and downhill (100 percent) relative row grade. This RUSLE2 contouring subfactor is comparable to AH537 contouring subfactor values computed as the ratio of measured average annual erosion with contouring to measured average annual erosion with up and downhill tillage. Values for this RUSLE2 contouring subfactor value differs from the RUSLE2 net contouring subfactor (see **Section 17.5.6** for a discussion of the reason for this difference).

A difficulty with RUSLE1 is that representative input values for the entire computational period must be chosen. RUSLE2 computes daily contouring subfactor values based on the daily values for cover-management variables. RUSLE2 and RUSLE1 should give similar contouring subfactor values but the values will not compare exactly.

All RUSLE versions describe how major variables affect contouring failure (critical slope length). AH537 values only vary with slope steepness and whether or not strip cropping is used. AH537 gives a single adjustment for conservation tillage conditions. All RUSLE versions were calibrated to give AH537 critical slope lengths for the base Columbia, MO condition (see **Section 14.1.2.5**).

RUSLE2 can be used to compute contouring subfactor values for use in the USLE. The value should be computed as a ratio of average annual erosion values with and without contouring computed by RUSLE2. Actually, RUSLE1.06c should be used rather than the USLE.

17.5.5.2. Strips/barriers

Although Table 14, AH537 list factor values for several rotational strip cropping conditions, AH537 provides no factor values for narrow strips of permanent vegetation or mechanical barriers like fabric (silt) fences. To compare RUSLE2 and RUSLE1 factor values with AH537 values, make RUSLE2 and RUSLE1 computations with and without rotational strip cropping for Columbia, MO using input values that represent farming practices, including yield, in the 1930' to mid 1950's. Compute ratio values using RUSLE2 estimated average annual sediment yield, not detachment or erosion, to compare with AH537 values that were computed as measured sediment yield with strip cropping to measured sediment yield without strip cropping. Similarly, RUSLE1 sediment yield values should be used rather than the P factor values. The RUSLE1 P factor values do not give full credit for deposition as soil saved, whereas the AH537 and RUSLE2 values give full credit for deposition as soil saved for rotational strip cropping.

The AH537 strip cropping factor values do not apply to modern farming practices, including conservation tillage, that leave rough soil surfaces and high residue cover that induce deposition much like dense vegetation strips. The effectiveness of strips is related to sediment production on the more erodible strips relative to transport capacity in the strips having a high hydraulic resistance (see *Section 14.2*).

All RUSLE versions capture how major variables affect the relationship between sediment yield and strips/barriers. RUSLE1 uses inputs for cover-management condition for each strip that represents each year of the computational period. RUSLE2 computes daily factor values as a function of daily cover-management variables. Just as with contouring, RUSLE2 and RUSLE1 factor values for strips/barriers will not agree because of this difference in input even though similar equations are used in both models. Another reason for differences is that RUSLE1.05 uses a single deposition coefficient value, RUSLE1.06 uses a deposition coefficient that is a function of soil texture, and RUSLE2 uses sediment characteristics that are a function of soil texture and upslope deposition.

See **Sections 14.2 and 17.5.5.3** for a discussion of RUSLE2's conservation planning soil loss that gives credit for deposition as soil saved.

RUSLE2 can compute factor values for strips/barriers that can be used in the USLE, but a better approach is to use RUSLE1.06c rather than the USLE.

17.5.5.3. Diversions/terraces/sediment basins

Factor values for diversions, terraces, and small sediment basins reported by Foster and Highfill and the RUSLE1.06 OSM manual are the best values for comparing with RUSLE values.[198] The value of terraces as a soil conservation practice has been debated for several years. The benefit of terraces for shortening the overland flow path length to reduce sediment production and deposition in terrace channels and small sediment basins reducing sediment yield reduction is universally accepted. However, the value of deposition as soil saved is debated. For example, credit was given to deposition in 1965 in AH282 as soil saved but no credit was given in 1978 in AH537. The credit given is a matter of judgment. USDA-NRCS agronomists tend to claim no credit for deposition with terraces but prefer to claim credit for deposition caused by narrow permanent vegetation strips, while USDA-NRCS engineers prefer to claim credit for deposition caused by terraces.[199]

---

[198] See:

Foster, G. R. and R. E. Highfill. 1983. Effect of terraces on soil loss: USLE P factor values for terraces. Journal of Soil and Water Conservation 38:48-51.

Toy, T.J. and G.R. Foster (coeditors). 1998. Guidelines for the use of the Revised Universal Soil Loss equation (RUSLE1.06) on mined lands, construction sites, and reclaimed lands. USDI-Office of Surface Mining. Denver. CO.

[199] This debate among these NRCS disciplines involves a certain amount of self-interest. NRCS agronomists have technical oversight for permanent vegetation strips while NRCS engineers have technical oversight for terraces.

The RUSLE2 developers consider deposition in terrace channels and above permanent vegetation strips to have a similar benefit as soil saved. In fact deposition in terrace channels could perhaps merit increased credit because tillage redistributes this deposited sediment over a larger landscape area than tillage redistributes sediment deposited by permanent vegetation strips. RUSLE2 gives consistent credit to deposition as soil saved between terraces and permanent vegetation strips based on location along the overland flow path, except for rotational strip cropping where full credit is given to deposition. Also, the credit given to deposition as soil saved with terraces decreases as terrace spacing increases (see **Section 14.3**). Giving full credit to deposition associated with rotational strip cropping is consistent with AH282 and AH537 values. The RUSLE2 soil conservation planning soil loss value is the RUSLE2 output that reflects credit for deposition as soil saved (see **Section 8.1.5.4**).

RUSLE1.05 computes sediment yield from diversion/terrace channels as a function of channel grade only. That is, the fraction of the sediment load that is deposited in a diversion/terrace channel is independent of the sediment load coming into the channel or transport capacity in the channel. RUSLE2 and RUSLE1.06 compute deposition as a function of sediment characteristics, sediment transport capacity in the channel, and sediment load reaching the channel. If incoming sediment load is less than transport capacity, no deposition is computed. RUSLE1.05 assumes that 95 percent of the sediment that reaches a small sediment basin is deposited. RUSLE2 and RUSLE1.06c compute deposition in small sediment basins as a function of characteristics of the incoming sediment.

RUSLE2 can be used to compute diversion/terrace/sediment basin P factor values for use in the USLE. However, a better approach than using the USLE is to use RUSLE1.06c, which computes diversion/terrace/sediment basin P factors using equations that are similar to those used in RUSLE2.

17.5.6. Computing erosion

RUSLE2 computes net values for the soil erodibility factor K, topographic factor LS, cover-management factor C without the ridging effect, ridge subfactor, ponding subfactor, and contouring subfactor by weighting daily values with the temporal erosivity distribution, exactly in the same way that these computations are made in the USLE for the C factor and in RUSLE1 for the K and C factors.

These RUSLE2 computed factor values can be compared with those for the USLE and RUSLE1. These comparisons give insight into differences among RUSLE2, RUSLE1, and the USLE. The comparisons should be properly made. For example, the RUSLE2 net factor values for cover-management and ridging should be multiplied to obtain a C factor that can be compared with the USLE and RUSLE1 C factor values. Also, the

proper RUSLE2 values for the contour and strip cropping factors is to divide the average annual sediment yield for contouring and contouring/contouring/strip cropping on a uniform overland flow path by estimated sediment yield without contouring or strip cropping. The RUSLE2 net contouring subfactor value differs from this RUSLE2 factor value for contouring because the net contouring subfactor only involves the temporal integration of the erosivity distribution while the ratio values involves the temporal integration of the product of all the RUSLE2 factors.

The RUSLE2 computed values for these factors can be multiplied as the USLE and RUSLE1 factor values are multiplied to estimate average annual erosion. However, this erosion value differs from the value computed by RUSLE2 because of differences in the mathematic integration among these models (see **Section 5.4**). RUSLE2 does not compute erosion by multiplying average annual values for individual factors; RUSLE2 computes average annual erosion by computing daily erosion as the product of the daily factor values and summing the daily erosion values. The difference in these mathematical procedures for computing average annual erosion can be as much as 15 percent, depending on cropping-management system and location.

Even if RUSLE2 were to produce net factor values that equaled USLE and RUSLE1 factor values, RUSLE2's computed average annual erosion would not match USLE and RUSLE1's computed average annual erosion. RUSLE2's mathematics properly integrate the temporally and spatially varying governing equations. The USLE and RUSLE1 procedures are approximations.

18. HOW RUSLE2 CAME TO BE

The Universal Soil Loss Equation (USLE) was developed in the late 1950s and became widely used in conservation planning on cropland in the 1960s. Beginning in the 1970s, the USLE was applied to many other land uses in addition to cropland and to other applications besides conservation planning.

The USLE was updated in 1978, but by 1985 the USLE needed another update with passage of the Farm Bill and to incorporate new research information. A project led by USDA-Agricultural Research Service was initiated at a workshop in Lafayette, Indiana in 1985 to update the USLE. This workshop attended by leading U.S. erosion research scientists and USLE users from the USDA-Natural Resources Conservation Service (formerly, Soil Conservation Service) and Forest Service, USDI-Bureau of Land Management, and U.S. Army Corps of Engineers set objectives and approaches for the update.

By 1987, much of the background work on updating the USLE was well underway and some had been completed. The project evolved into much more than an updating of the USLE. The USLE was undergoing a major revision, and hence the updated USLE became what is now referred to as **RUSLE1**, the **R**evised **USLE**. Also, another major addition to the project was the development of a computer program to implement RUSLE1.

Development of **RUSLE2** began in 1993 using RUSLE1 as the starting point. RUSLE2 uses the basic USLE equation structure to compute sediment detachment but differs greatly from the USLE in almost every other way. RUSLE2 is similar to RUSLE1, but RUSLE2 uses new equations, a new mathematical integration procedure, new database values, and is implemented in a modern graphical user interface computer program. Almost all of the mathematical relationships in RUSLE2 have been revised from corresponding relationships in RUSLE1.

RUSLE2 is much more powerful than either the USLE or RUSLE1. The interface for the RUSLE2 computer program, the underlying modeling engine of this computer program, its computational routines, and RUSLE2's mathematical equations make RUSLE2 the most modern, powerful, and easy-to-use erosion prediction technology available for use in conservation and erosion control planning at the local field office level.

RUSLE2 was developed by a group of experienced and nationally recognized erosion scientists, erosion control specialists, and soil conservationists. Data needed to develop and validate RUSLE were incomplete in some cases, which necessitated scientists and users using judgment to fill gaps. USDA-Agriculture Handbook 703 and other RUSLE1 publications, which was the starting point for RUSLE2, have been reviewed by peer scientists in a process typical of the reporting of rigorous research. Erosion scientists,

NRCS technical specialists, and many others have made many computations with RUSLE2 to ensure that RUSLE2 works well for every imaginable situation where RUSLE2 will be applied. The scientific documentation for RUSLE2 has been peer reviewed according to standard procedures of the USDA-Agricultural Research Service.

RUSLE2 can be used with full confidence that it meets high scientific standards and produces reliable results for conservation and erosion control planning for all lands where rill and interrill erosion occur by rainfall and Hortonian overland flow.

Assessment of erosion, sedimentation, and water quality impacts of the Mountain Valley Pipeline and Equitrans Expansion Project's proposed crossing of the Jefferson National Forest as it pertains to the U.S. Forest Service's Draft Supplemental Environmental Impact Statement dated December 2022

Prepared by Jonathan A. Czuba, Ph.D., Licensed Professional Engineer - February 9, 2023

REFERENCES
2

February 21, 2023

Formulas for Sediment Porosity and Settling Velocity

Weiming Wu, M.ASCE[1]; and Sam S. Y. Wang, F.ASCE[2]

Abstract: Several existing formulas for the initial porosity and settling velocity of sediment have been tested by using extensive data collected from different countries and regions, and modified to achieve better reliability or convenience in use.

DOI: 10.1061/(ASCE)0733-9429(2006)132:8(858)

CE Database subject headings: Sediment; Sediment deposit; Porosity; Settling velocity; Particle size; Shape.

Introduction

Sediment transport in rivers has been extensively studied since the early 20th century. Scientists and engineers have established theories and methodologies to give answers or solution methods for many important problems, such as quantification of sediment properties, determination of sediment transport rate under certain flow conditions, prediction of river morphological changes, etc. However, it is very hard for engineers to make a decision when several available empirical methods give different answers for the same problem. Thus, a review of the existing methods becomes necessary. Importantly, many empirical formulas were established decades ago based on a limited number of experimental and field data. Many new or rediscovered old data sets from different countries and regions may be used to enhance the reliability and accuracy of these established formulas and methods. With this intention, the authors have revisited two classical problems: initial porosity of sediment deposits and settling velocity of sediment particles. Several existing formulas have been tested by using the data collected from different sources, and newly modified formulas with more reliability and/or convenience have been proposed.

Initial Porosity of Sediment Deposits

The initial porosity of sediment deposits has been investigated by Hembree et al. (1952), Lane and Koelzer (1953), Colby (1963), Komura (1963), and Han et al. (1981). For the sediment deposits of one year or less, Komura (1963) related the porosity to the median diameter as

$$p'_m = 0.245 + \frac{0.0864}{(0.1d_{50})^{0.21}} \tag{1}$$

where p'_m = initial porosity of sediment deposit; and d_{50} = median diameter of sediment mixture (in millimeters).

Han et al. (1981) proposed the following semiempirical formula to calculate the initial porosity of uniform sediment deposits:

$$p'_m = \begin{cases} 1 - 0.525\left(\dfrac{d}{d + 4\delta_1}\right)^3 & d < 1 \text{ mm} \\ 0.3 + 0.175e^{-0.095(d-d_0)/d_0} & d \geq 1 \text{ mm} \end{cases} \tag{2}$$

where d = size of sediment (in millimeters); d_0 = reference size (set as 1 mm); and δ_1 = thickness of the water layer attaching to sediment particles, approximately set as 0.0004 mm.

As shown in Fig. 1, the authors revalidated the relationship between the initial porosity and the sediment size using more extensive data, including the laboratory data of Trask (1931) and Straub (1935) as well as the field data in Lake Clarmore, Moran Reservoir, Neosha County State Lake, Lake Marinuka, Tongue River Reservoir, and Powder River (Hembree et al. 1952), Lake Mead, Tone River, Pigeon Point Shelf, Nagara River, and Hatori Dam (Komura 1963), Sanmenxia Reservoir, Danjiangkou Reservoir, and another seven reservoirs in China (see CAHE Committee on Sedimentation 1992). The dry density, ρ'_s, in Fig. 1 is calculated from the porosity by using

$$\rho'_s = (1 - p'_m)\rho_s \tag{3}$$

where ρ_s = sediment density having a value of 2.65 t/m^3. Note that the international (SI) units are used here. It can be seen that Komura's formula is quite close to the trend of the data sets, slightly underestimating the dry density for sand and gravel and overestimating for silt and coarse clay. The semiempirical formula of Han et al. (1981) has significant errors, perhaps due to the fact that their formula was developed only for uniform-size sediment deposits. To match the measured data better, Komura's formula (1) is modified as

$$p'_m = 0.13 + \frac{0.21}{(d_{50} + 0.002)^{0.21}} \tag{4}$$

where d_{50} is in millimeters.

Compared with the measured data in Fig. 1, the mean relative errors of Eq. (4), Komura's formula and Han et al.'s formula are 12.7, 14.1, and 21.5%, respectively. The mean relative error is defined as $[(\Sigma_{i=1}^{m}|f_{\text{cal},i} - f_{\text{meas},i}|)/f_{\text{meas},i}]/m$, with m = number of

[1]Research Associate Professor, National Center for Computational Hydroscience and Engineering, Univ. of Mississippi, MS 38677 (corresponding author). E-mail: wuwm@ncche.olemiss.edu

[2]F.A.P. Barnard Distinguished Professor, Director, National Center for Computational Hydroscience and Engineering, Univ. of Mississippi, MS 38677. E-mail: wang@ncche.olemiss.edu

Note. Discussion open until January 1, 2007. Separate discussions must be submitted for individual papers. To extend the closing date by one month, a written request must be filed with the ASCE Managing Editor. The manuscript for this technical note was submitted for review and possible publication on October 13, 2004; approved on July 11, 2005. This technical note is part of the ***Journal of Hydraulic Engineering***, Vol. 132, No. 8, August 1, 2006. ©ASCE, ISSN 0733-9429/2006/8-858–862/ $25.00.

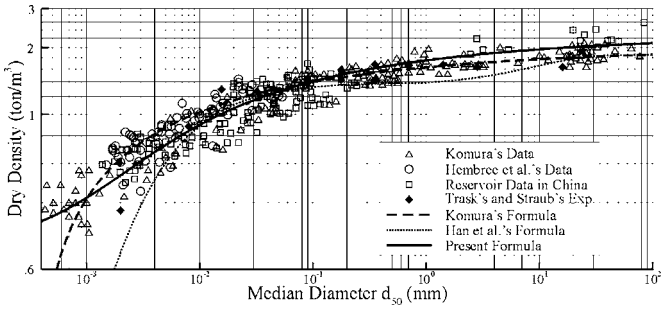

Fig. 1. Dry density of sediment deposit as function of d_{50}

samples, $f_{meas,i}$=measured value, and $f_{cal,i}$=predicted value. The porosities predicted by Eq. (4), Komura's formula, and Han et al.'s formula for 95.0, 87.3, and 77.8% of the samples, respectively, are within 30% error from the measured values. The modified formula (4) performs best.

Note that formula (4) is only for the initial porosity of sediment deposits. It does not consider the variation of deposit porosity with time and along depth due to the consolidation, especially for fine sediments (Lane and Koezler 1953), and the difference due to the effects of bed forms, organic matters (e.g., microalgae), etc. (Wheatcroft 2002).

Settling Velocity of Sediment Particles

Previous Studies

The terminal settling velocity of sediment particles, ω_s, can be derived by equating the effective weight force to the drag resistance as

$$\omega_s^2 = \frac{4}{3C_d}\frac{\rho_s - \rho}{\rho} gd \tag{5}$$

where ρ=water density; g=gravitational acceleration; and C_d=drag coefficient.

In 1851 Stokes solved the Navier–Stokes equations with the aid of a shear function and neglecting all inertia terms, and theoretically derived the drag coefficient for a spherical particle in the streamline settling region ($R<0.5$)

$$C_d = \frac{24}{R} \tag{6}$$

where R=particle Reynolds number, defined as $R=\omega_s d/\nu$, with ν being the kinematic viscosity of water. Oseen (1927) and Goldstein (1929) included more inertia terms in the Navier–Stokes equations and derived more complete analytical solutions that extend the application range a little further but are still in a limited range of Reynolds number ($R<2$). For higher R, the drag coefficient has to be determined by experiments. Rouse (1938) and Brown and Lawler (2003) summarized the available data and presented typical relations of C_d-R for spherical particles.

Because the particle shape and surface roughness affect the settling process, the C_d-R curve of natural sediment particles deviates from that of spheres. Rubey (1933), Cancharov [see Cheng 1997], Interagency Committee (1957), Zhang (1961), Sha (1965), Graf (1971), Zanke (1977), Hallermeier (1981), Van Rijn (1989), Raudkivi (1990), Julien (1995), Cheng (1997), and Ahrens (2000, 2003) have developed empirical or semiempirical relations for the settling velocity of sediment particles. Generally, the drag coefficient can be approximated as (Cheng 1997)

$$C_d = \left[\left(\frac{M}{R}\right)^{1/n} + N^{\frac{1}{n}}\right]^n \tag{7}$$

where M, N, and n=coefficients. Table 1 shows the values of these three coefficients given by different investigators in the case of naturally worn sediment particles, the shape factor of which usually is about 0.7. The coefficient M was given a value of 24 by Rubey (1933), Van Rijn (1989), and Julien (1995), and values between 32 and 34 by Zhang (1961), Raudkivi (1990), and Cheng (1997). The tests against measurement data performed by Cheng (1997) have shown that for natural sediment the values of 32–34 for M give better predictions than the value of 24. The latter corresponds to the Stokes' law, Eq. (6) for spherical particles. Rubey (1933) gave the coefficient N a value of 2.1, which yields a significant underestimation for the settling velocity of coarse sediment particles.

Table 1. Values of M, N, and n

Formula	Rubey (1933)	Zhang (1961)	Van Rijn (1989)	Raudkivi (1990)	Julien (1995)	Cheng (1997)
M	24	34	24	32	24	32
N	2.1	1.2	1.1	1.2	1.5	1
n	1	1	1	1	1	1.5

Krumbein (1942), Corey (1949), McNown et al. (1951), Wilde (1952), and Schulz et al. (1954) experimentally investigated the effect of sediment particle shape on the settling velocity, and the Subcommittee on Sedimentation of the U.S. Interagency Committee on Water Resources (Interagency Interagency Committee (1957) summarized the data measured by these investigators and published a graphical relation of the drag coefficient with sediment size, water temperature, and shape factor. This graphical relation has unique merits because it has considered the effect of particle shape on sediment settling that is ignored in many other popular formulas mentioned above. However, this graphical relation consists of a series of curves and tables, and several interpolations must be conducted to obtain the sought solution. It is not convenient to use. In addition, all the data used in the calibration were in the range of $R>3$, and the relation was extended in the range of $R<3$ based on the assumption that it approaches the Stokes' law Eq. (6) for spheres. Many experiments have shown that the settling velocity of fine sediment particles ($R<1$) somehow deviates from the Stokes' law Eq. (6) of spheres.

Romanovskii (1972) also performed experiments to investigate the effect of sediment particle shape on settling velocity, and obtained a formula of the settling velocity in the turbulent settling region. In Romanovskii's formula, the particles size was defined as $d_{cp}=(a+b+c)/3$ and the shape factor was $\Theta=d_{cp}^2/(ab)$, in which a, b, and c=lengths of the longest, intermediate, and shortest axes of the particle. Dietrich (1982) proposed an empirical formula to determine the settling velocity of sediment from laminar to turbulent settling regions, considering the effects of sediment size, density, shape factor, and roundness factor. However, the Powers roundness factor used in Dietrich's formula is rarely measured in practice, and his formula is very complicated and relatively difficult to use. Jimenez and Madson (2003) derived a simple formula from the relation of Dietrich. Jimenez and Madsen's formula determines the settling velocity of sediment particles when the shape and roundness factors are known, but two coefficients in their formula are still graphically related to the shape

J. Hydraul. Eng., 2006, 132(8): 858-862

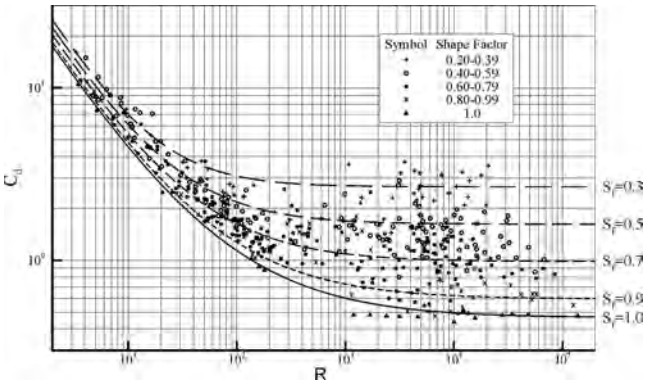

Fig. 2. Drag coefficient as function of Reynolds number and particle shape

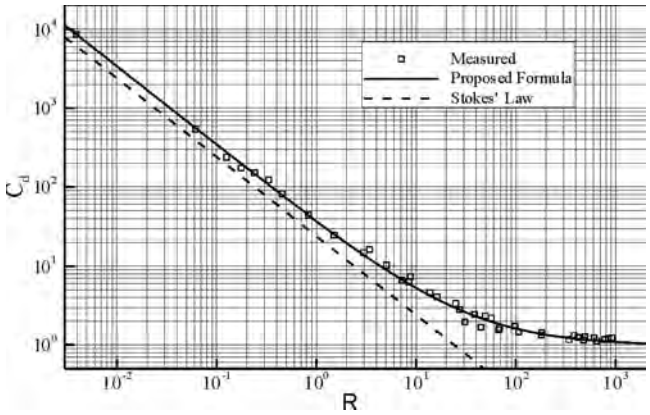

Fig. 3. Drag coefficient as function of Reynolds number for natural sediment (S_f=0.7)

factor. Swamee and Ojha's (1991) proposed formulas to represent Schulz et al.'s (1954) graphical relations of C_d–R for natural and crushed particles. Since the C_d–R curves of Schulz et al. have been replaced by the curves recommended by the Subcommittee on Sedimentation of the U.S. Interagency Committee on Water Resource (Interagency Committee 1957), Swamee and Ojha's (1991) formulas are less favorable. In addition, Gogus et al. (2001) experimentally studied the settling of angular particles and proposed a new factor to represent sediment particle shape. Because the range of the data used is very narrow, Gogus et al.'s finding still needs to be verified.

New Development

In this study, we have reevaluated the relation recommended by the U.S. Interagency Committee using a wider range of data and used Eq. (7) to replace the graphical relation. The data for the settling of natural sediment particles measured by Krumbein (1942), Corey (1949), Wilde (1952), Schulz et al. (1954), and Romanovskii (1972) are used. The sediment size is represented by the nominal diameter in the present analysis. For Romanovskii's data, the nominal diameter is approximated as $d=\sqrt[3]{abc}$, and only the data for coarse particles (R>1,000) are used due to lack of water temperature record. Based on these five groups of data, the coefficients M, N, and n in Eq. (7) are calibrated as

$$M = 53.5e^{-0.65S_f}; \quad N = 5.65e^{-2.5S_f}; \quad n = 0.7 + 0.9S_f \qquad (8)$$

where S_f=Corey shape factor defined as $c/\sqrt{ab}$.

Fig. 2 shows a comparison between the measured drag coefficients and those calculated using Eq. (7) with the coefficients given by Eq. (8). Because the data included in Fig. 2 are in the range of R>3, the trend of the C_d–R relation in the range of R<3 is determined by using the data of Russian scientists Zegzhda (1934), Arkhangel'skii (1935), and Sarkisyan (1958) compiled by Cheng (1997). The Corey shape factor of the sediment used in these three experiments is assumed to be 0.7, as suggested by Cheng (1997). For this value of shape factor, Eq. (8) corresponds to M=33.9, N=0.98, and n=1.33, which are in the ranges presented in Table 1. The relationship between C_d and R in the range of these data is shown in Fig. 3.

It should be noted that when S_f=1.0 the proposed Eq. (8) prescribes a C_d–R curve that deviates from the relation of spheres obtained by Rouse (1938). The reason is that the naturally worn sediment particles with a Corey shape factor of 1.0 may not be spheres and the particle angles and surface roughness also affect the settling process.

Inserting Eq. (7) into Eq. (5), one can derive the general relation of settling velocity as

$$\omega_s = \frac{M\nu}{Nd}\left[\sqrt{\frac{1}{4}+\left(\frac{4N}{3M^2}D_*^3\right)^{1/n}}-\frac{1}{2}\right]^n \qquad (9)$$

where $D_*=d[(\rho_s/\rho-1)g/\nu^2]^{1/3}$; and d=nominal diameter of sediment particles.

Eq. (9) is applied with the coefficients M, N, and n determined by Eq. (8). It is an explicit relation of the settling velocity for given sediment size and shape factor so that it can be easily used.

Comparison with Existing Methods

The predictions using Eq. (9) and the curves recommended by the U.S. Interagency Committee (1957) have been compared in Fig. 4. Here, the temperature is 24°C, the Corey shape factor is in the range of 0.3–0.9, and the sediment size is between 0.2 and 64 mm. It can be seen that these two methods give very close predictions. The average deviation between them is about 2.75%. However, a bigger deviation between these two methods is expected for fine sediment (less than 0.2 mm in diameter). The rea-

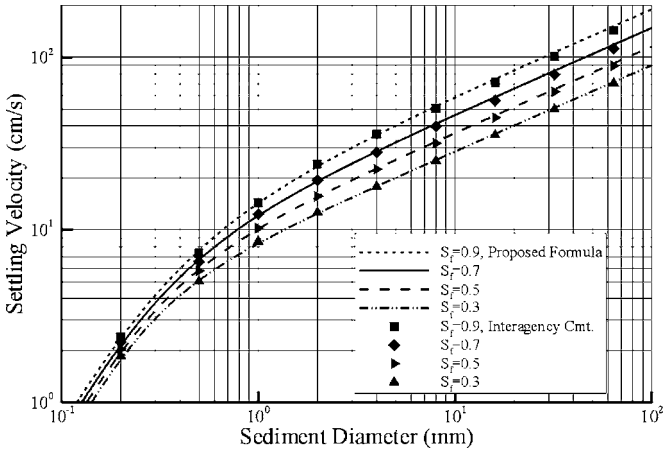

Fig. 4. Comparison of Eq. (9) and relation of Interagency Interagency Committee (1957)

J. Hydraul. Eng., 2006, 132(8): 858-862

Table 2. Comparison of Different Formulas against Data with Shape Factor

		Mean relative errors (%)			
Data range	Data number	Dietrich (1982)	Swamee and Ojha's (1991)	Jimenez and Madson (2003)	Wu and Wang (present)
Fine sediment ($D_* < 30$)	289	7.7	12.4	8.1	8.1
Coarse sediment ($D_* \geq 30$)	282	14.2	13.3	13.3	10.1
Total	571	10.9	12.8	10.7	9.1

son, which has been mentioned above, is that the Interagency Committee's curves approach the Stokes' law Eq. (6) that might have 30% error for the settling velocity of natural sediment particles as shown in Fig. 3. The present formula (9) has been validated by using the measurement data and should have better accuracy than the Interagency Committee's curves for fine sediment particles.

The newly proposed formula (9) has been also compared with those of Dietrich (1982), Swamee and Ojha's (1991), and Jimenez and Madson (2003), which all consider the effect of particle shape on the sediment settling. A total of 571 measurement data sets, including those in Fig. 2 and reported by Briggs et al. (1962), are used to test the four formulas. Briggs et al.'s data, which were for heavy mineral sands, were used to calibrate Dietrich's formula but not included in Fig. 2. Because the particle roundness information is not known in the data sets, a value of 3.5 is used for the Powers roundness index required in Dietrich's and Jimenez and Madsen's formulas. Table 2 shows the mean relative errors of the four compared formulas. The mean relative errors are 9.1, 10.7, 10.9, and 12.8% for the newly proposed formula, Jimenez and Madsen's formula, Dietrich's formula, and Swamee and Ojha's formula, respectively. Dietrich's formula gives slightly better prediction for fine sediment but worst prediction for coarse sediment. The newly proposed formula somehow performs better than the three existing formulas on average.

In the case where the sediment particle shape is not measured, the newly proposed formula (9) can be still used for naturally worn sediment particles by assuming the Corey shape factor as 0.7 (Interagency Committee 1957; Dietrich 1982; Cheng 1997) and setting the coefficients $M=33.9$, $N=0.98$, and $n=1.33$. This formula has been compared with nine existing formulas listed in Table 3 against the Russian data shown in Fig. 3, Hallermeier (1981) data, and Raudkivi (1990) data. Forty-three sets of Russian data and 13 sets of Raudkivi's data are taken from Cheng (1997). Because many of the data compiled by Hallermeier (1981) lack information on temperature or sediment density, only 44 sets of these data restricted for quartz sands (with a specific gravity of about 2.65) are selected. The sediment size in the Hallermeier's data is characterized by the sieve diameter, which is approximately converted to the nominal diameter by dividing by a factor of 0.9 (Raudkivi 1990). There are 100 data sets in total. All these data are for naturally worn sediment, assumed to have a Corey shape factor of 0.7 and a Powers roundness index of 3.5. Table 3 shows the mean relative errors of the ten compared formulas. It can be seen that the formula of Swamee and Ojha's (1991) has significant error, which occurs mainly for fine sediment particles ($d < 0.1$ mm). Rubey's (1933) formula and Van Rijn's (1989) formula also have large errors. The six formulas of Zhang (1961), Hallermeier (1981), Dietrich (1982), Cheng (1997), Ahrens (2000), and Jimenez and Madson (2003) perform well and have very close accuracies. The newly proposed formula predicts slightly better than these six formulas.

Conclusions

The formulas proposed by Komura (1963) and Han et al. (1981) for the initial porosity of sediment deposits have been tested using numerous data collected from different countries and regions. It is found that Komura's formula slightly underestimates the dry density for sand and gravel and overestimates for silt and coarse clay. Han et al.'s semiempirical formula, which was developed for uniform-size sediment mixture, exhibits more errors in comparison with the collected data. The coefficients in Komura's formula have been recalibrated by using the extended data set.

The relationship of the settling velocity with particle size and shape recommended by the Subcommittee on Sedimentation of the U.S. Interagency Committee on Water Resources (Interagency Committee 1957) has been reanalyzed. The original curves and tables are replaced by an explicit mathematical expression for the settling velocity that can be used more conveniently. The proposed formula has been tested by using not only the data used by the Interagency Committee, but also the data from other different sources. For the sediment particles coarser than 0.2 mm, the proposed formula has almost the same accuracy as the original curves recommended by the Interagency Committee. For the sediment finer than 0.2 mm, the proposed formula should have better accuracy than the original curves because it has been calibrated by using the measurement data rather than by the assumption that it approaches the Stokes' law of spheres. The proposed formula also exhibits better performance than nine existing formulas in the literature.

Acknowledgments

The present study is a part of the research project sponsored by the USDA-ARS Specific Research Agreement No. 58-6408-2-0062 (monitored by the USDA-ARS National Sedimentation Laboratory) and the University of Mississippi.

Table 3. Comparison of Different Formulas against Data without Shape Factor

Formula	Rubey (1933)	Zhang (1961)	Hallermeier (1981)	Dietrich (1982)	Van Rijn (1989)	Swamee and Ojha's (1991)	Cheng (1997)	Ahrens (2000)	Jimenez and Madson (2003)	Wu and Wang (present)
Mean relative error (%)	20.5	8.5	8.7	8.2	19.3	45.0	7.4	7.6	7.9	6.8

References

Ahrens, J. P. (2000). "The fall-velocity equation." *J. Waterw., Port, Coastal, Ocean Eng.*, 126(2), 99–102.

Ahrens, J. P. (2003). "Simple equations to calculate fall velocity and sediment scale parameter." *J. Waterw., Port, Coastal, Ocean Eng.*, 129(3), 146–150.

Arkhangel'skii, B. V. (1935). "Experimental study of accuracy of hydraulic coarseness scale of particles." *Izv. NIIG*, 15, Moscow, Russia (in Russian).

Briggs, L. I., McCulloch, D. S., and Moser, F. (1962). "The hydraulic shape of sand particles." *J. Sediment. Petrol.*, 32(4), 645–656.

Brown, P. P., and Lawler, D. F. (2003). "Sphere drag and settling velocity revisited." *J. Environ. Eng.*, 129(3), 222–231.

Cheng, N. S. (1997). "Simplified settling velocity formula for sediment particle." *J. Hydraul. Eng.*, 123(2), 149–152.

Chinese Association of Hydraulic Engineering (CAHE) Committee on Sedimentation. (1992). *Handbook of sedimentation engineering*, Environmental Science Press, Beijing, China (in Chinese).

Colby, B. R. (1963). "Discussion of 'Sediment transportation mechanics: Introduction and properties of sediment.'" *J. Hydraul. Div., Am. Soc. Civ. Eng.*, 89(1), 266–268.

Corey, A. T. (1949). "Influence of shape on the fall velocity of sand grains." Master's thesis, Colorado A&M College.

Dietrich, W. E. (1982). "Settling velocity of natural particles." *Water Resour. Res.*, 18(6), 1615–1626.

Gogus, M., Ipekci, O. N., and Kokpinar, M. A. (2001). "Effect of particle shape on fall velocity of angular particles." *J. Hydraul. Eng.*, 127(10), 860–869.

Goldstein, S. (1929). "The steady flow of viscous fluid past a fixed spherical obstacle at small Reynolds numbers." *Proc. R. Soc. London, Ser. A*, 123.

Graf, W. H. (1971). *Hydraulics of sediment transport*, McGraw-Hill, New York.

Hallermeier, R. J. (1981). "Terminal settling velocity of commonly occurring sand grains." *Sedimentology*, 28(6), 859–865.

Han, Q. W., Wang, Y. C., and Xiang, X. L. (1981). "Initial dry density of sediment deposit." *J. Sediment Res.*, 1 (in Chinese).

Hembree, C. H., Colby, B. R., Swenson, H. A., and Davis, J. R. (1952). "Sedimentation and chemical quality of water in the Powder River drainage basin, Wyoming and Montana." *Circular 170*, U.S. Geological Survey, Washington, D.C.

Interagency Committee. (1957). "Some fundamentals of particle size analysis: A study of methods used in measurement and analysis of sediment loads in streams." *Rep. No. 12*, Subcommittee on Sedimentation, Interagency Committee on Water Resources, St. Anthony Falls Hydraulic Laboratory, Minneapolis.

Jimenez, J. A., and Madsen, O. S. (2003). "A simple formula to estimate settling velocity of natural sediments." *J. Waterw., Port, Coastal, Ocean Eng.*, 129(2), 70–78.

Julien, P. Y. (1995). *Erosion and deposition*, Cambridge University Press, Cambridge, U.K.

Komura, S. (1963). "Discussion of 'Sediment transportation mechanics: Introduction and properties of sediment.'" *J. Hydraul. Div., Am. Soc. Civ. Eng.*, 89(1), 263–266.

Krumbein, W. C. (1942). "Settling velocities and flume behavior of nonspherical particles." *Trans., Am. Geophys. Union*, 41, 621–633.

Lane, E. W., and Koelzer, V. A. (1953). "Density of sediments deposited in reservoirs." *Rep. No. 9 of a Study of Methods Used in Measurement and Analysis of Sediment Loads in Streams*, Engineering District, St. Paul, Minn.

McNown, J. S., Malaika, J., and Pramanik, R. (1951). "Particle shape and settling velocity." *Trans., 4th Meeting of IAHR*, Bombay, India, 511–522.

Oseen, C. (1927). *Hydrodynamik*, Akademische Verlagsgesellschaft, Leipzig, Germany.

Raudkivi, A. J. (1990). *Loose boundary hydraulics*, 3rd Ed., Pergamon, Tarrytown, N.Y.

Romanovskii, B. B. (1972). *Experiments on settling velocity of sediment*, S. L. Zhang and Y. Y. Qian, translators, Yellow River Commission, Zhengzhou, China.

Rouse, H. (1938). *Fluid mechanics for hydraulic engineers*, Dover, New York.

Rubey, W. (1933). "Settling velocities of gravel, sand and silt particles." *Am. J. Sci.*, 225, 325–338.

Sarkisyan, A. A. (1958). "Deposition of sediment in a turbulent stream." *Izd. AN SSSR*, Moscow, Russia (in Russian).

Schulz, E. F., Wilde, R. H., and Albertson, M. L. (1954). "Influence of shape on the fall velocity of sedimentary particles." *Missouri River Division Sedimentation Series Rep. No. 5*, Corps of Engineers, U.S. Army, Omaha, Neb.

Sha, Y. Q. (1965). *Introduction to sediment dynamics*, Industry Press, Beijing, China (in Chinese).

Straub, L. G. (1935). "Missouri River report." *House Document 238*, Appendix XV, Corps of Engineers, U.S. Dept. of the Army to 73rd U.S. Congress, 2nd Session, 1156.

Swamee, P. K., and Ojha, C. S. P. (1991). "Drag coefficient and fall velocity of nonspherical particles." *J. Hydraul. Eng.*, 117(5), 660–667.

Trask, P. (1931). "Compaction of sediments." *Bull., Am. Assoc. Petroleum Geologists*, 15, 271–276.

Van Rijn, L. C. (1989). "Handbook: Sediment transport by current and waves." *Rep. No. H 461*, Delft Hydraulics, Delft, The Netherlands.

Wheatcroft, R. A. (2002). "In situ measurements of near-surface porosity in shallow-water marine sands." *Ocean Eng.*, 27(3), 561–570.

Wilde, R. H. (1952). "Effect of shape on the fall-velocity of gravel-sized particles." Master's thesis, Colorado A&M College, Colo.

Zanke, U. (1977). "Berechnung der sinkgeschwindigkeiten von sedimenten." Mitt. des Franzius-Instituts fuer Wasserbau, Heft 46, Seite 243, Technical Univ., Hannover, Germany.

Zegzhda, A. P. (1934). "Settlement of sand gravel particles instill water." *Izv. NIIG, 12*, Moscow, Russia (in Russian).

Zhang, R. J. (1961). *River dynamics*, Industry Press, Beijing, China (in Chinese).

J. Hydraul. Eng., 2006, 132(8): 858-862

Assessment of erosion, sedimentation, and water quality impacts of the Mountain Valley Pipeline and Equitrans Expansion Project's proposed crossing of the Jefferson National Forest as it pertains to the U.S. Forest Service's Draft Supplemental Environmental Impact Statement dated December 2022

Prepared by Jonathan A. Czuba, Ph.D., Licensed Professional Engineer - February 9, 2023

REFERENCES
3

February 21, 2023

HYDROLOGICAL PROCESSES
Hydrol. Process. **25**, 2112–2129 (2011)
Published online 1 February 2011 in Wiley Online Library
(wileyonlinelibrary.com) DOI: 10.1002/hyp.7965

Sediment targets for informing river catchment management: international experience and prospects

A. L. Collins,[1,2]* P. S. Naden,[3] D. A. Sear,[2] J. I. Jones,[4] I. D. L. Foster[5] and K. Morrow[1]

[1] *ADAS, Woodthorne, Wergs Road, Wolverhampton, West Midlands WV6 8TQ, UK*
[2] *Department of Geography, University of Southampton, Highfield, Southampton S017 1BJ, UK*
[3] *Centre for Ecology and Hydrology, Crowmarsh Gifford, Wallingford, Oxon OX10 8ED, UK*
[4] *School of Biological and Chemical Sciences, Queen Mary University of London, Mile End Road, London E1 4NS, UK*
[5] *School of Life Sciences, 115 New Cavendish Street, London W1W 6UW, UK*

Abstract:

Sediment plays a pivotal role in determining the physical, chemical and biological integrity of aquatic ecosystems. A range of factors influences the impacts of sediment pressures on aquatic biota, including concentration, duration of exposure, composition and particle size. In recognition of the need to assess environmental status for sediment and mitigate excessive sediment pressures on aquatic habitats, both water column and river substrate metrics have been proposed as river sediment targets. Water column metrics include light penetration, turbidity, sediment concentration summary statistics and sediment regimes. Substrate metrics include embeddedness, the fredle index and riffle stability. Identification of meaningful numeric targets along these lines has, however, been undermined by various issues including the uncertainty associated with toxicological dose-response profiles and the impracticalities of deploying statistically robust sampling strategies capable of supporting catchment-scale targets. Many of the thresholds reported are based on correlative relationships that fail to capture the specific mechanisms controlling sediment impacts on aquatic habitats and are stationary in nature. Temporal windows represented by the key life stages of specific species must be given greater emphasis. Given such issues and the need to support the revision of sediment targets for river catchment management, it is proposed that greater emphasis should be placed on developing generic modelling toolkits with the functionality for coupling current or future projected sediment regimes with biological response for a range of biota. Such tools should permit the identification of river catchment-specific targets within a national context, based on biological effect and incorporate sufficient flexibility for utilizing updated physical, chemical, biological and catchment attribute data. Confidence will continue to be required in compliance screening to ensure cost-effective management programmes for avoiding disproportionate investment in impacted river catchments. Copyright © 2011 John Wiley & Sons, Ltd.

KEY WORDS sediment targets; river catchment; ecology; water policy; mitigation; compliance

Received 16 April 2010; Accepted 17 November 2010

INTRODUCTION

Excessive sediment pressures on aquatic habitats constitute a significant ecosystem stressor. Enhanced sediment inputs impact adversely upon fluvial aquatic ecosystems by degrading habitat condition and directly impairing biota (Cordone and Kelly, 1961; Newcombe and MacDonald, 1991; Ryan, 1991; Bardonnet and Heland, 1994; Wood and Armitage, 1997; Bilotta and Brazier, 2008). Such impacts include the burial and suffocation of fish eggs and larvae in conjunction with spawning gravel siltation, gill clogging, impaired growth and histological changes, as well as reduced predatory or feeding efficiency and suppressed resistance to disease (Kemp, 1949; Cordone and Kelly, 1961; Bisson and Bilby, 1982; Whitman *et al*., 1982; Redding and Schreck, 1983; Berg and Northcote, 1985; Redding *et al*., 1987; Kondolf and Wolman, 1993; Bardonnet and Bagliniere, 2000; Harrod and Theurer, 2002; Milner *et al*., 2003; Sear *et al*., 2008). River channel sedimentation can also have a deleterious impact on macroinvertebrate populations (Ward *et al*., 1998; Sharley *et al*., 2008) and macrophyte communities (Clarke and Wharton, 2001). Fine sediment mobilization, transfers and delivery play a critical role in the dispersal and fate of nutrients (House, 2003; Collins *et al*., 2005; Jarvie *et al*., 2006; Ballantine *et al*., 2009) and contaminants (Rees *et al*., 1999; Kronvang *et al*., 2003). Elevated sediment inputs into watercourses from upstream erosion and sediment mobilization can also result in a range of undesirable so-called 'off-site' impacts, including reduced navigability, the infilling of dams and reservoirs and increased water treatment costs. Both climate and land use change represent important extrinsic drivers for sediment mobilization and delivery (Houben *et al*., 2006) and the expansion of agricultural land and intensification of farming practices have the potential to increase sediment pressures on watercourses (Dearing *et al*., 1987; Farnsworth and Milliman, 2003; Kasai *et al*., 2005).

Although enhanced sediment inputs to watercourses are considered to represent an important cause of water quality, habitat and biotic impairment, the impacts are

* Correspondence to: A. L. Collins, ADAS, Woodthorne, Wergs Road, Wolverhampton, West Midlands WV6 8TQ, UK.
E-mail: adrian.collins@adas.co.uk

complex and multidimensional, with such complexity being compounded by the natural requirement of aquatic biota for sediment. Given the key role of sediment in determining the river water quality, a range of policy drivers exist across the world for the control of sediment delivery to watercourses. Such drivers comprise international, national and sub-national commitments. In the European Union (EU), for instance, the adoption of the Water Framework Directive (WFD) (European Parliament, 2000), as the over-arching international water policy for Member States, is driving an increased focus on the biological effects of pollutant loadings, expressed in terms of ecological status, with a view to replacing guidelines in existing legislation for sediment due to be repealed in 2013. International obligations to achieve the targets set for designated Protected Areas (PAs) recognized by alternative European legislation are, in turn, overlain on the fundamental requirements of the WFD. Examples of such international legislation include the Habitats and Species Directives underpinning Special Areas of Conservation (SACs) and the Urban and Wastewater Treatment Directive underscoring Sensitive Areas (e.g. for eutrophication). National and sub-national obligations take various forms. In England and Wales, for example, a Public Service Agreement exists for protecting or improving the status of Sites of Special Scientific Interests (SSSIs), whereas in the USA, section 303(d) of the Clean Water Act (1972) requires States to identify and list impaired waters every 2 years and to establish total maximum daily loads (TMDLs) on a catchment-specific basis using a range of approaches including sediment rating curves or regression modelling (Hawkins, 2003).

A number of terms are used, sometimes interchangeably, in conjunction with sediment targets and it is useful to clarify these. Criteria represent scientific data that are evaluated and interpreted to derive guidelines, whereas the latter are narrative or numeric recommendations for protecting the aquatic environment. Objectives are narrative or numeric site-specific recommendations and standards are imperative guidelines or objectives that are recognized in enforceable laws (CCME, 1995). Existing recommended targets suffer from a number of inherent problems associated with the uncertainty in measuring or monitoring sediment pressures reliably, as well as uncertainty in experimental data describing impacts on biota, the diversity of environments to which guidelines are supposed to apply and a common over-simplification in the recommendation of 'global' targets. Ideally, sediment targets are required to protect all forms of aquatic biota and all aspects of their life cycles, but data availability and complexity mean that recommendations are most likely to be developed on the basis of biological response for key taxa (MacDonald *et al*., 2004). As the ecological status of freshwaters will be influenced by multiple stressors (Karr, 1991; Bedoya *et al*., 2009; Collins *et al*., 2009a), sediment targets should ultimately be seen as scientific benchmarks within broader river catchment managerial frameworks taking explicit account of additional pollutants and their concomitant ecological impacts.

Against the above background, the objectives of this paper are

- to review, briefly, the key factors (concentration, duration of exposure, quality and composition and grain size) controlling the impacts of sediment on aquatic biota, given the emphasis of current policy drivers on protecting or enhancing the ecological status of rivers,
- to review international approaches and experiences in setting sediment targets for rivers and
- to discuss future prospects for revising sediment targets for informing river catchment management.

Factors controlling the biological impacts of sediment in fluvial environments

As it is desirable to determine the sediment targets for informing river catchment management based on the biological effects, it is important to understand the nature of such impacts and their key controls. The biological impacts of sediment in rivers are dependent on a range of factors, including concentration, duration of exposure, sediment quality and particle size. Impacts may result directly from sediment in suspension or through the deposition of fine sediment either on, or within, the river bed, with the two being clearly related through the sediment transport process (Sear *et al*., 2008).

Sediment concentration. Existing international guidelines on water quality relating to critical sediment concentration thresholds (see examples in Table I) are founded on the assumption that there is a direct positive relationship between the concentration and ecological impact (Newcombe and MacDonald, 1991). The concept of a simple concentration–ecological response model is, however, undoubtedly an over-simplification. Aquatic biota can be adversely affected by extremely low concentrations and a recent synthesis of sediment dose–response relationships for reduced feeding, impaired growth and mortality pays testament to this complexity, suggesting very broad ranges of 4–330 000 mg l^{-1} for various fish species and 27–80 000 mg l^{-1} for mollusca (Berry *et al*., 2003). Examples of the results of sediment dose–response experiments for fish are presented in Table II. For macroinvertebrates, Gaugler and Molloy (1980) reported the reduced ingestion rate by blackfly larvae with increasing sediment concentrations, Kurtak (1978) suggested that feeding is curtailed in sediment concentrations >50 mg l^{-1} and Voelz and Ward (1992) noted behavioural changes in feeding by Trichoptera with a switch from filtering to grazing. Table III summarizes the findings of existing studies examining dose–response relationships for macroinvertebrates. Much existing work suggests that a number of additional factors interplay with, and complicate, the relationship between sediment concentration and resulting impacts on biota, including duration of exposure, sediment source and quality, particle size, species life history stage and the presence or absence of sediment sensitive species (Swietlik *et al*., 2003). As a result, toxicological data are

Table I. Examples of proposed sediment concentration thresholds (mg l^{-1}) for fish

Effects			Reference
Least effects: high protection, best conditions	Probable effects: moderate protection, moderate conditions	Definite effects: low protection, poor conditions	
<25	25–80	>80	EIFAC (1964)
<25	26–80	>80	Alabaster and Lloyd (1980)
<30	30–85	>83	Wilber (1983)
0	1–100	>100	DFO (1983)

Table II. Examples of the results of sediment dose–response experiments for fish

Organism	Sediment concentration (mg l^{-1})	Duration (h)	Impact	Reference
Atlantic salmon	20	—	Increased foraging	Robertson *et al*. (2007)
Atlantic salmon	60–180	—	Avoidance behaviour and reduced foraging	Robertson *et al*. (2007)
Arctic grayling	25	24	6% mortality for sac fry	Reynolds *et al*. (1988)
Arctic grayling	65	24	15% mortality for sac fry	Reynolds *et al*. (1988)
Arctic grayling	185	72	41% mortality of sac fry	Reynolds *et al*. (1988)
cyprinids	100 000	168	Some survival	Wallen (1951)
Rainbow trout	47	1152	10% mortaility of incubating eggs	Slaney *et al*. (1977)
Rainbow trout	Pulses	456	Reduced growth	Shaw and Richardson (2001)
Coho salmon	2000–3000	192	Reduced feeding efficiency and immunity	Redding *et al*. (1987)
Coho salmon	40 000	96	Physical damage to gills	Lake and Hinch (1989)
Chinook salmon	488	96	50% mortality of smolts	Stober *et al*. (1981)
Chinook salmon	207 000	1	100% mortality of juveniles	Newcomb and Flagg (1983)

Table III. Examples of the results of sediment dose–response experiments for macroinvertebrates

Organism	Suspended sediment concentration (mg l^{-1})	Impact	Reference
Ephemeroptera	2680	Increased drift	Ciborowski *et al*. (1977)
Diptera	>50	Feeding inhibition	Kurtak (1978); Gaugler and Molloy (1980)
Plecoptera	1·5	Feeding inhibition	Hornig and Brusven (1986)
Trichoptera	1·5	Feeding inhibition	Hornig and Brusven (1986)
Bivalvia	600	Feeding inhibition	Aldridge *et al*. (1987)
Bivalvia	600	Reduced metabolism	Aldridge *et al*. (1987)
Cladocera Copepoda	25 000	Feeding inhibition	Alabaster and Lloyd (1982)
Ephemeroptera	250–2000	Increased drift No effect on survival	Molinos and Donohue (2009)
Amphipoda Trichoptera	>2000	No effect No effect on survival	Molinos and Donohue (2009)
Diptera	300	Reduced density	Gray and Ward (1982)
Cladocera	82–392	Reduced survival	Robertson (1957)
Various benthic invertebrates	743	Reduced population (85%)	Wagener and LaPerriere (1985)
Various macroinvertebrates	133	Increased drift	Doeg and Milledge (1991)
Various invertebrates	25 000	Reduced density or elimination	Nutall and Bielby (1973)
Various benthic invertebrates	8	Increased drift	Rosenberg and Wiens (1978)
Various invertebrates	8–177	Reduced density	Quinn *et al*. (1992)
Various invertebrates	40 (above background)	25% increase in drift	Gammon (1970)
Various invertebrates	80 (above background)	90% increase in drift	Gammon (1970)

ideally required on a site-specific basis and should not be extrapolated to regional or larger scales. Furthermore, on account of the complex interplay of these different factors, it is highly unlikely that a comprehensive list of genus-based critical sediment concentration targets can be developed in the short-term (USEPA, 2003). Devising genus- or species-based targets would require substantial resource investment to support the identification of statistically robust thresholds. There remains a dearth of dose–response profiles describing the combined effects of interacting variables and the identification of robust relationships is further complicated by the

synergistic, additive or antagonistic interplay of multiple stressors present in the aquatic environment (Collins *et al*., 2009a). Such factors increase the dimensionality of the replicates required to disentangle sediment stressor-impact relationships. Dose–response experiments ideally require standardized methodologies accepted by a combination of regulatory, scientific and river catchment stakeholder communities. Experimental design and protocol frequently differ, hampering the comparison of studies (Cordone and Kelley, 1961) and the range of conditions to which findings can be extrapolated. Current legislation is aimed at both genus-specific (e.g. EU Habitats Directive, UK Biodiversity Action Plan) and community-level responses (e.g. EU WFD) with the latter focusing more on ecosystem goods and services as opposed to the preservation of individual species.

Duration of exposure. The duration of exposure of high sediment concentrations to aquatic biota is a fundamental factor with respect to detrimental impacts (Newcombe and MacDonald, 1991). Shorter duration exposures are likely to pose transitory effects, whereas prolonged doses can result in more severe and lasting impacts. Early attempts at documenting dose–response relationships for sediment and aquatic ecology were hampered by a number of shortcomings. Experiments tended to focus on pooled rather than taxon-based approaches and failed to investigate linkages with key life stages (Newcombe, 1986). Such work underscored the need to examine taxonomic groups, natural history, life stage and particle size (Newcombe, 1994). On the basis of these early lessons, Newcombe and Jensen (1996) used meta-analysis of 80 published reports to provide six empirical equations relating biological response to sediment dose and duration, with the 'severity of ill-effect' (SEV) being delineated semi-quantitatively along a scale describing four main responses. These comprised no behavioural effects (lowest on the scale), behavioural effects, sub-lethal and lethal effects (highest on the scale). The results clearly indicated that susceptible individuals exhibit more sensitivity to sediment dose and duration. In addition, the findings underscored the need for the identification of genus-based age-specific and sediment size-specific dose–response profiles, improved distinction of the sub-lethal and lethal thresholds and further investigation of grain size impacts (Servizi and Martens, 1991, 1992; Newcombe and Jensen, 1996). There remains a need for more information on the spatio-temporal variation in dose–response profiles (Dunlop and McGregor, 2007) and the application of this toxicological approach to setting critical sediment concentration thresholds will require a site-specific focus and meaningful dose–response relationships for a representative range (minimum of 20) of taxa (USEPA, 2003). Extrapolation of laboratory toxicological experiment data to field conditions does, nevertheless, remain highly problematic (Patten, 1984).

Sediment quality and composition. It is important to take account of sediment quality in developing targets. Although some studies have investigated the general impacts of contaminated sediments (Robertson, 1957; Lewis, 1973; Nuttall and Bielby, 1973; Wagener and LaPerriere, 1985), others have specifically correlated sediment contaminant content with measured biological impacts to develop toxicity thresholds (McCauley *et al*., 2000; den Besten *et al*., 2003). An abundance of useful data exists on account of the concurrent assessment of contamination and ecological risk at impaired sites. Such information has provided the basis for a variety of correlative approaches for sediment contamination and biological response, including the species screening level concentration (Neff *et al*., 1987), threshold and probable effects levels (MacDonald *et al*., 1996), apparent effects thresholds () (PTI Environmental Services, 1991) and the consensus approach based on various lines of evidence (Swartz, 1999). These approaches benefit from being founded on field evidence collected at a broad spectrum of sites, inclusion of a range of organisms and measurements of multiple effects (e.g. growth, reproduction, mortality). Furthermore, such approaches are readily applied in the regulatory context, as they provide reasonably robust predictive tools. It is, however, important to note that these tools are correlative and should not be used to identify priority substances other than contaminated sediment itself (McCauley *et al*., 2000). Sediment quality guidelines derived from these data are typically based on dry-weight concentrations in the particulate phase and so do not take explicit account of bioavailability and are susceptible to the toxicological sensitivity of individual organisms (Luoma and Carter, 1993). Sediment quality guidelines exist for a range of substances (MacDonald *et al*., 2000; McCauley *et al*., 2000; CCME, 2001; Burton, 2002; Simpson *et al*., 2005; Scrimshaw *et al*., 2007). The important role of sediment delivery in nutrient transfers through river catchments can impact on macrophyte growth by increasing the fertility of the rooting medium provided by material deposited on the channel substrate (Martinova, 1993; Trimmer *et al*., 2009).

It is also important to consider the organic component of sediment pressures on the aquatic environment. Optimal benthic habitat requires a sufficient dissolved oxygen gradient to ensure exchange across critical membranes under a range of environmental conditions (Turnpenny and Williams, 1980; Chevalier and Carson, 1984; Carling, 1985). Introduction of oxygen consumptive organic material into the benthic zone lowers available oxygen concentrations (Whitman and Clark, 1982; Chevalier and Carson, 1984; Sterba *et al*., 1992; Greig *et al*., 2005a,b, 2007; Macpherson *et al*., 2007). Organic material can be introduced into rivers from a variety of sources including livestock slurries or manures, silage liquor, steading washings, sewage effluent and decaying authochthonous or allochthonous vegetation (e.g. macrophytes or riparian trees). Recent work by Sullivan *et al*. (2010) has further elucidated the oxygen demand of organic material in rivers, suggesting the existence of two key pools: labile and refractory. In their study, the labile component was predominantly associated with the more rapid decay of

particulate organic matter, whereas the refractory component was associated with the dissolved organic fraction.

Particle size. Although the importance of particle size has been noted above in relation to dose–response profiles, its impact is perhaps more obvious through its effect on riverine habitat or substrate. Elevated quantities of fine sediment in the spawning substrate can have a detrimental impact on egg-to-emergence success (Beschta and Jackson, 1979; Lisle, 1989; Peterson and Quinn, 1996; O'Connor and Andrew, 1998; Soulsby *et al*., 2001). More specifically, enhanced fine sediment pressures on spawning gravels degrade two critical properties of the incubation environment, namely permeability and porosity. Permeability governs rates of oxygen supply to, and metabolic waste removal from, incubating progeny (Turnpenny and Williams, 1980; Brunke and Gonser, 1997; Fleming, 1998; Armstrong *et al*., 2003; Heywood and Walling, 2007). Fine sediment intrusion blocks interstitial pore spaces, thereby reducing interstitial flow velocities (Bjorn and Reiser, 1991; Acornley and Sear, 1999; Sear *et al*., 2008). Porosity controls the intra-gravel movement and eventual emergence of newly hatched fry (Phillips *et al*., 1975; Crisp, 1993). A large volume of work has examined the relationship between the granular characteristics of ingressed sediment and survival-to-emergence success (Tappel and Bjorn, 1983; Chapman, 1988; Reiser, 1998), highlighting the significance of the <2-mm size fraction (Carling and McCahon, 1987; Soulsby and Malcolm, 2001). However, such work has provided empirical relationships between sediment size and embryo survival that fail to elucidate the specific mechanisms influencing dissolved oxygen availability as a key habitat parameter. Accordingly, some work has reported that granular-based measures of survival are poor descriptors of incubation success (Greig *et al*., 2005a, 2007). Recent experimental work has demonstrated that the intrusion of clay particles post redd construction restricts oxygen consumption by incubating embryos by creating a film around the egg membrane and an associated zone of low dissolved oxygen supply and by blocking micropores in the egg chorion (Greig *et al*., 2005b). Grain size effects are also important in controlling sediment geochemistry (Horowitz, 1991; Stone and Droppo, 1996) and the transfer and fate of contaminants (Warren *et al*., 2003; Jeong *et al*., 2008; Naji *et al*., 2010; Sun *et al*., 2010) in fluvial systems which are potentially harmful to aquatic ecology. In addition to grain size, particle shape and angularity can be important in influencing biological impacts including gill damage (Stephan, 1953; Lake and Hinch, 1999).

Approaches to setting sediment targets for informing river catchment management

Approaches to setting sediment targets for the management of river catchments can be categorized into those based on water column or river substrate metrics (Figure 1).

Water column metrics. *Light penetration:* Inorganic and organic materials suspended in the water column reduce light penetration, thereby decreasing the depth of the photic zone and associated levels of primary production (Stross and Sokol, 1989; Kiffney and Bull, 2000; Rosemond *et al*., 2000; Devlin *et al*., 2008). Reduced light penetration can also impact negatively on organism abundance (Bricelj and Lonsdale, 1997; Gallegos and Bergstrom, 2005; Dobberfuhl, 2007) and reaction distances (Vogel and Beauchamp, 1999). Decreased light penetration can increase solar adsorption near the stream surface, resulting in stratification in the water column and reduced dispersion of dissolved oxygen and nutrients towards the benthic zone. Given the above, some countries have used Secchi disk readings as a basis for setting targets related to water clarity and light penetration (Effler, 1989; Bhargava and Mariam, 1991). For example, British Columbia has a clarity standard of >1·5 m based on the average of at least five readings over 30 days (Rowe *et al*., 2003). In the USA, the National Recommended Water Quality Criteria stipulate that suspended sediment levels should not reduce the depth of the compensation point for photosynthetic activity by more than 10% from the established seasonal norm for aquatic life (USEPA, 2007).

Turbidity: Turbidity is a measure of the optical scattering properties of water which are influenced by the

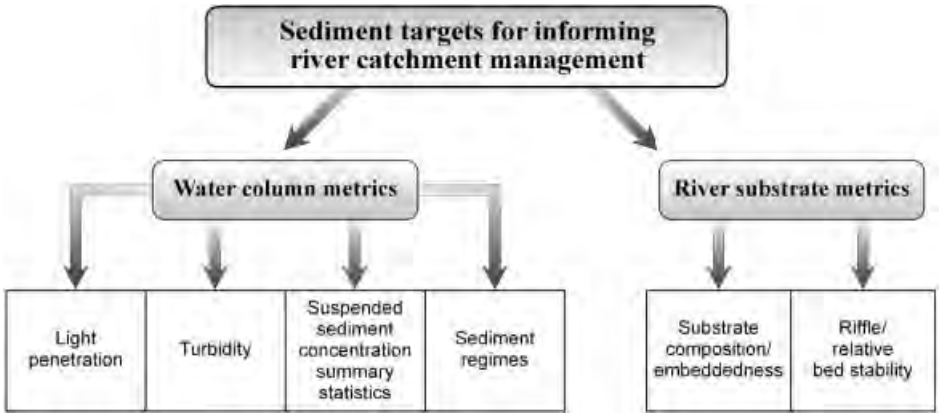

Figure 1. Approaches to setting sediment targets for informing river catchment management

Table IV. Examples of turbidity thresholds for impacts on aquatic biota

Organism	Effect	Turbidity range (NTU)	Reference
Juvenile coho	Increased coughing	3–30	Sevizi and Martens (1992)
Juvenile coho and steelhead	Emigration/avoidance	22–265	Sigler (1980)
Steelhead and coho	Emigration/avoidance	11–51	Sigler *et al.* (1984)
Juvenile coho	Reduced feeding rate	10–60	Berg and Northcote (1985)
Brown trout	Reduced feeing rate	7·5	Bachman (1958)
Cutthroat trout	Reduced feeding rate	3·5–25	Vinyard and Yuan (1996)
Juvenile coho and steelhead	Reduced growth	22–113	Sigler (1980)
Juvenile coho and steelhead	Reduced growth	As low as 25	Sigler *et al.* (1984)
Rainbow, lake and cutthroat trout	Reduced reaction distance	3·2–7·4	Vogel and Beauchamp (1999)
Brook trout	Reduced reaction distance	0–43	Sweka and Hartman (2001)
Various invertebrates	Reduced density	3·7	Quinn *et al.* (1992)
Various invertebrates	50% reduction in taxonomic richness	25	Quinn *et al.* (1992)
Trichoptera	Reduced survival	23	Strand and Merritt (1997)
Various invertebrates	Reduced densities	<4 (depended on primary production/allochthonous inputs)	Rosetta (2005)
Ephemeroptera, Trichoptera, Odonata, Decapoda	No effect	20 000	Suren *et al.* (2005)
Mayfly	No increased mortality	1000	Suren *et al.* (2005)
Various macroinvertebrates	Reduced richness	4·7	Evans-White *et al.* (2009)
Mayflies, Amphiphods, Midges	No effects	163–955	Anderson *et al.* (2006)
Damselfly	Reduced feeding efficiency	500–1500	Kefford *et al.* (2010)
Odonata	Reduced feeding efficiency	1000–1500	Kefford *et al.* (2010)
Odonata, Hemiptera	No effects on feeding	1000–1500	Kefford *et al.* (2010)
Thiaridae, Muscidae, Veliidae, and Aeshnidae	Reduced diversity	70–80	Dlamini *et al.* (2010)

content of sediment (>0·45 μm), dissolved humic and mineral substances (<0·45 μm), algal cells (>0·1 μm) and detrital organic matter. Monitoring for turbidity can be undertaken using a range of devices *in situ*, including attenuance or nephelometric turbidimeters, optical back scattering and acoustic back scattering instruments and fibre-optic in-stream transmissometers (Wren *et al*., 2000; Campbell *et al*., 2005). Existing literature has reported a number of detrimental impacts on aquatic biota resulting from increased turbidity including, amongst others, the decreased growth and predatory efficiency of fish (Sigler *et al*., 1984; Sweka and Hartman, 2001), as well as decreased secondary production and abundance of food organisms (Lloyd *et al*., 1987; Ward *et al*., 1998). Examples of turbidity thresholds for detrimental impacts on freshwater biota are illustrated in Table IV. The setting of absolute numerical standards (see examples in Table V) for turbidity has been hampered by the uncertainty evident in the findings of experimental and observational work aimed at linking turbidity thresholds to biological impacts such as avoidance, coughing, reduced feeding or growth and impaired reaction. Although in response to these uncertainties some turbidity-based water quality thresholds reflect a percentage above background, it is difficult to scale the percentage increase on the basis of existing understanding (McCarthy *et al*., 1974). In addition, protocols for assembling turbidity data records have not been standardized, whilst the relationship between turbidity and suspended sediment concentration is potentially confounded by variations in particle composition, grain size and water colour (Gippel, 1995). Ratings for converting turbidity into suspended sediment concentration need to be site-specific and reflect potential seasonal or even storm variations in the characteristics of the suspended sediment load. Despite these issues, some recent work by Dunlop and McGregor (2007) identified river water quality targets founded on modelled reference ranges for turbidity related to natural patterns, but with the effects of flow and catchment area factored out because both were found to influence turbidity data. These ranges, however, were not explicitly linked to ecological impacts.

Suspended sediment concentration summary statistics: A range of summary statistics has been used to define sediment targets using concentration as the primary metric. Care is required in interpreting the precise wording of such criteria (Smith *et al*., 2003). The EU Freshwater Fish Directive (78/659/EC), for example, cites a guideline annual mean suspended sediment concentration of 25 mg l^{-1} for salmonids (Reynolds *et al*., 2004; APEM, 2007; Collins and Anthony, 2008). The use of a single 'global' mean value is, however, highly questionable given the spatial and temporal variations in dose–response profiles, reflecting local sediment sources and composition and the contrasting ecological sensitivity of the receiving waters (Collins and Anthony, 2008).

Table V. Examples of turbidity-based water quality standards

Country	Standard	Reference
Australia (south east upand; <150–<1500 m altitude)	2–25 NTU	ANZECC (2000)
Australia (south east lowland; <150 m altitude)	6–50 NTU	ANZECC (2000)
Australia (south west upland)	10–20 NTU	ANZECC (2000)
Australia (south west lowland)	10–20 NTU	ANZECC (2000)
Australia (tropical upland)	2–15 NTU	ANZECC (2000)
Australia (tropical lowland)	2–15 NTU	ANZECC (2000)
Australia (south central upland)	1–50	ANZECC (2000)
Australia (south central lowland)	1–50	ANZECC (2000)
Canada (British Columbia)	Not to exceed 5 NTU over background if background is less than 50 NTU	Rowe *et al*. (2003)
Canada	Clear flow: maximum increase of 8 NTU over background for short-term (<24 h) exposure High flow: turbidity should not increase by >10% over background when background >8 NTU	CCME (2001)
New Zealand (upland)	4·1 NTU	ANZECC (2000)
New Zeland (lowland)	5·6 NTU	ANZECC (2000)
USA (Alaska)	Water supply: 5 NTU above natural conditions when background turbidity is 50 NTU or less, no more than 10% increase when the natural turbidity is >50 NTU	Rosetta (2005)
USA (California)	Central Valley Region: where natural turbidity is 0–5 NTU, increases shall not exceed 1 NTU. Where natural turbidity is 5–50 NTU, increases shall not exceed 20%	Rosetta (2005)
USA (Idaho)	Chronic turbidity not to exceed 10 NTU in summer baseflow	Rowe *et al*. (2003)
USA (Montana)	Class A1: no increase above naturally occurring turbidity except under short-term authorization	Rowe *et al*. (2003)
USA (Oregon)	<10% increase relative to an upstream control point	Rowe *et al*. (2003)
USA (Nevada)	10 NTU—cold water reaches; 50 NTU—warm water reaches	FWPCA (1968)
USA (Utah)	Classes 2A, 2B, 3A, 3D not to exceed 10 NTU (instantaneous) above background	Rowe *et al*. (2003)
USA (Wyoming)	Class 1 and 2 watersheds (outstanding waters and non-class 1 but supporting game fish) not to exceed 10 NTU (instantaneous) above background	Rowe *et al*. (2003)

Time-averaged, as opposed to flow-weighted, thresholds are more likely to provide a reliable index of the biological impacts of sediment as these depend, in part, on both concentration and duration of exposure. However, an annual mean or mean annual sediment concentration fails to capture the highly episodic nature of sediment transport whereby >90% of the sediment load can be transported in <10% of time (Walling and Webb, 1987). Suspended sediment concentrations are highly skewed and can range over three orders of magnitude during a single storm event, resulting in large standard deviations (Cooper *et al*., 2002; Naden *et al*., 2002). Substantial numbers of samples are therefore necessary to estimate the mean concentration with any degree of confidence. Example calculations based on 15-min data suggest that a minimum of daily sampling is required but that a stratified sampling approach to enable coverage of high flows reduces the number of samples required and, thus, for practical purposes, helps to reduce the uncertainty in estimating mean concentrations resulting from poor coverage of high flows.

Given the problems in trying to characterize sediment targets on the basis of a temporal mean, alternatives include the use of median or quantile descriptors (Cooper *et al*., 2002). Statistical approaches clearly need to be incorporated in any monitoring design for numerical sediment targets, as these permit unbiased estimates of population statistics. Useful experience can be gained from statistical approaches to assessing consent compliance in the UK and across Europe under, for example, the EC Bathing Water (76/160/EEC) and Urban Waste Water Treatment (92/271/EEC) Directives. Here, it is a common requirement that the 0·90 quantile for the concentration of a given determinand be less than some specified value and the statistical basis for monitoring and assessment is well-established (Ellis, 1989). Any statistical monitoring programme for similar numerical sediment targets needs to ensure random or stratified random sampling with sufficient sampling intensity in both space and time to provide population estimates within acceptable precision. Percentile estimation can be based on the use of parametric or non-parametric distribution fitting techniques (Crabtree *et al*., 1987). To date, however, sediment targets have not been expressed in terms of sediment duration curves and their quantiles.

Where relatively short-lived, high concentrations of sediment, such as those occurring during storm events, are the primary metric of interest, a peaks-over-threshold (POT) approach (Naden, 1992) can be used to estimate

the risk of occurrence in terms of an exceedance probability over specified durations. Analysis of this sort, however, requires either a continuous data record or a continuous series of modelled values covering at least 5–10 years in order to provide sufficient peaks for analysis. Thus, for example, Watts *et al*. (2003) produced maps of the risk of sediment harm to fish based on 1- and 4-day sediment concentrations exceeding the 80 mg l^{-1} limit for healthy freshwater fisheries in Europe proposed by Alabaster and Lloyd (1980) (Table I). Alternatively, Tramblay *et al*. (2007) fitted probability distributions to 149 series of annual sediment concentration maxima across Canada and the USA to estimate concentrations for different return periods. Risk exceedance mapping using POT or annual maximum approaches outside the USA is, however, hampered by the lack of continuous long-term data and of critical limits for individual fish species found outside the USA (Watts *et al*., 2003). It is also unknown whether ecological status is driven by the sediment concentration in these extreme events or by more frequent levels of concentration.

Whatever sediment concentration metric is chosen, there is a fundamental need to define associated protocols for spatio-temporal sampling frequencies, sample collection and processing in order to provide reliable and unbiased estimates. Given the magnitude of the temporal variation in sediment concentration, it remains unavoidable that investment in high-resolution monitoring programmes using commercially available equipment is necessary for assembling meaningful data sets (Gippel, 1989; Robertson and Richards, 2000; Naden *et al*., 2002). Measurement errors associated with the determination of sediment concentration can be significant and reflect a range of factors including the lack of mixing of sand-sized fractions throughout river channels (Horowitz, 1995; Edwards and Glysson, 2000; Gray and Glysson, 2002).

Table VI. Recently proposed target and critical suspended sediment yields for different catchment types across England and Wales (Cooper *et al*., 2008)

Catchment type	Target suspended sediment yield (t km^{-2} $year^{-1}$) (lower quartile)	Critical suspended sediment yield (t km^{-2} $year^{-1}$) (upper quartile)
High impermeable peat	50	>150
Low impermeable peat	No data	No data
Low impermeable (non-peat, non-Chalk)	40	>70
Low impermeable (non-peat, non-Chalk)	20	>50
High impermeable (non-peat, non-Chalk)	10	>20
High permeable (non-peat, non-Chalk)	No data	No data
Low Chalk	2	>5

Sediment regimes: Conventional river sediment thresholds based on simple numerical targets fail to represent the highly dynamic nature of water quality parameters such as sediment concentration (Poole *et al*., 2004). In contrast, regime standards aim to reflect the spatial and temporal dimensions of river water quality. The potential use of sediment regime standards is founded on the principle that natural regimes should be integrated into strategies for managing fluvial aquatic habitats (Poff *et al*., 1997; Fausch *et al*., 2002) in much the same way as hydrological regimes are used to plan reservoir operations. The development of regime standards explicitly recognizes that the variability of simple numerical statistics confounds the identification of thresholds to distinguish unimpaired and impaired aquatic ecosystems. Other major problems with threshold targets are an implicit assumption of stationarity (Milly *et al*., 2008) and high inter-annual variability. Managing the aquatic environment on the basis of single thresholds encourages potential homogenization of diverse fluvial habitats (Bisson *et al*., 1997). The adoption of regime standards helps to avoid the problem of thresholds typically describing the stress–response of individual organisms as opposed to those communities present. Regime standards encourage the efficient targeting and use of management resources by conceding that poor habitat can exist either spatially or temporally within a river catchment system. Application of regime standards helps to engage stakeholders by taking account of local natural conditions.

A good example of the sediment regime approach to target setting is provided by the recently proposed preliminary annual sediment yield targets (Table VI) for England and Wales (Cooper *et al*., 2008). These targets were empirically derived from over 100 available UK sediment yield estimates based on good quality measurements and a large number of potential catchment characteristics. A simple river catchment typology comprising five classes was identified. In each class, the distribution of sediment yields reflects both temporal and inherent variability and anthropogenic impact. Accordingly, the value of the lower quartile was chosen as a potential target value; the value of the upper quartile was taken to indicate cause for concern and the need to investigate further. Target values (Table VI) were also evaluated against historical sediment yields and other independent data. With the exception of the peat catchments that are all highly impacted, the target values are less than 25–35% higher than historical data. These preliminary targets go further than the 'global' targets discussed earlier, but are limited by the spatial and temporal coverages of available data, use of an annual time dimension and the lack of an explicit link to the ecology.

Fundamentally, there are a number of key constraints to setting meaningful critical river catchment sediment

yield targets. Catchment-specific conditions can be a confounding influence with the same sediment yield in retentive and non-retentive river systems having contrasting implications for aquatic ecology. The same is true with respect to individual river reaches. Sediment load composition is important in the context of taxa with differing sensitivities to sediment pressures and the timing of that load is important with respect to contrasting key life stage habitat requirements. Such considerations mean that although catchment suspended sediment annual yield is readily related to current measures of sediment pressure, it represents a poor metric for defining ecological requirements for sediment. Where continuous data are unavailable, quantification of suspended sediment yield involves a range of uncertainties (Phillips *et al*., 1999; Horowitz, 2008) meaning that identifying linkages between sediment delivery and ecological impacts requires careful interpretation and assessment, especially within the context of catchment compliance. Walling *et al*. (2008) suggest that the coefficient of variation of annual suspended sediment yields is typically 50–60% for UK rivers and use standard error statistics to suggest that 25 years of data would be required to estimate representative long-term mean annual suspended sediment yields to within ±20% of the true value. This poses problems not only for target setting but also for assessing whether those targets are being met. Thus, sediment yield targets are best used to represent an integrated measure of catchment response to climatic and anthropogenic drivers. Sediment yield provides a useful summary statistic for sediment mobilization, transfer and delivery and offers excellent potential for assessing the efficacy of mitigation strategies and for testing compliance in terms of deviation from reference or background conditions.

Aquatic sediment pressures are different to those arising from other substances, such as toxic chemicals, in that fluvial suspended sediment loads are a naturally occurring phenomenon, but one which has been enhanced greatly by human activities in river basins. Natural or intrinsic levels of sediment in fluvial systems are essential to habitat heterogeneity and ecological functioning (Yarnell *et al*., 2006). Sediment aggregates, in addition to inorganic mineral particles, comprise bacteria, algae, detritus and other organic material (Droppo, 2001) that are fundamental to the health of aquatic ecosystems (Swietlik *et al*., 2003). As a result, an understanding of the background sediment regimes should represent a basic premise for developing water quality targets. In this respect, the evaluation of historical catchment sediment yields represents an alternative form of the sediment regime approach to setting catchment management targets. Across England and Wales, rates of erosion and sediment delivery are generally accepted to have increased since the early part of the 20th century (Evans, 2006). Recent work by Foster (2006) summarizing the use of lake coring for the reconstruction of historical sediment yields has suggested that yields in lowland agricultural catchments in England and Wales have increased from 10–30 t km^{-2} year^{-1} to as much as 110 t km^{-2} year^{-1}.

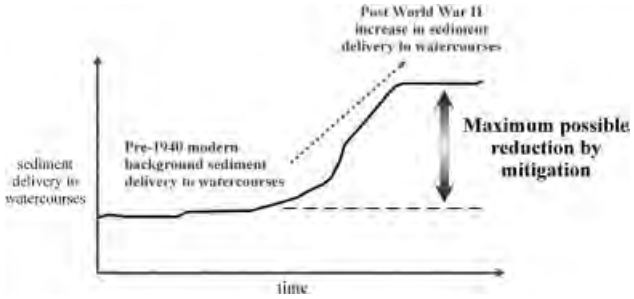

Figure 2. The use of estimated modern background sediment delivery to rivers (MBSDR) to inform water policy for sediment

An understanding of recent historical sediment pressures on aquatic environments and their use to estimate modern background sediment delivery to rivers is useful for informing policy makers on the upper ceiling of mitigation impact (Figure 2). A compliance approach aimed at establishing modern background sediment pressures on the basis of palaeolimnology overcomes some of the difficulties encountered in the selection of contemporary 'reference condition' sites to build predictive models of sediment stress—ecological condition. Reference condition catchments can be difficult to identify in areas with substantial anthropogenic activity, whereas in extensive tracts of undisturbed land, difficulties might be encountered with the selection of stringent criteria for isolating true reference sites. It is unrealistic to attempt to return to more historical sediment yields (i.e. truly intrinsic values), in the context of modern agricultural intensity and growing concerns over food security. Coulthard and Van De Weil (2007) have recently challenged the basis of inferring links between land use, climate and sediment yields either from lakes or from long-term data sets on the basis of self-organized criticality (SOC) exhibited by natural systems. SOC is a property of complex natural systems wherein fluctuations in sediment yields are highly nonlinear and depend as much on the structure of the sediment pathways and opportunities for storage within the catchment as they do on external pressures. Therefore, SOC raises important questions over the validity of setting standards on the basis of sediment regimes.

River substrate metrics. Stream bed measures have been widely used as a basis for proposing sediment guidelines and developing targets, as the characteristics of the substrate exert an important control on habitat availability especially for the key life stages of various organisms. Thus, for example, salmonids can encounter difficulties in constructing redds in situations where the bed matrix has been cemented or buried by excessive fines (Sear *et al*., 2008). Common stream bed measures used as a basis for proposing sediment guidelines or establishing regulatory targets include substrate composition/embeddedness, surface fines and riffle stability. Although these stream bed metrics are clearly interrelated, they are not interchangeable, because a river substrate can be partially embedded without having a significant amount of fines exposed.

When using these metrics, it is essential to designate specific reaches within the channel system and parts of the substrate therein used for particular life stages by important species such as riffles for spawning. Accordingly, applying river substrate metrics to guide catchment-scale sediment management is highly challenging.

Substrate composition/embeddedness: Numerous studies have cited river bed characteristics as a major control on aquatic species composition (Cummins, 1974; Platts *et al*., 1983; Witzel and MacCrimmon, 1983; Heggenes, 1988). Although human activities can modify substrate characteristics, catchment attributes such as geology, soils, slope and runoff result in natural variations in stream bed particle sizes (Morisawa, 1968). Sediment guidelines founded on substrate character (Table VII) have largely arisen because some evidence has suggested that salmon prefer spawning substrates with a characteristic bimodal grain size comprising coarse framework gravel and finer matrix material (Moir *et al*., 1998). But some studies have reported a general absence or low levels of bimodality in fish spawning gravels (Kondolf and Wolman, 1993). Crisp and Carling (1989) found that size distributions in gravels used for fish spawning were unimodal with a positive skew in northeast England and southwest Wales, but bimodal in the Chalk catchments of southern England. Other studies have reported a negative correlation between percent fines (<2 mm) in the river bed and periphyton biomass (Hill *et al*., 2000; Membane, 2001; Zweig and Rabeni, 2001). Regulatory thresholds have been established for percent fines in river substrates as part of the USEPA TMDL framework. Such targets are typically based on the literature review of optimum habitat conditions, followed by limited sampling of the river substrate in question. For example, USEPA TMDL studies for the Garcia and Navarro watersheds in northern Carolina set target values of 14% for <0·085 mm and 30% for <6·35 mm gravel, together with a median gravel particle size range of 37–69 mm (Rosser and O'Connor, 2007).

Embeddedness represents a measure of the degree to which cobble and coarse gravel matrix material are buried due to excessive fine sediment deposition. As a result, embedded substrates lack the interstitial spaces necessary for intra-gravel exchanges and fail to provide the habitat required by incubating or juvenile fish and for certain macroinvertebrate taxa. Excessive fine sediment retention and intrusion disrupts filter feeding (Lemly, 1982), impedes foraging and mobility (McClelland and Brusven, 1980) and increases drift (Doeg and Milledge, 1991) by macroinvertebrates. Ryder (1989) reported that a 12–17% increase in the interstitial fine sediment content of a relatively 'sediment-free' coarse substrate reduced the abundance of total macroinvertebrates by 16–40% and that of Ephemoptera by 27–55%. Table VIII presents some published thresholds for the impact of fine sediment deposition on macroinvertebrates in fluvial systems. Examples of sediment guidelines based on embeddedness are listed in Table IX. Working in Idaho, USA, Nelson *et al*. (1997) found an average embeddedness of 35% in spawning riffles. Bjornn *et al*. (1977) reported that an embeddedness of 67% resulted in detrimental changes to macroinvertebrate fauna. Chapman and McCleod (1987), however, found it impossible to generalize the relationship between embeddedness and salmon densities, although their review did suggest that embeddedness of 66–75% impacts detrimentally on macroinvertebrates.

Despite the apparent logic linking river substrate metrics and habitat suitability for aquatic biota, few studies relate such measures to functional biological impacts (Reiser, 1998). Instead, most investigations simply provide correlative evidence of substrate composition for those habitats used by a range of fish species. In using substrate metrics to define sediment guidelines, it is important to make the distinction between gravels that could potentially be used for spawning and actual redds

Table VII. Examples of sediment guidelines based on substrate composition

Organism	Substrate composition	Reference
Salmon	<8% fine sand, <15% fines	O'Connor and Andrew (1998)
Salmon	<20% combined sand and silt, 40–80% gravel, 10–40% cobble, <20% boulder	Semple (1991)
Salmon	Median grain size of 20–30 mm, 8–12% <1 mm	Crisp and Carling (1989)
Salmon	Median grain size of 22 mm	Kondolf and Wolman (1993)
Salmon	Mean particle size of 20·7 mm, 2·3–8% fines, 5·4% <1 mm	Moir *et al*. (1998)
Salmon	Gravel size range 16–256 mm	Symons and Heland (1978)
Salmonids	<12–14% <1 mm	Kondolf (2000)
Salmonids	~30% 3–6 mm	Kondolf (2000)
Salmonids	14% <0·085 mm, 30% < 6·35 mm	Rosser and O'Connor (2007)
Trout	Gravel size range 8–128 mm	Chapman (1988), Shirvall and Dungey (1983)
Brown trout	Mean grain size of 6·9 mm, range 8–128 mm	Witzel and MacCrimmon (1983)
Brown trout	Gravel size rang 50–70 mm	Heggenes (1988)
Brown trout	Gravel size range 10–90 mm	Bardonnet and Heland (1994)
Cutthroat trout	Mean particle size of 16·6 mm	Thurrow and King (1994)
Fish	<27% <6·35 mm	IDEQ (1991)

Table VIII. Examples of thresholds for sediment deposition impacts on macroinvertebrates

Organism	Deposition depth (mm) (particle size)	Effect	Reference
Ephemeroptera	5 (125 μm–4 mm)	Burial	Wood *et al*. (2005)
Isopoda	5 (>4 mm)	Burial	Wood *et al*. (2005)
Isopoda	10 (>2 mm)	Burial	Wood *et al*. (2005)
Trichoptera	10 (<500 μm)	Burial	Wood *et al*. (2005)
Ephemeroptera, Plecoptera, Trichoptera (EPT)	5 (volcanic ash)	Reduced colonization	Brusven and Hornig (1984)
Bivalvia	6–25 (silt)	Mortality	Ellis (1936)

Table IX. Examples of sediment guidelines based on embeddedness

Organism	% Embeddedness	Reference
Fish	<30 as a 3–5 year average	Nelson *et al*. (1997)
Fish	30–40 as a 3–5 year average	Nelson *et al*. (1997)
Fish	≤25	Rowe *et al*. (2003)
Fish	≤33	NMED (2002)
Fish	≤32	IDEQ (1991)

(Kondolf and Wolman, 1993). Attempts at relating substrate surface and subsurface metrics have generated contradictory results. For example, Platts *et al*. (1989) found a significant but weak relationship between the content of surface and subsurface fines, whereas the work of Nelson *et al*. (1997) reported a weak relationship between pebble counts and ingressed fines. Several authors report that a high degree of variability can be encountered in stream bed composition assessments of the same channel reach using different methods (Nelson *et al*., 2002; Sylte, 2002). Given the spatial and temporal variation in substrate composition, it is essential to adopt statistically robust sampling strategies when using such metrics to define sediment guidelines or regulatory targets (Rosser and O'Connor, 2007). Particle size sampling requires substantial effort and given the need for a critical evaluation of the sampling density necessary for characterizing the natural variability of substrate grain size, establishing meaningful numerical targets on the basis of substrate composition is highly challenging and not pragmatic at catchment scale.

Riffle stability: The Riffle Stability Index (RSI) has been used as a sediment metric and is based on the percentage of substrate particles that are smaller than the largest particles entrained in channel-forming flows (Kappeser, 2002). Riffle stability is important as riffle degradation results in detrimental impacts on the pools used as refugia by many aquatic species (Lisle, 1982; Kruzic *et al*., 2001; Stitchert *et al*., 2001). The stability of riffles is also a potentially significant factor in redd scour and the concomitant loss of incubating progeny during high flows, although some work has reported behavioural changes whereby salmonids deposit their eggs below the scour depth or avoid spawning during the periods of increased risk of river bed scour (Montgomery *et al*., 1999). Grain size analysis for the RSI is normally targeted on point bars. Similar metrics include relative bed stability (RBS) (Dingman, 1984; Swietlik *et al*., 2003) and the bed stability ratio (Dietrich *et al*., 1989). The former can be estimated by comparing the actual grain sizes of the substrate *in situ* with those of the mobilized wash and bed load. A high (100–1000) value of RBS is therefore indicative of an extremely stable substrate where sediment supply exceeds stream competence, whereas low values are indicative of more mobile substrates. In situations where sediment inputs to rivers have been enhanced by land use activities, textural fining of substrate results in very low RBS values (Kaufmann *et al*., 1999). River bed stability assessments using a comparison between the grain size range of bed sediments and erosive competence during typical flood events have been undertaken for a range of catchment scales, channel slopes and particle size compositions (Dietrich *et al*., 1989; Jowett, 1989; Montgomery *et al*., 1999; Kaufmann *et al*., 2008). Bed stability metrics have been used to examine the effects of sediment supply, bed forms, coarse woody debris and the frequency of competent flows (Cobb *et al*., 1992; Buffington and Montgomery, 1999; Bledsoe *et al*., 2007). The maintenance of riffles can also be assessed by coupling two-dimensional hydrodynamic models with sediment transport regime equations for predicting scour potential. In turn, these can be linked to habitat suitability curves to predict physical habitat quality for a range of biota (Hardy, 1998; Elkins *et al*., 2007; Pasternack *et al*., 2008).

Some US states (USEPA, 2002) have adopted the residual pool volume (Lisle and Hilton, 1992) as a comparable metric to the RSI. Residual pool volume is defined as the percentage of pool volume filled with fine sediment which is taken as a measure of mobile in-channel bed load. Quantitative assessments of riffle or bed stability are, however, typically hampered by a failure to adopt statistically robust sample sizes. Even if such metrics are adopted, it remains necessary to assess the relationship between sedimentation and biotic assemblages using a statistically sound number of sampling sites.

Prospects

Existing approaches to setting sediment targets for river catchments clearly face a number of problems and

constraints. However, given the important off-site environmental problems associated with accelerated erosion and sediment delivery and the threat to important catchment ecosystem services (e.g. erosion control and food provision, water quality/purification), resulting sediment pressures on watercourses and their ecological impacts need to be determined and mitigated. It is therefore necessary for government bodies to assess the gap between current and target status for sediment using appropriate standards and how best to reduce that gap using policy instruments and mitigation measures.

The definition of meaningful fluvial sediment targets continues to attract scientific debate (Collins and Anthony, 2008; Collins and McGonigle, 2008). Sediment target setting needs to consider the relationship between sediment pressures and ecological condition as defined by sediment impacts on key habitat parameters and especially dissolved oxygen availability. A sufficient supply of dissolved oxygen is essential for aquatic life, with oxygen depletion in the benthos being caused by a range of processes including the oxidation of organic sediment and respiration by aquatic organisms (Cox, 2003) and ground water–surface water interactions (Malcolm *et al*., 2003, 2004, 2006). Failure to characterize the impacts of sediment pressures on key processes and exchanges in the fluvial aquatic habitat renders the results of much existing work correlative, as opposed to causative, in nature.

The pressing need for revised sediment targets for informing river catchment water policy means that opportunities for constructing generic modelling toolkits capable of providing a catchment-specific focus within a national setting should be progressed. Toolkits will need to be founded on the coupling of sediment pressures and biological response (Collins and McGonigle, 2008) and should focus on fluvial sediment regimes to avoid the problems of stationarity and inter-annual varaiblity associated with thresholds. A range of deterministic and empirical modelling approaches has already been used to predict fluvial water quality compliance under various climate, land use and pollutant load reduction scenarios (McBride and Ellis, 2001, Gibbons, 2003; Jakeman and Letcher, 2003; Reckhow, 2003; Collins *et al*., 2007; Collins and Anthony, 2008, Collins *et al*., 2009b). There remains, however, a challenge for modeller communities to develop toolkits with the necessary functionality for linking the physico-chemical and biological components of river catchments (Horn *et al*., 2004; Collins and McGonigle, 2008). By being dynamic, such toolkits will help avoid some of the criticisms (Norris and Hawkins, 2000) frequently levied against previous attempts to link organism (e.g. fish) assemblage indices and environmental attributes (Hughes and Oberdorff, 1999; Olden and Jackson, 2001; An *et al*., 2002; FAME Consortium, 2004; Scardi *et al*., 2005). Generic modelling tools will need capacity to quantify key sediment sources and acceptable river sediment characteristics (mass, composition, timing) relative to ecological targets and represent the sensitivity of biological response to sediment pressure gradients. Indices of biological response will need to reflect the different forms of biota that can be used as indicators of environmental status, including fish (Fausch *et al*., 1990; Oberdorff and Hughes, 1992; Whitfield, 1996; Kurtz *et al*., 2001; Scardi *et al*., 2008) and macroinvertebrates (Wright *et al*., 1984; Simpson and Norris, 2000). On this basis, such tools could be used to provide estimates of the percentage reduction in current or future projected fluvial sediment pressures required to meet 'good ecological status' for sediment, taking account of key drivers including climate or land use change. Sediment compliance assessment modelling tools will need the flexibility to accommodate the latest physical and biological monitoring observations and key catchment attribute data. As such work progresses, careful consideration will need to be directed towards managing increased computational complexity associated with terrestrial and aquatic process representation, parameterization and output validation. Equally, it will be essential to acknowledge the 'confidence of compliance' given the inherent uncertainties in experimental or monitoring data used to inform models as well as in model structures and predictions (Borsuk *et al*., 2002; Gronewold *et al*., 2008; Liu *et al*., 2008; Collins *et al*., 2009b; Gronewold and Borsuk, 2009). Assessment methods for river catchment sediment compliance will need to be guided by minimum performance criteria and should be implemented with clear guidelines on data quality control and assurance. Identification of revised sediment targets will continue to require generic denominators that have clear and practical relevance to guiding cost-effective catchment management decisions. There remains a need to assess, restore and manage fluvial aquatic ecosystems with due consideration of their multiple components influenced by sediment, including hydromorphology, habitat, biota and chemistry. Improved sediment management is pivotal to the success of many catchment initiatives, including restoration projects.

ACKNOWLEDGEMENTS

The authors gratefully acknowledge the funding provided by the Department for Environment, Food and Rural Affairs (Defra) under project WQ0128 (Extending the evidence base on the ecological impacts of fine sediment and developing a framework for targeting mitigation of agricultural sediment losses). The draft manuscript benefitted from the comments of three anonymous reviewers. This manuscript represents a contribution to the SETAC SEDAG Working Group on Reviewing sediment targets used for water policy.

REFERENCES

Acornley RM, Sear DA. 1999. Sediment transport and sedimentation of Brown trout (*Salmo Trutta* L. spawning gravels in chalk streams. *Hydrological Processes* **13**: 447–458.

Alabaster JS, Lloyd R. 1980. *Water Quality Criteria for Freshwater Fish*. Butterworth: London; 297.

Alabaster JS, Lloyd DS. 1982. Finely divided solids. In *Water Quality Criteria for Freshwater Fish*, Alabaster JS, Lloyd DS (eds). Butterworth: London; 1–20.

Aldridge DW, Payne BS, Miller AC. 1987. The effects of intermittent exposure to suspended solids and turbulence on three species of freshwater mussels. *Environmental Pollution* **45**: 17–28.

An GK, Park SS, Shin JY. 2002. An evaluation of a river health using the index of biological integrity along with relations to chemical and habitat conditions. *Environment International* **28**: 411–420.

Anderson BS, Phillips BM, Hunt JW, Connor V, Richard N, Tjeerdema RS. 2006. Identifying primary stressors impacting macroinvertebrates in the Salinas River (California, USA): relative effects of pesticides and suspended particles. *Environmental Pollution* **141**: 402–408.

ANZECC. 2000. Aquatic ecosystems—rationale and background information, Chapter 8. *Australian and New Zealand Guidelines for Fresh and Marine Water Quality*. Paper no. 4, vol. 4. Australian and New Zealand Environment and Conservation Council and Agriculture and Resource Management Council of Australia and New Zealand.

APEM. 2007. Review of UKTAG proposed standard for suspended solids. Final report, APEM 410242 WWF-UK, Stockport, UK.

Armstrong JD, Kemp PS, Kennedy GJA, Ladle M, Milner NJ. 2003. Habitat requirements of Atlantic salmon and brown trout in rivers and streams. *Fisheries Research* **62**: 143–170.

Bachman RW. 1958. The ecology of four north Idaho streams with reference to the influence of forest road construction. MSc thesis, University of Idaho, Moscow, USA.

Ballantine DB, Walling DE, Collins AL, Leeks GJL. 2009. The content and storage of phosphorus in fine-grained channel bed sediment in contrasting lowland agricultural catchments in the UK. *Geoderma* **151**: 141–149.

Bardonnet A, Bagliniere JL, 2000. Freshwater habitat of Atlantic salmon (*Salmo salar*). *Canadian Journal of Fisheries and Aquatic Sciences* **57**: 497–506.

Bardonnet A, Heland M. 1994. The influence of potential predators on the habitat preferenda of emerging brown trout. *Journal of Fish Biology* **45**(Suppl. A): 131–142.

Bedoya D, Novotny V, Manolakos ES. 2009. Instream and offstream environmental conditions and stream biotic integrity: importance of scale and site similarities for learning and prediction. *Ecological Modelling* **220**: 2393–2406.

Berg L, Northcote TG. 1985. Changes in territorial, gill-flaring and feeding behaviour in juvenile coho salmon (*Oncorhynchus kisutch*) following short-term pulses of suspended sediment. *Canadian Journal of Fisheries and Aquatic Sciences* **42**: 1410–1417.

Berry W, Rubinstein N, Melzian B, Hill B. 2003. The Biological Effects of Suspended and Bedded Sediment (SABS) in Aquatic Systems: A Review. US Environment Protection Agency, National Health and Environmental Health Effects Laboratory, Rhode Island, Internal Report, 58.

Beschta RL, Jackson WL. 1979. The intrusion of fine sediment into a stable gravel bed. *Journal of the Fisheries Research Board Canada* **36**: 204–210.

Bhargava DS, Mariam DW. 1991. Effects of suspended particle size and concentration on reflectance measurements. *Photogrammetric Engineering and Remote Sensing* **57**: 519–529.

Bilotta GS, Brazier RE. 2008. Understanding the influence of suspended solids on water quality and aquatic biota. *Water Research* **42**: 2849–2861.

Bisson PA, Bilby RE. 1982. Avoidance of suspended sediment by juvenile Coho salmon. *North American Journal of Fisheries Management* **2**: 371–374.

Bisson PA, Reeves GH, Bilby RE, Naiman RJ. 1997. Watershed management and Pacific salmon: desired future conditions. In *Pacific Salmon and Their Ecosystems: Status and Future Options*, Stouder DJ, Bisson PA, Naiman RJ (eds). Chapman and Hall: New York, USA; 447–474.

Bjorn TC, Reiser DW. 1991. Habitat requirements of salmonids in streams. In *Influence of Forest and Rangeland Management on Salmonid Fishes and their Habitats*, Meehan WR (eds). Special Publication No. 19, American Fisheries Society: Bethesda, MA, USA.

Bjornn TC, Brusven MA, Molnau MP, Milligan JH, Klamt RA, Chacho E, Shaye C. 1977. *Transport of Granitic Sediment in Streams and its Effects on Insects and Fish. College of Forestry, Wildlife and Range Sciences Bulletin 17*. University of Idaho: Moscow, ID, USA.

Bledsoe BP, Brown MC, Raff DA. 2007. Geotools: a toolkit for fluvial system analysis. *Journal of the American Water Resources Association* **43**: 757–772.

Borsuk ME, Stow CA, Reckhow KH. 2002. Predicting the frequency of water quality standard violations: a probabilistic approach for TMDL development. *Environmental Science and Technology* **36**: 2109–2115.

Bricelj MA, Lonsdale DJ. 1997. Aureococcus anophagefferens: causes and ecological consequences of brown tides in US and mid-Atlantic coastal waters. *Limnology and Oceanography* **42**: 1023–1038.

Brunke M, Gonser T. 1997. The ecological significance of exchange processes between rivers and groundwater. *Freshwater Biology* **37**: 1–33.

Brusven MA, Hornig CE. 1984. Effects of suspended and deposited volcanic ash on survival and behavior of stream insects. *Journal of the Kansas Entomological Society* **57**: 55–62.

Buffington JM, Montgomery DR. 1999. Effects of sediment supply on surface textures of gravel-bed rivers. *Water Resources Research* **35**: 3523–3530.

Burton GA. 2002. Sediment quality criteria in use around the world. *Limnology* **3**: 65–76.

Campbell CG, Laycak DT, Hoppes W, Tran NT, Shi FG. 2005. High concentration suspended sediment measurements using a continuous fiber optic in-stream transmissometer. *Journal of Hydrology* **311**: 244–253.

Carling PA. 1985. Oxygen flux through salmonid gravels. Freshwater Biological Association Project 73.

Carling PA, McCahon CP. 1987. *Natural Sedimentation of Brown trout (Salmo Trutta L.) spawning gravels during low-flow conditions*. Plenum Publishing Corporation.

CCME. 1995. Protocol for the derivation of Canadian sediment quality guidelines for the protection of aquatic life. Canadian Council of Ministers of the Environment, Report CCME EPC-98E, Canada.

CCME. 2001. Canadian sediment quality guidelines for the protection of aquatic life. Canadian Council of Ministers of the Environment, Publication No. 1299, Guidelines and Standards Division, Hull, Canada.

Chapman DW. 1988. Critical review of variables used to define effects of fines in redds of large salmonids. *Transactions of the American Fisheries Society* **117**: 1–21.

Chapman DW, McCleod KP. 1987. Development of criteria for fine sediment in the northern Rockies ecoregion. Final Report to the Environment Protection Agency, Seattle, USA.

Chevalier BE, Carson C. 1984. Modelling the transfer of oxygen between the stream and the stream substrate with application to the survival rates of salmonid embryos. Colorado State University, Department of Agriculture and Chemical Engineering ARS Report 5602 208 13-008 A, 99.

Ciborowski JJH, Pointing PJ, Corkum LD. 1977. Effect of current velocity and sediment on drift of mayfly *Ephemerella subvaria* McDunnough. *Freshwater Biology* **7**: 567–572.

Clarke S, Wharton G. 2001. Sediment nutrient characteristics and aquatic macrophytes in lowland English rivers. *Science of the Total Environment* **266**: 103–112.

Cobb DG, Galloway TD, Flannagan JF. 1992. Effects of discharge and substrate stability on density and species composition of stream insects. *Canadian Journal of Fisheries and Aquatic Science* **49**: 1788–1795.

Collins AL, Anthony SG. 2008. Assessing the likelihood of catchments across England and Wales meeting 'good ecological status' due to sediment contributions from agricultural sources. *Environmental Science and Policy* **11**: 163–170.

Collins AL, McGonigle DF. 2008. Monitoring and modelling diffuse pollution from agriculture for policy support: UK and European experience. *Environmental Science and Policy* **11**: 97–101.

Collins AL, Walling DE, Leeks GJL. 2005. Storage of fine-grained sediment and associated contaminants within the channels of lowland permeable catchments in the UK. In *Sediment Budgets 1. International Association of Hydrological Sciences Publication No. 291*. IAHS Press: Wallingford, UK; 259–268.

Collins AL, Anthony SG, Turner T, Hawley J. 2007. Predicting the impact of projected change in agriculture by 2015 on annual mean fluvial suspended sediment concentrations across England and Wales. In *Water Quality and Sediment Behaviour of the Future: Predictions for the 21st Century. International Association of Hydrological Sciences Publication No. 314*. IAHS Press: Wallingford, UK; 28–37.

Collins AL, McGonigle DF, Evans R, Zhang Y, Duethmann D, Gooday R. 2009a. Emerging priorities in the management of diffuse pollution at catchment scale. *International Journal of River Basin Management* **7**: 179–185.

Collins AL, Anthony SG, Hawley J, Turner T. 2009b. The potential impact of projected change in farming by 2015 on the importance of the agricultural sector as a sediment source in England and Wales. *Catena* **79**: 243–250.

Cooper DM, Naden P, Smith B, Gannon B. 2002. Life in UK Rivers. *Methods for the Assessment and Monitoring of Siltation in SAC Rivers Part 2: A Minimum Monitoring Strategy for Two cSAC Rivers*. CEH: Wallingford, UK.

Cooper DM, Naden P, Old G, Laize C. 2008. Development of guideline sediment targets to support management of sediment inputs into aquatic systems. Natural England Research Report NERR008. Natural England, Sheffield.

Cordone AJ, Kelley DW. 1961. The influences of inorganic sediment on the aquatic life of streams. *California Fish Game* **47**: 189–228.

Coulthard TJ, Van De Weil MJ. 2007. Quantifying fluvial non linearity and finding self organised criticality? Insights from simulations of river basin evolution. *Geomorophology* **91**: 216–235.

Cox BA. 2003. A review of dissolved oxygen modelling techniques for lowland rivers. *Science of the Total Environment* **314–316**: 303–334.

Crisp DT. 1993. The ability of UK salmonid alevins to emerge through a sand layer. *Journal of Fish Biology* **43**: 656–658.

Crabtree RW, Cluckie ID, Forster CF. 1987. Percentile estimation for water quality data. *Water Research* **21**: 583–590.

Crisp DT, Carling P. 1989. Observations on siting, dimensions and structure of salmonid redds. *Journal of Fish Biology* **34**: 119–134.

Cummins KW. 1974. Structure and function of stream ecosystems. *Bioscience* **24**: 631–641.

Dearing JA, Hakanson H, Liedberg-Johnsson B, Persson A, Skansjo S, Widholm D, El Daoushy F. 1987. Lake sediments used to quantify the erosional response to land use change in southern Sweden. *Oikos* **50**: 60–78.

den Besten PJ, de Deckere E, Babut MP, Power B, Angel DelValls T, Zago C, Oen AMP, Heise S. 2003. Biological effects-based sediment quality in ecological risk assessment for European waters. *Journal of Soils and Sediments* **3**: 144–162.

Devlin MJ, Barry J, Mills DK, Gowen RJ, Foden J, Sivyer D, Tett P. 2008. Relationships between suspended particulate material, light attenuation and Secchi depth in UK marine waters. *Estuarine, Coastal and Shelf Science* **79**: 429–439.

DFO. 1983. Department of Fisheries and Oceans. A rationale for the suspended solids standards for Yukon streams subject to placer mining. Report to interdepartmental committee on placer mining, New Westminster, Canada.

Dietrich WE, Kirchner JW, Ikeda H, Iseya F. 1989. Sediment supply and the development of the coarse surface layer in gravel bed rivers. *Nature* **340**: 215–217.

Dingman SL. 1984. *Fluvial Hydrology*. W.H. Freeman: New York, USA; 383.

Dlamini V, Hoko Z, Murwira A, Magagula C. 2010. Response of aquatic macro invertebrate diversity to environmental factors along the Lower Komati River. *Physics and Chemistry of the Earth* **35**: 665–671.

Dobberfuhl DR. 2007. Light limiting thresholds for submerged aquatic vegetation in a blackwater river. *Aquatic Botany* **86**: 346–352.

Doeg TJ, Milledge GA. 1991. Effect of experimentally increasing concentration of suspended sediment on macro-invertebrate drift. *Australian Journal of Marine and Freshwater Research* **42**: 519–526.

Droppo IG. 2001. Rethinking what constitute suspended sediment. *Hydrological Processes* **15**: 1551–1564.

Dunlop J, McGregor G. 2007. Setting water quality guidelines for salinity and sediment in freshwater streams in Queensland: an applied approach within a natural resource management context. The State of Queensland Department of Natural Resources and Water, Australia.

Edwards TK, Glysson GD. 2000. Field methods for measurement of fluvial sediment. U.S. Geological Survey.

Effler SE. 1989. Secchi disk transparency and turbidity. *Journal of Environmental Engineering ASCE*. **114**: 1436–1447.

EIFAC. 1964. European Inland Fisheries Advisory Commission—Water quality criteria for European freshwater fish: report in finely divided solids and inland fisheries. United Nations, Food and Agriculture Organisation, EIFAC Technical Report No. 1, Rome, Italy.

Elkins EE, Pasternack GB, Merz JE. 2007. The use of slope creation for rehabilitating incised, regulated gravel-bed rivers. *Water Resources Research* **43**: W05432.

Ellis JC. 1989. *Handbook on the design and interpretation of monitoring programmes*. Water Research Centre; Marlow, UK.

Ellis MM. 1936. Erosion silt as a factor in aquatic environments. *Ecology* **17**: 29–42.

European Parliament. 2000. Parliament and Council Directive 2000/60/EC. Establishing a framework for community action in the field of water policy. Official Journal PE-CONS 3639/1/00 REV 1. European Union, Brussels, Belgium.

Evans R. 2006. Land use, sediment delivery and sediment yield in England and Wales. In *Soil Erosion and Sediment Redistribution in River Catchments*, Owens PN, Collins AJ (eds). CAB International: Wallingford, UK; 70–84.

Evans-White MA, Dodds WK, Huggins DG, Baker DS. 2009. Thresholds in macroinvertebrate biodiversity and stoichiometry across water-quality gradients in Central Plains (USA) streams. *Journal of the North American Benthological Society* **28**: 855–868.

FAME Consortium. 2004. Manual for the application of the European Fish Index—EFI. A fish-based method to assess the ecological status of European rivers in support of the Water Framework Directive. Available online at http://fame.boku.ac.at/downloads/manual Version Februar2005.pdf.

Farnsworth KL, Milliman JD. 2003. Effects of climatic and anthropogenic change on small mountainous rivers: the Salinas River example. *Global and Planetary Change* **39**: 53–64.

Fausch KD, Lyons J, Karr JR, Angermeier PL. 1990. Fish communities as indicators of environmental degradation. *American Fisheries Society Symposium* **8**: 123–144.

Fausch KD, Torgersen CE, Baxter CV, Li HW. 2002. Landscapes to riverscapes: bridging the gap between research and conservation of stream fishes. *BioScience* **52**: 483–498.

Fleming IA. 1998. Pattern and variability in the breeding system of Atlantic salmon (*Salmo salar*), with comparisons to other salmonids. *Canadian Journal of Fisheries and Aquatic Sciences* **55**(Suppl. 1): 59–76.

Foster IDL. 2006. Lakes in the sediment delivery system. In *Soil Erosion and Sediment Redistribution in River Catchments*, Owens PN, Collins AJ (eds). CAB International: Wallingford, UK; 128–142.

FWPCA. 1968. Federal Water Pollution Control Administration Report of the Committee on Water Quality Criteria (Green Book).

Gallegos CL, Bergstrom PW. 2005. Effects of a Prorocentrum minimum bloom on light availability for and potential impacts on submersed aquatic vegetation in upper Chesapeake Bay. *Harmful Algae* **4**: 553–574.

Gammon JR. 1970. The effect of inorganic sediment on stream biota. US Environmental Protection Agency, Water pollution control research series, 18050 DWC 12/70; 141.

Gaugler R, Molloy D. 1980. Feeding inhibition in black fly larvae (Diptera, Simuliidae) and its effects on the pathogenicity of *Bacillus thuringiensis* var israelensis. *Environmental Entomology* **9**: 704–708.

Gibbons RD. 2003. A statistical approach for performing water quality impairment assessments. *Journal of the American Water Resources Association* **39**: 841–849.

Gippel CJ. 1989. The use of turbidity instruments to measure stream water suspended sediment concentration. Department of Geography and Oceanography, University College, The University of New South Wales, Australia. Monograph Series.

Gippel CJ. 1995. Potential of turbidity monitoring for measuring the transport of suspended solids in streams. *Hydrological Processes* **9**: 83–97.

Gray LJ, Ward JV. 1982. Effects of sediment releases from a reservoir on stream macroinvertebrates. *Hydrobiologia* **96**: 177–184.

Gray JR, Glysson GD. 2002. *Proceedings of the Fifth Interagency Workshop on Turbidity and Other Sediment Surrogates Workshop*, Reno, USA.

Greig SM, Sear DA, Carling PA. 2005a. The impact of fine sediment accumulation on the survival of incubating salmon progeny: implications for sediment management. *Science of the Total Environment* **344**: 241–258.

Greig SM, Sear DA, Smallman DJ, Carling PA. 2005b. Impact of clay particles on the cutaneous exchange of oxygen across the chorion of Atlantic salmon eggs. *Journal of Fish Biology* **66**: 1681–1691.

Greig S, Sear D, Carling P. 2007. A field-based assessment of oxygen supply to incubating Atlantic salmon (*Salmo salar*) embryos. *Hydrological Processes* **21**: 3087–3100.

Gronewold AD, Borsuk ME. 2009. A software tool for translating deterministic model results into probabilistic assessments of water quality standard compliance. *Environmental Modelling and Software* **24**: 1257–1262.

Gronewold AD, Borsuk ME, Wolpert RL, Reckhow KH. 2008. An assessment of faecal indicator bacteria-based water quality standards. *Environmental Science and Technology* **42**: 4676–4682.

Hardy TB. 1998. The future of habitat modelling and instream flow assessment techniques. *Regulated Rivers: Research and Management* **14**: 405–420.

Harrod TR, Theurer FD. 2002. Sediment. In *Agriculture, Hydrology and Water Quality*, Haygarth PM, Jarvis SC (eds). CABI: Wallingford, UK.

Hawkins RH. 2003. Survey of Methods for Sediment TMDLs in Western Rivers and Streams of the the United States. Report to US EPA Office

of Water, Assessment and Watershed Protection Division, Washington DC.

Heggenes J. 1988. Substrate preferences of brown trout fry (*Salmo trutta*) in artificial stream channels. *Canadian Journal of Fisheries and Aquatic Sciences* **45**: 1801–1806.

Heywood MJT, Walling DE. 2007. The sedimentation of salmonid spawning gravelss in the Hampshire Avon catchment, UK: implications for the dissolved oxygen content of intragravel water and embryo survival. *Hydrological Processes* **21**: 770–788.

Hill BH, Herlihy AT, Kaufmann PR, Stevenson RJ, McCormick RJ, Johnson FH, Burch C. 2000. Use of periphyton assemblage data as an index of biotic integrity. *Journal of the North American Benthological Society* **19**: 50–67.

Horn AL, Rueda FJ, Horman G, Fohrer N, 2004. Implementing river water quality modelling issues in mesoscale watershed models for water policy demands—an overview on current concepts, deficits and future tasks. *Physics and Chemistry of the Earth* **29**: 725–737.

Hornig CE, Brusven MA. 1986. Effects of suspended sediment on leaf processing by *Hesperophylax occidentalis* (Trichoptera, Limnephilidae) and *Pteronarcys californica* (Plecoptera, Pteronarcidae). *Great Basin Naturalist* **46**: 33–38.

Horowitz AJ. 1991. *A Primer on Sediment-trace Element Chemistry*. Lewis Publishers: Boca Raton, FL, USA.

Horowitz AJ. 1995. *The Use of Suspended Sediment and Associated Trace Elements in Water Quality Studies*. International Association of Hydrological Sciences Special Publication 4. IAHS Press: Wallingford, UK.

Horowitz AJ. 2008. Determining annual suspended sediment and sediment-associated trace element and nutrient fluxes. *Science of the Total Environment* **400**: 315–343.

Houben P, Hoffmann T, Zimmermann A, Dikau R. 2006. Land use and climatic impacts on the Rhine system (RheinLUCIFS): quantifying sediment fluxes and human impact with available data. *Catena* **66**: 42–52.

House WA. 2003. Geochemical cycling of phosphorus in rivers. *Applied Geochemistry* **18**: 739–748.

Hughes RM, Oberdorff T. 1999. Application of IBI concepts and metrics to water outside the United States and Canada. In *Assessing the Sustainability and Biological Integrity of Water Resources using Fish Communities*, Simon TP (eds). CRC Press LLC: Boca Raton, FL, USA; 79–93.

IDEQ. 1991. *South Fork River TMDL*. Idaho Division of Environmental Quality: Boise, ID, USA.

Jakeman AJ, Letcher RA. 2003. Integrated assessment and modelling: features, principles and examples for catchment management. *Environmental Modelling and Software* **18**: 491–501.

Jarvie HP, Neal C, Jürgens MD, Sutton EJ, Neal M, Wickham HD, Hill LK, Harman SA, Davies JJL, Warwick A, Barrett C, Griffiths J, Binley A, Swannack N, McIntyre N. 2006. Within-river nutrient processing in Chalk streams: the Pang and Lambourn, UK. *Journal of Hydrology* **330**: 101–125.

Jeong BS, Wander MM, Kleineidam S, Grathwohl P, Ligouis B, Werth CJ. 2008. The role of condensed carbonaceous materials on the sorption of hydrophobic organic contaminants in subsurface sediments. *Environmental Science and Technology* **42**: 1458–1464.

Jowett IG. 1989. River hydraulic and habitat simulation, RHYHABSIM computer manual. New Zealand Fisheries Miscellaneous Report 49, Christchurch, New Zealand.

Kappeser GB. 2002. A riffle stability index to evaluate sediment loading to streams. *Journal of the American Water Resources Association* **38**: 1069–1081.

Karr JR. 1991. Biological integrity: a long-neglected aspect of water resource management. *Ecological Applications* **1**: 66–84.

Kasai M, Brierley GJ, Page MJ, Marutani T, Trustrum NA. 2005. Impacts of land use change on patterns of sediment flux in Weraamaia catchment, New Zealand. *Catena* **64**: 27–60.

Kaufmann PR, Levine P, Robison EG, Seeliger C, Peck P. 1999. Quantifying physical habitat in wadeable streams EPA 620/R-99/003. Environmental Monitoring and Assessment Program (EMAP), U.S. Environmental Protection Agency, Washington, DC. 102 pp + Appendices.

Kaufmann PR, Faustini JM, Larsen DP, Shirazi MA. 2008. A roughness-corrected index of relative bed stability for regional stream surveys. *Geomorphology* **99**: 150–170.

Kefford BK, Zalizniak L, Dunlop JE, Nugegoda D, Choy SC. 2010. How are macroinvertebrates of slow flowing lotic systems directly affected by suspended and deposited sediments? *Environmental Pollution* **158**: 543–550.

Kemp HA 1949. Soil pollution in the Potomac River basin. *American Water Works Association Journal* **41**: 792–796.

Kiffney PM, Bull JP. 2000. Factors controlling periphyton accrual during summer in headwater streams of southwestern British Columbia, Canada. *Journal of Freshwater Ecology* **15**: 339–351.

Kondolf GM. 2000. Assessing salmonid spawning gravel quality. *Transactions of the American Fisheries Society* **129**: 262–281.

Kondolf GM, Wolman MG. 1993. The sizes of salmonid spawning gravels. *Water Resources Research* **29**: 2275–2285.

Kronvang B, Laubel A, Larsen SE, Friberg N. 2003. Pesticides and heavy metals in Danish streambed sediment. *Hydrobiologia* **494**: 93–101.

Kruzic LM, Scarnecchi DL, Roper BB. 2001. Comparison of midsummer survival and growth of age-0 hatchery coho salmon held in polls and riffles. *Transactions of the American Fisheries Society* **130**: 147–154.

Kurtak DC. 1978. Efficiency of filter feeding of black fly larvae (Diptera Simuliidae). *Canadian Journal of Zoology* **56**: 1608–1623.

Kurtz JA, Jackson LE, Fisher WS. 2001. Strategies for evaluating indicators based on guidelines from the Environmental Protection Agency's Office of Research and Development. *Ecological Indicators* **1**: 49–60.

Lake RG, Hinch SG. 1999. Acute effects of suspended sediment angularity on juvenile Coho salmon. *Canadian Journal of Fisheries and Aquatic Sciences* **56**: 862–867.

Lemly AD. 1982. Modification of benthic insect communities in polluted streams: combined effects of sedimentation and nutrient enrichment. *Hydrobiologia* **87**: 229–245.

Lewis K. 1973. The effect of suspended coal particles on the life forms of the aquatic moss Eurhynchium riparіodus. 1. The gametophyte plant. *Freshwater Biology* **3**: 251–257.

Lisle TE. 1982. Effects of aggradation and degradation on riffle-pool morphology in natural gravel channels, northwestern California. *Water Resources Research* **90**: 1643–1651.

Lisle TE. 1989. Sediment transport and resulting deposition in spawning gravels, north coastal California. *Water Resources Research* **25**: 247–260.

Lisle TE, Hilton S. 1992. The volume of fine sediment in pools: an index of sediment supply in gravel-bed streams. *Water Resources Bulletin* **28**: 371–383.

Liu Y, Yang P, Hu C, Guo H. 2008. Water quality modelling for load reduction under uncertainty: a Bayesian approach. *Water Research* **42**: 3305–3314.

Lloyd DS, Koenings JP, LaPerriere JD. 1987. Effects of turbidity in fresh waters of Alaska. *North American Journal of Fisheries Management* **7**: 18–33.

Luoma SN, Carter JL. 1993. Understanding the toxicity of contaminants in sediments: beyond the bio-assay-based paradigm. *Environmental Toxicology and Chemistry* **12**: 793.

MacDonald DD, Carr RS, Calder FD, Long ER, Ingersoll CG. 1996. Development and evaluation of sediment quality guidelines for Florida coastal waters. *Ecotoxicology* **5**: 253–278.

MacDonald DD, Ingersoll CG, Berger TA. 2000. Development and evaluation of consensus-based sediment quality guidelines for freshwater ecosystems. *Archives of Environmental Contamination and Toxicology* **39**: 20–31.

MacDonald DD, Carr RS, Eckenrod D, Greening H, Grabe S, Ingersoll CG, Janicki S, Janicki T, Lindskoog RA, Long ER, Pribble R, Sloane G, Smorong DE. 2004. Development, evaluation and application of sediment quality targets for assessing and managing contaminated sediments in Tampa Bay, Florida. *Archives of Environmental Contamination and Toxicology* **46**: 147–161.

Macpherson TA, Cahoon LB, Mallin MA. 2007. Water column oxygen demand and sediment oxygen flux: patterns of oxygen depletion in tidal creeks. *Hydrobiologia* **586**: 235–248.

Malcolm IA, Youngson A, Soulsby C. 2003. Survival of salmonid eggs in gravel bed streams: effects of groundwater–surface water interactions. *River Research and Applications* **19**: 303–316.

Malcolm IA, Coulsby C, Youngson AF, Hannah DM, McLaren IS, Thorne A. 2004. Hydrological influences on hyporheic water quality: implications for salmon egg survival. *Hydrological Processes* **18**: 1543–1560.

Malcolm IA, Soulsby C, Youngson AF. 2006. High-frequency logging technologies reveal statedependent hyporheic process dynamics: implications for hydroecological studies. *Hydrological Processes* **20**: 615–622.

Martinova MV. 1993. Nitrogen and phosphor compounds in bottom sediments—mechanisms of accumulation, transformation and release. *Hydrobiologia* **252**: 1–22.

McBride GB, Ellis JC. 2001. Confidence of compliance: a Bayesian approach for percentile standards. *Water Research* **35**: 1117–1124.
McCarthy JC, Pyle TE, Griffin GM. 1974. Light transmissivity, suspended sediments and the legal definition of turbidity. *Estuarine and Coastal Marine Science* **2**: 291–299.
McCauley DJ, DeGraeve GM, Linton TK. 2000. Sediment quality guidelines and assessment: overview and research needs. *Environmental Science and Policy* **3**: S133–S144.
McClelland WT, Brusven MA. 1980. Effects of sedimentation on the behavior and distribution of riffle insects in a laboratory stream. *Aquatic Insects* **2**: 161–169.
Membane CA. 2001. Testing bioassessment metrics: macroinvertebrates, sculpin and salmonid responses to stream habitat, sediment and metals. *Environmental Monitoring and Assessment* **67**: 293–322.
Milly PC, Betancourt J, Falkenmark M, Hirsch RM, Kundzewicz ZW, Lettenmaier DP, Stouffer RJ. 2008. Stationarity is dead: whither water management? *Science* **319**: 573–574.
Milner NJ, Elliott JM, Armstrong JD, Gardiner R, Welton JS, Ladle M. 2003. The natural control of salmon and trout populations in streams. *Fisheries Research* **62**: 111–125.
Moir HJ, Soulsby C, Youngson A. 1998. Hydraulic and sedimentary characteristics of habitat utilized by Atlantic salmon for spawning in the Girnock Burn, Scotland. *Fisheries Management and Ecology* **5**: 241–254.
Molinos JG, Donohue I. 2009. Differential contribution of concentration and exposure time to sediment dose effects on stream biota. *Journal of the North American Benthological Society* **28**: 110–121.
Montgomery DR, Beamer EM, Press GR, Quinn TP. 1999. Channel type and salmonid spawning distribution and abundance. *Canadian Journal of Fisheries and Aquatic Sciences* **56**: 377–387.
Morisawa M. 1968. *Streams, Their Dynamics and Morphology*. McGraw-Hill Book Company: New York, USA; 175.
Naden PS. 1992. Analysis and use of peaks-over-threshold data in flood estimation. In *Floods and Flood Management*, Saul AJ (ed). Kluwer Academic Publishers: Dordrecht; 131–143.
Naden P, Smith B, Jarvie H, Llewellyn N, Matthiessen P, Dawson H, Scarlett P, Hornby D. 2002. Life in UK rivers. *Methods for the Assessment and Monitoring of Siltation in SAC Rivers. Part 1: Summary of Available Techniques*. CEH: Wallingford, UK; 133 pp.
Naji A, Ismail A, Ismail AR. 2010. Chemical speciation and contamination assessment of Zn and Cd by sequential extraction in surface sediment of Klang River, Malaysia. *Microchemical Journal* **95**: 285–292.
Neff JM, Word JQ, Gulbransen TC. 1987. Recalculation of screening level concentrations for non-polar organic contaminants in marine sediments. Final report. US Environmental Protection Agency, Washington, USA.
Nelson RL, Wagoner LJ, Bunrs DC, Newberry DD, Lund J. 1997. Deposition of fine sediment in selected streams on the Payette and Boise National Forests, Idaho: report of sediment trends and monitoring effects, 1977–1996. Payette and Boise National Forests, McCall and Boise, Idaho, USA.
Nelson RL, Burns DC, Newberry DD. 2002. Deposition of fine sediment in the Salmon River watershed, Payette and Boise National Forests, Idaho: interstitial conditions in Salmon River tributaries—report of sediment trends from cobble embeddedness and free matrix sampling 1981–2000. US Forest Service, Payette and Boise National Forest, McCall and Boise, USA.
Newcomb TW, Flagg TA. 1983. Some effects of Mount St. Helens ash on juvenile salmon smolts. US National Marine Service Review, Report No. 45, pp 8–12.
Newcombe CP. 1986. Fisheries and the problem of turbidity and inert sediment in water: a synthesis for environmental impact assessment. British Columbia Ministry of Environment, Environmental Impact Unit, Environmental Services Section, Waste Management Branch, Victoria, Canada.
Newcombe CP. 1994. Suspended sediment in aquatic ecosystems: ill effects as a function of concentration and duration of exposure. British Columbia Ministry of Environment, Land and Parks, Habitat Protection Branch, Victoria, Canada.
Newcombe CP, Jensen JOT. 1996. Channel suspended sediment and fisheries: a synthesis for quantitative assessment of risk and impact. *North American Journal of Fisheries Management* **16**: 693–727.
Newcombe CP, MacDonald DD. 1991. Effects of suspended sediments on aquatic ecosystems. *North American Journal of Fisheries Management* **11**: 72–82.
NMED, 2002. Protocol for the assessment of stream bottom deposits on wadeable streams. New Mexico Environment Department, Surface Water Quality Bureau, Santa Fe, New Mexico.
Norris RH, Hawkins CP. 2000. Monitoring river health. *Hydrobiologia* **435**: 5–17.
Nuttall PM, Bielby GH. 1973. The effect of china-clay wastes on stream invertebrates. *Environmental Pollution* **5**: 77–86.
Oberdorff T, Hughes RM. 1992. Modification of an index of biotic integrity based on fish assemblages to characterise rivers of the Seine Basin, France. *Hydrobiologia* **228**: 117–130.
O'Connor WCK, Andrew TE. 1998. The effects of siltation on Atlantic salmon, *Salmo salar* L., embryos in the river Bush. *Fisheries Management and Ecology* **5**: 393–401.
Olden JD, Jackson DA. 2001. Fish-habitat relationships in lakes: gaining predictive and explanatory insight by using artificial neural networks. *Transactions of the American Fisheries Society* **130**: 878–897.
Pasternack GB, Bounrisavong MK, Parikh KK. 2008. Backwater control on riffle-pool hydraulics, fish habitat quality and sediment transport regime in gravel-bed rivers. *Journal of Hydrology* **357**: 125–139.
Patten BC. 1984. System theory formulation of site-specific water quality standards and protocols. *Ecological Modelling* **23**: 313–340.
Peterson NP, Quinn TP. 1996. Spatial and temporal variation in dissolved oxygen in natural egg pockets of chum salmon, in Kennedy Creek, Washington. *Journal of Fish Biology* **48**: 131–143.
Phillips JM, Webb BW, Walling DE, Leeks GJL. 1999. Estimating the suspended sediment loads of rivers in the LOIS study area using infrequent samples. *Hydrological Processes* **13**: 1035–1050.
Phillips RW, Lantz RL, Claire LL, Moring WE. 1975. Some effects of gravel mixtures on emergence of coho salmon and steelhead trout fry. *Transactions of the American Fisheries Society* **104**: 461–465.
Platts WS, Megahan WF, Minshall GW. 1983. Methods for evaluating stream, riparian and biotic conditions. Gen. Tech. Rep. INT-138. U.S. Forest Service, Intermountain Forest and Range Experiment Station, Ogden, UT; 70 p.
Platts WS, Torquemada RJ, McHenry ML, Graham CK. 1989. Changes in salmon spawning and rearing habitat from increased delivery of fine sediment to the Soth Fork Salmon River, Idaho. *Transactions of the American Fisheries Society* **118**: 274–283.
Poff NL, Allan JD, Bain MB, Karr JR, Prestegaard KL, Richter BD, Sparks RE, Stromberg JC. 1997. The natural flow regime: a paradigm for river conservation and restoration. *BioScience* **47**: 769–784.
Poole GC, Dunham JB, Keenan DM, Sauter ST, Mccullough DA, Mebane C, Lockwood JC, Essig DA, Hicks MP, Sturdevant DJ, Materna EJ, Spalding SA, Risley J, Deppman M. 2004. The case for regime-based water quality standards. *Bioscience* **54**: 155–161.
PTI Environmental Services. 1991. Pollutants of concern in Puget Sound. US Environmental Protection Agency Report EPA/910-91-003, Seattle, USA.
Quinn JM, Davies-Colley RJ, Hickey CW, Vickers ML, Ryan PA. 1992. Effects of clay discharges on streams. *Hydrobiologia* **248**: 235–247.
Reckhow KH. 2003. On the need for uncertainty assessment in TMDL modelling and implementation. *Journal of Water Resources Planning and Management—ASCE* **129**: 245–246.
Redding JM, Schreck CB. 1983. Influence of ambient salinity on osmoregulation and cortisol concentration in yearling Coho salmon during stress. *Transactions of the American Fisheries Society* **112**: 800–807.
Redding JM, Schreck CB, Everest FH. 1987. Physiological effects on Coho salmon and steelhead of exposure to suspended solids. *Transactions of the American Fisheries Society* **116**: 737–744.
Rees JG, Ridgeway J, Know RWOB, Wiggans G, Breward N. 1999. Sediment-borne contaminants in rivers discharging into the Humber estuary, UK. *Marine Pollution Bulletin* **37**: 316–329.
Re'r DW. 1998. Sediment in gravel-bed rivers: ecological and biological considerations. In *Gravel-bed Rivers in the Environment*, Klingeman PC, Beschta RL, Komar PD, Bradley JB (eds). Water Resource Publications: Colorado, USA; 199–228.
Reynolds B, Norris DA, Hilton J, Bass JAB, Hornby DD. 2004. *The Current and Potential Impact of Diffuse Pollution on Water Dependent Biodiversity in Wales*. Centre for Ecology and Hydrology: Bangor, Wales.
Reynolds JB, Simmons RC, Burkholder AR. 1988. Effects of placer mining discharge on health and food habits of Arctic grayling. *Water Resources Bulletin* **25**: 625–635.
Robertson DM, Richards KD. 2000. Influence of different temporal sampling strategies on estimating loads and maximum concentrations in small streams. In *Proceedings of the 2000 Conference of the National Water Quality Council, US*.
Robertson M. 1957. The effects of suspended materials on the reproductive rate of Daphnia magna. Publication of the Institute of Marine Science, University of Texas 4; 265–277.

Robertson MJ, Scruton DA, Clarke KD. 2007. Seasonal effects of suspended sediment on the behaviour of juvenile Atlantic salmon. *Transaction of the American Fisheries Society* **136**: 822–828.

Rosemond AD, Mulholland PJ, Brawley SH. 2000. Seasonally shifting limitation of stream periphyton: response of algal populations and assemblage biomass and productivity to variations in light, nutrients and herbivores. *Canadian Journal of Fisheries and Aquatic Sciences* **57**: 66–75.

Rosenberg DM, Wiens AP. 1978. Effects of sedimentation on macrobenthic invertebrates on a northern Canadian river. *Water Research* **12**: 753–763.

Rosetta T. 2005. Technical basis for revising turbidity criteria. Water Quality Division, The Oregon Department of Environmental Quality, Oregon, USA.

Rosser B, O'Connnor M. 2007. Startistical analysis of streambed sediment grain size distributions: implications for environmental management and regulatory policy. USDA Forest Service General Technical Report PSW-GTR-194, pp 445–456.

Rowe M, Essig D, Jessup B. 2003. Guide to selection of sediment targets for use in Idaho TMDL's. Idaho Department of Environmental Quality Report, Idaho, USA.

Ryan PA. 1991. Environmental effects of sediment on New Zealand Streams: a review. *New Zealand Journal of Marine and Freshwater Research* **25**: 207–221.

Ryder GI. 1989. Experimental studies on the effects of fine sediment on lotic invertebrates. Unpublished PhD thesis, Department of Zoology, University of Otago: Dunedin, New Zealand; 216.

Scardi M, Cataudella S, Ciccotti E, Di Dato P, Maio G, Marconato E, Salviati S, Tancioni L, Turin P, Zanetti M. 2005. Optimizationof artificial neural networks for predicting fish assemblages in rivers. In *Modelling Community Structure in Freshwater Ecosystems*, Lek S, Scardi M, Verdonschot PF, Descy JP, Park YS (eds). Springer-Verlag: Berlin; 114–129.

Scardi M, Cataudella S, Dato PD, Fresi E, Tancioni L. 2008. An expert system based on fish assemblages for evaluating the ecological quality of streams and rivers. *Ecological Informatics* **3**: 55–63.

Scrimshaw MD, DelValls TA, Blasco J, Chapman PM. 2007. Sediment quality guidelines and weight of evidence assessments. *Sustainable Management of Sediment Resources* **1**: 295–309.

Sear DA, Frostick LB, Rollinson G, Lisle TE. 2008. The significance and mechanics of fine-sediment infiltration and accumulation in gravel spawning beds. In *Salmon Spawning Habitat in Rivers: Physical Controls, Biological Responses and Approaches to Remediation*, Sear DA, DeVries P (eds). American Fisheries Society: Bethesda, USA (Symposium 65); 149–174.

Semple JR. 1991. Atlantic salmon habitat survey: enhancement opportunities and problems in the Dunbar stream, Naswaak River, New Brunswick. Canadian Manuscript Reports of Fisheries and Aquatic Sciences No. 2076, pp 1–35.

Servizi JA, Martens DW. 1991. Effects of temperature, season and fish size on acute lethality of suspended sediments to coho salmon (*Oncorhynchus kisutch*). *Canadian Journal of Fisheries and Aquatic Sciences* **48**: 493–497.

Servizi JA, Martens DW. 1992. Sublethal reponses of coho salmon (Onchorhynchus kisutch) to suspended sediments. *Canadian Journal of Fisheries and Aquatic Sciences* **49**: 1389–1395.

Sharley DJ, Hoffmann AA, Pettigrove V. 2008. Effects of sediment quality on macroinvertebrates in the Sunraysia region of the Murray-Darling Rivers, Australia. *Environmental Pollution* **156**: 689–698.

Shaw EA, Richardson JS. 2001. Direct and indirect effects of sediment pulse duration on stream invertebrate assemblages and rainbow trout (*Oncorhynchus mykiss*) growth and survival. *Canadian Journal of Fisheries and Aquatic Sciences* **58**: 2213–2221.

Shirvell CS, Dungey RG. 1983. Microhabitats chosen by brown trout for feeding and spawning in rivers. *Transactions of the American Fisheries Society* **112**: 355–367.

Sigler JW. 1980. Effects of chronic turbidity on feeding, growth and social behaviour of steelhead trout and coho salmon. PhD thesis, University of Idaho, Moscow, USA.

Sigler JW, Bjornn TC, Everest FH. 1984. Effects of chronic turbidity on density and growth of steelheads and coho salmon. *Transactions of the American Fisheries Society* **113**: 142–150.

Simpson JC, Norris RH. 2000. Biological assessment of river quality: development of AUSRIVAS models and outputs. In *Assessing the Biological Quality of Freshwaters. RIVPACS and other Techniques*, Wright JF, Sutcliffe DW, Furse MT (eds). Freshwater Biological Association: Ambleside, UK; 125–142.

Simpson SL, Batley GE, Charlton AA, Stauber JL, King CK, Chapman JC, Hyne RV, Gate SA, Roach AC, Maher WA. 2005. *Handbook for Sediment Quality Assessment*. CSIRO: Bangor, NSW, Australia.

Slaney PA, Halsey TG, Tautz AF. 1977. Effect of forest harvesting practices on spawning habitats of stream salmonids in the Centennial Creek watershed in Vancouver. Province of British Columbia, Ministry of Recreation and Conservation, Fisheries Management, Report No. 73; 45.

Smith B, Naden P, Cooper D. 2003. Siltation in rivers. 3. Integrated assessment procedure. Conserving Natura 2000 Rivers Conservation Techniques Series. English Nature, Peterborough, UK.

Soulsby C, Malcolm IA. 2001. Fine sediment influence on spawning habitat in a lowland regulated stream: a preliminary assessment. *Science of the Total Environment* **265**: 295–307.

Soulsby C, Youngson AF, Moira HJ, Malcolm IA. 2001. Fine sediment influence on salmonid spawning habitat in a lowland agricultural stream: a preliminary assessment. *Science of the Total Environment* **265**: 295–307.

Stephan H. 1953. Seefishcerei und Hochwasser. Der Einfluss von anorganischen Schwebestoffen auf Cladoceren und Copepoder, Muchen.

Sterba O, Uvira V, Mathur P, Rulik M. 1992. Variations in the hyporheic zone through a riffle in the R. Moriva, Czechoslovakia. *Regulated Rivers: Research and Management* **7**: 31–44.

Stitchert ND, Hubert WA, Skinner D. 2001. A test of factors hypothesized to influence biomass of salmonids in Rocky Mountain streams. *Journal of Freshwater Ecology* **16**: 493–500.

Stober QJ, Ross BD, Melby CL, Dinnel PA, Jagielo TH, Salo EO. 1981. Effects of suspended volcanic sediment on Coho Chinook salmon in the Toule and Cowlitz rivers in Seattle. Technical Completion Report. FRI-UW-8124, Fisheries Research Institute, University of Washington: Seattle, Washington; 147.

Stone M, Droppo IG. 1996. Distribution of lead, copper and zinc in size-fractionated river bed sediment in two agricultural catchments of southern Ontario, Canada. *Environmental Pollution* **93**: 353–362.

Strand RM, Merritt RW. 1997. Effects of episodic sedimentation on the net-spinning caddisflies Hydropsyche betteni and Ceratopsyche sparna (Trichoptera : Hydropsychidae). *Environmental Pollution* **98**: 129–134.

Stross RG, Sokol RC. 1989. Runoff and flocculation modify underwater light environment of the Hudson River estuary. *Estuarine, Coastal and Shelf Science* **29**: 305–316.

Sullivan AB, Snyder DM, Rounds SA. 2010. Controls on biochemical oxygen demand in the upper Klamath River, Oregon. *Chemical Geology* **269**: 12–21.

Sun K, Gao B, Zhang Z, Zhang G, Liu X, Zhao Y, Xing B. 2010. Sorption of endocrine disrupting chemicals by condensed organic matter in soils and sediments. *Chemosphere* **80**: 709–715.

Suren AM, Martin ML, Smith BJ. 2005. Short-term effects of high suspended sediments on six common New Zealand stream invertebrates. *Hydrobiologia* **548**: 67–74.

Swartz RC. 1999. Concensus sediment quality guidelines for polycyclic aromatic hydrocarbon mixtures. *Environmental Toxicology and Chemistry* **18**: 780–787.

Sweka JA, Hartman KJ. 2001. Influence of turbidity on brook trout reactive distance and foraging success. *Transactions of the American Fisheries Society* **130**: 138–146.

Swietlik W, Berry W, Gardner T, Hill B, Jha M, Kaufmann P, Melzian B, Norton D, Paul J, Rubinstein N, Shippen R, Spehar R. 2003. Developing water quality criteria for suspended and bedded sediments (SABS). Potential approaches. US EPA Office of Water, Office of Science and Technology, Health and Ecological Criteria Division, USA.

Sylte TL. 2002. A comparison and evaluation of streambed embeddedness techniques. MSc thesis, Colorado State University, Fort Collins, USA.

Symons PEK, Heland M. 1978. Stream habitats and behavioural interactions of underyearling and yearling Atlantic salmon (*Salmo salar*). *Journal of the Fisheries Research Board of Canada* **35**: 175–183.

Tappel PD, Bjorn TC. 1983. A new way of relating size of spawning gravel to salmonid embryo survival. *North American Journal of Fisheries Management* **3**: 123–135.

Thurrow RF, King JG. 1994. Attributes of Yellowstone cutthroat trout redds in a tributary of the Snake River, Idaho. *Transactions of the American Fisheries Society* **123**: 37–50.

Tramblay Y, Saint-Hilaire A, Ouarda TBMJ. 2007. Modelling extreme suspended sediment concentrations in North America: frequency analysis and correlations with watershed characteristics. In *Water*

Quality and Sediment Behaviour of the Future: Predictions for the 21st Century, Webb BW, De Boer D (eds). International Association of Hydrological Sciences Publication No. 314, IAHS Press: Wallingford, UK; 20–27.

Trimmer M, Sanders IA, Heppell CM. 2009. Carbon and nitrogen cycling in a vegetated lowland chalk river impacted by sediment. *Hydrological Processes* **23**: 2225–2238.

Turnpenny AWH, Williams R. 1980. Effects of sedimentation on the gravels of an industrial river system. *Journal of Fish Biology* **17**: 681–693.

USEPA. 2002. *North Folk Eel River total maximum daily load for suspended sediment and temperature*. Office of Water: Washington DC, USA.

USEPA, 2003. Strategy for water quality standards and criteria: setting priorities to strengthen the foundation forprotecting and restoring the nation's waters. Office of Water (EPA-823-R-03-010), Washington DC, USA.

USEPA, 2007. www.epa.gov/waterscience/criteria/wqcriteria.html. #nonprioritySS.

Vinyard GL, Yuan AC. 1996. Effects of turbidity on feeding rates of Lahontan cutthroat trout (Oncorhynchus clarki henshawi) and Lahontan redside shiner (Richardsonius egregious). *Great Basin Naturalist* **56**: 157–161.

Voelz NJ, Ward JV. 1992. Feeding habits and food resources of filter-feeding Trichoptera in a regulated mountain stream. *Hydrobiologia* **231**: 187–196.

Vogel JL, Beauchamp DA. 1999. Effects of light, prey size, and turbidity on reaction distances of lake trout (*Salvelinus namaycush*) to salmonid prey. *Canadian Journal of Fisheries and Aquatic Sciences* **56**: 1293–1297.

Wagener SM, LaPerriere JD. 1985. Effects of placer mining on the invertebrate communities of interior Alaska. *Freshwater Invertebrate Biology* **4**: 208–214.

Ward JV, Bretschko G, Brunke M, Danielpol D, Gibert J, Gonser T, Hildrew AG. 1998. The boundaries of river systems: the metazoan perspective. *Freshwater Biology* **40**: 531–569.

Wallen IE. 1951. The direct effect of turbidity on fishes. *Bulletin of the Oklahoma Agricultural and Mechanical College* **2**: 48.

Walling DE, Webb BW. 1987. Suspended load in gravel-bed rivers: UK experience. In *Sediment Transport in Gravel-bed Rivers*, Thorne CR, Bathurst JC, Hey RD (eds). Wiley: Chichester, UK; 691–723.

Walling DE, Webb BW, Shanahan J. 2008. Investigations into the use of critical sediment yields for assessing and managing fine sediment inputs into freshwater ecosystems. Natural England Research Report NERR007. Natural England, Sheffield.

Warren N, Allan IJ, Cater JE, House WA, Parker A. 2003. Pesticides and other micro-organic contaminants in freshwater sedimentary environments—a review. *Applied Geochemistry* **18**: 159–194.

Watts CD, Naden PS, Cooper DM, Gannon B. 2003. Application of a regional procedure to assess the risk to fish from high sediment concentrations. *Science of the Total Environment* **314–316**: 551–565.

Whitfield AK. 1996. Fishes and the environmental status of South African estuaries. *Fisheries Management and Ecology* **3**: 45–57.

Whitman RL, Clark WJ. 1982. Availability of dissolved oxygen in interstitial waters of a sandy creek. *Hydrobiologia* **92**: 651–658.

Whitman RR, Quinn TP, Brannon EL. 1982. Influence of suspended volcanic ash on homing behaviour of adult Chinook salmon. *Transactions of the American Fisheries Society* **111**: 63–69.

Wilber CG. 1983. *Turbidity in the Aquatic Environment: An Environmental Factor in Fresh and Oceanic Waters*. Charles C. Thomas: Springfield, Illinois, USA.

Witzel L, MacCrimmon H. 1983. Redd-site selection by brook trout and brown trout in southwestern Ontario streams. *Transactions of the American Fisheries Society* **112**: 760–771.

Wood PJ, Armitage PD. 1997. Biological effects of fine sediment in the lotic environment. *Environmental Management* **21**: 203–217.

Wood PJ, Toone J, Greenwood MT, Armitage PD. 2005. The response of four lotic macroinvertebrate taxa to burial by sediments. *Archiv für Hydrobiologie* **163**: 145–162.

Wren DG, Barkdoll BD, Kuhnle RA, Derrow DW. 2000. Field techniques for suspended sediment measurement. *Journal of Hydraulic Engineering* **126**: 97–104.

Wright JF, Moss D, Armitage PD, Furse MT. 1984. A preliminary classification of running-water sites in Great Britain based on macroinvertebrate species and the prediction of community type using environmental data. *Freshwater Biology* **14**: 221–256.

Yarnell SM, Mount JF, Larsen EW. 2006. The influence of relative sediment supply on riverine habitat heterogeneity. *Geomorphology* **80**: 310–324.

Zweig LD, Rabeni CF. 2001. Biomonitoring for deposited sediment using benthic invertebrates: a test on four Missouri streams. *Journal of the North American Benthological Society* **20**: 643–657.

Assessment of erosion, sedimentation, and water quality impacts of the Mountain Valley Pipeline and Equitrans Expansion Project's proposed crossing of the Jefferson National Forest as it pertains to the U.S. Forest Service's Draft Supplemental Environmental Impact Statement dated December 2022

Prepared by Jonathan A. Czuba, Ph.D., Licensed Professional Engineer - February 9, 2023

REFERENCES
4

February 21, 2023

Advanced Review

The pernicious problem of streambed colmation: a multi-disciplinary reflection on the mechanisms, causes, impacts, and management challenges

Geraldene Wharton,[1]* Seyed Hossein Mohajeri[2] and Maurizio Righetti[3]

The accumulation of fine sediments in rivers is a pernicious problem with wide-ranging consequences for the healthy functioning of rivers throughout the world. It is linked to a range of landuse changes and human activities that have increased sediment inputs leading to elevated fine sediment loads that exceed the sediment transport capacities of rivers. Surficial deposits of fine material can also create the conditions for fine sediment to move into and accumulate *within* the coarser bed substrate, a process known as *colmation* and the focus of this review. Colmation, also referred to as clogging, fine sediment infiltration, fine sediment deposition, ingress, infilling, intrusion of fines, siltation, and the surface–subsurface exchange of particles, is particularly damaging to river habitats and ecosystems. It causes degradation through the physical effects of reduced porosity and flow connectivity and the biogeochemical changes arising from the hydraulic and hydrological impacts and the effects of sediment-bound contaminants, all of which can impact on river ecology. Different aspects of the phenomenon of colmation have been studied across a number of disciplines and over several decades and this paper synthesizes this wide literature to provide a multidisciplinary perspective on the mechanisms, causes, and impacts of colmation and discusses some key management challenges.

How to cite this article:
WIREs Water 2017, 4:e1231. doi: 10.1002/wat2.1231

INTRODUCTION

Fine sediment, defined as inorganic and organic material < 2 mm in diameter, plays an important role in the geomorphology, hydrology, and ecology of river systems not least because the healthy functioning of aquatic habitats is dependent upon the delivery of nutrients bound to fine sediments. The varying proportions of sand, silt, and clay in fine sediment will determine whether it is either granular or cohesive, and the organic matter component can comprise particulate organic matter, such as seeds and aggregates and/or flocs of organic and inorganic particles,[1,2] including invertebrate faecal pellets[3] or particles with biofilms.[4] In addition to the particulates (solids), fine sediment deposits also contain liquid and gaseous components resulting in a mixture that is physically, chemically, and biologically heterogeneous. Longitudinal, lateral, and vertical fluxes of fine sediment in the fluvial system link hillslopes to floodplains, riparian zones, the active channel, and

*Correspondence to: g.wharton@qmul.ac.uk

[1]School of Geography, Queen Mary University of London, London, UK

[2]Department of Civil Engineering, Science and Research Branch, Islamic Azad University, Tehran, Iran

[3]Hydraulic and Maritime Constructions and Hydrology, Faculty of Science and Technology, Free University of Bozen, Bozen, Italy

Conflict of interest: The authors have declared no conflicts of interest for this article.

the hyporheic and groundwater zones. Therefore, fine sediment can provide an important 'connectivity signature' of the river landscape as well possessing a distinctive 'biogeochemical signature' due to its heterogeneous nature.[5]

During recent decades, however, many river systems around the world have been experiencing rising inputs of fine sediment[6–8] resulting in fine sediment loadings far exceeding pre-industrial (background) conditions.[9,10] These increases have been linked to a large number of human activities and catchment disturbances[11–14] and have resulted in a wide range of environmental impacts. The same chemically active silts and clays that supply vital nutrients to aquatic habitats can also be a vector for pollutant transport because many inorganic and organic micro-pollutants including heavy and trace metals, polycyclic aromatic hydrocarbons (PAHs), pesticides, dioxins and radionuclides, have a high affinity for the fine-grained fraction of sediments[15] with fine sediment entrainment, transport, and deposition dictating the delivery of these sediment-bound contaminants to different parts of the river system and their subsequent residence times.[16] The enhanced sedimentation and accumulated surficial sediments (Figure 1) observed in many rivers[17] reflect elevated fine sediment loads exceeding the ability of streams to transport the material.[8] Permeable, groundwater-dominated streams are particularly prone to fine sediment deposition and colmation due to their distinctive hydrology which reduces the ability of fine surficial sediments to be eroded once deposited on the streambed. These accumulations of surficial fines affect the habitat for aquatic macrophytes,[18–20] benthic invertebrates, diatoms,[21] and fish.[22] Particles from these accumulated fine sediment deposits can also penetrate into the coarser materials (e.g., gravels and cobbles) forming the streambed and reduce its hydraulic conductivity[23] and also infiltrate further into the hyporheic zone. Thus, several aquatic interfaces will be affected.[24] In particular, the connectivity among surface water, the hyporheic zone,[25] and the underlying groundwater may be impeded thus altering the flux of dissolved and sediment-bound substances.[26–30]

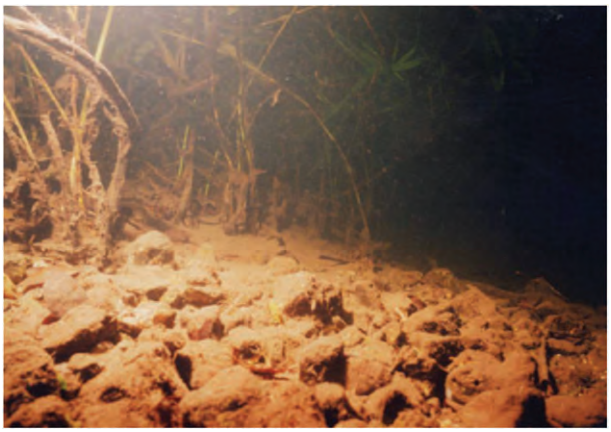

FIGURE 1 | Surficial fine sediments can create the conditions for streambed colmation (Photo: Lin Baldock).

There are fewer studies documenting elevated levels of sedimentation *within* streambeds and bed sediment storage compared to those showing increased sediment yields and suspended loads in rivers. However, studies of the infiltration of fine sediments into streambeds (colmation) and their re-release (decolmation) and an awareness of the environmental impacts can be traced back many decades, e.g., Refs 18,31–41. Since this early research, biologists, geomorphologists, hydrologists, and engineers have undertaken field measurements, laboratory experiments, and developed numerical models aimed at understanding how fine sediment enters the river bed, its causes, and its impacts with several terms emerging and being employed interchangeably in the research literature. These include siltation[42]; ingress[30]; clogging[43–50]; infilling[51,52]; fine sediment infiltration[53–58]; fine sediment deposition or sedimentation[8,46]; surface-subsurface exchange of particles[4]; intrusion of fines[59]; and colmation[60–63] the term used hereafter in this review because it has been used across disciplines and has a clear corresponding term (decolmation) for the reverse process by which fines leave the streambed. A more inter-disciplinary approach to the study of colmation has only started to emerge in recent years, e.g., Refs 4,63 and, in bringing together the literature on this topic, this review aims to provide some new perspectives and insights which might help inform the management of fine sediments in rivers. We first consider the processes and key factors controlling colmation before examining the main causes and impacts and concluding with a discussion of some of the challenges for river and catchment management.

COLMATION AND DECOLMATION: PROCESSES AND CONTROLLING FACTORS

Understanding how, why, and where colmation takes place is critical for assessing the environmental and economic impacts of upstream anthropogenic and natural fine sediment releases into rivers.[55] Streambed colmation has been observed in the field but laboratory studies have been particularly useful

in clarifying the mechanisms under different combinations of suspended particles, bed sediments, and hydrodynamic conditions,[4] and researchers have also developed theoretical, mathematical, and probabilistic models, e.g., the models by Lauck[64] and Herrero and Berni.[58]

The process of colmation encompasses the entry of finer material into the coarser matrix of the bed (normally sands, silts, and clays moving into gravels and/or cobbles; or silts and clays entering a sand substrate); its filtration to the hyporheic zone below; and the formation of a layer which reduces the permeability of a streambed compared to the initial conditions.[43,44,60] Colmation is more commonly associated with the intrusion of fine sediments into the coarser bed sediments from surficial deposits (Figure 2(a), external colmation) which arises due to increased fine sediment loads in combination with reduced flow velocities and water levels triggering sediment deposition and the subsequent infiltration of fine sediments into the streambed. Interestingly, Lisle[65] found that the largest proportion of infiltrated sediment originated from the finest fraction of the bedload rather than from settled suspended load showing the importance of bed material load and transport. External colmation can also arise due to increased sewage loading in rivers which causes sedimentation of an organic layer on the streambed and the development of dense algal mats.[60] However, the formation of a thin sealed layer below an armor layer (Figure 2(b), internal colmation) can occur when surficial fines that have been able to penetrate through a coarse armor layer are unable to pass through the smaller pore spaces of a finer sub-armor layer beneath or when fines move upwards from the underlying hyporheic zone and collect underneath an armor layer.[43,66,67] Fines can also penetrate into, and cause the clogging of, an armor layer (as distinct from the entry into a more open and mobile coarse streambed), a process known as *contact colmation*, *intermediate colmation*, or *armor layer colmation*.[44,62]

All three forms of colmation are dependent on a number of interconnected physical, chemical, and biological variables[37,43,68] including the flow velocity and shear stress of the river; the hydraulic gradient of the seepage flow and its direction; suspended sediment concentrations; grain size distributions and particle shapes of the infiltrating material and the bed substrate; the presence of algae and biofilms[4]; and the type and concentration of dissolved substances. Early experimental work by Beschta and Jackson[38] was valuable in showing the importance of the flow condition (as represented by the Froude number) as a key hydraulic parameter affecting fine particle infiltration, in combination with sediment input rate and its particle size distribution. They also showed how turbulent pulses generated at higher velocities inhibited fine sediment deposition. Subsequently, Carling[69] demonstrated, not surprisingly, that mean flow data have limited value in understanding a process that takes place on and within the streambed by showing how pore water velocity distribution and substrate porosity are important in controlling the movement of fine sediment into the gravel substrate. A macro-analysis by Huston and Fox[50] of 10 recently published studies also provided further insight by showing that whilst bed-to-grain ratio (defined as the grain size distribution of the bed sediments relative to those of the infiltrating grains) is reliable in predicting the initiation of colmation, the depth of ingress is determined more by the substrate porosity, roughness, and Reynolds number since together these better reflect the control of pore water velocity distribution on how fine sediment moves (infiltrates) into the gravel substrate.

Early detailed studies of the mechanism of infiltration, e.g., Refs 37,70 identified a *mechanical filtration* that occurs with larger fine particles (diameters > 30 μm) where particle size and shape are the most important factors; and a *physicochemical filtration* for smaller particles (<1 μm) where the surface charge of the particle and adhesion of colloidal particles and bacteria play a role. For medium-sized fine particles (diameters 3–30 μm) both mechanisms can determine particle entry and retention. For example, deposition of small biological particles into streambeds is increased if associated with larger inorganic particles or organic/inorganic aggregates and benthic and hyporheic biofilms increase particle retention.[71] Further research is thus needed on the role of biological factors and, in particular, the mechanism of particle capture in biofilms and how particles are released back to the water column.[4]

Streambeds that suffer from colmation are characterized by a more consolidated texture, and a reduced porosity and hydraulic conductivity[61] and an important consideration is the depth of ingress. Observations in the field have shown that there is a limit to the depth of fine sediment infiltration within gravel beds[43,69,72] with the grain size distribution of the streambed an important control. Cui and Parker[73] reported that the fine sediment fraction within gravel deposits is negatively correlated to the standard deviation of the particle diameters within the gravel matrix (which is a surrogate measure for available pore space). The grain size distribution of the bed sediments influences the available pore space of the substrate which in turn

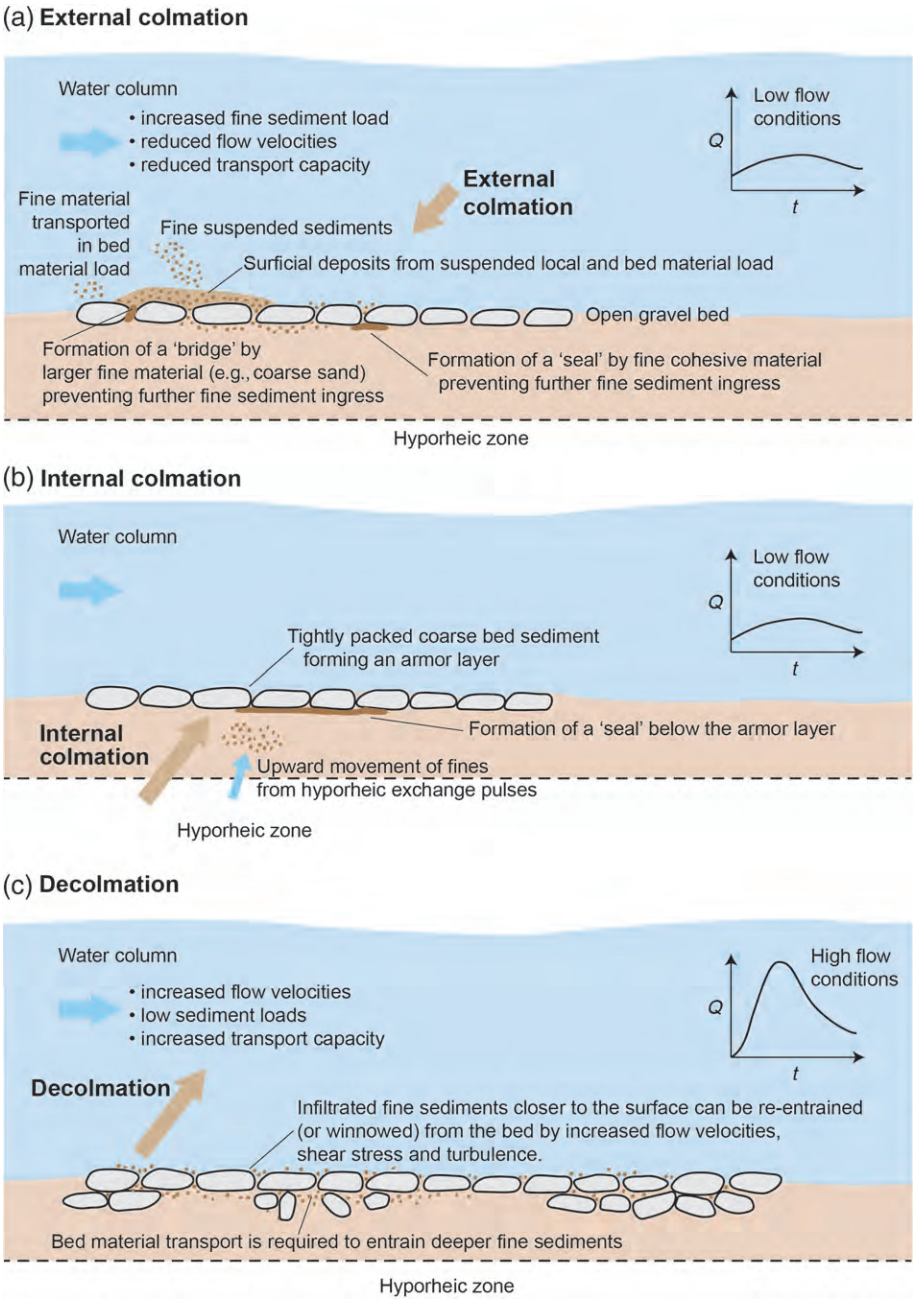

FIGURE 2 | Conceptual diagram showing the mechanisms of colmation and decolmation.

exerts a major control on the size of the particles that can infiltrate and the amount and depth of colmation.[43,57,74] Grain size distribution has been shown to be more important for initial particle intrusion,[38] whereas pore sizes are critical in determining infiltration depth.[66] A further important recent finding[57] is that larger grain sizes in a streambed offer more pore space to receive smaller infiltrating grains but a streambed with a wider range of particle sizes will have less available pore space because voids can be filled by variably sized particles. This supports earlier work by Wooster et al.[55] on the importance of the relative grain sizes of the substrate, the infiltrating material, and the pore spaces in the bed material and explains how silts and clays can still infiltrate a gravel bed already saturated or over-saturated with sand. And building on this, a new method has been proposed to predict the grain size distribution for a saturated gravel bed and the reduced porosity taking into account the changing characteristics of the bed and the supplied sediments during the filling process.[75]

Complementing the field observations and laboratory studies, theoretical and probabilistic models, e.g., the Lauck[64] model, have reproduced the general observations of Einstein[32] that fine sediment fills the pores in the gravel matrix from the bottom up when the size ratio of the bed material to fine sediment is large and the bed material is shallow. The Lauck[64] model has also reproduced the key observations from other studies[38,43,65,66,69] that fine sediment can only infiltrate to a finite depth if the bed material is sufficiently thick. Subsequently, Cui et al.[56] developed a theory to describe the processes of colmation based on Lauck,[64] and this states that the highest possible fine sediment fraction resulting from fine sediment infiltrating an immobile clean gravel deposit is an exponential decay function with depth into the bed material. Thus, well-sorted gravels with large pores are conducive to deeper colmation, whereas in poorly-sorted streambed sediments with smaller pore sizes the colmation depth is relatively shallow, although the presence of macropores can enable the movement of fines through poorly sorted sediments to deeper layers.[61]

During the process of colmation, larger infiltrating grains can also become trapped among the pore spaces of large bed grains near the surface of the bed substrate creating a 'bridge' or the accumulation of fine cohesive material can create a 'seal' both of which block further infiltration (Figure 2 (a) and (b)). Seals and bridges have been observed in both field and laboratory studies. Gibson et al.[76] suggest that they form when the ratio D_{15} substrate/D_{85} infiltrating sand is below 12–14, although a mobile bed substrate will limit seal formation and persistence even under conditions of high sand supply.[57] And laboratory flume experiments of clay infiltration into a sand bed[45] showed that clay particles caused the clogging of the surface of the streambed which isolated deeper sections of the bed from the streamflow. Thus, when seals or bridges form, streambeds do not always fill from the bottom upwards and even relatively low suspended sediment loads can degrade the habitat by reducing or preventing surface–subsurface exchanges).[77] Recent progress which will contribute to a growing understanding of the physics of streambed colmation has also been made in the development of a mathematical model which reproduces the two main infiltration mechanisms ('bridging' and 'unimpeded static percolation,' i.e., the infiltration of fines to an impermeable layer and subsequent filling).[58] In addition to the variations in bed substrate, spatial patterns of bed morphology (e.g., pool-riffle sequences), flow types, and suspended sediment characteristics along a river can create 'a three-dimensional mosaic of differentially colmated areas within the streambed.'[61] For example, Diplas[78] recorded how pools and the downstream side of bars were the first locations to experience colmation. Furthermore, temporal changes in flow and sediment conditions that arise, e.g., during periods of reduced river flow may exacerbate infiltration in locations of the streambed that are already prone to colmation including pools or low velocity areas in and around vegetation or large wood.[20,30,79]

In contrast, the higher flow velocities, shear stresses, and turbulent pulses experienced during flood conditions or the upwelling of groundwater[44,80] may not only inhibit the first stages of colmation[38] but may also trigger site-specific *decolmation* (Figure 2(c)). Decolmation, also known as *declogging* or *exfiltration*, locally re-establishes the permeability of the streambed as fines are flushed from the pore spaces.[81] Early work by Milhous[36] observed that during low flows the gravel bed acts as a sink for fine sediments (a 'silt reservoir') but during high flows the gravel bed becomes a source and releases fines into suspension. And a recent modeling study showed a doubling in the retention of clay particles within the streambed during low flow conditions.[82]

Schälchli[43] proposed four main phases to the decolmation process related to increasing dimensionless shear stress and this provides a valuable conceptual framework and starting point for understanding decolmation mechanisms. In Phase I, bedload transport is initiated as the shear stress increases and reaches a threshold level that triggers a partial decolmation. This is followed in Phase II by a further flushing out of fines and an increase in the hydraulic conductivity of the top layer of the streambed. In Phase III, the armor layer breaks up locally and the hydraulic conductivity increases up to a maximum level. Finally, at peak flow (Phase IV) the whole riverbed is mobilized and previously consolidated channel beds are broken up. As with the process of colmation, the spatial variations in streambed morphology and hydraulic conditions create areas with different levels of susceptibility to decolmation and those areas most prone to colmation (e.g., pools and the downstream side of bars) are the least prone to decolmation.[78] The colmation–decolmation cycle has also been linked to scour and fill events[65] with fill events leading to colmation but scour events responsible for both decolmation by winnowing fines from the bed but also colmation by exposing deeper portions of the bed to fine sediment infiltration.

Thus, decolmation of the upper layers can be achieved through increased flow velocities and shear stress,[60] but bedload movement is needed to open

deeper interstices to allow the flushing of fines from lower layers[83] without which *permanent colmation* will occur. More recently, Venditti et al.[84] and Evans and Wilcox[57] have linked the residence time of fine sediment in the bed to the frequency and depth of bed mobilization. A 'mortar effect' from the addition of fines has also been observed[85] which could reduce decolmation through the increased strength of the streambed. However, the mobility of coarse surface layers and associated feedbacks with infiltrated fines remains poorly understood[86] and further research is needed.

Building on the studies focusing on the hydraulic controls of decolmation, e.g., Ref 43 there is growing evidence from more recent research of the importance of biological processes and controls on colmation and decolmation. For example, bioturbation by fish, crayfish, and benthic invertebrates can be a pre-conditioning agent that promotes decolmation by increasing the exposure of sediments to increasing shear stress[87] and Nogaro et al.[88] in an experimental study showed how invertebrate bioturbation can reduce the clogging of sediment. In contrast, extracellular polymeric substances (EPS), such as those produced by diatoms[89] and biofilms,[90] may bind and strengthen ingressed sediments and thus slow both the rate of decolmation and the total amount of fine material flushed from the streambed. And the colonization of nutrient-rich fine sediments by filamentous green algae can also encourage the deposition of fine sediments.[91] Further research is thus needed to consider the interplay of physical, chemical, and biological controls which may also have a seasonal dimension as with the preliminary observations of temporal patterns in the erodibility and, therefore, the residence times of surficial fine cohesive sediments.[92]

Finally, it is important to emphasize that alternating phases of colmation and decolmation, linked to a river's flow regime and fluxes of fine sediment, are natural cyclical processes of sedimentation and erosion in streambeds[44,61] that contribute to habitat heterogeneity and the healthy functioning of river systems by giving rise, e.g., to the turnover of sediments and replenishment of sediment-bound nutrients. However, anthropogenic activity in many catchments has altered the natural flux of fine materials and resulted in elevated fine sediment loads, enhanced sedimentation, and thus the conditions for colmation leading to a wide range of environmental impacts.[61] The causes and effects of colmation are now discussed in more detail.

CAUSES OF COLMATION

A situation of sediment surplus in rivers arises when more sediment is present than can be transported by the available flow and this creates the surficial sediment deposits from which colmation may occur. Those processes and activities which increase the sediment loads of rivers and/or reduce the flow velocities or discharges are thus the triggers for colmation. Numerous studies have reported increasing sediment loads in river systems and enhanced sedimentation. For example, sediment yields in the Danube catchment have risen by 30–50% in the period 1950–1980,[93,94] annual sediment loads for the River Lech in Bavaria increased after 1965,[95] and future increases of 250% are anticipated in the annual sediment supply of the Rhine, e.g., Ref 96. These elevated fine sediment loads have been linked to a large number of in-stream and catchment-wide human activities, many of which have a long history and create a legacy effect (see Wohl[14] for a detailed review of the history and causes of enhanced sedimentation in river systems).

The main causes of elevated sediment loads in rivers have been changes to the catchment landuse, such as deforestation[97] and logging,[98] clearance of native vegetation in association with grazing or cropping,[12,99–102] and changes in agricultural practice, in particular a shift from grazing to tilled agriculture, and an increase in the amount of tillage, all of which have increased runoff and erosion of top soil.[10,12,103–106] Different types of crop production have also been linked to elevated fine sediment loads, e.g. the switch from grain to potato cultivation documented by Klimek,[107] as have farming practices, such as those that have led to overgrazing, trampling, and poaching by cattle. And increases in fine sediment production and delivery have been linked to the intensive cultivation of cereals and high livestock numbers during the second half of the 20th century in the River Frome Catchment, Dorset, UK.[108] Although the agricultural sector is a significant contributor to the fine sediment delivered to rivers, estimated to contribute approximately 76% nationally to the watercourses in England and Wales,[109] the urbanization of catchments increases runoff and can lead to increases in fine sediments from road-deposited sediment.[110,111] Further inputs of solids can derive from sewage treatment plants, with Carter et al.[112] estimating approximately 40% of fine sediments in urban rivers coming from sewage or road dust. A large number of in-stream human activities have also resulted in enhanced sedimentation including mining activities,[113,114] sediment 'flushing' from

hydro-electric power plants,[77,115,116] and the release of sediments in the construction phase of channelization schemes,[19] and as a consequence of dam removal.[117] A few studies have also shown increases in the bed storage of fine sediments in addition to the accumulation of surficial deposits linked to higher fine sediment loads and ultimately changes in catchment landuse and agricultural practices, e.g., the studies of the chalk streams of the Frome and Piddle catchments by Collins and Walling[104] and Heppell et al.[30]

Climate change will clearly have an impact on the sediment dynamics in rivers and therefore streambed colmation, but there is currently limited evidence available and it is difficult to isolate the influence of climate change from all the other changes that affect the condition of the catchment.[6] Furthermore, there is no clear emerging pattern in the changing sediment loads of the world's rivers.[6] For the alpine Rhine catchment, sediment supply is estimated to increase by 250% based on future scenarios of climate and landuse change.[84] However, large decreases have been reported in the sediment load delivered from the Huanghe (Yellow River) to the sea and the yield now represents only 14% of the widely cited estimate of 1.08 Gt/year.[118] This sharp reduction has been explained by decreased precipitation combined with human activities in the river and catchment. In addition to the challenge of isolating the effects of changes in climate and landuse, and understanding the response of different regions and catchments to climate changes, there is also a gap in research linking increases in sediment supply and load to surficial fine sediment deposits and streambed colmation. However, some insights into the effects of climate change on sediment inputs and streambed deposition with links to fish habitat and have been provided by a few studies of deglaciation in alpine countries.[82] This research has shown how rising air temperatures have indirectly affected river sediment loads through changed precipitation patterns, a decline in permafrost, snow melting and rising snow lines[82] and changes in snowmelt dynamics[108]; changes which are known to leave unconsolidated deposits exposed and result in increased runoff and erosion.[119] Further research is needed to establish clear cause and effect relationships between changing climate and catchment conditions, increases in sediment loads and sedimentation both on and within riverbeds, and how this impacts on river ecology.

Alongside the many human activities that increase the supply of sediments to rivers are those that modify river flows and therefore affect the sediment transport capacity. Widespread reductions in groundwater levels and river discharges have occurred due to human consumptive uses with abstractions for drinking water supply, agriculture and industry. In natural streams where the bed is permeable, exchanges (upwelling and downwelling) between surface and subsurface flows take place.[61,120,121] Lowering of groundwater levels reduces river baseflow and weakens these exchanges and promotes the development of a colmation layer.[122–124] Hydropower schemes have major impacts on the magnitude and timing of river flows (hydropeaking effects) and river water temperatures (thermopeaking effects)[125] and as a consequence sediment regimes and sediment deposition. Significantly, some studies have shown temporal variations in the deposition and colmation of fine sediments downstream of dams which differ from natural cycles[126] and the promotion of biocolmation processes due to the higher temperatures of the released water.[127] And with a global boom in dam-building activity,[128] the extent of these impacts is anticipated to increase.

IMPACTS OF COLMATION

Although colmation causes a relatively slow and insidious change to streambeds[7] because it is triggered in part by the frequent lower flows in contrast to the more dramatic changes that occur as a result of high magnitude discharges, the impacts are wide ranging and have been linked to the severe degradation of river environments. Colmation changes: the composition and structure of streambeds, which in turn modifies the flow conditions in the surface waters above the bed; the interconnections between surface water, interstitial pore water, the hyporheic zone and groundwater and the biogeochemical functioning in each of these zones; and the connectivity between the instream environment and the riparian and floodplain zones. In this section, we focus on the impacts of colmation on stream ecology as a result of the direct and indirect effects of these hydrological, hydraulic, and biogeochemical changes operating both vertically and laterally in the fluvial system.

The infilling of streambeds by fine sediments causes the compaction of the stream substratum and an increase in cementation,[129] which gradually alters the bed structure and morphology. Experimental studies have demonstrated how this has a significant impact upon the flow structure and turbulence[130–132] above the streambed by reducing the bed relief and effective roughness and Kuhnle et al.[133] have shown how the roughness geometry function[134] reduces

abruptly with increments in sand level. Furthermore, even if the streambed is not completely infilled and smothered with fines the protrusion of some coarse particles can create a hiding effect which will reduce fine sediment transport.[135] These studies indicate that sharp thresholds in flow structures may characterize areas of the streambed suffering from colmation and further research is now needed to consider the effects of streambed colmation upon vertical and streamwise velocity distributions and turbulence to inform understanding of fine sediment deposition and entrainment.

The physical changes to streambed structure and composition will have several direct effects on stream ecology by altering the function of different species and competition between them. In turn, this will affect species composition and diversity[47,87,136] and impacts have been observed on fish, e.g., Ref 22, macro-invertebrates, e.g., Ref 21, diatoms, e.g., Ref 91, and macrophytes, e.g., Ref 20 which comprise the biological elements used to assess the ecological quality of freshwaters under the EU Water Framework Directive.[137] Overall, colmation produces a more homogeneous streambed which reduces habitat and species diversity[60] and community composition can also be altered depending upon how different species respond and adapt to the changes caused by colmation. For example, the increased presence of fine sediments within the uppermost layers of the bed increases the possibility of abrasion which can damage unprotected, fine and fleshy body parts such as gills and filter-feeding apparatus.[21] Blackfly (*Simuliidae*) and caddis fly larvae are also sensitive to receiving particles[21,138] with blackfly larvae ingesting large amounts of inert material and the nets of caddis fly larvae becoming clogged with fine sediments necessitating increased energy expenditure on cleaning activities. Bivalave molluscs and Cladocera cope better in being able to reject unwanted particles from their gills and filter combs but in so doing they also spend time and energy cleaning these structures.[21,139]

Burial, and sometimes abrasion by fine sediment, can also be a problem for fish eggs in the streambed[22] and smaller individuals and certain life stages of invertebrates can be particularly vulnerable.[21] Additionally, the nymphal stage of species such as mayflies will be impacted because they prefer coarser, more stable, substrates for gripping.[21,140] The ingress of fine sediments also restricts the space for the movement and growth of macro-organisms such as mussels and reduces the ability of invertebrates to penetrate to deeper layers of the substrate to seek refugia from high flows and predators.[141] Non-motile diatoms can also be buried by fine sediment causing diatom assemblages to become dominated by motile taxa, where the rates of deposition and ingress of fine sediments are high but benthic diatoms can also thrive in the nutrient-rich deposits.[91] In contrast, some species, such as certain Chironomidae and Ephemeridae that perform bioturbation, are able to move sediment and create enough space for their continued survival and can thrive under colmation.[21,142] Bioturbators also increase water-sediment interactions which can initiate beneficial biogeochemical and microbial processes,[88] which further helps in adapting to colmation.

Colmation can have several direct and indirect effects on macrophytes with the level of impact determined by the rate of fine sediment deposition and ingress and the nature of the ingressed material.[20] For example, fine sediment ingress reduces the grain size distribution of the bed which potentially increases its erodibility and also encourages shallow rooting, both of which increase the likelihood that plants will be uprooted during high flow events. Fine sediment ingress will also smother seeds, turions, tubers, and other reproductive propagules, and affect the ability of macrophytes to establish. The composition of macrophyte communities can also be altered by colmation depending on the different levels of adaptability. For example, fast-growing emergent species (e.g., *Rorippa nasturtium-aquaticum*) can continue to grow through the fine sediment and thus competitively replace species such as *Ranunculus penicillatus* subsp. pseudofluitans which are unable to cope with being smothered[18] and the competitive ability of *Elodea nuttallii* (Planch.) St. John and *Myriophyllum spicatum* L. has been observed to increase in more nutrient-rich fine sediments.[143] But the benefits of growing in a more fertile substrate are eventually balanced by the negative aspects of being rooted in an unstable, anoxic medium.[20]

Colmation is particularly damaging to the health of rivers because the reduced hydraulic conductivity of the streambed[61,144] disturbs the spatial and temporal patterns in the exchanges of water, dissolved substances, and fine suspended particles between the surface water, interstitial water, the underlying hyporheic zone[145] and groundwater. This in turn alters the physical and chemical conditions and gradients important for supporting a healthy riverine flora and fauna with significant implications for stream metabolism and nutrient cycling. Thus, colmation will restrict the supply of oxygen to fish eggs buried in the streambed[22] and organisms in the streambed will be excluded from up-welling nutrients and down-welling oxygen with impacts observed on the taxa in the hyporheic zone.[87,144,146,147] Lowering

of dissolved oxygen levels leads to reductions in oxic processes such as respiration and nitrification but an intensification of bacterial activity and anoxic processes and a greater prevalence of denitrification and fermentation[88,144,146,148,149] stimulating the growth of biofilm and heterotrophic microbial processes.[144,150] These conditions also increase the reproduction of nitrate-reducing bacteria[147] which accelerates the process of biological colmation. The chemical conditions of the streambed are often further altered by the ingress of sediment-bound contaminants such as fertilizers and pesticides which can accumulate over time[62] and reduce species diversity.[90,105] However, this reduced vertical connectivity and increased resistance can sometimes helpfully prevent pollutants entering the groundwater and also improve purification by bank-filtration processes.[60,80,151]

River temperature regulation is also affected by colmation which has an impact on benthic and hyporheic habitat conditions.[25,60,152] Without up-welling groundwater the river is not able to benefit from the injection of cooler water in summer, especially important in counteracting the daytime heating of surface water[153] nor the flow of warmer water in winter. Water temperature has been shown to be critical for fish reproduction,[154] invertebrate development, and microbial activity in the hyporheic zone.[60,155] For example, the earlier than predicted hatching and alevin emergence of brown trout eggs reported by Acornley[154] was explained by the warmer river gravels because colmation weakens the intragravel temperature gradients and produces a more uniform spatial thermal distribution.

Finally, the effects of reduced surface–subsurface connectivity can extend beyond the instream and hyporheic zones to the riparian and floodplain environments since colmation can induce lower groundwater levels[60,156] and sometimes change a perennial river to an ephemeral one.[121] The riparian zone is an important area for biodiversity and productivity and lower groundwater can have detrimental effects on the riparian vegetation[121,157] which can have further impacts on other biota.[152]

CHALLENGES FOR MANAGEMENT AND FUTURE DIRECTIONS

Fine sediment is a natural and important component of fluvial systems but in recent decades a range of landuse changes and human activities in combination with some reported climate change effects have caused it to become a major ecosystem stressor. The increased delivery of fine sediments to rivers and reductions in sediment transport capacity have elevated suspended sediment loads far beyond background (pre-industrial) levels[9] and led to the accumulation of surficial fine deposits and streambed colmation with impacts on the physical, chemical, and biological condition of rivers (Figure 3). In England and Wales, e.g., the total loss of sediment in excess of the target modern 'background' sediment delivery to rivers has been estimated at an alarming 1,389,818 t/year, equating to environmental damage costs of up to £523 M/year.[10] Contaminants bind to fine sediments further degrading river habitats and fine sediment is now classified as a diffuse pollutant in Europe under the Water Framework Directive[126] and responsible for 23% of water bodies in England at risk of failing to reach good ecological status.[96,158] A key management challenge is thus to address these sediment quantity and quality issues and meet legislative requirements[159] without undermining the positive effects of fine sediment in sustaining ecosystem functions and services.[160] But the lack of routine monitoring of sediment runoff or in-channel siltation means that there is limited regional to national data to inform decision making and assess the effectiveness of implemented management options.[158] Data on streambed colmation are particularly limited but hydraulic conductivity, which is highly correlated with the percentage of subsurface fines, has been identified as an accurate and robust method that could be used for large scale and long-term colmation monitoring programs.[161]

Instream approaches to remediate excessive fine sediments in streambeds, such as mechanical removal (vacuuming) of fines from fish spawning beds or the use of clean 'flushing' flows,[162] can be prohibitively expensive, may impact on other biota, and are not sustainable because they treat the reach-scale symptoms of degradation rather than the causes. Thus, management and restoration strategies need to shift toward integrated solutions from the river through to the catchment scale[10] that seek to reduce the production of fine sediment and its delivery to rivers and promote the mobilization and removal of fines from the bed. Such source control methods, as part of strategic sediment management regimes[8] should be underpinned by sediment targets[163] (such as total maximum daily loads) which account for the ability of streams to transport or retain fine sediment[8] and quality guidelines.[164,165] Furthermore, the control measures should be informed by improved estimates of the nature and extent of fine sediments not just in the suspended load of rivers but also *on* and *within* streambeds. The latter is particularly difficult to identify and quantify if it is not accompanied by surficial

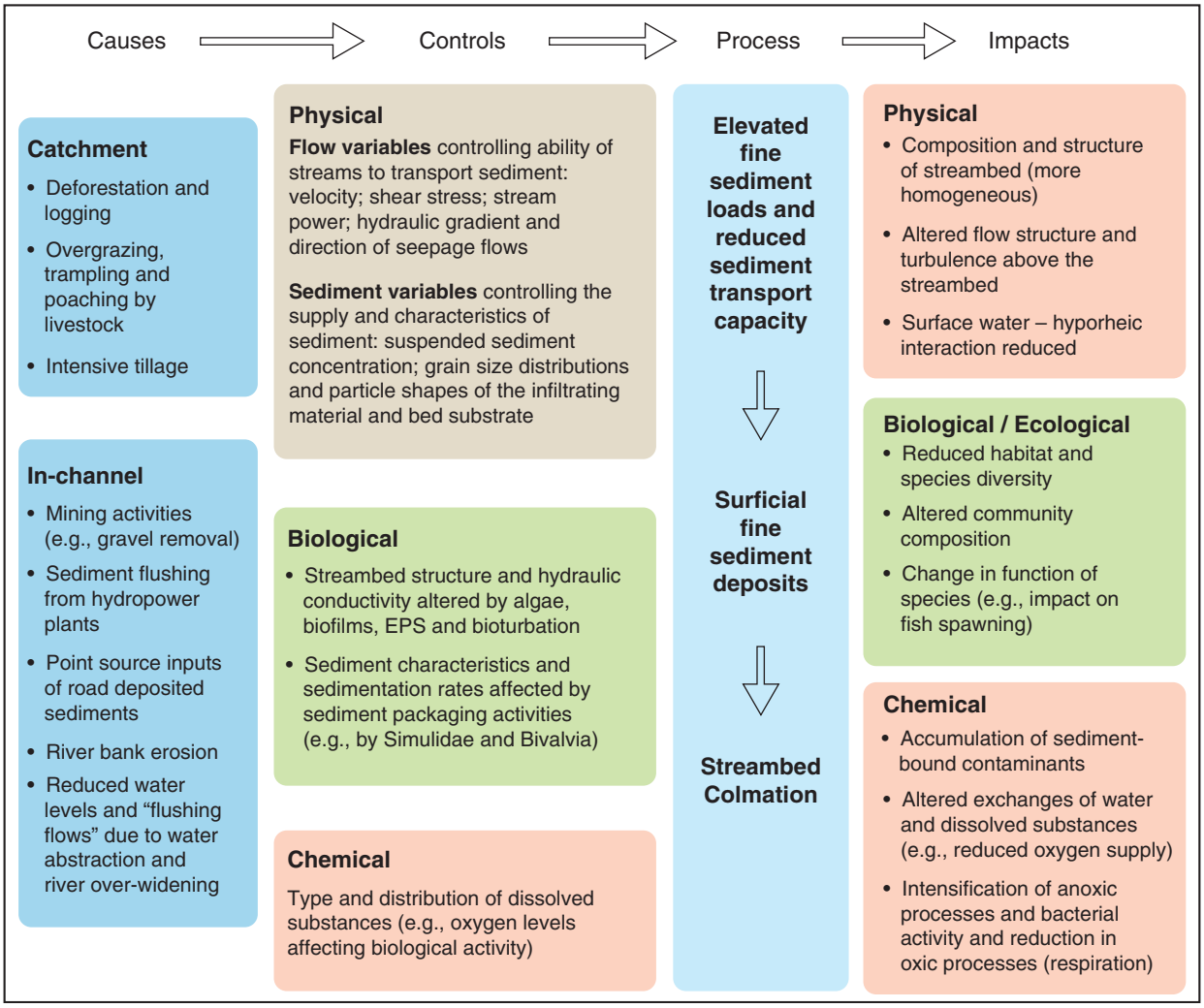

FIGURE 3 | Summary of the main causes, controls, and impacts of streambed colmation.

deposits, e.g., if colmation is caused by internal mechanisms or if fines have penetrated to deeper layers in the bed.

Fine sediment ingress is particularly damaging to river ecology but, despite recent advances in understanding the processes of colmation, further research is still needed to achieve a more comprehensive understanding of what sized sediment infiltrates into the subsurface under different sediment supply and shear stress conditions and the role of biological processes and controls.[57] Understanding the mechanism of fine sediment infiltration will also help develop more environmentally sensitive management operations, such as sediment flushing operations from hydropower schemes.[58] To improve the prediction of contaminant transport for the protection of human and aquatic health, Droppo et al.[159] have also called for the suspended and bed sediments to be combined with the biological components and stream energy. This could support the development of risk-based management approaches with river reaches or segments at risk of colmation identified from a combined knowledge of suspended sediment characteristics relative to the bed material characteristics set within the context of the energy conditions of the reach. As a starting point, more studies are needed to determine the spatial and temporal extent of bed sediment storage in rivers with river substrate metrics that capture substrate composition and embeddedness, mirroring calls for a rapid, cost-effective method for assessing the extent of surficial fine sediment deposits.[166] Furthermore, to begin to predict the residence times of ingressed sediments, a better understanding is needed of the mobility of coarse surface layers and associated feedbacks with infiltrated fines which are still poorly understood.

Another key challenge in managing fine sediment loads in rivers through the implementation of source control measures, such as catchment-sensitive farming, is determining an acceptable level of input and critical sediment yields from catchment and sub-catchment sources[167] that take into consideration the amount of fine sediment required for the healthy functioning of the system. Thus, targets need to recognise the dynamic nature of fine sediment transport, including colmation and decolmation, and be related to demonstrable impact based on biological effect data.[167] This approach should be based on new analyses of the linkages between fine sediment pressures and a range of freshwater biota and life stages for different river types. A desired outcome would be generic modeling toolkits that couple sediment stress and impacts on a range of biological quality elements to support a weight-of-evidence approach in fine sediment management.[91] Such toolkits have been proposed within a pressure-impact modeling framework[109] that could explore the expected benefit of sediment mitigation options in relation to improved targets for sediment compliance.

ACKNOWLEDGMENTS

This review was partially carried out during the doctoral research of Mohajeri within the SMART Joint Doctorate (Science for the MAnagement of Rivers and their Tidal systems) funded with the support of the Erasmus Mundus program of the European Union. The authors are grateful to Lin Baldock for supplying the photograph (Figure 1) and Ed Oliver for drawing Figures 2 and 3 and the graphical abstract. The authors also thank the reviewers for their valuable comments which have helped to improve the manuscript.

REFERENCES

1. Droppo I, Leppard G, Flannigan D, Liss S. The freshwater floc: a functional relationship of water and organic and inorganic floc constituents affecting suspended sediment properties. *Water Air Soil Pollut* 1997, 99:43–53.
2. Droppo I. Rethinking what constitutes suspended sediment. *Hydrol Process* 2001, 15:1551–1564.
3. Wotton R, Malmqvist B. Feces in aquatic ecosystems. *Bioscience* 2001, 51:537–544.
4. Arnon S, Marx LP, Searcy KE, Packman AI. Effects of overlying velocity, particle size, and biofilm growth on stream–subsurface exchange of particles. *Hydrol Process* 2010, 24:108–114.
5. Gurnell AM, Bertoldi W, Tockner K, Wharton G, Zolezzi G. How large is a river? Conceptualizing river landscape signatures and envelopes in four dimensions. *WIREs Water* 2016, 3:313–325.
6. Walling D, Fang D. Recent trends in the suspended sediment loads of the world rivers. *Global Planetary Change J* 2003, 39:111–126.
7. Owens PN, Batalla R, Collins AJ, Gomez B, Hicks DM, Horowitz AJ, Kondolf GM, Marden M, Page M, Peacock D, et al. Fine-grained sediment in river systems: environmental significance and management issues. *River Res Appl* 2005, 21:693–717.
8. Naden PS, Murphy JF, Old GH, Newman J, Scarlett P, Harman M, Duerdoth CP, Hawczak A, Pretty JL, Arnold A, et al. Understanding the controls on deposited fine sediment in the streams of agricultural catchments. *Sci Total Environ* 2016, 547:366–381.
9. Foster I, Collins A, Naden P, Zhang L. The potential for paleolimnology to determine historic sediment delivery to rivers. *J Paleolimnol* 2011, 45:287–306.
10. Collins AL, Zhang Y. Exceedance of modern 'background' fine-grained sediment delivery to rivers due to current agricultural land use and uptake of water pollution mitigation options across England and Wales. *Environ Sci Policy* 2016, 61:61–73.
11. Richards C, Host G, Arthur J. Identification of predominant factors structuring stream macroinvertebrate communities within a large agricultural catchment. *Freshwater Biol* 1993, 29:285–294.
12. Walling DE. Linking land use, erosion and sediment yields in river basins. *Hydrobiologia* 1999, 410: 223–240.
13. Owens P, Petticrew E, van der Perk M. Sediment response to catchment disturbances. *J Soil Sediment* 2010, 10:591–596.
14. Wohl E. Legacy effects on sediments in river corridors. *Earth Sci Rev* 2015, 147:30–53.
15. Droppo IG, D'Andrea L, Krishnappan BG, Jaskot C, Trapp B, Basuvaraj M, Liss SN. Fine-sediment dynamics: towards an improved understanding of sediment erosion and transport. *J Soil Sediment* 2015, 15:467–479.
16. Stone M, Droppo I. In channel surficial fine grained sediment laminae. Part II: chemical characteristics

and implications for contaminant transport in fluvial systems. *Hydrol Process* 1994, 8:113–124.

17. Wohl E. Particle dynamics: the continuum of bedrock to alluvial river segments. *Geomorphology* 2015, 241:192–208.
18. Brookes A. Response of aqutaic vegetation to sedimentation downstream of river channelization works in England and Wales. *Biol Conserv* 1986, 38:351–367.
19. Brookes A. *Channelized Rivers*. Chichester: John Wiley & Sons; 1988.
20. Jones JI, Collins AL, Naden PS, Sear DA. The relationship between fine sediment and macrophytes in rivers. *River Res Appl* 2012, 28:1006–1018.
21. Jones JI, Murphy JF, Collins AL, Sear DA, Naden PS, Armitage PD. The impact of fine sediment on macroinvertebrates. *River Res Appl* 2012, 28:1055–1071.
22. Kemp P, Sear D, Collins A, Naden P, Jones I. The impacts of fine sediment on riverine fish. *Hydrol Process* 2011, 25:1800–1821.
23. Boulton AJ. Hyporheic rehabilitation in rivers: restoring vertical connectivity. *Freshwater Biol* 2007, 52:632–650.
24. Marion A, Nikora V, Puijalon S, Bouma T, Koll K, Ballio F, Tait S, Zaramella M, Sukhodolov A, O'Hare M, et al. Aquatic interfaces: a hydrodynamic and ecological perspective. *J Hydraul Res* 2014, 52:744–758.
25. Krause S, Hannah DM, Fleckenstein JH, Heppell CM, Kaeser D, Pickup R, Pinay G, Robertson AL, Wood PJ. Inter-disciplinary perspectives on processes in the hyporheic zone. *Ecohydrology* 2011, 4:481–499.
26. Salomons W, Förstner U. *Metals in the Hydrocycle*. Berlin: Springer Verlag; 1984.
27. Horowitz A, Elrick K, Robbins J, Cook R. Effect of mining and related activities on the sediment trace element geochemistry of Lake Coeur D'Alene, Idaho, USA. Part II: subsurface sediments. *Hydrol Process* 1995, 9:35–54.
28. Foster I, Charlesworth S. Heavy metals in the hydrological cycle: trends and explanation. *Hydrol Process* 1996, 10:227–261.
29. Owens P, Walling D, Carton J, Meharg A, Wright J, Leeks G. Downstream changes in sediment-associated contaminant (P, Cr and PCBs) transport and storage in agricultural and industrialized drainage basins. *Sci Total Environ* 2001, 266:177–186.
30. Heppell C, Wharton G, Cotton J, Bass J, Roberts S. Sediment storage in the shallow hyporheic of lowland vegetated river reaches. *Hydrol Process* 2009, 23:2239–2251.
31. Cordone AJ, Kelly DW. The influence of inorganic sediment on the aquatic life of streams. *Calif Fish Game* 1961, 47:189–228.
32. Einstein H. Deposition of suspended particles in a gravel bed. *J Hydraulics Div (ASCE)* 1968, 94: 1197–1206.
33. Chutter FM. The effects of silt and sand on the invertebrate fauna of streams and rivers. *Hydrobiologia* 1969, 34:29–37.
34. Nuttall PM. The effects of sand deposition upon the macroinvertebrate fauna of the River Camel, Cornwall. *Freshwater Biol* 1972, 2:181–186.
35. Nuttall PM, Bielby GH. The effects of china-clay waste on stream invertebrates. *Environ Pollut* 1973, 5:77–86.
36. Milhous R. Sediment transport in a gravel-bottomed stream. PhD Thesis, *Civil Engineering*, 1973.
37. Beyer W, Banscher E. Zur Kolmation der Gewässerbetten bei der Uferfiltratgewinnung. *Z Angew Geol* 1975, 21:565–570.
38. Beschta R, Jackson W. The intrusion of fine sediments into a stable gravel bed. *J Fish Res Board Can* 1979, 36:204–210.
39. Petts GE. Sedimentation within a regulated river. *Earth Surf Process Landf* 1984, 9:125–134.
40. Ryan PA. Environmental effects of sediment on New Zealand streams: a review. *N Z J Mar Freshwater Res* 1991, 25:207–221.
41. Wood PJ, Armitage PD. Biological effects of fine sediment in the lotic environment. *Environ Manage* 1997, 21:203–217.
42. Acornley RM, Sear DA. Sediment transport and siltation of brown trout (*Salmo trutta* L.) spawning gravels in chalk streams. *Hydrol Process* 1999, 13:447–458.
43. Schälchli U. The clogging of coarse gravel river beds by fine sediment. *Hydrobiologia* 1992, 235-236:189–197.
44. Blaschke AP, Steiner K-H, Schmalfuss R, Gutknecht D, Sengschmitt D. Clogging processes in hyporheic interstices of an impounded river, the Danube at Vienna, Austria. *Int Rev Hydrobiol* 2003, 88:397–413.
45. Packman AI, MacKay JS. Interplay of stream-subsurface exchange, clay particle deposition, and streambed evolution. *Water Resour Res* 2003, 39:1097.
46. Rehg KJ, Packman AI, Ren J. Effects of suspended sediment characteristics and bed sediment transport on streambed clogging. *Hydrol Process* 2005, 19:413–427.
47. Bo T, Fenoglio S, Malacarne G, Pessino M, Sgariboldi F. Effects of clogging on stream macroinvertebrates: an experimental approach. *Limnol—Ecol Manage Inland Waters* 2007, 37:186–192.
48. Schneider J, Saueregger G. Model testing of clogging processes in a free-flowing section. In: *River flow 2008: Proceedings of the International Conference on Fluvial Hydraulics*, Çeşme, Izmir, Turkey, 2008.

49. Schneider J, Saueregger G. Physical model tests of clogging processes in a riverbed with unsaturated conditions downstream of a reservoir. In: *Proceedings of the 8th International Symposium on Ecohydraulics (ISE)*, Seoul, South Korea, 2010.
50. Huston D, Fox J. Clogging of fine sediment within gravel substrates: dimensional analysis and macroanalysis of experiments in hydraulic flumes. *J Hydraul Eng* 2015, 141:04015015.
51. McCloskey TF, Finnemore EJ. Estimating hydraulic conductivities in an alluvial basin from sediment facies models. *Ground Water* 1996, 34:1024–1032.
52. Li W, Zhou LS. Sedimentary facies and tectonic setting of the Cretaceous in the Suhongtu-Yingen basin. *Scientia Geol Sin* 1997, 32:387–396.
53. Sear D. Fine sediment infiltration into gravel spawning beds within a regulated river experiencing floods and the ecological implications for salmonids. *Regul Rivers: Res Manage* 1993, 8:373–390.
54. Julien HP, Bergeron NE. Effect of fine sediment infiltration during the incubation period on Atlantic Salmon (*Salmo salar*) embryo survival. *Hydrobiologia* 2006, 563:61–71.
55. Wooster JK, Dusterhoff SR, Cui Y, Sklar LS, Dietrich WE, Malko M. Sediment supply and relative size distribution effects on fine sediment infiltration into immobile gravels. *Water Resour Res* 2008, 44: W03424.
56. Cui Y, Wooster J, Baker P, Dusterhoff S, Sklar L, Dietrich W. Theory of fine sediment infiltration into immobile gravel bed. *J Hydraul Eng* 2008, 134: 1421–1429.
57. Evans E, Wilcox A. Fine sediment infiltration dynamics in a gravel-bed river following sediment pulse. *River Res Appl* 2014, 30:372–384.
58. Herrero A, Berni C. Sand infiltration into a gravel bed: a mathematical model. *Water Resour Res* 2016, 52:8956–8969.
59. Karna N, Prasad H, Giri S, Lodhi A. Intrusion of fine sediments into river bed and its effect on river environment—a research review. *ISH J Hydraul Eng* 2015, 21:142–150.
60. Brunke M, Gonser T. The ecological significance of exchange processes between rivers and groundwater. *Freshwater Biol* 1997, 37:1–33.
61. Brunke M. *The influence of hydrological exchange patterns on environmental gradients and community ecology in hyporheic interstices of a pre-alpine river*. PhD Thesis, *Natural Science*, 1998. Available at: http://books.google.com/books?id=hPKojwEACAAJ.
62. Velickovic B. Colmation as one of the processes in interaction between the groundwater and surface water. *Facta Univ* 2005, 3:165–172.
63. Noack M, Ortlepp J, Wieprecht S. Colmation-simulation of interstitial habitat conditions during the incubation phase of gravel-spawning fish. In: *Proceedings of the 10th International Symposium on Ecohydraulics (ISE)*, Trondheim, Norway, 2014.
64. Lauck T. *A simulation model for the infiltration of sediment into spawning gravel*. Master's Thesis, Mathematics Department, 1991.
65. Lisle TE. Sediment transport and resulting deposition in spawning gravels, north coastal California. *Water Resour Res* 1989, 25:1303–1319.
66. Frostick L, Lukas P, Reid I. The infiltration of fine matrices into coarse-grained alluvial sediments and its implications for stratigraphical integration. *J Geol Soc London* 1984, 141:955–965.
67. Cunningham A, Anderson C, Bouwer H. Effects of sediment-laden flow on channel bed clogging. *J Irrig Drain Eng (ASCE)* 1987, 113:106–118.
68. Hünken A, Mutz M. Field studies on factors affecting very fine and ultra fine particulate organic matter deposition in low-gradient sand-bed streams. *Hydrol Process* 2007, 21:525–533.
69. Carling P. Deposition of fine and coarse sand in an open-work gravel bed. *Can J Fish Aquat Sci* 1984, 41:263–270.
70. Herzig J, Leclerc D, LeGoff P. Flow of suspensions through porous media-application to deep bed filtration. *Ind Eng Chem* 1970, 62:8.
71. Battin T, Kaplan L, Newbold J, Cheng X, Hansen C. Effects of current velocity on the nascent architecture of stream microbial biofilms. *Appl Environ Microbiol* 2003, 69:5443–5452.
72. Sear D, Newson M, Brookes A. Sediment-related river maintenance: The role of fluvial geomorphology. *Earth Surf Process Landf* 1995, 20:629–647.
73. Cui Y, Parker G. The arrested gravel front: stable gravel-sand transitions in rivers. Part 2: general numerical solution. *J Hydraul Res* 1998, 36:159–182.
74. Toro-Escobar CM, Paola C, Parker G. Transfer function for the deposition of poorly sorted gravel in response to streambed aggradation. *J Hydraul Res* 1996, 34:35–53.
75. Núñez-González F, Martín-Vide JP, Kleinhans MG. Porosity and size gradation of saturated gravel with percolated fines. *Sedimentology* 2016, 63:1209–1232.
76. Gibson S, Abraham D, Heath R, Schoellhamer D. Bridging process threshold for sediment infiltrating into a coarse substrate. *J Geotech Geoenviron Eng* 2010, 136:402–406.
77. Brandt SA, Swenning J. Sedimentological and geomorphological effects of reservoir flushing: the Cachí reservoir, Costa Rica, 1996. *Geogr Ann Phys Geogr* 1999, 81:391–407.
78. Diplas P. Modeling of fine and coarse sediment interaction over alternate bars. *J Hydrol* 1994, 159:335–351.
79. Pilotto F, Bertoncin A, Harvey GL, Wharton G, Pusch MT. Diversification of stream invertebrate

communities by large wood. *Freshwater Biol* 2014, 59:2571–2583.

80. Hiscock KM, Grischek T. Attenuation of groundwater pollution by bank filtration. *J Hydrol* 2002, 266:139–144.
81. Banscher E. Gesetzmässigkeiten der Kolmation-sentwicklung. *Wasserwirtsch Wassertech* 1976, 9: 320–323.
82. Karwan DL, Saiers JE. Hyporheic exchange and streambed filtration of suspended particles. *Water Resour Res* 2012, 48:W01519.
83. Adams JN, Beschta RL. Gravel bed composition in Oregon coastal streams. *Can J Fish Aquat Sci* 1980, 37:1514–1521.
84. Venditti JG, Dietrich WE, Nelson PA, Wydzga MA, Fadde J, Sklar L. Effect of sediment pulse grain size on sediment transport rates and bed mobility in gravel bed rivers. *J Geophys Res Earth* 2010, 115: F03039.
85. Hodge RA, Sear DA, Leyland J. Spatial variations in surface sediment structure in riffle–pool sequences: a preliminary test of the Differential Sediment Entrainment Hypothesis (DSEH). *Earth Surf Process Landf* 2013, 38:449–465.
86. Vericat D, Batalla RJ. Sediment transport in a large impounded river: the lower Ebro, NE Iberian Peninsula. *Geomorphology* 2006, 79:72–92.
87. Statzner B, Sagnes P. Crayfish and fish as bioturbators of streambed sediments: assessing joint effects of species with different mechanistic abilities. *Geomorphology* 2008, 93:267–287.
88. Nogaro G, Mermillod-Blondin F, François-Carcaillet F, Gaudet J-P, Lafont M, Gibert J. Invertebrate bioturbation can reduce the clogging of sediment: an experimental study using infiltration sediment columns. *Freshwater Biol* 2006, 51:1458–1473.
89. Gerbersdorf SU, Westrich B, Paterson DM. Microbial extracellular polymeric substances (EPS) in freshwater sediments. *Microb Ecol* 2009, 58:334–349.
90. Grabowski RC, Droppo IG, Wharton G. Erodibility of cohesive sediment: the importance of sediment properties. *Earth Sci Rev* 2011, 105:101–120.
91. Jones JI, Duerdoth CP, Collins AL, Naden PS, Sear DA. Interactions between diatoms and fine sediment. *Hydrol Process* 2014, 28:1226–1237.
92. Grabowski RC, Wharton G, Davies GR, Droppo IG. Spatial and temporal variations in the erosion threshold of fine riverbed sediments. *J Soil Sediment* 2012, 12:1174–1188.
93. Summer W, Zhang W, Stritzinger W. Consequences of human impacts on the sediment transport process. *Z f Kulturtechnik und Landentwicklung* 1994, 35:382–389.
94. Scheurer K, Alewell C, Bänninger D, Burkhardt-Holm P. Climate and land-use changes affecting river sediment and brown trout in alpine countries—a review. *Environ Sci Pollut Res* 2009, 16:232–242.
95. Walling DE. The response of sediment yields to environmental change. *Human Impact Erosion Sedimentation* 1997, 245:77–89.
96. Asselman N, Middelkoop H, van Dijk P. The impact of changes in climate and land use on soil erosion, transport and deposition of suspended sediment in the River Rhine. *Hydrol Process* 2003, 17: 3225–3244.
97. Mohta J, Wallbrink P, Hairsine P, Grayson R. Determining the sources of suspended sediment in a forested catchment in southeastern Australia. *Water Resour Res* 2003, 39:1056.
98. Davies PE, Nelson M. The effect of steep slope logging on fine sediment infiltration into the beds of ephemeral and perennial streams of the Dazzler Range, Tasmania, Australia. *J Hydrol* 1993, 150:481–504.
99. Abernethy C. The use of river and reservoir sediment data for the study of regional soil erosion rates and trends conservation. In: *International Symposium on Water Erosion, Sedimentation and Resource,* Dehradun, India, 1990.
100. Walling DE. Sediment yields and sediment budgets. In: Anderson MG, McDonnell JJ, eds. *Encyclopaedia of Hydrological Sciences*. New York: John Wiley & Sons Inc.; 2005.
101. Clarke SJ, Wharton G. Sediment nutrient characteristics and aquatic macrophytes in lowland English rivers. *Sci Total Environ* 2001, 266:103–112.
102. Trimble S. *Historical Agriculture and Soil Erosion in the Upper Mississippi Valley Hill Country*. Boca Raton: CRC Press; 2013.
103. Collins A, Walling D, Leeks G. Fingerprinting the origin of fluvial suspended sediment in larger river basins: combining assessment of spatial provenance and source type. *Geogr Ann* 1997, 79A:239–254.
104. Collins AL, Walling DE. Fine-grained bed sediment storage within the main channel systems of the Frome and Piddle catchments, Dorset, UK. *Hydrol Process* 2007, 21:1448–1459.
105. Von Bertrab MG, Krein A, Stendera S, Thielen F, Hering D. Is fine sediment deposition a main driver for the composition of benthic macroinvertebrate assemblages? *Ecol Indicators* 2013, 24:589–598.
106. Walling DE, Amos CM. Source, storage and mobilisation of fine sediment in a chalk stream system. *Hydrol Process* 1999, 13:323–340.
107. Klimek K. Man's impact on fluvial processes in the Polish Western Carpathians. *Geogr Ann* 1987, 69A:221–226.
108. Grabowski RC, Gurnell AM. Diagnosing problems of fine sediment delivery and transfer in a lowland catchment. *Aquatic Sci* 2016, 78:95–106.

109. Collins AL, Jones JI, Sear DA, Naden PS, Skirvin D, Zhang YS, Gooday R, Murphy J, Lee D, Pattison I, et al. *Extending the evidence base on the ecological impacts of fine sediment and developing a framework for targeting mitigation of agricultural sediment losses*. 2015. Report of Defra Project WQ0128, September 2015, Rothamsted Research, UK, 103 pp.

110. Angermeier PL, Wheeler AP, Rosenberger AE. A conceptual framework for assessing impacts of roads on aquatic biota. *Fisheries* 2004, 29:19–29.

111. Taylor KG, Owens PN. Sediments in urban river basins: a review of sediment–contaminant dynamics in an environmental system conditioned by human activities. *J Soil Sediment* 2009, 9:281–303.

112. Carter J, Owens PN, Walling DE, Leeks GJL. Fingerprinting suspended sediment sources in a large urban river system. *Sci Total Environ* 2003, 314–316: 513–534.

113. Turnpenny A, Williams R. Effects of sedimentation on the gravels of an industrial river system. *J Fish Biol* 1980, 17:681–693.

114. Kondolf M. Application of the pebble count notes on purpose, method, and variants. *JAWRA* 1997, 33:79–87.

115. Wohl EE, Cenderelli DA. Sediment deposition and transport patterns following a reservoir sediment release. *Water Resour Res* 2000, 36:319–333.

116. Asaeda T, Rashid MH. The impacts of sediment released from dams on downstream sediment bar vegetation. *J Hydrol* 2012, 430–431:25–38.

117. Downs P, Cui Y, Wooster J, Dusterhoff S, Booth D, Dietrich W, Sklar L. Managing reservoir sediment release in dam removal projects: An approach informed by physical and numerical modelling of non-cohesive sediment. *International Journal of River Basin Management* 2009, 7:433–452.

118. Wang H, Yang Z, Saito Y, Liu JP, Sun X, Wang Y. Stepwise decreases of the Huanghe (Yellow River) sediment load (1950–2005): impacts of climate change and human activities. *Global and Planetary Change* 2007, 57:331–354.

119. Church M, Ryder JM. Paraglacial Sedimentation: a consideration of fluvial processes conditioned by glaciation. *Geol Soc Am Bull* 1972, 83:3059–3072.

120. Malard F, Tockner K, Dole-Olivier M-J, Ward JV. A landscape perspective of surface-subsurface hydrological exchanges in river corridors. *Freshwater Biol* 2002, 47:621–640.

121. Webb R, Leake S. Ground-water surface-water interactions and long-term change in riverine riparian vegetation in the southwestern United States. *J Hydrol* 2006, 320:302–323.

122. Bickerton M, Petts G, Armitage P, Castella E. Assessing the ecological effects of groundwater abstraction on chalk streams: three examples from Eastern England. *Regul Rivers: Res Manage* 1993, 8:121–134.

123. Wood PJ, Armitage PD. Sediment deposition in a small lowland stream-management implications. *Regul Rivers: Res Manage* 1999, 15:199–210.

124. Acreman MC, Adams B, Birchall P, Connorton B. Does groundwater abstraction cause degradation of rivers and wetlands? *Water Environ J* 2000, 14:200–206.

125. Bruno MC, Maiolini B, Carolli M, Silveri L. Impact of hydropeaking on hyporheic invertebrates in an Alpine stream (Trentino, Italy). *Ann Limnol* 2009, 45:157–170.

126. Zhang Y, Hubbard S, Finsterle S. Factors governing sustainable groundwater pumping near a river. *Ground Water* 2011, 49:432–444.

127. Carolli M, Bruno MC, Siviglia A, Maiolini B. Responses of benthic invertebrates to abrupt changes of temperature in flume simulations. *River Res Appl* 2012, 28:678–691.

128. Zarfl C, Lumsdon AE, Berlekamp J, Tydecks L, Tockner K. A global boom in hydropower dam construction. *Aquatic Sci* 2015, 77:161–170.

129. Sternecker K, Wild R, Geist J. Effects of substratum restoration on salmonid habitat quality in a subalpine stream. *Environ Biol Fishes* 2013, 96:1341–1351.

130. Sambrook Smith GH, Nicholas AP. Effect on flow structure of sand deposition on a gravel bed: results from a two-dimensional flume experiment. *Water Resour Res* 2005, 41:W10405.

131. Wren DG, Langendoen EJ, Kuhnle RA. Effects of sand addition on turbulent flow over an immobile gravel bed. *J Geophys Res Earth* 2011, 116:F01018.

132. Mohajeri SH, Righetti M, Wharton G, Romano GP. On the structure of turbulent gravel bed flow: implications for sediment transport. *Adv Water Resour* 2016, 92:90–104.

133. Kuhnle R, Wren D, Langendoen E, Rigby J. Sand transport over an immobile gravel substrate. *J Hydraul Eng* 2013, 139:167–176.

134. Nikora V, Goring D, McEwan I, Griffiths G. Spatially averaged open-channel flow over rough bed. *J Hydraul Eng* 2001, 127:123–133.

135. Grams PE, Wilcock PR. Equilibrium entrainment of fine sediment over a coarse immobile bed. *Water Resour Res* 2007, 43:W10420.

136. Maridet L, Philippe M. Influence of substrate characteristics on the vertical distribution of stream macroinvertebrates in the hyporheic zone. *Int Rev Hydrobiol* 1995, 91:101–105.

137. European Parliament. Establishing a framework for community action in the field of water policy, 2000.

138. Armitage PD, Blackburn JH. The macroinvertebrate fauna of the Holy Stream, a small tributary of the

River Frome, Dorset. *Proc Dorset Nat Hist Archeol Soc* 2001, 123:95–100.

139. MacIsaac HJ, Rocha R. Effects of suspended clay on zebra mussel (dreissena polymorpha) faeces and pseudofaeces production. *Archiv Hydrobiol* 1995, 135: 53–64.

140. Wood PJ, Vann AR, Wanless PJ. The response of Melampophylax mucoreus (Hagen) (Trichoptera: Limnephilidae) to rapid sedimentation. *Hydrobiologia* 2001, 455:183–188.

141. Lancaster J, Hildrew AG, Townsend CR. Invertebrate predation on patchy and mobile prey in streams. *J Animal Ecol* 1991, 60:625–641.

142. Armitage PD, Cannan CE. Annual changes in summer patterns of mesohabitat distribution and associated macroinvertebrate assemblages. *Hydrol Process* 2000, 14:3161–3179.

143. Angelstein S, Wolfram C, Rahn K, Kiwel U, Frimel S, Merbach I, Schubert H. The influence of different sediment nutrient contents on growth and competition of *Elodea nuttallii* and *Myriophyllum spicatum* in nutrient-poor waters. *Fundam Appl Limnol* 2009, 175:49–57.

144. Boulton A, Findlay S, Marmonier P, Stanley E, Valett M. The functional significance of the hyporheic zone in streams and rivers. *Annu Rev Ecol Syst* 1998, 29:59–81.

145. Krause S, Hannah DM, Fleckenstein JH. Hyporheic hydrology: interactions at the groundwater-surface water interface. *Hydrol Process* 2009, 23:2103–2107.

146. Pretty JL, Hildrew AG, Trimmer M. Nutrient dynamics in relation to surface–subsurface hydrological exchange in a groundwater fed chalk stream. *J Hydrol* 2006, 330:84–100.

147. Mueller M, Pander J, Wild R, Lueders T, Geist J. The effects of stream substratum texture on interstitial conditions and bacterial biofilms: methodological strategies. *Limnol Ecol Manage Inland Waters* 2013, 43:106–113.

148. Lefebvre S, Marmonier P, Pinay G. Stream regulation and nitrogen dynamics in sediment interstices: comparison of natural and straightened sectors of a third-order stream. *River Res Appl* 2004, 20:499–512.

149. Dong LF, Smith CJ, Papaspyrou S, Stott A, Osborn AM, Nedwell DB. Changes in benthic denitrification, nitrate ammonification, and anammox process rates and nitrate and nitrite reductase gene abundances along an estuarine nutrient gradient (the Colne Estuary, United Kingdom). *Appl Environ Microbiol* 2009, 75:3171–3179.

150. Nogaro G, Datry T, Mermillod-Blondin F, Descloux S, Montuelle B. Influence of streambed sediment clogging on microbial processes in the hyporheic zone. *Freshwater Biol* 2010, 55:1288–1302.

151. Doussan C, Poitevin G, Ledoux E, Detay M. River bank filtration: modelling of the changes in water chemistry with emphasis on nitrogen species. *J Contam Hydrol* 1997, 25:129–156.

152. Lambs L. Interactions between groundwater and surface water at river banks and the confluence of rivers. *J Hydrol* 2004, 288:312–326.

153. Webb BW, Hannah DM, Moore RD, Brown LE, Nobilis F. Recent advances in stream and river temperature research. *Hydrol Process* 2008, 22:902–918.

154. Acornley RM. Water temperatures within spawning beds in two chalk streams and implications for salmonid egg development. *Hydrol Process* 1999, 13:439–446.

155. Burkholder BK, Grant GE, Haggerty R, Khangaonkar T, Wampler PJ. Influence of hyporheic flow and geomorphology on temperature of a large, gravel-bed river, Clackamas River, Oregon, USA. *Hydrol Process* 2008, 22:941–953.

156. Kondolf M, Mathews W. Management of coarse sediment in regulated rivers of California. *UC Water Resources Center Technical Completion Report W-748*, 1991.

157. Stromberg JC, Tiller R. Effects of groundwater decline on riparian vegetation of semiarid regions: the San Pedro, Arizona. *Ecol Appl* 1996, 6:113–131.

158. Environment Agency. Updated River Basin Management Plans, Supporting Information: Pressure Narrative: Fine Sediment, 2015. Available at: www.gov.uk/environment-agency. (Accessed March 05, 2017).

159. Droppo I, Krishnappan B, Lawrence J. Microbial interactions with naturally occurring hydrophobic sediments: influence on sediment and associated contaminant mobility. *Water Res* 2016, 92:121–130.

160. Apitz SE. Conceptualizing the role of sediment in sustaining ecosystem services: Sediment-ecosystem regional assessment (SEcoRA). *Sci Total Environ* 2012, 415:9–30.

161. Descloux S, Datry T, Philippe M, Marmonier P. Comparison of different techniques to assess surface and subsurface streambed colmation with fine sediments. *Int Rev Hydrobiol* 2010, 95:520–540.

162. Wu F, Chou Y. Tradeoffs associated with sediment-maintenance flushing flows: a simulation approach to exploring non-inferior options. *River Res Appl* 2004, 20:591–604.

163. Walling DE, Webb B, Shanahan J. Investigations into the use of critical sediment yields for assessing and managing fine sediment inputs into aquatic ecosystems. Natural England Research Reports, 2007, Number 007.

164. Cooper D, Naden P, Old G, Laizé C. Development of guideline sediment targets to support management of sediment inputs into aquatic systems, Vol. NERR008, 2008, 84.

165. Crane C. Proposed development of sediment quality guidelines under the European Water Framework Directive: a critique. *Toxicol Lett* 2003, 142:195–206.

166. Duerdoth CP, Arnold A, Murphy JF, Naden PS, Scarlett P, Collins AL, Sear DA, Jones JI. Assessment of a rapid method for quantitative reach-scale estimates of deposited fine sediment in rivers. *Geomorphology* 2015, 230:37–50.

167. Collins AL, Naden PS, Sear DA, Jones JI, Foster IDL, Morrow K. Sediment targets for informing river catchment management: international experience and prospects. *Hydrol Process* 2011, 25: 2112–2129.

Assessment of erosion, sedimentation, and water quality impacts of the Mountain Valley Pipeline and Equitrans Expansion Project's proposed crossing of the Jefferson National Forest as it pertains to the U.S. Forest Service's Draft Supplemental Environmental Impact Statement dated December 2022

Prepared by Jonathan A. Czuba, Ph.D., Licensed Professional Engineer - February 9, 2023

REFERENCES
5

February 21, 2023

Transactions of the American Fisheries Society 145:1266–1281, 2016

ISSN: 0002-8487 print / 1548-8659 online
DOI: 10.1080/00028487.2016.1217929

ARTICLE

Development of Habitat Suitability Indices for the Candy Darter, with Cross-Scale Validation across Representative Populations

Corey G. Dunn*
Department of Fish and Wildlife Conservation, Virginia Tech, 100 Cheatham Hall, Blacksburg, Virginia 24061,USA; and Department of Fisheries and Wildlife Sciences, University of Missouri, 302 Anheuser-Busch Natural Resources Building, Columbia, Missouri 65201, USA

Paul L. Angermeier
U.S. Geological Survey, Virginia Cooperative Fish and Wildlife Research Unit, 100 Cheatham Hall, Virginia Tech, Blacksburg, Virginia 24061, USA

Abstract

Understanding relationships between habitat associations for individuals and habitat factors that limit populations is a primary challenge for managers of stream fishes. Although habitat use by individuals can provide insight into the adaptive significance of selected microhabitats, not all habitat parameters will be significant at the population level, particularly when distributional patterns partially result from habitat degradation. We used underwater observation to quantify microhabitat selection by an imperiled stream fish, the Candy Darter *Etheostoma osburni*, in two streams with robust populations. We developed multiple-variable and multiple-life-stage habitat suitability indices (HSIs) from microhabitat selection patterns and used them to assess the suitability of available habitat in streams where Candy Darter populations were extirpated, localized, or robust. Next, we used a comparative framework to examine relationships among (1) habitat availability across streams, (2) projected habitat suitability of each stream, and (3) a rank for the likely long-term viability (robustness) of the population inhabiting each stream. Habitat selection was characterized by ontogenetic shifts from the low-velocity, slightly embedded areas used by age-0 Candy Darters to the swift, shallow areas with little fine sediment and complex substrate, which were used by adults. Overall, HSIs were strongly correlated with population rank. However, we observed weak or inverse relationships between predicted individual habitat suitability and population robustness for multiple life stages and variables. The results demonstrated that microhabitat selection by individuals does not always reflect population robustness, particularly when based on a single life stage or season, which highlights the risk of generalizing habitat selection that is observed during nonstressful periods or for noncritical resources. These findings suggest that stream fish managers may need to be cautious when implementing conservation measures based solely on observations of habitat selection by individuals and that detailed study at the individual and population levels may be necessary to identify habitat that limits populations.

A clear understanding of habitat requirements is essential for effective species management (Rosenfeld 2003). In stream networks, habitat is hierarchically organized into discrete spatial scales spanning large river basins to microhabitats, which facilitate the persistence of populations as well as the growth and reproduction of individuals (Frissell et al. 1986). Incompatibility between a species' life history requirements and available resources can exclude that species from an area at any spatial scale within the habitat hierarchy (Schlosser and Angermeier 1995). Often, a clear (i.e., mechanistic) understanding of habitat requirements is obtained only after the integration of findings from numerous observational and experimental studies spanning multiple levels of ecological organization (Rosenfeld 2003).

*Corresponding author: cgd7n7@mizzou.edu
Received March 30, 2016; accepted July 19, 2016

The decline of North America's rich freshwater fish fauna over the past century partly reflects an inadequate understanding of basic habitat requirements and how anthropogenic changes to aquatic ecosystems impinge on those requirements (Jelks et al. 2008; Burkhead 2012). Regional declines of many species are characterized by the gradual dissolution of a network of populations. Individual populations are lost due to sudden anthropogenic or natural events or the accumulation of years of population declines owing to altered environmental conditions (Angermeier 1995). This process often results in a distributional pattern of disjunct populations that are scattered across the landscape in locations with sufficient habitat quality and quantity to support positive or neutral growth in the absence of immigration (Schlosser and Angermeier 1995). Predisturbance conditions are usually undocumented, and thus managers tasked with recovering a species are left without (1) a true reference of normal population function within affected areas, (2) critical knowledge of life history that applies across the species' range, or (3) both. However, remaining populations and associated environmental conditions can inform management. Within areas still supporting populations, information that is beneficial to species recovery includes an understanding of available habitat structure, how individuals interact with the environment, and which parameters influence individual fitness and population function.

Population-level metrics (e.g., presence, density, and demographic rates) are normally measured via extensive surveys across the distributional range of focal species. Extensive surveys provide a representative sample of possible physical habitat configurations across the species' range and therefore are less susceptible to site-specific biases (Newcomb et al. 2007). However, researchers must often balance the extent of surveys with the sampling intensity per site. In particular, extensive surveys may be infeasible for nongame species, which have historically received less attention (Loomis and White 1996; White 1996; Gabelhouse 2005). Furthermore, extensive surveys may merely reveal correlative population-level responses across space while missing the underlying mechanisms, particularly when rare habitats at specific life stages ultimately regulate populations (Torgersen et al. 1999; Fausch et al. 2002). Therefore, detailed study of individual habitat use is frequently employed to identify the factors limiting populations.

Fish–habitat relationships are frequently quantified in the form of habitat suitability models. Management uses of these models include characterizing important habitat types (Guay et al. 2000; Haxton et al. 2008; Midway et al. 2010); guiding habitat augmentation (Boavida et al. 2012); and, increasingly, identifying suitable habitat for species reintroduction (Mattingly and Galat 2002; Dixon and Vokoun 2009). Models vary in complexity, but most individual-level models assume that individuals actively select conditions that optimize fitness within the context of specific behavioral modes (e.g., reproduction, foraging, and refuge use). For example, foraging individuals try to maximize the ratio of energy intake to expenditure while minimizing mortality risk (Werner and Gilliam 1984; Grossman 2013). Habitat suitability models frequently use the density of individuals occupying a habitat type as a metric for habitat suitability (Rosenfeld 2003); however, this metric can be affected by plasticity of habitat use (Leftwich et al. 1997), resource availability (Dunham et al. 2002), biotic interactions (Orth 1987), ontogeny (Rosenberger and Angermeier 2003), and behavior mode (Kwak et al. 1992). Thus, individual-level models of habitat use frequently perform poorly outside the spatiotemporal context in which they were developed (Fausch et al. 1988; Leftwich et al. 1997; Hewitt et al. 2009). Further, individual-level habitat studies rarely examine links to population-level responses (Peckarsky et al. 1997). Although recent methodological advances allow researchers to explicitly link individual- and population-level patterns by using individual-based models (Grimm and Railsback 2005), these models may be infeasible—except for well-studied species—due to their extensive data requirements.

The primary goal of this study was to examine whether the predicted microhabitat suitability for an imperiled stream fish, the Candy Darter *Etheostoma osburni*, is consistent with population robustness across four streams. Herein, "robustness" reflects population size, density, and likely long-term viability. To accomplish this, we used a study design that revealed relationships among the three primary factors that are relevant to the development and application of individual-level habitat suitability models: (1) instream habitat gradients, (2) individual habitat selection, and (3) population robustness across streams. First, individual-level habitat selection (i.e., disproportional use) was estimated from two streams with robust populations and that presumably contained optimal habitat (i.e., "reference condition" approach; Stoddard et al. 2006; Newcomb et al. 2007). Next, we validated habitat selection by examining the predicted suitability of available habitat within streams where populations of Candy Darters were robust, localized, or extirpated. By comparing habitat gradients, predicted suitability, and actual population robustness, we examined a seldom-tested assumption of habitat suitability models developed from individual-level habitat selection: that patch quality perceived by individuals at the microhabitat scale can be "scaled up" to reflect population robustness at the stream segment scale.

METHODS

Focal Species

The Candy Darter is endemic to the New River drainage, where the species is patchily distributed across the Appalachian Plateau Physiographic Province and the Valley and Ridge Physiographic Province in Virginia and West Virginia (Chipps et al. 1993; Jenkins and Burkhead 1994). Candy Darters historically inhabited many stream types (Jenkins and Burkhead 1994); currently, however, most populations remain in cool, high-gradient to moderate-gradient streams within forested watersheds. The reduced range may be due to habitat degradation, but this hypothesis has received little investigation. Within streams, adults almost exclusively occupy patches with swift flow and coarse substrates (Chipps et al. 1994). Habitat use by immature

life stages of the Candy Darter has never been described (Supplementary Table S.1 available in the online version of this article) despite the importance of these life stages for population dynamics (Schlosser 1985, 1998), and little is known about habitat use and behavior in early spring during the spawning season. The current management of the species is similar to that of many nongame species, as managers must use a framework that is missing critical pieces of information and also suffers from a lack of cohesiveness among the patchwork of small-scale studies describing individual-level habitat associations from different portions of the species' distributional range. Coherent relationships between individual habitat selection and population robustness are needed to inform managers about which recovery actions are likely to be cost effective.

Field Sites

We selected four streams where Candy Darter populations were robust, localized, or extirpated (Figure 1). Two streams supporting large populations (hereafter, status = "robust populations") were selected to develop habitat suitability models based on the literature and preliminary sampling. The South Fork Cherry River (SFC) and East Fork Greenbrier River (EFG), West Virginia, are third- and fourth-order streams located in the Gauley River and Greenbrier River subbasins, respectively. Both streams primarily drain forested watersheds at high elevations (>700 m) within the Appalachian Mountains (Messinger and Hughes 2000). To examine microhabitat selection, we selected relatively undisturbed, accessible 5-km sections of stream in both EFG and SFC. Each study section was divided into five 1-km segments, and then 300-m sites from the first (downstream), third, and fifth (upstream) segments were randomly selected for survey. Due to prohibited access in the fifth segment of EFG, we randomly selected a 300-m site between the first and third segments. Randomization ensured that the 900 m of survey effort per stream and season (3.6 km in total) were spatially representative of the study sections within each stream.

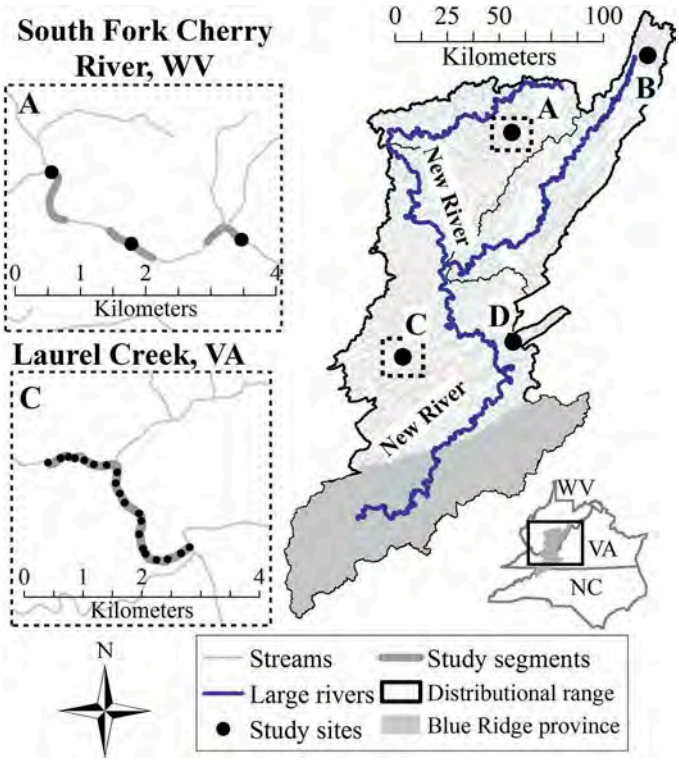

FIGURE 1. Map of the New River drainage and study sites: **(A)** South Fork Cherry River (SFC), West Virginia (contains a robust population of Candy Darters); **(B)** East Fork Greenbrier River, West Virginia (robust population); **(C)** Laurel Creek (LC), Virginia (localized population); and **(D)** Sinking Creek, Virginia (extirpated population). Insets depict the survey designs that were used to develop habitat suitability indices within streams supporting robust populations (e.g., SFC) and to systematically measure habitat availability in streams with localized (LC) or extirpated populations. Candy Darters have never been collected in the Blue Ridge province.

Laurel Creek (LC), Virginia, is a third-order stream within the Valley and Ridge Physiographic Province and contains a small, isolated population of Candy Darters (hereafter, status = "localized population"). The population in LC is likely self-sustaining, as the closest known population is approximately 50 fluvial kilometers away and there is no evidence of connectivity between the two populations. Systematic habitat surveys (described below) were conducted beginning at the mouth of LC and extending 4.2 km upstream to a series of small impoundments, encompassing the entire known range of the population in this system.

Sinking Creek (SC), Virginia (hereafter, status = "extirpated population"), is one of five systems in Virginia where Candy Darter are extirpated; it is a candidate site for reintroduction. Burton and Odum (1945) collected one individual over the summers of 1938–1941. However, there are no other records of Candy Darter occurrence in this heavily surveyed system (Jenkins and Burkhead 1994; Hitt and Roberts 2012). The collection of only one specimen in SC is consistent with early records from other streams where the species was extirpated. By the time of the first significant fish surveys in the Virginia portion of the New River drainage (1940s), Candy Darters were localized and always rare in streams where they are now extirpated (Jenkins and Kopia 1995). In the study segment, SC is a fourth-order stream with channel and land cover characteristics that are typical of a large stream in the Valley and Ridge Physiographic Province. Habitat surveys (described below) were conducted in SC at systematically spaced sites within a 5.5-km segment near the original collection locality.

Underwater Observation

We sampled microhabitat use and availability in spring and late summer–fall (hereafter, "fall") to examine possible behavioral changes and differences in habitat availability between seasons. Spring sampling occurred during high flows and the spawning season (May to early June 2011), whereas fall sampling corresponded with low flows and the nonspawning season (August–October 2011). Within EFG and SFC, we used direct underwater observation (snorkeling) during base flow to record the suite of microhabitat conditions that were

immediately associated with each individual. We ensured sufficient water clarity by only sampling when turbidity was less than 5.00 NTU. Beginning at the downstream-most point of a study site, the stream was longitudinally divided into two halves, and a snorkeler was assigned to survey each half. Snorkelers proceeded upstream at the same pace while searching under rocks and moving laterally between the center of the stream and the bank. When a snorkeler spotted a Candy Darter, the snorkeler used a ruler to estimate the fish's TL by either directly measuring the individual or by measuring a nearby rock of comparable size. Nearly all lengths were estimated less than 1 m from individual fish. If a snorkeler influenced an individual's initial position, the observation was omitted. While spring habitat use by adults reflected the areas occupied during the spawning season (staging areas for spawning), the exact microhabitat patches used for spawning within staging areas were not quantified because spawning followed courtship behavior, and observations of habitat use were restricted to the first sighting of individual darters.

Snorkelers classified each fish as belonging to one of three life stages based on the lengths at maturity reported by Jenkins and Burkhead (1994:827–830), our own observations of lengths at maturity from collected individuals, and pigmentation differences among life stages and sexes. Visual estimation of fish lengths and attribution of life stages during underwater observation have been previously used when examining habitat use by darters (Mattingly and Galat 2002; Ashton and Layzer 2010), including the Candy Darter (Chipps et al. 1994). Females that were 60 mm TL or larger and males that were 65 mm TL or larger were classified as adults. Individuals that were 46–59 mm TL were considered juveniles. Some individuals (60–64 mm TL) that were clearly juvenile males based on their pigmentation were classified as juveniles. All 45-mm-TL and smaller individuals were classified as age 0 regardless of the season. All age-0 individuals were postlarvae and ranged from 17 to 45 mm TL. A length frequency histogram constructed from estimated lengths contained three modes corresponding to the three life stages that we monitored (Figure S.1). After recording TL, the snorkeler placed a weighted fluorescent flag at the exact location of each fish and guided the individual downstream to prevent double counting.

After snorkelers finished flagging darter locations, five microhabitat variables were recorded at each flag. We measured depth with a top-setting wading rod and measured the average water column velocity at 60% depth by using a Marsh–McBirney Model 2000 flow meter. The nearest substrate particle was classified (based on its intermediate axis) into one of nine ordered substrate size categories according to a modified Wentworth scale: silt (<0.06 mm), sand (0.07–2.0 mm), gravel (3.0–16 mm), pebble (17–64 mm), small cobble (65–128 mm), large cobble (129–256 mm), boulder (257–1,000 mm), large boulder (>1,000 mm), and bedrock. Finally, within the 0.5-m^2 area surrounding each flag, we visually estimated the average depth of rocks that were embedded by fine substrates (hereafter, "embeddedness") and the surface area that was covered by silt (hereafter, "silt cover"). Percentages of both metrics were subsequently coded into five ordered categories (Newcomb et al. 2007:846): 0 = ≤5%, 1 = 6–25%, 2 = 26–50%, 3 = 51–75%, and 4 = 76–100%. Category 0 (≤5%) represented observations with no perceived embeddedness or silt cover.

Microhabitat Availability

Immediately after habitat use was recorded, the availability of microhabitats in EFG and SFC was measured by placing transects perpendicular to flow spanning the study site. In spring, 30 transects were placed every 10 m; in fall, 15 transects were placed every 20 m. We used data from spring to determine that the number of transects could be reduced to 15 per site without affecting the relative frequencies of available habitat categories. Beginning 1 m from the right descending bank, a field crew member recorded depth, average water velocity, substrate size, embeddedness, and silt cover every 2 m along each transect by using the same protocols employed for microhabitat use (described above). This ensured that the available habitat points were proportional to the area of each stream so as to reduce error when pooling observations across all sites and both streams (EFG and SFC). Observations were not pooled across seasons. Post hoc inspection of frequency distributions and multivariate space representing available microhabitats showed that physical habitats in the two streams were similar; therefore, error resulting from pooling across sites and streams was likely minimal. Furthermore, habitat selection (described below) showed no clear bimodality, which would have likely resulted from stream-specific differences in habitat availability rather than consistent responses to measured habitat gradients from separate streams.

We applied habitat suitability models developed from EFG and SFC to the available instream habitat in LC and SC to assess the ability of the models to predict suitable habitat for populations in a region outside the context of original model development. We employed a sampling design that systematically quantified available microhabitats throughout the 4.2-km section of LC, and we sampled a comparable extent (5.5 km) in SC. For LC and SC, we delineated sites by randomly selecting one of the first four riffles at the downstream-most point in each stream, and we systematically selected sites beginning at every fourth riffle extending upstream throughout the section (Dolloff et al. 1993). Therefore, sites in LC and SC consisted of all channel units between the bases of two consecutive riffles, and the number of sites per stream depended on the number of riffles within study sections. At each site, we placed transects perpendicular to flow and spaced every 10 m, beginning within the first 3 m of the base of the riffle and extending upstream to the base of the next upstream riffle. At five equidistant points along each transect, the same aforementioned microhabitat variables were recorded. We also snorkeled sites in LC to determine whether the microhabitats used there by Candy Darters were similar to those used in EFG and SFC.

The designs we used to quantify habitat availability in LC and SC differed from those used in EFG and SFC for multiple reasons. First, habitat data from LC and SC were not used for habitat suitability models, so it was not necessary to ensure that the observations of habitat availability were proportional to the area of each stream (discussed above). Second, although survey extents were similar across all streams (3.0–5.5 km), we distributed effort more evenly (i.e., more sites) in LC and SC to accomplish multiple management objectives (not reported here). The use of more systematically spaced sites in LC helped to clarify the distribution of Candy Darters within the stream, which could potentially be related to site-level habitat attributes, including rare—yet critical—habitat patches within LC (Torgersen et al. 1999; Fausch et al. 2002). A similar approach was used in SC to identify specific sites for potential restoration and reintroduction efforts. Because additional management objectives within LC and SC were focused at the site level (i.e., specific riffle–pool sequences), we used a fixed number of points for each transect in LC and SC to provide greater sample sizes and to improve estimates of habitat availability at each site.

Data Analysis

Habitat suitability criteria.—We estimated habitat suitability by first developing habitat selection curves. We use "selection" to refer to disproportionate use relative to availability across a single microhabitat gradient in an uncontrolled environment (i.e., a natural stream setting); in contrast, "preference," refers to disproportionate use in a controlled experimental setting (Rosenfeld 2003). Predictions from habitat selection curves are referred to as habitat suitability criteria (HSC), which were developed for each variable at each life stage within each season (hereafter, single-variable suitability unit = HSC). Habitat suitability criteria reflect the ratio of habitat use to availability for habitat bins or categories spanning each gradient (Newcomb et al. 2007:857–872). First, depth observations were categorized into 10-cm bins, and velocity observations were categorized into 0.2-m/s bins. To ensure that each bin contained at least one observation, all observations greater than 70 cm were combined into a single bin for depth, and all observations greater than 1.0 m/s were combined into a single bin for velocity. Bins for substrate, embeddedness, and silt cover were the same as the original categories described above. Bins for habitat use and availability were subsequently relativized and standardized so that a value of 1 corresponded with the most selected possible value, while a value of 0 corresponded with the least selected possible value. Finally, we used generalized additive models with a Gaussian error distribution to regress HSC values against the corresponding midpoint of each bin to aid visual interpretation of habitat selection. However, all estimates of suitability are from the original HSC.

Habitat suitability indices.—After developing HSCs from habitat use and availability in EFG and SFC, the HSCs were combined into multivariable and multiple-life-stage habitat suitability indices (HSIs; Newcomb et al. 2007). An HSI is a type of habitat suitability model that can be easily deconstructed to investigate the contributions of each life stage and variable to species-level estimates of instream suitability. Habitat suitability criteria and HSIs were used to predict the suitability of available habitat within each focal stream. Seasonal habitat suitability for each stream was the arithmetic mean of HSCs for each life stage (life stages l to L, where $L = 3$) based on the five habitat variables (variables v to V, where $V = 5$) for each habitat observation in a stream (n to N, where N = the total number of habitat availability observations per stream and season):

$$\mathrm{HSI}_{\mathrm{stream-season}} = \frac{\sum_{n=1}^{N}\sum_{l=1}^{L}\sum_{v=1}^{V}(\mathrm{HSC})_{nlv}}{N \times L \times V}. \quad (1)$$

Therefore, streamwide suitability within each season was the average HSI value of all measured 0.5-m^2 microhabitat patches based on habitat selection by multiple life stages. Overall habitat suitability for each stream ($\mathrm{HSI}_{\mathrm{stream}}$) was calculated as the arithmetic mean of spring and fall HSI values:

$$\mathrm{HSI}_{\mathrm{stream}} = \frac{\mathrm{HSI}_{\mathrm{stream-spring}} + \mathrm{HSI}_{\mathrm{stream-fall}}}{2}. \quad (2)$$

Finally, because life-stage-specific and variable-specific suitability values were nested within the calculation of seasonal suitability for each stream, we deconstructed stream-level HSIs into values for each combination of life stage, season, and habitat variable.

Multivariate habitat use and suitability.—We used nonmetric multidimensional scaling (NMDS) and biplots to visualize how microhabitat use and availability corresponded to predicted HSI values. For each season, microhabitat measurements from the four streams were organized into a Euclidian distance matrix, and the multivariate configuration with the lowest stress value after 20 runs was plotted using two axes. Convex-hull polygons were drawn around all observations of habitat availability in each stream. Next, each observation of habitat availability was color coded to reflect its HSI value. We also added NMDS points corresponding to the microhabitats used by Candy Darters in LC to examine the consistency of microhabitat use across streams. Finally, highly correlated Pearson's product-moment correlation coefficients (Pearson's $r \geq |0.50|$) between axes and instream habitat variables were added to biplots. The coefficients are also provided in Table S.2.

Cross-scale relationships.—We used a framework that examined the relationships between (1) instream habitat gradients across streams currently or formerly containing Candy Darter populations, (2) predicted individual-level suitability within each stream, and (3) observed population robustness across streams. The framework organized these components into a 3 × 3 correlation matrix in which each component was the heading of a single row and column (Figure 2). Analytically, the framework used the regional

	Stream-habitat gradient	Predicted individual suitability	Population robustness
Stream-habitat gradient	r = 1.0	r = Predicted individual response	ρ = Observed population relationship
Predicted individual suitability		r = 1.0	ρ = Cross-scale relationship
Population robustness			ρ = 1.0

FIGURE 2. Framework for examining relationships among stream habitat gradients, predicted individual habitat suitability, and observed robustness of Candy Darter populations across streams (r = Pearson's product-moment correlation coefficient; ρ = Spearman's rank-order correlation coefficient). The relationship between columns 1 and 3 is the observed population relationship to a habitat gradient. The relationship between columns 1 and 2 is the predicted response of individuals to a habitat gradient across streams. The relationship between columns 2 and 3 is the cross-scale relationship between predicted individual suitability and observed population robustness.

pattern of decline to generate a gradient of population robustness that could be compared to other columns of the matrix, thereby imposing the context of localization on relationships between the individual level and the population level.

The first relationship was Spearman's rank-order correlation (ρ) between the mean of each instream habitat variable within each stream and a rank corresponding with population robustness within each stream (i.e., columns 1 and 3). These relationships are typically the focus of distributional surveys aimed at observing population-level responses (e.g., site-level occupancy and abundance) across environmental gradients, which typically must sacrifice site-level intensity for larger spatial extents (i.e., more sites). Possible values of ρ ranged from 1 to –1, indicating positive and negative relationships, respectively, between population robustness and environmental gradients.

The second relationship was Pearson's product-moment correlation between the mean of each instream habitat variable within each stream and the predicted habitat suitability (i.e., HSC and HSI values) of each stream (i.e., columns 1 and 2). Correlations represented the predicted individual responses to habitat gradients at the stream level, and Pearson's r-values could range from 1 to –1. To trust these correlations is to assume that individual-level habitat selection reflects stream-level habitat suitability for populations—an assumption that is frequently not validated (Rosenfeld 2003).

Finally, the relationship between predicted stream-level suitability based on individual-level HSI values (column 2) and a rank of population robustness (column 3) represented the relationship between the individual and population levels. This correlation, the cross-scale relationship (CSR), will always be positive if individual-level HSIs can be scaled up to reflect population robustness. The CSR served as a form of validation in that negative or weak CSR coefficients indicated disconnects between the two ecological levels. The EFG, SFC, LC, and SC were given ranks of 3 (robust), 3 (robust), 2 (localized), and 1 (extirpated), respectively, which were corroborated by the observed population densities (Table S.3). The framework was inherently qualitative and was designed to facilitate detailed comparisons within and across representative systems. Correlation coefficients provided simple, objective measures of the strength of relationships. Different correlation coefficients were used because the estimated suitability and environmental gradients were ratio scale and normally distributed (i.e., appropriate for Pearson's r), whereas ranks for population status were ordinal and nonparametric (i.e., appropriate for ρ).

Hereafter, we use the term "CSR" to refer to consistent relationships observed at the microhabitat (individual) and stream segment (population) spatial scales. The concept of spatial scaling is well established in ecology (Wiens 1989; Levin 1992) and has catalyzed the proliferation of multiple-scale approaches aimed at identifying relationships among ecological levels of organization and the spatial scales at which habitat is organized (Schneider 2001). Rather than a top-down approach, which is frequently used in habitat suitability investigations, we used a bottom-up approach to examine the ability of microhabitat models to predict the suitability of habitat in stream segments. Figure 2 demonstrates important relationships among scales that are often overlooked when scaling up microhabitat suitability models to the spatial scales necessary to support populations.

RESULTS

Seasonal Habitat Availability across Streams (Columns 1 and 3 in Figure 2)

Streams with extant Candy Darter populations had similar instream habitat. The EFG, SFC, and LC contained many shallow areas (i.e., riffles and shallow runs), whereas SC had a meandering, lower-gradient channel with fewer and more isolated riffles composed of gravel, pebble, and cobble (Table 1). Embeddedness was consistently lower in streams with robust populations (<6%) than in LC or SC (6–25%).

Decreased rain and higher evapotranspiration throughout summer and fall resulted in shallower depths and slower water velocities for all streams in the fall. Seasonal differences in habitat availability were most apparent in EFG, where discharge was reduced by 92% from spring to fall. Despite being a heavily spring-fed system, the reduction in discharge in SC (–79%) was similar to that in LC (–82%) and greater than that in SFC (–73%). However, base flow (i.e., depth and velocity) remained higher in SC, likely due to greater groundwater contributions. Substrate size was the most constant of all variables. There were slightly higher levels of embeddedness and silt cover for most streams during fall, likely due to

TABLE 1. Means (±95% confidence interval in parentheses) and counts of observations of habitat availability for Candy Darters in four streams (EFG = East Fork Greenbrier River; SFC = South Fork Cherry River; LC = Laurel Creek; SC = Sinking Creek) and two seasons. Substrate categories are 1 = silt, 2 = sand, 3 = gravel, 4 = pebble, 5 = small cobble, 6 = large cobble, 7 = small boulder, 8 = large boulder, and 9 = bedrock. Embeddedness and silt categories are 0 = ≤5%, 1 = 6–25%, 2 = 26–50%, 3 = 51–75%, and 4 = >75%.

Stream	Population status	*N*	Depth (cm)	Velocity (m/s)	Substrate (rank)	Embeddedness (rank)	Silt cover (rank)
				Spring			
EFG	Robust	620	28.8 (1.5)	0.41 (0.02)	5.3 (0.1)	0.3 (0.0)	0.8 (0.1)
SFC	Robust	693	25.9 (1.3)	0.28 (0.02)	5.5 (0.1)	0.3 (0.1)	0.6 (0.1)
LC	Localized	435	26.2 (1.5)	0.35 (0.02)	5.6 (0.2)	1.1 (0.1)	1.0 (0.1)
SC	Extirpated	490	47.5 (2.3)	0.43 (0.02)	4.7 (0.1)	1.5 (0.1)	0.8 (0.1)
				Fall			
EFG	Robust	212	16.2 (2.2)	0.11 (0.02)	5.1 (0.2)	0.4 (0.1)	1.1 (0.1)
SFC	Robust	277	19.1 (1.7)	0.15 (0.02)	5.3 (0.2)	0.5 (0.1)	0.8 (0.1)
LC	Localized	440	17.6 (1.2)	0.15 (0.02)	5.1 (0.2)	1.0 (0.1)	0.9 (0.1)
SC	Extirpated	515	32.5 (1.6)	0.19 (0.02)	4.5 (0.1)	1.8 (0.1)	1.3 (0.1)

deposition of suspended sediment coinciding with reduced stream discharge. Higher fine-sediment levels from spring to fall were most pronounced for SC (embeddedness in spring = 1.5, ±95% confidence interval [CI] = 0.1; embeddedness in fall = 1.8, 95% CI = 0.1; silt in spring = 0.8, 95% CI = 0.1; silt in fall = 1.3, 95% CI = 0.1), which was relatively turbid in spring but clear in the fall (C.G.D., personal observation).

Relationships between population status and environmental gradients (columns 1 and 3 in Figure 2) tended to be strong and consistent across seasons (Table 2). We interpreted large coefficients ($\rho \geq |0.50|$) as indicators of strong population relationships with environmental gradients; consistency in the direction of coefficients across seasons indicated few seasonal effects on these relationships. Streams with more robust populations tended to be shallower ($\rho = -0.63$), to have less-embedded and less-silted substrates (embeddedness: $\rho = -0.95$, silt cover: $\rho = -0.42$), and to have slower water velocities ($\rho = -0.79$). The negative relationship between average stream-level water velocity and population robustness was higher in fall during low-flow conditions (spring: $\rho = -0.63$; fall: $\rho = -0.95$). Finally, there was a positive, albeit weak, correlation between substrate size and population robustness ($\rho = 0.47$).

TABLE 2. Spearman's rank-order correlation coefficients (ρ) between habitat variables and a rank representing the population status of Candy Darters in four study streams and two seasons (columns 1 and 3 in Figure 2). Streams with the highest Candy Darter densities were given the highest rank (East Fork Greenbrier River = 3 [robust]; South Fork Cherry River = 3 [robust]; Laurel Creek = 2 [localized]; Sinking Creek = 1 [extirpated]). Predictions are based on historical accounts of habitat use (Table S.1). The predicted relation for embeddedness was not applicable (NA) because there were no historical accounts. Values of ρ that were ≥ |0.50| and consistent with predictions are shown in bold to emphasize the strength of the relationship; ρ values that were ≥ |0.50| and inconsistent with predictions are italicized. The "Combined" column presents the averages of spring and fall values.

Variable	Predicted relationship	Spring	Fall	Combined
Depth	–	**–0.63**	**–0.63**	**–0.63**
Velocity	+	*–0.63*	*–0.95*	*–0.79*
Substrate	+	0.32	**0.63**	0.47
Embeddedness	NA	**–0.95**	**–0.95**	**–0.95**
Silt cover	–	–0.21	**–0.63**	–0.42

Individual Habitat Selection

We recorded 290 (EFG = 115; SFC = 175) and 508 (EFG = 286; SFC = 222) microhabitat use observations for multiple life stages in the spring and fall, respectively. Among the three life stages, counts of adults were the most consistent across systems (EFG = 135; SFC = 151) and seasons (spring = 137; fall = 149). Counts of subadult life stages (age-0 and juvenile fish) were higher in the fall, coinciding with new recruitment. We also observed Candy Darters at 8 (spring) and 14 (fall) of 20 total sites throughout LC. Adults and juveniles were observed during spring, and all three life stages were detected during fall.

Selection curves for all life stages across seasons were either approximately monotonic or unimodal, indicating that observed curves were consistent with the selection of habitat across environmental gradients (Figure 3). Clear, biologically sensible selection patterns aid interpretation of habitat associations and obviate the need to rely on *P*-values from tests of nonrandom habitat selection (Cherry 1998). Generally, most life stages selected microhabitats with at least moderate flow (>0.19 m/s), shallow depths (<0.5 m), coarse substrates (>sand), and nonembedded and nonsilted substrates (<26%). However, each life stage demonstrated more nuanced habitat selection patterns corresponding with age and body size. The most pronounced ontogenetic differences were for water velocity, with adults selecting the swiftest water velocities

available in spring (>1.20 m/s) and fall (>0.60 m/s). Juveniles selected intermediate water velocities (0.40–1.20 m/s) in both seasons, while age-0 fish selected slower water velocities (0.0–0.80 m/s). Similar ontogenetic patterns occurred for substrate, embeddedness, and silt cover. Adults selected larger substrates and avoided areas with fine sediments, resulting in near-zero HSC values for all microhabitats with embeddedness or silt cover scores greater than 25% (rank = 2). Younger life stages selected smaller substrates and were less averse to fine sediments.

Ontogenetic habitat selection patterns were similar across seasons. The most pronounced difference was that of juveniles, which selected velocities more similar to those of adults in fall than in spring (Figure 3). When individual variables were collectively viewed, the observed ontogenetic differences were attributable to habitat shifts from the pool margins and runs occupied by age-0 fish to the swift, turbulent riffles occupied by adults. Juveniles tended to select run channel units or riffle margins in spring and shifted to riffles by fall (i.e., intermediate habitat selection).

Our underwater observations enabled us to document the behavior underlying habitat selection patterns (Jordan et al. 2008). Individuals tended to segregate by life stage rather than behavior mode. For example, in spring, adults foraged, used cover, and displayed behavior associated with spawning (e.g., antagonistic behavior or courtship) within the most selected habitats. None of the habitat use observations revealed the exact locations selected by females for egg deposition, but spawning was observed during surveys and occurred near areas that were strongly selected by adults in spring.

Most of the Candy Darters inhabiting LC used habitat patches that were similar to those used in EFG and SFC (Figure 4; Figure S.2). Low sample sizes prevented us from developing selection curves for each life stage based on observations of habitat use and availability within LC; however, nearly all observations of habitat use were consistent with projected highly suitable habitat.

Individual-Level Habitat Suitability within and across Streams (Columns 1 and 2 in Figure 2)

In spring, two distinct groups of suitability values were apparent: streams with robust Candy Darter populations (EFG: HSI = 0.68, 95% CI = 0.01; SFC: HSI = 0.66, 95% CI = 0.02) and streams where Candy Darters were localized (LC: HSI = 0.58, 95% CI = 0.02) or extirpated (SC: HSI = 0.56, 95% CI = 0.01; Table S.4). The EFG had the highest overall HSI value as a result of having the highest HSC values for depth, velocity, and substrate size. Lower HSI values for LC and SC were attributable to their low HSC values for embeddedness and substrate size (Table S.4).

Habitat suitability values were lower in fall than in spring due to less-suitable depths, velocities, and fine-sediment levels. In the fall, HSI values also separated into two tiers; however, unlike spring, the highest tier comprised streams with extant populations (EFG: HSI = 0.51, 95% CI = 0.02; SFC: HSI = 0.56, 95% CI = 0.02; LC: HSI = 0.52, 95% CI = 0.02), while SC had markedly lower HSI values (HSI = 0.44, 95% CI = 0.01; Table S.4). Sinking Creek remained the least suitable stream due to its relatively low HSC values for embeddedness and silt cover.

These results were corroborated by NMDS plots of projected habitat suitability for each observation of available microhabitat within the four streams (Figure 4 for spring; Figure S.2 for fall). In both spring and fall, the most suitable microhabitats occurred in high-velocity areas composed of coarse substrates and few fine sediments. Although highly suitable habitat was within the environmental space enveloped by all four streams, SC contained more areas with low suitability, representing slower, more embedded, or more silted habitat patches.

Predicted habitat suitability across streams mirrored individual-level habitat selection. The strongest correlations between predicted suitability and habitat availability at the stream scale (i.e., Pearson's $r \geq |0.50|$) across seasons were negative relationships with embeddedness and silt cover for all life stages (Table 3). In other words, predicted individual-level suitability (i.e., selection) decreased with greater average embeddedness and silt cover across the four streams. Strong positive relationships with increasing water velocity were also observed for adults and juveniles across streams. Predicted suitability for both depth and substrate tended to be either weakly consistent or inconsistent with predicted relationships based on historical accounts of habitat selection by Candy Darters (Table S.1). Inconsistencies reflected seasonal differences in depth selection (spring: Pearson's r = –0.42; fall: Pearson's r = 0.01) and ontogenetic differences between adults and younger life stages for depth (adult: Pearson's r = 0.21; juvenile: Pearson's r = –0.12; age 0: Pearson's r = –0.37) and substrate (adult: Pearson's r = 0.21; juvenile: Pearson's r = −0.34; age 0: Pearson's r = –0.66), which demonstrates that temporal or ontogenetic habitat shifts can generate conflicting habitat suitability predictions across a species' life cycle.

Relationships between Predicted Individual-Level Habitat Suitability and Population Robustness across Streams (Columns 2 and 3 in Figure 2)

Overall, when averaged across two seasons and three life stages, predicted habitat suitability was positively correlated with population robustness (studywide CSR coefficient [ρ_{CSR}] = 0.95; Figure 5), indicating that the proportion of suitable microhabitats within a stream was related to population robustness. However, the strength of these relationships varied with life stage, season, and habitat variable. The HSIs had higher CSR coefficients in spring (ρ_{CSR} = 0.95) than in fall (ρ_{CSR} = 0.63) owing to weaker relationships for velocity and substrate size in the fall. All life stages had equal CSR coefficients after averaging HSI values across seasons (ρ_{CSR} = 0.95); however, coefficients for adults were consistently the

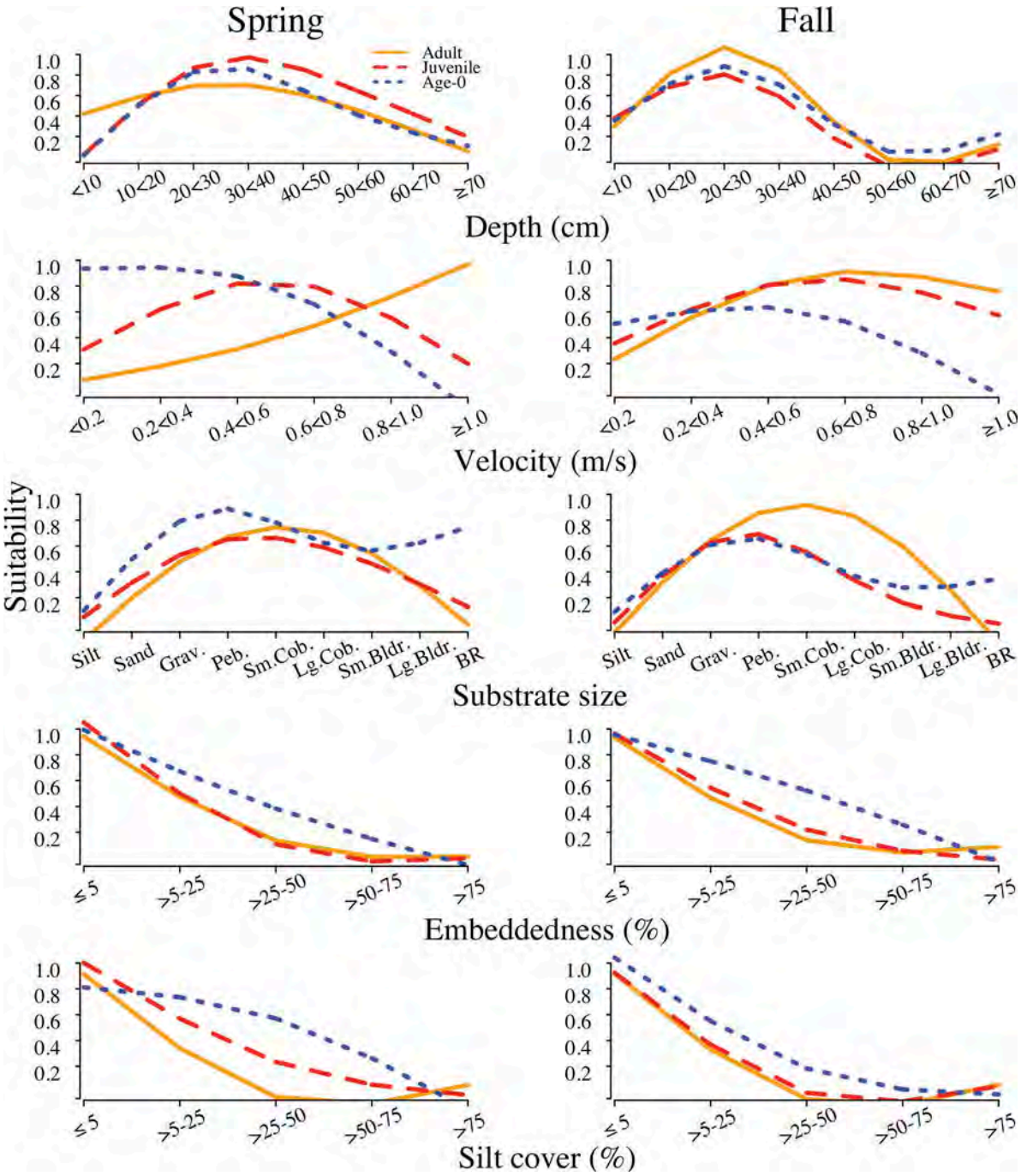

FIGURE 3. Habitat selection curves developed from habitat used by Candy Darters during three life stages and two seasons and the available habitat in two streams. Continuous curves, presented as visual aids, were obtained by regressing suitability values against the midpoint of each bin using generalized additive regression models (substrate abbreviations: Grav. = gravel; Peb. = pebble; Sm. Cob. = small cobble; Lg. Cob. = large cobble; Sm. Bldr. = small boulder; Lg. Bldr. = large boulder; BR = bedrock).

highest for both seasons (spring: $\rho_{CSR} = 0.96$; fall: $\rho_{CSR} = 0.96$), which may be due to the greater microhabitat specificity of adults. Coefficients for depth and substrate size were the most inconsistent, which indicates that these variables may only be important at the population level during certain life stages or seasons. In contrast, velocity consistently had the most negative CSR for all scenarios ($\rho_{CSR} = -1.0$), which indicates that despite strong selection of high-velocity habitat, streams with more high-velocity habitat patches did not support more robust populations. Velocity CSR coefficients were

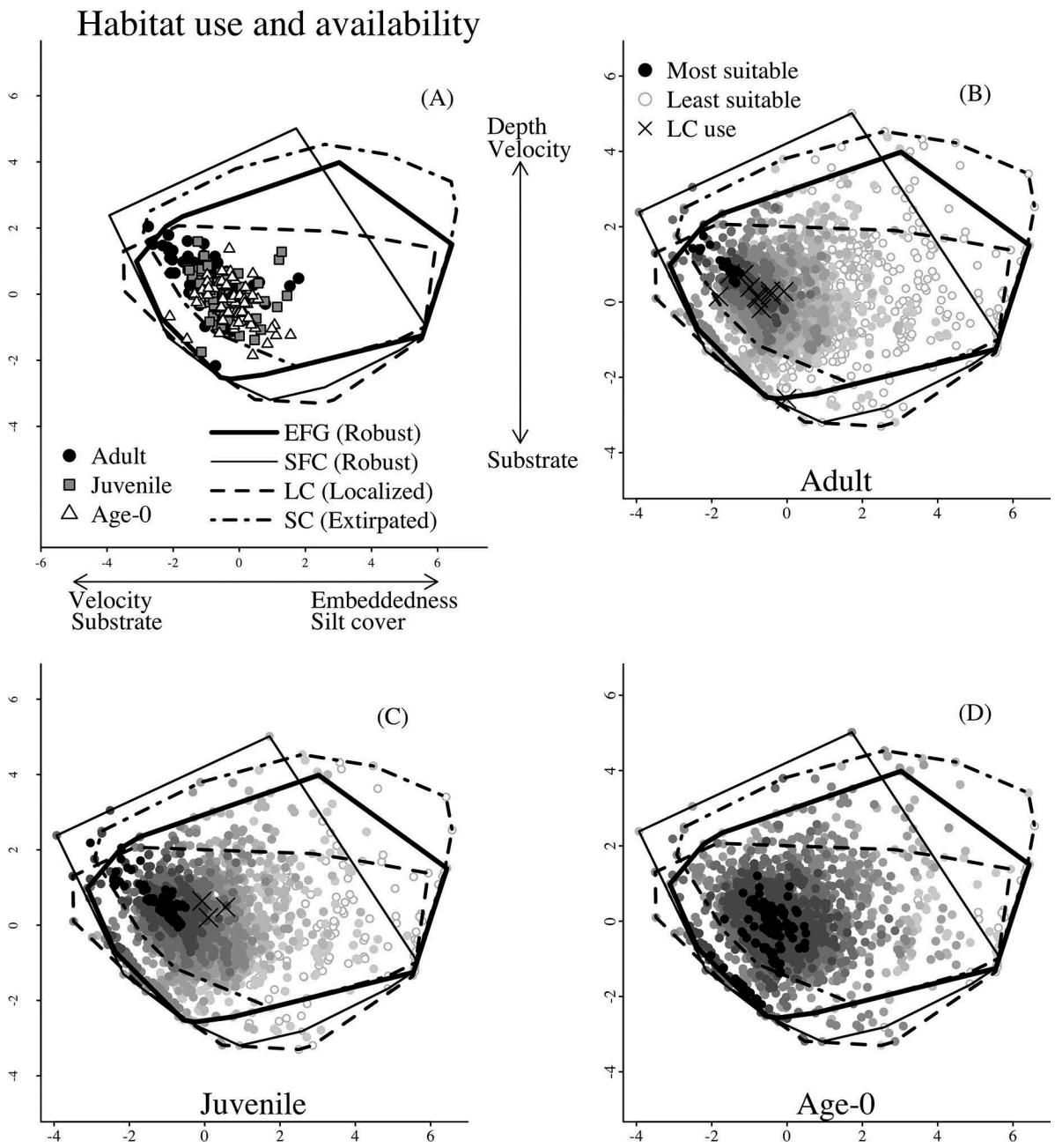

FIGURE 4. Nonmetric multidimensional scaling (NMDS) plots of habitat use, availability, and suitability for Candy Darters in spring: **(A)** habitat use by three life stages and availability in four streams (polygons; EFG = East Fork Greenbrier River; LC = Laurel Creek; SC = Sinking Creek; SFC = South Fork Cherry River); **(B)** predicted habitat suitability for adults; **(C)** predicted habitat suitability for juveniles; and **(D)** predicted habitat suitability for age-0 fish. Symbols for "LC use" represent locations used by Candy Darters in Laurel Creek during the spring. Variables that are highly correlated (Pearson's product-moment correlation coefficient [Pearson's r] ≥ 0.50) with axes are shown. All Pearson's r-values are presented in Table S.2. The NMDS stress value was 0.17. See Figure S.2 for NMDS plot for fall data.

more negative in fall, when all streams with extant populations had slower average velocities than SC, where Candy Darters were extirpated (spring: $\rho_{CSR} = -0.39$; fall: $\rho_{CSR} = -0.50$). The CSR correlations for silt cover were season specific and life stage specific but were positive overall ($\rho_{CSR} = 0.63$). Finally, embeddedness HSI values were highly correlated with population robustness regardless of season (spring: $\rho_{CSR} = 0.95$; fall: $\rho_{CSR} = 0.63$) or life stage (adult: $\rho_{CSR} = 0.95$; juvenile: $\rho_{CSR} = 0.95$; age 0: $\rho_{CSR} = 0.95$), which indicates that embeddedness is consistently the most important parameter for both the selection of microhabitats by individuals and the robustness of populations.

TABLE 3. Pearson's product-moment correlation coefficients (Pearson's *r*) between predicted individual habitat suitability for Candy Darters and averages of five instream habitat variables across four streams that varied in Candy Darter population status (columns 1 and 2 in Figure 2). Predictions are based on prior accounts of habitat use (Table S.1). The predicted relation for embeddedness was not applicable (NA) because there were no historical accounts. "Multi-stage" is the correlation between average suitability across multiple life stages (Table S.4) and habitat gradients (Table 1). Pearson's *r*-values that were ≥ |0.50| and consistent with predictions are shown in bold to emphasize the strength of the relationship. Pearson's *r*-values that were ≥ |0.50| and inconsistent with predictions are italicized. The "Combined" column presents the averages of spring and fall values.

Variable	Predicted relationship	Adults	Juveniles	Age 0	Multi-stage
Spring					
Depth	–	–0.10	0.21	**–0.74**	–0.42
Velocity	+	**0.97**	**0.99**	–0.19	**0.99**
Substrate	+	0.15	0.25	*–0.54*	0.06
Embeddedness	NA	**–1.00**	**–1.00**	**–1.00**	**–1.00**
Silt cover	–	–0.36	**–0.92**	**–0.69**	**–0.98**
Fall					
Depth	–	*0.52*	–0.45	–0.01	0.01
Velocity	+	**0.93**	**0.78**	**0.74**	**0.77**
Substrate	+	0.28	*–0.93*	*–0.78*	*–0.71*
Embeddedness	NA	**–1.00**	**–1.00**	**–1.00**	**–1.00**
Silt cover	–	**–0.91**	**–0.90**	**–0.99**	**–0.93**
Combined					
Depth	–	0.21	–0.12	–0.37	–0.20
Velocity	+	**0.96**	**0.89**	**0.28**	**0.88**
Substrate	+	0.21	–0.34	*–0.66*	–0.32
Embeddedness	NA	**–1.00**	**–1.00**	**–1.00**	**–1.00**
Silt cover	–	**–0.63**	**–0.91**	**–0.84**	**–0.96**

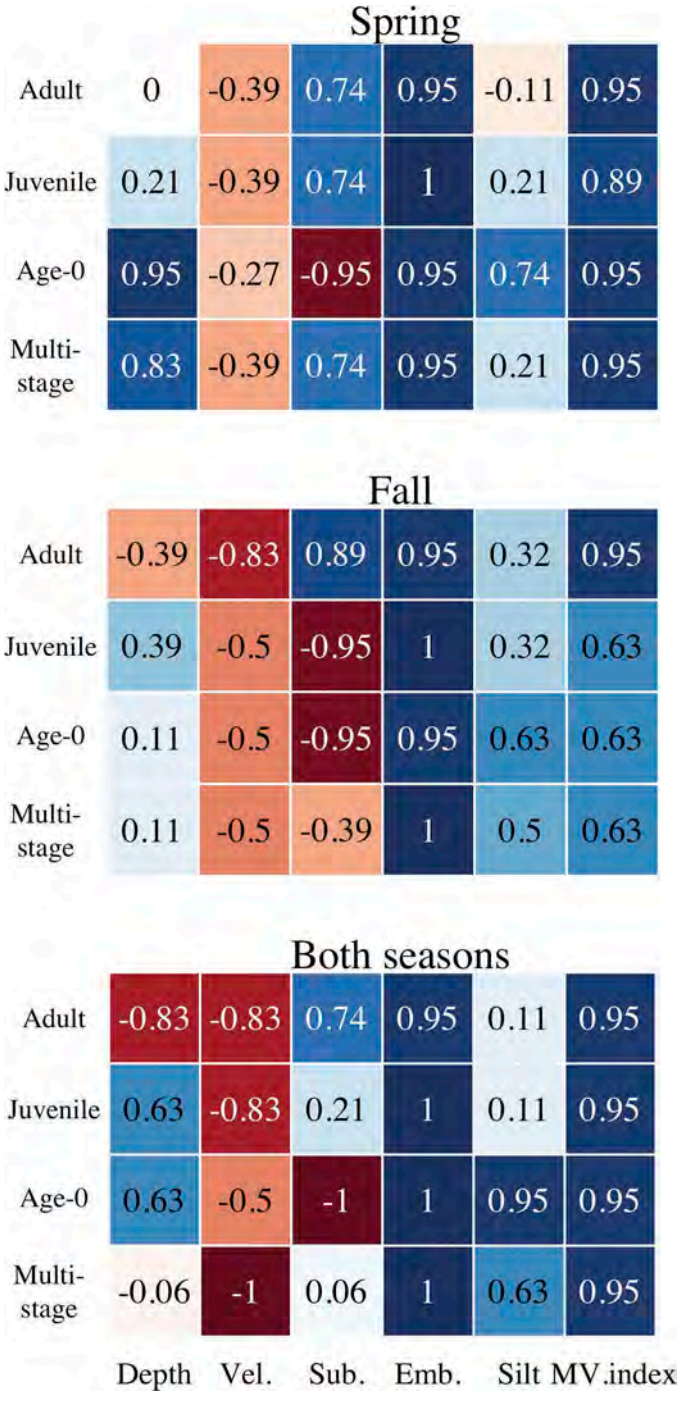

FIGURE 5. Spearman's rank-order correlation coefficients (ρ) between predicted individual microhabitat suitability and Candy Darter population robustness in four streams during two seasons (columns 2 and 3 in Figure 2; Multi-stage = multiple-life-stage habitat suitability index; MV.index = multiple-variable habitat suitability index; Vel. = velocity; Sub. = substrate size; Emb. = embeddedness). Positive coefficients (blue) indicate that individual habitat selection predicts population robustness, whereas negative coefficients (red) indicate disconnects between the individual level and the population level. Darker shading reflects greater absolute value of ρ. The lower far-right cell (ρ = 0.95) represents the studywide cross-scale relationship.

DISCUSSION

Much of North America's imperiled fish fauna has an unnatural distributional pattern marked by disjunct yet viable populations occupying a fraction of their historical range (Jelks et al. 2008). A key to fish conservation is the identification of habitat that promotes the resistance or resiliency of these populations to factors that diminish habitat quality. We used a comparative approach aimed at directly contrasting systems that are currently supporting Candy Darter populations and those that formerly supported populations. Often, the processes underlying the localization of populations are anthropogenic; therefore, this comparative approach may reflect the gradients leading to the decline of the Candy Darter.

Scaling Up Individual Habitat Selection to Populations

Many fishes exhibit complex life cycles that are marked by the use of distinctive habitat patches through ontogeny, yet much of the existing management is based solely on adult

habitat use (Copp and Vilizzi 2004; King 2004), which may not be as limiting as habitat for subadults. Although our observations of habitat selection by adult Candy Darters were largely consistent with previous accounts of adults, clear ontogenetic differences were documented, most notably for depth, substrate, and velocity. The most apparent ontogenetic shift by Candy Darters was for velocity, with age-0 fish selecting low-velocity to moderate-velocity areas and adults being largely restricted to high-velocity areas. These observations are consistent with habitat shifts observed in other species of darter (Rosenberger and Angermeier 2003; Skyfield and Grossman 2008; Ashton and Layzer 2010). For Candy Darters, it is unclear whether these shifts are structured by predation risk (Schlosser 1987; Werner and Hall 1988; Labeelund et al. 1993), the energetic costs of maintaining position in fast flows (Lobb and Orth 1991; Mann and Bass 1997; Moore and Thorp 2008), differing food sources (Schlosser 1990; King 2004), or intraspecific competition (Davey et al. 2005; Petty and Grossman 2007). In spring, adult males were highly territorial near areas where spawning occurred (i.e., staging areas), and this may have excluded juveniles from the high-velocity habitats. Our observations of adult male territoriality and lower spatial overlap between adults and juveniles in spring during the spawning season tentatively support intraspecific competition as one potential mechanism structuring observed ontogenetic habitat shifts.

Microhabitat use is a product of complex interactions among fish size, behavior mode, physiological state, intraspecific and interspecific interactions, and habitat availability. As a result of this complexity, selection could be a measure of the most suitable habitat available for individuals, but alternative habitat may be substitutable and therefore the resource may be less influential at the population level (Rabeni and Sowa 1996). If so, individual selection could mislead managers to incorporate nonessential resources into their guiding image of suitable habitat. For example, adult Candy Darters are flow specialists based on their specificity for high-velocity, shallow microhabitats (Chipps et al. 1994); however, the negative CSR coefficients for water velocity and depth demonstrated that suitable microhabitats for these variables were more available or similarly available in SC compared to the streams with viable populations. Seasonal decreases in suitable velocity and depth microhabitats were greatest in EFG, where discharge was the most reduced from spring to fall. Rather than observing lower abundances of adults as a result of mortality or emigration in fall during low-flow conditions, we found that all life stages—especially adults—compensated by shifting locations to the most suitable flows available. A hypothesis warranting further testing is that low fall flows enhance the survival of age-0 individuals, which frequent shallow, slow microhabitats, as observed in other stream fishes (Schlosser 1982; Rosenberger and Angermeier 2003). Additionally, periods of drought or low flows can have a disproportionate negative influence on the large piscivorous fishes that prey upon age-0 fish (Schlosser 1987). Low fall flows may have created nursery habitat that was unsuitable for predators, in turn allowing for expanded foraging in warmer, more productive habitat (Moore and Gregory 1988; Henderson and Johnston 2010) and less density dependence among the large age-0 year-classes we observed in both of the streams with robust populations (Schlosser 1990). Similarly, individuals selected certain substrate sizes during specific life stages, but the near-zero CSR coefficient indicated that substrate size may not be limiting at the population level within the context of localization. Overall, our results suggest that ontogenetic shifts and seasonal habitat plasticity may limit the management utility of a simple, generalized image of suitable habitat for a species based solely on the selection of habitat by a single life stage during a single season or potentially even a single year.

The largest and most consistent CSR coefficients indicated that both individual habitat selection and population robustness were negatively related to embeddedness. Embeddedness can profoundly alter the function of stream ecosystems and has been implicated in the declines of most imperiled fishes in North America (Jelks et al. 2008). The specific pathways through which elevated embeddedness may influence individuals and populations of Candy Darters remain unexamined. Potential hypotheses are the filling of interstitial spaces, which can alter food webs by reducing the microhabitats used by macroinvertebrates (Ryan 1991; Henley et al. 2000) and can eliminate structure used for cover and refugia. Alternatively, observed negative relationships could covary with life stages not studied herein, such as a loss of rearing habitat that is suitable for eggs and larvae. Future studies specifically aimed at identifying relationships among the characteristics, placement, and abundance of the exact habitat patches needed for egg incubation and larval survival would help to determine the role of these life stages in the population dynamics within each stream.

Additional research on several topics would help to clarify the mechanisms underlying the decline of the Candy Darter. For example, documenting fish responses to experimental manipulations of habitat would help to reduce any observational biases associated with habitat selection patterns and to control for multicollinearity among variables (Rosenfeld 2003). Moreover, the present study quantified habitat availability at a spatial scale that was large enough to be germane to Candy Darter population dynamics (i.e., stream segment), but additional research spanning relevant temporal scales (i.e., multiple years) could provide a better understanding of the consistency of habitat availability and the stability of predicted suitability under different conditions. However, until specific mechanisms influencing individual fitness and population dynamics are understood, managers could utilize our HSIs, and especially the embeddedness selection curves, to help identify sites with suitable habitat for the translocation or restoration of Candy Darters.

Hypothesized Ecological Processes among Instream Habitat Patches

Instream habitat, as perceived by small aquatic organisms, represents a landscape of microhabitat patches with varying quality (Palmer et al. 2000). For continued occupation within a region, nonsubstitutable resources must be abundant enough, accessible, and in harmony with the life cycle of a species. On average, habitat patches in SC had the lowest suitability for each of the three life stages investigated. However, the NMDS plots and HSIs indicated that highly suitable habitat patches existed in SC. It is unclear whether the prevalence of these patches, particularly unembedded substrate, is too low to support a Candy Darter population. Poor habitat suitability may interact with other population threats and further diminish population resistance to altered conditions. When suitable habitat is proportionally low and spatially diffuse, the suitability of habitat patches is likely reduced by neighborhood effects from the surrounding poor-quality habitat (Dunning et al. 1992; Schlosser 1995). Moreover, when navigating corridors between suitable patches, individuals may be exposed to fitness-reducing factors, such as an elevated risk of predation, which may be exacerbated by a reduction in benthic complexity in embedded systems (Roberts and Angermeier 2007). Many nonnative fishes, including piscivores, have colonized SC (Hitt and Roberts 2012) and now occupy likely corridor habitat. Although no information exists on the movements of Candy Darters among suitable patches or the predation rates by introduced piscivores, Labbe and Fausch (2000) found that nonnative piscivores influenced the demographic rates of the Arkansas Darter *E. cragini* due to predation in corridor habitat. Understanding interactions between multiple-scale habitat suitability and other factors, such as predation and movement, will require detailed demographic investigation. Nonetheless, findings suggest that the prevalence and harshness of the matrix of nonsuitable habitat could be as important as the presence of suitable habitat within an area. These findings are consistent with other multiple-scale investigations of darter habitat, which have reported that the presence of suitable habitat nested within a matrix of poor-quality habitat may not be enough to sustain populations (Freeman and Freeman 1994; Davis and Cook 2010; Compton and Taylor 2013). For species with uncertain habitat requirements, the incorporation of multiple scales into investigations may help to identify consistencies across populations and individuals (Torgersen et al. 1999; Fausch et al. 2002) and to refine hypotheses related to limiting habitat parameters.

Application to Imperiled Species Management and Recovery

Frameworks that employ realistic and validated benchmarks are staples of stream restoration and biomonitoring (Stoddard et al. 2006; Whittier et al. 2007) but are less common when defining fish habitat suitability at the site and population levels. We estimated the habitat suitability of streams where Candy Darter populations were robust (EFG and SFC) or localized (LC). Consequently, segment-scale suitability values for EFG and SFC are also ecologically derived benchmarks of optimal instream habitat conditions among known populations of the Candy Darter, while values for LC may meet the minimum habitat conditions necessary to sustain a population. In contrast, HSI values are often categorized into levels of suitability (e.g., "optimal" habitat ≥ 50th percentile of HSI [Thomas and Bovee 1993], HSI ≥ 0.40 [Freeman et al. 1997]), which may be meaningful benchmarks for predicting the habitats selected by individuals but may not have significance for populations. Attempts at validating individual habitat selection often examine the consistency of habitat selection across systems (Newcomb et al. 2007). However, even if habitat use is consistent, the approach still does not establish relationships between individual habitat selection and population function. Alternatively, the approach used here effectively rescaled suitability based on individual habitat selection to represent segment-level suitability for a population, which will likely be more meaningful for conservation efficacy.

Validating individual habitat selection at the stream scale may be particularly applicable for imperiled species management. For example, recovery plans often aim to re-establish extirpated populations (George et al. 2009), yet historical conditions within streams are rarely documented. Managers could reference suitability values from streams with robust populations when identifying streams with suitable habitat for reintroduction. Alternatively, potentially more realistic criteria may be the suitability values from streams supporting small populations (e.g., LC) given that additional (albeit small) populations can dilute the risk of regional extirpation.

Conclusions

The HSIs for Candy Darters should not be considered infallible or definitive. A correlative framework is no substitute for detailed study of the mechanisms influencing individuals or populations. However, more direct measures of individual fitness (e.g., growth and fecundity) or population function (e.g., demographic rates) across additional streams could be incorporated within the general framework described herein (Figure 2). A clear understanding of habitat requirements is typically gained through a progression of detailed investigation at multiple ecological levels (Rosenfeld 2003). Our approach is likely helpful in identifying the limiting habitat types at the beginning of this progression, which could potentially assist in directing future investigations and conservation measures.

Candy Darters are highly selective of specific instream habitat patches within occupied streams, and habitat selection varies through ontogeny. Habitat specificity may reflect adaptive benefits of certain patch types for growth, survival, and reproduction under natural conditions. However, when viewed across populations that were affected by anthropogenic disturbances, habitat specificity did not always indicate limiting conditions. Similar to many nongame species, the only habitat information available for Candy Darters prior to this investigation were descriptions of adult habitat use within short reaches (<150 m) in a few streams during a single season. While our findings

support some of these descriptions, ontogenetic shifts and seasonal habitat plasticity make habitat selection more complex than previously described. Such complexity demonstrates that studies aimed at the individual level could be potentially misleading when identifying habitat that is suitable to facilitate population persistence. This finding underscores the potential inadequacy of the information guiding management decisions for many of North America's freshwater fishes. Until rigorous study of relationships between individuals and populations becomes the norm for species with lower management priority, the framework used here may be a viable approach to identifying habitat parameters that are important at both levels of ecological organization.

ACKNOWLEDGMENTS

This study was partially funded by a State Wildlife Grant from the U.S. Fish and Wildlife Service and the Virginia Department of Game and Inland Fisheries (VDGIF). We thank Mike Pinder, Stuart Welsh, and Dan Cincotta for site recommendations. We also thank VDGIF and the West Virginia Division of Natural Resources for field collection permits and Greg Anderson for programming assistance. Field help was provided by Matt Bierlein, Joe Cline, David Crain, Laura Heironimus, Pat Kroboth, Josh Light, Vance Nepomuceno, Phil Pegelow, Jordan Richard, Chris Rowe, and Laura Zseleczky. Earlier versions of the paper were improved by recommendations from Nick Sievert and two anonymous reviewers. This work was carried out under the auspices of Institutional Animal Care and Use Committee Protocol 10-094-FIW at Virginia Tech. The Virginia Cooperative Fish and Wildlife Research Unit is jointly sponsored by the U.S. Geological Survey, Virginia Polytechnic Institute and State University, VDGIF, and Wildlife Management Institute. Use of trade, firm, or product names does not imply endorsement by the U.S. Government.

REFERENCES

Angermeier, P. L. 1995. Ecological attributes of extinction-prone species: loss of freshwater fishes of Virginia. Conservation Biology 9:143–158.

Ashton, M. J., and J. B. Layzer. 2010. Summer microhabitat use by adult and young-of-the-year Snail Darters (*Percina tanasi*) in two rivers. Ecology of Freshwater Fish 19:609–617.

Boavida, I., J. M. Santos, R. Cortes, A. Pinheiro, and M. T. Ferreira. 2012. Benchmarking river habitat improvement. River Research and Applications 28:1768–1779.

Burkhead, N. M. 2012. Extinction rates in North American freshwater fishes, 1900–2010. Bioscience 62:798–808.

Burton, G. W., and E. P. Odum. 1945. The distribution of stream fish in the vicinity of Mountain Lake, Virginia. Ecology 26:182–194.

Cherry, S. 1998. Statistical tests in publications of The Wildlife Society. Wildlife Society Bulletin 26:947–953.

Chipps, S. R., W. B. Perry, and S. A. Perry. 1993. Status and distribution of *Phenacobius teretulus, Etheostoma osburni*, and "*Rhinichthys bowersi*" in the Monongahela National Forest, West Virginia. Virginia Journal of Science 44:48–58.

Chipps, S. R., W. B. Perry, and S. A. Perry. 1994. Patterns of microhabitat use among four species of darters in three Appalachian streams. American Midland Naturalist 131:175–180.

Compton, M., and C. Taylor. 2013. Spatial scale effects on habitat associations of the Ashy Darter, *Etheostoma cinereum*, an imperiled fish in the southeast United States. Ecology of Freshwater Fish 22:178–191.

Copp, G. H., and L. Vilizzi. 2004. Spatial and ontogenetic variability in the microhabitat use of stream-dwelling Spined Loach (*Cobitis taenia*) and Stone Loach (*Barbatula barbatula*). Journal of Applied Ichthyology 20:440–451.

Davey, A. J. H., S. J. Hawkins, G. F. Turner, and C. P. Doncaster. 2005. Size-dependent microhabitat use and intraspecific competition in *Cottus gobio*. Journal of Fish Biology 67:428–443.

Davis, J. G., and S. B. Cook. 2010. Habitat use of the Tuxedo Darter (*Etheostoma lemniscatum*) at macrohabitat and microhabitat spatial scales. Journal of Freshwater Ecology 25:321–330.

Dixon, C. J., and J. C. Vokoun. 2009. Burbot resource selection in small streams near the southern extent of the species range. Ecology of Freshwater Fish 18:234–246.

Dolloff, C. A., D. G. Hankin, and G. H. Reeves. 1993. Basinwide estimation of habitat and fish populations in streams. U.S. Forest Service, Report SE-93, Asheville, North Carolina.

Dunham, J. B., B. S. Cade, and J. W. Terrell. 2002. Influences of spatial and temporal variation on fish–habitat relationships defined by regression quantiles. Transactions of the American Fisheries Society 131:86–98.

Dunning, J. B., B. J. Danielson, and H. R. Pulliam. 1992. Ecological processes that affect populations in complex landscapes. Oikos 65:169–175.

Fausch, K. D., C. L. Hawkes, and M. G. Parsons. 1988. Models that predict standing crop of stream fish from habitat variables: 1950–1985. U.S. Forest Service Report PNW-GTR-213.

Fausch, K. D., C. E. Torgersen, C. V. Baxter, and H. W. Li. 2002. Landscapes to riverscapes: bridging the gap between research and conservation of stream fishes. Bioscience 52:483–498.

Freeman, B., and M. Freeman. 1994. Habitat use by an endangered riverine fish and implications for species protection. Ecology of Freshwater Fish 3:49–58.

Freeman, M. C., Z. H. Bowen, and J. H. Crance. 1997. Transferability of habitat suitability criteria for fishes in warmwater streams. North American Journal of Fisheries Management 17:20–31.

Frissell, C. A., W. J. Liss, C. E. Warren, and M. D. Hurley. 1986. A hierarchical framework for stream habitat classification: viewing streams in a watershed context. Environmental Management 10:199–214.

Gabelhouse, D. W. 2005. Staffing, spending, and funding of state inland fisheries programs. Fisheries 30(2):10–17.

George, A. L., B. R. Kuhada, J. D. Williams, M. A. Cantrell, P. L. Rakes, and J. R. Shute. 2009. Guidelines for propagation and translocation for freshwater fish conservation. Fisheries 34:529–545.

Grimm, V., and S. F. Railsback. 2005. Individual-based modeling and ecology. Princeton University Press, Princeton, New Jersey.

Grossman, G. 2013. Not all drift feeders are trout: a short review of fitness-based habitat selection models for fishes. Environmental Biology of Fishes 97:465–473.

Guay, J. C., D. Boisclair, D. Rioux, M. Leclerc, M. Lapointe, and P. Legendre. 2000. Development and validation of numerical habitat models for juveniles of Atlantic Salmon (*Salmo salar*). Canadian Journal of Fisheries and Aquatic Sciences 57:2065–2075.

Haxton, T. J., C. S. Findlay, and R. W. Threader. 2008. Predictive value of a Lake Sturgeon habitat suitability model. North American Journal of Fisheries Management 28:1373–1383.

Henderson, A. R., and C. E. Johnston. 2010. Ontogenetic habitat shifts and habitat use in an endangered minnow, *Notropis mekistocholas*. Ecology of Freshwater Fish 19:87–95.

Henley, W., M. Patterson, R. Neves, and A. D. Lemly. 2000. Effects of sedimentation and turbidity on lotic food webs: a concise review for natural resource managers. Reviews in Fisheries Science 8:125–139.

Hewitt, A. H., T. J. Kwak, W. G. Cope, and K. H. Pollock. 2009. Population density and instream habitat suitability of the endangered Cape Fear Shiner. Transactions of the American Fisheries Society 138:1439–1457.

Hitt, N. P., and J. H. Roberts. 2012. Hierarchical spatial structure of stream fish colonization and extinction. Oikos 121:127–137.

Jelks, H. L., S. J. Walsh, N. M. Burkhead, S. Contreras-Balderas, E. Diaz-Pardo, D. A. Hendrickson, J. Lyons, N. E. Mandrak, F. McCormick, J. S. Nelson, S. P. Platania, B. A. Porter, C. B. Renaud, J. J. Schmitter-Soto, E. B. Taylor, and M. L. Warren Jr. 2008. Conservation status of imperiled North American freshwater and diadromous fishes. Fisheries 33:372–407.

Jenkins, R. E., and N. M. Burkhead. 1994. Freshwater fishes of Virginia. American Fisheries Society, Bethesda, Maryland.

Jenkins, R. E., and B. L. Kopia. 1995. Population status of the Candy Darter, *Etheostoma osburni*, in Virginia 1994–1995, with historical review. Roanoke College, Department of Biology, Final Report, Salem, Virginia.

Jordan, F., H. L. Jelks, S. A. Bortone, and R. M. Dorazio. 2008. Comparison of visual survey and seining methods for estimating abundance of an endangered, benthic stream fish. Environmental Biology of Fishes 81:313–319.

King, A. J. 2004. Ontogenetic patterns of habitat use by fishes within the main channel of an Australian floodplain river. Journal of Fish Biology 65:1582–1603.

Kwak, T. J., M. J. Wiley, L. L. Osborne, and R. W. Larimore. 1992. Application of diel feeding chronology to habitat suitability analysis of warmwater stream fishes. Canadian Journal of Fisheries and Aquatic Sciences 49:1417–1430.

Labbe, T. R., and K. D. Fausch. 2000. Dynamics of intermittent stream habitat regulate persistence of a threatened fish at multiple scales. Ecological Applications 10:1774–1791.

Labeelund, J. H., A. Langeland, B. Jonsson, and O. Ugedal. 1993. Spatial segregation by age and size in Arctic Charr: a trade-off between feeding possibility and risk of predation. Journal of Animal Ecology 62:160–168.

Leftwich, K. N., P. L. Angermeier, and C. A. Dolloff. 1997. Factors influencing behavior and transferability of habitat models for a benthic stream fish. Transactions of the American Fisheries Society 126:725–734.

Levin, S. A. 1992. The problem of pattern and scale in ecology. Ecology 73:1943–1967.

Lobb, M. D., and D. J. Orth. 1991. Habitat use by an assemblage of fish in a large warmwater stream. Transactions of the American Fisheries Society 120:65–78.

Loomis, J. B., and D. S. White. 1996. Economic values of increasingly rare and endangered fish. Fisheries 21(11):6–10.

Mann, R. H. K., and J. A. B. Bass. 1997. The critical water velocities of larval Roach (*Rutilus rutilus*) and Dace (*Leuciscus leuciscus*) and implications for river management. Regulated Rivers: Research and Management 13:295–301.

Mattingly, H. T., and D. L. Galat. 2002. Distributional patterns of the threatened Niangua Darter, *Etheostoma nianguae*, at three spatial scales, with implications for species conservation. Copeia 2002:573–585.

Messinger, T., and C. Hughes. 2000. Environmental setting and its relations to water quality in the Kanawha River basin. U.S. Geological Survey, Water-Resources Investigations Report 00-4020, Reston, Virginia.

Midway, S. R., T. J. Kwak, and D. D. Aday. 2010. Habitat suitability of the Carolina Madtom, an imperiled, endemic stream fish. Transactions of the American Fisheries Society 139:325–338.

Moore, K. M. S., and S. V. Gregory. 1988. Summer habitat utilization and ecology of Cutthroat Trout fry (*Salmo clarki*) in Cascade Mountain streams. Canadian Journal of Fisheries and Aquatic Sciences 45:1921–1930.

Moore, S. L., and J. H. Thorp. 2008. Coping with hydrogeomorphic variations in a prairie river: resiliency in young-of-the-year fishes. River Research and Applications 24:267–278.

Newcomb, T. J., D. J. Orth, and D. F. Stauffer. 2007. Habitat evaluation. Pages 843–886 *in* C. S. Guy and M. L. Brown, editors. Analysis and interpretation of freshwater fisheries data. American Fisheries Society, Bethesda, Maryland.

Orth, D. J. 1987. Ecological considerations in the development and application of instream flow habitat models. Regulated Rivers: Research and Management 1:171–181.

Palmer, M. A., C. M. Swan, K. Nelson, P. Silver, and R. Alvestad. 2000. Streambed landscapes: evidence that stream invertebrates respond to the type and spatial arrangement of patches. Landscape Ecology 15:563–576.

Peckarsky, B. L., S. D. Cooper, and A. R. McIntosh. 1997. Extrapolating from individual behavior to populations and communities in streams. Journal of the North American Benthological Society 16:375–390.

Petty, J. T., and G. D. Grossman. 2007. Size-dependent territoriality of Mottled Sculpin in a southern Appalachian stream. Transactions of the American Fisheries Society 136:1750–1761.

Rabeni, C. F., and S. P. Sowa. 1996. Integrating biological realism into habitat restoration and conservation strategies for small streams. Canadian Journal of Fisheries and Aquatic Sciences 53:252–259.

Roberts, J. H., and P. L. Angermeier. 2007. Movement responses of stream fishes to introduced corridors of complex cover. Transactions of the American Fisheries Society 136:971–978.

Rosenberger, A., and P. L. Angermeier. 2003. Ontogenetic shifts in habitat use by the endangered Roanoke Logperch (*Percina rex*). Freshwater Biology 48:1563–1577.

Rosenfeld, J. 2003. Assessing the habitat requirements of stream fishes: an overview and evaluation of different approaches. Transactions of the American Fisheries Society 132:953–968.

Ryan, P. A. 1991. Environmental effects of sediment on New Zealand streams—a review. New Zealand Journal of Marine and Freshwater Research 25:207–221.

Schlosser, I. J. 1982. Fish community structure and function along two habitat gradients in a headwater stream. Ecological Monographs 52:395–414.

Schlosser, I. J. 1985. Flow regime, juvenile abundance, and the assemblage structure of stream fishes. Ecology 66:1484–1490.

Schlosser, I. J. 1987. The role of predation in age-related and size-related habitat use by stream fishes. Ecology 68:651–659.

Schlosser, I. J. 1990. Environmental variation, life history attributes, and community structure in stream fishes: implications for environmental management and assessment. Environmental Management 14:621–628.

Schlosser, I. J. 1995. Critical landscape attributes that influence fish population dynamics in headwater streams. Hydrobiologia 303:71–85.

Schlosser, I. J. 1998. Fish recruitment, dispersal, and trophic interactions in a heterogeneous lotic environment. Oecologia 113:260–268.

Schlosser, I. J., and P. L. Angermeier. 1995. Spatial variation in demographic processes of lotic fishes: conceptual models, empirical evidence, and implications for conservation. Pages 392–401 *in* J. L. Nielsen, editor. Evolution and the aquatic ecosystem: defining unique units in population conservation. American Fisheries Society, Symposium 17, Bethesda, Maryland.

Schneider, D. C. 2001. The rise of the concept of scale in ecology. Bioscience 51:545–553.

Skyfield, J. P., and G. D. Grossman. 2008. Microhabitat use, movements and abundance of Gilt Darters (*Percina evides*) in southern Appalachian (USA) streams. Ecology of Freshwater Fish 17:219–230.

Stoddard, J. L., D. P. Larsen, C. P. Hawkins, R. K. Johnson, and R. H. Norris. 2006. Setting expectations for the ecological condition of streams: the concept of reference condition. Ecological Applications 16:1267–1276.

Thomas, J. A., and K. D. Bovee. 1993. Application and testing of a procedure to evaluate transferability of habitat suitability criteria. Regulated Rivers: Research and Management 8:285–294.

Torgersen, C. E., D. M. Price, H. W. Li, and B. A. McIntosh. 1999. Multiscale thermal refugia and stream habitat associations of Chinook Salmon in northeastern Oregon. Ecological Applications 9:301–319.

Werner, E. E., and J. F. Gilliam. 1984. Ontogenetic niche and species interactions in size-structured populations. Annual Review of Ecology and Systematics 15:393–425.

Werner, E. E., and D. J. Hall. 1988. Ontogenetic habitat shifts in Bluegill: the foraging rate-predation risk trade-off. Ecology 69:1352–1366.

White, R. J. 1996. Growth and development of North American stream habitat management for fish. Canadian Journal of Fisheries and Aquatic Sciences 53:342–363.

Whittier, T. R., J. L. Stoddard, D. P. Larsen, and A. T. Herlihy. 2007. Selecting reference sites for stream biological assessments: best professional judgment or objective criteria. Journal of the North American Benthological Society 26:349–360.

Wiens, J. A. 1989. Spatial scaling in ecology. Functional Ecology 3:385–397.

Assessment of erosion, sedimentation, and water quality impacts of the Mountain Valley Pipeline and Equitrans Expansion Project's proposed crossing of the Jefferson National Forest as it pertains to the U.S. Forest Service's Draft Supplemental Environmental Impact Statement dated December 2022

Prepared by Jonathan A. Czuba, Ph.D., Licensed Professional Engineer - February 9, 2023

REFERENCES
6

February 21, 2023

HYDROLOGICAL PROCESSES
Hydrol. Process. **25**, 1800–1821 (2011)
Published online 24 January 2011 in Wiley Online Library
(wileyonlinelibrary.com) DOI: 10.1002/hyp.7940

The impacts of fine sediment on riverine fish

Paul Kemp,[1]* David Sear,[2] Adrian Collins,[3] Pamela Naden[4] and Iwan Jones[5]

[1] *University of Southampton, International Centre for Ecohydraulics Research, Faculty of Engineering and the Environment, Southampton, Hampshire, UK*
[2] *University of Southampton, School of Geography, Highfield, Southampton SO17 1BJ, UK*
[3] *ADAS, Environment Systems, Woodthorne, Wergs Road, Wolverhampton WV6 8TQ, UK*
[4] *Centre for Ecology and Hydrology, Water, Crowmarsh Gifford, Wallingford OX10 8BB, UK*
[5] *Queen Mary University of London Biology, London, UK*

Abstract:

Elevated fine sediment input from terrestrial and aquatic sources as a result of anthropogenic activity is widely recognized to impact negatively on aquatic ecosystems. In rivers, freshwater fish are exposed to a range of impacts resulting from fine sediment pressures. To date, research on the effects of fine sediments on fish has been concentrated within relatively few families, notably the salmonidae. This paper reviews the literature describing indirect and direct impacts of fine sediment on freshwater fish as a contribution towards enhancing the understanding of the impacts of anthropogenic activities on freshwater ecosystems. We identify the causal mechanisms that underpin the observed negative response exhibited by fish populations to enhanced fine sediment loads, and the variability across different fish species. Copyright © 2011 John Wiley & Sons, Ltd.

KEY WORDS fine sediment; freshwater fish; anthropogenic impacts; casual mechanisms; river

Received 1 May 2010; Accepted 13 October 2010

INTRODUCTION

The transport of sediments by rivers to the oceans represents an important pathway in the global geochemical cycle, a key component of the global denudation system, and an important measure of land degradation and the associated reduction in the global soil resource (Walling and Fang, 2003). Fine sediments (defined in this paper as inorganic and organic particles finer than 1 mm diameter) are a natural and integral component of aquatic ecosystems (Wood and Armitage, 1997; Owens *et al.*, 2005; Walling *et al.*, 2008). Natural or intrinsic levels of sediment in fluvial systems are essential to habitat heterogeneity and ecological functioning (Yarnell *et al.*, 2006). Fine sediment aggregates comprise bacteria, algae, detritus and other organic material (Droppo, 2001) that is equally as critical to the health of aquatic ecosystems (Swietlik *et al.*, 2003). In natural ecosystems, the concentration of suspended sediments and rates of deposition are temporally and spatially variable depending on the seasonal changes in flow rates (e.g. drought, rainfall, snow-melt events) and the characteristics of the river network and surrounding catchment (Walling and Webb, 1987; Walling *et al.*, 2008). In addition, there can also be catastrophic events (e.g. volcanic eruptions, landslides) that can increase sediment levels significantly above normal variability (Major, 2004). Thus, fish and other aquatic organisms, adapt themselves to accommodate a range of sediment loads, although the evidence from palaeohydrological data (Foster *et al.*, in press; Macklin *et al.*, 2010) suggests that these loads were substantially lower than those at present. Nevertheless, fine (organic) sediment is a primary source of food and energy for riverine ecosystems. Furthermore, fine sediment is also an integral requirement within the lifecycles of some species, e.g. lamprey ameocetes and psammophilous fish (Maitland, 2003). Adaptation and behaviour of taxa to variability in suspended loads and turbidity under natural conditions are also characteristics of natural ecosystems, and create opportunities for some species (e.g. benthic feeders during phases of high turbidity; Gregory and Northcote, 1992; Henley *et al.*, 2000). Geographical and temporal variations in natural suspended sediment regimes are therefore likely to be reflected in the adaptation and structure of biological communities. It is against this background that the relationship between fine sediment dynamics and ecological response needs to be better understood so that management targets can be set.

Aquatic sediment pressures, however, differ from those arising from other substances, such as toxic chemicals, in that fluvial suspended sediment loads are a naturally occurring phenomenon, but one that has been enhanced greatly by human impacts in river basins (Walling and Fang, 2003; Bilotta and Brazier, 2008). Evidence from longer term records of sediment loads indicates that river sediment fluxes are sensitive to many influences, including land clearance and land use change, which tend to increase sediment delivery into watercourses (Foster *et al.*, in press), whereas others such as soil and water conservation measures, sediment control programmes and

* Correspondence to: Paul Kemp, University of Southampton, International Centre for Ecohydraulics Research, Faculty of Engineering and the Environment, Southampton, Hampshire, UK.
E-mail: p.kemp@soton.ac.uk

reservoir construction cause decreased sediment fluxes (Walling and Fang, 2003). For example, recent summaries of long-term fine sediment records from lakes in England and Wales have demonstrated that yields in lowland agricultural catchments have increased from 10 to 30 t km^{-2} $year^{-1}$ to as much as 110 t km^{-2} $year^{-1}$(Foster, 2006). When sediment concentrations and rates of deposition exceed natural background levels, aquatic biota can be negatively affected resulting in reduced abundance and diversity, and shifts in community composition. Collins *et al*. (2009a,b) have demonstrated that the agricultural sector within England and Wales dominates present-day (year 2000) sediment inputs to rivers (76%) compared with eroding channel banks (15%), diffuse urban sources (6%) and point source discharges (3%). Moreover, they concluded that projected changes in farming by 2015, represented by the 'Business As Usual' forecast of structural developments and predicted uptake of sediment mitigation methods, suggest only a 9% reduction in sediment losses from the agricultural sector across England and Wales. This projected pattern is likely to be common across much of northwest Europe and North America. Thus, the current state of anthropogenically enhanced sediment delivery to riverine ecosystems in many areas is set to continue or increase due to changes in rainfall patterns associated with climate change (Evans *et al*., 2008) and continued need to sustain intensive agriculture.

High sediment loads have a range of physical, chemical, and ecological effects on aquatic ecosystems (Figure 1). Sediment in suspension increases turbidity and light attenuation, and, when deposited, influences channel morphology and bed characteristics. Ecological responses ultimately include shifts in community assemblage and food chain structure (Wood and Armitage, 1997). Lowland river systems are often particularly vulnerable to the adverse effects of excessive sedimentation owing to their low energy and limited ability to recover to their natural form (Brookes, 1995), together with the sensitivity of specific life stages of the aquatic ecology they support. In turn, sediments have been suggested to be one of the most detrimental forms of aquatic pollution (Ritchie, 1972; Lemly, 1982; Wood *et al*., 2005; Izagirre *et al*., 2009).

In addition to elevated inputs of sediment, increased deposition also occurs as a result of altered flow regime, e.g. due to impoundment (whether anthropogenic or natural) or abstraction (Wood and Armitage, 1997). For example, increased deposition in impounded reaches as a result of beaver activity or logjams, can reduce dissolved oxygen (Bryant, 1984; Dolloff, 1987), and cause temporary hypoxia (Schlosser and Kallenmeyn, 2000), which under extreme conditions can result in significant fish mortalities (Fox and Keast, 1990). Further, the greater retention of organic-rich sediment may result in local declines in pH to levels below the lower tolerance range of trout species (Salyer, 1935), but as a result of creating a sediment trap, improve overall stream acidity levels and benefit fish communities in general (Cirmo and Driscoll, 1993; Halley, 1995).

Although several negative impacts of fine sediment on fluvial ecosystems have been described (Lenat, 1983; Richardson and Jowett, 2002; Kaller and Hartman, 2004),

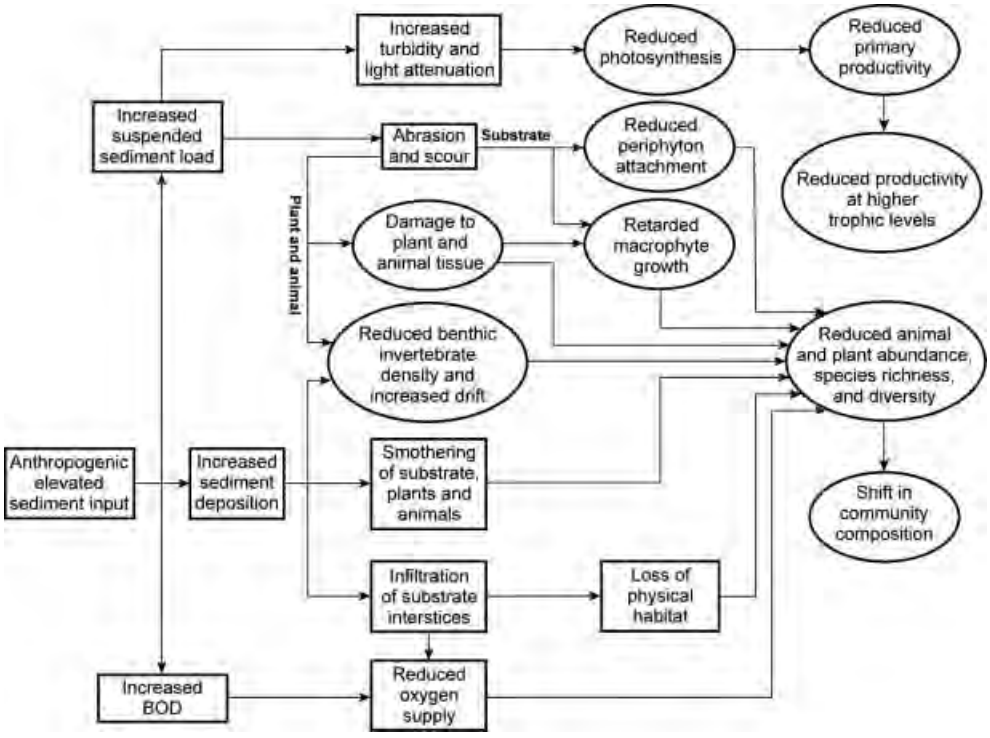

Figure 1. Negative impacts of anthropogenically enhanced sediment input to lotic aquatic systems on lower trophic levels. Rectangles and ovals respectively denote physicochemical effects and direct and long-term biological and ecological responses

the response of fish populations, particularly economically important salmonids, are most frequently considered. Fish are an important indicator group for assessing the ecological integrity of rivers (Karr, 1991). This value as an indicator results from the broad range of habitat requirements of different ecological guilds which integrate during their life cycle, a wide range of riverine conditions from the properties of bottom sediments relevant for egg development to the large scale longitudinal integrity required, e.g. for spawning migrations (Persat *et al*., 1994). Fish frequently occupy positions at the top of the food chain as apex predators and consequently respond to the indirect ecological impacts of fine sediment dynamics operating at lower trophic levels, and as such may be employed as indicators of biotic integrity (Karr, 1991). Fish are also directly affected by fine sediment either in suspension or deposited on the substrate. These effects operate via influencing food availability and foraging efficiency, physiology and behaviour, and habitat. This paper aims to review the literature describing indirect and direct impacts of fine sediment on freshwater fish as a contribution towards enhancing the understanding of the impacts of anthropogenic activities on lotic ecosystems and of the need to refine management targets. By identifying the causal mechanisms that underpin the observed negative response exhibited by fish populations to enhanced fine sediment loads, and the variability across different fish species, management actions may be better informed and targeted.

IMPACTS OF FINE SEDIMENT ON LOWER TROPHIC LEVELS

Sedimentation affects growth, reproduction and mortality rates at all trophic levels (Henley *et al*., 2000), and can impact the key components of the food chain, first influencing primary production (Izagirre *et al*., 2009), and then zooplankton (Hart, 1992), benthic invertebrates (Nuttall and Bielby, 1973; Bjerkli and LaPerriere, 1985; Suren and Jowett, 2001; Bo *et al*., 2007), and ultimately fish communities (Kent and Stelzer, 2008). Therefore, to understand how shifting fine sediment dynamics affect fish populations, it is important to first consider impacts on lower trophic levels (Figure 1).

High turbidity and light attenuation associated with excessive suspended sediment loading constrains photosynthesis to upper levels of the water column (Berry *et al*., 2003) and limits primary (Van Nieuwenhuyse and LaPerriere, 1986; Davies-Colley *et al*., 1992; Hoetzel and Croome, 1994; Izagirre *et al*., 2009) and higher trophic level production. Suspended sediments can reduce abundance of periphyton on stream substrate through abrasion (Steinman and McIntire, 1996; Luce *et al*., 2010) and deposits of fine sediment can block substrate attachment of, and smother, periphyton (Brookes, 1986). As a result, algal biomass is reduced. Further, fine sediment can directly alter the physical composition of periphyton and diminish its value and quality as a vital food source for invertebrates (Graham, 1990). For example, in relatively fast-flowing braided New Zealand streams, Graham (1990) reported that at suspended silt concentrations of 1–10 mg l^{-1}, the infiltration of fine sediment into the epilithic periphyton accounted for approximately 50% of its dry weight. As a result, the mean organic content of the periphyton was 22% compared with 52% in a reference stream (silt concentration: <1 mg l^{-1}). A recent experimental study assessed the impact of pulsed sediment (clay) deposition on periphyton (Izagirre *et al*., 2009). High sediment loads resulted in a reduction in algal photosynthetic efficiency, algal growth, and a change in community structure. Interestingly, considerable compensation as a result of periphyton adaptation was observed in terms of increased chlorophylla *a* contents and photosynthetic activity, although community composition did not recover over the timescale of the study.

Fine sediments, in suspension or when deposited, can negatively impact macrophytes (Yamada and Nakamura, 2002). Submerged and emergent macrophytes are an important component in the physical and ecological functioning of lowland river systems. Macrophytes influence river hydrodynamics (Dodds and Biggs, 2002; Cotton *et al*., 2006), provide substrate for periphyton growth (James *et al*., 2000), and food and cover for invertebrates and fish (Wood and Armitage, 1997). They trap sediments (Cotton *et al*., 2006), including organic matter and other debris, and facilitate nutrient cycling and processing through uptake and subsequent decay (Wood and Armitage, 1997; Sand-Jenson, 1998; Clarke and Wharton, 2001).

Macroinvertebrates provide an important food for many species of stream- and river-dwelling fish. Shifts in the quantity and composition of this resource can directly influence fish growth and community structure. The effects of increased fine sediment on invertebrate communities have been widely documented (Newcombe and MacDonald, 1991; Waters, 1995; Kefford *et al*., 2010). Fine sediment can directly smother invertebrates (Kefford *et al*., 2010), limit oxygen supply, reduce quantity and quality of periphyton, zooplankton, and macrophyte food sources, and alter the food chain (Theurer *et al*., 1998). Fine sediments also decrease habitat availability and suitability for some invertebrate species by infilling interstitial spaces and smothering the substrate (Theurer *et al*., 1998), which can disrupt and potentially block the supply of oxygen (Malcolm *et al*., 2008; Sear *et al*., 2008). Many studies have reported a decrease in invertebrate abundance and diversity and a change in community composition resulting from an increase in fine sediment load (Crisp and Gledhill, 1970; Lloyd *et al*., 1987; Ryan, 1991; Angradi, 1999; Wood and Armitage, 1999; Matthaei *et al*., 2006; Bo *et al*., 2007).

High loads of suspended sediment can increase the density of drift (Shaw and Richardson, 2001) either by dislodging invertebrates (Dobson and Frid, 1998; Curry *et al*., 2004) or reducing the availability of interstitial space (Walton *et al*., 1977). Drift has also been found to increase as invertebrates escape from the deposition of

sediment on the river substrate (Rosenberg and Wiens, 1978; Culp *et al*., 1986). Under experimental settings, measured rates of invertebrate drift increased in proportion to the concentrations of suspended sediment added (Gammon, 1970). Further, field manipulation in New Zealand rivers illustrated the negative and positive relationships between sediment concentrations and densities of benthic invertebrate and drift, respectively (Suren and Jowett, 2001). Elevated drift as a result of increased concentrations of fine sediment can cause changes in community composition (Fairchild *et al*., 1987). Culp *et al*. (1986) observed a greater than 50% reduction in benthic invertebrate diversity within riffles during a 24-h period as increased suspended sediment transfers scoured the stream substrate, even when corresponding water velocities were low.

Shifts in invertebrate community composition can result from increased concentrations of suspended and deposited fine sediments (Merritt and Cummins, 1984; Ryan, 1991), usually resulting in reductions in diversity and species richness. Changes in invertebrate diversity and abundance will inevitably result in a shift in fish community composition by altering the composition of the food resource. A study in Missouri, however, found that the response of fish communities to agriculturally derived siltation was poorly described by invertebrate diversity and species richness indices (Rabeni and Smale, 1995). Nevertheless, herbivorous and benthic insectivorous species were the most sensitive feeding guilds to siltation, as they responded negatively to the decline of riffle-dwelling invertebrates.

IMPACTS OF FINE SEDIMENT ON FISH PHYSIOLOGY AND PERFORMANCE

Fine sediment, either in suspension or when deposited, can have multiple impacts on fish (see Table I for characteristics of sediment that impact fish). Physiological effects can be both short term and local, such as elevated stress (e.g. as indicated by increased corticosteroid, glucose, and hemoatocrits, and by reduced leukocrit levels in salmonids; Redding and Schreck, 1982; Redding *et al*., 1987; Lake and Hinch, 1999) in response to a sediment pulse, or long-term and widespread shifts in sediment concentrations resulting in prolonged physiological stress (Anderson *et al*., 1996) Table II. This will ultimately lead to population level responses, which, under extreme circumstances, may result in loss of the fish community from impacted reaches (Birtwell *et al*., 1984).

Table I. Characteristics that influence the effects of fine sediment on freshwater fish (after Bash *et al*., 2001)

Factor	Effect
Source of sediment (natural, agricultural, urban, etc.)	Determines the physical and biogeochemical characteristics of the sediment (e.g. Sediment Oxygen Demand (SOD)) and the temporal dynamics of inputs to rivers
Temperature	Influences reactivity of biogeochemical processes, fitness of individual especially if close to lethal limit
Angularity of particles	Influences abrasion effects on soft/sensitive tissues (e.g. gills)
Size of particles	Blocks micropores in egg chorion, influences rate of sedimentation and reactivity and content of contaminants through surface area and associated substrates
Sediment oxygen demand	Competes for oxygen demanded by incubating larvae
Organic matter composition and source	Determines SOD, influences bacterial communties on sediment, influences sedimentation processes
Toxicity (associated pollutants)	Can result in lethal levels particularly at incubation stage
Concentration of particles	Influences rate of sedimentation, turbidity, and abrasion
Resulting turbidity	Influences light, ability to forage and feed (visual feeders)
Duration of exposure	Can result in fatalities if prolonged, and result in changes to fish populations. May result in adaptation over long periods of time
Frequency of exposure	Can result in fatalities if prolonged, and result in changes to fish populations. May result in adaptation over long periods of time
Natural background concentration/turbidity	Determines tolerance levels of fish populations to fine sediment pressures
Availability and access to refugia	Provides opportunity to escape sediment pressure particularly if pressure is of short exposure
Species/genotype of fish	Determines tolerance levels to fine sediment pressures
Life stage of fish	Determines nature of impact and sensitivity to sediment pressure
Time of occurrence (relative to life history stage)	Influences impact—e.g. high risk during immobile larval stages
Fitness/health of individual	Determines tolerance threshold and ability to move away from pressure
Presence of other stressors/pressures	Influences tolerance thresholds/behaviour and/or presence of refugia

Table II. Published responses of fish to fine sediment. Responses are broadly divided by immediacy of response, with population changes resulting in the longer term. Specific timescales will vary according to species, individual fitness, and magnitude and duration of sediment impact

Temporal	Impact	Reference
Scale		
Short term	Stress response as indicated by elevated corticosteroids, glucose, and hermatocrits and reduced leukocrit levels.	Redding and Schreck (1982) Redding *et al*. (1987) Lake and Hinch (1999)
	Reduced feeding	Henley *et al*. (2000)
	Reduced oxygen acquisition and fish mortalities due to hypoxia	Bruton (1985); Henley *et al*. (2000) Fox and Keast (1990)
Intermediate term	Reduced tolerance to toxicants	Lloyd *et al*. (1987)
	Lower resistance to disease	Redding *et al*. (1987), Sutherland and Meyer (2007)
	Physical damage to gills:	
	erosion of mucus lining	Redding and Schreck (1982)
	abrasion of tissue	Herbert and Merkins (1961)
	Interrupted gas exchange:	
	sediment binds directly to gill epithelium	Bond and Downes (2003)
	Disrupted and blocked oxygen supply and removal of metabolites to egg and larval life stages in the gravel	Giller and Malmqvist (1998) Greig *et al*. (2005); Sear *et al*. (2008)
	Interrupted osmoregulation	Bruton (1985); Bergstedt and Bergersen (1997) Waters (1995)
	Reduced pH below tolerance of some species	Salyer (1935)
	Prolonged physiological stress	Anderson *et al*. (1996)
	Retarded growth	Shaw and Richardson (2001) Sutherland and Meyer (2007)
	Disrupted development	Suttle *et al*. (2004)
	Reduced survival	Henley *et al*. (2000)
Long term	Population level response e.g. loss of fish from impacted reach	Birtwell *et al*. (1984)

Elevated fine sediment loads can impact fish directly, e.g. by causing physical damage to organs, or indirectly by adversely influencing water quality (Table I). Fine sediment in suspension can directly damage gills as a result of erosion of the mucus coating (Redding and Schreck, 1982) and abrasion of tissue (Herbert and Merkins, 1961); the extent being related to water velocity, suspended sediment concentrations and particle size and shape, with smaller and more angular clasts having the most negative impact (Servizi and Martens, 1987; but see Lake and Hinch, 1999). Further, gaseous exchange can be interrupted as fine particles bind directly to the gill epithelium (Bond and Downes, 2003) and clog rakers and filaments. Gill damage will also result in interruption of osmoregulation (Bruton, 1985; Waters, 1995; Bergstedt and Bergersen, 1997) resulting in the impairment of excretion which affects salt balance (Cordone and Kelley, 1961).

Suspended or deposited sediment can deplete oxygen in the surrounding water (Bruton, 1985; Henley *et al*., 2000), a factor that influences the tolerance of fish to the detrimental impacts of suspended sediments (Servizi and Martens, 1991). The biological oxygen demand exerted as the organic component of sediment is aerobically decomposed may result in severe depletion of oxygen, particularly under low flows (Ryan, 1991) and/or when temperatures are high. Infiltration of fine sediment in the interstitial spaces of river bed gravels can disrupt or block the supply of oxygen to developing eggs and embryonic stages of fish species that excavate gravel nests, particularly salmonids, resulting in a range of physiological impacts; these include reduced weight and length, morphological adaptations (e.g. extended yolk sac), and hypoxia.

Fine sediment can influence aspects of water quality other than oxygen concentrations as finer fractions represent an important vector for the transfer and fate of numerous contaminants. Fine sediment particles (<63 μm) are chemically the most active (Collins *et al*., 1997) and have a high affinity for soluble metals and organic contaminants and nutrients (Warren *et al*., 2003; Ballantine *et al*., 2009) that may be deposited (Lijklema *et al*., 1993; Maher *et al*., 1999; Collins *et al*., 2005) and consequently become bioavailable, resulting in influences on ecosystem processes. The deposition of fine sediment due to increased input from mining and deforestation can act as a sink for heavy metal contaminants (Trimble, 1981).

Elevated sediment concentrations may directly influence fitness of fish by increasing stress levels and reducing feeding (Redding *et al*., 1987) and growth rates (Shaw and Richardson, 2001; Sutherland and Meyer, 2007), disrupting developmental progress (e.g. age at smolting for salmonids; Suttle *et al*., 2004), and reducing

overall rates of survival (Henley *et al*., 2000). Inefficient respiration and associated physiological stress as a result of gill damage will elevate energetic costs (Cordone and Kelley, 1961), lower resistance to secondary factors such as bacterial and viral infections (Redding *et al*., 1987; Sutherland and Meyer, 2007) and toxicants (Lloyd *et al*., 1987). Nevertheless, fish are able to compensate physiologically for stressors to which they are exposed, enabling them to acclimatize to changes in fine sediment regime (Bunt *et al*., 2004). For example, mucus secretion may be increased (Strmac *et al*., 2002), and in extreme cases, the gill epithelium may thicken (Horkel and Pearson, 1976; Goldes *et al*., 1988; Sutherland and Meyer, 2007). Fish are also able to respond behaviourally as discussed in the following section.

IMPACTS OF FINE SEDIMENT ON FISH BEHAVIOUR

It is expected that environmental perturbations, including increases in fine sediment concentrations in excess of some critical threshold, will impact behaviours, either by altering the magnitude and efficacy of the response, or by inducing alternative responses. Examples of the former include impairment of visual communication by signalling under conditions of high turbidity, e.g. for courtship (Burkhead and Jelks, 2001), communicating with young (Keenleyside and Bietz, 1981), or hinderance of fish migration (Newcombe and Jensen, 1996; Wood and Armitage, 1997; but see Bruton, 1985). Fish that exhibit avoidance of turbid conditions, or are actively attracted to them (e.g. Gradall and Swenson, 1982 for creek chub *Semotilus atromaculatus*) illustrate the latter.

For visual foragers, elevated turbidity decreases the ability to obtain food (Berg and Northcote, 1985; Bruton, 1985; Vogel and Beauchamp, 1999; Sutherland and Meyer, 2007) as has been observed for bluegills *Lepomis macrochirus* (Gardener, 1981), smallmouth bass *Micropterus dolomieu* (Sweka and Hartman, 2003), striped bass larvae *Morone saxatilis* (Breitburg, 1988), and rosyside dace *Clinostomus funduloides* (Zamor and Grossman, 2007), and will ultimately reduce growth rates (e.g. Northcote, 1995, for sub-yearling Arctic grayling, *Thymallus arcticus;* Sigler *et al*., 1984 for coho salmon, *Oncorhynchus kisutch*), abundance (Gardener, 1981; Berkman and Rabeni, 1987), and distribution (Mol and Ouboter, 2004). The requirement for relatively clear water for visual foragers, such as salmonids (DeYoung, 2007), reflects the positive relationship between foraging efficiency and light intensity (Fraser and Metcalfe, 1997 for juvenile Atlantic salmon, *Salmo salar*) and the negative relationship between reactive distance and turbidity (Barrett *et al*., 1992). However, salmonids may become more active (Gregory, 1993) and potentially exhibit higher foraging rates (Sigler *et al*., 1984) in slightly turbid water if perceived predation risk is reduced. Interestingly, territorial behaviour of Atlantic salmon parr, exhibited principally to acquire food, declined with increasing suspended sediment concentration (Robertson *et al*., 1997). Mechanisms other than the relationship between turbidity and visual acuity have a role to play as illustrated by the energetic costs imposed by the ingestion of sediment on the armoured catfish (*Ancistrus spinosus*) as it grazes on periphyton on the substrate of neotropical streams (Power, 1984).

Benefits of elevated turbidity for some fish species include enhanced foraging efficiency and growth (Gregory and Northcote, 1992) if the visual acuity of their prey is reduced. Conversely, turbidity may provide cover from predators (Doan, 1941; Gregory and Levings, 1996), although when sufficiently high, it may prevent visual contact with other fish required to form the schools that offer protection from predation (Keenleyside, 1955). Intermittent and short-term increases in suspended sediment may benefit some species, such as the salmonids, due to the associated increase in density of drifting prey (Brittain and Eikland, 1988; DeYoung, 2007). In slow-flowing lotic environments, foraging of planktivorous fish may be facilitated under turbid conditions as zooplankton become concentrated close to the surface (Doan, 1941), although reduced feeding efficiency and reactive distances due to the lower contrast of the prey image have also been described (Liljendahl-Nurminen *et al*., 2008). Rowe and Dean (1998) showed that feeding success was reduced by increased turbidity but this was less so for fish with non-visual food-sensing ability. Increased foraging activity may result as fish attempt to compensate for the apparent reduction in prey availability: daily activity of the visual predator Ide, *Leuciscus idus*, increased with increasing turbidity (Kulíšková *et al*., 2009). Hence the adaptation of a species determines the biological impact of the sediment pressure (Rowe and Dean, 1998). Some species, e.g. *Sander lucioperca* (Zander) and *Gymnocephalus cernuus* (Ruffe), are equipped with visual adaptations that enhance their foraging capacity in turbid environments. Both species are physiologically adapted for low light conditions by the presence of a reflective layer, the *tapetum lucidum*, in the retina that enhances light sensitivity in dim conditions (Ahlbert, 1969; Ali *et al*., 1977), which in addition to well-developed lateral line organs enables them to feed efficiently even in darkness (Bergman, 1988). Cyprinids can also forage efficiently at low light intensities (Bergman, 1988). Many species forage using tactile or olfactory senses. The fish communities of turbid floodplain lakes connected to the Orinoco are dominated by catfish, whereas the communities of isolated clear lakes are dominated by visual predators (Rodriguez and Lewis, 1997).

Fish exhibit a range of avoidance strategies to mitigate potential negative impacts of fine sediments (Bisson and Bilby, 1982; Berg and Northcote, 1985; McLeay *et al*., 1987; Servizi and Martens, 1992; Newcombe and Jensen, 1996). This may involve seeking refugia or moving to unimpacted reaches (Barton, 1977). In laboratory experiments, it has been shown that salmonids will move to less turbid waters, if available, after a short-term pulse (Berg and Northcote, 1985). Bisson and Bilby (1982)

illustrated the displacement of salmonids in water with turbidities greater than 70 NTU (nephelometric turbidity units). These results suggest that salmonids in a river system might seek out turbidity refugia when subjected to short-term pulses of sediment. A similar affect was observed for non-salmonid fish species, where in general, elevated turbidity had less effect on prey consumption of species that are adapted to turbid environments.

Fish are not always able to avoid the impacts of elevated fine sediment loads. The combined influences of increased turbidity and restricted opportunities for escape from the effect (lack of refugia) constitute a cumulative effect (Reid, 1998). In such instances, fish may exhibit alternative behaviours to compensate for deleterious effects, e.g. damage to the gills by coughing or gill flaring (Carlson, 1984; Berg and Northcote, 1985; Servizi and Martens, 1992). Ultimately, community composition will shift as turbidity regimes change over greater temporal and spatial scales (Bonner and Wilde, 2002).

IMPACTS OF FINE SEDIMENT ON FISH HABITAT

The deposition of fine sediment can alter the morphology of the river bed and change habitat quality and quantity (Walling and Amos, 1999; Collins and Walling, 2007a). Low energy, lowland river ecosystems are particularly sensitive to deposition of sediments, and associated ecological impacts, which may be considered positive or negative depending on the species considered. Habitat requirements shift with ontogenetic development and are often described in terms of spawning, nursery, rearing, and adult components. The influence of sediment on different habitat types is briefly discussed in the following sections.

Spawning habitat

Spawning habitat of fish is suggested to be the most critical for determining the success or failure of a population (Schiemer *et al*., 2000; Kamler, 1992). This is because fish suffer the highest mortality during their early life history (Kamler, 1992). Sedimentation by fines can result in smothering of spawning habitat, which will particularly impact species that spawn on or in the bed substrate. Owing to their immobility, and the specific hydraulic conditions and substrate chosen for spawning, eggs have the most restrictive niche of all fish life stages (Cunjak *et al*., 1998). The majority of research on the influence of sediment on spawning habitat has focused on the implications for salmonids because of their economic significance and susceptibility to deleterious effects (Finn, 2007; Sear *et al*., 2008). To maximise fitness, the adult fish must choose suitable habitat that will ensure survival throughout embryonic development. The nature of spawning gravel is an important factor in this choice, where substrate suitability depends on several factors. However, it is important to consider the reproductive strategies of different species. For example, reproductive strategies that involve parental care such as fin fanning (e.g. bullhead *Cottus gobio*; Morris, 1955), appear to provide advantages in sedimented habitats, compared with substrate or pelagic broadcasting of eggs (Berkman and Rabeni, 1987).

The suitability of salmonid spawning substrate is dependent on mean dimensions of the particles relative to the size of the female fish, and proportion of fine material (Crisp and Carling, 1989). Typically, suitability of spawning substrate is based on categorization of substrate size (Semple, 1991). However, the average reported particle size (diameter) used by Atlantic salmon and brown trout (*Salmo trutta*) for redd construction is highly variable, ranging from 20 mm (Crisp and Carling, 1989; Moir *et al*., 1998) to 100 mm (Heggberget, 1991) for Atlantic salmon, and from 7 to 128 mm (Ottaway and Clarke, 1981; Shirvell and Dungey, 1983; Witzel and MacCrimmon, 1983; Chapman, 1988) for brown trout. This variability in spawning substrate size utilized by salmonids indicates plasticity in habitat selection, and suggests that some factor other than average size (e.g. gravel texture, packing, shape, permeability, and fines content) may be of primary importance. Grain size may not even be the main determinant of spawning habitat; with many studies identifying selection on the basis of local hydraulics and hyporheic flows (though these will both be a function of, and create a response in, the substrate) (Malcolm *et al*., 2008).

The influence of texture on two fundamental properties of spawning gravels, pore size and permeability, is a major determinant of substrate suitability. Large particles (gravel/cobble) also tend to be relatively loosely packed and porous. This is important for the successful development and survival of eggs, as the transport of solutes (the most important being dissolved oxygen), and the removal of metabolites is consequently facilitated. In addition, large gravel provides sufficient interstices to allow the movement of alevins towards the redd surface and eventual emergence.

A key determinant in the suitability of spawning substrate is the level of the fine sediment content. A high proportion of fine sediment can form an impermeable layer and entomb salmonid eggs and fry (Kondolf *et al*., 1993; Sear, 1993; Soulsby *et al*., 2001; Sear *et al*., 2008). Excessive fine sediment deleteriously impacts the incubation of salmonid embryos by preventing sufficient permeation of oxygen and the efficient removal of metabolic waste, particularly ammonia (Chapman, 1988; Crisp, 1996; Payne and Lapointe, 1997; Giller and Malmqvist, 1998; O'Connor and Andrew, 1998; Greig *et al*., 2005). Further, fine sediment, e.g. from agricultural runoff may also be composed of organic waste with high levels of sediment-bound nutrients, pesticides, and herbicides, which may have synergistic effects on aquatic biota in general (Lowrance *et al*., 1985; Collins *et al*., 2009c), and impact salmonid incubation in particular (Greig *et al*., 2005). The precise impact of fine sediments on egg incubation relates to the ability of the environment to support the oxygen demand of the developing embryo. Fine sediment can reduce the supply rate of oxygen

through three key proceses. First, fine sediment physically blocks the micropores in the egg surface (Greig *et al.*, 2005; Stuart, 1953a). For example, Stuart (1953b) found that the chorion (an acellular membrane that surrounds the mature fish egg) of brown trout eggs lost their smooth and glossy exterior by attracting the finer silt particles and became completely covered by a dark coat of sediment. All early ova in this condition died without hatching. More recently, Greig *et al.* (2005) have demonstrated how increasing quantities of fine, inert clay created a reduction in oxygen consumption by salmon eggs, which was caused by cloaking of the surface of the eggs. Secondly, fine sediment accumulation within the gravel framework reduces the porosity and permeability of the gravels which in turn reduces the intragravel flow velocity (Greig *et al.*, 2005; Sear *et al.*, 2008). For example, Greig *et al.* (2007) report a four orders of magnitude reduction in intragravel flow rates within Atlantic salmon redds as a result of fine sediment accumulation. The reduction in flow rates through the gravels results in a decrease in the supply rate of oxygen to the eggs. Thirdly, fine sediment creates an oxygen demand through the biological as well as chemical oxidation of organic matter (Theurer *et al.*, 1998; Greig *et al.*, 2007). Oxygen demands are increased during periods when the contact time of hyporheic water with organic matter increases; thus the combination of reduced intragravel flow rates and organic matter accumulation creates a high oxygen demand and low rates of oxygen supply.

Other impacts of fine sediments include a reduction in spawning activity (Saunders and Smith, 1965), reduced adhesiveness in some species eggs (Doan, 1941), accumulated toxic metabolites around incubating eggs (McCubbin *et al.*, 1990), and blocked fry emergence (McCubbin *et al.*, 1990; Crisp, 1993). Meyer *et al.* (1975) found that redds with a high abundance of fine sediments also contained a high abundance of a fish egg-eating worm, *Haplotaxis ichthyophagous*, an oligochaete that may have been attracted to fine sediment. Further, the exposed larval stage appears to be more sensitive than the egg or juvenile stages (Appleby and Scarratt, 1989; Lisle and Lewis, 1992; Zimmerman *et al.*, 2003).

The level of fines considered deleterious to spawning substrate quality is variable dependent on the definition of particle size (Crisp, 1996; Greig *et al.*, 2005). Poor quality gravels for salmonid early life stage survival have been described to have fines contents between 8% and 15% (O'Connor and Andrew, 1998), which is within the same range used to describe good spawning gravels where the mean percentage contents of fines (<1 mm) range from 5·4% to 20% (Crisp and Carling, 1989, Moir *et al.*, 1998; Theurer *et al.*, 1998). Figure 2 shows a compilation of published data on the range of survival to hatching stage of Atlantic salmon eggs in relation to the proportion of fine sediment (by mass) within the spawning gravels. In keeping with recent metadata analysis of survival data on Pacific salmon species, we found that a logistic regression model of survival provided the best fit to the data ($r^2 = 0{\cdot}614$); (Jensen *et al.*, 2009). In logistic regression, the analysis determines the probability that the dependent variable (the probability of mortality in this case) equals 1·0. Although a decrease in survival (increase in probability of mortality) with increasing proportion of fines is evident, there is a substantial range for a given level of fines. Jensen *et al.* (2009) argue that such variability is accounted for by a series of factors that influence the sensitivity of the eggs to fine sediments, including genetic predisposition, biological factors (e.g. small *vs* large eggs), oxygen supply rate to the egg zone, and the effects of other unmeasured factors. The model in Figure 2 suggests a limit to survival of around 90–95% irrespective of the level of fines, and a low level of survival (<5%) even in conditions of relatively high fine sediment content (>30% by mass). There is no statistically significant difference within the data to indicate any difference in the sensitivity to fine sediment between populations spawning within warmer groundwater-dominated rivers compared to those in colder runoff-dominated rivers.

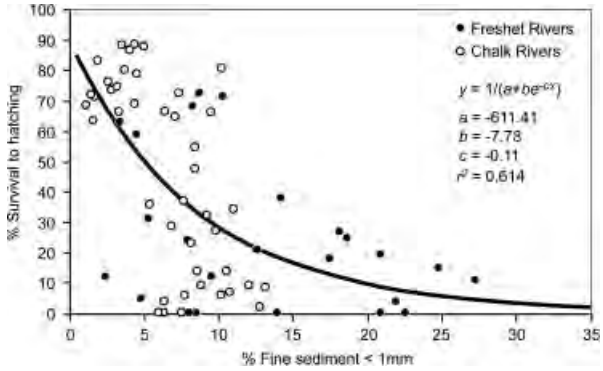

Figure 2. Variability in the survival rate of Atlantic salmon embryo relative to increasing levels of fine (<1 mm) sediments. The logistic model equates to an estimate of the probability of survival for a given increase in fine sediment (Jensen *et al.*, 2009). No statistically significant difference exists between survival in warmer groundwater-dominated rivers and runoff-dominated rivers. Data compiled from Greig *et al.* (2007)—artificial redds; O'Connor, and Andrew (1998)—instream incubators; Julian and Bergeron (2006)—artificial redds; Heywood and Walling (2007)—artificial redds

Local fines content measured at a given point in time is not a sufficient indicator of spawning substrate quality (Sear *et al.*, 2008). The hydraulic properties of the river must also be considered (Greig *et al.*, 2007). Even where inputs of cut-bank sediments are high, the hydraulic forces at work in a moderately powerful river can be quite efficient in preventing the build-up of excess fines thus maintaining good spawning substrates (Payne and Lapointe, 1997; Sear *et al.*, 2008). However, the erosional power of a river and the input of fine material may have other impacts on spawning gravels. During high flow events, a large input of coarse sediment to a spawning site modifies local hydraulic patterns resulting in greater scour and fill which in turn can deeply bury or scour eggs during the incubation period, resulting in increased mortality (Payne and Lapointe, 1997; Elliott *et al.*, 1998; DeVries, 2008).

It is suggested that salmonids have the ability to sense poor- quality spawning habitat based on hydraulic cues

and may thus avoid heavily silted gravels (Alabaster and Lloyd, 1982). During redd construction, the substrate is temporarily cleansed of fine sediment (Shirvell and Dungey, 1983; Witzel and MacCrimmon, 1983; Crisp and Carling, 1989; Peterson and Quinn, 1996). As much as 75% of fines were removed from the streambed sediment during the spawning activity of chum salmon, *Oncorhynchus keta* (Peterson and Quinn, 1996), and brown trout redds contained substantially lower levels of fine material than the adjacent undisturbed substrate (Shirvell and Dungey, 1983). However, the benefits of purging sediment of fines in this way can be short lived as redds may become re-infiltrated by fines, potentially to their former level, by the time emergence occurs (Sear, 1993; Acornley and Sear, 1999; Sear *et al*., 2008). The rate of fine sediment accumulation is strongly controlled by the near-bed suspended sediment flux and inversely correlated with bed mobility (Sear *et al*., 2008).

Non-salmonid species are also influenced by interactions between sediment dynamics and spawning habitat suitability. Coarse fish species can be grouped according to their spawning behaviours (Maitland, 2003). Lithophils stick their eggs to gravels and stones on the river bed (e.g. bullhead); phytophils stick their eggs to submerged plants (e.g. roach *Rutilus rutilus*; tench *Tinca tinca (L.)*, and psammophils lay their eggs on sand or fine roots associated with sand (e.g. gudgeon *Gobio gobio*). In Europe, bullhead (Mills and Mann, 1983), lamprey (*Lampetra* spp and *Petromyzon marinus*, Maitland and Campbell, 1992), and shad (allis shad: *Alosa alosa* and twaite shad *Alosa fallax*, Maitland and Hatton-Ellis, 2003), species protected under the EC Habitats Directive (92/43/EEC), and barbel (*Barbus barbus*), are similar to the salmonids in that they require relatively coarse and clean gravel substrate to spawn and will also suffer negative effects of high sediment deposition. The main difference is that these species tend to utilize broadcast spawning behaviour that results in the accumulation of eggs within the surface interstices of gravels and under gravel particles. The eggs are therefore susceptible to embedding and to accumulation of surface drapes of fine sediment. Negative effects have also been suggested elsewhere, e.g. reduced production of eggs associated with increased sediment concentrations (Burkhead and Jelks, 2001), and impaired reproduction due to infilling of nest sites, e.g. cavities in sunken logs (Mol and Ouboter, 2004). Conversely, the relative abundance of mound-building cyprinids and *centrarchids* that excavate nests in soft sediment was observed to be higher in turbid-disturbed streams in the United States relative to reference sites (Sutherland *et al*., 2002), highlighting the species-specific nature of sensitivity to fine sediment and the importance of strategies to utilize habitats apparently under pressure from sediment inputs. Rearing behaviours can offset some fine sediment impacts, e.g. the ventilation of eggs by adult bulheads with the use of fins (Morris, 1955; Maitland, 2003).

Aquatic macrophyte stands provide the substrate on which several species of fish spawn, including representatives of the *Cyprinidae*, whose larval and juvenile stages also associate with vegetation (Impson *et al*., 2007). Spawning fish may, therefore, be indirectly influenced by the relationship between plant growth and fine sediment concentrations. Although understanding of the interrelationships between sediment nutrients and macrophytes is incomplete (Clarke and Wharton, 2001), plants may be expected to benefit if the fine sediment is rich in organic material, although excessive nutrient enrichment that results in eutrophication will have other detrimental effects (e.g. on the food web). Interactions are likely to be complex. Macrophytes may be negatively impacted if suspended sediment loads and flows are sufficiently high to result in scouring or if deposition causes smothering. Therefore, in addition to lithophilous species spawning on gravel beds, those depositing eggs on macrophytes such as perch (*Perca fluviatilis*) and roach may also suffer from increased sediment loads within a watercourse. High suspended sediment concentrations during the incubation period of these species have been reported to result in high mortality through the adherence of silt particles to the egg surface preventing sufficient oxygen and carbon dioxide exchange (Stuart, 1953).

Nursery, rearing, and adult habitat

As is the case for spawning requirements, consideration of the impact of sediments on the key habitat for successive life stages has tended to focus on salmonids. Suitable substrate (Table III) is a significant habitat variable in salmonid ecology as it provides protection from predators (Heggenes, 1988a; Heggenes *et al*., 1993; Bardonnet and Heland, 1994; Mitchell *et al*., 1998), shelter from adverse currents (Heggenes, 1988a; Heggenes *et al*., 1993; Bardonnet and Heland, 1994), visual isolation from aggressive conspecifics (Kalleberg, 1958; Chapman, 1966; Imre *et al*., 2002), and habitat for invertebrates (Crowder and Cooper, 1982; Borchardt, 1993; Hegge *et al*., 1993; Langler and Smith, 2001); it also increases the availability and diversity of habitat (Heggenes, 1988b; Shirvell, 1990; Fausch, 1993; Huusko and Yrjana, 1997; Van Zyll de Jong, 1997; Mitchell *et al*., 1998; Harvey *et al*., 1999; Maki-Petays *et al*., 2000; Milan *et al*., 2000; Langler and Smith, 2001; Yarnell *et al*., 2006).

Increases in fine sediment deposition can affect the rearing habitat for juvenile salmonids. The infilling of interstitial spaces and loss of vegetation can potentially limit the amount of cover exposing juvenile salmonids to increased predation and reduced foraging efficiency. As is the case for eggs, larval and juvenile stages are more susceptible to the effect of fine sediment than adults that have greater propensity to move and avoid adverse conditions (Wood and Armitage, 1999).

Non-salmonid species and community structure will also be influenced by shifts in morphology of a habitat determined by the movement of sediment and fluid transfer processes. At the meso-habitat scale, increased

Table III. Spawning traits and incubation periods of benthic spawning freshwater fish detailing the spawning habitat, egg characteristics and incubation period. Potential impacts of fine sediments are reported. Coarse fish species tend to spawn later in the year when temperatures are warmer and embryos develop faster. Biological traits include broadcast spawning of larger numbers of smaller eggs compared to salmonidae. These eggs are often sticky and adhere to the bed and vegetation. Compared to salmonidae, research on the impacts of fine sediment on coarse fish embryo incubation is not as well developed

Species	Spawning time	Incubation time (days)	Eggs per female	Egg diameter (mm)	Spawning habitat	Threat from fine sediment	Source
Atlantic Salmon (*Salmo salar*) Anadromous	October (northern rivers)–January (southern groundwater rivers)	40 at 10 °C 145 at 3 °C 440 degree days	2500–8900	4·91–6·2	Depth 0–128 cm, velocity <5–75 cm s^{-1}. Temperature: 1·4–15 °C.	Infiltration and accumulation of fines within egg zone impacts oxygen supply. Sediment oxygen demand of organic materials and, potentially, pesticide/herbicides bound to fines critically influence survival. Development of fine sediment capping within surface of redds gravels can entomb embryos	Greig *et al.* (2005, 2007)Sear *et al.*, 2008) Mills (1989) Hendry and Cragg-Hine (2003) Crisp (2000)
Brown Trout/Sea Trout (*Salmo trutta*) Rheophilic A/Anadromous	Late Autumn–Winter.	40 at 10 °C 145 at 3 °C 440 degree days	5000–10,000	3·2–5·9	Substrate >10 mm <75 mm. Depth 6–91 cm, velocity <11–81 cm s^{-1}. Temperature: 0–12 °C.	Infiltration and accumulation of fines within egg zone impacts oxygen supply. Sediment oxygen demand of organic materials and potentially pesticide/herbicides bound to fines critically influence survival. Development of fine sediment capping within surface of redds gravels can entomb embryos.	Acornley and Sear (1999) Crisp (1989, 2000)
Grayling (*Thymallus thymallus*) Rheophilic A	March–May	20–30	2000–20 000	2·5-3·5	Bed of fine gravel, with water depth between 10 and 50 cm and water velocities between 23 and 92 cm s^{-1}. Temperature between 3·5 and 16·2 °C	Smothering by fine sediments and adhesion of fines to egg surface	Sempeski and Gaudin (1995.)

Table III. (*Continued*)

Species	Spawning time	Incubation time (days)	Eggs per female	Egg diameter (mm)	Spawning habitat	Threat from fine sediment	Source
Bullhead (*Cottus gobio*) Rheophilic A	February–June	20–30	400 per spawn, multiple spawning batches in warmer streams, one cold water (upland) stream	2–2·5	Riffles with coarse gravels. Water depths >0·05 m, velocity 0·1–0·8 m s^{-1} Thermal range −4·2–27·7 °C Excavates nest and eggs adhere to underside of large stones/wood	Embeddeness (smothering) reduces availability of nest sites	Tomlinson and Perrow (2003)
Stone loach ***(****Noemacheilus barbatulus****)***	April–June (Temp >10 °C)	14–16	10 000	1·0	Phytolithophilic sticks eggs to stones or plants. Spawns in gravel/pebble habitats	None mentioned but embedde-ness/smothering of egg deposition sites potentially critical	Smyly (1955, 1957) Freyhof and Kottelat (2008).
River/brook lamprey (*Lampetra fluviatilis/planeri)* Rheophilic A	March–April (when water temperature lies between 8·5 and 12 °C.)	15–30	1000–1500	0·8–1·25	Tail end of pools, where mixture of sands and gravels occur and water moves through substrate. Water depths typically 0·2–1·5 m, velocities of 0·3–0·5 m s^{-1}. Thermal range 8·5–12 at spawning, constructs oval nest (30–70 cm across, 2–10 cm deep for river lamprey, and 20–40 cm across and 2–10 cm deep for brook lamprey). Whitish eggs adhere to sand particles and become embedded within nest substrate	None mentioned but embedde-ness/smothering of egg deposition sites potentially critical	Hardisty and Potter (1971) Maitland (2003)
Allis Shad (*Alosa alosa*) Twaite shad (*Alsoa fallax*)	May–July	4–8 4–6	50 000–636 000 30 000–675 000	2·5–4·51·5–3·5	Tails of pools, sandy-gravels (2–20 mm), depth of 0·3–1·5 m, velocity range 0·5–1·5 m s^{-1}. Temperature regime at spawning >16 °C. Broadcast spawn, neutrally buoyant eggs drift downstream and catch in interstices of gravel beds	None mentioned but embedde-ness/smothering of egg deposition sites potentially critical	Maitland and Hatton-Ellis (2003)
Smelt (*Osmerus eperlanus*) Anadromous	February–March		40 000–106 000	1·0	Phytolithophilic Gravel riffles. Shallow fast-flowing water. Females broadcast spawn. Sticky eggs adhere to gravels, plants, and debris. Spawning temperature 4–7 °C	None mentioned but embedde-ness/smothering of egg deposition sites potentially critical.	Lyle and Maitland (1997). Nellbring (1989)

Table III. (*Continued*)

Species	Spawning time	Incubation time (days)	Eggs per female	Egg diameter (mm)	Spawning habitat	Threat from fine sediment	Source
Barbel (*Barbus barbus*) Rheophilic A	April–July	10–15	8000–12 000	2·0	Gravels, in shallow water. Eggs adhere to stones and crevices. Depth 15–40 cm. Temperature: >14 °C (optimum). A typical spawning site is several metres long and wide. with moderate to fast-flowing (28–43 cm s^{-1}) clear water, running over a substrate of small pebbles and gravels	None mentioned but embedde-ness/smothering of egg deposition sites potentially critical.	Philippart (1987); Baras (1992)
Chub (*Leuciscus cephalus*) Rheophilic A	May–late July	3–5	27 000–65 000	2·0	Lithophilic–phytolithophilic. Substrate 20–40 mm and occasional channel vegetation. Depth 10–128 cm, velocity <5–75 cm s^{-1}. Temperature: 14–20 °C (optimum)	None mentioned but embedde-ness/smothering of egg deposition sites potentially critical	Cragg-Hine and Jones (1969)
Dace (*Leuciscus leuciscus*) Rheophilic A	March–April	29	6550–9500	1·5–2·5	Lithophilic Substrate >30 mm <250 mm and channel vegetation, rootwad. Depth 25–40 cm, velocity 20–50 cm s^{-1}. Temperature: 6–9 °C (optimum)	Egg mortality is mainly due to silt deposition, which impedes gaseous exchange	(Mills, 1981); Mann and Mills (1985) Cowx (1990)
Bleak (*Alburnus alburnus*)	April–May		1700–12 284	1·0	Depth <1 m (0·2–0·5 m) Phytolithophilic Velocity <0·2 m s^{-1} 13–14 °C Eggs are deposited on sand, gravel,and rock bottom	None mentioned but smothering of eggs by silt/clay likely to be detrimental	Copp (1989) Vriese *et al*. (1994) Kestemont *et al.* (2001)
Rudd (*Scardinius erythrophthalmus*) Limno	May–July	4–5 at 17·5–21·5 °C 19–20 at 10·5–11·5 °C	50 000–120 000	1·4–1·7	Depth 10–90 cm, velocity <5 cm s^{-1}	None mentioned but embedde-ness/smothering of egg deposition sites potentially critical	USGS http://fisc.er.usgs.gov/Carp_ID/html/scardinius_erythrophthalmus.html Accessed 06/01/2010.
Gudgeon (*Gobio gobio*) Rheophilic B	Late May–late June	7–8	2300–6800	1·4–1·6	Gravel substrate >3 mm, 30 mm and occasionally channel vegetation. Depth 5–8 cm, velocity <2–80 cm s^{-1}. Temperature: >17 °C (optimum)	None mentioned but smothering of eggs by silt/clay likely to be detrimental	Kennedy and Fitzmaurice (1972)

Table III. (*Continued*)

Species	Spawning time	Incubation time (days)	Eggs per female	Egg diameter (mm)	Spawning habitat	Threat from fine sediment	Source
Bream (*Abramis brama*) Eurytopic	May–July	10–14	100 000–300 000	1·2	Gravel substrate >5 mm with Glyceria, Sagittaria, Nuphar. Depth 25–50 cm, Velocity <20 cm s^{-1}. Temperature: 12–20 °C	None mentioned but smothering of eggs by silt/clay likely to be detrimental	Cowx (1983)
Common Minnow (*Phoxinus phoxinus*) Rheophilic A	May–June	3–6	200–1000	1·0	Adhesive eggs. Spawns over gravels to which eggs stick. 10 °C.	None mentioned but smothering of eggs by silt/clay likely to be detrimental	Mills (1986)
Stickleback (Gasterosteus aculeatus)	May–June	20	10–100	1·3	Silty sand substrate in weeds. 16–20 °C, nest building out of vegetation and sand. Eggs are laid in nest. Male fans eggs to prevent silt accumulation and to supply oxygenated water	None mentioned but smothering of eggs by silt/clay likely to be detrimental	Wootton (1976). Banister (1986)

fine sediment deposition may reduce distinction between riffles, runs, and pools and the associated community composition (Berkman and Rabeni, 1987). Excessive fine sediment deposition (e.g. from logging) can reduce residual pool volumes (*cf* Lisle and Hilton, 1992).

In the UK and Europe, species such as eel (*Anguilla anguilla*), bream (*Abramis brama*), and gudgeon are better adapted to highly sedimented habitats than salmonids (Maitland and Campbell, 1992). Other species such as bullhead, however, that may on occasions associate with depositional habitat dominated by a silt bed, e.g. pools with woody debris (Perrow *et al*., 1997; Punchard *et al*., 2000), still require a coarse substrate with larger stones or cobbles that provide refuge against flow and predators, as well as for spawning (Maitland, 2003). Loss of preferred habitat due to prolonged elevated sediment loads can influence fish population structure. In a study of cyprinid and percivorous fish, recruitment areas for fish species preferring vegetated areas (roach and bream) decreased as an effect of increased turbidity that caused a die back in the vegetation due to suppressed light levels. Among those species, young-of-year cyprinids and ruffe, nevertheless, were favoured because of their ability to forage in the dim and turbid environments (Sandström and Karås, 2002).

FISH POPULATION RESPONSE TO ELEVATED FINE SEDIMENT REGIMES

The magnitude and nature of the effect of altered sediment regimes on fish populations will depend on the change in composition and concentration relative to background levels, degree of oxygenation, temperature (Servizi and Martens, 1991), species and life stage (Ryan, 1991), frequency and duration of exposure (Redding and Schreck, 1982; Newcombe and MacDonald, 1991; Anderson *et al*., 1996; Newcombe and Jensen, 1996), and degree of acclimation (Redding *et al*., 1997). Newcombe and MacDonald (1991) developed a stress index to quantify impact based on the natural logarithm of the product of the concentration of suspended sediment and duration of exposure, and categorized the effect as (1) behavioural (e.g. increased coughing rate, alarm/avoidance response, reduced feeding, impaired homing); (2) sublethal (e.g. physiological stress and histological changes, reduced growth rates); and (3) lethal (percentage mortality).

Although reductions in fish density occur in response to significant inputs of fine sediment, e.g. due to mining (Gammon, 1970; Brown *et al*., 1998), agriculture (Walser and Bart, 1999), and engineering practices (Doeg and Koehn, 1994), wild populations will most likely encounter sublethal concentrations (Boubee *et al*., 1997), and short-term population responses will usually be attributed to avoidance behaviour (Robertson *et al*., 1997) and dispersal. Deposited fine sediment resulting in habitat alterations and physical disturbance has a greater effect than short-lived suspended sediment fluxes from flood events when invertebrates and juvenile fish can seek refuge or be swept downstream (Suren and Jowett, 2001).

Long-term changes in habitat quality, however, will influence the carrying capacity of the system and changes in community composition. When suspended sediment inputs are high, direct mortality of fish can result (Newcombe and Jensen, 1996; Henley *et al*., 2000). Korstrom and Birtwell (2006) report results which suggested that even a relatively brief (48-h) exposure to elevated levels of suspended sediment could indirectly jeopardize survival of juvenile salmonids in the wild. Sub-lethal effects on behaviour were considered to render juvenile salmon more conspicuous and therefore more susceptible to avian and aquatic predators.

Sedimentation and turbidity can contribute towards short-term or local decreases in fish populations since many fish simply relocate when ambient sediment loads are increased (Barton, 1977). For example, avoidance of turbid waters has been observed in juvenile coho salmon *O. kisutch*, Arctic grayling, *Thymallus arcticus*, and rainbow trout, *O. mykiss* (Newcombe, 1994; Newcombe and Jensen, 1996). If high suspended sediment loads persist, a general shift in community composition will ultimately occur, e.g. from salmonid to non-salmonid fish communities. This may reflect a higher tolerance to turbidity of groups such as the cyprinids (Gradall and Swenson, 1992) due to their ability to utilize plants and detritus as a food resource (Persson, 1983; Vinni *et al*., 2000) and their large capacity and flexibility in reproduction (Barthelmes, 1983).

Recovery of a fish population from a sediment pressure depends on the magnitude and period of the perturbation, and composition of the sediment deposited. Fish populations are, however, capable of recovering from even the most devastating of catastrophic sediment input events. Despite the obliteration of several stocks of fish inhabiting the river systems on the slopes of Mount St. Helens immediately after the 1980 eruption, populations have been able to recover aided by straying of individuals from unaffected systems, survival of remnant populations in refugia environments, and abundant food resources, and limited competition in the years that followed (Bisson *et al*., 2005). However, the recovery was also influenced by fisheries management activities including restocking and the emplacement of sediment control structures.

DISCUSSION

The input of fine sediments into a river system is a natural and essential process, important for the hydrological, geomorphological, and ecological functioning of the river. However, fine sediments have been found to be highly damaging when manageable limits have been exceeded due to excessive inputs (Henley *et al*., 2000). It is clear that suspended and settled fine sediment has both positive and negative effects on freshwater ecosystems. The direct effects of increased sediments on fish will vary with the concentration of suspended matter (Zimmerman *et al*., 2003), duration and timing of exposure (Robertson *et al*., 1997), degree of sediment deposition (Chapman, 1988), particle size distribution and type of sediment (Lake and Hinch, 1999), and fish species and life stages at which the fish is exposed (Servizi and Martens, 1987) (Table I). Therefore, the propensity for accumulation of fine sediments within a given reach of channel becomes a critical measure of habitat suitability, but crucially this measure must be based on a knowledge of naturally occurring levels (and variability) of sediment concentrations and accumulation (Collins *et al*., 2009c).

The results of this review indicate that fine organic and inorganic sediments create a range of impacts on both coarse and salmonid fish species. These impacts can be defined in terms of lethal and sub-lethal effects that can occur across the different life stages, though these are typically poorly defined for most fish species. The main period of sensitivity to enhanced fine sediment loads is during the incubation stage when embryos are immobile (i.e. cannot move away from the pressure), and in the case of lithophils, in environments susceptible to surface sedimentation. Phytophils are similarly susceptible to high concentrations of suspended fine sediments. However, compared to salmonids, coarse fish species tend to produce high quantities of small eggs and have shorter incubation periods as a result of the generally warmer water temperatures at spawning (Table II). In addition many coarse fish species exhibit multiple spawning strategies. Hence the risk of exposure to fine sediments may be reduced. In addition, most of the coarse fish species spawn later than the salmonids, a period typically characterized by fewer high flow events and lower suspended sediment loads, except in areas with significant amounts of spring cultivation of cereals or alternative crops (Figure 3). Furthermore, later spawning tends to be associated with periods of relatively high crop cover in agricultural landscapes and a concomitant reduction in soil erosion and sediment mobilization (Figure 3). Conversely, the higher water temperatures typically utilized by spawning coarse fish, increases the rate of organic matter oxidation and hence the threat of hypoxia resulting from sediment oxygen demands.

At present, there is a dearth of research on the biological, physiological, and behavioural responses of different freshwater fish species to exposure to fine sediment *per se* and to fine sediment pressures resulting from inputs associated with specific sources (Collins *et al*., 2009c). Moreover, those studies that have been undertaken often utilize different measures of exposure, different definitions of fine sediment, and use different measures of response; thus making inter-comparisons and synthesis of results difficult to translate into practical generic management applications. This is particularly concerning in relation to recent attempts to develop revised sediment targets for freshwater environments (Collins and Anthony, 2008).

Given the interdependencies of the different biological communities highlighted in this paper (and others), there is a strong argument for considering whether the research agenda is better served by ecosystem studies of the effects of fine sediments rather than more fish

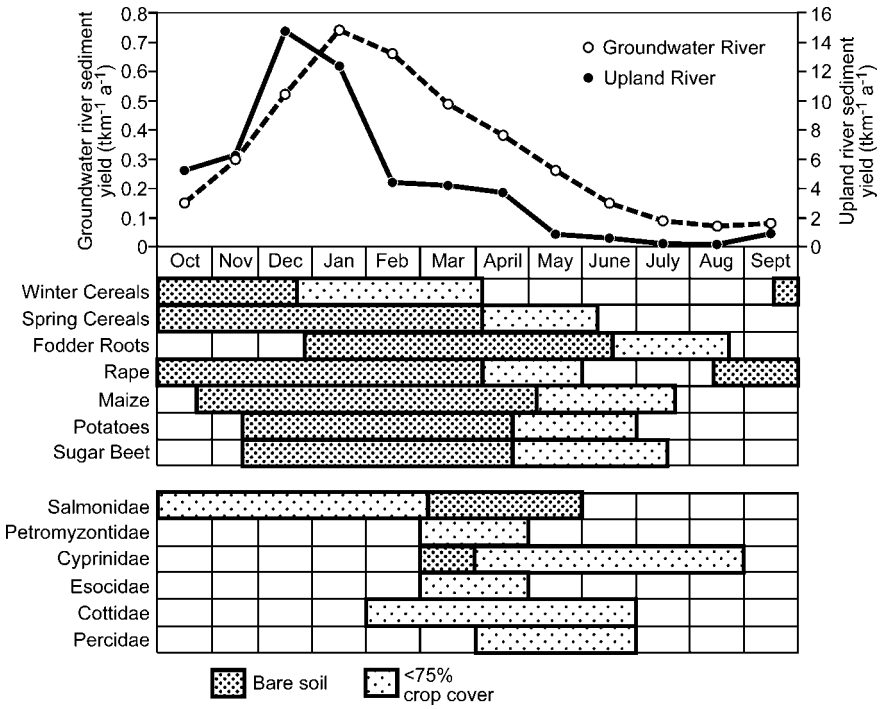

Figure 3. Fine sediment risk periods in river systems are mainly associated with the winter months when suspended sediment yields are highest and agricultural activity results in bare soils that are most susceptible to water erosion. The spawning period of major north European fish families is shown. Of these, the salmonidae (e.g. Atlantic salmon, brown/sea trout) and thymallidae (e.g. European grayling) are most at risk from fine sediment. Cottidae (e.g. bullhead) and petromyzontidae (e.g. river and brook lamprey) are also at risk when spawning in February and early March particularly in groundwater streams. The major coarse fish family; cyprinidae (e.g. dace, carp, chub, and minnow) tends to spawn after cover is established on the fields, and during the period of lowest suspended sediment yields in rivers. Cropping chart data provided by ADAS. Sediment regimes derived from data held by the authors

(or other taxa)-focussed research. However, we would argue that given our poor understanding of the biological impacts of fine sediments on even single fish species, approaches that focus on fish species can be justified when these are integrated within broader ecosystem/food web experimental or modelling frameworks (Anderson *et al*., 2007).

Setting targets for sediment management in relation to fish species

Given the pivotal role of sediment in determining water quality, countries have recommended corresponding targets to assist the management of freshwaters. For example, in the USA section 303(d) of the Clean Water Act (1972) requires states to identify and list impaired waters every 2 years and to establish total maximum daily loads (TMDLs) using a range of empirical and modelling approaches (Hawkins, 2003). In the European Union (EU), the introduction of the Water Framework Directive (WFD) (European Parliament, 2000), as the principal water policy, is driving an increased focus on the biological effects of pollutant loadings, with a view to replacing guidelines in the existing Freshwater Fish Directive legislation for sediment, which is due to be repealed in 2013 (Collins and Anthony, 2008).

Existing recommended targets for sediment management suffer from a number of inherent problems. These include the uncertainty in measuring or monitoring sediment pressures reliably, the need for and use of experimental data describing impacts on biota, the diversity of environments to which guidelines are supposed to apply, and a common oversimplification in the recommendation of 'global' targets regardless of localized factors (Collins and Anthony, 2008). The concept of a fine sediment concentration—fish response model is undoubtedly an oversimplification, especially since aquatic biota can be adversely affected by extremely low sediment concentrations. Rogers (1969) has suggested that the variability in tolerance to suspended sediment could be explained by species differences and nature of the stressor, e.g. sediment particle characteristics, water temperature, and their potential synergistic effects (Table I). It is clearly important to consider sediment stress in the context of additional stressors on aquatic environments and such interactions can be synergistic, additive, or antagonistic (Collins *et al*., 2009c).

With respect to setting sediment targets using loadings as a metric, there are five main constraints to identifying meaningful thresholds for freshwater fish, which can be summarized as follows:

1. *Catchment dependency*. For example, lowland groundwater-dominated (sensu Sear *et al*., 1999) streams accumulate and store more of their catchment yield in the channel network than higher energy upland rivers (Collins and Walling, 2007b). Catchment topography/lithology/land cover/climatic regime create different sediment supply regimes (Walling, 1995).
2. *Reach dependency*. Some reaches produce, others store (Collins and Walling, 2007b). At a catchment scale,

this may in itself constitute physical habitat diversity (e.g. 1000-year-old ponded mill reaches on lowland rivers interspersed with short steep reaches produce arguably more varied habitat than might result from natural processes).

3. *Sediment dependency*. Fine clays and silts are especially deleterious to early life stages of fish that require oxygen diffusion and that lie within stable gravel beds. Similarly, the organic matter and associated contaminants are especially important. Sand becomes important for entombing and embedding substrates, reducing refugia/habitat for benthic invertebrates, and thus reducing food availability for fish.
4. *Fish family dependency*. Different fish families have different tolerances/requirements for fine sediment (e.g. salmonids/lamprey) and are linked more or less through the food chain to other fine sediment specific biota (e.g. invertebrates). Furthermore, organisms can modify the fine sediments; e.g. by growth of biofilms or reworking through ingestion and excretion by invertebrates.
5. *Life stage dependency*. Different life stages are more/less sensitive to fine sediments within the river and floodplain ecosystem with an emphasis placed on the relatively immobile larval stages.

Thus a dynamic fine sediment load, interacting with a hydraulically variable river network, may result in a diverse range of habitats at the catchment scale. In contrast, excessive delivery of fines to, or excessive storage of fines within, the river network may reduce the heterogeneity of the substrate with implications for the diversity of hyporheic exchange as a result of substrate accumulation.

A final consideration is the type and magnitude of river management activity that may render reaches or the river network more or less sensitive to sedimentation. Abstraction of water can exacerbate low flow problems resulting in increased rates of silt accumulation (Wood and Armitage, 1997), whereas channel maintenance (e.g. deepening and over-widening) can create extensive marginal deadwater zones or a gross reduction in fine sediment transport rate resulting in accumulation of fines on the river bed (Sear, 1993; Sear *et al.*, 2000). Similarly, river restoration undertaken in the absence of catchment management of fine sediment sources, typically results in reaches with a higher capacity for fine sediment accumulation, causing Sear (1994) to argue against the reach-scale enhancements frequently undertaken for fisheries management (*cf* Walling *et al.*, 2003).

CONCLUSIONS

The impact of fine sediment on freshwater fish is complex and highly dependent on species and life stage. Fine sediments can impact freshwater fish populations and community structure by influencing food supply, behaviour, physiology, and habitat. Unlike other reviews, we have reported the sediment impacts across a broad range of fish families. This has highlighted a general dearth of information on the impacts of fine sediments on some families (e.g. petromyzontidae). In most cases, the research undertaken tends to be correlative, and does not provide causative understanding of the interactions between biological and physiological processes on the one hand, and robust and consistent descriptions of the fine sediment pressure on the other. Although we can conclude that fine sediments do generally impact all fish species across all of their life stages within freshwater, we are unable to defend existing approaches to setting singular sediment targets (e.g. EU Freshwater Fish Directive 78/659/EC). We also conclude that standardization of experimental reporting would increase the collective information content and transferable value of studies, enabling the scientific community to begin to quantify the cause of experimental and observational variability.

Ultimately, this review highlights that although the complexity and variability of biological response to fine sediment is appreciated, and conceptual models of impacts on fish species exist, we lack sufficient quantitative understanding of these relationships to be able to set robust and scientifically justifiable targets. Progress towards target setting must develop from a more robust understanding of what we mean by 'enhanced sediment loads' and a more complete analysis of the different impacts (both positive and negative) that sediments have on the different trophic levels within riverine ecosystems.

ACKNOWLEDGEMENTS

The authors gratefully acknowledge the funding provided by the Department for Environment, Food and Rural Affairs (Defra) under project WQ0128 (extending the evidence base on the ecological impacts of fine sediment and developing a framework for targeting mitigation of agricultural sediment losses). This paper represents a contribution to the SETAC SEDAG (Sediment Advisory Group) Working Group on Reviewing sediment targets used for water policy.

REFERENCES

Acornley RM, Sear DA. 1999. Sediment transport and siltation of brown trout (*Salmo trutta* L.) spawning gravels in chalk streams. *Hydrological Processes* **13**: 447–458.

Ahlbert IB. 1969. The organization of the cone cells in the retina of four teleosts with different feeding habits (*Perca fluviatilis* L., *Lucioperca lucioperca* L., *Acerina cernua* L., *Coregonus albula* L.). *Arkiv for zoologi* **22**: 445–481.

Alabaster JS, Lloyd R. 1982. *Water Quality Criteria for Freshwater Fish*. Butterworth: London; 361.

Ali MA, Ryder RA, Anctil M. 1977. Photoreceptors and visual pigments as related to behavioural responses and preferred habitats of perches (*Perca* spp.) and pike-perches (*Stizostedion* spp.). *Journal of the Fisheries Research Board of Canada* **34**: 1475–1480.

Anderson PG, Taylor BR, Balch GC. 1996. *Quantifying the Effects of Sediment Release on Fish and Their Habitats*. Canadian Manuscript Report Fisheries and Aquatic Sciences No. 2346; 110.

Anderson TM, Ritchie ME, Mayemba E, Eby S, Grace JB, McNaughton SJ. 2007. Forage nutritive quality in the Serengeti ecosystem: the roles of fire and herbivory. *American Naturalist* **170**: 343–357.

Angradi TR. 1999. Fine sediment and macroinvertebrate assemblages in Appalachian streams: a field experiment with biomonitoring applications. *Journal of the North American Benthological Society* **18**: 49–66.

Appleby JP, Scarratt DJ. 1989. Physical effects of suspended solids on marine and estuarine fish and shellfish with special reference to ocean dumping: a literature review. *Canadian Technical Report of Fisheries and Aquatic Sciences* **1**: 1681–1687.

Ballantine DJ, Walling DE, Collins AL, Leeks GJL. 2009. The content and storage of phosphorus in fine-grained channel bed sediment in contrasting lowland agricultural catchments in the UK. *Geoderma* **151**: 141–149.

Banister K. 1986. Gasterosteidae. In *Fishes of the north-eastern Atlantic and the Mediterranean*. PJP Whitehead, M-L Bauchot, J-C Hureau, J Nielsen and E Tortonese (eds.) volume 2. UNESCO: Paris; 640–643.

Baras E. 1992. Etude des strategies d'occupation du temps et de l'espace chez le barbeau fluviatile, *Barbus barbus* (L.). *Cahiers d'ethologie* **12**: 125–442.

Bardonnet A, Heland M. 1994. The influence of potential predators on the habitat preferenda of emerging brown trout. *Journal of Fish Biology* **45**(Suppl. A): 131–142.

Barrett JC, Grossman GD, Rosenfeld F. 1992. Turbidity induced changes in reactive distance of rainbow trout. *Transactions of the American Fisheries Society* **121**: 437–443.

Barthelmes D. 1983. Effects of eutrophication and fisheries management on fish faunas of cyprinid lakes. *Roczniki Nauk Rolniczych, Series H* **100**: 31–44.

Barton BA. 1977. Short-term effects of highway construction on the limnology of a small stream in southern Ontario. *Freshwater Biology* **7**: 99–108.

Bash J, Berman C, Bolton S. 2001. *Effects of Turbidity and Suspended Solids on Salmonids*, Washington State Transportation Center (TRAC) Report No.WA-RD 526·1, Olympia, Washington, USA; 50.

Berg L, Northcote TG. 1985. Changes in territorial, gill-flaring, and feeding behaviour in juvenile coho salmon (*Oncorhynchus kisutch*) following short-term pulses of suspended sediment. *Canadian Journal of Fisheries and Aquatic Sciences* **42**: 1410–1417.

Bergman E. 1988. Foraging abilities and niche breadths of two percids, *Perca fluviatilis* and *Gymnocephalus cernua*, under different environmental conditions. *Journal of Animal Ecology* **572**: 443–453.

Bergstedt LC, Bergersen EP. 1997. Health and movements of fish in response to sediment sluicing in the Wind River, Wyoming. *Canadian Journal of Fisheries and Aquatic Sciences* **54**: 312–319.

Berkman HE, Rabeni CF. 1987. Effects of siltation on stream fish communities. *Environmental Biology of Fishes* **18**: 285–295.

Berry W, Rubenstein N, Melzian B. 2003. *The biological effects of suspended and bedded sediment (SABS) in aquatic systems: a review*. United States Environmental Protection Agency Internal Report; 102.

Bilotta GS, Brazier RE. 2008. Understanding the influence of suspended solids on water quality and aquatic biota. *Water Research* **42**: 2849–2861.

Birtwell IK, Hartman GF, Anderson B, McLeay DJ, Malick JG. 1984. *A brief investigation of Arctic grayling (Thymallus arcticus) and aquatic invertebrates in the Minto Creek drainage, Mayo, Yukon territory: an area subjected to placer mining*. Canadian Technical Report of Fisheries and Aquatic Sciences No. **1287; 57.**

Bisson PA, Bilby RE. 1982. Avoidance of suspended sediment by juvenile coho salmon. *North American Journal of Fisheries Management* **2**: 371–374.

Bisson PA, Crisafulli CM, Fransen BR, Lucas RE, Hawkins CP. 2005. Response of fish to the 1980 eruption of Mount St. Helens. In *Ecological response to the 1980 eruption of Mount St. Helens*, Dale VD, Swanson FJ, Crisafulli CM (eds). Birkhauser: USA; 163–181.

Bjerkli DM, LaPerriere JD. 1985. Gold-mining effects on stream hydrology and water quality, Circle Quadrangle, Alaska. *Water Resources Bulletin* **21**: 235–243.

Bo T, Fenoglio S, Malacarne G, Pessino M, Sgariboldi F. 2007. Effects of clogging on stream macroinvertebrates: an experimental approach. *Limnologica—Ecology and Management of Inland Waters* **37**: 186–192.

Bond NR, Downes BJ. 2003. The independent and interactive effects of fine sediment and flow on benthic invertebrate communities characteristic of small upland streams. *Freshwater Biology* **48**: 455–465.

Bonner TH, Wilde GR. 2002. Effects of turbidity on prey consumption by prairie stream fishes. *Transactions of the American Fisheries Society* **131**: 1203–1208.

Borchardt D. 1993. Effects of flow and refugia on drift loss of benthic macroinvertebrates: implications for habitat restoration in lowland streams. *Freshwater Biology* **29**: 221–227.

Boubee JAT, Dean TL, West DW, Barrier DW. 1997. Avoidance of suspended sediment by the juvenile migratory stage of six New Zealand native fish species. *New Zealand Journal of Marine and Freshwater Research* **31**: 61–69.

Breitburg L. 1988. Effects of turbidity on prey consumption by striped bass larvae. *Transactions of the American Fisheries Society* **117**: 72–77.

Brittain JE, Eikland TJ. 1988. Invertebrate drift—a review. *Hydrobiologia* **166**: 77–93.

Brookes A. 1986. Response of aquatic vegetation to sedimentation downstream from river channelization works in England and Wales. *Biological Conservation* **38**: 352–367.

Brookes A. 1995. River channel restoration: theory and practice. In *Changing River Channels*, Gurnell A, Petts GE (eds). John Wiley & Son, Inc.: Chichester; 369–388.

Brown AV, Lyttle MM, Brown KB. 1998. Impacts of gravel mining on gravel bed streams. *Transactions of the American Fisheries Society* **127**: 979–994.

Bruton MN. 1985. The effects of suspensoids on fish. *Hydrobiologia* **125**: 221–241.

Bryant MD. 1984. The role of beaver dams as coho salmon habitat in southeast Alaska streams. In *Proceedings of the Olympic Wild Fish Conference. Fisheries Technology Programme*, Walton JM, Houston DB (eds). Peninsula College, Port Angeles: Washington, DC; 183–192.

Bunt CM, Cooke SJ, Schreer JF, Philipp DP. 2004. Effects of incremental increases in silt load on the cardiovascular performance of riverine and lacustrine rock bass, *Ambloplites rupestris*. *Environmental Pollution* **138**: 437–444.

Burkhead NM, Jelks H. 2001. Effects of suspended sediment on the reproductive success of the tricolour shiner, a crevice-spawning minnow. *Transactions of the American Fisheries Society* **130**: 959–968.

Carlson RW. 1984. The influence of pH, dissolved oxygen, suspended solids or dissolved solids upon ventilatory and cough frequencies in the bluegill (*Lepomis machrochirus*) and brook trout (*Salvelinus fontinalis*). *Environment Pollution Series A Ecological and Biological* **34**: 149–169.

Chapman DW. 1966. Food and space as regulators of salmonid populations in streams. *American Naturalist* **100**: 345–357.

Chapman DW. 1988. Critical review of variables used to define effects of fines in redds of large salmonids. *Transactions of the American Fisheries Society* **117**: 1–21.

Cirmo CP, Driscoll CT. 1993. Beaver pond biogeochemistry: acid neutralizing capacity generation in a headwater wetland. *Wetlands* **13**: 277–292.

Clarke SJ, Wharton G. 2001. Sediment nutrient characteristics and aquatic macrophytes in lowland English rivers. *The Science of the Total Environment* **266**: 103–112.

Collins AL, Anthony SG. 2008. Assessing the likelihood of catchments across England and Wales meeting 'good ecological status' due to sediment contributions from agricultural sources. *Environmental Science and Policy* **11**: 163–170.

Collins AL, Anthony SG, Hawley J, Turner T. 2009a. The potential impact of projected change in farming by 2015 on the importance of the agricultural sector as a sediment source in England and Wales. *Catena* **79**: 243–250.

Collins AL, Anthony SG, Hawley J, Turner T. 2009b. Predicting potential change in agricultural sediment inputs to rivers across England and Wales by 2015. *Marine and Freshwater Research* **60**: 626–637.

Collins AL, McGonigle DF, Evans R, Zhang Y, Duethmann D, Gooday R. 2009c. Emerging priorities in the management of diffuse pollution at catchment scale. *International Journal of River Basin Management* **7**: 179–185.

Collins AL, Walling DE. 2007a. The storage and provenance of fine sediment on the channel bed of two contrasting lowland permeable catchments, UK. *River Research and Applications* **23**: 429–450.

Collins AL, Walling DE. 2007b. Fine-grained bed sediment storage within the main channel systems of the Frome and Piddle catchments, Dorset, UK. *Hydrological Processes* **21**: 1448–1459.

Collins AL, Walling DE, Leeks GJL. 1997. Source type ascription for fluvial suspended sediment based on a quantitative composite fingerprinting technique. *Catena* **29**: 1–27.

Collins AL, Walling DE, Leeks GJL. 2005. Storage of fine-grained sediment and associated contaminants within the channels of lowland

permeable catchments in the UK. In *Sediment Budgets 1 (pp. 259–268)*, International Association of Hydrological Sciences Publication No. 291: Wallingford, UK; 363–382.
Copp GH. 1989. The habitat diversity and fish reproductive function of floodplain ecosystems. *Environmental Biology of Fishes* **26**: 1–27.
Cordone AJ, Kelley DW. 1961. The influence of inorganic sediment on the aquatic life of streams. *California Fish and Game* **47**: 189–228.
Cotton JA, Warton G, Bass JAB, Heppell CM, Wotton RS. 2006. The effects of seasonal changes to instream vegetation cover on patterns of flow and accumulation of sediment. *Geomorphology* **77**: 320–334.
Cowx IG. 1983. The biology of bream, *Abramis brama* (L), and its natural hybrid with roach, *Rutilus rutilus* (L), in the River Exe. *Journal of Fish Biology* **22**: 631–646.
Cowx IG. 1989. Interaction between roach (*Rutilus rutilus*) and dace (*Leuciscus leuciscus*) populations in a river catchment in the south-west of England. *Journal of Fish Biology* **35(Suppl. A)**:), 279–284.
Cowx IG. 1990. Growth and reproduction tactics of roach, *Rutilus rutilus* (L.), and dace, *Leuciscus leuciscus* (L.), populations in the Rives Exe and Culm, England. *Polskie Archiwum Hydrobiologii* **37**: 195–210.
Cragg-Hine D, Jones JW. 1969. The Growth of Dace *Leuciscus leuciscus* (L.), Roach *Rutilus rutilus* (L.) and Chub *Squalius cephalus* (L.) in Willow Brook, Northamptonshire. *Journal of Fish Biology* **1**: 59–82.
Crisp DT. 1989. Some impacts of human activities on trout, *Salmo trutta*, populations. *Freshwater Biology* **5**(1): 21–33.
Crisp DT. 1993. The ability of UK salmonid alevins to emerge through a sand layer. *Journal of Fish Biology* **43**: 656–658.
Crisp DT. 1996. Environmental requirements of common riverine European salmonid fish species in fresh water with particular reference to physical and chemical aspects. *Hydrobiologia* **323**: 201–221.
Crisp DT. 2000. *Trout and Salmon: Ecology, Conservation and Rehabilitation*. Fishing News Books: Oxford; 212.
Crisp DT, Carling P. 1989. Observations on siting, dimensions and structure of salmonid redds. *Journal of Fish Biology* **34**: 119–134.
Crisp DT, Gledhill T. 1970. A quantitative description of the recovery of the bottom fauna in a muddy reach of a mill stream in southern England after draining and dredging. *Hydrobiologia* **67**: 502–541.
Crowder LB, Cooper WE. 1982. Habitat structural complexity and the interaction between bluegills and their prey. *Ecology* **63**: 1802–1813.
Culp JM, Wrona FJ, Davies RW. 1986. Response of stream benthos and drift to fine sediment deposition versus transport. *Canadian Journal of Zoology* **64**: 1345–1351.
Cunjak R, Prowse T, Parrish D. 1998. Atlantic salmon (*Salmo salar*) in winter: "the season of parr discontent". *Canadian Journal of Fisheries and Aquatic Sciences* **55**(Suppl. 1): 161–180.
Curry R, Macneill A, Scott W. 2004. Population-level responses to sediment during early life in brook trout. *Journal of the North American Benthological Society* **23**: 140–150.
Davies-Colley RJ, Hickey CW, Quinn JM, Ryan PA. 1992. Effect of clay discharges on streams. 1. Optical properties and epilithon. *Hydrobiologia* **248**: 215–234.
DeVries P. 2008. Bed disturbance processes and the physical mechanisms of scour in salmonid spawning habitat. In *Salmonid Spawning habitat in Rivers; Physical controls, biological responses and approaches to Remediation*, Sear DA, DeVries PD (eds). AFS: Bethesda, MD; 121–147.
DeYoung CJ. 2007. Effects of turbidity on foraging efficiency and growth of salmonids in natural settings. Masters thesis. The Faculty of Natural Science, Humboldt State University; 89.
Doan KH. 1941. Relation of auger catch to turbidity in Lake Erie. *Ohio Journal of Science* **41**: 449–452.
Dobson M, Frid C. 1998. *Ecology of Aquatic Ecosystems*. Prentice Hall: UK; 390.
Dodds WK, Biggs BJF. 2002. Water velocity attenuation by stream periphyton and macrophytes in relation to growth form and architecture *Journal of the North American Benthological Society* **21**: 2–15.
Doeg TJ, Koehn JD. 1994. Effects of draining and desilting a small weir on downstream fish and macroinvertebrates. *Regulated Rivers-Research & Management* **9**: 263–277.
Dolloff CA. 1987. Seasonal population characteristics and habitat use by juvenile coho salmon in a small southeast alaska stream. *Transactions of the American Fisheries Society* **116**: 829–838.
Droppo IG. 2001. Rethinking what constitute suspended sediment. *Hydrological Processes* **15**: 1551–1564.
Elliott S, Coe T, Helfield J, Naiman R. 1998. Spatial variation in environmental characteristics of Atlantic salmon (*Salmo salar*) rivers. *Canadian Journal of Fisheries and Aquatic Sciences* **55**(Suppl. 1):; 267–280.
European Parliament. 2000. *Parliament and Council Directive 2000/60/EC. Establishing a framework for community action in the field of water policy*. Official Journal PE-CONS 3639/1/00 REV 1. European Union, Brussels, Belgium.
Evans EP, Simm JD, Thorne CR, Arnell NW, Ashley RM, Hess TM, Lane SN, Morris J, Nicholls RJ, Penning-Rowsell EC, Reynard NS, Saul AJ, Tapsell SM, Watkinson AR, Wheater HS. 2008. *An update of the Foresight Future Flooding 2004 Qualitative Risk Analysis*. Cabinet Office: London.
Fairchild JFT, Boyle T, English WR, Rabeni C. 1987. Effects of sediment and contaminated sediment on structural and functional components of experimental stream ecosystems. *Water Air and Soil Pollution* **36**: 271–293.
Fausch KD. 1993. Experimental analysis of microhabitat selection by juvenile steelhead (*Oncorhynchus mykiss*) and coho salmon (*O. kisutch*) in a British Columbia stream. *Canadian Journal of Fisheries and Aquatic Sciences* **50**: 1198–1207.
Finn RN. 2007. The physiology and toxicology of salmonid eggs and larvae in relation to water quality criteria. *Aquatic Toxicology* **81**: 337–354.
Foster IDL. 2006. Lakes in the sediment delivery system. In *Soil Erosion and Sediment Redistribution in River Catchments*, Owens PN, Collins AJ (eds). CAB International: Wallingford, CT; 128–142.
Foster IDL, Collins AL, Naden PN, Sear DA, Jones JI, Zhang Y. Palaeolimnology, policy and practice; the potential for lake-sediment based reconstructions to determine intrinsic sediment yields across England and Wales. *Journal of Palaeolimnology*, in press.
Fox MG, Keast A. 1990. Effects of winterkill on population structure, body size, and prey consumption patterns of pumpkinseed in isolated beaver ponds. *Canadian Journal of Zoology-Revue Canadienne De Zoologie* **68**: 2489–2498.
Fraser NHC, Metcalfe NB. 1997. The costs of becoming nocturnal: feeding efficiency in relation to light intensity in juvenile Atlantic salmon. *Functional Ecology* **11**: 385–391.
Freyhof J, Kottelat M. 2008. *Barbatula barbatula. IUCN 2010. IUCN Red List of Threatened Species. Version 2010.1*. www.iucnredlist.org (downloaded on 24 March 2010).
Gammon JR. 1970. *The Effect of Inorganic Sediment on Stream Biota*. Environmental Protection Agency: Washington, DC; 53.
Gardener MB. 1981. Effects of turbidity on feeding rates and selectivity of bluegills. *Transactions of the American Fisheries Society* **110**: 446–450.
Giller PS, Malmqvist B. 1998. *The Biology of Streams and Rivers*. Oxford University Press: UK; 425.
Goldes SA, Ferguson HW, Moccia RD, Daoust PY. 1988. Histological effects of the inert suspended clay kaolin on the gills of juvenile rainbow trout. *Salmo gairdneri* Richardson. *Journal of Fish Disease* **11**: 23–33.
Gradall KS, Swenson WA. 1982. Responses of brook trout and creek chub to turbidity. *Transactions of the American Fisheries Society* **111**: 392–395.
Graham AA. 1990. Siltation of stone-surface periphyton in rivers by clay sized particles from low concentrations in suspension. *Hydrobiologia* **199**: 107–115.
Gregory RS, Levings CD. 1996. The effect of turbidity and vegetation on the risk of juvenile salmonids, *Oncorhynchus* spp., to predation by adult cutthroat trout, *O. clarkii*. *Environmental Biology of Fishes* **47**: 279–288.
Gregory RS, Northcote TG. 1992. Surface, planktonic, and benthic foraging by juvenile Chinook salmon (*Oncorhynchus tshawytscha*) in turbid laboratory conditions. *Canadian Journal of Fisheries and Aquatic Sciences* **50**: 233–240.
Gregory RS. 1993. Effect of turbidity on the predator avoidance behaviour of juvenile Chinook salmon (*Oncorhynchus tshawytscha*). *Canadian Journal of Fisheries and Aquatic Sciences* **50**: 241–246.
Greig SM, Sear DA, Carling PA. 2007. A field-based assessment of oxygen supply to incubating Atlantic salmon embryos. *Hydrological Processes* **22**: 3087–3100.
Greig SM, Sear DA, Carling PA. 2005. The impact of fine sediment accumulation on the survival of incubating salmon progeny: Implications for sediment management. *The Science of the Total Environment* **344**: 241–258.
Halley D. 1995. The Proposed Re-Introduction of Beavers to Britain—In Reply. *Reintroduction News* **10**: 17–18.
Hart RC. 1992. Experimental studies of food and suspended sediment effects on growth and reproduction of six planktonic cladocerans. *Journal of Plankton Research* **14**: 1425–1448.
Harvey BC, Nakamoto RJ, White JL. 1999. Influence of large woody debris and a bankfull flood on movement of adult resident coastal cutthroat trout (*Onchorhynchus clarki*) during fall and winter. *Canadian Journal of Fisheries and Aquatic Sciences* **56**: 2161–2166.

Hawkins RH. 2003. *Survey of Methods for Sediment TMDLs in Western Rivers and Streams of the the United States*. Report to US EPA Office of Water, Assessment and Watershed Protection Division, Washington DC, 143.

Heggberget TG. 1991. Some environmental requirements of Atlantic salmon. *American Fisheries Society Symposium* **10**: 132–135.

Hegge O, Hesthagen T, Skurdal J. 1993. Vertical distribution and substrate preference of brown trout in a littoral zone. *Environmental Biology of Fishes* **36**: 17–24.

Heggenes J. 1988a. Substrate preferences of brown trout fry (*Salmo trutta*) in artificial stream channels. *Canadian Journal of Fisheries and Aquatic Sciences* **45**: 1801–1806.

Heggenes J. 1988b. Effects of short-term flow fluctuations on displacement of, and habitat use by, brown trout in a small stream. *Transactions of the American Fisheries Society* **117**: 336–344.

Heggenes J, Krog O, Lindas O, Dokk J, Bremnes T. 1993. Homeostatic behavioural responses in a changing environment: brown trout (*Salmo trutta*) become nocturnal during winter. *Journal of Animal Ecology* **62**: 295–308.

Hendry K, Cragg-Hine D. 2003. Ecology of Atlantic Salmon *Salmo salar*. *Conserving Natura Rivers Ecology Series No. 7*. English Nature: Peterborough; 32.

Henley WF, Patterson MA, Neves RJ, Lemly AD. 2000. Effects of sedimentation and turbidity on lotic food webs: a concise review of natural resource managers. *Reviews in Fisheries Science* **8**: 125–139.

Herbert DW, Merkins JC. 1961. The effect of suspended mineral solids on the survival of trout. *International Journal of Air and Water Pollution* **5**: 46–55.

Heywood MJT, Walling DE. 2007. The sedimentation of salmonid spawning gravels in the Hampshire Avon catchment, UK: Implications for the dissolved oxygen content of intragravel water and embryo survival. *Hydrological Processes* **21**: 770–788.

Hoetzel G, Croome R. 1994. Long-term phytoplankton monitoring of the Darling River at Burtundy, New South Wales: incidence and significance of cyanobacterial blooms. *Australian Journal of Marine and Freshwater Research* **45**: 747–759.

Horkel JD, Pearson WD. 1976. Effects of turbidity on ventilation rates and oxygen consumption of green sunfish, *Lepomis cyanellus*. *Transactions of the American Fisheries Society* **105**: 107–113.

Huusko A, Yrjana T. 1997. Effects of instream enhancement structures on brown trout, *Salmo trutta* L., habitat availability in a channelized boreal river: a PHABSIM approach. *Fisheries Management and Ecology* **4**: 453–466.

Impson ND, Marriott MS, Bills IR, Skelton PH. 2007. Conservation biology and management of a critically endangered cyprinid, the Twee River redfin, *Barbus erubescens* (Teleostei: Cyprinidae), of the Cape Florisitic Region, South Africa. *African Journal of Aquatic Science* **32**: 27–33.

Imre I, Grant JWA, Keeley ER. 2002. The effect of visual isolation on territory size and population density of juvenile rainbow trout (*Oncorhynchus mykiss*). *Canadian Journal of Fisheries and Aquatic Sciences* **59**: 303–309.

Izagirre O, Serra A, Guasch H, Elosegi A. 2009. Effects of sediment deposition on periphytic biomass, photosynthetic activity and algal community structure. *Science of the Total Environment* **407**: 5694–5700.

James MR, Hawes I, Weathermead M. 2000. Removal of settled sediments and periphyton from macrophytes by grazing invertebrates in the littoral zone of a large oligotrophic lake. *Freshwater Biology* **44**: 311–326.

Jensen DW, Steel EA, Fullerton AH, Pess GR. 2009. Impact of fine sediment on egg-to-fry survival of Pacific salmon: a meta-analysis of published studies. *Reviews in Fisheries Science* **17**(3): 348–359.

Julian HP, Bergeron NE. 2006. Effects of fine sediment infiltration during the incubation period on Atlantic Salmon (*Salmo salar*) embryo survival. *Hydrobiologia* **563**: 61–71.

Kalleberg H. 1958. Observations in a stream tank of territoriality and competition in juvenile salmon and trout (*Salmo salar* L. and *S. trutta* L.). *Republic Institute Freshwater Research Drottningholm* **39**: 55–98.

Kaller MD, Hartman KJ. 2004. Evidence of a threshold level of fine sediment accumulation for altering benthic invertebrate communities. *Hydrobiologia* **518**: 95–104.

Kamler E. 1992. *Early Life History of Fish: An Energetic Approach*. Chapman and Hall: London. 330p.

Karr JR. 1991. Biological integrity: a long neglected aspect of water resource management *Ecological Applications* **1**: 66–84.

Keenleyside MHA. 1955. Some aspects of the schooling behaviour of fish. *Behaviour* **8**: 183–248.

Keenleyside MHA, Bietz BF. 1981. The reproductive behaviour of *Aequidens vittatus* in Surinam, S. America. *Environmental Biology of Fishes* **6**: 87–94.

Kefford BJ, Zalizniak L, Dunlop JE, Nugegoda D, Choy SC. 2010. How are macroinvertebrates of slow flowing lotic systems directly affected by suspended and deposited sediments. *Environmental Pollution* **158**: 543–550.

Kennedy M, Fitzmaurice P. 1972. Some aspects of the biology of gudgeon *Gobio gobio* (L.) in Irish waters. *Journal of Fish Biology* **4**: 425–440.

Kent TR, Stelzer RS. 2008. Effects of deposited fine sediment on life history traits of *Physa integra* snails. *Hydrobiologia* **596**: 329–340.

Kestemont P, Rinchard J, Damoiseau F, Tans M. 2001. Seasonal variations in egg and larval quality in two multiple-spawner cyprinid fish, the bleak *Alburnus alburnus* and the white bream *Blicca bjoerkna*. *Archiv für Hydrobiologie* **12**(2–4): 357–371.

Kondolf GM, Wolman MG. 1993. The sizes of salmonid spawning gravels. *Water Resources Research* **29**: 2275–2285.

Korstrom JS, Birtwell IK. 2006. Effects of suspended sediment on the escape behavior and cover-seeking response of juvenile Chinook salmon in freshwater. *Transactions of the American Fisheries Society* **135**(4): 1006–1016.

Kulíšková P, Slavik O, Horky P, Jones JI. 2009. Factors influencing movement behaviour and home range size in ide *Leuciscus idus*. *Journal of Fish Biology* **74**: 1269–1279.

Lake RG, Hinch SG. 1999. Acute effects of suspended sediment angularity on juvenile coho salmon (*Oncorhynchus kisutch*). *Canadian Journal of Fisheries and Aquatic Sciences* **56**: 862–867.

Langler GJ, Smith C. 2001. Effects of habitat enhancement on 0-group fishes in a lowland river. *Regulated Rivers-Research & Management* **17**: 677–686.

Lemly AD. 1982. Modification of benthic insect communities in polluted streams: combined effects of sedimentation and nutrient enrichment. *Hydrobiologia* **87**: 229–245.

Lenat DR. 1983. Chironomid taxa richness: natural variation and use in pollution assessment. *Freshwater Invertebrate Biology* **2**: 192–198.

Lijklema L, Koelmans AA, Portielje R. 1993. Water quality impacts of sediment pollution and the role of early diagenesis. *Water Science and Technology* **28**: 1–12.

Liljendahl-Nurminen A, Horppila J, Lampert W. 2008. Physiological and visual refuges in a metalimnion: an experimental study of the effects of clay turbidity and an oxygen minimum on fish predation *Freshwater Biology* **53**: 945–951.

Lisle TE, Hilton S. 1992. The volume of fine sediment in pools: an index of sediment supply in gravel-bed streams. *Water Resources Bulletin* **28**: 371–383.

Lisle TE, Lewis J. 1992. Effects of sediment transport on survival of salmonid embryos in a natural stream: a simulation approach. *Canadian Journal of Fisheries and Aquatic Sciences* **49**: 2337–2344.

Lloyd DS, Koenings JP, LaPierre JD. 1987. Effects of turbidity in freshwaters of Alaska. *North American Journal of Fisheries Management* **7**: 18–33.

Lowrance R, Leonard R, Sheridan J. 1985. Managing riparian ecosystems to control non-point pollution. *Journal of Soil and Water Conservation* **18**: 87–91.

Luce JJ, Steele R, Lapointe MF. 2010. A physically based statistical model of sand abrasion effects on periphyton biomass. *Ecological Modelling* **221**: 353–361.

Lyle AA, Maitland P. 1997. The spawning migration and conservation of Smelt *Osmerus eperlanus* in the River Cree, Southwest Scotland. *Biological Conservation* **80**: 303–311.

Macklin MG, Jones AF, Lewin J. 2010. River response to rapid Holocene environmental change: evidence and explanation in British catchments. *Quaternary Science Reviews*. DOI:10.1016/j.quascirev.2009.06.010.

Maher W, Batley GE, Lawrence I. 1999. Assessing the health of sediment ecosystems: use of chemical measurements. *Freshwater Biology* **41**: 361–372.

Maitland PS, Hatton-Ellis TW. 2003. *Ecology of the Allis and Twaite Shad; Alosa alosa and Alos fallax. Conserving Natura Rivers Ecology Series No. 3*, English Nature: Peterborough; 28.

Maitland PS. 2003. *Ecology of the River, Brook and Sea Lamprey; Lampetra fluviatilis, Lampetra planeri and Petromyzon marinus. Conserving Natura Rivers Ecology Series No. 5*. English Nature: Peterborough; 52.

Maitland P, Campbell RN. 1992. *British Freshwater Fishes*. Collins: London; 453pp.

Major JJ. 2004. Post-eruption suspended sediment transport at Mount St. Helens: Decadal-scale relationships with landscape adjustments and river discharges. *Journal of Geophysical Research* **109**: 1–22.

Maki-Petays A, Vehanen T, Muotka T. 2000. Microhabitat use by Age-0 brown trout and grayling: Seasonal responses to streambed restoration under different flows. *Transactions of the American Fisheries Society* **129**: 771–781.

Malcolm IA, Greig SM, Youngson AF, Soulsby C. 2008. Hyporheic influences on salmon embryo survival and performance In *Salmonid Spawning habitat in Rivers; Physical Controls, Biological Responses and Approaches to Remediation*, Sear DA, DeVries P (eds). AFS: Bethesda, MD; 225–248.

Mann RHK, Mills CA. 1985. Variations in the sizes of gonads, eggs and larvae of the dace, *Leuciscus leuciscus*. *Environmental Biology of Fishes* **13**(4): 277–187.

Matthaei CD, Weller F, Kelly DW, Townsend CR. 2006. Impacts of fine sediment addition to tussock, pasture, dairy and deer farming streams in New Zealand. *Freshwater Biology* **51**: 2154–2172.

McCubbin RN, Case AB, Rowe DA, Scruton DA. 1990. Environmental effects of sediments on aquatic habitats and suggested mitigation. Appendix IV In *Resource Road Construction: Fish Habitat Protection Guidelines*. Canadian Forest Service and Department of Fisheries and Oceans: St. John's, New Foundland; 65pp.

McLeay DJ, Birtwell IK, Hartman GF, Ennis GL. 1987. Response of Arctic grayling (*Thymallus arcticus*) to acute and prolonged exposure to Yukon placer mining sediment. *Canadian Journal of Fisheries and Aquatic Sciences* **44**: 658–673.

Merritt RW, Cummins KW. 1984. The role of aquatic insects in the processing and cycling of nutrients. *Canadian Journal of Fisheries and Aquatic Science* **34**: 56–75.

Meyer GJ, Schoeneberger PJ, Huddleston JH. 1975. Sediment yields from roadsides: an application of the universal soil loss equation. *Journal of Soil and Water Conservation* **30**: 289–291.

Milan DJ, Petts GE, Sambrook H. 2000. Regional variations in the sediment structure of trout streams in southern England: benchmark data for siltation assessment and restoration. *Aquatic Conservation: Marine and Freshwater Ecosystems* **10**: 407–420.

Mills CA. 1981. Egg population dynamics of naturally spawning dace. *Leuciscus leuciscus (L.) Environmental Biology of Fishes* **6**(2): 151–158.

Mills CA. 1986. The life history of the minnow *Phoxinus phoxinus* (L.) in a productive stream. *Freshwater Biology* **17**(1): 53–67.

Mills D. 1989. *Ecology and Management of Atlantic Salmon*. Chapman & Hall: London; 315pp.

Mills CA, Mann RHK. 1983. The bullhead *Cottus gobio*, a versatile and successful fish. *Annual Reports of the freshwater Biological Association* **51**: 76–88.

Mitchell J, McKinley R, Power G, Scruton D. 1998. Evaluation of Atlantic salmon parr responses to habitat improvement structures in an experimental channel in Newfoundland, Canada. *Regulated Rivers-Research & Management* **14**: 25–39.

Moir H, Soulsby C, Youngson A. 1998. Hydraulic and sedimentary characteristics of habitat utilized by Atlantic salmon for spawning in the Girnock Burn, Scotland. *Fisheries Management and Ecology* **5**: 241–254.

Mol JH, Ouboter PE. 2004. Downstream effects of erosion from small-scale gold mining on the instream habitat and fish community of a small neotropical rainforest stream. *Conservation Biology* **18**: 201–214.

Morris D. 1955. The reproductive behaviour of the river bullhead (*Cottus gobio* L.), with special reference to the fanning activity. *Behaviour* **7**: 1–32.

Nellbring S. 1989. The ecology of smelts (Genus *Osmerus*) a literature review. *Nordic Journal of Freshwater Research* **65**: 116–145.

Newcombe CP. 1994. *Suspended sediment in aquatic ecosystems; ill effects as a function of concentration and exposure*. Habitat Protection Branch, Ministry of Environment: Lands and Parks, Victoria B.C., Canada; 180pp.

Newcombe CP, MacDonald DD. 1991. Effects of suspended sediments on aquatic ecosystems. *North American Journal of Fisheries Management* **11**: 72–82.

Newcombe CP, Jensen JOT. 1996. Channel suspended sediment and fisheries: a synthesis for quantitative assessment of risk and impact. *North American Fisheries Management* **16**: 693–727.

Northcote TG. 1995. Comparative biology and management of Arctic and European grayling (Salmonidae, *Thymallus*). *Reviews in Fish Biology and Fisheries* **5**: 141–194.

Nuttall PM, Bielby GH. 1973. The effects of china clay waste on stream invertebrates. *Environmental Pollution* **5**: 77–86.

O'Connor WC, Andrew TE. 1998. The effects of siltation on Atlantic salmon, *Salmo salar* L., embryos in the River Bush. *Fisheries Management and Ecology* **5**: 393–401.

Ottaway E, Clarke A. 1981. A preliminary investigation into the vulnerability of young trout (*Salmo trutta* L.) and Atlantic salmon (*S. salar* L.) to downstream displacement by high water velocities. *Journal of Fish Biology* **19**: 135–145.

Owens PN, Batalla RJ, Collins AJ, Gomez B, Hicks DM, Horowitz AJ, Kondolf GM, Marden M, Page MJ, Peacock DH, Petticrew EL, Salomons W, Trustrum NA. 2005. Finegrained sediment in river systems: environmental significance and management issues. *River Research and Applications* **21**: 693–717.

Payne BA, Lapointe MF. 1997. Channel morphology and lateral stability: effects on distribution of spawning and rearing habitat for Atlantic salmon in a wandering cobble-bed river. *Canadian Journal of Fisheries and Aquatic Sciences* **54**: 2627–2636.

Perrow MR, Punchard NT, Jowitt AJD. 1997. *The Habitat Requirements of Bullhead (Cottus gobio) and Brown Trout (Salmo trutta) in the Headwaters of Selected Norfolk Rivers: Implications for Conservation and Fisheries*. Environment Agency: Eastern Area, Ipswich; 48.

Persat H, Olivier JM, Pont D. 1994. Theoretical habitat templets, species traits, and species richness: fish in the Upper Rhône river and its floodplain. *Freshwater Biology* **31**: 439–454.

Persson L. 1983. Effects of intra- and interspecific competition on dynamics and size structure of a perch (*Perca fluviatilis*) and roach (*Rutilus rutilus*) population. *Oikos* **41**: 126–132.

Peterson NP, Quinn TP. 1996. Persistence of egg pocket architecture in redds of chum salmon, *Oncorhynchus keta*. *Environmental Biology of Fishes* **46**: 243–253.

Philippart JC. 1987. Population ecology, conservation and restoration of the barbel, *Barbus barbus* (Linné) (Teleostei, Cyprinidas) in the Meuse River and its tributaries—15 years of research. *Annales de la Societe Royale Zoologique de Belgique* **117**(1): 49–61.

Power ME. 1984. The importance of sediment in the grazing ecology and size class interactions of an armored catfish, *Ancistrus spinosus*. *Environmental Biology of Fishes* **10**: 173–181.

Punchard NT, Perrow MR, Jowitt AJD. 2000. Fish habitat associations, community structure, density and biomass in natural and channelized lowland streams in the catchment of the River Wensum, UK. *Management and Ecology of River Fisheries*. Blackwell Science: Oxford; 143–157.

Rabeni CF, Smale MA. 1995. Effects of siltation on stream fishes and the potential mitigating role of the buffering riparian zone. *Hydrobiologia* **303**: 211–219.

Redding JM, Schreck CB. 1982. Mount St. Helens ash causes sublethal stress response in steelhead trout. In *Washington Water Research Centre proceeding from the Conference, Mt. St. Helens–effects on water resources: Report 41*. Washington Water Research Center: Pullman, WA; 300–307.

Redding JM, Schreck CB, Everest FH. 1987. Physiological effects on coho salmon and steelhead of exposure to suspended solids. *Transactions of the American Fisheries Society* **116**: 737–744.

Reid LM. 1998. Forest roads, chronic turbidity, and salmon. *EOS Transactions-American Geophysical Union* **79** (45): F285. Abstract from www.rsl.psw.fs.fed.us/people/lreid.html.

Richardson J, Jowett IG. 2002. Effects of sediment on fish communities in East Cape streams. *New Zealand Journal of Marine and Freshwater Research* **36**: 431–442.

Ritchie JC. 1972. Sediment, fish, and fish habitat. *Journal of Soil and Water Conservation* **27**: 124–125.

Robertson MJ, Scruton DA, Clarke KD. 1997. Seasonal effects of suspended sediment on the behaviour of juvenile Atlantic salmon. *Transactions of the American Fisheries Society* **16**: 822–828.

Rodriguez MA, Lewis WM. 1997. Structure of fish assemblages along environmental gradients in floodplain lakes of the Orinoco River. *Ecological Monographs* **67**: 109–128.

Rogers BA. 1969. Tolerance levels of four species of estuarine fishes to suspended mineral solids. MS thesis, Univ. Rhode Island, Kingston, RI; 60.

Rosenberg DM, Wiens AP. 1978. Effects of sediment addition on macrobenthic invertebrates in a northern Canadian River. *Water Research* **12**: 753–763.

Rowe DK, Dean TL. 1998. Effects of turbidity on the feeding ability of the juvenile migrant stage of six New Zealand freshwater fish species New Zealand. *Journal of Marine and Freshwater Research* **32**: 21–29.

Ryan PA. 1991. Environmental effects of sediment on New Zealand streams: a review. *New Zealand Journal of Marine and Freshwater Research* **25**: 207–221.

Salyer JC. 1935. Preliminary report on the beaver trout investigation. *American Game* **24**: 6–15.

Sand-Jenson K. 1998. Influence of submerged macrophytes on sediment composition and near-bed flow in lowland streams. *Freshwater Biology* **39**: 663–679.

Sandström A, Karås P. 2002. Effects of eutrophication on young-of-the-year freshwater fish communities in coastal areas of the Baltic. *Environmental Biology of Fishes* **63**: 89–101.

Saunders JW, Smith MW. 1965. Changes in a stream population of trout associated with increased silt. *Journal of the Fisheries Research Board of Canada* **22**: 395–404.

Schlosser IJ, Kallenmeyn LW. 2000. Spatial variation in fish assemblages across a beaver-influenced successional landscape. *Ecology* **81**: 1371–1382.

Sear DA. 1993. Fine sediment infiltration into gravel spawning beds within a regulated river experiencing floods: ecological implications for salmonids. *Regulated Rivers-Research & Management* **8**: 373–390.

Sear DA. 1994. River restoration and geomorphology. *Aquatic Conservation*. **4**: 169–177.

Sear DA, Armitage PD, Dawson FDH. 1999. Groundwater dominated rivers. *Hydrological Processes* **11**(14): 255–276.

Sear DA, Frostick LB, Rollinson G, Lisle TE. 2008. The significance and mechanics of fine sediment infiltration and accumulation in gravel spawning beds. In *Salmonid Spawning Habitat in Rivers; Physical Controls, Biological Responses and Approaches to Remediation*, Sear DA, DeVries PD (eds). AFS: Bethesda, MD; 149–174.

Sear DA, Wilcock D, Robinson MR, Fisher KR. 2000. Channel modifications and impacts. In *The Changing Hydrology of the UK*, Acreman M (eds). Routledge: London; 55–81.

Sempeski P, Gaudin P. 1995. Habitat selection by Grayling:1. Spawning habitats. *Journal of Fish Biology* **47**(2): 256–265.

Semple R. 1991. Atlantic salmon habitat survey: Enhancement opportunities and problems in the Dunbar stream, Naswaak river, New Brunswick. Canadian Manuscript Report Fisheries Aquatic. *Science* **2076**: 1–35.

Servizi JA, Martens DW. 1991. Effect of temperature, season, and fish size on acute lethality of suspended sediments to coho salmon, *Oncorhynchus kisutch*. *Canadian Journal of Fisheries and Aquatic Science* **48**: 493–497.

Servizi JA, Martens DW. 1992. Sublethal responses of coho salmon (*Oncorhynchus kisutch*) to suspended sediments. *Canadian Journal of Fisheries and Aquatic Sciences* **49**: 1389–1395.

Servizi JA, Martens DW. 1987. Some effects of suspended Fraser River sediments on sockeye salmon (*Oncorhynchus nerka*). *Canadian Special Publication Fisheries Aquatic Science* **96**: 254–264.

Shaw EA, Richardson JS. 2001. Direct and indirect effects of sediment pulse duration on stream invertebrate assemblages and rainbow trout (*Oncorhynchus mykiss*) growth and survival. *Canadian Journal of Fisheries and Aquatic Science* **58**: 2213–2221.

Shirvell CS. 1990. Role of instream rootwads as juvenile coho salmon (*Oncorhynchus kisutch*) and steelhead trout (*O. mykiss*) cover habitat under varying streamflows. *Canadian Journal of Fisheries and Aquatic Sciences* **47**: 852–861.

Shirvell C, Dungey R. 1983. Microhabitats chosen by brown trout for feeding and spawning in rivers. *Transactions of the American Fisheries Society* **112**: 355–367.

Sigler JW, Bjornn TC, Everest FH. 1984. Effects of chronic turbidity on density and growth of steelhead and coho salmon. *Transactions of the American Fisheries Society* **113**: 142–150.

Smyly WJP. 1957. The life history of the bullhead or Miller's thumb (*Cottus gobio* L.). *Proceedings of the Zoological Society of London* **128**: 431–453.

Smyly WJP. 1955. On the biology of the stone-loach *Nemacheilus barbatula* (L.). *Journal of Animal Ecology* **24**(1): 167–186.

Soulsby C, Youngson AF, Moir HJ, Malcolm IA. 2001. Fine sediment influence on salmonid spawning habitat in a lowland agricultural stream: a preliminary assessment. *The Science of the Total Environment* **265**: 295–307.

Strmac M, Oberemm A, Braunbeck T. 2002. Effects of sediment eluates and extracts from differently polluted small rivers on zebrafish embryos and larvae. *Journal of Fish Biology* **61**: 24–38.

Stuart TA. 1953a. Spawning migration, reproduction and young stages of loch trout (*Salmo trutta*). *Freshwater Salmonid Fisheries Research* **5**: 1–39.

Stuart TA. 1953b. Water currents through permeable gravels and their significance to spawning salmonids etc. *Nature* **172** (4374): 407–408.

Suren AM, Jowett IG. 2001. Effects of deposited sediment on invertebrate drift: an experimental study. *New Zealand Journal of Marine and Freshwater Research* **35**: 725–737.

Sutherland AB, Meyer JL. 2007. Effects of increased suspended sediment on growth rate and gill condition of two southern Appalachian minnows. *Environmental Biology of Fish* **80**: 389–403.

Sutherland AB, Meyer JL, Gardiner EP. 2002. Effects of land cover on sediment regime and fish assemblage structure in four southern Appalachian streams. *Freshwater Biology* **47**: 1791–1805.

Suttle KB, Power ME, Levine JM, McNeely C. 2004. How fine sediment in riverbeds impairs growth and survival of juvenile salmonids. *Ecological Applications* **14**: 969–974.

Sweka JA, Hartman KJ. 2003. Reduction of reaction distance and foraging success of smallmouth bass, *Micropterus dolomieu*, exposed to elevated turbidity levels. *Environmental Biology of Fishes* **67**: 341–347.

Swietlik W, Berry W, Gardner T, Hill B, Jha M, Kaufmann P, Melzian B, Norton D, Paul J, Rubinstein N, Shippen R, Spehar R. 2003. Developing water quality criteria for suspended and bedded sediments (SABS). Potential approaches. US EPA Office of Water, Office of Science and Technology, Health and Ecological Criteria Division, USA; 134.

Theurer FD, Harrod TR, Theurer M. 1998. *Sedimentation and Salmonids in England and Wales*. Environment Agency: Bristol; 24.

Tomlinson ML, Perrow MR. 2003. *Ecology of the Bullhead Cottus gobio*, *Conserving Natura Rivers Ecology Series* No. 4. English Nature: Peterborough; 16.

Trimble SW. 1981. Changes in sediment storage in the Coon Creek Basin, Driftless area, Wisconsin. *Science* **214**: 181–183.

United States Geological Survey. 2010. http://fisc.er.usgs.gov/Carp_ID/html/scardinius_erythrophthalmus.html(accessed 06 January 2010).

Van Nieuwenhuyse EE, LaPerriere JD. 1986. Effects of placer gold mining on primary production of subarctic streams of Alaska. *Water Resource Bulletin* **22**: 91–99.

Van Zyll de Jong MC, Cowx IG, Scruton DA. 1997. An evaluation of instream habitat restoration techniques on salmonid populations in a Newfoundland stream. *Regulated Rivers-Research & Management* **13**: 603–614.

Vinni M, Horppila J, Olin M, Ruuhijärvi J, Nyberg K. 2000. The food, growth and abundance of five co-existing cyprinids in lake basins of different morphometry and water quality. *Aquatic Ecology* **34**: 421–431.

Vogel JL, Beauchamp DA. 1999. Effects of light, prey size, and turbidity on reaction distances of lake trout (*Salvelinus namaycush*) to salmonid prey. *Canadian Journal of fisheries and Aquatic Sciences* **56**: 1293–1297.

Vriese FT, Semmekrot S, Raat AJP. 1994. Assessment of spawning and nursery area in the river Meuse. *Water Science Technology* **29** (3): 297–299.

Walling DE. 1995. Suspended sediment yields in a changing environment. In *Changing River Channels*, Gurnell AM, Petts GE (eds). John Wiley & Sons, Inc.: Chichester; 149–176.

Walling DE, Amos CM. 1999. Source, storage and mobilisation of fine sediment in a chalk stream system. *Hydrological Processes* **13**: 323–340.

Walling DE, Collins AL, McMellin G. 2003. A reconnaissance survey of the source of interstitial fine sediment recovered from salmonid spawning gravels in England and Wales. *Hydrobiologia* **497**: 91–108.

Walling DE, Fang D. 2003. Recent trends in the suspended sediment loads of the world's rivers. *Global and Planetary Change* **39** (1-2111-126).

Walling DE, Webb BW. 1987. Suspended load in gravel-bed rivers: UK experience. In *Sediment Transport in Gravel-bed Rivers*, Thorne CR, Bathurst JC, Hey RD (eds). Wiley: Chichester; 691–723.

Walling DE, Webb BW, Shanahan J. 2008. Investigations into the use of critical sediment yields for assessing and managing fine sediment inputs into freshwater ecosystems. Natural England Research Report NERR007. Natural England, Sheffield; 63.

Walser CA, Bart HL Jr. 1999. Influence of agriculture on in-stream habitat and fish community structure in Piedmont watersheds of the Chattahoochee River system. *Ecology of Freshwater Fish* **8**: 237–246.

Walton OE, Reice SR, Andrews RW. 1977. The effects of density, sediment size and velocity on drift of *Acroneuria abnormis* (Plecoptera). *Oikos* **28**: 291–298.

Warren N, Allan IJ, Cater JE, House WA, Parker A. 2003. Pesticides and other micro-organic contaminants in freshwater sedimentary environments–a review. *Applied Geochemistry* **18**: 159–194.

Waters TF. 1995. *Sediment in Streams: Sources, Biological Effects, and control American Fisheries Society Monograph 7*. American Fisheries Society: Bethesda, MD; 268.

Witzel L, MacCrimmon H. 1983. Redd-site selection by brook trout and brown trout in southwestern Ontario streams. *Transactions of the American Fisheries Society* **112**: 760–771.

Wood PJ, Armitage PD. 1997. Biological effects of fine sediment in the lotic environment. *Environmental Management* **21**: 203–217.

Wood PJ, Armitage PD. 1999. Sediment deposition in a small lowland stream–management implications. *Regulated Rivers-Research & Management* **15**: 199–210.

Wood PJ, Toone J, Greenwood MT, Armitage PD. 2005. The response of four lotic macroinvertebrate taxa to burial by sediments. *Archives Hydrobiology* **163**: 145–162.

Wootton RJ. 1976. *The Biology of the Sticklebacks*. Academic Press: New York.

Yamada H, Nakamura F. 2002. Effect of fine sediment deposition and channel works on periphyton biomass in the Makomanai River, northern Japan. *River Research and Applications* **18**: 481–493.

Yarnell SM, Mount JF, Larsen EW. 2006. The influence of relative sediment supply on riverine habitat heterogeneity. *Geomorphology* **80**: 310–324.

Zamor RM, Grossman GD. 2007. Turbidity affects foraging success of drift-feeding rosyside dace. *Transactions of the American Fisheries Society* **136**: 167–176.

Zimmerman JKH, Vondracek B, Westra J. 2003. Agricultural land use effects on sediment loading and fish assemblages in two Minnesota (USA) watersheds. *Environmental Management* **32**: 93–105.

Assessment of erosion, sedimentation, and water quality impacts of the Mountain Valley Pipeline and Equitrans Expansion Project's proposed crossing of the Jefferson National Forest as it pertains to the U.S. Forest Service's Draft Supplemental Environmental Impact Statement dated December 2022

Prepared by Jonathan A. Czuba, Ph.D., Licensed Professional Engineer - February 9, 2023

REFERENCES
7

February 21, 2023

Biological Effects of Fine Sediment in the Lotic Environment

PAUL J. WOOD*
School of Geography
The University of Birmingham
Edgbaston, Birmingham B15 2TT, UK

PATRICK D. ARMITAGE
Institute of Freshwater Ecology
River Laboratory
East Stoke, Wareham
Dorset, BH20 6BB, UK

ABSTRACT / Although sedimentation is a naturally occurring phenomenon in rivers, land-use changes have resulted in an increase in anthropogenically induced fine sediment deposition. Poorly managed agricultural practices, mineral extraction, and construction can result in an increase in suspended solids and sedimentation in rivers and streams, leading to a decline in habitat quality. The nature and origins of fine sediments in the lotic environment are reviewed in relation to channel and nonchannel sources and the impact of human activity. Fine sediment transport and deposition are outlined in relation to variations in streamflow and particle size characteristics. A holistic approach to the problems associated with fine sediment is outlined to aid in the identification of sediment sources, transport, and deposition processes in the river catchment. The multiple causes and deleterious impacts associated with fine sediments on riverine habitats, primary producers, macroinvertebrates, and fisheries are identified and reviewed to provide river managers with a guide to source material. The restoration of rivers with fine sediment problems are discussed in relation to a holistic management framework to aid in the planning and undertaking of mitigation measures within both the river channel and surrounding catchment area.

The deleterious effects of high suspended solid loads and sedimentation on riverine habitats have been well documented (Berkman and Rabeni 1987, Carling and McCahon 1987). The terms fine sediment and sedimentation used herein describe sediments less than 2 mm in size, thus encompassing sand ($<$2000 to $>$62 µm), silt ($<$62 to $>$4 µm) and clay ($<$4 µm) (Chang 1988, Church and others 1987). Fine sediments in the water column increase turbidity, limit light penetration, and potentially reduce primary productivity with resultant impacts on the rest of the food chain (Davies-Colley and others 1992, Van Nieuwenhuyse and LaPerriere 1986). Sedimentation modifies the substrate by altering its surface conditions (Graham 1990) and the volume of fine sediment within the hyporheos (Richards and Bacon 1994). In extreme cases, fine sediments smother the entire riverbed, changing channel morphology (Doeg and Koehn 1994, Nuttall 1972, Wright and Berrie 1987), killing aquatic flora (Brookes 1986, Edwards 1969), clogging the interstices between substrate clasts, increasing invertebrate drift, and reducing the available habitat for benthic organisms (Petts 1984a, Richards and Bacon 1994, Schälchi 1992).

KEY WORDS: Sedimentation; Fine sediment; Holistic approach; Ecological impact; River restoration

*Author to whom correspondence should be addressed.

This review aims to provide information on the causes and extent of sedimentation in the lotic environment and in particular the impact on riverine ecology. We aim to examine the whole range of sizes and types of sediment (inorganic and organic) that have been referred to as fine sediments or implicated in sedimentation studies. We recognize that the effects of different types of fine sediment and sedimentation will vary, and where possible distinctions will be made between them. By considering the river holistically (Figure 1) the generation and passage of fine sediment to the stream and its transport, deposition, and storage in the channel can be elucidated. This is important in terms of both natural and anthropogenically induced processes because the extent of sedimentation varies spatially and temporally. Individual rivers respond in different ways to both natural and human impacts according to their catchment characteristics, although the latter tends to accelerate natural processes. There is a need to recognize and identify the physiochemical effects of sedimentation and their impact on riverine biota before mitigation measures are implemented (Figure 1).

Nature and Origins of Fine Sediment

The characteristics of fine sediment in rivers at a global scale are highly variable, reflecting variations in climate, catchment geology, basin scale, and sediment

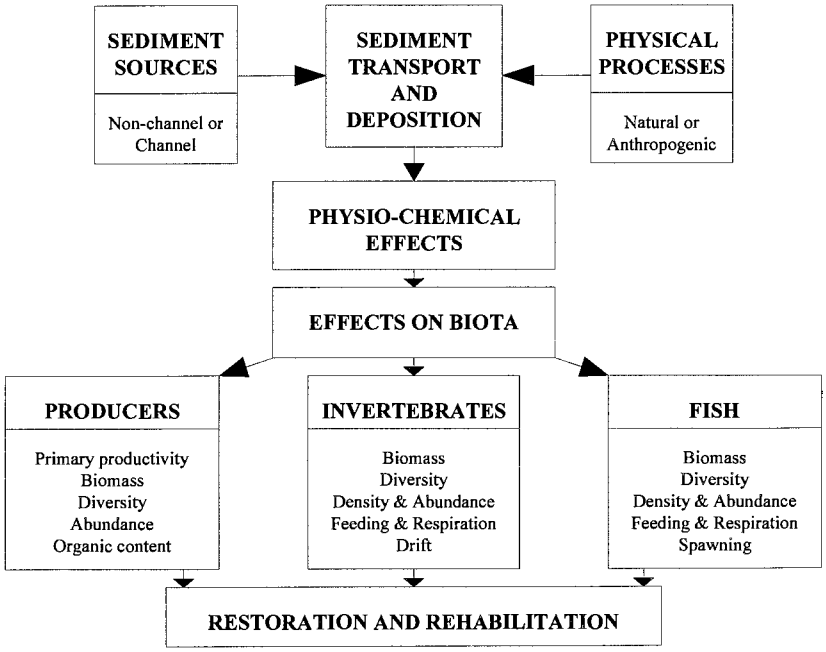

Figure 1. A holistic overview of fine sediment in the lotic ecosystem.

erosion and delivery process (Walling and Moorehead 1989). Frequently the terms ''fines'' and ''sedimentation'' are used in their broadest sense by many freshwater scientists. For examples, Pinder and others (1987) refer to ''soft sediments'' to characterize the entire range of fine particles in riverine deposits. Wright and others (1983) adopt an even broader definition, which encompasses sand and silt (as determined by physical size) as well as fine and coarse organic material such as leaves.

The term sedimentation has similarly been widely applied to the deposition of a whole range of fine sediments. In laboratory flumes the term has been used to describe the deposition of inorganic sediments, ranging from coarse sand to clay (Beschta and Jackson 1979, Carling 1984, Einstein 1968, Jopling and Forbes 1979, Schälchli 1992, 1995). Studies in natural streams and rivers have also examined this wide range of sediment sizes with a varying level of attention given to organic material (Graham 1990, Petts 1988, Sear 1993). The organic matter component of fine sediments has often been ignored, despite the fact it is increasingly being considered a major descriptor of benthic sediments (Gagnier and Bailey 1994) and communities (Boulton and Lake 1992, Culp and Davies 1985). The organic fraction of silt deposits is biodegradable and may be selectively resuspended as flow velocity increases (Carling and McCahon 1987). As a result, the impact of this material may vary seasonally depending on the river in question.

It is widely recognized that sediments less than 63 μm in size are the most important fraction for contaminant adsorption and transport, due to their relatively large surface area and geochemical composition (Stone and Droppo 1994). Silt and clay are particularly important in heavy-metal transport and their storage within fluvial sediments (Thoms 1987). However, the association of toxic materials with fine sediments is beyond the scope of this current review.

At its most basic level, sedimentation is controlled by natural variations in river flow. It is possible to identify two main sources of sediment available to the river: (1) channel sources, which are principally derived from the bed and banks of the stream and its tributaries; and (2) nonchannel sources within the catchment, such as bare soils that are susceptible to erosion (Grimshaw and Lewin 1980). The supply of sediment from channel sources is strongly related to stream discharge and the stability of the channelbed and banks. In marked contrast, the supply of sediment from nonchannel sources may be highly variable depending on its mode of production and transport into the stream. The principle sources of fine particles available to a stream from channel sources are: (1) river banks subject to erosion due to high shear, long exposure to water, and location (e.g., on a meander bend); (2) mid-channel and point bars subject to erosion; (3) fine bed material stored within the interstices or from surficial deposits; (4) natural backwaters where sediment may accumulate during base flow conditions; (5) fine particles trapped within aquatic macrophyte stands or associated with the seasonal growth and decline of aquatic vegetation; and

(6) other biotic particles including phytoplankton and zooplankton. In some instances there may be some on-site generation of fine particles due to the decay of aquatic macrophytes, bioflims and invertebrate material. Benthic invertebrate fecal material has been shown to constitute a significant source of fine particulate matter (Ladle and Griffiths 1980, Ward and others 1994).

However, much of this material would initially be derived from nonchannel sources and may only be stored within the channel temporarily. The main nonchannel sources of fine sediment supplied to a stream are: (1) exposed soils subject to erosion—this material is transported to the channel via gullies, rills, and other features associated with runoff erosion; (2) mass failures within the catchment, such as landslides and soil creep; (3) urban areas, which markedly increase sediment delivery by increasing both the volume and timing of runoff; (4) anthropogenic activities; (5) litter fall, principally leaf material from vegetation adjacent to the channel; and (6) atmospheric deposition, due to aeolian processes and precipitation.

The processes involved are controlled by a number of factors such as land use, soil type, and ground/vegetation cover (Table 1). The influence of these factors may vary depending on the time of year and the nature of individual runoff events. The dynamics of the catchment sediment budget may thus provide important insights into the downstream impact of changing rates of erosion, conveyance, or storage within the river channel (Walling and Quine 1993).

Humans can increase the mobilization of large volumes of sediment into streams and rivers by activities such as agriculture (Richards and others 1993, Walling 1990), mining (Davies-Colley and others 1992), forestry operations (Scrivener and Brownlee 1989), construction of roads (Extence 1978) and reservoirs (Boon 1988, Marchant 1989), and flow regulation (Hellawell 1988, Petts 1988) (see Table 2 for more detail). However, the nature of the river and the environment around it strongly influence the volume of sediment transported to the river, the degree of sedimentation, and its impact on both fauna and flora. Anthropogenic activities have important hydrological, geomorphological, and ecological implications, altering the physical environment of the stream by increasing runoff and affecting both the volume and timing of sediment delivery to the stream.

The most widespread impacts of sedimentation are associated with the fines eroded from agricultural land (Walling 1990). Typically, the deleterious impact of fines associated with forestry activities are less than those in agricultural areas. However, when poorly managed on steep slopes, forestry operations potentially mobilize large volumes of sediment from freshly exposed soils, landslides, surface scour from roads, and sediment stored in the bed and banks of the river (Murphy and Milner 1996). This is primarily the result of a decrease in slope stability as a result of the removal of trees and the decomposition of roots, which help protect the soil and bind it together (Scrivener and Brownlee 1989).

The effect of river regulation via impoundment on benthic substrate is complex and largely depends on the purpose of the dam. A dam used for hydroelectric

Table 1. Factors controlling volume of fine sediment reaching channel from nonchannel sources[a]

Factor	Level of impact	Comment
Topography	Variable	High on steep slopes, low on gentle slopes
Soil type	Variable	Dependent on erodability of soil and ground cover
Ground cover	Variable	Impact decreases with increasing ground cover
Sediment delivery	High	No buffer zone or if disturbance adjacent to watercourse
	Moderate	Some form of buffer zone or impact not adjacent to watercourse
	Low	Extensive control measures/buffer zones or impact some distance away from watercourse
Landuse		
Agriculture	High	>50% arable or poorly managed land
	Moderate	<25% arable or pasture
	Low	Fallow, orchards or effective soil conservation
Forestry	High	Clear cut, bare soil and/or no buffer zone adjacent to watercourse
	Moderate	Clear cut but with some soil conservation and buffer zones
	Low	Well-managed harvesting and effective soil conservation and/or buffer zones
Urban	Variable	Increases both the volume and speed of runoff to the channel
Disturbance (i.e., surface mines and construction activities)	Variable	Highly variable depending on the extent, timing and location of disturbance in relation to watercourse and implementation of preventative measures

[a]Adapted from Coleman and Scatena (1986).

Table 2. Conditions of flow, physical impact, and cause of increase in suspended sediment and sedimentation in rivers and streams

Flow	Location	Impact	Cause	Author
Flume	Washington (USA)	Development of fine sediment clog	Induced	Beschta and Jackson (1979)
Flume	Cumbria (UK)	Infiltration of fine sediment to base of substrate	Induced	Carling (1984)
Flume	California (USA)	Infiltration of fine sediment to base of substrate	Induced	Einstein (1968)
Flume	Washington (USA)	Development of fine sediment clog	Induced	Jackson and Beschta (1984)
Flume	Idaho (USA)	Clogging of the surface of substrate	Induced	McClelland and Brusven (1980)
Flume	Zurich (Switzerland)	Development of fine sediment clog	Induced	Schälchli (1992)
Flume	Zurich (Switzerland)	Development of fine sediment clog	Induced	Schälchli (1995)
Compensation	UK rivers	Thin surficial deposits of silt	Impoundment	Armitage (1987)
Compensation	South Island (N. Zealand)	Siltation of stone surface biofilm/periphyton community	Impoundment	Graham (1990)
Compensation	2 rivers (UK)	Infiltration of fines (<2 mm) into gravel bed	Impoundment	Petts (1988)
Compensation	Northumberland (UK)	Infiltration of fines (<2 mm) into gravel bed	Impoundment	Sear (1993)
0.2–0.6 m/s	3 streams Missouri (USA)	Increase in the proportion of fines within the substrate	Agriculture	Berkman and Rabeni (1987)
0.05–0.38 m/s	British Columbia (Canada)	Experimental sediment deposition and transport (0.5–2 mm)	Induced	Culp and others (1985)
0.15–0.85 m/s	Virginia (USA)	Storage of fine sediment in channel and at margins	Natural	Miller and Shoemaker (1986)
0.86–1.18 m/s	2 streams (USA)	Siltation of experimental cages	Natural	Peckarsky (1984)
0.2–0.4 m/s	Hess (Germany)	Artificial smothering of bed by sand	Induced	Wagner (1984)
0.2–0.4 m/s	Hess (Germany)	Artificial smothering of bed by sand	Induced	Wagner (1989)
Variable	South African rivers	Silt and sand suspension and deposition	Natural/induced	Chutter (1969)
Variable	Colorado (USA)	Fine sediment infiltration into substrate	Road construction	Cline and others (1982)
Variable	California (USA)	Inorganic sediment suspension and deposition	Natural, human impact	Cordone and Kelly (1961)
Variable	Michigan (USA)	Assessment of silted and clean substrates	Induced	Cummins and Lauff (1969)
Variable	South Island (N. Zealand)	Fine sediment suspension and deposition	Placer gold mining	Davies-Colley and others (1992)
Variable	Dorset (UK)	Siltation within macrophyte stands	Natural	Dawson (1978)
Variable	South African streams	Siltation on and within macrophytes	Natural, human impact	Edwards (1969)
Variable	USA rivers	Erosion silt suspension and deposition	Natural, human impact	Ellis (1936)
Variable	Essex (UK)	Smothering of substrate by sand and silt	Road construction	Extence (1978)
Variable	London (UK)	Development of fine sediment clog	Natural	Frostick and others (1984)

Table 2. (Continued)

Flow	Location	Impact	Cause	Author
Variable	Wyoming (USA)	Sediment in suspension and deposition at margins of river	Reservoir release	Gray and Ward (1982)
Variable	N. Carolina (USA)	Filling of substrate interstices and surficial silts	Logging and enrichment	Lemly (1982)
Variable	California (USA)	Infiltration of fines in to gravel bed	Natural	Lisle (1989)
Variable	California (USA)	Filling of pools with fine sediment	Regulation and logging	Lisle and Hilton (1992)
Variable	Cornwall (UK)	Sediment suspension and deposition of sand	China clay extraction	Nuttall (1972)
Variable	Cornwall (UK)	Sediment suspension and deposition of sand and silt	China clay extraction	Nuttall and Bielby (1973)
Variable	South Island (N. Zealand)	Fine sediment suspension and deposition	Placer gold mining	Quinn and others (1992)
Variable	New Zealand streams	Fine sediment suspension and deposition	Natural, human impact	Ryan (1991)
Variable	Birmingham (UK)	Infiltration of fines into gravel bed	Urbanisation	Thoms (1987)
Variable	Shropshire (UK)	Deposition and resuspension in a natural backwater / dead zone	Natural	Tipping and others (1993)
Variable	Wales (UK)	Infiltration of fines into gravel bed	Coal mining	Turnpenny and Williams (1980)
Variable	Alaska (USA)	Fine sediment suspension and deposition	Placer gold mining	Van Nieuwenhuyse and LaPerriere (1986)
Variable	Dorset (UK)	Deposits at margins of river and within macrophytes	Natural	Welton (1980)
Base Flow	Ontario (Canada)	Deposition of up to 0.61 g dry weight / cm / day	Road construction	Barton (1977)
Base Flow	Alaska (USA)	Fine sediment suspension and surficial deposition	Placer gold mining	Bjerklie and La Perriere (1985)
Base Flow	4 rivers (UK)	Sediment suspension and varying degrees of siltation	Channelisation	Brookes (1986)
Base Flow	Durham (UK)	Infiltration of fines into gravel bed	Natural	Carling and McCahon (1987)
Base Flow	3 upland streams (UK)	Surficial fine particle deposition	Natural	Carling and Reader (1982)
Base Flow	Victoria (Australia)	Sand and silt deposition up to 2 km downstream of weir	Desilting operations	Doeg and Koehn (1994)
Base Flow	Ontario (Canada)	Surficial fine particle deposition	Natural	Droppo and Stone (1994)
Base Flow	Devon (UK)	Surficial fine particle deposition	Natural	Lambert and Walling (1988)
Base Flow	California (USA)	Storage of fines (<210 µm) in gravel bed	Natural, Logged	Mahoney and Erman (1984)
Base Flow	Idaho (USA)	Infiltration of sand (>150 µm) into gravel bed	Natural, Human impact	Richards and Bacon (1994)
Base Flow	Alaska (USA)	Infiltration of sand into gravel bed	Induced	Shapley and Bishop (1965)
Base Flow	Kent (UK)	Extensive siltation of river bed and margins	Drought and abstraction	Wood and Petts (1994)
Base Flow	Berkshire (UK)	Extensive siltation of river bed and margins	Drought and abstraction	Wright and Berrie (1987)

power generation will have a highly variable discharge, whereas one used for the storage of water for a public water supply will vary moderately. The general effect of a dam is to reduce pre-regulation peak discharge and to increase low flows (Petts 1984b). Almost all sediment transported by the river upstream of the impoundment will be deposited within the reservoir, and this reduction in sediment load downstream can lead to significant main channel degradation and armoring of substrates where the river retains its erosive power (Donnely 1993). However, downstream of non-regulated tributaries, sedimentation has been widely recognized as a consequence of the elimination or reduction in the magnitude and frequency of mainstream floods that would naturally act as flushing flows for these sediments (Petts 1984b, 1988). In their absence, sedimentation may occur on both the surface and within the substrate, leading to the development of a finer gravel matrix infill than in comparable unregulated tributaries and rivers (Armitage 1987, Petts 1988, Sear 1993).

Suspension and Deposition

Artificial or experimental manipulations of fine sediment have been more widely reported than natural increases in deposition as a result of low flows, primarily because in most cases they are easier to monitor. It is generally difficult to predict natural events that will result in fine sediment deposition due to the relatively infrequent nature of droughts and low flows.

The initiation of particle motion from the bed and banks of a river occurs when a threshold flow intensity is exceeded. The critical flow intensity controlling the initiation of particle movement is measured by shear stress, velocity, or stream power, and this critical flow has the minimum intensity capable of initiating the movement of a sediment grain (Richards 1982, Schälchli 1992). Well-sorted sand grains (0.2–0.5 mm) have the lowest threshold velocity and critical bed shear. Greater velocities and shear stress values are required to transport larger particles and also smaller particles that are protected by submergence within the laminar sublayer. However, many fine sediments are cohesive and are normally eroded as floccules rather than individual particles, further discouraging their detachment (Richards 1982). Two types of fine sediment transport can be identified: (1) along the surface of the substrate as bedload by rolling, sliding, or saltating; and (2) as turbulence increases, the weight of the particle may be upheld as suspended load by a succession of eddy currents (Petts and Foster 1985).

The deposition of fine sediments occurs when tractive forces are less than the settling velocity (gravitational forces) exerted upon the grain, as expressed by Stokes's Law (Richards 1982). However, this only holds for silts and clays. For particles larger than 0.1 mm, the relationship between grain diameter and fall velocity is nonlinear due to the influence of inertial forces. Several other factors such as particle shape, water temperature, flocculation of particles, and the turbulent nature of flow in rivers also influences particle deposition (Carling 1992, Norwell and Jumars 1984). The assumption that fine sediment deposition only occurs in areas of slow flowing water is a common misunderstanding. During spates, an increase in the volume of suspended sediment and fine bedload occurs. Some of this material is carried into interstitial spaces reducing substrate porosity and hydrostatic permeability, leading to a decline in the volume of water within the substratum and reduced concentrations of dissolved oxygen (Crisp 1989, Moring 1982, Turnpenny and Williams 1980).

Experimental studies, principally in flumes, have identified many of the physical effects of sedimentation, although the outcome largely depends on the nature of the fines and the substrate. Froude numbers have been used to help characterize the flow conditions that influence the intrusion of fines into the bed (Beschta and Jackson 1979, Carling 1984). This dimensionless variable represents the ratio of inertial to gravitational forces in fluid flow (Chow 1959). At low Froude values, 0.5-mm sand grains have been observed to develop a seal or clog in the uppermost layer of previously clean gravels, thus preventing the infiltration of fines deeper in to the substrate. At higher values, associated with greater velocity and turbulence, the seal has been observed to develop at greater depth within the substrate (Beschta and Jackson 1979, Schälchli 1992). This process can be divided into three phases. In phase 1, coarser particles effectively bridge and close interstitial pores and crevices. During phase 2, the pores are filled by medium-sized particles, and in the final phase, the accumulation of fine particles leads to the development of an almost impermeable layer between the surface and subsurface layers of the substrate (Schälchli 1995). However, in flume studies of finer ($<$0.5-mm) sediments, the development of clogs has not been recorded. These sediments, through a combination of turbulent pulses and gravitational settling, have been observed to fill interstitial spaces from the base of the substrate upwards (Carling 1984, Einstein 1968).

Sedimentation occurs under a number of flow conditions and in different areas of the channel, resulting in distinct types of sedimentation and characteristic deposits (Table 2). A reduction in flow velocity, particularly during low flow conditions during the summer months, can lead to large volumes of fines and decaying organic

matter being deposited onto the riverbed (Giles and others 1991). This problem is particularly acute in groundwater-fed streams, which rely on precipitation for aquifer recharge (Wright and Berrie 1987).

During baseflow conditions, the development of ephemeral surficial fine particle deposits up to 20 mm thick have been reported (Carling and Reader 1982, Droppo and Stone 1994, Lambert and Walling 1988). The influence of these predominantly inorganic deposits have been difficult to gauge due to their temporary nature, although they do not appear to consolidate into a compact layer and are easily disturbed and resuspended when flow increases. It has been noted, however, that almost all of these sediments have a grain size <1 mm and are similar to the substrate matrix material. Some of these sediments may therefore infiltrate into the bed and constitute an important source of particles for replacing matrix material winnowed from the interstices of the substrate during high flows.

Even under normal flow conditions, natural sedimentation occurs in backwaters or dead zones, such as clearly defined pools, regions of retarded flow close to the bank, the water within macrophyte beds, and sheltered areas behind individual cobbles and boulders. Anthropogenic structures, such as the lee behind a groin, may also be considered to be dead zones. Large volumes of sediment accumulate in these areas due to reduced resuspension and enhanced deposition, except at high discharge when turbulent flow mobilizes these sediments (Tipping and others 1993). An experimental reduction in flow from 0.5 m/s to <0.01 m/s in an artificial dead zone resulted in complete coverage of a gravel substrate by fine organic material within two days (Armitage unpublished data).

Effects on Biota

The causes and deleterious effects of fine sediment suspension and deposition on the ecology of running waters have been widely reported (Table 3), with the most marked impact on primary productivity, faunal diversity, and abundance. The influence of fine sediment on fisheries has historically been particularly well documented (Cordone and Kelly 1961, Shapley and Bishop 1965) as have the effects on benthic invertebrates (Chutter 1969, Cordone and Kelly 1961, Cummins and Lauff 1969), although there have been relatively few studies on the effects of sedimentation on aquatic macrophytes (Edwards 1969).

Primary Producers

The impact of sedimentation on producers in streams and rivers has far reaching consequences since periphyton and aquatic macrophytes form the base of the food chain and any deleterious impacts will probably also be manifested in the invertebrate and fish communities. Fine sediment suspension and deposition affects producers in four main ways: (1) by reducing the penetration of light and, as a result, reducing photosynthesis and primary productivity within the stream (Van Nieuwenhuyse and LaPerriere 1986); (2) by reducing the organic content of periphyton cells (Cline and others 1982, Graham 1990); (3) by damaging macrophyte leaves and stems due to abrasion (Lewis 1973a,b); and (4) by preventing attachment to the substrate of algal cells, and by smothering and eliminating periphyton and aquatic macrophytes in extreme instances (Brookes 1986).

Aquatic macrophyte growth has important implications for the hydraulic conditions within a stream. Seasonal growth of both marginal and instream macrophytes influences flow velocity and secondary flow patterns, creating areas of slow and fast flowing water, increasing channel roughness (Manning's n) and water depth (Hearne and Armitage 1993, Watson 1987), and increasing habitat diversity (Armitage 1995). Macrophyte stands can therefore enhance the deposition and accumulation of fine sediments (Carpenter and Lodge 1986, Dawson 1978, Welton 1980) and effectively act as sieves, trapping sediment particles that settle out and are deposited beneath them.

In extreme instances, high suspended solid concentrations or sediment deposition may exclude periphyton and rooted macrophytes from reaches where they historically occurred or would naturally be expected (Nuttall and Bielby 1973, Van Nieuwenhuyse and LaPerriere 1986). Lewis (1973a) found that suspended coal particles seriously damaged the aquatic moss, *Eurhynchium riparioides*. Deleterious abrasion of the plants' leaves was evident within three weeks at a sediment concentration of 100 mg/liter and the development of new side shoots only occurred at concentrations below 500 mg/liter. As the volume of suspended coal particles increased to 5000 mg/liter germination of spores was reduced by 42% (Lewis 1973b).

Brookes (1986, 1988) examined the effects of channelization, involving the straightening, widening, or deepening of the channel, on the macrophytes in four rivers in southern England. Twenty-four hours after operations ceased in Wallop Brook, Hampshire (UK), the deposition of sediment reached a maximum of 130 cm in pools and 5 cm in riffles. Stands of *Ranunculus penicillatus* var. *calcareus* (Butcher), were smothered and eliminated in pools since the plant is unable to vary its rooting level. In contrast *Nasturtium officinale* only declined by 60%, reflecting its ability to adjust its

Table 3. Ecological impact and cause of an increase in suspended sediment and sedimentation in rivers and streams

Impact	S/D[a]	Cause	Author
Primary producers			
Elimination of macrophytes—no effect	D	Channelisation	Brookes (1986)
Reduced species diversity and organic content	S & D	Road construction	Cline and others (1982)
Reduced productivity, biomass, and organic content	S & D	Placer gold mining	Davies-Colley and others (1992)
Reduced organic content	D	Impoundment	Graham (1990)
Reduced primary productivity	S & D	Placer gold mining	Van Nieuwenhuyse and LaPerriere (1986)
Macroinvertebrates			
Impaired filter-feeding and reduced metabolic rate of mussels	S	Induced	Aldridge and others (1987)
Reduced density, abundance, and diversity	S & D	Road construction	Cline and others (1982)
Reduced density (>50%) and increased drift	S & D	Induced	Culp and others (1985)
Reduced abundance and diversity	S & D	Desilting operations	Doeg and Koehn (1994)
Reduced density and diversity	D	Water filtration facility	Erman and Ligon (1988)
Change in community structure	D	Road construction	Extence (1978)
Change in community structure	S & D	Reservoir release	Gray and Ward (1982)
Reduced diversity and biomass	D	Logging and nutrient enrichment	Lemly (1982)
Reduced diversity	D	China clay extraction	Nuttall (1972)
Reduced diversity and relative abundance of taxa	D	China clay extraction	Nuttall and Bielby (1973)
Reduced density and effect of predation	D	Natural	Peckarsky (1984)
Reduced density and diversity	S & D	Placer gold mining	Quinn and others (1992)
Change in community structure	S & D	Agriculture	Richards and others (1993)
Change in community structure and an increase in drift	S & D	Induced	Rosenberg and Wiens (1978)
Decline in abundance of emerging taxa	D	Induced	Wagner (1984)
Decline in abundance of emerging Ephemeroptera	D	Induced	Wagner (1989)
Change in community structure	D	Induced	Walentowicz and McLachlan (1980)
Reduced abundance	D	Drought—Abstraction	Wood and Petts (1994)
Reduced abundance and diversity	D	Drought—Abstraction	Wright and Berrie (1987)
Fish			
Reduced standing crop	S & D	Road construction	Barton (1977)
Reduced abundance of benthic insectivores, herbivores, and lithophilous spawners	D	Agriculture	Berkman and Rabeni (1987)
Decline in quality of salmonid spawning habitat	D	Natural	Carling and McCahon (1987)
Reduced abundance	D & S	Desilting operations	Doeg and Koehn (1994)
Reduced survival of salmonid eggs	D	Water filtration facility	Erman and Ligon (1988)
Decline in quality of salmonid spawning habitat	D	Natural	Lisle (1989)
Decline in quality of salmonid spawning habitat	D	Impoundment	Sear (1993)
Decline in quality of salmonid spawning habitat	D	Induced	Shapley and Bishop (1965)
Decline in quality of salmonid spawning habitat and reduced survival of eggs	D	Coal mining	Turnpenny and Williams (1980)

[a]S = suspended sediment, D = deposition of sediment.

rooting level. In Ober Water, Hampshire, and the River Cale, Somerset, surficial deposits were never more than 10 cm thick. In the River Wylye, Wiltshire, sediment deposition was negligible because operations coincided with a period of high water flow, resulting in most of the sediment remaining in suspension; because construction took place before the start of the growing season, there was no damage to riverine macrophytes. In all of the river's post-operation deposits were short-lived and were removed during the next spate. This demonstrates that the timing of channel management activities is vitally important in the management of fine sediments.

Benthic Macroinvertebrates

The natural variability of river flow, from the extremes of flood to low flows, results in variations in the concentration of suspended solids and their deposition. Therefore, benthic faunal communities should be able to withstand short-term increases in suspended and benthic sediments. Additions of fine particulate material due to human disturbance over a short duration may also result in a rapid recovery. However, continuous high levels of sediment input, generally associated with agriculture and surface mining activity, may completely change the natural faunal assemblage.

Fine sediment suspension and deposition affects benthic invertebrates in four ways: (1) by altering substrate composition and changing the suitability of the substrate for some taxa (Erman and Ligon 1988, Richards and Bacon 1994); (2) by increasing drift due to sediment deposition or substrate instability (Culp and others 1985, Rosenberg and Wiens 1978); (3) by affecting respiration due to the deposition of silt on respiration structures (Lemly 1982) or low oxygen concentrations associated with silt deposits (Eriksen 1966); and (4) by affecting feeding activities by impeding filter feeding due to an increase in suspended sediment concentrations (Aldridge and others 1987), reducing the food value of periphyton (Cline and others 1982, Graham 1990) and reducing the density of prey items (Peckarsky 1984).

An increase in the volume of fine sediments clearly favors some benthic invertebrates at the expense of others. Some taxa, such as Chironomidae, utilize fine sediments in the construction of cases and tubes (Dudgeon 1994), and Oligochaeta and Sphaeriidae are frequently associated with fine sediment (Armitage 1995). However, there have been relatively few studies on the effects of fine sediment deposition on individual taxa. Eriksen (1963, 1966) examined the oxygen consumption of two burrowing mayfly larvae in different sized substrates. *Ephemera simulans* displayed a preference for coarse substrates since its gills are inefficient at the low O_2 concentrations found in silt deposits. *Hexagenia limbata,* in contrast, is more common in silt deposits, into which it burrows. Both taxa display morphological and physiological adaptations for the preferred environment, emphasizing the need to understand specific faunal habitat requirements and their response to fine sediment deposition.

The most serious and obvious ecological and physical effects of sedimentation occur as a result of human activity close to river channels. Placer gold-mining on the West Coast of the South Island of New Zealand resulted in a deterioration of the optical properties of the water and the deposition of fine onto and within the riverbed (Davies-Colley and others 1992). The resulting low densities of benthic flora and macroinvertebrates were attributed to the high level of suspended solids and associated turbidity (Quinn and others 1992). Similar results were recorded in streams in Alaska subject to placer gold mining (Bjerkli and LaPerriere 1985) and several streams in Cornwall, England, subject to china clay wastes (Nuttall 1972, Nuttall and Bielby 1973).

The deposition of sand is a particular problem highlighted in many studies (see Tables 1 and 3). Leudtke and Brusven (1976) suggested that its deposition indirectly affects benthic fauna by impeding their upstream migration, even at low current velocities. Sand is an inherently unstable substrate (ASCE 1992) with most benthic taxa being found in the uppermost layers of the substrate (Strommer and Smock 1989) and some small taxa reach very high densities (Soluk 1985). It has also been recognized that the timing of sand deposition, peaking during base flow conditions, coincides with the period of dispersion and colonization by young benthic macroinvertebrates (Extence 1978).

Fish

The effects of fine particle suspension and deposition on fish are better documented than for other organisms. There are several reasons for this; fish are economically important both commercially and recreationally. Other organisms do not offer such tangible benefits, although in some countries, such as the UK, there is government legislation that requires river authorities to protect the flora and fauna in the waters under their control (Armitage and Petts 1992). It has also been suggested that the effects of anthropogenic activity will ultimately be reflected in the fish community, due to direct impacts and/or food-chain-related events (Ryan 1991).

At least five ways in which high concentrations of fine sediment adversely affect lotic fisheries have been

identified. (1) by adversely acting on the fish swimming in the water and either reducing their rate of growth, reducing their tolerance to disease or killing them; lethal concentrations primarily kill by clogging gill rakers and gill filaments (Bruton 1985); (2) by reducing the suitability of spawning habitat and hindering the development of fish eggs, larvae and juveniles; all of these stages appear to be more susceptible to suspended solids than adult fish (Chapman 1988, Moring 1982); (3) by modifying the natural migration patterns of fish (Alabaster and Lloyd 1982); (4) by reducing the abundance of food available to fish due to a reduction in light penetration and as a result photosynthesis, primary production, and a reduction of habitat available for insectivore prey items (Bruton 1985, Doeg and Koehn 1994, Gray and Ward 1982); and (5) by affecting the efficiency of hunting, particularly in the case of visual feeders (Bruton 1985, Ryan 1991).

Salmonids deposit their eggs in a shallow pit or redd excavated by the female at the head of a riffle and then bury them under 10–40 cm of bed material. The location and construction of the redd winnows out fine sediments, thus increasing gravel permeability and intergravel flow to oxygenate the eggs (Kondolf and others 1993, Milner and others 1981, Sear 1993). However, incubation requires between two and six months and during this period the redds are vulnerable to the deposition of fine sediments (Chapman 1988, Lisle 1989). Experimental studies have shown that the concentration of fines is a critical factor in the embryonic development of salmonids. A significant increase in the volume of fines can result in reduced egg survival, an increase in the number of premature alevins, and an increase in the likelihood of predation (Olsson and Petersen 1986, Reiser and White 1990). Lisle (1989) found that the infiltration of fine bedload material (0.25–2 mm) into salmonid spawning gravels accounted for 70%–78% of the total sediment deposited within experimental gravels, implanted in a river in California. In extreme cases, when the surface layers of the substrate become clogged, developing eggs and fry may be entombed (Kondolf and others 1993, Moring 1982, Petts 1988).

Sedimentation of salmonid spawning gravels as a result of coal industry effluent on the Ebbw Fawr, an industrial river in South Wales, seriously suppressed reproductive success and the natural recovery of trout (*Salmo trutta* L.) populations (Turnpenny and Williams 1980). In reaches affected by mining waste, a decline in dissolved oxygen and gravel permeability occurred. During incubation in seriously affected reaches 98%–100% of eyed salmonid eggs died compared to 9% at a nearby control site. A survival threshold for dissolved oxygen of 16 $\mu g/cm^2/h$ was calculated with a medium lethal supply rate of 50 $\mu g/cm^2/h$. Even if dissolved oxygen levels are above this critical threshold, however, the removal of metabolic wastes may not occur from within the substrate, leading to a fatal increase in carbon dioxide and ammonia levels.

The negative effects of sedimentation on fisheries are not confined to salmonids. The deposition of fines on the bed of a river in northeast Missouri (USA) resulted in identifiable impacts on both fish feeding and reproductive guilds (Berkman and Rabeni 1987). As the percentage of fine substrate increased, the difference between fish assemblages in riffles, runs, and pools decreased, largely due to a decline in the abundance of riffle taxa. Benthic insectivores and herbivores declined, as did lithophilous/gravel spawners, as the volume of $<$62.5-µm sediment increased within the bed. The results of this study suggested an overall degradation of fish habitat, due to sedimentation, as a result of erosion from adjacent agricultural land.

Discussion

The causes and negative effects of increased suspended sediment and sedimentation on the physical environment and the flora and fauna in streams and rivers around the world are highly variable (Tables 2 and 3). This reflects the different sediment sources, types of sediment, and the factors influencing its transport and deposition into and within the channel (Table 1). Human activities have greatly increased the natural sedimentation processes. In some instances this has been difficult to quantify, particularly in the case of agriculture. This is largely due to the lack of information relating to natural baseline conditions and the cumulative effect of fine sediments from headwaters on downstream areas.

The recovery of flora and fauna after an impact associated with fine sediments is controlled by the nature of the impact and the survival of organisms in refugia from which recolonization can take place (Sedell and others 1990); as a result recovery times vary greatly (Niemi and others 1990). Natural recovery processes may operate quickly following short-duration pulse disturbances: 21 days as a result of sediment released due to reservoir cleaning operations (Gray and Ward 1982), 45 days as a result of desilting a weir (Doeg and Koehn 1994). It is important to distinguish between different types and magnitudes of disturbance (Gore and Milner 1990). When an impact is extended over several months or years, as in the case of mineral extraction, impoundment, urbanization, and agricultural practice, the morphology and ecology of the

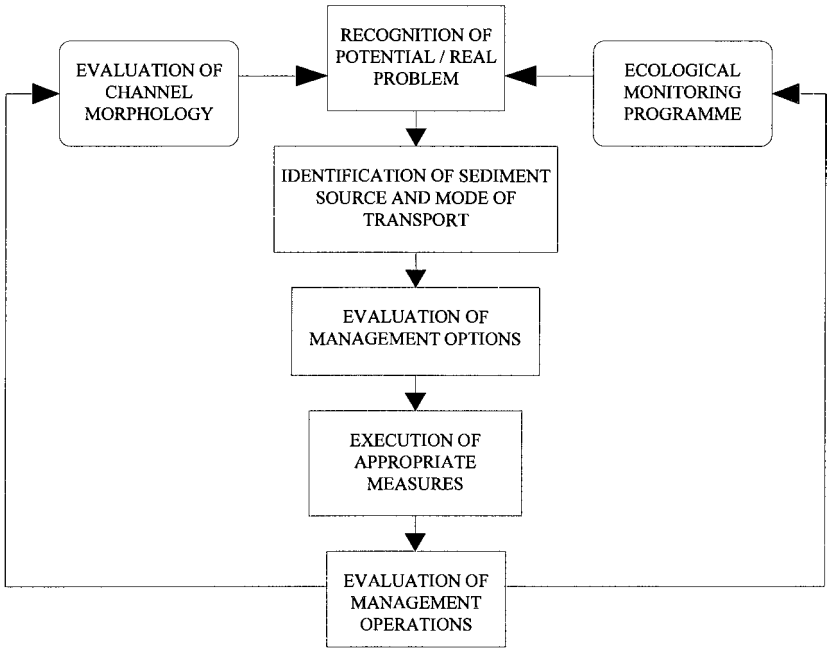

Figure 2. A holistic management framework for fine sediment in streams and rivers.

channel may be completely altered. Press disturbances such as these may require many months or years for the morphology and ecology of the channel to recover and may require human intervention to restore the system to a natural state.

Recognition of the need for river restoration has been widely accepted (Brookes 1988, Gardiner 1991), and there are an ever increasing number of terms used to describe restoration activities, including rehabilitation, revitalization, renaturation, reconversion, and restructuring (Muhar and others 1995). These terms encompass a wide range of activities at different scales, from the creation of an individual pool or riffle to the long-term management of entire river systems. However, there is a need to undertake such operations within a holistic framework. Figure 2 shows a pathway through which the monitoring of riverine ecology and channel characteristics can be utilized by river managers to aid in the identification of potential and existing problems within the catchment associated with fine sediment. This in turn can be used to evaluate different management options, undertake appropriate mitigation measures, and form the basis of an ongoing ecological and physically based monitoring program.

Many measures exist to control sediment deposition and transport in streams. In catchments with high sediment loads it may be necessary to install sediment traps, stabilize river banks, and introduce instream devices such as groins and willow posts (Brookes 1988, Jungwirth and others 1995, Sear and others 1994, Shields and others 1995). These measures reduce sediment input into the channel and/or help remove fine sediment accumulations from key locations at the margin and within the bed of the river. The main aim of such projects is usually to increase instream morphological diversity and ecological value, primarily directed at fish habitat, while at the same time maintaining flood defense properties. Results have been promising, with several projects reporting improvements in the physical environment and an increase in the number of fish taxa present as well as an increase in density and biomass (Jungwirth and others 1995, Shields and others 1995). However, in the case of some of the most degraded rivers, short- and medium-term management options may not offer any perceptible benefit, despite substantial economic expenditure. In such situations it may be necessary to accept the dereliction of a river so that resources can be directed to rivers where restoration projects have a chance to succeed (Boon 1992). This emphasizes the need for further research and long-term studies to assess the temporal and spatial variability of sedimentation.

Probably the most desirable, although often impractical, aim of restoration activities involves the prevention of fine sediment influx to the stream. The primary aim of such a project is to address the causal factors at their source within the catchment rather than cure the symptoms within the stream. Reforestation or the establishment of riparian vegetation is increasingly common (Jungwirth and others 1995) despite the time lag of up to 30 years between its establishment and observable recovery (Bryant 1995). Other options involve the

careful development of best management practices for human activities such as agriculture, construction, and forestry to minimize erosion and sediment delivery to the channel. The proposed holistic approach to the management of fine sediments within river catchments (Figures 1 and 2) should enable river managers, hydrologists, geographers, and ecologists alike to identify sediment sources, the impact of sedimentation, and an increase in suspended sediments in both the physical environment and the flora and fauna within the channel. Through the identification and consideration of these factors the deleterious impact of sedimentation may be mitigated allowing the river to recover.

Acknowledgments

This paper was produced while one of the authors (P.J.W.) was in receipt of a School of Geography Studentship from The University of Birmingham. Thanks to M. A. Bickerton, J. Couperthwaite, D. Hannah, Dr. A. M. Milner, Prof. G. E. Petts, Dr. J. P. Sadler, and three reviewers who provided helpful and constructive comments on drafts of this manuscript.

Literature Cited

Alabaster, J. S., and R. L. Lloyd. 1980. Water quality criteria for freshwater fish. Butterworths, London, 297 pp.

Aldridge, D. W., B. S. Payne, and A. C. Miller. 1987. The effects if intermittent exposure to suspended solids and turbulence on three species of freshwater mussel. *Environmental Pollution* 45:17–28.

Armitage, P. D. 1987. The classification of tailwater sites receiving residual flows from upland reservoirs in Great Britain, using macroinvertebrates. Pages 131–144 *in* J. F. Craig and J. B. Kemper (eds.), Regulated streams: Advances in ecology. Plenum Press, New York.

Armitage, P. D. 1995. Faunal community change in response to flow manipulation. Pages 59–78 *in* D. M. Harper and A. J. D. Ferguson (eds.), The ecological basis for river management. Wiley, Chichester.

Armitage, P. D., and G. E. Petts. 1992. Biotic score and prediction to assess the effects of water abstraction on river macroinvertebrates for conservation purposes. *Aquatic Conservation: Marine and Freshwater Ecosystems* 2:1–17.

ASCE (Task Committee on Sediment Transport and Aquatic Habitats, Sedimentation Committee). 1992. Sediment and aquatic habitat in river systems. *Journal of Hydraulic Engineering.* 118:669–687.

Barton, B. A. 1977. Short-term effects of highway construction on the limnology of a small stream in southern Ontario. *Freshwater Biology* 7:99–108.

Berkman, H. E., and C. F. Rabeni. 1987. Effects of siltation on stream fish communities. *Environmental Biology of Fishes* 18:285–294.

Beschta, R. L., and W. L. Jackson. 1979. The intrusion of fine sediment into a stable gravel bed. *Journal of the Fisheries Research Board of Canada* 36:204–210.

Bjerklie, D. M., and J. D. LaPerriere. 1985. Gold-mining effects on stream hydrology and water quality, Circle Quadrangle, Alaska. *Water Resources Bulletin* 21:235–243.

Boon, P. J. 1988. The impact of river regulation on invertebrate communities in the UK. *Regulated Rivers: Research and Management* 2:389–409.

Boon, P. J. 1992. Essential elements in the case for river conservation. Pages 11–13 *in* P. J. Boon, P. Calow, and G. E. Petts (eds.), River conservation and management. John Wiley, Chichester.

Boulton, A. J., and P. S. Lake. 1992. Benthic organic matter and detritivorous macroinvertebrates in two intermittent streams in south-eastern Australia. *Hydrobiologia* 241:107–118.

Brookes, A. 1986. Response of aquatic vegetation to sedimentation downstream from river channelisation works in England and Wales. *Biological Conservation* 38:352–367.

Brookes, A. 1988. Channelized rivers: Perspectives for environmental management. John Wiley, Chichester, 326 pp.

Bruton, M. N. 1985. The effects of suspensoids on fish. *Hydrobiologia* 125:221–241.

Bryant, M. D. 1995. Pulsed monitoring for watershed and stream restoration. *Fisheries* 20:6–13.

Carling, P. A. 1984. Deposition of fine and coarse sand in an open-work gravel bed. *Canadian Journal of Fisheries and Aquatic Sciences* 41:263–270.

Carling, P. A. 1992. The nature of the fluid boundary layer and the selection of parameters for benthic ecology. *Freshwater Biology* 28:273–284.

Carling, P. A., and C. P. McCahon. 1987. Natural siltation of brown trout (*Salmo trutta* L.) spawning gravels during low-flow conditions. Pages 229–244 *in* J. F. Craig and J. B. Kemper (eds.), Regulated streams: Advances in ecology. Plenum Press, New York.

Carling, P. A., and N. A. Reader. 1982. Structure, composition and bulk properties of upland stream gravels. *Earth Surface Processes and Landforms* 7:349–365.

Carpenter, S. R., and D. M. Lodge. 1986. Effects of submerged macrophytes on ecosystem processes. *Aquatic Botany* 26:341–370.

Chang, H. H. 1988. Fluvial processes in river engineering. Krieger Publishing, Malabar, Florida, 432 pp.

Chapman, D. W. 1988. Critical review of variables used to define effects of fines in redds of large salmonids. *Transactions of the American Fisheries Society* 117:1–21.

Chow, V. T. 1959. Open channel hydraulics. McGraw-Hill, Singapore, 680 pp.

Church, M. A., D. G. Mclean, and J. F. Wolcott. 1987. River bed gravels: Sampling and analysis. Pages 43–79 *in* C. R. Thorne, J. C. Bathurst, and R. D. Hey (eds.), Sediment transport in gravel-bed rivers. John Wiley, Chichester.

Chutter, F. M. 1969. The effects of silt and sand on the invertebrate fauna of streams and rivers. *Hydrobiologia* 34: 29–37.

Cline, L. D., R. A. Short, and J. V. Ward. 1982. The influence of highway construction on the macroinvertebrates and epilithic algae of a high mountain stream. *Hydrobiologia* 96: 149–159.

Coleman, D. J., and F. N. Scatena. 1986. Identification and evaluation of sediment sources. Pages 3–18 *in* R. F. Hadley (ed.), Proceedings of the drainage basin sediment delivery symposium held in Albuquerque, New Mexico, USA, 4–8 August 1986, IAHS Publ. No. 159.

Cordone, A. J., and D. W. Kelly. 1961. The influence of inorganic sediment on the aquatic life of streams. *California Fish and Game* 47:189–228.

Crisp, D. T. 1989. Some impacts of human activities on trout, *Salmo trutta*, populations. *Freshwater Biology* 21:21–33.

Culp, J. M., and R. W. Davies. 1985. Responses of benthic macroinvertebrate species to manipulation of interstitial detritus in Carnation Creek, British Columbia. *Canadian Journal of Fisheries and Aquatic Sciences* 42:139–146.

Culp, J. M., F. J. Wrona, and R. W. Davies. 1985. Response of stream benthos and drift to fine sediment deposition versus transport. *Canadian Journal of Zoology* 64:1345–1351.

Cummins, K. W., and G. H. Lauff. 1969. The influence of substrate particle size on the microdistribution of stream macrobenthos. *Hydrobiologia* 34:145–181.

Davies-Colley, R. J., C. W. Hickey, J. M. Quinn, and P. A. Ryan. 1992. Effects of clay discharges on streams: 1. Optical properties and epilithon. *Hydrobiologia* 248:215–234.

Dawson, F. H. 1978. The seasonal effects of aquatic plant growth on the flow of water in a stream. Pages 71–78 *in* Proceedings European Weed Research Society 5th symposium on aquatic weeds, 5–8 September, 1978. Amsterdam, Netherlands.

Doeg, T. J., and J. D. Koehn. 1994. Effects of draining and desilting a small weir on downstream fish and macroinvertebrates. *Regulated Rivers: Research and Management* 9:263–278.

Donnely, T. W. 1993. Impoundment of rivers: Sediment regime and its effect on benthos. *Aquatic Conservation: Marine and Freshwater Ecosystems* 3:331–342.

Dudgeon, D. 1994. The functional significance of selection of particles by aquatic animals during building behaviour. Pages 289–312 *in* R. S. Wotton (ed.), The biology of particles in aquatic systems, 2nd ed. Lewis Publishers, London.

Droppo, I. G., and M. Stone. 1994. In-channel surficial fine-grained sediment laminae. Part 1: Physical characteristics and formational processes. *Hydrological Processes* 8:101–111.

Edwards, D. 1969. Some effects of siltation upon aquatic macrophyte vegetation in rivers. *Hydrobiologia* 34:29–37.

Einstein, H. A. 1968. Deposition of suspended particles in a gravel bed. *Journal of the Hydraulic Division of the American Society of Civil Engineers* 94:1197–1205.

Ellis, M. M. 1936. Erosion silt as a factor in aquatic environments. *Ecology* 17:29–42.

Eriksen, C. H. 1963. The relation of oxygen consumption to substrate particle size in two burrowing mayflies. *Journal of Experimental Biology* 40:447–453.

Eriksen, C. H. 1966. Ecological significance of respiration and substrate for burrowing Ephemeroptera. *Canadian Journal of Zoology* 46:93–103.

Erman, D. C., and F. K. Ligon. 1988. Effects of discharge fluctuation and the addition of fine sediment on stream fish and macroinvertebrates below a water-filtration facility. *Environmental Management* 12:85–97.

Extence, C. A. 1978. The effects of motorway construction on an urban stream. *Environmental Pollution* 17:245–252.

Frostick, L. E., P. M. Lucas, and I. Reid. 1984. The infiltration of fine matrices into coarse-grained alluvial sediments and its implications for stratigraphical interpretation. *Journal of the Geological Society of London* 141:955–965.

Gagnier, D. L., and R. C. Bailey. 1994. Balancing loss of information and grains in efficiency in characterizing stream sediment samples. *Journal of the North American Benthological Society* 13:170–180.

Gardiner, J. L. 1991. River projects and restoration; A manual for holistic appraisal. John Wiley, Chichester, 236 pp.

Giles, N., V. E. Phillips, and S. Barnard. 1991. Ecological effects of low flows on chalk streams. Report compiled for the Wiltshire Trust for Nature Conservation, 34 pp.

Gore, J. A., and A. M. Milner. 1990. Island biogeographical theory: Can it be use to predict lotic recovery rates. *Environmental Management* 14:737–753.

Graham, A. A. 1990. Siltation of stone-surface periphyton in rivers by clay-sized particles from low concentrations in suspension. *Hydrobiologia* 199:107–115.

Gray, L. J., and J. V. Ward. 1982. Effects of sediment releases from a reservoir on stream macroinvertebrates. *Hydrobiologia* 96:177–184.

Grimshaw, D. L., and J. Lewin. 1980. Source identification for suspended sediments. *Journal of Hydrology* 47:151–162.

Hearne, J. W., and P. D. Armitage. 1993. Implications of the annual macrophyte growth cycle on habitat in rivers. *Regulated Rivers: Research and Management* 8:313–322.

Hellawell, J. M. 1988. River regulation and nature conservation. *Regulated Rivers: Research and Management* 2:425–443.

Jackson, W. L., and R. L. Beschta. 1984. Influence of increased sand delivery on the morphology of sand a gravel channels. *Water Resources Bulletin* 20:527–533.

Jopling, A. V., and D. L. Forbes. 1979. Flume study of silt transportation and deposition. *Geografiska Annaler* 61A: 67–85.

Jungwirth, M., S. Muhar, and S. Schmutz. 1995. The effects of recreated instream and ecotone structures on the fish fauna of an epipotamal river. *Hydrobiologia* 303:195–206.

Kondolf, G. M., M. J. Sale, and M. G. Wolman. 1993. Modification of fluvial gravel size by spawning salmonids. *Water Resources Research* 29:2265–2274.

Ladle, M., and B. S. Griffiths. 1980. A study on the faeces of some chalk stream invertebrates. *Hydrobiologia* 74:161–171.

Lambert, C. P., and D. E. Walling. 1988. Measurement of channel storage of suspended sediment in a gravel-bed river. *Catena* 15:65–80.

Lemly, A. D. 1982. Modification of benthic insect communities in polluted streams: Combined effects of sedimentation and nutrient enrichment. *Hydrobiologia* 87:229–245.

Leudtke, R. J., and M. A. Brusven. 1976. Effects of sand sedimentation on colonization of stream insects. *Journal of the Fisheries Research Board of Canada* 33:1881–1886.

Lewis, K. 1973a. The effect of suspended coal particles on the life forms of the aquatic moss *Eurhynchium riparioides* (Hedw.). I. The gametophyte plant. *Freshwater Biology* 3:251–257.

Lewis, K. 1973b. The effect of suspended coal particles on the life forms of the aquatic moss *Eurhynchium riparioides* (Hedw.). II. The effect on spore germination and regeneration of apical tips. *Freshwater Biology* 3:391–395.

Lisle, T. E. 1989. Sediment transport and resulting deposition in spawning gravels, North Coastal California. *Water Resources Research* 25:1303–1319.

Lisle, T. E., and S. Hilton. 1992. The volume of fine sediment in pools: An index of sediment supply in gravel-bed streams. *Water Resources Bulletin* 28:371–383.

Mahoney, D., and D. C. Erman. 1984. An index of stored fine sediment in gravel bedded streams. *Water Resources Bulletin* 20:343–349.

Marchant, R. 1989. Changes in the benthic invertebrate communities of the Thomson River, southeastern Australia, after dam construction. *Regulated Rivers: Research and Management* 4:71–89.

McClelland, W. T., and M. A. Brusven. 1980. Effects of sedimentation on the behaviour and distribution of riffle insects in a laboratory stream. *Aquatic Insects* 2:161–169.

Miller, A. J., and L. L. Shoemaker. 1986. Channel storage of fine-grained sediment in the Potomac River. Pages 287–303 *in* R. F. Hadley (ed.), Proceedings of the drainage basin sediment delivery symposium held in Albuquerque, New Mexico, USA, 4–8 August 1986, IAHS Publ. No. 159.

Milner, N. J., J. Scullion, P. A. Carling, and D. T. Crisp. 1981. The effects of discharge on sediment dynamics and consequent effects on invertebrates and salmonids in upland rivers. *Advances in Applied Biology* 6:154–220.

Moring, J. R. 1982. Decrease in stream gravel permeability after clear-cut logging: An indication of intergravel conditions for developing salmonid eggs and alevin. *Hydrobiologia* 88:295–298.

Muhar, S., S. Schmutz, and M. Jungwirth. 1995. River restoration concepts—goals and perspectives. *Hydrobiologia* 303:183–194.

Murphy, M. L., and A. M. Milner. 1996. Alaska timber harvest and fish habitat. *In* A. M. Milner and M. W. Oswood (eds.), Alaska fresh waters. Springer-Verlag, New York (in press).

Niemi, G. J., P. DeVore, N. Detenbeck, D. Taylor, A. Lima, J. Pastor, J. D. Yount, and R. J. Naiman. 1990. Overview of case studies on recovery of aquatic systems from disturbance. *Environmental Management* 14:571–587.

Norwell, A. R. M., and P. A. Jumars. 1984. Flow environments of aquatic benthos. *Annual Reviews of Ecology and Systematics* 15:303–328.

Nuttall, P. M. 1972. The effects of sand deposition upon the macroinvertebrate fauna of the River Camel, Cornwall. *Freshwater Biology* 2:181–186.

Nuttall, P. M., and G. H. Bielby. 1973. The effects of china-clay waste on stream invertebrates. *Environmental Pollution* 5: 77–86.

Olsson, T. I., and B. Petersen. 1986. Effects of gravel size and peat material on embryo survival and alevin emergence of brown trout, *Salmo trutta* L. *Hydrobiologia* 135:9–14.

Peckarsky, B. L. 1984. Do predaceous stoneflies and siltation affect the structure of stream insect communities colonizing enclosures? *Canadian Journal of Zoology* 63:1519–1530.

Petts, G. E. 1984a. Impounded rivers: Perspectives for ecological management. John Wiley, Chichester, 326 pp.

Petts, G. E. 1984b. Sedimentation within a regulated river. *Earth Surface Processes and Landforms* 9:125–134.

Petts, G. E. 1988. Accumulation of fine sediment within substrate gravels along two regulated rivers, UK. *Regulated Rivers: Research and Management* 2:141–153.

Petts, G., and I. Foster. 1985. Rivers and landscape. Edward Arnold, London, 274 pp.

Pinder, L. C. V., M. Ladle, T. Gledhill, J. A. B. Bass, and A. M. Matthews. 1987. Biological surveillance of water quality—1. A comparison of macroinvertebrate surveillance methods in relation to assessment of water quality, in a chalk stream. *Archiv für Hydrobiologie* 109:207–226.

Quinn, J. M., R. J. Davies-Colley, C. W. Hickey, M. L. Vickers, and P. A. Ryan. 1992. Effects of clay discharges on streams: 2. Benthic invertebrates. *Hydrobiologia* 248:235–247.

Reiser, D. W., and R. G. White. 1990. Effects of streamflow reduction on Chinook salmon egg incubation and fry quality. *Rivers* 1:110–118.

Richards, C., and K. L. Bacon. 1994. Influence of fine sediment on macroinvertebrate colonization of surface and hyporheic stream substrates. *Great Basin Naturalist* 54:106–113.

Richards, C., G. H. Host, and J. W. Arthur. 1993. Identification of predominant environmental factors structuring stream macroinvertebrate communities within a large agricultural catchment. *Freshwater Biology* 29:285–294.

Richards, K. 1982. River: Form and process in alluvial channels. Methuen, London, 361 pp.

Rosenberg, D. M., and A. P. Wiens. 1978. Effects of sediment addition on macrobenthic invertebrates in a northern Canadian stream. *Water Research* 12:753–763.

Ryan, P. A. 1991. Environmental effects of sediment on New Zealand streams: A review. *New Zealand Journal of Marine and Freshwater Research* 25:207–221.

Schälchli, U. 1992. The clogging of coarse gravel river beds by fine sediment. *Hydrobiologia* 235/236:189–197.

Schälchli, U. 1995. Basic equations for siltation of riverbeds. *Journal of Hydraulic Engineering* 121:274–287.

Scrivener, J. C., and M. J. Brownlee. 1989. Effects of forest harvesting on spawning gravel and incubation survival of chum (*Oncorhynchus keta*) and coho salmon (*O. kisutch*) in Carnation Creek, British Columbia. *Canadian Journal of Fisheries and Aquatic Sciences* 46:681–696.

Sear, D. A. 1993. Fine sediment infiltration into gravel spawning beds within a regulated river experiencing floods: Ecological implications for salmonids. *Regulated Rivers: Research and Management* 8:373–390.

Sear, D. A., S. E. Darby, C. R. Thorne, and A. B. Brookes. 1994. Geomorphological approach to stream stabilization and restoration: Case study of the Mimmshall Brook, Hertford-

shire, UK. *Regulated Rivers: Research and Management* 9: 205–223.

Sedell, J. R., G. H. Reeves, F. H. Hauer, J. A. Stanford, and C. P. Hawkins. 1990. Role of refugia in recovery from disturbances: Modern fragmented and disconnected river systems. *Environmental Management* 14:711–724.

Shapley, S. P., and D. M. Bishop. 1965. Sedimentation in a salmon stream. *Journal of the Fisheries Research Board of Canada* 22:919–929.

Shields, F. D., C. M. Cooper, and S. S. Knight. 1995. Experiments in stream restoration. *Journal of Hydraulic Engineering* 121:494–502.

Soluk, D. A. 1985. Macroinvertebrate abundance and production of psammophilous Chironomidae in shifting sand areas of a lowland river. *Canadian Journal of Fisheries and Aquatic Sciences* 42:1296–1302.

Stone, M., and I. G. Droppo. 1994. In-channel surficial fine-grained sediment laminae. Part II: Chemical characteristics and implications for contaminant transport in fluvial systems. *Hydrological Processes* 8:113–124.

Strommer, J. L., and L. A. Smock. 1989. Vertical distribution and abundance of invertebrates within the sandy substrate of a low-gradient headwater stream. *Freshwater Biology* 22: 263–274.

Thoms, M. C. 1987. Channel sedimentation within the urbanized River Tame, UK. *Regulated Rivers: Research and Management* 1:229–246.

Tipping, E., C. Woof, and K. Clarke. 1993. Deposition and resuspension of fine particles in a riverine ''dead zone.'' *Hydrological Processes* 7:263–277.

Turnpenny, A. W. H., and R. Williams. 1980. Effects of sedimentation on the gravels of an industrial river system. *Journal of Fish Biology* 17:681–693.

Van Nieuwenhuyse, E. E., and J. D. LaPerriere. 1986. Effects of placer gold mining on primary production in subarctic streams of Alaska. *Water Resources Bulletin* 22:91–99.

Wagner, R. 1984. Effects of an artificially changed stream bottom on emerging insects. *Verhandlungen Internationale Vereinigung für Theoretische und Angewandte Limnologie* 22:2042–2047.

Wagner, R. 1989. The influence of artificial stream bottomsiltation on Ephemeroptera in emergence traps. *Archiv für Hydrobiologie* 115:71–80.

Walentowicz, A. T., and A. J. McLachlan. 1980. Chironomidae and particles: A field experiment with peat in an upland stream. Pages 179–185 *in* D. A. Murray (ed.), Chironomidae: Ecology, systematics and physiology. Pergamon Press, Oxford.

Walling, D. E. 1990. Linking the field to the river: Sediment delivery from agricultural land. Pages 129–152 *in* J. Boardman, I. D. L. Foster, and J. A. Dearing (eds.), Soil erosion on agricultural land. John Wiley, Chichester.

Walling, D. E., and P. W. Moorehead. 1989. The particle size characteristics of fluvial suspended sediment: An overview. *Hydrobiologia* 176 / 177:125–149.

Walling, D. E., and T. A. Quine. 1993. Using Chernobyl-derived fallout radionuclides to investigate the role of downstream conveyance losses in the suspended sediment budget of the River Severn, United Kingdom. *Physical Geography* 14:239–253.

Ward, G. W., A. K. Ward, C. N. Dahm, and N. G. Aumen. 1994. Origins and formation of organic and inorganic particles in aquatic systems. Pages 45–73 *in* R. S. Wotton (ed.), The biology of particles in aquatic systems, 2nd ed. Lewis Publishers, London.

Watson, D. 1987. Hydraulic effects of aquatic weeds in UK rivers. *Regulated Rivers: Research and Management* 1:211–227.

Welton, J. S. 1980. Dynamics of sediment and organic detritus in a small chalk stream. *Archiv für Hydrobiologie* 90:162–181.

Wood, P. J., and G. E. Petts. 1994. Low flows and recovery of macroinvertebrates in a small regulated chalk stream. *Regulated Rivers: Research and Management* 9:303–316.

Wright, J. F., and A. D. Berrie. 1987. Ecological effects of groundwater pumping and a natural drought on the upper reaches of a chalk stream. *Regulated Rivers: Research and Management* 1:145–160.

Wright, J. F., P. D. Hiley, A. C. Cameron, M. E. Wigham, and A. D. Berrie. 1983. A quantitative study of macroinvertebrate fauna of five biotopes in the River Lambourn, Berkshire, England. *Archiv für Hydrobiologie* 96:271–292.

Assessment of erosion, sedimentation, and water quality impacts of the Mountain Valley Pipeline and Equitrans Expansion Project's proposed crossing of the Jefferson National Forest as it pertains to the U.S. Forest Service's Draft Supplemental Environmental Impact Statement dated December 2022

Prepared by Jonathan A. Czuba, Ph.D., Licensed Professional Engineer - February 9, 2023

REFERENCES
8

February 21, 2023

JGR Oceans

RESEARCH ARTICLE
10.1029/2021JC017354

Key Points:

- Suspended sand and mud can be distinguished by their different optical and acoustic backscatter signatures
- We define a sediment composition index (SCI) from relative optical and acoustic backscatter and verify it with lab and field measurements
- SCI can be used to estimate the fraction of suspended sand, adding interpretive value to measurements in mixed sediment environments

Supporting Information:

Supporting Information may be found in the online version of this article.

Correspondence to:

S. G. Pearson,
s.g.pearson@tudelft.nl

Citation:

Pearson, S. G., Verney, R., van Prooijen, B. C., Tran, D., Hendriks, E. C. M., Jacquet, M., & Wang, Z. B. (2021). Characterizing the composition of sand and mud suspensions in coastal and estuarine environments using combined optical and acoustic measurements. *Journal of Geophysical Research: Oceans*, *126*, e2021JC017354. https://doi.org/10.1029/2021JC017354

Received 21 MAR 2021
Accepted 16 JUN 2021

Characterizing the Composition of Sand and Mud Suspensions in Coastal and Estuarine Environments Using Combined Optical and Acoustic Measurements

Stuart G. Pearson[1,2], Romaric Verney[3], Bram C. van Prooijen[1], Duc Tran[3], Erik C. M. Hendriks[1,4], Matthias Jacquet[3], and Zheng Bing Wang[1,2]

[1]Faculty of Civil Engineering and Geosciences, Delft University of Technology, Delft, The Netherlands, [2]Department of Applied Morphodynamics, Deltares, Delft, The Netherlands, [3]DYNECO/DHYSED Laboratory, IFREMER, Plouzane, France, [4]Department of Ecosystems and Sediment Dynamics, Deltares, Delft, The Netherlands

Abstract Quantifying and characterizing suspended sediment is essential to successful monitoring and management of estuaries and coastal environments. To quantify suspended sediment, optical and acoustic backscatter instruments are often used. Optical backscatter systems are more sensitive to mud particles (<63 μm) and flocs, whereas acoustic backscatter systems are more responsive to larger sand grains (>63 μm). It is thus challenging to estimate the relative proportion of sand or mud in environments where both types of sediment are present. The suspended sediment concentration measured by these devices depends on the composition of that sediment, thus it is also difficult to confidently measure concentration with a single instrument when the composition varies and extensive calibration is not possible. The objective of this paper is to develop a methodology for characterizing the relative proportions of sand and mud in mixed sediment suspensions by comparing the response of simultaneous optical and acoustic measurements. We derive a sediment composition index (SCI) that is used to directly predict the relative fraction of sand in suspension. Here, we verify the theoretical response of these optical and acoustic instruments in laboratory experiments and successfully apply this approach to field measurements from Ameland ebb-tidal delta (the Netherlands). Increasing sand content decreases SCI, which was verified in laboratory experiments. A reduction in SCI appears during more energetic conditions when sand resuspension is expected. Conversely, the SCI increases in calmer conditions when sand settles out, leaving behind mud. This approach provides crucial knowledge of suspended sediment composition in mixed sediment environments.

Plain Language Summary Sand and mud particles are the building blocks of our coastlines. Counting and describing sand and mud particles floating through the water is essential to managing coasts. We commonly do this with devices that send out a sound (acoustic) or light (optical) signal into the water. The sensors measure the strength of the signal reflecting back off of any sand and mud particles passing by. Optical instruments are better at "seeing" mud than sand, and acoustic instruments are better at "hearing" sand than mud. If both sand and mud are present, a single instrument will not accurately estimate the total amount of sediment because of these different sensitivities. Instead, we can use both types of instrument together and compare what we "see" with what we "hear." This comparison allows us to estimate whether there are more sand or mud particles floating through the water. The relationship between "seeing" and "hearing" can be described in a single number, the sediment composition index (SCI). We successfully tested this approach in laboratory experiments and then applied it to a site on the coast of the Netherlands. This approach gives us a new way to understand environments that are both sandy and muddy.

1. Introduction

1.1. Background

Estuaries and coastal seas are characterized by strong morphological and sedimentary gradients, from shallow beaches and intertidal shoals or flats, to deeper foreshore and channel areas or other subtidal features. Furthermore, the sediment composition at a given site may vary widely in both particle size and mineralogy (Flemming & Ziegler, 1995; Son et al., 2011; Winkelmolen & Veenstra, 1974). The size and material

properties of mud (aka "fines" or "fine sediment") and sand are different: sand particles are individual quasi-spherical grains (with typical density $\rho_s = 2{,}650$ kg/m^3 for quartz particles), between 63 and 2,000 μm in diameter, d. Muddy sediments, especially clay particles ($d < 2$ μm), have the ability to flocculate and often bond with organic matter. The resulting flocs vary widely in diameter (from 10 to 1,000 μm) and have relatively low densities ($\rho_{floc} = O(1{,}100 - 2{,}000$ kg/m$^3)$) with irregular shapes and lower settling velocities than sand (Chapalain et al., 2019; Dankers & Winterwerp, 2007; Eisma, 1993; Fugate & Friedrichs, 2002; P. S. Hill et al., 2000; Khelifa & Hill, 2006; Manning et al., 2006; Many et al., 2019; McCave, 1984; Milligan & Hill, 1998). The spatial distribution of these different types of sediment is a function of morphology, supply, and hydrodynamic conditions.

Due to episodic (storms and floods) and persistent (tides) hydrometeorological forcing and human influences, estuarine and coastal sediment are highly dynamic. Bed sediments are mobilized and transported, through bed load (rolling, sliding, and saltating near the surface of the seabed) or suspended load (held aloft in the water column by turbulence). In this paper, we focus on transport in suspension, dealing with mud ($d < 63$ μm) and very fine to medium sand $d = 63$–500 μm, the latter being found in suspension (relatively close to the bed) during energetic conditions. Depending on local and remote bed composition and hydrodynamic forcing, the concentration, characteristics, and fluxes of suspended particulate matter (SPM) will drastically change.

The morphological changes resulting from these fluxes may threaten or enhance coastal infrastructure and ecosystems. Quantifying these sediment fluxes is critical for sustainable coastal management (Hanley et al., 2014; Hendriks et al., 2020; Mulder et al., 2011). Measurements of these fluxes can be used to derive sediment budgets (Wang et al., 2018), better understand the physical processes underlying sediment transport (White, 1998), and quantify sediment pathways and connectivity (Pearson et al., 2020). They also allow us to calibrate and improve numerical sediment transport models (Amoudry & Souza, 2011; Roelvink & Reniers, 2012). Of critical importance is not just quantifying total sediment fluxes but also sediment fluxes as a function of particle size. For example, overestimating sand concentration could lead to underestimates of an estuary's ability to import sediment and evolve in equilibrium with accelerating sea level rise (e.g., Lodder et al., 2019).

The main challenge faced in understanding coastal sediment dynamics and quantifying associated fluxes is to make continuous observations of total (sand and mud) suspended sediment and their related mass concentration (SSC). Continuous in situ measurements are possible with acoustic or optical instruments (Fettweis et al., 2019). Optical backscatter (OBS) sensors have been used successfully to measure suspended sediment in a wide range of environments, from estuaries and embayments (Bass et al., 2002, 2007; Fettweis et al., 2019; Fugate & Friedrichs, 2002; Green et al., 2000; Li et al., 2018; Lin et al., 2020; Lunven & Gentien, 2000) to mud flats and salt marshes (Guo et al., 2018; Voulgaris & Meyers, 2004) to sandy beaches (Aagaard et al., 2002; J. P. Downing et al., 1981). Acoustic backscatter sensors have also been successfully used to measure suspended sediment in many different coastal and estuarine settings (Bass et al., 2007; Chanson et al., 2008; Fugate & Friedrichs, 2002; Green et al., 2000; Hoitink & Hoekstra, 2005; Li et al., 2018; Lin et al., 2020; Thorne et al., 1993; Voulgaris & Meyers, 2004) and beyond (Hawley, 2004; D. C. Hill et al., 2003).

The measurement capabilities of optical and acoustic backscatter instruments are inextricably tied to the material properties of the sediment they observe. Each type of instrument responds with different sensitivity to muddy or sandy sediment because of a dependence on particle size and density. Hence, in practice, empirical calibration models for optical or acoustic sensors are built via regression against laboratory or in situ samples, the latter providing reference gravimetric concentrations (Fettweis et al., 2019; J. Gray & Elliott, 2009). Once the calibration for a given instrument has been developed, the calibrated relationship can be applied to the recorded signal from the field (e.g., voltage, nephelometric turbidity units [NTU], counts, or signal-to-noise ratio [SNR]) and translated into a time series of mass concentration. This concentration can then be interpreted in light of other measurements such as velocity.

However, these calibration models are representative of a given condition (e.g., calm, moderate tidal flows with SPM dominated by mud) and may not be well adapted for observing a succession of low- and high-energy conditions when the SPM sand and mud content (f_{sand} and f_{mud}) can vary strongly in time (Bass et al., 2007). The most appropriate methodology would require sampling and recalibrating sensors as fast as

SPM composition changes, but this is neither easily predictable nor realistic. A library of population-adapted calibration models could be built following Green and Boon (1993), but knowledge about SPM composition dynamics is a prerequisite for their application.

In this paper, we develop an original sediment composition index (SCI) derived from optical and acoustic measurements to quantitatively and dynamically evaluate the relative fraction of sand or mud in suspension. The concept is first validated using laboratory measurements, and then applied to field measurements. The SCI index provides researchers with a way to more accurately quantify *SSC*, especially during high-energy events when calibration with physical samples is not possible.

1.2. Optical Backscatter Measurements

OBS sensors are widely used to indirectly measure suspended sediment concentration. Near-infrared light (typical wavelength $\lambda = 0.780–0.865$ μm) is emitted from the instrument, backscattered by suspended particles, and then recorded by photoreceptors. In a Mie scattering regime, backscatter is strongest when the light wavelength and particle size are similar, so *OBS* are more sensitive to mud particles $O(1\ \mu m)$ than sand particles $O(100\ \mu m)$ (Conner & De Visser, 1992; Green & Boon, 1993; Voulgaris & Meyers, 2004). According to Sutherland et al. (2000), the photon flux received by the sensor is given as

$$F = VNE\frac{\pi d^2}{4}Q_s \tag{1}$$

where F is photon flux (W), V is scattering volume (cm^3), N is the number concentration of scatters (cm^{-3}), E emitted irradiance (W/cm^2), d is the particle diameter (μm), Q_s the (back)scattering efficiency of the particles. Relating the number concentration to the mass concentration *SSC* (mg/L), this relationship can be modified as follows (Sutherland et al., 2000):

$$F = \frac{3}{2}\frac{V(SSC)E}{\rho_s d}Q_s \tag{2}$$

where ρ_s is the particle (dry) density (kg/m^3). This flux is then translated to a voltage output by the sensor.

Equation 2 can then be reworked as

$$OBS = \alpha_{OBS}\frac{Q_s}{\rho_s d}SSC \tag{3}$$

where *OBS* is the optical backscatter signal (V) and α_{OBS} is approximated as a constant for the range of *SSC* investigated.

Due to the dependency on $1/(\rho_s d)$, for the same concentration of sediment, the flux observed for 200 μm sand ($\rho_s \approx 2{,}600\ kg/m^3$) will be 10 times smaller than for muddy flocs of the same size ($\rho_{floc} \approx 1{,}100\ kg/m^3$), and even smaller in presence of microflocs. However, this sensitivity to size may be as low as a factor of 2 when intercomparing floc particles with a continuous size distribution from microflocs to macroflocs, rather than the sandy and muddy end members considered in this study (Boss, Slade, & Hill, 2009; Boss, Slade, Behrenfeld, et al., 2009; P. S. Hill et al., 2011).

1.3. Acoustic Backscatter Measurements

Analogously to *OBS* devices, an acoustic signal is emitted and backscattered by particles in suspension, then recorded by transducers. The estimation of *SSC* from acoustic measurements depends on the properties of sediment in suspension. For well-characterized particles (e.g., a well-sorted sand population) and electronically/acoustically calibrated sensors, backscattering models and representative diameters can be used to evaluate *SSC* from the theory (Thorne & Hanes, 2002). Otherwise, similarly to optical sensors, the acoustic response can be calibrated against samples from field or laboratory experiments, with similar limitations regarding calibration representativity.

Acoustic devices typically used in coastal sediment studies can loosely be grouped into (a) single-frequency acoustic Doppler velocimeters (ADVs) which measure at a single point; (b) single-frequency acoustic Doppler current profilers (ADCPs) which measure over multiple points in the water column; and (c) multifrequency acoustic backscatter devices. Only the latter is specifically designed to measure suspended sediment concentration; ADCPs and ADVs were originally intended to measure velocity, but their operating principles mean that inferring sediment concentration from acoustic backscatter is a useful side benefit. In this study, we mainly consider acoustic backscatter from ADVs, which are widely used to measure suspended sediment concentrations (Fugate & Friedrichs, 2002; Lin et al., 2020; Öztürk, 2017).

We can mathematically describe acoustic backscatter using the sonar equation, which balances the difference between energy emitted and received by the sensor with energy lost on the return trip of an acoustic pulse (Hoitink & Hoekstra, 2005). The sonar equation is presented here in form similar to (Chmiel et al., 2018; Hoitink & Hoekstra, 2005; Salehi & Strom, 2011)

$$SNR = C - \underbrace{20\log_{10}(\psi R^2)}_{Spherical\ Spreading} - \underbrace{\int_0^R \left(\alpha_w(r) + \alpha_s(r)\right)dr}_{Attenuation} + BI \tag{4}$$

SNR (dB) is the signal-to-noise ratio recorded directly by the ADV, which indicates the intensity of acoustic backscatter. *C* (dB) is a constant including instrument-related and geometrical terms. The spherical spreading term ($20\log_{10}(\psi R^2)$) is a function of *R* (m), the one-way distance that the acoustic pulse travels from the transmitter to the measurement volume. The attenuation of the acoustic pulse can be decomposed into absorption by the water α_w (dB/m) and attenuation by sediment α_s (dB/m), integrated over the travel distance. *BI* is the volume backscatter strength (dB) and is a function of *SSC* and particle characteristics:

$$BI = 10\log_{10}\left(\frac{SSC\bar{\sigma}}{\rho_s \overline{V_s}}\right) \tag{5}$$

where $\bar{\sigma}$ is the mean backscattering cross section (m^2), ρ_s is the dry particle density (kg/m^3), and $\overline{V_s}$ is the scattering volume (m^3).

The attenuation terms (α_s and α_w) are higher at larger concentrations and greater distances (Thorne et al., 1993) but can be neglected below 1,000 mg/L (Chmiel et al., 2018) and *O*(10 cm) from the sensor (Pomázi & Baranya, 2020). In this study, we thus neglect attenuation, given the small distance between source and measuring volume (15 cm) and low concentrations expected at our study site in Ameland (<1,000 mg/L). All terms except *BI* can be reorganized and set in a global constant *C*′ [dB]. Equation 5 then becomes

$$SNR = 10\log_{10}(SSC) + 10\log_{10}\left(\frac{\bar{\sigma}}{\rho_s \overline{V_s}}\right) + C' \tag{6}$$

Equation 6 can be further simplified as

$$SNR = 10\log_{10}(SSC) + b' + c' \tag{7}$$

where *c*′ is a constant depending on instrument characteristics and *b*′ is a variable depending on suspended particle properties (e.g., size, shape, density, and elasticity). The log linear relation between *SNR* and *SSC* is only valid for concentrations less than 1,000 mg/L (Chmiel et al., 2018; Salehi & Strom, 2011); beyond this threshold, particle absorption losses reduce the recorded backscattering signal.

The interaction between an acoustic pulse and particles (scattering) is optimal for coarser individual (unflocculated) particles, with a dependency on the acoustic frequency such as $kd/2 \approx 1$ (or $< d$) where *k* is the wave number ($2\pi/\lambda$, and λ is the wavelength) and *d* the diameter of the particle (Salehi & Strom, 2011). Hence, for a 1 MHz acoustic signal, the optimal backscattering size (diameter) is around 480 μm, while for a 6 MHz signal, the optimal size is around 80 μm. Flocculated particles are characterized by lower backscattering efficiency (1–2 order of magnitude lower) (Thorne & Hurther, 2014). Acoustic instruments are

thus more sensitive to fine to coarse sands than flocculated mud particles (Salehi & Strom, 2011): for similar concentrations, the *SNR* will be stronger for sand than for mud.

1.4. Combining Optical and Acoustic Measurements: Toward the SCI

In coastal and estuarine environments where suspended particles are often characterized by a mixture of mud (including flocs) and sand particles, *SSC* measurements relying on a single technique (optical or acoustic) are ambiguous with respect to sediment composition. This can lead to misestimates of particle size and concentration (Thorne et al., 2021) and limits the interpretability and representativeness of the recorded signal. The objective of the present paper is to combine the use of optical and acoustic backscatter sensors to estimate the relative fraction of sand in suspension.

Bass et al. (2007) note that although optical and acoustic backscatter systems are routinely used together, few studies have taken advantage of using them together to estimate suspended sediment composition in mixed environments. There is a salient difference in the response of optical and acoustic instruments to changes in suspended particle size (Ha et al., 2009), which may be exploited to resolve ambiguities.

In some cases, it has been assumed that optical or acoustic instruments only observe a single class of sediment. Bass et al. (2002) disregard locally resuspended sand in their *OBS* measurements of mud. In studies of tidal channels flanked by intertidal mud flats, both Green et al. (2000) and van de Kreeke and Hibma (2005) assumed that optical sensors detected only silt, while acoustic sensors detected only sand. The interpretation of a single instrument depends on the assumptions behind its calibration (e.g., an *OBS* calibrated to sandy sediment will overestimate total *SSC* when mud is also present). However, instead of ignoring the presence of sand in optical measurements or the presence of mud in acoustic measurements, paired instruments can more beneficially be used concurrently and compared (Conner & De Visser, 1992; Green & Boon, 1993; Hawley, 2004). In this study, we take advantage of these paired instruments to derive a SCI that quantitatively discriminates the presence of suspended sand from mud.

This relative optical-acoustic backscatter response can be analyzed by combining Equations 3 and 7 to obtain:

$$SNR = 10\log_{10}(OBS) + b_{particle} + c_{instr} \tag{8}$$

where $b_{particle}$ is a variable parameter function of SPM characteristics and c_{instr} is a global (optical/acoustic) instrument-related constant. In our study, as instruments were not calibrated, $b_{particle} + c_{instr}$ are considered as a single constant, the SCI. SCI is therefore dependent on the characteristics of the sediment particles being measured and of the instruments being used. Equation 8 can be rearranged to present SCI:

$$SCI = 10\log_{10}(OBS) - SNR \tag{9}$$

Considering the high sensitivity of the acoustic sensor to sand and of the optical sensor to mud, SCI is relatively smaller when suspended sand particles dominate and relatively larger when mud dominates suspensions. SCI can thus be used as an indicator of sand or mud dominance.

2. Methods

Laboratory measurements were used as a proof of concept for the SCI and to quantify the relationship between SCI and the fraction of sand in suspension (f_{sand}). The fraction of mud in suspension can also be directly calculated via $f_{mud} = 100\% - f_{sand}$. We then analyze in situ measurements to demonstrate the added value of SCI for investigating the dynamics of mixed sediment environments. We compared optical/acoustic signals measured on Ameland ebb-tidal delta in the Netherlands during a 40-day period featuring storms and calm conditions. From these signals, we calculated SCI and f_{sand} and put them into context with other simultaneous measurements (tidal stage) and derived parameters (bed shear stress due to waves and currents). By interpreting these measurements, we can test whether SCI is a valid and useful indicator of relative suspended sand or mud dominance in estuarine environments.

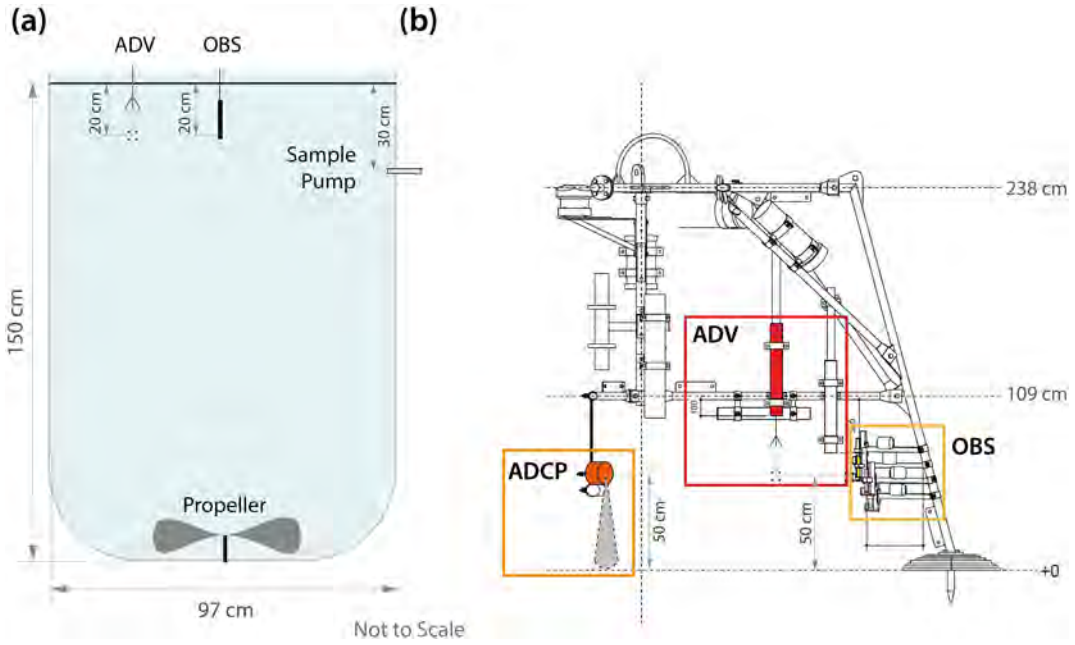

Figure 1. Overview of the DEXMES tank used in the laboratory experiments. (a) Schematic of instrument setup. During the experiments, the tank contained an acoustic Doppler velocimeter (ADV) and an Optical Backscatter (*OBS*) sensor mounted just below the surface. An external pump was connected to the tank to extract suspended sediment samples. (b) Frame used to conduct field measurements (Amelander Zeegat [Ameland Inlet] Frame #4 [AZG F4]), featuring ADVs, *OBS*s, and an downward-facing acoustic Doppler current profiler (ADCP) sensors. The ADV and *OBS* measured sample volumes 50 cm above the base of the frame, and the ADCP measured a 50-cm profile between the instrument and the bed. DEXMES, Dispositif EXpérimental de quantification des Matières En Suspension.

2.1. Laboratory Experiments

We used the DEXMES (Dispositif EXpérimental de quantification des Matières En Suspension) tank for our experiments. DEXMES is operated by Ifremer and managed together with Géosciences Océan, Géosciences Rennes and SHOM (French Hydrographic Service). The glass-walled tank has a volume of approximately 1 m^3 and internal diameter of 0.97 m (Figure 1) and was filled with fresh water.

Two sets of similar experiments were conducted to evaluate SCI at various total sediment concentration ranges and sand/mud contents. In Experiment 1, pure bentonite (d_{50} = 17 μm) and two classes of well-sorted pure quartz sand (ρ_s = 2,650 kg/m^3) with median grain sizes d_{50} = 100 and 220 μm were used. Conversely, Experiment 2 used estuarine mud (d_{50} = 15 μm) instead of bentonite, and the same sources of sand but without further sieving (d_{50} = 93 and 210 μm). The estuarine mud contained organic matter, but this was not quantified. For simplicity, we hereafter refer to $d_{50} \approx$ 100 μm and $d_{50} \approx$ 200 μm sand for both experiments. In the context of these experiments, "mud" refers to bentonite and estuarine mud ($d_{50} <$ 63 μm), while "coarse sediment" or "sand" refers to both size classes of sand ($d_{50} >$ 63 μm).

Five sediment composition conditions were investigated for both 100 and 200 μm sand in Experiment 1: pure bentonite, pure sand, and three intermediate mixtures: 25%, 50%, and 75% sand content (f_{sand}). For each condition, six total concentrations were tested stepwise from 15 to 200 mg/L (see Appendix A). In Experiment 2, the (estuarine mud) concentration was held constant at approximately 130 mg/L and sand concentration (100 or 200 μm) incrementally varied between 0 and 1,460 mg/L (see Appendix A), in order to approximate an estuarine environment with a sandy local bed composition and steady background presence of mud (e.g., Green et al., 2000; van de Kreeke & Hibma, 2005). Concentrations of both classes of sediment were kept within the linear range of response for each instrument (<5,000 mg/L of mud and <50,000 mg/L of sand for the *OBS* (J. Downing, 2006) and <5,000 mg/L for the ADV (Salehi & Strom, 2011) to avoid ambiguity in the readings. Precise details of the suspended sediment concentrations and sand fractions in each experiment are provided in Appendix A and experimental protocols are outlined in Supporting Information.

Figure 2. Overview of measurements during the September 2017 field measurement campaign at Ameland Inlet, including the frame (AZG-F4) bearing the instruments used in this study. Bathymetry source: Rijkswaterstaat Vaklodingen. Elevation source: Actueel Hoogtebestand Nederland (AHN), Rijkswaterstaat. Basemap sources: Esri, HERE, Garmin, ©OpenStreetMap contributors, and the GIS user community.

Vertical concentration gradients were observed within the tank for 200 μm sand, but all instruments and samples measured within 10 cm of the same elevation, leading to comparable sample and sensor data. The propeller at the bottom of the tank was set to a speed of 175 rpm to provide high turbulent shear between $G = 30$ and 100 s^{-1}, maximizing resuspension and mixture homogeneity while minimizing the formation of bubbles.

In Experiments 1 and 2, acoustic backscatter was measured using a Nortek Vector ADV (Nortek AS, 2005), operating at a frequency of 6 MHz, and sampling at 32 Hz (8 Hz in Experiment 2), 20 cm beneath the water surface (25 cm in Experiment 2). *OBS* was measured in Experiment 1 using a Wetlabs combined FLuorometer and turbidity sensor (Nephelometric Turbidity Units) (FLNTU) WET Labs Inc (2019), sampling at 1 Hz, 20 cm beneath the water surface. In order to exclude data points below the sensor's detection limits for coarser particles, turbidity data below 0.9 NTU are discarded from the study. In Experiment 2, a Campbell OBS-3+ (Campbell Scientific Inc., 2014) was used instead, with similar properties to the Wetlabs FLNTU. To calibrate the optical and acoustic measurements, an external pump was connected to the tank 30 cm beneath the surface to extract suspended sediment samples. The instruments were arranged to avoid mutual interference but while sampling a similar elevation and hence similar sediment concentrations. All sensors were operated in continuous recording mode for the duration of each experiment, and statistics were computed over a 10–11-min period at each sediment concentration level. The median *SNR* of the three ADV beams and median *OBS* output were then used to calculate the relative optical-acoustic backscatter index SCI from Equation 9.

2.2. In Situ Measurements

Ameland Inlet is located in the Netherlands between the sandy barrier islands of Terschelling and Ameland, connecting the North Sea with the Dutch Wadden Sea (Figure 2). The inlet is characterized by a 30-m deep main channel (the "Borndiep") on its eastern side and a shifting complex of shoals and channels on its west side. There is a large and highly dynamic ebb-tidal delta complex on the seaward side of the inlet and a shallow backbarrier basin environment of intertidal shoals and flats on the landward side (the Wadden Sea) (Elias et al., 2019; Lenstra et al., 2019). The seabed of the ebb-tidal delta of the inlet is mainly well-sorted sand (mean $d_{50} = 211$ μm, $n = 165$) with mud content generally <1%, whereas the Wadden Sea has a mud

content up to 20% at its landward edge and on the intertidal flats separating Ameland Inlet from adjacent tidal basins (Pearson et al., 2019; Rijkswaterstaat, 1999). Samples with mud content of ~5% can also be found on the North Sea bed beyond the distal end of the ebb-tidal delta.

A field measurement campaign was carried out from August 29 to October 9, 2017, with the goal of characterizing hydrodynamic and sediment transport processes in the inlet and on its ebb-tidal delta (Brakenhoff et al., 2020; De Wit et al., 2019; Reniers et al., 2019; van der Werf et al., 2019; Van Prooijen et al., 2020). Measurements of flow, waves, SPM, bedform dynamics, and water quality were made at four locations across the site. Measurements considered in this study were obtained at frame AZG-F4 (Figure 2), at the distal end of the ebb-tidal delta, approximately 8 m deep.

As with the laboratory experiments in Section 2.1, acoustic backscatter was measured using three Nortek Vector ADVs (Nortek AS, 2005), operating at a frequency of 6 MHz, and sampling at 16 Hz, 20, 50, and 78 cm above the seabed. The median *SNR* of acoustic backscatter was taken over 30 min bursts for the deployment period as per Ha et al. (2009).

OBS was measured using four Campbell OBS-3+ (Campbell Scientific Inc., 2014), sampling at 16 Hz, 20, 30, 50, and 78 cm above the seabed. The *OBS* was initially calibrated using sandy sediment obtained from the seabed adjacent to the measurement frame, as is frequently done in practice (Fettweis et al., 2019; Paphitis & Collins, 2005). However, there is still concern that calibration using bed material can be inappropriate and error-prone if there are significant differences between the bed sediment and material in suspension (Bass et al., 2007; Beamsley et al., 2001; Kineke & Sternberg, 1992; Öztürk, 2017; Su et al., 2016), as expected at our field site. On this basis, the original calibration was discarded when it was recognized that the additional presence of suspended sediment significantly finer than the bed sediment made interpretation ambiguous. Thus, the uncalibrated *OBS* signal is presented here in volts. The median *OBS* signal over 30 min bursts was used.

Near-bed hydrodynamic conditions during the monitoring period were measured using a high-resolution downward-looking Nortek Aquadopp acoustic doppler current profiler (ADCP-HR) (Nortek AS, 2008). The ADCP sampled at a rate of 4 Hz in 30 min bursts. These measurements were averaged over the water column between the sensor and the bed (approximately 0.5 m, depending on field conditions) and then median velocities were calculated for each 30 min burst interval. Bed shear stresses due to the influence of waves and currents were calculated separately using the method of Soulsby (1997) (with default parameter settings) to give an indication of the potential for local bed material to be resuspended at the frame. For simplicity, we do not consider the effect of combined wave-current bed shear stresses here, which likely underestimates the frequency of sediment resuspension.

To assess the intratidal variation of the field measurements, we classified each 30 min burst into flood tide, high water slack (HWS), ebb tide, and low water slack (LWS) based on an analysis of tidal currents (Pearson et al., 2019). At the measurement site, the major axis of flow is almost exactly in an east-west direction. Thus, eastward (0°–179°) currents exceeding 0.1 m/s were classified as flood, and westward (180°–359°) currents exceeding that threshold as ebb. Velocities below that threshold with positive water surface elevations (with respect to mean water level) were classified as HWS, and with negative water surface elevations as LWS.

3. Results

3.1. Laboratory Experiments

3.1.1. Optical and Acoustic Backscatter

We consider the joint response of the optical and acoustic sensors to various sand/fine sediment mixtures: from purely mud suspensions to purely sand suspensions and with varying total concentrations (Figure 3). Optical turbidity values are recorded in NTU or volts (Experiments 1 and 2, respectively) depending on the instrument deployed. Readings in volts are first normalized in equivalent NTU using an offset value in log space (constant for all Experiment 2 *OBS* data), so that their values are aligned in Experiments 1 and 2 for purely mud suspension conditions.

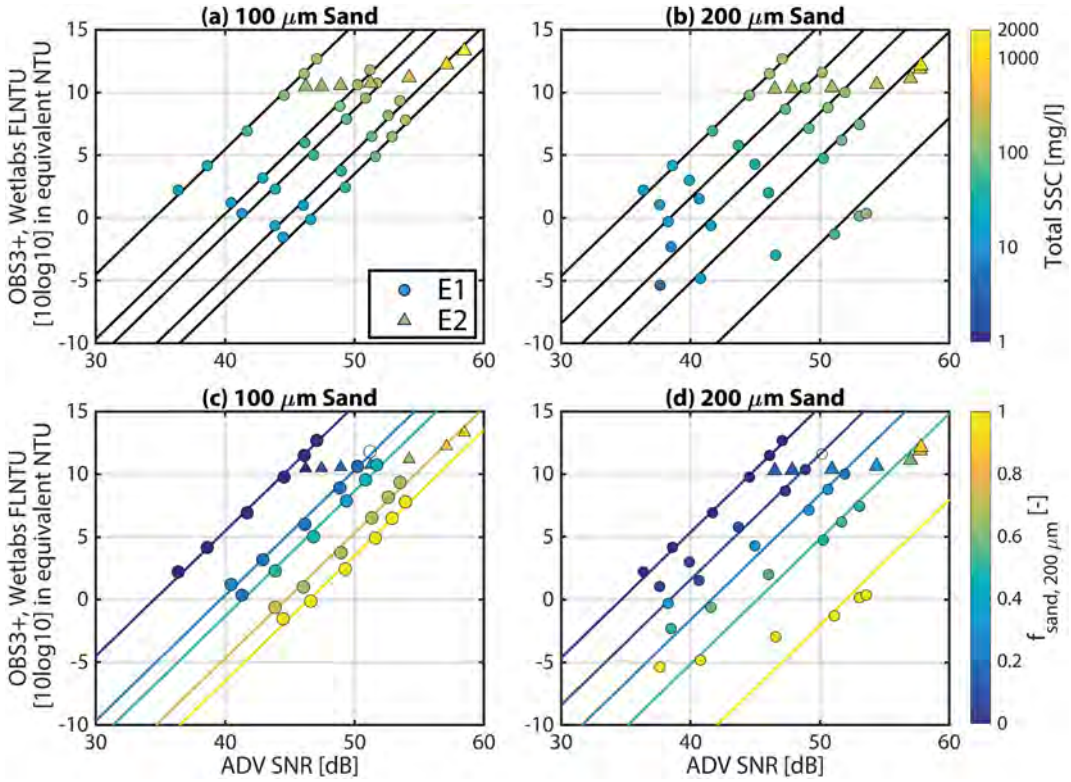

Figure 3. Median acoustic (ADV *SNR*) and optical backscatter (*OBS*) as a function of total suspended sediment concentration (a, b) and suspended sand fraction (f_{sand}) in the laboratory experiments (c, d). (a, c) Experiments with 100 μm sand. (b, d) Experiments with 200 μm sand. Data from Experiment 1 (E1) measured with a Wetlabs FLNTU are marked with circles ($n = 30$), while data from Experiment 2 (E2), measured with an OBS-3+, are marked with triangles ($n = 7$). Black and colored lines indicate constant f_{sand} contours. ADV, acoustic Doppler velocimeter; *SNR*, signal-to-noise ratio.

Results from Experiment 1 for 100 μm sand (Figures 3a and 3c) show that the sensors' response is linear in $\log_{10}(OBS)$/ADV *SNR* space. This is valid for a range of total sediment concentration (from 15 to 200 mg/L), such that $10\log_{10}(OBS) = SNR + \text{SCI}$, confirming the theoretical relationship (Equation 9). Increasing the sand fraction (f_{sand}) leads to a shift in the data alignment for the different conditions, but lines are still parallel (Figure 3c). That is, for a given ADV *SNR* value, the optical turbidity value increases as SPM becomes finer. Conversely, for a given optical turbidity value, ADV *SNR* increases as SPM become sandier. Experiment 2 independently tested a larger total *SSC* gradient, increasing the sand content from 0% to 100% and total sediment concentration from 135 to 1603 mg/L, while progressively adding sand (Figures 3a and 3c). These results are in full agreement with Experiment 1, with their data points matching the corresponding sand/mud ratio contours as sand content increases.

Similar results are observed for 200 μm sands: $\log_{10}(OBS)$/ADV pairs are aligned for a given sand content, and these lines are organized parallel to each other (Figures 3b and 3d). For similar turbidity values, the *SNR* signal is stronger for 200 μm sand than for 100 μm sand (Figures 3a and 3b). However, deviations from alignment are observed when sand content dominates (i.e., $f_{sand} > 50\%$) and total concentration is low (i.e., $SSC \leq 50$ mg/L) (Figures 3b and 3d). This bias corresponds to the poor sensitivity of the optical sensor to detect low 200 μm particle concentrations, when there are few scatterers in suspension. In such conditions, recorded NTU values range from 0.1 to 0.9 NTU, close to the sensor resolution and lower detection limit.

The measurements in Figure 3 are time-averaged values (see Supporting Information for full protocols), and we describe signal variability using the coefficient of variation ($CV = \sigma/\mu$). In Experiment 1, Wetlabs FLNTU signals are more variable when sand particles get coarser (from $CV = 2\%$–3% for pure mud to 3%–16% for pure 100 μm sand and 5%–22% for pure 200 μm sand) and 2%–9% for sand–mud mixtures. ADV *SNR*

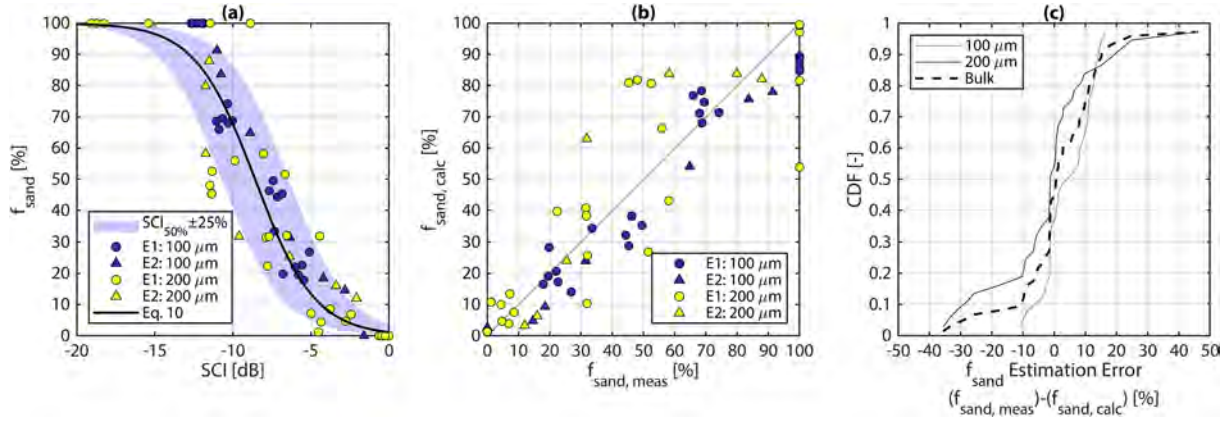

Figure 4. Fraction of sand in total suspended sediment (f_{sand}), calculated from the sediment composition index (SCI). (a) f_{sand} as a function of SCI, with Equation 10 fit to both grain sizes in bulk ($SCI_{50\%} = -8.58$). Blue bands indicate the envelope of uncertainty in f_{sand}, varying $SCI_{50\%}$ by ±25%. Experiments 1 and 2 (E1 and E2, respectively) are indicated, along with the sand grain size used in each experiment ($R^2_{100} = 0.957$, $R^2_{200} = 0.806$, and $R^2_{bulk} = 0.884$). (b) Comparison of experimentally measured $f_{sand,\,meas}$ with $f_{sand,\,calc}$ determined using Equation 10. (c) Cumulative distribution function (CDF) of sand fraction estimation error ($f_{sand,\,meas} - f_{sand,\,calc}$) for each sand grain size class and for all classes combined in bulk.

variability is less ($CV < 6\%$ for mud, 100 μm sand, and 100 μm sand–mud mixtures) and generally decreases with increasing concentration. The highest ADV *SNR* variability was seen for low concentrations of pure 200 μm sand (*CV* up to 20%). Sand–mud mixtures (200 μm) have *CV* ranging from 5% to 13% in Experiment 1. For sand–mud mixtures in Experiment 2, *OBS* signal variability is between 6% and 12% and ADV *SNR* variability is between 2% and 5%. As with Experiment 1, mixtures with 200 μm sand showed higher signal variability than mixtures with 100 μm sand in Experiment 2.

3.1.2. Sediment Composition Index

We derived the SCI for the laboratory measurements using Equation 9, and it is shown to be an appropriate proxy for evaluating the sand content (Figure 4a). As a first step toward a generic SCI, we propose to normalize SCI such that SCI = 0 in purely muddy conditions.

To understand the relationship between the derived SCI and the actual sediment composition, we compare f_{sand} with SCI from both experiments and grain size classes and find a negative correlation (Figure 4a). A hyperbolic tangent was fit to the data (Equation 10) because f_{sand} should asymptotically reach 0% for maximum SCI (minimum acoustic response, maximum optical response, no sand, only mud) and should tend asymptotically toward 100% for minimum SCI (maximum acoustic response, minimum optical response, only sand, no mud).

$$f_{sand} = \left(\frac{1}{2} + \frac{1}{2}\tanh\left[\frac{-(SCI - SCI_{50\%})}{\Delta SCI}\right]\right) \cdot 100\% \tag{10}$$

where $SCI_{50\%}$ is a constant corresponding to a mixture of 50% sand and 50% mud. It is equal to −8.03 when fitting only 100 μm sand ($R^2_{100\mu m} = 0.954$), −9.63 for 200 μm sand ($R^2_{200\mu m} = 0.848$), and −8.58 when both grain sizes are fit in bulk ($R^2_{bulk} = 0.884$). For the analyses in the rest of this study, we consider $SCI_{50\%} = -8.58$, $\Delta SCI = 3.85$ and indicates the width in variation. Equation 10 allows us to deepen the interpretation of SCI by directly predicting f_{sand} (and by extension, $f_{mud} = 1 - f_{sand}$). It shows good predictive skill when compared with measured f_{sand} for both experiments and grain size classes ($R^2_{100} = 0.957$, $R^2_{200} = 0.806$, and $R^2_{bulk} = 0.884$) (Figure 4b). The bulk prediction is accurate for 200 μm sands, as 70% of the calculated sand fractions are associated with an absolute error lower than ±10%. Results are the best for 100 μm sand, with more than 85% of the samples estimated with an absolute error below ±10%. In case the sand distribution is not known, we also investigated the SCI response to sand content when merging all experimental data

(Figure 4c). This bulk index still performs well, with 70% of the calculations with errors within ±10%, although the error range is slightly larger, between −30% and +20%.

3.2. In Situ Measurements

3.2.1. Hydrodynamic Conditions

The measurements from Ameland ebb-tidal delta span 40 days (August 29 to October 8, 2017) or approximately 2.5 spring–neap cycles (Figure 5a). There are two minor storms ($H_s \approx 1$ m) on August 30 and September 7 and two major storms ($H_s > 4$ m), *Sebastian* (September 14, during neap tide) and *Xavier* (October 6, during spring tide).

Spring tide occurs around September 10, 20, and October 7 (corresponding to the larger tidal range in Figure 5a). Under calmer conditions, bed shear stresses due to currents ($\tau_{b,c}$) exceed the critical threshold for local sand ($\tau_{cr,211\ \mu m} = 0.18$ Pa, derived using Soulsby, 1997) only during spring flood tides (Figures 5c and 6f). These periods with currents strong enough to resuspend or advect sand correspond to flood and ebb stages of the tidal cycle (Figures 5a and 6b).

Wave-induced bed shear stress $\tau_{b,w}$ is greatest during the storms (Figures 5b and 6c), exceeding $\tau_{cr,211\ \mu m}$. High bed shear stresses due to currents ($\tau_{b,c}$) are also observed during the two major storms, likely due to wind-induced storm surge and wave-driven currents (Figure 5b). During *Storm Sebastian* on September 14, eastward currents during the peak of the storm were so strong and persistent that the tide did not reverse (no ebb occurred for nearly 24 h). During storm periods, $\tau_{b,w}$ is greatest at low tide.

3.2.2. Optical and Acoustic Backscatter

Over the total deployment period, *OBS* measurements show strong tidal variation and a response to individual storm events (Figures 5d and 6h). The largest ADV readings occur during spring tide and the peaks of the two largest storms (Figures 5e, 6i, and 6j), while the lowest ADV *SNR* readings tend to correspond to calmer periods with low wave stress (Figures 5e and 6j).

During Storm Sebastian on September 12–16, both *SNR* and *OBS* signals strongly increase and tidal variation is weak for the next two tidal cycles (Figures 6g and 6i). Both signals remain relatively high but noisy, and higher background (minimum) readings persist for about a week after the storm.

During the calm spring tidal period from September 21 to 25, the influence of waves is minimal and the intratidal dynamics are clear (Figures 6h and 6j). The *OBS* signal shows strong M2 (semidiurnal) tidal oscillations peaking around LWS. Conversely, ADV *SNR* shows mixed M2 and M4 (quarter-diurnal) tidal variation, peaking at flood tide and to a lesser degree at ebb. ADV *SNR* is lowest at HWS. The calm period from September 28 to October 2 coincides with neap tide and exhibits similar dynamics to the prestorm period at the beginning of the monitoring period, albeit with lower background *OBS* and ADV *SNR* levels and reduced intratidal variability.

3.2.3. Sediment Composition Index and f_{sand}

Suspended sediment composition was estimated from the optical and acoustic backscatter readings. SCI was calculated with Equation 9, using the *OBS* and ADV *SNR* measurements 50 cm above the bed. SCI was offset to zero by subtracting its 99th percentile value. As in the laboratory experiments, this corresponds to a condition when sand is not likely present. This assumption is corroborated by the calm hydrodynamic conditions during moments of high SCI. We then applied Equation 10 with $SCI_{50\%} = -8.58$ (fit to both 100 and 200 μm sand) to the SCI time series including the confidence bands to approximate the fraction of sand in suspension (f_{sand}).

At subtidal time scales, SCI is lower during storms and spring tides (e.g., Figures 6k and 6l). SCI reaches its lowest observed values during spring tide, during both calm and stormy periods (Figure 5b). By contrast, it is highest during calm conditions and neap tide (e.g., Figure 5f from September 28 to October 2). SCI is much more dynamic at spring tide, its standard deviation nearly doubling when compared to neap tide.

Over the course of a tidal cycle, SCI typically followed a mixed M2 and M4 pattern. The M4 signal has minima at flood and ebb tide and is especially pronounced during spring tidal conditions. Superimposed on this

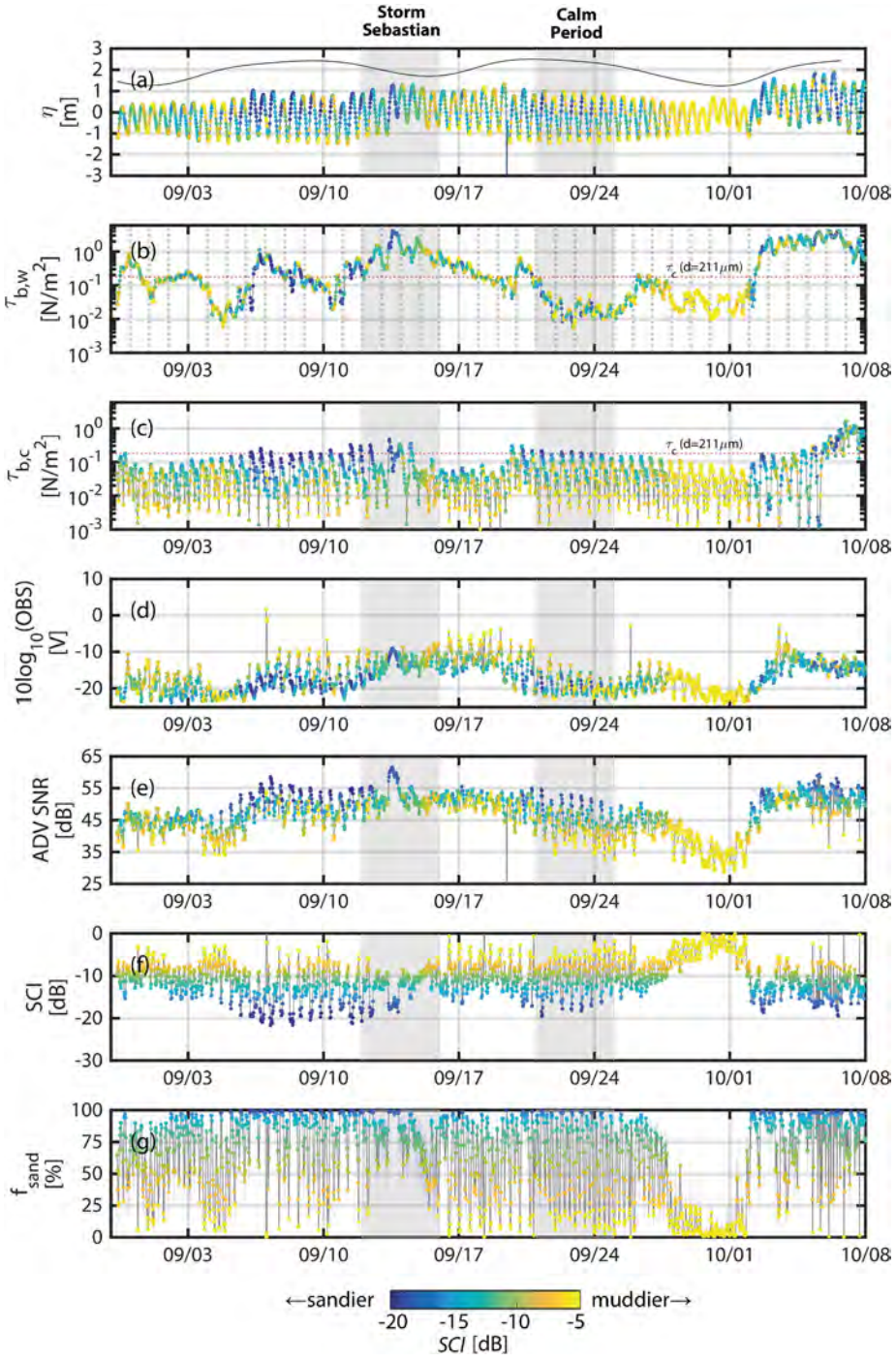

Figure 5. Time series of hydrodynamic conditions and backscatter at Ameland ebb-tidal delta Frame 4, with dot color indicating relative optical-acoustic backscatter index SCI. Higher SCI (lighter yellow colors) suggest relatively higher mud content, and lower SCI (darker blue colors) suggest relatively higher sand content. (a) Water level relative to the mean depth during the deployment period (8.3 m). The tidal range (indicated with a solid black line) shows spring tide (high values) and neap tide (low values). (b) Bed shear stress due to waves ($\tau_{b,w}$). The critical shear stress for local sand ($\tau_{cr,211\,\mu m} = 0.18$ Pa) is indicated with a dashed line. (c) Bed shear stress due to currents ($\tau_{b,c}$). (d) Log of optical backscatter measured 50 cm above the bed. (e) Acoustic backscatter (signal-to-noise ratio, *SNR*) measured 50 cm above the bed. (f) Relative optical-acoustic backscatter index SCI. (g) Fraction of sand in total suspended sediment (f_{sand}) calculated from SCI using Equation 10. SCI, sediment composition index.

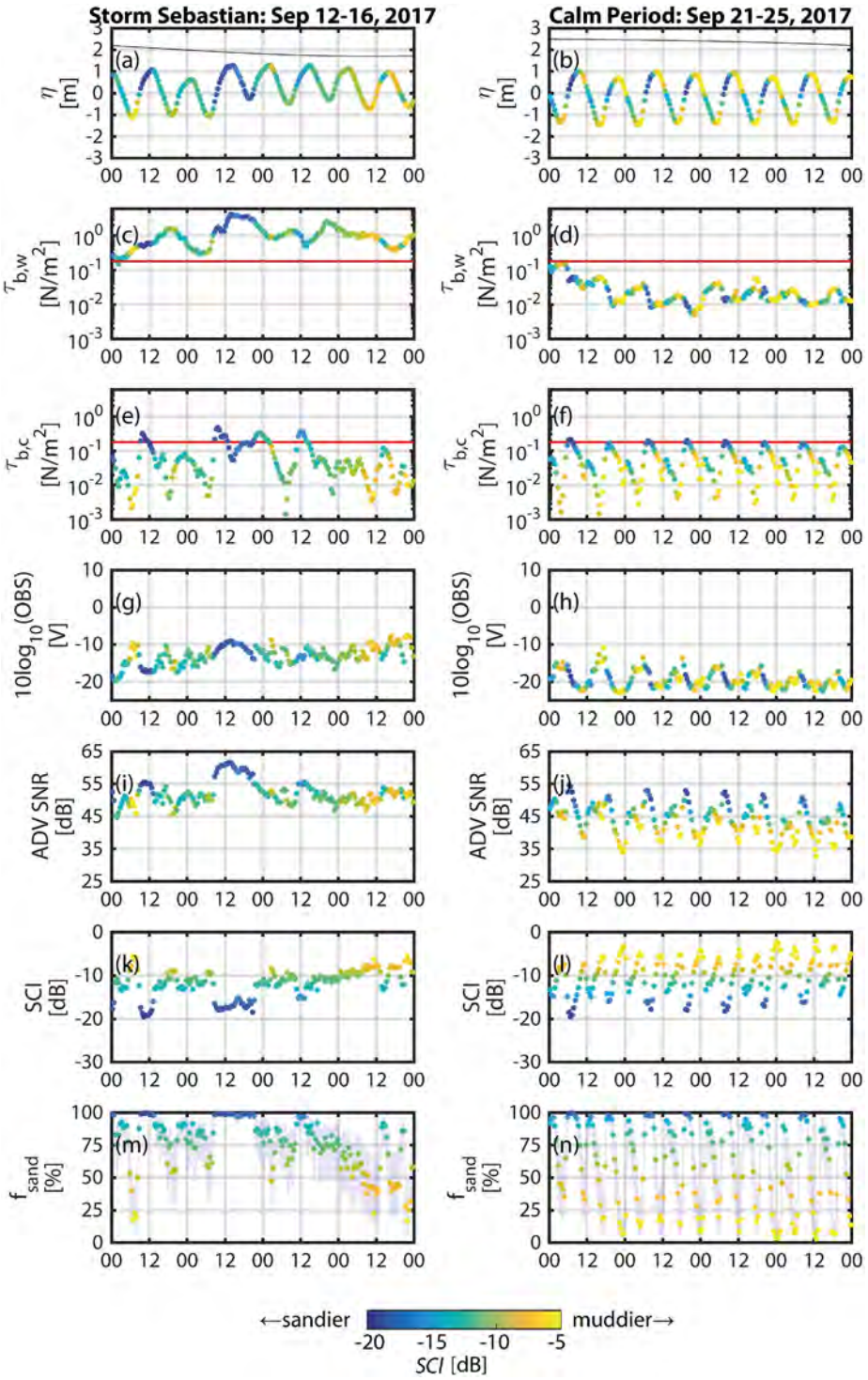

Figure 6. Time series of hydrodynamic conditions and backscatter at Ameland ebb-tidal delta Frame 4, focusing on Storm Sebastian (September 12–16) and a calmer period during spring tide (September 21–25). Dot color indicates relative optical-acoustic backscatter index SCI. Higher SCI (lighter yellow colors) suggest relatively higher mud content, and lower SCI (darker blue colors) suggest relatively higher sand content. (a, b) Water level (η) relative to the mean depth during the deployment period (8.3 m). The tidal range (indicated with a solid black line) shows spring tide (high values) and neap tide (low values). (c, d) Bed shear stress due to waves ($\tau_{b,w}$). The critical shear stress for local sand ($\tau_{cr,211\ \mu m} = 0.18$ Pa) is indicated with a dashed line. (e, f) Bed shear stress due to currents ($\tau_{b,c}$). (g, h) Log of optical backscatter. (i, j) Acoustic backscatter (signal-to-noise ratio, *SNR*). (k, l) Relative optical-acoustic backscatter index SCI. (m, n) Fraction of sand in total suspended sediment (f_{sand}) calculated from SCI using Equation 10. SCI, sediment composition index.

is an M2 variation with its peak centered at ebb tide. The combination of these two signals results in minimal SCI at flood tide when $\tau_{b,c}$ is high, then a peak at HWS when $\tau_{b,c}$ is low (Figure 6l). This is followed by a sharp drop to a secondary minimum at ebb tide (when $\tau_{b,c}$ increases again), and then a gradual rise to another peak at LWS. The cycle completes with another rapid decline in SCI at flood tide as currents strengthen. Although SCI nearly always peaks at slack water, the maximum varies between LWS (e.g., September 8–10) and HWS (e.g., September 21–25).

SPM composition varied throughout the tidal cycle, with distinct differences observed between periods of higher flow (i.e., ebb and flood) and periods of lower flow (i.e., slack water). SPM is dominated by sand at ebb and flood tide, when $f_{sand} > 75\%$ (Figure 6n). Conversely, the suspension consists primarily of mud at high and LWS ($f_{sand} < 25\%$). f_{sand} follows an M4 signal, with only weak M2 variations compared to SCI.

The presence of waves (indicated by higher wave-induced bed shear stress $\tau_{b,w}$) was often associated with lower SCI (Figure 5b). During Storm Sebastian on September 13, SCI drops during the peak in the storm and loses its characteristic M2–M4 tidal variation for several days (Figure 6k). This corresponds to a period of mainly sand in suspension ($f_{sand} > 75\%$), with f_{sand} approaching 100% at the peak of the storm (Figure 6m). The proportion of mud in suspension increases toward the end of the storm, and tidal variations in f_{sand} begin to return.

To further explore the influence of waves on tidal variations in relative optical-acoustic response, SCI is plotted as a function of wave ($\tau_{b,w}$) and current-related bed shear stresses ($\tau_{b,c}$) at each stage of the tidal cycle (Figure 7). We summarize the variability of SCI relative to wave and current forcings (shear stresses), separating results into flood and ebb-tidal phases. In this shear stress space, the dynamics of SCI are clearly structured. During calm flood tides ($\tau_{b,w} < \tau_{cr,211\ \mu m}$), SCI ranges from 0 dB during weak currents to −22 dB during stronger currents. A similar pattern is observed during ebb, although generally SCI > −15 dB. This can be explained by the weaker $\tau_{b,c}$ during maximum ebb compared with during maximum flood. Both high and LWS are characterized by relatively high SCI (>−10 dB). SCI reaches <−12 dB during slack periods during wavy conditions. Larger wave-induced stresses are generally associated with SCI < −5 dB, although brief peaks in SCI can sometimes be observed during storms (Figure 5).

4. Discussion

4.1. Interpreting the Dynamics of the SCI

The SCI is a useful indicator of the relative fractions of sand and mud in suspension, as validated in laboratory experiments. Application of this index was demonstrated by interpreting the sediment dynamics on Ameland ebb-tidal delta in light of two main processes: resuspension of local sandy bed material by waves and strong tides and tidal advection of mud from locations outside the ebb-tidal delta. These processes explain the response of optical and acoustic backscatter measurements, and hence the corresponding dynamics of SCI.

At subtidal time scales (>24 h), the dynamics of SCI can be explained in part by a fortnightly spring–neap cycle. The larger intratidal variation of SCI at spring tide is likely due to the increased resuspension of sand by stronger currents (Figure 5c) and to the greater advection of mud from nearby intertidal flats at late ebb and LWS, similarly to the observations of Weeks et al. (1993) and Fettweis et al. (1998) at other sites. Conversely, high SCI (and thus higher relative proportions of mud in suspension) coincides with the neap tide (e.g., September 28 to October 1) and with lower values of $\tau_{b,w}$ and $\tau_{b,c}$. Without sufficiently strong forcing to resuspend local sand ($\tau_b < \tau_{cr,211\ \mu m} = 0.18$ Pa, derived using Soulsby, 1997), only mud can remain in suspension (Figure 5c).

The observed intratidal variation in SCI (Figure 6l) can be explained by the local hydrodynamics and sedimentary environment and is summarized conceptually for a generic sandy tidal inlet or ebb-tidal delta with a muddy inner basin in Figure 8. At flood and ebb tide, strong currents are capable of resuspending sand from the local seabed or advecting it from elsewhere nearby, so the corresponding SCI values decrease. Conversely, when sand settles out at slack water, only the suspended mud remains in the water column, explaining the increase in SCI value at that time. The result is an M4 signal with minima at flood and ebb

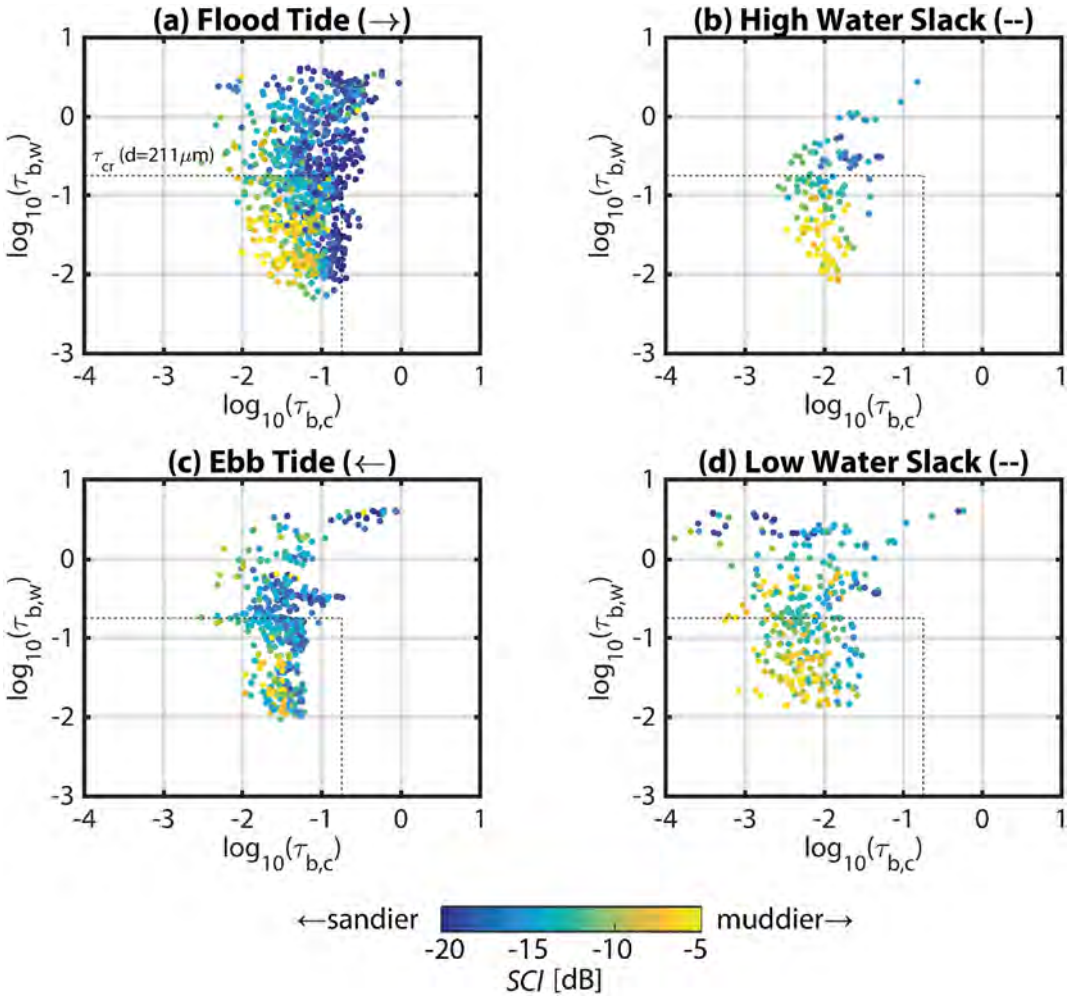

Figure 7. Sediment composition index SCI (in color) as a function of wave shear stress (vertical axes) and current shear stress (horizontal axes), at four different stages of the tidal cycle. (a) Flood tide ($u > 0.1$ m/s and to the east), (b) high water slack ($u < 0.1$ m/s and at high water), (c) ebb tide ($u > 0.1$ m/s and to the west), and (d) low water slack ($u < 0.1$ m/s and at low water). The critical shear stress for local 211 μm sand (0.18 Pa) is plotted for reference as a dotted line. Bed shear stresses were computed using Soulsby (1997).

tide. This relationship between local resuspension and local current velocities is also observed by Lavelle et al. (1984), Weeks et al. (1993), Bass et al. (2002), and van de Kreeke & Hibma (2005).

Modulating the M4 SCI signal is an M2 signal with its maximum centered at ebb tide. This M2 signal can be explained by the semidiurnal migration of a strong landward mud concentration gradient in the channels of Ameland basin (Postma, 1961). Remote sensing indicates that this turbid water mass can be ejected several kilometers seaward of the inlet and across the ebb-tidal delta at ebb (Pearson et al., 2019), which causes the corresponding SCI to increase. This muddy water mass is then displaced by less turbid oceanic water on the flood tide, so SCI decreases again. This semidiurnal transport pattern is widely observed at other sites where there is a persistent gradient in suspended mud concentration (Bass et al., 2002; Green et al., 2000; van de Kreeke & Hibma, 2005; Weeks et al., 1993).

To fully explain the SCI dynamics at Ameland, the episodic influence of storms must also be accounted for. If waves are sufficiently large ($\tau_{b,w} > \tau_{cr,211\ \mu m}$), then the majority of local sand can be mobilized, which can result in low values of SCI regardless of the tidal stage. Conversely, the periods with the lowest SCI (suggesting lower proportions of sand in suspension and relatively more mud) coincide mainly with periods of low wave action (e.g., September 28 to October 1).

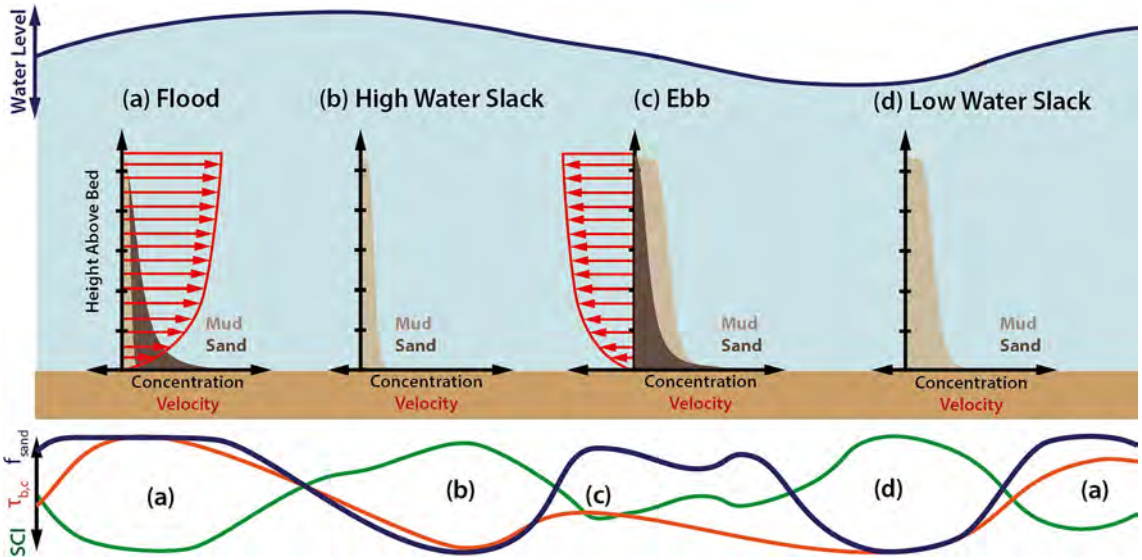

Figure 8. Conceptual model of tidally driven mixed sand–mud sediment transport at a sandy tidal inlet or ebb-tidal delta with a muddy inner basin. A normalized example time series of sediment composition index (SCI), bed shear stress due to currents ($\tau_{b,c}$), and fraction of sand in suspension (f_{sand}) over a tidal cycle are indicated below. (a) At flood tide, strong currents locally resuspend sand but carry few mud particles from the sea, so SCI is low. (b) At HWS, currents are too weak to mobilize sand, so total concentrations are relatively low and consist only of mud, so SCI is higher. (c) At ebb tide, strong currents locally resuspend sand, though less than at flood tide, so SCI decreases again. These ebb currents also carry with them mud particles from the muddy and biologically productive inner basin. (d) At low water slack, currents are too weak to mobilize sand, leaving only the mud advected from the inner basin at ebb, which begins to settle, resulting in higher SCI.

During periods with large waves, SCI may be influenced not just by an increased capacity for local resuspension of sand but also by wind and wave-induced mud resuspension. This is reflected in the SCI signal during Storm Sebastian (Figure 6). Even when bed shear stresses due to waves and currents greatly exceed $\tau_{cr,211\ \mu m}$, SCI seldom drops below −15 dB and f_{sand} remains between 50% and 90% for most of the storm. In the latter half of the storm, f_{sand} decreases as sand settles out, while mud remains in suspension. This mud can originate from two locations: the Wadden Sea tidal basin and the bed of the North Sea. During storms, tidal flats in Ameland basin may easily lose the surface layers of sediment deposited in calm periods (Postma, 1961). In a similar case study, Green et al. (2000) found that wave activity on nearby intertidal flats was the principal determinant of suspended mud load advected through a tidal channel. However, storms may also remobilize mud which accumulates in the bed of the North Sea (Flores et al., 2017; Hendriks et al., 2020; Van Der Hout et al., 2017). Instantaneous bed shear stress does not tell the whole story of suspended sediment composition: it is also necessary to account for spatial and temporal variations in the supply of mud.

Our interpretation of SCI based on theoretical considerations and the laboratory results are fully supported by the local hydrodynamics and sedimentological context. SCI thus provides a novel and valuable characterization of the suspended sediment dynamics on Ameland ebb-tidal delta. This metric is especially useful for mixed sediment environments like Ameland where optical and acoustic measurements are otherwise ambiguous when viewed in isolation.

4.2. Limitations and Outlook

Having been conceptually validated by laboratory and field measurements, there are many opportunities for further developing the SCI and improving its applicability. The next steps toward a more quantitative evaluation of sediment composition lie in the accumulation of larger data sets and in quantifying the component of SCI specific to the instruments being used (the c_{instr} term of Equation 8, which is invariant with SPM).

For a more generic SCI, we propose a reference calibration of optical and acoustic sensors to evaluate the instrument constant c_{instr} (Equation 8), using NTU/BTU (formazin calibration) for optical systems, and monodispersed glass beads for acoustic particles, similarly to the calibration procedure for an acoustic backscatter system (e.g., Thorne & Meral, 2008). With calibrated scatterers, the sonar equation (Equation 4) can be fully

evaluated, the instrument constant c_{instr} is the only unknown. Acoustic backscatter is sensitive to the acoustic frequency of the transducers: the SCI dynamics will be different from 1 to 6 MHz sensors, because each sensor will respond differently to sediment of a given grain size and concentration. Similarly, optical sensors will provide different NTU values depending on whether the optical sensor is based on backscatter (e.g., OBS-3+ [Campbell Scientific Inc., 2014], Seapoint [Seapoint Sensors Incorporated, 2013], or Wetlabs [WETLabs, 2010]) or side scattering (e.g., YSI 6600 [YSI Incorporated, 2012]). Many additional laboratory experiments would be required in order to determine c_{instr} and make a full set of conversion factors for each type of instrument. By applying these calibrations, SCI could become generic, at least for similar instruments. However, even without quantifying c_{instr} directly, SCI provides useful information on suspended sediment composition when its dynamics are considered in the context of local hydrodynamic and sedimentological conditions.

Additional laboratory experiments must be carried out with a wider variety of sediment mixtures and concentrations. We expect that most of the variability of SCI is caused to first order by the presence of sand in suspension, because sand has a relatively stronger influence on acoustic backscatter than flocs of comparable size (Thorne & Hurther, 2014). However, the influence of flocculation on the variability of SCI requires further investigation. Estimating how SCI would change in response to organic matter also remains an open question. Organic matter has different optical and acoustic backscatter characteristics from inorganic sediment (Boss et al., 2018; Hoitink & Hoekstra, 2005), so its presence will potentially affect SCI.

Field measurements should also be collected from sites with different sedimentary characteristics under a range of hydrodynamic conditions in order to generalize the conclusions of the present study and SCI $- f_{sand}$ relationships like Equation 10. Samples pumped at regular intervals (e.g., Beamsley et al., 2001) or better yet, at moments triggered by specific turbidity levels, would provide a more representative basis for calibrating optical and acoustic measurements. Fortunately, analyzing SCI dynamics of additional field sites is already possible, since optical and acoustic instruments are frequently paired together in the field (e.g., Colosimo et al., 2020; de Vet et al., 2020; Flores et al., 2018; Fugate & Friedrichs, 2002; Lin et al., 2020; Moura et al., 2011; Pomeroy et al., 2021; Voulgaris & Meyers, 2004; Zhu et al., 2019). Our approach thus gives added value to existing data sets by providing an additional, simple-to-calculate metric for interpreting sediment dynamics.

These additional efforts to make SCI more general and to better understand the underlying physics will strengthen the usefulness and applicability of the metric. This will lead to new insights into the dynamics of mixed sediment environments where ambiguity due to suspended sediment composition previously limited the information that could be obtained from optical and acoustic measurements.

This approach is most valuable in settings where it cannot be assumed that suspended sediment always has the same properties as the seabed. The majority of the world's coasts are heterogeneous sedimentary environments where these conditions may be found (Holland & Elmore, 2008). Even if ADV and OBS measurements are not available, the general principle of using differential optical and acoustic backscatter to disambiguate mixed sediment suspensions should still apply to pairs of other similar instruments. This would however require SCI-specific calibration experiments with the dedicated pair, similar to those performed in the present study. If applied in conjunction with instruments using different measurement principles (e.g., Laser In-Situ Scattering and Transmissometry [Agrawal & Pottsmith, 2000; Chapalain et al., 2019; P. S. Hill et al., 2011; Mikkelsen & Pejrup, 2001] or multifrequency acoustic backscatter sensors [J. R. Gray & Gartner, 2009; Moate & Thorne, 2009, 2012; Wilson & Hay, 2015]), SCI could yield even more insight into suspended sediment composition.

5. Conclusions

The SCI derived in this study quantifies the suspended sediment composition in mixed sediment environments. It does so using the relative intensity of optical and acoustic backscatter signals, as these two measurement techniques have different sensitivities to sand and mud (Equation 9). SCI can be used to estimate the fraction of sand and mud in suspension (f_{sand} and f_{mud}) in marine environments. Here, we verify the theoretical response of these optical and acoustic instruments in laboratory experiments. SCI is negatively correlated with the fraction of sand in suspension (Equation 10).

The SCI approach was successfully applied to in situ measurements on the ebb-tidal delta of Ameland Inlet in the Netherlands. SCI shows a clear M4 variation associated with suspension of local sand, modulated by

an M2 variation associated with suspended mud advected from the nearby Wadden Sea. Lower values of SCI (indicating a stronger acoustic response) and higher f_{sand} are observed under more energetic conditions when sand is expected to dominate the suspension (e.g., spring flood tide or strong wave conditions). Conversely, SCI increases (indicating a stronger optical response) and f_{sand} reduces in calmer conditions and at slack water, when the suspended sediment consists mainly of mud.

This approach reduces the ambiguity of suspended sediment composition in mixed sediment environments. Furthermore, it adds value to existing sets of measurements since simultaneous optical/acoustic measurements have frequently been carried out together in sediment transport studies. Being able to discern between different types of sediment in suspension will increase confidence in the interpretation of suspended sediment concentration measurements. This can ultimately improve estimates of sediment fluxes, leading to deeper understanding of coastal systems and enable better informed coastal management decision making.

Appendix A: Experimental Concentrations and Sand Fractions

A complete record of the sediment concentrations and sand fractions measured in Experiment 1 is provided in Table A1.

A complete record of the sediment concentrations and sand fractions measured in Experiment 2 is provided in Table A2.

Table A1
Summary of Sediment Concentrations in Experiment 1 (Bentonite With 100 and 200 μm Sand)

	SSC_{actual}		f_{sand}	
SSC_{target}	100 μm	200 μm	100 μm	200 μm
15	15.0	15.0	0.0	0.0
25	25.0	25.0	0.0	0.0
50	50.0	50.0	0.0	0.0
100	100.0	100.0	0.0	0.0
150	150.0	150.0	0.0	0.0
200	200.0	200.0	0.0	0.0
15	15.4	12.1	26.9	6.9
25	24.2	19.7	22.6	4.7
50	48.1	41.0	22.1	8.5
100	93.2	75.9	19.5	1.2
150	137.0	117.7	17.9	4.4
200	NaN	149.6	NaN	NaN
15	9.4	11.0	19.8	31.9
25	24.8	13.5	49.5	7.2
50	46.5	36.8	46.2	32.1
100	75.2	73.0	33.5	31.5
150	134.7	109.9	44.3	31.8
200	182.8	128.8	45.3	22.3
15	14.5	7.7	74.2	51.6
25	18.4	14.9	66.0	58.1
50	39.8	28.4	68.6	55.9
100	81.9	45.7	69.5	45.3
150	117.2	79.0	68.0	52.5
200	160.0	96.2	68.7	48.0

Table A1
Continued

	SSC_{actual}		f_{sand}	
SSC_{target}	100 μm	200 μm	100 μm	200 μm
15	14.0	4.8	100.0	100.0
25	20.5	15.6	100.0	100.0
50	45.5	27.8	100.0	100.0
100	85.7	52.8	100.0	100.0
150	126.2	76.9	100.0	100.0
200	175.6	115.1	100.0	100.0

Note. The left column indicates the target for each test, and the center column the actual *SSC* measured from pumped samples. The right columns indicate the sand content (f_{sand}) measured from pumped water samples.

Table A2
Summary of Sediment Concentrations in Experiment 2 (Estuarine Mud With 100 and 200 μm Sand)

	f_{sand} (%)							
	Measured		SSC_{fine}		SSC_{sand}		SSC_{total}	
Target	100 μm	200 μm	100 μm	200 μm	100 μm	200 μm		100 μm
0.0	0.0	12.0	134.9	127.9	0.0	17.4	134.9	145.3
10.0	14.6	16.0	128.1	127.1	21.9	24.2	150.0	151.3
25.0	18.5	25.4	133.0	123.9	30.1	42.2	163.1	166.1
50.0	31.5	31.8	134.0	125.8	61.6	58.7	195.6	184.5
75.0	64.9	58.2	132.4	123.6	244.3	172.2	376.7	295.8
90.0	83.7	79.9	131.4	124.6	674.2	494.5	805.6	619.1
95.0	91.4	87.9	138.6	128.6	1,464.4	936.0	1,603.0	1,064.6

Note. The left columns indicate the target and measured sand content (f_{sand}) for each test. The right columns indicate the fine sediment (≤63 μm), sand (≥63 μm), and total concentration in mg/L measured from pumped water samples.

Notation

b'	suspended particle property variable, dB
$b_{particle}$	variable function of SPM characteristics, dB
BI	volume backscatter strength, dB
c'	instrument characteristic constant, dB
c_{instr}	global (optical/acoustic) instrument-related constant, *dB*
C	constant including acoustic instrument-related and geometrical terms dB
C'	global acoustic constant, dB
CV	coefficient of variation
d	particle diameter, μm
d_{25}	particle diameter at 25th percentile, μm
d_{50}	median particle size, μm
d_{75}	particle diameter at 75th percentile, μm
E	emitted irradiance, W/cm^2
f_{mud}	fraction of mud in suspension (100% – f_{sand})
f_{sand}	fraction of sand in suspension (100% – f_{mud})
$f_{sand,\,calc}$	fraction of sand in suspension calculated using Equation 10
$f_{sand,\,meas}$	fraction of sand in suspension measured via water sample analysis
F	photon flux, W

G	turbulent shear, s^{-1}
H_s	significant wave height, m
k	wave number, m^{-1}
n	number of samples
N	number concentration of scatters, cm^{-3}
OBS	optical backscatter, V
Q_s	(back)scattering efficiency of the particles
r	one-way distance along path of acoustic pulse, m
R	one-way distance from acoustic transmitter to measurement volume, m
$R^2_{100\mu m}$	coefficient of determination for 100 μm sand
$R^2_{200\mu m}$	coefficient of determination for 200 μm sand
R^2_{bulk}	coefficient of determination for bulk sample of 100 and 200 μm sand
SCI	sediment composition index, dB
$SCI_{50\%}$	constant corresponding to a mixture of 50% sand and 50% mud, dB
SNR	signal-to-noise ratio (indicator of acoustic backscatter intensity), dB
SSC	suspended sediment mass concentration, kg/m^3
V	scattering volume, cm^3
$\overline{V_s}$	mean scattering volume, m^3
α_s	attenuation by suspended sediment, dB/m
α_w	absorption by water, dB/m
α_{OBS}	optical backscatter constant, V · m
Δ_{SCI}	the width in variation of SCI, dB
η	water level relative to mean depth during measurement period, m
λ	light wavelength, μm
μ	mean
ρ_{floc}	floc density, kg/m^3
ρ_s	solid particle (dry) density, kg/m^3
σ	standard deviation
$\overline{\sigma}$	mean backscattering cross section, m^2
τ_b	bed shear stress, Pa
$\tau_{b,c}$	bed shear stress due to currents, Pa
$\tau_{b,w}$	bed shear stress due to waves, Pa
$\tau_{cr,211\ \mu m}$	critical bed shear stress for 211 μm sand, Pa
ψ	spherical spreading constant

Acknowledgments
This work is part of the research program "Collaboration Program Water" with project number 14489 (SEAWAD), which is (partly) financed by NWO Domain Applied and Engineering Sciences. Special thanks to the Dutch Ministry of Infrastructure and Water Management (Rijkswaterstaat and Rijksrederij) for their ongoing support as part of the Kustgenese2.0 project. This work was also supported by ISblue project, Interdisciplinary graduate school for the blue planet (ANR-17-EURE-0015) and cofunded by a grant from the French government under the program "Investissements d'Avenir." DT was partly funded by the research project PHRESQUES 2, coordinated by the GIP Seine Aval and financed by the CPIER Vallée de Seine program. We are grateful to the two anonymous reviewers for their positive and constructive feedback, which has improved the quality of the manuscript.

Data Availability Statement

Data archiving for this study are currently underway, with some data already publicly available at 4TU. Centre for Research Data at https://doi.org/10.4121/collection:seawad Delft University of Technology et al. (2019). Details of this data set can be found in Van Prooijen et al. (2020) and van der Werf et al. (2019). Additional files from this study including laboratory experimental data are publicly available at: https://doi.org/10.4121/14815893.v1.

References

Aagaard, T., Black, K. P., & Greenwood, B. (2002). Cross-shore suspended sediment transport in the surf zone: A field-based parameterization. *Marine Geology*, *185*(3–4), 283–302. https://doi.org/10.1016/S0025-3227(02)00193-7

Agrawal, Y. C., & Pottsmith, H. C. (2000). Instruments for particle size and settling velocity observations in sediment transport. *Marine Geology*, *168*(1–4), 89–114. https://doi.org/10.1016/S0025-3227(00)00044-X

Amoudry, L. O., & Souza, A. J. (2011). Deterministic coastal morphological and sediment transport modeling: A review and discussion. *Reviews of Geophysics*, *49*, RG2002. https://doi.org/10.1029/2010RG000341

Bass, S. J., Aldridge, J. N., McCave, I. N., & Vincent, C. E. (2002). Phase relationships between fine sediment suspensions and tidal currents in coastal seas. *Journal of Geophysical Research*, *107*(10), 3146. https://doi.org/10.1029/2001JC001269

Bass, S. J., McCave, I. N., Rees, J. M., & Vincent, C. E. (2007). Sand and mud flux estimates using acoustic and optical backscatter sensors: Measurements seaward of the Wash, southern North Sea. *Geological Society, London, Special Publications*, *274*, 25–35. https://doi.org/10.1144/GSL.SP.2007.274.01.04

Beamsley, B. J., Black, K. P., & Healy, T. (2001). Micro-scale pumped measurements of suspended sediment over a mixed sand/mud bed: Profiles, grain sizes and sediment diffusivity. *Journal of Coastal Research*, *34*, 342–356.
Boss, E., Sherwood, C. R., Hill, P., & Milligan, T. (2018). Advantages and limitations to the use of optical measurements to study sediment properties. *Applied Sciences*, *8*(12), 2692. https://doi.org/10.3390/app8122692
Boss, E., Slade, W., & Hill, P. (2009). Effect of particulate aggregation in aquatic environments on the beam attenuation and its utility as a proxy for particulate mass. *Optics Express*, *17*(11), 9408. https://doi.org/10.1364/oe.17.009408
Boss, E., Slade, W. H., Behrenfeld, M., & Dall'Olmo, G. (2009). Acceptance angle effects on the beam attenuation in the ocean. *Optics Express*, *17*(3), 1535. https://doi.org/10.1364/oe.17.001535
Brakenhoff, L., Kleinhans, M., Ruessink, G., & Vegt, M. (2020). Spatio-temporal characteristics of small-scale wave–current ripples on the Ameland ebb-tidal delta. *Earth Surface Processes and Landforms*, *45*, 1248–1261. https://doi.org/10.1002/esp.4802
Campbell Scientific Inc. (2014). *OBS-3+ and OBS300 suspended solids and turbidity monitors* (Tech. Rep.). Logan, UT: Campbell Scientific Inc.
Chanson, H., Trevethan, M., & Aoki, S.-i. (2008). Acoustic Doppler velocimetry (ADV) in small estuary: Field experience and signal post-processing. *Flow Measurement and Instrumentation*, *19*, 307–313. https://doi.org/10.1016/j.flowmeasinst.2008.03.003
Chapalain, M., Verney, R., Fettweis, M., Jacquet, M., Le Berre, D., & Le Hir, P. (2019). Investigating suspended particulate matter in coastal waters using the fractal theory. *Ocean Dynamics*, *69*(1), 59–81. https://doi.org/10.1007/s10236-018-1229-6
Chmiel, O., Baselt, I., & Malcherek, A. (2018). Applicability of acoustic concentration measurements in suspensions of artificial and natural sediments using an acoustic Doppler velocimeter. *Acoustics*, *1*(1), 59–77. https://doi.org/10.3390/acoustics1010006
Colosimo, I., de Vet, P. L., van Maren, D. S., Reniers, A. J., Winterwerp, J. C., & van Prooijen, B. C. (2020). The impact of wind on flow and sediment transport over intertidal flats. *Journal of Marine Science and Engineering*, *8*(11), 1–26. https://doi.org/10.3390/jmse8110910
Conner, C. S., & De Visser, A. M. (1992). A laboratory investigation of particle size effects on an optical backscatterance sensor. *Marine Geology*, *108*(2), 151–159. https://doi.org/10.1016/0025-3227(92)90169-I
Dankers, P. J., & Winterwerp, J. C. (2007). Hindered settling of mud flocs: Theory and validation. *Continental Shelf Research*, *27*(14), 1893–1907. https://doi.org/10.1016/j.csr.2007.03.005
Delft University of Technology, Utrecht University, & University of Twente. (2019). *SEAWAD: SEdiment supply At the WAdden Sea ebb-tidal Delta*. 4TU.Centre for Research Data. https://doi.org/10.4121/collection:seawad
de Vet, P. L., van Prooijen, B. C., Colosimo, I., Steiner, N., Ysebaert, T., Herman, P. M., & Wang, Z. B. (2020). Variations in storm-induced bed level dynamics across intertidal flats. *Scientific Reports*, *10*(1), 1–15. https://doi.org/10.1038/s41598-020-69444-7
de Wit, F., Tissier, M., & Reniers, A. J. (2019). Characterizing wave shape evolution on an ebb-tidal shoal. *Journal of Marine Science and Engineering*, *7*(10), 1–20. https://doi.org/10.3390/jmse7100367
Downing, J. (2006). Twenty-five years with OBS sensors: The good, the bad, and the ugly. *Continental Shelf Research*, *26*(17–18), 2299–2318. https://doi.org/10.1016/j.csr.2006.07.018
Downing, J. P., Sternberg, R. W., & Lister, C. R. (1981). New instrumentation for the investigation of sediment suspension processes in the shallow marine environment. *Developments in Sedimentology*, *32*(C), 19–34. https://doi.org/10.1016/S0070-4571(08)70292-9
Eisma, D. (1993). *Suspended matter in the aquatic environment*. New York: Springer.
Elias, E. P., Van Der Spek, A. J. F., Pearson, S. G., & Cleveringa, J. (2019). Understanding sediment bypassing processes through analysis of high-frequency observations of Ameland Inlet, the Netherlands. *Marine Geology*, *415*, 10596. https://doi.org/10.1016/j.margeo.2019.06.001
Fettweis, M., Riethmüller, R., Verney, R., Becker, M., Backers, J., Baeye, M., et al. (2019). Uncertainties associated with in situ high-frequency long-term observations of suspended particulate matter concentration using optical and acoustic sensors. *Progress in Oceanography*, *178*, 102162. https://doi.org/10.1016/j.pocean.2019.102162
Fettweis, M., Sas, M., & Monbaliu, J. (1998). Seasonal, neap–spring and tidal variation of cohesive sediment concentration in the Scheldt Estuary, Belgium. *Estuarine, Coastal and Shelf Science*, *47*(1), 21–36. https://doi.org/10.1006/ecss.1998.0338
Flemming, B. W., & Ziegler, K. (1995). High-resolution grain size distribution patterns and textural trends in the backbarrier environment of Spiekeroog Island (Southern North Sea). *Senckengbergiana Maritima*, *26*, 1–24.
Flores, R. P., Rijnsburger, S., Horner-Devine, A. R., Souza, A. J., & Pietrzak, J. D. (2017). The impact of storms and stratification on sediment transport in the Rhine region of freshwater influence. *Journal of Geophysical Research: Oceans*, *122*, 4456–4477. https://doi.org/10.1002/2016JC012362
Flores, R. P., Rijnsburger, S., Meirelles, S., Horner-Devine, A. R., Souza, A. J., Pietrzak, J. D., et al. (2018). Wave generation of gravity-driven sediment flows on a predominantly sandy seabed. *Geophysical Research Letters*, *45*, 7634–7645. https://doi.org/10.1029/2018GL077936
Fugate, D. C., & Friedrichs, C. T. (2002). Determining concentration and fall velocity of estuarine particle populations using. ADV, OBS and LISST, *Continental Shelf Research*, *22*(11–13), 1867–1886. https://doi.org/10.1016/S0278-4343(02)00043-2
Gray, J., & Elliott, M. (2009). *Ecology of marine sediments* (2nd ed., 241 pp.). Oxford: Oxford University Press.
Gray, J. R., & Gartner, J. W. (2009). Technological advances in suspended-sediment surrogate monitoring. *Water Resources Research*, *46*, W00D29. https://doi.org/10.1029/2008WR007063
Green, M. O., Bell, R. G., Dolphin, T. J., & Swales, A. (2000). Silt and sand transport in a deep tidal channel of a large estuary (Manukau Harbour, New Zealand). *Marine Geology*, *163*(1–4), 217–240. https://doi.org/10.1016/S0025-3227(99)00102-4
Green, M. O., & Boon, J. D. (1993). The measurement of constituent concentrations in nonhomogeneous sediment suspensions using optical backscatter sensors. *Marine Geology*, *110*(1–2), 73–81. https://doi.org/10.1016/0025-3227(93)90106-6
Guo, C., He, Q., van Prooijen, B. C., Guo, L., Manning, A. J., & Bass, S. (2018). Investigation of flocculation dynamics under changing hydrodynamic forcing on an intertidal mudflat. *Marine Geology*, *395*, 120–132. https://doi.org/10.1016/j.margeo.2017.10.001
Ha, H. K., Hsu, W. Y., Maa, J. P., Shao, Y. Y., & Holland, C. W. (2009). Using ADV backscatter strength for measuring suspended cohesive sediment concentration. *Continental Shelf Research*, *29*(10), 1310–1316. https://doi.org/10.1016/j.csr.2009.03.001
Hanley, M. E., Hoggart, S. P., Simmonds, D. J., Bichot, A., Colangelo, M. A., Bozzeda, F., et al. (2014). Shifting sands? Coastal protection by sand banks, beaches and dunes. *Coastal Engineering*, *87*, 136–146. https://doi.org/10.1016/j.coastaleng.2013.10.020
Hawley, N. (2004). A comparison of suspended sediment concentrations measured by acoustic and optical sensors. *Journal of Great Lakes Research*, *30*(2), 301–309. https://doi.org/10.1016/S0380-1330(04)70348-2
Hendriks, H. C. M., van Prooijen, B. C., Aarninkhof, S. G., & Winterwerp, J. C. (2020). How human activities affect the fine sediment distribution in the Dutch Coastal Zone seabed. *Geomorphology*, *367*(107), 314. https://doi.org/10.1016/j.geomorph.2020.107314
Hill, D. C., Jones, S. E., & Prandle, D. (2003). Derivation of sediment resuspension rates from acoustic backscatter time-series in tidal waters. *Continental Shelf Research*, *23*(1), 19–40. https://doi.org/10.1016/S0278-4343(02)00170-X

Hill, P. S., Boss, E., Newgard, J. P., Law, B. A., & Milligan, T. G. (2011). Observations of the sensitivity of beam attenuation to particle size in a coastal bottom boundary layer. *Journal of Geophysical Research*, *116*, C02023. https://doi.org/10.1029/2010JC006539

Hill, P. S., Milligan, T. G., & Geyer, W. R. (2000). Controls on effective settling velocity of suspended sediment in the Eel River flood plume. *Continental Shelf Research*, *20*(16), 2095–2111. https://doi.org/10.1016/S0278-4343(00)00064-9

Hoitink, A. J., & Hoekstra, P. (2005). Observations of suspended sediment from ADCP and OBS measurements in a mud-dominated environment. *Coastal Engineering*, *52*(2), 103–118. https://doi.org/10.1016/j.coastaleng.2004.09.005

Holland, K. T., & Elmore, P. A. (2008). A review of heterogeneous sediments in coastal environments. *Earth-Science Reviews*, *89*(3–4), 116–134. https://doi.org/10.1016/j.earscirev.2008.03.003

Khelifa, A., & Hill, P. S. (2006). Models for effective density and settling velocity of flocs. *Journal of Hydraulic Research*, *44*(3), 390–401. https://doi.org/10.1080/00221686.2006.9521690

Kineke, G., & Sternberg, R. (1992). Using the optical backscatterance sensor. *Marine Geology*, *108*, 253–258. https://doi.org/10.1016/0025-3227(92)90199-r

Lavelle, J. W., Mofjeld, H. O., & Baker, E. T. (1984). An in situ erosion rate for a fine-grained marine sediment. *Journal of Geophysical Research*, *89*(C4), 6543–6552. https://doi.org/10.1029/JC089iC04p06543

Lenstra, K. J., Pluis, S. R., Ridderinkhof, W., Ruessink, G., & Van Der Vegt, M. (2019). Cyclic channel-shoal dynamics at the Ameland inlet: The impact on waves, tides, and sediment transport. *Ocean Dynamics*, *69*(4), 409–425. https://doi.org/10.1007/s10236-019-01249-3

Li, Y., Jia, J., Zhu, Q., Cheng, P., Gao, S., & Wang, Y. P. (2018). Differentiating the effects of advection and resuspension on suspended sediment concentrations in a turbid estuary. *Marine Geology*, *403*, 179–190. https://doi.org/10.1016/j.margeo.2018.06.001

Lin, J., He, Q., Guo, L., van Prooijen, B. C., & Wang, Z. B. (2020). An integrated optic and acoustic (IOA) approach for measuring suspended sediment concentration in highly turbid environments. *Marine Geology*, *421*(October 2019), 106062. https://doi.org/10.1016/j.margeo.2019.106062

Lodder, Q. J., Wang, Z. B., Elias, E. P., Van Der Spek, A. J., de Looff, H., & Townend, I. H. (2019). Future response of the Wadden Sea tidal basins to relative sea-level rise—An aggregated modeling approach. *Water*, *11*(10), 2198. https://doi.org/10.3390/w11102198

Lunven, M., & Gentien, P. (2000). Suspended sediments in a macrotidal estuary: Comparison and use of different sensors. *Oceanologica Acta*, *23*(3), 245–260. https://doi.org/10.1016/S0399-1784(00)00126-2

Manning, A. J., Bass, S. J., & Dyer, K. R. (2006). Floc properties in the turbidity maximum of a mesotidal estuary during neap and spring tidal conditions. *Marine Geology*, *235*(1–4 SPEC. ISS.), 193–211. https://doi.org/10.1016/j.margeo.2006.10.014

Many, G., Durrieu de Madron, X., Verney, R., Bourrin, F., Renosh, P. R., Jourdin, F., & Gangloff, A. (2019). Geometry, fractal dimension and settling velocity of flocs during flooding conditions in the Rhône ROFI, *Estuarine, Coastal and Shelf Science*, *219*, 1–13. https://doi.org/10.1016/j.ecss.2019.01.017

McCave, I. N. (1984). Erosion, transport and deposition of fine-grained marine sediments. *Geological Society, London, Special Publications*, *15*(1), 35–69. https://doi.org/10.1144/GSL.SP.1984.015.01.03

Mikkelsen, O. A., & Pejrup, M. (2001). The use of a LISST-100 laser particle sizer for in-situ estimates of floc size, density and settling velocity. *Geo-Marine Letters*, *20*(4), 187–195. https://doi.org/10.1007/s003670100064

Milligan, T. G., & Hill, P. S. (1998). A laboratory assessment of the relative importance of turbulence, particle composition, and concentration in limiting maximal floc size and settling behavior. *Journal of Sea Research*, *39*(3–4), 227–241. https://doi.org/10.1016/S1385-1101(97)00062-2

Moate, B. D., & Thorne, P. D. (2009). Measurements and inversion of acoustic scattering from suspensions having broad size distributions. *Journal of the Acoustical Society of America*, *126*(6), 2905–2917. https://doi.org/10.1121/1.3242374

Moate, B. D., & Thorne, P. D. (2012). Interpreting acoustic backscatter from suspended sediments of different and mixed mineralogical composition. *Continental Shelf Research*, *46*, 67–82. https://doi.org/10.1016/j.csr.2011.10.007

Moura, M. G., Quaresma, V. S., Bastos, A. C., & Veronez, P. (2011). Field observations of SPM using ADV, ADP, and OBS in a shallow estuarine system with low SPM concentration-Vitória Bay, SE Brazil. *Ocean Dynamics*, *61*(2–3), 273–283. https://doi.org/10.1007/s10236-010-0364-5

Mulder, J. P. M., Hommes, S., & Horstman, E. M. (2011). Ocean & Coastal Management Implementation of coastal erosion management in the Netherlands. *Ocean & Coastal Management*, *54*(12), 888–897. https://doi.org/10.1016/j.ocecoaman.2011.06.009

Nortek AS. (2005). *Vector current meter—User manual* (Tech. Rep. N 300-10 Rev. H). Vangkroken, Norway: Nortek Group.

Nortek AS. (2008). *Aquadopp high resolution—User manual* (Tech. Rep. AHR00-0101-0508). Vangkroken, Norway: Nortek AS.

Öztürk, M. (2017). Sediment size effects in acoustic Doppler velocimeter-derived estimates of suspended sediment concentration. *Water (Switzerland)*, *9*(7), 529. https://doi.org/10.3390/w9070529

Paphitis, D., & Collins, M. B. (2005). Sand grain threshold, in relation to bed 'stress history': An experimental study. *Sedimentology*, *52*(4), 827–838. https://doi.org/10.1111/j.1365-3091.2005.00710.x

Pearson, S. G., Prooijen, B. C., Elias, E. P. L., Vitousek, S., & Wang, Z. B. (2020). Sediment connectivity: A framework for analyzing coastal sediment transport pathways. *Journal of Geophysical Research: Earth Surface*, *125*, e2020JF005595. https://doi.org/10.1029/2020JF005595

Pearson, S. G., van Prooijen, B., de Wit, F., Meijer-Holzhauer, H., de Looff, A., & Wang, Z. B. (2019). Observations of suspended particle size distribution on an energetic ebb-tidal delta. *Coastal sediments 2019* (pp. 1991–2003). St. Petersburg, Florida: World Scientific. https://doi.org/10.1142/9789811204487_0172

Pomázi, F., & Baranya, S. (2020). Comparative assessment of fluvial suspended sediment concentration analysis methods. *Water*, *12*(3), 873. https://doi.org/10.3390/w12030873

Pomeroy, A. W., Storlazzi, C. D., Rosenberger, K. J., Lowe, R. J., Hansen, J. E., & Buckley, M. L. (2021). The contribution of currents, sea-swell waves, and infragravity waves to suspended-sediment transport across a coral reef-lagoon system. *Journal of Geophysical Research: Oceans*, *126*, e2020JC017010. https://doi.org/10.1029/2020JC017010

Postma, H. (1961). Suspended matter and Secchi disc visibility in coastal waters. *Netherlands Journal of Sea Research*, *1*(3), 359–390. https://doi.org/10.1016/0077-7579(61)90009-6

Reniers, A. J., de Wit, F. P., Tissier, M. F. S., Pearson, S. G., Brakenhoff, L. B., Van Der Vegt, M., et al. (2019). Wave-skewness and current-related ebb-tidal sediment transport: Observations and modeling. In *Coastal sediments 2019* (pp. 2018–2028). St. Petersburg, Florida: World Scientific. https://doi.org/10.1142/9789811204487_0174

Rijkswaterstaat. (1999). *Sedimentatlas Waddenzee* (pp. 36–38). Haren, The Netherlands: Rijkswaterstaat.

Roelvink, D., & Reniers, A. J. (2012). *A guide to modeling coastal morphology*. Singapore: World Scientific. https://doi.org/10.1142/9789814304269

Salehi, M., & Strom, K. (2011). Using velocimeter signal to noise ratio as a surrogate measure of suspended mud concentration. *Continental Shelf Research*, *31*(9), 1020–1032. https://doi.org/10.1016/j.csr.2011.03.008

Seapoint Sensors Incorporated. (2013). *Seapoint turbidity meter user manual* (Tech. Rep.). Exeter, NH: Seapoint Sensors, Inc.
Son, C. S., Flemming, B. W., & Bartholomä, A. (2011). Evidence for sediment recirculation on an ebb-tidal delta of the East Frisian barrier-island system, southern North Sea. *Geo-Marine Letters*, *31*(2), 87–100. https://doi.org/10.1007/s00367-010-0217-8
Soulsby, R. L. (1997). *Dynamics of marine sands: A manual for practical applications*. London: Thomas Telford.
Su, M., Yao, P., Wang, Z. B., Zhang, C., Chen, Y., & Stive, M. J. (2016). Conversion of electro-optical signals to sediment concentration in a silt–sand suspension environment. *Coastal Engineering*, *114*, 284–294. https://doi.org/10.1016/j.coastaleng.2016.04.014
Sutherland, T. F., Lane, P. M., Amos, C. L., & Downing, J. (2000). The calibration of optical backscatter sensors for suspended sediment of varying darkness levels. *Marine Geology*, *162*(2–4), 587–597. https://doi.org/10.1016/S0025-3227(99)00080-8
Thorne, P. D., & Hanes, D. M. (2002). A review of acoustic measurement of small-scale sediment processes. *Continental Shelf Research*, *22*(4), 603–632. https://doi.org/10.1016/S0278-4343(01)00101-7
Thorne, P. D., Hardcastle, P. J., & Soulsby, R. L. (1993). Analysis of acoustic measurements of suspended sediments. *Journal of Geophysical Research*, *98*(92), 899–910. https://doi.org/10.1029/92JC01855
Thorne, P. D., & Hurther, D. (2014). An overview on the use of backscattered sound for measuring suspended particle size and concentration profiles in non-cohesive inorganic sediment transport studies. *Continental Shelf Research*, *73*, 97–118. https://doi.org/10.1016/j.csr.2013.10.017
Thorne, P. D., Lichtman, I. D., & Hurther, D. (2021). Acoustic scattering characteristics and inversions for suspended concentration and particle size above mixed sand and mud beds. *Continental Shelf Research*, *214*, 104320. https://doi.org/10.1016/j.csr.2020.104320
Thorne, P. D., & Meral, R. (2008). Formulations for the scattering properties of suspended sandy sediments for use in the application of acoustics to sediment transport processes. *Continental Shelf Research*, *28*(2), 309–317. https://doi.org/10.1016/j.csr.2007.08.002
van de Kreeke, J., & Hibma, A. (2005). Observations on silt and sand transport in the throat section of the Frisian Inlet. *Coastal Engineering*, *52*(2), 159–175. https://doi.org/10.1016/j.coastaleng.2004.10.002
Van Der Hout, C. M., Witbaard, R., Bergman, M. J. N., Duineveld, G. C. A., Rozemeijer, M. J. C., & Gerkema, T. (2017). The dynamics of suspended particulate matter (SPM) and chlorophyll-*a* from intratidal to annual time scales in a coastal turbidity maximum. *Journal of Sea Research*, *127*, 105–118. https://doi.org/10.1016/j.seares.2017.04.011
Van Der Werf, J., Antolínez, J. A. Á., Brakenhoff, L., Gawehn, M., den Heijer, K., de Looff, H., et al. (2019). *Datareport Kustgenese 2.0* (Tech. Rep. 1220339-015-ZKS-0004). Delft, The Netherlands: Rijkswaterstaat.
van Prooijen, B. C., Tissier, M. F., de Wit, F. P., Pearson, S. G., Brakenhoff, L. B., van Maarseveen, M. C., et al. (2020). Measurements of hydrodynamics, sediment, morphology and benthos on Ameland ebb-tidal delta and lower shoreface. *Earth System Science Data*, *12*(4), 2775–2786. https://doi.org/10.5194/essd-12-2775-2020
Voulgaris, G., & Meyers, S. T. (2004). Temporal variability of hydrodynamics, sediment concentration and sediment settling velocity in a tidal creek. *Continental Shelf Research*, *24*(15), 1659–1683. https://doi.org/10.1016/j.csr.2004.05.006
Wang, Z. B., Elias, E. P., Van Der Spek, A. J., & Lodder, Q. J. (2018). Sediment budget and morphological development of the Dutch Wadden Sea: Impact of accelerated sea-level rise and subsidence until 2100. *Netherlands Journal of Geosciences*, *97*(3), 183–214. https://doi.org/10.1017/njg.2018.8
Weeks, A. R., Simpson, J. H., & Bowers, D. (1993). The relationship between concentrations of suspended particulate material and tidal processes in the Irish Sea. *Continental Shelf Research*, *13*(12), 1325–1334. https://doi.org/10.1016/0278-4343(93)90086-D
WETLabs. (2010). *ECO 3-measurement sensor user's guide* (Tech. Rep.). Philomath, OR: WET Labs, Inc.
WET Labs Inc. (2019). *User manual: ECO fluorometers and scattering sensors* (Tech. Rep.). Philomath, OR: WET Labs Inc.
White, T. E. (1998). Status of measurement techniques for coastal sediment transport. *Coastal Engineering*, *35*(1–2), 17–45. https://doi.org/10.1016/S0378-3839(98)00033-7
Wilson, G. W., & Hay, A. E. (2015). Measuring multi-phase particle flux with a multi-frequency acoustic profiler. *Proceedings of the Institute of Acoustics*, *37*, 343–3819. https://doi.org/10.1121/1.4938219
Winkelmolen, A. M., & Veenstra, H. J. (1974). Size and shape sorting in a Dutch tidal inlet. *Sedimentology*, *21*(1), 107–126. https://doi.org/10.1111/j.1365-3091.1974.tb01784.x
YSI Incorporated. (2012). *6-Series multiparameter water quality Sondes user manual* (revision j ed., 374 pp.). Yellow Springs, OH: YSI Incorporated.
Zhu, Q., van Prooijen, B. C., Maan, D. C., Wang, Z. B., Yao, P., Daggers, T., & Yang, S. L. (2019). The heterogeneity of mudflat erodibility. *Geomorphology*, *345*, 106834. https://doi.org/10.1016/j.geomorph.2019.106834

Reference From the Supporting Information

Aminot, A., & Kérouel, R. (2004). *Hydrologie des écosystèmes marins: Paramètres et analyses* (1 ed., 336 pp.). IFREMER.

Assessment of erosion, sedimentation, and water quality impacts of the Mountain Valley Pipeline and Equitrans Expansion Project's proposed crossing of the Jefferson National Forest as it pertains to the U.S. Forest Service's Draft Supplemental Environmental Impact Statement dated December 2022

Prepared by Jonathan A. Czuba, Ph.D., Licensed Professional Engineer - February 9, 2023

REFERENCES
9

February 21, 2023

Technological advances in suspended-sediment surrogate monitoring

John R. Gray[1] and Jeffrey W. Gartner[2]

Received 22 April 2008; revised 26 November 2008; accepted 30 December 2008; published 6 March 2009.

[1] Surrogate technologies to continuously monitor suspended sediment show promise toward supplanting traditional data collection methods requiring routine collection and analysis of water samples. Commercially available instruments operating on bulk optic (turbidity), laser optic, pressure difference, and acoustic backscatter principles are evaluated based on cost, reliability, robustness, accuracy, sample volume, susceptibility to biological fouling, and suitable range of mass concentration and particle size distribution. In situ turbidimeters are widely used. They provide reliable data where the point measurements can be reliably correlated to the river's mean cross section concentration value, effects of biological fouling can be minimized, and concentrations remain below the sensor's upper measurement limit. In situ laser diffraction instruments have similar limitations and can cost 6 times the approximate $5000 purchase price of a turbidimeter. However, laser diffraction instruments provide volumetric-concentration data in 32 size classes. Pressure differential instruments measure mass density in a water column, thus integrating substantially more streamflow than a point measurement. They are designed for monitoring medium-to-large concentrations, are generally unaffected by biological fouling, and cost about the same as a turbidimeter. However, their performance has been marginal in field applications. Acoustic Doppler profilers use acoustic backscatter to measure suspended sediment concentrations in orders of magnitude more streamflow than do instruments that rely on point measurements. The technology is relatively robust and generally immune to effects of biological fouling. Cost of a single-frequency device is about double that of a turbidimeter. Multifrequency arrays also provide the potential to resolve concentrations by clay silt versus sand size fractions. Multifrequency hydroacoustics shows the most promise for revolutionizing collection of continuous suspended sediment data by instruments that require only periodic calibration for correlation to mean concentrations in river cross sections. Broad application of proven suspended sediment surrogate technologies has the potential to revolutionize fluvial sediment monitoring. Once applied, benefits could be enormous, providing for safer, more frequent and consistent, arguably more accurate, and ultimately less expensive sediment data for managing the world's sedimentary resources.

Citation: Gray, J. R., and J. W. Gartner (2009), Technological advances in suspended-sediment surrogate monitoring, *Water Resour. Res.*, *45*, W00D29, doi:10.1029/2008WR007063.

1. Introduction

[2] Fluvial sediment and sorbed materials are the most widespread pollutants affecting United States (U.S.) rivers and streams (http://iaspub.epa.gov/waters/national_rept.control#TOP_IMP). The need for reliable, comparable, cost-effective, spatially and temporally consistent data to quantify the clarity and sediment content of waters of the U.S. has never been greater. The number of sites at which the U.S. Geological Survey (USGS) collected nationally consistent daily sediment data in 2006 was about a quarter of the number operated in 1981 (D. W. Stewart, personal communication, 2008). This precipitous decrease in sediment monitoring over a quarter century by the USGS, the federal agency responsible for collecting, archiving, and disseminating the nation's water data, including fluvial sediment [*Glysson and Gray*, 1997], is due to a number of factors, principally cost [*Gray*, 2003a, 2003b]. The decrease in monitoring is of particular concern, given that the physical, chemical, and biological damages attributable to fluvial sediment in North America alone are estimated to range between $20 billion and $50 billion annually [*Pimentel et al.*, 1995; *Osterkamp et al.*, 1998, 2004]. Given this dearth in adequate, consistent, and reliable data describing fluvial sediment fluxes, decision makers responsible for mitigating its deleterious effects are at best hard-pressed to develop technically supportable management and remedial plans.

[3] Historically, riverine suspended sediment data in the U.S. have been produced by gravimetric analyses performed on water sediment samples collected manually or by automatic samplers [*Edwards and Glysson*, 1999; *Bent et al.*,

[1]U.S. Geological Survey, Reston, Virginia, USA.
[2]U.S. Geological Survey, Tucson, Arizona, USA.

2003; *Nolan et al.*, 2005; *Davis*, 2005; *Gray et al.*, 2008]. These data collection methods tend to be expensive, difficult, labor intensive, and hazardous under some conditions. Specialized equipment and considerable training are prerequisites for obtaining reliable samples and results. The characteristic paucity of the derived data may be inadequate for defining the variability in suspended sediment concentrations (SSC) and particle size distributions (PSD), particularly for periods of storm runoff. Consequently, temporal interpolations and calibrations along with spatial corrections to the data are commonly required to develop the requisite SSC time series used with an associated time series of water discharge data to produce subdaily and daily records of suspended sediment discharges [*Porterfield*, 1972; *Koltun et al.*, 2006].

[4] Existing and emerging sediment surrogate technologies may provide the types and density of fluvial sediment data needed to improve sediment discharge computations in a range of river types and sedimentological conditions [*Gray and Gartner*, 2004]. Potentially useful instruments and methods for inferring selected physical characteristics of fluvial sediments [*Gartner et al.*, 2003; *Bogen et al.*, 2003; *Gray*, 2005; *Gray et al.*, 2003b, 2003c] are being developed and tested around the world. Through the informal Sediment Monitoring Instrument and Analysis Research Program [*Gray*, 2003a, 2003b], the USGS is testing instruments operating on bulk optic (turbidity), laser optic, pressure difference, and acoustic backscatter principles in U.S. rivers and in laboratory settings for measuring selected characteristics of suspended sediment, bed load, and bed material. To make the transition from research to operational applications, these new technologies must be rigorously tested with respect to accuracy and reliability in different physiographic settings, and their performances must be compared to the aforementioned traditional techniques. The performance comparisons should include concurrent collection of data by traditional and new techniques for a sufficient ''shake-out'' period, probably years, to identify and minimize changes in bias and precision between the old and new technologies.

[5] Even after the ''shake-out'' period, each of the four in situ technologies will require periodic calibration in field applications to define the relation of the surrogate measurement to the mean value in the cross section [*Porterfield*, 1972]. However, the need for routine calibration is expected to diminish over time.

[6] None of the technologies examined herein represents a panacea for sediment monitoring at all rivers under all flow and sediment transport conditions. However, with careful matching of proven monitoring technologies to the physical and sedimentological characteristics of selected river reaches, it may be possible in the coming years to remotely and continuously monitor suspended sediment discharges, in some cases by particle size class, with sufficient reliability to store the information as public-releasable data in the USGS National Water Information System (http://waterdata.usgs.gov/nwis). Calculation and publication of some uncertainties associated with variables used in computations of SSC and suspended sediment discharge records in a variety of river types over a large range of flow and sedimentary regimes may also be possible (http://ks.water.usgs.gov/Kansas/rtqw/sites/06892350/htmls/2005/p63680_2005_all_uv.shtml).

[7] The prospect of large-scale application of proven suspended sediment surrogate technologies is a revolutionary concept in fluvial sedimentology when considered from a worldwide or even national perspective. The benefits of such applied capability could be enormous, providing for safer, more frequent and consistent, arguably more accurate, and ultimately less expensive fluvial sediment data collection for use in managing the world's sedimentary resources.

[8] This paper describes four commercially available surrogate technologies that operate on bulk optic (turbidity), laser optic, pressure difference, or acoustic backscatter principles for monitoring SSC and in some cases PSD. These technologies are being evaluated in field settings by the USGS with varying degrees of promise toward providing continuous, largely automated subdaily time series of SSC data in rivers. The paper begins with a description of traditional techniques for suspended sediment sampling, against which the surrogate technologies are evaluated. Descriptions of the theory, applications, evaluations, and some advantages and limitations of each technology are presented and compared.

1.1. Background: Traditional Suspended Sediment Sampling Techniques in the United States

[9] Instruments and methods for collecting fluvial-sediment data in the U.S. have evolved considerably since 1838 when Captain Andrew Talcott of the U.S. Army Corps of Engineers first sampled the Mississippi River [*Federal Interagency Sedimentation Project*, 1940]. The earliest suspended sediment samples were collected by use of instantaneous samplers, such as open containers or pails. By 1939, at least nine different types of sediment samplers were being used by U.S. agencies. Most of the samplers had been developed by independent investigators, lacked calibrations, and were deployed using a variety of methods. A 1930s survey of sediment sampling equipment used in the U.S. indicated that the 30 instantaneous samplers studied had limited usefulness either because of poor intake velocity characteristics or because of the short filament of water-sediment mixture sampled [*Federal Interagency Sedimentation Project*, 1940; *Nelson and Benedict*, 1950; *Glysson*, 1989].

[10] In 1939, six federal agencies and the Iowa Institute of Hydraulic Research organized a committee to consider the development of sediment samplers, sampling techniques, and laboratory procedures and to coordinate such work among the federal agencies ''actively concerned with the sedimentation problem'' [*U.S. Department of Agriculture*, 1965]. This committee has evolved into the present-day Subcommittee on Sedimentation, Technical Committee, and Federal Interagency Sedimentation Project (FISP) [*Skinner*, 1989; *Glysson and Gray*, 1997; http://acwi.gov/sos/]. The purpose of the FISP is to study methods and equipment used in measuring the sediment discharge of streams and to improve and standardize equipment and methods where practicable.

[11] The bulk of suspended-sediment data obtained by federal agencies using traditional sampling techniques are collected by isokinetic samplers and methods developed by the *Federal Interagency Sedimentation Project* [2008] and described by *Edwards and Glysson* [1999], *Davis* [2005], *Nolan et al.* [2005], and *Gray et al.* [2008]. These include

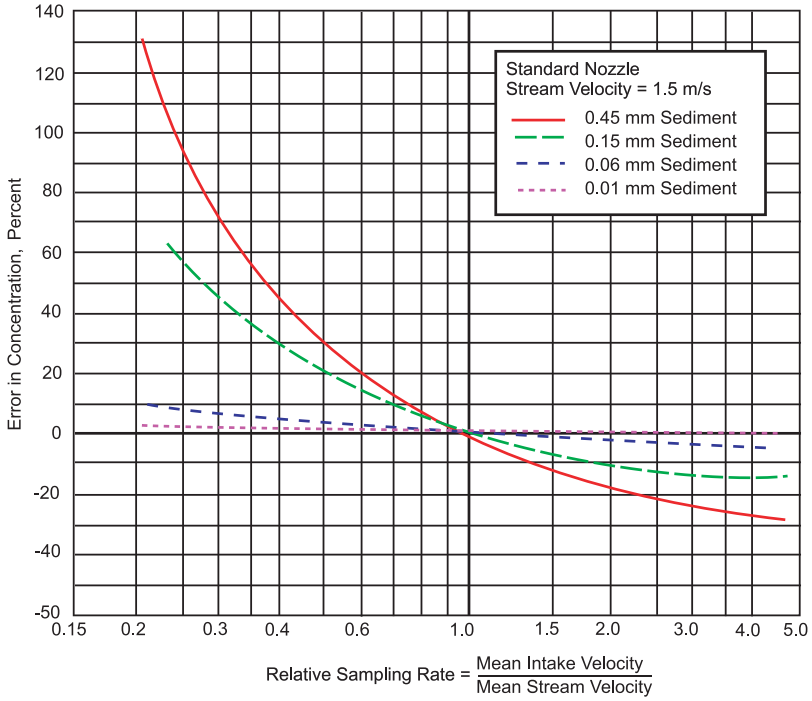

Figure 1. Effect of sampling rate on measured suspended-sediment concentrations for four sediment-size distributions. From *Gray et al.* [2008]; adapted from the *Federal Interagency Sedimentation Project* [1941].

samplers with rigid sample bottles (bottle samplers) and flexible bags (bag samplers) that fill at a rate determined by the product of the ambient stream velocity at the sampler nozzle and the nozzle's area. These samplers, ranging in mass from 2 to 125 kg, are designed to collect a representative velocity-weighted sample of the water-sediment mixture at the deployment location within the sampler's flow velocity and transit rate limits. FISP isokinetic samplers are designed to ensure that the water velocity entering the nozzle is within about 10 percent of the stream velocity incident on the sampler throughout the samplers′ operable velocity range to minimize bias in SSC and PSD measurements. Figure 1 shows the effect of sampling rate on measured SSCs for four PSDs [*Gray et al.*, 2008].

[12] A list of FISP samplers and selected attributes is provided by *Davis* [2005] and *Gray et al.* [2008]. Examples of a rigid-bottle sampler, the U.S. D-74, and a bag sampler, the U.S. D-96, are shown in Figure 2.

[13] When deployed using either the equal discharge increment (EDI) or equal width increment (EWI) sampling method [*Edwards and Glysson*, 1999; *Nolan et al.*, 2005], an isokinetic sampler integrates a sample proportionally by velocity and area, resulting in a discharge-weighted sample that contains a concentration and size distribution representative of the suspended material in transport throughout the cross section at the time that the sample is collected.

[14] Although manual isokinetic samplers have considerable benefits, most notably the acquisition of demonstrably reliable suspended-sediment data from rivers, they have consequential drawbacks. For example, total noncapital costs associated with manual deployment of isokinetic samplers (about a half-person day for consecutive EDI or EWI samples per site excluding transportation) and subsequent analytical costs (typically tens to hundreds of dollars depending on types of analyses) can be substantial with respect to available resources. Safety issues are paramount whenever a hydrographer works in, over, or near a stream. The time and effort required to collect manual samples by traditional methods precludes their use to resolve high-frequency sediment transport dynamics. The sparse temporal distribution of the derivative data, often a single observation or less per day, requires that daily load computations be based on estimated concentration values and (or) stochastically indexed to another more plentiful if imperfect predictive data source such as river discharge through sediment transport curves [*Glysson*, 1987; *Gray and Simões*, 2008].

1.2. Performance Criteria for Data Produced by Sediment Surrogate Technologies

[15] A number of advances in surrogate technologies used to compute SSCs and in some cases PSDs have been made in recent decades. However, verification data, particularly certifiably reliable verification data covering the broad range of flow and sedimentological conditions, are often lacking.

[16] Validation of a sediment surrogate technology requires evaluation criteria and a well-conceived and well-administered testing program [*Gray et al.*, 2002; *Gray and Glysson*, 2005]. Following are some qualitative criteria for selecting and deploying a surrogate technology:

[17] 1. Capital, operating, and analytical costs should be affordable with respect to the objectives of the program in which the monitoring instrument is deployed.

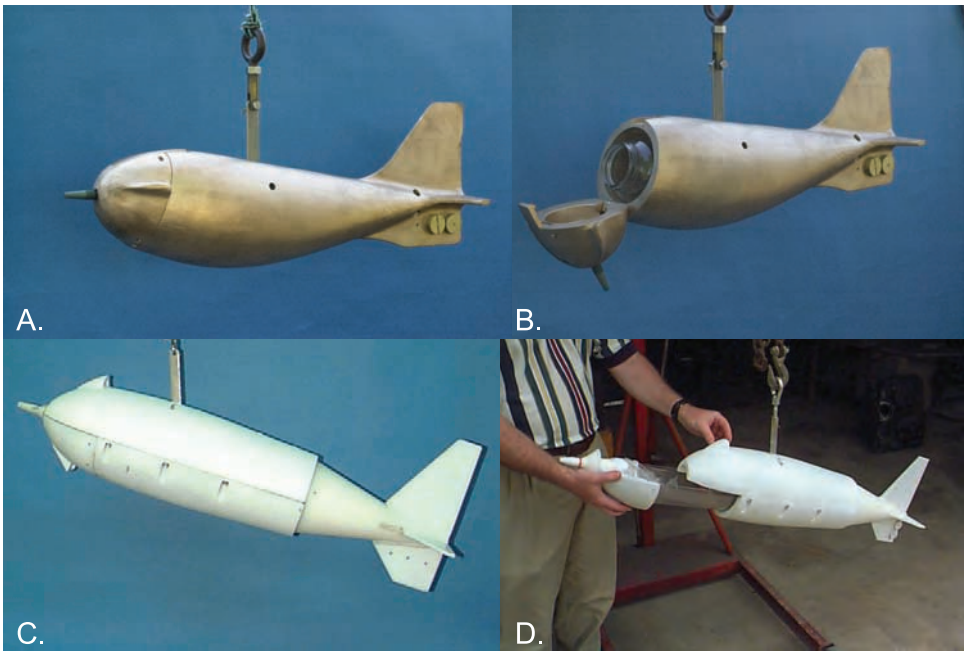

Figure 2. Two Federal Interagency Sedimentation Project suspended-sediment samplers: A U.S. D-74 suspended-sediment rigid bottle sampler (a) closed and (b) open; a U.S. D-96 flexible-bag suspended-sediment sampler (c) closed and (d) with tray containing flexible bag partially open.

[18] 2. The technology should be able to measure SSC, and in some cases PSD, throughout the range of interest.

[19] 3. The instrument should be robust and reliable; that is, prone to neither failure nor signal drift.

[20] 4. The technology should be sufficiently simple to deploy and operate by a field technician with a reasonable amount of appropriate training.

[21] 5. The derived data should be relatively simple and straightforward to use in subsequent computations and (or) accompanied by standard analytical procedures as computational routines for processing the derived data.

[22] Quantitative criteria for acceptable accuracies of the derived data are difficult to develop for all potential applications, in part because of significant differences in river sedimentary and flow regimes. For example, accuracy criteria for rivers transporting mostly silt and clay in suspension should be set more stringently (intolerant of larger-magnitude uncertainties) than those for rivers that transport comparatively large fractions of sand. However, there is a clear need for consistency in PSD and SSC criteria on the part of instrument developers, marketers, and users.

[23] To this end, acceptance criteria developed for PSD and SSC data produced by a laser diffraction instrument [*Gray et al.*, 2002] have been generalized for evaluating data from any suspended sediment surrogate instrument. At least 90% of PSD values between 0.002 and 0.5 mm median diameter are required to be ±25% of true median diameters. Absent a more rigorous evaluation, this criterion has been applied to all particle sizes in suspension.

[24] SSC acceptance criteria range from ±50% uncertainty at lowest SSCs to ±15% uncertainty for SSC's exceeding 1 g/L. The criteria presented in Table 1 are adapted from *Gray et al.* [2002].

[25] These criteria pertain solely to the performance of a surrogate technology within its physical realm of measurement. Routine calibrations to correlate instrument signals to mean cross-sectional SSC values are required for all of the in situ instruments presented herein.

[26] Because of the spatial and temporal variability in river sedimentological regimes, only generalities regarding the expected range of SSCs and PSDs in rivers can be made in the absence of site-specific data. *Rainwater* [1962] produced an empirically derived map of the 48 conterminous U.S showing mean SSCs for rivers (generalized for the entire land area) over seven logarithmically based SSC ranges. The SSC ranges were computed from measurements of the annual suspended sediment load divided by the annual streamflow. Computed SSC values in the largest range exceeded about 48 g/L. Using a similar computational scheme, *Meade and Parker* [1985] and the U. S. Geological Survey (http://co.water.usgs.gov/sediment/conc.frame.html) simplified the *Rainwater* [1962] map to show areas characterized by SSC in the following ranges: less than 0.3 g/L;

Table 1. Acceptance Criteria for Suspended-Sediment Concentrations[a]

Suspended-Sediment Concentration Minimum, g/L	Suspended-Sediment Concentration Maximum, g/L	Acceptable Uncertainty, %
0	<0.01	50
0.01	<0.1	50–25 computed linearly
0.1	<1.0	25–15 computed linearly
1.0	–	15

[a]Suspended-sediment data produced are considered acceptable when they meet these criteria 95 percent of the time [*Gray et al.*, 2002].

0.3–2 g/L; 2–6 g/L; and more than 6 g/L. These maps can serve as initial, general indicators of the suitability of a selected sediment surrogate technology in a river reach of interest.

[27] Additional information on the range of SSCs in U.S. rivers is available from *Smith et al.* [1987], who computed percentile values for SSC data collected at 267 USGS streamgages in medium and large river basins as part of the original USGS National Stream Quality Accounting Network (NASQAN) (http://water.usgs.gov/nasqan/). The 25th, 50th, and 75th SSC percentiles were 0.02, 0.07, and 0.19 g/L, respectively. In 1995, the NASQAN network was redesigned to focus on the nation's largest rivers basins, the Mississippi (including the Missouri and Ohio), Columbia, and Colorado rivers and the Rio Grande. A. Horowitz (personal communication, 2008) calculated the 10th, 25th, 50th, 75th, and 90th SSC percentiles for the 41 NASQAN streamgages in these large river basins for the period 1994–2006 as 0.01, 0.03, 0.12, 0.32, and 0.74 g/L, respectively.

[28] Many streams transport near-zero SSCs at various times. On the other extreme, SSCs measured during surface runoff from 1989 to 1991 in the Little Colorado River basin, Arizona and New Mexico, commonly exceeded 100 g/L [*Graf et al.*, 1995]. Maximum SSC values measured at the USGS streamgage on the Paria River at Lees Ferry, Arizona, have exceeded 1000 g/L [*Beverage and Culbertson*, 1964].

[29] In general, most of a river's annual sediment budget is transported during infrequent high-flow periods concomitant with high SSCs. Any proposed suspended sediment surrogate technology deployment should take into consideration not only the statistics quoted above but also the potential maximum SSC and, where appropriate, maximum particle sizes that might be transported in the period of interest.

[30] After surrogate technology efficacy is resolved, cost considerations are often of penultimate interest. The cost of producing reliable, quality-assured suspended sediment data can be separated into four categories: (1) the purchase price of the instrument; (2) other capital costs associated with installation and initial operation of the instrument; (3) operational costs to maintain and calibrate the instrument; and (4) analytical costs to evaluate, reduce, compute, review, store, and publish the derivative data.

[31] Of these four categories, only the current purchase price is straightforward to quantify. The others are dependent on a number of factors, including site location and physical characteristics, hydrological and sedimentological regime, availability of electrical power, limitations associated with accessibility, safety considerations, and the time and complexity associated with data analysis. Additionally, any such cost information inevitably becomes obsolete due, in part, to technological advances, marketing competition, and changes in currency valuation. Hence, the relative purchase prices are proffered for the surrogate instruments described herein versus the actual (summer 2008) purchase price for the most common of the instruments, an in situ fully equipped turbidimeter. In some instances, other relevant cost information for a given technology that is considered reliable is provided. That information may be considered in light of the fact that the cost to compute, store, and provide daily sediment discharge data at a USGS streamgage in 2001 (adjusted for inflation in 2008 dollars) ranged from $24,000 to $78,000 [*Gray*, 2003a].

2. Technological Advances in Suspended Sediment Surrogate Monitoring

[32] The need for more affordable time series data representing an expanded suite of measurements recorded on subdaily intervals at less risk to field personnel, coupled with advanced technological capabilities, is leading to a new era in fluvial sediment monitoring. The following sections describe theoretical principles [*Gray and Gartner*, 2004], selected examples of field applications, and advantages and limitations of four technologies considered by the USGS to hold varying degrees of promise for use in large-scale monitoring programs.

2.1. Bulk Optics (Turbidity)

2.1.1. Background and Theory

[33] Turbidity is an expression of the optical properties of a sample that causes light rays to be scattered and absorbed rather than transmitted in straight lines through the sample [*Ziegler*, 2003; *Anderson*, 2005]. Measurements of turbidity are the most common means for determining water clarity and computing SSCs in U.S. rivers [*Pruitt*, 2003].

[34] A number of commercially available optical instruments operate on one of two basic bulk-optic (hereafter referred to as turbidity) principles: transmissometry and nephelometry. Transmissometers employ a light source beamed directly at a light detector. The instrument measures the fraction of visible light from a collimated light source (typically at about 660 nm) that reaches the detector. The fraction of light reaching the detector is converted to a beam attenuation coefficient, which is related to SSC.

[35] Nephelometry is the measurement of light scattering usually with a light detector at 90° from the incident light (adapted from *U.S. Environmental Protection Agency* [1999]) in visible or infrared (IR) spectra. Most laboratory turbidimeters measure 90° scattering. According to *D&A Instrument Company* [1991], optical backscatterance (OBS) instruments collectively are a type of nephelometer designed to measure backscattered (140°–165°) IR in a small (concentration-dependent) volume on the order of a few cubic centimeters. Transmittance and scatterance are functions of the number, size, color, index of refraction, and shape of suspended particles [*Conner and De Visser*, 1992; *Sutherland et al.*, 2000]. Figure 3 shows examples of five types of nephelometry sensors.

[36] A wide variety of turbidimeters are available for calculating SSC. For example, *Landers* [2003] describes bench tests as part of a workshop at which variances in measurements from nine different types of turbidimeters using blind reference samples were evaluated. One instrument that was first described in the early 1980s [*Downing et al.*, 1981; *Downing*, 1983] and is now widely used for in situ applications is the OBS-3 (originally manufactured by the D&A Instrument Company, now Campbell Scientific, Inc.). (Use of any trade or firm names in this report is for identification purposes only and does not constitute endorsement by the U.S. Government.)

[37] Turbidity instruments lack moving parts (unless outfitted with optical wipers), can be deployed in situ, and provide rapid-sampling capability. Site-specific empirical

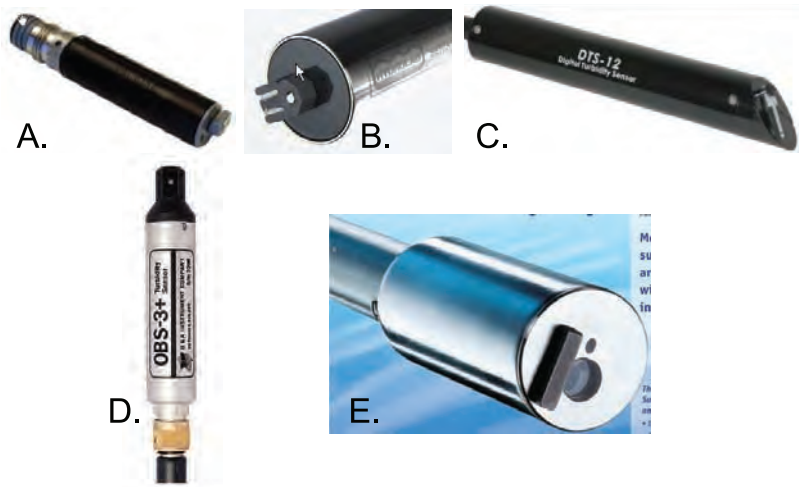

Figure 3. Photographs showing nephelometry sensors: (a) YSI model 6136, (b) Hydrolab turbidity sensor with wiper, and (c) Forrest Technology Systems model DTS-12. (d) D&A Instrument Company model OBS 3+, and (e) Hach OptiQuant with wiper.

calibrations are required to convert measurements to reliable cross-sectional SSC estimates. The technology is relatively mature and has been shown to provide reliable data at a number of USGS streamgages [*Schoellhamer and Wright*, 2003; *Melis et al.*, 2003; *Uhrich*, 2002; *Uhrich and Bragg*, 2003; *Rasmussen et al.*, 2005] and other sites [*Pratt and Parchure*, 2003; *Lewis*, 2002]. The cost of an in situ turbidimeter with sonde (sensor), wiper, and controller in 2008 was about $5000. The purchase price of an OBS without a wiper but with cable was about equal to the fully equipped in situ nephelometric turbidimeter cost.

[38] Maximum SSC limits for these instruments depend in part on PSDs. The OBS has a generally linear response at SSC less than about 2 g/L for clay and silt and 10 g/L for sand [*Ludwig and Hanes*, 1990], although *Kineke and Sternberg* [1992] describe the capability to measure SSC up to about 320 g/L (in the nonlinear region of the OBS response curve). The specification sheet for the OBS-5+ manufactured by Campbell Scientific (http://www.campbellsci.com/index.cfm) lists an applicable range of up to 500 g/L (specific gravity 1.3). The upper SSC limit for transmissometers depends on optical path length, but may be as low as about 0.05 g/L [*D&A Instrument Company*, 1991]. Thus, transmissometers are more sensitive at low SSC whereas optical backscatter sensors have superior linearity in turbid water [*Downing*, 1996]. In general, the wider a turbidimeter's turbidity measurement range, the less precise the within-range derived turbidity data, and vice versa.

[39] Biological fouling of sensor optical windows remains a problem. Biological fouling results in a tendency for the output to shift from the calibration curve to spuriously larger values over timescales of days or more, particularly in warmer, microbiologically active waters. Commercially available mechanical wiper systems available with some sensors may alleviate this problem.

[40] Because of the relation between OBS signal response and PSD, OBS (like all single-frequency optical instruments) is best suited for application at sites with relatively stable PSDs. For a given mass SSC, OBS response increases with decreasing particle size [*Conner and De Visser*, 1992; *Downing*, 1996; *Sutherland et al.*, 2000]. OBS signal response is minimally affected by changes in PSD in the range of 200–400 μm and greatly affected by changes when particles are smaller than about 44 μm [*Conner and De Visser*, 1992]. *Conner and De Visser* [1992] caution against using OBS in environments where changes in PSDs occur and particle sizes are less than 100μm. Additionally, the OBS signal can vary as a function of particle color. *Sutherland et al.* [2000] found a strong correlation between observed and predicted OBS measurements of varying SSC and ratios of black and white suspended sediment. They found the smallest OBS signal-gain response for black sediment and the largest for white sediment, with responses from other colors falling between. They suggest that the level of blackness of particles acts to absorb the near-infrared signal of the OBS, thus modifying its output. Hence, caution should be exercised in deployments under varying particle size and particle color conditions, unless the instrument is recalibrated for ambient conditions.

2.1.2. Example Field Evaluation

[41] Continuous turbidity measurements have been shown to provide reliable continuous SSC values with a quantifiable uncertainty at the USGS streamgage on the Kansas River at DeSoto, Kansas since the 1990s. Simple linear regression analysis explained by *Christensen et al.* [2000] was used to develop a site-specific univariate model using turbidity to compute SSC (Figure 4). The model explains about 93% of the variance in SSC. Continuous suspended sediment discharge values computed from the model and subdaily time series water discharge data are available online (http://ks.water.usgs.gov/Kansas/rtqw/sites/06892350/htmls/2005/p63680_2005_all_uv.shtml). The advantages of regression-based estimates using continuous turbidity measurements over discrete sample collection are that regardless of flow conditions, SSC and sediment discharge values are obtained essentially continuously at the interval in which water discharges are recorded.

[42] Some researchers are using variables in addition to turbidity to compute time series of SSC. J. D. Jastram et al. (A comparison of streamflow-based and turbidity-based estimates of suspended sediment concentrations in three

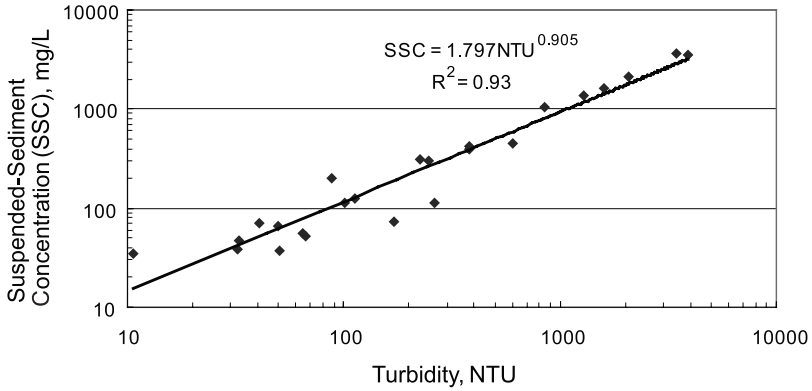

Figure 4. Linear regression comparing field turbidity in nephelometric turbidity units and instantaneous suspended-sediment concentrations in milligrams per liter for the Kansas River at DeSoto, Kansas, 1999 through 2002. From *Gray et al.* [2003a].

Chesapeake Bay tributaries, submitted to *U.S. Geological Survey Scientific Investigations Report*, 2009) have monitored turbidity at a USGS streamgage on the James River at Cartersville, Virginia, since 2003. Figure 5 shows a time series of computed SSC, sampled SSC, and streamflow data for this station from 22 October 2006 to 30 April 2007. The continuous SSC data were computed by a multiple regression technique from square root-transformed time series data describing turbidity, streamflow, and water temperature. The model explains about 97% of the variance in SSC.

[43] *Schoellhamer et al.* [2002] describe a multistation, multiyear field investigation to continuously monitor SSC in California's San Francisco Bay and Delta system that began in 1991. As of 2002, the program consisted of 13 monitoring stations (with OBS sensors at multiple depths) at which a cumulative 159 years of sensor data have been collected. OBS sensors are calibrated with water samples

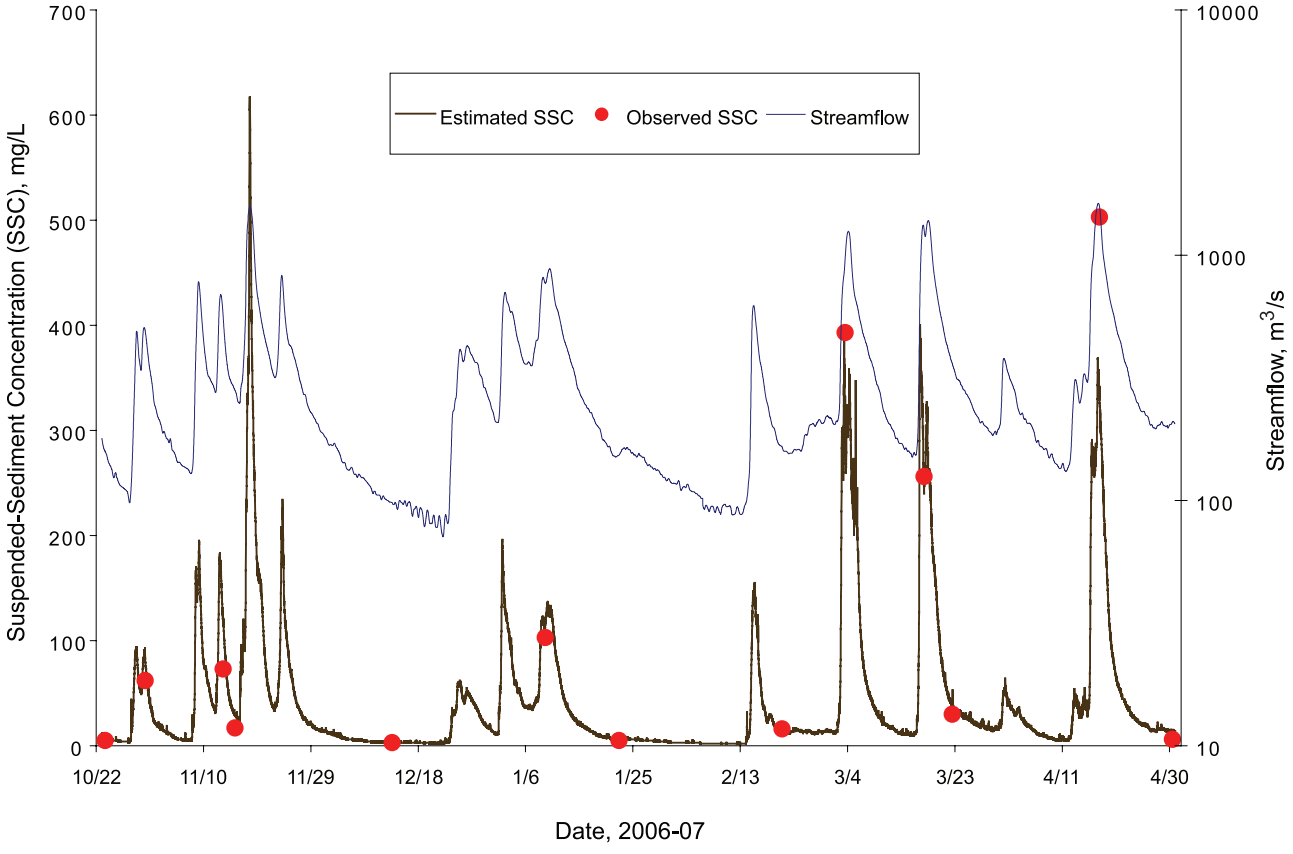

Figure 5. Time series plot of continuous suspended-sediment concentrations (computed by multiple linear regression from square root-transformed time series of turbidity, streamflow, and water temperature data), sampled SSCs in milligrams per liter, and streamflow in cubic meters per second for the James River at Cartersville, Virginia, 22 October 2006 to 30 April 2007. From Jastram et al. (submitted manuscript, 2009).

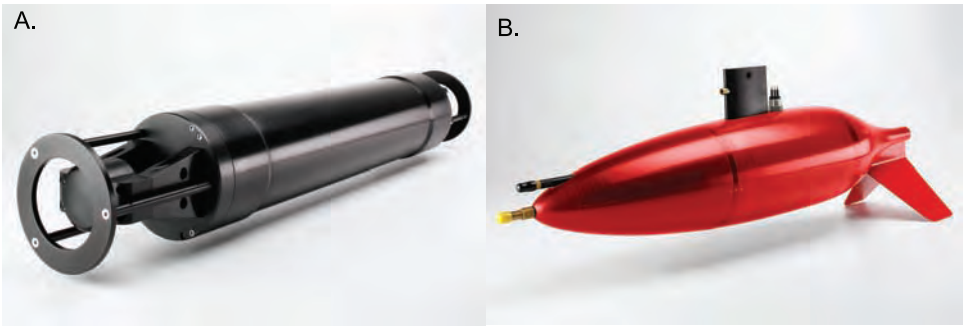

Figure 6. Laser in situ scattering and transmissometers: (a) a LISST-100 in situ instrument; (b) a LISST-SL (streamlined) manually deployable instrument. Photographs courtesy of Sequoia Scientific, Inc.

collected by Van Dorn sampler (or U.S. P-72 point sampler prior to 1994) [*Davis*, 2005] before and after sensor cleaning at each sensor location. As an example of data quality, results from the 1997 water year from 15 records at eight stations in San Francisco Bay had an average of about 59% data considered acceptable (after deletion of records compromised by biological fouling and other factors). Calibration curves indicated generally good correlations between SSC samples and OBS voltage readings. The mean value for the correlation coefficient, r^2, for the 15 records was 0.87 and ranged between 0.56 and 0.99. Prior to October 1997, calibrations were performed using ordinary least squares regressions; starting with water year 1998, a robust, nonparametric, repeated median method was used (see *Buchanan and Ruhl* [2000] for a description of the method). San Francisco Bay sensors are calibrated to point measurements and Delta sensors are calibrated to discharge-weighted, cross-sectionally averaged SSC values. Suspended sediment discharge is determined by multiplying the discharge-weighted, cross-sectionally averaged SSC by water discharge, accounting for tide-driven bidirectional flow [*Schoellhamer et al.*, 2002].

[44] Advantages of turbidity technology are summarized as follows:

[45] 1. As the most ubiquitous of the field-deployed surrogate technologies, results from a large number of field settings are available for evaluation.

[46] 2. The technology is relatively mature and reliable.

[47] 3. Calibration techniques are documented and largely straightforward.

[48] 4. At a cost for a fully equipped turbidimeter of about $5000, this is one of the more affordable sediment surrogate technologies.

[49] Limitations of the technology are summarized below:

[50] 1. The at-a-point turbidity time series data may not be representative of the sedimentary conditions in the river cross section.

[51] 2. Saturation of the turbidimeter signal can occur resulting in erroneous (constant) values for all SSC values that exceed a maximum value.

[52] 3. Biological fouling or damage to optical windows may require frequent site visits to service the instrument.

[53] 4. Instrument response to grain size, composition, color, shape, and coating can be variable and hence can reduce the accuracy of derived SSC values without additional calibration.

[54] 5. A lack of consistency in measurement characteristics among commercially available instruments impinges on the comparability of turbidity measurements.

2.2. Laser Diffraction

2.2.1. Background and Theory

[55] Laser diffraction instruments exploit the principles of small-angle forward scattering to infer PSDs. At small forward scattering angles, laser diffraction by spherical particles is essentially identical to diffraction by an aperture of equal size [*Agrawal and Pottsmith*, 1994]. Thus, this method of determining PSDs (and, by inference, volumetric SSC values) is mostly insensitive to changes in particle color or composition although departure from sphericity produces a bias in the computed PSD (compared to that for sieving). For example, *Agrawal et al.* [2008] have shown that natural particles measured by laser diffraction are inferred to be about 20–40% larger than identically sieved spheres.

[56] At present, an in situ version of this type of instrument is commercially available from only one manufacturer. First used in the early 1990s [*Agrawal and Pottsmith*, 1994], the present version of a laser diffraction instrument that can be deployed unattended to provide a time series of PSD and volume SSC values is the LISST-100, shown in Figure 6 (http://www.sequoiasci.com/default.aspx?SectionName=home). The Laser in Situ Scattering and Transmissometry (LISST) instrument uses a 32-ring detector to sense a laser beam defracted by sediment particles at small forward angles. These data are inverted to determine PSDs in 32 size classes between 1.25 and 250 μm, 2.5–500 μm, or 7.5–1500 μm (LISST-FLOC). The standard sample path of this device is a cylindrical volume with a diameter of approximately 6 mm and a length of 50 mm (essentially a point measurement). An isokinetic, cable-suspended, streamlined version of the LISST-100, the LISST-SL shown in Figure 6, features the capability of real-time velocity measurement that is in turn used to control a pump to withdraw a filament of water and route it through the laser beam at the ambient current velocity [*Gray et al.*, 2002; *Gray and Gartner*, 2004; *Gray et al.*, 2004; *Agrawal and Pottsmith*, 2006]. The performance of the LISST-SL was evaluated by the Federal Interagency Sedimentation Project (http://fisp.wes.army.mil/) in a laboratory, a flume, and in the field. The purchase price of one of the LISST instruments (in situ or manually deployed) described in this section ranges from about 5 to

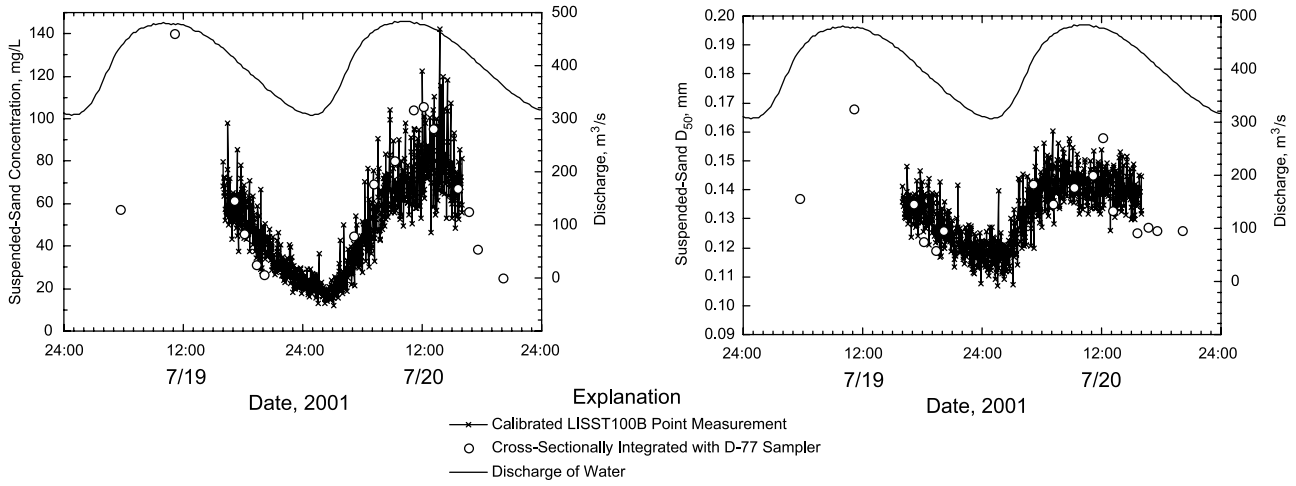

Figure 7. Comparison of sand concentrations in milligrams per liter and median grain sizes in millimeters measured at the USGS streamgage at the Colorado River near Grand Canyon, Arizona, using a LISST-100B and a U.S. D-77 bag sampler. From *Melis et al.* [2003].

6 times that for a fully equipped turbidimeter, depending on the instrument of interest.

[57] Because a LISST determines PSD for all measurements, it is not subject to potential inaccuracies in the calculation of SSC associated with single frequency (optical and acoustic) instruments in the presence of changes in particle size distributions as long as particle sizes fall within the instrument measurement range [*Agrawal and Pottsmith*, 2000].

[58] Field and laboratory tests have shown the LISST-100 to be capable of determining PSDs of natural materials and the size of monosized particle suspensions with an accuracy of about 10% [*Traykovski et al.*, 1999; *Gartner et al.*, 2001]. The LISST-100 can also be used to determine mass SSC from volume SSC if mean particle density is known from field calibrations or some other means [*Gartner et al.*, 2001].

[59] As is the case with all types of in situ optical instruments, biological fouling can degrade measurements. Antifouling shutters for some LISST instruments are available from the manufacturer. In addition, the technology has a SSC range limitation associated with multiple scattering in the presence of high SSCs. The LISST-100 requires about 30% or more laser optical transmission. The range limitation is a function of the laser path length, PSDs, and SSCs. For SSC, the useable limits range from tenths of a g/L (small particle sizes) to several g/L (larger particle sizes). Optical blocks that reduce the path length by 50, 80, or 90% are available; reducing the optical path from the standard 5 cm to 5 mm can theoretically extend measurement limits from about 0.5 g/L to about 5 g/L for 25 μm particles (Y. Agrawal, personal communication, 2008) [*Agrawal et al.*, 2008]. A prototype LISST-INFINITE is being tested by the USGS [*Konrad et al.*, 2006] for application in very high SSCs. The system pumps a water-sediment sample to the instrument and then uses automated multistage dilution (as necessary) before measuring PSDs and SSCs with a built-in LISST-100. However, the process of pumping the water sample from a point in the channel may alter the original PSD.

[60] A somewhat simpler and less expensive version of the LISST-100 instrument, the LISST-25, measures mean SSC and a mean particle size (Sauter mean size) in two size classes (2.5–63 μm and 63–500 μm) (http://www.sequoiasci.com/default.aspx?SectionName=home). This device is also based on the same small-angle scattering principles as the LISST-100, but it obtains the SSC through a weighted summation of the output of ring detectors, bypassing the inversion to PSD. The cost of the LISST-25 is about double that of a fully equipped in situ turbidimeter.

2.2.2. Example Field Evaluation

[61] Laser sensors are being investigated as an alternative monitoring protocol for tracking reach-scale suspended sediment supply at a USGS streamgage on the Colorado River near Grand Canyon, Arizona, located 164 km downstream from Glen Canyon Dam [*Topping et al.*, 2004]. A canyon wall-mounted LISST-100B provides continuous suspended sediment transport data (SSCs, and PSDs in the range of 1.25–250 μm) that may reduce uncertainty in estimates of the transport of sand and finer material. An example of data collected by a LISST-100B at a fixed-depth, near-bank site on the Colorado River is shown in Figure 7. Data were obtained averaging 16 measurements at 2-min intervals during a 24-h deployment in July 2001. The time series of 720 LISST at-a-point measurements are compared with cross-sectional data obtained by U.S. D-77 isokinetic bag sampler concurrent with some of the LISST measurements using techniques described by *Nolan et al.* [2005]. In addition to accurately tracking sand-size SSCs, the LISST-100B also recorded the increase of variance in the SSCs of sand-size particles expected with increasing flows; peak sand-size SSC values ranged up to 0.15 g/L (Figure 7).

[62] The FISP has performed laboratory bench tests of the sedimentological characteristics of a LISST-SL. The range in SSC used in tests was 0.01–3 g/L. Material used for testing was primarily less than 150 μm although some tests included coarser material that was difficult to keep suspended in the test system. Sedimentological results from these LISST-SL tests fall within the acceptable uncertainty

values for the corresponding SSC levels shown in Table 1 (B. Davis, personal communication, 2008).

[63] Advantages of laser optic technology are summarized as follows:

[64] 1. The instrument provides in situ or real-time PSD measurement in 32 size classes.

[65] 2. Calculated volumetric SSC values are not affected by changes in PSD.

[66] 3. A manually deployed isokinetic version of the LISST technology is available.

[67] The limitations of the technology are summarized below:

[68] 1. The at-a-point laser measurements may not be representative of sedimentary conditions in the river cross section.

[69] 2. Deviation of particle shape from spherical may bias results.

[70] 3. Saturation of the laser optic signal can occur at a SSC level of about half of that at which a standard in situ turbidimeter saturates.

[71] 4. Frequent field visits may be required to clean the optics if antifouling shutters are not used.

[72] 5. The cost of a LISST instrument is 2–6 times that for a fully equipped in situ turbidimeter depending on the instrument of interest.

2.3. Pressure Difference

2.3.1. Background and Theory

[73] The pressure difference technique for monitoring SSC relies on simultaneous measurements from two exceptionally sensitive pressure transducer sensors arrayed at different fixed elevations in a water column. The difference in pressure readings is converted to a water density value, from which SSC is inferred after correcting for water temperature (dissolved solids concentrations in fresh water systems are rarely of consequence in the density computation). Implicit assumptions are that the same water surface location is measured by both sensors and that the density of the water-sediment mixture above the lower sensor is more or less equal to that above the higher sensor. The technology has both laboratory and field applications [*Lewis and Rasmussen*, 1999]. One of the first uses of the pressure-difference technique was for monitoring the density of crude oil in pipes (W. Fletcher, personal communication, 1999).

[74] The 1999 purchase prices of the in situ field version of this technology and a fully equipped in situ turbidimeter were similar. The instrument evaluated by the USGS is no longer manufactured (http://www.waterlog.com/). However, the essential parts of the technology, precision pressure sensors, remain available from several commercial sources.

[75] The technique has been applied in the laboratory with promising results of better than 3% accuracy (0.543 ± 0.014 g/L) for determining mass concentrations of suspensions of glass microspheres [*Lewis and Rasmussen*, 1999]. However, application of this technique in the field can be complicated by low signal-to-noise ratios associated with low SSC, turbulence, significantly large dissolved solids concentrations, and water temperature variations. Additionally, analyses may be complicated by density variations in the suspended material. These complications coupled with the sensitivity limitations of the pressure-transducer sensors may render this technology unreliable at concentrations below 10–20 g/L.

2.3.2. Example Field Evaluation

[76] Information on the field performance of the pressure-difference technology is available from USGS streamgages on the lower Río Caguitas in Puerto Rico [*Larsen et al.*, 2001] and the Paria River in Arizona. Continuous pressure-difference data were collected during October–December 1999 at the Río Caguitas streamgage using a Double Bubbler Pressure Differential Instrument, composed of a digital recorder, bubbler system, and two precision pressure sensors with orifices anchored at fixed depths in a vertical (http://www.waterlog.com/) (Figure 8). Most of the annual sediment discharge in the lower Rio Caguitas occurs as runoff from a few storms during which SSCs exceed about 0.5 g/L. The maximum SSC measured at the streamgage during the Puerto Rico Double Bubbler tests based on water samples collected by an autosampler [*Edwards and Glysson*, 1999] was 17.7 g/L.

[77] Data analyses involved data smoothing and removal of outliers. To calculate the weight density of suspended sediment and dissolved solids, the weight density of pure water at 27°C was subtracted from the smoothed data values. Even with these manipulations, the tests of the Double Bubbler instrument at the Puerto Rico site during October–December 1999 showed relatively poor agreement with discharge, SSC, and water density (Figure 9). The Double Bubbler data contained a large amount of signal noise, making interpretation difficult. Lacking a thermistor for temperature compensation, 12 of 15 base flow instrument measurements inferred negative SSC values (an impossibility) concomitant with in-stream measured SSC values of 0.01–0.1 g/L. However, all but two of the samples collected during seven higher-flow periods showed concomitant increases in inferred positive SSC values.

[78] A complicating factor in the pressure-difference method is in-stream turbulence, which introduces noise about equal to the magnitude of the signal of interest, particularly during high flows that occur more or less concomitant with the largest SSCs. Additionally, diel- and storm-related fluctuations in water temperatures resulted in a daily range as much as 10°C. The high relative humidity characteristic of this humid tropical site may also complicate the use of the Double Bubbler because of the sensitivity of the narrow diameter bubbler gas lines to moisture, unless the gas lines are equipped with dryer tubes. This test of the Double Bubbler instrument showed the need for temperature compensation and possibly the need to deploy the instrument at a site where the range in the density of the water-sediment mixture is substantially larger than the 1.00–1.02 range occurring at the Río Caguitas streamgage during the Double Bubbler tests.

[79] In 2004, the Puerto Rico Double Bubbler system was transferred to the USGS streamgage on the Paria River at Lees Ferry, Arizona, where SSCs as high as 10^3 g/L have been measured during storm runoff. Deployment of the Double Bubbler in the Paria River was predicated on the hypothesis that Paria River SSC's, commonly exceeding peak measured Rio Caguitas concentrations by a factor of at least three and in some cases by 1–2 orders of magnitude, would subject the instrument to a substantially larger density range than that inferred for higher flows at the Rio Caguitas streamgage in Puerto Rico. Even with the

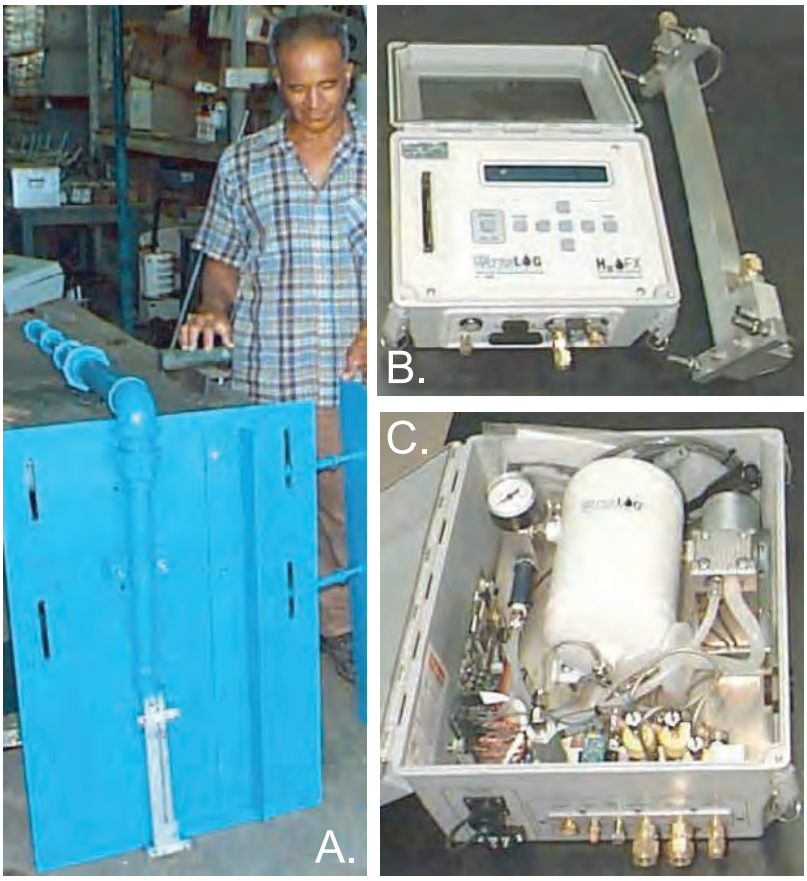

Figure 8. Double Bubbler Pressure Differential Instrument (a) in-stream components before installation, (b) controller and orifice bar, and (c) air compressor and tank assembly. Figures 8b and 8c courtesy of Design Analysis Associates, Inc.

addition of a thermistor for monitoring water temperatures, results to date have been mixed.

[80] Double Bubbler data were collected, at 5-min intervals, during periods of elevated flow at the Paria River streamgage from July 2004 through September 2006. Double Bubbler data collected from over 14 storm runoff hydrographs were examined and compared to SSCs from samples collected during storm runoff. The elevated flows had peaks ranging from about 7 to 90 m^3/s; the maximum SSC measured was 382 g/L from a sample collected using an autosampler. Of the 261 suspended sediment samples collected during the 14 periods storm runoff periods, 86% had SSC values larger than 50 g/L (N. Hornewer, personal communication, 2008).

[81] Similar to data collected at the Rio Caguitas in Puerto Rico and contrary to the aforementioned hypothesis, the Double Bubbler data collected at the Paria River at Lees Ferry streamgage seemed to have a large amount of signal noise, also making interpretation difficult. The Double Bubbler data were collected only during periods of elevated stages (discharges) because the instrument was not fully submerged during normal shallow flows. Data were filtered in a manner similar to that for the Río Caguitas data but not smoothed. Relations were between measured SSCs and those calculated from Double Bubbler data tended to be inconsistent. It is likely that bed movement caused the lower orifice to become partially or fully blocked at times, contributing to erroneous data. Also, the paired stage readings necessary for the density calculation could not always be obtained because both orifices were only submerged during infrequent periods of high flow.

[82] The performance of the Double Bubbler neither has been proven inadequate nor adequate for USGS data collection purposes. Because of this, its strong theoretical underpinnings, continuous monitoring capability, and, not unimportantly, a lack of any other proven technology for monitoring SSCs in high-concentrated and hyperconcentrated streamflow conditions, the pressure difference technique continues to be evaluated by the USGS.

[83] Advantages of the pressure differential technology are summarized as follows:

[84] 1. The pressure difference technology's inference of SSC in a single vertical is an improvement over at-a-point measurements but still may not provide SSC data representative of mean cross-sectional values.

[85] 2. The technology is relatively robust, being prone to neither signal drift nor biological fouling.

[86] 3. The technology doubles as a redundant stage sensor for the site.

[87] 4. The technology may be unique in that the accuracy of its measurements theoretically improves with concentrations increasing above about 10–20 g/L.

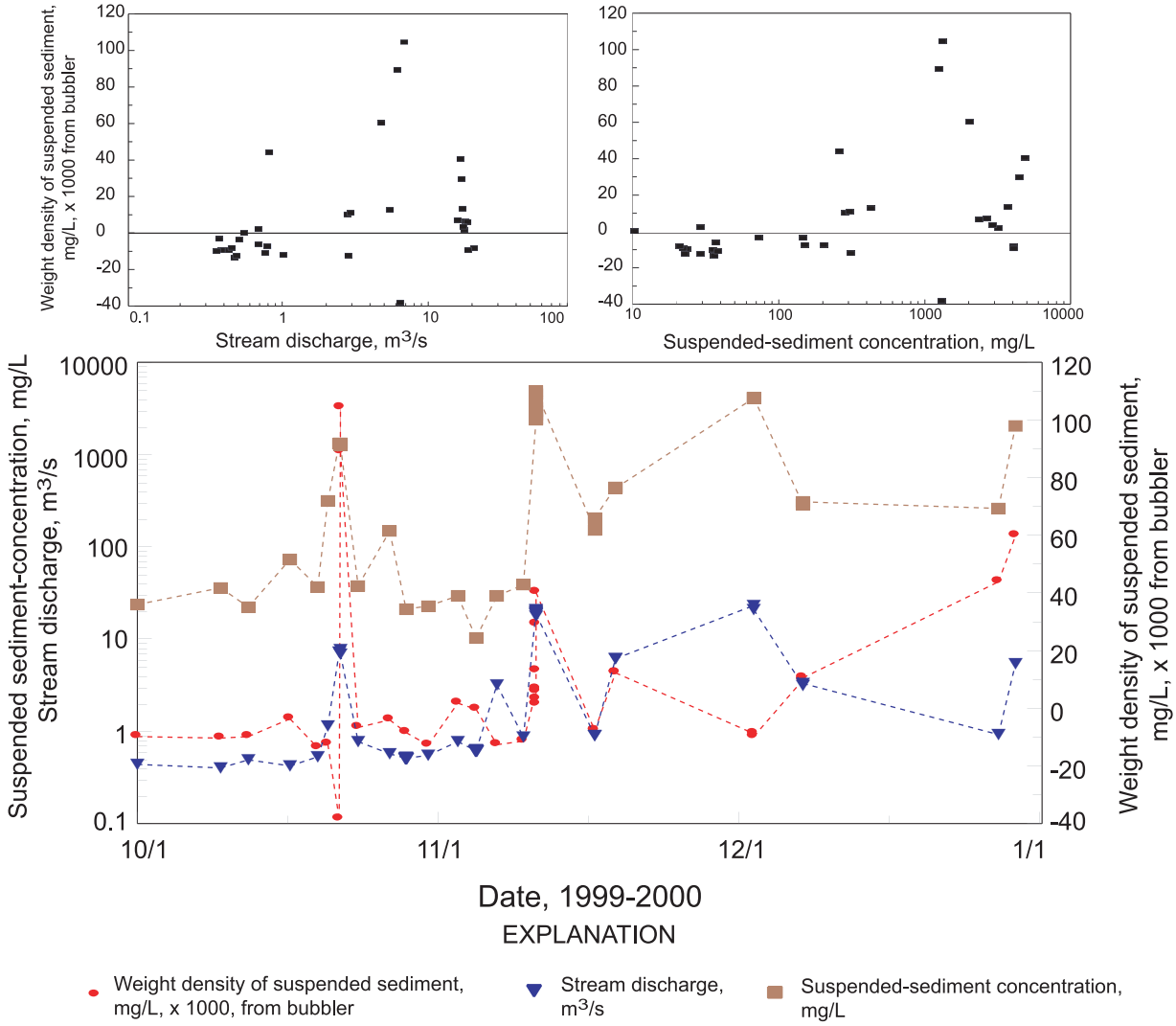

Figure 9. Scatterplots and time series of stream discharges, SSCs, and weight density of suspended-sediments and dissolved solids measured with a Double Bubbler (Design Analysis Associates, Inc.), 1 October 1999 to 1 January 2000, lower Rio Caguitas, Puerto Rico. Discharge and sediment data are instantaneous values in cubic meters per second and milligrams per liter, respectively; Double Bubbler weight density values are expressed in milligrams per liter as 30-min mean values of measurements made at 5-min intervals. From *Larsen et al.* [2001].

[88] 5. The theoretical underpinnings of the technology are relatively simple and straightforward.

[89] The limitations of the technology are summarized below:

[90] 1. The required computational scheme presupposes that the concentration in the vertical profile above the lower pressure sensor is more or less constant to the surface. This assumption, which is difficult to verify, may not be valid.

[91] 2. The technology may be incapable of measuring SSCs below about 10–20 g/L in turbulent flows and where the bed forms cover one or both orifices. The field performance of the technology has yet to be adequately resolved at any SSC.

[92] 3. The technology is incapable of measuring SSC when the top orifice is not submerged or the bottom orifice is buried in sediment.

[93] 4. Spurious data are numerous and are believed to be associated with flow turbulence.

[94] 5. The Double Bubbler is no longer marketed, and no other commercial source of this device is known by the authors. Those seeking to deploy this technology may have to construct their own system from commercially available parts.

2.4. Acoustic Backscatter

2.4.1. Background and Theory

[95] Attempts to characterize suspended sediments from acoustic backscatter measurements by prototype and commercial acoustic backscatter (ABS) instruments have increased in recent years. Utilization of acoustic backscatter measured by portable acoustic Doppler current profilers (ADCP), a byproduct of ADCP velocity measurements, is also appealing. In addition to being virtually immune to

biological fouling, acoustic sensors such as commercially available ADCPs can provide nonintrusive estimates of SSC profiles concurrent with measurements of three-dimensional velocity data from the same instrument. As of 2008, such Doppler velocity instruments are available from about a half dozen manufacturers.

[96] The method of converting acoustic backscatter measured by ADCP to SSC has its basis in the sonar equation [*Urick*, 1975]. Theoretical aspects of the technique have been well documented [e.g., *Thevenot et al.*, 1992; *Reichel and Nachtnebel*, 1994; *Deines*, 1999]. As with turbidity measurements, empirical calibrations are required to convert measurements to estimates of SSCs representative of the cross-sectional value. Postprocessing algorithms are complex, requiring compensations for physical properties of ambient water such as temperature, salinity, pressure, and suspended materials as well as instrument characteristics such as frequency, power, and transducer design [*Thorne et al.*, 1991; *Downing et al.*, 1995]. The information is necessary to properly account for acoustic signal transmission losses from the water (including nonspherical spreading in the transducer near field [*Downing et al.*, 1995]) and, in some cases, attenuation from suspended materials in the water. Some commercial software products are available to convert backscatter to SSC [*Land and Jones*, 2001; *Mol*, 2003] although not yet widely used. Some researchers have written their own postprocessing software.

[97] The purchase price of a commercially available single-frequency Doppler in situ horizontal-looking instrument is about double to triple that of a fully equipped turbidimeter (no self-contained situ Doppler multifrequency version of this technology is yet commercially available). The purchase price of a bed-deployed upward looking instrument is about fourfold that for the turbidimeter. Because biological fouling has little if any effect on the performance of the sensor, field-maintenance costs are probably less than that for a turbidimeter. However, complexities in calibrating the acoustic signal to SSC and perhaps also PSD may increase analytical costs.

[98] Initial studies utilizing acoustics to estimate SSCs in the mid-1980s provided qualitative results, for example, *Schott and Johns* [1987], *Flagg and Smith* [1989], and *Heywood et al.* [1991]. Subsequent work attempted to quantify SSC estimates through laboratory or field calibrations of acoustic backscatter. *Thevenot et al.* [1992] developed calibration parameters as part of a study to monitor dredged material near Tylers Beach, Virginia, using Broadband-ADCPs (BB-ADCPs). *Thevenot and Kraus* [1993] compared optical and acoustic methods using a 2.4-MHz BB-ADCP in the Chesapeake Estuary and *Lohrman and Huhta* [1994] undertook a sediment calibration experiment in the laboratory to determine the fate of suspended sediments during dredging operations. *Jay et al.* [1999] incorporated a correction function for improved calculation of beam spreading losses in the ADCP transducer near field to account for the complex acoustic beam pattern, and *Holdaway et al.* [1999] accounted for sediment attenuation in their evaluation of ADCPs to estimate SSC. More recently, *Gartner* [2004] estimated SSCs in San Francisco Bay using 1.2- and 2.4-MHz ADCPs, *Lorke et al.* [2004] applied acoustic backscatter to the distribution and movement of zooplankton, *C. flavicans*, populations in lakes, and *Wall et al.* [2006] used ADCP backscatter data to compute suspended-sediment discharges in the lower Hudson River, New York. Comparisons of SSCs computed from acoustic backscatter with SSC determined from water samples have been found to agree within about 10–20% [*Thevenot et al.*, 1992; *Thorne et al.*, 1991; *Hay and Sheng*, 1992].

[99] General limitations of the technique (especially when using single-frequency instruments) are also well described in the literature [e.g., *Reichel and Nachtnebel*, 1994; *Hamilton et al.*, 1998]. *Gartner* [2004] provides a discussion of the theoretical background of the technique and some inherent limitations. One critical limitation is the fact that it is impossible to differentiate between a change in mass concentration and a change in PSD (without sufficient calibrations) when using a single-frequency instrument, as changes in both SSC and PSD can result in a change in the backscatter signal strength. In addition, there is an appropriate or optimum acoustic frequency for a given PSD. Errors in estimates of SSC will increase if a significant fraction of the suspended material includes particles that are too large or too small for a given frequency. For these reasons, techniques or instruments that utilize more than one acoustic frequency are preferable to single-frequency methods.

[100] Corrections for attenuation from suspended materials must be accounted for in the presence of significant SSCs of very small particles (where viscous losses may be substantial) or very large particles (where scattering losses may be high) [*Flammer*, 1962]. The method appears appropriate for use in SSCs up to several g/L depending on acoustic frequencies and PSDs. Quantification of high SSCs may be problematic, especially when using high acoustic frequencies that are more prone to attenuation from sediment. The result is a nonlinear (backscatter intensity) response at high SSCs [*Hamilton et al.*, 1998]. Although a function of frequency, attenuation from sediment should be accounted for in the presence of as little as 0.1 g/L [*Libicki et al.*, 1989; *Thorne et al.*, 1991]; multiple scattering produces nonlinear response when SSC is on the order of 10 g/L [*Hay*, 1991; *Sheng and Hay*, 1988].

2.4.2. Example Field Application

[101] A multiinstrument, multifrequency system has been established at the USGS streamgage Colorado River near Grand Canyon, Arizona, to produce data from which continuous SSCs and discharges can be computed [*Topping et al.*, 2007]. The system utilizes three single-frequency side-looking acoustic Doppler profilers (1.0 and 2.0 MHz, and 600 kHz) (Figure 10) set to record 4 out of every 15 min. For sand-size SSCs, the 1 MHz acoustic data were calibrated with 345 EDI measurements between February 2003 and September 2005, the 2 MHz acoustic data were calibrated with 74 EDI measurements between September 2004 and September 2005, and the 600 kHz acoustic data were calibrated with 65 EDI measurements between September 2004 and September 2005. EDI measurements prior to April 2003 utilized U.S. D-77 bag samplers; subsequent measurements were made with U.S. D-96-A1 or U.S. D-96 depth-integrating bag samplers [*Topping et al.*, 2007; *Davis*, 2005]. Calibrations were done with EDI measurements augmented by automatic pump samples collected under conditions of high silt and clay SSCs.

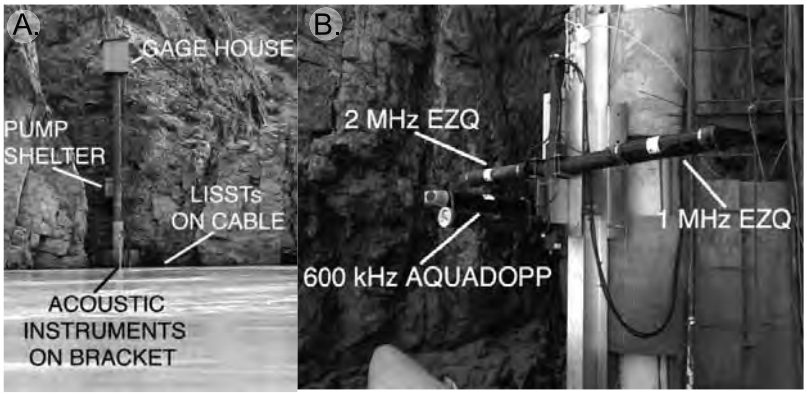

Figure 10. Photographs of (a) instrument locations and (b) an array of the three bracket-mounted acoustic Doppler profiler used to estimate suspended-sediment concentrations by silt-, clay-, and sand-size classes, at the USGS streamgage Colorado River near Grand Canyon, Arizona. From *Topping et al.* [2007].

[102] A postprocessing technique was employed for analyzing acoustic attenuation to compute the suspended silt- and clay-size fraction and acoustic backscatter to compute the suspended sand fraction in a size range applicable for each frequency. *Topping et al.* [2007] indicate that the approach is applicable for monitoring SSCs over the ranges of 0.01–20 g/L (silt and clay) and 0.01–3 g/L (sand), with results within 5% of those computed by conventional means [*Porterfield*, 1972]. In addition, the method calculates median grain size within 10% of that measured by conventional means. *Topping et al.* [2007] infer a greater accuracy with this technique than with a conventional sampling regime (±10% for suspended silt and clay concentrations; ±22% for suspended sand concentrations) largely due to the substantially greater sample frequency. Figure 11 shows comparisons of SSCs from three-frequency acoustic backscatter, calibrated pump, and LISST measurements.

[103] *Wall et al.* [2006] describe an ongoing study begun in July 2002 to use acoustic backscatter to compute suspended sediment discharge in the Hudson River near Poughkeepsie, New York. At that location, the Hudson River is about 18 m deep and 800 m wide; it is usually fresh water but experiences a mean tidal range of 0.95 m. A 600 kHz ADCP, set to average 100 acoustic pings for a measurement of velocity profile and acoustic backscatter every 15 min, is deployed on the riverbed in an up-looking orientation. Vertical resolution (ADCP bin size) is set at 0.5 m. Computation of SSC from the ADCP backscatter measurement is based on the exponential form of the sonar equation [see, e.g., *Reichel and Nachtnebel*, 1994; *Deines*, 1999; *Gartner*, 2004] but includes a variable for water temperature that *Wall et al.* [2006] found significant. As part of the postprocessing, they describe their process for normalizing echo intensity to account for variations in instrument transmit power and variations in acoustic beams. Measurements from a vessel-mounted ADCP and SSCs from water samples collected with a U.S. P-61 point-integrating isokinetic sampler [*Davis*, 2005] have been used to relate acoustic backscatter to SSC. Analysis of water samples showed that particle sizes are generally smaller than 62 μm. Regression between Log_{10} $SSC_{measured}$ and Log_{10} $SSC_{computed}$ is considered acceptable with a coefficient of determination, R^2, of 0.86 and a standard deviation of residuals equal to 7.9 mg/L. The range of SSCs is about 5–65 mg/L. Estimates of SSCs in the full river cross section made from moving boat are used to adjust estimates from the upward ADCP at fixed location in the river that continuously recorded measurements every 15 min. Sus-

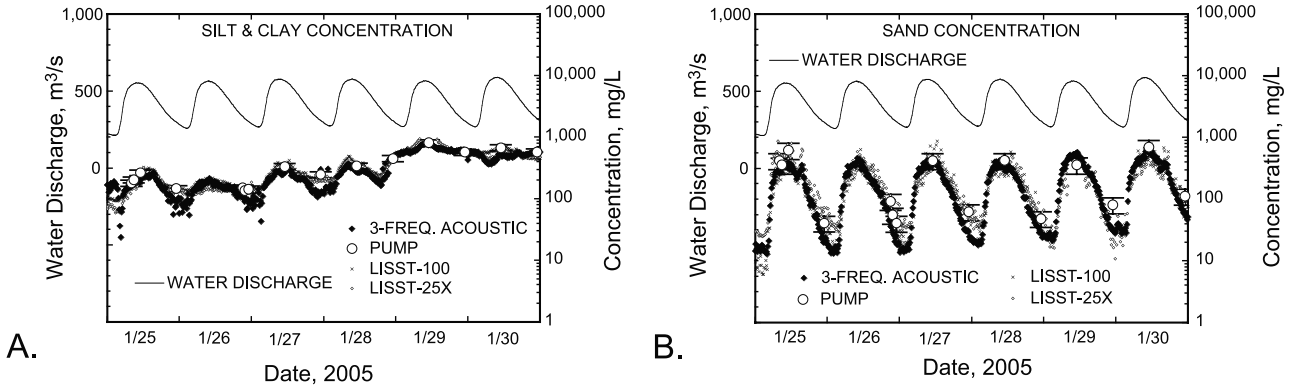

Figure 11. Comparisons of suspended-sediment concentrations in milligrams per liter from three-frequency acoustic backscatter, calibrated pump, and LISST-100 and LISST-25X measurements: (a) suspended silt- and clay-size concentrations and (b) suspended sand concentrations. From *Topping et al.* [2007].

Table 2. Summary of Selected Attributes of Four Suspended-Sediment Surrogate Technologies

Technology	Turbidity (Bulk Optics)		Laser		Pressure Difference	Hydroacoustics	
Instrument or Type	In Situ Turbidimeter	In Situ OBS	In Situ LISST-100	Manually deployed LISST-SL	In Situ Double Bubbler	In Situ Single-Frequency Acoustic Doppler Profiler	In Situ Multiple-Frequency Acoustic Doppler Profiler
Price Relative to In Situ Turbidimeter	Ca $5,000 (Summer 2008)	About 1X	About 5X	About 6X	About 1X	About 2X-4X	Unknown
Approximate Concentration Measurement Range	Standard 0–2 g/L Available at larger ranges	Standard 0–5 g/L Available at larger ranges	Depending on versions: 0–2 g/L (particle size dependent)	About 0–2 g/L (particle size dependent)	Larger than about 10 g/L, but needs more research; no upper limit	Signal attenuation limited as function of PSD and frequency	Signal attenuation limited as function of PSD and frequency
Approximate Measurement Range, PSD in mm	Does not measure PSD	Does not measure PSD	0.0025–0.5 or 0.00125–0.25	0.0025–0.5 or 0.00125–0.25	Does not measure PSD	Does not measure PSD. Particle-size dependent. Ratio circumference to wavelength < 1	May measure sand versus silt/clay content. Particle-size dependent. Ratio circumference to wavelength < 1
Measurement Metric Basis to Routinely Compute Mean Cross-Sectional Values	Calibrated to concentrations from physical samples in mass units	Calibrated to concentrations from physical samples in mass units	Calibrated to concentrations from physical samples in mass units; PSD in 32 size classes; volume concentration, converted to mass concentration if density known	Calibration may be unnecessary; PSD in 32 size classes; volume concentration, converted to mass concentration if density known	Calibrated to concentrations from physical samples in mass units	Calibrated to concentrations from physical samples in mass units	Calibrated to concentrations from physical samples in mass units; If PSD, by variable response to selected frequencies
Ancillary Measurements	None	None	Depth and water temperature	Depth, ambient velocity, water temperature	Stage	Index velocity. Depth if oriented down	Index velocity. Depth if oriented down
Reliability And Robustness	Optical window may foul, causing signal to drift with time; sensor may saturate at larger concentrations	Optical window may foul, causing signal to drift with time; sensor may saturate at larger concentrations	Requires anti-fouling device BioBlock. Sensor may saturate at larger concentrations; PSD larger than 0.5 mm not included in calculation.	PSD larger than 0.5 mm not included in calculation.	Low concentration data unreliable; veracity of higher concentrations unresolved	More or less unaffected by fouling, responds almost solely to entrained sediment	More or less unaffected by fouling, responds almost solely to entrained sediment
Region of Measurement	Fixed point	Fixed Point	Fixed Point; device may be used in profiling mode from a wire	Point, vertical, or multiple verticals	Single fixed vertical, mean concentration value	Conic beam with data available at selected distances from the sensor	Conic beam with data available at selected distances from the sensor
Accuracy for Derivation of Suspended-Sediment Data	When within measurement range has been used to develop reliable SSC-turbidity regression relations	When within measurement range has been used to develop reliable SSC-turbidity regression relations	Deemed reliable in some field applications	Sedimentological and isokinetic test results pending, 2009	Unresolved based on two field tests; additional work planned	Shown useful in field applications where size distribution does not change dramatically	Shown to provide accurate silt-clay versus sand-size fractions
Potential for Meeting USGS Accuracy Standards	High for mass SSC	High for mass SSC	High for volume SSC and for PSD	High for volume SSC and for PSD	Low for mass SSC	Moderate for mass SSC	High for mass SSC; moderate for silt-clay versus sand-size fractions

Table 2. (continued)

Technology	Turbidity (Bulk Optics)		Laser	Pressure Difference	Hydroacoustics	
Potential for Application in Large-Scale Monitoring Programs	Very high (given appropriate in-stream sedimentological conditions, calibration, and ability to maintain instruments)	Very high (given appropriate in-stream sedimentological conditions, calibration, and ability to maintain instruments)	High (given appropriate in-stream sedimentological conditions, known density, and ability to maintain instruments)	High (used for calibrating in situ instruments in addition to routine data collection)	Unknown pending additional testing using modifications of the physical system and algorithms	Moderate (given appropriate in-stream sediment-ological conditions, and calibration)	High for SSC; moderate for silt-clay versus sand-size fractions

pended sediment discharge is determined from water discharge and computed, cross-sectional average SSC values.

[104] Advantages of the acoustic-backscatter technology are summarized as follows:

[105] 1. Unlike point measurements, acoustic backscatter measurements can cover a substantial part of the water depth or river cross section; they integrate orders of magnitude more flow than other methods that rely on at-a-point or single vertical measurements.

[106] 2. Sediment fluxes in the beam can be computed and empirically indexed to the mean cross-sectional SSC value. These data in turn can be used with continuous water discharge data to compute unit and daily value sediment fluxes at the monitoring site.

[107] 3. Unlike optic-based surrogate instruments, biological fouling is not a problem.

[108] 4. The approach is applicable for monitoring SSCs over the ranges of 0.01–20 g/L for silt and clay and 0.01–3 g/L for sand.

[109] 5. Concentrations have been measured up to 2 g/L by this technique.

[110] The limitations of the technology are summarized below:

[111] 1. Similar to optical surrogate techniques, a single-frequency source cannot differentiate between changes in PSDs and changes in SSCs without calibration.

[112] 2. There is an optimal frequency for a given particle size and a somewhat narrow frequency range for which the method is appropriate for a given PSD.

[113] 3. Complex software is required for the reduction and analysis of the acoustic signals.

[114] 4. The purchase price of an in situ horizontally looking instrument is about double to triple that for a fully equipped in situ turbidimeter and about fourfold the price of a turbidimeter for an upward looking instrument.

[115] 5. Until standard operating procedures are developed and adopted for this technique, time requirements for the hydrographer to resolve the continuous SSC trace will not be trivial.

3. Summary and Conclusions

[116] Four advanced in situ technologies for monitoring fluvial suspended sediment transport are among instruments and techniques being tested by the USGS: turbidity (bulk optics), laser optics, pressure difference, and acoustic backscatter. Although none is a panacea for sediment monitoring needs in all rivers, the capability for consistent, large-scale monitoring of suspended sediment transport in many of the world's rivers may be possible.

[117] Table 2 summarizes selected attributes of the four technologies that are germane to their potential use as a sediment surrogate technology. Each technology, with the possible exceptions of manually deployed laser optic instruments, requires periodic calibration with data produced from traditionally collected water samples to calculate the mean value in the cross section. When properly configured and deployed, each is capable of providing a dense and continuous time series of SSC for use in computation of continuous suspended sediment transport. Laser optics and possibly multifrequency acoustic backscatter may provide the added capability of sediment discharge computations by particle size class. The ability to determine

continuous, high-frequency, time series of SSC is a major advantage over traditional data collection techniques, obviating the need for routine, potentially subjective interpolations between sample values, and providing the capability to determine high-frequency SSC and PSD fluctuations not revealed by traditional measurements. Calibrations with somewhat larger uncertainty bounds might be considered more acceptable in that the vastly increased derived data density preclude the routine need for sediment trace interpolations.

[118] The applicability of each technology is dictated in part based on the physical and hydrological characteristics of the monitoring site; monitoring objectives; and the instrument's advantages and limitations. Each deployed surrogate instrument provides time series data representative of the sedimentological characteristics in but a fraction of the cross section. Both optical technologies provide at-a-point SSC data during periods that in-stream SSC values remain below the instrument's saturation limit. The SSC data provided by laser optics are computed from PSDs associated with each measurement.

[119] An instrument's measurement realm is an important factor in correlating the measurements to mean cross-sectional SSC values. Assuming production of reliable data collected from the instrument realm, SSCs computed utilizing acoustic backscatter technology (employing a profile of vertical or horizontal measurements) may correlate better with the mean SSC value for the river cross section than those computed with the pressure difference method, which in turn may be better than those computed from at-a-point turbidity or laser optic measurements.

[120] Nevertheless, the most ubiquitous in situ surrogate technology utilizes turbidimeters, which have been shown to provide useful data for computing SSCs in a number of field settings. However, issues associated with instrument sensor saturation can result in failure to record reliable data at the higher values of SSCs that tend to be the most influential in sediment transport. SSCs computed from at-a-point turbidity data may not be representative of the mean cross-sectional SSC, particularly when sand-size material composes an appreciable fraction of total suspended sediment transport. Biological fouling can reduce signal integrity in the absence of a mechanical wiper or manual cleaning to keep the optical window clean. Turbidimeter costs are a small fraction of the annual cost of monitoring suspended sediment transport using traditional techniques, but the potential for increased site visits for maintenance may result in increased operating costs.

[121] In situ laser optic instruments also suffer from the drawbacks associated with sensor saturation, biological fouling, and at-a-point measurement limitation characteristics of in situ turbidimeters. Additionally, laser data are in the form of volume SSC; mass SSC may be calculated only if particle density is known or can be reliably inferred. The purchase price of an in situ laser optical instrument (LISST-100) is about 5 times the cost of a fully equipped in situ turbidimeter. However, these instruments have the major advantage in providing continuous PSDs from which the volumetric SSCs are inferred.

[122] The pressure difference technology is designed for monitoring SSCs exceeding about 10 g/L in a single vertical, which is near or above the maximum range of the other technologies examined herein. The purchase price of this relatively uncomplicated technology is similar to that for a turbidimeter. It is relatively robust in that it integrates the density of a water column as opposed to a single vertical, and it is not subject to biological fouling. The theoretical underpinnings of this technology are straightforward. However, performance of the pressure difference technology has been marginal at best in field tests in Puerto Rico (maximum concentrations of about 18 g/L) and Arizona (maximum concentrations of about 380 g/L). Because this technology addresses a unique monitoring niche for measurements in highly concentrated or hyperconcentrated flows, and because of large benefits associated with the production of a dense time series of surrogate measurements, it is remains under consideration for future testing and use.

[123] Acoustic backscatter technology shows the most promise for meeting the needs of large-scale fluvial sediment monitoring programs. The technology integrates several orders of magnitude more flow than those technologies associated with point measurements. SSC data computed from backscatter data obtained using a three-frequency instrument array and appropriate postprocessing techniques ranged from 0.01 to 20 g/L (silt- and clay-size material) and 0.01–3 g/L (sand-size material). These data were deemed by the principal investigators to be at least as accurate, within 5%, as measurements by traditional techniques. At present, the cost of using a three-frequency Doppler array (three separate instruments) is about sixfold that of a fully equipped in situ turbidimeter. Although at least one multifrequency ABS is commercially available, it lacks Doppler velocity capability. Until a multifrequency Doppler velocity profiler becomes commercially available, the cost of such an array will probably remain comparatively high. Fortunately, there are indications that development of such self-contained, multifrequency Doppler velocity units are planned, making more economic monitoring of sediment transport possible in the future, at least under some hydrological and sedimentological conditions.

[124] Most suspended sediment data obtained by federal agencies today have their underpinnings in instruments and techniques conceived before the mid-1940s. Hence, the prospect of broad application of one or more suspended-sediment surrogate technologies presented herein, and perhaps others in development, is a revolutionary concept in fluvial sedimentology. The benefits of such applied capability could be enormous, providing for safer, more frequent and consistent, arguably more accurate, and ultimately less expensive fluvial data collection for use in managing the world's sedimentary resources.

References

Agrawal, Y. C., and H. C. Pottsmith (1994), Laser diffraction particle sizing in STRESS, *Cont. Shelf Res.*, *14*, 1101–1121, doi:10.1016/0278-4343(94)90030-2.

Agrawal, Y. C., and H. C. Pottsmith (2000), Instruments for particle size and settling velocity observations in sediment transport, *Mar. Geol.*, *168*(1–4), 89–114, doi:10.1016/S0025-3227(00)00044-X.

Agrawal, Y. C., and H. C. Pottsmith (2006), The isokinetic streamlined suspended-sediment profiling LISST-SL: Status and field results, paper presented at 8th Federal Interagency Sedimentation Conference, Advisory Comm. on Water Inf., Reno, Nevada. (Available at http://pubs.usgs.gov/misc_reports/FISC_1947-2006/pdf/1st-7thFISCs-CD/8thFISC/Session%202C-1_Agrawal.pdf)

Agrawal, Y. C., A. Whitmire, O. A. Mikkelsen, and H. C. Pottsmith (2008), Light scattering by random shaped particles and consequences on measuring suspended sediments by laser diffraction, *J. Geophys. Res.*, *113*, C04023, doi:10.1029/2007JC004403.

Anderson, C. A. (2005), Turbidity, in *National Field Manual for the Collection of Water-Quality Data*, *U.S. Geol. Surv. Tech. of Water Resour. Invest.*, Book 9, U. S. Geol. Surv., Reston, Va. (Available at http://water.usgs.gov/owq/FieldManual/Chapter6/6.7_contents.html)

Bent, G. C., J. R. Gray, K. P. Smith, and G. D. Glysson (2003), A synopsis of technical issues for monitoring sediments in highway and urban runoff, in *The National Highway Runoff Data and Methodology Synthesis*, *Publ. FHWA-EP-03–054*, edited by G. E. Granato et al., pp. 113–163, U. S. Dept. of Transportation, Washington, D. C. (Available at http://ma.water.usgs.gov/fhwa/products/ofr00497.pdf)

Beverage, J. P., and J. K. Culbertson (1964), Hyperconcentrations of suspended sediment, *Proc. Am. Soc. Civ. Eng.*, *90*, 117–128.

Bogen, J., T. Fergus, and D. E. Walling (2003), Erosion and sediment transport in rivers, technological and methodological advances, *Int. Assoc. Hydrol. Sci. Publ. 283*, 238 pp.

Buchanan, P. A., and C. A. Ruhl (2000), Summary of suspended-solids concentration data, San Francisco Bay, California, Water Year 1998, *U.S. Geol. Surv. Open File Rep.*, 00–88, 41 pp.

Christensen, V. G., J. Xiaodong, and A. C. Ziegler (2000), Regression analysis and real-time water-quality monitoring to estimate constituent concentrations, loads, and yields in the Little Arkansas River, south-central Kansas, 1995–99, *U.S. Geol. Surv. Water Resour. Invest. Rep.*, 00–4126, 36 pp. (Available at http://ks.water.usgs.gov/Kansas/pubs/reports/wrir.00-4126.html)

Conner, C. S., and A. M. De Visser (1992), A laboratory investigation of particle size effects on optical backscatterance sensor, *Mar. Geol.*, *108*, 151–159, doi:10.1016/0025-3227(92)90169-I.

D&A Instrument Company (1991), *OBS-1 & 3 Instruction Manual*, 41 pp., Port Townsend, Wash.

Davis, B. E. (2005), A guide to the proper selection and use of Federally approved sediment and water-quality samplers, *U. S. Geol. Surv. Open File Rep.*, 2005–1087, 20 pp. (Available at http://pubs.usgs.gov/of/2005/1087/)

Deines, K. L. (1999), Backscatter estimation using broadband acoustic Doppler current profilers, paper presented at Sixth Working Conference on Current Measurement, IEEE, San Diego, Calif.

Downing, A., P. D. Thorne, and C. E. Vincent (1995), Backscattering from a suspension in the near field of a piston transducer, *J. Acoust. Soc. Am.*, *97*(3), 1614–1620, doi:10.1121/1.412100.

Downing, J. P. (1983), An optical instrument for monitoring suspended particles in ocean and laboratory, paper presented at OCEANS 1983, Inst. of Electr. and Electron. Eng., San Francisco, Calif.

Downing, J. P. (1996), Suspended sediment and turbidity measurements in streams: What they do and do not mean, paper presented at Automatic Water Quality Monitoring Workshop, B. C. Water Quality Monitor. Agree. Coord. Comm., Richmond, British Columbia, Canada.

Downing, J. P., R. W. Sternberg, and C. R. B. Lister (1981), New instrumentation for the investigation of sediment suspension processes in the shallow marine environment, *Mar. Geol.*, *42*, 19–34, doi:10.1016/0025-3227(81)90156-0.

Edwards, T. E., and G. D. Glysson (1999), Field methods for collection of fluvial sediment, in *Techniques of Water-Resources Investigations*, Book 3, 89 pp., U.S. Geol. Surv., Reston, Va. (Available at http://water.usgs.gov/osw/techniques/Edwards-TWRI.pdf)

Federal Interagency Sedimentation Project (1940), Field practice and equipment used in sampling suspended sediment, *Interagency Rep. 1*, 175 pp., Hydraul. Lab., Univ. of Iowa, Iowa City. (Available at http://fisp.wes.army.mil/Report%20)

Federal Interagency Sedimentation Project (1941), Laboratory investigation of suspended-sediment samplers, *Interagency Rep. 5*, 99 pp., Hydraul. Lab., Univ. of Iowa, Iowa City. (Available at http://fisp.wes.army.mil/Report%205.pdf.

Flagg, C. N., and S. L. Smith (1989), On the use of the acoustic Doppler current profiler to measure zooplankton abundance, *Deep Sea Res.*, *36*(3), 455–474, doi:10.1016/0198-0149(89)90047-2.

Flammer, G. H. (1962), Ultrasonic measurement of suspended sediment, *U.S. Geol. Surv. Bull. 1141-A*, 48 pp., Govt. Printing Off., Washington, D.C.

Gartner, J. W. (2004), Estimating suspended solids concentrations from backscatter intensity measured by acoustic Doppler current profiler in San Francisco Bay, California, *Mar. Geol.*, *211*, 169–187, doi:10.1016/j.margeo.2004.07.001.

Gartner, J. W., R. T. Cheng, P. F. Wang, and K. Richter (2001), Laboratory and field evaluations of LISST-100 instrument for suspended particle size determinations, *Mar. Geol.*, *175*(1–4), 199–219, doi:10.1016/S0025-3227(01)00137-2.

Gartner, J. W., D. S. Mueller, G. R. Wall, and J. R. Gray (2003), Breakout session 4: Other fluvial-sediment surrogates, paper presented at Federal Interagency Workshop on Turbidity and Other Sediment Surrogates, Fed. Interagency Subcomm. on Sediment., Reno, Nevada. (Available at http://pubs.usgs.gov/circ/2003/circ1250/)

Glysson, G. D. (1987), Sediment-transport curves, *U.S. Geol. Surv. Open File Rep.*, 87–218, 47 pp. (Available at http://pubs.er.usgs.gov/usgspubs/ofr/ofr87218)

Glysson, G. D. (1989), 100 years of sedimentation study by the USGS, in *Proceedings of the International Symposium, Sediment Transport Modeling*, edited by S. S. Y. Wang, pp. 260–265, Am. Soc. of Civ. Eng., New Orleans, La.

Glysson, G. D., and J. R. Gray (1997), Coordination and standardization of Federal sedimentation activities, in *Expanding Sediment Research Capabilities in Today's U.S. Geological Survey*, edited by J. R. Gray, 3 pp., U. S. Geol. Surv., St. Petersburg, Fla. (Available at http://water.usgs.gov/osw/techniques/sedtech21/gray.html)

Graf, J. B., L. Wirt, E. K. Swanson, G. G. Fisk, and J. R. Gray (1995), Streamflow transport of radionuclides in the Puerco and Little Colorado River basins, Arizona and New Mexico, *U. S. Geol. Surv. Water Supply Pap.*, 2459, 89 pp. (Available at http://pubs.er.usgs.gov/usgspubs/wsp/wsp2459)

Gray, J. R. (2003a), The need for sediment surrogate technologies to monitor fluvial-sediment transport, in *Proceedings of the Federal Interagency Sedimentation Workshop on Turbidity and Other Sediment Surrogates*, edited by J. R. Gray and G. D. Glysson, *U. S. Geol. Surv. Circ.*, vol. 1250, 4 pp. (Available at http://water.usgs.gov/osw/techniques/TSS/gray.pdf)

Gray, J. R. (2003b), U.S. Geological Survey suspended-sediment surrogate research, Part I: Call for a sediment monitoring instrument and analysis research program, paper presented at Virginia Water Research Symposium 2003, Water Resource Management for the Commonwealth, Va. Polytech. Inst. and State Univ., Blacksburg.

Gray, J. R. (Ed.) (2005), Proceedings of the Federal Interagency Sediment Monitoring Instrument and Analysis Research Workshop, Flagstaff, Arizona, 9–11 September, *U.S. Geol. Surv. Circ.*, 1276, 46 pp. (Available at http://pubs.usgs.gov/circ/2005/1276/)

Gray, J. R., and J. W. Gartner (2004), Surrogate technologies for continuous suspended-sediment monitoring in the United States, paper presented at 9th International Symposium on River Sedimentation, Tsinghua Univ., Yichang, China.

Gray, J. R., and G. D. Glysson (2005), Attributes of a sediment monitoring instrument and analysis research program, paper presented at Federal Interagency Sediment Monitoring Instrument and Analysis Research Workshop, U. S. Geol. Surv., Flagstaff, Ariz. (Available at http://water.usgs.gov/osw/techniques/sediment/sedsurrogate2003workshop/gray_glysson.pdf)

Gray, J. R., and F. J. M. Simões (2008), Estimating sediment discharge, in *Sedimentation Engineering–Processes, Measurements, Modeling, and Practice, Manual 110*, edited by M. Garcia, pp. 1067–1088, Am. Soc. of Civ. Eng., Reston, Va.

Gray, J. R., G. D. Glysson, and D. S. Mueller (2002), Comparability and accuracy of fluvial-sediment data–a view from the U.S. Geological Survey, in *paper presented at Specialty Conference, Hydraulic Measurements and Experimental Methods*, Am. Soc. of Civ. Eng., Estes Park, Colo. (Available at http://water.usgs.gov/osw/techniques/asce.pdf)

Gray, J. R., T. S. Melis, E. Patiño, M. C. Larsen, D. J. Topping, P. P. Rasmussen, and C. Figueroa-Alama (2003a), U.S. Geological Survey research on surrogate measurements for suspended sediment, in *Proceedings of the 1st Interagency Conference on Research in Watersheds*, edited by K. Renard et al., pp. 95–100, U. S. Dept. of Agric., Benson, Ariz.

Gray, J. R., D. J. Gooding, T. S. Melis, D. J. Topping, and P. P. Rasmussen (2003b), U.S. Geological Survey suspended-sediment surrogate research, Part II: Optic technologies, paper presented at Virginia Water Research Symposium 2003, Water Resource Management for the Commonwealth, Va. Polytech. Inst. and State Univ., Blacksburg.

Gray, J. R., E. Patiño, and M. C. Larsen (2003c), U.S. Geological Survey suspended-sediment surrogate research, Part III: Acoustic and pressure-differential technologies, paper presented at Virginia Water Research Symposium 2003, Water Resource Management for the Commonwealth, Va. Polytech. Inst. and State Univ., Blacksburg.

Gray, J. R., Y. C. Agrawal, and H. C. Pottsmith (2004), The LISST-SL streamlined isokinetic suspended-sediment profiler, paper presented at 9th International Symposium on River Sedimentation, Tsinghua Univ., Yichang, China. (Available at http://water.usgs.gov/osw/techniques/Lisst_Gray_Agrawal_Pottsmith.pdf)

Gray, J. R., G. D. Glysson, and T. K. Edwards (2008), Suspended-sediment samplers and sampling methods, in *Sedimentation Engineering, Manual 110*, chap. 5.3, pp. 318–337, Am. Soc. of Civ. Eng., Reston, Va.

Hamilton, L. J., Z. Shi, and S. Y. Zhang (1998), Acoustic backscatter measurements of estuarine suspended cohesive sediment concentration profiles, *J. Coastal Res.*, *14*(4), 1213–1224.

Hay, A. E. (1991), Sound scattering from a particle-laden, turbulent jet, *J. Acoust. Soc. Am.*, *90*(4), 2055–2074.

Hay, A. E., and J. Sheng (1992), Vertical profiles of suspended sand concentration and size from multi-frequency acoustic backscatter, *J. Geophys. Res.*, *97*(C10), 15,661–15,677, doi:10.1029/92JC01240.

Heywood, K. J., S. Scrope-Howe, and E. D. Barton (1991), Estimation of zooplankton abundance from shipborne ADCP backscatter, *Deep Sea Res.*, *38*(6), 677–691, doi:10.1016/0198-0149(91)90006-2.

Holdaway, G. P., P. D. Thorne, D. Flatt, S. E. Jones, and D. Prandle (1999), Comparison between ADCP and transmissometer measurements of suspended sediment concentration, *Cont. Shelf Res.*, *19*, 421–441, doi:10.1016/S0278-4343(98)00097-1.

Jay, D. A., P. Orton, D. J. Kay, A. Fain, and A. M. Baptisa (1999), Acoustic determination of sediment concentrations, settling velocities, horizontal transports and vertical fluxes in estuaries, paper presented at 6th Working Conference on Current Measurement, IEEE, San Diego, Calif.

Kineke, G. C., and R. W. Sternberg (1992), Measurements of high concentration suspended sediments using the optical backscatterance sensor, *Mar. Geol.*, *108*, 253–258, doi:10.1016/0025-3227(92)90199-R.

Koltun, G. F., M. Eberle, J. R. Gray, and G. D. Glysson (2006), User's manual for the Graphical Constituent Loading Analysis System (GCLAS), in *Techniques and Methods, Book 4*, chap. C1, 50 pp., U.S. Geol. Surv., Reston, Va. (Available at http://pubs.er.usgs.gov/usgspubs/tm/tm4C1)

Konrad, C., H. C. Pottsmith, T. S. Melis, and D. M. Rubin (2006), Real-time analysis of concentrated fluvial suspended sediments, paper presented at 8th Federal Interagency Sedimentation Conference, U. S. Geol. Surv., Reno, Nev. (Available at http://pubs.usgs.gov/misc_reports/FISC_1947-2006/pdf/1st-7thFISCs-CD/8thFISC/Session%208C-2_Konrad.pdf)

Land, J. M., and P. D. Jones (2001), Acoustic measurement of sediment flux in rivers and near-shore waters, paper presented at 7th Federal Interagency Sedimentation Conference, U. S. Geol. Surv., Reno, Nev. (Available at http://pubs.usgs.gov/misc_reports/FISC_1947-2006/pdf/1st-7thFISCs-CD/7thFISC/7Fisc-V1/7FISC1-3.pdf)

Landers, M. N. (2003), Summary of blind sediment reference sample measurement session, in *Proceedings of the Federal Interagency Workshop on Turbidity and Other Sediment Surrogates*, edited by J. R. Gray and G. D. Glysson, *U.S. Geol. Surv. Circ.*, vol. 1250, pp. 29–30. (Available at http://water.usgs.gov/osw/techniques/turbidity.html)

Larsen, M. C., C. Figueroa-Alamo, J. R. Gray, and W. Fletcher (2001), Continuous automated sensing of streamflow density as a surrogate for suspended-sediment concentration sampling, paper presented at 7th Federal Interagency Sedimentation Conference, U. S. Geol. Surv., Reno, Nev. (Available at http://pubs.usgs.gov/misc_reports/FISC_1947-2006/pdf/1st-7thFISCs-CD/7thFISC/7Fisc-V1/7FISC1-3.pdf)

Lewis, J. (2002), Estimation of suspended sediment flux in streams using continuous turbidity and flow data coupled with laboratory concentrations, in *Proceedings of the Federal Interagency Workshop on Turbidity and Other Sediment Surrogates*, edited by J. R. Gray and G. D. Glysson, *U.S. Geol. Surv. Circ.*, *1250*, 3 pp. (Available at http://water.usgs.gov/osw/techniques/TSS/LewisTSS.pdf)

Lewis, A. J., and T. C. Rasmussen (1999), Determination of suspended sediment concentrations and particle size distributions using pressure measurements, *J. Environ. Qual.*, *28*, 1490–1496.

Libicki, C., K. W. Bedford, and J. F. Lynch (1989), The interpretation and evaluation of a 3-MHz acoustic backscatter device for measuring benthic boundary layer sediment dynamics, *J. Acoust. Soc. Am.*, *85*(4), 1501–1511, doi:10.1121/1.397351.

Lohrman, A., and C. Huhta (1994), Plume measurement system (Plumes) calibration experiment, dredging research program, *Tech. Rep. DRP-94–3*, 152 pp., U. S. Army Corps of Eng., Washington, D.C.

Lorke, A., D. F. McGinnis, P. Spaak, and A. Wuest (2004), Acoustic observations of zooplankton in lakes using Doppler current profiler, *Freshwater Biol.*, *49*, 1280–1292, doi:10.1111/j.1365-2427.2004.01267.x.

Ludwig, K. A., and D. M. Hanes (1990), A laboratory evaluation of optical backscatterance suspended solids sensors exposed to sand-mud mixtures, *Mar. Geol.*, *94*, 173–179, doi:10.1016/0025-3227(90)90111-V.

Meade, R. H., and R. S. Parker (1985), Sediment in rivers of the United States, *U.S. Geol. Surv. Water Supply Pap.*, *2275*, 49–60.

Melis, T. S., D. J. Topping, and D. M. Rubin (2003), Testing laser-based sensors for continuous in situ monitoring of suspended sediment in the Colorado River, Arizona, in *Erosion and Sediment Transport Measurement in Rivers, Technological and Methodological Advances, Publ.*, vol. 203, edited by J. Bogen et al., pp. 21–27, Int. Assoc. of Hydrol. Sci., Geneva.

Mol, J.-W. (2003), Sedimentation estimation from ADCP measurements, *Hydro Int.*, *7*(6). (Available at http://www.hydro-international.com/issues/articles/id17-Sedimentation_Estimation_from_ADCP_Measurements.html)

Nelson, M. E., and P. C. Benedict (1950), Measurement and analysis of suspended sediment loads in streams, *Am. Soc. Civ. Eng. Trans.*, *2450*, 891–918.

Nolan, K. M., J. R. Gray, and G. D. Glysson (2005), Introduction to suspended-sediment sampling [CD-ROM], *U.S. Geol. Surv. Sci. Invest. Rep.*, *2005–5077*. (Available at http://pubs.er.usgs.gov/pubs/sir/sir20055077)

Osterkamp, W. R., P. Heilman, and L. J. Lane (1998), Economic considerations of a continental sediment-monitoring program, *Int. J. Sediment. Res.*, *13*(4), 12–24.

Osterkamp, W. R., et al. (2004), An invitation to participate in a North American sediment-monitoring network, *Eos Trans. AGU*, *84*(40), 386.

Pimentel, D., et al. (1995), Environmental and economic costs of soil erosion and conservation benefits, *Science*, *267*, 1117–1123, doi:10.1126/science.267.5201.1117.

Porterfield, G. (1972), Computation of fluvial-sediment discharge, in *Techniques of Water-Resource Investigations, Book 3*, chap. C3, 66 pp., U. S. Geol. Surv., Reston, Va. (Available at http://water.usgs.gov/pubs/twri/twri3-c3/)

Pratt, T., and T. Parchure (2003), OBS calibration and field measurements, in *Proceedings of the Federal Interagency Workshop on Turbidity and Other Sediment Surrogates*, edited by J. R. Gray and G. D. Glysson, *U.S. Geol. Surv. Circ.*, *1250*, 31–46. (Available at http://pubs.usgs.gov/circ/2003/circ1250/)

Pruitt, B. A. (2003), Uses of turbidity by States and Tribes, in *Proceedings of the Federal Interagency Workshop on Turbidity and Other Sediment Surrogates*, edited by J. R. Gray and G. D. Glysson, *U.S. Geol. Surv. Circ.*, *1250*, 31–46. (Available at http://pubs.usgs.gov/circ/2003/circ1250/)

Rainwater, F. H. (1962), Stream composition of the conterminous United States, *Hydrol. Invest. Atlas HA-61*, U.S. Geol. Surv., Reston, Va.

Rasmussen, T. J., A. C. Ziegler, and P. P. Rasmussen (2005), Estimation of constituent concentrations, densities, loads, and yields on Lower Kansas River, Northeast Kansas, using regression models and continuous water-quality modeling, January 2000 through December 2003, *U.S. Geol. Surv. Sci. Invest. Rep.*, 2005–5165, 117 pp. (Available at http://pubs.usgs.gov/sir/2005/5165/)

Reichel, G., and H. P. Nachtnebel (1994), Suspended sediment monitoring in a fluvial environment: Advantages and limitations applying an acoustic Doppler current profiler, *Water Res.*, *28*(4), 751–761, doi:10.1016/0043-1354(94)90083-3.

Schoellhamer, D. H., and S. A. Wright (2003), Continuous measurement of suspended-sediment discharge in rivers by use of optical backscatterance sensors, in *Erosion and Sediment Transport Measurement in Rivers, Technological and Methodological Advances, Publ. 283*, edited by J. Bogen et al., pp. 28–36, Int. Assoc. of Hydrol. Sci., Geneva.

Schoellhamer, D. H., P. A. Buchanan, and N. K. Ganju (2002), Ten years of continuous suspended sediment concentration monitoring in San Francisco Bay and Delta, paper presented at Turbidity and Other Sediment Surrogates Workshop, U. S. Geol. Surv., Reno, Nev. (Available at http://water.usgs.gov/osw/techniques/TSS/schoelhamer.pdf)

Schott, F., and W. Johns (1987), Half-year-long measurements with a buoy-mounted acoustic Doppler current profiler in the Somali Current, *J. Geophys. Res.*, *92*(C5), 5169–5176, doi:10.1029/JC092iC05p05169.

Sheng, J., and A. E. Hay (1988), An examination of the spherical scatter approximation in aqueous suspensions of sand, *J. Acoust. Soc. Am.*, *83*(2), 598–610, doi:10.1121/1.396153.

Skinner, J. V. (1989), History of the Federal Interagency Sedimentation Project, in *Proceedings of the International Symposium, Sediment Transport Modeling*, edited by S. S. Y. Wang, pp. 266–271, Am. Soc. of Civ. Eng., New Orleans, La.

Smith, R. A., R. B. Alexander, and M. G. Wolman (1987), Water-quality trends in the nation's rivers, *Science*, *235*, 1607–1615, doi:10.1126/science.235.4796.1607.

Sutherland, T. F., P. M. Lane, C. L. Amos, and J. Downing (2000), The calibration of optical backscatter sensors for suspended sediment of varying darkness levels, *Mar. Geol.*, *162*, 587–597, doi:10.1016/S0025-3227(99)00080-8.

Thevenot, M. M., and N. C. Kraus (1993), Comparison of acoustical and optical measurements of suspended material in the Chesapeake Estuary, *J. Mar. Environ. Eng.*, *1*, 65–79.

Thevenot, M. M., T. L. Prickett, and N. C. Kraus (1992), Tylers Beach, Virginia, dredged material plume monitoring project 27 September to 4 October 1991, *Tech. Rep. DRP-92–7*, 204 pp., U. S. Army Corps of Eng., Washington, D.C.

Thorne, P. D., C. E. Vincent, P. J. Harcastle, S. Rehman, and N. Pearson (1991), Measuring suspended sediment concentrations using acoustic backscatter devices, *Mar. Geol.*, *98*, 7–16, doi:10.1016/0025-3227(91)90031-X.

Topping, D. J., T. S. Melis, D. M. Rubin, and S. A. Wright (2004), High-resolution monitoring of suspended-sediment concentration and grain size in the Colorado River in Grand Canyon using a laser acoustic system, paper presented at 9th International Symposium on River Sedimentation, Tsinghua Univ., Yichang, China.

Topping, D. J., S. A. Wright, T. S. Melis, and D. M. Rubin (2007), High-resolution measurement of suspended-sediment concentrations and grain size in the Colorado River in Grand Canyon using a multi-frequency acoustic system, paper presented at 10th International Symposium on River Sedimentation, World Assoc. for Sediment. and Erosion Res., Moscow, Russia.

Traykovski, P., R. J. Latter, and J. D. Irish (1999), A laboratory evaluation of the LISST instrument using natural sediments, *Mar. Geol.*, *159*, 355–367, doi:10.1016/S0025-3227(98)00196-0.

Uhrich, M. A. (2002), Determination of total and clay suspended-sediment loads from instream turbidity data in the North Santiam River Basin, Oregon, 1998–2002, in *Proceedings of the Federal Interagency Workshop on Turbidity and Other Sediment Surrogates*, edited by J. R. Gray and G. D. Glysson, *U. S. Geol. Surv. Circ.*, *1250*, 3 pp. (Available at http://water.usgs.gov/pubs/circ/2003/circ1250/)

Uhrich, M. A., and H. M. Bragg (2003), Monitoring instream turbidity to estimate continuous suspended-sediment loads and yields and clay-water volumes in the Upper North Santiam River Basin, Oregon, 1998–2000, *U.S. Geol. Surv. Water Resour. Invest. Rep.*, 03–4098, 44 pp. (Available at http://pubs.usgs.gov/wri/WRI03-4098/)

Urick, R. J. (1975), *Principles of Underwater Sound*, 2nd ed., 384 pp., McGraw Hill, New York.

U. S. Department of Agriculture (1965), Proceedings of the Federal Inter-Agency Sedimentation Conference, *Misc. Publ. 970*, 933 pp., Washington, D. C.

U.S. Environmental Protection Agency (1999), Guidance manual for compliance with the Interim Enhanced Surface Water Treatment rule–Turbidity provisions, *Rep. EPA 815-R-99–010*, Washington, D.C.

Wall, G. R., E. A. Nystrom, and S. Litten (2006), Use of an ADCP to compute suspended-sediment discharge in the tidal Hudson River, New York, *U.S. Geol. Surv. Sci. Invest. Rep.*, 2006–5055, 16 pp. (Available at http://pubs.usgs.gov/sir/2006/5055/)

Ziegler, A. C. (2003), Breakout session 1–Definition of optical methods for turbidity and data reporting, in *Proceedings of the Federal Interagency Workshop on Turbidity and Other Sediment Surrogates*, edited by J. R. Gray and G. D. Glysson, *U.S. Geol. Surv. Circ.*, *1250*, 9–13. (Available at http://water.usgs.gov/pubs/circ/2003/circ1250/)

J. W. Gartner, U.S. Geological Survey, 520 North Park Avenue, Tucson, AZ 85719, USA.

J. R. Gray, Office of Surface Water, U.S. Geological Survey, 12201 Sunrise Valley Drive, Reston, VA 20192, USA. (jrgray@usgs.gov)

Assessment of erosion, sedimentation, and water quality impacts of the Mountain Valley Pipeline and Equitrans Expansion Project's proposed crossing of the Jefferson National Forest as it pertains to the U.S. Forest Service's Draft Supplemental Environmental Impact Statement dated December 2022

Prepared by Jonathan A. Czuba, Ph.D., Licensed Professional Engineer - February 9, 2023

REFERENCES
10

February 21, 2023

USGS
science for a changing world

Revised Methods for Characterizing Stream Habitat in the National Water-Quality Assessment Program

U.S. Geological Survey
Water-Resources Investigations Report 98-4052

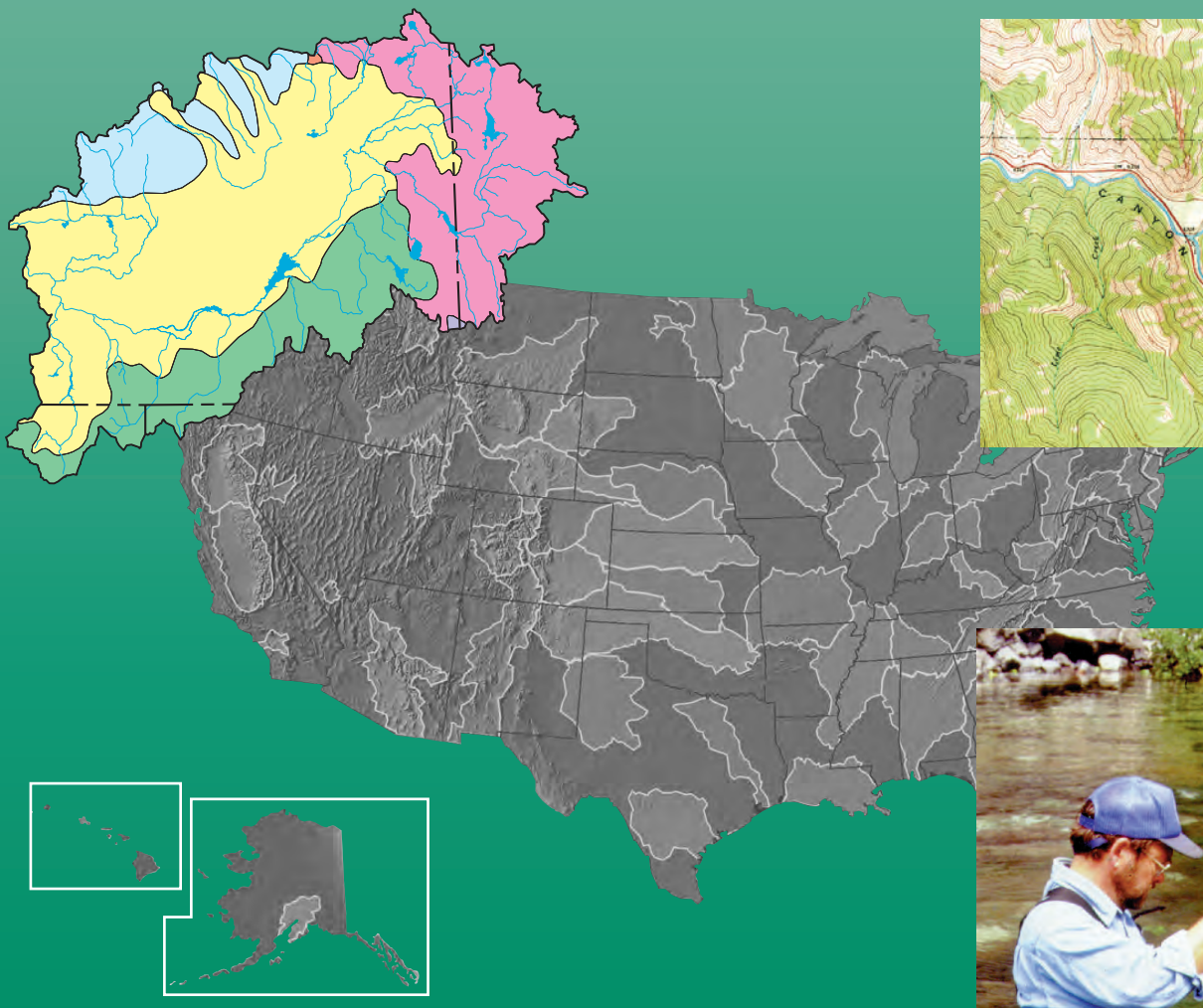

U.S. Department of the Interior
U.S. Geological Survey

ACKNOWLEDGMENTS

Technical Support

Thomas F. Cuffney, Ecologist, U.S. Geological Survey, Raleigh, N.C.
Terry M. Short, Physical Scientist, U.S. Geological Survey, Menlo Park, Calif.
Steven L. Goodbred, Biologist, U.S. Geological Survey, Sacramento, Calif.
Paul L. Ringold, Ecologist, U.S. Environmental Protection Agency, Corvallis, Oreg.

Technical Reviewers

Janet S. Heiny, Hydrologist, U.S. Geological Survey, Denver, Colo.
Cliff R. Hupp, Botanist, U.S. Geological Survey, Reston, Va.
Robert B. Jacobson, Research Hydrologist, U.S. Geological Survey, Columbia, Mo.
Peter M. Ruhl, Hydrologist, U.S. Geological Survey, Raleigh, N.C.
Charles A. Peters, Supervisory Hydrologist, U.S. Geological Survey, Madison, Wis.

Editorial and Graphics

Rebecca J. Deckard, Supervisory Writer/Editor, U.S. Geological Survey, Raleigh, N.C.
Kay E. Hedrick, Writer/Editor, U.S. Geological Survey, Raleigh, N.C.
Jeffrey L. Corbett, Scientific Illustrator, U.S. Geological Survey, Raleigh, N.C.
Michael Eberle, Technical Publications Editor, U.S. Geological Survey, Columbus, Ohio
Betty B. Palcsak, Technical Publications Editor, U.S. Geological Survey, Columbus, Ohio

Approving Official

Chester Zenone, Reports Improvement Advisor, U.S. Geological Survey, Reston, Va.

Revised Methods for Characterizing Stream Habitat in the National Water-Quality Assessment Program

By Faith A. Fitzpatrick, Ian R. Waite, Patricia J. D'Arconte, Michael R. Meador, Molly A. Maupin, and Martin E. Gurtz

---

U.S. GEOLOGICAL SURVEY

Water-Resources Investigations Report 98-4052

Raleigh, North Carolina
1998

U.S. DEPARTMENT OF THE INTERIOR
BRUCE BABBITT, Secretary

U.S. GEOLOGICAL SURVEY
Thomas J. Casadevall, Acting Director

For additional information write to:

District Chief
U.S. Geological Survey
3916 Sunset Ridge Road
Raleigh, NC 27607-6416

Copies of this report can be purchased from:

U.S. Geological Survey
Branch of Information Services
Box 25286, Federal Center
Denver, CO 80225-0286

FOREWORD

The mission of the U.S. Geological Survey (USGS) is to assess the quantity and quality of the earth resources of the Nation and to provide information that will assist resource managers and policymakers at Federal, State, and local levels in making sound decisions. Assessment of water-quality conditions and trends is an important part of this overall mission.

One of the greatest challenges faced by water-resources scientists is acquiring reliable information that will guide the use and protection of the Nation's water resources. That challenge is being addressed by Federal, State, interstate, and local water-resource agencies and by many academic institutions. These organizations are collecting water-quality data for a host of purposes that include compliance with permits and water-supply standards; development of remediation plans for a specific contamination problem; operational decisions on industrial, wastewater, or water-supply facilities; and research on factors that affect water quality. An additional need for water-quality information is to provide a basis on which regional and national-level policy decisions can be based. Wise decisions must be based on sound information. As a society we need to know whether certain types of water-quality problems are isolated or ubiquitous, whether there are significant differences in conditions among regions, whether the conditions are changing over time, and why these conditions change from place to place and over time. The information can be used to help determine the efficacy of existing water-quality policies and to help analysts determine the need for, and likely consequences of, new policies.

To address these needs, the Congress appropriated funds in 1986 for the USGS to begin a pilot program in seven project areas to develop and refine the National Water-Quality Assessment (NAWQA) Program. In 1991, the USGS began full implementation of the program. The NAWQA Program builds upon an existing base of water-quality studies of the USGS, as well as those of other Federal, State, and local agencies. The objectives of the NAWQA Program are to

- Describe current water-quality conditions for a large part of the Nation's freshwater streams, rivers, and aquifers.
- Describe how water quality is changing over time.
- Improve understanding of the primary natural and human factors that affect water-quality conditions.

This information will help support the development and evaluation of management, regulatory, and monitoring decisions by other Federal, State, and local agencies to protect, use, and enhance water resources.

The goals of the NAWQA Program are being achieved through ongoing and proposed investigations of 60 of the Nation's most important river basins and aquifer systems, which are referred to as Study Units. These Study Units are distributed throughout the Nation and cover a diversity of hydrogeologic settings. More than two-thirds of the Nation's freshwater use occurs within the 60 Study Units and more than two-thirds of the people served by public water-supply systems live within their boundaries.

National synthesis of data analysis, based on aggregation of comparable information obtained from the Study Units, is a major component of the program. This effort focuses on selected water-quality topics using nationally consistent information. Comparative studies will explain differences and similarities in observed water-quality conditions among study areas and will identify changes and trends and their causes. The first topics addressed by the national synthesis are pesticides, nutrients, volatile organic compounds, and aquatic biology. Discussions on these and other water-quality topics will be published in periodic summaries of the quality of the Nation's ground and surface water as the information becomes available.

This report is an element of the comprehensive body of information developed as part of the NAWQA Program. The program depends heavily on the advice, cooperation, and information from many Federal, State, interstate, Tribal, and local agencies and the public. The assistance and suggestions of all are greatly appreciated.

Robert M. Hirsch
Chief Hydrologist

CONTENTS

FIGURES

TABLES

CONVERSION FACTORS

Multiply	By	To obtain
	Length	
millimeter (mm)	0.03937	inch
centimeter (cm)	0.3937	inch
meter (m)	3.281	foot
kilometer (km)	0.6214	mile
	Area	
square meter (m^2)	10.76	square foot
square kilometer (km^2)	0.38361	square mile
	Volume per unit time (flow)	
cubic meter per second (m^3/s)	35.31	cubic foot per second

GLOSSARY

The terms in this glossary were compiled from numerous sources. Some definitions have been modified in accordance with the usage of the National Water-Quality Assessment (NAWQA) Program and may not be the only valid definitions for these terms.

Aggradation—A long-term, persistent rise in the elevation of a streambed by deposition of sediment. Aggradation can result from a reduction of discharge with no corresponding reduction in sediment load, or an increase in sediment load with no change in discharge.

Bank—The sloping ground that borders a stream and confines the water in the natural channel when the water level, or flow, is normal. It is bordered by the flood plain and channel.

Bankfull stage—Stage at which a stream first overflows its natural banks formed by floods with 1- to 3-year recurrence intervals (Langbein and Iseri, 1960; Leopold and others, 1964).

Base flow—Sustained, low flow in a stream; ground-water discharge is the source of base flow in most streams.

Basic fixed sites—Sites on streams at which streamflow is measured and samples are collected for measurements of temperature, salinity, and suspended sediment, and analyses for major ions and metals, nutrients, and organic carbon to assess the broad-scale spatial and temporal character and transport of inorganic constituents of streamwater in relation to hydrologic conditions and environmental settings.

Canopy angle—Generally, a measure of the openness of a stream to sunlight. Specifically, the angle formed by an imaginary line from the highest structure (for example, tree, shrub, or bluff) on one bank to eye level at mid-channel to the highest structure on the other bank.

Channel—The channel includes the thalweg and streambed. Bars formed by the movement of bedload are included as part of the channel.

Channelization—Modification of a stream, typically by straightening the channel, to provide more uniform flow. Channelization is often done for flood control or for improved agricultural drainage or irrigation.

Confluence—The flowing together of two or more streams; the place where a tributary joins the main stream.

Contributing area—The area in a drainage basin that contributes runoff to a stream.

Crenulation—A “V” or “U” shaped indentation in a contour line that represents a course for flowing water (ephemeral, intermittent, or perennial stream) on a topographic map. The point forming the crenulation faces upstream.

Cross section—A line of known horizontal and vertical elevation across a stream perpendicular to the flow. Measurements are taken along this line so that geomorphological characteristics of the section are measured with known elevation from bank to bank. Compare to transect.

Diversion—A turning aside or alteration of the natural course of flowing water, normally considered to physically leave the natural channel. In some States, this can be a consumptive use directly from another source, such as by livestock watering. In other States, a diversion must consist of such actions as taking water through a canal, pipe, or conduit.

Drainage area—An area of land that drains water, sediment, and dissolved materials to a common outlet along a stream channel. The area is measured in a horizontal plane and enclosed by a drainage divide.

Drainage basin—A part of the surface of the Earth that is occupied by a drainage system, which consists of a surface stream or a body of impounded surface water, including all tributary surface streams and bodies of impounded surface water.

Ecoregion—An area of similar climate, landform, soil, potential natural vegetation, hydrology, or other ecologically relevant variables.

Embeddedness—The degree to which gravel-sized and larger particles are surrounded or enclosed by finer-sized particles.

Ephemeral stream—A stream that carries water only during periods of rainfall or snowmelt events (Leopold and Miller, 1956).

Flood—Any relatively high streamflow that overtops the natural or artificial banks of a stream.

Flood plain—The relatively level area of land bordering a stream channel and inundated during moderate to severe floods. The level of the flood plain is generally about the stage of the 1- to 3-year flood.

Geomorphic channel units—Fluvial geomorphic descriptors of channel shape and stream velocity. Pools, riffles, and runs are three types of geomorphic channel units considered for National Water-Quality Assessment (NAWQA) Program habitat sampling.

Habitat—In general, aquatic habitat includes all nonliving (physical) aspects of the aquatic ecosystem (Orth, 1983), although living components like aquatic macrophytes and riparian vegetation also are usually included. Measurements of habitat are typically made over a wider geographic scale than measurements of species distribution.

Hydrography—Surface-water drainage network.

Hypsography—Elevation contours.

Indicator sites—Stream sampling sites located at outlets of drainage basins with relatively homogeneous land use and physiographic conditions. Most indicator-site basins have drainage areas ranging from 52 to 520 square kilometers.

Integrator or mixed-use sites—Stream sampling sites located at outlets of drainage basins that contain multiple environmental settings. Most integrator sites are on major streams with relatively large drainage areas.

Intensive fixed sites—Basic fixed sites with increased sampling frequency during selected seasonal periods and analysis of dissolved pesticides for 1 year. Most NAWQA Study Units have one to two integrator intensive fixed sites and one to four indicator intensive fixed sites.

Intermittent stream—A stream in which, at low flow, dry reaches alternate with flowing ones along the stream length (Leopold and Miller, 1956).

Lattice elevation model—A file of terrain elevations stored in a grid format.

Perennial stream—A stream that carries some flow at all times (Leopold and Miller, 1956).

Physiography—A description of the surface features of the Earth, with an emphasis on the origin of landforms.

Pool—A small part of the reach with little velocity, commonly with water deeper than surrounding areas.

Reach—A length of stream that is chosen to represent a uniform set of physical, chemical, and biological conditions within a segment. It is the principal sampling unit for collecting physical, chemical, and biological data.

Recurrence interval—The average time period within which the size (magnitude) of a given flood will be equaled or exceeded.

Reference location—A geographic location that provides a link to habitat data collected at different spatial scales. It is often a location with known geographic coordinates, such as a gaging station or bridge crossing.

Reference site—A NAWQA sampling site selected for its relatively undisturbed conditions.

Retrospective analysis—Review and analysis of existing data in order to address NAWQA objectives, to the extent possible, and to aid in the design of NAWQA studies.

Riffle—A shallow part of the stream where water flows swiftly over completely or partially submerged obstructions to produce surface agitation.

Riparian—Pertaining to or located on the bank of a body of water, especially a stream.

Riparian zone—Area adjacent to a stream that is directly or indirectly affected by the stream. The biological community or physical features of this area are different or modified from the surrounding upland by its proximity to the river or stream.

Run—A relatively shallow part of a stream with moderate velocity and little or no surface turbulence.

Segment—A section of stream bounded by confluences or physical or chemical discontinuities, such as major waterfalls, landform features, significant changes in gradient, or point-source discharges.

Sideslope gradient—The representative change in elevation in a given horizontal distance (usually about 300 meters) perpendicular to a stream; the valley slope along a line perpendicular to the stream.

Sinuosity—The ratio of the channel length between two points on a channel to the straight-line distance between the same two points; a measure of meandering.

Stage—The height of a water surface above an established datum; same as gage height.

Stream—The general term for a body of flowing water. Generally, this term is used to describe water flowing through a natural channel as opposed to a canal.

Streamflow—A general term for water that flows through a channel.

Stream order—A ranking of the relative sizes of streams within a watershed based on the nature of their tributaries.

Study Unit—A major hydrologic system in the United States in which NAWQA studies are focused. Study Units are geographically defined by a combination of ground- and surface-water features and generally encompass more than 4,000 square miles of land area.

Synoptic sites—Sites sampled during a short-term investigation of specific water-quality conditions during selected seasonal or hydrologic conditions to provide improved spatial resolution for critical water-quality conditions.

Terrace—An abandoned flood-plain surface. A terrace is a long, narrow, level or slightly inclined surface that is contained in a valley and bounded by steeper ascending or descending slopes, and it is always higher than the flood plain. A terrace may be inundated by floods larger than the 1- to 3-year flood.

Thalweg—The line formed by connecting points of minimum streambed elevation (deepest part of the channel) (Leopold and others, 1964).

Transect—A line across a stream perpendicular to the flow and along which measurements are taken, so that morphological and flow characteristics along the line are described from bank to bank. Unlike a cross section, no attempt is made to determine known elevation points along the line.

Wadeable—Sections of a stream where an investigator can wade from one end of the reach to the other, even though the reach may contain some pools that cannot be waded.

Revised Methods for Characterizing Stream Habitat in the National Water-Quality Assessment Program

By Faith A. Fitzpatrick, Ian R. Waite, Patricia J. D'Arconte, Michael R. Meador, Molly A. Maupin, *and* Martin E. Gurtz

ABSTRACT

Stream habitat is characterized in the U.S. Geological Survey's National Water-Quality Assessment (NAWQA) Program as part of an integrated physical, chemical, and biological assessment of the Nation's water quality. The goal of stream habitat characterization is to relate habitat to other physical, chemical, and biological factors that describe water-quality conditions. To accomplish this goal, environmental settings are described at sites selected for water-quality assessment. In addition, spatial and temporal patterns in habitat are examined at local, regional, and national scales.

This habitat protocol contains updated methods for evaluating habitat in NAWQA Study Units. Revisions are based on lessons learned after 6 years of applying the original NAWQA habitat protocol to NAWQA Study Unit ecological surveys. Similar to the original protocol, these revised methods for evaluating stream habitat are based on a spatially hierarchical framework that incorporates habitat data at basin, segment, reach, and microhabitat scales. This framework provides a basis for national consistency in collection techniques while allowing flexibility in habitat assessment within individual Study Units. Procedures are described for collecting habitat data at basin and segment scales; these procedures include use of geographic information system data bases, topographic maps, and aerial photographs. Data collected at the reach scale include channel, bank, and riparian characteristics.

INTRODUCTION

The U.S. Geological Survey's (USGS) National Water-Quality Assessment (NAWQA) Program is designed to assess the status of and trends in the Nation's water quality (Gilliom and others, 1995) and to develop an understanding of the major factors that affect observed water-quality conditions and trends (Hirsch and others, 1988; Leahy and others, 1990). This assessment is accomplished by collecting physical, chemical, and biological data at sites that represent major natural and human factors (for example, ecoregion, land use, stream size, hydrology, and geology) that are thought to control water quality. These data are used to provide an integrated assessment of water quality within selected environmental settings, assess trends in water quality, and investigate the influence of major natural and human factors on water quality.

Study Unit investigations in the NAWQA Program are done on a staggered time scale in approximately 59 of the largest and most significant hydrologic systems across the Nation (Gilliom and others, 1995). These investigations, which consist of 4 to 5 years of intensive assessment followed by 5 years of low-intensity assessment, consist of four main components—(1) retrospective analysis; (2) occurrence and distribution assessment; (3) assessment of long-term trends and changes; and (4) case studies of sources, transport, fate, and effects (Gilliom and others, 1995). Occurrence and distribution assessments are done in a nationally consistent and uniform manner for identification of spatial and temporal trends in water quality at a national scale (Gilliom and others, 1995).

Characterization of stream habitat is an essential component of many water-quality assessment programs (Osborne and others, 1991) and an important element in the NAWQA Program (Gurtz, 1994).

Habitat assessment is critical in determining the limiting natural and human factors that affect water chemistry and aquatic biological communities. These limiting factors exist at many different spatial scales, from drainage-basin characteristics to streambed conditions within a small area of the stream. Thus, habitat assessments consist of measuring a wide range of characteristics. For example, fish-species distribution is affected by climate (Tonn, 1990), stream gradient (Sheldon, 1968), and particle size of substrate within a specific section of a stream (Hynes, 1975). Habitat assessment provides baseline information on stream conditions so that trends resulting from natural and human causes can be identified, estimated, or predicted. Habitat assessments also are done to determine the physical, chemical, and biological consequences of alterations of stream conditions, such as stream impoundment or channelization, or of changes in land use in the drainage basin. Hence data collected as part of the habitat assessment can be used to help interpret physical (for example, channel characteristics) and chemical (for example, transport of sediment-associated contaminants) properties in addition to supporting investigations of biological communities.

Many State and regional assessment programs incorporate habitat data (Osborne and others, 1991) using guidelines with a regional or single-purpose focus (for example, Bovee, 1982; Platts and others, 1983; Hamilton and Bergersen, 1984; Platts and others, 1987); however, little national uniformity in concept or methodology currently exists (Osborne and others, 1991). Because no current habitat evaluation procedures meet national objectives of the NAWQA Program, a NAWQA habitat protocol was developed (Meador, Hupp, and others, 1993).

The goal of the NAWQA stream habitat protocol (Meador, Hupp, and others, 1993) is to measure habitat characteristics that are essential in describing and interpreting water-chemistry and biological conditions in many different types of streams studied within the NAWQA Program. To accomplish this goal, various habitat characteristics are measured at different spatial scales; some characteristics are important at the national scale, whereas others might be equally important at the Study Unit or regional scale.

The original NAWQA habitat protocol (Meador, Hupp, and others, 1993) was written at the start of the NAWQA Program with the idea that the methods described in that document were to be continuously tested and refined and new methods evaluated. After application of the protocol by approximately 37 NAWQA Study Units over 6 years, it was determined that a revision of the NAWQA protocol was necessary. This revised protocol incorporates the experiences of NAWQA Study Units under a wide range of environmental conditions and contains examples of how the habitat data were used by the Study Units while retaining the goals of the original protocol. The revised protocol also incorporates links to the NAWQA habitat data dictionary, which provides the framework for a relational data base for storing computer files of habitat data.

The purpose of this report is to provide revised procedures for characterizing stream habitat as part of the NAWQA Program. These procedures allow for appropriate habitat descriptions and standardization of measurement techniques to facilitate unbiased evaluations of habitat influences on stream conditions at local, regional, and national scales.

This report describes the methods for collecting and analyzing habitat data at three spatial scales. Data at the basin and segment scales are collected by using a geographic information system (GIS) data base, topographic maps, and aerial photographs. Data collected at the reach scale include measurements and observations of channel, bank, and riparian characteristics. Habitat characteristics from each scale that are needed for NAWQA national data aggregation are distinguished from optional characteristics that might be important for specific Study Units. Forms for recording the habitat data are presented, and guidance on data management and analysis is provided. Examples of how the data were used in two NAWQA Study Unit investigations also are included. The glossary includes brief definitions of habitat terms found throughout the report.

SUMMARY OF REVISIONS TO ORIGINAL PROTOCOL

The revised NAWQA habitat protocol contains both major and minor updates to the original protocol. The following is a general list of major additions or changes.

Updates or changes affecting the entire protocol:

1. Highlighted habitat measurements in **bold** if required for NAWQA national data aggregation.
2. Expanded discussion of the usefulness of habitat data and how the data may correlate to aquatic community and water-chemistry data.
3. Added data-analysis section that describes how habitat data can be analyzed statistically.
4. Added examples of how habitat data were used in aquatic community and water-chemistry analyses for two NAWQA Study Units.
5. Added data-management section that links habitat data with files in the NAWQA habitat data dictionary.
6. Included several habitat characteristics from the NAWQA habitat data dictionary.
7. Updated hard-copy forms for recording habitat measurements.
8. Updated protocol on collection of habitat data on the basis of the results from a survey filled out by NAWQA Study Unit biologists.
9. Added explanation for collecting habitat data at nonwadeable sites.

Updates or changes specific to reach scale:

1. Added a description for identifying bankfull stage.
2. Added step-by-step instructions for conducting a reach characterization.
3. Increased the number of transects from six transects in the center of geomorphic channel units to 11 equidistant transects and, by reducing the number of data elements collected along each transect, kept the time requirements similar.
4. Dropped the requirements for channel cross sections and point-quarter vegetation at all basic fixed sites and converted these to Study Unit options.
5. Dropped the previous terminology of "Level I" and "Level II."

HABITAT-SAMPLING DESIGN

Relations among physical, chemical, and biological components of streams are determined not only within the context of a stream but also within the broader context of the surrounding watershed (Hynes, 1975). Therefore, to adequately examine the relations among physical, chemical, and biological attributes of streams, evaluating stream habitat must be accomplished within a systematic framework that accounts for multiple spatial scales.

Conceptual Framework for Characterizing Stream Habitat

A framework for evaluating stream habitat must be based on a conceptual understanding of how stream systems are organized in space and how they change through time (Lotspeich and Platts, 1982; Frissell and others, 1986). Among physiographic regions, or among streams within a region, different geomorphic processes control the form and development of basins and streams (Wolman and Gerson, 1978). In addition, geomorphic conditions may be different depending on the position of the stream within the hierarchy of the stream network. Therefore, researchers have recognized the importance of placing streams and stream habitats in a geographic, spatial hierarchy (Godfrey, 1977; Lotspeich and Platts, 1982; Bailey, 1983; Frissell and others, 1986).

NAWQA uses a modification of the spatially hierarchical approach proposed by Frissell and others (1986) for describing environmental settings and evaluating stream habitat. Frissell and others (1986) included five spatial systems—stream, segment, reach, pool/riffle, and microhabitat. The modified approach used in the NAWQA Program consists of a framework that integrates habitat data at four spatial scales—basin, segment, reach, and microhabitat (fig. 1). This approach differs from the scheme proposed by Frissell and others (1986) in that (1) the term "system" is not used, (2) basin is used to refer to stream system, and (3) the pool/riffle system is omitted as a separate scale to be evaluated because measurements are incorporated into the reach scale. The microhabitat scale has been found to provide insight to patterns of relations between biota and habitat at larger scales (Hawkins, 1985; Biggs and others, 1990). Procedures for collection of microhabitat data are described in the NAWQA protocols for the collection of invertebrate (Cuffney and others, 1993) and algal (Porter and others, 1993) samples.

Basin and segment data are collected by using GIS, topographic maps, or aerial photographs, whereas

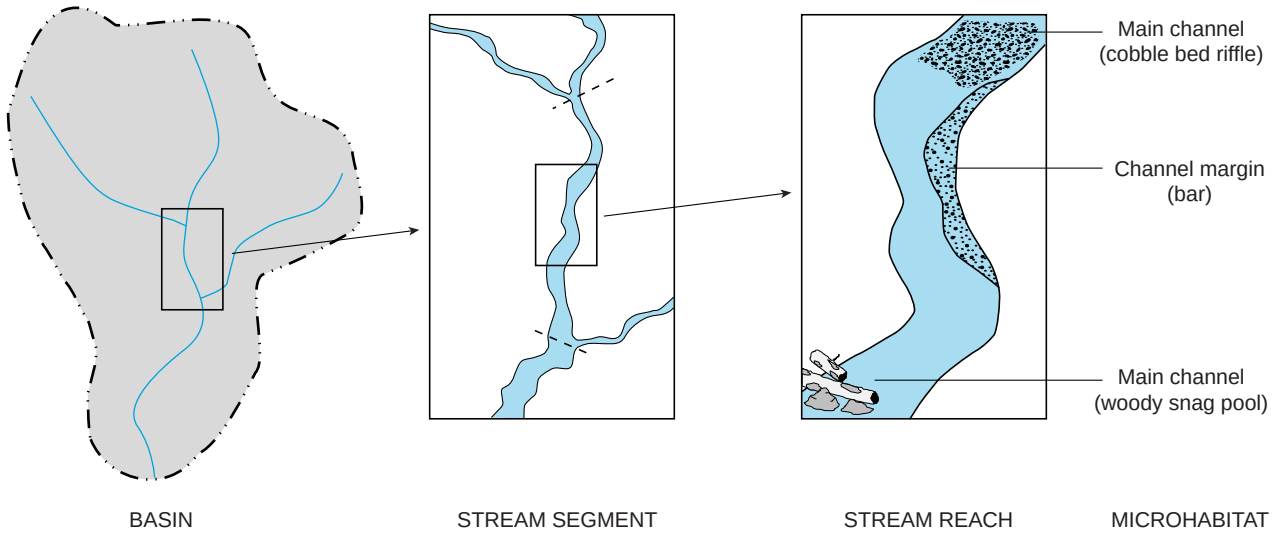

Figure 1. Spatial hierarchy of basin, stream segment, stream reach, and microhabitat (modified from Frissell and others, 1986).

reach data require site visits. The collection of a core part of the reach-scale data is based on the systematic placement of equally spaced transects; the distance between these transects depends upon stream width. This approach was adopted to maximize repeatability and precision of measurements while minimizing observer bias; it is based in part on results from a study of optimal transect spacing and sample size for fish habitat (Simonson and others, 1994b).

Relevance and Application to Other Habitat-Assessment Techniques

Within the past couple of decades, the number of systems for habitat assessment and classification has increased substantially, and new ones are continually being published. Each assessment or classification scheme differs in goals, spatial scale, quantitativeness, the effort and time required, and applicability to different-sized streams. For example, some may be specifically designed to quantify fish habitat in wadeable streams (Simonson and others, 1994a), or to qualitatively classify State or regional stream use or potential (Ball, 1982; Michigan Department of Natural Resources, 1991). Others are more focused on channel characteristics from a geomorphic perspective (Montgomery and Buffington, 1993; Rosgen, 1994). Some have been designed for national use but are qualitative, such as the habitat component of the U.S. Environmental Protection Agency's (USEPA's) Rapid Bioassessment Protocol (Plafkin and others, 1989), which is currently being revised. The habitat assessment for the USEPA's Environmental Monitoring and Assessment Program (Kaufmann and Robison, 1994) contains goals similar to the NAWQA reach-scale characterization (quantitative, national scope; consideration of time; systematic placement of transects) but does not include basin or segment characterization.

The NAWQA protocol balances qualitative and quantitative measures of habitat. Qualitative measures of habitat are often advantageous because they reduce the amount of time needed to collect data at a site. However, qualitative measures often incorporate observer bias; thus, they may lack repeatability (Roper and Scarnecchia, 1995). Although quantitative measures may be more precise, they increase the amount of time needed to collect data. The procedures described in this document represent a balance of qualitative and quantitative measures judged necessary to adequately ensure national consistency, minimize observer bias, and maximize repeatability. Individual NAWQA Study Units may find additional data collection useful for comparison with State or regional assessments. Many local or regional assessments rely on qualitative data to generate stream habitat indices for classification and interpretation of stream conditions. Such approaches may not be applicable everywhere (Stauffer and Goldstein, 1997). Data collected for local purposes (for example, to link with State assessments) should be obtained concurrently with measurements made for nationally consistent characterizations, thereby providing an opportunity to

compare different methods or to support qualitative indices with quantitative measurements.

Selection of Sampling Sites

Sampling sites are generally chosen to represent the set of environmental conditions deemed important to controlling water quality in the Study Unit (Gilliom and others, 1995). Sites should represent combinations of natural and human factors thought to influence collectively the physical, chemical, and biological characteristics of water quality in the Study Unit and to be of importance locally, regionally, or nationally. Two distinct types of sampling sites are established as part of the NAWQA Program—basic fixed sites and synoptic sites.

Basic fixed sites are used to characterize the spatial and temporal distribution of general water quality and constituent transport in relation to hydrologic conditions and contaminant sources (Gilliom and others, 1995). At these sites, broad suites of physical and chemical characteristics are measured, along with characteristics of fish, benthic-invertebrate, and algal assemblages. Basic fixed sites are typically at or near USGS gaging stations where continuous discharge measurements are available. Synoptic sites are typically nongaged sites where one-time measurements of a limited number of physical, chemical, and biological characteristics are made with the objective of answering questions regarding source, occurrence, effects, or spatial distribution.

Sampling Strategy for Fixed and Synoptic Sites

The type of habitat characterization to be done depends on the type of site (basic fixed or synoptic), NAWQA national data-aggregation requirements, and individual Study Unit goals. Intensive ecological assessments are done at a subset of basic fixed sites to provide information on spatial and temporal variability of biological communities and habitat characteristics (Gilliom and others, 1995). At this subset of sites, reach-to-reach variability is estimated by sampling multiple reaches (minimum of three) that are located so as to represent similar water-quality conditions. Year-to-year variability is described by sampling one of the three reaches during each year of the 3-year high-intensity phase (HIP) data collection. Low-intensity phase (LIP) ecological assessments are done every year during the 6-year period between HIP data-collection cycles.

At basic fixed sites, a full complement of basin, segment, and reach data are required at the national scale to consistently characterize stream conditions at local, regional, and national scales (table 1). These characteristics are listed in **bold** in table 1. Basin and segment data are collected at each basic fixed site once during the HIP. Reach data are collected concurrently with biological data and, at a subset of basic fixed sites, are collected at multiple reaches and in multiple years during the HIP. During the LIP, reach characteristics are measured concurrently with biological sample collection. Additional characteristics that are useful for Study Unit interpretation of chemical and biological data listed in table 1 are suggested.

The type of habitat characterization at synoptic sites may differ from that at basic fixed sites. The design of synoptic sites offers Study Units an opportunity to address various specific local questions. Some habitat data-collection efforts at synoptic sites can be tailored to be consistent with other local efforts, such as qualitative approaches leading to locally derived habitat-quality indices. However, significant differences in data-collection approaches between synoptic and basic fixed sites will decrease the ability to combine data from the two types of sites to provide greater interpretive capability across the Study Unit. Therefore, a subset of the variables required for NAWQA national data aggregation for basic fixed sites (using the procedures required for collecting these variables) is required at synoptic sites. Variables that are required at all synoptic sites (reach water-surface gradient, wetted channel width, depth, velocity, and bed substrate) are those that are considered to have the greatest potential value in comparing sites across a wide variety of environmental settings. In addition to the subset of variables, additional variables and procedures consistent with local or regional habitat data-collection efforts may increase the ability to combine NAWQA data with habitat data from other sources.

Preferred Units of Measure

For the purpose of stream habitat characterization, metric units are the units of choice for collecting, storing, and analyzing habitat data. For some measurements, such as velocity, discharge, and

Table 1. Sampling strategy for habitat measurements at National Water-Quality Assessment (NAWQA) Program basic fixed sites and synoptic sites

[Multiple-year sites include intensive ecological assessment sites during the high-intensity phase (HIP), plus those sites designated for continued sampling during the low-intensity phase (LIP). Items in **bold** are required for NAWQA Program national data aggregation; items not in bold are suggested for Study Unit consideration. PBS, per biological sample—measurements in conjunction with biological-community samples, made at or near the time of biological sampling]

Habitat characteristic	Basic fixed site			Synoptic site [1]
	Single reach	Multiple reach	Multiple year	
Basin				
Drainage boundaries	—	**Once per HIP**	—	**Once**
Drainage area	—	**Once per HIP**	—	**Once**
Runoff	—	Once per HIP	—	Once
Climate (precipitation, temperature, evaporation)	—	Once per HIP	—	Once
Basin length	—	Once per HIP	—	Once
Basin relief	—	Once per HIP	—	Once
Drainage shape	—	Once per HIP	—	Once
Stream length	—	Once per HIP	—	Once
Cumulative perennial stream length	—	Once per HIP	—	Once
Drainage density	—	Once per HIP	—	Once
Drainage texture	—	Once per HIP	—	Once
Entire stream gradient	—	Once per HIP	—	Once
Flow characteristics (floods, low-flow)	—	Once per HIP	—	Once
Segment				
Sinuosity	—	**Once per HIP**	—	Once
Gradient	—	**Once per HIP**	—	Once
Segment length	—	**Once per HIP**	—	Once
Water-management features	—	**Once per HIP**	—	Once
Stream order	—	Once per HIP	—	Once
Link	—	Once per HIP	—	Once
Downstream link	—	Once per HIP	—	Once
Sideslope gradient	—	Once per HIP	—	Once
Reach				
Discharge	**Continuous**	**All reaches PBS**	**All years PBS**	**PBS**
Channel modification	**Once**	**All reaches PBS**	**All years PBS**	**PBS**
Reach length	**Once**	**All reaches PBS**	**All years PBS**	**PBS**
Reach water-surface gradient	**Once**	**All reaches PBS**	**All years PBS**	**PBS**
Geomorphic channel units	**Once**	**All reaches PBS**	**All years PBS**	PBS
Wetted channel width	**Once**	**All reaches PBS**	**All years PBS**	**PBS**
Bankfull channel width	**Once**	**All reaches PBS**	**All years PBS**	PBS
Channel features	**Once**	**All reaches PBS**	**All years PBS**	PBS
Canopy angles	**Once**	**All reaches PBS**	**All years PBS**	PBS
Dominant riparian land use	**Once**	**All reaches PBS**	**All years PBS**	PBS
Riparian canopy closure (densiometer)	**Once**	**All reaches PBS**	**All years PBS**	PBS
Bank angle	**Once**	**All reaches PBS**	**All years PBS**	PBS
Bank height	**Once**	**All reaches PBS**	**All years PBS**	PBS
Bank vegetative cover	**Once**	**All reaches PBS**	**All years PBS**	PBS
Bank stability index	**Once**	**All reaches PBS**	**All years PBS**	PBS
Habitat cover	**Once**	**All reaches PBS**	**All years PBS**	PBS

Table 1. Sampling strategy for habitat measurements at National Water-Quality Assessment (NAWQA) Program basic fixed sites and synoptic sites—Continued

[Multiple-year sites include intensive ecological assessment sites during the high-intensity phase (HIP), plus those sites designated for continued sampling during the low-intensity phase (LIP). Items in **bold** are required for NAWQA Program national data aggregation; items not in bold are suggested for Study Unit consideration. PBS, per biological sample—measurements in conjunction with biological-community samples, made at or near the time of biological sampling]

Habitat characteristic	Basic fixed site			Synoptic site [1]
	Single reach	Multiple reach	Multiple year	
Depth	**Once**	**All reaches PBS**	**All years PBS**	**PBS**
Velocity	**Once**	**All reaches PBS**	**All years PBS**	**PBS**
Dominant bed substrate	**Once**	**All reaches PBS**	**All years PBS**	**PBS**
Embeddedness	**Once**	**All reaches PBS**	**All years PBS**	PBS
Bank erosion	Once	All reaches PBS	All years PBS	PBS
Siltation	Once	All reaches PBS	All years PBS	PBS
Channel cross sections	Once	Primary reach	Once[2]	PBS
Pebble counts	Once	All reaches PBS	All years PBS	PBS
Sediment laboratory analyses	Once	All reaches PBS	All years PBS	PBS
Point-quarter vegetation	Once	Primary reach	Once	PBS
Vegetation plots	Once	Primary reach	Once	PBS

[1]Additional elements may be considered at synoptic sites in conjunction with biological-community sampling, depending on specific Study Unit objectives.

[2]Once per NAWQA cycle (HIP + LIP), preferably early during the HIP; measurements may be repeated following extremely high-flow conditions thought to have caused major geomorphic changes.

measurements of length and elevation gathered from USGS 7.5-minute topographic maps, data may need to be collected in inch-pound units because of equipment limitations; however, inch-pound units should be converted into metric units when the data are entered into the computer data base.

BASIN CHARACTERIZATION

The characteristics of a stream are dependent in large part upon the downstream transfer of water, sediment, nutrients, and organic material. In order to characterize a stream, it is important to know the geologic, climatic, hydrologic, morphologic, and vegetational setting of a stream within its basin (Schumm and Lichty, 1965; Frissell and others, 1986; Klingeman and MacArthur, 1990). Geology influences the shapes of drainage patterns, channel bed materials, and water chemistry. Soils influence infiltration rates, erosion potential, and vegetation types. Climate affects hydrologic, morphologic, and vegetational characteristics. Vegetation affects a number of factors, including water loss through evapotranspiration, runoff, and channel bank stability. Thus, the basin serves as a fundamental ecosystem unit and an important basis from which to understand the characteristics of streams (Leopold and others, 1964; Schumm and Lichty, 1965; Frissell and others, 1986; Gordon and others, 1992). Evaluation of basin characteristics also enhances an understanding of the comparative biogeographic patterns in biological communities (Biggs and others, 1990; Quinn and Hickey, 1990).

Background

Basin characterization consists of a combination of (1) geomorphic descriptors using index or ratio data derived from USGS 7.5-minute topographic maps (table 2), (2) climate and potential runoff characteristics, (3) streamflow characteristics for various recurrence intervals, and (4) land-cover data from thematic maps. For NAWQA national data aggregation, the Study Unit is required to delineate and digitize basin boundaries and record methodology. From this information, many of the land-cover data from thematic maps and climate data will be derived by NAWQA national synthesis teams. Although not required for NAWQA national data aggregation, many of the geomorphic descriptors and streamflow

Table 2. Commonly measured geomorphic descriptors of drainage basins from 7.5-minute topographic maps

[km^2, square kilometer; km, kilometer; dimen., dimensionless unit; m, meter]

Attribute	Derivation or definition	Unit	Source
Drainage area	For a specified stream location, that area, measured in a horizontal plane, enclosed by a drainage divide.	km^2	Horton (1945)
Cumulative perennial stream length	Sum of the length of all perennial streams within a drainage basin.	km	Horton (1945)
Drainage density	Ratio of the cumulative perennial stream length and drainage area.	km/km^2	Leopold and others (1964)
Basin length	Length of the line, parallel to the main drainage line, from the headwater divide to a specified stream location.	km	Schumm (1956)
Drainage shape	Ratio of drainage area and the square of the basin length.	dimen.	Horton (1932)
Basin relief	Highest elevation on the headwater divide minus the elevation at a specified stream location.	m	Schumm (1956)
Basin relief ratio	Ratio of basin relief and basin length.	dimen.	Schumm (1956)
Drainage texture	Ratio of the number of crenulations on the contour line on a topographic map with the most crenulations and the length of the perimeter of the basin.	km^{-1}	Smith (1950)
Entire stream gradient	Ratio of the difference between elevation at 85 and 10 percent of stream length and stream length between these two points.	dimen.	Craig and Rankl (1978)

characteristics are needed at the Study Unit scale for interpretation of water-quality and biological data. Study Unit personnel should seriously examine the potential usefulness of these additional geomorphic basin characteristics within the context of their Study Unit goals and measure those characteristics that will help interpret variations observed in water-quality and biological data.

Many geomorphic descriptors (for example, drainage area, drainage density, basin relief, and drainage shape) have been developed and applied to the measurement of basins and the network of streams within basins (table 2). Geomorphic descriptors represent relatively simple approaches to describe basin processes and to compare and contrast basin characteristics. The effect of data calculation methods on geomorphic descriptors is significant (Gandolfi and Bischetti, 1997). Thus, to ensure the utility of these measures for analyses beyond the Study Unit scale, consistency is required in the approach used to calculate the selected descriptors.

Drainage area is one of the most important characteristics of a basin and serves as a component of many other basin descriptors. Drainage area is dependent on the boundaries of the basin and may be subdivided into contributing and noncontributing parts (Novak, 1985). National evaluation of NAWQA data focuses on total drainage area. However, an evaluation of contributing and noncontributing components of drainage area may be useful at local or regional scales, especially in areas with karst, poorly defined **drainage boundaries**, or discontinuous stream networks.

Cumulative perennial stream length determines the amount of stream habitat within a basin and the availability of sediment for transport and is measured as the total length of solid blue lines (representing perennial streams) on USGS 7.5-minute topographic maps. Ephemeral or intermittent streams should not be included in stream-length calculations. It should be noted that the actual length of a channel changes over time, and the establishment of blue lines on topographic maps is based on approximation rather than hydrologic criteria (Leopold, 1994). However, measurement of blue lines on a map represents a standardized approach to determining stream length.

Drainage density is a basin descriptor that represents the amount of stream required to drain the basin. It is a length/area ratio based on the total length of all perennial streams in the basin divided by the drainage area. Because the density of a stream network reflects climate patterns, geology, soils, basin vegetation, and age of the stream network, drainage density is perhaps the single most useful index to describe basin processes (Gregory and Walling, 1973).

High drainage density may indicate high flood peaks, high sediment production, steep hillslopes, general difficulty of access, low suitability for agriculture, and high construction costs. Drainage density ranges from about 1 to 1,000 (Leopold and others, 1964).

There are many methods used to measure basin length (Gardiner, 1975). The definition given by Schumm (1956) is used here, where a line is drawn from the mouth of the basin following the main stream valley to the drainage divide. Basin length is used for calculating drainage shape.

Drainage shape is a ratio designed to convey information about the elongation of a basin. Drainage shape is difficult to express unambiguously and has been measured several different ways (Gordon and others, 1992). The definition for basin shape as originally proposed by Horton (1932) is used here, where drainage shape is a simple dimensionless ratio of drainage area divided by the square of basin length. In general, with increasing drainage area, basins tend to increase in length faster than in width. Given two drainage basins of the same size, an elongated basin will tend to have smaller flood peaks but longer lasting floodflows than a round basin (Gregory and Walling, 1973).

Basin relief can have a significant effect on drainage density and stream gradient. Hadley and Schumm (1961) demonstrated that annual sediment yields increase exponentially with basin relief. The basin relief ratio (basin relief divided by basin length) (Schumm, 1956) is helpful for eliminating the effects of differences in basin size when comparing data from drainage basins of different size.

Drainage texture represents a measure of the proximity of streams in a basin. Although two basins may have the same or similar drainage densities, the basins may differ in texture or the dissection of streams within the basin. For example, the cumulative length of streams may be the same in two basins, but the number of streams may be different. Smith (1950) developed a ratio by dividing the number of crenulations (taken from the contour with the most crenulations in the basin on a USGS 7.5-minute topographic map) by the length of the perimeter of the basin. The crenulations are an indication of channel crossing and, thus, a measure of the closeness of the spacing between streams. It is recognized that the determination of drainage texture from 7.5-minute maps can be difficult for relatively large drainage areas.

A measurement of the entire stream gradient (Craig and Rankl, 1978) is used in estimations of flood characteristics. Along with drainage area, this characteristic is one of the most important characteristics used to estimate the size of floods. It may be quite different from channel gradient, which is measured at the segment scale. To measure entire stream gradient, points at 85 percent and 10 percent of the basin length, as measured from the mouth of the basin, are determined. Elevations at these points are determined and subtracted. The resulting difference is then divided by 75 percent of the basin length.

A computer program called "Basinsoft" has been developed by the USGS to quantify a number of basin characteristics, such as the ones described above, by using GIS information (Eash, 1994; Harvey and Eash, 1996). Basinsoft uses four digital maps (drainage-basin boundary, hydrography extracted from digital line-graph data, hypsography generated from digital elevation-model data, and a lattice elevation model generated from digital elevation-model data) to quantify 27 basin characteristics (table 3). Comparison tests indicate that, for most characteristics, Basinsoft-generated descriptors of basins are not significantly different from those calculated manually from 7.5-minute topographic maps. However, comparison tests indicate that descriptors that rely on measures of slope, such as basin relief, are underestimated by Basinsoft. Additional information regarding the Basinsoft processing steps is provided by Harvey and Eash (1996).

Even though all the geomorphic descriptors except **drainage area** are optional for NAWQA data aggregation, most descriptors will be important for Study Unit analyses of relations among drainage basin geomorphology, instream channel characteristics, biotic assemblages, and water chemistry. For example, in a study of the relations of geomorphology to trout populations in Rocky Mountain streams, Lanka and others (1987) demonstrated significant correlations among measures of drainage basin geomorphology, instream habitat, and trout abundance. These investigators reported significant univariate correlations among basin relief, drainage density, stream length, and reach-scale habitat characteristics in both high-elevation forest and low-elevation rangeland streams (Lanka and others, 1987). They also found that multiple-regression equations predicting fish abundance were often dominated by basin geomorphic descriptors, with some descriptors predicting fish

Table 3. Drainage-basin and stream-network characteristics that can be measured with Basinsoft software

[Software described in Harvey and Eash (1996)]

Basin measurements		Stream or channel measurements	
Quantifications	**Computations**	**Quantifications**	**Computations**
Total drainage area	Contributing drainage area	Main-channel length	Main-channel sinuosity ratio
Noncontributing drainage area	Effective basin width	Total stream length	Stream density
Basin length	Shape factor	Main-channel slope	Constant of channel maintenance
Basin perimeter	Elongation ratio	Stream order at basin outlet	Main-channel slope proportion
Average basin slope	Rotundity of basin	Number of first-order streams	Ruggedness number
Basin relief	Compactness ratio		Slope ratio of main channel slope to basin slope
Basin azimuth	Relative relief		Drainage frequency
			Relative stream density

abundance as accurately as reach-scale habitat characteristics.

The climatic characteristics (precipitation, temperature, and evaporation) of a basin affect habitat characteristics at all scales. Precipitation and temperature characteristics determine evaporation, evapotranspiration, and runoff. Climate and runoff data can be gathered from a variety of sources at different temporal and spatial scales. Gebert and others (1987) contains runoff data for hydrologic units in the United States. Local, basin, State, or regional runoff data also may be available. Temperature and precipitation data may be obtained from the National Weather Service. Regional summary data, for example Wendland and others (1992), also may be available. Estimates of long-term evaporation for the 48 contiguous United States can be found in Farnsworth and others (1982).

Three types of estimated streamflow characteristics are useful in describing flood and low-flow characteristics of a basin. These are estimated peak flow, flood volume, and 7-day low-flow for various exceedance probabilities. If long-term streamflow data are available for the site, these characteristics may be directly calculated from site data. Otherwise, State- or regional-scale equations are available for estimating these characteristics at ungaged sites. For example, Jennings and others (1994) gives equations for estimating peak flows at several recurrence intervals for the United States. Using State or regional equations (availability dependent on State or region), flood volume and 7-day low flows can be estimated for 2-, 5-, 10-, 25-, 50-, and 100-year recurrence intervals.

Thematic maps provide a simple means of describing a basin in terms of geology, soils, land use, and vegetation. From basin-boundary information provided by the Study Unit, drainage area and several types of basin-scale thematic data are determined for each Study Unit by NAWQA national synthesis teams by using national coverages of themes, such as ecoregion, physiographic province, geology, soils, land use, and potential natural vegetation. Scales for national coverage maps generally range from 1:250,000 to 1:7,500,000 for many of these data bases. Local or regional maps may be available to the Study Unit and may provide better resolution and more recent data than national maps.

Description and List of Basin Characteristics

A basin characterization for fixed and synoptic sites is done usually once during the NAWQA intensive sampling phase. Except for delineation of basin boundaries, the choice of parameters is determined by the Study Unit. Field form 1 (see Field Forms at back of report) provides an example of how a Study Unit might document a basin characterization. Instructions for completing the example

form are given below, with the numbers corresponding to the items listed in field form 1. Abbreviations in parentheses refer to the codes used for the parameter in the USGS National Water Information System (NWIS) or the NAWQA habitat data dictionary file called "Basin." If streamflow or water-quality data were collected previously by the USGS at a site, many of the items coded with a "C" can be obtained from NWIS. Items in **bold** are required for NAWQA national data aggregation. The following items are used to describe the location of the site and to record the data:

1. Study Unit (SUID)—Use the 4-character code (Meador, Hupp, and others, 1993) designated for each Study Unit.
2. Site type (SITYPE)—Record type of site: BFS, NAWQA basic fixed site; IFS, NAWQA intensive fixed site; SYN, synoptic site.
3. **Station identification number (C001 or STAID)**—List the USGS station identification number for the site.
4. Hydrologic unit code (C020)—Record the 8-digit hydrologic unit code for the basin. See Seaber and others (1984) for a description of State hydrologic unit maps. This code is useful for linking information with other data bases.
5. Station name (C900)—List the USGS station name (may already be available if the site was a previously established USGS sampling site).
6. Reference location (C010, C009, C016)—Record the longitude and latitude (in degrees, minutes, and seconds) and elevation (in meters) of the reference location. The reference location is a geographic marker that provides a link to habitat data collected at different spatial scales. It is often a location with known geographic coordinates, such as a gaging station or bridge crossing.
7. State FIPS code (C007)—There are Federal Information Processing Standards codes for each State. See your district NWIS specialist for more information or consult Appendix B in Hutchinson (1975). These codes are useful for linking information with other data bases.
8. County FIPS code (C008)—There are Federal Information Processing Standards codes for each county in every State. See your district NWIS specialist for more information or consult Appendix C in Hutchinson (1975). These codes also are useful for linking information with other data bases.
9. State (STATE)—Record name of State for reference location.
10. County (COUNTY)—Record name of county or parish for reference location.
11. Township (TWN)—Record the township designation, if available, for the reference location.
12. Range (RANGE)—Record the appropriate range designation, if available, for the reference location.
13. Section (SEC)—Provide the appropriate 1- or 2-digit number of the section, if available, for the reference location.
14. Quad name(s) (QUAD)—Record the name, scale (for example, 1:24,000), and year of the appropriate 7.5-minute maps that included the reference location and were used to measure basin characteristics. This is helpful for future data checking.
15. File names and path—Record the directory path and file names for appropriate data files.
16. Contact person—Record the person in charge of the data in case questions arise later.

The following basin characteristics can be computed by using GIS, Basinsoft, or manual methods, and most are stored in the data dictionary file called "Basin":

17. **Total drainage area (C808)**—Delineate basin boundaries and calculate the total drainage area in square kilometers (> 0.0) of the basin upstream from the site. Both manual and GIS methods are possible, using various map scales. It is worthwhile to record contributing (C809) area, if applicable.

18. **Drainage area method (DRAREAMD)**—This pertains to the method used to determine drainage area. Record the map year, computation method, source map scale used for the assessment.

19. Average annual runoff (RUNOFF)—Runoff information can be gathered from a variety of sources at different scales. Maps of runoff for the hydrologic units in the United States have been produced by Gebert and others (1987). Average annual runoff (reported in centimeters) usually is estimated by dividing average streamflow (cubic meters per second) by the drainage area (square meters) and multiplying by the number of seconds in a year (60 x 60 x 24 x 365) and the conversion from centimeters to meters (100 cm/m). Numerous publications also have been published by the USGS for major river basins (one example for Wisconsin is Skinner and Borman, 1973). More local data may also be available.

20. Average annual runoff method (RUNOFFMD)—Record the method used. Methods include GAGE, calculations from long-term streamflow record (gaging station) at the station; WTGAGE, area weighting multiple gaging stations; REFERENCE, value from published source; or OTHER.

21. Beginning and ending years of record for runoff data (BYRUNOFF and EYRUNOFF)—Record the beginning and ending years for runoff calculations. Because these data are based on average annual streamflow, it is important to know the length of record used for the calculations.

22. Average annual air temperature (TEMP)—Data for average annual temperature (degrees Celsius) can be gathered from some National Weather Service precipitation gages across the United States. Consult your State climatologist or the nearest National Weather Service office for more information. Regional summary data also may be available (for example, Wendland and others, 1992). At the highest scale of detail, data from several weather stations are averaged for a given drainage basin. Collect data from stations within and surrounding the drainage basin. Several methods can be used:

    a. Construct Thiessen polygons by connecting nearest-neighbor stations and drawing lines perpendicular to them, and weight temperature at a station by the proportion of area covered in the drainage basin;
    b. Calculate grid-weighted average created from nearest-neighbor computation;
    c. Draw contour lines of equal temperature (isohyets);
    d. Obtain value from published sources;
    e. Calculate the arithmetic mean temperature for all the weather stations in the basin;
    f. Calculate a grid-weighted average created from kriging computation; and
    g. Other.

    See Dunne and Leopold (1978, p. 37–42) for more detailed instructions.

23. Average annual air temperature method (TEMPMD)—The domain for this variable includes THIESSEN, area-weighted average from irregularly spaced points; NEIGHBOR, grid-weighted average created from nearest-neighbor computation; ISOHYET, value from contour lines; REFERENCE, value from published source; AVG, arithmetic mean from all stations in basin;

KRIG, grid-weighted average created from kriging computation; OTHER, method used was not one of the choices listed.

24. Beginning and ending years of record for temperature data (BYTEMP and EYTEMP)—This is very important information to record because results will vary depending on the time period used.
25. Average annual precipitation (PRECIP)—An area-weighted average in centimeters obtained from most recent (or most accurate) reports or studies describing the basin or data gathered from National Weather Service precipitation stations. For calculating averages, see discussion above on average annual air temperature. The sources, scale, and quality of these data will vary among Study Units and basins.
26. Average annual precipitation method (PRECIPMD)—Pertains to the method used to determine average annual precipitation in the basin. The domain for this variable includes THIESSEN, area-weighted average from irregularly spaced points; NEIGHBOR, grid-weighted average created from nearest-neighbor computation; ISOHYET, value from contour lines; REFERENCE, value from published source; AVG, arithmetic mean from all stations in the basin; KRIG, grid-weighted average created from kriging computation; OTHER, method used was not one of the choices listed.
27. Beginning and ending years of record for precipitation data (BYPRECIP and EYPRECIP)—This is very important information to record, because results will vary depending on the time period used.
28. Average annual Class A pan evaporation (EVAPAN)—This value is often an area-weighted average, in centimeters. Available data will vary in source, scale, and quality for each Study Unit. Estimates of long-term evaporation and free-water surface evaporation for the contiguous 48 United States are found in Farnsworth and others (1982).
29. Average annual Class A pan evaporation method (EVAPANMD)—Pertains to the method used to determine average annual evaporation in the basin. The domain for this variable includes THIESSEN, area-weighted average from irregularly spaced points; NEIGHBOR, grid-weighted average created from nearest-neighbor computation; ISOHYET, value from contour lines; REFERENCE, value from published source; AVG, arithmetic mean from all stations in basin; KRIG, grid-weighted average created from kriging computation; OTHER, method used was not one of the choices listed.
30. Beginning and ending years of record for evaporation data (BYEVAPAN and EYEVAPAN)—Record beginning and ending dates of data sets, because results will vary depending on the time period used.
31. Basin length (BLENG)—Measure the length of the basin in kilometers (> 0.0) by drawing a line from the mouth of the basin following the main stream valley to the drainage divide. See Gardiner (1975) for examples of how to calculate basin length.
32. Basin length method (BLENGMD)—This pertains to the method used to determine basin length. Record the map year, computation method, source map scale used for the assessment.
33. Minimum elevation in the basin (MNELEV)—Determine the minimum elevation in meters above the 1929 National Geodetic Vertical Datum (NGVD) (above datum > 0.0; below datum < 0.0).
34. Minimum elevation method (MNELEVMD)—This pertains to the method used to determine minimum elevation in the basin. Record the map year, computation method, source map scale used for the assessment.

35. Maximum elevation in the basin (MXELEV)—Determine the maximum elevation in meters above NGVD (above datum > 0.0; below datum < 0.0).

36. Maximum elevation method (MXELEVMD)—This pertains to the method used to determine maximum elevation in the basin. Record the map year, computation method, source map scale used for the assessment.

37. Basin relief ratio (RELRAT)—Determine the difference between the MXELEV and MNELEV. Divide the difference by BLENG.

38. Drainage shape (DRNSHAPE)—Divide the drainage area by the square of the basin length. Units are dimensionless.

39. Stream length (SLENG)—Measure the longest stream length in kilometers (> 0.0) from the headwaters to the site.

40. Stream length method (SLENGMD)—This pertains to the method used to determine stream length. Record the map year, computation method, source map scale used for the assessment.

41. Cumulative perennial stream length (PSLENG)—Measure the cumulative length in kilometers (> 0.0) of all perennial streams and canals in the basin.

42. Cumulative perennial stream length method (PSLENGMD)—This pertains to the method used to determine cumulative perennial stream length. Record the map year, computation method, source map scale used for the assessment.

43. Drainage density (DRNDENS)—Divide the cumulative stream length by the drainage area. Units are kilometer^{-1}.

44. Drainage texture (DRNTEX)—Determine the basin contour with the most crenulations, as noted by inspection of a 7.5-minute map. Count the number of crenulations on that contour. Divide the number of crenulations by the length of the perimeter of the basin. Units are contours/kilometer.

45. Entire stream gradient (SLOPE)—A ratio of the difference between elevation at 85 and 10 percent of stream length as measured from the reference location and stream length between these two points (Craig and Rankl, 1978). Units are recorded in meters per kilometer.

46. Estimated flow characteristics—At least three types of estimated streamflow characteristics are useful for describing flood and low-flow characteristics of a basin. They are estimated peak flow, flood volume, and 7-day low-flow for given recurrence intervals. If the site has long-term streamflow data (5–15 years of data, depending on the recurrence interval), these characteristics can be directly calculated. USGS District offices also can provide statistical analyses for flow characterization at USGS gaging stations. Otherwise, State- or regional-scale equations are available for estimating these characteristics (for example, Jennings and others (1994) to obtain equations for estimating peak flows for specific hydrologic regions within a State). Peak flows can be estimated for 1-, 2-, 5-, 10-, 25-, 50-, and 100-year recurrence intervals (QP1, QP2, QP5, QP10, QP25, QP50, QP100). Flood volume can be estimated for 2-, 5-, 10-, 25-, 50-, and 100-year intervals (QV2, QV5, QV10, QV25, QV50, QV100). In addition, 7-day low flows can be estimated for 2-, 5-, 10-, 25-, 50-, and 100-year intervals (Q7L2, Q7L5, Q7L10, Q7L25, Q7L50, Q7L100). Be sure to record beginning (QBDATE) and ending (QEDATE) dates of streamflow record used to estimate these characteristics, if applicable.

47. Method used to estimate flow characteristics (FLOWMD)—Record method used to estimate flow

characteristics, such as streamflow data from a gaging station or reference source for equations.

Many types of ancillary basin data in a GIS may be associated with water quality. A short description and some sources for GIS data that can be collected but are not included on the basin form are listed below. Two useful measurements are percentage of basin covered and absolute area (such as square kilometers). Even though these data may be in a computerized format from the start, it is very important to record data sources, scale, category definitions, date, and spatial extent. These data are stored in the habitat dictionary files called "Giscat" and "Cover." Data for several of the thematic maps listed below may be provided to the Study Unit by a NAWQA national synthesis team.

Land use/land cover—Land-use/land-cover information for the Nation is available from USGS high-altitude color-infrared aerial photography generally taken in the 1970's at a scale of 1:250,000. The land-use/land-cover classification scheme used is based on Anderson and others (1976). Additional land-use/land-cover GIS maps from other sources are available at a higher resolution for some areas.

Soils—The State soil geographic data base (STATGO) is available for the United States and contains general information on soil texture, permeability, and erodibility at a scale of 1:250,000. See U.S. Department of Agriculture (1991) for more details.

Geology—GIS coverages are available for bedrock and surficial geology but will differ in spatial extent and scale for each Study Unit. A national map of bedrock geology (King and Beikman, 1974) at a scale of 1:2,500,000 is available from GIS data bases. Consult applicable State geological surveys for more information.

Physiography—A national GIS coverage of physiography for the United States is available at a scale of 1:7,000,000. Provinces and sections are based on common topography, bedrock type and structure, and geologic and geomorphic history (Fenneman, 1946).

Ecoregions—A national GIS coverage of ecoregions in the United States is available at a scale of 1:7,500,000, based on overlays of land use, major land-resource areas, and natural vegetation types. See Omernik (1987) and Hughes and Larsen (1988) for more information. Revised and regional maps also may be available. Be sure to record the date of the map.

Potential natural vegetation—A national GIS coverage of vegetation before European settlement (Küchler, 1970) for the United States is available at a scale of 1:7,500,000.

Land-resource areas—A national GIS coverage of land-resource areas for the United States is available at a scale of 1:7,500,000. The land-resource areas are based on the interrelation of land use, climate, water resources, and soils (U.S. Department of Agriculture, 1972).

Wetlands—The U.S. Fish and Wildlife Service's National Wetlands Inventory is designed to determine the status of and trends in wetlands throughout the United States (Frayer and others, 1983; Dahl and Johnson, 1991). Wetlands are defined on the basis of plant types, soils, and frequency of flooding. Approximately 80 percent of wetlands in the United States have been mapped at 1:24,000-scale resolution. Approximately 20 to 30 percent of the maps have been digitized and are available in the Map Overlay Statistical System (MOSS) format.

SEGMENT CHARACTERIZATION

A segment is a length of stream that is relatively homogeneous with respect to physical, chemical, and biological properties. Boundaries of a segment may be tributary junctions that contain different streamflow or water-quality characteristics or substantial changes in basin characteristics (fig. 1) or major hydrologic discontinuities, such as waterfalls, landform features, significant changes in gradient, or point-source discharges (Frissell and others, 1986). Water-chemistry patterns (Teti, 1984) and benthic-invertebrate communities (Burns and others, 1984) have been shown to vary where tributaries converge.

Background

Gradient, **sinuosity**, and **water-management features** are required elements for NAWQA national data aggregation. Additional information, including Strahler stream order, link (Shreve stream order), downstream link, sideslope gradient, and riparian

vegetation, may be important for Study Unit analyses of biological and water-quality conditions.

Gradient is the ratio of channel-elevation drop divided by the curvilinear channel length. It is an indication of the amount of energy available for movement of water and sediment through the reach; thus, it has a direct influence on streamflow and channel substrate characteristics and on the type of aquatic habitat present. Gradient can be an important determinant in the distribution of fish (Maret and others, 1997) and invertebrates (Tate and Heiny, 1995).

Sinuosity describes the channel pattern. It is the ratio of curvilinear channel length to the valley centerline length (Schumm, 1963; Platts and others, 1983) (fig. 2). For sinuous channels tightly confined in V-shaped valleys, straight-line segments that follow the broad-scale changes in channel direction can be substituted for the valley centerline length (Gordon and others, 1992). It is important to note that sinuosity is dependent on the length of stream measured. For most situations, the segment length should be used. If the segment is very short, a curvilinear channel length of at least 20 times the bankfull width of the stream should be measured (Gordon and others, 1992). In meandering streams, 20 times the bankfull width incorporates at least 1 meander wavelength (Leopold and others, 1964). Straight streams will have a sinuosity of 1, whereas meandering streams generally have a sinuosity of 1.5 or more (Leopold and others, 1964). Sinuosity is helpful in describing energy conditions and is related to gradient and the diversity of habitat. In general, low sinuosity indicates a steep channel gradient, uniform cross sections, and few pools. High sinuosity is associated with flat gradients, asymmetrical cross sections, overhanging banks, and pools on the outside bend of meanders.

Water-management features are local hydrologic features that may cause temporal or spatial variability of habitat and water-quality characteristics in the segment. They include bridges, channelization, diversions, point sources, tile drains, bank stabilization, lakes, dams, and any other features that may be important. These features may form the boundaries of the segment. In addition, features outside of the segment boundaries should be noted if they might be affecting habitat or water quality within the segment.

Stream order, or classification of streams based on the number and type of tributary junctions, has proven to be a useful indicator of stream size, discharge, and drainage area (Strahler, 1957). There are several methods for determining stream order. Two commonly used methods are the Strahler method (Strahler, 1957) and the link, or Shreve method

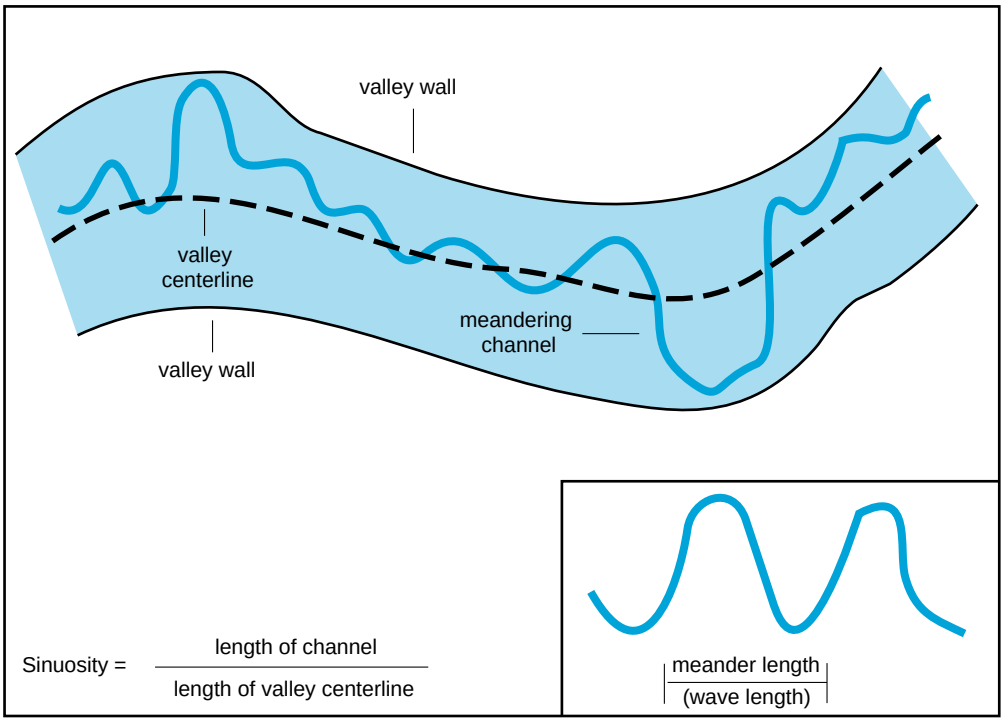

Figure 2. Example of how to measure sinuosity.

(Shreve, 1967). For Strahler stream order, all of the smallest, unbranched tributaries are designated order 1. Where two first-order streams join, a second-order segment is formed; where two second-order segments join, a third-order segment is formed, and so on (fig. 3A). For the link method, the orders of upstream tributaries are summed. For example, if a second- and fifth-order segment come together a seventh-order segment is formed (fig. 3B).

The downstream link number describes the relation of a given segment to upstream and downstream influences within a basin and, therefore, indicates the spatial location of a stream within a basin (Osborne and Wiley, 1992). This information can be important for analyses of fish data. For example, if a segment is located in a small tributary stream that feeds into the Mississippi River, the downstream link would be large, indicating that although the size of the stream is small, large river species may be present. The downstream link number is the magnitude of the link of the next downstream confluence (fig. 3).

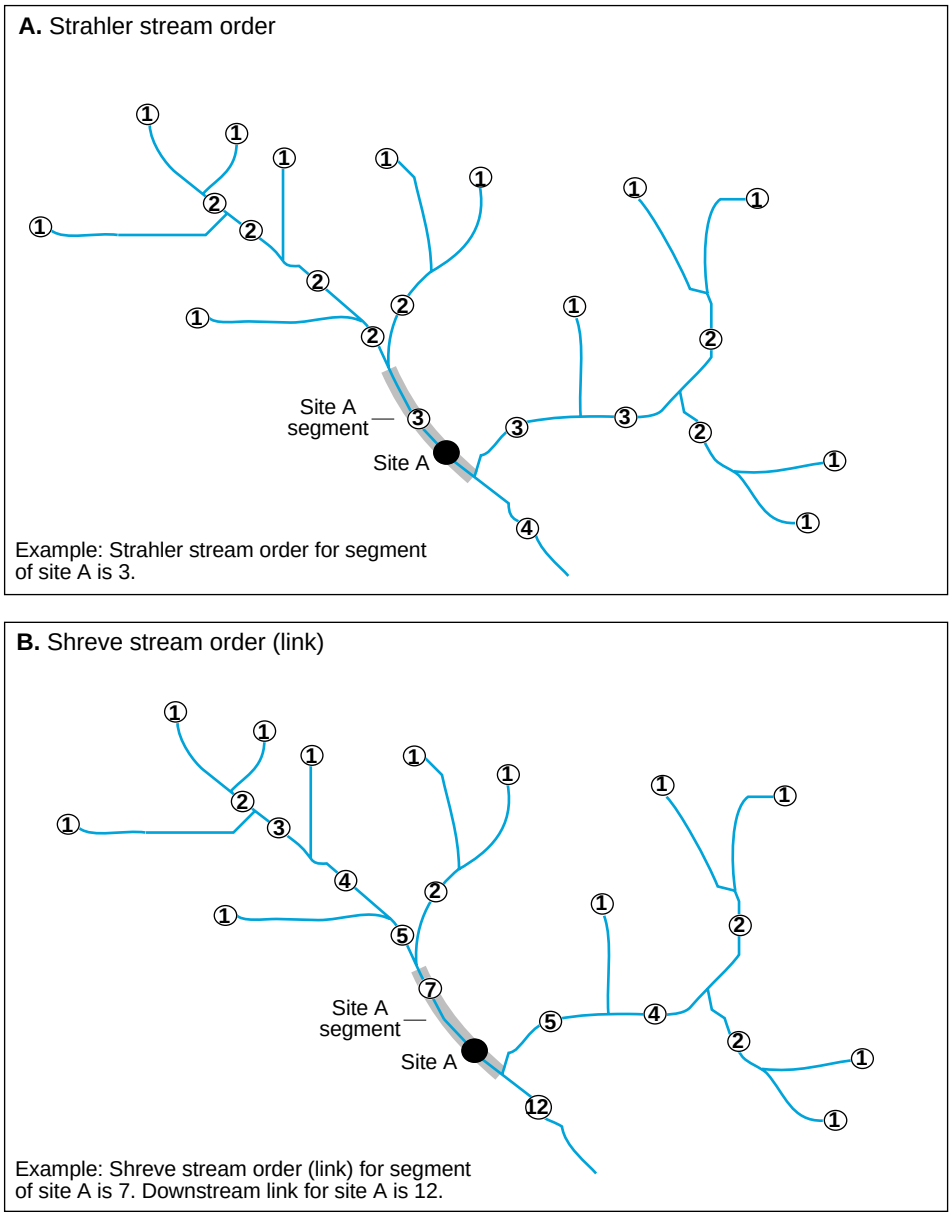

Figure 3. Examples of how to calculate (A) Strahler stream order and (B) Shreve stream order (link) and downstream link.

All stream ordering methods are dependent on the source and scale of maps used to count tributaries, and the same map series should be used for consistency and comparison. The major difficulty in determining stream order is deciding what constitutes a first-order stream. The USGS 7.5-minute quadrangle maps are used here, and both intermittent and perennial streams are counted (Leopold and others, 1964). Digital elevation data also may be used to develop a drainage network (Harvey and Eash, 1996) from which stream order can be calculated. Results may be different from those obtained from use of stream network delineations on USGS 7.5-minute topographic maps.

Valley sideslope gradient is a measure of the slope of valley walls. Differences in the sideslope gradient may be indicative of differences in lithology or geologic structure (Hack, 1957).

Specific information about land cover along the segment riparian zone also may be important to the Study Unit for special situations—for example, where land cover along the segment differs from that along the reach, or where riparian vegetation is suspected of being an important factor in determining stream conditions and aquatic community characteristics in the segment. Important aspects of the riparian buffer zone include width, length, and spatial continuity or heterogeneity. Traditionally, measurements have been made from GIS, aerial photographs, or field work. For some studies, it may be useful to extend measurements of the riparian buffer zone outside of the segment boundaries.

Description and List of Segment Characteristics

A segment characterization is done for fixed and synoptic sites using 7.5-minute topographic maps, recent aerial photographs, or a GIS. An example form is given in field form 2 (see Field Forms at back of report). Instructions for completing the form are detailed below. There is no space on the form to record riparian land-use information because of the variety of methods and scales that could be used for data collection. Items in **bold** are required for NAWQA national data aggregation, either for characterizing the segment or to link segment data with other habitat data. Abbreviations in parentheses are parameter codes in the NAWQA data dictionary files called "Segment" and "Wmf." A record of the method is particularly important for segment characteristics because a variety of methods can be used.

1. Study Unit (SUID)—Use the 4-letter code designated for each Study Unit.
2. **Station identification number (C001 or STAID)**—List the USGS station identification number for the site.
3. Station name (C900)—List the USGS station name.
4. Segment code (SEGCODE)—The USEPA's River Reach data base (RF3) is a GIS national hydrographic data base of surface-water features that contains code numbers for each segment. Record the segment code number that corresponds to the study segment, if one exists. This information is used to link these data with other data bases. Segment boundaries in RF3 may not always correspond to Study Unit segment boundaries.
5. **Location of segment boundaries (USLAT, USLONG, DSLAT, DSLONG)**—Record the latitude and longitude, in degrees, minutes, and seconds, of the upstream and downstream ends of the segment. This information is needed to locate the segment in the future.
6. **Method for locating segment boundaries (LOCMD)**—Record method used to locate segment boundaries. If a map is used, record map year and scale. If a GIS is used, also record scale and map year, if applicable. Field measure refers to use of a global positioning system. If different methods

were used to measure longitude and latitude, record differences at the end of the field form in item no. 26. “Comments about segment data.”

7. **Segment (valley) length (SEGLENG)**—Using a map wheel (or GIS), record the straight-line length of the segment, in kilometers, by following a relatively straight line through the centerline of the valley (fig. 2). For sinuous channels tightly confined in V-shaped valleys, straight-line segments that follow the broad-scale changes in channel direction can be substituted for the valley centerline length (Gordon and others, 1992).

8. **Method used to measure segment length (SEGLENMD)**—Record method used to measure segment length. If a map is used, record map year and scale. If a GIS is used, also record scale and map year, if applicable. Field measure refers to use of a global positioning system.

9. **Curvilinear channel length and distance to reference location (SEGCUR, USDIST, DSDIST)**—Using a map wheel (or GIS), record the approximate length, in kilometers, of the channel in the segment by following a line through the thalweg of the main channel (or midpoint of channel if thalweg is not known). Record the curvilinear distance from the reference location to the upstream and downstream boundaries of the segment. If the boundary is upstream from the reference location, record it as a negative number. If the boundary is downstream from the reference location, record it as a positive number.

10. **Method used to measure curvilinear channel length (SEGCURMD)**—Record method used to measure curvilinear channel length. If a map is used, record map year and scale. If a GIS is used, also record scale and map year, if applicable. Field measure refers to use of a global positioning system.

11. **Upstream and downstream elevation (USELEV, DSELEV)**—Record elevation, in meters, of a segment at upstream and downstream boundaries using the National Geodetic Vertical Datum (NGVD).

12. **Method used to measure upstream and downstream elevation (SELEVMD)**—Record method used to measure upstream and downstream elevation. If a map is used, record map year and scale. If a GIS is used, also record scale and map year, if applicable. Field measure refers to use of a global positioning system.

13. **Sinuosity (SINUOS)**—To calculate sinuosity, divide the curvilinear channel length by the valley length (fig. 2). If the segment is very short, a curvilinear channel length of at least 20 times the bankfull width of the stream should be measured. In meandering streams, 20 times the bankfull width incorporates at least one meander wavelength (Leopold and others, 1964). Straight streams will have a sinuosity of 1, whereas meandering streams generally have a sinuosity of 1.5 of more (Leopold and others, 1964).

14. **Segment gradient (GRADIENT)**—Determine the gradient of the segment by subtracting the downstream elevation from the upstream elevation and dividing the difference by the segment channel length.

15. **Water management feature (WMFID, WMFTYPE, WMFDES,** WMFBDATE, WMFEDATE, **WMFDIST)**—Record the type(s) of water management feature(s) that is(are) likely to influence habitat conditions in the segment. Include a short description and give starting and ending dates, if appropriate. Record distance from the reference location; distances upstream from the reference location are negative, and those downstream are positive. Include as many water-management features as appropriate. Features upstream or downstream from the segment should be noted if they might be affecting habitat or water quality within the segment. Use the following 12-letter codes for WMFTYPE:

Bridge	Natural Lake	Gw Inflow
Diversion	Bank Stabiliz	Hydropower
Return Flow	Tile Drain	Industrial
Stp > 5	None	Mining
Ips > 5	Channelized	Storm Sewer
Impoundment	Feedlot	Thermal
Low-head Dam	Sewage Treat	Other

16. Strahler stream order (ORDER)—On a USGS 7.5-minute topographic map showing all intermittent and perennial streams in a basin, the smallest unbranched tributaries are designated order 1 (Leopold and others, 1964). Where two first-order streams join, a second-order segment is formed; where two second-order segments join, a third-order segment is formed, and so on (fig. 3). For irrigation canals and other "artificial" systems, "-1" is recorded for stream order.
17. Strahler stream-order method (ORDERMD)—Record method used to measure Strahler stream order. Data sources include maps or GIS; record year and scale for either type.
18. Link (Shreve stream order) (LINK)—Calculating the link, or Shreve stream order, for a segment is done by summing the orders of upstream tributaries (Shreve, 1967) (fig. 3). For example, the joining of a second-order and third-order stream produces a fifth-order stream. This method may be a better indicator of the approximate size of a drainage basin than the Strahler method, especially if a drainage basin has a large number of minor tributaries that intersect a higher order stream. For irrigation canals and other manmade systems, "-1" is recorded for link.
19. Link (Shreve stream order) method (LINKMD)—Record method used to measure link. Data sources include maps or GIS. Record year and scale for either type.
20. Downstream link (DSTRLINK)—Calculate the link of the stream downstream from the segment and below the next tributary junction. Downstream link number is the magnitude of the link of the next downstream confluence (fig. 3). For example, the segment immediately downstream from the confluence of two headwater tributaries has a downstream link of 2. If a headwater tributary flows into a stream with a downstream link of 2, then the segment immediately downstream from the confluence of these two streams has a downstream link of 3, and so on. For irrigation canals and other manmade systems, "-1" is recorded for downstream link.
21. Downstream link method (DSLINKMD)—Record method used to measure downstream link. Data sources include maps or GIS; record year and scale for either type.
22. Valley sideslope gradient (SIDEGRAD)—Sideslope gradient is based on the cross-sectional profile of the segment valley. Make three gradient measurements within 300 m of the horizontal distance of the channel at positions representative of the valley sideslope gradient along the segment. These measurements and their mean are recorded.
23. Method used to measure valley sideslope gradient (SIDEGRMD)—Record method used to measure sideslope gradient. Possible methods include map-derived data, field data, or GIS data; record map year and scale, if applicable.
24. File names and path name where data can be found—Record the directory path and file names for appropriate data files.
25. Contact person for segment data—Record the name of the person responsible for the data.
26. Comments about segment data (SEGCOM)—Note special circumstances for measurements or data limitations.

REACH CHARACTERIZATION

A reach (fig. 1) is the least clearly defined unit in the spatial hierarchy; however, it is the most useful scale for describing long-term effects of human activities and determining population and distribution of aquatic communities (Frissell and others, 1986). Although a segment is a discrete unit that should represent a uniform set of physical, chemical, and biological conditions within a stream, its length (often more than several kilometers) prohibits effective collection of field data. The reach is the principal sampling unit for collecting physical, chemical, and biological data that represent conditions within the segment.

Selection of a Reach

The selection of a reach depends on a combination of four criteria—stream width, stream depth (wadeable or nonwadeable), geomorphology (type and distribution of **geomorphic channel units** (GCU's)), and local habitat disturbance. Wadeable reaches are those reaches where an investigator can wade from one end of the reach to the other, even though the reach may contain some pools that cannot be waded. Nonwadeable reaches are those reaches where an investigator cannot wade from one end of the reach to the other through the deepest part of the stream, and a boat is needed.

In general, the **reach length** is determined by multiplying the mean **wetted channel width** (MCW) by 20. The width is multiplied by 20 because, in meandering streams, 20 times the channel width typically encompasses at least one complete meander wavelength (Leopold and others, 1964). This ensures that all habitat types are represented within the reach. A minimum reach length is necessary to ensure the collection of representative samples of biological communities, and a maximum reach length is needed to prevent unnecessary sampling and to minimize crew fatigue (and associated reduction of sampling efficiency). Therefore, minimum and maximum reach lengths for wadeable streams are the same as for biota sampling, 150 and 300 m, respectively (Meador, Cuffney, and Gurtz, 1993). For nonwadeable streams, recommended minimum and maximum reach lengths are 500 and 1,000 m, respectively.

The type and distribution of GCU's (often called habitat types) are important factors in selecting a reach. GCU's are fluvial geomorphic descriptors of channel shape and scour pattern that are widely used in habitat assessment surveys (Orth, 1983; Ohio Environmental Protection Agency, 1989). The development of specific sequences of GCU's is a fundamental stream process (Ying, 1971; Beschta and Platts, 1986), and identification of GCU's is important because it classifies stream habitat at a spatial scale relevant to most biota in streams (Frissell and others, 1986). Three types of GCU's are considered when selecting a reach—pools, riffles, and runs (fig. 4). From an instream perspective in large, nonwadeable rivers, inside meander bends (convex side of a meander bend), outside meander bends (concave side of a meander bend), crossovers (areas carrying the greatest water volume between two river bends), and possibly forewater and backwater side habitats replace pools, riffles, and runs as the important geomorphic units.

Pools are areas of the channel with reduced velocity, little surface turbulence, and deeper water than surrounding areas. Pools can form downstream from depositional bars, in backwater areas around boulders or woody debris, or in trenches or chutes. Eddies may be present. Pools also can form behind channel blockages, such as beaver dams or logjams, where water is impounded. Because a pool can form from a variety of hydraulic processes, there are many different types of pools (Bisson and others, 1982; McCain and others, 1990). Plunge pools form at the base of a nickpoint or channel obstruction that creates a hydraulic drop. Lateral scour pools form beside a bank or against a partial channel obstruction.

Riffles are relatively shallow areas of the channel where water flows swiftly over completely or partially submerged obstructions to produce surface turbulence (fig. 4). Usually, riffles have relatively coarser substrates than pools and runs and occur in straight reaches. During flooding, a riffle can look like a run. Riffles include low-gradient riffles, rapids, and cascades (Bisson and others, 1982). Low-gradient riffles have a gradient less than 0.04 m/m, are shallow with moderate velocities, moderate turbulence, and gravel to cobble substrates. Rapids have gradients greater than 0.04 m/m with fast velocity, significant turbulence, and typically boulder substrate. Cascades have very steep gradients and are distinguished from rapids by having alternating small waterfalls and

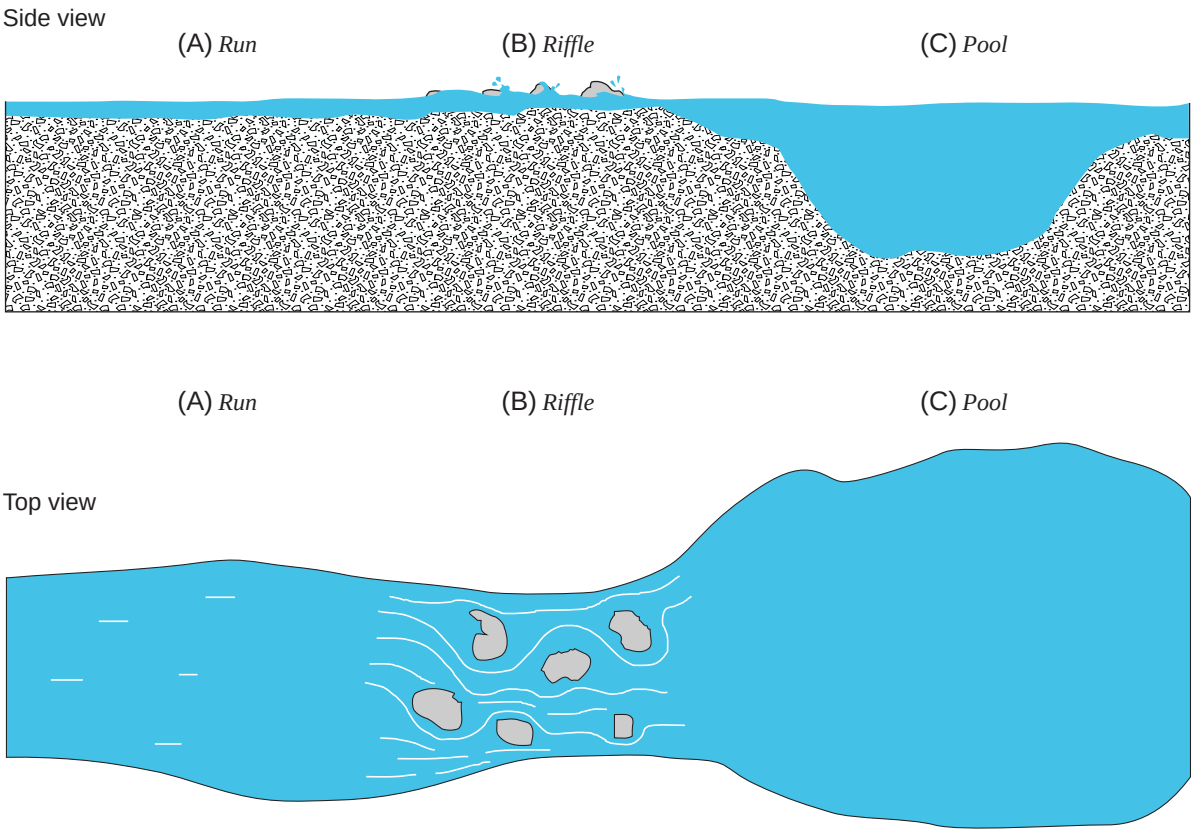

Figure 4. Diagram of the three main geomorphic channel units. (A) Run—A slow moving, relatively shallow body of water with moderately low velocities and little or no surface turbulence; (B) Riffle—A part of the stream where the water flows swiftly over completely or partially submerged obstructions to produce surface agitation; (C) Pool—A part of the stream with reduced velocity, commonly with deeper water than surrounding areas (modified from Bisson and others, 1982).

shallow pools, usually with bedrock or boulder substrate.

Runs are areas with moderate depth and little or no surface turbulence (fig. 4). Velocities can be high or low, but the key feature is little apparent surface turbulence. The term "glide" also has been applied to runs (Bisson and others, 1982). Runs typically are found in the transition zone between riffles and pools and in low-gradient reaches with no flow obstructions. Typical substrate in runs ranges from cobble to sand. Runs may become riffles during low-flows or droughts.

If possible, the reach should include at least two examples each of two types of GCU's. Only those GCU's that are greater than 50 percent of the channel width are considered. The composition of GCU's included in the reach should reflect the sequence of GCU's in the segment. For example, the GCU's near the reference location may include a pool and a sequence of riffles and runs. If the pool is present only at the reference location and nowhere else in the segment, the pool is not included in the selected reach. If two examples of two geomorphic units are not present, a reach should be selected that contains a balance of geomorphic units most representative of the segment.

If the representative reach selected must be located near a bridge or other manmade alteration, it should be located upstream from the structure in order to minimize its influence on habitat. When compelling reasons dictate that the reach must be downstream from a bridge or other feature, then the reach must be established far enough downstream from the bridge to avoid local hydraulic effects, such as scour holes and overwidened channels.

Collection of General Reach Data and Placement of Transects

Once the general reach location has been selected, the boundaries of the reach are established

and information about the reach is gathered. Permission must be obtained from the local landowner before proceeding with data collection and the establishment of semipermanent markers. Again, habitat data should be collected during base flow to minimize the variability caused by measuring habitat at different flow conditions.

At the beginning of data collection, the general condition of the reach (evidence of recent floods; unusual storm events; manmade alterations; point sources for sediment, contaminants, nutrients; beaver activity; or other events that might affect the overall reach) is noted. Next, **discharge** is measured if no streamgage is located at the reference location, or gage height recorded if a gaging station is operated at the reference location. Evidence of **channel modification** is noted. The reference location should be selected near a permanent structure that provides a geographic marker to link the habitat data collection to data collected at other scales of spatial hierarchy, such as segment and basin characteristics. At fixed sites, the reference location is often a bridge crossing. The reference location is described and photodocumented.

If there are well-developed sequences of GCU's in the reach, the first boundary and first transect of the reach is placed approximately one-half of the MCW upstream or downstream from the boundary of a GCU (fig. 5). Boundaries between GCU's may be hard to identify and, in practice, are more like zones than lines in the channel and can be identified by changes in depth or surface turbulence. If there are no well-developed sequences of GCU's, the reach boundary and first transect are located about 10 times the MCW from the reference location to maintain objectivity. For general guidance in wadeable streams, the reach boundary and first transect should be at least 10 times the MCW distance away from bridges, dams, waterfalls, and major tributaries to avoid any influence from these disturbances. This distance may need to be shortened or lengthened, depending on reach-specific circumstances and the size of the stream. The reach boundaries should be the same as those used for fish sampling.

Once a boundary of the reach has been determined, a semipermanent marker is installed on a surface that is not subject to frequent scour or sediment deposition. The marker may consist of a capped iron pipe or concrete reinforcing bar driven about 60 cm into the ground. Do not use reinforcing bars in pastures or fields, as they may damage farm equipment or injure animals. The part extending out of the ground is painted a bright waterproof color to facilitate location at a later date. A hand-held metal detector also may be useful for locating the marker in the future if thick vegetation or sediment accumulation makes it difficult to locate visually. If conditions do not permit the use of a marker driven into the ground, a hole can be drilled in an adjacent rock or tree, and a standard carriage bolt can be inserted and painted as the marker. This technique is not recommended in areas with the potential for logging (commercial or by a local landowner); growth around the bolt can hide it, which becomes a serious hazard for a logger with a chain saw. A large metal washer (inscribed with appropriate information) also may be glued to a large rock. Under certain conditions, only brightly colored flagging may be appropriate for marking a reach.

The semipermanent boundary marker location is noted on the map, and the type of marker and its location relative to the channel are described. Additional information also is collected to help locate the reach boundary in case the semipermanent marker cannot be found in the future. If not done previously, three measurements of representative wetted channel width are collected, and the average of the three measurements, the MCW, is used to determine the reach length.

Eleven equidistant transects are established throughout the reach to collect information on channel, bank, and riparian characteristics (fig. 5). Transects are placed equidistantly and systematically to statistically represent habitat characteristics within the entire reach and to eliminate observer bias. Eleven transects are used to maintain repeatability and precision (sampling 11 equidistant transects provides approximately 80-percent accuracy of estimates of means for selected habitat characteristics (Simonson and others, 1994b)), while keeping time commitments realistic (Kaufmann and Robison, 1994). Transects are oriented perpendicular to the streamflow direction as it occurs at base flow. The distance between transects is determined by dividing the total reach length by 10. Sometimes, small but important GCU's, such as a small riffle or deep pool, may be missed by placing the transects equidistantly. If warranted, these unique features should be noted with additional field notes, and their locations recorded on the diagrammatic map.

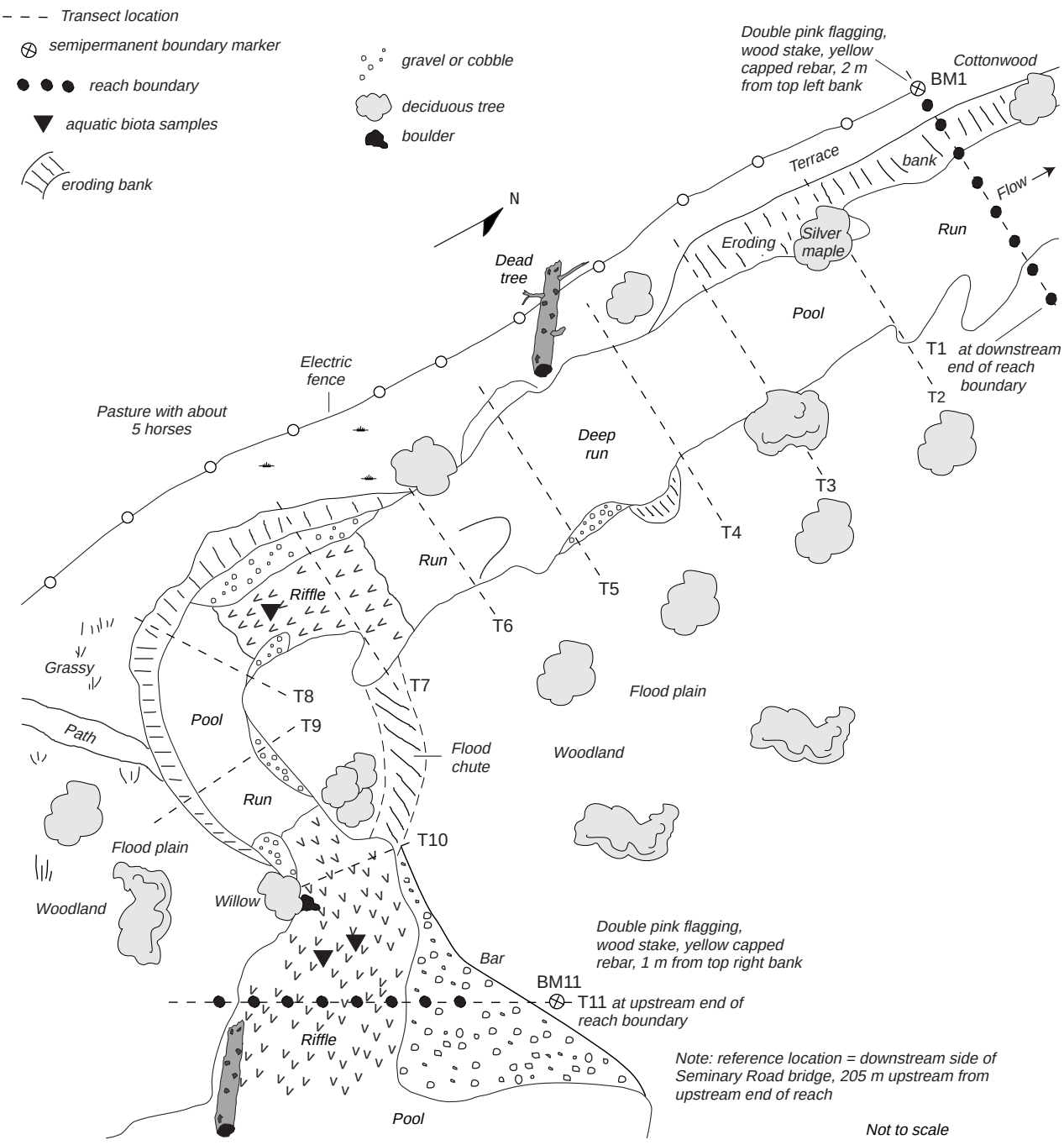

Figure 5. Example of a diagrammatic stream map showing transect locations, reach boundary markers, and other important stream characteristics.

After establishing the lower reach boundary and determining the length between transects, the crew proceeds upstream, flags transect locations by using flagging tape or surveying flags (Do not leave surveying flags behind; cows like to eat them!), measures the **length of each GCU**, and maps the reach (fig. 5). (If the area of each type of GCU is needed for other habitat classifications, measure two to three wetted channel widths per GCU in addition to length to calculate the area of each GCU.) The length of a GCU is an important determinant of habitat diversity that can affect the type and amount of instream biota. The diagrammatic map of the reach (fig. 5) should show the approximate area and type of each GCU, and the locations of major habitat features, reach boundaries, reference locations, discharge measurements, transects, semipermanent markers, and the flood plain, bars, islands, and shelves.

At the top of the reach, the upper permanent boundary marker is established at the last transect location. Channel, bank, and riparian features of each transect are measured as the crew moves back downstream. For nonwadeable reaches, collection of these types of data requires (at a minimum) a boat, a rangefinder or other long-range distance measurer, a surveying scale or laser-level survey system, and a depth-finder. Edsall and others (1997) contains more information on techniques and equipment for collecting habitat data in large streams.

The **reach water-surface gradient** is calculated by measuring the change in elevation of the water surface along the known length of the reach (distance from the upstream reach boundary to the downstream reach boundary). The water-surface gradient provides a good estimation of the energy gradient, which is an important parameter in the hydraulic power of the stream and, therefore, an important influence on a variety of other habitat measurements. The elevation change of the water surface can be determined by measuring the elevation of the left and(or) right edge of water directly or by measuring the water-surface elevation indirectly by recording the water depth and the elevation of the channel bed in the thalweg. If the latter method is used, two gradients can be calculated—one for the water surface and the other for the thalweg. In addition, the latter method may be more accurate in streams where the water's edge is soft and the surveying rod could sink during the measurement. It may also be useful to measure the gradient of the flood plain, which is the same as the water-surface gradient during bankfull flow.

Depending on the number of people in the sampling crew, the **gradient** measurements may be done while the transects are flagged and the GCU's are measured or during transect-data collection. The number of points used to measure the gradient along the reach and the type of equipment used varies, depending on the size and gradient of the stream. Usually, elevation data are collected at a spacing similar to the spacing between the 11 transects or at about a distance of one channel width (Emmett, 1975). In high-gradient streams, the reach gradient can be determined by measuring the angle between transects by using a clinometer or compass and surveying staff rod, or by measuring the elevation change with a hand level and surveying staff rod (fig. 6). For low-gradient streams, a hand level or clinometer may not provide the accuracy needed, in which case the gradient should be determined with a surveying level on a tripod and a surveyor's rod. For large, nonwadeable rivers, water-surface elevations are determined along one or both banks, and thalweg elevations can be determined by use of a hydroacoustic system.

For measuring gradient with a clinometer (fig. 6), the first step is to measure and flag the eye height of the person who is sighting on the surveying rod. Next, the sighting person stands at the water's edge at one transect while the person with the surveying rod moves upstream or downstream to the next transect and holds the survey rod at the water's edge. The sighting person sights to the mark on the survey rod and records the angle between the transects. This procedure is done for each set of transects.

For measuring gradient with a hand level or a surveyor's level (fig. 6), differential leveling is done to measure the elevation drop and the distance between selected transects along the reach. For example, the person who is sighting stands between transect 1 and transect 2, and backsights (BS) to the semipermanent marker established at the reach boundary and transect 1. This marker is considered a benchmark and has a known or assumed elevation. From this measurement, the height of the instrument (HI) is obtained. Next, sightings are done to the rod placed at the water's edge at both transects and at a turning point (TP). These readings are called foresights (FS), or readings obtained from an unknown elevation. A turning point is a temporary reference point, such as a rock or wooden stake. As mentioned previously, instead of placing the

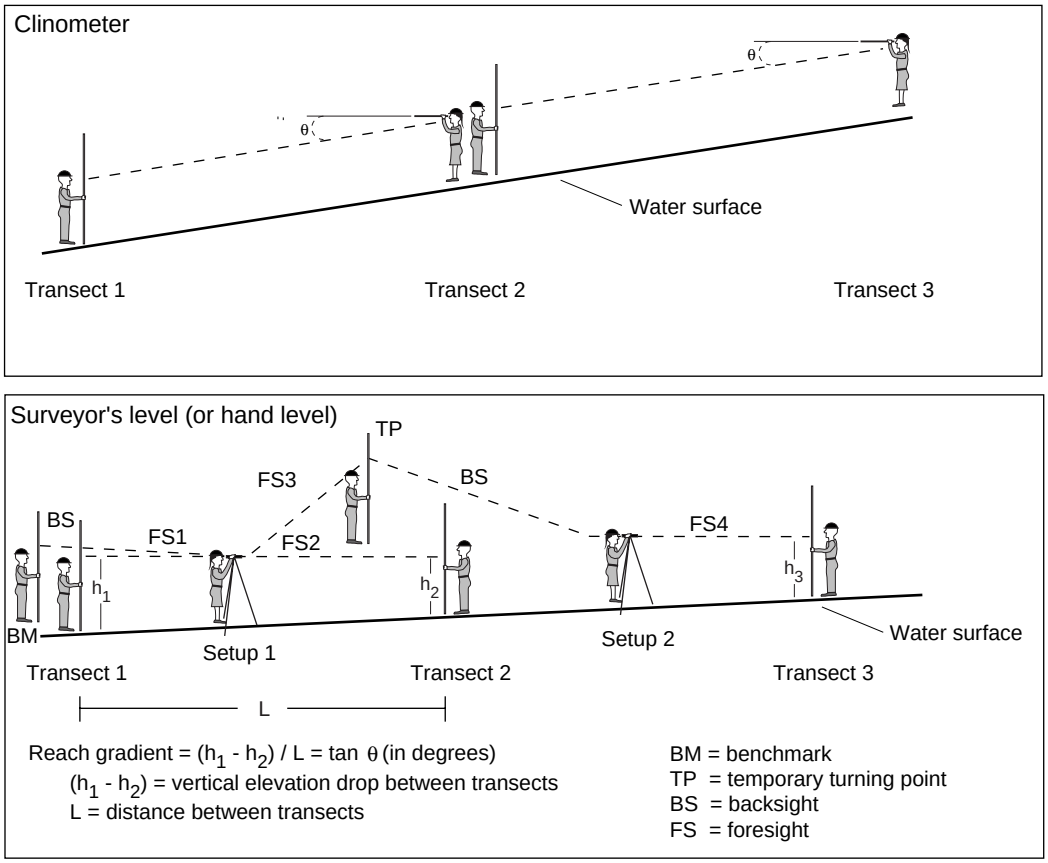

Figure 6. Diagram of how to measure water-surface gradient with a clinometer or surveyor's level.

rod at the water's edge, the rod also can be placed at the thalweg and a water-depth reading recorded. With this information, both the water-surface gradient and thalweg gradient can be calculated. After the foresights are done at both transects, the person who is sighting moves to a new location between transect 2 and transect 3. A backsight is taken from the rod at the turning point to establish the new height of instrument, and foresights are made to additional transects. This process is continued until the elevation drop along the entire reach has been measured. See Harrelson and others (1994) for more details.

Identification of Banks and Bankfull Stage

Several reach measurements require an understanding of some basic geomorphic concepts and definitions because the measurements are based on identifying the boundary between the flood plain, bank, and channel. The boundaries between these features are important because they are morphological indicators that can be associated with flood and sediment characteristics. The first step in defining the boundaries between flood plain, bank, and channel is to have a clear definition of each geomorphic feature.

The flood plain (fig. 7) is generally a flat to gently sloping depositional surface adjacent to a stream channel and is under construction by the modern stream. The surface of and the sediment under the flood plain relate to the activity of the present river (Wolman and Leopold, 1957). The elevation of this "active" flood plain under construction is considered here to be the same as bankfull stage, as originally defined by Wolman and Leopold (1957). The change in the bankfull stage along the reach (flood-plain gradient) represents the water-surface gradient during bankfull flow. The flood plain is subject to periodic flooding approximately every 1 to 3 years (Wolman and Leopold, 1957; Wolman and Miller, 1960; Leopold and others, 1964), although considerable variability in the recurrence interval of floods has been found among different streams (Williams, 1978). It is important to note that not all streams have flood plains, especially

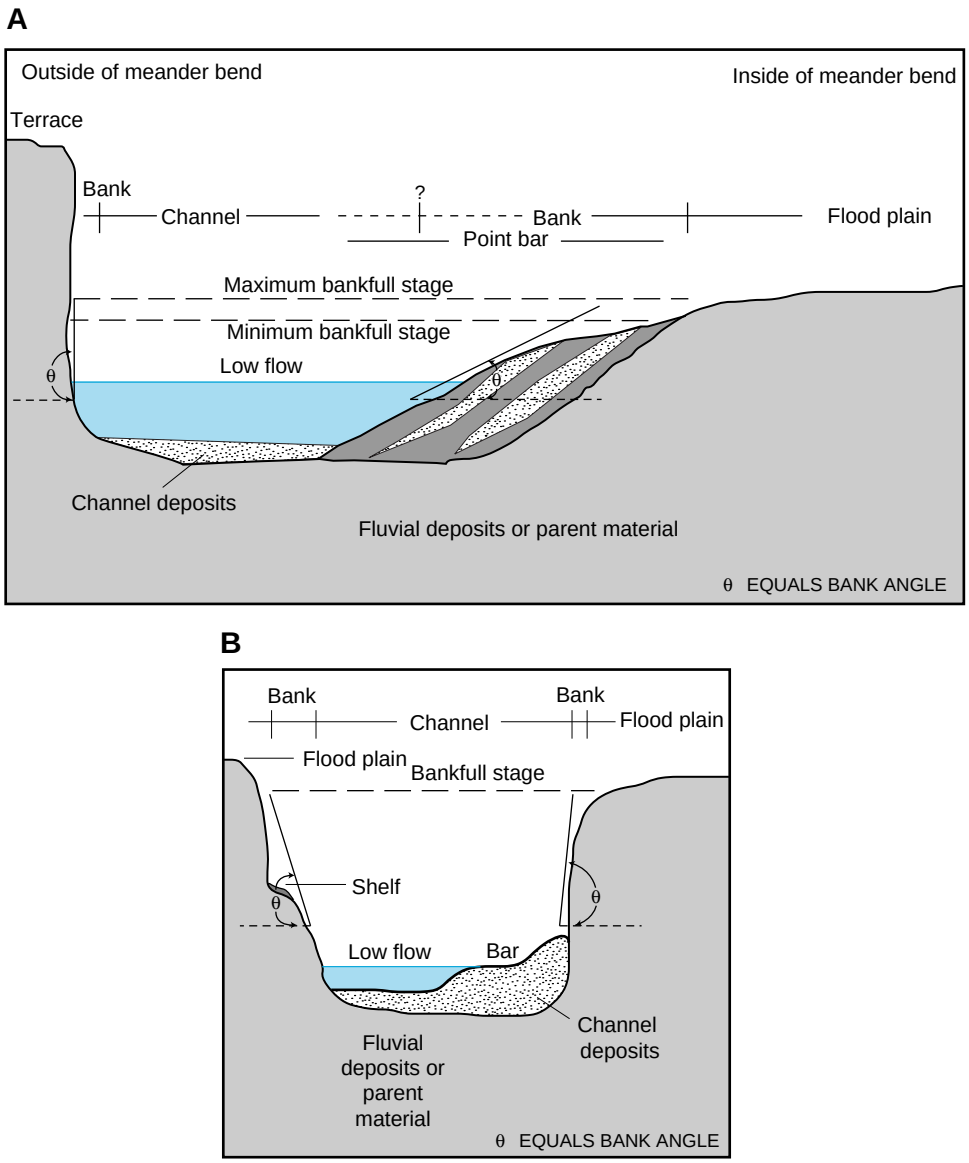

Figure 7. Examples of the relative position of geomorphic features, bankfull stage, and bank angle from (A) a bend in a meandering stream, and (B) a straight reach.

those with steep gradients, those that are geologically young, or those that are downcutting.

Terraces (fig. 7) are abandoned flood plains that formed when the stream flowed at a higher level than at present. Terraces are no longer related to the modern hydrology of the stream (Ritter, 1978); however, terraces also may be adjacent to the channel and be difficult to distinguish from the flood plain if little is known about the stream hydrology. Sometimes a terrace can be distinguished from the flood plain by its morphologic and sedimentologic characteristics if flow and sediment characteristics have changed over time.

In general, banks are defined by the steep or sloping ground that borders a stream and confines the water in the natural channel when the water level, or flow, is normal (fig. 7). Banks are located between the channel and flood plain. The channel of a perennial stream is the surface that is wholly or partly covered by flows below the mean discharge.

The presence of bars and shelves (fig. 7) may complicate distinguishing the boundary between channel and bank. Shelves may be present in high-gradient mountain streams and may be depositional or erosional. Shelves are usually considered to be part of the bank (Hupp, 1986). If the flood plain contains trees, a shelf sometimes can be distinguished from a flood plain by the presence of shrubs and the absence of trees (Hupp and Osterkamp, 1985). Bars may be part of the

channel or bank and are formed by deposition of suspended load and(or) bedload. Bars can form in the middle or near the sides of a channel and typically are covered by flows slightly larger than low flow. Typically, they are devoid of woody vegetation and composed of relatively coarse-grained sediment (Hupp and Osterkamp, 1985). Point bars, which form on the inside bend of a meandering stream, usually extend through part of the channel and most of the bank (fig. 7A).

In stable reaches with a wide flood plain, the boundary between flood plain and bank may be easy to determine. However, in many cases the boundary between flood plain and bank is not easy to determine if flood characteristics are unknown, even for experienced geomorphologists. Thus, several types of indirect evidence are used to determine the bankfull stage and ultimately determine the height of a bank. These indicators rely on sedimentary and vegetative characteristics, as well as regional or State empirical relations and(or) gaging-station data.

Below is a list of some of the techniques that can be helpful in identifying bankfull stage. The order of importance for each indicator will vary according to local conditions; best results will be achieved if a combination of indicators is employed. Empirical relations and streamflow data should be examined before field data collection. When in the field, use as many field indicators as possible, marking the boundary with pin flags on both banks along the entire reach. Field evidence for bankfull stage in erosional reaches may be ambiguous because of continuous downcutting of the channel; in this situation it is best to have some knowledge of flood characteristics and geomorphic history of the reach before going out into the field. Finding field evidence for bankfull stage in leveed and confined systems also can be difficult; again, having prior knowledge of flooding characteristics through empirical relations is helpful. Harrelson and others (1994) and the videotape by U.S. Department of Agriculture (1995) also have some useful descriptions of field indicators for identifying bankfull stage.

Empirical Relations for Identifying Bankfull Stage

1. Regional curves—Four regional curves (Dunne and Leopold, 1978, p. 615) are available for estimating average bankfull depth, width, and cross-sectional area for a stream with a given drainage area (fig. 8). These curves should be consulted to help estimate the probable location of the boundary between flood plain and bank. Average bankfull depth is defined as the cross-sectional area divided by the width and, therefore, represents the depth of a rectangular channel of the same area (Dunne and Leopold, 1978).
2. State flood-frequency equations—Some States have developed flood-frequency equations for specific hydrologic regions within a State (Jennings and others, 1994). These equations are based on data from gaging stations, and they work best if used for streams of the same size. Equations for the 2-year flood can be used to estimate the upper limit of bankfull discharge, which in turn can be used to estimate bankfull depth by using indirect discharge calculations, such as the slope-area method (Rantz and others, 1982) and estimates of channel roughness.
3. Recurrence interval at gaged site—If the reach is located near a long-term streamflow gaging station with more than 5 years of data, sometimes bankfull depth can be estimated as the stage for the 1.5-year flood based on an annual-maximum series of streamflow data (data set of the largest instantaneous discharge for a given year). However, even though bankfull discharge has an average recurrence interval of about 1.5 years, data from 36 streams across the United States indicated that the distribution of recurrence intervals for bankfull discharge among sites can range from 1 to 32 years (Williams, 1978). Thus, this method must be used with extreme caution.

Field Indicators of Bankfull Stage

1. Point bars—Point bars are accumulations of sediment on the inside of meander bends (Ritter, 1978) (fig. 7A). This sediment is deposited laterally by the stream and represents active building of the flood plain. Usually, the texture of the point-bar sediment is different from sediment in the bank (may be coarser or finer). The top of the point bar (top of the laterally accreted sediment) provides a minimum estimate for bankfull stage (Knox, 1985).
2. Slope changes—There may be several changes in slope along a line drawn perpendicular from the direction of streamflow in the channel bed to the flood plain and terraces. Bankfull stage is at the

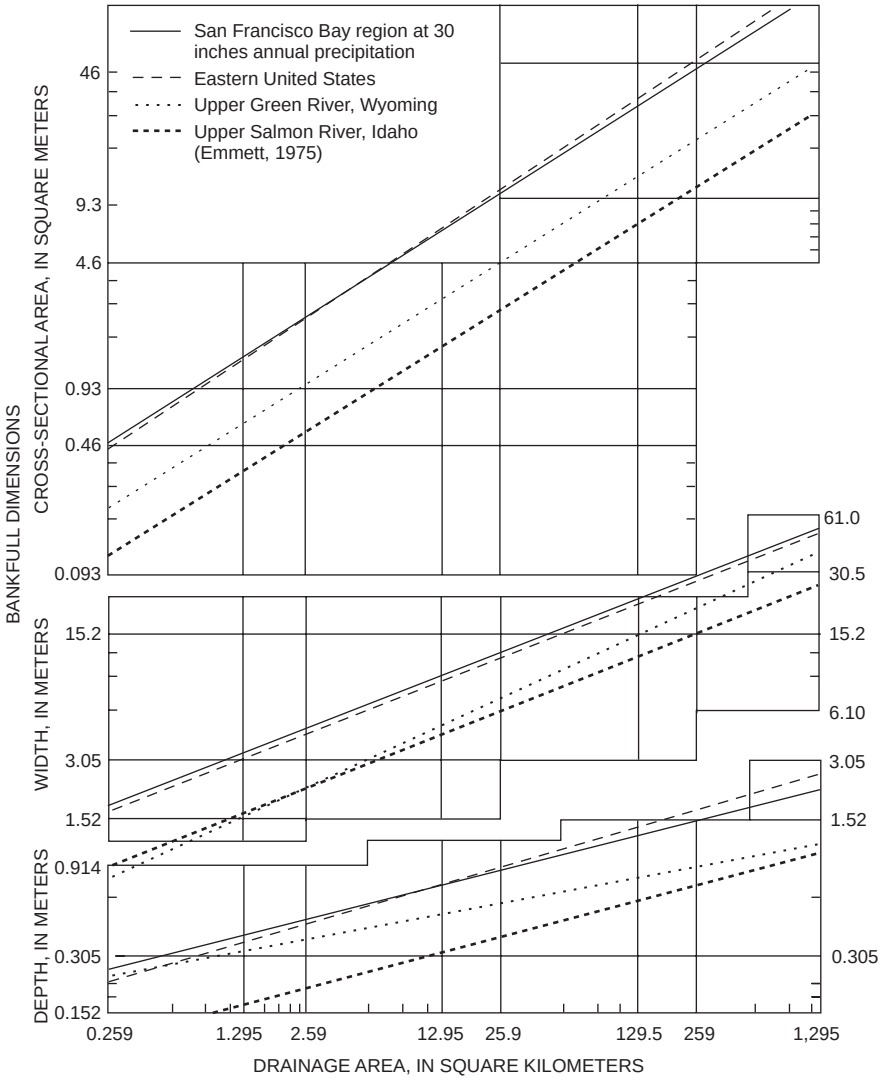

Figure 8. Average values for bankfull channel features in relation to drainage area for four regions of the United States (modified from Dunne and Leopold, 1978).

first point where the slope changes from vertical to more horizontal. If examining width-to-depth ratios, bankfull stage would be the first instance where the width-to-depth ratio increases significantly (Williams, 1978). In unstable, incised streams or in streams with shelves, there may be several such breaks in slope, so caution must be used. Three terraces have been identified for many western United States streams (Harrelson and others, 1994). However, some streams may have more or less than three terraces, and a "counting down" of breaks in slope in order to determine bankfull stage is not reliable.

3. Vegetation patterns—Patterns in the types and density of riparian vegetation can be helpful in distinguishing the boundary between bank and flood plain (Hupp and Osterkamp, 1985; Harrelson and others, 1994). Sudden changes in density as well as changes from herbaceous and(or) shrub vegetation to trees may be an indication (Schumm, 1960). Identifying the lower limit of mosses and lichens on rocks or banks also may be helpful (Harrelson and others, 1994). Recent catastrophic floods may alter significantly the vegetation; therefore, an understanding of the flood history of the reach also is important.

4. Undercut banks—In streams with undercut banks topped with dense, herbaceous perennial vegetation, the top of the undercut beneath a dense root mat is usually slightly below bankfull

stage (Harrelson and others, 1994). This method is best used as a last resort in steep channels lacking flood plains.

Collection of Transect Data

Transect data consist of quantitative information about channel width, bank features, water depth, velocity, substrate, habitat features, and riparian vegetation. Techniques for collecting transect data are different for wadeable and nonwadeable streams.

The first task in a wadeable stream is to extend a measuring tape perpendicular to the channel at a transect from the left bank to the right bank (the left side of a stream is usually considered "0"). The **wetted channel width** and **bankfull channel width** are measured, and the width of any **channel features** (bars, shelves, or islands) intersected by the tape are measured. The wetted channel width, along with depth, is used for estimating the water surface area and volume at low flow, which are useful for determining fish density or standing crop. The bankfull channel width is independent from streamflow conditions and is useful for determining the channel shape and the size of small frequent floods (floods with a recurrence interval of about 1.5 years). The bankfull channel width and bankfull depth (bank height) also are related to the size and type of transported sediment and the channel bed and bank substrate.

Two types of measurements for riparian vegetation near the stream are made—open canopy angle and riparian canopy closure. These measurements provide an estimate of the amount of shading in a reach, an important habitat feature for many fish, invertebrate, and algal species (Gorman and Karr, 1978; Byl and Carney, 1996). Riparian vegetation influences the amount of sunlight entering a stream, which controls photosynthesis and stream temperature, and also can affect streamflow and bank erosion (Platts and others, 1987). In addition to its influence on shading and temperature, riparian areas are important sources of organic material for aquatic organisms and can help create and maintain complex instream habitat. Riparian areas also can act as important buffers between upslope land use and the stream.

The amount of open canopy is determined by standing at the center of the channel at each transect and measuring the right and left canopy angle with a clinometer or compass (fig. 9). The angle is measured from mid-channel to the tallest object on each bank. The right and left angles are subtracted from 180 degrees to give the open canopy angle, which can be converted to percentage of open canopy by dividing by 180 and multiplying by 100. The distance from the water surface to eye level should be noted, especially for very narrow streams where canopy angle can be grossly underestimated by recording the angle from eye level.

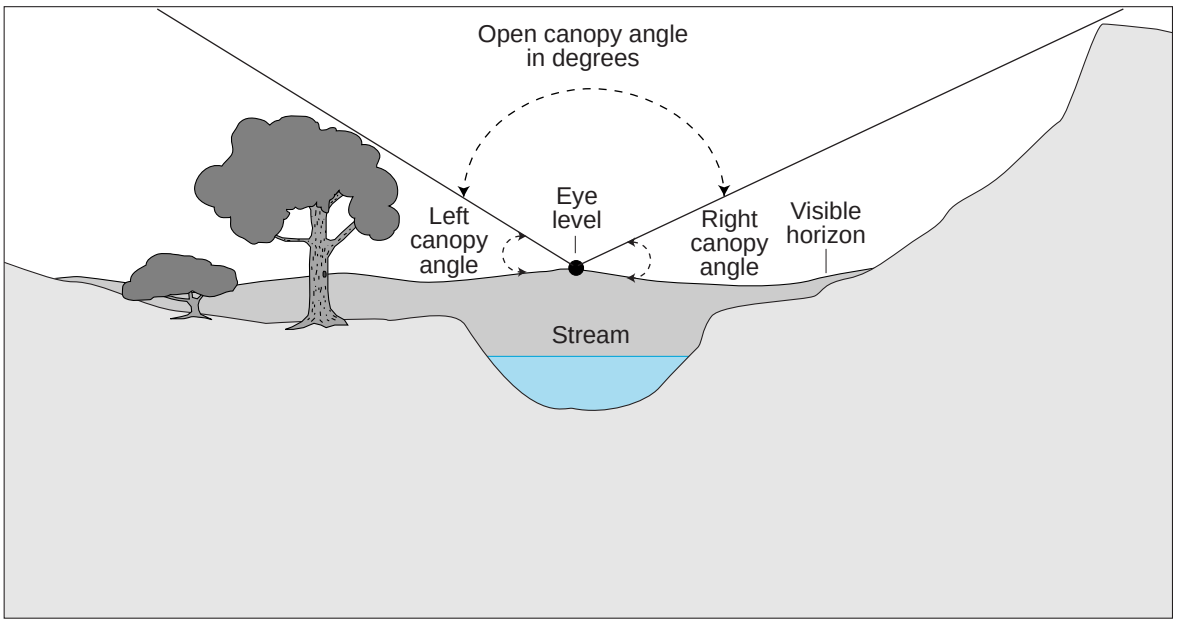

Figure 9. Measurement of open canopy angle (modified from Platts and others, 1983).

Riparian canopy closure is measured with a concave spherical densiometer by use of techniques outlined in Platts and others (1987). Measurement of canopy closure (the area of sky bracketed by vegetation) is preferred over measurement of canopy density (the area of sky blocked within the closure by vegetation) because measurements of canopy closure are less affected by seasonality than canopy density (Strichler, 1959). The densiometer is modified by taping a "V" on the mirrored surface (fig. 10). This modification uses only 17 of the possible 37 line intersections (points) and helps eliminate bias introduced by the overlap of vegetation reflected in the concave mirror when more than one reading is taken at the same position. At transects with woody vegetation in wadeable streams, riparian canopy closure is measured with a spherical densiometer at the water's edge along both sides of the stream. At the water's edge, the densiometer is held on the transect line perpendicular to the bank 30 cm from and 30 cm above the shoreline. The number of line intersections surrounded by vegetation are counted for canopy closure (fig. 10).

For consistency and repeatability of measurements, it is extremely important to maintain the same position for densiometer measures. This low position accounts for vegetation most directly over the banks and also incorporates any low overhead vegetation that overhangs the water (Platts and others, 1987). Thus, a total of two readings (34 points) is made

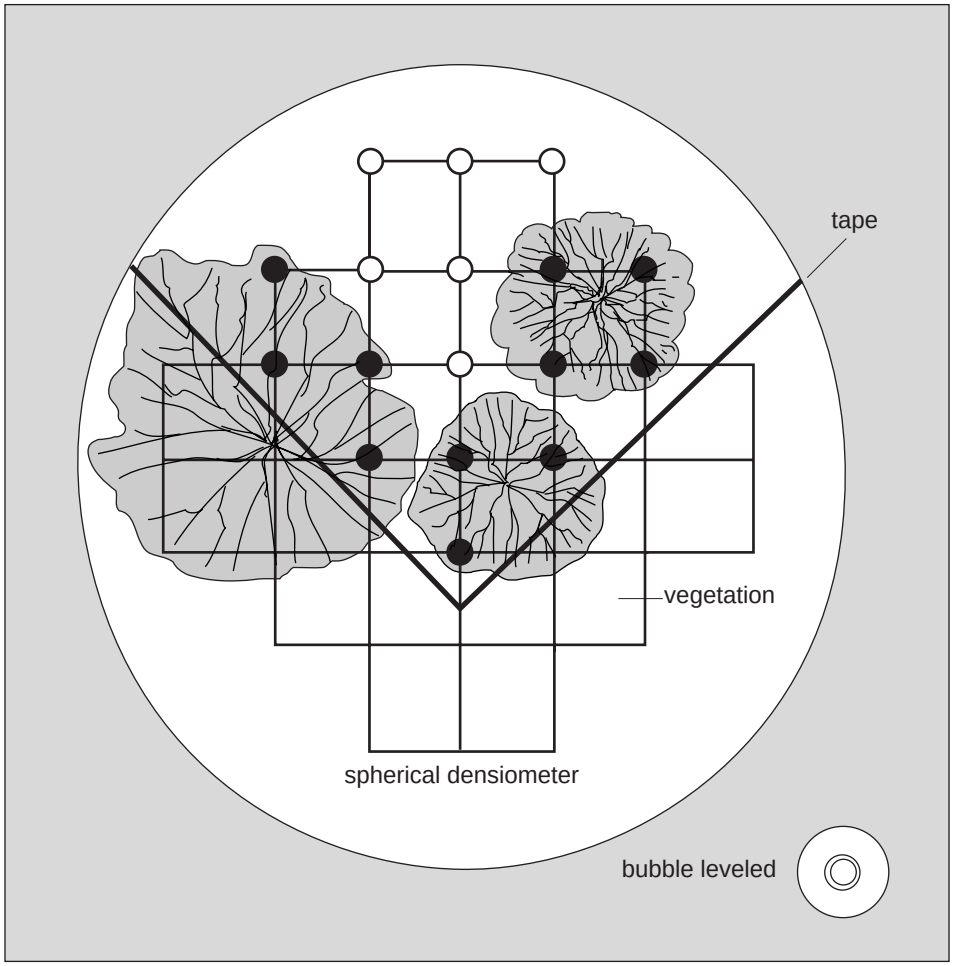

Figure 10. A concave spherical densiometer with bubble level, tape, and 17 points of observation. Line of intersections at both open and closed circles are examined. Closed circles represent line intersections counted in measurement of canopy closure (11 out of 17 points).

along each transect. To convert the readings to percentage of canopy closure for the reach, readings from all transects are summed, divided by 374 (34 x 11 possible points), and multiplied by 100. A solar pathfinder (Platts and others, 1987) also may be useful for more detailed measurements of seasonal or monthly solar radiation at a site.

The **dominant riparian land use** in the flood plain is determined by extending an imaginary transect line 30 m into the flood plain, perpendicular to the channel, and recording the major type of land use or land cover within a 30-m zone. More quantitative methods are highly suggested for characterizing the flood-plain vegetation, especially for sites that will be resampled over time. Detailed information on how to collect these types of data is presented in the following section.

Several characteristics are recorded for the left and right banks. The presence or absence of bank erosion (potential for sediment in the bank to fall into the stream) is recorded at each transect end. Other bank measurements consist of **angle**, **height**, dominant substrate, and **vegetative cover**. These four bank measurements are used to calculate a **bank stability index** modified from Simon and Hupp (1992) (table 4), which is a useful indicator of overall bank conditions and can be correlated to land use and habitat evaluation scores (Fitzpatrick and Giddings, 1997). The index is calculated by using scores for each category (table 4), which add to a maximum possible value of 22. In general, banks with scores of 4 to 7 tentatively can be considered stable, scores of 8 to 10 are at risk, scores of 11 to 15 are unstable, and scores of 16 to 22 are very unstable. It also is useful to calculate a bankfull channel width to depth (bank height) ratio that may be related to reach gradient, sediment type and load, degree of entrenchment, bank erodibility, and the distribution of energy in the channel (Rosgen, 1997).

Table 4. Explanation of the bank stability index

[>, greater than; >, less than]

Bank characteristic	Measurement	Score
Angle (degrees)	0–30	1
	31–60	2
	> 60	3
Vegetative cover (percent)	> 80	1
	50–80	2
	20–< 50	3
	< 20	4
Height (meters)	0–1	1
	1.1–2	2
	2.1–3	3
	3.1–4	4
	> 4	5
Substrate (category)	Bedrock, artificial	1
	Boulder, cobble	3
	Silt	5
	Sand	8
	Gravel/sand	10

For water depth, mean water-column velocity, dominant bed substrate, and embeddedness, data are collected at three points along the transects—the thalweg and two locations that are equally spaced along the transect from the thalweg to the channel margin. If the thalweg is at a channel margin, as may be the case on the outside bend of a meandering channel, then the two remaining points should be equally spaced between the thalweg and the opposite stream margin. At each point, record the distance from the left edge of water.

Water **depth** and **velocity** are measured at each point by using a wading rod and current meter for wadeable reaches and either a sounding line or hydroacoustic system for nonwadeable reaches. For wadeable reaches with high banks, a telescoping leveling rod works well for measuring bank height and elevations for gradient. **Dominant bed substrate** type also is determined at the three points by using the modified Wentworth scale. A field scale for substrate is provided in figure 11. Substrate **embeddedness** is determined by estimating the percentage (to the nearest 10 percent) of the surface area of gravel or larger substrate that is covered by sand or finer sediment. If the dominant substrate is sand or finer, record the embeddedness as 100 percent. The use of a graded ruler or calipers to measure the height of the embedding mark on the substrate as a percentage of the total height of the substrate can aid in accurately estimating the percentage of embeddedness. It also may be useful to record the presence or absence of silt at each point.

The presence of instream **habitat cover** is determined at five points (presence/absence within about a 1-m^2 area around the point) along the transect—at the three depth/velocity/substrate points, and at two additional points at both stream margins. Habitat cover consists of any mineral or organic matter that produces shelter for aquatic organisms to rest, hide, or feed. Habitat cover also includes natural features, such as large boulders, natural debris piles,

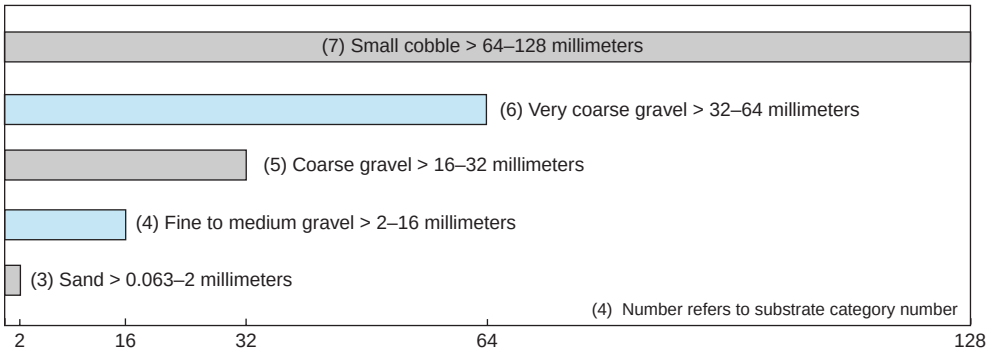

Figure 11. Field scale for identifying particle-size classes from sand to small cobble.

undercut banks, aquatic macrophyte beds, and overhanging vegetation, as well as structures such as discarded tires, appliances, and automobile parts. All habitat-cover categories present at each 1-m^2 point are recorded. The abundance of each type of habitat cover (in percent) is calculated from the 55 possible measurements for the 11 transects (5 points per transect).

For large, nonwadeable streams, transects are established as for wadeable streams. However, data cannot be collected along the transects in the same fashion as in wadeable streams. In nonwadeable streams, a paper-trace hydroacoustic system is attached to a boat, and the boat is moved along the transect. The depth finder produces a depth profile of the stream along the transect. From the paper printout of the depth finder, three measures of depth are made, corresponding to the three points along the transect as measured in wadeable streams. Samples of bottom substrate may be collected at each point with a sediment coring device, a Ponar sampler, or an Ekman dredge. However, collection of bottom substrate may be impossible on many large rivers. Habitat cover data are collected only at 22 points along the shoreline. For NAWQA national data-aggregation requirements, Study Unit personnel should attempt to collect depth, width, riparian canopy closure, canopy angle, and habitat cover at nonwadeable sites, if possible.

Bottom substrate, embeddedness, and velocity data are not required at nonwadeable sites. Individual Study Units may desire to collect additional information on bottom substrate, velocity, and habitat features in nonwadeable streams. Collection of habitat characteristics from large rivers should reflect the most important features that are thought to be affecting biota sampled at a site. A variety of equipment has been used in such streams, including side-scan sonar, acoustic doppler current profilers, and remotely operated underwater camera systems. Edsall and others (1997) provide information on the applicability and use of these kinds of equipment in large rivers. Aerial videography is a relatively inexpensive, easy-to-use alternative to other remote sensing techniques for measuring macrohabitat features in streams greater than 15-m wide (Jennings and others, 1994; Seibert and others, 1996).

Additional Optional Measurements

Depending on Study Unit goals, it may be useful to collect additional information on channel stability, riparian vegetation, and bottom- and bank-substrate characteristics, especially if there is the potential for changes in habitat caused by changes in land use, hydrology, or sediment input. If collected, these data can be stored in the habitat data dictionary files called "Chansect" for cross sections, "Veg" for riparian vegetation data, and "Substrat" for bottom- and bank-substrate quantification. In the original habitat protocol (Meador, Hupp, and others, 1993), channel cross sections and point-quarter riparian vegetation were elements required for national data aggregation. Elements of the channel cross-section survey, such as reach gradient, have been separated from the overall channel cross-section effort; only these selected elements are listed as required in the present document. Evaluation of point-quarter sampling techniques has suggested that the methods may not be applicable nationally. Thus, the point-quarter vegetation sampling was changed from a required to an optional measurement. While densiometer measures are not

intended to replace point-quarter sampling, they do provide a broadly applicable assessment of riparian vegetation characteristics.

Surveys of Channel Cross Sections

An understanding of how stream channels adjust and respond to natural and manmade environmental conditions requires baseline data on channel geometry. Surveys of channel cross sections provide the means for quantitative assessments of patterns in channel adjustments. Cross sections provide a graphic display of channel form that is referenced to known elevations. Through repeated measures of cross sections over time, these graphic displays can be compared to determine changes in the vertical and horizontal positions of the channel, changes in cross-sectional area (aggradation, degradation, or lateral migration), and movement of streambed or bank material (Olson-Rutz and Marlow, 1992). Evaluating cross-section data over time also provides the opportunity to assess channel incision and channel widening (Simon and Hupp, 1992; Dose and Roper, 1994; James, 1997), both typical responses to natural and manmade changes in stream channels. Cross-section data also provide the means to quantify fish habitat (Hogan and Church, 1989). Optimally, at least five cross sections are established in a reach. Thus, conducting cross-section measurements is encouraged at sites that are to be revisited over time.

Surveying techniques can provide accurate and precise measures of vertical and horizontal locations of given points along a reach. The procedures required to obtain vertical and horizontal locations vary somewhat depending on available equipment. For this reason, detailed procedures for all possible types of equipment are not covered in this document. Surveying references include Higgins (1965), Brinker and Wolf (1977), and Uren and Price (1984). Additional information on applying surveying techniques to measure stream channels is provided in Gordon and others (1992) and Harrelson and others (1994). USGS form 9-276 or a surveying field book with waterproof paper can be used to record surveying notes. An example of how data are recorded by using a standard surveyor's level and USGS level notes is shown in figure 12.

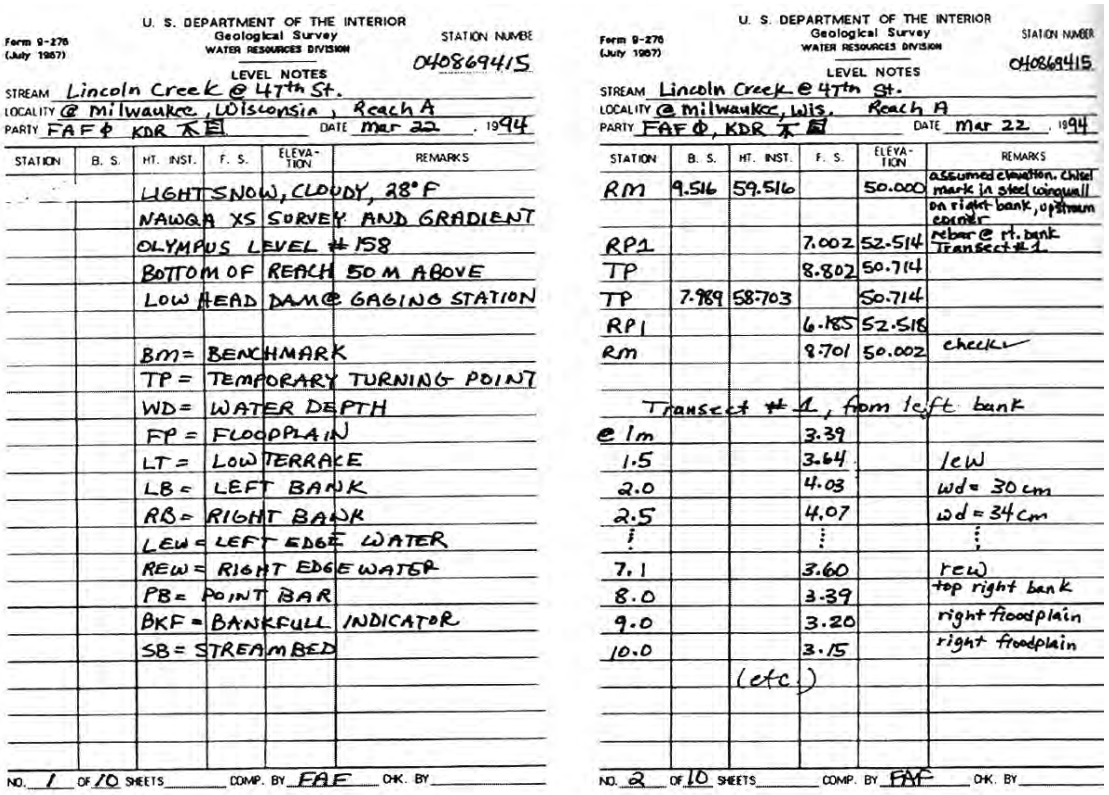

U. S. DEPARTMENT OF THE INTERIOR
Geological Survey
WATER RESOURCES DIVISION
Form 9-276 (July 1967)
STATION NUMBE 04086941S

LEVEL NOTES
STREAM Lincoln Creek @ 47th St.
LOCALITY @ Milwaukee, Wisconsin, Reach A
PARTY FAF & KDR DATE Mar 22, 1994

STATION	B. S.	HT. INST.	F. S.	ELEVATION	REMARKS
		LIGHT SNOW, CLOUDY, 28° F			
		NAWQA XS SURVEY AND GRADIENT			
		OLYMPUS LEVEL #158			
		BOTTOM OF REACH 50 M ABOVE			
		LOW HEAD DAM @ GAGING STATION			
		BM = BENCHMARK			
		TP = TEMPORARY TURNING POINT			
		WD = WATER DEPTH			
		FP = FLOODPLAIN			
		LT = LOW TERRACE			
		LB = LEFT BANK			
		RB = RIGHT BANK			
		LEW = LEFT EDGE WATER			
		REW = RIGHT EDGE WATER			
		PB = POINT BAR			
		BKF = BANKFULL INDICATOR			
		SB = STREAMBED			

NO. 1 OF 10 SHEETS COMP. BY FAF CHK. BY

U. S. DEPARTMENT OF THE INTERIOR
Geological Survey
WATER RESOURCES DIVISION
Form 9-276 (July 1967)
STATION NUMBER 04086941S

LEVEL NOTES
STREAM Lincoln Creek @ 47th St.
LOCALITY @ Milwaukee, Wis. Reach A
PARTY FAF, KDR DATE Mar 22, 1994

STATION	B. S.	HT. INST.	F. S.	ELEVATION	REMARKS
RM	9.516	59.516		50.000	assumed elevation. Chisel mark in steel wingwall on right bank, upstream corner
RP1			7.002	52.514	Nbar @ rt. bank Transect #1.
TP			8.802	50.714	
TP	7.989	58.703		50.714	
RP1			6.185	52.518	
RM			8.701	50.002	check
	Transect #1, from left bank				
@ 1m			3.39		
1.5			3.64		lew
2.0			4.03		wd = 30 cm
2.5			4.07		wd = 34 cm
⋮			⋮		⋮
7.1			3.60		rew
8.0			3.39		top right bank
9.0			3.20		right floodplain
10.0			3.15		right floodplain
		(etc.)			

NO. 2 OF 10 SHEETS COMP. BY FAF CHK. BY

Figure 12. Sample notes for channel cross-section survey and water-surface gradient.

To determine profiles of channel cross sections, five transects that best represent the geomorphic features of the reach should be selected. Two of the cross sections should be located at the reach boundaries, one at the upstream end and one at the downstream end. Endpoints of each cross section should be above bankfull height; it is preferable to have at least two or more points in the flood plain or on higher surfaces. Permanent markers and elevation benchmarks for one or both endpoints of the cross section should be established. Details for establishing elevation benchmarks and permanent markers are provided in Harrelson and others (1994). Benchmarks should be referenced to known elevation points. In some cases, known elevations can be the elevation benchmarks of a USGS gaging station, a bridge, a nearby highway, or a benchmark for recent urban development. It is very helpful to establish this information before going into the field. Local surveying firms may provide additional useful information.

To define the cross-section profile, the left endpoint is measured first, and bed elevations at each change in an important feature are measured, including the edge of water, the water surface, and the channel bed (fig. 13). The left side of the channel is determined when facing downstream. In general, the spacing of elevation measurements along the transect is determined by the shape of the channel; however, elevation measurements should be done at every point where the slope changes. If the surface is flat, elevations should be determined about every 0.5 m or at regular intervals equal to the channel width divided by 20 (Harrelson and others, 1994). Elevations at isolated features, such as boulders or logs, are avoided. As elevations are taken from left to right, the horizontal distance between endpoints and water-depth measurements also is recorded. The survey must be closed by taking a reading back to the elevation benchmark.

Riparian-Vegetation Characterization

Densiometer measurements provide quantitative information on overhead canopy closure above the channel and along channel margins; however, they do not provide information on the density, dominance, and species of woody vegetation in the riparian zone. Woody vegetation in the riparian zone may directly influence channel conditions, water chemistry, the amount of large woody debris, and aquatic communities in the reach (Lowrance and others, 1984; Gurtz and others, 1988; Sweeney, 1993; Large and Petts, 1994; Trimble, 1997) and, in turn, may be affected by flooding characteristics and the presence of

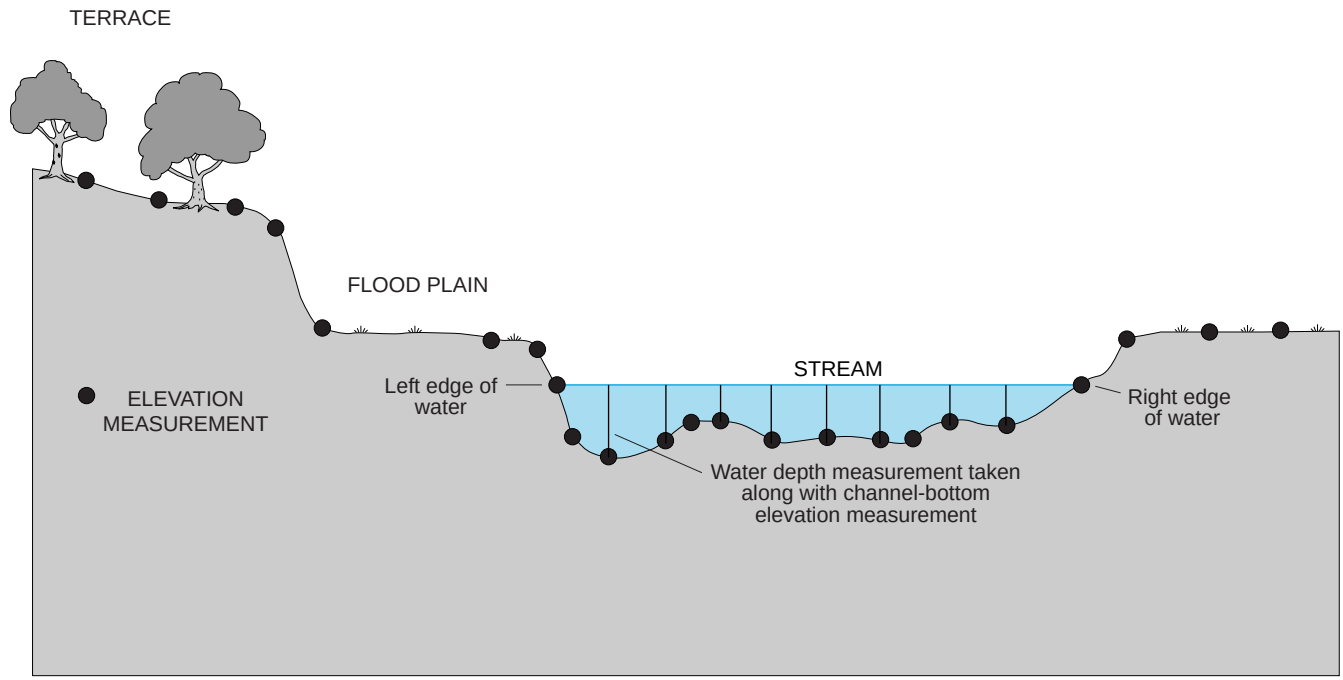

Figure 13. Example of measurement points for cross-section profiles.

fluvial landforms (Hupp and Osterkamp, 1985, 1996; Johnson and others, 1995). For example, high densities of vegetation at one site compared to low densities of vegetation at another could be explained by a predominance of mature cypress trees at one site compared to a predominance of young red maples at the other. Because red maples are more likely to populate an area after disturbance, knowledge of species and basal area information may be very important to aid interpretation of differences in conditions among sites (Simon and Hupp, 1992).

The point-centered quarter method (Mueller-Dombois and Ellenberg, 1974) provides quantitative estimates of stem density and basal area (biomass), and a permanent record of the woody species supported by the riparian zone. For the point-centered quarter method, sampling points usually are established at a point in the flood plain along a transect that is most representative of the dominant woody vegetation that has the most influence on channel conditions. This point is usually located in the flood plain but also may be along the bank in entrenched streams with little or no flood plain or along braided streams that have wide banks. A minimum of 10 points is measured along the reach, selecting among the most representative of the 22 possible points at the ends of the 11 transects. The same geomorphic surface (flood plain or bank) should be sampled for all points. At each point, four quarters are established, formed by the intersection of two perpendicular lines, one of which is the transect line (fig. 14). Trees and shrubs are included in the measurement if they are at least breast height (1.5 m). Trees are distinguished from shrubs in that trees are at least 2 m high and have a diameter at breast height (dbh) of at least 3 cm. The sampled trees or shrubs are identified to species, and the distance from the sampling point to the nearest tree or shrub in each quarter is measured, along with the dbh (fig. 14). Measurement of the same tree twice should be avoided, otherwise it may cause over-representation of certain

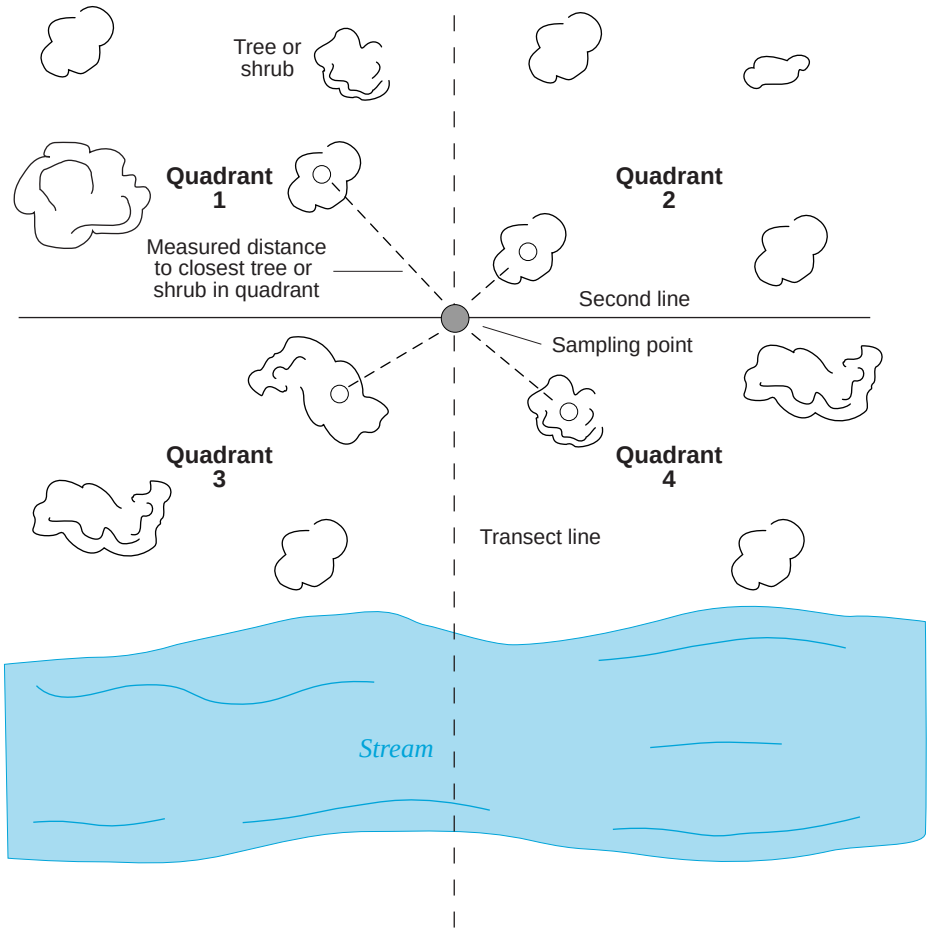

Figure 14. Point-centered quarter method used to evaluate density and dominance of bank woody vegetation.

species. Where bank woody vegetation is growing in narrow strips or rows, the two closest trees or shrubs on either side of the sampling point (a total of four trees or shrubs) are measured. In open sites with a potential for less than four trees or shrubs per point, the quarter-point method should not be used. Where a single tree or shrub has developed many separate trunks, an average dbh for three trunks is recorded, along with the total number of trunks. (The average dbh is multiplied by the number of trunks to calculate total basal area and biomass.) Measurements are recorded in a field notebook. Pertinent information to record includes transect number, left or right side of channel, geomorphic surface (flood plain, bank, bar), species, distance to species (in meters), dbh, and number of trunks. It also is important to record local conditions that prevent quarter-point measurements, such as a clearcut or pasture. To record the species, use a four-letter code based on the first two letters of the scientific name for the genus and the first two letters of the species (for example, "BENI" is recorded for *Betula nigra*).

Stem density of all woody species combined is calculated by dividing a unit area by the square of the mean point-to-tree distance. Unit area refers to the size of the area, in the same units as those for the mean area per tree, on the basis of which density is to be expressed. Typically, 100 m^2 is chosen as the unit area. Several steps are required to calculate stem density for all woody species:

1. Calculate a total for all point-to-tree distances per reach.
2. Calculate the mean point-to-tree distance per reach.
3. Calculate the square of the mean point-to-tree distance per reach. (This value gives the mean area per plant, representing the average area of ground surface on which one plant occurs.)
4. Divide the unit area (100 m^2) by mean point-to-tree distance per reach squared.

To determine the mean basal area for all woody species combined, calculate the basal area for each tree using the following formula:

$$\text{Area} = \frac{\pi(dbh)^2}{4} \qquad (1)$$

or Area = 0.7854 $(dbh)^2$. A mean basal area can then be determined for the entire reach.

Permanent vegetation plots are established to document trends in riparian vegetation over time. Plots are established where stability or change in the riparian vegetation is particularly important for water-quality analyses. For example, it may be useful to establish plots along urbanizing reaches, forested streams with the potential for logging, or reference sites. To construct a permanent vegetation plot, an area at the end of each surveyed cross section is selected. A 20- by 20-m plot is identified by using a tape measure for distance and a compass to establish 90-degree angles at the corners of the plot. The corners are marked with semipermanent boundary markers. The edge of the plot nearest the bank should be at least several meters from the bank. Sample the vegetation by determining the diameter and species of all trees and shrubs within the plot. Record only living trees and shrubs. If the riparian zone is narrow such that a 20- by 20-m plot cannot be established, then two or more smaller plots are established so that the total area sampled equals 400 m^2. Where herbaceous vegetation is clearly dominant, then a 10- by 10-m square plot is established. At herbaceous vegetation plots, the aerial coverage of up to five species is measured, and the percentage of these species within the plot is calculated. Vegetation plots are usually established at the ends of surveyed cross sections.

Substrate Characterization

Quantitative measurement of channel-substrate particle size can be made by means of Wolman pebble counts (Wolman, 1954) in wadeable reaches where substrates are coarse or by the collection of sediment for laboratory analysis where substrates are composed of sand or finer material. Both types of data provide a more quantitative measure of substrate characteristics than can be obtained through categorical observations. Quantitative data gathered from pebble counts are particularly useful for fish and invertebrate community analyses. A pebble count is done as follows:

1. Begin the count at each transect at bankfull elevation on the left bank and proceed to bankfull elevation on the right bank.
2. Proceed one step at a time, with each step constituting a sampling point.
3. At each step, reach down to the tip of your boot and, with your finger extended, pick up the first

pebble-size particle touched by the extended finger.

4. To reduce sampling bias, look across and not down at the channel bottom when taking steps or retrieving bed material.
5. As you retrieve each particle, measure the intermediate axis. If the intermediate axis cannot be determined easily, measure the long diameter and the short diameter of the particle, and determine the average of the two numbers. The transect may have to be traversed several times to measure 100 pebbles.

Thus, the size distribution of particles is determined and expressed in percentage by number of particles. A count of 100 particles is recommended; however, 50 or 25 particles can be measured.

To obtain a quantitative determination of fine-grained substrate, three samples of the bed material are collected along each transect and composited. In addition, samples of the bank-substrate material can be collected from one or both banks. These samples are returned to the laboratory for sieve analysis. Size fractions are determined by the Study Unit; however, at a minimum, analyses should be conducted for sand, silt, and clay fractions.

Description and List of Reach-Scale Habitat Characteristics

Detailed descriptions and lists are given below for collecting general reach information and transect data. Two example field forms for use at wadeable sites are shown in field forms 3 and 4 (see Field Forms at back of report). An example for recording reach gradient channel cross-section data on USGS level notes is shown in figure 12. Optional information on riparian vegetation (point-quarter and vegetation plots) and sediment characteristics (Wolman counts and sediment collection) should be recorded on waterproof paper in field note books.

General Reach Information

Detailed field methods for collecting general reach data are listed below. An example form is shown in field form 3. Items listed in **bold** are required for NAWQA national data aggregation. Abbreviations in parentheses are parameter codes for the NAWQA habitat data dictionary. These data are stored in files called "Reach" and "Gcu" in the habitat data dictionary.

1. **Study Unit (SUID)**—Use the 4-letter code designated for each Study Unit.
2. **Station identification number (C001 or STAID)**—List the USGS station identification number for the site.
3. **Date (DATE)**—Record the date as month, day, and year (4-digit year).
4. **Reach (REACHSEQ)**—Reach sequence letter, usually an "A." If more than one reach is characterized at the station, then assign sequential letters.
5. Station name (C900)—Record the USGS stream name.
6. Description of reference location (REFLOC)—Provide a general description of the reference location (for example, "gage on left bank just below Highway 1462 bridge" or "Highway 1462 bridge, upstream edge"). The reference location should be a permanent structure. If no permanent structure is present, a semipermanent marker (such as an iron pipe) should be installed at the location. The reference location provides the geographic link to habitat data collected at the segment and basin scale. Photos of the reference location should be taken. If the reference location is a bridge, a photograph of the reach from the bridge will be useful for documenting changes in the overall character of the reach over time.

7. **Investigators (INVEST)**—Names of the investigators are useful if followup information is necessary. The team leader's name is logged in the NAWQA habitat data dictionary.
8. **Quality of habitat sampling effort (RCHQUAL)**—This is used to denote the quality of the data.
9. **Comments on habitat sampling or conditions (REACHCOM)**—Note the general conditions of the reach. Be sure to note factors, such as recent flood history, beaver activity, and weather conditions.
10. Stage (STAGE)—Record water level as measured to a known point at the time of habitat sampling. Usually, at fixed sites, this information will come from the gaging station. If no gaging station is present and data may be collected at the site more than once, measure from a known point on a bridge or other permanent object. Be sure to note units of measure.
11. Stage method (STAGEMD)—The method used to measure stage, such as automatic data recorder (ADR), staff, or tape-down.
12. **Instantaneous discharge (DISCH)**—If no gaging station is present, measure discharge by using USGS techniques (Rantz and others, 1982). Use USGS form 9-275-F. Habitat data should be collected during stable low-flow conditions. This discharge measurement reflects base flow, which is an important habitat feature (Johnson and others, 1995) and is useful for comparing sites.
13. **Discharge method (DISCHMD)**—Record method used for discharge measurement: gaging station, wading rod, estimated (describe how), other.
14. **Channel modification at reach (CHMOD)**—Note any amount of channel modification at the reach. Choose from categories of concrete lined, stabilized, dredged, channelized but not stabilized, wing dams, lightly affected, or not modified. If only a small section is modified, use "lightly affected."
15. Mean channel width (MCW)—The wetted channel width is measured from the left edge of water to the right edge of water along the existing water surface. This channel-width measurement is used for estimating the needed reach length. Select the appropriate location that represents the average reach width. Make three measurements of wetted channel width and calculate the mean channel width. To provide consistency in measurement, protruding logs, boulders, stumps, or debris surrounded by water are included in the measurement of the water surface. Islands are not included in the measurement. Any solid accumulation of inorganic sediment particles protruding above the water and supporting woody vegetation is considered an island.
16. **Curvilinear reach length (REACHLEN)**—The curvilinear reach length is measured by following the path of the thalweg (the part of the stream with the deepest water and most flow). If there is no distinct thalweg (a possibility in a run), then follow the center of the channel. The reach length is computed by multiplying the mean channel width by 20. For wadeable streams, the minimum and maximum reach lengths are 150 and 300 m, respectively; for nonwadeable streams, the minimum and maximum reach lengths are 500 and 1,000 m, respectively.
17. Distance between transects (TRANDIS)—Eleven equidistant transects are spaced evenly within the reach. The distance between transects is the reach length divided by 10. The distance between transects is measured by following the thalweg of the channel. If no thalweg is observable, follow the center of the channel.
18. **Curvilinear distance from reference location to reach ends (USRCHEND and DSRCHEND)**—Measure the curvilinear distance (follow the thalweg) from the reference location to the upstream and downstream reach boundaries by using a range finder or tape measure. If either

boundary is upstream from the reference location, its value is negative; otherwise, it is positive. This information will be used to locate the reach in the future.

19. Location of boundary markers (USBMBK, DSBMBK)—Note the location of the boundary markers to aid in locating them in the future. Record whether the semipermanent boundary marker is on the left bank, the right bank, or both banks (looking downstream).

20. Boundary marker descriptions (USBMDESC, DSBMDESC)—Describe the type of boundary marker and measure the distance from the channel (top of bank or water's edge) (for example, "iron bar, painted orange, about 2 m from the wetted channel") and the distance and compass direction to other landmarks that may help in locating the boundary marker in the future. A record of this information is key to finding the location of the reach in the future.

21. **Reach water-surface gradient (RCHGRAD)**—Reach water-surface gradient is the difference between the water-surface elevation at the top and bottom of the reach divided by the curvilinear reach length. The water-surface gradient provides a good estimation of the energy gradient, which is an important parameter in the hydraulic power of the stream and, therefore, an important influence on a variety of other habitat measurements. This measurement is made with a surveyor's level for low-gradient streams, or can be estimated with a clinometer or Abney hand level for high-gradient streams (fig. 6). For a clinometer measurement, first mark a pole or use a stadia rod to get "eye height" of the person who is holding the clinometer. Flag this mark so that it can be viewed from a distance. Next, have each person stand at the water's edge, preferably at each transect or at observable breaks in the water surface. Look through the clinometer with one eye and view the staff or rod with the other, raising or lowering the clinometer until the cross hairs line up with the correct mark on the pole or rod. Record the slope in dimensionless units. If the clinometer measures percentage, divide the values by 100 to get dimensionless units. Make sure you know what scale you are using on the clinometer! The number of sightings also can be reduced by skipping transects and moving to the farthest transect that can still be sighted effectively; however, there can be a lot of variability in just a few measurements of water's edge, so be sure enough measurements are made. For double-checking, it could be advantageous to take measurements at the same distance along both right and left edges of water. Also, some reaches may be too flat to get an accurate estimation by using this technique. Note that the gradient of the channel bed may be very different from the water surface; thus, one cannot be substituted for the other. Also, the water-surface gradient at low flow will not always be the same as the water-surface gradient at bankfull flow. Depending on Study Unit goals, it may be useful to measure water-surface gradient, gradient of the channel bed thalweg (THGRAD), and gradient at bankfull (flood-plain gradient). Record data on USGS field notes or in a field book. Use the reach field form (field form 3) to record final calculations of reach water-surface gradient.

22. **Method used to measure reach gradient (RCHGRAMD)**—Record the method used, such as surveying level, clinometer, hand level, or other.

23. **Geomorphic channel units (GCUSEQ, GCUTYPE, GCULEN)**—While mapping the reach, draw (see diagrammatic mapping) and record all riffles, runs, or pools that are greater than 50 percent of the channel width, and measure and record the length of each. These data provide information on spatial dominance and diversity of habitat types. See previous discussion for information about identifying GCU's. Use additional space as needed.

24. Diagrammatic mapping (not in data dictionary)—Draw a schematic or representative map of the reach (see, for example, fig. 5). The mapping of all GCU's and habitat features can provide critical information needed to evaluate temporal trends in habitat. The map should include the

locations of GCU's, habitat features, and bank and flood-plain land use and land cover to approximate scale. Include the reference location, bridges, road names, reach boundaries, locations of semipermanent boundary markers, and transect locations relative to the geomorphic units. Draw the approximate aspect of the reach. Include a north arrow and the direction of streamflow. For reference, paste an example map or explanation to the clipboard used for drawing the maps.

Transect Information

An example transect form is shown in field form 4 (see Field Forms at back of report) for recording information for wadeable streams. One form is filled out for each transect. Items in **bold** are required for NAWQA national data aggregation. Other features listed are helpful to the Study Unit for documenting long-term changes and revisiting the site. These data are stored in files called "Transect," "Chfeat," "Habfeat," and "Tranpnt" in the habitat data dictionary.

1. **Station identification number (C001 or STAID)**—List the USGS station identification number for the site.
2. **Reach (REACHSEQ)**—Reach sequence letter, usually an "A." If more than one reach is characterized at the station, then assign sequential letters to additional reaches.
3. **Date (DATE)**—Record the beginning date of reach and transect sampling as month, day, and year (4-digit year).
4. **Transect number (TCTNO)**—The sequential number of each transect is recorded (usually 1 through 11) for each site.
5. Habitat type (HABTYPE)—Record whether the transect is located in a riffle, pool, or run. Sometimes it is useful to analyze features in each type of habitat, and this information will help in grouping transect information on the basis of habitat type. For example, it might be useful to distinguish between substrate type in riffles and substrate type in pools.
6. Photodocumentation (not in data dictionary)—Note whether or not photos were taken at the transect. Record the exposure number in the blank. Optimally, stream conditions at each transect, especially those at the reach boundaries, are photographed. Photographs are taken facing upstream, perpendicular to the channel, and downstream, from either the left or right banks, and they should include a scale reference. Color slide film is preferred. Use of the same type of film at all sites and at the same site over time increases comparability of repeat photographs and reduces variability related to film development. The inclination and aspect of the camera lens are important and can be measured with a compass. A level camera is preferred because inclination complicates the perspective of the view and makes accurate duplication of repeat photographs difficult. The aspect of the camera can be noted by pointing a compass at the central aiming point in the view and recording the compass reading. Camera lens size, camera type, exposure, film type, and other appropriate documentation information for taking 35-mm color photographs should be recorded. Semipermanent markers can be established at these locations to facilitate taking repeat photographs.
7. **Wetted channel width (CHWIDTH)**—Measure the wetted-channel width along the transect from the left edge of the water to the right edge of the water. Do not include bars, shelves, or islands in width.

8. **Bankfull channel width (BFWIDTH)**—Measure bankfull channel width along the transect from the top edge of the left bank to the top edge of the right bank. See previous discussion for useful indicators of banks and bankfull stage.

9. **Channel width method (CHWIDRM)**—Record the method used to measure wetted and bankfull channel width.

10. **Channel features (CHFEAT, CFWIDTH)**—If channel bars, shelves, or islands are present, measure width using a tape measure or rangefinder. Channel bars are the lowest prominent geomorphic feature higher than the channel bed (fig. 7). Channel bars are typically devoid of woody vegetation and consist of relatively coarse sand, gravel, and cobbles. Shelves are bank features extending nearly horizontally from the flood plain to the lower limit of persistent woody vegetation (Hupp and Osterkamp, 1985). Shelves are most common along relatively high-gradient streams. Islands are mid-channel bars that have permanent woody vegetation, are flooded once a year on average, and remain stable except during large flood events.

11. Aspect (CHANHEAD)—The aspect of the downstream flow is recorded in degrees (0 to 360) using a compass. At the midpoint of the transect, face downstream and point a compass parallel to streamflow.

12. **Canopy angles (LCANANG, RCANANG, CANANG)**—Open canopy angle or sun angle is formed by the angles from midpoint of the transect (midpoint of the channel width) to the visible horizon at either bank. It is a measure of the amount of sunlight potentially reaching the stream. From the midpoint of the transect, use a clinometer to determine the angle from the line of sight of the investigator to the tallest structure (for example, tree, shrub, building, or grass) on the left bank; this is called the left canopy angle (in the general area of the transect). The same procedure is done for the right bank (right canopy angle). The sum of these angles is computed and subtracted from 180 degrees. The result, the open canopy angle or sun angle (fig. 9), also can be converted to percentage of open canopy ((sun angle/180) x 100) or percentage of shade ((right canopy angle + left canopy angle/180) x 100). On narrow streams, note the measurement at eye height. A solar pathfinder (Platts and others, 1987) may be useful for more detailed measurements of seasonal or monthly solar radiation at a site.

13. **Riparian canopy closure (LBSHAD, RBSHAD, CANCLOSR)**—Riparian canopy closure is measured with a concave spherical densiometer by use of techniques outlined in Platts and others (1987). Measurement of canopy closure (the sky area that includes vegetation) is preferred over measurement of canopy density (the sky area that is blocked by vegetation), because measurements of canopy closure are less affected by seasonality than canopy density. The densiometer is modified by taping a right angle on the mirror surface (fig. 10). This modification uses only 17 of the possible 37 points and helps eliminate bias introduced by the overlap of vegetation reflected in the concave mirror when readings are taken at the same position. At transects with woody vegetation in wadeable streams, riparian canopy closure is measured with a spherical densiometer at two positions along the transect—at the water's edge and along both sides of the stream. At the water's edge, the densiometer is held on the transect line perpendicular to the bank 30 cm from and 30 cm above the shoreline. The number of line intersections surrounded by vegetation are counted for canopy closure (fig. 10). For consistency and repeatability of measurements, it is extremely important to maintain the same position for the densiometer. This position accounts for vegetation most directly over the banks and also incorporates any vegetation that overhangs the water (important for fish habitat (Platts and others, 1987)). A total of two readings (34 points) is made per transect. To convert the readings to percentage of canopy closure

for the reach, readings from each transect are summed, divided by 374 (34 x 11), and multiplied by 100. If no woody vegetation is present, a value of "0" is recorded.

14. **Dominant riparian land use/land cover (LBLULC, RBLULC)**—At each transect, the dominant riparian land use is recorded for each bank within an approximate 30-m distance (use a rangefinder or other method for approximating 30 m) from the top of the bank into the flood plain. Only one land-use category should be recorded for each bank for each transect, representing a visual band on either side of the transect. The percentage of each type of land use for the reach can be estimated by summing the number of occurrences of each land use, dividing by 22 (2 each at 11 transects) and multiplying by 100. The categories are modified from Simonson and others (1994a):

Agricultural:	
Cropland (annually harvested row crops, hay fields, or orchards)	CR
Pasture (regularly grazed by livestock, wooded, or open)	PA
Farmstead/barnyard (feedlots, confined livestock areas, farm buildings)	FM
Silviculture (tree plantation or logged woodland)	SI
Developed:	
Urban residential/commercial (houses, apartments, commercial buildings, parking lots)	UR
Urban industrial (industrial buildings and parking lots)	UI
Rural residential (low-density housing development in a rural setting)	RR
Right-of-way (paved or unpaved roads, railroads, paved paths, powerlines)	RW
Less disturbed:	
Grassland (grass/hedges not subject to regular mowing or grazing)	GR
Shrubs or woodland (woody plants)	SW
Wetland (covered by water much of the year; may be forested, shrubby, or open)	WE
Other (exposed rock, desert, and so on)	OT

If the 30-m riparian zone is a slumped bank or bluff, record the land use at the top of the bank or bluff. For national consistency, a riparian distance of 30 m was selected to encompass the majority of riparian conditions across a wide range of environmental settings. At the local or regional scale, however, effects of riparian width on water quality are varied and depend on the type of vegetation and geologic setting. The Study Unit may use additional methods to characterize riparian vegetation or human disturbance depending on Study Unit issues and environmental setting. Depending on Study Unit goals, more quantitative data on species dominance, frequency, and distribution can be collected through point-quarter techniques and vegetation plots (refer to discussion of point-quarter techniques for more details).

15. **Bank angle (LBANGLE, RBANGLE)**—A clinometer is used to measure the angle formed by the downward-sloping bank as it meets the stream bottom. The angle is determined directly from a clinometer placed on top of a surveyor's rod or meter stick that is aligned parallel to the bank along the transect. If the height and shape of the bank are such that more than one angle is produced, an average of three readings is recorded. If the bank is undercut, the bank angle may be more than 90 degrees. Both left bank and right bank (facing downstream) angles are recorded. A flat bank will have a reading close to 0 degrees.

16. **Bank height (LBHIGH, RBHIGH)**—Determine the left and right vertical distance from the channel bed (thalweg) to the top of the bank. If the distance can be measured directly, use a surveyor's rod and a hand level. If the bank height cannot be measured directly, estimate the height. Note that the bottom of the bank is the deepest part of the channel. At large, nonwadeable reaches, topographic maps may be useful in determining bank height. See previous section on identification of banks and bankfull stage for more information.

17. **Bank substrate (LBSUB, RBSUB)**—Record type of dominant bank substrate. In streams with flood plains, the texture of bank substrate may vary based on the depositional environment of the sediment and the current location of the channel. Also, a coating of sediment from the top of the bank may cover the entire bank during low flow, and the substrate may not be the same beneath the coating. Thus, determination of what best represents the overall bank material may be difficult and requires some consideration of sampling the material most available to the stream. Coring of flood-plain sediment may be useful depending on Study Unit goals. Choose from the following categories for substrate type:

Smooth bedrock/concrete/hardpan	1
Silt, clay, marl, muck, organic detritus	2
Sand (>0.063–2 mm)	3
Fine/medium gravel (>2–16 mm)	4
Coarse gravel (>16–32 mm)	5
Very coarse gravel (>32–64 mm)	6
Small cobble (>64–128 mm)	7
Large cobble (>128–256 mm)	8
Small boulder (>256–512 mm)	9
Large boulder, irregular bedrock, irregular hardpan, irregular artificial surface (>512 mm)	10

18. **Bank vegetative cover (LBVEG, RBVEG)**—Bank vegetation acts to resist erosion and contributes to bank stability (Platts and others, 1987). Bank vegetative cover is evaluated by visually estimating the percentage of the bank covered by vegetation to the nearest 10 percent. Roots usually are considered part of the vegetation cover. If the bank is completely covered with vegetation, it receives a value of 100 percent. If the bank is not vegetated, it receives a value of 0 percent.

19. **Bank erosion (LBEROS, RBEROS)**—Record the presence or absence of bank erosion at each end of the transect.

20. **Habitat cover features (WD, OV, UB, BO, AM, MS, TB, NO)**—Determine the presence/absence of all types of habitat cover that are found at five locations (within about a 1-m zone) along the transect at the three points where velocity, depth, substrate, and embeddedness measurements are made and also at the left and right water edges. Habitat cover consists of any mineral or organic matter that produces shelter for aquatic organisms (mainly fish) to rest, hide, or feed and includes natural features of a stream, such as large boulders, woody debris, undercut banks, and aquatic macrophyte beds, as well as artificial structures, such as discarded tires, appliances, and parts of automobiles. For fish cover, these features need to be at least 0.3 m long, 0.3 m wide, 0.3 m high, and in or just above (<0.1 m) water that is at least 0.3 m deep (Simonson and others, 1994a). For example, a woody debris accumulation in 5 cm of water is not considered to be a significant habitat cover for fish. However, small features in shallow water may be important for invertebrates; thus,

size limitations are given only as a guide and not as a rule. In turbid wadeable reaches and in nonwadeable reaches, only those habitat cover features that are easily determined are recorded. Note the presence/absence of the following habitat cover types:

Natural woody debris pile	WD
Overhanging vegetation (terrestrial)	OV
Undercut banks	UB
Boulders	BO
Aquatic macrophytes (emergent, submergent, and floating)	AM
Manmade structure	MS
Too turbid to determine	TB
None	NO

21. Transect point (TCTPNO, THALWEG)—The numbers of the three transect points are recorded and the thalweg is noted.

22. Distance from left edge of water (LEWDIST)—The distance from the transect point to the left edge (facing downstream) of water is recorded. This is useful for checking data.

23. Depth (DEPTH)—In wadeable reaches, water depth between the water surface and the bed substrate is measured with a wading rod and recorded. In nonwadeable reaches, a sounding line or hydroacoustic system may be necessary to determine depth. When using a hydroacoustic system, the investigator maneuvers the boat along the transect with the meter operating, so as to produce a continuous recording of water depth along the transect.

24. Velocity (VELOCITY)—In wadeable reaches, record the average water-column velocity using a Price AA current meter, pygmy meter, or Gurley meter. In nonwadeable reaches, use a velocity meter appropriate for velocity determinations at that site. Velocity is recorded at 60-percent depth where depth is less than 1 m. At depths greater than or equal to 1 m, two velocity measurements, one at 20-percent depth and the other at 80-percent depth, are taken and the average is recorded.

25. Dominant bed substrate (BEDSUB)—Determine dominant substrate at each transect point by using the same categories listed for bank substrate. In turbid wadeable reaches and in all nonwadeable reaches, a sample of the substrate can be obtained by using an appropriate device, such as a sediment corer, Ponar sampler, or Ekman dredge. In turbid wadeable reaches where sampling devices cannot yield a sample, the substrate type can be determined by touch. In nonwadeable reaches where sampling devices cannot yield a substrate sample, acoustic recording of the stream bottom along the transect can detect boulders and bedrock. An average and standard deviation from the 33 substrate measurements can be calculated and used in analyses. Edsall and others (1997) has more information on alternative methods for characterizing substrate in nonwadeable reaches. Alternative methods include side-scan sonar, RoxAnn, or remotely operated underwater camera systems. Bed substrate data at nonwadeable streams are not required for NAWQA national data aggregation.

26. Embeddedness (EMBED)—The attribute of embeddedness refers to the degree to which the larger substrate particles (boulder, cobble, or gravel) are surrounded or covered by fine-grained sediment (sand, or finer). As the percentage of embeddedness decreases, biotic productivity is thought to decrease (Platts and others, 1983). Embeddedness is estimated by determining the percentage of the surface area of the larger-sized particles (by visual estimation) covered by fine

sediment. Five relatively large (gravel to boulder size) substrate particles are examined at the three transect points. The percentage (to the nearest 10 percent) of each particle's height that was buried in sediment is noted by the extent of discoloration of the particle surface. The percentage of fine sediment covering the large substrate particles is determined from calculating the average percentage of coverage for the five particles. In turbid wadeable reaches and in nonwadeable reaches, a sample of the substrate may be obtained by use of a shovel, Ponar sampler, or Ekman dredge, but data from nonwadeable reaches are not required for NAWQA national data aggregation.

27. Silt present (SILT)—Record the presence or absence of significant areas of silt at each of the three points. A percentage for the presence of silt in a reach can be calculated by dividing the number of occurrences of silt by 33 (3 points in channel per 11 transects) and multiplying by 100.

Equipment List

Suggested equipment for reach characterization required for national NAWQA data aggregation is detailed in table 5. Much of the equipment can be purchased from mail-order environmental supply catalogs and sporting equipment stores.

DATA MANAGEMENT

Habitat data may be recorded initially on paper field forms (field forms 1–4 at back of report) and later entered into an electronic format. Eventually, for purposes of NAWQA national aggregation, these electronic data will need to be entered into a nationally consistent format.

Forms

Example forms for recording basin, segment, and reach data are provided for Study Unit use (field forms 1–4), but may be modified to meet local needs. The basin form is for organizing manually collected data for a single site from a variety of data sources. To avoid redundancy, information already compiled in NWIS or calculated from a GIS are not included on the form. Land-use/land-cover data can be extracted from data sets available from a NAWQA National Synthesis Team or from local coverages. Much of the remaining basin and segment data are derived directly from USGS 7.5-minute maps or GIS.

Elements of each form that are in boldface type are required for national aggregation. Basin and segment forms are filled out in the office, whereas reach and transect forms are intended for field use. The basin and segment forms contain space for noting the names of corresponding electronic files after the data have been entered. The name of a contact person for these electronic files also should be noted.

Habitat Data Dictionary

The habitat data dictionary was created to provide a uniform template for organizing data. Its overall structure is text-based, tab-delimited tables, but similar tables can be created in a spreadsheet and exported as text for national aggregation. Table templates with field/cell names and formats also are available on the world wide web and can be imported to a variety of spreadsheet and data-base software packages for manipulation and data entry. Data-dictionary documents describe the structure, relations, and contents of the various habitat tables and should be referenced during data entry. Descriptions of each table include field/cell names, units, domains, storage types, and priorities of table elements. Study Units can always add fields/cells to the ends of these tables for data that are not described in the protocol or data dictionary, but these fields/cells will not be included in the national data aggregation. The tables of the data dictionary, their interrelations, and their linking fields are diagrammed in figure 15. The table names, their contents, their

Table 5. Equipment and supplies for measuring reach and transect characteristics

[m, meter; in., inch; ft, foot]

Wadeable sites
Reach and transect forms
Flagging tape
Surveying flags
60-m engineering measuring tape (longer tape may be needed for wide rivers)
Meter sticks or metric leveling rod
Sledge hammer
Wooden stakes or lath
Concrete reinforcement steel bar, 0.5-in. diameter, steel post, or pipe at least 1.5 m long, depending on local frost conditions
Plastic caps for concrete reinforcement bar or pipe
Spray marking paint
Shovel
Hand level (if needed, for gradient or bank height measurements)
Surveyor's level and tripod or laser level survey station (for measuring gradient of low-gradient streams)
Leveling rod, metric or prism
Clinometer
Concave spherical densiometer
Clipboard
Camera and film
Wading rod, pygmy velocity meter, Price AA velocity meter, headset
USGS discharge-measurement forms
Pencils and permanent markers
USGS leveling notes or field book for recording gradient measurements
Rangefinder (may be useful for estimating long distances)
Sunscreen and insect repellent
Insulated shoulder-length gloves (for cold water)
Waders
Rain gear
Plastic ruler (if needed, for Wolman pebble counts)
Tree diameter tape (if needed, for point-quarter measurements or vegetation plots)
Additional equipment for nonwadeable sites[1]
Boat with motor
Depth finder with strip chart
Ponar clam-shell sampler
Surveyor's level and tripod or laser level survey station (for measuring gradient of low-gradient streams)
Global Positioning System

[1]At a bare minimum, equipment at nonwadeable sites should consist of a boat with motor, a depth finder with strip chart, and a surveyor's level and tripod or laser level survey station (total station). Additional state-of-the-art equipment for sampling habitat at nonwadeable sites will change and improve over time as new techniques are developed. For more background information on the equipment listed for nonwadeable sites consult Edsall and others (1997).

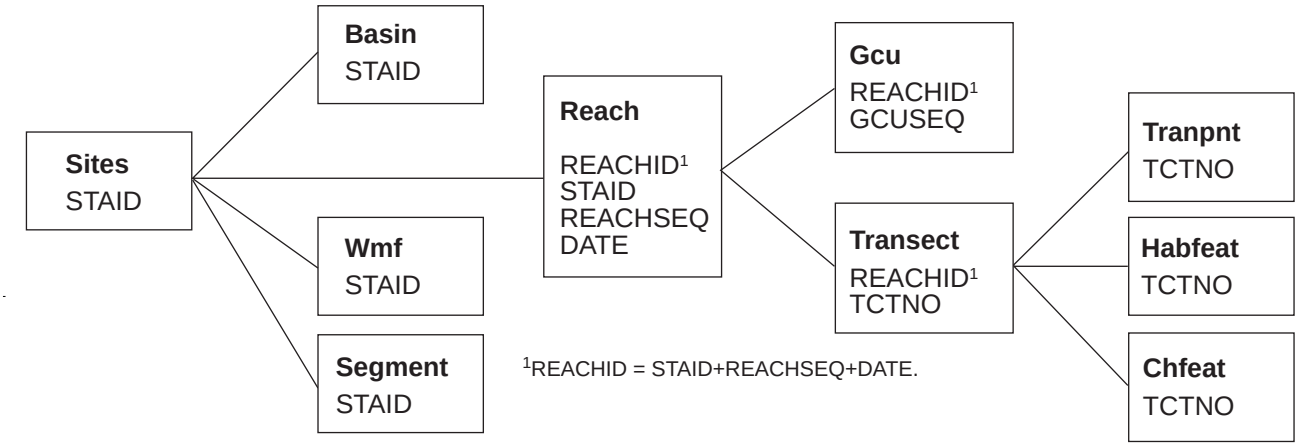

Figure 15. Tables in the habitat data dictionary.

relation to habitat protocol sections, and comments on their use are listed in table 6.

Priorities listed in the data dictionary describe the importance of each characteristic to the data structure itself and to users of the data. In the data dictionary, priority 1 items are required in order to link tables and to ensure uniqueness of records in tables; these items are known as “keys." Priority 2 items are needed for a uniform national synthesis data base. Boldface items in this protocol description are either priority 1 or priority 2. Priority 3 items are considered optional, but they may be very useful to individual Study Units.

DATA ANALYSIS

The overall goals of habitat analysis are to (1) determine whether there are relations among habitat variables that help in the understanding of stream conditions and (2) determine whether there are relations among habitat variables and dependent biological variables, such as fish, invertebrate, or algal composition and relative abundances. Analyses of habitat data can be separated into three general types—(1) exploratory analyses and site assessment using only habitat data, (2) gradient analyses using habitat data along with species data to determine relations of biological assemblages to physical

Table 6. Habitat data dictionary tables and their contents

[NWIS, National Water-Information System; GIS, geographic information system]

Table name	Contents	Related habitat protocol section	Comments
Sites	NWIS sitefile	Basin characterization	NWIS “sitefile”
Basin	Basin data	Basin characterization	Data available from NWIS and others
Wmf	Water management features data	Segment characterization—water-management features	None
Segment	Segment-level data	Segment characterization	None
Reach	Reach-level data	Reach characterization	None
Gcu	Geomorphic channel unit data	Reach characterization—geomorphic channel units	None
Transect	Transect-level data	Transect characterization	None
Chfeat	Bar-shelf-island data	Transect characterization	None
Tranpnt	Transect-point-level data	Transect characterization	None
Habfeat	Transect habitat feature data	Transect characterization	None

variables, and (3) analyses of variance among sites or groups of data. After the habitat data are entered into the computer by means of a software package, such as a spreadsheet or data base, the first task is to edit the data to correct any mistakes. Though this task may be tedious and may likely require data-point-by-data-point checking, it can save much time in the future by eliminating incorrect data analysis runs.

General data exploration is done by graphically plotting and(or) completing correlation analyses of habitat variables with respect to the response variables of interest. Computer spreadsheets provide a simple means for the plotting of two variables to enable visual assessment of their relation and to determine whether there are any outliers or errors in the data. Boxplots also are useful for showing visual summaries of medians and means, as well as the distribution of the data and outliers and skewness. Before any parametric statistical analysis is performed, the habitat variables (which commonly are measured on many different scales) need to be standardized and possibly transformed to near normality (Jongman and others, 1995). A common method is to standardize each variable to a mean of 0 and a variance of 1. This is done by subtracting the mean from each observation and then dividing by the standard deviation. If the data also are highly skewed, additional transformation may be needed; however, standardization is often all that is necessary. Log transformations are often used for hydrologic data, such as discharge or chemical concentrations, which tend to have right-skewed distributions.

Correlation analysis is useful to identify habitat characteristics that follow similar distributions among sites. Spearman rank correlations usually are done on habitat data because the Spearman technique is nonparametric (Iman and Conover, 1983; Johnson and Wichern, 1992). This analysis can show which variables are highly correlated with each other and which habitat variables are associated with biotic abundances or land use. For example, Spearman correlation analysis could be done on a data set containing nutrient and pesticide concentrations, percentage of irrigated and nonirrigated agricultural land use, median streambed substrate size, embeddedness, percentage of riffles, percentage of open canopy, bank stability index, and fish community data. Significant correlations usually are considered to be those that have *p*-values less than 0.05.

Principal component analysis (PCA) is often used to determine the primary factors that explain the greatest amount of variation among sites based on the habitat data alone. This process also can help to identify redundant variables that commonly are used to explain the same characteristic, function, or process. For example, there are often many variables that describe stream size, such as mean discharge, stream width, stream order, drainage area, and others that are highly correlated. Ideally, only one or two variables that best describe the variation among sites for stream size are retained. There may be other redundant characteristics for geomorphic channel units (percentage of riffles, velocity, gradient, substrate), bank characteristics (bank stability, bank height, bank erosion), and riparian characteristics (sun angle, percentage of shade, tree density, canopy cover). Thus, it should be possible to reduce significantly the number of variables while keeping a high percentage of explained variation. Results of the PCA can be interpreted according to the stream functions or processes that best explain variations among sites based on the physical habitat data.

Another objective of collecting quantitative habitat data is to relate the condition of the physical habitat among sites to the biota that are sampled at these sites. Two methods are commonly used to accomplish this—indirect and direct gradient analysis; several statistical computer software programs are available to perform these types of analysis. For indirect gradient analysis, ordination of the sites by using the relative abundances of biota can be related indirectly to the physical variables through correlation analyses. An example of this is a detrended correspondence analysis (DCA) (Hill, 1979) of relative abundances of fish followed by a Spearman rank correlation of selected habitat variables to the ordination scores for each axis. The DCA ordination reveals the patterns among sites based on the fish assemblages, and the Spearman rank correlation allows an indirect interpretation of the physical variables that are related to these patterns in fish assemblages (gradients) along each axis. A direct gradient analysis can be performed by canonical correspondence analysis (CCA). This technique allows a direct comparison of the biotic assemblages among sites and the environmental variables. The general "rule of thumb" is three times the number of sites as

environmental variables are needed. Through the forward selection process, the variables that best describe variations among sites are selected and are correlated to the species makeup at the sites. The final number of retained variables should be no more than one-third the number of sites.

Analysis of variance (ANOVA) techniques also can be used to compare two or more independent groups of data and identify statistically significant spatial or temporal differences among sites or samples. These tests determine if all groups have the same mean or median (depending on whether it is a parametric or nonparametric test), or whether at least one of the groups differs from the others. ANOVA techniques require parametric data (normally distributed with equal variances). Other nonparametric techniques include the Kruskal-Wallis test (Iman and Conover, 1983) and the Tukey standardized range test (Neter and others, 1985) on ranked data. The Wilcoxon sign-ranks procedure (Iman and Conover, 1983) is another nonparametric test that is similar to a t-test, except that the test is done on the signed ranks of the differences between paired data points. Like correlation analyses, *p*-values also should be reported for ANOVA tests.

DATA-APPLICATION EXAMPLES

The following two examples of how habitat data were used in NAWQA Study Units were chosen to help represent a range of conditions found in the NAWQA Study Units, such as those conditions characteristic of the northwestern United States (Willamette Basin) and the Midwest (Western Lake Michigan Drainages). These examples are provided as a starting point for the individual Study Units as they determine the best methods of data analysis for fulfilling Study Unit goals. For additional examples of how habitat data were used in NAWQA Study Units, see Maret and others (1997) and Maret (1997) for the Upper Snake River; Goldstein and others (1996) for the Red River of the North Basin; Baker and Frey (1997) for the White River Basin; and Tate and Heiny (1995) for the South Platte River Basin.

Willamette Basin

Using a combination of Spearman rank correlation analysis and PCA, the number of environmental variables (physical habitat and water chemistry) was reduced from more than 120 variables to 22 surrogate variables. Spearman rank correlation analysis was used to explore general relations between habitat variables and relations between habitat variables and relative abundance of fish (based on families). On the basis of results from the correlation analyses, the 120 environmental variables were reduced to 68 variables to start the PCA. Through iterations of PCA, many redundant variables were removed until 22 surrogate variables remained. Using the 22 variables for 24 stream sites, five factors were retained in the PCA at an eigenvalue greater than 1 (table 7). The first factor explained 38 percent of the variance among sites and was heavily loaded by variables related to land use (for example, percentage of agriculture in the basin, silt, embeddedness, maximum water temperature, total phosphorus and pesticide concentrations, percentage of forest, percentage of riffles, elevation, dominant substrate, and riparian score). The second and third factors accounted for 16 and 12 percent of the variance, respectively. These factors together describe the relations among autotrophic production, nutrients, water-quality characteristics, and percentage of open canopy above the channel. The fourth and fifth factors explain an additional 9 and 5 percent of the variance, respectively. These factors are dominated by environmental characteristics, such as bank score, percentage of open canopy, chlorophyll *a*, riparian score, percentage of agriculture in the basin, drainage area, dominant substrate, silt, and embeddedness. Overall, on the basis of the correlation of environmental data alone in the PCA, land use was the dominant factor describing the differences among stream sites.

A direct gradient analysis was done by using CCA and the 22 environmental variables. Through forward selection in CCA and many iterations, five surrogate variables were selected that best described the relation of fish assemblages among sites—percentage of riffles, maximum water temperature, percentage of forest in the basin,

Table 7. Results from principal components analysis of habitat data from the Willamette Basin, 1994

[Numbers in **bold** have the highest loadings in each component]

Environmental variable	Principal component				
	1	2	3	4	5
Silt	**0.830**	0.173	-0.077	-0.031	-0.292
Embeddedness	**.800**	-.006	.079	-.304	-.375
Total phosphorus	**.710**	.033	**.528**	-.069	.181
Percentage of agriculture in the basin	**.705**	-.249	-.043	.398	.082
Maximum water temperature	**.666**	**.496**	-.289	.161	.161
Pesticides	**.640**	-.370	**.465**	-.068	.228
Percentage of irrigated agriculture	**.614**	**-.521**	.207	-.028	.230
Total nitrogen	.490	**-.704**	-.230	.222	.019
Percentage of macrophytes	.460	.458	**.615**	.104	.111
Chlorophyll *a*	.457	.145	-.275	**-.592**	.155
Percentage of open canopy	.404	**.667**	-.167	**.459**	.150
Nitrite plus nitrate minus nitrogen	.371	**-.753**	-.309	.246	.075
Drainage area	.280	.451	**-.559**	-.266	**.481**
Maximum dissolved oxygen	.236	**.730**	.306	-.051	.021
Percentage of forest in the basin	**-.822**	.224	.055	-.299	-.126
Percentage of riffles in the reach	**-.772**	-.228	.185	-.022	.314
Elevation	**-.744**	.178	.166	.181	-.174
Dominant substrate	**-.742**	.136	-.243	.340	**.425**
Riparian score	**-.684**	-.263	.192	**-.425**	.054
Percentage of instream habitat	**-.616**	-.174	**.421**	-.123	.289
Minimum dissolved oxygen	-.492	-.033	**-.717**	.107	-.156
Percentage of bank score	-.421	.108	**.439**	**.651**	-.151
Eigenvalue	8.3	3.5	2.7	1.9	1.2
Percentage of variation explained	37.7	15.8	12.3	8.7	5.2

percentage of open canopy (canopy angle) above the channel, and minimum dissolved oxygen (fig. 16). Four clusters of sites are evident in the CCA and are displayed as forested (F), agricultural or urban (A), large river (L), and heavily impacted (H). These groups of individual sites can be related to the fish species that are dominant at the sites and related to the five environmental variables (arrows). For example, the three forested sites had high abundances of cutthroat and rainbow trout, coho salmon, and mottled and Paiute sculpin. These three sites also plot at high values for percentage of forest in the basin and riffles, and at low values for percentage of open canopy (small canopy angle) and maximum water temperature. On the other hand, the heavily impacted and large river sites had high abundances of introduced species (yellow bullhead, carp, smallmouth and largemouth bass, and warmouth) and plot at high values of percentage of open canopy (high canopy angle), maximum water temperature, and minimum dissolved oxygen concentrations. The agricultural sites had high abundances of native but tolerant species (reticulate sculpin, redside shiner, and largescale sucker) and plot at low values of percentage of riffles (high amounts of run GCU), minimum dissolved oxygen concentrations, and at relatively low values of water temperature and percentage of open canopy. Overall, habitat variables that were related to land use (basin scale), GCU, and riparian canopy (reach characteristics) were important

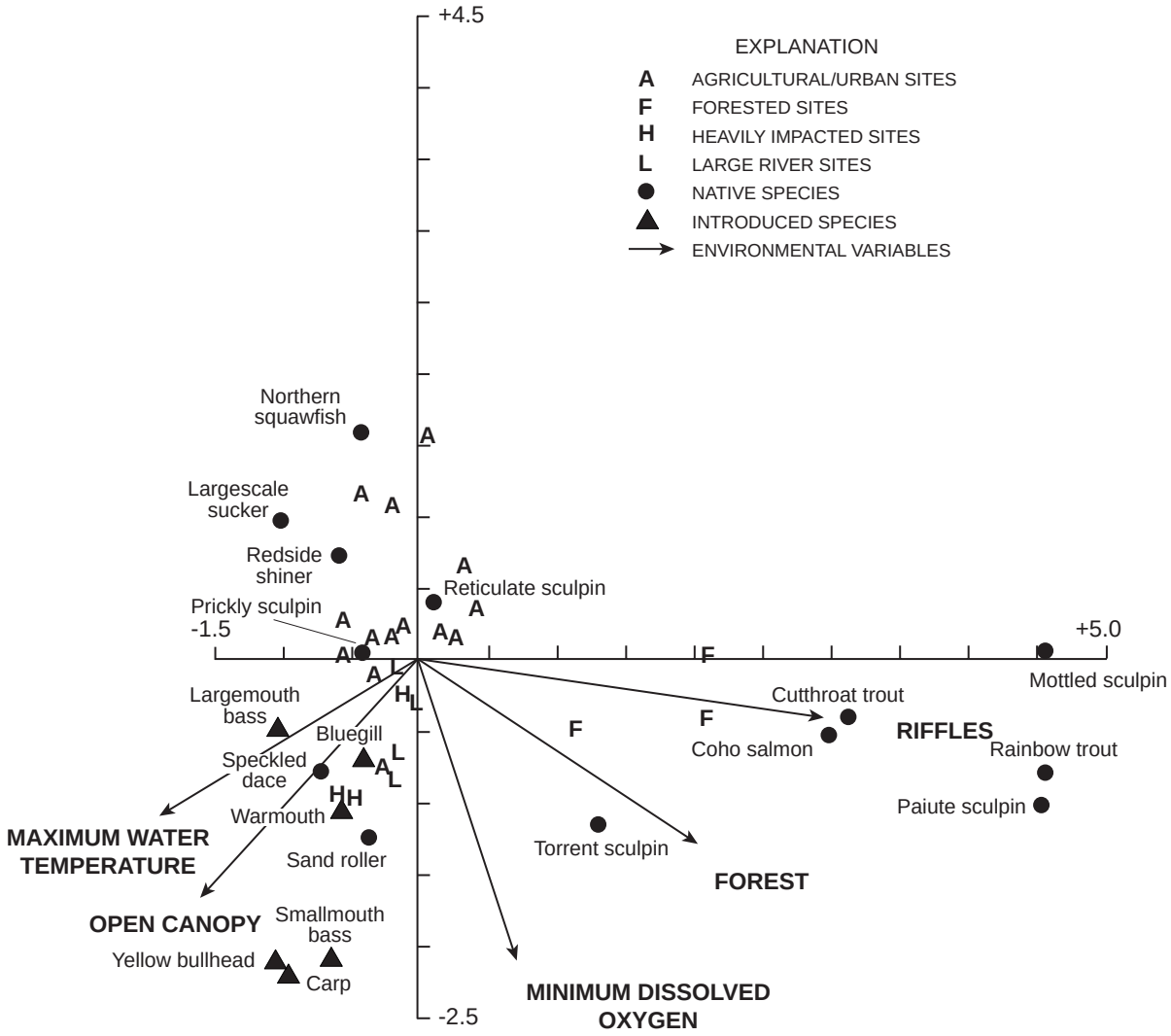

Figure 16. Results from canonical correspondence analysis of fish relative abundance and five environmental variables in the Willamette Basin, Oregon.

in describing the variations in fish abundances among sites in the Willamette Basin.

Western Lake Michigan Drainages

Analysis of habitat and aquatic community data from synoptic sites and basic fixed sites in the Western Lake Michigan Drainages (WMIC) NAWQA Study Unit has shown that habitat characteristics from all spatial scales are important in determining the natural and human factors that influence aquatic communities and overall stream quality. A summary of significant findings is given below.

Synoptic Study

As part of the ecological synoptic survey of the WMIC Study Unit, 20 "benchmark" stream sites in agricultural areas of eastern Wisconsin were surveyed for habitat, algae, invertebrates, and fish. These streams were designated benchmark streams because of their potential use as regional references for healthy streams in agricultural areas. The selected agricultural streams were from four physical settings that differ in bedrock type and texture of surficial deposits. Of the 20 sites, 19 are classified as trout (salmonid) streams.

The first step in analyzing the data involved summarizing the habitat data and identifying the most important environmental factors (Fitzpatrick and others, 1996). (Additional habitat data that were not included in the original NAWQA protocol but were

found to be useful included data from STATSGO [texture, erodibility factor, soil drainage, and permeability] and width of the wooded riparian zone at the segment and reach scale.) Next, the data were checked for normality. Various distributions were found—some normal, some log-normal, some neither. Thus, nonparametric statistical methods were employed. Spearman correlation analysis was used to identify habitat characteristics that followed similar distributions among sites. Habitat characteristics that were significantly correlated (Spearman's rho > 0.50 and *p*-values < 0.1) were plotted against each other by site identification number to identify site groupings. Next, PCA was done on a subset of characteristics (both raw and ranked data) to explain the overall variance seen in the combination of habitat characteristics. For exploratory purposes, the PCA was done on four subsets of habitat data: (1) 17 habitat characteristics from all scales and three nutrient constituents, (2) 16 basin and segment characteristics, (3) 13 reach characteristics, and (4) 8 water-quality constituents. Axis scores were plotted by physical setting to identify potential groupings of sites. A Kruskal-Wallis test, a nonparametric analysis of variance on rank-transformed data (Iman and Conover, 1983), and the Tukey studentized range test on ranks (Neter and others, 1985) were used to identify significant differences in habitat characteristics between the four physical settings. Finally, using the habitat data, streams were ranked according to Michigan's qualitative habitat classification system (Michigan Department of Natural Resources, 1991), which is designed to evaluate the effects of nonpoint sources of pollution.

Results from the PCA on all scales of habitat data indicate that the most important habitat characteristics for the benchmark sites are at the basin scale and include land use, soil characteristics, bedrock type, drainage area, and basin storage. Streams that have undergone habitat restoration for fish formed a distinct group on PCA ordination plots of the reach-scale components, indicating that the variability of possible habitat types is reduced when streams are modified by humans to meet the needs of specific aquatic species.

Michigan habitat classification scores (indicators of overall stream condition) indicated that 16 of the 20 sites were suitable reference streams for habitat. No significant differences in scores were found between streams that have undergone habitat restoration and those that have not. All four physical settings had the same range of scores.

Indirect gradient analysis was used to compare fish species and habitat data at the benchmark sites (Sullivan and Peterson, 1997). First, fish community data were ordinated using DCA. The DCA showed three site groupings, each one associated with one of three trout species. The DCA axis 1 and 2 scores correlated with average velocity and percentage of pool, as well as basin-scale characteristics of percentage of sandy surficial deposits, wetland, agriculture, and bedrock type.

In contrast, several community measures for invertebrate data at the benchmark streams such as Hilsenhoff's Biotic Index, did not correlate to bedrock geology, texture of surficial deposits, or amount of agricultural land use (Rheaume and others, 1996). A PCA analysis indicated that 18 of the 20 streams could be divided into three groups relative to stream size, available habitat, and water chemistry: (1) large, warmer streams with slight pollution, (2) deep, mixed-temperature streams with minimal pollution, and (3) small, cold, pristine, headwater streams. Two streams were identified as poor representations of benchmark conditions (overlapped with two of the four from habitat data analyses alone).

Basic Fixed Sites

Habitat characteristics also were measured at 11 WMIC basic fixed sites during 1993–95. Multiple-reach comparison surveys were done at 3 of the 11 sites. Each of the 11 sites had a unique combination of geology and land use; thus, habitat characteristics from these sites represented a range of conditions influenced by both natural and human factors (Fitzpatrick and Giddings, 1997). Results from Spearman correlation analysis indicate that, for basin-scale characteristics, significant correlations were found among land use, soil permeability and erodibility, drainage density, basin shape, stream gradient, flood characteristics, annual mean flow, and base flow. In addition, several basin-scale characteristics, such as land use, basin storage, and soil texture and erodibility, correlated with the NAWQA bank stability index. Soil erodibility correlated with dominant substrate type and embeddedness. Habitat evaluation scores correlated with riparian zone width and the bank stability index. These correlations indicate the importance of understanding how landscape-scale features in the

drainage basin ultimately affect local habitat conditions along a reach.

The availability of temporal and multiple-reach data prompted analyses of significant differences among years and reaches at three sites. In general, most of the significant temporal variability observed was attributed to variable streamflow conditions or problems in identifying bankfull stage. The WMIC sampling strategy required habitat sampling to be done during the spring with invertebrate and algal sampling, after snowmelt runoff but before summer storms. Optimally, this was during low-flow or base-flow conditions, but in some cases base flow was greater during sampling than during the summer months because of prolonged effects from snowmelt on base flow. Even though field conditions appeared similar from year to year, slight variations in streamflow were apparent in measurements that depend on water level, such as depth and velocity.

Comparison of data from the multiple-reach sites indicated whether or not the reach was representative of the segment characteristics. Statistically significant within-segment variability (at the 95-percent confidence level) was found for velocity, embeddedness, bank angle, bank height, and bank vegetative stability. Causes for these differences were thought to be that (1) the reaches were not representative of the segment for these characteristics, or (2) too few measurements were made. These results suggest that there is the potential for variability among multiple reaches for algae, invertebrate, and fish community data as well.

SUMMARY

The NAWQA Program is designed to assess the status of and trends in the Nation's water quality and to develop an understanding of the major factors that affect observed water-quality conditions and trends. Stream habitat is characterized as part of an integrated physical, chemical, and biological assessment of the Nation's water quality. The goal of the stream habitat characterization is to provide information on the physical characteristics that, together with chemical and biological characteristics, describe water-quality conditions. Spatial and temporal patterns in habitat characteristics are examined at local, regional, and national scales. The NAWQA stream habitat characterization is based on a spatially hierarchical framework that incorporates habitat data at basin, segment, reach, and microhabitat scales. This framework provides a basis for national consistency in collection techniques while allowing flexibility in habitat assessment within individual Study Units.

The spatially hierarchical framework of NAWQA habitat characterization requires several methods for data collection. Basin and segment characterization are done by using a GIS data base or data that are derived manually from USGS 7.5-minute topographic maps. Reach and microhabitat data are collected from measurements made in the field. A subset of reach characteristics is collected at synoptic sites, with some flexibility to address local questions and sample a large number of sites while maintaining consistent methods so that data from basic fixed sites and synoptic sites can be compared. Lastly, these revised methods reflect the experiences of a subset of NAWQA Study Units. Data-collection techniques will continue to evolve as experience grows and technology advances.

REFERENCES CITED

Anderson, J.R., Hardy, E.E., Roach, J.T., and Witmer, R.E., 1976, A land use and land cover classification system for use with remote sensor data: U.S. Geological Survey Professional Paper 964, 28 p.

Bailey, R.G., 1983, Delineation of ecosystem regions: Environmental Management, v. 7, p. 365–373.

Baker, N.T., and Frey, J.W., 1997, Fish community and habitat data at selected sites in the White River Basin, Indiana, 1993–95: U.S. Geological Survey Open-File Report 96–653A, 44 p.

Ball, Joseph, 1982, Stream classification guidelines for Wisconsin: Wisconsin Department of Natural Resources Technical Bulletin, 14 p.

Beschta, R.L., and Platts, W.S., 1986, Morphological features of small streams—Significance and function: Water Resources Bulletin, v. 22, p. 369–379.

Biggs, B.J.F., Duncan, M.J., Jowett, I.G., Quinn, J.M., Hickey, C.W., Davies-Colley, R.J., and Close, M.E., 1990, Ecological characterization, classification, and modeling of New Zealand rivers—An introduction and synthesis: New Zealand Journal of Marine and Freshwater Research, v. 24, p. 277–304.

Bisson, P.A., Nielsen, J.L., Palmason, R.A., and Grove, L.E., 1982, A system of naming habitat types in small streams, with examples of habitat utilization by salmonids during low streamflow, *in* Armantrout, N.B., ed., Acquisition and utilization of aquatic habitat inventory information: Western Division, American Fisheries Society, p. 62–73.

Bovee, K.D., 1982, A guide to stream habitat analysis using the Instream Flow Incremental Methodology: Fort Collins, Colo., U.S. Fish and Wildlife Service Instream Flow Information Paper 12, FWS/OBS–82/26, 258 p.

Brinker, R.C., and Wolf, P.R., 1977, Elementary surveying (6th ed.): New York, IEP–A Dun-Donnelley Publishers, 568 p.

Burns, D.A., Minshall, G.W., Cushing, C.E., Cummings, K.W., Brock, J.T., and Vannote, R.L., 1984, Tributaries as modifiers of the river continuum concept—Analysis by polar ordination and regression models: Archives of Hydrobiology, v. 99, p. 208–220.

Byl, T.D., and Carney, K.A., 1996, Instream investigations in the Beaver Creek watershed in West Tennessee: U.S. Geological Survey Water-Resources Investigations Report 96–4186, 34 p.

Craig, G.S., and Rankl, J.G., 1978, Analysis of runoff from small drainage basins in Wyoming: U.S. Geological Survey Water-Supply Paper 2056, 70 p.

Cuffney, T.F., Gurtz, M.E., and Meador, M.R., 1993, Methods for collecting benthic invertebrate samples as part of the National Water-Quality Assessment Program: U.S. Geological Survey Open-File Report 93–406, 66 p.

Dahl, T.E., and Johnson, C.E., 1991, Status and trends of wetlands in the conterminous United States, mid-1970's to mid-1980's: Washington, D.C., U.S. Fish and Wildlife Service, 28 p.

Dose, J.J., and Roper, B.B., 1994, Long-term changes in low-flow channel widths within the South Umpqua watershed, Oregon: Water Resources Bulletin, v. 30, no. 6, p. 993–1000.

Dunne, Thomas, and Leopold, L.B., 1978, Water in environmental planning: San Francisco, W.H. Freeman and Co., 818 p.

Eash, D.A., 1994, A geographic information system procedure to quantify drainage-basin characteristics: Water Resources Bulletin, v. 30, no. 1, p. 1–8.

Edsall, T.A., Behrendt, T.E., Cholwek, Gary, Frey, J.W., Kennedy, G.W., and Smith, S.B., 1997, Use of remote-sensing techniques to survey the physical habitat of large rivers: U.S. Geological Survey Great Lakes Science Center, Contribution 983, 20 p.

Emmett, W.W., 1975, The channels and waters of the upper Salmon River area, Idaho: U.S. Geological Survey Professional Paper 870–A, 116 p.

Farnsworth, R.K., Thompson, E.S., and Peck, E.L., 1982, Evaporation atlas for the contiguous 48 United States: Office of Hydrology, National Weather Service, National Atmospheric and Oceanic Administration Report NWS 33, 26 p., 4 pls.

Fenneman, N.M., 1946, Physical divisions of the United States: U.S. Geological Survey, scale 1:7,000,000.

Fitzpatrick, F.A., and Giddings, E.M.P., 1997, Stream habitat characteristics of fixed sites in the Western Lake Michigan Drainages, Michigan and Wisconsin, 1993–95: U.S. Geological Survey Water-Resources Investigations Report 95–4211–B, 58 p.

Fitzpatrick, F.A., Peterson, E.M., and Stewart, J.S., 1996, Habitat characteristics of benchmark streams in agricultural areas of eastern Wisconsin: U.S. Geological Survey Water-Resources Investigations Report 96–4038–B, 35 p.

Frayer, W.E., Monahan, T.J., Bowden, D.C., and Graybill, F.A., 1983, Status and trends of wetlands and deep-water habitats in the conterminous United States, 1950's to 1970's: Fort Collins, Colorado State University, 31 p.

Frissell, C.A., Liss, W.J., Warren, C.E., and Hurley, M.D., 1986, A hierarchical framework for stream habitat classification—Viewing streams in a watershed context: Environmental Management, v. 10, p. 199–214.

Gandolfi, C., and Bischetti, G.B., 1997, Influence of the drainage network identification on geomorphological properties and hydrological response: Hydrological Processes, v. 11, p. 353–375.

Gardiner, V., 1975, Drainage basin morphometry: Norwich, England, British Geomorphological Research Group, Technical Bulletin 14, 48 p.

Gebert, W.A., Graczyk, D.J., and Krug, W.R., 1987, Average annual runoff in the United States, 1951–80: U.S. Geological Survey Hydrologic Investigations Atlas HA–710, scale 1:2,000,000.

Gilliom, R.J., Alley, W.M., and Gurtz, M.E., 1995, Design of the National Water-Quality Assessment Program—Occurrence and distribution of water-quality conditions: U.S. Geological Survey Circular 1112, 33 p.

Godfrey, A.E., 1977, A physiographic approach to land use planning: Environmental Geology, v. 2, p. 43–50.

Goldstein, R.M., Stauffer, J.C., Larson, P.R., and Lorenz, D.L., 1996, Relation of physical and chemical characteristics of streams to fish communities in the Red River of the North Basin, Minnesota and North Dakota, 1993–95: U.S. Geological Survey Water-Resources Investigations Report 96–4227, 57 p.

Gordon, N.D., McMahon, T.A., and Finlayson, B.L., 1992, Stream hydrology, An introduction for ecologists: Chichester, U.K., John Wiley & Sons, Ltd., 526 p.

Gorman, O.T., and Karr, J.R., 1978, Habitat structure and stream fish communities: Ecology, v. 59, no. 3, p. 507–515.

Gregory, K.J., and Walling, D.E., 1973, Drainage basin form and process, a geomorphological approach: New York, John Wiley & Sons, Inc., 456 p.

Gurtz, M.E., 1994, Design of biological components of the National Water-Quality Assessment (NAWQA) Program, *in* Loeb, S.L., and Spacie, A., eds., Biological

monitoring of aquatic systems, chap. 15: Boca Raton, Fla., Lewis Publishers, p. 323–354.
Gurtz, M.E., Marzolf, R.G., Killingbeck, K.T., Smith, D.L., and McArthur, J.V., 1988, Hydrologic and riparian influences on the import and storage of coarse particulate organic matter in a prairie stream: Canadian Journal of Fisheries and Aquatic Sciences, v. 45, p. 655–665.
Hack, J.T., 1957, Studies of longitudinal stream profiles in Virginia and Maryland: U.S. Geological Survey Professional Paper 294–B, p. 45–97.
Hadley, R.F., and Schumm, S.A., 1961, Sediment sources and drainage basin characteristics in upper Cheyenne River Basin: U.S. Geological Survey Water-Supply Paper 1531–B, 198 p.
Hamilton, Karen, and Bergersen, E.P., 1984, Methods to estimate aquatic habitat variables: Denver, Colo., U.S. Bureau of Reclamation, Environmental Evaluation Project Report DPTS–35–9.
Harrelson, C.C., Rawlins, C.L., and Potyondy, J.P., 1994, Stream channel reference sites—An illustrated guide to field techniques: U.S. Department of Agriculture, Forest Service, Rocky Mountain Forest and Range Experiment Station, General Technical Report RM–245, 61 p.
Harvey, C.A., and Eash, D.A., 1996, Description, instructions, and verification for Basinsoft, a computer program to quantify drainage-basin characteristics: U.S. Geological Survey Water-Resources Investigations Report 95–4287, 25 p.
Hawkins, C.P., 1985, Substrate associations and longitudinal distributions in species of Ephemerellidae (Ephemeroptera: Insecta) from western Oregon: Freshwater Invertebrate Biology, v. 4, p. 181–188.
Higgins, A.L., 1965, Elementary surveying: London, Longmans, Green, and Co.
Hill, M.O., 1979, DECORANA—A Fortran program for detrended correspondence analysis and reciprocal averaging: Ithaca, N.Y., Cornell University.
Hirsch, R.M., Alley, W.M., and Wilber, W.G., 1988, Concepts for a National Water-Quality Assessment Program: U.S. Geological Survey Circular 1021, 42 p.
Hogan, D.L., and Church, Michael, 1989, Hydraulic geometry in small, coastal streams—Progress toward quantification of salmonid habitat: Canadian Journal of Fisheries and Aquatic Sciences, v. 46, no. 5, p. 844–852.
Horton, R.E., 1932, Drainage basin characteristics: Transactions of the American Geophysical Union, v. 13, p. 350–361.
———1945, Erosional development of streams and their drainage basins—Hydrophysical approach to quantitative morphology: Bulletin of the Geological Society of America, v. 56, p. 275–370.
Hughes, R.M., and Larsen, D.P., 1988, Ecoregions—An approach to surface water protection: Journal of Water Pollution Control Federation, v. 60, no. 4, p. 486–493.
Hupp, C.R., 1986, Upstream variation in bottomland vegetation patterns, northwestern Virginia: Bulletin of the Torrey Botanical Club, v. 113, p. 421–430.
Hupp, C.R., and Osterkamp, W.R., 1985, Bottomland vegetation distribution along Passage Creek, Virginia, in relation to fluvial landforms: Ecology, v. 66, p. 670–681.
———1996, Riparian vegetation and fluvial geomorphic processes: Geomorphology, v. 14, p. 277–295.
Hutchinson, N.E., 1975, WATSTORE user's guide, National Water Data Storage and Retrieval System: U.S. Geological Survey, v. 1, p. B–1—C–9.
Hynes, H.B.N., 1975, The stream and its valley: Verhandlungen Internationale Vereinigung für Theoretische und Angewandte Limnologie, v. 19, p. 1–15.
Iman, R.L., and Conover, W.J., 1983, A modern approach to statistics: New York, John Wiley & Sons, Inc., 497 p.
James, L.A., 1997, Channel incision on the lower American River, California, from streamflow gage records: Water Resources Research, v. 33, no. 3, p.485–490.
Jennings, M.E., Thomas, W.O., Jr., and Riggs, H.C., 1994, Nationwide summary of U.S. Geological Survey regional regression equations for estimating magnitude and frequency of floods for ungaged sites, 1993: U.S. Geological Survey Water-Resources Investigations Report 94–4002, 196 p.
Johnson, R.A., and Wichern, D.W., 1992, Applied multivariate statistical analysis (3d ed.): Englewood Cliffs, N.J., Prentice-Hall, p. 356–395.
Johnson, W.C., Dixon, M.D., Simons, Robert, Jenson, Susan, and Larson, Kevin, 1995, Mapping the response of riparian vegetation to possible flow reductions in the Snake River, Idaho: Geomorphology, v. 13, p. 159–173.
Jongman, R.H.G., ter Braak, C.J.F., and van Tongeren, O.F.R., 1995, Data analysis in community and landscape ecology: Cambridge, U.K., Cambridge Univ. Press, 299 p.
Kaufmann, P.R., and Robison, E.G., 1994, Physical habitat assessment, *in* Klemm, D.J., and Lazorchak, J.M., eds., Environmental monitoring and assessment program, 1994 pilot field operations manual for streams: U.S. Environmental Protection Agency EPA/620/R–94/004, p. 6–1—6–38.
King, P.B., and Beikman, H.M., 1974, Explanatory text to accompany the geologic map of the United States: U.S. Geological Survey Professional Paper 901, 40 p.
Klingeman, P.C., and MacArthur, R.C., 1990, Sediment transport and aquatic habitat in gravel-bed rivers, *in* Chang, H.H., and Hill, J.C., eds., Hydraulic engineering: New York, American Society of Civil Engineers, p. 1116–1121.

Knox, J.C., 1985, Responses of floods to Holocene climatic change in the upper Mississippi valley: Quaternary Research, v. 23, p. 287–300.

Küchler, A.W., 1970, Potential natural vegetation, *in* The national atlas of the United States of America: U.S. Geological Survey, p. 89–91.

Langbein, W.B., and Iseri, K.T., 1960, General introduction and hydrologic definitions—Manual of hydrology—Part 1. General surface-water techniques: U.S. Geological Survey Water-Supply Paper 1541–A, 29 p.

Lanka, R.P., Hubert, W.A., and Wesche, T.A., 1987, Relations of geomorphology to stream habitat and trout standing stock in small Rocky Mountain streams: Transactions of the American Fisheries Society, v. 116, no. 1, p. 21–28.

Large, A.R.G., and Petts, G.E., 1994, Rehabilitation of river margins, *in* Lalow, Peter, and Petts, G.E., eds., The rivers handbook—Hydrological and ecological principles, v. 2: Boston, Mass., Blackwell Scientific Pub., p. 401–418.

Leahy, P.P., Rosenshein, J.S., and Knopman, D.S., 1990, Implementation plan for the National Water-Quality Assessment Program: U.S. Geological Survey Open-File Report 90–174, 10 p.

Leopold, L.B., 1994, A view of the river: Cambridge, Mass., Harvard University Press, 298 p.

Leopold, L.B., and Miller, J.P., 1956, Ephemeral streams—Hydraulic factors and their relation to the drainage net: U.S. Geological Survey Professional Paper 282–A, 37 p.

Leopold, L.B., Wolman, M.G., and Miller, J.P., 1964, Fluvial processes in geomorphology: San Francisco, W.H. Freeman, 522 p.

Lotspeich, F.B., and Platts, W.S., 1982, An integrated land-aquatic classification system: North American Journal of Fisheries Management, v. 2, p. 138–149.

Lowrance, Richard, Todd R.L., Fail, Joseph, Jr., Hendrickson, Ole, Jr., Leonard, R.A., and Asmussen, L.E., 1984, Riparian forests as nutrient filters in agricultural watersheds: BioScience, v. 34, no. 6, p. 374–377.

Maret, T.R., 1997, Characteristics of fish assemblages and related environmental variables for streams of the Upper Snake River Basin, Idaho and Western Wyoming, 1993–95: U.S. Geological Survey Water-Resources Investigations Report 97–4087, 50 p.

Maret, T.R., Robinson, C.T., Minshall, G.W., 1997, Fish assemblages and environmental correlations in least-disturbed streams of the Upper Snake River Basin: Transactions of the American Fisheries Society v. 126, no. 2, p. 200–216.

McCain, M., Fuller, D., Decker, L., and Overton, K., 1990, Stream habitat classification and inventory procedures for northern California: U.S. Department of Agriculture, R–5's Fish Habitat Relationships Technical Bulletin 1, 15 p.

Meador, M.R., Cuffney, T.F., and Gurtz, M.E., 1993, Methods for sampling fish communities as part of the National Water-Quality Assessment Program: U.S. Geological Survey Open-File Report 93–104, 40 p.

Meador, M.R., Hupp, C.R., Cuffney, T.F., and Gurtz, M.E., 1993, Methods for characterizing stream habitat as part of the National Water-Quality Assessment Program: U.S. Geological Survey Open-File Report 93–408, 48 p.

Michigan Department of Natural Resources, 1991, Qualitative biological and habitat survey protocols for wadable streams and rivers: Great Lakes and Environmental Assessment Section Procedure 51, 40 p.

Montgomery, D.R., and Buffington, J.M., 1993, Channel classification, prediction of channel response, and assessment of channel condition: Timber, Fish, and Wildlife TFW–SH10–93–002 [variously paged].

Mueller-Dombois, Dieter, and Ellenberg, Heinz, 1974, Aims and methods of vegetation ecology: New York, John Wiley & Sons, Inc., 547 p.

Neter, J., Wasserman, W., and Kutner, M.H., 1985, Applied linear statistical models—Regression, analysis of variance, and experimental designs (2d ed.): Homewood, Ill., R.D. Irwin Publishers, 1,127 p.

Novak, C.E., 1985, WRD data reports preparation guide: U.S. Geological Survey Water Resources Division, p. 43–46.

Ohio Environmental Protection Agency, 1989, Biological criteria for the protection of aquatic life, v. III, Standardized biological field sampling and laboratory methods for assessing fish and invertebrate communities: Ohio Environmental Protection Agency, 58 p.

Olson-Rutz, K.M., and Marlow, C.B., 1992, Analysis and interpretation of stream channel cross-sectional data: North American Journal of Fisheries Management, v. 12, no. 1, p. 55–61.

Omernik, J.M., 1987, Ecoregions of the conterminous United States: Annals of the Association of American Geographers, v. 77, p. 118–125.

Orth, D.J., 1983, Aquatic habitat measurements, *in* Nielsen, L.A., and Johnson, D.L., eds., Fisheries techniques, Chapter 4: Bethesda, Md., American Fisheries Society, p. 61–84.

Osborne, L.L., Dickson, B., Ebbers, M., Ford, R., Lyons, J., Kline, D., Rankin, E., Ross, D., Sauer, R., Seelbach, P., Speas, C., Stefanavage, T., Waite, J., and Walker, S., 1991, Stream habitat assessment programs in states of the American Fisheries Society North Central Division: Fisheries, v. 16, p. 28–35.

Osborne, L.L., and Wiley, M.J., 1992, Influence of tributary spatial position on the structure of warmwater fish communities: Canadian Journal of Fisheries and Aquatic Sciences, v. 49, p. 671–681.

Plafkin, J.L., Barbour, M.T., Porter, K.D., Gross, S.K., and Hughes, R.M., 1989, Rapid bioassessment protocols for use in streams and rivers—Benthic macroinvertebrates and fish: U.S. Environmental Protection Agency EPA/444/4–89–001 [variously paged].

Platts, W.S., Armour, Carl, Booth, G.D., Bryant, Mason, Bufford, J.L., Cuplin, Paul, Jensen, Sherman, Lienkaemper, G.W., Minshall, G.W., Monsen, S.B., Nelson, R.L., Sedell, J.R., and Tuhy, J.S., 1987, Methods for evaluating riparian habitats with applications to management: Ogden, Utah, U.S. Forest Service, General Technical Report INT–221, 177 p.

Platts, W.S., Megahan, W.F., and Minshall, G.W., 1983, Methods for evaluating stream, riparian, and biotic conditions: Ogden, Utah, U.S. Forest Service, General Technical Report INT–138, 70 p.

Porter, S.G., Cuffney, T.F., Gurtz, M.E., and Meador, M.R., 1993, Methods for collecting algal samples as part of the National Water-Quality Assessment Program: U.S. Geological Survey Open-File Report 93–409, 39 p.

Quinn, J.M., and Hickey, C.W., 1990, Characterization and classification of benthic invertebrate communities in 88 New Zealand rivers in relation to environmental factors: New Zealand Journal of Marine and Freshwater Research, v. 24, p. 387–409.

Rantz and others, 1982, Measurement and computation of streamflow—v. 1 Measurement of stage and discharge: U.S. Geological Survey Water-Supply Paper 2175, p. 273–284.

Rheaume, S.J., Lenz, B.N., and Scudder, B.C., 1996, Benthic invertebrates of benchmark streams in agricultural areas of eastern Wisconsin—Western Lake Michigan Drainages: U.S. Geological Survey Water-Resources Investigations Report 96–4038–C, 39 p.

Ritter, D.F., 1978, Process geomorphology: Dubuque, Iowa, Wm. C. Brown, 603 p.

Roper, B.B., and Scarnecchia, D.L., 1995, Observer variability in classifying habitat types in stream surveys: North American Journal of Fisheries Management, v. 15, no. 1, p. 49–53.

Rosgen, D.L., 1994, A classification of natural rivers: Catena, v. 22, p. 169–199.

———1997, Applied river morphology: Pagosa Springs, Colo., Wildland Hydrology [variously paged].

Schumm, S.A., 1956, Evolution of drainage systems and slopes in badlands at Perth Amboy, New Jersey: Geological Society of America Bulletin, v. 67, p. 597–646.

———1960, The shape of alluvial channels in relation to sediment type: U.S. Geological Survey Professional Paper 352–B, 30 p.

———1963, Sinuosity of alluvial channels on the Great Plains: Geological Society of America Bulletin, v. 74, p. 1089–1100.

Schumm, S.A., and Lichty, R.W., 1965, Time, space, and causality in geomorphology: American Journal of Science, v. 263, p. 110–119.

Seaber, P.R., Kapino, F.P., and Knapp, G.L., 1984, State hydrologic unit maps: U.S. Geological Survey Open-File Report 84–708, 198 p.

Seibert, T.F., Sidle, J.G., and Savidge, J.A., 1996, Inexpensive aerial videography acquisition, analysis, and reproduction: Wetlands, v. 16, no. 2, p. 245–250.

Sheldon, A.L., 1968, Species diversity and longitudinal succession in stream fishes: Ecology, v. 49, p. 193–198.

Shreve, R.L., 1967, Infinite topologically random channel networks: Journal of Geology, v. 75, p. 178–186.

Simon, Andrew, and Hupp, C.R., 1992, Geomorphic and vegetative recovery processes along modified stream channels of west Tennessee: U.S. Geological Survey Open-File Report 91–502, 142 p.

Simonson, T.D., Lyons, John, and Kanehl, P.D., 1994a, Guidelines for evaluating fish habitat in Wisconsin streams: U.S. Department of Agriculture, North Central Forest Experiment Station, General Technical Report NC–164, 36 p.

———1994b, Quantifying fish habitat in streams—Transect spacing, sample size, and a proposed framework: North American Journal of Fisheries Management, v. 14, no. 3, p. 607–615.

Skinner, E.L., and Borman, R.G., 1973, Water resources of Wisconsin—Lake Michigan Basin: U.S. Geological Survey Hydrologic Investigations Atlas HA–432, 4 sheets.

Smith, K.G., 1950, Standards for grading texture of erosional topography: American Journal of Science, v. 248, p. 655–668.

Stauffer, J.C., and Goldstein, R.M., 1997, Comparison of three qualitative habitat indices and their applicability to prairie streams: North American Journal of Fisheries Management, v. 17, no. 2, p. 348–361.

Strahler, A.N., 1957, Quantitative analysis of watershed geomorphology: Transactions of the American Geophysical Union, v. 38, p. 913–920.

Strichler, G.S., 1959, Use of the densiometer to estimate density of forest canopy on permanent sample plots: U.S. Department of Agriculture, Forest Service, Research Note INT–180, 5 p.

Sullivan, D.J., and Peterson, E.M., 1997, Fish communities of benchmark streams in agricultural areas of eastern Wisconsin: U.S. Geological Survey Water-Resources Investigations Report 96–4038–D, 23 p.

Sweeney, B.W., 1993, Effects of streamside vegetation on macroinvertebrate communities of White Clay Creek in eastern North America: Proceedings of the Academy of Natural Sciences of Philadelphia, v. 144, p. 291–340.

Tate, C.M., and Heiny, J.S., 1995, The ordination of benthic invertebrate communities in the South Platte River Basin in relation to environmental factors: Freshwater Biology, v. 33, p. 439–454.

Teti, Patrick, 1984, Time-variant differences in chemistry among four smaller streams: Water Resources Research, v. 20, p. 347–359.

Tonn, W.M., 1990, Climate change and fish communities—A conceptual framework: Transactions of the American Fisheries Society, v. 119, p. 337–352.

Trimble, S.W., 1997, Stream channel erosion and change resulting from riparian forests: Geology, v. 25, no. 5, p. 467–469.

Uren, J., and Price, W.F., 1984, Calculations for engineering surveys: New York, Van Nostrand Reinhold, 309 p.

U.S. Department of Agriculture, 1972, Land resource regions and major land resource areas of the United States: U.S. Department of Agriculture Handbook 296, 156 p.

———1991, State soil geographic data base (STATSGO), data user's guide: U.S. Department of Agriculture, Soil Conservation Service Miscellaneous Publication 1492, 88 p., scale 1:250,000.

———1995, A guide to field identification of bankfull stage in the western United States: Rocky Mountain Forest and Range Experiment Station Stream Systems Technology Center, Forest Service videotape, approx. 30 minutes.

Wendland, W.M., Kunkel, K.E., Conner, G., Decker, W.L., Hillaker, H., Nabor-Knox, P., Nurnberger, F.V., Rogers, J., Scheeringa, K., and Zandlo, J., 1992, Mean 1961–1990 temperature and precipitation over the upper Midwest: Midwest Climate Center Research Report 92–01, 27 p.

Williams, G.P., 1978, Bank-full discharge of rivers: Water Resources Research, v. 14, no. 6, p. 1141–1154.

Wolman, M.G., 1954, A method for sampling coarse river-bed material: Transactions of the American Geophysical Union, v. 35, p. 951–956.

Wolman, M.G., and Gerson, R., 1978, Relative scales of time and effectiveness of climate in watershed geomorphology: Earth Surface Processes, v. 3, p. 189–208.

Wolman, M.G., and Leopold, L.B., 1957, River flood plains—Some observations on their formation: U.S. Geological Survey Professional Paper 282–C, p. 87–109.

Wolman, M.G., and Miller, J.P., 1960, Magnitude and frequency of forces in geomorphic processes: Journal of Geology, v. 68, p. 54–57.

Ying, T.C., 1971, Formation of riffles and pools: Water Resources Research, v. 7, p. 1567–1574.

FIELD FORMS

USGS Field Form 1. Basin Characterization

[Fill out one form for each site. Items in **bold** are required for NAWQA national data aggregation. Circle units of measure where appropriate. Abbreviations in parentheses refer to parameter codes in NWIS or the NAWQA data dictionary file]

1. Study Unit (SUID): __ __ __ __
2. Site type (SITYPE): BFS IFS SYN
3. **Station ID (C001 or STAID): _____**
4. HUC code (C020): _____
5. Station name (C900):_____

6. Reference location: longitude (C010): _____ latitude (C009): _____
   elevation (meters above NGVD) (C016): _____

7. State FIPS code (C007):_____
8. County FIPS code (C008): _____
9. State (STATE): _____
10. County (COUNTY):_____
11. Township (TWN): _____ 12. Range (RANGE): _____ 13. Section (SEC): _____

14. Quad topographic sheets covering basin (QUAD):

Quad name	Scale	Year

15. File name(s) and path where these data can be found:
_____

16. Contact person for site and basin data: _____

17. Total drainage area (C808): _____ square kilometers square miles
Contributing drainage area (C809): _____
18. Drainage area method (DRAREAMD): map year _____
Computation method list (circle one): manual vector raster
Source-map-scale list (circle one): 1:24k 1:48k 1:100k 1:250k
19. Average annual runoff (RUNOFF): _____ centimeters inches
20. Average annual runoff method (RUNOFFMD): GAGE WTGAGE REFERENCE OTHER _____
21. Length of record for average annual runoff: Beginning year (BYRUNOFF) _____
Ending year (EYRUNOFF) _____
22. Average annual air temperature (TEMP): _____ °C
23. Average annual air temperature method (TEMPMD): THIESSEN NEIGHBOR ISOHYET REFERENCE AVG KRIG OTHER _____
24. Length of record for average annual air temperature:
Beginning year (BYTEMP) _____
Ending year (EYTEMP) _____
25. Average annual precipitation (PRECIP): _____ centimeters
26. Average annual precipitation method (PRECIPMD): THIESSEN NEIGHBOR ISOHYET REFERENCE AVG KRIG OTHER _____
27. Length of record for average annual precipitation:
Beginning year (BYPRECIP) _____
Ending year (EYPRECIP) _____

28. Average annual Class A pan evaporation (EVAPAN): _____ centimeters inches
29. Average annual evaporation method (EVAPANMD): THIESSEN NEIGHBOR ISOHYET REFERENCE AVG KRIG OTHER _____
30. Length of record for average annual Class A pan evaporation:
    Beginning year (BYEVAPAN): _____ Ending year (EYEVAPAN): _____

31. Basin length (BLENG): _____ kilometers miles
32. Basin length method (BLENGMD): map year _____
    Computation-method list (circle one): manual vector raster
    Source-map-scale list (circle one): 1:24k 1:48k 1:100k 1:250k
33. Minimum elevation in the basin (MNELEV):_____ meters above NGVD (above datum > 0.0; below datum < 0.0)
34. Minimum elevation method (MNELEVMD): map year _____
    Computation-method list (circle one): manual vector raster
    Source-map-scale list (circle one): 1:24k 1:48k 1:100k 1:250k
35. Maximum elevation in the basin (MXELEV): _____meters above NGVD (above datum > 0.0; below datum < 0.0)
36. Maximum elevation method (MXELEVMD): map year _____
    Computation-method list (circle one): manual vector raster
    Source-map-scale list (circle one): 1:24k 1:48k 1:100k 1:250k
37. Basin relief ratio (RELRAT): _____
38. Drainage shape (DRNSHAPE): _____
39. Stream length (SLENG): _____ kilometers (> 0.0)
40. Stream length method (SLENGMD): map year _____
    Computation-method list (circle one): manual vector raster
    Source-map-scale list (circle one): 1:24k 1:48k 1:100k 1:250k
41. Cumulative perennial stream length (PSLENG): _____ kilometers (> 0.0)
42. Cumulative perennial stream length method (PSLENGMD): map year _____
    Computation-method list (circle one): manual vector raster
    Source-map-scale list (circle one): 1:24k 1:48k 1:100k 1:250k
43. Drainage density (DRNDENS): _____ $kilometers^{-1}$
44. Drainage texture (DRNTEX): _____ contours/kilometer (> 0.00)
45. Entire stream gradient (SLOPE): _____ meters/kilometer
46. Estimated flow characteristics:
    Beginning period of record (QBDATE): _____ Ending period of record (QEDATE): _____

Recurrence interval (in years)	Peak flow (m^3/s ft^3/s)		Flood volume (m^3 ft^3)		7-day low flow (m^3/s ft^3/s)	
1	_____	(QP1)				
2	_____	(QP2)	_____	(QV2)	_____	(Q7L2)
5	_____	(QP5)	_____	(QV5)	_____	(Q7L5)
10	_____	(QP10)	_____	(QV10)	_____	(Q7L10)
25	_____	(QP25)	_____	(QV25)	_____	(Q7L25)
50	_____	(QP50)	_____	(QV50)	_____	(Q7L50)
100	_____	(QP100)	_____	(QV100)	_____	(Q7L100)

47. Method(s) for estimating streamflow characteristics, such as from gaging-station data or list references if State or regional equations were used (FLOWMD):

_____

USGS Field Form 2. Segment Characterization

[Fill out one form for each site. Items in **bold** are required for NAWQA national data aggregation. Circle units of measure where appropriate. Abbreviations in parentheses refer to parameter codes in the NAWQA data dictionary]

1. Study Unit (SUID): __ __ __ __ **2. Station ID (C001 or STAID):** _____

3. Station name (C900): _____

4. EPA RF3 segment code (SEGCODE): _____

5. Location of segment boundaries (degrees, minutes, seconds):
Upstream end: latitude (USLAT) _____ longitude (USLONG) _____
Downstream end: latitude (DSLAT) _____ longitude (DSLONG) _____

6. Segment boundary location method (LOCMD): map year _____
Computation-method list (circle one): manual field GIS-vector GIS-raster
Source-map-scale list (circle one): 1:24k 1:48k 1:100k 1:250k

7. Segment length (SEGLENG): _____ kilometers meters miles feet

8. Segment length method (SEGLENMD): map year _____
Computation-method list (circle one): manual field GIS-vector GIS-raster
Source-map-scale list (circle one): 1:24k 1:48k 1:100k 1:250k

9. Curvilinear channel length and distance to reference locations (upstream is negative, downstream is positive):
Upstream end (USDIST): _____ kilometers meters miles feet
Downstream end (DSDIST): _____ kilometers meters miles feet
Total curvilinear channel length (SEGCUR): _____ kilometers meters miles feet

10. Curvilinear channel length method (SEGCURMD): map year _____
Computation-method list (circle one): manual field GIS-vector GIS-raster
Source-map-scale list (circle one): 1:24k 1:48k 1:100k 1:250k

11. Upstream and downstream elevation above NGVD:
Upstream end (USELEV): _____ meters feet
Downstream end (DSELEV): _____ meters feet

12. Elevation method (SELEVMD): map year _____
Computation-method list (circle one): manual field GIS-vector GIS-raster
Source-map-scale list (circle one): 1:24k 1:48k 1:100k 1:250k

13. Channel sinuosity (SINUOS): _____ (dimensionless)

14. Segment gradient (GRADIENT): _____ (dimensionless)

15. Water management features (in "Wmf" file):

Identification (WMFID)	**Type (WMFTYPE)**	**Description (WMFDES)**	Start date (WMFBDATE)	End date (WMFEDATE)	**Distance[1] (WMFDIST) (km mi)**

[1]Distance, in kilometers, from reference location—upstream is negative and downstream is positive.

16. Strahler stream order (ORDER): _____

17. Strahler stream-order method (ORDERMD): map year _____
Computation-method list (circle one): manual field GIS-vector GIS-raster
Source-map-scale list (circle one): 1:24k 1:48k 1:100k 1:250k

18. Link (Shreve stream order) (LINK): _____

19. Link method (LINKMD): map year _____
    Computation-method list (circle one): manual field GIS-vector GIS-raster
    Source-map-scale list (circle one): 1:24k 1:48k 1:100k 1:250k

20. Downstream link (DSTRLINK): _____
21. Downstream link method (DSLINKMD): map year _____
    Computation-method list (circle one): manual field GIS-vector GIS-raster
    Source-map-scale list (circle one): 1:24k 1:48k 1:100k 1:250k

22. Valley sideslope gradient (SIDEGRAD): Mean _____ (dimensionless)

Top elevation	Bottom elevation	Elevation difference	Distance	Gradient

23. Sideslope gradient method (SIDEGRMD): map year _____
    Computation-method list (circle one): manual field GIS-vector GIS-raster
    Source-map-scale list (circle one): 1:24k 1:48k 1:100k 1:250k

24. File name(s) and path where these data can be found: _____
    _____

25. Contact person for segment data: _____

26. Comments about segment data (SEGCOM): _____
    _____
    _____

USGS Field Form 3. Reach Characterization

[Fill out one form for each reach. Items in **bold** are required for NAWQA national data aggregation. Circle units of measure where appropriate. Abbreviations in parentheses refer to parameter codes in the NAWQA data dictionary]

1. **Study Unit (SUID):** _____ **2**. **Station ID (C001** or **STAID):** _____

3. **Date (DATE):** _____ - _____ - _____ (mm-dd-yyyy) **4**. **Reach (REACHSEQ): A B C D E**

5. Station name (C900): _____

6. Description of reference location (REFLOC): _____

7. **Investigators (INVEST): _____**

8. **Quality of habitat sampling effort (RCHQUAL): (circle one) excellent good fair poor**

9. **Comments on habitat sampling or conditions (REACHCOM):** _____

_____

_____

10. Stage (STAGE): _____ meters feet 11. Method (STAGEMD): ADR staff tape-down

12. **Instantaneous discharge (DISCH): _____ m^3/s ft^3/s**

13. **Method (DISCHMD): gage wading rod estimated _____ other _____**

14. **Channel modification at reach (CHMOD): concrete lined stabilized dredged channelized, not stabilized wing dams lightly affected not modified**

15. Mean channel width (MCW): 1 ____ 2 _____ 3 _____ mean _____ meters feet

16. **Curvilinear reach length (REACHLEN): _____ meters feet**

17. Distance between transects (TRANDIS): _____ meters feet

18. **Curvilinear distance from reference location to reach (upstream is negative, downstream is positive): Upstream end (USRCHEND) _____ meters feet**

Downstream end (DSRCHEND) _____ meters feet

19. Location of boundary markers (circle one for each):

Upstream boundary (USBMBK) left right both

Downstream boundary (DSBMBK) left right both

20. Boundary marker descriptions (USBMDESC, DSBMDESC): _____

_____

_____

21. **Water-surface gradient (RCHGRAD):** _____ thalweg gradient (THGRAD): _____

22. **Method for reach gradient (RCHGRAMD): surveying level clinometer hand level other**

23. **Geomorphic channel units (in "Gcu" file), length measured in (circle one): meters feet**

Sequence (GCUSEQ)	Type (circle one) (GCUTYPE)	Length (GCULEN)	Sequence (GCUSEQ)	Type (circle one) (GCUTYPE)	Length (GCULEN)
1	pool riffle run		11	pool riffle run	
2	pool riffle run		12	pool riffle run	
3	pool riffle run		13	pool riffle run	
4	pool riffle run		14	pool riffle run	
5	pool riffle run		15	pool riffle run	
6	pool riffle run		16	pool riffle run	
7	pool riffle run		17	pool riffle run	
8	pool riffle run		18	pool riffle run	
9	pool riffle run		19	pool riffle run	
10	pool riffle run		20	pool riffle run	

24. Diagrammatic map: Station ID _____ Reach A B C D E Date ___-___-___

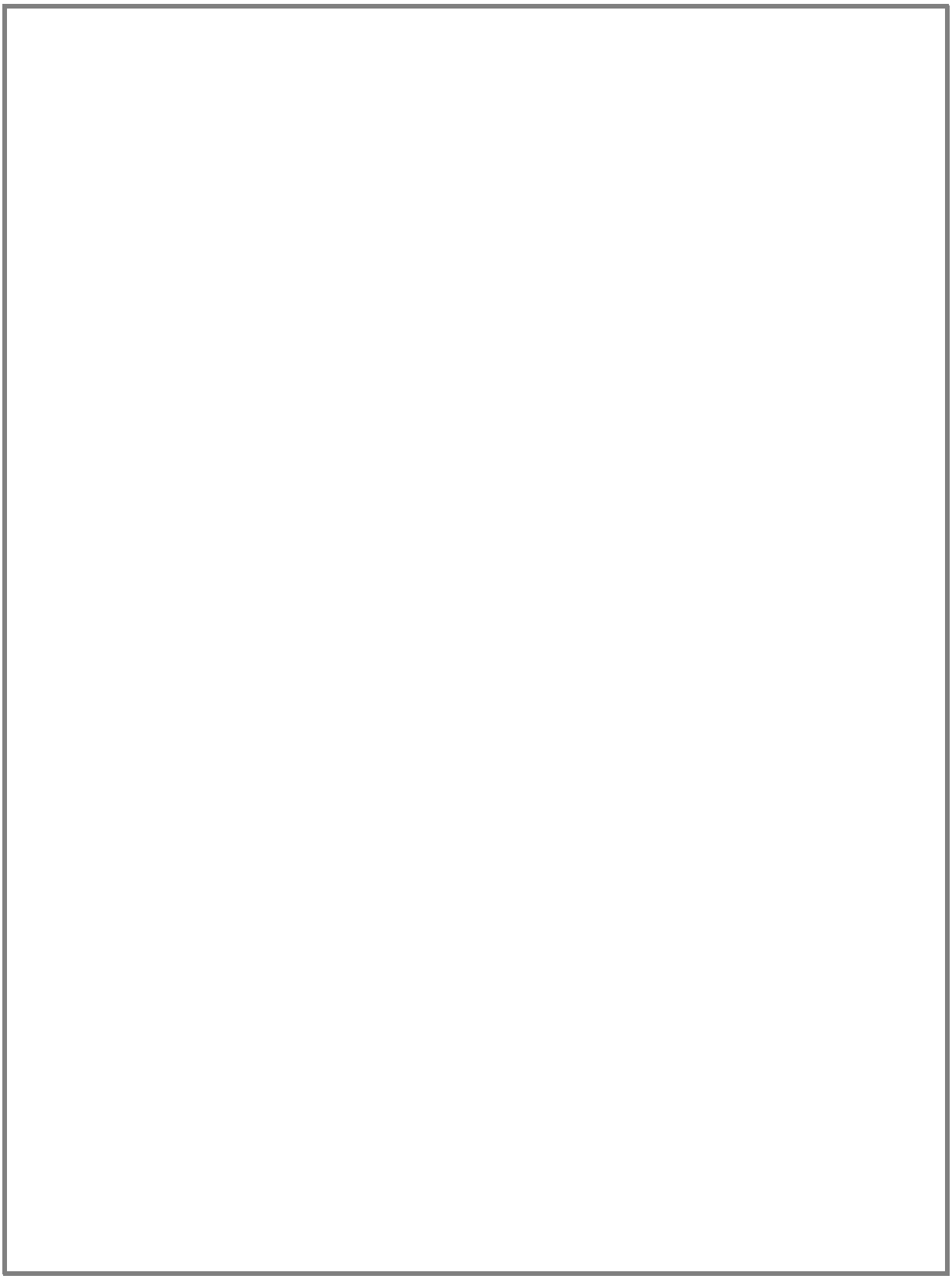

USGS Field Form 4. Transect Characterization

[Fill out one form for each transect (11 forms per reach). Items in **bold** are required for NAWQA national data aggregation. Circle units of measure where appropriate. Abbreviations in parentheses refer to parameter codes in the NAWQA data dictionary]

1. Station ID (C001 or STAID): _____ **2. Reach (REACHSEQ): A B C D E**
3. Date (DATE): ___ - ___ - _____ (mm-dd-yyyy) **4. Transect number (TCTNO): _____**
5. Habitat type (HABTYPE): riffle pool run
6. Photodocumentation of transect: looking upstream _____ looking downstream _____ other _____
7. Wetted channel width (CHWIDTH): _____ meters feet 8. Bankfull channel width (BFWIDTH): _____ meters feet
9. Channel width method (CHWIDRM): tape rangefinder from map estimated
10. Channel features (in "Chanfeat" file) (CHFEAT, CFWIDTH): (circle one and record width) meters feet
bar shelf island _____ bar shelf island _____
bar shelf island _____ bar shelf island _____
bar shelf island _____ bar shelf island _____
11. Aspect (CHANHEAD): _____ **12. Canopy angles: left (LCANANG) _____ right (RCANANG) _____**
open canopy angle (CANANG) _____ eye height _____
13. Riparian canopy closure (# of intersections): left (LBSHAD) _____ right (RBSHAD) _____ CANCLOSR _____

14-19. Bank characteristics:

Bank	14. Dominant riparian land use/ land cover <30 m (LBLULC, RBLULC)[1]	15. Bank angle (LBANGLE, RBANGLE)	16. Bank height (LBHIGH, RBHIGH) (m ft)	17. Bank substrate (LBSUB, RBSUB)[2]	18. Bank vegetative cover (LBVEG, RBVEG) (nearest 10%)	19. Bank erosion (LBEROS, RBEROS) (Y or N)
Left					%	
Right					%	

[1]Riparian land-use categories for column 14:

CR	Cropland	RR	Rural residential
PA	Pasture	RW	Right-of-way
FM	Farmstead/barnyard	GR	Grassland
SI	Silviculture	SW	Shrubs or woodland
UR	Urban residential / commercial	WE	Wetland
UI	Urban industrial	OT	Other

[2]Bank and bed substrate categories for columns 17 and 25:

1	Smooth bedrock/concrete/hardpan	6	Very coarse gravel (>32–64 mm)
2	Silt/clay/marl/muck/organic detritus	7	Small cobble (>64–128 mm)
3	Sand (> 0.063–2 mm)	8	Large cobble (>128–256 mm)
4	Fine/medium gravel (>2–16 mm)	9	Small boulder (>256–512 mm)
5	Coarse gravel (>16–32 mm)	10	Large boulder, irregular bedrock, irregular hardpan, irregular artificial surface (>512 mm)

20. Habitat cover (in "Habfeat" file): (circle all that apply)

[WD, natural woody debris pile; OV, overhanging vegetation; UB, undercut banks; BO, boulders; AM, emergent, submergent, and floating aquatic macrophytes; MS, manmade structure; TB, too turbid to determine; NO, none]

Left edge of water	**WD**	**OV**	**UB**	**BO**	**AM**	**MS**	**TB**	**NO**
Point 1	**WD**	**OV**	**UB**	**BO**	**AM**	**MS**	**TB**	**NO**
Point 2	**WD**	**OV**	**UB**	**BO**	**AM**	**MS**	**TB**	**NO**
Thalweg	**WD**	**OV**	**UB**	**BO**	**AM**	**MS**	**TB**	**NO**
Right edge of water	**WD**	**OV**	**UB**	**BO**	**AM**	**MS**	**TB**	**NO**

21-27. Transect point measurements (in "Tranpnt" file):

21. Point (TCTPNO)	Thalweg (Y or N)	22. Distance from LEW (LEWDIST) (m ft)	23. Depth (DEPTH) (m ft)	24. Velocity (VELOCITY) Type meter (circle one): AA pygmy other (rev/s m/s ft/s)		25. Bed substrate (BEDSUB)[2]	26. Embeddedness (EMBED) (nearest 10%)	27. Silt present? (SILT) (Y or N)
1							%	
2							%	
3							%	

Assessment of erosion, sedimentation, and water quality impacts of the Mountain Valley Pipeline and Equitrans Expansion Project's proposed crossing of the Jefferson National Forest as it pertains to the U.S. Forest Service's Draft Supplemental Environmental Impact Statement dated December 2022

Prepared by Jonathan A. Czuba, Ph.D., Licensed Professional Engineer - February 9, 2023

REFERENCES
11

February 21, 2023

8 Universal Soil Loss Equation and Revised Universal Soil Loss Equation

K.G. RENARD[1], D.C. YODER[2], D.T. LIGHTLE[3] AND S.M. DABNEY[4]

[1]*USDA-ARS, Southwest Watershed Research Center, Tucson, AZ, USA*
[2]*Biosystems Engineering and Soil Science, University of Tennessee, Knoxville, TN, USA*
[3]*USDA-NRCS, National Soil Survey Center, Lincoln, NE, USA*
[4]*USDA-ARS, National Sedimentation Laboratory, Oxford, MS, USA*

8.1 Introduction

8.1.1 History of the USLE (Universal Soil Loss Equation)

Conservation of soil and water requires both knowledge of the factors affecting these resources, and methods for controlling those factors to preserve those resources. Over the years, field, plot and small watershed studies have provided much valuable information regarding the complex factors and interactions involved in the environmental operations of land use and farming. These studies are the basis of the Universal Soil Loss Equation (USLE), which is a conservation planning tool that has been demonstrated to do a reasonably good job of estimating erosion for many disturbed-land uses. Predicting soil loss associated with modern land use is based on guidelines developed from research information in combination with additional experience from many sources. Information from empirical experiments and physically-based principles both assist in effective conservation planning.

The process of pulling together research results and experiences from agricultural practices began with Hugh Hammond Bennett (Helms, 2008), who was undoubtedly the most influential soil conservationist in the US. His early efforts led to his recognition as the 'father of soil conservation'. Bennett's early preaching against the menace of soil erosion led to Congressional action in 1929 establishing ten experimental stations, primarily in the cultivated agricultural areas of the US (Meyer & Moldenhauer, 1985; Renard, 1985). Later expansion of the research programmes included a large number of plots, crops, and management conditions that ultimately resulted in over 10,000 plot-years of data, collected over seven decades. Most of the plots involved the familiar dimensions 6.0 ft (1.8 m) wide by 72.6 ft (22.1 m) long, or a plot 35 ft (10.7 m) long used for some rainfall simulator studies. These plots simplified the computing of runoff and erosion on a per unit area basis (0.01 acre for the 6 × 72.6 ft or nominally 40 m^2 for the 1.8 × 22.1 m). Typical plot configurations were described in Brakensiek *et al.* (1979) and Laflen and Moldenhauer (2003).

In 1954, the National Runoff and Soil Loss Data Center was established by the US Department of Agriculture – Agricultural Research Service (USDA-ARS) at Purdue University in West Lafayette, Indiana. The Center was established to provide a central location for compiling and analysing soil erosion data collected from studies throughout the US. The Center, under the direction of W.H. Wischmeier, was responsible

Handbook of Erosion Modelling, 1st edition. Edited by R.P.C. Morgan and M.A. Nearing.

for summarizing and analysing the more than 10,000 plot-years of soil erosion and runoff data mentioned above, which resulted in the USLE (Wischmeier & Smith, 1965, 1978).

It has now been more than 50 years since the first releases of erosion prediction technology based on what have become widely known as the factors affecting sheet and rill erosion and, ultimately combining those in the USLE. Table 1 in Laflen and Moldenhauer (2003) gives an excellent synopsis of the published chronology of soil erosion prediction technology in the US.

The USLE and its predecessors were meant as field-level conservation planning rather than research tools, and were therefore structured to be 'user friendly' for USDA programmes in the Soil Conservation Service (SCS) (now the Natural Resources Conservation Service (NRCS)), and designed for tailoring erosion-control practices to the needs of specific fields and farms. The USLE was a 'paper-based' model where factors were found in printed tables and charts, and calculations were done by hand.

> "Had digital computers been available in the 1940s when erosion became recognized as a national problem, current prediction methods might more closely mimic the theory contained in Ellison's classic paper (1947) than the current empiricisms of the USLE." (Renard, 1985: 5)

What follows is a description of the evolution of the USLE–RUSLE effort, beginning with the improvements over the USLE leading to the RUSLE1 computer program and publication of the USDA Agriculture Handbook No. 703 (Renard *et al.*, 1997). We will then describe the development of RUSLE2, leading to its release in 2004 and its continuing documentation. The final section of this chapter will examine continuing and possible future developments of the technology.

8.1.2 USLE/RUSLE factor values

The fundamental concept in establishing factor values in the USLE was the Unit Plot. This conceptual plot was composed of a land parcel 72.6 feet (22.1 m) in length with a 9% slope, maintained in a continuous, regularly tilled fallow condition with up-and-down hill tillage, thereby representing a condition very near the worst-case management. Such a plot was used as a base condition to which all other topographic, cropping, management and conservation practices were compared. Data from plots with different slopes, lengths and crops were adjusted to the unit plot, and compared across locations to establish reliable factor values. Benchmark soil erodibility and other terms (rainfall, slope length, slope steepness, cover-management and the support practice factors) used in the USLE/RUSLE have evolved over the years from data derived for varied conditions. Few if any unit plots were ever actually developed, but the concept was used to determine how the conditions of actual plots related to the unit plot.

The USLE soil loss equation is:

$$A = R\,K\,L\,S\,C\,P \qquad (8.1)$$

where A is the computed soil loss per unit area, expressed in the units selected for K and for the period selected for R (in common practice these are usually selected such that they compute A, soil loss in US tons per acre per year); R, the rainfall and runoff factor, is the number of rainfall erosion index units, plus a factor for runoff from snowmelt or applied water where such runoff is significant; K, the soil erodibility factor, is the soil loss rate per rainfall erosion index unit for the specified soil under Unit Plot conditions; L and S are the slope length and steepness factors in relation to the conditions on a unit plot; C, the cover and management factor, is the ratio of soil loss from an area with specified cover and management to that from an identical area under the tilled continuous fallow Unit Plot conditions (C thus ranges from a value of zero for completely non-erodible conditions, to a value of 1.0 for the worst-case Unit Plot conditions); and P, the support practice factor, is the ratio of soil loss with a support practice like contouring, stripcropping, or terracing to that with straight-row farming up and down slope.

Because the USLE was based on empirical erosion data collected from relatively small plots or subwatersheds on relatively uniform hillslopes, the resulting erosion estimates were limited to similar situations. In essence, these results did not

include any impact (either erosion or deposition) of the concentrated flow channels that form in the natural swales at the bottom of the roughly planar hillslopes, and certainly did not address classical gullying processes that often occur at steep boundaries such as headcuts and sidewall sloughing.

Use of the plot data to establish values for the factors above began with an analysis of rainfall erosivity by correlating the erosion measured under Unit Plot conditions with a whole series of measured rainfall values. A very strong correlation was found between this worst-case erosion and a combination of two rainfall factors, namely the total storm energy E and the maximum storm 30-minute intensity, or I_{30} (Wischmeier, 1959). The R factor was then calculated by summing over the calendar year the $E \cdot I_{30}$ values for all storms of over 12 mm (0.5 in.) or with more than 6.5 mm (0.25 in.) falling in 15 minutes, and taking the average of those annual values over all years of record. The soil erodibility (K) values were then determined for Unit Plot conditions ($C = P = LS = 1.0$) solving for K using measured A and R values. With the K values in hand, the values for C, P and LS could be determined by replicated plot studies on similar soils using different management practices or topographies.

Techniques for determining factor values to insert in the USLE (Equation (8.1)) were first presented for general use in the USDA's Agriculture Handbook No. 282 (Wischmeier & Smith, 1965). As use of this technology expanded and new studies were carried out to fill gaps and address weaknesses, new data were incorporated into the USLE, resulting in the second and most widely known release of the USLE technology in the USDA's Agriculture Handbook No. 537 (AH537) (Wischmeier & Smith, 1978). The values for the USLE factors as presented in AH537 were generally created to represent an average annual basis, although the form of the relationship does not demand that. The exception to this was the C factor, which was recognized as changing substantially through the year, leading to the cropping-period approach presented in AH537.

Following the release of AH537, the USLE became very widely used, both within the US and internationally. Perhaps its most common use was as one of the primary tools of the USDA Soil Conservation Service for conservation planning on agricultural lands. As use of the USLE expanded and it was applied in other situations, like disturbed forest lands (Dissmeyer & Foster, 1981, 1984), limitations of the technology became apparent. At the same time, continuing soil erosion research on both natural plots and under simulated rainfall led to improved understanding of the physical processes involved in hillslope sheet and rill erosion. Recognized limitations and advancements in erosion science pointed to the need for updating the USLE.

8.2 RUSLE

8.2.1 RUSLE1 development

In 1985, scientists and engineers from the USDA-ARS and the USDA Soil Conservation Service and affiliated academics with expertise in soil erosion assembled in West Lafayette, Indiana. At that workshop, two important decisions evolved, including the need to (1) develop technology to replace the USLE with a physically-based model (subsequently called the Water Erosion Prediction Project or WEPP); and (2) to computerize and update the 1978 version of the USLE with an improved model, subsequently called the Revised USLE or RUSLE. All subsequent material in this chapter is directed to a description and analysis of the various portions of the RUSLE effort, including both RUSLE1 and RUSLE2.

The first version of RUSLE1, a software program designed to operate in a DOS-based computer environment, was released in 1997. RUSLE1 was supported by USDA-ARS through Agriculture Handbook No. 703 (AH703) (Renard *et al.*, 1997). The computer system soil erosion model described therein was a major conversion of the factor approach presented in AH537. Perhaps the most significant change was the subfactor approach to the calculation of the cover-management factor C, thereby allowing use of RUSLE1 for any land use that could be adequately addressed by these subfactors. This broke the previous bonds of the

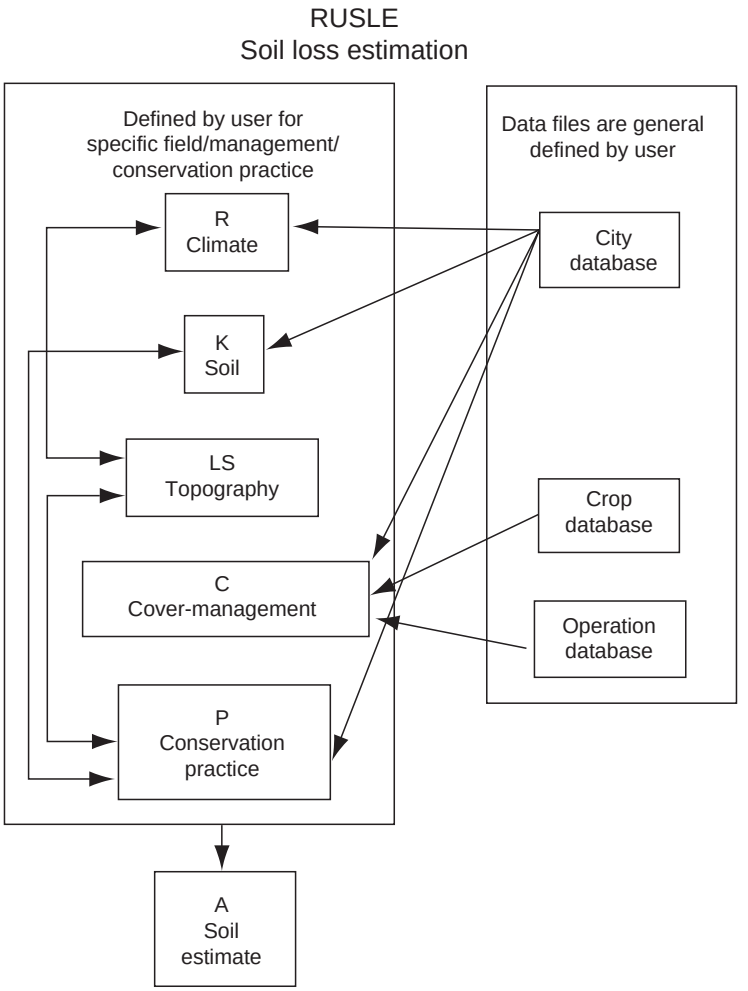

Fig. 8.1 RUSLE1 software flow chart (from AH703).

USLE to agricultural settings, as described in some detail below. The new AH703 development took an appreciable amount of effort involving scientists and engineers with experience in areas of knowledge representing each factor. It also involved a significant amount of testing by SCS-NRCS personnel in various locations, each having specific expertise in the crops, soils and climates involved. The DOS program developed for the 1997 RUSLE1 version permitted English unit calculations only. To input or output metric units required hand conversions of individual factor values using conversion factors (Foster *et al.*, 1981) which were included in Appendix B of AH703.

Another change in the RUSLE1 approach was to begin grouping the expanded list of required user inputs into a crude database, defined as shown in Fig. 8.1. This allowed for saving and re-use of sets of inputs corresponding to, for example, a specific location. In addition to the computerization of the model, every USLE factor underwent significant changes in moving to RUSLE1. These changes are generally described in the paragraphs that follow.

(i) Rainfall erosivity factor (*R*) The most common way of presenting rainfall erosivity information in the US has been through the use of isoerodent maps, allowing the reader to interpolate the corresponding *R* value for a specific location. The isoerodent maps in AH703 were calculated using the same criteria as in AH537, namely summing the storm kinetic energy times the maximum 30-minute intensity for storms larger than 0.5 in (12 mm), unless at least 0.25 in (6.5 mm) fell in 15 min. These calculations were computed for all non-snow storms within a period of *N* years. Normally at least 22 years of storms were included for the calculations (see AH537 for details), but longer periods are advisable when the coefficient of variation of annual precipitation is large. A total of 181 key precipitation locations with 15-min data were used for the map in AH537, and a few additional locations to fill in gaps were added to produce Figure 2.1 in AH703. AH537 included very little erosivity information for the western US, with only 11 western station isoerodent values used to estimate the two-year 6-h precipitation amount. A power relationship developed by Wischmeier (1974) to fit those values provided some measure of the expected erosivity, but the results were not thought to be very accurate, or to reflect adequately the known intermontane climate variability. Through an agreement between Oregon State University, USDA-ARS, USDA-SCS and the National Weather Service, data from 713 stations with 15-min measurement intervals were used to calculate *EI* values, and thereby to construct new isoerodent maps for the western US in AH703, although all storms were included in the western erosivity calculations (excluding snow). Analysis of these records showed that 225 precipitation-measuring locations had records longer than 12 years and precipitation resolutions of 0.01 in. (0.25 mm). Values of the coefficient of determination (R^2) in excess of 0.8 were obtained with the model $EI_{15} = b(EI_{60})$. Values of the regression parameter *b* ranged from 1.08 to 3.16, varying widely among climate zones.

To supplement this work, 1082 hourly stations were used to calculate EI_{60}. Of these stations, 790 had record lengths of 20 years or longer. These data were adjusted to a 15-min measurement interval using the cited correction. *R* factors were also adjusted to equivalent break-point data using the Weiss (1964) relationship $R = 1.0667\ (R_{15})$. The isoerodent map was prepared by hand contouring on large-scale maps, reflecting the major topographic influences in mountain and range topography. The newer isoerodent maps (Figures 2-2, 2-3 and 2-4 of AH703) were thus felt to be a significant improvement over those in AH537.

In addition, seasonal *EI* distributions were developed for 84 climate zones in the western US (Fig. 2-7, AH703). The distributions were developed for calculating the time-varying *C* factor in RUSLE1, building on the crop growth stage approach found in AH537.

City database files were then developed in RUSLE1 to provide the climatic data needed for erosion calculations. This included the *R*-factor value, the *EI* distribution values for 24 bimonthly periods, and the 10-yr frequency storm maximum *EI* that was needed for calculating the *P* factor credit for contour farming. Maps of these values were calculated for precipitation gauge locations and are presented in Figures 2-9 to 2-12 in AH703.

Two additional modifications to the classical USLE *R*-factor approach were included in RUSLE1 to address specific geographical needs. In areas with very low relief and high rainfall intensities (such as in the Mississippi River delta), research has found that runoff ponds to substantial depths before running off, and that this ponded water absorbs some of the raindrop impact that could cause detachment (Mutchler, 1970). Based on these data, RUSLE1 included a term to adjust downwards the erosivity experienced by the soil, based on slope steepness and rainfall erosivity (taken as a surrogate for intensity). The other modification to the *R* factor was for frozen and thawing soils, encountered in the Pacific Northwest (Northwest Wheat and Range Region (Austin, 1981)), and in some of the southern plains of Canada. In these cases, a soil with much weakened structure exposed to even a low-erosivity event will experience high erosion rates, so an

alternative means of selecting an equivalent *R* value for these conditions was included in RUSLE1.

(ii) Soil erodibility factor (*K*) The soil erodibility factor (*K*) represents the effect of soil properties and soil profile characteristics on soil loss (see Chapter 2 in Renard *et al.*, 1997). In a practical sense, *K* is a lumped parameter representing an integrated annual average of the soil and profile reaction to erosion and hydrological processes. The processes consist of soil detachment and transport by raindrop impact and surface flow, deposition due to topography and tillage roughness and rain infiltration into the soil profile.

The best erodibility factors are obtained from long-term direct soil-loss measurement on natural plots. Rainfall simulation data has also been used, but is recognized as being less accurate (Römkens, 1985). Only inherent soil properties are considered determinants of the USLE soil erodibility factor, which means that soil erodibility must be measured under the Unit Plot conditions described earlier. The minimum adequacy of the observation period for soil erodibility was usually taken as two years, but longer periods provide better results due to the likelihood of experiencing a broader range of climatic and soil conditions. Most of the plots used in measuring soil erodibility were in the Midwestern cropping areas of the US (see Table 3.1 in Renard *et al.*, 1997).

In most cases, US RUSLE1 users will have little trouble in selecting specific *K* values, because NRCS has identified values for most major soil mapping units. Site-specific values can be obtained from the widely available NRCS soil surveys, or directly from USDA soil databases. If such data are not available, the erodibility nomograph (Fig. 8.2), based on a relationship fitting the data as described above, is the most commonly used tool to estimate *K*, although there are some soils where it does not apply, and one of the site-specific relationships for specific soils (Renard *et al.*, 1997: 75) may be a better choice in the US. Users should contact their NRCS state soil scientist or other local soil specialist to certify the value to be used for their location. In other areas of the world, users may have to resort to soil sampling and the use of Fig. 8.2.

(iii) Topography factors (*LS*) There are more questions and concerns about the *LS* topographic factor than for any other term in RUSLE. The primary reason for these concerns is that the choice of slope length involves substantial judgment; different users choose different slope lengths for similar situations. The two primary questions here are what hillslope (downslope runoff path) to use to represent an area, and how then to define that hillslope in terms of specific length and steepness values. The first question is really one of policy rather than science (do we choose the worst-case hillslope, or the median slope, or some other?), while the second question is a more technical yet qualitative one of how to define where runoff begins, the path it takes down the slope and when it reaches a concentrated flow channel, thus ending the hillslope. The attention given to slope length is not always warranted because soil loss is often less sensitive to slope length than to any other USLE/RUSLE factor. For typical slope conditions, a 10% error in slope length results in a 5% error in computed soil loss. In contrast, soil loss is much more sensitive to changes in slope steepness than to errors in slope length. In the USLE, for example, a 10% error in slope steepness will usually give about a 20% error in computed soil loss. RUSLE has a more linear slope steepness relationship than did the USLE. Improvements in the relationship for steep slopes mean that computed soil loss for slopes less than 20% are similar in RUSLE and USLE, but on steep slopes, computed soil loss in RUSLE is just over half that predicted by the USLE, whose relationship did not include data for steep slopes. In addition, RUSLE makes more explicit the reliance of the length relationship on the susceptibility of the soil to rilling, which may be influenced by the slope steepness, soil characteristics, and management impacts. Finally, RUSLE includes a slope relationship specifically for the frozen soil region of the Northwest Wheat and Range Region (Austin

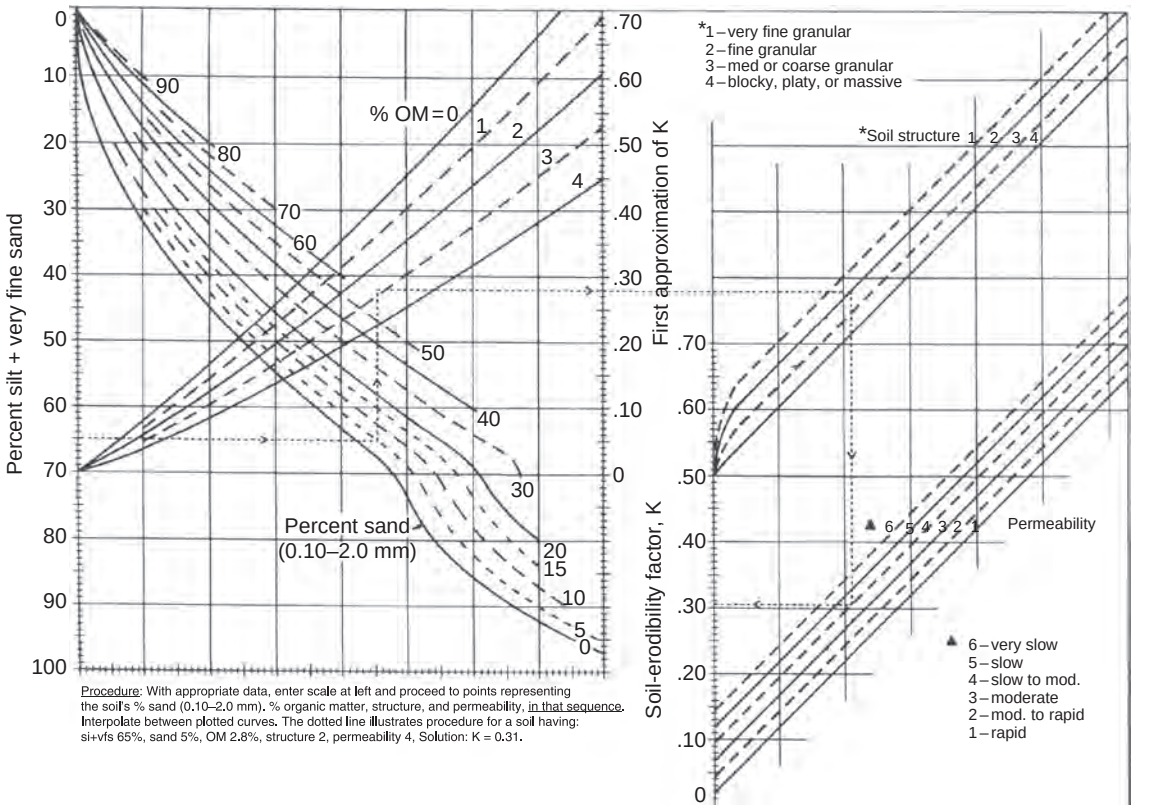

Fig. 8.2 The soil erodibility nomograph that gives *K* in US Customary Units (see Wischmeier & Smith, 1978).

1981). Detailed information on the selection of slope calculations is given in AH703 Chapter 4.

The difficulty in defining slope length is, however, substantial enough to have served as the primary impediment for employing GIS-based systems in using RUSLE. The topographic data available to populate GIS databases generally does not have the spatial resolution necessary to pick out the small concentrated flow channels commonly found at the bottom of a USLE/RUSLE hillslope. As a result, slope lengths computed using these data are almost always far too long. In fact, most attempts to use GIS with USLE/RUSLE recognize this and simply cut off the slope lengths at some arbitrary value. This poor resolution also causes the GIS system to miss the flat floodplains often found at the bottom of a hillslope, where substantial deposition may occur. This may change as higher-resolution topographic data (such as those collected using Lidar) become available, although how best to use these extensive datasets must still be decided.

In using the USLE, the slope length was defined as beginning at the top of the hillslope where runoff starts, and extending down to where the sheet and rill flow reaches either a concentrated flow channel or a depositional area. This limit of the depositional area was required because such deposition rarely occurred on the plots used to collect USLE data. Deposition can be caused by anything that slows the runoff and causes sediment to deposit, such as an increase in roughness caused by a management change (e.g. a strip of dense vegetation), or a decrease in slope grade.

In RUSLE1, this definition was expanded slightly to include areas of deposition caused by management changes on the hillslope, which was accomplished by including some of the more process-based routines used in CREAMS (Foster *et al.*, 1980).

Slope length factor (L) Plot data used to derive slope length (L) show that erosion for slope length λ (ft) varies as:

$$L = (\lambda/72.6)^m \qquad (8.2)$$

where 72.6 = the RUSLE unit plot length (ft) and m is a variable slope length exponent. The slope length λ is the horizontal projection. The value for m can be found from $m = \beta/(1 + \beta)$, where the slope-length exponent β is related to the ratio of rill erosion (caused by overland flow) to inter-rill erosion (principally caused by raindrop impact). The ratio of rill to inter-rill erosion when the soil is susceptible to both rill and inter-rill erosion is:

$$\beta = (\sin\theta/0.0896)/[3.0(\sin\theta)^{0.8} + 0.56] \qquad (8.3)$$

where θ is the slope angle. For a value of β, the slope-length exponent m is calculated using the relation above. When runoff, soil, cover, and management conditions indicate that the soil is highly susceptible to rill erosion, the exponent should be increased (see AH703, Chapter 4). These conditions are expected, for example, for steep, freshly prepared construction slopes. In such cases where the soil is highly susceptible to rilling, AH703 recommended doubling the value of β resulting from Equation (8.3). When conditions favour more inter-rill and less rill erosion, as in cases of consolidated soils like those found in no-till agriculture, m should be decreased by halving the β value. A low rill to inter-rill erosion ratio is typical of conditions on rangelands. With thawing, and cultivated soils dominated by surface flow, a constant value of 0.5 should be used (McCool *et al.*, 1989, 1993). In RUSLE1 the choice between these alternatives was made by selecting a general land-use category; in RUSLE2 the program automatically and continuously adjusts the m value based on slope steepness, soil type and management impacts.

Slope steepness factor (S) Soil loss increases more with steepness than with slope length. In RUSLE, the slope steepness has changed from that used by the USLE, and is evaluated with the relationship (McCool *et al.*, 1987):

$$S = 10.8 \sin\theta + 0.03 \quad S<9\% \qquad (8.4)$$

$$S = 16.8 \sin\theta - 0.50 \quad S>9\% \qquad (8.5)$$

The relationship is based on the assumption that runoff is not a function of slope steepness for slopes greater than 9%. Slope effect on runoff and erosion as a result of mechanical disturbance, cover and vegetation is considered in the cover-management (C) or support practice factor (P). For slopes shorter than 4.6 m (15 ft), use:

$$S = 3.0 (\sin\theta)^{0.8} + 0.56 \qquad (8.6)$$

Equation (8.6) applies to conditions where the water drains freely from the slope end. For the slope steepness factor above, it is assumed that rill erosion is insignificant on slopes shorter than 4.6 m (15 ft), and that inter-rill erosion is independent of slope length.

When freshly tilled soil is thawing, in a weakened state and primarily subjected to surface flow, use the following (McCool *et al.*, 1993):

$$S = 10.8 \sin\theta + 0.03 \quad S<9\% \qquad (8.7)$$

$$S = (\sin\theta/0.0896)^{0.6} \quad S>9\% \qquad (8.8)$$

In most practical applications, a single plane or uniform slope can be a poor representation of the hillslope topography, and erosion can vary greatly between concave or convex slopes of equal average steepness. Users are cautioned and encouraged to use the complex slope calculations, because differences can be significant when contrasted with a uniform plane.

Actual selection of the hillslope used to represent a field can be a complicated choice, and is best done through examples rather than verbiage. Additional detail and guidance for field measurement of the *LS* factor for varying field scenarios is given in AH703.

Cover-management Factor (C) The cover-management factor, *C*, is possibly the most important of the RUSLE/USLE factors because it represents the most readily managed condition for reducing erosion. In the USLE, the *C* factor was described as providing a measure of how erosion from the current condition compares with that for the Unit Plot condition, which is considered as nearly worst-case. The individual values of *C* vary between 0 for a completely non-erodible condition, to a value somewhat greater than 1.0. Values greater than 1.0 imply conditions more erodible than those normally experienced under Unit Plot conditions, which can occur for conditions with very extensive tillage (e.g. roto-tilling), leaving a very smooth surface that produces much runoff and makes the soil especially susceptible to erosion. *C* values are weighted average soil-loss ratios (SLRs), each of which represents the ratio of soil loss under current conditions for a short period of time to the expected soil loss under Unit Plot conditions during that same period. The SLRs vary throughout the year as soil and cover conditions change with soil disturbance and plant growth. The *C* value then represents the average of the time-varying SLR values, each weighted by the portion of rainfall erosivity during that same time period.

In contrast to the tables of *C* factors presented in AH282 and AH537, RUSLE1 uses a subfactor method to compute SLRs as a function of five factors:

$$C = PLU \cdot CC \cdot SC \cdot SR \cdot SM \qquad (8.9)$$

where *C* is the overall cover-management factor, *PLU* is the prior landuse subfactor, *CC* is the canopy cover subfactor, *SC* is the surface cover subfactor, *SR* is the surface roughness subfactor, and *SM* is the soil moisture subfactor (used only in the Northwest Wheat and Range Region area (Austin, 1981), otherwise unity). Expanded details for evaluating *C* factors are presented in AH703.

Although ground cover is known to affect erosion more than the other subfactors, it is wrong to give it exclusive attention without considering within-soil effects such as those associated with root mass and tillage. A 30% surface cover after planting is the criterion frequently used for conservation tillage; the USLE relationships predict that this 30% cover will reduce soil loss by about 72%. By comparison, the soil loss for a freshly ploughed meadow is reduced by about 75% from that for Unit Plot conditions, showing that within-soil effects can have a substantial impact. Although the effects are not as pronounced, the impacts of canopy cover and surface roughness can also provide substantial benefits, especially in the absence of surface cover.

The structure of Equation (8.9) implies that the effects of subfactors in reducing erosion are multiplicative. For example, if there is a canopy cover that reduces erosion by 45% from Unit Plot conditions, this means that $CC = 0.55$. If there is also enough surface cover to reduce erosion by 60% from Unit Plot conditions ($SC = 0.4$), then assuming all other factors are under Unit Plot conditions ($PLU = SR = SM = 1.0$), the overall factor value would be $C = 0.55 \times 0.4 = 0.22$, or a 78% reduction in erosion from Unit Plot conditions.

The subfactor approach in RUSLE1 was designed to break the dependence of the USLE structure on specific land-use data. Without this break, calculations would require separate complete and expensive datasets for each possible combination of land uses. The subfactor analytical approach was carried out under the basic assumption that the erosion impact of various factors such as surface cover and roughness is really independent of the type of land management controlling that factor. For example, the impact of covering the surface with straw mulch and of growing grass should be relatively independent of whether this is done as part of normal agricultural field operations or to control erosion on construction sites. Under this assumption, we start with the relationships to estimate erosion

based on the parameters that control the subfactors for surface cover, biomass and roots in the soil, surface roughness, vegetative canopy cover, and soil moisture. Once those relationships are developed using field data, if the RUSLE1 program can model the effect of any field management operation on those parameters (soil, vegetation, biomass), it should be able to model the resulting erosion.

The subfactor approach and the equations controlling it are described in great detail in AH703. What follows is a brief introduction to the subfactors included in RUSLE1.

Prior land-use subfactor (PLU) The *PLU* subfactor is calculated in RUSLE as the product of soil consolidation and soil biomass effects:

$$PLU = C_f \cdot C_b \cdot \exp\text{-}[(c_{ur} \cdot B_{ur}) + (c_{us} \cdot B_{us}/C_f^{cuf})] \quad (8.10)$$

where *PLU* is the prior land-use subfactor (ranging from 0 to 1), C_f is a surface-soil-consolidation factor, C_b represents the relative effectiveness of subsurface residue in consolidation, B_{ur} is the mass density of live and dead roots in the upper 100 mm (lb acre^{-1} in^{-1}), B_{us} is the mass density of incorporated surface residue in the upper 100 mm of soil (lb acre^{-1} in^{-1}), C_{uf} represents the soil consolidation impact on the effectiveness of incorporated residue, and c_{ur} and c_{us} are calibration coefficients indicating subsurface residue impacts.

The B_u variables calculate the impact on erosion rates of live and dead roots and incorporated residue. The effectiveness of such materials can take two forms. Firstly, roots and residue can control erosion directly by physically binding soil particles together and acting as mechanical barriers to soil and water movement. Secondly, roots and residue exude binding agents and serve as a food source for micro-organisms that produce other organic binding agents. These serve to increase soil aggregation and thereby reduce susceptibility to erosion. The RUSLE software keeps track of the biomass in each layer, continuously adjusting the rootmass and subsurface residue to account for residue additions or losses by decomposition.

Canopy cover subfactor (CC) The canopy-cover subfactor indicates the effectiveness of the vegetative canopy in reducing the energy of rainfall striking the soil surface. Although most of the rainfall intercepted by canopy eventually reaches the soil surface, it usually does so with much less energy than rainfall directly striking the ground. The intercepted drops fracture into smaller drops, or drip from leaf edges, or travel down crop stems to the ground. The canopy-cover effect is given as:

$$CC = 1 - F_c \cdot \exp(-0.1 \cdot H) \quad (8.11)$$

where *CC* is the canopy-cover subfactor ranging from 0 to 1, F_c is the fraction of land surface covered by canopy, and H (ft) is the distance that raindrops fall after striking the canopy.

Surface cover subfactor (SC) Surface cover affects erosion by reducing the transport capacity of runoff, by causing deposition in ponded areas, and by decreasing the surface area susceptible to raindrop impact. This is perhaps the single most important factor in lowering SLR values. Surface cover includes crop residue, rocks, cryptogams, and other non-erodible and non-mobile material in direct contact with the soil surface. The effect of surface cover on soil erosion is given as:

$$SC = \exp[-b \cdot S_p (0.24 / R_u)^{0.08}] \quad (8.12)$$

where *SC* is the surface cover subfactor, b is a coefficient, S_p is the percentage of land area covered by surface cover, and R_u is the surface roughness, as will be defined later.

Land area percentage covered by residue can be estimated from residue weight by the relationship of Gregory (1982):

$$S_p = [1 - \exp(-\alpha \cdot B_s)] \cdot 100 \quad (8.13)$$

where S_p is percentage residue cover, α is the ratio of the area covered by a piece of residue to its

mass (acre lb^{-1}), and B_s is the dry weight of crop residue on the surface (lb ac^{-1}). If more than one type of residue is present, the resulting total surface area cover is calculated as:

$$S_p = \{1 - \exp[-\Sigma (\alpha_i \cdot B_{si})]\} \cdot 100 \qquad (8.14)$$

where α_i is the ratio of area covered to the mass of that residue for each type encountered. The summation is for each type of residue, as each residue type may have a unique α_i value.

Surface roughness subfactor (SR) Surface roughness has been shown to affect soil erosion directly, and also to affect it indirectly through the impact of residue effectiveness as controlled by the *b* value in Equation (8.12). The surface roughness subfactor is a function of the surface random roughness, which is defined as the standard deviation of surface elevations across the slope, when changes due to land slope or non-random tillage marks (such as dead furrows, traffic marks, and/or disk marks) are removed from consideration. A rough surface has many depressions and barriers. During a precipitation event, these trap water and sediment, causing rough surfaces to erode at lower rates than do smooth surfaces under similar conditions. Increasing surface roughness decreases transport capacity and runoff detachment by reducing flow velocity.

Roughness and cloddiness of soils also affect the degree and rate of soil sealing from raindrop impact. Soils that are left rough and cloddy typically have greater infiltration rates. Soils that are finely pulverized are usually smooth, seal rapidly, and have low infiltration rates. RUSLE assumes that roughness decreases with the time since tillage by the relationship:

$$D_r = \exp[\ ½(-0.14\ P_t) + 1/2(-0.012 \cdot EI_t)] \qquad (8.15)$$

where D_r is the dimensionless roughness decay coefficient, P_t is the total inches of rainfall since the most recent soil-disturbing surface operation, and EI_t is the total *EI* amount since that operation.

If the initial roughness is defined as R_i, then surface roughness just before a new tillage operation (R_u) can be defined as:

$$R_u = 0.24 + [D_r (R_i - 0.24)] \qquad (8.16)$$

where R_u is in inches. Since many field operations affect only a portion of the surface, R_u is also the roughness of that field portion left undisturbed by the current operation.

For that surface portion affected by the field operation, the resulting roughness has been found to be a function of subsurface biomass present in the top 4 in. of soil. The relationship is:

$$R_a = 0.24 + (R_t - 0.24) \{0.8\ [1 - \exp\ (-0.0012\ B_u)] + 0.2\} \qquad (8.17)$$

where R_a is the roughness after biomass adjustment (in.), R_t is the original roughness based on the assumption of ample subsurface biomass such as is found with high-yielding US-type corn, and B_u is total subsurface biomass density in the top inch of soil (lb ac^{-1} in^{-1}), with $B_u = B_{ur} + B_{us}$ as used in Equation (8.10).

The adjusted tillage roughness is then combined with that of the undisturbed portion of the surface as follows:

$$R_n = R_a F_d + R_u F_u \qquad (8.18)$$

where R_n is the net roughness following the field operation (in.) and F_d and F_u are respectively the fractions of the surface disturbed and undisturbed, such that their sum equals one.

Similarly, the roughness decay coefficient must be adjusted to reflect that only a portion of the field is disturbed using the relation:

$$D_e = D_r F_u + 1.0 F_d \qquad (8.19)$$

where D_e is the equivalent roughness decay coefficient. RUSLE then reorganizes the relationships described above to calculate the R_t, P_t and EI_t values corresponding to the equivalent roughness decay coefficients, under the assumption of a constant EI_t/P_t ratio. If a site is clean-tilled and left without human intervention, two things will happen: (1) the tillage roughness will decrease as defined previously; and (2) as time passes, vegetation will tend towards its climax

community, with attendant roughness caused by protruding roots, soil pushing up around old basal areas, rocks, and so on. RUSLE assumes that the formation of this vegetative roughness follows a typical sigmoidal growth curve, increasing from the minimum roughness (r_{min} with a default of 0.24 in.) to the total roughness when soil is consolidated (r_{max}) over the time required for consolidation (t_{con}).

Once the current roughness R_u has been defined based on the tillage roughness and all the roughness decay calculations described above, the surface roughness subfactor for this time period is then:

$$SR = \exp\left[-0.66\,(R_u - 0.24)\right] \qquad (8.20)$$

Soil moisture subfactor (SM) In non-irrigated portions of the Northwest Wheat and Range Region (NWRR; Austin, 1981), soil moisture during critical crop periods depends upon crop rotation and management. In such cases, the addition of a soil-moisture subfactor (*SM*) is suggested. *SM* reflects dry fall conditions and increasing soil moisture over winter. The soil moisture decrease during the growing season depends upon crop rooting depth and soil depth, and the soil moisture replenishment during the winter and spring depends upon precipitation amount and soil depth. Research to make such a correction is needed. In most instances this factor is assumed to be unity, which means that there is no substantial impact of soil moisture extraction by the vegetation on erosion. This assumption of $SM = 1.0$ is probably valid for all areas except those experiencing erosion caused by light rains on frozen-thawing soils.

(iv) Conservation practice factor (*P*) It is not always clear how the conservation practice factor (*P*) differs from the cover management factor (*C*), because both are meant to indicate the impact of management practices on erosion. In general terms, the basic difference is that the *C* factor reflects the positive impact over the larger portion of the management area, through factors like vegetation, biomass on the surface or within the soil, and roughness. The *P* factor is generally seen as reflecting the positive impacts of management through the control of runoff, with special emphasis on how the management changes the direction and speed of that runoff, but also reflecting to some degree management practices that control the amount of runoff. Traditionally the *P* factor has been used to reflect the impact of agricultural practices such as the various forms of strip-cropping (buffer strips, filter strips, rotational strip-cropping), terraces, contour tillage, and subsurface drainage. In other land uses, *P* would reflect the impact of analogous practices, such as filter strips for water quality control, or the use of diversions on construction sites. RUSLE1 brought to the USLE structure a subfactor approach for the *P* factor as well as the *C* factor, with separate subfactors for contouring, strips, terraces, and subsurface drainage. As with the *C* factor, these subfactor values are multiplied together to give the overall *P* factor.

Contouring subfactor Data on the effect of contouring show a tremendous amount of scatter, but there are some trends, as shown in Figure 6-2 of AH703. These indicate that higher ridges give more benefit than lower ridges, that contouring is more effective for areas with lower rainfall intensities, and that the effectiveness reaches a peak at about 9% slope, losing effectiveness at lower slopes due to less inherent erosion, and at higher slopes due to potential breakover of the ridges by ponded runoff. In addition, contouring is most effective when the ridges are perfectly on the contour, with its impact decreasing rapidly as the furrows have more grade.

RUSLE1 fits the scattered contouring data with a series of equations used to describe the base contouring *P* value for different slope steepnesses. It then adjusts these for climate and storm intensity using a runoff scaling factor based on the 10-year storm *EI* compared with a value for the central part of the US, and finally adjusts the results based on the contour furrow grade, using the relationship (AH703 eqn. 6-11):

$$P_g = P_o + (1 - P_o)(s_f / s_l)^{1/2} \qquad (8.21)$$

where P_g is the P factor for off-grade contouring, P_o is the P factor for on-grade contouring calculated using the sequence described above, s_f is the grade along the contour furrow, and s_l is the slope grade.

As reflected in the data summarized in tables in AH537, contouring tends to lose effectiveness on very long slopes, as runoff tends to build up behind the contour ridges and cause breakover of the ridges, which can be assumed to make the lower contour ridges ineffective. RUSLE estimates the maximum slope length over which contouring is effective (called the 'critical slope length' in AH703) using a variation on a relationship developed by Foster *et al.* (1982) for mulch stability. Once again, this relationship depends on slope steepness and runoff, and it is calibrated against the critical slope lengths shown in the tables in AH537. RUSLE then gives *P*-factor credit (i.e. reduces the erosion estimate) for the area upslope of the critical length, but not for the downslope area.

Strip-cropping subfactor The impact of management on runoff and its ability to carry sediment is probably the single factor that has changed most in the USLE/RUSLE evolutionary process. As described above, this has included substantial changes in how the hillslope is defined. RUSLE1 included a process-based approach to estimating the amount of deposition caused by changes in management and the resulting slowing of runoff. This started with the definition of a slope segment as being a portion of the topography with constant soil, management, and steepness. The approach taken was a simplified version of the CREAMS approach (Foster *et al.*, 1980), which looks at four possible cases for each slope segment, where a segment is defined: (1) where there is no runoff leaving the segment, so all incoming sediment is deposited; (2) where there is erosion throughout the segment; (3) where there is deposition throughout the segment; and (4) where deposition occurs at the top of the segment and erosion at the bottom. These four cases are examined by calculating the increase in transport capacity within the segment, and comparing that with the amount of additional sediment added by erosion within the segment. This requires estimation of a runoff rate, which in RUSLE1 is based on the ten-year *EI* storm erosivity.

The impact of the deposited sediment on the *P* factor is somewhat subjective, as the *P* factor is meant primarily as a measure of soil resource conservation, while the primary effect of deposition is on sediment delivery. Because sediment deposition does not preserve the soil resource as much as preventing erosion in the first place, RUSLE1 does not give as much conservation credit for practices that cause sediment deposition as for practices that prevent soil erosion. RUSLE1 gives credit for deposition that occurs based on its location on the slope, using the relationship:

$$B = M\,(1 - x^{1.5}) \tag{8.22}$$

where B is the benefit, M is the mass of sediment deposited, and x is the location of the deposition as a fraction of the total distance downslope. This benefit is calculated into the P factor as:

$$P_s = (g_p - B)/g_p \tag{8.23}$$

where P_s is the P factor for strip-cropping, and g_p is the potential sediment load that would occur if there was no deposition.

Terracing subfactor Within RUSLE, terraces (or diversions on construction sites) provide two benefits: (1) they break the hillslope profile into a combination of multiple shorter profiles, thereby reducing erosion; and (2) they cause some deposition to occur up on the hillslope, thereby providing some benefit in conserving the soil resource. The first of these benefits is taken into account through the *LS* topographic factor described above. For the second benefit, RUSLE uses sediment yield data collected on watersheds with terraces to estimate the amount of sediment deposition that will take place, then gives that a credit benefit identical to that described above for the benefit of deposition in strip-cropping.

Subsurface drainage subfactor There are some data that suggest subsurface drainage can be effective in reducing erosion, presumably by reducing soil moisture and thereby decreasing runoff during a storm event (Formanek *et al.*, 1987; Bengtson & Sabbage, 1988). These data show substantial scatter, but indicate an average erosion reduction of about 40% for a subfactor $P = 0.6$.

Sediment delivery estimate As the first step in the evolution from the USLE, RUSLE1 is still primarily geared towards planning based on soil conservation. In spite of this, using the techniques described above for strip-cropping, it does provide a crude sediment delivery estimate. This is done by using a value of $B = M$ in Equation (8.22), providing the ratio of sediment delivered over sediment eroded, or essentially a sediment delivery ratio. Multiplying this P factor for sediment delivery by the other factors then provides the hillslope sediment delivery for evaluating off-site impacts.

8.2.2 RUSLE1 program implementation

The RUSLE1 computer code was written in the C programming language. Chapter 7 in AH703 included a fairly detailed description of the RUSLE1 program layout and operation. This was deemed necessary because as dissemination of and training in RUSLE1 proceeded, it quickly became apparent that a program with this level of complexity could not be assumed to be intuitive to a first-time user. Part of this complexity was inherent in the level of input information required from the user, while an additional portion was due to the program structure. This structure was based on the USLE 'paper' implementation, and hid nothing from the user.

8.2.3 RUSLE1 implementation history and experience

Perhaps the two primary lessons learned from the USDA-NRCS implementation of RUSLE1 were: (1) the importance of an iterative feedback process in developing the program; and (2) the sheer scale of the effort necessary to implement such a model on the national scale. Although these lessons were partially due to the specifics of the situation, they are also broad enough to be instructive to other individuals and groups within or outside the US who are implementing a program like RUSLE. One of the key elements in the development of the RUSLE1 computer program was the close contact between the program developers and a variety of user representatives. Although the development began with defined user requirements, these underwent substantial changes as the program was presented to users through a variety of feedback and training sessions, involving a mixture of skilled and novice users. Only through that iterative feedback process did the program begin to meet the true user needs, as these needs often only became apparent when users were exposed to the program. Based on the RUSLE experience, it simply does not work to introduce a new model under the presumed process of setting initial user requirements and declaring success once those are met.

Although the RUSLE1 computer program itself was first deemed ready for full review and delivery in 1991, the process of developing the database information necessary to allow full implementation took an additional 4–5 years. This included a strong collaborative research effort sponsored by USDA-NRCS and carried out by researchers at North Carolina A&T University, Alcorn State University, and Alabama A&M University to collect the data required for the vegetation descriptions, including especially time-varying data on vegetative canopy cover, rootmass and biomass.

Substantial effort also went into determining exactly how the program would be implemented in the USDA-NRCS field offices, with special attention paid to consistency of results across political boundaries, and consistency of use patterns. One of the important concepts developed during this period was the development of *C*-Factor Zones, which recognized that climatic differences rather than political boundaries controlled the possible management scenarios, leading to shared management descriptions across state lines. National, state and regional NRCS

personnel developed the required management descriptions to describe the bulk of schemes used in these areas, which in turn defined the operation and vegetation descriptions that had to be developed. In other words, broad implementation required both local expertise and substantial cooperation and oversight.

In spite of all the work that needed to be done and all the decisions that needed to be made (and remade!), full NRCS implementation of RUSLE1 began in 1993, using version 1.04 of the program, which is the version represented and documented in far more detail in AH703. This was actively used for conservation planning throughout the US, and for the Conservation Compliance portion of NRCS responsibilities associated with the 1985 and 1990 US Farm Bills.

8.2.4 Science problems with RUSLE1

As the USLE came into general use, it quickly became apparent that the impact of management on erosion could vary greatly among periods within a year or among years within a rotation. This was recognized by the later USLE methods, with AH537 using a time-varying SLR based on cropping periods. RUSLE1 carried this further, using a daily time-step for the *C*-factor calculations, and also for some of the *P*-factor calculations. However, due to user requirements that the structure of RUSLE1 reflect that of a 'paper implementation' of the USLE, this was not carried to its logical extreme. The time-varying values of each of the individual factors were aggregated over the year, and the resulting annual values were multiplied as shown in Equation (8.1). Unfortunately, this aggregated approach is not correct, as the sum of products is not equal to the product of sums, which can be seen in the simple calculation $(2 + 3) \times (4 + 5) = 45 \neq (2 \times 4) + (3 \times 5) = 23$. Clearly, the proper approach was to take any time-varying values and multiply these for each day or period, then add the daily products to get the total erosion. This was recognized as a problem early in RUSLE1 development, but it could not be dealt with while retaining the 'paper implementation' capability. Calculations showed that the erosion results could vary by up to 30% between the two approaches.

8.2.5 RUSLE1 program weaknesses

In addition to the weaknesses inherent in the RUSLE1 science development, some more general weaknesses in the program operation became apparent during implementation.

The first program weakness was that the RUSLE1 structure was based on science rather than on how the user saw things. For example, one parameter used in the *LS* calculations is the soil texture, which affects the susceptibility of the soil to develop rills, thereby impacting the *LS* β value (Equation (8.2)). In spite of this, the user will clearly think of texture as a soil property, and not as something related to topography. This is one of many examples in RUSLE1 where there was a need to approach things more from the user's viewpoint, and not from the modelling viewpoint.

Another weakness of the RUSLE1 approach is that any user could change any database value. Although NRCS had put substantial effort into developing specific databases for climates and vegetations, any user could change the values, either intentionally or by accident. This resulted in many implementation headaches, such that two users using the same inputs would get very different results because one of the underlying database files had been modified.

Finally, the DOS-based interface used in RUSLE1 was already dated at the time of its delivery, and users repeatedly asked for a Windows®-based or similar graphical user interface, with which they were becoming increasingly familiar.

8.3 RUSLE2

As RUSLE1 developed, it quickly became apparent that there were some scientific weaknesses with the approach taken that were primarily caused by its close linkage to the methodology used in the USLE. In addition, through the training and implementation process, some lessons were learned about how the general program

could be improved. Work began to address these issues in 1996, culminating in the release of a first RUSLE2 version in 2001 and the beginning of a US-wide NRCS implementation with actual distribution of the program to the field offices beginning in 2004. Based on some of the lessons learned in RUSLE1 implementation, this included a much earlier push to begin establishing the required databases, as well as to begin the iterative process of developing and modifying the program based on user feedback.

A primary change in the RUSLE2 implementation of the USLE relationships could be described as downplaying the importance of the individual factors. In the original USLE concept, these factors (except perhaps for C and P) were generally considered to be independent. This was clearly no longer the case in RUSLE1, as exemplified by the dependence of the β term in the LS relationship (Equation (8.3)) on various soil and management factors, which also impact the K and LS values. The factor-based RUSLE1 implementation caused both science and user problems. Inconsistent values could be entered in the various factors (a science error) and the program required the user to jump back and forth between factors in order to enter relevant and related data.

Implementation of RUSLE1 also made clear many places where the science was not specifically in error, but could be greatly enhanced. The most obvious of these was in full implementation within RUSLE2 of the CREAMS (Foster *et al.*, 1980) sediment transport and deposition approach, allowing the definition of the RUSLE2 hillslope to include depositional zones all the way down to the concentrated flow channel, and making RUSLE2 much more applicable to water quality problems. Other places where it was thought that the science could be enhanced by smaller improvements were many, especially in reducing the need for user selection of values by developing ways for the program to calculate needed values from information already available in databases. For example, in RUSLE1 the user needed to describe in several places the susceptibility of the soil to rilling; but this would vary with time, and can be estimated using parameters such as the soil texture, slope steepness, and management parameters already calculated within RUSLE2.

As with RUSLE1, many scientists and engineers were involved in producing and delivering the RUSLE2 technology, including those involved in data collection and preparation for analysis. Most of these individuals are acknowledged in the references for the corresponding documents.

8.3.1 General approach to RUSLE2 science problems

The following summary brings up to date earlier and more extensive summaries of science improvements in RUSLE2 (Foster *et al.* 2000, 2003; USDA-ARS, 2008a,b). In this treatment, distinctions are drawn between RUSLE2 and RUSLE1 version 1.04, as documented in AH703. Some of the science enhancements in RUSLE2 exist in later versions of RUSLE1, specifically in RUSLE1.05 and RUSLE1.06, which were developed with the support of the US Department of Interior Office of Surface Mining (Foster *et al.*, 2003).

RUSLE2 retains the conceptual use of the USLE factors, makes computations that are based on soil loss estimates referenced to unit plot conditions, and uses ratios to adjust predictions to other conditions. However, RUSLE2 goes beyond the USLE. It uses process-based equations derived from fundamental erosion science and professional judgment to make RUSLE2 applicable to situations beyond the scope of USLE or RUSLE1. As scientific approaches improved, RUSLE2 was calibrated to reproduce the core SLRs for different cropping systems and crop growth stages listed in Table 5 of Agriculture Handbook 537 (Wischmeier & Smith, 1978). This calibration ensured that RUSLE2 erosion estimates for common situations would be similar to the established and accepted values that have been used for decades in the US for conservation compliance assessment.

A major change in RUSLE2 was the de-emphasis of the USLE factors, and the organization of information into 'objects'. This object-oriented

organization applies to both the computer programming and the way that data are input by the user. The RUSLE2 developers made an effort to group and consolidate information needed by RUSLE2 into objects or descriptions that reflected how users think about the USLE factors. In the example mentioned above, with RUSLE1 the user had to use soil-related information not only in determining the *K* factor, but also in determining the *LS* factor, where the user chose among soil classes differing in their relative susceptibility to rill or inter-rill erosion (Table 4-5, Renard *et al*., 1997). In RUSLE2, all soil-related information is included in a soil description, and all management information is contained in a management description. RUSLE2 combines these descriptions with the topographic description to define another description, that of a hillslope profile object, and extracts the information it needs from the descriptions to make erosion computations based on climate information contained in a location description.

Databases are maintained at the object level. Objects may contain other objects and subobjects. For example, a management object is composed of the dates of occurrence of operation objects (like tillage, planting, or other soil-disturbing operations) and vegetation objects. Vegetation objects contain descriptions of growth patterns, and canopy and residue characteristics needed by RUSLE2 to compute the vegetation's influence on erosion. RUSLE2 does not simulate the growth of vegetation, but rather takes the information contained in the vegetation description and accounts for its effect on the *L*, *C* and *P* factors through numerous influences on variables tracked or calculated internally by RUSLE2, including soil biomass, surface residue cover, surface roughness, canopy cover, Manning's roughness, and the runoff curve number. In the USLE, all the factors were independent of each other; the *K*, *L*, *S* and *P* factors were annual constants, while the *R* and *C* factors were broken down into crop growth phases. In RUSLE1, the *R*, *K* and *C* factors varied among 24 half-month periods but remained largely independent of each other, although the *LS* and ground-cover effects varied with the ratio of rill to inter-rill erosion, which in turn varied with soil texture, slope steepness and cover-management variables. In RUSLE2, all factors except *S* vary on a daily basis, and there are numerous interactions among the factors (USDA-ARS, 2008a). Annual averages of the RUSLE2 factors can be calculated, but the products of these averages will not equal the average annual erosion predicted by RUSLE2.

A major improvement in RUSLE2 is that the user can now define any number of steepness, soil, or management breaks along the slope, and the program will accordingly break the slope into segments representing each combination, and complete the calculations on those. RUSLE2 overcame limitations in describing complex hillslopes that existed in USLE and RUSLE1 by conceiving of hillslopes as being composed of three layers: topography, soil, and management. Each of these layers can be segmented independently to represent any complex one-dimensional hillslope situation. RUSLE2 then defines slope segments as each unique combination of topography, soil, and management layers. Because of the inclusion of deposition routines that were not part of the USLE or RUSLE1, RUSLE2 applies to hillslopes that include concave areas where sediment deposition occurs. Also, channels at the slope bottom, terraces with channels within hillslopes, impoundments, and sediment basins may all be described. These features allow RUSLE2 to compute sediment deposition and fine-particle enrichment of delivered sediment using process-based equations. Currently RUSLE2 does not simulate erosion in channels.

This ability to consider slope segments has also enabled RUSLE2 to deal nicely with the application of terraces or diversions as a management alternative. From a USLE/RUSLE perspective, the terrace channel becomes the concentrated flow channel defining the bottom of an upper hillslope profile, while the top of the terrace itself defines the beginning of a new lower profile. Within RUSLE2 this is handled automatically, defining not only the profiles, but allowing the user to specify the type of concentrated flow

channel transferring water down from the terrace/diversion to the hillslope bottom. This channel can currently be modelled to cause deposition, but cannot currently be modelled as experiencing erosion. The ability to easily add or remove terraces for the hillslope description is important because it allows these to be approached as another management alternative, rather than requiring redefinition by the user of the hillslope profile itself.

(i) Changes in the climate description The climate data required to calculate soil loss in RUSLE2 are monthly averages for precipitation, temperature and erosivity, plus the desired location's ten-year 24-h precipitation amount ($P_{10y,24h}$). Climate description changes from RUSLE1 to RUSLE2 include: specification of $P_{10y,24h}$ rather than the ten-year *EI* event; updating the underlying record to the period from 1960 to 1989 (1960 to 1999 in many cases); and development of the erosivity density concept. Specification of monthly average precipitation and monthly average erosivity density is the preferred way of describing monthly erosivity in RUSLE2, and these values are contained in all the NRCS location climate files (USDA-NRCS, 2008). Erosivity density is defined as the amount of rainfall erosivity per unit of precipitation. Erosivity density has units of energy per unit area per unit time (e.g. MJ ha^{-1} h^{-1}), and when multiplied by the depth of precipitation over an interval (event, day, month, year) yields the appropriate average erosivity value. Using erosivity density has several advantages over directly calculated rainfall erosivity: (1) because it is the ratio of storm erosivity to storm precipitation, missing data have less impact on monthly means; (2) a shorter period of record is needed to arrive at a stable value of this ratio than a stable absolute value of erosivity; (3) because erosivity density was found to be relatively independent of elevation up to 3000 m, it was possible to interpolate a smoothly-varying erosivity density surface for the entire nation, making it possible to calculate erosivity for each county (common use in the US) or each precipitation zone (USDA-ARS, 2008a,b). The effect of elevation on erosivity was reflected by defining precipitation zones within counties of 11 mountainous western US states. The erosivity density approach allows geographically consistent erosion predictions needed for a conservation/erosion planning tool, and maximizes information that can be extracted from available 15-min precipitation data.

(ii) Changes in the soil description Changes in the soil description and *K*-factor computations include the development of a modified nomograph for highly disturbed soils, the development of new routines to describe time-variation in the *K* factor based on location temperature and precipitation data, and the ability to reflect the impact of subsurface drainage by specifying a soil hydrological class. RUSLE2 contains equations representing both the standard nomograph (Fig. 8.2) and a modified nomograph that applies to disturbed soils such as construction sites or reclaimed mine soils. The modified nomograph is the same as the standard nomograph for fine granular soils ($S = 2$), but the structural trend in erodibility is reversed in the modified nomograph, so that erodibility decreases as structure varies from very fine granular to massive. In the modified nomograph, the labels for class 1 and 3 structures would be exchanged and the line for class 4 structure would be to the left of all structure lines shown in Fig. 8.2. The modified nomograph is recommended for highly disturbed lands such as reclaimed mined land and construction sites, whereas the standard nomograph is recommended for agricultural soils because of its empirical support. For equivalent soil properties, both the standard and modified nomograph return a base *K* factor for Columbia, MO, which is a reference location and the centre of the RUSLE2 domain.

RUSLE1 included a time-varying *K* factor that was based on a few data points collected in the central US that indicated a time-varying change in Unit Plot erosion from storms with similar erosivity. New relationships in RUSLE2 capture the effect of temperature and precipitation on the likelihood of runoff and hence the *K*

factor. For example, during cool and wet periods, higher antecedent soil water is likely to increase runoff and soil erosion, thus K should be higher. Similarly, increased temperature is expected to increase evapotranspiration, leading to lower antecedent soil moisture, lower runoff, and reduced K values. Relationships in RUSLE2 capture the main effects of seasonal variation in K at each location based on the ratio of temperature and precipitation values at each location to the average annual values at the reference location (Columbia, MO). For identical soil descriptions, these adjustments will increase the annual effective K at locations that are cooler and wetter than Columbia, MO, while average K values will be lower than the nomograph value at locations that are hotter and drier than Columbia, MO.

In RUSLE2, inclusion of the CREAMS (Foster *et al.*, 1980) sediment transport and deposition relationships requires knowledge of the sediment size distribution at the point of detachment, so the diameter, specific gravity, and primary particle composition of each of five size classes is calculated as a function of soil clay using equations similar to those in CREAMS (Foster *et al.*, 1985). The effect of drainage on runoff and sediment transport is discussed below with regard to the P factor.

(iii) Changes to the topographic description Whereas the rill to inter-rill erosion ratio in RUSLE1 was selected by the user, in RUSLE2 this ratio is calculated internally based on soil texture, prior land use (soil biomass and soil consolidation) effects, ground cover and slope steepness. This ratio determines the slope length exponent, m, in Equation (8.2), which controls the sensitivity of sheet and rill erosion to slope length. Instead of using Equation (8.3), the ratio of rill to inter-rill erosion in RUSLE2 is computed from (USDA-ARS, 2008a):

$$\beta = \left(\frac{K_r}{K_i}\right)\left(\frac{c_{pr}}{c_{pi}}\right)\left(\frac{\exp(-b_r f_g)}{\exp(-0.025 f_g)}\right)\left(\frac{s/0.0896}{3s^{0.8}+0.56}\right) \quad (8.24)$$

where the ratio K_r/K_i is the inherent rill to inter-rill soil erodibility ratio computed as a function of soil texture (as discussed in the text following Equation (8.3)); the term c_{pr}/c_{pi} reflects the effect of prior land use on the rill to inter-rill erosion ratio; the ratio $\exp(-b_r f_g)/\exp(-0.025 f_g)$ reflects how ground cover affects rill erosion more than it affects inter-rill erosion, b_r and 0.025 are coefficients ($\%^{-1}$) that express the relative effectiveness of ground cover for reducing rill erosion and inter-rill erosion, and f_g is ground cover expressed as a percentage. The last term is the same as Equation (8.3). Equation (8.24) shows how RUSLE2 takes the information stored in the topographic, management, and soil objects and uses it to calculate needed coefficients, thus reducing the need for users to specify unfamiliar parameters. The fact that the rill to inter-rill erosion ratio, as calculated from Equation (8.24), is independent of slope length (when it really is not) illustrates the price that RUSLE2 pays for the ability to retain the simple and familiar USLE equation structure.

Complex slopes can be represented in RUSLE2 to provide a better approximation of topography. A broad range of process-based routines allows for calculation of deposition caused by either management or topographic changes. This means that, for RUSLE2, the hillslope is defined as from where runoff begins until it enters a concentrated flow channel, which is the same definition as for WEPP.

(iv) Changes to the management description One significant change from RUSLE1 to RUSLE2 was the grouping of field operations and vegetations into a separate management object or description. Management objects comprise descriptions of field operations (their dates of occurrence, and their effects on surface cover and surface roughness) with vegetation descriptions whose growth is begun by the operation (if any) and the yield expected for that vegetation, and the amount and type of external residue added to the surface if a mulching operation. Management descriptions result in daily tracking of an extensive suite of variables that affect sheet and rill erosion, including canopy cover, standing residue,

surface residue, surface roughness, ridge height, and the depth distribution of buried residue and soil biomass. Some of these, like standing stubble and ridge height, are variables that did not exist as USLE or RUSLE1 subfactors, but even the more familiar variables have received new and more detailed treatment in RUSLE2. In addition to surface and standing residue, RUSLE2 tracks dead biomass in 24 2.5-cm-thick soil layers in the soil profile. By default, standing residue decays at a rate that is a fraction of that of the surface residue, buried residue, or dead roots, which all decay at a rate controlled by climatic and residue variables using the same relationships as in RUSLE1. Mechanical tillage operations are described much more fully in RUSLE2 database files than in RUSLE1, in terms of the impact they have on flattening standing residues, disturbing the soil, or affecting the growth of vegetation. Soil disturbance is described in terms of the fraction of the soil disturbed, the intensity and depth of soil disturbance, the creation of ridges and random roughness, and the effect on burying, redistributing, or re-surfacing residues.

In a vegetation description, users define the base crop yield, the time course of canopy and root mass development (a 'growth chart'), and the characteristics of the residue produced when the crop dies. RUSLE2 uses this information once a 'begin growth' operation in a management description calls for that vegetation. The growth of the vegetation in RUSLE2 is independent of the location's climate data, so it must be properly described by the user for the situation being analysed. Several 'wizards' are available in the RUSLE2 interface to help users to develop vegetation descriptions, to define canopy/biomass relationships, canopy shape and intercepted raindrop fall height, and yield/flow retardance relationships. A new portion of the program specifically designed to help the database developer and program user properly to account for residue and root production in perennial vegetation systems is being developed, and is discussed subsequently.

One key feature added to the vegetation/operation/management descriptions in RUSLE2 is the ability of the user to vary crop yield. Vegetation is described for a specific assumed base yield, but when the vegetation is actually used within a management regime, the user can specify a higher or lower yield value. The vegetation description includes how the biomass varies with yield, allowing adjustment of all of the vegetation parameters by the program.

(v) Changes to the support practice factor

Whereas the RUSLE1 user selects a cover management condition that, together with the soil hydrological group, defines a 'runoff index' analogous to the runoff curve number (*CN*), RUSLE2 calculates a *CN* internally as a function of soil hydraulic class, soil biomass, soil consolidation, soil roughness, and soil residue cover, thus reflecting the combined effects of soil, management and climate. RUSLE2 calculates runoff for the $P_{10y,24h}$ rainfall event every day. It also calculates sheet and rill erosion for this index event, and uses process-based equations to determine sediment transport, deposition, and fines enrichment. 'Infiltration' is calculated on slope segments with a low *CN* as the difference between $P_{10y,24h}$ precipitation depth and the 'initial abstraction', taken as 0.2 times the 'maximum retention' parameter, a transform of the *CN* (USDA-ARS, 2008a). The RUSLE2 equations for sediment transport capacity and deposition, and robust simplifications of the equations used in CREAMS, give RUSLE2 the ability to reflect the effects of spatial variation of soil erodibility, slope steepness, and cover management along a slope on detachment, transport and deposition. This approach results in estimates of the long-term average sediment production, erosion rate, transport capacity, deposition, and sediment characteristics along the slope, as well as the sediment amount and characteristics of sediment leaving the slope (Foster *et al.*, 2000). In fact, RUSLE2 goes further than other 'process-based' models, in that it approximates backwater effects when it determines the effectiveness of dense narrow vegetative buffers on sediment trapping (USDA-ARS, 2008a). RUSLE2 also includes the ability to approximate the effect of simple impoundments and channels on sediment delivery and fines enrichment.

8.3.2 RUSLE2 implementation and lessons learned

(i) RUSLE2 websites There are two 'official' RUSLE2 web sites: an ARS site, http://www.ars.usda.gov/Research/docs.htm?docid=6010, and an NRCS site, http://fargo.nserl.purdue.edu/rusle2_dataweb/RUSLE2_Index.htm. Both sites offer the same model, but with different databases, permission (access) levels, and templates. The ARS site provides a minimal database and access levels that allow scientists and engineers to see and change more parameters. The NRCS site includes much more extensive databases, and templates including a wide variety of additional tools, but the permissions for database manipulation are more restricted. The USDA-NRCS website is the single national point of delivery for the NRCS-approved RUSLE2 management templates and database components. Both websites contain documentation and training materials.

The NRCS website is remotely maintained and kept current by the NRCS database manager, who posts frequent database updates, revised soils data in RUSLE2 format, and updates to the 24,000+ management templates. Although the current version installer is posted for downloading and installation by private sector users, the NRCS has recently begun using an automatic software installation process for new releases of RUSLE2. This minimizes the amount of support time necessary to remove and install RUSLE2 on NRCS field office computers.

(ii) RUSLE2 interface: plasticity and security An internal NRCS oversight and evaluation review of RUSLE1 implementation uncovered significant differences in soil loss estimates from RUSLE1 across county lines in adjacent states and regions due to a lack of consistent RUSLE1 databases within NRCS. With this past experience in mind, RUSLE2 was implemented with a hierarchical approach that allows users to see and change only those factors they fully understand. In RUSLE1, any user could change any parameter, sometimes leading to a very unlikely combination of inputs that gave them the output they desired. In RUSLE2 inappropriate changes are controlled by three mechanisms. The first is the user interface, which is very user-configurable. This allows more complicated inputs or outputs to be removed from the visible set, simplifying the model to a degree matching the user's interests and abilities. Since in the RUSLE2 calculation engine a parameter that is not needed is not calculated, removing unnecessary parameters also accelerates calculations. The second control mechanism is called access control, which limits what the user is allowed to see or edit. Access must be granted to the user by a higher-level user, providing a very flexible control structure that can be modified as a user is trained and needs greater control over the program. The third control mechanism is protection of specific records or groups of records within the database. For example, records created by a user with a high access level can only be edited and re-saved by a user with that access level or a higher one in the same access chain. Other users can edit the record, but can only save it as another record, over which they can exert control. As a result, once NRCS creates and locks a record, they can distribute it with the confidence that it cannot be modified by less knowledgeable users.

(iii) RUSLE2 database development and management RUSLE2 is supported by databases that store factor data and data entered by users. The climatic data are held in a location/climate description stored in the database, as are the soil data in their own separate description. These can then be accessed for re-use simply by calling for them by name. The most extreme example of this approach is in the management descriptions. A management description is a list of the field operations and associated dates, including what vegetation is planted or residue added (if any). These field operation, vegetation, and residue descriptions are each stored in their own named database descriptions for potential re-use by other managements, which in turn can also be stored.

Database development began in early 2000 with the designation of a USDA-NRCS National Database Manager or 'czar' who was given the

task of expanding the initial minimal core vegetation and operation descriptions for NRCS use on cropland and pastureland, as well as assisting with the development of detailed climate descriptions, and directing and managing the importing of soils data for all available soil surveys. Working with many colleagues, the database czar populated a single nationally-coordinated database of climate, soils, operations, vegetations, residue and support practice descriptions. For consistency, field office users were 'locked out' of editing the data in these parts of the database.

Because the national database was vast, it was organized into sections that could be downloaded from the NRCS website for use in local conservation planning. Soils data were organized by state and county or soil survey area. Thus, only the soils data that a particular field office or user needed would be contained in the local database, although another soils description could be imported as needed. Climate data were organized by state for use in the same way. Management records were organized by Crop Management Zones (CMZs), 75 regions of the country with similar crops and tillage systems.

Climate records. Climate data were populated for the entire US, including Alaska, Hawaii and the Pacific islands, Puerto Rico and the Virgin Islands. The effort included extraction of the monthly parameters from the national 1960–1989 dataset (1960–1999 in some cases), with calculation of monthly *EI* values for stations with recording intervals of 15 min or shorter. These data were smoothed using several routines and visual inspection to provide a relatively smooth erosivity density 'surface', which was then used to provide point values or, more commonly, an average value over a county.

Soil records. Creation of soil descriptions in RUSLE2 was eased by making direct use of the NRCS NASIS/SURGO soil database and tools, available online at http://soils.usda.gov/technical/nasis/. This is based on an NRCS soils expert (usually the State Agronomist) downloading from NASIS all of the necessary soil descriptions, then running those through a RUSLE2 utility that extracts the necessary information, tests it for consistency, and puts it into the required RUSLE2 format. Most RUSLE2 soils databases include some generic soil descriptions based on soil texture, and these are often more appropriate for use with highly disturbed and mixed soils like those on construction sites and mine reclamation projects.

Management records. The RUSLE1 experience used the approach of organizing the US by *C* factor or *EI* distribution zones in order to develop and coordinate the issuance of *C*-factor sets for common single crop and crop rotation scenarios. With RUSLE2 implementation, this cropping region concept was built upon with the creation of 75 Crop Management Zones (CMZs), in which common crops and tillage systems were described in detail and saved as 'locked' RUSLE2 management templates. CMZs are zones in which the climate and other factors thought to control management are assumed to be constant and unaffected by political boundaries. In other words, within a CMZ the crops are likely to be grown with very similar planting and harvest dates, as well as similar tillage systems, and so on. For example, one CMZ representing the central Corn Belt stretches east from the southeastern corner of Nebraska and northwestern corner of Kansas through northern Missouri, and across central Illinois, Indiana and Ohio. Another CMZ stretches south along the eastern side of the Appalachian range from Maryland into Alabama.

With national coordination, this effort involved significant coordination among NRCS state agronomists in setting typical dates of operations and creating these management templates to represent the typical tillage systems used in growing the important crops in each CMZ. Once a set of crop management template descriptions was created by a CMZ coordinator, it was submitted to the database manager for inclusion in the national NRCS RUSLE2 database. Each CMZ set was contained in a separate RUSLE2 export file so it could be imported into the local RUSLE2 database in each field office located within the boundaries of that CMZ. This provided a starting point for field offices as they implemented RUSLE2, and also provided consistency in the use of RUSLE2 since the locked management templates were based on typical

dates and typical tillage systems used in the CMZ. Internally, the vegetations, operations and residues used by these managements all came from the same national NRCS RUSLE2 database. Users could copy templates into a local management file and change or edit the tillage system details, yields, crops and dates of operations to tailor them for use locally in specific runs, whereas the locked templates remained unedited for future use.

(iv) RUSLE2 database status Although the data developed for RUSLE1 (especially the vegetation and operation descriptions) proved invaluable in the NRCS database development efforts, development of the RUSLE2 database was still a tremendous effort. The USDA-NRCS, with initial guidance from ARS and aided by university and other cooperators, has compiled a database that includes (as of 21 July 2008): (1) 105 residues, describing how much cover each provides and how fast it decomposes; (2) 917 vegetations, from asparagus to zucchini, with each describing how the vegetation grows in terms of providing canopy cover and biomass; (3) 438 field operations, describing what happens to the soil, residue and vegetation as a result of the operation; (4) 10,976 climate descriptions; (5) 1,048,659 soil component descriptions, representing 649,032 soil map units in 3100 soil survey areas; (6) 467 special descriptions describing saved descriptions of strip-cropping, contouring, terracing, and sediment control basin practices; and (7) 26,361 managements for 75 CMZs, describing how the field operations, vegetations and residues fit together into management schemes.

8.3.3 Implementation needs and training requirements

(i) Preliminary training Initial RUSLE2 training was conducted by NRCS with assistance from the RUSLE2 development team in regional testing sessions during the period from 1999 to 2000. A minimal database, which included generic soils and only a few major crops and operations, was used for testing RUSLE2. As the training sessions progressed, it became clear that there were several background requirements that would be required of the trainees prior to full-scale training, including:

- enough background in the underlying USLE/RUSLE science to allow the trainee to understand the conceptual approach, the use of the inputs, and the meaning of the results; and
- a general understanding of how the computer program organizes information and reflects the 'conceptual model' behind RUSLE. This was enhanced by the flexibility of the program in developing very simple user interface templates, which allowed the program to be introduced at a rather basic level.

In addition, a fuller database adequately reflecting the broad range of situations that users would need to address was required for full-scale training.

(ii) NRCS RUSLE2 training Beginning in the summer of 2001, USDA-NRCS conducted regional 'train the trainer' sessions for NRCS state and area agronomists and others with erosion prediction responsibilities. These sessions were conducted by the NRCS Water Erosion cooperating scientist, national database manager, and the RUSLE2 development team. Training focused on the erosion science on which RUSLE2 is based, how to navigate the user interface, how the database structure is organized, the content of records in the various parts of the database, and hands-on experience in creating management scenarios and making simple RUSLE2 runs. One or two individuals from each state attended and began learning the model as well as learning how to train field office employees within their states. Each of these trainers then went back and conducted a series of 1–2 day RUSLE2 model training sessions to allow field office staff to develop sufficient skills such that they could make soil loss estimates using a relatively simple user template.

The regional 'train the trainer' sessions proved very valuable not only to the NRCS state personnel but also to the RUSLE2 development team, in that several NRCS user needs were identified that eventually led to enhancements and modifications

to the RUSLE2 user interface. One enhancement was the development of a rotation builder module to allow creation of multi-year and multi-crop rotations from concatenation of single-year management scenarios. This also allows rapid substitution of individual tillage system years as treatment alternatives are explored during conservation planning with producers. NRCS users also expressed a need to group RUSLE2 runs for these different alternative treatments into a 'worksheet screen', and to assemble the worksheets for multiple fields within RUSLE2, thereby representing an entire farm. This need was addressed through the development of the 'plan view' in the interface. As states began to conduct field office training sessions, an NRCS User Guide for the RUSLE2 interface was developed and distributed. Additional 'how to' guides and references were prepared for specific tasks, such as importing and exporting database components, importing soils data from NASIS soils descriptions, installing new versions, and performing database updates.

As implementation and use of RUSLE2 expanded, and as NRCS and private sector users gained experience in the model, regional advanced RUSLE2 training sessions were conducted in all regions of the US. These sessions built on the initial training and provided more in-depth training, resulting in a deeper understanding of operations, vegetations, and support practice records, of modelling erosion and sediment deposition on complex slopes, of database management, of more complex screen views, and of organizing outputs and dealing with complex management scenarios. Additionally, as users became more sophisticated, more complicated screen views and printing templates that included more detailed outputs and analysis were developed and released.

(iii) Day-to-day support A significant amount of day-to-day support was provided to states and field offices by the NRCS water erosion cooperating scientist and the national database manager during the implementation years of 2001 through to the present. This was provided through a combination of telephone and e-mail support, and direct computer-to-computer sharing of software applications. Several 1–3 hour training sessions were conducted via this latter method to provide training to multiple states on new enhancements and timely topics. Support personnel also processed hundreds or even thousands of individual requests for additional vegetations, operations and support practices, as RUSLE2 use expanded across the US.

As various other applications were being developed, access to the 24,000 + RUSLE2 crop management templates became necessary. A common file exchange format was used so that these files could be exported and utilized by the Wind Erosion Prediction System (WEPS) model (Hagen, 1996). Several other applications have used this file exchange format to utilize all subsets of the RUSLE2 management templates.

8.3.4 Most significant application enhancements

RUSLE2 includes a user convenience called the 'worksheet view' that allows comparisons or combinations of a series of hillslope profiles, each of which represents a single RUSLE2 erosion/delivery calculation. For example, the management alternative worksheet uses a single climate, soil and topographic description, but below that shows a table of management alternatives and resulting erosion and sediment delivery (Plate 4). Each line in the table represents a single RUSLE2 calculation, and all lines share the common climate, soil and topography. The idea is that each worksheet in this case represents a field, with a list of likely management options and resulting erosion values. A group of worksheets can then be combined/compared in a 'plan', which can represent a farm, with each worksheet representing a field within that farm or land parcel. Within the worksheet, the user can control which management alternatives are brought into the plan for each field, allowing for comparison of all the alternatives. Once the planning decision is made, yes/no toggles can be set to display only the scenarios representing the 'before' and 'after' management

alternatives. Thus they provide documentation of the 'before' and 'after' soil losses.

As indicated earlier, a feature added to the RUSLE2 program that greatly eased the database development effort was the inclusion of the Rotation Builder. This allowed the management scenarios to be developed as single crops, allowing the user within the program to 'paste' these together into the desired sequence. For example, the long growing seasons in the southeast US allows for multiple vegetable crops to be grown in sequence, resulting in a huge number of permutations requiring a large number of database descriptions. The Rotation Builder allows for limiting the descriptions to the single vegetations, which the RUSLE2 user can then combine within the program run as desired. If a specific combination is used frequently, the program allows users to save the combination as a single management, allowing for easy re-use.

Another RUSLE2 enhancement, developed with the support of the Wisconsin Department of Natural Resources and Dane County Land Conservation, is that the erosion and sediment delivery no longer need to be summed for the year. Conservationists working on construction sites are often interested in what happens only during some accounting period, over which the site operator is liable for erosion and sediment control. For example, the Wisconsin project defined a successful management plan as that which would keep the total sediment delivered from the site under 11 Mg ha^{-1} (5 US t ac^{-1}) during the period from the time of first soil disturbance until either placement of some non-erodible cover, or 60 days of growth of a permanent perennial vegetation. RUSLE2 allows for flexible definition of the accounting period, and of the target that must be achieved.

RUSLE2 also allows for printing a report describing the inputs and outputs of a RUSLE2 calculation. The form of the report is user-configurable, allowing users to define what they would like to see and in what form in a Microsoft Word® document. The resulting document can then be locked so that the user cannot change the results, and the associated RUSLE2 inputs can be saved into the document, allowing for a regulator to inspect the underlying information.

8.3.5 NRCS tools added to the NRCS RUSLE2 interface

Several additional calculations have been added to the NRCS RUSLE2 interface. The most prominent of these is calculation of the Soil Conditioning Index (SCI) (USDA-NRCS, 2002, examined by Zobeck *et al.*, 2007), which provides a rough estimate of whether a specific location/management/soil combination will tend to cause an increase or decrease in soil organic matter. One component of the SCI that has also proved useful is the Soil Tillage Intensity Rating (STIR), which makes use of the tillage type, tillage depth, operation speed, and percentage surface disturbance as a rough estimate of the soil disturbance cause by the operation. The STIR value is used as a criterion for NRCS's National Residue Management Practice Standards (available for download at http://www.nrcs.usda.gov/Technical/Standards/nhcp.html, accessed 3 September 2008). The STIR and SCI calculations have no impact on the RUSLE2 erosion/delivery calculations, but make use of the management operation and erosion results.

NRCS has added a calculation of management fuel usage based on the sequence of operations to the RUSLE2 interface. Several state phosphorus index calculations have also been added to the interface. Other tools were added to the NRCS RUSLE2 interface to compute a Nitrogen Leaching Index and an Energy and Fuel Use Calculator based on the tillage operations. Examples of the SCI and the Fuel Use Calculator results are shown in Plate 4.

8.3.6 Future of the technology

The science supporting RUSLE2 continues to advance and will be incorporated into future releases of the model. Two active areas of research include (1) residue production in perennial systems, and (2) ephemeral gully erosion estimation.

In most USDA erosion models (e.g. WEPP, WEPS, RUSLE1), residue production occurs only during senescence of a crop and is calculated from the decline in live biomass. This is equivalent to the assumption that there is no dead biomass production during periods of increasing biomass, and no additional growth after the peak biomass is reached. This is probably a reasonable and acceptable assumption for the treatment of annual crops. However, in perennial vegetation and in mixed stands where different components mature at different times, death and growth usually occur simultaneously. A new type of vegetation description is being developed for RUSLE2 in which residue production is more continuous, based on the assumption that live biomass has an effective life span. In the absence of forage harvest or biomass removal, the daily change in live biomass amount is calculated as the difference between new growth and the death of old growth. Live biomass that is not harvested is added to a dead biomass pool after its lifespan is reached, thereby providing the soil the benefits of additional residue cover. Users input monthly potential growth patterns and shoot and root life-spans, and RUSLE2 calculates corresponding residue production patterns. Growth patterns are altered in response to management operations involving biomass removal. Daily changes in residue biomass are then calculated as the difference between death and decomposition or residue harvest. RUSLE2's new routines will simplify the creation of vegetation descriptions for perennial systems, providing more realistic estimates of residue creation throughout the year, and thereby improving runoff and erosion estimation for pastures, hay fields, and other systems dominated by perennial vegetation.

To predict average annual ephemeral gully erosion is challenging because there is no existing long-term database of ephemeral gully erosion rates comparable to the plot database underlying the USLE, which in turn underlies RUSLE. Ephemeral gully erosion is a process inherently driven by larger-than-average runoff events (see Chapter 19). Many process-based models have developed climate-generators (e.g. CREAMS: Knisel, 1980) that reproduce the stochasticity of weather. Applying these long-term weather records to an ideal runoff and erosion model would create a distribution of runoff and erosion events. Taking the monthly means of this population of ephemeral gully erosion events would represent the long-term average values needed to complement RUSLE2 sheet and rill erosion estimates and to estimate long-term average ephemeral gully erosion. The RUSLE2 developers proposed that modelling the correct storm amount and sequence of storms could reproduce the mean values. Toward this end, techniques to predict a sequence of index storms for any combination of soil and management anywhere within the continental US (and elsewhere, with appropriate calibration) have been developed, and require only RUSLE2 climate and profile-level information. The results approximate the mean monthly runoff, annual runoff event frequency, and a gamma distribution function scale parameter that characterizes 30-year stochastic runoff predictions generated using the AnnAGNPS (annualized Agricultural Non-Point Source) model (Bingner & Theurer, 2001).

By taking the largest in a series of runoff events as a 6-month return period event, and scaling the magnitudes of the periodic runoff events proportional to the long-term average disaggregated daily runoff amounts on event days, these parameters allow estimation of the date and size of a series of index runoff events that are proposed as the basis for an ephemeral gully calculation capability within RUSLE2. Index event RUSLE2 hillslope runoff, sediment yield, and sediment size distribution will be coupled with a physically-based ephemeral gully erosion model, possibly that used in CREAMS, to predict annual average ephemeral gully erosion.

8.3.7 RUSLE2 examples

RUSLE2 is so flexible that it is very difficult to decide which capabilities to show in a few examples, and in which form to display those. In narrowing the possibilities, it was decided to concentrate on three examples. The first example

is included especially to dispel the notion that RUSLE2 is difficult and complicated to use. The other examples represent two common uses of RUSLE2. The second example compares management alternatives on a single field, as would probably be done by a conservation planner working with an agricultural producer. The third example demonstrates planning to meet a specific sediment delivery target on a construction site. In both of these latter cases the figure will appear relatively complex, but this complexity was added so that specific features could be highlighted.

(i) Example 1. Very simple view One of the complaints sometimes lodged against RUSLE2 is that it is too complex and difficult for a novice user. As described in the sections above, the complexity the user sees in RUSLE2 is totally controlled by what the user asks to see and how they ask to see it. The calculations are exactly the same for a simple view (Plate 5) as for a more complex one, except that fewer calculations may be needed because fewer outputs are requested. The user views are completely user-configurable, so there is an infinite number of possible views, not just some pre-specified simple, medium and complex views. The RUSLE2 screen capture (Plate 5) shows one of the simpler views, which could be used by someone with a minimal understanding of soil erosion. In order to get an erosion and sediment delivery result, the user need only select a location (climate), a soil, and a management from pre-existing lists in the database. They then enter a slope length and steepness (which assumes a uniform slope), and can immediately see the resulting erosion and sediment delivery. If desired, this view also allows the user to select from pre-defined contour or cross-slope tillage systems, to put in pre-defined vegetated barriers on or at the bottom of the slope, or to see what happens if pre-defined terrace systems are installed. If the trainer or program supplier believes that even these few conservation practices will not be understood by the target user, even these entries associated with Step 5 in the view above may be easily removed.

In this access level and view, the user has no way of directly modifying any of the inputs except slope length and steepness. Everything else must be selected from pre-defined descriptions in the database, presumably placed there by someone with the training and knowledge to do so. Most users are not long satisfied with so little flexibility. For example, they may want to be able to see the impact of a complex slope shape rather than being forced to assume a uniform slope. This increased power comes at the cost of increased complexity, as the user must now be faced with a user template allowing them to enter length and steepness values for the slope segments. This constant desire for more power and flexibility results in what the RUSLE2 development team calls 'template creep', which is the tendency of user templates to become increasingly complex over time in order to provide additional power. The RUSLE2 complexity that some users complain of is not built into the RUSLE2 program, but rather exists because other users who developed that user template thought those entries and outputs were necessary.

Finally, notice that Plate 5 shows the inputs and results in metric units, while the values shown in Plate 4 were in Imperial units. This demonstrates some of the additional flexibility of the RUSLE2 interface, which allows for any desired mixing and matching of units, and also for selecting the desired units within a system (e.g. cm or mm for height).

(ii) Example 2. Agricultural conservation planning The RUSLE2 screen capture shown earlier in Plate 4 presents the results of conservation planning on a hypothetical field. In this view the field is defined as having a single climate, soil, and uniform slope. Each line in the table then represents a single RUSLE2 erosion calculation, using the climate, soil and topography defined above, and combining it with a unique combination of contouring, terraces and cropping sequence to yield erosion, fuel use, and Soil Conditioning Index (SCI) results. In order from the top of the table, the lines represent: (1) corn with moldboard ploughing in the fall and disking in the spring,

tilled and planted up-and-down the slope; (2) the same tillage, but close to the contour; (3) the same as (2), but with a single terrace in the middle of the slope; (4) fall chisel ploughing up-and-down the slope; (5) fall chisel ploughing, but close to the contour; and (6) fall strip tillage, where in the fall only a narrow strip is disturbed in knifing in nitrogen. The results for each line show the planner not only the erosion and sediment yield associated with each alternative, but also the estimated fuel cost and the SCI value for that option, with values > 0 indicating a net increase in soil organic carbon over time. These generally show the expected results, with the reduced tillage option resulting in the lowest erosion, fuel cost, and highest SCI values.

The graphs shown in Plate 4 indicate some of RUSLE2's capability in graphically representing results. In this case the graphs are of the percentage of soil surface covered by crop residue, with the graph on the left for the fall moldboard plough scenario, and that on the right for the strip till management. In addition, although it is not displayed here, the crop yields for each of the management alternatives can be set by the user, if it is thought that the management sequence has an effect on those.

(iii) Example 3. Construction site sediment control As described above, although the RUSLE2 calculations for estimating erosion and sediment yield for construction sites are no different from those for agricultural settings, the RUSLE2 flexibility allows for a substantially different look and feel, which makes it easier to use in construction settings. Several of these differences are shown in Plate 6.

One primary difference seen here is that for construction sites the primary output of interest is not the soil erosion on the hillslope, but rather the sediment delivery to the receiving channel, representing the off-site impact. In fact, it is often comparison of this value to some defined standard rather than comparison of average annual soil loss with the soil loss tolerance (*T*) (Johnson, 1987) that indicates the success or failure of a construction plan.

Another difference is the look and feel of the screen itself, including especially the visible icons and the text. These can be things as trivial as using a bulldozer icon instead of a tractor to represent field operations, or as substantial as completely different text shown on the screen for the same parameter, reflecting differences in terminology. For example, in agricultural settings we generally speak of crops and of crop residues added to the surface, while in construction settings we would use the more generic vegetation and surface cover materials, including synthetic blankets and added mulches as well as residues from the vegetation grown on the site.

Another difference mentioned above is the ability of RUSLE2 to aggregate results not only on an average annual basis, but over a user-defined accounting period. For example, in the situation shown here, the accounting period is defined as beginning from the time of the first soil disturbance until either the application of some non-erodible permanent material (e.g. pavement, sod, or landscaping materials) or 60 days of growth of perennial vegetation, with days whose average temperature falls below 35°F not counted. In Plate 6, the two bottommost results in the lower left-hand corner indicate whether the system meets the definition of the accounting period, and a green or red colour in the rectangle indicates whether the system did or did not meet the allowable sediment delivery threshold, in this case set by the regulatory body as a total of no more than 5 Mg ha^{-1} (2 US t ac^{-1}) over the entire accounting period.

Users indicated that for construction site use – unlike for agricultural use – there would be little need for the capability to save and re-use management descriptions, as the timing of field operations would vary tremendously due to many factors. Because of this, the view in Plate 6 shows the management scenario description (dates and descriptions of field operations) directly within the general RUSLE2 profile view, rather than named and stored as a separate database record.

These users also indicated a need to define complex slope topography, as they wanted to be able to account for the deposition occurring on

the flatter portion at the bottom of an S-shaped slope: thus the complexity of Step 3 in Plate 6, which in the previous views was shown simply as single uniform slope length and steepness. The slope schematic in the upper-right corner of the view displays this complexity. The upper (management) layer of this schematic shows a management break about 55 ft (16.8 m) down the slope. This is caused by the selection in Step 5 of a pre-defined strip-barrier system, which in this case puts a single 20-ft strip of poor stand cool-season grass at the bottom of the slope. In addition, Step 5 sets that the runoff from the bottom of the slope feeds to a sediment basin, which is pre-defined as having an 80% settling efficiency for a silt loam soil that has not experienced previous deposition. This last clause is important because any deposition occurring before the runoff hits the sediment basin will cause the coarse material to settle out, thereby reducing the actual efficiency of the basin. In the specific case shown here, there will be deposition at the bottom of the slope caused by both the decreased slope steepness and the grass strip, so the basin will not provide 80% efficiency. If they had so desired, the users could have added additional complexity to the view to show where the deposition actually occurred, but this was not deemed worthwhile.

8.4 Summary

Soil erosion has long been recognized as a serious problem. Considerable efforts have been expended to address this problem, beginning in Missouri in 1923 and supported by the US Congress in a 1929 appropriation that initiated intensive soil erosion research. Early efforts to preserve soil and prevent erosion through the work of pioneers like H.H. Bennett led to an early period of plot scale conservation research at sites representing the ten major farming regions in the US. The 6 ft (1.8 m) wide by 72.6 ft (22.1 m) long (0.01 acre, 40 m^2) research plots were constructed to represent various crops and rotations. Primary measurements included precipitation, runoff and soil loss (erosion). The results from this research, in combination with additional crops and cultural practices data, ultimately provided a repository of data widely used by engineers and scientists to evaluate conservation practices. These data were the foundation of the empirical erosion prediction technologies and ultimately the Universal Soil Loss Equation (USLE).

The USLE was developed at Purdue University under the direction of Walter Wischmeier, with able assistance from Dwight Smith, and was published in 1965 and 1978 in two handbooks (AH282 and AH537). The handbooks became widely accepted for conservation farming (and especially soil erosion by water) in the US. In the early 1980s a program to develop technology to replace the USLE was initiated. The computer-based RUSLE (Revised Universal Soil Loss Equation) model was published in 1997. RUSLE incorporated significant advances over the USLE and permitted application of soil erosion estimation for a greater variety of crops and management practices beyond those in the original USLE database.

RUSLE was subsequently revised to include advanced scientific and interface technology and subsequently delivered as RUSLE2, along with expanded databases and more control over the parameters that specific users could see and change. The USDA-NRCS has accepted responsibility for the underlying databases within the US, which include descriptions of climates, vegetations and soils, along with extensive files describing common management practices. RUSLE2 is widely recognized as a major advance in erosion prediction and conservation technology, and provides a very flexible tool allowing resource conservationists, managers and developers to compare a broad range of management alternatives in deciding on an optimum resource use.

References

Austin, M.E. (1981) Land resource regions and major land resource areas of the United States. *USDA Agricultural Handbook No.* 296. 156 pp.

Bengtson, R.L. & Sabbage, G. (1988) *USLE P-factors for subsurface drainage in a hot, humid climate*. ASAE

Paper 88-2122, American Society of Agricultural Engineers, St. Joseph, MI.

Bingner, R.L. & Theurer, F.D. (2001) AnnAGNPS: estimating sediment yield by particle size for sheet and rill erosion. *Proc. 7th Federal Interagency Sedimentation Conference*, Reno, NV, 25–29 March 2001. I-1–I-7.

Brakensiek, D.L., Osborn, H.B. & Rawls, W.J. (Coordinators) (1979) Field manual for research in agricultural hydrology. *USDA Agriculture Handbook* No. 224. 550 pp.

Dissmeyer, G.E. & Foster, G.R. (1981) Estimating the cover-management factor (C) in the Universal Soil Loss Equation for forest conditions. *Journal of Soil and Water Conservation* **36**: 235–40.

Dissmeyer, G.E. & Foster, G.R. (1984) *A Guide for Predicting Sheet and Rill Erosion on Forest Land*. USDA-Forest Service Technical Publication R8-TP.

Ellison, W.D. (1947) Soil erosion studies. *Agricultural Engineering* **28**: 145–6, 197–201, 245–8, 297–300, 349–51, 402–5, 442–4.

Formanek, G.E., Ross, E. & Istok, J. (1987) Subsurface drainage for erosion reduction on croplands in northwestern Oregon. In *Irrigation Systems for the 21st Century*. Proceedings of the Irrigation and Drainage Division Special Conference, American Society of Civil Engineers, New York: 25–31.

Foster, G.R., Lane, L.J., Nowlin, J.D., *et al.* (1980) A model to estimate sediment from field-sized areas. In *CREAMS, A field scale model for chemicals, runoff, and erosion from agricultural management systems*. USDA, Conservation Research Report No. 26, pp. 36–64.

Foster, G.R., McCool, D.K., Renard, K.G. & Moldenhauer, W.C. (1981) Conversion of the USLE to SI metric units. *Journal of Soil and Water Conservation* **36**: 355–9.

Foster, G.R., Johnson, C.B. & Moldenhauer, W.C. (1982) Hydraulic failure of unanchored cornstalk and wheat straw mulches for erosion control. *Transactions of the American Society of Agricultural Engineers* **25**: 940–47.

Foster, G.R., Young, R.A. & Neibling, W.H. (1985) Sediment composition for nonpoint source pollution analyses. *Transactions of the American Society of Agricultural Engineers* **28**: 133–9, 146.

Foster, G.R., Yoder, D.C., McCool, D.K., *et al.* (2000) *Improvements in science in RUSLE2*. 2000 ASAE Annual International Meeting, Technical Papers; Engineering Solutions for a New Century **2**: 2871–89 (paper no. 00-2147).

Foster, G.R., Toy, T.J. & Renard, K.G. (2003) Comparison of the USLE, RUSLE1.06c, and RUSLE2, for application to highly disturbed land. In *First Interagency Conference on Research in the Watersheds*. USDA-ARS Agricultural Research Service. Washington, DC: 154–60.

Gregory, J.M. (1982) Soil surface prediction with various amounts and types of crop residue. *Transactions of the American Society of Agricultural Engineers* **25**: 1333–7.

Hagen, L.J. (ed.) (1996) *Wind Erosion Prediction System technical documentation*. USDA-ARS. Available at http://www.weru.ksu.edu/weps/docs/weps_tech.pdf [accessed 4 October 2008].

Helms, D. (2008) *Hugh Hammond Bennett and the Creation of the Soil Erosion Service*. USDA Natural Resources Conservation Service. Historical Insights No. 8. 13 pp.

Knisel, W.G. (1980) A field scale model for chemicals, runoff and erosion from agricultural management systems. *USDA Conservation Research Report No.* 26. USDA, Washington, DC. 643 pp.

Johnson, L.C. (1987) Soil loss tolerance: fact or myth? *Journal of Soil and Water Conservation* **42**: 155–60.

Laflen, J.M. & Moldenhauer, W.C. (2003) *Pioneering soil erosion prediction: the USLE story*. Special Publication No. 1, World Association of Soil & Water Conservation. Beijing, China. 54 pp.

McCool, D.K., Foster, G.R., Mutchler, C.K. & Meyer, L.D. (1987) Revised slope steepness factor for the Universal Soil Loss Equation. *Transactions of the American Society of Agricultural Engineers* **30**: 1387–96.

McCool, D.K., Foster, G.R., Mutchler, C.K. & Meyer, L.D. (1989) Revised slope length factor for the Universal Soil Loss Equation. *Transactions of the American Society of Agricultural Engineers* **32**: 1571–6.

McCool, D.K., George, G.E., Freckleton, M., *et al.* (1993) Topographic effect of erosion from cropland in the Northwestern Wheat Region. *Transactions of the American Society of Agricultural Engineers* **36**: 771–5.

Meyer, L.D. & Moldenhauer, W.C. (1985) Soil erosion research: a historical perspective. In *Agricultural History*. University of California Press, Berkeley, CA: 192–204.

Mutchler, C.K. (1970) Splash of a waterdrop at terminal velocity. *Science* **169**: 1311–12.

Renard, K.G. (1985) Rainfall simulators and USDA erosion Research; history, perspective, and future.

In Lane, L.J. (ed.), *Proceedings of the Rainfall Simulator Workshop*, Tucson, AZ. Society for Range Management, Denver, CO: 3–6.

Renard, K.G., Foster, G.R., Weesies G.A., *et al*. (Coordinators). (1997) *Predicting Soil Erosion by Water: A guide to conservation planning with the Revised Universal Soil Loss Equation (RUSLE)*. USDA Agricultural Handbook No. 703, 404 pp. Available at http://www.ars.usda.gov/SP2UserFiles/Place/64080530/RUSLE/AH_703.pdf [accessed 3 September 2008].

Römkens, M.J.M. (1985) The soil erodibility factor: a perspective. In El-Swaify, S.A., Moldenhauer, W.C. & Lo, A. (eds), *Soil Erosion and Conservation*. Soil and Water Conservation Society, Ankeny, IA: 445–61.

USDA-ARS (2008a) Draft science documentation, Revised Universal Soil Loss Equation, Version 2. Available at http://www/ars.usda.gov/sp2UserFiles/Place/64080510/RUSLE/RUSLE2_Science_Doc.pdf [accessed 3 September 2008].

USDA-ARS (2008b) Draft user's reference guide, Revised Universal Soil Loss Equation, Version 2. Available at http://www.ars.usda.gov/sp2UserFiles/Place/64080510/RUSLE/RUSLE2_User_Ref_guide.pdf [accessed 3 September 2008].

USDA-NRCS (2002) National agronomy manual, section 508. Available at http://www.info.usda.gov/media/pdf/M_190_NAM.pdf [accessed 3 September 2008].

USDA-NRCS (2008) ftp://fargo.nserl.purdue.edu/pub/RUSLE2/NRCS Base Database/ [accessed 3 September 2008].

Weiss, L.L. (1964) Ratio of true to fixed-interval maximum rainfall. *Journal of the Hydraulics Division ASCE* **90**(HY1): 77–82.

Wischmeier, W.H. (1959) A rainfall erosion index for a universal soil-loss equation. *Soil Science Society of America Proceedings* **23**: 246–9.

Wischmeier, W.H. (1974) *New developments in estimating water erosion*. Proceedings, 29th Annual Meeting of the Soil Science Society of America, Madison, WI: 179–86.

Wischmeier, W.H. & Smith, D.D. (1965) *Predicting rainfall-erosion losses from cropland east of the Rocky Mountains: a guide for selecting practices for soil and water conservation*. USDA Agricultural Handbook No. 282. Available at http://www.ars.usda.gov/SP2UserFiles/Place/64080530/RUSLE/AH_282.pdf [accessed 3 September 2008].

Wischmeier, W.H. & Smith, D.D. (1978) *Predicting rainfall-erosion losses – a guide to conservation farming*. USDA Agricultural Handbook No. 537. Available in scanned pdf format at http://www.ars.usda.gov/SP2UserFiles/Place/64080530/RUSLE/AH_537.pdf [accessed 3 September 2008].

Zobeck, T.M., Crownover, J., Dollar, M., *et al*. (2007) Investigation of Soil Conditioning Index values for Southern High Plains agroecosystems. *Journal of Soil and Water Conservation* **62**: 433–43.

Assessment of erosion, sedimentation, and water quality impacts of the Mountain Valley Pipeline and Equitrans Expansion Project's proposed crossing of the Jefferson National Forest as it pertains to the U.S. Forest Service's Draft Supplemental Environmental Impact Statement dated December 2022

Prepared by Jonathan A. Czuba, Ph.D., Licensed Professional Engineer - February 9, 2023

REFERENCES
12

February 21, 2023

PREDICTING RAINFALL EROSION LOSSES

A GUIDE TO CONSERVATION PLANNING

UNITED STATES DEPARTMENT OF AGRICULTURE

AGRICULTURE HANDBOOK NUMBER 537

PREPARED BY SCIENCE AND EDUCATION ADMINISTRATION

PREDICTING RAINFALL EROSION LOSSES

A GUIDE TO CONSERVATION PLANNING

Supersedes Agriculture Handbook No. 282,
"Predicting Rainfall-Erosion Losses From Cropland East of the Rocky Mountains"

Science and Education Administration
United States Department of Agriculture
in cooperation with
Purdue Agricultural Experiment Station

December 1978

ABSTRACT

Wischmeier, W. H., and Smith, D.D. 1978. Predicting rainfall erosion losses—a guide to conservation planning. U.S. Department of Agriculture, Agriculture Handbook No. 537.

The Universal Soil Loss Equation (USLE) enables planners to predict the average rate of soil erosion for each feasible alternative combination of crop system and management practices in association with a specified soil type, rainfall pattern, and topography. When these predicted losses are compared with given soil loss tolerances, they provide specific guidelines for effecting erosion control within specified limits. The equation groups the numerous interrelated physical and management parameters that influence erosion rate under six major factors whose site-specific values can be expressed numerically. A half century of erosion research in many States has supplied information from which at least approximate values of the USLE factors can be obtained for specified farm fields or other small erosion prone areas throughout the United States. Tables and charts presented in this handbook make this information readily available for field use. Significant limitations in the available data are identified.

The USLE is an erosion model designed to compute longtime average soil losses from sheet and rill erosion under specified conditions. It is also useful for construction sites and other nonagricultural conditions, but it does not predict deposition and does not compute sediment yields from gully, streambank, and streambed erosion.

Keywords: Conservation practices, conservation tillage, construction sites, crop canopy, crop sequence, delivery ratios, erosion factors, erosion index, erosion prediction, erosion tolerances, erosivity, gross erosion, minimum tillage, no-till, rainfall characteristics, rainfall data, residue mulch, runoff, sediment, sediment delivery, slope effect, water quality, soil erodibility.

For sale by the Superintendent of Documents, U.S. Government Printing Office
Washington, D.C. 20402

Stock Number 001-000-03903-2

CONTENTS

TABLES

FIGURES

PREDICTING RAINFALL EROSION LOSSES— A GUIDE TO CONSERVATION PLANNING

Walter H. Wischmeier and Dwight D. Smith[1]

PURPOSE OF HANDBOOK

Scientific planning for soil and water conservation requires knowledge of the relations between those factors that cause loss of soil and water and those that help to reduce such losses. Controlled studies on field plots and small watersheds have supplied much valuable information regarding these complex factor interrelations. But the greatest possible benefits from such research can be realized only when the findings are converted to sound practice on the numerous farms and other erosion prone areas throughout the country. Specific guidelines are needed for selecting the control practices best suited to the particular needs of each site.

The soil loss prediction procedure presented in this handbook provides such guidelines. The procedure methodically combines research information from many sources to develop design data for each conservation plan. Widespread field experience for more than two decades has proved it highly valuable as a conservation planning guide.

The procedure is founded on an empirical soil loss equation that is believed to be applicable wherever numerical values of its factors are available. Research has supplied information from which at least approximate values of the equation's factors can be obtained for specific farm fields or other small land areas throughout most of the United States. Tables and charts presented in this handbook make this information readily available for field use.

This revision of the 1965 handbook (*64*) updates the content and incorporates new material that has been available informally or from scattered research reports in professional journals. Some of the original charts and tables are revised to conform with additional research findings, and new ones are developed to extend the usefulness of the soil loss equation. In some instances, expanding a table or chart sufficiently to meet the needs for widespread field application required projection of empirical factor relationships appreciably beyond the physical limits of the data from which the relationships were derived. Estimates obtained in this manner are the best information available for the conditions they represent. However, the instances are identified in the discussions of the specific erosion factors, tables, and charts. Major research needs are suggested by these discussions and were recently summarized in an available publication by Stewart and others (*42*).

HISTORY OF SOIL LOSS EQUATIONS

Developing equations to calculate field soil loss began about 1940 in the Corn Belt. The soil loss estimating procedure developed in that region between 1940 and 1956 has been generally referred to as the slope-practice method. Zingg (*64*)[2] published an equation in 1940 relating soil loss rate to length and percentage of slope. The following year, Smith (*38, 39*) added crop and conservation practice factors and the concept of a specific soil loss limit, to develop a graphical method for

[1] Retired. Former research statistician (water management), Science and Education Administration (SEA), and professor emeritus, agricultural engineering, Purdue University, West Lafayette, Ind.; and agricultural engineer, SEA, Beltsville, Md.

[2] Numbers in parentheses refer to References p. 48.

determining conservation practices on Shelby and associated soils of the Midwest. Browning and associates (*6*) added soil and management factors and prepared a set of tables to simplify field use of the equation in Iowa. Research scientists and operations personnel of the Soil Conservation Service (SCS) in the North Central States worked together in developing the slope-practice equation for use throughout the Corn Belt.

A national committee met in Ohio in 1946 to adapt the Corn Belt equation to cropland in other regions. This committee reappraised the Corn Belt factor values and added a rainfall factor. The resulting formula, generally known as the Musgrave Equation (*31*), has been widely used for estimating gross erosion from watersheds in flood abatement programs. A graphical solution of the equation was published in 1952 (*19*) and used by the SCS in the Northeastern States.

The soil loss equation presented in this handbook has become known as the Universal Soil Loss Equation (USLE). Regardless of whether the designation is fully accurate, the name does distinguish this equation from the *regionally* based soil loss equations. The USLE was developed at the National Runoff and Soil Loss Data Center established in 1954 by the Science and Education Administration (formerly Agricultural Research Service) in cooperation with Purdue University. Federal-State cooperative research projects at 49 locations[3] contributed more than 10,000 plot-years of basic runoff and soil loss data to this center for summarizing and overall statistical analyses. After 1960, rainfall simulators (*23*) operating from Indiana, Georgia, Minnesota, and Nebraska were used on field plots in 16 states to fill some of the gaps in the data needed for factor evaluation.

Analyses of this large assembly of basic data provided several major improvements for the soil loss equation (*53*): (a) a rainfall erosion index evaluated from local rainfall characteristics; (b) a quantitative soil erodibility factor that is evaluated directly from soil property data and is independent of topography and rainfall differences; (c) a method of evaluating cropping and management effects in relation to local climatic conditions; and (d) a method of accounting for effects of interactions between crop system, productivity level, tillage practices, and residue management.

Developments since 1965 have expanded the use of the soil loss equation by providing techniques for estimating site values of its factors for additional land uses, climatic conditions, and management practices. These have included a soil erodibility nomograph for farmland and construction areas (*58*); topographic factors for irregular slopes (*12, 55*); cover factors for range and woodland (*57*); cover and management effects of conservation tillage practices (*54*); erosion prediction on construction areas (*61, 24, 25*); estimated erosion index values for the Western States and Hawaii (*5, 21, 55*); soil erodibility factors for benchmark Hawaii soils (*9*); and improved design and evaluation of erosion control support practices (*17, 36*).

Research is continuing with emphasis on obtaining a better understanding of the basic principles and processes of water erosion and sedimentation and development of fundamental models capable of predicting specific-storm soil losses and deposition by overland flow (*10, 11, 22, 26, 32*). The fundamental models have been helpful for understanding the factors in the field soil loss equation and for interpreting the plot data.

SOIL LOSS TOLERANCES

The term "soil loss tolerance" denotes the maximum level of soil erosion that will permit a high level of crop productivity to be sustained economically and indefinitely.

---

[3] The data were contributed by Federal-State cooperative research projects at the following locations: Batesville, Ark.; Tifton and Watkinsville, Ga.; Dixon Springs, Joliet, and Urbana, Ill.; Lafayette, Ind.; Clarinda, Castana, Beaconsfield, Independence, and Seymour, Iowa; Hays, Kans.; Baton Rouge, La.; Presque Isle, Maine; Benton Harbor and East Lansing, Mich.; Morris, Minn.; Holly Springs and State College, Miss.; Bethany and McCredie, Mo.; Hastings, Nebr.; Beemerville, Marlboro, and New Brunswick, N.J.; Ithaca, Geneva, and Marcellus, N.Y.; Statesville and Raleigh, N.C.; Coshocton and Zanesville, Ohio; Cherokee and Guthrie, Okla.; State College, Pa.; Clemson and Spartanburg, S.C.; Madison, S.Dak.; Knoxville and Greeneville, Tenn.; Temple and Tyler, Tex.; Blacksburg, Va.; Pullman, Wash.; LaCrosse, Madison, and Owen, Wis.; and Mayaguez, P.R.

The major purpose of the soil loss equation is to guide methodical decisionmaking in conservation planning on a site basis. The equation enables the planner to predict the average rate of soil erosion for each of various alternative combinations of crop system, management techniques, and control practices on any particular site. When these predicted losses can be compared with a soil loss tolerance for that site, they provide specific guidelines for effecting erosion control within the specified limits. Any cropping and management combination for which the predicted erosion rate is less than the tolerance may be expected to provide satisfactory erosion control. From the satisfactory alternatives indicated by this procedure, the one best suited to a particular farm or other enterprise may then be selected.

Soil loss tolerances ranging from 5 to 2 t/A/year for the soils of the United States were derived by soil scientists, agronomists, geologists, soil conservationists, and Federal and State research leaders at six regional workshops in 1961 and 1962. Factors considered in defining these limits included soil depth, physical properties and other characteristics affecting root development, gully prevention, on-field sediment problems, seeding losses, soil organic matter reduction, and plant nutrient losses. A deep, medium-textured, moderately permeable soil that has subsoil characteristics favorable for plant growth has a greater tolerance than soils with shallow root zones or high percentages of shale at the surface. Widespread experience has shown these soil loss tolerances to be feasible and generally adequate for sustaining high productivity levels indefinitely. Some soils with deep favorable root zones may exceed the 5-t tolerance without loss of sustained productivity.

Soil loss limits are sometimes established primarily for water quality control. The criteria for defining field soil loss limits for this purpose are not the same as those for tolerances designed to preserve cropland productivity. Soil depth is not relevant for offsite sediment control, and uniform limits on erosion rates will allow a range in the quantities of sediment per unit area that are delivered to a river. Soil material eroded from a field slope may be deposited in the field boundaries, in terrace channels, in depressional areas, or on flat or vegetated areas traversed by the overland flow before it reaches a river. The erosion damages the cropland on which it occurs, but sediment deposited near its place of origin is not directly relevant for water quality control.

If the soil loss tolerance designed for sustained cropland productivity fails to attain the desired water quality standard, flexible limits that consider other factors should be developed rather than uniformly lowering the soil loss tolerance. These factors include distance of the field from a major waterway, the sediment transport characteristics of the intervening area, sediment composition, needs of the particular body of water being protected, and the probable magnitude of fluctuations in sediment loads (*42*). Limits of sediment yield would provide more uniform water quality control than lowering the limits on soil movement from field slopes. They would also require fewer restrictions on crop system selection for fields from which only small percentages of the eroded soil become off-farm sediment.

SOIL LOSS EQUATION

The erosion rate at a given site is determined by the particular way in which the levels on numerous physical and management variables are combined at that site. Physical measurements of soil loss for each of the large number of possible combinations in which the levels of these variable factors can occur under field conditions would not be feasible. Soil loss equations were developed to enable conservation planners to project limited erosion data to the many localities and conditions that have not been directly represented in the research.

The USLE is an erosion model designed to predict the longtime average soil losses in runoff from specific field areas in specified cropping and management systems. Widespread field use has substantiated its usefulness and validity for this purpose. It is also applicable for such nonagricultural conditions as construction sites.

With appropriate selection of its factor values, the equation will compute the average soil loss for a multicrop system, for a particular crop year in a rotation, or for a particular cropstage period within a crop year. It computes the soil loss for a given

site as the product of six major factors whose most likely values at a particular location can be expressed numerically. Erosion variables reflected by these factors vary considerably about their means from storm to storm, but effects of the random fluctuations tend to average out over extended periods. Because of the unpredictable short-time fluctuations in the levels of influential variables, however, present soil loss equations are substantially less accurate for prediction of specific events than for prediction of longtime averages.

The soil loss equation is

$$A = R K L S C P \qquad (1)$$

where

A is the computed soil loss per unit area, expressed in the units selected for **K** and for the period selected for **R**. In practice, these are usually so selected that they compute **A** in tons per acre per year, but other units can be selected.

R, the rainfall and runoff factor, is the number of rainfall erosion index units, plus a factor for runoff from snowmelt or applied water where such runoff is significant.

K, the soil erodibility factor, is the soil loss rate per erosion index unit for a specified soil as measured on a unit plot, which is defined as a 72.6-ft length of uniform 9-percent slope continuously in clean-tilled fallow.

L, the slope-length factor, is the ratio of soil loss from the field slope length to that from a 72.6-ft length under identical conditions.

S, the slope-steepness factor, is the ratio of soil loss from the field slope gradient to that from a 9-percent slope under otherwise identical conditions.

C, the cover and management factor, is the ratio of soil loss from an area with specified cover and management to that from an identical area in tilled continuous fallow.

P, the support practice factor, is the ratio of soil loss with a support practice like contouring, stripcropping, or terracing to that with straight-row farming up and down the slope.

The soil loss equation and factor evaluation charts were initially developed in terms of the English units commonly used in the United States. The factor definitions are interdependent, and direct conversion of acres, tons, inches, and feet to metric units would not produce the kind of integers that would be desirable for an expression of the equation in that system. Therefore, only the English units are used in the initial presentation of the equation and factor evaluation materials, and their counterparts in metric units are given in the Appendix under **Conversion to Metric System.**

Numerical values for each of the six factors were derived from analyses of the assembled research data and from National Weather Service precipitation records. For most conditions in the United States, the approximate values of the factors for any particular site may be obtained from charts and tables in this handbook. Localities or countries where the rainfall characteristics, soil types, topographic features, or farm practices are substantially beyond the range of present U.S. data will find these charts and tables incomplete and perhaps inaccurate for their conditions. However, they will provide guidelines that can reduce the amount of local research needed to develop comparable charts and tables for their conditions.

The subsection on **Predicting Cropland Soil Losses**, page 40 illustrates how to select factor values from the tables and charts. Readers who have had no experience with the soil loss equation may wish to read that section first. After they have referred to the tables and figures and located the values used in the sample, they may move readily to the intervening detailed discussions of the equation's factors.

The soil loss prediction procedure is more valuable as a guide for selection of practices if the user has a general knowledge of the principles and factor interrelations on which the equation is based. Therefore, the significance of each factor is discussed before presenting the reference table or chart from which local values may be obtained. Limitations of the data available for evaluation of some of the factors are also pointed out.

RAINFALL AND RUNOFF FACTOR (R)

Rills and sediment deposits observed after an unusually intense storm have sometimes led to the conclusion that the significant erosion is associated with only a few storms, or that it is solely a function of peak intensities. However, more than 30 years of measurements in many States have shown that this is not the case (*51*). The data show that a rainfall factor used to estimate average annual soil loss must include the cumulative effects of the many moderate-sized storms, as well as the effects of the occasional severe ones.

The numerical value used for **R** in the soil loss equation must quantify the raindrop impact effect and must also provide relative information on the amount and rate of runoff likely to be associated with the rain. The rainfall erosion index derived by Wischmeier (*49*) appears to meet these requirements better than any other of the many rainfall parameters and groups of parameters tested against the assembled plot data. The local value of this index generally equals **R** for the soil loss equation and may be obtained directly from the map in figure 1. However, the index does not include the erosive forces of runoff from thaw, snowmelt, or irrigation. A procedure for evaluating **R** for locations where this type of runoff is significant will be given under the topic **R Values for Thaw and Snowmelt.**

Rainfall Erosion Index

The research data indicate that when factors other than rainfall are held constant, storm soil losses from cultivated fields are directly proportional to a rainstorm parameter identified as the **EI** (defined below) (*49*). The relation of soil loss to this parameter is linear, and its individual storm values are directly additive. The sum of the storm **EI** values for a given period is a numerical measure of the erosive potential of the rainfall within that period. The average annual total of the storm **EI** values in a particular locality is the rainfall erosion index for that locality. Because of apparent cyclical patterns in rainfall data (*33*), the published rainfall erosion index values were based on 22-year station rainfall records.

Rain showers of less than one-half inch and separated from other rain periods by more than 6 hours were omitted from the erosion index computations, unless as much as 0.25 in of rain fell in 15 min. Exploratory analyses showed that the **EI** values for such rains are usually too small for practical significance and that, collectively, they have little effect on monthly percentages of the annual **EI.** The cost of abstracting and analyzing 4,000 location-years of rainfall-intensity data was greatly reduced by adopting the 0.5-in threshold value.

EI Parameter

By definition, the value of **EI** for a given rainstorm equals the product, total storm energy (**E**) times the maximum 30-min intensity ($\mathbf{I}_{30}$), where **E** is in hundreds of foot-tons per acre and $\mathbf{I}_{30}$ is in inches per hour (in/h). **EI** is an abbreviation for energy-times-intensity, and the term should not be considered simply an energy parameter. The data show that rainfall energy, itself, is not a good indicator of erosive potential. The storm energy indicates the volume of rainfall and runoff, but a long, slow rain may have the same **E** value as a shorter rain at much higher intensity. Raindrop erosion increases with intensity. The $\mathbf{I}_{30}$ component indicates the prolonged-peak rates of detachment and runoff. The product term, **EI,** is a statistical interaction term that reflects how total energy and peak inensity are combined in each particular storm. Technically, it indicates how particle detachment is combined with transport capacity.

The energy of a rainstorm is a function of the amount of rain and of all the storm's component intensities. Median raindrop size increases with rain intensity (*62*), and terminal velocities of free-falling waterdrops increase with increased dropsize (*13*). Since the energy of a given mass in motion is proportional to velocity-squared, rainfall energy is directly related to rain intensity. The relationship is expressed by the equation,

$$\mathbf{E} = 916 + 331 \log_{10} \mathbf{I}, \qquad (2)$$

where **E** is kinetic energy in foot-tons per acre-inch and **I** is intensity in inches per hour (*62*). A limit of 3 in/h is imposed on **I** by the finding that median dropsize does not continue to increase when intensities exceed 3 in/h (*7, 15*). The energy

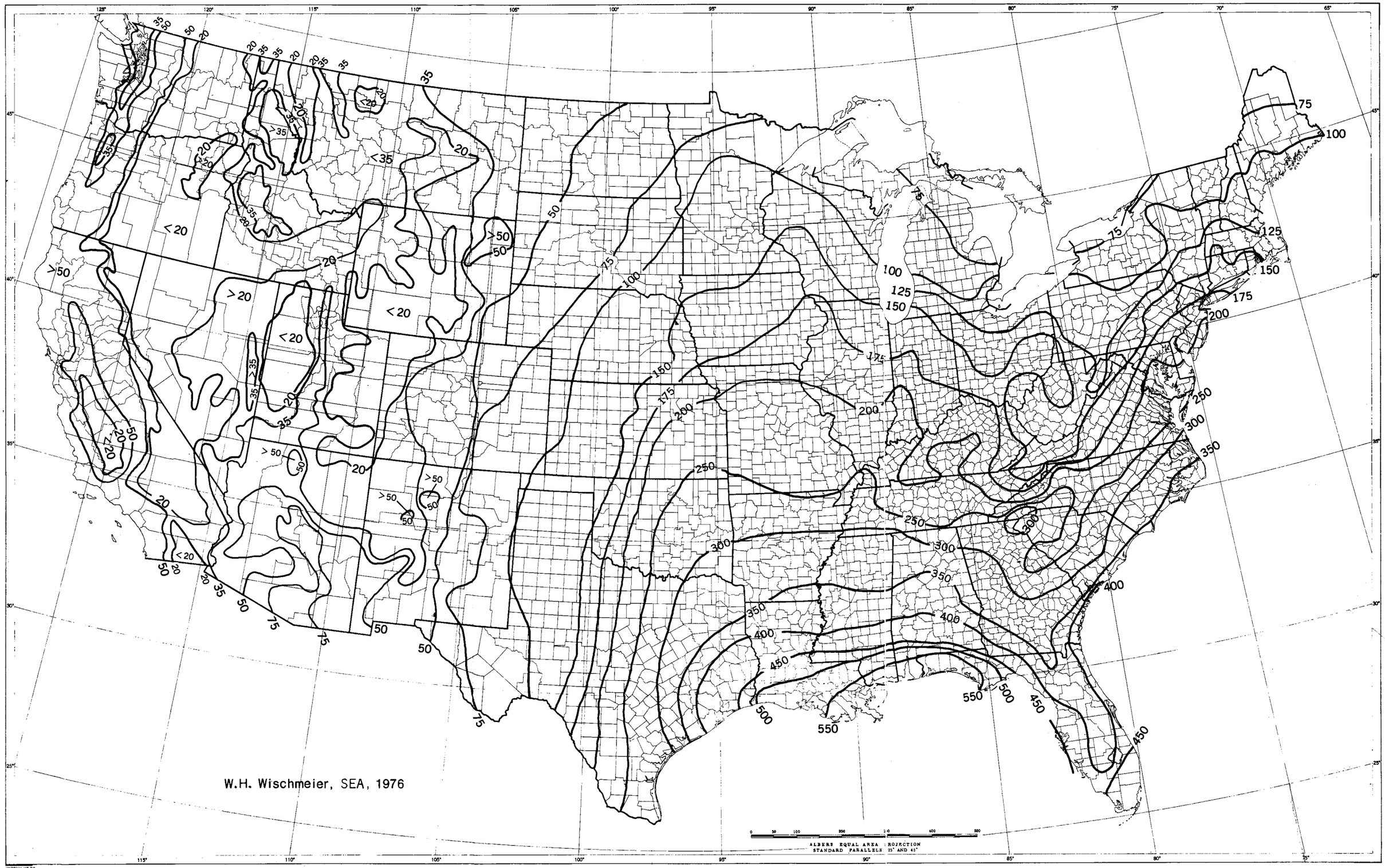

FIGURE 1.—Average annual values of the rainfall erosion index.

of a rainstorm is computed from recording-rain gage data. The storm is divided into successive increments of essentially uniform intensity, and a rainfall energy-intensity table derived from the above formula (app., table 19) is used to compute the energy for each increment. (Because the energy equation and energy-intensity table have been frequently published with energy expressed in foot-tons per acre-inch, this unit was retained in table 19. However, for computation of **EI** values, storm energy is expressed in hundreds of foot-tons per acre. Therefore, energies computed by the published formula or table 19 must be divided by 100 before multiplying by I_{30} to compute **EI**.)

Isoerodent Maps

Local values of the rainfall erosion index may be taken directly from the isoerodent maps, figures 1 and 2. The plotted lines on the maps are called isoerodents because they connect points of equal rainfall erosivity. Erosion index values for locations between the lines are obtained by linear interpolation.

The isoerodent map in the original version of this handbook (*64*) was developed from 22-year station rainfall records by computing the **EI** value for each storm that met the previously defined threshold criteria. Isoerodents were then located between these point values with the help of published rainfall intensity-frequency data (*47*) and topographic maps. The 11 Western States were omitted from the initial map because the rainfall patterns in this mountainous region are sporadic and not enough long-term, recording-rain gage records were available to establish paths of equal erosion index values.

The isoerodent map was extended to the Pacific Coast in 1976 by use of an estimating procedure. Results of investigations at the Runoff and Soil Loss Data Center at Purdue University showed that the known erosion index values in the Western Plains and North Central States could be approximated with reasonable accuracy by the quantity $27.38\ P^{2.17}$, where **P** is the 2-year, 6-h rainfall amount (*55*). This relationship was used with National Weather Service isopluvial maps to approximate erosion index values for the Western States. The resulting isoerodents are compatible with the few point values that had been established within the 11 Western States and can provide helpful guides for conservation planning on a site basis. However, they are less precise than those computed for the 37-State area, where more data were available and rainfall patterns are less eratic. Also, linear interpolations between the lines will not always be accurate in mountain regions because values of the erosion index may change rather abruptly with elevation changes. The point values that were computed directly from long-term station rainfall records in the Western States are included in table 7, as reference points.

Figure 2 was developed by computing the erosion index for first-order weather stations in Hawaii and deriving the relation of these values to National Weather Service intensity-frequency data for the five major islands. When the present short-term, rainfall-intensity records have been sufficiently lengthened, more point values of the index should be computed by the standard procedure.

Figure 1 shows that local, average-annual values of the erosion index in the 48 conterminous States range from less than 50 to more than 500. The erosion index measures the combined effect of rainfall and its associated runoff. If the soil and topography were exactly the same everywhere, average annual soil losses from plots maintained in continuous fallow would differ in direct proportion to the erosion index values. However, this potential difference is partially offset by differences in soil, topography, vegetative cover, and residues. On fertile soils in the high rainfall areas of the Southern States, good vegetal cover protects the soil surface throughout most of the year and heavy plant residues may provide excellent cover also during the dormant season. In the regions where the erosion index is extremely low, rainfall is seldom adequate for establishing annual meadows and the cover provided by other crops is often for relatively short periods. Hence, serious soil erosion hazards exist in semiarid regions as well as in humid.

Frequency Distribution

The isoerodent maps present 22-year-average annual values of **EI** for the delineated areas. However, both the annual and the maximum-storm values at a particular location vary from year to year. Analysis of 181 station rainfall records showed that they tend to follow log-normal frequency distributions that are usually well defined by continu-

ous records of from 20 to 25 years (*49*). Tables of specific probabilities of annual and maximum-storm **EI** values at the 181 locations are presented in the appendix (tables 17 and 18).

R Values for Thaw and Snowmelt

The standard rainfall erosion index estimates the erosive forces of the rainfall and its directly associated runoff. In the Pacific Northwest, as much as 90 percent of the erosion on the steeply rolling wheatland has been estimated to derive from runoff associated with surface thaws and snowmelt. This type of erosion is not accounted for by the rainfall erosion index but is considered either predominant or appreciable in much of the Northwest and in portions of the central Western States. A linear precipitation relationship would not account for peak losses in early spring because as the winter progresses, the soil becomes increasingly more erodible as the soil moisture profile is being filled, the surface structure is being broken down by repeated freezing and thawing, and puddling and surface sealing are taking place. Additional research of the erosion processes and means of control under these conditions is urgently needed.

In the meantime, the early spring erosion by runoff from snowmelt, thaw, or light rain on frozen soil may be included in the soil loss computations by adding a subfactor, $\mathbf{R}_s$, to the location's erosion index to obtain **R**. Investigations of limited data indicated that an estimate of $\mathbf{R}_s$ may be obtained by taking 1.5 times the local December-through-March precipitation, measured as inches of water. For example, a location in the North-

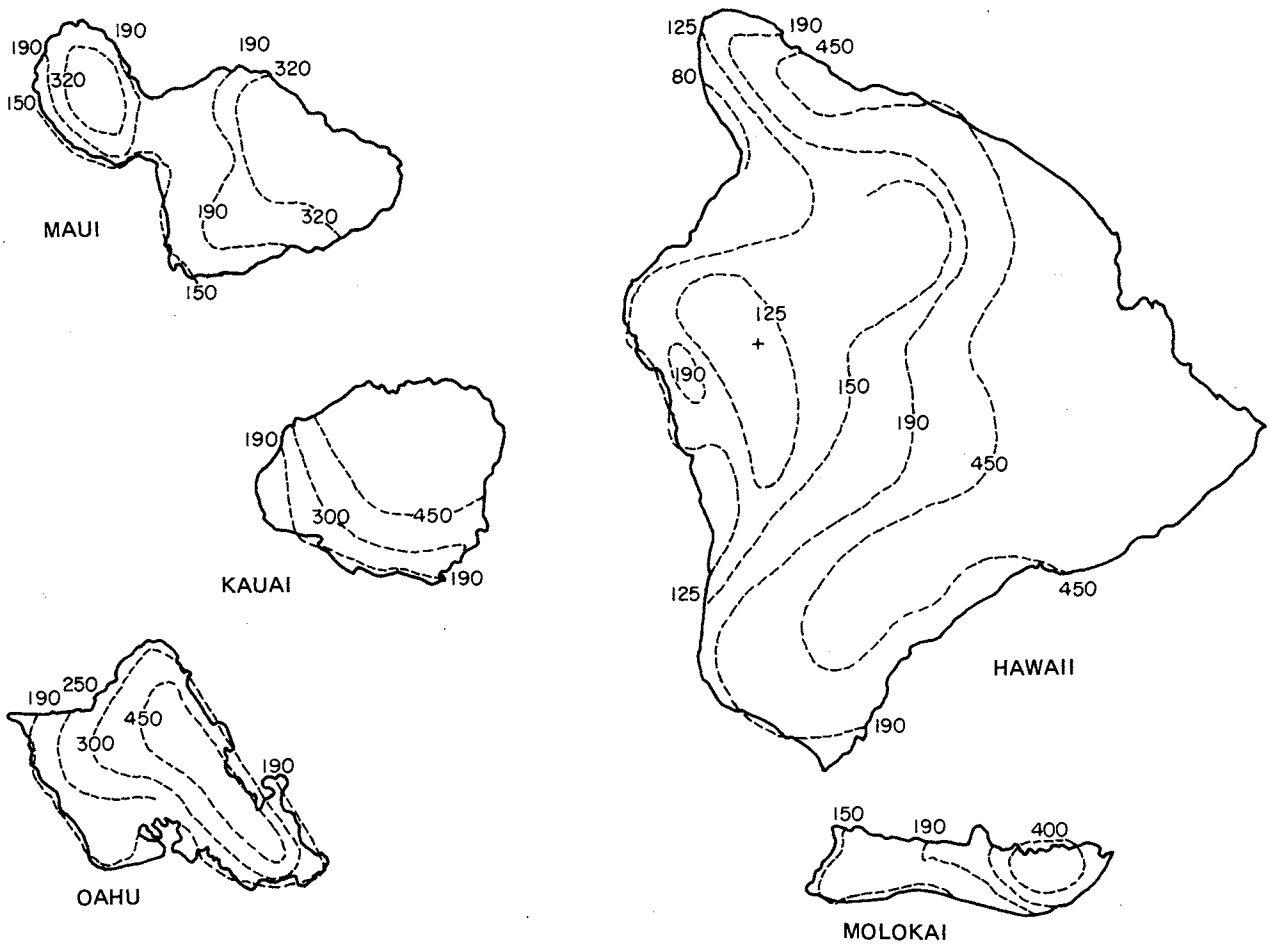

FIGURE 2.—Estimated average annual values of the rainfall erosion index in Hawaii.

west that has an erosion index of 20 (fig. 1) and averages 12 in of precipitation between December 1 and March 31 would have an estimated average annual **R** of 1.5(12) + 20, or 38.

This type of runoff may also be a significant factor in the northern tier of Central and Eastern States. Where experience indicates this to be the case, it should be included in **R** and also in the erosion index distribution curves as illustrated on page 27.

SOIL ERODIBILITY FACTOR (K)

The meaning of the term "soil erodibility" is distinctly different from that of the term "soil erosion." The rate of soil erosion, **A**, in the soil loss equation, may be influenced more by land slope, rainstorm characteristics, cover, and management than by inherent properties of the soil. However, some soils erode more readily than others even when all other factors are the same. This difference, caused by properties of the soil itself, is referred to as the soil erodibility. Several early attempts were made to determine criteria for scientific classifications of soils according to erodibility (*6, 18, 28, 35*), but classifications used for erosion prediction were only relative rankings.

Differences in the natural susceptibilities of soils to erosion are difficult to quantify from field observations. Even a soil with a relatively low erodibility factor may show signs of serious erosion when it occurs on long or steep slopes or in localities with numerous high-intensity rainstorms. A soil with a high natural erodibility factor, on the other hand, may show little evidence of actual erosion under gentle rainfall when it occurs on short and gentle slopes, or when the best possible management is practiced. The effects of rainfall differences, slope, cover, and management are accounted for in the prediction equation by the symbols **R, L, S, C,** and **P**. Therefore, the soil erodibility factor, **K**, must be evaluated independently of the effects of the other factors.

Definition of Factor K

The soil erodibility factor, **K**, in the USLE is a quantitative value experimentally determined. For a particular soil, it is the rate of soil loss per erosion index unit as measured on a "unit" plot, which has been arbitrarily defined as follows:

A unit plot is 72.6 ft long, with a uniform lengthwise slope of 9 percent, in continuous fallow, tilled up and down the slope. Continuous fallow, for this purpose, is land that has been tilled and kept free of vegetation for more than 2 years. During the period of soil loss measurements, the plot is plowed and placed in conventional corn seedbed condition each spring and is tilled as needed to prevent vegetative growth and severe surface crusting. When all of these conditions are met, **L, S, C,** and **P** each equal 1.0, and **K** equals **A/EI**.

The 72.6 ft length and 9 percent steepness were selected as base values for **L, S,** and **K** because they are the predominant slope length and about the average gradient on which past erosion measurements in the United States had been made. The designated management provides a condition that nearly eliminates effects of cover, management, and land use residual and that can be duplicated on any cropland.

Direct measurements of **K** on well-replicated, unit plots as described reflect the combined effects of all the soil properties that significantly influence the ease with which a particular soil is eroded by rainfall and runoff if not protected. However, **K** is an average value for a given soil, and direct measurement of the factor requires soil loss measurements for a representative range of storm sizes and antecedent soil conditions. (See **Individual Storm Soil Losses** under **APPLYING THE SOIL LOSS EQUATION**.) To evaluate **K** for soils that do not usually occur on a 9-percent slope, soil loss data from plots that meet all the other specified conditions are adjusted to this base by **S**.

Values of K for Specific Soils

Representative values of **K** for most of the soil types and texture classes can be obtained from tables prepared by soil scientists using the latest available research information. These tables are available from the Regional Technical Service Centers or State offices of SCS. Values for the exact

TABLE 1.—*Computed* **K** *values for soils on erosion research stations*

Soil	Source of data	Computed K
Dunkirk silt loam	Geneva, N.Y.	[1]0.69
Keene silt loam	Zanesville, Ohio	.48
Shelby loam	Bethany, Mo.	.41
Lodi loam	Blacksburg, Va.	.39
Fayette silt loam	LaCrosse, Wis.	[1].38
Cecil sondy clay loam	Watkinsville, Ga.	.36
Marshall silt loam	Clarinda, Iowa	.33
Ida silt loam	Castana, Iowa	.33
Mansic clay loam	Hays, Kans.	.32
Hagerstown silty clay loam	State College, Pa.	[1].31
Austin clay	Temple, Tex.	.29
Mexico silt loam	McCredie, Mo.	.28
Honeoye silt loam	Marcellus, N.Y.	[1].28
Cecil sandy loam	Clemson, S.C.	[1].28
Ontorio loam	Geneva, N.Y.	[1].27
Cecil clay loam	Watkinsville, Ga.	.26
Boswell find sandy loam	Tyler, Tex.	.25
Cecil sandy loom	Watkinsville, Ga.	.23
Zaneis fine sandy loam	Guthrie, Okla.	.22
Tifton loamy sand	Tifton, Ga.	.10
Freehold loamy sand	Marlboro, N.J.	.08
Bath floggy silt loam with surface stones > 2 inches removed	Arnot, N.Y.	[1].05
Albia gravelly loam	Beemerville, N.J.	.03

[1] Evaluated from continuous follow. All others were computed from rowcrop data.

soil conditions at a specific site can be computed by use of the soil erodibility nomograph presented in the next subsection.

Usually a soil type becomes less erodible with decrease in silt fraction, regardless of whether the corresponding increase is in the sand fraction or the clay fraction. Overall, organic matter content ranked next to particle-size distribution as an indicator of erodibility. However, a soil's erodibility is a function of complex interactions of a substantial number of its physical and chemical properties and often varies within a standard texture class.

Values of **K** determined for 23 major soils on which erosion plot studies under natural rain were conducted since 1930 are listed in table 1. Seven of these values are from continuous fallow. The others are from row crops averaging 20 plot-years of record and grown in systems for which the cropping effect had been measured in other studies. Other soils on which valuable erosion studies have been conducted[4] were not included in the table because of uncertainties involved in adjustments of the data for effects of cropping and management.

Direct measurement of the erodibility factor is both costly and time consuming and has been feasible only for a few major soil types. To achieve a better understanding of how and to what extent each of various properties of a soil affects its erodibility, an interregional study was initiated in 1961. The study included the use of field-plot rainfall simulators in at least a dozen States to obtain comparative data on numerous soils, laboratory determinations of physical and chemical properties, and operation of additional fallow plots under natural rain. Several empirical erodibility equations were reported (*3, 60*). A soil erodibility nomograph for farmland and construction sites (*58*) provided a more generally applicable working tool. Approximate **K** values for 10 benchmark soils in Hawaii are listed in table 2.

[4] See footnote 3, p. 2.

TABLE 2.—*Approximate values of the soil erodibility factor,* **K**, *for 10 benchmark soils in Hawaii*

Order	Suborder	Great group	Subgroup	Family	Series	K
Ultisols	Humults	Tropohumults	Humoxic Tropohumults	Clayey, kaolinitic, isohyperthermic	Waikane	0.10
Oxisols	Torrox	Torrox	Typic Torrox	Clayey, kaolinitic, isohyperthermic	Molokai	.24
Oxisols	Ustox	Eutrustox	Tropeptic Eutrustox	Clayey, kaolinitic, isohyperthermic	Wahiawa	.17
Vertisols	Usterts	Chromusterts	Typic Chromusterts	Very fine, montmorillonitic, isohyperthermic	Lualualei	.28
					Kawaihae (Extremely stony phase)	.32
Aridisols	Orthids	Camborthids	Ustollic Camborthids	Medial, isohyperthermic		
Inceptisols	Andepts	Dystrandepts	Hydric Dystrandepts	Thixotropic, isothermic	Kukaiau	.17
Inceptisols	Andepts	Eutrandepts	Typic Eutrandepts	Mediol, isohyperthermic	Naolehu (Variant)	.20
Inceptisols	Andepts	Eutrandepts	Entic Eutrandepts	Medial, isohyperthermic	Pakini	.49
Inceptisols	Andepts	Hydrandepts	Typic Hydrondepts	Thixotropic, isohyperthermic	Hilo	.10
Inceptisols	Tropepts	Ustropepts	Vertic Ustropepts	Very fine, kaolinitic, isohyperthermic	Waipahu	.20

SOURCE: El-Swaify and Dangler (*9*).

Soil Erodibility Nomograph

The soil loss data show that very fine sand (0.05-0.10 mm) is comparable in erodibility to silt-sized particles and that mechanical-analysis data are much more valuable when expressed by an interaction term that describes the proportions in which the sand, silt, and clay fractions are combined in the soil. When mechanical analysis data based on the standard USDA classification are used for the nomograph in figure 3, the percentage of very fine sand (0.1-0.05 mm) must first be transferred from the sand fraction to the silt fraction. The mechanical analysis data are then effectively described by a particle-size parameter **M**, which equals percent silt (0.1-0.002 mm) times the quantity 100-minus-percent-clay. Where the silt fraction does not exceed 70 percent, erodibility varies approximately as the 1.14 power of this parameter, but prediction accuracy is improved by adding information on organic matter content, soil structure, and profile permeability class.

For soils containing less than 70 percent silt and very fine sand, the nomograph (fig. 3) solves the equation:

$$100\,K = 2.1\,M^{1.14}\,(10^{-4})\,(12 - a) + 3.25\,(b - 2) + 2.5\,(c - 3) \quad (3)$$

where

M = the particle-size parameter defined above,
a = percent organic matter,
b = the soil-structure code used in soil classification, and
c = the profile-permeability class.

The intersection of the selected percent-silt and percent-sand lines computes the value of **M** on the unidentified horizontal scale of the nomograph. (Percent clay enters into the computation as 100 minus the percentages of sand and silt.)

The data indicate a change in the relation of **M** to erodibility when the silt and very fine sand fraction exceeds about 70 percent. This change was empirically reflected by inflections in the percent-sand curves at that point but has not been described by a numerical equation.

Readers who would like more detail regarding the data and relationships underlying the nomograph equation may obtain this from journal articles (*58*, 60).

Nomograph Solution

With appropriate data, enter the scale at the left and proceed to points representing the soil's percent sand (0.10-2.0 mm), percent organic matter, structure code, and permeability class as illustrated by the dotted line on the nomograph. The horizontal and vertical moves must be made in the listed sequence. Use linear interpolations between plotted lines. The structure code and permeability classes are defined on the nomograph for reference.

Many agricultural soils have both fine granular topsoil and moderate permeability. For these soils, **K** may be read from the scale labeled "first approximation of **K**," and the second block of the graph is not needed. For all other soils, however, the procedure must be completed to the soil erodibility scale in the second half of the graph.

The mechanical analysis, organic matter, and structure data are those for the topsoil. For evaluation of **K** for desurfaced subsoil horizons, they pertain to the upper 6 in of the new soil profile. The permeability class is the profile permeability. Coarse fragments are excluded when determining percentages of sand, silt, and clay. If substantial, they may have a permanent mulch effect which can be evaluated from the upper curve of the chart on mulch and canopy effects (p. 19, fig. 6) and applied to the number obtained from the nomograph solution.

Confidence Limits

In tests against measured **K** values ranging from 0.03 to 0.69, 65 percent of the nomograph solutions differed from the measured **K** values by less than 0.02, and 95 percent of them by less than 0.04. Limited data available in 1971 for mechanically exposed **B** and **C** subsoil horizons indicated about comparable accuracy for these conditions. However, more recent data taken on desurfaced high-clay subsoils showed the nomograph solution to lack the desired sensitivity to differences in erodibilities of these soil horizons. For such soils the content of free iron and aluminum oxides ranks next to particle-size distribution as an indicator of erodibility (*37*). Some high-clay soils form what has been called irreversible aggregates on the surface when tilled. These behave like larger primary particles.

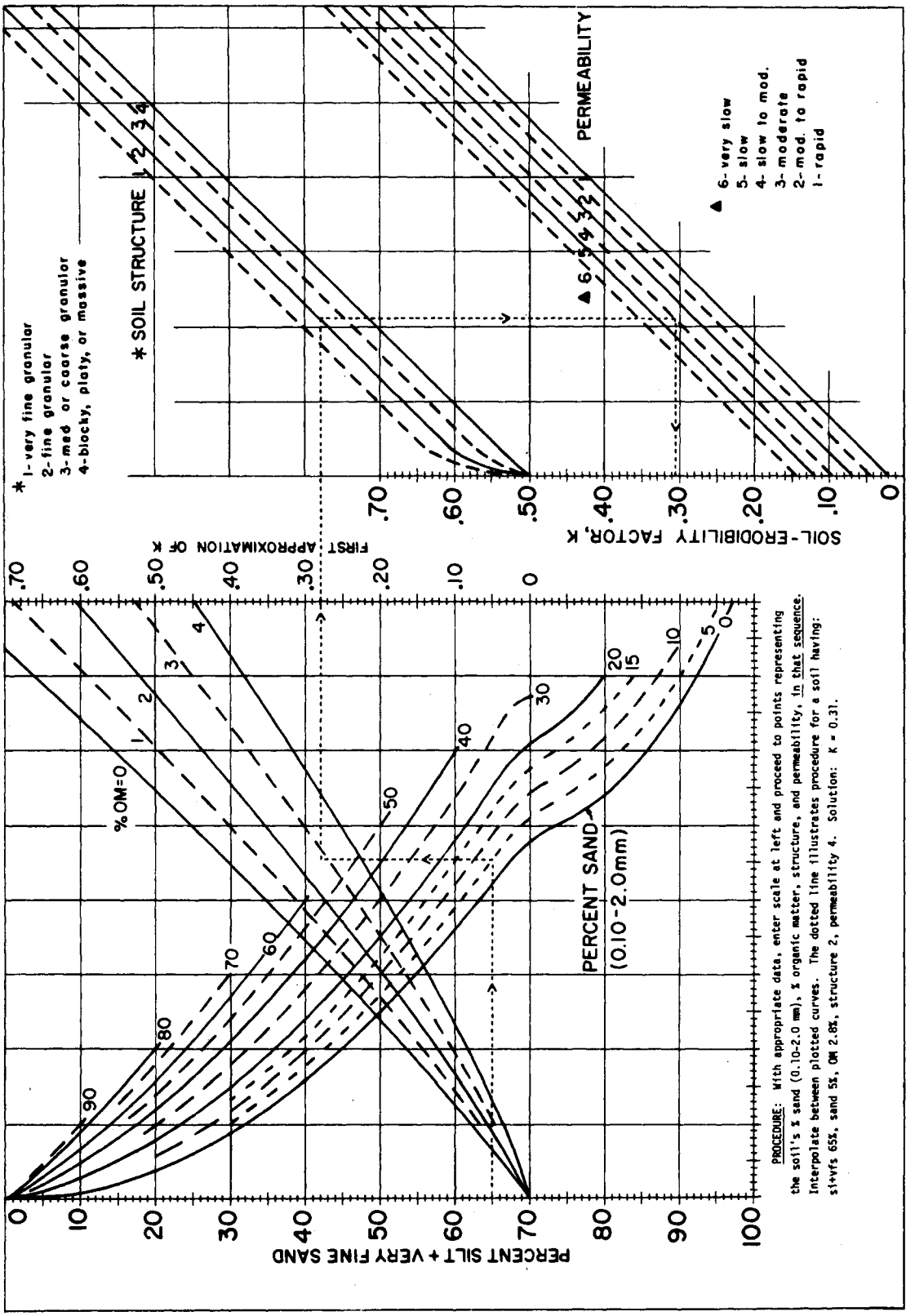

FIGURE 3.—The soil-erodibility nomograph. Where the silt fraction does not exceed 70 percent, the equation is $100\ K = 2.1\ M^{1.14}\ (10^{-4})\ (12 - a) + 3.25\ (b - 2) + 2.5\ (c - 3)$ where M = (percent si + vfs) (100 — percent c), a = percent organic matter, b = structure code, and c = profile permeability class.

TOPOGRAPHIC FACTOR (LS)

Both the length and the steepness of the land slope substantially affect the rate of soil erosion by water. The two effects have been evaluated separately in research and are represented in the soil loss equation by **L** and **S**, respectively. In field applications, however, considering the two as a single topographic factor, **LS**, is more convenient.

Slope-Effect Chart

LS is the expected ratio of soil loss per unit area from a field slope to that from a 72.6-ft length of uniform 9-percent slope under otherwise identical conditions. This ratio for specified combinations of field slope length and uniform gradient may be obtained directly from the slope-effect chart (fig. 4). Enter on the horizontal axis with the field slope length, move vertically to the appropriate percent-slope curve, and read **LS** on the scale at the left. For example, the **LS** factor for a 300-ft length of 10-percent slope is 2.4. Those who prefer a table may use table 3 and interpolate between listed values.

To compute soil loss from slopes that are appreciably convex, concave, or complex, the chart **LS** values need to be adjusted as indicated in the section **LS Values for Irregular Slopes.** Figure 4 and table 3 assume slopes that have essentially uniform gradient. The chart and table were derived by the equation

$$LS = (\lambda/72.6)^m \ (65.41 \sin^2 \theta + 4.56 \sin \theta + 0.065) \quad (4)$$

where λ = slope length in feet;
θ = angle of slope; and
m = 0.5 if the percent slope is 5 or more, 0.4 on slopes of 3.5 to 4.5 percent, 0.3 on slopes of 1 to 3 percent, and 0.2 on uniform gradients of less than 1 percent.

The basis for this equation is given in the subsection discussing the individual effects of slope length and steepness. However, the relationships expressed by the equation were derived from data obtained on cropland, under natural rainfall, on slopes ranging from 3 to 18 percent in steepness and about 30 to 300 ft in length. How far beyond these ranges in slope characteristics the relationships derived from the data continue to be accurate has not been determined by direct soil loss measurements.

The Palouse Region of the Northwest represents

TABLE 3.—*Values of the topographic factor,* **LS,** *for specific combinations of slope length and steepness*[1]

Percent slope	Slope length (feet)											
	25	50	75	100	150	200	300	400	500	600	800	1,000
0.2	0.060	0.069	0.075	0.080	0.086	0.092	0.099	0.105	0.110	0.114	0.121	0.126
0.5	.073	.083	.090	.096	.104	.110	.119	.126	.132	.137	.145	.152
0.8	.086	.098	.107	.113	.123	.130	.141	.149	.156	.162	.171	.179
2	.133	.163	.185	.201	.227	.248	.280	.305	.326	.344	.376	.402
3	.190	.233	.264	.287	.325	.354	.400	.437	.466	.492	.536	.573
4	.230	.303	.357	.400	.471	.528	.621	.697	.762	.820	.920	1.01
5	.268	.379	.464	.536	.656	.758	.928	1.07	1.20	1.31	1.52	1.69
6	.336	.476	.583	.673	.824	.952	1.17	1.35	1.50	1.65	1.90	2.13
8	.496	.701	.859	.992	1.21	1.41	1.72	1.98	2.22	2.43	2.81	3.14
10	.685	.968	1.19	1.37	1.68	1.94	2.37	2.74	3.06	3.36	3.87	4.33
12	.903	1.28	1.56	1.80	2.21	2.55	3.13	3.61	4.04	4.42	5.11	5.71
14	1.15	1.62	1.99	2.30	2.81	3.25	3.98	4.59	5.13	5.62	6.49	7.26
16	1.42	2.01	2.46	2.84	3.48	4.01	4.92	5.68	6.35	6.95	8.03	8.98
18	1.72	2.43	2.97	3.43	4.21	3.86	5.95	6.87	7.68	8.41	9.71	10.9
20	2.04	2.88	3.53	4.08	5.00	5.77	7.07	8.16	9.12	10.0	11.5	12.9

[1] $LS = (\lambda/72.6)^m \ (65.41 \sin^2 \theta + 4.56 \sin \theta + 0.065)$ where λ = slope length in feet; **m** = 0.2 for gradients < 1 percent, 0.3 for 1 to 3 percent slopes, 0.4 for 3.5 to 4.5 percent slopes, 0.5 for 5 percent slopes and steeper; and θ = angle of slope. (For other combinations of length and gradient, interpolate between adjacent values or see fig. 4.)

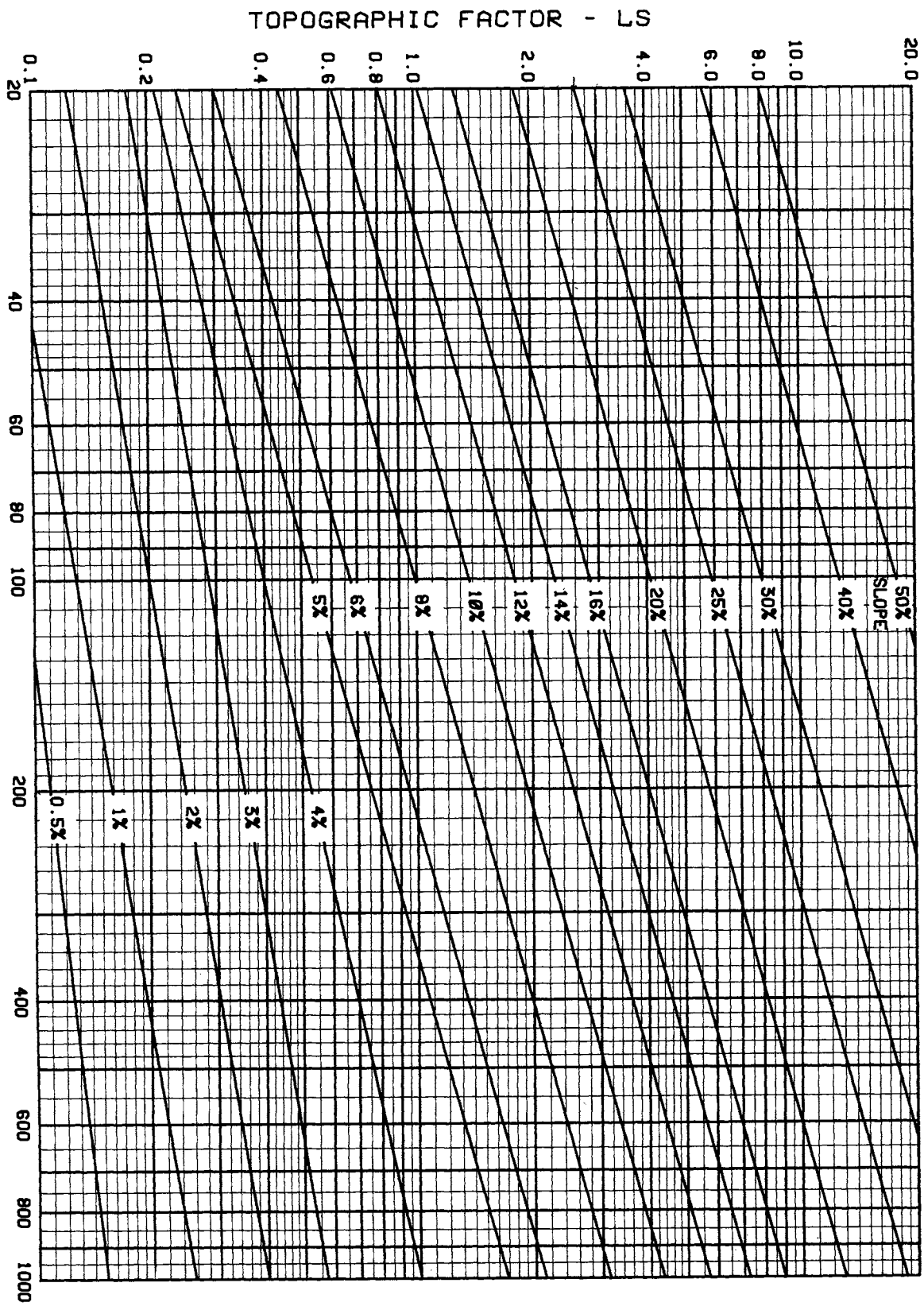

FIGURE 4.—Slope-effect chart (topographic factor, LS). $LS = (\lambda/72.6)^m$ $(65.41 \sin^2\theta + 4.56 \sin\theta + 0.065)$ where λ = slope length in feet; θ = angle of slope; and $m = 0.2$ for gradients < 1 percent, 0.3 for 1 to 3 percent slopes, 0.4 for 3.5 to 4.5 percent slopes, and 0.5 for slopes of 5 percent or steeper.

a different situation. The rainfall erosion index is quite low because most of the rain comes as small drops and at low intensities. But many of the cropland slopes are long or steep, and substantial erosion occurs because of runoff from snowmelt or light rains over saturated soil surfaces. Limited erosion data from this region, mostly observational, strongly indicate that for this type of runoff (not accompanied by raindrop impact) the effects of percent and length of slope are of lower magnitude than indicated by the humid region data. Investigations designed to develop a more accurate **LS** equation for this region are underway at Pullman, Wash. (*21*). In the meantime, the researchers are temporarily recommending using a modified equation which computes **LS** values that are close to those that would be calculated by the equation given above if $\sin^{1.5}\theta$ were substituted for $\sin^{2}\theta$ and the length-exponent, **m**, were assumed to equal 0.3. Intuitively, these changes seem reasonable for the conditions under which about 90 percent of the erosion in this region occurs.

Slope-Length Effect

Slope length is defined as the distance from the point of origin of overland flow to the point where either the slope gradient decreases enough that deposition begins, or the runoff water enters a well-defined channel that may be part of a drainage network or a constructed channel (*40*). A change in land cover or a substantial change in gradient along a slope does not begin a new slope length for purposes of soil loss estimation.

The effect of slope length on annual *runoff* per unit area of cropland may generally be assumed negligible. In some of the studies runoff per unit area was slightly lower on the longer slopes during the growing season and slightly higher during the dormant season, but the differences were relatively small and neither of the relationships was consistent (*52*).

However, the *soil loss* per unit area generally increases substantially as slope length increases. The greater accumulation of runoff on the longer slopes increases its detachment and transport capacities.

The plot data showed average soil loss per unit area to be proportional to a power of slope length. Because **L** is the ratio of field soil loss to the corresponding loss from 72.6-ft slope length, its value may be expressed as $\mathbf{L} = (\lambda/72.6)^{\mathbf{m}}$, where λ is the field slope length in feet, and **m** assumes approximately the values given in the **LS** equation in the preceding section. These are average values of **m** and are subject to some variability caused by interaction effects which are not now quantitatively predictable.

The existing field plot data do not establish a general value greater than 0.5 for **m** on slopes steeper than 10 percent, as was suggested in 1965 (*64*). Although apparent values up to 0.9 were observed in some of the data (*63*), the higher values appear to have been related to soil, crop, and management variables rather than to greater slope steepness. However, basic modeling work has suggested that **m** may appreciably exceed 0.5 on steep slopes that are highly susceptible to rilling, like some construction slopes (*10*). Additional research data are greatly needed to quantify the significant interaction effects so that specific site values of **m** can be more precisely computed. Subdividing erosion between interrill (or sheet) erosion and rill erosion, being done in recent modeling work (*10, 11, 22*), promises to be quite helpful for solving this problem.

Some observations have indicated that the values of the length exponent that were derived from the plot data may overestimate soil loss when applied to lengths in the range of a quarter of a mile or more. This is logical because slopes of such lengths would rarely have a constant gradient along their entire length, and the slope irregularities would affect the amount of soil movement to the foot of the slope. By the definition of slope length quoted earlier, such slopes would usually consist of several lengths, between points where deposition occurs.

Slope length is difficult to determine for long slopes with an average gradient of less than 1 percent, unless they are precisely formed with a land leveler. On flat slopes, reflecting both the erosion and the deposition accurately by a length factor may not be possible. However, on a nearly zero-percent slope, increased length would have minor effect on runoff velocity, and the greater depths of accumulated runoff water would cushion the raindrop impact. An exponent of 0.2 for gradients of less than 1 percent is compatible with the

scarce data available for such slopes and was used to derive figure 4 and table 3.

Distribution of Length Effect

LS values from figure 4 or table 3 predict the *average* erosion over the entire slope. But this erosion is not evenly distributed over the entire length. The rate of soil loss per unit of area increases as the m^{th} power of the distance from the top of the slope, where **m** is the length exponent in the preceding equation.

An equation by Foster and Wischmeier (*12*) estimates the relative amounts of soil loss from successive segments of a slope under conditions where there is no deposition by overland flow. When the gradient is essentially uniform and the segments are of equal length, the procedure can be shortened (*55*). Table 4, derived by this procedure, shows the proportionate amounts of soil detachment from successive equal-length segments of a uniform slope.

Table 4 is entered with the total number of equal-length segments, and the fraction of the soil loss for each segment is read beneath the applicable value of **m**. For example, three equal-length segments of a uniform 6-percent slope would be expected to produce 19, 35, and 46 percent, respectively, of the loss from the entire slope.

TABLE 4.—*Estimated relative soil losses from successive equal-length segments of a uniform slope*[1]

Number of segments	Sequence number of segment	Fraction of soil loss		
		m = 0.5	m = 0.4	m = 0.3
2	1	0.35	0.38	0.41
	2	.65	.62	.59
3	1	.19	.22	.24
	2	.35	.35	.35
	3	.46	.43	.41
4	1	.12	.14	.17
	2	.23	.24	.24
	3	.30	.29	.28
	4	.35	.33	.31
5	1	.09	.11	.12
	2	.16	.17	.18
	3	.21	.21	.21
	4	.25	.24	.23
	5	.28	.27	.25

[1] Derived by the formula:

$$\text{Soil loss fraction} = \frac{i^{m+1} - (i-1)^{m+1}}{N^{m+1}}$$

where **i** = segment sequence number; **m** = slope-length exponent (0.5 for slopes $\geq$ 5 percent, 0.4 for 4 percent slopes, and 0.3 for 3 percent or less); and **N** = number of equal-length segments into which the slope was divided.

Four segments would produce 12, 23, 30, and 35 percent, respectively. Segment No. 1 is always at the top of the slope.

Percent Slope

Runoff from cropland generally increases with increased slope gradient, but the relationship is influenced by such factors as type of crop, surface roughness, and profile saturation. In the natural rain slope-effect studies, the logarithm of runoff from row crops was linearly and directly proportional to percent slope. With good meadow sod and with smooth bare surfaces, the relationship was insignificant. The effect of slope on runoff decreased in extremely wet periods.

Soil loss increases much more rapidly than runoff as slopes steepen. The slope-steepness factor, **S**, in the soil loss equation is evaluated by the equation

$$S = 65.41 \sin^2 \theta + 4.56 \sin \theta + 0.065 \qquad (5)$$

where θ is the angle of slope.

This equation was used to develop the slope-effect chart. The values reflect the average effect of slope steepness on soil loss in the plot studies. The relation of percent slope to soil loss is believed to to be influenced by interactions with soil properties and surface conditions, but the interaction effects have not been quantified by research data. Neither are data available to define the limits on the equation's applicability.

This equation can be derived from the formerly published equation for **S**. Expressing the factor as a function of the sine of the angle of slope rather than the tangent is more accurate because raindrop-impact forces along the surface and runoff shear stress are functions of the sine. Substituting 100 sin θ for percent slope, which is 100 tan θ, does not significantly affect the initial statistical derivation or the equation's solutions for slopes of less than 20 percent. But as slopes become steeper, the difference between the sine and the tangent becomes appreciable and projections far beyond the range of the plot data become more realistic. The numerator was divided by the constant denominator for simplification.

Irregular Slopes

Soil loss is also affected by the shape of a slope. Many field slopes either steepen toward the lower end (convex slope) or flatten toward the lower end (concave slope). Use of the average gradient to enter figure 4 or table 3 would underestimate soil movement to the foot of a convex slope and would overestimate it for concave slopes. Irregular slopes can usually be divided into segments that have nearly uniform gradient, but the segments cannot be evaluated as independent slopes when runoff flows from one segment to the next.

However, where two simplifying assumptions can be accepted, **LS** for irregular slopes can be routinely derived by combining selected values from the slope-effect chart and table 4 (*55*). The assumptions are that (1) the changes in gradient are not sufficient to cause upslope deposition, and (2) the irregular slope can be divided into a small number of equal-length segments in such a manner that the gradient within each segment for practical purposes can be considered uniform.

After dividing the convex, concave, or complex slope into equal-length segments as defined earlier, the procedure is as follows: List the segment gradients in the order in which they occur on the slope, beginning at the upper end. Enter the slope-effect chart with the total slope length and read **LS** for each of the listed gradients. Multiply these by the corrresponding factors from table 4 and add the products to obtain **LS** for the entire slope. The following tabulation illustrates the procedure for a 400-ft convex slope on which the upper third has a gradient of 5 percent; the middle third, 10 percent; and the lower third, 15 percent:

Segment	*Percent slope*	*Table 3*	*Table 4*	*Product*
1	5	1.07	0.19	0.203
2	10	2.74	.35	.959
3	15	5.12	.46	2.355
				LS = 3.517

For the concave slope of the same length, with the segment gradients in reverse order, the values in the third column would be listed in reverse order. The products would then be 0.973, 0.959, and 0.492, giving a sum of 2.42 for **LS.**

Research has not defined just how much gradient change is needed under various conditions for deposition of soil particles of various sizes to begin, but depositional areas can be determined by observation. When the slope breaks are sharp enough to cause deposition, the procedure can be used to estimate **LS** for slope segments above and below the depositional area. However, it will not predict the total sediment moved from such an interrupted slope because it does not predict the amount of deposition.

Changes in Soil Type or Cover Along the Slope

The procedure for irregular slopes can include evaluation of changes in soil type within a slope length (*55*). The products of values selected from table 3 or figure 4 and table 4 to evaluate **LS** for irregular slopes are multiplied by the respective values of **K** before summing. To illustrate, assume the **K** values for the soils in the three segments of the convex slope in the preceding example were 0.27, 0.32, and 0.37, respectively. The average **KLS** for the slope would be obtained as follows:

Segment No.	*Table 3*	*Table 4*	K	*Product*
1	1.07	0.19	0.27	0.055
2	2.74	.35	.32	.307
3	5.12	.46	.37	.871
				KLS = 1.233

Within limits, the procedure can be further extended to account for changes in cover along the slope length by adding a column of segment **C** values. However, it is not applicable for situations where a practice change along the slope causes deposition. For example, a grass buffer strip across the foot of a slope on which substantial erosion is occurring induces deposition. The amount of this deposition is a function of transport relationships (*10*) and cannot be predicted by the USLE.

Equation for Soil Detachment on Successive Segments of a Slope

This procedure is founded on an equation (*12*) that can be applied also when the slope segments are not of equal length. Concepts underlying this equation include the following:

Sediment load at a location on a slope is controlled either by the transport capacity of the runoff and rainfall or by the amount of detached soil material available for transport. When the amount of detached material exceeds the transport capacity, deposition occurs and the sediment load is determined primarily by the transport capacity of the runoff at that location. Where upslope detachment has not equaled the transport capacity, sediment load at a given location is a function of erosion characteristics of the upslope area and can be computed by the USLE. Soil loss from a given segment of the slope can then be computed as the difference between the sediment loads at the lower and upper ends of the segment.

Foster and Wischmeier (12) present a procedure for using this equation to evaluate **LS** for irregular slopes and to account for the effects of the soil or coverage changes along a slope, so long as the changes do not cause deposition to occur.

COVER AND MANAGEMENT FACTOR (C)

Cover and management effects cannot be independently evaluated because their combined effect is influenced by many significant interrelations. Almost any crop can be grown continuously, or it can be grown in rotations. Crop sequence influences the length of time between successive crop canopies, and it also influences the benefits obtained from residual effects of crops and management. The erosion control effectiveness of meadow sod turned under before a row crop depends on the type and quality of the meadow and on the length of time elapsed since the sod was turned under. Seedbeds can be clean tilled, or they can be protected by prior crop residues. They can be left rough, with much available capacity for surface storage and reduction of runoff velocity, or they can be smoothed by secondary tillage.

Crop residues can be removed, left on the surface, incorporated near the surface, or plowed under. When left on the surface, they can be chopped or dragged down, or they can be allowed to remain as left by the harvesting operation. The effectiveness of crop residue management will depend on the amount of residue available. This, in turn, depends on the amount and distribution of rainfall, on the fertility level, and on the management decisions made by the farmer.

The canopy protection of crops not only depends on the type of vegetation, the stand, and the quality of growth, but it also varies greatly in different months or seasons. Therefore, the overall erosion-reducing effectiveness of a crop depends largely on how much of the erosive rain occurs during those periods when the crop and management practices provide the least protection.

Definition of Factor C

Factor **C** in the soil loss equation is the ratio of soil loss from land cropped under specified conditions to the corresponding loss from clean-tilled, continuous fallow. This factor measures the combined effect of all the interrelated cover and management variables.

The loss that would occur on a particular field if it were continuously in fallow condition is computed by the product of **RKLS** in the soil loss equation. Actual loss from the cropped field is usually much less than this amount. Just how much less depends on the particular combination of cover, crop sequence, and management practices. It also depends on the particular stage of growth and development of the vegetal cover at the time of the rain. **C** adjusts the soil loss estimate to suit these conditions.

The correspondence of periods of expected highly erosive rainfall with periods of poor or good plant cover differs between regions or locations. Therefore, the value of **C** for a particular cropping system will not be the same in all parts of the country. Deriving the appropriate **C** values for a given locality requires knowledge of how the erosive rainfall in that locality is likely to be distributed through the 12 months of the year and

how much erosion control protection the growing plants, crop residues, and selected management practices will provide at the time when erosive rains are most likely to occur. A procedure is presented for deriving local values of **C** on the basis of available weather records and research data that reflect effects of crops and management in successive segments of a rotation cycle. The cropping and weather data needed for this purpose appear in reference form in the subsections entitled, **Soil Loss Ratios** and **Erosion Index Distribution Data.**

Cropstage Periods

The change in effectiveness of plant cover within the crop year is gradual. For practical purposes, the year is divided into a series of cropstage periods defined so that cover and management effects may be considered approximately uniform within each period.

Initially, five periods were used, with the seedling and establishment periods defined as the first and second months after crop seeding (*50*). Because of the existing ranges in soil fertility, row spacing, plant population, and general growing conditions, however, soil loss prediction accuracy is improved when the cropstage periods are defined according to percentage of canopy cover rather than for uniform time periods. The lengths of the respective periods will then vary with crop, climate, and management and will be determined by conditions in a particular geographic area.

The soil loss ratios presented in the next subsection for computation of **C** were evaluated for six cropstage periods defined as follows:

Period F (rough fallow)—Inversion plowing to secondary tillage.

Period SB (seedbed)—Secondary tillage for seedbed preparation until the crop has developed 10 percent canopy cover.

Period 1 (establishment)—End of *SB* until crop has developed a 50 percent canopy cover. (Exception: period 1 for cotton ends at 35 percent canopy cover.)

Period 2 (development)—End of period 1 until canopy cover reaches 75 percent. (60 percent for cotton.)

Period 3 (maturing crop)—End of period 2 until crop harvest. This period was evaluated for three levels of final crop canopy.

Period 4 (residue or stubble)—Harvest to plowing or new seeding.

Quantitative Evaluations of Crop and Management Effects

More than 10,000 plot-years of runoff and soil loss data from natural rain,[5] and additional data from a large number of erosion studies under simulated rainfall, were analyzed to obtain empirical measurements of the effects of cropping system and management on soil loss at successive stages of crop establishment and development. Soil losses measured on the cropped plots were compared with corresponding losses from clean-tilled, continuous fallow to determine the soil loss reductions ascribable to effects of the crop system and management. The reductions were then analyzed to identify and evaluate influential subfactors, interactions, and correlations. Mathematical relationships observed for one crop or geographic region were tested against data from other research sites for consistency. Those found compatible with all the relevant data were used to compute soil loss reductions to be expected from conditions not directly represented in the overall plot studies.

The value of **C** on a particular field is determined by many variables, one of which is weather. Major variables that can be influenced by management decisions include crop canopy, residue mulch, incorporated residues, tillage, land use residual, and their interactions. Each of these effects may be treated as a subfactor whose numerical value is the ratio of soil loss with the effect to corresponding loss without it (*57*). **C** is the product of all the pertinent subfactors.

Crop Canopy

Leaves and branches that do not directly contact the soil have little effect on amount and velocity of runoff from prolonged rains, but they reduce the effective rainfall energy by intercepting falling raindrops. Waterdrops falling from the canopy may regain appreciable velocity but usually less than the terminal velocities of free-falling

[5] See footnote 3, p. 2.

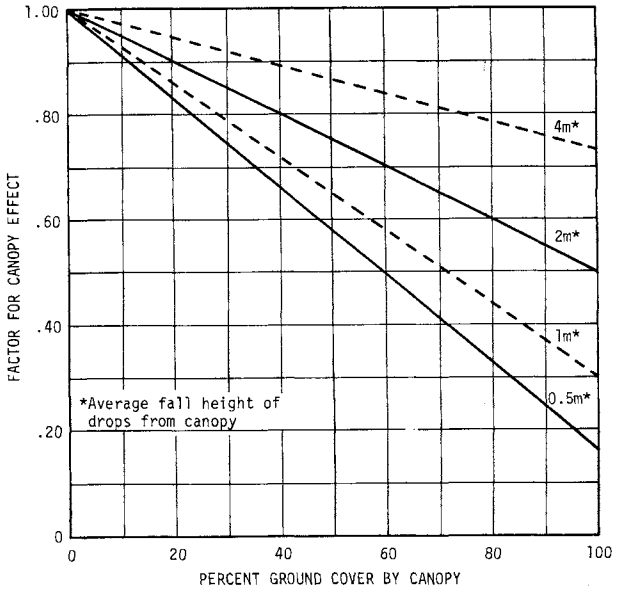

FIGURE 5.—Influence of vegetative canopy on effective EI values. Canopy factor is a subfactor of C.

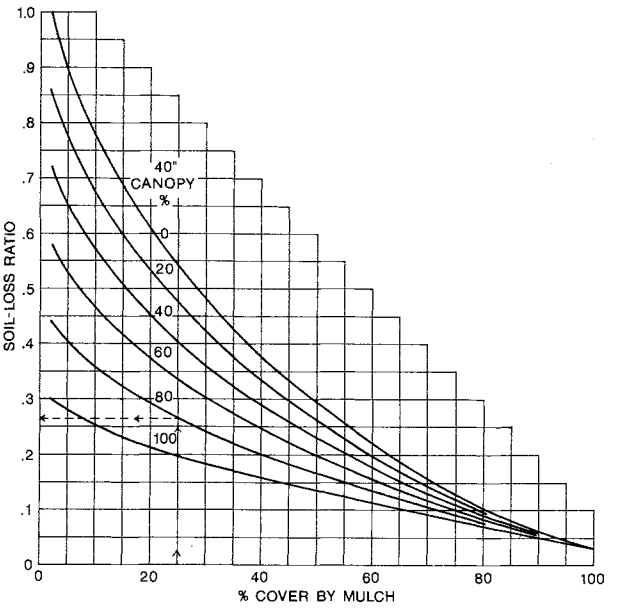

FIGURE 6.—Combined mulch and canopy effects when average fall distance of drops from canopy to the ground is about 40 inches (1 m).

raindrops. The amount by which energy expended at the soil surface is reduced depends on the height and density of the canopy. The subfactor for canopy effect can be estimated for specified conditions by reference to figure 5.

Residue Mulch

Residue mulches and stems from close-growing vegetation are more effective than equivalent percentages of canopy cover. Mulches intercept falling raindrops so near the surface that the drops regain no fall velocity, and they also obstruct runoff flow and thereby reduce its velocity and transport capacity. Measurements of the effectiveness of several types and rates of mulch have been published (*1, 2, 20, 27, 43*). Average subfactors for specific percentages of surface cover by plant materials at the soil surface are given by the upper curve of figure 6. Guides for estimating percent cover are given in the appendix.

If the cover includes both canopy and mulch, the two are not fully additive; the impact energy of drops striking the mulch is dissipated at that point regardless of whether canopy interception has reduced its velocity. The expected effects of mulch and canopy combinations have been computed and are given in figures 6 and 7. Figure 6 applies to corn, sorghum, and cotton in the maturing stage. Figure 7 applies to small grain, soybeans, potatoes, and the establishment period for taller row crops. Enter either figure 6 or 7 along the horizontal scale, move vertically to the appro-

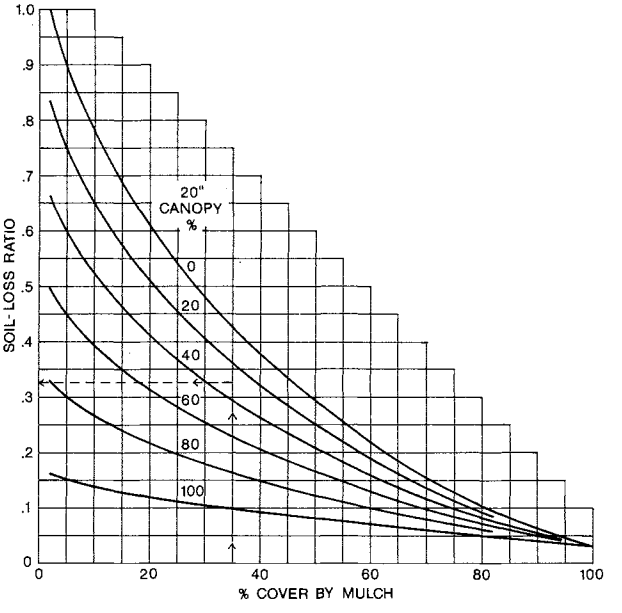

FIGURE 7.—Combined mulch and canopy effects when average fall distance of drops from canopy to the ground is about 20 inches (0.5 m).

priate percent-canopy curve, and read at the left the soil loss ratio from cover effect. This ratio is a subfactor that may be combined with other pertinent subfactors to account for the cropstage soil loss of table 5 or to estimate others.

Incorporated Residues

The plot data indicate that, at least during the seedbed and establishment periods, the erosion-reducing effectivensss of residues mixed into the upper few inches of soil by shallow tillage is appreciably greater than the residual effect of long-term annual incorporation with a moldboard plow. However, the incorporated residues are less effective than if left on the surface.

Tillage

The type, frequency, and timing of tillage operations influence porosity, roughness, cloddiness, compaction, and microtopography. These, in turn, affect water intake, surface storage, runoff velocity, and soil detachability, all of which are factors in potential erosion. These effects are highly correlated with cropland residual effects.

Land Use Residuals

These include effects of plant roots; long-term residue incorporation by plowing; changes in soil structure, detachability, density, organic matter content, and biological activity; and probably other factors. The residual effects are most apparent during seedbed and establishment periods.

Some residual effect will be apparent on nearly any cropland, but the magnitude of its erosion-reducing effectiveness will differ substantially with crops and practices. Tillage and land use residuals are influenced by so many factor interrelations that development of charts like those for canopy and mulch has not been feasible. However, apparent values of these subfactors for some situations were derived from the data and used for expansion of the soil loss ratio table to include conditions somewhat different from those directly represented in the plot studies.

Plowing residues down is far less effective than leaving them on the surface but better than burning them or removing them from the land. After several years of turning the crop residues under with a moldboard plow before row crop seeding in plot studies under natural rainfall, both runoff and soil loss from the row crops were much less than from similar plots from which cornstalks and grain straw were removed at harvesttimes (*52*, *54*, *59*).

Short periods of rough fallow in a rotation will usually lose much less soil than the basic, clean-tilled, continuous fallow conditions for which **C** = 1. This is largely because of residual effects and is also partly because of the roughness and cloddiness.

The most pronounced residual effect is that from long-term sod or forest. The effect of a grass-and-legume rotation meadow turned under diminishes gradually over about 2 years. In general, the erosion-reducing effectiveness of sod residual (from grass or grass-and-legume meadows) in the plot studies was directly proportional to hay yields. Site values of the subfactor for sod residuals in rotations can be obtained from soil loss ratio table 5-D. The effectiveness of virgin sod and of long periods of alfalfa in which grass became well established was longer lasting. Mixtures of grasses and legumes were more effective than legumes alone.

Residual effectiveness of winter cover crops plowed under in spring depends largely on the type and quality of the crop and its development stage at the time it is plowed under. The effectiveness of grass-and-legume catch crops turned under in spring was less and of shorter duration than that of full-year rotation meadows. Covers such as vetch and ryegrass seeded between corn or cotton rows before harvest and turned under in April were effective in reducing erosion during the winter and showed some residual effect in the following seedbed and establishment periods. Small grain seeded alone in corn or cotton residues showed no residual effect under the next crop. Small grain or vetch on fall-plowed seedbed and turned at spring planting time lost more soil than adjacent plots with undisturbed cotton residues on the surface.

Soil Loss Ratios

Factor **C** is usually given in terms of its average annual value for a particular combination of crop system, management, and rainfall pattern. To derive site values of **C**, soil loss ratios for the indi-

vidual cropstage periods must be combined with erosion-index distribution data, as demonstrated later. Ratios of soil losses in each cropstage period of specified cropping and management systems to corresponding losses from the basic long-term fallow condition were derived from analysis of about a quarter million plot soil loss observations. The ratios are given in table 5 as percentages.

The observed soil loss ratios for given conditions often varied substantially from year to year because of influences of unpredictable random variables and experimental error. The percentages listed in table 5 are the best available averages for the specified conditions. To make the table inclusive enough for general field use, expected ratios had to be computed for cover, residue, and management combinations that were not directly represented in the plot data. This was done by using empirical relationships of soil losses to the subfactors and interactions discussed in the preceding subsection. The user should recognize that the tabulated percentages are subject to appreciable experimental error and could be improved through additional research. However, because of the large volume of data considered in developing the table, the listed values should be near enough to the true averages to provide highly valuable planning and monitoring guidelines. A ratio derived locally from 1-year rainfall simulator tests on a few plots would not necessarily represent the true average for that locality more accurately. Small samples are more subject to bias by random variables and experimental error than larger samples.

Table for Cropland

Table 5, with its supplements 5A, B, C, and D, replaces tables 2, 3, and 4 in the 1965 edition. The supplements had to be separated from the main table to accommodate changes in format requirements. The ratios are expressed as percentages in the tables to eliminate decimal points.

More than half the lines in table 5 are for conditions associated with conservation tillage practices (65), which were not included in the 1965 edition. Also, it provides a direct means of crediting effects of faster and more complete canopy development by improved fertility, closer row spacing, and greater plant population. Because the table includes several times as many specific conditions as the table in the 1965 edition and defines applicable field conditions more accurately, some simplicity has been sacrificed. However, it is not intended for direct use by each field technician or farmer.

Table 5 as presented here is designed to provide the details needed by a trained agronomist to develop simple handbook tables of **C** values for conditions in specific climatic areas. It is designed for use of the revised definitions of cropstage periods given in the preceding section. The agronomist will first determine, for the particular climatic area, the number of weeks normally required for the crop canopies to attain 10, 50, and 75 percent surface cover, respectively. The table will then be used as illustrated in the next major section. Linear interpolation between ratios listed in the table is recommended where appropriate.

Semiarid Regions

Water erosion is a serious problem also in subhumid and semiarid regions. Inadequate moisture and periodic droughts reduce the periods when growing plants provide good soil cover and limit the quantities of plant residue produced. Erosive rainstorms are not uncommon, and they are usually concentrated within the season when cropland is least protected. Because of the difficulty of establishing rotation meadows and the competition for available soil moisture, sod-based rotations are often impractical. One of the most important opportunities for a higher level of soil and moisture conservation is through proper management of available residues. The effects of mulch-tillage practices in these areas can be evaluated from lines 129 to 158 of table 5 and item 12 of 5-B.

Erosion Index Distribution Data

The rainfall factor, **R**, in the soil loss equation does not completely describe the effects of local differences in rainfall pattern on soil erosion. The erosion control effectiveness of a cropping system on a particular field depends, in part, on how the year's erosive rainfall is distributed among the six cropstage periods of each crop included in the system. Therefore, expected monthly distribution

TABLE 5.—*Ratio of soil loss from cropland to corresponding loss from continuous fallow*

Line No.	Cover, crop sequence, and management[1]	Spring residue[2]	Cover after plant[3]	Soil loss ratio[4] for cropstage period and canopy cover[5] F	SB	1	2	3:80	90	96	4L[6]
		Lb	Pct	Pct	Pct	Pct	Pct	Pct	Pct	Pct	Pct
	CORN AFTER C, GS, G OR COT IN MEADOWLESS SYSTEMS										
	Moldboard plow, conv till:										
1	RdL, sprg TP	4,500	—	31	55	48	38	—	—	20	23
2		3,400	—	36	60	52	41	—	24	20	30
3		2,600	—	43	64	56	43	32	25	21	37
4		2,000	—	51	68	60	45	33	26	22	47
5	RdL, fall TP	HP[2]	—	44	65	53	38	—	—	20	—
6		GP	—	49	70	57	41	—	24	20	—
7		FP	—	57	74	61	43	32	25	21	—
8		LP	—	65	78	65	45	32	26	22	—
9	RdR, sprg TP	HP	—	66	74	65	47	—	—	22	56
10		GP	—	67	75	66	47	—	27	23	62
11		FP	—	68	76	67	48	35	27	—	69
12		LP	—	69	77	68	49	35	—	—	74
13	RdR, fall TP	HP	—	76	82	70	49	—	—	22	—
14		GP	—	77	83	71	50	—	27	23	—
15		FP	—	78	85	72	51	35	27	—	—
16		LP	—	79	86	73	52	35	—	—	—
17	*Wheeltrack pl, RdL, TP*[8]	4,500	—	—	31	27	25	—	—	18	23
18		3,400	—	—	36	32	30	—	22	18	30
19		2,600	—	—	43	36	32	29	23	19	37
20		2,000	—	—	51	43	36	31	24	20	47
21	*Deep off-set disk or*	4,500	10	—	45	38	34	—	—	20	23
22	*disk plow*	3,400	10	—	52	43	37	—	24	20	30
23		2,600	5	—	57	48	40	32	25	21	37
24		2,000	—	—	61	51	42	33	26	22	47
25	*No-till plant in crop residue*[9]	6,000	95	—	2	2	2	—	—	2	14
26		6,000	90	—	3	3	3	—	—	3	14
27		4,500	80	—	5	5	5	—	—	5	15
28		3,400	70	—	8	8	8	—	8	6	19
29		3,400	60	—	12	12	12	12	9	8	23
30		3,400	50	—	15	15	14	14	11	9	27
31		2,600	40	—	21	20	18	17	13	11	30
32		2,600	30	—	26	24	22	21	17	14	36
	Chisel, shallow disk, or fld cult, as only tillage:										
33	On moderate slopes	6,000	70	—	8	8	7	—	—	7	17
34			60	—	10	9	8	—	—	8	17
35			50	—	13	11	10	—	—	9	18
36			40	—	15	13	11	—	—	10	19
37			30	—	18	15	13	—	—	12	20
38			20	—	23	20	18	—	—	16	21
39	Do.	4,500	70	—	9	8	7	—	—	7	18
40			60	—	12	10	9	—	—	8	18
41			50	—	14	13	11	—	—	9	19
42			40	—	17	15	13	—	—	10	20
43			30	—	21	18	15	—	—	13	21
44			20	—	25	22	19	—	—	16	22
	CORN AFTER WC OF RYEGRASS OR WHEAT SEEDED IN C STUBBLE										
	WC reaches stemming stage:										
79	No-till pl in killed WC	4,000	—	—	7	7	7	—	7	6	[13]
80		3,000	—	—	11	11	11	11	9	7	
81		2,000	—	—	15	15	14	14	11	9	
82		1,500	—	—	20	19	18	18	14	11	
	Strip till one-fourth raw space										
83	Rows U/D slope	4,000	—	—	13	12	11	—	11	9	[13]
84		3,000	—	—	18	17	16	16	13	10	
85		2,000	—	—	23	22	20	19	15	12	
86		1,500	—	—	28	26	24	22	17	14	
87	Rows on cantour[11]	4,000	—	—	10	10	10	—	10	8	[13]
88		3,000	—	—	15	15	15	15	12	9	
89		2,000	—	—	20	20	19	19	15	12	
90		1,500	—	—	25	24	23	22	17	14	
91	TP, conv seedbed	4,000	—	36	60	52	41	—	24	20	[13]
92		3,000	—	43	64	56	43	31	25	21	
93		2,000	—	51	68	60	45	33	26	22	
94		1,500	—	61	73	64	47	35	27	23	
	WC succulent blades only:										
95	No-till pl in killed WC	3,000	—	—	11	11	17	23	18	16	[13]
96		2,000	—	—	15	15	20	25	20	17	
97		1,500	—	—	20	20	23	26	21	18	
98		1,000	—	—	26	26	27	27	22	19	
99	Strip till one-faurth row space	3,000	—	—	18	18	21	25	20	17	[13]
100		2,000	—	—	23	23	25	27	21	18	
101		1,500	—	—	28	28	28	28	22	19	
102		1,000	—	—	33	33	31	29	23	20	
	CORN IN SOD-BASED SYSTEMS										
	No-till pl in killed sod:										
103	3 to 5 tons hay yld	—	—	—	1	1	1	—	1	1	1
104	1 to 2 tons hay yld	—	—	—	2	2	2	2	2	2	2
	Strip till, 3-5 ton M:										
105	50 percent cover, tilled strips	—	—	—	2	2	2	—	2	2	4
106	20 percent cover, tilled strips	—	—	—	3	3	3	—	3	3	5
	Strip till, 1-2 ton M:										
107	40 percent cover, tilled strips	—	—	—	4	4	4	4	4	4	6
108	20 percent cover, tilled strips	—	—	—	5	5	5	5	5	5	7
	Other tillage after sod:			[14]	[14]	[14]	[14]	[14]	[14]	[14]	[14]
	CORN AFTER SOYBEANS										
109	*Sprg TP, conv till*	HP	—	40	72	60	48	—	—	25	29
110		GP	—	47	78	65	51	—	30	25	37
111		FP	—	56	83	70	54	40	31	26	44
112	*Fall TP, conv till*	HP	—	47	75	60	48	—	—	25	—
113		GP	—	53	81	65	51	—	30	25	—
114		FP	—	62	86	70	54	40	31	26	—

45	Do.	3,400	60	—	13	11	10	—	10	8	20
46			50	—	16	13	12	—	12	9	24
47			40	—	19	17	16	—	14	11	25
48			30	—	23	21	19	—	17	14	26
49			20	—	29	25	23	—	21	16	27
50			10	—	36	32	29	—	24	20	30
51	Do.	2,600	50	—	17	16	15	15	13	10	29
52			40	—	21	20	19	19	15	12	30
53			30	—	25	23	22	22	18	14	32
54			20	—	32	29	28	27	22	17	34
55			10	—	41	36	34	32	25	21	37
56	Do.	2,000	40	—	23	21	20	20	15	12	37
57			30	—	27	25	24	23	19	15	39
58			20	—	35	32	30	28	22	18	42
59			10	—	46	42	38	33	26	22	47
	On slopes > 12 percent.										
60	Lines 33-59 times factor of:	—	—	—	1.3	1.3	1.1	1.0	1.0	1.0	1.0
	Disk or harrow after spring chisel or fld cult:										
	Lines 33-59 times factor of:										
61	On moderate slopes	—	—	—	1.1	1.1	1.1	1.0	1.0	1.0	1.0
62	On slopes > 12 percent	—	—	—	1.4	1.4	1.2	1.0	1.0	1.0	1.0
	Ridge plant:[10]										
	Lines 33-59 times factor of:										
63	Rows on contour[11]	—	—	—	.7	.7	.7	.7	.7	.7	.7
64	Rows U/D slope < 12 percent	—	—	—	.7	.7	1.0	1.0	1.0	1.0	1.0
65	Rows U/D slope > 12 percent	—	—	—	.9	.9	1.0	1.0	1.0	1.0	1.0
	Till plant:										
	Lines 33-59 times factor of:										
66	Rows on contour[11]	—	—	—	.7	.85	1.0	1.0	1.0	1.0	1.0
67	Rows U/D slope < 7 percent	—	—	—	1.0	1.0	1.0	1.0	1.0	1.0	1.0
	Strip till one-fourth of row spacing:										
68	Rows on contour[11]	4,500	[12]60	—	12	10	9	—	—	8	23
69		3,400	50	—	16	14	12	—	11	10	27
70		2,600	40	—	22	19	17	17	14	12	30
71		2,000	30	—	27	23	21	20	16	13	36
72	Rows U/D slope	4,500	[12]60	—	16	13	11	—	—	9	23
73		3,400	50	—	20	17	14	—	12	11	27
74		2,600	40	—	26	22	19	17	14	12	30
75		2,000	30	—	31	26	23	20	16	13	36
	Vari-till:										
76	Rows on contour[11]	3,400	40	—	13	12	11	—	—	11	22
77		3,400	30	—	16	15	14	14	13	12	26
78		2,600	20	—	21	19	19	19	16	14	34

115	Fall & sprg chisel or cult	HP	[15]30	—	40	35	29	—	—	23	29
116		GP	25	—	45	39	33	—	27	23	37
117		GP	20	—	51	44	39	34	27	23	37
118		FP	15	—	58	51	44	36	28	23	44
119		LP	10	—	67	59	48	36	28	23	54
120	*No-till pl in crop res'd*	HP	[15]40	—	25	20	19	—	14	11	26
121		GP	30	—	33	29	25	22	18	14	33
122		FP	20	—	44	38	32	27	23	18	40
	BEANS AFTER CORN										
123	*Sprg TP, RdL, conv till*	HP	—	—	33	60	52	38	—	20	17	[16]
124		GP	—	—	39	64	56	41	—	21	18	
125		FP	—	—	45	68	60	43	29	22	—	
126	*Fall TP, RdL, conv till*	HP	—	—	45	69	57	38	—	20	17	[16]
127		GP	—	—	52	73	61	41	—	21	18	
128		FP	—	—	59	77	65	43	29	22	—	
	Chisel or fld cult:				[17]	[17]	[17]	[17]	[17]	[17]	[17]	[16]
	BEANS AFTER BEANS				[18]	[18]	[18]	[18]	[18]	[18]	[18]	[16]
	GRAIN AFTER C, G, GS, COT[19]										
129	*In disked residues:*	4,500	70	—	12	12	11	7	4	2	[20]
130		3,400	60	—	16	14	12	7	4	2	
131			50	—	22	18	14	8	5	3	
132			40	—	27	21	16	9	5	3	
133			30	—	32	25	18	9	6	3	
134			20	—	38	30	21	10	6	3	
135	Do.	2,600	40	—	29	24	19	9	6	3	[20]
136			20	—	43	34	24	11	7	4	
137			10	—	52	39	27	12	7	4	
138	Do.	2,000	30	—	38	30	23	11	7	4	[20]
139			20	—	46	36	26	12	7	4	
140			10	—	56	43	30	13	8	5	
141	*In disked stubble, RdR*	—	—	—	79	62	42	17	11	6	[20]
142	*Winter G after fall TP, RdL*	HP	—	—	31	55	48	31	12	7	5	[20]
143		GP	—	—	36	60	52	33	13	8	5	
144		FP	—	—	43	64	56	36	14	9	5	
145		LP	—	—	53	68	60	38	15	10	6	
	GRAIN AFTER SUMMER FALLOW										
146	*With grain residues*	200	10	—	70	55	43	18	13	11	[21]
147		500	30	—	43	34	23	13	10	8	
148		750	40	—	34	27	18	10	7	7	
149		1,000	50	—	26	21	15	8	7	6	
150		1,500	60	—	20	16	12	7	5	5	
151		2,000	70	—	14	11	9	7	5	5	
152	*With row crop residues*	300	5	—	82	65	44	19	14	12	[21]
153		500	15	—	62	49	35	17	13	11	
154		750	23	—	50	40	29	14	11	9	
155		1,000	30	—	40	31	24	13	10	8	
156		1,500	45	—	31	24	18	10	8	7	
157		2,000	55	—	23	19	14	8	7	5	
158		2,500	65	—	17	14	12	7	5	4	
	POTATOES										
159	*Rows with slope*	—	—	—	43	64	56	36	26	19	16	
160	*Contoured rows, ridged when canopy cover is about 50 percent*[11]	—	—	—	43	64	56	18	13	10	8	

See footnotes, p. 24.

Footnotes for table 5.

[1] Symbols: B, soybeans; C, corn; conv till, plow, disk and horrow for seedbed; cot, cotton; F, rough fallow; fld cult, field cultivator; G, small grain; GS, grain sorghum; M, gross and legume meadow, at least 1 full year; pl, plant; RdL, crop residues left on field; RdR, crop residues removed; SB, seedbed period; sprg, spring; TP, plowed with moldboard; WC, winter cover crop; —, insignificant or an unlikely combination of variables.

[2] Dry weight per acre after winter loss and reductions by grazing or partial removal: 4,500 lbs represents 100 to 125 bu corn; 3,400 lbs, 75 to 99 bu; 2,600 lbs, 60 to 74 bu; and 2,000 lbs, 40 to 59 bu; with normal 30-percent winter lass. For RdR or fall-plow practices, these four productivity levels are indicated by HP, GP, FP and LP, respectively (high, good, fair, and low productivity). In lines 79 to 102, this column indicates dry weight of the winter-cover crop.

[3] Percentage of soil surface covered by plant residue mulch *after* crop seeding. The difference between spring residue and that on the surface after crop seeding is reflected in the soil loss ratios as residues mixed with the topsoil.

[4] The soil loss ratios, given as percentages, assume thot the indicoted crop sequence and practices are followed consistently. One-year deviotions from normal practices do not have the effect of a permanent change. Linear interpolation between lines is recommended when justified by field conditions.

[5] Cropstage periods are as defined on p. 18. The three columns for cropstage 3 are for 80, 90, and 96 to 100 percent canopy cover at maturity.

[6] Column 4L is for all residues left on field. Corn stalks partially stonding as left by some mechanical pickers. If stalks are shredded and spread by picker, select ratio from table 5-C. When residues are reduced by grazing, take ratio from lower spring-residue line.

[7] Period 4 values in lines 9 to 12 are for corn stubble (stover removed).

[8] Inversion plowed, no secondary tillage. For this practice, residues must be left and incorporated.

[9] Soil surface and chopped residues of *matured* preceding crop undisturbed except in narrow slots in which seeds are planted.

[10] Top of old row ridge sliced off, throwing residues and some soil into furrow areas. Reridging assumed to occur near end of cropstage 1.

[11] Where lower soil loss rotios ore listed for rows on the contour, this reduction is in addition to the standard field contouring credit. The *P* value for contouring is used with these reduced loss ratios.

[12] Field-average percent cover; probably about three-fourths of percent cover on undisturbed strips.

[13] If again seeded to WC crop in corn stubble, evaluate winter period as a winter grain seeding (lines 132 to 148). Otherwise, see table 5-C.

[14] Select the appropriate line for the crop, tillage, and productivity level and multiply the listed soil loss ratios by sod residual factors from table 5-D.

[15] Spring residue may include carryover from prior corn crop.

[16] See table 5-C.

[17] Use values from lines 33 to 62 with appropriate dates and lengths of cropstage periods for beans in the locality.

[18] Values in lines 109 to 122 are best available estimates, but planting dates and lengths of cropstages may differ.

[19] When meadow is seeded with the grain, its effect will be reflected through higher percentages of cover in cropstages 3 and 4.

[20] Ratio depends on percent cover. See table 5-C.

[21] See item 12, table 5-B.

TABLE 5-A.—*Approximate soil loss ratios for cotton*

Expected final canopy percent cover:	65	80	95
Estimated initial percent cover from defoliation + stalks down:	30	45	60
Practice Number — Tillage operation(s)	Soil loss ratio[1]		
	Percent		
COTTON ANNUALLY:			
1....*None:*			
Defoliation to Dec. 31	36	24	15
Jan. 1 to Feb. or Mar. tillage:			
Cot Rd only	52	41	32
Rd & 20 percent cover vol veg[2]	32	26	20
Rd & 30 percent cover vol veg	26	20	14
2....*Chisel plow soon after cot harvest:*			
Chiseling to Dec. 31	40	31	24
Jan. 1 to sprg tillage	56	47	40
3....*Fall disk after chisel:*			
Disking to Dec. 31	53	45	37
Jan. 1 to sprg tillage	62	54	47
4....*Chisel plow Feb-Mar, no prior tillage:*			
Cot Rd only	50	42	35
Rd & 20 percent vol veg	39	33	28
Rd & 30 percent vol veg	34	29	25
5....*Bed ("hip") Feb-Mar, no prior tillage:*			
Cot Rd only	100	84	70
Rd & 20 percent vol veg	78	66	56
Rd & 30 percent vol veg	68	58	50
Split ridges & plant after hip, or Disk & plant after chisel (SB):			
Cot Rd only	61	54	47
Rd & 20 percent vol veg	53	47	41
Rd & 30 percent vol veg	50	44	38
Cropstage 1:			
Cot Rd only	57	50	43
Rd & 20 percent vol veg	49	43	38
Rd & 30 percent vol veg	46	41	36
Cropstage 2	45	39	34
Cropstage 3	40	27	17
6....*Bed (hip) after 1 prior tillage:*			
Cot Rd only	110	96	84
Rd & 20 percent veg	94	82	72
Rd & 30 percent veg	90	78	68
Split ridges after hip (SB):			
Cot Rd only	66	61	52
Rd & 20 to 30 percent veg	61	55	49
Cropstage 1:			
Cot Rd only	60	56	49
Rd & 20 to 30 percent veg	56	51	46
Cropstage 2	47	44	38
Cropstage 3	42	30	19
7....*Hip after 2 prior tillages:*			
Cot Rd only	116	108	98
Rd & 20-30 percent veg	108	98	88
Split ridges after hip (SB)	67	62	57
8....*Hip after 3 or more tillages:*	120	110	102
Split ridges after hip (SB)	68	64	59
9....*Conventional moldboard plow and disk:*			
Fallow period	42	39	36
Seedbed period	68	64	59
Cropstage 1	63	59	55
Cropstage 2	49	46	43
Cropstage 3	44	32	22
Cropstage 4 (See practtices 1, 2, and 3)			

COTTON AFTER SOD CROP:

For the first or second crop after a grass or grass-and-legume meadow has been turnplowed, multiply values given in the last five lines above by sod residual factors from table 5-D.

COTTON AFTER SOYBEANS:

Select values from above and multiply by 1.25.

See footnotes at right.

of erosive rainfall at a particular location is an element in deriving the applicable value of cover and management, **C**.

Central and Eastern States

A location's erosion index is computed by summing **EI** values of individual rainstorms over periods from 20 to 25 years. Thus, the expected monthly distribution of the erosion index can be computed from the same data. For each rainfall record abstracted for development of the isoerodent map, the monthly **EI** values were computed and expressed as percentages of the location's average annual erosion index. When the monthly percentages are plotted cumulatively against time, they define **EI** distribution curves such as illustrated in figure 8 for three locations. The three contrasting curves are presented to demonstrate how drastically the normal **EI** distribution can differ among climatic regions.

On the basis of observed seasonal distributions of **EI**, the 37 States east of the Rocky Mountains were divided into the 33 geographic areas delineated in figure 9. The changes in distribution are usually gradual transitions from one area to the next, but the average distribution within any one of the areas may, for practical purposes, be considered applicable for the entire area. The **EI** distributions in the 33 areas, expressed as cumulative percentages of annual totals, are given in table 6. The area numbers in the table correspond to those in figure 9. The data in the table were

[1] *Alternate procedure for estimating the soil loss ratios:*

The ratios given above for cotton are based on estimates for reductions in percent cover through normal winter loss and by the successive tillage operations. Research is underway in Mississippi to obtain more accurate residue data in relation to tillage practices. This research should provide more accurate soil loss ratios for cotton within a few years.

Where the reductions in percent cover by winter loss and tillage operations are small, the following procedure may be used to compute soil loss ratios for the preplant and seedbed periods: Enter figure 6 with the percentage of the field surface covered by residue mulch, move vertically to the upper curve, and read the mulch factor on the scale at the left. Multiply this factor by a factor selected from the following tabulation to credit for effects of land-use residual, surface roughness and porosity.

Productivitty level	No tillage	Rough surface	Smoothed surface
High	0.66	0.50	0.56
Medium	.71	.54	.61
Poor	.75	.58	.65

Values for the bedded period on slopes of less than 1 percent should be estimated at twice the value computed above for rough surfaces.

[2] Rd, crop residue; vol veg, volunteer vegetation.

TABLE 5-B.—*Soil loss ratios for conditions not evaluated in table 5*

COTTON:
See table 5-A.

CROPSTAGE 4 FOR ROWCROPS:
Stalks broken and partially standing: Use col. 4L.
Stalks standing after hand picking: Col. 4L times 1.15.
Stalks shredded without soil tillage: See table 5-C.
Fall chisel: Select values from lines 33-62, seedbed column.

CROPSTAGE 4 FOR SMALL GRAIN:
See table 5-C.

DOUBLE CROPPING:
Derive annual C value by selecting from table 5 the soil loss percentages for the successive cropstage periods of each crop.

ESTABLISHED MEADOW, FULL-YEAR PERCENTAGES:

Grass and legume mix, 3 to 5 t hay	0.4
Do. 2 to 3 t hay	.6
Do. 1 t hay	1.0
Sericea, after second year	1.0
Red clover	1.5
Alfalfa, lespedeza, and second-year sericea	2.0
Sweetclover	2.5

MEADOW SEEDING WITHOUT NURSE CROP:
Determine appropriate lengths of cropstage periods SB, 1, and 2 and apply values given for small grain seeding.

PEANUTS:
Comparison with soybeans is suggested.

PINEAPPLES:
Direct data not available. Tentative values derived analytically are available from the SCS in Hawaii or the Western Technical Service Center at Portland, Oreg. (Reference 5).

SORGHUM:
Select values given for corn, on the basis of expected crop residues and canopy cover.

SUGARBEETS:
Direct data not available. Probably most nearly comparable to potatoes, without the ridging credit.

SUGARCANE:
Tentative values available from sources given for pineapples.

SUMMER FALLOW IN LOW-RAINFALL AREAS, USE GRAIN OR ROW CROP RESIDUES:
The approximate soil loss percentage after each successive tillage operation may be obtained from the following tabulation by estimating the percent surface cover after that tillage and selecting the column for the appropriate amount of initial residue. The given values credit benefits of the residue mulch, residues mixed with soil by tillage, and the crop system residual.

Percent cover by mulch	Initial residue (lbs/A)			
	>4,000	3,000	2,000	1,500
90	4	—	—	—
80	8	[1]8	—	—
70	12	13	[1]14	—
60	16	17	[1]18	[1]19
50	20	22	24	[1]25
40	25	27	30	32
30	29	33	37	39
20	35	39	44	48
10	47	55	63	68

[1] For grain residue only.

WINTER COVER SEEDING IN ROW CROP STUBBLE OR RESIDUES:
Define cropstage periods based on the cover seeding date and apply values from lines 129 to 145.

TABLE 5-C.—*Soil loss ratios (percent) for cropstage 4 when stalks are chopped and distributed without soil tillage*

Mulch cover[1]	Corn or Sorghum		Soybeans		Grain Stubble[4]
	Tilled seedbed[2]	No-till	Tilled seedbed[2]	No-till in corn rd[3]	
20	48	34	60	42	48
30	37	26	46	32	37
40	30	21	38	26	30
50	22	15	28	19	22
60	17	12	21	16	17
70	12	8	15	10	12
80	7	5	9	6	7
90	4	3	—	—	4
95	3	2	—	—	3

[1] Part of a field surface directly covered by pieces of residue mulch.
[2] This column applies for all systems other than no-till.
[3] Cover after bean harvest may include an appreciable number of stalks carried over from the prior corn crop.
[4] For grain with meadow seeding, include meadow growth in percent cover and limit grain period 4 to 2 mo. Thereafter, classify as established meadow.

abstracted from the published **EI** distribution curves.

The percentage of the annual erosion index that is to be expected within each cropstage period may be obtained by reading from the appropriate line of table 6, the values for the last and first date of the period, and subtracting. Interpolate

TABLE 5-D.—*Factors to credit residual effects of turned sod*[1]

Crop	Hay yield	Factor for cropstage period:				
		F	SB and 1	2	3	4
	Tons					
First year after mead:						
Row crop or grain ...	3-5	0.25	0.40	0.45	0.50	0.60
	2-3	.30	.45	.50	.55	.65
	1-2	.35	.50	.55	.60	.70
Second year after mead:						
Row crop	3.5	.70	.80	.85	.90	.95
	2-3	.75	.85	.90	.95	1.0
	1-2	.80	.90	.95	1.0	1.0
Spring grain	3-5	—	.75	.80	.85	.95
	2-3	—	.80	.85	.90	1.0
	1-2	—	.85	.90	.95	1.0
Winter grain	3-5	—	.60	.70	.85	.95
	2-3	—	.65	.75	.90	1.0
	1-2	—	.70	.85	.95	1.0

[1] These factors are to be multiplied by the appropriate soil loss percentages selected from table 5. They are directly applicable for sod-forming meadows of at least 1 full year duration, plowed not more than 1 month before final seedbed preparation.

When sod is fall plowed for spring planting, the listed values for all cropstage periods are increased by adding 0.02 for each additional month by which the plowing precedes spring seedbed preparation. For example, September plowing would precede May disking by 8 months and 0.02(8—1), or 0.14, would be added to each value in the table. For nonsod-forming meadows, like sweetclover or lespedeza, multiply the factors by 1.2. When the computed value is greater than 1.0, use as 1.0.

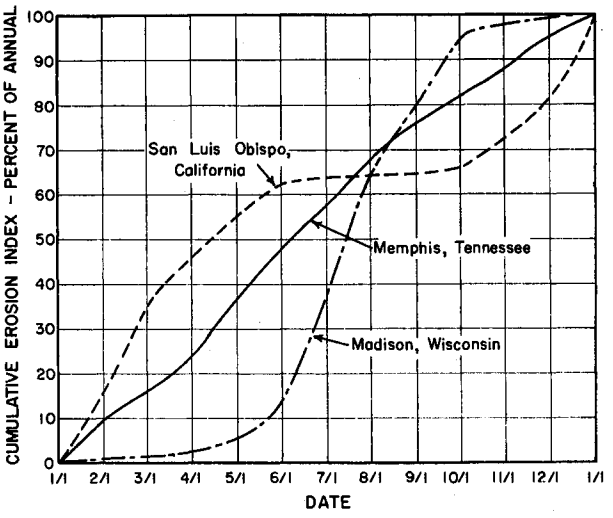

FIGURE 8.—Typical **EI**-distribution curves for three rainfall patterns.

between values in the selected line when the desired dates are not listed.

Western States, Hawaii, and Puerto Rico

Normal rainfall patterns in these mountainous States often change abruptly within a short distance. Figure 9 was not extended to include these States because long-term intensity data were not available for enough locations to delineate boundaries of homogeneous areas. However, **EI** distributions indicated by station records that were abstracted are given in table 7 for reference.

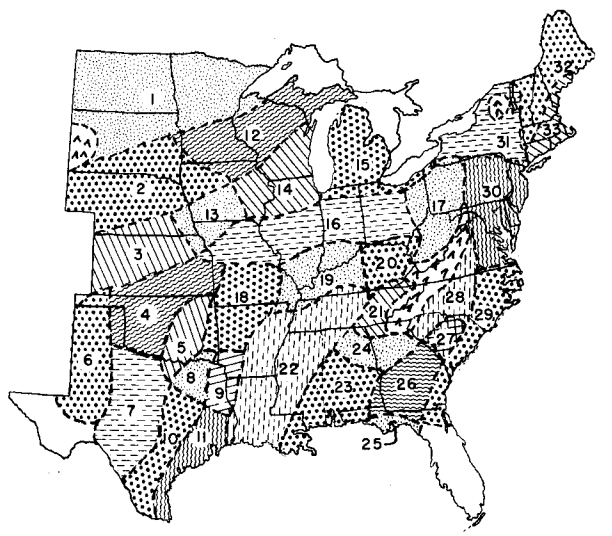

FIGURE 9.—Key map for selection of applicable **EI**-distribution data from table 6.

Winter Periods

Site **EI** values reflect only rain falling at erosive intensities. Where the winter precipitation comes as snow or light rain, **EI** distribution curves may show insignificant percentages for several winter months. Yet, snowmelt and low intensity rains on frozen soil may cause appreciable runoff that is erosive even though the associated maximum 30-minute rainfall intensity is extremely low or zero. The section on **Isoerodent Maps** pointed out that where this type of runoff is significant its erosive force must be reflected in an $\mathbf{R}_s$ value that is added to the **EI** value to obtain **R**. This additional erosive force must also be reflected in the *monthly distribution* of **R**. Otherwise, poor management during the winter period will not be reflected in the USLE estimate of annual soil loss because a zero crop-stage **R** value would predict zero soil loss regardless of the relevant soil loss ratio.

Soil erosion by thaw runoff is most pronounced in the Northwest, where $\mathbf{R}_s$ values often exceed the average annual **EI**. However, it may also be significant in other Northern States. Probable amounts of thaw runoff were not available for inclusion in the calculations of the **EI** distributions given in tables 6 and 7, but the significance and probable time of occurrence of such runoff can be estimated by local people. The procedure for adjusting table 6 cumulative percentages to include this erosive potential will be illustrated.

Based on the previously described estimating procedure, $\mathbf{R}_s$ values in area No. 1, figure 9, appear to equal about 8 percent of the annual **EI**. Assuming that the thaw runoff in that area normally occurs between March 15 and April 15, the percentage in table 6 for April 1 is increased by 4, the April 15 and all subsequent readings are increased by 8, and all the adjusted readings are then divided by 1.08. This procedure corrects the data given in line 1, table 6, for dates April 1 to September 1 to the following cumulative percentages listed in chronological sequence: 5, 9, 10, 13, 18, 29, 41, 53, 66, 79, 91. The other values are unchanged. Such adjustments in monthly distribution of **R** where thaw runoff is significant will be particularly helpful when the USLE is used to estimate seasonal distribution of sediment from agricultural watersheds.

TABLE 6.—*Percentage of the average annual* **EI** *which normally occurs between January 1 and the indicated dates.*[1] *Computed for the geographic areas shown in figure 9*

Area No.	Jan.		Feb.		Mar.		Apr.		May		June		July		Aug.		Sept.		Oct.		Nov.		Dec.	
	1	15	1	15	1	15	1	15	1	15	1	15	1	15	1	15	1	15	1	15	1	15	1	15
1	0	0	0	0	0	0	1	2	3	6	11	23	36	49	63	77	90	95	98	99	100	100	100	100
2	0	0	0	0	1	1	2	3	6	10	17	29	43	55	67	77	85	91	96	98	99	100	100	100
3	0	0	0	0	1	1	2	3	6	13	23	37	51	61	69	78	85	91	94	96	98	99	99	100
4	0	0	1	1	2	3	4	7	12	18	27	38	48	55	62	69	76	83	90	94	97	98	99	100
5	0	1	2	3	4	6	8	13	21	29	37	46	54	60	65	69	74	81	87	92	95	97	98	99
6	0	0	0	0	1	1	1	2	6	16	29	39	46	53	60	67	74	81	88	95	99	99	100	100
7	0	1	1	2	3	4	6	8	13	25	40	49	56	62	67	72	76	80	85	91	97	98	99	99
8	0	1	3	5	7	10	14	20	28	37	48	56	61	64	68	72	77	81	86	89	92	95	98	99
9	0	2	4	6	9	12	17	23	30	37	43	49	54	58	62	66	70	74	78	82	86	90	94	97
10	0	1	2	4	6	8	10	15	21	29	38	47	53	57	61	65	70	76	83	88	91	94	96	98
11	0	1	3	5	7	9	11	14	18	27	35	41	46	51	57	62	68	73	79	84	89	93	96	98
12	0	0	0	0	1	1	2	3	5	9	15	27	38	50	62	74	84	91	95	97	98	99	99	100
13	0	0	0	1	1	2	3	5	7	12	19	33	48	57	65	74	82	88	93	96	98	99	100	100
14	0	0	0	1	2	3	4	6	9	14	20	28	39	52	63	72	80	87	91	94	97	98	99	100
15	0	0	1	2	3	4	6	8	11	15	22	31	40	49	59	69	78	85	91	94	96	98	99	100
16	0	1	2	3	4	6	8	10	14	18	25	34	45	56	64	72	79	84	89	92	95	97	98	99
17	0	1	2	3	4	5	6	8	11	15	20	28	41	54	65	74	82	87	92	94	96	97	98	99
18	0	1	2	4	6	8	10	13	19	26	34	42	50	58	63	68	74	79	84	89	93	95	97	99
19	0	1	3	6	9	12	16	21	26	31	37	43	50	57	64	71	77	81	85	88	91	93	95	97
20	0	2	3	5	7	10	13	16	19	23	27	34	44	54	63	72	80	85	89	91	93	95	96	98
21	0	3	6	10	13	16	19	23	26	29	33	39	47	58	68	75	80	83	86	88	90	92	95	97
22	0	3	6	9	13	17	21	27	33	38	44	49	55	61	67	71	75	78	81	84	86	90	94	97
23	0	3	5	7	10	14	18	23	27	31	35	39	45	53	60	67	74	80	84	86	88	90	93	95
24	0	3	6	9	12	16	20	24	28	33	38	43	50	59	69	75	80	84	87	90	92	94	96	98
25	0	1	3	5	7	10	13	17	21	24	27	33	40	46	53	61	69	78	89	92	94	95	97	98
26	0	2	4	6	8	12	16	20	25	30	35	41	47	56	67	75	81	85	87	89	91	93	95	97
27	0	1	2	3	5	7	10	14	18	22	27	32	37	46	58	69	80	89	93	94	95	96	97	99
28	0	1	3	5	7	9	12	15	18	21	25	29	36	45	56	68	77	83	88	91	93	95	97	99
29	0	1	2	3	4	5	7	9	11	14	17	22	31	42	54	65	74	83	89	92	95	97	98	99
30	0	1	2	3	4	5	6	8	10	14	19	26	34	45	56	66	76	82	86	90	93	95	97	99
31	0	0	0	1	2	3	4	5	7	12	17	24	33	42	55	67	76	83	89	92	94	96	98	99
32	0	1	2	3	4	5	6	8	10	13	17	22	31	42	52	60	68	75	80	85	89	92	96	98
33	0	1	2	4	6	8	11	13	15	18	21	26	32	38	46	55	64	71	77	81	85	89	93	97

[1] For dates not listed in the table, interpolate between adjacent values.

Procedure for Deriving Local C Values

Factor **C** in the USLE measures the combined effect of all the interrelated cover and management variables and is defined as the ratio of soil loss from land cropped under specified conditions to the corresponding loss from clean-tilled continuous fallow. It is usually expressed as an annual value for a particular cropping and management system. Soil loss ratios, as used in table 5, express a similar ratio for a short time interval within which cover and management effects are relatively uniform. The cropstage soil loss ratios must be combined in proportion to the applicable percentages of **EI** to derive annual **C** values.

To compute the value of **C** for any particular crop and management system on a given field, one needs first to determine the most likely seeding and harvest dates, rate of canopy development, and final canopy cover. Also, the system to be evaluated must be carefully defined with regard to crop and residue management details. Within the broad limits of tables 5 and 6, these tables then supply the research data needed to complete

TABLE 7.—*Monthly distribution of* **EI** *at selected raingage locations*

Location[1]	Average percentage of annual EI occurring from 1/1 to:											
	2/1	3/1	4/1	5/1	6/1	7/1	8/1	9/1	10/1	11/1	12/1	12/31
California												
Red Bluff (69)	18	36	47	55	62	64	65	65	67	72	82	100
San Luis Obispo (51)	19	39	54	63	65	65	65	65	65	67	83	100
Colorado												
Akron (91)	0	0	0	1	18	33	72	87	98	99	100	100
Pueblo (68)	0	0	0	5	14	23	40	82	84	100	100	100
Springfield (98)	0	0	1	4	26	36	60	94	96	99	100	100
Hawaii												
Hilo (770)	9	23	34	44	49	51	55	60	65	72	87	100
Honolulu (189)	19	33	43	51	54	55	56	57	58	62	81	100
Kahului (107)	14	32	49	62	67	68	69	70	71	76	86	100
Lihue (385)	19	29	36	41	44	45	48	51	56	64	80	100
Montana												
Billings (18)	0	0	1	6	22	49	86	88	96	100	100	100
Great Falls (17)	1	1	2	6	20	56	74	93	98	99	100	100
Miles City (28)	0	0	0	1	10	32	65	93	98	100	100	100
New Mexico												
Albuquerque (15)	1	1	2	4	10	21	52	67	89	98	99	100
Roswell (52)	0	0	2	7	20	34	55	71	92	99	99	100
Oregon												
Pendleton (6)	8	12	15	22	56	64	67	67	74	87	96	100
Portland (43)	15	27	35	37	40	45	46	47	54	65	81	100
Puerto Rico												
Mayaguez (600)	1	2	3	6	15	31	47	63	80	91	99	100
San Juan (345)	5	8	11	17	33	43	53	66	75	84	93	100
Washington												
Spokane (8)	5	9	11	15	25	56	61	76	84	90	94	100
Wyoming												
Casper (11)	0	0	1	6	32	44	70	90	96	100	100	100
Cheyenne (32)	0	1	2	5	17	42	73	90	97	99	100	100

[1] Numbers in parentheses are the observed average annual **EI**.

the computation of **C**. The procedure will be explained by an example that, for illustration purposes, was selected to include many changes in field conditions.

Problem. Evaluate **C** for a 4-year rotation of wheat-meadow-corn-corn on moderately sloping land in Central Illinois or Indiana, assuming the following management details and dates: Wheat is seeded October 15 in a 40-percent cover of disked corn residue, and a grass and legume meadow mix is seeded with the wheat. The wheat would normally develop a 10-percent cover by November 1, 50 percent by December 1, 75 percent by April 15, and nearly 100 percent in the maturing stage. It is harvested July 15, leaving an 80-percent surface cover of straw and small grass. The sod developed under 1 full year of meadow, yielding more than 3 t of hay, is turned under in April. The field is disked May 5 and is harrowed and planted to corn May 10. The first-year corn, harvested October 15, is followed by fall chiseling about November 15 and spring disking for second-year corn. Residue cover is 50 percent after fall chiseling and 30 percent after corn planting on May 10. Fertility, row spacing, and plant population for both corn years are such that 10, 50, and 75 percent canopy covers will be developed in 20, 40, and 60 days, respectively, from planting, and final canopy cover is more than 95 percent.

Procedure. Set up a working table similar to the one illustrated in table 8, obtaining the needed information as follows:

Column 1. List in chronological sequence all the land-cover changes that begin new cropstage periods, as previously defined.

Column 2. List the date on which each cropstage period begins.

Column 3. Select the applicable area number

TABLE 8.—*Sample working table for derivation of a rotation* **C** *value*

(1) Event	(2) Date	(3) Table 6, area 16	(4) Cropstage period	(5) EI in period	(6) Soil loss ratio[1]	(7) Sod Factor	(8) Cropstage C value	(9) Crop year
Pl W[2]	10/15	92	SB	0.03	0.27(132)	0.95	0.0077	
10 percent c	11/1	95	1	.03	.21	.95	.0060	
50 percent c	12/1	98	2	.12	.16	1.0	.0192	
75 percent c	4/15	10	3	.46	.03		.0138	
Hv W	7/15	56	4	.28	.07(5C)		.0196	0.066
Meadow	9/15	84		1.26	.004(5B)	1.0	.0050	.005
TP	4/15	10	F	.05	.36(2)	.25	.0045	
Disk	5/5	15	SB	.10	.60	.40	.0240	
Pl C	5/10	—						
10 percent c	6/1	25	1	.13	.52	.40	.0270	
50 percent c	6/20	38	2	.14	.41	.45	.0258	
75 percent c	7/10	52	3	.40	.20	.50	.0400	
Hv C	10/15	92	4L	.05	.30	.60	.0090	.130
Chisel	11/15	97	4c	.17	.16(46)	.60	.0163	
Disk	5/1	14	SB	.11	.25(48 & 61)	.80	.0220	
Pl C	5/10	—						
10 percent c	6/1	25	1	.13	.23	.80	.0239	
50 percent c	6/20	38	2	.14	.21	.85	.0250	
75 percent c	7/10	52	3	.40	.14(48)	.90	.0504	.138
Hv C & pl W	10/15	92						
Rotation totals				4.0			0.3392	
Average annual C value for rotation							.085	

[1] Numbers in parentheses are line numbers in table 5.

[2] Abbreviations: c, canopy cover; C, corn; hv, harvest; pl, plant; TP, moldboard plow; W, wheat.

from figure 9, and from the line in table 6 having the corresponding area number (in this case, 16), read the cumulative percentage of **EI** for each date in column 2. Values for the corn planting dates were omitted in table 8 because the seedbed periods had begun with the spring diskings. The **EI** percentage for May 5 was obtained by interpolating between readings from May 1 and 15.

Column 4. Identify the cropstage periods.

Column 5. Subtract the number in column 3 from the number in the next lower line. If the cropstage period includes a year end, subtract from 100 and add the number in the next lower line. The differences are percentages and may be pointed off as hundredths.

Column 6. Obtain from table 5. Enter the table with crop and management, pounds of spring residue or production level, and percent mulch cover after planting, in that sequence. The data in the selected line are percentages and are used as hundredths in the computation of **C**. For cropstage 3, use the column whose heading corresponds with expected final canopy. For conditions not listed in the primary table, consult supplements 5-A to D. Lines used for the examples are given in parentheses in column 6.

Column 7. From table 5-D.

Column 8. The product of values in columns 5, 6 and 7. The sum of these products is the value of **C** for the entire rotation. Because **C** is usually desired as an average annual value, this sum is divided by the number of years in the rotation.

Column 9. The subtotals in this column are **C** values for the individual crop-years. They also show the relative contributions of the four crops to the rotation **C** value.

Changes in geographic area or in planting dates would affect the **C** value by changing columns 3 and 5. Changes in amount or disposition of residues, tillage practices, or canopy development would change column 6. Thus **C** can vary substantially for a given crop system.

Values of **C** for one-crop systems are derived by the same procedure but would require only a few lines. Also, column 7 is omitted for meadowless systems.

C-Value Tables for Cropland

It will rarely, if ever, be necessary for a field technician or farmer to compute values of **C**. Persons experienced in the procedures outlined above have prepared **C** value tables for specific geographic areas. Such a table will list all the one-crop and multicrop systems likely to be found within the designated area and will list the **C** values for each system for each of the combinations of management practices that may be associated with it. They are usually listed in ascending or descending order of magnitude of the **C** values. The user can then quickly determine all the potential combinations of cropping and management that have **C** values smaller than any given threshold value. Persons in need of **C** values for a particular locality can usually obtain a copy of the applicable table from the nearest SCS state office.

C Values for Construction Areas

Site preparations that remove all vegetation and also the root zone of the soil not only leave the surface completely without protection but also remove the residual effects of prior vegetation. This condition is comparable to the previously defined continuous fallow condition, and **C** = 1. Roots and residual effects of prior vegetation, and partial covers of mulch or vegetation, substantially reduce soil erosion. These reductions are reflected in the soil loss prediction by **C** values of less than 1.0.

Applied mulches immediately restore protective cover on denuded areas and drastically reduce **C** (*1, 2, 20, 27, 43*). Soil loss ratios for various percentages of mulch cover on field slopes are given by the upper curve of figure 6. Where residual effects are insignificant, these ratios equal **C**. The percentage of surface cover provided by a given rate of uniformly spread straw mulch may be estimated from figure 10 (appendix).

Straw or hay mulches applied on steep construction slopes and not tied to the soil by anchoring and tacking equipment may be less effective than equivalent mulch rates on cropland. In Indiana tests on a 20 percent slope of scalped subsoil, a 2.3-t rate of unanchored straw mulch allowed soil loss of 12 t/A when 5 in of simulated rain was applied at 2.5 in/h on a 35-ft plot (*61*). There was evidence of erosion from flow beneath the straw. Mulches of crushed stone at 135 or more t/A, or wood chips at 7 or more t/A, were more effective. (Broadcast seedings of grass after the tests gave good stands on the plots mulched with 135 or 240 t crushed stone, 70 t road gravel, 12 t wood chips, or 2.3 t straw. Stands were poor on the no-mulch and the 15-t rate of crushed stone mulch.)

Table 9 presents approximate **C** values for straw, crushed stone, and woodchip mulches on construction slopes where no canopy cover exists, and also shows the maximum slope lengths on which these values may be assumed applicable.

Soil loss ratios for many conditions on construc-

TABLE 9.—*Mulch factors and length limits for construction slopes*[1]

Type of mulch	Mulch Rate	Land Slope	Factor C	Length limit[2]
	Tons per acre	*Percent*		*Feet*
None	0	all	1.0	—
Straw or hay,	1.0	1-5	0.20	200
tied down by	1.0	6-10	.20	100
anchoring and				
tacking	1.5	1-5	.12	300
equipment[3]	1.5	6-10	.12	150
Do.	2.0	1-5	.06	400
	2.0	6-10	.06	200
	2.0	11-15	.07	150
	2.0	16-20	.11	100
	2.0	21-25	.14	75
	2.0	26-33	.17	50
	2.0	34-50	.20	35
Crushed stone,	135	<16	.05	200
¼ to 1½ in	135	16-20	.05	150
	135	21-33	.05	100
	135	34-50	.05	75
Do.	240	<21	.02	300
	240	21-33	.02	200
	240	34-50	.02	150
Wood chips	7	<16	.08	75
	7	16-20	.08	50
Do.	12	<16	.05	150
	12	16-20	.05	100
	12	21-33	.05	75
Do.	25	<16	.02	200
	25	16-20	.02	150
	25	21-33	.02	100
	25	34-50	.02	75

[1] From Meyer and Ports (*24*). Developed by an interagency workshop group on the basis of field experience and limited research data.

[2] Maximum slope length for which the specified mulch rate is considered effective. When this limit is exceeded, either a higher application rate or mechanical shortening of the effective slope length is required.

[3] When the straw or hay mulch is not anchored to the soil, **C** values on moderate or steep slopes of soils having **K** values greater than 0.30 should be taken at double the values given in this table.

tion and developmental areas can be obtained from table 5 if good judgment is exercised in comparing the surface conditions with those of agricultural conditions specified in lines of the table. Time intervals analogous to cropstage periods will be defined to begin and end with successive construction or management activities that appreciably change the surface conditions. The procedure is then similar to that described for cropland.

Establishing vegetation on the denuded areas as quickly as possible is highly important. A good sod has a **C** value of 0.01 or less (table 5-B), but such a low **C** value can be obtained quickly only by laying sod on the area, at a substantial cost. When grass or small grain is started from seed, the probable soil loss for the period while cover is developing can be computed by the procedure outlined for estimating cropstage-period soil losses. If the seeding is on topsoil, without a mulch, the soil loss ratios given in line 141 of table 5 are appropriate for cropstage **C** values. If the seeding is on a desurfaced area, where residual effects of prior vegetation are no longer significant, the ratios for periods SB, 1 and 2 are 1.0, 0.75 and 0.50, respectively, and line 141 applies for cropstage 3. When the seedbed is protected by a mulch, the pertinent mulch factor from the upper curve of figure 6 or table 9 is applicable until good canopy cover is attained. The combined effects of vegetative mulch and low-growing canopy are given in figure 7. When grass is established in small grain, it can usually be evaluated as established meadow about 2 mo after the grain is cut.

C Values for Pasture, Range, and Idle Land

Factor **C** for a specific combination of cover conditions on these types of land may be obtained from table 10 (*57*). The cover characteristics that must be appraised before consulting this table are defined in the table and its footnotes. Cropstage periods and **EI** monthly distribution data are generally not necessary where perennial vegetation has become established and there is no mechanical disturbance of the soil.

Available soil loss data from undisturbed land were not sufficient to derive table 10 by direct comparison of measured soil loss rates, as was done for development of table 5. However, analyses of the assembled erosion data showed that the research information on values of **C** can be extended to completely different situations by combining subfactors that evaluate three separate and distinct, but interrelated, zones of influence: (a) vegetative cover in direct contact with the soil surface, (b) canopy cover, and (c) residual and tillage effects.

Subfactors for various percentages of surface cover by mulch are given by the upper curve of

TABLE 10.—*Factor* **C** *for permanent pasture, range, and idle land*[1]

Vegetative canopy			Cover that contacts the soil surface					
			Percent ground cover					
Type and height[2]	Percent cover[3]	Type[4]	0	20	40	60	80	95+
No appreciable canopy		G	0.45	0.20	0.10	0.042	0.013	0.003
		W	.45	.24	.15	.091	.043	.011
Tall weeds or short brush with average drop fall height of 20 in	25	G	.36	.17	.09	.038	.013	.003
		W	.36	.20	.13	.083	.041	.011
	50	G	.26	.13	.07	.035	.012	.003
		W	.26	.16	.11	.076	.039	.011
	75	G	.17	.10	.06	.032	.011	.003
		W	.17	.12	.09	.068	.038	.011
Appreciable brush or bushes, with average drop fall height of 6½ ft	25	G	.40	.18	.09	.040	.013	.003
		W	.40	.22	.14	.087	.042	.011
	50	G	.34	.16	.08	.038	.012	.003
		W	.34	.19	.13	.082	.041	.011
	75	G	.28	.14	.08	.036	.012	.003
		W	.28	.17	.12	.078	.040	.011
Trees, but no appreciable low brush. Average drop fall height of 13 ft	25	G	.42	.19	.10	.041	.013	.003
		W	.42	.23	.14	.089	.042	.011
	50	G	.39	.18	.09	.040	.013	.003
		W	.39	.21	.14	.087	.042	.011
	75	G	.36	.17	.09	.039	.012	.003
		W	.36	.20	.13	.084	.041	.011

[1] The listed **C** values assume that the vegetation and mulch are randomly distributed over the entire area.

[2] Canopy height is measured as the average fall height of water drops falling from the canopy to the ground. Canopy effect is inversely proportional to drop fall height and is negligible if fall height exceeds 33 ft.

[3] Portion of total-area surface that would be hidden from view by canopy in a vertical projection (a bird's-eye view).

[4] G: cover at surface is grass, grasslike plants, decaying compacted duff, or litter at least 2 in deep.

W: cover at surface is mostly broadleaf herbaceous plants (as weeds with little lateral-root network near the surface) or undecayed residues or both.

TABLE 11.—*Factor* **C** *for undisturbed forest land*[1]

Percent of area covered by canopy of trees and undergrowth	Percent of area covered by duff at least 2 in deep	Factor C[2]
100-75	100-90	.0001-.001
70-45	85-75	.002-.004
40-20	70-40	.003-.009

[1] Where effective litter cover is less than 40 percent or canopy cover is less than 20 percent, use table 6. Also use table 6 where woodlands are being grazed, harvested, or burned.

[2] The ranges in listed **C** values are caused by the ranges in the specified forest litter and canopy covers and by variations in effective canopy heights.

figure 6. Subfactors for various heights and densities of canopy cover are given in figure 5. The subfactor for residual effects of permanent pasture, range, idle land, or grazed or harvested woodland has been estimated to vary from 0.45 to 0.10 (*57*). Major influences on this subfactor are plant roots, organic matter buildup in the topsoil, reduced soil compaction, and surface stabilization after long periods without soil disturbance. The **C** values given in table 10 were derived by combining subfactors for specified combinations of type, height, and density of canopy cover; type and density of cover at the soil surface; and probable residual effects of longtime existence of the specified cover on the land. They are compatible with the rather scarce existing soil loss data from undisturbed land areas.

C Values for Woodland

Three categories of woodland are considered separately: (1) undisturbed forest land; (2) woodland that is grazed, burned, or selectively harvested; and (3) forest lands which have had site preparation treatments for re-establishment after harvest.

In undisturbed forests, infiltration rates and organic matter content of the soil are high, and much or all of the surface is usually covered by a layer of compacted decaying forest duff or litter several inches thick. Such layers of duff shield the soil from the erosive forces of runoff and of drop impact and are extremely effective against soil erosion. Where cover by trees and litter is incomplete, the spots with little or no litter cover are partially protected by undergrowth canopy. Factor **C** for undisturbed forest land may be obtained from table 11. These estimated **C** values are supported by the quite limited existing data and also by the subfactor-evaluation procedure discussed in the preceding subsection.

Woodland that is grazed or burned, or has been recently harvested, does not merit the extremely low **C** values of table 11. For these conditions, **C** is obtained from table 10. However, the buildup of organic matter in the topsoil under permanent woodland conditions is an added factor that should be accounted for by a reduction in the **C** value read from table 10. An earlier publication (*57*) recommended a factor of 0.7 for this purpose.

Site preparation treatments for re-establishing trees on harvested forest land usually alter the erosion factors substantially. Canopy effect is initially greatly reduced or lost entirely, and its restoration is gradual. Some of the forest litter is incorporated in the soil, and it may be entirely removed from portions of the area. A surface roughness factor is introduced. Windrowed debris, if across slope, may function as terraces by reducing effective slope length and inducing deposition above and in the windrows. The amount of residual effect retained depends on the amount and depth of surface scalping. Some of the changes are analogous to cropland situations. Some of the relationships available from tables 5 and 10 can be used to evaluate **C** for these conditions, but neither table is directly applicable.

Table 12 presents **C** values computed for Southern Pine Forests that have had site preparation treatments after harvesting. This table was jointly developed (in 1977) by representatives of SEA, SCS, and Forest Service, using factor relationships from tables 5, 10, and 11 as basic guides. Its application on forest lands in other climatic regions may require some modifications of factor values. Research designed to refine and improve tables 10, 11, and 12 is underway.

Tree plantings on converted cropland should, in the initial years, be evaluated similarly to cropland because the forest residual effect which underlies tables 10 to 12 will not be applicable. The subfactor for residual effects may be estimated by selecting from lines 1 to 16 of table 5 the line that most nearly describes the condition of the converted cropland and assuming a residual subfactor equal to the seedbed-period value given in that line. If the cropland has most recently been in

TABLE 12.—*Factor* **C** *for mechanically prepared woodland sites*

Site preparation	Mulch cover[1]	Soil condition[2] and weed cover[3]							
		Excellent		Good		Fair		Poor	
		NC	WC	NC	WC	NC	WC	NC	WC
	Percent								
Disked, raked, or bedded[4]	None	0.52	0.20	0.72	0.27	0.85	0.32	0.94	0.36
	10	.33	.15	.46	.20	.54	.24	.60	.26
	20	.24	.12	.34	.17	.40	.20	.44	.22
	40	.17	.11	.23	.14	.27	.17	.30	.19
	60	.11	.08	.15	.11	.18	.14	.20	.15
	80	.05	.04	.07	.06	.09	.08	.10	.09
Burned[5]	None	.25	.10	.26	.10	.31	.12	.45	.17
	10	.23	.10	.24	.10	.26	.11	.36	.16
	20	.19	.10	.19	.10	.21	.11	.27	.14
	40	.14	.09	.14	.09	.15	.09	.17	.11
	60	.08	.06	.09	.07	.10	.08	.11	.08
	80	.04	.04	.05	.04	.05	.04	.06	.05
Drum chopped[5]	None	.16	.07	.17	.07	.20	.08	.29	.11
	10	.15	.07	.16	.07	.17	.08	.23	.10
	20	.12	.06	.12	.06	.14	.07	.18	.09
	40	.09	.06	.09	.06	.10	.06	.11	.07
	60	.06	.05	.06	.05	.07	.05	.07	.05
	80	.03	.03	.03	.03	.03	.03	.04	.04

[1] Percentage of surface covered by residue in contact with the soil.

[2] *Excellent* soil condition—Highly stable soil aggregates in topsoil with fine tree roots and litter mixed in.

Good—Moderately stable soil aggregates in topsoil or highly stable aggregates in subsoil (topsoil removed during raking), only traces of litter mixed in.

Fair—Highly unstable soil aggregates in topsoil or moderately stable aggregates in subsoil, no litter mixed in.

Poor—No topsoil, highly erodible soil aggregates in subsoil, no litter mixed in.

[3] NC—No live vegetation.

WC—75 percent cover of grass and weeds having an average drop fall height of 20 in. For intermediate percentages of cover, interpolate between columns.

[4] Modify the listed C values as follows to account for effects of surface roughness and aging:

First year after treatment: multiply listed C values by 0.40 for rough surface (depressions >6 in); by 0.65 for moderately rough; and by 0.90 for smooth (depressions <2 in).

For 1 to 4 years after treatment: multiply listed factors by 0.7.

For 4+ to 8 years: use table 6.

More than 8 years: use table 7.

[5] For first 3 years: use C values as listed.

For 3+ to 8 years after treatment: use table 6.

More than 8 years after treatment: use table 7.

meadow, the selected seedbed soil loss ratio is multiplied by a factor from table 5-D. If mulch is applied, a subfactor read from the upper curve of figure 6 is multiplied by the residual subfactor to obtain **C**. When canopy develops, a canopy subfactor from figure 5 is also included.

SUPPORT PRACTICE FACTOR (P)

In general, whenever sloping soil is to be cultivated and exposed to erosive rains, the protection offered by sod or close-growing crops in the system needs to be supported by practices that will slow the runoff water and thus reduce the amount of soil it can carry. The most important of these supporting cropland practices are contour tillage, stripcropping on the contour, and terrace systems. Stabilized waterways for the disposal of excess rainfall are a necessary part of each of these practices.

By definition, factor **P** in the USLE is the ratio of soil loss with a specific support practice to the corresponding loss with up-and-down-slope culture. Improved tillage practices, sod-based rotations, fertility treatments, and greater quantities of crop residues left on the field contribute materially to erosion control and frequently provide the major control in a farmer's field. However, these are considered conservation cropping and management practices, and the benefits derived from them are included in **C**.

Contouring

The practice of tillage and planting on the contour, in general, has been effective in reducing erosion. In limited field studies, the practice provided almost complete protection against erosion from storms of moderate to low intensity, but it provided little or no protection against the occasional severe storms that caused extensive breakovers of the contoured rows. Contouring appears to be the most effective on slopes in the 3- to 8-percent range. As land slope decreases, it approaches equality with contour row slope, and the soil loss ratio approaches 1.0. As slope increases, contour row capacity decreases and the soil loss ratio again approaches 1.0.

Effectiveness of contouring is also influenced by the slope length. When rainfall exceeds infiltration and surface detention in large storms, breakovers of contour rows often result in concentrations of runoff that tend to become progressively greater with increases in slope length. Therefore, on slopes exceeding some critical length the amount of soil moved from a contoured field may approach or exceed that from a field on which each row carries its own runoff water down the slope. At what slope length this could be expected to occur would depend to some extent on gradient, soil properties, management, and storm characteristics.

P Values for Contouring

A joint SEA and SCS workshop group, meeting at Purdue University in 1956, adopted a series of contour **P** values that varied with percent slope. The **P** values were based on available data and field observations supplemented by group judgment. Subsequent experience indicated only a few minor changes. Current recommendations are given in table 13. They are average values for the factor on the specified slopes. Specific-site values may vary with soil texture, type of vegetation, residue management, and rainfall pattern, but data have not become available to make the deviations from averages numerically predictable.

Full contouring benefits are obtained only on fields relatively free from gullies and depressions other than grassed waterways. Effectiveness of this practice is reduced if a field contains numerous small gullies and rills that are not obliterated by normal tillage operations. In such instances, land smoothing should be considered before contouring. Otherwise, a judgment value greater than shown in table 13 should be used when computing the benefits for contouring.

TABLE 13.—**P** *values and slope-length limits for contouring*

Land slope percent	P value	Maximum length[1]
		Feet
1 to 2	0.60	400
3 to 5	.50	300
6 to 8	.50	200
9 to 12	.60	120
13 to 16	.70	80
17 to 20	.80	60
21 to 25	.90	50

[1] Limit may be increased by 25 percent if residue cover after crop seedlings will regularly exceed 50 percent.

Slope-Length Limits

After the 1956 workshop, the SCS prepared reference tables for use with the Corn Belt slope-practice procedure. They included guides for slope-length limits for effective contouring, based largely on judgment. These limits, as modified with later data and observations (*16, 42*), are also given in table 13. Data to establish the precise limits for specific conditions are still not available. However, the **P** values given in table 13 assume slopes short enough for full effectiveness of the practice. Their use for estimating soil loss on unterraced slopes that are longer than the table limits specified is speculative.

Contour Listing

Contour listing, with corn planted in the furrows, has been more effective than surface planting on the contour (*29*). However, the additional effectiveness of the lister ridges applies only from the date of listing until the ridges have been largely obliterated by two corn cultivations. Therefore, it can be more easily credited through **C** than through **P**. This is done by a 50-percent reduction in the soil loss ratios (table 5) that apply to the time interval during which the ridges are intact. The standard **P** value for contouring is applicable in addition to the **C** value reduction.

Potato rows on the contour present a comparable condition from lay-by time until harvest. However, this ridging effect has been already credited in table 5, line 160, and should not be duplicated.

Controlled-Row Grade Ridge Planting

A method of precise contouring has been developed that provides effective conservation on farm fields where the land slope is nearly uniform, either naturally or by land smoothing, and runoff from outside the field can be diverted. The practice uses ridge planting with undiminished channel capacity to carry water maintained throughout the year. It is being studied in Texas (*36*), Arkansas, Mississippi (*8*), and Iowa (*30*). In Texas, the channel cross section, with 40-in row spacing, was nearly 0.5 ft^2, and row grades varied from nearly zero at the upper end to 1 percent at the lower end

of a 1,000-ft length. Measured soil loss compared favorably with that from an adjacent terraced watershed. Soil loss measurements in Mississippi and Iowa showed similar effectiveness during the test periods.

Because each furrow functions as an individual terrace, **P** values similar to those for terracing seem appropriate. Slope-length limits for contouring would then not apply, but the length limits would be applicable if the channel capacity were only sufficient for a 2-year design storm.

Contoured-Residue Strips

Contoured strips of heavy crop-residue mulch, resembling contour stripcropping without the sod, may be expected to provide more soil loss reduction than contouring alone. **P** values equal to about 80 percent of those for contouring are recommended if fairly heavy mulch strips remain throughout the year. If the strips are maintained only from harvest until the next seedbed preparation, the credit should be applied to the soil loss ratio for cropstage 4 rather than the **P** value.

Contour Stripcropping

Stripcropping, a practice in which contoured strips of sod are alternated with equal-width strips of row crops or small grain, is more effective than contouring alone. Alternate strips of grain and meadow year after year are possible with a 4-year rotation of corn-wheat with meadow seeding-meadow-meadow. This system has the added advantage of a low rotation **C** value. A stripcropped rotation of corn-corn-wheat-meadow is less effective. Alternate strips of winter grain and row crop were effective on flat slopes in Texas (*14*), but alternate strips of spring-seed grain and corn on moderate to steep slopes have not provided better erosion control than contouring alone.

Observations from stripcrop studies showed that much of the soil eroded from a cultivated strip was filtered out of the runoff as it was slowed and spread within the first several feet of the adjacent sod strip. Thus the stripcrop factor, derived from soil loss measurements at the foot of the slope, accounts for off-the-field soil movement but not for all movement within the field.

P Values, Strip Widths, and Length Limits

Recommended **P** values for contour stripcropping are given in table 14. The system to which each column of factors applies is identified in the table footnotes. The strip widths given in column 5 are essentially those recommended by the 1956 slope-practice workshop and are to be considered approximate maximums. Reasonable adjustments to accommodate the row spacing and row multiple of the planting and harvesting equipment are permissible. Slope-length limit is generally not a critical factor with contour stripcropping except on extremely long or steep slopes. The lengths given in column 6 are judgment values based on field experience and are suggested as guides.

Buffer Stripcropping

This practice consists of narrow protective strips alternated with wide cultivated strips. The location of the protective strips is determined by the width and arrangement of adjoining strips to be cropped in the rotation and by the location of steep, severely eroded areas on slopes. Buffer strips usually occupy the correction areas on sloping land and are seeded to perennial grasses and legumes. This type of stripcropping is not as effective as contour stripcropping (*4*).

TABLE 14.—**P** *values, maximum strip widths, and slope-length limits for contour stripcropping*

Land slope percent	P values[1]			Strip width[2]	Maximum length
	A	B	C		
				Feet	*Feet*
1 to 2	0.30	0.45	0.60	130	800
3 to 5	.25	.38	.50	100	600
6 to 8	.25	.38	.50	100	400
9 to 12	.30	.45	.60	80	240
13 to 16	.35	.52	.70	80	160
17 to 20	.40	.60	.80	60	120
21 to 25	.45	.68	.90	50	100

[1] **P** values:

A For 4-year rotation of row crop, small grain with meadow seeding, and 2 years of meadow. A second row crop can replace the small grain if meadow is established in it.

B For 4-year rotation of 2 years row crop, winter grain with meadow seeding, and 1-year meadow.

C For alternate strips of row crop and small grain.

[2] Adjust strip-width limit, generally downward, to accommodate widths of farm equipment.

Terracing

The most common type of terrace on gently sloping land is the broadbase, with the channel and ridge cropped the same as the interterrace area. The steep backslope terrace is most common on steeper land. Difficulty in farming point rows associated with contoured terraces led to developing parallel terracing techniques (*16*). Underground outlets, landforming, and variable channel grades help establish parallel terraces. The underground outlets are in the low areas along the terrace line. The ridge is constructed across these areas. Another type of terrace, using a level and broad channel with either open or closed ends, was developed to conserve moisture in dryland farming areas.

Terraces with underground outlets, frequently called impoundment terraces, are highly effective for erosion control. Four-year losses from four such terrace systems in Iowa (*17*) averaged less than 0.4 t/A/year, which was less than 5 percent of the calculated soil movement to the channel. Comparable losses were measured from installations in Nebraska.

Terracing combined with contour farming and other conservation practices is more effective than those practices without the terraces because it positively divides the slope into segments equal to the horizontal terrace interval. The horizontal terrace interval for broadbase terraces is the distance from the center of the ridge to the center of the channel for the terrace below. For steep backslope terraces with the backslope in sod, it is the distance from the point where cultivation begins at the base of the ridge to the base of the frontslope of the terrace below (*44*). With terracing, the slope length is this terrace interval; with stripcropping or contouring alone, it is the entire field slope length.

P Values

Values of **P** for contour farming terraced fields are given in table 15. These values apply to contour farmed broadbase, steep backslope, and level terraces. However, recognize that the erosion control benefits of terraces are much greater than indicated by the **P** values. As pointed out earlier, soil loss per unit area on slopes of 5 percent or steeper is approximately proportional to the square root of slope length. Therefore, dividing a field slope into **n** approximately equal horizontal terrace intervals divides the average soil loss per unit area by the square root of **n**. This important erosion control benefit of terracing is not included in **P** because it is brought into the USLE computation through a reduced **LS** factor obtained by using the horizontal terrace interval as the slope length when entering figure 4 or table 3.

Erosion control between terraces depends on the crop system and other management practices evaluated by **C**. The total soil movement within a contour-farmed terrace interval may be assumed equal to that from the same length of an identical slope that is contoured only. Therefore, if a control level is desired that will maintain soil movement between the terraces within the soil loss tolerance limit, the **P** value for a contour-farmed terraced field should equal the contour factor (col. 2, table 15), and use of these values for farm planning purposes is generally recommended.

With contour stripcropping, the soil deposited in the grass strips is not considered lost because it remains on the field slope. With terraces, most of the deposition occurs in the terrace channels, but research measurements have shown that this deposition may equal 80 percent of the soil moved from the contour-farmed slopes between the terraces (*67*). Use of the contour factor as the **P** value for terracing assumes that all of the eroded soil deposited in the terrace channels is lost from the productive areas of the field. With broadbase terraces, the channels and ridges are cropped the same as

TABLE 15.—**P** *values for contour-farmed terraced fields*[1]

Land slope (percent)	Farm planning		Computing sediment yield[3]	
	Contour factor[2]	Stripcrop factor	Graded channels sod outlets	Steep backslope underground outlets
1 to 2	0.60	0.30	0.12	0.05
3 to 8	.50	.25	.10	.05
9 to 12	.60	.30	.12	.05
13 to 16	.70	.35	.14	.05
17 to 20	.80	.40	.16	.06
21 to 25	.90	.45	.18	.06

[1] Slope length is the horizontal terrace interval. The listed values are for contour farming. No additional contouring factor is used in the computation.

[2] Use these values for control of interterrace erosion within specified soil loss tolerances.

[3] These values include entrapment efficiency and are used for control of offsite sediment within limits and for estimating the field's contribution to watershed sediment yield.

the interterrace slopes, and some of the material deposited in the channels is moved to the ridges in terrace maintenance. The 1956 slope-practice group felt that some of the deposition should be credited as soil saved and recommended use of a terracing practice factor equal to the stripcrop factor (*64*). However, the more conservative values given in column 2 are now commonly used in conservation planning.

When the USLE is used to compute a terraced field's contribution to offsite sediment or watershed gross erosion, the substantial channel deposition must be credited as remaining on the field area. For this purpose, the **P** values given in the last two columns of table 15 are recommended unless an overland flow deposition equation based on transport relationships is used with the USLE.

With widespread use of large multirow equipment, farming with field boundaries across nonparallel terraces is not uncommon in some regions. When terraces are not maintained and overtopping is frequent, $P = 1$ and the slope length is the field slope length. However, if the terraces are periodically maintained so that overtopping occurs only during the most severe storms, **LS** is based on the horizontal terrace interval. If farming across terraces is at an angle that approximates contour farming, **P** values less than 1.0 but greater than the contour factors would be appropriate.

Soil Loss Terrace Spacing

Traditionally, terrace spacing has been based on slope gradient; however, some recent spacing guides have included modifying factors for severity of rainfall and for favorable soil and tillage combinations. A major objective of cropland conservation planning is to hold the productive topsoil in place. Extending this objective to terrace system design suggests limiting slope lengths between terraces sufficiently so that specified erosion tolerances will not be exceeded. Using the USLE in developing spacing guides will make this possible.

The USLE may be written as $LS = T/RKCP$, where **T** is the tolerance limit. If $T/RKP = Z$, then $LS = Z/C$, and $C = Z/LS$. The values **T**, **R**, **K** and **P** are constant for a given location and can be obtained from handbook tables and charts as illustrated in the section **Predicting Cropland Soil Losses.** Factor **C** can be selected as the **C** value of the most erosion-vulnerable crop system that a farmer is likely to use on the terraced field. **LS** can be computed by solving the equation as written above and, with the percent slope known, the maximum allowable length can be read from the slope-effect chart, figure 4.

To illustrate the procedure, assume a 6-percent slope at a location where $R = 175$, $K = 0.32$, $T = 5$, $P = 0.5$, and the most erodible crop expected to occur on the field has a **C** value of 0.24. (An assumption that the field will always be in a sod based rotation or that the operator will always make the best possible use of the crop residues would be too speculative to serve as a guide for terrace spacing.) With these assumptions, $Z = 5/175(0.32)(0.5) = 0.179$ and $LS = 0.179/0.24$, or 0.744. Enter the slope-effect chart, figure 4, on the **LS** scale with a value of 0.744, move horizontally to intersect the 6 percent-slope line and read the corresponding slope length, 120 ft, on the horizontal scale. Add to this value the width of the terrace frontslope and compute the vertical interval: $\left(\frac{120 + 12}{100}\right)6 = 7.9$ ft. However, the horizontal interval should not exceed the slope-length limit for effectiveness of contouring. From table 13 the length limit for contouring on a 6-percent slope is 200 ft, so the computed terrace interval is satisfactory. A small modification in spacing may be made to adjust to an even multiple of machinery width.

The maximum **C** value that will allow a horizontal terrace spacing equal to the length limit for effective contouring on the given slope can also be determined by using figure 4 and table 13. For the conditions in the illustration above, $C = 0.179/LS$. The maximum acceptable length for contouring is 200 ft. From figure 4, the **LS** value for a 200-ft length of 6-percent slope is 0.95. Therefore, the maximum allowable $C = 0.179/0.95$, which is 0.188. With terraces spaced at 200-ft intervals, any cropping and management system with a **C** value of less than 0.188 should provide the level of conservation prescribed by the assumed soil loss tolerance limit of 5 t/A/year.

One additional consideration is important. For a terrace to function satisfactorily, the channel

capacity must be sufficient to carry the runoff safely to a stabilized outlet without excessive channel scour or overtopping of the ridge. SCS engineering practice standards specify a capacity sufficient to control the runoff from a 10-year-frequency, 24-hour storm without overtopping. Some SCS practice standards may require a shorter terrace interval than would be indicated by the foregoing procedure.

The discussion of the topographic factor pointed out that the erosion rate increases as slope length increases. Table 4 lists the relative soil losses for successive equal-length increments of a uniform slope divided into 2, 3, 4, or 5 segments. The third column of table 4 shows that if a uniform 6-percent slope were controlled at a tolerance of 5 t average soil loss, the average loss per unit area from the lower third of the slope would exceed the tolerance by about 38 percent. Soil loss from the upper third would be 43 percent less than the tolerance limit. To have an average rate of 5 t from the lower third, the **T** values used in the spacing calculation would need to be 1/1.38 times the 5-t tolerance, or 3.6 t. This is an approach that can be used to calculate terrace spacings for a higher level of conservation.

Effect of Terraces on Amount and Composition of Offsite Sediment

By reducing runoff velocity and inducing deposition of sediment in the channels, terraces have a profound effect on the amount and composition of offsite sediments from cultivated fields. The type of terrace, the channel grade, and the type of outlet influence the magnitude of the effect.

The greatest reduction in sediment is attained with the impoundment type terrace systems that use underground outlets. With the outlets in the lower areas of the field and terrace ridges built across these areas, temporary ponds are created around the risers of the outlet tile. The outlets are designed to drain the impounded runoff in 1 to 2 days. Thus, the ponds provide a maximum stilling effect, and only the smallest and lightest soil particles are carried off the field in the runoff water. The increased time for infiltration also reduces runoff.

Sediments collected from four impoundment terrace systems over 4 years in Iowa (*17*) showed the following percentages of fine materials:

Soil type	< 0.002 mm	< 0.008 mm
	Percent	*Percent*
Fayette silt loam	78	91
Sharpsburg silty clay loam	68	96
Floyd loam	31	82
Clarion loam	35	78

Sediment concentrations in the runoff ranged from about 1,300 p/m on the Fayette soil to 6,300 p/m on the Clarion. Average annual sediment from the outlets was less than 800 lb/A for all four systems.

Farm chemical losses in runoff vary with type and formulation, amount, placement, and time of rainfall in relation to time of application, as well as with the usual runoff and erosion factors. Principal chemicals are the fertilizers, insecticides, fungicides, and herbicides. Losses are by solution and by suspension of chemical granules or adsorption on soil particles suspended in the runoff water.

Terracing exerts its greatest influence in reducing offsite pollution from those chemicals that are adsorbed on soil particles. Examples of these are the phosphates, organic nitrogen, and persistent organochlorine insecticides. Reductions in offsite *sediment* by terrace systems with contouring are estimated to range from 82 to 95 percent. However, the reductions in chemical transport are generally not proportional to reductions in soil loss because of an enrichment process that applies to the suspensions. The nutrient content of sediments is often 50 percent greater than that of the soil. Offsite delivery of sediment is also affected by watershed characteristics, particularly size of the drainage area. This reduction is measured by a "delivery ratio" that ranges from 0.33 for an area of one-half square mile to 0.08 for a 200-mi^2 area (*45*).

Terracing has the least effect on offsite pollution from those chemicals transported primarily in solution. Annual runoff reductions by terracing and contour farming, at 21 locations throughout the United States, have been estimated to vary only from 9 to 37 percent (*42*). Examples of farm chemicals transported primarily in solution are the nitrates and some herbicides such as 2,4-D ((2,4-dichlorophenoxy) acetic acid). The predominate transport modes for an extensive list of pesticides are listed in volumes 1 and 2 of "Control of Water Pollution From Cropland" (*42*).

APPLYING THE SOIL LOSS EQUATION

The major purpose of the soil loss prediction procedure is to supply specific and reliable guides for selecting adequate erosion control practices for farm fields and construction areas. The procedure is also useful for computing the upland erosion phase of sediment yield as a step in predicting rates of reservoir sedimentation or stream loading, but the USLE factors are more difficult to evaluate for large mixed watersheds. Specific applications of the soil loss equation are discussed and illustrated below.

Predicting Cropland Soil Losses

The USLE is designed to predict longtime-average soil losses for specified conditions. This may be the average for a rotation or for a particular crop year or cropstage period in the rotation. Where the term "average loss" is used below, it denotes the average for a sufficient number of similar events or time intervals to cancel out the plus and minus effects of short-time fluctuations in uncontrolled variables.

Rotation Averages

To compute the average annual soil loss from a particular field area, the first step is to refer to the charts and tables discussed in the preceding sections and select the values of **R, K, LS, C,** and **P** that apply to the specific conditions on that field. For example, assume a field on Russell silt loam soil in Fountain County, Ind. The dominant slope is about 8 percent with a length of 200 ft. Fertility and crop management on this field are such that crop yields are rarely less than 85 bu corn, 40 bu wheat, or 4 t alfalfa-brome hay. The probability of meadow failure is slight.

Factor **R** is taken from the isoerodent map (fig. 1). Fountain County, in west-central Indiana, lies between isoerodents of 175 and 200. By linear interpolation, $R = 185$. **K** is taken from a table of **K** values that were derived either by direct research measurement or by use of the soil erodibility nomograph (fig. 3). For the Russell silt loam soil, $K = 0.37$. The slope-effect chart, figure 4, shows that an 8 percent slope 200 ft long has an **LS** of 1.41. If the field were continuously in clean-tilled fallow, the average annual soil loss from the dominant slope would equal the product **RKLS;** that is, $185(0.37)(1.41) = 96.5$ t/A.

Next, we need to know the effect of the cropping and management system and support practices existing on the field. This effect is represented by factors **C** and **P**. The **C** value for the field may either be derived by the procedure previously presented, using data from tables 5 and 6, or it may be obtained from a centrally prepared **C** value table available from the SCS. For convenience, assume the same crop system and management as were assumed for the problem illustrating the derivation of locality **C** values. From table 8, **C** then equals 0.085. If rows and tillage are in the direction of the land slope, factor $P = 1.0$. The computed average soil loss is then $96.5(0.085)(1.0) = 8.2$ t/A/year.

From table 13, contour farming on 8 percent slopes not exceeding 200 ft in length has a **P** value of 0.5. Therefore, if farming were on the contour, the computed average soil loss for the field would be $96.5(0.085)(0.5) = 4.1$ t. If the length of 8-percent slope was appreciably greater than 200 ft, the effectiveness of contouring could not be assumed, and the **P** value of 0.5 would not be applied unless the slope length was broken by terraces or diversions. Any change in either the crop sequence or the management practices would likely increase or decrease soil loss. This would be reflected in the USLE solution through a change in the **C** value.

When **C** is used at its average annual value for a rotation that includes a sod crop, as was done in the example given in table 8, the heavier losses experienced during row crop years are diluted by trivial losses in the meadow year(s). For holding longtime-average soil losses below some prescribed tolerance limit, this dilution poses no problem. But from the viewpoint of offsite water quality, it may not be desirable. The USLE may also be used to compute the average soil loss for each crop in the rotation or for a particular cropstage period.

Crop-Year Averages

The subtotals in column 9 of table 8 show that

with the assumed management system, **C** for the first-year corn would be 0.130 and for the second-year, 0.138. For the second-year corn, without contouring, the expected average soil loss would equal 185(0.37)(1.41)(0.138), or 13.3 t. If, in the same crop system, the corn residues were plowed down in fall, the **C** value for second-year corn would be 0.29, and the soil loss would average 28 t. On the other hand, no-till planting the second-year corn in a 70-percent cover of shredded cornstalks would reduce the **C** value for this crop to 0.08 and the soil loss to about 8 t. This would also reduce the rotation average for straight row farming to 7 t. Killing the meadow instead of turning it under, and no-till planting, would reduce the **C** value for the first-year corn to 0.01 and the soil loss to less than 1 t. Thus, crop-year **C** values can be helpful for sediment control planning.

Cropstage Averages

Additional information can be obtained by computing the average annual soil loss for each cropstage period. First, the computed cropstage soil losses will show in which portions of the crop year (or rotation cycle) improved management practices would be most beneficial. Second, they provide information on the probable seasonal distribution of sediment yields from the field. When a tabulation like table 8 has been prepared, the values in column 8 will be directly proportional to the cropstage soil losses. They can be converted to tons per acre for a specific field by multiplying them by the product of factors **R**, **K**, **LS**, and **P**.

To estimate the average soil loss for a particular cropstage when such a table has not been prepared, the cropstage soil loss ratio from table 5 is used as **C**. The annual **EI** fraction that is applicable to the selected period is obtained from table 6 and is multiplied by the location's annual erosion index value (fig. 1) to obtain the relevant **R** value. **K**, **LS**, and **P** will usually be assumed to have the same values as for computation of average annual soil losses.

Suppose, for example, that one wishes to predict the average soil loss for the seedbed and establishment periods of corn that is conventionally planted about May 15 on spring plowed soybean land in southwestern Iowa (area No. 13, fig. 9). Suppose also that the corn is on a field for which the combined value of factors **K**, **LS**, and **P** is 0.67 and the fertility and crop management are such that corn planted by May 15 usually develops a 10 percent canopy cover by June 5, 50 percent by June 25, and a final canopy cover of more than 95 percent. Interpolating between values in line 13 of table 6 shows cumulative **EI** percentages of 12, 23, and 43 for these three dates. Therefore, on the average, 11 percent of the annual **EI** would occur in the seedbed period, and 20 percent would occur in the establishment period. From line 109 of table 5, the soil loss ratios for these two cropstage periods under the assumed management are 0.72 and 0.60. From figure 1, the average annual **EI** is 175. The soil loss would be expected to average $0.11(175)(0.72)(0.67) = 9.3$ t/A in the seedbed period and $0.20(175)(0.60)(0.67) = 14$ t in the establishment period. The cropping assumed for this example represents an extremely erodible condition. For second-year corn with good residue management, the applicable soil loss ratios and the predicted soil losses would be much lower.

Individual Storm Soil Losses

The USLE factors derived from tables and charts presented herein compute longtime-average soil losses for specified cover and management on a given field. The USLE is not recommended for prediction of specific soil loss events.

If it is applied to a specific rainstorm, using the storm **EI** for **R** and the relevant cropstage soil loss ratio for **C**, it will estimate the *average* soil loss for a large number of storms of this size occurring on that field and in that cropstage period. However, the soil loss from any one of these events may differ widely from this average because of interactions with variables whose values fluctuate randomly over time (*56*).

When rain falls on relatively dry, freshly tilled soil, most of the water may infiltrate before runoff begins, resulting in a low-average soil loss per unit of **EI** for that storm. When rain falls on presaturated soil, runoff begins quickly, and most of the rain becomes runoff. Such rains usually produce above-average soil loss per **EI** unit. Some rains are accompanied by high winds that increase the impact energy of raindrops; others occur in a fairly calm atmosphere. Some storms begin with a high intensity and seal the surface quickly so that trailing lower intensities encounter a low infiltration rate. In other storms the moderate intensities

precede the high ones. In some seasons the soil is cultivated when wet and remains cloddy; in other seasons it is cultivated when soil moisture is ideal for fine pulverization. A claypan or fragipan subsoil may substantially influence permeability in early spring or in a wet growing season and yet have no significant effect on infiltration rates during intense thunderstorms on dry soil.

The soil loss ratios of table 5 are averages for cropstage periods that cover several weeks to several months. Early in a cropstage period, the ratio will usually be higher than the average because the development of cover is gradual. Later in the period it will be lower than average. In a poor growing season the ratio will be above average because cover and water use by transpiration are below normal. In a favorable growing season, the ratio will be below average. Cover effect in a specific year may be substantially influenced by abnormal rainfall. A crop canopy or conservation tillage practice may delay the start of runoff long enough to be 100 percent effective for moderate storms on a given field and yet allow substantial erosion by prolonged runoff periods.

The irregular fluctuations in these and other variables can greatly influence specific-storm soil losses. However, they do not invalidate the USLE for predicting long-term-average soil losses for specific land areas and management conditions. Their positive and negative effects tend to balance over a longtime period, and their average effects are reflected in the factor-evaluation tables and charts.

Two recent research reports are recommended references for those who find it necessary to estimate specific-storm soil losses (*34, 10*). The authors present modifications of **R** and **LS** that are designed to account for some random effects discussed.

Specific-Year Soil Losses

In any given year, both the annual **EI** and its monthly distribution may differ substantially from the location averages. Therefore, **R** values from figure 1 and **EI** distribution data from table 6 will not correctly reflect specific-year values of these variables. The most accurate procedure is to compute the **EI** value for each storm from a recording-rain gage record for the location and year by the method given in the appendix. The storm values are summed for each cropstage period, and the subtotals are combined with soil loss ratios from table 5 to estimate the soil loss for each cropstage period. The sum of the cropstage soil losses then reflects the effects of possible abnormal **EI** distribution, as well as the corrected **R** value for the specific year. However, the irregular fluctuations in variables discussed in the preceding subsection are often related to abnormalities in rainfall. The plus and minus effects on soil loss may not average out within 1 year but may appreciably bias specific-year soil losses. These biases will not be evaluated by the USLE. Therefore, specific-year estimates of soil loss will be less accurate than USLE estimates of long-term, crop-year averages.

Soil Loss Probabilities

Soil loss probabilities are a function of the combination of the probabilities for annual **EI**, seasonal distribution of the erosive rains, abnormal antecedent soil moisture conditions, favorable or unfavorable conditions for soil tillage and crop development, and other factors. The section on the **Rainfall Erosion Index** pointed out that a location's annual and maximum storm **EI** values tend to follow log-normal frequency distributions and that specific probability values are listed in tables 17 and 18 for 181 key locations. When these probabilities of **EI** are used for **R** in the USLE, the equation will estimate the soil loss that would occur if all the other factors were at their normal levels. However, the seasonal distribution of erosive rains, and the surface conditions in the field, may also be abnormal in years of rainfall extremes. Deriving probable relationships of these variables to extremes in annual **EI** would require longer records than were available.

Stochastic modeling techniques (*66*) are available that could be used to generate synthetic data having the same statistical properties as historical data. Such data could be used to estimate the probable range in specific-year soil losses in a particular rainfall area.

Determining Alternative Land Use and Treatment Combinations

The soil loss prediction procedure supplies the practicing conservationist with concise reference tables from which he can ascertain, for each particular situation encountered, which specific land

use and management combinations will provide the desired level of erosion control. A number of possible alternatives are usually indicated. From these, the farmer will be able to make a choice in line with his desires and financial resources.

Management decisions generally influence erosion losses by affecting the factor **C** or **P** in the erosion equation. **L** is modified only by constructing terraces, diversions, or contour furrows with sufficient capacity throughout the year to carry the runoff water from the furrow area above. **R, K,** and **S** are essentially fixed as far as a particular field is concerned.

When erosion is to be limited within a predetermined tolerance, **T,** the term **A** in the equation is replaced by **T,** and the equation is rewritten in the form **CP** = **T/RKLS.** Substituting the site values of the fixed factors in this equation and solving for **CP** give the maximum value that the product **CP** may assume under the specified field conditions. With no supporting practices, **P** = 1, and the most intensive cropping plan that can be safely used on the field is one for which **C** just equals this value. When a supporting practice like contouring or stripcropping is added, the computed value of **T/RKLS** is divided by the practice factor, **P,** to obtain the maximum permissible cover and management factor value. Terracing increases the value of **T/RKLS** by decreasing the value **L.**

A special USLE calculator, originally designed in Tennessee (*41*) and recently updated, enables rapid and systematic calculation of either average annual soil loss or **T/RKLS** for any specific situation.

Many practicing conservationists prefer to use handbook tables. **C**-value tables for specific geographic areas (fig. 9) are centrally prepared by persons who are experienced in the procedures outlined in a preceding section and who obtain the needed data from tables 5 and 6. Values of **T/RKLS** are also centrally computed and arranged in two-way classification as illustrated in table 16 for **R** = 180, **K** = 0.32, and **T** = 5. Similar tables are prepared for other combinations of **R, K,** and **T.**

A conservationist working in the field usually carries a pocket-sized handbook which includes the **R** value(s), **T** and **K** soil values, applicable tables of **T/RKLS** values, and a table of **C** values for the area. These items will provide all the information needed to use this procedure as a guide

TABLE 16.—*Maximum permissible* **C** *values* (**T/RKLS**) *for* **R** = *180,* **K** = *0.32 and* **T** = *5*

Gradient percent	Values for slope lengths (feet)							
	50	75	100	150	200	250	300	400
	STRAIGHT ROW							
2 ..	0.53	0.47	0.43	0.38	0.35	0.33	0.31	0.28
4 ..	.29	.24	.22	.18	.16	.15	.14	.12
6 ..	.18	.15	.13	.11	.091	.082	.074	.064
8 ..	.12	.10	.087	.072	.062	.055	.050	.044
10 ..	.090	.073	.063	.052	.045	.040	.037	.032
12 ..	.068	.056	.048	.039	.034	.030	.028	.024
14 ..	.054	.044	.038	.031	.027	.024	.022	.019
16 ..	.043	.035	.030	.025	.022	.019	.018	.015
	CONTOURED[1]							
2 ..	0.89	0.78	0.72	0.64	0.58	0.55	0.52	0.47
4 ..	.57	.49	.43	.37	.33	.30	.28	.25
6 ..	.36	.30	.26	.21	.18	.16	([2])	—
8 ..	.25	.20	.17	.14	.12	.11	—	—
10 ..	.15	.12	.11	.086	([2])	—	—	—
12 ..	.11	.093	.080	.065	—	—	—	—
14 ..	.077	.062	.054	([2])	—	—	—	—
16 ..	.062	.050	.044	—	—	—	—	—

[1] The values for contour farming are **T/RKLSP**, where **P** is dependent on percent slope (see table 13).

[2] Omission of values indicates that the slope-lengths exceed the limits for effectiveness of contouring. Use corresponding values from upper half of table.

for selecting conservation practices in each field. Solving the equation or performing field computations rarely will be necessary.

Example. The first step is to ascertain the soil type, percent slope, and slope length for the field being planned. From his handbook data, the conservationist can then obtain the values of **R, K,** and **T.** To complete the illustration, assume that **R** = 180, **K** = 0.32, **T** = 5, and the field slope is 400 ft long with a nearly uniform gradient of 6 percent. For this combination, the **T/RKLS** table shows a value of 0.064 for straight-row farming with the land slope (table 16). This is the maximum **C** value that will hold the average annual soil loss from that field within the 5-t tolerance limit, if no supporting practices are used. Consulting the **C** value table will show that a **C** as low as 0.064 can be attained only with well-managed, sod-based crop systems, or with no-till planting in residue covers of at least 70 percent.

A logical improvement is to add contouring. Table 13 shows a slope-length limit of 200 ft (250 ft if residue cover after seeding exceeds 50 percent) for contouring on 6-percent slope. Therefore,

the **P** value of 0.5 for contouring will not be applicable on the 400-ft slope without terracing. Construction of three, equally spaced terraces across the slope would divide it into four 100-ft slope lengths. Shortening the slope lengths to 100 ft will assure contour effectiveness and will also reduce the site value of **L**. For a 100-ft length of 6-percent slope farmed on the contour, table 16 shows a **T/RKLSP** value of 0.26. Any combination of cropping and management practices having a **C** value less than 0.26 will now be acceptable. Consulting the table of **C** values will show that with the terraces and contouring, the conservationist can recommend a range of possibilities for land use and management. If a system with a **C** value appreciably less than 0.26 is selected, a higher level of conservation will be attained than required by the 5-t tolerance limit.

Had the slope length in the example been only 200 ft, the contour **P** value of 0.5 (table 13) would have been applicable without the terraces. Table 16 shows that this combination would have permitted use of any system having a **C** value less than 0.18.

Thus, by this procedure a conservationist can list all the alternative crop system and management combinations that would control erosion on a field at an acceptable level. Study of this list will show how an erosion control program can be improved and still increase crop yields or decrease labor and fuel costs. In making a selection from this list, practices needed for control of nutrient and pesticide losses in the runoff (*42*) should also be considered.

Construction Sites

Procedures and data have been presented for predicting erosion losses from specific cropland areas and logically determining alternative ways in which the losses from each field may be held below given tolerance limits. These procedures and data can also be adapted to conditions on highway, residential, and commercial developing areas. The USLE will show under which development plan the area will produce the least sediment, and it will also show about how much sediment the developer will need to trap in sediment basins (*46*) during construction to prevent excessive soil movement to streams or reservoirs.

Evaiuating the erosion factors for construction site conditions is discussed below. However, those primarily concerned with this particular phase of sediment control should also read the preceding discussions of the USLE factors and the procedures for predicting cropland soil losses.

Factor R. For a construction project extending over several years, the average annual **R** value for the site is obtained directly from figure 1. Probabilities of **EI** values greater than average are given in table 17. Using **EI** probabilities for **R** was discussed in the subsection **Soil Loss Probabilities.**

For construction periods of less than 1 year, the procedure outlined for predicting cropland soil losses for specific cropstage periods is appropriate. The portion of the annual **R** value that is applicable to the construction period is obtained from table 6 as illustrated on p. 41 for cropstage averages.

Factor K. Because the soil surface is often unprotected during construction, this factor assumes even greater importance than for cropland. The soil erodibility nomograph (fig. 3) can be especially helpful for sediment prediction and erosion control planning on construction sites because it can predict the changes in erodibility when various subsoil horizons are exposed in the reshaping process. Some subsoils are substantially more erodible than the original topsoil, and others are less erodible. The planner can usually obtain a detailed description of the successive horizons of his soil from published soil survey data. By using the data for each soil horizon separately to follow the steps of the nomograph solution, the **K** value can be determined after various depths of desurfacing. Soil losses from the successive soil horizons, if exposed on similar slopes, would be directly proportional to the horizon **K** values. Information on the subsoil **K** values not only shows the depths of cut that would result in the most or the least soil erosion but also indicates whether return of stockpiled topsoil on the exposed subsoil would be profitable on the particular site.

When a chemical soil additive is used that stabilizes the soil and makes it less erodible, the **K** value is the nomograph solution times a factor for the effectiveness of the chemical additive.

Factor LS. Within limits, the **LS** value for a given length and steepness of uniform slope can be obtained directly from figure 4 or table 3. When the

slope is concave or convex, the figure 4 value needs to be adjusted by the procedure outlined for irregular slopes in the section on **The Topographic Factor.**

Development planning may include measures designed to reduce sediment yield by lowering **LS.** The effect of shortening slope lengths by diversions or stabilized drainageways is credited by entering figure 4 with the reduced slope length. A slope graded to flatten toward the bottom (concave) will lose less soil than an equivalent uniform slope whereas one that steepens toward the bottom (convex) will lose more. Reduction or increase in soil loss can be predicted by the procedure illustrated in the subsection **Irregular Slopes.**

Data are not available to evaluate **LS** on very steep slopes, like 2:1 and 3:1 roadbank slopes, in relation to soil and rainstorm characteristics. The best presently available estimates of **LS** for these slopes can be obtained by the **LS** equation presented earlier. However, values projected by this equation for steep slopes are speculative because the equation was derived from data obtained on slopes of less than 20 percent.

Factor C. Procedures for selecting **C** values for construction sites were given in the **Cover and Management Factor** section.

Factor P. This factor as used for soil conservation planning on cropland would rarely have a counterpart during construction on development areas, and **P** will usually equal 1.0. Erosion-reducing effects of shortening slopes or reducing slope gradients are accounted for through the **LS** factor.

If the lower part of a grass or woodland slope on a development area can be left undisturbed while the upper part is being developed, the procedure outlined for computing the value of **LSC** on irregular slopes is applicable, and sediment deposition on the undisturbed strip must be accounted for separately. For prolonged construction periods, buffer strips of grass, small grain, or high rates of anchored mulch may also be feasible to induce deposition within the area. Such deposition is important for water quality or offsite sediment control, but it should be evaluated from soil-transport factors rather than by a **P** factor.

Alternative plans. When appropriate numerical values of the six erosion factors are combined, their product is the soil loss estimate for the particular area in tons per acre and for the time interval for which **R** was evaluated. With the information supplied by the tables and charts in this handbook, the six factor values can be derived for each feasible alternative plan. Successive solutions of the equation will then provide comparative soil loss estimates to help guide decisions by the developer.

Estimating Upslope Contributions to Watershed Sediment Yield

The importance of predicting watershed sediment yields and identifying the major sediment sources was increased by the Federal Water Pollution Control Act Amendments of 1972, Public Law 92-500. Sources, causes, and potentials of sediment, nutrient, and pesticide losses from cropland, and measures that may be necessary to control these pollutants, are dealt with in depth in a two-volume manual developed by SEA and the Environmental Protection Agency (EPA) (*42*). Volume II, "An Overview," also includes an extensive list of other relevant publications. Only sediment yield prediction will be considered here.

Estimates show that about one-fourth of the amount of sediment moved by flowing water in the United States annually reaches major streams (*42*). The USLE can be used to compute average sheet and rill erosion in the various parts of a watershed, but deposition and channel-type erosion must be estimated by other means. A fully tested equation for sediment transport to use on agricultural land is not now available. One presented by Neibling and Foster (*32*) is perhaps the best now available for use with the USLE. It estimates transport capacity for sand and large silt-sized particles and does not consider the transport of clay particles.

Of the several methods now used for estimating sediment yield, the Gross Erosion-Sediment Delivery Method uses the USLE. A brief description of this method follows. More details are available from the SCS National Engineering Handbook (*45*). The equation is

$$Y = E(DR)/W_s \qquad (6)$$

where **Y** is sediment yield per unit area,

E is the gross erosion,

DR is the sediment delivery ratio, and

W_s is the area of the watershed above the point for which the sediment yield is being computed.

Gross Erosion

Gross erosion is the summation of erosion from all sources within the watershed. It includes sheet and rill erosion from tilled cropland, meadows, pastures, woodlands, construction sites, abandoned acreages, and surface-mined areas; gully erosion from all sources; and erosion from streambeds and streambanks. The relative importance of each of these sources of gross erosion will vary between watersheds.

The USLE can be used to estimate the sediment generated by sheet and rill erosion that is usually, but not always, the major portion of a watershed's gross erosion. Sediment from gully, streambank and streambed erosion, and from uncontrolled roadsides must be added to the USLE estimates. Methods for estimating sediment yields from these sources are discussed in Section 3 of the SCS National Engineering Handbook (*45*).

For small areas like farm fields or construction sites, the six USLE factors can usually be evaluated directly from the information presented in this handbook. For a large heterogeneous watershed, the factors are more difficult to define. Several methods of computing the average slope length and gradient for a large drainage area are available. Using **LS** values based on such averages, together with estimated watershed-average soil and cover factors, simplifies the computing procedure, but the saving in time is at the expense of substantial loss in accuracy. Erosion hazards are highly site specific. The parameters that determine the USLE factor values vary within a large watershed, and the variations are often not interrelated. Combining overall averages in the equation does not reflect the particular way in which the factors are actually combined in different parts of the watershed. Neither does it show which portions of the drainage area are contributing most of the sediment.

A more accurate procedure is to divide the heterogeneous drainage area into subareas for which representative soil type, slope length, gradient, cover, and erosion-control practice factors can be defined. The USLE is then used to compute the sheet and rill erosion on each subarea. For this purpose, eroded soil that is entrapped within the field area by terrace systems is not soil loss. An estimate of the entrapped sediment can be excluded from the USLE soil loss estimates by using values from the last two columns of table 15 as the **P** values. An alternate procedure is to estimate the channel deposition by sediment-transport relationships and subtract this amount from the soil loss computed by using the standard terracing factor (col. 2, table 15) in the USLE. By this procedure, the subarea soil loss computations identify the portions of the drainage area that contribute most of the sediment and also show how much of the sediment derives from tracts that receive heavy applications of agricultural chemicals.

Procedures for computing soil losses from cropped, idle, pasture, range, or wooded areas and from construction or development areas were outlined in the preceding sections. Factor values derived by the prescribed procedures are assumed applicable also for surface-mined areas. However, the effect of mining processes on soil erodibility, **K**, has not been determined. Length and percent slope and deposition within the area also are hard to determine for rugged strip mine spoils. Sometimes nearly all the sediment may be trapped within the bounds of the area. The USLE can be quite useful for predicting the effectiveness of each feasible reclamation plan for such areas.

Sediment Delivery Ratio

Eroded soil materials often move only short distances before a decrease in runoff velocity causes their deposition. They may remain in the fields where they originated or may be deposited on more level slopes that are remote from the stream system. The ratio of sediment delivered at a given location in the stream system to the gross erosion from the drainage area above that location is the sediment delivery ratio for that drainage area. A general equation for computing watershed delivery ratios is not yet available, but the ratios for some specific drainage areas have been computed directly from local data. Helpful guides for estimating this factor for other drainage areas were published by SCS in Section 3 of their National Engineering Handbook (*45*), and most of these guides were also included in a publication by SEA and EPA (*42*). Therefore, the relationships involved will be only briefly summarized here.

Available watershed data indicate that the delivery ratio varies approximately as the 0.2 power of drainage-area size, with representative values of about 0.33 for 0.5 mi^2; 0.18 for 10 mi^2; and 0.10 for 100 mi^2. There were indications that the exponent in this relationship may be as small as 0.1 for very large areas. But the ratio may vary substantially for any given size of drainage area. Other important factors include soil texture, relief, type of erosion, sediment transport system, and areas of deposition within the watershed. Fine soil texture, high channel density, and high stream gradients generally indicate delivery ratios that are above average for the drainage-area size.

A substantial reduction in sediment delivered to a stream may sometimes result in a compensatory increase in channel erosion. Channel erosion produces sediment that is immediately available to the transport system and that may remain in motion as bedload and suspended sediment. The composition of sediment derived from channel erosion will usually differ substantially from that derived from cropland erosion. This is particularly important from the viewpoint of transported chemical pollutants.

With reference to a field-sized area, the delivery ratio can closely approach 1.0 if the runoff drains directly into a lake or stream system with no intervening obstructions or flattening of the land slope. On the other hand, a substantial width of forest litter or dense vegetation below the eroding area may cause deposition of essentially all the sediment except colloidal material. Anything that reduces runoff velocity (such as reduction in gradient, physical obstructions, vegetation, and ponded water) reduces its capacity to transport sediment. When the sediment load exceeds the transport capacity of the runoff, deposition occurs.

From analysis of runoff and soil loss data from small single-cropped watersheds, Williams (*48*) concluded that the need for a sediment delivery ratio could be eliminated by using the watershed runoff times peak rate as the storm **R** value in the USLE.

Accuracy of USLE Predictions

Soil losses computed with the USLE are best available estimates, not absolutes. They will generally be most accurate for medium-textured soils, slope lengths of less than 400 ft, gradients of 3 to 18 percent, and consistent cropping and management systems that have been represented in the erosion plot studies. The farther these limits are exceeded, the greater will be the probability of significant extrapolation error.

An indication of the accuracy of the equation, tables, and charts presented herein was obtained by using them to compute longtime average soil losses for plots in past erosion studies and comparing these with the actually measured losses on each plot. About 53 percent of the differences were less than 1 t/A, 84 percent were less than 2 t, and 5 percent were as much as 4.6 t (*53*). The mean annual soil loss for this 2,300 plot-year sample was 11.3 t. Of those differences that exceeded 1 t/A, 67 percent were from comparisons with plot records whose duration was less than half of a normal 22-year rainfall cycle (*33*). Such short records are subject to bias by cyclical effects and random fluctuations in uncontrolled variables whose effects are averaged in the USLE factor values (*56*). Testing the complete equation against the assembled plot data was statistically valid because the equation for each factor, as a function of several parameters, was independently derived from only selected portions of the data.

The accuracy of a predicted soil loss will depend on how accurately the physical and management conditions on the particular piece of land are described by the parameter values used to enter the factor-evaluation tables and charts. An error in the selection of a factor value will produce an equivalent percentage error in the soil loss estimate. Large-scale averaging of parameter values on mixed drainage areas will usually also reduce accuracy. For reasons previously pointed out and discussed in depth in another publication (*56*), specific-storm or specific-year soil losses and short-term averages may differ substantially from the longtime average predicted by the USLE for the specified physical and management conditions.

REFERENCES

(1) Adams, J. E. 1966. Influence of mulches on runoff, erosion, and soil moisture depletion. Soil Science Society of Americo Proceedings 30:110-114.

(2) Barnett, A. P., Diseker, E. G., and Richardson, E. C. 1967. Evaluation of mulching methods for erosion control on newly prepared and seeded highway backslopes. Agronomy Journal 59:83-85.

(3) ——— and Rogers, J. S. 1966. Soil physical properties related to runoff ond erosion from artificial rainfall. Americon Society of Agricultural Engineers Transactions 9:123-125.

(4) Blokely, B. D., Coyle, J. J., and Steele, J. G. 1957. Erosion on cultivated land. *In* Soil, Yearbook of Agriculture, pp. 290-306.

(5) Brooks, F. L. 1976. Use of the universol soil loss equotion in Hawaii. *In* Soil Erosion: Prediction ond Control. Soil Conservation Society of America, pp. 29-30.

(6) Browning, G. M., Porish, C. L., and Glass, J. A. 1947. A method for deterrmining the use and limitation of rotation and conservotion practices in control of soil erosion in Iowa. Soil Science Society of America Proceedings 23:246-249.

(7) Corter, C. E., Greer, J. D., Braud, H. J., and Floyd, J. M. 1974. Raindrop characteristics in South Central United States. American Society of Agricultural Engineers Transactions 17:1033-1037.

(8) ——— ond Carreker, J. R. 1969. Controlling water erosion with graded furrows. American Society of Agricultural Engineers Tronsactions 12:677-680.

(9) El-Swaify, S. A., and Dangler, E. W. 1976. Erodibility of selected tropical soils in relotion to structural and hydrological porometers. *In* Soil Erosion: Prediction and Control, Soil Conservation Society of America, pp. 105-114.

(10) Foster, G. R., Meyer, L. D., and Onstod, C. A. 1977. A runoff erosivity factor ond variable slope length exponents for soil loss estimates. American Society of Agricultural Engineers Transactions 20:683-687.

(11) ——— Meyer, L. D., and Onstod, C. A. 1977. An erosion equation derived from basic erosion principles. American Society of Agricultural Engineers Transactions 20:678-682.

(12) ——— and Wischmeier, W. H. 1974. Evaluating irregular slopes for soil loss prediction. Americon Society of Agriculturol Engineers Transoctions 17:305-309.

(13) Gunn, R., and Kinzer, G. D. 1949. The terminal velocity of fall for water droplets. Journal Met. 6:243-248.

(14) Hill, H. O., Peevy, W. J., McCall, A. G., and Bell, F. G. 1944. Investigations in erosion control and reclamation of eroded land at the Blackland Conservation Experiment Stotion, 1931-41. U.S. Department of Agriculture, Technicol Bulletin 859, 109 pp.

(15) Hudson, N. W. 1971. Raindrop size. *In* Soil Conservation: Cornell University Press, Ithaca, New York, pp. 50-56.

(16) Jamison, V. C., Smith, D. D., and Thornton, J. F. 1968. Soil and Water research on a claypon soil. U.S. Department of Agriculture, Technical Bulletin 1379.

(17) Laflen, J. M., and Johnson, H. P. 1976. Soil and water loss from impoundment terroce systems. 3d Federal Inter-Agency Sedimentation Conference Proceedings 2:20-41.

(18) Lillard, J. H., Rogers, H. T., and Elson, Jesse. 1941. Effects of slope, character of soil, rainfall, and cropping treatments on erosion losses from Dunmore silt loam. Virginia Agricultural Experiment Stotion Technical Bulletin 72, 32 pp.

(19) Lloyd, C. H., and Eley, G. W. 1952. Graphical solution of probable soil loss formula for Northeastern Region. Journal of Soil and Woter Conservation 7:189-191.

(20) Mannering, J. V., and Meyer, L. D. 1963. Effects of various rates of surface mulch on infiltration ond erosion. Soil Science Society of America Proceedings 27:84-86.

(21) McCool, D. K., Papendick, R. I., ond Brooks, F. L. 1976. The universal soil loss equotion as adapted to the Pocific Northwest. 3d Federal Inter-Agency Sedimentation Conference Proceedings 2:135-147.

(22) Meyer, L. D., Foster, G. R., ond Romkens, M. J. M. 1975. Source of soil eroded by water from upland slopes. Sediment Prediction Workshop Proceedings, Oxford, Miss. ARS-S-40:177-189.

(23) ——— and McCune, D. L. 1958. Rainfoll simulotor for runoff plots. Agricultural Engineering 39:644-648.

(24) ——— ond Ports, M. A. 1976. Prediction and control of urban erosion and sedimentation. Notional Symposium on Urban Hydrology, Hydraulics, ond Sedimentation Proceedings, University of Kentucky, Lexington, Bulletin 111, pp. 323-331.

(25) ——— and Romkens, M. J. M. 1976. Erosion and sediment control on reshoped land. 3d Federol Inter-Agency Sedimentation Conference Proceedings 2:65-72.

(26) ——— and Wischmeier, W. H. 1969. Mathemotical simulotion of the process of soil erosion by woter. Americon Society of Agricultural Engineers Transactions 12:754-758, 762.

(27) ——— Wischmeier, W. H., and Foster, G. R. 1970. Mulch rates required for erosion control on steep slopes. Soil Science Society of Americo Proceedings 34:928-931.

(28) Middleton, H. E., Slater, C. S., and Byers, H. G. 1932-1934. Physical and chemical characteristics of the soils from the erosion experiment stations. U.S. Department of Agriculture, Technical Bulletin No. 316 and 430.

(29) Moldenhauer, W. C., and Wischmeier, W. H. 1960. Soil and water losses and infiltration rates on Ida silt loom os influenced by cropping systems, tillage practices ond roinfoll chorocteristics. Soil Science Society of America Proceedings 24:409-413.

(30) ——— Lovely, W. G., Swanson, N. P., and Currence, H. D. 1971. Effect of row grades ond tillage systems on soil and water losses. Journal of Soil ond Water Conservation 26(5): 193-195.

(31) Musgrave, G. W. 1947. The quontitotive evoluotion of foctors in water erosion, a first approximation. Journal of Soil ond Water Conservotion 2(3):133-138.

(32) Neibling, W. H., and Foster, G. R. 1977. Estimating deposition and sediment yield from overland flow processes. 1977 International Symposium on Urban Hydrology, Hydraulics, and Sediment Control Proceedings, University of Kentucky, Lexington.

(33) Newman, J. E. 1970. Climate in the 1970's. American Society of Agronomy, Crops and Soils 22(4):9-12.

(34) Onstad, C. A., and Foster, G. R. 1975. Erosion modeling on a watershed. American Society of Agricultural Engineers Transactions 18:288-292.

(35) Peele, T. C., Latham, E. E., and Beale, O. W. 1945. Relation of the physical properties of different soil types to erodibility. South Carolina Agricultural Experiment Station Bulletin No. 357.

(36) Richardson, C. W. 1973. Runoff, erosion and tillage efficiency on graded furrows and terraced watersheds. Journal of Soil and Water Conservation 28(4):162-164.

(37) Roth, C. B., Nelson, D. W., and Romkens, M. J. M. 1974. Prediction of subsoil erodibility using chemical, mineralogical and physical parameters. U. S. Environmental Protection Agency Report No. 660/2-74-043. 111 pp.

(38) Smith, D. D. 1941. Interpretation of soil conservation data for field use. Agricultural Engineering 22:173-175.

(39) ——— and Whitt, D. M. 1947. Estimating soil losses from field areas of claypan soils. Soil Science Society of America Proceedings 12:485-490.

(40) ——— and Wischmeier, W. H. 1957. Factors affecting sheet and rill erosion. American Geophysical Union Transactions 38:889-896.

(41) Springer, D. L., Breinig, C. B., and Springer, M. E. 1963. Predicting soil losses in Tennessee. Journal of Soil and Water Conservation 18(4):157-158.

(42) Stewart, B. A., Wischmeier, W. H., Woolhiser, and others. 1975. Control of water pollution from cropland: Vol. I, a manual for guideline development; Vol. II, an overview. U.S. Department of Agriculture, ARS-H-5-1 and ARS-H-5-2.

(43) Swanson, N. P., Dedrick, A. R., Weakley, H. E., and Haise, H. R. 1965. Evaluation of mulches for water-erosion control. American Society of Agricultural Engineers Transactions 8: 438-440.

(44) U.S. Department of Agriculture. 1977. Terracing Code 600. *In* National Engineering Handbook. U.S. Department of Agriculture, Soil Conservation Service.

(45) ——— 1971. Sediment sources, yields and delivery ratios. *In* National Engineering Handbook, Section 3, Sedimentation. U.S. Department of Agriculture,Soil Conservation Service.

(46) ——— 1975. Standards and specifications for soil erosion and sediment control in developing areas, approved by Maryland Water Resources Administration. U.S. Department of Agriculture, Soil Conservation Service. 200 pp.

(47) U. S. Weather Bureau. 1958. Rainfall intensity-frequency regime. Technical Paper No. 29, 5 parts.

(48) Williams, J. R. 1975. Sediment-yield prediction with the universal equation using a runoff energy factor. U.S. Department of Agriculture, ARS-S-40:244-252.

(49) Wischmeier, W. H. 1959. A rainfall erosion index for a universal soil-loss equation. Soil Science Society of America Proceedings 23:246-249.

(50) ——— 1960. Cropping-management factor evaluations for a universal soil-loss equation. Soil Science Society of America Proceedings 23:322-326.

(51) ——— 1962. Storms and soil conservation. Journal of Soil Water and Conservation 17(2):55-59.

(52) Wischmeier, W. H. 1966. Relation of field-plot runoff to management and physical factors. Soil Science Society of America Proceedings 30:272-277.

(53) ——— 1972. Upslope erosion analysis. *In* Environmental Impact on Rivers. Water Resources Publications, Fort Collins, Colo.

(54) ——— 1973. Conservation tillage to control water erosion. National Conservation Tillage Conference Proceedings, Soil Conservation Society of America, pp. 133-141.

(55) ——— 1974. New developments in estimating water erosion. 29th Annual Meeting of the Soil Conservation Society of America Proceedings, pp. 179-186.

(56) ——— 1976. Use and misuse of the universal soil loss equation. Journal of Soil and Water Conservation 31(1): 5-9.

(57) ——— 1975. Estimating the soil loss equation's cover and management factor for undisturbed areas. Sediment Yield Workshop Proceedings, Oxford, Miss. U.S. Department of Agriculture, ARS-S-40.

(58) ——— Johnson, C. B., and Cross, B. V. 1971. A soil erodibility nomograph for farmland and construction sites. Journal of Soil and Water Conservation 26:189-193.

(59) ——— and Mannering, J. V. 1965. Effect of organic matter content of the soil on infiltration. Journal of Soil and Water Conservation 20:150-152.

(60) ——— and Mannering, J. V. 1969. Relation of soil properties to its erodibility. Soil Science Society of America Proceedings 33:131-137.

(61) ——— and Meyer, L. D. 1973. Soil erodibility on construction areas. Highway Research Board, National Academy of Science Special Report 135:20-29.

(62) ——— and Smith, D. D. 1958. Rainfall energy and its relationship to soil loss. American Geophysical Union Transactions 39:285-291.

(63) ——— Smith, D. D., and Uhland, R. E. 1958. Evaluation of factors in the soil loss equation. Agricultural Engineering 39:458-462, 474.

(64) ——— and Smith, D. D. 1965. Predicting rainfall-erosion losses from cropland east of the Rocky Mountains—Guide for selection of practices for soil and water conservation. Agricultural Handbook No. 282.

(65) Witmuss, H. D., Triplett, G. B., Jr., and Creb, B. W. 1973. Concepts of conservation tillage systems using surface mulches. National Conservation Tillage Conference Proceedings, Soil Conservation Society of America 5-12.

(66) Woolhiser, D. G. 1975. Simulation of unsteady overland flow. *In* Unsteady Flow in Open Channels. Water Resources Publications, Fort Collins, Colo. Vol. II, Ch. 12, pp. 485-508.

(67) Zingg, R. W. 1940. Degree and length of land slope as it affects soil loss in runoff. Agricultural Engineering 21:59-64.

APPENDIX

Estimating Percentages of Canopy and Mulch Covers

"Percent canopy cover" is the percentage of the field area that could not be hit by vertically falling raindrops because of canopy interception. It is the portion of the soil surface that would be covered by shadows if the sun were directly overhead. Because the blades from adjacent rows intertwine does not necessarily indicate 100 percent canopy cover.

"Percent mulch cover" is the percentage of the field area that is covered by pieces of mulch lying on the surface. Researchers in Indiana attempted to relate percent cover to mulch rate by photographing numerous small, equal-sized areas in harvested corn fields. The residues on the photographed areas were carefully picked up, dried, and weighed to measure mulch rates, and the photographs were projected on grids to determine percent cover. The indicated average relation of percent cover to dry weight of well-distributed corn stover mulch is shown by the solid-line curve in figure 10. However, observed differences between samples were appreciable. The average relation of percent cover to dry weight of straw mulch uniformly distributed over research plots is shown by the broken-line curve.

A simple method of estimating percent mulch cover on a field is with a cord, preferably not shorter than 50 ft, that has 100 equally spaced knots or other readily visible markings. The cord is stretched diagonally across several rows, and the knots that contact a piece of mulch are counted. This procedure is repeated at randomly selected spots on the field, and the data are averaged to obtain a representative value for the field.

Probability Values of EI in the United States

The annual and maximum-storm values of **EI** at any given location differ substantially from year to year. The observed ranges and 50 percent, 20 percent and 5 percent probabilities of annual **EI** values from 22-year precipitation records at 181 locations in 44 States are listed in table 17. Other probabilities can be derived by plotting the 50 percent and 5 percent values on log-probability paper and joining the two points by a straight line. Annual maxima storm probabilities for the same locations are given in table 18.

Computing the Erosion Index from Recording-Rain Gage Records

Soil loss prediction by the method presented in this handbook does not require computation of **EI** values by application personnel, but the procedure is included here for the benefit of those who may wish to do so.

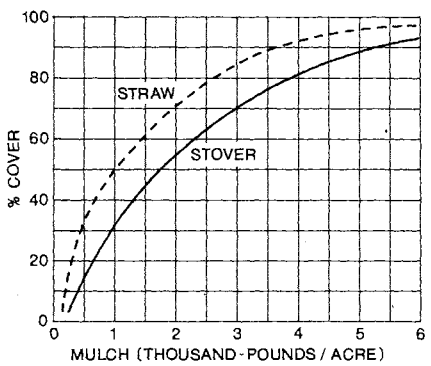

FIGURE 10.—Relation of percent cover to dry weight of uniformly distributed residue mulch.

The kinetic energy of a given amount of rain depends on the sizes and terminal velocities of the raindrops, and these are related to rainfall intensity. The computed energy per inch of rain at each intensity is shown in table 19. The energy of a given storm depends on all the intensities at which the rain occurred and the amount that occurred at each intensity. A recording-rain gage record of the storm will provide this information. Clock time and rain depth are read from the chart at each point where the slope of the pen line changes and are tabulated as shown in the first two columns of the sample computation below. Clock times (col. 1) are subtracted to obtain the time intervals given in column 3, and the depths (col. 2) are subtracted to obtain the incremental amounts tabulated in column 4. The intensity for each increment (col. 5) is the incremental amount times 60, divided by column 3.

Chart readings		For each increment			Energy	
Time	Depth (inch)	Duration (minute)	Amount (inch)	Intensity (in/hr)	Per inch	Total
4:00	0					
:20	0.05	20	0.05	0.15	643	32
:27	.12	7	.07	.60	843	59
:36	.35	9	.23	1.53	977	225
:50	1.05	14	.70	3.00	1074	752
:57	1.20	7	.15	1.29	953	143
5:05	1.25	8	.05	.38	777	39
:15	1.25	20	0	0	0	0
:30	1.30	15	.05	.20	685	34
Totals		90	1.30			1,284
Kinetic energy of the storm = $1{,}284(10^{-2}) = 12.84$						

The energy per inch of rain in each interval (col. 6) is obtained by entering table 19 with the intensity given in column 5. The incremented energy amounts (col. 7) are products of columns 4 and 6. The total energy for this 90-minute rain is 1,284 foot-tons per acre. This is multiplied by a constant factor of 10^{-2} to convert the storm energy to the dimensions in which **EI** values are expressed.

The maximum amount of rain falling within 30 consecutive minutes was 1.08 in, from 4:27 to 4:57. I_{30} is twice 1.08, or 2.16 in/h. The storm **EI** value is $12.84(2.16) = 27.7$. When the duration of a storm is less than 30 minutes, I_{30} is twice the amount of the rain.

The **EI** for a specified time is the sum of the computed values for all significant rain periods within that time. The average annual erosion index for a specific locality, as given in figures 1 and 2, is the sum of all the significant storm **EI** values over 20 to 25 years, divided by the number of years. For erosion index calculations, 6 h or more with less than 0.5 in of precipitation was defined as a break between storms. Rains of less than 0.5 in, separated from other showers by 6 h or more, were omitted as insignificant unless the maximum 15-min intensity exceeded 0.95 in/h.

Recent studies showed that the median dropsize of rain does not continue to increase for intensities greater than about 2.5 to 3 in/h (*7*, *15*). Therefore, energy per unit of rainfall also does not continue to increase, as was assumed in the derivation of the energy-intensity table published in 1958 (62). The value given in table 19 for rain at 3 in/h (7.6 cm/h in table 20) should be used for all greater intensities. Also, analysis of the limited soil loss data available for occasional storms with 30-min intensities greater than 2.5 in/h showed that placing a limit of 2.5 in (6.35 cm)/h on the I_{30} component of **EI** improved prediction accuracy for these storms. Both of these limits were applied in the development of figure 1. They slightly lowered previously computed erosion index values in the Southeast, but average-annual **EI** values for the U.S. mainland other than the Southeast were not significantly affected by the limits because they are rarely exceeded.

Conversion to Metric System

Metric equivalents were not included in the procedures and tables presented in this handbook because direct conversion of each English unit would produce numbers that would be awkward and undesirable. Converting the USLE as a whole is more appropriate. Metric units can then be selected so that each of the interdependent factors will have a metric counterpart whose values will be expressed in numbers that are easy to visualize and to combine in computations.

A convenient unit for measuring cropland soil losses is metric tons per hectare per year. **EI** values of convenient magnitude can be obtained by expressing rainfall energy in metric ton-meters per hectare, expressing intensities in centimeters per hour, and retaining the constant factor of 10^{-2} that has been used consistently for **EI** calculations in English units. Factor **K** will then be in metric tons per hectare per metric **EI** unit. If 22 meters is taken as the basic slope length and 9 percent is retained as the basic slope gradient, the **LS** factor will not be significantly affected. Using these units is recommended and is assumed in the following paragraphs.

The USLE factors will normally be derived directly in these units by procedures outlined below. However, the following conversion factors will facilitate comparisons of the metric factor values with the English values published in this handbook. Factors expressed in the recommended metric units are identified by the subscript, **m**.

Text continues on page 56.

TABLE 17.—*Observed range and 50-, 20-, and 5- percent probability values of erosion index at each of 181 key locations*

Location	Values of erosion index (*EI*)			
	Observed 22-year range	50-percent probability	20-percent probability	5-percent probability
Alabama:				
Birmingham	179-601	354	461	592
Mobile	279-925	673	799	940
Montgomery	164-780	359	482	638
Arkansas:				
Fort Smith	116-818	254	400	614
Little Rock	103-625	308	422	569
Mountain Home	98-441	206	301	432
Texarkana	137-664	325	445	600
California:				
Red Bluff	11-240	54	98	171
San Luis Obispo	5-147	43	70	113
Colorado:				
Akron	8-247	72	129	225
Pueblo	5-291	44	93	189
Springfield	4-246	79	138	233
Connecticut:				
Hartford	65-355	133	188	263
New Haven	66-373	157	222	310
District of Columbia	84-334	183	250	336
Florida:				
Apalachicola	271-944	529	663	820
Jacksonville	283-900	540	693	875
Miami	197-1225	529	784	1136
Georgia:				
Atlanta	116-549	286	377	488
Augusta	148-476	229	308	408
Columbus	215-514	336	400	473
Macon	117-493	282	357	447
Savannah	197-886	412	571	780
Watkinsville[1]	182-544	278	352	441
Illinois:				
Cairo	126-575	231	349	518
Chicago	50-379	140	212	315
Dixon Springs[1]	89-581	225	326	465
Moline	80-369	158	221	303
Rantoul	73-286	152	201	263
Springfield	38-315	154	210	283
Indiana:				
Evansville	104-417	188	263	362
Fort Wayne	60-275	127	183	259
Indianapolis	60-349	166	225	302
South Bend	43-374	137	204	298
Terre Haute	81-413	190	273	389
Iowa:				
Burlington	65-286	162	216	284
Charles City	39-308	140	205	295
Clarinda[1]	75-376	162	220	295
Des Moines	30-319	136	198	284
Dubuque	54-389	175	251	356
Sioux City	56-336	135	205	308
Rockwell City	40-391	137	216	335
Kansas:				
Burlingame	57-447	176	267	398
Coffeyville	66-546	234	339	483
Concordia	38-569	131	241	427
Dodge City	16-421	98	175	303
Goodland	10-166	76	115	171
Hays[1]	66-373	116	182	279
Wichita	42-440	188	292	445
Kentucky:				
Lexington	54-396	178	248	340
Louisville	84-296	168	221	286
Middlesboro	107-301	154	197	248
Louisiana:				
Lake Charles	200-1019	572	786	1063
New Orleans	273-1366	721	1007	1384
Shreveport	143-707	321	445	609
Maine:				
Caribou	26-120	58	79	106
Portland	36-241	91	131	186
Skowhegan	39-149	78	108	148
Maryland:				
Baltimore	50-388	178	263	381
Massachusetts:				
Boston	39-366	99	159	252
Washington	65-229	116	153	198
Michigan:				
Alpena	14-124	57	85	124
Detroit	56-179	100	134	177
East Lansing	35-161	86	121	166
Grand Rapids	33-203	84	123	178
Minnesota:				
Alexandria	33-301	88	147	240
Duluth	7-227	84	127	189
Fosston	22-205	62	108	184
Minneapolis	19-173	94	135	190
Rochester	46-338	142	207	297
Springfield	37-290	96	154	243
Mississippi:				
Meridian	216-820	416	557	737
Oxford	131-570	310	413	543
Vicksburg	165-786	365	493	658
Missouri:				
Columbia	98-419	214	297	406
Kansas City	28-361	170	248	356
McCredie[1]	64-410	189	271	383
Rolla	105-415	209	287	387
Springfield	97-333	199	266	352
St. Joseph	50-359	178	257	366
St. Louis	59-737	168	290	488
Montana:				
Billings	2-82	12	26	50
Great Falls	3-62	13	24	44
Miles City	1-101	21	40	72
Nebraska				
Antioch	18-131	60	86	120
Lincoln	44-289	133	201	299
Lynch	34-217	96	142	205
North Platte	14-236	81	136	224
Scribner	69-312	154	205	269
Valentine	4-169	64	100	153

See footnote at end of table.

TABLE 17.—*Observed range and 50-, 20-, and 5- percent probability values of erosion index at each of 181 key locations*—Continued

Location	Values of erosion index (*EI*)			
	Observed 22-year range	50-percent probability	20-percent probability	5-percent probability
New Hampshire:				
Concord	52-212	91	131	187
New Jersey:				
Atlantic City	71-318	166	229	311
Marlboro[1]	58-331	186	254	343
Trenton	37-382	149	216	308
New Mexico:				
Albuquerque	0-46	10	19	35
Roswell	5-159	41	73	128
New York:				
Albany	40-172	81	114	159
Binghamton	20-151	76	106	146
Buffalo	20-148	66	96	139
Geneva[1]	33-180	73	106	152
Marcellus[1]	24-241	74	112	167
Rochester	22-180	66	101	151
Salamanca	31-202	70	106	157
Syracuse	8-219	83	129	197
North Carolina:				
Asheville	76-238	135	175	223
Charlotte	113-526	229	322	443
Greensboro	102-357	184	244	320
Raleigh	152-569	280	379	506
Wilmington	196-701	358	497	677
North Dakota:				
Bismarck	9-189	43	73	120
Devils Lake	21-171	56	90	142
Fargo	5-213	62	113	200
Williston	4-71	30	45	67
Ohio:				
Cincinnati	66-352	146	211	299
Cleveland	21-186	93	132	185
Columbiana	29-188	96	129	173
Columbus	45-228	113	158	216
Coshocton[1]	72-426	158	235	343
Dayton	56-245	125	175	240
Toledo	32-189	83	120	170
Oklahoma:				
Ardmore	100-678	263	395	582
Cherokee[1]	49-320	167	242	345
Guthrie[1]	69-441	210	316	467
McAlester	105-741	272	411	609
Tulsa	19-584	247	347	478
Oregon:				
Pendleton	2-28	4	8	16
Portland	16-80	40	56	77
Pennsylvania:				
Erie	11-534	96	181	331
Franklin	50-228	97	135	184
Harrisburg	48-232	105	146	199
Philadelphia	72-361	156	210	282
See footnote at end of table.				
Pittsburgh	43-201	111	148	194
Reading	84-308	144	204	285
Scranton	52-198	104	140	188
Puerto Rico:				
San Juan	203-577	345	445	565
Rhode Island:				
Providence	53-225	119	167	232
South Carolina:				
Charleston	174-1037	387	559	795
Clemson[1]	138-624	280	384	519
Columbia	81-461	213	298	410
Greenville	130-589	249	350	487
South Dakota:				
Aberdeen	19-295	74	129	219
Huron	18-145	60	91	136
Isabel	16-141	48	78	125
Rapid City	10-140	37	64	108
Tennessee:				
Chattanooga	163-468	269	348	445
Knoxville	64-370	173	239	325
Memphis	139-595	272	384	536
Nashville	116-381	198	262	339
Texas:				
Abilene	27-554	146	253	427
Amarillo	33-340	110	184	299
Austin	59-669	270	414	624
Brownsville	46-552	267	386	549
Corpus Christi	124-559	237	330	451
Dallas	93-630	263	396	586
Del Rio	19-405	121	216	374
El Paso	4-85	18	36	67
Houston	176-1171	444	674	1003
Lubbock	17-415	82	158	295
Midland	35-260	82	139	228
Nacogdoches	153-769	401	571	801
San Antonio	77-635	220	353	556
Temple[1]	81-644	261	379	542
Victoria	108-609	265	385	551
Wichita Falls	79-558	196	298	447
Vermont:				
Burlington	33-270	72	114	178
Virginia:				
Blacksburg[1]	81-245	126	168	221
Lynchburg	64-366	164	232	324
Richmond	102-373	208	275	361
Roanoke	78-283	129	176	237
Washington:				
Pullman[1]	1-30	6	12	21
Spokane	1-19	7	11	17
West Virginia:				
Elkins	43-223	118	158	209
Huntington	56-228	127	173	233
Parkersburg	69-303	120	165	226
Wisconsin:				
Green Bay	17-148	77	107	147
LaCrosse[1]	61-385	153	228	331
Madison	38-251	118	171	245
Milwaukee	31-193	93	139	202
Rice Lake	24-334	122	202	327
Wyoming:				
Casper	1-24	9	15	26
Cheyenne	8-66	28	43	66

Computations based on SEA rainfall records. All others are based on Weather Bureau records.

TABLE 18.—*Expected magnitudes of single-storm erosion index values*

Location	Index values normally exceeded once in—				
	year 1	years 2	years 5	years 10	years 20
Alabama:					
Birmingham	54	77	110	140	170
Mobile	97	122	151	172	194
Montgomery	62	86	118	145	172
Arkansas:					
Fort Smith	43	65	101	132	167
Little Rock	41	69	115	158	211
Mountain Home	33	46	68	87	105
Texarkana	51	73	105	132	163
California:					
Red Bluff	13	21	36	49	65
San Luis Obispo	11	15	22	28	34
Colorado:					
Akron	22	36	63	87	118
Pueblo	17	31	60	88	127
Springfield	31	51	84	112	152
Connecticut:					
Hartford	23	33	50	64	79
New Haven	31	47	73	96	122
District of Columbia	39	57	86	108	136
Florida:					
Apalachicola	87	124	180	224	272
Jacksonville	92	123	166	201	236
Miami	93	134	200	253	308
Georgia:					
Atlanta	49	67	92	112	134
Augusta	34	50	74	94	118
Columbus	61	81	108	131	152
Macon	53	72	99	122	146
Savannah	82	128	203	272	358
Watkinsville	52	71	98	120	142
Illinois:					
Cairo	39	63	101	135	173
Chicago	33	49	77	101	129
Dixon Springs	39	56	82	105	130
Moline	39	50	89	116	145
Rantoul	27	39	56	69	82
Springfield	36	52	75	94	117
Indiana:					
Evansville	26	38	56	71	86
Fort Wayne	24	33	45	56	65
Indianapolis	29	41	60	75	90
South Bend	26	41	65	86	111
Terre Haute	42	57	78	96	113
Iowa:					
Burlington	37	48	62	72	81
Charles City	33	47	68	85	103
Clarinda	35	48	66	79	94
Des Moines	31	45	67	86	105
Dubuque	43	63	91	114	140
Rockwell City	31	49	76	101	129
Sioux City	40	58	84	105	131

Location	Index values normally exceeded once in—				
	year 1	years 2	years 5	years 10	years 20
Kansas:					
Burlingame	37	51	69	83	100
Coffeyville	47	69	101	128	159
Concordia	33	53	86	116	154
Dodge City	31	47	76	97	124
Goodland	26	37	53	67	80
Hays	35	51	76	97	121
Wichita	41	61	93	121	150
Kentucky:					
Lexington	28	46	80	114	151
Louisville	31	43	59	72	85
Middlesboro	28	38	52	63	73
Louisiana:					
New Orleans	104	149	214	270	330
Shreveport	55	73	99	121	141
Maine:					
Caribou	14	20	28	36	44
Portland	16	27	48	66	88
Skowhegan	18	27	40	51	63
Maryland:					
Baltimore	41	59	86	109	133
Massachusetts:					
Boston	17	27	43	57	73
Washington	29	35	41	45	50
Michigan:					
Alpena	14	21	32	41	50
Detroit	21	31	45	56	68
East Lansing	19	26	36	43	51
Grand Rapids	24	28	34	38	42
Minnesota:					
Duluth	21	34	53	72	93
Fosston	17	26	39	51	63
Minneapolis	25	35	51	65	78
Rochester	41	58	85	105	129
Springfield	24	37	60	80	102
Mississippi:					
Meridian	69	92	125	151	176
Oxford	48	64	86	103	120
Vicksburg	57	78	111	136	161
Missouri:					
Columbia	43	58	77	93	107
Kansas City	30	43	63	78	93
McCredie	35	55	89	117	151
Rolla	43	63	91	115	140
Springfield	37	51	70	87	102
St. Joseph	45	62	86	106	126
Montana:					
Great Falls	4	8	14	20	26
Miles City	7	12	21	29	38
Nebraska:					
Antioch	19	26	36	45	52
Lincoln	36	51	74	92	112
Lynch	26	37	54	67	82
North Platte	25	38	59	78	99
Scribner	38	53	76	96	116
Valentine	18	28	45	61	77

TABLE 18.—*Expected magnitudes of single-storm erosion index values*—Continued

Location	Index values normally exceeded once in—				
	year 1	years 2	years 5	years 10	years 20
New Hampshire:					
Concord	18	27	45	62	79
New Jersey:					
Atlantic City	39	55	77	97	117
Marlboro	39	57	85	111	136
Trenton	29	48	76	102	131
New Mexico:					
Albuquerque	4	6	11	15	21
Roswell	10	21	34	45	53
New York:					
Albany	18	26	38	47	56
Binghamton	16	24	36	47	58
Buffalo	15	23	36	49	61
Marcellus	16	24	38	49	62
Rochester	13	22	38	54	75
Salamanca	15	21	32	40	49
Syracuse	15	24	38	51	65
North Carolina:					
Asheville	28	40	58	72	87
Charlattte	41	63	100	131	164
Greensboro	37	51	74	92	113
Raleigh	53	77	110	137	168
Wilmingtan	59	87	129	167	206
North Dakata:					
Devils Lake	19	27	39	49	59
Fargo	20	31	54	77	103
Williston	11	16	25	33	41
Ohio:					
Cincinnati	27	36	48	59	69
Cleveland	22	35	53	71	86
Columbiana	20	26	35	41	48
Columbus	27	40	60	77	94
Coshocton	27	45	77	108	143
Dayton	21	30	44	57	70
Toledo	16	26	42	57	74
Oklahoma:					
Ardmare	46	71	107	141	179
Cherokee	44	59	80	97	113
Guthrie	47	70	105	134	163
McAlester	54	82	127	165	209
Tulsa	47	69	100	127	154
Oregon:					
Portland	6	9	13	15	18
Pennsylvania:					
Franklin	17	24	35	45	54
Harrisburg	19	25	35	43	51
Philadelphia	28	39	55	69	81
Pittsburgh	23	32	45	57	67
Reading	28	39	55	68	81
Scranton	23	32	44	53	63
Puerta Rico:					
San Juan	57	87	131	169	216
Rhode Island:					
Providence	23	34	52	68	83
South Carolina:					
Charleston	74	106	154	196	240
Clemsan	51	73	106	133	163
Columbia	41	59	85	106	132
Greenville	44	65	96	124	153
South Dakota:					
Aberdeen	23	35	55	73	92
Huron	19	27	40	50	61
Isabel	15	24	38	52	67
Rapid City	12	20	34	48	64
Tennessee:					
Chattanooga	34	49	72	93	114
Knoxville	25	41	68	93	122
Memphis	43	55	70	82	91
Nashville	35	49	68	83	99
Texas:					
Abilene	31	49	79	103	138
Amarillo	27	47	80	112	150
Austin	51	80	125	169	218
Brownsville	73	113	181	245	312
Corpus Christi	57	79	114	146	171
Dallas	53	82	126	166	213
Del Rio	44	67	108	144	182
El Pasa	6	9	15	19	24
Houston	82	127	208	275	359
Lubbock	17	29	53	77	103
Midland	23	35	52	69	85
Nacogdoches	77	103	138	164	194
San Antonio	57	82	122	155	193
Temple	53	78	123	162	206
Victoria	59	83	116	146	178
Wichita Falls	47	63	86	106	123
Vermont:					
Burlington	15	22	35	47	58
Virginia:					
Blacksburg	23	31	41	48	56
Lynchburg	31	45	66	83	103
Richmond	46	63	86	102	125
Roanoke	23	33	48	61	73
Washington:					
Spokane	3	4	7	8	11
West Virginia:					
Elkins	23	31	42	51	60
Huntington	18	29	49	69	89
Parkersburg	20	31	46	61	76
Wisconsin:					
Green Bay	18	26	38	49	59
LaCrosse	46	67	99	125	154
Madison	29	42	61	77	95
Milwaukee	25	35	50	62	74
Rice Lake	29	45	70	92	119
Wyoming:					
Casper	4	7	9	11	14
Cheyenne	9	14	21	27	34

$$1\ t/ha = 2.242 \text{ tons per acre} \quad (7)$$
$$1\ t\text{-}m/ha/cm = 0.269 \text{ ft-tons per ocre per inch}$$
$$1\ E_m = 0.683\ E$$
$$1\ I_{30m} = 2.54\ I_{30}$$
$$1\ (EI)_m = 1.735\ EI$$
$$1\ K_m = 1.292\ K$$

Factor R. The procedure for computing $(EI)_m$ for a given rain period is similar to that described in the preceding section for computation of **EI,** but the input data will be in different units. If the rain gage chart used for the preceding example had been calibrated in millimeters, the computation would have been as follows:

Chart readings		Storm increments			Energy	
Time	Depth (mm)	Duration (min)	Amount (cm)	Intensity (cm/h)	Per cm	For increment
4:00	0					
:20	1.2	20	0.12	0.36	175	21
:27	3.0	7	.18	1.54	226	41
:36	8.8	9	.58	3.87	263	153
:50	26.6	14	1.78	7.68	289	514
:57	30.4	7	.38	3.26	256	97
5:05	31.7	8	.13	.98	220	29
:15	31.7	10	0	0	0	0
:30	33.0	15	.13	.52	184	24
Totals		90	3.30			879

Kinetic energy of the storm = $879(10^{-2}) = 8.79$

TABLE 19.—*Kinetic energy of rainfall expressed in foot-tons per acre per inch of rain*[1]

Intensity inch per hour	0.00	0.01	0.02	0.03	0.04	0.05	0.06	0.07	0.08	0.09
0	—	254	354	412	453	485	512	534	553	570
0.1	585	599	611	623	633	643	653	661	669	677
.2	685	692	698	705	711	717	722	728	733	738
.3	743	748	752	757	761	765	769	773	777	781
.4	784	788	791	795	798	801	804	807	810	814
.5	816	819	822	825	827	830	833	835	838	840
.6	843	845	847	850	852	854	856	858	861	863
.7	865	867	869	871	873	875	877	878	880	882
.8	884	886	887	889	891	893	894	896	898	899
.9	901	902	904	906	907	909	910	912	913	915
	0	0.1	0.2	0.3	0.4	0.5	0.6	0.7	0.8	0.9
1	916	930	942	954	964	974	984	992	1000	1008
2	1016	1023	1029	1036	1042	1048	1053	1059	1064	1069
3	[2]1074									

[1] Computed by the equation, $E = 916 + 331 \log_{10} I$, where **E** = kinetic energy in foot-tons per acre per inch of rain, and **I** = rainfall intensity in inches per hour.

[2] The 1074 value also applies for all intensities greater than 3 in/h (see text).

TABLE 20.—*Kinetic energy of rainfall expressed in metric ton-meters per hectare per centimeter of rain*[1]

Intensity cm/h	.0	0.1	0.2	0.3	0.4	0.5	0.6	0.7	0.8	0.9
0 ..	0	121	148	163	175	184	191	197	202	206
1 ..	210	214	217	220	223	226	228	231	233	235
2 ..	237	239	241	242	244	246	247	249	250	251
3 ..	253	254	255	256	258	259	260	261	262	263
4 ..	264	265	266	267	268	268	269	270	271	272
5 ..	273	273	274	275	275	276	277	278	278	279
6 ..	280	280	281	281	282	283	283	284	284	285
7 ..	286	286	287	287	288	288	[2]289			

[1] Computed by the equation $E = 210 + 89 \log_{10} I$, where **E** = kinetic energy in metric-ton meters per hectare per centimeter of roin, and **I** = rainfoll intensity in centimeters per hour.

[2] The 289 value also applies for all intensities greater than 7.6 cm/h.

Values for column 6 are obtained by entering table 20 with the intensities listed in column 5, and their sum, 879, is the kinetic energy (E_m) of the 3.30 cm of rain expressed in metric ton-meters per hectare. The constant factor of 10^{-2} used for the English system should be applied here also so that storm $(EI)_m$ values will usually not exceed 100. The maximum amount of rain in any 30-minute period was 2.74 cm, from 4:27 to 4:57. Therefore $I_{30m} = 2(2.74 = 5.48$ cm/h. $(EI)_m = 8.79(5.48) = 48.17$

The procedure for combining storm **EI** values for local erosion index values was fully described in the preceding section. For predicting average annual soil losses from rainfall and its associated runoff, **R** equals the erosion index. Where runoff from thaw, snowmelt, or irrigation is significant, an R_s factor must be added to the **EI** value as previously discussed.

Where adequate rainfall intensity data are not available, the erosion index cannot be estimated solely from annual precipitation data. It is a function of the sizes and intensities of the individual rainstorms, and these are not closely related to annual precipitation. Therefore a given annual rainfall will indicate only a broad range of possible values of the local erosion index. However, the United States data indicate that the range of likely values can be somewhat narrowed by knowledge of the general climatic conditions in the particular geographic area.

In the U.S. Northern and Northeastern States, the winter precipitation generally comes as snow and low-intensity rains, but erosive intensities occur during the spring and summer. There, the local erosion index values, $(\mathbf{EI})_m$, have ranged from 2**P**-52 to 2.6**P**, where **P** is the average annual precipitation expressed in centimeters. In several Northwestern States, where rain intensities rarely exceed 2.5 cm/h, the annual $(\mathbf{EI})_m$ is generally less than **P**, but $\mathbf{R}_s$ values are high. Near the Gulf of Mexico and along the southern half of the Atlantic Coast, the rainfall characteristics are substantially influenced by coastal storms, 24-h rainfall exceeds 10 cm at least once in 2 years, on the average, and erosive rains occur in nearly every month of the year. There, erosion index values range between 4.2**P** and 6.7**P**. Values computed from the few long-term, recording-raingage records available for the islands of Hawaii and Puerto Rico were also within this range. In the large region between the northern and southern extremes mentioned above, the annual $(\mathbf{EI})_m$ values range from 2.5**P** to 4.5**P**. Brief, high-intensity thunderstorms are common in this region during the summer months, but general rains of longer duration also occur.

Where data are adequate to determine 2-year probabilities of 6-hour rainfall, these probabilities may provide more specific estimates of the local erosion index values. In the U.S. data, local erosion index values were approximately equal to the quantity $27.38\ \mathbf{P}^{2.17}$, where **P** = the 2-year, 6-hour precipitation in inches. Converted to the recommended metric units, $(\mathbf{EI})_m$ equals approximately $6.28\mathbf{P}^{2.17}$, where **P** is expressed in centimeters. However, this estimating procedure should not be substituted for the standard erosion index calculation procedure where adequate intensity data are available.

Factor K. This factor is the average soil loss in metric tons per hectare per unit of $(\mathbf{EI})_m$, measured on unit plots of the given soil. A unit plot is a 22-m length of uniform 9 percent slope that has been in clean fallow for more than 2 years and is tilled to prevent vegetative growth and surface crusting during the period of soil loss measurement. If a gradient other than 9 percent must be used, the data are adjusted by an **LS** factor available from figure 11. If the soil-erodibility nomograph (fig. 3) is used to evaluate $\mathbf{K}_m$, the **K** value read from the nomograph is multiplied by a conversion factor of 1.292.

The most accurate direct measurement of **K** for a given soil is obtained by measuring soil losses from unit plots under natural rain for at least 5 years, beginning 2 years after the clean-fallow condition was established. This permits averaging the interactions of soil erodibility with antecedent soil moisture, storm size, and other randomly distributed variables. The fallow plots receive the same annual tillage as conventionally tilled row crops.

Using rainfall simulators to evaluate **K** is quicker and less costly, but it requires caution. A one-time simulator test, even though replicated on several plots, measures soil loss from only one storm size and rain intensity, on one set of antecedent conditions, and these may or may not represent natural rainfall patterns. When simulated rainfall is used to evaluate **K**, measuring the soil losses for four or five successive 30-minute periods is helpful so that the segmented data can be rearranged to represent small, intermediate, and large storms beginning at various antecedent soil moisture levels. These can be weighted according to their probability of occurrence in natural rainfall (*58*).

Factor LS. Selecting 22 m as the basic slope length and retaining 9 percent as the basic slope gradient leaves the **LS** values essentially unchanged from those used in the English system of units. For uniform slopes, **LS** may be obtained by entering figure 11 with the field slope length expressed in meters. For concave or convex slopes, the value read from figure 11 should be modified by the procedure given in the subsection **Irregular Slopes.**

Factors C and P. Soil loss ratios (table 5) and **P** values (tables 13, 14, 15) are not affected by the units selected for the other factors. However, in countries where crops and farming techniques are different from those reflected in table 5, measurements of soil loss reductions attainable with feasible changes in crop system, tillage methods, and residue management may merit priority over establishing **EI** and **K** values.

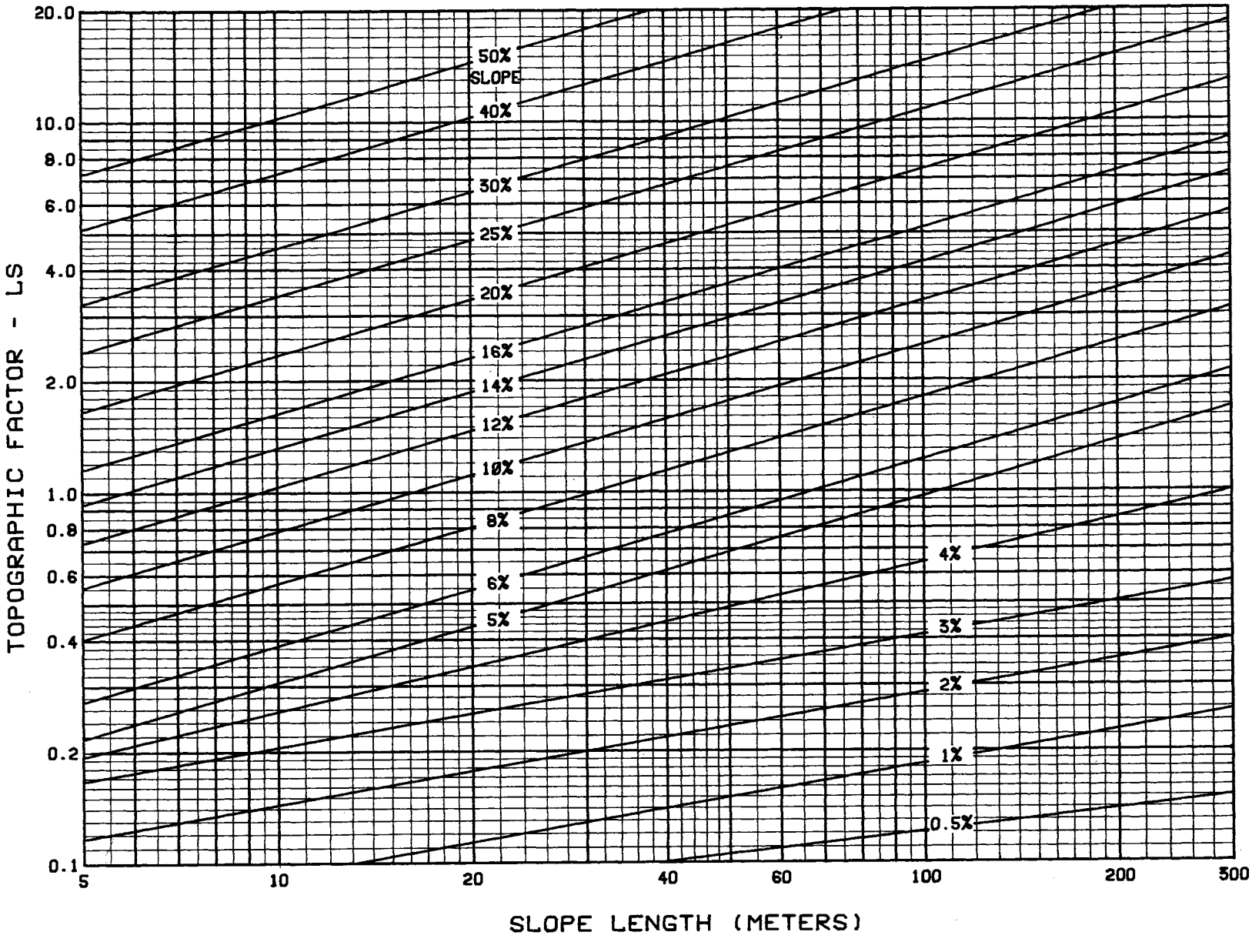

FIGURE 11.—Slope-effect chart for metric system.

☆U.S. GOVERNMENT PRINTING OFFICE: 1978 O—278-995/6583

PREDICTING RAINFALL EROSION LOSSES— A GUIDE TO CONSERVATION PLANNING

Supplement to Agriculture Handbook No. 537

METRICATION OF THE USLE IN THE INTERNATIONAL SYSTEM OF UNITS (SI)

The metric conversion originally presented in this handbook and in prior publications (*53, 60*) is not completely in the International System of Units (SI), which is expected to gain widespread usage. This supplement presents an alternative conversion in which all the Universal Soil Loss Equation (USLE) factors are expressed in standard SI units or approved multiples thereof, and the order of magnitude of each new unit is similar to the old.

Both conversion systems are authentic, and conservationists who have adopted the originally recommended metric units would not improve their USLE accuracy by changing to the new units. For future conversions, however, the revised procedure, which is fully outlined below, is recommended because its use will facilitate standardization of units.

The USLE terms **A, LS, C,** and **P** need no change from the recommendations in the preceding section. Strictly, the **SI** units for mass and area are kilograms and square meters. Because of common use, however, metric ton (a special name for megagram) and hectare (a special name for square hectometer) will be used. Soil loss (**A**) wil be expressed in metric tons per hectare, and factor **K** in metric tons per hectare per metric **EI** unit. Factors **LS, C,** and **P** are dimensionless. **L** is expressed relative to slope lengths measured in meters, but selecting 22 m as the basic slope length and retaining 9 percent as the basic slope gradient leaves the **LS** values essentially unchanged. **C** and **P** are not affected by the units selected for the other factors.

Factor **R** will be in different units than previously recommended. In the **SI** system, energy is measured in joules and rainfall in millimeters. The use of "centi" as a multiple is minimized. Metric **EI** values can be obtained in standard **SI** units by expressing rainfall energy in megajoules (**MJ**) per hectare and maximum 30-minute intensity (I_{30}) in mm/h, but use of cm/h to express I_{30} is more expedient for the following reasons: With I_{30} expressed in mm/h, the metric **EI** values would be 17 times the magnitude of **EI** in U.S. customary units. Annual erosion index values would be in four- or five-digit numbers, which are harder to visualize and compare mentally than the present smaller numbers. Of greater importance, the large metric **EI** values would result in extremely small metric **K** values, ranging downward from a maximum of about 0.09. Absolute differences between **K** values would be so small that many casual users of the USLE would tend to neglect important soil differences as insignificant.

Reducing the magnitude of I_{30} by a factor of 10 alleviates these disadvantages and does not preclude the use of mm as the unit for rainfall amounts and incremental intensities in energy computations. The energy equation or table will also be expressed in MJ/ha per mm of rain. Only I_{30} will be converted to cm as a matter of expedience. This is directly comparable to the U.S. customary procedure of computing energy in ft-tons/acre and dividing by 100 to obtain more convenient magnitudes. The metric **EI** will then equal storm energy in MJ/ha times I_{30} in cm/h.

Assuming use of the metric units specified above, a comparison of U.S. customary and **SI** dimensions for the terms in the USLE is as follows:

Term	*US customary dimensions*	*SI dimensions*	*Symbol*
A	ton/acre	metric ton/hectare	t/ha
R	$\frac{\text{100 foot-ton inch}}{\text{acre hour}}$	$\frac{\text{megajoule centimeter}}{\text{hectare hour}}$	$\frac{\text{MJ cm}}{\text{ha h}}$
K	$\frac{\text{.01 ton ocre hour}}{\text{ocre foot-ton inch}}$	$\frac{\text{metric ton hectare hour}}{\text{hectare megajoule centimeter}}$	$\frac{\text{t ha h}}{\text{ha MJ cm}}$
L,S,C,P	dimensionless	dimensionless	

The USLE terms will usually be derived directly in the **SI** units by procedures outlined below. However, the following conversion factors will facilitate comparisons of the metric factor values with the U.S. customary values published in this handbook. Terms expressed in metric units are identified by the subscript $_m$.

To convert from:	*multiply by:*	*to obtain:*
A in tons/acre	2.242	A_m in t/ha
E in 100 ft-tons/acre	0.670	E_m in MJ/ha
I_{30} in in/h	2.540	I_{30m} in cm/h
EI in $\frac{\text{100 ft-ton in}}{\text{ocre h}}$	1.702	$(EI)_m$ in $\frac{\text{MJ cm}}{\text{ha h}}$
K in $\frac{\text{.01 ton acre h}}{\text{acre ft-ton in}}$	1.313	K_m in $\frac{\text{t ha h}}{\text{MJ ha cm}}$

UNITED STATES DEPARTMENT OF AGRICULTURE

AGRICULTURE HANDBOOK NUMBER 537

PREPARED BY SCIENCE AND EDUCATION ADMINISTRATION

Factor R. The procedure for computing $(EI)_m$ for a given rain period is similar to that described in the preceding section for computing **EI**, but the input data will be in different units. If the raingage chart used for the example on page 51 had been calibrated in millimeters, the computation would have been as follows:

Chart readings		*Storm increments*			*Energy*	
Time	Depth (mm)	Duration (min)	Amount (mm)	Intensity (mm/h)	Per mm of rain (MJ/ha mm)	Increment total (MJ/ha)
(1)	(2)	(3)	(4)	(5)	(6)	(7)
4:00	0					
:20	1	20	1	3	0.161	0.161
:27	3	7	2	17	.226	.452
:36	9	9	6	40	.259	1.554
:50	27	14	18	77	.283	5.094
:57	30	7	3	26	.242	.726
5:05	32	8	2	15	.222	.444
:15	32	10	0	0	0	0
:30	33	15	1	4	.172	.172
Totals		90	33			8.603

Kinetic energy of the storm: 8.60 MJ/ha

Values for column 6 are obtained by entering the revised table 20 with the intensities listed in column 5. The sum of the products of corresponding values from columns 4 and 6 (8.60) is the kinetic energy, E_m, of the 33 mm of rain expressed in megajoules per hectare. The maximum amount of rain in any 30-minute period was 27 mm, from 4:27 to 4:57. Therefore the maximum 30-minute intensity was 2×27, or 54, mm/h, and $I_{30m} = 54/10 = 5.4$ cm/h. $(EI)_m = 8.60 \times 5.4 = 46.4$ (MJ cm)/(ha h).

For the **EI** computations, the rain occurring between two successive periods of 6 hours or more with less than 1.3 mm (0.05 in) of precipitation is considered one storm. Rain showers of less than 12 mm are omitted as insignificant unless they include a 15-minute intensity of at least 25 mm/h. The erosion index at a given location, as mapped in figures 1 and 2, is the average annual total of storm **EI** values over 20 to 25 years. For predicting average annual soil losses from rainfall and its associated runoff, **R** equals the erosion index. Where runoff from thaw, snowmelt, or irrigation is significant, **R** equals the **EI** plus an R_s value as discussed on page 7.

The erosion index cannot be reliably estimated from annual-rainfall data alone. It is a function of the sizes and intensities of the individual rainstorms, and these have no common relationship to annual rainfall totals. However, later analyses of the U.S. annual erosion index values that had been derived by the above procedure indicated that they were roughly equal to the quantity $27.38\ P^{2.17}$, where **P** = the 2-year, 6-hour rainfall expressed in inches. By direct conversion, the average annual $(EI)_m$ would be roughly estimated by $0.0416\ P^{2.17}$, where **P** is expressed in mm. This estimating formula is appreciably less accurate than the standard erosion index calculation procedure and should not be substituted for it where intensity data are available.

Factor K. The soil-erodibility factor **K** is the average soil loss in metric tons per hectare per unit of metric **EI**, measured on unit plots of the given soil. A unit plot (see p. 8) is a 22-m length of uniform 9 percent slope that has been in clean fallow for more than 2 years and is tilled to prevent vegetative growth and surface crusting during the period of soil loss measurement. If a gradient other than 9 percent must be used, the data are adjusted by the appropriate **LS** factor. If the soil-erodibility nomograph (fig. 3) is used to evaluate K_m, the **K** value read from the nomograph must be multiplied by a conversion factor of 1.313.

The basic slope length used for **K** and **L** in this handbook is 72.6 ft, which equals 22.134 m. For experimental evaluation of factor **K** in metric units, rounding this to 22.0 m is more convenient and introduces no error when 22.0 m is also used as the basic length for **L**, as in figure 11. The slight reduction in basic length increases factor **L** by 0.3 of 1 percent and decreases factor **K** by the same percentage, so the product of **K** and **L** is unchanged. For conversion of the U.S. customary **K** values in this handbook to metric **K** values based on a 22.0 m length, the relatively insignificant potential error is avoided by including an **L**-value of 0.997 in the conversion factor. The **K**-conversion factor of 1.313 given above has been so adjusted.

Factor LS. The preceding paragraph applies here, also. For uniform slopes, **LS** may be obtained by entering figure 11 with the field slope length expressed in meters or it may be computed by the equation

$$LS = (\lambda/22)^m\ (65.41\ \sin^2\theta + 4.56\ \sin\theta + 0.065)$$

where λ = slope length in m; θ = angle of slope; and m = 0.5 if the percent slope is 5 or more, 0.4 on slopes of 3.5 to 4.5 percent, 0.3 on slopes of 1 to 3 percent, and 0.2 on uniform gradients of less than 1 percent. For concave, convex, or mixed-gradient slopes, the value so computed or read from figure 11 should be modified by the procedure outlined on page 16.

Factor C and P. Soil loss ratios (table 5) and **P** values (tables 13, 14, 15) are not affected by the units selected for the other factors and therefore need no conversion.

TABLE 20. (revised).—*Kinetic energy of rainfall at specified intensities, expressed in megajoules per hectare per millimeter of rain*[1]

Intensity (mm/h)	0	1	2	3	4	5	6	7	8	9
0 ..	0	0.119	0.145	0.161	0.172	0.180	0.187	0.193	0.198	0.202
10 ..	.206	.210	.213	.216	.219	.222	.224	.226	.229	.231
20 ..	.233	.234	.236	.238	.240	.241	.242	.244	.245	.247
30 ..	.248	.249	.250	.252	.253	.254	.255	.256	.257	.258
40 ..	.259	.260	.261	.262	.262	.263	.264	.265	.266	.267
50 ..	.267	.268	.269	.270	.270	.271	.272	.272	.273	.274
60 ..	.274	.275	.276	.276	.277	.277	.278	.278	.279	.280
70 ..	.280	.281	.281	.282	.282	.283	.283[2]			

[1] Computed by the equation $e = 0.119 - 0.0873 \log_{10} i$, where e = kinetic energy in megajoules/(hectare millimeter) and i = rainfall intensity in mm/h.

[2] The value of 0.283 also applies for all intensities greater than 76 mm/h.

U.S. DEPARTMENT OF AGRICULTURE
SCIENCE AND EDUCATION ADMINISTRATION
HYATTSVILLE, MARYLAND 20782

OFFICIAL BUSINESS
PENALTY FOR PRIVATE USE $300

POSTAGE AND FEES PAID
U. S. DEPARTMENT OF
AGRICULTURE
AGR 101

Assessment of erosion, sedimentation, and water quality impacts of the Mountain Valley Pipeline and Equitrans Expansion Project's proposed crossing of the Jefferson National Forest as it pertains to the U.S. Forest Service's Draft Supplemental Environmental Impact Statement dated December 2022

Prepared by Jonathan A. Czuba, Ph.D., Licensed Professional Engineer - February 9, 2023

REFERENCES
13

February 21, 2023

USDA

United States
Department of
Agriculture

Agricultural
Research
Service

Agriculture
Handbook
Number 703

Predicting Soil Erosion by Water: A Guide to Conservation Planning With the Revised Universal Soil Loss Equation (RUSLE)

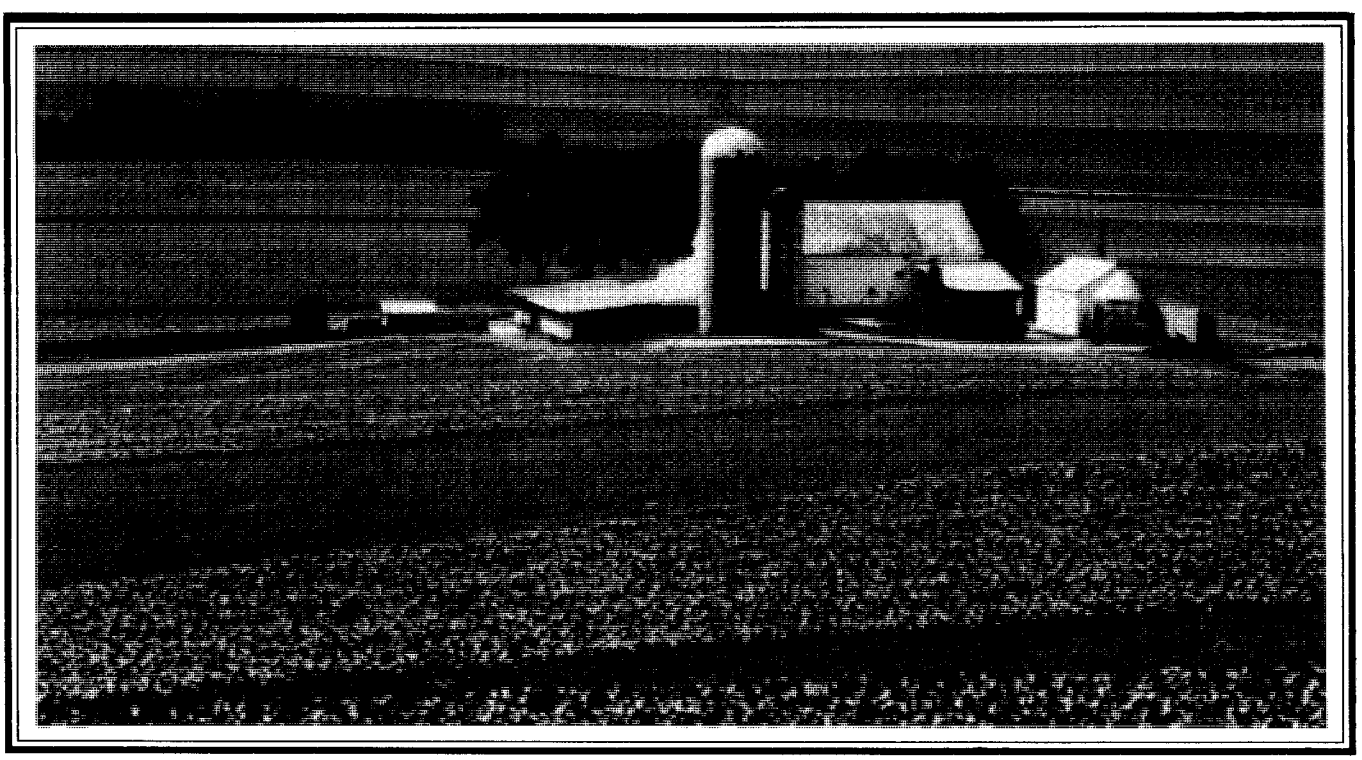

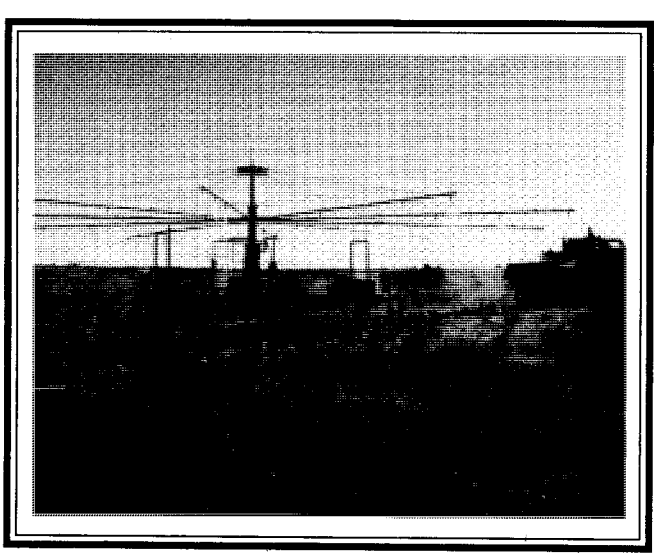

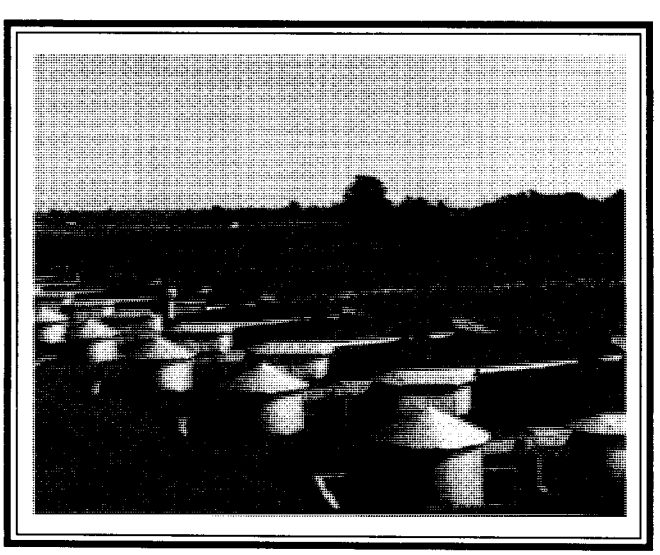

Cover: A conservation-designed farm *(top)* in York County, PA, showing stripcropping. The farm conservation plan was developed using rainfall and runoff plot data from research plots like the ARS plots near Kingdom City, MO *(lower right)*, and from rotating-boom rainfall simulators like that on a grassland site on the ARS Walnut Gulch Experimental Watershed near Tombstone, AZ *(lower left)*.

PREDICTING SOIL EROSION BY WATER: A GUIDE TO CONSERVATION PLANNING WITH THE REVISED UNIVERSAL SOIL LOSS EQUATION (RUSLE)

K.G. Renard, G.R. Foster, G.A. Weesies, D.K. McCool, and D.C. Yoder, Coordinators*

Note: See the errata at the end of the document

*Renard (retired) was research hydraulic engineer, USDA-ARS, Southwest Watershed Research Center, 2000 East Allen Road, Tucson, AZ. Foster is director, USDA-ARS, Sedimentation Laboratory, Oxford, MS. Weesies is conservation agronomist, USDA-NRCS, National Soil Erosion Research Laboratory, Purdue University, Building SOIL, West Lafayette, IN. McCool is agricultural engineer, USDA-ARS, Washington State University, Pullman, WA. Yoder is assistant professor, Agricultural Engineering Department, University of Tennessee, Knoxville, TN.

For sale by the U.S. Government Printing Office
Superintendent of Documents, Mail Stop: SSOP, Washington, DC 20402-9328
ISBN 0-16-048938-5

ABSTRACT

Renard, K.G., G.R. Foster, G.A. Weesies, D.K. McCool, and D.C. Yoder, coordinators. 1997. Predicting Soil Erosion by Water: A Guide to Conservation Planning With the Revised Universal Soil Loss Equation (RUSLE). U.S. Department of Agriculture, Agriculture Handbook No. 703, 404 pp.

The Revised Universal Soil Loss Equation (RUSLE) is an erosion model predicting longtime average annual soil loss (A) resulting from raindrop splash and runoff from specific field slopes in specified cropping and management systems and from rangeland. Widespread use has substantiated the RUSLE's usefulness and validity. RUSLE retains the six factors of Agriculture Handbook No. 537 to calculate A from a hillslope. Technology for evaluating these factor values has been changed and new data added. The technology has been computerized to assist calculation. Thus soil-loss evaluations can be made for conditions not included in the previous handbook using fundamental information available in three data bases: CITY, which includes monthly precipitation and temperature, front-free period, annual rainfall erosivity (R) and twice monthly distributions of storm erosivity (E); CROP, including below-ground biomass, canopy cover, and canopy height at 15-day intervals as well as information on crop characteristics; and OPERATION, reflecting soil and cover disturbances that are associated with typical farming operations.

KEYWORDS: soil erosion, cropland, rangeland, rill erosion, interrill erosion, rainfall-runoff erosivity, soil erodibility, slope length, slope steepness, prior land use, surface cover, crop canopy, surface roughness, soil moisture, contouring, stripcropping, terracing, personal computer, residue decomposition

While supplies last, single copies of this publication may be obtained at no cost from USDA-ARS, Southwest Watershed Research Center, 2000 East Allen Road, Tucson, AZ 85719.

Copies of this publication may be purchased from the National Technical Information Service, 5285 Port Royal Road, Springfield, VA 22161.

Issued January 1997

This publication supersedes Agriculture Handbook No. 537, titled "Predicting Rainfall Erosion Losses: A Guide to Conservation Planning."

CONTENTS

SYMBOLS

A	average annual soil loss (ton· acre^{-1}· yr^{-1})
A	coefficient used to describe the shape of the residue decomposition response to temperature (°C) (ch. 5)
A_{wr}	winter soil loss from rills alone (ton· acre^{-1}· yr^{-1})
a	- coefficient used in unit rainfall energy relation (ch. 2) - location-dependent constant (ch. 3) - coefficient dependent on residue characteristics and climate variables (ch. 5) - coefficient dependent on contour ridge height (ch. 6)
a_1, a_2	coefficients used in determination of the discharge rate when deposition ends within a strip
B	amount of deposition considered to benefit the long-term maintenance of the soil resource (ton· acre^{-1}· yr^{-1})
B_a	above-ground biomass (lb· acre^{-1})
B_b	below-ground root biomass (lb· acre^{-1})
B_s	weight of residue on the surface (lb· acre^{-1})
B_{si}	weight of a particular type of residue (lb· acre^{-1})
B_{ur}	mass density of live and dead roots in the upper layer of soil (lb· acre^{-1}· in^{-1})
B_{us}	mass density of incorporated surface residue in the upper layer of soil (lb· acre^{-1}· h^{-1})

b	- coefficient used in unit rainfall energy relation (ch. 2) - location dependent constant (ch. 3) - coefficient describing effectiveness of surface cover (dimensionless) (ch. 5) - coefficient dependent on contour ridge height (ch. 6)
C	cover-management factor (dimensionless)
CC	canopy-cover subfactor (dimensionless)
C_B	coefficient representing the relative effectiveness of the total subsurface biomass in controlling erosion (dimensionless)
C_f	surface-soil-consolidation factor (dimensionless)
c	- location-dependent constant (ch. 3) - coefficient dependent on contour ridge height (ch. 6)
c_d	consolidation factor dependent on a decay parameter and time since the soil was disturbed (dimensionless)
c_{uf}	coefficient representing the impact of soil consolidation on the effectiveness of incorporated surface residue (dimensionless)
c_{ur}	coefficient describing the effectiveness of live and dead root mass in controlling erosion (acre· in· lb^{-1})
c_{us}	coefficient describing the effectiveness of incorporated surface residue in controlling erosion (acre· in· lb^{-1})
D	- period length (d) (ch. 5) - if > 0, erosion rate at a point (mass· $area^{-1}$· $time^{-1}$) (ch. 6) - if < 0, deposition rate (mass· $area^{-1}$· $time^{-1}$) (ch. 6)
D_b	minimum value of detachment as it decreases over time after consolidation relative to the detachment immediately after disturbance (dimensionless)

D_e	- equivalent roughness decay coefficient (dimensionless) (ch. 5) - sediment produced on the slope by detachment (ton· acre^{-1}· yr^{-1}) (ch. 6)
D_g	mean geometric particle diameter (mm)
D_n	net erosion (ton· acre^{-1}· yr^{-1})
D_r	roughness decay coefficient (dimensionless)
D_y	sediment transported from slope (ton· acre^{-1}· yr^{-1})
d	coefficient dependent on contour ridge height (ch. 6)
d_t	decay parameter (d^{-1})
E	storm energy (ft· tonf· acre^{-1})
EI	storm erosivity (ft· tonf· in· acre^{-1}· h^{-1}, or hundreds of ft· tonf· in· acre^{-1}· h^{-1}). Also a percentage of annual R
$(EI)_{10}$	storm erosivity of single storm with 10-yr return frequency (hundreds of ft· tonf· in· acre^{-1}· h^{-1})
EI_{30}	storm erosivity, interchangeable with EI (hundreds of ft· tonf· in· acre^{-1}· h^{-1})
EI_t	total storm erosivity since the most recent complete tillage operation; adjusted proportionately for operations disturbing less than 100% of the surface (hundreds of ft· tonf· in· acre^{-1}· h^{-1})
e	rainfall kinetic energy per unit of rainfall (ft· tonf· acre^{-1}· in^{-1})
e_m	rainfall kinetic energy (metric) (MJ· ha^{-1}· mm^{-1})
e_{max}	a maximum unit energy as intensity approaches infinity (ft· tonf· acre^{-1}· in^{-1})
F	coefficient dependent on temperature characteristics and shape of the residue decomposition response to temperature

F_c	fraction of land surface covered by canopy (dimensionless)
F_d	fraction of the soil surface disturbed by a field operation
F_u	fraction of the soil surface undisturbed by a field operation
f	function of ( )
f_i	primary particle size fraction (%)
f_r	runoff reduction factor (dimensionless)
f_{ri}	initial runoff reduction factor (dimensionless)
G	soil loss for a slope length (ton· ft^{-1}· yr^{-1})
g	sediment load (ton· ft^{-1}· yr^{-1})
g_{db}	sediment load at location where deposition begins within strip (ton· ft^{-1}· yr^{-1})
g_{de}	sediment load at location where deposition ends within strip (ton· ft^{-1}· yr^{-1})
g_p	sediment load at the end of the slope that would occur if the strips caused no deposition (ton· ft^{-1}· yr^{-1})
g_λ	sediment load at the end of the slope (ton· ft^{-1}· yr^{-1})
H	distance raindrops fall after striking the crop canopy (ft)
I	precipitation intensity (in· h^{-1})
I_{30}	maximum 30-min intensity (in· h^{-1})
i	- rainfall intensity (in· h^{-1}) - subscript indicating a particular segment or strip
i_m	rainfall intensity (metric) (mm· h^{-1})
K	soil erodibility factor (ton· acre· h· [hundreds of acre-ft· tonf· in]$^{-1}$)

K_{av}	EI weighted average annual soil-erodibility value (ton· acre· h· [hundreds of acre-ft· tonf· in] $^{-1}$)
K_b	saturated hydraulic conductivity of the soil with rock fragments (in· h^{-1})
K_f	saturated hydraulic conductivity of the fine soil (< 2 mm) fraction (in· h^{-1})
K_i	soil erodibility factor at any time, t_i (in calendar days) (ton· acre· h· [hundreds of acre-ft· tonf· in] $^{-1}$)
K_{max}	maximum value of soil erodibility for a given soil (ton· acre· h· [hundreds of acre-ft· tonf· in] $^{-1}$)
K_{min}	minimum value of soil erodibility for a given soil (ton· acre· h· [hundreds of acre-ft· tonf· in] $^{-1}$)
K_{nom}	soil erodibility as determined from the nomograph (ton· acre· h· [hundreds of acre-ft· tonf· in] $^{-1}$)
K_r	ratio of average seasonal (monthly) K-factor value over the average annual K value (dimensionless)
K_{wr}	rill soil erodibility for winter period (ton· acre· h· [hundreds of acre-ft· tonf· in] $^{-1}$)
k_t	sediment transport coefficient (ton· ft^{-1}· yr^{-1})
L	slope length factor (dimensionless)
$(LS)_{wr}$	rill slope length and steepness relationship for winter period (dimensionless)
M	- product of primary particle size fractions (dimensionless) (ch. 3) - amount of deposition on a strip (ton· $acre^{-1}$· yr^{-1}) (ch. 6)
M_a	average residue mass during a time period (lb· $acre^{-1}$)

M_b	residue mass at beginning of a time period ($lb \cdot acre^{-1}$)
M_e	residue mass at end of a time period ($lb \cdot acre^{-1}$)
m	slope length exponent (dimensionless) (ch. 4 and 6)
m_i	arithmetic mean of particle size limits of particular particle size (mm)
N	- number of residue types (ch. 5) - runoff index (dimensionless) (ch. 6)
n	- number of slope segments (ch. 4) - number of time periods used in summation (ch. 5) - number of strips (ch. 6)
n_i	ratio of root mass in the upper 4 in of soil to the total below-ground root biomass (dimensionless)
n_t	Manning's n
OM	organic matter (%)
P	support practice factor (dimensionless)
P	annual precipitation (in)
PLU	prior land use subfactor (dimensionless)
P_b	base value of the P factor for contouring (dimensionless)
P_{eff}	effective P-factor value for irregular slopes (dimensionless)
P_g	off-grade contouring P factor (dimensionless)
P_m	minimum P-factor value (dimensionless)
P_{mb}	minimum P-factor value for a given ridge height with base conditions (dimensionless)
P_o	on-grade contouring P factor (dimensionless)
P_s	P-factor value for stripcropping (dimensionless)

P_t	total rainfall since most recent field operation (in)
P_{wr}	winter conservation practice factor (dimensionless)
P_y	sediment delivery ratio of a slope under stripcropping or terracing (dimensionless)
P_1	calculated values of climate variable for first half-month period within a month
P_2	calculated values of climate variable for second half-month period within a month
p	- code for soil permeability (ch. 3) - coefficient dependent on residue characteristics (ch. 5)
Q	runoff amount from the 10-yr storm EI (in)
Q_k	computed runoff amount for the soil and cover-management condition indicated by subscript k (in)
q	runoff discharge rate ($ft^3 \cdot sec^{-1} \cdot ft^{-1}$)
q_{de}	runoff discharge rate for condition where sediment load equals transport capacity and deposition within strip ends ($ft^3 \cdot sec^{-1} \cdot ft^{-1}$)
R	average annual erosivity factor (hundreds of $ft \cdot tonf \cdot in \cdot acre^{-1} \cdot yr^{-1}$)
R	rainfall in the 15-d period (in)
R_a	roughness after biomass adjustment (in)
R_c	rainfall erosivity adjustment factor (hundreds of $ft \cdot tonf \cdot in \cdot acre^{-1} \cdot yr^{-1}$) (ch. 2)
R_{eq}	equivalent average annual erosivity factor (hundreds of $ft \cdot tonf \cdot in \cdot acre^{-1} \cdot yr^{-1}$)
$(R_{eq})_{wr}$	equivalent R factor of rills for winter period (hundreds of $ft \cdot tonf \cdot in \cdot acre^{-1} \cdot yr^{-1}$)

$(R_{eq})_{wt}$	total equivalent R factor for winter period (hundreds of ft· tonf· in· $acre^{-1}$· yr^{-1})
R_i	calculated initial roughness immediately following the previous field operation (in)
r_{max}	maximum surface random roughness; caused by protruding roots, rocks, and other effects of the long-term climate vegetative community when the soil is fully reconsolidated (in)
r_{min}	minimum surface random roughness; caused by rainfall-induced decay of tillage clods (in)
r_{nat}	for the current time period, the calculated surface random roughness caused by the factors creating r_{max} (in)
R_o	minimum average 15-day rainfall required for optimum decomposition (in)
R_n	net roughness following a field operation (in)
R_{np}	net roughness following the previous field operation (in)
R_u	roughness of surface before disturbance and roughness of the undisturbed portion of surface (in)
R_v	volume of rock fragments > 2 mm (%)
R_t	random roughness after most recent field operation (in)
R_w	weight of rock fragments > 2 mm (%)
r	excess rainfall depth (in)
r_f	roughness factor
r_i	roughness index
S	slope steepness factor (dimensionless)
SC	surface-cover subfactor (dimensionless)
SLR	soil-loss ratio (dimensionless)

$(SLR)_{wr}$	winter soil-loss ratio for rilling (dimensionless)
SM	soil-moisture subfactor (dimensionless)
S_p	land area covered by surface cover (%)
SR	surface-roughness subfactor (dimensionless)
s	- code for soil structure (ch. 3) - slope steepness (%) (ch. 4 and 6) - slope steepness (sine of slope angle) (ch. 6)
s_c	slope steepness for which a value of P_b is desired (sine of slope angle)
s_e	slope steepness above which contouring is ineffective (sine of slope angle)
s_{eb}	slope steepness for a given ridge height on base conditions at which contouring loses its effectiveness (sine of slope angle)
s_f	slope steepness along the furrows (sine of slope angle)
s_l	steepness of the land (sine of slope angle)
s_m	slope steepness at which contouring is most effective (sine of slope angle)
T	- soil-loss tolerance (ton· $acre^{-1}$) - transport capacity of runoff (ton· ft^{-1}· yr^{-1})
T_a	average temperature in 15-day decomposition period (°F)
T_{av}	average daily air temperature (°F)
T_o	optimum temperature in 15-day decomposition period (°F)
t	mean monthly temperature (°F)
t_c	time for 95% of disturbance effect to disappear by consolidation (yr)

t_{con}	amount of time required for the soil to fully reconsolidate following disturbance (yr)
t_d	time since soil was disturbed (yr)
t_i	any time (calendar days)
t_{max}	time of year when the soil erodibility factor is at a maximum (calendar days)
t_{min}	time of year when the soil erodibility factor is at a minimum (calendar days)
u_i	ratio of root mass to above-ground biomass (dimensionless)
V_f	fall velocity of sediment ($ft \cdot sec^{-1}$)
V_r	rainfall amount (in)
W	ratio of the rainfall in a 15-d period to the minimum average 15-d rainfall required for optimum residue decomposition
x	- length of each slope segment (ft) (ch. 4) - relative distance from top of the slope to the lower edge of a strip (absolute distance/slope length) (dimensionless) (ch. 6)
x_c	distance along slope length where contouring is assumed to be fully effective (ft)
x_{de}	location where deposition within strip ends (ft)
x_*	normalized distance along slope length (dimensionless)
x_1	unstable aggregate size fraction less than 0.250 mm (%)
x_2	product of modified silt fraction (0.002 to 0.1 mm) and modified sand fraction (0.1 to 2 mm)
x_3	base saturation (dimensionless)
x_4	silt fraction (0.002 to 0.050 mm) (%)
x_5	sand fraction (0.1 to 2 mm) (%)

x_6	aggregation index (dimensionless)
x_7	montmorillonite in soil (%)
x_8	bulk density of the 50- to 125-mm depth ($g \cdot cm^{-3}$)
x_9	dispersion ratio (dimensionless)
x_{10}	parameter M (product of primary particle size fractions) (dimensionless)
x_{11}	citrate-dithionite-bicarbonate extractable percentage of Al_2O_3 plus Fe_2O_3 (%)
α	ratio of the area covered by a piece of residue to the mass of that residue ($acre \cdot lb^{-1}$)
β	ratio of rill to interrill erosion (dimensionless)
Δt	length of frost-free period or growing period (calendar days)
δ	constant with value of either 0 or 1
ζ	transport capacity factor ($ton \cdot ft^{-1} \cdot yr^{-1}$)
θ	slope angle (degrees)
λ	slope length (ft)
λ_c	critical slope length (ft)
ξ	erosion factor ($ton \cdot acre^{-1} \cdot yr^{-1}$)
σ	excess rainfall rate ($length \cdot time^{-1}$)
ϕ	ratio of sediment fall velocity to excess runoff rate (dimensionless)

PREFACE

The Revised Universal Soil Loss Equation (RUSLE) is an update of Agriculture Handbook No. 537, containing a computer program to facilitate the calculations. RUSLE also includes the analysis of research data that were unavailable when Agriculture Handbook No. 537 was completed. Although the original Universal Soil Loss Equation (USLE) has been retained in RUSLE, the technology for factor evaluation has been altered and new data have been introduced with which to evaluate the terms for specified conditions.

The rainfall-runoff erosivity factor (R) database has been expanded in the western United States, and a correction has been developed for the portion of rain falling on ponded water. The soil erodibility factor (K) has been made time varying to reflect freeze-thaw conditions and consolidation caused by moisture extraction of a growing crop, an alternative regression equation was developed for volcanic tropical soils, and a correction was developed for rock fragments in the soil profile. The topographic factors, slope length and steepness (LS), have been revised and algorithms developed to reflect the ratio of rill to interrill erosion. The cover-management factor (C) has been altered from the seasonal soil-loss ratios to a continuous function that is the product of four subfactors representing prior land use (PLU), surface cover (SC), crop canopy (CC), surface roughness (SR), and (for cropland in the Northwestern Wheat and Range Region) soil moisture (SM). These subfactors include consideration of the root mass in the upper 4 in of the soil profile, as well as changes in crop cover and root mass with time, tillage, and residue decomposition. Climatic data that include monthly precipitation and temperature, the frost-free period, rainfall-runoff erosivity, and twice monthly distributions for the EI (product of kinetic energy and maximum 30-min precipitation intensity) are used for consideration of the seasonal variations in K, C, and the support practice factor (P). P has been expanded to consider conditions for rangelands, contouring, stripcropping, and terracing.

The calculations in RUSLE are more involved than those in USLE and are facilitated with a computer program.

CHAPTER 1. INTRODUCTION AND HISTORY

Contributors:

K.G. Renard
L.D. Meyer
G.R. Foster

CHAPTER 1. CONTENTS

PURPOSE OF HANDBOOK

Scientific planning for soil conservation and water management requires knowledge of the relations among those factors that cause loss of soil and water and those that help to reduce such losses. Controlled studies on field plots and small watersheds have supplied much valuable information on these complex interrelations of factors. But the maximum benefits from such research can be realized only when the findings are applied as sound practices on the farms, ranches, and other erosion-prone areas throughout the United States. Specific guidelines are needed for the selection of the control practices best suited to the particular needs of each site.

Such guidelines are provided by the procedure for soil-loss prediction presented in this handbook. The procedure methodically combines research information from many sources to develop design data for each conservation plan. Widespread field experience for more than four decades has proved that this technology is valuable as a conservation-planning guide.

The procedure is founded on the empirical Universal Soil Loss Equation (USLE) (described in handbooks by Wischmeier and Smith 1965, 1978) that is believed to be applicable wherever numerical values of its factors are available. Research has supplied information from which at least approximate values of the equation's factors can be obtained for specific farm or ranch fields or other small land areas throughout most of the United States. Tables and charts or the personal-computer program presented in this handbook makes information readily available for field use.

The Revised Universal Soil Loss Equation (RUSLE) includes analyses of data not available when the previous handbooks were prepared. The analyses are documented so that users can review, evaluate, and repeat them in the process of making local analyses. Debate on this revision of USLE is important. Any such debate should be focused on the data, theory, and concepts described in the chapters. Many reviewers have helped with the debate. Their reviews were essential, and they should help to establish the credibility of this revision.

Judgments were necessary during the revision because some data were limited and inconclusive, and a few were conflicting. The decisions were made by the use of the collective knowledge of a number of erosion scientists. Furthermore, the technology was revised to permit the addressing of problems

not included or inadequately addressed in earlier versions of USLE. The current revision is intended to provide the most accurate estimates of soil loss without regard to how the new values compare with the old values.

This revision updates the content of the earlier handbooks (Wischmeier and Smith 1965, 1978) and incorporates new material that has been available informally or in scattered research reports and professional journals. Some of the original charts and tables have been revised to conform with additional research findings, and new charts and tables have been developed to extend the usefulness of RUSLE. In some instances, expanding a table, chart, or computer program sufficiently to meet the needs for widespread field application required the projection of empirical factor relationships appreciably beyond the physical limits of the data from which the relationships were derived. Estimates obtained in this manner are the best information available for the conditions they represent. These instances are identified in the chapter discussions of the specific erosion factors, tables, charts, and computer program.

The background material for each RUSLE factor value is presented in the text that helps the user select correct values of individual factor parameters. This revision, with its background chapters, user's guide, and associated computer program, will provide erosion technology for use in addressing problems being proposed in the last decade of the 20th century or until new technology becomes available, such as that from USDA's Water Erosion Prediction Project (WEPP) (Foster and Lane 1987, Lane and Nearing 1989).

HISTORY OF EROSION-PREDICTION EQUATIONS

Efforts to mathematically predict soil erosion by water started only about a half century ago. The development of erosion-prediction technology began with analyses such as those by Cook (1936) to identify the major variables that affect soil erosion by water. Cook listed three major factors: susceptibility of soil to erosion, potential erosivity of rainfall and runoff, and soil protection afforded by plant cover. A few years later, Zingg (1940) published the first equation for calculating field soil loss. That equation described mathematically the effects of slope steepness and slope length on erosion. Smith (1941) added factors for a cropping system and support practices to the equation. He also added the concept of a specific annual soil-loss limit, and he used the resulting equation to develop a graphic method for selecting conservation practices for certain soil conditions in the midwestern United States.

Progress continued on methods to predict erosion during World War II, but publication of the research was delayed until after the war. Browning and associates (1947) added soil erodibility and management factors to the Smith (1941) equation and prepared more extensive tables of relative factor values for different soils, crop rotations, and slope lengths. This approach emphasized the evaluation of slope-length limits for different cropping systems on specific soils and slope steepness with and without contouring, terracing, or stripcropping. Smith and Whitt (1947) presented a method for estimating soil losses from fields of claypan soils. Soil-loss ratios at different slopes were given for contour farming, stripcropping, and terracing. Recommended limits for slope length were presented for contour farming. Relative erosion rates for a wide range of crop rotations were also given. Then Smith and Whitt (1948) presented a "rational" erosion-estimating equation, $A = C \cdot S \cdot L \cdot K \cdot P$, which broadened the application to principal soils of Missouri. The C factor was the average annual soil loss from claypan soils for a specific rotation, slope length, slope steepness, and row direction. The other factors for slope steepness (S), slope length (L), soil erodibility (K), and support practice (P) were dimensionless multipliers used to adjust the value of C to other conditions. P-factor values were discussed in detail. Smith and Whitt acknowledged the need for a rainfall factor to make this equation applicable over several states.

The Milwaukee, Wisconsin, regional office of USDA's Soil Conservation Service (SCS) recognized the value of a soil-loss equation for farm planning and teamed with researchers in that region to develop a system for regional application. The result was the slope-practice method of estimating soil loss for use in the Corn Belt. To adapt the Corn Belt equation for use in other regions, a workshop for erosion specialists from throughout the United States was held in Ohio in 1946. Workshop participants reviewed soil-loss data from all over the United States, reappraised the factors previously used, and added a rainfall factor. The resulting so-called Musgrave equation included factors for rainfall, flow characteristics of surface runoff as affected by slope steepness and slope length, soil characteristics, and vegetal cover effects (Musgrave 1947).

Graphs to solve the Musgrave equation were prepared by Lloyd and Eley (1952). They tabulated values for many major conditions in the northeastern states. Van Doren and Bartelli (1956) proposed an erosion equation for Illinois soils and cropping conditions that estimated annual soil loss as a function of nine factors. One of the factors was soil loss as measured on research plots; soil loss was adjusted to site conditions by several factors used by previous researchers and also factors for prior erosion and management levels.

The state and regional erosion-prediction equations were so useful that soil conservation leaders recommended that an effort be initiated to develop a national equation. As a result, the Agricultural Research Service (ARS) established the National Runoff and Soil Loss Data Center at Purdue University (West Lafayette, Indiana) in 1954. The Data Center was given the responsibility of locating, assembling, and consolidating all available data from runoff and erosion studies throughout the United States for further analyses (Wischmeier 1955). During subsequent years, Federal-state cooperative research projects at 49 U.S. locations contributed more than 10,000 plot-years of basic runoff and soil-loss data to this Center for summarizing and overall statistical analyses.

To hasten the development of a national equation, joint conferences of key researchers and users were held at Purdue University in February and July of 1956. The participants concentrated their efforts on reconciling the differences among existing soil-loss equations and on extending the technology to regions where no measurements of erosion by rainstorms had been made. The equation that resulted had seven factors; they were for crop rotation, management, slope steepness, slope length, conservation practice, soil erodibility, and previous erosion. The group established the maximum permissible loss for any soil as 5 ton$\cdot$ acre$^{-1}\cdot$ yr^{-1} but set lower limits for many soils. Workshop participants concluded that insufficient data were

available to justify adding a rainfall factor; subsequent analyses at the Data Center led to a rainfall factor for the states east of the Rocky Mountains. Subsequent study also showed that the equation's crop rotation and management factors could be combined into one factor (Wischmeier et al. 1958).

Using the data assembled at the Data Center along with conclusions from deliberations at the 1956 conferences and subsequent analyses, Wischmeier, Smith, and others developed USLE as described in earlier handbooks (Wischmeier and Smith 1965, 1978). USLE quantifies soil erosion as the product of six factors representing rainfall and runoff erosiveness, soil erodibility, slope length, slope steepness, cover-management practices, and support conservation practices.

USLE was designed to provide a convenient working tool for conservationists. A relatively simple technique was needed for predicting the most likely average annual soil loss in specific situations. A goal for the equation was that each factor (1) could be represented by a single number; (2) could be predicted from meteorological, soil, or erosion research data for each location; and (3) must be free from any geographically oriented base. The term "Universal" in USLE distinguishes this prediction model from the regionally based models that preceded it. However, the use of USLE should be limited to situations in which its factors can be accurately evaluated and to conditions for which it can be reliably applied (Wischmeier 1976).

USLE overcame many of the deficiencies of its predecessors. The form of USLE is similar to that of previous equations, but the concepts, relationships, and procedures underlying the definitions and evaluations of the erosion factors are distinctly different. Major changes include (1) more complete separation of factor effects so that results of a change in the level of one or several factors can be more accurately predicted; (2) an erosion index that provides a more accurate, localized estimate of the erosive potential of rainfall and associated runoff; (3) a quantitative soil-erodibility factor that is evaluated directly from research data without reference to any common benchmark; (4) an equation and nomograph that are capable of computing the erodibility factor for numerous soils from soil survey data; (5) a method of including the effects of interactions between cropping and management parameters; and (6) a method of incorporating the effects of local rainfall patterns throughout the year and specific cropping conditions in the cover and management factor (Wischmeier 1972).

Regression analysis of the assembled data determined the mathematical relationship between each USLE factor and soil loss. Effects of slope length and steepness, crop sequence, and soil- and crop-management practices were

most accurately described as percentage increases or decreases in soil loss. A multiplicative model was selected for the equation. It uses four dimensionless factors to modify soil loss as described by dimensioned rainfall and soil factors.

USLE was introduced at a series of regional workshops on soil-loss prediction in 1959-62 and by a U.S. Department of Agriculture special report (USDA 1961). Several years of trial use by SCS and others plus extensive interaction between the developers and users resulted in improved factor values and the evaluation of additional conditions. Finally, USLE was presented in Agriculture Handbook No. 282 (Wischmeier and Smith 1965).

Widespread acceptance of USLE took time but came progressively as more regions and groups began to use this equation. During the same period, important improvements in USLE expanded its usefulness by providing techniques for estimating site values of its factors for additional land uses, climatic conditions, and management practices. These include a soil-erodibility nomograph for farmland and construction areas, topographic factors for irregular slopes, cover factors for range and woodland, effects of tillage practices on cover and management, prediction of erosion in construction areas, estimated erosion index values for the western states and Hawaii, soil erodibility factors for benchmark Hawaiian soils, and improved design and evaluation of erosion-control-support practices. These improvements were incorporated in an updated version of USLE, published as Agriculture Handbook No. 537 (Wischmeier and Smith 1978).

The erosion-research history that led to the development of USLE (Smith and Wischmeier 1962, Meyer 1984, Meyer and Moldenhauer 1985) shows that USLE was the logical culmination of several decades of innovative effort by scientists having unusual expertise and dedication. Since its introduction, USLE has had a tremendous impact and has become the major soil conservation planning tool in the United States and abroad.

Since the publication of Agriculture Handbook No. 537, additional research and experience have resulted in improvements in USLE. These include new and (in some instances) revised isoerodent maps; a time-varying approach to reflect freeze-thaw conditions and consolidation caused by extraction of moisture by a growing crop for the soil erodibility factor (K); a subfactor approach for evaluating the cover-management factor (C) for cropland, rangeland, and disturbed areas; a new equation to reflect slope length and steepness (LS) (the new terms also reflect the ratio of rill to interrill erosion); and new conservation-practice values (P) for both cropland and rangeland practices. Finally, the computations are now implemented using a personal

computer. These changes are detailed in this revision in the chapters for each RUSLE factor.

The revision of USLE described in this handbook incorporates the latest information available for using this erosion-prediction approach. Research on the principles and processes of erosion and sedimentation by water is continuing in order to improve the methods of predicting and controlling erosion. Knowledge from such research has been used in developing physically based models such as the erosion and sedimentation components of CREAMS (Knisel 1980, Foster et al. 1981a). Development of a new generation of technology for predicting water erosion is under way by a USDA team in WEPP working with other agencies and academic institutions (Foster and Lane 1987). The goal of this WEPP effort is a process-oriented model or family of models that are conceptually superior to the lumped-model RUSLE and are more versatile as to the conditions that can be evaluated. The WEPP technology is expected to replace RUSLE sometime in the future.

SOIL-LOSS TOLERANCE

A major purpose of the soil-loss equation is to guide the making of methodical decisions in conservation planning. The equation enables the planner to predict the average rate of soil erosion for each of various alternative combinations of cropping systems, management techniques, and erosion-control practices on any particular site. The term "soil-loss tolerance" (T) denotes the maximum rate of soil erosion that can occur and still permit crop productivity to be sustained economically. The term considers the loss of productivity due to erosion but also considers rate of soil formation from parent material, role of topsoil formation, loss of nutrients and the cost to replace them, erosion rate at which gully erosion might be expected to begin, and erosion-control practices that farmers might reasonably be able to implement. When predicted soil losses are compared with the value for soil-loss tolerance at that site, RUSLE provides specific guidelines for bringing about erosion control within the specified limits. Any combination of cropping, ranching, and management for which the predicted erosion rate is less than the rate for soil-loss tolerance may be expected to provide satisfactory control of erosion. Of the satisfactory alternatives offered by this procedure, the alternative(s) best suited to a particular farm or other enterprise may then be selected.

Values of soil-loss tolerance ranging from 1 to 5 ton$\cdot$ acre$^{-1}\cdot$ yr^{-1} for the soils of the United States were derived by soil scientists/conservationists, agronomists, engineers, geologists, and Federal and state researchers at six regional workshops between 1959 and 1962. Factors considered in defining these limits include soil depth, physical properties and other characteristics affecting root development, gully prevention, on-field sediment problems, seeding losses, reduction of soil organic matter, and loss of plant nutrients. Since the early discussions, several reports have been produced in which soil-loss tolerance is discussed (Schmidt et al. 1982, Johnson 1987). The passage of Public Law 95-192 and the 1977 Soil and Water Resources Conservation Act (RCA) prompted considerable interest in the effect of soil erosion on crop productivity. New experimental research and computer simulation models have furthered the interest in soil-loss tolerances. Two symposia proceedings of note that resulted from this activity are "Erosion and Soil Productivity" (ASAE 1985) and "Soil Erosion and Crop Productivity" (Follett and Stewart 1985). Needless to say, many issues about soil-loss tolerance remain unresolved.

A deep, medium-textured, moderately permeable soil that has subsoil characteristics favorable for plant growth has a greater tolerable soil-loss rate than do soils with shallow root zones or high percentages of shale at the surface. Widespread experience has shown that the concept of soil-loss tolerance may be feasible and generally adequate for indefinitely sustaining productivity levels.

Soil-loss limits are sometimes established to prevent or reduce damage to offsite water quality. The criteria for defining the tolerance limits of field soil-loss tolerance limits for this purpose are ***not*** the same as those for tolerances designed to preserve cropland productivity. Soil depth is not relevant for offsite sediment control, and uniform limits on erosion rates still allow a range in the amount of sediment per unit area that is delivered to a stream. Soil material eroded from a field slope may be deposited along field boundaries, in terrace channels, in depressional areas, or on flat or vegetated areas traversed by overland flow before it reaches a watercourse. Erosion damages the cropland on which it occurs, but sediment deposited near its place of origin does not directly affect water quality.

If the soil-loss tolerance established for sustained cropland productivity fails to attain the desired water-quality standard, other limits that consider other factors should be established rather than altering the value for soil-loss tolerance. Other factors may include distance of the field from a major waterway, sediment-transport characteristics of the intervening area, sediment composition, needs of the particular body of water being protected, and the probable magnitude of fluctuations in sediment loads (Stewart et al. 1975). Placing limits on sediment yield might provide more uniform water-quality control than would lowering the limits on soil movement from field slopes. The sediment-yield criteria would also require fewer restrictions on the selection of crop system for fields in which only small percentages of eroded soil become off-farm sediment.

As currently used in conservation-planning activities, T values are often an issue of policy. We recommend that T values remain as originally defined and intended: namely, the erosion rate that can occur and yet permit crop productivity to be sustained economically. If issues of water quality, economics, and policy are to be addressed for erosion control, we recommend that they be designated T_{WQ} (soil loss for water-quality concerns), T_{EP} (soil loss for economic planning), and T_{POL} (soil loss for policy concerns).

SOIL-LOSS EQUATION

The erosion rate for a given site results from the combination of many physical and management variables. Actual measurements of soil loss would not be feasible for each level of these factors that occurs under field conditions. Soil-loss equations were developed to enable conservation planners, environmental scientists, and others concerned with soil erosion to extrapolate limited erosion data to the many localities and conditions that have not been directly represented in the research.

Erosion and sedimentation by water involve the processes of detachment, transport, and deposition of soil particles (Foster 1982). The major forces are from the impact of raindrops and from water flowing over the land surface. Erosion may be unnoticed on exposed soil surfaces even though raindrops are eroding large quantities of sediment, but erosion can be dramatic where concentrated flow creates extensive rill and gully systems. Factors affecting erosion can be expressed in an equation of the form (Renard and Foster 1983)

$$E = f\,(C, S, T, SS, M) \qquad [1\text{-}1]$$

where

E = erosion,
f = function of ( ),
C = climate,
S = soil properties,
T = topography,
SS = soil surface conditions, and
M = human activities.

Sediment yield should not be confused with erosion; the terms are not interchangeable. Sediment yield is the amount of eroded soil that is delivered to a point in the watershed that is remote from the origin of the detached soil particles. In a watershed, sediment yield includes the erosion from slopes, channels, and mass wasting, minus the sediment that is deposited after it is eroded but before it reaches the point of interest (fig. 1-1). USLE and RUSLE do not estimate sediment yield.

USLE is essentially an expression of the functional relationship shown in equation [1-1] (Wischmeier and Smith 1965, 1978). Both USLE and RUSLE compute the average annual erosion expected on field slopes as

$$A = R \cdot K \cdot L \cdot S \cdot C \cdot P \qquad [1\text{-}2]$$

where

A = computed spatial average soil loss and temporal average soil loss per unit of area, expressed in the units selected for K and for the period selected for R. In practice, these are usually selected so that A is expressed in ton· $acre^{-1}$· yr^{-1}, but other units can be selected (that is, t· ha^{-1}· yr^{-1}).

R = rainfall-runoff erosivity factor—the rainfall erosion index plus a factor for any significant runoff from snowmelt.

K = soil erodibility factor—the soil-loss rate per erosion index unit for a specified soil as measured on a standard plot, which is defined as a 72.6-ft (22.1-m) length of uniform 9% slope in continuous clean-tilled fallow.

L = slope length factor—the ratio of soil loss from the field slope length to soil loss from a 72.6-ft length under identical conditions.

S = slope steepness factor—the ratio of soil loss from the field slope gradient to soil loss from a 9% slope under otherwise identical conditions.

C = cover-management factor—the ratio of soil loss from an area with specified cover and management to soil loss from an identical area in tilled continuous fallow.

P = support practice factor—the ratio of soil loss with a support practice like contouring, stripcropping, or terracing to soil loss with straight-row farming up and down the slope.

RUSLE is an erosion model designed to predict the longtime average annual soil loss (A) carried by runoff from specific field slopes in specified cropping and management systems as well as from rangeland. Widespread use has substantiated the usefulness and validity of RUSLE for this purpose. It is also applicable to nonagricultural conditions such as construction sites.

RUSLE users need to be aware that A (in addition to being a longtime average annual soil loss) is the average loss over a field slope and that the losses at various points on the slope may differ greatly from one another. On a long uniform slope, the loss from the top part of the slope is much lower than the slope average, and the loss near the bottom of the slope is considerably higher. For instance, a 360-ft uniform slope that averages 20

ton· acre^{-1} will have an average of less than 7 ton· acre^{-1} loss on the first 40 ft but over 29 ton· acre^{-1} loss on the last 40 ft. If the slope steepness changes within that length, the variation can be even greater. This suggests that even if a field soil loss is held to "T," soil loss on some portion of the slope may reach or exceed 2T, even when the ephemeral gully and other types of erosion that are not estimated by RUSLE are ignored. These higher-than-average rates generally occur at the same locations year after year, so excessive erosion on any part of the field may be damaging the soil resource.

With appropriate selection of its factor values, RUSLE will compute the average soil loss for a multicrop system, for a particular crop year in a rotation, or for a particular crop stage period within a crop year. Erosion variables change considerably from storm to storm about their means. But the effects of the random fluctuations such as those associated with annual or storm variability in R and the seasonal variability of the C tend to average out over extended periods. Because of the unpredictable short-time fluctuations in the levels of influential variables, however, present soil-loss equations are substantially less accurate for the prediction of specific events than for the prediction of longtime averages.

USLE has also been used for estimating soil loss from disturbed forested conditions. RUSLE does not address this particular application. Users of such technology are referred to Dissmeyer and Foster (1980, 1981).

Some recent research addresses the application of USLE technology to mine spoils and reconstructed topsoil (Barfield et al. 1988). The effects of compaction on erosion are significant in such instances and are treated as an integral part of the subfactor for calculating C (see ch. 5). Furthermore, slope steepness effects on soil loss from disturbed lands (McIsaac et al. 1987a) are treated specifically in chapter 4 with the application of an LS table (see table 4-3). Other RUSLE terms remain unchanged by massive land disturbance such as that associated with construction. It is important to realize that the amount of research on effects of land disturbance on RUSLE technology is not as extensive as that associated with most other applications.

The soil-loss equation was initially developed in U.S. customary units. The factor definitions are interdependent, and the direct conversion of acres, tons, inches, and feet to metric units produces integers that are best suited for expressing equations in that system. Only U.S. customary units are used in the equation and factor-evaluation materials, but the metric equivalents are given in appendix A.

Numerical values for each of the six factors were derived from analyses of research data and from National Weather Service precipitation records. For most conditions in the United States, the approximate values of the factors for any particular site may be obtained from charts and tables in this handbook or by use of the computer program developed to assist with the RUSLE evaluation. Users in localities or countries where the rainfall characteristics, soil types, topographic features, or farm practices are substantially beyond the range of present U.S. data will find these charts, tables, and computer program incomplete and perhaps inaccurate for their conditions. However, RUSLE provides guidelines that can reduce the amount of local research needed to develop appropriate technology for their conditions.

The RUSLE User Guide (ch. 7) illustrates how to select factor values either with the computer program or by use of data from the tables and charts. Users who have no experience with the soil-loss equation may wish to read chapter 7 next. After users have referred to the computer program and have located the values used therein, they may readily move to the intervening chapters (ch. 2-6), which define the technical details associated with the factors. The soil-loss-prediction procedure is more valuable as a guide for the selection of practices if the user has general knowledge of the principles on which the equation is based. Therefore, the significance of each factor is discussed before the introduction of the computer program and before the reference table or chart from which local values may be obtained. Limitations of the data available for evaluation of some of the factors are also discussed.

Chapters 2-6 are written as background for the development of the technology to permit evaluation of the individual RUSLE factors. Although liberal use is made of material from previous versions of USLE (Agriculture Handbooks No. 282 in 1965 and No. 537 in 1978), direct quotes from that material are not always noted. The computer program, intended to assist the user of this technology, is a new development that was not a part of earlier versions.

The authors acknowledge the efforts of Laura J. Yohnka for processing the many drafts prior to completion and E. Sue Anderson for finishing work on the final copy.

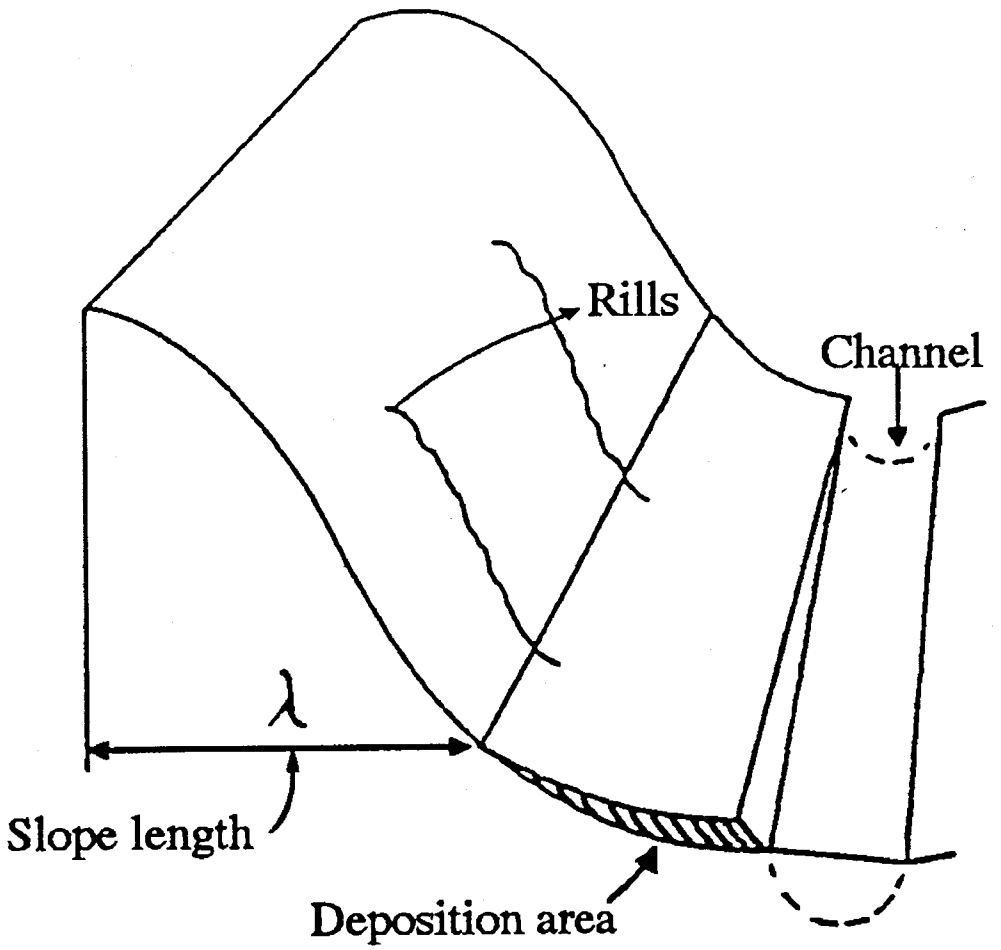

Figure 1-1. Schematic slope profile for RUSLE applications for interrill and rill erosion. λ is the RUSLE slope length (to the point where deposition occurs). Sediment yield is the sediment transported out of the channel section summed for time periods such as a storm event, month, crop stage, or year.

CHAPTER 2. RAINFALL-RUNOFF EROSIVITY FACTOR (R)

Contributors:

K.G. Renard
D.K. McCool
K.R. Cooley
G.R. Foster
J.D. Istok
C.K. Mutchler

CHAPTER 2. CONTENTS

The rainfall and runoff factor (R) of the Universal Soil Loss Equation (USLE) was derived (Wischmeier 1959, Wischmeier and Smith 1958) from research data from many sources. The data indicate that when factors other than rainfall are held constant, soil losses from cultivated fields are directly proportional to a rainstorm parameter: the total storm energy (E) times the maximum 30-min intensity (I_{30}).

Rills and sediment deposits observed after an unusually intense storm have sometimes led to the conclusion that significant erosion is associated with only a few severe storms--that significant erosion is solely a function of peak intensities. However, more than 30 yr of measurements in many states have shown that this is not the case (Wischmeier 1962). The data show that a rainfall factor used to estimate average annual soil loss must include the cumulative effects of the many moderate-sized storms as well as the effects of the occasional severe ones.

The numerical value used for R in USLE and in RUSLE must quantify the effect of raindrop impact and must also reflect the amount and rate of runoff likely to be associated with the rain. The erosion index (R) derived by Wischmeier appears to meet these requirements better than any of the many other rainfall parameters and groups of parameters tested against the plot data. The local value of this index may be obtained directly from maps. However, the index does not include the erosive forces of runoff from snowmelt, rain on frozen soil, or irrigation. A procedure for evaluating R for locations where this type of runoff is significant is given in this chapter under "R Equivalent (R_{eq}) for Cropland in the Northwestern Wheat and Range Region."

In RUSLE, the computational scheme is identical to that used in USLE, with a few exceptions (as noted later).

EI PARAMETER

The value of EI for a given rainstorm equals the product of total storm energy (E) times the maximum 30-min intensity (I_{30}), where E is in hundreds · ft· tonf · $acre^{-1}$, and I_{30} is in in · h^{-1}. EI is an abbreviation for energy times intensity, and the term should *not* be considered simply an energy parameter. Data show that rainfall energy itself is not a good indicator of erosive potential. The storm energy indicates the volume of rainfall and runoff, but a long, slow rain may have the same E value as a shorter rain at much higher intensity. Raindrop erosion increases with intensity. The I_{30} component reflects the prolonged peak rates of detachment and runoff. The product term EI is a statistical interaction term that reflects how total energy and peak intensity are combined in each particular storm. Technically, the term indicates how particle detachment is combined with transport capacity. Appendix B illustrates how the calculations are made from recording-raingage data.

The relation of soil loss to the EI parameter is assumed to be linear, and the parameter's individual storm values are directly additive. The sum of the storm EI values for a given period is a numerical measure of the erosive potential of the rainfall within that period. The average annual total of the storm EI values in a particular locality is the rainfall erosion index (R) for that locality. Because of apparent cyclical patterns in rainfall data, early published values for rainfall erosion indices (for example, in Agriculture Handbook No. 537) were based on 22-yr station rainfall records. Longer records are advisable, especially when the coefficient of variation of annual precipitation is large.

Rain showers of less than 0.5 in were omitted from the erosion index computations, unless at least 0.25 in of rain fell in 15 min. Furthermore, a storm period with less than 0.05 in over 6 h was used to divide a longer storm period into two storms. Exploratory analyses showed that erosion from these light rains is usually too small for practical significance and that, collectively, they have little effect on the distribution of the annual EI or erosion. The cost of abstracting and analyzing 4,000 location-years of rainfall-intensity data used to develop the initial R-factor map was greatly reduced by adopting the threshold value of 0.5 in.

The energy of a rainstorm is a function of the amount of rain and of all the storm's component intensities. The median raindrop size generally increases

with greater rain intensity (Wischmeier and Smith 1958), and the terminal velocities of free-falling waterdrops increase with larger drop size (Gunn and Kinzer 1949). Since the energy of a given mass in motion is proportional to velocity squared, rainfall energy is directly related to rain intensity. The relationship, based on the data of Laws and Parsons (1943), is expressed by the equation

$$e = 916 + 331 \log_{10} i, \qquad i \leq 3 \text{ in} \cdot h^{-1} \qquad [2\text{-}1]$$

$$e = 1074 \qquad i > 3 \text{ in} \cdot h^{-1} \qquad [2\text{-}2]$$

where e is kinetic energy in ft· tonf · $acre^{-1}$ · in^{-1}, and i is intensity in in· h^{-1} (Wischmeier and Smith 1958). A limit of 3 in · h^{-1} is imposed on i because median drop size does not continue to increase when intensities exceed 3 in · h^{-1} (Carter et al. 1974).

The corresponding SI metric-unit version of the equations are (Foster et al. 1981b, app. A)

$$e_m = 0.119 + 0.0873 \log_{10}(i_m) \qquad i_m \leq 76 \text{ mm} \cdot h^{-1} \qquad [2\text{-}3]$$

$$e_m = 0.283 \qquad i_m > 76 \text{ mm} \cdot h^{-1} \qquad [2\text{-}4]$$

where e_m has units of megajoule per hectare per millimeter of rainfall (MJ · ha^{-1} · mm^{-1}).

Other investigators have also presented algorithms for computing the kinetic energy for drop distributions in other geographic areas of the continental United States [for example, McGregor and Mutchler (1977) in Mississippi, Carter et al. (1974) in the South Central United States, Tracy et al. (1984) in southeastern Arizona, and Rosewell (1983, 1986) in Australia].

Brown and Foster (1987) used a unit energy relationship of the form

$$e = e_{max} [1 - a \exp (-b \cdot i)] \quad [2\text{-}5]$$

where

e_{max} = a maximum unit energy as intensity approaches infinity, and

a and b = coefficients.

Kinnell (1981, 1987) showed that this distribution described unit energy-intensity relationships in Zimbabwe and Florida. Additional work by Rosewell (1983, 1986) showed that the relationship also fit data in Australia, the McGregor and Mutchler (1977) data, and the Laws and Parsons (1943) data. Unfortunately, these applications showed some variability in the a and b coefficients. Brown and Foster stated in their analysis that they recommended

$$e_m = 0.29 [1 - 0.72 \exp (-0.05 i_m)] \quad [2\text{-}6]$$

for calculating unit energy, where e_m has units of MJ $\cdot$ ha^{-1} $\cdot$ mm^{-1} of rain and i_m has units of mm $\cdot$ h^{-1}. Brown and Foster also stated that this equation is a superior analytical form by having a finite positive value at zero intensity as data show and approaching an asymptote at high intensities as a continuous function. The U.S. customary units equivalent of equation [2-6] is

$$e = 1099[1 - 0.72 \exp (-1.27 i)] \quad [2\text{-}7]$$

where i has units of in $\cdot$ h^{-1} and e has units of ft $\cdot$ tonf $\cdot$ acre^{-1} $\cdot$ in^{-1}.

Then

$$R = \frac{\sum_{i-1}^{j} (EI_{30})_i}{N} \quad [2\text{-}8]$$

where $(EI_{30})_i = EI_{30}$ for storm i, j = number of storms in an N year period.

These equations were used for developing the isoerodent maps of figures 2-1 to 2-4.

The isoerodent maps of figures 2-1 and 2-9 were developed from equations [2-1] and [2-2]. We recommend that all future calculations be made using equation [2-6] or equation [2-7], especially in other countries where RUSLE technology is being developed.

Sample calculations of EI_{30} are given in appendix B.

ISOERODENT MAPS

Local values of the rainfall erosion index may be taken directly from isoerodent maps or from the CITY database in the computer program as explained in chapter 7. The plotted lines on the maps are called isoerodents because they connect points of equal rainfall erosivity. Erosion index values for locations between the lines can be obtained by linear interpolation.

The original isoerodent map (Wischmeier and Smith 1965) was developed from 22-yr station rainfall records by computing the EI value for each storm that met the previously defined threshold criteria. Isoerodents were then located between these point values with the help of published rainfall intensity-frequency data (U.S. Weather Bureau 1958) and topographic maps. The 11 western states were omitted from the initial map because sufficient long-term recording-raingage records were not available for establishing lines of equal erosion index values.

The isoerodent map was extended with an estimation procedure to the Pacific Coast in 1976 and was printed in Agriculture Handbook No. 537. Results of investigations at the USDA-ARS National Soil Erosion Research Laboratory at Purdue University showed that the known erosion index values in the Western Plains States and the North Central States are approximated with reasonable accuracy by the equation $R = 27.38P^{2.17}$ where P is the 2-yr frequency, 6-h rainfall amount (Wischmeier 1974). Although the isoerodents developed were compatible with the few point values that had been established in the western United States, the isoerodents were not sufficiently accurate to reflect the known spatial variability of the mountain and valley topography of the region.

In an agreement between Oregon State University, U.S. Department of Agriculture's Soil Conservation Service (SCS) and Agricultural Research Service (ARS), and the National Weather Service, 713 stations were used to determine relationships between values of EI calculated on a 15-min measurement interval basis and on values of EI calculated for the same storm on a 60-min measurement interval basis. In contrast to the calculations in the eastern United States, all storms were included to calculate EI. Of these stations, 225 had record periods of 12 yr or longer and precipitation measurement resolutions of 0.01 in. Values of coefficient of determination (r^2) in excess of 0.8 were obtained by use of the model $(EI)_{15} = b[\ (EI)_{60}\ ]$.

Values of the regression parameter b ranged from 1.08 to 3.16, varying widely from one climatic zone to the next.

To supplement this work, 1,082 stations were used to calculate $(EI)_{60}$. Of these stations, 790 had 20-yr record lengths or longer. These data values were adjusted to a 15-min measurement interval using the correction cited above. Computed values of $(EI)_{60}$ for each 60-min station were multiplied by the average regression parameter b (computed for all 15-min stations in the climatic zone containing the 60-min station) to obtain equivalent 15-min values, $(EI)_{15}$. These values were then adjusted to an equivalent breakpoint basis by use of $R = 1.0667\ (R)_{15}$ (Weiss 1964). The resulting isoerodent map (R) was prepared by hand contouring the adjusted R values for stations with record periods of at least 20 yr. The resulting isoerodent maps for the West is a significant improvement over that available in Agriculture Handbook No. 537 (Wischmeier and Smith 1978). Seasonal EI distributions were developed for 84 climate zones in the western States. The maximum storm 10-yr-frequency EI values were calculated as part of the project. In this analysis, for areas where winter precipitation is predominantly snowfall, the snowfall months were excluded from the EI development. Thus, in the CITY database, the winter months show zero percent EI.

In Hawaii, isoerodent maps of figure 2-5 were computed by the use of class-A weather stations to compute R and by relating these values to National Weather Service intensity-frequency data for Hawaii. EI distribution data were also calculated for select Hawaiian stations to use in the calculation of seasonally weighted K values (ch. 3) and C values (ch. 5).

If the soil and topography were exactly the same everywhere, average annual soil losses from plots maintained in continuous fallow would be in direct proportion to these erosion index values.

R Values for Flat Slopes

Although the R factor is assumed to be independent of slope in the structure of RUSLE, splash erosion is less on low slopes. On flat surfaces, raindrops tend to be more buffered by water ponded on the soil surface than on steep slopes. Higher rainfall intensities that are correlated with higher R factors also tend to increase the depth of ponded surface water, which in turn protects the soil from rainfall impact (Mutchler 1970). To account for this soil protection by a ponded water layer on low slopes under high rainfall rates, the R factor should be adjusted using a relationship having the form (modified from Mutchler and Murphree 1985)

$$R_c = f(I, S) = f(R, S) \quad [2\text{-}9]$$

where

R_c = rainfall erosivity adjustment factor,
f = function of ( ),
I = precipitation intensity,
S = slope steepness, and
R = RUSLE rainfall erosivity term.

To compute R_c assume that the 10-yr-frequency storm EI value provides an indication of storm intensity and therefore the amount of water ponded on the land surface. In this procedure, the 10-yr EI value of a CITY database is used with a runoff index (a constant CN = 78 was used) and Manning's equation to compute a flow depth ratio, y. This flow depth ratio is then used in the equation $R_c = \exp(-0.49 \cdot [y-1])$. Figure 2-6 is the result of such calculations for a variety of land slopes. For further discussion, refer to chapter 6.

EI DISTRIBUTION USED IN CALCULATION OF K FACTOR AND C FACTOR

To calculate the seasonal or average annual soil erodibility factor (K) and the seasonal or average annual cover-management factor (C), the distribution of EI is needed. In RUSLE, the EI distribution (as a percentage of the annual value) is used for twenty-four 15-d periods, corresponding with the 1st and 16th days of the month.

Figure 2-7 shows the 120 homogeneous climatic zones in the contiguous United States used in RUSLE. The EI distribution values for each of these zones have been determined and are available in the computer code. Table 2-1 shows the EI distributions for the 120 zones and 19 Hawaiian zones, as well as the equivalent EI distribution for the frozen soil area of the Northwestern Wheat and Range Region.

Most of the climatic zones in figure 2-7 also have a single station containing information on precipitation and temperature (by month), the frost-free period, and the annual R. For example, about 140 climate stations (including 19 in Hawaii) are in the computer files. A user of the computer files may want to enter additional climate data for a zone. In other instances, a user may have to enter a climate station into the program before making soil-loss estimates in that region. The climate zones of figure 2-7 represent uniform EI distributions rather than uniform precipitation data or temperature data or both. Thus, in the western United States, orographic trends may pose problems within many of the zones and the user may need to input the additional data to reflect the orographic differences.

Although 19 stations are included in the Hawaiian climatic data files, the tremendous variability in precipitation, R, and temperature are only partially included. Therefore, caution must be used when making soil-loss estimates with RUSLE in Hawaii.

EI DATA FOR 10-YR-FREQUENCY STORMS

In the P-factor calculation for contour farming (ch. 6), the 10-yr-frequency storm EI value is required. These 10-yr EI data are used to credit the effect of contour practices on the support practice value. The values were obtained from the data originally calculated for Agriculture Handbook No. 537 (Wischmeier and Smith 1978) involving 181 stations in the eastern United States and from about 1,000 stations used to develop the isoerodent values in the western United States. The maps of these isoerodent values are given in figures 2-9 to 2-12 for the eastern and western United States.

Site-specific data can be obtained by interpolation from these figures. In the RUSLE computer program (see ch. 7 for the subroutine CITY), these values are given for most stations or they can be obtained by interpolation using the figures.

R EQUIVALENT (R_{eq}) FOR CROPLAND IN THE NORTHWESTERN WHEAT AND RANGE REGION

In the dryfarmed cropland areas of the Northwestern Wheat and Range Region (Austin 1981) shown in figure 2-8, the effect of melting snow, rain on snow, and/or rain on thawing soil poses unique problems. Generally, measured soil-loss values in the regions devoted to winter wheat, spring wheat, spring barley, peas, and lentils are much greater than the value that might be expected from R values calculated with the conventional kinetic energy times maximum 30-min intensity (EI). Observations indicate that much of the soil loss occurs by rilling phenomena when the surface part of the soil profile thaws and snowmelt or rain occurs on the still partially frozen soil. To more accurately predict soil losses for this condition, an R_{eq} value has been calculated using the following procedures:

$$(R_{eq})_{wr} = \frac{A_{wr}}{K_{wr}\,(LS)_{wr}\,(SLR)_{wr}\,P_{wr}} \qquad [2\text{-}10]$$

where

$(R_{eq})_{wr}$ = equivalent R factor for winter rilling,
A_{wr} = soil loss over winter in rills alone (measured),
K_{wr} = rill soil erodibility for winter period (estimated),
$(LS)_{wr}$ = LS relationship,
$(SLR)_{wr}$ = soil loss ratio for rilling in winter period (estimated for field condition), and
P_{wr} = supporting practices factor.

The soil loss from rills (A_{wr}) was measured after the winter erosion season from strips on selected fields along a 45- to 50-mi transect across eastern Washington and northern Idaho for a period of 10 yr. This area was subsequently divided into four zones for presentation and interpretation. Similar soil-loss measurements were made in five counties in north-central Oregon for 5 yr (although data were not collected for each county every year). Soil-loss measurements in southeastern Idaho were made for 4 yr. Thus, the rill soil-loss measurements represent a potential of 10 data points.

The winter erodibility value might be obtained by use of the variable K procedure (ch. 3) and by use of the average value of K for the winter period.

However, in RUSLE, K_{av} (EI-weighted average annual K value) is used throughout the entire year; there is no provision for use of an average K value for a particular portion of the year. Therefore, for consistency, K_{av} was used to calculate $(R_{eq})_{wr}$.

The Northwestern Wheat and Range Region LS relationships in RUSLE (ch. 4) were developed from only the Palouse transect data (eastern Washington and northern Idaho). The following LS relationships were used for $(R_{eq})_{wr}$ calculation:

$$(LS)_{wr} = \left[\frac{\lambda}{72.6}\right]^{0.5} (10.8 \sin \theta + 0.03) \qquad s < 9\% \qquad [2\text{-}11]$$

$$(LS)_{wr} = \left[\frac{\lambda}{72.6}\right]^{0.5} \left[\frac{\sin \theta}{0.0896}\right]^{0.6} \qquad s \geq 9\% \qquad [2\text{-}12]$$

Values of $(LS)_{wr}$ were calculated for each segment of the measured slope based on the contributing area above the segment and the segment steepness.

The soil-loss ratio $(SLR)_{wr}$ was calculated from the following factors:

(1) The rotation was assigned a soil-moisture factor using (see ch. 5) ww/p = 0.88, ww/sf = 1.0, wr = 0.5, and ww/sb = 0.72.

(2) Surface residue effect was calculated from a residue effectiveness curve [exp (-0.05 · % cover)].

(3) Growing cover effect was obtained from [1 - fraction of land surface covered by canopy]. Growing cover was generally less than 10% and often less than 5%.

(4) Surface roughness effect was assigned values from 0.7 to 1.2 based on field observations. Most values used were about 1.1.

(5) Incorporated residue effect was obtained from [exp (-0.00045 · lb $acre^{-1}$ residue incorporated at a shallow depth)]. Shallow incorporated residue was assumed to be half of the residue incorporated less decomposition.

The soil-loss ratio $(SLR)_{wr}$ was then computed as the product of these five factors.

The winter support practices factor (P_{wr}) was assumed to be unity. Thus, $(R_{eq})_{wr}$ was calculated for each year for each zone or county by averaging all segment values.

The individual zone $(R_{eq})_{wr}$ was averaged over the years of record to obtain a zonal average value. The data points were reduced from 10 to 7 based on the number of segments and strips in a zone or county in a given year and on the number of years of data in a zone or county. The three points deleted were all from north-central Oregon. These average values were subsequently correlated against published annual precipitation for corresponding zones to obtain

$$(R_{eq})_{wr} = -110.3 + 10.78\ P \qquad r^2 = 0.98 \qquad [2\text{-}13]$$

where P = annual precipitation (in).

Adjustment for Interrill and Non-Winter Soil Loss

Measurements of the rill to interrill ratio soil loss in the Northwestern Wheat and Range Region vary greatly. For example, rill-erosion measurements near the Columbia Plateau Conservation Research Center near Pendleton, Oregon, indicate about a 95% rill soil loss. A rule of thumb based on the old Pullman Conservation Field Station (PCFS) plots near Pullman, Washington, was that 75% of the soil loss came from rill erosion. Recent measurements over a 4-yr period from continuous fallow plots at the PCFS indicate that 85-90% of the soil loss came from rill erosion. In other instances (and varying with treatments), the attempts to separate interrill losses from total soil loss have been essentially unsuccessful. Thus, a somewhat arbitrary ratio of 90% rill loss and 10% interrill soil loss was assumed to adjust the $(R_{eq})_{wr}$ to estimate the total winter equivalent R, $(R_{eq})_{wt}$.

Then

$$(R_{eq})_{wt} = (R_{eq})_{wr} \cdot \frac{100}{90} \qquad [2\text{-}14]$$

The nonwinter component of soil loss was estimated in two ways, each of which gives a ratio of roughly 5% of the annual R_{eq} occurring during the nonwinter periods. Thus, we estimate total annual soil loss as

$$R_{eq} = (R_{eq})_{wr} \cdot \frac{100}{90} \cdot \frac{100}{95} \qquad [2\text{-}15]$$

and finally

$$R_{eq} = -129.0 + 12.61P \qquad [2\text{-}16]$$

For lower precipitation areas of the Northwest Wheat and Range Region with a frozen soil erosion problem, the following relationship will provide a smooth transition from the R_{eq} to the non-R_{eq} zone:

$$R_{eq} = 1.602 \exp(0.2418\ P) \qquad 7.5 < P < 15.0 \qquad [2\text{-}17]$$

Equation 2-17 should be used for $P \leq 15.0$.

The P and R_{eq} maps for the cultivated areas farmed with winter wheat, spring wheat, spring barley, peas, or lentils in the Northwestern Wheat and Range Region are shown in figures 2-13 to 2-16. The small-grain areas include higher elevation forest and grazing land as well as the cultivated valleys and lower slopes. In general, winter wheat is not grown where P is greater than about 35 in. Thus, no R_{eq} values greater than 320 (P = 35.6 in) are plotted in figures 2-15 and 2-16.

It was necessary to distribute the R_{eq} throughout the year. The nonwinter component (5% of the total) was distributed uniformly from April 1 through September 30. The winter component (95% of the total) was distributed from October 1 through March 31. Based on historical soil-loss data from PCFS, the period of major erosivity was assigned to late January and early February. Erosivity then tapered gradually to October 1 and more steeply to March 31 (see Pullman, WA, CITY database for the R_{eq} distribution data).

RAINFALL EROSIVITY IN A COLD MOUNTAINOUS CLIMATE

Data analysis from the precipitation network in southwestern Idaho indicate major problems in assessing the erosivity index. The problems are not uniquely different from those in the Northwestern Wheat and Range Region (area of winter wheat, spring barley, peas, and lentils). RUSLE (and also its predecessor USLE) was designed to account for the effects of raindrop impact and subsequent overland flow on soil erosion (Cooley et al. 1988). In much of the western United States, precipitation occurring as snow should also be accounted for if representative EI estimates are to be produced.

Cooley et al. (1988) found that snowfall accounted for only a minor portion (4%) of EI based on annual precipitation values at low-elevation valley sites. However, at high elevation sites, snowfall accounted for most (up to 71%) of the annual precipitation. Therefore, it is important to use only the rainfall portion of annual precipitation when determining EI in areas where snowfall is significant, rather than using total annual precipitation.

Elevation was observed to have a relatively minor influence on summer (rain) EI values. Summer storms are mainly produced by air-mass thunderstorms and tend to be more random in location and smaller in areal extent than are frontal storms.

The consideration of all storms in estimating EI, rather than only storms that result in more than 0.5 in rainfall [per Wischmeier and Smith (1978) procedure], increased EI by 28-59% on the Reynolds Creek watershed. However, runoff and erosion data for evaluating the significance of these increases were not available.

Cooley et al. (1988) also tested several methods of computing average annual R involving 2-yr-frequency, 6-h-duration precipitation for comparison with long-term breakpoint-data R values (table 2-2). In mountain and range topography like that of southwestern Idaho, caution must be exercised in selecting storm values because snow events can affect the value. Cooley et al. (1988) observed that the storm value decreased by 5-34% when snowfall was eliminated from the annual data set. R decreased by 4-42% when snowfall was removed; that is, summer values were used instead of annual values.

SOUTHWESTERN AIR-MASS THUNDERSTORM

Precipitation gages operated by ARS in Arizona and New Mexico were used to compute EI data for areas dominated by air-mass thunderstorms. Of particular interest is the fact that EI during the summer period amounted to 85-93% of the annual total, which was 50-81 hundreds · ft· tonf · (acre · in · yr)$^{-1}$ (Renard and Simanton 1975).

In still other efforts, Simanton and Renard (1982) calculated the EI for a storm on the 57.7-sq-mi Walnut Gulch Experimental watershed in southeastern Arizona. Figure 2-17 shows the isohyetal values of precipitation determined for the 100 recording raingages for the event of July 22, 1964, and the corresponding isoerodent map. It should be noted that the isoerodent lines have little correlation with the isohyetal lines. An intense air-mass thunderstorm near the upper end of the area caused nearly 100 units of EI whereas only a short distance away (about 5 mi), the EI was less than 50% of the storm maximum.

Figure 2-18 illustrates the annual isohyetal map and the annual isoerodent (R) map, including the data of figure 2-17 plus the other storms occurring during the year. The highly variable rainfall illustrated in figures 2-17 and 2-18 is very typical of air-mass-thunderstorm country as shown on the isoerodent map. The 1.9 ratio of maximum to minimum annual precipitation and the 4.0 ratio of maximum to minimum R are normal occurrences.

The significance of these illustrations is that a single raingage and the EI calculations from it may be inadequate indicators of the soil loss at any specific point unless the precipitation record is collected at that site.

LIMITATIONS IN WINTER R FACTORS

Agriculture Handbook No. 537 suggests that the rainfall erosivity value (R) might be adjusted by multiplying the precipitation falling in the form of snow by 1.5 and then adding the product to EI, the kinetic energy times maximum 30-min intensity. This calculation has been used in the past at some locations, but we currently do not support this approach in RUSLE. The redistribution of snow by drifting, sublimation, and reduced sediment concentrations in snowmelt confuses the problem tremendously. But data are not presently available to support this approximation. Therefore, the developers of RUSLE recognized the weakness of ignoring the problem (except in the cropland areas of the Northwestern Wheat and Range Region where the R_{eq} data are being used).

ACKNOWLEDGMENT

The authors appreciate the assistance of Joe M. Sheridan, ARS, in Tifton, GA, who assisted in preparing portions of the data in this chapter.

Table 2-1.
EI as percentage of average annual value computed for geographic areas shown in figure 2-7[1,2]

EI number	Periods																							
	1	2	3	4	5	6	7	8	9	10	11	12	13	14	15	16	17	18	19	20	21	22	23	24
1	0.0	4.3	8.3	12.8	17.3	21.6	25.1	28.0	30.9	34.9	39.1	42.6	45.4	48.2	50.8	53.0	56.0	60.8	66.8	71.0	75.7	82.0	89.1	95.2
2	0.0	4.3	8.3	12.8	17.3	21.6	25.1	28.0	30.9	34.9	39.1	42.6	45.4	48.2	50.8	53.0	56.0	60.8	66.8	71.0	75.7	82.0	89.1	95.2
3	0.0	7.4	13.8	20.9	26.5	31.8	35.3	38.5	40.2	41.6	42.5	43.6	44.5	45.1	45.7	46.4	47.7	49.4	52.8	57.0	64.5	73.1	83.3	92.3
4	0.0	3.9	7.9	12.6	17.4	21.6	25.2	28.7	31.9	35.1	38.2	42.0	44.9	46.7	48.2	50.1	53.1	56.6	62.2	67.9	75.2	83.5	90.5	96.0
5	0.0	2.3	3.6	4.7	6.0	7.7	10.7	13.9	17.8	21.2	24.5	28.1	31.1	33.1	35.3	38.2	43.2	48.7	57.3	67.8	77.9	86.0	91.3	96.9
6	0.0	0.0	0.0	0.5	2.0	4.1	8.1	12.6	17.6	21.6	25.5	29.6	34.5	40.0	45.7	50.7	55.6	60.2	66.5	75.5	85.6	95.9	99.5	99.9
7	0.0	0.0	0.0	0.0	0.0	1.2	4.9	8.5	13.9	19.0	26.1	35.4	43.9	48.8	53.9	64.5	73.4	77.5	80.4	84.8	89.9	96.6	99.2	99.7
8	0.0	0.0	0.0	0.0	0.0	0.9	3.6	7.8	15.0	20.2	27.4	38.1	49.8	57.9	65.0	75.6	82.7	86.8	89.4	93.4	96.3	99.1	100.0	100.0
9	0.0	0.8	3.1	4.7	7.4	11.7	17.8	22.5	27.0	31.4	36.0	41.6	46.4	50.1	53.4	57.4	61.7	64.9	69.7	79.0	89.6	97.4	100.0	100.0
10	0.0	0.3	0.5	0.9	2.0	4.3	9.2	13.1	18.0	22.7	29.2	39.5	46.3	48.8	51.1	57.2	64.4	67.7	71.1	77.2	85.1	92.5	96.5	99.0
11	0.0	5.4	11.3	18.8	26.3	33.2	37.4	40.7	42.5	44.3	45.4	46.5	47.1	47.4	47.8	48.3	49.4	50.7	53.6	57.5	65.5	76.2	87.4	94.8
12	0.0	3.5	7.8	14.0	21.1	27.4	31.5	35.0	37.3	39.8	41.9	44.3	45.6	46.3	46.8	47.9	50.0	52.9	57.9	62.3	69.3	81.3	91.5	96.7
13	0.0	0.0	0.0	1.8	7.2	11.9	16.7	19.7	24.0	31.2	42.4	55.0	60.0	60.8	61.2	62.6	65.3	67.6	71.6	76.1	83.1	93.3	98.2	99.6
14	0.0	0.7	1.8	3.3	6.9	16.5	26.6	29.9	32.0	35.4	40.2	45.1	51.9	61.1	67.5	70.7	72.8	75.4	78.6	81.9	86.4	93.6	97.7	99.3
15	0.0	0.0	0.0	0.5	2.0	4.4	8.7	12.0	16.6	21.4	29.7	44.5	56.0	60.8	63.9	69.1	74.5	79.1	83.1	87.0	90.9	96.6	99.1	99.8
16	0.0	0.0	0.0	0.5	2.0	5.5	12.3	16.2	20.9	26.4	35.2	48.1	58.1	63.1	66.5	71.9	77.0	81.6	85.1	88.4	91.5	96.3	98.7	99.6
17	0.0	0.0	0.0	0.7	2.8	6.1	10.7	12.9	16.1	21.9	32.8	45.9	55.5	60.3	64.0	71.2	77.2	80.3	83.1	87.7	92.6	97.2	99.1	99.8
18	0.0	0.0	0.0	0.6	2.5	6.2	12.4	16.4	20.2	23.9	29.3	37.7	45.6	49.8	53.3	58.4	64.3	69.0	75.0	86.6	93.9	96.6	98.0	100.0
19	0.0	1.0	2.6	7.4	16.4	23.5	28.0	31.0	33.5	37.0	41.7	48.1	51.1	52.0	52.5	53.6	55.7	57.6	61.1	65.8	74.7	88.0	95.8	98.7
20	0.0	9.8	18.5	25.4	30.2	35.6	38.9	41.5	42.9	44.0	45.2	48.2	50.8	51.7	52.5	54.6	57.4	58.5	60.1	63.2	69.6	76.7	85.4	92.4
21	0.0	7.5	13.6	18.1	21.1	24.4	27.0	29.4	31.7	34.6	37.3	39.6	41.6	43.4	45.4	48.1	51.3	53.3	56.6	62.4	72.4	81.3	88.9	94.7
22	0.0	1.2	1.6	1.6	1.6	1.6	1.6	2.2	3.9	4.6	6.4	14.2	32.8	47.2	58.8	69.1	76.0	82.0	87.1	96.7	99.9	99.9	99.9	99.9
23	0.0	7.9	15.0	20.9	25.7	31.1	35.7	40.2	43.2	46.2	47.7	48.8	49.4	49.9	50.7	51.8	54.1	57.7	62.8	65.9	70.1	77.3	86.8	93.5
24	0.0	12.2	23.6	33.0	39.7	47.1	51.7	55.9	57.7	58.6	58.9	59.1	59.1	59.2	59.2	59.3	59.5	60.0	61.4	63.0	66.5	71.8	81.3	89.6
25	0.0	9.8	20.8	30.2	37.6	45.8	50.6	54.4	56.0	56.8	57.1	57.1	57.2	57.6	58.5	59.8	62.2	65.3	67.5	68.2	69.4	74.8	86.6	93.0

Table 2-1—Continued

EI number	Periods 1	2	3	4	5	6	7	8	9	10	11	12	13	14	15	16	17	18	19	20	21	22	23	24
26	0.0	2.0	5.4	9.8	15.6	21.5	24.7	26.6	27.4	28.0	28.7	29.8	32.5	36.6	44.9	55.4	65.7	72.6	77.8	84.4	89.5	93.9	96.5	98.4
27	0.0	0.0	0.0	1.0	4.0	5.9	8.0	11.1	13.0	14.0	14.6	15.3	17.0	23.2	39.1	60.0	76.3	86.1	89.7	90.4	90.9	93.1	96.6	99.1
28	0.0	0.0	0.0	0.0	0.2	0.5	1.5	3.3	7.2	11.9	17.7	21.4	27.0	37.1	51.4	62.3	70.6	78.8	84.6	90.6	94.4	97.9	99.3	100.0
29	0.0	0.6	0.7	0.7	0.7	1.5	3.9	6.0	10.5	17.9	28.8	36.6	43.8	51.5	59.3	68.0	74.8	80.3	84.3	88.8	92.7	98.0	99.8	99.9
30	0.0	0.0	0.0	0.0	0.0	0.2	0.8	2.8	7.9	14.2	24.7	35.6	45.4	52.2	58.7	68.5	77.6	84.5	88.9	93.7	96.2	97.6	98.3	99.6
31	0.0	0.0	0.0	0.0	0.0	0.2	1.0	3.5	9.9	15.7	26.4	47.2	61.4	65.9	69.0	77.2	86.0	91.6	94.8	98.7	100.0	100.0	100.0	100.0
32	0.0	0.1	0.1	0.1	0.1	0.6	2.2	4.3	9.0	14.2	23.3	34.6	46.3	54.2	61.7	72.9	82.5	89.6	93.7	98.2	99.7	99.9	99.9	99.9
33	0.0	0.0	0.0	0.0	0.0	0.6	2.3	4.2	8.8	16.1	30.0	46.9	57.9	62.8	66.2	72.1	79.1	85.9	91.1	97.0	98.9	98.9	98.9	98.9
34	0.0	0.0	0.0	0.0	0.0	1.8	7.3	10.7	15.5	22.0	29.9	35.9	42.0	48.5	56.9	67.0	76.9	85.8	91.2	95.7	97.8	99.6	100.0	100.0
35	0.0	0.0	0.0	0.0	0.0	2.5	10.2	15.9	22.2	27.9	34.7	43.9	51.9	56.9	61.3	67.3	73.9	80.1	85.1	89.6	93.2	98.2	99.8	99.8
36	0.0	0.0	0.0	0.0	0.0	0.9	3.4	6.7	12.7	18.5	26.6	36.3	46.0	53.5	60.2	68.3	75.8	82.6	88.3	96.3	99.3	99.9	100.0	100.0
37	0.0	0.0	0.0	0.0	0.0	0.0	0.0	1.0	3.9	9.1	19.1	26.7	36.3	47.9	61.4	75.1	84.5	92.3	96.0	99.1	100.0	100.0	100.0	100.0
38	0.0	0.0	0.0	1.1	4.3	7.2	11.0	13.9	17.9	22.3	30.3	43.1	55.1	61.3	65.7	72.1	77.9	82.6	86.3	90.3	93.8	98.4	100.0	100.0
39	0.0	0.0	0.0	0.0	0.0	1.6	6.5	11.0	17.8	24.7	33.1	42.8	50.3	54.9	59.7	68.9	78.1	83.6	87.5	93.0	96.5	99.2	100.0	100.0
40	0.0	0.0	0.0	0.0	0.0	1.5	6.2	10.1	16.3	23.3	32.5	42.2	50.1	55.6	60.5	67.5	74.3	79.4	84.1	91.1	95.8	99.1	100.0	100.0
41	0.0	0.1	0.2	0.2	0.2	0.2	0.2	0.4	1.1	6.8	22.9	40.1	54.9	63.8	70.7	81.5	89.8	96.3	98.7	99.2	99.3	99.4	99.4	99.7
42	0.0	0.0	0.0	0.0	0.0	0.0	0.0	0.2	0.9	5.2	17.3	33.8	53.2	66.5	75.9	87.6	93.7	97.5	99.0	99.7	100.0	100.0	100.0	100.0
43	0.0	0.0	0.0	0.0	0.0	0.0	0.0	0.1	0.4	2.7	9.5	21.9	42.7	58.6	71.1	84.6	91.9	97.1	99.0	99.8	100.0	100.0	100.0	100.0
44	0.0	1.7	2.3	2.4	2.4	2.4	2.4	2.7	3.5	7.6	18.5	34.3	52.5	64.0	72.3	83.3	90.0	95.1	97.3	98.5	98.9	98.9	98.9	99.2
45	0.0	0.2	0.2	0.3	0.3	0.4	0.6	0.8	1.4	3.7	10.2	22.6	41.8	54.0	64.5	78.7	88.4	96.0	98.7	99.4	99.7	99.7	99.8	99.9
46	0.0	0.0	0.0	0.0	0.0	0.0	0.0	0.6	2.6	7.5	19.6	32.9	48.9	63.0	73.5	83.3	89.5	95.6	98.3	99.6	100.0	100.0	100.0	100.0
47	0.0	0.0	0.0	0.0	0.0	0.0	0.0	0.4	1.6	5.8	17.0	33.0	52.5	66.4	75.7	85.5	91.3	96.5	98.8	100.0	100.0	100.0	100.0	100.0
48	0.0	0.0	0.0	0.0	0.0	0.0	0.0	0.0	0.0	2.0	8.1	15.4	27.8	40.7	52.6	61.1	69.3	82.6	92.0	98.0	100.0	100.0	100.0	100.0
49	0.0	0.0	0.0	0.0	0.0	0.0	0.0	0.7	2.7	8.3	20.0	27.5	35.6	44.6	46.0	70.2	81.3	89.2	93.6	98.5	100.0	100.0	100.0	100.0
50	0.0	0.0	0.0	0.0	0.0	0.1	0.4	2.4	8.2	13.7	23.8	38.8	55.1	66.1	73.6	81.8	87.7	93.8	97.0	99.4	100.0	100.0	100.0	100.0

Table 2-1—Continued

EI number	Periods 1	2	3	4	5	6	7	8	9	10	11	12	13	14	15	16	17	18	19	20	21	22	23	24
51	0.0	0.0	0.0	0.0	0.0	0.3	1.0	3.1	8.7	18.8	35.8	49.6	60.4	70.2	77.0	84.0	88.8	93.8	96.6	99.1	100.0	100.0	100.0	100.0
52	0.0	0.0	0.0	0.0	0.0	0.0	0.0	0.6	2.5	6.8	17.5	29.8	46.1	60.5	72.7	86.0	92.8	96.8	98.4	99.7	100.0	100.0	100.0	100.0
53	0.0	0.0	0.0	0.0	0.0	0.0	0.0	0.8	3.0	9.5	24.2	35.3	48.0	63.1	76.1	87.7	93.5	97.2	98.6	99.5	99.8	99.9	100.0	100.0
54	0.0	0.0	0.0	0.0	0.0	0.2	0.7	2.4	7.2	14.7	27.2	37.2	47.3	58.8	67.6	74.0	79.2	86.7	92.6	97.9	99.8	99.9	100.0	100.0
55	0.0	0.0	0.0	0.0	0.0	0.0	0.0	1.3	5.4	13.3	25.5	31.6	38.8	52.5	66.8	75.5	81.2	87.9	92.8	98.3	100.0	100.0	100.0	100.0
56	0.0	0.0	0.0	0.0	0.0	0.0	0.0	1.3	5.1	11.4	22.3	29.5	38.5	51.1	65.2	77.8	85.6	91.7	95.0	98.7	100.0	100.0	100.0	100.0
57	0.0	0.0	0.0	0.0	0.0	0.0	0.1	1.0	3.5	9.2	21.5	31.0	43.5	60.4	75.1	86.1	91.6	96.2	98.1	99.4	99.9	99.9	100.0	100.0
58	0.0	0.0	0.0	0.0	0.0	0.2	0.9	2.9	8.0	13.2	21.0	29.1	38.0	45.9	54.5	65.4	74.8	82.1	87.5	95.4	98.8	99.7	100.0	100.0
59	0.0	0.0	0.0	0.0	0.0	0.0	0.0	2.2	8.9	15.6	24.2	31.1	38.3	46.0	54.9	64.2	73.2	81.9	88.5	95.7	98.6	99.4	99.7	99.7
60	0.0	0.0	0.0	0.0	0.0	0.0	0.0	0.4	1.5	4.0	9.5	13.3	20.5	33.6	52.8	66.5	76.7	88.1	94.2	98.6	100.0	100.0	100.0	100.0
61	0.0	0.0	0.0	0.0	0.0	0.0	0.0	1.3	5.0	8.5	15.5	29.8	41.8	46.0	49.2	56.0	65.1	71.6	78.6	91.1	97.3	99.3	100.0	100.0
62	0.0	0.0	0.0	0.1	0.3	0.8	2.1	3.6	6.5	9.7	13.7	16.5	20.8	27.3	40.1	56.9	72.6	83.4	89.4	95.5	98.1	99.6	100.0	100.0
63	0.0	0.0	0.0	0.0	0.0	0.0	0.0	0.9	3.7	7.8	13.3	15.8	19.9	29.0	46.8	64.7	78.3	88.8	93.9	98.5	100.0	100.0	100.0	100.0
64	0.0	0.0	0.0	0.7	2.8	7.4	12.4	14.4	15.6	17.3	19.4	21.0	24.4	32.3	48.0	61.4	72.1	81.9	87.0	90.1	92.4	98.1	100.0	100.0
65	0.0	3.6	7.0	9.6	11.4	13.0	14.4	16.3	17.7	18.4	19.3	20.5	23.6	32.0	50.0	66.2	77.2	85.4	88.8	90.4	91.3	92.7	94.8	97.0
66	0.0	0.0	0.0	0.0	0.0	0.1	0.5	1.1	2.2	3.6	6.0	7.6	11.1	19.8	38.9	59.7	74.4	83.2	88.1	94.6	97.7	99.4	100.0	100.0
67	0.0	0.0	0.0	0.0	0.0	0.1	0.4	0.9	1.6	1.9	2.4	5.0	12.1	24.8	48.3	73.6	86.5	92.0	94.3	96.6	97.9	99.5	100.0	100.0
68	0.0	2.3	4.5	7.8	10.4	12.0	13.3	16.3	17.7	18.1	18.2	18.3	18.4	19.9	24.5	35.0	54.4	69.4	78.6	85.7	89.2	91.9	93.9	97.0
69	0.0	2.0	3.7	5.7	7.8	10.5	12.4	13.7	14.3	14.7	15.1	15.7	17.1	22.7	36.7	50.4	63.6	75.0	81.8	87.8	90.8	93.2	94.9	97.5
70	0.0	0.5	0.7	1.0	1.3	1.7	2.2	2.8	3.4	3.9	4.7	5.4	7.4	15.7	36.5	55.8	70.3	80.9	86.4	90.9	93.4	96.4	98.1	99.4
71	0.0	0.7	1.2	1.6	2.1	2.8	3.3	3.6	4.0	4.5	5.6	6.5	9.1	18.5	40.6	59.7	74.0	86.3	91.7	94.7	96.0	96.7	97.3	98.8
72	0.0	0.0	0.0	0.0	0.0	0.0	0.1	0.2	0.7	0.8	1.3	3.5	9.9	24.7	51.4	71.5	83.6	93.8	97.7	99.2	99.8	99.9	99.9	100.0
73	0.0	0.0	0.1	0.1	0.2	0.2	0.3	0.6	1.3	4.1	11.5	18.1	28.3	40.2	54.1	67.0	77.2	87.7	93.3	97.5	99.1	99.6	99.8	100.0
74	0.0	0.0	0.0	0.0	0.0	0.1	0.2	0.5	1.2	2.7	6.4	10.2	18.4	31.0	50.7	68.7	81.2	91.6	96.1	98.4	99.2	99.8	100.0	100.0
75	0.0	0.1	0.1	0.1	0.2	0.5	1.3	1.9	3.0	4.1	6.6	10.0	17.6	28.3	44.7	59.4	71.6	83.9	90.3	94.7	96.7	98.8	99.6	99.9

Table 2-1—Continued

EI number	Periods																							
	1	2	3	4	5	6	7	8	9	10	11	12	13	14	15	16	17	18	19	20	21	22	23	24
76	0.0	0.0	0.0	0.0	0.0	0.1	0.2	0.6	1.3	2.0	3.5	4.9	8.4	17.4	37.3	57.5	72.9	83.7	89.5	95.8	98.4	99.6	100.0	100.0
77	0.0	0.2	0.3	0.3	0.4	0.8	1.5	2.0	2.8	3.9	5.9	7.2	10.3	21.5	46.5	66.3	78.3	86.5	90.8	96.0	98.2	99.1	99.5	99.8
78	0.0	0.0	0.0	0.0	0.0	0.0	0.2	0.5	1.6	3.8	8.9	13.2	21.8	35.8	56.6	75.4	86.0	92.9	95.9	98.2	99.2	99.8	100.0	100.0
79	0.0	0.0	0.0	0.0	0.0	0.2	0.7	1.3	2.7	5.8	12.7	18.8	28.8	41.6	58.4	75.7	86.5	94.2	97.3	98.9	99.5	99.9	100.0	100.0
80	0.0	0.6	1.2	1.6	2.1	2.5	3.3	4.5	6.9	10.1	15.5	19.7	26.6	36.4	51.7	67.5	79.4	88.8	93.2	96.1	97.3	98.2	98.7	99.3
81	0.0	0.1	0.1	0.2	0.4	0.5	0.8	0.9	1.5	3.9	9.9	12.8	18.2	30.7	54.1	77.1	89.0	94.9	97.2	98.7	99.3	99.6	99.7	99.9
82	0.0	0.0	0.1	0.1	0.2	0.2	0.5	1.2	3.1	6.7	14.4	20.1	29.8	44.5	64.2	83.1	92.2	96.4	98.1	99.3	99.7	99.8	99.8	99.9
83	0.0	0.0	0.1	0.1	0.1	0.3	0.9	1.6	3.5	8.3	19.4	30.0	44.0	59.2	72.4	84.6	91.2	96.5	98.6	99.5	99.8	99.9	100.0	100.0
84	0.0	0.0	0.1	0.1	0.2	0.3	0.6	1.7	4.9	9.9	19.5	27.2	38.3	52.8	68.8	83.9	91.6	96.4	98.2	99.2	99.6	99.8	99.8	99.9
85	0.0	0.0	0.0	0.0	0.0	0.0	1.0	2.0	3.0	6.0	11.0	23.0	36.0	49.0	63.0	77.0	90.0	95.0	98.0	99.0	100.0	100.0	100.0	100.0
86	0.0	0.0	0.0	0.0	0.0	0.0	1.0	2.0	3.0	6.0	11.0	23.0	36.0	49.0	63.0	77.0	90.0	95.0	98.0	99.0	100.0	100.0	100.0	100.0
87	0.0	0.0	0.0	0.0	1.0	1.0	2.0	3.0	6.0	10.0	17.0	29.0	43.0	55.0	67.0	77.0	85.0	91.0	96.0	98.0	99.0	100.0	100.0	100.0
88	0.0	0.0	0.0	0.0	1.0	1.0	2.0	3.0	6.0	13.0	23.0	37.0	51.0	61.0	69.0	78.0	85.0	91.0	94.0	96.0	98.0	99.0	99.0	100.0
89	0.0	0.0	1.0	1.0	2.0	3.0	4.0	7.0	12.0	18.0	27.0	38.0	48.0	55.0	62.0	69.0	76.0	83.0	90.0	94.0	97.0	98.0	99.0	100.0
90	0.0	1.0	2.0	3.0	4.0	6.0	8.0	13.0	21.0	29.0	37.0	46.0	54.0	60.0	65.0	69.0	74.0	81.0	87.0	92.0	95.0	97.0	98.0	99.0
91	0.0	0.0	0.0	0.0	1.0	1.0	1.0	2.0	6.0	16.0	29.0	39.0	46.0	53.0	60.0	67.0	74.0	81.0	88.0	95.0	99.0	99.0	100.0	100.0
92	0.0	0.0	0.0	0.0	1.0	1.0	1.0	2.0	6.0	16.0	29.0	39.0	46.0	53.0	60.0	67.0	74.0	81.0	88.0	95.0	99.0	99.0	100.0	100.0
93	0.0	1.0	1.0	2.0	3.0	4.0	6.0	8.0	13.0	25.0	40.0	49.0	56.0	62.0	67.0	72.0	76.0	80.0	85.0	91.0	97.0	98.0	99.0	99.0
94	0.0	1.0	2.0	4.0	6.0	8.0	10.0	15.0	21.0	29.0	38.0	47.0	53.0	57.0	61.0	65.0	70.0	76.0	83.0	88.0	91.0	94.0	96.0	98.0
95	0.0	1.0	3.0	5.0	7.0	9.0	11.0	14.0	18.0	27.0	35.0	41.0	46.0	51.0	57.0	62.0	68.0	73.0	79.0	84.0	89.0	93.0	96.0	98.0
96	0.0	2.0	4.0	6.0	9.0	12.0	17.0	23.0	30.0	37.0	43.0	49.0	54.0	58.0	62.0	66.0	70.0	74.0	78.0	82.0	86.0	90.0	94.0	97.0
97	0.0	1.0	3.0	5.0	7.0	10.0	14.0	20.0	28.0	37.0	48.0	56.0	61.0	64.0	68.0	72.0	77.0	81.0	86.0	89.0	92.0	95.0	98.0	99.0
98	0.0	1.0	2.0	4.0	6.0	8.0	10.0	13.0	19.0	26.0	34.0	42.0	50.0	58.0	63.0	68.0	74.0	79.0	84.0	89.0	93.0	95.0	97.0	99.0
99	0.0	0.0	0.0	1.0	1.0	2.0	3.0	5.0	7.0	12.0	19.0	33.0	48.0	57.0	65.0	72.0	82.0	88.0	93.0	96.0	98.0	99.0	100.0	100.0
100	0.0	0.0	0.0	0.0	1.0	1.0	2.0	3.0	5.0	9.0	15.0	27.0	38.0	50.0	62.0	74.0	84.0	91.0	95.0	97.0	98.0	99.0	99.0	100.0

Table 2-1—Continued

EI number	Periods																							
	1	2	3	4	5	6	7	8	9	10	11	12	13	14	15	16	17	18	19	20	21	22	23	24
101	0.0	0.0	0.0	1.0	2.0	3.0	4.0	6.0	9.0	14.0	20.0	28.0	39.0	52.0	63.0	72.0	80.0	87.0	91.0	94.0	97.0	98.0	99.0	100.0
102	0.0	0.0	1.0	2.0	3.0	4.0	6.0	8.0	11.0	15.0	22.0	31.0	40.0	49.0	59.0	69.0	78.0	85.0	91.0	94.0	96.0	98.0	99.0	100.0
103	0.0	1.0	2.0	3.0	4.0	6.0	8.0	10.0	14.0	18.0	25.0	34.0	45.0	56.0	64.0	72.0	79.0	84.0	89.0	92.0	95.0	97.0	98.0	99.0
104	0.0	2.0	3.0	5.0	7.0	10.0	13.0	16.0	19.0	23.0	27.0	34.0	44.0	54.0	63.0	72.0	80.0	85.0	89.0	91.0	93.0	95.0	96.0	98.0
105	0.0	1.0	3.0	6.0	9.0	12.0	16.0	21.0	26.0	31.0	37.0	43.0	50.0	57.0	64.0	71.0	77.0	81.0	85.0	88.0	91.0	93.0	95.0	97.0
106	0.0	3.0	6.0	9.0	13.0	17.0	21.0	27.0	33.0	38.0	44.0	49.0	55.0	61.0	67.0	71.0	75.0	78.0	81.0	84.0	86.0	90.0	94.0	97.0
107	0.0	3.0	5.0	7.0	10.0	14.0	18.0	23.0	27.0	31.0	35.0	39.0	45.0	53.0	60.0	67.0	74.0	80.0	84.0	86.0	88.0	90.0	93.0	95.0
108	0.0	3.0	6.0	9.0	12.0	16.0	20.0	24.0	28.0	33.0	38.0	43.0	50.0	59.0	69.0	75.0	80.0	84.0	87.0	90.0	92.0	94.0	96.0	98.0
109	0.0	3.0	6.0	10.0	13.0	16.0	19.0	23.0	26.0	29.0	33.0	39.0	47.0	58.0	68.0	75.0	80.0	83.0	86.0	88.0	90.0	92.0	95.0	97.0
110	0.0	1.0	3.0	5.0	7.0	9.0	12.0	15.0	18.0	21.0	25.0	29.0	36.0	45.0	56.0	68.0	77.0	83.0	88.0	91.0	93.0	95.0	97.0	99.0
111	0.0	1.0	2.0	3.0	4.0	5.0	6.0	8.0	11.0	15.0	20.0	28.0	41.0	54.0	65.0	74.0	82.0	87.0	92.0	94.0	96.0	97.0	98.0	99.0
112	0.0	0.0	0.0	1.0	2.0	3.0	4.0	5.0	7.0	12.0	17.0	24.0	33.0	42.0	55.0	67.0	76.0	83.0	89.0	92.0	94.0	96.0	98.0	99.0
113	0.0	1.0	2.0	3.0	4.0	5.0	6.0	8.0	10.0	13.0	17.0	22.0	31.0	42.0	52.0	60.0	68.0	75.0	80.0	85.0	89.0	92.0	96.0	98.0
114	0.0	1.0	2.0	4.0	6.0	8.0	11.0	13.0	15.0	18.0	21.0	26.0	32.0	38.0	46.0	55.0	64.0	71.0	77.0	81.0	85.0	89.0	93.0	97.0
115	0.0	1.0	2.0	3.0	4.0	5.0	6.0	8.0	10.0	14.0	19.0	26.0	34.0	45.0	56.0	66.0	76.0	82.0	86.0	90.0	93.0	95.0	97.0	99.0
116	0.0	1.0	3.0	5.0	7.0	9.0	12.0	15.0	18.0	21.0	25.0	29.0	36.0	45.0	56.0	68.0	77.0	83.0	88.0	91.0	93.0	95.0	97.0	99.0
117	0.0	1.0	2.0	3.0	4.0	5.0	7.0	9.0	11.0	14.0	17.0	22.0	31.0	42.0	54.0	65.0	74.0	83.0	89.0	92.0	95.0	97.0	98.0	99.0
118	0.0	1.0	2.0	3.0	5.0	7.0	10.0	14.0	18.0	22.0	27.0	32.0	37.0	46.0	58.0	69.0	80.0	89.0	93.0	94.0	95.0	96.0	97.0	97.0
119	0.0	2.0	4.0	6.0	8.0	12.0	16.0	20.0	25.0	30.0	35.0	41.0	47.0	56.0	67.0	75.0	81.0	85.0	87.0	89.0	91.0	93.0	95.0	97.0
120	0.0	1.0	2.0	4.0	6.0	7.0	9.0	12.0	15.0	18.0	23.0	31.0	40.0	48.0	57.0	63.0	72.0	78.0	88.0	92.0	96.0	97.0	98.0	99.0
[2]121	0.0	8.0	16.0	25.0	33.0	41.0	46.0	50.0	53.0	54.0	55.0	56.0	56.5	57.0	57.8	58.0	58.8	60.0	61.0	63.0	66.5	72.0	80.0	90.0
122	0.0	7.0	14.0	20.0	25.5	33.5	38.0	43.0	46.0	50.0	52.5	54.5	56.0	58.0	59.0	60.0	61.5	63.0	65.0	68.0	72.0	79.0	86.0	93.0
123	0.0	4.0	8.0	12.0	17.0	23.0	29.0	34.0	38.0	44.0	49.0	53.0	56.0	59.0	62.0	65.0	69.0	72.0	75.0	79.0	83.0	88.0	93.0	96.0
124	0.0	4.0	9.0	15.0	23.0	29.0	34.0	40.0	44.0	48.0	50.0	51.0	52.0	53.0	55.0	57.0	60.0	62.0	64.0	67.0	72.0	80.0	88.0	95.0
125	0.0	7.0	12.0	17.0	24.0	30.0	39.0	45.0	50.0	53.0	55.0	56.0	57.0	58.0	59.0	61.0	62.0	63.0	64.0	66.0	70.0	77.0	84.0	92.0

Table 2-1—Continued

EI number	Periods 1	2	3	4	5	6	7	8	9	10	11	12	13	14	15	16	17	18	19	20	21	22	23	24
126	0.0	9.0	16.0	23.0	30.0	37.0	43.0	47.0	50.0	52.0	54.0	55.0	56.0	57.0	58.0	59.0	60.0	62.0	64.0	67.0	71.0	77.0	86.0	93.0
127	0.0	8.0	15.0	22.0	28.0	33.0	38.0	42.0	46.0	50.0	52.0	53.0	53.0	53.0	53.0	54.0	55.0	57.0	59.0	63.0	68.0	75.0	83.0	92.0
128	0.0	8.0	15.0	22.0	29.0	34.0	40.0	45.0	48.0	51.0	54.0	57.0	59.0	62.0	63.0	64.0	65.0	66.0	67.0	69.0	72.0	76.0	83.0	91.0
129	0.0	9.0	16.0	22.0	27.0	32.0	37.0	41.0	45.0	48.0	51.0	53.0	55.0	56.0	57.0	57.0	58.0	59.0	61.0	64.0	68.0	73.0	79.0	89.0
130	0.0	10.0	20.0	28.0	35.0	41.0	46.0	49.0	51.0	53.0	55.0	56.0	56.0	57.0	58.0	59.0	60.0	61.0	62.0	65.0	69.0	74.0	81.0	90.0
131	0.0	8.0	15.0	22.0	28.0	33.0	38.0	41.0	44.0	47.0	49.0	51.0	53.0	55.0	56.0	58.0	59.0	60.0	63.0	65.0	69.0	75.0	84.0	92.0
132	0.0	10.0	18.0	25.0	29.0	33.0	36.0	39.0	41.0	42.0	44.0	45.0	46.0	47.0	48.0	49.0	51.0	53.0	56.0	59.0	64.0	70.0	80.0	90.0
133	0.0	8.0	16.0	24.0	32.0	40.0	46.0	51.0	54.0	56.0	57.0	58.0	58.0	59.0	59.0	60.0	60.0	61.0	62.0	64.0	68.0	74.0	83.0	91.0
134	0.0	12.0	22.0	31.0	39.0	45.0	49.0	52.0	54.0	55.0	56.0	56.0	56.0	56.0	57.0	57.0	57.0	57.0	58.0	59.0	62.0	68.0	77.0	88.0
135	0.0	7.0	15.0	22.0	30.0	37.0	43.0	49.0	53.0	55.0	57.0	58.0	59.0	60.0	61.0	62.0	63.0	65.0	67.0	70.0	74.0	79.0	85.0	92.0
136	0.0	11.0	21.0	29.0	37.0	44.0	50.0	55.0	57.0	59.0	60.0	60.0	60.0	60.0	61.0	61.0	61.0	62.0	63.0	64.0	67.0	71.0	78.0	89.0
137	0.0	10.0	18.0	25.0	30.0	39.0	46.0	51.0	54.0	57.0	58.0	59.0	59.0	60.0	60.0	60.0	61.0	62.0	63.0	64.0	67.0	72.0	80.0	90.0
138	0.0	11.0	22.0	31.0	39.0	46.0	52.0	56.0	58.0	59.0	60.0	61.0	61.0	61.0	61.0	62.0	62.0	62.0	63.0	64.0	66.0	71.0	78.0	89.0
139	0.0	8.0	14.0	20.0	25.0	32.0	37.0	42.0	47.0	50.0	53.0	55.0	56.0	58.0	59.0	61.0	63.0	64.0	66.0	68.0	71.0	76.0	85.0	93.0
[3]140	0.0	13.0	28.0	43.0	56.0	65.0	69.0	69.4	69.7	70.1	70.4	70.8	71.1	71.5	71.9	72.2	72.6	73.0	73.3	73.6	74.0	76.0	81.0	89.0

[1] Periods are 15-d beginning January 1.
[2] Zones 121-139 are for stations in Hawaii.
[3] Zone 140 is the R_{eq} distribution for Pullman, WA.

Table 2-2.
Average annual and summer EI and 2-yr-frequency 6-h-duration precipitation computed from actual data in southwestern Idaho. Data for EI are compared with data in methods of Wischmeier (1974), Simanton and Renard (1982), Cooley (1980), and Cooley et al. (1988).

	R (hundreds ft · tonf · acre^{-1} · yr^{-1})											
	Precipitation 2-yr 6-h storm[2] (inches)		Observed EI		Wischmeier (1974)[3] $27.38P^{2.17}$		Simanton and Renard (1982) $27.38P^{1.62}$		Cooley (1980)[4] $13.00P^{2.15}$		Cooley et al. (1988) $22.17P^{2.56}$	
Site[1]	Summer	Annual	Summer	Annual	Summer	Annual	Summer	Annual	Summer	Annual	Summer	Annual
057	0.71	0.75	10.5	10.9	12.6	14.3	15.6	17.0	6.2	6.9	9.2	10.6
127	.75	.83	9.5	11.3	14.3	17.7	17	20	6.9	8.6	10.6	13.8
116	.79	.91	10	14.6	16	21.7	18.5	23.2	7.8	10.5	12.1	17.4
155	.83	1.06	16	31	17.7	30.9	20	30.1	8.6	14.8	13.8	36.9
176	.83	1.22	14.2	45.3	17.7	41.8	20	37.7	8.6	19.9	13.8	36.9
163	.91	1.38	17.3	59.3	21.7	54.6	23.2	45.8	10.5	25.9	17.4	50.6

[1] Site elevation: 057 is 3,885; 127 is 5,410; 116 is 4,770; 155 is 5,410; 176 is 6,802, and 163 is 7,100 ft above m.s.l.
[2] Determined from actual gage data. NOAA Atlas 2 (Miller et al. 1973) would not permit defining the orographic results shown.
[3] Wischmeier (1974) and Ateshian (1974) agree within about 2%.
[4] Includes precipitation during winter periods in the form of snow, a questionable computation according to Cooley et al. (1988).

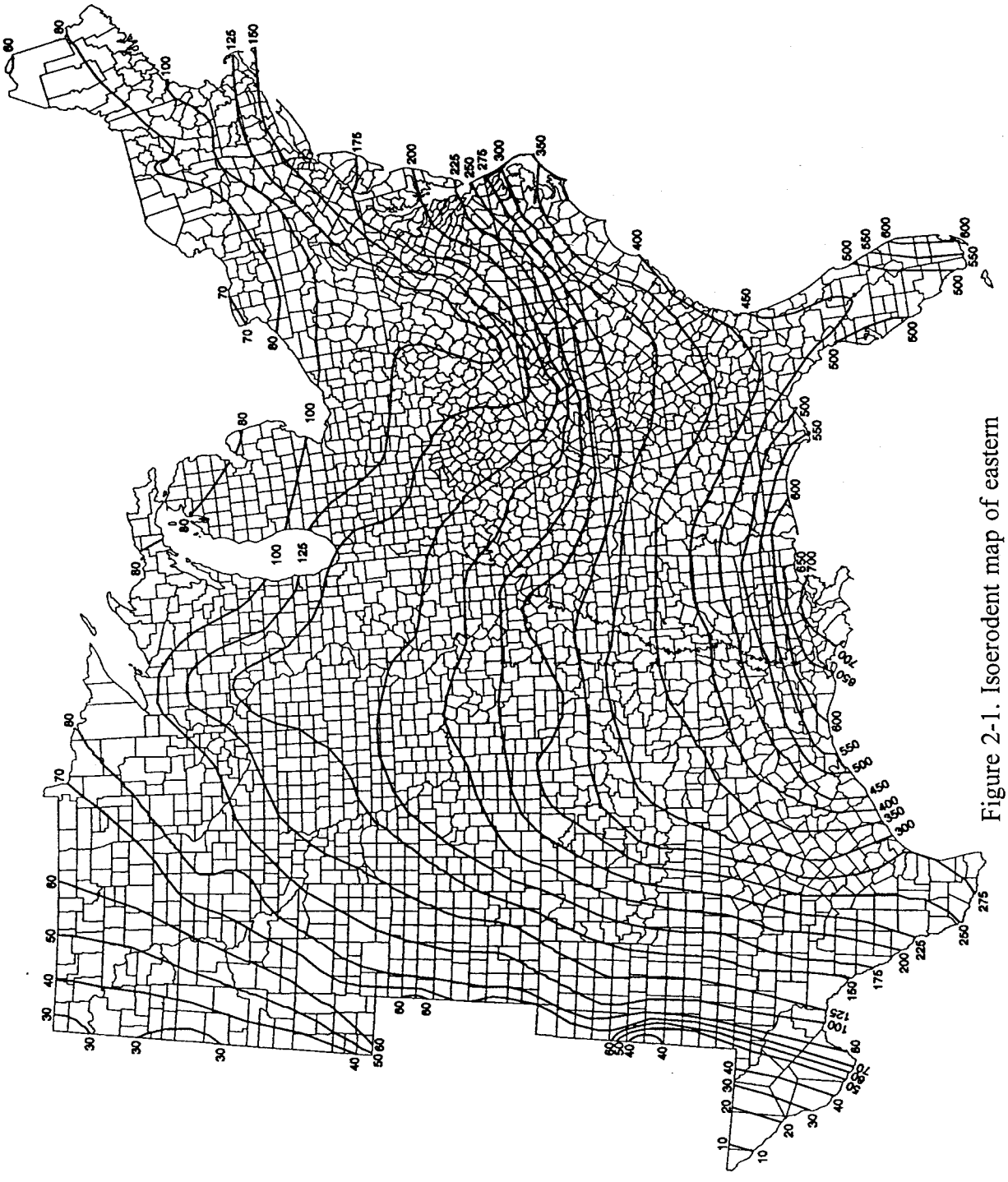

Figure 2-1. Isoerodent map of eastern United States. Units are hundreds ft·tonf·in(ac·h·yr)$^{-1}$.

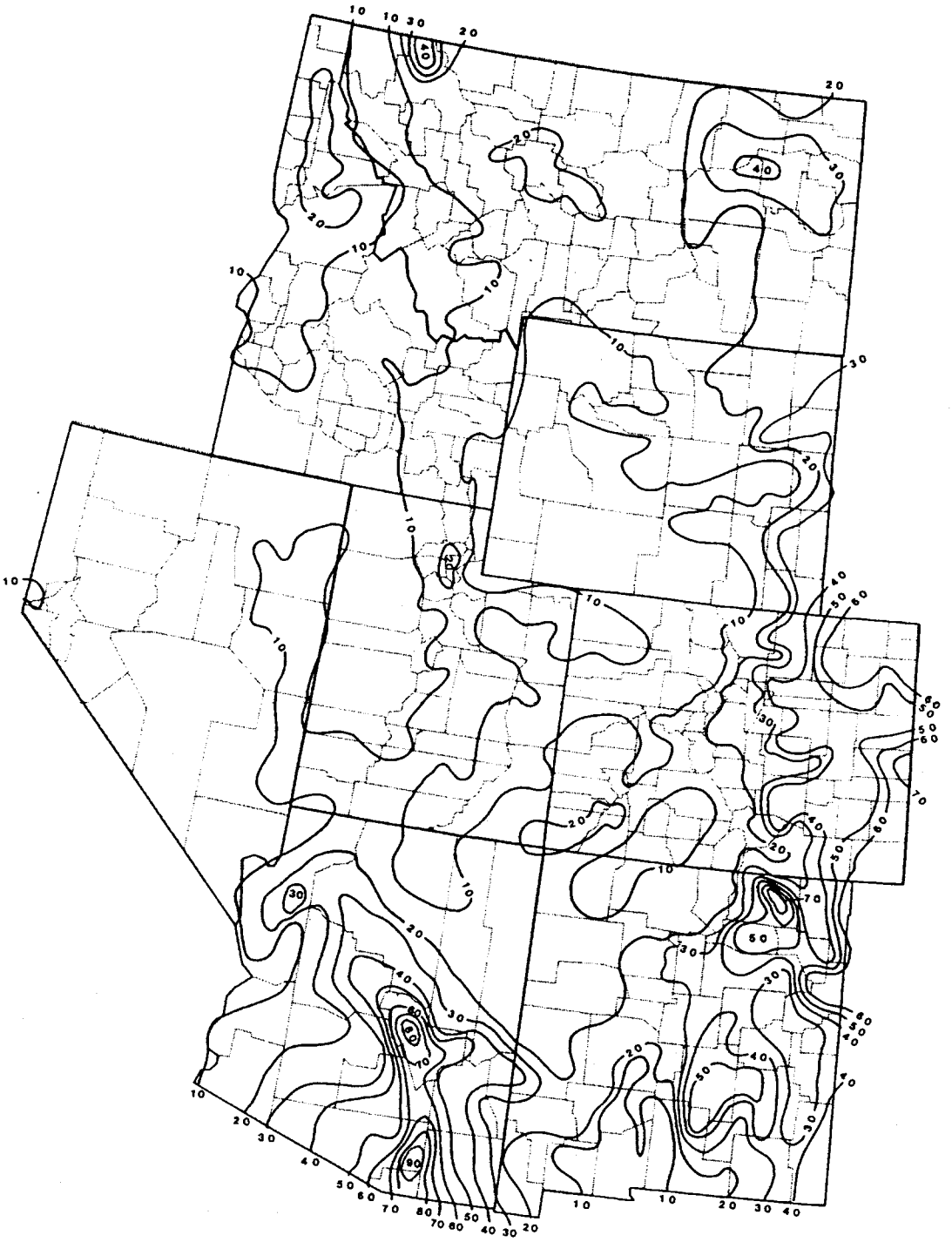

Figure 2-2. Isoerodent map of western United States. Units are hundreds ft·tonf·in(ac·h·yr)$^{-1}$.

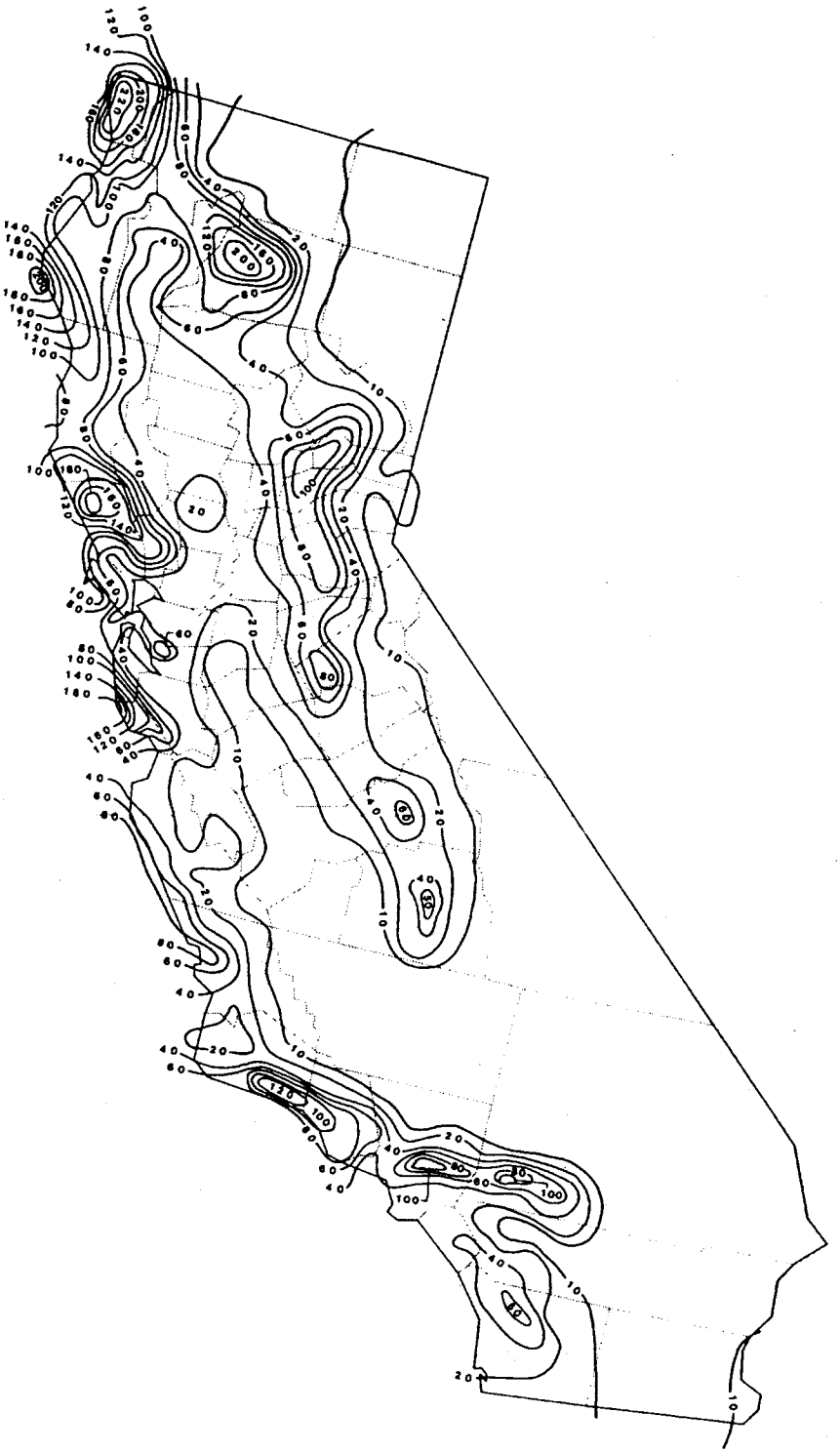

Figure 2-3. Isoerodent map of California. Units are hundreds ft·tonf·in(ac·h·yr)$^{-1}$.

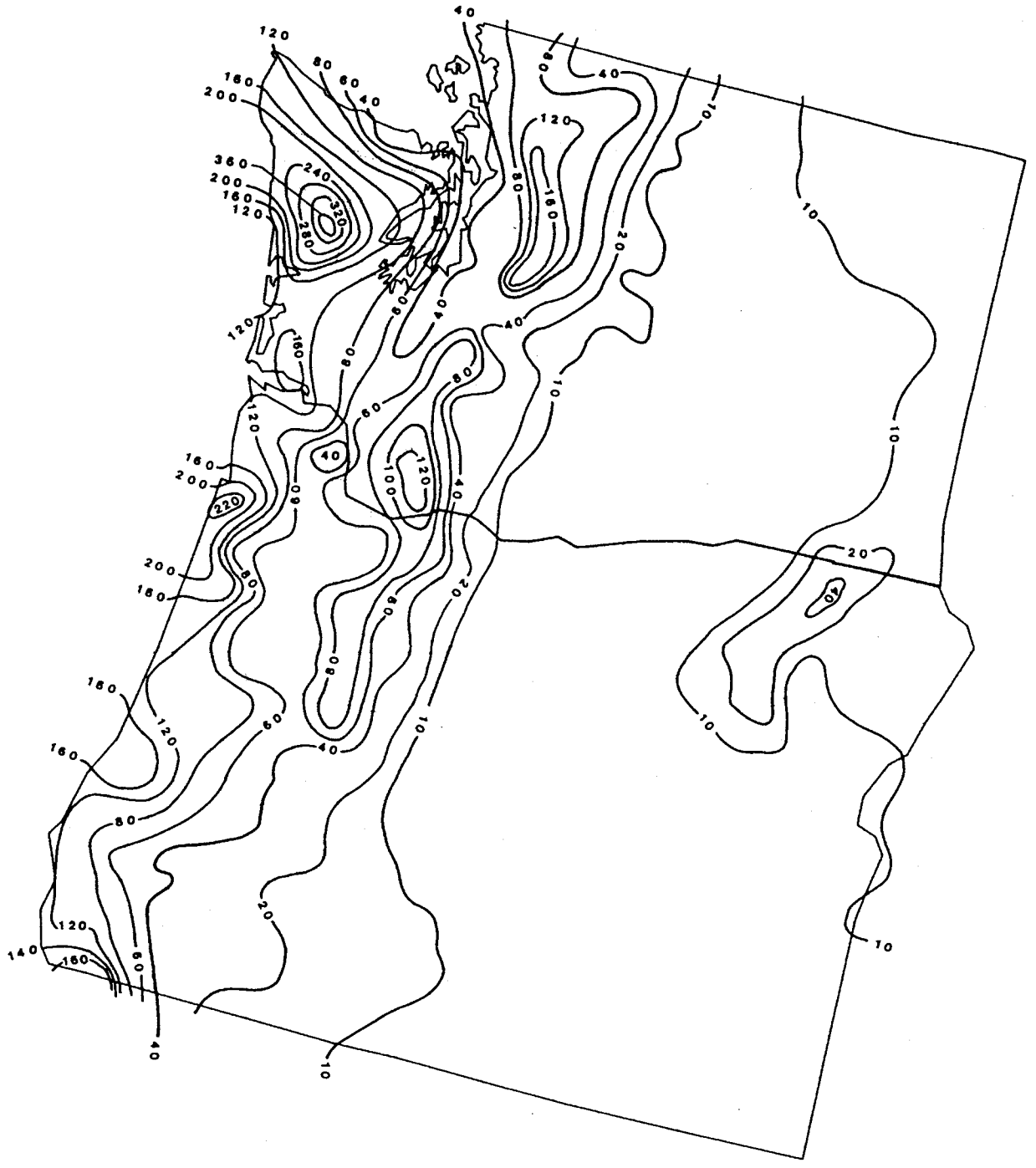

Figure 2-4. Isoerodent map of Oregon and Washington. Units are hundreds ft·tonf·in(ac·h·yr)$^{-1}$.

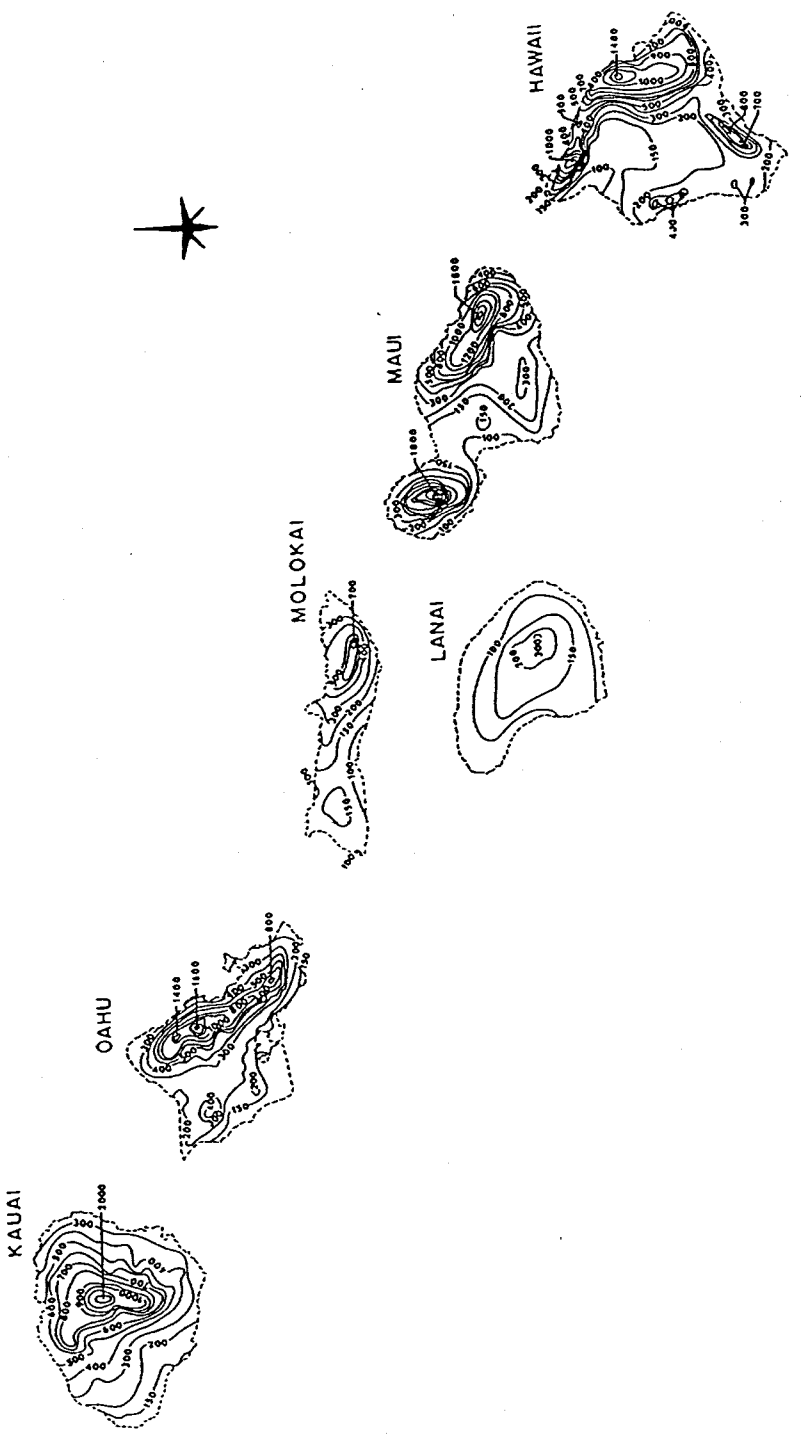

Figure 2-5. Isoerodent map of Hawaii. Units are hundreds $ft \cdot tonf \cdot in(ac \cdot h \cdot yr)^{-1}$.

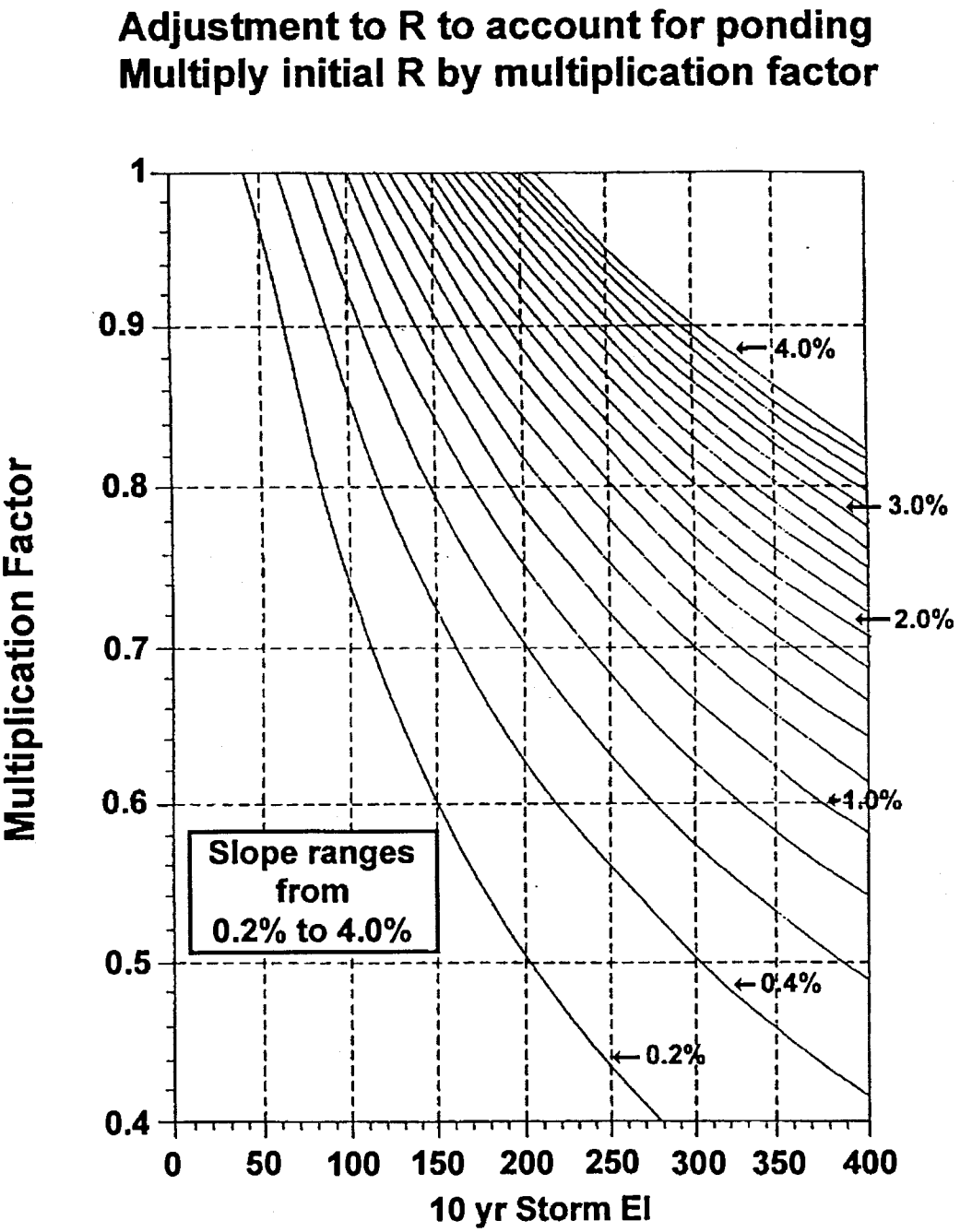

Figure 2-6. Corrections for R factor for flat slopes and large R values to reflect amount of rainfall on ponded water

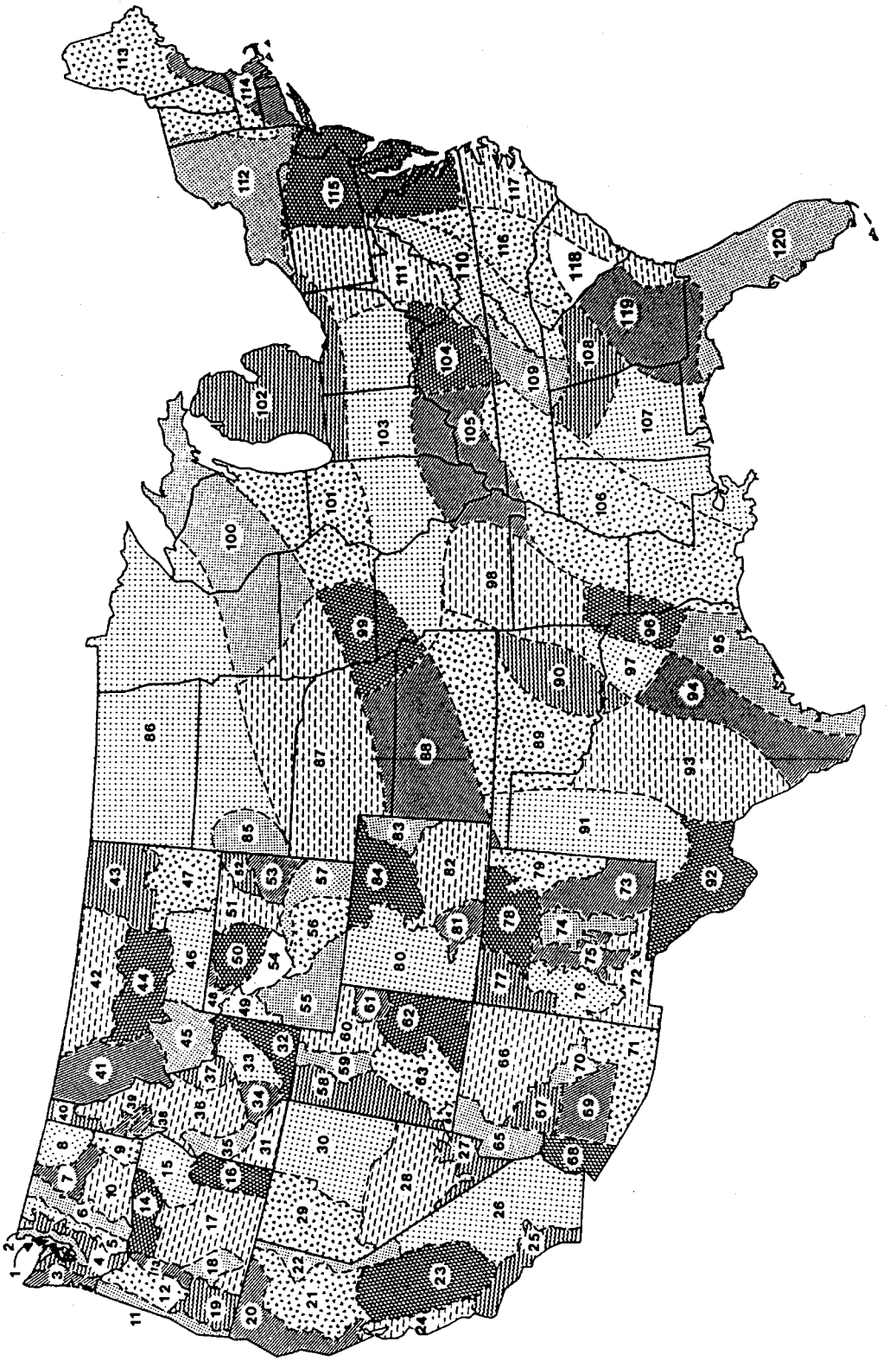

Figure 2-7. EI distribution zones for contiguous United States

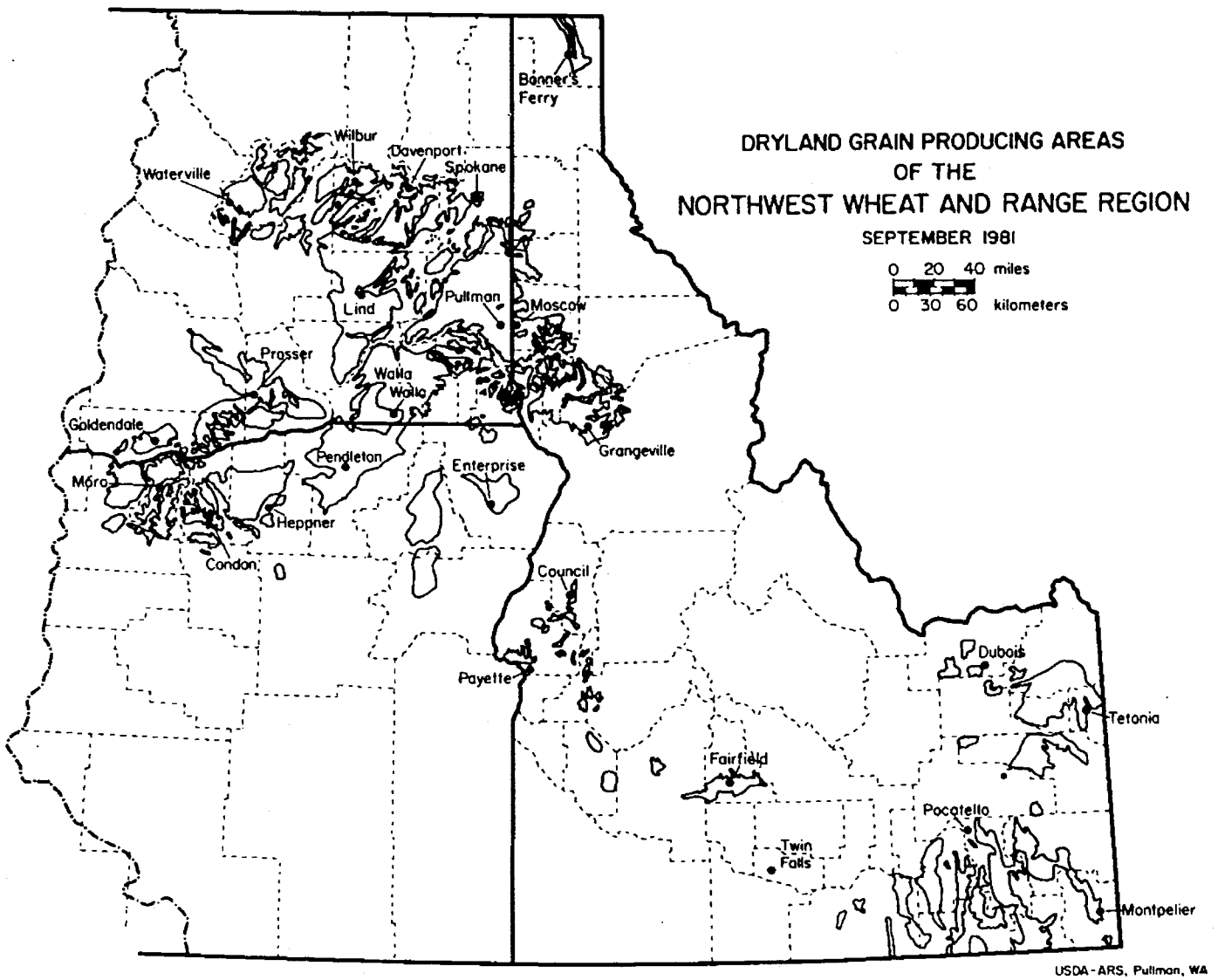

Figure 2-8. Location map of the cropland area of Northwestern Wheat and Range Region (adapted from Austin 1981)

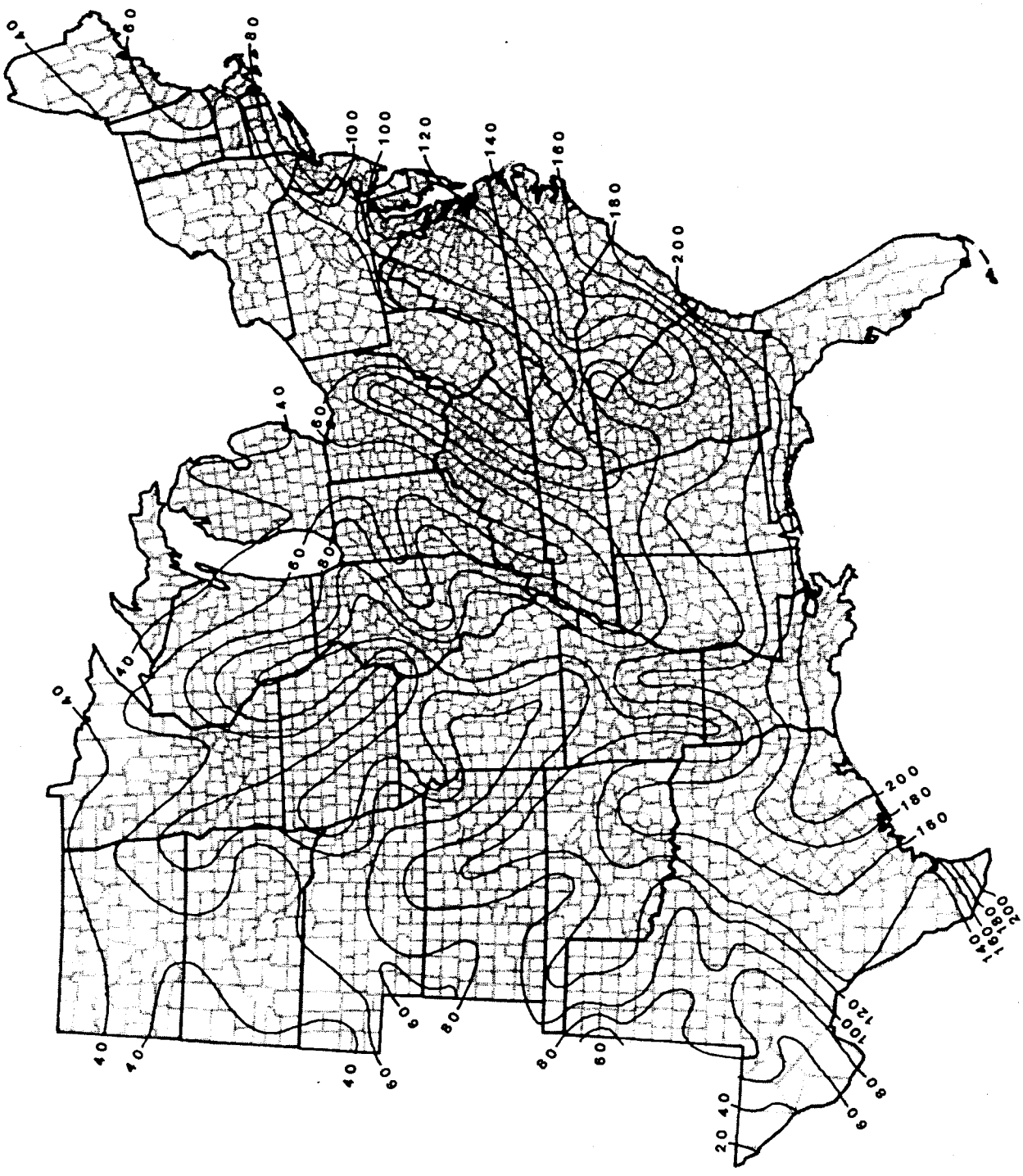

Figure 2-9. Ten-yr-frequency single-storm erosion index for eastern United States. Units are hundreds ft·tonf·in(ac·h)$^{-1}$.

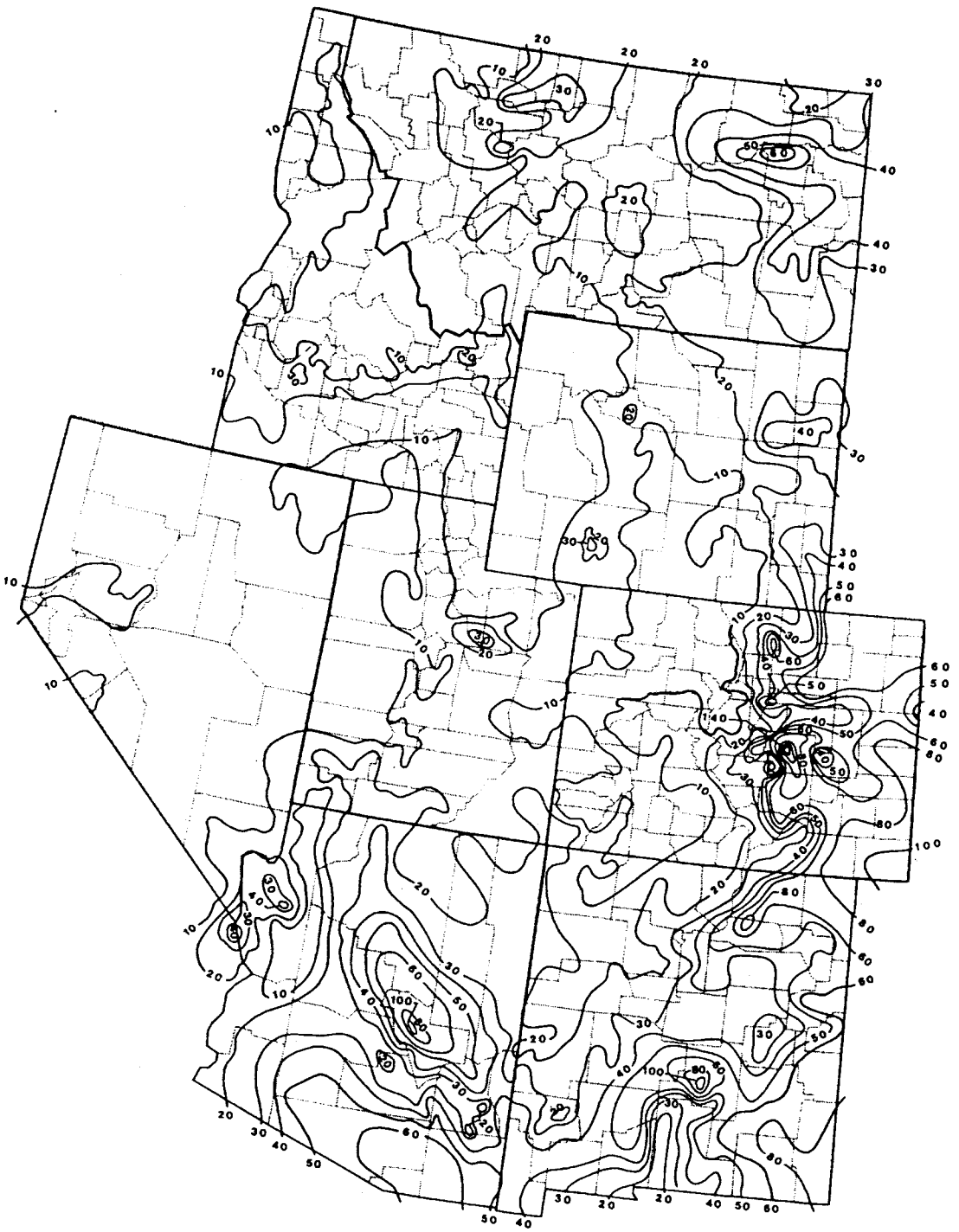

Figure 2-10. Ten-yr-frequency single-storm erosion index for western United States. Units are hundreds ft·tonf·in(ac·h)$^{-1}$.

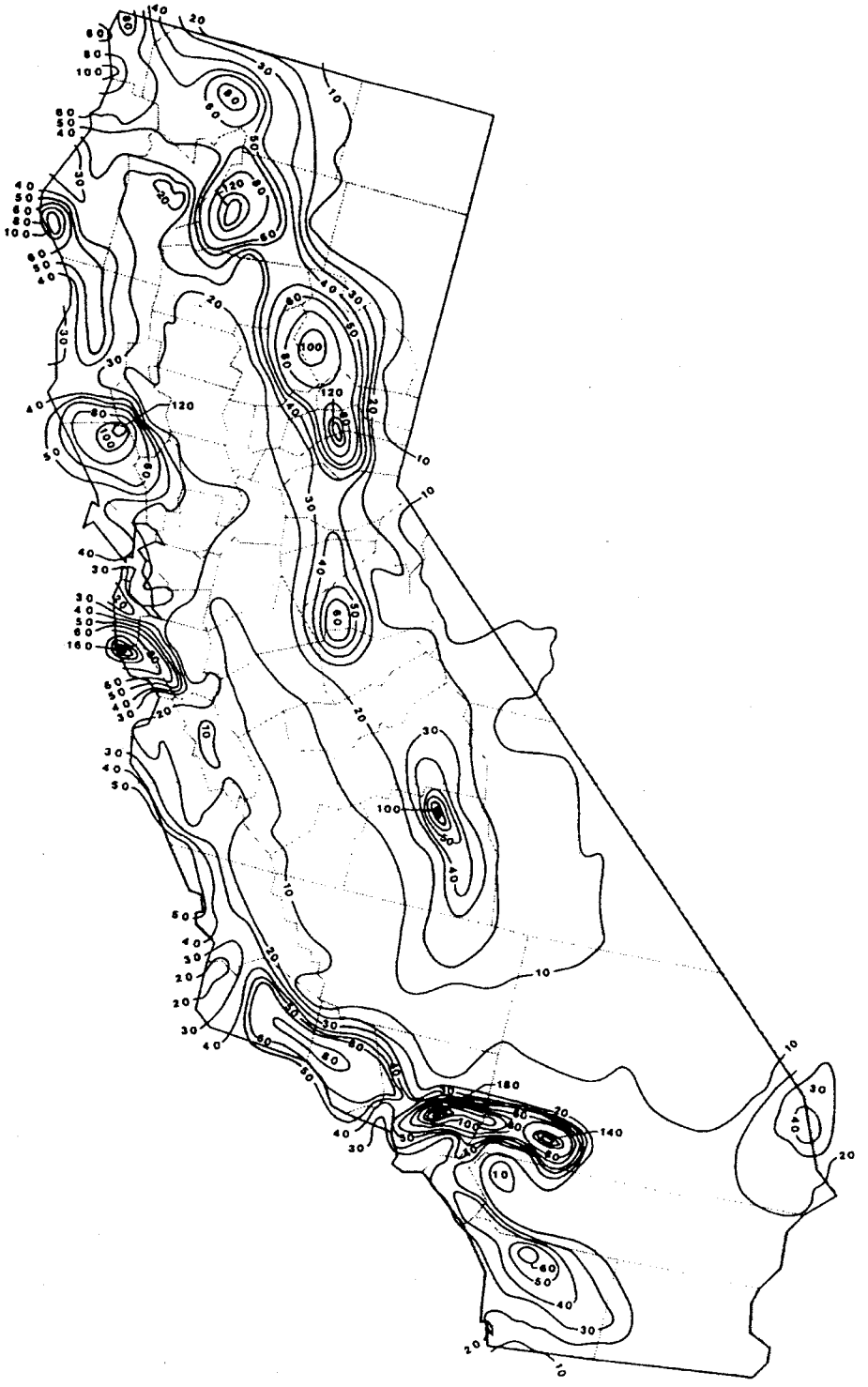

Figure 2-11. Ten-yr-frequency single-storm erosion index for California. Units are hundreds ft·tonf·in(ac· h)$^{-1}$.

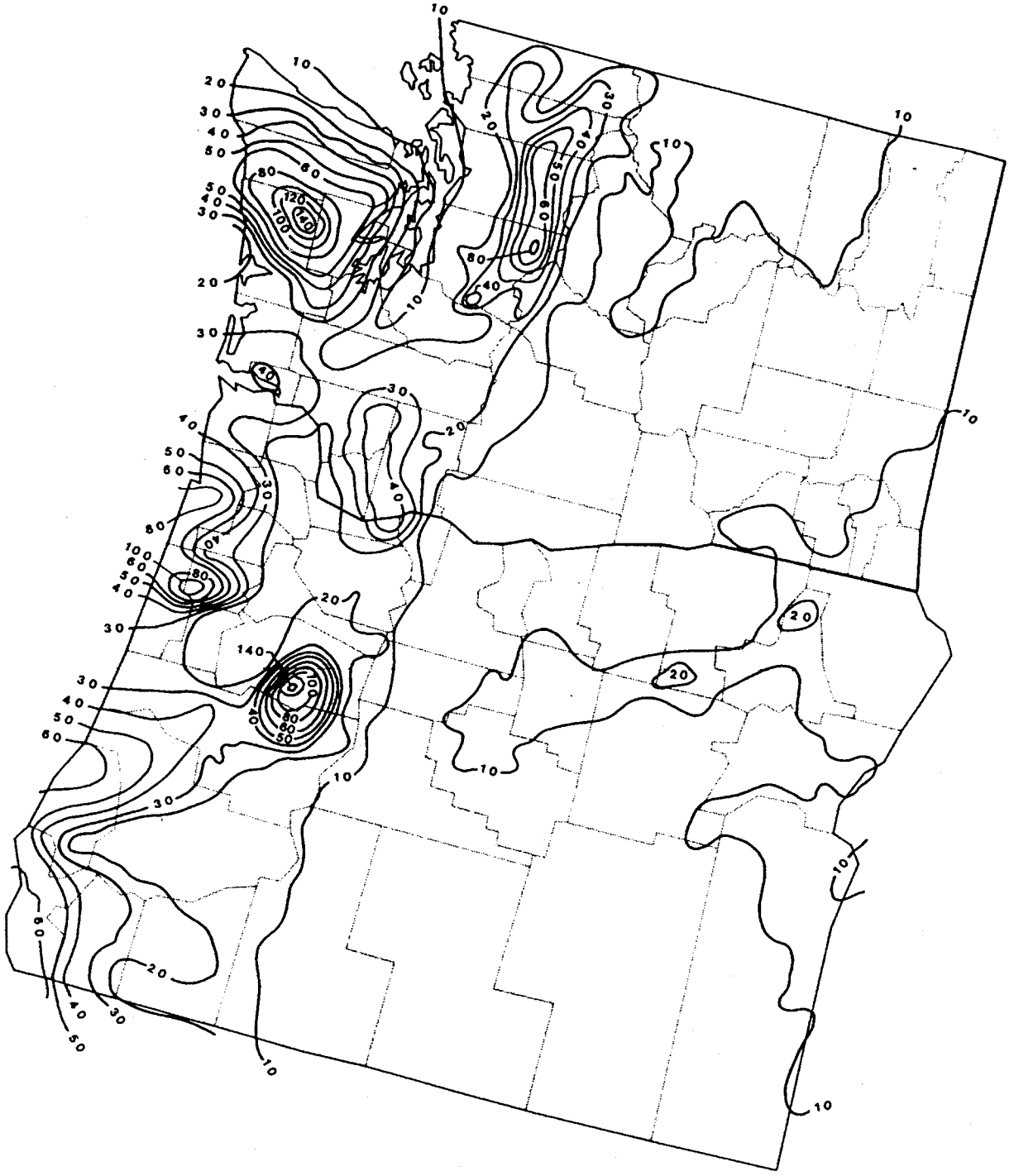

Figure 2-12. Ten-yr-frequency single-storm erosion index for Oregon and Washington. Units are hundreds ft·tonf·in(ac·h)$^{-1}$.

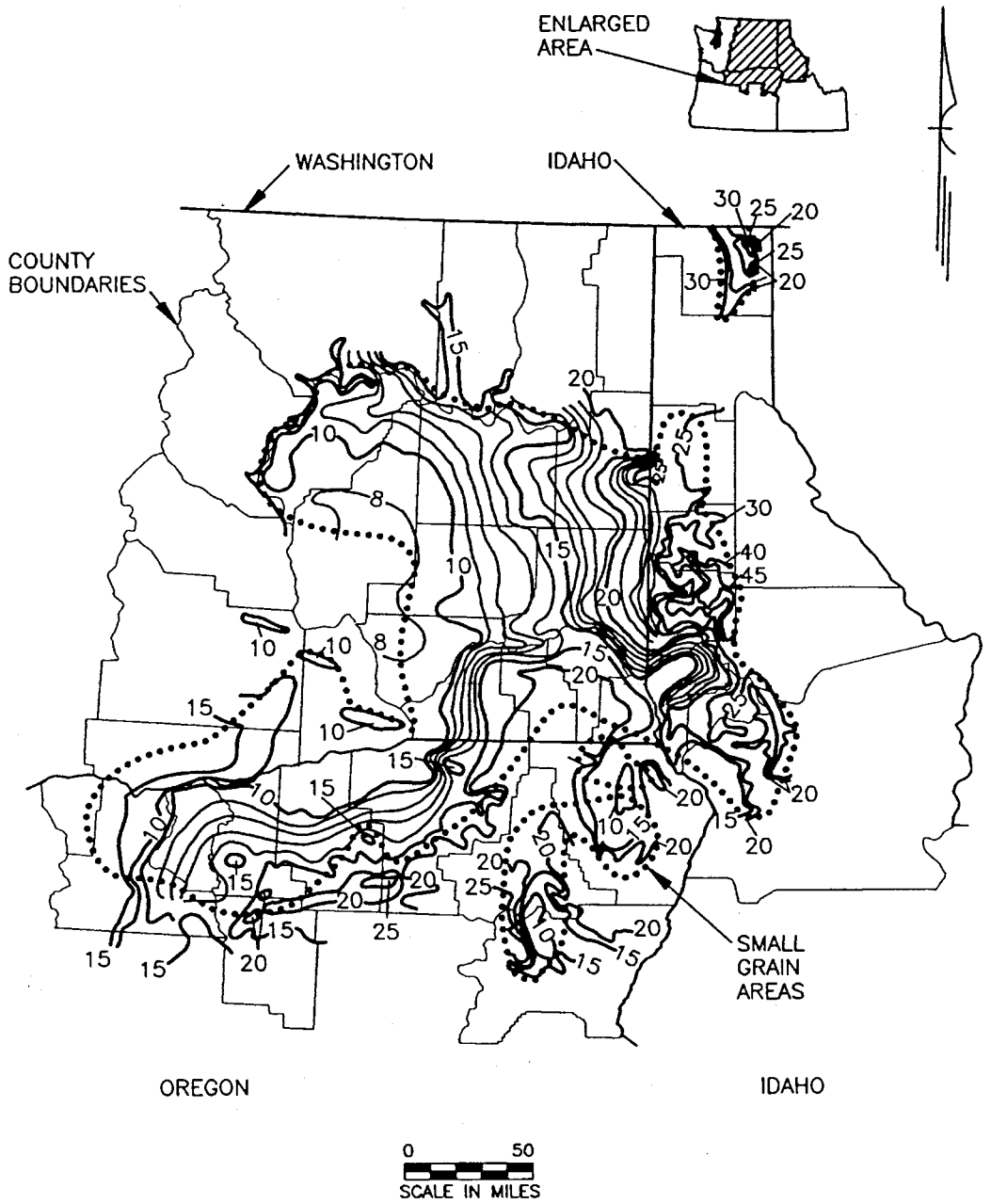

Figure 2-13. Precipitation map (inches) used to calculate R_{eq} in Washington, Oregon, and northern Idaho for small-grain areas of Northwestern Wheat and Range Region. Precipitation units are inches.

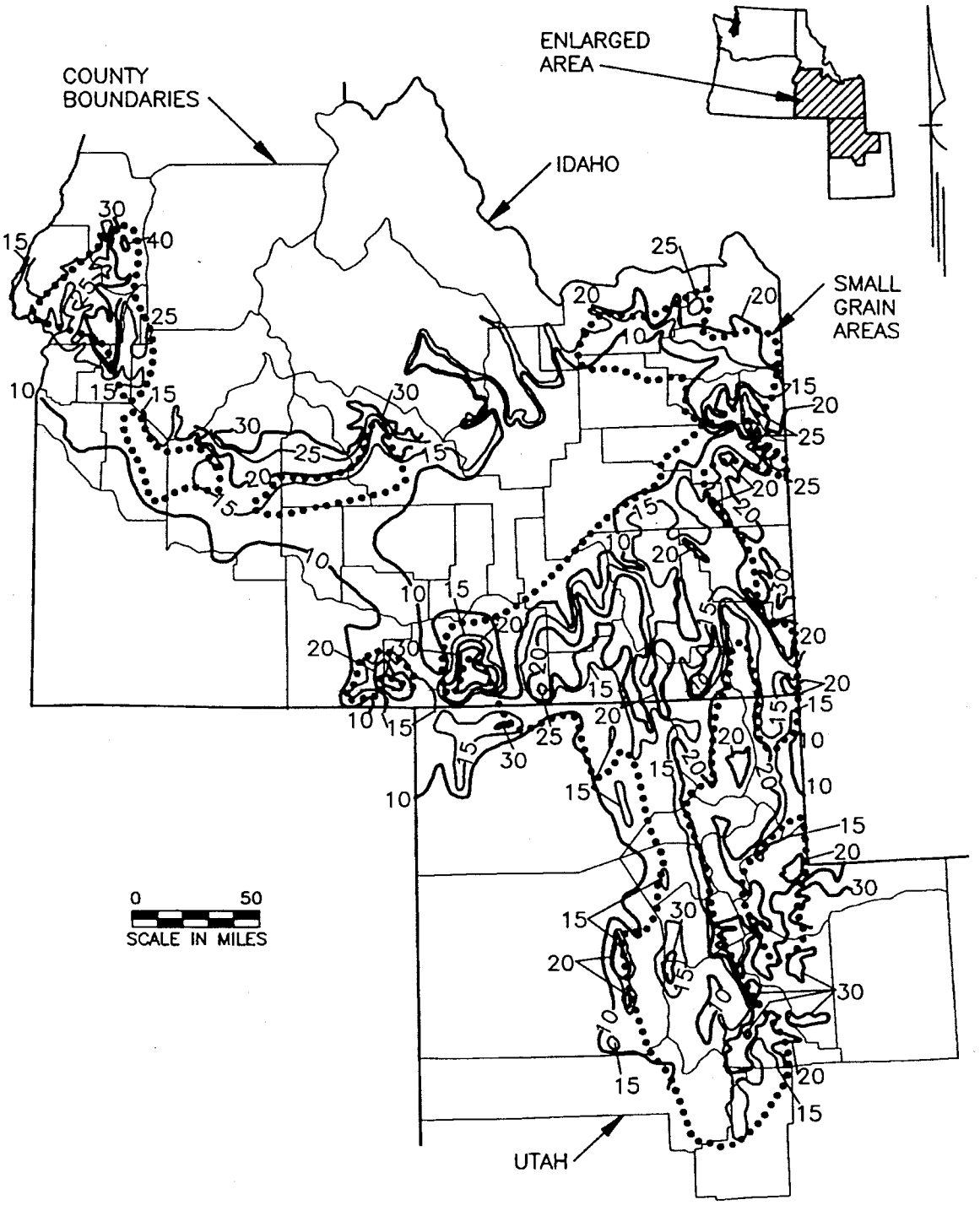

Figure 2-14. Precipitation map (inches) used to calculate R_{eq} in southern Idaho and Utah for small-grain areas of Northwestern Wheat and Range Region. Precipitation units are inches.

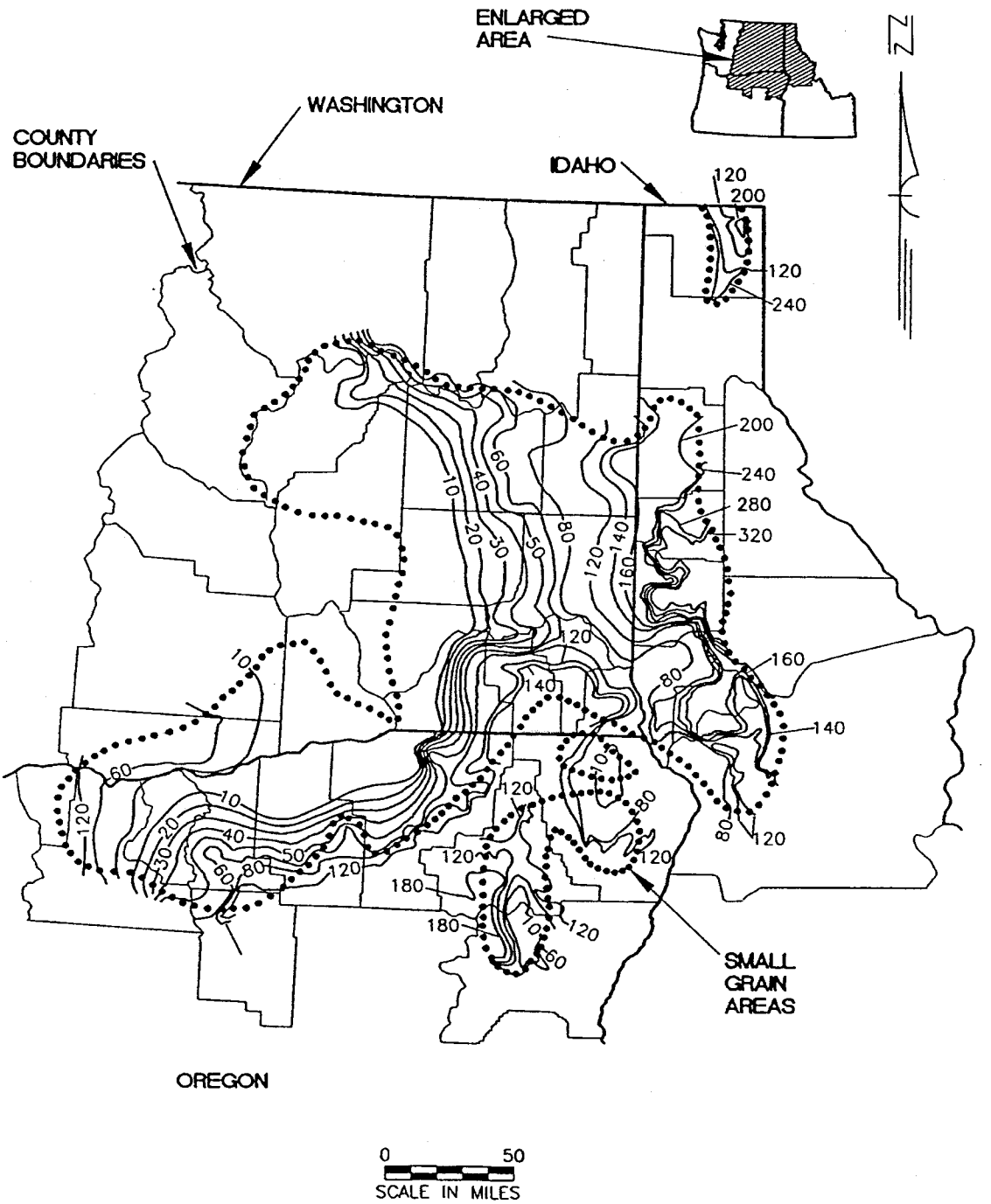

Figure 2-15. R_{eq} for cropland areas of Washington, Oregon, and northern Idaho in and adjacent to Northwestern Wheat and Range Region (Note: Some irregular contour intervals are used to preserve clarity). R_{eq} units are hundreds ft·tonf·in(ac·h)$^{-1}$.

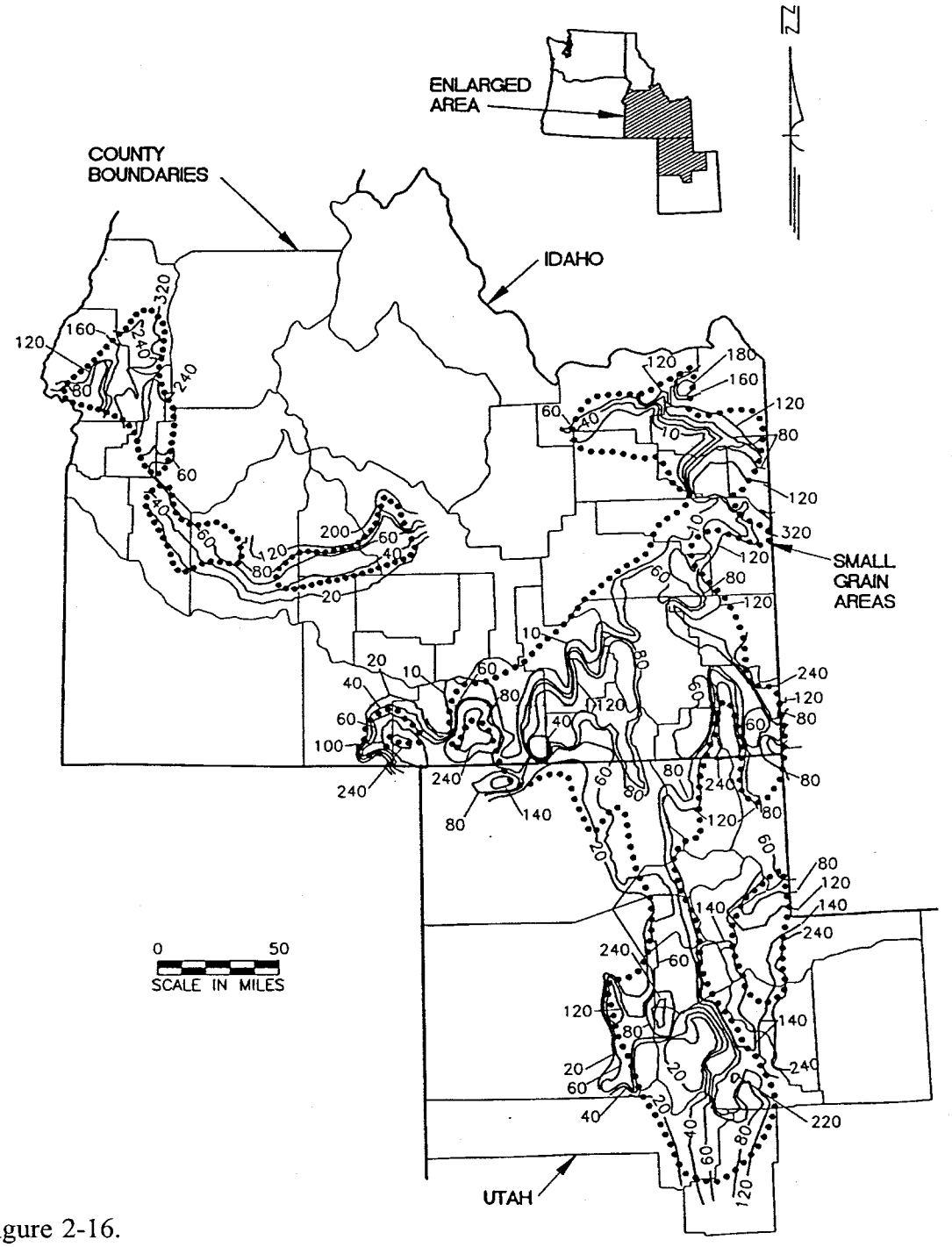

Figure 2-16.
R_{eq} for cropland areas of southern Idaho and Utah in and adjacent to Northwestern Wheat and Range Region (Note: Some irregular contour intervals are used to preserve clarity). R_{eq} units are hundreds ft·tonf·in(ac·h)$^{-1}$.

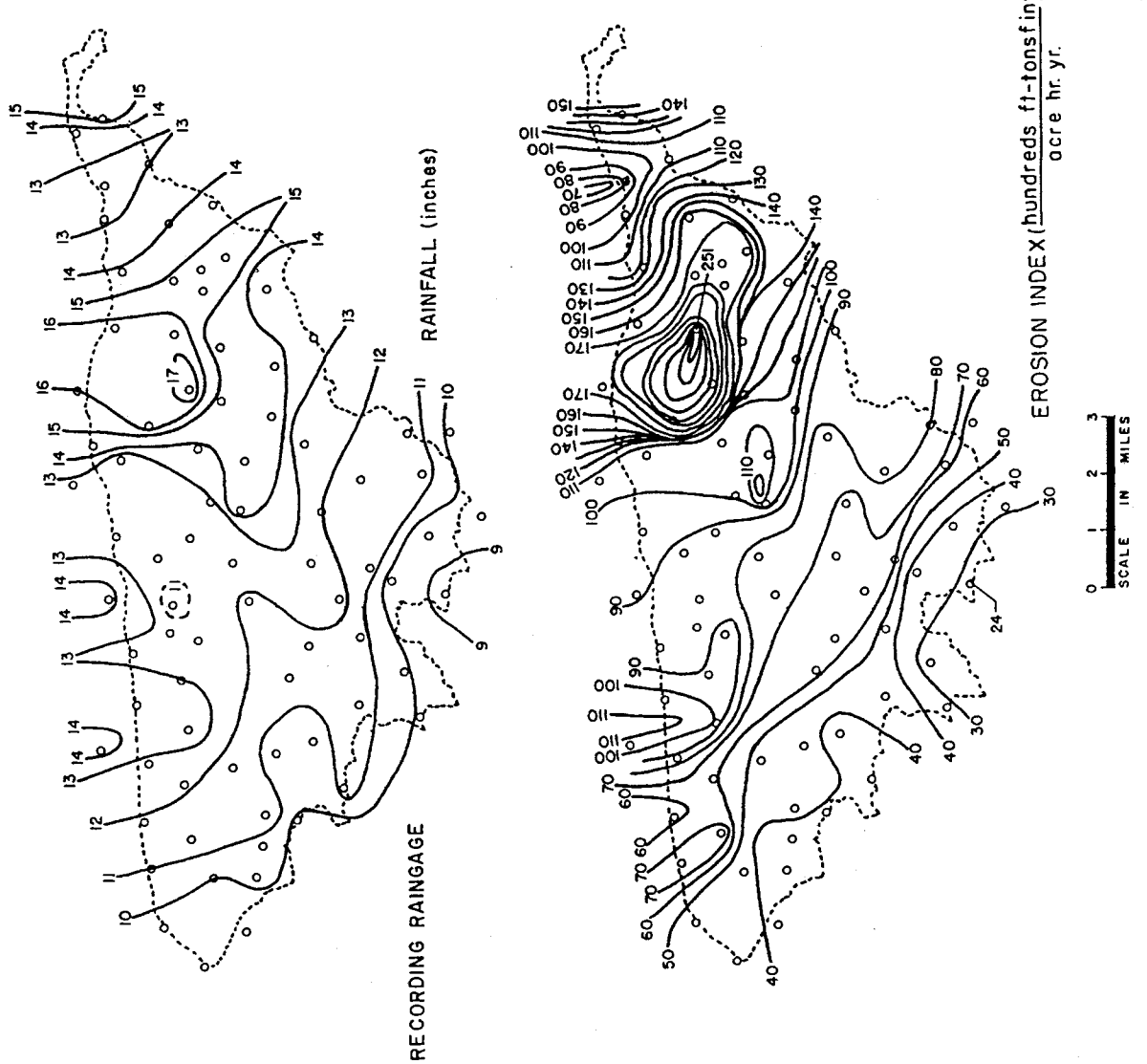

Figure 2-17. Storm precipitation (top) and isoerodent (bottom) values for storm of 7/22/64 on Walnut Gulch Experimental Watershed

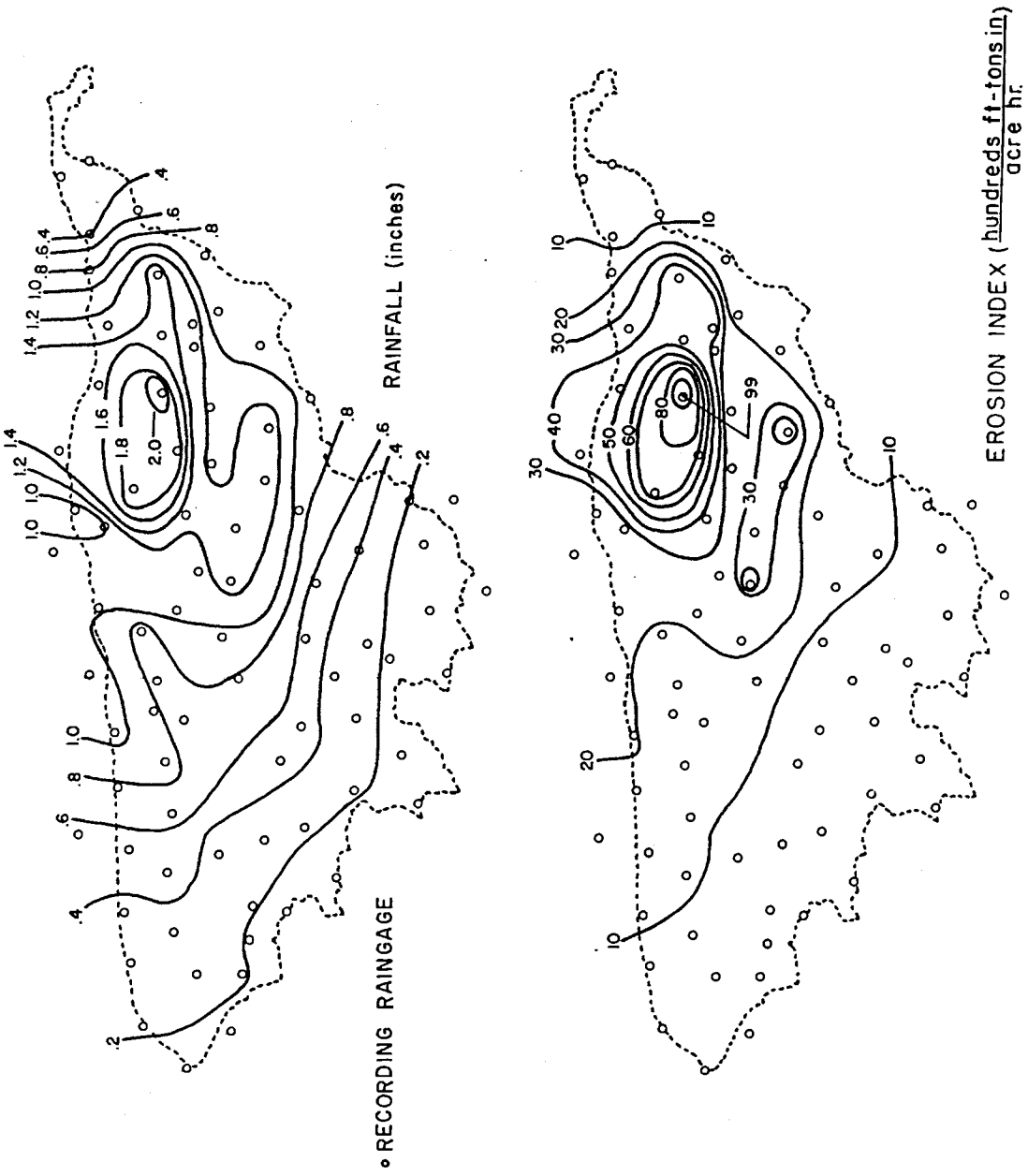

Figure 2-18. Annual precipitation (top) and isoerodent (bottom) maps for 1964 on Walnut Gulch Experimental Watershed

CHAPTER 3. SOIL ERODIBILITY FACTOR (K)

Contributors:

M.J.M. Römkens
R.A. Young
J.W.A. Poesen
D.K. McCool
S.A. El-Swaify
J.M. Bradford

CHAPTER 3. CONTENTS

Soil erodibility is a complex property and is thought of as the ease with which soil is detached by splash during rainfall or by surface flow or both. From a fundamental standpoint, however, soil erodibility should be viewed as the change in the soil per unit of applied external force or energy. Just as in USLE, RUSLE uses a restrictive and applied definition of soil erodibility. Soil erodibility is related to the integrated effect of rainfall, runoff, and infiltration on soil loss and is commonly called the soil-erodibility factor (K). The soil-erodibility factor (K) in RUSLE accounts for the influence of soil properties on soil loss during storm events on upland areas. In this chapter, the current state of knowledge of K-factor measurements and prediction technology is summarized. Background information is given to facilitate the estimation of K values for soils for which no direct K-value measurements are available. Specific areas of concern in evaluations of soil-erodibility factor are discussed, including seasonal variation of soil-erodibility factors (especially of soils subjected to freezing and thawing) and the evaluation of the soil-erodibility factor for soils with rock fragments.

DEFINITION AND EXPERIMENTAL GUIDELINES

The soil-erodibility factor (K) is the rate of soil loss per rainfall erosion index unit [ton· acre· h(hundreds of acre· ft-tonf· in) $^{-1}$] as measured on a unit plot. The unit plot is 72.6 ft (22.1 m) long, has a 9% slope, and is continuously in a clean-tilled fallow condition with tillage performed upslope and downslope (Wischmeier and Smith 1978). Recommended minimum plot width is 6 ft (1.83 m). Guidelines for preparation and maintenance of natural runoff plots in the United States were issued in 1961 by D.D. Smith (Römkens 1985). They are as follows: "Plow to normal depth and smooth immediately by disking and cultivating two or more times, except for areas where wind erosion during the winter poses a serious hazard. In the latter case, disking or cultivating should be delayed until spring. Plowing shall be each year at the time continuous row crop plots are plowed. Cultivation shall be at new crop planting, routine cultivating times, and when necessary to eliminate serious crust formations. Chemical weed control may be used, if cultivation does not control weed-growth. Plowing and cultivation should be upslope and downslope and should not be on an excessively wet soil."[1]

[1]Administrative communication from D.D. Smith to runoff plot managers (January 1, 1961), "Instructions for establishment and maintenance of cultivated fallow plots."

PRACTICAL INTERPRETATION

In practical terms, the soil-erodibility factor is the average long-term soil and soil-profile response to the erosive powers of rainstorms; that is, the soil-erodibility factor is a lumped parameter that represents an integrated average annual value of the total soil and soil profile reaction to a large number of erosion and hydrologic processes. These processes consist of soil detachment and transport by raindrop impact and surface flow, localized deposition due to topography and tillage-induced roughness, and rainwater infiltration into the soil profile.

INTERACTIONS WITH OTHER SOIL-LOSS FACTORS

The soil-erodibility factor (K) represents the effect of soil properties and soil profile characteristics on soil loss. Some interdependency exists between the K factor and other RUSLE factors. For instance, the traditional topographic relationships for slope length and steepness factors (LS) (Wischmeier and Smith 1978) were derived from soil-loss measurements on mostly medium-textured, poorly aggregated surface soils. It is to be expected that errors and shortcomings in the relationships for topographic effects will carry over into K values if these relationships are used to determine K values.

Similar problems exist for the rainfall-erosivity factor (R). Storm energy may vary substantially among storms due to variations in drop size and due to updraft or downdraft of wind. Some of these variations occur in areas where certain storm types prevail for part of the year (heavy thunderstorms versus gentle rains). Calculations of rainfall energy from rainfall breakpoint data for natural runoff plots using a relationship of specific intensity versus energy (Wischmeier and Smith 1978) may lead to "errors" in the computed K. Seasonal K values may offer some compensation for errors in R values computed from rainfall breakpoint data.

Interactions with the cover-management factor (C) are primarily due to the effect of organic matter or organic carbon on soil loss. The organic-carbon content of soils depends on the annual additions of surface and subsurface crop residue and manure and on their decomposition rate. No sharp delineation can be made where the effects of crop residue cease to be part of a C factor and instead become part of the K factor. Moreover, the processes of organic conversions are related to environmental factors (temperature, wetness, and so on) and thus vary among physiographic regions. A discussion of these processes is beyond the scope of this chapter. Short-term effects such as from the protective cover of mulch or from the mechanical constraints such as disturbance of surface and subsurface residues are related to the C factor, whereas long-term effects such as soil changes or soil structural alterations by organic compounds should be considered part of the K factor.

DETERMINATION OF K FACTOR

Soil-erodibility factors are best obtained from direct measurements on natural runoff plots. Rainfall simulation studies are less accurate, and predictive relationships are the least accurate (Römkens 1985). In each of these methods of determination, requirements for soil and plot conditions as well as methods of evaluation have to be met. These requirements are designed to eliminate the influence of variations in antecedent soil-water and soil-surface conditions and of variations in the rainstorm regimes on the soil-erodibility factor. Only inherent soil properties are considered determinants of the erodibility factor.

Natural Runoff Plots

The major requirement in a study using a natural runoff plot is a database that is large enough and that was obtained over a sufficiently long period. Very few studies exist for which long-term observations are available. For the eastern United States, this period is assumed to be 20-22 yr (Wischmeier 1976). Time and economic factors have limited the establishment of long-term runoff plots and therefore have promoted the development of plot research with simulated rainfall. However, simulated-rainfall procedures often fall short of the requirement of a sufficiently long fallow condition. Table 3-1 lists the soils in the United States on which natural runoff plots for K-factor determinations were established. Note that the observation period on all of these soils fell considerably short of the stated period of 20-22 yr. However, K values of many soils were obtained from long-term runoff data on cropped plots that had been adjusted for the C factor.

The second requirement for soil-erodibility-factor determinations on natural runoff plots is a fallow, tilled surface immediately before and during the observation period. This requirement stipulates the removal or natural degradation of all surface and subsurface plant residue that remained after cropping. The adequacy of this observation period should be determined relative to the climatic conditions in the United States but is usually taken to be 2 yr.

The third requirement for reliable K-value determinations is uniformity of soil and topography within the plot and also adherence to plot-size standards. Topographic uniformity is essential to avoid soil deposition or accelerated soil erosion in localized areas. The selection of plots having a standard length and steepness is important to avoid errors in soil-loss adjustments with topographic factors. Many soils do not occur with slopes of 9%, but standards, once formulated, must be adhered to in order to avoid ambiguities. Actually, the 9%-slope steepness is not rationally based, but was selected as being an average gradient of runoff plots on which early erosion studies in the United States were conducted. Similarly, the 72.6-ft (22.1-m) plot length was the result of the selection of a 1/100-acre (1/250-ha) plot area, given a two-row or 6-ft (1.83-m) plot width.

Rainfall-Simulation Plots

K-factor determinations in simulated-rainfall studies require plot standards that are the same as those for natural runoff plots with respect to size, slope, and preparation. However, the usually very short timespan allowed between cropping and rainfall-simulation runs is insufficient for the adequate degradation of surface or subsurface organic residue. Therefore, in the simulation, surface residue is often removed mechanically or manually before tillage, and corrections for subsurface-crop-residue effects are made through the C factor. Errors may be introduced in K-factor determinations for soils with incomplete removal or degradation of surface and subsurface residues or for soils with incorrect C-factor adjustments.

A second difficulty with the use of rainfall simulation in K-factor evaluations is the selection of weighting factors for soil losses on different antecedent soil-water conditions. Römkens (1985) and Barnett et al. (1965) observed that K values for different antecedent moisture levels need to be weighted in proportion to the occurrence of runoff and erosion in different climates to determine the average annual K value.

RELATIONSHIPS OF K FACTOR AND SOIL PROPERTIES

The physical, chemical, and mineralogical soil properties and their interactions that affect K values are many and varied. Moreover, several erosion mechanisms are operating at the same time, each one relating differently to a specific soil property. It is therefore unlikely that a relatively few soil characteristics will accurately describe K values for each soil. Yet several attempts have been made to relate measured K values to soil properties. Table 3-2 lists the principal studies in the United States and a summary of the results.

Of these studies, the most widely used and frequently cited relationship is the soil-erodibility nomograph (Wischmeier et al. 1971). The nomograph, shown in figure 3-1, comprises five soil and soil-profile parameters: percent modified silt (0.002-0.1 mm), percent modified sand (0.1-2 mm), percent organic matter (OM), and classes for structure (s) and permeability (p). The structure and permeability classes and groups of classes were taken from the Soil Survey Manual (USDA 1951). A useful algebraic approximation (Wischmeier and Smith 1978) of the nomograph for those cases where the silt fraction does not exceed 70% is

$$K = \left[2.1 \cdot 10^{-4}(12-OM)\, M^{1.14} + 3.25(s-2) + 2.5(p-3)\right] / 100 \qquad [3\text{-}1]$$

where M is the product of the primary particle size fractions: (% modified silt or the 0.002-0.1 mm size fraction) · (% silt + % sand). K is expressed as ton· acre^{-1} per erosion index unit with U.S. customary units of ton· acre· h (hundreds of acre· ft-tonf · in)$^{-1}$. Division of the right side of this and subsequent K-factor equations with the factor 7.59 will yield K values expressed in SI units of t· ha· h· ha^{-1}· MJ^{-1}· mm^{-1}.

The nomograph relationship is derived from rainfall-simulation data from 55 midwestern, mostly (81%) medium-textured, surface soils. More than 60% of these soils had an aggregation index smaller than 0.3 (Mannering 1967). The nomograph is well suited for the less aggregated, medium-textured surface soils of the Midwest. Attempts by other investigators to apply the nomograph to other classes of soils have met with limited success. Figure 3-2 shows the relationship between the observed and nomograph-predicted soil-erodibility

factors for the nomograph database and selected U.S. data sets of other soil classes. In most of these studies, aggregate sizes or aggregation indices were the most significant parameters. For details of the relationship between the soil-erodibility factor and soil properties, the reader is referred to the original publications (see table 3-2) or to a review paper by Römkens (1985).

Regression equations for specific classes of soils in the United States are those listed in table 3-2. Unfortunately, substantial intercorrelations exist among many of these variables, thereby affecting the true significance of each property in predicting K values. The relationship for volcanic soils in Hawaii (El-Swaify and Dangler 1976) is given by the expression

$$K = -0.03970 + 0.00311x_1 + 0.00043x_2 + 0.00185x_3 + 0.00258x_4 - 0.00823x_5 \quad [3\text{-}2]$$

where x_1 is the unstable aggregate size fraction in percent less than 0.250 mm, x_2 is the product of % modified silt (0.002-0.1 mm) and % modified sand (0.1-2 mm), x_3 is the % base saturation, x_4 is the silt fraction (0.002-0.050 mm) in percent, and x_5 is the modified sand fraction (0.1-2 mm) in percent. The applicability of equation [3-2] has not been demonstrated for all tropical soils of volcanic origin. Equation [3-2] should be considered for only those soils that are similar to soils found in Hawaii.

For soils in the upper Midwest, the following relationship was developed (Young and Mutchler 1977):

$$K = -0.204 + 0.385x_6 - 0.013x_7 + 0.247x_8 + 0.003x_2 - 0.005x_9 \quad [3\text{-}3]$$

where x_6 is an aggregation index, x_7 is the percentage montmorillonite in the soil, x_8 is the bulk density of the 50-125 mm depth in $g \cdot cm^{-3}$, and x_9 is the dispersion ratio. The presence of the montmorillonite term suggests that this clay mineral significantly impacted the aggregation and granulation characteristics of these soils--the latter by facilitating detachment during drying and transport in subsequent storm events.

For clay subsoils in the Midwest, the following relationship may be useful (Römkens et al. 1977):

$$K = 0.004 + 0.00023x_{10} - 0.108x_{11} \quad [3\text{-}4]$$

where x_{10} is the parameter M (Wischmeier et al. 1971) and x_{11} is the citrate-dithionite-bicarbonate (= CDB) extractable percentage of Al_2O_3 plus Fe_2O_3. This relationship again suggests the importance of the particle size between 0.002 and 0.1 mm in soil-erodibility-factor evaluations for subsoils. The importance of the CDB-extractable amount of the hydrous oxides of iron and aluminum as a predictor for the soil-erodibility factor should be tempered, in view of the small amounts (<3.76%) of these substances present in the soils tested. For highly weathered or cemented soils, equation [3-4] has not been tested and presumably needs modification.

Recently, all available published global data (225 soils) of measured K values, obtained from both natural- and simulated-rainfall studies, were pooled and grouped into textural classes. Only soils with less than 10% of rock fragments by weight (>2 mm) were considered. The mean values of the soil-erodibility factor for soils within these size classes were then related to the mean geometric particle diameter of that class. The resulting relationship, shown in figure 3-3A, can be expressed as

$$K = 7.594\left\{0.0034+0.0405\exp\left[-\frac{1}{2}\left\{\frac{\log(Dg)+1.659}{0.7101}\right\}^2\right]\right\} \quad [3\text{-}5]$$

where

$$Dg(mm) = \exp\left(0.01\sum f_i \ln m_i\right) \text{ with } r^2 = 0.983 \quad [3\text{-}6]$$

and

Dg = geometric mean particle diameter.

Here, f_i is the primary particle size fraction in percent, and m_i is the arithmetic mean of the particle size limits of that size (Shirazi and Boersma 1984). A similar relationship, shown in figure 3-3B with $r^2 = 0.945$, was derived for 138 U.S. soils only. This relationship is

$$K = 7.594\left\{0.0017+0.0494\exp\left[-\frac{1}{2}\left\{\frac{\log(Dg)+1.675}{0.6986}\right\}^2\right]\right\} \quad [3\text{-}7]$$

Figure 3-3 also indicates the variability in K values for each particle size class.

Relationships [3-5] and [3-7] are very useful for predicting K values of soils for which (1) data are limited (for instance, no information about the very-fine-sand fraction or organic-matter content) and (2) the textural composition is given in a different classification system. Also, equations [3-5] and [3-7] are useful for predicting K values of classes of soils other than those on which the nomograph was based, such as soils of textural extremes and well-aggregated soils. Of course, prediction equations [3-5] and [3-7] give an estimate of the K factor based on limited data and therefore yield less accurate values than those obtained from direct measurements or indirectly from regression data for soil types similar to those indicated in table 3-2.

CONSIDERATIONS IN SELECTION OF K VALUES

Several methods can be used to obtain estimates of the average annual value of the soil-erodibility factor. For medium-textured soils—certainly for the poorly aggregated ones of the temperate zones—the nomograph appears to be the best predictive relationship. For tropical soils of volcanic origin, relationship [3-2] may be helpful. For soils or subsoils that contain clay minerals with 2:1 expanding lattices, relationships [3-3] or [3-4] can be used. If K values are to be obtained for soils that do not readily fit any of these categories or for soils with incomplete information (that is, particle-size distribution and organic matter content), the broadly based relationships [3-5] and [3-7] can be selected.

SPECIFIC PROBLEM AREAS

Rill and Interrill Erodibility

Physically based models are being developed to explain the dynamic relationships of the erosion process (detachment, transport, deposition), and the models provide a great opportunity to improve the estimation of erosion. These models are incompatible with the empirically based RUSLE, which predicts long-term average values (effects of subprocesses are lumped). Thus, improved soil-erodibility estimates using soil properties and relating them to erosion processes are not included in this revision (Römkens et al. 1986).

Soils With Rock Fragments

In NRCS's map unit use file (MUUF), 15.6% of land area in the continental United States consists of soils with rock fragments on or in the soil surface (Miller and Guthrie 1984). These rock fragments, when present on the soil surface, significantly reduce soil detachment by rainfall. When present in a coarse-textured-soil profile (having sand and loamy sand textures), the fragments can appreciably reduce infiltration.

To account for these effects, one view has been to include the effect of rock fragments on soil loss solely in the C factor (Box and Meyer 1984, Römkens 1985), and another practice has been to include the effects solely in the K factor. Surface cover by rock fragments varies from site to site on otherwise identical soils. The fragments act as a surface mulch by protecting the soil surface from raindrop impact in a manner similar to that of surface mulches of straw and chopped stalks. Rock fragments are usually not moved by water from interrill areas but remain behind on the soil surface and act as an "armor" (Jennings and Jarrett 1985).

Subsurface rock fragments affect infiltration and thus runoff in a manner similar to that of subsurface residue by reducing the soil void space and soil hydraulic conductivity in coarse-textured soils. Moreover, because soil-mechanical-analysis procedures are based on particle-size fractions smaller than 2 mm, rock fragments larger than 2 mm are usually excluded when estimating K-factor values. However, rock fragments are part of a continuum of particle sizes in the mineral phase of the soil and therefore can be considered as part of the soil-erodibility factor.

This Agriculture Handbook separates the influence of rock fragments on soil loss into two components: (1) a surface cover component that represents the surface-protecting effect of rock fragments and that is accounted for in the C factor in a manner similar to that of crop residue and vegetative mulch, and (2) a subsurface component for sand and loamy-sand textures that represents the soil-loss increase due to the reduction in water infiltration. This latter effect is accounted for in the K factor through adjustments of the permeability class. It is shown below, however, that the subsurface effect of rock fragments can be relatively minor compared to the surface effect. Soil-profile descriptions with permeability classes that include the effect of rock fragments on permeability should not receive such an adjustment.

The hydraulic-conductivity-reducing effect of rock fragments can be determined from the relationship of the saturated hydraulic conductivity and permeability class given in the National Soils Handbook No. 430 (USDA 1983). Some clarification[2] is needed concerning the terminology and tables in that handbook. Rawls et al. (1982) proposed a relationship between the permeability class and the saturated hydraulic conductivity for different soil textures (table 3-3). Many factors other than texture determine the permeability class: for instance, structure, mineralogy, fragipans, sodium, and salinity. However, this relationship provides an estimate for relating changes in the effective hydraulic conductivity due to the presence of rock fragments to changes in the permeability class.

The rate of reduction in the saturated hydraulic conductivity with the presence of increasing amounts of coarse fragments in the soil profile was theoretically derived by Peck and Watson (unpublished data) and later verified for sand columns with inclusions of glass spheres and gravel by Dunn and Mehuys (1984). The relationship is

$$K_b / K_f = 2(1-R_v) / (2+R_v) \qquad [3\text{-}8]$$

[2]Permeability class as defined in the Soil Survey Manual of 1951 and in the USDA-SCS National Soils Handbook No. 430 is actually a hydraulic conductivity class. The relationship between permeability K_p (an intrinsic soil matrix property with dimensions L^2) and the saturated hydraulic conductivity K_h (a property that includes fluid properties of dimensions $L \cdot T^{-1}$) is $K_h = K_p \cdot \rho g \cdot \mu^{-1}$, where μ is fluid viscosity, ρ is fluid density, and g is gravitational acceleration.

where K_b is saturated hydraulic conductivity of the soil with rock fragments, K_f is saturated hydraulic conductivity of the fine soil fraction (<2 mm), and R_v is percent by volume of rock fragments >2 mm.

Brakensiek et al. (1986) simplified equation [3-8] to show that K_b of soil containing rock fragments can be reasonably related to K_f by using only the weight percent of rock fragments >2 mm. This relationship is

$$K_b/K_f = (1 - R_w) \qquad [3\text{-}9]$$

where R_w is percent by weight of rock fragments >2 mm. Using equation [3-9], a given percentage weight of rock fragments in a soil profile will result in an equal percentage reduction in the saturated hydraulic conductivity of the soil. Hence, the corresponding change in the permeability class can be estimated from table 3-3.

For example, a 40% volume of rock fragments in a severely eroding medium-textured soil (K = 0.50) will cause at best a change of one step in the permeability class or a maximum increase of 0.025 units in the soil-erodibility factor. This represents a 5% increase in soil loss. On the other hand, a 40% surface cover with rock fragments causes a reduction in soil loss of about 65% (Box 1981). For a less erodible soil (K = 0.10), a 40% volume of rock fragments represents a maximum increase of 25% in soil loss as reflected through the K value.

Seasonal K Values

K values are difficult to estimate mainly because of antecedent soil-water and soil-surface conditions and because of seasonal variations in soil properties. Because the value of these conditions and properties tends to be consistent for a season, it is thought that seasonal K values can reduce errors in soil-loss estimates. Based on this reasoning, Mutchler and Carter (1983) in the United States and Zanchi (1983) in Italy computed monthly K values. They independently proposed a periodic function of the type

$$K_r = 1 + a \cos(bt - c) \qquad [3\text{-}10]$$

where K_r is the ratio of the average seasonal (monthly) K value over the average annual K value; t is the mean monthly temperature; and a, b, and c are location-dependent constants. Similar reasoning by El-Swaify and

Dangler (1976) and Hosoyamada (1986) led to the introduction of wet/dry K values in Hawaii and cold/warm K values in Japan, respectively.

Variations in K through the seasons seem to be primarily related to three factors: soil freezing, soil texture, and soil water. Of these, the soil-freezing effect is probably the most difficult to evaluate. The effects of all three are now included in the average annual value.

The ability to more accurately predict the soil-erodibility factor for soils that are subjected to freeze-thaw cycles has been hampered by the limited understanding of the processes and temporary changes occurring in soil properties and in the soil profile during the cycles. Although no relationships have been developed, studies have shown that soil freezing and thawing can change properties that affect soil erodibility. These properties include soil structure, hydraulic conductivity, bulk density, aggregate stability, and soil strength (Benoit 1973, Benoit et al. 1986, Sillanpaa and Webber 1961, Formanek et al. 1984, Van Klaveren 1987, Kok and McCool 1990). It has been shown that the soil-water content at the time of initial freezing, the rate of soil freezing, and the number of freeze-thaw cycles can significantly affect soil aggregation and aggregate stability in spring at the time of thawing (Mostaghimi et al. 1988). Freeze-thaw cycling generally leads to low bulk density of the surface soil (Pall et al. 1982). Conditions of low density and high soil water provide a soil surface that is very susceptible to soil detachment and transport. Differences in soil density may persist even after frost layers have thawed. This, combined with intense spring rains, often results in large soil losses. Thus, freezing and thawing tend to increase the soil-erodibility factor.

High soil-water content can lead to the formation of concrete frost that is generally impermeable. Soil erodibility is then at a minimum, due to the soil's frozen conditions. When soil with a concrete frost layer thaws from the surface, drainage is almost nonexistent. Although the soil is not apt to be exposed to many freeze-thaw cycles in these areas, the spring melt period of 3 days to a month or more may still affect soil erodibility. During this period, a thawed surface layer of soil underlaid by a frost lens may exist, thereby impeding infiltration and water movement. Soil-erosion resistance is at a minimum immediately after the soil has thawed and tends to increase with time after thawing (Formanek et al. 1984). The greater the number of freeze-thaw cycles, the longer the erosion resistance of a soil is at a minimum. Because soil during the thawing period is extremely susceptible to erosion caused by snowmelt and rainfall, the soil loss is more likely to occur in that period. In regions where winter soil temperatures hover around the freezing point (such as in much of the Northwest Wheat and Range Region), the soil

surface is apt to undergo many freeze-thaw cycles throughout the winter, which tends to keep erosion rates high during this period. Reductions in surface-shear strength of 50% have been measured in a Palouse silt loam immediately after one freeze-thaw cycle, resulting in increased soil detachability in rills (Formanek et al. 1984).

In the portions of the United States where frozen soil is not a problem, the value for soil erodibility gradually decreases over the course of the growing season until it reaches a minimum sometime near the end of the growing season. Then the erodibility value gradually increases until it again reaches the maximum value. This pattern generally follows the rainfall pattern for many areas. Although the actual length of the growing season varies in warmer areas, a value of 6 mo (183 d) appears to be a reasonable approximation of the time between maximum and minimum values of soil erodibility for many soils in the United States. In areas where the growing season or wet-dry periods are significantly different from 6 mo, the values must be adjusted accordingly.

An approach to modifying K values for a given soil based on seasonal variation in erodibility is to assume an exponential decay function for the rate of decrease in erodibility as the growing season progresses. The rate of change in soil erodibility would vary with different types of soil or soil textures (Kirby and Mehuys 1987). The relationship of soil erodibility to soil texture is adequately determined from the soil-erodibility nomograph (Wischmeier et al. 1971) and has already been determined for most of the significant soil series of the United States. By letting the ratio of K_{max} (the maximum value of soil erodibility for a given soil) to K_{nom} (soil erodibility as determined from the nomograph) be constant for a given soil texture, the magnitude of K_{max} also becomes a function of soil texture.

The time span between K_{max} and K_{min} (minimum value of soil erodibility) varies with location and soil. The limited available data suggest that in the North, maximum values of soil erodibility generally occur at or near the beginning of the frost-free growing season and gradually decline to a minimum value at the end of the frost-free growing season. Data also indicate that t_{max} (time of year at which the soil-erodibility factor is at a maximum) occurs progressively earlier from north to south, whereas t_{min} (time of minimum erodibility) occurs progressively later. This is especially true where frost conditions exist during the winter months. In frost-free areas or areas with only minor frost activity, the time from maximum to minimum soil erodibilities corresponds more closely with periods of high and low rainfall, but seldom exceeds 6 mo.

The magnitude of the range of soil erodibility appears to vary, at least partially, with the soil water at the time of a rainfall event. The probability of the soil being wet at any time is a function of the timing and amount of annual precipitation which, for much of the United States, is reflected in the distribution of annual R values (Wischmeier and Smith 1978). Where average R values are low and monthly R values are less uniformly distributed (as in the northern United States), the range between K_{max} and K_{min} is usually wide (>7). Where R values are high and monthly values are more uniformly distributed (as in the southern United States), the range is usually narrower (<3). Where R values exceed 400, the range approaches unity. Data from long-term natural runoff plots at Morris, Minnesota, and Holly Springs, Mississippi, indicate that in northern Mississippi, K_{max} occurs in about mid-December and K_{max}/K_{min} is approximately 3.7, whereas in central Minnesota, K_{max} occurs in about mid-April and K_{max}/K_{min} is approximately 7.6.

Using data from one eastern Canadian province and from seven states in the midwestern and eastern United States, the following relationships were derived:

Case 1: $t_{max}<t_{min}$

If $t_{max} < t_i < t_{min}$, then

$$K_i = K_{max} \left(K_{min} / K_{max}\right)^{\left(t_i - t_{max}\right)/\Delta t} \qquad [3\text{-}11]$$

where K_i = soil-erodibility factor at any time (t_i in calendar days), K_{max} and K_{min} = soil-erodibility factors at times t_{max} and t_{min}, respectively; Δt = length of frost-free period or growing period (≤183 d); and T_{av} = average daily air temperature.

If $t_i < t_{max}$ or $t_i > t_{min}$, then for $T_{av} > 27°F$,

$$K_i = K_{min} \exp\left[0.009\left(t_i - t_{min} + 365\delta\right)\right] \qquad [3\text{-}12]$$

with $\delta = 1$ if $(t_i - t_{min}) \leq 0$ and $\delta = 0$ if $(t_i - t_{min}) > 0$ and for $T_{av} \leq 27°F$, $K_i = K_{min}$.

Case 2: $t_{max} > t_{min}$

If $t_{max} > t_i > t_{min}$, then for $T_{av} > 27°F$,

$$K_i = K_{min} \exp\left[0.009\ (t_i - t_{min})\right] \quad [3\text{-}13]$$

and for $T_{av} \leq 27°F$, $K_i = K_{min}$.

If $t_i > t_{max}$ or $t_i < t_{min}$, then

$$K_i = K_{max}\ (K_{min}/K_{max})^{\left(t_i - t_{max} + 365\delta\right)/\Delta t} \quad [3\text{-}14]$$

with $\delta = 1$ if $(t_i - t_{max}) \leq 0$ and $\delta = 0$ if $(t_i - t_{max}) > 0$.

However, if equation [3-11], [3-12], [3-13], or [3-14] yields

$K_i > K_{max}$, then put $K_i = K_{max}$, or if $K_i < K_{min}$, then put $K_i = K_{min}$.

The constant 0.009 of equations [3-12] and [3-13] was obtained upon fitting this relationship to the database. Based on data from four southern, four midwestern, and four northern soils, the ratios of K_{max}/K_{min} and K_{max}/K_{nom} and the value of t_{max} for areas where R does not exceed 400 are as follows:

$$K_{max}/K_{min} = 8.6 - 0.019R, \quad [3\text{-}15]$$

$$K_{max}/K_{nom} = 3.0 - 0.005R, \text{ and} \quad [3\text{-}16]$$

$$t_{max} = 154 - 0.44R. \quad [3\text{-}17]$$

If $t_{max} < 0$, then $t_{max} = t_{max} + 365$.

These values, plotted against the distribution of annual-erosivity values, are shown in figure 3-4. Using this method, the average annual value of

erodibility (K_{av}) will normally differ slightly from K_{nom} and can be estimated from the relationship

$$K_{av} = \sum (EI_i)K_i /100 \quad [3\text{-}18]$$

The annual EI distribution for any location in the United States can be found using figure 2-7 and table 2-1. The data from which the above relationships were derived were from the central and eastern United States and Canada. These are areas where isoerodent lines are approximated with reasonable accuracy and generally parallel each other as shown in figure 2-1 of chapter 2. There were no erodibility data available from the western states to include in the analysis. In the western United States there is a great deal more spatial variability of rainfall due to orographic effects caused by the mountain and valley topography, combined with the Pacific maritime influence. Erosivity values calculated from rainfall amount and intensity in most of the cropland areas of the western United States are lower than the ones in the central and eastern United States and Canada, where the variable K relationships were developed. Also in the western states, topography and orographic influences result in large fluctuations in local average air temperatures and length of growing season which are difficult to quantify. More research is needed on the effect of R values and fluctuations in temperature and growing season length on seasonal variation of K values in the western states. Thus it is recommended that K values for the region west of the line shown in figure 3-5 be estimated much as they have been in the past, from either the soil-erodibility nomograph or soil properties and the relationship shown in equation [3-1].

Data from volcanic soils in Hawaii suggest a somewhat different soil erodibility relationship than the one discussed above. There is little seasonal variation of K for these soils since they are not normally subject to freeze-thaw cycles. Thus, for volcanic soils in tropical areas, it is recommended that K values be estimated based on soil properties and the relationship shown in equation [3-2].

Following is an example of calculations for K_i and K_{av} for a Barnes loam (Udic Haploboroll) near Morris in west-central Minnesota with an annual EI of 90 and K_{nom} of 0.28. The frost-free period, or timespan between K_{max} and K_{min}, in west-central Minnesota is slightly less than 5 mo, or about 140 d (U.S. Department of Commerce 1968).

From figure 3-4 we arrive at

$t_{max} = 154\text{-}0.44(90)=114$ days (4/24) $\quad t_{min} = 114+140=254$ days (9/11)

$K_{max}/K_{nom} = 3.00\text{-}0.005(90)=2.55 \quad K_{max} = 2.55(0.28)=0.714$

$K_{max}/K_{min} = 8.60\text{-}0.019(90)=6.89 \quad K_{min} = 0.714/6.89=0.104$

Then, for the period from November 16 through March 15, when $T_{av} \leq 27°F$ (see fig. 3-5), $K_i = 0.104$; from March 16 through April 15 and September 1 through November 15 ($t_i < t_{max}$ and $t_i > t_{min}$), $K_i = 0.104\exp[0.009(t_i\text{-}254+365\delta)]$; and from April 15 through August 31 ($t_{max} < t_i < t_{min}$), $K_i = 0.714\ (0.146)^{(t_i-114)/140}$

From figure 3-5

$$K_{av} = \sum (EI_i)K_i /100 = 28.507 /100 = 0.285$$

Calculation of K_{av} by use of this method provides an annual average value for soil erodibility closely resembling the nomograph value (0.28) but reflecting a more realistic representation of seasonal fluctuations in the value of K. This value is similar to an average annual value of 0.24 for Barnes soil measured from long-term natural runoff plots at Morris (Mutchler et al. 1976).

Figure 3-6 shows a plot of K versus time of year for a Barnes loam from the example shown above and for a Loring silty-clay-loam soil (Glossic Fragiudalf) near Holly Springs, Mississippi (using EI distribution values from Memphis, Tennessee). Calculated values for figure 3-6 are shown in figures 3-7 and 3-8. Figure 3-6 indicates a slight increase in soil erodibility for a Barnes loam in early November. This behavior is due to the fact that once K reaches its minimum value at about the end of the growing season (sometime in early September), erodibility begins to increase again until complete soil freezing occurs (usually in November). Once the soil is frozen, erodibility goes back to a minimum value and remains at that value until spring thawing occurs. The Loring silty-clay-loam soil from Mississippi does not reflect this behavior because complete soil freezing does not occur in that area of the country.

ACKNOWLEDGMENT

The helpful suggestions from and discussions with G.R. Foster, USDA-ARS National Sedimentation Laboratory, W. Lafayette, IN, are acknowledged and appreciated.

Table 3-1.
K values obtained from natural fallow runoff plots

Soil type[1]	Location	Family	Period	Slope (%)	Length (ft)	K $\frac{ton}{acre \cdot eros.index}$	Source[2]
Bath sil.	Arnot, NY	Typic Fragiochrept	1938-45	19	72.6	0.05	(a)
Ontario l.	Geneva, NY	Glossoboric Hapludalf	1939-46	8	72.6	.27	(a)
Cecil sl.	Clemson, SC	Typic Hapludult	1940-42	7	180.7	.28	(a)
Honeoye sil.	Marcellus, NY	Glossoboric Hapludalf	1939-41	18	72.6	.28	(a)
Hagerstown sicl.	State College, PA	Typic Hapludalf	[3]NA	NA	NA	.31	(b)
Fayette sil.	LaCrosse, WI	Typic Hapludalf	1933-38	16	72.6	.38	(a)
Dunkirk sil.	Geneva, NY	Glossoboric Hapludalf	1939-46	5	72.6	.69	(a)
Shelby l.	Bethany, MO	Typic Arguidoll	1931-40	8	72.6	.53	(a)
Loring sicl.	Holly Springs, MS	Typic Fraguidalf	1963-68	5	72.6	.49	(c)
Lexington sicl.	Holly Springs, MS	Typic Paleudalf	1963-68	5	72.6	.44	(c)
Marshall sil.	Clarinda, IA	Typic Hapludoll	1933-39	9	72.6	.43	(d)
Tifton ls.	Tifton, GA	Plinthic Paleudult	1962-66	3	83.1	[4]n.c.	(d)
Caribou grav. l.	Presque Isle, ME	Alfic Haplorthod	1962-69	8	72.6	n.c.	(d)
Barnes l.	Morris, MN	Udic Haploboroll	1962-70	6	72.6	.23	(e)
Ida sil.	Castana, IA	Typic Udorthent	1960-70	14	72.6	.27	(d)
Kenyon sil.	Independence, IA	Typic Hapludoll	1962-67	4.5	72.6	n.c.	(d)
Grundy sicl.	Beaconsfield, IA	Aquic Arguidoll	1960-69	4.5	72.6	n.c.	(d)

[1]si l. = silt loam, l. = loam, sl. = sandy loam, sicl. = silty clay loam, ls. = loamy sand, grav. l. = gravelly loam
[2](a) = Olson and Wischmeier 1963
(b) = Wischmeier and Smith 1978
(c) = McGregor et al. 1969
(d) = Lombardi 1979
(e) = Mutchler et al. 1976
[3]NA = Not available.
[4]n.c. = Not calculated. However, soil-loss data for K-value computations are available from National Soil Erosion Laboratory, West Lafayette, Indiana.

Table 3-2.
Regression data of K values on soil properties

Study[1]	Number of Soils	Variables tested	Variables in regression equation	Coefficient of determination	Most significant variable	Dominant soil texture
1	17	34	8	0.87	Slope	Sand
2	55	24	24	0.98	Clay ratio/OM	Silt loam
3	13	10	5	0.90	Agg.	Loam
4	55	NA[3]	5	NA	M	Silt loam
5	7	35	2	0.95	M	Clay
6	10	20	5	0.97	0-0.25mm	Clay

[1] 1 = Barnett and Rogers 1966;
2 = Wischmeier and Mannering 1969;
3 = Young and Mutchler 1977;
4 = Wischmeier et al. 1971;
5 = Römkens et al. 1977;
6 = El-Swaify and Dangler 1976.

[2] Clay ratio = % clay/(% silt + % sand); OM = organic matter; Agg. = an aggregation index; M = (% modified silt) (% silt + % sand), where modified silt is the particle size fraction between 0.002 and 0.100 mm (Wischmeier et al. 1971)

[3]NA = Not available.
Source: Römkens (1985).

Table 3-3.
Soil-water data for major USDA soil textural classes

Texture	Permeability code[1]	Saturated hydraulic conductivity[2] (in/hr)	Hydrologic soil group[3]
Silty clay, clay	6	<0.04	D
Silty clay loam, sand clay	5	0.04-0.08	C-D
Sandy clay loam, clay loam	4	0.08-0.2	C
Loam, silt loam[4]	3	0.2-0.8	B
Loamy sand, sandy loam	2	0.8-2.4	A
Sand	1	>2.4	A+

[1]Permeability codes used in figure 3-1. See National Soils Handbook No. 430 (USDA 1983) for permeability classes.
[2]Rawls et al. (1982)
[3]See National Engineering Handbook (USDA 1972).
[4]Note: Although silt texture is missing because of inadequate data, this should be in permeability class 3.

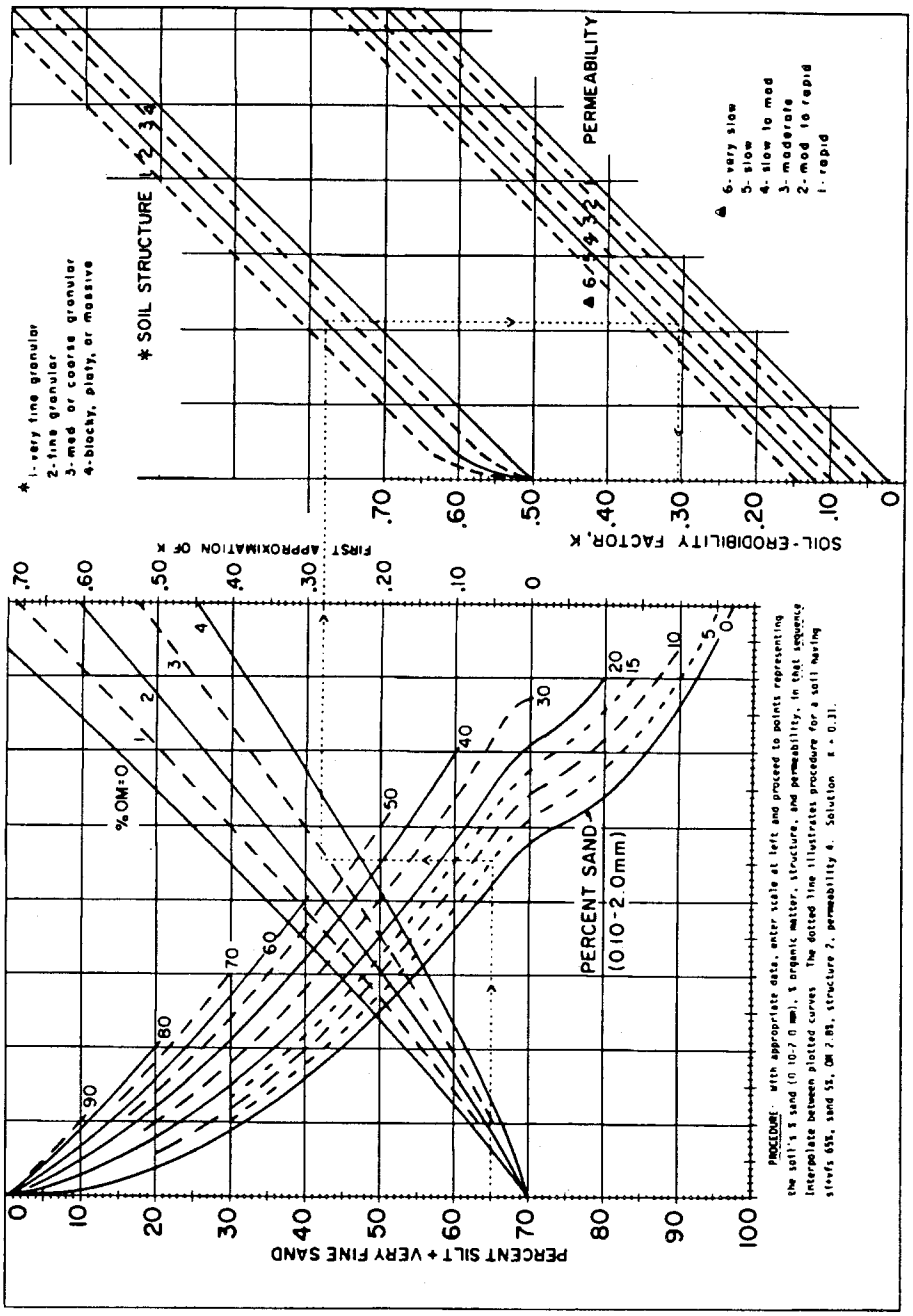

Figure 3-1. Soil-erodibility nomograph (after Wischmeier and Smith 1978). For conversion to SI divide K values of this nomograph by 7.59. K is in U.S. customary units.

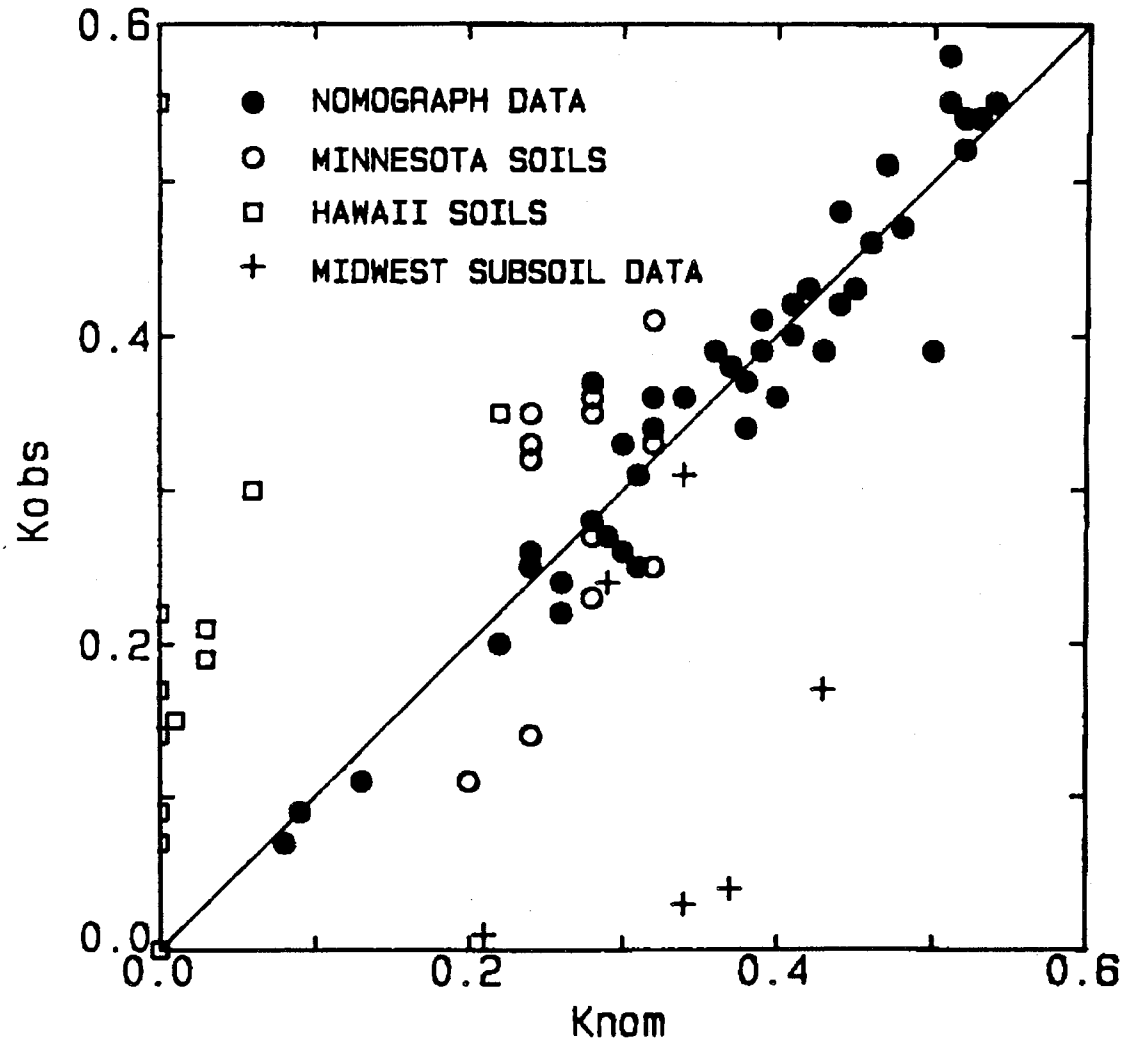

Figure 3-2. Relationship between observed and nomograph-predicted soil-erodibility factor values of several U.S. data sets (● Wischmeier et al. 1971; ○ Young and Mutchler 1977; □ El-Swaify and Dangler 1976; + Römkens et al. 1975). K_{nom} and K_{obs} have units of ton · acre · h (hundreds of acre-ft · tonf · in)$^{-1}$.

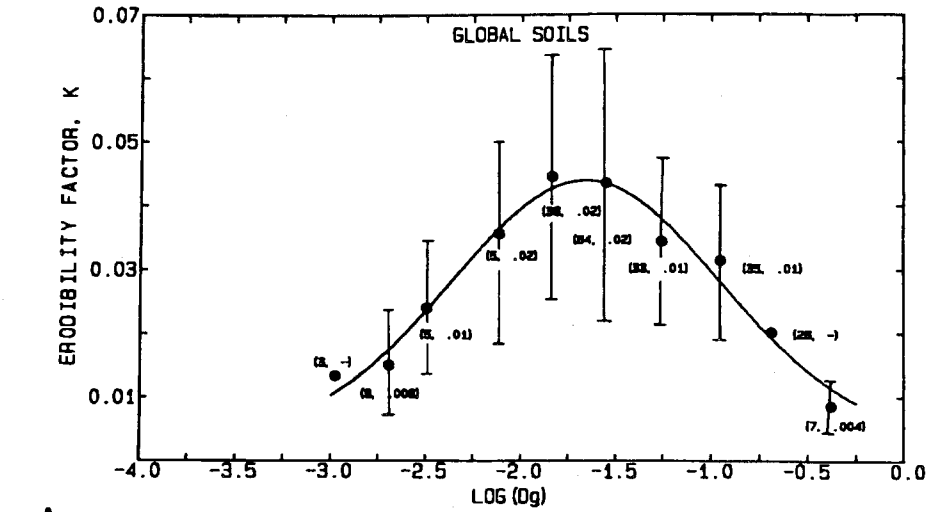

A

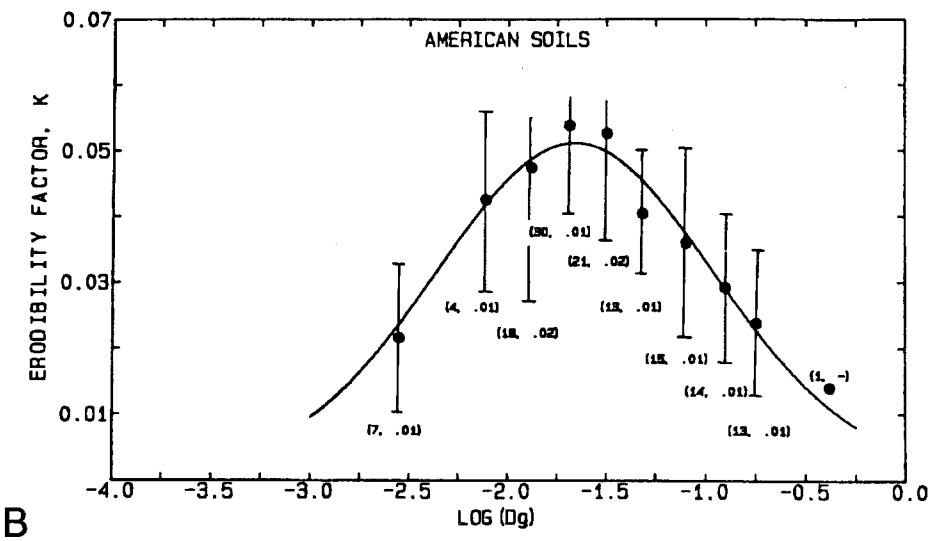

B

Figure 3-3. Soil-erodibility factor (K) as a function of the mean geometric particle diameter (Dg) (in mm). Values are given in SI units and should be multiplied by 7.59 to obtain U.S. customary units. Figure 3-3A represents global soil data, and figure 3-3B represents only U.S. data. Solid line was computed for averages of Dg classes with normal distribution. Vertical lines represent K values in each Dg class plus or minus 1 standard deviation. Numbers in parentheses represent number of observations and standard deviations for each Dg class.

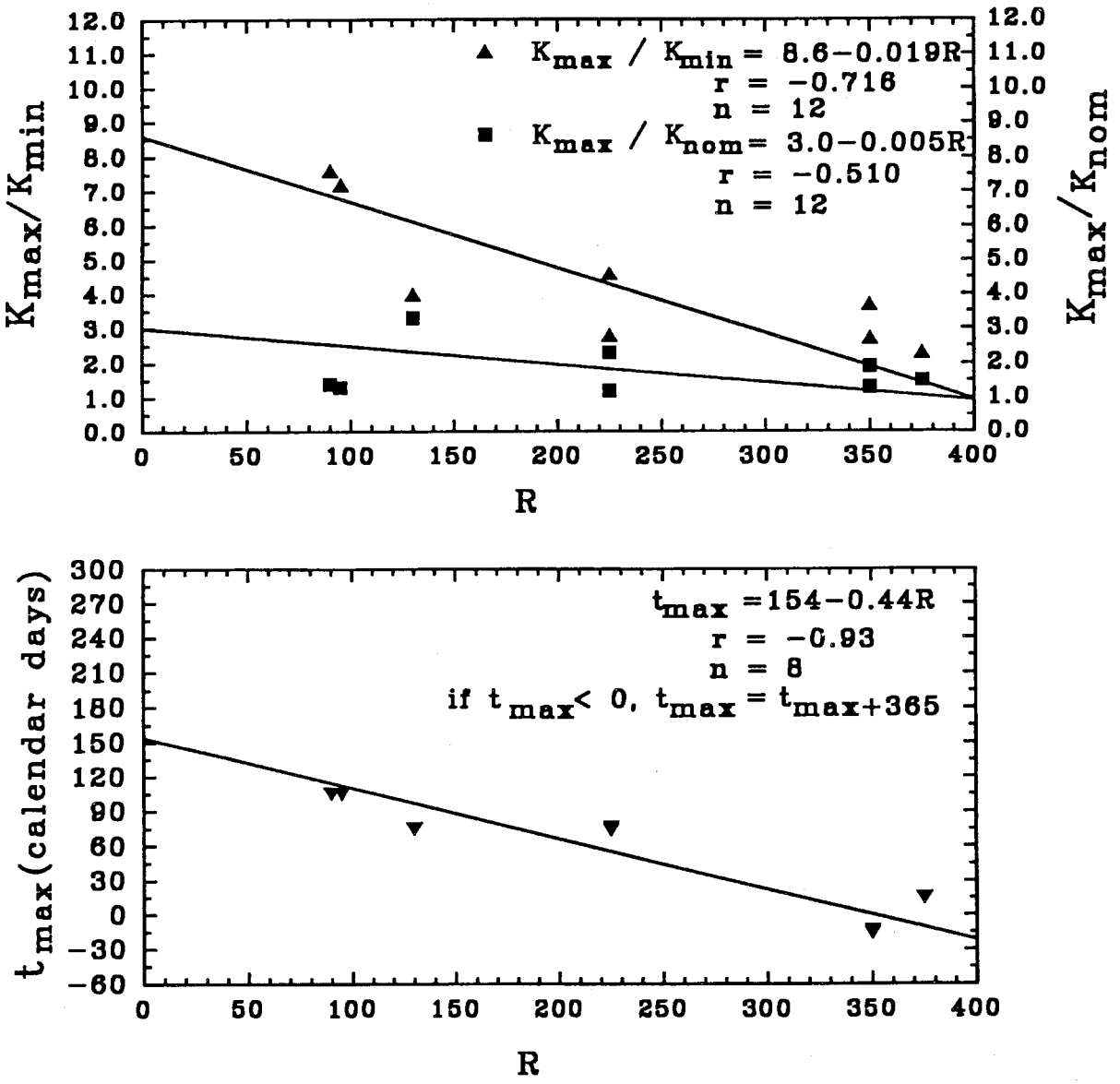

Figure 3-4. K_{max}/K_{min}, K_{max}/K_{nom}, and t_{max} relationships as a function of R for computing seasonal K-values. R is given in U.S. customary units.

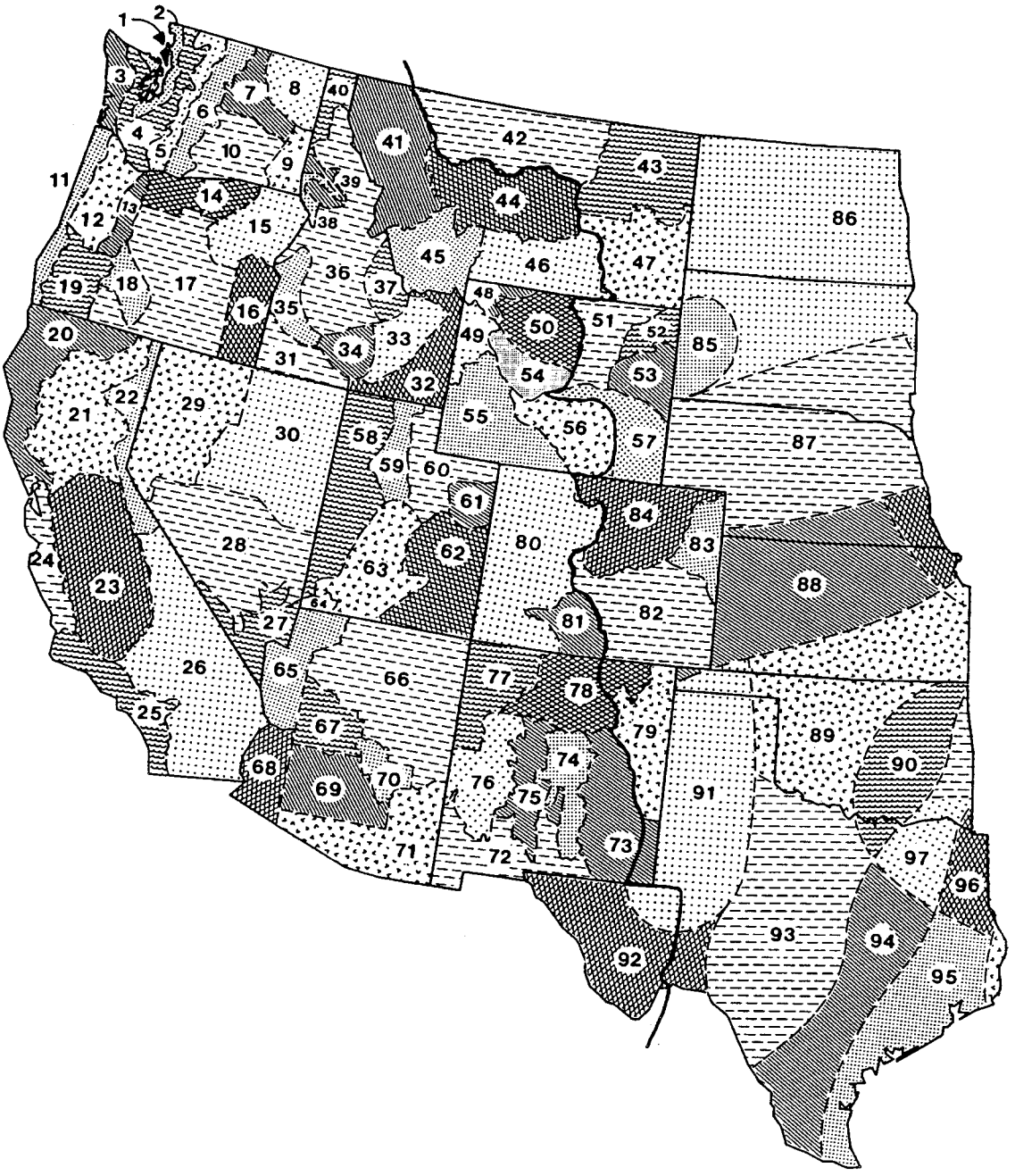

Figure 3-5. Map showing areas for which time-varying K should not be applied. Do not use time-varying K west of the dark line.

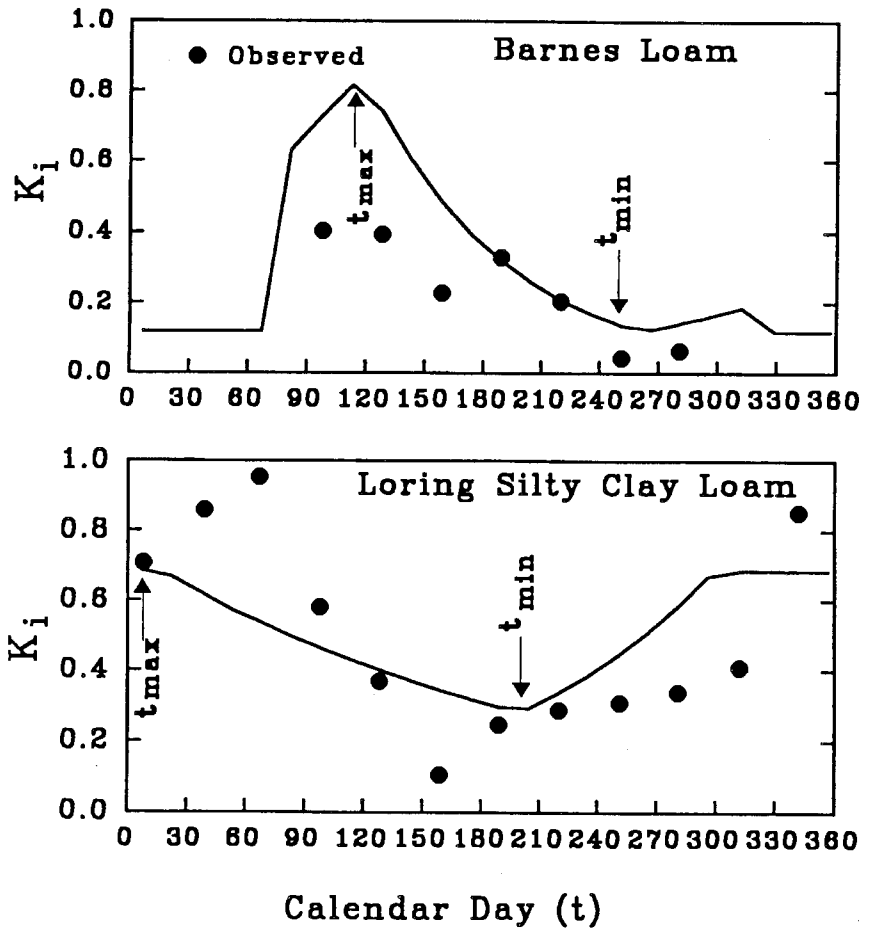

Figure 3-6. Relationship of K_i to calendar days for a Barnes loam soil near Morris, Minnesota, and a Loring silty clay loam soil near Holly Springs, Mississippi. K is given in U.S. customary units.

```
        File          Exit          Help          Screen
-----------------< Seasonally Variable K Factor SWCS1.02 >-----------------
    city code: 23003   MORRIS                MN       estimated K: 0.28
 hyd. group: 1              % surface covered by rock fragments: 0
 soil series: Barnes       surface texture: 1
-----DATE----------%EI----------K-----------DATE----------%EI----------K-----
  1/1-1/15          0.0        0.104         7/1-7/15         13.0        0.254
  1/16-1/31         0.0        0.104         7/16-7/31        14.0        0.206
  2/1-2/15          0.0        0.104         8/1-8/15         14.0        0.166
  2/16-2/28         0.0        0.104         8/16-8/31        13.0        0.135
  3/1-3/15          0.0        0.104         9/1-9/15          5.0        0.108
  3/16-3/31         1.0        0.589         9/16-9/30         3.0        0.115
  4/1-4/15          1.0        0.68          10/1-10/15        1.0        0.132
  4/16-4/30         1.0        0.714         10/16-10/31       1.0        0.151
  5/1-5/15          3.0        0.589         11/1-11/15        0.0        0.175
  5/16-5/31         5.0        0.479         11/16-11/30       0.0        0.104
  6/1-6/15         12.0        0.384         12/1-12/15        0.0        0.104
  6/16-6/30        13.0        0.312         12/16-12/31       0.0        0.104
                                                                          -----
   EI DIST.: 86          FREEZE-FREE DAYS: 140    AVERAGE ANNUAL K:     0.262
    R VALUE: 90      Kmin = 0.104 on 9/11    Kmax = 0.714 on 4/24
                                  < Esc exits >
Tab  Esc F1   F2  F3   F4   F6   F9
FUNC esc help clr cont call list info
```

```
        File          Exit          Help          Screen
-----------------< Create/Edit City Database Set SWCS1.02 >-----------------

  city code: 23003    city: MORRIS_____________      state: MN
  total P: 23.9"      EI curve #: 86          Freeze-Free days/year: 140
  elevation: 0        10 yr EI: 80                      R factor: 90
-------Mean P-----------Tav (deg. F)-----------%EI----------%EI-------
      1: 0.69            1: 10                1: 0          13: 36
      2: 0.72            2: 15                2: 0          14: 49
      3: 1.15            3: 26.5              3: 0          15: 63
      4: 2.45            4: 40                4: 0          16: 77
      5: 2.91            5: 57                5: 0          17: 90
      6: 3.91            6: 66                6: 0          18: 95
      7: 3.29            7: 72                7: 1          19: 98
      8: 3.13            8: 71                8: 2          20: 99
      9: 1.91            9: 60                9: 3          21: 100
     10: 1.85           10: 50               10: 6          22: 100
     11: 1.13           11: 30               11: 11         23: 100
     12: 0.74           12: 17               12: 23         24: 100


                  < F7 Saves, Esc Returns to CITY Main Menu >
Tab  Esc F1   F2  F7   F9   Del
FUNC esc help clr save info del
```

Figure 3-7. Computer screen showing calculated semimonthly K values for a Barnes loam soil near Morris, Minnesota (R = 90, K_{nom} = 0.28, freeze-free days = 140, Δt = 140).

```
        File          Exit          Help          Screen
──────────────< Seasonally Variable K Factor SWCS1.02 >──────────────
    city code: 42003   MEMPHIS              TN       estimated K: 0.498
 hyd. group: 1                % surface covered by rock fragments: 0
 soil series: Loring          surface texture: Sicl
──DATE──────%EI──────K──────┬──DATE──────%EI──────K──
  1/1-1/15       3.0     0.747 │  7/1-7/15      6.0     0.281
  1/16-1/31      3.0     0.738 │  7/16-7/31     6.0     0.258
  2/1-2/15       3.0     0.673 │  8/1-8/15      4.0     0.297
  2/16-2/28      4.0     0.617 │  8/16-8/31     4.0     0.34
  3/1-3/15       4.0     0.572 │  9/1-9/15      3.0     0.393
  3/16-3/31      4.0     0.524 │  9/16-9/30     3.0     0.45
  4/1-4/15       6.0     0.477 │  10/1-10/15    3.0     0.515
  4/16-4/30      6.0     0.437 │  10/16-10/31   2.0     0.59
  5/1-5/15       5.0     0.401 │  11/1-11/15    4.0     0.681
  5/16-5/31      6.0     0.367 │  11/16-11/30   4.0     0.747
  6/1-6/15       5.0     0.335 │  12/1-12/15    3.0     0.747
  6/16-6/30      6.0     0.307 │  12/16-12/31   3.0     0.747
                                                        -----
   EI DIST.: 106        FREEZE-FREE DAYS: 237    AVERAGE ANNUAL K:   0.478
    R VALUE: 300    Kmin = 0.258 on 7/23    Kmax = 0.747 on 1/21
                              < Esc exits >
Tab  Esc F1   F2  F3   F4   F6   F9
FUNC esc help clr cont call list info
```

```
        File          Exit          Help          Screen
──────────────< Create/Edit City Database Set SWCS1.02 >──────────────

  city code: 42003    city: MEMPHIS_____________      state: TN
  total P: 51.6"      EI curve #: 106      Freeze-Free days/year: 237
  elevation: 263      10 yr EI: 90                      R factor: 300
──Mean P──────────Tav (deg. F)──────────%EI──────────%EI──
     1: 4.61          1: 41.6          1: 0          13: 55
     2: 4.33          2: 44.5          2: 3          14: 61
     3: 5.44          3: 52            3: 6          15: 67
     4: 5.77          4: 61.75         4: 9          16: 71
     5: 5.06          5: 70.05         5: 13         17: 75
     6: 3.58          6: 78.3          6: 17         18: 78
     7: 4.03          7: 81.2          7: 21         19: 81
     8: 3.74          8: 80.25         8: 27         20: 84
     9: 3.62          9: 74.25         9: 33         21: 86
    10: 2.37         10: 63.55        10: 38         22: 90
    11: 4.17         11: 50.6         11: 44         23: 94
    12: 4.85         12: 43.25        12: 49         24: 97


                < F7 Saves, Esc Returns to CITY Main Menu >
Tab  Esc F1   F2  F7   F9   Del
FUNC esc help clr save info del
```

Figure 3-8. Computer screen showing calculated semimonthly K values for a Loring silty clay loam soil near Holly Springs, Mississippi (R = 300, K_{nom} = 0.50, freeze-free days = 237, Δt = 183). Nearby Memphis climate data used in Holly Springs.

CHAPTER 4. SLOPE LENGTH AND STEEPNESS FACTORS (LS)

Principal contributors:

D.K. McCool
G.R. Foster
G.A. Weesies

CHAPTER 4. CONTENTS

The effect of topography on erosion in RUSLE is accounted for by the LS factor. Erosion increases as slope length increases, and is considered by the slope length factor (L). Slope length is defined as the horizontal distance from the origin of overland flow to the point where either (1) the slope gradient decreases enough that deposition begins or (2) runoff becomes concentrated in a defined channel (Wischmeier and Smith 1978). Surface runoff will usually concentrate in less than 400 ft, which is a practical slope-length limit in many situations, although longer slope lengths of up to 1,000 ft are occasionally found. Unless the surface has been carefully graded into ridges and furrows that maintain flow for long distances, few slope lengths as long as 1,000 ft should be used in RUSLE. Slope length is best determined by pacing or measuring in the field. For steep slopes, these lengths should be converted to horizontal distance for use in RUSLE. Slope lengths estimated from contour maps are usually too long because most maps do not have the detail to indicate all concentrated flow areas that end RUSLE slope lengths. Figure 4-1 illustrates some typical slope lengths. Hints and guidelines for choosing slope lengths are given in a following section.

The slope steepness factor (S) reflects the influence of slope gradient on erosion. Slope is estimated in the field by use of an inclinometer, Abney level, or similar device. Slope may be estimated from contour maps having 2-ft contour intervals if considerable care is used.

Both slope length and steepness substantially affect sheet and rill erosion estimated by RUSLE. The effects of these factors have been evaluated separately in research using uniform-gradient plots. However, in erosion prediction, the factors L and S are usually evaluated together, and values can be selected from tables 4-1, 4-2, 4-3, or 4-4 for uniform slopes. The following sections give the relationships used to develop these tables. Also, a section explains how to apply RUSLE to nonuniform slopes.

SLOPE LENGTH FACTOR (L)

Plot data used to derive the slope length factor (L) have shown that average erosion for the slope length λ (in ft) varies as

$$L = (\lambda/72.6)^m \quad [4\text{-}1]$$

where 72.6 = the RUSLE unit plot length in ft and m = a variable slope-length exponent (Wischmeier and Smith 1978). The slope length λ is the horizontal projection, not distance parallel to the soil surface.

The slope-length exponent m is related to the ratio β of rill erosion (caused by flow) to interrill erosion (principally caused by raindrop impact) by the following equation (Foster et al. 1977):

$$m = \beta/(1 + \beta) \quad [4\text{-}2]$$

Values for the ratio β of rill to interrill erosion for conditions when the soil is moderately susceptible to both rill and interrill erosion were computed from (McCool et al. 1989)

$$\beta = (\sin \theta/0.0896) / [3.0(\sin \theta)^{0.8} + 0.56] \quad [4\text{-}3]$$

where θ = slope angle. Given a value for β, a value for the slope-length exponent m is calculated from equation [4-2].

The middle column in table 4-5, calculated from equations [4-3] and [4-2], gives values for m that are typical of agricultural fields in seedbed condition. When runoff, soil, cover, and management conditions indicate that the soil is highly susceptible to rill erosion, the exponent m should be increased as shown in the right column of table 4-5. This condition is most likely to occur on steep, freshly prepared construction slopes. These values for m were determined by doubling the β values from equation [4-3] before applying equation [4-2].

Conversely, when the conditions favor less rill erosion than interrill erosion, m should be decreased as shown in the left column of table 4-5. Values for m and LS for rangelands are usually taken from tables for the low ratio of rill to interrill erosion; those values were computed by halving the β values from equation [4-3] before applying equation [4-2]. Values in table 4-5 are based on an analysis by McCool et al. (1989).

When deposition occurs in furrows between ridges and in depressions, soil loss is independent of slope length; therefore the slope-length exponent is zero. Chapter 6 on the RUSLE P factor describes how to apply RUSLE to these conditions.

The slope-length exponent for the erosion of thawing, cultivated soils by surface flow (common in the Northwestern Wheat and Range Region described in ch. 2) differs from the values given in table 4-5. For the erosion of thawing soil by surface flow alone (McCool et al. 1989, 1993), a constant value of 0.5 should be used for the slope length exponent m, and LS values from table 4-4 should be used. When runoff on thawing soils is accompanied by rainfall sufficient to cause significant interrill erosion, values from table 4-5 for the low ratio of rill to interrill erosion should be used for the slope-length exponent m, and LS values from table 4-1 should be used.

SLOPE STEEPNESS FACTOR (S)

Soil loss increases more rapidly with slope steepness than it does with slope length. The slope steepness factor (S) is evaluated from (McCool et al. 1987)

$$S = 10.8 \sin \theta + 0.03 \qquad s < 9\% \qquad [4\text{-}4]$$

$$S = 16.8 \sin \theta - 0.50 \qquad s \geq 9\% \qquad [4\text{-}5]$$

Equation [4-5] is based on the assumption that runoff is not a function of slope steepness, which is strongly supported by experimental data for steepness greater than about 9%. The extent of the effect of slope on runoff is highly variable on cultivated soils. Runoff is assumed to be unaffected by slope steepness on rangelands not recently treated with mechanical practices such as ripping. The effect of slope on runoff and erosion as a result of mechanical disturbance is considered in the support practices factor (P) (ch. 6).

McIsaac et al. (1987a) examined soil-loss data from several experiments on disturbed lands at slopes of up to 84%. They recommended an equation of a form similar to that of equations [4-4] and [4-5]. Their coefficient of sin θ was a range that encompassed equations [4-4] and [4-5]. Thus these equations should also be valid for disturbed-land applications.

Equations [4-4] and [4-5] are not applicable to slopes shorter than 15 ft. For those slopes, the following equation should be used to evaluate S (McCool et al. 1987):

$$S = 3.0 (\sin \theta)^{0.8} + 0.56 \qquad [4\text{-}6]$$

This equation applies to conditions where water drains freely from the end of the slope.

For the slope steepness factor given by equation [4-6], it is assumed that rill erosion is insignificant on slopes shorter than 15 ft and that interrill erosion is independent of slope length. Therefore, equation [4-6] should not be applied to slopes where rill erosion is expected to occur. Rill erosion is assumed to begin with a slope length of 15 ft, although it will occur on shorter slopes that are especially susceptible. Conversely, rill erosion will not begin until longer slope lengths are reached on soils that are consolidated and resistant to detachment by flow.

When recently tilled soil is thawing, in a weakened state, and subjected primarily to surface flow, the following equations for S of McCool et al. (1987, 1993) should be used:

$$S = 10.8 \sin \theta + 0.03 \qquad s < 9\% \qquad [4\text{-}7]$$

$$S = (\sin \theta / 0.0896)^{0.6} \qquad s \geq 9\% \qquad [4\text{-}8]$$

Equations [4-7] and [4-8] were used to construct table 4-4.

TOPOGRAPHIC FACTOR (LS)

The combined LS factor in RUSLE represents the ratio of soil loss on a given slope length and steepness to soil loss from a slope that has a length of 72.6 ft and a steepness of 9%, where all other conditions are the same. LS values are not absolute values but are referenced to a value of 1.0 at a 72.6-ft slope length and 9% steepness.

Procedures are developed in this section for predicting soil loss on uniform slopes, where steepness is the same over their entire length; on irregular or nonuniform slopes that may be concave, convex, or complex; and on a particular segment of a slope.

LS Factor Values for Uniform Slopes

Tables 4-1, 4-2, 4-3, and 4-4 give LS values for uniform slopes. These tables should be used for RUSLE-type slopes with a fairly uniform surface. Table 4-1 is used for rangeland and pasture where the ratio of rill to interrill erosion is low. Table 4-2 is used for cropland where the ratio of rill to interrill erosion is moderate. Table 4-3 is used for construction sites where the ratio of rill to interrill erosion is high and the soil has a strong tendency to rill. Table 4-4 is used for thawing soil where most of the erosion is caused by surface flow.

In tables 4-1, 4-2, and 4-3 for slopes longer than 15 ft, S is calculated from equations [4-4] and [4-5]. For slope lengths of 3-15 ft and steepness greater than or equal to 9%, LS values were calculated for the 3-ft slope length using the short-slope equation [4-6] for S and equations [4-3], [4-2], and [4-1] with λ = 15 ft for L. Then for a given slope length of 3-15 ft and a given steepness, a linear relationship (based on the logarithm of length) was used to interpolate between the logarithm of LS at 3 ft and the logarithm of LS at 15 ft to provide intermediate LS values. For slopes of less than 9%, equation [4-4] was used for S, and equations [4-3], [4-2], and [4-1] with λ = 15 ft were used for L. The short-slope equation [4-6] was not used because for very low slopes, the criterion of free draining would not be met. The inapplicability of equation [4-6] is illustrated by the fact that for very low slopes, the use of equation [4-6] indicates a larger LS value at 3 ft than does the use of equation [4-4] at 20 ft.

The range of LS values for slope lengths of 15-1,000 ft is much greater in table 4-3 than in table 4-1, indicating that the range in L is smaller when interrill erosion is dominant than when rill erosion is dominant. Use of the

72.6-ft slope length and 9% steepness as unit conditions in RUSLE leads to the unexpected result that LS values on short slopes for highly erodible conditions (table 4-3) are smaller than those for less erodible conditions (table 4-1). The difference in overall soil loss is accounted for in the K and C factors. Conditions where soil loss varies little with slope length generally have relatively low C-factor values: less than 0.15. Conditions where soil loss varies greatly with slope length typically have high C-factor values. No LS values for slopes shorter than 15 ft are given in table 4-4. At this time, there are no data to use to develop relationships for short slopes under thawing soil conditions.

Irregular and Segmented Slopes

The shape of a slope affects the average soil loss and the soil loss along the slope. For example, the average soil loss from a convex slope can easily be 30% greater than that for a uniform slope with the same steepness as the average steepness of the convex slope. The difference in soil loss is much greater for maximum erosion on the slopes. The average erosion on a concave slope that does not flatten enough to cause deposition is less than that on a uniform slope that is equivalent to the average concave-slope steepness. Maximum erosion along a concave slope, which occurs about one-third of the way along the slope, may nearly equal the maximum erosion on a uniform slope. Therefore, when the slope shape is significantly curved, use of the procedure for an irregularly shaped slope (outlined below) should be considered (Foster and Wischmeier 1974).

If a nonuniform slope of unit width is broken into a number of segments, each with similar characteristics, an equation for sediment yield from the ith segment is (Foster and Wischmeier 1974)

$$E_i = RK_iC_iP_iS_i \left(\lambda_i^{m+1} - \lambda_{i-1}^{m+1}\right) / (72.6)^m \qquad [4\text{-}9]$$

where

E_i = sediment yield from ith segment from top of slope,
R = rainfall and runoff factor,
K_i = soil erodibility for ith segment,
C_i = cover-management factor for ith segment,
P_i = support practice factor for ith segment,
S_i = slope steepness factor for ith segment, and
λ_i = length (ft) from top of slope to lower end of ith segment.

The soil loss per unit area, A_i, for the ith segment is then the sediment yield from that segment divided by the segment length, as follows:

$$A_i = RK_iC_iP_iS_i\left(\lambda_i^{m+1} - \lambda_{i-1}^{m+1}\right) / \left(\lambda_i - \lambda_{i-1}\right) (72.6)^m \qquad [4\text{-}10]$$

The term $S_i \left(\lambda_i^{m+1} - \lambda_{i-1}^{m+1}\right) / \left(\lambda_i - \lambda_{i-1}\right) (72.6)^m$ in equation [4-10] is the effective LS for the segment.

These relationships are applicable to any slope that meets the criteria for the application of RUSLE. The slope segments can be of unequal length. Computations with unequal slope lengths are most easily handled with a digital computer, for example, by use of the RUSLE computer program. However, to illustrate application of the method, slopes of equal segment length will be used. The term for effective segment LS becomes

$$\begin{aligned} LS_i &= S_i\left\{(ix)^{m+1} - [(i-1)x]^{m+1}\right\} / \left[ix - (i-1)x\right] (72.6)^m \\ &= S_i x^m \left[i^{m+1} - (i-1)^{m+1}\right] / (72.6)^m \end{aligned} \qquad [4\text{-}11]$$

where

LS_i = effective LS for ith segment, and
x = length in ft of each segment.

An additional relationship that proves useful is the soil loss per unit area, A_i, from any segment of a uniform slope, as follows:

$$A_i = RK_iC_iP_iS_i\left\{(ix)^{m+1} - [(i-1)x]^{m+1}\right\} / (72.6)^m \; x \qquad [4\text{-}12]$$

The total soil loss per unit area from a uniform slope of n segments of length x is

$$A = RKCPS(nx)^m / (72.6)^m \qquad [4\text{-}13]$$

If equal RKCP values along the slope are assumed, the ratio of soil loss from any segment to soil loss from the total slope is

$$A_i/A = \left\{ \left[(ix)^{m+1} - ((i-1)x)^{m+1}\right] / (72.6)^m \, x \right\} \cdot \left\{(72.6)^m/(nx)^m\right\}$$
$$= \left[i^{m+1} - (i-1)^{m+1}\right] / (n)^m \qquad [4\text{-}14]$$

Values of A_i/A for a range of values of m appear in table 4-6.

The simplest irregular-slope case is for soil and cover to be constant along the slope. To apply the irregular-slope procedure, the convex, concave, or complex slope is divided into equal-length segments and the segments are listed in the order in which they occur on the slope, beginning at the upper end (as shown in table 4-7). The number of segments depends on how many are required to treat each segment as uniform for practical purposes. In many situations, three segments are sufficient, and more than five are seldom needed.

The segments and their slopes are listed in order from the top of the slope, columns 1 and 2 of table 4-7. Then the LS values for the entire slope length at the segment slopes are selected from tables 4-1, 4-2, 4-3, or 4-4 and are listed in column 3. In this example, a moderate ratio of rill to interrill erosion is assumed; thus table 4-2 is used. The ratio of soil loss from the segment to total soil loss is selected from table 4-6, based on the m value from table 4-5, and listed in column 4. Interpolation may be required. (If the evaluation is from a thawing soil, an m value of 0.5 is used.) Column 5 is the product of columns 3 and 4 divided by the number of segments. The total of the values in column 5 is the LS value for the entire slope. The segment LS is given in column 6 as the product of columns 3 and 4. This value will predict average soil loss in a given segment.

In this example, the LS value that gives the average soil loss for the convex slope is 3.76 versus a value of 2.84 for a 400-ft-long uniform slope with a gradient of 10%, the average steepness of the convex slope. Average soil loss on the convex slope is about 32% greater than that on the uniform slope.

The maximum erosion in this example occurs at the end of both the uniform and convex slopes. From table 4-7, the maximum segment LS is 7.58 for the convex slope and (2.84 x 1.38 =) 3.92 for the uniform slope (enter table 4-6 with an exponent value of 0.52 for segment 3). That is, soil loss over the lower third of the convex slope is almost double that for the lower third of the uniform slope.

For a concave slope of the same length with the segments in reverse order, the values in column 3 would be listed in reverse order. The data for a concave slope are given in table 4-8. The weighted average LS for the concave slope is about 15% smaller than that for an equivalent uniform slope. The maximum soil loss for a segment, as indicated by the segment LS values in column 6, is greatest from the middle segment of the slope. Maximum erosion on this segment is about 76% of maximum erosion on the lower length of the uniform slope. Average soil loss on the concave slope is about 85% of that on the uniform slope.

CHANGES IN SOIL TYPE OR COVER ALONG THE SLOPE

The procedure for irregular slopes can include the evaluation of changes in soil type along a slope. The values in column 5 of table 4-7 or 4-8 are multiplied by the respective values of the soil erodibility factor (K) before summing. The procedure is illustrated in table 4-9. In the example, by use of the data from table 4-7, the erosion on the last segment is seen to be 14 times that on the first segment, whereas it was only 10 times that when K was uniform along the convex slope. This example illustrates how erosion can be great if an erodible soil occurs on the lower end of a convex slope. Average soil loss for the convex slope, based on the sum of values in column 6, is 45% greater than that estimated for the average K (0.32) on an equivalent uniform slope.

Within limits, the procedure can be further extended to account for changes in the C and P factors along the slope by adding a column of segment C and P values. The procedure applies to the segments experiencing net erosion but not to the segments experiencing net deposition. The amount of deposition cannot be estimated by RUSLE.

The soil loss from any segment of a slope can be estimated by the irregular-slope procedure previously presented (column 6 in tables 4-7 and 4-8 is the segment LS). This value can be used with the pertinent RKCP value for the slope to estimate average soil loss from the particular segment. Similarly, column 7 in table 4-9 is the segment KLS and can be used with the RCP value for the slope to estimate average soil loss from the particular segment.

ALTERNATIVE METHOD FOR ESTIMATING LS FOR A SEGMENT

One application of the irregular-slope procedure is to estimate soil loss on a slope segment and compare that against a soil-loss-tolerance value. The irregular-slope procedure was illustrated previously to show how average erosion for segments along a slope can be computed.

A modification of the procedure can also be used. The slope is divided into equal-length segments like the three segments for the convex slope in table 4-7. Assume that a soil-loss estimate is needed for segment 3. Find the LS value from table 4-2 for a uniform slope having the steepness of the segment and total slope length to the lower end of the segment (400 ft). In this example, this LS value is 5.34. Multiply this value by the soil loss factor, 1.42, in table 4-6 using the value for the third segment in a three-segment slope. The product is 7.58, which is the LS value to use for computing erosion for the segment.

Computation of LS for the second segment requires obtaining the LS value for the uniform slope based on the segment steepness and the length to the lower end of the particular segment (267 ft). The LS value is 2.29 in this example. The third segment has no effect on what happens on the upslope segments; when the user is working on the second segment with this approach, the problem becomes a two-segment slope. Therefore, the factor value, 1.30, chosen from table 4-6 is for the end segment of a two-segment slope. The LS for the second segment is (2.29 x 1.30 =) 2.98, which is the same value obtained earlier in table 4-7.

RELATION OF SOIL-LOSS-TOLERANCE VALUES TO SEGMENT EROSION

Soil-loss-tolerance values given in soil surveys are based on average soil loss along a uniform slope (Schertz 1983). Even on a uniform slope, soil loss on the lowest segment of the slope may be as much as 70% greater than the average value for the slope. Slope-average soil-loss-tolerance values must first be adjusted before soil-loss values for segments along an irregular slope are compared to them. This adjustment takes into account the position on the slope and is made by multiplying the slope-average soil-loss-tolerance value by soil-loss-factor values from table 4-6. The procedure is illustrated for a uniform slope on cropland where RKCP = 1.0 is assumed and the soil-loss- tolerance value, T, is 2.0 ton· acre^{-1}· yr^{-1}. The adjusted soil-loss-tolerance values for three segments along a 10% uniform slope of 400-ft length are 2.0 x 0.57 = 1.14 ton · acre^{-1}· yr^{-1} for segment 1, 2.0 x 1.05 = 2.10 ton · acre^{-1}· yr^{-1} for segment 2, and 2.0 x 1.38 = 2.76 ton· acre^{-1}· yr^{-1} for segment 3. The soil-loss-adjustment factor for each segment is determined by entering table 4-5 with the appropriate slope and rill to interrill ratio, obtaining an m value (0.52 for a 10% slope and moderate rill/interrill ratio), and then selecting the appropriate factor for each segment from table 4-5. In this example, interpolation is required. The average soil loss for this slope is the product of (LS)(RKCP) or (2.84)(1.0) = 2.84 ton · acre^{-1}· yr^{-1}. Soil-loss values along the slope are found by multiplying this value by the same factor values from table 4-6 that are used to adjust T values for position on the slope. These products give the values of 1.62, 2.98, and 3.92 ton· acre^{-1}· yr^{-1} for segments 1, 2, and 3, respectively. The soil-loss values are now uniform with respect to the adjusted soil-loss-tolerance values along the slope.

For the convex slope in table 4-7, the initial adjusted T values are 1.28, 2.10, and 2.84 ton· acre^{-1}· yr^{-1} for segments 1, 2, and 3, respectively. The mean of these initial segment values is 2.07 ton· acre^{-1}· yr^{-1}, greater than the tolerance for a uniform slope of steepness equal to the average of the segment steepness. Therefore, the user should multiply each segment adjusted T value by the ratio of 2.00/2.07 = 0.96 to produce an average slope tolerance of 2.0 ton· acre^{-1}· yr^{-1}. The final segment adjusted tolerance values are then 1.23, 2.03, and 2.74 ton· acre^{-1}· yr^{-1} for segments 1, 2, and 3, respectively, whereas the soil-loss values for the segments are 0.72, 2.98, and 7.58 ton· acre^{-1}· yr^{-1}. The user should note that soil loss on the upper segment is much less than the adjusted T value;

therefore, erosion on the first segment is considered to be within allowable limits. However, the soil loss on the last segment is much greater than the adjusted T value, so soil loss is judged to be excessive on the last segment of the convex slope.

For the concave slope in table 4-8, the initial adjusted T values are 1.06, 2.10, and 2.60 ton· acre^{-1}· yr^{-1} for segments 1, 2, and 3, respectively. The mean of these initial segment values is 1.92 ton· acre^{-1}· yr^{-1}, less than the tolerance for a uniform slope of steepness equal to the average of the segment steepness. Therefore, the user should multiply each initial segment adjusted T value by the ratio of 2.00/1.92 = 1.04 to produce an average slope tolerance of 2.00 ton· acre^{-1}· yr^{-1}. The final segment adjusted tolerance values are then 1.10, 2.19, and 2.71 ton· acre^{-1}· yr^{-1} for segments 1, 2, and 3, respectively, whereas the soil losses along the slope are 2.83, 2.98, and 1.47 ton· acre^{-1}· yr^{-1}. The soil-loss values for the upper two segments exceed the adjusted T value, and management practices are chosen to reduce these values to the adjusted T value.

GUIDES FOR CHOOSING SLOPE LENGTHS

In training sessions, more questions are asked about slope length than about any other RUSLE factor. Slope length is the factor that involves the most judgment, and length determinations made by users vary greatly. Figure 4-1 illustrates the major slope-length situations that are found in the field. However, additional guides are useful, especially for rangelands and forest lands.

Actually, an infinite number of slope lengths exist in the field. To apply RUSLE, erosion can be calculated for several of them and the results averaged according to the area represented by each slope length. Sometimes a particular position on the landscape is chosen as the location for a slope length. To establish the ends of the slope length, the user walks upslope from that position, moving perpendicular to the contour, until the origin of overland flow is reached. Often this point is not at the top of the hill but at a divide down the nose of a ridge (illustrated in fig. 4-2).

The lower end of the slope length is located by walking downslope perpendicular to the contour until a broad area of deposition or a natural or constructed waterway is reached. These waterways are not necessarily eroded or incised channels, and this lack of channels can make it difficult to determine the end of slope. One aid is to visualize the locations on the landscape where eroded channels or gullies would naturally form. Figure 4-2 illustrates one area where such waterways are located.

If a slope flattens enough near its end, deposition may occur. When erosion and deposition rates are low and erosion has not recently occurred, deposition begins at the point where slope has decreased to about 5%. Deposition does not necessarily occur everywhere a slope flattens.

Sometimes slope decreases as shown in figure 4-3. On those slopes, deposition can end and erosion can occur on the lower end of the slope. To approximate where deposition ends, the user should do the following: First calculate the ratio of the slope steepness at the end to the slope steepness where deposition begins. Subtract that ratio from 1.0, multiply that difference by the distance from where deposition begins to the end of the slope, and add that product to the distance where deposition begins. To illustrate, assume a 400-ft-long slope with a 2% slope at the end. Assume that deposition begins at 250 ft, where the slope is 5%.

The ratio of the slope steepness is 0.40, and the distance from where deposition begins to the end of the slope is 150 ft. The location where deposition ends is 250+(1.0-0.40)(150) = 340 ft. This procedure, an approximation to results of CREAMS simulations, is for gently curving slopes. When the change of slope is very abrupt, deposition may occur over only a 20- to 40-ft distance.

In the case just described, the water is assumed to flow uniformly as broad sheet flow over the depositional area and onto the downslope eroding area, or from a relatively flat area at the top of the slope onto a steep area. The distance to the origin of flow must be considered in computing soil loss. To compute average erosion for the slope, only the segments experiencing erosion are used in the computations. In this case, RUSLE does not compute sediment yield for the slope. Of course, a diversion ditch across the slope would end the slope length and a new one would begin immediately below the ditch. Also, broad sheet flow does not occur in natural riparian vegetation.

All the situations discussed previously have been simplified. A few specific examples may help the user visualize field slope length. Figure 4-4 is a photo of rill erosion on a steep small-grain field in the Pacific Northwest. Although the small watershed is concave, a relatively straight, closely spaced rill pattern has resulted on most of the slope. The pattern is from the top to the bottom of the slope or to the flow concentration at the bottom of the swale. For these particular conditions alone, slope length can be obtained fairly accurately from U.S. Geological Survey (USGS) 7½-min contour maps with a 20-ft contour interval.

Figure 4-5A shows a row cropped watershed after a series of storms during the early stages of crop growth. The concentrated flow channels are spaced rather closely together, leading to fairly short slope lengths for RUSLE computation. Even with the 1-ft contour interval map in figure 4-5B, realistic slope lengths are difficult to estimate without the aerial photograph for guidance.

The effect of different crop managements on the upper and lower portions of a slope is illustrated in figure 4-6. The boundary between the two managements occurs at about the middle of the slope. Presence of the snow drift on the upper part of the slope causes measured slope length to be a poor predictor of soil loss; the distance to the top of the ridge does not provide a realistic estimate of the length that actually provides the snowmelt. Other than the area where a drill wheel track diverts the runoff and creates a flow concentration, the rill pattern is fairly straight and closely spaced. The bottom of the slope where the runoff collects into a larger channel, or deposits sediment at the toe of the slope, is not shown.

Determination of slope lengths on rangeland and forested watersheds is generally more difficult than determination of slope lengths on cropland because of the permanent vegetation and the frequently irregular topography of the former. Three selected small watersheds from the Lydle Gulch and Blacks Creek drainages east of Boise, Idaho, are shown on a portion of the 7½-min USGS quad sheet for Indian Creek Reservoir in figure 4-7. Figure 4-8 is an example of a steep rangeland watershed with little shrubby permanent vegetation. Because of the steepness of the watershed, there are few depositional areas. However, the hillslopes are rough and the ridgetops rounded, slightly complicating the determination of slope length. Even for this simple case, the determination of slope lengths by inspecting a 7½-min quad sheet with a 20-ft contour interval would lead to slope lengths longer than those determined in the field or from a low-level aerial photograph. The slopes of the transects are irregular, but to conserve space in this publication, LS in figure 4-8 was calculated from the total horizontal slope length and total fall.

Figure 4-9 is a photograph of a more complex rangeland watershed. The slope is flatter than that on the area in figure 4-8, and numerous large mounds make the topography very uneven. The drainage channels are rather broad, vegetated, and poorly defined, and the watershed boundaries are difficult to delineate. The shrubby permanent vegetation is more prevalent than that on figure 4-8, obscuring the flow paths on aerial or oblique photographs. Slope lengths are best determined by field inspection. The use of maps with even a 2-ft contour interval will lead to slope lengths much longer than those determined in the field.

The complex and irregular rangeland watershed that appears on figure 4-10 exemplifies conditions frequently found in the field. The watershed is of low slope, has undulating topography with numerous hummocks or mounds, and has shrubby permanent vegetation that masks the drainages. The determination of slope lengths even by field inspection is difficult, particularly when the grass cover is at its maximum and not yet reduced by grazing.

Figure 4-10 shows a complicated flow system where shrubs, grass clumps, and litter are isolated in hummocks scattered over rangeland, and in effect where water flows down a local slope to a locally concentrated flow area. This flow system may be treated as follows: If flow patterns around and among the hummocks are basically parallel, do not treat the flow concentrations as the end of a short slope length. Choose slope lengths by visualizing the surface as being smooth without the hummocks. If, however, major deposition occurs upstream of the hummocks and/or the flow pattern meanders without a direction, treat the slope lengths as short. Note that on figure 4-10, some of the transects pass through clumps of shrubby vegetation.

ACKNOWLEDGMENT

The assistance of Clifton W. Johnson (retired), hydraulic engineer, USDA-ARS, Northwest Watershed Research Center, Boise, ID, in obtaining photographs and field documentation is gratefully acknowledged.

Table 4-1.
Values for topographic factor, LS, for low ratio of rill to interrill erosion.[1]

Slope (%)	Horizontal slope length (ft)																
	<3	6	9	12	15	25	50	75	100	150	200	250	300	400	600	800	1000
0.2	0.05	0.05	0.05	0.05	0.05	0.05	0.05	0.05	0.05	0.05	0.05	0.05	0.05	0.05	0.05	0.05	0.05
0.5	0.08	0.08	0.08	0.08	0.08	0.08	0.08	0.08	0.09	0.09	0.09	0.09	0.09	0.09	0.09	0.09	0.09
1.0	0.12	0.12	0.12	0.12	0.12	0.13	0.13	0.14	0.14	0.15	0.15	0.15	0.15	0.16	0.16	0.17	0.17
2.0	0.20	0.20	0.20	0.20	0.20	0.21	0.23	0.25	0.26	0.27	0.28	0.29	0.30	0.31	0.33	0.34	0.35
3.0	0.26	0.26	0.26	0.26	0.26	0.29	0.33	0.36	0.38	0.40	0.43	0.44	0.46	0.48	0.52	0.55	0.57
4.0	0.33	0.33	0.33	0.33	0.33	0.36	0.43	0.46	0.50	0.54	0.58	0.61	0.63	0.67	0.74	0.78	0.82
5.0	0.38	0.38	0.38	0.38	0.38	0.44	0.52	0.57	0.62	0.68	0.73	0.78	0.81	0.87	0.97	1.04	1.10
6.0	0.44	0.44	0.44	0.44	0.44	0.50	0.61	0.68	0.74	0.83	0.90	0.95	1.00	1.08	1.21	1.31	1.40
8.0	0.54	0.54	0.54	0.54	0.54	0.64	0.79	0.90	0.99	1.12	1.23	1.32	1.40	1.53	1.74	1.91	2.05
10.0	0.60	0.63	0.65	0.66	0.68	0.81	1.03	1.19	1.31	1.51	1.67	1.80	1.92	2.13	2.45	2.71	2.93
12.0	0.61	0.70	0.75	0.80	0.83	1.01	1.31	1.52	1.69	1.97	2.20	2.39	2.56	2.85	3.32	3.70	4.02
14.0	0.63	0.76	0.85	0.92	0.98	1.20	1.58	1.85	2.08	2.44	2.73	2.99	3.21	3.60	4.23	4.74	5.18
16.0	0.65	0.82	0.94	1.04	1.12	1.38	1.85	2.18	2.46	2.91	3.28	3.60	3.88	4.37	5.17	5.82	6.39
20.0	0.68	0.93	1.11	1.26	1.39	1.74	2.37	2.84	3.22	3.85	4.38	4.83	5.24	5.95	7.13	8.10	8.94
25.0	0.73	1.05	1.30	1.51	1.70	2.17	3.00	3.63	4.16	5.03	5.76	6.39	6.96	7.97	9.65	11.04	12.26
30.0	0.77	1.16	1.48	1.75	2.00	2.57	3.60	4.40	5.06	6.18	7.11	7.94	8.68	9.99	12.19	14.04	15.66
40.0	0.85	1.36	1.79	2.17	2.53	3.30	4.73	5.84	6.78	8.37	9.71	10.91	11.99	13.92	17.19	19.96	22.41
50.0	0.91	1.52	2.06	2.54	3.00	3.95	5.74	7.14	8.33	10.37	12.11	13.65	15.06	17.59	21.88	25.55	28.82
60.0	0.97	1.67	2.29	2.86	3.41	4.52	6.63	8.29	9.72	12.16	14.26	16.13	17.84	20.92	26.17	30.68	34.71

[1]Such as for rangeland and other consolidated soil conditions with cover (applicable to thawing soil where both interrill and rill erosion are significant).

Table 4-2.
Values for topographic factor, LS, for moderate ratio of rill to interrill erosion.[1]

Slope (%)	Horizontal slope length (ft)																
	3	6	9	12	15	25	50	75	100	150	200	250	300	400	600	800	1000
0.2	0.05	0.05	0.05	0.05	0.05	0.05	0.05	0.05	0.05	0.05	0.05	0.05	0.05	0.05	0.06	0.06	0.06
0.5	0.07	0.07	0.07	0.07	0.07	0.08	0.08	0.08	0.09	0.09	0.09	0.09	0.09	0.10	0.10	0.10	0.10
1.0	0.11	0.11	0.11	0.11	0.11	0.12	0.13	0.14	0.14	0.15	0.16	0.17	0.17	0.18	0.19	0.20	0.20
2.0	0.17	0.17	0.17	0.17	0.17	0.19	0.22	0.25	0.27	0.29	0.31	0.33	0.35	0.37	0.41	0.44	0.47
3.0	0.22	0.22	0.22	0.22	0.22	0.25	0.32	0.36	0.39	0.44	0.48	0.52	0.55	0.60	0.68	0.75	0.80
4.0	0.26	0.26	0.26	0.26	0.26	0.31	0.40	0.47	0.52	0.60	0.67	0.72	0.77	0.86	0.99	1.10	1.19
5.0	0.30	0.30	0.30	0.30	0.30	0.37	0.49	0.58	0.65	0.76	0.85	0.93	1.01	1.13	1.33	1.49	1.63
6.0	0.34	0.34	0.34	0.34	0.34	0.43	0.58	0.69	0.78	0.93	1.05	1.16	1.25	1.42	1.69	1.91	2.11
8.0	0.42	0.42	0.42	0.42	0.42	0.53	0.74	0.91	1.04	1.26	1.45	1.62	1.77	2.03	2.47	2.83	3.15
10.0	0.46	0.48	0.50	0.51	0.52	0.67	0.97	1.19	1.38	1.71	1.98	2.22	2.44	2.84	3.50	4.06	4.56
12.0	0.47	0.53	0.58	0.61	0.64	0.84	1.23	1.53	1.79	2.23	2.61	2.95	3.26	3.81	4.75	5.56	6.28
14.0	0.48	0.58	0.65	0.70	0.75	1.00	1.48	1.86	2.19	2.76	3.25	3.69	4.09	4.82	6.07	7.15	8.11
16.0	0.49	0.63	0.72	0.79	0.85	1.15	1.73	2.20	2.60	3.30	3.90	4.45	4.95	5.86	7.43	8.79	10.02
20.0	0.52	0.71	0.85	0.96	1.06	1.45	2.22	2.85	3.40	4.36	5.21	5.97	6.68	7.97	10.23	12.20	13.99
25.0	0.56	0.80	1.00	1.16	1.30	1.81	2.82	3.65	4.39	5.69	6.83	7.88	8.86	10.65	13.80	16.58	19.13
30.0	0.59	0.89	1.13	1.34	1.53	2.15	3.39	4.42	5.34	6.98	8.43	9.76	11.01	13.30	17.37	20.99	24.31
40.0	0.65	1.05	1.38	1.68	1.95	2.77	4.45	5.87	7.14	9.43	11.47	13.37	15.14	18.43	24.32	29.60	34.48
50.0	0.71	1.18	1.59	1.97	2.32	3.32	5.40	7.17	8.78	11.66	14.26	16.67	18.94	23.17	30.78	37.65	44.02
60.0	0.76	1.30	1.78	2.23	2.65	3.81	6.24	8.33	10.23	13.65	16.76	19.64	22.36	27.45	36.63	44.96	52.70

[1]Such as for row-cropped agricultural and other moderately consolidated soil conditions with little-to-moderate cover (not applicable to thawing soil)

Table 4-3.
Values for topographic factor, LS, for high ratio of rill to interrill erosion.[1]

Slope (%)	Horizontal slope length (ft)																
	<3	6	9	12	15	25	50	75	100	150	200	250	300	400	600	800	1000
0.2	0.05	0.05	0.05	0.05	0.05	0.05	0.05	0.05	0.05	0.05	0.06	0.06	0.06	0.06	0.06	0.06	0.06
0.5	0.07	0.07	0.07	0.07	0.07	0.07	0.08	0.08	0.09	0.09	0.10	0.10	0.10	0.11	0.12	0.12	0.13
1.0	0.09	0.09	0.09	0.09	0.09	0.10	0.13	0.14	0.15	0.17	0.18	0.19	0.20	0.22	0.24	0.26	0.27
2.0	0.13	0.13	0.13	0.13	0.13	0.16	0.21	0.25	0.28	0.33	0.37	0.40	0.43	0.48	0.56	0.63	0.69
3.0	0.17	0.17	0.17	0.17	0.17	0.21	0.30	0.36	0.41	0.50	0.57	0.64	0.69	0.80	0.96	1.10	1.23
4.0	0.20	0.20	0.20	0.20	0.20	0.26	0.38	0.47	0.55	0.68	0.79	0.89	0.98	1.14	1.42	1.65	1.86
5.0	0.23	0.23	0.23	0.23	0.23	0.31	0.46	0.58	0.68	0.86	1.02	1.16	1.28	1.51	1.91	2.25	2.55
6.0	0.26	0.26	0.26	0.26	0.26	0.36	0.54	0.69	0.82	1.05	1.25	1.43	1.60	1.90	2.43	2.89	3.30
8.0	0.32	0.32	0.32	0.32	0.32	0.45	0.70	0.91	1.10	1.43	1.72	1.99	2.24	2.70	3.52	4.24	4.91
10.0	0.35	0.37	0.38	0.39	0.40	0.57	0.91	1.20	1.46	1.92	2.34	2.72	3.09	3.75	4.95	6.03	7.02
12.0	0.36	0.41	0.45	0.47	0.49	0.71	1.15	1.54	1.88	2.51	3.07	3.60	4.09	5.01	6.67	8.17	9.57
14.0	0.38	0.45	0.51	0.55	0.58	0.85	1.40	1.87	2.31	3.09	3.81	4.48	5.11	6.30	8.45	10.40	12.23
16.0	0.39	0.49	0.56	0.62	0.67	0.98	1.64	2.21	2.73	3.68	4.56	5.37	6.15	7.60	10.26	12.69	14.96
20.0	0.41	0.56	0.67	0.76	0.84	1.24	2.10	2.86	3.57	4.85	6.04	7.16	8.23	10.24	13.94	17.35	20.57
25.0	0.45	0.64	0.80	0.93	1.04	1.56	2.67	3.67	4.59	6.30	7.88	9.38	10.81	13.53	18.57	23.24	27.66
30.0	0.48	0.72	0.91	1.08	1.24	1.86	3.22	4.44	5.58	7.70	9.67	11.55	13.35	16.77	23.14	29.07	34.71
40.0	0.53	0.85	1.13	1.37	1.59	2.41	4.24	5.89	7.44	10.35	13.07	15.67	18.17	22.95	31.89	40.29	48.29
50.0	0.58	0.97	1.31	1.62	1.91	2.91	5.16	7.20	9.13	12.75	16.16	19.42	22.57	28.60	39.95	50.63	60.84
60.0	0.63	1.07	1.47	1.84	2.19	3.36	5.97	8.37	10.63	14.89	18.92	22.78	26.51	33.67	47.18	59.93	72.15

[1]Such as for freshly prepared construction and other highly disturbed soil conditions with little or no cover (not applicable to thawing soil)

Table 4-4.
Values for topographic factor, LS, for thawing soils where most of the erosion is caused by surface flow.

Slope (%)	Horizontal slope length (ft)												
	15	25	50	75	100	150	200	250	300	400	600	800	1000
0.2	0.02	0.03	0.04	0.05	0.06	0.07	0.09	0.10	0.10	0.12	0.15	0.17	0.19
0.5	0.04	0.05	0.07	0.09	0.10	0.12	0.14	0.16	0.17	0.20	0.24	0.28	0.31
1.0	0.06	0.08	0.11	0.14	0.16	0.20	0.23	0.26	0.28	0.32	0.40	0.46	0.51
2.0	0.11	0.14	0.20	0.25	0.29	0.35	0.41	0.46	0.50	0.58	0.71	0.82	0.91
3.0	0.16	0.21	0.29	0.36	0.42	0.51	0.59	0.66	0.72	0.83	1.02	1.17	1.31
4.0	0.21	0.27	0.38	0.47	0.54	0.66	0.77	0.86	0.94	1.08	1.33	1.53	1.71
5.0	0.26	0.33	0.47	0.58	0.67	0.82	0.94	1.06	1.16	1.34	1.64	1.89	2.11
6.0	0.31	0.40	0.56	0.69	0.79	0.97	1.12	1.26	1.38	1.59	1.95	2.25	2.51
8.0	0.41	0.52	0.74	0.91	1.05	1.28	1.48	1.65	1.81	2.09	2.56	2.96	3.31
10.0	0.48	0.62	0.88	1.08	1.25	1.53	1.77	1.98	2.16	2.50	3.06	3.54	3.95
12.0	0.54	0.70	0.98	1.21	1.39	1.71	1.97	2.20	2.41	2.78	3.41	3.94	4.40
14.0	0.59	0.76	1.08	1.32	1.53	1.87	2.16	2.41	2.64	3.05	3.74	4.31	4.82
16.0	0.64	0.82	1.17	1.43	1.65	2.02	2.33	2.61	2.86	3.30	4.04	4.67	5.22
20.0	0.73	0.94	1.33	1.63	1.88	2.30	2.66	2.97	3.25	3.76	4.60	5.31	5.94
25.0	0.83	1.07	1.51	1.85	2.13	2.61	3.02	3.37	3.69	4.27	5.23	6.03	6.75
30.0	0.91	1.18	1.67	2.05	2.36	2.89	3.34	3.73	4.09	4.72	5.78	6.68	7.47
40.0	1.07	1.38	1.95	2.39	2.75	3.37	3.90	4.36	4.77	5.51	6.75	7.79	8.71
50.0	1.19	1.54	2.18	2.67	3.08	3.77	4.35	4.87	5.33	6.16	7.54	8.71	9.74
60.0	1.30	1.67	2.37	2.90	3.35	4.10	4.74	5.30	5.80	6.70	8.20	9.47	10.59

Table 4-5.
Slope-length exponents (m) for a range of slopes and rill/interrill erosion classes[1]

Slope (%)	Rill/interrill ratio		
	Low	Moderate	High
0.2	0.02	0.04	0.07
0.5	0.04	0.08	0.16
1.0	0.08	0.15	0.26
2.0	0.14	0.24	0.39
3.0	0.18	0.31	0.47
4.0	0.22	0.36	0.53
5.0	0.25	0.40	0.57
6.0	0.28	0.43	0.60
8.0	0.32	0.48	0.65
10.0	0.35	0.52	0.68
12.0	0.37	0.55	0.71
14.0	0.40	0.57	0.72
16.0	0.41	0.59	0.74
20.0	0.44	0.61	0.76
25.0	0.47	0.64	0.78
30.0	0.49	0.66	0.79
40.0	0.52	0.68	0.81
50.0	0.54	0.70	0.82
60.0	0.55	0.71	0.83

[1]Not applicable to thawing soils

Source: McCool et al. (1989).

Table 4-6.
Soil loss factor to estimate soil loss on a segment of a uniform slope.

Number of segments	Sequential number of segments	Slope-length exponent (m)								
		.05	.1	.2	.3	.4	.5	.6	.7	.8
2	1	0.97	0.93	0.87	0.81	0.76	0.71	0.66	0.62	0.57
	2	1.03	1.07	1.13	1.19	1.24	1.29	1.34	1.38	1.43
3	1	0.95	0.90	0.80	0.72	0.64	0.58	0.52	0.46	0.42
	2	1.01	1.02	1.04	1.05	1.06	1.05	1.05	1.04	1.03
	3	1.04	1.08	1.16	1.23	1.30	1.37	1.43	1.50	1.55
4	1	0.93	0.87	0.76	0.66	0.57	0.50	0.44	0.38	0.33
	2	1.00	1.00	0.98	0.96	0.94	0.92	0.88	0.85	0.82
	3	1.03	1.05	1.09	1.13	1.16	1.18	1.2	1.22	1.23
	4	1.04	1.08	1.17	1.25	1.33	1.40	1.48	1.55	1.62
5	1	0.92	0.85	0.73	0.62	0.53	0.45	0.38	0.32	0.28
	2	0.99	0.97	0.94	0.90	0.86	0.82	0.77	0.73	0.69
	3	1.01	1.03	1.04	1.05	1.06	1.06	1.06	1.05	1.03
	4	1.03	1.06	1.12	1.17	1.21	1.25	1.29	1.32	1.35
	5	1.05	1.09	1.17	1.26	1.34	1.42	1.50	1.58	1.65

Soil-loss factors = $[i^{m+1} - (i - 1)^{m+1}]/n^m$
where i = sequential number of segment, m = slope length exponent, and n = number of segments. Values are forced to give a factor total equal to number of segments. Values from RUSLE computer program may differ slightly due to round-off.

Table 4-7.
Illustration of irregular-slope procedure where only gradient changes along a 400-ft convex slope of n segments on cropland

Column (1)	Column (2)	Column (3)	Column (4)	Column (5)	Column (6)
Segment	Gradient (%)	LS from table 4-2	Soil-loss factor from table 4-6	[1](3)· (4)/n	LS for segment (3)· (4)
1	5	1.13	0.64	0.24	0.72
2	10	2.84	1.05	0.99	2.98
3	15	5.34	1.42	2.53	7.58

[1]Total LS for slope = 3.76.

Table 4-8.
Illustration of irregular slope procedure where only gradient changes along a 400-ft concave slope of n segments on cropland

Column (1)	Column (2)	Column (3)	Column (4)	Column (5)	Column (6)
Segment	Gradient (%)	LS from table 4-2	Soil-loss factor from table 4-6	[1](3)· (4)/n	LS for segment (3)· (4)
1	15	5.34	0.53	0.94	2.83
2	10	2.84	1.05	0.99	2.98
3	5	1.13	1.30	0.49	1.47

[1]Total LS for slope = 2.42.

Table 4-9.
Evaluation of a change in K along a 400-ft convex slope of n segments on cropland

Column (1)	Column (2)	Column (3)	Column (4)	Column (5)	Column (6)	Column (7)
Segment	Gradient (%)	LS from table 4-2	Soil-loss factor from table 4-6	K	[1](3)·(4)·(5)/n	KLS for segment (3)·(4)·(5)
1	5	1.13	0.64	0.27	0.065	0.20
2	10	2.84	1.05	0.32	0.318	0.95
3	15	5.34	1.42	0.37	0.935	2.81

[1]Total KLS for slope = 1.32.

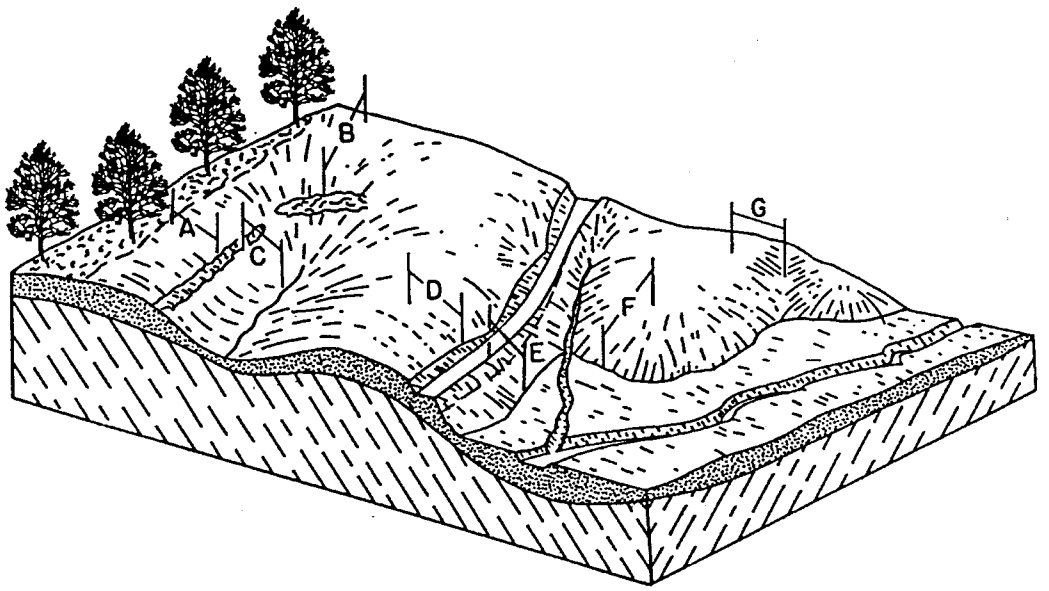

Figure 4-1. Typical slope lengths (Dissmeyer and Foster 1980). Slope A— If undisturbed forest soil above does not yield surface runoff, the top of slope starts with edge of undisturbed forest soil and extends down slope to windrow if runoff is concentrated by windrow. Slope B—Point of origin of runoff to windrow if runoff is concentrated by windrow. Slope C—From windrow to flow concentration point. Slope D—Point of origin of runoff to road that concentrates runoff. Slope E—From road to flood plain where deposition would occur. Slope F—On nose of hill, from point to origin of runoff to flood plain where deposition would occur. Slope G—Point of origin of runoff to slight depression where runoff would concentrate.

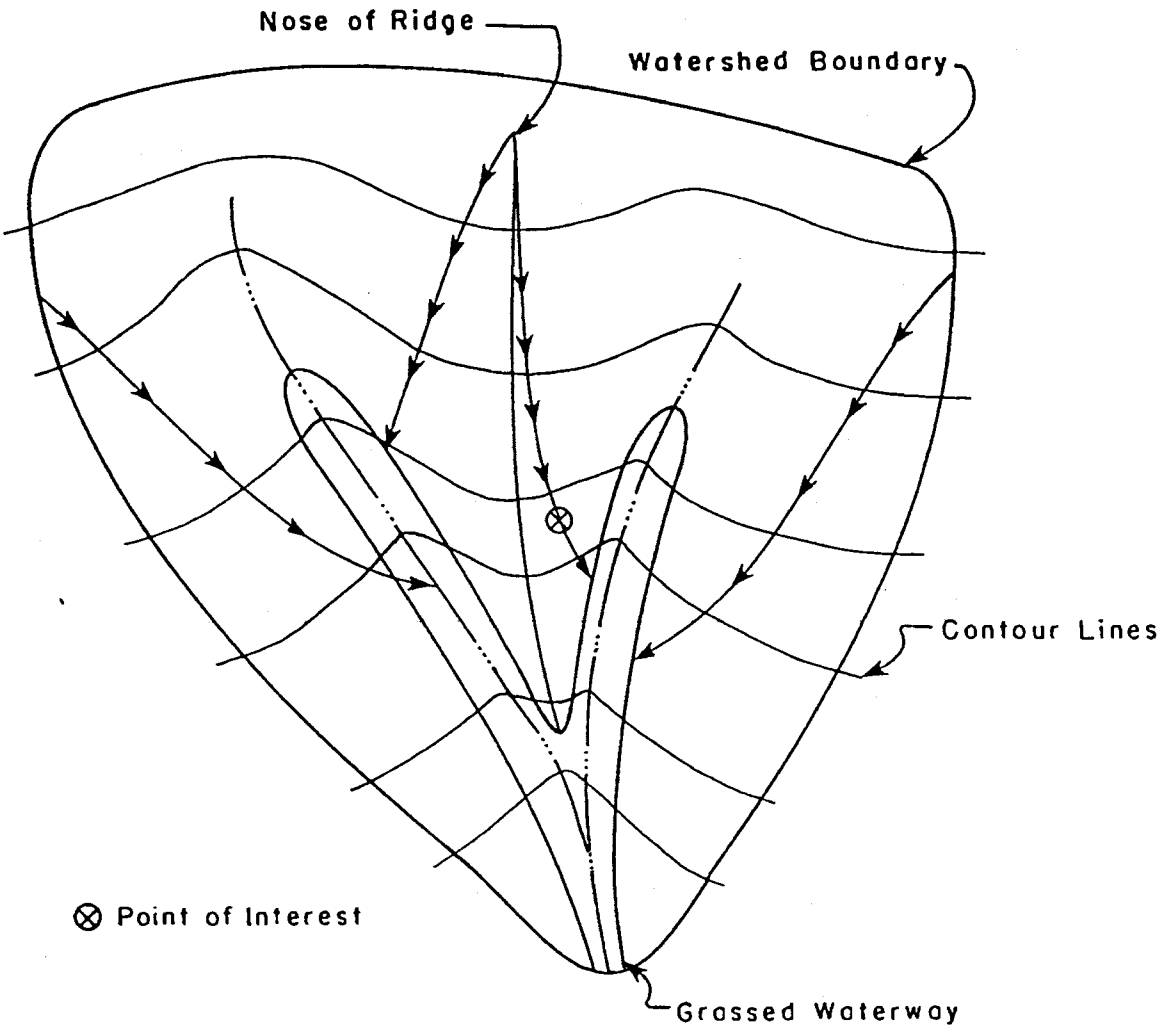

Figure 4-2. Illustration of some RUSLE slope lengths

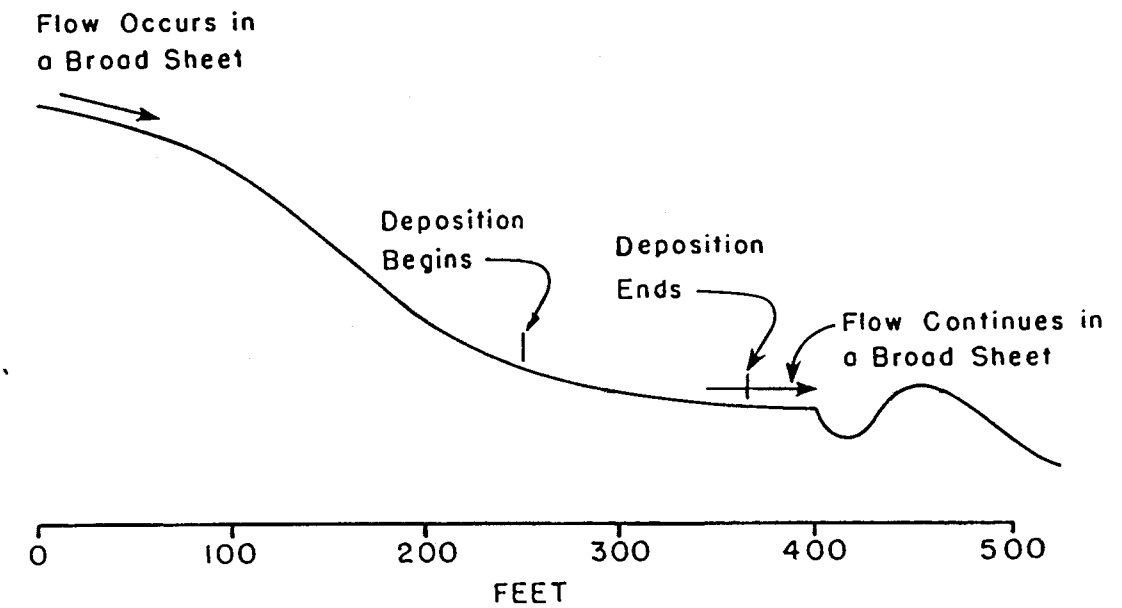

Figure 4-3. Illustration of deposition beginning and ending on a slope

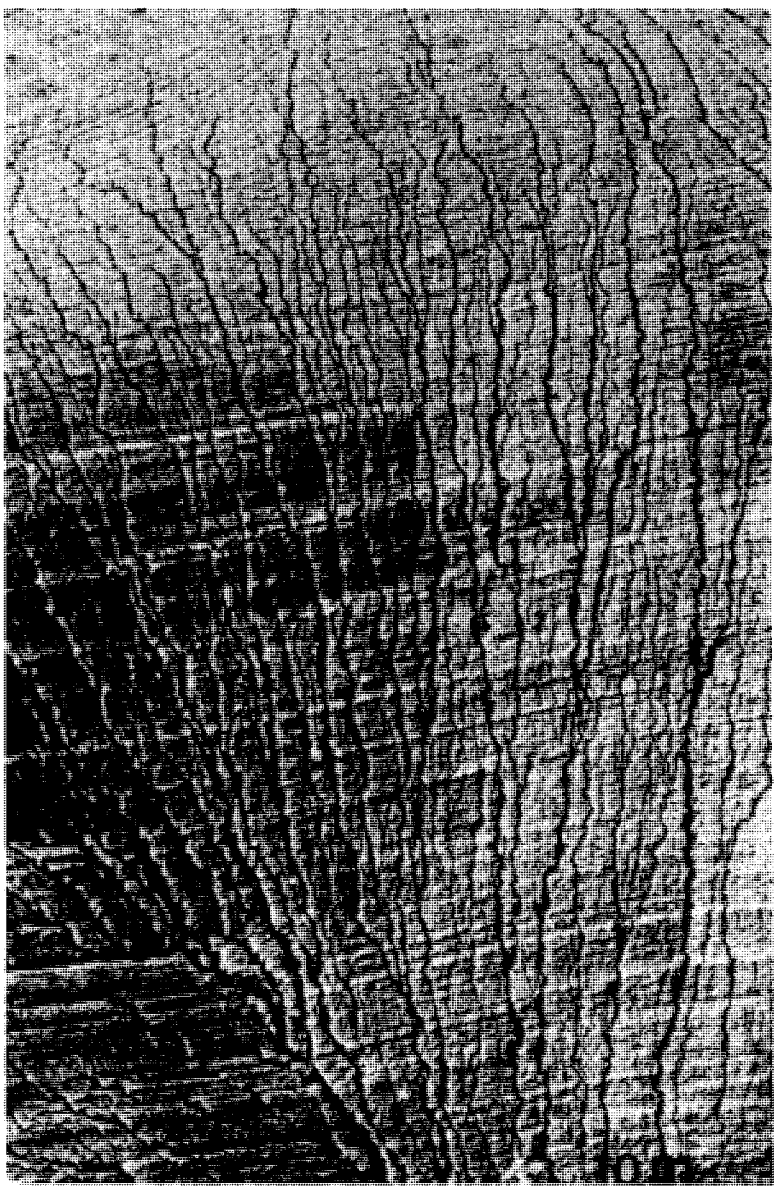

Figure 4-4. Dendritic rill pattern on a concave, north-facing slope. Estimated soil loss was 82 ton · acre^{-1}. From Frazier et al. (1983), reprinted by permission of Soil and Water Conservation Society.

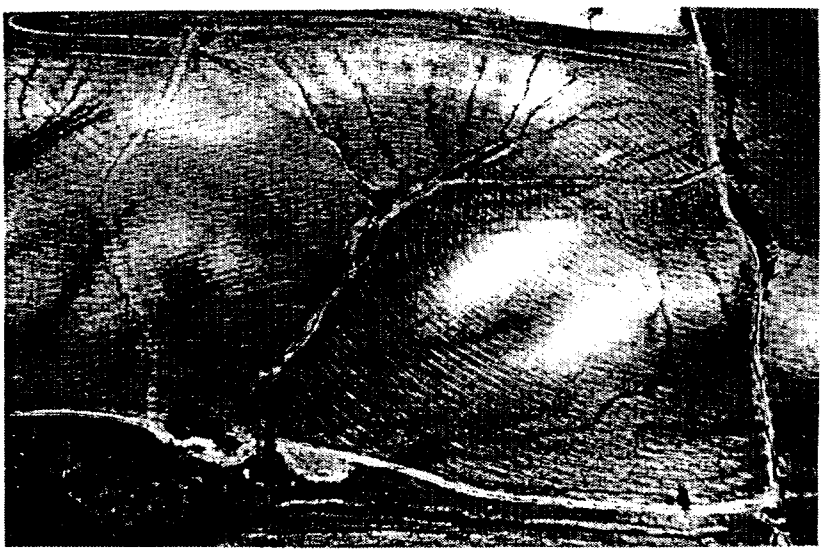

Transect	Slope length (λ) (ft)	Slope steepness (s) (%)	LS
1	280	12	3.14
2	325	13	3.84
3	240	11	2.53
4	205	13	2.97

Figure 4-5A. Erosion resulting from a series of storms on a row crop field during early stages of crop growth

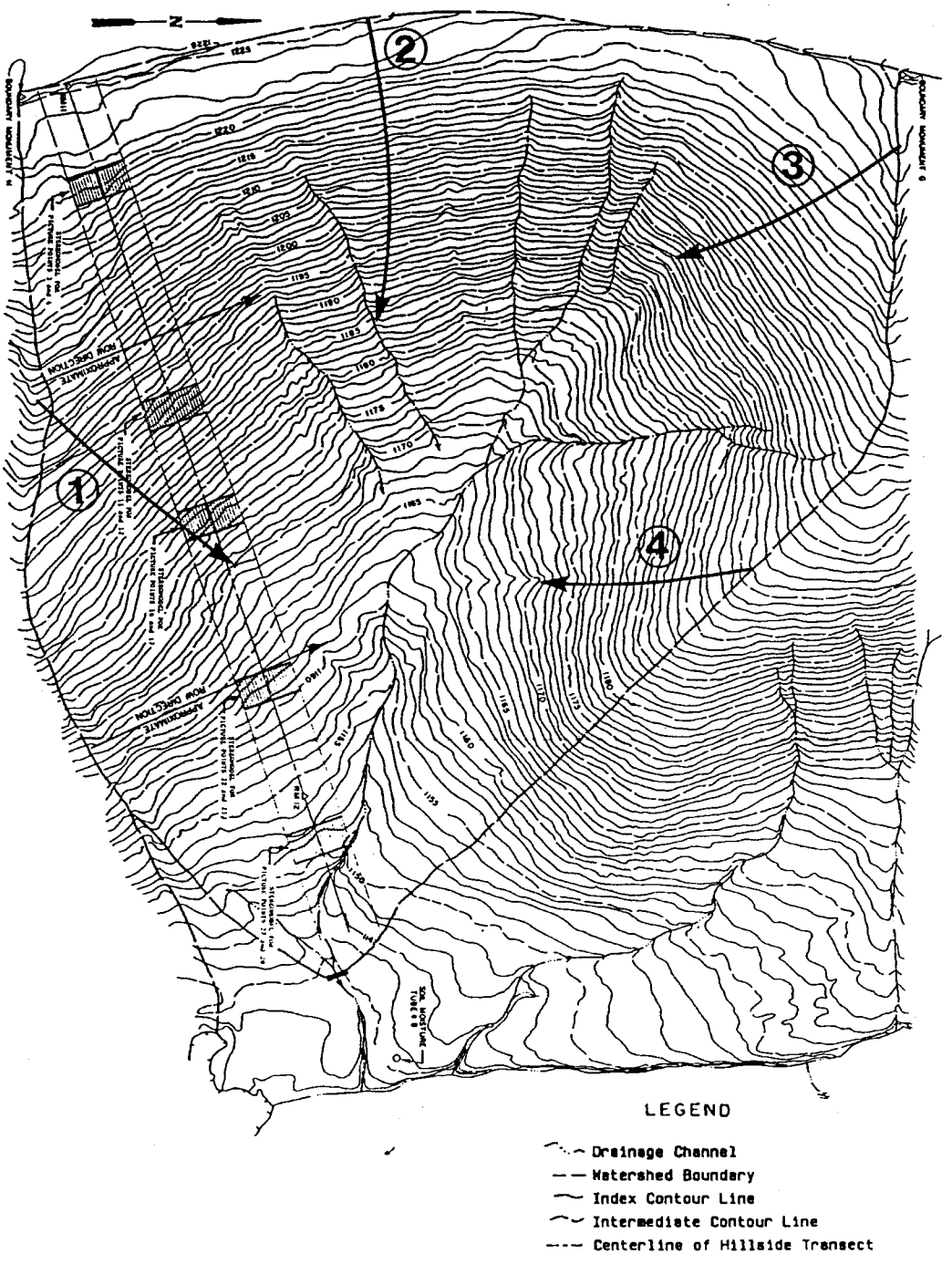

Figure 4-5B. One-ft contour interval map of the row crop field shown in figure 4-5A

Figure 4-6. Erosion from different crop managements on upper and lower halves of a slope. A large snow drift complicated the situation. From Frazier et al. (1983), reprinted by permission of Soil and Water Conservation Society.

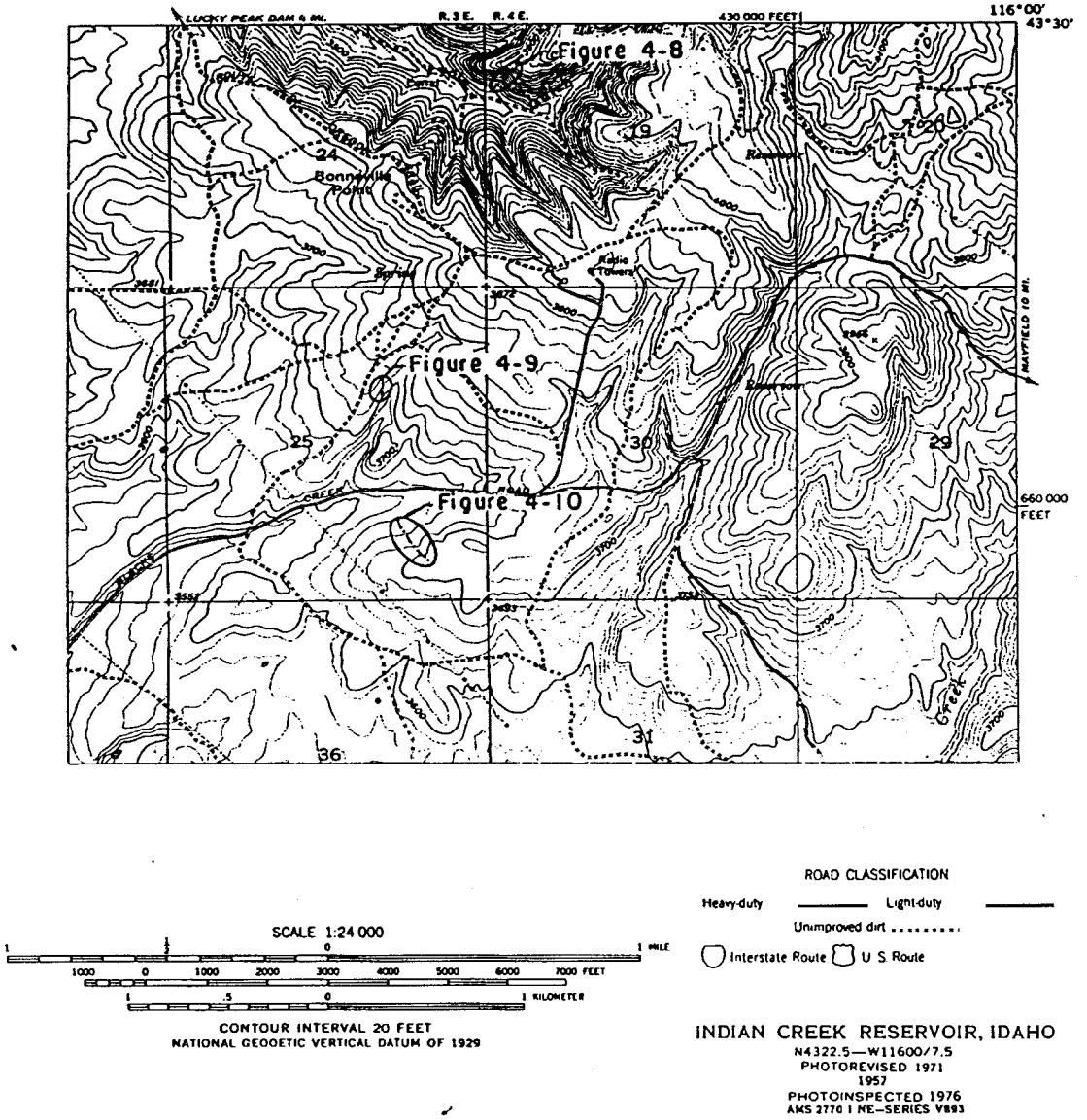

Figure 4-7. Portion of Indian Creek Reservoir USGS 7½-min Quad Sheet showing an area east of Boise, Idaho

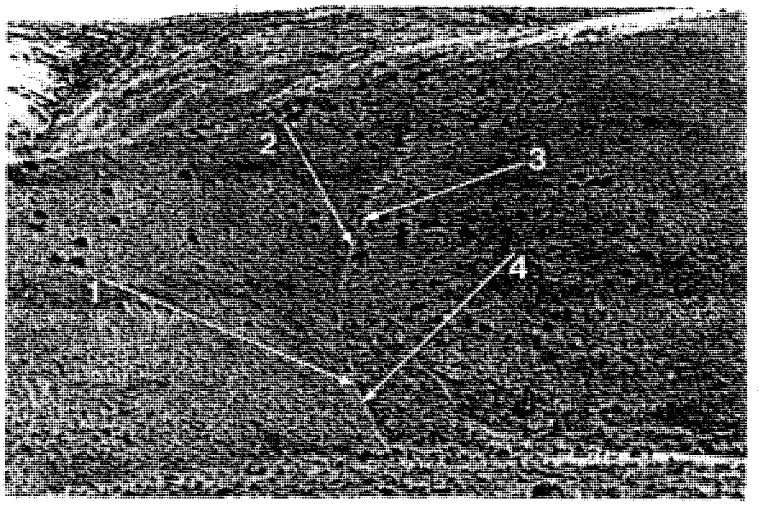

Transect	Slope length (λ) (ft)	Slope steepness (s) (%)	LS
1	225	61	15.44
2	135	53	10.32
3	150	45	9.39
4	375	60	20.18

Figure 4-8. Small rangeland watershed on Lydle Creek east of Boise, Idaho

Transect	Slope length (λ) (ft)	Slope steepness (s) (%)	LS
1	165	14	2.53
2	30	6	0.53
3	50	16	1.85
4	60	14	1.70

Figure 4-9. Small rangeland watershed on Blacks Creek east of Boise, Idaho

Transect	Slope length (λ) (ft)	Slope steepness (s) (%)	LS
1	135	10	1.46
2	45	14	1.51
3	65	21	2.81
4	100	11	1.50
5	40	10	0.95

Figure 4-10. Small rangeland watershed on Blacks Creek east of Boise, Idaho

CHAPTER 5. COVER-MANAGEMENT FACTOR (C)

Principal contributors:

D.C. Yoder
J.P. Porter
J.M. Laflen
J.R. Simanton
K.G. Renard
D.K. McCool
G.R. Foster

CHAPTER 5. CONTENTS

The C factor is used within both the Universal Soil Loss Equation (USLE) and the Revised USLE (RUSLE) to reflect the effect of cropping and management practices on erosion rates, and is the factor used most often to compare the relative impacts of management options on conservation plans. The C factor indicates how the conservation plan will affect the average annual soil loss and how that soil-loss potential will be distributed in time during construction activities, crop rotations, or other management schemes.

As with most other factors within RUSLE, the C factor is based on the concept of deviation from a standard, in this case an area under clean-tilled continuous-fallow conditions. The soil loss ratio (SLR) is then an estimate of the ratio of soil loss under actual conditions to losses experienced under the reference conditions. Work by Wischmeier (1975) and Mutchler et al. (1982) indicated that the general impact of cropping and management on soil losses can be divided into a series of subfactors. Within RUSLE, this technique is used as modified by Laflen et al. (1985) and Weltz et al. (1987). In this approach the important parameters are the impacts of previous cropping and management, the protection offered the soil surface by the vegetative canopy, the reduction in erosion due to surface cover and surface roughness, and in some cases the impact of low soil moisture on reduction of runoff from low-intensity rainfall. As used in RUSLE, each of these parameters is assigned a subfactor value, and these values are multiplied together to yield a SLR.

An individual SLR value is thus calculated for each time period over which the important parameters can be assumed to remain constant. Each of these SLR values is then weighted by the fraction of rainfall and runoff erosivity (EI) associated with the corresponding time period, and these weighted values are combined into an overall C factor value.

USE OF TIME-VARYING OR AVERAGE ANNUAL VALUES

For areas such as pasture or rangeland that have reached a relative equilibrium, the parameters used in computing SLR values may change very slowly with time, so calculated SLR values will also change little. In these cases, it may prove adequate to calculate a C factor based on a single average SLR representing the entire year. RUSLE provides this option to simplify calculations, but this capability must be used with caution, as the result will no longer reflect changes in the climate's erosive potential through the year.

In almost all cropland scenarios and in many cases where rangeland or pasture are being managed, the crop and soil parameters change with time due to either specific management practices or natural cyclic effects such as winter knockdown and spring growth. This demands that the SLR values be calculated frequently enough over the course of a year or a crop rotation to provide an adequate measure of how they change. This is especially important because the erosion potential is also changing with time, as indicated by the EI distributions discussed in chapter 2. The calculated average annual soil loss should be high if a cropping or management scheme happens to leave the soil susceptible to erosion at a time of high rainfall erosivity. USLE incorporated this effect into calculations of SLR values based on crop-growth stages (Wischmeier and Smith 1978). These values were usually assigned based on tillage type, elapsed time since a tillage operation, canopy development, and date of harvest.

Following the lead of the USLE approach, RUSLE calculations are based on a 15-day time step. This means that SLR values are calculated every 15 days throughout the year, and that the important parameters are assumed to remain constant during those 15 days. In order to maintain a total of 24 periods in a year, the first 15 days of each month are placed in one period, and the remainder in another. Period lengths thus range from 13 days for the second period in February to 16 days for the second period in any month having 31 days.

If a management operation occurs within the period, the parameters can no longer be assumed constant; the half-month period is then broken into two segments and two SLR values are calculated. These segments can in turn be broken into smaller time increments by other management operations. A recalculation of the SLR can therefore be forced by either of two occurrences. The first is the end of a half-month period, because conditions are presumed to

have changed sufficiently to require new calculations. The other occurrence is any field operation or sudden climatic change that affects the soil/vegetation/ residue system, thereby changing the value of the SLR. These are handled by dividing the entire time period of interest into time *segments*. Each segment is bracketed by two *events*, which are defined as either a field operation or the beginning of a new half-month period. A segment can therefore range in length from 0 days (if two events occur on the same day) to a 16-day maximum if a month has 31 days and there are no field operations within a period. A zero-length segment is kept track of for accounting purposes, but requires no SLR calculation because there is no associated EI.

Calculations of the SLR for the average annual and time-varying approaches are the same and require the same input parameters; the difference lies in how often the calculation is performed. In the time-varying approach, the SLR value is calculated at a date in the middle of each time segment, and this value is then weighted by the percentage of EI associated with that segment. In the average annual approach, everything is assumed constant, so the calculation is made once.

COMPUTATION OF HALF-MONTH CLIMATE VARIABLES

Calculation of the time-varying SLR requires values for the rainfall, average air temperature, and fraction of total EI associated with each of the half-month periods throughout the year. This forces additional calculations in order to get smooth half-month values when the available data are supplied on a monthly basis.

Known: M, (M-1), and (M+1), which are monthly values for the month of interest (M), the previous month (M-1), and the subsequent month (M+1).

Wanted: P_1 and P_2, which are calculated values of the variable for the first and second half-month periods in the month, respectively.

For the temperature variables,

$$P_1 = 2 \cdot M \left(\frac{.75(M-1)+.25(M+1)}{(M-1)+(M+1)} \right) ;$$

$$P_2 = 2 \cdot M \left(\frac{.25(M-1)+.75(M+1)}{(M-1)+(M+1)} \right) \qquad [5\text{-}1]$$

This works out so that the average of the two period temperatures is equal to the monthly average. For rainfall,

$$P_1 = M \left(\frac{.75(M-1)+.25(M+1)}{(M-1)+(M+1)} \right) ;$$

$$P_2 = M \left(\frac{.25(M-1)+.75(M+1)}{(M-1)+(M+1)} \right) \qquad [5\text{-}2]$$

This leaves the sum of the two period rainfalls equal to the monthly rainfall.

COMPUTATION OF SOIL-LOSS RATIOS

Based on new descriptions of cropping and management practices and their influence on soil loss (Laflen et al. 1985), soil-loss ratios are computed as

$$SLR = PLU \cdot CC \cdot SC \cdot SR \cdot SM \qquad [5\text{-}3]$$

where SLR is the soil-loss ratio for the given conditions, PLU is the prior-land-use subfactor, CC is the canopy-cover subfactor, SC is the surface-cover subfactor, SR is the surface-roughness subfactor, and SM is the soil-moisture subfactor.

Each subfactor contains cropping and management variables that affect soil erosion. Individual subfactors in equation [5-3] are expressed as functions of one or more variables, including residue cover, canopy cover, canopy height, surface roughness, below-ground biomass (root mass plus incorporated residue), prior cropping, soil moisture, and time.

RUSLE uses a CROP database to store the values required to calculate the impact on soil loss of any vegetation within the management plan. These user-defined sets of values specify the growth characteristics of the vegetation, the amount of residue the vegetation will produce, and the characteristics of that residue. The program uses that information to calculate the change with time of the variables listed above and their impact on the subfactors. RUSLE contains another database to store user-supplied information defining the impacts of management operations on the soil, vegetation, and residues, and uses that information to modify the variables accordingly. The relationships of these databases to the subfactor calculations are explained in more detail in the following sections. Published values used in defining some basic crop and operation database sets are shown in tables 5-1 through 5-7. These values are not suitable for all conditions and will need to be adjusted accordingly. This adjustment can be readily accomplished within the RUSLE program by use of procedures described in chapter 7, using estimates as described in appendix D.

The RUSLE program contains a third database that represents the climate for the area of interest. This is important to the C-factor calculations in two ways: first,

the EI distribution within the database set is used to weight each SLR value in calculating the overall C-factor value. Second, the set also contains temperature and rainfall data, which are needed to calculate the rate of residue decomposition. Note that the climatic data are not used to modify the crop growth characteristics, because these are already defined in the crop database.

In addition to the databases, the RUSLE program contains a module that is important to several of the subfactor calculations. This is a subroutine that calculates the rate of residue decomposition as a function of residue characteristics and climate variables. Based on work by Stott et al. (1990) and Stott and Barrett (1991), this is derived as a first-order rate equation, and is calculated as

$$M_e = M_b \exp(-a D) \quad [5\text{-}4]$$

where M_e is residue mass at end of a time period, M_b is mass at beginning of the period, D is period length in days, and

$$a = p \cdot [\text{minimum of } (W, F)] \quad [5\text{-}5]$$

where p is a coefficient depending on residue characteristics (taken from the CROP database), and W and F are precipitation and temperature factors defined subsequently. The database sets provided with the RUSLE program contain empirically derived values of p for specific crops; new values of p must be found either by experimentation or by modifying existing values to reflect known differences in decomposition rates. See appendix D for more information on this modification. The decomposition relationships continue with

$$W = \frac{R}{R_o} \quad [5\text{-}6]$$

and

$$F = \frac{2\left(T_a + A\right)^2 \cdot \left(T_o + A\right)^2 - \left(T_a + A\right)^4}{\left(T_o + A\right)^4} \qquad [5\text{-}7]$$

where R is rainfall in the half-month period, R_o is minimum average half-month rainfall required for optimum decomposition, T_a is average temperature in the half-month period, T_o is optimum temperature for decomposition, and A is a coefficient used to describe the shape of the decomposition response to temperature. Calibration of these constants against decomposition data yields the values $R_o = 2.6$ in, $T_o = 90$ °F, and $A = 46$ °F. These values provide decomposition rates that seem to accurately reflect data from various regions of the United States, including the Pacific Northwest, Texas, Indiana, and Mississippi. The corresponding values of the crop decomposition constant p are shown in table 5-1. There are not sufficient data to distinguish between the decomposition rates of residue under surface and subsurface conditions, so the values shown in table 5-1 can be used for both. These values can be changed when further tests yield more complete information on p values for surface and subsurface conditions. The program treats the two values separately to allow for these changes.

Because SLR values are for half-month periods, they are calculated for the average residue level during the period, which is defined as

$$M_a = \left[\frac{M_b}{a\ D}\right]\left[\ 1\ -\ \exp(-a\ D)\right] \qquad [5\text{-}8]$$

where M_a is average residue mass during the time period, and the other terms are as defined above. Note that D may be up to 16 days but can be smaller if the half-month period is divided by one or more management operations. Note also that the units of mass need not be specified as long as they are consistent. The RUSLE program calculates residue mass in units of (lb · acre^{-1}).

The RUSLE program separately calculates the amount of residue both on the surface and within the soil, and decomposes each according to climatic conditions and residue characteristics. It also accounts for additions of residue to the surface by harvests, senescence, or other management operations, and for incorporation of residue by tillage operations.

The calculations within RUSLE include three additional assumptions concerning residue incorporation and decomposition. First, it is assumed that residue incorporation cannot occur within a soil depth of less than 2 in, regardless of the depth of tillage defined for the field operation. Next, it is assumed that the residue is evenly incorporated throughout the depth of tillage. Finally, it is assumed that all subsurface residue will decompose at the same rate, without regard for the depth to which it is buried. While these assumptions are of limited validity, they provide an appropriate simplified basis on which to make the calculations.

The effectiveness of both surface and incorporated residues in controlling erosion rates has been found to depend on the mechanism by which the soil tends to erode. In general, soils that erode primarily through the formation of rills are substantially more protected by both surface and buried residues than are soils that erode primarily through sheet erosion in the interrill areas. Examples of soils that rill easily include those with naturally weak structure and those whose structure has been destroyed by disturbance and are in an unconsolidated state. Consolidated soils, or those with good structure, usually have a low ratio of rill to interrill erosion.

For permanent pasture or rangeland, the amounts of canopy cover, surface and subsurface residues, and root mass are relatively constant when compared to the widely varying amounts seen with most agronomic crops. This is especially true for permanent pasture or grassland, where the changes in residue and root mass are likely to be a small fraction of the total masses. If the assumption of constant values for these variables is thought to be adequate, RUSLE allows for calculation of the SLR values based on their average annual values. In this case, there are assumed to be no residue additions or decomposition. The program does allow for some disruption by tillage or other practices on a one-time basis and calculates an exponential decay of this effect.

Prior-Land-Use Subfactor (PLU)

The prior-land-use subfactor (PLU) expresses (1) the influence on soil erosion of subsurface residual effects from previous crops and (2) the effect of previous tillage practices on soil consolidation. The relationship is of the form

$$PLU = C_f \cdot C_b \cdot \exp[(-c_{ur} \cdot B_{ur}) + (c_{us} \cdot B_{us} / C_f^{c_{uf}})] \qquad [5\text{-}9]$$

where PLU is the prior-land-use subfactor (which ranges from 0 to 1), C_f is a surface-soil-consolidation factor, C_b represents the relative effectiveness of subsurface residue in consolidation, B_{ur} is mass density of live and dead roots found in the upper inch of soil (lb · acre^{-1} · in^{-1}), B_{us} is mass density of incorporated surface residue in the upper inch of soil (lb · acre^{-1} · in^{-1}), c_{uf} represents the impact of soil consolidation on the effectiveness of incorporated residue, and c_{ur} and c_{us} are calibration coefficients indicating the impacts of the subsurface residues.

The variable C_f expresses the effect of tillage-induced surface density changes on soil erosion. Tillage operations tend to break soil aggregate bonds, increasing the potential for erosion. This is reflected in the lower erosion rates associated with the undisturbed soils of rangeland or no-till systems. Based on the work of Dissmeyer and Foster (1981), the value of C_f for freshly tilled conditions is 1.0. If the soil is left undisturbed, this value decays exponentially to 0.45 over 7 yr, or over some other length of time specified by the user. The impact of a field operation on this factor is determined by the portion of the surface disturbed. For example, if a planting operation disturbs only 30% of the surface that had already consolidated to the point where $C_f = 0.6$, then 70% of the field would have a value of $C_f = 0.6$, and the disturbed 30% would have a value of $C_f = 1.0$; the overall value would be $[(70\%)(0.6) + (30\%)(1.0)]/(100\%) = 0.72 = C_f$.

The B_u variables are used to calculate the impact on erosion rates of live and dead roots and incorporated residue. The effectiveness of such materials can take two forms. First, roots and residue can control erosion directly by physically binding soil particles together and by acting as mechanical barriers to soil and water movement. Second, roots and residue exude binding agents and serve as a food source for microorganisms that produce other organic binding agents. These serve to increase soil aggregation and thereby reduce its susceptibility to erosion.

It is the subsurface biomass (incorporated residue and roots) near the surface that is most effective in resisting erosion, so the values of B_u are in terms of biomass density (lb · acre^{-1} · in^{-1}) in the top inch of soil. The depth of soil that has these biomass densities will be defined by the pattern of field operations. If the most recent operation affects 100% of the surface and has a disturbance depth of 6 in, the B_u values will be the subsurface biomass densities to a depth of 6 in. It is assumed in RUSLE that residue cannot be mixed into a soil depth of less than 2 in, which makes this the least depth to which the B_u values can apply.

The surface residue is assumed to be evenly incorporated into the soil to the depth of tillage, and the root mass at that depth is also assumed to be mixed in.

Inputs provide information on root mass to a depth of only 4 in, but the assumption of no roots below this will lead to incorrect dilution of the residue if mixing occurs to a depth greater than 4 in. RUSLE therefore includes the assumption that the soil depth of 4-8 in contains a root mass equal to 80% of that in the layer at 0-4 in. Note here that soil layers are defined not by soil characteristics or morphology, but by where the roots grow and how deeply the soil is disturbed.

This concept of the B_u values and soil layers can best be clarified with an example, beginning with 6,000 lb · acre^{-1} of surface residue and 1,000 lb · acre^{-1} of root mass in the top 4 in. This gives B_{ur} = 1,000/4 = 250 lb · acre^{-1} · in^{-1} throughout the top 4 in, a biomass density of (1,000 · 0.8)/(8-4) = 200 lb · acre^{-1} · in^{-1} for the layer at 4-8 in, and B_{us} = 0 because no surface residue has been buried. Assume then a field operation that disturbs 100% of the surface, leaves 70% of the surface residue on the surface, and has a tillage depth (and therefore an incorporation depth) of 6 in. Following the operation, there are two soil layers; the top layer is from the surface down to 6 in, below which is a layer from 6 to 8 in. The top layer has a total root mass of (250 · (4-0)) + (200 · (6-4)) = 1,400 lb · acre^{-1}, or B_{ur} = 1,400/6=233 lb · acre^{-1} · in^{-1}, while the bottom layer still has a root mass density of 200 lb · acre^{-1} · in^{-1}. The top layer also contains (6,000 · 0.3) = 1,800 lb · acre^{-1} of incorporated surface residue, leaving (6,000 · 0.7) = 4,200 lb · acre^{-1} on the surface, and yielding B_{us} = 1,800/6 = 300 lb · acre^{-1} · in^{-1}. If this is followed immediately with another tillage that disturbs 100% of the surface, leaves 75% of the residue on the surface, and has a tillage depth of 2 in, we end up with three soil layers: one from 0-2 in, one from 2-6 in, and one from 6-8 in. The top layer has a total root mass of 233 · 2 = 466 lb · acre^{-1} and a total incorporated residue of (300 · 2) + (4,200 · 0.25) = 1,650 lb · acre^{-1}, resulting in B_{ur} = 466/2 = 233 lb · acre^{-1} · in^{-1} and B_{us} = 1,650/2 = 825 lb · acre^{-1} · in^{-1}. The layers at 2-6 and 6-8 in will still have root mass biomass densities of 233 and 200 lb · acre^{-1} · in^{-1}, and incorporated biomass densities of 300 and 0 lb · acre^{-1} · in^{-1}, respectively.

The RUSLE program keeps track of the biomass in each soil layer, continuously adjusting the root mass and subsurface residue to account for additions and decomposition.

Additional complications arise when a field operation does not disturb 100% of the surface, because the residue incorporation and mixing will vary over the field. The program needs to account for the fact that some portions of the field will be protected by additional subsurface biomass, while other portions will not. As it handles the field operation for B_{ur}, the program calculates three values: one overall without considering spatial variability, one for just those areas with

the added incorporation and mixing, and one for the areas without the additional incorporation and mixing. Equation [5-9] is used to calculate the PLU values associated with each of these last two densities, which are then weighted by the associated surface fraction and added. This average PLU value is put back into equation [5-9] to calculate an equivalent weighted B_{ur}. This is divided by the first overall B_{ur}, which yields an adjustment ratio. Until it is changed by the next tillage operation, this ratio is used to adjust the calculated overall B_{ur} (which changes with residue decay and root growth); B_{ur} is multiplied by the ratio before it is put into equation [5-9]. This simplifies calculations during the time between operations by requiring only calculation of the overall B_{ur}, and by accounting for spatial variability with the adjustment ratio. If this procedure is followed, an operation that disturbs 100% of the surface simply yields an adjustment ratio of 1.0. A similar adjustment is used for B_{us}.

As an example of this adjustment, assume that an operation disturbs 20% of the surface, that in the disturbed area $B_{ur} = 500$ lb · acre^{-1} · in^{-1}, in the undisturbed area $B_{ur} = 200$ lb · acre^{-1} · in^{-1}, and that the overall $B_{ur} = 260$ lb · acre^{-1} · in^{-1}. If the first two values are put back into equation [5-9] with an assumed c_{ur} = 0.0014 acre · in · lb^{-1}, the weighted average PLU is PLU = (0.2 · 0.497) + (0.8 · 0.756) = 0.70. This corresponds to an equivalent density of 251 lb · acre^{-1} · in^{-1}, which yields an adjustment ratio of 251 / 260 = 0.97. This indicates that in this case the uneven residue incorporation is only slightly less effective at controlling erosion than if it were incorporated evenly.

The coefficients C_b, c_{ur}, c_{us}, and c_{uf} describe the relative effectiveness of subsurface biomass in reducing erosion. These were calibrated using information from Van Liew and Saxton (1983), values from table 5 and 5-D in Agriculture Handbook 537 (Wischmeier and Smith, 1978), and an extensive data set collected from a broad series of no-till experiments. This analysis yields C_b = 0.951, c_{ur} = 0.00199 acre · in · lb^{-1}, c_{us} = 0.000416 acre · in · lb^{-1}, and c_{uf} = 0.5. For soils that erode primarily as a result of rainfall and snowmelt on frozen or thawing soils (such as many in the Northwest Wheat and Range Region), subsurface residue has been found to be even more effective, yielding c_{ur} = 0.00398 acre · in · lb^{-1}, c_{us} = 0.000832 acre · in · lb^{-1}, and c_{uf} = 0.5.

The amount of incorporated residue is calculated from the additions of residue to the surface and its subsequent burial by tillage operations. The total subsurface biomass is made up of this incorporated surface residue (B_{us} in equation [5-9]), and the total live and dead root mass (B_{ur} in equation [5-9]). The program keeps track of the live roots as described later, and adds this amount to the root residue when the vegetation is killed. The root residue is decayed through use of the decomposition subroutine.

The impact of surface residue on soil organic matter is described by adding a portion of the decayed surface residue mass to the root-mass residue. Based on analysis of no-till erosion data, this fraction is defined as 0.5.

The amount of live roots in the top 4 in is usually taken directly from the CROP database set. The user is responsible for supplying these values, but estimates of root mass at various times in the growing season for selected agronomic crops are given in table 5-2, and suggested values for pasture and meadow crops are shown in table 5-3. In addition, the program assumes that the soil layer at 4-8 in will contain a root mass concentration equal to 80% of that in the top 4 in. This assumption is required to reflect the mixing of soil layers by tillage operations and the resulting redistribution of root mass.

For many rangeland conditions, values of live root mass are not available. Weltz et al. (1987) developed data for estimating root biomass on rangelands. The effective below-ground root biomass (B_b) is given as

$$B_b = B_a \cdot n_i \qquad [5\text{-}10]$$

where B_a is total average annual site production potential ($lb \cdot acre^{-1}$), and n_i is the ratio of effective root mass to annual site production potential. Suggested values of n_i for many plant communities in western U.S. rangelands and eastern pastures are found in table 5-4. Estimates of B_a can be made using standard production potential techniques, or by use of such guides as Natural Resources Conservation Service (NRCS) range-site descriptions.

On croplands, the amount of above- and below-ground biomass present at a given time depends on initial mass of the residue, root mass, fraction of crop residue incorporated by field operations, and decomposition rate of residue and roots. If the initial residue mass at harvest is not known, it can be estimated by multiplying the grain yield by the residue-to-yield ratio (table 5-1). The percentages of residue cover left on the soil surface after various field operations are shown in table 5-5. These values may vary considerably, depending on crop type, implement speed, and soil and residue conditions. If more than one type of residue cover exists on the surface, this percentage of each of the residues will be left after the field operation.

Canopy-Cover Subfactor (CC)

The canopy-cover subfactor expresses the effectiveness of vegetative canopy in reducing the energy of rainfall striking the soil surface. Although most rainfall intercepted by crop canopy eventually reaches the soil surface, it usually does so

with much less energy than does rainfall that strikes the ground without having been intercepted. The intercepted raindrops fracture into smaller drops with less energy, or drip from leaf edges, or travel down crop stems to the ground. The canopy-cover effect is given as

$$CC = 1 - F_c \cdot \exp(-0.1 \cdot H) \qquad [5\text{-}11]$$

where CC is the canopy-cover subfactor ranging from 0 to 1, F_c is fraction of land surface covered by canopy, and H (ft) is distance that raindrops fall after striking the canopy.

This relationship was given graphically by Wischmeier and Smith (1978) and is shown in figure 5-1 for several heights. It is based on the assumptions that the rainfall fraction intercepted by the canopy is equal to the fraction of the land surface beneath the canopy, and that any rainfall intercepted will leave the canopy at a height H (ft) with a mean drop diameter of 0.1 in. Although Quinn and Laflen (1983) found that stem flow was quite significant and that drop sizes differed from those assumed by Wischmeier and Smith, they did find that the relationship given in equation [5-11] was satisfactory for corn. Others have noted the different effects of various kinds of crops (Armstrong and Mitchell 1987, 1988; Finney 1984; Haynes 1940). Values for F_c and H for each crop are defined by the user. Some suggested values for several crops are listed in table 5-2.

Surface-Cover Subfactor (SC)

Surface cover affects erosion by reducing the transport capacity of runoff water (Foster 1982), by causing deposition in ponded areas (Laflen 1983), and by decreasing the surface area susceptible to raindrop impact. It is perhaps the single most important factor in determining SLR values. Surface cover includes crop residue, rocks, cryptogams, and other nonerodible material that is in direct contact with the soil surface (Simanton et al. 1984, Box 1981, Meyer et al. 1972). The effect of surface cover on soil erosion is given by

$$SC = \exp\left[-b \cdot S_p \cdot \left(\frac{0.24}{R_u} \right)^{0.08} \right] \qquad [5\text{-}12]$$

where SC is the surface-cover subfactor, b is an empirical coefficient, S_p is percentage of land area covered by surface cover, and R_u is surface roughness (in) as defined by equation [5-16].

The b value indicates the effectiveness of surface cover in reducing soil erosion. Laflen et al. (1980) and Laflen and Colvin (1981) found that b values ranged from 0.030 to 0.070 for row crops, and Dickey et al. (1983) found b values of 0.024-0.032 in a rainfall-simulation study on small grains. Within the Northwestern Wheat and Range Region, b values greater than 0.050 have been found for small grains. Simanton et al. (1984) recommended a b value of 0.039 for rangeland conditions with the impact of subsurface biomass removed. The relationship given in equation [5-12] is shown in figures 5-2 and 5-3 for several values of R_c and b.

Even though experimental data reflect a wide variance in b values, additional analyses using modeling techniques have indicated that the selection of an appropriate b value can be made more accurately if the dominant erosion process is known. When rill erosion is the primary mechanism of soil loss (such as for irrigation or snowmelt or for highly disturbed soils), b values should be about 0.050. Fields dominated by interrill erosion have a b value of around 0.025. For typical cropland erosion conditions, a b value of 0.035 is suggested. For rangeland and permanent pasture communities, the b value depends on the general type of vegetation.

The percentage of land area covered by residue can be estimated from residue weight by use of the relationship developed by Gregory (1982), as follows:

$$S_p = \left[1 - \exp \left(-\alpha \cdot B_s \right) \right] \cdot 100 \qquad [5\text{-}13]$$

where S_p is percent residue cover, α is the ratio of the area covered by a piece of residue to the mass of that residue (acre $\cdot$ lb^{-1}), and B_s is the dry weight of crop residue on the surface (lb $\cdot$ acre^{-1}). Typical values for α are given in table 5-1. Percent residue covers for various residue weights from the use of equation [5-13] are illustrated in figure 5-4. If more than one type of residue is present, the resulting total surface cover is calculated by modifying equation [5-13] as

$$S_p = \left\{ 1 - \exp \left[- \sum_{i=1}^{N} \left(\alpha_i B_{si} \right) \right] \right\} \cdot 100 \qquad [5\text{-}14]$$

where N is number of residue types and α_i is ratio of the area covered to the mass of that residue for each type encountered.

Within RUSLE, rather than entering a value for α, the program asks for residue weights associated with specific values of residue cover and calculates the corresponding α value. The program asks for residue weights at 30%, 60%, and 90% surface cover. Only one of these needs to be entered to calculate an α value. If more than one weight is entered, the program will calculate an α value for each and then average them.

Surface-Roughness Subfactor (SR)

Surface roughness has been shown to directly affect soil erosion (Cogo et al. 1984), and to indirectly affect it through the impact on residue effectiveness, implied in equation [5-12]. In either case, this is a function of the surface's random roughness, which is defined as the standard deviation of the surface elevations when changes due to land slope or nonrandom tillage marks (such as dead furrows, traffic marks, and disk marks) are removed from consideration (Allmaras et al. 1966). A rough surface has many depressions and barriers. During a rainfall event, these trap water and sediment, causing rough surfaces to erode at lower rates than do smooth surfaces under similar conditions. Increasing the surface roughness decreases the transport capacity and runoff detachment by reducing the flow velocity.

Roughness and cloddiness of soils also affect the degree and rate of soil sealing by raindrop impact. Soils that are left rough and cloddy typically have higher infiltration rates. Soils that are finely pulverized are usually smooth, seal rapidly, and have low infiltration rates (Sumner and Stewart 1992).

Values of random roughness vary, depending on the type and degree of surface disturbance. Typical values are given in table 5-5 for cropland and table 5-6 for rangeland conditions. These core values may be modified as described in appendix D. Roughness conditions for a given field operation may vary, depending on previous tillage, implement speed, and field conditions.

The impact of surface roughness on erosion is defined by a baseline condition, which sets SR equal to 1 for unit plot conditions of clean cultivation smoothed by extended exposure to rainfall of moderate intensity. These conditions yield a random roughness of about 0.24 in. This makes it possible to get SR values of greater than 1 for practices in which the soil is very finely pulverized and smoothed to a smaller random roughness, as might be the case for some rototilling operations or for repeated cultivations of silt loam soils under dry fallow conditions. For conditions in which repeated disturbance leaves a rougher surface (for example, for continuous cattle-grazing), this final roughness value of 0.24 can be replaced. Chapter 7 describes how this is done.

Except in these cases of fine pulverization, it is assumed that the roughness left after field operations is smoothed by the effects of raindrop impact, approaching a random roughness of 0.24 in as the cumulative rainfall increases. This smoothing is modeled by expanding on the relationship described by Onstad et al. (1984)

$$D_r = \exp\,[1/2\ (-0.14 \cdot P_t) + 1/2\ (-0.012 \cdot EI_t)] \qquad [5\text{-}15]$$

where D_r is the dimensionless roughness decay coefficient, P_t is the total inches of rainfall since the most recent operation that disturbed the entire surface, and EI_t is the total EI amount since that same operation. The value of D_r ranges exponentially from a value of 1.0 for a surface that has experienced no rainfall to a value approaching 0.0 for a surface that has experienced extensive rainfall and has lost most of its roughness.

If the initial roughness is defined as R_i (in inches), the surface roughness just before the current tillage operation (R_u) can be defined as

$$R_u = 0.24 + [D_r\ (R_i - 0.24)] \qquad [5\text{-}16]$$

where R_u is in inches. Since many field operations affect only a portion of the surface, R_u is also the roughness of the portion of the field that is undisturbed by the current field operation.

For that portion of the surface that is affected by the field operation, the resulting roughness has been found to be a function of subsurface biomass present in the top 4 in of soil. This relationship is described by

$$R_a = 0.24 + (R_t - 0.24)\{0.8\ [1 - \exp(-0.0012\ B_u)] + 0.2\} \qquad [5\text{-}17]$$

where R_a is the roughness after biomass adjustment (in), R_t is the original tillage roughness based on the assumption of ample subsurface biomass such as that found with high-yielding midwestern corn (in), and B_u is total subsurface biomass density in the top inch of soil (lb $\cdot$ acre^{-1} $\cdot$ in^{-1}). $B_u = B_{ur} + B_{us}$ as defined for equation [5-9]. Researchers in the Northwestern Wheat and Range Region indicate that the strong relationship of tillage roughness to subsurface biomass does not hold for their conditions (D.K. McCool, personal communication 1994). In that area of the country, equation [5-17] is not used, leaving simply $R_a = R_t$.

This adjusted tillage roughness is then combined with that of the undisturbed portion of the surface as

$$R_n = R_a F_d + R_u F_u \quad [5\text{-}18]$$

where R_n is the net roughness following the field operation (in). F_d and F_u are the fractions of the surface disturbed and undisturbed, respectively, so their sum equals one.

Similarly, the decay coefficient must be adjusted to reflect the fact that only a portion of the field was disturbed. This is done using the relationship

$$D_e = D_r F_u + 1.0 F_d \quad [5\text{-}19]$$

where D_e is the equivalent roughness decay coefficient. Under the assumption that the ratio EI_t/P_t before the operation equals that after, the P_t and EI_t values corresponding to the equivalent roughness decay coefficient are

$$P_t = -2 \cdot \ln(D_e) \Big/ \left[0.14 + 0.012 \left(\frac{EI_{t,b}}{P_{t,b}}\right)\right]; \quad [5\text{-}20]$$

$$EI_t = EI_{t,b} \cdot P_t/P_{t,b}$$

where the subscript b indicates the value before the operation.

These values for the decay coefficient and corresponding precipitation and EI describe a point on a new roughness decay curve, asymptotic to zero at infinite amounts of precipitation, and with a new initial roughness at $P_t = 0$. This new initial roughness R_i (in) is calculated from

$$R_i = 0.24 + \frac{(R_n - 0.24)}{D_e} \quad [5\text{-}21]$$

thereby completely describing the decay curve.

As the computer program steps through each time segment in the rotation, the total rainfall and EI since tillage (P_t and EI_t) are incremented by the amounts in that segment. The value of the roughness decay coefficient for that segment is then calculated by use of equation [5-15], and the current surface roughness is calculated by equation [5-16].

The surface random roughness is affected not only by the soil clods resulting from tillage, but also by the vegetation. If a site is clean-tilled and then left without human intervention, two things will happen: (1) the tillage roughness will decrease as defined previously, and (2) as the years go by, the vegetation will trend toward its climax community, with attendant roughness caused by protruding roots, soil mounded around old basal areas, rocks, and so on.

RUSLE assumes that the formation of this vegetative roughness follows a typical sigmoidal growth curve increasing from the minimum soil roughness (r_{min}, with a default of 0.24 in) to the total roughness when the soil is fully consolidated (r_{max}) over the time required for consolidation (t_{con}). At any time after disturbance (t_d), the relationship will be

$$r_{nat} = r_{min} + \left[\frac{(r_{max} - r_{min})}{1 + \exp \dfrac{\left(0.5 - \dfrac{t_d}{t_{con}}\right)}{0.1}} \right] \qquad [5\text{-}22]$$

where r_{nat} is the roughness caused by the community (in). For each time period the program calculates r_{nat}, and compares its value to R_u as calculated for that same period. If r_{nat} is larger, then R_u is set equal to r_{nat}. In general, this will only occur if the site has not been disturbed for quite some time.

The surface roughness subfactor is then

$$SR = \exp[-0.66(R_u - 0.24)] \qquad [5\text{-}23]$$

Soil-Moisture Subfactor (SM)

Antecedent soil moisture has a substantial influence on infiltration and runoff and hence on soil erosion. In general, antecedent moisture effects are an inherent component of continuous-tilled fallow plots, and these effects are reflected in variation in soil erodibility throughout the year. In most of the continental United States, soil moisture is usually high during susceptible crop stages in spring and early summer, when much of the erosion occurs. Hence the

antecedent soil moisture on cropped plots parallels that on the continuous-tilled fallow plots from which soil-erodibility factors are derived, so no adjustment is made for changes in soil moisture.

In the nonirrigated portions of the Northwestern Wheat and Range Region (Austin 1981) (including eastern Oregon, eastern Washington, and Idaho), soil moisture during critical crop periods depends on crop rotation and management. Winter wheat may be seeded after a previous crop of winter wheat, or after a more shallow-rooted crop, or after summer fallow. When a full year of fallow is used in the rotation, part of the moisture stored over the previous winter is retained in the soil profile. This is particularly true when an effective mulch system is used: either a loose soil and residue mulch in conjunction with a rodweeder, or an untilled residue mulch with direct stubble seeding. These systems are in contrast to continuous cropping, in which soil moisture is at or below the wilting point in the fall before the fall and winter precipitation. Addition of a soil-moisture subfactor (SM) is suggested for this region of the Northwestern Wheat and Range Region (McCool, personal communication 1994). SM reflects these dry fall conditions and the increase in soil moisture over the winter. The soil moisture decrease over the summer depends on the crop rooting depth and soil depth, and the soil moisture replenishment depends on the precipitation amount and soil depth.

When the soil profile is at or near field capacity, SM is 1.0 (such as on April 1 of fig. 5-5), indicating response equivalent to that of a continuous-fallow plot. When the profile is near wilting point to a 6-ft depth, the SM value is 0 (as on September 1 in fig. 5-5), indicating that no runoff and erosion are expected. This assumes that infiltration is not limited by surface conditions. SM increases over the winter from October 1 to March 31. Suggested replenishment-rate relationships are given in figure 5-6. Growing-season (April 1 to July 31) depletion rates for typical crops appear in table 5-7. These relationships and values are typical and may need adjustment for shallow-soil conditions or other considerations.

COMPUTATION OF C FACTOR

Once the SLR's have been calculated for each time interval, they are multiplied by their corresponding percentage of annual EI (Wischmeier and Smith 1978) as seen in table 2-1. These values are then summed and divided by the total percentage of annual EI value for the entire time period being investigated, as

$$C = \left(SLR_1\ EI_1 + SLR_2\ EI_2 + \ldots\ SLR_n\ EI_n\right) / EI_t \qquad [5\text{-}24]$$

where C is average annual or crop value, SLR_i is the value for time period i, EI_i is percentage of the annual or crop EI occurring during that time period, n is number of periods used in the summation, and EI_t is sum of the EI percentages for the entire time period.

For those systems where conditions are not rapidly changing (such as for rangeland, or continuous pasture or meadow), the PLU, CC, SC, and SR subfactor values are assumed to be annual averages, and are simply multiplied together to yield the overall C-factor value. If the assumption of nearly steady-state conditions does not hold, the weighted procedure used for cropland is more appropriate.

COMPUTATION OF C FACTORS FOR SINGLE DISTURBANCES AND FOR ROTATIONS

RUSLE technology can be used to estimate erosion under two very different sets of circumstances. The first circumstance is the one-time disturbance of an area, such as for a construction site, a rangeland under an improvement plan, or a disturbed forest site. In this case, the soil/vegetation/residue system is drastically disturbed but is then allowed to reconsolidate and return to more stable conditions.

The other general circumstance under which RUSLE can be used is a normal cropping rotation, in which the soil/vegetation/residue system is disturbed repeatedly in a cycle of one or more years. For example, a conventionally tilled corn-soybean rotation would have the same field operation (for example, planting of corn) at roughly the same time of year (perhaps May 15) every second year.

For the situation of a single disturbance, proper use of the RUSLE program requires definition of all the important soil/vegetation/residue parameters immediately after the disturbance. This process is described in more detail in chapter 7. For a crop rotation, matters are somewhat more complicated, because the disturbance is usually not so severe and the previous crops and field operations can still have a significant impact. The RUSLE program handles this by running three times through the calculations for the entire rotation, and by returning the calculated SLR values on only the third time through. This procedure allows the system to stabilize and minimizes the impact of the assumed initial conditions on the resulting SLR values.

COMPUTATION OF C FACTORS FOR HILLSLOPES UNDER STRIPCROPPING OR BUFFER STRIPS

For management schemes such as those modeling stripcropping and buffer strips, the vegetation and cropping schemes cause the SLR values to vary not only with time but also with position on the hillslope. For example, in a stripcropping scheme with alternating strips of conventionally tilled corn and good sod-forming grass, at any time half of the field would be under each crop.

The impact of such a scheme on the movement of runoff and the deposition of sediment is taken into account in the P factor (see ch. 6), but this does not account for the protection given the soil by the important parameters within the C factor: things such as random roughness, root mass, surface residue cover, and canopy cover. These must still be represented through the C factor.

This is done by calculating an individual C factor for each strip, and then weighting these by their area on the hillslope. For example, in any true stripcropping rotation scheme, each strip is rotated through the same pattern, so we need make only one C-factor calculation. On the other hand, for buffer strips, we can calculate a C factor for the buffer strips themselves and then calculate a C factor for the cropped areas between the buffer strips. We then calculate an overall C factor by multiplying each of the C factors by the percentage of the hillslope under that practice.

ACKNOWLEDGMENT

The authors acknowledge the kind assistance of Jim Cropper, NRCS, Chester, PA, for his extensive work in developing the CROP database information for forage crops.

Table 5-1.
Parameter values of typical crops[1]

Crop	Residue/yield ratio[2]	Surface p[3]	α[4] (acre · lb^{-1})	Residue at 30% cover[5] (lb · acre^{-1})	Yield	Row spacing[6] (in)	Plant population[6] (plants acre^{-1})
Alfalfa	0.15	0.020	0.00055	650	6 ton · acre^{-1}	(drilled)	180,000
Bromegrass	0.15	0.017	0.00055	650	5 ton · acre^{-1}	7 (drilled)	330,000
Corn	1.00	0.016	0.00038	950	130 bu · acre^{-1}	30	25,000
Cotton	1.00	0.015	0.00022	1,600	900 lb · acre^{-1}	38	35,000
Oats	2.00	[7]0.008	0.00059	600	65 bu · acre^{-1}	7 (drilled)	890,000
Peanuts	1.30	0.015	0.00030	1,200	2,600 lb · acre^{-1}	36	558,000
Rye	1.50	[7]0.008	0.00055	650	30 bu · acre^{-1}	(drilled)	890,000
Sorghum	1.00	0.016	0.00036	1,000	65 bu · acre^{-1}	30	41,000
Soybeans	1.50	0.025	0.00059	600	35 bu · acre^{-1}	30	110,000
Sunflowers	1.50	0.016	0.00024	1,500	1,100 lb · acre^{-1}	30	20,000
Tobacco	1.80	0.015	0.00036	1,000	2,200 lb · acre^{-1}	48	6,000
Wheat (spring)	1.30	[7]0.008	0.00059	600	30 bu · acre^{-1}	7 (drilled)	890,000
Wheat (winter)	1.70	[7]0.008	0.00059	600	45 bu · acre^{-1}	7 (drilled)	890,000

[1] Values in table are taken from Alberts et al. (1989), Ghidey et al. (1985), Gregory (1982), Gregory et al. (1985), Larson et al. (1978), National Research Council (1975), USDA (1990), and USDA-SCS (1991).

[2] Weight ratio of crop residue at harvest to crop yield,

[3] A constant that controls the exponential decomposition rate or surface residue from this crop. There are not enough data to justify different values for subsurface decay p values, so default values in program show identical decay rates for surface and buried residue. This can be changed by user.

[4] Ratio of area covered by a piece of residue to its mass.

[5] Mass of residue required to cover 30% of the surface area, corresponding to given value of α.

[6] Not currently used in program; is simply an aid in defining cropping patterns and likely residue levels

[7] Use 0.017 for the Northwestern Wheat and Range Region, or for small grain cover killed in the vegetative state.

Table 5-2.
Typical values of root mass, canopy cover, and canopy-droplet-fall-height for row crops and small-grain crops

	Root mass in upper 4 in of soil ($lb \cdot ac^{-1}$)						Land surface covered by canopy (%)						Canopy-droplet-fall-height (ft)					
Number of days after planting	Corn[1]	Soybeans[2]	Cotton[3]	Sorghum[4]	Winter small grain[5,6]	Spring small grain[5,7]	Corn	Soybeans	Cotton	Sorghum	Winter small grain	Spring small grain	Corn	Soybeans	Cotton	Sorghum	Winter small grain	Spring small grain
15	50	20	30	50	30	100	5	5	5	5	5	10	0.1	0.1	0.1	0.1	0.1	0.1
30	180	50	60	180	120	300	10	20	15	10	20	35	0.5	0.2	0.2	0.5	0.2	0.3
45	350	90	90	350	300	500	50	40	35	50	35	60	1.0	0.5	0.5	1.0	0.2	0.8
60	530	180	180	530	320	700	80	70	55	80	35	90	1.7	1.0	1.0	1.5	0.2	1.3
75	840	360	310	800	320	900	100	100	85	100	35	100	2.5	1.3	1.4	2.0	0.2	1.5
90	1060	360	360	1060	320		100	100	100	100	35		3.0	1.6	1.8	2.2	0.2	
105	1060	360	360		320		100	90	100		35		3.0	1.6	1.8		0.2	
120	1060	360	360		320		100	50	60		35		3.0	1.6	1.8		0.2	
135	1060	360	360		320		100	35	20		35		3.0	1.6	1.8		0.2	
150	1060				320		90				35		3.0				0.2	
165	1060				320		70				35		3.0				0.2	
180					340						40						0.5	
195					400						60						1.0	
210					660						90						1.3	
225					1000						100						1.5	
240					1200						100						1.5	

[1] 125 bu/ac yield, 30 in rows, 120 d, adjust duration of full canopy for different lengths of growing season
[2] 35 bu/ac yield, 30 in rows, full season
[3] 750 lbs/ac lint yield, 30 in rows, solid seeded
[4] 65 bu/ac yield, 30 in rows
[5] These are specific to areas with a spring and summer precipitation regime, a winter dormant period, and are not applicable to the Northwest Wheat and Range Region, adjust period of dormancy and growth of crop during dormant period according to growth patterns typical of region
[6] 45 bu/ac yield
[7] 60 bu/ac yield

Table 5-3.
Typical values for established forage stands[1]

Common name	Root mass in top 4 in (lbs·acre^{-1})	Canopy cover just prior to harvest (%)	Effective fall height (ft)	Average annual yield (tons·acre^{-1})
Grasses:				
Bahiagrass	1,900	95	0.1	4
Bermudagrass, coastal	3,900	100	0.2	8
Bermudagrass, common	2,400	100	0.1	3
Bluegrass, Kentucky	4,800	100	0.1	3
Brome grass, smooth	4,500	100	0.1	5
Dallisgrass	2,500	100	0.1	3
Fescue, tall	7,000	100	0.1	5
Orchardgrass	5,900	100	0.1	5
Timothy	2,900	95	0.1	5
Legumes:				
Alfalfa	3,500	100	0.2	6
Clover, ladino	1,400	100	0.2	3
Clover, red	2,100	100	0.1	4
Clover, sweet	1,200	90	2.0	2
Clover, white	1,900	100	0.1	2
Lespedeza, sericea	1,900	100	0.5	3
Trefoil, birdsfoot	2,400	100	0.3	4

[1]These values are for mature, full pure stands on well-drained nonirrigated soils with moderate-to-high available water-holding capacity. These values hold for species shown only within their range of adaptation. Except for biennials, most forages do not attain a fully-developed root system until end of second growing season. Root mass values listed can be reduced by as much as half on excessively drained or shallow soils and in areas where rainfall during growing season is less than 18 in. The values listed are from Bennett and Doss (1960), Denison and Perry (1990), Doss et al. (1960), Holt and Fisher (1960), Kramer and Weaver (1936), Lamba et al. (1949), MacDonald (1946), and Pavlychenko (1942).

Table 5-4.
Parameter values for estimating below-ground root mass in western U. S. rangelands

Vegetation type	Ratio of root mass in upper 4 in to total root mass		Ratio of root mass to above-ground biomass		Ratio of effective root mass to annual site production potential [1](n_i)
	Best estimate	Range	Best estimate	Range	
Southern mixed grass prairie	0.50	NA[2]	4.0	NA	1.1
Northern mixed grass prairie	0.34	0.22-0.77	30.0	0.64-119.6	1.5
Tallgrass prairie	0.74	0.73-0.75	7.4	0.23-20.3	0.3
Shortgrass prairie	0.41	0.24-0.64	3.2	1.12-10.7	1.0
Desert grasslands	0.60	0.36-0.73	3.4	2.0-4.9	2.7
Southeastern grasses and forbs	0.40	0.23-0.68	0.7	0.4-1.5	5.6
Cold desert shrubs	0.46	NA	5.0	4.09-11.0	3.25
Sandy shinnery oak with herbaceous interspaces	0.45	0.20-0.70	5.5	3.44-18.6	0.9
Southern desert shrubs	0.56	0.20-0.72	2.5	0.20-18.4	2.84
Chaparral	[3]0.13	0.08-0.30	0.8	0.30-1.9	6.5
California annual grassland	0.33	NA	3.0	NA	1.2
Pasture, bunchgrass	NA	NA	NA	NA	0.8
Pasture, sod-forming grass	NA	NA	NA	NA	1.3
Pasture, weeds	NA	NA	NA	NA	0.5

[1]Based on calibration against WEPP plot erosion data.
[2]NA = Data are not available.
[3]Root crowns and burls were excluded from root-biomass calculations.

Table 5-5.
Parameter values of typical cropland field operations

Field operations[1]	Random roughness[2] (in)	Residue left on surface[3,4] (%)	Depth of incorporation[5] (in)	Soil surface disturbed (%)
Chisel, sweeps	1.2	70	6	100
Chisel, straight point	1.5	60	6	100
Chisel, twisted shovels	1.9	45	6	100
Cultivator, field	0.7	75	3	100
Cultivator, row	0.7	80	2	85
Cultivator, ridge till	0.7	40	2	90
Disk, 1-way	1.2	30	4	100
Disk, heavy plowing	1.9	35	6	100
Disk, tandem	0.8	50	4	100
Drill, double disk	0.4	90	2	85
Drill, deep furrow	0.5	70	3	90
Drill, no-till	0.4	80	2	60
Drill, no-till into sod	0.3	90	2	20
Fertilizer applicator, anhydrous knife	0.6	80	2	15
Harrow, spike	0.4	80	2	100
Harrow, tine	0.4	85	2	100
Lister	0.8	20	4	100
Manure injector[5]	1.5	50	6	40
Moldboard plow	1.9	5	8	100
Mulch treader	0.4	75	2	100
Planter, no-till	0.4	85	2	15
Planter, row	0.4	90	2	15
Rodweeder	0.4	90	2	100
Rotary hoe	0.4	85	2	100
Vee ripper	1.2	80	3	20

[1]See American Society of Agricultural Engineers Standards 414 and 477.
[2]Zobeck and Onstad 1987.
[3]Stott and Barrett 1991.
[4]Percentage of before-operation cover for nonfragile residue. Values will be lower for fragile residues.
[5]The depth in which 75% of the residue is buried.

Table 5-6.
Roughness values for rangeland field conditions

Condition	Random roughness (in)
California annual grassland	0.25
Tallgrass prairie	0.30
Clipped and bare	0.60
Pinyon/Juniper interspace	0.60
Cleared	0.70
Natural shrub	0.80
Seeded rangeland drill	0.80
Shortgrass, desert	0.80
Cleared and pitted	1.00
Mixed grass, prairie	1.00
Pitted	1.10
Sagebrush	1.10
Root-plowed	1.30

Table 5-7.
Growing-season soil-moisture depletion rates for use in calculation of soil moisture subfactor for use in the Northwestern Wheat and Range Region.

Crop	Depletion rate
Winter wheat and other deep-rooted crops	1.00
Spring wheat and barley	0.75
Spring peas and lentils	0.67
Shallow-rooted crops	0.50
Summer fallow	0.00

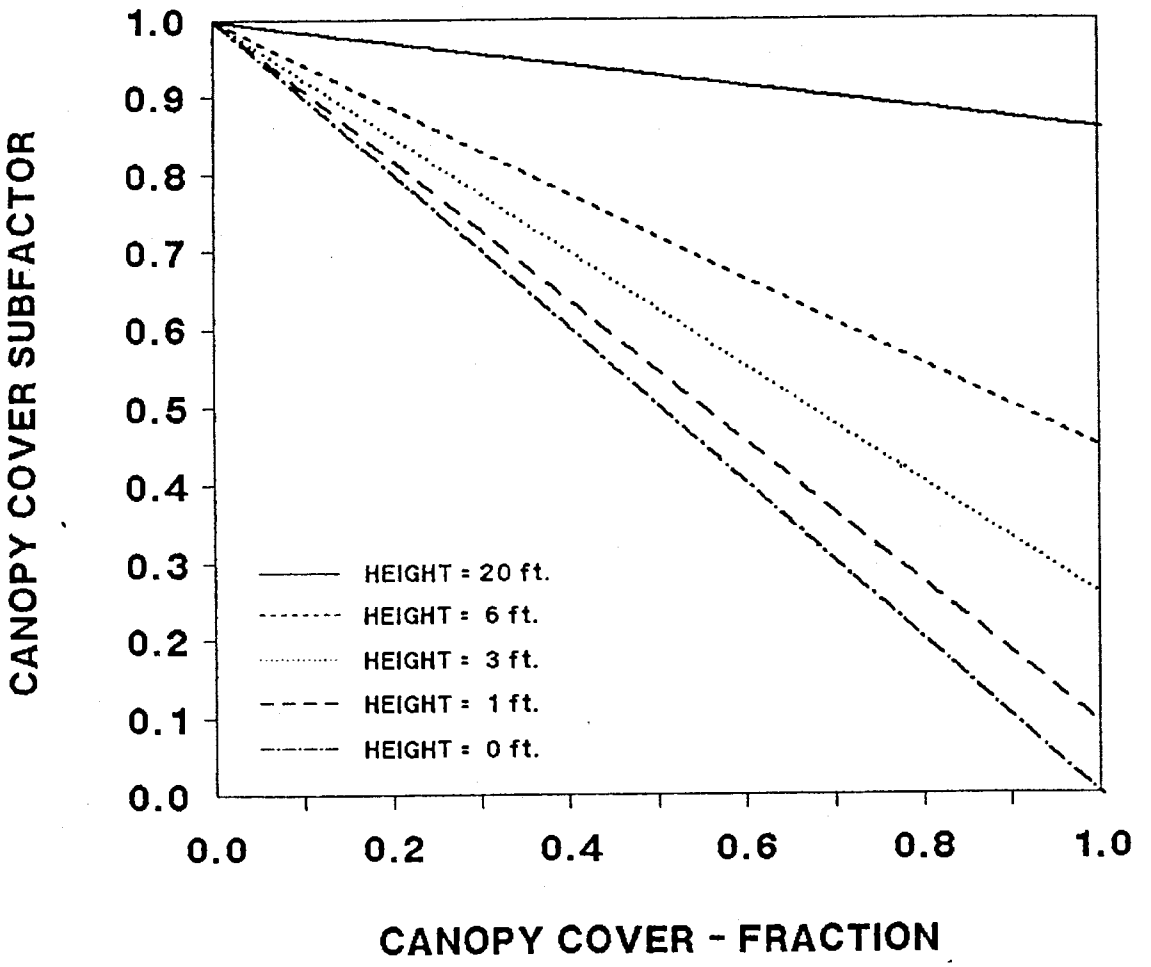

Figure 5-1.
Effect of canopy cover and canopy height on the canopy-cover subfactor

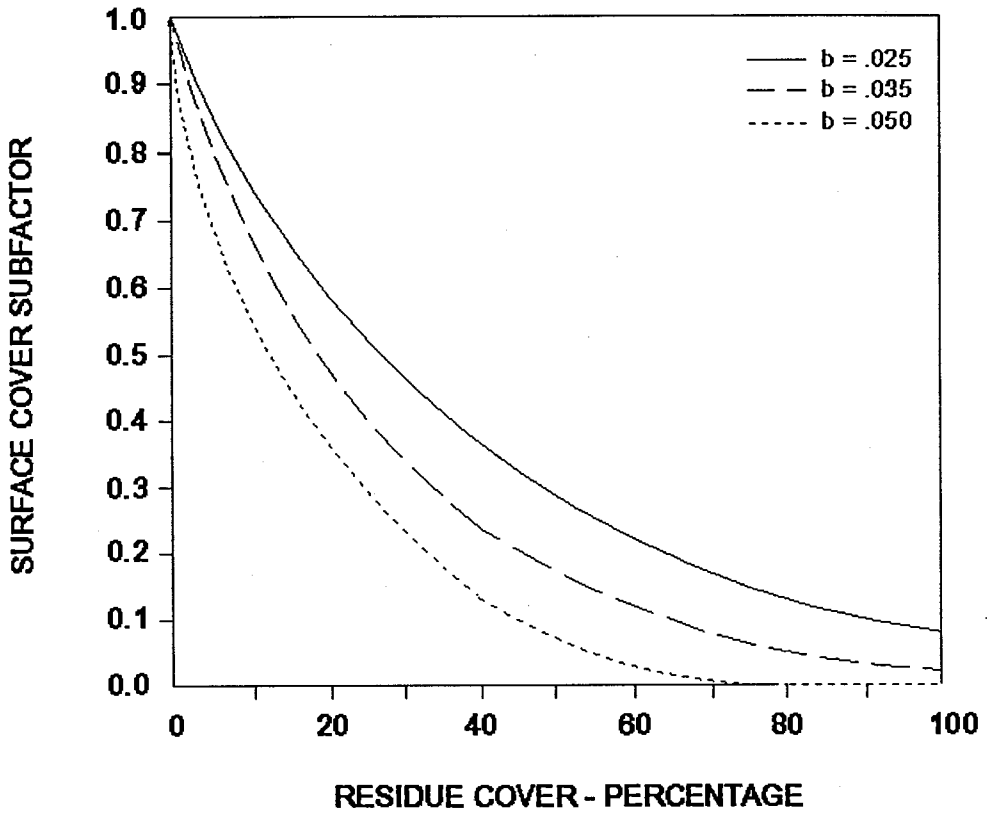

Figure 5-2.
Effect of residue cover and b values on the surface-cover subfactor for smooth field surfaces

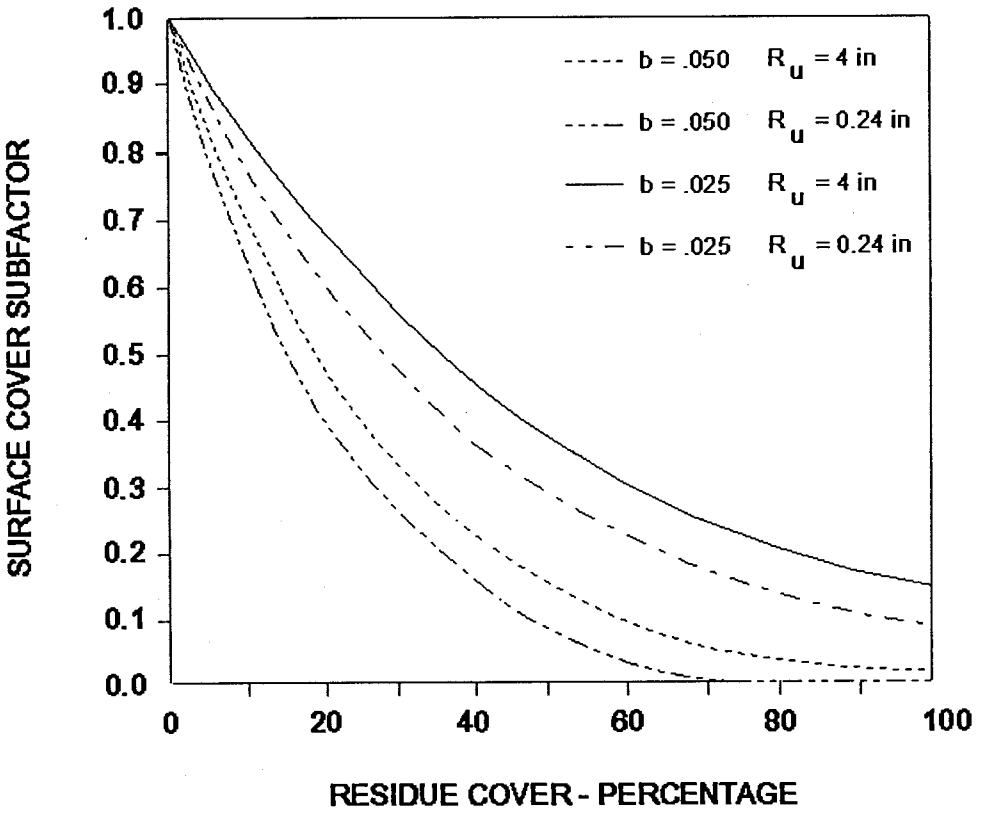

Figure 5-3.
Effect of residue cover, b values, and surface roughness on the surface-cover subfactor. An R_u value of 0.24 in is typical of a field in seedbed condition. An R_u value of 4 in indicates more roughness than from most primary tillage operations.

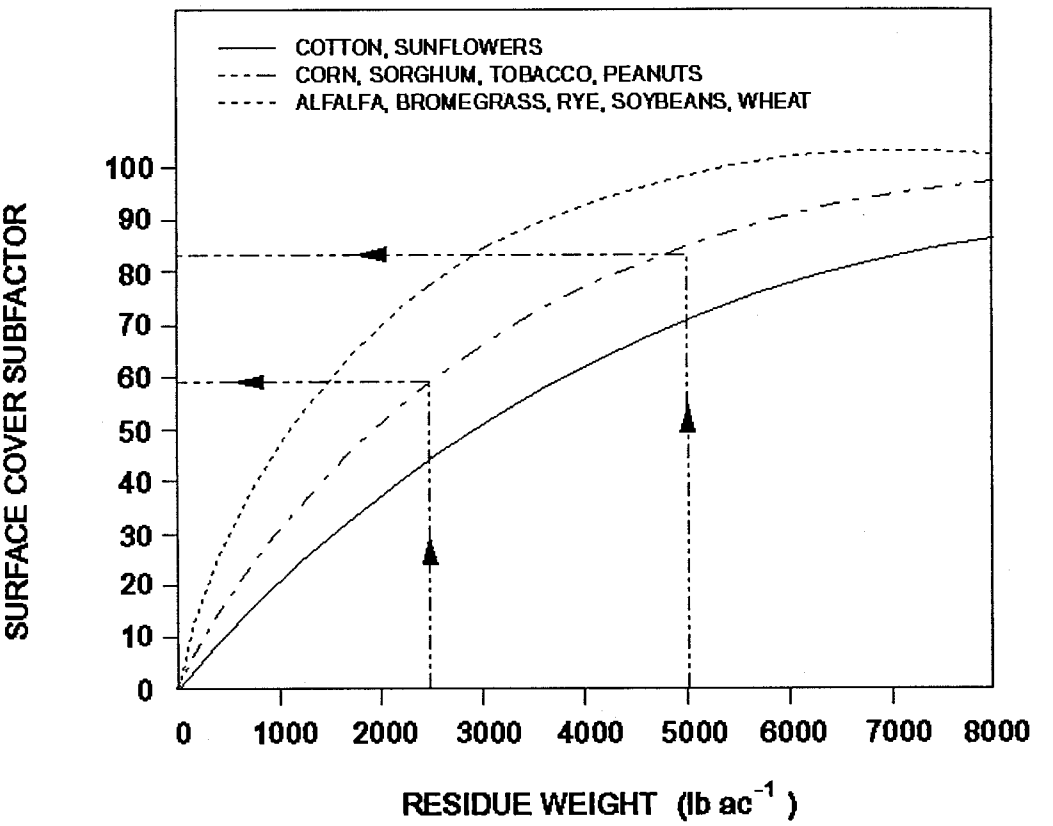

Figure 5-4.
Relationship of residue weight to percent residue cover for various crops.

Example: Dashed lines with arrows illustrate the procedure to convert weight to percent residue cover. Corn residue weighing 5,000 lb · acre^{-1} at harvest leaves 82% residue cover, and 2,500 lb · acre^{-1} leaves 57% cover. Note that, in this example, a 50% reduction in residue weight results in a 25% reduction in residue cover.

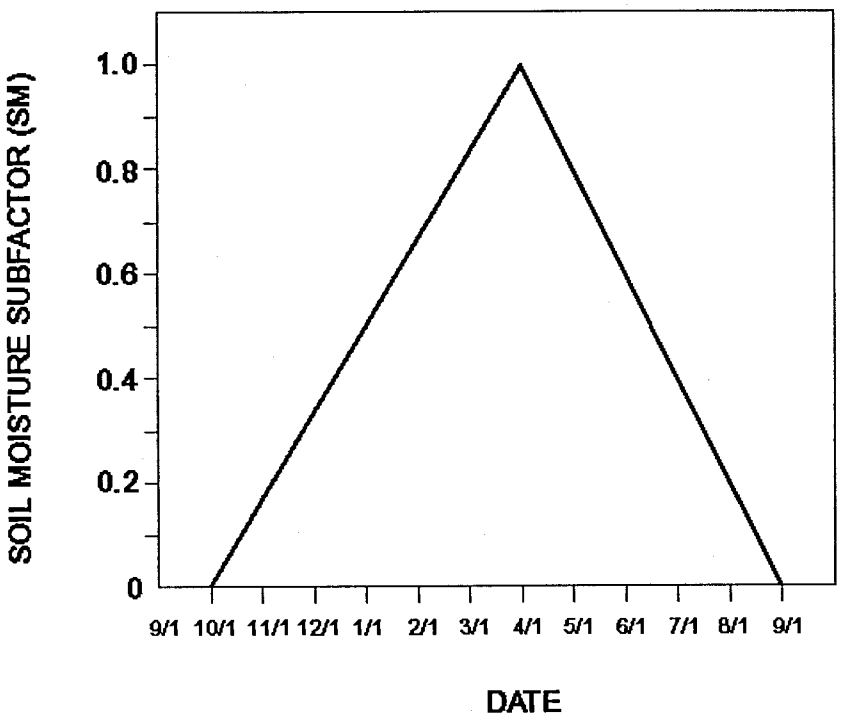

Figure 5-5.
Maximum range in soil-moisture subfactor as affected by profile replenishment and depletion for the Northwestern Wheat and Range Region

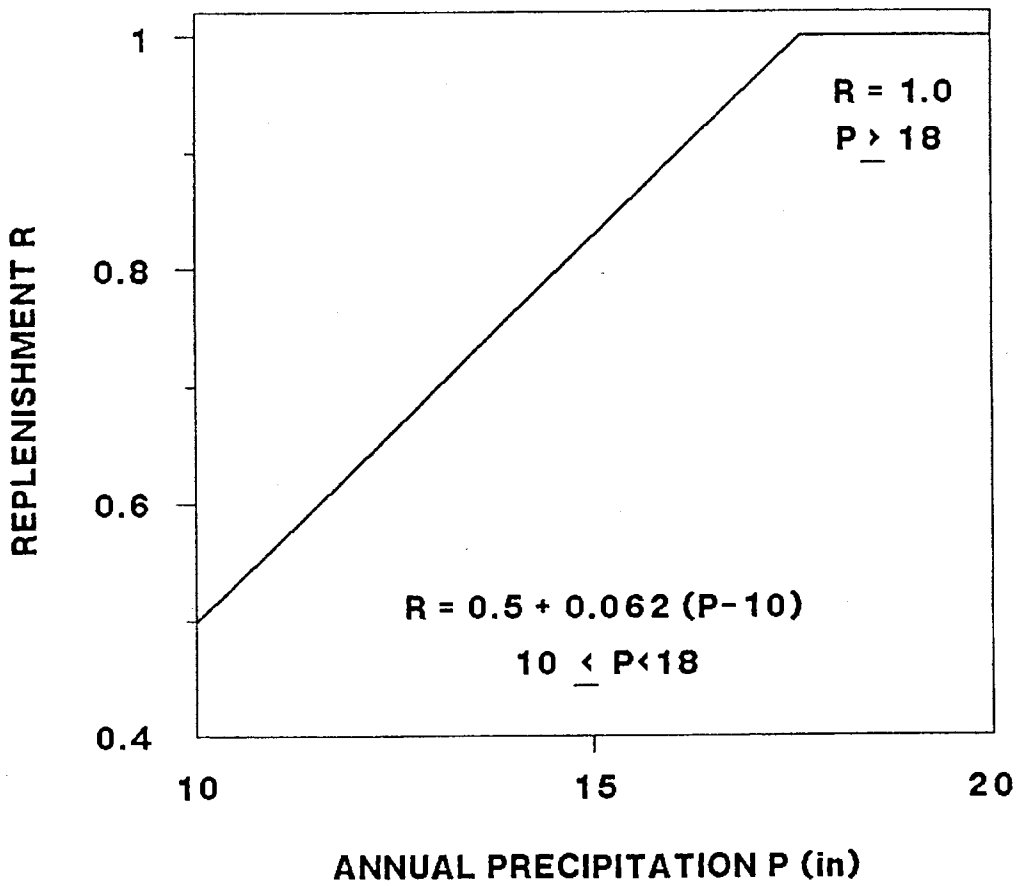

Figure 5-6.
Fraction of soil moisture replenished over winter versus annual precipitation for calculation of a soil-moisture subfactor for the Northwestern Wheat and Range Region

CHAPTER 6. SUPPORT PRACTICE FACTOR (P)

Principal contributors:

G.R. Foster
G.A. Weesies
K.G. Renard
D.C. Yoder
D.K. McCool
J.P. Porter

CHAPTER 6. CONTENTS

By definition, the support practice factor (P) in RUSLE is the ratio of soil loss with a specific support practice to the corresponding loss with upslope and downslope tillage. These practices principally affect erosion by modifying the flow pattern, grade, or direction of surface runoff and by reducing the amount and rate of runoff (Renard and Foster 1983). For cultivated land, the support practices considered include contouring (tillage and planting on or near the contour), stripcropping, terracing, and subsurface drainage. On dryland or rangeland areas, soil-disturbing practices oriented on or near the contour that result in storage of moisture and reduction of runoff are also used as support practices.

P does not consider improved tillage practices such as no-till and other conservation tillage systems, sod-based crop rotations, fertility treatments, and crop-residue management. Such erosion-control practices are considered in the C factor.

Values for P factors contained in this chapter were obtained from experimental data, supplemented by analytical experiments involving scientific observations of known cause-and-effect relationships in physically based models such as CREAMS (Knisel 1980). Recommended factor values are generally rounded to the nearest five-hundredth.

An overall P-factor value is computed as a product of P subfactors for individual support practices, which are typically used in combination. For example, contouring almost always accompanies stripcropping and terraces.

SUPPORT PRACTICE FACTOR (P) FOR CONTOURING

The effect of contour tillage on soil erosion by water is described by the contour P factor in the Revised Universal Soil Loss Equation (RUSLE). If erosion by flow occurs, a network of small eroded channels or rills develops in the areas of deepest flow. On relatively smooth soil surfaces, the flow pattern is determined by random natural microtopography. When tillage is oriented along the contour, the ridges or oriented roughness will partially or completely redirect the runoff, thereby modifying the flow pattern. When tillage leaves high ridges, runoff stays within the furrows between the ridges, and the flow pattern is completely determined by the tillage marks. High ridges from tillage on the contour cause runoff to flow around the slope, significantly reducing the grade along the flow path and reducing the flow's detachment and transport capacity compared to runoff directly downslope.

When grade is sufficiently flat along the tillage marks, much of the sediment eroded from the ridges separating the furrows is deposited in the furrows (Meyer and Harmon 1985). However, tillage is seldom exactly on the contour. Runoff collects in the low areas on the landscape and if accumulated water overtops the ridges, then rill and concentrated flow erosion usually occur, especially in recently tilled fields (Hill et al. 1944). Runoff from contoured fields is often less than that from fields tilled upslope-downslope (Van Doren et al. 1950). Contour tillage reduces erosion by reducing both the runoff and the grade along the flow path.

Values currently used in USLE (Wischmeier and Smith 1978) for the contour P factor are almost identical to those developed by Smith and Whitt (1947, 1948). At a 0% slope, Smith and Whitt reasoned that the value for the contouring subfactor should be 1.0 because no flow direction is defined. For steep slopes, they reasoned that the contouring subfactor value should be 1.0 for slopes steeper than 25% because a typical ridge 6 in high would store no water. At intermediate slopes, they chose a value of 0.6 for a 2% slope from the plot study of Van Doren et al. (1950) and a value of 0.5 for a 7% slope from the study of Smith et al. (1945).

This handbook recommends values for the RUSLE contour P factor based on erosion theory and analyses of experimental data. Data were from three sources: plots, small watersheds, and solutions of equations derived from erosion theory.

Data Analyses

Plot Data

Data from plot studies on the effect of contouring were found for the 18 locations identified in table 6-1. Plot dimensions varied from study to study with widths as narrow as 6 ft to as wide as 150 ft and lengths of 70 to 400 ft. Six studies were conducted with simulated rainfall, and 12 studies were on natural-runoff plots. The duration of the natural-runoff-plot studies ranged from a few days to 10 yr. Cropping and ridge height varied among the studies.

Contouring affected both runoff and erosion, but erosion was affected more than runoff. The ratio of (1) runoff and soil loss from a treatment tilled on the contour to (2) the runoff and soil loss from the same treatment tilled uphill-downhill was calculated for the period of record at a location. The results for runoff are shown in figure 6-1. The results for soil loss, the RUSLE contour P factor, are shown in figure 6-2.

Watershed Data

Soil-loss data collected from watersheds of 0.15-5 acres at four locations (table 6-2) were analyzed and plotted in figure 6-2. Straightforward comparisons of soil loss from uphill-downhill tillage with soil loss from contour tillage were impossible for many of the watershed studies. For example, the crop rotation at Clarinda, Iowa (Browning et al. 1948), differed among the watersheds. Data from a plot were compared against data from a watershed at LaCrosse, Wisconsin (Hays et al. 1949), to estimate a value for the contouring subfactor. At Bethany, Missouri (Smith et al. 1945), extensive gully erosion in the noncontoured watershed produced sediment that was measured at the watershed outlet but is not estimated with RUSLE. Also, the contoured watershed at Bethany had an extensive network of grassed waterways on 20% of the watershed, resulting in an unusually low sediment yield for this watershed. Therefore, the ratio of sediment yield to erosion from these two watersheds at Bethany gave a value for the contouring subfactor that was probably too low, in general. At Temple, Texas (Hill et al. 1944), areas of the watersheds were not equal. For example, the area of the watershed in the up-and-down tillage was 0.15 acre whereas the area of the contoured watershed was 1.5 acres. Such watershed differences result in appreciable differences in runoff, erosion, and sediment yield, so the data must be appropriately considered.

Analysis With CREAMS

The erosion component of the CREAMS model (Foster et al. 1981a) was used to compute erosion and sediment yield on several hypothetical watersheds under two levels of soil susceptibility to rill and concentrated flow erosion. The configuration of these watersheds was two planes that formed a V with a concentrated flow channel in the middle. Runoff on the planes was analyzed as flow in a series of furrows between ridges spaced 2.5 ft apart. An overland flow channel-channel hydrologic sequence was used in CREAMS to represent the watersheds. The overland-flow element represented the row side slopes, the first channel represented flow in furrows, and the second represented concentrated flow in the V between the planes. The maximum length of the concentrated flow channel in the V was 500 ft. Widths of the planes from their upper edge to the concentrated flow channel were 40 ft and 120 ft for two steep watersheds and 40 ft and 200 ft for two flat watersheds. The steepness of the planes on the steep watersheds was 12%, and the grade along the channel in the V was 6%. The steepness of the planes for the flat watersheds was 6%, and the grade along the channel was 4%. A critical shear stress value of 0.10 lb $\cdot$ ft^{-2} represented a field immediately after secondary tillage—a condition of high susceptibility to erosion by flow (Foster et al. 1980a). A critical shear stress value of 0.20 lb $\cdot$ ft^{-2} represented a field about a month or two after the last secondary tillage—a condition of moderate susceptibility to erosion by flow (Foster et al. 1980a).

Storm characteristics assumed in the analysis were 2.5 in for rainfall amount, 1.6 in for runoff amount, 2.0 in $\cdot$ h^{-1} for peak runoff rate, and 50 ft$\cdot$ tonf$\cdot$ in(acre-h)$^{-1}$ EI units for rainfall erosivity, which represent typical simulated rainstorms used in plot studies (Meyer 1960). These runoff values were not varied by watershed condition even though contouring affects runoff as shown in figure 6-1. Therefore, the computer analysis with CREAMS underestimated the effect of contouring.

Furrow grades in the analysis were 0.5%, 1%, 2%, and 4% for the flat watershed and 6% for the steep watersheds. As the grade of the furrows was increased, the upslope drainage area at the head of the concentrated flow channel was increased and the channel length of the concentrated flow in the V was shortened. The results from furrows on a 0.5% grade were assumed to represent excellent contouring and were plotted in figure 6-2.

Results

Figure 6-2 presents the basic data available in the literature. However, the application of RUSLE to contouring problems requires consideration of the storm erosivity and grade along the tillage marks when RUSLE is used in its standard way of taking slope length and steepness directly downslope.

Effect of Ridge Height

Five curves, drawn by inspection through the data shown in figure 6-2, represent the effectiveness of contouring where ridge heights are very low, low, moderate, high, and very high and where the ridges follow the contour so closely that runoff spills over the ridges uniformly along their length. Data showing the greatest effectiveness of contouring were generally from plots having high ridges (Borst et al. 1945, Moldenhauer and Wischmeier 1960). Conversely, data showing the least effectiveness of contouring were from plots having low ridge heights (Van Doren et al. 1950). The end points of the curves at the steep slopes were based on the steepness where typical ridge heights and row spacings would store no runoff.

These curves were described by the following equations:

$$P_b = a(s_m - s_c)^b + P_{mb} \qquad s_c < s_m \qquad [6\text{-}1]$$

$$P_b = c(s_c - s_m)^d + P_{mb} \qquad s_c \geq s_m \qquad [6\text{-}2]$$

$$P_b = 1.0 \qquad s_c \geq s_e \qquad [6\text{-}3]$$

where P_b = base values of the P factor for contouring, s_m = slope (expressed as sine of the slope angle) at which contouring has its greatest effectiveness, s_c = slope (expressed as sine of the slope angle) for which a value of P_b is desired, s_e = slope steepness (expressed as sine of the slope angle) above which contouring is ineffective, and P_{mb} = the minimum P value for a given ridge height with base conditions. The coefficients a, b, c, and d also vary with ridge height.

The curves described by equations [6-1] and [6-2] pass through P_m at the slope s_m, which varies with ridge height shown in table 6-3, and have a zero slope at s_m. In addition, values for the coefficients a and b must be chosen so that

equation [6-1] passes through 1 at $s_c = 0$ and equation [6-2] passes through 1 at $s_c = s_e$. To meet these boundary conditions, a is given by the equation

$$a = \frac{1 - P_m}{s_m^b} \qquad [6\text{-}5]$$

and c is given by the equation

$$c = \frac{1 - P_m}{(s_e - s_m)^d} \qquad [6\text{-}5]$$

Values for b, d, s_m, and s_e, chosen by inspection to give good fits to the data shown in figure 6-2, are listed along with values for a and c given in table 6-3.

The data in figure 6-2 are assumed to be for the base condition of a 10-yr-frequency storm EI of 100 ft · tonf · in(acre · hr)$^{-1}$ and for a row crop with clean tillage on a soil classified as being in the hydrologic soil group C.

Effect of Storm Severity

Data from field studies indicate that contouring is less effective for large storms than for small storms (Moldenhauer and Wischmeier 1960, Jasa et al. 1986). The reduced effectiveness depends on both amount of runoff and peak rate of runoff. These runoff variables are directly related to rainfall amount and intensity, which are the principal variables that determine EI (storm energy times maximum 30-min intensity), the erosivity factor in RUSLE. Therefore, values for the contouring subfactor should be near 1 (little effectiveness) when EI is high and infiltration into the soil is low, and should be small (greater effectiveness) when EI is low and infiltration is high (Moldenhauer and Wischmeier 1960). Loss of contouring effectiveness is likely to occur from a few major storms (Hill et al. 1944, Jamison et al. 1968). Therefore, erosivity of a single storm, such as the storm having a 10-yr return frequency, should be a better indicator of loss of contouring effectiveness than is average annual erosivity.

In figure 6-2, the highest 10-yr storm EI for the locations represented in figure 6-2 was 165 ft · tonf · in(acre · hr)$^{-1}$ at Temple, Texas (Wischmeier and Smith

1978), where contouring had little effectiveness. Conversely, the lowest 10-yr storm EI was 50 ft · tonf · in(acre · hr)$^{-1}$ at Arnot, New York (Lamb et al. 1944), where contouring was most effective. The contouring P-factor values were also low at Clarinda, Iowa (Moldenhauer and Wischmeier 1960), where the 10-yr storm EI was 76 ft · tonf · in(acre · hr)$^{-1}$. Erosivity was high—140 ft · tonf · in(acre · hr)$^{-1}$ at Batesville, Arkansas (Hood and Bartholomew 1956), where ridge breakovers occurred and the contouring P-factor value was high.

A linear regression analysis using the complete data set showed an increase in the contouring P factor with an increase in the 10-yr single-storm EI [$(EI)_{10}$]. The analysis also showed that effectiveness of contouring increased with increasing ridge height (Moldenhauer and Wischmeier 1960).

The effectiveness of contouring in RUSLE is assumed to vary with runoff, which is a function of both rainfall and infiltration. Runoff, computed using the Natural Resource Conservation Service (NRCS) runoff curve number method and the rainfall amount estimated from the 10-yr single-storm EI, is used as a guide in RUSLE to adjust P-factor values for changes in effectiveness of contouring that result from runoff differences among locations, soils, and cover-management conditions.

Values for the 10-yr storm EI are obtained from the Citycode files in the computer program of RUSLE. These EI values are converted to storm rainfall amounts using the equation (Foster et al. 1980b)

$$V_r = 0.255\ [(EI)_{10}\ ]^{0.662} \qquad [6\text{-}6]$$

where V_r = rainfall amount in inches. Values for rainfall amount, V_r, are used in the NRCS runoff curve method to compute a runoff amount. Cover-management conditions for cropland are grouped in the seven categories described in table 6-4. The runoff index values, equivalent to curve numbers, used to compute runoff for each of these conditions are given in table 6-5. (For Northwestern Wheat and Range conditions and runoff index values, see tables 6-25 and 6-26.)

Runoff was assumed to affect P-factor values for contouring in two ways: the minimum value of the P factor was assumed to vary directly with computed runoff, and the slope steepness above which contouring loses its effectiveness was also assumed to vary directly with runoff. The basis for these assumptions is that the effectiveness of contouring is assumed to be directly proportional to

the shear stress applied to the soil by the runoff. This shear stress is directly proportional to runoff rate and slope steepness to the 1.167 power (Foster et al. 1982). Runoff rate was assumed to be directly proportional to runoff amount. Thus the slope steepness (s_e) at which contouring loses its effectiveness was computed as

$$s_e = s_{eb}\left(\frac{3.72}{Q_k}\right)^{0.857} \qquad [6\text{-}7]$$

where s_{eb} = slope steepness for a given ridge height on base conditions at which contouring loses its effectiveness, Q = computed runoff amount (in) for the given soil and cover-management condition indicated by subscript k, and 3.72 = runoff amount (in) computed for cover-management condition 6, hydrologic soil group C, and a 10-yr storm EI of 100 ft · tonf · in(acre · hr)$^{-1}$. This storm EI is typical of much of the central part of the eastern United States, and the hydrologic soil group C is assumed to be typical of many of the soils in the contouring experiments that produce the data shown in figure 6-2. Similarly, the minimum P-factor value (P_m) is computed from

$$P_m = P_{mb}\left(\frac{Q_k}{3.72}\right) \qquad [6\text{-}8]$$

where P_{mb} = minimum P-factor value for a ridge height on base conditions.

Equations [6-1], [6-2], and [6-3] give P-factor values for base conditions. These curves shift as field conditions vary from the assumed base conditions. The following approach was used to take into account these differences:

The first step is to compute a scaled slope steepness. For a slope steepness of less than s_m, the actual slope steepness is used directly in equation [6-1] to compute a P_b value. For slopes steeper than s_m, the slope used in equation [6-2] is computed from

$$s_c = \frac{(s - s_m)(s_{eb} - s_m)}{(s_e - s_m)} + s_m \qquad [6\text{-}9]$$

The computed P_b value is then scaled as

$$P = 1 - \frac{(1 - P_b)(1 - P_m)}{1 - P_{mb}} \qquad [6\text{-}10]$$

If the steepness exceeds s_e computed from equation [6-7], then P = 1.0. If the value computed by equation [6-10] is less than an absolute minimum value (P_z) given in table 6-3, the absolute minimum P_b value for that ridge height is assigned to P.

Effect of Off-Grade Contouring

Contouring alone is often inadequate for effective erosion control (Hill et al. 1944, Smith et al. 1945, Jamison et al. 1968). Runoff frequently flows along the furrows to low areas on the landscape, where breakovers occur. Grassed waterways are needed in conjunction with contouring to safely dispose of the runoff that collects in natural waterways at the breakovers (Smith et al. 1945).

Erosion in the concentrated flow areas occurs even if contouring is not used, although eroded concentrated flow channels extend farther upslope with contouring. Our analysis with CREAMS showed that if row grade is slight, 0.5% or less, deposition in the furrows more than offsets the erosion in the concentrated flow areas.

As grade along the furrows increases from tillage being off contour, the effectiveness of contouring decreases. Results from CREAMS and experimental data (McGregor et al. 1969, Meyer and Harmon 1985) showed a rapid loss of effectiveness of contouring as grade along the furrows increased. The furrows in these situations were for clean-tilled row crops.

Soil loss estimated with RUSLE using the slope length measured downslope and the contouring factor in figure 6-2 includes the erosion in concentrated flow (ephemeral gully) areas for about 500 ft of a concentrated flow channel. The reason for the inclusion of ephemeral gully erosion by concentrated flow in the P factor is that the watershed data used in the derivation of figure 6-2 were collected on small watersheds that contained eroding ephemeral gully areas.

The equation used in RUSLE to compute P-factor values for off-grade contouring is

$$P_g = P_o + (1 - P_o)\left(\frac{s_f}{s_l}\right)^{1/2} \qquad [6\text{-}11]$$

where P_g = P factor for off-grade contouring, P_o = P factor for on-grade contouring (as computed by equation [6-10]), s_f = grade (expressed as sine of the slope angle) along the furrows, and s_l = steepness (expressed as sine of the slope angle) of the land. This equation is similar to the relationship assumed by Dissmeyer and Foster (1980) for application of USLE to disturbed forest lands. The data collected by McGregor et al. (1969) seem to be the only field data available that can be used to directly evaluate equation [6-11]. Grade along furrows in that study varied between 0.2% and 0.4%. The P-factor value in the McGregor et al. (1969) study was 0.39 for 150-ft wide plots on a 5% slope with off-contour tillage whereas the P-factor value was 0.10 when the furrows were perfectly on the contour. Given a value of $P_o = 0.10$, the value of P_g computed by equation [6-11] for a 0.3% furrow grade is 0.32, slightly less than the 0.39 measured value.

ESTIMATING SOIL LOSS WITH CONTOURING WHEN SLOPE LENGTH EXCEEDS CRITICAL SLOPE LENGTH

Critical Slope Limits

At long slope lengths, contouring loses its effectiveness. Wischmeier and Smith (1978) gave a table of values for critical slope lengths for USLE that represented slope lengths beyond which contouring was assumed to lose much of its effectiveness. These critical slope-length limits were given only as a function of slope steepness, but Wischmeier and Smith suggested that critical slope length increased if residue cover exceeded 50%.

Foster et al. (1982) investigated the hydraulic conditions under which surface residue failed and allowed serious erosion to occur. Their analysis considered the shear stress exerted by the runoff on the soil and the residue. When the shear stress exerted on the residue exceeded a critical value, the residue was assumed to move. Similarly, when the shear stress exerted on soil exceeded a critical shear stress, flow was assumed to erode the soil.

The equation derived by Foster et al. (1982) for movement of mulch used discharge as the principal hydraulic input variable. Critical slope-length limits in RUSLE are computed with a simplification of the Foster et al. (1982) equation for mulch stability. The equation is

$$\lambda_c = \frac{20182 n_t^{1.5}}{s^{1.1667} Q} \qquad [6\text{-}12]$$

where λ_c = critical slope length, n_t = Manning's n, s = slope (expressed as sine of the slope angle), and Q = runoff amount from the 10-yr storm EI. The value 20,182 was obtained by calibrating equation [6-12] to compute a critical slope length of 200 ft for a 7% slope, moderately high ridges, clean-tilled row crops, a soil classified in the hydrologic soil group C, and a 10-yr storm EI of 100 ft · tonf · in(acre · hr)$^{-1}$. This critical slope-length value agrees with Wischmeier and Smith (1978). Values for Manning's n_t are given in table 6-6 and were chosen from those suggested for the CREAMS model (Foster et al. 1980a) and from field research on the movement of mulch (Foster et al. 1982).

Existing recommended values for critical slope length (Wischmeier and Smith 1978) were based on judgment and field observations. The condition chosen for calibration seems to best represent the typical condition that would have been observed in the field. Values for a range of slopes were computed with equation [6-12] and are shown in table 6-7 along with values from Wischmeier and Smith (1978). The values computed by equation [6-12] are very close to those from Wischmeier and Smith (1978) except for slopes less than 4%. A value of 1,000 ft is set in RUSLE as a maximum critical slope length. Values for critical slope length for a range of conditions are given in tables 6-8, 6-9, and 6-10.

Derivation of RUSLE Equation for Effective P

The procedure for applying RUSLE to irregular slopes (Foster and Wischmeier 1974) was used to develop the equations to calculate effective P-factor values. The beginning point in the derivation is RUSLE applied to a point, as follows:

$$D = (m + 1)\, RKSCP \left(x_* \frac{\lambda}{72.6} \right)^m \qquad [6\text{-}13]$$

where D = erosion rate at a point, m = slope-length exponent, R = rainfall-runoff erosivity factor, K = soil erodibility factor, S = slope steepness factor, C = cover-management factor, and P = support-practice factor for contouring.

The normalized distance x_* is x/λ, where x is distance along the slope length λ and 72.6 is length (ft) of the RUSLE unit plot. All factor values apply to conditions at the point x. The derivation is for a uniform slope. If a more complex situation is being analyzed, the full irregular slope procedure should be used.

Equation [6-13] can be rearranged to give

$$D = (m + 1)\, RKSCP \left(\frac{\lambda}{72.6} \right)^m (x_*)^m \qquad [6\text{-}14]$$

where the term $(\lambda/72.6)^m$ is the slope length factor of RUSLE.

Soil loss, G, for the slope length is obtained by integrating equation [6-14] for the two parts of the slope: the upper part where contouring is assumed to be

fully effective and the lower part where no effectiveness of contouring is assumed. The equations for this soil loss are

$$G = \int_0^{x_c} D dx + \int_{x_c}^{1} D dx \qquad [6\text{-}15]$$

Substitution of equation [6-14] into equation [6-15] gives:

$$G = (m+1)\,\lambda \left(\frac{\lambda}{72.6}\right)^m \left(P \int_0^{x_c} x_*^m \, dx_* + \int_{x_c}^{1} x_*^m \, dx_* \right) \qquad [6\text{-}16]$$

Soil loss expressed in units of mass per unit area is obtained by dividing sediment yield G from the slope by slope length λ. Completion of the integration and division by λ gives the equation for soil loss A of

$$A = RKLSC\,[P_{eff}] \qquad [6\text{-}17]$$

where

$$P_{eff} = \left[1 - x_c^{\,m+1}(1 - P)\right] \qquad [6\text{-}18]$$

is the effective P factor to compute average soil loss for the slope length λ. Values for P_{eff} were computed using equation [6-18]. Slope-length exponent values for a range of slopes and rill-to-interrill erosion classes are in table 4-5.

Discussion

Use of the effective P-factor values from table 6-10 gives an estimate of the average soil loss for the slope length λ. Soil loss on the lower part of the slope where contouring has been assumed to fail can be considerably greater than the

average soil loss for the entire slope. When using this method in conservation planning, the conservationist must consider whether it is permissible to allow soil losses on the lower part of the slope in excess of the soil loss tolerance. Chapter 4 describes how to use RUSLE to compute soil loss on segments and how to adjust segment values to compare with soil-loss tolerances to provide for consistency in RUSLE applications.

SUPPORT PRACTICE FACTOR (P) FOR CROSS-SLOPE STRIPCROPPING, BUFFER STRIPS, AND FILTER STRIPS

Stripcropping is a support practice where strips of clean-tilled or nearly clean-tilled crops are alternated with strips of closely growing vegetation such as grasses and legumes. Another form of stripcropping used on cropland in the Northwestern Wheat and Range Region is very rough, tilled strips instead of strips of closely growing vegetation. The crops are generally rotated sequentially so that at some time in the rotation cycle, every crop will have been grown on every strip. To be compatible with the crop rotation, the width of all strips in the system is usually the same. Stripcropping performs best when the upper edge of each strip is perfectly on the contour.

Stripcropping for the control of water erosion is variously described as contour stripcropping, cross-slope stripcropping, and field stripcropping. Each of these practices has the common characteristic of crops in rotation forming strips of nearly equal width. The difference between the practices is the degree of deviation from the contour. All of them, including contour stripcropping, involve some degree of off-grade contouring. The effectiveness of all of them can be determined with the same equations in the RUSLE computer model. All are versions of the same technology with no sharp distinction despite the wide variation in effectiveness, depending on grade of the row. Therefore, the term "cross-slope stripcropping" is used to refer to the various conditions described above.

Buffer strips, located at intervals up the slope, are resident strips of perennial vegetation laid out across the slope. Like the strips in cross-slope stripcropping, they may or may not be on the contour. These strips, predominantly composed of grass species, are not in the crop rotation, are usually much narrower than the adjacent strips of clean-tilled crops, and may be left in place for several years or permanently. The effectiveness of buffer strips in trapping sediment and reducing erosion can also be evaluated by the RUSLE model.

Vegetated filter strips are bands of vegetation at the base of a slope. Riparian filter strips are located along stream channels or bodies of water. These conservation practices are designed to reduce the amount of sediment reaching offsite water bodies. Neither practice traps eroded sediment on the hillslope and therefore has minimal benefit as a P factor.

Densely vegetated strips or very rough strips that induce deposition of eroded sediment are assigned a P-factor value. Deposition must occur on the hillslope in areas where crops are routinely grown to deserve a low P factor indicative of greatest value to soil conservation. Therefore, P-factor values for maintenance of soil productivity are lowest for cross-slope stripcropping, moderate for buffer strips, and highest for filter strips. A P value of 1.0 is often assigned to filter strips because they provide little protection to the majority of the field where crops are grown.

A major advantage of stripcropping is the rotation of crops among the strips. By rotating crops among strips, each clean-tilled crop receives benefit from the sediment deposited in a previous year by the closely growing crop or the rough strip. Stripcropping significantly reduces the rate of sediment moving down the slope. Because filter strips are located at the base of slopes, the strips do not greatly affect this rate. In general, the benefit of deposition depends on the amount of deposition and its location. Sediment deposited far down the slope provides less benefit than does sediment deposited on the upper parts of the slope. With buffer strips, the sediment is trapped and remains on small areas of the slope, such as terraces; thus the entire slope does not benefit as much as it does in stripcropping.

A strip is effective in reducing soil loss when it significantly reduces the transport capacity of the runoff as it leaves one strip and enters the next strip. For deposition to occur, the transport capacity must be reduced to less than the sediment load being transported by the runoff. If no deposition occurs, the P value is 1.0. The following examples illustrate the basis for assigning P-factor values.

Examples

The first example is the situation of strips of a clean-tilled row crop separated by strips of grass hay. It is assumed that the uppermost strip is in corn and that erosion occurs at a high rate on this strip. Sediment load will be large in the runoff at the lower edge of the corn strip. The hay strip has a much greater hydraulic resistance to flow than does the clean-tilled area, and this resistance greatly reduces the transport capacity of the runoff as it enters the hay strip. If transport capacity is reduced at the upper edge of the hay strip to a level much less than the sediment load of the runoff entering the hay strip, much deposition occurs and gives a P-factor value of less than 1. As the runoff moves through a sufficiently wide hay strip, deposition reduces the sediment load to less than the transport capacity of the flow in the hay strip. The flow can be erosive as it exits the lower edge of the hay strip.

The relationship of erodibility of a clean-tilled strip to the transport capacity in the densely vegetated strip is illustrated by the extreme example of strips of concrete separated by dense grass strips. It is assumed that the uppermost strip is concrete. Flow over the concrete has great transport capacity, but its sediment load is very low (and approaches zero) because the concrete is not erodible. Even though the grass strip at the lower edge of the concrete greatly reduces the transport capacity of the flow, no deposition occurs because the transport capacity was not reduced to a level less than the sediment load in the flow. Therefore, the value of the P factor for this case is 1.0.

Another example more realistic than the above concrete-grass example illustrates the same principle. This example involves strips of no-till corn interspersed among strips of grass. It is assumed that the uppermost strip is no-till corn with a very heavy cover of residue. Very little erosion occurs on the strip of no-till corn. When the runoff reaches the grass strip, little reduction in the transport capacity of the runoff occurs because that of the grass is only slightly greater than the hydraulic resistance of the no-till corn. Therefore, since the sediment load in the runoff leaving the strip of no-till corn is very low because of little erosion on the no-till corn, no deposition will occur because the grass strip did not reduce the transport capacity of the runoff to a level less than the sediment load in the flow from the no-till strip. In this case, the P-factor value is 1.0.

In summary, the effectiveness of stripcropping, buffer strips, and filter strips as support practices depends on the sediment load generated from the erodible strips relative to the transport capacity of the strips that have greater hydraulic resistance.

Development of P-Factor Values for Strips

The first step in developing RUSLE P-factor values for strips was to review the literature. Unfortunately, most of the experimental research on stripcropping was conducted from 1930 to 1960 and did not include modern conservation tillage systems (Hill et al. 1944, Borst et al. 1945, Smith et al. 1945, Hays et al. 1949, Hood and Bartholomew 1956, Hays and Attoe 1957). Also, crop yields during that period were much less than modern yields, and canopy cover and residue amounts were less than those with modern practices.

Therefore, published experimental data alone are inadequate for developing the necessary P-factor values for the wide range of current practices. The approach taken was to develop a simple erosion-deposition model based on fundamental erosion concepts (Renard and Foster 1983, Flanagan et al. 1989) that could be used in RUSLE to estimate P-factor values for strips. Steps in addition to developing the model included developing parameter values based on theory and

experimental data from fundamental erosion studies and adjusting parameter values to obtain an adequate fit of the model to the limited field data. The model is included in RUSLE to compute values for the P factor for stripcropping, buffer strips, and filter strips for a wide variety of situations.

A value for the P factor for strips is computed from

$$P_s = \frac{(g_p - B)}{g_p} \qquad [6\text{-}19]$$

where P_s = value for P factor for strips, g_p = sediment load at end of slope that would occur if the strips caused no deposition, and B = credit for deposition.

Table 6-11 shows values for sediment yield from experimental data for stripcropping found in the literature, along with values computed by the model.

The model computes erosion, sediment transport, and deposition on a strip-by-strip basis, routing the sediment from the top to the bottom of the slope. One of the four following conditions exists on each strip:

(1) Net erosion occurs everywhere along the strip.

(2) Net deposition occurs everywhere along the strip.

(3) Net deposition occurs on an upper area of the strip and net erosion occurs on a lower area of the strip.

(4) Runoff ends within a strip, and no runoff or sediment leaves the strip.

The objective in each case is to compute the amount of deposition (M_i) on each strip and the sediment load (g_i) leaving each strip.

Case 1. Net Erosion Occurs Everywhere Along the Slope

For this case to apply, one condition is that the rate of increase in transport capacity along the strip must be greater than the detachment rate along the strip. For this condition, net erosion is computed by

$$D_{ni} = \xi_i \left(x_i^{\,n} - x_{i-1}^{\,n} \right) \qquad [6\text{-}20]$$

where ξ = an erosion factor, x = relative distance from the top of the slope to the lower edge of a strip (absolute distance/slope length), n = an exponent set to 1, and I = subscript indicating a particular strip. Values of ξ are given in table 6-12. Sediment load at the lower edge of the strip is given by

$$g_i = g_{i-1} + D_{ni} \qquad [6\text{-}21]$$

where g = sediment load.

The exponent n is set to 1 for all conditions. The reasoning for this value is that contouring is an integral part of stripcropping. When contouring is completely effective, it eliminates rill erosion. Much of the effectiveness of contouring is because of deposition in the furrows left by tillage. Erosion on strips where cover is dense is minimal and is mostly interrill erosion rather than rill erosion. In both situations, the appropriate value of the exponent is 1 (Renard and Foster 1983). The value of the exponent should be about 1.5 where rill erosion is significant. A single value of 1 is used in RUSLE because the principal intent of equation [6-21] is to provide an index of net erosion.

Local deposition, such as in depressions left by tillage, can occur within a strip because the detachment rate exceeds the rate of increase in transport capacity along the strip. For this condition, the deposition equation developed by Renard and Foster (1983) is used to compute net erosion as

$$D_{ni} = \left[\frac{\left(\frac{\phi dT_i}{dx} + \xi_i \right)}{(1 + \phi)} \right] \left(x_i - x_{i-1} \right) \qquad [6\text{-}22]$$

where $\phi = V_f/\sigma$, V_f = fall velocity of the sediment, and σ = excess runoff rate (rainfall intensity - infiltration rate). A value of 15 was selected by calibration for ϕ. Although the value for ϕ varies with sediment size and density, the single value of 15 is used in RUSLE. Equation [6-23] is based on the following equation for deposition (Renard and Foster 1983):

$$D = \left(\frac{V_f}{q}\right)(T - g) \qquad [6\text{-}23]$$

where D = deposition rate, q = discharge rate, and T = transport capacity of the runoff.

Case 2. Deposition Occurs Everywhere Along Strip

Deposition occurs at the upper edge of a strip if the transport capacity at the upper edge of a strip is less than the sediment load reaching the upper edge. Deposition will occur over the entire strip if the strip is narrow or if runoff rate decreases with distance within the strip. This latter condition occurs where the infiltration rate in a particular strip is much greater than the infiltration rates on upslope areas.

The basic equation used for strips where deposition occurs is equation [6-23]. Discharge rate q is given by the equation

$$q = q_{i-1} + \sigma_i \left(x - x_{i-1}\right) \qquad [6\text{-}24]$$

In RUSLE, the excess runoff rate is computed as the ratio of runoff amount, expressed as a depth, for the given strip condition to the runoff amount from a clean-tilled row-crop strip, which is condition 6 in table 6-4. Runoff amounts are computed by use of the NRCS runoff curve number method and runoff index values given in table 6-5.

When the infiltration rate on a strip is greater than the rainfall intensity, discharge rate decreases within the strip; if the strip is wide, runoff ends within the strip. Because the NRCS runoff curve number method would ordinarily compute no runoff for this condition, the method was modified to compute the rainfall amount that would just produce runoff. This equation is

$$r = V_r - 0.2\left[\left(\frac{1000}{N}\right) - 10\right] \qquad [6\text{-}25]$$

where r = excess runoff depth (in), V_r = rainfall amount, and N = runoff index. The equation for transport capacity (T) is

$$T = \zeta q \qquad [6\text{-}26]$$

where ζ = a sediment transport capacity factor. Values of ζ are relative and were chosen based on the Manning's n_t recommended for the CREAMS model (Foster et al. 1980a), the relation of runoff velocity to Manning's n_t, and the assumed relationship that transport capacity varies with the cube of runoff velocity (Foster and Meyer 1975). Values for ζ are given in table 6-12.

The equation derived from equations [6-24], [6-25], and [6-27] to compute sediment load where deposition occurs along the entire strip is

$$g_i = \left(\frac{\phi dT_i}{dx} + \xi_i \right) q_i \left[\sigma_i (1 + \phi) \right]^{-1} + \left(\frac{q_{i-1}}{q_i} \right)^{\phi} \left\{ g_{i-1} - \left(\frac{\phi dT_i}{dx} + \xi_i \right) q_{i-1} \left[\sigma_i (1 + \phi) \right]^{-1} \right\} \qquad [6\text{-}27]$$

The change of transport capacity with distance dT_i/dx is given by

$$\frac{dT_i}{dx} = \zeta_i \sigma_i \qquad [6\text{-}28]$$

The amount (M) of deposition on the strip is computed from

$$M_i = g_i - g_{i-1} + D_{ni} \qquad [6\text{-}29]$$

Case 3. Both Deposition and Erosion Within a Strip

If the sediment load at the upper edge of a strip is greater than the transport capacity at that location, deposition occurs over an upper area of the strip.

Deposition ends within a strip if the rate of increase in the transport capacity, dT/dx, exceeds the detachment rate ξ, and if the strip is wide. The location where deposition ends is the location where the sediment load equals the transport capacity. The discharge rate (q_{de}) for this condition is given by

$$q_{de} = \left(\frac{a_2 \phi \sigma_i}{a_1 \sigma_i + \xi_i} \right)^{\frac{1}{1+\phi}} \left[q_i \right]^{\frac{\phi}{1+\phi}} \qquad [6\text{-}30]$$

where coefficients a_1 and a_2 are given by

$$a_1 = \frac{\left(\frac{\phi dT_i}{dx} + \xi_i \right)}{\left[\sigma_i \, (1 + \phi) \right]} \qquad [6\text{-}31]$$

$$a_2 = g_{i-1} - a_1 q_{i-1} \qquad [6\text{-}32]$$

The location x_{de} where deposition ends is computed from

$$x_{de} = \frac{\left(q_{de} - q_{i-1} + \sigma_i \, x_{i-1} \right)}{\sigma_i} \qquad [6\text{-}33]$$

The sediment load at the location where deposition ends is given by

$$g_{de} = \zeta_i \, q_{de} \qquad [6\text{-}34]$$

If $dT_i / dx > \xi_i$, sediment load at the lower edge of the strip is given by

$$g_i = g_{de} + \xi_i \left(x_i^{\,n} - x_{de}^{\,n} \right) \qquad [6\text{-}35]$$

If $dT/dx < \xi_i$, sediment load at the lower edge of the strip is given by

$$g_i = g_{de} + \left[\frac{\left(\frac{\phi dT_i}{dx} + \xi_i\right)}{(1 + \phi)}\right](x_i - x_{de}) \quad [6\text{-}36]$$

The amount of deposition (M) is given by

$$M_i = g_i - g_{de} + \left[\frac{\left(\frac{\phi dT_i}{dx} + \xi_i\right)}{(1 + \phi)}\right](x_{de} - x_{i-1}) \quad [6\text{-}37]$$

Another possibility is for net erosion to occur on the upper area of a strip and local deposition to begin within the strip. This condition occurs when the sediment load is less than the transport capacity at the upper edge of a strip and the rate of increase in the transport capacity is less than the detachment rate, $dT_i/dx < \xi_i$. The location where local deposition begins is where sediment load (g_i) equals transport capacity (T). The sediment load at the lower edge of the strip is given by

$$g_i = g_{db} + \left[\frac{\left(\frac{\phi dT_i}{dx} + \xi_i\right)}{(1 + \phi)}\right](x_i - x_{db}) \quad [6\text{-}38]$$

where g_{db} = sediment load where local deposition begins and x_{db} = location where deposition begins. The amount of deposition (M) is zero for this condition if $g_i > g_{db}$. If $g_d < g_{db}$, then $M = g_{db} - g_i$.

Case 4. Runoff Ends Within a Strip

Sometimes the difference in infiltration can be so great between strips that all runoff from upslope is infiltrated within a strip having high infiltration rates. No runoff or sediment leaves these strips.

The location where runoff ends is calculated by use of equations [6-24] and [6-25]. The amount of deposition is the amount of sediment in the runoff entering the strip plus the amount of sediment detached within the strip between the upper edge of the strip and the location where runoff ends.

Application

Computation of P-Factor Value

The P-factor value for stripcropping is computed from

$$P_s = \frac{g_p - B}{g_p} \qquad [6\text{-}39]$$

where P_s = a P-factor value for conservation planning; g_p = potential sediment load if no deposition, other than local deposition, would have been caused by the strips; and B = amount of deposition considered to benefit the long-term maintenance of the soil resource. This benefit is computed by

$$B = \sum_{i=1}^{n} M_i \left(1 - x_{i-1}^{1.5}\right) \qquad [6\text{-}40]$$

where n = number of strips. The potential sediment load (g_p) is computed from

$$g_p = \sum_{i=1}^{n} D_{ni} \qquad [6\text{-}41]$$

where D_{ni} is computed for each strip according to equation [6-20] or [6-22].

The model also computes a sediment delivery ratio (P_y) for the slope by use of the equation

$$P_y = \frac{g_\lambda}{g_p} \qquad [6\text{-}42]$$

where g_λ = sediment load at the end of the slope.

Values for P computed for several stripcrop systems are shown in table 6-13.

The above equations and parameter values given in table 6-12 are used in RUSLE to compute a P-factor value and a sediment-delivery-factor value for any combination of strips, including buffer and filter strips. The parameter values in table 6-12 were developed to produce average annual P-factor values. The data used to determine the parameter values were heavily weighted by erosion in late spring and early summer, conditions when most erosion occurs with row crops in the eastern United States. Thus, the parameter values in table 6-12 most represent these conditions, but other conditions can be represented by choosing parameter values from table 6-12 based on surface conditions at a given time. The model can be applied several times during the year to compute an average P-factor value for the year, or the model can be applied over several years to compute a rotational P-factor value.

The equations used to compute deposition by strips do not take into account deposition in the ponded runoff on the upper side of the grass strip. The effect of the ponded runoff can be partially taken into account by adding the width of the ponded area to the width of the grass strip.

The effectiveness of strips as a soil conservation practice primarily results from the deposition induced at the upper edge of heavily vegetated or rough strips. In traditional applications of stripcropping, uniform-width strips are moved up the slope according to a crop rotation such as corn-wheat-1st yr hay-2d yr hay. In buffer strip applications, permanent vegetated strips that are much narrower than the cropped strips are installed. In rotational stripcropping, clean-tilled crops are grown on the strips where deposition occurred in prior years. In contrast, the benefit of narrow, permanent strips is that sediment is trapped and kept on the slope, but the immediate benefit is localized. The benefit to the entire slope is very little if a permanent strip is narrow and located at the end of the slope. If a single, narrow strip is placed high on the slope, none of the slope segment above the strip benefits from the deposition. This portion of the slope continues to erode at the same rate as if the strip were not present. The strip does, however, decrease the rate at which sediment moves off the slope over the long term; thus

the slope segment below the strip benefits from the deposition induced at the upper edge of the strip.

The P-factor values and the resulting soil-loss values computed by RUSLE are intended to be used in conservation planning for maintenance of the soil resource base. Full credit is not taken for the total amount of deposition for conservation planning. The benefit assigned by equation [6-40] to the deposition depends on the location of deposition. The degree of benefit increases as the location of deposition moves up the slope; conversely, little benefit is assigned when the strip is near the end of the slope. This approach is conceptually consistent with the way that P-factor values are assigned to terraces (Foster and Highfill 1983).

RUSLE also computes a sediment delivery factor. Multiplication of this factor by the product RKLSC gives an estimate of sediment yield leaving the slope. Sediment-yield values are typically less than the soil loss computed with RUSLE because RUSLE does not give full credit to deposition as a benefit for maintenance of the soil resource over the entire slope.

The effectiveness of stripcropping is assumed to be independent of strip width up to the point that rilling begins. Results were varied in experimental studies on the effect of strip width. Once strips become so wide or slope lengths become so long that rilling occurs, stripcropping begins to lose its effectiveness. Because of the complexity of the problem, no approach is suggested to estimate a P-factor value representing the lost effectiveness of stripcropping due to excessively long slope lengths. Critical slope lengths for conservation planning for stripcropping are assumed to be 1.5 times the critical slope length for contouring. Critical slope lengths for stripcropping are related to the maximum slope lengths for contouring because contouring is an integral part of stripcropping. Computation of soil loss when slope lengths exceed critical slope lengths is the same as computation of soil loss for contouring.

For maximum effectiveness, stripcropping is installed with the upper edge of the strips on the contour. However, strips are sometimes installed off contour, resulting in a grade along the upper edge of the strips. The effectiveness of these strips is difficult to evaluate. Deposition occurring at the upper edge of the densely vegetated strips builds up a ridge of soil that can cause runoff to flow along the upper edge of the strip and not pass through the strips. On tilled strips, runoff can flow along the tillage marks and never reach the strip if tillage is on a grade. The net result is that the system behaves no differently than off-grade contouring with a weighted C factor based on the area occupied by the various strips. This approach produces a P-factor value that represents the minimum

effectiveness of strips. The maximum effectiveness can be estimated by use of the stripcrop model by choosing a designation for the cropped strips having an erodibility greater than that for the contour tilled condition, to represent the reduced effectiveness of off-grade contouring. The overall P factor is a combination of two P factors: one for off-grade contouring, and one for stripcropping with an adjusted surface designation because of increased sediment (resulting from off-grade contouring) reaching the densely vegetated strips.

The stripcrop model in RUSLE estimates the amount of deposition induced by a strip by representing the main factors that affect sediment transport and deposition. However, even though the parameter $\phi = V_f/\sigma$ represents the effect of sediment characteristics, a single value is used for all conditions. Therefore, actual deposition will be greater and sediment delivery will be less than that computed with RUSLE for soils high in either clay or sand content compared to typical silt loam soils. The converse is true for soils whose silt content is higher than that in silt loam soils. Furthermore, upslope localized deposition in depressions left by tillage or deposition by upslope strips reduces the particle size and thus the amount of sediment deposited by downslope strips. In estimating sediment passing through strips that induce deposition, the CREAMS model (Foster et al. 1980a) or the SEDIMOT II model (Wilson et al. 1986) considers more factors over a wider range of conditions than does RUSLE.

SUPPORT PRACTICE FACTOR (P) FOR TERRACING

Terraces reduce sheet and rill erosion on the terrace interval by breaking the slope into shorter slope lengths. Also, deposition along the terraces may trap much of the sediment eroded from the interterrace interval, particularly if the terraces are level and include closed outlets, have underground outlets, or have a very low grade. Deposited sediment remains on the field and is redistributed over a significant portion of the field, thus reducing soil deterioration caused by erosion. In this way, terraces help to maintain the soil resource much as contour stripcropping does. Furthermore, properly designed terraces and outlet channels collect surface runoff and convey it off the field at nonerosive velocities. Without the terraces and outlet channels, runoff in natural waterways on unterraced fields can cause significant erosion.

Deposition Behind Terraces

The amount and location of sediment deposited on terraced fields are important in assigning P-factor values to calculate soil loss for conservation planning. If no soil is trapped, none is saved by deposition. Even if deposition traps all sediment eroded from the interterrace interval, the area benefiting directly is that near the terraces. Some of the interterrace interval is still degraded as if no deposition occurs. The P factor for computing soil loss for conservation planning to maintain the soil resource is computed as a function of spacing between terraces. The maximum benefit assigned to deposition is that half of the deposition directly benefits maintenance of the soil resource at spacings of less than 110 ft. At spacings of greater than 110 ft, the benefit is assumed to decrease to the point that no benefit is assigned for spacings of 300 ft and greater.

Erosion of the upslope and deposition on the downslope portion, within the terrace interval, cause a flatter slope that can be permanently maintained above storage-type terraces. On deep soils, a permanent bench can be formed, resulting in less erosive topography and easier farming (Jacobson 1981).

Measured elevations on gradient terraces (Borst et al. 1945, Copley et al. 1944, Daniel et al. 1943, Pope et al. 1946, Smith et al. 1945) showed that after 8 yr, deposited soil accumulated on terrace ridges, channel bottoms, and front and back slopes. The sediment accumulation on ridges and backslopes was produced by displacement during tillage and terrace maintenance. With closed

outlet and underground outlet terraces, sediment accumulates where runoff enters standing water.

Effect of Grade

An analysis of terrace data from the 1930's and 1940's showed that deposition varies greatly with terrace grade (Foster and Ferreira 1981). Sediment yield from single-terrace watersheds with a range of grades was measured for about 8 yr at several locations. Results of this analysis show that the sediment yield from uniform-grade terraces increases according to the following exponential relationship:

$$P_y = 0.1e^{2.4s} \qquad s<0.9\% \qquad [6\text{-}43]$$

$$P_y = 1.0 \qquad s\geq 0.9\% \qquad [6\text{-}44]$$

where P_y = sediment delivery factor and s = terrace-slope grade (%). The P factor for conservation planning is computed as

$$P = 1 - B(1-P_y) \qquad [6\text{-}45]$$

where B = the benefit assigned to deposition, and the quantity $1-P_y$ = that amount of deposition, comparable to M in the stripcropping computations. Values for B are given in table 6-14.

Terrace P Factor for Conservation Planning

The P factor for terraces for use in conservation planning considers both the benefit of deposition and the amount of sediment deposited. This net soil loss is the soil loss on the interterrace interval minus the amount of deposited soil that is credited for helping to maintain the soil resource. Table 6-15 gives terrace P-factor values for use in conservation planning (Foster and Highfill 1983). Table 6-16 gives values for use in estimating sediment yield from terraces.

To compute soil loss with RUSLE for conservation planning, values for the terrace P factor are multiplied by other factor values for contouring and stripcropping on the interterrace interval.

SUPPORT PRACTICE FACTOR (P) FOR SUBSURFACE DRAINED AREAS

Limited field data indicate that subsurface drainage is effective in reducing overland flow and erosion (Formanek et al. 1987, Bengtson and Sabbage 1988). Both the Formanek and the Bengtson and Sabbage studies reported P values with an average of about 0.6, although individual annual values and storm values varied appreciably.

Because of limited information and differences in procedures among studies, further research is needed to develop a range of P-factor values for subsurface drained areas that are applicable across many conditions of climate, soil, crop, and slope. The technique needing development may well include a procedure similar to that reported by Skaggs et al. (1982). This technique may involve estimating runoff volume, peak runoff rate, and storm EI by use of a physically based model like CREAMS (Knisel 1980) to estimate P-factor values for simulations with and without subsurface drainage situations over a wide range of field conditions.

SUPPORT PRACTICE FACTOR (P) FOR RANGELANDS

The support practice factor (P) in RUSLE reflects the effect on rangeland erosion of mechanical practices such as ripping, root plowing, contour furrowing, and chaining. Some common mechanical practices applied on rangelands are listed in tables 6-17, 6-18, and 6-19. These practices affect erosion in several ways, including the removal of surface cover, which is perhaps the most important single factor affecting erosion. However, that effect is considered by the cover-management factor C in RUSLE. Mechanical practices described by the P factor can affect runoff amount, runoff rate, flow direction of runoff, and hydraulic forces exerted by runoff on the soil.

Almost every mechanical practice that disturbs rangeland soils increases infiltration, which in turn reduces runoff and erosion. An exception is the compaction and smoothing used for water harvesting. The degree to which infiltration is increased depends on the soil. The increase in infiltration and the reduction in runoff can be very large on the coarse-textured soils of the southwestern United States, whereas the increase in infiltration and the reduction in runoff can be slight on fine-textured soils like those in South Dakota. In fact, the crusting of fine-textured soils after mechanical practices that expose the soil can cause decreased infiltration. The ratings for runoff reduction given in tables 6-16, 6-17, and 6-18 are general. More precise ratings are possible from knowledge of the hydrologic properties of local soils.

A practice like contour furrowing that produces ridges and furrows will redirect surface runoff from flowing directly downhill to a flow path around the hill on a reduced grade. The reduced grade can greatly decrease the erosivity of the runoff. A practice like ripping at right angles to the slope, which leaves a very rough surface, also slows the runoff and reduces its erosivity. Depressions formed by the roughness provide areas where sediment is deposited, thus reducing soil loss.

The effectiveness of mechanical practices decreases over time as the soil surface seals and the depressions and furrows are filled with sediment. The rate at which a practice loses its effectiveness depends on the climate, soil, slope, and cover. The estimated times of effectiveness for practices listed in table 6-19 are general and should be adjusted for local conditions. Values for P should be

increased over time from the minimum value immediately after treatment, because the practices are estimated to lose their effectiveness.

Runoff Reduction and Surface Roughness

The effect of increased infiltration and surface roughness are considered together when selecting a value for P because the influence of runoff and surface roughness are interrelated with slope steepness. The effect of surface roughness on the reduction of soil loss will decrease as the slope steepness increases.

Values for the P factor for rangelands for the effect of roughness, infiltration, and slope are computed in RUSLE with the equation

$$P = \frac{D_y}{D_e} \qquad [6\text{-}46]$$

where D_y = sediment transported from the slope, and D_e = sediment produced on the slope by detachment.

The P factor considers that the roughness is assumed to cause some of the sediment produced by detachment to be deposited in the depressions left by the roughness. The amount of sediment leaving the slope (D_y) is computed by the deposition equation used to compute values for P with stripcropping (Renard and Foster 1983), as follows:

$$D_y = \left(\phi \; dT/dx + D_e\right) / \left(1 + \phi\right) \qquad [6\text{-}47]$$

where ϕ = a parameter that indicates how readily sediment is deposited, and dT/dx = change in transport capacity with distance.

A value of 15 was assigned to ϕ, the same as in the stripcropping computations. The equation for dT/dx is based on the transport capacity equation used in WEPP (Foster et al. 1989), as follows:

$$dT/dx = k_t \; s \; \sigma \; r_f \qquad [6\text{-}48]$$

where k_t = a transport coefficient, s = sine of the slope angle, σ = excess rainfall rate (rainfall rate minus infiltration rate), and r_f = a roughness factor.

The parameter k_t was assigned a value of 33.28, which was chosen so that the model would fit experimental data for deposition as a function of slope (Meyer and Harmon 1985). Excess runoff rate is computed from

$$\sigma = 1 - f_r \qquad [6\text{-}49]$$

where f_r is a runoff reduction factor that varies between an initial value at the time of disturbance and zero after decaying over time as the soil consolidates after the disturbance according to

$$f_r = f_{ri}\, c_d \qquad [6\text{-}50]$$

where f_{ri} = the initial runoff reduction, and c_d = the consolidation factor that is given by

$$c_d = \exp\left(-d_t\, t_d\right) \qquad [6\text{-}51]$$

where d_t = a decay parameter, and t_d = time (yr) since the soil was disturbed.

Consolidation is assumed to begin immediately. The decay parameter is computed from

$$d_t = -\ln(0.05) \,/\, t_c \qquad [6\text{-}52]$$

where t_c = time (yr) for 95% of effect of disturbance to have disappeared by consolidation.

Runoff reduction at the time of disturbance is computed by use of the 10-yr frequency single-storm erosivity, and the NRCS runoff index method. Values for runoff index as a function of cover roughness are described in table 6-20; cover roughness conditions are shown in table 6-21. The runoff index values are

a function of the rainfall intensity pattern in a storm. Runoff index values are greater for thunderstorm-type rains than for long-duration, gentle, frontal-activity rains. The ratio of 10-yr storm erosivity, $(EI)_{10}$, to average annual precipitation (P) is used as an index to determine curve number values. For $(EI)_{10}/P > 3$, values for thunderstorm-dominated areas are used; for $(EI)_{10}/P < 1$, values for areas dominated by frontal activity are used. Linear interpolation is used for values of $(EI)_{10}/P$ between 1 and 3.

The roughness factor (r_f) is computed from

$$r_f = 0.23\ r_i^{-1.18} \qquad [6\text{-}53]$$

where r_i is a roughness index (in). The coefficient 0.23 and exponent -1.18 were selected to give values for the roughness factor (r_f), which are similar to the values used for ζ in the stripcropping computations.

The value used for r_i is the value that represents the current surface condition. That value is determined by interpolating between the roughness immediately after disturbance and the roughness after consolidation. Equations [6-50] and [6-51] are used in this interpolation. Roughness values for the RUSLE range condition classes are given in tables 6-21 through 6-24.

Detachment (D_e) is assumed to be the same for all conditions except for the effect of disturbance. Detachment is computed with the equation

$$D_e = D_b + \left(1 + D_b\right) c_d \qquad [6\text{-}54]$$

where D_b is the minimum value of detachment after it decreases over time after consolidation relative to the detachment immediately after disturbance. A value of 0.45 is assumed for D_b, the same as used in the C-factor computations.

Redirection of Runoff

When applied on rangelands, practices like contour furrowing are effective because they redirect surface runoff from a downslope path to a less erosive path around the hill. Any rangeland practice that leaves ridges sufficiently high to redirect runoff in this manner has an effect that is considered in the P factor.

Slope Length and Steepness Taken Downhill

Ideally, the grade along the furrows between the ridges should be flat or near flat so that runoff may spill uniformly over the length of the ridges. Ridges perfectly on the contour ensure maximum runoff storage and infiltration and also minimize runoff and erosion. P values for this condition are computed using equations [6-1] through [6-10] by use of the parameter values given in tables 6-21 through 6-24. Slope length is then taken directly down the hill perpendicular to the contour.

The effectiveness of contouring depends on the storm erosivity and the reduction in runoff caused by mechanical practices. Because a few major storms determine the overall effectiveness of contouring, the erosivity (EI_{10}) of the storm with a 10-yr return interval is recommended as the basis for adjusting contour factor values to account for the influence of storm erosivity.

The effectiveness of contouring depends on the ridge height, as indicated by the contour factor values in figure 6-2. A low-height ridge (2-3 in) is like that left by a typical rangeland drill or light disk. Moderately high ridges are those that are left by an agricultural chisel plow with twisted shanks. Very high ridges (>6 in) are like those left by typical contour furrowing on rangelands.

To get the ridges exactly on the contour is practically impossible. When the ridges are off-contour, runoff flows along the furrows to low places in the landscape. As water accumulates, breakovers in these depressed areas often occur and cause concentrated flow erosion. The effectiveness of contouring is rapidly lost as grade along the furrows increases.

The same relationships used in the cropland section and the parameter values given in tables 6-21 through 6-24 are used to compute the effect of storm erosivity, increased infiltration, ridge height, and grade along the ridges for contouring on rangeland.

Terraces, Diversions, and Windrows

Terrace and diversion channels on a slight grade across a slope will intercept surface runoff and direct it around the slope on a slight grade. As a part of chaining, brush and other debris are sometimes pushed into windrows that are on the approximate contour. If these windrows intercept surface runoff and direct it around the hill, they too should be treated as terraces.

Terraces and similar practices usually reduce the slope length. Therefore, when RUSLE is applied to terraced land, the slope length is taken from the origin of surface runoff on the upslope terrace ridge or other watershed divide to the edge of the flow in the terrace channel. Slope steepness used in the S factor is the slope of the interterrace area. This procedure for selecting slope length is used when the terraces are on a uniform grade. Sometimes the terraces may be on a nonuniform grade and may be so far apart that concentrated flow areas develop on the interterrace interval. When this situation exists, terraces may have little effect on slope length, and the slope is taken in the same way as if the terraces were not present.

Terrace, diversion, or windrow channels on a sufficiently flat grade cause considerable deposition, with the amount deposited being a function of erosion between terraces and channel grade. Sediment yield from the terrace outlets may be obtained by multiplying the RUSLE soil-loss estimate for the interterrace area by the sediment delivery ratio values in table 6-16.

Conservationists debate the value of deposition in terraces for maintaining soil productivity. It is usually given some credit on cropland because tillage is assumed to partially redistribute the deposited sediment. Because tillage is infrequent, if ever, on rangelands, no credit should be given for a benefit of deposition. However, if this credit is taken for conservation planning purposes, the suggested values in table 6-15 may be used.

Undisturbed Strips

Undisturbed strips of land adjacent to channels are sometimes left to minimize the sediment yield into a channel and the accelerated channel erosion. If the undisturbed strips have heavy ground cover, the deposition of sediment can occur when water flows through the strips from the disturbed areas. The effectiveness of these practices on rangeland are judged to be highly variable, and a procedure for applying RUSLE to these strips is not provided.

P-FACTOR VALUES FOR STRIPCROPPING ON CROPLAND IN THE NORTHWESTERN WHEAT AND RANGE REGION

Runoff and erosion processes occur very differently on cropland in the Northwestern Wheat and Range Region than on cropland in other parts of the United States. Much of the erosion occurs during the winter from rain or snowmelt on thawing soils. These soils remain wet and highly erodible over several weeks from repeated freezing and thawing. A transient frost layer near the surface allows little infiltration, producing high amounts and rates of runoff for given amounts and intensities of rainfall.

The definition of cover-management conditions and the values for the runoff indices used in RUSLE for cropland in the Northwestern Wheat and Range Region for these winter conditions differ from values used for other locations. These definitions and the adjusted values for winter are shown in table 6-25 and 6-26, respectively.

Strips with residue and stubble that are rough tilled with implements similar to chisel plows and moldboard plows that turn the soil uphill can have high infiltration rates—often so large that runoff from upslope completely infiltrates within the strip if the strip exceeds about 50 ft. No runoff or sediment leaves the rough-tilled strip. The soil must be left in a rough-tilled condition with residue from the previous crop for these high infiltration rates to occur. Infiltration on these rough strips seems to be greater than that for permanent grass strips.

The cover and roughness of this rough-tilled condition is represented by condition VR in table 6-25. The rough-tilled strip is assumed to behave the same during the winter as at other times during the year. Values for the runoff index for the remaining strips where frost affects infiltration are selected from table 6-26. Values for runoff indices for periods not influenced by frost are selected from table 6-5.

The choice of slope length must be considered where all upslope runoff infiltrates on a strip. Two approaches may be used. The preferred approach is to use the entire slope length as if infiltration did not differ among the strips. The effect of all sediment reaching a strip being deposited within the strip is considered by RUSLE in the computation of P.

The alternative approach is to assume that the effect of the stripcropping system is like that of terraces. A slope length equal to the width of the strip is selected and a P-factor value is computed for terraces assuming a closed-outlet terrace.

Table 6-1.
Summary of data from plot studies on the effect of contouring on runoff and soil loss

Study number	Location	Reference	Plot dimensions			Type of study[1]
			Length (ft)	Width (ft)	Slope (%)	
1	Auburn, Alabama	Diseker and Yoder (1936)	50	15.1	0, 5, 10, 15, 20	Both
2	Urbana, Illinois	Van Doren et al. (1950)	180	53	2	Nat
3	Temple, Texas	Hill et al. (1944)	[2]—	[2]—	3.5	Nat
4	McCredie, Missouri	Jamison et al. (1968)	420	104	3.5	Nat
5	Morris, Minnesota	Young et al. (1964)	75	13.5	4, 7.5, 10.5	Sim
6	Batesville, Arkansas	Hood and Bartholomew (1956)	90	30	4	Nat
7	Central, Illinois	McIsaac et al. (1987)	35	10	5	Sim
8	Lincoln, Nebraska	Jasa et al. (1986)	35	10	5	Sim
9	Bethany, Missouri	Smith et al. (1945)	270	45	7	Nat
10	Guthrie, Oklahoma	Daniel et al. (1943)	[3]—	[3]—	7	Nat
11	Clarinda, Iowa	Browning et al. (1948)	158	84	9	Nat
12	Auburn, Alabama	Nichols and Sexton (1932)	50	15	10, 15	Sim
13	Concord, Nebraska	Jasa et al. (1986)	35	10	10	Sim
14	Arnot, New York	Lamb et al. (1944)	310	21	11	Nat
15	Sioux City, Iowa	Moldenhauer and Wischmeier (1960)	726	10	12	Nat
16	Zanesville, Ohio	Borst et al. (1945)	726	6	13	Nat
17	Sussex, New Jersey	Knoblauch and Haynes (1940)	70	13.5	16	Nat
18	Holly Springs, Mississippi	McGregor et al. (1969)	70	150	4.2	Nat

[1]Nat = study with natural rainfall, Sim = study with simulated rainfall, Both = study involving both natural and simulated rainfall.
[2]These are 0.01-, 0.03-, and 0.084-acre plots; other plot dimensions not available.
[3]A 0.25-acre plot; other dimensions not available.

Table 6-2.
Summary of data from watershed studies on effect of contouring on runoff and soil loss

Study number	Location	Reference	Watershed dimensions	
			Area (acre)	Average slope (%)
1	Temple, Texas	Hill et al. (1944)	0.15, 1.5, 2.2	3, 5
2	Bethany, Missouri	Smith et al. (1945)	4.5, 7.4	7
3	Clarinda, Iowa	Browning et al. (1948)	2, 3.2	8
4	LaCrosse, Wisconsin	Hays et al. (1949)	2.2	15

Table 6-3.
Values for coefficients in equations [6-1] and [6-2]
used to fit the base data for the P factor for contouring

Ridge height	Coefficient							
	a	b	c	d	s_m (%)	s_{eb} (%)	P_{mb}	P_z
Very low[1]	24,120	4	10.36	1.5	5	11	0.85	0.50
Low	27,201	4	13.31	1.5	6	15	0.65	0.3
Moderate	23,132	4	12.26	1.5	7	20	0.45	0.15
High	18,051	4	10.24	1.5	8	26	0.27	0.08
Very high	22,255	4	6.83	1.5	8	36	0.1	0.05

[1]See fig. 6-2 for ridge height definitions.

Table 6-4.
Description of cropland cover-management conditions used in RUSLE for estimating P-factor values

Categories of conditions	Description of condition
C1. Established meadow (very dense cover)	Grass is dense and runoff is very slow, about the slowest under any vegetative condition. Becomes condition 2 when mowed and baled.
C2. 1st yr meadow, hay (moderately dense cover)	Hay is a mixture of grass and legume just before cutting. Meadow is a good stand of grass that is nearing the end of 1st yr. Becomes condition 4 when mowed and baled.
C3. Heavy (dense) cover or very rough or both	Ground cover for this condition is about 75-95%. Roughness is like that left by a high-clearance moldboard plow on a heavy-textured soil. Roughness depressions appear 7 in or more deep. Vegetative hydraulic roughness like that from a good legume crop (such as lespedeza) that has not been mowed.
C4. Moderate cover or rough or both	Ground cover for this condition is about 40-65%. Roughness is like that left by a moldboard plow in a medium-textured soil. Depressions appear 4-6 in deep. Vegetative hydraulic roughness is similar to that produced by winter small grain at full maturity.
C5. Light cover or moderate roughness or both	Ground surface cover is 10-30%. Surface roughness is like that left by first pass of tandem disk over a medium-textured soil that has been moldboard plowed. This roughness could also be similar to that left after a chisel plow through a medium-textured soil at optimum moisture conditions for tillage. Roughness depressions appear 2-3 in deep. In terms of hydraulic roughness produced by vegetation, this condition is similar to that produced by spring small grain at about 3/4 maturity.
C6. No cover or minimal roughness or both	This condition closely resembles the condition typically found in row cropped fields after the field has been planted and exposed to a moderately intense rainfall. Ground cover is less than about 5%. Roughness is like that of a good seedbed for corn or soybeans. Surface is rougher than that of a finely pulverized seedbed for seeding vegetables.
C7. Clean-tilled, smooth, fallow	Surface is essentially bare, 5% or less of cover. Soil has not had a crop grown on it in the last 6 mo or more, so much of the residual effects of previous cropping has disappeared. Surface is smooth, similar to the surface that develops on a very finely pulverized seedbed exposed to several intense rainfalls. This condition is most likely found in fallow and vegetable fields.

Table 6-5.
Values of runoff index used to compute runoff to estimate P-factor values for cropland

Cropland cover-management condition	Hydrologic soil group			
	A	B	C	D
C1	30	58	71	78
C2	46	66	78	83
C3	54	69	79	84
C4	55	72	81	85
C5	61	75	83	87
C6	64	78	85	88
C7	77	86	91	94

Table 6-6.
Values of Manning's n_t used in RUSLE cropland conditions

Cover-management condition[1]	Manning's n_t
C1	0.200
C2	0.110
C3	0.070
C4	0.040
C5	0.023
C6	0.014
C7	0.011

[1]Refer to table 6-4 for a description of cover-management conditions.

Table 6-7.
Critical slope length values computed by equation [6-12] and critical slope length values from AH 537

Slope (%)	From Equation [6-1][1] (ft)	From AH 537 (ft)
1.5	1000	400
4.0	384	300
7.0	200	200
10.5	125	120
14.5	80	86
18.5	60	64
23.0	50	50

[1]Moderate ridge height, hydrologic soil group C, C6 cover-management condition (defined in table 6-4), 100 ft·tonf·in (acre h)$^{-1}$ $(EI)_{10}$ storm

Source: Wischmeier and Smith (1978).

Table 6-8.
Computed critical slope length as a function of $(EI)_{10}$ storm erosivity and cover-management conditions[1]

$(EI)_{10}$ Storm erosivity	For cover-management condition[2]						
	C1 (ft)	C2 (ft)	C3 (ft)	C4 (ft)	C5 (ft)	C6 (ft)	C7 (ft)
10	1,000	1,000	1,000	1,000	1,000	1,000	933
25	1,000	1,000	1,000	1,000	1,000	824	348
50	1,000	1,000	1,000	1,000	885	387	184
100	1,000	1,000	1,000	1,000	446	201	104
200	1,000	1,000	1,000	579	243	111	61

[1] 7% slope, hydrologic soil group C
[2] Cover-management conditions are defined in table 6-4.

Table 6-9.
Critical slope length computed as a function of hydrologic soil group and $(EI)_{10}$ storm erosivity[1]

$(EI)_{10}$ storm	For hydrologic soil group			
	A (ft)	B (ft)	C (ft)	D (ft)
10	1,000	1,000	1,000	1,000
25	1,000	1,000	1,000	1,000
50	1,000	1,000	1,000	1,000
100	1,000	1,000	1,000	969
200	1,000	700	579	537

[1]7% slope, cover-management condition C4

Table 6-10.
Critical slope length computed as a function of hydrologic soil group and $(EI)_{10}$ storm erosivity[1]

$(EI)_{10}$ storm	For hydrologic soil group			
	A (ft)	B (ft)	C (ft)	D (ft)
10	1,000	1,000	1,000	1,000
25	1,000	1,000	824	687
50	1,000	525	387	343
100	407	246	201	185
200	178	127	111	106

[1]7% slope, cover-management condition C6

Table 6-11.
Values for sediment delivery for stripcropping as determined from experimental data

Location	Rotation	Sediment delivery	
		Observed	Model
Bethany, Missouri (Smith et al. 1945)	C-W-M	0.44	0.53
Zanesville, Ohio (Borst et al. 1945)	C-W-M	0.36	0.53
Owen, Wisconsin (Hays and Attoe 1957)	C-W-M-M	0.42	0.48
LaCrosse, Wisconsin (Hays et al. 1949)	C-W-M-M	0.55	0.48
Batesville, Arkansas (Hood and Bartholomew 1956)	C-Ct-O/L	0.80	0.68
Temple, Texas (Watershed 1) (Hill et al. 1944)	C-Ct-O	0.52	0.51
Temple, Texas (Watershed 2) (Hill et al. 1944)	C-Ct-O	0.30	0.51

C = corn, Ct = cotton, W = wheat, O = oats, O/L = oats/lespedeza mixture, M = meadow.

Table 6-12.
Erosion and sediment transport factor values for P factor model for strips

	Cover-management condition[1]	Factor values		Length exponent (n)
		Erosion (ξ)	Transport (ζ)	
C1	Very dense cover	0.005	0.02	1.0
C2	Dense cover or extreme roughness or both	0.02	0.05	1.0
C3	Moderately dense cover	0.03	0.10	1.0
C4	Moderate cover or roughness or both	0.12	0.14	1.0
C5	Light cover or moderate roughness or both	0.25	0.25	1.0
C6	Clean row crop tillage, no cover or minimal roughness or both	0.50	0.50	1.0
C7	Clean-tilled, smooth, fallow	1.00	1.50	1.5

[1]Cover-management conditions defined in table 6-4.

Table 6-13.
Values for P factor for sediment delivery and conservation planning computed with model for selected stripcropping, buffer, and filter strip systems[1]

System[2]	Sediment delivery (P_y)	Conservation planning (P_s)
RC-WSG-M1-M2[3]	0.53	0.78
RC-RC-WSG-M1[4]	0.54	0.80
RC-RC-WSG-M1-M2	0.47	0.77
RC-SSG-RC-SSG	0.75	0.91
RC-SSG[5]	0.83	0.93
RC-WSG[6]	0.71	0.86
RC-M1	0.58	0.78
RC-M1-RC-M1 (year 1)[7]	0.39	0.69
SSG-M2-SSG-M2 (year 2)		
M1-RC-M1-RC (year 3)		
M2-SSG-M2-SSG (year 4)		
RC-RCrt-RCrt-M1	0.65	0.84
Cnt-SBrt-SBnt	1.00	1.00
Crt-SBrt-Crt-WSGrt	0.89	0.96
0.5 filter[8]	0.06	0.51
0.1 filter[9]	0.24	0.91
Buffer strips[10]	0.15	0.67
Buffer strips[11]		0.71
Buffer strips[12]		0.75

[1]Values for filter strip systems are primarily for illustration as filter strips are usually not used to protect upslope areas from productivity loss.
[2]RC = row crop, WSG = winter small grain, SSG = spring small grain, M1 = 1st yr meadow, M2 = 2d yr meadow, C = corn, SB = soybeans, rt = reduced tillage, nt = no till.
[3]Wischmeier and Smith (1978) P = 0.50.
[4]Wischmeier and Smith (1978) P = 0.75.
[5]Wischmeier and Smith (1978) P = 1.00.
[6]Wischmeier and Smith (1978) P = 1.00, but they note that winter small grain can be effective in some cases.
[7]Location of strips by year in rotation; that is, Y1 is year of rotation.
[8]Permanent meadow filter strip that covers 0.5 of slope below row crop.
[9]Permanent meadow filter strip that covers 0.1 of slope below row crop.
[10]Permanent meadow buffer strips located at 0.4-0.5 and 0.9-1.0, separated by row crop strips.
[11]Permanent meadow buffer strips located at 0.35-0.40 and 0.65-0.70, separated by row crop strips.
[12]Permanent meadow buffer strip at 0.4-0.5, separating two row crop strips.

Table 6-14. Benefit assigned to deposition behind terraces

Terrace spacing (ft)	Benefit (B)
≤110	0.5
125	.6
160	.7
200	.8
260	.9
≥300	1.0

Table 6-15.
Terrace P-factor values for conservation planning[1]

Horizontal terrace interval (ft)	Terrace P-factor values			
	Closed outlets[2]	Open outlets, with percent grade of[3]		
		0.1-0.3	0.4-0.7	>0.8
Less than 110	0.5	0.6	0.7	1.0
110-140	.6	.7	.8	1
140-180	.7	.8	.9	1
180-225	.8	.8	.9	1
225-300	.9	.9	1	1
More than 300	1	1	1	1

[1]Multiply these values by other P-subfactor values for contouring, stripcropping, or other support practices on interterrace interval to obtain composite P-factor value.

[2]Values for closed-outlet terraces also apply to terraces with underground outlets and to level terraces with open outlets.

[3]Channel grade is measured on the 300 ft of terrace closest to outlet or 1/3 of total length, whichever distance is less.

Table 6-16.
Sediment delivery subfactor (P_y) for terraces[1]

Terrace grade	Sediment delivery subfactor
%	
Closed outlet	[2]0.05
0 (level)	.10
.1	.13
.2	.17
.4	.29
.6	.49
.8	.83
.9	1
[3]>1	1

[1]Includes terraces with underground outlet.
[2]From Foster and Highfill 1983. All other values from $P_y = 0.1e^{2.64g}$, where e = natural logarithm and g = terrace grade (%).
[3]Potential for net erosion in terrace channels, depending on flow hydraulics and soil erodibility in the channels. If net erosion occurs, $P_y > 1$.

Source: Foster and Highfill (1983).

Table 6-17.
Runoff and erosion effects from mechanical practices on rangelands

Rangeland treatment	Data source	Runoff and erosion changes after treatment for indicated years[1]		
		Runoff (%)	Erosion (%)	Years
Pitting	Hickey and Dortignac (1963)	-18	-16	1
		-10	0	3
Ripping	Hickey and Dortignac (1963)	-96	-85	1
		-85	-31	3
Moldboard plowing	Gifford and Skau (1967), Blackburn and Skau (1974)	+U	0	1
		0	0	5
Contour furrowing (model B)	Branson et al. (1966), Wein and West (1973)	-U	-U	1
		-U	-U	10
Root plowing	Simanton et al. (1977)	+50	-54	1
		-80	-45	4
Land imprinting	Unpublished, Walnut Gulch Experimental Watershed (1978)	0	-90	1

[1]Relative to pretreatment level; (-) = decrease, (+) = increase, and U = unknown.

Source: Simanton (1988, personal communication).

Table 6-18.
Ratings[1] of possible effects of rangeland treatment and implement use

Possible effect	Treatment or implement[2]											
	LP	PT	CH	BP	RP	RI	CF	BR	RD	TR	FL	BU
Incr. infiltration	3	3	1	2	3	1	3	2	1	3	1	0
Incr. percolation	2	2	1	1	3	3	3	1	0	3	0	0
Incr. pore space	2	2	1	2	2	3	3	1	0	1	0	0
Incr. water holding cap.	3	3	1	2	2	3	3	2	1	3	1	0
Incr. surface porosity	1	2	0	2	3	1	2	2	1	1	0	0
Incr. surface stability	3	2	1	2	2	1	1	3	1	1	1	0
Incr. roughness	3	3	1	2	2	1	2	3	1	1	0	0
Incr. seedling establish.	3	2	0	1	2	0	2	1	2	1	0	1
Decr. surface compaction	0	2	0	3	3	1	2	0	2	1	0	0
Decr. soil water evap.	2	1	1	1	1	0	1	2	0	0	3	0
Decr. surface runoff	2	2	1	1	2	1	3	1	1	2	1	0
Decr. erosion	2	2	1	1	3	2	2	1	1	2	1	0
Decr. canopy cover	3	2	2	2	2	1	1	3	0	0	3	3
Decr. competition	1	1	2	2	3	0	1	1	0	0	1	2
Treatment or implement used on:	LP	PT	CH	BP	RP	RI	CF	BR	RD	TR	FL	BU
Steep slopes	3	1	3	1	2	3	1	3	2	3	3	3
Rocky soils	3	1	3	1	2	1	2	3	2	3	3	3
Clay soils	2	2	3	1	3	3	2	2	3	3	3	3
Shallow soils	3	3	3	3	3	2	3	3	3	3	3	3
Woody shrubs	3	2	3	2	3	3	2	3	1	3	3	3
Herbaceous plants	3	3	0	3	0	0	3	0	1	3	0	3
Treatment longevity	3	1	3	2	3	3	2	1	1	3	0	2
Return/cost	3	1	3	1	2	1	2	1	3	3	1	2
Treatment or implement totals:	53	43	34	38	51	34	46	39	27	43	28	28

[1]LP = Land imprinter, broadcast seeding
PT = Pitting, broadcast seeding
CH = Chaining, cabling
BP = Brushland plow
RP = Rootplow, rangeland drill seeding
RI = Ripping
CF = Contour furrow, broadcast seeding
BR = Brush roller
RD = Rangeland drill (seeding)
TR = Terrace, broadcast seeding
FL = Flail
BU = Burning

[2] Ratings range from 0 = no effect, to 3 = greatest effect.

Source: Simanton (1988, personal communication).

Table 6-19.
Common mechanical practices applied to rangelands

Practice	Degree of disturbance	Surface configuration	Estimated duration of effectiveness (yr)	Runoff reduction
Rangeland drill	Minimal tillage except in furrow	Low ridges (<2 in) and slight roughness	1–2	None to slight
Contour furrow/pitting	Major tillage 8-12 in deep	High ridges, about 6 in	5–10	Slight to major
Chaining	Severe surface but shallow	Slight to moderate random roughness	3–5	Slight to moderate
Land imprinting	Moderate-sized shallow depressions	Short channels (40 in) and small to moderate	2–3	Slight to moderate
Disk plows, offset disks	Major tillage, about 4-8 in deep	Moderate ridges 2-4 in	3–4	Slight to moderate
Ripping, grubbing, root plowing	Minimal but often deep, 8+ in	Slight to very rough, especially when done at right angles	4–7	Moderate to major

Table 6-20.
Definition of cover-roughness conditions for rangeland

Condition identification	Description
R1	Very rough; plant plus rock cover greater than 50%
R2	Very rough; plant plus rock cover less than 50%
R3	Rough; plant plus rock cover greater than 50%
R4	Rough; plant plus rock cover less than 50%
R5	Moderately rough; plant plus rock cover less than 50%
R6	Moderately rough; established vegetation; plant plus rock cover less than 40%
R7	Slightly rough; plant plus rock cover less than 25%
R8	Slightly rough; established vegetation; plant plus rock cover less than 35%
R9	Smooth; established vegetation; plant plus rock cover less than 25%

Table 6-21.
Runoff indices for cover-roughness conditions at disturbance in areas dominated by thunderstorms

Cover-roughness condition[1]	Hydrologic soil group				Manning's n_t	Roughness index (in)
	A	B	C	D		
R1	47	50	53	56	0.10	2.0
R2	52	55	58	61	0.08	2.0
R3	57	60	63	66	0.07	1.4
R5	62	65	68	71	0.04	0.9
R7	67	70	73	76	0.023	0.5

[1]Defined in table 6-20

Table 6-22.
Runoff indices for cover-roughness conditions at disturbance in areas dominated by frontal activity

Cover-roughness condition[1]	Hydrologic soil group				Manning's n_t	Roughness index (in)
	A	B	C	D		
R1	32	35	38	41	0.20	2.0
R2	37	40	43	46	0.10	2.0
R3	42	45	48	51	0.07	1.4
R5	47	50	53	56	0.04	0.9
R7	52	55	58	61	0.023	0.5

[1]Defined in table 6-20

Table 6-23.
Runoff indices after consolidation for cover-roughness conditions at disturbance in areas dominated by thunderstorms

Cover-roughness condition[1]	Hydrologic soil group				Manning's n_t	Roughness index (*in*)
	A	B	C	D		
R3	67	70	73	76	0.10	1.4
R4	72	75	78	81	0.08	1.4
R6	77	80	83	86	0.07	0.9
R8	82	85	88	90	0.04	0.5
R9	87	90	92	94	0.023	0.2

[1]Defined in table 6-20

Table 6-24.
Values for runoff index after consolidation for cover-roughness conditions in areas dominated by frontal activity

Cover-roughness condition[1]	Hydrologic soil group				Manning's n_t	Roughness index (in)
	A	B	C	D		
R3	47	50	53	56	0.10	1.4
R4	52	55	58	61	0.08	1.4
R6	57	60	63	66	0.07	0.9
R8	62	65	68	71	0.04	0.5
R9	67	70	73	76	0.023	0.2

[1]Defined in table 6-20

Table 6-25.
Description of cropland cover-management conditions used in RUSLE for estimating P-factor values in the Northwestern Wheat and Range Region.

Categories of conditions	Description of condition
C1. Established sod-forming grass (very dense cover)	The grass is dense and runoff is very slow; about the slowest under any vegetative condition. When moved and baled, this changes to condition 2.
C2. Standing stubble, 1st year grass, or meadow to be cut for hay (moderately dense cover)	The stubble is from a good stand with few rills or flow concentrations. The hay is a mixture of grass and legumes just before cutting. When mowed and baled, this becomes condition 4.
C3. Heavy (dense) cover or very rough or both	Ground cover is about 75 to 95%. Roughness depressions appear to be 5 or more inches deep (Random Roughness >2 ½ inches). Vegetative hydraulic roughness is like that of a good legume crop that has not been mowed.
C4. Moderate cover or roughness or both	Ground cover is about 40 to 65%. Roughness depressions appear to be about 3 to 5 inches deep (Random Roughness 1 ½ to 2 ½ inches), and vegetative hydraulic roughness is like that of a good stand of winter small grain at full maturity.
C5. Light cover or moderate roughness or both	Ground cover is from 10 to 30%. Roughness depressions appear to be 1 to 3 inches deep (Random Roughness ½ to 1 ½ inches), and the vegetative hydraulic roughness is like that of a typical stand of spring small grain at 3/4 maturity.
C6. Minimal cover or minimal roughness or both	Ground cover is 5 to 10% and the roughness is that of a moderately tilled seedbed. The surface is rougher than that of a finely pulverized seedbed for seeding vegetables. Roughness depressions appear to be ½ to 1 inch deep (Random Roughness 1/4 to ½ inch).
C7. Clean, tilled, smooth, fallow	The surface is essentially bare, with less than 5% cover. A crop has not been grown for some time so that the residual effects of previous cropping have disappeared. The surface is smooth, similar to that of a finely pulverized seedbed exposed to one or more intense rainfalls. Roughness depressions appear to be less than ½ inch deep (Random Roughness < 1/4 inch). This condition is most likely found in a fallowed field, but could exist in a vegetable field as well.
VR. Very rough primary tillage	Very rough primary tillage across slope that leaves the soil fractured below normal frost depth. The fractures are expected to last through the winter erosion season, preventing surface sealing and formation of impermeable frost, thus allowing a high rate of infiltration. Roughness depressions are greater than 7 inches deep (Random Roughness > 3 inches).

Table 6-26.
Values for runoff index used to compute runoff to estimate P-factor values for cropland in the Northwestern Wheat and Range Region for conditions where frost in soil significantly reduces infiltration

Cropland cover-management condition	Hydrologic soil group			
	A	B	C	D
C1	40	67	78	86
C2	65	76	84	88
C3	69	82	85	89
C4	75	92	92	92
C5	81	93	93	93
C6	85	94	94	94
C7	89	95	95	95
VR	30	58	71	78

[1]Defined in table 6-25

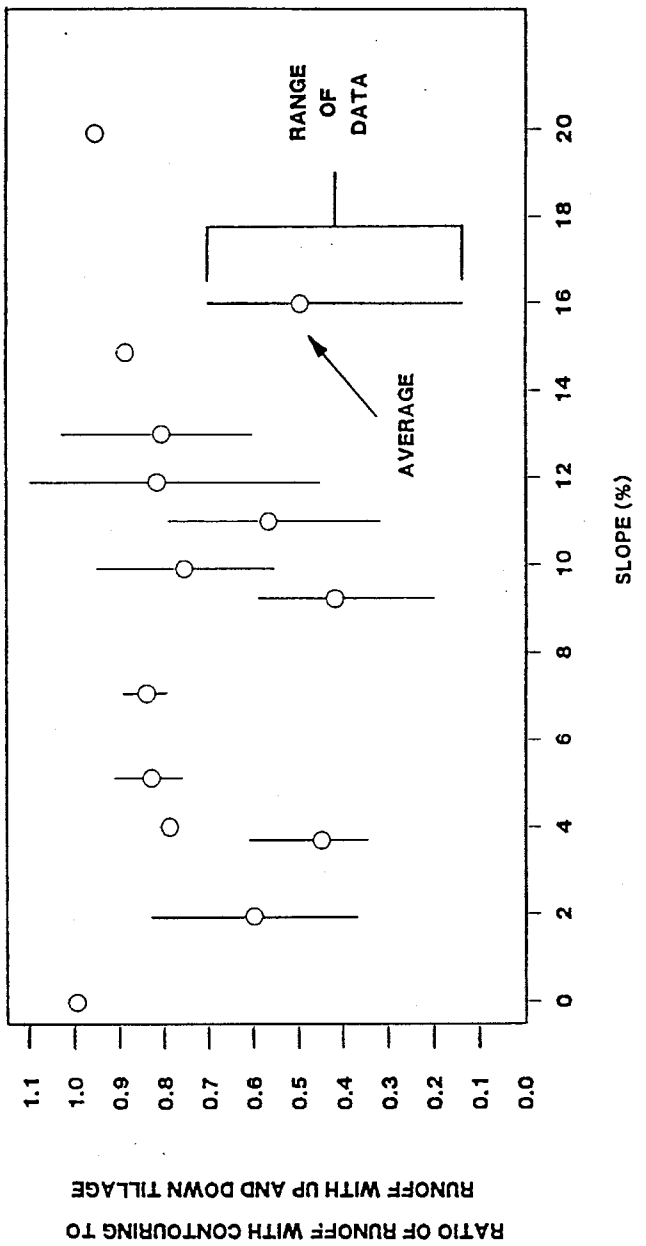

Figure 6-1. Effect of contouring on runoff.

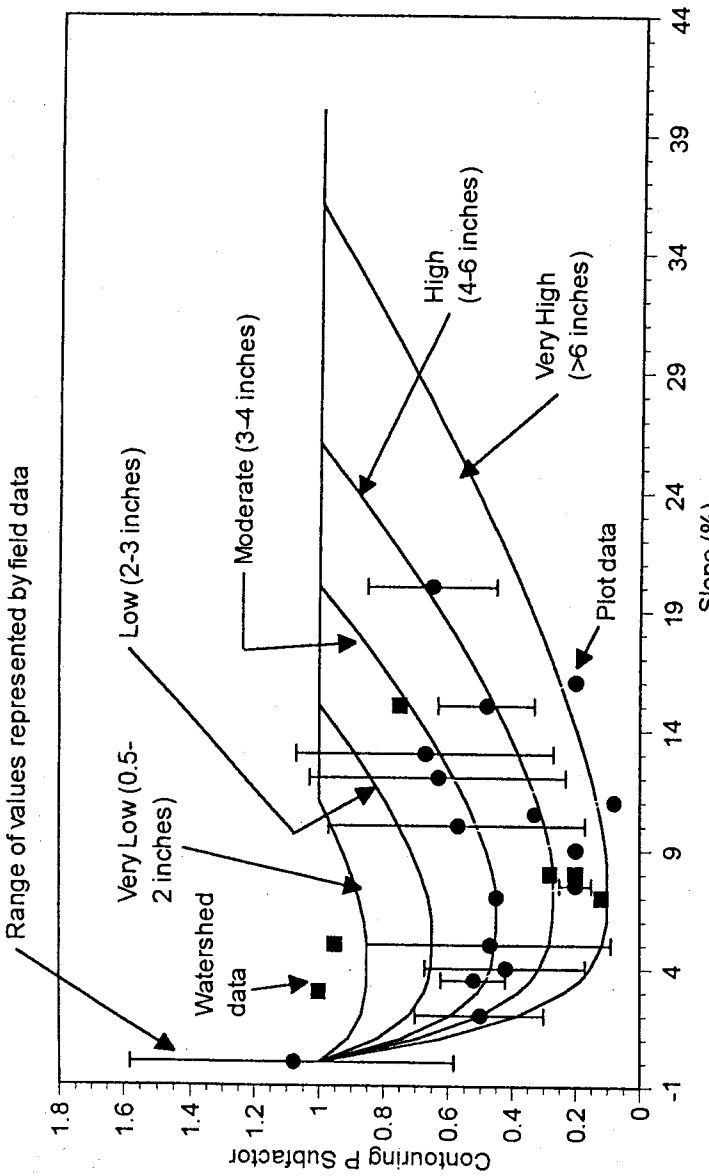

Figure 6-2. Effect of contouring on soil loss.

CHAPTER 7. RUSLE USER GUIDE

Principal contributors:

D.C. Yoder
A.J. Ketchem
D.A. Whittemore
J.P. Porter
G.A. Weesies
K.G. Renard

CHAPTER 7. CONTENTS

WELCOME TO THE RUSLE COMPUTER PROGRAM

Purpose of the User Guide

This User Guide is designed to teach the first-time user how to run the RUSLE computer program, and to answer the questions most frequently asked by more experienced users. Because the program itself provides online help screens that describe the expected user responses, this Guide focuses instead on the reasoning and mechanics behind the responses. The background theory and equations used in soil-loss calculations are described in chapters 1 through 6 of this handbook.

Introduction to the User Guide

The first portion of this User Guide is meant for first-time users. It explains in general terms how RUSLE works and introduces the terminology that will be used in the following sections. This introductory section is not long, and we strongly recommend that novice users read it to familiarize themselves with the program.

The remainder of the User Guide gives specific information on the different parts of the program, including answers to frequently asked questions. This reference section of the User Guide assumes familiarity with the terminology of the program, and may be confusing if you have not read the introductory section.

Within the User Guide, a command or entry that you type in is shown in brackets, [ ], and the name given that command or entry is placed in braces, { }.

INFORMATION FOR FIRST-TIME USERS

Getting RUSLE To Work on Your Machine

Background

The RUSLE computer code was written in the C programming language. Since C is portable, the program can be run on a variety of machines. RUSLE has been tested on IBM-compatible machines with 640 kilobytes of RAM memory using the MS-DOS operating system (version 2.0 or later). It has also been used on large systems under the UNIX operating system, and on the ATT 6386 under both DOS and UNIX. The executable program will run only on the type of machine on which it was compiled; if this is something other than DOS, the machine type will be specifically noted on the diskette labels.

The RUSLE executable program is large and does not have the capability of using expanded memory. It therefore may cause problems if used at the same time as other programs that reside in lower memory, possibly including some shell programs or peripheral drivers. This problem most often shows up as an "out of memory" error message. This can be minimized by not using these memory-resident packages when running RUSLE. Consult your DOS or program manuals or your site consultant for more details.

Loading RUSLE From Supplied Diskette(s) Onto Computer

The RUSLE program can be run directly from the supplied diskette in the floppy drive. As with most other programs, however, RUSLE can be run much faster and more efficiently by loading it onto the hard disk drive.

For DOS systems, RUSLE can be loaded by copying all the files from the diskette(s) onto the hard disk. These files include the RUSLE executable program, the Database files, the files used to create the Help screens, and some miscellaneous system files. These files should be copied into a directory created specifically to run RUSLE, as this will speed execution and make the program easier to use. Consult your DOS system manual for instructions on creating a directory and on copying files from the diskette drive to that directory.

Copying all the files onto the hard disk should also be done when using the RUSLE computer program from within a DOS window environment. The files should still be copied from the supplied diskette(s) into a directory, although this

will be done through use of a file manager. If desired, the windowing package can then be used to link the execution of the RUSLE code to an icon through use of a command line containing one of the commands specified below.

For UNIX systems, the technique for loading the program from the diskette(s) onto the hard disk depends greatly on the system. Consult your system manuals or specialist for instructions.

Running RUSLE

Once the RUSLE files have been loaded into a directory on the hard drive, begin operation by moving into that directory and typing one of the commands listed below. The command [rusle] puts you into the main program and brings up a menu that lists the options for the program. If you want to run only one of the factors or options, simply enter its command. For example, to have access to the CROP Database, the command is [rusle crop]; to run the C-factor subprogram, the command is [rusle c]. The options for the command string are as follows:

[rusle]	to get the RUSLE Main Menu, giving access to all the options
[util]	the three Database Utility programs
[city]	the CITY Database Utility program
[crop]	the CROP Database Utility program
[op]	the OPERATIONS Database Utility program
[r]	R-factor routine only
[k]	K-factor routine only
[ls]	LS-factor routine only
[c]	C-factor routine only
[p]	P-factor routine only

If you choose any option other than [rusle], you will not be able to reach all the other options.

How RUSLE Works

Background

The computer code within RUSLE is responsible only for calculations based on information that you give it; you are responsible for the quality of that information, and most of your time using the program will be spent describing your situation in terms that the program understands.

RUSLE is based on a routine that waits for your response. There are two basic types of responses. The first is to answer the question that the program is

asking–a fill-in-the-blank answer. We call this response an "input." The second type of response is a "command," which tells the program what to do next. For example, commands are used to direct the program to carry out the calculations or to move to the next screen. Inputs and commands are often used together. For instance, if the program prompts you for the name of a CROP, you might type in [cotton] as the input, and then give a command by pressing the [ENTER] key.

In most cases, you can respond with either an input or a command, but there are a few cases when only a command is appropriate. For instance, in looking at results, all the program needs to know is when and how you want to move on; the input type of response is not available.

Description of RUSLE Screen

All your interaction with RUSLE will be through screens that have the same general pattern as shown

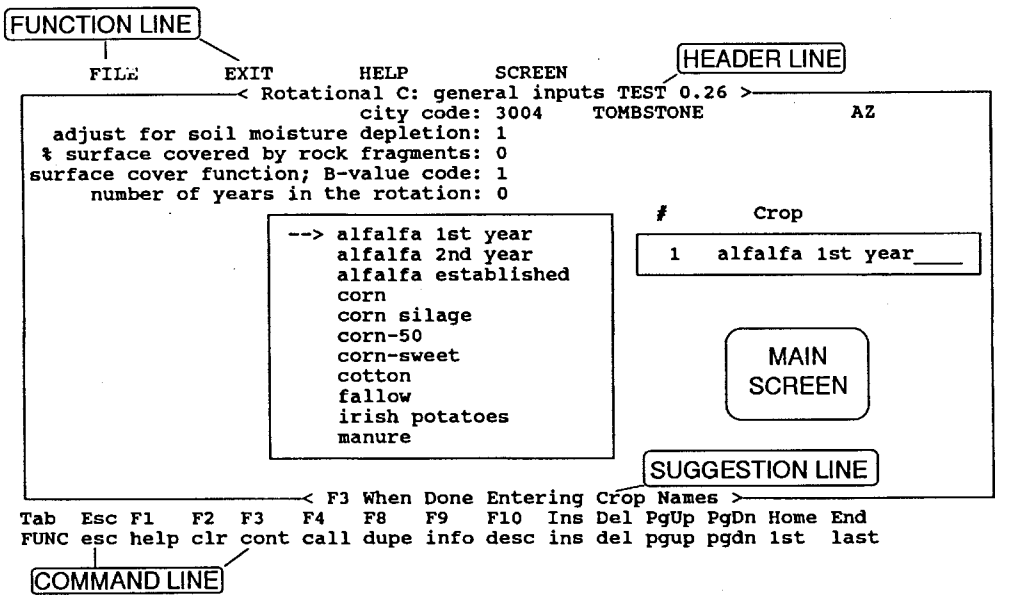

The screen can be divided into five parts, as follows:

(1) Main Screen

The main portion of the screen is the area in the center, which contains the list of questions and comments. It is here that inputs are entered and results displayed.

(2) Command Line

The bottom two lines of the screen make up the Command Line. Whenever the program is awaiting your response, commands will tell it what to do next. The available commands are listed here on the screen. The upper of these two lines shows which key to press to execute each command; on the lower line below each key is listed a three- or four-letter command description. The section "Giving Program Commands" later in this chapter lists all possible commands and what they do.

(3) Function Line

The top line on the screen is called the Function Line; it defines RUSLE Functions. These are subroutines that perform the housekeeping chores for the program. The FILE Function provides all the options for manipulating Input Files and the Current Input List (see "Input Lists And Files"). The EXIT Function provides options for leaving the program. The HELP Function provides several options for general help on running RUSLE. The SCREEN Function gives the user control over how the screen looks. "The Functions: Program Housekeeping" explains the use of the Function Line.

(4) Header Line

The second line down from the top of the screen is the Header Line, which tells the user the version of RUSLE that is running and the name of the current screen.

(5) Suggestion Line

The third line up from the bottom of the screen is the Suggestion Line, which lists the most likely command or course of action. This displays the suggested response or course of action as you go through the logical sequence of the program.

Input Field

An Input Field is a place where the cursor sits as the program waits for you to answer a question. As mentioned above, your response can be either an answer to the question (input), or a command telling the program what to do next. An input can take any of three forms:

(1) *Filling in a blank.* For example, when the program asks for a CROP name, the appropriate response may be to type [cotton].

(2) *Selecting an option.* The program shows a numbered list of options and asks you to select one. If you have not already chosen one of the options, the entire list will be shown. There are two ways to select an option: Type in the number shown next to the desired option and then press [ENTER] to select it, or use the [ARROW] keys to move through the list and then press [ENTER] to choose the marked option. If one of the options was chosen earlier, the list may not be shown, but the {list} command will display the options again. See "Giving Program Commands" for more information on this command. In some cases the list is always shown, but the marking arrow may not appear within it. In this instance, use of the {list} command will move the arrow into the list.

(3) *Selecting an item from a list.* This works in the same way as the option selection described above, but is based on a list of named items rather than on a numbered list of options. The box in the center of the example screen shown previously contains such a list.

Giving a Command

The second way to respond to an input field is to give the program a command, which tells it what to do next. There are several commands to which the program will always respond, so they are not displayed on the screen. These are the [ARROW] keys and [ENTER]. A list of all possible commands and what they do can be found in the section titled "Program Commands and Controls." Not all of the commands can be used at every place in the program, so the list of commands that are available for use from the current Input Field is shown on the Command Line at the bottom of the screen. A command is given by pressing the key listed on the Command Line.

Calling a Function

One command that is usually available is {FUNC}, which moves the cursor onto the Function Line (the top line of the screen). This allows you to perform the general housekeeping chores shown on that line. These include the FILE routines (see "How RUSLE Gets, Uses, and Saves Information" for an overview or "Input Lists and Files" for complete information), the EXIT routines that allow the user to leave the program, the HELP routines for assistance in using the program (see "Help"), and the SCREEN routine for changing screen colors.

When {FUNC} has been used to move the cursor to the Function Line, use the [RIGHT ARROW] or [LEFT ARROW] keys to move it through the functions. As the cursor moves to a function, the list of associated routines is displayed. [ARROW] up or down through the list until the routine you want is marked, or type in the number of the desired function. Press [ENTER] to select that routine and begin its execution. With the cursor on the Function Line, use the {esc}ape command to return to the Main Screen.

"The Functions: Program Housekeeping" gives more information on calling and using the Function routines.

Getting Help

RUSLE provides two general types of help. The first is additional information on the current input field, describing what sort of input is expected and why. This is always available through the {help} command. The second is made up of general descriptions of RUSLE and its operation, available through the HELP routines of the Function Line.

How RUSLE Gets, Uses, and Saves Information

Background

RUSLE requires a lot of information telling it which calculations to make and what values to use for the variables in each equation. It can get that information from one of three sources: values you enter directly, data that you have stored in Databases, or information that you entered earlier and then stored.

Current Input List

RUSLE maintains a record of all responses to the program questions in a list called the Current Input List. This is updated every time you respond to a question by either entering an input or selecting an option or item. The list does

not include the commands given to the program. When the program begins, this list is cleared (everything is set to 0).

The section titled "Input Lists and Files" provides more information on the Current Input List and its manipulation.

Input Files

Entering information by hand is tedious and inefficient. In order to make it easier to enter information and also to provide a record of the values used, you can save the Current Input List into an Input File. Each Input File thus contains a copy of the Current Input List at the time it was saved, along with a unique name and identifying comments. "Input Lists and Files" explains how to save the Current Input List into an Input File, and how to load one of these files back in as the new Current Input List.

Databases

The RUSLE Databases provide another way of entering data more efficiently by associating a large amount of information with a single Identifier. For example, all the weather information for a specific city can be associated with a city code, which from then on serves as the Identifier for all that information. You need to enter the weather information for that city only once; from then on, you can retrieve any part of that information by just giving the Citycode Identifier.

RUSLE contains three Databases. The CITY Database includes all necessary climatic data identified with a specific city or region. The CROP Database provides information on the growth and residue characteristics of specific crops or other vegetation. The OPERATIONS Database defines how field operations affect the soil, crop, and residue and, through those, the erosion rates. General information on using the Databases can be found in the section titled "Databases," and information unique to an individual Database can be found in the sections "CITY Database," "CROP Database," and "OPERATIONS Database."

You should change the information in the Databases to meet your specific situation and needs. Remember that the Databases exist to make it easier to enter the required information but that the users are still responsible for the validity of the information used in their computations. Appendix D provides valuable advice on how to modify the existing core database information to match your specific situation.

PROGRAM COMMANDS AND CONTROL

From any input field within RUSLE, you have the option of either answering the question or giving the program a command. In general, these commands control the flow of the program by telling it when to move on to the next step or screen, telling it that you want to get back out of the current section, telling it to leave the program altogether, and so on.

Giving Program Commands

There are several commands to which the program will always respond, so these are not shown on the screen. One such command is {ENTER}, given using the [ENTER] key ([RETURN] or [NEW LINE] on some machines). This command tells the program to accept the current value as the answer to the question being asked and to move on to the next question. The other commands not displayed are the [ARROW] commands, which are used to move the cursor. When a [RIGHT ARROW] or [LEFT ARROW] doesn't make sense (as in a vertical list of questions), using either [ARROW] will have the same effect as using [ENTER].

The [ARROW] commands have one additional peculiarity. As described in "Input Field," some questions ask you to choose from a list of options. When no choice has been made, moving the cursor onto that question will automatically display the list and put the cursor in the list. Using [ARROW]'s at this point will move the cursor within the list rather than between questions on the main screen. Once you have answered the question, the list will not be displayed unless you ask for it with the {list} command, so the [ARROW]'s will move the cursor on the Main Screen without interruption.

In addition to [ENTER] and [ARROW], there are usually several other commands to which the program will respond. These vary from screen to screen and question to question, but the available commands will always be listed on the Command Line. The Command Line actually comprises the bottom two lines of the screen. The upper line shows which key to use, and the lower line gives a three- or four-letter description of the command. "Description of RUSLE Screen" shows an example of how this appears on the screen.

List of Commands

A complete list of all possible commands and a brief description of what each does is given below. The command description or name is given within braces, { }, and the associated DOS key for each command is shown within brackets, [ ]. The keys may differ on some machines, but the command description is always as shown here.

{FUNC} [TAB]	places the cursor onto the Function Line to let you do the required housekeeping chores (see "Calling a Function" or "The Functions: Program Housekeeping"). When the cursor is on the Function Line, use {esc}ape to bring it back to the Main Screen.
{esc} [ESC]	allows you to {esc}ape from the current screen or question without giving an answer. This is most commonly used in three places: (1) if you have gotten into a screen or series of screens and want to get back out; (2) after an error or warning message has been displayed, and you want to continue; (3) to continue the program after a result has been displayed.
{help} [F1]	shows one or more screens of additional information to help answer the current question (see "Help"). This usually includes a brief description of how the variable is used in the calculations and also suggestions for possible answers.
{clear} [F2]	{clear}s (sets to 0) all variables associated with the current screen. This is most useful when you want to get a fresh start on a screen containing several mistakes.
{cont} [F3]	{cont}inues program movement to the next logical screen in the sequence. For example, when you have answered all the questions on one screen, this command moves you to the next screen or initiates the calculations. For screens that require only one input or command, the {cont}inue command acts just like an [ENTER], telling the program to accept the current value and to move on.
{call} [F4]	{call}s a subroutine on which the answer might depend. Use of this command will automatically put you into the

required subroutine; when you exit from that, you will return to the current question.

The {call} command is used in three different instances.

(1) When an answer is calculated from the results of several different factors. An example is in estimation of soil loss from the factor values. Each factor is {call}ed individually by use of this command.

(2) When the question asks for the Identifier of a Database Set, as when entering a city code, a crop name, or an operation name. Use of the {call} from one of these locations allows you to examine or modify the information within the associated Database. "Databases" gives more detail.

(3) When the calculation requires information entered in another portion of the program. An example of this is the value of average field slope, which is used in several places but is calculated within the LS factor. If this value has already been calculated, it will be shown; if not, the {call} command must be used to move to that calculation.

{list} [F6] displays a list from which you can select an option or item, as explained in "Input Field." If you have previously selected one of the choices, the list may not be shown but this command will appear as an option. Use of this command displays the list and allows you to move through it using the [ARROW] keys.

There are places in the program where the list is also shown but the marker arrow is not visible. In these cases, a {list} command will move the marker arrow into the list, where the marker can be controlled with the [ARROW] keys.

{save} [F7] {save}s the data shown on the screen into a Database Set named by the Identifier at the top of the screen. Changes

made within the CITY, CROP, or OPERATIONS Database routines will not be saved into those Databases unless this command is used before exiting those routines. If changes have been made, you will be asked whether or not you want to save them before you are allowed to exit.

{dupe} [F8] — used only in the crop listing on the initial C factor input screen, this duplicates an entire operation listing screen into another location within the list. For example, if I {dupe} "corn" from the first place on the list into the fifth, the program will duplicate all operations associated with that first corn onto the fifth screen. It will not change the dates, so this must be done by moving to that screen and modifying them individually.

{info} [F9] — gives information on the Current Input List. When you {save} a Current Input List into an Input File, you are also saving a series of comments describing that List. Use of this command allows you to look at (and change) the descriptive information for the Current Input List.

{desc} [F10] — gives information on the current CROP or OPERATIONS Database Set. These sets also contain a series of descriptive comments, which can be viewed and/or changed from almost anywhere this command is available.

{ins} [INS] — used to insert a line of information just above the line on which the cursor is resting.

{del} [DEL] — used to delete the line of information on which the cursor is resting.

{1st} [HOME] — used to jump to the first in a series of screens or to the beginning of a list.

{last} [END] — used to jump to the last in a series of screens or to the end of a list.

{pgup} [PGUP] — used to move forward one screen in a series of screens or up one screen in a long list of information.

{pgdn} [PGDN]	used to move back one screen in a series of screens or down one screen in a long list of information.

Giving a Command

A command is given by pressing the key listed above the desired command. This directs the program to immediately execute that command.

THE FUNCTIONS: PROGRAM HOUSEKEEPING

Several components of the RUSLE program are not part of the actual program workings but are needed to make the program easier to use. These are called Functions and are used to manipulate Input Files, to exit the program, to manipulate the screen coloring, or to get additional help. They are displayed on the Function Line, which is the top line on the screen. See "How RUSLE Works" for explanation of a sample screen.

Calling a Function

Functions are called by use of the {FUNC} command to move the cursor to the Function Line. Then use the [RIGHT ARROW] or [LEFT ARROW] key to move the cursor to the desired Function. The list of routines associated with that Function will be shown automatically. Either use the [UP ARROW] or [DOWN ARROW] key to select a routine or type in the option number. Press [ENTER] to execute the routine.

Once the cursor has been moved to the Function Line, you can return it to the Main Screen by using {esc}.

The FILE Function

The most commonly used Function in RUSLE is the FILE Function. From here, the Current Input List (see "How RUSLE Gets, Uses, and Saves Information" or "Input Lists and Files") can be cleared (all values set to zero), it can be SAVEd into an Input File, or it can be replaced by values LOADed from an Input File. As described in "Input Lists and Files," the purposes of this function are to allow you to save information so that you don't have to reenter it later, and to keep a record of the inputs used to reach a specific answer.

The EXIT Function

The EXIT Function provides a quick and easy way to get out of RUSLE from anywhere in the program. This Function is not the only way out (a series of {esc} commands will give the same result), but it is the fastest.

The HELP Function

The HELP Function provides general help in operating RUSLE, including such options as introductory information for the novice user and definitions of the various commands. This Function does not give information about the current question, because that role is filled by the {help} command. "Help" gives more detail on the HELP Function and the {help} command.

The SCREEN Function

The SCREEN Function gives the user some control over the appearance of the screen, including a color option for computers with color screens and a black-and-white option for monochrome screens.

HELP

Two types of help are available within the RUSLE program. The first is help for a specific question, available by using the {help} command. This is meant to provide you with information on how the variable fits into the general scheme of RUSLE calculations and with an idea of the expected type and size of answer. The second type of help available is more general information on the workings of RUSLE, available through the HELP Function.

Help for a Specific Question

It is often difficult to know what sort of response is expected when faced with a specific question. The {help} command provides that information. Help information is available for almost every response within the program, such as a blank to fill in, a list to select from, or even a warning message. If you don't know how to respond, try the {help} command.

Information on giving commands is found in "Program Commands and Control."

General Help

If you need more general information on running RUSLE, you can almost always call in the HELP Function. This provides information on the following:

guide to RUSLE
- how RUSLE works
- principal contributors

how to use help

Command keys
- ENTER
- ARROW keys
- Command keys

guide for first-time user

Information on using the Functions is found in "The Functions: Program Housekeeping."

INPUT LISTS AND FILES

As explained briefly in "How RUSLE Gets, Uses, and Saves Information," RUSLE maintains a set of the current values of all important variables used by the program, and this is called the Current Input List. This List is updated every time one of these variables is changed.

The calculated values of the R, K, LS, C, and P factors and of the average annual soil loss are also saved in the Current Input List. This can cause a situation in which some of the inputs have been changed but new results have not been calculated. The results in the Current Input List may thus be meaningless, because they no longer correspond to the inputs in that List. RUSLE keeps track of such potential errors and gives warnings in the Soil Loss Prediction Table when they occur.

To facilitate the use of RUSLE, the FILE Function has been included to store the Current Input List for later use. When the Current Input List is stored (SAVEd), it becomes an Input File. This File contains all the values from the Current Input List at the time of SAVEing, plus any descriptive comments that you added through use of the {info} command. This File can later be LOADed back into the program, replacing all values in the Current Input List with the values in the File. This capability allows you to use that Current Input List later as a template, changing only the necessary input values before calculating another answer. It also gives you a record of the inputs associated with a particular result.

SAVEing the Input List to an Input File

The Current Input List is SAVEd to an Input File through the FILE Function of the Function Line. Refer to "Calling a Function" or "The FILE Function" for detailed information on the Function Line and on how to call a Function. Briefly, you move the cursor to the Function Line with the {FUNC} command. Because the FILE Function is the first one listed on the Function Line, its options will be shown automatically. Select the SAVE option either by marking it with the arrow (using the [UP ARROW] and [DOWN ARROW] keys) or by typing in the number of the SAVE option. [ENTER] to begin the SAVE routine.

This routine will bring up a list of the existing Input Files. To SAVE the Current Input List to an existing Input File, type in its name or move the marker

with the [UP ARROW] and [DOWN ARROW] keys, and then press [ENTER]. *If you SAVE to an existing file, the information previously in it will be lost.*

You can SAVE the Current Input List to a new Input File by typing in a new name, using a maximum of eight characters. All alphanumeric characters (including the underscore, "_") may be used in the name. The program will not allow you to use blank spaces or a period within the name.

It is important that you choose an Input File name that will give you enough information so that you can pick it out of a list, because you may create many of these Files. This is difficult to do within the eight-character limit, but most users have found it helpful to include single-letter descriptions of each crop (for instance, *c* for corn, *b* for soybeans, *a* for alfalfa) followed by a single letter describing the tillage system. As an example of this sort of scheme, we describe a rotation of 4 yr of alfalfa followed by 1 yr of conventionally tilled corn and then 2 yr of no-till corn. One possible name is "4accc2cn," where the *4a* indicates 4 yr of alfalfa, the first *c* indicates that the alfalfa is planted after conventional tillage, the *cc* stands for conventional corn, followed by *2cn*, which describes the 2 yr of corn under no-till. The name you choose depends on which information that you are saving is most important to you. If you are most concerned with location, then the file name should include that. If you are comparing rotations, the location is probably not as important.

Finally, you will be allowed to enter up to five lines of file description, or to modify the comments entered previously through the {info} command. This may include such information as location, rotation, tillage practices–anything that might help you later to identify the file. Once you have entered all the information you want, use the {cont} command to force the actual SAVE to occur.

LOADing an Input File Into the Input List

A new Current Input List can be LOADed from an existing Input File. This allows you to take a File with values close to the ones you want and to change just the variables that differ. This is especially useful when you are making multiple runs under fairly similar conditions.

An Input File is LOADed into the Current Input List by use of the same procedure as for SAVEing, but by choosing the LOAD rather than the SAVE option of the FILE Function. Refer to "Calling a Function" or "The FILE Function" for detailed information on the Function Line and how to call a Function, or to the section immediately preceding this one for a brief description of the procedure.

LOADing an Input File into the Current Input List will replace all values in the List. These values will be lost unless they were SAVEd earlier.

Deleting Unnecessary Input Files

When Input Files are no longer needed, they can be removed using the Delete routine of the FILE Function. Either type in the file name or [ARROW] to the file you want; then [ENTER] to remove it. You can also use the {del}ete command from inside this routine or the LOAD and SAVE routines to erase files.

Using an Input File Created Earlier or Elsewhere

Input Files can be stored and shared with other users. When it is SAVEd, an Input File is stored in the directory in which the program is being run, and the Input File's name is the one you gave it when SAVEing plus a ".rus" suffix. If, for example, you gave the Input File the name "c-b-conv" when SAVEing, it would show up in the directory as the file "c-b-conv.rus."

The File can then be shared by copying it onto a diskette from which other users can copy it into their RUSLE directory. If your Input File has the same name as one already in their directory, they should change the name before copying it. After it is copied into the RUSLE directory, the new Input File will be treated like any of their other Input Files. Refer to your system manuals if you need help in copying or renaming files.

Files created on an older version of RUSLE can usually be used with newer versions of the program. Changes between versions may alter the number, names, and types of variables used by the program, but the program routines can adapt. If the program is looking for a variable that is not found within the old Input File, the variable will be set to zero or left blank. Extra values within the old Input File are ignored. If you are using an Input File created under an earlier program version, go through the program carefully the first time to make sure that all variables are set correctly.

DATABASES

Much of the information needed by the RUSLE calculations comes from a group of three Databases. The CITY Database contains information on climate, the CROP Database holds the parameters defining the characteristics of vegetative growth and residue, and the OPERATIONS Database defines the effects of field operations on the soil, crop, and residues.

Databases provide a way of associating a large amount of data with a single name or number, called the "Identifier." For instance, the CITY Database takes all the information necessary to describe for RUSLE the weather of a specific city or area, and associates that information with a single code number. One Identifier (city code, crop name, or operation name) is assigned to each Database Set, which includes all associated information.

In most cases, the data in each Database are independent of other available information. For example, the CITY Database's weather information is not likely to be affected by which crop is grown or which field operations are used. This independence holds to a lesser degree for the OPERATIONS Database and CROP Database. For example, a crop's growth characteristics will change with weather but likely will not vary as much from location to location as does weather. A corn Database Set may well apply to a fairly large part of the midwestern United States, although the weather within that area may vary considerably.

One key to using the Databases is to decide how many different Sets are required. For example, for how large an area of the Midwest are a set of corn-growth characteristics appropriate, and when will you have to add another CROP Database Set to show differences? How many CITY Database Sets are required to describe an area, given its particular weather patterns? How significant do crop varietal differences have to be to justify another CROP Set? You must answer these questions, and your responses will likely be based on the available data and the difference these changes seem to make in the final results.

Validity of Default Database Information

The values given in the default CROP and OPERATIONS Databases supplied with the program are supported by published literature cited in chapter 5. These values generally apply to the specific combination of location, crop variety,

expected yield, row spacing, planting density, tillage practices, equipment speed, soil conditions, and so forth, used in the studies. The values should therefore be thought of as typical base values designed to give general guidance.

You, the user, are ultimately responsible for ensuring that the information within the Databases fits your local conditions. In general, you should modify the values in the Databases so that the results match your conditions. For instance, if you have seen in field observations and measurements that your soybean residue decays more quickly (or more slowly) than that predicted by RUSLE, you should change the residue decay parameter in the CROP Database until the model matches the information you have. The default Databases provide a strong basis in actual measured values, but these default values should be modified to reflect measured values under your specific conditions. Appendix D describes how to carry out these modifications.

The CITY Database is somewhat different, because the default Database values are based on the same information you are likely to find. You may, however, need to create additional Sets to describe your local conditions.

Calling the Database Utility Routines

The Database Utility routines are used to manipulate the information stored in the Databases. One way to reach these routines is by selecting the Database Utility from the RUSLE Main Menu. More commonly, you can get into the Utility routines for a specific Database from anywhere the Database is used. You can {call} the CITY Database routines from wherever you are asked for a city, the CROP Database routines from wherever you enter a crop name, and the OPERATIONS Database routines from wherever you give a field operation name. Practically speaking, you can {call} the CITY routines from the R, K, C, and P factors, whereas the CROP and OPERATIONS routines can be {call}ed from the input screens of the C factor. "Program Commands and Control" gives details on using commands such as {call}.

When you return from the Utility routines, the program should put you back at the same Input Field from which you {call}ed the routines.

Using the Database Utility Routines

The CITY, CROP, and OPERATIONS Databases are created and maintained by four major subroutines known as Utility routines. There are routines to edit the Database Sets or to create new ones, to print Database Sets, to delete unnecessary Sets from a Database, and to bring in (merge) new Database Sets.

Editing Existing Sets or Creating New Ones

The Edit routine is the most commonly used of the Database routines, and serves to review or revise an existing Database Set or to create a new one. After you choose this option, the program will respond with a list of available Sets, listed by Identifier. Select the desired Database Set by either typing in the Identifier or by [ARROW]ing to the one you want. Then press [ENTER]. The program will respond with a screen of information associated with that Identifier. Use {esc} to return from this option.

To edit an existing Database Set, move the cursor around on the screen to make the changes and then save the changed Set into the Database with the {save} command. See "Program Commands and Control" for how to give commands. Note that the new values will not be kept unless the modified Database Set is specifically {save}d into the Database.

The most efficient way to create a new Database Set is to begin with an existing Set that is similar to the one you want. Type in the new Identifier and then change only the values that need to be changed. To keep the new Database Set, {save} it before you {esc}ape from this Utility routine.

This routine can also be used to rename Database Sets. Call up the Set to be changed, then create a new Database Set by changing the Identifier and {save}ing. This gives you two Sets that are identical except for the Identifiers. You can then bring up the list and {del}ete the original Database Set as described below.

To delete an unnecessary Database Set, type in the name of the Set or use the [UP ARROW] and [DOWN ARROW] keys to move the marker to the Set Identifier; then give the {del}ete command. You will be asked to confirm this request.

Printing Database Sets

The second Utility routine is used to print information in the Database. This gives two options: The first option prints a list of available Sets within the Database, and the second option provides a complete printout of all information associated with a chosen Identifier. If, for some reason, the program cannot find an attached printer or cannot send the information to the printer, a warning will be displayed on the screen.

Background on Database Files

The RUSLE program uses three different computer files for each Database. The Original File contains only those Database Sets supplied with the program. The program will read from this file but cannot write to it, so it remains unchanged. The Working File is the one that you actually use. When you {save} a Set, it is copied here, and the list of Identifiers you usually see is made up from the Sets in this file. Finally, the Delete File contains all sets you didn't need and removed from the Working File. This serves as a file of last resort, allowing you an opportunity to bring back files that you wrongly deleted.

Every time the program is run, it checks to see if a Working File exists. If not, it creates one that is a clone of the Original File. If a Working File does exist, the program leaves it alone; this allows you to put new program versions in the same directory without destroying your Working File.

Deleting Unnecessary Database Sets

The speed and efficiency of the RUSLE program is improved by deleting extraneous information. Since Database Sets are designed to fit local conditions, it is likely that you will want to remove Sets that cannot possibly apply to your conditions. When one of the lists of Database Sets is shown, or when you are within the Create/Edit option of the Database Utility routines, you can do one of the following: Use the [ARROW] keys to mark the correct Set in the list, or type in the name of the Database Set, or move into that Set as if you are going to Edit. Giving the {del}ete command will then bring up a confirmation message, to prevent accidental removals. If you confirm your intentions, the Database Set will be removed from the list. As mentioned in the section below, it is still possible to recover that information.

You may also {del}ete Sets more quickly by using the Delete Database Utility routine. This option is faster because the program does not prompt you to confirm your decision to remove Sets.

Because of the large number of CITY Database Sets and because they are divided by state, the CITY Database Utility contains a special routine that allows you to remove large numbers of Sets from the CITY Database by indicating the names (abbreviations) of the states whose cities you wish to keep. It is then possible to {del}ete specific cities within those states by the procedure described above.

Sets {del}eted from the Working File are simply moved into the Delete File, but Sets removed from the Delete File are permanently deleted.

Restoring Information Deleted From a Database

You can use the "bring new Sets" routine of the Database Utilities to recover Database Sets that were mistakenly {del}eted. Simply specify that you want to bring the Sets in from the list of deleted Database Sets.

Information will be lost if you {save} to an existing Database Set. For example, if you make changes to the "corn" CROP Database Set and then {save} it, the information previously there will be lost, and will be replaced by the new information that will now be stored in the Working File. If there is any chance that you may want to keep this old information, either give the new Set a slightly different name or first {save} the old Set under a different name.

Using Database Sets Created Earlier or Elsewhere

The "bring new Sets" routine of the Database Utilities can also be used to copy Sets created on another computer or by another user. The procedure to do this is as follows:

(1) Before entering RUSLE (from the operating system):

(a) You need to know that the names of the Working, Original, and Delete Files end with the ".dat," ".org," and ".del" suffixes, respectively. The prefixes are "croplist," "oplist," and "citylist" for the CROP, OPERATIONS, and CITY Database Sets, respectively. If you want to copy a CROP Database Set, for example, you are looking for the "croplist.dat" file.

(b) Copy that file into another with a different name and with no suffix.

(c) You need to make this available to your machine. In most cases, this means having a copy of the file on a diskette, but it can also mean having access to it over a network.

(d) Copy that new file into your RUSLE directory. Do NOT copy "croplist.dat" into your RUSLE directory under that name, because doing so will erase your "croplist.dat" file.

(e) Refer to your system manuals for assistance if you have questions about copying files.

(2) After entering RUSLE:

(a) Enter the Utility routines for the Database you want to merge.

(b) Begin the "bring new Sets" routine.

(c) Enter the name of the file from which to merge; this is the name you gave it in step 1.b above. The routine will bring in the Sets within that new file. If a Set in the new file has the same Identifier as one already contained in your Database, you will be asked which to keep.

USING THE RUSLE SOIL LOSS PREDICTION TABLE

Although the individual factors and routines of RUSLE can be run separately, the heart of the erosion prediction package is the RUSLE Soil Loss Prediction Table. This table shows the R, K, LS, C, and P values calculated from the Current Input List as well as the annual soil-loss estimate (A) in tons · acre^{-1}.

Each line of the table corresponds to a single set of inputs. For instance, the top line may contain the results of a conventional tillage rotation on a specific field, the next line may be for the same rotation but using reduced tillage, and the third and fourth lines may examine what happens with different rotations on the same field. As this example shows, one main purpose of the table is to show the effects of alternative management systems, although the table may also be used to make other comparisons.

Relationship of Input Lists and Files to Lines of the RUSLE Table

NOTE: See "How RUSLE Gets, Uses, and Saves Information" and "Input Lists and Files" for a description of the Current Input List and of Input Files.

Each line of the RUSLE table corresponds to a set of inputs. When you enter the table, RUSLE creates a temporary Input File for each table line. This permits you to move freely between lines. The values from the Current Input List will be automatically SAVEd into the temporary Input File for the line you are leaving, and the values from the temporary Input File for the new line are automatically LOADed into the Current Input List.

You can also SAVE the Current Input List into an Input File. This replaces the temporary Input File assigned to that table line with the permanent Input File given whatever name you have assigned.

If you have made changes to the temporary Input Files but have not SAVEd these, the program will warn you of this before allowing you to exit.

You can move the cursor between factors on a single line without changing any values. To compute a factor, move the cursor to that column and use the {call} command. When the computations are complete, the new factor value will be shown on the table.

Entering Values Directly Into the RUSLE Table

You can also enter values into the RUSLE Soil Loss Prediction Table directly. For example, if you know that the R Factor associated with your location is 120, you can type that number in the R Factor column in the table. The program will use any combination of typed and computed results to calculate an estimated annual erosion rate.

Warning Footnotes on the RUSLE Table

Because of the complicated relationships between the RUSLE Soil Loss Prediction Table, the Current Input List, and the Input Files, RUSLE keeps track of potential problems and gives warning messages. These show up as flags placed near the values in the RUSLE table and as warnings in footnotes to the table.

In general, these warnings indicate that the factor values in the table may no longer correspond to the numbers in the Current Input List, which can happen in three instances: (1) if you go into one of the factor routines and make some changes but do not carry through with the calculations, (2) if you enter a factor value directly from the keyboard, and (3) if information used several places in the program is changed in one location without being changed everywhere. For example, the city of interest can be specified within the C factor, but the information is used in the C, R, K, and P factors. If the citycode is changed only in the C factor, the results shown in the other factors may no longer correspond to the Current Input List (with its new citycode). To resolve this, move to each of the other factors and use the {call} command to perform the calculations. A similar difficulty arises when the field slope is changed, because the R, LS, and P factors all use this value.

SPECIFIC GUIDELINES AND ANSWERS TO COMMON QUESTIONS

CITY Database

The CITY Database contains all the climate information used in RUSLE. This information is divided into Database Sets, each of which represents a specific location. You, as the user, must determine the size of area to which that information applies. Areas where climatic patterns change quickly with distance will require more Sets (for instance, in the mountainous regions of the western United States).

Each Set has a unique name called the Citycode Identifier. This is an integer number unique to that Set and may range from 1 to 99,999. Citycode Identifiers may be assigned in any arbitrary order, although a specific ordering scheme is used within the default Database. Each CITY Database Set also has a Block Identifier of two upper-case letters. This is used to group the cities into blocks. In the default Database, the state abbreviation is used.

"How RUSLE Gets, Uses, and Saves Information" gives some background, and "Databases" gives specific details on changing and manipulating this information.

Answers to Common Questions About the CITY Database

How do I name/number a new city?

(1) Select a Citycode Identifier. Although any numbering or naming scheme may be used, the one for the default CITY Database is recommended because changes in the numbering scheme may make it more difficult to share your Database Sets with others, or to incorporate their Sets into your program (see "Using Database Sets Created Earlier or Elsewhere"). The default Database uses a five-digit Citycode Identifier for each Set.

(a) An alphabetical list of states is numbered from 1 (Alabama) to 50 (Wyoming), and the District of Columbia is assigned number 51. The first two digits of the five-digit number indicate the number of the state within that list. Under this scheme, cities in Arizona (the third state in the list) have Citycodes of the form 3XXX (same as 03XXX), and cities in number 14 (Indiana) look like 14XXX.

(b) The three rightmost digits refer to the cities within that state. The default scheme places cities within a state in the order in which they were created, with the first city given the description 001, the next 002, and so on.

(2) Type in the name of the city or area. The name associated with a CITY Database Set is by no means limited to the name of an actual city. In fact, the Set is likely to be applied to a larger area, so the name can be that of a county or anything that identifies the Set. In the default Database, this is the city by which the original weather information was identified.

Note: The default scheme uses the two-letter state abbreviation as the Block Identifier.

When is the Equivalent R value used? Much of the erosion in portions of the Pacific Northwestern Wheat and Range Region is the result of rainfall and runoff on frozen or thawing soils, and erosion rates in that area far exceed those predicted using the standard R values. Also, the distribution of this erosion over the year does not match that expected from the standard EI distribution. These considerations make it necessary to use Equivalent R values to describe the erosivity, rather than the standard values of R.

Within RUSLE, the EI distribution you select for a city determines whether the equivalent R can be used. Figure 2-7 of chapter 2 shows all the distribution areas. The program currently recognizes EI distribution areas 6-10, 14-18, 20-22, 29-41, 45, 58-60, and 63 as those for which the Equivalent R value can be used. If you select one of these areas, you are given the choice of using either the standard EI distribution for that area, a "frozen soil 95-5" default distribution that researchers have found works well for the area, or your own distribution. If you choose one of the options containing a "frozen soil" distribution, an equivalent R value will need to be chosen from figures 2-13 through 2-16 of chapter 2.

How do I select and enter an EI distribution? The EI distribution defines how the precipitation energy-intensity varies over the course of the year. Every area within the continental United States has been assigned a standard distribution, numbered as shown in figure 2-7.

In general, two options are available in the selection of an EI distribution: (1) use of one of the standard distributions, with the number selected from figure 2-7; or (2) creation of a new distribution to meet specific local conditions. If the

latter is done, the distribution will not be given a number, as it no longer corresponds to the numbering in the figure. Instead, it will be given the label "NEW." You then need to enter the EI values for the new distribution.

The exception to the rule is for the cities of the Northwestern Wheat and Range Region, where it is possible to include the effect of rainfall and runoff on frozen or thawing soils. In this case, four options are presented: (1), (2) the options mentioned above; (3) use of the standard 95-5 frozen soil distribution, which will be given the label "REQ"; and (4) manually entering a new frozen soil distribution, given the label "NEW REQ." The use of either of these last two options requires selection of an Equivalent R value.

For what is the city elevation used? The CITY Database Set includes an entry for the city elevation. The elevation is for information only and is not currently used within the RUSLE program.

CROP Database

The CROP Database contains all the information on growth and residue for the vegetation of interest. The information is divided up into Database Sets, each representing a specific crop or plant community. You must decide how many Sets are required to adequately reflect the differences caused by region, variety, or crop stress. This decision can be made only by noting the sensitivity of the outputs to differing inputs.

The information in each Set is associated with a Crop Identifier, which may be any name up to 20 characters long. This may be anything that makes the crop unique and describes it in a way that is meaningful to you. You cannot use some special characters reserved by the program or the operating system, but the program will warn you of these or will not allow you to enter them.

"How RUSLE Gets, Uses, and Saves Information" gives some background, and "Databases" gives specific details on changing and manipulating this information.

Answers to Common Questions About the CROP Database

How do I choose a vegetation/land use category? The crop category is critical in deciding how RUSLE gets and treats the crop information. The possible categories and what they mean to the program are:

(1) *time-varying vegetation:* This category is used for all vegetation where seasonal or cultivation effects cause significant changes in root mass,

canopy cover, or canopy height. This should be used for all cases except where the changes are so small or gradual that they can be ignored.

(2) *time-invariant vegetation:* If there are few seasonal changes in cover, residue, or root mass at the site, choosing this category greatly simplifies calculations. In this case, you need to enter only the average annual values. The use of this information is described in more detail in "C factor."

RUSLE uses these categories in displaying lists of crops. For example, in the calculation of an average annual C-factor value, RUSLE will show the list containing only the crops designated as "permanent"; when asking for a time-varying vegetation, RUSLE will show a list containing only those.

How does the database information control residue levels? Vegetative residue is a basic component of erosion control, and the information in the CROP Database Set determines the amount of residue and how it behaves. Each Set contains residue-decay rate parameters, which are used along with weather data to estimate the decay rates of the surface and subsurface residue.

RUSLE keeps track of the amount of residue by weight, although its effectiveness in controlling erosion is computed as a function of the percentage of cover. To convert between the two, each CROP Database Set contains as many as three values defining the relationship between cover and weight. You must supply at least one of these values, but giving two or three values will yield better results. Each supplied value is used to define a relationship between cover and weight; if you give more than one value, the relationships are averaged.

RUSLE contains routines that make it easier for you to decide how much residue has been added to the surface by a harvest operation. Within the CROP Database you enter the harvest yield and a few other constants, from which RUSLE will calculate a residue weight.

Surface residue is added to the field only by field operations (see "OPERATIONS Database") or by senescence, which is described in the next section. Surface residue is removed only through decay or by a field operation. Subsurface residue, on the other hand, can be added in one of two ways: (1) by the burial of surface residue during a tillage operation, or (2) by the death of the root biomass of vegetation.

The RUSLE program looks for two possible scenarios in adding root biomass to the subsurface residue. The first of these occurs when the vegetation is

completely killed, as might occur with tillage or application of a knock-down herbicide. The second scenario occurs whenever the CROP Database Set indicates a drop in live root biomass, which the program takes as an indication of the conversion of that much root biomass from live roots to subsurface residue.

What is the crop senescence option? In RUSLE, senescence is defined as leaf loss after the plant has reached maturity. The senescence option in the C-factor calculations calls on the CROP Database Set to provide information that may not be readily apparent. If this option is chosen, the crop is assumed to add residue to the surface when the leaves fall. RUSLE handles this by treating a decrease in canopy cover as a similar increase in surface cover. For example, if the canopy cover decreases from 90% to 75%, the total weight of surface residue is presumed to increase by an amount equal to the weight that would give 15% surface cover as defined by the cover-weight relationship.

Do I have to enter all those values for root mass, canopy cover, and canopy fall height? You do not have to enter values for root mass, canopy cover, and canopy height for the entire year. The program searches for the last value of root mass greater than zero and then assigns all remaining root mass, canopy cover, and fall height to the values they have at that point.

How do I handle crops with growth cycles lasting longer than a year? There are two ways of handling a crop whose growth cycle lasts longer than 1 yr: (1) Leave it as a single crop. When the crop goes beyond 1 yr, the program will continue to use the last values of root mass, canopy cover, and canopy height for the rest of the time. (2) Call in a regrowth file, either under an operation within the original crop or as a completely separate crop.

OPERATIONS Database

Field operations are important to the RUSLE program in how they affect the soil, vegetation, and residue. Operations disturb the soil, begin vegetative growth, kill the vegetation, add residue to the surface, or incorporate residue. They may also affect the way the vegetation grows.

This information is divided into Database Sets, with each Set representing a specific operation. You must decide how many Database Sets are required to adequately reflect the differences in the type, speed, and method of use of implements. This decision can be made only by noting the sensitivity of the outputs to differing inputs.

The information in each Set is associated with an Operation Identifier, which may be any name up to 20 characters long. You cannot use some special

characters reserved by the program or the operating system, but the program will warn you of these or will not allow you to enter them. The Operation Identifier may be anything that makes the name of the operation unique and that describes it in a way that is meaningful to you.

The OPERATIONS Database is currently used only in the C-factor calculations.

Answers to Common Questions About the OPERATIONS Database

What are the "effects"? The information in an OPERATIONS Database Set consists of a list of effects of the operation on the soil/vegetation/residue system and any additional information required to define them. The program goes through the effects in the order in which they are given (first #1, then #2, and so on) and calculates the impact of the effect on the soil, vegetation, and residue.

RUSLE allows up to five effects for any field operation, and these are chosen from a list of nine possible effects. If a field operation has more than five effects, these may be split between two operations scheduled to occur on the same day.

The program does not allow you to have more than one residue addition or removal in an operation. For instance, you may not add both residue from the current crop and some other residue within a single operation. This limitation exists because you can enter only a single number to tell the program how much residue you are adding. This also means that you cannot add and remove residue within the same operation.

The nine possible effects are listed below, along with a brief description of their place in the program and the calculations.

(1) *no effect:* The program requires five effects. Actual operation effects are listed first, and any remaining spaces are filled with this null value.

(2) *soil surface disturbed:* A field operation disturbs the soil surface in ways that affect erosion rates: (a) disturbing the soil is the only way to incorporate some of the surface residue; (b) the surface of the soil is loosened, which changes the degree of soil consolidation seen in the prior-land-use subfactor of the soil-loss-ratio (see ch. 5); (c) the surface roughness is altered, changing its impact on erosion rates. Including this effect in the list for an operation automatically brings forward questions that are used to define these changes.

(3) *current crop residue added to surface:* This effect specifies residue from the current crop, which means that the residue and decomposition parameters are taken from the current CROP Database Set. If a regrowth crop has been called in, the parameters are taken from there. If there is no current crop, the program adds residue from the most recent current crop.

The program will ask you to define in one of two ways how much residue is added to the surface. If the operation is a harvest operation (see below), the program will automatically pull in from the CROP Database Set the amount of residue added at harvest. If the operation is not defined as a harvest, you must enter the amount of residue added when you fill in the list of operations within the C-factor inputs.

(4) *other residue added to field:* This effect is used to model the impact of material coming from other sources, such as straw mulch used on a vegetable crop or manure spread on a field. This effect brings up questions asking you to define the cover and decomposition parameters for that residue, as well as what percentage of the applied material is left on the surface.

Because the only way to apply a material to the subsurface region (as with a manure injection) is to disturb the surface, this effect must be followed by a (2) within the same operation. When this is done, the percentage of residue buried by the (2) will be for the residue on the surface before the operation. The (2) effect will not bury any of the residue added to the surface by this operation.

(5) *residue removed/added to field:* This is the only effect that considers the removal of residue from the field. You need to specify whether it is from only the current or most recent crop (for instance, baling of corn stover) or from all previous crops (such as burning of residue). Within the list of operations in the C-factor inputs, you will need to specify how much residue is removed.

(6) *current crop harvested:* Information in the CROP Database Set for each crop indicates how much residue is added to the surface when the crop is harvested. Use of this effect automatically brings in that value as residue added to the surface. Refer to the earlier description of effect (3) for more information.

(7) *crop growth begins:* This effect tells RUSLE to begin the growth cycle found in the CROP Database Set for the vegetation listed at the top of the C-factor input screen, and to set "day 0" in that vegetation's cycle as the date of this operation.

(8) *current crop is killed:* This effect does two things: (a) the canopy cover and fall height are automatically set to 0 because the crop is no longer growing, and (b) the root mass is converted into a subsurface residue and begins to decay. The crop can be killed without adding residue to the surface, but from that point on there is no canopy effect.

(9) *call in a new crop growth set:* This effect begins growth of a regrowth crop whose name you are asked to specify when you define the cropping sequence and field operations. This effect should be used when growth patterns change because of an operation or weather, or simply to bring in a new crop as the current crop. The growth, decomposition, and weight-cover values are all replaced by those of the new growth Set, as are the root mass and canopy values.

In what order should I enter the effects? The effects of an operation must be entered in the order in which they occur. For example, operations that add residue either before or after disturbing the soil will give different results. Adding the residue before the soil disturbance will incorporate some of the residue, whereas adding it afterward will not.

How are residues buried or uncovered? The "% left" variable is defined as the percentage of original residue left on the surface following the operation. This can be defined as a "% wt", which is the percentage of the original surface-residue weight. If defined instead as a "% cov", it is the percentage of surface cover left after the operation. For example, if the residue covered 50% of the surface before the operation and the operation leaves 90% cover, the cover after the operation is $50\% \cdot 90\% = 45\%$.

If there is more than one residue type on the surface, it is assumed that the specified "% cov" refers to each residue type individually and not to the overall cover. For example, if before the operation there was on the surface a weight of wheat residue equivalent to 60% cover plus a weight of soybean residue equivalent to 40% cover, then after an operation leaving 30% cover there would remain on the surface weights of residue equivalent to 18% and 12% cover for the wheat and soybeans, respectively. Depending on the specified residue characteristics, this might well yield an overall percent cover not equal to 30% of the original cover.

You can also use this term to uncover buried residue by specifying that more than 100% of the residue be left on the surface. For example, if before the operation the surface has 50% cover and the operation leaves 120%, the surface cover after the operation is 50% · 120% = 60%. The program is set to limit the total amount of residue cover to 99.99%, and will not bring up more residue than actually exists. The option of uncovering residue can be used with either the percent weight or percent cover options.

R Factor

The RUSLE R factor defines the total annual erosive potential that is due to climatic effects. This factor reflects the impact of geographical location on erosion, including such factors as localized impacts of lakes or mountain ranges and the dominance of frontal or cyclonic activity.

Options

Initial R-factor value. The first option in selecting an R value is to take it directly from the isoerodent maps of figures 2-1 through 2-5 of chapter 2. The R values in the default CITY Database Sets are taken from these. This information is currently available for all locations in the contiguous United States and Hawaii.

Adjusted R value. For fields with very low slopes and in areas with high rainfall, the R value will be modified to reflect the absorption of raindrop impact energy by ponded water. Note that this changes the R factor to a value that applies to only a specific field rather than to a general geographical region, and does not change the R value in the CITY Database Set.

You are asked to indicate whether or not you want this correction. If your field has a very rough surface or has moderate-to-high ridges, more of the surface will be exposed to raindrop impact, thereby increasing detachment. Under these circumstances, do not use the adjustment.

Equivalent R value. As explained in "Answers to Common Questions About the CITY Database" and chapter 2, erosion in parts of the Northwestern Wheat and Range Region far exceeds the amount predicted by the simple R value because much of the erosion occurs on frozen or thawing soils subjected to gentle rains but erosive runoff. If the CITY Database Set you specify was defined as being for such an area, the Equivalent R value can be entered. You are not required to enter this value, because you are not forced to have this effect for cities in this area. "Answers to Common Questions About the CITY Database" explains how to use this effect.

K Factor

The K factor of RUSLE defines the soil erodibility under a set of standard conditions.

Options

Seasonal K value. The seasonal K value attempts to include the effects of freeze-thaw cycles and other factors affecting the temporal variation of soil erodibility. This option requires an original estimate of K, which may be either entered directly or calculated through use of the soil-erodibility nomograph.

Volcanic K value. Data collected in Hawaii for volcanic soils have shown a somewhat different relationship between soil properties and erodibility. If this option is used, K is calculated for the entered data. No seasonal variation of K is needed for these soils, because they are in general not subject to freeze-thaw cycles. These data have not been tested for soils outside Hawaii.

Answers to Common Questions About the K factor

What are the dates of maximum and minimum K for the seasonal K option? The time-varying K calculations yield a K value for each half-month period through the year, with the calculations made at the middle of each period. The date shown for the maximum or minimum K may not correspond to the period with the highest or lowest value if that date is very early or very late in the period.

Why can't I use the time-varying K for the western United States? As described in chapter 3, the algorithms used to calculate the time-varying K work well for the eastern United States, but not for the area west of approximately longitude 105°W. The RUSLE program determines your location by use of the EI distribution zone number, and will not allow the calculations for any areas west of that line.

How is the K nomograph used? The calculation of seasonal K variability uses an original estimate of K. If a Soil Interpretation Record exists, you may enter the K value from it as your estimate. The other option is to develop an initial estimate of K using the K-nomograph method. You get access to the K-nomograph method by {call}ing the subroutine from the Input Field for the original estimate.

What is the soil hydrologic group? Because the soil hydrologic group is a soil property, it is entered within the inputs for the K factor even though it is not

used in the K-factor calculations. It is used solely within the P factor to indicate the effect of runoff on support practices.

How is the # years to consolidate used? The C factor also requires the length of time it takes for the soil to fully reconsolidate in the calculation of the PLU subfactor. Since this is primarily a soil property, it is entered here in the K factor.

How is the % surface covered by rocks used? RUSLE treats rocks on the surface as surface cover rather than through their impact on the K factor. This value is therefore not used in the K-factor calculation, but rather is called in from here for the C-factor routines. However, since surface rock cover is generally a soil characteristic, this input is included here with the other soil inputs.

LS Factor

The RUSLE LS factor accounts for the effects of slope length and slope steepness on soil loss.

Answers to Common Questions About the LS factor

Which LS table should I use? The selection of an LS table depends on the condition of the soil and its susceptibility to rill erosion, presented as a ratio of rill to interrill erosion rates. This susceptibility can be a function of either the innate soil properties (such as texture, aggregation, and structure) or the degree to which the soil is modified by mechanical disturbance. In general, a disturbed soil shows a higher rill-interrill erosion ratio than does an undisturbed soil.

Table 4-1 is used for soils with low rill-interrill erosion ratios, usually including those not disturbed for some time. Table 4-2 applies to soils with a moderate percentage of erosion coming from the formation of rills, including soils that are disturbed relatively frequently. Most agricultural soils fall into this category.

Table 4-3 is used for soils that undergo high degrees of rill erosion, including highly disturbed soils such as those on construction sites. This category also contains agricultural soils that by their nature are susceptible to large amounts of rilling.

Finally, table 4-4 contains LS values for soils subject to thawing, runoff from snowmelt, and rain on frozen soil or snow. This changes the importance of the LS factor in relation to overall erosion rates. In general, these values will be used only for slopes in the Northwestern Wheat and Range Region.

What is the equivalent slope? Several routines within RUSLE require an estimate of the average steepness of the downhill slope, called the "equivalent slope." This estimation is easy for a uniform slope because uniform slope = average slope = equivalent slope. For a complex slope, RUSLE defines the equivalent slope steepness as the uniform slope steepness that gives the same LS value as that calculated for the complex slope. For example, if the complex slope has an overall length of 200 ft and an overall LS = 2.34, the equivalent slope steepness is that for which a uniform slope of 200 ft has an LS = 2.34.

The equivalent slope is calculated automatically in the LS routines. When needed by other parts of the program, these calculations may be {call}ed from there.

How do I get LS printouts? The Print option of the LS factor gives a printout of the tables showing LS values corresponding to a broad range of uniform slope lengths and steepnesses. The output tables are 132 characters wide and do not fit on most printers (which use 8½" x 11" paper), unless the printers can be specially configured to do this. Check your printer manuals.

C Factor

The RUSLE C factor describes the effects of cover and management on average annual soil loss.

Options

Time-varying vs. continuous. The C-factor calculations are used to determine the soil-loss ratio (SLR) subfactors for half-month time periods over which conditions are assumed to remain constant. The exception to this is cases of continuous pasture, meadow, or rangeland, for which conditions are likely to change very little over the course of an entire year. For these cases it would be of little value to make the calculations every half month, because the numbers would change only slightly.

The time-varying option must be used whenever the cropping or plant community changes significantly over a year, or when field operations disturb the soil or plant residues.

Single disturbance vs. rotation. Within the time-varying C option there are also two very different options. The first assumes that there is a single disturbance of the system, with subsequent long-term restabilization. You therefore need to define for the program the condition of the soil, vegetation, and residue immediately after the disturbance, and how the site changes over the years as the soil reconsolidates and vegetation regrows. This alternative fits best for

construction sites, mine spoils, or many of the mechanical rangeland improvement techniques.

The single-disturbance option is selected by placing a zero (0) in the field for the number of years in the rotation. This brings up additional questions concerning the final surface roughness expected for the site, since this number will be a function of the expected long-term vegetation. For the rotation option, it is assumed that there is repeated soil disturbance, which keeps this natural long-term roughness from ever having a significant influence.

The other alternative is to assume a rotation, where the operations are repeated in a cycle through many years. For example, the list of operations for a corn-soybean rotation would be only 2 yr long, but this list would be expected to repeat itself every 2 yr. If the rotation option best fits the system you are describing, the RUSLE program runs through the calculations three times. The program uses the results from the first two times as the initial conditions for the third run. The rotation option is chosen by specifying the number of calendar years in the rotation.

Concepts of the Time-Varying C Factor, With Examples

At first glance it may appear complex, but the time-varying option for calculating a C factor is simple if several basic concepts are understood. Since these concepts are crucial to an understanding of the power and flexibility of the C-factor calculations, they are illustrated through the use of examples. *Values and Database Sets included in the examples are meant solely as illustrations.*

Important parameters in the time-varying C option. The time-varying C option is based on a listing of the field operations, which in turn call in information from the CITY, CROP, and OPERATIONS Databases. The combination of information from these sources defines the changes in crop root mass and canopy cover, in soil roughness and consolidation, and especially in surface and subsurface residue.

Defining the current crop in the time-varying C option. The RUSLE program keeps track of only one set of CROP Database parameters at a time: root mass, canopy cover and height, and residue amount and decay variables. These values are taken from a single CROP Database Set, and the Set in use at a specific time is referred to as the current crop. When a CROP Database Set becomes the current crop, the program automatically pulls in all the information associated with that crop name, replacing the root mass, canopy, and residue values that had been linked to the previous current crop.

There are two ways to identify the current crop, and both of these require the use of a field operation. The first option is to have a planting operation, which instructs the program to install as the current crop the Set named at the top of the operations list screen. The second option is to have a field operation that asks for a regrowth crop. The program will prompt you for the name of that new Set, which it then pulls in as the current crop.

Note that the crop listed at the top of the screen never becomes the current crop unless an operation tells the program to begin its growth. In spite of this, when the results are shown, they will be displayed under this crop name. This means that the crops you list on the initial C-factor screen and that are shown atop each operations list screen serve two purposes: (1) they are used in accounting, defining over what time period the SLR values are summed; and (2) if called on by a planting operation, they can become the current crop.

It is essential that you keep track of which is the current crop, as this defines all the crop and residue parameters. For instance, unless you specifically direct the program otherwise, any residue added to the surface will have the decay and cover characteristics associated with the CROP Database Set for the current crop.

Defining a Set as the current crop causes one additional hidden impact. The date of the operation defining a new current crop (either a planting operation or one requesting a new Set) automatically becomes day zero in the growth cycle in that Set.

Use of regrowth crops within the time-varying C option. Some events drastically alter the growth patterns of the vegetation without killing it completely, such as mowing hay or cutting rangeland brush. In RUSLE, these changes in growth patterns are handled through CROP Database Sets called in as regrowth crops. The regrowth Set is meant to reflect the crop growth and residue patterns as the crop rebounds from the effects of some operation or event that drastically changes those patterns. The date when an operation calls in a regrowth crop becomes day zero in the crop growth cycle, and that Set becomes the current crop.

When you use regrowth crops, you must make sure that proper transition is made between crops. For example, if there is a sudden drop between the last root mass value for the first Set and the first root mass for the second, the program will assume that you meant for this drop to occur, and will add that difference to the subsurface residue. Changes in residue cover and decay

parameters as you move from one crop to the next indicate that subsequent residue additions will have those new characteristics.

How the time-varying option handles root mass. The root mass for the current crop begins growing at either the time of planting or when the crop is called in as a regrowth file. When an operation is defined as killing the current crop, the root mass becomes part of the subsurface residue and begins to decompose at a rate controlled by the decay parameter from the CROP Database Set in which the root mass was defined.

The program will also recognize a drop in root mass either within a CROP Database Set or between crops, as in the transition to a regrowth crop. Any drop in root mass is taken as a similar increase to the subsurface residue pool. If the drop in root mass occurs between Sets, the decay parameter for this residue will be that from the first Set.

Definition of canopy cover in the time-varying option. For the most part, the handling of canopy cover is very straightforward; the program simply takes the values from the current crop Set and uses them to make the calculations. The single possible complication occurs when you choose the senescence option for a crop. This indicates that a drop in canopy cover should cause an increase in residue on the soil surface. The program calculates this effect by looking at the percentage drop in residue cover, and then adding to the surface cover a mass of residue equal to that which would give the same percentage of cover to a bare surface. This amount is defined by the residue cover parameters from the CROP Database Set.

The program does not keep track of drops in canopy cover when you switch to a regrowth crop, because this type of change is usually caused by an operation, which often involves removing canopy material from the field.

How RUSLE handles surface residues. RUSLE keeps track individually of every residue you add to the field, and calculates its cover and decay relationships based on the specific parameters assigned to that residue when it was still associated with a current crop or when it was added as a "foreign" residue. Most residue additions are for the current crop, so you must be aware of which crop that is and whether its residue parameters are the ones you want.

Residue additions to the soil surface are specified on the screen where you list the operations. In general, you are responsible for telling the program how much residue is being added to the surface, but there is one exception. If you specify that the operation harvests the current crop, this tells the program to look

in the CROP Database Set associated with that crop to find the residue added at harvest. The program then automatically enters that value into the correct place in the list of operations.

Example 1: Five years of Eastern alfalfa cut for hay followed by 3 yr of corn. Many of these concepts become more clear when dealing with specific examples. The first example is for an alfalfa-corn rotation in eastern Pennsylvania, with 5 yr of alfalfa followed by 3 yr of corn.

The first screen describes the location and gives general information about the rotation. The number of years in the rotation is set at 8 since, as we will see later, the first operation in the rotation will not be repeated for 8 yr. The crops indicated in the list were selected from the CROP Database File, and for each crop in the list the program will display a screen on which you will be asked to enter the field operations associated with that crop. The crops in this list need not correspond to calendar years; there can be either more or fewer crops in the list than years in the rotation. This list also does not need to include all CROP Database Sets used in the rotation.

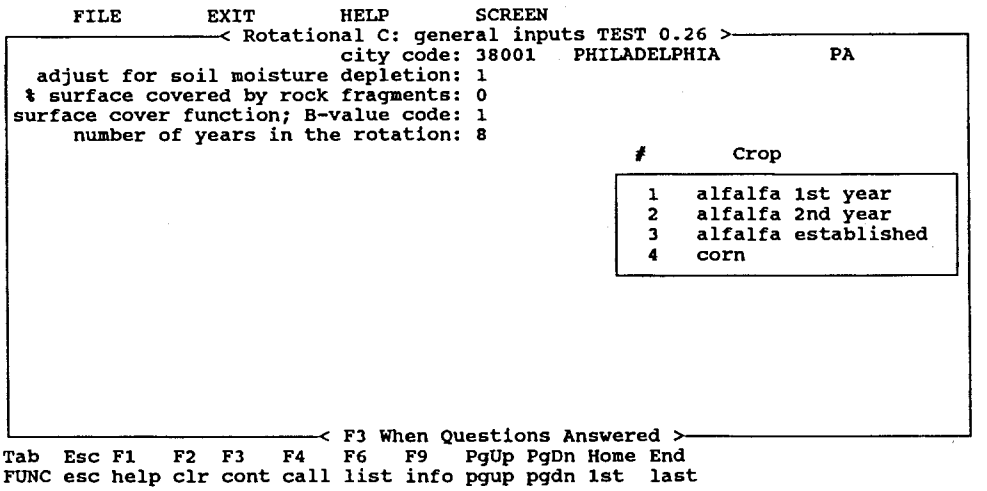

Below is the first screen of information describing the field operations associated with the rotation. All operations that we want included in the calculation for "alfalfa 1st year" are listed here.

```
     FILE        EXIT        HELP        SCREEN
                 < Rotational C: field operations TEST 0.26 >

 1/4   crop: alfalfa 1st year      senescence code: 2
---Date-------Field Operation-----Res. Add. (#/A)----------New Growth Set-------
 3/30/1       chisel (3 in. twist)
 4/5/1        disk; tandem
 4/6/1        harrow (tine)
 4/10/1       drill; conventional
 6/30/1       hay harvest              600                alf. 1st yr regrowth
 8/15/1       hay harvest              450                alf. 1st yr regrowth
 9/30/1       hay harvest              450                alf-1st yr.sen clrso

                          < F3 When Questions Answered >
Tab  Esc F1   F2  F3   F4   F6   F9   F10  Ins Del PgUp PgDn Home End
FUNC esc help clr cont call list info desc ins del pgup pgdn 1st  last
```

The first three operations in this list are tillage operations, which disturb the soil surface and incorporate some of the surface residue. Since the corn crop came just before these operations in the rotation, the operations will be burying corn residue. The tillage operations will also affect the soil surface random roughness.

The drill operation on April 10 includes an effect entitled "crop growth begins." This takes the CROP Database Set listed at the top of the screen (alfalfa 1st year), installs it as the current crop, and begins its growth cycle.

The hay harvests scheduled in this first year do two things: (1) they completely change the alfalfa growth characteristics, requiring a regrowth Database Set to show how the crop responds after being cut, and (2) they add some alfalfa residue to the field through wastage in the harvest process. There are two ways of handling this residue addition. The first way is as shown above, which uses the OPERATIONS Database Set below.

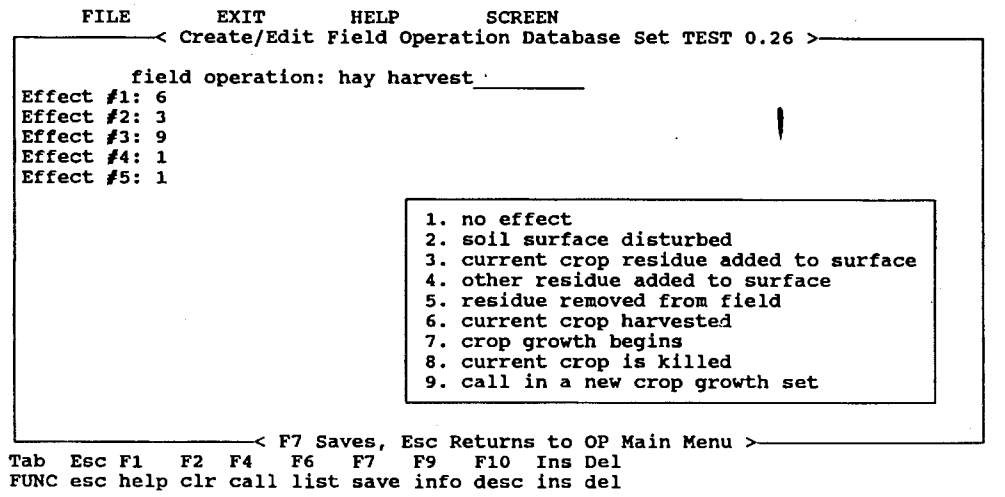

This Set specifies that the operation harvests the current crop, which causes the program to automatically go into the CROP Database Set for the current crop (in this case, "alfalfa 1st year") and to extract the information required to calculate residue added at harvest. The OPERATIONS Set also specifies that the operation adds residue from the current crop to the field: this is redundant because this is assumed by the program when it sees the harvest effect, but this may be included for the sake of completeness. Finally, the Set states that the operation will significantly affect the crop growth characteristics, requiring a new CROP Database Set to model that regrowth.

The operations list is repeated below for convenience. In it we see the regrowth CROP Database Sets listed in the far right column. Note that from 6/30/1 to 8/15/1, the current crop is "alf. 1st yr regrowth," which once again becomes the current crop with the hay harvest of 8/15/1. This means that on 8/15, the program brings this Set in to replace itself, and once again sets the days of growth to zero and restarts the growth cycle all over again.

```
     FILE        EXIT        HELP        SCREEN
                 < Rotational C: field operations TEST 0.26 >

 1/4   crop: alfalfa 1st year      senescence code: 2
--Date-------Field Operation----Res. Add. (#/A)----------New Growth Set-------
 3/30/1      chisel (3 in. twist)
 4/5/1       disk; tandem
 4/6/1       harrow (tine)
 4/10/1      drill; conventional
 6/30/1      hay harvest              600               alf. 1st yr regrowth
 8/15/1      hay harvest              450               alf. 1st yr regrowth
 9/30/1      hay harvest              450               alf-1st yr.sen clrso

                          < F3 When Questions Answered >
Tab  Esc F1   F2  F3   F4   F6   F9   F10  Ins Del PgUp PgDn Home End
FUNC esc help clr cont call list info desc ins del pgup pgdn 1st  last
```

The values in the third column, Res. Add., indicate the amount of residue added to the surface by each operation. Since the "hay harvest" Set listed the operation as a harvest, these values are calculated automatically from information in the CROP Database Set for the current crop. The 600 is calculated from the Set for "alfalfa 1st year" since it is the current crop to that point, and the 450 comes from the "alf. 1st yr regrowth" Set.

The second way of handling the residue additions is to specify the hay harvest simply as adding residue to the surface but not harvesting the crop. The program would then ask you to enter a value in the Res. Add. column rather than automatically calculating a value.

The senescence code for this crop is set at 2, which indicates that the program should consider a drop in canopy cover as an increase in surface cover. The CROP Database Set "alf-1st yr.sen clrso" includes such an effect to model the impact of winter on alfalfa growth, as shown below.

```
     FILE       EXIT       HELP       SCREEN
──────────────< Create/Edit Crop Database Set TEST 0.26 >──────────────
          crop: alf-1st yr.sen clrso        category: 1
res. @ harv. (lb/A): 200     row spacing (in): 6___ plant pop. (#/A): 900000
surf. res. decomp. cons.: 0.01500      sub. res. decomp. cons.: 0.01500
res. at 30% cover (#/A): 640     at 60% cover: 1650     at 90% cover: 4100
  days    root mass  canopy    fall       days    root mass  canopy    fall
   of     #/Ac (in   cover     height      of     #/Ac (in   cover     height
 growth    top 4")    (%)      (ft)     growth    top 4")    (%)      (ft)
 0        2600       0         0         180      0          0         0
 15       2650       65        0.1       195      0          0         0
 30       2700       80        0.1       210      0          0         0
 45       2700       70        0.1       225      0          0         0
 60       2700       60        0.1       240      0          0         0
 75       2700       10        0.1       255      0          0         0
 90       0          0         0         270      0          0         0
 105      0          0         0         285      0          0         0
 120      0          0         0         300      0          0         0
 135      0          0         0         315      0          0         0
 150      0          0         0         330      0          0         0
 165      0          0         0         345      0          0         0
──────────────< F7 Saves, Esc Escapes to CROP Main Menu >──────────────
Tab  Esc F1   F2  F7   F9   F10  Del
FUNC esc help clr save info desc del
```

The drop in canopy cover from 70% to 60% from day 45 to day 60 demonstrates the use of the senescence option. The program will use the residue weight/cover relationship from this Set to determine the weight of residue equivalent to 70 - 60 = 10% cover. This weight will then be added to the surface, with the addition distributed evenly over the 15 d in the period.

This completes the information required for the first crop listed on the first general information screen. The second crop listed is "alfalfa 2nd year," which requires the operations listing shown below.

```
     FILE       EXIT       HELP       SCREEN
──────────────< Rotational C: field operations TEST 0.26 >──────────────

 2/4   crop: alfalfa 2nd year      senescence code: 2
──Date─────Field Operation────Res. Add. (#/A)──────New Growth Set──────
 3/15/2    begin alfalfa growth
 5/15/2    hay harvest              525              alfalfa 2nd year
 6/29/2    hay harvest              525              alfalfa 2nd year
 8/13/2    hay harvest              525              alfalfa 2nd year
 9/27/2    hay harvest              525              alf-2nd y senescence
──────────────────────────< F3 When Questions Answered >──────────────
Tab  Esc F1   F2  F3   F4   F6   F9   F10  Ins Del PgUp PgDn Home End
FUNC esc help clr cont call list info desc ins del pgup pgdn 1st  last
```

The "begin alfalfa growth" in this listing calls in "alfalfa 2nd year" as the current crop and begins its growth. The hay harvest operations are the same as in the first screen, adding residue to the surface and calling in regrowth crops. As before, the hay harvest operation calculates the amount of residue added based on information in the CROP Database Set of the current crop.

Up to this point we have had a single year's worth of operations on each screen, but this is not a requirement. The screen below shows 3 yr of crops and operations intended to model the alfalfa crop once it has reached fairly stable growth.

```
     FILE        EXIT        HELP        SCREEN
                 < Rotational C: field operations TEST 0.26 >

 3/4   crop: alfalfa established   senescence code: 2
--Date---------Field Operation-----Res. Add. (#/A)----------New Growth Set-------
 3/15/3____  begin alfalfa growth
 5/15/3      hay harvest              1800               alfalfa established
 6/29/3      hay harvest              1800               alfalfa established
 8/13/3      hay harvest              1800               alfalfa established
 9/27/3      hay harvest              1800               alf. est. senescence
 3/15/4      begin alfalfa growth
 5/15/4      hay harvest              1800               alfalfa established
 6/29/4      hay harvest              1800               alfalfa established
 8/13/4      hay harvest              1800               alfalfa established
 9/27/4      hay harvest              1800               alf. est. senescence
 3/15/5      begin alfalfa growth
 5/15/5      hay harvest              1800               alfalfa established
 6/29/5      hay harvest              1800               alfalfa established
 8/13/5      hay harvest              1800               alfalfa established
 9/27/5      hay harvest              1800               alf. est. senescence
 3/15/6      begin alfalfa growth
                 < F3 When Questions Answered >
Tab  Esc F1   F2  F3   F9   Ins Del PgUp PgDn Home End
FUNC esc help clr cont info ins del pgup pgdn 1st  last
```

A single screen can contain any number of years' worth of operations, as long as the total number of operations on the screen does not exceed 16. Similarly, a screen may contain operations representing a fraction of a year. The only difference comes in the final accounting. The program calculates an overall rotation C factor and a C factor for the time associated with each screen. For this rotation, the program would calculate separate C factors for each of the first 2 yr, but would lump these 3 yr together into a single C factor.

Note also that the program is not limited to working with calendar years; but it will allow you to divide the time up in any convenient fashion simply by which screen contains which operations.

The screens shown above take care of the 5 yr of alfalfa in the rotation, but we must still handle the 3 yr of corn. In the initial crop listing there was only one corn, so all operations associated with these 3 yr will also have to be lumped together on a single screen, as shown below.

The first operation in this listing is used to kill the alfalfa and also to prepare the soil for the corn-planting operation. The information for this operation is listed below.

```
     FILE        EXIT        HELP        SCREEN
              < Rotational C: field operations TEST 0.26 >

 4/4   crop: corn_____________  senescence code: 1
 Date      Field Operation     Res. Add. (#/A)     New Growth Set
 4/15/6    chisel alfalfa          2500
 4/20/6    disk; tandem
 4/25/6    planter; no-till
 6/10/6    fert. applicator
 10/10/6   harvest                 7280
 4/15/7    chisel (3 in. twist)
 4/20/7    disk; tandem
 4/25/7    planter; no-till
 6/10/7    fert. applicator
 10/10/7   harvest                 7280
 4/15/8    chisel (3 in. twist)
 4/20/8    disk; tandem
 4/25/8    planter; no-till
 6/10/8    fert. applicator
 10/10/8   harvest                 7280

                        < F3 When Questions Answered >
Tab  Esc F1   F2  F3   F4   F6   F9   F10  PgUp PgDn Home End
FUNC esc help clr cont call list info desc pgup pgdn 1st  last
```

```
     FILE        EXIT        HELP        SCREEN
          < Create/Edit Field Operation Database Set TEST 0.26 >

        field operation: chisel alfalfa_____
Effect #1: 3
Effect #2: 2  % disturb.:100   roughness:1.5   % cov. left:50    depth:8
Effect #3: 8
Effect #4: 1
Effect #5: 1

                                  1. no effect
                                  2. soil surface disturbed
                                  3. current crop residue added to surface
                                  4. other residue added to surface
                                  5. residue removed from field
                                  6. current crop harvested
                                  7. crop growth begins
                                  8. current crop is killed
                                  9. call in a new crop growth set

                    < F7 Saves, Esc Returns to OP Main Menu >
Tab  Esc F1   F2  F4   F6   F7   F9   F10  Ins Del
FUNC esc help clr call list save info desc ins del
```

This case is one where the order of the operation's effects is critical. This operation first adds residue to the soil surface. Since the operation is not specified as a harvest, the amount added will not be calculated from information in the CROP Database Set, but will instead have to be entered manually in the Res. Add. column of the operations listing.

After the residue is added, the soil surface is disturbed, thereby incorporating some of that newly added residue. If these effects had been entered in the opposite order, none of this new residue would have been buried by the

operation, because the soil disturbance would have occurred before the residue was added.

Finally, the current crop is killed, immediately removing the effects of crop canopy and turning the root mass into subsurface residue.

The remainder of the operations in the "corn" listing are relatively straightforward, and are shown below. The "harvest" operation behaves like the "hay harvest" we saw earlier, in that it calculates the amount of residue added to the surface from the CROP Database Set. It does not call in a regrowth Set because harvesting corn also kills it.

The information needed by the rotation is now complete, because the next operation in the series would be the primary tillage before planting alfalfa, which is a repeat of the first operation in the sequence. Note that this would occur on 3/30 of year 9, which is 8 yr after its first occurrence. This is what determined the rotation length of 8 yr. If the rotation length had been entered as 9 yr, the program would assume a fallow period from 10/10/8 to 3/30/10.

Example 2: Continuously cropped conventional soybeans in Indiana with an aerially seeded rye winter cover crop. This example demonstrates how to handle two crops grown simultaneously. The example is based on a continuous conventionally tilled soybean crop, into which rye is aerially seeded when the soybeans are mature. The rye grows as an understory to the soybeans until they are harvested, at which time the rye begins vigorous growth until the onset of winter. The rye is tilled under in the spring before the planting of the next crop of soybeans. Because every operation is repeated every year, the rotation is 1 yr long.

The critical concept is that RUSLE can handle only one current crop, so the CROP Database Set associated with that crop must reflect everything that is growing in the field.

The general information screen for this rotation is shown below.

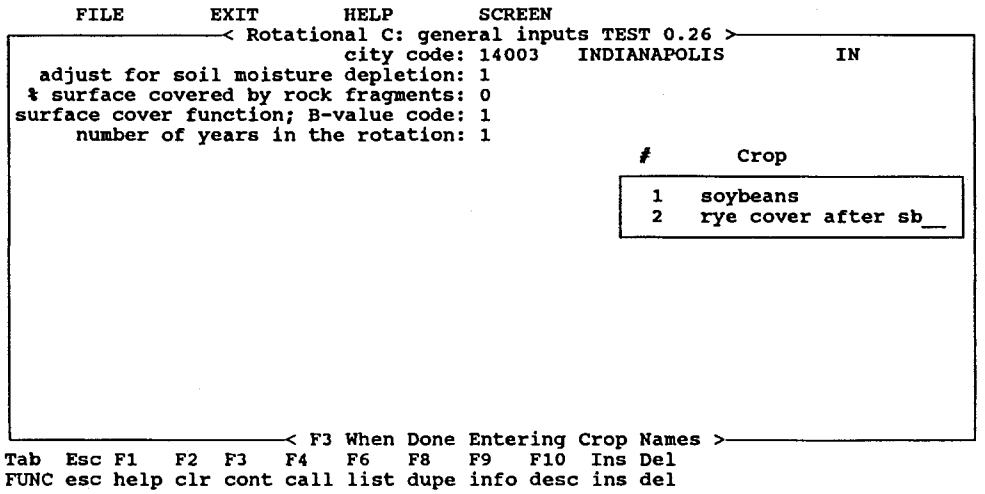

We could vary the list of crops, depending on how we want the accounting to be done. For instance, if we want only a total rotation value, we could list just soybeans. Another option is as shown above, where we separate the time that the soybeans are growing from the rest of the time.

The operations listing associated with the soybean accounting time is shown below. This includes the planting of the standard soybean file and its growth up to the time of the aerial seeding of the rye. From this point on, the current crop must reflect the root mass and canopy characteristics of not only the soybeans but the combined soybean/rye mixture. These characteristics will be shown in the CROP Database Set "sb and aerial rye" as an increase in root mass and canopy cover and a decrease in canopy height to show the effect of the low-growing rye. The residue characteristics of this Set will still be those of the soybeans, as this is the type of residue that will be added.

At the time of harvest we must not kill the crop, because the rye will continue to grow. Instead, we add the soybean residue to the surface and then call in a regrowth crop to simulate the vigorous rye growth after soybean harvest. The root mass value in this Set will be much lower than that in the combined soybean/rye Set, which the program will recognize as an addition of the soybean roots to the subsurface soybean residue pool. This new Set will have the residue characteristics of the rye, because any residue added to the surface now will be rye residue.

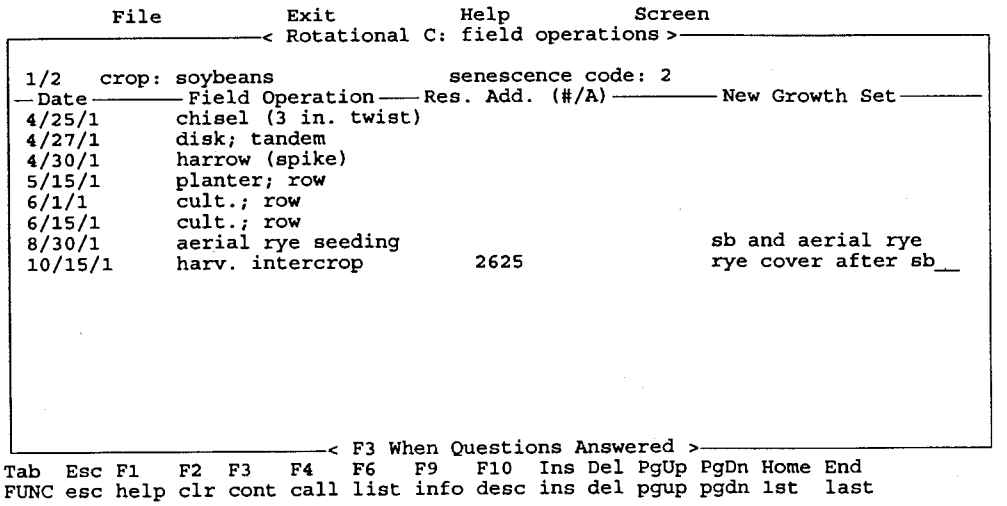

The rye crop is called in as the current crop with the last operation of the soybean listing, but recall that we wanted to account for the time from the soybean harvest to the next planting of soybeans under the rye cover crop. We do this with the first operation shown on the screen above. This "no operation" has no effects on the soil, crop, or residue, but is used to tell the program to begin the accounting under this crop name on this date. (See next figure.)

There are two ways of modeling the impact of a natural phenomenon like winter or drought conditions. First, if the impact is very sudden (as perhaps the first frost that kills tomatoes), you will want to model the impact as an operation. On the other hand, if the effect is more gradual (as it would be for the rye example), it is probably better to develop a CROP Database Set that shows the reduction in canopy cover and live root mass that can be caused by winter damage. Note in the listing below that nowhere within this screen is there an operation that begins the growth of the "rye cover after sb" crop. A current crop is still growing based on information in the previous screen, so there is no need to plant this crop.

```
     FILE        EXIT        HELP        SCREEN
                 < Rotational C: field operations TEST 0.26 >

 2/2   crop: rye cover after sb    senescence code: 2
--Date---------Field Operation-----Res. Add. (#/A)----------New Growth Set-------
 10/15/1      no operation
 11/15/1      begin winter impact                          rye cover overwinter
 3/1/2        begin spring growth                          rye cover spring ___









                          < F3 When Questions Answered >
Tab  Esc F1   F2  F3   F4   F6   F9   F10  Ins Del PgUp PgDn Home End
FUNC esc help clr cont call list info desc ins del pgup pgdn 1st  last
```

Example 3: Grazing of rangeland or pasture. The grazing of rangeland or pasture can be handled as the impact of winter on crops was handled. If the grazing is high intensity and can be thought of as occurring at a specific time, it can be treated as an operation, as with the hay harvests shown above. The vegetation would be harvested by the cattle, leaving a rough surface and trampling some residue onto the soil. The grazed area would then begin to regrow, so the high-intensity grazing operation would call in a regrowth crop Set.

On the other hand, if the grazing is long term and low intensity, it is probably best to treat it as a change in the crop growth patterns and to develop a CROP Database Set to reflect these conditions.

Answers to Common Questions About the C Factor

For a single disturbance, how do I define the initial conditions? Remember the factors that you must define: (1) amount of residue on the surface; (2) amount of buried residue; (3) surface roughness; and (4) any vegetative regrowth. This is done by beginning the growth of vegetation whose CROP Database Set reflects that found at the site before its disturbance. This should be grown for several years to reflect the soil consolidation found before the disturbance. The operations used in the disturbance are then listed, making sure that the effects of each operation reflect all of its impacts on the factors listed above.

How do I specify that the operations sequence is a rotation? You command the program to assume a rotation by specifying on the initial C-factor screen the number of years in the rotation. You calculate this by determining how many years it takes before the first operation will occur again. For example, if the first operation in the rotation takes place on May 1 of the first year and will not occur again until May 1 of the fourth year, then there will be 4 - 1 = 3 yr in the rotation. If you want a single disturbance rather than a rotation, simply place a zero in the input field for number of years in the rotation.

For the time-invariant C option, should I use the CROP Database or enter values directly? The C calculations for RUSLE require values from the CROP Database for canopy cover, fall height, and root mass. For continuous crops, these values are assumed to remain relatively constant through the year, so the only entries needed are average annual values. To specify these values, you can either enter them directly within the C factor or use the CROP Database Utility routines (see "Databases" and "CROP Database") to create a Set with these values. Do this with the "permanent" option for the crop/land use category, and then {save} the set under some unique Identifier name.

If you decide to use the CROP Database, the list of all {save}d "continuous" crops will be shown. Select an Identifier to automatically bring in the values from that Set for root mass, canopy cover, and fall height.

Within this time-invariant C option, the values of surface cover and roughness must be typed in directly.

What inputs are required for the time-invariant C option? The variables of surface cover, canopy cover, and fall height are relatively easy to deduce from experience. It is much harder to estimate the mass of roots in the top 4 in of soil. If you choose to not put the required data into a CROP Database Set (see section above), RUSLE will go through a series of questions to help you define the root-mass variable. You will be asked to define the type of plant community and the annual site production potential. The program will use these to calculate a root-mass value directly and, in that case, the program will calculate a corresponding site potential.

What general information is required for the time-varying C option? The first screen within the time-varying C-factor option defines all the general information for the rotation. Soil-moisture depletion should be taken into account only for those areas in which the rainfall is of low amounts and intensities and the soil surface characteristics do not limit infiltration. Thus far, this is supported only by data from the Northwestern Wheat and Range Region,

although there may be other areas to which this option can be applied. The "rock cover" variable should reflect the presence of all rocks and similar "permanent" surface cover, and is changed by {call}ing the K factor. Choose the b-value option that best describes your conditions. For well-consolidated soils dominated by interrill erosion, a low b value should be used; for highly disturbed or thawing soils dominated by rilling, a high b value is more appropriate. All other cases should use the moderate b value.

The crop list on the first screen of this option makes it easy to change an existing Input File. Crops can be {dupe}licated to new spots in the rotation, old crops can be {del}eted from the list, and new crops can be {Ins}erted. When you move a crop within the list, its operations will tag along, but the dates of the operations may need to be changed to show their new place within the rotation.

What information is needed on the operations screens of the time-varying C option? The rotation information screen contains general information about the crop and a list of all associated field operations. Also included is a question on whether a decrease in canopy cover should be seen as a contribution to surface cover. If you specified in the general information that you wanted to account for soil moisture depletion, the depletion rate value associated with the crops on this screen is entered here.

You must enter the dates (using xx/xx/xx to represent month/day/year) and names of all field operations, as well as any additional information required by the effects listed in the OPERATIONS Database Sets for those operations. You have great flexibility in entering the year. You can enter it as a calendar year (1995), as an abbreviated calendar year (95), or as the number of the year in the crop sequence. The program calculates the relative time elapsed, so all of these will be treated the same.

There are some limitations on the operations that you can enter, as follows:

(1) You can have only one current crop. Since there will be interactions between interplanted crops, RUSLE does not allow you to use two separate CROP Database Sets and to have them both growing at once. You must instead combine the Sets into one that reflects the total values of the combined crops. The residue parameters should be for the crop whose residue is added to the surface by a harvest operation; you can call in a regrowth CROP Database Set containing the parameters of the second crop before harvesting it.

(2) If an operation has a "harvest" effect, the program will automatically enter the weight of residue added. For other effects, you will be asked to specify the amount of residue added.

(3) The operation can also ask for the name of a regrowth crop. In this case, a list of the crops is shown, and you must either pick from this list or go into the CROP Database Utility routines to create a new crop.

(4) There are few restrictions on the order in which the operations may be listed, but one restriction is that the current crop must exist in order to be able to do anything with it. The program will issue a warning if you try to do anything with the current crop without having specified something to tell the program just what that crop is.

How are all the different roughness values set and used? The time-varying C-factor calculations use three different random roughness values. The first is the roughness immediately after a soil disturbance operation; this value is defined within the OPERATIONS Database Set for that operation, and is a function of soil condition and of the implement that is used.

The second roughness value is that to which the tillage roughness decays as it is acted upon by raindrop impact and surface flow. The default setting for this roughness is 0.24 in, which is the roughness found on experimental fallow plots exposed to natural rainfall. If desired, this value can be set to reflect continuous re-roughening of the surface, as can happen with cattle grazing. In this case, the initial and final roughness values can be set equal to indicate a constant roughness, or can be adjusted as desired to indicate increasing or decreasing roughness. The final decay roughness value is set in the OPERATIONS Database Set.

The third random roughness value used in this part of RUSLE reflects the impact of the vegetation on soil surface roughness; this will be a function of protruding roots, basal mounding, and so on. This variable represents the site roughness several years in the future (as defined by the number of years to soil consolidation), under the assumption that the site will not be disturbed during that time. The value, therefore, also reflects the assumption of some vegetative community that will come to dominate the undisturbed site over this time period. The program uses this value only for runs with a single disturbance, and uses a sigmoidal growth curve to increase the natural roughness to this value from the minimum value defined in the previous paragraph. The long-term site roughness is set in the general information screen of the time-varying C-factor option if the length of the rotation is set to zero.

What outputs are available for the time-varying C option? The options for showing the results of the rotational C-factor calculations vary primarily in the degree of detail shown. The "Rotation C" option divides the results into the SLR · %EI associated with each crop, whereas the "Operation C" option breaks this down further into the SLR · %EI associated with each operation. The "Half-Month Subfactor" option shows the finest division, displaying each of the SLR subfactors for each calculation period.

There is one difference between the "Operation C" results and the "Half-Month" results that might cause confusion. In Operation C, the values shown for percent surface cover are calculated immediately after the operation, whereas the Half-Month surface cover values are calculated in the middle of the time period.

P Factor

The RUSLE P factor reflects the impact of support practices on the average annual erosion rate.

Options

As with the other factors, the P factor differentiates between cropland and rangeland or permanent pasture. Both options allow for terracing or contouring, but the cropland option contains a stripcropping routine whereas the rangeland/permanent-pasture option contains an "other mechanical disturbance" routine. For the purposes of this factor, the rangeland/permanent-pasture option is based on the support operation being performed infrequently, whereas in the cropland option, the support operation is part of the annual management practice.

One variable seen in the contouring, mechanical-disturbance, and stripcropping routines is a site description. RUSLE asks you to choose from a list of descriptions the one that best fits your conditions. This information is used in several ways, as follows:

(1) The site description is used to assign a runoff index and roughness value to the situation. The runoff index is a measure of the percentage of available precipitation that will be seen as runoff, and is a function of soil type, soil structure, soil surface condition, and surface vegetative cover. The runoff index value is similar to the curve number used in the NRCS Direct Runoff method of calculating runoff volume, and is used here for roughly the same purpose. Runoff index values associated with specific soil hydrologic groups and site descriptions can be changed by

using the {call} command from the Input Field where the site description is requested.

(2) The site description is also used to estimate the effect of surface roughness and vegetative cover on erosion and transport from the slope. A qualitative view of the roughness is given in the site descriptions, but the actual roughness values associated with the descriptions are assigned internally.

Answers to Common Questions About the P Factor

What is the variable ridge height option on the contouring subfactor (cropland or pasture/rangeland option)? This option allows you to define how the contour ridge heights change with time during the rotation. The program calculates a P value for each ridge height and then multiplies that by the percentage of annual EI associated with each period to derive an average annual contouring subfactor.

What is the critical slope length in the contouring subfactor (cropland or pasture/rangeland option)? The effectiveness of contouring breaks down when the slope is so long that runoff causes break-over and subsequent gullying. This point is defined by the critical slope length, which is a function of the slope steepness, ridge height, residue cover, and runoff potential. When the slope is longer than this calculated maximum, the contour credit applies only to the portion above the critical length. The portion below has a P contour subfactor of 1. RUSLE will give you a warning that this is occurring, and will adjust the overall P factor accordingly.

Why are there dual site descriptions in the contour subfactor (pasture/rangeland option only)? After a disturbance, a pasture/rangeland soil will take some years to reconsolidate to a point similar to that before the disturbance. In order to look at this consolidation effect, it is necessary to detail just how the site responds to consolidation and what effect this has on runoff. This information is given by describing the site both immediately after disturbance and after enough time has passed for relatively complete consolidation. The program then assumes an exponential decay function, and allows you to look at any year within that range.

What is the stripcropping subfactor (cropland option only)? The stripcropping P subfactor defines the effectiveness of contoured or cross-slope strips in causing deposition where it might benefit future productivity, and in slowing

and spreading the runoff. These strips can be any combination of crops and/or tillage practices that would affect the surface roughness, infiltration rates, or hydraulic roughness seen by the runoff.

Why does the stripcropping subfactor require {call}ing the contouring routine (cropland option only)? Because stripcropping is closely linked to contouring, the RUSLE program uses the contouring routines to provide information on row grade and critical slope length. If it is needed, the call to the contouring subroutine occurs automatically. When the contouring routine is called from the stripcropping routine, the site description used should be for the "smoothest" strip within the stripcropping rotation.

What is the stripcropping subfactor strip width (cropland option only)? The stripcropping subfactor program requires a complete description of the slope, including the condition and width of each strip. There are two ways of specifying strip width. The first is to indicate the position of the bottom of the strip as a percentage of the total slope length. For example, if a 120-ft slope is divided into four 30-ft strips, their relative positions would be at (30/120), (60/120), (90/120), and (120/120), or 25%, 50%, 75%, and 100%, respectively. The other option is to specify the actual strip widths in feet, which in the above example would be 30, 30, 30, and 30. The disadvantage of this second style is that the total slope length has already been specified in the LS factor. If the total length calculated by adding these strip widths varies from that entered in LS by more than 10%, the RUSLE program issues a warning and requires a response before proceeding.

What is the Other Mechanical Disturbance subfactor (pasture/rangeland option only)? Mechanical disturbance of the soil takes two possible forms: (1) disturbance on the contour, which results in roughness on the contour and redirection of runoff along the rows; and (2) a more random mechanical disturbance, which results in a rough surface that can slow runoff and in depressional areas that can store runoff and increase infiltration. The option chosen depends on whether the roughness that is left after the disturbance is primarily oriented or random. If the roughness has a definite orientation (ridges), choose the contouring option, even though the ridges may not be directly on the contour. If the roughness is more random, choose the Other Mechanical Disturbance option.

SYSTEM CONSIDERATIONS: USING RUSLE WITH YOUR EQUIPMENT

All computer requirements and instructions for loading and running RUSLE are described in detail in "Getting RUSLE To Work on Your Machine."

Using a Printer

RUSLE is meant primarily to be a tool to make it easy to compare cropping and management alternatives, and to speed up these repeated calculations. Although RUSLE will print out some results and inputs, it is not designed to generate documents.

For machines that use DOS, RUSLE looks for an attached printer, as it does also for the 3B2 and 6386 machines running either DOS or UNIX. When run under BSD UNIX, the print routines will look in a file named "printer.use" for the name of the network printer. Check your manuals or consult with a site specialist if problems arise.

Most of the printouts are meant to fit on 8½" x 11" paper. The exception is the printout of LS tables, which may be up to 132 characters wide. If your printer cannot be configured to handle this many characters within 8½ in, you must use wider paper. Note that copies of the tables are available in chapter 4 of this handbook.

Making Copies of RUSLE To Share With Others

RUSLE contains a routine that allows you to copy the program onto a diskette(s) to share with others. This routine is available from the RUSLE Information option of the RUSLE Main Menu, and works only on DOS. This option is not available in UNIX.

Refer to "Using an Input File Created Earlier or Elsewhere" and to "Using Database Sets Created Earlier or Elsewhere" for information on how to send information you have entered to another user.

Reporting Problems and Trouble

RUSLE is a relatively new and complex computer program. A user may find problems that did not arise in preliminary testing. It will greatly help the developers and programmers of RUSLE if you report problems that you find, giving as much information as possible about when and how the problems occurred. This information includes the following:

- screen you were on and question being answered
- command you gave just before the problem showed up
- what (if anything) showed up on the screen
- how the problem manifested itself (program locked up, gave unreasonable answer, and so on.)

Please send this information to:

George R. Foster
USDA-ARS, National Sedimentation Laboratory
P.O. Box 1157, 598 McElroy Drive
Oxford, Mississippi 38655
Telephone (601) 232-2900
FAX (601) 232-2915

Glenn A. Weesies
USDA-NRCS, National Soil Erosion Research Laboratory
Purdue University, Building SOIL
West Lafayette, Indiana 47907
Telephone (317) 494-8692

Daniel C. Yoder
Department of Agricultural Engineering
University of Tennessee
PO Box 1071
Knoxville, Tennessee 37901-1071
Telephone (615) 974-7266

or

Kenneth G. Renard
USDA-ARS, Southwest Watershed Research Center
2000 E. Allen Road
Tucson, Arizona 85719-1596
Telephone (520) 670-6481
FAX (520) 670-5550

SUMMARIES

Command Keys

A complete list of all possible commands and a brief description of what each does are given below. The command description or name is given in braces, { }, and the associated DOS key for each command is given in brackets, [ ]. The keys may differ on some machines, but the command description is always as shown here.

{FUNC} [TAB] places the cursor onto the Function Line to let you do the required housekeeping chores (see "Calling a Function" or "The Functions: Program Housekeeping"). When the cursor is on the Function Line, use {esc}ape to bring it back to the Main Screen.

{esc} [ESC] allows you to {esc}ape from the current screen or question without giving an answer. This is most commonly used in three places: (1) if you have gotten into a screen or series of screens and want to get back out; (2) after an error or warning message has been displayed, and you want to continue; and (3) to continue the program after a result has been displayed.

{help} [F1] shows one or more screens of additional information to help answer the current question (see "Help"). This usually includes a brief description of how the variable is used in the calculations and also suggestions for possible answers.

{clear} [F2] {clear}s (sets to 0) all variables associated with the current screen. This is most useful when you want to get a fresh start on a screen containing several mistakes.

{cont} [F3] {cont}inues program movement to the next logical screen in the sequence. For example, when you have answered all the questions on one screen, this command moves you to the next screen or initiates the calculations. For screens that require only one input or command, the {cont}inue command acts just like an [ENTER], telling the program to accept the current value and to move on.

{call} [F4] {call}s a subroutine on which the answer might depend. Use of this command will automatically put you into the required subroutine; when you exit from that, you will return to the current question.

The {call} command is used in three different instances, as follows:

(1) When an answer is calculated from the results of several different factors. An example is in estimation of soil loss from the factor values. Each factor is {call}ed individually by use of this command.

(2) When the question asks for the Identifier of a Database Set, as when entering a city code, a crop name, or an operation name. Use of the {call} from one of these locations allows you to examine or modify the information within the associated Database. "Databases" gives more detail.

(3) When the calculation requires information entered in another portion of the program. An example of this is the value of average field slope, which is used in several places but is calculated within the LS factor. If this value has already been calculated, it will be shown; if not, the {call} command must be used to move to that calculation.

{list} [F6] displays a list from which you can select an option or item, as explained in "Input Field." If you have previously selected one of the choices, the list may not be shown but this command will appear as an option. Use of this command displays the list and allows you to move through it using the [ARROW] keys.

There are places in the program where the list is also shown but the marker arrow is not visible. In these cases a {list} command will move the marker arrow into the list, where the marker can be controlled with the [ARROW] keys.

{save} [F7] {save}s the data shown on the screen into a Database Set named by the Identifier at the top of the screen. Changes made within the CITY, CROP, or OPERATIONS

Database routines will not be saved into those Databases unless this command is used before exiting those routines. If changes have been made, you will be asked whether or not you want to save them before you are allowed to exit.

{dupe} [F8] is used only in the crop listing on the initial C-factor input screen; this duplicates an entire operation listing screen into another location within the list. For example, if I {dupe} "corn" from the first place on the list into the fifth, the program will duplicate all operations associated with that first corn onto the fifth screen. It will not change the dates, so this must be done by moving to that screen and modifying them individually.

{info} [F9] gives information on the Current Input List. When you {save} a Current Input List into an Input File, you are also saving a list of comments describing that List. Use of this command allows you to look at (and change) the descriptive information for the Current Input List.

{desc} [F10] gives information on the current CROP or OPERATIONS Database Set. These Sets also contain a series of descriptive comments, which can be viewed or changed from anywhere this command is available.

{ins} [INS] is used to insert a line of information just above the line on which the cursor is resting.

{del} [DEL] is used to delete the line of information on which the cursor is resting.

{1st} [HOME] is used to jump to the first in a series of screens or to the beginning of a list.

{last} [END] is used to jump to the last in a series of screens or to the end of a list.

{pgup} [PG UP] is used to move to the previous screen in a series of screens or up one screen in a long list of information.

{pgdn} [PG DN] is used to move to the next screen in a series of screens or down one screen in a long list of information.

Terminology

command :	is an instruction given to RUSLE to control the flow of the program. A *command* is usually given by pressing a key. At any point in the program, the available *commands* are shown on the *Command Line.*
Command Line:	is made up of the bottom two lines of the screen, and contains a list of all the available *commands* at any point in the program. The bottom line shows the three- or four-letter description of the *command,* and the upper line shows the keystroke used to execute it.
Current Input List:	is a list of the current values for all answers to the questions. This is updated every time a new value is entered or a new selection is made from a list, such as the entering or selection of a new city.
Database Set:	is all of the CROP, CITY, or OPERATIONS information associated with a specific *Identifier.* For instance, for the CITY Database, this is all the climatic data for a specific city or region.
file(s):	is an operating system file. See your manual or site specialist for a more complete description.
Function:	is a set of routines used by RUSLE to perform housekeeping tasks. For RUSLE, these consist of the FILE Function to move information back and forth between the *Current Input List* and the *Input Files*, the EXIT Function to leave the program quickly, the HELP Function to obtain general information about the program, and the SCREEN Function to change screen coloring.
Function Line:	is a list of the available *Functions,* shown on the top line of the screen. These can be reached with the {FUNC} *command* to move the cursor to the *Function Line*, using the [ARROW] keys to get the correct *Function* and option, and pressing [ENTER].
Header Line:	is the top line of the *Main Screen*, and the second line down from the top of the actual screen. This shows the program version and the screen name.

Identifier: is a name or number with which to associate the information in a particular *Database Set.* When a list of the names or numbers is shown, selection of the one you want brings in all associated information.

input: is a response typed into an *Input Field* or chosen from a list in response to a program question.

Input Field: is the place where the cursor rests while waiting for your response to a question. You can respond with either an *input* or a *command.*

Input File: is a copy of the *Current Input List* that has been SAVEd. This copy is stored as a file with the name it was given in SAVEing, along with a ".rus" suffix.

Main Screen: is the central part of the screen. It contains all the questions and areas for response.

Suggestion Line: is seen within the line forming the bottom of the *Main Screen.* This line displays the suggested *command* or course of action.

APPENDIX A. CONVERSION TO SI METRIC SYSTEM

SI metric equivalents are not included in the procedures and tables presented in this handbook because direct conversion of each English unit is awkward in many instances and undesirable for a procedure used in the United States. Converting the RUSLE as a whole may be more appropriate. SI metric units can then be selected so that each of the interdependent factors will have a metric counterpart whose values will be expressed in numbers that are easy to visualize and to combine in computations.

A convenient unit for measuring cropland soil losses is metric tons per hectare (table A-1). **EI** values can be obtained by expressing rainfall energy in megajoule· millimeter per hectare· h· yr and expressing intensities in millimeters per hour. Factor **K** will then be in metric tons· hectare· hour per hectare· megajoule· millimeter or metric tons per hectare per unit **EI**. If 22.1 meters is taken as the basic slope length and 9 percent is retained as the basic slope gradient, the **LS** factor will not be affected. Using these units is recommended and is assumed in the following paragraphs.

The RUSLE factors will normally be derived directly in the English units by procedures outlined in Foster et al. (1981). However, the conversion factors in table A-2 will facilitate comparisons of the metric factor values with the English values published in this handbook. Details of the conversions are shown in Foster et al. (1981).

Table A-1.
Dimensions of universal soil loss equation (USLE) factors

Factor	Symbol	Dimensions		Typical U.S. customary units
Rainfall intensity	i or I	[1] $\frac{length}{time}$	$\frac{L}{T}$	$\frac{inch}{hour}$
Rainfall energy per unit of rainfall	e	$\frac{length \cdot force}{area \cdot length}$	$\frac{LF}{L^2L}$	[2] $\frac{foot \cdot tonf}{acre \cdot inch}$
Storm erosivity	EI	$\frac{length \cdot force \cdot length}{area \cdot time}$	$\frac{LFL}{L^2T}$	[3] $\frac{hundreds\ of\ foot \cdot tonf \cdot inch}{acre \cdot hour}$
Soil loss	A	$\frac{mass}{area \cdot time}$	$\frac{M}{L^2T}$	$\frac{ton}{acre \cdot year}$
Annual erosivity	R	$\frac{length \cdot force \cdot length}{area \cdot time \cdot time}$	$\frac{LFL}{L^2TT}$	$\frac{hundreds\ of\ foot \cdot tonf \cdot inch}{acre \cdot hour \cdot year}$
Soil erodibility	K	$\frac{mass \cdot area \cdot time}{area \cdot length \cdot force \cdot length}$	$\frac{ML^2T}{L^2LFL}$	$\frac{ton \cdot acre \cdot hour}{hundreds\ of\ acre \cdot foot \cdot tonf \cdot inch}$
Slope length	L	$\left(\frac{length}{length}\right)^m$	$\left(\frac{L}{L}\right)^m$	
Slope steepness	S	Dimensionless		
Cover-management	C	Dimensionless		
Supporting practices	P	Dimensionless		

[1]F=forces, L=length, M=mass, T=time, m=exponent that varies from 0.2 to 0.5
[2]Tonf indicates ton force. Ton without a subscript indicates ton.
[3]This notation, "hundreds of," means that the numerical value of the factor is 0.01 times its true value. That is, if R=125, its true value is 12,500 ft· tonf· in (acre· h· yr)$^{-1}$. The converse is true for "hundreds of" in the denominator of a fraction.

Source: Foster et al., 1981.

Table A-2.
Conversion factors for universal soil loss equation (USLE) factors.

To convert from	U.S. customary units	Multiply by	To obtain:	SI Units
Rainfall intensity, i or I	$\frac{inch}{hour}$	25.4	$\frac{millimeter}{hour}$	[1] $\frac{mm}{h}$
Rainfall energy per unit of rainfall, e	$\frac{foot \cdot tonf}{acre \cdot inch}$	$2.638 \cdot 10^{-4}$	$\frac{megajoule}{hectare \cdot millimeter}$	[2] $\frac{MJ}{ha \cdot mm}$
Storm energy, E	$\frac{foot \cdot tonf}{acre}$	0.006701	$\frac{megajoule}{hectare}$	[3] $\frac{MJ}{ha}$
Storm erosivity, EI	$\frac{foot \cdot tonf \cdot inch}{acre \cdot hour}$	0.1702	$\frac{megajoule \cdot millimeter}{hectare \cdot hour}$	$\frac{MJ \cdot mm}{ha \cdot h}$
Storm erosivity, EI	[4] $\frac{hundreds\ of\ foot \cdot tonf \cdot inch}{acre \cdot hour}$	17.02	$\frac{megajoule \cdot millimeter}{hectare \cdot hour}$	$\frac{MJ \cdot mm}{ha \cdot h}$
Annual erosivity, R[5]	$\frac{hundreds\ of\ foot \cdot tonf \cdot inch}{acre \cdot hour \cdot year}$	17.02	$\frac{megajoule \cdot millimeter}{hectare \cdot hour \cdot year}$	$\frac{MJ \cdot mm}{ha \cdot h \cdot y}$
Soil erodibility, K[6]	$\frac{ton \cdot acre \cdot hour}{hundreds\ of\ acre \cdot foot \cdot tonf \cdot inch}$	0.1317	$\frac{metric\ ton \cdot hectare \cdot hour}{hectare \cdot megajoule \cdot millimeter}$	$\frac{t \cdot ha \cdot h}{ha \cdot MJ \cdot mm}$
Soil loss, A	$\frac{ton}{acre}$	2.242	$\frac{metric\ ton}{hectare}$	$\frac{t}{ha}$
Soil loss, A	$\frac{ton}{acre}$	0.2242	$\frac{kilogram}{meter^2}$	$\frac{kg}{m^2}$

[1]Hour and year are written in U.S. customary units as h and yr and in SI units as h and y. The difference is helpful for distinguishing between U.S. customary and SI units.
[2]The prefix mega (M) has a multiplication factor of $1 \cdot 10^6$.
[3]To convert ft · tonf to megajoule, multiply by $2.712 \cdot 10^{-3}$. To convert acre to hectare, multiply by 0.4071.
[4]This notation, "hundreds of," means numerical values should be multiplied by 100 to obtain true numerical values in given units. For example, R=125 (hundreds of ft · ton · in (acre · h)$^{-1}$=12,500 ft · tonf h. The converse is true for "hundreds of" in the denominator of a fraction.
[5]Erosivity, EI or R, can be converted from a value in U.S. customary units to a value in units of Newton/hour (N/h) by multiplying by 1.702.
[6]Soil erodibility, K, can be converted from a value in U.S. customary units to a value in units of metric ton · ha (Newton · h)$^{-1}$ [t · h(ha · N)$^{-1}$] by multiplying by 1.317.
Source: Foster et al. 1981

APPENDIX B. CALCULATION OF EI FROM RECORDING-RAINGAGE RECORDS

The energy of a rainstorm can be computed from recording-raingage data. The storm is divided into successive increments of essentially uniform intensity, and a rainfall energy-intensity equation (for example, equations [B-3] and [B-5]) is used to compute the energy for each increment. Because the energy equation and energy-intensity table have been frequently published with energy expressed in ft · tonf · acre^{-1}, this unit was retained in table B-1. However, for computation of EI values, storm energy is expressed in hundreds of foot-tons per acre. Therefore, energies computed by the published formula or by table B-1 must be divided by 100 before multiplying by I_{30} to compute EI.

Soil-loss prediction with USLE does not require the computation of EI values by application personnel, but the procedure is included here for the benefit of those who may wish to compute them.

Mathematically, R is

$$R = \frac{1}{n} \sum_{j=1}^{n} \left[\sum_{k=1}^{m} (E) \left(I_{30}\right)_k \right] \qquad [B\text{-}1]$$

where

E = total storm kinetic energy,
I_{30} = maximum 30-min rainfall intensity,
j = index of number of years used to produce average,
k = index of number of storms in each year,
n = number of years used to obtain average R,
m = number of storms in each year, and
R = average annual rainfall erosivity.

$$EI = (E)\left(I_{30}\right) = \left(\sum_{k=1}^{m} e_r \, \Delta V_r \right) I_{30} \qquad [B\text{-}2]$$

where

e_r = rainfall energy per unit depth of rainfall per unit area ft · tonf · acre^{-1} · in^{-1}, and

ΔV_r = depth of rainfall for the rth increment of the storm hyetograph which is divided into m parts, each with essentially constant rainfall intensity (in).

Unit energy, e, is a function of rainfall intensity and is computed as

$$e_k = 1099 \left[1 - 0.72 \exp \left(-1.27 i_r \right) \right] \quad [B\text{-}3]$$

and

$$i_r = \frac{\Delta V_r}{\Delta t_r} \quad [B\text{-}4]$$

where

Δt_r = duration of the increment over which rainfall intensity is considered to be constant (h), and

i_r = rainfall intensity (in · h^{-1}).

The unit energy equation [B-3] was suggested by Brown and Foster (1987) as a replacement to the relationship used in Agriculture Handbook 537 because the equation not only includes more data for its development but also has a better functional form at low intensities. Equation [B-3] was used for the preparation of the isoerodent maps in the western United States whereas the isoerodent maps in the eastern United States were calculated using the following equation:

$$e_k = 916 + 331 \log_{10}(i_r) \quad [B\text{-}5]$$

We do not recommend using equation [B-5] for future calculations of unit energy.

The EI for a specified time period (such as the annual value) is the sum of the computed value for all rain periods within that time. Thus

$$R = \sum EI_{30}(10^{-2}) \qquad [B\text{-}6]$$

where

R = average annual rainfall erosivity in

$$\frac{\text{hundreds of ft} \cdot \text{tonf} \cdot \text{in}}{\text{acre} \cdot \text{h} \cdot \text{yr}}$$

and the division by 100 is made for convenience of expressing the units.

In the western United States, all storms were included in the calculation of R, except storms where the precipitation occurred as snow. Erosion index calculations in the eastern United States were computed for storms exceeding 0.5 in of precipitation. Rains of less than 0.5 in, separated from other showers by 6 h or more, were omitted as insignificant unless the maximum 15-min intensity exceeded 0.95 in $\cdot$ h^{-1}.

Sample Calculation of EI From Recording-Raingage Records

The kinetic energy of a given amount of rain depends on the sizes and terminal velocities of the raindrops, and these are related to rainfall intensity. The computed energy per inch of rain at each intensity is obtained by solving equations [B-3] and [B-4], or by using table B-1 and reading energy values for the intensity obtained from the recording raingage. The energy of a given storm depends on all the intensities at which the rain occurred and the amount that occurred at each intensity. A recording-raingage record of the storm will provide this information. Clock time and rain depth are read from the chart at each point where the slope of the pen line (from a cumulative record) changes, and are tabulated as shown in the first two columns of the sample computation in table B-2. Clock times (col. 1) are subtracted to obtain the time intervals given in column 3, and the depths (col. 2) are subtracted to obtain the incremental amounts tabulated in column 4. The intensity for each increment (col. 5) is the incremental amount times 60, divided by column 3.

The energy per inch of rain in each interval (col. 6) is obtained by entering table B-2 with the intensity given in column 5 or by solving equations [B-3] and [B-4]. The incremented energy amounts (col. 7) are products of columns 4 and 6. The total energy for this 90-min rain is 1,254 ft $\cdot$ tonf $\cdot$ $acre^{-1}$. This is

multiplied by a constant factor of 10^{-2} to convert the storm energy to the dimensions in which EI values are expressed.

The maximum amount of rain falling within 30 consecutive minutes was 1.08 in, from 4:27 to 4:57. I_{30} is twice 1.08, or 2.16 in $\cdot$ h^{-1}. The storm EI value is 12.54(2.16) = 27.1. When the duration of a storm is less than 30 min, I_{30} is twice the amount of rain.

Comparison of the new unit energy relationship (eq. [B-3]) with the one from Agriculture Handbook 537 (eq. [B-5]) shows less than a 1% difference in the energy of some sample storms (see tables B-3 and B-4).

Table B-1.
Kinetic energy of rainfall expressed in ft · tonf · $acre^{-1}$ · in^{-1}

Intensity (in/h)	0	0.01	0.02	0.03	0.04	0.05	0.06	0.07	0.08	0.09
0	308	318	328	337	347	356	366	375	384	393
0.1	402	411	420	428	437	445	453	461	469	477
.2	485	493	501	508	516	523	530	537	545	552
.3	558	565	572	579	585	592	598	604	611	617
.4	623	629	635	641	646	652	658	663	669	674
.5	680	685	690	695	700	705	710	715	720	725
.6	730	734	739	743	748	752	757	761	765	770
.7	774	778	782	786	790	794	798	801	805	809
.8	813	816	820	823	827	830	834	837	840	843
.9	847	850	853	856	859	862	865	868	871	874
1.0	877	903	927	947	956	981	995	1,008	1,019	1,028
2.0	1,037	1,044	1,051	1,056	1,061	1,066	1,070	1,073	1,076	1,079
3.0	1,081									

Table B-2.
Sample calculation of storm EI_{30}

Chart readings		For each increment			Energy	
Time	Depth (in)	Duration (min)	Amount (in)	Intensity ($in \cdot h^{-1}$)	Per inch	Total
4:00	0.00					
:20	.05	20	0.05	0.15	445	22
:27	.12	7	.07	.6	730	51
:36	.35	9	.23	1.53	985	227
:50	1.05	14	.7	3	1081	757
:57	1.2	7	.15	1.29	945	142
5:50	1.25	8	.05	.38	611	31
:15	1.25	20	0	0	308	0
:30	1.3	15	.05	.2	485	24
Total		90	1.30			1,254

Total storm $EI_{30} = 1{,}254(10^{-2})(2.16) =$
27.09 hundred ft · tonf · in · $acre^{-1}$ · h^{-1}.

Table B-3.
Sample calculation of storm EI for storm of July 22, 1964, at raingage 63.056, using revised equation [B-3] for computing rainfall energy

Chart readings		For each increment			Energy	
Time	Depth (in)	Duration (min)	Amount (in)	Intensity ($in \cdot h^{-1}$)	Per inch	Total
18:15	0					
:19	.35	4	0.35	5.25	1,081	378
:22	.47	3	.12	2.4	1,061	127
:27	1	5	.53	6.36	1,081	573
:30	1.62	3	.62	12.4	1,081	670
18:45	2.06	15	.44	1.76	1,015	447
Total		30	2.06			2,195

Table B-4.
Sample calculation of storm EI for storm of July 22, 1964, at raingage 63.056, using original equation [B-5] for computing rainfall energy

Chart readings		For each increment			Energy	
Time	Depth (in)	Duration (min)	Amount (in)	Intensity ($in \cdot h^{-1}$)	Per inch	Total
18:15	0					
:19	.35	4	0.35	5.25	1,074	376
:22	.47	3	.12	2.4	1,042	125
:27	1	5	.53	6.36	1,074	569
:30	1.62	3	.62	12.4	1,074	666
18:45	2.06	15	.44	1.76	997	439
Total		30	2.06			2,175

APPENDIX C. ESTIMATING RANDOM ROUGHNESS IN THE FIELD

Random roughness is the nonoriented surface roughness that is sometimes referred to as cloddiness (Allmaras et al. 1966, Römkens and Wang 1986). Such roughness is usually created by the action of tillage implements. Random roughness is an important component in computing the soil-loss ratio (ch. 5). It can be contrasted with oriented roughness such as the ridges and furrows created by the passage of a tillage implement through the field. Oriented roughness in ridges and furrows is a component of the P factor (ch. 6).

Random roughness is defined as the standard deviation of elevation from a plane across a tilled area, after oriented roughness is accounted for by appropriate statistical procedures. Random roughness can be determined by mechanical profile meters or by more sophisticated devices such as laser profilers. At this time, no rapid, inexpensive technique is available to measure random roughness in the field. Frequently roughness is estimated as either a mean or a range in clod size. It has also been estimated in terms of the number of hits on clods of greater than a given size using a beaded line. Neither technique provides a value of random roughness as needed by RUSLE or other models.

Based on the need for rapid field assessment of random roughness and the lack of a suitable field technique, photographs of areas of selected random roughness conditions were taken to be used as visual guides to estimate random roughness in the field.

Procedure

It was thought essential to document a wide range of surface conditions, from very fine to very rough. Plot areas on the Palouse Conservation Field Station near Pullman, WA, were inspected for suitable conditions. By conducting additional tillage on selected plots, a wide range of roughness conditions was established on nine plot areas. A 6-ft-wide mechanical profile meter with pins on 1/2-in spacing was used to obtain roughness measurements. A 35-mm single-lens-reflex camera with a wide-angle lens was used to record the pin-top heights against a grid background (McCool et al. 1981). The profile meter was set up parallel to the tillage direction, and 10 lines were taken across a 1-m-deep plot. No attempt was made to establish a common datum elevation for all lines. This research differed from that of Allmaras et al.

(1966), in which all points on a rectangular grid were measured from a common datum. Hence, only random roughness parallel to tillage lines is considered in this study.

Black-and-white enlargements, 8x12 in, were obtained from the profile meter photos, and the pin-top elevations were digitized. A regression line was fitted to each set of readings for use as a reference datum, and the standard deviation was calculated for each cross section. The average standard deviation or random roughness was calculated for each plot by averaging these 10 values.

An undisturbed area measuring 1x1 m beside the profile meter transect was photographed at an oblique angle to provide an image similar to that seen by an observer standing a few feet from the plot. These photographs were taken at right angles to the tillage direction.

Results

The nine plot areas yielded random roughness values, R_t, ranging from 0.25 to 2.15 in. Photos of these plots are presented in figures C-1 through C-9. These figures can be used in the field to estimate random roughness. The soil-loss ratio is moderately sensitive to random roughness. Estimating random roughness as 0.50 when it is actually 0.25 results in a 15% error in the soil-loss ratio.

During the data analysis, it was found that the R_t value was linearly related to the difference in elevation between the highest and lowest pin-top reading (i.e., range) for a given cross section. The data from each of the cross sections is plotted in figure C-10. The R_t values were linearly fitted to the range in pin-top elevations as shown by the line in figure C-10, with a coefficient of determination of 0.93.

Thus random roughness can also be estimated by determining the distance from the highest to the lowest point along a furrow or ridge. Averaging a number of these readings in a field provides an average value to use with figure C-10 to obtain a value of R_t.

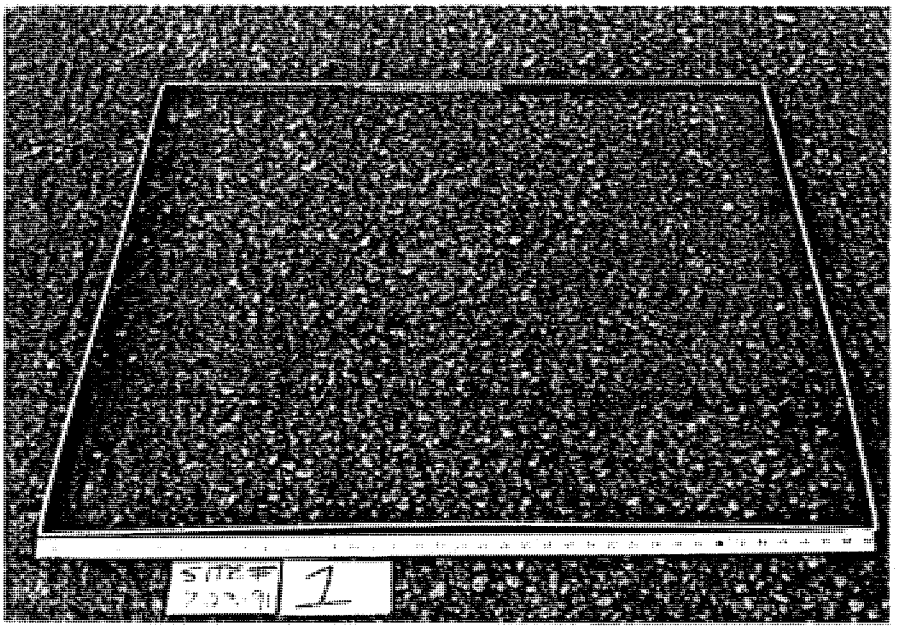

Figure C-1. Random roughness, R_t, of 0.25 in, site 1

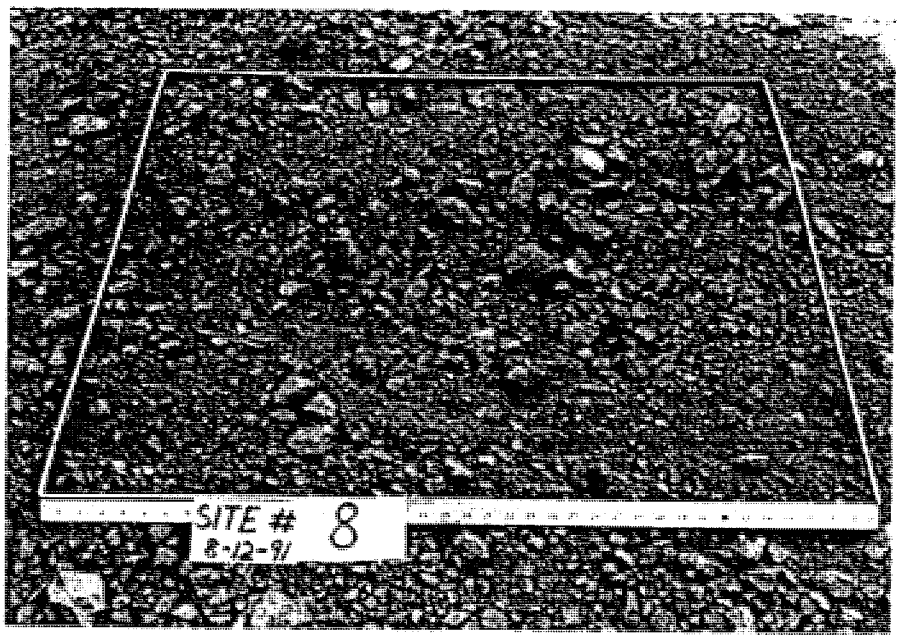

Figure C-2. Random roughness, R_t, of 0.40 in, site 8

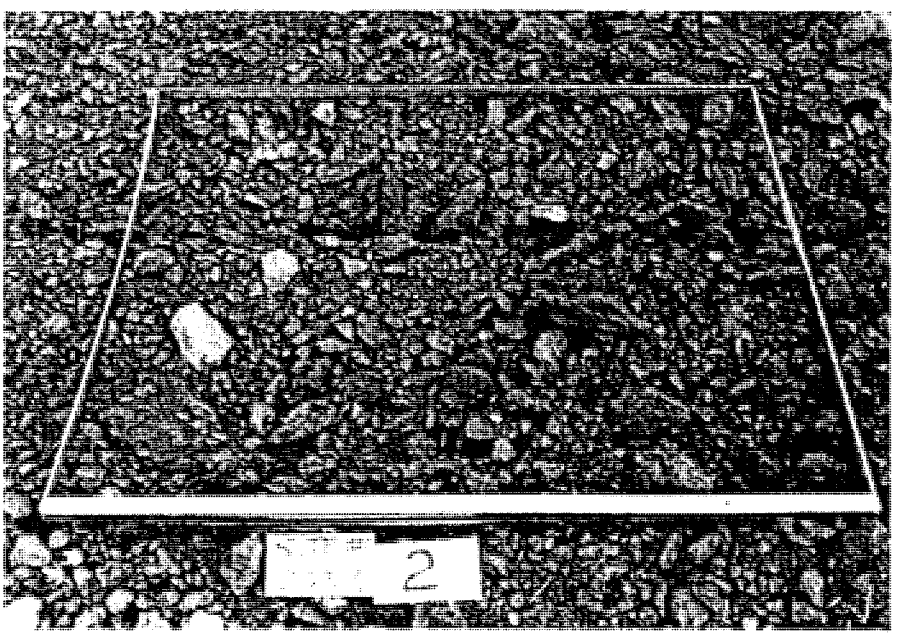

Figure C-3. Random roughness, R_t, of 0.65 in, site 2

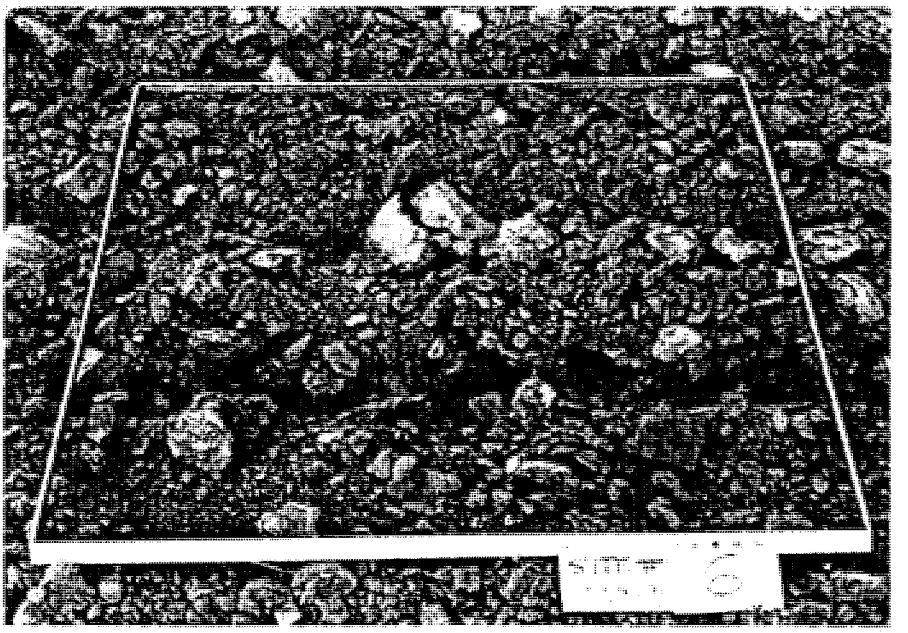

Figure C-4. Random roughness, R_t, of 0.75 in, site 6

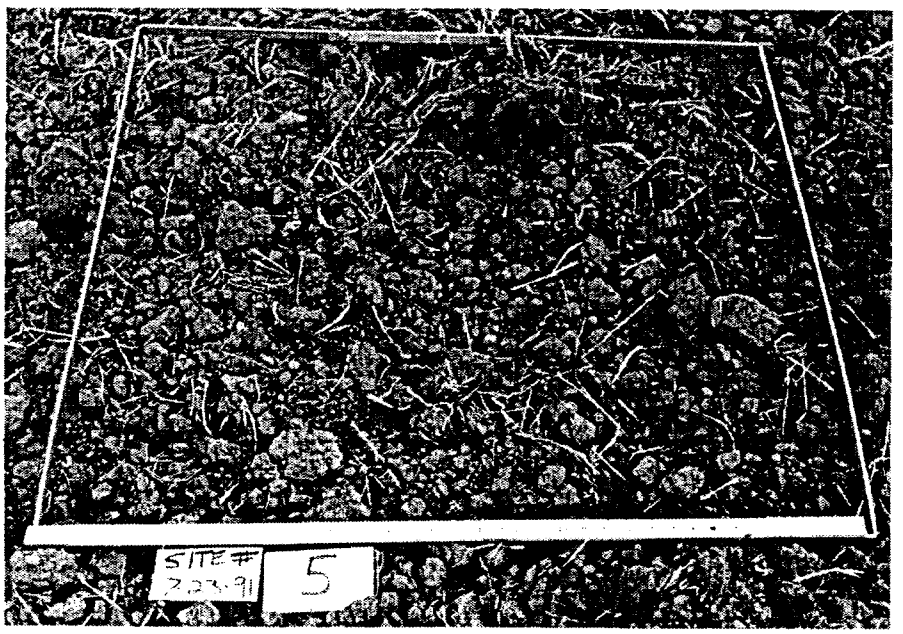

Figure C-5. Random roughenss, R_t, of 0.85 in, site 5

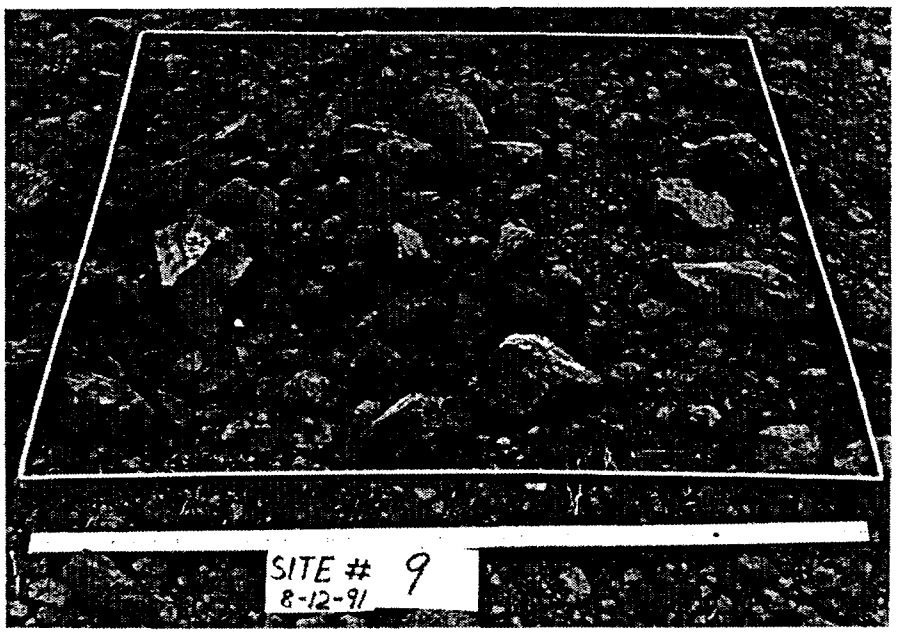

Figure C-6. Random roughness, R_t, of 1.05 in, site 9

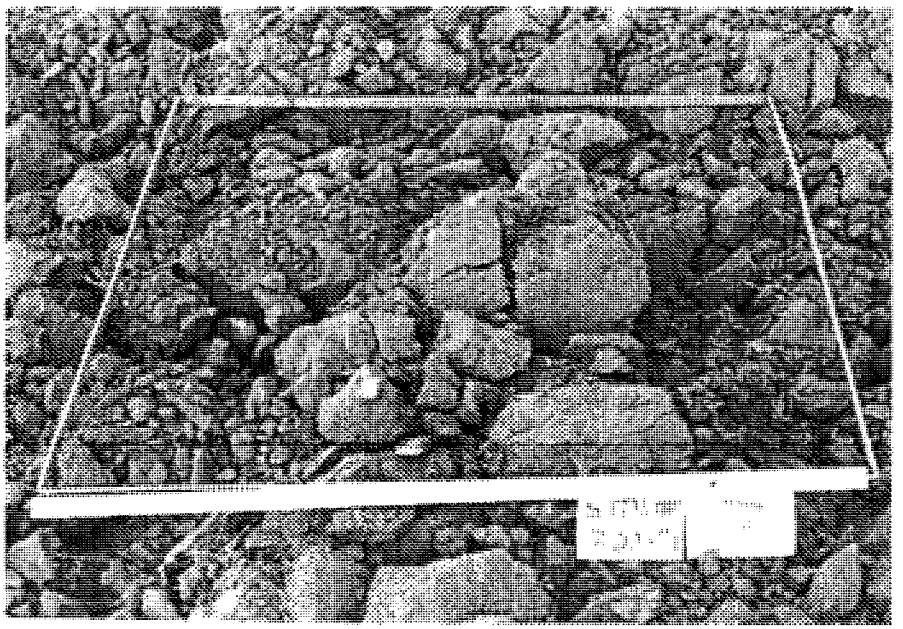

Figure C-7. Random roughness, R_t, of 1.60 in, site 7

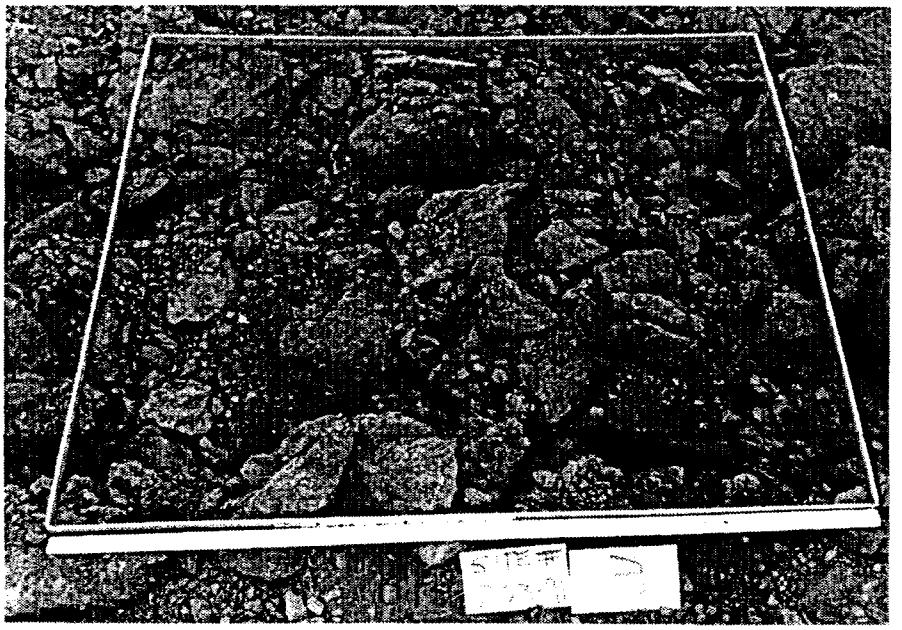

Figure C-8. Random roughness, R_t, of 1.70 in, site 3

Figure C-9. Random roughness, R_t, of 2.15 in, site 4

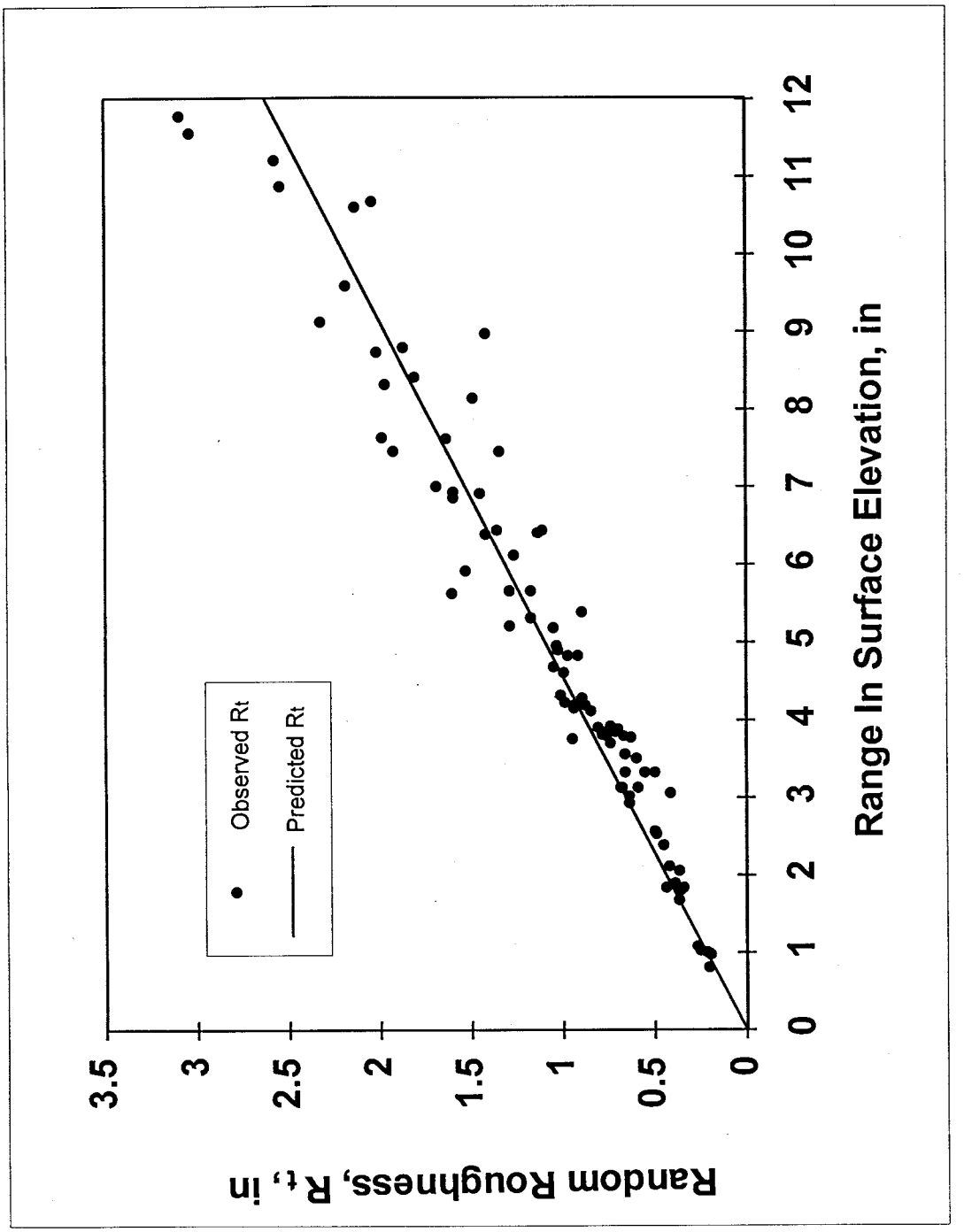

Figure C-10. Random roughness, R_t, versus range in surface elevation along a 6-ft transect

APPENDIX D. PARAMETER VALUES FOR MAJOR AGRICULTURAL CROPS AND TILLAGE OPERATIONS

The following information and data are to be used to prepare data files for crops and tillage operations used in application of RUSLE to cropland. Data presented for the crops and tillage operations represent "core" values that are to be used as starting points. Procedures are given that can be used to adjust the core values to represent conditions that differ from those described by the core data. Guidelines are also given on how to develop parameter values for crops and tillage operations not listed in the tables by extracting data from the literature or by comparing characteristics of the given crop or operation to crops and operations listed in the "core" data.

Data presented in the following tables were developed by the USDA Agricultural Research Service (ARS) and the Natural Resources Conservation Service (NRCS) for use by NRCS in its national implementation of RUSLE. The values and procedures are based on a review of data in the literature and on the judgment of numerous technical specialists in NRCS and the ARS RUSLE development team.

Use of these values and procedures can greatly help to ensure consistency in the application of RUSLE. If you get inconsistent results with RUSLE, first make checks using "core" values. Then carefully evaluate adjustments to the "core" values to ensure that reasonable adjustments have been made and that RUSLE is responding as expected to each adjustment.

Procedure for Adjusting Values for a "Core" Crop

If RUSLE is being applied to a crop included in the "core" data but the yield differs from the yield of the core crop, adjustments to the parameter values given for the core crop in table 5-1 or 5-2 are needed.

Residue:Yield Ratio

RUSLE has been designed to use a constant residue:yield ratio over the range of yields given in table D-1. If the yield of the given crop falls outside of the range given for the core crop, the residue:yield ratio can be varied with yield. In general, assumption of a constant residue:yield ratio for yields above the upper limit is acceptable. However, this ratio increases significantly as yield

decreases below the lower limit. If the residue:yield ratio is varied as a function of yield outside of the given range, the ratios should be chosen to match the constant ratio value at the upper and lower limits.

The residue:yield ratios given in table D-1 are based on commonly accepted, typical values for this ratio. However, this ratio can vary with crop variety, region, and other factors. A value for this ratio can be selected that differs from the "core" value given in table D-1, but the assumption of a constant value must be observed within the yield range given in table D-1.

Root Mass

Root biomass is adjusted using multiplication factors in table D-2 where root biomass is assumed to be linearly adjusted as a function of aboveground biomass. If yield is within the range where the residue:yield ratio is assumed to be constant, root biomass can be adjusted linearly with yield. One way to make the adjustment is to first determine the multiplication factor based on a ratio of the aboveground biomass. Each root biomass value for the core crop can be multiplied by this factor to determine values for the given crop.[3] The procedure is illustrated in table D-3.

Canopy

Canopy cover (percentage) is adjusted according to the square root (0.5 power) of the ratio of aboveground biomass for the given crop to that for the core crop. The multiplication factors are given in table D-2. If the resulting canopy value exceeds 100%, a value of 100% should be assigned to the canopy value. If the yield is within the range where a constant residue:yield is assumed, yield values can be used to form the ratio of biomass values to determine a multiplication factor. All canopy values of the core crop are multiplied by the adjustment factor to obtain the new set of canopy values. The procedure is illustrated in table D-3.

Effective Fall Height

Effective fall height is adjusted according to the 0.2 power of the ratio of aboveground biomass for the given crop to that for the core crop. The multiplication factors are given in table D-2. If the yield is within the range

[3]The following guide should be used in rounding numbers. Root biomass values are rounded to nearest 10 lb/acre per 4 in depth, canopy percentage to nearest 5 percent, and fall height to the nearest 0.1 ft.

where a constant residue:yield is assumed, yield values can be used to form the ratio of biomass values to determine a multiplication factor. All effective fall height values of the core crop are multiplied by the adjustment factor to obtain the new set of canopy values. The procedure is illustrated in table D-3.

Length of Growing Season and Dormancy

Adjustments may be needed for length of growing season for crops like corn and soybeans and length of the dormancy season for crops like winter wheat. The adjustment made for length of growing season is to add or subtract days from the period of full canopy before senescence begins. Length of the dormancy period is adjusted by adding or subtracting days to the dormancy period. In the southern part of the United States, reduced growth can continue throughout the dormancy period. The core data should be adjusted to account for this effect.

Crops Not Listed Among Core Crops

Situations will arise where RUSLE will be applied to crops not listed in the core data set. Several options are available for obtaining values for these crops. Key variables are amount of aboveground biomass, amount of root biomass at harvest, amount of canopy, and fall height at harvest.

Obtain Data From the Literature

The first option involves selecting published values in the literature. Try to find as much published data as possible. Variations among the sources can be large. The ratio of aboveground biomass to root biomass is not constant during the growing season. Select the root biomass value at maturity as the starting point. Choose values during the growing season that form an S-shaped curve similar to the data shown for the core crops. The same applies for canopy and effective fall height. Choose a residue:yield ratio value that can be assumed to be constant over the mid 50% yield range of the crop.

Obtain Data From NRCS

The second option is to contact the State Agronomist in an office of the Natural Resources Conservation Service (NRCS) of the USDA. Very likely NRCS has already developed a data set for a crop that can be used directly or that can be modified.

Compare Crop Characteristics to Characteristics of a Core Crop

The third alternative is to compare characteristics of the given crop to those of a similar core crop and adjust parameter values accordingly. For example, peanuts might be compared to soybeans.

Relation of Ground Cover Percent to Mass

In many cases, ground cover is the single most important factor affecting erosion. Therefore, the single most important crop variable is amount of residue at harvest and at planting time. Table D-4 lists values for the "core" crops for relating percent ground cover to mass.

Percent ground cover is not an accurate indicator of amount of biomass when percent cover exceeds 90%, as at harvest. The exponential shape of the curve that describes the relation of residue cover to residue mass is not sensitive to mass at high percent cover values. Mass can change greatly with little detectable change in cover above 90%, especially for covers greater than 95%. However, percent cover for values less than 75% is a reliable indicator of cover mass on the surface.

Even though percent cover is the single most important variable affecting erosion, loss of residue is on a mass basis. While cover is readily measured, mass of cover is not easily measured. Soil particles must be carefully washed from the residue, and leaves and stems must be carefully recovered. Also, the residue rapidly loses mass shortly after harvest, which is not reflected in a corresponding loss of cover.

If RUSLE is using the proper mass of residue at harvest but is giving a poor estimate of cover before spring tillage, two possibilities should be checked. One is that the decomposition parameter value used to compute loss of residue is in error; the other possibility is that the relationship of residue cover to residue mass is in error.

If the residue cover after planting is not correct but was correct before the first tillage operation at planting time, the most likely cause is that the value of residue left by the tillage operation is incorrect. If the residue after planting is correct but is not correct at the end of the growing season, the decomposition parameter value is incorrect.

Be Cautious

Because erosion is sensitive to cover, care should be taken to ensure that cover values are reasonable. However, when adjustments are needed, analyze

the reason for the problem and make adjustments carefully and methodically. Sometimes the problem is not as it appears.

Decomposition Parameter Values

Loss of residue over time is computed in RUSLE as a function of temperature and rainfall. Parameter values for decomposition are given in table D-5.

Data used in RUSLE to evaluate the adequacy of the decomposition parameter values should be field measurements of the loss of residue cover. Obviously, other factors such as soilborne organisms can affect residue loss. These effects are empirically captured in the decomposition parameter values. Thus, a decomposition parameter value should be based on field measurements and not laboratory decomposition tests.

The decomposition computations in RUSLE do not consider standing stubble separate from biomass on the soil. As a consequence, RUSLE may overestimate the loss of standing stubble. However, a decomposition parameter value can be applied to the biomass in the soil that is different from the parameter value for biomass on the soil.

RUSLE does not treat the plant components of leaves, stems, and roots separately. All components are assumed to be lost at the same rate. Furthermore, RUSLE does not vary the decomposition parameter value based on the state of decomposition to consider, for example, that decomposition may initially proceed more rapidly than in later stages.

Decomposition is related more closely to soil moisture than to the rainfall values used in RUSLE to compute loss of residue. Also, temperature varies within a day, and both temperature and rainfall vary from day to day. Monthly values in RUSLE are disaggregated into smoothed daily values for the RUSLE computations. The result is that decomposition parameter values for a given crop may need adjustment by climatic region. For example, a much larger decomposition parameter value is needed for wheat in the Northwestern Wheat and Range Region than in other parts of the United States.

Given these considerations and the limitations of the simple equations used in RUSLE to compute loss of biomass, decomposition parameter values are chosen to provide the best overall results.

Adjusting Parameter Values for Operations in the Core List

Table 5-5 contains parameter values for the core list of field implements used in many cropland operations. When an operation in the core list does not match the operation as applied in your situation, the following adjustments can be made.

Depth of Incorporation

For a given type of implement, a single value is used for depth of incorporation. For example, a value of 6 in is used for all chisel plows regardless of actual depth of tillage. Values for depth of incorporation are chosen based on information given in table D-6.

Roughness

A roughness value assigned to a tillage operation can be adjusted up or down one roughness step as shown in table D-7. For example, a moldboard plow has a roughness value of 1.9 in for its core value. It could be assigned a value of 2.3 for a clay soil that is very rough or a value of 1.5 for a sandy soil that is relatively smooth after plowing. The roughness index as used in RUSLE represents both the effects of depressional storage and the degree of pulverization.

Amount of Residue Left

Since surface cover has such a great effect on erosion, the value for the amount of residue left by an operation should be selected carefully. In general, values should be rounded to the nearest 10% or perhaps to the nearest 5%. Consideration should be given to whether the residue is fragile or nonfragile. Nonfragile residues are assumed in table 5-5. A very important consideration, especially if information is obtained from the literature, is whether or not residue mass or percent cover was used to indicate how much residue was left by the tillage operation.

Obtaining Parameter Values for Operations Not in the Core List

If a particular operation is not in the core list, values for the operation can often be obtained from the NRCS, which has developed values for an array of operations. This approach is preferred because the NRCS values have been tested and evaluated for consistency with other operations. The next best alternative is to choose values based on data in literature. The third and last desirable option is to compare characteristics of the particular operation against those of operations in the core list. If values are obtained from the literature or by comparison with operations in the core list, the following must be observed. The depth of incorporation is based on type of tillage operation as described in table D-6. The value of roughness that is assigned to a tillage operation is based on the tillage occurring in a medium-textured soil at a high level of management, meaning that large amounts of residue from a high yielding crop like corn has been routinely incorporated into the soil.

Table D-1. Residue:yield ratio and yield range over which to use a constant residue:yield ratio

Crop	Residue:yield ratio	Range[1]
Corn	1.0	50 to 150 bu(acre)$^{-1}$
Soybeans	1.5	15 to 45 bu(acre)$^{-1}$
Cotton	[2]4.5	300 to 1000 lbs(acre)$^{-1}$lint
Sorghum	1.0	40 to 90 bu(acre)$^{-1}$
Winter wheat	1.7	25 to 60 bu(acre)$^{-1}$
Spring wheat	1.3	25 to 60 bu(acre)$^{-1}$
Spring oats	2.0	30 to 80 bu(acre)$^{-1}$

[1]If yield is less than the minimum value in the range, the residue:yield ratio may need to be increased. If yield is greater than the maximum value in the range, the residue:yield ratio may need to be decreased.
[2]Value given is for shredding stalks in the fall. Use 3.0 for stalks shredded in the spring.

Table D-2. Multiplication factors to adjust RUSLE plant data from core data

Ratio of biomass at maturity of given crop to biomass of core crop	Multiplication factor for root biomass[1]	Multiplication factor for canopy percent[2]	Multiplication factor for fall height[3]
0.1	0.1	0.32	0.63
.2	.2	.45	.72
.3	.3	.55	.79
.4	.4	.63	.83
.5	.5	.71	.87
.6	.6	.77	.90
.7	.7	.84	.93
.8	.8	.89	.96
.9	.9	.95	.98
[4]1.0	1.0	1.00	1.00
1.1	1.1	1.05	1.02
1.2	1.2	1.10	1.04
1.3	1.3	1.14	1.05
1.4	1.4	1.18	1.07
1.5	1.5	1.22	1.08
1.6	1.6	1.26	1.10
1.7	1.7	1.30	1.11
1.8	1.8	1.34	1.12
1.9	1.9	1.38	1.14
2.0	2.0	1.41	1.15

[1]Adjustment factor for roots = (M_g / M_c), where M_g is aboveground biomass for given crop and M_c is aboveground biomass for core crop.
[2]Adjustment factor for canopy percenter = $(M_g / M_c)^{0.5}$
[3] Adjustment factor for fall height = $(M_g / M_c)^{0.2}$
[4]Represents core crop

Table D-3. Data adjustment examples for root biomass, percentage of canopy cover, and fall height[1].

	Root biomass percent adjustments		Canopy percent adjustments		Fall height adjustment in feet	
Days	Core crop	Given crop	Core crop	Given Crop	Core Crop	Given Crop
30	180	110	10	10	0.5	0.4
45	350	210	50	40	1.0	0.9
60	530	320	80	60	1.7	1.5
75	840	500	100	80	2.5	2.2
90	1060	640	100	80	3.0	2.7
150	1060	640	70	55	3.0	2.7

[1]The following example is used:

- Core crop is corn at 125 bu(acre)$^{-1}$
- Given crop is corn at 75 bu(acre)$^{-1}$. Ratio of biomass at maturity for given crop to that core crop = 0.6.

Table D-4. Percent cover to mass relationship for core crops.

	Mass (lbs(acre)$^{-1}$) at various percentages of residue cover		
Crop	30	60	90
Corn	950	2400	6050
Soybeans	600	1600	—
Cotton	1600	4150	—
Sorghum	1050	2700	6750
Winter wheat	600	1550	3850
Spring oats	600	1550	3850

Table D-5. Decomposition coefficient values

Crop	Coefficient
Alfalfa	0.020
Brome grass	.017
Corn	.016
Cotton	.015
Peanuts	.015
Small grain	[1].008
Small grain cover crop killed while in vegetative stage	.017
Sorghum	.016
Soybeans	.025
Sunflowers	.016
Tobacco	.015

[1] Use 0.017 for the Northwestern Wheat and Range Region.

Table D-6. Depth of incorporation according to type of tillage operation

Operation	Depth of incorporation (in)
Primary tillage operations that invert soil, such as moldboard plow	8
Primary tillage operations that do not invert soil, such as chisel plows and heavy plowing disks	6
Operations involving widely spaced shanks that inject significant amounts of biomass into the soil, such as manure injectors	6
Secondary tillage operations involving disks, such as tandem disk	4
Bedding and ridging operations, such as listers, hippers, and similar tools (cultivators used in ridge-till cropping are not included in this category)	4
Secondary tillage operations involving shank type tools that mix the soil significantly, such as field cultivators	3
Shank type operations using widely spaced shanks where minimal mixing occurs, such as subsoilers and anhydrous fertilizer knife-type applicators	2
Secondary tillage operations and other operations that disturb only a shallow upper layer or that leave crop residue in a shallow upper layer, such as harrows, planters, row cultivators, and tools where minimal mixing occurs	2

Table D-7. Adjustments to random roughness index in inches to represent smoother and rougher surfaces than represented by "core" value

Smoother surface	Core roughness value	Rougher surface
0	0.1	0.2
0.1	.2	.4
.2	.4	.8
.4	.8	1.2
.8	1.2	1.6
1.2	1.6	2.0
1.6	2.0	2.4
2.0	2.4	2.8

Procedure: Identify a "core" roughness value. If the site specific condition is significantly smoother than the core surface, use the roughness value from the "smoother surface" column, and conversely for a rougher surface.

APPENDIX E. CONTRIBUTORS AND AFFILIATIONS

J.M. Bradford, soil scientist
USDA-ARS, Plant Stress and Water Conservation Research
Route 3, Box 215
Lubbock, Texas
(formerly at USDA-ARS, National Soil Erosion Laboratory)

K.R. Cooley, research hydrologist
USDA-ARS, Northwest Watershed Research Center
800 Park Blvd., Plaza IV, Suite 105
Boise, Idaho

S.A. El-Swaify, professor and chairman
Department of Agronomy
University of Hawaii at Manoa
Honolulu, Hawaii

G.R. Foster, director
USDA-ARS, National Sedimentation Laboratory
P.O. Box 1157
Oxford, Mississippi
(formerly at Department of Agricultural Engineering,
University of Minnesota)

J.M. Gregory, associate professor
Agricultural Engineering Department
Texas Tech University
Lubbock, Texas

J.D. Istok, professor
Department of Civil Engineering
Oregon State University
Corvalis, Oregon

A.J. Ketchem, agricultural engineer
USDA-NRCS
San Luis Valley Water Quality Demonstration Project
723 First Avenue
Monte Vista, Colorado
(formerly at USDA-ARS, National Soil Erosion Research Laboratory)

J.M. Laflen, research leader and agricultural engineer
USDA-ARS, National Soil Erosion Research Laboratory
Purdue University
West Lafayette, Indiana

D.K. McCool, agricultural engineer
USDA-ARS, Land Management and Water Conservation Research Unit
Biological Systems Engineering Department
Washington State University
Pullman, Washington

L.D. Meyer, (retired) agricultural engineer
USDA-ARS, National Sedimentation Laboratory
P.O. Box 1157
Oxford, Mississippi

C.K. Mutchler, (retired) research agricultural engineer
USDA-ARS, National Sedimentation Laboratory
P.O. Box 1157
Oxford, Mississippi

J.W.A. Poesen, research scientist
Belgium National Fund for Scientific Research
Laboratory of Experimental Geomorphology
University of Leuven
Leuven, Belgium

J.P. Porter, agricultural engineer
USDA-NRCS, Flint Area Office
G-4312 S. Dort Hwy., Suite B
Burton, Michigan
(formerly at USDA-ARS, National Soil Erosion Research Laboratory)

K.G. Renard, (retired) research hydraulic engineer
USDA-ARS, Southwest Watershed Research Center
2000 East Allen Road
Tucson, Arizona

M.J.M. Römkens, soil physicist/agricultural engineer
USDA-ARS National Sedimentation Laboratory
P.O. Box 1157
Oxford, Mississippi

J.M. Sheridan, research hydraulic engineer
USDA-ARS, Southeast Watershed Research Laboratory
P.O. Box 946
Tifton, Georgia

J.R. Simanton, hydrologist
USDA-ARS, Southwest Watershed Research Center
2000 East Allen Road
Tucson, Arizona

G.A. Weesies, agronomist
USDA-NRCS, National Soil Erosion Research Laboratory
Purdue University
West Lafayette, Indiana

D.A. Whittemore, software engineer
USDA-ARS, National Soil Erosion Research Laboratory
Purdue University
West Lafayette, Indiana

D.C. Yoder, agricultural engineer and assistant professor
Department of Agricultural Engineering
University of Tennessee
Knoxville, Tennessee
(formerly with USDA-ARS, National Soil Erosion Research Laboratory)

R.A. Young, (retired) agricultural engineer
USDA-ARS, North Central Soil Conservation Research Laboratory
North Iowa Avenue
Morris, Minnesota

APPENDIX F. REFERENCES

Alberts, E.E., M.A. Weltz, and F. Ghidey. 1989. Plant growth component, ch. 8. *In* L.J. Lane and M.A. Nearing, eds., USDA-Water Erosion Prediction Project: Hillslope Profile Model Documentation, pp. 8.1-8.38. NSERL Rep. No. 2, USDA-ARS Nat. Soil Eros. Res. Lab., West Lafayette, Indiana.

Allmaras, R.R., R.E. Burwell, W.E. Larson, et al. 1966. Total porosity and random roughness of the interrow zones influenced by tillage. U.S. Dep. Agric., Conserv. Res. Rep. 7.

American Society of Agricultural Engineers (ASAE). 1985. Erosion and soil productivity. Amer. Soc. Agric. Engr. Publ. No. 8-85.

Armstrong, C.L., and J.K. Mitchell. 1987. Transformation of rainfall by plant canopy. Trans. ASAE 30:688-696.

Armstrong, C.L., and J.K. Mitchell. 1988. Plant canopy characteristics and processes which affect transformation of rainfall properties. Trans. ASAE 31:1400-1409.

Ateshian, J.K.H. 1974. Estimation of rainfall erosion index. J. Irrig. Drain. Div., ASCE 100:293-307.

Austin, M.E. 1981. Land resource regions and major land resource areas of the United States. U.S. Dep. Agric., Agric. Handbook No. 296.

Barfield, B.J., R.I. Barnhisel, M.C. Hirschi, and I.D. Moore. 1988. Compaction effects on erosion of mine spoil and reconstructed topsoil. Trans. ASAE 31:447-452.

Barnett, A.P., and J.S. Rogers. 1966. Soil physical properties related to runoff and erosion from artificial rainfall. Trans. ASAE 9:123-125, 128.

Barnett, A.P., J.S. Rogers, J.H. Holladay, and A.E. Dooley. 1965. Soil erodibility factors for selected soils in Georgia and South Carolina. Trans. ASAE 8:393-395.

Bengtson, R.L., and G. Sabbage. 1988. USLE P-factors for subsurface drainage in a hot, humid climate. ASAE Paper 88-2122, Am. Soc. Agric. Eng., St. Joseph, Michigan.

Bennett, O.L., and B.D. Doss. 1960. Effect of soil moisture level on root distribution of cool-season forage species. Agron. J. 52:204-207.

Benoit, G.R. 1973. Effect of freeze-thaw cycles on aggregate stability and hydraulic conductivity of three soil aggregate sizes. Soil Sci. Soc. Am. Proc. 37:3-5.

Benoit, G.R., S. Mostaghimi, R.A. Young, and M.J. Lindstrom. 1986. Tillage-residue effects on snow cover, soil water, temperature, and frost. Trans. ASAE 29:473-479.

Blackburn, W.H., and C.M. Skau. 1974. Infiltration rates and sediment production of selected plant communities in Nevada. J. Range Manage. 27:476-480.

Borst, H.L., A.G. McCall, and F.G. Bell. 1945. Investigations in erosion control and the reclamation of eroded land at the Northwest Appalachian Conservation Experiment Station, Zanesville, Ohio, 1934-42. U.S. Dep. Agric. Tech. Bull. 888.

Box, J.E., Jr. 1981. The effects of surface slaty fragments on soil erosion by water. Soil Sci. Soc. Am. J. 45:111-116.

Box, J.E., Jr., and L.D. Meyer. 1984. Adjustment of the Universal Soil Loss Equation for cropland soils containing coarse fragments. *In* Erosion and Productivity of Soils Containing Rock Fragments, pp. 23-90. Spec. Publ. No. 13, Soil Sci. Soc. Am., Madison, Wisconsin.

Brakensiek, D.L., W.J. Rawls, and G.R. Stephenson. 1986. Determining the saturated hydraulic conductivity of a soil containing rock fragments. Soil Sci. Soc. Am. J. 50:834-835.

Branson, F.A., R.F. Miller, and I.S. McQueen. 1966. Contour furrowing, pitting, and ripping on rangelands of the Western United States. J. Range Manage. 19:182-190.

Brown, C.B. 1943. The control of reservoir silting. U.S. Dep. Agric. Misc. Publ. 521.

Brown, L.C., and G.R. Foster. 1987. Storm erosivity using idealized intensity distributions. Trans. ASAE 30:379-386.

Browning, F.M., R.A. Norton, A.G. McCall, and F.G. Bell. 1948. Investigation in erosion control and the reclamation of land at the Missouri Valley Loess Conservation Experiment Station, Clarinda, Iowa, 1931-42. U.S. Dep. Agric. Tech. Bull. 959.

Browning, G.M., C.L. Parish, and J.A. Glass. 1947. A method for determining the use and limitation of rotation and conservation practices in control of soil erosion in Iowa. Soil Sci. Soc. Am. Proc. 23:249-264.

Carter, C.E., J.D. Greer, H.J. Braud, and J.M. Floyd. 1974. Raindrop characteristics in South Central United States. Trans. ASAE 17:1033-1037.

Cogo, N.D., W.C. Moldenhauer, and G.R. Foster. 1984. Soil loss reduction from conservation tillage practices. Soil Sci. Soc. Am. J. 48:368-373.

Cook, H.L. 1936. The nature and controlling variables of the water erosion process. Soil Sci. Soc. Am. Proc. 1:60-64.

Cooley, K.R. 1980. Erosivity values for individual design storms. J. Irrig. Drain. Div., ASCE 106:135-145.

Cooley, K.R., C.L. Hanson, and C.W. Johnson. 1988. Precipitation erosivity index estimates in cold climates. Trans. ASAE 31:1445-1450.

Copley, T.L., L.A. Forrest, A.G. McCall, and F.G. Bell. 1944. Investigations in erosion control and the reclamation of eroded land of the Central Piedmont Conservation Experiment Station, Statesville, North Carolina, 1930-40. U.S. Dep. Agric. Tech. Bull. 873.

Daniel, H.A., H.M. Elwell, and M.B. Cox. 1943. Investigations in erosion control and reclamation of eroded land at the Red Plains Conservation Experiment Station, Guthrie, Oklahoma, 1930-40. U.S. Dep. Agric. Tech. Bull. 837.

Denison, R.F., and H.D. Perry. 1990. Seasonal growth rate patterns for orchardgrass and tall fescue on the Appalachian Plateau. Agron. J. 82:869-873.

Dickey, E.C., C.R. Fenster, J.M. Laflen, and R.H. Mickelson. 1983. Effects of tillage on soil erosion in a wheat-fallow rotation. Trans. ASAE 26:814-820.

Diseker, E.G., and R.E. Yoder. 1936. Sheet erosion studies on Cecil clay. Univ. Alabama Agric. Exp. Stn. Bull. 245.

Dissmeyer, G.E., and G.R. Foster. 1980. A guide for predicting sheet and rill erosion on forest land. U.S. Dep. Agric., Forest Serv. Tech. Publ. SA-TP-11.

Dissmeyer, G.E., and G.R. Foster. 1981. Estimating the cover-management factor (C) in the universal soil loss equation for forest conditions. J. Soil Water Conserv. 36:235-240.

Doss, B.D., D.A. Ashley, and O.L. Bennett. 1960. Effect of soil moisture regime on root distribution of warm season forage species. Agron. J. 52:569-572.

Dunn, A.J., and G.R. Mehuys. 1984. Relationship between gravel content of soils and saturated hydraulic conductivity in laboratory tests. *In* Erosion and Productivity of Soils Containing Rock Fragments, pp. 55-63. Spec. Publ. No. 13, Soil Sci. Soc. Am., Madison, Wisconsin.

El-Swaify, S.A., and E.W. Dangler. 1976. Erodibilities of selected tropical soils in relation to structural and hydrologic parameters. *In* Soil Erosion: Prediction and Control, pp. 105-114. Soil Conserv. Soc. Am., Ankeny, Iowa.

Finney, H.J. 1984. The effect of crop covers on rainfall characteristics and splash detachment. J. Agric. Eng. Res. 29:337-343.

Flanagan, D.C., G.R. Foster, W.H. Neibling, and J.P. Burt. 1989. Simplified equations for filter strip design. Trans. ASAE 32:2001-2007.

Follett, R.F., and B.A. Stewart, eds. 1985. Soil erosion and crop productivity. Am. Soc. Agron., Crop Sci. Soc. Am., and Soil Sci. Soc. Am., Madison, Wisconsin.

Formanek, G.E., D.K. McCool, and R.I. Papendick. 1984. Freeze-thaw and consolidation effects on strength of a wet silt loam. Trans. ASAE 27:1749-1752.

Formanek, G.E., E. Ross, and J. Istok. 1987. Subsurface drainage for erosion reduction on croplands of northwestern Oregon. *In* Irrigation Systems for the 21st Century, Proc. Irrig. Drain. Div. Spec. Conf., pp. 25-31. Am. Soc. Civil Eng., New York.

Foster, G.R. 1982. Modeling the erosion process, ch. 8. *In* C.T. Haan, H.D. Johnson, and D.L. Brakensiek, eds., Hydrologic Modeling of Small Watersheds. ASAE Monogr. No. 5., Am. Soc. Agric. Eng., St. Joseph, Michigan.

Foster, G.R., and V.A. Ferreira. 1981. Deposition in uniform grade terrace channels. *In* Crop Production With Conservation in the 80's, pp. 185-197. Am. Soc. Agric. Eng., St. Joseph, Michigan.

Foster, G.R., and R.E. Highfill. 1983. Effect of terraces on soil loss: USLE P-factor values for terraces. J. Soil Water Conserv. 38:48-51.

Foster, G.R., C.B. Johnson, and W.C. Moldenhauer. 1982. Hydraulic failure of unanchored cornstalk and wheat straw mulches for erosion control. Trans. ASAE 25:940-947.

Foster, G.R., and L.J. Lane. 1987. User requirements USDA-Water Erosion Prediction Project (WEPP). U.S. Dep. Agric., Agric. Res. Serv. NSERL Rep. No. 1, West Lafayette, Indiana.

Foster, G.R., L.J. Lane, M.A. Nearing, et al. 1989. Erosion component, ch. 10. *In* USDA-Water Erosion Prediction Project: Hillslope Profile Model Documentation, pp. 10.1-10.12. NSERL Rep. No. 2, U.S. Dep. Agric., Agric. Res. Serv., Nat. Soil Eros. Res. Lab., West Lafayette, Indiana.

Foster, G.R., L.J. Lane, and J.D. Nowlin. 1980a. A model to estimate sediment yield from field sized areas: Selection of parameter values. *In* CREAMS--A Field Scale Model for Chemicals, Runoff, and Erosion From Agricultural Management Systems: Volume 2, User Manual, pp. 193-281. U.S. Dep. Agric. Conserv. Res. Rep. 26.

Foster, G.R., L.J. Lane, J.D. Nowlin, et al. 1980b. A model to estimate sediment yield from field sized areas: Development of model. *In* CREAMS--A Field Scale Model for Chemicals, Runoff, and Erosion From Agricultural Management Systems: Volume 1, Model Documentation, pp. 36-64. U.S. Dep. Agric. Conserv. Res. Rep. 26.

Foster, G.R., L.J. Lane, J.D. Nowlin, et al. 1981a. Estimating erosion and sediment yield on field sized areas. Trans. ASAE 24:1253-1262.

Foster, G.R., D.K. McCool, K.G. Renard, and W.C. Moldenhauer. 1981b. Conversion of the universal soil loss equation to SI metric units. J. Soil Water Conserv. 36:355-359.

Foster, G.R., and L.D. Meyer. 1975. Mathematical simulation of upland erosion by fundamental erosion mechanics. *In* Present and Prospective Technology for Predicting Sediment Yields and Sources, pp. 190-204. U.S. Dep. Agric. ARS-S-40.

Foster, G.R., L.D. Meyer, and C.A. Onstad. 1977. A runoff erosivity factor and variable slope length exponents for soil loss estimates. Trans. ASAE 20:683-687.

Foster, G.R., and W.H. Wischmeier. 1974. Evaluating irregular slopes for soil loss prediction. Trans. ASAE 17:305-309.

Frazier, B.E., D.K. McCool, and C.F. Engle. 1983. Soil erosion in the Palouse: An aerial perspective. J. Soil Water Conserv. 38: 70-74.

Ghidey, F., J.M. Gregory, T.R. McCarty, and E.E. Alberts. 1985. Residue decay evaluation and prediction. Trans. ASAE 28:102-105.

Gifford, G.F., and C.M. Skau. 1967. Influence of various rangeland cultural treatments on runoff and sediment production from the big sage type, Eastgate Basin, Nevada. *In* Proc. 3d Am. Water Resources Conf., pp. 137-148. Am. Water Resour. Assoc.

Gregory, J.M. 1982. Soil cover prediction with various amounts and types of crop residue. Trans. ASAE 25:1333-1337.

Gregory, J.M., T.R. McCarty, F. Ghidey, and E.E. Alberts. 1985. Derivation and evaluation of a residue decay equation. Trans. ASAE 28:98-101, 105.

Gunn, R., and G.D. Kinzer. 1949. Terminal velocity of fall for water droplets in stagnant air. J. Meteorol. 6:243-248.

Haynes, J.L. 1940. Ground rainfall under vegetative canopy of crops. J. Am. Soc. Agron. 32:176-184.

Hays, O.E., and O.J. Attoe. 1957. Control of runoff and erosion on Almena silt loam in Wisconsin. U.S. Dep. Agric., Agric. Res. Serv. ARS 41-16.

Hays, O.E., A.G. McCall, and F.G. Bell. 1949. Investigations in erosion control and the reclamation of eroded land at the Upper Mississippi Valley Conservation Experiment Station near La Crosse, Wisconsin, 1933-43. U.S. Dep. Agric. Tech. Bull. 973.

Hickey, W.C., Jr., and E.J. Dortignac. 1963. An evaluation of soil ripping and soil pitting on runoff and erosion in the semiarid Southwest. *In* Int. Assoc. Sci. Hydrol. Publ. 65, pp. 22-33.

Hill, H.O., W.J. Peevy, A.G. McCall, and F.G. Bell. 1944. Investigations in erosion control and reclamation of eroded land at the Blackland Conservation Experiment Station, Temple, Texas, 1931-41. U.S. Dep. Agric. Tech. Bull. 859.

Holt, E.C., and F.L. Fisher. 1960. Root development of coastal bermudagrass with high fertilization. Agron. J. 52:593-595.

Hood, G.W., and R.P. Bartholomew. 1956. Soil and water conservation studies in the Ozark Highlands of Arkansas. Agric. Exp. Stn., Univ. Arkansas Bull. 563.

Horner, G.M., A.G. McCall, and F.G. Bell. 1944. Investigations in erosion control and the reclamation of eroded land at the Palouse Conservation Experiment Station, Pullman, Washington, 1931-42. U.S. Dep. Agric., Soil Conserv. Serv. Tech. Bull. No. 860.

Hosoyamada, K. 1986. The effects of rainfall and soil properties on farmland conservation. Irrig. Eng. and Rural Planning Jpn. Soc. Irrig., Drainage, and Reclamation Eng. 9:5-14.

Jacobson, P. 1981. Terrace planning for runoff control for deep Loess soil. Trans. ASAE 24:699-704.

Jamison, V.C., D.D. Smith, and J.F. Thornton. 1968. Soil and water research on a claypan soil. U.S. Dep. Agric. Tech. Bull. 1379.

Jasa, P.J., E.C. Dickey, and D.P. Shelton. 1986. Soil erosion from tillage and planting systems used in soybean residue: Part 2. Influences of row direction. Trans. ASAE 29:761-766.

Jennings, G.D., and A.R. Jarrett. 1985. Laboratory evaluation of mulches in reducing erosion. Trans. ASAE 28:1466-1470.

Johnson, L.C. 1987. Soil loss tolerance: Fact or myth? J. Soil and Water Conserv. 42:155-160.

Kinnell, P.I.A. 1981. Rainfall-kinetic energy relationships for soil loss prediction. Soil Sci. Soc. Am. J. 45:153-155.

Kinnell, P.I.A. 1987. Rainfall kinetic energy in eastern Australia. Intensity-kinetic energy relationships for Canberra, A.C.T. Aust. J. Soil Res. 25:547-553.

Kirby, P.C., and G.R. Mehuys. 1987. Seasonal variation of soil erodibilities in southwestern Quebec. J. Soil Water Conserv. 42:211-215.

Knisel, W.G., ed. 1980. CREAMS: A field scale model for chemicals, runoff, and erosion from agricultural management systems. U.S. Dep. Agric., Conserv. Res. Rep. No. 26.

Knoblauch, H.C., and J.L. Haynes. 1940. The effect of contour cultivation on runoff. Trans. AGU 21:499-504.

Kok, H., and D.K. McCool. 1990. Quantifying freeze/thaw-induced variability of soil strength. Trans. ASAE 33:501-506.

Kramer, J., and J.E. Weaver. 1936. Relative efficiency of roots and tops of plants in protecting the soil from erosion. Bull. No. 12, Conserv. Dep., Conserv. Survey Div., Univ. Nebraska.

Laflen, J.M. 1983. Tillage and residue effect on erosion from cropland. *In* D.A. DeCoursey, ed., Natural Resources Modeling Symposium, pp. 438-441. U.S. Dep. Agric., Agric. Res. Serv., Pingree Park, Colorado.

Laflen, J.M., and T.S. Colvin. 1981. Effect of crop residues on soil loss from continuous row cropping. Trans. ASAE 24:605-609.

Laflen, J.M., G.R. Foster, and C.A. Onstad. 1985. Simulation of individual-storm soil loss for modeling the impact of soil erosion on crop productivity. *In* S.A. El-Swaify, W.C. Moldenhauer, and A. Lo, eds., Soil Erosion and Conservation, pp. 285-295. Soil Conserv. Soc. Am., Ankeny, Iowa.

Laflen, J.M., H.P. Johnson, and R.C. Reeve. 1972. Soil loss from tile outlet terraces. J. Soil Water Conserv. 27:74-77.

Laflen, J.M., W.C. Moldenhauer, and T.S. Colvin. 1980. Conservation tillage and soil erosion on continuously row-cropped land. *In* Crop Production With Conservation in the 80's, pp. 121-133. Am. Soc. Agric. Eng., St. Joseph, Michigan.

Lamb, J., Jr., J.S. Andrews, and A.F. Gustafson. 1944. Experiment in the control of soil erosion in southern New York. Cornell Univ. Exp. Stn. Bull. 811, Ithaca, New York.

Lamba, P.S., H.L. Algren, and R.J. Muckenhirn. 1949. Root growth of alfalfa, medium red clover, bromegrass, and timothy under various soil conditions. Agron. J. 41:451-458.

Lane, L.J., ed. 1986. Erosion on rangelands: Emerging technology and data base. *In* Proc. Rainfall Simulator Workshop. Soc. Range Manage., Denver, Colorado.

Lane, L.J., and M.A. Nearing, eds. 1989. USDA-Water Erosion Prediction Project: Hillslope Profile Version. NSERL Rep. No. 2, U.S. Dep. Agric., Agric. Res. Serv., West Lafayette, Indiana.

Larson, W.E., R.F. Holt, and C.W. Carlson. 1978. Residue for soil conservation, ch. 1. *In* W.R. Oschwald, M. Stelly, D.M. Kral, and J.H. Nauseef, eds., Crop Residue Management Systems, pp. 1-15. ASA Spec. Publ. No. 31, Am. Soc. Agron., Crop Sci. Soc. Am., and Soil Sci. Soc. Am., Madison, Wisconsin.

Laws, O.J., and D.A. Parsons. 1943. The relation of raindrop-size to intensity. Trans. AGU 24:452-460.

Lloyd, C.H., and G.W. Eley. 1952. Graphical solution of probable soil loss formula for Northeastern Region. J. Soil and Water Conserv. 7:189-191.

Lombardi, F. 1979. Universal soil loss equation (USLE), runoff erosivity factors, slope length exponent, and slope steepness exponent for individual storms. Purdue Univ. Dissertation.

MacDonald, H.A. 1946. Birdsfoot trefoil (*Lotus corniculatus* L.): Its characteristics and potentialities as a forage legume. Cornell Univ. Agric. Exp. Stn. Memoir 261.

Mannering, J.V. 1967. The relationships of some physical and chemical properties of soils to surface sealing. Purdue Univ. Dissertation.

McCool, D.K., L.C. Brown, G.R. Foster, et al. 1987. Revised slope steepness factor for the Universal Soil Loss Equation. Trans. ASAE 30:1387-1396.

McCool, D.K., M.G. Dossett, and S.J. Yecha. 1981. A portable rill meter for measuring field soil loss. *In* Erosion and Sediment Transport Measurement, Proc. Florence Symp., pp. 479-484. Int. Assoc. Hydrol. Sci. Publ. No. 133.

McCool, D.K., G.R. Foster, C.K. Mutchler, and L.D. Meyer. 1989. Revised slope length factor for the Universal Soil Loss Equation. Trans. ASAE 32:1571-1576.

McCool, D.K., G.E. George, M. Freckleton, C.L. Douglas, Jr., and R.I. Papendick 1993. Topographic effect of erosion from cropland in the Northwestern Wheat Region. Trans. ASAE 36:771-775.

McGregor, K.C., J.D. Greer, G.E. Gurley, and G.C. Bolton. 1969. Runoff and sediment production from north Mississippi Loessial soils. Mississippi Agric. Exp. Stn., Mississippi State College, Bull. 777.

McGregor, K.C., and C.K. Mutchler. 1977. Status of the R factor in northern Mississippi. *In* Soil Erosion: Prediction and Control, pp. 135-142. Spec. Publ. No. 21, Soil Conserv. Soc. Am., Ankeny, Iowa.

McIsaac, G.F., J.K. Mitchell, and M.C. Hirschi. 1987a. Slope steepness effects on soil loss from disturbed lands. Trans. ASAE 30:1005-1013.

McIsaac, G.F., J.K. Mitchell, J.C. Siemens, and J.W. Hummel. 1987b. Row cultivation effects on runoff, soil loss and corn yield. Trans. ASAE 30:125-128, 136.

Meyer, L.D. 1984. Evolution of the universal soil loss equation. J. Soil and Water Conserv. 39:99-104.

Meyer, L.D., and C. Harmon. 1985. Sediment losses from cropland furrows of different gradients. Trans. ASAE 28:448-453, 461.

Meyer, L.D., C.B. Johnson, and G.R. Foster. 1972. Stone and woodchip mulches for erosion control on construction sites. J. Soil Water Conserv. 27:264-269.

Meyer, L.D., and W.C. Moldenhauer. 1985. Soil erosion by water: The research experience. Agric. Hist. 59:192-204.

Miller, F.T., and R.L. Guthrie. 1984. Classification and distribution of soils containing rock fragments in the United States. *In* Erosion and Productivity of Soils Containing Rock Fragments, pp. 1-12. Spec. Publ. No. 13, Soil Sci. Soc. Am., Madison, Wisconsin.

Miller, J.F., R.H. Frederick, and R.J. Tracey. 1973. Precipitation-frequency atlas of the Western United States, vol. 1-9, NOAA Atlas 2. U.S. Dep. Commerce, Nat. Oceanic Atmos. Admin., Silver Spring, Maryland.

Moldenhauer, W.C., and W.H. Wischmeier. 1960. Soil and water losses and infiltration rates on Ida silt loam as influenced by cropping systems, tillage practices and rainfall characteristics. Soil Sci. Soc. Am. J. 24:409-413.

Mostaghimi, S., R.A. Young, A.R. Wilts, and A.L. Kenimer. 1988. Effects of frost action on soil aggregate stability. Trans. ASAE 32:435-439.

Musgrave, G.W. 1947. The quantitative evaluation of factors in water erosion: A first approximation. J. Soil Water Conserv. 2:133-138.

Musgrave, G.W., and R.A. Norton. 1937. Soil and water conservation investigations at the Soil Conservation Experiment Station Missouri Valley Loess Region, Clarinda, Iowa, Progress Report, 1931-35. U.S. Dep. Agric. Tech. Bull. 558.

Mutchler, C.K. 1970. Splash of a waterdrop at terminal velocity. Science 169:1311-1312.

Mutchler, C.K., R.E. Burwell, and L.C. Staples. 1976. Runoff and soil losses from Barnes soils in the Northwestern Corn Belt. U.S. Dep. Agric., Agric. Res. Serv. ARS NC-36.

Mutchler, C.K., and C.E. Carter. 1983. Soil erodibility variation during the year. Trans. ASAE 26:1102-1104, 1108.

Mutchler, C.K., and C.E. Murphree, Jr. 1985. Experimentally derived modification of the USLE. *In* S.A. El-Swaify, W.C. Moldenhauer, and A. Lo, eds., Soil Erosion and Conservation, pp. 523-527. Soil Conserv. Soc. Am., Ankeny, Iowa.

Mutchler, C.K., C.E. Murphree, and K.C. McGregor. 1982. Subfactor method for computing C-factors for continuous cotton. Trans. ASAE 25:327-332.

National Research Council. 1975. Agricultural production efficiency. Commission on Natural Resources, Nat. Acad. Sci., Washington, DC.

Neibling, W.H., and E.E. Alberts. 1979. Composition and yield of soil particles transported through sod strips. ASAE Paper 79-2065, Am. Soc. Agric. Eng., St. Joseph, Michigan.

Nichols, M.L., and H.D. Sexton. 1932. A method of studying soil erosion. Agric. Eng. 13:101-103.

Olson, T.C., and W.H. Wischmeier. 1963. Soil erodibility evaluations for soils on the runoff and erosion stations. Soil Sci. Soc. Am. Proc. 27:590-592.

Onstad, C.A., M.C. Wolfe, C.L. Larson, and D.C. Slack. 1984. Tilled soil subsidence during repeated wetting. Trans. ASAE 27:733-736.

Pall, R., W.T. Dickenson, D. Green, and R. McGirr. 1982. Impact of soil characteristics on soil erodibility. *In* Recent Developments in the Explanation and Prediction of Erosion and Sediment Yield. Int. Assoc. Hydraul. Sci. Publ. 137.

Pavlychenko. 1942. From A. Troughton, 1957. The underground organs of herbage grasses. Bull. No. 44, Commonwealth Bureau of Pasture and Field Crops, Aberystwyth, Wales.

Pope, J.B., J.C. Archer, P.R. Johnson, et al. 1946. Investigation in erosion control and reclamation of eroded sandy clay lands of Texas, Arkansas, and Louisiana at the Conservation Experiment Station, Tyler, Texas, 1931-40. U.S. Dep. Agric. Tech. Bull. 916.

Quinn, M.W., and J.M. Laflen. 1983. Characteristics of raindrop throughfall under corn canopy. Trans. ASAE 26:1445-1450.

Rawls, W.J., D.L. Brakensiek, and K.E. Saxton. 1982. Estimation of soil water properties. Trans. ASAE 25:1316-1320.

Renard, K.G., and G.R. Foster. 1983. Soil conservation: Principles of erosion by water. *In* H.E. Dregne and W.O. Willis, eds., Dryland Agriculture, pp. 155-176. Agronomy Monogr. 23, Am. Soc. Agron., Crop Sci. Soc. Am., and Soil Sci. Soc. Am., Madison, Wisconsin.

Renard, K.G., and J.R. Simanton. 1975. Thunderstorm precipitation effects on the rainfall-erosion index of the universal soil loss equation. Hydrology and Water Resources in Arizona and the Southwest, No. 5, pp. 47-55. Office of Arid Land Studies, Univ. Arizona, Tucson.

Römkens, M.J.M. 1985. The soil erodibility factor: A perspective. *In* S.A. El-Swaify, W.C. Moldenhauer, and A. Lo, eds., Soil Erosion and Conservation, pp. 445-461. Soil Water Conserv. Soc. Am., Ankeny, Iowa.

Römkens, M.J.M., D.W. Nelson, and C.B. Roth. 1975. Soil erosion on selected high clay subsoils. J. Soil and Water Conserv. 30:173-176.

Römkens, M.J.M., S.N. Prasad, and J.W.A. Poesen. 1986. Soil erodibility and properties. *In* Proc. 13th Congr. Int. Soil Sci. Soc., Vol. 5, pp. 492-504. Hamburg, Germany.

Römkens, M.J.M., C.B. Roth, and D.W. Nelson. 1977. Erodibility of selected clay subsoils in relation to physical and chemical properties. Soil Sci. Soc. Am. J. 41:954-960.

Römkens, M.J.M., and J.Y. Wang. 1986. Effect of tillage on surface roughness. Trans. ASAE 29:429-433.

Roth, C.B., A.W. Nelson, and M.J.M. Römkens. 1974. Prediction of subsoil erodibility using chemical, mineralogical and physical parameters. U.S. Environ. Protection Agency EPA-660/2-74-043, Washington, DC.

Rosewell, C.J. 1983. Characteristics of high intensity rainfall. Univ. New England, Armidale, Australia. Master's thesis.

Rosewell, C.J. 1986. Rainfall kinetic energy in Eastern Australia. J. Climate Applied Meteorol. 25:1695-1701.

Schertz, D.L. 1983. The basis for soil loss tolerances. J. Soil and Water Conserv. 38:10-14.

Schmidt, B.L., R.R. Allmaras, J.V. Mannering, and R.I. Papendick, eds. 1982. Determinants of soil loss tolerance. Am. Soc. Agron. Spec. Publ. No. 45, Madison, Wisconsin.

Shirazi, M.A., and L. Boersma. 1984. A unifying quantitative analysis of soil texture. Soil Sci. Soc. Am. J. 48:142-147.

Sillanpaa, N., and L.R. Webber. 1961. Effect of freezing-thawing and wetting-drying cycles on soil aggregates. Can. J. Soil Sci. 41:82-87.

Simanton, J.R., C.W. Johnson, and J.W. Nyhan. 1986. Rainfall simulation on rangeland erosion plots. *In* L.J. Lane, ed., Proc. Rainfall Simulator Workshop, pp. 11-17. Soc. Range Manage., Denver.

Simanton, J.R., H.B. Osborn, and K.G. Renard. 1977. Effects of brush-to-grass conversion on the hydrology and erosion of a semiarid Southwestern rangeland watershed. Hydrol. Water Resources Assoc., AZ Section--AZ Acad. Sci., Hydrol. Sect. 7:249-256.

Simanton, J.R., E. Rawitz, and E.D. Shirley. 1984. The effects of rock fragments on erosion of semiarid rangeland soils, ch. 7. *In* Erosion and Productivity of Soils Containing Rock Fragments, pp. 65-72. SSSA Spec. Publ. 13, Soil Sci. Soc. Am., Madison, Wisconsin.

Simanton, J.R., and K.G. Renard. 1982. The USLE rainfall factor for Southwestern U.S. Rangelands. *In* Proceedings of Workshop on Estimating Erosion and Sediment Yield on Rangelands, pp. 50-62. U.S. Dep. Agric., Agric. Res. Serv., Agric. Rev. and Man. ARM-W-26.

Skaggs, R.W., A. Nassehzadeh-Tabrizi, and G.R. Foster. 1982. Subsurface drainage effects on erosion. J. Soil and Water Conserv. 37:167-172.

Smith, D.D. 1941. Interpretation of soil conservation data for field use. Agric. Eng. 22:173-175.

Smith, D.D., and D.M. Whitt. 1947. Estimating soil losses from field areas of claypan soil. Soil Sci. Soc. Am. 12:485-490.

Smith, D.D., and D.M. Whitt. 1948. Evaluating soil losses from field areas. Agric. Eng. 29:394-398.

Smith, D.D., D.M. Whitt, A.W. Zingg, et al. 1945. Investigations in erosion control and reclamation of eroded Shelby and related soils at the Conservation Experiment Station, Bethany, Missouri, 1932-42. U.S. Dep. Agric. Tech. Bull. 883.

Smith, D.D., and W.H. Wischmeier. 1962. Rainfall erosion. Adv. Agron. 14:109-148.

Stewart, B.A., W.H. Wischmeier, D.A. Woolhiser, et al. 1975. Control of water pollution from cropland: Vol. 1, A manual for guideline development; Vol. 2, An overview. U.S. Dep. Agric., ARS-H-5-1 and ARS-H-5-2.

Stott, D.E. 1991. RESMAN: A tool for soil conservation education. J. Soil and Water Conserv. 46:332-333.

Stott, D.E., H.F. Stroo, L.F. Elliott, et al. 1990. Wheat residue loss in fields under no-till management. Soil Sci. Soc. Am. J. 54:92-98.

Sumner, M.E., and B.A. Stewart, eds. 1992. Soil crusting: Chemical and physical processes. Lewis Publishers, Boca Raton, Florida.

Thomas, H., and A.M. Grano. 1971. Agricultural land and water resource base and productivity, Pacific Northwest. U.S. Dep. Agric., Econ. Res. Serv., Nat. Res. Econ. Div., Corvallis, Oregon.

Tracy, F.C., K.G. Renard, and M.M. Fogel. 1984. Rainfall energy characteristics for southeastern Arizona. *In* J.A. Replogle and K.G. Renard, eds., Water Today and Tomorrow, pp. 449-566. Proc. ASCE, Irrig. Drain. Div. Spec. Conf., Flagstaff, Arizona.

U.S. Department of Agriculture. 1951. Soil survey manual. Agric. Handb. No. 18.

U.S. Department of Agriculture. 1990. Agricultural statistics. U.S. Gov. Printing Office, Washington, DC.

U.S. Department of Agriculture, Agricultural Research Service. 1961. A universal equation for predicting rainfall-erosion losses. ARS Spec. Rep. 22-66.

U.S. Department of Agriculture, Soil Conservation Service. 1972. Nat. Eng. Handb., Sec. 4, Hydrology.

U.S. Department of Agriculture, Soil Conservation Service. 1983. National Soils Handb. No. 430.

U.S. Department of Agriculture, Soil Conservation Service. 1984. Users' guide for the CREAMS computer model, Washington Computer Center version. USDA-SCS Tech. Release 72.

U.S. Department of Agriculture, Soil Conservation Service. 1991. Agricultural Waste Management Field Handbook Part 651.

U.S. Department of Commerce, Environmental Science Services Administration. 1968. Climatic atlas of the United States. Environ. Data Serv., Washington, DC.

U.S. Weather Bureau. 1958. Rainfall intensity-frequency regime. Tech. Paper No. 29, 5 parts, Washington, DC.

Van Doren, C.A., and L.J. Bartelli. 1956. A method of forecasting soil losses. Agric. Eng. 37:335-341.

Van Doren, C.A., R.S. Stauffer, and E.H. Kidder. 1950. Effect of contour farming on soil loss and runoff. Soil Sci. Soc. Am. Proc. 15:413-417.

Van Klaveren, R.W. 1987. Hydraulic erosion resistance of thawing soil. Washington State Univ. Dissertation.

Van Liew, M.W., and K.E. Saxton. 1983. Slope steepness and incorporated residue effects on rill erosion. Trans. ASAE 26:1738-1743.

Wein, R.W., and N.E. West. 1973. Soil changes caused by erosion control treatment on a salt desert area. Soil Sci. Soc. Am. Proc. 37:98-103.

Weiss, L.L. 1964. Ratio of true to fixed-interval maximum rainfall. J. Hydraul. Div., ASCE 90(HY1):77-82.

Weltz, M.A., K.G. Renard, and J.R. Simanton. 1987. Revised universal soil loss equation for western rangelands, pp. 104-111. *In* US/Mexico Symposium on Strategies for Classification and Management of Native Vegetation for Food Production in Arid Zones. U.S. Forest Serv. Gen. Tech. Rep. RM-150.

Wilson, B.N., B.J. Barfield, and R.C. Warner. 1986. Simple models to evaluate non-point pollution sources and controls. *In* A. Giorgini and F. Zingales, eds., Agricultural Nonpoint Source Pollution: Model Selection and Application, pp. 231-263. Elsevier, New York.

Wischmeier, W.H. 1955. Punched cards record runoff and soil-loss data. Agric. Eng. 36:664-666.

Wischmeier, W.H. 1959. A rainfall erosion index for a universal soil loss equation. Soil Sci. Soc. Am. Proc. 23:246-249.

Wischmeier, W.H. 1962. Storms and soil conservation. J. Soil and Water Conserv. 17:55-59.

Wischmeier, W.H. 1972. Upslope erosion analysis. *In* Environmental Impact on Rivers, pp. 15-1 to 15-26. Water Resour. Publ., Ft. Collins, Colorado.

Wischmeier, W.H. 1974. New developments in estimating water erosion. *In* Proc. 29th Annu. Meet. Soil Sci. Soc. Am., pp. 179-186. Madison, Wisconsin.

Wischmeier, W.H. 1975. Estimating the soil loss equations cover and management factor for undisturbed lands. *In* Present and Prospective Technology for Predicting Sediment Yields and Sources, pp. 118-125. U.S. Dep. Agric., Agric. Res. Serv., ARS-S-40.

Wischmeier, W.H. 1976. Use and misuse of the universal soil loss equation. J. Soil and Water Conserv. 31:5-9.

Wischmeier, W.H., and J.V. Mannering. 1969. Relation of soil properties to its erodibility. Soil Sci. Soc. Am. Proc. 33:131-137.

Wischmeier, W.H., and D.D. Smith. 1958. Rainfall energy and its relationship to soil loss. Trans. AGU 39:285-291.

Wischmeier, W.H., and D.D. Smith. 1965. Predicting rainfall-erosion losses from cropland east of the Rocky Mountains: Guide for selection of practices for soil and water conservation. U.S. Dep. Agric., Agric. Handb. No. 282.

Wischmeier, W.H., and D.D. Smith. 1978. Predicting rainfall erosion losses: A guide to conservation planning. U.S. Dep. Agric., Agric. Handb. No. 537.

Wischmeier, W.H., C.B. Johnson, and B.V. Cross. 1971. A soil erodibility nomograph for farmland and construction sites. J. Soil and Water Conserv. 26:189-193.

Wischmeier, W.H., D.D. Smith, and Uhland, R.E. 1958. Evaluation of factors in the soil loss equation. Agric. Eng. 39:458-462, 474.

Young, R.A., and C.K. Mutchler. 1977. Erodibility of some Minnesota soils. J. Soil and Water Conserv. 32:180-182.

Young, R.A., C.K. Mutchler, and W.H. Wischmeier. 1964. Influence of row direction and type of vegetal cover on the soil-loss relationship. Trans. ASAE 7:316-317, 320.

Zanchi, C. 1983. Influenza dell'azione battente della pioggia e del ruscellamento nel processo erosivo e variazioni dell'erodibilitta del suolo nei diversi periodi stagionali. Annali Istituto Sperimentale Studio e Difesa Suolo 14:347-358. Florence, Italy (in Italian).

Zingg, A.W. 1940. Degree and length of land slope as it affects soil loss in runoff. Agric. Eng. 21:59-64.

Zobeck, T.M., and C.A. Onstad. 1987. Tillage and rainfall effects on random roughness: A review. Soil Tillage Res. 9:1-20.

Technical and Grammatical Problems in AH703

March 1, 2001

Don McCool

Page #	Problem
vii	B_{us} should be $lb \cdot acre^{-1} \cdot in^{-1}$
xv	T should be $ton \cdot acre^{-1} \cdot yr^{-1}$
22	It is implied that Req includes irrigation. This is incorrect.
28	"Maps------is"
33	The abbreviations "ww/p", etc need to be defined.
34, last par.	Change to "measurements of the ratio of rill to interrill soil loss".
89	Presenting K without units is extremely misleading. This implies that K is numerically the same regardless of the EI system used.
152	For equation 5-7, it should be indicated that temperatures must be in degrees C. The text presents values for T_o and A in degrees F, but using T_a in degrees F gives erroneous answers.
153	Equation 5-9 is incorrect. The minus sign should be before the brace "[" instead of before the "c_{ur}".

Assessment of erosion, sedimentation, and water quality impacts of the Mountain Valley Pipeline and Equitrans Expansion Project's proposed crossing of the Jefferson National Forest as it pertains to the U.S. Forest Service's Draft Supplemental Environmental Impact Statement dated December 2022

Prepared by Jonathan A. Czuba, Ph.D., Licensed Professional Engineer - February 9, 2023

REFERENCES
14

February 21, 2023

Revised Slope Steepness Factor for the Universal Soil Loss Equation

D. K. McCool, L. C. Brown, G. R. Foster, C. K. Mutchler, L. D. Meyer

MEMBER ASAE | ASSOC. MEMBER ASAE | MEMBER ASAE | MEMBER ASAE | FELLOW ASAE

ABSTRACT

A reanalysis of historical and recent data from both natural and simulated rainfall soil erosion plots has resulted in new slope steepness relationships for the Universal Soil Loss Equation. For long slopes on which both interrill and rill erosion occur, the relationships consist of two linear segments with a breakpoint at 9% slope. These relationships predict less erosion than current relationships on slopes steeper than 9% and slopes flatter than about 1%. A separate equation is proposed for the slope effect on short slopes where only interrill erosion is present. For conditions where surface flow over thaw-weakened soil dominates the erosion process, two relationships with a breakpoint at 9% slope are presented.

INTRODUCTION

The slope steepness factor S in the Universal Soil Loss Equation (USLE) (Wischmeier and Smith, 1978) expresses the effect of slope gradient on sheet and rill erosion. The equation published for S in Agriculture Handbook (AH) 537 (Wischmeier and Smith, 1978), the main guideline manual for the USLE is:

$$S = 65.4 \sin^2 \theta + 4.56 \sin \theta + 0.0654 \quad \ldots\ldots\ldots [1]$$

where: θ = angle of the slope. The factor S evaluated for a given steepness is the ratio of soil loss on the particular slope to that from a nine percent slope, when all other conditions are the same. Nine percent slope is the steepness of the USLE unit plot (Wischmeier and Smith, 1978), and equations for S are normalized to give a value of 1.0 at this steepness. This report covers our review and analysis of data on the effect of slope on sheet and rill erosion and presents revised relationships for the USLE slope factor S.

Article was submitted for publication in September, 1986; reviewed and approved for publication by the Soil and Water Div. of ASAE in June, 1987.

Contribution from USDA-ARS, Land Management and Water Conservation Research, Pullman, WA; National Soil Erosion Research Laboratory, W. Lafayette, IN; and USDA Sedimentation Laboratory, Oxford, MS in cooperation with College of Agriculture and Home Economics Research Center, Washington State University, Pullman, WA and Purdue Agricultural Experiment Station, W. Lafayette, IN.

Washington State University Scientific Paper No. 7563.

The authors are: D. K. MCCOOL, Agricultural Engineer, USDA-ARS, Washington State University, Pullman; L. C. BROWN, Graduate Research Assistant, Agricultural Engineering Dept., Purdue University, W. Lafayette, IN; G. R. FOSTER, Hydraulic Engineer, USDA-ARS, W. Lafayette, IN; C. K. MUTCHLER, Hydraulic Engineer, USDA-ARS, Oxford, MS and L. D. MEYER, Agricultural Engineer, USDA-ARS, Oxford, MS.

BACKGROUND

Zingg (1940) was one of the early researchers to relate erosion to slope steepness. He analyzed simulated rainfall data from Kansas (Duley and Hays, 1932) and Alabama (Diseker and Yoder, 1936), which indicated that soil loss varied with slope steepness to the 1.49 power, and from simulated rainfall plots at Bethany, MO, which indicated that soil loss varied with slope steepness to the 1.37 power. The plots at Bethany were 2.4 and 4.8 m long and 1.1 m wide on slope steepnesses of 4, 8, and 12%. For application, Zingg recommended:

$$S = (s/9)^{1.4} \quad \ldots\ldots\ldots [2]$$

where: s = slope steepness in percent. The 9 in the denominator of equation [2] normalizes Zingg's original equation to 9% steepness for consistency with the USLE unit plot concept.

The next slope factor equation in the series of soil loss equations that preceded the USLE was Smith and Whitt's (1947) equation which, when normalized to 9% steepness, can be written as:

$$S = 0.025 + 0.052\, s^{4/3} \quad \ldots\ldots\ldots [3]$$

Smith and Whitt derived their slope equation from Neal's (1938b) data from laboratory plots 3.7 m long by 1.1 m wide under simulated rainfall. Earlier, Neal (1938a,b) concluded from his data that soil loss from saturated soil varied with steepness to the 0.7 power.

The slope factor in the empirical equation developed by the Musgrave (1947) committee was:

$$S = (s/9)^{1.35} \quad \ldots\ldots\ldots [4]$$

Musgrave (1947) did not specifically identify the data used to derive equation [4], but evidently they came from studies reported by Borst et al., (1945); Browning et al.,(1948); Dickson et al., (1940); Diseker and Yoder, (1936); Duley and Hays, (1932); Lamb et al., (1944); Hays et al.,(1949); Hill et al., (1944); Knoblauch and Brill, (1940); Krusekopf, (1943); Lillard, (1941); Lillard et al., (1941); Neal, (1938a); Pope et al., (1946) and Smith et al., (1945).

Smith and Wischmeier (1957) reported a slope steepness function in their review of factors affecting sheet and rill erosion. When normalized to a 9% slope, their equation was:

$$S = 0.00650\, s^2 + 0.0453\, s + 0.0650 \quad \ldots\ldots\ldots [5]$$

which is identical to equation [1] except that percent slope, s, was used instead of sine of the slope angle. Equation [5] was derived primarily from data collected at

La Crosse, WI from natural rainfall plots on slopes of 3, 8, 13, and 18% (Hays et al., 1949). The plots were 11.1 and 22.1 m long by 4.3 m wide. Smith and Wischmeier (1957) used data from Zingg's rainfall simulator study at Bethany, MO and from studies on natural rainfall plots on two slope steepnesses at Dixon Springs, IL (Gard and Van Doren, 1949) and Zanesville, OH (Borst et al., 1945) to validate the slope effect relationship derived from the La Crosse data*. They also derived another slope effect equation from analysis of data from Blacksburg, VA where plots were 17.7 m long and 4.6 m wide on slope steepnesses of 5, 10, 15, 20, and 25% (Lillard et al., 1941)*. Smith and Wischmeier's equation for the Blacksburg data, when normalized to a 9% slope, was:

$$S = 0.044 + 0.10\,s - 0.00073\,s^2 \quad \ldots\ldots\ldots\ldots [6]$$

The effect of slope steepness on erosion is nearly linear in this equation. However, Smith and Wischmeier gave this relationship minor treatment in their 1957 article and in later major USLE publications (Wischmeier and Smith, 1965, 1978).

Agriculture Handbook 282 (Wischmeier and Smith, 1965), the first major, widely distributed, guideline manual for the USLE, used equation [5] for the S factor, while its revision, AH537 (Wischmeier and Smith, 1978), used equation [1]. The only change from 1965 to 1978 in the S factor was to change slope percent (actually tangent of the slope angle) to sine of the slope angle, which is consistent with the relationship for the shear force of surface flow on its boundary (Chow, 1959):

$$\tau = \gamma\, R \sin\theta \quad \ldots\ldots\ldots\ldots\ldots\ldots\ldots [7]$$

where: τ = shear stress of the flow on the boundary, γ = weight density of the runoff, and R = hydraulic radius. On slopes less than about 20%, values for sine and tangent of the slope angle are nearly equal, and therefore the change from tangent to sine had little impact on lower slopes. Above 20%, tangent of the slope angle increases rapidly and approaches infinity for a vertical slope whereas sine of the angle approaches one. The change from tangent to sine reduced S from about 19 to 15 for a 50% slope. For slopes of such steepness, no field data are available to test these values. However, flume tests at the Utah Water Research Laboratory (Israelsen et al., 1980) produced similar results at slopes of up to 84%.

Another major USLE slope factor equation is the one recommended for application of the USLE to steep slopes in the Pacific Northwest Wheat and Range Region (McCool et al., 1987):

$$S = (\sin\theta/0.0896)^{0.6} \quad \ldots\ldots\ldots\ldots\ldots [8]$$

This equation was derived from measured cross sections of rills on slopes ranging from 1.5 to 56%. Since most of the erosion was caused by surface flow over thawing soils that have a high silt content, little accuracy was lost by omitting estimates of interrill erosion.

*Smith and Wischmeier used data from these locations that were collected after the cited reports were published. Those data are on file at the USDA-National Soil Erosion Research Laboratory (NSERL).

ANALYSIS

General

Data on the effect of slope on erosion were assembled from reports on about 20 studies summarized in Table 1. Most of the data we used are available in the reports identified in the References and Data Sources Section except for data from a Mississippi study and the complete data sets from La Crosse, WI and Blacksburg, VA, which are on file at the USDA-National Soil Erosion Research Laboratory (NSERL). The data were analyzed to derive a revised slope factor equation for the USLE.

Even though the USLE estimates long term, average annual soil loss, it accounts for the seasonal variation in climate and cover. A specific procedure is used to derive a weighted value for the USLE's cover-management factor C to account for the average seasonal variation in climate's erosivity and cover, tillage, and other similar cropping-management effects (Wischmeier and Smith, 1978). However, no such weighting is used for the other USLE factors even though S and other factors vary with climate, season, crop, soil condition, and tillage direction and type (Lombardi, 1979). We were unable to develop equations for S to account for these variations, partly because the equation structure of the USLE is inconvenient for varying the S factor according to current theory based on erosion processes (Foster et al., 1977). Consequently, we chose relationships that, in our judgment, best described the entire data set and erosion theory in general. For purposes of clarity for the remainder of this report, the terms low slopes and steep slopes will designate slope steepnesses of relatively low, less than about 9%, and relatively high, greater than about 9%, gradients, respectively.

Steep Slopes

The largest and most complete single data set was from the natural rainfall plots at La Crosse, WI and covered 25 years from 1939 through 1963. Only the first 5 years of the data were reported by Hays et al. (1949); the remaining data are on file at the NSERL. Plot management for the first 5 years was continuous small grain, tilled up and down hill. During the remaining 20 years, the plots were cropped across slope on the contour, with a 3-year rotation of corn-small grain-hay. Year to year variation in soil loss was much less from the continuous small grain than it was from the rotation cropping.

Analysis of the complete La Crosse data set gave a slope effect equation that was almost identical to equation [1]. However, when the up and down hill data were analyzed separately from the contour data, the two resulting slope effect relationships differed significantly, as Fig. 1 shows. The up and down hill tillage matched the USLE unit plot definition whereas contour tillage did not (Wischmeier and Smith, 1978). The additional slope effect from contouring is considered in the USLE's supporting practices factor P, and therefore, the effect of contouring should be excluded from the slope steepness factor.

At La Crosse, runoff was slightly affected by slope for up and down hill tillage, but, runoff increased significantly with slope for the contour tillage. The increase of runoff with slope was apparently caused by the reduction in surface storage of the contour tillage as slope increased. Therefore, the increase in runoff with

TABLE 1. SUMMARY OF SLOPE STEEPNESS DATA FOR LONG PLOTS

Study no.	Location	Data source	Rainfall		Plot characteristics			
			Type*	Length of record†	Length, m	Steepness, %	Tillage‡ direction	Cropping and other surface conditions
1	Petersburg, IN	Hahn et al., 1985	SIM	1982	10.7	6,10,13	U&D	Freshly prepared, surface mine topsoil
2	Evansville, IN	Hahn et al., 1985	SIM	1981	10.7	6,11,13,15	U&D	Freshly prepared, surface mine topsoil
3	Coshocton, OH	Bonta & Sutton, 1983	NAT	2 yr	22.1	9,16,23,30	U&D	Freshly prepared, surface mine topsoil
4	Jonestown, MS	Murphree & Mutchler, 1981	SIM	NS§	22.9	0.1,0.2,0.5,1,2,3	U&D	Freshly prepared, tilled, smooth
5	Oahu, HI	El-Swaify et al., 1982	SIM	1.5 yr	10.7	3 to 18	U&D	Residual soils, freshly prepared, tilled, smooth
6	Oahu, HI	El-Swaify et al., 1982	SIM	1.5 yr	22.9	3 to 18	U&D	Residual soils, freshly prepared, tilled, smooth
7	Hawaii, HI	El-Swaify et al., 1982	SIM	1.5 yr	10.7	4 to 15	U&D	Volcanic soils, freshly prepared, tilled, smooth
8	Dixon Springs, IL	Gard & Van Doren, 1949	NAT	7 yr	21.3	5,9	CON	Corn-winter wheat-lespedeza rotation
9	Temple, TX	Hill et al., 1944	NAT	11 yr	22.1	2,4	U&D	2% plots, cotton-corn-oat rotation
							NS	4% plots, continuous corn
10	St. George, KS	Duley & Hays, 1932	SIM	1931	7.6	1,2,4,6	NS	Handworked, fallow, silty clay loam
11	St. George,KS	Duley & Hays, 1932	SIM	1931	7.6	0.6,2,4,8,12	NS	Handworked, fallow, sandy loam
12	St. George, KS	Duley & Hays, 1932	SIM	1931	7.6	0.6,2.4,8,12	NS	Handworked, fallow, sandy loam
13	State College, MS	Unpublished data‖	NAT	6 yr	18.3	2.5,5,7.5,10,12.5	CON	Continuous cotton with vetch cover crop
14	State College, MS	Unpublished data	NAT	6 yr	18.3	2.5,5,7.5,10,12.5	CON	Continuous cotton, no cover crop
15	Auburn, AL	Nichols & Sexton, 1932	SIM	1931	15.2	0,5,10,15,20	U&D	Bare, fallow
16	Auburn, AL	Nichols & Sexton, 1932	SIM	1931	15.2	0,5,10,15,20	U&D	Plowed, fallow
17	Wasatch Mt., UT	Hart, 1984	SIM	1980	22.1	10,32	U&D	Bare, fallow, tilled
18	Wasatch Mt., UT	Hart, 1984	SIM	1980	22.1	10,32	U&D	Bare, fallow, tilled
19	Wasatch Mt., UT	Hart, 1984	SIM	1980	22.1	10,32	U&D	Bare, fallow, tilled
20	Wasatch Mt., UT	Hart, 1984	SIM	1980	22.1	10,32	U&D	Bare, fallow, tilled
21	Spur, TX	Conner et al., 1930	NAT	3 yr	29.5	0,1,2,3	NS	Handworked cotton
22	Auburn, AL	Diseker & Yoder, 1936	NAT	4 mo	15.2	0,5,10,15,20	U&D	Cotton, April-July
23	Auburn, AL	Diseker & Yoder, 1936	NAT	4 mo	15.2	0,5,10,15,20	CON	Cotton, April-July
24	Auburn, AL	Diseker & Yoder, 1936	SIM	1935	15.2	0,5,10,15,20	CON	Wet strip vetch, 3.8 m plowed, 11.4 m vetch
25	Auburn, AL	Diseker & Yoder, 1936	SIM	1935	15.2	0.5,10,15,20	CON	Wet strip vetch, 7.6 m plowed, 7.6 m vetch
26	Auburn, AL	Diseker & Yoder, 1936	SIM	1935	15.2	0,5,10,15,20	CON	Wet strip vetch, 11.4 m plowed, 3.8 m vetch
27	Auburn, AL	Diseker & Yoder, 1936	SIM	1935	15.2	0,5,10,15,20	CON	No vetch, plowed
28	Auburn, AL	Diseker & Yoder, 1936	SIM	1935	15.2	0,5,10,15,20	CON	No vetch, fallow
29	Auburn, AL	Diseker & Yoder, 1936	NAT	3 mo	15.2	0,5,10,15,20	CON	Corn, beans, rough cloddy beds, June-August
30	Auburn, AL	Diseker & Yoder, 1936	NAT	3 mo	15.2	0,5,10,15,20	U&D	Smooth, compact, fallow, June-August
31	Auburn, AL	Diseker & Yoder, 1936	NAT	6 mo	15.2	0,5,10,15,20	CON	Vetch cover crop, November-June
32	Auburn, AL	Diseker & Yoder, 1936	NAT	5 mo	15.2	0,5,10,15,20	CON	Rye, November-April
33	Auburn, AL	Diseker & Yoder, 1936	SIM	NS	15.2	0,5,10,15,20	CON	Freshly cultivated, cotton
34	Auburn, AL	Diseker & Yoder, 1936	SIM	NS	15.2	0,5,10,15,20	U&D	Smooth, fallow
35	Zanesville, OH	Borst et al., 1945	SIM	1938	22.1	3,4,9,15,18,22	U&D	Muskingum soil, bare, dry run
36	Zanesville, OH	Borst et al., 1945	SIM	1938	22.1	3,4,9,15,18,22	U&D	Muskingum soil, bare, wet run
37	Zanesville, OH	Borst et al., 1945	SIM	1938	22.1	3,4,9,15,18,22	U&D	Muskingum soil, average of studies 35 and 36
38	Zanesville, OH	Borst et al., 1945	NAT	9 yr	22.1	8,12	U&D	Continuous corn
39	Arnot, NY	Lamb et al., 1944	NAT	9 yr	NS	9,18	CON	Cultivated corn
40	Blacksburg, VA**	Unpublished data	NAT	10 yr	17.7	5,10,15,20,25	CON	Corn-wheat-clover rotation
41	Blacksburg, VA	Unpublished data	NAT	7 yr	17.7	5,15,25	CON	Corn-wheat-clover rotation
42	Blacksburg, VA	Unpublished data	NAT	7 yr	17.7	10,20	U&D	Corn-wheat-clover rotation
43	Blacksburg, VA	Unpublished data	NAT	17 yr	17.7	5,15,25	CON	Corn-wheat-clover rotation
44	La Crosse, WI	Unpublished data	NAT	5 yr	22.1	3,8,13,18	U&D	Small grain
45	La Crosse, WI	Unpublished data	NAT	20 yr	22.1	3,8,13,18	CON	Corn-small grain-hay rotation
46	Bethany, MO	Krusekopf, 1943	NAT	6 yr	27.4	3.7,6,8.5	NS	Corn-wheat-clover rotation
47	Bethany, MO	Krusekopf, 1943	NAT	6 yr	27.4	3.7,6,8.5	NS	Continuous corn
48	Marcellus, NY	Free et al., 1946	NAT	2 yr	11.1	4.7,9.3,16.3	CON	Continuous corn
49	Marcellus, NY	Free et al., 1946	NAT	2 yr	22.1	4.7,9.3,16.3	CON	Continuous corn
50	Marcellus, NY	Free et al., 1946	NAT	2 yr	64.0	4.7,9.3,16.3	CON	Continuous corn

*Simulated rainfall (SIM), natural rainfall (NAT)
†Approximate time period of the natural rainfall studies or the year for a simulated rainfall study.
‡Up and down hill (U&D), contour (CON) or not specified (NS).
§(NS) not specified.
‖Unpublished data on file at the National Soil Erosion Research Laboratory.
**1937-1946, all plots on contour; 1947-1953, 5, 15, 25% plots remained on contour while 10, 20% plots were on up and down hill.

slope partially caused the greater slope effect on erosion with contouring.

Break in Slope Effect Equation

A trend that emerged from the data collected at the other locations (Nichols and Sexton, 1932; Diseker and Yoder, 1936) was that erosion increased at a slower rate for the low slopes than for the steep slopes, as Fig. 2 illustrates. One possible reason for these two regions in the slope effect relationship is that little or no rill erosion occurs on the low slopes, and interrill erosion, the other major component of total soil loss is not greatly affected by slope (Foster, 1982). When the slope exceeds a critical steepness, rill erosion begins, which causes total soil loss to increase rapidly with slope (Meyer and Harmon, 1985). The idea of rill erosion beginning at a particular slope is consistent with rill erosion theory where the shear stress of runoff must exceed a critical shear stress value for the particular soil condition before the flow begins to detach sediment (Meyer et al., 1976; Foster and Lane, 1983).

Another factor is that runoff varied more with steepness on the low slopes than on the steep slopes. Above a slope of about 8%, runoff did not vary significantly with steepness, as the data in Table 2 show.

As Meyer and Harmon (1985) showed for a ridge-furrow surface configuration, transport capacity of runoff controls soil loss when slope steepness is slight.

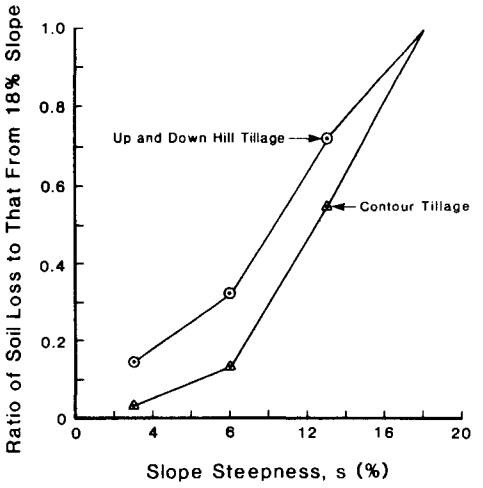

Fig. 1—Effect of tillage direction on the relation of soil loss to slope steepness at La Crosse, WI.

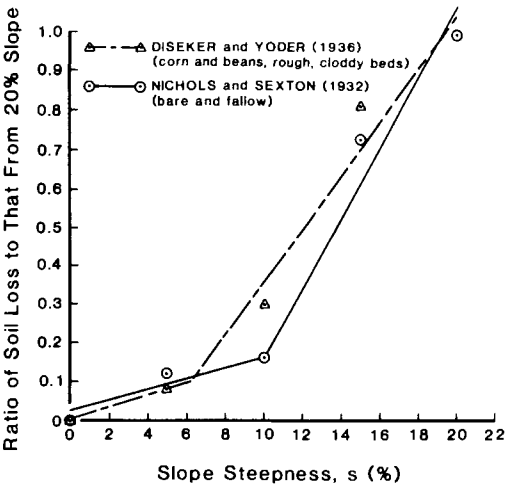

Fig. 2—Erosion increases more rapidly on steep slopes than on low slopes.

TABLE 2. EFFECT OF SLOPE STEEPNESS ON RUNOFF

Study no.*	Location	Data source	Steepness, %	Increase of runoff with steepness†			Slope where runoff tends to a constant value or decreases with increased steepness, %
				Lower 1/3 of slope range	Middle 1/3 of slope range	Upper 1/3 of slope range	
				Relative change in runoff per unit‡ change in slope percent			
10	St. George, KS	Duley and Hays, 1932	1,2,4,6	0.313	0.107	0.006	4
11	St. George, KS	Duley and Hays, 1932	1,4,8,11	0.240	-0.071	0.016	4
15	Auburn, AL	Nichols and Sexton, 1932	0,5,10,15	0.096	0.021	-0.015	10
21	Spur, TX	Conner et al., 1930	0,1,2,3	0.333	NV§	NV	
35	Zanesville, OH	Borst et al., 1945	3,9,15,22	-0.015	0.040	-0.056	3
36	Zanesville, OH	Borst et al., 1945	3,9,15,22	0.003	-0.002	0.002	3
37	Zanesville, OH	Borst et al., 1945	3,9,15,22	-0.0047	0.015	-0.0117	4
44	La Crosse, WI	Unpublished data‖	3,8,13,18	0.034	0.021	0.028	18
45	La Crosse, WI	Unpublished data	3,8,13,18	0.052	0.071	0.039	18
46	Bethany, MO	Krusekopf, 1943	3.5,6,8.5	0.170	0.099	NV	8.5
47	Bethany, MO	Krusekopf, 1943	3.5,6,8.5	-0.023	0.163	NV	3.5
48	Marcellus, NY	Free et al., 1946	4.7,9.3,16.3	NV	0.094	-0.008	4.7
49	Marcellus, NY	Free et al., 1946	4.7,9.3,16.3	NV	0.125	-0.013	4.7
50	Marcellus, NY	Free et al., 1946	4.7,9.3,16.3	NV	0.053	0.047	

Study no.*	Location	Data source	Steepness, %	Increase of runoff with steepness†				Slope where runoff tends to a constant value or decreases with increased steepness, %
				First 1/4 of slope range	Second 1/4 of slope range	Third 1/4 of slope range	Fourth 1/4 of slope range	
				Relative change in runoff per unit‡ change in slope percent				
13	State College, MS	Unpublished data‖	2.5,5,7.5,10,12.5	0.125	0.153	-0.342	0.175	10
14	State College, MS	Unpublished data	2.5,5,7.5,10,12.5	0.084	0.173	-0.060	-0.027	10
15	Auburn, AL	Nichols and Sexton, 1932	0,5,10,15,20	0.096	0.021	-0.015	NV	10
16	Auburn, AL	Nichols and Sexton, 1932	0,5,10,15,20	0.170	0.013	0.021	0.007	15
24	Auburn, AL	Diseker and Yoder, 1936	0,5,10,15,20	0.026	0.021	0.020	-0.009	15
25	Auburn, AL	Diseker and Yoder, 1936	0,5,10,15,20	0.027	0.018	0.017	-0.030	15
26	Auburn, AL	Diseker and Yoder, 1936	0,5,10,15,20	0.018	0.003	0.004	-0.022	5
27	Auburn, AL	Diseker and Yoder, 1936	0,5,10,15,20	0.106	-0.014	0.010	0.039	5
28	Auburn, AL	Diseker and Yoder, 1936	0,5,10,15,20	0.083	0.001	0.011	-0.011	5
29	Auburn, AL	Diseker and Yoder, 1936	0,5,10,15,20	0.109	0.043	0.057	-0.022	15
30	Auburn, AL	Diseker and Yoder, 1936	0,5,10,15,20	0.178	0.001	-0.020	0.023	5
31	Auburn, AL	Diseker and Yoder, 1936	0,5,10,15,20	0.161	-0.018	0.007	-0.013	5
32	Auburn, AL	Diseker and Yoder, 1936	0,5,10,15,20	0.068	0.022	-0.001	-0.008	10
33	Auburn, AL	Diseker and Yoder, 1936	0,5,10,15,20	0.148	0.038	0.008	0.030	10
34	Auburn, AL	Diseker and Yoder, 1936	0,5,10,15,20	0.062	0.007	0.010	0.014	5
40	Blacksburg, VA	Unpublished data‖	5,10,15,20,25	0.158	-0.152	0.063	-0.033	10

*Study number refers to Table 1.

†Slope ranges were broken down into thirds or quarters depending on the specific data set.

‡$(V_{i+1} - V_{i-1})/[\bar{V}(s_{i+1} - s_i)]$ where V_{i+1} = runoff volume for the slope steepness s_{i+1}, in percent, V_{i-1} = runoff volume for the slope steepness s_i in percent, and $\bar{V}$ = average runoff volume for all steepnesses.

§Slope and runoff data not considered valid over this range.

‖Unpublished data on file at the National Soil Erosion Research Laboratory.

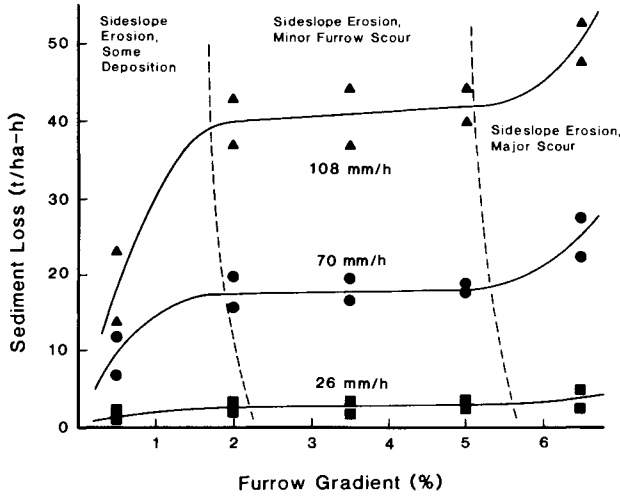

Fig. 3—Effect of row furrow gradient and rain intensity on sediment losses from the ends of bedded rows (from Meyer and Harmon, 1985).

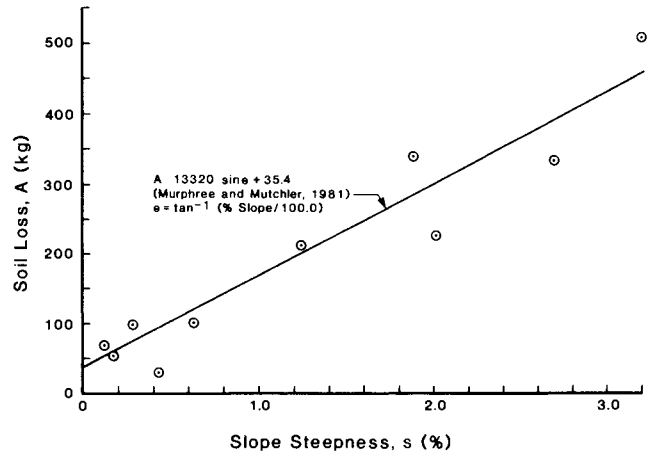

Fig. 4—Effect of slope steepness on soil loss for low gradient slopes (from Murphree and Mutchler, 1981).

Therefore, soil loss increases with steepness on low slopes as steepness increases transport capacity of runoff. When slope steepness had increased to about 2%, Meyer and Harmon (1985) observed that the flow in the furrows could transport all of the sediment eroded from the ridges by interrill erosion. However, the flow did not cause rill erosion in the furrows until a steepness of about 5% was reached, as Fig. 3 shows.

According to erosion theory and the data of Meyer and Harmon (1985), the S factor relationship can be divided into three steepness regions: (a) where soil loss is limited by transport capacity of the runoff and deposition of rainfall detached sediment occurs, (b) where flow is sufficient to transport most sediment from interrill erosion, but is not sufficient to cause rill erosion, and (c) where flow is sufficient to transport all sediment from interrill erosion and also cause rill erosion. No deposition occurs with cases (b) and (c). However, the location of these regions varies with many factors and we judged that derivation and use of such a three region S relationship was beyond the practicality of the USLE equation strucure.

In the data analyzed, breaks in the soil loss-steepness relationship between low slopes and steep slopes were not always abrupt. The value of the steepness separating low slopes from steep slopes in the steepness relationship varied with runoff rate, soil erodibility, critical shear stress, cover, and other factors. Over the 14 data sets that exhibited a break in slope, on the average, the break occurred at about 8%.

As stated previously, the La Crosse data set was the most complete set analyzed, particularly for steep slopes. The La Crosse data exhibited a break in slope at 8% (Fig. 1). Therefore, we concluded that the La Crosse data for up and down hill tillage on the 8, 13, and 18% slopes (Fig. 1) were in the region where rill erosion was occurring and that the La Crosse data from the 3% slope was either in the region where transport capacity limited soil loss or where rill erosion was insignificant. Then, we fitted a straight line through the data points for the steeper three slopes and normalized the resulting equation to 9% slope:

$$S = 16.8 \sin \theta - 0.50 \quad \ldots\ldots\ldots\ldots\ldots\ldots [9]$$

Low Slopes

The largest and most complete data set for the low slopes was collected by Murphree and Mutchler (1981) on rainfall simulator plots that were 22.9 m long by 3.7 m wide with a range in steepness from 0.1 to 3%. The plot surface was smooth without ridges. Murphree and Mutchler (1981) published an equation that expressed the linear relationship of soil loss with slope steepness for low slopes ($r^2 = 0.97$). The metric equivalent of this linear relationship is shown in Fig. 4. Based on the size and completeness of the data set, we considered this relationship to be representative of low slopes.

Three alternatives were considered to develop a relationship for the steepness effect of low slopes: (a) The relationship of Murphree and Mutchler could be normalized to intersect the La Crosse steep slope relationship, equation [9], at 8% slope; (b) The Murphree and Mutchler relationship could be normalized and forced to give the same value as the La Crosse data at 3% slope; or (c) The Murphree and Mutchler data could be normalized to give a value of 1.0 at 9% slope. If the first approach were chosen, the S value at 8% slope would be 0.83 and at 3% slope would be 0.33. If the second alternative were selected, the S value at 3% slope would be 0.35, at 8% slope would be 0.88, and at 9% slope would be 0.98. The third alternative would give an S value of 0.35 at 3% slope and 0.89 at 8% slope, quite similar to the results of the second alternative. Using alternative three, the percent difference between the observed and fitted value at 8% slope is about the same as that at 3% slope if the alternative one is used; the breakpoint at 9% slope is compatible with the unit plot concept and the lumped equation structure of the USLE. Thus alternative three was selected. The resulting equation for low slopes from the relationship of Murphree and Mutchler is:

$$S = 10.8 \sin \theta + 0.03 \quad \ldots\ldots\ldots\ldots\ldots\ldots [10]$$

Comparison with other Data

The remaining data were analyzed to determine the fit of equations [9] and [10]. Fig. 5 illustrates how well linear relationships fit selected data sets. By inspection, the slope factor relationships were judged to be linear provided separate equations were fitted to the low and steep slopes. The breakpoint steepness between the

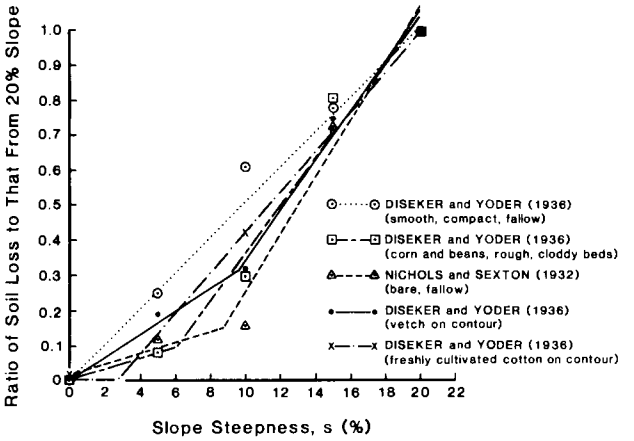

Fig. 5—Linear relationships of soil loss to slope steepness.

regions varied greatly between data sets (5 to 10%) and some data sets did not require a breakpoint.

The data in Fig. 5 represented up and down hill tillage or contoured tillage where ridges were low and runoff was not greatly affected by slope above 8%. Soil conditions ranged from freshly tilled, where critical shear stress is low, to consolidated, where critical shear stress can be large (Foster and Lane, 1983). However, no data were from thawing soils where critical shear stress is extremely low (Formanek et al., 1984).

Table 3 gives values of S estimated for an 18% steepness for the data considered in the study. Even though the values vary considerably with treatment and location, equations [9] and [10] satisfactorily represent the data as a whole. For example, the mean value for S for the 18% steepness was 3.53 (standard deviation = ± 3.08). However, some S values like those from the data of Hart (1984) and Nichols and Sexton (1932) were unrealistically high because of very low soil loss at the 9% unit plot steepness. When S values greater than 5.01 were omitted, the average S value was 2.35 (standard deviation = ± 0.79). Since most erosion is caused by the moderate to high intensity storms (Wischmeier, 1962) that would cause significant erosion on a 9% slope, deletion of the high values was justified. Therefore, the value of 2.48 for S for an 18% slope from equation [9] is reasonable in comparison with the data as a whole.

The average S value for the 3% slope was 0.32 (standard deviation = ±0.16) when the negative values in Table 3 were counted as zeroes. When the negative values were not included, the average S was 0.36 (standard deviation = 0.13). The value of 0.35 from the proposed S factor, equation [10], is therefore reasonable.

At the 0.5% slope, the average of all S values, including a zero for each negative value in Table 3, was 0.13 (standard deviation = ± 0.12), and when the negative values were excluded, the average S value was 0.17 (standard deviation = ± 0.11). These values are somewhat greater than the value of 0.08 from equation [10]. If the contention of Murphree and Mutchler (1981) that the USLE S factor overestimates for very low slopes is correct, then equation [10] is acceptable. Variability in the soil loss-steepness relationships for low slopes seemed to be caused by soil, recency of tillage, roughness, contouring, and cover affecting both runoff amount and rate.

The variation in S values for the experimental data for the low slopes was sometimes related to whether the breakpoint between the low and steep regions occurred below or above 9% steepness. When the data contained no slope steepness greater than 9% or no breakpoint occurred within the range of the slopes in a study, S values at the low slopes were typically large. Problems caused by the position of the breakpoint with respect to

TABLE 3. SLOPE FACTOR VALUES FROM THE EXPERIMENTAL DATA FOR LONG SLOPES

Number*	Study Reference	S factor for slopes of: 0.5%	3.0%	18%
Equations [9] and [10]		0.08	0.35	2.48
1	Hahn et al., 1985	0.11	0.37	1.93
2	Hahn et al., 1985	neg†	0.27	2.09
3	Bonta and Sutton, 1983	0.45	0.61	1.58
4	Murphree and Mutchler, 1981	0.08	0.35	–‡
5	El-Swaify et al., 1982	neg	0.15	2.24
6	El-Swaify et al., 1982	neg	0.26	2.09
7	El-Swaify et al., 1982	neg	0.22	2.14
8	Gard and Van Doren, 1949	0.31	0.48	–
9	Hill et al., 1944	0.14	0.39	–
10	Duley and Hays, 1932	0.13	0.39	–
11	Duley and Hays, 1932	0.16	0.41	–
12	Duley and Hays, 1932	neg	0.19	–
13	Unpublished data§	neg	0.13	3.55
14	Unpublished data	neg	0.17	2.65
15	Nichols and Sexton, 1932	0.38	0.57	12.50
16	Nichols and Sexton, 1932	0.28	0.50	13.40
17	Hart, 1984	–	–	3.58
18	Hart, 1984	–	–	2.42
19	Hart, 1984	–	–	9.50
20	Hart, 1984	–	–	1.66
21	Conner et al., 1930	0.16	0.41	–
22	Diseker and Yoder, 1936	–	neg	2.12
23	Diseker and Yoder, 1936	–	neg	2.36
24	Diseker and Yoder, 1936	0.06	0.34	1.98
25	Diseker and Yoder, 1936	0.15	0.40	1.89
26	Diseker and Yoder, 1936	0.28	0.50	1.74
27	Diseker and Yoder, 1936	0.10	0.37	8.26
28	Diseker and Yoder, 1936	0.06	0.34	1.97
29	Diseker and Yoder, 1936	0.08	0.35	2.76
30	Diseker and Yoder, 1936	0.07	0.34	1.97
31	Diseker and Yoder, 1936	0.18	0.42	2.11
32	Diseker and Yoder, 1936	0.32	0.52	1.71
33	Diseker and Yoder, 1936	0.17	0.41	2.84
34	Diseker and Yoder, 1936	0.07	0.36	2.06
35	Borst et al., 1945	0.08	0.35	2.82
36	Borst et al., 1945	–	0.23	2.13
37	Borst et al., 1945	neg	0.28	2.55
38	Borst et al., 1945	–	–	1.80
39	Lamb et al., 1944	–	–	1.77
40	Unpublished data‖	0.14	0.40	1.89
41	Unpublished data	0.17	0.42	1.86
42	Unpublished data	0.27	0.49	1.75
43	Unpublished data	0.09	0.36	1.93
44	Unpublished data**	–	0.35	2.42
45	Unpublished data	–	0.14	4.76
46	Krusekopf, 1943	neg	0.21	–
47	Krusekopf, 1943	–	0.17	–
48	Free et al., 1946	–	0.67	8.06
49	Free et al., 1946	–	neg	10.77
50	Free et al., 1946	–	neg	5.01

*Study number is referenced in Table 1.
†neg means that slope relationship from the data gave a negative value when extrapolated to this slope.
‡– means that the relationship from the data clearly could not be extrapolated to this slope.
§State College, MS studies 13 and 14.
‖Blacksburg, VA studies 40, 41, 42 and 43.
**La Crosse, WI studies 44 and 45.

9% steepness in the soil loss-steepness relationships can not be easily resolved with the lumped equation structure of the USLE.

Thawing Soils

The largest data set was that collected in the Palouse Region of the Pacific Northwest by McCool (McCool et al., 1987). The data were collected by measuring rills in cooperators' fields along an 80-km transect at the end of the winter erosion season. The project covered an 11-year period with one year excluded because of drought. Several hundred data points were obtained on slopes ranging from 1.5 to 56% steepness. The mean slope was 28.4%, and 95% of the data points were collected from slopes between approximately 9 and 48% steepness. For slopes of 9% or greater steepness we recommend use of equation [8].

For slopes of less than 9% steepness we recommend equation [10]. The difference between equations [8] and [10] is less than 10% for slopes between 7 and 9%. For lesser slopes the low shear strength of thawing soil and the relatively low runoff rates of the Palouse Region create a condition where transport capacity apparently limits soil loss. Thus the large S values obtained by extrapolating equation [8] to slopes of 5% or less appear unrealistic.

Short Slopes

The USLE does not apply to slope lengths shorter than about 4 m (Foster et al., 1981). Little rill erosion occurs on such short slope lengths and most of the soil loss is by interrill erosion. The equation derived by Foster (1982) from analysis of data from Lattanzi et al. (1974) is recommended for estimating interrill erosion:

$$S = 3.0 (\sin \theta)^{0.8} + 0.56 \quad \ldots\ldots\ldots\ldots\ldots\ldots [11]$$

Lattanzi et al. (1974) used 0.61 m long slopes under simulated rainfall. Data in Table 4 from the studies of Singer and Blackard (1982), Evett and Dutt (1985), and Rubio-Montoya and Brown (1984) show that equation [11] is reasonable.

DISCUSSION

Table 5 gives values from our revised S factor (equations [9] and [10]), AH537's S factor (equation [1]), thawing soil S factor (equations [8] and [10]), Zingg's S factor (equation [2]), and one S factor for short slopes (equation [11]). As expected, our S values for slopes steeper than 9% are less than those from AH537. For example, at a 50% slope, the AH537 S value is over twice that from equation [9]. The lower values are consistent with the linear treads in erosion as a function of slope that are evident in most of the data.

Hart (1984) concluded that AH537 S values are too large on slopes as steep as 30%. Although the increase in erosion with steepness on the contour tilled plots at La Crosse was greater than that for the up and down hill tilled plots, erosion still increased linearly with slope above a steepness of 8%, as Fig. 1 shows. However, this increased slope effect is caused by contouring and is

TABLE 4. SUMMARY OF SLOPE FACTOR VALUES FOR INTERRILL EROSION DATA, NORMALIZED TO NINE PERCENT SLOPE STEEPNESS

Slope	Equation* [11]	Data source†											
		(1a)	(1b)	(2)	(3)	(4)	(5a)	(5b)	(5c)	(5d)	(5e)	(6a)	(6b)
0	0.56	—	—	0.56	—	—	—	—	—	0.17	—	—	—
1	0.64	—	—	—	—	—	—	0.20	—	0.19	—	—	—
2	0.69	—	—	—	0.66	—	—	0.20	0.28	0.24	0.43	—	—
3	0.76	0.54	0.57	0.72	—	—	—	—	—	—	—	—	—
4	0.79	—	—	—	—	0.36	0.18	0.46	0.45	0.54	0.55	—	—
7	0.92	—	0.86	0.92	—	—	—	—	—	—	—	—	—
8	0.96	—	—	—	—	0.83	0.83	0.91	0.93	0.91	0.91	0.91	0.97
9	1.00	1.00	1.00	1.00	1.00	1.00	1.00	1.00	1.00	1.00	1.00	1.00	1.00
12	1.11	1.13	2.42	1.17	—	1.52						—	—
16	1.25	1.30	3.56	1.25	—							1.65	1.23
18	1.31	—	—		1.34							—	—
20	1.38	—	4.12									—	—
24	1.50	1.89	5.50									—	4.32
28	1.61	—	5.94									—	—
32	1.72	2.15	6.97									—	—
33	—	—	—									2.91	5.72
36	1.82	—	6.82									—	
40	1.91	2.08	7.56									—	
44	—		—									4.82	
50	2.13		7.55										

*Equation based on data from Lattanzi et al. (1974)

†Data sources:

(1) Singer and Blackard (1982), 1.2 m long plots: (a) Contra costa soil (clayey), (b) Hillgate soil (sandy).
(2) Evett and Dutt (1985), 3.0 and 6.0 m long plots.
(3) Rubio-Montoya and Brown (1984), 0.61 m long plots.
(4) Zingg (1940), 2.4 m long plots.
(5) Neal (1938a), No values were used from slopes greater than nine percent because rill erosion was reported, 3.6 m long plots. Intensity (mm/h): (a) 25, (b) 38, (c) 51, (d) 76, (e) 102.
(6) Gabriels et al. (1975), 60 mm/h intensity, 0.3 m long plots, silt loam soils: (a) soil 1, (b) soil 2.

TABLE 5. VALUES FROM VARIOUS SLOPE FACTOR RELATIONSHIPS

Slope, %	Equations [9] & [10]*	USLE† AH537	Equations [8] & [10]‡	Equation [2]§	Equation [11]‖
0.2	0.050	0.075	0.050	0.005	0.581
0.5	0.083	0.090	0.083	0.018	0.603
1.0	0.137	0.118	0.137	0.046	0.635
2.0	0.245	0.183	0.245	0.122	0.691
3.0	0.354	0.261	0.354	0.216	0.741
4.0	0.462	0.352	0.462	0.323	0.788
5.0	0.570	0.456	0.570	0.441	0.833
6.0	0.678	0.573	0.678	0.569	0.876
8.0	0.893	0.845	0.893	0.849	0.957
10.0	1.165	1.167	1.065	1.158	1.034
12.0	1.494	1.538	1.186	1.490	1.107
14.0	1.820	1.955	1.299	1.843	1.178
16.0	2.144	2.419	1.405	2.212	1.246
20.0	2.783	3.476	1.600	2.994	1.375
25.0	3.560	5.020	1.817	4.031	1.526
30.0	4.311	6.777	2.012	5.111	1.666
40.0	5.719	10.782	2.346	7.320	1.918
50.0	6.989	15.188	2.623	9.495	2.136

*Our recommendation for the slope factor for long slopes.
†Slope factor in Agriculture Handbook 537 (Wischmeier and Smith, 1978).
‡Our recommendation for erosion of thawing soils.
§Zingg's (1940) slope factor.
‖Our recommendation for short slopes.

taken into account in the USLE P factor. When only data from up and down hill tillage from La Crosse are considered, the erosion-slope relationship is linear with little indication of the trend that the quadratic equation in AH537 gives for very steep slopes. Our recommendation for reduced S values for steep slopes is consistent with the general consensus among field users of the USLE that AH537 S values for steep slopes are too high.

Values for S from equation [10] differ from AH 537 values for slopes less than 9%. The value from equation [10] is 36% greater than the AH537 value at a 3% slope and 18% greater at a 6% slope. Slope factor values from AH537 for slopes less than 3% are questionable because they are an extrapolation of a quadratic equation fitted to a section of data showing an apparent curved trend that seems uncharacteristic of the soil loss-steepness relationship at both low and steep slopes. The soil loss-steepness effect in the data of Murphree and Mutchler (1981) is linear for slopes ranging from 0.1% to 3% steepness. The S value for the La Crosse data from the 3% slope with up and down hill tillage is 0.35, while the AH537 value is 0.26 and the value from equation [10] is 0.35. These differences result from our analysis being limited to data from the up and down hill tillage at La Crosse while Smith and Wischmeier (1957) apparently combined the up and down hill and contoured data sets. We believe that the S factor should be derived from data where tillage was up and down hill, which justifies our larger S values for slopes lower than 9%.

As Table 5 shows, the McCool et al. (1987) S factor equation gives lower S values at steep slopes than does equation [9]. The exact reason for this difference is not known, but it may be related to the low resistance of thawing soil to rill detachment and the relatively low runoff rates of the major thawing soil areas. Extrapolation of equation [8] to slopes of less than 5% would give S values considerably larger than either those from AH537 or equation [10]. For slopes of less than 9%, equation [10] appears more realistic than equation [8].

Equation [11], the S equation for short slopes, applies where runoff occurs as broad sheet flow at the end of the slope. As Table 5 shows, soil loss increases much more slowly with slope on interrill areas than it does on long slopes. Researchers studying interrill erosion have noted the great difference between their results and the USLE slope factor (Harmon and Meyer, 1978; Lattanzi et al., 1974; Meyer et al., 1975; Singer and Blackard, 1982).

The USLE slope length factor does not apply to short slopes because most of the soil loss on them is from interrill erosion, which does not vary greatly with slope length (Foster et al., 1981; Foster, 1982). A short slope is therefore defined as one where erosion is caused principally by raindrop impact. In theory, erosion per unit area on such slopes should be independent of slope length (Meyer et al., 1975; Foster, 1982). Erosion did not vary between the 3 and 6 m long plots used in a natural runoff study by Evett and Dutt (1985).

For the most part, equation [11] applied well to all of the short slope data indicating that slope length is not a major factor on short slopes. When slope exceeded 8%, erosion increased rapidly from rill erosion on Neal's (1938a,b) 3.7 m long plots. This added contribution from rill erosion steepened the slope factor relationships as slope increased above 8%. When slope exceeded about 10%, erosion of the sandy soil on a 1.2 m long slope in Singer and Blackard's (1982) study rapidly increased. This increase in soil loss may have been caused by greater transport capacity that carried large sand particles that could not be transported on lower slopes. Also, Monke et al. (1977) observed increased soil loss when they added flow to a 0.61 m slope length, which also suggests that increased transport capacity resulted in greater soil loss. The significant increase of erosion on the steep slopes of Gabriels et al. (1975) may have been caused by rill erosion. Up to a 16% slope, these results do not differ greatly from equaton [11]. Therefore, equation [11] principally describes conditions where detachment by raindrop impact limits soil loss rather than transport capacity of the thin interrill flow and raindrop impact.

The reason for the low S factor values from Neal's (1938a,b) lower slopes is not apparent. One possible explanation is that his rainfall simulator did not enhance sediment transport capacity as much as did rainfall in the other studies (Moss et al., 1979). Therefore, soil loss in Neal's study could have been controlled by transport capacity at the low slopes, while detachment by raindrop impact controlled soil loss in other studies like Lattanzi et al. (1974), Singer and Blackard (1982), Evett and Dutt (1985), and Rubio-Montoya and Brown (1984). The effect of transport capacity controlling soil loss would have been more important on Neal's 3.7 m long slopes versus the approximate 1 m slopes in other studies. Soil loss also varied more in Zingg's (1940) study than it did in the studies of Lattanzi et al. (1974), Singer and Blackard (1982), Evett and Dutt (1985), and Rubio-Montoya and Brown (1984). The difference may have been caused by a rougher surface and rill erosion on Zingg's plots. On short rough field slopes and soils with higher susceptibility to rill erosion, equation [11] could be adjusted to be consistent with Zingg's data.

A value of 4 m is suggested as a general value for the shortest slope length for use in the USLE (Foster et al., 1981). This slope length value is based on the length where soil loss values from a fundamentally based erosion equation having separate components for rill and

interrill erosion begins to depart from USLE values as slope length is decreased (Foster et al., 1981). Neal (1938a,b) in his study of erosion on 3.7 m long beds in the laboratory under simulated rainfall observed rill erosion when steepness was greater than 8%. Likely his soil was easily eroded by flow, or rainfall detachment was low.

Data were insufficient to eliminate discontinuities between equation [11] and equations [9] and [10]. Much of the difficulty is related to the equation structure of the USLE, which lumps rill and interrill erosion. A model structure having separate rill and interrill components would eliminate the discontinuities.

SUMMARY

Field data from about 20 studies on the effect of slope on sheet and rill erosion were analyzed to revise the relationship for the slope steepness factor in the Universal Soil Loss Equation (USLE). Slopes studied ranged from 0.1 to 32% steepness. Data sets used to develop the revised relationships included a slope range of 0.1 to 18%. The two relationships derived from the analysis apply respectively to ranges of slope steepness less than 9% and equal to or greater than 9%. Application to slopes greater than 18% represents an extrapolation beyond the observed data.

These relationships more reasonably predict soil loss values from research studies on both low and steep slopes as compared to those values computed with the present USLE slope steepness relationship. Therefore, the following equations are recommended for use in the USLE:

$$S = 10.8 \sin \theta + 0.03 \qquad s < 9\% \quad \ldots\ldots\ldots\ldots [10]$$

$$S = 16.8 \sin \theta - 0.50 \qquad s \geq 9\% \quad \ldots\ldots\ldots\ldots [9]$$

where: S = USLE slope steepness factor and θ = angle of slope having a steepness of s expressed in percent. These equations apply best to relatively smooth surfaces where tillage is up and down hill, and runoff does not vary with slope for steepnesses above 8%. The effect of contour tillage on the soil loss-slope steepness relationship is considered in the USLE supporting practices factor P.

For conditions when erosion is principally by surface flow over thawing soil the following equations are recommended:

$$S = 10.8 \sin \theta + 0.03 \qquad s < 9\% \quad \ldots\ldots\ldots\ldots [10]$$

$$S = (\sin \theta / 0.0896)^{0.6} \qquad s \geq 9\% \quad \ldots\ldots\ldots\ldots [8]$$

where: 0.0896 = the sine of the angle of a 9% slope.

None of the above equations apply to short slopes where all of the erosion is caused by raindrop impact and runoff freely discharges from the end of the slope. For these short slopes, the recommended slope factor equation is:

$$S = 3.0(\sin \theta)^{0.8} + 0.56 \quad \ldots\ldots\ldots\ldots\ldots\ldots [11]$$

This equation does not apply to slopes longer than 4 m.

The above equations represent a summary of the data. Among data sets, the soil loss-slope steepness relationships varied greatly with soil, slope length, steepness, tillage, cover, runoff, and other factors. Also, discontinuities exist between the slope effect equation for short slope lengths and that for long slopes. However, the USLE equation form, which lumps rill and interrill erosion components, greatly complicates considering the variety of factors that affect the S factor relationships. A more fundamentally based model structure of separate components for rainfall and runoff detachment on interrill and rill areas, and the transport and deposition of sediment by flow would greatly facilitate consideration of these other factors. However, at present the USLE represents the best available practical technology for estimating sheet and rill erosion.

References

1. Bonta, J. V. and P. Sutton. 1983. Erosion and reclamation plots: Research on the hydrology and water quality of watersheds subjected to surface mining. Bureau of Mines, U.S. Dept. Interior, 60 pp.

2. Borst, H. L., A. G. McCall and F. G. Bell. 1945. Investigations in erosion control and the reclamation of eroded land at the Northwest Appalachian Conservation Experiment Station, Zanesville, OH, 1934-42. USDA Tech. Bull. No. 888, 95 pp.

3. Browning, G. M., R. A. Norton, A. G. McCall and F. G. Bell. 1948. Investigations in erosion control and the reclamation of eroded land at the Missouri Valley Loess Conservation Experiment Station, Clarinda, IA, 1931-42. USDA Tech. Bull. No. 959, 88 pp.

4. Chow, V. T. 1959. Open-channel hydraulics. McGraw-Hill Book Co. 680 pp.

5. Conner, A. B., R. E. Dickson and D. Scoates. 1930. Factors influencing runoff and soil erosion. Texas Agr. Exp. Sta. Bull. No. 411, 50 pp.

6. Dickson, R. E., B. C. Langley and C. E. Fisher. 1940. Water and soil conservation experiments at Spur, Texas. Texas Agr. Exp. Sta. Bull. No. 587, 67 pp.

7. Diseker, E. G. and R. E. Yoder. 1936. Sheet erosion studies on Cecil clay. Agr. Exp. Sta. Ala. Polytech. Inst. Bull. No. 245, 52 pp.

8. Duley, F. L. and O. E. Hays. 1932. The effect of the degree of slope on run-off and soil erosion. Jour. Agr. Res. 45(6):349-360.

9. El-Swaify, S. A., E. W. Dangler and C. L. Armstrong. 1982. Soil erosion by water in the tropics. HITAHR, College of Tropical Agr. and Hum. Res., University of Hawaii, Res. Ext. Ser. 024, 168 pp.

10. Evett, S. R. and G. R. Dutt. 1985. Effect of slope and rainfall intensity on erosion from sodium dispersed, compacted earth microcatchments. Soil Sci. Soc. Amer. Jour. 49(1):202-206.

11. Formanek, G. E., D.K. McCool and R. I. Papendick. 1984. Freeze-thaw and consolidation effects on strength of a wet silt loam. TRANSACTIONS of the ASAE 27(6):1749-1752.

12. Foster, G. R. 1982. Modeling the erosion process. In: Hydrologic Modeling of Small Watersheds. Edited by C. T. Haan et al. Chaper 8. ASAE Monograph No. 5, St. Joseph, MI 49085, pp 297-380.

13. Foster, G. R. and L. J. Lane. 1983. Erosion by concentrated flow in farm fields. In: Proceedings of the D. B. Simons Symposium on Erosion and Sedimentation. Colorado State University. Ft. Collins, pp 9.65-9.82.

14. Foster, G. R., L. D. Meyer and C. A. Onstad. 1977. An erosion equation derived from basic erosion principles. TRANSACTIONS of the ASAE 20(4):678-682.

15. Foster, G. R., J. R. Simanton, K. G. Renard, L. J. Lane and H. B. Osborn. 1981. Discussion of "Application of the Universal Soil Loss Equation to rangeland on a per-storm basis." Jour. of Range Manage. 34(2):161-165.

16. Free, G. R., E. A. Carleton, J. Lamb, Jr. and A. F. Gustafson. 1946. Experiments in the control of soil erosion in Central New York. Cornell Univ. Agr. Exp. Sta. Bull. 831, 30 pp.

17. Gabriels, D., J. M. Pauwels and M. De Boodt. 1975. The slope gradient as it affects the amount and size distribution of soil loss material from runoff on silt loam aggregates. Mededelingen Fakulteit Landbouwwetenschappen. State Univ. Ghent, Belgium. 40:1333-1338.

18. Gard, L. E. and C. A. Van Doren. 1949. Soil losses as affected by cover, rainfall, and slope. Soil Sci. Soc. Proc. 14:374-378.

19. Hahn, D. T., W. C. Moldenhauer and C. B. Roth. 1985. Slope

gradient effect on erosion of reclaimed soil. TRANSACTIONS of the ASAE 28(3):805-808.

20. Harmon, W. C. and L. D. Meyer. 1978. Cover, slope, and rain intensity affect interrill erosion. Proc. Mississippi Water Resources Conference. Water Res. Res. Inst., Mississippi State University, Mississippi State, pp. 9-15.

21. Hart, G. E. 1984. Erosion from simulated rainfall on mountain rangeland in Utah. Jour. Soil and Water Cons. 39(5):330-334.

22. Hays, O. E., A. G. McCall and F. G. Bell. 1949. Investigations in erosion control and the reclamation of eroded land at the Upper Mississippi Valley Conservation Experiment Station near La Crosse, WI 1933-43. USDA Tech. Bull. 973, 87 pp.

23. Hill, H. O., W. J. Peevy, A. G. McCall and F. G. Bell. 1944. Investigations in erosion control and reclamation of eroded land at the Blackland Conservation Experiment Station, Temple, TX. 1931-41. USDA Tech. bull. 859, 109 pp.

24. Israelsen, C. E., C. G. Clyde, J. E. Fletcher, E. K. Israelsen, F. W. Haws, P. E. Packer, and E. E. Farmer. 1980. Erosion Control During Highway Construction — Manual on Principles and Practices. National Cooperative Highway Research Program Report 221. Transportation Research Board, National Research Council, Washington, DC. 23 pp.

25. Knoblauch, H. C. and G. D. Brill. 1940. Preliminary report of investigations at the Marlboro Soil Conservation Experiment Station. (New Jersey), 21 pp.

26. Krusekopf, H. H. 1943. The effect of slope on soil erosion. University of Missouri Agr. Exp. Sta. Res. Bull. 363, 24 pp.

27. Lamb, J., Jr., J. S. Andrews and A. F. Gustafson. 1944. Experiments in the control of soil erosion in southern New York. Cornell University Agr. Exp. Sta. Bull. 811, 32 pp.

28. Lattanzi, A. R., L. D. Meyer and M. F. Baumgardner. 1974. Influence of mulch rate and slope steepness on interrill erosion. Soil Sci. Soc. Amer. Proc. 38 (6):946-950.

29. Lillard, J. H. 1941. Effect of crops and slopes on rates of run-off and total soil loss. AGRICULTURAL ENGINEERING 22(11):396-398, 406.

30. Lillard, J. H., H. T. Rogers and J. Elson. 1941. Effects of slope, character of soil, rainfall, and cropping treatments on erosion losses from Dunmore silt loam. Va. Agr. Exp. Sta. Tech. Bull. 72, 32 pp.

31. Lombardi, F. 1979. Universal soil loss equation, runoff erosivity factor, slope length exponent, and slope steepness exponent for individual storms. PhD Thesis. Purdue University, W. Lafayette, IN, 128 pp.

32. McCool, D. K., J. F. Zuzel, J. D. Istok, G. E. Formanek, M. Molnau, K. E. Saxton and L. F. Elliott. 1987. Erosion processes and prediction for the Pacific Northwest. Proceedings of the 1986 National STEEP Symposium. Spokane, WA, May 20-21. pp. 187-204.

33. Meyer, L. D., D. G. DeCoursey and M. J. M. Romkens. 1976. Soil erosion concepts and misconceptions. Proceedings of the Third Federal Interagency Sedimentation Conference. Denver, CO. Sedimentation Committee of the Water Resources Council. PB-245 100, pp. 2-1 to 2-12.

34. Meyer, L. D., G. R. Foster and M. J. M. Romkens. 1975. Source of soil eroded by water from upland slope. In: Present and prospective technology for predicting sediment yields and sources. US Agr. Res. Ser. ARS-S-40, 285 pp.

35. Meyer, L. D. and W. C. Harmon. 1985. Sediment losses from cropland furrows of different gradients. TRANSACTIONS of the ASAE 28(2):448-453,461.

36. Monke, E. J., H. J. Marelli, L. D. Meyer and J. F. DeJong. 1977. Runoff, erosion, and nutrient movement from interrill areas. TRANSACTIONS of the ASAE 20(1):58-61.

37. Moss, A. J., P. H. Walker and J. Hutka. 1979. Raindrop-stimulated transportation in shallow water flows: An experimental study. Sediment. Geol. 22(3-4):165-184.

38. Murphree, C. E. and C. K. Mutchler. 1981. Verification of the slope factor in the universal soil loss equation for low slopes. Jour. Soil and Water Cons. 36(5):300-302.

39. Musgrave, G. W. 1947. The quantitative evaluation of factors in water erosion—A first approximation. Jour. Soil and Water Xons. 2(3):133-138, 170.

40. Neal, J. H. 1938a. Effect of degree of slope and rainfall characteristics on runoff and soil erosion. AGRICULTURAL ENGINEERING 19(5):213-217.

41. Neal, J. H. 1938b. The effect of the degree of slope and rainfall characteristics on runoff and soil erosion. Univ. Missouri Agr. Exp. Sta. Res. Bull. 280, 47 pp.

42. Nichols, M. L. and H. D. Sexton. 1932. A method of studying soil erosion. AGRICULTURAL ENGINEERING 13(4):101-103.

43. Pope, J. B., J. C. Archer, P. R. Johnson, A. G. McCall and F. G. Bell. 1946. Investigations in erosion control and reclamation of eroded sandy clay lands of Texas, Arkansas, and Louisiana at the Convservation Experiment Station, Tyler, TX, 1931-40. USDA Tech. Bull. 916, 76 pp.

44. Rubio-Montoya, D. and K. W. Brown. 1984. Erodibility of strip-mine spoils. Soil Sci. 138(5):365-373.

45. Singer, M. J. and J. Blackard. 1982. Slope angle-interrill soil loss relationships for slopes up to 50%. Soil Sci. Soc. Amer. Jour. 46(6):1270-1273.

46. Smith, D. D. and D. M. Whitt. 1947. Estimating soil losses from field areas of claypan soil. Soil Sci. Soc. Proc. 12:485-490.

47. Smith, D. D. and W. H. Wischmeier. 1957. Factors affecting sheet and rill erosion. Trans. Amer. Geophys. Union. 38(6):889-896.

48. Smith, D. D., D. M. Whitt, A. W. Zingg, A. G. McCall and F. G. Bell. 1945. Investigations in erosion control and the reclamation of eroded Shelby and related soils at the Conservation Experiment Station, Bethany, MO. 1930-42. USDA Tech. Bull. 883, 175 pp.

49. Wischmeier, W. H. 1962. Storms and soil conservation. Jour. Soil and Water Cons. 17(2):55-59.

50. Wischmeier, W. H. and D. D. Smith. 1965. Predicting rainfall-erosion losses from cropland east of the Rocky Mountains. Agriculture Handbook 282. USDA-ARS,47 pp.

51. Wischmeier, W. H. and D. D. Smith. 1978. Predicting rainfall erosion losses. Agriculture Handbook 537. USDA-SEA, 58 pp.

52. Zingg, A. W. 1940. Degree and length of land slope as it affects soil loss in runoff. AGRICULTURAL ENGINEERING 21(2):59-64.

Assessment of erosion, sedimentation, and water quality impacts of the Mountain Valley Pipeline and Equitrans Expansion Project's proposed crossing of the Jefferson National Forest as it pertains to the U.S. Forest Service's Draft Supplemental Environmental Impact Statement dated December 2022

Prepared by Jonathan A. Czuba, Ph.D., Licensed Professional Engineer - February 9, 2023

REFERENCES
15

February 21, 2023

Slope Steepness Effects on Soil Loss from Disturbed Lands

G. F. McIsaac, J. K. Mitchell, M. C. Hirschi
ASSOC. MEMBER ASAE | MEMBER ASAE | ASSOC. MEMBER ASAE

ABSTRACT

THERE was close agreement between observed slope steepness effect on soil loss from disturbed lands and that predicted by the USLE slope steepness factors in two categories: (a) for slopes less than 4 m in length, and (b) for slopes greater than 4 m in length but less than 9% steepness. For slopes greater than 4 m in length and between 9 and 33% steepness, the USLE tended to over estimate the observed slope steepness effect. A slope steepness factor equation for this slope range was developed which provides a range of slope steepness factors for a given slope corresponding to the range of slope steepness effects that have been observed experimentally.

INTRODUCTION

There is considerable potential for soil erosion by rainfall and runoff on reclaimed mine lands, construction sites and other "disturbed lands." In these settings, plants, roots and topsoil are commonly removed leaving the exposed soil or subsoil in a highly erodible condition. Quantifying erosion from these areas is necessary to manage on-site and off-site impacts of soil erosion.

The most extensively researched and commonly used method of estimating erosion from rainfall and runoff is the Universal Soil Loss Equation (USLE) (Wischmeier and Smith, 1978). The USLE uses empirically derived relationships and, therefore, is expected to give the most reliable estimates of erosion for conditions which closely resemble those from which the model relationships were developed: medium textured agricultural soils with slopes from 3 to 18% and less than 122 m in length.

Gilley et al. (1977), Stein et al. (1983) and Hahn et al. (1985) observed that the USLE tended to over estimate the effect of slope steepness on soil loss from various reclaimed mine lands. Disturbed lands, such as reclaimed mine soils, may have significantly different characteristics than cropland, such as the lack of soil structure (Thomas and Jansen, 1985), an abundance of gravel and stones (Ashby et al., 1984 and Bonta and Sutton, 1983), surface sealing (Gilley et al., 1977) and a lack of roots or organic matter. These factors may lead to significantly different erosion rates than predicted by the USLE. The presence of stone fragments in soil has been shown to reduce the rate of erosion (McCormack et al., 1984) and runoff (Edwards et al., 1984) from cropland and rangeland.

The objective of this study was to determine whether the USLE slope steepness factors are in agreement with observed slope steepness effects on soil loss from distrubed lands and, if necessary, to develop a slope steepness factor equation that is more appropriate for disturbed land yet which is compatible with the present USLE equation structure.

THE USLE SLOPE STEEPNESS FACTORS

The slope steepness factor of the USLE is defined as the ratio of soil loss from a field slope to that from a uniform, nine percent slope under otherwise identical conditions (Wischmeier and Smith, 1978). Wischmeier and Smith (1978) recommended the following relation between slope steepness and slope steepness factor, which was derived from a Fayette soil under crop production in Wisconsin:

$$S = 65.4\sin^2\theta + 4.56\sin\theta + 0.0654 \quad \ldots\ldots\ldots\ldots [1]$$

where S is the slope steepness factor and θ is the angle of inclination of the land from the horizontal. At this writing, McCool et al. (1987) are proposing a revision of the USLE slope steepness factor. Based on a reanalysis of the Fayette soil data, McCool et al. (1987) recommend the following equation for slopes greater than 9%:

$$S = 16.8\sin\theta - 0.5 \quad \ldots\ldots\ldots\ldots\ldots\ldots [2]$$

For slopes less than 9%, McCool et al. (1987) recommend:

$$S = 10.8\sin\theta + 0.03 \quad \ldots\ldots\ldots\ldots\ldots\ldots [3]$$

which is based upon erosion from the Fayette soil under natural rainfall, and a Dubbs silt loam soil under simulated rainfall.

Equations [1] through [3] were developed from plots 22 m in length. McCool et al. (1987) contend that equations [1] through [3] do not apply to slopes less than 4 m in length. They argue that rill erosion is negligible in areas less than 4 m in length and to estimate the slope steepness effect on soil loss from slopes in this range, McCool et al. (1987) recommend the following slope factor equation:

$$S = 3.0\sin^{0.8}\theta + 0.56 \quad \ldots\ldots\ldots\ldots\ldots\ldots [4]$$

Article was submitted for publication in June, 1986; reviewed and approved for publication by the Soil and Water Div. of ASAE in April, 1987. Presented as ASAE Paper No. 86-2037.

This study was part of Project No. 10-309 of the Agricultural Experiment Station, College of Agriculture, University of Illinois at Urbana-Champaign.

Reclaimed mine land data were collected as part of Project 10-344 of the Illinois Agricultural Experiment Station.

The authors are: G. F. McISAAC, Agricultural Engineer, J. K. MITCHELL, Professor, and M. C. HIRSCHI, Assistant Professor, Agricultural Engineering Dept., University of Illinois, Urbana-Champaign.

Acknowledgment: We acknowledge the cooperation of W. C. Moldenhauer in providing additional data for this study.

  0001-2351/87/3004-1005$02.00

In this study, we compared slope steepness effects predicted by equations [1] through [4] to observed slope steepness effects on soil loss from distrubed lands.

PROCEDURE

We conducted a review of published and unpublised studies in which soil loss was measured from disturbed soils over a range of slopes. Using these reported erosion measurements, ratios of soil loss at a various slope steepness to the soil loss measured or estimated for 9% sloe under otherwise identical conditions were calculated. This ratio is consistent with the definition of the USLE slope factor (Wischmeier and Smith, 1978). For convenience and clarity, this ratio is referred to as the soil loss ratio in this study.

In studies where soil loss was measured at 9% slope (Israelsen et al., 1980; Bonta and Sutton, 1983; Lang et al., 1984; Andrews, 1981 and Watts, 1982), the measured soil losses at various slopes were divided by the mean soil loss measured at 9% slope.

If soil loss was not measured at 9% slope, we estimated a mean soil loss at 9% slope for the given experimental conditions using regression analysis. Various linear and non-linear regression models were tested with soil loss (or soil loss per unit of EI if the data were available) as the dependent variable and a measure of slope steepness as the independent variable. The measures of slope steepness tested were percent slope and sine of the angle of inclination (sin θ). From the regress model with the greatest coefficient of determination, we estimated soil loss at 9% slope, and then divided observed losses by this value to obtain the soil loss ratio for various slopes.

In order to reduce the variability in soil loss due to rainfall, soil loss was divided by the rainfall erosivity factor (EI) as described by Wischmeier and Smith (1978) or as reported by the individual investigators. In these cases, the calculated soil loss ratio was actually a ratio of soil loss per EI at the given slope to the soil loss per EI at 9% slope.

We conducted regression analyses to identify relationships between soil loss ratio and slope steepness under various conditions. Separate regression analyses were conducted for each soil type and rain source (natural or simulated). In these regressions, soil loss ratio was the dependent variable and percent slope and sin θ were tested as independent variables. For slopes less than 4 m in length, we also conducted regressions with sin θ to the 0.8 power as the independent variable.

Finally, regression analyses were conducted with various combinations of experimental conditions in order to identify equations which best describe the slope steepness effect on soil loss from the entire sample of disturbed soils analyzed in this study.

TABLE 1. SOIL LOSS PER EI FOR A SANDY CLAY LOAM SPOIL MATERIAL UNDER SIMULATED AND NATURAL RAINFALL (GILLEY ET AL., 1977 AND 1981).

Rain type	Tillage	Slope, %	Soil Loss x 10^3 per EI, Mg h/MJ mm	Annual soil loss, Mg/ha
simulated	roto-tilled	4.6	5.3	–
simulated	roto-tilled	17.0	8.7	–
simulated	untilled	4.6	9.2	–
simulated	untilled	17.0	12.6	–
natural (1975)	roto-tilled	0.7	1.3	0.6
		4.8	19.3	1.23
		17.6	77.0	6.93
natural (1976)	untilled	0.7	1.3	0.26
		4.8	66.0	12.63
		17.6	337.0	82.87

DATA SOURCES

Gilley et al. (1977 and 1981) reported soil loss from sodic, surface sealing mine spoil under simulated and natural rainfall. Plots 4 m wide and 22.1 m long were established on a sandy clay loam spoil. Rainfall simulations following the method of Meyer (1960) were conducted on one roto-tilled and one untilled plot at 4.6 and 17% slope. Plots for the natural rainfall study were maintained at 0.7, 4.8 and 17.6% slope. In the first year (1975) the natural rainfall plots were roto-tilled four times. In the second year (1976) the plots were not tilled. annual soil loss and EI values (considering only those storms which produced more than 0.25 mm of runoff) appear in Table 1.

Israelsen et al. (1980) measured soil loss from slopes of 9, 25, 50 and 84% in a tilting soil bin 5.9 m long and 1.2 m wide. We considered these soils disturbed since they were reconstructed in the soil bin for the experiment. Three soil materials were tested: a washed sand, a Nibley silty clay loam, and a Cecil gravelly clay loam. The soils were tilled up and down the slope to approximate a crop

TABLE 2. SOIL LOSS FROM SIMULATED RAINFALL ON THREE SOIL TREATMENTS (ISRAELSEN ET AL., 1980).

Slope, %	Rainfall intensity, mm/h	Duration, min	Reported EI, MJ-mm / ha-h	Soil Loss, t/ha		
				Nibley (tilled)	Cecil (tilled)	Nibley (not tilled)
9	64	30	549	0.05	0.17	0.15
9	100	15	339	0.91	0.35	0.43
9	194	8	362	2.03	0.39	0.25
25	64	30	514	0.11	0.31	0.09
25	100	15	318	0.93	0.99	1.10
25	194	10	339	2.38	1.75	10.11
50	64	30	457	0.72	2.13	12.95
50	100	15	284	0.27	4.58	6.29
50	194	10	302	0.35	0.86	12.68
84	64	30	364	9.64	4.79	15.40
84	100	15	226	11.62	4.23	7.82
84	194	10	240	10.68	5.47	18.75

TABLE 3. MEAN RUNOFF VOLUME, PEAK FLOW, AND SOIL LOSS FROM FALLOW RECLAIMED TOPSOIL AND SURFACE MINE SPOIL PLOTS AT VARIOUS SLOPES (BONTA AND SUTTON, 1983).

	Surface mine spoil				Reclaimed topsoil			
Slope, %	Soil* texture	Mean runoff volume, mm	Mean peak runoff rate, mm/h	Mean soil loss, t/ha	Soil* texture	Mean runoff volume, mm	Mean peak runoff rate, mm/h	Mean soil loss, t/ha
9	loam	11.9	63.5	2.2	loam	7.4	40.6	0.66
16	loam	16.2	71.1	6.6	fsl	16.0	63.5	3.3
21	sl	12.9	55.9	3.3	fsl	12.2	58.4	3.7
33	loam	12.7	71.1	7.0	fsl	7.4	33.0	4.0

*sl = sandy loam, fsl = fine sandy loam.

management factor (C) of 1.0. For an additional treatment, the Nibley soil was compacted and not tilled. Simulated rainfall was applied at intensities of 64, 100 and 144 mm/h. Soil loss from the sand was not affected by slope steepness. Soil loss reported by Israelsen et al. (1980) for the three other soil treatments appear in Table 2.

The rainfall erosivity in the study of Israelsen et al. (1980) appears to have been affected by the slope steepness since the fall distance of the rain drops varied from 5.3 to 1.1 m depending upon slope steepness and location in the soil bin. Israelsen et al. (1980) addressed this variation and reported an RLS factor (rainfall erosivity times the slope steepness and slope length factors) for each slope steepness and rainfall intensity.

TABLE 4. SLOPE, RAINFALL INTENSITY AND SOIL LOSS FROM SIMULATED RAINFALL ON RECLAIMED A HORIZON SILT LOAM SOIL AT THE SOLAR SOURCES RECLAIMED STRIP MINE (MOLDENHAUER AND HAHN PERSONAL COMMUNICATION).

Plot ID	Rainfall simulator run*	Slope, %	Rainfall intensity, mm/h	EI, MJ-mm/ha-h	Soil loss, Mg/ha
S6A1	d	5.50	61	790	39.42
S6A1	w	5.50	65	456	31.45
S6A1	v	5.50	64	432	27.26
S6A2	d	5.95	70	1037	63.32
S6A2	w	5.95	69	514	31.87
S6A2	v	5.95	71	541	33.13
S6A3	d	6.05	63	851	40.54
S6A3	w	6.05	63	425	31.87
S6A3	v	6.05	57	344	31.31
S12A1	d	9.70	61	804	85.82
S12A1	w	9.70	60	388	44.87
S12A1	v	9.70	60	382	37.46
S12A2	d	9.40	59	758	62.62
S12A2	w	9.40	61	395	49.48
S12A2	v	9.40	58	366	43.61
S12A3	d	10.15	64	878	88.76
S12A3	w	10.15	64	432	38.30
S12A3	v	10.15	67	481	35.08
S18A1	d	13.10	63	857	85.68
S18A1	w	13.10	63	425	39.42
S18A1	v	13.10	64	432	30.89
S18A2	d	13.40	59	758	93.37
S18A2	w	13.40	64	442	43.75
S18A2	v	13.40	61	395	33.13
S18A3	d	16.40	60	771	120.49
S18A3	w	16.40	60	385	48.50
S18A3	v	16.40	63	428	36.20

*d = dry run, rain applied for 1h on relatively dry soil.
w = wet run, rain applied for ½h, 1h after the conclusion of the dry run.
v = very wet run, rain applied for ½h, approximately ½h after the wet run.

We calculated EI values for eahc storm and slope steepness by dividing the reported RLS by the LS factor (Wischmeier and Smith, 1978) for the experimental conditions. These values also appear in Table 2.

Bonta and Sutton (1983) measured runoff and soil loss from natural rainfall on surface mined land for two years with slopes ranging from 9 to 33%. Plots were 22 m long, 4.6 m wide and prepared with a bulldozer and a road grader. Treatments consisted of 0 and 20 cm of reclaimed topsoil on mine spoil which were maintained in a fallow condition. The mean soil loss from several sampling intervals in Bonta's study appear in Table 3.

Hahn et al. (1985) measured soil loss from simulated rainall (following the method of Meyer and McCune, 1958) on two mine reclamation sites (Ayreshire and Solar Sources) with slopes ranging from 5 to 16% and a constant slope length of 11 m. Both sites were reclaimed with topsoil that had been stockpiled during the mining operation. The reclamation area was smoothed with a bulldozer and the experimental plots were disked up-and-down hill before rainfall simulation.

Hahn et al. (1985) did not report measured soil loss but reported soil loss normalized by the method described by Meyer (1960) in which soil loss is divided by the square of the ratio of the mesured rainfall intensity to the target rainfall intensity. However, due to uncertainty

TABLE 5. SLOPE, RAINFALL INTENSITY AND SOIL LOSS FROM SIMULATED RAINFALL ON RECLAIMED B HORIZON SILT LOAM SOIL AT THE SOLAR SOURCES RECLAIMED STRIP MINE (MOLDENHAUER AND HAHN PERSONAL COMMUNICATION).

Plot ID	Rainfall simulator run*	Slope, %	Rainfall intensity, mm/h	EI, MJ-mm/ha-h	Soil loss, Mg/ha
S6B1	d	5.85	62	830	32.71
S6B1	w	5.85	64	442	26.84
S6B1	v	5.85	64	442	25.72
S6B2	d	6.75	66	920	10.48
S6B2	w	6.75	62	408	13.28
S6B2	v	6.75	59	369	19.57
S6B3	d	6.45	64	871	25.16
S6B3	w	6.45	64	442	23.76
S6B3	v	6.45	63	425	25.02
S12B1	d	8.85	62	823	81.35
S12B1	w	8.85	64	432	55.49
S12B1	v	8.85	65	456	39.98
S12B2	d	9.50	63	857	69.33
S12B2	w	9.50	61	402	38.16
S12B2	v	9.50	63	425	27.26

*d = dry run, rain applied for 1h on relatively dry soil.
w = wet run, rain applied for ½h, 1h after the conclusion of the dry run.
v = very wet run, rain applied for ½h, approximately ½h after the wet run.

TABLE 6. SLOPE, RAINFALL INTENSITY AND SOIL LOSS FROM RAINFALL SIMULATIONS ON RECLAIMED A HORIZON SILT LOAM SOIL AT THE AYRESHIRE RECLAIMED STRIP MINE (MITCHELL ET AL., 1983 AND MITCHELL AND MOLDENHAUER, 1981).

Plot ID	Rainfall simulator run*	Slope, %	Rainfall intensity, mm/h	EI, MJ-mm/ha-h	Soil loss, Mg/ha
A6A1	d	5.78	61	782	12.72
A6A1	w	5.78	61	391	19.67
A6A1	v	5.78	62	408	19.26
A6A2	d	4.99	57	697	15.10
A6A2	w	4.99	56	340	10.28
A6A2	v	4.99	57	340	7.66
A6A3	d	5.82	61	782	1.45
A6A3	w	5.82	61	391	1.76
A6A3	v	5.82	62	408	2.91
A12A1	d	10.90	55	612	50.62
A12A1	w	10.90	55	306	44.35
A12A1	v	10.90	64	425	38.30
A12A2	d	10.70	64	851	26.66
A12A2	w	10.70	55	323	21.44
A12A2	v	10.70	55	323	21.17
A12A3	d	11.50	54	629	35.17
A12A3	w	11.50	54	306	29.79
A12A3	v	11.50	56	340	31.72
A18A1	d	15.65	64	851	47.00
A18A1	w	15.65	61	408	20.63
A18A1	v	15.65	57	340	16.80
A18A2	d	15.09	53	578	68.28
A18A2	w	15.09	54	306	39.54
A18A2	v	15.09	55	306	25.85
A18A3	d	13.10	61	782	55.62
A18A3	w	13.10	58	357	47.26
A18A3	v	13.10	64	425	25.54

*d = dry run, rain applied for 1h on relatively dry soil.
w = wet run, rain applied for ½h, 1h after the conclusion of the dry run.
v = very wet run, rain applied for ½h, approximately ½h after the wet run.

about their rain gauge measurements, Hahn calculated the rainfall intensity from the runoff in the final 20 min of the simulated rainfall. Neither the measured nor the calculated rainfall intensities were reported by Hahn et al. (1985).

Moldenhauer and Hahn (personal communication, 1985) provided the rain gauge and soil loss measurements and the calcuated rainfall intensities used in the study of Hahn et al., 1985. In our judgment, the calculated rainfall intensities used by Hahn et al. (1985) were too variable for simulated rainfall. We calculated soil loss per EI ratios using the actual rain gauge measurements. Soil loss and rainfall erosivity data for a reclaimed A horizon silt loam soil at the Solar Sources location appear in Table 4. Data provided by Moldenhauer and Hahn from a reclaimed B horizon silt loam soil at the Solar Sources site appear in Table 5 and were also used in our regression analyses.

Soil loss and rainfall erosivity data from reclaimed A horizon silt loam soils at the Ayreshire location appear in Table 6. Some of these data were taken from Mitchell et al. (1983). Data from reclaimed B horizon silt loam soil at the Ayreshire site appear in Table 7. These data were provided by Mitchell and Moldenhauer (1981).

Andrews (1981) measured soil loss from 1-m square plots of two reclaimed mine soils (Mecco and Sunspot) under simulated rain at 63 mm/h at 4.5 and 9% slope. Andrews conducted these tests over a 2-h period and these data appear in Table 8. Soil was packed in the bin to approximate average bulk density observed at the

TABLE 7. SLOPE, RAINFALL INTENSITY AND SOIL LOSS FROM RAINFALL SIMULATIONS ON RECLAIMED B HORIZON SILT LOAM SOIL AT THE AYRESHIRE RECLAIMED STRIP MINE (MITCHELL AND MOLDENHAUER, 1981).

Plot ID	Rainfall simulator run*	Slope, %	Rainfall intensity, mm/h	EI, MJ-mm/ha-h	Soil loss, Mg/ha
A6B1	d	6.33	61	816	29.93
A6B1	w	6.33	62	408	12.19
A6B1	v	6.33	62	408	11.02
A6B2	d	5.42	70	1038	32.66
A6B2	w	5.42	75	612	13.13
A6B2	v	5.42	70	527	9.48
A6B3	d	7.11	66	936	32.03
A6B3	w	7.11	63	425	10.75
A6B3	v	7.11	62	408	9.32
A12B1	d	9.88	59	748	61.82
A12B1	w	9.88	55	323	25.24
A12B1	v	9.88	62	408	22.18
A12B2	d	10.3	56	663	40.54
A12B2	w	10.3	54	306	14.67
A12B2	v	10.3	54	306	12.72
A12B3	d	9.68	57	680	48.83
A12B3	w	9.68	52	289	18.82
A12B3	v	9.68	54	289	14.49

*d = dry run, rain applied for 1h on relatively dry soil.
w = wet run, rain applied for ½h, 1h after the conclusion of the dry run.
v = very wet run, rain applied for ½h, approximately ½h after the wet run.

reclamation sites.

Watts (1982) measured soil loss from 1-m square plots of reclaimed mine soil under simulated rainfall at 64 mm/h. One mine soil (Captain) was tested at 4.5 and 9% slope, and the other (Ayreshire) was tested at 6 and 12% slope. Measured soil losses after 2 h of rainfall for three replicates of each slope appear in Table 9.

Lang et al. (1984) measured soil loss from 1-m square plots of surface mined topsoil at 9 and 3% slope under simulated rainfall. Two surface mined topsoils (Falkirk and Indian Head mines) which had been stockpiled were air dried, rolled, passed through a 1.27 cm sieve, and packed to a bulk density of 1.18 g/cc, except for the top 2 cm of soil which was not packed. The two soils were tested at 2 levels of antecedent moisture content, two slopes and three levels of surface cover. These data appear in Table 10.

RESULTS

Regression analyses indicated that in nearly all cases the effect of slope steepness on soil loss, soil loss per EI

TABLE 8. CUMULATIVE SOIL LOSS FROM 120 MIN OF SIMULATED RAINFALL ON 1-m SQUARE PLOTS OF TWO RECLAIMED SURFACE MINE TOPSOILS (ANDREWS, 1981).

Surface mine name	Slope, %	Cumulative rainfall erosivity, MJ-mm/ha-h	Cumulative soil loss, t/ha
Mecco	9	2463	12.5
	9	2463	9.9
	9	2463	10.7
	4.5	2463	9.0
	4.5	2463	10.3
	4.5	2463	6.6
Sunspot	9	2463	11.8
	9	2463	10.8
	4.5	2463	8.0
	4.5	2463	7.0

TABLE 9. CUMULATIVE SOIL LOSS FROM 120 MIN OF SIMULATED RAINFALL ON 1-m SQUARE PLOTS OF TWO RECLAIMED MINE TOPSOILS (WATTS, 1982).

Surface mine name	Slope, %	Cumulative rainfall erosivity, MJ-mm/ha-h	Cumulative soil loss, t/ha
Captain	9	2553	21.1
	9	2345	51.4
	9	2414	16.3
	4.5	2491	14.1
	4.5	2221	16.2
	4.5	2138	26.5
Ayreshire	12	2483	17.5
	12	2437	19.5
	12	2468	31.0
	6	2514	13.4
	6	2499	18.4
	6	2562	12.6

and soil loss ratio was best described as a linear function of either percent slope or sine of the angle of inclination (sin θ). Regressions with percent slope as the independent variable tended to have a slightly greater coefficient of determination than the corresponding regression using sin θ as the independent variable, but the differences were not significant.

The linear regression results with soil loss ratio as the dependent variable and sin θ as the independent variable for individual soil types and experimental conditions appear in Table 11. The regression coefficients ranged

TABLE 10. MEAN SOIL LOSS AND RUNOFF RATES FROM SIMULATED RAIN ON 1-m SQUARE PLOTS OF TWO RECLAIMED SURFACE MINE SOILS AT TWO ANTECEDENT MOISTURE CONDITIONS AND THREE LEVELS OF RESIDUE COVER (LANG ET AL., 1984).

Surface mine name	Slope, %	Mulch rate, t/ha	Antecedent moisture condition	Water loss* kg/m^2-h	Soil loss* kg/m^2-h
Falkirk	3	0	dry	30.5	0.33
	3	0	wet	48.1	0.35
	3	1.12	dry	21.9	0.13
	3	1.12	wet	39.8	0.18
	3	2.24	dry	17.4	0.07
	3	2.24	wet	48.3	0.17
	9	0	dry	32.5	0.47
	9	0	wet	44.9	0.46
	9	1.12	dry	26.1	0.17
	9	1.12	wet	50.4	0.34
	9	2.24	dry	20.7	0.11
	9	2.24	wet	46.2	0.20
Indian Head	3	0	dry	27.4	0.17
	3	0	wet	44.8	0.26
	3	1.12	dry	24.6	0.09
	3	1.12	wet	47.9	0.19
	3	2.24	dry	22.5	0.07
	3	2.24	wet	48.2	0.10
	9	0	dry	28.3	0.27
	9	0	wet	43.7	0.36
	9	1.12	dry	25.6	0.13
	9	1.12	wet	50.2	0.28
	9	2.24	dry	25.1	0.09
	9	2.24	wet	48.6	0.16

*Values are averages of two replications.

TABLE 11. DATA SOURCES, EXPERIMENTAL CONDITIONS, AND RESULTS OF LINEAR REGRESSIONS WITH SOIL LOSS RATIO AS THE DEPENDENT VARIABLE AND SIN θ AS THE INDEPENDENT VARIABLE, WHERE EROSION PLOTS WERE GREATER THAN 4 m IN LENGTH.

Data source	Soil texture*	Rain source†	Slope steepness, %	Regression coefficient	Standard error‡	Intercept	n§	r^2
Gilley et al. (1977)								
tilled	scl	S	4.6, 17	4.3	—	0.61	2	—
not tilled	scl	S	4.6, 17	2.6	—	0.76	2	—
both tillage treatments	scl	S	4.6, 17	3.5	0.6	0.68	4	0.94
Gilley et al. (1981)								
tilled	scl	N	0.7, 4.8, 17.6	12.8	1.0	−0.06	3	0.99
not tilled	scl	N	0.7, 4.8, 17.6	13.2	1.3	−0.13	3	0.99
both tillage treatments	scl	N	0.7, 4.8, 17.6	13.0	0.6	−0.16	6	0.99
Israelsen et al. (1980)								
Nibley soil, compacted	sicl	S	9, 25, 50, 84	146.7	26.0	−6.5	4	0.94
Nibley soil, tilled	sicl	S	9, 25, 50, 84	24.4	14.0	−4.0	4	0.60
Cecil soil, tilled	grcl	S	9, 25, 50, 84	40.9	8.5	−4.9	4	0.92
Israelsen et al. (1980)								
Nibley soil, compacted	sicl	S	9, 25	7.6	—	0.32	2	—
Nibley soil, tilled	sicl	S	9, 25	1.4	—	0.87	2	—
Cecil soil, tilled	grcl	S	9, 25	16.9	—	−0.53	2	—
Bonta and Sutton (1983)	fsl	N	16, 21, 33	1.4	0.5	0.90	3	0.89
	l	N	9, 16, 33	8.4	6.5	0.83	3	0.62
Hahn et. al. (1985), and Moldenhauer and Hahn (personal communications)								
A horizon	sil	S	5.5 to 16.4	6.9	1.3	0.38	9	0.80
B horizon	sil	S	5.8 to 9.5	18.8	8.0	−0.68	5	0.64
Mitchell et al. (1983), and Mitchell and Moldenhauer (1981)								
A horizon	sil	S	5.0 to 15.6	13.9	4.5	−0.25	9	0.57
B horizon	sil	S	5.4 to 10.3	16.3	3.9	−0.46	6	0.81

* scl = sandy clay loam, fsl = fine sandy loam, sicl = silty clay loam, grcl = gravely clay loam, l = loam, sil = silt loam.
† S = simulated rain, N = natural rain.
‡ Standard error of the regression coefficient.
§ Number of observations in regression analysis.

TABLE 12. RESULTS OF LINEAR REGRESSION WITH SELECTED SOIL LOSS RATIOS AS THE DEPENDENT VARIABLE AND SIN θ AS THE INDEPENDENT VARIABLE, WHERE EROSION PLOT LENGTHS WERE GREATER THAN 4 m.

Selection criteria	Slope range, %	Regression coefficient	Standard error*	Intercept	n†	r^2
Ayreshire and solar sources reclamation sites						
dry runs‡	5 to 16.4	15.8	2.0	−0.44	29	0.69
wet runs		10.3	2.2	0.04	29	0.45
very wet runs		6.7	1.9	0.37	29	0.38
cumulative soil loss§		11.8	1.8	−0.09	29	0.61
Central data set‖	0.7 to 33	12.1	0.9	−0.09	42	0.80
Central data set, slopes > 8%	8.0 to 33	10.7	1.6	0.14	26	0.66
All data	0.7 to 33	8.2	1.0	0.22	51	0.57

* Standard error of regression coefficient.
† Number of observations in regression analysis.
‡ Dry run, wet run, and very wet runs are simulated rain storms which have been previously described.
§ Soil loss ratios calculated from cumulative soil loss from three simulated rain storms (dry, wet and very wet runs).
‖ Central data set includes all soil loss ratios calculated for slopes greater than 4 meters in length and less than 33% steepness excluding the data of Gilley et al. (1977), the fine sandy loam reclaimed topsoil of Bonta and Sutton (1983) and the tilled Nibley soil of Israelsen et al. (1980).

from 147 to 1.4. The mean value of the regression coefficients was 23.8 with a standard deviatio of 36.8.

The three largest regression coefficients (147, 40.9 and 24.4) were all from data of Israelsen et al. (1980) and describe the slope steepness effect for slopes from 9 to 84%. The maximum slope in the other studies was 33%. Regresssion analysis considering only the 9 and 25% sloeps of the Israelsen et al. (1980) gives coefficients of 7.6, 16.9 and 1.4 for the compacted Nibley, tilled Cecil, and the tilled Nibley soils, respectively, which are similar to regression coefficients observed for the other studies. The greater regression coefficients for steeper sloeps may reflect the initiation of mechanisms of soil movement which do not occur at lesser slopes. Sidle et al. (1985) report that slopes greater than 47% are subject to avalanches and earth slumps.

For slopes of 33% or less, the smallest regression coefficients were observed from the tilled Nibley soil (Israelsen et al., 1980), the reclaimed fine sandy loam soil (Bonta and Sutton, 1983) and the sandy clay loam spoil under simulated rainfall (Gilley et al., 1981).

The regression coefficients for the sandy clay loam of Gilley et al. under simulated rainfall (1977) were significantly less than the regression coefficients for the same soil under natural rainfall (Gilley et al. 1981). The cause of this difference is unknown. For the simulated rainfall experimetns, a total of 128 mm of rain was applied in 2 days. In the natural rainfall study, erosion measurements were based on 233 mm of rainfall over the 2-yr period. It would appear that a greater portion of the natural rain fell on initially dry soil, a condition which appears to lead to a greater effect of slope steepness on soil loss, as observed by Hahn et al. (1985).

Results of regressions with selected combinations of soil loss ratios for slopes longer than 4 m appear in Table 12.

Considering soil loss ratios from individual simulated rain storms at the Ayreshire and Solar Sources locations, the regression coefficient decreases from 15.8 for the initial rain storm (dry run) to 6.7 for the third rain storm (very wet run). For most plots, the dry run was the first rainfall after disking, the soil was relatively dry and rain was applied for approximately 1 h. The wet and very wet runs were ½ h storms which followed the dry runs. The trend for the regression coefficient to decrease from the dry to the very wet run indicates that the slope steepness effect for an individual storm is influenced by antecedent moisture content, duration of rainfall and/or cumulative rainfall effects on the soil surface. Therefore, an annual slope steepness factor may be influenced by annual distribution of rainfall and tillage.

For slopes of 33% or less, we observed that most of the regression coefficients were between 6.9 and 18.8 (Table 11). We refer to the soil loss ratios from the studies with regression coefficients within this range as the central data set, which includes all of the calculated soil loss ratios except for those of the tilled Nibley soil (Israelsen et al., 1980), the reclaimed fine sandy loam soil (Bonta and Sutton, 1983). Regression coefficients for these conditions were considerably less than 6.9. When these data are omitted from the regression analyses, the following linear regression equation is the best fit of the data with a coefficient of determination of 0.80:

$$SLR = 12.1 \sin \theta - 0.10 \quad \ldots\ldots\ldots\ldots\ldots\ldots [5]$$

When only slopes greater than 8% in the central data set are considered in the regression analysis, the regression coefficient decreases to 10.7 and the regression coefficient of determination decreases to 0.66. This result suggests a lesser regression coefficient as slope steepness increases which is in contradiction to the slope steepness effect observed for the Fayette soil (equations [1], [2] and [3]).

The soil loss ratios calculated for all soil textures with slope lengths greater than 4 m and slopes of 33% or less were best described as a quadradic function of sin θ:

$$SLR = -24.8 \sin^2 \theta + 15.7 \sin \theta - 0.19 \qquad r^2 = 0.61$$

$$\ldots\ldots\ldots\ldots\ldots\ldots\ldots\ldots\ldots\ldots\ldots\ldots [6]$$

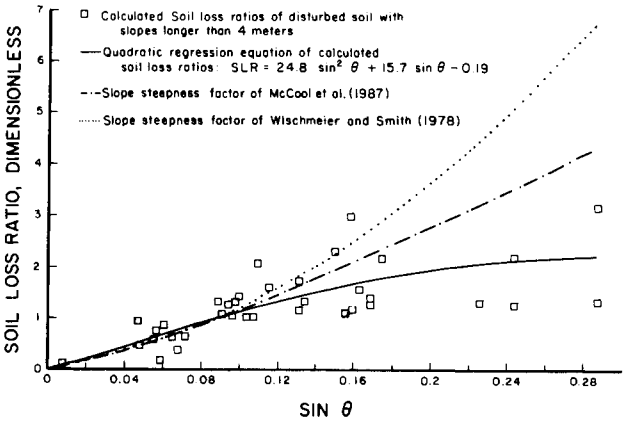

Fig. 1—Calculated soil loss ratios for disturbed lands with slopes greater than 4 m in length, quadratic regression equation [6] from this study, and USLE slope steepness factors of Wischmeier and Smith (1978) and McCool et al. (1987).

where SLR is the soil loss ratio as previously defined. Equations [1], [2], [3], [6] and the calculated soil loss ratios appear in Fig. 1. For slopes less than 9% there is close agreement between all slope factor equations. For slopes greater than 9%, there is considerable divergence.

McCool et al. (1987) reported some conditions in which the slope steepness effect could be expressed as a single linear equation for slopes up to 20%. Lillard et al. (1941) observed a linear effect of slope steepness on soil loss from contoured cropland at slopes up to 25%. Normalization to 9% slope of the soil loss vs. slope steepness relation of Lillard et al (1941) results in a coefficient of sin θ of 11.0.

McCool et al. (1987) argue that the effect of slope steepness increases for steeper slopes due to initiation of soil detachment by runoff. According to Meyer (1985), soil loss at low slopes is mostly interrill erosion limited by the transport capacity of the runoff. As slope steepness increases, soil erosion becomes limited by the rainfall detachment rate. As slopes exceed 5 to 10%, the runoff develops enough energy to detach particles and cause substantial rill erosion.

We offer two hypotheses which, if correct, may explain why lesser soil loss ratios were observed for disturbed lands than predicted by equations [1] and [2]. First, at steep slopes, soil detachment by runoff may have been limited by stone fragments, or a compacted layer caused by the action of bulldozers and road graders used in the mine reclamation process. Thus, reclaimed mine land may be less susceptable to rill erosion than cropland. Secondly, erosion at steep slopes might have been further limited by the quantity of rainfall and runoff, which, due to the relatively short periods of observation, may not have included very high intensity rainfall and therefore, may not reflect the long term slope steepness effects of these soils.

Soil loss ratios for slopes less than 4 m were equally well described by linear functions of percent slope, sin θ, or sin θ to the 0.8 power. The results of the later regression are presented in Table 13. The regression coefficients ranged from 1.8 to 5.7. The mean regression coefficient is 3.9, and soil loss ratios from all of these studies were best described by the following equation:

$$SLR = 4.0 \sin^{0.8} \theta + 0.4 \quad \ldots\ldots\ldots\ldots\ldots\ldots [7]$$

TABLE 13. DATA SOURCES, EXPERIMENTAL CONDITION WHERE EROSION PLOTS WERE LESS THAN FOUR METERS IN LENGTH, AND RESULTS OF LINEAR REGRESSION WITH SOIL LOSS RATIO AS THE DEPENDENT VARIABLE AND SIN θ TO THE 0.8 POWER AS THE INDEPENDENT VARIABLE.

Data source		Slope steepness, %	Regression coefficient	Standard error*	Intercept	n†	r^2
Andrews (1981)							
Mecco mine		4.5, 9	3.5	1.9	0.49	6	0.45
Sunspot mine		4.5, 9	5.5	1.0	0.20	4	0.93
Watts (1982)							
Captain mine		4.5, 9	5.1	6.9	0.26	6	0.12
Ayreshire mine		6, 12	5.7	3.2	0.17	6	0.44
Lang et al. (1984)							
Falkirk							
bare surface	dry	3, 9	3.5		0.49	2	
	wet	3, 9	2.8		0.59	2	
1.1 t/ha mulch	dry	3, 9	2.8		0.59	2	
	wet	3, 9	5.6		0.19	2	
2.2 t/ha mulch	dry	3, 9	4.3		0.37	2	
	wet	3, 9	1.8		0.74	2	
Indian Head							
bare surface	dry	3, 9	4.4		0.36	2	
	wet	3, 9	3.3		0.52	2	
1.1 t/ha mulch	dry	3, 9	3.6		0.48	2	
	wet	3, 9	3.8		0.45	2	
2.2 t/ha mulch	dry	3, 9	2.6		0.62	2	
	wet	3, 9	4.4		0.36	2	
Grand mean			3.9				

*Standard error of the regression coefficient.
†Number of observations in regression analysis.

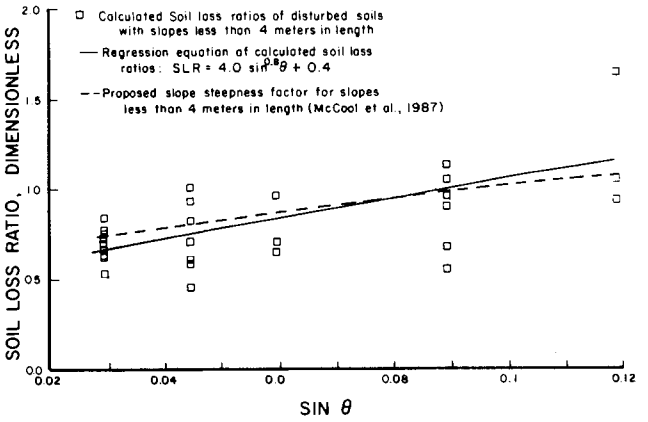

Fig. 2—Calculated soil loss ratios for disturbed lands with slopes less than 4 m in length, linear regression equation [7] from this study, and the slope steepness factor for short slopes of McCool et al. (1987).

Equation [7] is not significantly different from equation [4], as illustrated in Fig. 2.

RECOMMENDATIONS

To estimate the effect of slope steepness on soil erosion from disturbed lands for slopes less than 4 m in length, we recommend equation [4]. For slopes greater than 4 m in length and less than 9% steepness we recommend equation [3]. Between 9 and 30% steepness for slopes greater than 4 m in length, we recommend the following equation:

$$S = (12 \pm 7)\sin\theta + B \quad \ldots\ldots\ldots\ldots\ldots\ldots [8]$$

where S is the slope steepness factor, θ is the angle of inclination of the land from the horizontal, and B is an intercept chosen such that S = 1.0 at 9% slope.

A regression coefficient of 12 represents a median value of the conditions tested in this study. However, for various experimental conditions, regression coefficients ranged from 1.4 to 18.8. Thus, the range of regression coefficients provided in equation [8] expresses much of the variation in slope steepness effects which has been observed experimentally.

Equation [8] is based upon soil loss from research plots at slopes up to 33%. For slopes greater than 33%, soil may be transported by mechanisms other than sheet and rill erosion (Sidle et al., 1985). Consequently, even the maximum slope factor extrapolated from equation [8] may underestimate soil loss.

Additional research is needed to evaluate the effect of slope steepness on soil loss from disturbed lands. Our results indicate that slope steepness effects are influenced by antecedent moisture content and/or cumulative effects of rainfall on the soil surface. The variation in slope steepness effects may also be influenced by soil texture and the presence of stone fragments. The avilable data are insufficient to quantify exact slope steepness effects for given conditions of soil texture, compaction or rainfall distribution pattern. Reserach is needed which addresses the interactions of slope steepness, tillage, rainfall intensity, antecedent moisture content and soil texture on soil erosion by rainfall on distrubed land.

SUMMARY AND CONCLUSIONS

The effect of slope steepness on soil loss from disturbed lands was evaluated. From soil erosion measurements, we calculated ratios of soil loss from disturbed land at various slopes to soil loss measured or estimated for 9% slope under otherwise identical conditions.

Results indicate close agreement between observed soil loss ratio and that predicted by the USLE slope steepness factors for two slope categories: (a) slopes less than 4 m in length, and (b) slopes greater than 4 m in length and less than 9% steepness. For slopes between 9 and 33% and slope lengths greater than 4 m, the USLE tended to overestimate the observed soil loss ratios. The relationship between slope steepness and soil loss ratio varied considerably across experimental conditions, however most of the soil loss ratios fell within a central range.

For slopes greater than 4 m in length and between 9 and 30% steepness we developed a slope steepness factor equation for estimating soil erosion from disturbed land. This equation provides a range of possible slope steepness factors, corresponding to those observed under experimental conditions.

Further research is recommended on the influence of soil texture, antecedent moisture content, and cumulative rainfall effects on slope steepness effects.

References

1. Andrews, J. E. 1981. Erosion characteristics of reclaimed surface mined topsoil under rainfall simulation at 9% and 4.5% slope. Unpublished AE 299 Research Report. Department of Agricultural Engineering, University of Illinois at Urbana-Champaign.

2. Ashby, W. C., W. G. Vogel, C. A. Kolar and G. R. Philo. 1984. Productivity of stony soils on strip mines. p. 31-44. In: Nichols, J. D. (ed.). Erosion and productivity of soils containing rock fragments. Soil Science Society of America, Madison, WI.

3. Bonta, J. V. and P. Sutton. 1983. Erosion and reclamation plots: research on the hydrology and water quality of watersheds subjected to surface mining. Report for Grant No. 50166054, December 1983. U.S. Bureau of Mines, Department of the Interior.

4. Edwards, W. M., P. F. Germann, L. B. Owens, and C. A. Amerman. 1984. Watershed studies of factors influencing infiltration, runoff, and erosion on stony and non-stony soils. p. 45-54. In: Nichols, J. D. (ed.). Erosion and productivity of soils containing rock fragments. Soil Science Society of America, Madison, WI.

5. Gilley, J. E., G. W. Gee, A. Bauer, W. O. Willis, and R. A. Young. 1977. Runoff and erosion characteristics of surface-mined sites in Western North Dakota. TRANSACTIONS of the ASAE 20(4):697-700.

6. Gilley, J. E., F. W. Schroer, and L. Zimmerman. 1981. Suspended and dissolved solids in runoff from rangeland and surface mined sites in Western North Dakota. North Dakota Research Report No. 88. N.D. Agricultural Experiment Station, Fargo.

7. Hahn, D. T., W. C. Moldenhauer, and C. B. Roth. 1985. Slope gradient effect on erosion of reclaimed soil. TRANSACTIONS of the ASAE 28(3):805-808.

8. Israelsen, C. E., C. G. Clyde, J. E. Fletcher, E. K. Israelsen, F. W. Han, P. E. Packer, and E. E. Farmer. 1980. Erosion control during highway construction, manual on principles and practices. National Cooperative Highway Research Program Report No. 221, Transportation Research Board, National Research Council, Washington, D.C.

9. Lang, J. K., L. Prunty, S. A. Schroeder, and L. A. Disrud. 1984. Interrill erosion as an index of mined land erodibility. TRANSACTIONS of the ASAE 27(1):99-104.

10. Lillard, J. H., H. T. Rogers and J. Elson. 1941. Effects of slope, character of soil, rainfall, and cropping treatments on erosion losses from Dunmore silt loam. Technical Bulletin 72. Virginia Agricultural Experiment Station, Blacksburg.

11. McCool, D. K., L. C. Brown, G. R. Foster, C. K. Mutchler, and L. D. Meyer. 1984. Revised slope steepness factor for the Universal Soil Loss Equation. TRANSACTIONS of the ASAE (in press).

12. McCormack, D. E., K. K. Young, and G. M. Darby. Rock fragments and the K factor of the Universal Soil Loss Equation. p. 73-82. In: Nichols, J. D. (ed.). Erosion and productivity of soils containing rock fragments. Soil Science Society of America, Madison, WI.

13. Meyer, L. D. 1960. Use of rainulator on runoff plot research. SSSA Proc. 24(4):319-322.

14. Meyer, L. D. and D. L. McCune. 1958. Rainfall simulator for runoff plots. AGRICULTURAL ENGINEERING 39(10):644-648.

15. Meyer, L. D., W. H. Wischmeier, and W. H. Daniel. 1971. Erosion, runoff, and revegetation of denuded construction sites. TRANSACTIONS of the ASAE 14(1):139-141.

16. Mitchell, J. K. and W. C. Moldenhauer. 1981. Unpublished data collected as a part of Project 10-344 of the Illinois Agricultural Experiment Station.

17. Mitchell, J. K., W. C. Moldenhauer, and D. D. Gustavson. 1983. Erodibility of selected reclaimed surface mined soils. TRANSACTIONS of the ASAE 26(5):1413-1417.

18. Stein, O. R., C. B. Roth, W. C. Moldenhauer, and D. T. Hahn. 1983. Erodibility of selected Indiana reclaimed strip mined soils. Proceedings of the 1983 Symposium on Surface Mining, Hydrology, Sedimentology and Reclamation. University of Kentucky, Lexington, pp. 101-106.

19. Thomas, D., and I. Jansen. 1985. Soil development in coal mine spoils. Journal of Soil and Water Conservation 40(5):439-442.

20. Watts, S. R. 1982. Erosion characteristics of four surface mined soils using laboratory rainfall simulation. Unpublished AE 299 Research Report. Department of Agricultural Engineering, University of Illinois at Urbana-Champaign.

21. Wischmeier, W. H. and D. D. Smith. 1978. Predicting rainfall erosion losses. Agriculture Handbook No. 537. USDA-Science and Education Administration, Washington, D.C.

Assessment of erosion, sedimentation, and water quality impacts of the Mountain Valley Pipeline and Equitrans Expansion Project's proposed crossing of the Jefferson National Forest as it pertains to the U.S. Forest Service's Draft Supplemental Environmental Impact Statement dated December 2022

Prepared by Jonathan A. Czuba, Ph.D., Licensed Professional Engineer - February 9, 2023

REFERENCES
16

February 21, 2023

Published September, 2000

Slope Length Effects on Soil Loss for Steep Slopes

B. Y. Liu, M. A. Nearing,* P. J. Shi, and Z. W. Jia

ABSTRACT

Empirical soil erosion models continue to play an important role in soil conservation planning and environmental evaluations around the world. The effect of hillslope length on soil loss, often termed the *slope length factor*, is one of the main and most variable components of any empirical model. In the most widely used model, the Universal Soil Loss Equation (USLE), normalized soil loss, *L*, is expressed as a power function of slope length, λ, as $L = (\lambda/22.1)^m$, in which the slope exponent, *m*, is 0.2, 0.3, 0.4, and 0.5 for different, increasing slope gradients. In the Revised Universal Soil Loss Equation (RUSLE), the exponent, *m*, is defined as a continuous function of slope gradient and the expected ratio of rill to interrill erosion. When the slope gradient is 60% and the ratio of rill to interrill erosion is classified as moderate, the exponent *m* has the value of 0.71 in RUSLE, as compared with 0.5 for the USLE. The purpose of this study was to evaluate the relationship between soil loss and slope length for slopes up to 60% in steepness. Soil loss data from natural runoff plots at three locations on the Loess Plateau in China and data from a previous study were used. The results indicated that the exponent, *m*, for the relationship between soil loss and the slope length for the combined data from the three stations in the Loess Plateau was 0.44 ($r^2 = 0.95$). For the data as a whole, the exponent did not increase as slope steepness increased from 20 to 60%. We also found that the value of *m* was greater for intense storms than for less intense storms. These experimental data indicate that the USLE exponent, $m = 0.5$, is more appropriate for steep slopes than is the RUSLE exponent, and that the slope length exponent varies as a function of rainfall intensity.

BECAUSE PHYSICALLY BASED MODELS are either not well tested or require many input parameters, empirical soil loss models still play an important role in soil conservation planning. This is especially true for those areas where extensive soil and biological data that are required by process-based models are not readily available. The USLE (Wischmeier and Smith, 1978) is the most widely used empirical erosion model worldwide. The USLE was revised recently as the RUSLE (Renard et al., 1997). The slope length factor is one of the main factors for soil loss predictions in both the USLE and RUSLE. It is also one of the most variable factors, as we discuss below.

The slope length factor has often been expressed as (Zingg, 1940):

$$L' = a\lambda^m \quad [1]$$

where L' is soil loss (mass per unit area per unit time), λ (m) is slope length, and *a* and *m* are empirical coefficients. Normalizing to a unit plot of length 22.13 m, both the USLE and RUSLE use the equation

$$L = (\lambda/22.13)^m \quad [2]$$

where *L* is soil loss normalized to the 22.13-m-long slope. The differences of slope length factors from the literature can be compared directly by comparing the *m* values. Zingg (1940) proposed 0.6 as the slope length exponent. Musgrave (1947) suggested 0.3. A study conducted at Purdue University in 1956 recommended 0.5 ± 0.1 (Wischmeier et al., 1958). In the USLE (Wischmeier and Smith, 1978), the *m* values recommended were 0.2, 0.3, 0.4, and 0.5 for slope gradients <1, 1 to 3, 3.5 to 4.5, and 5% or greater, respectively. Thus, when the slope gradient is >5%, the slope length factor for the USLE does not change with slope steepness. However, in RUSLE, *m* increases continuously with the slope steepness according to (Renard et al., 1997)

$$m = \beta/(1 + \beta) \quad [3]$$

and

$$\beta = (\sin\theta/0.0896)/3.0\ \sin\theta^{0.8} + 0.56) \quad [4]$$

where β is the ratio of rill erosion to interrill erosion, and θ is the angle of the slope. When slope steepness is equal to 9%, the slope length exponent for both USLE and RUSLE is 0.5. When the slope is <9%, the USLE has a greater slope length factor than RUSLE. When the slope is steeper than 9%, USLE has a lesser slope length factor than RUSLE. The greatest differences are for the steepest slopes (Fig. 1). According to Eq. [3] and [4], the slope length exponent, *m*, is 0.71 for a 60% a 60-m-long slope with a moderate rill/interrill erosion ratio. Under these conditions, RUSLE will have a slope length factor, *L*, which is 23% greater than that for the USLE.

Many classifications of slope steepness for soil and land surveys take 30% as a starting point for "steep" slopes (McDonald et al., 1984; Liu and Tang, 1987). The data used to develop the USLE and RUSLE involved slopes only up to 18% (McCool et al., 1989). However, McCool et al. (1993) studied the effect of both slope length and slope steepness on cropped slopes up to 56% gradient in the northwestern wheat (*Triticum aestivum* L.) region of the United States by performing field surveys of rill networks. Several hundred data points were used in their study. Mean slope steepness was 28.4%, with 95% of the data points collected on slopes ranging from 9 to 48%. The authors concluded by recommending a slope length exponent, *m*, of 0.5.

The purpose of our study was to analyze experimental data for slopes up to nearly 60% in steepness to evaluate the relationship between soil loss and slope length for

Bao Y. Liu, Beijing Normal Univ., Beijing, China; Mark A. Nearing, National Soil Erosion Research Lab., USDA-ARS, 1196 SOIL Bldg., Purdue Univ., West Lafayette, IN 47907-1196; Pei J. Shi, Open Research Lab. of Environment Change and Disaster of the State Education Commission, Beijing, China; and Zhi W. Jia, Institute of Soil and Water Conservation, Chinese Academy of Sciences, Yangling, Shaanxi, China. Received 15 July 1999. *Corresponding author (mnearing@purdue.edu).

Published in Soil Sci. Soc. Am. J. 64:1759–1763 (2000).

Abbreviations: RUSLE, Revised Universal Soil Loss Equation; USLE, Universal Soil Loss Equation.

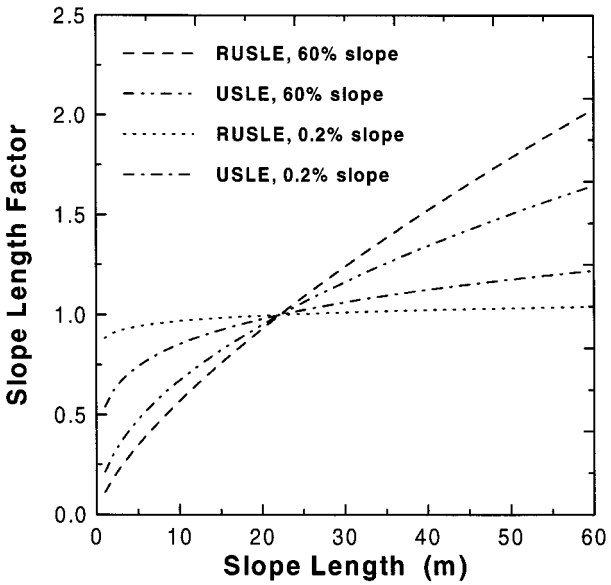

Fig. 1. Slope length factor of Universal Soil Loss Equation (USLE) and Revised Universal Soil Loss Equation (RUSLE). For the 60% slope: $m = 0.5$ for USLE and $m = 0.71$ for RUSLE. For the 0.2% slope: $m = 0.20$ for USLE and $m = 0.04$ for RUSLE.

steep slopes. The results were compared with USLE and RUSLE slope length factors. The data we chose are from three field stations with slope gradients steeper than 30%, which we consider here to be classified as steep.

MATERIALS AND METHODS

Natural rainfall soil loss data from three locations on the Loess Plateau of China were used: the Ansai (36°56′N, 109°16′E), Zizhou (37°31′N, 109°47′E), and Suide (37°29′N, 110°08′E) experimental stations. Soil texture in the Loess Plateau region changes from south to north (Liu, 1966). The plateau is divided into three zones: clayey loess in the southern part, typical loess in the middle, and sandy loess in the north. Stations used in this study were located in the typical loess and sandy loess zones. Two of the soils were fine-silty, mixed mesic Typic Udorthents, and the soil at Zizhou was a fine-loamy, mixed mesic Typic Udorthents (Table 1). The region is semiarid with annual rainfall ranging from 485 to 541mm. More than 60% of the precipitation occurs from June through September. Most of the soil losses were caused by these heavy storms. Soil loss caused by storms with >45mm h^{-1} maximum 30-min intensity (I_{30}) was 80.4% of the total soil loss for the 20-m-long plot in the Ansai station. All of the soils at these three stations were susceptible to rill erosion. After each storm, extensive rilling would be seen in the fields. Rills in this area tend to be rectangular in cross section and generally develop within, but not to the bottom of, the tillage layer. Plots at Zizhou were 15 m wide, and for the other two sites the plot widths were 5 m. The slope lengths, measured horizontally, ranged from 10 to 60 m. The slope steepness was 57.7% for Ansai station and ≈40% for other two stations (Table 2). The plots were selected from a larger database using the criteria of 30% slope or steeper with all other conditions identical. Soil loss was measured by sampling the sediment concentration of the runoff, which was collected in either metal tanks and divisors or concrete pools.

Table 2. Average annual runoff and soil loss from the three experiment sites.

Plot number	Slope length	Slope gradient	Annual runoff	Annual soil loss	Annual soil loss normalized to 22.1 m
	m	%	mm	Mg ha^{-1}	Mg ha^{-1}
			Ansai		
1	10	57.7	46.8	92.66	0.72
2	20	57.7	43.1	128.56	1.00
3	30	57.7	38.7	142.20	1.10
4	40	57.7	39.5	162.85	1.26
			Suide		
12	10	40.0	20.6	15.59	0.70
29	40	42.8	17.9	28.00	1.26
34	60	40.4	14.0	36.59	1.64
			Zizhou		
4	20	40.4	23.9	91.84	0.90
2	40	40.4	27.5	153.14	1.51
3	60	40.4	24.1	143.11	1.41

The data collected from the Ansai site (Jiang et al., 1991) were from 5 yr of fallow conditions from 1985 to 1989. The slope lengths were 10, 20, 30, and 40 m. Data from the Suide site were for 4 yr from 1957 to 1960 and for the Zizhou site were 5 yr from 1963 to 1967. The latter two sites were conventionally tilled farmland. Generally, the crop cover was very sparse due to insufficient soil moisture and the steep slope. The plots were cropped in a 3-yr rotation of millet [*Setaria italica* (L.) Beuv.], soybean [*Glycine max* (L.) Merr.], and potato (*Solanum tuberosum* L.). The slope lengths at Suide were 10, 40, and 60 m, and at Zizhou they were 20, 40, and 60 m.

Since the data used in this study were collected at three field stations, the soil loss was different from site to site. In order to compile and compare the data together, the soil loss was normalized to 22.13 m for all the sites. Because no soil loss was measured at a slope exactly 22.13 m long, regression equations were fitted for each of the data sets according to Eq. [1]. Regression analysis was conducted on each data set individually to calculate the soil loss on the 22.13-m-long slope, then that value was used to normalize the measured values for each site.

RESULTS AND DISCUSSION

We used the average annual soil loss data to analyze the slope length relationships. Average annual soil loss and normalized values are presented in Table 2. The steepest slope of 57.7% was at the Ansai station, for which, according to the RUSLE equations, the slope

Table 1. Soil properties for the upper 10 cm of the three sites on the Loess Plateau of China.

Location	Sand	Silt	Clay	Cation–exchange capacity	Organic matter	1/3 Bar gravimetric	15 Bar gravimetric
	%			cmol kg^{-1}	%		
Ansai	19.0	70.3	10.7	8.6	0.63	17.2	4.5
Suide	32.1	60.5	7.5	6.7	0.47	15.8	4.0
Zizhou	46.1	48.7	5.2	5.3	0.47	14.8	3.5

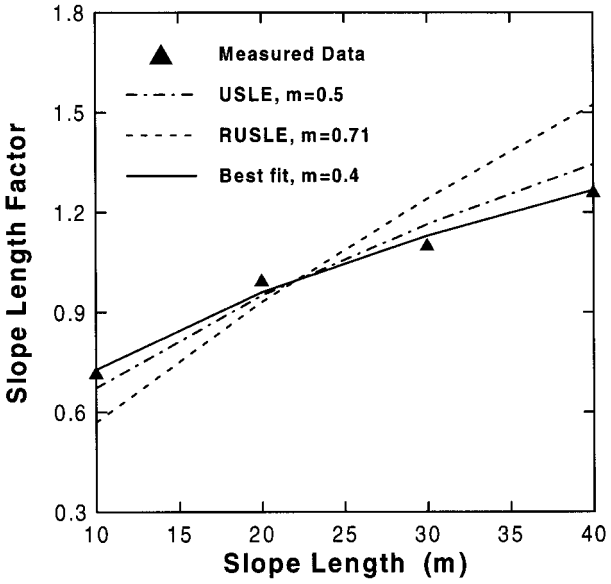

Fig. 2. Slope length factors for measured data on a 57.7% slope at the Ansai station compared with the Universal Soil Loss Equation (USLE; m = 0.5) and Revised Universal Soil Loss Equation (RUSLE) slope length factor (m = 0.71) curves.

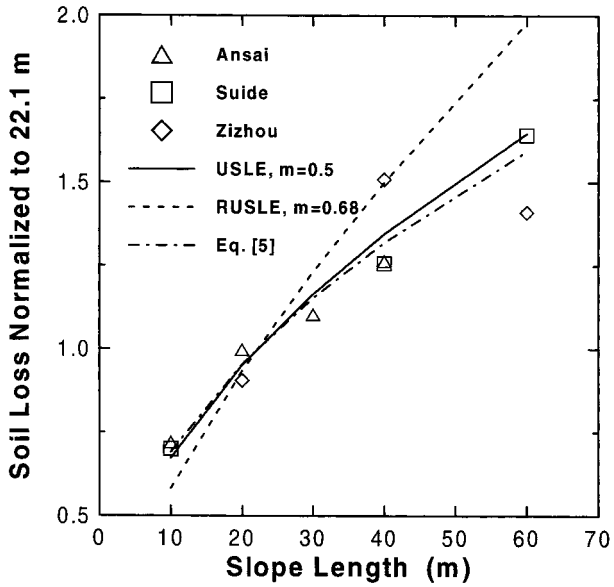

Fig. 3. Soil loss normalized to 22.13-m length from the natural rainfall plot data used in this study and the best-fit curve (m = 0.44) for all measured data combined.

length exponent, m, would be 0.71. As seen in Fig. 2, we found that the RUSLE L factor was greater than that from the measured data. The RUSLE overpredicted soil loss by 20% compared with the best-fit equation (m = 0.4) for the 40-m slope (Table 3) and underpredicted data for the 10-m slope by 21.8%. In contrast, the USLE overpredicted the measured soil loss by only 6% for the 40-m plot and underpredicted by 7.6% for the 10-m plot compared with the best-fit equation for the data. The other two data sets were collected on ≈40% slopes. The best-fit slope length exponents for the measured data at Suide and Zizhou were 0.46 and 0.44, respectively (Table 3). In summary, the data from these three stations did not indicate that the slope length exponent increased with a slope steepness increase from ≈40 to 60%.

Compiling all of the normalized soil loss data from the three stations together, Eq. [5] was derived for the combined data set (r^2 = 0.95):

$$L = (\lambda/22.13)^{0.44} \quad [5]$$

From Fig. 3 we can see that the USLE relationship and Eq. [5] for slope length fit the measured data reasonably well (r^2 = 0.91). Interestingly, the average length exponent for the steep Loess Plateau slopes was 0.44, while the average of the 10 exponents from studies in the USA was 0.46 (McCool et al., 1989). The results from our data also compare very well with the results of McCool et al. (1993) for slopes with an average steepness of 28.4% and a maximum steepness of 56%.

In China, and in other parts of the world, slopes up to 60% are not unusual for cropped farmland. Thus, it is important to know and use the best relationship between slope length and soil loss for steep slopes. The RUSLE uses Eq. [3] and [4] to calculate the ratio of rill/interrill erosion (β) and the length exponent (m). Equation [3] was based on the Foster and Meyer's analyses (Foster and Meyer, 1975; Foster et al., 1977). The basic assumption was that if soil loss is primarily from rills, the exponent will approach one, but it will approach zero where erosion is dominantly from interrill processes (Meyer et al., 1975). For slopes where both rill and interrill erosion occurred, the exponent, m, can be

Table 3. Slope length exponents, m, and parameters, a, from Eq. [1] for the three sites on the Loess Plateau of China.

Location	Parameter a	Slope length exponents, m	Determination coefficients, R^2
Ansai	1.58	0.40	0.988
Suide	0.73	0.46	0.991
Zizhou	1.42	0.44	0.771

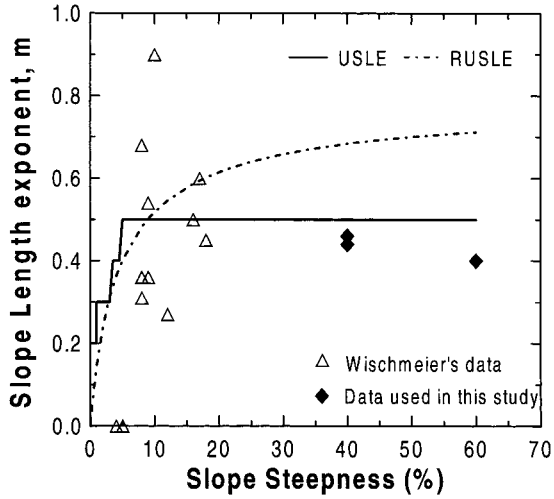

Fig. 4. Slope length exponents from the data of Wischmeier et al. (1958) and from the Loess Plateau of China compared with relationships from the Universal Soil Loss Equation (USLE) and Revised Universal Soil Loss Equation (RUSLE) as a function of slope steepness.

Table 4. Average soil loss at the Ansai station cataloged according to maximum 30-min rainfall intensity. The numbers of storms measured were 23, 9, 3, and 4 for intensities of <15, 15–30, 30–45, >45 mm h^{-1}, respectively.

Slope length	Maximum 30-min rainfall intensity (mm h^{-1})							
	<15		15–30		30–45		>45	
	Runoff	Soil	Runoff	Soil	Runoff	Soil	Runoff	Soil
m	mm	Mg ha^{-1}	mm	Mg ha^{-1}	mm	Mg ha^{-1}	mm	Mg ha^{-1}
10	1.18	0.35	2.12	4.04	14.72	15.49	35.58	93.16
20	0.85	0.37	2.08	5.83	13.30	21.60	34.14	129.17
30	0.66	0.31	1.42	4.69	10.38	20.63	33.46	149.87
40	0.56	0.28	1.50	7.40	12.30	27.30	33.35	164.76

calculated by Eq. [3]. The ratio β (Eq. [4]) was developed by McCool et al. (1989) by dividing Foster's interrill equation into his rill equation (Foster et al., 1977) and then simplifying with several assumptions to obtain Eq. [4]. According to Eq. [3] and [4], the slope length exponent is continually increasing with slope gradient. The USLE relationship, on the other hand, is constant when slopes are greater than 5%.

The fitted exponent of slope length from this study at 57.7% slope was 0.40, and at 40% slope values were 0.46 and 0.44. Several measured data distributed at a joint ARS-SCS workshop held in 1956 at Purdue University by W.H. Wischmeier (McCool et al., 1989) show that when slope steepness was 16% at Lacrosse, WI; 17% at Marcellas, NY; and 18% at Arnot, NY, the slope length exponent was 0.5, 0.6, and 0.45, respectively. These results, together with our data, indicate that when slope steepness is increased from 20 to 40 and 60%, the slope length exponent does not increase (Fig. 4).

The USLE plot data (McCool et al., 1989) showed that the slope length exponent may vary from 0 to 0.9. Wischmeier et al. (1958) point out that at the majority of locations, runoff did not differ significantly with plot length for the 15 studies. However, three of them showed decreasing runoff with increased slope length. For these three studies, the length-exponent was zero. For the studies in Guthrie, OK, and in Bethany, MO, runoff showed a significant increase with increased slope length. For these two studies, the length exponent was high: 0.68 and 0.9. From these data, we might surmise that the two high values, which were collected at 8 and 10% slopes, were caused by the runoff increasing with slope rather than by increasing slope steepness per se.

The data separated by a maximum 30-min storm intensity from the Ansai station (Table 4) showed that the slope length exponent was a function of the maximum 30-min rainfall intensity (I_{30}) (Table 5). Tables 4 and 5 also provide further evidence that runoff rates may be the controlling factor for the slope length factor. The group of storms with I_{30} >45 mm h^{-1} showed the greatest effect of slope length on erosion and also showed an essentially unchanging runoff depth as a function of slope length (Table 4). Low intensity storms of <15 mm h^{-1} actually showed a negative value of slope length exponent *m* and exhibited a large decrease in runoff depth as a function of slope length increase.

Table 5. Results of regression analyses on slope loss as a function of slope length at different rainfall intensities according to Eq. [1] for the Ansai station.

Rainfall intensity	*a*	*m*	R^2
mm h^{-1}			
<15	0.54	−0.16	0.61
15–30	1.88	0.34	0.59
30–45	6.86	0.36	0.86
>45	36.43	0.41	0.99

CONCLUSIONS

Soil loss data from natural runoff plots at three sites on the Loess Plateau of China were reported in this study. The experimental data for slope lengths from 10 to 60 m on steep slopes showed that the relationship between slope length and soil loss was well approximated by the USLE equation, and not as well by the RUSLE equations. The exponent, *m*, for the relationship between soil loss and the slope length for the combined data from the three stations in the Loess Plateau was 0.44 ($r^2 = 0.95$). The three data sets from the slopes of 57.7, 40.4, and 40.4%, together with the USLE plot data distributed at Purdue University by Wischmeier et al. (1958), indicate that the slope length exponent does not increase with slope gradient increase from ≈20 to 60%. Rainfall intensity and runoff influenced the slope length exponent greatly. The slope length exponent showed greater sensitivity to differences in rainfall and runoff than to slope length per se.

ACKNOWLEDGMENTS

This study was funded by National Science Foundation of China for Distinguished Young Scholars. We also thank Zhongshan Jiang for contributing the data of Ansai station.

REFERENCES

Foster, G.R., and L.D. Meyer. 1975. Mathematical simulation of upland erosion by fundamental erosion mechanics. p. 190–207. *In* Present and prospective technology for predicting sediment yield and sources. Proc. of the 1972 Sediment-Yield Workshop, USDA Sedimentation Lab., Oxford, MS. 28–30 Nov. 1972. U.S. Agric. Res. Ser. Rep. ARS-S-40. U.S. Gov. Print. Office, Washington, DC.

Foster, G.R., L.D. Meyer, and C.A. Onstad. 1977. A runoff erosivity factor and variable slope length exponents for soil loss estimates. Trans. ASAE 20:683–687.

Jiang, Z.S., Z.W. Jia, X.L. Hou, and Z. Liu. 1991. Monitoring of soil loss and researches results from the Ansai experiment station. Research Report of the Ansai Ecological Station, Northwestern Inst. of Soil and Water Conservation. Chinese Academy of Sciences and Ministry of Water Resources, Yangling Shaansi, China.

Liu, D.S. 1966. Components and structures of loess. Chinese Scientific Press, Beijing, China.

Liu, B.Y., and K.L. Tang. 1987. Slope gradient classification and distribution of the slope gradient of Wangdog Watershed. (In Chinese.) Bull. Soil Water Conserv. 7(3):59–64.

McCool, D.K., G.R. Foster, C.K. Mutchler, and L.D. Meyer. 1989. Revised slope length factor for the Universal Soil Loss Equation. Trans. ASAE 32:1571–1576.
McCool, D.K., G.O. George, M. Freckleton, C.L. Douglas, and R.I. Papendick. 1993. Topographic effect on erosion from cropland in the northwestern wheat region. Trans. ASAE 36:1067–1071.
McDonald, R.C., R.F. Isbell, J.G Speight, J. Walker, and M.S. Hopkins. 1984. Australian soil and land survey. Field Handbook. Inkata Press, Melbourne, Australia.
Meyer, L.D., G.R. Foster, and M.J.M. Romkens. 1975. Source of soil eroded by water from upland slopes. p. 177–189. *In* Present and prospective technology for predicting sediment yield and sources. Proc. of the 1972 Sediment-Yield Workshop, USDA Sedimentation Lab., Oxford, MS. 28–30 Nov. 1972. U.S. Agric. Res. Ser. Rep. ARS-S-40. U.S. Gov. Print. Office, Washington, DC.
Musgrave, G.W. 1947. The quantitative evaluation of factors in water erosion—A first approximation. J. Soil Water Conserv. 2:133–138.
Renard, K.G., G.R. Foster, G.A. Weesies, D.K. McCool, and D.C. Yoder (coordinators). 1997. Predicting soil erosion by water: A guide to conservation planning with Revised Universal Soil Loss Equation (RUSLE). USDA Agric. Handb. 703. U.S. Gov. Print. Office, Washington, DC.
Wischmeier, W.H., and D.D. Smith. 1978. Predicting rainfall erosion losses: A guide to conservation planning. USDA Agric. Handb. 537. U.S. Gov. Print. Office, Washington, DC.
Wischmeier, W.H., D.D. Smith, and R.E. Uhland. 1958. Evaluation of factors in the soil-loss equation. Agric. Eng. 39:458–462.
Zingg, A.W. 1940. Degree and length of land slope as it affects soil loss in runoff. Agric. Eng. 21:59–64.

Characteristics and Modeling of Runoff Hydrographs for Different Tillage Treatments

B. Yu,* S. Sombatpanit, C. W. Rose, C. A. A. Ciesiolka, and K. J. Coughlan

ABSTRACT

Surface runoff rate is a critical variable in determining the rate of soil erosion and sediment transport. Rainfall and runoff data at 1-min intervals from an experiment site at Khon Kaen, Thailand, were used to test a three-parameter runoff model originally developed for bare plots in relation to soil erosion studies. The site has a sandy soil with a slope of 3.6%. Plot length and width were 30 and 5 m, respectively. Four tillage treatments with three replicates each were considered: up- and down-slope cultivation, two contour cultivation treatments with tillage depth of 25 and 50 cm, respectively, and no tillage. Runoff data for 200 individual runoff hydrographs showed that runoff amount and peak runoff rate for the no tillage treatment were significantly less than those for other treatments at the site. On average, runoff amount and peak runoff rate for the no tillage treatment were 37 and 44%, respectively, of those for the up- and down-slope cultivation. Results for contour cultivation practices are between the two extremes, although the water retention was not greater with greater tillage depth as we originally thought would be the case at the site. For these 200 runoff events for the four treatments, the model for runoff hydrographs worked well, with an average coefficient of efficiency of 0.90 and an average standard error of 0.88 mm h^{-1}. The model performance is particularly good for large storm events with high volumetric runoff coefficient. The three model parameters vary considerably from event to event and from treatment to treatment. The initial infiltration amount was found to be inversely related to prior 10-d rainfall at the site; the spatially averaged maximum rate of infiltration can be related to the maximum retention or the Soil Conservation Service (SCS) Curve Number, and the hydrologic lag time is least variable among different storm events and tillage treatments, but tends to decrease with peak runoff rate.

Surface runoff rate plays a critical role in determining the rate of soil loss from agricultural lands. This is especially the case during large events with high stream power (Proffitt and Rose, 1991). In the Universal Soil Loss Equation (Wischmeier and Smith, 1978), the effect of rainfall and runoff is encapsulated in a rainfall and runoff factor, known as the *R*-factor, to represent the long-term climatic influence on soil erosion. As such, the *R*-factor should not be used to determine the soil loss on an event basis. In process-based water erosion models, runoff rate is explicitly required in order to determine the rate of soil loss. For example, in the Water Erosion Prediction Project (WEPP; Laflen et al., 1991; Flanagan and Nearing, 1995), which represents a new generation of process-based erosion models, the peak runoff rate is used to determine the rate of both interrill and rill erosion (Foster et al., 1995). In GUEST (Rose, 1993; Misra and Rose, 1996), a theoretical expression is derived for sediment concentration at the transport limit based on the stream power, which is in turn a function of the runoff rate. It is important therefore to predict runoff rates for given rainfall intensity, soil, and topographical characteristics.

As part of projects funded by the Australian Centre for International Agricultural Research (ACIAR), rainfall intensity and runoff rate were measured at 1-min intervals at a number of sites in Australia and Southeast Asia. One of the research objectives was to develop hydrologic models to predict runoff rates from rainfall rates for a range of soil types, slopes, slope lengths, and management practices in the tropical and subtropical regions of Australia and Southeast Asia. A three-parameter infiltration and runoff routing model was developed and validated using data from bare plots from six sites in Southeast Asia and Australia (Yu et al., 1997b). Apart from satisfactory performance of the model in terms of modeled hydrographs for these sites, two subsequent studies gave further support of the model as a tool for predicting runoff rate. Yu (1998) showed that one of the infiltration parameters is implicitly related to the widely used SCS Curve Number method for runoff estimation (Soil Conservation Ser-

B. Yu and C.W. Rose, Faculty of Environmental Sciences, Griffith Univ., Nathan QLD 4111, Australia; S. Sombatpanit, Dep. of Land Development, Bangkok, 10900 Thailand; C.A.A. Ciesiolka, Queensland Natural Resources, Toowoomba, QLD 4350, Australia; K.J. Coughlan, Australian Centre for International Agricultural Research, ACT 2601, Australia. Received 17 Sept. 1999. *Corresponding author (b.yu@mailbox.gu.edu.au).

Published in Soil Sci. Soc. Am. J. 64:1763–1770 (2000).

Abbreviations: ACIAR, Australian Centre for International Agricultural Research; DSM, downhill simplex method; SCS, Soil Conservation Service.

Assessment of erosion, sedimentation, and water quality impacts of the Mountain Valley Pipeline and Equitrans Expansion Project's proposed crossing of the Jefferson National Forest as it pertains to the U.S. Forest Service's Draft Supplemental Environmental Impact Statement dated December 2022

Prepared by Jonathan A. Czuba, Ph.D., Licensed Professional Engineer - February 9, 2023

REFERENCES
17

February 21, 2023

MethodsX 6 (2019) 219–229

Contents lists available at ScienceDirect

MethodsX

journal homepage: www.elsevier.com/locate/mex

Method Article

Modification of the RUSLE slope length and steepness factor (LS-factor) based on rainfall experiments at steep alpine grasslands

Simon Schmidt[a,*], Simon Tresch[b,c,d], Katrin Meusburger[e]

[a] Environmental Geosciences, University of Basel, Bernoullistrasse 30, CH-4056 Basel, Switzerland
[b] Department of Soil Sciences, Research Institute of Organic Agriculture (FiBL), Ackerstrasse 113, CH-5070 Frick, Switzerland
[c] Functional Ecology Laboratory, Institute of Biology, University of Neuchâtel, Rue Emile-Argand 11, CH- 2000 Neuchâtel, Switzerland
[d] Biodiversity and Conservation Biology, Swiss Federal Institute for Forest, Snow and Landscape Research (WSL), Zürcherstrasse 111, CH-8903 Birmensdorf, Switzerland
[e] Forest Soils and Biogeochemistry, Swiss Federal Institute for Forest, Snow and Landscape Research (WSL), Zürcherstrasse 111, CH-8903 Birmensdorf, Switzerland

A B S T R A C T

The slope length and slope steepness factor (LS-factor) is one of five factors of the Universal Soil Loss Equation (USLE) and its revised version (RUSLE) describing the influence of topography on soil erosion risk. The LS-factor was originally developed for slopes less than 50% inclination and has not been tested for steeper slopes. To overcome this limitation, we adapted both factors slope length L and slope steepness S for conditions experimentally observed at Swiss alpine grasslands. For the new L-factor (L_{alpine}), a maximal flow path threshold, corresponding to 100 m, was implemented to take into account short runoff flow paths and rapid infiltration that has been observed in our experiments. For the S-factor, a fitted quadratic polynomial function (S_{alpine}) has been established, compiling the most extensive empirical studies. As a model evaluation, uncertainty intervals are presented for this modified S-factor. We observed that uncertainty increases with slope gradient. In summary, the proposed modification of the LS-factor to alpine environments enables an improved prediction of soil erosion risk including steep slopes.

- Empirical experiments (rainfall simulation, sediment measurements) were conducted on Swiss alpine grasslands to assess the maximal flow length and slope steepness factor (S-factor).
- Flow accumulation is limited to a maximal flow threshold (100 m) at which overland runoff is realistic in alpine grassland.
- Slope steepness factor is modified by a fitted S-factor equation from existing empirical S-factor functions.

* Corresponding author.
E-mail addresses: simon@simonschmidt.de, si.schmidt@unibas.ch, simon.schmidt@bgr.de (S. Schmidt), simon.tresch@fibl.org (S. Tresch), katrin.meusburger@wsl.ch (K. Meusburger).

https://doi.org/10.1016/j.mex.2019.01.004

ARTICLE INFO
Method name: L_{alpine}, S_{alpine}, LS_{alpine}
Keywords: Revised Universal Soil Loss Equation, Erosion modeling, Switzerland, Terrain features, Maximal, Flow length
Article history: Received 13 November 2018; Accepted 19 January 2019; Available online 26 January 2019

Specifications Table

Subject area	*Environmental Science*
More specific subject area	*Soil erosion modeling*
Method name	- L_{alpine} - S_{alpine} - LS_{alpine}
Name and reference of original method	USLE LS-factor: Wischmeier, W.H., & Smith, D.D. (1978). Predicting rainfall erosion losses. Washington. S-factor: McCool, D.K., Brown, L.C., Foster, G.R., Mutchler, C.K., & Meyer, L.D. (1987). Revised Slope Steepness Factor for the Universal Soil Loss Equation. Transactions of the ASAE, 30, 1387–1396. https://doi.org/doi:10.13031/2013.30576. S-factor: Smith, D.D., & Whitt, D. (1948). Estimating soil losses from field areas. Agricultural Engineering, 29, 394–396.
Resource availability	- *SAGA GIS* (http://www.saga-gis.org; [31]) - *RSAGA* (https://cran.r-project.org/web/packages/RSAGA/index.html; [30])

Method details

Existing approaches for S- and L-factor parametrization

The LS-factor is a product of the slope length (L-) and the slope steepness (S-factor). The most widely used slope length factor represents the ratio of observed soil loss related to the soil loss of a standardized plot (22.13 m). Originally Wischmeier and Smith [1] defined the L-factor as Eq. (1):

$$L = \left(\frac{\lambda}{22.13}\right)^{m} \tag{1}$$

where λ represents the length of the slope in meters and m the different slope steepness. Later, Eq. (2) was adapted for the RUSLE-approach to better describe soil loss with increasing slope steepness. Desmet and Govers [2] transformed the original L-factor (Eq. (1)) into a GIS-approach (Eq. (2)) considering the flow accumulation and adding a ratio of rill to interrill erosion (Eq. (3)):

$$L_{i,j} = \frac{\left(A_{i,j-in} + D^2\right)^{m+1} - A_{i,j-in}^{m+1}}{D^{m+2} * X_{i,j}^{m} * 22.13^{m}} \tag{2}$$

where $A_{i,j-in}$ is the flow accumulation in m^2 at the inlet of a grid cell (i,j). D is the grid cell size in m and $X_{i,j}$ equals to $\sin a_{i,j} + \cos a_{i,j}$ where $a_{i,j}$ is the aspect of the grid cell (i,j). The coefficient m (Eq. (3)) represents the ratio of rill and interrill erosion and is calculated by the β-value (Eq. (4)):

$$m = \frac{\beta}{\beta + 1} \tag{3}$$

with a range between 0 (ratio of rill to interrill erosion close to 0) and 1.

$$\beta = \frac{\frac{\sin\theta}{0.0896}}{\left[0.56 + 3 * (\sin\theta)^{0.8}\right]} \tag{4}$$

where θ is the slope angle in degrees.

For the S-factor, most often the empiric function proposed by McCool et al. [3] is used to determine the slope steepness factor in the Revised Universal Soil Loss Equation (RUSLE). McCool et al. [3] differentiate the relation between soil loss and slope steepness in radians (s) with two functions. One for slopes with an inclination less than 9% and the other greater or equal 9%. The functions are as follows:

$$S = 10.8s + 0.03 \qquad for \quad slope \quad steepness \quad in \quad percent < 9\% \tag{5}$$

$$S = 16.8s - 0.50 \qquad for \quad slope \quad steepness \quad in \quad percent \geq 9\% \tag{6}$$

The S-factor after McCool et al. [3] is particular recommended for areas with low summer rainfall amounts [4]. Many other empirical S-factors were developed since the 1940s (Table 1) but all S-factors have in common that empirical evidence and thus validity is limited to slope gradients less than 50%.

Proposed adaption of the L-factor

Often, GIS modeled potential flow path length on slopes, expressed as flow accumulation in a GIS-environment, is driven by gravity and theoretically unlimited [13]. In particular cases, these potential flow path lengths can reach many kilometers and enormous runoff volumes. The flow accumulation can be constrained by streets or houses as ending points of the potential flow paths as discussed by Winchell et al. [14].

In 2016, we conducted 19 different rainfall simulation experiments on south facing slopes in an alpine environment (Val Piora, Switzerland) with different conditions regarding soil moisture (dry, moist), steepness (36°–82°), and vegetation (low, medium, full vegetation cover) to observe the flow path lengths. The rainfall simulations were realized with an Eijkelkamp mini rainfall simulator (type M1.09.06. E, Eijkelkamp, NL; Fig. 1) for erosion tests with a rainfall intensity of 640 mm/h and an energy of 4 J mm^{-1} m^{-2}. This rainfall energy is comparable with the average rainfall energy of Val Piora (station Piotta; 5.6 J mm^{-1} m^{-2}; [15]). Regardless of the conditions, our observations revealed short surface flow path lengths at the scale of meters with a rapid infiltration into shallow alpine soils (see Appendix A.

Table 1
Review of selected S-factors (S).

Source	function	Description
Zingg [5]	$S = \left(\frac{s}{9}\right)^{1.4}$	s = slope steepness in percent
Musgrave [6]	$S = \left(\frac{s}{9}\right)^{1.35}$	s = slope steepness in percent
Smith and Whitt [7]	$S = 0.025 + 0.052s^{\frac{4}{3}}$	s = slope steepness in percent
Smith [8]	$S = 0.00650s^2 + 0.0453s + 0.065$	s = slope steepness in percent
Smith [8]	$S = 0.044 + 0.10s - 0.00073s^2$	s = slope steepness in percent
Wischmeier and Smith [1]	$S = 65.4\sin\theta^2 + 4.56\sin\theta + 0.0654$	θ = slope steepness in radians
McCool et al. [9]	$S = \left(\frac{\sin\theta}{0.00896}\right)^{0.6}$	θ = slope steepness in radians
Foster [10]	$S = 3(\sin\theta)^{0.8} + 0.56$	θ = slope steepness in radians
McCool et al. [3]	$S = 16.8\sin\theta - 0.5$	θ = slope steepness in radians
McCool et al. [3]	$S = 10.8\sin\theta + 0.03$	θ = slope steepness in radians
Nearing [11]	$S = -1.5 + \frac{17}{1+e^{2.3-6.1\sin\theta}}$	θ = slope steepness in radians
Liu et al. [12]	$S = 21.91\sin\theta - 0.96$	θ = slope steepness in radians
S_{alpine} present study	$S = 0.0005s^2 + 0.1795s - 0.4418$	s = slope steepness in percent

Fig. 1. Different set ups and preconditions of the rainfall simulation experiment on steep slopes in Val Piora, Ticino, Switzerland.

supplementary material). Our measurements and observations show, that potential flow paths without considering infiltration is not realistic for alpine environments and thus, requesting a maximal flow threshold for the estimation of the slope length factor L. McCool et al. [16] and Winchell et al. [14] limited the slope length to a maximal threshold of 333 m (1000 feet) as longer slope length appear only occasionally. According to McCool et al. [16], the usual threshold in many cases is 121 m (400 feet). As a compromise of their suggestion and our observed short flow path lengths in the Swiss Alps, we decided to limit the maximal flow length to 100 m.

The threshold is implemented as a condition either directly in SAGA GIS or in RSAGA after creating the flow accumulation grid:

$$A_{alpine\,i,j-in} = ifelse(A_{i,j-in} > thresh,\ thresh,\ A_{i,j-in}) \tag{7}$$

where $A_{alpine\,i,j-in}$ is the constraint flow accumulation in m^2 at the inlet of a grid cell (i,j) considering a threshold value *thresh*. That constraint flow accumulation value is inserted into the L-factor equation for the alpine environment (Eq. (8)):

$$L_{alpine\,i,j} = \frac{\left(A_{alpine\,i,j-in} + D^2\right)^{m+1} - A_{alpine\,i,j-in}^{m+1}}{D^{m+2} * X_{i,j}^{m} * 22.13^{m}} \tag{8}$$

Likewise to Eq. (2), D is the grid cell size in m and $X_{i,j}$ equals to $\sin a_{i,j} + \cos a_{i,j}$ where $a_{i,j}$ is the aspect of the grid cell (i,j). The coefficient m is the ratio of rill (β-value) to interrill erosion according to the above mentioned Eqs. (3) and (4).

For our calculation of L-factor using a 2 m resolution Digital Elevation Model, the maximal flow length of 100 m, corresponds to a threshold of 50 cells multiplied by the cell size of 2 m (Fig. 2).

Additionally, maximal flow path length was constrained by a field block cadaster. The cadaster defines hydrological units of continuous agricultural land, that are separated by landscape elements acting as flow boundaries (e.g., forests, streets, urban areas, water bodies, or ditches) following the approach of Winchell et al. [14].

Proposed adaption of the S-factor

In 2014, we conducted a total of 16 rainfall simulations on alpine slopes to assess the soil loss rates related to different slope inclinations (Table 2; [17]). The experiments were conducted at a north and south facing slope both with grassland cover in the mountains of the Urseren Valley, Switzerland. At each slope two transects were selected with slope gradient ranging from 20 to 90%. We used a field hybrid rainfall simulator modified after Schindler Wildhaber et al. [18] with an intensity of 60 mm $h^{-}1$, which is comparable to a high rainfall event in this area.

The experimental sites showed small variation in vegetation cover, soil erodibility, and slope length (due to the effect of slope angle), therefore all experimental plots were normalized to average values of

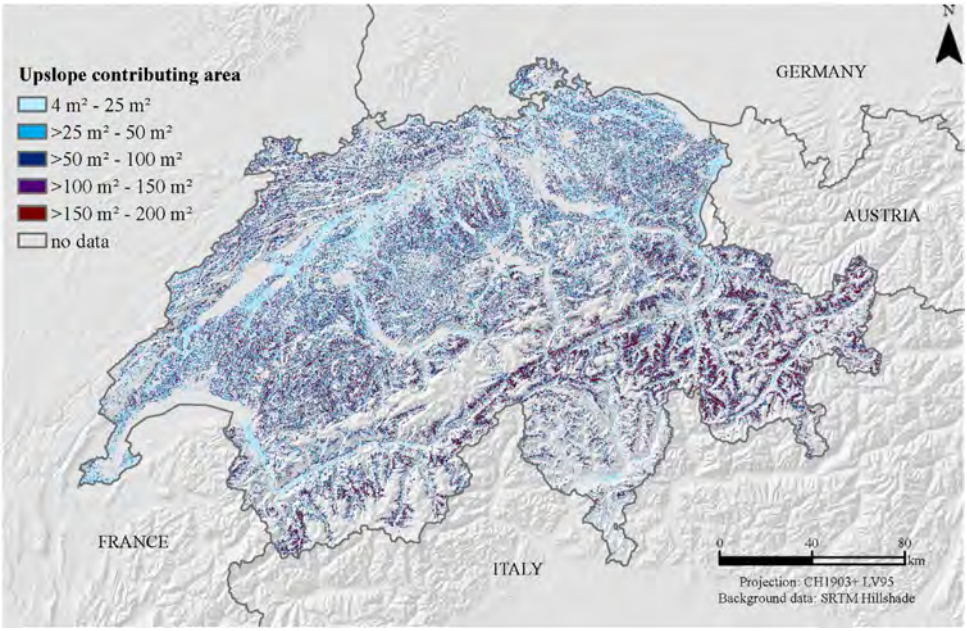

Fig. 2. Constraint flow accumulation grid with a maximal flow path length of 100 m.

Table 2
Rainfall simulation measurements at the two study sites on steep alpine slopes in Switzerland under consideration of different inclinations and vegetation cover.

N°	inclination (°)	vegetation cover (%)	measured sediment rate ($t\,ha^{-1}\,yr^{-1}$)	normalized[a] sediment rate ($t\,ha^{-1}\,yr^{-1}$)	normalized[a] sediment rate without outliers ($t\,ha^{-1}\,yr^{-1}$)
1	17	23	13.8	8.5	8.5
2	22	33	0.6	0.7	0.7
3	11	27	0.0	0.0	0.0
4	27	41	1.2	1.6	1.6
5	31	35	0.2	0.2	0.2
6	35	34	6.8	5.6	5.6
7	42	53	9.4	19.0	19.0
8	39	26	31.0	17.4	17.4
9	11	33	0.6	0.7	0.7
10	17	36	1.4	1.8	1.8
11	22	47	1.3	2.0	2.0
12	27	33	34.3	40.6	
13	31	63	26.1	111.3	
14	35	38	11.1	13.1	13.1
15	39	34	40.2	26.0	26.0
16	42	40	75.4	69.8	

[a] By C-factor with 35% vegetation cover, L-factor of 1.2, and K-factor of 0.031.

the respective factors. S-factors were fitted to observed soil loss versus sine of the slope angle using an exponential, power, and polynomial equation to the original dataset with all observation and a dataset excluding one outlier (N° 13), and three outliers (N° 12, 13, 16). The nine regression lines yield R^2 estimates between 0.18 and 0.70, but differ largely with increasing slope steepness. This range of S-factors with increasing steepness is comparable to previous developed empirical S-factor equations (Table 1,Fig. 1). Therefore, we decided that a fitted function (S_{alpine} in Table 1, Fig. 3) complying the most important S-factors from the literature would be most suitable to describe the soil loss behavior

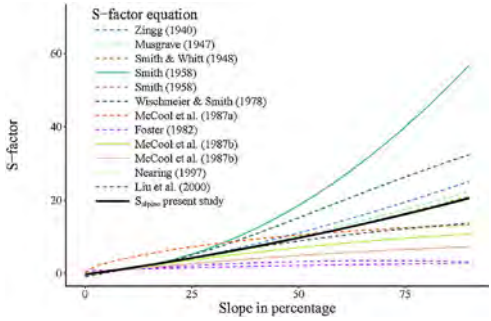

Fig. 3. Review and behavior of different empirical S-factor functions and the fitted function for steep alpine environments (S_{alpine}).

at steep slopes. The aggregated S function and is a quadratic polynomic function with progressive growth (Eq. (9)):

$$S_{alpine} = 0.0005s^2 + 0.7956s - 0.4418 \quad (9)$$

where s is the slope steepness in percent.

S_{alpine} is very close to the empirical normalized function proposed by Musgrave [6] for a slope steepness of 9%.

The Swiss LS-factor map including the Alps

The resulting modeled mean LS_{alpine}-factor of Switzerland is 14.8. The LS-factor increases with elevation gradient from a mean of 7.0 in the zone <1500 m a.s.l. to 30.4 in the zone >1500 m a.s.l. A cluster of highest mean LS-factors can be found across the Alps (Fig. 4). The lowest mean LS-factors are

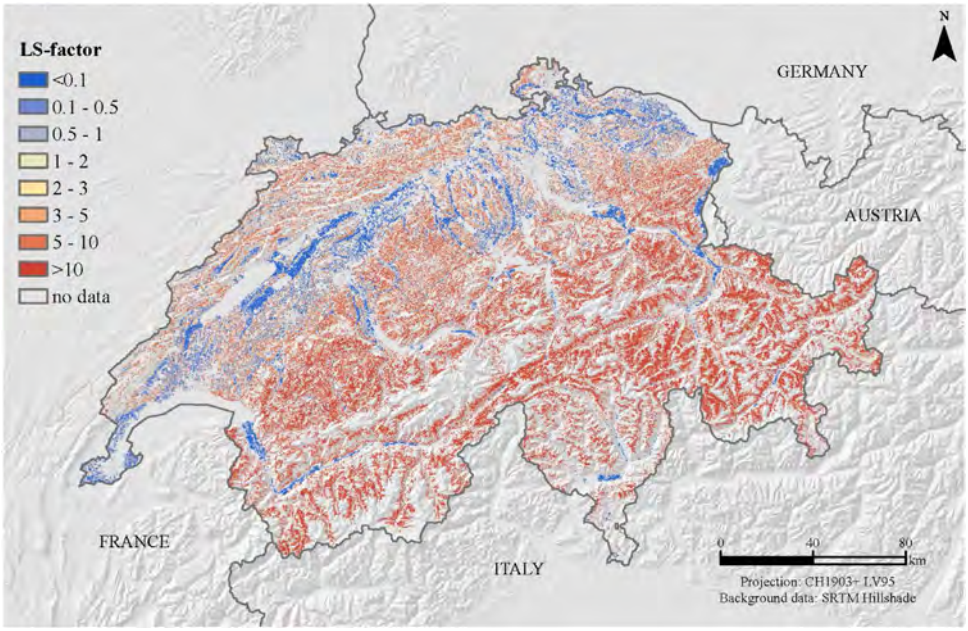

Fig. 4. LS_{alpine}-factor map (spatial resolution 2 m) for Switzerland derived by the digital elevation model SwissAlti3D.

in the Swiss lowlands. South-western facing slopes have higher LS-factors (17.6) compared to plain surfaces (0.04) and north facing slopes (12.5).

Quality assessment and method uncertainties

The original LS-factor has its origin in empirical field experiments and is developed for a maximum slope steepness of 50%. Validation of existing equations for slopes that are steeper than 50% is a challenge. However, while previous studies at inclinations >25% with approximately 20 plot measurements ([19], 24 plots; [20], 19 plots; [12], 9 plots; [21], 22 plots; [18], 6 plots) were successful in delineating and S-factor equation, in our case the variability of the data impeded a unique solution of the S-factor equation. To account for this high variability and still existing uncertainty, the way forward is to include the variability in the LS-factor calculation.

We investigated the deviation in percentage of our proposed S_{alpine} to a conservative function and a rather progressive function. The conservative function (S_{cons}) is based on the translated and scaled sine functions of Eqs. (5) and (6) by McCool et al. [3] with a proportional and slightly digressive growth. The progressive function (S_{prog}) is a quadratic polynomic function according to Smith and Whitt [7] with a progressive growth, but a higher coefficient than the here presented fitted function S_{alpine} (Eq. (10)) for S_{alpine}.

$$S_{prog} = 0.00650s^2 + 0.0453s + 0.065 \tag{10}$$

where s is the slope steepness in percent.

Low uncertainty has a deviation close to 0%. Higher percentages equals to a higher deviation of $S_{cons/prog}$ to S_{alpine}.

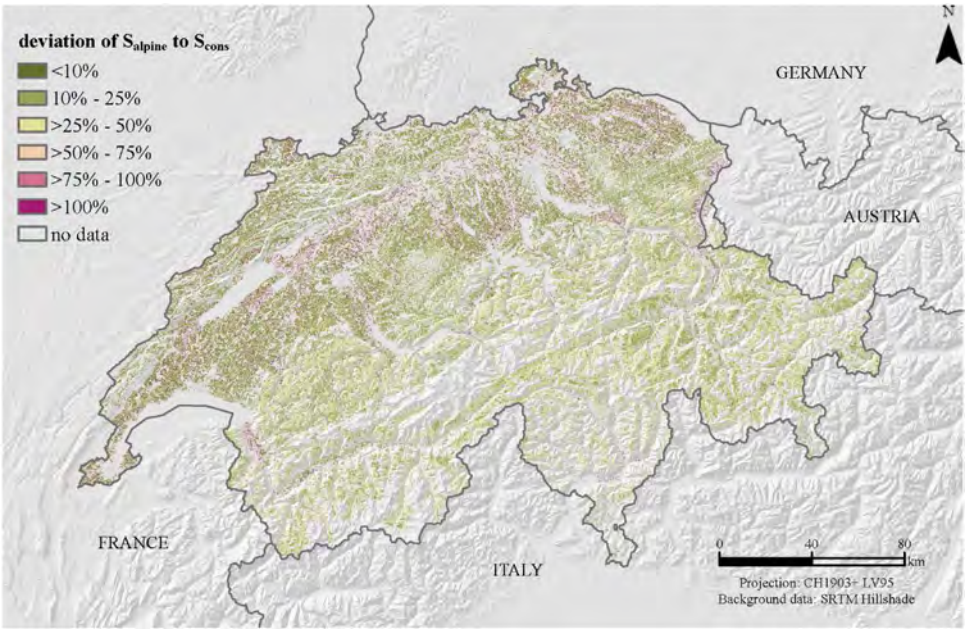

Fig. 5. Deviation in percentage of S_{alpine} to S_{cons} as an indicator of quality for the proposed S_{alpine}-factor. S_{alpine} is a lumped S-factor of a total of 12 empiric S-factor equations of the literature (Eq. (9)). It can be seen as an approximation to the high slope gradients in alpine environments. S_{cons} complies with the proposed S-factor of McCool et al. [3] (Eqs. (5) and (6)). The deviation is presented in percentage.

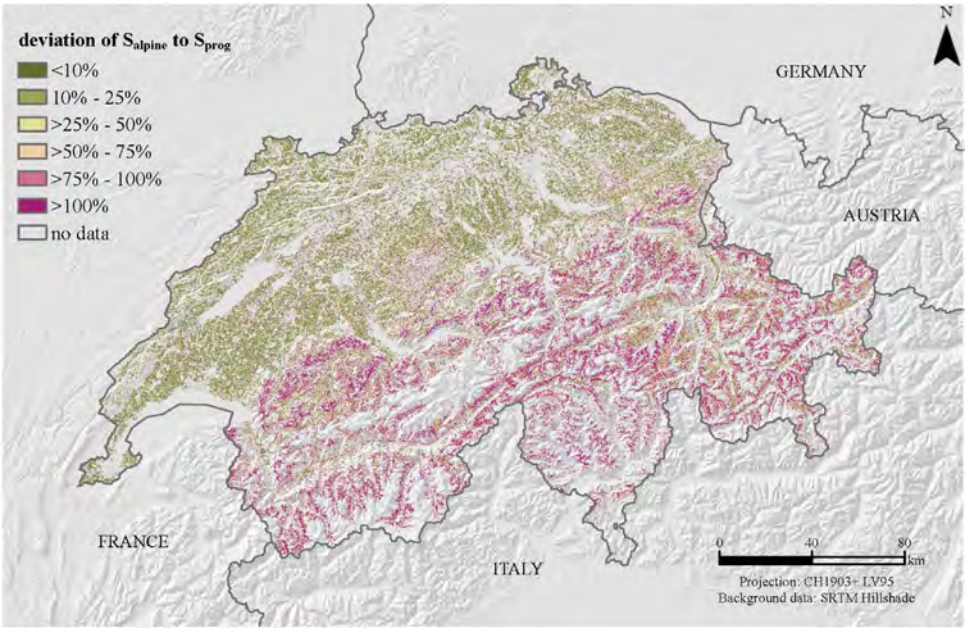

Fig. 6. Deviation in percentage of S_{alpine} to S_{prog} as an indicator of quality for the proposed S_{alpine}-factor. S_{alpine} is a lumped S-factor of a total of 12 empiric S-factor equations of the literature (Eq. (9)). It can be seen as an approximation to the high slope gradients in alpine environments. S_{prog} complies with the proposed S-factor of Smith and Whitt [7] (Eq. (10)). The deviation is presented in percentage.

The deviation of S_{alpine} to S_{cons} shows higher deviations in areas with less slope gradiants (parts of Swiss midland) (Fig. 5). The steep slope areas in the Alps have deviations of 25%–50%. Both functions, S_{alpine} and S_{cons} predict the steep alpine environment in a comparable way. The deviation of the progressive S-factor (Sprog) and S_{alpine} diverge much more in the Alps whereas the equations are rather fitting in flatter regions (Fig. 6). A sharp edge of low divergence to high divergence is marked by the northern Alpine foothill with increasing slope gradients.

This relationship of deviation and slope gradient is not surprising as the uncertainty of many equations rises with slope steepness (cf. Fig. 3). García-Ruiz et al. [22] identified an increasing trend of uncertainty for 624 measured erosion rates and slope gradients across the world for slope steepness >11°.

The LS-Factor map of the Swiss agricultural land use unit is visually compatible with the LS-factor maps of the European Union provided by Panagos et al. [23] (Fig. 7). In contrast to the modeling of the total country area by Panagos et al. [23] we constrained the LS-factor to agricultural soils incl. grasslands using a field cadaster. The main differences are found on steeper slopes >50%, which have been excluded in the European approach. Furthermore, the European map relies on the conservative Eqs. (5) and (6) by McCool et al. [3]. Additionally, different spatial resolutions of Digital Elevation Models (2 m versus 25 m) are influencing the slope and aspect mapping and thus the LS-factor [24–26].

It should be considered that the number of rainfall experiments for the L-factor (n = 19) and the S-factor (S = 16) is short and limited only to grasslands which are the predominant land use at Swiss alpine slopes [27]. Rainfall simulations in alpine environments are difficult to conduct due to the harsh terrain and climate conditions. Often, the temporal period for measurements is limited by the late melt out of snow cover and the short vegetation period [28]. To better model the S-factor for steep

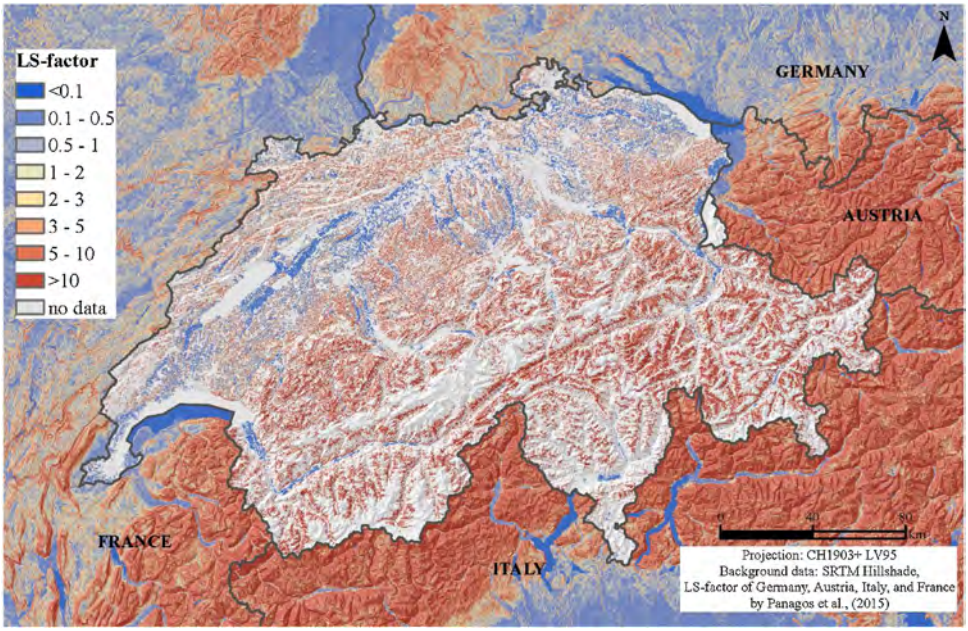

Fig. 7. LS-factor for the Swiss agricultural area (incl. Liechtenstein) embedded in the European Union's LS-factor map (for total country area) by Panagos et al. [23].

alpine slopes further measurements (e.g., rainfall simulation experiments) are needed to constrain S-factor assessment for steep slopes.

Additional information

Introduction

The slope length factor L and slope steepness factor S, often lumped together as the topographic factor LS. The LS-factor is one of the factors (R rainfall erosivity, C cover and management factor, K soil erodibility, P support practices) of the Universal Soil Loss Equation (USLE) and its revised version (RUSLE) [1,29]. LS is a factor that describes the influence of the topography to the soil erosion risk by considering the length of a slope and the influence of surface runoff which can be active on eroding soil material before it infiltrates or continuous as interflow. Furthermore, it includes the steepness of a slope as runoff on steeper slopes has a higher gravity and therefore is more relevant for erosion.

With the availability of Digital Elevation Models the calculation of LS-factors in GIS environments was made possible even for large-scale erosion modeling approaches. Winchell et al. [14] revealed a reasonable agreement of GIS-based LS-factor and field measured LS-factors of the US Natural Resource Inventory database for the Mississippi Catchment.

Originally, the LS-factor was assessed on a 9% steep slope with a length of 22.13 m (72.6 feet) [1]. Owing to its empirical character, LS-factors are usually limited to a maximum slope angle of 50% (26.6°) [3,12]. As Switzerland is a country with a high elevation gradient from 192 m a.s.l. to 4633 m a.s.l. (mean elevation 1288 m a.s.l.) and a mean slope gradient of up to 36% (20°), a not negligible fraction of slopes (4.7%) exceeds the limitation of 50%. Yet, no uniform equation to assess the LS-factor for steep slopes like in the alpine environment of Switzerland was presented to the scientific community. Only a few studies are dealing with LS-factors on steep slopes (e.g. [12]). For example, slopes >50% were disregarded in the most recent European Union's LS-factor map by Panagos et al. [23].

To overcome that limitation in LS-factor modeling on steep slopes, we (i) limited the potential flow path length to a maximal flow and (ii) choose the most representative equation for Swiss steep slopes.

Data statement

Raw data were generated at Swisstopo and provided only for scientific purposes. Derived data supporting the findings of this study are available from the corresponding author SS on request.

Acknowledgments

This work was supported by the Swiss Federal Office for the Environment (FOEN) (grant numbers N° N222-0350 and N° P182-1535). The authors would like to thank Christine Alewell for the methodological support and Pascal Bircher for the advice in data handling with SAGA GIS/RSAGA and the upgrade of the existing field block cadaster of Switzerland. Our thank goes to M. Schulthess, C. Keller, N. Bongni, S. Rothenbühler, and A. Aeschbach for the support in the field and the footage. The authors thank Swisstopo for making their data available for this research. The authors would like to thank two anonymous referees for their valuable comments and suggestions to improve the quality of the paper.

Appendix A. Supplementary data

Supplementary material related to this article can be found, in the online version, at doi:https://doi.org/10.1016/j.mex.2019.01.004.

References

[1] W.H. Wischmeier, D.D. Smith, Predicting Rainfall Erosion Losses Washington, (1978) .
[2] P.J.J. Desmet, G. Govers, A GIS procedure for automatically calculating the USLE LS factor on topographically complex landscape units, J. Soil Water Conserv. 51 (1996) 427–433.
[3] D.K. McCool, L.C. Brown, G.R. Foster, C.K. Mutchler, L.D. Meyer, Revised slope steepness factor for the universal soil loss equation, Trans. ASAE 30 (1987) 1387–1396, doi:http://dx.doi.org/10.13031/2013.30576.
[4] K. Auerswald, Eignung der Hangneigungsfaktoren verschiedener Erosionsmodelle unter bayerischen Anbauverhältnissen, Zeitschrift für Kulturtechnik und Flurbereinigung 27 (1986) 218–224.
[5] A. Zingg, Degree and length of land slope as it affects soil loss in run-off, Agric. Eng. (1940) 59–64.
[6] G.W. Musgrave, The quantitative evaluation of factors in water erosion—a first approximation, J. Soil Water Conserv. (1947) 133–138.
[7] D.D. Smith, D. Whitt, Estimating soil losses from field areas, Agric. Eng. 29 (1948) 394–396.
[8] D.D. Smith, Factors affecting rainfall erosion and their evaluation, Int. Assoc. Sci. Hydrol. Publ. 43 (1958) 97–107.
[9] D. McCool, L. Brown, G.R. Foster, C. Mutchler, L. Meyer, Revised slope steepness factor for the universal soil loss equation, Trans. ASAE 30 (1987) 1387–1398.
[10] G.R. Foster, Modeling the erosion process, in: I.C.T. Haan, H.P. Johnson, D.L. Brakenslek (Eds.), Hydrologic Modeling of Small Watersheds, St. Joseph, 1982, pp. 297–382.
[11] M.A. Nearing, A single, continuous function for slope steepness influence on soil loss, Soil Sci. Soc. Am. J. 61 (1997) 917, doi:http://dx.doi.org/10.2136/sssaj1997.03615995006100030029x.
[12] B.Y. Liu, M.A. Nearing, P.J. Shi, Z.W. Jia, Slope length effects on soil loss for steep slopes, Soil Sci. Soc. Am. J. 64 (2000) 1759, doi:http://dx.doi.org/10.2136/sssaj2000.6451759x.
[13] S. Orlandini, G. Moretti, M.A. Corticelli, P.E. Santangelo, A. Capra, R. Rivola, J.D. Albertson, Evaluation of flow direction methods against field observations of overland flow dispersion, Water Resour. Res. 48 (2012) 412, doi:http://dx.doi.org/10.1029/2012WR012067.
[14] M.F. Winchell, S.H. Jackson, A.M. Wadley, R. Srinivasan, Extension and validation of a geographic information system-based method for calculating the revised universal soil loss equation length-slope factor for erosion risk assessments in large watersheds, J. Soil Water Conserv. 63 (2008) 105–111, doi:http://dx.doi.org/10.2489/jswc.63.3.105.
[15] MeteoSwiss, Automatic Monitoring Network, (2018) . https://www.meteoswiss.admin.ch/home/measurement-and-forecasting-systems/land-based-stations/automatisches-messnetz.html.
[16] D.K. McCool, G. Foster, G. Weesies, Slope length and steepness factor (LS). Chapter 4, in: K.G. Renard, G.R. Foster, G.A. Weesies, D.K. McCool, D.C. Yoder (Eds.), Predicting Soil Erosion by Water: A Guide to Conservation Planning with the Revised Universal Soil Loss Equation (RUSLE), USDA, Washington, D.C, 1997, pp. 101–142.
[17] S. Tresch, Influence of the Slope Steepness on Soil Erosion Modelling Measured with Rainfall Simulations in the Urseren Valley. Master Thesis Basel, (2014), doi:http://dx.doi.org/10.13140/RG.2.2.15260.54409.
[18] Y. Schindler Wildhaber, D. Bänninger, K. Burri, C. Alewell, Evaluation and application of a portable rainfall simulator on subalpine grassland, Catena 91 (2012) 56–62, doi:http://dx.doi.org/10.1016/j.catena.2011.03.004.
[19] A.W. Kilinc, E.V. Richardson, Mechanics of Soil Erosion from Overland Flow Generated by Simulated Rainfall, Colorado State University, 1973.
[20] B.Y. Liu, M.A. Nearing, L.M. Risse, Slope gradient effects on soil loss for steep slopes, Trans. ASAE 37 (1994) 1835–1840.

[21] A. Merz, C. Alewell, E. Hiltbrunner, D. Bänninger, Plant-compositional effects on surface runoff and sediment yield in subalpine grassland, J. Plant Nutr. Soil Sci. 172 (2009) 777–788, doi:http://dx.doi.org/10.1002/jpln.200800231.
[22] J.M. García-Ruiz, S. Beguería, E. Nadal-Romero, J.C. González-Hidalgo, N. Lana-Renault, Y. Sanjuán, A meta-analysis of soil erosion rates across the world, Geomorphology 239 (2015) 160–173, doi:http://dx.doi.org/10.1016/j.geomorph.2015.03.008.
[23] P. Panagos, P. Borrelli, K. Meusburger, A new european slope length and steepness factor (LS-factor) for modeling soil erosion by water, Geosciences 5 (2015) 117–126, doi:http://dx.doi.org/10.3390/geosciences5020117.
[24] K.-t. Chang, B.-w. Tsai, The effect of DEM resolution on slope and aspect mapping, Cartogr. Geogr. Inf. Syst. 18 (1991) 69–77, doi:http://dx.doi.org/10.1559/152304091783805626.
[25] M.F. Ramli, M.K. Yusoff, S. Mustapha, T.S. Hiang, The effect of digital elevation model scale factor on soil erosion studies. Case study in Cameron Highlands, Malaysia, J. Environ. Hydrol. 14 (2006) 1–9.
[26] Q. Zhu, X. Yang, Q. Yu, Assess the topographic resolution impact on soil loss, 2016 IEEE International Geoscience and Remote Sensing Symposium (IGARSS) (2016) 6055–6058.
[27] S. Schmidt, C. Alewell, K. Meusburger, Swiss national grassland map and change (1996–2015) of permanent grasslands extent in Switzerland, Data Brief 20 (2018) 1992–1998, doi:http://dx.doi.org/10.1016/j.dib.2018.09.039.
[28] S. Schmidt, C. Alewell, K. Meusburger, Mapping spatio-temporal dynamics of the cover and management factor (C-factor) for grasslands in Switzerland, Remote Sens. Environ. 211 (2018) 89–104, doi:http://dx.doi.org/10.1016/j.rse.2018.04.008.
[29] K. Renard, G. Foster, G. Weesies, J. Porter, RUSLE. Revised universal soil loss equation, J. Soil Water Conserv. 46 (1991).
[30] A. Brenning, D. Bangs, M. Becker, Package 'RSAGA', (2018) . https://cran.r-project.org/web/packages/RSAGA/RSAGA.pdf.
[31] O. Conrad, B. Bechtel, M. Bock, H. Dietrich, E. Fischer, L. Gerlitz, J. Wehberg, V. Wichmann, J. Böhner, System for automated geoscientific analyses (SAGA) v. 2.1.4, Geosci. Model. Dev. Discuss. 8 (2015) 1991–2007, doi:http://dx.doi.org/10.5194/gmd-8-1991-2015.

Assessment of erosion, sedimentation, and water quality impacts of the Mountain Valley Pipeline and Equitrans Expansion Project's proposed crossing of the Jefferson National Forest as it pertains to the U.S. Forest Service's Draft Supplemental Environmental Impact Statement dated December 2022

Prepared by Jonathan A. Czuba, Ph.D., Licensed Professional Engineer - February 9, 2023

REFERENCES
18

February 21, 2023

Science Documentation

Revised Universal Soil Loss Equation
Version 2

(RUSLE2)

(for the model with release date of May 20, 2008)

USDA-Agricultural Research Service

Washington, D.C.

August 2013

Table of Contents

Acknowledgements

RUSLE2 was developed cooperatively by the USDA-Agricultural Research Service (ARS), the USDA-Natural Resources Conservation Service (NRCS), and the Biosystems Engineering and Environmental Science Department of the University of Tennessee. Each project participant maintains a RUSLE2 Internet site directed toward their specific interests. Consult these sites for a list of the employees of these organizations who contributed to the development of RUSLE2. Contributors from several other organizations also participated in the development of RUSLE2.

The USDA-ARS was responsible for providing the erosion science on which RUSLE2 is based including the mathematical equations used in RUSLE2, core data values used to calibrate RUSLE2, scientific documentation, and a user's reference guide for RUSLE2.

The USDA-NRCS was the principal client for RUSLE2. The NRCS provided information to ensure that RUSLE2 could be easily used in their local field (district) offices. The NRCS also developed an extensive RUSLE2 operational (working) database, primarily for cropland. The NRCS has developed RUSLE2 templates and user guides specifically for their purposes.

The University of Tennessee participated in the development of the mathematical equations used in RUSLE2, developed the computer science used in RUSLE2, and developed the RUSLE2 computer program. They also developed user guides and other RUSLE2 information for their clients.

The interests and needs of a wide variety of other users were considered during RUSLE2's development. RUSLE2 was developed to be land-use independent to give RUSLE2 the widest applicability range possible and to accommodate the needs of these users.

This RUSLE2 Science Documentation was reviewed by USDA-Natural Resources Conservation Service technical specialists from several disciplines; Kenneth G. Renard (retired), USDA-Agricultural Research Service, Tucson, Arizona; and Seth Dabney, USDA-Agricultural Research Service, Oxford, Mississippi.

Preface

The Revised Universal Soil Loss Equation, Version 2 (RUSLE2) is used to guide conservation and erosion control planning at the local field office level. RUSLE2 estimates average annual rill and interrill erosion based on site-specific conditions. In a typical application, the planner identifies several potential erosion control alternatives for the site and estimates erosion for each alternative. The planner then chooses the alternative that provides adequate erosion control and best meets other requirements.

RUSLE2 is computer-based technology that involves a computer program, mathematical equations, and a large database. The RUSLE2 user describes a specific site by making selections from the database. RUSLE2 uses this information in its mathematical equations to compute erosion estimates for alternative erosion control practices for the site.

RUSLE2 can be used to estimate rill and interrill erosion where mineral soil is exposed to the erosive forces of impacting raindrops and water drops falling from vegetation and surface runoff produced by Hortonian overland flow. RUSLE2 is land use independent and can be applied wherever these conditions exist. RUSLE2 can be used on cropland, pastureland, rangeland, constructions site, reclaimed mine land, landfills, mine tailings, mechanically disturbed and burned forestlands, military training sites, and similar lands.

This document describes the RUSLE2 science, which is primarily embodied in the mathematical equations used in RUSLE2. The RUSLE2 User's Reference Guide, a companion document, describes how RUSLE2 works, how to interpret values computed by RUSLE2, how to select and enter values into the RUSLE2 database, and how to judge the adequacy of RUSLE2. Additional information is available on the RUSLE2 Internet site maintained by the USDA-Agricultural Research Service: http://www.ars.usda.gov/Research/docs.htm?docid=6010. Additional information is also available on RUSLE2 Internet sites maintained by the USDA-Natural Resources Conservation Service and the University of Tennessee.

Each chapter in this document stands alone with its own list of symbols given at the end of the chapter. Symbols are defined on their occurrence. Refer to the list of symbols at the end of each chapter because symbol usage differs between chapters.

RUSLE2 uses mathematical equations from several disciplines. In most cases, the symbols that are common in a given discipline are used in this document, which results in the same symbol being used for multiple variables, even within the same chapter. Using the typical symbol for a given variable was considered to be more useful than having a unique symbol for each variable.

Also, topics overlap between chapters. The topics within and between chapters are organized according to the mathematical structure of RUSLE2 rather than along a user oriented structure, which is followed in the RUSLE2 User Reference Guide. Consequently, the mathematical representation of key variables such as residue may be discussed in several places in this document. Cross references to other sections where this variable is discussed are included for the major variables.

Disclaimer

The purpose of RUSLE2 is to guide and assist erosion-control planning. Erosion-control planners should consider information generated by RUSLE2 to be only one set of information used to make an erosion-control decision. RUSLE2 has been verified and validated, and every reasonable effort has been made to ensure that RUSLE2 works as described in RUSLE2 documentation available from the USDA-Agricultural Research Service. However, RUSLE2 users should be aware that errors may exist in RUSLE2 and exercise due caution in using RUSLE2.

Similarly, this RUSLE2 Science Documentation has been reviewed by erosion scientists and RUSLE2 users. These reviewers' comments have been faithfully considered in the revision of this document.

Every reasonable effort has been made to ensure that this document is accurate. The USDA-Agricultural Research Service alone is responsible for this document's accuracy and how faithfully the RUSLE2 computer program represents the information in this document.

Glossary of Terms

Term	Description
10 yr EI	Storm EI with a 10-year return period
10 yr-24 hr EI	Storm EI for the 10 yr-24 hr precipitation amount
10 yr-24 hr precipitation	24 hour precipitation amount having a 10 year return period
Antecedent soil moisture subfactor	See cover-management subfactors
Average annual, monthly, period, and daily erosion	RUSLE2 computes average daily erosion for each day of the year, which represents the average erosion that would be observed if erosion was measured on that day for a sufficiently long period. Average period, monthly, and annual erosion are sums of the average daily values
Average erosion	Average erosion is the sediment load at a given location on the overland flow path divided by the distance from the origin of overland flow path to the location
b value	Coefficient in equation for effect of ground cover on erosion, values vary daily with rill-interrill erosion ratio and residue type
Buffer strips	Dense vegetation strips uniformly spaced along overland flow path; can cause much deposition
Burial ratio	Portion of existing surface (flat) cover mass that is buried by a soil disturbing operation (dry mass basis-not area covered basis)
Calibration	Procedure of fitting an equation to data to determine numerical values for equation's coefficients
Canopy cover	Cover above soil surface; does not contact runoff; usually vegetation
Canopy shape	Standard shapes used to assist selection of fall height values
Canopy subfactor	See cover-management subfactors
Climate description	Input values for variables used to represent climate, stored under a location name in the climate component of RUSLE2 database

Concentrated flow area	Area on landscape where channel flow occurs; ends overland flow path
Conservation planning soil loss	A conservation planning erosion value that gives partial credit to deposition as soil saved, credit is function of location on overland flow path where deposition occurs
Contouring	Support erosion control practice involving ridges-furrows that reduces erosion by redirecting runoff around hillslope
Contouring failure	Contouring effectiveness is lost where runoff shear stress exceeds a critical value
Contouring description	Row grade used to describe contouring; stored in contouring component of RUSLE2 database; ridge height in *operation* description used in cover-*management* description also key input
Core database	RUSLE2 database that includes values for base conditions used to validate RUSLE2; input values for a new condition must be consistent with values in core database for similar conditions
Cover-*management* description	Values for variables that describe cover-management, includes dates, *operation* descriptions, *vegetation* descriptions, vegetation production levels (yields), external *residue* descriptions and amount applied, cover-*management* descriptions named and saved in the management component of RUSLE2 database
Cover-management subfactors	Cover-management subfactor values used to compute detachment (sediment production) by multiplying subfactor values; subfactor values vary through time as cover-management conditions vary temporally
Canopy	Represents how canopy affects erosion; function of canopy cover and fall height, canopy varies through time
Ground cover	Represents how ground cover affects erosion; function of portion of soil surface covered
Surface roughness	Represents how soil surface roughness affects erosion; function of roughness index
Soil biomass	Represents how live and dead roots in upper 10 inches and buried residue in upper 3 inches and less affect erosion
Soil consolidation	Represents how a mechanical disturbance affects erosion;, erosion decreases over time after last disturbance as the soil consolidates (soil consolidation as used in RUSLE2 represents soil particles rebonding during soil wetting and drying; rebonding process is not

	to occur by mechanical compaction)
Ridging	Represents how ridges increase detachment (sediment production)
Ponding	Represents how a water layer on soil surface reduces erosion
Antecedent soil moisture	Represents how previous vegetation affects erosion by reducing soil moisture; used only in Req zone
Critical slope length	Location where contouring fails on a uniform overland flow path
Cultural practice	Erosion control practice such as no-till cropping where cover-management variables are used to reduce erosion
Curve number	An index used in NRCS curve number method to compute runoff; RUSLE2 computes curve number values as a function of hydrologic soil group and cover-management conditions
Database	RUSLE2 database stores both input and output information in named descriptions
Dead biomass	Represents live above ground and root biomass converted to dead biomass by *kill vegetation* process in an *operation* description; dead biomass decomposes
Dead root biomass	A *kill vegetation* process in an *operation* description converts live root biomass to dead root biomass; dead roots decompose at the same rate as surface and buried residue
Decomposition	Loss of dead biomass as a function of material properties, precipitation, and temperature; decomposition rate for all plant parts and buried and surface biomass is equal; decomposition rate for standing residue is significantly decreased because of no soil contact
Deposition	Process that transfers sediment from sediment load transported by runoff to soil surface; net deposition causes sediment load to decrease with distance along overland flow path; depends on sediment characteristics and degree that sediment load exceeds sediment transport capacity; enriches sediment load in fines; computed as a function of sediment particle class fall velocity, runoff rate, and difference between sediment load and transport capacity
Deposition portion	Portion of overland flow path where net deposition occurs
Detachment	Separates soil particles from soil mass by raindrops, waterdrops falling from vegetation, and surface runoff; net detachment causes

	sediment load to increase along overland flow path; detachment is non-selective with respect to sediment characteristics; computed as function of erosivity, soil erodibility, distance along overland flow path, steepness of overland flow path, cover-management condition, and contouring
Disaggregation	Mathematical procedure used to convert monthly precipitation and temperature values to daily values assuming that daily values vary linearly; daily precipitation values sum to equal monthly values, average daily monthly temperature values equals average monthly temperature value
Diversion/terrace/ sediment basin	A set of support practices that intercept overland flow to end overland flow path length.
Diversions	Intercepts overland flow and directs it around hillslope in channelized flow, grade is sufficiently steep that deposition does not occur but not so steep that erosion occurs
EI_{30}	Storm (rainfall) erosivity; product of storm energy and maximum 30 minute intensity; storm energy closely related to rain storm amount and partly to rainfall intensity
Enrichment	Deposition is selective, removing the coarse and dense particles and leaving the sediment load with increased portion of fine and less dense particles
Enrichment ratio	Ratio of specific surface area of sediment after deposition to specific surface area of soil subject to erosion
Eroding portion	Portion of overland flow path where net detachment (erosion) occurs
Erosivity	Index of average annual rainfall erosivity at a location; closely related to rainfall amount and intensity; monthly erosivity is average sum of individual storm values in month, annual erosivity is average sum of values in year; storm rainfall amount must be ½ inch or more to be included in sum
Erosivity density	Ratio of monthly erosivity to monthly precipitation amount
External residue	Material, usually biomass, added to soil surface or placed in the soil; affects erosion as surface residue and buried residue produced by vegetation
Fabric (silt) fence	Fabric about 18 inches wide placed against upright posts on the contour; porous barrier that ponds runoff and causes deposition;

	widely used on construction sites
Fall height (effective)	Effective fall height is the effective height from which waterdrops fall from canopy; depends on canopy shape, canopy density gradient from bottom to top of canopy, and top and bottom canopy heights
Filter strip	A single strip of dense vegetation at the end of an overland flow path; can induce high amounts of deposition
Final roughness	Soil surface roughness after roughness has decayed to unit-plot conditions; primarily represents roughness provided by soil resistant clods
Flattening ratio	Describe how much standing residue that an operation flattens; ratio of standing residue before operation to standing residue after operation; values depend on operation and residue dry mass basis.
Flow interceptors	Topographic features (ridge or channel) on an overflow path that collects overland flow and directs the runoff around hillslope; ends overland flow path; diversions, terraces, and sediment basins are flow interceptors
Gradient terraces	Terraces on a uniform grade (steepness)
Ground cover	Represents the portion of the soil surface covered by material in direct contact with soil; includes plant litter, crop residue, rocks, algae, mulch, and other material that reduces both raindrop impact and surface flow erosivity
Ground cover subfactor	See cover-management subfactors
Growth chart	The collection of values that describe the temporal vegetation variables of live root biomass in upper 4 inches, canopy cover, effective fall height, and live ground cover; values are in a *vegetation* description in the vegetation component of the RUSLE2 database
Hortonian overland flow	Overland flow generated by rainfall intensity being greater than infiltration rate; although flow may be concentrated in micro-channels (rills), runoff is uniformly distributed around hillslope
Hydraulic (roughness) resistance	Degree that ground cover, surface roughness, and vegetation retardance slow runoff; daily values vary as cover-management conditions change
Hydraulic element	RUSLE2 hydraulic elements are a channel and a small

	impoundment
Hydraulic element flow path description	Describes the flow path through a sequence of hydraulic elements; named and saved in hydraulic element flow path component of RUSLE2 database
Hydraulic element system description	Describes a set of hydraulic element paths that are uniformly spaced along the overland flow path described without the hydraulic element system being present, named and saved in the hydraulic element system component of the RUSLE2 database
Hydrologic soil group	Index of runoff potential for a soil profile at a given geographic location, at a particular position on the landscape, and the presence or absence of subsurface drainage
Impoundment	A flow interceptor; impounds runoff; results in sediment deposition; represents impoundments typical of impoundment terraces on cropland and sediment basins on construction sites
Impoundment parallel terrace	Parallel terraces; impoundments occur where terraces cross concentrated flow areas; impoundments drains through risers into underground pipe
Incorporated biomass	Biomass incorporated (buried) in the soil by a *soil disturbing* operation; also biomass added to the soil by decomposition of surface biomass; amount added by decomposition of surface material is function of soil consolidation subfactor
Inherent organic matter	Soil organic matter content in unit-plot condition
Inherent soil erodibility	Soil erodibility determined by inherent soil properties, measured under unit-plot conditions (see soil erodibility)
Initial conditions	Cover-management conditions at the beginning of a no-rotation cover-*management* description
Initial input roughness	Roughness index value assigned to *soil disturbing* operation for the base condition of a silt loam soil having a high biomass on and in the soil; actual initial roughness value used in computations is a function of soil texture, soil biomass, existing roughness at time of soil disturbance, and tillage intensity
Injected biomass	Biomass placed in the soil using an *add other residue/cover* process in a *soil disturbing operation* description; biomass placed in lower half of disturbance depth (see operation processes)
Interrill erosion	Erosion caused by water drop impact; not function of distance along overland flow path unless soil, steepness, and cover-

	management conditions vary, interrill areas are the spaces between rills; very thin flow occurs on interrill areas
Irrigation	Water artificially added to the soil to enhance seed germination and vegetation production
Land use independent	RUSLE2 applies to all situations where Hortonian overland flow occurs and where raindrop impact and surface runoff cause rill and interrill erosion of exposed mineral soil; the same RUSLE2 equations are used to compute erosion regardless of land use
Live above ground biomass	Live above ground biomass provided by vegetation (dry matter basis); converted to standing residue (dead biomass) by a *kill vegetation* process in an *operation* description.
Live ground (surface) cover	Parts of live above ground biomass that touches the soil surface to reduce erosion.
Live root biomass	RUSLE2 distributes input values for live root biomass in upper four inches over a constant rooting depth of 10 inches for all vegetation types and plant growth stages; a *kill vegetation* process in an *operation* description converts live root biomass to dead root biomass. Primarily refers to fine roots that are annually produced, RUSLE2 uses live and dead root biomass in the upper 10 inches to compute a value for the soil biomass subfactor
Local deposition	Deposition that occurs very near, within a few inches, the point of detachment in surface roughness depressions and in furrows between ridges; given full credit for soil saved
Long term roughness	Roughness that naturally develops over time; specified as input in cover-*management* description; depends on vegetation characteristics (e.g., bunch versus sod forming grasses, root pattern near soil surface) and local erosion and deposition, especially by wind erosion; RUSLE2 computes roughness over time; fully developed by *time to soil consolidation*
Long term vegetation	Permanent vegetation like that on pasture, range, reclaimed mined land, and landfills; vegetation description can include temporal values starting on seeding date through maturity, any arbitrary date, or only for the annual cycle of vegetation at maturity
Management alignment offset	Used to sequence cover-management descriptions along an overland flow path to create alternating strips
Mass-cover relationship	Equation used to compute portion of soil surface covered by a

	particular residue mass (dry basis)
Mass-yield relationship	Equation used to compute standing biomass (dry basis) as a function of vegetation production (yield) level
Maximum 30 minute intensity	Average rainfall intensity over the continuous 30 minutes that contains the greatest amount in a rain storm
Non-erodible cover	Cover such as plastic, standing water, snow, and other material that completely eliminates erosion; material can be porous and disappear over time
Non-uniform overland flow path	Soil, steepness, and/or cover-management vary along an overland flow path; path is divided into segments where input selections are made for each segment
NRCS curve number method	Mathematical procedure used in RUSLE2 to compute runoff; a daily runoff value is computed using the 10 yr-24 hr precipitation amount and temporally curve number values that vary as cover-management varies
NWWR	Northwest Wheat and Range Region, a region in the Northwestern US covering eastern Washington and Oregon, northern Idaho (see Req zone)
Operation	An operation changes soil, vegetation, or residue; typically used to represent common farm and construction activities such as plowing, blading, vehicular or animal traffic, and mowing; also used to represent burning and natural processes such as killing frost and germination of volunteer vegetation.
Operation disturbance depth	Surface residue buried by a *soil disturbing* operation is a function of operation disturbance depth
Operation description	Information used to describe an operation, named and stored in the operations component of the RUSLE2 database
Operation processes	An operation is described by a sequence of processes; used to describe how an operation changes cover-managements conditions that affect erosion
No effect	Has no effect on computations; commonly used to reference dates in a cover-management description and to cause RUSLE2 to display information for a particular set of dates
Begin growth	Tells RUSLE2 when to begin using data from a particular *vegetation* description

Kill vegetation	Converts live above ground biomass to standing residue and to convert live root biomass to dead root biomass
Flatten standing residue	Converts a portion of the standing residue to surface residue
Disturb (soil) surface	Mechanically disturbs soil; required to bury surface residue; resurfaces buried residue; required to create roughness and ridges; required to place material (external residue) directly into the soil
Add other cover	Adds material (external residue) to the soil surface and/or places it in the soil
Remove live above ground biomass	Removes a portion of the live above ground biomass; leaves a portion of the affected biomass as surface (flat) residue and standing residue
Remove residue/cover	Removes a portion of standing and surface (flat) residue
Add nonerodible cover	Adds nonerodible cover such as plastic, water depth, snow, or other material that allows no erosion for portion of soil surface covered, cover disappears over time; cover can be porous; cover has no residual effect; not used to represent erosion control blankets and similar material
Remove nonerodible cover	Removes portion of nonerodible cover
Operation speed	Surface residue buried by a soil disturbing operation is a function of operation speed
Overland flow path	Path taken by overland flow on a smooth soil surface from its point of origin to the concentrated flow area that ends the overland flow path; runoff is perpendicular to hillslope contours
Overland flow path (profile) description	Includes values for steepness, names for *soil* and cover-*management* descriptions for segments along an overland flow path; a uniform overland flow path (profile) is where steepness, soil, or cover-management does not vary with distance along overland flow path; a convex profile is where steepness increases with distance; a concave profile is where steepness decreases with distance; a complex profile is a combination of convex, concave, and/or uniform sub-profiles or where soil and/or cover-management vary along the overland flow path

Overland flow path length	Distance along the overland flow path from the origin of overland flow to the concentrated flow area (channel) that intercepts runoff to terminate overland flow;, does not end where deposition begins (see USLE slope length and steepness)
Overland flow path segments	Overland flow path is divided into segments to represent spatial variability along an overland flow path; conditions are considered uniform within each segment
Overland flow path steepness	Steepness along the overland flow path, not hillslope steepness (see USLE slope steepness)
Permeability index	Index for the runoff potential of the soil under the unit-plot condition; used in RUSLE2's soil erodibility nomographs, similar to inverse of hydrologic soil group
Plan description	Collection of RUSLE2 *profile* descriptions used to computed weighted averages for a complex area based on the portion of the area that each profile represents; named and saved in plan component of RUSLE2 database
Ponding subfactor	See cover-management subfactors
Porous barriers	Runoff flows through a porous barrier; does not affect overland flow path; typically slows runoff to cause deposition; examples are stiff grass hedges, fabric (silt) fences, gravel dams, and straw bales
Precipitation amount	Includes all forms of precipitation; RUSLE2 disaggregates input monthly values into daily values to compute decomposition and temporal soil erodibility
Production (yield) level	A measure of annual vegetation live above ground biomass production; user defines yield measure and preferred units on any moisture content basis; input value used to adjust values in a vegetation description at a base yield; maximum canopy cover in base vegetation description must be less than 100 percent
Profile description	Information used to describe profile (overland flow path); includes names for location, topography, soil, cover-management, and support practices used to make a particular RUSLE2 computation, named and stored in profile component of RUSLE2 database
Profile shape	See overland flow path description
Rainfall (storm) energy	Computed as sum of products of unit rainfall energy and rainfall amount in storm intervals where rainfall intensity is assumed uniform; storm energy is closely related to rain storm amount

Rainfall intensity	Rainfall rate express as depth (volume of rainfall/per unit area) per unit time
Remote deposition	Deposition that occurs a significant distance (tens of feet) from the point where the sediment was detached; examples include deposition by dense vegetation strips, terraces, impoundments, and toe of concave overland flow paths; only partial credit given to remote deposition as soil saved; credit depends on location of deposition along overland flow path; very little credit given for deposition near end of overland flow path
Req	Equivalent erosivity for the winter months in the Req zone; used to partially represent Req effect
Req effect	Refers to Req equivalent erosivity; erosion per unit rainfall erosivity in the winter period in the Req zone is much greater than in summer period; winter effect is much greater than in other regions because of a greatly increased soil erodibility; effect partially results from an elevated soil water content, increased runoff, and soil thawing
Req zone	Region where erosion is elevated in the winter months because of the Req effect; region primarily in eastern WA and OR, portions of ID, CA, UT, CO, and limited area in other western US states
Residue	Has multiple meanings in RUSLE2; generally refers to dead biomass, such as crop residue, created when vegetation is killed; plant litter from senescence; and applied mulch material (external residue) such as straw, wood fiber, rock, and erosion control blankets used on construction sites; material is generally assumed to be biomass that decomposes; also used to represent applied material like rock that does not decompose
Residue description	Values used to describe residue, named and stored in the residue component of the RUSLE2 database
Residue type	Refers to fragility and geometric residue characteristics; affects residue amount buried and resurfaced by an operation; affects degree that residue conforms to surface roughness; affects erosion control on steep slopes like those on construction sites
Resurfacing ratio	Portion (dry mass basin) of the buried residue in the soil disturbance depth that a soil disturbing operation brings to the soil surface; function of residue and operation properties
Retardance	Degree that vegetation (live above ground biomass) and standing residue slows runoff; varies with canopy cover; function of

	production (yield) level; part of *vegetation* description
Ridge height	Height of ridges created by a *soil disturbing* operation; major variable along with row grade that determines contouring effectiveness; decays as a function of precipitation amount and interrill erosion
Ridge subfactor	See cover-management subfactors
Rill erosion	Caused by overland flow runoff; increases with distance along the overland flow path
Rill to interrill erosion ratio	Function of slope steepness, rill to interrill soil erodibility, and how cover-management conditions affect rill erosion different from interrill erosion
Rock cover	Rock cover entered in the *soil* description; represents naturally occurring rock on soil surface; operations do not affect this rock cover; rock cover created by an operation that *adds other cover* (rock residue) is treated as external residue; soil disturbing operations bury and resurface rock added as external residue
Root biomass	See dead and live root biomass
Root sloughing	Annual decrease in root biomass, RUSLE2 adds the decrease in live root biomass to dead residue biomass pool
Rotation	Refers to whether a list of operation descriptions in a cover-*management* description are repeated in a cycle; length of cycle is rotation duration; list of operation descriptions are repeated in RUSLE2 until computed average annual erosion value stabilizes; eliminates need to specify initial conditions; *operation* descriptions in a no-rotation cover-*management* descriptions are sequentially processed in a single pass, first *operation* descriptions in cover-*management* description establish initial conditions
Rotation duration	Time (length of cycle) before the list of *operation* descriptions in a rotation type cover-*management* description repeats; time period over which RUSLE2 makes its computation in a no-rotation cover-*management* description
Rotational strip cropping	A rotation type cover-management description that involves periods of dense vegetation that are sequenced along the overland flow path to create strips of alternating dense vegetation that cause deposition
Row grade	Grade along furrows separated by ridges; usually expressed as

	relative row grade, which is the ratio of grade along the furrows to steepness of the overland flow path
Runoff	RUSLE2 computes runoff using NRCS curve number method and the 10 yr-24 hour precipitation amount; used to compute contouring effect, contouring failure (critical slope length), and deposition by porous barriers, flow interceptors, and concave overland flow path profiles
Sediment basin	Small impoundment typical of those used on cropland and construction sites; discharge is usually through a perforated riser that completely drains basin in about 24 hours
Sediment characteristics	Deposition is computed as a function of sediment characteristics, which are particle class diameter and density and the distribution of sediment among particle classes
Sediment particle classes	RUSLE2 uses sediment particle classes of primary clay, silt, and sand and small and large aggregate classes, diameter of aggregate classes and the distribution of sediment among particle classes at point of detachment is function of soil texture; RUSLE2 computes how deposition changes the distribution of sediment particle classes
Sediment load	Mass of sediment transported by runoff per unit hillslope width
Sediment transport capacity	Runoff's capacity for transporting sediment; depends on runoff rate, overland flow path steepness, and hydraulic roughness; deposition occurs when sediment load is greater than runoff's transport capacity
Sediment yield	Sediment load at the end of the flow path represented in a RUSLE2 computation; flow path ends at overland flow path unless hydraulic elements (channel or impoundment) are present; sediment yield for site only if RUSLE2 flow path ends at site boundary
Segments	The overland flow path divided into segments based on topography, soil, and cover-management to represent spatial variation
Senescence	Decrease in vegetation canopy cover; senescence adds biomass to surface (flat) residue unless RUSLE2 is instructed that a decrease in canopy cover, such as leaves drooping, does not add to surface residue
Shear stress	Total runoff shear stress is divided into two parts of that acting on the soil (grain resistance) and that acting on surface residue, surface

	roughness, live vegetation, and standing residue (form resistance); shear stress acting on the soil is used to compute sediment transport capacity; total shear stress is used to compute contouring failure; also function of runoff rate and steepness of overland flow path
Short term roughness	Roughness created by a soil disturbing operation, decays over time as a function of precipitation amount and interrill erosion
Slope length exponent	Exponent in equation used to compute rill-interrill erosion as a function of distance along overland flow path, function of rill to interrill erosion ratio.
Soil biomass subfactor	See cover-management subfactors
Soil consolidation effect	Represents how wetting/drying and other processes cause soil erodibility to decrease over time following a mechanical soil disturbance; increase in soil bulk density (mechanical compaction) not the major cause of reduced soil erodibility; affects runoff, accumulation of biomass in upper 2 inch soil layer, and soil biomass effectiveness
Soil consolidation subfactor	See cover-management subfactors
Soil description	Describes inherent soil properties that affect erosion, runoff, and sediment characteristics at point of detachment on unit plot conditions, named and saved in the soil component of the RUSLE2 database
Soil disturbance width	Portion of the soil surface disturbed; weighted effects of disturbance computed as a function of erosion on disturbed and undisturbed area to determine an effective time since last disturbance, effective surface roughness, and effective ground cover
Soil disturbing operation	*Operation* description that contains *disturb soil* process
Soil erodibility	RUSLE2 considers two soil erodibility effects, one based on inherent soil properties and one based on cover-management; inherent soil erodibility effect represented by K factor value empirically determined from erosion on unit plot; part related to cover-management is represented in cover-management subfactors
Soil erodibility nomograph	Mathematical procedure used to compute a K factor value, i.e., inherent soil erodibility
Soil loss	Proper definition is the sediment yield from a uniform overland

	flow path divided by the overland flow path length; loosely used as the net removal of sediment from an overland flow path segment
Soil loss from eroding portion	Net removal of sediment from the eroding portion of the overland flow path
Soil loss tolerance (T)	Erosion control criteria, objective is that "soil loss" be less than soil loss tolerance T value, special considerations must be given to non-uniform overland flow paths to avoid significantly flawed conservation and erosion control plans
Soil mechanical disturbance	Mechanical soil disturbance resets soil consolidation effects; *disturb soil* process must be included in an *operation* description to create surface roughness and ridges and to place biomass into the soil
Soil saved	Portion of deposited sediment that is credited as soil saved; computed erosion is reduced by soil saved to determine a conservation planning soil loss value; credit depends on location of deposition along overland flow path
Soil structure	Refers to the arrangement of soil particles in soil mass; used to compute soil erodibility (K) factor values
Soil texture	Refers to the distribution of primary particles of sand, silt, and clay in soil mass subject to erosion
Standing residue	Created when live vegetation is *killed*, decomposes at a reduced rate; falls over at a rate proportional to decomposition of surface residue
Strip/barrier *description*	Support practice, describes porous barriers, named and stored in the strip/barrier component of RUSLE2 database
Subfactor method	See cover-management subfactors
Subsurface drainage description	Support practice that lowers water table to reduce soil water content, runoff, and reduces erosion; RUSLE2 uses difference between hydrologic soil groups for drained and undrained conditions to compute erosion as affected by subsurface drainage, named and save in subsurface drainage component of RUSLE2 database
Support practices	Erosion control practice used in addition to cultural erosion control practice, hence a support practice; includes contouring, filter and buffer strips, rotational strip cropping, silt (fabric) fences, stiff grass hedges, diversions/terraces, gravel dams, and sediment basins

Surface (flat) residue	Material in direct contact with the soil surface; main source is plant litter, crop residue, and applied mulch (external residue).
Surface roughness	Random soil surface roughness; combination of soil peaks and depressions that pond runoff; created by a *soil disturbing* operation, decays as a function of precipitation amount and interrill erosion
Surface roughness index	A measure of soil surface roughness; standard deviation of surface elevations measured on a 1 inch grid about mean elevation; effect of ridges and land steepness removed from measurements
Surface roughness subfactor	See cover-management subfactors
Temperature	Input as average monthly temperature; disaggregated into daily values, used to compute biomass decomposition and temporal soil erodibility
Template	Determines the computer screen configuration of RUSLE2 and inputs and outputs; determines the complexity of field situations that can be described with RUSLE2
Terraces	Flow interceptors (channels) on a sufficiently flat grade to cause significant deposition
Three layer profile schematic	Some RUSLE2 templates include an overland flow path schematic having individual layers to represent cover-management, soil, and topography; used to graphically divide the overland flow path into segments to represent complex conditions
Tillage intensity	Degree that existing soil surface roughness affects roughness left by a soil disturbing operation
Tillage type	Identifies where a soil disturbing operation initially places buried residue in soil, also refers to how operation redistributes buried residue and dead roots
Time to soil consolidation	Time required for 95 percent of the soil consolidation effect to be regained following a soil disturbing operation
Topography	Refers to steepness along the overland flow path and the length of the overland flow path
Uniform slope	Refers to an overland flow path where soil, steepness, and cover-management along the overland flow path do not vary along flow path

Unit rainfall energy	Energy content of rainfall per unit of rainfall; function of rainfall intensity
Unit plot	Base condition used to determine soil erodibility; reference for effects of overland flow path steepness and length; cover-management, and support practices; continuous tilled fallow (no vegetation; tilled up and downhill, maintained in seedbed conditions; topographic, cover-management, support practice factor values equal 1 for unit-plot condition
USLE slope length and steepness	USLE slope length is distance to a concentrated flow (e.g., terrace or natural waterway) or to the location where deposition occurs; USLE soil loss is sediment yield from this length divided by length (mass/area); USLE steepness is steepness of the slope length, uniform steepness often assumed
Validation	Process of ensuring that RUSLE2 serves its intended purpose as a guide to conservation and erosion control planning.
Vegetation description	Information used by RUSLE2 to represent the effect of vegetation on erosion; includes temporal values in growth chart, flow retardance, and biomass-yield information; named and stored in the vegetation component of the RUSLE2 database
Verification	Process of ensuring RUSLE2 correctly solves the mathematical procedures in RUSLE2
Worksheet description	A form in RUSLE2 program; used to compare conservation and erosion control practices for a given site; used to compare erosion computer for profile descriptions; named and saved in the worksheet component of the RUSLE2 database

Rusle 2 Science Documentation

1. ABOUT RUSLE2

1.1. Introduction

The Revised Universal Soil Loss Equation, Version 2 (RUSLE2) is a computer program that estimates rill and interrill erosion by solving a set of mathematical equations (Toy et al., 2002). RUSLE2 makes estimates based on site specific conditions, which allows erosion control practices to be tailored to each specific site. The RUSLE2 user describes the site by making selections from the RUSLE2 database. RUSLE2 uses this information to compute its erosion estimates. The purpose of RUSLE2 is to serve as a guide to conservation and erosion control planning. RUSLE2 is land use independent and applies to all conditions where rill and interrill erosion occurs when mineral soil is exposed to the erosive forces of impacting raindrops and water drops falling from vegetation and runoff produced by Hortonian overland flow. RUSLE2 computes erosion and deposition along a single overland flow path. RUSLE2 also computes deposition in channels and small impoundments that end overland flow paths.

RUSLE2 has three major components. One component is the science component that includes the mathematical equations that RUSLE2 uses to compute erosion and deposition. Inputs to the equations are user selected to represent the four major factors that affect erosion at a specific site. Those factors are climate (determined by location), inherent soil properties including soil erodibility, topography, and land use.

The second major RUSLE2 component is the RUSLE2 database. The RUSLE2 user makes selections from the database to describe site-specific conditions. The database contains information that describes climate (weather) at various locations, soils, cover-management systems, vegetations, residues, operations, porous strips and barriers, flow interceptors including diversions and terrace channels and small impoundments, subsurface drainage systems, irrigation systems, overland flow paths, worksheets, and plan views (collections of overland flow paths). A single overland flow path is the basic RUSLE2 computational unit. Erosion can be compared in a worksheet for multiple erosion control alternatives for a single overland flow path or multiple overland flow paths. A plan view is used to compute erosion on overland flow areas in spatially complex landscapes.

The third major RUSLE2 component is the computer program. The program includes a powerful computational engine that organizes and solves the mathematical equations, database maintenance tools, and an interface (computer screen) that accepts user inputs and displays computed values.

The USDA-Agricultural Research Service had overall lead responsibility for developing RUSLE2 and lead responsibility for developing the science (i.e., mathematical equations used in RUSLE2). The University of Tennessee had lead responsibility for developing

the RUSLE2 computer program including its interface and computational engine. The USDA-Natural Resources Conservation Service had lead responsibility for developing user requirements as the principal RUSLE2 client and the RUSLE2 database for cropland. Other organizations developed database information, user guides, and instructional material for RUSLE2. For example, the University of Denver developed database information and other materials for application of RUSLE2 to construction sites, reclaimed mined land, landfills, and other highly disturbed lands.

This document describes the RUSLE2 science, which is primarily embodied in the mathematical equations used in RUSLE2 to compute erosion and deposition estimates.

1.2. Major requirements

The RUSLE2 erosion prediction technology was designed to meet several requirements, many of which affected RUSLE2's science and the equations. These requirements included:

1) Purpose of RUSLE2 is to serve as a guide to conservation and soil erosion control planning at the local field office level.

2) Be easy to use.

3) Be robust so that computed erosion values are not overly sensitive to small changes in variables where input values involve considerable uncertainty. Helps ensure good estimates when extrapolated beyond range of data used to derive RUSLE2.

4) Input values are physically meaningful to typical RUSLE2 users and directly measurable where possible.

5) Not require resources beyond those available at the field office level, especially for the USDA-Natural Resources Conservation Service that is the primary RUSLE2 user.

6) Produce useful information for conservation and erosion control planning that is consistent with the resources (i.e., expertise, time, effort, and other costs) required to implement and use RUSLE2.

7) Lead to desired conservation and erosion control planning decisions as expected based on available erosion research data, accepted erosion science, field experience, and professional judgment.

8) Apply to Hortonian overland flow where rill and interrill erosion is caused by mineral soil being exposed to the erosive forces of surface runoff and impacting waterdrops from rainfall and rainwater falling from vegetation.

9) Be land-use independent by using relationships based on the fundamental variables that affect erosion.

10) Produce accurate erosion estimates comparable to measured research values and estimated by the Universal Soil Loss Equation (USLE).

11) Be an evolution of the USLE and RUSLE1.

12) Be thoroughly and carefully reviewed and evaluated to ensure that RUSLE2 performs acceptably.

13) Recommendations on how to best apply RUSLE2 would be a part of the RUSLE2 development and documentation.

1.3. Major guiding principles used to develop RUSLE2 science

The following principles guided the development of the RUSLE2 science according to the requirements listed in **Section 1.2**.

1) The USLE is accepted in term of its conceptual basis, equation structure, empirical derivation, and computed values by both the scientific and user communities.

2) The USLE is valid (i.e., serves its intended purpose) for conservation and soil erosion control planning.

3) RUSLE2 development will start from the USLE structure and extend that structure and empirical derivation.

4) RUSLE2 will represent main effects that can be considered in the conservation and erosion control planning. These main effects are those established by empirical data and fundamental erosion science.

5) Erosion data available for empirically deriving RUSLE2 equations are very limited. The data set is small in relation to the many variables and their many complex interactions that affect erosion. The dataset is not a statistically robust data set because of non-uniform coverage of important variables. The data contain much unexplained variability that can not be resolved.

6) Equations will be chosen to best represent established main effects rather than using regression procedures to fit equations to data to provide the best overall statistical fit. Equations will be chosen based on main effects conclusively established by empirical data, fundamental erosion science, practical experience, professional judgment, and overall good judgment (common sense).

7) First establish mathematical relationships empirically using experimental data and then use process-based equations based on fundamental erosion science to extend the RUSLE2 beyond the available research data.

8) Start from a mean, typical, or accepted value consistent with the USLE unit-plot concept and use normalized variables to compute values that deviate about the

value for a base condition to capture main effects. Equations and limits will be selected to produce a robust erosion prediction technology.

9) Minimize use of geographic zones and variable classes to avoid step changes (discontinuities) between zones and classes.

10) Achieve land-use independence by having a single set of equations that vary as a continuous function of the major variables that affect erosion across all land uses.

11) Make judgments in the context of reasonableness and appropriateness for conservation and erosion planning and implementation. Do the results make good overall sense? If one had perfect knowledge, what would be the planning decision? RUSLE2 is a tool for conservation and erosion control planning, not a scientific product designed to produce new scientific knowledge and understanding.

2. BASIC MATHEMATICAL STRUCTURE

RUSLE2 computes values for the three fundamental erosion processes of detachment (sediment production), transport, and deposition.[1] The empirical equation form of the USLE is used to compute detachment while process-based equations are used to compute sediment transport and deposition. These equations, which are written for a point in time and a location on an overland flow path, are integrated in both time and distance to produce average annual and spatial estimates for segments along the overland flow path and for the entire overland flow path.

2.1. Detachment (Sediment Production) Equation

The USLE in its original form is:

$$A = RKLSCP \qquad [2.1]$$

where: A = average annual erosion rate (mass/area·year) for the slope length λ, R = erosivity factor (erosivity unit/area·year), K = soil erodibility factor (mass/ erosivity unit), L = slope length factor (dimensionless), S = slope steepness factor (dimensionless), C = cover-management factor (dimensionless), and P = support practice factor (dimensionless).[2] The USLE, equation 2.1, has two parts, the part that computes unit-plot erosion and the part that adjusts unit plot-erosion to represent actual field conditions. The part that computes unit-plot erosion is:

---

[1] Refer to the RUSLE2 User's Reference Guide for detailed explanations of RUSLE2 terms. Also, see **Glossary of Terms** section in this document.

[2] See List of symbols at end of this chapter.

$$A_u = RK \quad [2.2]$$

where: A_u = average annual erosion (mass/area·year) for the unit plot (mass/area·year).[3] The terms LSCP are normalized with respect to the unit plot and, therefore, have a value of 1 for unit plot conditions.[4] In effect, the USLE computes erosion for unit plot conditions with the product RK and then uses the terms LSCP to adjust the unit plot erosion to account for differences between unit plot conditions and actual field conditions.

Equation 2.2 is a temporal integration of the basic USLE equation that computes unit-plot erosion for individual storms as:

$$a_{us} = (EI_{30})K \quad [2.3]$$

where: a_{us} = the unit-plot erosion (mass/area) from the storm that has the rainfall erosivity EI_{30} (force·length/area)(length/time), E = rain storm energy (force·length/area), and I_{30} = average intensity (length/time) over the continuous 30 minutes with the most rainfall in the storm. The linear relationship between unit plot erosion and storm erosivity EI_{30} means that the erosivity factor R can be computed for a locations as:

$$R = \sum_{j=1}^{M_r} \sum_{m=1}^{M_{s(j)}} (EI_{30})_m \Big/ M_r \quad [2.4]$$

where: EI_{30} = storm erosivity for storm events greater than 0.5 inches (12 mm), $M_{s(j)}$ = the number of storms in the *jth* year, M_r = number of years in the record being used to compute erosivity.[5]

The linear relationship between erosion on the unit plot and erosivity mathematically means that average daily erosion can be computed as:[6]

$$a_u = rK \quad [2.5]$$

---

[3] The unit plot is 72.6 ft (22.1 m) long on a 9 percent slope, maintained in continuous fallow, tilled up and down hill to a seedbed condition periodically to control weeds and break crusts that form on the soil surface.

[4] The terms A_u, R, and K have dimensions and units. The terms LSCP are ratios of erosion from a given field condition to erosion for the unit-plot condition, and these terms are, therefore, dimensionless and have no units.

[5] See RUSLE2 User's Reference Guide for a detailed description of the computation of RUSLE2 erosivity values.

[6] Daily erosion computed by RUSLE2 is a long-term average erosion for that day.

where: a_u = daily erosion from the unit plot on the *ith* day and r = the average daily erosivity on the *ith* day. Average daily erosivity values are determined by the disaggregation of average monthly erosivity input values into daily values (see **Section 3.1**).

Although the terms LSCP vary with time as field conditions change, the cover-management factor C is the only one of these USLE terms that is mathematically integrated with time. An average annual representative value is selected for the other terms. The mathematical equation used in the USLE to compute erosion for a crop stage period is:

$$a_k = KLS \, \mathrm{Pr}_k \, c_k \qquad [2.6]$$

where: a, r, and c = the erosion, erosivity, and cover-management (soil loss ratio) factors, respectively, for the *kth* crop stage.[7] The erosivity for the *kth* crop stage is given by:

$$r_k = f_k R \qquad [2.7]$$

where: f_k = the portion of the average annual erosivity that occurs during the *kth* crop stage.[8] Therefore, the average annual cover management C factor in the USLE is computed as:

$$C = \left(\sum_{k=1}^{M_k} f_k c_k \right) \Big/ N_c \qquad [2.8]$$

where: M_k = the number of crop stages over the period of N_c years involved in the computation, such as years in a crop rotation or years after disturbance of a construction site, used to compute erosion.

The mathematics of the USLE equation structure, therefore, allows RUSLE2 to compute an average daily erosion as:

$$a = rklScp_p \, p_c \, p_d \qquad [2.9]$$

---

[7] A crop stage period is a time interval over which a constant soil loss ratio can be assumed. The soil loss ratio is the ratio of erosion with a given cover-management condition to the unit plot erosion for the same period, with all other conditions being the same between the two cover-management conditions.

[8] Erosivity varies during the year. The empirical curve that describes this temporal distribution is referred to as the EI distribution.

where: r = daily erosivity (erosivity unit/area·day), k = daily soil erodibility factor (mass/erosivity unit), l = daily slope length factor dimensionless, c= daily cover-management (soil loss ratio) factor (dimensionless), p_p = daily ponding subfactor (dimensionless), p_c = daily contouring subfactor (dimensionless), and p_d = daily subsurface drainage subfactor (dimensionless).[9] The average daily erosion computed by equation 2.9 is the average erosion (mass/area) for the slope length λ. All terms in equation 2.9 use average daily values except for the slope steepness factor that is assumed to be constant in RUSLE2 for all conditions except for variations in slope steepness.[10]

2.1.1. Equation for rill and interrill detachment combined

Equation 2.9 is converted to an equation that computes rill and interrill erosion combined at a point so that RUSLE2 can be applied to non-uniform overland flow paths where soil, steepness, and cover-management vary along the overland flow path. This equation is (Foster and Wischmeier, 1974):

$$D = (m+1) r k (x/\lambda_u)^m S c p_p p_c p_d \qquad [2.10]$$

where: D = average daily net detachment by both rill and interrill erosion (mass/area) at a point at the distance x from the origin of the overland flow path, λ_u = the unit plot length (72.6 ft, 22.1 m), and m = daily slope length exponent. The value for each term, except erosivity r, is the value for the term at the location x on the overland flow path.

2.1.2. Equation for interrill erosion

Interrill erosion is assumed to occur even when RUSLE2 computes deposition (see **Sections 2.3.1, 2.3.6, and 2.3.8**). The RUSLE2 equation for interrill erosion is:

$$D_i = 0.5 r k S_i c p_r p_c p_d \qquad [2.11]$$

where: D_i = daily interrill erosion (mass/area·day), and S_i = the slope steepness factor for interrill erosion. Equation 2.11 for interrill erosion is similar to equation 2.10 for rill and interrill erosion combined except that equation 2.11 has no distance (x) term, has a slope steepness factor specifically for interrill erosion, and has a 0.5 factor. The reason for not having a distance term is that detachment on interrill areas is caused by impacting

---

[9] RUSLE2 describes the effect of other support practices besides contouring on erosion. Those effects are described using process-based equations that compute deposition rather than a P factor value as in the USLE.

[10] Lower case symbols are used in equation 2.9 to distinguish between the daily factor values used in RUSLE2 and the average annual factor values used in the USLE. An upper case symbol is used for the slope steepness factor because a constant value is used in RUSLE2 that is equivalent to the USLE slope steepness factor value.

raindrops and waterdrops falling from vegetation. Detachment on interrill areas is assumed to be uniform along the overland flow path provided soil, steepness, or cover-management does not change along the overland flow path (Foster and Meyer, 1975; Foster et al., 1977a; Toy et al., 2002).

The slope steepness factor for interrill erosion differs from the slope steepness for rill erosion because the detachment forces produced by impacting waterdrops differ from the detachment forces produced by flow in rill areas. The interrill erosion slope steepness factor in equation 2.11 was empirically derived from experimental data (Lattanzi et al., 1974; Foster, 1982; McGregor et al., 1990). The slope steepness factor in the equation 2.10 represents the effect of slope steepness on rill and interrill erosion combined. The 0.5 factor in equation 2.11 results from the assumption that interrill erosion and rill erosion are equal for unit plot conditions (Foster and Meyer, 1975; Foster et al., 1977b; McCool et al., 1989).

2.1.3. Ratio of rill to interrill erosion

The slope length exponent m in equation 2.10 is a function of the ratio of rill to interrill erosion. RUSLE2 computes the slope length exponent m as (Foster et al., 1977b; McCool et al., 1989):

$$m = \beta/(1+\beta) \qquad [2.12]$$

where: β = ratio of rill to interrill erosion. The typical slope length exponent in the USLE is 0.5, which is the value computed by equation 2.12 when rill and interrill erosion are equal. The slope length exponent m computed by equation 2.12 varies about 0.5 as the ratio of rill erosion to interrill erosion varies about 1. The base condition for rill erosion equaling interrill erosion is for unit plot conditions.

The ratio of rill to interrill erosion is computed from:[11]

---

[11] Equations 2.11 and 2.13 illustrate an important design principle in RUSLE2. The terms that represent interrill erosion in equation 2.13 differ from those in equation 2.11 used to compute absolute interrill erosion, which seems inconsistent. The design philosophy in RUSLE2 is that RUSLE2 starts from accepted empirical values, which is 0.5 for the slope length exponent for unit plot conditions. Empirical values are used to the extent that they can be determined from experimental data, especially to represent main effects. The best possible empirical value is determined from the experimental data, and then the accepted empirical value is adjusted using process-based equations. The adjustment is up or down about the accepted empirical value, which is almost always a ratio in RUSLE2 because the LSCP variables are non-dimensional ratios. This approach of adjusting up or down about an accepted empirical ratio value rather than computing absolute values gives RUSLE2 increased robustness and avoids RUSLE2 giving seriously erroneous values when it is extrapolated. The ratio of rill to interrill ratio can be computed more accurately than can an absolute value for interrill erosion. The advantage of equation 2.11 is that it computes values that are close to erosion values computed by the USLE, which is a more conservative and robust approach than computing an absolute value of interrill erosion using variables from equation 2.13.

$$\beta = \left(\frac{K_r}{K_i}\right)\left(\frac{c_{pr}}{c_{pi}}\right)\left(\frac{\exp(-b_r f_g)}{\exp(-0.025 f_g)}\right)\left(\frac{s/0.0896}{3s^{0.8}+0.56}\right) \quad [2.13]$$

The ratio K_r/K_i = the inherent rill to interrill soil erodibility ratio (see **Section 4.3**), which is computed as a function of soil texture to reflect that some soils are inherently more susceptible to rill erosion than to interrill erosion than are other soils. The term c_{pr}/c_{pi} = the rill to interrill erosion ratio for prior land use soil erodibility (see **Section 6.2.2**), which reflects how soil consolidation and soil biomass affect rill erosion differently from how it affects interrill erosion. The ratio $\exp(-b_r f_g)/\exp(-0.025 f_g)$ reflects how ground cover affects rill erosion more than it affects interrill erosion, where b_r and 0.025 = coefficients (percent^{-1}) that express the relative effectiveness of ground cover for reducing rill erosion and interrill erosion, respectively (see **Section 6.2**), and f_g = ground cover expressed as a percent (see **Section 6.2.2**).

The term $(s/0.0896)/(3s^{0.8}+0.56)$ [where s = steepness of overland flow path (sine of slope angle)] reflects how steepness affects rill erosion differently than it does interrill erosion (Foster, 1982). This term assumes that rill erosion varies linearly with steepness.

The assumption in equation 2.12 that rill erosion varies with a slope length exponent of 1 (McCool et al., 1989) is consistent with the maximum slope length exponent of 1 observed in the experimental plot data used to derive the USLE [AH537 (Wischmeier and Smith, 1978)]. The maximum exponent of 1 is also consistent with the variation of erosion with discharge on steep slopes (Meyer et al., 1972) but is less than a value of 0.75 reported in other field research (Govers, 1991; McCool et al., 1989) where rill erosion is the dominant erosion process.

The slope length exponent base value is 0.5. Equation 2.12 increases or decreases this value as rill erosion increases or decreases relative to interrill erosion. The terms in equation 2.13 represent the main variables that affect rill erosion relative to interrill erosion.

Given that rill erosion varies with a slope length exponent of 1, the rill erosion term in equation 2.13 should have included a slope length term. The reason that a slope length term is not in equation 2.13 is because of mathematical limitations in devolving the USLE equation structure into rill and interrill erosion terms. If a slope length term had been included in equation 2.13, RUSLE2 could not have met the requirement that erosion computed for the entire overland flow path length be independent of how many overland flow path segments are used in the computations when other conditions are uniform along the overland flow path (see **Section 5.Appendix 1**).

2.2. Spatial and Temporal Integration

RUSLE2 requires both a spatial and temporal integration. The spatial integration is made by solving the governing equations along the overland flow path each day. Temporal integration is made by summing daily values to obtain totals for the computation

duration.[12] The average annual erosion is the sum of the daily values divided by the number of years (duration) in the computation.

If RUSLE2 were applied to only spatially uniform overland flow paths, equation 2.9 could be analytically solved for each day and the values summed to compute total erosion for a **rotation duration**. However, the solution is complex when soil, steepness, and cover-management vary along the overland flow path (i.e., spatially non-uniform overland flow paths), especially when deposition occurs.[13] RUSLE2 performs a spatial integration each day to compute daily spatially-distributed erosion, deposition, and sediment load values along the overland flow path. The spatial integration process in RUSLE2 is referred to as **sediment routing**, a common term used in hydraulic analyses.

2.3. Sediment Routing (Spatial Integration)

2.3.1. Continuity equation

The RUSLE2 governing equation that is spatially integrated is the steady state continuity (conservation of mass equation) given by (Foster, 1982):

$$dg / dx = D_i + D_{rorp} \qquad [2.14]$$

where: g = sediment load (mass/unit overland flow width·time), x = distance along the overland flow path from its origin, and D_{rorp} = either rill erosion rate (D_r) (mass/area· time) or deposition (D_p) (mass/area· time) by runoff in rill areas.

Equation 2.14 is solved numerically because it can not be analytically solved except for the special case of a uniform overland flow path where neither soil, steepness, nor cover-management vary along the overland flow path. RUSLE2 applies in the general case where any or all of these variables change along the overland flow path. The numerical solution requires that the overland flow path be divided into segments as illustrated in Figure 2.1 where the soil, steepness, and cover-management conditions are uniform over each segment. The numerical form of equation 2.14 for this computation is:

$$g_i = D_i\left(x_{(i)} - x_{(i-1)}\right) + \int_{x_{(i-1)}}^{x_{(I)}} D_{rorp}\,dx + g_{(i-1)} \qquad [2.15]$$

---

[12] Computation duration is the rotation duration (cycle length) for a **rotation** type cover-management description. The computation duration is the length of time specified for the duration of a no-rotation type cover-management description.

[13] RUSLE2 is much more powerful than the USLE because the USLE can not be applied to spatially non-uniform conditions that cause deposition (Foster and Wischmeier, 1974).

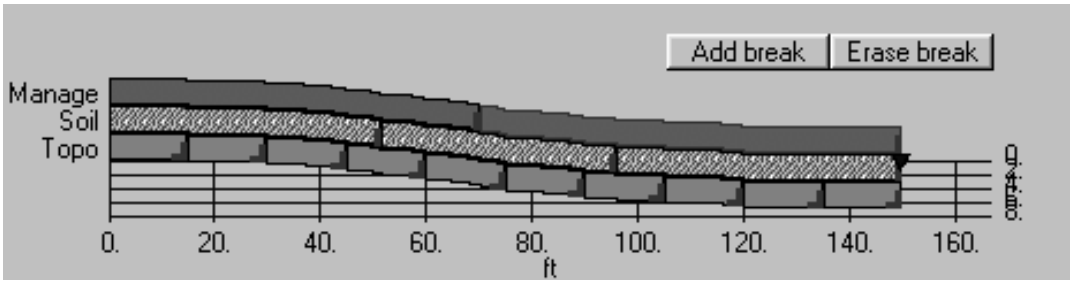

Figure 2.1. Schematic of the three layers that represent an overland flow path (a RUSLE2 hillslope(overland flow path) profile).

The lower and upper ends of the segment are delineated by $x_{(i)}$ and $x_{(i-1)}$, respectively, and the segment length is the difference $x_{(i)} - x_{(i-1)}$. Equation 2.12 is applied sequentially along the overland flow path starting at x = 0, which is the origin of the overland flow path. The incoming sediment load $g_{(i-1)}$ to the first segment at x = 0 is zero because no runoff enters at the origin of the overland flow path. The sediment load, g_{i-1}, entering the *ith* segment is known from the computation for the upslope *(i-1)th* segment. The sediment load g_i is the sediment load leaving the *ith* segment.

Rill and interrill erosion combined are computed with equation 2.10 rather computing interrill erosion and rill erosion separately as implied in equation 2.15. Equation 2.10 is solved analytically over the segment by assuming that soil, steepness, and cover-management are uniform over the segment. If deposition occurs, interrill erosion D_i is computed with equation 2.11 and the integral for deposition D_p is solved numerically (see **Section 2.3.6**).

The RUSLE2 assumption of uniformity within a segment causes step changes in input variables and certain computed variables where segments adjoin. Each soil, steepness, and cover-management variable is constant over a segment, but these variables make step changes at the common point between two segments. For example, the steepness values for two segments are not averaged to obtain a single steepness value at the intersection of two segments. Consequently, computed detachment and deposition values are discontinuous (i.e., step change) across segment intersections where soil, steepness, or cover-management changes between segments. However, runoff rate and sediment load are continuous at adjoining segment points. These step changes require sufficiently short segments to represent variables that vary continuously along the overland flow path. An example is a concave overland flow path (profile) where steepness continuously decreases from its upper end to lower end. A preliminary sensitivity analysis can be conducted to determine appropriate segment lengths for developing an erosion control plan for a specific site.

RUSLE2 could have been constructed to accommodate both step and continuous changes with distance. However, the benefits of representing both continuous and step changes were judged insufficient to merit the increased complexity in the equations, inputs, and programming for most RUSLE2 applications in erosion control planning. Step changes seem to occur more frequently than continuous changes in variables along an overland

flow path in most field situations. RUSLE2 represents these step changes, such as those associated with buffer strips and intersection of land slopes on construction sites.

2.3.2. Transport capacity-detachment limiting concept

RUSLE2 uses the transport capacity-detachment limiting concept to compute rill detachment or deposition (Foster et al., 1981a). The assumption is that rill erosion occurs where runoff transport capacity exceeds sediment load. Rill erosion is assumed not to be affected by the degree that sediment load fills runoff's sediment transport capacity, except where rill erosion would overfill transport capacity if rill erosion were to occur at its capacity rate. In this situation, rill erosion occurs at the rate that just fills transport capacity.[14]

A very important RUSLE2 assumption is that detachment and deposition by flow in rill areas at a location on an overland flow path can not occur simultaneously. Another important assumption is that both rill and interrill erosion are non-selective (Foster et al., 1985b). When rill and interrill detachment occur, the detached sediment contains all of the sediment classes having a distribution and size based solely on soil texture (see **Section 4.7**). That is, neither rill nor interrill detachment processes can "reach into the soil" and selectively remove sediment from particular sediment classes and not remove sediment from other particle classes. The basis of this assumption is that most soils are cohesive. Detachment is a process that separates soil particles from the soil mass by breaking cohesive bonds within the soil. This separation process produces sediment in all sediment classes because not all bonds in the soil are uniformly broken, much like striking a piece of concrete with a hammer produces a mixture of particles.[15]

Another important RUSLE2 assumption is that interrill erosion and deposition in rill areas occur simultaneously. When flow causes rill erosion, small incised channels are eroded. When deposition by runoff in rill areas occurs, the deposition is spread across the slope so that deposition covers the entire local area unless ridges are present (Toy et al., 2002). Therefore, a case can be made that no interrill erosion occurs on depositional areas, especially where deposition rates are high and flow is deep to protect the underlying soil surface from raindrop impact. However, even in these cases, deposition and water depths are quite spatially non-uniform, resulting in local areas that are not

---

[14] The concept of the interaction between rill erosion, sediment load, and transport capacity is valid, especially in ideal conditions and has advantages for RUSLE2 (Foster and Meyer, 1975; Foster, 1982). However, rill erosion in most field conditions is highly variable along rills where very intense local erosion occurs (e.g., at headcuts) and intervening areas of very low rill erosion. Because the hydraulic equations used in RUSLE2 do not represent this high degree of spatial non-uniformity, RUSLE2 can not adequately capture this important interaction.

[15] Soils can contain gravel that runoff does not transport. Conceptually, those particles are not assumed in RUSLE2 to be a part of the cohesive soil mass. The reason that gravel particles are not transported is that the runoff does not have sufficient transport capacity to move these particles. The effect of gravel and rock fragments on erosion is taken into account in RUSLE2 (see **Section 4.6**).

protected by deposited sediment or deep water. Also, many soil disturbing operations, such as tillage, leave surface roughness and ridges where soil protrudes above the flow and is directly exposed to interrill erosion. The RUSLE2 assumption is that interrill erosion and deposition by rill flow occurs simultaneously has the important benefit of allowing RUSLE2 to compute local deposition in soil surface roughness, furrows between ridges, and similar local roughness features.[16]

2.3.3. Basic deposition equation

RUSLE2 computes deposition when sediment load exceeds transport capacity using (Foster et al., 1981a; Foster, 1982):

$$D_p = (\alpha_d V_f / q)(T_c - g) \qquad [2.16]$$

where: D_p = deposition rate (mass/area·time), α_d = a deposition coefficient determined by calibration, V_f = fall velocity of the sediment in still water (length/time), q = overland flow (runoff) rate (volume/overland flow width·time) where flow depth is assumed to be uniform across the slope, T_c = transport capacity (mass/overland flow width·time). Equation 2.16 is solved for each sediment class (see **Section 4.7**). The distribution of the total transport capacity among the sediment classes is assumed to equal the distribution of the total sediment load among the classes. Equation 2.16 gives RUSLE2 its capability for computing deposition's selectivity where coarse, dense sediment is deposited more readily than fine, less dense sediment. The orders of magnitude variation in sediment fall velocity among the sediment classes is the major factor in computing selective deposition.

2.3.4. Sediment transport capacity equation

The RUSLE2 equation for sediment transport capacity of runoff in the rill areas is (Foster and Meyer, 1972; Foster and Meyer, 1975; Nearing et al., 1989, Finkner et al., 1989):

$$T_c = K_T \zeta q s \qquad [2.17]$$

where: the coefficient K_T coefficient for sediment transportability (mass/volume) and the ζ = coefficient for effect of hydraulic resistance on sediment transport capacity (dimensionless).

---

[16] Equation 2.11, which computes interrill erosion, actually computes sediment load delivered to rill flow rather than detachment on interrill areas. An improved approach is to use separate equations to compute detachment, deposition, and sediment transport on interrill areas, but that approach was judged to be too complex for RUSLE2. The RUSLE2 limitation regarding interrill erosion is that RUSLE2 does not compute sufficient enrichment of fines in the sediment although interrill erosion is appropriately computed. However, this limitation can be overcome by using the procedure described by Foster (1982) that can be used to compute distribution of sediment by sediment class delivered from interrill areas as a function of soil surface roughness.

A RUSLE2 assumption is that all sediment regardless of its composition is equally transportable, and therefore, a single value for sediment transportability is used in RUSLE2 (see **Section 4.7**). This assumption is questionable because the transportability of coarse sediment is much less than for fine sediment. Sediment transport capacity equations are available that could be used to vary sediment transportability as a function of sediment characteristics, but these equations were judged not to be sufficiently robust for RUSLE2 (Foster and Meyer, 1972; Alonso et al., 1981). For example, slight changes in fine sediment properties significantly affect overland flow's sediment transport capacity computed with sediment transport equations. Slight spatial variations in overland flow hydraulics that can not be described in RUSLE2 also dramatically affect overland flow's sediment transport capacity. Using a complex sediment transport equation is not warranted when RUSLE2 does not capture important details in describing flow hydraulics. Furthermore, the effect of sediment transportability is partially captured by RUSLE2's soil erodibility factor (see **Section 4.1**).[17]

A value for the transportability coefficient K_T was obtained by fitting RUSLE2 to experimental data where deposition occurred on a concave profile overland flow path (Foster et al., 1980c). Sediment transport capacity equals sediment load at the location where deposition begins. Values for K_T were adjusted until computed sediment transport capacity matched the measured sediment load at the location where deposition began in the field study. The K_T value was validated by computing deposition along on the same overland flow path used to determine the K_T value the point where deposition started. The K_T value was also validated by computing deposition for other laboratory and field experimental data (Foster et al., 1980; Neibling and Foster, 1982; Lu et al., 1988). Deposition was computed with RUSLE2 for a wide range of field conditions and those values were inspected for reasonableness and consistency with field observations (see the **RUSLE2 User's Reference Guide**).

The RUSLE2 calibrated value for K_T is 250,000 (lbs_m/ft^3). This value is based on the following set of units. T_c: $lbs_m/(sec \cdot ft\ width)$, ζ: dimensionless, q: $ft^3/(sec \cdot ft\ width)$, s: dimensionless.

The coefficient ζ represents the effect of hydraulic resistance on runoff's sediment transport capacity. This coefficient, which is the ratio of transport capacity with a hydraulic rough surface to transport capacity for a hydraulic smooth surface, varies from essentially 0 for a very hydraulic rough surface to 1 for a hydraulically smooth surface. Hydraulic resistance (roughness) is provided by soil surface roughness, ground cover (material in direct contact with the soil surface), and vegetation retardance. Flow over a soil surface applies a total shear stress. Part of the shear stress is applied to form

---

[17] RUSLE2 is a hybrid empirical/process-based model. Many of the variables and equations used in RUSLE2 are not nice and crisp where elemental properties and processes are described. For example, the RUSLE2 soil erodibility factor represents both detachability and transportability. RUSLE2 has been validated to ensure that it acceptably computes erosion over the vast majority of situations where RUSLE2 is applied. See the RUSLE2 User's Reference Guide for a discussion of RUSLE2's validation.

roughness (soil surface roughness, ground cover, and vegetation retardance) and the other part is applied to grain roughness (the individual soil particles and aggregates at the soil-flow interface). The shear stress exerted on grain roughness is assumed to be responsible for sediment transport (Foster et al., 1981a; Foster, 1982). The grain roughness shear stress decreases as form roughness increases, and consequently values for ζ decrease as form roughness increase (see **Section 3.4.1**). RUSLE2 computes a change in ζ, and thus sediment transport capacity, as cover-management conditions change.

2.3.5. Runoff

RUSLE2 uses flow rate values for runoff to compute sediment transport capacity (see **Section 2.3.4**), contouring effectiveness (see **Section 7.1**), and contouring failure (see **Section 3.4.3**). Discharge rate at a location along an overland flow path is computed with:

$$q = q_{(i-1)} + \sigma\left(x - x_{(i-1)}\right) \qquad [2.18]$$

where: q = discharge rate at the location x between the segment ends x_{i-1} and x_i, q_{i-1} = discharge rate at x_{i-1}, and σ = excess rainfall rate (rainfall rate minus infiltration rate) on the *ith* segment. Excess rainfall rate is computed using the NRCS runoff curve number method that computes runoff depth (see **Section 3.3.1.1**). The RUSLE2 assumption is that excess rainfall rate equals runoff depth divided by one hour. The difference between the two is accounted for in calibration coefficients including the K_T value for sediment transport capacity in equation 2.17. The RUSLE2 principle is to capture runoff's main effects sufficiently well for erosion control planning. RUSLE2 computes excess rainfall rate as a function of hydrologic soil group, surface roughness, ground cover, soil biomass, and soil consolidation to represent cover-management's effect on runoff.

In most cases, runoff rate q increases within each segment, where the rate of increase depends on infiltration within the segment. RUSLE2 computes a decreasing runoff rate within a segment if infiltration rate in the segment is sufficiently high (see **Sections 2.3.8.3.3 and 3.3.1.1**).

2.3.6. Numerical solution of deposition equation

The deposition equation (equation 2.16) combined with the continuity equation (equation 2.14) must be integrated to compute deposition over a segment of an overland flow path. RUSLE2 solves these equations numerically because an analytical solution was not found. Equations 2.15 and 2.16 along with an equation for transport capacity were written in discrete form for each sediment class as:

$$\frac{D_{pk(1)} + D_{pk(2)}}{2} = \frac{\alpha_d V_{fk}}{[(q_{(1)} + q_{(2)})/2]}\left(\frac{T_{ck(1)} + T_{ck(2)}}{2} - \frac{g_{k(1)} + g_{k(2)}}{2}\right) \qquad [2.19]$$

$$g_{k(2)} = g_{k(1)} + D_{ik}\Delta x + \left(\frac{D_{pk(1)} + D_{pk(2)}}{2}\right)\Delta x \qquad [2.20]$$

and

$$T_{ck} = (g_k / g)T_c \qquad [2.21]$$

where: D_{ik} = interrill erosion for the *kth* sediment class, D_{pk} = deposition rate of the *kth* sediment class, α_d = a deposition coefficient, V_{fk} = fall velocity for the *kth* sediment class, T_{ck} = transport capacity for the *kth* sediment class, T_c = the total sediment transport capacity for all sediment classes, g_k = sediment load for the *kth* sediment class, g = total sediment load, and Δx = the length of the distance step used in the numerical integration. The subscript (1) refers to the upstream end of the distance step and the subscript (2) refers to the downstream end of the distance step.

These equations are combined and solved for the deposition rate D_2, which is the only unknown, at the lower end of the distance step. The solution is by trial and error because a value for sediment transport capacity for a sediment class is not known until a value for the total sediment load is computed. The total sediment load can not be computed until sediment load is computed for each sediment class. The trial-and-error solution starts with the sediment load distribution computed in the previous distance step. This distribution is updated with each trial-and-error iteration until the total sediment load becomes stable.

An alternative approach and perhaps simpler approach is to numerically solve equations 2.15 as:

$$g_{k(2)} = D_{ik}\Delta x + \left(\frac{D_{pk(1)} + D_{pk(2)}}{2}\right)\Delta x + g_{k(1)} \qquad [2.22]$$

Substitution for D_2 using equation 2.14 in equation 2.22 gives:

$$g_{k(2)} = D_{ik}\Delta x + \left(\frac{D_{pk(1)} + (\alpha_d V_{fk} / q_2)(T_{ck(2)} - g_{k(2)})}{2}\right)\Delta x + g_{k(1)} \qquad [2.23]$$

Equation 2.23 is solved for the sediment load $g_{k(2)}$, the only unknown in equation 2.23, at the end of the distance step. A trial-and-error solution is also required for this procedure as well because transport capacity for a single sediment class computed with equation 2.21 depends on the total sediment load.

Regardless of the numerical procedure, the boundary condition must the determined for each segment (see **Section 2.3.8.2)**. This boundary condition is the deposition rate of each sediment class determined at the upper end of the *ith* segment to start the step by step solution of the equations. The deposition rate at the lower end of the *(i-1)th* segment can not be used as the boundary condition for the upper end of the *ith* segment because deposition values are not continuous at common points of segments. Deposition rates change stepwise at these points even though discharge rate and sediment load are continuous at these points. Steepness makes a step change at common segment points.

The deposition rate at the upstream end of the *ith* segment is computed from:

$$D_{puk(i)} = \left(\alpha_d V_{fk} / q_{(i-1)}\right)\left(T_{cuk(i)} - g_{k(i-1)}\right) \quad [2.24]$$

where: equation 2.24 is solved for each sediment class using sediment transport capacity computed for each class using equation 2.21. The sediment load $g_{k(i-1)}$ is the sediment load at the end of the upslope *(i-1)th* segment, which is the same as the sediment load at the upper end of the *ith* segment because sediment load is continuous along the overland flow path.

A value of 3 was determined by calibration for the deposition coefficient. Values for α_d were adjusted until the computed sediment distribution matched observed distributions for situations where deposition occurred (Foster et al., 1980c). This calibration coefficient is partly needed to adjust for runoff depth rather than excess rainfall rate being used to compute runoff rate.

The numerical procedure used to compute deposition must be carefully chosen so that computed values are not affected by arbitrary division of a segment. Segments by definition are uniform in soil, steepness, and cover-management. Dividing a portion of the overland flow path where conditions do not change into segments as illustrated in Figure 2.2 should not affect the detachment and erosion computations. Also, the computations for a segment must not be affected by downslope conditions, including overland flow path length beyond the segment.

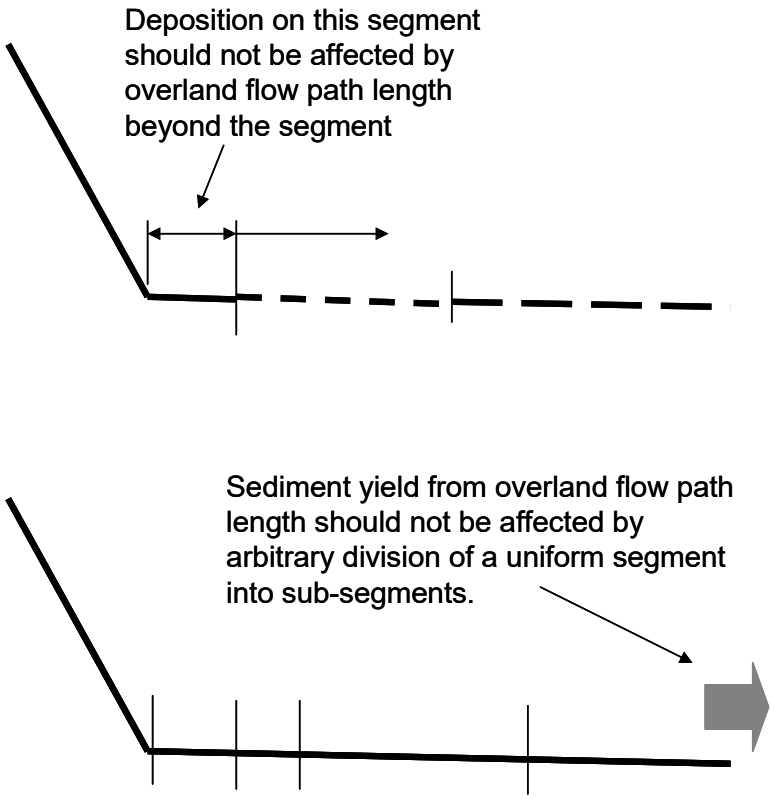

Figure 2.2. Situations where overland flow path lengths and segment divisions should have no effect on computed deposition.

The RUSLE2 procedure avoids these problems by dividing the entire overland flow path into a particular number of segments. The number of sub-segments used in RUSLE2 for an overland flow path length is 200. The sub-segments are only used in the segments having deposition. Thus, the density of sub-segments within a particular segment is the same for all segments. The number of sub-segments within a segment x_{i-1} to x_i is:

$$n_i = \left[\left(x_i - x_{i-1}\right)/\lambda_o\right] n_o \qquad [2.25]$$

where: n_i = an integer number of sub-segments within the *ith* segment, λ_o = the overland flow path length, and n_o = 200, the number of sub-segments for the entire overland flow path length. The length of the sub-segment Δx used in the numerical solution of the deposition equations is:

$$\Delta x = \left(x_{(i)} - x_{(i-1)}\right)/n_i \qquad [2.26]$$

These equations ensure that the end sub-segments within a particular segment begin and end on the segment ends.

A sensitivity analysis was conducted to determine how the sediment delivery ratio (sediment yield/sediment production) for an overland flow path like the ones in Figure

2.2 varied as a function of n_o, the number of sub-segment for the entire overland flow path length. The variation in sediment delivery ratio was about 5 percent as the number of sub-segments for the overland flow path length varied from 100 to 10,000. The value of 200 was chosen, which gives acceptable accuracy while minimizing computer run time.

2.3.7. Concept of a representative storm

Runoff is a key RUSLE2 variable used to compute erosion reduction by support practices including contouring, porous barriers, and flow interceptors and deposition on concave overland flow paths. The intent for using RUSLE2 as a guide to erosion control planning is that RUSLE2 compute the relative erosion control effectiveness of support practices by location. For example, support practices like contouring are less effective in the southern US than in the northern US because of differences in storm severity (Foster et al., 1997). RUSLE2 is calibrated to compute the effectiveness of support practices at the base Columbia, Missouri location. RUSLE2 compute the deviation in support practice effectiveness by the degree that climatic conditions at a specific location vary from those at the base Columbia, Missouri location. This approach gives RUSLE2 increased robustness.

RUSLE2 uses the 10 year (return period-frequency), 24 hour (storm duration) P_{10y24h} precipitation amount to capture the climatic variation by location to compute erosion control by support practices.[18] This precipitation variable is used as an index of storm severity. A more erosive storm than an average annual storm is used as a storm severity index because support practice effectiveness, especially for contouring, depends on storm severity (Foster et al., 1997). For example, contouring can greatly reduce erosion for small storms but fail completely for large storms.

The effect of support practices and concave overland flow path profile shape on erosion and deposition depends much more on runoff than the combination of raindrop impact and runoff. RUSLE2 uses a representative storm in process-based equations to compute runoff that in turn is used to compute deposition. The daily erosion and deposition values computed with this representative storm are scaled to match the daily detachment values computed with equation 2.10 (**see Section 2.3.9**). The same representative storm is used in the process-based equations for each day, but the computed daily runoff values vary as cover-management conditions change daily. The representative storm is used as an index for storm severity at a location. The intent is not to compute actual runoff on each day but to compute runoff values that show the how relative effectiveness of support practices and concave overland flow path profiles changes daily for the index storm. The index storm captures main-effect differences between locations. RUSLE2 computes comparable P-factor type effects for each day rather than using a single temporally constant P factor value like the USLE and RUSLE1.

---

[18] The 10 year-24 hour precipitation procedure used in RUSLE2 is a replacement for the 10 year EI procedure used in RUSLE1.

RUSLE2 also computes an erosivity value for the P_{10y24h} index storm in addition to runoff. The storm erosivity r_{10y24h} for the 10 year-24 precipitation amount P_{10y24h} is computed from:

$$r_{10y24h} = 2\gamma_m P_{10y24h} \quad [2.27]$$

where: γ_m = the maximum monthly erosivity density at the location. Monthly erosivity density is the ratio of average monthly erosivity to average monthly precipitation amount (see **Section 3.2.1.4.1**).

2.3.8. Solving the sediment routing equations segment by segment

The sediment routing equations are solved using the value for the 10 year-24 hour precipitation amount P_{10y24h} used as an index storm. Although the same storm is used each day, computed sediment load changes daily as cover-management conditions temporally change. Daily sediment load values computed using the representative index storm are scaled to compute daily sediment load values appropriate for the daily erosivity values (see **Section 2.3.9**).

2.3.8.1. Inconsistency between slope effect in detachment and sediment transport capacity equations

Inconsistencies occur between the empirical detachment equation (equation 2.10) and the process-based sediment transport capacity equation (equation 2.17) because of differences in the steepness terms in the equations. The steepness effect in equation 2.10 for detachment is a two piece linear equation (see **Section 5.6**), whereas the steepness effect in equation 2.17 for sediment transport capacity is a single linear term. Equations 2.10 and 2.17 are calibrated to be close at the unit-plot nine percent steepness. However, the steepness effect in equation 2.10 can exceed the steepness effect in equation 2.17 at both flat and steep slopes depending on values for the other terms in the equations. Although equation 2.10 is generally assumed to represent detachment limiting conditions in RUSLE2, this empirical equation reflects a mixture of both detachment and transport capacity limiting at low steepness. The assumption used to deal with this and other similar inconsistencies that occur between the empirical USLE formulation and the process-based equations is that RUSLE2 gives the empirical USLE erosion estimate for uniform overland flow paths.[19]

The inconsistencies between these two steepness effects could not be reconciled for non-uniform overland flow paths at low steepness, but RUSLE2 was very carefully evaluated to ensure that the inconsistencies have little effect in conservation planning.

---

[19] These inconsistencies could be eliminated by developing RUSLE2 so that it uses all process-based equations rather than combining the empirical USLE equation with process-based equations. However, the RUSLE2 hybrid approach combines the best of the empirical USLE approach with the best of the process-based approach (see **Section 1.2 and 1.3**).

2.3.8.2. Boundary values

Boundary values must be determined for each segment to solve the sediment routing equations. The equations are solved sequentially starting with the first segment at the origin of the overland flow path and then moving downslope segment by segment. The computed values for runoff and sediment load at the end of the last segment become boundary values for the next segment. The major boundary values for the first segment at x = 0 is that no inflow of either runoff or sediment occurs (i.e., $q_0 = 0$ and $g_0 = 0$).

2.3.8.3. Special boundary conditions cases

Five special cases were used to organize the sediment routing computations and to set boundary values.

2.3.8.3.1. Case 1: First segment

The first segment is a special case because of the no-inflow boundary condition and because the sediment load leaving this segment must equal the sediment load computed by the USLE (i.e., equation 2.10), (assuming the RUSLE2 factor values are used in the USLE). The first segment directly matches the USLE uniform slope assumptions.

Many RUSLE2 conservation and erosion control planning applications involve a uniform overland flow path. In these situations, RUSLE2 uses a single uniform overland flow path segment and only the equations for the Case 1: First Segment special case in its sediment routing computations.

An important logic check for the first segment is to determine if local deposition is computed within the segment. RUSLE2 computes no deposition if the rate of increase in sediment transport capacity with distance dT_c/dx is greater than the interrill erosion rate D_i within the first segment. The rate of increase in transport capacity in the first segment is computed as:

$$dT_c / dx = K_T \zeta \sigma s \qquad [2.28]$$

Excess rainfall rate σ is computed using the 10 year-24 hour representative storm P_{10y24h} and the interrill erosion rate D_i is computed with equation 2.11 using the representative (index) storm erosivity r_{10y24h} (see **Section 3.2.4**).

2.3.8.3.1.1. $dT_c/dx > D_i$ - No local deposition

RUSLE2 computes no local deposition in the first segment when the rate of increase in sediment transport capacity with distance dT_c/dx is greater than the interrill erosion rate D_i. No local deposition occurs because runoff's sediment transport capacity is sufficient to transport the sediment load produced by interrill erosion. The interrill erosion rate $D_{i10y24h}$ in the first segment is computed using the erosivity r_{10y24y} value computed with equation 2.27 for the P_{10y24h} representative storm. In that case, the sediment load leaving

the segment is given by equation 2.15 after rill and interrill erosion are combined into a single term as:[20]

$$g = r_{10y24h} k S c p_p p_c p_d x_{(1)}^{m_i+1} / \lambda_u^{m_i} \quad [2.29]$$

where: g = the total sediment load for all sediment classes and $x_{(1)}$ = distance to downstream of the first segment.[21] The sediment load g_k of each sediment class at the end of the first segment is given by:

$$g_k = \psi_k g \quad [2.30]$$

where: ψ_k = sediment mass in the *kth* sediment class (fraction). This special case is detachment limiting. Therefore, the distribution of sediment classes in the sediment load at the end of segment 1 for Case 1 where $dT_c/dx > D_i$ equals the distribution of the sediment classes at the point of detachment (see **Section 4.7.5**). The enrichment ratio is one (1) for this case because no deposition is computed (see **Section 4.7.6**).

2.3.8.3.1.2. $dT_c/dx < D_i$ - Local deposition occurs

When the interrill erosion rate D_i within the first segment exceeds the rate of increase in transport capacity with distance dT_c/dx, local deposition is computed. Even though local deposition is computed, equation 2.29 is used to compute sediment load at the end of the first segment to ensure that RUSLE2 gives the USLE result for the first segment. However, local deposition enriches the sediment in fines. RUSLE2 computes quasi-deposition and -sediment load values to estimate the distribution of the sediment classes for the sediment leaving the first segment. The sole purpose of this computation is to obtain the sediment distribution; this computation does not affect the value computed for sediment load at the end of the first segment, which is computed with equation 2.29.

Equations 2.14, 2.16, 2.17, and 2.18 were solved in closed form to compute the quasi-deposition and -sediment load values in segment 1 (Renard and Foster, 1983). The equation used to compute deposition is:

---

[20] The units for sediment load depend on the units used for erosivity r, soil erodibility k, distance x, and length λ_u. For example, in the US customary units system for the USLE, the typical units for sediment load g would be ($tons_m$/acre·day)·ft. These set of units are multiplied by (2000 lbs_m/ton)/(43560 ft^2/acre) to obtain a consistent set of units of lbs for mass and ft for length. In RUSLE2, erosion values are computed for each day using a daily erosivity value (see **Sections 2.1 and 3.1**), which is the reason for the day unit in sediment load. The sediment amount values have mass units. In the US customary USLE units, lbs-mass and lbs-force are equal. In the SI system, kg is the recommended unit for sediment mass, although the output would likely be displayed in metric tonnes. See AH703 (Renard et al., 1997) for additional discussion of USLE/RUSLE units.

[21] Equation 2.29 is the USLE equation form when the slope length λ is substituted for x_i and the equation is divided by slope length λ to compute average erosion for the slope length.

$$D_{qk} = \left[\left(a_d V_{fk} / \sigma\right)/\left(1 + a_d V_{fk} / \sigma\right)\right]\left[\left(dT_c / dx - D_i\right)\psi_k\right] \quad [2.31]$$

$$g_{qk} = \psi_k T_c - qD_{qk} / \left(a_d V_{fk}\right) \quad [2.32]$$

$$q = \sigma x_{(1)} \quad [2.33]$$

$$T_c = K_T \zeta q s \quad [2.34]$$

where: D_{qk} and g_{qk} are the quasi-deposition and -sediment load variables used specifically to compute the distribution of the sediment load among the sediment classes for the first segment when local deposition occurs and $x_{(1)}$ = the distance to the end of the first segment. The subscript k refers to sediment class. Equations 2.31-2.34 are solved for each sediment class. The fraction of the sediment load in each sediment class for the sediment load at the end of the first segment is computed as:

$$\omega_k = g_{qk} / \sum_{k=1}^{5} g_{pk} \quad [2.35]$$

where: ω_k = the portion of the total sediment load leaving the first segment that is composed of sediment in the *kth* sediment class and 5 is the number of sediment classes used in RUSLE2. The sediment load in each sediment class at the end of the first segment is computed as:

$$g_k = \omega_k g \quad [2.36]$$

The enrichment ratio for the sediment at the end of the first segment is greater than 1 based on the portion of the interrill erosion that RUSLE2 computes as deposited in the first segment. Enrichment ratio is based on specific surface area of the sediment (see **Section 4.7.6**).

2.3.8.3.2. Case 2: Detachment over entire segment

Two boundary conditions must be met for detachment to be computed over an entire segment. The incoming sediment load at the upper end of the segment must be less than transport capacity at the upper end of the segment. The mathematical condition for this check is that $g_{i-1} < T_{cu(i)}$ where $T_{cu(i)}$ = transport capacity at the upstream end of the *ith* segment. This transport capacity is computed using the runoff discharge rate q_{i-1}, the slope steepness s_i, and sediment transport capacity coefficient ζ_i for the ith segment. Therefore, transport capacity at the upstream end of the *ith* segment $T_{cu(i)}$ does not equal the transport capacity $T_{cl(i-1)}$ at the downstream end of the *(i-1)th* segment if steepness and/or cover-management changes between the segments.

The second condition is that the potential sediment load at the end of the segment computed as the sum of the incoming sediment load plus the sediment produced by interrill erosion within the segment is less than the transport capacity at the lower end of the segment. This potential sediment load is computed as:

$$g_{p(i)} = g_{(i-1)} + D_{i(i)}\left(x_{(i)} - x_{(i-1)}\right) \quad [2.37]$$

where: g_p = potential sediment load. The boundary condition is that this potential sediment load be less than transport capacity at the downstream end of the segment, i.e., $g_{p(i)} < T_{cl(i)}$.

2.3.8.3.2.1. Sediment load when rill erosion occurs at capacity rate

A subsequent check must also be made to determine if rill erosion can occur at its capacity over the segment. A second potential sediment load is computed as:

$$g_{p(i)} = g_{(i-1)} + r_{10y24h} k_{(i)} S_{(i)} c_{(i)} p_{p(i)} p_{c(i)} p_{d(i)} \left(x_{(i)}^{m_i+1} - x_{(i-1)}^{m_i+1}\right) / \lambda_u^{m_i} \quad [2.38]$$

where rill erosion is assumed to occur at its capacity rate. If this potential sediment load is less than sediment transport capacity at the lower end of the segment, rill erosion is assumed to occur at its capacity rate and the sediment load leaving the segment is given by equation 2.38.

The distribution of the sediment load among the sediment classes is computed by:

$$g_{k(i)} = g_{k(i-1)} + \psi_k \left(g_{(i)} - g_{(i-1)}\right) \quad [2.39]$$

which results from detachment being non-selective.[22] That is, the distribution of the sediment added within the sediment load, $g_{(i)} - g_{(i-1)}$, is assumed to be the same as sediment at the point of detachment.

2.3.8.3.2.2. Sediment load when rill erosion at less than capacity rate

If potential load computed by equation 2.39 exceeds the transport capacity at the downstream end of the segment, rill erosion is limited to the rate that will just fill transport capacity, which means that sediment load at the end of the segment is given by:

$$g_{(i)} = T_{Cl(i)} \quad [2.40]$$

Even though rill erosion is not computed at its capacity rate, some rill erosion is computed, and, therefore, no local deposition is computed. The distribution of the sediment load at the end of the segment is given by equation 2.39.

---

[22] Sediment characteristics at the point of detachment change as soil texture changes by segment. RUSLE2 starts at the first segment with the five sediment classes for that segment based on soil texture. RUSLE2 adds sediment classes to represent soil texture changes in the segments along the overland flow path.

2.3.8.3.3. Case 3: Detachment on upper portion of segment, deposition on lower portion of segment

An example where detachment occurs on the upper portion of a segment and deposition occurs on the lower portion of the segment is illustrated in Figure 2.3. Infiltration rate on the *ith* (second) segment is greater than the rainfall rate, which causes the runoff rate to decrease within the segment. Sediment load increases within the segment while sediment transport capacity decreases within the *ith* segment. Deposition begins at the point where sediment load equals transport capacity.

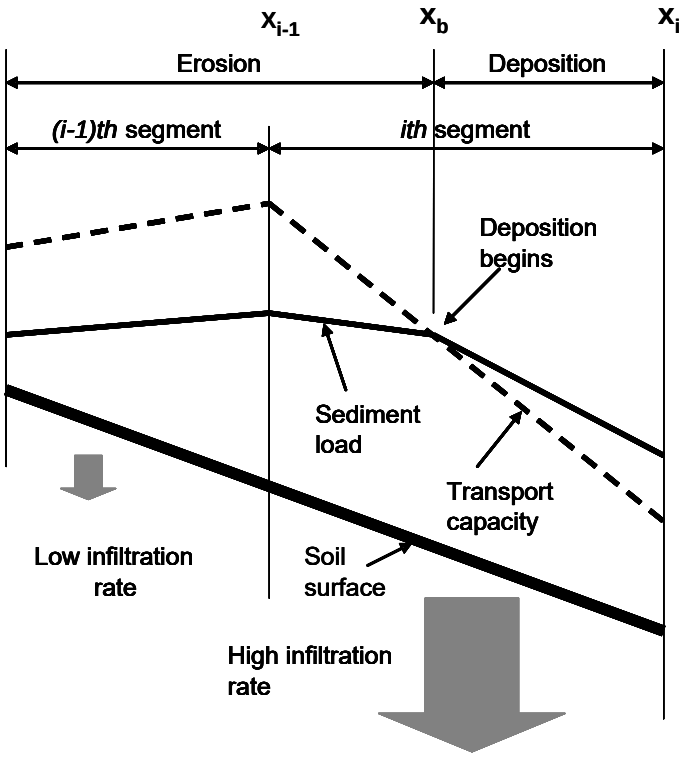

Figure 2.3. Illustration where detachment ends and deposition begins within the ith segment

Two conditions must be met for this case. The first condition is that the incoming sediment load is less than sediment transport capacity at the upstream end of the segment, i.e., $g_{(i-1)} < T_{cu(i)}$. The second condition is that the potential sediment load at the lower end of the segment computed with equation 2.37 is greater than the transport capacity at the downstream end of the segment.

When this condition is met, deposition begins at the location where the sediment load equals transport capacity. The sediment load where deposition begins is given by:

$$g_b = g_{(i-1)} + D_{i(i)}\left(x_b - x_{(i-1)}\right) \qquad [2.41]$$

where: g_b = sediment load at the location x_b = where deposition begins. The sediment transport capacity T_{cb} where deposition begins is given:

$$T_{cb} = K_T \zeta_{(i)} s_{(i)} \left\lfloor q_{(i-1)} + \sigma_i \left(x_b - x_{(i-1)} \right) \right\rfloor \quad [2.42]$$

where: σ = the excess rainfall rate (rainfall rate minus infiltration rate).[23] Equations 2.41 and 2.42 are combined and solved to determine a value for the location x_b where deposition begins.

The sediment load by sediment class at the location where deposition begins is given by:

$$g_{bk} = g_{k(i-1)} + \psi_k \left(g_b - g_{(i-1)} \right) \quad [2.43]$$

Deposition is computed on the portion of the segment from x_b to x_i using equations 2.19-2.21. The main boundary values are that deposition rate is zero and sediment load equals sediment transport capacity at $x = x_b$. These equations compute values for total sediment load and sediment load for each sediment class at the lower end of the segment.

2.3.8.3.4. Case 4: Deposition over entire segment

Figure 2.4 illustrates deposition occurring over an entire segment. In this case, the width of the vegetation strip is so narrow that sediment transport capacity does not increase within the strip to where it exceeds sediment load. The first boundary condition for this case is that the incoming sediment load is greater than sediment transport capacity at the upper end of the segment. The second condition is that the interrill erosion rate D_i within the segment is greater than the increase in sediment transport capacity with distance dT_c/dx within the segment. This boundary condition is the same as the incoming sediment load plus sediment production by interrill erosion within the segment being greater than sediment transport capacity at the lower end of the segment.

Equation 2.24 is used to compute the deposition rate at the upper end of the segment, which is a boundary value along with the incoming discharge rate $q_{(i-1)}$ and sediment load $g_{(i-1)}$ from the immediate upslope segment. These boundary values are used in equations 2.19-2.21 to compute deposition within the segment and values for total sediment load and sediment load by sediment class at the lower end of the segment.

---

[23] Excess rainfall rate is negative for situations where RUSLE2 computes a decreasing runoff rate within a segment (see **Section 3.3.1.1**).

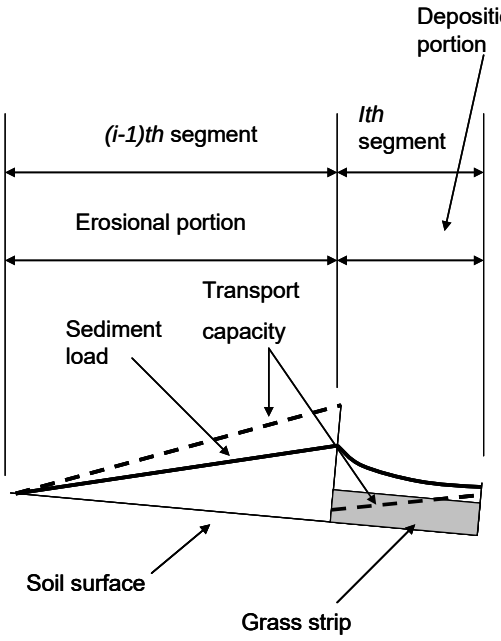

Figure 2.4. Narrow grass where deposition occurs over entire segment

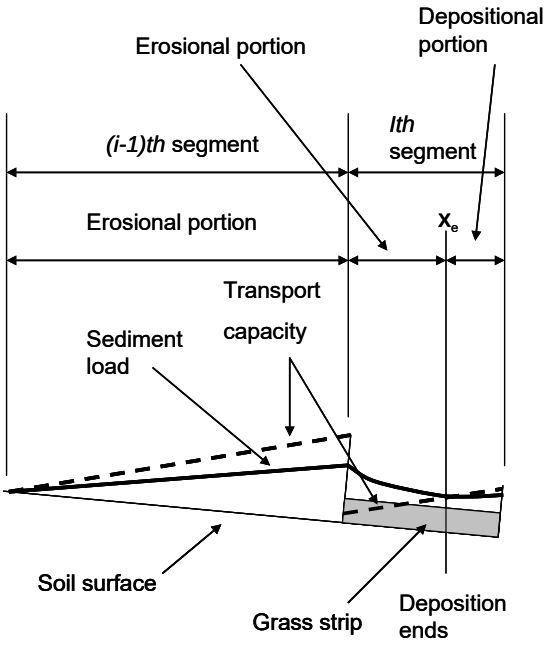

Figure 2.5. Grass strip sufficiently wide that deposition ends within segment and erosion occurs on lower portion of segment

2.3.8.3.5. Case 5: Deposition over upper part of segment, detachment over lower part of segment

Figure 2.5 illustrates deposition ending within a segment. Another example of deposition ending within a segment is illustrated in Figure 2.2 provided the segment is sufficiently long. As discussed in **Section 5.3**, RUSLE2 assumes that segments are discontinuous, even when used to represent a smooth, continuous concave overland flow path profile. The result is that RUSLE2 computes deposition on the upper portion of the segment and detachment on the lower portion of the segment if the segment is sufficiently long. This result is opposite from that for a smooth, continuously decreasing slope steepness where detachment occurs on the upper portion of the segment and deposition occurs on the lower portion of the segment where deposition begins. The error from not properly computing the location of the deposition is minimized by choosing short segment lengths to represent smooth, continuous overland flow path profiles.

The first boundary condition is that incoming sediment load is greater than the transport capacity at the upper end of the segment. The second boundary condition is that the incoming sediment load plus the sediment produced by interrill erosion within the segment is less than the transport capacity at the lower end of the segment. This boundary condition is the same as the boundary condition that the rate of increase in transport capacity with distance dT_c/dx is greater than the interrill erosion rate D_i within the segment. These boundary conditions are required but are not sufficient to determine

that deposition ends within the segment if the segment length is short. The location x_e where deposition ends within the segments is determined by solving equations 2.19-2.21 and 2.24. Deposition ends at the location where computed deposition rate becomes zero. These equations compute the total sediment load g_e and the sediment load of each sediment class $g_{e(k)}$ at the location that deposition ends.

Detachment occurs on the lower portion of the segment. The potential sediment load at the end of the segment is computed from:

$$g_{p(i)} = g_e + r_{10y24h} k_{(i)} S_{(i)} c_{(i)} p_{p(i)} p_{c(i)} p_{d(i)} \left(x_i^{m_i+1} - x_e^{m_i+1} \right) / \lambda_u^{m_i} \qquad [2.44]$$

This potential sediment load is checked against sediment transport capacity at the lower end of the segment. If the sediment transport capacity at the lower end of the segment exceeds this sediment load, then the sediment load leaving the segment is the potential sediment load computed by equation 2.44, i.e, $g_{(i)} = g_{p(i)}$. However, if the potential sediment load computed with equation 2.44 exceeds the transport capacity at the end of the segment, then rill erosion is limited to the rate that will just fill sediment transport capacity. In that case, the sediment load at the end of the segment equals sediment transport capacity at the lower end of the segment, i.e., $g_{(i)} = T_{cl(i)}$.

The sediment load for each sediment class at the end of the segment is given by:

$$g_{k(i)} = g_{ek} + \psi_k \left(g_{(i)} - g_e \right) \qquad [2.45]$$

2.3.9. Scaling values computed with representative storm to create daily values

The daily sediment load values computed using the sediment routing equations and the representative storm P_{10y24h} must be scaled to compute daily sediment load values appropriate for the daily erosivity values. This scaling factor is computed as the ratio of sediment load computed at the end of each segment with the sediment routing equations and the sediment load at the lower end of each segment that would be produced if detachment occurs at detachment capacity for the representative storm. That sediment load g_{detcap} is computed as:

$$g_{\det cap(i)} = r_{10y24h} k_{(i)} S_{(i)} c_{(i)} p_{p(i)} p_{c(i)} p_{d(i)} \left(x_{(i)}^{m_i+1} - x_{(i-1)}^{m_i+1} \right) / \lambda_u^{m_i} \qquad [2.46]$$

The scaling factor δ_i for each *ith* segment is computed as:

$$\delta_{(i)} = g_{(i)} / g_{\det cap(i)} \qquad [2.47]$$

A sediment load based on detachment capacity comparable to $g_{detcap(i)}$ is computed using daily values for erosivity and the other factors as:

$$g_{daily\,\det cap(i)} = r k_{(i)} S_{(i)} c_{(i)} p_{p(i)} p_{c(i)} p_{d(i)} \left(x_{(i)}^{m_i+1} - x_{(i-1)}^{m_i+1} \right) / \lambda_u^{m_i} \qquad [2.48]$$

where: $g_{dailydetcap(i)}$ = daily sediment load at end of *ith* segment that would be produced if full detachment occurred in each segment, r = the daily erosivity value determined from the disaggregation of the monthly erosivity values (see **Section 3.1**), and all of the other values in equation 2.48 are the same daily values used in the sediment routing equations.

The daily sediment load value is computed as the product of this daily detachment sediment load and the sediment load scaling factor as:

$$g_{daily(i)} = \delta_{(i)} g_{daily\,\det cap(i)} \qquad [2.49]$$

where: $g_{daily(i)}$ = average daily sediment load at the end of the *ith* segment. The average daily net erosion rate $D_{daily(i)}$for the *ith* segment is computed as:

$$D_{daily(i)} = \left(g_{daily(i)} - g_{daily(i-1)}\right) \Big/ \left(x_{(i)} - x_{(i-1)}\right) \qquad [2.50]$$

2.3.10. Computing average annual erosion values for conservation and erosion control planning[24]

RUSLE2 computes average annual values for four variables used in conservation and erosion control planning. These variables are: (1) average annual erosion rate for the entire overland flow path (sediment yield from the overland flow path), (2) average annual detachment rate for the entire overland flow path, (3) average annual erosion rate for the eroding portion of the overland flow path, and (4) an average annual conservation planning soil loss for the overland flow path that gives partial credit to deposition as soil saved.

2.3.10.1. Average annual erosion rate for entire overland flow path (sediment yield)

The average annual erosion rate for the entire overland flow path is the ratio of the average annual sediment amount leaving the overland flow path divided by the overland flow path length. The sediment load at the end of the last segment on the overland flow path is also known as sediment yield or sediment delivery from the overland flow path.

The average annual sediment load at the end of the overland flow path is given by:

$$G_{\lambda} = \left(\sum_{j=1}^{J_d} g_{daily\lambda(j)} \right) \Big/ M_d \qquad [2.51]$$

where: G_{λ} = the average annual sediment load (i.e., sediment yield, sediment delivery) at the end of the overland flow path, $gdaily\lambda_{(j)}$ = the daily sediment load at the end of the overland flow path on the *jth* day, M_d = the number of years in the computation period

---

[24] See the RUSLE2 User's Reference Guide for detailed information on these variables and how they are used in conservation and erosion control planning.

(duration entered in cover-management description, see **Section 2.2**), and J_d = the total number of days in the computation period (i.e., $J_d = 365 \cdot M_d$). The subscript n refers to each day in the computation period and the subscript I is the index value of the last segment used to describe the overland flow path.

The average annual erosion rate (sediment yield, sediment delivery) for the overland flow path is given by:

$$A_{sedyld} = G_\lambda / \lambda_o \qquad [2.52]$$

where: A_{sedyld} = the average annual erosion rate for the overland flow path length, λ_o.

2.3.10.2. Average annual detachment rate (sediment production) for entire overland flow path

The average annual detachment rate for the entire overland flow path represents a measure of total sediment production on the overland flow path. This variable is a measure of local erosion and sediment that has been moved away from its local point of origin. RUSLE2 computes detachment on each segment in its sediment routing computations and a sediment load value based on detachment. That sediment load is given by:

$$g_{\det(i)} = g_{\det(i-1)} + D_{i(i)}\left(x_{(i)} - x_{(i-1)}\right) + \Delta g_{r(i)} \qquad [2.53]$$

where: g_{det} = the sediment load produced by detachment at the lower end of the *ith* segment and ΔG_r = the sediment amount produced by rill erosion within the segment. Interrill erosion D_i is assumed to occur over an entire segment regardless of whether deposition occurs. If deposition does not occur, rill detachment occurs. Rill detachment in each segment is computed as described for each of the special cases in **Section 2.3.8.3**.

The average annual sediment load produced by detachment at the end of the overland flow path is given by:

$$G_{\det\lambda} = \left(\sum_{j=1}^{J} g_{\det\lambda(j)}\right) \Big/ M_d \qquad [2.54]$$

where: $G_{det\lambda}$ = the average annual sediment load at the end of the overland flow path. The average annual detachment rate for the entire overland flow path is given by:

$$A_{\det} = G_{\det\lambda} / \lambda_o \qquad [2.55]$$

where: A_{det} = the average annual detachment rate for the entire overland flow path.

2.3.10.3. Average annual erosion rate for eroding portions of the overland flow path

The average annual sediment load is computed for each segment as:

$$G_{(i)} = \left(\sum_{j=1}^{J_d} g_{daily(i,j)} \right) \Big/ M_d \qquad [2.56]$$

The average annual erosion rate for each segment is given by:

$$D_{aseg(i)} = \left(G_{(i)} - G_{(i-1)}\right)/(x_{(i)} - x_{(i-1)})/\left(x_{(i)} - x_{(i-1)}\right) \qquad [2.57]$$

where: $D_{aseg(i)}$ = the average annual erosion rate for the *ith* segment. Positive values for $D_{aseg(i)}$ values indicate net erosion and negative values indicate deposition. The eroding portions of the overland flow path are the segments where $D_{aseg(i)}$ is positive. The value for average annual erosion rate for the eroding portions of the overland flow path is computed as:

$$A_{erod} = \left[\left(G_{(l1)} - G_{(u1)}\right) + \left(G_{(l2)} - G_{(u2)}\right) + \left(G_{(l3)} - G_{(u3)}\right) + \ldots\right] / \qquad [2.58]$$

$$\left[\left(x_{(l1)} - x_{(u1)}\right) + \left(x_{(l2)} - x_{(u2)}\right) + \left(x_{(l3)} - x_{(u3)}\right) + \ldots\right]$$

where: A_{erod} = average annual erosion rate for the eroding portions of the overland flow path, the subscript l refers to the downstream end of an eroding portion of the overland flow path, the subscript u refers to the upstream end of an eroding portion of the overland flow path, and the subscript 1, 2, 3, and ... refers to individual eroding portions of an overland flow path.

2.3.10.4. Conservation planning soil loss

The conservation planning soil loss variable gives partial credit for remote deposition as soil saved. The credit that is given to remote deposition along an overland flow path as soil saved is computed as (Foster et al., 1997):[25]

$$b_{d(i)} = 1 - \left(x_{du(i)} / \lambda_o\right)^{1.5} \qquad [2.59]$$

where: $b_{d(i)}$ = the fraction of the deposition in the *ith* segment that is credited as soil saved (i.e., deposition benefit) and $x_{du(i)}$ = the location of the upper edge of deposition in the

---

[25] Remote deposition is the deposition of sediment some distance from the location on the overland flow path that the sediment is detached. Examples of remote deposition are deposition upslope of dense vegetation strips, on the toe of concave overland flow path profiles, and in terrace channels. Local deposition is deposition very near the point of detachment such as deposition in the depressions created by random roughness and in the furrows between ridges on a low grade. Local deposition is given full credit as soil saved, which is implicit in the empirical equation structure for computing detachment. Local deposition associated with random roughness is explicitly computed only for the first segment in an overland flow path description. Deposition computed for segments other than the first segment for overland flow paths involving multiple segments is considered to be remote deposition and is given partial credit as soil saved according to equation 2.59.

segment in which the deposition occurs. A significantly reduced benefit is computed when the deposition occurs close to the overland flow path end, which is the location x = λ. The credited deposition in a segment is computed as:[26]

$$\Delta g_{pb(i)} = \Delta g p_{a(i)} b_{d(i)} \quad [2.60]$$

where: $\Delta g_{pb(i)}$ = daily deposited sediment credited as soil saved (mass/width) and $\Delta g_{pa(i)}$ = the daily computed total deposition for the segment before any credit is taken (mass/width). The daily conservation planning sediment load along the overland flow path is computed as:

$$g_{cp(i)} = g_{cp(i-1)} + \Delta g_{pb(i)} + \Delta g_{i(i)} + \Delta g_{r(i)} \quad [2.61]$$

where: g_{cp} = daily conservation planning sediment load along the overland flow path, $\Delta g_{i(i)}$ = total interrill detachment within the segment (mass/width) and $\Delta g_{r(i)}$ = total rill detachment within the segment (mass/width). Interrill erosion D_i is assumed to occur over an entire segment regardless of whether deposition occurs. If deposition does not occur, rill detachment occurs. Rill detachment in each segment is computed as described for each of the special cases in **Section 2.3.8.3**.

The average annual conservation planning sediment load at the end of the overland flow path or at the end of terrace channels for the computation period is given by:

$$G_{cp\lambda} = \left(\sum_{j=1}^{J_d} g_{cp\lambda(j)} \right) \Big/ M_d \quad [2.62]$$

where: $G_{cp\lambda}$ = the average annual sediment load for conservation planning.

The conservation planning soil loss is given by:

$$A_{cp} = G_{cp\lambda} / \lambda_o \quad [2.63]$$

where: A_{cp} = the average annual conservation planning soil loss.

Deposition occurs in terrace channels that are on a sufficiently low grade. The credit for soil saved computed for this deposition is computed with (Foster and Highfill, 1983; Foster et al., 1997):

$$a_{cpt} = a_{ty} \exp\left[-0.011\left(\lambda_t - 100\right)\right] \quad \lambda_t > 100 \quad [2.64]$$

---

[26] These computations are made using the scaled values that match the daily erosivity values.

$$a_{cpt} = 0.45 a_{ty} \quad \lambda_t \le 100 \qquad [2.65]$$

where: a_{cpt} = the daily conservation planning sediment yield [average erosion for area (mass/area)] when deposition occurs in terrace channels, a_{yt} = daily sediment yield [average erosion for area (mass/area)] from terrace channels, and λ_t = terrace spacing (feet). The average annual conservation planning soil loss for conservation planning is:

$$A_{cp} = \left(\sum_{j=1}^{J_d} a_{cp(j)} \right) \Big/ M_d \qquad [2.66]$$

2.3.10.5. Comments on conservation and erosion control planning variables

The values for all four of these conservation and erosion control planning variables are equal for a uniform overland flow path. If a dense vegetation strip is located at the end of the overland flow path, the value for average erosion rate for the entire overland flow path (sediment yield) will be much lower than the other values because of deposition caused by the grass strip and its backwater. The highest value of the four will be the average erosion rate for the eroding portion of the overland flow path. In this example, this part of the overland flow path is from its origin to the location where deposition begins at the upper edge of the backwater created by the vegetation strip. The value for the average detachment rate for the entire overland flow path will be less than the average erosion rate for the eroding portion of the overland flow path because of the greatly reduced detachment in the backwater and in the vegetation strip itself. The conservation planning soil loss will be less than the detachment value but greater than the sediment yield value because of the partial credit taken for deposition as soil saved. In this example, the conservation planning soil loss value will be closer to the detachment value than to the sediment yield value. Not much credit (benefit) is given to the deposition because it occurs near the end of the overland flow path (see the RUSLE2 User's Reference Guide).

2.4. List of symbols

a = daily erosion (mass/area·day)

a_{cpt} = daily conservation planning soil loss for terraces (mass/area·day)

a_{yt} = daily average sediment yield expressed for terrace interval expressed as average erosion for area (mass/area·day)

a_k = erosion in *kth* crop stage (mass/area)

a_u = unit plot daily erosion (mass/area·day)

a_{us} = unit plot erosion for a single storm (mass/area)

A = average annual erosion (mass/area·year)

A_{cp} = average annual conservation planning soil loss (mass/area·year)

A_{det} = average annual detachment rate for the entire overland flow path (mass/time·year)

A_{erod} = average annual erosion for the eroding portions of the overland flow path (mass/area·year)

A_{sedyld} = average annual erosion rate for the overland flow path length (mass/area·year)

A_u = unit plot average annual erosion (mass/area·year)

b_d = deposition in a segment credited as soil saved (i.e., deposition benefit) (fraction)

b_r = **b** value, coefficient for ground surface) cover effectiveness for rill erosion ($percent^{-1}$)

c = daily cover-management factor (soil loss ratio) (dimensionless)

c_k = cover-management factor (soil loss ratio) for *kth* crop stage (dimensionless)

c_{pr}/c_{pi} = rill to interrill prior land use soil erodibility ratio

C = average annual cover-management factor (dimensionless)

D = daily detachment by rill and interrill erosion combined (mass/area·day)

D_{aseg} = average annual erosion for a segment (mass/area·day)

D_i = daily detachment by interrill erosion (mass/area·day)

D_i = interrill erosion rate (mass/area·time)

D_{daily} = average daily net erosion for a segment (mass/area·day]

D_p = deposition rate in rill areas (mass/area· time)

D_{pk} = deposition rate for the *kth* sediment class (mass/area·time)

D_{puk} = deposition rate at the upstream end of a segment for the *kth* sediment class (mass/area·day)

D_{qk} = quasi-deposition rate in first segment for *kth* sediment (mass/area· time)

D_r = rill erosion rate(mass/unit area· time)

D_{rorp} = either rill erosion (D_r) or deposition (D_p) in rill areas (mass/area·time)

$\exp(-b_r f_g)/\exp(-0.025 f_g)$ = rill erosion surface cover effect to interrill erosion surface cover effect ratio

E = rain storm energy (force·length/area)

EI_{30} = rain storm erosivity (force·length/area)·(length/time)

f_g = ground (surface) cover (percent)

f_k = portion of average annual erosivity that occurs during *kth* crop stage (fraction)

g = sediment load (mass/unit overland flow width· time)

g_b = sediment load at the location where deposition begins within segment (mass/width· time)

g_{bk} = sediment load for the *kth* sediment class at the location where deposition begins within segment (mass/width· time)

g_{cp} = daily conservation planning sediment load (mass/width·day)

$g_{cp\lambda}$ = daily conservation planning sediment load at end of overland flow path (mass/width·day)

g_{daily} = daily sediment load (mass/width· day)

$g_{daily\lambda}$ = daily sediment load at end of overland flow path (mass/width· day)

$g_{dailydetcap}$ = daily sediment load that would be produced if detachment occurred at detachment capacity (mass/width· day)

g_{det} = daily sediment load produced by detachment (mass/width· day)

g_{detcap} = daily sediment load that would result from detachment at capacity rate (mass/width· day)

g_{ek} = sediment load where deposition ends for *kth* sediment class (mass/width· time)

g_k = sediment load for *kth* sediment class (mass/width· time)

g_0 = 0, sediment load at x = 0 (mass/width· time)

g_p = potential sediment load at end of segment (mass/width· time)

g_{qk} = quasi-sediment load for *kth* sediment class rate for first segment (mass/width·time)

$G_{cp\lambda}$ = average annual conservation planning sediment load at end of overland flow path (mass/width·year)

$G_{det\lambda}$= average annual sediment load produced by detachment at end of overland flow path (mass/width·year)

G_λ = average annual sediment load (i.e., sediment yield, sediment delivery) at end of overland flow path (mass/width·year)

I_{30} = average intensity over the continuous 30 minutes with most rainfall in storm (distance/time)

J_d = number of days in computation period (J_d =365M_d)

k = daily soil erodibility factor (mass/erosivity unit)

K = average annual soil erodibility factor (mass/erosivity unit)

K_r/K_i = inherent rill to interrill soil erodibility ratio

K_T = sediment transportability coefficient (mass/volume)

l = daily slope length factor (dimensionless)

L = average annual slope length factor (dimensionless)

m = daily slope length exponent (dimensionless)

M_c = number of year in computation for cover-management computation

M_d = number of years in the computation period

M_k = number of crop stages in computation period

M_r = number of years in the record being used to compute erosivity

$M_{s(j)}$ = the number of storms in the *jth* year

n_i = number of sub-segments within the *ith* segment (integer)

n_o = 200, number of sub-segments for the entire overland flow path length, used to solve numerical deposition equation

p_c = daily contouring subfactor dimensionless)

p_d = daily subsurface drainage subfactor (dimensionless)

p_p = daily ponding subfactor (dimensionless)

P = average annual support practice factor (dimensionless)

P_{10y24h} = 10 year(return period)-24 hour (storm duration) precipitation amount (length)

q = overland flow (runoff) rate (volume/width·time)

q_0 = 0, discharge rate at x = 0 (mass/width·time)

r = daily erosivity (erosivity unit/area·day)

r_k = erosivity during *kth* crop stage (erosivity unit/area)

r_{10y24h} = storm erosivity associated with 10 year-24 hour precipitation amount P_{10y24h} (erosivity unit)

R = average annual erosivity factor (erosivity unit/area·year)

$(s/0.0896)/(3s^{0.8}+0.56)$ = steepness effect for rill erosion to interrill erosion ratio

s = overland flow path steepness (sine of slope angle)

S = average annual slope steepness factor (dimensionless)

S_i = slope steepness factor for interrill erosion

T_c = sediment transport capacity in rill areas (mass/overland flow width·time)

T_{ck} = transport capacity for *kth* sediment class (mass/width·time)

T_{clk} = sediment transport capacity at the downstream (lower) end of segment (mass/width·time)

T_{cuk} = sediment transport capacity at the upstream (upper) end segment (mass/width·time)

T_{cb} = sediment load where deposition begins (mass/width·time)

V_f = sediment fall velocity (length/time)

V_{fk} = sediment fall velocity for *kth* sediment class (length/time)

x = distance from origin of overland flow path (length)

x_b = location where deposition begins (length)

x_e = location where deposition ends (length)

x_{ud} = location of upper edge of deposition in a segment in which deposition occurs (length)

α_d = deposition coefficient (dimensionless)

β = daily ratio of rill to interrill erosion for unit plot length

δ = scaling factor used to compute daily sediment load

Δg_i = daily sediment load produced by interrill erosion in a segment (mass/width·day)

Δg_{pa} = daily sediment load deposited in a segment before any credit is taken for deposition benefit (mass/width·day)

Δg_{pb} = daily sediment load deposited in a segment credited as soil saved (mass/width·day)

Δg_r = daily sediment load produced by rill erosion in a segment (mass/width·day)

Δx = length of the distance step used in the numerical integration to compute deposition (length)

γ_m = the maximum monthly erosivity density at the location (erosivity unit/length)

ζ = coefficient for effect of hydraulic resistance on sediment transport capacity

K = the number of crop stages

λ = slope length (length)

λ_o = overland flow path length (length)

λ_u = unit plot length (length)

σ = excess rainfall length rate (rainfall rate - infiltration rate) (length/time)

ψ_k = sediment mass in *kth* sediment class (fraction)

indices

i = segment along overland flow path

j = year

k = crop stage

k = sediment class

m = storm

1 and 2 = subscript 1 for upstream (upper) end of distance step and subscript 2 for downstream (lower) end of distance step in numerical integration of deposition equation

3. CLIMATE (WEATHER), RUNOFF, AND HYDRAULICS

The major weather variables used by RUSLE2 are monthly erosivity, precipitation, and temperature and the 10 year (return period)-24 hour (storm duration) precipitation amount. Erosivity values are an index of erosive rainfall at a location for causing rill and interrill erosion. Erosivity is a major variable in the equations used to compute detachment (e.g., see Section **2.1**). Precipitation and temperature influence the loss of biomass on and in the soil and how that loss varies among locations (e.g., see **Section 10.4.1**). Precipitation and temperature also affect the temporal distribution of soil erodibility and how that distribution varies by location (see **Section 4.5**). The 10 year-24 hour precipitation amount is a representative (index) storm that is used to compute the effect of ponding on erosivity, deposition on concave overland flow path profiles, deposition by dense vegetation strips, deposition in terrace channels, and the effectiveness of contouring (e.g., see **Section 7.1**). These computations are made using runoff and flow hydraulics based equations.

3.1. Disaggregation of monthly values into daily values

RUSLE2 uses daily values for erosivity, precipitation, and temperature to compute daily erosion (see **Section 2.1**). The RUSLE2 disaggregation procedure converts (disaggregates) the input monthly erosivity, precipitation, and temperature into daily values.

3.1.1. Basic disaggregation procedure

The same basic disaggregation procedure is used for monthly temperature, precipitation, and erosivity. The procedure assumes that daily values vary linearly within each month according to a two-piece linear equation. A requirement is that the average of the daily values in a month equals the input monthly value.

The daily value at the beginning of a month is assumed to equal the mean of the monthly values for the current and immediately preceding month and the daily value at the end of the month equals the mean of the monthly values for the current and next month as illustrated in Figure 3.1. That is:

$$Y_b = (M_{(j)} + M_{(j-1)})/2 \qquad [3.1]$$

and

$$Y_e = (M_{(j+1)} + M_{(j)})/2 \qquad [3.2]$$

where: M = the average monthly value of the variable being disaggregated, Y_b = the daily value at the beginning of the *jth* month, Y_e = the daily value at the end of the month, and the index j refers to the month.

Figure 3.1 illustrates an example of increasing monthly values. The same equations apply to both increasing and decreasing values. A second set of equations apply for local maximums and local minimums illustrated in Figure 3.2.

3.1.1.1. Increasing or decreasing monthly values

The third major value is the time t_c where the two linear lines in Figure 3.1 equal the average monthly value M_j. The value for t_c is determined so that the total area under the two linear lines equals the average monthly value M_j. The area under the two lines is given by:

$$M_{(j)} = t_c(Y_b + M_{(j)})/2 + (1 - t_c)(M_{(j)} + Y_e)/2 \quad [3.3]$$

A value for t_c is determined by rearranging equation 3.3 as:

$$t_c = [M_{(j)} - (Y_e + M_{(j)})/2]/[(Y_b + M_{(j)})/2 - (Y_e + M_{(j)})/2] \quad [3.4]$$

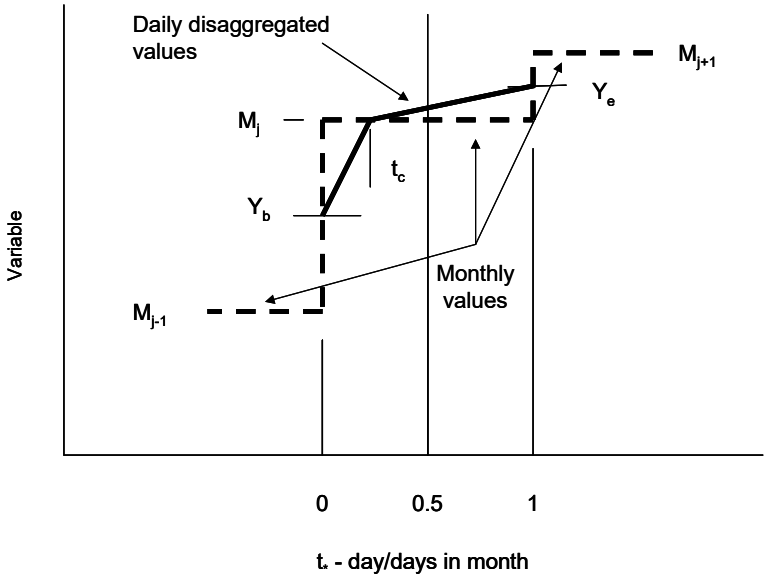

Figure 3.1. Illustration of two linear equations used to disaggregate monthly values into daily values for increasing or decreasing monthly values.

The equation used to compute daily values for times less than t_c is given by:

$$y_d = (d / D_{(j)})[(M_{(j)} - Y_b)/t_c] + Y_b \quad [3.5]$$

where: y_d = the daily value on day d of the month and D_j = the number of days in the month. The equation to compute daily values for times greater than t_c is given by:

$$y_d = (1 - d / D_{(j)})[(M_{(j)} - Y_e)/(1 - t_c)] + Y_e \quad [3.6]$$

3.1.1.2. Local maxima and minima

Figure 3.2 illustrates a local maximum. The equations apply both to local maximums and minimums.

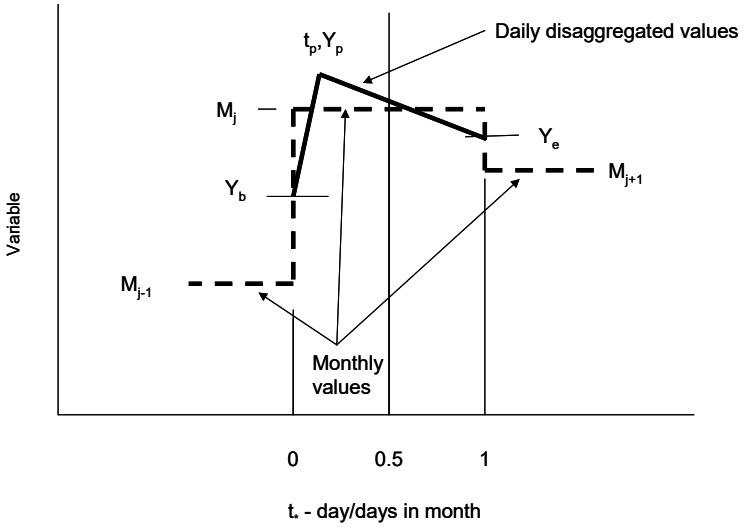

Figure 3.2. Illustration of two linear equations used to disaggregate monthly values for a local maxima or minima.

The daily value at the beginning and end of the month are computed using equations 3.1 and 3.2. The total area under the two lines must equal the average monthly value as:

$$M_{(j)} = (Y_b + Y_p)t_p / 2 + (Y_p + Y_e)(1 - t_p) / 2 \quad [3.7]$$

where: Y_p = the maximum value during the month that occurs at time t_p. Equation 3.7 is rearranged so that a value for the maximum value Y_p can be computed from:

$$Y_p = 2M_{(j)} + t_p(Y_e - Y_b) - Y_e \quad [3.8]$$

The equation for the time of the peak t_p is given by:

$$t_p = 1 - (M_{(j)} - Y_b)/(2M_{(j)} - Y_b - Y_e) \quad [3.9]$$

The equation for daily values for times less than the time of the peak is given by:

$$y_d = (d / D_{(j)})(Y_p - Y_b)/t_p + Y_b \quad [3.10]$$

and the equation for times after the time to peak is given by:

$$y_d = [(Y_p - Y_e)/(1 - t_p)](1 - d / D_{(j)}) + Y_e \quad [3.11]$$

3.1.2. Disaggregation procedure for temperature and erodibility

The disaggregation procedure is applied directly as described in **Section 3.1.1** for temperature. Figure 3.3 illustrates disaggregation of monthly temperature values into daily values for Columbia, Missouri. Notice that the date of the minimum daily temperature occurs in the third week of January as expected.

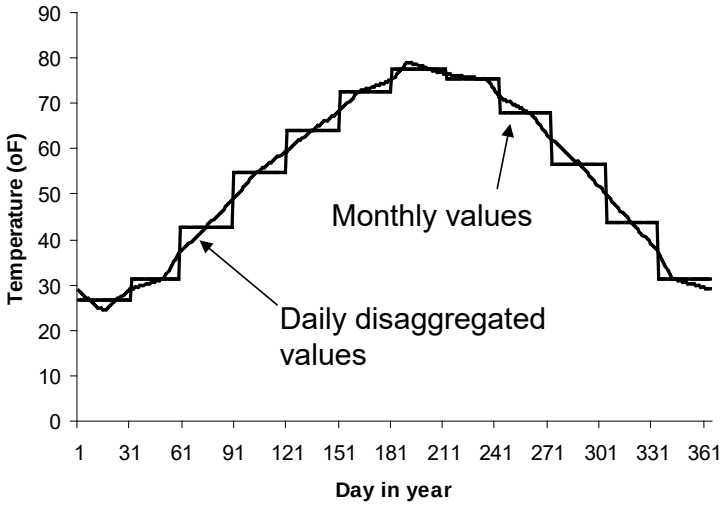

Figure 3.3. Daily temperature values obtained by disaggregating monthly temperature values at Columbia, Missouri.

3.1.3. Disaggregation procedure for precipitation and erosivity

When the disaggregation procedure is applied to monthly precipitation and erosivity, the average monthly value is divided by number of days in the month to obtain a mean daily value for the month. The disaggregation procedure is applied to the mean daily value in each month. Daily precipitation and erosivity values must be checked for negative values in very low rainfall areas like Yuma, Arizona. Daily precipitation and erosivity values are set to zero when negative values are computed. Setting these values to zero results in the sum of the disaggregated daily values being slightly greater than the monthly values in the months when the negative values occur. This adjustment has an insignificant effect on computed erosion values. Figure 3.4 shows daily disaggregated precipitation values for Columbia, Missouri.

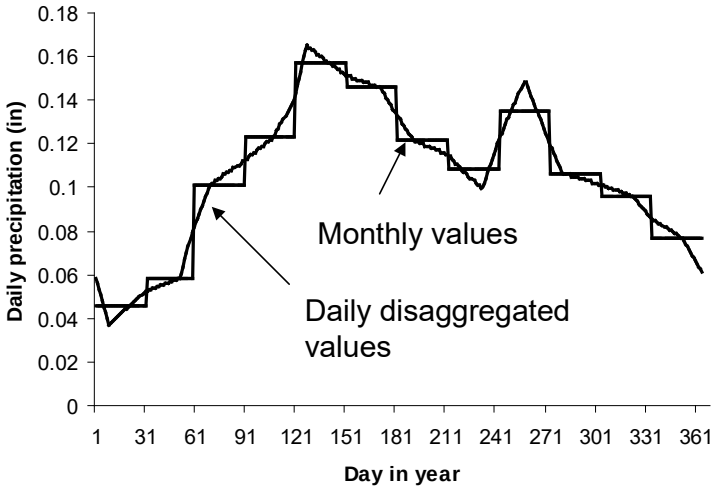

Figure 3.4. Daily precipitation values obtained from disaggregating monthly precipitation values at Columbia, Missouri.

3.2. Climate (weather) variables

The four basic RUSLE2 weather variables are monthly erosivity, precipitation, and temperature and the 10 year-24 hour precipitation amount. Selection of values for these variables is described in the RUSLE2 User's Reference Guide. This section describes underlying concepts, principles, and equations for processing weather data to develop input values consistent with RUSLE2 procedures and RUSLE2's purpose as a guide to conservation and erosion control planning.

3.2.1. Erosivity

RUSLE2 disaggregates average monthly erosivity values to obtain daily erosivity values used to compute daily erosion (see **Section 3.1**). Monthly erosivity values can be input directly into RUSLE2 in three ways, the recommended procedure for the Continental US is to input average monthly values for erosivity density.[27] Erosivity density, which is the ratio of monthly erosivity to monthly precipitation, is multiplied by monthly precipitation to obtain monthly erosivity values. The first step in developing average monthly erosivity density values is to compute erosivity values for individual storms using measured weather data.

[27] RUSLE2 can uses monthly erosivity values (1) computed by multiplying monthly erosivity density and precipitation values (see **Section 3.2.1.4.1**), (2) input directly, or (3) determined from input values for annual erosivity and the biweekly temporal distribution of erosivity.

3.2.1.1. Storm erosivity

Erosivity, the product of a storm's energy and its maximum 30 minute intensity, for an individual storm is computed as (Wischmeier and Smith,1978):

$$r_s = EI_{30} \quad [3.12]$$

where: r_s = storm erosivity, E = storm energy, and I_{30} = maximum 30-minute intensity. Maximum 30 minute intensity is the average intensity over the continuous 30 minutes in the storm with the most rainfall. Storm energy is computed using (Renard et al., 1997):

$$E = \sum_{k-1}^{m} e_k \Delta V_k \quad [3.13]$$

where: e = unit energy (energy content per unit area per unit rainfall depth) in the *kth* period, and ΔV = the amount (depth) of rainfall in the *kth* period, k = index for periods during the rainstorm where rainfall intensity is considered uniform, and m = the number of periods in the rainstorm. Unit energy is computed from (Brown and Foster, 1987; McGergor et al., 1995; Renard et al., 1997):

$$e_k = 0.29[1 - 0.72\exp(-0.082 i_k)] \quad [3.14]$$

where: e_k = the unit energy [MJ/(mm·ha)] for the *kth* period and i_k = rainfall intensity (mm/h) for the *kth* period.[28]

Data for storms less than 0.5 inch (12 mm), non-rainfall precipitation events, and extreme storm erosivity events with a return period greater than 50 years are excluded in the RUSLE2computation of storm erosivity.

3.2.1.2. Determining average annual erosivity values from measured precipitation data

Data from 15-minute precipitation gages that provide rainfall intensity values are required to compute storm erosivity values using equations 3.12-3.14. Modern data from 1960 through 1989 (1960-1999 in several cases) were analyzed to determine rainstorm erosivity and precipitation values at approximately 3700 15-minute precipitation gage locations across the Continental US (Hollinger et al., 2002). Erosivity values computed for the qualifying storms (i.e., rain events where amount was 0.5 inch or greater) were summed over the record length and divided by the years of record to determine an average annual erosivity value for each 15-minute precipitation station.

---

[28] See Foster et al. (1981) and AH703 (Renard et al., 1997) for a discussion of RUSLE2 units and how to convert between customary US units and SI units.

The plan was to develop an average annual erosivity contour map based on values computed from measured data at as many 15-minute precipitation gage locations as possible. Initial maps had many "bull's eyes" and irregular spatial trends rather than smooth trends required for RUSLE2 application as a guide for conservation planning. Data analysis showed that short and differing record lengths among locations greatly contributed to undesired spatial variability. The analysis also showed that the record length should be at least 18 years for directly computing average annual erosivity from measured 15-minute precipitation gage data. Even then the spatial variability among precipitation gage locations was sometimes too great.

3.2.1.3. Need for consistency in conservation and erosion control planning

Consistency in computed erosion estimates (hence, consistency in erosivity values) between locations within geographic regions and between regions is just as important as the absolute erosion estimates computed with RUSLE2. Land users impacted by erosion prediction perceive inconsistency and variability in erosion estimates for no apparent reason to be unfair, especially when the results negatively affect them. The probability distribution (return periods) of storms in a measured precipitation record used to compute erosivity values should be the consistent among locations. To illustrate, the average annual erosivity values at Wink, Texas and Pecos, Texas, towns in West Texas, computed from measured 15-minute precipitation data differed by a factor of two for no obvious reason. Inspection of the data showed that a 600-year return period storm caused the much larger average annual erosivity at one location.

The benefits or costs incurred by land users impacted by RUSLE2 should not be determined by the "luck of the draw" based on where they happen to be located. Furthermore, extreme events, such as a 100-, 200-, and 600-year storms, in the last 30 years are a very poor indicator of events likely to occur in the next 30 years. An average annual record that excludes extreme events is the best predictor of the immediate future for conservation planning where the objective is to protect the on-site soil resource from excessive degradation by erosion. However, other erosion prediction applications such as protecting highly sensitive water bodies and designing sediment storage in reservoirs may well require a different consideration of extreme events and a different set of input erosivity values than those developed for RUSLE2. Most erosion control practices are not designed or expected to withstand extreme events because in most cases failure does not cause catastrophic damages and the practices can be reinstalled without great costs.

Therefore, all storms with a return greater than 50 years were deleted from the measured data used in the RUSLE2 analysis to develop erosivity values.

3.2.1.4. Erosivity density approach to developing erosivity values

3.2.1.4.1. Erosivity density analysis

The RUSLE2 erosivity density approach for determining monthly erosivity values was developed in consideration of RUSLE2's consistency requirements for conservation planning and to maximize the information that could be extracted from the measured 15-minute precipitation data. RUSLE2 multiplies input values for average monthly erosivity

density by input values for average monthly precipitation to compute monthly erosivity values as:

$$R_{m(j)} = \alpha_{(j)} P_{md(j)} \quad [3.15]$$

where: R_m = average monthly erosivity, α = average monthly erosivity density, and P_{md} = average monthly precipitation determined from daily precipitation gage data, all for the *jth* month. Erosivity density refers to the erosivity content per unit precipitation. Erosivity density for a month is computed from measured 15-minute precipitation data as:

$$\alpha = \frac{\sum_{i=1}^{n} E_{(i)} I_{30(i)}}{\sum P_{15}} \quad [3.16]$$

where: all values were determined from 15-minute precipitation gage data including precipitation amount P_{15} from all storms and storm energy E is computed using equations 3.13 and 3.14, i = the index for storm in a month and n = total number of storms greater than 12 mm but smaller than a 50-yr event in a given month. Unit energy e_k for each *kth* period is computed from the average intensity for each 15-minute period in the storm (i.e., $i_k = \Delta V_k/15$ minutes and V_k = the rainfall amount in the *kth* 15-minute period). The I_{30} values used in equation 3.16 using 15-minute precipitation data were multiplied by a 1.04 factor to account for the fact that maximum intensity values from the 15-minute precipitation data are slightly lower than those computed with breakpoint rainfall (Hollinger et al., 2002). Breakpoint rainfall data are data divided into non-uniform periods where constant rainfall intensity can be assumed for each period. Breakpoint data are preferred rather than 15-minute precipitation data for computing storm erosivity.[29]

Approximations can be made in Equation 3.16 to aid the interpretation of erosivity density. Unit energy e does not vary greatly with intensity such that storm energy can be approximated with $\hat{e}P_{15}$ where $\hat{e}$ = effective unit energy for a month (Foster et al., 1982d). By assuming a representative $\bar{I}_{30}$ for the month, erosivity density is approximated by:

[29] The storm data including computed storm erosivity values were provided by the Illinois State Water Survey. The analysis of erosivity data was a joint effort between the Illinois State Water Survey, the USDA-ARS and NRCS, and the University of Tennessee.

$$\alpha \approx \frac{\bar{I}_{30}\hat{e}\sum_{i=1}^{n} P_{15(i)}}{\sum_{i=1}^{n} P_{15(i)}} \qquad [3.17]$$

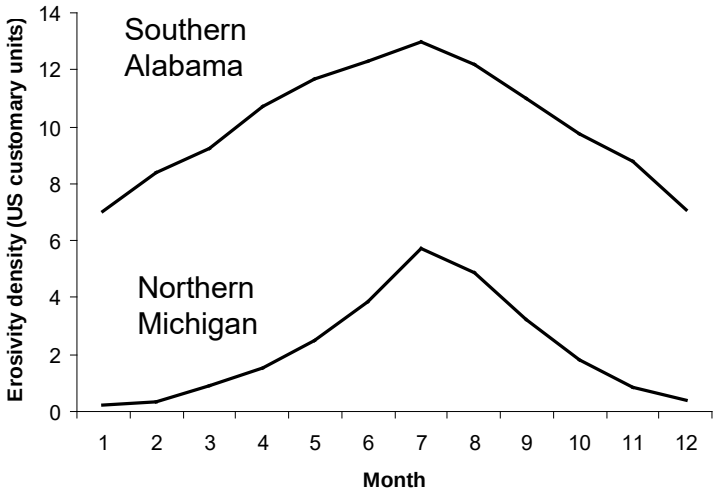

Figure 3.5. Erosivity density values for two locations.

where: $\bar{I}_{30}$ = the representative maximum 30-minute intensity for the month. Equation 3.17 in turn reduces to:

$$\alpha \approx \hat{e}\bar{I}_{30} \qquad [3.18]$$

Equation 3.18 shows that erosivity density varies directly with 30-minute rainfall intensity.

Erosivity density varies by location as illustrated in Figure 3.5 that shows that erosivity is higher in Southern Alabama than in Northern Michigan. In both locations, erosivity density is higher in the summer months than in the winter months, which according to equation 3.18, is caused by rainfall intensity varying with season. Rainfall intensity is greater in the summer than in the winter, resulting in erosivity being greater in the summer than in the winter for a given amount of rainfall. Also, most of the precipitation in Northern Michigan in the winter is snow and, therefore, is not included in the rainfall erosivity index.[30]

[30] The storm precipitation and erosivity values used in this analysis were provided by the Illinois State Water Survey and the USA-Natural Resources Conservation Service Water and Climate Center. These

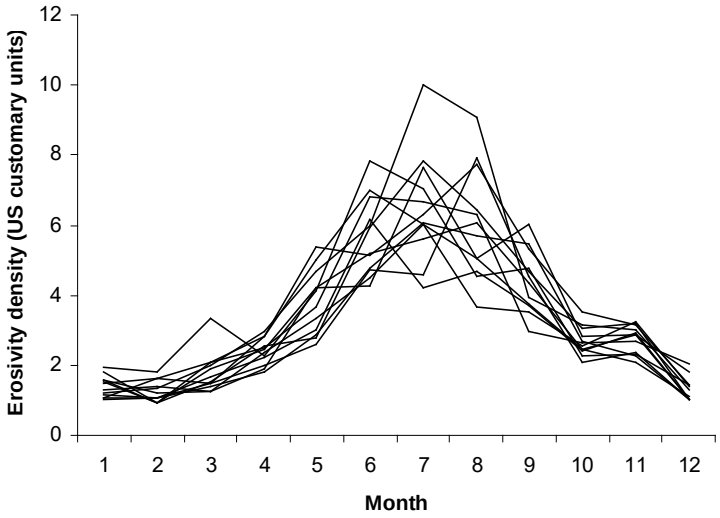

Figure 3.6. Spatial and temporal variability in erosivity density for locations in Southwestern Indiana.

Spatial and temporal variation in the erosivity density values computed from the 15-minute precipitation data was a major problem. Erosivity density values computed directly from the 15-minute precipitation data, as illustrated in Figure 3.6 for 15-minute gage locations in the southwest quadrant of Indiana, do not provide the smooth temporal and spatial trends required for RUSLE2 as a conservation and erosion control planning tool. Spatially averaging the erosivity density values by quadrant in Indiana smoothed the erosivity density values, both temporally and spatially, across Indiana as illustrated in Figure 3.7.

Geographic information systems (GIS) techniques, including kriging, were used to spatially average the erosivity density values computed from 15-minute precipitation data measured at the various gage locations. The procedure is similar to a spatial, moving average fitting technique and produced results similar to that illustrated in Figure 3.7.[31] Before kriging was applied, the monthly erosivity density values computed from the measured data in a relatively small region, such as a quadrant of Indiana, were inspected and analyzed for outliers. Monthly erosivity density values that departed from the mean in this local region by more than two times the standard deviation were considered outliers. Rather than excluding the entire dataset for a location (i.e., deleting the location from the entire data set), the outlier data point was adjusted to be consistent with other

---

values are computed from measured weather data collected by the National Weather Service. See (Hollinger et al., 2002) for additional information.

[31] The GIS and kriging analysis was conducted by the Department of Biosystems Engineering and Environmental Science, University of Tennessee, Knoxville.

monthly erosivity density values at the location. Adjusting individual monthly data points kept the number of locations in the dataset as large as possible. In most cases, the same outliers at a location identified by the statistical test could also be identified by inspection. Outliers were monthly erosivity density value outside the smooth trend obtained by averaging the data points in the local region as was done in Figure 3.7. This process of identifying and adjusting outliers typically involved two or three iterations.

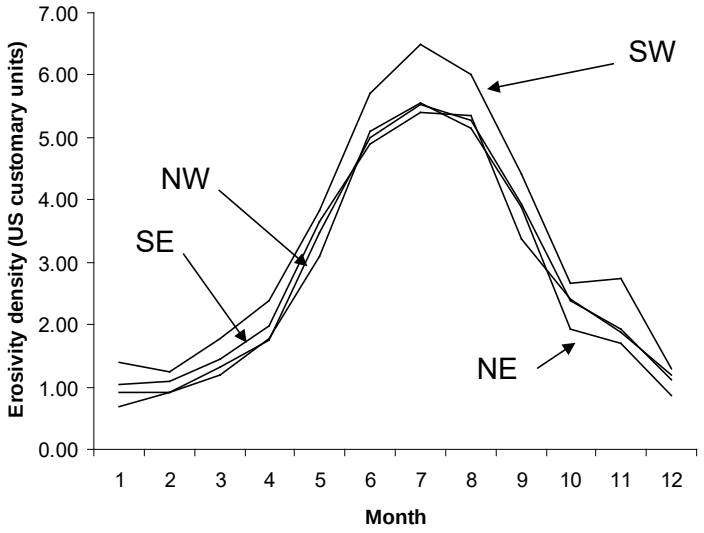

Figure 3.7. Erosivity density values spatially averaged for the four quadrants in Indiana.

A compromise was made in the number of nearest neighbors used in the kriging analysis. Using the 10 nearest neighbors worked well in the eastern US, but it did not work well along the eastern side of the Cascade Mountains in Washington and Oregon where erosivity density values decrease very rapidly with distance in this area. This rapid decrease necessitated using five rather than 10 nearest neighbors. This problem was also related to a very low density of 15-minute precipitation stations in the region. Using the five nearest neighbors also worked better than 10 nearest neighbors along coastlines and borders between Canada and Mexico where no precipitation data were available.

This procedure produced erosivity density values that varied smoothly over the Continental US, including mountainous regions. The hypothesis that erosivity density was not affected by mountainous terrain was tested in two ways. The first test involved fitting a linear equation to erosivity density values as a function of elevation at the 15-minute precipitation gage locations in a local region. The region had to relatively small, such as a quadrant of Utah, to avoid cross and spurious correlations. For example, the linear equation could not be fitted to erosivity density values for the entire state of Montana. When erosivity density values for all of Montana were included in the analysis, erosivity density values appeared to be a function of elevation, but that correlation was spurious. Elevation decreases from west to east across Montana while erosivity density increases across Montana. The increase in erosivity density across

Montana was not caused by elevation but by a west to east broad geographic increase in erosivity density.

Measured precipitation data from the 15-minute precipitation gages were available to compute erosivity density values for elevations up to about 10,000 ft. Statistical analysis for eleven local regions in mountainous areas throughout the western US and two local regions in the eastern US were conducted to determine if the hypothesis that erosivity density varied with elevation could be rejected. The analysis involved fitting a linear equation to the erosivity density values as a function of elevation. The data for three regions are shown in Figure 3.8-3.10. The result of the analysis was that the hypothesis that erosivity density values are independent of elevation could not be rejected. This test was not especially robust because of data variability. Elevation clearly affects erosivity density in the winter months because an increasing fraction of the precipitation occurs as snow at higher elevations. However, the assumption of no effect of elevation on erosivity density values in the summer months is considered acceptable.

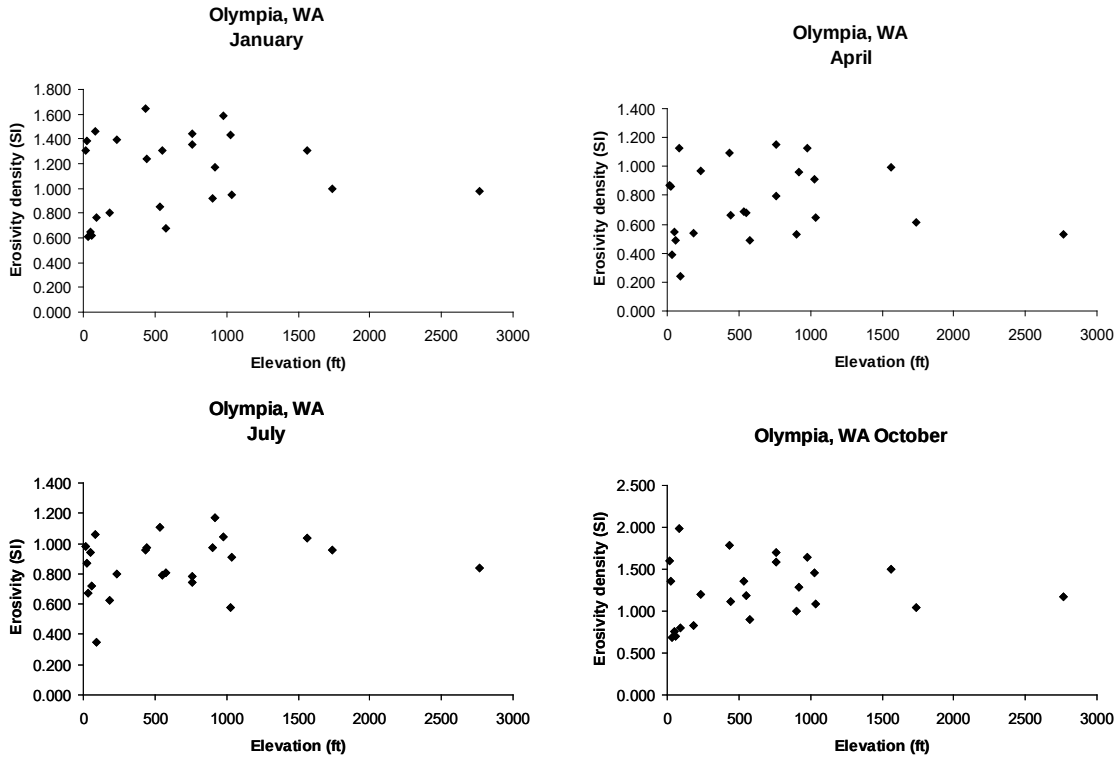

Figure 3.8. Variation of erosivity density with elevation in the Olympia, Washington region.

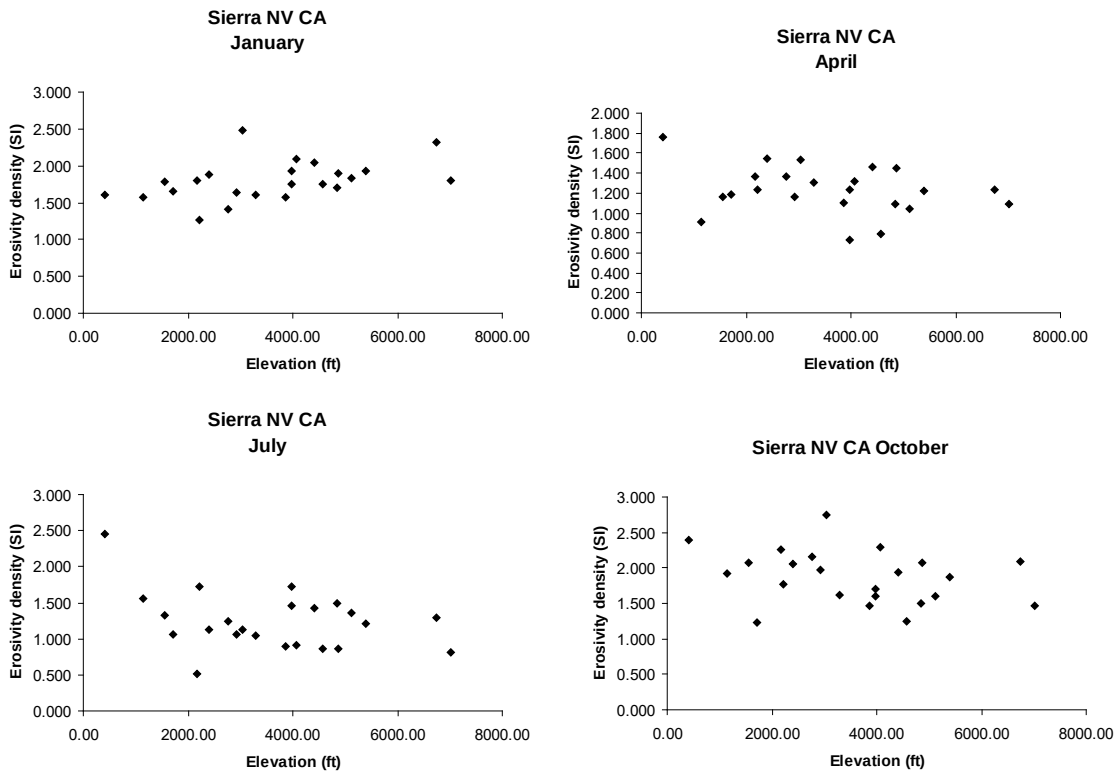

Figure 3.9. Variation of erosivity density with elevation in Sierra NV-CA region.

Another test of the hypothesis that erosivity density values are independent of elevation was to inspect a map, shown in Figure 3.11, of average 30 minute intensity for all storms in the data set (Hollinger et al., 2002). Even though these data were extensively smoothed as a part of the contouring process, the map shows no effect of mountainous terrain in the Western US on maximum 30-minute intensity. Equation 3.18 shows that erosivity density is approximately proportional to maximum 30-minute rainfall intensity. Therefore, if 30-minute intensity is independent of elevation in mountainous regions, as indicated in Figure 3.11, then erosivity density is independent of elevation. This result means that the effect of mountainous terrain on erosivity can be fully captured in how terrain affects monthly precipitation. While these tests are not especially robust, the erosivity density approach is a major improvement over previously available erosivity values in AH703 (Renard et al., 1997) for the Western US.

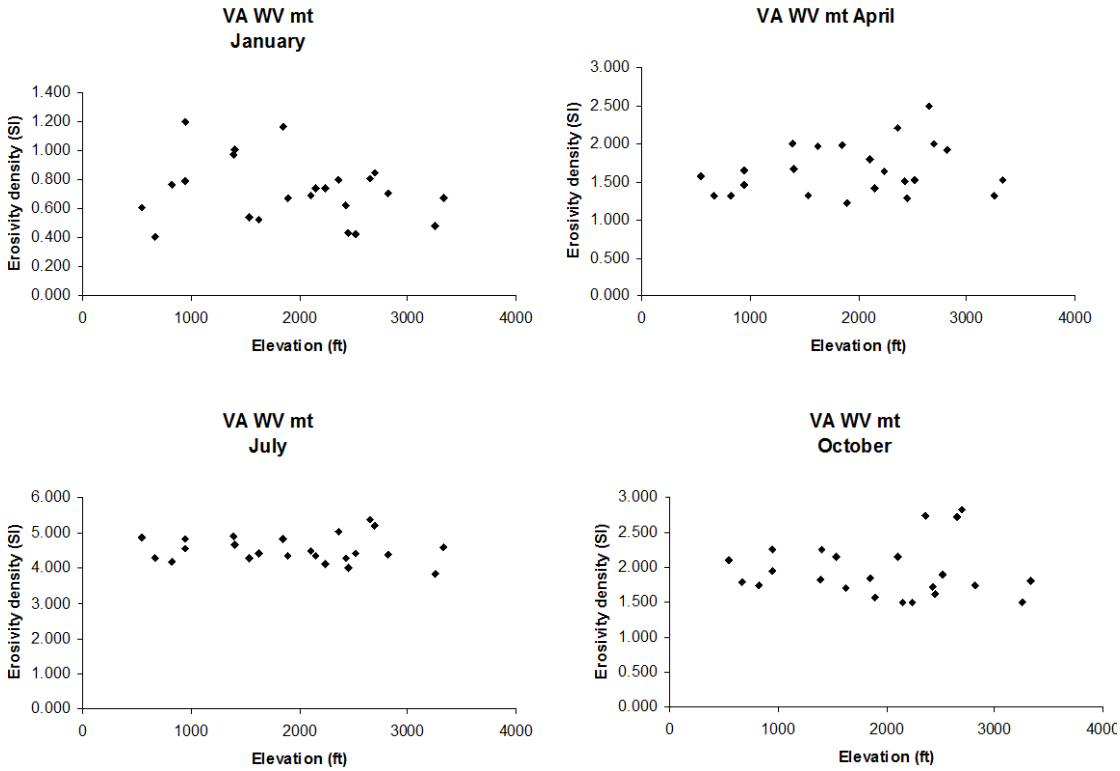

Figure 3.10. Variation of erosivity density with elevation in the West Virginia and Virginia mountainous region.

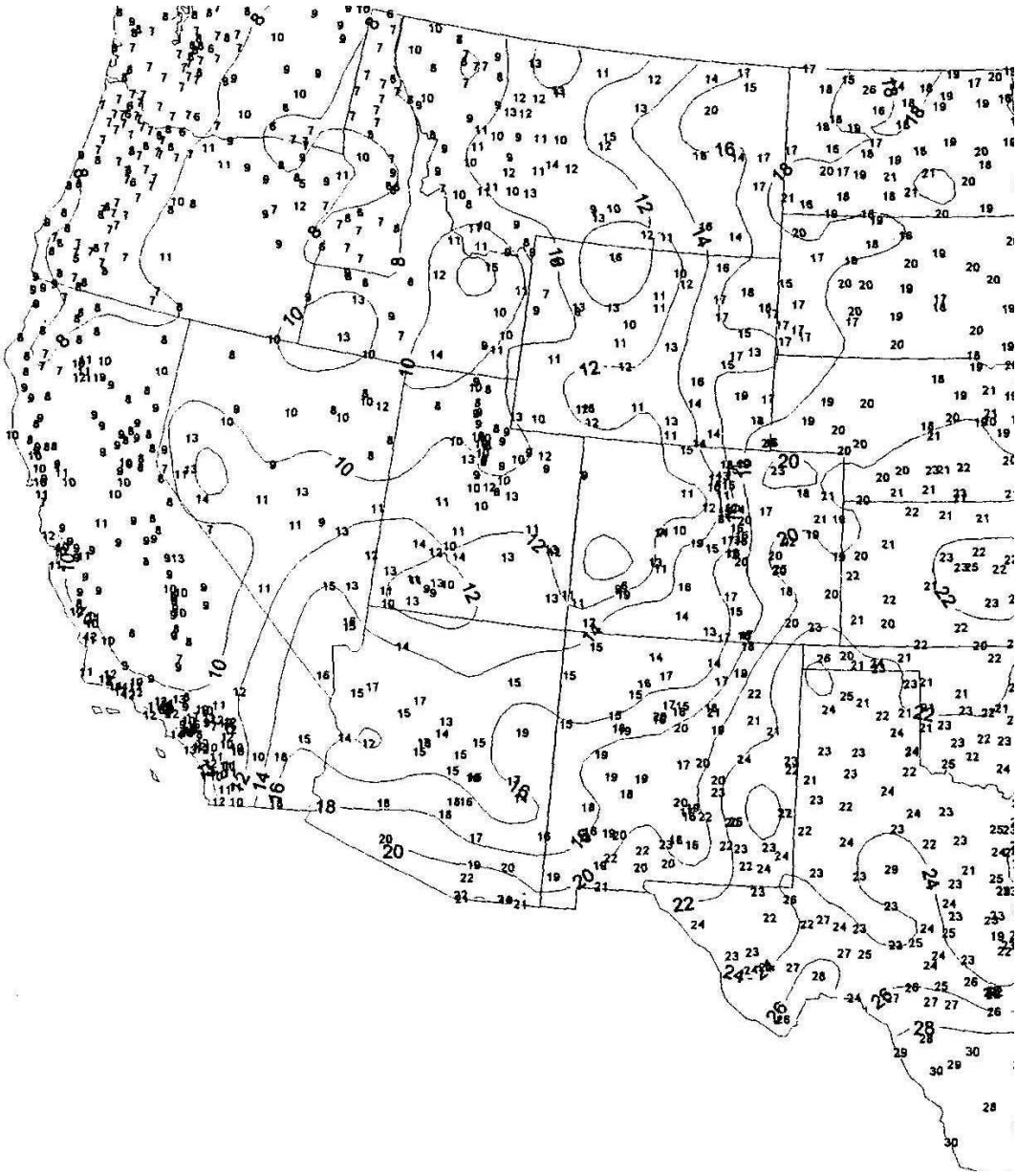

Figure 3.11. Average maximum 30 minute intensity computed for all storms. Source: Illinois State Water Survey (Hollinger et al., 2002).

3.2.1.4.2. Advantages of erosivity density approach

The erosivity density approach has major advantages. It produces consistent, smoothly varying erosivity density values across the US as desired for conservation and erosion control planning. The erosivity density approach uses data from daily precipitation gage stations, which are far more numerous than the 15-minute precipitation stations, to fill in erosivity values between the 15-minute precipitation gage locations where erosivity was computed from measured precipitation data. The erosivity maps for the Eastern US in AH282 (Wischmeier and Smith, 1965) and AH537 (Wischmeier and Smith, 1978) were based on approximately 2000 data points (see AH282). However, storm erosivity was computed from detailed intensity precipitation data comparable to the 15-mintue

precipitation data at only 181 locations. An equation involving 2 year-6 hour precipitation amount and other variables was fitted to average annual erosivity values computed from the measured detailed precipitation data at the 181 locations (AH282, AH537). This equation was then used to estimate average annual erosivity values at the approximately 2000 locations used to draw the AH282 and AH537 erosivity maps for the Eastern US. The erosivity density approach using monthly precipitation measured by daily precipitation gages to compute erosivity at any particular location serves this function in RUSLE2.

The USLE and RUSLE1 use EI distribution zones in the US to describe the spatial variations in the temporal distribution of erosivity during the year. The temporal distribution of erosivity is assumed to be constant within a zone. Differences in temporal erosivity distributions between zones resulted in major differences in erosion estimates across certain zone boundaries. For example, Little Rock, Arkansas is very close to a EI zone boundary. The USLE and RUSLE1 compute a 25 percent change in erosion across the EI zone boundary at this location for a conventionally tilled corn cropping system. The impact of this step change is that a client should not be expected to change management practices unless estimated erosion changes by at least 25 percent. RUSLE2's estimated erosion values vary smoothly across the US because RUSLE2 does not use such zones. See RUSLE2 User's Reference Guide for a discussion on how aggregating input weather data by counties affects estimated erosion across county boundaries.

Precipitation data measured by daily precipitation gages are much more stable and reliable and have much less missing data than precipitation data measured with the 15-mintue precipitation gages. That is, the quality of the 15-minute precipitation data is less than the quality of the daily precipitation data. The erosivity density approach computes a ratio in contrast to the standard approach that computes an absolute sum. The data requirements for computing a ratio of monthly erosivity to monthly precipitation amount are less demanding than for computing an absolute erosivity sum. An absolute sum is greatly affected by missing data, unless the missing data are so small that the missing values have little effect on the sum. In contrast, missing data have no effect on the ratio if the missing data are not biased. Although the missing 15-minute precipitation data were surely biased, problems caused by missing data and errors in reconstructing missing data are much less in the ratio erosivity density approach than in the absolute standard approach.

The erosivity density approach also reconciles differences in precipitation amounts measured by the daily and 15-minute precipitation gages. The Illinois State Water Survey provided precipitation data for 14 locations in West Texas and Eastern New Mexico where daily and 15-minutes precipitation gages were located sufficiently close so that annual precipitation measured by the two gages types could be compared. Overall, the annual precipitation measured by the 15-minute gages was 85 percent of that measured by the daily gages. The annual precipitation measured by the 15-minute gages was less than that measured by the daily gages for all 14 locations. The ratio of the precipitation amounts for the two gage types ranged from 0.76 to 0.94. This disparity between gage types affects erosivity density values much less than it does absolute

erosivity values. The erosivity density approach computes monthly erosivity values, determined from 15-minute precipitation gage data that are consistent with the monthly precipitation values, determined from daily precipitation gage data, used in RUSLE2.

A shorter record length and a record with more missing data can be used to compute erosivity density values than can be used to directly compute erosivity values with the standard method. Record length, including both number of years and number of storms, is especially critical in the Western US where spatial density of 15-minute precipitation gages is low, spatial and temporal variability is great, and records are often short with missing data. Twenty years was the minimum data record length considered to be acceptable for computing erosivity values for the Eastern US. That record length was actually too short using the standard procedure, but it was a compromise to include as many stations as possible. A data record length of 15 years was judged to be satisfactory for computing erosivity density values in the Eastern US. This conclusion was based on analysis of precipitation data collected by the USDA-Agricultural Research Service in Northern Mississippi in a research environment where data quality was very carefully maintained (McGregor et al. 1995). As Table 3.1 shows, a record length of 10 years was acceptable for these data using the erosivity density approach. Most important, the analysis showed that a shorter length of record could be used in the erosivity density approach than in the standard approach.

Table 3.1. Percent error in estimating monthly R from measured preciptiation data. Ratio refers to erosivity density approach. Abs refers to standard approach that computes absolute values.

record length	jan		feb		mar		apr		may		jun	
(yrs)	ratio	abs	ratio	abs	ratio	abs	ratio	abs	ratio	abs	ratio	abs
11	-21	-32	1	25	-5	3	-9	11	1	32	-10	-6
12	-21	-32	1	16	-4	-4	-5	6	-4	24	-8	-12
13	-12	-25	1	14	-8	-3	-5	2	-8	15	-8	-8
14	-9	-22	1	9	-1	0	-8	-3	-3	10	-7	-4
15	-2	-18	0	2	0	1	-6	0	0	4	-12	-2
16	-2	-11	3	3	2	0	-8	-3	-2	6	2	8
17	-7	-7	3	5	-3	-2	0	-1	-2	0	0	2
18	0	0	0	0	0	0	0	0	0	0	0	0

record length	jul		aug		sep		oct		nov		dec		ann		aver	
yrs	ratio	abs	ratio	abs	ratio	abs	ratio	abs	ratio	abs	ratio	abs	ratio	abs	ratio	abs
11	-4	17	10	19	7	-10	11	17	11	31	16	18	3	13	1	11
12	-5	8	4	27	4	-14	9	12	10	25	16	14	2	7	0	6
13	-6	10	4	18	0	-13	1	13	9	26	11	12	-1	6	-2	5
14	-8	9	1	13	-1	-16	5	9	6	22	10	5	0	3	-1	3
15	3	8	-3	5	-5	-9	6	16	5	19	7	5	1	3	-1	3
16	0	5	2	5	-3	13	3	11	3	11	3	4	2	5	1	4
17	0	0	0	-1	-3	6	2	4	1	5	0	-1	0	1	-1	1
18	0	0	0	0	0	0	0	0	0	0	0	0	0	0	0	0

The length of record in years and number of storms in the record are more important in the Western US than in the Eastern US. Figure 3.12 shows the effect of record length for a precipitation gage located in Beaver County, Utah. The example in Figure 3.12 is not very robust, but it represents typical conditions for the 15-minute precipitation data in the Western US where the data record was short, the data was highly variable and contained relatively few storms, and number of the 15-minute gage locations was sparse. The erosivity density approach much more effectively uses the limited data in the Western US than does the standard procedure.

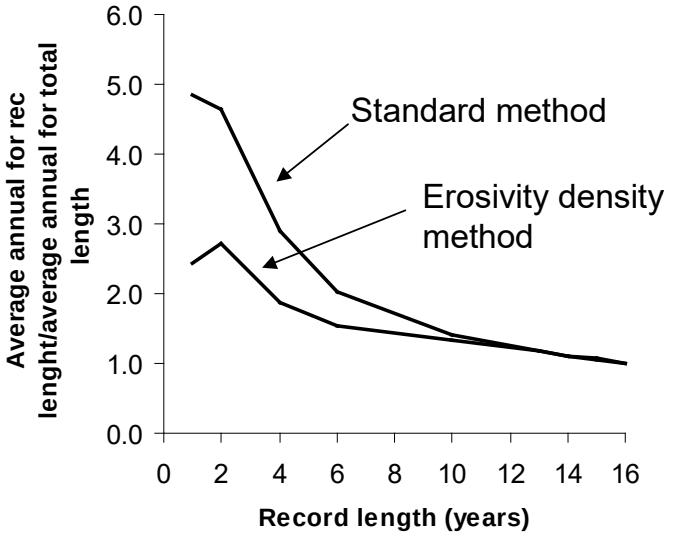

Figure 3.12. Effect of record length on variation of average annual values for erosivity and erosivity density for Beaver County, Utah.

Data for a gage location were not automatically discarded because of a short record length in the Western US in order to include as many stations as possible. The overall curve of monthly erosivity density by month computed by averaging erosivity density values in a local region was examined (e.g., see Figures 3.6 and 3.7), and the data for the location were left in the analysis if the trend at the location matched the local regional trend. When the trends in a dataset at a location did not match the overall trend, the record length at the location was almost always short.

3.2.1.4.3. Comments on erosivity density approach

Precipitation amount is a very poor indicator of erosivity (Wischmeier, 1958; Foster et al., 1982). Measures of both rainfall intensity and amount are required in erosivity measures and indices. Monthly erosivity values computed using the erosivity density method have the immediate appearance of being solely a function of monthly precipitation amount. The erosivity density value for each month depends strongly on intensity as shown by equation 3.18. The erosivity density method also seems to conflict with the empirical result that storm erosivity is a nonlinear function of storm amount (Richardson et al., 1983). The empirical erosivity density values account for this nonlinearity. Nonlinear mathematical relationships can be linearized by dividing the solution space into sufficiently small intervals so that linear equations can be assumed within each interval. The erosivity density approach is a linearized procedure that captures the effect of both intensity and nonlinearity between storm erosivity and storm amount.

Care must be taken in developing and applying the erosivity approach in other situations, especially when it is used where only very limited precipitation data are available. The erosivity density method can be quite useful in these situations, but sufficient data must be available and analysis must be conducted to determine the variation of erosivity density values over the region where the method is being applied. Assuming constant erosivity density values over too large of a region can produce very erroneous results.

3.2.1.4.4. Alternative procedures for estimating erosivity involving precipitation amount

Lack of adequate precipitation data to derive RUSLE2 erosivity values is a major limitation in applying RUSLE2 in many countries. Erosivity values are estimated from storm, monthly, and annual precipitation amounts. Rainfall intensity is a critical element in erosivity indices and any estimation procedure must account for how intensity varies over space and time in relation to precipitation amount. The effect of intensity on erosivity varies by location and by month as Figure 3.5 and equation 3.18 indicate.

A procedure to estimate storm or daily erosivity from storm or daily precipitation, respectively, uses the equation (Richardson et al., 1983):

$$r_s = a_p P_s^b \qquad [3.19]$$

where: r_s = storm or daily erosivity, P_s = storm or daily precipitation amount, and a and b are coefficients that vary by location and month. Values for a_p and b are determined by empirically fitting equation 3.19 to observed data. The procedure requires sufficient data and analysis to determine values for a_p and b over space and by month or season. The Illinois State Water Survey (ISWS) attempted to apply this procedure to US data but concluded they had insufficient data to properly compute a and b values (Hollinger et al., 2002). Another problem was that they used a logarithmic transformation and linear regression in fitting equation 3.19 to the data rather than a nonlinear fitting procedure. The logarithmic transformation-linear regression procedure returns the mean of the logarithms of the observed values rather than the mean of the absolute observed values. Erosivity values that would be used in RUSLE2 produced by the ISWS procedure had a systematic error by being too low by about 10 percent. Use of equation 3.19 can work if the proper precautions are followed and sufficient data are available to determine values for a_p and b in equation 3.19 over space and time by month or season.

Another procedure is to compute storm erosivity using a design storm that has a particular intensity distribution (Cooley, 1980; Brown and Foster, 1987). The requirement for this procedure is that design storm intensity distributions vary over space and time. A few design storms are available that vary intensity distributions over space in the US, but no design storms seem to be available that vary intensity distributions by month or season.

A modified Fournier index is widely used to estimate erosivity where precipitation data are very limited. A value for the modified Fournier index is computed from (Renard and Freimund, 1994):

$$F = \frac{\sum_{j=1}^{12} P_{m(j)}^2}{\sum_{j=1}^{12} P_{m(j)}} \qquad [3.20]$$

where: F = the modified Fournier index, P_m = average monthly precipitation, and j = index for each month. The usual procedure is to fit a linear equation involving average annual erosivity as a function of the modified Fournier index (Fournier, 1960). Values of the modified Fournier index were computed at the US locations listed in Table 3.2. Average annual erosivity values at these locations are plotted as a function of the modified Fournier index in Figure 3.13.

Table 3.2. Locations where modified Fournier index computed
Minneapolis, MN
Des Monies, IA
Columbia, MO
Oklahoma City. OK
Bryan, TX
Oxford, MS
Mobile, AL
Atlanta, GA
Norfolk, VA
Boston, MA
Scotfsbluff, NE
Houston, TX
Gulfport, MS
Miami, FL
Montgomery, AL
Denver, CO
Bismark, SD
Tombstone, AZ
Lincoln, NE
Lafayette, IN
San Francisco, CA
Bakesfield, CA
Jackson, MI
Pittsburg, PA

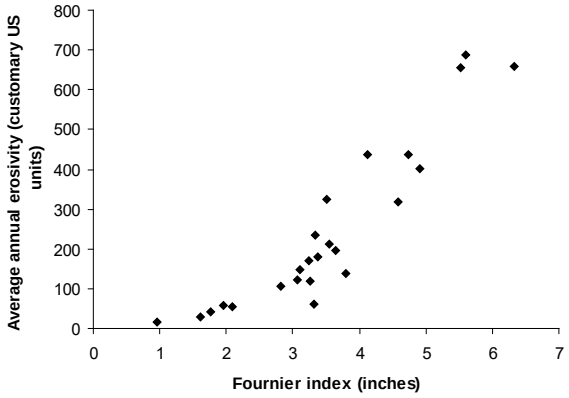

Figure 3.13. Relation of average erosivity to modified Fournier index for several US locations.

These results show that the relation between average annual erosivity and the modified Fournier index is nonlinear rather than linear. Renard and Freimund (1994) also found that the relationship of average annual erosivity to the modified Fournier index was nonlinear where erosivity varied with the index raised to the 1.85 power for US data that are comparable to data represented in Figure 3.13. That equation is given by:

$$R = a_F F^{1.85} \qquad [3.21]$$

where: R = average annual erosivity. When this equation form is fitted to the data represented by Table 3.2, the exponent is 2.24. The difference in these exponent values is caused by differences in datasets and fitting procedures.

Another concern with the modified Fournier index is whether the square of monthly precipitation in equation 3.20 is the appropriate value for the exponent. A modified Fournier index with a generalized value for the exponent would be computed as:

$$F_r = \frac{\sum_{j=1}^{12} P_{m(j)}^{z}}{\sum_{j=1}^{12} P_{m(j)}} \qquad [3.22]$$

$$R = a_r F_r \qquad [3.23]$$

where: F_r = the modified Fournier index where a value for the exponent z is determined by fitting equations 3.22 and 3.23 to observed data. In this formulation, the relationship between average annual erosivity and the generalized modified Fournier index is linear as shown in equation 3.23. The value for the exponent b most likely varies with the dataset. A value of 3.02 was obtained when equations 3.22 and 3.23 were fitted to the data represented in Table 3.2. Figure 3.14 shows a comparison between the values computed by equations 3.20 and 3.21 and equations 3.22 and 3.23. The values computed by equation 3.21 are slightly better than the values computed with equations 3.22 and 3.23. Using equations 3.20 and 3.21 or equations 3.22 and 3.23 is an improvement over fitting a linear equation to the standard modified Fournier index with the square exponent.

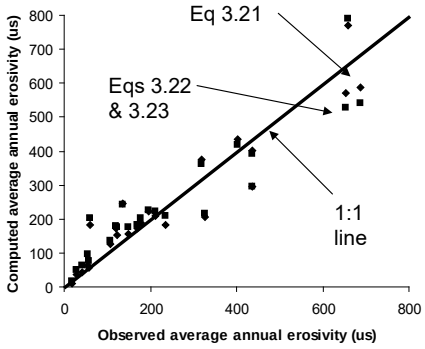

Figure 3.14 Comparison of alternate ways of using a modified Fournier index to estimate average annual erosivity.

The best approach for fitting either equations 3.20 or 3.21 or equations 3.22 and 3.23 is to divide the data into subsets by geographic region where the relationship between precipitation amount and intensity is constant over the region. A separate equation is fitted to the sub-dataset for each region. If the regions are too large, the variation in the relationship of intensity to precipitation amount over geographic space will be too large. Otherwise, the error in estimated erosivity will be very large. For example, the range in average annual erosivity in Figure 3.13 is from about 50 to 325 (US units) for a modified Fournier index value of about 3.5 inches. Obviously this great difference in erosivity for a particular value of the modified Fournier index results in very large errors in estimated erosion.

The implicit assumption in the modified Fournier procedure is that the monthly precipitation distribution coincides with the monthly intensity distribution. That is, the monthly precipitation distribution must coincide with the monthly erosivity density distribution. These distributions coincide well at Minneapolis, Minnesota but not at Oxford, Mississippi. The effect of the coincidence of the distributions on the monthly erosivity distribution is illustrated in Figure 3.15. The monthly erosivity distribution computed from the Fournier index, assuming a square power as in equation 3.20, compares reasonably well with the observed distribution at Minneapolis but compares very poorly at Oxford. Therefore, if the Fournier index is used to estimate monthly erosivity for the USLE, RUSLE1, or RUSLE2, the monthly erosivity density distribution must correspond closely to the monthly precipitation distribution.

Another procedure to estimate erosivity from monthly or annual precipitation amounts is to empirically fit equations involving these variables to observed data (Renard and Freimund, 1994). These procedures work satisfactorily only if the spatial and temporal

variations in the relationship between precipitation amount and intensity are taken into account. For example, average annual erosivity ranged from 88 (US units) to 470 (US units) for an average annual precipitation of 39 inches in the data analyzed by Renard and Freimund (1994). This variation in average annual erosivity for a particular average annual precipitation is much too great to be useful in erosion prediction used for

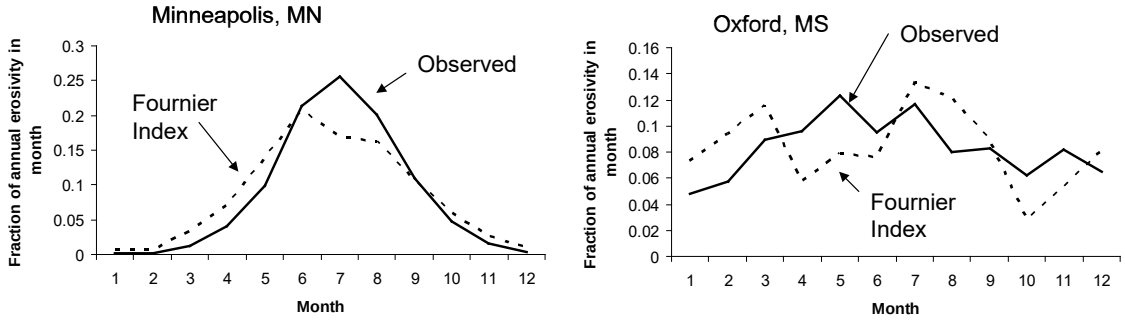

Figure 3.15. Comparison of monthly erosivity distributions computed with the modified Fournier index with observed monthly erosivity distributions.

conservation and erosion control planning. The data should be divided into subsets according to the relation of intensity to precipitation amount.

Any method used to estimate erosivity from precipitation amount MUST take into account how the relationship between precipitation and intensity varies over space and time.

3.2.2. Precipitation

RUSLE2 uses average monthly precipitation values as input values for precipitation. RUSLE2 uses the disaggregation procedure described in **Section 3.1** to disaggregate average monthly precipitation values into daily values. A consistent and sufficient record length should be used to determine average monthly precipitation values from measured data. A 22-year record length was used to develop erosivity values for the USLE (Wischmeier and Smith, 1958, 1965, 1978) because climate was thought to vary in a 22-year cycle. The modern accepted record length seems to be 30 years for hydrologic modeling. The National Weather Service has assembled 30-year data records for the locations where daily precipitation was measured. These data have been reviewed to correct erroneous and missing data. In addition, the USDA-NRCS, National Weather Service, and other agencies used the PRISM (Daly et al., 1997) computer program that extrapolates the measured data at each weather station to compute monthly precipitation values across the US on a 4 km grid. This mathematical procedure adjusts measured values for the effect of elevation, proximity to a coastline, and other variables that spatially affect precipitation. RUSLE2 users should contact their USDA-NRCS state office for precipitation data to use in RUSLE2.

The data available from the NRCS, referred to as the PRISM data, were analyzed to ensure that the probability distribution of the data is uniform for all locations. For example, extreme summer precipitation events can be highly localized. The PRISM data

should be reviewed to ensure that the return periods for the precipitation input data are uniform among locations where RUSLE2 is being applied so that a land user is not unfairly affected by the happenstance of extreme precipitation occurring at their location and not at other locations (See RUSLE2 User's Reference Guide). In general, events having a return period greater than 50 years should be excluded when using RUSLE2 for conservation and erosion control planning.

3.2.3. Temperature

RUSLE2 uses average monthly values for input temperature values. RUSLE2 uses the disaggregation procedure described in **Section 3.1** to compute average daily temperature values from average monthly input values. The time period used to obtain monthly precipitation values should be the same as that used to obtain average monthly temperature values so that precipitation and temperature input values will be consistent. The most recent 30 years is an acceptable period over which to obtain average monthly temperature values. However, the data should be reviewed to ensure that the data record does not contain unusually extreme events that would have extraordinary effect on RUSLE2's computations. Extreme events in the observed temperature data do not seem be as severe as in the precipitation record.

The best source of temperature values for use in RUSLE2 is from the USDA-NRCS. Their data have been produced with the PRISM program that takes into account how elevation and other variables affect temperature. Like precipitation, the USDA-NRCS PRISM temperature values are available on a 4 km grid across the US.

3.2.4. 10 year-24 hour precipitation

RUSLE2 uses the precipitation amount for a 24-hour event that has a 10-year return period as a representative storm to compute the effect of ponding on rainfall erosivity, runoff's sediment transport capacity, and the location along an overland flow path length that contouring fails (e.g., see **Section 3.4.3**). The fundamental structure of RUSLE2 computes daily erosion for unit plot conditions (see **Section 2.1**), which in turn is multiplied by non-dimensional ratios to account for effects of topography, cover-management, and support practices. A single storm is used to compute values for these non-dimensional ratios that involve ponding and runoff. The RUSLE2 intent is to capture main effects related to runoff as they vary with location, soil, and cover-management. RUSLE2 starts with accepted USLE values and uses runoff computations to adjust the ratio values up or down as runoff departs from a base condition. An advantage of this approach is ratio values vary less temporally than erosivity, which allows a single precipitation event to be used to compute runoff. Most of the temporal variation is captured by the temporal varying erosivity. Other temporal differences are captured by computing daily runoff for the representative storm as cover-management variables change temporally. The 10 year-24 hour precipitation was chosen to make the runoff computations because most of the rill-interrill erosion at a site is caused by moderate to large rainfall events (Wischmeier and Smith, 1958, 1978).

The 10-year EI storm was used for the same purpose in RUSLE1 [Foster et al., 1997; AH703 (Renard et al., 1997)]. The procedure in RUSLE1 computed a precipitation amount for the 10 year-EI storm using an empirical equation. This equations was derived by fitting storm erosivity values as a function of storm precipitation amount (Richardson et al., 1983). The RUSLE1 procedure worked satisfactory for the eastern US but not for the Western US, especially in the Northwest Wheat and Range Region (NWRR) that includes the eastern portions of Washington and Oregon and northern portion of Idaho. Winter precipitation causes most of the erosion in the NWRR. This precipitation occurs at a very low intensity, which has low unit energy whereas most of the erosion in the Eastern US is caused by summer precipitation at high unit energy. Directly using the 10 year-24 hour precipitation values more accurately computes runoff for RUSLE2 purposes than computing runoff from a precipitation value computed from an erosivity-precipitation equation empirically derived from eastern US data as was done in RUSLE1.

An erosivity value is needed for the 10 year-24 hour precipitation amount. This erosivity value should reflect the 10 year-24 hour precipitation amount and unit energy at the location. The equation used in RUSLE2 to compute the erosivity for the 10 year-24 hour precipitation amount is:

$$EI_{10y24h} = 2\alpha_m P_{10y24h} \qquad [3.24]$$

where: EI_{10y24h} = the storm erosivity associated with the 10 year-24 hour precipitation amount, α_m = the maximum monthly erosivity density at the location, and P_{10y24h} = the 10 year-24 hour precipitation amount. The 2 coefficient in equation 3.24 was obtained by calibrating equation 3.24 to observed values for the 10-year EI from modern precipitation data in the Eastern US (Hollinger et al., 2002).

Equation 3.24 is consistent with the procedure used to compute monthly erosivity using monthly precipitation amount and monthly erosivity density (see **Section 3.2.1.4.1**). The implicit assumption is that the 10 year-24 hour precipitation event occurs in the month having the maximum erosivity density. A procedure that uses the erosivity density from the month with the maximum precipitation was evaluated. That procedure gave inconsistent results because of spatial variability in the month with the maximum precipitation. The month having the maximum precipitation varies greatly within a relatively small region, which in turn results in relatively large variations in the monthly erosivity density values used in equation 3.24.

The main role of using the 10 year-24 hour precipitation event in RUSLE2 and the 10 year EI in RUSLE1 was to compute the variation in the effectiveness of support practices, especially contouring and strip cropping, across the US. The 10-year EI map published in AH703 (Renard et al., 1997) shows numerous narrow ridges and valleys for the 10-year EI contours. Those narrow ridges and valleys were judged to represent unexplained variability in the measured data used to compute 10-year EI values rather than trends in precipitation important in support practice effectiveness. The smooth trends in the widely accepted maps of the 10 year-24 hour precipitation for the Eastern

US were judged to much more accurately represent precipitation trends important in support practice effectiveness.

3.2.5. Req

In the Northwest Wheat and Range Region (NWRR), erosion per unit erosivity is much greater during the winter months than during the summer months and much greater than for the Eastern US. A unique set of conditions in the NWRR related to highly saturated thawing soil produces a highly erodible soil condition (McCool et al. 1995). The approach used in RUSLE2 computes erosion using standard soil erodibility values (see **Section 4.1**) and adjusted erosivity, i.e., Req for the effective (equivalent) average annual erosivity. Also, a special monthly erosivity distribution is used to distribute the annual Req erosivity over each month.

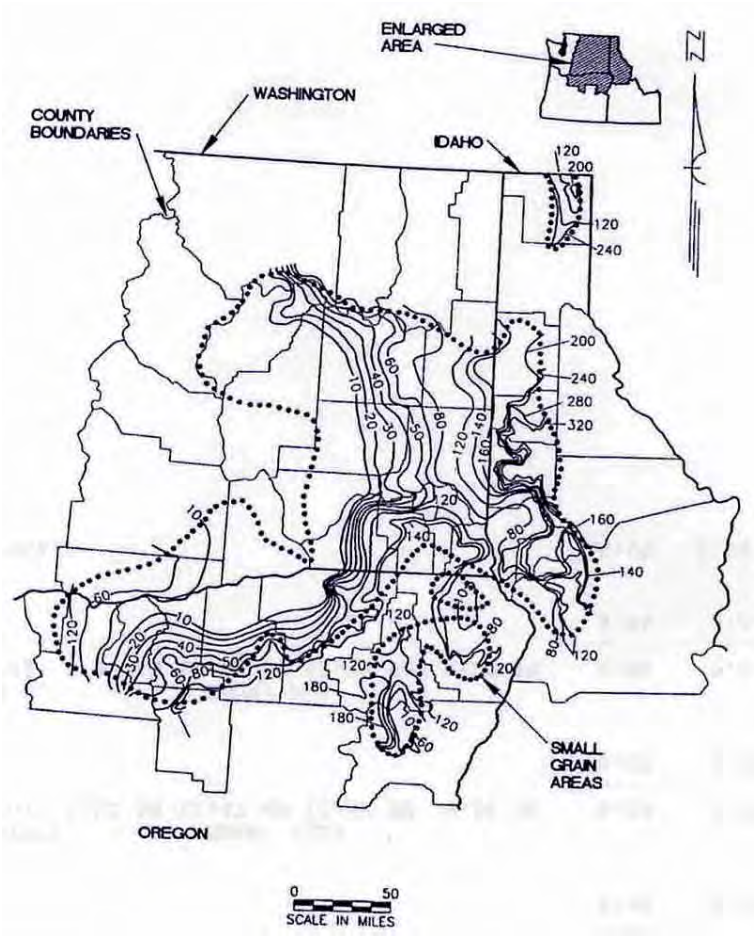

Figure 3.16. Area in Oregon, Washington, and Oregon where RUSLE2 Req procedure works best. Ignore contour lines.

The principal source of data for determining Req has been from research erosion plots operated by the USDA-ARS at Pullman, WA and Pendleton, OR. The procedure is to measure erosion on plots having the unit plot cover-management condition (see **Section 2.1** and **Footnote 3**) and to adjust measured erosion values for the effect of length and steepness to account for differences between the actual plots and unit plots. The adjusted average annual erosion value is divided by the standard soil erodibility value to produce an Req value. The distribution of measured erosion on unit-plot conditions by month is used to obtain an Req erosivity distribution.

The RUSLE2 Req procedure works well for the region shown in Figure 3.16, which is mainly northeastern Oregon, eastern Washington and northern Idaho. The Req effect

occurs in other parts of the Western US, but the Req relationships for these regions have not been well determined. RUSLE2 compute Req as a function of average annual precipitation based on conditions across eastern Washington. Whether that relationship applies in other regions where the precipitation and temperature differs from that in eastern Washington is a concern. Certainly the monthly distribution for Req differs in other regions where the monthly distribution of precipitation differs from that in eastern Washington. The Req distribution for eastern Washington should not be used at other locations without making adjustments for differences in monthly precipitation and temperature distributions.

Another consideration is that winter temperatures are so low at some locations that soil freezing significantly decreases erosion, which is represented by a decreased soil erodibility value during that period. Also, snow covers the soil at high elevations to prevent winter erosion. Another factor is erosion by snowmelt in late winter and early spring, but RUSLE2 is not designed to estimate erosion by snowmelt. Erosion research at Morris, Minnesota showed that only about seven percent of the erosion occurred by snowmelt (Knisel, 1980). Thawing and recently thawed soil can be highly erodible in late winter and early spring in all locations, including the eastern US. Even though soil erodibility can be greatly increased for a short time, less than three weeks, not much erosion occur if little erosivity occurs during this period, which is the case in Minnesota. A similar effect occurs in the Mid-South region. This effect is partially captured in the temporal soil erodibility equation for the mid-south US and similar regions (see **Section 4.5**).

The Req effect is described in detail in the **RUSLE2 User's Reference Guide**. Additional information can be obtained by contacting D.K. McCool, USDA-ARS, Pullman, WA, and by reviewing his scientific publications.

3.3. Runoff

RUSLE2 uses the 10 year-24 hour index (representative) storm to compute runoff depth, which is subsequently used as an index to compute deposition, erosion control effectiveness of support practices, and effect of water depth (ponding) on erosion (see **Sections 2.3.3, 7 and 3.4.5**). This procedure captures runoff's main effects but not every detail. For example, RUSLE2 uses this approach to estimate how contouring effectiveness differs between the Northern and Southern US.

Both runoff amount and rate are important for computing erosion. RUSLE2's equations for runoff hydraulics (see **Section 3.4**) are based on runoff rate. RUSLE2 computes a daily sediment load to erosivity ratio, which RUSLE2 multiplies by daily erosivity to estimate daily erosion, deposition, and sediment load (see **Section 2.3.9**). The RUSLE2 assumption is that excess rainfall rate (depth/time) equals runoff depth divided by one hour. Rainfall depth is the major determinant of excess rainfall rate. The 10 year-24 hour precipitation amount is used each day to compute daily runoff depth as cover-management conditions temporally vary. The resulting runoff values are indices of how runoff varies by location as a function of soil and cover-management.

3.3.1. Computation of runoff

RUSLE2 uses the NRCS curve number method to compute runoff depth as a function of precipitation amount and curve number (Haan et al., 1994). Curve number values vary with cover-management, hydrologic soil group, and antecedent soil moisture. A moderate antecedent soil moisture condition is used in RUSLE2.

3.3.1.1. NRCS curve number method

The NRCS curve number equation computes runoff depth as:

$$Q = \frac{(P - 0.2S)^2}{P + 0.8S} \qquad [3.25]$$

where: Q = runoff depth, P = precipitation depth, and S = a variable computed with:

$$S = 1000 / N - 10 \qquad [3.26]$$

where: N = curve number and inches are the units for P, Q, and S.

A requirement for equation 3.25 is that precipitation depth P is greater than 0.2S. Equation 3.25 was modified so that RUSLE2 computes decreasing runoff rate with distance along the overland flow path where a segment has a much higher infiltration rate than do upslope segments. The modified equation computes the additional precipitation amount that would be needed to just produce runoff for the precipitation depth P as:

$$P_a = P - 0.2\left[\left(\frac{1000}{N}\right) - 10\right] \qquad [3.27]$$

where: P_a = the additional precipitation (inches) needed to produce runoff.

Excess rainfall rate σ (inches/hour) in equation 2.18 is set equal to Q (inches) in equation 3.25 or to P_a (inches) in equation 3.27 if P < 0.2S (see **Section 2.3.5**). The negative excess rainfall rate causes RUSLE2 to compute a decreasing discharge rate along the overland flow path.

3.3.1.2. Curve number as function of cover-management variables

RUSLE2 uses equations that are functions of cover-management variables to compute curve number N values. Curve number values vary daily as cover-management variables including ground cover, soil surface roughness, soil biomass, and soil consolidation, change daily (see **Section 6**).

Equations were derived for RUSLE2 that compute curve number values as a function of cover-management variables and hydrologic soil group. First, curve number values was assigned to each hydrologic soil group for a wide range of cover-management conditions based on standard NRCS procedures for non-Req conditions and measured runoff from USDA-ARS research plots at Pullman, Washington for Req conditions. These curve

number values are comparable to those used in RUSLE1. The equations used to compute RUSLE2 curve numbers were empirically derived using equation forms chosen to represent the trend of curve number values as a function of key cover-management variables. Coefficient values for these equations were obtained by fitting the equations to the assigned curve number values.

3.3.1.2.1. Standard conditions – no Req, no non-erodibile cover, no irrigation, no adjustment made for subsurface drainage

Curve number N represents the effect of cover-management on runoff and the inherent potential of the soil for producing runoff. Hydrologic soil group is the variable used in RUSLE2 to represent the inherent runoff potential of the soil. Cover-management affects runoff in several ways. For example, improved soil management, which is represented in RUSLE2 by increased soil biomass, decreases runoff. Mechanical soil disturbance like tillage reduces runoff on soils having no biomass in comparison to the soils not disturbed for several years. Soil biomass and soil consolidation interact to affect runoff. Soil consolidation increases runoff when soil biomass is very low, typical of construction sites not recently mechanically disturbed. Conversely, soil consolidation decreases runoff when soil biomass is very high, typical of undisturbed, high production pasture. Increased soil surface roughness and ground cover decrease runoff depending on soil biomass levels. Curve numbers and how they are affected by cover-management are also a function of soil properties as represented by hydrologic soil group. For example, cover-management decreases runoff more on soils having a high infiltration potential, hydrologic soil group A, than on soils having a low infiltration potential, hydrologic soil group D.

RUSLE2 curve number equations were calibrated to curve number values commonly used by NRCS (Haan et al., 1994). Indices in these empirical equations reflect how cover-management is known to affect infiltration and runoff.

The main RUSLE2 equation used to compute curve number values is:

$$N = [N_{u100} - s_u(1 - s_c)]\, f_B \exp(b_D B_s) \qquad [3.28]$$

where: N = curve number used in equations 3.25, 3.26, and 3.27 to compute runoff, N_{u100} = a curve number value that represents the effect of ground cover and soil roughness on curve number on a soil recently mechanically disturbed (i.e., $s_c = 1$), s_u = the change in curve number per unit change in the soil consolidation subfactor (see **Section 6.6**), f_B = a fraction, which along with the term $\exp(b_D B_s)$, describes the main effect of soil biomass and its interaction with soil consolidation on curve number, b_D = a coefficient that is a function of the soil consolidation subfactor s_c, and B_s = soil biomass. Soil biomass B_s is the sum of buried residue averaged over the residue accounting depth (see **Section 6.2**) and the live and dead root biomass averaged over the upper 10 inch soil depth (see **Section 6.2.1**). Units for B_s are biomass on a dry basis/(land area·unit soil depth). The accounting depth for buried residue decreases from 3 inches to 1 inch as the soil consolidation subfactor s_c decreases from 1 to 0.45 (see Section **6.6**).

The curve number N_{u100} is determined by starting with a base curve number for a recently mechanically tilled soil. This curve number is decreased for increases in both ground cover and adjusted soil surface roughness r_a greater than 0.24 inch, which is the base roughness value assumed for unit plot conditions (see **Section 2.1** and **Footnote 3**). Curve number values increase when adjusted roughness is less than 0.24 inch, which represents a condition where runoff is greater than from the unit plot condition. The adjusted soil surface roughness is used in equation 6.26 to compute a soil surface roughness subfactor value (see **Section 6.3**).

The equations used to compute N_{u100}, which do not consider any effect of soil biomass or soil consolidation on curve number, are given by:

Table 3.3. Curve number and coefficient values used in standard RUSLE2 curve number equations (not Req)

Hydrologic soil group	N_{s100}	N_{uB}	N_{lB}	N_{u45}	N_{lb45}	b_B (in ac/lbs$_m$)	a_{cu}	a_{cl}	a_{ru}	a_{rl}	a_{45}
A	87.0	87.0	53.0	94.0	70.0	0.00219	-12.0	-6.5	-12.0	6.5	-0.12
B	92.0	92.0	68.0	98.0	82.0	0.00174	-12.0	-6.5	-12.0	6.5	-0.12
C	93.0	93.0	75.0	98.6	84.6	0.00200	-7.0	-5.0	-7.0	5.0	-0.07
D	94.0	94.0	79.0	98.7	88.4	0.00153	-5.0	-3.0	-5.0	4.0	-0.05

$$N_{u100} = N_{s100} + a_{cu}(f_g/100) + a_{ru}\{1-\exp[-1.7(r_a-0.24)]\} \quad [3.29]$$

$$N_{u100} = N_{s100} + a_{cl}(f_g/100) + a_{rl}[(0.24-r_a)/0.24] \ \ r_a \le 0.24 \text{ in} \quad [3.30]$$

where: N_{u100} = a curve number for a recently mechanically disturbed soil (i.e., s_c = 1) with no soil biomass, N_{s100} = a starting curve number value for unit plot conditions that are recently mechanically disturbed, adjusted soil surface roughness r_a = 0.24 in, and no soil biomass, a_{cu} = a coefficient for the effect of ground cover when surface roughness is greater than 0.24 inches, a_{cl} = a coefficient for the effect of ground cover when surface roughness is less than 0.24 inches, f_g = ground cover (percent), a_{ru} = a coefficient for the effect of soil surface roughness when roughness is greater than 0.24 inches, a_{rl} = a coefficient for the effect of adjusted soil surface roughness when the adjusted soil surface roughness is less than 0.24 inches, and r_a = adjusted soil surface roughness index (inches) (see **Section 6.3**). Values for starting curve number N_{s100} and the coefficients a_{cl}, a_{clu}, a_{rl}, and a_{ru}, which vary with hydrologic soil group, are given in Table 3.3.

The main effect of soil consolidation is represented in the terms involving s_u, which is the rate of change in the curve number per unit change in the soil consolidation subfactor s_c. The equation for s_u is given by:

$$s_u = (N_{u100} - N_{u45})/0.55 \quad [3.31]$$

where: N_{u45} = the curve number for a fully consolidated soil with no ground (surface) cover or soil biomass and soil surface roughness = 0.24 inches, 0.55 = the range in the

soil consolidation subfactor s_c from 1 for a recently mechanically disturbed soil to 0.45 for a fully consolidated soil. Values for the curve number N_{u45}, given in Table 3.3, are for a fully consolidated soil with no ground cover and soil biomass.

The fraction f_B represents the main effect of soil biomass on curve number. A value for f_B is computed with:

$$f_B = [(N_{uB} - N_{lB})\exp(-b_B B_s) + N_{lB}] / N_{uB} \quad [3.32]$$

where: N_{uB} = the curve number value when no biomass is present in the soil and the soil has been recently mechanically disturbed, N_{lB} = the curve number for a very high soil biomass (i.e., when $\exp(-b_B B_s)$ is near zero) and the soil has been recently mechanically disturbed, and b_B = a decay coefficient that represents how the curve number decreases exponentially as a function of soil biomass. Curve number values for N_{uB} and N_{lB} are given in Table 3.3. The effect of soil biomass on curve number is assumed to be greater in soils having a low runoff potential, i.e., hydrologic soil group A, than soils having high runoff potential, i.e., hydrologic soil group D. Values for the decay coefficient b_B, are also given in Table 3.3.

The term $\exp(b_D B_s)$ in equation 3.28 represents how the interaction between soil biomass and soil consolidation affect curve number values. A value for the coefficient b_D is computed from:

$$b_D = \ln(N_l / N_u) / 1750 \quad [3.33]$$

where: N_l and N_u = lower and upper curve numbers, respectively, that represent the difference in curve numbers for a soil with no soil biomass and one with a high soil biomass of 1750 lbs_m/(acre·in) value. The value for N_u is computed from:

$$N_u = N_{u100} - s_u(1 - s_c) \quad [3.34]$$

A value for the lower curve number that is comparable to the upper curve number N_u is computed as:

$$N_l = N_{u100} - s_l(1 - s_c) \quad [3.35]$$

where: s_l is computed from:

$$s_l = (N_{l100} - N_{l45}) / 0.55 \quad [3.36]$$

The curve number N_{l45} is adjusted for ground cover is computed as:

$$N_{l45} = N_{lb45}(1 + a_{45} f_g / 100) \quad [3.37]$$

where: a_{45} = a coefficient having values given in Table 3.3. Soil surface roughness is assumed not to affect curve number for a fully consolidated soil with high soil biomass.

Values for the index curve number N_{lb45} used to calculate curve numbers for fully consolidated soil at high soil biomass with no ground cover are also given in Table 3.3.

Table 3.4. RUSLE2 (R2) curve numbers computed for Columbia, Missouri compared with curve numbers used in RUSLE1 (R1) for A, B, C, and D hydrologic soil groups

Cover-management condition		A		B		C		D	
R1 class	Description	R1	R2	R1	R2	R1	R2	R1	R2
C1	Established meadow, very dense cover with high soil biomass	30	45	58	64	71	71	78	78
C2	Mixed grass-legume hay, moderate cover, and moderate to high soil biomass	46	61	66	75	78	80	83	85
C3	Heavy cover (75-95%) or very rough with moderate biomass	54	46	69	62	79	70	84	77
C4	Moderate cover (40-65%) or rough with moderate soil biomass	55	54	72	66	81	75	85	81
C5	Light cover (10-30%), moderate roughness, and low to moderate soil biomass	56	61	75	70	83	76	87	82
C6	Essentilly no cover (5%), minimal roughness and low to moderate soil biomass	64	67	78	78	85	82	89	84
C7	Very little soil biomass and smooth	77	84	86	90	91	91	94	93
	Cut soil, no soil biomass without mulch		94		98		99		99
	Cut soil, no soil biomass with 4000 lbs/ac straw mulch		94 - 63		98 - 77		98 - 82		99 - 87
	Fill soil, graded smooth with no mulch		87 - 88		92 - 93		93 - 94		94 - 95
	Fill soil, graded smooth with 4000 lbs/ac straw mulch		81 - 85		86 - 90		89 - 92		91 - 94

Notes:
The curve numbers from RUSLE2 were taken at planting time because theRUSLE1 curve numbers are most applicable for that period.
The range in RUSLE2 curve numbers for the construction site conditions are for the 12 month period

A-hydrologic soil group (lowest runott potential) to D-hydrologic soil group (highest runoff potential)

RUSLE2 computed curve number values as shown in Table 3.4 along with the curve number values used in RUSLE1. RUSLE2 adequately captures the trends in curve numbers for land use that varies from construction sites to dense grass. RUSLE2

computes higher curve number values for the A-hydrologic soil group soils (low runoff potential) than those used in RUSLE1. However, the higher curve numbers are considered more appropriate for RUSLE2 applications. RUSLE2 also computes curve number values that are consistent with those reported for a wide range of land uses (Haan et al. 1994).

3.3.1.2.2. Req conditions, no irrigation, no adjustment made for subsurface drainage

The procedure described in Section 3.3.1.2.1 is also used to compute runoff for Req conditions, but different runoff curve number and coefficient values are used. A major effect in the Req zone is that infiltration is very low during the winter unless residue cover, soil biomass, and soil surface roughness is very high. The soil becomes highly saturated resulting in a very high portion of the precipitation becoming runoff during the winter period. High residue cover, soil biomass, and surface roughness seem to keep open macro-pores for significantly increased infiltration. The values given in Table 3.5 are used during by RUSLE2 for the winter Req period to compute runoff while the values given in Table 3.3 can be used for the summer months.

Table 3.5. Curve number and coefficient values used in RUSLE2 curve number equations for Req conditions

Hydrologic soil group	N_{s100}	N_{uB}	N_{lB}	N_{u45}	N_{lb45}	b_B (in ac/lbs$_m$)	a_{cu}	a_{cl}	a_{ru}	a_{rl}	a_{45}
A	92.0	92.0	22.0	94.0	70.0	0.00024	-12.0	-6.5	-25	2.0	-0.12
B	97.0	97.0	58.0	98.0	82.0	0.00020	-12.0	-6.5	-25	2.0	-0.12
C	98.0	98.0	73.0	98.6	84.6	0.00025	-7.0	-5.0	-15	2.0	-0.07
D	98.0	98.0	78.0	98.7	88.4	0.00020	-5.0	-3.0	-10	2.0	-0.05

3.3.1.2.3. Effect of non-erodible cover on runoff

RUSLE2 assumes no detachment for the portion of the soil surface covered by non-erodible cover. However, RUSLE2 assumes that non-erodible cover can be permeable. A RUSLE2 input value used to describe non-erodible cover is the fraction of the non-erodible cover that is fully permeable so that infiltration is controlled by the underlying soil. All of the precipitation is assumed to become runoff for the remaining portion of the non-erodible cover. The overall effective curve number for this condition is computed by RUSLE2 as:

$$N = N_b(1 - f_\mu) + f_\mu[N_b f_\rho + 100(1 - f_\rho)] \quad [3.38]$$

where: N = overall, effective curve number used in equation 3.25 or 3.27 to compute runoff, f_μ = fraction of the soil surface covered by non-erodible cover, f_ρ = fraction of the non-erodible cover that is permeable, N_b = the curve number for the portion of the soil not covered by the non-erodible cover, and 100 = the curve number for the non-permeable portion of the non-erodible cover. A 100 curve number means that all of the precipitation becomes runoff.

3.3.1.2.4. Effect of subsurface drainage on runoff

The RUSLE2 procedure for adjusting for subsurface drainage is to select a hydrologic soil group that describes runoff potential for the undrained condition and one that describes runoff potential for the drained condition (see **Sections 7.4** and the RUSLE2 User's Reference Guide). RUSLE2 uses the hydrologic soil group assigned to the drained and undrained soil conditions to compute runoff using the values in either Table 3.3 or 3.4.

A RUSLE2 input for subsurface drainage is the portion of the area represented by the overland flow path that is subsurface drained. RUSLE2 uses this input to compute an effective curve number value for the entire overland flow path. The effective curve number is computed with:

$$N = N_d f_d + N_{ud}(1 - f_d) \quad [3.39]$$

where: N = effective curve number used in equation 3.25 or 3.27 to compute runoff, N_d = curve number for the drained condition, N_{ud} = the curve number for the undrained condition, and f_d = the fraction of the area represented by an overland flow path that is drained.

3.3.1.2.5. Effect of irrigation on runoff

RUSLE2 computes the effect of irrigation on erosion when rainfall occurs. RUSLE2 does not compute erosion caused by the applied water. RUSLE2 computes increased erosion on irrigated areas because increased soil moisture increases soil erodibility and residue decomposition and decreases soil surface roughness. However, RUSLE2 does not compute increased runoff caused by irrigation.

3.4. Hydraulics

RUSLE2 uses shear stress as the hydraulic variable to compute sediment transport capacity and locations where contouring fails. Runoff's total shear stress is applied to surface soil particles, ground cover, soil surface roughness elements, and stems of live and standing dead vegetation. Total shear stress is computed with (Chow, 1959):

$$\tau_t = \gamma y s \quad [3.40]$$

where: τ_t = total shear stress (force/unit area), γ = weight density of water (force/volume), y = flow depth (length), and s = overland flow path steepness (sine of slope angle). Flow depth is computed with the Manning equation as (Chow, 1959):

$$y = \left(\frac{q n_t}{1.49 s^{1/2}} \right)^{3/5} \quad [3.41]$$

where: q = discharge rate, n_t = total Manning's n (index for hydraulic roughness-resistance), and the 1.49 is used when US customary units [q - ft3/(sec·ft width), y – ft] are used.

3.4.1. Concept of grain and form roughness

The total shear stress can be divided into two parts (Graf, 1971), the part referred to as grain roughness shear stress that acts on surface soil particles and the part referred to as form roughness shear stress that acts on ground cover, stems of live and dead standing vegetation, and soil surface roughness elements. Grain roughness shear stress is assumed to be responsible for sediment transport while form roughness shear stress is assumed to be responsible for contouring failure (Foster, 1982; Foster et al., 1982b).

3.4.2. Grain roughness shear stress for computing sediment transport capacity

RUSLE2 uses Equation 2.17 to compute sediment transport capacity. That equation is based on the assumption that sediment transport capacity can be computed as:

$$T_c = K_T \tau_g^{3/2} \qquad [3.42]$$

where: T_c = sediment transport capacity (mass/width·time), and τ_g = grain roughness shear stress(force/aea). By using the concept that flow depth can be divided into parts associated with grain and form roughness, equations 3.41 and 3.42 can be combined with a Manning's n for grain roughness to give equation 2.17 where the coefficient ζ is given by (Foster et al., 1982b):

$$\zeta = 0.0008 n_t^{-1.5} \qquad [3.43]$$

where: the coefficient ζ has absorbed γ and the Manning's n_g value for grain roughness, which is assumed to be 0.01.[32] Total Manning's n_t is computed by RUSLE2 as a function of soil surface roughness, ground cover, live vegetation biomass, and standing residue biomass (see **Section 3.4.6**).

3.4.3. Form roughness shear stress for computing contouring failure

3.4.3.1. Main equations

RUSLE2 computes form roughness shear stress as a function of discharge rate as:

$$\tau_f = a_f q^{0.85714} s / n_t^{1.2857} \qquad [3.44]$$

---

[32] This equation is based on US customary units of ft^3/sec per ft width for discharge rate (q), ft for flow depth (y), and lbs_f/ft^2 for shear stress (τ).

where: τ_f = grain roughness shear stress and a_f =a coefficient that includes γ in equation 3.40, 1.49 in equation 3.41, and other empirical coefficients. RUSLE2 assumes contouring failure where form roughness shear stress computed with equation 3.44 exceeds a critical shear stress. A value for critical shear stress for contouring failure was determined by calibrating equation 3.44 to critical slope length values given in AH537 (Wischmeier and Smith, 1978). The resulting critical shear stress for contour failure is 3619 value when US customary units are used in the equations. The value for a_f in equation 3.44 is absorbed in the critical shear stress value along with conversion factors that would be used to convert excess rainfall rate to ft/sec rather than using inches/hour. Form roughness shear stress for contouring failure is computed with:

$$\tau_f = q_i^{0.85714} s / n_t^{1.2857} \qquad [3.45]$$

where: the discharge rate q_i is computed using excess rainfall rate (σ_i) in inches/hour rather than ft/sec as $q_i = x\sigma_i$ and x = distance (feet) along overland flow path.[33]

The critical slope length values beyond which contouring failure is assumed were based on judgment of soil conservation technical specialists and were not determined by research. These values were developed at a 1956 workshop (Wischmeier and Smith, 1978) and therefore represented observations from research studies and field observations from the early 1930's to the mid 1950's The base condition used in calibrating the critical shear stress for contouring failure represents those conditions rather than modern conditions. The assumed base condition is conventionally tilled, low yield (50 bu/ac), continuous corn at Columbia, Missouri. The operations assumed for this cropping system include a moldboard plow in the spring for primary tillage, two secondary tillage operations to prepare the seedbed, row planter to seed the crop, row cultivator to control weeds, and harvest. Table 3.6 shows a comparison between the values computed with RUSLE2 and those given in AH537 (Wischmeier and Smith, 1978). The values compare well except at very flat steepness where RUSLE2 computed values are much longer than those given in AH537. The values computed by RUSLE2 are considered acceptable.

Table 3.6. Critical slope lengths

	Critical slope length (ft)	
Slope steepness (%)	AH537	RUSLE2
1.5	400	>1000
4.0	300	384
7.0	200	200
10.5	120	125
14.5	80	86
18.5	60	66
23.0	50	51

RUSLE2 sets the contouring subfactor value to 1 for those portions of the overland flow path where form roughness shear stress exceeds the critical shear stress for contouring failure (see **Section 7.1**). No adjustments are made in the cover-management subfactors used to compute detachment in equation 2.10. RUSLE2 also computes the location

[33] Mixed units are given in these equations for consistency with the equations used in the RUSLE2 computer program to facilitate a comparison of computer code with this documentation.

where runoff shear stress acting on form roughness equals the critical shear stress for contour failure. That equation is:

$$q_c = 13900 n_t^{1.5} / s^{1.1667} \quad [3.46]$$

where: q_c = the discharge rate (where excess rainfall rate in equation 2.18 is in units of in/hr) at which contouring fails. The location of this discharge rate can be determined from equation 2.18.

RUSLE2 computes where contouring fails along overland flow paths as a function of location (i.e., as reflected by the $P_{10y\text{-}24h}$ precipitation amount), runoff, soil infiltration potential, overland flow path steepness, and cover-management conditions. For example, RUSLE2 computed critical slope length values are a function of crop yield. Increased crop yield increases critical slope length. The increased biomass improves soil properties that increase infiltration and reduce runoff, increases soil surface roughness, and increases ground cover provided by crop residue. The critical slope length increases from 103 to 151 ft for an increase in corn yield from 50 to 115 bu/ac in a grain corn-silage corn-alfalfa hay-alfalfa hay-alfalfa hay crop rotation for an overland flow path on a silt loam soil at 20 percent steepness at LaCrosse, Wisconsin. Tillage systems that leave increased surface soil roughness and surface crop residue cover also increase RUSLE2 computed critical slope length as illustrated in Table 3.7.

Table 3.7. RUSLE2 computed critical slope lengths for three tillage systems for continuous 50 bu/ac corn.

	RUSLE2 computed critical slope length (ft)		
Slope steepness (%)	Conv till	Mulch till	No-till
1.5	>1000	>1000	>1000
4.0	384	594	837
7.0	200	310	436
10.5	125	194	273
14.5	86	134	188
18.5	66	101	143
23.0	51	79	112

RUSLE2 does not compute contouring failure as a function of how soil properties affect the soil's critical shear stress for contouring failure. This capability is desirable, but sufficient empirical data are not available to develop the required critical shear stress values as a function of soil properties. Contouring failure in RUSLE2 is assumed not to be a function of ridge height or grade along the ridges-furrows. Clearly contouring failure is a function of ridge height because ridge height affects storage of runoff water and the likelihood of ridge breakover especially in low areas. However, accurately describing flow hydraulics and water storage on a specific field site is very difficult because of imperceptible variations of row grade and ridge heights along the ridges-furrows. Although RUSLE2 has these shortcomings, it was developed to guide conservation planning, and in that context, RUSLE2 is a major improvement over the USLE and RUSLE1.

3.4.3.2. Form roughness shear stress below segment having a high hydraulic roughness

RUSLE2 assumes a gradual rather than a step decrease in total hydraulic roughness where total hydraulic roughness decreases from one overland flow path segment to the

next segment. Consequently, the form roughness shear stress increases gradually rather than abruptly between segments. An example is runoff exiting from dense vegetation onto a relatively smooth, bare soil surface. The dense vegetation spreads the runoff so that the flow has a laterally uniform depth as it exits the vegetation. Form roughness shear stress is assumed to be less when flow depth is laterally uniform than when concentrated in rills. A distance is required below the dense vegetation for the runoff to become concentrated in rills with increased form roughness shear stress.

This concept is implemented in RUSLE2 by assuming that the effective total hydraulic roughness decreases exponentially below a segment having a high total hydraulic roughness. The equation for the total Manning's n_t in the transitional region is:

$$n_{et} = n_{tl} + (n_{tu} - n_{tl}) \exp[-0.065(x - x_u)] \qquad [3.47]$$

where: n_{et} = Manning's n_t in the transitional zone, n_{tl} = the total Manning's n_t in the lower segment, Manning's n_{tu} = the Manning n_t in the upper segment, x = distance along the overland flow path (ft), and x_u = the distance to the upper end of the lower segment (ft). Figure 3.17 shows the RUSLE2 computed decrease in Manning's n_t below a hay strip in a typical strip cropping system used in LaCrosse, Wisconsin and evaluated in research studies (Hays and Attoe, 1957; Hays et al., 1949). Also, erosion from other strip cropping systems was also studied at other locations (Borst et al., 1945; Hill et al.,. 1944; Hood and Bartholomew, 1956; Smith et al. 1945). RUSLE2 gives similar results for these systems discussed in AH703 (Renard et al., 1997; Foster et al., 1997).

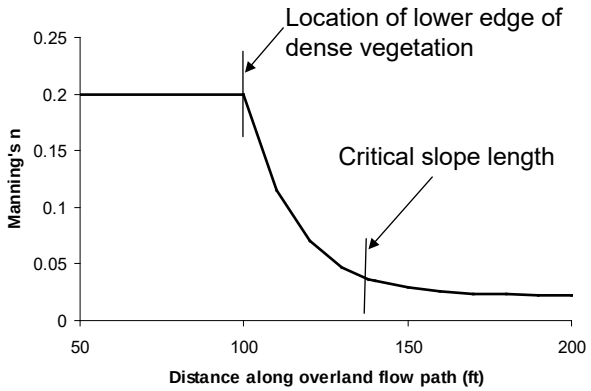

Figure 3.17. Decrease in Manning's n_t along overland flow path below a segment having a high Manning's n_t.

The reduction in form roughness shear stress by runoff spreading reduces the portion of an overland flow path where form roughness shear stress can exceed critical shear stress for contouring failure. The result is that contour strip cropping increases computed critical slope length (i.e., the location where contouring fails). The assumption that contour strip cropping increases critical slope length has long been accepted and used in conservation planning [e.g., see AH282 (Wischmeier and Smith, 1965) and AH537 (Wischmeier and Smith, 1978)]. In AH537, the critical slope length (referred as slope length limits in AH537) is doubled for contour strip cropping without regard to cover-management condition such as type, quality, and density of vegetation on each overland flow path segment. However, the AH537 contouring factor values for contour strip cropping do vary with cover-management condition.

Data from research in Wisconsin (Hays and Attoe,1957; Hays et al., 1949) were the best available in the 1950's to guide development of critical slope length concepts and values by erosion scientist and soil conservation specialists for use in the USLE (AH282, AH537). The RUSLE1 developers judged that critical slope length with strip cropping was 1.5 times the critical slope length without strip cropping [AH703 (Renard et al., 1997)]. A major RUSLE2 improvement is that RUSLE2 computes how location (i.e., $P_{10y\text{-}24h}$ precipitation), runoff, overland flow path steepness, cover-management conditions, number of strips, and relative placement of strips along an overland flow path affect critical slope length. The RUSLE2 procedure is far more comprehensive that previous USLE and RUSLE1 procedures.

The 0.065 ft^{-1} value in equation 3.47 was selected to give critical slope length values considered appropriate for the LaCrosse, Wisconsin experimental contour strip cropping (Hays et al., 1949). For example, RUSLE2 computes a critical slope length of 103 ft on a 20 percent steep overland flow path for the crop rotation used in the contour stripping studies without the crops being arranged in strips. That is, cover-management along the overland flow path is uniform at any particular time although cover-management temporally changes during the crop rotation. The crop rotation is a year of grain corn and a year of silage corn conventionally tilled with a moldboard plow, and three years of alfalfa hay fall seeded immediately after the silage corn is harvested. The assumed corn yield is 50 bu/acre, a typical yield in the 1930's and 1940's. The RUSLE2 computed critical slope length is 191 ft when the crops are arranged in a four strip contour strip cropping system.

The RUSLE2 computed critical slope length is a function of number of strips along the overland flow path. For example, the RUSLE2 computed critical slope length is 153 ft for the LaCrosse, Wisconsin crop rotation placed in two rather than four strips. Strip width is 50 ft for the four-strip system on a 200 ft overland flow path length while it is 100 ft for the two-strip system. As Figure 3.17 shows, about 38 ft is required for total effective hydraulic roughness computed with equation 3.47 to decrease to where form roughness shear stress exceeds the critical shear stress for contouring failure. Strip width should be no wider than 38 ft, according to Figure 3.17 for these conditions, to prevent form roughness shear stress from exceeding the critical shear stress for contour failure. The 100 ft strip width in the two-strip contouring strip cropping system greatly exceeds 38 ft. In contrast, the 50 ft wide strip in the four-strip contour strip cropping system is sufficiently narrow that the form roughness shear stress only exceeds critical shear stress for contouring failure over the last 9 ft of the overland flow path length.

3.4.3.3. Determining location where contouring failure occurs

RUSLE2 uses rules to determine where the form roughness shear stress exceeds critical shear stress for contouring failure within an overland flow path segment.

3.4.3.3.1. Discharge rate increases within segment

If discharge rate increases within a segment and form roughness shear stress at both the upper and lower ends of the segment is less than the critical shear stress for contouring failure, contouring failure does not occur within the segment. If form roughness shear

stress exceeds the critical shear stress for contouring failure at both the upper and lower ends of the segment, contouring failure occurs over the entire segment. However, if form roughness shear stress at the upper end of the segment is less than the critical shear stress for contouring failure, and form roughness shear stress at the lower end of the segment exceeds critical shear stress for contouring failure, contouring failure occurs over the lower portion of the segment beginning at the location where form roughness shear stress equals the critical shear stress for contouring failure. This location is computed with equations 2.18 and 3.46.

3.4.3.3.2. Discharge rate decreases within segment

If discharge rate decreases within a segment and form roughness shear stress at both the upper and lower ends of the segment is less than the critical shear stress for contouring failure, contouring failure does not occur within the segment.

If form roughness shear stress at the upper end of the segment is less than the critical shear stress for contouring failure but exceeds critical shear stress for contouring failure at the lower end of the segment, contouring failure occurs over the lower portion of the segment beginning at the location where form roughness shear stress equals the critical shear stress for contouring failure. This location is computed with equations 2.18 and 3.46.

If form roughness shear exceeds the critical shear stress for contouring failure at both the upper and lower ends of the segment, the possibility exists for contouring failure on upper and lower portions of the segment without contouring failure in the middle portion of the segment. RUSLE2 determines where the form roughness shear stress is a maximum within the segment and if that shear stress is greater than the critical shear stress for contouring failure, then contouring failure occurs over the entire segment. If the minimum form roughness shear stress within the segment is less than the critical shear stress for contouring failure, then form roughness shear stress equals the critical shear stress at two locations within the segment. These locations are determined with equations 2.18 and 3.46.

If form roughness shear stress is less than the critical shear stress for contouring failure at both the upper and lower ends of the segment, the possibility exists that form roughness shear stress increases to a value greater than the critical shear stress for contouring failure within the segment and then decreases to below this critical shear stress above the lower end of the segment. Contouring failure occurs on a middle portion within the segment. This check can be made by computing the maximum form roughness shear stress within the segment, and if it exceeds the critical shear stress for contouring failure, this condition exists. The portion where contouring fails lies in the middle of the segment between the two locations where form roughness shear stress equals the critical shear stress for contouring failure, which are determined from equations 2.18 and 3.46.

3.4.3.4. Runoff rate used to compute contouring failure

To compute contouring failure, RUSLE2 computes a daily runoff rate that varies with both cover-management and the probability of an intense storm occurring when

contouring is susceptible to failure. The daily precipitation amount used to compute contouring failure is assumed to vary linearly with the temporal daily erosivity distribution (see **Sections 3.1 and 3.2.1**) with the maximum daily precipitation occurring on same day that the maximum daily erosivity occurs. This daily precipitation amount is computed as:

$$P_{cf} = (f_{Rd} / f_{Rmx}) P_{10y24h} \quad [3.48]$$

where: P_{cf} = the daily precipitation amount used to compute contouring failure, f_{Rdj} = the fraction of the annual erosivity that occurs on the *jth* day, and f_{Rmx} = the fraction of the annual erosivity that occurs on the day when maximum daily erosivity occurs.[34] **The time varying precipitation computed with equation 3.48 is only used to compute contouring failure. It is not used anywhere else in RUSLE2.**

3.4.4. Backwater

Backwater occurs at locations on an overland path where total hydraulic roughness makes a step increase, such as at the upper edge of a dense vegetation strip. This backwater is especially important because most of the deposition caused by dense vegetation strips occurs in the backwater (Dabney et al., 1995; Flanagan et al., 1989; Foster et al., 1980a; Hayes et al., 1984; McGregor et al., 1999). Ignoring backwater length would cause RUSLE2 to greatly underestimate deposition when computing deposition caused by narrow, dense vegetation strips.

The Manning equation is used in RUSLE2 to compute flow depth at the upper edge of segments where Manning's n_t makes a step increases. An effective backwater length is computed from this flow depth assuming that the backwater is level. The combined equation for computing backwater length is:

$$\Delta x_b = 3.44[n_t q_u / (1.49 s_{lh}^{0.5})]^{0.6} / s_{uh} \quad [3.49]$$

where: Δx_b = the backwater length (ft), q_u = discharge rate (ft^2/s) at the upper edge of the segment having the high total Manning's n_t, s_{lh} = the steepness of the segment having the high Manning's n (**sine** of the slope angle), and s_{uh} = steepness of the immediately upslope segment (the **tangent** of the slope angle). The 3.44 value in equation 3.49 was determined by calibration. The coefficient was adjusted until RUSLE2 computed the observed sediment yield from plots having a dense 1.5 ft wide dense stiff grass hedge below conventionally tilled cotton on a 5 percent steepness at Holly Springs, Mississippi (McGregor et al., 1999). The RUSLE2 computed backwater length was compared to

---

[34] In an early version of RUSLE2, contouring failure was computed with the single precipitation P10y,24h precipitation amount. Runoff rate varies temporally only as cover-management variables varied temporally. Although RUSLE2 was calibrated to give the correct critical slope length, the timing of contouring failure was out of phase with precipitation during the year. Use of Equation 3.48 gave the correct timing for contouring failure.

measured backwater values and locations of deposited sediment above the stiff grass hedge. Although the upper edge of deposition moves upslope as deposited sediment accumulates (Dabney et al., 1995), this dynamic effect is not considered in RUSLE2. The RUSLE2 computed backwater length is an index that captures the effects of location through the 10 year-24 hour precipitation amount, runoff, hydraulic roughness, and overland flow path steepness. The maximum computed backwater length is limited to 15 ft to prevent RUSLE2 from computing excessively long backwater lengths on relatively flat overland flow paths. Also, RUSLE2 assumes a 3 ft minimum for special cases like fabric filter fence on construction sites (see **Section 7.2**). RUSLE2 adds the computed backwater length to the lower edge of the segment having the high total Manning's n_t and decreases the length of the immediate downslope segment by the same amount except for the segment at the end of the overland-flow path.

3.4.5. Ponding

Water deeper than about 3 mm reduces raindrop impact erosivity (Mutchler, 1970; Mutchler and Murphree, 1985; Mutchler and Young. 1975). The judgment of soil conservation specialists is that water depth reduces erosion on flat overland flow paths in high erosivity locations, such as the lower Mississippi Delta [AH703 (Renard et al., 1997)]. Erosivity (R) values along the Gulf Coast Region were reduced to consider this effect in the USLE (e.g., compare erosivity values between AH282 (Wischmeier and Smith, 1965) and AH537 (Wischmeier and Smith, 1978). RUSLE1 uses a ponding subfactor that reduces effective erosivity based on flow depth if ridges are not present. Water depth (ponding) was assumed to have no effect on erosivity in RUSLE1 when high ridges are present. However, in RUSLE2, the ponding effect is assumed to reduce erosivity regardless of the presence or absence of ridges.

The 10 year-24 hour precipitation amount is used to compute a runoff amount using equation 3.25. A normalized flow depth is computed using the Manning equation as:

$$y_n = (v_r / 3.03)^{0.6} (0.01/s)^{0.3} \qquad [3.50]$$

where: y_n = the normalized flow depth, v_r = the runoff amount (inches), computed with P10y24h precipitation amount, 3.03 = a reference runoff depth (inches) selected to represent runoff and 0.01 = a reference overland flow path steepness to represent slopes typical of cotton production in the Mississippi Delta where the water depth effect is most highly important. This ponding effect has been studied by Mutchler et al. (1982), Mutchler and McGregor (1983), Mutchler and Murphree (1985), and McCool et al. (1987). This normalized flow depth is then used to compute a ponding subfactor value using:

$$p_r = \exp[-0.49(y_n - 1)] \text{ if } p_r < 0.4, p_r = 0.4 \text{ if } p_r > 1, p_r = 1 \qquad [3.51]$$

where: p_r = the ponding subfactor for the effect of water depth on raindrop impact erosivity. The minimum value for the ponding subfactor is 0.4. The 0.49 value in equation 3.51 was chosen by calibration to represent the judgment of erosion scientists and soil conservationists regarding the ponding effect [AH537 (Wischmeier and Smith,

1978), AH703 (Renard et al., 1997)]. Example values for the average annual ponding factor are given in Table 3.8 where daily ponding values have been weighted by the temporal erosivity distribution (see **Sections 3.1** and **3.2.1**).

Table 3.8. Example values for the ponding subfactor

Location, 0.5% steepness	Value	Steepness (%), at Jackson, MS	Value
New Orleans, LA	0.58	0.001	0.45
Baton Rouge, LA	0.63	0.005	0.73
Jackson, MS	0.73	0.01	0.85
Memphis, TN	0.82	0.02	0.96
Columbia, MO	0.86	0.04	1.00

3.4.6. Manning's n_t as a function of cover-management and row grade

RUSLE2 computes total Manning's n_t values as a function of soil surface roughness, ground cover, live vegetation, and standing residue using:

$$n_t = 0.11[1-\exp(-0.6r_n)] + [0.075(f_g/100)/\exp(0.35r_n)] + n_v + n_s \text{ if } n_t < 0.01,\ n_t = 0.01 \quad [3.52]$$

$$r_n = r_a \text{ if } r_n > 5, r_n = 5 \text{ inches} \quad [3.53]$$

where: n_t = total Manning's n_t, $r_n = r_a$ = adjusted roughness index value (inches) used to compute roughness subfactor values (see **Section 6.3**), f_g = net ground (surface) cover (percent) (see **Section 6.2**), n_v = Manning's n contributed by live vegetation (see **Section 9.2.6**), and n_s = the Manning's n contributed by standing residue (see **Section 10.4.3**). Equation 3.52 was derived from multiple data sets where overland flow velocity was measured for a wide variety of conditions. Manning's n values derived from these measurements have been compiled and used in numerous models including CREAMS, RUSLE1, and scientific articles (Foster et al., 1980b; Foster, 1982; Foster et al., 1982a; Foster et al., 1997; Gilley and Finkner, 1991; Gilley and Kottwitz, 1994; Gilley and Kottwitz, 1995).

Equation 3.52 represents form and form roughness combined rather than representing them as two separate terms. The condition on n_t in equation 3.52 is to prevent total Manning's n_t from being less than the grain roughness Manning's n_g of 0.01.

The ground (surface) cover and soil surface roughness combination term in equation 3.52 reduces the effect of ground cover on hydraulic roughness as soil surface roughness increases. Ground cover in depressions is inundated by ponded water and deposited sediment so that ground cover has reduced effect on runoff hydraulics as soil surface roughness increases.

The condition that adjusted roughness not be greater than 5 inches is primarily because no research data were available at high roughness values to derive equation 3.52. Actually the high soil surface roughness condition has little effect on computed Manning's n_t values. For example, the first term in equation 3.52 is 0.105 for $r_a = 5$ inches and 0.11 for $r_a = 10$ or more inches.

Net ground cover is (1 – the fraction of soil surface not covered by ground cover). Net ground cover takes into account surface residue overlapping rock cover and live ground cover overlapping both surface residue and rock cover.

The maximum Manning's n value for vegetation in rows perpendicular to the overland flow path (i.e., on the contour) is computed with:

$$n_{vmxc} = 0.017154 R_v + 3.82 \times 10^{-5} R_v^5 \quad [3.54]$$

where: n_{mvxc} = the Manning's n for live vegetation in rows on the contour at maximum canopy cover and R_v = vegetation retardance at maximum canopy cover for vegetation in rows on the contour, which is a measure of how much vegetation and porous barriers like fabric fences slow runoff. Input retardance values are chosen to represent the combined hydraulic roughness of the vegetation in rows and bare soil between the rows for vegetation at its maximum growth in the RUSLE2 vegetation description.[35] Using these input retardance values listed in Table 3.9, RUSLE2 computes a retardance value based on vegetation production (yield) level (see **Section 9.3.1**). The Manning's n_{mvc} represents the effect of stems and any vegetation component, besides live ground cover, that slows runoff. Live ground cover values in the RUSLE2 vegetation description are used to represent the effect of leaves and similar plants components touching the soil surface and slowing runoff.

Table 3.9. Retardance classes used in RUSLE2

Class	Retardance index
no retardance (wide plant spacing in strip-row)	0
low retardance (corn)	1
moderate low (soybeans, cotton)	2
moderate (dense wheat)	3
moderate high (legume hay before mowing)	4
high (legume-grass hay before mowing)	5
very high (dense sod)	6
extreme (stiff grass hedge, silt fence)	7

Table 3.10. Factor values used to multiply Manning's vegetation n on contour to obtain Manning's n value for orientation parallel to overland flow path

Row width	Factor
Vegetation on ridges	0.063
Wide row	0.125
Moderate row spacing	0.250
Narrow row spacing	0.500
Very narrow row spacing	0.750
No rows (broadcast)	1.000

The hydraulic roughness for vegetation rows oriented parallel to the overland flow path (up and down hill) differs from the hydraulic roughness for the vegetation's rows on the contour. RUSLE2 computes a value for the Manning's n_{mvud} for vegetation in rows parallel to the overland flow path by multiplying the contour vegetation Manning's n_{vmxc}

[35] Assignment of retardance values considers the geometrical arrangement of the vegetation rows. For example, retardance for small grain represents the net retardance for multiple grain rows whereas the retardance for a narrow stiff grass hedge considers only a single row of the vegetation. In the case of the stiff grass hedge, the overland flow path is divided into segments to represent the bare soil separately from the vegetation in a situation where backwater created by the dense vegetation has an important effect on deposition.

by a factor based on the user entered row width. Values for this factor are given in Table 3.10. The **No rows (broadcast)** input means that the vegetation is randomly spaced in both directions so that no row orientation exists. Manning's n is the same in all directions. The **Vegetation on ridges** represents vegetation rows so widely spaced or the vegetation being on ridges so that the vegetation stems have no effect on hydraulic roughness.

Depending on row grade (steepness along the vegetation rows), vegetation Manning's n varies between the Manning's n for vegetation rows on the contour and the Manning's n for the vegetation rows oriented up and down hill. The RUSLE2 equation used to compute vegetation Manning's n for intermediate row orientations is:

$$n_{vrg} = n_{vud} + (n_{vc} - n_{vud})[1 - (s_r / s_{ud})^{1/2}] \quad [3.55]$$

where: n_{vrg} = vegetation Manning's n for the row grade s_r, n_{vc} = vegetation Manning's n for rows on the contour (perpendicular to the overland flow path), n_{vud} = vegetation Manning's n for rows parallel to overland flow path (i.e., up and down slope), s_r = row grade (tangent of slope angle), and s_{ud} = overland flow path steepness (tangent of slope angle).

RUSLE2 assumes that vegetation Manning's n varies temporally as the vegetation's effective fall height varies (see **Section 6.1**). The equation used to compute vegetation Manning's n values through time is:

$$n_v = n_{vmx}(h_f / h_{fmx})^{0.3} \quad [3.56]$$

where: n_{vm} = the vegetation Manning's n at maximum growth in the vegetation description, h_f = the daily effective fall height for a particular vegetation description and h_{fmx} = the maximum daily effective fall height for the vegetation description (see **Section 9**).

When live vegetation is killed in RUSLE2, it becomes standing residue that continues to provide hydraulic roughness. The hydraulic roughness caused by standing residue is assumed to vary through time as:

$$n_s = n_{sk}(B_{td} / B_{tk}) \quad [3.57]$$

where: n_s = Manning's n for standing residue on day d, n_{sk} = Manning's n for the standing residue on the day that the live vegetation is killed, B_{td} = standing residue biomass (dry matter basis) on day d, and B_{tk} = the live vegetation biomass (dry matter basis) on the day that the vegetation is killed (see **Section 9.2.5**).

3.5. List of symbols

a_{cl} = a coefficient used to compute curve number values as a function of ground (surface) cover when surface roughness is less than 0.24 inches

a_{cu} = a coefficient used to compute curve number values as a function of ground (surface) cover when surface roughness is greater than 0.24 inches

a_f = coefficient used to compute form roughness shear stress

a_F = coefficient used to compute average annual erosivity from Fournier index

a_p = coefficient in equation that computes storm or daily erosivity from storm or daily precipitation

a_r = coefficient used to average annual erosivity from RUSLE2 modified Fournier index

a_{rl} = a coefficient used to compute curve number values as a function of soil surface roughness when soil surface roughness is less than 0.24 inches

a_{ru} = a coefficient used to compute curve number values as a function of soil surface roughness when soil surface roughness is greater than 0.24 inches

a_{45} = coefficient used to compute curve number values for fully consolidated soils as a function of ground (surface) cover

b= exponent in equation that computes storm or daily erosivity from storm or daily precipitation

b_B = a decay coefficient used how the curve number values decreases exponentially as a function of soil biomass

b_D = a decay coefficient used to compute how curve number values are affected by the interaction of the soil consolidation factor and soil biomass

B_s = soil biomass per unit depth (dry mass/area·soil depth)

B_{tk} = live above ground biomass on day that vegetation is killed (mass/area)

B_{td} = live above ground biomass on day d (mass/area)

D = number of days in the month

e = unit storm energy (energy content per unit area per unit rainfall depth) [force-distance/(area·length)]

$\hat{e}$ = effective unit storm energy directly (force-length)/(area·length)

E = storm energy (force-distance/area)

EI_{10y24h} = the storm erosivity associated with the 10 year-24 hour precipitation amount (erosivity units)

EI_{30} = storm erosivity (erosivity units)

f_B = a fraction that represents the main effect of soil biomass on curve number values

f_d = fraction of area represented by an overland flow path that is subsurface drained

f_g = net ground (surface) cover (percent)

f_{Rd} = fraction of the annual erosivity that occurs on *jth* day

f_{Rmx} = fraction of the annual erosivity that occurs on day when maximum daily erosivity occurs

f_μ = portion of the soil surface covered by non-erodible cover (fraction)

f_ρ = portion of the non-erodible cover that is permeable (fraction)

F = the modified Fournier index

F_r = the RUSLE2 modified Fournier index

h_f = daily effective fall height for a particular vegetation description (length)

h_{fmx} = maximum daily effective fall height for the vegetation description (length)

i = rainfall intensity for a period during rainstorm (length/time)

I_{30} = maximum 30-minute intensity for a rain strom (length/time)

$\bar{I}_{30}$ = representative maximum 30 minute intensity for rain storms occurring in amonth (length/time)

m = number of periods in a storm used to compute storm energy

M = monthly value of climate variable being disaggregated

n = number of rainstorms in a month

n_{et} = Manning's n_t in the transitional zone below a high hydraulic resistance segment

n_g = grain roughness Manning's n

n_k = Manning's n for standing residue on day that live vegetation is killed

n_s = Manning's n contributed by standing residue

n_{sk} = Manning's n contributed by standing residue on the day that live vegetation is killed

n_t = total Manning's n

n_{tl} = total Manning's n_t in segment downslope of high hydraulic resistance segment

n_{tu} = Manning n_t in upslope high hydraulic resistance segment

n_v = Manning's n contributed by live vegetation

n_{vc} = vegetation Manning's n for rows (strips) on the contour (perpendicular to the overland flow path)

n_{vmx} = vegetation Manning's n at maximum growth in the vegetation description

n_{vmxc} = Manning's n for live vegetation in rows (strips) on the contour at maximum canopy cover

n_{vrg} = vegetation Manning's n for row grade s_r

n_{vud} = vegetation for Manning's n for rows up and down slope (parallel to overland flow path)

N = curve number in NRCS curve number method used to compute runoff

N_b = curve number for the portion of the soil not covered by the non-erodible cover

N_d = curve number for the drained condition

N_l = lower curve numbers that represents difference in curve numbers for a soil with no soil biomass and one with a high soil biomass of 1750 lbs_m/(acre·in) value

N_{lb45} = index curve number for fully consolidated soil at high soil biomass with no ground cover

N_{lB} = the curve number for a very high soil biomass and the soil has been recently mechanically disturbed

N_{l45} = N_{lB} curve number adjusted for ground cover

N_{s100} = a starting curve number value for unit plot conditions

N_u = upper curve numbers that represents difference in curve numbers for a soil with no soil biomass and one with a high soil biomass of 1750 lbs_m/(acre·in) value

N_{uB} = curve number value when no biomass is present in the soil and the soil has been recently mechanically disturbed

N_{ud} = curve number for the undrained condition

N_{u45} = the curve number for a fully consolidated soil with no ground (surface) cover or soil biomass and soil surface roughness = 0.24 inches

N_{u100} = curve number value that represents the effect of ground cover and soil roughness on curve number on a soil recently mechanically disturbed with no soil biomass

p_r = daily ponding subfactor

P = precipitation depth (length)

P_a = additional precipitation required so that zero runoff would be computed when infiltration is greater than precipitation (length)

P_{cf} = daily precipitation amount used to compute contouring failure (length)

P_{md} = average monthly precipitation from daily precipitation gage data (length)

P_m = average monthly precipitation (length)

P_s = storm or daily precipitation amount (length)

P_{10y24h} = the 10 year-24 hour precipitation amount (length)

P_{15} = storm precipitation amount determined from 15-minute precipitation gage data (length)

q = discharge rate (volume/width·time)

q_c = discharge rate (where excess rainfall rate is in units of in/hr) at which contouring fails (volume/width·time)

q_i = discharge rate $q_i = x\sigma_i$ computed using excess rainfall rate in inches/hour rather than ft/sec

q_u = discharge rate at upper edge of segment having high hydraulic resistance (volume/width·time)

Q = runoff depth computed with NRCS curve number method (length)

r_a = adjusted soil surface roughness index (length)

r_n = adjusted soil surface roughness index used to compute Manning n for soil surface roughness (length)

r_s = storm erosivity (erosivity units)

R = average annual erosivity (erosivity units)

R_m = average monthly erosivity (erosivity units)

R_v= vegetation retardance at maximum canopy cover for vegetation in rows (strips) on contour, which is a measure of how much vegetation and porous barriers like fabric fences slow runoff

s = overland flow path steepness (sine of slope angle)

s_c = soil consolidation subfactor

s_l = change in lower curve numbers per unit change in soil consolidation subfactor

s_{lh} = steepness of segment having high hydraulic resistance (**sine** of slope angle)

s_r = row grade (**tangent** of slope anagle)

s_u = change in upper curve number per unit change in the soil consolidation

s_{ud} = steepness of overland flow path (**tangent** of soil angle)

s_{uh} = steepness of segment immediately upslope of high hydraulic resistance segment (**tangent** of slope angle)

S = a variable in NRCS curve number equation used to compute runoff

t_c = time during month that disaggregated value equals monthly value

t_p = time during month of peak or minimum of climate variable being disaggregated

T_c = sediment transport capacity (mass/width·time)

x = distance along overland flow path (length)

x_u = the distance to the upper end of segment immediately downslope of high hydraulic resistance segment (length)

y = flow depth (length)

y_d = daily value of climate variable being disaggregated

v_r = runoff amount used to compute ponding subfactor (length)

y_n = normalized flow depth used to compute ponding subfactor

Y_b = daily value of climate variable being disaggregated at beginning of month

Y_e = daily value at end of month

Y_p = maximum value of climate variable being disaggregated when peak or minimum occurs within month

z = exponent in RUSLE2 modified Fournier index

α = average monthly erosivity density (erosivity units/length)

α_m = maximum monthly erosivity density

Δx_b = backwater length upslope of a segment having a high hydualic resistance (length)

ΔV = rainfall depth during a period in a rainstorm (length)

γ = weight density of water (force/volume)

σ_i = excess rainfall rate in inches/hour (length/time)

τ_f = form roughness shear stress (force/area)

τ_g = grain roughness shear stress (force/area)

τ_t = total shear stress (force/area)

ζ = coefficient that has absorbed γ and the Manning's n_g for grain roughness

Indices

i – storm

j - month

k – period during a rainstorm

4. SOIL

4.1. Erodibility

The major RUSLE2 soil variable is the soil erodibility factor. A value for the soil erodibility factor for soils that have their soil horizons in place and have not been disturbed other than for cultivation can be selected from the USDA-NRCS soil survey database. However, soil erodibility values are not available for all soils, especially highly disturbed soils where the original soil layers have been mixed. RUSLE2 includes two sets of equations referred to as the standard soil erodibility nomograph and the RUSLE2 modified soil erodibility nomograph. These nomographs can be used to estimate soil erodibility factor values for most situations (See RUSLE2 User's Reference Guide), especially where the original soil profile has been disturbed.

The RUSLE2 soil erodibility factor is a measure of soil erodibility under unit plot conditions. These conditions empirically measure soil erodibility where cover-management effects are removed so that the measured erosion represents how inherent soil properties and local climate affect soil erodibility as defined in RUSLE2. The RUSLE2 soil erodibility factor is not an inherent soil property like soil texture. It is defined in terms of the RUSLE2 erosivity variable and, therefore, should not be used in other erosion prediction technologies that use a different erosivity factor than the RUSLE2 erosivity factor. Conversely, soil erodibility factor values from other erosion models that use an erosivity factor that differs from the RUSLE2 erosivity factor can not be used in RUSLE2.

The RUSLE2 soil erodibility factor, which is the same as the USLE and RUSLE1 soil erodibility factor (Wischmeier and Smith, 1965 and 1978; Römkens et al,, 1997), is a measure of erosion per unit erosivity EI for unit plot conditions. The RUSLE2 soil erodibility factor is a function of local climate in addition to soil properties because erosion per unit erosivity is greater where runoff is increased per unit erosivity. For example, if the same soil properties were to occur in two locations, the RUSLE2 soil erodibility factor would be increased in locations where frequent, high, intense rainfall occurs that produces increased runoff per unit precipitation. Unfortunately, the soil erodibility nomograph commonly used to estimate soil erodibility factor values, including those in RUSLE2, is not a function of climate variables. However, the RUSLE2 temproal soil erodibility equation described below takes location into account.

4.1.1. Standard soil erodibility nomograph

The standard soil erodibility nomograph (Wischmeier et al., 1971) was derived from erosion data produced by applying simulated rainfall to about 55 agricultural soils, primarily in Indiana (Wischmeier. and Mannering, 1969). Although these soils

represented a range of inherent soil properties, the standard nomograph best fits medium textured soils.

The equation for the standard soil erodibility nomograph is:[36]

$$K = (k_t k_o + k_s + k_p)/100 \qquad [4.1]$$

where: K = soil erodibility factor, k_t = texture subfactor, k_o = organic matter subfactor, k_s = soil structure subfactor, and k_p =soil profile permeability subfactor.

4.1.1.1. Texture subfactor

The soil texture subfactor equation is (Wischmeier et al., 1971):

$$k_{tb} = 2.1[(P_{sl} + P_{vfs})(100 - P_{cl})]^{1.14}/10000 \qquad [4.2]$$

$$k_t = k_{tb} \qquad \text{if} \quad P_{sl} + P_{vfs} \le 68\% \qquad [4.3]$$

where: P_{sl} = percent silt, P_{vfs} = percent very fine sand based on the total soil primary particles and not just the portion of the sand content, and P_{cl} = percent clay. Although equation 4.2 was derived using regression analysis, Wischmeier et al. (1971) used judgment to graphically draw the k_t relationship for $P_{sl} + P_{vfs}$ percentage above 68 percent. The RUSLE2 equations fitted to the Wischmeier et al. (1971) graphical curves are:

$$k_{t68} = 2.1[68(100 - P_{cl})]^{1.14}/10000 \qquad [4.4]$$

$$k_t = k_{tb} - [0.67(k_{tb} - k_{t68})^{0.82}] \qquad \text{if} \quad P_{sl} + P_{vfs} > 68\% \qquad [4.5]$$

where: k_{t68} = base soil texture subfactor in soil erodibility nomograph when $P_{sl} + P_{vfs} > 68\%$.

4.1.1.2. Organic matter subfactor

The equation for the soil erodibility nomograph organic matter subfactor is:

$$k_o = (12 - O_m) \qquad [4.6]$$

where: O_m = percent inherent soil organic matter. Inherent organic matter is the organic matter content of the soil in unit plot conditions. The experimental plots used to develop the soil erodibility nomograph were not in unit plot condition (Wischmeier and

---

[36] Units for K and associated variables are US customary units

Mannering, 1969). Above ground biomass was removed but the plots were not maintained in a tilled fallow condition for more than a few months. Soil organic matter had not reached inherent soil organic matter levels for unit plot conditions, which resulted in measured soil organic matter being higher than it would have been in unit plot conditions. However, measured erosion values were adjusted to remove land use residual effects from previous cover-management conditions (see **Section 6**), but organic matter content values were not adjusted to unit plot conditions.

The organic matter relationship in the soil erodibility nomograph ***can not be used*** to evaluate how biomass additions and organic farming practices affect rill and interrill erosion. Those effects are considered in RUSLE2's cover-management relationships (see **Section 6**). Furthermore, the experimental conditions used to derive the soil erodibility nomograph were very dissimilar to organic matter conditions associated with organic farming or application of manure, biological waste, or other biological soil amendments.

4.1.1.3. Soil structure subfactor

The soil erodibility nomograph soil structure subfactor refers to how the arrangements of soil primary particles in aggregates and the arrangement of aggregates in the soil affect erosion under unit plot conditions. Four structural classes are used in the nomograph. These classes are 1-very fine granular, 2-fine granular, 3-medium or coarse granular, and 4-blocky, platy, or massive. These classes are defined in the USDA-NRCS soil survey manual. The classes used to derive the soil erodibility nomograph were those in use in the mid-1960's when the experiments were conducted. The definitions for those classes should be used to assign RUSLE2 values for soil structure.

The equation for the soil erodibility nomograph soil structure subfactor is:

$$k_s = 3.25(S_s - 2) \qquad \text{if } (k_t k_o + k_s) \geq 7 \qquad [4.7]$$

$$k_t k_o + k_s = 7 \qquad \text{if } (k_t k_o + k_s) < 7 \qquad [4.8]$$

where: S_s = the soil structure class. The graphical soil structure relationship in the soil erodibility nomograph has a slight "knee" close the origin of the subfactor (Wischmeier et al., 1971), which is represented with equation 4.8.

4.1.1.4. Soil profile permeability subfactor

The soil permeability subfactor is a measure of the potential of the soil profile in unit-plot conditions for generating runoff. Six permeability classes that range from 1-rapid (very low runoff potential) to 6-very slow (very high runoff potential) are used to rate the soil profile for infiltrating precipitation and reducing runoff. The USDA-NRCS soil survey definitions for soil profile permeability used in the mid-1960's should be used to assign a soil permeability class in applying the soil erodibility nomograph. ***The assigned permeability class must not be based on a permeability measurement of the surface soil layer.*** The permeability rating should take into account the presence of restricting layers such as rock, claypan, or fragipan. Also, the rating should consider landscape position.

For example, the permeability rating for a sandy soil underlain by a restricting layer might be moderate for the soil at the top of a hillslope but be very slow if the soil is at the bottom of the hillslope. The input permeability rating should consider the presence of rock fragments. ***The permeability rating should not reflect current or past cover-management on runoff; it is a rating for the soil in unit plot condition*** (see **Sections 4.6 and 7.4** and RUSLE2 User's Reference Guide). The RUSLE2 temporal soil erodibility equation described in **Section 4.5** takes into account how the permeability rating varies as climate varies among locations.

The equation for the permeability subfactor is given by:

$$k_p = 2.5(P_r - 3) \qquad [4.9]$$

where: P_r = the soil profile permeability class.

4.1.2. RUSLE2 modified soil erodibility nomograph

Soil erodibility factor values computed with the standard soil erodibility nomograph do not show the expected range or trend for very high sand soils and very high clay soils typical of highly disturbed lands, such as reclaimed mined land and construction sites. This problem seemed most associated with the soil structure subfactor. Soil erodibility is expected to decrease as soil structure changes from very fine granular to blocky, platy, or massive because of the role of clay as a bonding agent and its effect on soil structure.

The unexpected trend in the soil structure subfactor most likely resulted from the empirical derivation of the standard soil erodibility nomograph from a relatively small database where the soils were predominantly medium texture (Wischmeier and Mannering, 1969; Wischmeier et al., 1971). Consequently, the data points were not uniformly distributed among the major variables that affect soil erodibility. Furthermore, all of the nomograph variables are correlated with each other, which can result in empirical equations derived from a small database not reflecting proper trends for how major variables affect soil erodibility. For example, soil structure is related to soil texture. The soil structure subfactor in the standard soil erodibility nomograph may well represent an interactive effect rather than a main effect in the particular dataset used to derive the standard soil erodibility nomograph.

After reviewing measured erosion data from high clay soils typical of construction sites (Römkens et al., 1975; Römkens et al., 1977; Roth et al., 1974), the judgment was made to modify the soil structure subfactor in the standard nomograph. The modification results in the RUSLE2 modified nomograph computing soil erodibility values that decrease as soil structure goes from fine granular to blocky, platy, and massive and decrease as soil structure goes from fine granular to coarse granular. Soil erodibility factor values computed with the RUSLE2 modified soil erodibility nomograph are smaller than those computed with the standard nomograph for high clay and high sand soils.

4.1.2.1. Soil structure subfactor

The soil structure subfactor equation used in the RUSLE2 modified soil erodibility nomograph is:

$$k_s = 3.25(2 - S_s) \quad [4.10]$$

The difference between this equation and the comparable equation, equation 4.7, in the standard soil erodibility nomograph is the algebraic sign on the variables in the second term in equations 4.7 and 4.10. A nice feature of both the standard and the RUSLE2 modified nomographs is that they use equations referenced to a midpoint. The equations compute values about the midpoint well established by the experimental data. The midpoint for the soil structure subfactor is the fine granular structure. Both soil erodibility nomographs give the same soil erodibility factor values for the fine granular soil structure, but the two nomographs give different trends for departures from this midpoint soil structure.

4.1.2.2. Other subfactors in RUSLE2 modified soil erodibility nomograph

All other subfactors in the RUSLE2 modified soil erodibility nomograph are the same as those used in the standard nomograph.

4.1.3. Special soil erodibility cases

Special cases, described in the RUSLE2 User's Reference Guide, exist where neither RUSLE2 soil erodibility nomograph applies. Equations are available in AH703 (Renard et al., 1997) and elsewhere (El-Swaify and Dangler, 1976; Mutchler et al., 1976; Young and Mutchler. 1977; Roth et al., 1974) to estimate soil erodibility for some of these special conditions. However, these equations were not included in RUSLE2 even though some of them were included in RUSLE1 [AH703 (Renard et al., 1997)]. The equations were judged to give poor results or to use variables that were not properly defined or could not be easily measured for input in typical RUSLE2 applications. Soil erodibility values can be user determined outside of RUSLE2 and entered in RUSLE2.

4.2. Very fine sand

Soil texture is the single most important variable in estimating soil erodibility. In many cases, the standard soil texture such as clay loam, silt loam, or sandy loam based on the USDA classification may be known or can be estimated. However, as Wischmeier et al. (1971) found, this standard classification does not work as well as including the very fine sand fraction with the silt fraction. Unfortunately, the sand, silt, and clay content may be known for a soil, but information on the very fine sand fraction may not be available. A mechanical analysis of the soil is required to determine the very fine sand fraction. The following RUSLE2 equation was developed to estimate the very fine sand fraction from sand, silt, and clay content:

$$P_{vfs} = (0.74 - 0.62P_{sd}/100)P_{sd} \quad [4.11]$$

where: P_{vfs} and P_{sd} are in percent. Regression analysis was used to fit equation 4.11 to the USDA-NRCS soil survey data for Lancaster County, Nebraska.

4.3. Rill to interrill soil erodibility

RUSLE2 computes a ratio of rill to interrill erosion used to compute a slope length exponent in equation 2.10 (e.g., see **Section 2.1.3**) and a **b** value in the subfactor equation for the ground cover effect on erosion (see **Section 6.2**). The RUSLE2 equation used to compute a value for the rill to interrill soil erodibility ratio is:

$$K_r / K_i = (P_{sd}/100)[(1-\exp(-0.05P_{sd})] + 2.7(P_{sl}/100)^{2.5}[1-\exp(-0.05P_{sl})] \quad [4.12]$$

$$+ 0.35(P_{cl}/100)[1-\exp(-0.05P_{cl})]$$

where: K_r/K_i = the rill to interrill soil erodibility ratio and all soil texture values are in percent. Rill to interrill soil erodibility ratio values computed with equation 4.12 are shown in Table 4.1 at the central point of the textural classes.

Table 4.1. Rill to interrill soil erodibility ratio as a function of soil texture

Soil textural class	Rill to interrill soil erodibility ratio
Clay	0.36
Clay loam	0.50
Loam	0.65
Loamy sand	0.82
Sand	0.89
Sandy clay	0.61
Sandy clay loam	0.65
Sandy loam	0.7
Silt	1.91
Silt loam	1.04
Silty clay	0.53
Silty clay loam	0.73

Equation 4.12, like many RUSLE2 equations, is based on computing variations about a mid or central point that is well established by experimental data. As shown in Table 4.1, equation 4.12 gives a value of 1 for the reference silt loam soil. Equation 4.12 computes values that vary about one as soil texture deviates from silt loam. Although soil erodibility data from the Water Erosion Prediction Project (WEPP) were reviewed as the basis for deriving equation 4.12 (Elliot et al., 1989; Laflen et al., 1991a), the equation was derived based on judgment.

For example, increased clay content is assumed to reduce rill erosion much more rapidly than it reduces interrill erosion. Conversely, soils very high in silt are assumed to have increased rill erosion relative to interrill erosion. Increased rill erosion relative to interrill erosion is expected because of reduced clay content that reduces soil cohesiveness, which increases rill erosion more than interrill erosion. In addition, soils high in silt produce increased runoff, which increases rill erosion more than interrill erosion.

Soils high in sand are more susceptible to rill erosion than interrill because of low clay content and reduced cohesiveness. However, offsetting the increase in rill erosion susceptibility is decreased runoff, which would reduce rill erosion more than interrill erosion because rill erosion is directly related to runoff. Overall, the rill to interrill soil erodibility ratio is assumed to be reduced for soils high in sand but not as much as for soils high in clay.

Equation 4.12 quantifies concepts and advice that users were expected to consider in RUSLE1 for selecting LS and ground cover effect relationships [(AH703 (Renard et al., 1997)]. Equation 4.12 is considered to be a significant improvement over RUSLE1 procedures.

4.4. Geographic soil erodibility variability

Even when soil properties are identical, RUSLE2 soil erodibility factor values should vary with location because of climatic differences among locations. For example, erosion is greater per unit rainfall erosivity in locations such as the southern US, where frequent, high, and intense rainfall occurs, than in the northern Great Plains. Average annual soil erodibility factor values also vary with the temporal distribution of erosive precipitation because of the interaction between the temporal variation of erosive precipitation and the temporal variation of soil erodibility values [(AH703 (Renard et al., 1997)]. The temporal variation of erosive precipitation varies among locations

The RUSLE2 standard and modified soil erodibility nomographs do not take these factors into consideration. The data used to derive the standard soil erodibility nomographs were produced by uniform intensity simulated rainfall applied in a sequence of three events. The first simulated storm was 60 minutes of rainfall at 2.5 in/hr on dry soil conditions. The second storm was 30 minutes of rainfall at 2.5 in/hr approximately 24 hour later. The third storm was also 30 minutes long at 2.5 in/hr that occurred approximately 15 minutes after the second storm. When Wischmeier et al. (1971) developed the standard soil erodibility nomograph, they weighted measured erosion values produced by each simulated storm to compute an average annual soil erodibility factor value. This sequence of storms reflects a greater likelihood of a storm on dry conditions than on wet conditions.

This weighting procedure was assumed to apply at all locations, which is probably satisfactory for conservation planning on cropland in the eastern US. However, major questions arise about applying the soil erodibility nomograph to the western US where the precipitation patterns and rainfall amounts and intensities differ significantly from that used to derive the soil erodibility nomograph.

Although questions can be raised about the applicability of the soil erodibility nomograph for these and other reasons, the RUSLE2 assumption is that the nomographs provide soil erodibility values suitable for conservation and erosion control planning. Some of the nomograph issues are not significant with respect to conservation planning when uncertainty in the RUSLE2 soil erosion estimates are considered (See Section 17, RUSLE2 User's Reference Guide) because other factors have a much greater effect on rill-interrill erosion than does the soil erodibility factor.

The temporal soil erodibility equation described in **Section 4.5** takes into account soil erodibility factor values vary with location as temperature and precipitation var with location. Also, the effect of rainfall amount, intensity, and temporal climate patterns are considered in RUSLE2 equations for estimating rill-interrill erosion from rainfall on irrigated lands (see **Section 7.5**).

4.5. Temporal soil erodibility factor values

Along with factors for slope length, cover-management, and supporting practices, the RUSLE2 soil erodibility factor varies temporally (Mutchler and Carter, 1983). Erosion is significantly increased if peak soil erodibility occurs, for example, when cover-management conditions are most susceptible to erosion. An equation is needed to compute daily soil erodibility so that daily erosion can be computed to improve the mathematical accuracy of the RUSLE2 (see **Section 2.1**).

Soil erodibility is high for thawing soil and for the immediate period after the soil has thawed because the soil's susceptibility to detachment is increased (Van Klaveren and McCool, 1998.). Also, soil erodibility is high when soil moisture is high, which increases runoff per unit rainfall and hence erosion per unit erosivity. Erosion on the unit plot per unit erosivity is soil erodibility in RUSLE2. Runoff per unit rainfall is increased on the unit plot, and hence rill erosion is increased, when rainfall is frequent and soil evaporation is low. Soil erodibility may also be related to biological activity in the soil, which is a function of soil moisture and temperature (Vigil and Sparks, 2004).[37]

Although the reasons for soil erodibility varying temporally are partially known, adequate equations for temporal soil erodibility are lacking. The pattern for temporally varying soil erodibility seems well defined for plots at Morris, Minnesota and Holly Springs, Mississippi but not at other locations (Mutchler and Carter, 1983). A complication in making soil erodibility measurements is the coincidence of plot maintenance with highly erosive rains. The unit plots used to experimentally determine soil erodibility factor values are periodically tilled to break the soil crust and to control weeds. Erosion per unit erosivity, hence RUSLE2's soil erodibility factor, can be very high if a highly erosive rain occurs immediately after plot tillage.

The RUSLE1 temporal soil erodibility equations were reexamined and found to work poorly at most of the 11 locations where temporal soil erodibility data are available. Also, the equations performed very poorly in Minnesota and northern Iowa where computed temporal soil erodibility factor values varied too much with slight differences in weather between adjacent counties. Furthermore, the empirically derived RUSLE1 temporal soil erodibility equations are not applicable in the Western US. Consequently, a new temporal soil erodibility equation was derived for RUSLE2 using data collected at the locations listed in Table 4.2. The record length for these data is about 10 years.

---

[37] The RUSLE2 soil erodibility factor is solely related to unit plot conditions. Soil erodibility is also influenced by cover-management conditions but those effects, such as related to soil moisture and runoff, are considered in cover-management variables (see **Section 6**).

Table 4.2. Locations where unit plot conditions were used to determine monthly soil erodibility factor values

Location
Tifton, GA
Watkinsville, GA
Holly Springs, MS
Bethany, MO
Independence, IA
Beaconsfield, IA
Castana, IA
Clarinda, IA
Morris, MN
LaCrosse, WI
Presque Isle, ME

Temporal soil erodibility values grouped by geographic area are shown in Figure 4.1. A similar pattern in the temporal erodibility values by location was expected for each geographic area, especially for the four Iowa locations. The patterns are similar for the two northern Midwestern US and Northern Maine locations where almost no rill-interrill erosion occurs during the winter. The patterns are mostly similar for the two Georgia locations but differ significantly from the pattern at Holly Springs, Mississippi. The difference in patterns, especially among the Iowa locations, indicates that other variables besides weather, such as timing of plot maintenance with erosive rains, affect temporal soil erodibility.

With the exception of the southern locations, the data do not capture the increased soil erodibility in late winter and early spring during and immediately after soil thawing. The very few data available for these conditions are not usable because of very large variability. In many cases, measurements were not made during late winter and early spring because measuring equipment was difficult to operate during cold weather. Also, increased soil erodibility during the thawing and recently thawed period seems to be related to a unique set of conditions that do not occur every year.

Regardless of these limitations, a temporal soil erodibility equation seemed advisable for

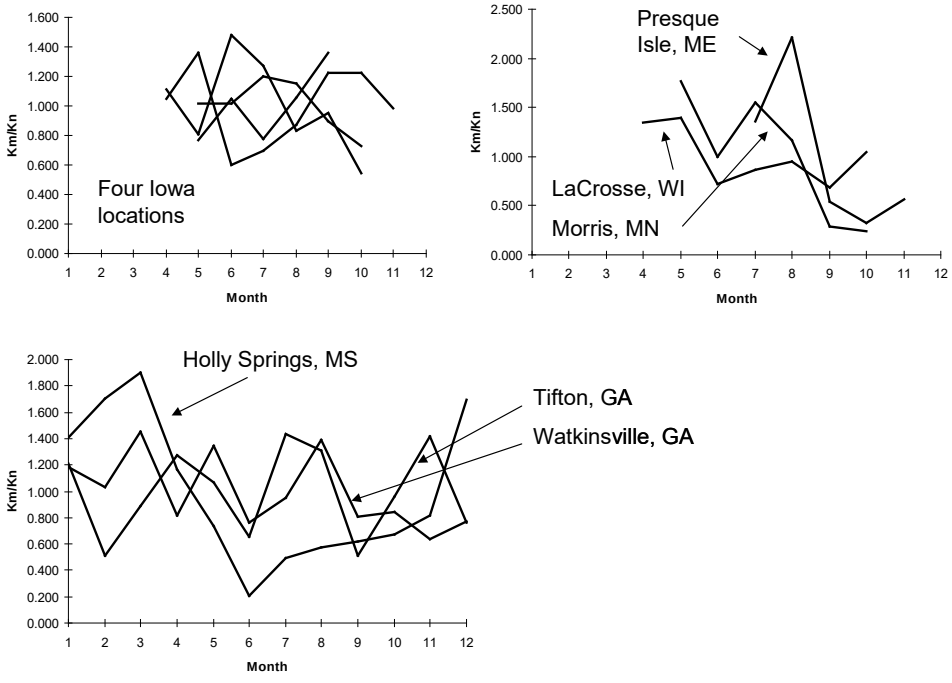

Figure 4.1. Monthly variation in soil erodibility at several locations.

RUSLE2. An equation for RUSLE2was empirically derived from these data.

4.5.1. Basic assumptions

The RUSLE2 assumption is that the soil erodibility value entered in RUSLE2, whether user entered or computed with either of the RUSLE2 soil erodibility nomographs, represents average soil erodibility for a summer period. The RUSLE2 summer period is defined for temporal soil erodibility purposes as the period when average daily temperature exceeds 40 ^{o}F. Analysis of soil erodibility data at Pullman, WA indicates that a better definition is the time between when average daily temperature reaches 45 ^{o}F early in the year to when it decreases to 35 ^{o}F late in the year.

The major assumption used to derive the RUSLE2 temporal soil erodibility equation is that monthly precipitation and temperature can be used as indices to estimate the temporal variability in soil erodibility during the RUSLE2 summer period.

4.5.2. Temporal soil erodibility for the summer period referenced to summer conditions at location

Average values for the ratio of monthly soil erodibility to average soil erodibility for the RUSLE2 summer period were computed for the data collected at the locations listed in Table 4.2. Average soil erodibility for the RUSLE2 summer period was computed as the total erosion for the period of record divided by total erosivity, excluding storms less than 0.5 inches (see **Section 3.2.1**). The period of record at all locations closely corresponded to the RUSLE2 summer definition because the plots were not operated during the winter as can be seen in Figure 4.1. However, the plots were operated throughout the year in the southern US locations and the total data for the year were used to compute an average erodibility value for the southern locations.

The resulting equation from fitting the data is:

$$K_j / K_n = 0.591 + 0.732(P_j / P_s) - 0.324(T_j / T_s) \qquad [4.13]$$

where: K_j = average daily soil erodibility factor value for the *jth* day, K_n = soil erodibility value from the RUSLE2 soil erodibility nomographs or user entered into RUSLE2, T_j = average daily temperature for the *jth* day (^{o}F), T_s = the average temperature for the RUSLE2 summer period defined above, P_j = the average daily precipitation, and P_s = the average precipitation for the RUSLE2 summer period. This equation follows the expected trends of increased soil erodibility when precipitation is high and decreased soil erodibility when temperature is high. Equation 4.13 does not describe increased soil erodibility during or immediately after soil thawing.

The fit of equation 4.13 to the observed data at three locations is shown in Figure 4.2, which also represents the fit at the other locations. Equation 4.13 is a major improvement over the RUSLE1 equations as can be seen by inspection and by comparing the sum of squares of differences between observed and computed values. However, the fit of

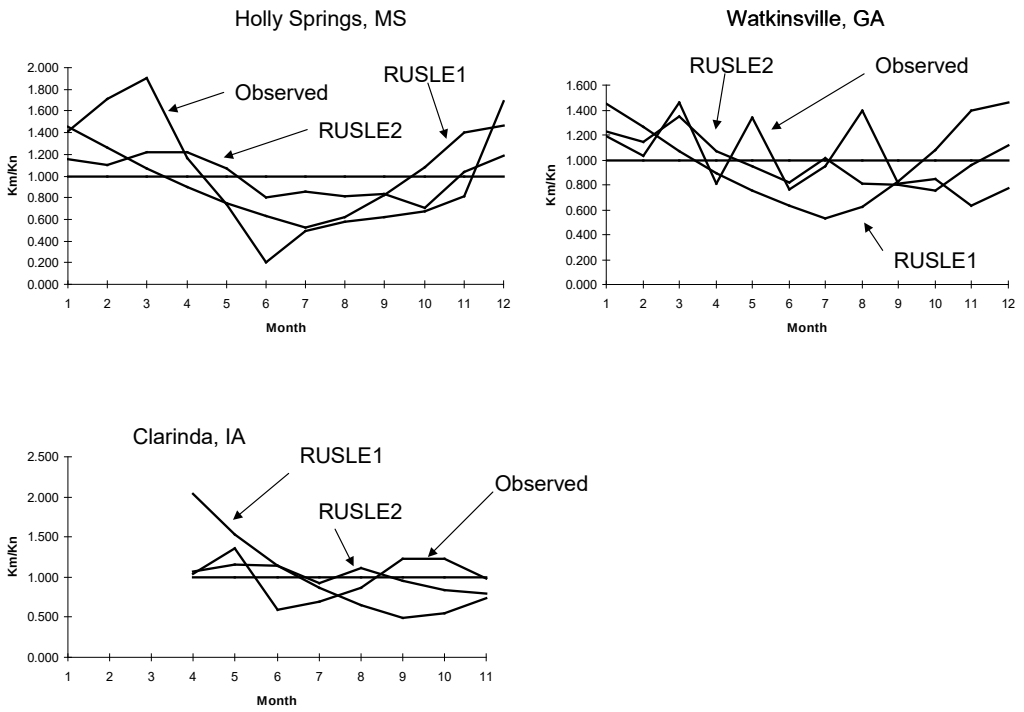

Figure 4.2. Fit of RUSLE2 temporal erodibility equation (equation 4.13), RUSLE1 equation, and constant value to observed data.

equation 4.13 is only slightly better than assuming a time invariant soil erodibility factor value for the summer period.

Computed values from equation 4.13 are shown in Figure 4.3 for Tombstone, Arizona and compared to values computed with the RUSLE1 equations and observed values. Very clearly, equation 4.13 performs much better than the RUSLE1 equations, which illustrates why a time invariant soil erodibility factor value should be assumed when applying RUSLE1 to the western US. The observed values shown in Figure 4.3 were obtained by applying rainfall each month with a rainfall simulator.[38] The observed values are not

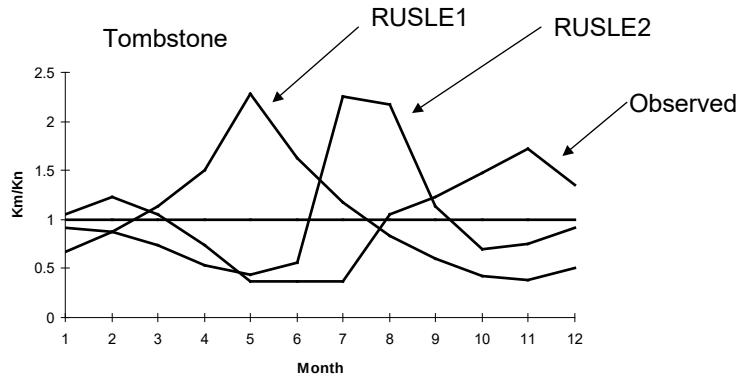

Figure 4.3. Fit of temporal erodibility equations to data from simulated rainfall on rangeland plots at Tombstone, Arizona.

[38] USDA-Agricultural Research Service, Tucson, Arizona.

directly comparable to soil erodibility values produced by natural precipitation because of temporal differences between natural precipitation and the uniform precipitation of the simulated rainfall. Nevertheless, the fit of equation 4.13 to the observed Tombstone, Arizona data is comparable to the fit of equation 4.13 to soil erodibility values produced by natural rainfall in the eastern US.

Therefore, the recommendation is that the RUSLE2 temporal soil erodibility equation be used for all locations in the US except for Req periods (see **Section 3.2.5** and RUSLE2 User's Reference Guide).

4.5.3. Temporal soil erodibility for the summer period referenced to summer conditions at Columbia, Missouri

Equation 4.13 does acceptably well in capturing the relative temporal variations in soil erodibility at a location. Equation 4.13 is an improvement over using a constant soil erodibility factor at a location.

However, equation 4.13 gives exceptionally high soil erodibility values that do not seem reasonable in many western US locations. For example, equation 4.13 computes summer soil erodibility values at Tombstone, Arizona that are twice the average erodibility for summer period (i.e, the period that average daily temperature exceed 100 ^{o}F). The soil erodibility nomograph gives the same average erodibility for both Columbia, Missouri and Tombstone when soil properties are the same at the two locations.. However, the absolute July soil erodibility at Tombstone should not be higher than the absolute July soil erodibility at Columbia.

The root cause of the problem is that the soil erodibility nomograph is not a function of climate at a location. This deficiency does not cause major problems in the Eastern US, but it does cause great problems in the Western US.

To fix this problem, the P_s and T_s variables in equation 4.13 were changed from location values to values at Columbia, MO. The temporal soil erodibility equation referenced to Columbia, Missouri is:

$$K_j / K_n = 0.591 + 0.732(P_j / 0.123) - 0.324(T_j / 62.8) \qquad [4.14]$$

$$If\ (K_j / K_n) > 2.0\ \text{ then }\ (K_j / K_n) = 2.0$$

$$If\ (K_j / K_n) < 0.4\ \text{ then }\ (K_j / K_n) = 0.4$$

where: P_j = daily precipitation (inches), 0.123 (inches) = the daily average reference precipitation at Columbia, Missouri, T_j = the daily temperature (^{o}F), and 62.8 (^{o}F) = the daily average reference temperature at Columbia, Missouri. The j subscript is for the *jth* day. The reference precipitation and temperature value for Columbia, Missouri are for the time period that the average daily temperature is above 40 ^{o}F.

Either the standard or RUSLE2 soil erodibility nomographs can be used to determine a value for the nominal soil erodibility factor K_n, or another soil erodibility value can be used if values computed by the RUSLE2 soil erodibility nomographs are not applicable. The upper limit of 2 and the lower limit of 0.4 for the ratio K_j/K_n provides robustness by preventing extreme precipitation and temperature from excessively affecting daily soil erodibility factor values.

4.5.4. Temporal soil erodibility for the winter period

Equation 4.14 is used to compute temporal RUSLE2 soil erodibility factor values in the winter period as well as the summer period, except when average daily temperature is less than 30 ^{o}F. The RUSLE2 temporal soil erodibility equation for average daily temperature less than 30 ^{o}F is:

$$K_{(j)} / K_n = (K_{s(j)} / K_n) \exp[-0.2(30 - T_{(j)})] \qquad [4.15]$$

where: $K_{s(j)}$ = the soil erodibility factor value computed with equation 4.14 on the *jth* day, T_j = the average daily temperature on the *jth* day (^{o}F), and 30 = the average daily temperature below which soil erodibility is reduced because of soil freezing (^{o}F). The *exp* term in equation 4.15 computes a K_j/Kn value less than 0.05 when average daily temperature is less than 15 ^{o}F. The exponential decay term in equation 4.15 takes into account the fact that temperature in some years on a given day will not be less than freezing even though average daily temperature is below freezing. Also, the temperature used in equation 4.15 is air temperature rather than soil temperature.

Equation 4.15 does not compute increased erosion during and immediately after soil thawing.

4.5.5. Temporal soil erodibility for winter and summer periods combined

Figure 4.4 shows temporal soil erodibility factor values computed for the entire year at selected locations. Note the difference in the mean soil erodibility factor value among the locatins for the same base soil erodibility factor value.

4.5.6. Temporal soil erodibility for the Req regions

Winter erosion processes differ greatly from summer erosion processes in the Northwest Wheat and Range Region (NWRR) and other areas in the Western US (McCool et al., 1995). Soil erodibility is very high during the winter in these regions, resulting in very high erosion. This winter effect is accounted for in RUSLE2 by assuming an equivalent erosivity known as Req. Equation 4.14 can be used to estimate temporal erodibility for the summer period defined as the time between the day when average daily temperature reaches 45 ^{o}F early in the year and decreases to 35 ^{o}F late in the year. Equation 4.15 does not apply where Req effects are assumed to occur (see **Section 3.2.5** and RUSLE2 User's Reference Guide).

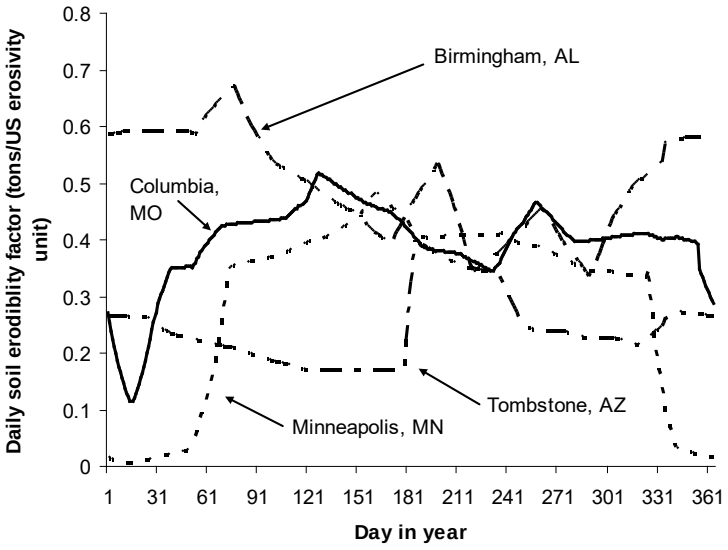

Figure 4.4. RUSLE2 computed temporal soil erodibility factor values for the same base soil erodibility factor value. The temporal soil erodibility factor equations are referenced to Columbia, Missouri.

4.6. Effect of rock on soil erodibility

Rock on and in the soil affects rill-interrill erosion. RUSLE2 treats rock on the soil surface as ground cover (see **Section 6.2**). Rock in the soil is assumed to affect runoff and this effect on erosion is represented by choosing a soil erodibility factor value based on how rock in the soil profile is assumed to affect runoff under unit plot conditions. **User entered soil erodibility values should reflect how rock in the soil profile affects erosion but not account for any effect of rock on the soil surface.**

The permeability class input should reflect how rock in the soil profile affects runoff when a RUSLE2 soil erodibility nomograph is used to compute a soil erodibility factor value. Although RUSLE2 includes the RUSLE1 soil erodibility nomograph equations used to estimate how rock in the soil profile affect soil erodibility (Römkens et al., 1997), these equations should not be used in RUSLE2, especially for construction sites and reclaimed surface mine lands. Toy and Foster (1998) describes how to adjust input values to the RUSLE2 modified soil erodibility nomograph to estimate the effect of large rock fragments in the soil on soil erodibility. 20-40=+1; 40-60=+2; 60-80=+3; >80=+4; max permeability is class=6 (very slow).

A value for soil surface cover provided by rock that is a natural part of the soil can be entered in RUSLE2's soil input. RUSLE2 assumes that this rock cover is not affected by mechanical soil disturbing operations. Rock cover can also be represented in RUSLE2 as an operation that adds surface cover, but RUSLE2 handles this rock cover differently from how it handles rock cover entered in the soil input. Rock cover represented as surface cover added by an operation is affected by soil disturbing operations and

RUSLE2 treats this rock as an organic material. Special inputs are required when rock cover is represented in this way (see **Section 10.1** and RUSLE2 User's Reference Guide).

The USDA-NRCS soil survey database includes soil erodibility factor values that have been adjusted for rock cover on the soil surface. **NRCS soil erodibility factors values adjusted for rock surface cover must not be used in RUSLE2.** The ground cover subfactor relationship used by NRCS to adjust for rock surface cover differs from the comparable RUSLE2 relationship (see **Section 6.2.1**). The surface cover relationship used by the NRCS is the USLE mulch cover subfactor [AH537 (Wischmeier and Smith, 1978)], which has an approximate 0.026 **b** value whereas the approximate RUSLE2 **b** value is 0.035. The error in estimated erosion from this difference for a 20 percent rock cover is 20 percent.

Also, RUSLE2 uses a net ground cover that takes into account surface residue and live ground cover overlapping rock surface cover. This overlap is not taken into account when NRCS soil erodibility factor values adjusted for rock surface cover are used, which can result in serious errors because the ground (mulch) cover relationships are highly non-linear (see RUSLE2 User's Reference Guide). The error in estimated erosion from neglecting the overlap for a 50 percent residue cover and a 20 percent rock cover is 30 percent even when if the proper **b** value had been used in the NRCS adjustment.

4.7. Sediment characteristics

RUSLE2 computes deposition and enrichment ratio as a function of sediment characteristics (see **Sections 2.3.3** and **4.7.6**). Diameter, specific gravity, distribution among sediment particle classes, and composition of sediment particle classes are the RUSLE2 variables used to describe sediment characteristics. RUSLE2 uses only soil texture and inherent soil organic matter content to compute values for sediment characteristics at the point of detachment although soil management affects these sediment characteristics. Sufficient information was not available to develop equations for the effect of soil management on sediment characteristics at the point of detachment.

The RUSLE2 equations used to compute sediment characteristics at the point of detachment are described by (Foster et al., 1985b). The RUSLE2 intent in representing sediment characteristics is to capture main effects rather than precisely representing all variables that affect sediment characteristics at the point of detachment. Also, more detail, such as more than the five sediment particle classes used in RUSLE2 equations is desired for computing deposition. However, the desired information is not readily available for most RUSLE2 applications as a conservation planning tool in local field offices. The RUSLE2 approach is far better than assuming that sediment characteristics at the point of detachment are the same as the characteristics of dispersed samples of the soil subject to detachment. A critically important point is that sediment is eroded as a mixture of aggregates and primarily particles. Assuming that sediment is composed entirely of primary particles produces serious errors when computing deposition. RUSLE2 computes how deposition changes sediment characteristics so that the characteristics of sediment leaving an overland flow path, terrace/diversion channels, and

small impoundments can be quite different from the characteristics of the soil being eroded, especially where RUSLE2 computes a high degree of deposition.

4.7.1. Definition of sediment particle classes

Five sediment particle classes are used to represent the sediment produced by detachment for each soil along an overland flow path. The five classes are primary clay, primary silt, small aggregate, large aggregate, and primary sand. Sediment from cohesive soils is eroded as a mixture of primary particles (small mineral particles that the soil can be divided into) and aggregates (conglomerates of primary particles) (Foster et al., 1985b). Also, the sediment distribution for many cohesive soils is bimodal, having a peak in the silt-size range and a peak in the sand-size range (Meyer et al., 1980). The two aggregate sediment particle classes represent these two peaks in the sediment distribution. The three primary sediment particle classes represent primary particles in the sediment while the two aggregate classes represent aggregates in the sediment.

4.7.2. Density of sediment particle classes

Densities, expressed as specific gravity, of the sediment particle classes are given in Table 4.3. The slightly reduced density for the primary clay class relative to the primary silt and sand classes is because of the platy nature of clay particles. The difference is of no consequence in RUSLE2. The significantly reduced densities of the aggregate classes from the primary particle classes reflect how aggregates are conglomerates of primary particles with internal open spaces in them that are partially or fully filled with water. Sediment particle density is especially important for sediment sizes larger than 0.1 mm because density seems to affect deposition by overland flow as much as size (Lu et al., 1988; Neibling and Foster, 1982). A smaller density is assigned to the large aggregate class than to the small aggregate class because density decreases as aggregate size increases (Foster et al., 1985b).

Table 4.3. Densities of sediment particle classes

Particle class	Density (specific gravity)
Primary clay	2.60
Primary silt	2.65
Small aggregate	1.80
Large aggregate	1.60
Primary sand	2.65

4.7.3. Diameters of sediment particle classes

The diameters of the sediment particle classes are given in Table 4.4. The diameter of each primary particle class is fixed. However, the diameter for each aggregate sediment particle class varies with soil clay content, which reflects the role of clay as a bonding agent.

Table 4.4. Diameter of sediment particle classes.

Particle class	Diameter		
	Symbol	Size (mm)	Condition where equation applies
Primary clay	d_{cl}	0.002	
Primary silt	d_{sl}	0.010	
Small aggregate	d_{sa}	0.030	$P_{cl} < 25$
	d_{sa}	$0.2(P_{cl}/100 - 0.25) + 0.03$	$25 \le P_{cl} \le 60$
	d_{sa}	0.100	$P_{cl} > 60$
Large aggregate	d_{la}	0.300	$P_{cl} \le 15$
	d_{la}	$2P_{cl}/100$	$P_{cl} > 15$
Primary sand	d_{sd}	0.200	

The diameter of each aggregate class is a function of soil clay content for certain ranges of clay content. RUSLE2 adds aggregate sediment particle classes as necessary along the overland flow path where soil clay differs by segment to represent unique particle classes having different diameters. The same primary sediment particle classes are used for all soils along an overland flow path because the diameters used for these classes do not vary with soil.

4.7.4. Distribution of sediment mass among particle classes at point of detachment

As shown in Table 4.5, the distribution of sediment mass among the sediment particle classes at the point of detachment depends mainly on the soil's clay content. Seventy four percent of the clay in the sediment at the point of detachment is in the aggregate sediment particle classes while only 26 percent is in the primary clay sediment particle class.

Table 4.5. Distribution of sediment mass among particle classes at the poi				
Particle class	Fraction			
	Symbol		Condition	Comment
Primary clay	F_{cl}	$0.26P_{cl}/100$		
Primary silt	F_{sl}	$P_{sl}/100 - F_{sa}$		
Small aggregate	F_{sa}	$1.8P_{cl}/100$	$P_{cl} < 25$	
	F_{sa}	$0.45 - 0.6(P_{cl}/100 - 0.25)$	$25 \le P_{cl} \le 50$	If $F_{sl} < 0$, F_{sl} =0.0001 and
	F_{sa}	$0.6P_{cl}/100$	$P_{cl} > 50$	$F_{sa} = P_{sl}/100 - F_{sl}$
Large aggregate	F_{la}	$1 - F_{cl} - F_{sl} - F_{sa} - F_{sd}$		If $F_{la} < 0$, each fraction is multiplied by the same fraction to give F_{la} = 0.0001
Primary sand	F_{sd}	$(P_{sd}/100)(1 - P_{cl}/100)^5$		
Note:				
If the clay content of the large aggregate class is less than $0.5P_{cl}$, the value for F_{sa} must be reduced to meet this condition.				

Soil clay content determines the fraction of the sediment mass that is in the small aggregate sediment particle class at the point of detachment. The fraction of the sediment in the primary silt class at the point of detachment is the soil's silt content less the silt fraction computed to be in the small aggregate class. The fraction of sediment mass in the small aggregate class at the point of detachment can not be larger than the silt content in the soil.

Both clay and sand content in the soil determine the fraction of the sediment mass that is in the primary sand sediment particle class at the point of detachment. The role of soil clay content in determining this fraction increases rapidly as soil clay content increases. The fraction of sediment mass in the large aggregate sediment particle class at the point of detachment is computed as 1 minus the sum of the fractions of the other four sediment particle classes. The fractions for the other four classes are adjusted when the fraction of the large aggregate sediment particle class is computed as being less than zero.

4.7.5. Composition of each sediment particle class

Detachment in RUSLE2 is assumed to be non-selective. Consequently, the sediment's primary particle composition at the point of detachment is the same as the composition of the surface soil subject to detachment.

4.7.5.1. Primary clay sediment particle class

The primary sediment particle is composed of primary clay and the organic matter associated with the clay.[39] The RUSLE2 assumption is that the ratio of organic matter to clay on a mass basis is the same for all sediment particle classes where clay is present. That ratio is given by:

$$r_{om,cl} = P_{om} / P_{cl} \quad [4.16]$$

where: $r_{om,cl}$ = the fraction (mass) of the primary clay sediment particle class that is composed of organic matter and P_{om} = 100 times the ratio of mass of organic matter in the soil to the mass of soil mineral particles.

4.7.5.2. Primary silt sediment particle class

The primary silt sediment particle class is composed solely of silt. This particle class contains no organic matter because the class contains no clay.

4.7.5.3. Small aggregate sediment particle class

The small aggregate sediment particle class is composed of clay, silt, and organic matter. This particle class contains no sand by definition. The size of the small aggregate particle class is too small to contain any sand except very fine sand. However, the RUSLE2 assumption is that this particle class does not contain even very fine sand. The distribution of the clay and silt is assumed to equal the proportion of clay and silt in the soil subject to detachment. That is,

$$f_{cl,sa} = P_{cl} /(P_{cl} + P_{sl}) \quad [4.17]$$

where: $f_{cl.sa}$ = the fraction (mass) of the small aggregate that is composed of clay. The fraction of the small aggregate that is composed of silt is given by:

$$f_{sl,sa} = P_{sl} /(P_{cl} + P_{sl}) \quad [4.18]$$

where: $f_{sl,sa}$ = the fraction (mass) of the small aggregate that is composed of silt. The fraction of the small aggregate that is composed of organic matter is given by:

$$f_{om,sa} = r_{om,cl} f_{cl,sa} \quad [4.19]$$

where: $f_{om,sa}$ = fraction (mass) of the small aggregate sediment class composed of organic matter.

---

[39] The terms clay, silt, and sand sometimes refer to particle sizes. However, as used herein, clay, silt, and sand refer to mineral particles in the clay, silt, and sand sizes. The fractions of the primary particles sum to 1. Organic matter is not considered in determining fraction of the particles classes.

4.7.5.4. Large aggregate sediment particle class

The large aggregate sediment particle class is assumed to be composed of clay, silt, sand, and organic matter. The total of each constituent among the sediment particles classes must equal the constituent's amount in the soil. The mass of a constituent, except organic matter, in the large aggregate is computed as the total minus the sum of that constituent in the other sediment particle classes That is:

$$f_{cl,la} = (P_{cl}/100 - F_{cl} - f_{cl,sa}F_{sa})/F_{la} \quad [4.20]$$

$$f_{sl,la} = (P_{si}/100 - F_{si} - f_{sl,sa}F_{sa})/F_{la} \quad [4.21]$$

$$f_{sd,la} = (P_{sd}/100 - F_{sa})/F_{la} \quad [4.22]$$

Equations 4.20-4.22 directly result from the RUSLE2 assumption that detachment is a non-selective process, which requires that the distribution of the constituents in the sediment at the point of detachment be the same as that in the soil subject to detachment. A check is made of the clay content in the large aggregate sediment particle class. Because clay and the organic matter associated with it are assumed to be bonding agents for the two aggregate classes, clay must be sufficient in the large aggregate class to give those particles stability. To meet this requirement, the RUSLE2 assumption is that the clay content in the large aggregate class must be at least half of the soil's clay content. If the clay content in the large aggregate particle class computed with equation 4.20 is less than half the soil's clay content, the fraction F_{sa} of the small aggregate sediment particle class is reduced to meet this requirement.

The fraction of the organic matter in the large aggregate sediment particle class is given by:

$$f_{om,la} = f_{cl,la}r_{om,cl} \quad [4.23]$$

4.7.5.5. Primary sand sediment particle class

The primary sand class is solely composed of sand. It contains no organic matter because it contains no clay.

4.7.6. Specific surface area

Table 4.6. Specific surface area of soil/sediment constituents.

Constituent	Specific surface area (m^2/g)
Clay	20
Silt	4
Sand	0.05
Organic matter	1000

Each constituent of clay, silt, sand, and organic matter is assigned a specific surface area so that RUSLE2 can compute an enrichment ratio based on specific area of the soil subject to detachment and the computed sediment yield from the overland flow path, terrace/diversion channel, or small impoundment, represented in a RUSLE2 computation. Specific surface area is the total surface area of the soil or sediment per unit mass. The specific surface areas used in RUSLE2 are given in Table 4.6,

which were used in the CREAMS model (Foster et al.1980a, 1980b; Foster et al., 1981a). As Table 4.6 shows, most of the surface area is associated with organic matter and clay with almost no specific surface area associated with sand. Because organic matter is directly associated with the clay, the specific surface of both the soil and the sediment is directly related to clay content in each.

Specific surface area of the soil subject to detachment and the sediment leaving the RUSLE2 flow path is used to compute an enrichment ratio as:

$$E_r = S_{sed} / S_{soil} \qquad [4.24]$$

where: E_r = enrichment ratio, S_{sed} = the specific surface area of the sediment and S_{soil} = the specific surface area of the soil. The enrichment ratio is a measure of the degree that RUSLE2 computes that deposition enriches the sediment in fine particles, especially clay. Deposition is a selective process that first deposits particles that are coarse and dense, which have a low specific surface area, leaving the sediment enriched in fine particles that have a high specific surface area. The enrichment ratio increases as deposition increases. A sediment delivery ratio can be computed as the ratio of sediment yield at the end of the RUSLE2 flow path divided by the total amount of sediment produced by detachment. Enrichment ratio increases as the sediment delivery ratio decreases. A low sediment delivery ratio represents a high degree of deposition. Enrichment ratio is a relative term and not an absolute term. A high enrichment ratio means that the specific area of the sediment is greater than that of the soil that produced the sediment, but the specific surface area of the sediment may still be low if the soil being eroded has a high sand content and a low inherent organic matter content.

Table 4.7. RUSLE2 computed enrichment ratios for a filter strip

Soil textural class	Enrichment ratio
Clay	1.95
Clay loam	2.23
Loam	2.65
Loamy sand	7.56
Sand	11.50
Sandy clay	2.13
Sandy clay loam	3.07
Sandy loam	3.47
Silt	0.94
Silt loam	1.58
Silty clay	1.19
Silty clay loam	1.44

The enrichment ratio computed by RUSLE2 is strongly affected by soil texture as shown in Table 4.7. Interestingly, the highest enrichment ratio is for a sand soil while the lowest enrichment ratio is for a high silt soil. Enrichment ratio values are moderate for high clay soils. These results are directly related to the sediment being a mixture of aggregates and primary particles, the role of clay as a bonding agent in determining size of the large the aggregates, and the distribution of sediment between the small aggregate and large aggregate sediment particle classes. An important point to remember when interpreting and using the RUSLE2 computed enrichment ratio values is that about 74 percent of the clay is in the small and large aggregate particle classes at the point of detachment. RUSLE2 computes that a moderate sized large aggregate class is deposited at a rate comparable to the primary sand sediment particle class. Because much of the clay is assumed to be in the large aggregate class, a significant amount of clay is deposited when the large aggregate class is deposited.

The enrichment ratio values computed by RUSLE2 are very different from those that would be computed if the sediment at the point of detachment was assumed to be composed entirely of primary particles. High sand soils have very low clay contents such that the portion of the sediment in the aggregates classes at the point of detachment is low. The aggregate classes, which contain most of the clay, have small diameters for high sand soils and are, therefore, less readily deposited. Consequently, the enrichment ratio for sediment from high sand soils is generally high as illustrated in Table 4.7. In contrast, the diameters of both the small and large aggregate classes, which contain most of the clay, are very large for the high clay soils. These aggregates classes are more readily deposited than the aggregate classes produced by high sand soils. The result is that a higher fraction of the clay in a high sand soil remains in the sediment after deposition than for a high clay soil.

Essentially no enrichment occurs with the high silt soil because of the very low clay content and a very high portion of the sediment at the point of detachment being in the primary silt class that is not readily deposited. Most of the clay is in the aggregate classes that are more readily deposited than the primary silt class where most the sediment is concentrated at the point of detachment.

Although specific surface area of clay varies significantly with clay mineralogy, RUSLE2 does not consider that effect. Also, RUSLE2 uses the inherent soil organic matter content under unit plot conditions in these computations. Soil organic matter content as influence by cover-management is a more appropriate measured than inherent soil organic matter content.

The enrichment ratio values computed by RUSLE2 represent an index. The enrichment ratio value indicates the concentration of sediment associated chemicals in the sediment relative to their concentration in the soil. Calibration should be used to empirically relate the concentration of chemicals on sediment to the RUSLE2 enrichment ratio values because the values computed by RUSLE2 are lower than expected (Knisel et al., 1980).

4.8. Time to soil consolidation

Soil consolidation refers to the soil becoming resistant to erosion over time after a mechanical soil disturbance and not to a mechanical increase in bulk density of the soil (see **Section 6.6**). RUSLE2 computes time to soil consolidation as function of annual precipitation using:

$$t_c = 20 \quad P_a < 10 \qquad [4.25]$$

$$t_c = 26.5 - 0.65P_a + 0.5 \quad 10 \le P_a \le 30 \qquad [4.26]$$

$$t_c = 7 \quad 30 < P_a \qquad [4.27]$$

where: t_c = the time to soil consolidation (years) and P_a = annual precipitation (inches). The equation that computes values for the soil consolidation subfactor uses the ratio of

time since last mechanical soil disturbance to time to soil consolidation and computes subfactor values that asymptotically approach the 0.45 final value (see **Section 6.6.2**). The time to soil consolidation is defined as the time for 95 percent of the reduction in the soil consolidation subfactor to occur. The time to soil consolidation occurs when the soil consolidation factor equals 0.4775, which is 95 percent of the decrease from 1 for the soil consolidation subfactor immediately after a mechanical soil disturbance to the final 0.45 value.

After a mechanical soil disturbance, the soil becomes resistant to detachment by the soil experiencing wetting and drying cycles in the presence of soil moisture and bonding agents including clay and organic matter (Foster et al., 1985b). Mechanical compaction of the soil is assumed to have little effect on this increase in erosion resistance in RUSLE2. The seven year time to soil consolidation is based on analysis of fallow plot data from Zanesville, Ohio (Borst et al., 1945), which are the only sufficient data available to empirically determine time to soil consolidation. This seven year period is assumed to apply to all areas where annual precipitation is greater than 30 inches. The increase of time to soil consolidation based on average annual precipitation is an approximate way to capture the idea that soil consolidation occurs more slowly in the western US than in the eastern US because of reduced rainfall amount and reduced number of rainfall events. Equations 4.25 and 4.26 are based on judgment.

4.9. List of symbols

b = coefficient used to compute ground cover subfactor values

d_{cl} = diameter of primary clay sediment class (mm)

d_{la}= diameter of large aggregate sediment class (mm)

d_{sa}= diameter of small aggregate sediment class (mm)

d_{sd} = diameter of primary sand sediment class (mm)

d_{sl} = diameter of primary silt sediment class (mm)

E_r = enrichment ratio

$f_{cl.la}$ = mass portion of large aggregate sediment class composed of clay (fraction)

$f_{cl.sa}$ = mass portion of small aggregate sediment class composed of clay (fraction)

$f_{om,la}$ = mass portion of large aggregate sediment class composed of organic matter (fraction)

$f_{om,sa}$ = mass portion of the small aggregate sediment class composed of organic matter (fraction)

$f_{sd,la}$ = mass portion of large aggregate sediment class composed of sand (fraction)

$f_{sl,la}$ = mass portion of large aggregate sediment class composed of silt (fraction)

$f_{sl,sa}$ = mass portion of small aggregate sediment class composed of silt (fraction)

F_{cl} = mass portion of sediment at point of detachment composed of primary clay sediment class (fraction)

F_{la} = mass portion of sediment at point of detachment composed of large aggregate sediment class (fraction)

F_{sa} = mass portion of sediment at point of detachment composed of small aggregate sediment class (fraction)

F_{sd} = mass portion of sediment at point of detachment composed of primary sand sediment class (fraction)

F_{sl} = mass portion of sediment at point of detachment composed of primary silt sediment class (fraction)

k_o = organic matter subfactor in soil erodibility nomograph

k_p =soil profile permeability subfactor in soil erodibility nomograph

k_s = soil structure subfactor in soil erodibility nomograph

k_t = texture subfactor in soil erodibility nomograph

k_{tb} = base soil texture subfactor in soil erodibility nomograph for all soil textures

k_{t68} = base soil texture subfactor in soil erodibility nomograph when $P_{sl} + P_{vfs} > 68\%$.

K = soil erodibility factor[40]

K_j = average daily soil erodibility factor value for the *jth* day

K_n = soil erodibility value from RUSLE2 soil erodibility nomographs or user entered for summer periods

K_r/K_i = rill to interrill soil erodibility ratio

$K_{s(j)}$ = soil erodibility factor computed with equation 4.14

O_m = inherent soil organic matter (percent)

P_a = annual precipitation (inches)

P_{cl} = portion of soil mass composed of clay based on total soil primary particles (percent)

P_j = average daily precipitation (inches)

P_{om} = 100 times ratio of mass of organic matter in soil to mass of soil mineral particles

P_r = soil profile permeability class used in soil erodibility nomograph

P_s = average precipitation for the RUSLE2 summer period (inches)

P_{sd} = portion of soil mass composed of sand based on total soil primary particles (percent)

P_{sl} = portion of soil mass composed of silt based on total soil primary particles (percent)

P_{vfs} = portion of soil mass composed of very fine sand based on total soil primary particles, not the portion of sand content (percent)

---

[40] US customary units used for K and associated variables

$r_{om,cl}$ = mass portion of the primary clay sediment class composed of organic matter (fraction)

S_s = soil structure class used in soil erodibility nomograph

S_{sed} = specific surface area of sediment

S_{soil} = specific surface area of soil subject to erosion

t_c = time to soil consolidation (years)

T_j = average daily temperature for the *jth* day (^oF)

T_s = average temperature for the RUSLE2 summer period (^oF)

Indices

j - day

5. TOPOGRAPHY

This section describes mathematical consequences of RUSLE2's equation structure rather than providing additional equations except for the steepness factor and adjusting soil loss tolerance values for position along the overland flow path.

Equations that describe how topography affects rill-interrill erosion where the overland flow streamlines are parallel are described in **Section 2**. Those equations provide RUSLE2's fundamental, underlying mathematical structure. Those equations accommodate spatial variability in soil, steepness, cover-management, and support practices along the overland flow path. Those equations compute whether detachment or deposition occurs along the overland flow path. RUSLE2 computes its erosion and sediment load values using a numerical solution of the governing RUSLE2 equations written as a function of distance along the overland flow path. The numerical solution is a spatial integration of the governing equations. Furthermore, RUSLE2 performs a temporal integration of the governing equations, where the slope length exponent m in equation 2.10, along with soil erodibility and cover-management relationships change daily.

5.1. Converging-diverging streamlines on overland flow areas

The RUSLE2 assumption is that overland flow streamlines are parallel. Consequently, RUSLE2 does not estimate how converging or diverging overland flow affects rill-interrill erosion. An analysis based on a simple process-based erosion model showed that rill-interrill erosion with converging overland flow is about 7/6 times that where the streamlines are parallel (Toy and Foster, 2000). The same analysis showed that rill-interrill erosion with diverging overland flow is about 5/6 times that where the streamlines are parallel.

5.2. Topographic equations for overland flow having parallel streamlines on uniform overland flow paths

RUSLE1 requires users to select a slope length exponent value, m in equation 2.10, based on land use classes [AH703, (Renard et al., 1997); Toy and Foster, 1998]. The RUSLE1 slope length exponent is time invariant and thus does not change as cover-management conditions change temporally. Overland flow path steepness is the only variable considered in adjusting the slope length exponent in the USLE [AH537 (Wischmeier and Smith, 1978)].

A RUSLE2 major improvement is that it computes slope length exponent values as a function of overland flow path steepness, soil, and cover-management conditions. Consequently, the RUSLE2 slope length exponent varies as cover-management conditions vary temporally. RUSLE2 automatically computes slope length exponent values from basic input data rather than the user selecting a value as required by RUSLE1.

The slope length exponent should vary with position along the overland flow path according to erosion theory (Foster and Meyer, 1975). However, equation 2.10 is based on the assumption that the slope length exponent is a not a function of position x. The slope length exponent not varying with position greatly simplifies RUSLE2 mathematics and numerical procedures (see **Section 2.3**) and gives RUSLE2 increased robustness for overland flow paths longer than 150 ft (see **Section 5-Appendix I**).

If equation 2.10 is used to compute erosion for a slope length exponent that varies with position, RUSLE2 computes erroneous erosion values for a uniform overland flow path divided into segments, even if conditions are the same for all segments. Computed erosion should be independent of the number and length of segments used to represent a uniform overland flow path.

Some of the sediment produced by interrill erosion is deposited in "rill" areas when overland flow path steepness is low and interrill erosion is sufficiently high. RUSLE2 computes no rill erosion when it computes deposition. RUSLE2 computes this local deposition[41] when interrill erosion rate is greater than the increase in transport capacity with distance along the overland flow path (i.e., $D_i > dT_c/dx$ where D_i = interrill erosion rate, T_c = runoff's sediment transport capacity, and x = distance). Interrill erosion is computed with equation 2.11, dT_c/dx is computed using equation 2.17, and deposition and net erosion is computed using equation 2.16 and its companion equations. RUSLE2-computed net erosion does not vary with distance along the overland flow path as expected (Renard and Foster, 1983; Meyer and Harmon, 1985).

Erosion values computed with equations 2.16 and 2.17 differ from values computed by the empirical USLE, which is equation 2.10. This inconsistency, which should not occur, results from RUSLE2 combining the empirical USLE equation with a process-based sediment transport capacity equation. These equations do not work well together for this condition. A choice must be made as to whether the USLE based erosion value or the process-based erosion value will be the RUSLE2-computed value.

A RUSLE2 development principle is that RUSLE2 compute erosion values agree with USLE computed values (see **Section 1**). The conflict between equation 2.16 and the USLE equation forms, therefore, is resolved by having RUSLE2 produce the same results as the USLE. However, RUSLE2 uses equation 2.16 to compute how local deposition change sediment characteristics.

This procedure works well for local deposition on a uniform overland flow path not subdivided into segments. Subdivision without changing any of the segment variable values should not affect computed erosion and sediment values. Subdivision does not

---

[41] Local deposition is where sediment is deposited almost adjacent to the point of detachment such as in soil surface roughness depressions and in furrows between ridges. Remote deposition is where sediment is deposited a significant distance from the point detachment such as at the upper edge of dense vegetation strips and on the toe of concave-shaped overland flow path profiles.

affect computed erosion values but does affect computed enrichment ratio values when RUSLE2 computes local deposition. The RUSLE2-computed enrichment ratio value is correctly computed when a uniform overland flow path is not subdivided.

RUSLE2 was constructed so that its remote deposition computations are independent of segment subdivision. An example of remote deposition is the deposition that occurs at the upper end of a 0.5 percent segment downslope from a one percent steep segment. RUSLE2 also computes local deposition on the 1 percent steep segment if interrill erosion is sufficiently great.

RUSLE2 makes these computations correctly if the upper one percent segment is not subdivided. However, if that segment is subdivided, it will compute erroneous enrichment ratio values, especially if the subdivision is near the upper end of the segment. The erosion values are affected only very slightly by subdivision of the upslope segment.

The error in the enrichment ratio values caused by subdividing the overland flow path is a RUSLE2 flaw. This flaw can not be eliminated because of differences in equation structure between the USLE and the process-based sediment transport capacity equation used in RUSLE2. The enrichment ratio error could have been prevented by developing RUSLE2 entirely from process-based equations. However, RUSLE2's power of giving the well-accepted, empirically derived USLE values would have been lost. RUSLE2 was derived, developed, and evaluated to ensure that inconsistencies, which can not be totally eliminated, are acceptable for the purpose of conservation and erosion control planning. Fortunately, most RUSLE2 conservation planning applications assume a uniform overland flow path without subdivision.

5.3. Topographic equations for overland flow having parallel streamlines on non-uniform overland flow paths

RUSLE2 uses the equations described in **Section 2** to compute erosion and sediment load on non-uniform overland flow paths. The overland flow path is divided into segments where soil, steepness, or cover-management change along the overland flow path. The governing equations are numerically solved along the overland flow path starting at the upper end of the overland flow path where overland flow originates (see **Section 2.3**).

Each soil, steepness, and cover-management variable that changes between segments is treated as a step rather than a continuous change (see **Section 2.3.1**). Assuming step changes is appropriate for most cover-management changes, whereas continuous change is appropriate for changes in soil and steepness for overland flow paths on most natural landscapes.

Steepness at the intersection of two segments could be treated as the average of the steepness of the two segments, which is appropriate for describing an overland flow path where steepness changes continuously along the overland flow path, such as a concave overland flow path profile. However, a continuous change in steepness is not appropriate for constructed slopes where steepness makes a step change. Examples include the

intersection a landfill's top with a sideslope and the intersection of a hillslope cut with a flat area. RUSLE2 assumes a step change in steepness to accommodate step changes in steepness common to constructed slopes. The effect of step changes in representing gradual soil and steepness changes along an overland flow path is minimized by dividing the overland flow path into several segments (see the RUSLE2 User's Reference Guide).

A concern in applying RUSLE2 to non-uniform overland flow paths is dealing with changes in infiltration caused by soil and cover-management changes along the overland flow path. RUSLE2 considers how changes in infiltration along an overland flow path affect contouring failure, sediment transport capacity, and deposition. RUSLE2 does not consider how changes in infiltration along an overland flow path affect detachment on a downslope segment. While interrill erosion on a particular segment is only affected by infiltration rate on that segment, rill erosion on a segment is affected by both the runoff generated on that segment and by the runoff that arrives from the upslope area of the overland flow path. This effect can be partially represented by adjusting the upslope overland flow path length to reflect runoff coming into a downslope segment.

Nevertheless, a conflict exists in RUSLE2 between the way that overland flow path distance is treated for computing runoff and the way that overland flow path distance is treated for computing detachment. An example situation is runoff from an upslope pasture draining onto a cultivated field where infiltration on the pasture area is much higher than on the cultivated area. If the actual overland flow length is entered, RUSLE2 computes detachment values that are too high on the cultivated area because runoff reaching the cultivated area will be much less than is implicitly assumed in RUSLE2. If an effective overland flow path length is entered to correctly compute detachment on the cultivated area, RUSLE2 computes runoff rates that are too low on the cultivated area and incorrectly computes detachment on the pasture area. See the RUSLE2 User's Reference Guide for recommendations for selecting overland flow path lengths where infiltration varies greatly along an overland flow path.

The resolution to this problem is to have derived RUSLE2 using process-based erosion equations. Given that most RUSLE2 conservation planning applications involve uniform overland flow paths or overland flow paths where infiltration does not vary greatly along the path, RUSLE2 is considered to produce satisfactory results for most conservation planning applications.

5.4. Applying RUSLE2 to complex topography with converging and diverging overland flow

The RUSLE2 User's Reference Guide describes the proper procedure for applying RUSLE2 to complex topography. The effect of converging and diverging overland flow on RUSLE2 computed erosion is discussed in **Section 5.1**.

The USLE and RUSLE1 are used in GIS applications to compute erosion on topographically complex areas where overland flow converges and diverges. In these

applications, overland flow path distance is considered equivalent to upslope drainage area (Desmet and Govers, 1996). This assumption is questionable as discussed in **Sections 5.2** and **5.Appendix I**. The slope length exponent should be a function of upslope drainage area. If the slope length exponent is used as a function of upslope drainage area, the proper numerical procedure must be used. The irregular slope procedure derived by Foster and Wischmeier (1974) assumes that the slope length exponent does not vary with position along the overland flow path. If the slope length exponent is varied with the Foster and Wischmeier irregular slope procedure, erroneous erosion values will be computed (see **Sections 5.3** and **5.Appendix I**).

RUSLE2 is much more complex than the USLE or RUSLE1 regarding the rill to interrill erosion ratio used to compute slope length exponent values. RUSLE2 may be used in GIS applications to represent complex topography where distance along an overland flow path is assumed to be comparable to upslope drainage area. Such applications should be made ***only*** **where infiltration rate varies little spatially and where convergence or divergence of overland flow is minimal.**

A much better approach than using the RUSLE2 equations is to derive separate rill erosion, interrill erosion, and deposition equations using RUSLE2 assumptions, concepts, and equations. In this approach, a discharge rate can be properly computed from upslope drainage area. The discharge rate can be used to compute rill erosion, sediment transport capacity, deposition, and contouring failure. Interrill erosion is computed independent of upslope drainage area.

A common error in using the USLE and RUSLE1 in GIS applications is that excessively long overland flow path lengths are assumed. Inadequate resolution in topographic data, results in excessively long overland flow paths and poor representation of steepness along the overland flow path (Toy and Foster, 2000). The maximum overland flow path length allowed in RUSLE2 is 1,000 ft (see RUSLE2 User's Reference Guide). In fact, overland flow is collected in concentrated flow areas within 200 ft on most farm fields (Foster, 1985).

When using GIS applications to compute erosion, deposition, and sediment yield, separate relationships should be used to compute sediment production and sediment transport capacity needed to compute deposition. Desmet and Govers (1996) illustrate this procedure.

5.5. Slope length exponent

5.5.1. Slope length exponent for standard (non-Req) conditions

The slope length exponent is the exponent m in equations 2.10 and 5.1. The RUSLE2 slope length exponent is a function of the rill to interrill erosion ratio just is it was in RUSLE1 [Foster and Meyer, 1975; McCool et al., 1989; AH703 (Renard et al., 1997)]. However, in contrast to RUSLE1 where the slope length exponent is time invariant, the RUSLE2 slope length exponent varies daily as cover-management conditions change. A

value for the RUSLE2 slope length exponent for standard, non-Req conditions is computed daily using equations 2.12 and 2.13 (see **Section 5.2**).

5.5.2. Slope length exponent for Req conditions

The erosion processes that occur during the winter Req conditions (see **Section 3.2.5** and RUSLE2 User's Reference Guide) differ from those that occur with standard rill-interrill erosion. Most of the erosion during Req conditions is by surface runoff. The empirically derived RUSLE2 soil length exponent for Req conditions is m = 0.5 (McCool et al., 1989, 2002); [AH703, (Renard et al., 1997)]. The slope length exponent for Req conditions is time invariant and does not vary with the rill to interrill erosion ratio.

The slope length exponent (equations 2.12 and 2.13) for standard, non-Req rill-interrill erosion can be used for the non-Req period (summer period) at Req locations. Standard rill-interrill erosion can be assumed for the summer months at Req locations. This summer period defined for RUSLE2 as the time between the day when average daily temperature becomes greater than 45 ^{o}F early in the year to the day average daily temperature falls to 35 ^{o}F late in the year (see **Section 4.5.1**).

5.6. Steepness effect on rill-interrill erosion

5.6.1. Steepness factors for standard (non-Req) conditions

An interrill erosion steepness factor is used in equation 2.11 and 6.13 to compute interrill erosion and to compute the rill to interrill erosion ratio in several equations (e.g., equations 2.13). A steepness relation for rill erosion is needed to compute rill erosion (e.g., equation 6.13) and the rill to interrill ratio in several equations including equations 2.13. Also, a steepness factor equation is needed to compute rill-interrill erosion combined in equation 2.10.

The same equation used for interrill erosion in RUSLE1 is also used in RUSLE2 [Foster, 1982; AH703 (Renard et al., 1997)]:

$$S_i = 3s_i^{0.8} + 0.56 \qquad [5.1]$$

where: S_i = the interrill erosion steepness factor, s_i = steepness of the interrill area (sine of slope angle). Equation 5.1 is referenced to the unit-plot steepness so that the equation gives a value of 1 for nine percent steepness. The interrill steepness is the same as the overland flow path steepness in RUSLE2. However, the overland flow path steepness and the interrill steepness are not always the same as the land steepness. An example is when RUSLE2 is used to compute erosion on ridge side slopes, where the interrill and overland flow path steepness equals the steepness of the ridge side slopes (see RUSLE2 User's Reference Guide).

A simple rill erosion equation is assumed to compute the rill to interrill erosion ratio (Foster and Meyer, 1975). The steepness factor for rill erosion is:

$$S_r = s_r / 0.0896 \qquad [5.2]$$

where: S_r = the rill erosion steepness factor and s_r = steepness of the rill area (sine of slope angle). This steepness factor is normalized to the nine steepness of the unit plot. The steepness of the rill area is the same as the overland flow path steepness, which can differ from the land steepness.

A third steepness factor is used to compute rill-interrill erosion in equation 2.10. The relationship of rill-interrill erosion for a wide range of studies is shown in Figure 5.1 (McCool et al., 1987). These erosion data were normalized to the erosion for 20 percent steepness rather than to the unit plot nine percent steepness.

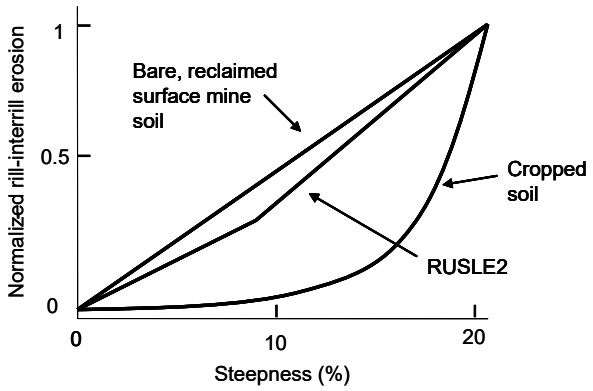

Figure 5.1. Effect of slope steepness on rill-interrill erosion.

The steepness factor for rill-interrill differed greatly among cover-management conditions. At one extreme is where erosion varied linearly for a bare reclaimed, surface mine soil. Steepness had little effect on runoff in this case. At the other extreme is erosion for a cropped soil where the relationship between erosion and steepness is very non-linear. In this case, runoff increased as steepness increased. Most of the erosion for the cropped soil at low steepness is caused by interrill erosion with little or no rill erosion. Once the overland flow path steepness exceeds a critical steepness, rill erosion begins, which results in rill-interrill erosion increasing rapidly. Runoff's shear stress must exceed a critical shear stress for rill erosion to begin, much like contouring failure. The resulting rill erosion equation would have rill erosion being proportional to the difference between shear stress applied to the soil and a critical shear stress related to soil conditions (Meyer et al., 1975b; Foster, 1982; Graf, 1971; Foster et al., 1980a).

The relation of rill-interrill erosion to overland flow path steepness should be a function of the rill to interrill erosion ratio and a critical shear stress at which rill erosion begins. However, in contrast to the temporally varying slope length effect, RUSLE2 uses an invariant slope steepness factor. Although erosion theory indicates reasons why the steepness factor should vary, the experimental plot data were not sufficient to develop a RUSLE2 steepness factor as a function of the rill to interrill erosion ratio, critical shear stress, or other variables. Consequently, RUSLE2 uses the invariant steepness relationship illustrated by the middle curve in Figure 5.1. The equation for that curve is given by [McCool et al., 1987; AH703 (Renard et al., 1997)]:

$$S = 10.8s + 0.03 \quad s_p < 9\% \qquad [5.3]$$

$$S = 16.8s - 0.50 \quad s_p \geq 9\% \qquad [5.4]$$

where: S = steepness factor in equation 2.10, s = overland flow path steepness (sine of slope angle) and s_p = overland flow path steepness (100 times tangent of slope angle). Equations 5.3 and 5.4 give a value of 1 referenced to the unit plot 9 percent steepness rather than the 20 percent steepness in Figure 5.1.

5.6.2. Steepness factor for Req conditions

A special steepness factor relationship is used for Req winter conditions because erosion processes for the Req condition differ significantly from the standard rill-interrill erosion conditions. Most of the erosion is caused by surface runoff during the Req conditions. The empirically derived steepness factor for Req conditions is given by [McCool et al., 1987; McCool et al., 1997; AH703 (Renard et al., 1997)]:

$$S = 10.8s + 0.03 \quad s_p < 9\% \qquad [5.5]$$

$$S = (s / 0.0896)^{0.6} \quad s_p \geq 9\% \qquad [5.6]$$

where: 0.0896 = the sine of the angle for 9 percent unit plot steepness. Equations 5.4 and 5.6 are also referenced to the unit plot steepness.

Equations 5.3 and 5.4 can be used for the summer period at locations where the Req winter effects occur.

5.7. Topographic relationships for short overland flow paths (x ≤ 15 ft)

Equation 2.10 does not apply for short overland flow path distances because these equations compute a zero erosion rate for a zero overland flow path length. Erosion rate should equal the interrill erosion rate at the origin of overland flow (x = 0). Experimental interrill erosion studies show that overland flow path length must be about 15 feet before rill erosion begins to occur (Meyer and Harmon, 1989), a distance that is also consistent with field observations, including rainfall simulator studies of the variables that affect rill-interrill erosion (Meyer et al., 1975ab). Therefore, equation 2.10 is assumed not to apply to short overland flow path distances less than 15 ft.

5.7.1. Overland flow steepness < 9 percent

The overland flow path distance x is set to 15 ft when the actual overland flow path distance is less than 15 ft to represent the concept that interrill erosion is independent of distance. The preferred steepness factor for interrill erosion is equation 5.1, but his equation conflicts with the empirically derived rill-interrill erosion S factor given by equation 5.3 for steepness less than 9 percent. Therefore, the rill-interrill erosion steepness factor, equation 5.3, is used for all overland flow distances less than 15 ft if the overland flow path steepness is less than 9 percent. The variables used for $(x/\lambda_u)^m S$ in equation 2.10 are $(15/72.6)^m S_i$ where S_i is the rill-interrill steepness factor computed from

equation 5.3, 15 = 15 ft, the overland flow path length assumed for all overland flow path lengths less than 15 ft, and 72.6 = 72.6 ft, the unit plot length.

5.7.2. Overland flow path steepness ≥ 9 percent

5.7.2.1. Overland flow path length ≤ 3 ft

The inconsistency between the interrill steepness factor, equation 5.1, and the rill-interrill steepness, equation 5.4, does not occur when overland flow path steepness exceeds 9 percent. If the overland flow path length is less than or equal to 3 ft, the rill-interrill steepness factor in equation 2.10 equals the interrill steepness factor, equation 5.1. The overland flow path distance is set to 15 ft regardless of actual overland flow path distance. The variables used for $(x/\lambda_u)^m S$ in equation 2.10 are $(15/72.6)^m S_i$ where S_i is the interrill steepness factor computed from equation 5.1, 15 = 15 ft, the overland flow path length assumed for all overland flow path lengths less than 15 ft, and 72.6 = 72.6 ft, the unit plot length.

5.7.2.2. Overland flow path 3 ft < x ≤ 15 ft

A logarithmic interpolation is used to transition between the interrill steepness factor, equation 5.1, at a 3 ft overland flow distance to the rill-interrill steepness factor, equation 5.4, at a 15 ft overland flow distance. This interpolation is computed as:

$$\alpha_3 = (3/72.6)^m S_i \qquad [5.7]$$

$$\alpha_{15} = (15/72.6)^m S \qquad [5.8]$$

where: α_3 and α_{15} = the combined distance and steepness factor for 3 ft and 15 ft overland flow path lengths, respectively, at the given steepness, 15 = 15 ft, the assumed overland flow path distance for all actual overland flow path distances less than 15 ft. The interrill steepness factor S_i, equation 5.1, is used to compute and S = the rill-interrill steepness factor, equation 5.3, is used to compute the steepness effect at a 15 ft overland flow distance. A logarithmic interpolation is made between α_3 in equation 5.7 and α_{15} in equation 5.8 as:

$$\ln(\alpha_x) = [\ln(\alpha_{15}) - \ln(\alpha_3)][(\ln(x) - \ln(15)]/[\ln(15) - \ln(3)] + \ln(\alpha_3) \qquad [5.9]$$

$$\alpha_x = \exp[\ln(\alpha_x)] \qquad [5.10]$$

where: α_x = the combined length and steepness factor at the overland flow distances between 3 and 15 ft and an overland flow path steepness greater than 9 percent. This distance and steepness factor value is used in equation 2.10 for the variables $(x/\lambda_u)^m S$.

5.8. Effect of position along overland flow path on soil loss tolerance (T) factor

The powerful conservation planning approach of comparing an estimated erosion rate to an allowable erosion rate developed in the mid 1940's (Mannering, 1981; McCormack and Young, 1981; Toy et al., 2002). Erosion control practices resulting in an estimated erosion rate that is less than the allowable erosion rate are considered to provide adequate erosion control for the site. Soil loss tolerance (T) values assigned to soil mapping units in the USDA-NRCS Soil Survey are widely used for allowable erosion rate on croplands.[42] Other values for the erosion control criteria are used when RUSLE2 is applied to other lands including construction sites and rangelands. For example, very low soil loss tolerance values are used for very fragile soils that are easily damaged by erosion. Soil loss tolerance values larger than those used for cropland are often used for construction sites for the disturbance and reclamation periods. However, cropland soil loss tolerance values are used for the after-reclamation period where maintenance of the soil for long-term vegetation production is the primary erosion control concern.

Erosion is not considered excessive if the estimated erosion rate is less than the T value. The procedure implicitly assumes a uniform overland flow path, which is common practice in most erosion prediction applications and in research used to determine soil loss tolerance (T) values. The average erosion rate for the entire overland flow path, rather than maximum erosion rate, is compared to the soil loss tolerance (T) value.

The erosion rate computed with RUSLE2 varies along even a uniform overland flow path from an interrill erosion rate at the origin of overland flow ($x = 0$) to $(m+1)$ times the average erosion rate for the entire overland flow path length at the end of the path ($x = \lambda$). Therefore, erosion rate over the approximate lower one half of uniform overland flow paths exceeds T when the average erosion rate for the overland flow path equals T. That is, the conservation planning criteria does not require that maximum erosion rate along an overland flow path be less than soil loss tolerance; only that average erosion rate for a uniform overland flow path be less than soil loss tolerance [AH703 (Renard et al., 1997); Toy et al., 2002].

Comparing average erosion rate for the overland flow path to soil loss tolerance is not appropriate for overland flow paths on non-uniform shape profiles, especially convex profiles. To make these comparisons, RUSLE2 computes an adjusted soil loss tolerance value that is compared against the RUSLE2 estimated erosion rate for each segment along a non-uniform overland flow path (see the RUSLE2 User's Reference Guide). The comparison with the adjusted T value puts conservation planning on the same basis for non-uniform overland flow paths as for a uniform overland flow path. The adjusted soil

---

[42] Soil loss tolerance (T) values have a specific definition in the NRCS Soil Survey and NRCS RUSLE2 applications. However, T in general RUSLE2 applications refers to the erosion control criteria used in a specific RUSLE2 application. This value can be quite different from the assigned NRCS T value depending on the application. See the RUSLE2 User's Reference Guide.

loss tolerance values are the T factor values for the soil on *jth* segment times a factor value computed with [(AH703 (Renard et al., 1997)]:

$$F_j = (x_j^{m_i+1} - x_{j-1}^{m_i+1}) / [(x_j - x_{j-1})\lambda^{m_i}] \quad [5.11]$$

where: F_j = the factor that is used to multiply the soil loss tolerance (T) value to obtain a soil loss tolerance value adjusted based on the position of the *jth* segment along the overland flow path, x_j = distance to the lower end of the *jth* segment, m_j = slope length exponent for the *jth* segment, and λ = the entire length of the overland flow path. The ratio of computed erosion rate to the adjusted soil loss tolerance value is the same for all segments along a uniform overland flow path.

5.9. Conservation planning soil loss

RUSLE2 computes a conservation planning soil loss where deposition is given partial credit based on the location where the deposition occurs along the overland flow path. This type of deposition, which is referred to as remote deposition, occurs on concave overland flow path profiles and at the upper edge of dense vegetations strips. The use of conservation planning soil loss in conservation planning is discussed in the RUSLE2 User's Reference Guide, and the equations used to compute a value for conservation planning soil loss are given in **Section 2.3.10.4**.

Partial credit for deposition as soil saved also is taken with terraces. The deposition credit decreases as terrace spacing increases beyond 90 ft. However, the credit for deposition remains constant for terrace spacing closer than 90 ft.

High ridges spaced about 3 ft apart on a uniform, nearly flat grade act like small terraces. RUSLE2 can be applied to the ridge side slopes just like RUSLE2 is applied to the inter-terrace interval. The furrows between the ridges act like terrace channels. The deposition in the furrows should be treated as local deposition rather than remote deposition. The conservation planning soil loss that RUSLE2 computes for this case incorrectly assumes that this deposition is remote deposition. The user should ignore the conservation planning soil loss and use sediment yield as the conservation planning soil loss.

5.10. List of symbol

a = coefficient that is product of terms that do not vary with x in $D = ax^m$

a_e = product of terms that do not vary with x in $D = a_e x_e^m$ when x_e is the overland flow distance adjusted in proportion to upslope drainage area for converging runoff surface

a_p = product of terms that do not vary with x in equation $D = a_p x^m$ when runoff streamlines are parallel

a_T = product of terms that do not vary with x in sediment transport capacity equation $T_c = a_T q$

A = average combined rill-interrill erosion rate for the slope length λ (mass/area·time)

D = combined rill-interrill erosion (detachment) rate at location x along an overland flow path (mass/area·time)

D_i = interrill erosion rate (mass/area·time)

D_r = rill erosion rate (mass/area·time)

D_{rc} = capacity rill erosion rate (mass/area·time)

F = factor used to multiply soil loss tolerance (T) to obtain adjusted soil loss tolerance value based on position of segment along overland flow path

g = sediment load (mass/width·time)

g_λ = sediment load at end of overland flow path

k_c = product of terms that do not vary with x in equation $A = k_c \lambda^m$

k_r = product of terms that do not vary with x in rill erosion equation $D_r = k_r x$

m = slope length exponent

q = discharge rate (volume/width·time)

q_c = discharge rate at which runoff shear stress applied to soil equals the soil's critical shear stress

s = overland flow path steepness (sine of slope angle)

s_i = interrill area steepness (sine of slope angle)

s_p = overland flow path steepness (100 times tangent of slope angle)

s_r = rill area steepness (sine of slope angle)

S = combined rill-interrill erosion steepness factor

S_i = interrill erosion steepness factor

S_r = rill erosion steepness factor

T = soil loss tolerance (mass/area·time)

T_c = runoff's sediment transport capacity (mass/width·time)

$T_{c\lambda}$ = runoff's sediment transport capacity at end of overland flow path (mass/width·time)

W = width of runoff surface at location x (length)

x = distance along overland flow path (length)

x_e = distance along overland flow path that is proportional to upslope drainage area for converging runoff surface (length)

α_x = combined length and steepness factor at overland flow distances between 3 and 15 ft and overland flow path steepness greater than 9 percent

α_3 = combined distance and steepness factor for 3 ft overland flow path length at a particular steepness

α_{15} = combined distance and steepness factor for 15 ft overland flow path length at a particular steepness

Δ = change in a variable

β = ratio of rill erosion sediment load to interrill erosion sediment load

λ = overland flow path length

λ_u = unit plot overland flow path length (72.6 ft, 22.1 m)

ρ = term in equation $\beta = \rho x$

σ = excess rainfall rate (length/time)

Indices

j – segment

5.Appendix 1. Slope length exponent that varies with position

5.Appendix 1.1. Derivation of equations

The RUSLE2 slope length exponent m does not vary with position along the overland flow path. The topographic equations for the slope length exponent m varying with position along the overland flow path are much more complex than the equations used in RUSLE2. The additional complexities and reduced robustness did not warrant their use in RUSLE2 for routine erosion-control planning in local field offices. However, a variable slope length exponent m that varies with position along the overland flow path is very important for applying RUSLE2 to landscapes where surface runoff converges or diverges. Representation of flow convergence/divergence must be considered when RUSLE2 equations are used in GIS models applied to three dimensional landscapes.

In the 1940's when erosion prediction was first developed as an erosion-control planning tool, the following simple empirical equation became widely accepted for describing how erosion varies with overland flow path length for uniform slopes (Zingg, 1940).[43]

$$A = k_c \lambda^m \qquad [V.1]$$

where: A = average erosion rate (mass/area·time) for the slope length λ, k_c = a term that combines the other terms used to compute A that are not a function of λ, and m = the slope length exponent. Equation V.1 is a derived equation. The equation that actually represents the measured field data is:

$$g_\lambda = k_c \lambda^{m+1} \qquad [V.2]$$

where: g_λ = the sediment load (mass/width·time) at the end of the slope length λ, which was the measured sediment discharge from the plots used to measure erosion. The term A in equation V.1 was determined by dividing equation V.2 by the slope length λ. Soil loss A was the variable needed in erosion-control planning.

Equation V.2, not equation V.1, is the starting point for developing RUSLE2 (and the USLE and RUSLE1) equations that represent spatial variability along overland flow paths (Foster and Wischmeier, 1974). The equation for detachment at any point along a uniform overland flow path can be derived by differentiating equation V-2 as:

$$D = dg / dx \qquad [V.3]$$

where: D = detachment rate (mass/area·time) at the location x along an overland flow path. The derivation of a detachment equation is simple where the slope length exponent m is not a function of position x along the overland flow path. By inspection, equation

---

[43] Uniform means that steepness does not vary with x and the surface runoff streamlines are parallel.

V.2 is recognized to compute sediment load g (mass/width·time) at any position x along a uniform slope as well as sediment load at the end of the overland flow path. If m does not vary with position, the detachment equation is:

$$D = (m+1)k_c x^m \qquad [V.4]$$

Equation V.4 is equation 2.10 with terms except x and m combined in k_c. **Thus, equation 2.10 is based on the assumption that m does not vary with x**. Consequently, the rill to interrill erosion ratio term in equation 2.13 does not contain a distance (x or λ) term. Equation V.4 does not correctly compute detachment if m is varied by segment. If that computation is attempted, sediment load values at the end of the overland flow path for a uniform overland flow path become a function of how many segments and their lengths that are used to divide the overland flow path even if conditions do not vary between segments. **Therefore, if the slope length exponent m is to vary with position x, a new detachment equation must be derived to replace equation 2.10**.[44]

The slope length exponent m was observed to vary from about 0 to 1 for measured ersion data (McCool et al., 1989). Other than m increasing with slope steepness up to five percent steepness, possible reasons for m varying did not seem to be understood when the USLE was developed (Wischmeier and Smith, 1975; Foster and Meyer, 1975).

As early as the mid 1940's, detachment on overland flow areas was recognized to be caused by raindrop impact and surface runoff (Ellison, 1947). Detachment by flow varied much more along the overland flow path than detachment by raindrop impact. These terms are written as (Meyer and Wischmeier, 1969; Foster and Meyer, 1975):

$$D = D_r + D_i \qquad [V.5]$$

where: D_r = rill erosion (mass/area·time), D_i = interrill erosion (mass/area·time), and D = the total of rill and interrill erosion (mass/area·time) at the location x. Interrill erosion is assumed not to vary along a uniform overland flow path, while rill erosion is assumed to vary with (Foster and Meyer, 1975):

$$D_r = k_r x \qquad [V.6]$$

where: k_r = a product of terms that do not vary with x. The combined equation for rill-interrill erosion is therefore:

---

[44] RUSLE2 did not have the slope length exponent m as a function of x to avoid extrapolation too far beyond the experimental data. Only two sets of plots used to derive RUSLE2 had overland flow path lengths greater than 150 ft. Not having the slope length exponent vary with position x significantly increases RUSLE2's robustness, which is important for an erosion control planning tool.

$$D = k_r x + D_i \quad [V.7]$$

Equation V.4 was chosen as the basic RUSLE2 detachment equation because a wide array of empirically derived and **accepted** factor values are available for that form (see **Section 1**). Equation V.7 was used to extrapolate equation V.4 to conditions beyond that represented in the USLE plot data.

The RUSLE2 approach was to start with equation V.4 and mold it to equation V.7 as much as possible. However, the difference in equation form between equations V.4 and V.7 causes conflict within RUSLE2. Rules were established to deal with those conflicts (see **Section 2.3.8.3**).

The m value for equation V.7 increases from 0 at x = 0 to 1 as either x or k_r becomes large or D_i becomes small (McCool et al., 1989). Mathematical analysis of equation V.7 shows that the slope length exponent m varies from 0 to 1 and is a function of the rill to interrill erosion ratio as (Foster and Meyer, 1975):

$$m = \beta/(\beta + 1) \quad [V.8]$$

where: β = the ratio of rill sediment load to interrill erosion sediment load, which is equation 2.12. The equation for β from equation V.7 is:

$$\beta = \frac{(k_r x / 2)}{D_i} \quad [V.9]$$

which is equation 2.13 with an x term in the numerator.

Equation V.9 can be simplified to:

$$\beta = \rho x \quad [V.10]$$

where: $\rho = k_r/2D_i$. Substitution of equation V.10 into equation V.8 gives:

$$m = \rho x/(\rho x + 1) \quad [V.11]$$

Substitution of equation V.11 into equation V.2 gives:

$$g = k_c x^{[\rho x/(\rho x+1)]+1} \quad [V.12]$$

The equation form for sediment load when the slope length exponent m varies with position x differs significantly from equation V.2, which is the RUSLE2 form. An equation for D can be derived by differentiating equation V.12 with respect to x. The resulting equation is much more complicated than equation V.4 used in RUSLE2. However, equation V.12 can be solved numerically to determine values for average detachment for a segment to route sediment downslope as described in **Section 2.3**. However, equation V.12 was not used in RUSLE2 because of concerns about its robustness.

Equation V.12 is based on the assumption that equation V.6 describes rill erosion. Equation V.6 could be written as:

$$D_r = k_r q \qquad [V.13]$$

where: q = discharge rate (volume/width·time), q = σx where σ = excess rainfall rate (length/time) that is assumed to be constant along the overland flow path, and k_r = a collection of terms that do not vary with x.

A case can be made for two other rill erosion equation forms. One form is (Meyer et al., 1975):

$$D_r = k_r (q - q_c) \qquad if\,(q \le q_c) D_r = 0 \qquad [V.14]$$

where: q_c = the discharge rate where runoff shear stress applied to soil exceeds the soil's critical shear stress and rill erosion begins and k_r = the collection of terms that do no vary with x.

A case can also be made for (Foster and Meyer, 1975):

$$D_r = D_{rc}(1 - g / T_c) \qquad [V.15]$$

where: D_{rc} = detachment capacity (mass/area·time) computed with equation V.6 or V.14 and T_c = runoff's sediment transport capacity (mass/width·time). Transport capacity is computed with:

$$T_c = a_T q \qquad [V.16]$$

where: the term a_T is the product of terms that do not vary with position x. Equation V.15 reduces rill erosion as transport capacity becomes filled with sediment on long overland flow paths or where sediment production rate by rill or interrill erosion is very high.

As Figure V.1 shows, the ax^m form (equation 2.10) fits well the equation form D_i+k_rx except for short overland flow paths. This deficiency is corrected as described in Section 5.7. However, neither of these two equation forms fits V.14 or V.15, an equation form that involves a critical shear stress term for estimating rill erosion.

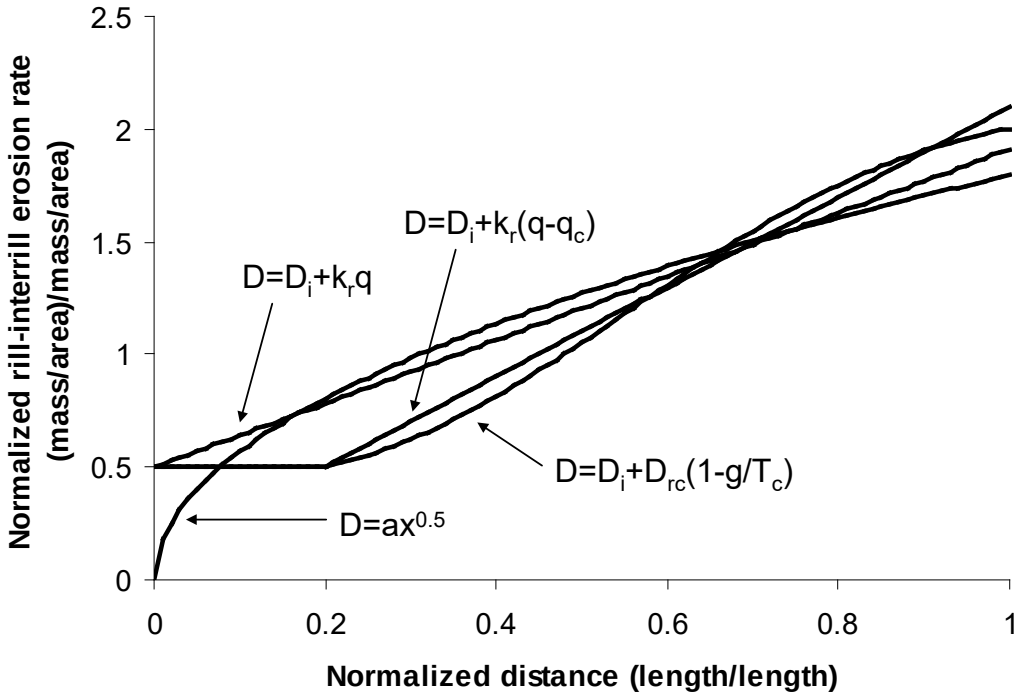

Figure V.1. Variation of detachment along an overland flow path for various rill erosion equation forms.

These advanced rill erosion equation forms greatly complicate RUSLE2 mathematics and further reduce RUSLE2's robustness of. A questionable gain in accuracy while losing robustness is not a wise choice for RUSLE2 as an erosion control planning tool. Choices were made in RUSLE2 that favor robustness for erosion control planning. RUSLE2 may not be as accurate as it could be but it is less likely to give poor results because of uncertainties when extrapolated.

5.Appendix 1.2. Implications for use of RUSLE2 in GIS models

A sediment transport capacity equation should be included with RUSLE2 detachment equations when RUSLE2 is used in a GIS model that computes that computes the spatial variability in erosion and deposition over the landscape. Equation 2.10 is used to compute sediment production (detachment) and equation 2.17 and other equations are used to compute deposition. A sediment transport capacity is required to compute deposition, and a deposition equation like equation 2.16 should be used also. The RUSLE2 sediment production equation (i.e., equation 2.10) does not and can not be used to compute deposition that occurs on the toe of many natural hillslopes.

Also, the RUSLE2 detachment equation 2.10 should be modified to compute how erosion varies with either converging or diverging surface runoff. Applying equation 2.10

without varying the slope length exponent m can result in significant error, even when the overland flow path length is varied in proportion to upslope drainage area.

5.Appendix 1.2.1. Computing detachment and sediment transport capacity

RUSLE2 computes sediment transport capacity per unit width as a function of discharge rate per unit width. An equivalent overland flow path length can be used to represent a converging or diverging landscape to compute discharge rate per unit width and sediment transport capacity per unit width. However, RUSLE2 does not compute the proper sediment production (detachment) values because equation 2.10 does not contain a runoff term. The equivalent overland flow path length that works for computing sediment transport capacity is not the equivalent length required to compute detachment. Furthermore, even though the overland flow path length is adjusted, the slope length exponent m also should be varied with position along the overland flow path to properly represent convergence/divergence in computing detachment with equation 2.10.

5.Appendix 1.2.2. Equations for RUSLE2 in a GIS model

A simple erosion model can be used to evaluate the behavior of RUSLE2 equations in a GIS model. The watershed for a single rill on a hillslope where the streamlines are parallel is a rectangle of width W and length λ. The watershed for a single rill on a converging surface is pie (wedge) shaped. The width at the upper end is 2W and 0 at the lower end. Figure V.2 shows a plot of computed erosion along the overland flow path where streamlines are parallel and where streamlines converge. Erosion was computed with the equation form D_i+k_rq using discharge rate computed by multiplying the excess rainfall rate by the upslope area divided by the watershed width at x. This equation form is assumed to give the desired values, and thus the other equation forms are compared against this one.

The x in the ax^m equation form in Figure V.2 is proportional to upslope drainage area. As Figure V.2 shows, the ax^m approximation does well where streamlines are parallel except for short overland flow paths. In contrast, the ax^m approximation does not work well where the streamlines converge.

When discharge is assumed to be a broad sheet flow across the individual rill watersheds, discharge rate rapidly increases and approach infinity as x approaches λ, the overland flow path length. A corresponding increase in rill erosion is computed. An infinite discharge rate per unit width at $x = \lambda$ computes an infinite rill erosion rate. Such high erosion rates near the end of converging surfaces are not observed in the field. Consequently, the broad sheet flow assumption should not be used without carefully constructed limits on converging surfaces. This problem does not exist on diverging surfaces.

A better approach than assuming broad sheet flow across the entire rill watershed is to assume that surface runoff is concentrated in defined rills. The overland flow path ends where the interrill path length becomes zero, which is where the rill edges meet. Discharge rate (volume; not volume per unit width) does not go to infinity, which means that rill erosion rate does not go to infinity (Toy and Foster, 2000).

The other equation form evaluated in Figure V.2 is equation V.12 where the slope length exponent varies with distance along the overland flow path. This equation was solved numerically to compute detachment along the overland flow path. In these computations, the slope length exponent m was varied with discharge rate rather actual distance to reflect the increase in rill erosion as the surface runoff converges. This approach, while improved, is less than satisfactory.

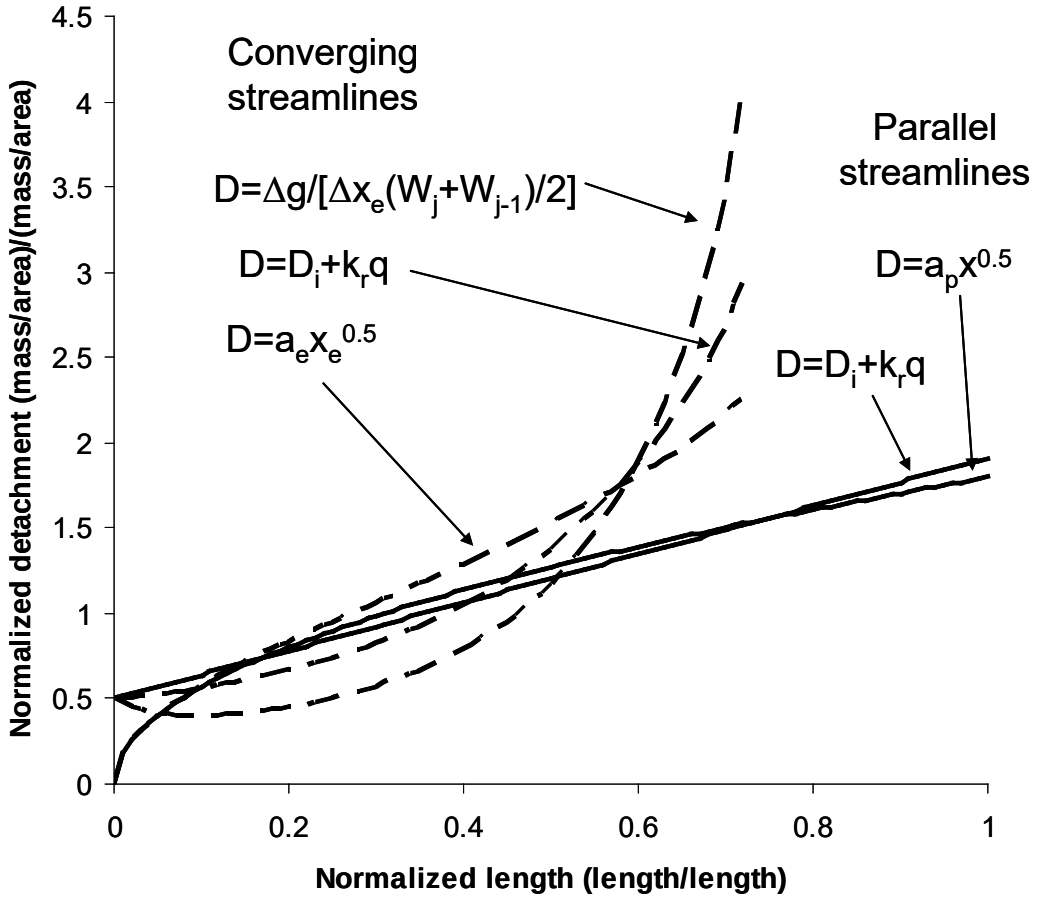

Figure V.2. Erosion along the overland flow paths for parallel and for a converging streamlines.

None of the approximations compare well to the preferred erosion equation that has separate terms for rill and interrill erosion. The best approach in applying RUSLE2 in a GIS model is to devolve the equation 2.10 into separate terms for rill and interrill erosion. Discharge rate can be computed and used directly in both the detachment and sediment transport equations without having to make the overland flow path length proportional to

upslope drainage area. This approach would significantly simplify RUSLE2 and would remove the inconsistencies between equation forms.

6. COVER-MANAGEMENT

Equation 2.10 includes the term c used to compute the main effect of cover-management on detachment. The c factor is the product of subfactors as:[45]

$$c = c_c g_c s_r r_h s_b s_c s_m \quad [6.1]$$

where: c = daily cover-management factor, c_c = daily canopy subfactor, g_c = daily ground (surface) cover subfactor, daily s_r =soil surface roughness subfactor, r_h = daily ridge height subfactor, s_b = daily soil biomass subfactor, s_c = daily soil consolidation subfactor, and s_m = daily antecedent soil moisture subfactor used when RUSLE2 is applied in Req zones (see RUSLE2 User's Reference Guide). A daily cover-management c factor value is computed using daily values for each of the subfactors in equation 6.1.[46]

6.1. Canopy subfactor

Canopy is live and dead vegetative cover above the soil surface that intercepts raindrops but does not contact the surface runoff. The portion of the above ground plant biomass touching the soil surface is treated as live ground cover. The canopy subfactor equation is (Wischmeier, 1975; Yoder et al. 1997):

$$c_c = 1 - f_{ec} \exp(-0.1 h_f) \quad [6.2]$$

where: f_{ec} = daily effective canopy cover (fraction) and h_f = daily effective fall height (ft). Equation 6.2 is based on how canopy cover affects the impact energy of waterdrops falling from canopy that has intercepted rainfall. The impact energy of a waterdrop striking the soil surface is:

$$e_d = m_d V^2 / 2 \quad [6.3]$$

where: e_d = impact energy of the waterdrop, m_d = waterdrop mass, and V_d = the waterdrop impact velocity.

Canopy cover affects waterdrop impact energy in several ways. Canopy cover increases the size of waterdrops falling from the canopy. Waterdrops falling from canopy have

---

[45] The RUSLE2 subfactor procedure is an extension of the RUSLE1 procedure [AH703 (Renard et al., 1997)]. The RUSLE2 procedure has several scientific improvements and added capability, and it uses of a daily time step rather than the RUSLE1 half-month time step. The RUSLE1 and RUSLE2 subfactor procedures are patterned after ones developed and used by Wischmeier (1975); (Wischmeier, 1978); Dissmeyer and Foster (1981); Mutchler et al. (1982); and Laflen et al. (1985).

[46] This section describes the subfactor relationships. Other sections describe how RUSLE2 computes values for variables used by the subfactor equations.

about a 3 mm drop diameter compared to 1.5 mm for median drop diameter of raindrops (Wischmeier, 1975). Therefore, canopy must be sufficiently close to the ground surface for waterdrops falling from canopy to have reduced impact velocity to offset the increased mass of waterdrops falling from canopy in comparison to raindrops. Because of the increased drop size, the impact energy of water drops falling from tall canopies, (e.g., 30 ft high) exceeds the impact energy of raindrops (Chapman, 1948). Equation 6.2 is based on an assumed 3 mm diameter for waterdrops falling from canopy and empirical fall velocities of waterdrops based on effective fall height h_f (Gunn and Kinzer. 1949).

Equation 6.2 should be interpreted as empirically representing the main effects of canopy cover on detachment with a particular equation form rather than describing how a physical variable, impact energy, affects detachment. Equation 6.2 does not directly represent all of the ways that canopy affects detachment. For example, some of the intercepted rainfall becomes stem flow and reaches the soil surface without falling from the canopy. Also, some of the intercepted rainfall evaporates from the vegetation, never to reach the soil surface by drop impact or stemflow. Also, RUSLE2 does not consider how wind driven rainfall in conjunction with vegetation affects erosion.[47]

Input effective fall height values are chosen based on judgment of how canopy of a particular plant type affects erosion (see RUSLE2 User's Reference Guide). The reference fall height, illustrated in Figure 6.1, is one third of the distance from the bottom of the canopy to the top of a canopy for a cylindrical shaped canopy where the vegetative surface area is uniformly distributed along the vertical axis of the canopy.

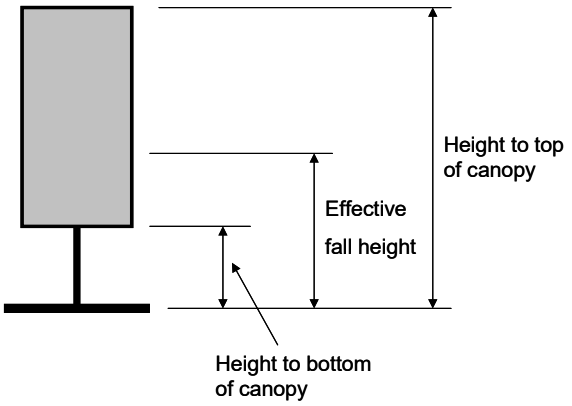

Figure 6.1. Effective fall height for a cylindrical shaped, uniform gradient canopy.

RUSLE2 also includes an equation that can be used to compute effective fall height. The equation is a function of canopy shape, vertical gradient of vegetative surface area, and heights to the bottom and top of the canopy. The effective fall height equation is:

$$h_f = h_b + a_s a_g (h_t - h_b) \qquad [6.4]$$

where: h_b = the height to the bottom of the canopy, h_t = the height to the top of the canopy, and a_s = a coefficient that is a function of canopy shape, and a_g = a coefficient

[47] An improved approach would be to divide equation 6.2 into two parts, one part related to interrill erosion and one part related to rill erosion.

Table 6.1. Values for the coefficient a_s used to estimate effective fall height as a function of canopy

Canopy shape	Value
Inverted trianagle	0.5
Rectangle	0.33
Diamond	0.29
Round	0.29
Triangle	0.25

Table 6.2. Values for coefficient a_g used to estimate fall height as a function of concentration of surface area within canopy.

Location of surface surface area concentration	Value
Top	1.33
Toward top	1.17
Uniform	1.00
Toward bottom	0.88
Bottom	0.75

related to the height within the canopy where vegetative surface area is concentrated. Values for the coefficient a_s and a_g are given in Tables 6.1 and 6.2, respectively.

Some vegetation communities involve multiple plant types that produce over and under stories. RUSLE2 uses only a single set of variables to represent the net effect of canopy on erosion. RUSLE2 does not mathematically combine sets of values for over and under stories nor does RUSLE2 separately compute how each canopy type affects erosion. RUSLE2 uses a single set of values in equation 6.2 to compute the net canopy effect for the vegetation that exists on any given day.

In addition to varying with plant community type, effective fall height varies with production (yield) level and with time as vegetation emerges, grows, matures, and experiences senescence. The RUSLE2 computes effective fall height as a function of production (yield) level and time (see **Sections 9.1** and **9.3.3.3)**.

Canopy cover directly above ground cover is assumed not to affect erosion. The equation used to compute daily effective canopy cover f_{ec} is:

$$f_{ec} = f_c(1 - f_g) \qquad [6.5]$$

where: f_c = daily canopy cover (fraction) and f_g = daily net ground cover, which takes into account the overlap of different types of ground (surface) cover (see **Section 10.2.4**). Net ground cover equals 1 – fraction of the soil surface exposed to direct waterdrop impact from either rainfall or waterdrops falling from canopy.

Furthermore, the RUSLE2 assumption is that canopy cover affects erosion the same way as does ground cover when effective fall height becomes zero. Therefore, the value for the canopy subfactor c_c can not be less than the ground cover subfactor g_c when ground cover equals the effective canopy cover value f_{ec}.

6.2. Ground cover subfactor

Ground cover is provided by material directly in contact with the soil surface. Ground cover affects both waterdrop impact, which in turn affects interrill erosion, and surface runoff, which in turn affects rill erosion. The RUSLE2 equation for the ground cover subfactor is given by (Foster and Meyer, 1975; Laflen et al., 1985; Yoder et al., 1997):

$$g_c = \exp[-bf_g(0.24/R_a)^{0.08}] \qquad [6.6]$$

where: **b** = a coefficient (percent^{-1}) that describes the relative effectiveness of the ground (surface) cover for reducing erosion, f_g = net ground cover (percent), R_a = adjusted roughness used to compute the soil surface roughness subfactor (inches) (see **Section 6.3**), and 0.24 is the assumed adjusted soil surface roughness value (inches) for unit plot conditions. Research has shown that a single variable, portion of the soil surface covered by material directly in contact with the soil surface, describes how all types of ground (surface) cover affects rill-interrill erosion. Analysis based on fundamental erosion mechanics shows that large diameter, long pieces of material, such as intact corn stalks, perpendicular to the overland flow path should affect rill-interrill erosion per unit of soil surface covered more than small diameter, flat pieces (Brenneman and Laflen, 1982). A special concern is how rock fragments on the soil surface affects rill-interrill erosion (see **Section 4.6**). However, when data from various types and rates of surface cover are combined, portion of the soil surface covered seems adequate as a single ground cover variable to use in the ground cover subfactor, equation 6.6 (Box, 1981; Dickey et al., 1983; Dickey et al., 1985; Laflen and Colvin, 1981; Meyer et al., 1972; Simanton et al., 1984; Meyer et al., 1970; Swanson et al., 1965; 1970; Mannering and Meyer, 1963; Meyer and Mannering, 1967).

Net ground cover used in equation 6.6 takes into account the overlap of ground cover materials. For example, applied materials, such as mulch and erosion control blankets, and plant residue are assumed to lie on top of rock cover entered in the RUSLE2 soil input. Live ground cover is assumed to lie on top of applied material and plant residue. Thus, net ground cover (percent) is 100 – bare ground (percent).

The soil surface roughness term in equation 6.6 computes a reduced effect of ground cover on rough soil surfaces. The RUSLE2 assumption is that ground cover in soil depressions is covered by water and deposited sediment, and therefore has no effect on erosion.

The RUSLE2 ground cover subfactor computed with equation 6.6 only partially captures the effect of ground (surface) cover material on rill-interrill erosion. A RUSLE2 ground cover subfactor value is primarily the ratio of rill-interrill erosion at a given point in time with ground (surface) cover to rill-interrill erosion from the same soil in unit plot conditions. The effect most represented by the RUSLE2 ground cover subfactor is how the physical presence of surface cover material affects the erosive forces applied to the soil by impacting raindrops and waterdrops falling from canopy and surface runoff. Other subfactors, such as soil surface roughness and soil biomass, are affected by ground (surface) cover materials (see **Sections 6.3 and 6.5**).

Many of the **b** values reported in the literature were determined by plotting erosion solely a function of ground cover. The RUSLE2 **b** values used in equation 6.6 are not the same as the literature **b** values. The RUSLE2 **b** values are smaller than the literature values because the literature **b** values include other effects not included in equation 6.6. Erosion values were computed with RUSLE1 for a range of corn yields for mulch-till and no-till cropping systems to illustrate this difference. The net **b** value for equation 6.6 without the surface roughness terms fitted to erosion values plotted as a function as cover immediately after planting was 0.058. In comparison, the **b** values used in equation 6.6

as used in RUSLE1 were 0.031 for the mulch till systems and 0.04 for the no-till systems. The conclusion of this preliminary analysis using RUSLE1, which uses a similar but simpler cover-management subfactor method, is that **b** values used in the RUSLE2 subfactor method can not be compared to widely reported literature values. Also, terms in addition to ground cover are needed in the RUSLE2 subfactor procedure to adequate how cover-management affects erosion, even for the same cover-management practice.

6.2.1. b value (ground cover effectiveness index)

6.2.1.1. Literature b values

Research shows that **b** values derived from measured erosion data range from approximately 0.025 to greater than 0.1 (Box, 1981; Colvin and Gilley. 1987; Dickey et al., 1983; Gilley et al., 1986; Laflen et al., 1980; Laflen and Colvin, 1981; Mannering and Meyer, 1963; Meyer and Mannering, 1967; Meyer et al., 1970; Meyer et al., 1972; Simanton et al., 1984). The reason for a variation in **b** is obvious in some cases. For example, Mannering and Meyer (1963) and Meyer and Mannering (1967) conducted two similar studies involving wheat straw applied to recently tilled soil. In one case, infiltration increased significantly as mulch rate increased, which in turn gave a larger **b** value than was the case where mulch rate did not affect infiltration. In some cases, large **b** values resulted when other effects of a tillage system including soil surface roughness and residue incorporation were lumped with the ground cover effect.

6.2.1.2. Rill-interrill effect on b values

Another reason for a range of **b** values is related to the erosion mechanics of rill and interrill erosion. A given amount of ground cover reduces rill erosion more than interrill erosion as illustrated in Figure 6.2 (Foster and Meyer, 1975). The term in equation 2.13 that represents the effect of ground cover on the rill to interrill erosion ratio is:

$$\frac{g_{cr}}{g_{ci}} = \left[\frac{\exp(-b_r f_g)}{\exp(-0.025 f_g)} \right] \qquad [6.7]$$

where: g_{cr} = the surface cover subfactor for rill erosion, g_{ci} = the surface cover subfactor for interrill erosion, b_r = the coefficient for how ground cover affects rill erosion and 0.025 = the value for the coefficient for how ground cover affects interrill erosion.[48] Consequently, RUSLE2 **b** values range between the **b** value (0.025) for interrill erosion and the **b** value (b_r) for rill erosion. The **b** value of 0.025 used in RUSLE2 for interrill

[48] Although not used in RUSLE2 an improved approach would be to assume that the **exp** expression for ground cover effect on interrill erosion should end where it becomes tangent to the linear line in Figure 6.2, where values follow the linear line to zero for a completely covered surface.

erosion was derived from the Lattanzi et al. (1974) and McGregor et al. (1988) data (Foster, 1982).

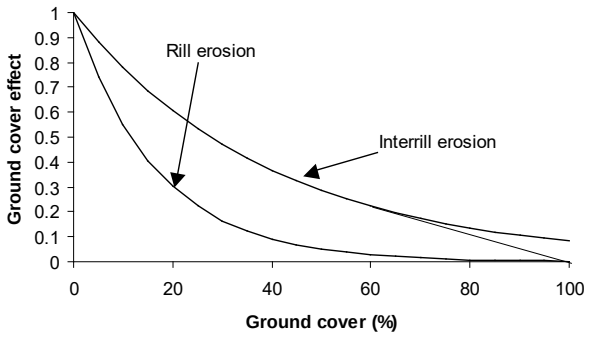

Figure 6.2. Effect of ground cover on rill and interrill erosion

The **b** value for rill erosion is the upper limit for the range of **b** values computed by RUSLE2. A 0.05 b_r value was chosen for soil conditions where ground (surface) cover does not affect infiltration, and the largest values used for b_r by RUSLE2 is 0.06 for situations where increased ground (surface) has a major effect on infiltration. RUSLE2's upper limit on **b** values is less than values reported in the literature, partly because RUSLE2 accounts for other subfactor effects that researchers included in a ground-cover type effect. Also, the reduced upper limit for **b** values was chosen so that RUSLE2 would be conservative in its computations of how much mulch, crop residue, and other ground cover materials reduce erosion for conservation planning purposes.

The coefficient b_r is assumed to increase in RUSLE2 from 0.05 to a maximum of 0.06 as ground cover increases, buried residue in the soil accounting depth increases, and the soil consolidation subfactor decreases. Mechanical soil disturbance is assumed to disrupt macro-pores and large aggregates, which increases runoff and increases erosion for a given ground cover. Conversely, biomass accumulates in a shallow, undisturbed soil surface layer with time after a mechanical soil disturbance increases infiltration, which in turn reduces runoff and rill erosion. The equation for the rill erosion ground cover effectiveness coefficient is given by:

$$b_r = 0.05 + 0.01 c_a \qquad [6.8]$$

where: c_a = coefficient for the combined effect of buried residue and soil consolidation on ground (surface) cover effectiveness in relation to rill erosion. The equation for c_a is:

$$c_a = 3.52 \times 10^{-6} B_{rs}^2 (1 - s_c) \text{ if } c_a > 1 : c_a = 1 \qquad [6.9]$$

where: B_{rs} = buried residue mass (dry basis) density [$lbs_m/(ac \cdot in)$] in the accounting soil depth d_{rs}. The value for the coefficient c_a varies between 0 and 1. A value of zero is computed when the soil has been recently mechanically disturbed, which sets b_r to a value of 0.05 and a value of 1 for the combination of high buried residue and low soil consolidation subfactor. If a value greater than 1 is computed for c_a, the value is set to 1.

The equation for the soil accounting depth for the effect of buried residue on erosion is given by:

$$d_{rs} = 1 + 2(s_c - 0.45)/0.55 \quad [6.10]$$

where: d_{rs} = the soil depth (inches) over which the density of buried residue mass is computed, 1 = the minimum accounting depth (inches) when the soil is fully consolidated (i.e., $s_c = 0.45$), 2 = the range (inches) over which the accounting depth varies as a function of the soil consolidation subfactor s_c (see **Section 6.6**), and 0.55 = the range of the soil consolidation subfactor. The maximum accounting depth is 3 inches when the soil has just been mechanically disturbed (i.e., s_c =1).

Values computed by equation 6.10 are rounded to the nearest 1 inch. RUSLE2 divides the soil depth into 1-inch intervals and accounts for soil biomass within these 1-inch intervals. RUSLE2 does not subdivide soil depth intervals further in making its buried residue density computations.

6.2.1.3. RUSLE2 b value equations

RUSLE2 uses a series of equations to compute a **b** value for equation 6.6 based on the fundamental concept that **b** values are a function of the rill to interrill erosion ratio. The starting point for developing these equations is the simple equation that computes erosion when ground cover is present as:

$$D_c = D_b \exp(-bf_g) \quad [6.11]$$

where: D_c = rill-interrill erosion when ground (surface) cover is present and D_b = rill and interrill erosion when ground cover is not present (bare soil). Therefore, a **b** value is computed by rearranging equation 6.11:

$$b = -\ln(D_c / D_b)/ f_g \quad [6.12]$$

The equation for rill-interrill erosion D_c when ground cover is present is:

$$D_c = D_{ib}(3s^{0.8} + 0.56)\exp(-0.025 f_g) + D_{rb}(s/0.0896)\exp(-b_r f_g) \quad [6.13]$$

where: D_{rb} and D_{ib} = rill and interrill erosion, respectively, when ground cover in not present (bare soil). A value for rill erosion for bare soil is computed from:

$$D_{rb} = [\alpha/(\alpha + 1)] \quad [6.14]$$

where: the term α in equation 6.14 represents a rill to interrill erosion ratio for bare soil. Equation 6.14 is the same as β in equation 2.13 without the ground cover effect. The term $(3s^{0.8} + 0.56)$ adjusts for the effect of overland flow path steepness on interrill erosion and the term s/0.0896 adjusts for the effect of overland flow path steepness on rill

erosion.[49] Rill and interrill erosion D_{rb} and D_{ib} are normalized so that they sum to 1 for a base, reference condition. Consequently, interrill erosion D_{ib} is computed from:

$$D_{ib} = 1 - D_{rb} \quad [6.15]$$

The term D_b in equations 6.11 and 6.12 is computed as:

$$D_b = D_{ib}(3s^{0.8} + 0.56) + D_{rb}(s / 0.0896) \quad [6.16]$$

The next step is to compute a value for the rill to interrill erosion ratio for bare soil as:

$$\alpha = (K_r / K_i)a_2 a_4 \quad [6.17]$$

where: the rill to interrill soil erodibility ratio (K_r/K_i) is computed using equation 4.12 and the coefficients a_2 and a_4 describe how soil consolidation, soil biomass, and conformance of the ground cover to the soil surface affect the rill to interrill erosion ratio for the purpose of computing a **b** value.

The coefficient a_2 is given by:

$$a_2 = a_1 + a_b \text{ if } a_2 > 8 : a_2 = 8 \quad [6.18]$$

where: the coefficient a_1 is given by:

$$a_1 = 1 - \{0.9[(1 - s_c) / 0.55][1 - \exp(-0.0022 B_{rt})]\} \quad [6.19]$$

where: B_{rt} = mass (dry basis) density (lbs_m/acre·inch) of the total of the live and dead roots in the soil accounting depth (10 inches) for roots. The a_1 coefficient represents how the rill to interrill erosion ratio changes as the soil becomes consolidated and as live and dead root biomass in the soil increases. This coefficient reflects how soil consolidation and root biomass affect rill erosion differently than it does interrill erosion.

The coefficient a_b, which represents how soil consolidation and buried residue affects the rill to interrill erosion ratio, is given by:

$$a_b = 1.76x10^{-5} B_{rs}^2 (1 - s_c) \quad [6.20]$$

---

[49] No adjustment is made for overland flow path length because of mathematical limitations in devolving the USLE equation structure into rill and interrill terms while meeting the requirement that erosion computed for the entire overland flow path be independent of how many overland flow path segments are used in the computations when other conditions are uniform along the overland flow path.

The a_b coefficient computes the effect of buried residue on the b value increasing as soil consolidation increases, such as for no-till crop, pasture, range, and similar lands that are not mechanically disturbed and B_{rs} = buried residue mass density in the soil accounting depth for buried residue.

Research shows that straw mulch cover is less effective at reducing rill-interrill erosion on steep overland flow paths characteristic of construction sites where mulch is applied to a smooth cut or graded soil in comparison to mulch applied to steep cropland soils [Meyer and Ports, 1976; AH537 (Wischmeier and Smith, 1978), Meyer et al., 1970; 1971; 1972].

RUSLE2 computes this effect assuming that the lost of ground (surface) effectiveness is determined by how well the mulch material conforms to the soil surface and stays in place. The coefficient a_4 describes how conformance of ground cover to the soil surfaces affects the rill to interrill erosion ratio. Poor conformance of ground cover to the soil surface affects rill erosion more than it does interrill erosion. The equation for a_4 is:

$$a_4 = a_3 + (1 - a_3)[1 - \exp(-0.0055 B_{rt})] \quad [6.21]$$

where: the equation for a_3 is given by:

$$a_3 = \exp[-\psi(\lambda / s^{1/2})^{0.6} s] \quad [6.22]$$

where: λ = the overland flow path length and ψ = a coefficient that describes conformance of ground cover to the soil surface.

Three classes of ground (surface) cover conformance that vary with material properties are used in RUSLE2 (see RUSLE2 User's Reference Guide). The values used for the conformance coefficient ψ are 0.0 for material like gravel that very closely conforms to the soil surface, 0.15 for materials that conform to the soil surface much like typical pieces of soybean stems and wheat straw after having passed through a combine, and 0.3 for corn stalks and woody debris that do not conform well to the soil surface.

Equations 6.21 and 6.22 compute reduced effectiveness of mulch, erosion control blankets, and similar materials applied on construction sites where overland flow paths are steep and long and no roots or plant stems are present. Both live and dead roots provide plant stems that help hold ground cover in place so that runoff does not dislodge and move mulch downslope or undercut erosion control blankets (Foster et al., 1982a). The tendency for mulch failure and rill erosion under erosion control blankets increases when these materials bridge soil surface roughness elements.

6.2.2. Slope length exponent m

Equations 2.12 and 2.13 are the equations used to compute the slope length exponent **m**. Values for the prior land use residual effect term in equation 2.13 are computed with:

$$c_{pr} / c_{pi} = 0.45 + 1.55(s_c s_b)^2 \quad [6.23]$$

Equation 6.23 is based on the assumption that soil consolidation and soil biomass have a greater relative effect on rill erosion than on interrill erosion. The term for effective ground cover in equation 2.13 is computed from:

$$f_{ge} = f_g(0.4 + 0.6\delta) \quad [6.24]$$

where: the cover adjustment term δ is given by:

$$\delta = (b_r - 0.05)/0.01 \quad [6.25]$$

Equations 6.24 and 6.25 reflects how ground cover has a greater effect on rill erosion than on interrill erosion when the soil has not been mechanically disturbed recently and soil biomass is high in the soil surface layer (e.g., no-till type crop, pasture, range, and similar undisturbed lands).

6.2.3. Non-uniform ground cover

The user can divide the overland flow path into segments to partially represent spatial variability of ground cover. However, RUSLE2 assumes that ground cover is spatially uniform within a segment. When a soil disturbing operation occurs that disturbs only a portion of the soil surface, RUSLE2 computes detachment on both the undisturbed and disturbed portions, and it then determines the overall detachment based on the relative areas of the undisturbed and disturbed portions. An effective ground cover that gives the overall detachment is then back calculated using equation 6.6. The effective surface residue mass associated with that ground cover is determined (see **Section 10.2**). The ratio between this effective mass and the actual mass is maintained as surface residue is lost by decomposition.

6.2.4. b and m values for Req conditions

Most of the erosion during the winter Req period in Req areas is caused by rill erosion. Constant values of 0.50 and 0.046 are used for the slope length exponent **m** and the ground cover effectiveness index **b** for these conditions. These values are based on analysis of experimental research data (McCool et al., 2002).

6.2.5. Comments on b and m equations

The equations used to describe how ground cover affects erosion are empirically based on the RUSLE2 developers' judgment of how various factors affect the ratio of rill to interrill erosion. These empirical equations replace user inputs of selecting LS tables and **b** values [AH703 (Renard et al., 1997)] or land use classes (Toy and Foster, 2000). Although the equations were not fitted to experimental research data, the equations qualitatively represent both laboratory and field research findings.

These equations for **b** and **m** values, along with other cover-management equations, give RUSLE2 its **land use independence**. RUSLE2 uses fundamental variables common to all land uses to compute how cover-management affects rill-interrill erosion.

6.3. Soil surface roughness subfactor

6.3.1. How surface roughness created by mechanical soil disturbance affects erosion

The soil surface roughness subfactor represents how random soil surface roughness created by mechanical soil disturbance affects rill-interrill erosion. Soil surface roughness includes depressions where local deposition occurs and soil peaks of large, stable soil aggregates that are resistant to detachment depending on soil biomass content. Infiltration is increased, which reduces runoff and rill erosion. Also, soil surface roughness slows surface runoff, which reduces its erosivity.

The RUSLE2 equation for the soil surface roughness subfactor is:

$$s_r = \exp[-0.66(R_a - 0.24)] \qquad [6.26]$$

where: R_a = daily adjusted roughness value (inches) and 0.24 inches (6 mm) = the adjusted roughness value assigned to unit plot conditions. Equation 6.26 was derived from research measurements of roughness and erosion (Cogo et al., 1984).

The reference condition where the soil roughness subfactor s_r equals 1 is the unit plot condition during and after intense rainfall. The reference unit plot soil surface roughness of 0.24 (6 mm) is produced by a harrow or similar soil finishing tool after disking or similar tools used to prepare seedbeds. Most soil surface conditions are rougher than the unit plot conditions, which give s_r values less than 1. However, some soil surfaces are smoother than the unit plot. Equation 6.26 gives s_r values up to 1.17 for soil surface roughness smoother than 0.24 inches, the roughness value assumed for unit-plot conditions. Mechanical soil disturbing operation such as roto-tilling that finely pulverizes soil, cutting and filling with a blade, and rolling a finely pulverized soil surface produces a surface that is smoother than the unit plot soil surface.

6.3.2. Random roughness as affected by soil biomass

Biomass production (yield) level affects the soil surface roughness subfactor. The effect of biomass production level on the roughness subfactor, as seen in experimental soil loss ratio values [AH537 (Wischmeier and Smith, 1978)] is illustrated in Table 6.3. The roughness subfactor values in Table 6.3 were computed by dividing the soil loss ratio for the fallow crop stage period by the soil loss ratio for the seedbed period.[50] The only essential difference in soil conditions between these two short periods is soil surface roughness.

---

[50] Crop stages are periods where soil loss ratio values are considered constant in the USLE [AH537 (Wischmeier and Smith, 1978)]. The fallow period is for the time between when the soil is first tilled with a primary tillage tool such as a moldboard plow and when the soil is first tilled afterwards with a secondary tillage tool to prepare a seedbed. The seedbed period is the time between the first secondary tillage following primary tillage to when canopy cover of the planted crop reaches 10 percent.

Table 6.3. Effect of corn production level and soil biomass on soil surface roughness subfactor s_r

		Soil loss ratio		
Yield (bu/acre)	Management	Fallow	Seedbed	Roughness subfactor
112	Grain	0.31	0.55	0.56
87	Grain	0.36	0.60	0.60
67	Grain	0.43	0.64	0.67
49	Grain	0.51	0.68	0.75
112	Silage	0.66	0.74	0.89
87	Silage	0.67	0.75	0.89
67	Silage	0.68	0.76	0.89
49	Silage	0.69	0.77	0.90

Experimental roughness subfactor values increased as production (yield) level decreased as shown in Table 6.3. Similarly, experimental roughness subfactor values [AH537 (Wischmeier and Smith, 1978)], as shown in Table 6.4, were significantly reduced when a corn grain crop followed an established meadow (sod), which has a very high soil biomass. Roughness subfactor values increased as hay yield decreased and increased in the second year of corn following sod. Residual soil biomass was less in the second year after the sod than in the first year immediately after the meadow. Also, roughness subfactor values were higher when corn followed small grain than when it followed sod. The small grain provided less soil biomass than did the sod.

Table 6.4 Effect of sod on soil surface roughness subfactor s_r for moldboard plow period

Hay yield (tons/acre)	Year after sod	Roughness subfactor
4	1	0.35
2.5	1	0.38
1.5	1	0.39
4	2	0.49
2.5	2	0.50
1.5	2	0.50

Roughness subfactor values are interpreted as being a function of soil biomass level caused by different yield levels, soil biomass level determined by whether crop residue is removed such as with silage or left with grain harvest, and the difference in biomass level caused by type of preceding crop such as hay, small grain, or row crop grain. Recommendations for the USLE [AH537 (Wischmeier and Smith, 1978)] are that non-sod forming meadows such as sweet clover or lespedeza have less effect on rill-interrill erosion than does sod forming vegetation, which is explained by the difference in soil biomass production between these vegetation types.

RUSLE2 computes initial soil roughness after a mechanical soil disturbance as a function of the soil biomass in the soil disturbance depth using:

$$R_{ib} = 0.24 + (R_{it} - 0.24)\{0.8[1 - \exp(-0.0015 B_{td})] + 0.2\} \qquad [6.27]$$

where: R_{ib} = the initial roughness adjusted for the soil texture and biomass effect, R_{it} (inches) = the initial roughness after the input roughness value is adjusted for soil texture and B_{td} = the total mass (dry basis) [$lbs_m/(acre \cdot inch)$] of buried residue and live and dead roots averaged over the soil disturbance depth after the operation. The 0.24-inch value is the roughness value assumed for unit plot conditions. The 0.2 value reflects the portion of the roughness value that is not affected by soil biomass.

6.3.3. Adjusting roughness input values for soil texture

Input roughness entered in the RUSLE2 database for a soil disturbing operation is adjusted for soil texture before equation 6.27 is used to adjust for the soil biomass effect on roughness. The equation that adjusts input roughness values for soil texture is:

$$R_{it} = R_{in}[0.16(P_{sl}/100)^{0.25} + 1.47(P_{cl}/100)^{0.27}] \quad [6.28]$$

where: R_{in} = the input roughness value entered for a soil disturbing operation in the RUSLE2 database, P_{sl} = percent silt in the soil, and P_{cl} = percent clay in the soil. The roughness values R_{it} adjusted for soil texture are the same as roughness input R_{in} values for the reference silt loam soil texture. Roughness values computed by equation 6.28 are greater than the roughness input values for soils high in clay and less than roughness input values for soils high in sand. Equation 6.28 was developed based on judgment and field observations of how soil surface roughness varies with soil texture when mechanically disturbed.

6.3.4. Assigning input roughness values for operations

Input values entered in the RUSLE2 database for soil surface roughness created by a mechanical soil disturbing operation are assigned according to the soil surface roughness that the operation creates for a base, reference condition. This condition is a smooth, silt loam soil (clay = 15%, silt = 65%) having a very high soil biomass (dry basis) density of greater than 1000 $lbs_m/(acre \cdot inch)$ in the soil disturbance depth, which includes both buried residue and dead roots. These soil biomass levels occur where crop yield exceeds 200 bu/acre corn, 70 bu/acre wheat, and 4 tons/acre hay or pasture land (see RUSLE2 User's Reference Guide).

The roughness index used in RUSLE2 for input values assigned to soil disturbing operations in the RUSLE2 database is the standard deviation soil surface elevations measured on a 1-inch grid. The elevations are relative to a plane that removes elevation differences caused by land steepness and ridges.

6.3.5. Effect of existing roughness at time of soil disturbance (tillage intensity effect)

Roughness left by a soil disturbing operation is a function of the operation itself and existing roughness at the time of the operation. The RUSLE2 assumption is that existing roughness has no effect if the roughness, adjusted for soil texture and biomass, left by a soil disturbing operation is greater than the existing soil roughness at the time of the operation. However, the RUSLE2 assumption is that the roughness left by a soil disturbing operation is a function of existing roughness if the adjusted roughness created by an operation is less than existing roughness. In this case, the resulting roughness is a function of the initial adjusted roughness, existing roughness, and tillage intensity of the soil disturbing operation. Tillage intensity is a measure of the aggressiveness of the soil disturbing operation for obliterating existing roughness. The equation for how existing roughness and tillage intensity affect soil roughness is:

$$R_{aa} = (1 - \xi)(R_{ae} - R_{ib}) + R_{ib} \quad [6.29]$$

where: R_{aa} = the adjusted roughness immediately after a soil disturbing, ξ = tillage intensity for the operation, R_{ae} = existing adjusted roughness immediately before the operation, and R_{ib} = the input roughness for the soil disturbing operation after adjustment for soil biomass and soil texture, which is computed with equation 6.27.

A tillage intensity of 1 means that the soil disturbing operation is so aggressive that existing roughness has no effect on the roughness left by the operation. Examples of these operations include moldboard plows and roto-tillers. Conversely, a tillage intensity of 0 means roughness after the soil disturbing operation is the same as existing roughness before the operation. Harrows that have a tillage intensity of 0.4 are examples of operations where existing roughness has a significant effect on roughness left after a soil disturbing operation.

6.3.6. Roughness decay

Roughness diminishes (decays) after a mechanical soil disturbance because of soil slumping (i.e., settlement and subsidence) caused by the presence of moisture, interrill erosion wearing away roughness peaks, and local deposition in roughness depressions. The RUSLE2 equation used to represent this effect is given by [AH703 (Renard et al., 1997)]:

$$f_r = \exp[-0.07(P_d + I) - 0.006 r_d c_c g_{ci})] \quad [6.30]$$

where: f_r = the fraction of the current roughness greater than 0.24 inch that remains, P_d = the daily precipitation amount (inches), I = daily amount (inches) of water added by irrigation, r_d = the daily erosivity (US customary units), and g_{ci} = the interrill ground cover factor. The term in equation 6.30 associated with precipitation amount represents roughness loss by settlement and subsidence and the term associated with erosivity represents roughness loss by interrill erosion. The RUSLE2 assumption is that half of the roughness loss is by settlement and the other half is by interrill erosion. Roughness loss by local deposition is not explicitly represented. Roughness decay is not computed as a function of soil properties including texture and soil biomass. The adjustment made to initial roughness by equations 6.27 and 6.28 is assumed to adequately represent the effect of soil texture and soil biomass on roughness at any time.

The interrill ground cover factor is given by:

$$g_{ci} = \exp(-0.025 f_g) \quad [6.31]$$

where: f_g = the net ground cover (percent). Daily adjusted roughness used in equation 6.26 is computed as:

$$R_a = 0.24 + f_r (R_{ap} - 0.24) \quad [6.32]$$

where: R_{ap} = adjusted roughness on the previous day. The RUSLE2 assumption is that roughness is not decayed when the input initial roughness in the RUSLE2 database for a soil disturbing operation is less than the unit plot roughness of 0.24 inch.

6.3.7. Base roughness value

The 0.24-inch value in equations 6.27 and 6.32 represents a base roughness value for unit plot conditions. The assumption is that soil clods persist so that the unit-plot surface never becomes perfectly smooth. The unit plot final roughness value is not varied as a function of soil texture because that effect is empirically accounted for in the RUSLE2 soil erodibility factor. However, RUSLE2 allows the user to enter a "final" roughness value for an operation that is greater than 0.24 inch to represent conditions where roughness decays to a final value greater than 0.24 inch. If an input final roughness value greater than 0.24 inch is entered in the RUSLE2 database for a soil disturbing operation, RUSLE2 uses that value instead of the 0.24 value in equations 6.27 and 6.32. RUSLE2 does not allow roughness to decay to a value less than 0.24 inch, even if the input final roughness is less than 0.24 inches. The input initial and final roughness values can be used force RUSLE2 to use a particular roughness in its computations (see RUSLE2 User's Reference Guide).

6.3.8. Long term roughness development

A natural soil roughness develops over time after the last mechanical soil disturbance. The final natural roughness is a function of soil properties, vegetation characteristics, and local erosion and deposition. RUSLE2 assumes that the time required for this long-term roughness to develop equals the time to soil consolidation (see **Section 4.8**). The RUSLE2 equation used to compute long term roughness is given by:

$$R_l = 0.24 + (R_{alf} - 0.24) / \{1 + \exp[(0.5 - t_d / t_c) / 0.1]\} \qquad [6.33]$$

where: R_l = daily long term roughness, R_{alf} = the adjusted final long term roughness value, t_d = number of days since the last mechanical soil disturbance, and t_c = the time to soil consolidation (days). A value for R_{alf} is computed using equations 6.27and 6.28 using the input long-term natural roughness values entered in the RUSLE2 database. The biomass value used in equation 6.27 is based on total soil biomass including buried residue and dead and live roots in the upper 4 inches of the soil. The value input for final long-term roughness for a given cover-management description is relative to the reference condition for short term roughness associated with mechanical soil disturbance (see **Section 6.3.4** and RUSLE2 User's Reference Guide). RUSLE2 adjusts this input value for soil texture and soil biomass just as it does roughness created by mechanical disturbance. The assumption is that vegetation must be present for long term surface roughness to develop and be effective. Equation 6.33 is illustrated in Figure 6.3 where the time to soil consolidation is 7 years.

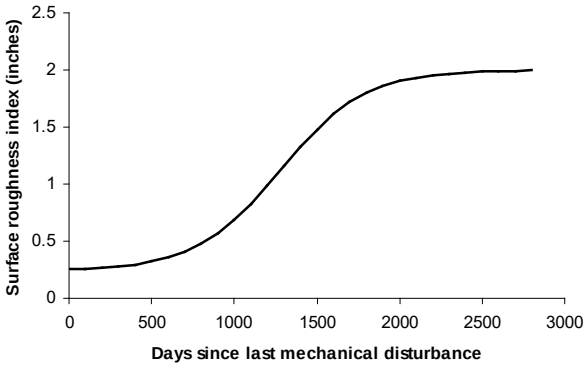

Figure 6.3. Development of long term roughness as a function of time since last mechanical soil disturbance.

RUSLE2 tracks both short term roughness resulting from mechanical soil disturbance and long term roughness development. RUSLE2 uses the maximum of the two roughness values in equation 6.26 to compute a soil surface roughness subfactor value.

6.3.9. Accounting for spatial variability in roughness

RUSLE2 can take soil surface roughness spatial variability partially into account by dividing the overland flow path into segments. However, roughness is assumed to be uniform within a segment. Some mechanical soil disturbing operations disturb the soil in strips. For these operations, RUSLE2 computes soil surface roughness subfactor values for both the undisturbed and disturbed areas and the overall soil surface roughness subfactor value based on the portion of the soil surface that the operation disturbs. RUSLE2 then back-calculates an effective roughness using equation 6.26 that gives the effective roughness subfactor value. This single effective roughness value is assigned to the segment and decayed over time using equation 6.30.

6.3.10. Comments on roughness subfactor

RUSLE2 captures the main effects of roughness on rill-interrill erosion. The intent is not to explicitly model soil roughness to produce roughness values comparable to field measured values except for input values determine from the reference condition (see **Section 6.3.4**). For example, internal RUSLE2 computed roughness values are less than those measured in the field on construction sites where soil clay content is high. The roughness effect on erosion is more than the geometric effect of soil surface roughness slowing runoff, ponding water, and depositing sediment. It also includes an infiltration effect that is less related to soil surface roughness than are the other erosion processes. The adequacy of the soil roughness relationships in RUSLE2 should be judged on the basis of how well RUSLE2 computes rill-interrill erosion as affected by soil disturbing operations that create soil surface roughness.

6.4. Ridge height subfactor

6.4.1. Effect of ridges on rill-interrill erosion

Ridges affect erosion primarily in two ways. When the ridges are oriented parallel to the overland flow path, ridges increase rill-interrill erosion because of increased interrill erosion on the ridge sideslopes. This effect is represented by the ridge height subfactor. When ridges are nearly perpendicular to the overland flow path, ridges alter the runoff

flow path by partially redirecting runoff around the hillslope or by ponding runoff behind the ridges if the ridges are perfectly on the contour. This effect of ridges is considered in the contouring subfactor (see **Section 7.1**).

Increased ridge height increases ridge sideslope (interrill) steepness, which in turn increases interrill erosion steepness (Lattanzi et al., 1974). RUSLE2 uses only ridge height to compute ridge height subfactor values although both ridge height and spacing determine interrill steepness. Accurately identifying ridge spacing or number of ridges per unit overland flow path width is difficult whereas ridge height can be easily visualized and measured.

6.4.2. Reference condition for ridge height subfactor

The reference condition for the ridge height subfactor, as with all cover-management subfactors, is the unit plot condition. Unit plots are prepared to a seedbed condition (see **Section 2.1** and **Footnote 3**) using tools like spike tooth harrow that leave small ridges up and down slope. The RUSLE2 ridge subfactor must be 1 for the unit plot condition. Unit plot conditions are not static because the unit plots are periodically tilled to break soil crusts and to control weeds. A ridge subfactor value of 1 for unit plot conditions represents an average over time because of periodic ridge formation and decay.

The ridge subfactor equations are also derived for the reference condition of the ridges being parallel to the overland flow path (i.e., up and down slope).

6.4.3. Ridge height subfactor for low steepness

The RUSLE2 ridge height subfactor is constant for overland flow path steepness less than six percent as determined from experimental data and the judgment of scientists who experimentally measured the effect of ridges on rill-interrill erosion from almost flat slopes (<1%) to land steepness as great as 5 percent (Young and Mutchler, 1969; Mutchler and Murphree, 1985; McGregor et al., 1999).[51] The RUSLE2 ridge height subfactor equations derived from experimental data are:

$$r_{h6} = 0.9(1 + 0.0582H^{1.84}) \quad H \le 3 \text{ inches} \qquad [6.34]$$

$$r_{h6} = 2.136[1 - \exp(-0.484H)] - 0.336 \quad H > 3 \text{ inches} \qquad [6.35]$$

where: r_{h6} = daily ridge height subfactor when the overland flow path steepness is less than or equal to 6 percent and H = daily ridge height (inches). The significance of the 0.9 in equation 6.34 is that the minimum ridge height subfactor is 0.9 for a flat soil surface and the maximum ridge height subfactor from equation 6.35 is 1.8, which is consistent

[51] C.K. Mutchler and K.C. MCGregor. 1999. Effect of ridge height on erosion on low slopes. Personal communication. Scientists (retired) at the USDA-National Sedimentation Laboratory, Oxford, Mississippi.

with the values given in AH537 (Wischmeier and Smith, 1978) for applying the USLE to cotton production on high ridges [Mutchler et al., 1982; Mutchler and Murphree, 1985, AH537 (Wischmeier and Smith, 1978)]. Also, equation 6.34 gives a subfactor value of 1 for a ridge height of 1.42 inch, which represents unit plot conditions except for the difference between six percent steepness and the unit plot nine percent steepness.

6.4.4. Adjustment for effect of overland flow path steepness

Interrill steepness is affected by land steepness. Interrill steepness is much greater than land steepness on flat slopes than on steep slopes. For example, local interrill steepness with high ridges (about 8 inches high when formed) like those used in cotton production in the Mississippi Delta is about 20 percent (Meyer and Harmon, 1985; Mutchler and Murphree, 1985), which is the interrill steepness when the land is flat (about 0.5%). As land steepness increases, local interrill steepness increases but much more slowly than does land steepness. Local interrill steepness of the ridge sideslope almost equals land steepness on steep slopes. For example, the same ridges that give a 20 percent steep ridge sideslope on a 6 percent land steepness give a 54 percent interrill steepness on a land steepness of 50 percent. The ridge height subfactor, therefore, approaches 1 for steep overland flow paths.

A simple rill-interrill erosion model was used to develop equations for the ridge height subfactor for overland flow path steepness greater than six percent. That simple equation is:

$$D_t = 0.5[(s/0.0896) + (3s_i^{0.8} + 0.56)] \qquad [6.36]$$

where: the 0.5 represents the assumption that rill and interrill erosion are equal for unit plot conditions (Foster and Meyer, 1975; Foster et al., 1977a, 1977b; Foster, 1982), the term s/0.0896 represents the effect of steepness on rill erosion, and the term $(3s_i^{0.8} + 0.56)$ represents the effect of steepness on interrill erosion. Steepness s_i of the interrill area is greater than the steepness s of the rill area because ridge height increases interrill steepness (i.e., the ridge sideslope steepness).

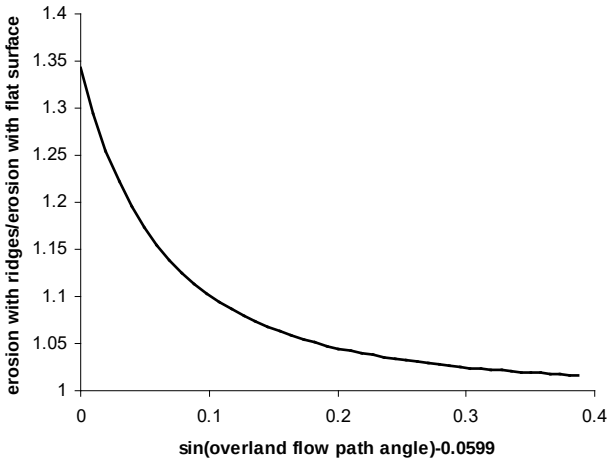

Figure 6.4. Effect of overland flow path steepness on the ratio of erosion with a 20% ridge sideslope to erosion from a flat surface.

Equation 6.36 was solved for overland flow path steepness between and 6 and 50 percent for a range of ridge side slope steepness and for a flat (i.e., non-ridged soil surface). Erosion computed for a given ridge sideslope steepness for a

particular flow path steepness was divided by erosion for a flat soil surface at that same overland flow path steepness. An example of those values is shown in Figure 6.4 for a ridge sideslope of 20 percent. The RUSLE2 equations used to represent this effect are:

$$r_h = r_{h6} \quad s_p < 6\% \qquad [6.37]$$

$$r_h = 1 + (r_{h6} - 1)\exp[-a_h(s - 0.05989)] \quad s_p \geq 6\% \qquad [6.38]$$

where: s_p = overland flow path steepness (100 times tangent of slope angle) and a_h is computed from:

$$a_h = 16.02 - 0.927H \quad H \leq 10 \text{ inches} \qquad [6.39]$$

$$a_h = 6.75 \quad H > 10 \text{ inches} \qquad [6.40]$$

where: ridge height H has units of inches.

6.4.5. Effect of row grade on ridge height subfactor

The ridge height subfactor equations given above apply to the reference condition of the ridges being parallel to the overland flow path (i.e., up and down slope). As relative row grade (i.e., ratio of grade along the ridges to overland flow path steepness) decreases from 1 (up and down slope) to 0 (on contour), the ridge subfactor value should become 1. The effect of ridge height on rill-interrill erosion is represented in the contouring subfactor when the ridges are on the contour (see **Section 7.1**). However, this requirement can not be met because of RUSLE2's mathematical structure. Instead, the ridge subfactor value is 0.9 when ridges are perfectly on the contour, which is the ridge height subfactor value for a flat soil surface.

The equations that compute ridge height subfactor values as a function of ridge orientation (i.e., relative row grade) are:

$$r_h = 0.9 - (0.9 - r_{h,u\&d})g_r^2 \quad r_{h,u\&d} \leq 1 \qquad [6.41]$$

$$r_h = 0.9 + (r_{h,u\&d} - 0.9)g_r^2 \quad r_{h,u\&d} > 1 \qquad [6.42]$$

where: $r_{h,u\&d}$ = the ridge height subfactor value when ridge orientation is parallel to the overland flow path, which are computed equations 6.37 and 6.38 and g_r = relative row grade (grade along the ridges/overland flow path steepness).

6.4.6. Ridge height decay

Ridge height decays because of settlement and interrill erosion. Settlement occurs quickly after the ridges are formed when water is presence. The RUSLE2 assumption is that forty percent of the initial ridge height is lost by settlement while the remaining sixty percent is lost by interrill erosion based on analysis of experimental data (Lyles and.

Tatarko. 1987).[52] Thus, the initial ridge height left by a soil disturbing operation is divided into two parts as:

$$H = H_s + H_e \quad [6.43]$$

where: H_s = daily ridge height component associated with settlement and H_e = daily ridge height component associated with interrill erosion. The initial value for H_s is 0.4 times the ridge height left by the soil disturbing operation, while the initial value for H_e is 0.6 times the ridge height left by the soil disturbing operation. The daily settlement component ridge height is computed as:

$$H_s = H_{sp} \exp = [-0.2343(P_d + I)] \quad [6.44]$$

where: H_{sp} = the daily ridge height associated with settlement from the previous day. The daily interrill erosion ridge height is computed as:

$$H_e = H_{ep} - a_e r_d c_c g_{ci} \quad [6.45]$$

where: H_{ep} = ridge height associated with interrill erosion for the previous day and the coefficient a_e is computed as:

$$a_e = 0.033 - 0.002 H_i \quad H_i \leq 10 \text{ inches} \quad [6.46]$$

$$a_e = 0.013 \quad H_i > 10 \text{ inches} \quad [6.47]$$

where: the units for a_e are inches/(US customary EI unit) and H_i = initial ridge height left by the soil disturbing operation (inches). The reason for the coefficient a_e is a function of ridge height is the RUSLE2 assumption that high ridges have a wide base so that the overall loss of ridges having a wide base occurs more slowly than does the loss of ridges with a narrow base. The minimum allowable ridge height is zero. These equations and their coefficients were derived from research data (Lyles and Tatarko, 1987) and from field observations in cotton fields in the Mississippi Delta.[53]

6.4.7. Effect of existing ridge height, soil, and cover-management on ridge height when new ridges are formed

The RUSLE2 assumption is that existing ridges have no effect on the ridges created by a soil disturbing operation. Also, the RUSLE2 assumption is that initial ridge height.

---

[52] K.C. McGregor. 1999. Field observations of ridge height decay in the Mississippi Delta. Personal communtation. Scientist (retired), USDA-National Sedimentation Laboratory, Oxford, Mississippi.

[53] McGregor, K.C. 1999. Loss of ridge heights in the spring in the Mississippi Delta. Personal communication. Scientist (retired), USDA-National Sedimentation Laboratory, Oxford, Mississippi.

Ridge height at formation is determined entirely by the soil disturbing operation. The effect of existing ridges and soil and cover-management conditions on ridge height can be taken into account in RUSLE2 by creating multiple soil disturbing operation decriptions having a range of ridge height values. The user then selects a particular operation description for RUSLE2 input that gives the desired ridge height for the given situation.

6.4.8. Comments on ridge height subfactor

The intent in RUSLE2 is to capture the main effect of ridge height on rill-interrill erosion as ridge height interacts with land steepness and to capture the main effect of variables that cause ridge height to decay. The intent is not to explicitly model ridge height. The adequacy of the RUSLE2 ridge height subfactor equations should be judged on the basis of how well RUSLE2 computes rill-interrill erosion as a function of soil disturbing operations that create ridges.

RUSLE2 not giving 1 for the ridge subfactor when ridges are perfectly on the contour is a limitation of RUSLE2's empirical mathematical structure not being consistent with process-based equations. RUSLE2 was constructed so that these problems do not significantly affect RUSLE2's utility as a conservation and erosion control planning tool.

6.5. Soil biomass subfactor

6.5.1. Soil biomass effect

The RUSLE2 soil biomass subfactor estimates how soil biomass affects rill-interrill erosion [Mannering et al., 1968; Foster et al., 1985c; McGregor et al., 1990; Brown et al., 1989; Toy et al., 2002; Van Liew and Saxton, 1983, AH537 (Wischmeier and Smith, 1978)]. Soil biomass represented by RUSLE2 includes buried residue, live roots, and dead roots.

Live roots produce exudates that reduce soil erodibility. Also, live root biomass is a measure of plant transpiration, which reduces soil moisture that in turn increases infiltration and decreases runoff. Dead roots add organic matter to the soil that increases infiltration and decrease soil erodibility. Both live and dead roots mechanically hold the soil in place, hold soil in "clumps" when the soil is mechanically disturbed, and reduce waterdrop impact and runoff erosivity if the roots are exposed.

Buried residue is biomass that has been mechanically incorporated into the soil. RUSLE2 also "incorporates" up to 25 percent of the daily decomposition of surface residue into the soil to represent the accumulation of high organic matter at the soil surface for no-till and other conditions where little or no soil disturbance occurs (Kay and VanderBygaart, 2002; Shelton and Bradley, 1987). Incorporated biomass, such as crop residue, manure, or bio-solids in sewage waste, provides organic compounds that increase infiltration and decrease soil erodibility [Browning et al., 1948; Copley et al., 1944; Hays et al., 1949; AH537 (Wischmeier and Smith, 1978)]. Also, pieces of organic material,

such as incorporated crop residue, can be sufficiently large to mechanically reduce rill erosion (Brown et al., 1989).

6.5.2. Soil biomass subfactor equation

The equation for the RUSLE2 soil biomass subfactor is:

$$s_b = 0.951\exp(-0.0026B_{rt} - 0.0006B_{rs} / s_c^{0.5}) \quad s_b \le 0.9035 \qquad [6.48]$$

$$s_b = \exp[-1.9785(0.0026B_{rt} + 0.0006B_{rs} / s_c^{0.5})] \quad s_b > 0.9035 \qquad [6.49]$$

Equation.6.49 is used for very low soil biomass where the soil biomass subfactor s_b is greater than 0.9035. Equation 6.48 does not give the required value of 1 for unit plot conditions that has no soil biomass (i.e., B_{rt} and $B_{rs} = 0$). The common point of s_b = 0.9035 results from the product of 0.951 in equation 6.48 and 0.95, the upper value for which the exp(…) term in equation 6.48 is assumed to apply.

The coefficient values in equation 6.48 were obtained by fitting the equation to soil biomass subfactor values estimated from research-based soil loss ratio values. The values points for no-till and mulch (reduced) till were obtained from the literature.[54] The other values selected from AH537 (Wischmeier and Smith, 1978). These values are given in Table 6.5, and the fit of equation 6.48 to the observed values is shown in Figure 6.5. The data points (soil loss ratio values) shown in Table 6.5 were selected across the range of soil biomass represented by Table 5, AH537. Equation 6.48 fits the observed values well except for the 112 bu/acre corn following 1.5 tons/acre meadow.

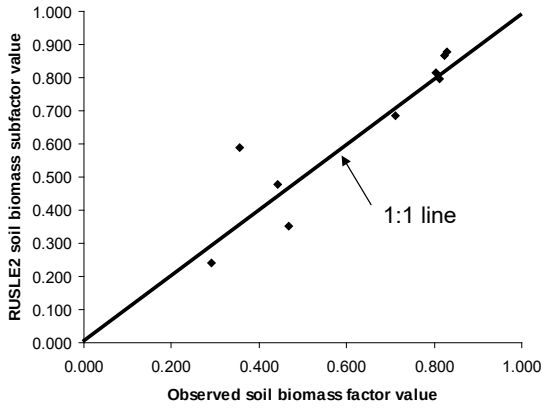

Figure 6.5. Comparison of RUSLE2 soil biomass values to observed values

Observed soil biomass subfactor values were estimated from the soil loss ratio values given in Table 6.5. Soil biomass subfactor values were computed from soil loss ratio values by rearranging equation 6.1 to solve for the soil biomass subfactor and substituting RUSLE2 estimated values for the other subfactors. Soil loss ratio values were substituted for cover-management factor c in equation 6.1.

Using soil loss ratios in Table 5, AH537 for the seedbed crop stage period for conventional, clean tillage,

[54] More than 100 articles were reviewed to evaluate the effect of no-till and mulch till cropping on rill-interrill erosion. Those articles are listed in the **Additional References Section**.

which is most like the unit plot condition, minimizes the error in estimated subfactor values used in equation 6.1 to estimate soil biomass subfactor values. The major subfactor affecting soil loss ratio values for the seedbed crop stage for conventional, clean tillage is soil biomass although some ground (surface residue) cover is present and soil surface roughness is rougher than for unit-plot conditions.

Soil loss ratio values given in Table 5, AH537 are assumed to apply to the reference silt loam soil at Columbia, Missouri. RUSLE2 was used to compute subfactor values for ground cover (surface residue) and surface roughness for all conditions listed in Table 6.5 and soil consolidation for the no-till data condition. The canopy subfactor value was 1 for all conditions and the soil consolidation subfactor was 1 except for no-till. RUSLE2 was used to compute soil biomass values using values in the RUSLE2 **core database** (see RUSLE2 User's Reference Guide).

Table 6.5. Soil biomass subfactor values used to derive RUSLE2 subfactor equation

			Soil biomass factor	
Cover-management (yield)	Data source	Seedbed soil loss ratio	Obs	RUSLE2
conv corn 112 bu/ac	AH537	0.55	0.71	0.69
conv corn 50 bu/ac	AH537	0.68	0.80	0.82
conv corn sillage 112 bu/ac	AH537	0.74	0.81	0.79
conv corn sillage 50 bu/ac	AH537	0.77	0.83	0.88
conv corn 112 bu/ac soybeans 25 bu/ac	AH537	0.72	0.82	0.87
conv corn 112 bu/ac after meadow 4 tons/acre	AH537	0.18	0.29	0.24
conv corn 112 bu/ac after meadow 1.5 tons/acre	AH537	0.29	0.35	0.59
no till corn 112 bu/ac	literature	0.028	0.47	0.35
mulch till corn 112 bu/ac	literature	0.24	0.44	0.48

The soil consolidation term s_c in equation 6.48 gives increased credit for buried residue to represent no-till cropping and other undisturbed soil conditions. For example, a given amount of buried residue at the soil surface decreased rill-interrill erosion more with no-till than with clean tillage. Increased soil macro-pores and aggregation develop in the upper few inches of soil under no-till cropping and other undisturbed soil conditions (Kay and VanderBygaart, 2002). Frequent, routine tillage and other mechanical soil disturbance prevent these conditions from developing. Mechanical soil disturbance disrupts these favorable soil conditions for reducing rill-interrill erosion, and time is required for these soil conditions to become reestablished. The term $1/s_c^{0.5}$ in equation 6.48 and 6.49is used as an index for the development of these favorable soil properties.

Values for the accounting depths d_{rs}, described in **Section 6.2** for buried residue, and d_{rt} for roots were determined during the fitting of equation 6.48 and 6.49. The best fit was obtained with a buried residue accounting depth of three inches for conventional, clean tillage, which is represented by s_c =1. The accounting depth is reduced to 1 inch as the soil consolidation subfactor value decreases from 1 for a soil recently mechanically disturbed to 0.45 for a fully consolidated soil (see equation 6.10). The accounting depth for buried residue reflects the soil depth over which buried residue has its major effect on infiltration, soil erodibility, and runoff erosivity.

The accounting depth determined for roots was 10 inches. This depth contains the bulk of roots for most vegetation, especially major agricultural crops like corn, soybeans, and wheat. The apparent depth over which roots affect erosion is greater than that for buried residue because live roots affect infiltration by extracting soil water. The 10-inch accounting depth for roots is also influenced by the common depth of 10 inches for modern moldboard plows, which invert the soil. Moldboard plow bring roots near the bottom of the plow depth to near the soil surface. Moldboard plows also move surface residue and buried residue near the soil surface to near the bottom of the plow depth, where the buried residue has little effect on rill-interrill erosion. Although the case can be made that live roots and dead roots should be treated differently in RUSLE2 because of moisture extraction, the effect of live roots and dead roots per unit mass are considered to be the same for both live and dead roots.

See **Sections 8.2** and **9.2.1** for additional comments.

6.5.3. Soil biomass subfactor equation for Req conditions

When RUSLE2 is applied to Req conditions (see **Section 3.2.5** and the RUSLE2 User's Reference Guide), soil biomass values are multiplied by 1.65 to give increased erosion reduction per unit biomass. Most of the rill-interrill erosion for Req conditions is rill erosion, and soil biomass has a greater relative effect on rill erosion than on interrill erosion (Van Liew and Saxton,1983; Brown et al., 1989; McGregor et al., 1990). The 1.65 value was determined by fitting RUSLE2 to data collected at Pullman, Washington (McCool et al., 2002).

6.5.4. Applicability of soil biomass subfactor equation for biomass additions

The data used to derive equations 6.48 and 6.49 were for cropped conditions where the biomass source was vegetation grown on-site. RUSLE2 must also represent the effect of incorporation of applied biomass from other sources including animal manure, compost, bio-solids in sewage and similar waste, and forest litter. The applicability of RUSLE2 for these conditions was evaluated by computing and comparing rill-interrill RUSLE2 erosion estimates with measured erosion in research studies. Tables 6.6 and 6.7 show estimated and observed erosion values for surface application of manure and its incorporation into the soil using primary tillage at Clarinda, Iowa and La Crosse, Wisconsin (Browning et al, 1948; Hays et al., 1949). Table 6.8 shows erosion values for various biomass types applied and incorporated in the soil for cotton grown at Statesville, North Carolina (Copley et al., 1944). RUSLE2 is judged to adequately estimate how surface applied and soil incorporated biomass affects rill-interrill erosion.

Table 6.6. Effect of manure additions on erosion at Clarinda, Iowa

			Ratio of erosion with manure to erosion without manure	
Cover	Yield (bu/ac)	Manure application (tons/acre wet basis)	Obs	RUSLE2
Corn	22	0	1.00	1.00
Corn	30	8	0.42	0.39
Corn	36	16	0.21	0.20
Fallow		0	-	-
Fallow		8	0.79	0.42
Fallow		16	0.63	0.24

Table 6.7. Effect of manure additions on erosion at La Crosse, Wisconsin

			Ratio of erosion with manure to erosion without manure	
Cover	Yield (bu/ac)	Manure application (tons/acre wet basis)	Obs	RUSLE2
Corn	30	0	1.00	1.00
Corn, manure spring applied	30	8	0.82	0.42
Corn, manure fall applied	30	8	0.80	0.42
Fallow		0	1.00	1.00
Fallow, manure spring applied		5	0.85	0.75

Several factors complicate this analysis. One factor is data variability. Incorporated animal manure decreased erosion much more at Clarinda, Iowa than at La Crosse, Wisconsin. RUSLE2 seems to seriously over estimate the effect of manure applied to fallow conditions at both Clarinda and La Crosse. A comparison of observed erosion with manure applied to corn with erosion for manure applied to fallow soil at Clarinda indicates a much greater effect of the corn biomass than is supported by data in Table 5, AH537 (Wischmeier and Smith, 1978). Another problem with the experimental data is that manure applied to the corn at La Crosse did not reduce erosion as much as expected based on the results for the fallow soil. Such unexplained variability in erosion data is common.

Another complicating factor is how well the biomass was incorporated into the soil by the 6-inch deep manual spading operation used on the research plots to replicate moldboard plowing. The RUSLE2 inputs were based on the assumption that the spading incorporated the biomass more like a chisel plow than like a moldboard plow. Assuming that the incorporation was like a moldboard plow rather than a chisel plow results in RUSLE2 estimating that the ratio of erosion with incorporated biomass to erosion without incorporated biomass increases from 0.42 to 0.48 for applying 8 tons/acre of manure at Clarinda, Iowa. Consequently, the uncertainty in how the spading operation incorporated the biomass does not seem to account for the large difference between the RUSLE2 values and the measured values for fallow conditions.

Table 6.8. Effect of biomass additions on erosion with cotton at Statesville, North Carolina

Yield (lbs/acre seed cotton)	Biomass type	Biomass application (tons/acre wet basis)	Ratio of erosion with biomass to erosion without manure	
			Obs	RUSLE2
800	-	none	1.00	1.00
1800	Animal manure	8	0.19	0.27
1800	Compost	12	0.39	0.21
1800	Compost	18	0.13	0.16
1800	Compost	60	0.03	0.04
1800	Wood litter	24	0.09	0.13
1800	Pine needles	24	0.10	0.13

Another complicating factor is that the reported application rates were on a wet basis rather than a dry basis required as input to RUSLE2. The dry biomass was assumed to be 25 percent of the wet basis application rates for all biomass types. The erosion ratios for fallow conditions at La Crosse assuming a 6 inch deep moldboard plowing are 0.65, 0.48, and 0.29 for the dry biomass inputs of 2000, 4000, and 8000 lbs/acre, respectively. Errors in estimating the dry biomass can have a significant effect on the RUSLE2 estimate erosion.

RUSLE2 assumes that the effect of all types of buried residue on rill-interrill erosion is described solely by biomass amount on a dry basis. Mechanical characteristic, such as diameter and length of individual pieces, of buried residue are assumed not to affect rill-interrill erosion in RUSLE2. This assumption is supported by the experimental and RUSLE2 results for the Statesville, North Carolina data.

The experimental results given in Tables 6.6 - 6.8 do not indicate the effect of biomass addition on rill-interrill erosion with modern farming practices. The depth of incorporation in these studies, which were conducted primarily in the late 1930's, was six inches while common modern moldboard plows incorporate material to 10 inches deep. Changing incorporation depth affects the RUSLE2 estimated ratio of erosion with incorporated biomass to erosion without biomass incorporation. Increasing incorporation depth from 10 to 6 inches increases the erosion ratio from 0.42 assuming a chisel plow type incorporation in the soil (0.48 assuming a moldboard plow incorporation) to 0.82 assuming incorporation with a modern moldboard plow for the 8 tons/acre manure spring application to corn at La Crosse, Wisconsin. The reason for the major difference is the effect of machine operation depth on the fraction of the biomass that is incorporated (see **Section 8.2.4.2**) and the biomass density in the surface 3-inch soil depth.

6.5.5. Soil biomass subfactor for pasture, range, and similar undisturbed lands

The equations for the soil biomass subfactor, equations 6.48 and 6.49, are considered to apply to all land use conditions (i.e., that is RUSLE2 is land-use independent). Range, pasture, and other undisturbed lands are highly variable in both time and space. Accurately measuring root biomass is extremely difficult, if not impossible for undisturbed lands because of temporal and spatial variability. Reliable measurements of

root biomass and buried residue are not available to either directly validate equations 6.48 and 6.49 or derive alternative equations for these lands.[55] Therefore, erosion data from research plots under simulated rainfall were used to derive effective root biomass values for rangeland plant communities rather than use measured root biomass values. [56]

The common approach for applying the USLE [AH537 (Wischmeier and Smith, 1978)] and RUSLE1 [AH703 (Renard et al., 1997)] to undisturbed lands is to input values that represent average annual conditions to make a single erosion computation using subfactors similar to those in equation 6.1 to for the year rather than to compute daily erosion. This approach can also be used in RUSLE2, although a better approach is to use time varying inputs to represent temporal effects on rill-interrill erosion (see RUSLE2 User's Reference Guide). The lack of both measured soil biomass data and research that establishes how soil biomass and its characteristics affect rill-interrill erosion required derivation of effective root biomass ratio values, which is defined as the ratio of effective root biomass to average annual above ground biomass production on a dry basis. Values for this ratio vary by plant community and were determined directly from experimental soil erosion research data (See RUSLE2 User's Reference Guide; Simanton et al., 1991). This derivation empirically accounts for differences between cropland and undisturbed land conditions and overcomes the impossibility of measuring root biomass on undisturbed lands.

First, a **c** factor value was computed for each site from measured erosion data by rearranging equation 2.1 as:

$$c_p = A_p / [R_p K_n (\lambda_p / \lambda_u)^m S_p] \qquad [6.50]$$

where: c_p = the c factor value for the measured erosion data obtained from applying simulated rainfall to field plots 12 ft wide by 35 ft long, A_p = measured erosion, R_p = the erosivity for the simulated rainfall, K_n = the soil erodibility value determined by applying the standard soil erodibility nomograph (see **Sections 4.1.1** and **4.1.2**) using soil property values measured at each site, λ_p = the plot length, λ_u = unit plot length, and S_p = the slope steepness factor computed from the measured plot steepness. Next an observed soil biomass subfactor value s_c was computed for each experimental site by rearranging

---

[55] An extensive review of measured root biomass for rangeland plant communities was conducted during the development of RUSLE1. The variability in these values, as indicated in Table 5-4, [AH703 (Renard et al., 1997) , is far too great to use these values as either input to RUSLE2 or to develop a soil biomass subfactor, especially a temporally varying one, for these conditions.

[56] Data from the WEPP study (Simanton et al., 1991) were used in the analysis to compute effective root biomass values. Data from the USDA Range Study Team study Spaeth et al., 2003) were considered for use in the development of RUSLE2. However, the data were not used because of inconsistencies in the data, which were not resolved by the researchers who collected the data (see the RUSLE2 User's Reference Guide).

equation 6.1, substituting c_p values for c and values for the subfactors, and solving for the soil biomass subfactor s_b value.

An effective root biomass value was computed by rearranging equation 6.48 and assuming no buried residue effect (i.e., assuming $B_{rs} = 0$). RUSLE2 does not consider a buried residue effect when using a single average annual input for root biomass. This RUSLE2 application method also requires using RUSLE2 inputs that add surface residue that does not decompose (see RUSLE2 User's Reference Guide). The value for the effective root biomass was divided by the average annual dry matter above ground biomass production to compute a value for effective root biomass ratio for the site. These values were averaged where the same plant community occurred at multiple sites. RUSLE2 multiplies the input value for above ground annual production by the effective root biomass ratio to obtain a value for effective root biomass B_{rt} that is used in equation 6.48 or 6.49 to compute a value for the soil biomass subfactor. Derivation of RUSLE2 effective root biomass values was the same as that used to derive comparable values for RUSLE1 [Yoder et al., 1997; AH703 (Renard et al., 1997)], except that RUSLE2 equations and procedures were used for equations 6.1, 6.48, and 6.50.

The RUSLE2 User's Reference Guide discusses how time varying inputs can be used in RUSLE2 to represent changes in time during the establishment of permanent cover on mechnanically disturbed lands such as construction sites, reclaimed mined lands, rangelands, military training grounds, and logged and burned forest lands. This Guide also describes how time varying inputs can be used in RUSLE2 to represent long-term vegetation that has reached maturity on undisturbed land. Using time varying inputs for canopy and root biomass allows RUSLE2 to compute a litter cover produced by senescence, soil biomass produced by dead (soughed) roots, and soil biomass produced by buried residue that are a function of plant community, production level, and location (Reeder et al., 2001).

RUSLE2 was fitted directly to the measured erosion data for rangelands to determine the soil biomass effect for these lands. However, RUSLE2 erosion estimates for undisturbed lands, especially rangelands, are much more uncertain than erosion estimates for cropland. This increased uncertainty exists for all erosion prediction technologies and is not unique to RUSLE2. Reasons for this uncertainty and its magnitude are discussed in detail in the RUSLE2 User's Reference Guide.

6.5.6. Sources of soil biomass in RUSLE2

The sources of soil biomass in RUSLE2 are biomass applied to the soil surface or directly injected into the soil, above ground biomass from vegetation grown on site, and roots from vegetation grown on-site. The amount of applied biomass is a direct input to RUSLE2 (see **Section 10**). The amounts of above ground and root biomass for vegetation grown on-site are directly related to RUSLE2 inputs (see **Section 9**). Once live above ground biomass becomes dead biomass (i.e., residue) by senescence or killed by an operation such as mowing, it disappears by decomposition discussed in **Section 10.3.** Similarly, once live roots become dead roots either by the plants being killed or by root sloughing, this biomass disappears by decomposition. Operations, including soil

disturbing operations, move biomass between the various biomass pools and redistribute biomass within the soil (see **Section 8**). The RUSLE2 User's Reference Guide describes the RUSLE2 biomass pools in detail and how these pools are manipulated in RUSLE2.

6.5.7. Transfer of surface residue to soil biomass by decomposition in RUSLE2

The organic matter content of the approximate 2-inch soil depth for no-till cropped soil is about twice that for conventional, clean-till cropping (Kay and VanderBygaart, 2002; Shelton and Bradley, 1987). A RUSLE2 assumption is that biomass occurs in the soil only by roots grown in the soil or a mechanical soil disturbing operation incorporating biomass. To accommodate the accumulation of high organic matter level in a shallow soil surface layer where little or no mechanical soil disturbance occurs, such as for no till croplands and undisturbed lands, RUSLE2 assumes that a portion of the daily surface residue decomposition is added to the top 2-inch soil layer. Once in this soil layer, this biomass is treated as any other buried residue that is subject to decomposition and has the same effect on rill-interrill erosion as any other buried residue.

This empirical procedure is used as a mechanism for increasing soil biomass in the upper soil layer when the soil is minimally disturbed. The equation used to compute this buried residue addition is:

$$f_b = 0.25[(1/s_c) - 1] \qquad [6.51]$$

where: f_b = the fraction of the daily biomass decomposed from surface residue that is added to the buried residue biomass in the upper 2-inch soil layer. The 0.25 value was determined during the fitting of equation 6.48 to observed data. The 0.25 variable was adjusted so that RUSLE2 computes a soil biomass in the top 2-inch soil layer for the no-till data point that is approximately twice the soil biomass for conventional, clean tillage. The structure of equation 6.51 was chosen so that the rate of change in the effect of soil consolidation is least immediately after a mechanical soil disturbance (i.e., $s_c = 1$). The rate of increase in f_b increases as the soil approaches full soil consolidation (i.e., $s_c = 0.45$).

The soil consolidation s_c subfactor term in equation 6.51 and the time to soil consolidation (see **Section 4.8**) determine the time required after a conversion from conventional, clean tillage to no tillage for soil biomass to come to a new equilibrium. Seven years is used for the time to soil consolidation in the eastern US, which is too short for all of the soil biomass changes to occur (Kay and VanderBygaart, 2002). However, seven years for time to soil consolidation is sufficient for RUSLE2 to represent particulate organic matter, and seven years seems sufficiently long for most major land use changes that affect rill-interrill erosion in the context of conservation planning. The time to soil consolidation is also used to compute change in soil erodibility when no biomass is present. Consequently, thus the RUSLE2 time to soil consolidation variable is a compromise for describing multiple effects.

Equation 6.51 computes no transfer of biomass from the surface residue to the buried residue when the soil has been recently mechanically disturbed, which is indicated by s_c =

1, which gives $f_b = 0$ from equation 6.51. If the soil is totally undisturbed where $c_s = 0.45$, $f_b = 0.31$, which means that for each day, approximately 30 percent of the surface residue that is lost by decomposition on that day is added to the buried residue in the upper 2-inch soil depth. In no-till corn cropping where the only soil disturbing operation is a planter that disturbs 15 percent of the soil surface, the c_s ranges from 0.54 to 0.61 during the year. The approximate annual average is 0.58, which gives a value of 0.18 from equation 6.51. That is, approximately 18 percent of the daily surface residue decomposition is added to the upper 2-inch soil depth for typical no-till corn cropping in comparison to almost 30 percent being added for a completely undisturbed soil condition (e.g., a pasture or rangeland).

6.5.8. Spatial variability in the soil biomass subfactor

Soil biomass and the soil biomass subfactor are assumed to be spatially uniform within a segment along the overland flow path, even when the soil is disturbed in strips. Non-uniformity in soil biomass along the overland flow path can be represented by dividing the overland flow path into segments.

6.5.9. Comments on soil biomass subfactor

The purpose of the soil biomass subfactor is to capture the main effect of live and dead roots and buried residue on rill-interrill erosion. The RUSLE2 soil biomass relationships are not meant to be a model of soil biomass that stands alone from how it used in RUSLE2 to estimate rill-interrill erosion for conservation and erosion control planning. The soil biomass subfactor does not capture all interactions, such as how the effect of soil biomass on erosion is affected by soil texture.

The importance of the soil biomass subfactor is often overlooked in evaluating how cover-management practices affect rill-interrill erosion. For example, large amounts of biomass added to the soil can greatly reduce rill-interrill erosion as indicated in Table 6.8. Similarly, large amounts of live and dead root biomass also greatly reduce erosion.

RUSLE2 only uses biomass amount as the variable to capture how soil biomass affects erosion. For example, RUSLE2 makes no distinction between how small and larges roots affect erosion. However, preference in selecting root biomass input values is given to fine roots instead of coarse roots (see RUSLE2 User's Reference Guide). Not much of the mass of coarse roots is entered for root biomass because coarse roots are assumed to have relatively little effect on erosion. Fine roots are assumed to have much greater effect on erosion per unit biomass than do coarse roots. Fine roots have greater surface area per unit mass than coarse roots and often are very close to the soil surface where they have a greater effect on runoff and erosion than coarse roots. Fine roots are readily sloughed and become a part of the soil organic matter pool.

Research to directly determine the effect of buried residue on rill-interrill erosion has been limited and incomplete (Van Liew and Saxton, 1983; Brown et al., 1989; McGregor et al., 1990; Box, Jr. and Bui, 1993). Research to measure soil buried residue and its characteristics as they affect rill-interrill erosion is difficult and is very incomplete.

However, research, such as that summarized in AH537 (Wischmeier and Smith, 1978), conclusively shows that root biomass reduces erosion. No studies have shown how root characteristics affect rill-interrill erosion.

Getting good results from RUSLE2 requires that instructions in the RUSLE2 User's Reference Guide for selecting input values be carefully followed. RUSLE2's soil biomass subfactor equation and other subfactor equations were calibrated using the data in the RUSLE2 **core database**. When those values and the procedures described in the RUSLE2 User's Reference Guide are followed, RUSLE2 users can expect good results from RUSLE2 for conservation and erosion control planning. If one disagrees with the soil biomass values used by RUSLE2, one can not simply change RUSLE2 input values because of RUSLE2 having been calibrated using values from the RUSLE2 **core database**. If soil biomass values are changed, the soil biomass subfactor equation must be re-derived because the RUSLE2 equation was derived using RUSLE2 computed soil biomass values.

The importance of this point can not be over emphasized.

6.6. Soil consolidation subfactor

6.6.1. Soil consolidation effect

The RUSLE2 assumption is that mechanical soil disturbance by tillage, construction activities, and other soil loosening operations significantly increases soil susceptibility to erosion. Rill-interrill erosion immediately after a mechanical soil disturbance is assumed to be about twice that when the soil has not been disturbed for an extended period. The effect is much greater for rill erosion than for interrill erosion (Foster, 1982; Foster et al., 1982c).

The term soil consolidation does not accurately connote the process by which soil becomes less susceptible to erosion over time. The reduction in soil erodibility over time represented by the soil consolidation subfactor is related to internal cohesive soil bonding increasing over time rather than to a mechanical increase in soil bulk density. Cohesive bonding increases as the soil experiences wetting and drying cycles in the presence of organic matter and chemical bonding agents in the soil (Foster et al., 1985c; Toy et al., 2002). The important role of soil moisture is the reason for the time to soil consolidation being a function of average annual precipitation between 10 and 30 inches (see **Section 4.8**).

The soil consolidation effect is based on a comparison of erosion from a soil in the unit plot condition to erosion of the same soil that has not been mechanically disturbed for some time after being left in unit-plot condition by the last mechanical soil disturbance. Soil disturbance also affects the ground cover, soil surface roughness, and soil biomass subfactors in addition to the soil consolidation subfactor. The soil consolidation subfactor represents solely the effects of soil loosening on erosion relative to time since the last mechanical soil disturbance that left unit plot conditions. The soil consolidation

subfactor variable is also used to compute values for the soil biomass subfactor, rill to interrill erosion ratio, and runoff curve number. Therefore, the effect of soil loosening computed by RUSLE2 can be significantly greater than the effect represented by the soil consolidation subfactor.

6.6.2. Soil consolidation subfactor equation

The equation for the RUSLE2 soil consolidation subfactor is:

$$s_c = 0.45 + \exp\{-3.314[0.1804 + (t_d / t_c)^{1.439}]\} \quad [6.52]$$

where: t_d = days since last mechanical soil disturbance and t_c = the time to soil consolidation The 0.45 value in equation 6.52 represents the minimum soil consolidation subfactor value that occurs for time exceeding the time to soil consolidation.[57] The soil consolidation subfactor value is 1 for $t_d = 0$, which is immediately after a mechanical soil disturbance. A plot of equation 6.52 is shown in Figure 6.6 for two times to soil consolidation.

Equation 6.52 was derived from experimental erosion data collected from natural runoff plots at Zanesville, Ohio (Borst et al., 1945). Erosion was measured for a few years from a plot periodically tilled to maintain unit plot conditions. Tillage was stopped and erosion measurements were continued for several years after tillage stopped. Measured annual erosion values were adjusted based on the annual erosivity to account for weather differences between years. Observed soil consolidation subfactor values were computed by dividing the adjusted annual erosion values after tillage stopped by adjusted average annual erosion before tillage stopped.

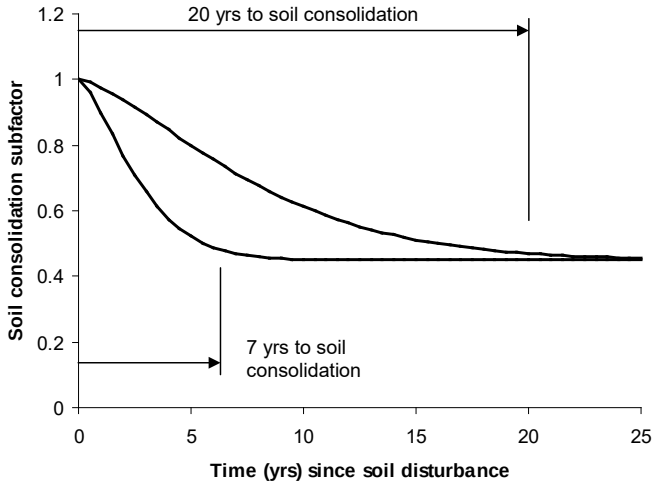

Figure 6.6. Variation of the soil consolidation subfactor as a function of time after last mechanical soil disturbance.

Experimental erosion studies on mine spoil and reconstructed shoed that compaction can increase rill-interrill erosivity by as much as 40 percent (Barfield et al.,

[57] Equation 6.52 approaches 0.45 asymptotically. The time to soil consolidation is defined as the time when 95 percent of the decrease in the soil consolidation subfactor has occurred (see **Section 4.8**).

1988). About half of this effect can be captured in RUSLE2 by inputting a 0 soil surface roughness value for the soil disturbing operation used to describe the compaction. The 0 input value for soil surface roughness represents a smooth soil surface that is assumed to result from the compaction. This value is increased to represent the roughness effect left by a compactor such as a sheep's foot roller that leaves some soil surface roughness.

6.6.3. Spatial variability effect on soil consolidation subfactor

RUSLE2 accommodates spatial variability along the overland flow path when the overland flow path is divided into segments. RUSLE2 also represents the effect of operations that disturb only a portion of the soil surface (e.g., strip tillage) based on the fraction of the soil surface that the operation disturbs. An effective value for the soil consolidation subfactor is computed as the weighted average of $s_c = 1$ for the portion disturbed and the s_c value for the undisturbed portion at the time of the mechanical soil disturbance. An effective time since soil disturbance is calculated by rearranging equation 6.52 and solving for the time t_d that gives the effective s_c value (see **Section 8.3.1**). The time since last soil disturbance is reset to this effective time, and time accounting for soil consolidation begins again from the effective time value.

6.6.4. Comments on soil consolidation subfactor

The RUSLE2 soil consolidation subfactor only captures the soil loosening effect on rill-interrill erosion in the broadest terms. The soil consolidation subfactor is the most poorly defined of all the RUSLE2 cover-management subfactors. Very little empirical and not much fundamental research has been conducted to determine how the soil consolidation effect varies with climate, soil texture, and other factors. The RUSLE2 soil consolidation subfactor is determined from a single set of data collected at a single location on a single soil texture. The effect is greater for rill erosion than for interrill erosion (Foster et al., 1982c). However, the soil consolidation effect on rill erosion can be quite variable. In one study, rill erosion of a silt loam soil decreased by about 75 percent over about a year's time (Dissmeyer and Foster, 1981). In another study, sediment eroded from ridges and deposited in furrows became quite resistant to erosion in just four weeks (Foster et al., 1982c).

The soil consolidation effect surely must be a function of soil texture. For example, the range in the soil consolidation subfactor for soils high in sand is assumed to be less than for silt loam soils. Also, the time to soil consolidation is assumed to be a function of soil texture. However, available research information is not sufficient to include these effects in the RUSLE2 soil consolidation subfactor.

The RUSLE2 assumption is that mechanical soil compaction (i.e., mechanical increases in soil bulk density) does not affect rill-interrill erosion. Soil compaction has two offsetting effects. One is to decrease infiltration, which increases runoff and hence rill-interrill erosion. The other effect is to decrease erosion by decreasing the detachability of soil particles by raindrop and runoff forces. The assumption of no effect of soil compaction on erosion is false for a high clay soil being mechanically compacted at optimum soil moisture. Soil compaction of a high clay soil can greatly reduce rill erosion

(Graf, 1971). Available research information was not sufficient to include a RUSLE2 relationship that computes erosion as a function of soil bulk density. An input value less tha 0.24 inches for soil surface roughness can be used to represent increase in erosion caused by compaction. Also, the soil erodibility factor value can be reduced to represent decreased erosion caused by compaction of high clay soils.

RUSLE2 does represent the effect on rill-interrill erosion of subsoiling, scarifying, and similar mechanical soil disturbances designed to break up soil to increase infiltration, which in turn decreases runoff and erosion. RUSLE2 represents this effect though the soil surface roughness subfactor (see the RUSLE2 User's Reference Guide).

The RUSLE2 soil erodibility factor does not represent the effect of soil compaction. Soil compaction is a cover-management effect. Changing a soil erodibility input value to represent soil compaction is for convenience only in RUSLE2 because no other input method is available to represent the effect of compaction. RUSLE2 soil erodibility are based on the tilled unit plot condition.

6.7. Antecedent soil moisture subfactor

The antecedent soil moisture subfactor is used only when RUSLE2 is applied to Req conditions (see **Section 3.2.5**).

6.7.1. Antecedent soil moisture effect

Rill-interrill erosion under Req conditions is highly sensitive to soil moisture [AH703 (Renard et al., 1997); Van Klaveren and McCool,1998]. High soil moisture significantly increases erosion during the winter Req period. Freezing and thawing cycles in the presence of very high soil moisture and other processes dramatically increase soil erodibility during the winter months at Req locations [see RUSLE2 User's Reference Guide, AH703 (Renard et al., 1997); Van Klaveren and McCool,1998). Highly saturated soil in the tilled surface layer plays a major role in Req processes that do not occur to nearly the same degree or regularity in non-Req locations.

6.7.2. Antecedent soil moisture subfactor equations

The RUSLE2 antecedent soil moisture subfactor equations are a refinement of those in RUSLE1 [Yoder et al., 1997; AH703 (Renard et al., 1997); McCool et al., 2002]. The year is divided into periods of soil moisture replenishment (October 1 – March 31), stable at maximum soil moisture (April 1 – April 30), depletion (May 1 – July 31), and stable at minimum soil moisture (August 1 – September 30).

6.7.2.1. Replenishment (October 1 – March 31)

The average daily soil moisture replenishment rate is computed as:

$$R_m = 0.5/182 \quad P_a \le 10 \text{ inches} \qquad [6.53]$$

$$R_m = [0.5 + 0.062(P_a - 10)]/182 \quad 10 < P_a \leq 18 \text{ inches} \qquad [6.54]$$

$$R_m = 1/182 \quad P_a > 18 \text{ inches} \qquad [6.55]$$

where: R_m = an index (dimensionless) for daily moisture replenishment rate, P_a = average annual precipitation (inches), and 182 = number of days over which replenishment occurs.

$$s_m = s_{mp} + R_m \quad if\,(s_m > 1) : s_m = 1 \qquad [6.56]$$

where s_m = daily antecedent soil moisture subfactor and s_{mp} = the soil moisture subfactor on the previous day.

6.7.2.2. Depletion (May 1 – July 31)

The daily soil moisture depletion rate is computed as:

$$D_m = \phi_m / 91 \qquad [6.57]$$

where: D_m = an index (dimensionless) for daily moisture depletion rate, ϕ_m = the total soil moisture depletion as a function of vegetation, and 91 is the number of days over which depletion is assumed to occur. Example values for ϕ_m are given in Table 6.9.

$$s_m = s_{mp} - D_m \quad if\,(s_m < 0) : s_m = 0 \qquad [6.58]$$

6.7.2.3. Minimum and maximum periods (April 1 – April 30) and (August 1 – September 30)

The soil moisture subfactor is assumed not to change during the minimum period between the depletion and replenishment periods and the maximum period between the replenishment and depletion periods. That is:

$$s_m = s_{mp} \qquad [6.59]$$

6.7.2.4. Initial s_m value

Table 6.9. Soil moisture depletion index for vegetation grown in Req location

Vegetation	Depletion index
Winter wheat and other deep rooted crops	1.00
Spring wheat and barley	0.75
Spring peas and lentils	0.67
Shallow rooted crops	0.50
Summer fallow	0.00
Vegetation that has been killed	0.00

The initial default value for the antecedent soil moisture subfactor s_m is 1. The initial condition is not important when cover-management practice are rotations (i.e., the set of operations is repeated in cycles). RUSLE2 runs until dynamically stable conditions are reached. However, when the cover-management practice is not a rotation, the initial operations in the cover-management description are used to set the desired initial

condition (see RUSLE2 User's Reference Guide). Specific values can not be entered in the RUSLE2 computer program to set initial values of RUSLE2 variables.

6.7.2.5. Applicability of RUSLE2 antecedent soil moisture subfactor equations

The RUSLE2 antecedent soil moisture subfactor equations (equations 6.53 - 6.59) strictly apply only to the portion of the Req zone from central Washington across northern Idaho and in northeastern Oregon illustrated in Figure 3.16 (also, see RUSLE2 User's Reference Guide). Although Req conditions occur in other locations, equations 6.53 – 6.59 do not apply to those locations because of differences in precipitation patterns.

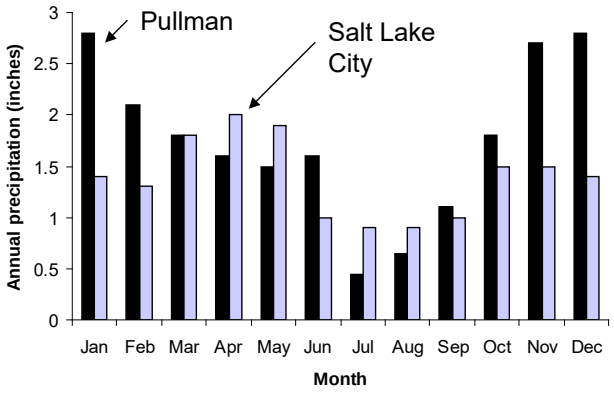

Figure 6.7. Distribution of monthly precipitation at Pullman, Washington (P_a = 20.9 inches) and Salt Lake City, Utah (P_a = 16.9 inches)

These equations were empirically derived from data collected at Pullman, Washington. Differences in monthly precipitation distributions between Pullman Washington and Salt Lake City, Utah are illustrated in Figure 6.7. Equation 6.53 – 6.55 do take into account differences in annual precipitation between locations but not differences in monthly precipitation and vegetation extraction patterns. Replenishment and depletion rates are expected to differ among locations as monthly precipitation distributions vary.

6.7.3. Comments on antecedent soil moisture subfactor

The antecedent soil moisture subfactor is a very important variable at Req locations. For example, changing the moisture depletion variable ϕ_m from 1, its standard value, to 0 for no moisture depletion, increased estimated erosion from 8.9 to 14 tons/acre per year for a typical conventional, clean-till continuous wheat crop at Pullman, Washington. Given that the antecedent soil moisture subfactor has a major effect on rill-interrill erosion emphasizes the need for improved equations for this subfactor as a function of monthly precipitation distribution.

The RUSLE2 antecedent soil moisture subfactor should be used only for Req locations. The antecedent soil moisture subfactor equations were empirically derived from data collected at Pullman, Washington where climatic conditions are very different from those in other US regions. Antecedent soil moisture affects rill-interrill erosion in all locations. Those effects are empirically described by the canopy and soil biomass subfactors and by the precipitation and temperature variables used to compute temporal soil erodibility factor values (see **Section 4.5**). Using the antecedent soil moisture subfactor in non-Req location causes serious errors in RUSLE2 estimated erosion.

6.8. Validation of cover-management factor values

RUSLE2 should represent the effect of cover-management on rill-interrill erosion better than it does for any other major factor. Rill-interrill erosion varies more as cover-management varies over its likely range than it does for the likely range of any other factor. Cover-management type erosion control practices are used more widely than any other type of erosion control practice. RUSLE2 must accurately estimate how cover-management affects erosion to avoid excessive expense of installing more erosion control than necessary. Likewise, RUSLE2 must accurately estimate how cover-management affects erosion to ensure adequate erosion control and prevention of excessive damages. The RUSLE2 User's Reference Guide extensively discusses the validity of RUSLE2 for estimating how cover-management affects rill-interrill erosion.

Tables 6.10 – 6.12 illustrate how well the RUSLE2 cover-management subfactors compute soil loss ratios in relation to summarized experimental data taken from AH537 (Wischmeier and Smith, 1978) and other sources. As these tables show, RUSLE2 estimates very well the variation in soil loss ratios as a function of crop stage periods and as a function of the major cover-management variables that affect rill-interrill erosion.

In addition, an extensive set of literature was reviewed and analyzed in validating RUSLE2 for conservation tillage especially no till (see **Section 12.23**).

Table 6.10. Soil loss ratios for conventional clean tilled continuous 112 bu/ac from AH537 and RUSLE2 computed values.

Crop stage (defined in AH537)	AH537 soil loss ratio	RUSLE2 computed soil loss ratio
Fallow	0.31	0.28
Seedbed	0.55	0.54
1 - 10% < canopy cover < 50%	0.48	0.52
2 - 50% < canopy cover < 75%	0.38	0.3
3 - 75% < canopy cover to maturity	0.23	0.18
4 after harvest (stalks spread)	0.06	0.06

Table 6.11. Soil loss ratio values for conventional clean till flat planted continuous 750 lbs/acre cotton at Holly Springs, Mississippi.

Crop stage (defined in AH537)	AH537 soil loss ratio	RUSLE2 computed soil loss ratio
Fallow	0.39	0.54
Seedbed	0.64	0.74
1- 10% canopy cover < 35%	0.59	0.74
2 - 35% < canopy cover < 60%	0.46	0.49
3 - 60% canopy cover to maturity	0.32	0.23
Defoliation to Dec 31	0.26	0.24
Jan 1 to Feb. tillage	0.32	0.32

Table 6.12. Soil loss ratio values for conventional clean till ridge (hipped) continuous planted 750 lbs/acre cotton at Holly Springs, Mississippi.

Crop stage (defined in AH537)	AH537 soil loss ratio	RUSLE2 computed soil loss ratio
1st hip, no prior tillage	0.84	0.88
Split ridges with a “do-all”	0.54	0.52
Hip after 2 prior tillages	1.08	1.01
Split ridges with a “do all”	0.62	0.58
Hip after 3 or more tillages	1.1	1.12
Split ridges with a “do all”	0.64	0.64
Seedbed	0.64	0.64
1 - 10% canopy cover < 35%	0.59	0.64
2 - 35% < canopy cover < 60%	0.46	0.45
3- 60% canopy cover to maturity	0.32	0.21
Defoliation to Dec 31	0.22	0.23
Jan 1 to Feb. tillage	0.32	0.27

6.9. List of symbols

a_b = coefficient related to buried residue and soil consolidation used to compute a_2

a_e = coefficient used to compute loss of ridge height by interrill erosion (inch/customary US erosivity unit)

a_g = coefficient related to height within the canopy where vegetative surface area is concentrated, used to compute effective fall height

a_h = coefficient used to compute ridge subfactor values

a_s = coefficient that is a function of canopy shape, used to compute effective fall height

a_1 = coefficient related to soil biomass and soil consolidation used to compute a_2

a_2 = coefficient, along with a_4, for how soil consolidation, soil biomass, and conformance of ground cover to the soil surface affect rill to interrill erosion ratio

a_3 = coefficient related overland flow path length and steepness and conformance of ground cover to soil used to compute a_4

a_4 = coefficient, along with a_2, for how soil consolidation, soil biomass, and conformance of ground cover to the soil surface affect rill to interrill erosion ratio

A_p = measured erosion from simulated rainfall applied to plots used to determine c_p factor values (mass/area)

b = coefficient for how ground (surface) cover affects rill-interrill erosion ($percent^{-1}$)

b_r = coefficient for how ground cover affects rill erosion ($percent^{-1}$)

B_{rs} = buried residue mass (dry basis) density in soil accounting depth for buried residue (mass/area·length)

B_{rt} = live and dead root mass (dry basis) density in soil accounting depth for roots (mass/area·length)

B_{td} = total mass (dry basis) density of buried residue and live and dead roots averaged over soil disturbance depth after the operation (lbs_m/acre·inch)

c = daily cover-management factor

c_a = coefficient for combined effect of buried residue and soil consolidation on ground cover effectiveness in relation to rill erosion

c_c = daily canopy subfactor

c_p = c factor value for measured erosion data obtained from applying simulated rainfall to field plots

c_{pr}/c_{pi} = rill to interrill prior land use soil erodibility ratio

d_{rs} = accounting soil depth for buried residue (inches)

D_b = rill-interrill erosion when ground cover is not present (bare soil) (mass/area)

D_c = rill-interrill erosion when ground cover is present (mass/area)

D_{ib} = interrill erosion when ground cover is not present (bare soil) (mass/area)

D_m = index for daily moisture depletion rate

D_{rb} = rill erosion when ground cover in not present (bare soil) (mass/area)

D_t = normalized rill-interrill erosion

e_d = waterdrop impact energy (force-distance)

f_b = fraction of the daily biomass decomposed from surface residue added to buried residue biomass in upper 2-inch soil layer

f_c = daily canopy cover (fraction)

f_{ec} = daily effective canopy cover (fraction)

f_g = ground (surface) cover (fraction or percent when used to compute g_c)

f_{ge} = effective ground cover used to compute values for slope exponent m (percent)

f_{gn} = net ground cover, portion of soil surface covered

f_r = fraction of today's soil surface roughness greater than 0.24 inch that remains after today's loss of roughness

g_c = daily ground (surface) cover subfactor

g_{ci} = interrill erosin ground (surface)cover subfactor

g_{cr} = rill erosion ground (surface)cover subfactor

g_r = relative row grade (grade along the ridges/overland flow path steepness)

h_b = height to canopy bottom (length)

h_f = daily effective fall height (feet)

h_t = height to canopy top (length)

H = daily ridge height (inches)

H_e = ridge height component associated with interrill erosion (inches)

H_{ep} = previous day ridge height component associated with interrill erosion (inches)

H_s = ridge height component associated with settlement (inches)

H_{sp} = previous day ridge height component associated with settlement (inches)

I = daily amount of water added by irrigation (inches)

K_n = soil erodibility value determined from standard soil erodibility nomograph using soil property values measured at each site (mass/erosivity unit)

K_r/K_i = rill to interrill soil erodibility ratio

m = slope length exponent

m_d = waterdrop mass

P_a = average precipitation (inches)

P_{cl} = mass portion of soil composed of clay (percent)

P_d = daily precipitation (inches)

P_{sl} = mass portion of soil composed of silt (percent)

r_d = daily erosivity (erosivity units)

r_h = daily ridge height subfactor

$r_{h,u\&d}$ = ridge height subfactor value when ridge orientation is parallel to overland flow path

r_{h6} = daily ridge height subfactor when overland flow path steepness is less than or equal to 6 percent

R_a = daily adjusted sil surface roughness roughness used to compute soil surface roughness subfactor values (inches)

R_{aa} = adjusted soil surface roughness immediately after soil disturbing operation (inches)

R_{ae} = existing adjusted soil surface roughness before a soil discturbing operation (inches)

R_{alf} = adjusted final long term soil surface roughness value after input value for long term roughness adjusted for soil texture and soil biomass (inches)

R_{ap} = adjusted soil surface roughness on previous day (inches)

R_{ib} = initial soil surface roughness after input roughness adjusted for soil texture and biomass (inches)

R_{in} = input soil surface roughness value for reference condition for soil disturbing operation (inches)

R_{it} = initial soil surface roughness after input roughness value adjusted for soil texture (inches)

R_l = daily adjusted long long term soil surface roughness (inches)

Req = equivalent erosivity related to greatly increased soil erodibility during winter months in Nrthwestern US

R_m = index for daily moisture replenishment rate

R_p = erosivity for simulated rainfall applied to plots used to determine c_p factor values (erosivity units)

s = overland flow path steepness (sine of slope angle)

s_b = daily soil biomass subfactor

s_c = daily soil consolidation subfactor

s_i = interrill area steepness (sine of slope angle)

s_m = daily antecedent soil moisture subfactor used in Req zone

s_p = overland flow path steepness (100 times tanget of slope angle)

s_r = daily soil surface roughness subfactor

S_p = slope steepness factor computed from steepness of plots used with simulated rainfall to determine c_p factor values

t_c = time to soil consolidation (days)

t_d = time since the last mechanical soil disturbance (days)

V = waterdrop impact velocity (length/time)

α = rill to interrill erosion ratio for bare soil

δ = cover adjustment term used to compute slope length exponent

ξ = tillage intensity

λ = overland flow path length (length)

λ_p = length of plots used with simulated rainfall to determine c_p factor values

λ_u = unit plot length (72.6, 22.1 m)

ϕ_m = the total soil moisture depletion as a function of vegetation

ψ = coefficient related to conformance ground (surface) cover to soil surface

7. SUPPORT PRACTICES

7.1. Contouring (ridging)

7.1.1. Description of contouring (ridging)

Contouring is an erosion control practice where ridges are placed on the contour around the hillslope perpendicular to the overland flow path. Runoff flows uniformly over the ridges along their length when the ridges are perfectly on the contour and the ridge top is level. Ponded water in the furrows between the ridges reduces detachment and causes a major portion of the sediment eroded from the ridges to be deposited in the furrows.

These ideal conditions seldom occur in the field. Breakovers occur in low ridge areas and where the soil is susceptible to rill erosion. Erosion reduction with contouring is reduced when breakovers occur. However, erosion reduction occurs even with breakovers if furrow (row) grade is sufficiently flat to cause deposition in the furrows or to cause reduced rill erosion in relation to the rill-interrill erosion that occurs when the ridges are parallel to the overland flow path. Runoff travels long distances in the furrows between high ridges to concentrated flow areas where ephemeral gully erosion occurs. RUSLE2 does not explicitly estimate ephemeral gully erosion (see RUSLE2 User's Reference Guide), although ephemeral gully erosion occurred in the small watersheds used to derive the RUSLE2 contour subfactor relationships. Thus, ephemeral gully erosion is partially included in RUSLE2 erosion estimates for contoured conditions.

The effect of ridging (contouring) on rill-interrill erosion must be considered even when ridging is not used explicitly as an erosion control practice. For example, tillage direction in an agricultural field is often parallel to a field boundary, which results in ridges at an angle to the overland flow path. Rill-interrill erosion varies between the extremes of being minimal when the ridges are perfectly on the contour and maximum when the ridges are parallel to the overland flow path.

The base, reference unit plot condition is that ridges-furrows are parallel to the overland flow path. Thus, the RUSLE2 contouring subfactor represents the effect of ridge-furrow orientation with respect to the overland flow path on rill-interrill erosion.

7.1.2. Contouring (ridging) effect

Figure 7.1 is a graph of experimental data that shows how contouring affects rill-interrill erosion on plots that ranged in width from12 to 150 ft and small watersheds that were about 5 acres in area (Foster et al., 1997; see other references in **Section 7.1** and **Section 12.2.1**).

Each type of measurement area has shortcomings. A shortcoming of watersheds is that measured sediment from watersheds includes sediment produced by ephemeral gully erosion, which is not estimated by RUSLE2. A shortcoming of plots narrower than about

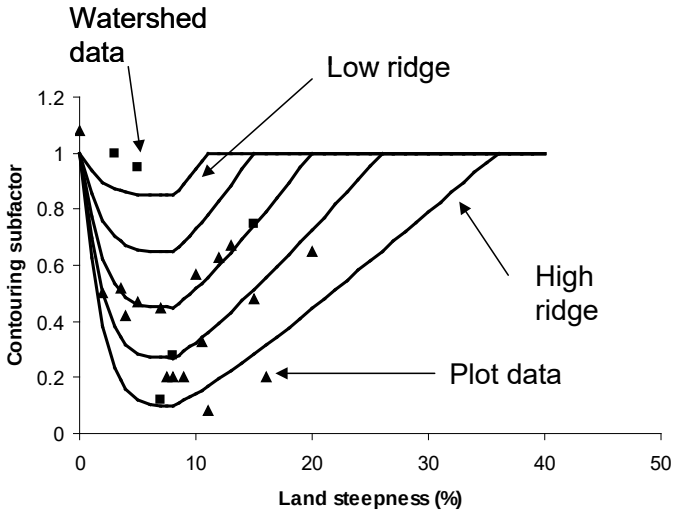

Figure 7.1. Experimental data from plots and small watershed (~ 5 acres) for effect of contouring (ridging) on rill-interrill erosion and fitted lines for effect of ridge height on contouring.

20 ft is that runoff rates are too low at the ridge breakovers. Several plot widths exceeded 20 ft with some as wide as 150 ft, which are sufficiently wide to represent field contouring. Although, neither plot nor watershed data are entirely satisfactory, data from both plots and watersheds were combined to derive RUSLE2 contouring subfactor equations.

The well accepted general contouring subfactor relationship is an upward concave curve that starts at 1 for a zero steepness, decreases to a minimum as land steepness increases to an approximate 8 percent steepness and then increases to 1 at an upper steepness beyond which contouring is assumed not to reduce erosion [AH537 (Wischmeier and Smith, 1978)]. Contouring has no effect at zero land steepness because no flow direction is defined. Contouring has no effect beyond a maximum steepness that is a function of ridge height because the land is so steep that no water can be stored by the ridges.

The range in the data illustrated in Figure 7.1 for the effect of contouring on rill-interrill erosion is assumed to be caused primarily by a ridge height variation. Experimental data show that contouring's erosion reduction increases as ridge height increases (Moldenhauer and Wischmeier, 1960). Increased ridge height increases storage of runoff, decreases interrill detachment, and increases deposition in the furrows, which is the basis for the curves in Figure 7.1 being a function of ridge height. Also, dense plant stems in narrow rows on the contour have the same effect on rill-interrill erosion as ridges on the contour (Daniel et al., 1943; Van Doren et al., 1950). Experimental data show that contouring is less effective for large intense runoff events than for small ones (Moldenhauer and Wischmeier, 1960). In some cases, erosion on watersheds was greater with contouring than with tillage up and down hill as illustrated in Figure 7.1 (Hill et al., 1944). These examples of increased erosion are associated with concentrated flow erosion where ridge-breakovers occurred. Thus, the effective of contouring on rill-interrill erosion depends on storm, soil, and cover-management characteristics that affect runoff.

A long accepted principle by soil conservationists is that contouring fails if the overland flow path length exceeds a critical length that is a function of land steepness [(AH282 (Wischmeier and Smith, 1965); AH537 (Wischmeier and Smith, 1978)]. That critical length is assumed in RUSLE2 to be a function of the shear stress applied to the soil by

runoff, which in turn is a function of storm characteristics, inherent potential of the soil for generating runoff, and how cover-management affects runoff and the shear stress that runoff applies to the soil.

The RUSLE2 contouring subfactor equations are very similar to the comparable RUSLE1 equations [Foster et al, 1997, AH703 (Renard et al., 1997)] except for the RUSLE2 equations being a function of daily ridge height, runoff, and cover-management conditions.

7.1.3. Contouring (ridging) subfactor equations

The RUSLE2 contouring equations were developed to give accepted values for a base, reference condition of conventional, clean tilled 50 bu/ac corn grown on a silt loam hydrologic C soil group soil located at Columbia, Missouri.[58] This management practice was common when the contouring data were collected from the mid 1930's to the mid 1950's for much of the data represented in Figure 7.1.

The RUSLE2 equations vary contouring subfactor values about base, reference values as climate, soil, and cover-management conditions depart from the base, reference condition. The RUSLE2 equations were structured to meet required boundary conditions and were calibrated to experimental data to give similar contouring subfactor values used by the USLE and computed by RUSLE1 for base, reference conditions. In contrast to the RUSLE1 equations that used a representative ridge height and cover-management condition to represent the cover-management practice to compute an average annual contouring subfactor value (Foster et al, 1997), the RUSLE2 equations compute daily contouring subfactor values as climate, cover-management, runoff, and ridge height vary daily.

7.1.3.1. Base equations

The data shown in Figure 7.1 were collected from several locations in the eastern US. However, the data were insufficient for directly deriving explicit equations and coefficient values that consider all of the major variables related to contouring's effect on rill-interrill erosion. The data in Figure 7.1 were assumed to represent the overall effect of contouring for the base, reference condition described in **Section 7.1.3**.

The first step in deriving the RUSLE2 contouring equations was to develop a set of equations that represent the base, reference condition. Those equations, which follow similar RUSLE1 equations, are given by:

---

[58] These farming conditions differ from current farming practices. Also, these farming practices are not typical of rangelands, surface mine reclamation, construction sites, and other conditions where ridging (contouring) is used to control rill-interrill erosion. RUSLE2 includes procedures to account for these differences.

$$p_b = a_c(s_m - s_c)^4 + p_{bm} \quad s_c < s_m \qquad [7.1]$$

$$p_b = c_c(s_c - s_m)^{1.5} + p_{bm} \quad s_m \le s_c < s_{be} \qquad [7.2]$$

$$p_b = 1 \qquad s_{be} \le s_c \qquad [7.3]$$

where: p_b = base contouring subfactor value, s_c = a scaled land steepness (sine of slope angle), s_m = the land steepness (sine of slope angle) at which $p_b = p_{bm}$, the minimum base contouring value and s_{be} = the steepness (sine of slope angle) at which the contouring subfactor reaches 1. Values for the coefficients a_c and c_c are computed from:

$$a_c = (1 - p_{bm}) / s_m^4 \qquad [7.4]$$

$$c_c = (1 - p_{bm}) / (s_{be} - s_m)^{1.5} \qquad [7.5]$$

These equations satisfy the boundary conditions that $p_b = 1$ at $s_c = 0$, $p_b = p_m$ at $s_c = s_m$, $p_b = 1$ at $s_c = s_{be}$, and the slope of equations 7.1 and 7.2 is zero at $s_c = s_m$.

7.1.3.2. Ridge height adjustments

The minimum contouring subfactor value p_{bm}, which occurs at $s = s_m$, is assumed to be a function of ridge height as (Moldenhauer and Wischmeier, 1960):

$$p_{bm} = 0.05 + 0.95\exp(-0.5512H_e) \;\; if\,(H_e > 8) : H_e = 8 \text{ inches} \qquad [7.6]$$

where: H_e = daily effective total ridge height (inches), which is the sum of the daily soil ridge height H (see **Sections 6.4.6 and 8.3.5**) and the daily effective vegetation ridge height H_{vr} (see **Section 9.2.7**). The steepness s_{bm} at which the base contouring subfactor is minimum (i.e., $p_b = p_{bm}$) is also assumed to be a function of effective ridge height as:

$$s_{bm} = 4[1 - \exp(-0.7903H_e)] + 4 \;\; if\,(H_e > 8) : H_e = 8 \text{ inches} \qquad [7.7]$$

The steepness s_{be} at which the contouring subfactor p_b becomes 1 as steepness increases is assumed to be a function of effective ridge height as:

$$s_{be} = \sin\{\tan^{-1}[(9 + 53.09H_e / 8) / 100]\} \; if\,(H_e > 8) : H_e = 8 \text{ inches} \qquad [7.8]$$

where: s_{be} = the steepness (sine of slope angle) that the contouring subfactor becomes 1. Maximum effective ridge height for equations 7.6, 7.7, and 7.8 is limited to 8 inches.[59]

---

[59] The uncertainty of contouring's erosion control effectiveness at any specific site is greater than for all other erosion control practices. Also, data for the effect of ridge height and other factors on the erosion control effectiveness of contouring are very limited for a wide range of conditions. Contouring using high ridges can be highly effective, especially in low rainfall areas, but result in very high erosion for rarely

7.1.3.3. Runoff adjustments

The minimum contouring subfactor values p_{rm} at s_m are assumed to vary directly with the ratio of runoff with the given climate, soil, and cover-management condition to the runoff for the base, reference condition as:

$$p_{rm} = p_{bm}(d_r / 4.16) \quad [7.9]$$

where: p_{rm} = the minimum contouring subfactor value adjusted for runoff, d_r = runoff depth (inches) for the 10 year-24 hour precipitation amount P_{10y24h} at the given location, soil, and cover-management condition on the day that a contouring factor value is computed, and 4.16 (inches) = runoff computed with the 10 year-24 hour storm for the base, reference condition (see **Section 2.3.7**).

The steepness at which the contouring subfactor becomes 1 for a given condition is assumed to be related to the shear stress that the runoff applies to the soil. It is computed from:

$$s_{re} = s_{be} /(d_r / 4.16)^{0.8571} \quad [7.10]$$

where: s_{re} = the runoff adjusted steepness (sine of slope angle) above which the contouring subfactor equals 1.

7.1.3.4. Steepness scaling

A scaled steepness s_c is used to compute a base contouring p_b subfactor value using equation 7.1, 7.2, or 7.3. The equation for the scaled steepness at low steepness is given by:

$$s_c = s \quad s \le s_m \quad [7.11]$$

where: s = the steepness (sine of slope angle) of the overland flow path. The scaled steepness for $s > s_m$ is given by:

$$s_c = s_{bm} + \frac{(s - s_{bm})(s_{be} - s_{bm})}{s_{re} - s_{bm}} \quad s > s_m \quad [7.12]$$

The reason that steepness used to compute a p_b value must be scaled is that the upper steepness where the contouring subfactor becomes equal to 1 varies as conditions vary from the base, reference condition.

---

occurring intense storms. The 8 inch limit in these equations was chosen based on professional judgment and experience (see **Section 7.1.5**). See the RUSLE2 User's Reference Guide for guidance on using RUSLE2 to evaluate the erosion control effectiveness of contouring (ridging).

7.1.3.5. Contouring subfactor scaling

The contouring subfactor value must also be scaled because the contouring factor value at s_m for the given condition differs from the contouring subfactor value for the base, reference conditions. The contouring subfactor value for level furrow (row) is computed from the scaling equation as:

$$p_{c0} = 1 - \frac{(1 - p_b)(1 - p_{rm})}{1 - p_{bm}} \quad if\,(p_{c0} > 1) : p_{c0} = 1 \qquad [7.13]$$

where: p_{c0} = the contouring subfactor for a zero row grade (grade along furrows separating the ridges).

7.1.3.6. Contouring subfactor limits

Contouring subfactor values computed by equation 7.13 must be within certain limits. The upper limit is that contouring subfactor values can not be greater than 1. The other limit is a lower limit assumed to be acceptable for conservation and erosion control planning. RUSLE2 must account for the possibility of an extreme storm occurring even when annual erosivity and the P_{10y24h} precipitation amounts are low. The lower limit for contouring subfactor values is computed from:

$$p_{c0,\min} = 0.05 + 0.95 \exp(-h_e) \qquad [7.14]$$

$$if\,(p_{c0} > p_{c0,\min}) : p_{c0} = p_{c0,\min} \qquad [7.15]$$

where: $p_{c0,min}$ = minimum contouring subfactor value for a given ridge height.

7.1.3.7. Adjusting for row grade

The RUSLE2 assumption, which is the same as the RUSLE1 assumption, is that contouring rapidly loses its effectiveness as row grade increases (Foster et al., 1997).

$$p_c = p_{c0} + (1 - p_{c0})(s_f / s_p)^{1/2} \qquad [7.16]$$

where: p_c = the daily contouring subfactor and s_f = grade along the furrows separating the ridges (row grade) (100·tangent of slope angle). The variable s_f/s_p is designated as the relative row grade and sp =land steepness (100·tangent of slope angle). Measured erosion on 150 ft wide plots on a 5 percent land steepness showed that the contouring subfactor values vary with row grade (McGregor et al., 1969). The observed contouring subfactor values were 0.10 and 0.39 for the ridges perfectly on the contour and ridges on a 0.3 percent row grade, respectively. Given the observed p_{c0} = 0.10 contouring subfactor value for ridges perfectly on the contour (i.e., row grade = 0), the computed contouring subfactor value from equation 7.16 is 0.32, which is slightly less than the 0.39 observed value.

7.1.4. Contouring failure

The RUSLE2 assumption is that contouring fails when the shear stress applied to the soil by runoff exceeds a critical shear stress. The contouring subfactor is set to 1 for those portions of the overland flow path where contouring failure is computed. The equations used in these computations are described in **Section 3.4.3**.

Once contouring failure occurs at a location on an overland flow path, the daily contouring subfactor remains at 1 until the next soil disturbing operation. The RUSLE2 assumption is that contouring failure results from runoff breaking through the ridges, and thus the contouring effect can be regained only after ridges are re-established to fill the breakthrough areas. The RUSLE2 procedure is that only a soil disturbing operation creates ridges that repair the ridge breakthroughs that represent contouring failure (see RUSLE2 User's Reference Guide).

7.1.5. Comments on contouring subfactor

RUSLE2 allows row grade to be input as absolute row grade or as relative row grade. In most applications, relative row grade should be used as the input for consistency with the concepts behind equation 7.16 for the effect of row grade on the contouring subfactor. Using relative row grade implicitly results in the quality of contouring being treated equally regardless of land steepness (see RUSLE2 User's Reference Guide).

RUSLE2 accurately represents the general trends of how major variables affect contouring's reduction on rill-interrill erosion. However, local conditions that can not be easily measured or visualized, especially before a storm event, greatly affect contouring's effectiveness. For example, slight and imperceptible variations in ridge height and furrow grade along the ridges greatly affect the number and locations of breakovers. Therefore, while RUSLE2 accurately represents the overall effect of contouring on rill-interrill erosion, the uncertainty in how contouring affects rill-interrill erosion on a specific site is greater than for any other major RUSLE2 variable (see RUSLE2 User's Reference Guide).

7.2. Porous barriers

7.2.1. Description of porous barriers

A porous barrier is a portion of the overland flow path that has a significantly higher hydraulic resistance than the overland flow path immediately upslope of the barrier. The RUSLE2 assumption is that runoff passes through porous barriers. That is, porous barriers do not end the overland flow path. Porous barriers include strips of dense vegetation used in rotational strip cropping; grass buffers, filter strips, and stiff grass hedges; a strip of dense vegetation left undisturbed along a channel on construction and logging sites; and fabric fences and gravel bag dams used on construction sites (see RUSLE2 User's Reference Guide).

7.2.2. Processes associated with porous barriers

The significantly increased hydraulic resistance of the porous barrier slows and ponds runoff in backwater at the upper edge of the barrier. Runoff's sediment transport capacity is greatly reduced in both the backwater and within the porous barrier. Deposition occurs if the sediment transport capacity is reduced to less than the sediment load coming into the backwater and barrier. Most of the deposition caused by porous barriers actually occurs in the backwater. The upper edge of deposited sediment and backwater advance upslope as deposition occurs in the backwater, which increases transport capacity within the backwater. Eventually the backwater becomes filled with sediment and most of the incoming sediment load is then transported into the barrier itself. However, RUSLE2 does not account for sediment accumulation within the backwater and change in sediment transport capacity as sediment accumulates in the backwater.

Runoff is assumed to pass through porous barriers. Infiltration rate within the barrier can be much higher than that on the overland flow path immediately upslope of the barrier, which reduces runoff downslope of the barriers. The high hydraulic resistance in a porous barrier can eliminate rill erosion and spread runoff within the barrier so that runoff exits the barrier as a thin uniform depth flow along the lower edge of the barrier. Spreading of the runoff reduces its erosivity immediately downslope of a porous barrier.

7.2.3. RUSLE2 equations used to describe porous barriers

The RUSLE2 equations used to compute deposition caused by porous barriers and the sediment load leaving porous barriers are described in **Sections 2.3 and 3.4**. This section describes key features of these equations.

RUSLE2 uses the same cover-management values to compute detachment within the backwater as it uses to compute detachment within the porous barrier. The RUSLE2 assumption is that detachment downslope of a porous barrier is not affected by the barrier except as the barrier affects contouring failure. RUSLE2 does not compute how increased infiltration on an overland flow path segment affects detachment on downslope segments because of reduced runoff. That is, RUSLE2 computes the same detachment, except for contouring failure, immediately downslope of a porous barrier regardless of the presence or absence of the barrier.

The conceptual basis for this assumption is that spreading the overland flow by the porous barrier reduces runoff erosivity. However, the very low sediment concentration in the runoff leaving the barrier increases runoff erosivity. Flow has greater erosivity when it has a very low sediment load in contrast to when the runoff's sediment transport capacity is nearly filled with sediment (Foster and Meyer, 1975; Foster, 1982). The RUSLE2 assumption is that these two effects on runoff erosivity offset each other.

The assumption that downslope detachment is unaffected by high infiltration on an upslope segment is obviously invalid where a porous barrier is sufficiently wide and has a sufficiently high infiltration rate to significantly reduce the runoff that leaves the barrier.

The RUSLE2 User's Reference Guide describes how to choose RUSLE2 inputs to partially represent conditions where high infiltration and reduced runoff affects downslope detachment.

RUSLE2 computes reduced runoff from segments, including those with porous barriers, having high infiltration rates. RUSLE2 computes reduced sediment yield from these segments if transport capacity is less than sediment load within the segment because of reduced runoff. Also, reduced runoff from high infiltration segments affects downslope sediment transport capacity and deposition computations. For example, computed deposition and sediment load on a concave shaped overland flow profile is affected by high infiltration and reduced runoff for an upslope segment.

RUSLE2 computes how reduced runoff caused by high infiltration within a porous barrier and runoff spreading by the barrier affects shear stress applied by runoff to the soil immediately downslope from the barrier. Contouring failure is assumed to occur if this shear stress exceeds a critical shear stress (see **Section 3.4.3**). RUSLE2 computes reduced erosion below a porous barrier where RUSLE2 computes no contouring failure below the barrier but computes contouring failure without the barrier.

Hydraulic resistance is a major variable that affects the amount of deposition caused by a porous barrier. A Manning's n value, RUSLE2's measure of hydraulic resistance, is computed as a function of retardance (see **Section 3.4.6**), which varies temporally as vegetation changes through time. All porous barriers are represented in RUSLE2 as strips of vegetation, even when the barriers are non-vegetative including fabric fences, gravel bags, and similar behaving barriers. Non-vegetative porous barriers slow runoff as do vegetative porous barriers.

Eight retardance classes are used to describe porous barriers based on the degree that a barrier slows runoff (see **Section 3.4.6** and RUSLE2 User's Reference Guide). The eighth retardance class is a special case used to describe barriers such as stiff grass hedges and silt fences that provide maximum retardance. The minimum backwater length that RUSLE2 uses for this retardance class is 3 ft, whereas no minimum backwater length is used for the other retardance classes (see **Section 3.4.4**). The maximum backwater length allowed by RUSLE2 is 15 ft for all retardance classes.

7.2.4. Effect of row grade

Runoff must pass through porous barriers for them to reduce sediment load. A ridge of soil at the upper side of porous barriers left by tillage or deposited sediment or debris collected on a fabric fence causes runoff to flow along the upper edge of the barrier and never enter the barrier if the grade along the upper edge of the barrier is too steep. The barrier acts as a flow interceptor (see **Section 7.3**) that ends the overland flow path.

Inputs used to describe porous barriers can be entered in two ways. One way is to select porous barriers from a list of supporting practices. When this input method is used, RUSLE2 requires that the relative row grade for the barrier be less than 10 percent. RUSLE2 assumes that trapping efficiency is independent of row grade for relative row

grade less than 10 percent. The RUSLE2 assumption with this input method is that runoff does not enter the barrier but runs along the upper edge of the barrier if the relative row grade along the upper edge of the barrier exceeds 10 percent. In that case, the barriers operate as a flow interceptor barrier.

The other way to input information to describe porous barriers in RUSLE2 is to divide the overland flow path into segments and enter information for each segment, including those segments used to represent the porous barriers. When this input method is used, RUSLE2 assumes that runoff enters the porous barrier regardless of the relative row grade along the upper edge of the porous barrier (see RUSLE2 User's Reference Guide).

7.2.5. Spatial variability

When the RUSLE2 input method of selecting a support practice is used to represent porous barriers, RUSLE2 assumes that multiple barriers are spaced uniformly along the overland flow path length. Also, the conditions are assumed to be the same for each barrier. When the input method of dividing the overland flow path into segments is used, each segment can be described individually and barriers can be spaced non-uniformly. Conditions are assumed to be uniform within a segment.

7.2.6. Validation of RUSLE2 computed values

7.2.6.1. Strip cropping

RUSLE2 computed values for the effect of strip cropping and narrow stiff grass hedges on sediment yield from an overland flow path were compared with measured data reported in the literature (Foster et al., 1997, see references this section). Because strip cropping data are highly variable, many more years of data and/or experimental plots and small watersheds are required to accurately evaluate strip cropping than for any other soil conservation practice. Sediment yield from strip cropping is closely related to the storm events that occur when the erodible strips are at the end of the overland flow path. Data must be recorded over a sufficiently long duration for representative storms to occur on the erodible strips in all positions along the overland flow path. Sediment yield is much less when an extreme event occurs when an erodible strip is near the upper end of the overland flow path than at the lower end of the overland flow path. Data from such a storm would indicate that strip cropping is much more effective than it actually is. Very little of the available strip cropping data are for an adequate duration. Also, much of the strip cropping data are inconsistent. In one study, erosion with a small grain in a rotation in a strip cropping system was much less than when in the same crop rotation was not in strip cropping.

Priority was given to ensuring that RUSLE2 fits strip cropping data from Wisconsin (Hays et al., 1949; Hays and Attoe,1957) and to values given in AH282 and AH537 (Wischmeier and Smith, 1965, 1978) for a base, reference condition. Strip cropping has been used extensively and highly successfully since the 1930's in the La Crosse, Wisconsin region. The support practice factor values given in AH282 and AH537 have been well accepted in conservation planning by USDA-NRCS personnel for this region. Also, the Wisconsin data seem to be of higher quality than most of the other available

data. Wischmeier and Smith (1965, 1978) and technical and scientific personnel from the USDA-Agricultural Research Service and Soil Conservation Service reviewed these same data and developed recommendations included in AH282 and 537. These values are established and accepted based on many years of field applications of the USLE.

The values in AH282 and AH537 are that strip cropping reduces sediment yield from the end of an overland flow path by 50 percent "For 4-year rotation of row crop, small grain with meadow (mixture of legume and grass hay), and 2 years of meadow. A second row crop can replace the small grain if meadow is established in it [AH537 (Wischmeier and Smith, 1978)]." The comparable RUSLE2 computed value is 0.43 for the base, reference condition of a 150 ft long, six percent steep overland flow path on a silt loam soil at Columbia, Missouri for crops and yields comparable to those represented in the data on which the AH282 and 537 values are based. The comparable measured values from research in Wisconsin are 0.42 and 0.55 (Hays et al, 1949; Hays and Attoe, 1957).

The AH282/537 values for the ratio of sediment yield with strip cropping to sediment yield without strip cropping is 0.75 "For 4-year rotation of 2 years row crop, winter grain with meadow seeding, and 1-year meadow." The RUSLE2 computed value is 0.54.

The AH282/537 values for the ratio of sediment yield with strip cropping to sediment yield without strip cropping is 1 "For alternate strips of row crop and small grain." RUSLE2 also computes a value of 1 for this condition.

7.2.6.2. Stiff grass hedges

RUSLE2 computed value of 0.25 for fraction of the incoming sediment load from a conventional, clean tilled cotton that is trapped by a stiff grass hedge at Holly Springs, MS is very close to the measured value of 0.25 (McGregor et al., 1999). RUSLE2 computes a value of 0.20 for no-till cotton upslope of the stiff grass hedge while the measured value was 0.43. The study was run for three years. The hedges were much better established and uniform in the third year of the experiment than in the first year. The fraction of the incoming sediment load that was trapped by the hedges in the third year was 0.29 and 0.33 for the conventional and no-till managements, respectively, which are close to the RUSLE2 computed values.

7.2.7. Comments on porous barriers

The RUSLE2 intent for computing how porous barriers affect erosion is for the purpose of conservation and erosion control planning where the main effects of the major variables are captured. The equations are based on well accepted hydraulic principles. The performance of porous barriers is highly dependent on how well the barriers are installed and maintained. For example, fabric fences are widely used on construction sites to control sediment leaving the site. However, very poor sediment control occurs in far too many cases because of substandard installation and/or maintenance. The actual sediment trapping of fabric in a typical field situation is much less than the sediment trapping measured in laboratory studies.

A comparable situation exists with vegetative strips that are poorly established and/or maintained. For example, non-uniform grass stands within a strip or damage caused by tillage, construction activities, or other soil disturbing operations can significantly reduce sediment trapping efficiency.

RUSLE2 does not represent the variations that result from poor installation and maintenance. RUSLE2 represents the performance of porous barriers that are installed and maintained according to specifications and inspections.

The RUSLE2 equations and input values were chosen to represent barriers that perform well in the field but less than would be measured in carefully controlled laboratory hydraulic studies.

7.3. Interceptor barriers

7.3.1. Characteristics of interceptor barriers

Interceptor barriers are topographic features that end the overland flow path. Examples of interceptor barriers represented by RUSLE2 include terraces, diversions, and small impoundments. Terraces are defined as channels on a sufficiently flat grade to cause deposition while diversions are channels are on a sufficiently steep grade that deposition does not occur in them but are not on such a steep grade that erosion occurs in them. Impoundments are water bodies where flow velocities are almost negligible. RUSLE2 represents typical impoundments comparable to those used with impoundment terraces in farm fields [e.g., parallel tile outlet (PTO) terraces] and small sediment basins used on construction sites.

Interceptor barriers reduce erosion by cutting overland flow path length and causing deposition. RUSLE2 also computes how deposition by interceptor barriers affects sediment characteristics. RUSLE2 does not compute ephemeral gully erosion that occurs in concentrated flow areas (channels) (Foster, 1985).

7.3.2. Channels (Terraces/diversions)

7.3.2.1. Deposition and sediment load equations

Deposition occurs in a channel when the incoming sediment load exceeds sediment transport capacity of flow in the channel (Foster, 1982; Foster et al., 1980a). Deposition rate is computed in RUSLE2 using (Renard and Foster, 1983):

$$D_{p(k)} = f_{(k)}\left(\frac{\phi_{(k)}}{1+\phi_{(k)}}\right)\left(\frac{dT_c}{dx} - g_o\right) \quad dT_c / dx < g_o \qquad [7.17]$$

$$D_{p(k)} = 0 \quad dT_c / dx \geq g_o \qquad [7.18]$$

$$\phi_{(k)} = 400000 V_{f(k)} / q_o \qquad [7.19]$$

where: $D_{p(k)}$ = deposition rate for the *kth* particle class [mass/(unit channel length·time)], $f_{(k)}$ = fraction, based on mass, of the total incoming sediment load g_0 (mass/unit channel length·time) from the overland flow area made up of the *kth* particle class, T_c = sediment transport capacity of the flow in the channel (mass/time), x = distance along the channel $V_{f(k)}$ = the fall velocity (ft/sec) of the *kth* sediment particle class, and q_o = the discharge rate at the end of the overland flow path (ft^3/sec per ft channel length). Equation 7.17 is derived from equation 2.16 and the assumptions of uniform channel grade, uniform sediment input from the overland flow area along the channel length, incoming sediment load for each particle class exceeds the sediment transport capacity in the channel for that particle class, and channel sediment transport capacity for each particle is proportional to the distribution (mass basis) of the incoming sediment load.

The change in sediment load with distance along the channel is computed using:

$$dT_c / dx = 450 s_{ch}^{1.16} q_0 \qquad [7.20]$$

where: T_c = transport capacity (lbs_m/sec), s_{ch} = grade (steepness) of the channel (sine of channel slope angle), and x = distance along the channel (ft). Equation 7.20 was derived from the assumptions that transport capacity is directly proportional to the 3/2 power of shear stress applied to the channel boundary by the flow and that Manning's equation is used to compute hydraulic radius for flow in the channel (Foster and Meyer, 1975; Foster, 1982; Foster et al., 1980). The channel's hydraulic roughness is assumed to be that of deposited sediment that covers soil surface roughness, surface residue, and standing vegetation. The effect of standing live or dead vegetation on deposition in channels is not considered in RUSLE2 because most of the deposition is assumed to occur when little vegetation is present, such as at seedbed time when crops are planted. The 450 coefficient value in equation 7.20 was determined by calibrating RUSLE2 to compute values similar to those given by the RUSLE1 sediment delivery ratio equation, which was empirically derived from field data [AH703(Renard, 1997); Foster et al., 1997; Foster and Ferreira, 1981; Foster and Highfill, 1983).

Equation 7.17 and its companion equations compute a uniform deposition rate along the channel. The sediment leaving the channel is computed with:

$$g_{ch(k)} = g_{o(k)} - D_{p(k)} \qquad [7.21]$$

where: $g_{ch(k)}$ = the sediment load (mass/unit channel length·time) leaving the end of the channel for the *kth* particle class. The sediment load leaving the channel expressed as the ratio of sediment load at the end of the channel to unit drainage area for the channel is computed with:

$$A_{ch(k)} = g_{ch(k)} / \lambda_o \qquad [7.22]$$

where: $A_{ch(k)}$ = the sediment load for the *kth* particle class leaving the end of the channel expressed as mass/time per unit drainage area and λ_o = the length of the overland flow path that discharges into the channel. The sediment delivery ratio for the channel for the *kth* particle class is given by:

$$\omega_{(k)} = 1 - D_{p(k)} / g_{o(k)} \quad [7.23]$$

where: $\omega_{ch(k)}$ = sediment delivery ratio for a channel for the *kth* sediment particle class. Total sediment load is computed by summing the sediment load values for the five RUSLE2 particle classes (see **Section 4.7**).

7.3.2.2. Comments on channels

When flow interceptors are represented in RUSLE2 as a support practice, the spacing between flow interceptors is the same for all flow interceptors represented by the support practice. However, non-uniform spacing among flow interceptors can be represented by manually entering appropriate spacing values. Similarly, the grade is assumed the same for all channels when flow interceptors are represented as a support practice. However, separate grade values for each channel can be entered in RUSLE2.

RUSLE2 requires that a representative channel grade be chosen for channels on a non-uniform grade. This limitation can be of consequence for parallel terraces where grade varies along the channel. In most of these situations, channel grade is flattest at the upper channel end with grade increasing along the channel. RUSLE2's estimates for deposition for these conditions are less accurate than for uniform grade channels. A grade flatter than the average channel grade for its length is the appropriate input grade.

RUSLE2 does not represent channels where sediment inflow varies along the channel length. Not many field situations occur where this limitation is of consequence.

The RUSLE2 equations used to compute deposition in channels are based on commonly used equations for channel hydraulics. However, RUSLE2 is a conservation and erosion control planning tool, not a hydraulic design tool. Appropriate hydraulic equations should be used to design the channels represented in RUSLE2. Channels are usually designed to accommodate runoff rate from a particular design storm under particular soil and cover conditions whereas most conservation and erosion control planning is based on average annual erosion rates for the range of cover-management conditions expected over the time period being represented in the RUSLE2 computation. See the RUSLE2 User's Reference Guide for information on the types of channels represented by RUSLE2.

7.3.3. Impoundments

7.3.3.1. Sediment delivery ratio equation

The RUSLE2 assumption is that sediment transport capacity in impoundments is essentially zero. Impoundments are treated as a fixed length settling basin in RUSLE2. The RUSLE2 equation for computing sediment deliver ratio for an impoundment is:

$$\omega_{(k)} = \exp(-c_i V_{f(k)}) \quad [7.24]$$

where: $\omega_{i(k)}$ = the sediment delivery ratio for an impoundment for the *kth* sediment particle class. Sediment delivery ratio is the ratio of sediment mass leaving the sediment basin to incoming sediment mass.

A 10000 $(ft/sec)^{-1}$ value for the coefficient c_i for a base reference silt loam soil was determined by fitting equation 7.24 to experimental data for impoundments used in parallel tile outlet terraces (Laflen et al., 1972). The average trapping efficiency of those impoundments was 94 percent. Literature reporting measured trapping efficiency of sediment basins on construction sites was reviewed during the development of RUSLE1.06 (Toy and Foster, 2000; Bonta and Hamon, 1980, Fennessey and Jarret, 1997; USEPA, 1976 a, 1976b). The trapping efficiency of these basins is comparable to that for impoundment terraces when the sediment basins are well designed, constructed, and maintained and perform at maximum efficiency. Also, no deposition is assumed to occur between the point that the sediment is detached and where the sediment reaches the impoundment. If deposition occurs along the overland flow path upstream of the impoundment, trapping efficiency will be less than computed by RUSLE2 (see **Section 7.3.3.2**).

Many sediment basins on construction sites do not perform at maximum efficiency because of poor design, the basins being partly filled with sediment, and water/sediment chemistry that keeps fine sediments highly dispersed.

The RUSLE2 user can select a base sediment delivery ratio for the reference silt loam soil texture to accommodate trapping efficiency variations by specific site. The c_i coefficient values used in RUSLE2 for a range of sediment delivery ratios are given in Table 7.1.

Table 7.1. Values for the coefficient c_i used to compute sediment delivery ratio for deposition of sediment from reference silt loam soil in impoundments.

Sediment trapping ratio (%)	c_i $(ft/sec)^{-1}$
6.4	10000 (1)
10	5900
15	3500
20	2300
25	1700

Note (1): Coefficient value determined by fitting RUSLE2 equation to experimental data for impoundment terraces

7.3.3.2. Effect of incoming sediment characteristics

RUSLE2 computes trapping efficiency for impoundments solely as a function of incoming sediment characteristics. RUSLE2 does not consider basin geometry or flow withdrawn characteristics in these computations. However, RUSLE2 computes sediment delivery ratios as a function of texture of the soil that produces the sediment, upslope deposition amount, and the feature that produces the upslope deposition as shown in Table 7.2 because these variables affect sediment characteristics. As a point of reference, the RUSLE2 computed sediment characteristics leaving the uniform overland flow path represented in Table 7.2 are the same as the sediment characteristics at the point of detachment because

RUSLE2 computed no local deposition for this particular overland flow path.

Table 7.2. RUSLE2 computed sediment delivery ratio for sediment basin in various flow sequence.

	Flow path			
Soil texture	uniform overland flow path into basin	steep flow segment onto low steepness segment into basin	uniform flow path into grass strip into basin	uniform overland flow path into basin into basin
silt loam	0.064	0.469	0.317	0.678
silt	0.068	0.157	0.101	0.216
silty clay	0.119	0.612	0.581	0.825
clay	0.105	0.741	0.905	0.902
loamy sand	0.014	0.125	0.531	0.890
sand	0.009	0.127	0.333	0.900

The primary particle distribution of the soil producing the sediment does not accurately indicate the RUSLE2 computed sediment delivery ratio for impoundments. Sediment is eroded as a mixture of primary particles and aggregates (see **Section 4.7**). The size and density distributions of the sediment do not parallel the distribution of primary particles in the soil. Clay is assumed in RUSLE2 to be a bonding agent that influences aggregate sizes and densities and the mass distribution between the particle classes, especially the small and large aggregates. Consequently, sediment eroded from high clay soils has a large portion of the sediment in aggregates of increased size. Conversely, soils very high in silt produce poorly aggregated sediment that is almost entirely in small-sized primary silt particles that are not rapidly deposited. Soils high in sand produce poorly aggregated sediment that is almost entirely in sand-sized primarily particles that are readily deposited. Consequently, the sediment delivery ratio computed for sediment eroded from high clay soils is not proportionally higher than that for silt loam soils when no upslope or local deposition occurs. **Expecting RUSLE2 computed sediment delivery ratio values for an impoundment to be directly related to the primary particle distribution of either the soil or sediment is a very serious error.**

As illustrated in Table 7.2, RUSLE2 computed sediment delivery ratio values for impoundments also vary with the type of upslope feature that causes deposition. Even though the sediment delivery ratios for the overland flow path with a low steepness segment, a grass strip, and a sediment basin are comparable, the characteristics of the sediment leaving each of these flow paths and entering a sediment basin are quite different because of differences in upslope erosion and deposition processes. RUSLE2 computes a relatively high interrill erosion rate for the overland flow path that has the low steepness segment in comparison to the one with a dense grass strip at the end of the overland flow path. Interrill erosion is very low in the grass strip, which adds very little sediment to the sediment load in the grass strip in contrast to interrill erosion adding sediment to the sediment load on the low steepness segment. The sediment leaving the grass strip is finer than the sediment leaving the low steepness segment. Consequently, the RUSLE2 computed sediment delivery ratio values for impoundments are generally larger for the grass strip overland flow path than for the low steepness segment overland flow path. Sediment delivery ratios for sediment eroded from high silt soils are not affected as much as for the other soil textures because sediment eroded from the high silt soils is poorly aggregated and has a very narrow size range in a relative small size range.

Sediment delivery ratio values are high for a basin downstream of another sediment basin. That is, much less sediment trapping occurs in the second basin than in the first basin, except for the sediment eroded from the high silt soils. The upstream sediment basin removes almost all of the sediment that is easily deposited.

7.3.3.3. Design

RUSLE2 should not be used to design sediment basins unless regulations explicitly state that RUSLE2 can be used. The RUSLE2 values computed for impoundments are for the purpose of conservation and erosion control planning. The accuracy of RUSLE2's computations for sediment trapping by small impoundments is comparable to that for other erosion and sediment control practices. The specific hydraulic and sediment trapping performance of impoundments depends on many complex, interactive variables. Accepted design procedures should be used to design impoundments (e.g., see Haan et al., 1994).

7.3.3.4. Comments

RUSLE2 results for sediment trapping by impoundments must be interpreted very carefully. The flow path up to the sediment basin must be properly represented. For example, RUSLE2 seriously under-computes sediment delivery by an impoundment if a uniform steepness overland flow path is assumed when in fact the overland flow path has a segment at the lower end of the overland flow path that causes a high degree of deposition. Likewise, when RUSLE2 computed values are compared to research and field measurements, the RUSLE2 inputs must be very carefully selected to accurately represent measurement conditions. The characteristics of the sediment entering the experimental basin must match those assumed in RUSLE2. For example, as Table 7.2 shows, if upstream deposition is not considered, the sediment delivery values computed by RUSLE2 will be much less than is measured.

Another consideration is that RUSLE2 does not represent basin geometry, degree that the basin is filled, and other factors. The assumption in RUSLE2 is that the basin is well designed and maintained. Standards and specifications for design, construction, and maintenance of impoundments should be a principal tool used to ensure expected results.

7.3.4. Hydraulic flow paths

Simple channels and impoundments can be combined into simple hydraulic flow paths. RUSLE2 can represent an overland flow area discharging into a channel from a single side and the channel in turn discharging into an impoundment or a series of impoundments. Non-uniform conditions along the channel can not be represented. RUSLE2 can not represent a channel on a particular grade discharging into a channel on a different grade. That is, RUSLE2 can not represent channels in series nor can RUSLE2 represent an impoundment discharging into a channel. However, RUSLE2 can represent overland areas discharging into a channel from both sides. Also, RUSLE2 can represent an overland flow area discharging directly into an impoundment without involving a channel. (See the RUSLE2 User's Reference Guide)

7.3.5. Benefit of deposition caused by porous barriers and flow interceptors

7.3.5.1. Concepts

Deposited sediment trapped on the hillslope by porous barriers and by flow interceptors including channels/impoundments (e.g., terraces) is assumed to be a soil conservation benefit. Landscape quality is degraded less when sediment is retained by deposition on the hillslope.

Partial credit is taken for deposition on the hillslope as soil saved based on the location of the deposition along the overland flow path (see Section **2.3.10.4)**. The credit taken for deposition caused by flow interceptors is less than the credit taken for porous barriers because most flow interceptors are much more permanent and the deposition more localized than with porous barriers. Porous barriers such as grass strips are assumed to be periodically removed and reestablished in new locations. An increased portion of the hillslope benefits from deposition with these barriers than occurs with flow interceptor such as impoundment-type terraces. Full credit for deposition as soil saved is taken for rotational strip cropping (see Section **2.3.10.4**).

Partial credit is given to deposition as soil saved with flow interceptors (e.g., channels/impoundments in farm fields) because the deposition is localized although the deposited sediment is spread over a significant-sized area on either side of channels/impoundments in farm fields. The absolute size of this area is the same regardless of channel/impoundment spacing. Consequently, the fraction of the total field area over which the sediment is spread becomes less as channel/impoundment spacing increases.

Deposition near the end of the original overland flow path before porous/interceptor barriers were placed is assumed to be less valuable for maintaining landscape quality than sediment deposited near the upper end of the overland flow path. This concept is consistent with that used to compute the benefit of deposition on the overland flow area (see **Section 2.3.10.4**).

Deposition is a selective process that enriches the deposited sediment in coarse particles. Even though coarse sediment is deposited first, clay and silt primary particles are deposited because sediment is assumed to be a mixture of primary particles and aggregates so that fine primary particles are deposited along with sand particles (see **Section 4.7.5**). The assumption that deposition on overland flow areas is predominantly sand is erroneous. Thus, deposition is assumed to be beneficial because deposited sediment includes clay and silt particles even though the deposited sediment is partially enriched in sand.

7.3.5.2. Equations for benefit of deposition caused by flow interceptors

The RUSLE2 equation for the benefit of deposition by a flow interceptor is:

$$b_{s(i)} = 0.45 \exp[-0.011(\delta_{s(i)} - 100)] \quad \delta_{s(i)} \geq 100 \text{ ft} \qquad [7.25]$$

$$b_{s(i)} = 0.45 \quad \delta_{s(i)} < 100\,\text{ft} \qquad [7.26]$$

where: $b_{s(i)}$ = the fraction of the deposition that is credited as soil saved for the *ith* flow interceptor and δ_s = flow interceptor spacing (ft). The credit $b_{p(i)}$ for deposition as affected by the *ith* flow interceptor location along the original overland flow path is computed with:

$$b_{p(i)} = 1 - (\lambda_{s(i)} / \lambda_o)^{1.5} \qquad [7.27]$$

where: $\lambda_{s(i)}$ = distance from the origin of overland flow for the original overland flow path to the *ith* flow interceptor and λ_o = the overland flow path length without flow interceptors. The conservation planning sediment load (see **Section 2.3.10.4**) for each channel is computed from:

$$g_{cp(i)} = g_{o(i)}[1 - (b_{s(i)} + 0.2b_{p(i)})(1 - \omega_{(i)})] \qquad [7.28]$$

where: $g_{cp(i)}$ = the conservation planning sediment load per unit channel length for the *ith* channel, the $g_{o(i)}$ = the sediment load for conservation planning from the overland flow area immediately above the *jth* channel, and ω = sediment delivery ratio. The conservation planning soil loss in term of mass per unit area for the area represented by the overland flow path without channels is:

$$A_{cp} = \left(\sum_{i=1}^{J} g_{cp(i)} \right) \Big/ \lambda_o \qquad [7.29]$$

where: A_{cp} = the conservation planning soil loss (mass/area) for the area represented by λ_o and i = the index for each flow interceptor along the original overland flow path, and J = number of flow interceptors.

7.4. Subsurface drainage

The effect of subfactor drainage on detachment is represented by the subsurface drainage subfactor p_d in equation 2.10.[60] In general, research has shown that subsurface drainage reduces rill-interrill erosion by approximately 40 percent (Bengston and Sabbage, 1988; Formanek et al., 1987; Schwab and Fouss, 1967; Schwab, 1976; Skaggs et al., 1982). The reduction is caused by reduced runoff and an increased vegetation production (yield) level. The input value for production (yield) level in vegetation descriptions should reflect production level under subsurface drained conditions. RUSLE2 does not adjust production (yield) level as a function of environmental inputs.

---

[60] The effect of subsurface drainage on runoff is discussed in **Section 3.3.1.2.4**.

The runoff effect on erosion with subsurface drainage is assumed to be same as the soil erodibility factor being a function of a soil's runoff potential. Therefore, equation 4.9, the permeability subfactor equation used to compute soil erodibility factor values, is used to compute how subsurface drainage affects detachment. The subsurface drainage subfactor is computed as:

$$p_d = K_d / K_u \quad if\,(p_d < 0.2) : p_d = 0.2 \qquad [7.30]$$

where: K_d and K_u = soil erodibility factors (US customary units) for the drained and undrained conditions, respectively (see **Section 4.1**). A minimum value of 0.2 is set for the subsurface drainage subfactor. A base soil erodibility factor value without the permeability subfactor is computed as:

$$K_b = K_u - 0.025(P_{ru} - 3) \qquad [7.31]$$

where: K_b = a base soil erodibility factor value (US customary units) computed without the permeability subfactor and P_{ru} = the soil profile permeability class for the undrained condition. The soil erodibility factor with subsurface drainage is computed with:

$$K_d = K_b + 0.025(P_{rd} - 3) \qquad [7.32]$$

where: P_{rd} = the soil profile permeability class for the drained condition.

Hydrologic soil group (see **Section 3.3.1 and** RUSLE2 User's Reference Guide) used in NRCS soil survey descriptions is used as the RUSLE2 input to describe how subsurface drainage affects soil profile permeability class. The RUSLE2 relationship between hydrologic soil group and the soil profile permeability class is given in Table 7.3.

Table 7.3. Relation between hydroligc soil groups and permeabiltiy classes.

Hydrologic soil group	Permeability class
A	1
B	2.67
C	4.33
D	6

RUSLE2 computed subsurface drainage subfactor values are shown in Table 7.4. As expected, subsurface drainage reduces the subsurface drainage subfactor the greatest when subsurface drainage causes the greatest change in hydrologic soil group from D to A in contrast to a change from D to C. The erosion reduction is also related to the soil erodibility (K factor) value. The subsurface drainage subfactor reduction is greatest when soil erodibility factor values are low. This effect results from the additive equation form used to compute soil erodibility factor values (See **Section 4.1.1**). Location has only a slight effect on the RUSLE2 subsurface drainage subfactor and probably should be greater than is computed by RUSLE2. However, the values computed by RUSLE2 are considered adequate for conservation and erosion control planning. Other erosion estimation procedures can be used when increased accuracy is desired (Skaggs et al., 1982).

Table 7.4. Subsurface drainage subfactor values as affected by soil erodibility factor value (US customary units) for undrained soil condition and for a change in hydrologic soil group by hydrologic soil group.

	subsurface drainage subfactor p_d			
Location	K = 0.20 D to A	K = 0.20 D to C	K = 0.30 D to A	K = 0.55 D to A
Ft Wayne, IN	0.38	0.83	0.58	0.77
Raleigh, NC	0.38	0.78	0.57	0.76
Jackson, MS	0.38	0.75	0.60	0.77

7.5. Irrigation

RUSLE2 computes how irrigation affects rill-interrill erosion caused by precipitation, but RUSLE2 does not compute erosion caused by water drop impact and surface runoff directly produced by the applied irrigation water. The increase soil moisture from irrigation affects rill-interrill erosion by precipitation during the irrigation period because of increased soil erodibility, increased biomass decomposition, decreased soil surface roughness and ridge height, and increased vegetation production (yield). The effect of irrigation on production (yield) level is accounted for by inputting yield values appropriate for production under irrigated conditions. RUSLE2 does not adjust production (yield) level as a function of environmental inputs.

7.5.1. Effect on soil erodibility

The effect of increased soil moisture on soil erodibility during the irrigation period is computed using equation 4.14 that computes temporal (daily) values for the soil erodibility factor. This equation is modified by adding the daily amount of water added by irrigation to the daily precitation amount as:

$$K_{(j)} / K_n = 0.591 + 0.732[(P_{(j)} + I_{(j)}) / 0.123] - 0.324(T_{(j)} / 62.8) \qquad [7.33]$$

$$If\,(K_{(j)} / K_n) > 2.0 \quad \text{then} \quad (K_{(j)} / K_n) = 2.0$$

$$If\,(K_{(j)} / K_n) < 0.4 \quad \text{then} \quad (K_{(j)} / K_n) = 0.4$$

where: $K_{(j)}$= the soil erodibility factor on the *jth* day, K_n = the soil erodibility factor value computed with a RUSLE2 soil erodibility nomograph for the frost free period defined as the period that average daily temperature $T_{(j)}$ is above 40 ^{o}F, 62.8 = the average temperature during the frost free period (^{o}F), $P_{(j)}$ = daily precipitation (inches), $I_{(j)}$ = average daily water added by irrigation (inches), and 0.123 = average daily precipitation during the frost free period (inches).

The average daily water added by irrigation on the *jth* day is computed from:

$$I_{(j)} = V_{w(j)} - P_{(j)} \;\; if\,(I_{(j)} < 0) : I_{(j)} = 0 \qquad [7.34]$$

where: $V_{w(j)}$ = consumption use (inches) by the vegetation on the *jth* day (Schwab et al., 1966). Plant consumption use values are input for the vegetation descriptions that represent irrigated conditions.

7.5.2. Effect on soil surface roughness, ridge height, and decomposition

The daily amount of water added by irrigation is added to the daily precipitation amount to compute the effect of irrigation on soil surface roughness (see **Section 6.3.6** and equation 6.30), ridge height (see **Section 6.4.6** and equation 6.43), and decomposition (see **Section 10.3.1** and equation 10.5).

7.5.3. Effect on vegetation

Individual vegetation descriptions must be created to describe vegetation under irrigated conditions. These descriptions include values for consumptive water use that are a function of the soil properties and location and location where the RSULE2 computation is being made. Figure 7.2 illustrative consumptive use values for a particular corn crop grown at Lincoln, Nebraska.

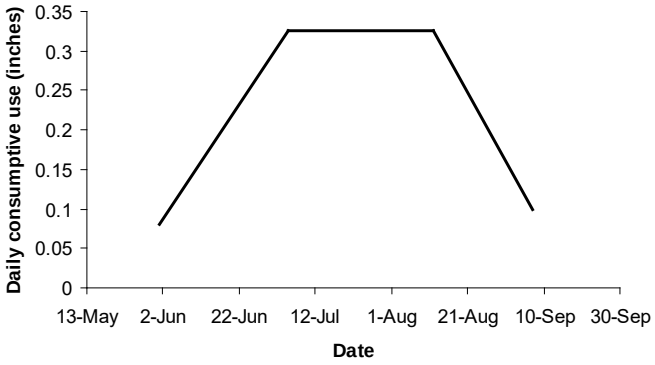

Figure 7.2. Daily consumptive water use for a 120 day corn crop grown at Lincoln, Nebraska.

The input yield for the vegetation description is the yield expected for the consumptive use water values entered because RUSLE2 does not compute how environmental conditions affect yield. RUSLE2 adjusts consumptive use values in its yield adjustment procedures directly in proportion to live above ground biomass (see **Section 9.3**).

7.6. List of symbols

a_c = coefficient used to compute values for base contouring subfactor values

$A_{ch(k)}$ = sediment load for *kth* particle class leaving end of the channel (mass/ unit drainage area·time)

A_{cp} = conservation planning soil loss for the area having channels (mass/area)

$b_{p(i)}$ = deposition credit as affected by the *ith* flow interceptor location along the original overland flow path

$b_{s(i)}$ = fraction of the deposition that is credited as soil saved for the *ith* flow interceptor

c_c = coefficient used to compute values for base contouring subfactor values

c_i = coefficient used to sediment delivery ratio in an impoundment for base reference silt loam soil

d_r = runoff depth for P_{10y24h} storm (inches)

$D_{p(k)}$ = deposition rate for *kth* sediment class (mass/unit channel length·time)

$f_{(k)}$ = mass fraction of the incoming sediment load g_0 from the overland flow area made up of *kth* sediment class

$g_{ch(k)}$ = sediment load leaving end of the channel for *kth* particle class (mass/unit channel length·time)

$g_{cp(i)}$ = conservation planning sediment load for the *jth* channel (mass/unit channel length)

g_o =total incoming sediment load from overland flow area (mass/unit channel length·time)

$g_{o(k)}$ = incoming sediment load from overland flow area (mass/unit channel length·time)

$g_{o(i)}$ = sediment load for conservation planning from overland area immediately above the *jth* channel (mass/unit channel length·time)

H = daily soil ridge height (inches)

H_e = daily effective total ridge height, which is sum of soil ridge height and effective vegetation ridge height (inches)

H_{vr} = daily effective vegetation ridge height (inches)

I_j = average water added by irrigation on *jth* day (length)

J = number of flow interceptors along an overland flow path

K_b = base soil erodibility factor value computed without the permeability subfactor (US customary units)

K_d = soil erodibility factor for drained condition (US customary units)

K_j = soil erodibility factor on the *jth* day (US customary units)

K_n = soil erodibility factor computed with a RUSLE2 soil erodibility nomograph for frost free period (US customary units)

K_u = soil erodibility factor for undrained condition (US customary units)

p_b = base contouring subfactor value

p_{bm} = minimum base contouring subfactor value

p_c = the daily contouring subfactor

p_{c0} = contouring subfactor for a zero row grade

$p_{c0,min}$ = minimum contouring subfactor value for a given ridge height

p_d = subsurface drainage subfactor

p_{rm} = minimum contouring subfactor value adjusted for runoff

P_j = daily precipitation (length)

P_{rd} = the soil profile permeability class for the drained condition

P_{ru} = the soil profile permeability class for the undrained condition

P_{10y24h} = 10 year-24 hour precipitation amount (length)

q_o = discharge rate at end of the overland flow path (volume/ unit channel length·time)

s = overland flow path steepness (sine of slope angle)

s_{be} = land steepness at which the contouring subfactor reaches 1 (sine of slope angle)

s_{bm} = land steepness at which contouring subfactor value is minimum (sine of slope angle)

s_c = scaled land steepness (sine of slope angle)

s_{ch} = grade of the channel (sine of channel angle with horizontal)

s_f = grade along the furrows separating the ridges (row grade) (100 time tangent of slope angle)

s_f/s_p = relative row grade

s_m = land steepness at which $p_b = p_{bm}$ (sine of slope angle)

s_p = land steepness (100 time tangent of slope angle)

s_{re} = runoff adjusted land steepness above which contouring subfactor equals 1 (sine of slope angle)

T_c = total sediment transport capacity for all sediment classes of the flow in the channel (mass/time)

$V_{w(j)}$ = daily consumption watercuse by vegetation (length)

$V_{f(k)}$ = fall velocity of *kth* sediment class (length/time)

x = distance along the channel (length)

$\delta_{s(i)}$ = *ith* flow interceptor spacing (feet)

λ_o = overland flow path length without flow interceptors (length)

$\lambda_{s(i)}$ = distance from origin of overland flow for the original overland flow path to the *ith* flow interceptor (length)

$\phi_{(k)}$ = a deposition coefficient for the *kth* sediment class ($length^{-1}$)

$\omega_{(k)}$ = sediment delivery ratio for *kth* sediment class

$\omega_{(i)}$ = total sediment delivery ratio for the *ith* flow interceptor

Indices

i – flow interceptor

j - day

k – sediment class

8. OPERATIONS

A RUSLE2 operation is an event that changes vegetation, residue, or soil conditions. RUSLE2 uses a set of rules and 10 processes to represent how operations affect rill and interrill erosion (see the RUSLE2 User's Reference Guide). RUSLE2 computes erosion based on user supplied descriptions of the variables that affect rill-interrill erosion. For example, RUSLE2 does not use simulation modeling to compute how environmental conditions affect vegetation. This section discusses the RUSLE2 equations used to describe how operations affect vegetation, residue, and soil variables.

8.1. Effect on vegetation

RUSLE2 uses **begin growth**, **kill vegetation**, and **remove live vegetation processes** to describe how operations affect vegetation variables.

8.1.1. Begin growth

The **begin growth** process tells RUSLE2 to stop using data in the current vegetation description and start using data from another vegetation description. The change occurs on the date of the operation that uses the **begin growth** process (See RUSLE2 User's Reference Guide).

RUSLE2 uses only a single vegetation description on any particular date. RUSLE2 does not combine data from multiple vegetation descriptions to represent a composite of vegetations having different properties. For example, a single vegetation description is used to describe a rangeland plant community that involves multiple plant types such as shrubs that provide an over-story and grasses that provide an under-story under the shrubs with open space between the individual shrub-grass clumps.

8.1.2. Kill vegetation

The **kill vegetation** process transfers the biomass (dry mass basis) of live vegetation to the dead standing residue pool and transfers live root biomass to the dead root biomass pool in the soil. Both the standing residue and dead root biomass pools disappear by daily decomposition.

8.1.3. Remove live vegetation

The purpose of the **remove live vegetation** process is to determine the amount of residue left by a field operation like a hay harvest that removes live biomass and leaves both standing and surface residue. The standing and surface residue biomass left by a remove live vegetation process is computed as:

$$\Delta B_{tr} = f_{tl}(f_{lr} B_{al}) \quad [8.1]$$

$$\Delta B_{sr} = f_{sl}(f_{lr} B_{al}) \quad [8.2]$$

where: ΔB_{tr} = the biomass left as standing residue that is added to the existing standing biomass pool, $f_{lr}B_{al}$ = the live biomass that is affected by the operation, f_{tl} = the fraction of the affected biomass that is left as standing residue, f_{lr} = the fraction of the above ground live biomass that is affected by the operation, B_{al} = existing live vegetation biomass, ΔB_{sr} = the biomass left as surface residue that is added to the existing surface residue biomass pool, and f_{sl} = the fraction of the affected biomass that is left as surface residue. These residue biomass values are added to the existing biomass values in the respective residue pools.

The amount of live aboveground biomass left after a remove live biomass process is computed from:

$$B_{al} = (1 - f_{lr})B_{alp} \qquad [8.3]$$

where: Bal = the mass (dry basis) of the above bround live biomass that is left after the operation and Balp = the mass (dry basis) of the above bround live biomass that exists immediately before the operation.

8.2. Effect on residue/dead roots

RUSLE2 tracks the three residue pools of standing residue, surface residue, and buried residue. Operations that include a **flatten standing residue** process transfer biomass from the standing residue pool to the surface residue pool. Operations that include a **disturb soil** process bury transfer surface residue to the buried residue pool and transfers buried residue to the surface residue pool. RUSLE2 rules are that standing residue can not be buried without first being flattened and live above ground biomass can not be flattened or buried without first being killed (i.e., transferred from the live above ground biomass pool to the standing residue pool).

8.2.1. Flatten standing residue

The **flatten standing residue** process transfers biomass from the standing residue pool to the surface residue pool using:

$$\Delta B_{tr} = f_f B_{tr} \qquad [8.4]$$

where: f_f = the fraction of the existing standing residue that is flattened (i.e., added to the surface biomass pool).[61] The standing residue biomass pool after the operation is computed as:

---

[61] Flattening, burial, and resurfacing ratios are based on mass, not portion of the soil surface covered (see RUSLE2 User's Reference Guide).

$$B_{tr} = B_{trp}(1 - f_f) \quad [8.5]$$

where: B_{tr} = mass (dry basis) of the standing residue immediately after the operation and B_{trp} = the mass (dry basis) that existed immediately before the operation.

8.2.2. Burial of surface residue

Burial of surface residue is the transfer of biomass from the surface residue pool to the buried residue pool. The amount of surface residue that is buried is computed by:

$$\Delta B_{sr} = f_b B_{sr} \quad [8.6]$$

where: ΔB_{sr} = the mass of the surface residue that is transferred to the buried residue pool and f_b = the fraction of the surface residue that is buried.

The surface residue mass is computed by (Wagner and Nelson, 1995):

$$B_{sr} = (B_{trp} f_f + B_{srp})(1 - f_b) + B_{brp} f_u \quad [8.7]$$

where: B_{sr} = the surface residue mass (dry basis) immediately after the operation, B_{srp} = the surface mass immediately before the operation, f_u = the fraction of the buried residue mass that is resurfaced and B_{brp} is the amount of buried biomass in the soil disturbance depth immediately before the operation. Note that the surface residue mass in equation 8.7 is the sum of the existing surface residue mass plus the mass added by flattening of standing residue and the mass of buried residue that is resurfaced.

8.2.3. Resurfacing of buried residue

The mass of buried residue that is resurfaced by the operation is computed from:

$$\Delta B_u = f_u B_{br} \quad [8.8]$$

where: ΔB_u = residue that is resurfaced from soil disturbance depth, f_u = the resurfacing ratio, and B_{br} = the mass of buried residue in the soil disturbance depth. RUSLE2 does not consider the resurfacing of dead roots.

8.2.4. Determining values for the flattening, burial, and resurfacing ratios

8.2.4.1. Base reference values

A single data point can be used to determine a value for the flattening ratio. However, equation 8.7 involves the two unknowns of burial and resurfacing ratios, which requires at least two data points to determine values for these two ratios. The proper data for determining values for these ratios is where the same operation is repeated multiple times, preferably at least four times. Only two data sets were found that meet this requirement (Brown et al., 1992; Wagner and Nelson, 1995) and even then the (Brown et al., 1992) data set did not include standing residue. Most data previously used to

determine burial ratio values are not usable because they are from situations where a particular operation was used a single time.

Base reference values for the flattening ratio were determined by fitting equation 8.5 to observed data reported by (Wagner and Nelson, 1995). Values for the burial and resurfacing ratios were determined by fitting equation 8.7 to observed data reported by (Brown et al., 1992; Wagner and Nelson, 1995). Surface residue biomass values were estimated for the (Brown et al., 1992) data from measured surface residue cover values using equation 10.1 that estimates surface cover as a function of surface biomass (see **Section 10.2**).

The minimization function that was minimized to fit equations 8.5 and 8.7 to measured data to determine flattening, burial, and resurfacing ratio values is:

$$\delta = \left\{ \sum_{n=1}^{N} \left[\ln(y_{e(n)} - \ln(y_{o(n)} \right]^2 \right\} \Big/ N \qquad [8.9]$$

where: δ = the function that is minimized, $y_{e(n)}$ = estimated value for the *nth* data point, $y_{o(n)}$ = observed value for the *nth* data point, and N = number of observations. A minimization function using logarithms rather than absolute values gives a more uniform relative error among the observations in comparison to a minimization function that uses absolute values. A minimization function using absolutes values gives flattening, burial, and resurfacing ratio values that are biased to the large surface biomass values. Equations 8.5 and 8.7 were fitted by the soil disturbing implement types represented in the observed data. The flattening, burial, and resurfacing ratio values obtained by fitting equations 8.5 and 8.7 were used to guide assign values in the RUSLE2 core database (see the RUSLE2 User's Reference Guide).

8.2.4.2. Effect of soil disturbance depth on residue burial

The input value for burial ratio is for a reference depth, which is assumed to the manufacturer recommended or normal operating depth for the implement, machine, tool, or other residue burial process.

The effect of operation depth (i.e., soil disturbance depth) on the residue burial ratio is computed using:

$$\alpha_d = [1 - (1 - y_d / y_m)^{2.7}] / [1 - (1 - y_{rc} / y_m)^{2.7}] \qquad [8.10]$$

where: α_d = an adjustment factor for depth, y_{rc} = reference soil disturbance depth, y_d = the soil disturbance depth of the operation, and y_m = the maximum soil disturbance depth for

the operation. The fit of equation 8.10 to observed data is shown in Figure 8.1 (Hanna et al., 1995; Hill and Stott, 2000; Johnson, 1988).[62]

8.2.4.3. Effect of speed on surface residue burial

The effect of operation speed on residue burial ratio values is computed using:

$$\alpha_s = [0.6 + 0.4(v_s / v_m)^{1/2}] / [0.6 + 0.4(v_r / v_m)^{1/2}] \quad [8.11]$$

where: α_s = an adjustment factor for speed, v_r = reference speed, v_s = operation speed, and v_m = maximum operation speed. The fit of equation 8.11 to observed data is shown in Figure 8.2 (Hanna et al., 1995; Hill and Stott, 2000; Johnson, 1988).

8.2.4.4. Combined effect of soil disturbance depth and speed on surface residue burial

The burial ratio for the effect of both depth and speed is computed from:

$$f_b = \alpha_d \alpha_s f_{br} \quad [8.12]$$

where: f_{br} = the burial ratio for the given residue type for the reference soil disturbance depth y_{rc} and reference operation speed v_r.

8.2.5. Distribution of buried residue and dead roots by soil disturbing operations

Soil disturbing operations resurface buried residue but not dead roots, redistribute existing buried residue in the soil, redistribute dead roots in the soil, and bury surface residue. RUSLE2 makes these computations in three steps. The first step computes inversion of the burial material. The second step computes the redistribution of existing buried residue and dead roots and resurfacing of buried residue from the upper soil layer(s). The third step computes the mass distribution by soil layer of the material buried by the

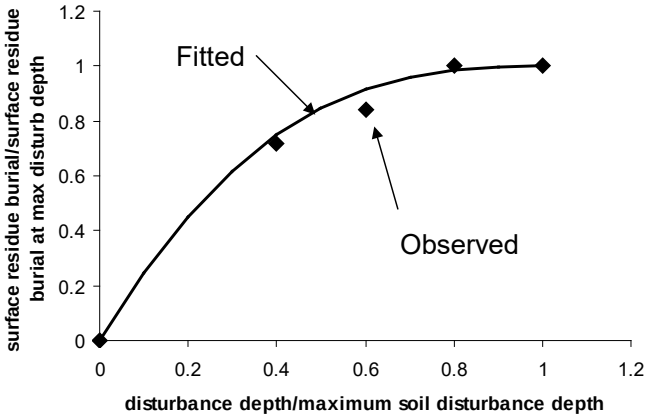

Figure 8.1. Effect of soil disturbance depth on surface residue burial.

[62] R.L. Raper, USDA-Agricultural Research Service, researched the literature and assembled the data used to derive the equations for effect of soil disturbance depth and operation speed on residue burial and equations for distribution of buried material by soil layer.

operation.

8.2.5.1. Types of soil disturbance operations

Types types of soil disturbing operations are used in RUSLE2 to describe how these operations distribute bury residue and dead roots in the soil. These types are: inversion, mixing with some inversion, and mixing. The *inversion* type represents machines like moldboard plows and soil disturbances (e.g., hand tillage with a spading fork) that primarily bury and mix material in the soil by inverting the disturbed soil layer. The *mixing with some inversion* type represents machines like field cultivators, chisel plows, tandem disks, and scarifiers and soil disturbances that bury material in the soil primarily by mixing with some inversion. The *mixing* type represents machines like rotary powered machines (e.g., rototillers); shank machines used to inject manure, fertilizers, and other materials into the soil; and soil disturbances that incorporate material by mixing with essentially no inversion. The mixing type also represents materials pressed into the soil by cattle trampling, sheep's foot compactors, and similar operations. Burial of residue by compression does not involve soil disturbance.

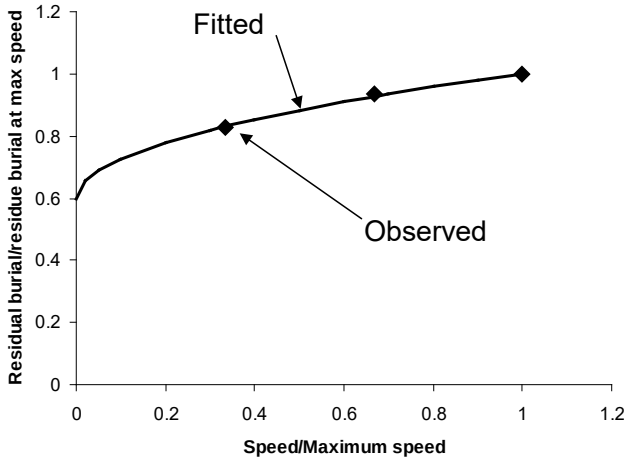

Figure 8.2. Effect of speed on surface residue burial.

8.2.5.2. Equations for redistribution of buried residue and dead roots

A sifting concept is used in RUSLE2 to compute redistribution of buried material by soil disturbing operations. RUSLE2 computes separately the redistribution of buried residue and dead roots. Conceptually, soil disturbance "sifts" each soil layer so that some of the buried material (i.e., buried residue or roots) is retained in each layer and the remainder moves downward to the next soil layer.[63]

RUSLE2 assumes that no material moves upward except by inversion-type soil disturbances. The first step is to compute inversion of the buried material for inversion type soil disturbing operations. This computation assigns the existing buried material

[63] The RUSLE2 equations used to redistribute buried residue and dead roots are based on empirical data reported in the literature cited in **Section 12.2.4.**

mass in the bottom soil layer to the top soil layer, the existing material in the top layer to the bottom layer, the existing material in the next to bottom soil layer is assigned to the soil layer next to top layer, and so forth. For example, the buried material mass in the top soil layer after inversion is set equal to the material mass in the bottom soil layer before inversion and the mass in the bottom layer after inversion is set equal to the mass in the top soil layer before inversion.

The next step for all soil disturbing operations is to "sift" the soil layers to compute the buried material that leaves each soil layer using:

$$\Delta B_{(i)} = (1 - \phi_{k(i)})(B_{p(i)} + \Delta B_{(i-1)} - R_{(i)}) \qquad [8.13]$$

where: $\Delta B_{(i)}$ = the buried material (dry mass/area) that moves from the *ith* soil layer to the *(i+1)th* layer, $\Delta B_{(i-1)}$ = the buried material (dry mass/area) that moves from the *(i-1)th* soil layer to the *)th* layer ϕ_k = the mass fraction of the buried material in the *ith* layer that is retained for the *kth* type soil disturbance operation, $B_{p(i)}$ = existing buried material (mass/area) in the *ith* soil layer, $R_{(i)}$ = the buried residue (dry mass/area) that is resurfaced for the *ith* layer. The soil disturbance depth is divided into 10 layers to make these computations where i = index for the soil layers (i = 1 for surface soil layer). The computations start with the top layer and proceed downward. The inflow to the top layer is set to zero in this step. The amount of material that enters the top layer by burial is added in the third step described below.

The fine roots tightly bound to soil particles dead roots are assumed to have the greatest effect on erosion. Therefore, the RUSLE2 assumption is that dead roots are not resurfaced.[64]

Values for R in equation 8.13 are zero when equation 8.13 is used to compute the redistribution of dead roots. The total mass of buried residue that is resurfaced is computed using equation 8.8. The value for R in the top soil layer (i.e., R_1) in equation 8.13 is set to the value computed by 8.8. If the value computed by equation 8.8 exceeds the buried residue mass in layer 1, the value for the mass removed is set equal to the buried residue in layer 1 before sifting. The remainder of the buried residue mass needed to provide the mass computed by equation 8.8 is removed from layer 2. If the buried residue mass in layer 2 is insufficient, the entire buried residue before sifting is removed from layer 2. The check moves to subsequent layers until the total resurfaced residue mass computed by equation 8.8 is satisfied.

---

[64] The fact that soil disturbing operations surface dead roots is recognized. However, the fraction of dead roots in the soil that is resurfaced is considered to be much smaller than the fraction of buried residue that is resurfaced.

Table 8.1. Retention coefficient Φ values for redistributing buried material among soil layers

	Type soil disturbance operation		
Layer	Inversion w/mixing	Mixing w/inversion	Mixing
1 (top)	0.40	0.32	0.50
2	0.40	0.39	0.56
3	0.40	0.47	0.61
4	0.40	0.54	0.67
5	0.40	0.62	0.72
6	0.40	0.69	0.78
7	0.40	0.77	0.83
8	0.40	0.84	0.89
9	0.50	0.92	0.94
10	1.00	1.00	1.00

Values for the retention coefficient ϕ are given in Table 8.1. The value of 1 for the *10th* layer denotes that no buried material passes through the bottom layer in the soil disturbance depth. Retention values for the mixing-type soil disturbing operations are assumed to increase linearly from the value for the top layer to 1 for the bottom layer. This increase with depth means that buried material is more likely to move downward in the upper part of the disturbed soil layer than in the lower part. The increased retention coefficient values with depth indicate greater retention because of less stirring and mixing in the bottom of the soil disturbed layer. In contrast, stirring, mixing, and retention are assumed to be nearly uniform with depth for inversion-type soil disturbing operations as shown in Table 8.1.

The retention ϕ values in Table 8.1 were determined by fitting equation 8.13 to measured data where the same operation was repeated multiple times. These data conclusively show that buried material redistributed by multiple events of mixing with some inversion and mixing types soil disturbing operations forms a bulge that moves downward in the soil rather than producing a uniform distribution (see RUSLE2 User's Reference Guide). In contrast, the distribution of buried material becomes nearly uniform with multiple events of an inversion-type soil disturbing operation. Retention values were independent of characteristics of the buried material.

The third step is to distribute surface residue by soil layer when it is buried by a soil disturbing operation. That mass is added to the buried residue mass after sifting as computed with equation 8.13 for redistribution and resurfacing of existing buried residue. The equation used to compute the distribution of surface residue when it is buried in the soil by mixing-type soil disturbing operations is:

$$M = (y / y_d)^b \qquad [8.14]$$

where: M = cumulative normalized mass (cumulative mass above depth in soil/total mass buried in soil depth disturbed by operation) of buried residue with depth (i.e., M = 0 at y = 0 and M =1 at y = y_d), y = depth in soil, y_d = soil disturbance depth for a specific soil disturbing operation, and b = 0.5 for *mixing with some inversion* type soil disturbing operations and b = 0.3 for *mixing* type soil disturbing operations.

The comparable equations for inversion-type soil disturbing operations are:

$$M = 0.28\{\exp[1.83(y / y_d) - 1]\} \quad y / y_d \le 0.6 \qquad [8.15]$$

$$M = 1 - 0.441\{[1 - (y / y_d)] / 0.4\}^{1.4} \quad y / y_d > 0.6 \qquad [8.16]$$

Equations 8.14 - 8.16 were derived from observed data where surface material was buried by a single occurrence of an operation when no buried residue existed in the soil. The distributions of buried residue computed by equations 8.14 – 8.16 are shown in Figure 8.3.

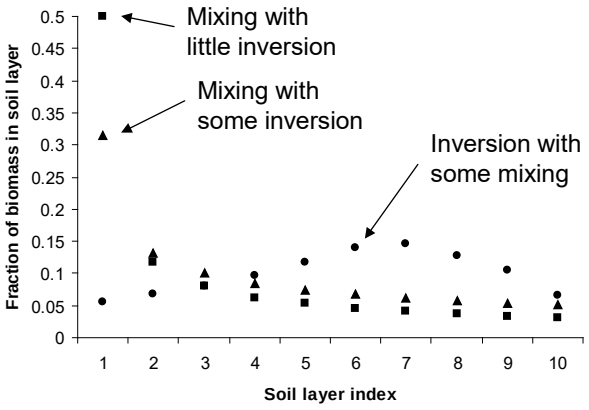

Figure 8.3. Distribution of residue by soil layer when initially buried by a soil disturbing operation.

In summary, RUSLE2 computes buried residue mass in each soil layer after an operation by (1) computing inversion of buried residue biomass if the operation is an inversion-type operation, (2) using equation 8.13 to compute redistribution of existing buried residue mass caused by stirring and mixing (i.e., sifting), and (3) using equations 8.14 – 8.16 to distribute the surface biomass among soil layers that is buried by the operation, which is added to the buried residue mass computed in step 2. The steps for computing redistribution of dead roots is to (1) add the dead roots produced by the kill live vegetation process to the existing dead roots in each soil layer if the operation includes a kill vegetation process, (2) invert the dead roots by soil layer if the operation is an inversion type operation, and (3) compute the sifting of dead roots using equations 8.13.

8.2.6. Add other cover

The **add other cover** process is used to apply material to the soil surface and/or place (inject) material into the soil.

8.2.6.1. Add cover to soil surface

The **add other cover** process has the inputs of the residue, amount (dry mass basis) added as well as the portion added to the soil surface and the portion placed (injected) in the soil. The mass of the material added to the soil surface is added to the surface residue pool.

8.2.6.2. Injection of material (residue) into the soil by a soil disturbing operation

The **add other cover** process along with a **disturb soil** process are used together to inject material into the soil. This material is assumed to be added in the lower half of the disturbed soil depth in a parabolic distribution. The equations for cumulative mass with depth for material injected into the soil are:

$$M = 6\left[\frac{(2y/y_d - 1)^2}{2} - \frac{(2y/y_d - 1)^3}{3}\right] \quad y/y_d \geq 0.5 \qquad [8.17]$$

$$M = 0 \quad y/y_d < 0.5 \ [8.18] \qquad [8.18]$$

where: m = cumulative normalized mass (cumulative mass above depth in soil/total mass), y = depth in soil, and y_d = soil disturbance depth. The mass placed in the soil is added to the buried residue pool.

8.2.7. Remove residue cover

The **remove residue cover** process is used to describe removal of standing and surface residue. Inputs for this process include the portions of the standing and surface residue masses that are removed. The masses of standing and surface residue are reduced by these portions. Another input is whether the residue removal applies to all residues involved in the RUSLE2 computation or only the last residue added to the soil surface in the computation. An example is where corn and wheat grain crops are grown in sequence. The harvest of each crop leaves residue. The straw is baled (removed) but the corn residue is left in the field. The input to remove the last residue is selected in this situation. Another example is burning where all residues is selected.

8.2.8. Add/remove non-erodible cover

8.2.8.1. Description of add/remove non-erodible cover processes

The **add non-erodible** cover process sets detachment to zero for the portion of the soil surface covered with non-erodible cover. That is:

$$c = c_\omega(1 - f_\mu) \qquad [8.19]$$

where: c = the c in equations 2.10 and 6.1 used to compute detachment, c_ω = the c term in equation 2.10 without the non-erodible cover effect, and f_μ = the portion of the soil surface covered by non-erodible cover. Equation 8.19 in effect adds a non-erodible cover subfactor to equation 6.1.

Non-erodible cover also affects runoff. The equations used to adjust cover number values used to compute runoff when non-erodible cover is present are given in **Section 3.3.1.2.3**.

The **remove non-erodible cover** process removes non-erodible cover. The input value is the portion of the existing non-erodible cover that is removed by the operation. A 100 percent input value removes all of the existing non-erodible cover. A 40 percent input value removes 40 percent of the existing non-erodible cover. For example, assume that the existing non-erodible cover is 72 percent on the day of an operation that removes 40

percent of the non-erodible cover. The remaining non-erodible cover is 43 percent [72·(100-40)/100] after the operation.

8.2.8.2. Loss of non-erodible cover over time

RUSLE2 assumes that non-erodible cover disappears over time because of photo-chemical and other processes. The equation for the loss of non-erodible cover is given by:

$$f_\mu = f_0 \exp(-\alpha_\mu \Delta t_\mu) \quad [8.20]$$

where: f_0 = the fraction of the soil surface covered by non-erodible cover immediately after an operation affects non-erodible cover (i.e., added or removed) and Δt_μ = the days since the non-erodible cover was affected. The coefficient α_μ = a coefficient (days^{-1}) that describes the rate of loss of non-erodible cover. Equation 8.20 is not written as a function of environmental conditions. To consider the effect of environmental conditions on this cover loss, users select α_μ values that reflect both material properties and local environmental conditions. Consequently, α_μ values can differ among locations for the same material based on variation of environmental conditions between locations.

8.3. Effect on soil

The **disturb soil** process is used to describe how operations affect the soil. An operation that includes a disturb soil process is referred to as a soil disturbing operation. Soil disturbing operations loosen the soil, buries surface residue, resurfaces buried residue, redistributes buried residue and dead roots, affects soil roughness, and affects ridges. Some operations such as planting disturb only a portion of the soil surface.

8.3.1. Loosen soil

The effect of an operation loosening the soil is described by the soil consolidation subfactor. The equation for the soil consolidation subfactor is given in **Section 6.6.2**.

For those operations that do not disturb the entire soil surface area, RUSLE2 computes a net soil consolidation subfactor as:

$$s_{cn} = f_d + (1 - f_d) s_{cu} \quad [8.21]$$

where: $s_{c,n}$ = the net soil consolidation subfactor for the overall soil surface, f_d = the fraction of the soil surface that is disturbed, $s_{c,u}$ = the soil consolidation subfactor for the portion of the soil surface not disturbed by the operation, and 1 = the consolidation subfactor value for the soil surface portion that is disturbed.

An effective soil consolidation time t_{de} since last soil disturbance is computed by solving equation 6.52 for the time that gives the value for the net soil consolidation subfactor value computed with equation 8.21. The time used in equation 6.52 to compute the soil consolidation subfactor starts from this effective soil consolidation time.

8.3.2. Burying and resurfacing residue

Soil disturbing operations bury surface residue and resurface buried residue. The RUSLE2 assumption is that surface residue can only be buried by disturbing the soil. The equations used to compute residue mass buried and resurfaced by soil disturbing operations are given in **Section 8.2**. Important variables used in these computations are the fraction of the surface residue mass that the operation buries and the faction of the buried residue mass in the soil disturbance depth that is resurfaced. **The burial and resurfacing ratios apply to the entire soil surface and not just to the portion of the soil surface that is disturbed** (see the RUSLE2 User's Reference Guide).

Some soil disturbing operations that disturb only a portion of the soil surface. The RUSLE2 procedure that determines an effective surface residue biomass for the entire surface is described in **Section 6.2.3**.

8.3.3. Redistribution of buried residue and dead roots

Soil disturbing operations redistribute existing buried residue and dead roots on the date of the operations. The equations used in these computations are given in **Section 8.2.5**.

The RUSLE2 assumption is that soil disturbance is required to place material in the soil (e.g., manure and fertilizer injection). The equations used to compute the distribution of material placed in the soil by an **add other cover** process are given in **Section 8.2.6.1**.

8.3.4. Soil surface roughness

A soil disturbing operation affects soil surface roughness. An operation can either smooth the soil surface (i.e., reduce soil surface roughness) or roughen the soil (i.e., increase soil surface roughness). Roughness decays over time because of subsidence (settlement), interrill erosion, and local deposition.

The RUSLE2 assumption is that soil surface roughness can only be created by a soil disturbing operation. Consequently, operations with a disturb soil process must be used to represent soil surface roughness creation.

8.3.4.1. Inputs for soil surface roughness in an operation description

Three inputs are used in a **disturb soil** process to describe soil surface roughness. One input is initial roughness, which is the roughness created by the operation when performed on a smooth surface under the base, reference condition of high biomass and silt loam soil (see **Section 6.3.1** and **6.3.6** and RUSLE2 User's Reference Guide). Equations given in **Sections 6.3.2, 6.3.3,** and **6.3.5** are used to adjust this initial roughness value for soil texture, biomass, and existing soil surface roughness to represent site specific conditions where RUSLE2 is being applied.

RUSLE2 computes soil surface roughness decay over time as a function of precipitation and interrill erosion using equations given in **Section 6.3.6**. RUSLE2 computes roughness decay to the final roughness value input for the particular operation. The final

roughness value is usually set to 0.24 inches and not adjusted for soil texture or soil biomass. This final roughness value represents persistent, highly stable soil clods that remain even after extensive erosivity applied to the reference silt loam soil in unit plot conditions. The roughness subfactor value is 1 for unit plot conditions (see **Section 6.3.1**). Final roughness on unit plots varies by soil texture, but that effect on rill-interrill erosion is captured in the soil erodibility factor (see **Section 4.1**).

In special cases such as construction sites where a high clay soil is scarified, a final roughness value greater than 0.24 inches can be entered to represent an increased roughness effect (see the RUSLE2 User's Reference Guide). A final roughness value less than 0.24 inches is entered for operations, such as for fine seedbeds typical of vegetable production or smooth surfaces left by a blading operation on a construction site, that create roughness smoother than that for unit-plot conditions (see **Section 2.1**). When the final roughness value is less than 0.24 inches, the initial roughness input value should be the same as the final roughness input value. RUSLE2 computes no roughness decay when the final roughness input is less than 0.24 inches.

8.3.4.2. Partial soil disturbance

In contrast to the assumption made for burying and resurfacing residue, the RUSLE2 assumption is that the input roughness values only apply to the portion of the soil surface disturbed. A net soil surface roughness value is computed as:

$$s_{rn} = f_d s_{rd} + (1 - f_d) s_{ru} \qquad [8.22]$$

where: s_{rn} = the net soil surface roughness subfactor immediately after a soil disturbing operation that occurs on day t, s_{rd} = the soil surface roughness subfactor for the disturbed portion of the soil surface immediately after the operation on day t, and s_{ru} = the soil surface roughness subfactor for the undisturbed portion of the soil surface on day of the operation. The starting value in equation 6.26 for the roughness subfactor immediately after the operation that is decayed is the s_{rn} value computed with equation 8.22.

RUSLE2 assumes that an operation that disturbs only a portion of the soil surface disturbs some of the undisturbed soil. Consequently, multiple occurrences of an operation that disturbs only a portion of the soil surface ultimately disturb most of the soil surface. That is, RUSLE2 can not represent an operation that disturbs the same area with each occurrence of the operation.

8.3.4.3. Tillage intensity (effect of existing roughness)

The RUSLE2 assumption is that the roughness left by a soil disturbing operation can depend on existing roughness. The input for this effect is a **tillage intensity** value assigned to the disturb soil process (see RUSLE2 User's Reference Guide). Tillage intensity refers to the degree that a soil disturbing operation obliterates existing roughness (i.e., conversely the degree that existing roughness affects roughness left by the soil disturbing operation). A tillage intensity value of 1 means that the soil disturbing operation is so aggressive that existing roughness has no effect on roughness left by the

operation. For example, the tillage intensity value of 1 is used to describe moldboard plows and rototillers. A tillage intensity of 0 means that the operation does not affect existing roughness. Harrows used as secondary tillage to create a seedbed are assigned 0.4 for tillage intensity to reflect that existing roughness has a significant effect on the roughness left by harrows. For example, the soil surface roughness after a harrow is greater when it follows a moldboard plow than when it follows a tandem disk used for secondary tillage. The tillage intensity effect is computed using:

$$R_a = (R_{ae} - R_{ao})(1 - \xi) + R_{ao} \quad R_{ao} \le R_{ae} \qquad [8.23]$$

$$R_a = R_{ao} \quad R_{ao} > R_{ae} \qquad [8.24]$$

where: R_a = adjusted roughness after a soil disturbing operation, R_{ae} = existing adjusted roughness immediately before the operation, ξ = tillage intensity, and R_{ao} = the adjusted roughness left by the operation when applied to a smooth surface. Roughness values used in equations 8.23 and 8.24 have been adjusted for soil texture and biomass effects using the procedures described in **Section 6.3**.

8.3.5. Ridges

The RUSLE2 assumption is that only soil disturbing operations create ridges. Consequently, operations with a disturb soil process must be used to represent ridge creation.

The ridge input for the **disturb soil** process is initial ridge height. In contrast to soil surface roughness, the input ridge height is not adjusted for soil texture, soil biomass, existing ridges, or portion of the soil surface disturbed. For example, the ridge height left by a planter run on top of existing ridges depends on the existing ridge height. This effect is represented in RUSLE2 by having a set of planter descriptions in the RUSLE2 database for a range of ridge heights. A particular planter entry is selected from this input set based on the operations that precede the planter operation (see the RUSLE2 User's Reference Guide).

8.4. List of symbols

b = exponent in equation for distribution of buried residue left by an operation

$B_{(i)}$ = buried material in *ith* soil layer (mass/area)

B_{al} = live vegetation biomass (mass/area)

B_{br} = buried biomass in soil disturbance depth (mass/area)

B_{sr} = surface residue (mass/area)

B_{tr} = stading residue biomass (mass/area)

c = daily cover-management factor value in equation 2.10 with non-erodible cover effect

c_{ω} = daily cover-management factor in equation 2.10 without non-erodible cover effect

f_b = portion of surface residue that is buried (fraction)

f_{br} = burial ratio for given residue type for reference soil disturbance depth and speed

f_d = portion of the soil surface that is disturbed (fraction)

f_f = portion of existing standing residue biomass that is flattened a flatten standing residue process operation (fraction)

f_{lr} = portion of above ground live biomass that is affected by a **remove live vegetation** process operation (fraction)

f_n = faction of soil surfaced by non-erodible cover

f_{sl} = portion of affected biomass that is left as surface residue by a **remove live vegetation** process operation (fraction)

f_{tl} = portion of affected biomass that is left as standing residue by a **remove live vegetation** process operation (fraction)

f_u = portion of the buried residue biomass in soil disturbance depth that is resurfaced that is resurfaced (fraction)

f_0 = portion of soil surface covered by non-erodible cover immediately after an operation affects non-erodible cover (i.e., added or removed) (fraction)

f_{μ} = portion of soil surface covered by non-erodible cover (fraction)

M = cumulative buried residue normalized with depth (cumulative mass above depth in soil/total mass buried in soil disturbance depth) bured by a **soil disturb** process operation

N = number of data points

$R_{(i)}$ = buried residue niomass that is resurfaced from a soil layer (mass/area)

R_a = roughness after a soil disturbing operation (length)

R_{ae} = existing roughness immediately before the operation (length)

R_{ao} = the roughness left by the operation when applied to a smooth surface (length)

s_{cn} = net soil consolidation subfactor

s_{cu} = soil consolidation subfactor for the portion of soil surface not disturbed by operation

s_{rn} = net soil surface roughness subfactor immediately after a soil disturbing operation that occurs on day t

s_{rd} = soil surface roughness subfactor for disturbed portion of the soil surface immediately after the operation

s_{ru} = soil surface roughness subfactor for undisturbed portion of the soil surface on day t

v_m = maximum operation speed (length/time)

v_r = reference speed (length/time)

v_s = operation speed (length/time)

y = depth in soil (length)

y_d = soil disturbance depth of operation (length)

y_{en} = estimated value for the *nth* data point

y_m = the maximum soil disturbance depth for operation (length)

y_{on} = observed value for the *nth* data point

y_{rc} = reference soil disturbance depth (length)

α_d = adjustment factor for depth

α_s = adjustment factor for speed

α_μ = coefficient that describes rate of loss of non-erodible cover ($days^{-1}$)

δ = function that is minimized

$\Delta B_{(i)}$ = buried material that moves from *ith* soil layer to *(i+1)th* layer (mass/area)

$\Delta B_{(i-1)}$ = buried material that moves from (*i-1)th* soil layer to *i)th* layer (mass/area)

ΔB_{sr} = standing residue added to surface residue biomass pool by a **remove live vegetation** operation process or surface residue biomass transferred to the buried residue pool by a **soil disturb** process operation (mass/area)

ΔB_{tr} = live above ground biomass added to standing biomass pool added by a **remove live vegetation** process operation or biomass lost from standing residue bimass and added to surface bimass by a **flatten standing residue** process in an operation (mass/area)

$\Delta B_{u(i)}$ = residue biomass that is resurfaced from soil disturbance depth by a **soil disturb** process operation (mass/area)

Δt_{μ} = time since non-erodible cover was affected (days)

ξ = tillage intensity

$\phi_{k(i)}$ = portion of buried material in the *ith* layer that is retainedby a *kth* type soil disturbance operation (fraction)

Indices

i – soil layer

j – day

k - type of soil disturbance operation

n – data point

9. VEGETATION

The input variables used to describe vegetation are biomass (dry basis) at maximum canopy cover and the temporal variables of root biomass (dry basis) in the upper 4-inch (100 mm) soil depth, canopy cover, effective fall height, and live ground cover. These variables are used to compute values for the temporal variables of the live root biomass by soil layer, dead root biomass produced by root sloughing, live above ground biomass, biomass produced by senescence that falls to the soil surface, and retardance. All of these variables are used to compute values for the cover-management subfactors (see **Section 6**), curve numbers used to compute runoff (see **Section 3.3.1.2**), and hydraulic resistance (see **Section 3.4.6**). The RUSLE2 User's Reference Guide describes selection of input values for variables used to describe vegetation.

9.1. Input of temporal variables

Input values for the temporal vegetation variables are often manually constructed and entered in RUSLE2 using values in the RUSLE2 core database as a guide (see RUSLE2 User's Reference Guide). This procedure works satisfactorily for simple vegetation descriptions for annual agricultural and horticultural crops and annual descriptions for mature perennial plant communities. However, creating and entering values for vegetation descriptions for long term vegetation from seeding to maturity is cumbersome and time consuming. RUSLE2 includes a long term vegetation tool that can be used to create long term vegetation descriptions (see RUSLE2 User's Reference Guide).

Temporal variables used to describe vegetation are assumed to vary linearly between the times in the data points entered for these variables. The time between data points should be sufficiently small to accurately represent non-linear variations.

9.2. Computed temporal vegetation variables

9.2.1. Live root biomass by soil layer

RUSLE2 uses input values for live root biomass in the upper 4-inch soil depth to compute daily live root biomass values in individual soil layers.

The literature was reviewed to obtain measured data for root biomass and its distribution in the soil at plant maturity for the major agricultural crops of corn, soybeans, cotton, and wheat; several vegetable crops; and several pasture/range plant communities (see **Section 12.2.5**). The RUSLE2 equations for the distribution of live root biomass in the soil were derived from these data, especially the data by Long (1959). These equations are:

$$M_r = y[24.24y\exp(-5.50y) + 0.778] \quad y \le 0.533333 \qquad [9.1]$$

$$M_r = 0.783391 + 0.147688(y - 0.533333) \quad 0.533333 < y \le 2 \qquad [9.2]$$

$$M_r = 0 \quad 2 < y \qquad [9.3]$$

where: M_r = cumulative root biomass (dry basis) above the depth y, y = Y/15, Y = depth (inches) in soil (Y = 0 at soil surface), and 15 = a reference depth (inches) used to normalize the depth variable y. A plot of these equations by 1 inch layer is shown in Figure 9.1.

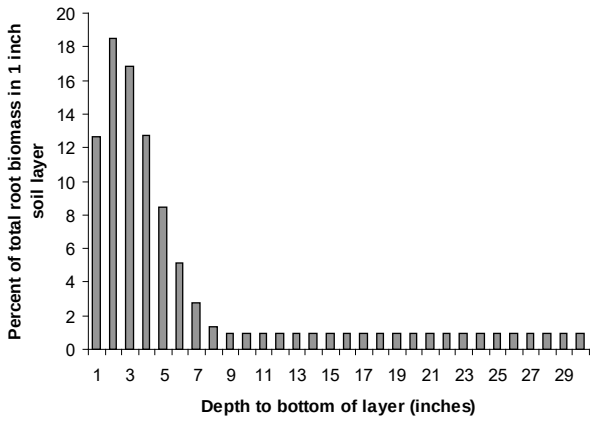

Figure 9.1. Fraction of total root biomass in 1 inch soil layers.

No data were found for measured root biomass in 1-inch soil layers. Accurately measuring roots is very difficult in soil layers as thin as 1-inch, especially near the soil surface. Preference was given to data where root biomass was measured in soil layers sufficiently thick to obtain accurate measurements, which is one of the reasons why the input value for root biomass is based on the upper 4-inch soil layer. This depth also contains the bulk of the roots that significantly affect rill-interrill erosion as discussed below.

The shape of the curve in Figure 9.1 within the upper 4-inch soil layer is based on judgment. A power equation gave the best fit to the observed data, but it was not used because a power equation form gives maximum root biomass density at the soil surface. The judgment is that root mass in the upper 1-inch layer is less than that at a slightly deeper soil depth. Soil moisture at the soil surface is reduced because of evaporation when soil surface (residue) cover is minimal, which in turn results in reduced root biomass near the soil surface. Increased surface residue reduces evaporation, which increases soil moisture at the soil surface. The form of equation 9.1, which represents reduced root biomass near the soil surface, was judged more appropriate overall for RUSLE2 than the power equation form. The shape of the curve in the upper 4-inch soil depth is of minimal consequence because RUSLE2 uses the average root biomass density in the upper 10-inch soil depth to compute runoff curve values, b values for effect of ground (surface) cover, slope length exponent, soil surface roughness, and soil biomass subfactor values (see **Sections 3.3.1.2, 6.2.1, 6.2.2, 6.3, and 6.5**).

A major result from the literature review and data analysis was that rooting depth for the roots judged to have the greatest effect on rill-interrill erosion do not vary greatly among agricultural crops and pasture/range plant communities. However, the rooting depths for most vegetable crops were about one half of that for agricultural crops. A rooting depth of 30 inches was assumed in RUSLE2 for all plant communities, including vegetable crops. Other RUSLE2 assumptions based on data analysis were that 85 percent of live root biomass was above the 15-inch depth, the live root biomass distribution by depth was the same for all plant communities, and rooting depth does not temporally vary.

The adequacy of these RUSLE2 assumptions must be judged in terms of RUSLE2's stated purpose of being an easily used guide for erosion control planning. Do RUSLE2's erosion estimates adequately represent the effect of temporal variability in root biomass for purposes of erosion control planning? Such an evaluation described in the RUSLE2 User's Reference Guide shows that RUSLE2 meets that criterion. Capturing the main effects of root biomass rather than all of the details is adequate for RUSLE2 purposes.

RUSLE2 uses average live root biomass density in the upper 10 inch soil depth to compute values for the soil biomass subfactor (see **Section 6.5.2**). The RUSLE2 live root distribution described by equations 9.1 and 9.2 compute that 61 percent of the total live root biomass is in the upper 4-inch soil depth and 80 percent is in the upper 10-inch soil depth. The constant rooting depth assumption does not result in large errors for estimating the soil biomass subfactor because the input variable is the root biomass in the upper 4-inch soil depth that contains more than half of the total root biomass.[65] Temporal live root biomass values given in the RUSLE2 Core Database (see the RUSLE2 User's Guide) were scaled from measured values at plant maturity. RUSLE2 accurately computes expected erosion estimates for times before the vegetation reaches maturity for major agricultural crops (see RUSLE2 User's Reference Guide), which strongly indicates that these assumptions are adequate for RUSLE2 purposes.

These assumptions are in accordance with the RUSLE2 objective to provide a system where the major vegetation variables affecting rill-interrill erosion can be easily described and measured and values for variables used to describe vegetation can be easily entered in RUSLE2. The objective is to sufficiently represent vegetation for RUSLE2 to estimate the effects of vegetation for conservation and erosion control planning. The adequacy of RUSLE2 for conservation and erosion control planning is the criteria for judging these RUSLE2 relationships. **The RUSLE2 User's Reference Guide guidelines must be followed to ensure accurate RUSLE2 erosion estimates.**

9.2.2. Live root biomass becoming dead root biomass

RUSLE2 uses a single vegetation description on any particular day (see **Section 8.1.1**). An operation that includes a **kill vegetation** process transfers the entire live root biomass in each soil layer to the dead root biomass in the corresponding soil layer. RUSLE2 does not allow killing a portion of the live root biomass. That effect can be accomplished by using an operation that includes a **begin growth** process that instructs RUSLE2 to begin using values for a new vegetation description. RUSLE2 assumes that the difference between the live root biomass on the last day that a vegetation description is used and the live root biomass on day zero in the new vegetation description represents dead root biomass that is added to the existing root biomass. RUSLE2 assumes that a decrease in

---

[65] A possible RUSLE2 improvement would be to temporally vary rooting depth according to plant community. Similarly, the root distribution should also be varied with plant community and plant growth stage. These improvements were judged to excessively complicate RUSLE2.

root biomass from one day to the next represents root sloughing (Reeder et al., 2001). Each daily decrease in live root biomass is added that day to the dead root biomass.

9.2.3. Live above ground biomass

RUSLE2 vegetation descriptions are divided into new growth, senescence, and regrowth periods, illustrated in Figure 9.2, to compute temporal values for live above ground biomass as a function of canopy cover.[66]

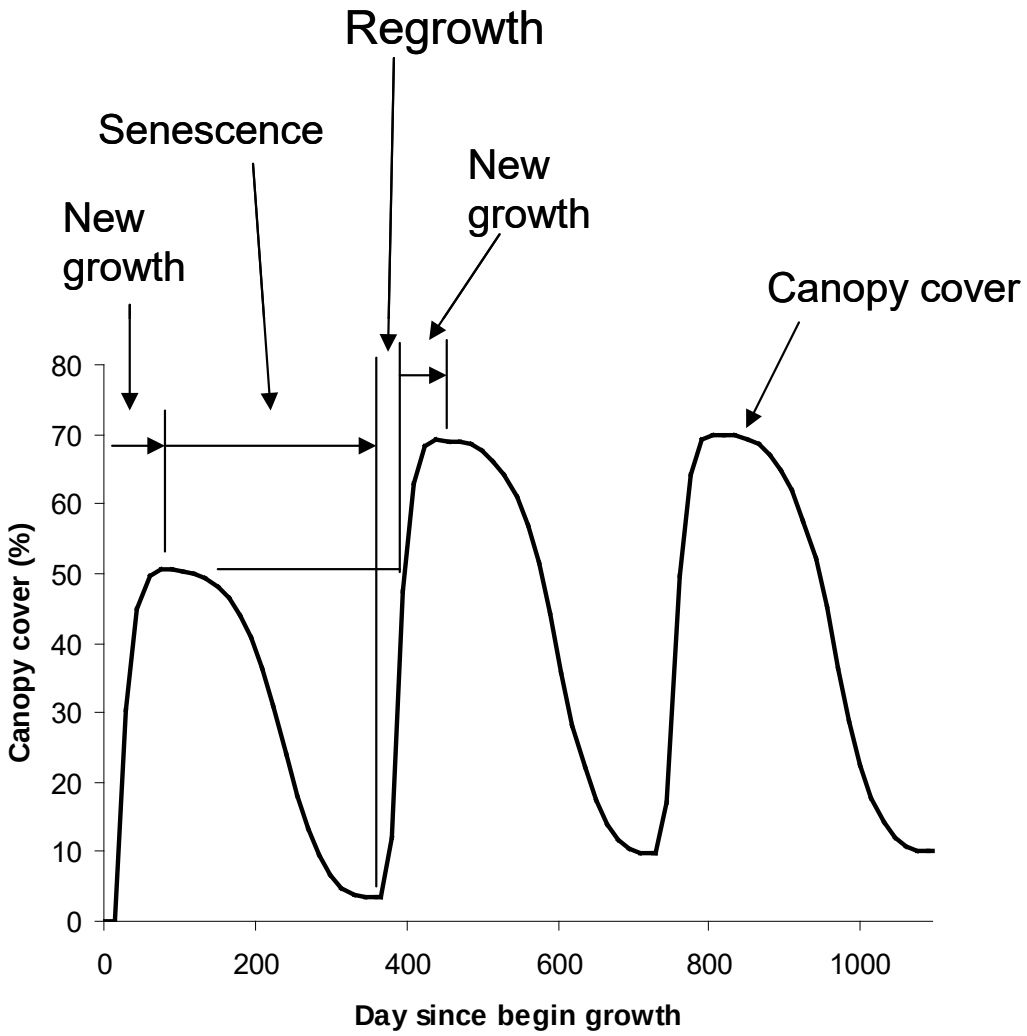

Figure 9.2. Vegetation growth periods used to compute live above ground biomass as a function of canopy cover.

9.2.3.1. New growth period

A **new growth** period is the time during which particular canopy cover values are first reached in a vegetation description. For example, the canopy cover from the seeding date to the first canopy cover maxima is a new growth period as illustrated in Figure 9.2. A second new growth period occurs in the second year over the time that canopy cover increases from the value of the first local canopy cover maxima in the first year to the local canopy cover maxima in the second year, also illustrated in Figure 9.2. A similar third new growth period, not illustrated, occurs in the third year. A composite of plant materials including leaves and stems is assumed to be produced during new growth periods.

The local canopy cover maxima that occurs in the third year for the vegetation description illustrated in Figure 9.2 is also the absolute canopy cover maxima for the vegetation description. The local canopy cover minima that occurs immediately after the absolute local canopy cover maxima is defined in RUSLE2 as the local absolute canopy cover minima for the vegetation description, even though other local canopy cover minima are less than this canopy cover. Values for the absolute canopy maxim and minima and the corresponding live above ground biomass values for these canopy values are user RUSLE2 inputs.

Live above ground biomass is computed from canopy cover during a new growth period using:

$$B_l = B_{lamx}(C / C_{amx})^{1.5} \qquad [9.4]$$

where: B_l = daily live above ground biomass during a new growth period, B_{lamx} = the live above ground biomass at absolute maximum canopy cover for a vegetation description, C = daily canopy cover, and C_{amx} = canopy cover at absolute maximum canopy cover for a vegetation description.

9.2.3.2. Senescence period

A **senescence** period is the time over which canopy cover decreases in a vegetation description from a local canopy cover maxima to a local canopy cover minima as illustrated in Figure 9.2. The equation used to compute live above ground biomass for a senescence period is:

$$B_l = B_{lmn(k)} + (B_{lmx(k)} - B_{lmn(k)})[(C - C_{mn(k)}) / (C_{mx(k)} - C_{mn(k)})]^{1.5} \qquad [9.5]$$

where: $B_{lmn(k)}$ = live above ground biomass at the *kth* local canopy cover minima, $B_{lmx(k)}$ = live above ground biomass at the *kth* local canopy cover maxima, $C_{mn(k)}$ = canopy cover at the *kth* local minima, and $C_{mx(k)}$ = canopy cover at the *kth* local maxima. The index k refers to canopy cover maxima-canopy cover minima combinations where canopy cover minima occur after the corresponding canopy cover maxima.

The live above ground biomass and canopy cover at local canopy cover minima must be on the curve given by:

$$B_{lmn(k)} = B_{lamn}(C_{mn(k)} / C_{mn(1)})^{1.5} \quad [9.6]$$

where: B_{lamn} = the absolute minimum live above ground biomass which occurs at $C_{mn(1)}$ = the first minimum canopy cover defined in **Section 9.2.3.1.** Values for live above ground biomass and canopy cover at local maxima must fall along the curve defined by equation 9.4.

The live above ground biomass-canopy cover curves for the new growth and the senescence periods are illustrated in Figure 9.3 for the first year of the vegetation description represented in Figure 9.2. The live above ground biomass for a given canopy cover during the senescence period is greater than that during the new growth period. Canopy cover loss during the senescence period is primarily by leaves falling to the soil surface. The biomass per unit canopy cover is much less for leaves than for the material, primarily stems, left standing during senescence. Each daily decrease in live above ground biomass is assumed to be biomass that falls and reaches the soil surface. This daily above ground biomass loss is added to the daily surface residue pool.

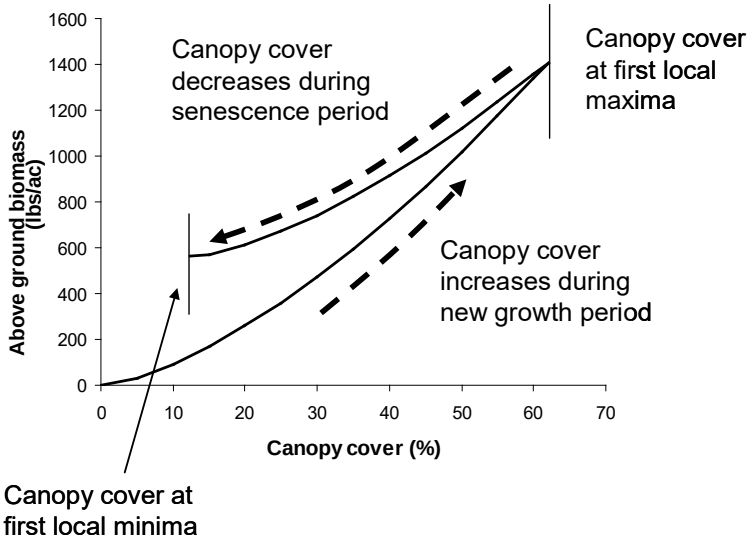

Figure 9.3. Live above ground biomass-canopy cover relationships for new growth and senescence periods during first year.

Equations 9.4 and 9.5 compute a decrease in live above ground biomass for a decrease in canopy cover. However, a decrease in live above ground biomass can occur with some plant communities with canopy cover remaining at 100 percent. An exponential equation form was evaluated to describe these plant communities. However, an exponential type equation was not used in RUSLE2 because such an equation can not be easily calibrated using the desired RUSLE2 inputs. Also, the exponential equation form did not give desired values for low canopy cover values.

Multiple vegetation descriptions are used in a RUSLE2 cover-management description to describe significant changes in live above ground biomass during periods when canopy cover changes very little. The inputs for these vegetation descriptions are selected so that

RUSLE2 computes a significant change in live above ground biomass for very little change in canopy cover such as from 99.9 percent to 99.5 percent. Such small changes in canopy cover have essentially no effect on canopy subfactor values (see **Section 6.1**). Additional vegetation descriptions are used for times during the cover-management description that canopy cover changes rapidly.

9.2.3.3. Regrowth period

The **regrowth** period starts from the canopy cover and live above ground biomass at the last local minima that was reached in the RUSLE2 computations as illustrated in Figure 9.2. Equation 9.5 is used to compute live above ground biomass values for the regrowth period as the live above ground biomass-canopy cover relationship retraces the senescence curve as illustrated in Figure 9.4. Most of the live biomass added during this period is assumed to be leaves and other material that has low biomass for the canopy cover that it provides. The regrowth period ends when canopy cover becomes equal to the canopy cover value of the last local maxima. A new growth period begins at this

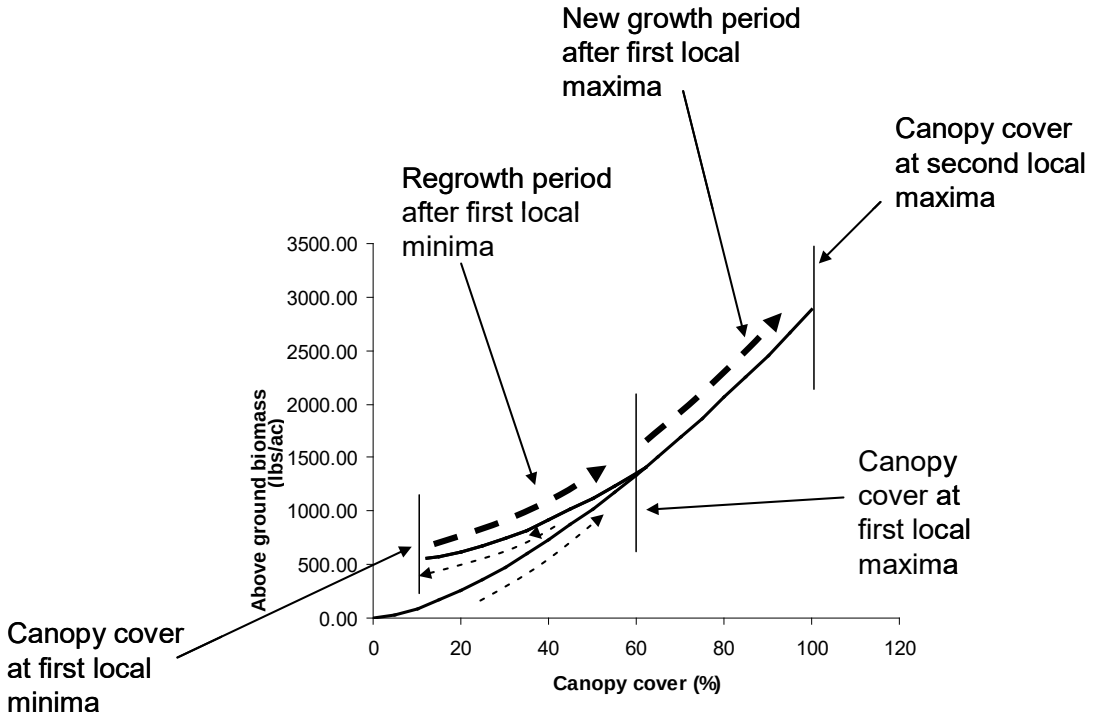

Figure 9.4. Live above ground biomass-canopy cover relationships for regrowth and new growth periods during second year.

point and continues until canopy cover becomes equal to the canopy cover of the next local maxima as illustrated in Figures 9.2 and 9.4. Equation 9.4 is used to compute values for live above ground biomass from canopy cover values during this new growth period. Once the next local maximum is reached, the next senescence period begins where equation 9.5 is used to compute live above ground biomass values.

Computations for this sequence of vegetation periods are repeated until the end of the RUSLE2 computation period.

9.2.3.4. Special cases

9.2.3.4.1. Annual plant communities that experience senescence

Most agricultural crops are annual and are described with either a single new growth period or by a single new growth period and a senescence period. Soybeans and cotton are examples of crops that experience senescence.

9.2.3.4.2. Annual plant communities that experience a decrease in canopy cover without a corresponding decrease in live above ground biomass

RUSLE2 also represents vegetation (e.g., corn and wheat) where canopy cover decreases by leaves drooping instead of falling to the soil surface. In this special case, the live above ground biomass does not decrease as canopy cover decreases. However, RUSLE2 can not represent perennial (long term) vegetation (i.e., multiple sequences of new growth-senescence-regrowth periods in the vegetation description) that has these characteristics.

9.2.4. Litter fall by other processes than senescence

9.2.4.1. Simultaneous birth and death of live above ground biomass

Litter is produced during the increase in growth period before canopy cover begins to decrease by senescence (Dubeux et al., 2005; Thomas and Asakawa, 1993). The litter produced during this period adds substantially to the surface residue produced by litter fall during senescence.

The amount of litter fall during the increase in growth period and into the first part of the senescence period is computed using:

$$L_f = c_f (B_l - B_{lmn(k)}) \;\; if\,(B_l < B_{lmn(k)}) : L_f = 0 \qquad [9.7]$$

where: L_f = day litter fall rate (mass/area·day) during the birth-death period and c_f = coefficient for birth-death litter fall (day^{-1}). A single value of 0.01 day^{-1} probably can be used almost all vegetation types (Dubeux et al. 2005; Thomas and Asakawa, 1993). However, this conclusion needs further research.

Litter fall is computed using equation 9.7 into the senescence period until the rate of litter falls computed by the difference in above ground biomass in a day exceeds the litter fall rate computed by equation 9.7.

9.2.4.2. Litter fall caused by mechanical traffic

Mechanical traffic by humans, animals, and vehicles can transfer biomass from the canopy to the soil surface that adds to surface residue. That biomass transfer is estimated by:

$$L_m = c_m(B_l - B_{lmn(k)}) \;\; if\,(B_l < B_{lmn(k)}) : L_f = 0 \qquad [9.8]$$

where: L_m = litter fall rate (mass/area·day) caused by mechanical traffic and c_m = a litter fall coefficient (day^{-1}) for the litter fall caused by mechanical traffic. The input value for c_m is based on the user's judgment.

9.2.4.3. Adjustment in above ground biomass for litter fall

RUSLE2 does not adjust live above ground biomass for litter fall. The user entered input values for canopy cover are assumed to represent the canopy that exists in the field regardless of what affects canopy cover. RUSLE2 converts those values to biomass, which like the canopy cover values are the live above ground biomass that exists regardless of how it came to be. RUSLE2's litter fall computations describe the disposition of live above ground biomass.

9.2.5. Operations that affect live vegetation

Operations that include **begin growth**, **kill vegetation**, **remove live biomass, and Process: Perennial biomass & current standing res removal** processes affect live above ground biomass. A **begin growth** process instructs RUSLE2 to begin using values from a new vegetation description. RUSLE2 assumes no relationship between live above ground biomass for the two vegetation descriptions although a relationship is assumed for live root biomass (see **Section 9.2.2**). The RUSLE2 assumption is that a decrease in live root biomass between the last day that a vegetation description is used to compute daily erosion and the live root biomass on day zero in the new vegetation description is biomass added to the existing dead root biomass pool. In contrast, no such connections are assumed for live above ground biomass. The RUSLE2 user explicitly use operations, such as **remove live biomass**, to describe the fate of live above ground biomass between vegetation descriptions when a begin growth process is executed. Within the period represented by a vegetation description, the RUSLE2 assumption is that a decrease in canopy cover represents a senescence period and the decrease in live above ground biomass during a senescence period is daily added to the surface residue biomass pool.

Consequently, RUSLE2 assumes that a new growth vegetation period begins on day zero for a new vegetation description when a begin growth process is executed. This assumption applies to transplanted crops and to vegetation that regrows after hay harvest or mowing where canopy and live above ground biomass are greater than zero on day zero in the vegetation description. Similarly, an operation that includes the **remove live biomass** process can leave live above ground biomass after the operation. RUSLE2 assumes that a new growth period begins immediately after the remove live biomass process is executed. The increase in live above ground biomass is assumed to be a composite of above ground plant components, including stems and leaves, during a new growth vegetation period in contrast to the increase in live above ground biomass being primarily leaves during the regrowth period that follows a senescence period.

A **kill vegetation** process transfers the entire live above ground biomass that exists on the day that the process is executed to the standing residue pool. The relation between standing residue biomass and canopy cover is given in **Section 9.2.3**.

9.2.6. Temporal standing live vegetation Manning's n

Standing vegetation contributes to total hydraulic resistance (see **Section 3.4**). The temporal contribution of standing live vegetation, not including live ground cover, to Manning's n is computed using:

$$n_v = n_{vmx}(h_f / h_{fmx})$$

where: n_v = daily Manning's n contributed by live standing vegetation not including live ground cover, n_{vmx} = maximum Manning's n contributed by live standing vegetation, not including live ground cover, during the period represented by the vegetation description, h_f = daily effective fall height, h_{fmx} = maximum effective fall height during the vegetation description, and i = subscript for day. Manning's n contributed by standing live vegetation is most affected by stems. Of the temporal input or computed variables used in a RUSLE2 vegetation description, Manning's n for standing live vegetation was assumed to be best related to effective fall height. The Manning's n contributed by live ground (surface) cover is consider in the relation of Manning's n to net ground (surface) cover (see **Section 3.4.6**)

Table 9.1. Coefficient a_H values used to multiply maximum effective vegetation ridge height on contour to obtain effective vegetation ridge height for effect of row spacing

Row width	Coefficient a_H
Vegetation on ridges	0.25
Wide row (≥ 30 inches)	0.50
Moderate row spacing (15 to 20 inches)	0.75
Narrow row spacing (7 to 10 inches)	1.00
Very narrow row spacing (≤5 inches)	0.50
No rows (broadcast)	0.00

Maximum Manning's n for live standing vegetation for a vegetation description is computed from the user input vegetation retardance at maximum canopy cover. Vegetation retardance is a function of vegetation stem density and orientation of vegetation strips (rows) to the overland flow path (see **Section 3.4.6**). The live vegetation Manning's n when vegetation strips (rows) are on the contour (i.e., perpendicular to the overland flow path) is computed using equation 3.54. A Manning's n value for live standing vegetation for vegetation in rows up and downhill (i.e., parallel to the overland flow path) is computed using values in Table 3.10. The live standing vegetation Manning's n for the actual orientation of vegetation rows to the overland flow path (i.e., row grade) is computed using equation 3.55.

9.2.7. Temporal effective vegetation ridge height

Densely spaced stems of vegetation rows on the contour affect rill-interrill erosion much like soil ridges (see **Section 7.1.3**). An effective live vegetation ridge height is added to the soil ridge height to obtain an effective total ridge height used to compute values for the contouring subfactor in equation 7.6. The effect of live standing vegetation rows on erosion depends on row spacing. If row spacing is zero (i.e., the vegetation is not in rows and the plant stems are randomly spaced over the entire soil surface), orientation of vegetation rows to the overland flow path and row spacing has no meaning or effect on

the contouring subfactor. The erosion reduction (i.e., contouring effect) for effective live standing vegetation ridge height increases as vegetation row spacing increases to a maximum at the narrow row width of approximately 8 inches). Erosion reduction by effective vegetation ridge height decreases as row spacing widens beyond the narrow row spacing. This effect is represented by the coefficient α_h values given in Table 9.1.

The maximum effective live standing vegetation ridge height for contour vegetation strips (rows) for a vegetation description is computed using:

$$H_{vmx} = 0.5 a_H R_v \quad if\,(R_v > 7) : R_v = 7 \qquad [9.10]$$

where: H_{vmx} = maximum effective live standing vegetation ridge height (inches) for the vegetation description when vegetation strips (rows) are on the contour, a_H = the coefficient that adjusts for row spacing (inches), and R_v = the retardance class at maximum canopy cover in the vegetation description (see **Section 9.3.1**).

Daily effective live standing vegetation ridge height H_v is computed using:

$$H_v = H_{vmx} (h_f / h_{fmx})^{0.3} \qquad [9.11]$$

Like Manning's n for live standing vegetation, of the temporal vegetation variables, effective live vegetation ridge height is assumed to be most related to effective fall height.

9.3. Adjust input values for vegetation production (yield) level

Input values in RUSLE2 vegetation descriptions are functions of vegetation production (yield) level, and each RUSLE2 vegetation description applies to a particular production (yield) level. RUSLE2 computes values in a vegetation description for a new production (yield) level by adjusting values in a base vegetation description. The maximum canopy cover in the base vegetation description must be less than 100 percent for RUSLE2 to make the proper mathematical computations. RUSLE2 can use a base vegetation description that has a maximum canopy cover of 100 percent to adjust for production (yield) levels greater than the production (yield) level for the base vegetation description, but RUSLE2 can not use a base vegetation description with a 100 percent maximum canopy cover to adjust to a lower production (yield) level.

Biomass values used in RUSLE2 computations are on a dry basis, but input values for vegetation production (yield) level are on a user defined basis. The user inputs information that RUSLE2 uses to convert production (yield) level value on the user defined basis to the dry basis needed for RUSLE2's computations (see RUSLE2 User's Reference Guide).

Multiple RUSLE2 vegetation descriptions can be used to compute erosion for a particular plant community over the period represented in the RUSLE2 computation (i.e., rotation duration). For example, vegetation descriptions are used to describe a multiple year alfalfa hay production system. The first vegetation description describes the alfalfa crop

from seeding to first hay harvest, the second vegetation description describes regrowth after each hay harvest in the first harvest year, the third vegetation description describes senescence and regrowth after senescence to the first hay harvest in the second harvest year, and so on. Input values such for live above ground biomass at maximum canopy apply to that particular vegetation description and not to the vegetation as a whole over the RUSLE2 computation period, such as the example alfalfa crop.

9.3.1. Live above ground biomass at maximum canopy cover

A major vegetation input is live above ground biomass at maximum canopy cover for a particular vegetation description. When multiple vegetation descriptions are used to represent a particular vegetation, the live above ground biomass entered for each vegetation description is for the maximum canopy cover in that particular vegetation description.

The RUSLE2 assumption is that live above ground biomass at maximum canopy varies linearly as a function of production (yield) level. That is:

$$B_{lamx} = a_y + b_y Y_d \qquad [9.12]$$

where: B_{lamx} = live above ground biomass (dry basis, mass/area) at maximum canopy cover for the vegetation description and Y_d = production (yield) level (dry basis, mass/area). The user provides inputs that RUSLE2 uses to convert production (yield) level in user units to biomass on a dry basis. These equations have the form:

$$Y_d = b_u Y_u \qquad [9.13]$$

where: Y_u = production level (yield) in user defined units and b_u = a conversion factor that RUSLE2 computes from user inputs. The values for the coefficients a_y and b_y in equation 9.12 are computed from user inputs for two live above ground biomass at maximum canopy cover-production (yield level) data points (see RUSLE2 User's Reference Guide).

9.3.2. Retardance at maximum canopy cover

Retardance for live vegetation at maximum canopy cover is computed from:

$$R_v = c_R + d_R Y_u \qquad [9.14]$$

where: R_v = retardance at maximum canopy cover for a vegetation description and Y_u = production (yield) level in user defined units for the vegetation description. The user enters two input data points for retardance-production (yield) level that RUSLE2 uses to determine values for the coefficients c_R and d_R in equation 9.14. RUSLE2 uses eight retardance classes that vary with the degree that vegetation grown in strips (rows) on the contour slows runoff (see Table 3.9). Equation 9.14 computes continuous values that are used in equation 3.54 to compute Manning's n values.

Vegetation descriptions are used to describe both live vegetation and porous barriers (fabric fences, gravel bag dams, and similar mechanical devices used on construction sites to trap and retain sediment on site) (see **Section 7.2** and RUSLE2 User's Reference Guide). The yield input for the vegetation description selected to describe these devices is used to represent the degree that the installed device retards runoff. The eighth retardance class is reserved for conditions that provide extremely high retardance such as stiff grass hedges, fabric (silt) fences and gravel bag dams. RUSLE2 computes backwater length caused by vegetation strips and flow retarding devices as a function of Manning's n, which are computed from the retardance class for the vegetation description (see **Section 3.4.4**). RUSLE2 assigns a minimum backwater length of 3 ft for the extremely high retardance class but uses the backwater length computed for the other retardance classes. RUSLE2 assumes a maximum backwater length of 15 ft for all vegetation/mechanical retarding strips.

9.3.3. Temporal input vegetation variables

Simple equations based on values computed by the EPIC model (Williams et al., 1989) are used in RUSLE2 to compute values for the temporal variables of root biomass, canopy cover, effective fall height, live ground cover, and consumptive water use.

9.3.3.1. Root biomass

Live root biomass values are assumed to vary linearly with live above ground biomass at maximum canopy cover. Live root biomass values for a new vegetation are computed as a function of production level (yield) using:

$$B_{rn(j)} = B_{rb(j)}(B_{lamxn} / B_{lamxb}) \qquad [9.15]$$

where: $B_{rn(j)}$ = root biomass value in the new vegetation description for the *jth* data point, $B_{rb(j)}$ = root biomass value for the *jth* data point in the base vegetation description, and B_{lamxb} = absolute maximum live above ground biomass in the base vegetation description. A value for the live above ground biomass at absolute maximum canopy B_{lamxn} in the new vegetation description is computed using equation 9.12 and the production (yield) level value for the new vegetation description.

9.3.3.2. Canopy cover

The equation used to adjust canopy cover values for production (yield) level is:

$$C_{n(j)} = C_{b(j)}(B_{lamxn} / B_{lamxb})^{0.5} \qquad [9.16]$$

where: $C_{n(j)}$ = canopy cover for *jth* data point the new vegetation description and $C_{b(j)}$ = the corresponding canopy cover value for the *jth* data point in the base vegetation description.

9.3.3.3. Effective fall height

The equation used to adjust effective fall height values for production (yield) level is:

$$h_{fn(j)} = h_{fb(j)}(B_{lamxn} / B_{lamxb})^{0.2} \quad [9.17]$$

where: $h_{fn(j)}$ = effective fall value for the *jth* data point in the new vegetation description and $h_{fb(j)}$ = corresponding effective fall height value for the *jth* data point in the base vegetation description.

9.3.3.4. Live ground cover

The equation used to adjust live ground cover values as a function of production (yield) level is:

$$f_{lgcn(j)} = f_{lgcb(j)}(B_{lamxn} / B_{lamxb})^{0.5} \quad [9.18]$$

where: $f_{lgcn(j)}$ = live ground cover value for the *jth* data point in the new vegetation description (percent) and $f_{lgcb(j)}$ = corresponding live ground cover value for the *jth* data point in the base vegetation description (percent).

9.3.3.5. Consumptive water use

Consumptive water use is used to compute how irrigation affects rill-interrill erosion by precipitation (see **Section 7.5**). Consumption water use is a function of production (yield) level. The equation used to adjust consumptive water use values as a function of production (yield) level is:

$$V_{wn(j)} = V_{wb(j)}(B_{lamxn} / B_{lamxb}) \quad [9.19]$$

where: $V_{wn(j)}$ = consumptive water use value for the *jth* data point in the new vegetation description and $V_{wb(j)}$ = corresponding values for consumptive water use value for the *jth* data point in the base vegetation description.

9.4. List of symbols

a_y = coefficient used to compute live above ground biomass at absolute maximum canopy cover for a vegetation description

a_H = coefficient used to computed effective vegetation ridge height from vegetation retardance (inches)

b_u = coefficient used to convert user defined yield units to dry mass

b_y = coefficient used to compute live above ground biomass at absolute maximum canopy cover for a vegetation description

B_l = daily live above ground biomass (dry basis) during a new growth period (mass/area)

B_{lamn} = live above ground biomass (dry basis) at first minimum canopy cover $C_{mn(1)}$ for a vegetation description (mass/area)

B_{lamx} = absolute maximum live above ground biomass (dry basis) at absolute maximum canopy cover for a vegetation description (mass/area)

$B_{lmn(k)}$ = live above ground biomass (dry basis) at *kth* local canopy cover minina in a vegetation description (mass/area)

$B_{lmx(k)}$ = live above ground biomass (dry basis) at *kth* local canopy cover maxima in a vegetation description (mass/area)

B_{lamxb} = live above ground biomass at absolute maximum canopy cover in base vegetation description (mass/area)

B_{lamxn} = live above ground biomass at absolute maximum canopy cover in new vegetation description (mass/area)

$B_{rb(j)}$ = root biomass value for the *jth* data point in the base vegetation description (mass/area in upper 4-inch depth)

$B_{rn(j)}$ = root biomass value for the *jth* data point in the new vegetation description (mass/area in upper 4-inch depth)

$B_{t,mn}$ = live above ground biomass (dry basis) at a local canopy cover minima (mass/area)

$B_{t,mx}$ = live above ground biomass (dry basis) at a local canopy cover maxima (mass/area)

c_f = coefficient for birth-death litter fall (day^{-1})

c_m = cooefficient fr litter fall caused by mechanical traffic (day^{-1})

c_R = coefficient used to compute retardance from user input yield

C = daily canopy cover (fraction)

C_{amx} = canopy cover at absolute maximum canopy cover for a vegetation description (fraction)

$C_{mn(k)}$ = canopy cover at the *kth* local canopy minima (fraction)

$C_{mx(k)}$ = canopy cover at the *kth* local canopy maxima (fraction)

$C_{b(j)}$ = canopy cover value for *jth* data point in base vegetation description (fraction)

$C_{n(j)}$ = canopy cover for *jth* data point in new vegetation description (fraction)

d_R = coefficient used to compute retardance from user input yield

$f_{lgcb(j)}$ = live ground cover value for *jth* data point in base vegetation description (percent)

$f_{lgcn(j)}$ = live ground cover value for *jth* data point in new vegetation description (pecent)

h_f = daily effective fall height (length)

$h_{fb(j)}$ = effective fall height value for the *jth* data point in the base vegetation description (length)

$h_{fn(j)}$ = effective fall value for *jth* data point in new vegetation description (length)

h_{fmx} = maximum effective fall height for a vegetation description (length)

H_v = daily effective live standing vegetation ridge height (inches)

H_{vmx} = maximum effective live standing vegetation ridge height for a vegetation description

L_f = daily litter fall during birth-death period (mass/area·day)

L_m = daily litter fall caused by mechanical traffic (mass/area·day)

M_r = cumulative root biomass (dry basis) above the depth y (mass/area)

n_v = daily Manning's n contributed by live standing vegetation not including live ground cover

n_{vmx} = maximum Manning's n contributed by live standing vegetation not including live ground cover for a vegetation description

R_v = vegetation retardance class at maximum canopy cover for a vegetation description

$V_{wb(j)}$ = corresponding values for consumptive water use value for *jth* data point in base vegetation description (inches)

$V_{wn(j)}$ = consumptive water use value for *jth* data point in the new vegetation description (inches)

y = normalized depth in soil from soil surface Y/15 inches

Y = depth in soil from soil surface (inches)

Y_d = production (yield) level (dry basis) (mass/area)

Y_u = production level (yield) in user defined units

15 = reference depth in inches for determining root mass distribution in soil

Indices

j – data point

k - refers to canopy cover maxima-canopy cover minima combination where canopy cover minima occur after a canopy cover maxima

10. RESIDUE AND DEAD ROOTS

10.1. Description of residue and dead roots

Residue and dead roots are materials lost by decomposition. RUSLE2 includes standing, surface, and buried residue pools that account for material produced when live above ground biomass is converted to standing residue (**Sections 6.1, 6.2, 6.5, and 9.2.5**). RUSLE2 accounts for the movement of residue mass between these pools by harvest, tillage, ripping, and other operations that affect vegetation, residue, and soil (see **Section 8.2**). The RUSLE2 surface residue pool also includes material such as mulch, manure, and erosion control blankets applied to the soil surface (see **Section 6.2**). The RUSLE2 buried residue pool includes material such as manure and bio-solids in sewage sludge that are injected or incorporated into the soil (see **Sections 6.3 and 6.5**).

Mass in the RUSLE2 dead root residue pool results from live root biomass associated with a vegetation description being transferred to the dead root biomass pool (see **Sections 6.5.6 and 9.2.2**).

The general RUSLE2 assumption is that residue and dead roots are organic materials that decompose. RUSLE2 also describes the effects of non-organic material such as erosion control blankets and rock placed on the soil surface or incorporated into the soil. However, special inputs are used to represent non-organic material (see **Section 10.2.5**).

Crop residue and plant litter are composed of diverse components including stems, leaves, seed pods, and chaff. Similarly, dead roots vary from very fine to coarse roots. A single residue description is used to represent a composite of these components for a particular vegetation description

10.2. Relation of portion of soil surface covered to surface residue mass

10.2.1. Size criteria for counting residue

To be counted as ground cover, soil surface material must remain in place, not be moved downslope by surface runoff during a rainstorm, and not be moved away by wind. The minimum size required to be counted as ground cover for RUSLE2 purposes must meet this criteria. **No single size should be used for all ground cover material in all situations**. For example, small pieces of residue will stay in place at the upper end of an overland flow path that would be moved at the lower end of a long overland flow path. Similarly, residue will be stable on a very flat overland flow path that would be moved on a steep overland flow path. Small residue pieces can be stable among a gradation of residue sizes but be unstable when the residue is uniformly composed of the small pieces. Small residue pieces that are stable at high residue surface covers may be unstable at low residue surface covers.

Equations that compute the hydraulic stability of mulch and crop residue were considered for RUSLE2 but were rejected because the equations were judged not to be sufficiently robust for RUSLE2 purposes (Foster et al., 1982a, 1982b).

Rock fragments on the soil surface require special consideration. The same stability considerations for other surface residue also apply to counting surface rock fragments as surface cover. Another factor is whether the rock fragments are a part of the soil matrix or simply "loose" rock on the soil surface that acts like surface cover. An approximate guideline is that rock fragments must be larger than 5 mm on coarse textured soils in arid and semi-arid regions where runoff is low and larger than 10 mm in other regions to be counted as ground cover.

10.2.2. Equation for computing residue cover from residue mass

RUSLE2 tracks surface residue (material in direct contact with the soil surface) on a dry mass basis (mass/area). However, the portion of the soil surface covered is the major variable used in equation 6.6 to compute how ground cover (surface residue) affects rill-interrill erosion. The RUSLE2 equation that computes portion of the soil surface covered by surface residue is:

$$f_g = 1 - \exp(-\alpha B_s) \qquad [10.1]$$

where: f_g = fraction of the soil surface covered by residue when no other residue type is present and B_s = surface residue mass (dry mass/area). RUSLE2 computes a value for the coefficient α using equation 10.1 rearranged and user entered values for the residue mass that provides 30, 60, or 90 percent soil cover.

A typical example of surface residue mass-cover data is illustrated in Figure 10.1. A common feature of these data is their high variability, which in turn greatly affects the variability in computed erosion estimates. For example, cover ranges from 0.70 to 1.0 percent in Figure 10.1 at a mass of 150 g/m^2. This range in cover gives ground cover subfactor values for g_c in equation 6.6 (**b** = 0.04 percent^{-1} and R_a = 0.24 inches) that range from 0.018 to 0.061. The portion of the soil surface covered ranges from 0.55 to 0.85 percent for a residue mass of 50 g/m^2, which gives values of 0.033 to 0.11 for g_c. In both cases, erosion

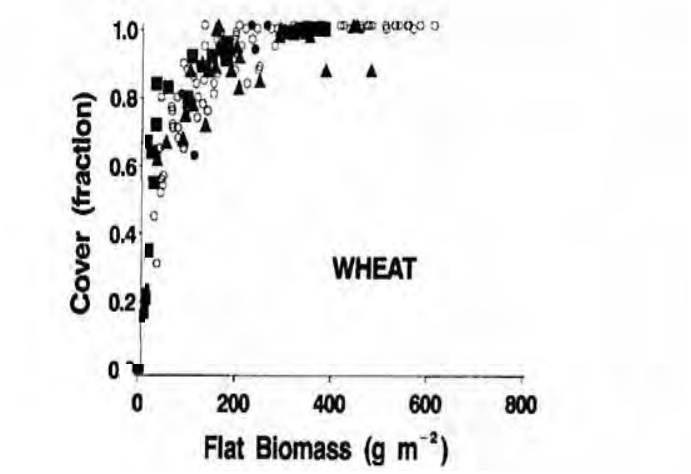

Figure 10.1. Measured data for relationship of residue cover to surface residue mass. (Source: Steiner et al., 2000).

can differ by a factor of 3 for a given surface residue mass. Therefore, even if RUSLE2 could estimate surface residue mass perfectly, RUSLE2's estimated portion of the soil surface covered, and its corresponding estimated erosion, could be significantly in error when compared to an individual measurement of soil surface cover.

Given this variability, the best that RUSLE2 can represent is differences in major residue types. Expecting RUSLE2 to accurately estimate percent residue cover at a particular location on a landscape at a particular point in time is unreasonable.

Data reported in the literature for residue cover as a function of residue mass vary greatly from study to study and even within a particular study as illustrated in Figure 10.1. The values used in the RUSLE2 Core Database were chosen as representative values for conservation and erosion control planning, realizing that numerous studies give values that differ from the RUSLE2 values. For example, surface cover ranged from about 65 percent to 100% for a flat wheat residue mass of about 1500 lbs/acre (168 g/m^2) in the Steiner et al. (2000) study, which is significantly greater than the 58 percent that the RUSLE2 Core Database values compute for the same residue mass. The RUSLE2 Core Database values for wheat straw are based on AH537 (Wischmeier and Smith, 1978) values, which were primarily derived from data reported by Mannering and Meyer (1963), Meyer and Mannering (1967) and Meyer et al. (1970).

The variation among some plant varieties is so great than different mass-cover relationships should be used for major variety types. For example, Stott (1995) noted that α values for corn varied from about 0.00023 to 0.00045 $(lbs/acre)^{-1}$ for corn residue based on her measurements and data reported in the literature. Stott recommended that the 0.00023 acre/lbs value (60 percent cover at 4000 lbs/acre flat corn residue mass) be used for corn grown after the mid 1980's and that the RUSLE2 Core Database value of 0.00038 $(lbs/acre)^{-1}$ (60 percent cover at 2400 lbs/acre corn residue mass) be used for corn grown before the mid 1980's. RUSLE2 satisfactorily estimates flat residue cover at planting for a wide range of soil and conservation tillage methods as Table 10.1 shows, with the recognition that the corn in these studies was grown before the mid 1980's.

Another example is that soybean varieties grown in the Midwest US differ from those grown in the Mid-South US. The RUSLE2 Core Database mass-cover value for soybeans varieties grown in the Midwestern US is that 600 lbs/acre of soybean residue gives 30 percent soil surface cover [AH703 (Renard et al., 1997)] while the mass-cover value for the variety of soybeans grown in the Mid-South US is that 1460 lbs/acre of soybean residue gives 30 percent soil surface cover (Mutchler and Greer, 1984).[67]

---

[67] K.C. McGregor. 1994. Mass-cover data for soybeans grown at Holly Springs, Mississippi. Personal communication. Scientist (retired) at the USDA-National Sedimentation Laboratory, Oxford, Mississippi.

Table 10.1. Measured and RUSLE2 estimated residue cover (percent) immediately after planting (Source: RUSLE2 User's Reference Guide)

Crop	Tillage system	Observed cover	Estimated cover	Reference
corn	spring disk	15	21	1
corn	fall chisel, spring disk	13	12	1
corn	spring disk, spring disk	27	18	2
corn	spring chisel, spring disk	22	11	2
corn	spring disk	15	21	2
corn	fall chisel, spring disk	13	12	2
soybeans	spring disk, spring disk	27	18	2
soybeans	spring chisel, spring disk	22	11	2
corn	spring disk	8	20	2
corn	spring disk, spring disk	5	7	2
corn	spring chisel, spring disk	7	3	2
corn	field cultivator	24	20	2
soybeans	spring disk, spring disk	11	8	2
soybeans	spring disk	15	22	2
soybeans	spring chisel, spring disk	11	4	2
corn	fall chisel, spring disk	33	26	3
corn	spring chisel, spring disk	19	19	4
corn	spring disk, spring disk	30	27	4
corn	fall chisel, spring disk, spring field cultivator	9	14	5
soybeans	fall chisel, spring field cultivator, spring field cultivator	9	5	5
corn	fall chisel, spring disk, spring field cultivator	16	14	6
soybeans	fall chisel, spring field cultivator, spring field cultivator	3	5	6
soybeans	spring disk, spring disk	9	7	7
soybeans	spring disk, spring disk	9	7	8
soybeans	spring disk	13	18	8

Table 10.1 (continued). Measured and RUSLE2 estimated residue cover (percent) immediately after planting			
References:			
1. Siemens and Oschwald (1976)			
2. Dickey et al. (1985)			
3. Lindstrom and Onstad (1984)			
4. Laflen et al. (1978)			
5. McIsacc et al. (1990)			
6. McIsaac et al. (1991)			
7. Shelton et al, (1986)			
8. Jasa et al. (1986)			

The RUSLE2 Core Database values for surface residue mass-cover relationships should be used for routine RUSLE2 applications. When RUSLE2 users wish to use values for residue mass-cover other than those in the RUSLE2 Core Database, users should review and analyze data from multiple sources because of the great variability in these data within a study as illustrated in Figure 10.1 and between studies. RUSLE2 was calibrated to measured erosion values using the values in the RUSLE2 Core Database. That is, RUSLE2 was calibrated to give expected erosion values. **Unexpected serious error in RUSLE2 computed erosion estimates can occur when input residues values are improperly changed from those in the RUSLE2 Core Database (see the RUSLE2 User's Reference Guide). If a change is made in residue input values, RUSLE2 computed erosion values with the new input values should be compared against erosion measured with the residue represented in the new input values.**

10.2.3. Reasons for variability in the surface residue mass-residue cover relationship

A major reason for the variability in the residue mass-residue cover relationship is that crop residue, plant litter, and similar materials are composed of multiple plant components (e.g., leaves, stems, seed pods, and chaff) and pieces that vary in composition, geometry, size, mass, and surface area covered per unit dry mass. RUSLE2 uses a single residue description to represent residue as a composite of multiple components. Consequently, α in equation 10.1 is a function of the relative mass of each residue component in the composite and varies temporally as the relative mass of each residue component varies temporally. For example, the α value for corn and soybean residue immediately after harvest differs significantly from the α value several months later because leaves cover more area than do stems per unit mass and leaves decompose much more rapidly than do the stems. In contrast to corn and soybeans, field measured data at Bushland, Texas showed that α values for barley, oats, spring wheat, and winter wheat did not vary from 24 to 400 days after harvest (Steiner et al., 2000). However, data variability, as in all studies of residue mass-residue cover, may have masked temporal changes in the residue mass-residue cover relationship.

The RUSLE2 assumption is that residue properties such as α in equation 10.1 are time invariant for the period represented by a residue description in a RUSLE2 computation. Consequently, equation 10.1 is a compromise and the values in the RUSLE2 Core Database used to compute α were chosen to compute erosion values appropriate for conservation and erosion control planning (see RUSLE2 User's Reference Guide). The input values that RUSLE2 uses to compute α values should be carefully selected to ensure that equation 10.1 gives the best erosion estimates for the time periods that have the greatest effect on average annual erosion. User entered values for a new residue description being added to a RUSLE2 database should be consistent with values in the RUSLE2 Core Database. Procedures described in the RUSLE2 User's Reference Guide must be followed.

In some cases, temporal changes in residue properties can be represented in RUSLE2 by using multiple residue descriptions during the RUSLE2 computation period. Using multiple residue descriptions requires using an operation that includes a **remove residue/cover process** to remove the existing material and another operation that includes an **add other cover process** that adds the removed material back to the soil surface using a new residue description. The computer mechanics of using RUSLE2 in this way are not convenient for routine conservation and erosion control planning. However, the procedure is mentioned to illustrate RUSLE2's capability for computing the effects of temporal variations of residue properties. Technical specialists for agencies using RUSLE2 in routine conservation planning can use this technique to evaluate the uncertainty in RUSLE2 erosion estimates resulting from the assumption that residue properties do not vary temporally (see RUSLE2 User's Reference Guide).

10.2.4. Overlap of residue

The user assigns a single residue description to each vegetation description and to each operation description in a cover-management description that adds material to the soil surface (see RUSLE2 User's Reference Guide). For example, a corn-soybeans crop rotation involves two residue descriptions, one for corn and one for soybeans. The mass for each residue description is tracked separately. A daily ground cover value is computed with equation 10.1 for each residue description. A net ground cover value is used in equation 6.6 to compute a value for the ground cover subfactor, not the sum of the ground cover values computed with equation 10.1 for each residue description when multiple residue descriptions are involved. RUSLE2 takes into account the overlap of residue applications to compute net ground cover. The RUSLE2 assumption is that the portion of material that overlaps underlying material has no effect on rill-interrill erosion. The computation of net ground cover is illustrated for crop residue or mulch applied to a soil surface with existing rock cover. The net ground cover for these two residue descriptions (e.g., crop residue or mulch and rock) is computed as:

$$f_{gn} = f_{gr} + f_{gm}(1 - f_{gr}) \qquad [10.2]$$

where: f_{gn} = net ground cover (fraction), f_{gr} = ground cover (fraction) computed with equation 10.1 provided by the rock surface residue cover assuming no other material is present, and f_{gm} = ground cover (fraction) computed with equation 10.1 for crop residue or mulch assuming no other material is present. Equations 10.1 and 10.2 are used repeatedly to account for each residue description used in a particular RUSLE2 computation to compute a net ground cover value. The overall net ground cover value is used in equations 6.6, 6.7, and related equations to compute the effect of surface residue cover on rill and interrill erosion. A ground cover subfactor g_c is not computed for each residue description.

10.2.5. Inputs for non-organic residue

In some cases, a material is applied to the soil surface that significantly affects erosion but has less effect on erosion when incorporated into the soil than routine plant residue. The mass values entered in the residue description for cover-mass data points can be scaled to be so small that the mass values used for the material when incorporated in the soil are so small that they have no effect on soil biomass subfactor values (see **Section 6.5**). Input values for mass of these materials applied to the soil must be accordingly scaled. The objective in these RUSLE2 applications is that RUSLE2 uses desired ground cover values to compute ground cover subfactor values using equation 6.6 but uses such small residue mass values that soil biomass factor values computed with equation 6.48 are hardly affected if the material is incorporated into the soil (see RUSLE2 User's Reference Guide**)**.

The importance of using recommended RUSLE2 inputs and following RUSLE2 procedures described in the RUSLE2 User's Reference Guide can not be over-emphasized, especially when making comparisons with the USLE, RUSLE1, and much of the historical data used to develop those models as well as RUSLE2. However, crop characteristics and yield, especially for corn, has changed greatly from the 20 bu/ac corn yield common in the 1930's data used to determine the AH282 and 537 soil loss ratio values, which were used to calibrate RUSLE2, to modern 200 bu/ac high production corn yields. The values in the RUSLE2 Core Database are considered adequate for evaluating modern crops and cropping practices, especially when RUSLE2 erosion computed values are being compared with values computed with the USLE or RUSLE1.

Consideration should be given to changing input values to represent modern crops and cropping practices in certain RUSLE2 applications. In doing so, the procedures described in the RUSLE2 User's Reference Guide should be carefully followed, and input values must be based on multiple data sources, not a single source. RUSLE2 was calibrated to compute expected erosion rates as a function of the principal variables affecting erosion. Therefore, RUSLE2's computation of what appears to be an erroneous cover value does not necessarily mean that RUSLE2's computed erosion values are erroneous.

Improper inputs without consideration of RUSLE2's calibration can result in very serious errors in RUSLE2 computed erosion values.

10.3. Decomposition of residue and dead roots

10.3.1. Description of equations

Both residue and dead roots are assumed to be lost over time as a result of decomposition and other processes related to precipitation and temperature. The basic RUSLE1 decomposition equations are used in RUSLE2 [AH703 (Renard et al., 1997); Yoder et al., 1997; Stott et al., 1990; Stott et al., 1995], which are a simplification of the decomposition equations used in the erosion prediction model WEPP (Laflen et al., 1991b; Flanagan and Nearing, 1995).[68] The main decomposition equation is:

$$B = B_p \exp(-\beta D) \qquad [10.3]$$

where: B = the mass in a particular residue/dead root pool after decomposition B_p= the mass in the pool on the previous day, and D = the number of days in the period over

[68] Also, see references listed in the **Decomposition Subsection** of the **References Section**.

which decomposition is being computed, which is a single day in RUSLE2 (i.e., D = 1 day). A daily value for the coefficient β is computed from:

$$\beta = \phi[\min(W_f, T_f)] \qquad [10.4]$$

where: ϕ = a decomposition coefficient (day^{-1}) that is a function of biomass type, W_f = a moisture function, and T_f = a temperature function. Equation 10.4 is based on the assumption that decomposition on a particular day is limited by either moisture or temperature on that date.

Moisture must be present for decomposition to occur. Daily precipitation is used in RUSLE2 as an indicator of moisture available for decomposition. RUSLE2 does not compute moisture in residue/dead root pieces or in the soil that contacts residue/dead roots. Decomposition rate decreases if moisture decreases below the moisture content for optimum decomposition. RUSLE2 does not take into account reduced decomposition at excessively high moisture contents. Daily values for the moisture function W_f are computed from:

$$W_f = (P + I)/P_b \;\; if[(P + I)/P_b > 1] : W_f = 1 \qquad [10.5]$$

where: P = daily precipitation (inches), I = daily amount (inches) of water added by irrigation, and P_b = base daily precipitation (inches) at which optimum decomposition occurs. A value of 0.173 inch (4.4 mm) was determined by fitting the RUSLE2 decomposition equations to the field data identified in Table 10.2.

Decomposition also varies with temperature. Decomposition decreases as temperature decreases below 32 ^{o}C, the optimum temperature at which decomposition rate is maximum. Similarly, decomposition decreases as temperature increases above 32 ^{o}C. Daily values for the temperature function are computed from:

$$T_f = \frac{2(T + A)^2 (T_o + A)^2 - (T + A)^4}{(T_o + A)^4} \;\; if(T < -10) : T_f = 0 \qquad [10.6]$$

where: T = daily air temperature (^{o}C), T_o = the optimum temperature (^{o}C) for decomposition (32 ^{o}C), and A = 8 ^{o}C. The value for A was set so that when air temperature becomes less than – 10 ^{o}C, the temperature function is set to zero.[69] The reason that the temperature function does not become zero at a higher temperature, such as near 0 ^{o}C, is that temperature varies between a minimum and maximum during the day and average temperature on a given day varies about the long-term average temperature for that day. Air temperature rather than soil temperature is used in the temperature

[69] An adjustment should have been made to equation 10.6 to flatten the top of the curve around the 32 ^{o}C temperature for maximum decomposition to account for within day and year-to-year variation in temperature about the average daily temperature used in RUSLE2. See Schomberg et al. (2002).

function because soil temperature data are not readily available for use in RUSLE2. Like precipitation, air temperature is an indicator variable rather than the actual temperature that the decomposing material experiences. Values for the RUSLE2 decomposition coefficient ϕ differ from values for decomposition coefficient in similar equations used in other erosion prediction models such as WEPP (Stott et al., 1995), WEPS (Steiner et al., 1995), and RWEQ (Schomberg and Steiner, 1997).

The RUSLE2 composition coefficient ϕ can be expressed in terms of residue half life, which is defined as the time required for half of the residue mass to decompose at optimum temperature and moisture (i.e., $W_f = 1$ and $T_f = 1$). The relation of residue half life $D_{1/2}$ to the decomposition coefficient ϕ is given by:

$$D_{1/2} = -\ln(0.5)/\phi \qquad [10.7]$$

where: $D_{1/2}$ = residue half life (days) and ln(0.5) = 0.693.

The same decomposition coefficient ϕ values and moisture (W_f) and temperature (T_f) functions are used in RUSLE2 for buried and surface residue and dead roots (see **Section 10.3.3** for discussion of the reasons for this decision). Also, RUSLE2 decomposition coefficient ϕ values and the W_f and T_f functions are assumed not to vary with depth in the soil, soil texture, soil management, or residue mass. The same W_f and T_f functions are used to estimate decomposition of standing residue, but the RUSLE2 decomposition coefficient ϕ value for standing residue is 0.3 of that for surface and buried residue because moisture available for decomposition of standing residue is assumed to be much less than moisture available for decomposition of surface and buried residue (Douglas et al., 1980; Ghidey and Alberts, 1993; Steiner et al., 1994) (see **Section 10.3.3** for discussion of the reasons for this decision).

10.3.2. Calibration of equations

Values for the daily base precipitation P_b in equation 10.5 and values for the decomposition coefficient ϕ were determined by fitting the decomposition equations to measured data. Resulting P_b and ϕ values are given in Table 10.2.

The decomposition equations were fitted to the field data using daily average precipitation and temperature values disaggregated (see **Section 3.1**) from long term average monthly precipitation and temperature rather than actual precipitation and temperature values. Using long term-averages in these computations had a smoothing effect. Also, RUSLE2 uses average daily precipitation regardless of whether precipitation actually occurs, and thus values determined for P_b and ϕ are a function of RUSLE2's mathematical structure. Furthermore, the RUSLE2 purpose is to

Table 10.2. Values for P_b and Φ determined by fitting decomposition equations to measured data

Location	Crop	Daily precipition above which W_f = 1 P_b (mm)	Decomposition coefficient Φ (day^{-1})	Placement	Reference
Columbia, MO	corn	4.4 assumed	0.016	buried, in bags	(1)
Columbia, MO	corn	4.4 assumed	0.010	surface, in bags	(1)
Columbia, MO	corn	4.4 assumed	0.010	buried, in bags	(2)
W. Lafayette, IN	corn, conventional till	4.4 assumed	0.016	surface, determined from surface samples removed from plots, not in bags	(3)
W. Lafayette, IN	corn, no-till	4.4 assumed	0.016	same	(3)
Treynor, IA	corn, till plant	4.4 assumed	0.011	same	(4)
Bushland, Tx	corn	4.4 assumed	0.006	surface, in bags	(5)
Columbia, MO	soybeans	3.6	0.029	buried, in bags	(2)
W. Lafayette, IN	soybeans	4.4 assumed	0.025	surface, determined from surface samples removed from plots, not in bags	(3)
W. Lafayette, IN	soybeans	4.4 assumed	0.025	same	(3)
Griffin, GA	soybeans	4.4 assumed	0.025	same	(5)
Holly Springs, MS	soybeans	10.0	0.015	estimated from measured portion of soil surface covered and mass-cover equations	(6)
Holly Springs, MS	soybeans	2.7	0.013	same	(6)

Table 10.2. Values for P_b and Φ determined by fitting decomposition equations to measured data (continued)

Location	Crop	Daily precipition above which W_f = 1 P_b (mm)	Decomposition coefficient Φ (day^{-1})	Placement	Reference
W. Lafayette, IN	wheat	4.2	0.0064	surface, determined from surface samples removed from plots, not in bags	(7)
W. Lafayette, IN	wheat	4.4	0.008	same	(7)
Bushland, TX	wheat	3.7	0.0081	same	(7)
Bushland, TX	wheat	4.4	0.008	same	(7)
Griffin, GA	wheat	4.4 assumed	0.008	same	(5)
Twin Falls, ID	wheat	1.8	0.012	buried, in bags	(8)
Twin Falls, ID	wheat	4.4 assumed	0.021	same	(8)
Pullman, WA	wheat	0.5	0.0099	surface, determined from surface samples removed from plots, not in bags	(7)
Pullman, WA	wheat	0.5	0.0098	same	(7)
Pullman, WA	wheat	0.5	0.0097	same	(7)
Pullman, WA	wheat	4.4 assumed	0.019	same	(7)
Pullman, WA	wheat	4.4 assumed	0.019	same	(7)
Pullman, WA	wheat	4.4 assumed	0.019	same	(7)
Holly Springs, MS	cotton	4.4 assumed	0.015	estimated from measured portion of soil surface covered and mass-cover equations	(9)
Holly Springs, MS	cotton	10.0	0.029	same	(10)
Holly Springs, MS	cotton	3.0	0.010	same	(10)
Holly Springs, MS	cotton	2.7	0.026	same	(10)
Holly Springs, MS	cotton	6.3	0.011	same	(10)
Holly Springs, MS	cotton	5.4	0.017	same	(10)
Holly Springs, MS	cotton	6.6	0.03	same	(10)
Holly Springs, MS	cotton	5.0	0.012	same	(10)

Table 10.2. Values for P_b and Φ determined by fitting decomposition equations to measured data (continued)

Location	Crop	Daily precipition above which W_f = 1 P_b (mm)	Decomposition coefficient Φ (day^{-1})	Placement	Reference
Bushland, TX	grain sorghum	4.4 mm assumed	0.007	surface, in bags	(11)
Griffin, GA	alfalfa	4.4 mm assumed	0.015	surface, determined from surface samples removed from plots, not in bags	(5)
Melfort, SK	alfalfa	4.4 mm assumed	0.015	same	(12)
Akron, CO	blue stem hay	4.4 mm assumed	0.015	surface, in bags	(13)
Akron, CO	blue stem hay	4.4 mm assumed	0.015	buried, in bags	(13)
SW Australia	Eucalypt litter	4.4 mm assumed	0.002	surface, determined from samples	(14)

References:
(1) Parker (1962)
(2) Broder and Wagner (1988)
(3) Stott (1995)
(4) Alberts and Schrader (1980)
(5) Schomberg and Steiner (1997)
(6) Mutchler and Greer (1984)
(7) Stott et al. (1990)
(8) Smith and Peckenpaugh (1986)
(9) Mutchler et al. (1985)
(10) Mutchler, personal communiction
(11) Schomberg et al. (1994)
(12) Schomberg et al. (1996)
(13) Hunt (1977)
(14) Birk and Simpson (1980)

capture the main differences in decomposition between locations rather than to precisely compute decomposition as a function of soil and cover-management. Furthermore, empirical data available to calibrate RUSLE2's decomposition equations were not sufficient to empirically determine coefficient values that are functions of soil and cover-management.

The RUSLE2 decomposition equations should be calibrated with several years of data at a location for a particular residue type and placement so that the data represent the expected range of climatic conditions at that site over a 10 to 30 year period. Unfortunately, most residue decomposition studies involve only a single year. Even when only single years of data were available, the RUSLE2 average daily precipitation and temperature values were used to calibrate the RUSLE2 decomposition equations.

Data sets were assembled from as many locations for each residue type as were available. Field residue mass-area and decomposition data are highly variable. Multiple sets of data

for the same residue type were used as much as possible. The RUSLE2 decomposition equations were fitted to averages of these data by residue type and location.

Calibration of the RUSLE2 decomposition equations involved fitting them to field data to determine values for the base precipitation P_b and the decomposition coefficient ϕ. The first step in the fitting was to allow both P_b and ϕ to vary. The results for some of those fittings are shown in Table 10.2 for the P_b entries other than "4.4 assumed." A consideration was whether both P_b and ϕ varied by residue type and location. Based on an inspection of the fitted P_b and ϕ values, the conclusion was that a constant value of 4.4 mm (0.173 inches) could be used for P_b for the entire US except in the Palouse region (Req region, see **Section 3.2.5**) in the Northwestern US.

The use of a constant P_b = 4.4 mm value also was evaluated qualitatively by making computations for numerous locations across the US for several residue types. The 4.4 mm value worked well everywhere except for the Req region where a 0.5 mm value worked better. As Table 10.2 shows for the Pullman, WA location, use of the 0.5 mm P_b value gave ϕ values of 0.01 day^{-1} for wheat residue that are comparable to 0.008 day^{-1} values determined in other parts of the country. The reason for the low P_b values in the Req region is that the soil is highly saturated during the winter months when almost all of the erosion occurs and moisture does not limit decomposition even though daily precipitation is not high. If the 4.4 mm P_b value is used in the Req region, the ϕ value for wheat is 0.017 day^{-1} rather than the 0.008 day^{-1} for other parts of the US (see **Section 10.3.3.9**).

Table 10.3. Recommended values for the decomposition coefficient Φ in RUSLE2 with A = 8 °C and P_b = 4.4 mm (0.173 inches) based on fitting decomposition equations to measured data.

Crop	Decomposition Coefficient Φ (day^{-1})
Alfalfa	0.015
Blue stem hay	0.012
Corn	0.016
Cotton	0.015
Sorghum	0.016
Soybeans (Midwest US)	0.025
Soybeans (Mid South US)	0.015
Wheat in Eastern US (soft white wheat)	0.008
Wheat in Northwest Wheat and Range Region (NWRR) (hard red wheat)	0.017

Note: If P_b = 0.5 mm, then Φ = 0.01 day^{-1} for NWRR wheat

Once the P_b value was set at 4.4 mm, the calibration was repeated where values of ϕ were determined by fitting the decomposition equations to the field data. Table 10.2 entries for the "4.4 assumed" value for P_b are where the decomposition equations were fitted to the data with the P_b value fixed at 4.4 mm. The fitted values for ϕ were inspected and the ϕ values chosen for the RUSLE Core Database are shown in Table 10.3. Figure 10.2 shows how well RUSLE2 decomposition equations fit field data using the 4.4 mm P_b value and Table 10.2 ϕ values for surface residue. Decomposition of buried residue is discussed in **Section 10.3.3.3**.

The ϕ value for the Eucalypt litter was determined using a different calibration approach from the one used to determine the ϕ values shown in Table 10.2.

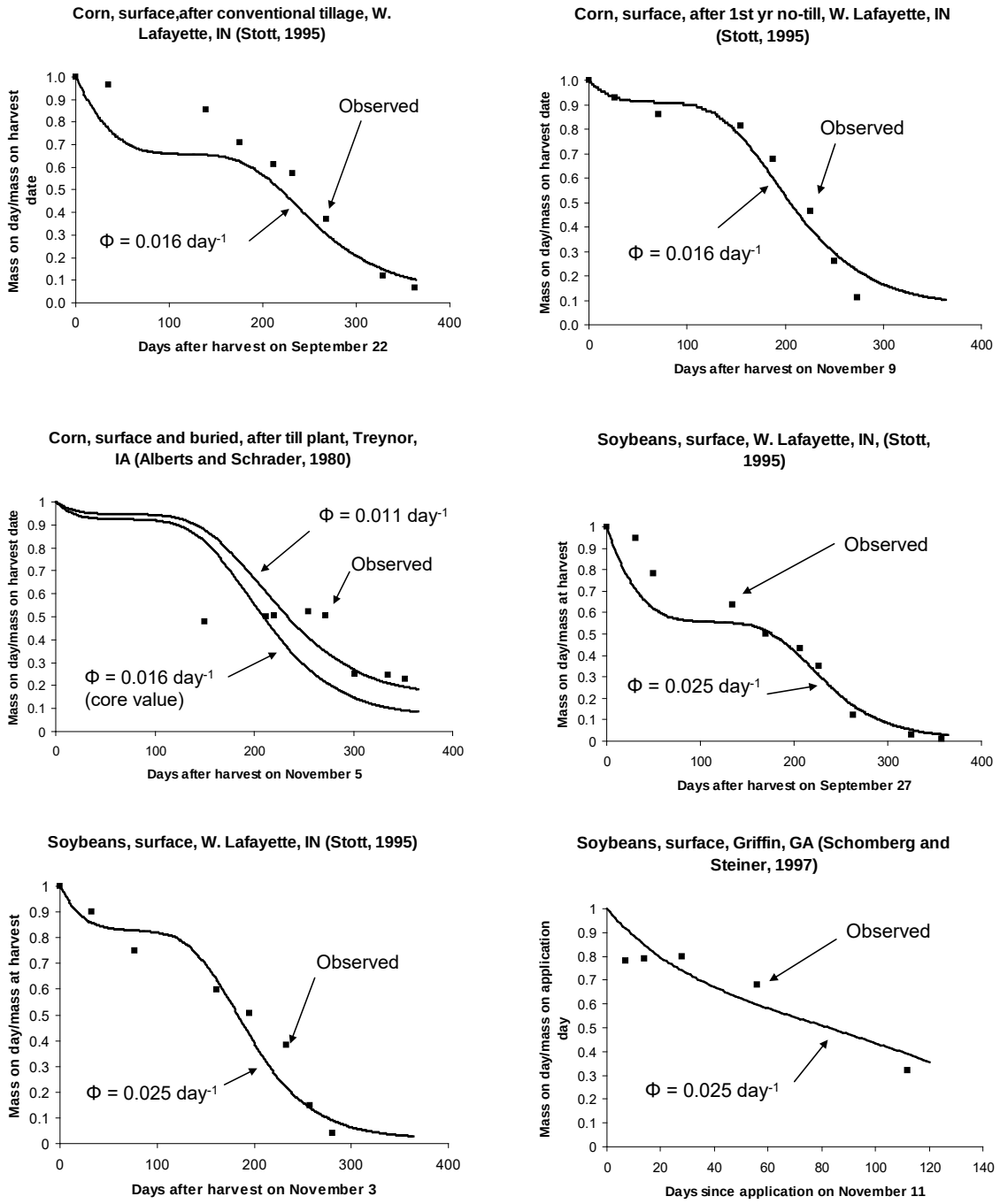

Figure 10.2. Comparison of RUSLE2 decomposition estimates using RUSLE2 Core Database values in comparison with field data.

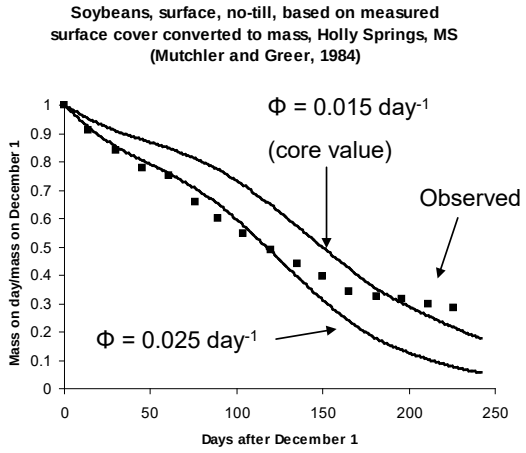

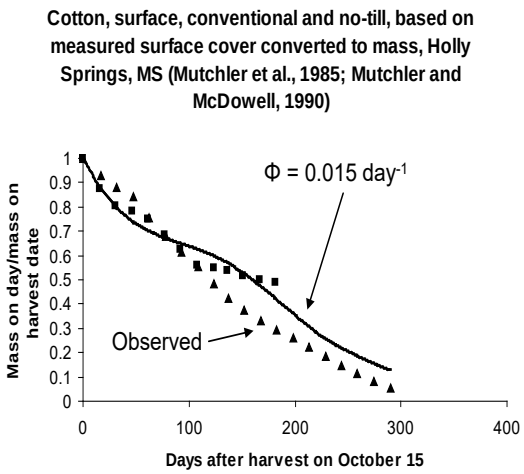

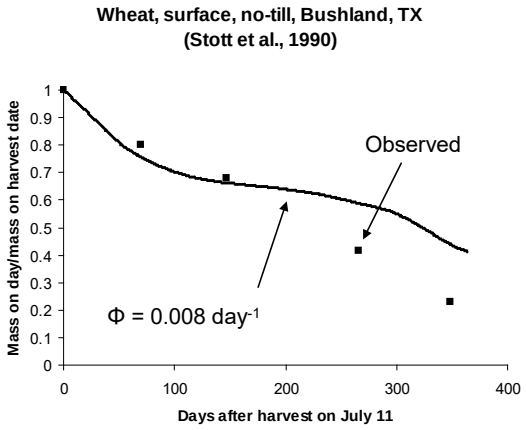

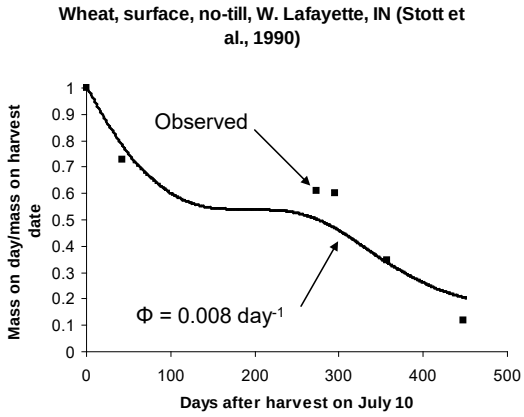

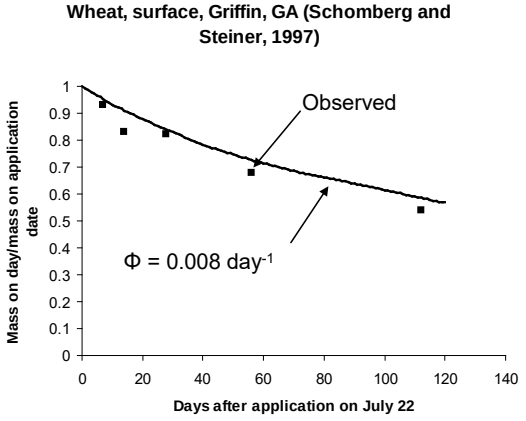

Figure 10.2. Comparison of RUSLE2 decomposition estimates using RUSLE2 Core Database values in comparison with field data. (continued)

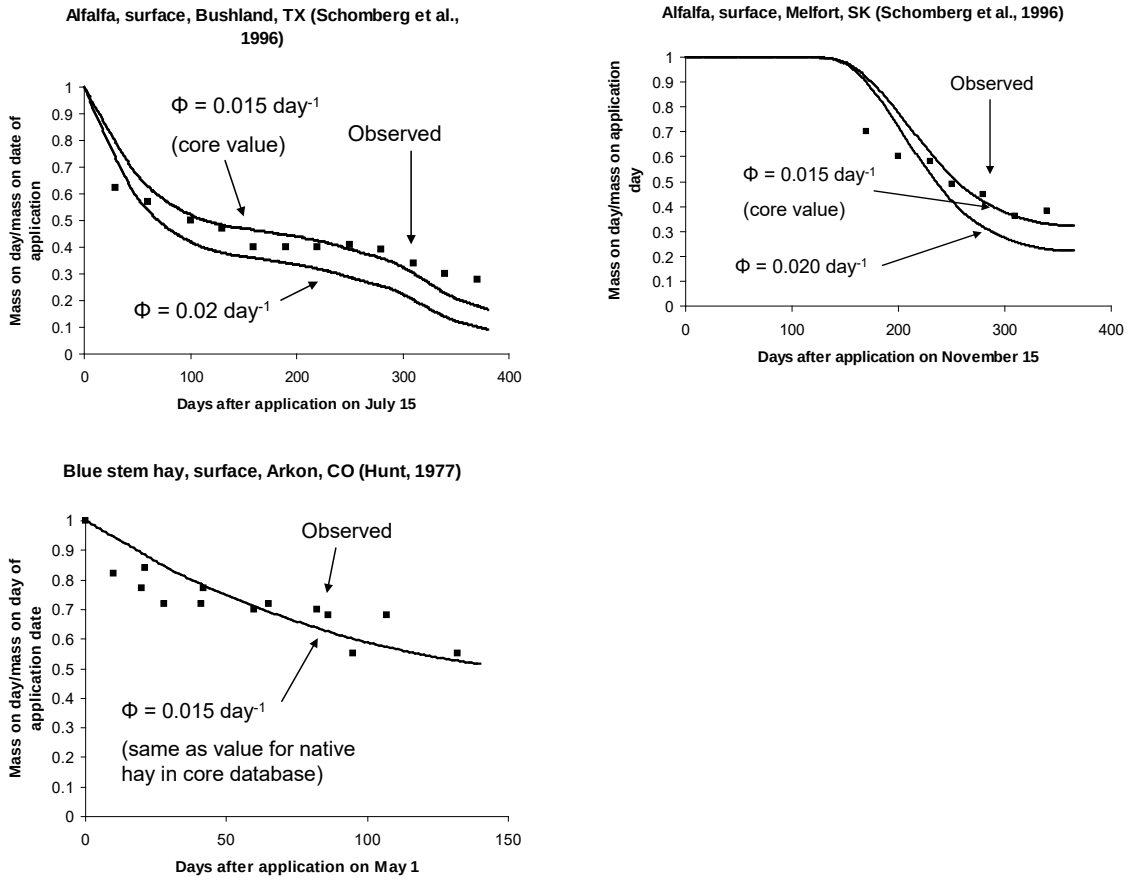

Figure 10.2. Comparison of RUSLE2 decomposition estimates using RUSLE2 Core Database values in comparison with field data. (continued)

Rather than fitting the RUSLE2 decomposition equations to the loss of residue mass over time, a ϕ value was determined for the Eucalypt litter by fitting RUSLE2 decomposition equations to an increasing residue mass over time until the mass reached a stable maximum. The Eucalypt litter data shown in Figure 10.3 are for surface residue (litter) accumulation following a forest fire in the Southwestern Australian Eucalypt forest (Birk and Simpson, 1980). This application illustrates RUSLE2's capability for computing both the accumulation of a surface litter layer where the biomass input is produced by aboveground senescence and the accumulation of a similar below ground biomass pool produced by root growth and death (root senescence, turnover).

An inspection of Figure 10.2 shows that RUSLE2 captures well the effect of location and material type on residue decomposition over time. A constant P_b value over almost all of the US works surprisingly well. Also, assuming the same ϕ value for a residue type works well for locations where climate differs greatly. For example, compare the results for alfalfa at both Griffin, Georgia and Melfort, Saskatchewan.

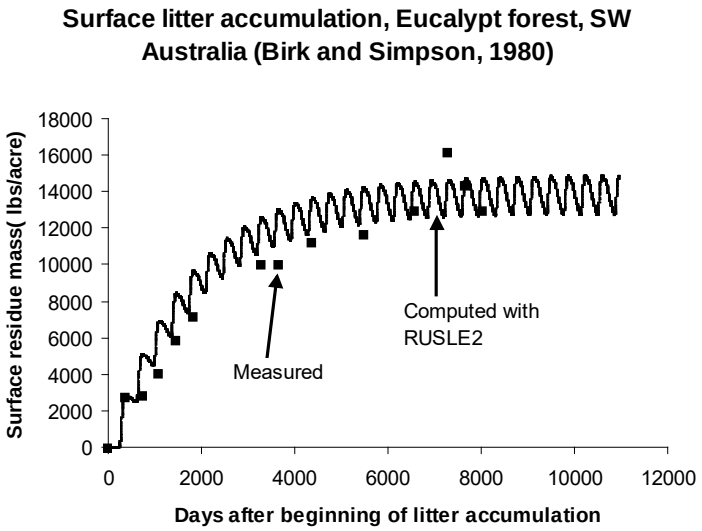

Figure 10.3. Computing the accumulation of a litter layer for an Eucalypt forest in Southwestern Australia.

An expectation is that RUSLE2 database developers can use values in the RUSLE2 Core Database to guide assignment of decomposition coefficient ϕ values for other residue types based on a comparison of residue characteristics. This procedure works but it requires more thought that initially expected. For example, a ϕ value of 0.02 day^{-1} was originally assigned for alfalfa before the ϕ value of 0.015 day^{-1} illustrated in Figure 10.2 was obtained by fitting measured field data. A ϕ value of 0.012 day^{-1} was assigned for native hay before the same ϕ value was determined by fitting measured data for the blue stem hay illustrated in Figure 10.2. The procedure of using values in the RUSLE2 Core Database as a guide in selecting decomposition coefficient values for other residue types will give reasonable RUSLE2 results for erosion control planning provided a careful comparison is made between residue types. The role of stems seems to be a major factor to consider in selecting ϕ values.

10.3.3. Basis for RUSLE2 decomposition decisions

RUSLE2's computation of residue loss is based on decomposition principles even though residue loss occurs by other processes besides decomposition. RUSLE2 is calibrated to field data representative of actual conditions as much as possible. RUSLE2 computations of residue and soil biomass loss are consistent with RUSLE2's purpose to be a **guide** to erosion control planning. Many decisions involved judgment during the formulation and calibration of RUSLE2's residue loss (decomposition) equations. This section describes the basis for those decisions.

10.3.3.1. User expectations

RUSLE2 computes residue decomposition and portion of the soil surface covered essentially using RUSLE1 procedures. Based on the RUSLE1 experience, some users will scrutinize RUSLE2's computed values for ground (surface, flat) residue cover more closely than RUSLE2's computed erosion values. RUSLE2 users are well aware of the importance of ground cover for controlling erosion. RUSLE2 users can not visually estimate erosion rates but they can visually measure ground (surface) cover. If RUSLE2's computed ground cover values do not meet their expectations, they assume

that RUSLE2's erosion computations must also be wrong, which is often a false assumption.

Surface residue cover is a major variable used in judging the adequacy of cropland erosion control measures. USDA-Natural Resources Conservation Service (NRCS) standards and specifications for certain conservation practices require a minimum surface residue cover at planting (e.g., 30 percent). The RUSLE2 decomposition procedures were carefully constructed to ensure that RUSLE2 computes appropriate surface residue cover values for conservation planning, as demonstrated by the values shown in Table 10.1. The RUSLE2 decomposition procedures were designed specifically for RUSLE2's use as a conservation planning tool, not for residue management and certainly not to advance residue decomposition science and modeling. The RUSLE2 intent is to capture main differences in loss of residue/dead roots between material types and locations in the context of estimating average annual erosion rates for comparison against a criteria such as the USDA-NRCS soil loss tolerance (T) values (Toy et al., 2002).

While RUSLE2 users can easily measure residue cover, which they can compare with RUSLE2 computed values, they must exercise great caution in their measurements and evaluations of RUSLE2's adequacy for computing residue cover and corresponding erosion estimates. Residue mass-cover data are highly variable as illustrated in Figure 10.1. The cotton data in Table 10.2 illustrates the variability in decomposition data among multiple data sets collected under near identical conditions for the same residue type. Making a few field measurements is not the proper way to evaluate RUSLE2's computed residue cover values. The RUSLE2 User's Reference Guide provides information on how to adjust RUSLE2 inputs to obtain particular RUSLE2 computed residue cover values.

10.3.3.2. Residue sampling method

RUSLE2's computation of residue loss is based on dry mass, which requires field measurements of residue mass over time are needed to calibrate RUSLE2. The mesh bag and the "grab" sample are the two techniques used most often to determine surface residue mass in decomposition experiments. The mesh bag method involves inserting residue in a mesh bag and placing the bag on the soil surface or in the soil. The grab sample method involves removing amd unconfined residue from a sample area. Each method has significant drawbacks (Dabney, 2005).

The residue loss measured by the mesh bag method is a function of mesh size (Dabney, 2005). The mesh bag method tends to underestimate residue loss. The residue loss determined using the common 1 mm mesh bags has to be multiplied by a factor that ranges from 1 to greater than 2 to represent the loss of unconfined residue.

Conversely, the grab sample method tends to overestimate residue loss and has its own shortcomings including the difficulty of removing soil particles attached to the residue. Another difficulty is retrieving the entire residue from the sample area because fragile residue pieces can be broken and not recovered.

The difference in measured residue loss by sampling methods is very significant as illustrated in Figure 10.4. Using the RUSLE2 Core Database values, RUSLE2 computes that a 150 bu/acre corn crop produces 8200 lb/acre of residue. The corn residue mass remaining after 12 months at Bushland, Texas measured by the bag method would be 4100 lbs/acre (Schomberg et al., 1995, 1997) (see Figure 10.4). The percent soil surface cover provided by this residue mass is 79 percent and the ground cover subfactor value computed with equation 6.6 is 0.042.

The RUSLE2 decomposition equations were fitted to corn residue loss at W. Lafayette, Indiana measured using the grab sample method (Stott, 1995). The RUSLE2 computed value for residue mass remaining after 12 months using climate data for Bushland, Texas is 1480 lbs/acre. The percent soil surface cover provided by this residue mass is 43 percent and the ground cover subfactor value is 0.18, which is four times the value based on mesh bag measurements. Consequently, RUSLE2 computes greatly different erosion estimates depending on which set of data is used to calibrate RUSLE2's residue loss (decomposition) equations.

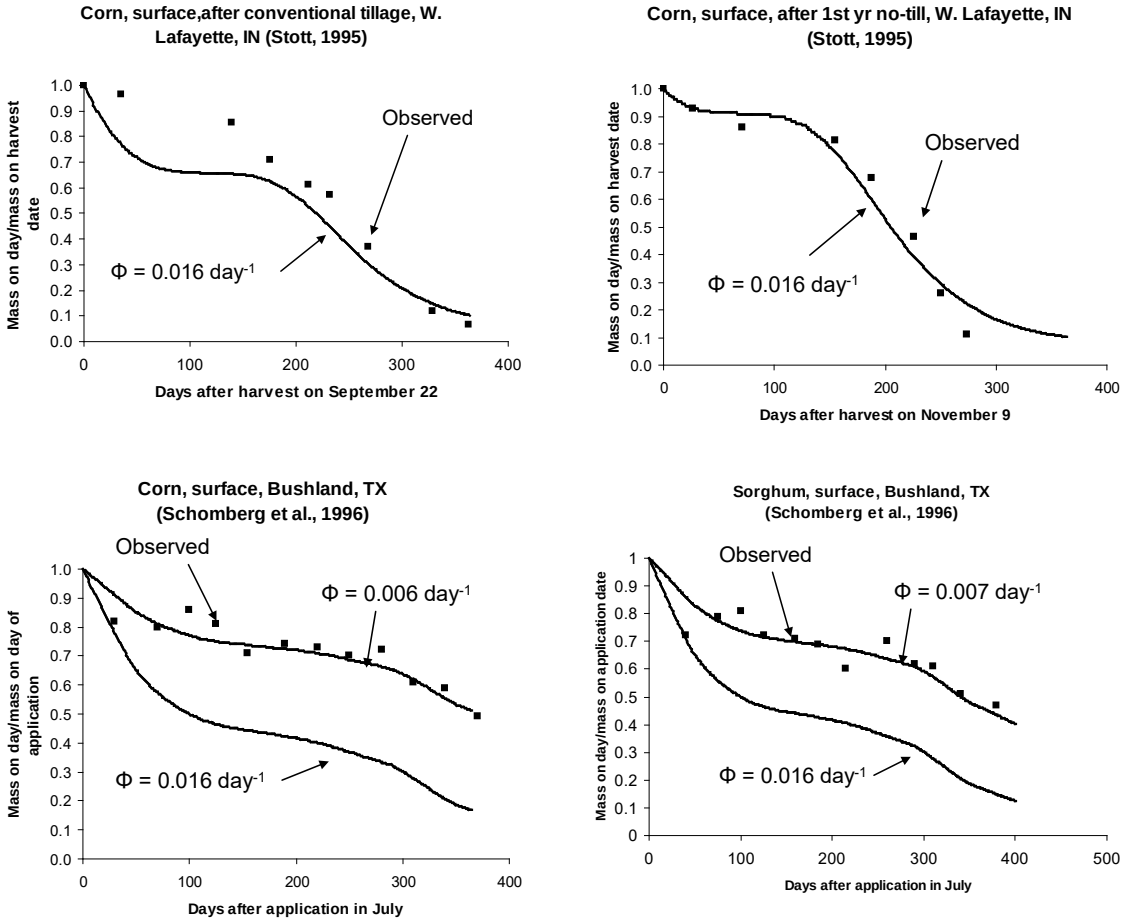

Figure 10.4. Comparison of observed and RUSLE2 computed decomposition of corn residue at W. Lafayette, Indiana and corn and sorghum residue at Bushland, Texas.

The difference in the measured Bushland, Texas data for corn and the RUSLE2 computed values based on a calibration to corn data measured at W. Lafayette, Indiana is not attributable to the RUSLE decomposition equations not performing equally well at the two locations. When wheat straw decomposition was measured by grab sampling from the soil surface (Stott et al., 1990; Stott, 1995; Stenier et al., 1999), measured decomposition at Bushland, Texas was consistent with data collected at W. Lafayette, Indiana and the RUSLE2 decomposition equations performed equally well at both locations (see Figure 10.2).

The difference in measured residue loss between the mesh bag and the grab sampling method is too large too ignore, which required a choice of one sampling method over the other. The grab sampling method was chosen for the development of RUSLE2. The conditions represented by this method, including the loss of residue by wind and other processes besides decomposition, better represent actual field conditions than does the mesh bag method. The differences between the two sampling methods seemed to be greatest for corn and wheat and much less for soybeans and forage crops. Decomposition coefficient ϕ values were determined for corn and wheat from the grab sample method while decomposition coefficient values were determined for forage crops from the mesh bag method.

Surface residue cover data were used to determine decomposition coefficient ϕ values for cotton and soybeans at Holly Springs, Mississippi. These data are field measured values for ground cover, which are the values most important in computing the effect of surface residue on rill-interrill erosion. These field data were considered to be superior to residue loss data measured with the mesh bag method.

The RUSLE2 decomposition coefficient ϕ value determined for corn is assumed to apply to grain sorghum based on the similarity in decomposition of corn and sorghum residue measured at Bushland, Texas by the mesh bag method. While the absolute decomposition values determined by the mesh bag method are not considered acceptable for RUSLE2 use, the mesh bag method is useful for determining relative differences in decomposition among residue types.

Other experimental procedures besides use of the mesh bag can affect decomposition results. The Ghidey and Alberts (1993) dataset includes decomposition values for roots and buried, surface, and above surface residue. Their data differ significantly from data considered best for RUSLE2 as illustrated in Figure 10.5. Oven drying the residue at 65 ^{o}C for 24 hours before placing the residue in the field may have contributed to the differences illustrated in Figure 10.5 in addition to mesh bags being used to measure residue loss.

10.3.3.3. Residue placement

RUSLE2 considers three placements of residue: (1) standing above ground, (2) soil surface, and (3) buried in the soil.

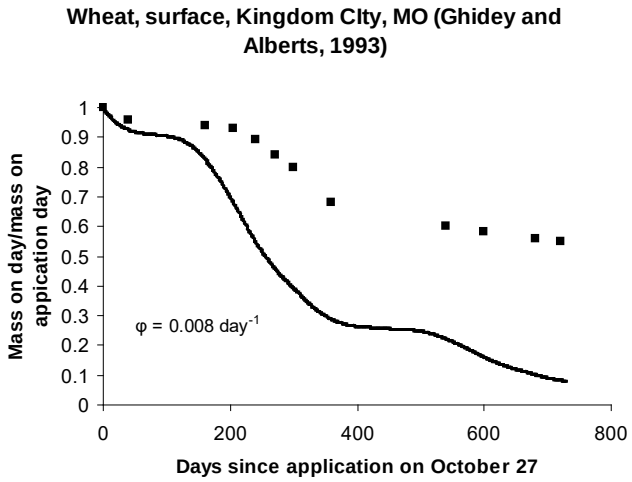

Figure 10.5. Difference in decomposition between that measured by Ghidey and Alberts (1993) and other data considered better for RUSLE2.

The RUSLE2 decomposition coefficient ϕ value used for above ground biomass is 0.3 times the ϕ value used for surface and buried residue. The decomposition coefficient ϕ value for above ground residue should be about 0.75 times the surface/buried residue ϕ value based on data collected by Douglas et al. (1980) and Ghidey and Alberts (1993). However, these data are questionable because the bundled residue samples used in these experimental studies do not represent individual pieces of standing stubble residue. Standing residue would retain much less moisture than the bundled residue samples. The 0.3 value performed satisfactorily in RUSLE2's computation of loss of standing residue (see **Section 10.4.1**)

The RUSLE2 assumption is that buried residue is lost at the same rate that soil surface residue is lost, although the common assumption is that buried residue decomposes more rapidly than does surface residue (Dabney, 2005). An example of measured data illustrating this apparent difference is shown in Figure 10.6. Like other residue aspects, the difference in decomposition rates for surface and buried residue varied greatly in the data reviewed by Dabney (2005) with no clear trend. Overall, the apparent decomposition rate for buried residue, regardless of residue type, was 1.3 times the decomposition rate of surface residue. Additional adjustment is required to obtain decomposition estimates of unconfined residue because the mesh bag sampling method was used in 10 out of 12 studies reviewed by Dabney (2005).

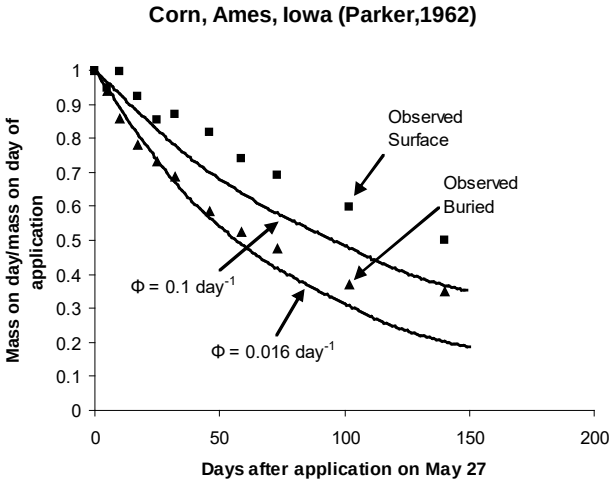

Figure 10.6. Difference in decomposition of residue in bags buried in the soil and placed on the soil surface.

Just as discussed in **Section 10.3.3.2** for surface residue, an adjustment also must be made for the mesh size effect on measured buried residue decomposition.

Instead of multiplying the mesh bag measured residue loss by 2 to obtain an estimate of unconfined surface residue loss, the measured mesh bag buried residue loss should be multiplied by 1.3 to estimate unconfined buried residue loss. Assume that the mesh bag measured surface residue loss is 1000 lbs/acre. The estimated actual loss is 2·1000 = 2000 lbs/acre. The measured mesh bag loss for buried residue is 1.3·1000 = 1300 lbs/acre based on the data reviewed by Dabney (2005), where the 1.3 factor accounts for the apparent higher decomposition rate for buried residue than for surface residue. Next, the 1300 value needs to be multiplied by the 1.3 factor to account for mesh bags underestimating the loss of unconfined buried residue. The buried residue loss of unconfined residue is therefore 1.3·1300 = 1700 lbs/acre. Consequently, these computations show that surface residue is lost at a greater rate (2000 lbs/acre versus 1700 lbs/acre) than is buried residue when the different effect of mesh size on decomposition of surface and buried residue is properly considered. The problem with these computations and with the mesh bag sampling method is the uncertainty involved in adjusting for mesh size and other factors related to how well decomposition in mesh bags represents actual field conditions.

The RUSLE2 intent is not to capture soil differences or placement within soil differences because RUSLE2 does not use soil moisture accounting routines. The buried residue studies cited by Dabney (2005) involved residue mesh bags placed 6 inches deep, which only partly simulates residue burial with a moldboard plow. A moldboard plow distributes residue throughout the disturbed soil layer even though most of the residue is buried in the lower half of the disturbed soil depth (see **Section 8.2.5.2**). Conservation tillage tools like disks, chisel plows, and field cultivators used for primary tillage leave most of the residue in the upper half of the disturbed soil depth (see **Section 8.2.5.2**), which residue buried at six inches does not represent. Furthermore, RUSLE2 uses the residue mass buried in the upper two or three inches to compute the effect of buried residue on erosion (see **Section 6.5**). The soil is drier at this shallow depth than at the six-inch measurement depth, and thus decomposition in this surface layer would be more like decomposition of surface residue than decomposition of residue buried at six inches. Therefore, mesh residue bags buried six inches deep do not represent typical field conditions.

Similarly, the placement of residue filled mesh bags on the soil surface does not represent typical field conditions. As Parker (1962) noted, a distinct boundary between surface residue and the soil surface does not exist in many cropland situations. For example, many residue pieces are both partially buried and exposed in conventional and mulch-till forms of cropping systems where tillage buries a portion of the residue left from the previous year's harvest. Soil splash by raindrop impact and local deposition behind residue pieces bonds the residue to the soil (Brenneman and Laflen, 1982; Toy et al., 2002). Also, the boundary between residue and the soil is not distinct in long-term no-till cropping systems. These effects are not captured by mesh bags placed on the soil surface.

The RUSLE2 objective is to produce reliable erosion estimates for conservation and erosion control planning. Increasing RUSLE2's decomposition rate for buried residue would not improve its erosion estimates but in fact would degrade them. The RUSLE2

computed ratio of erosion during the seedbed period for cropland going from turned sod to conventionally tilled 112 bu/ac yield corn to erosion for the same yield corn continuously cropped is 0.42, whereas the observed value is 0.40 [Table 5-D. AH537 (Wischmeier and Smith, 1978)].[70] However, the RUSLE2 computed ratio value is 0.95 for the second year while the observed value is 0.85. RUSLE2 computes this residual effect from turned sod using buried residue and dead root biomass values in equations 6.48 and 6.49. The first year erosion ratio value is computed well as a function of soil biomass before significant soil biomass loss by decomposition is computed. The fact that an accurate erosion ratio value is computed for the first year indicates that RUSLE2 is computing the proper effect of soil biomass when the estimated soil biomass is accurate. However, the fact that RUSLE2 computes too little soil biomass effect the second year indicates that RUSLE2 is computing too little soil biomass and a corresponding erosion that is too high. Consequently, increasing the decomposition coefficient ϕ value to represent buried residue decomposing more rapidly than surface residue will further degrade RUSLE2's performance for computing the effect of soil biomass.

These RUSLE2 erosion ratio values were computed using a decomposition coefficient ϕ value of 0.0017 day^{-1} for permanent grass vegetation residue. This decomposition coefficient value was originally selected based on comparison with other decomposition coefficient values in the RUSLE2 Core Database. However, recent analysis shown in Figure 10.2 for the blue stem hay shows that 0.012 day^{-1} is an appropriate value for decomposition coefficient ϕ value for blue stem hay. The erosion ratios computed with this ϕ value are now 0.36 compared to the observed 0.4 for the first year and 0.84 compared to the 0.85 observed for the second year, which is a significant improvement.

These results illustrate that the greater requirement is to accurately capture main effects before trying to capture minor effects. No basis exists for RUSLE2 computing decomposition of buried residue at a faster rate than surface residue. The RUSLE2 assumption that surface and buried residue decomposes at the same rate is strongly supported by both data, consideration of actual field conditions, increased accuracy of computed erosion values, and increased RUSLE2 robustness.

10.3.3.4. Roots

Fine roots are the most important roots in RUSLE2. A reasonable assumption is that the decomposition of fine roots is the same as buried residue. This assumption may need

---

[70] In this case, conventional tillage refers to a spring moldboard plow used for primary tillage followed two weeks later with a tandem disk and harrow or a tandem disk and field cultivator for secondary tillage used to create a seedbed.

reconsideration. Having the decomposition coefficient values the same for residue and roots gives RUSLE2 increased robustness, especially until additional information is learned about the distribution of root sizes and other root properties in the soil, the birth and death of roots, and how roots affect rill-interrill erosion. The RUSLE2 intent is to empirically capture the main effect of roots as an index rather than be a full description of how roots affect erosion.

10.3.3.5. Interdependence among calibration inputs for residue

No reliable data were found where both soil biomass and erosion were measured in the same experiment. Consequently, observed values for buried residue, dead root, and live root biomass were not used to calibrate the soil biomass subfactor equations 6.48 and 6.49 (see **Section 6.5**). Instead, RUSLE2 computed values for soil biomass were used to calibrate the soil biomass subfactor equations. In addition, "observed" soil biomass subfactor values were back-calculated from observed soil loss ratio values given in Table 5, AH537 (Wischmeier, and Smith, 1978) using RUSLE2 computed subfactor values for ground cover, soil surface roughness, ridge height, and soil consolidation for the seedbed crop stage of a silt loam soil at Columbia, Missouri, the RUSLE2 reference (base) location. Equation 6.1 was rearranged to compute values for s_b, the soil biomass subfactor. Soil loss ratio values from Table 5, AH537 are substituted for c in equation 6.1. Values for the other subfactors in equation 6.1 were RUSLE2 computed for the conditions listed in Table 6.5.

This soil biomass subfactor calibration approach has several consequences. The soil biomass subfactor absorbs the error and uncertainty in the other subfactors for the calibration conditions. The seedbed crop stage is the best crop stage for calibrating the soil biomass subfactor. Calibrating the soil biomass subfactor for this crop stage minimizes errors in the other subfactors because they deviate less from unit-plot conditions for the seedbed crop stage than for any other crop stage.

The only independent cover-management input in the calibration of the soil biomass subfactor, equations 6.48 and 6.49, is crop yield. All other cover-management inputs involved in the calibration are derived from yield, RUSLE2 Core Database values, and RUSLE2 procedures such as residue loss by decomposition and redistribution of soil biomass by mechanical soil disturbance. Therefore, a change in either RUSLE2 Core Database values or a RUSLE2 procedure used to compute subfactor values involved in the soil biomass subfactor calibration invalidates the calibration. **Consequently, a change in one of these items without recalibration produces erroneous RUSLE2 computed erosion estimates**.

The RUSLE2 assumption is that buried residue and dead roots decompose at the same rate as surface residue. This calibration approach has the advantage that it is partially self correcting if these assumptions are wrong. The empirically determined coefficient values in equations 6.48 and 6.49 compensate for erroneous soil biomass estimates used in the calibration as long as the relative values are accurate.

RUSLE2 has been developed and carefully validated to ensure that it computes the desired erosion values across the full range of conditions where RUSLE2 is expected to be used. Therefore, a change made to one RUSLE2 procedure, such as residue decomposition, requires a second change to ensure that RUSLE2 continues to compute expected erosion values.

Interdependence among RUSLE2 residue variables must be considered when changes are made so that RUSLE2 computes different ground (surface) cover values. To illustrate, What if RUSLE2 computed surface cover values seem questionable (see the **RUSLE2 User's Reference Guide** for additional discussion)? What RUSLE2 variable should be changed to improve surface cover estimates? The first step is to ensure that the data or observations being used as the basis for a change represent main effects rather than a minor effect or unexplained variability that RUSLE2 is not designed to capture.

The next step is to assess RUSLE2's computed erosion estimates to determine if these values should be changed along with the change in surface cover values. RUSLE2 was calibrated to give expected erosion estimates with an assumed set of values. A difference between an observed surface cover value and a RUSLE2 computed surface cover value does not necessarily mean that RUSLE2 is computing erroneous erosion estimates. What evidence, other than surface cover values, shows that RUSLE2 erosion estimates also need changing? An independence assessment should be made to determine if different erosion values should also be computed.

Changing decomposition coefficient ϕ values changes RUSLE2 computed surface cover values, but changing ϕ values also affects RUSLE2 computed soil biomass values and even soil surface roughness values that are a function of soil biomass. Therefore, a change in a ϕ value affects erosion in more ways than just changing surface cover. The question that should be asked before changing a ϕ value is: What evidence indicates that different soil biomass values should be computed along with different surface cover values?

Another way to change RUSLE2 computed surface cover values is to change above ground biomass as a function of yield. In addition to changing surface cover values, this change also affects soil biomass and soil surface roughness values. Once again, RUSLE2 computed erosion values are affected by changes in other variables besides surface cover.

The simplest way to change RUSLE2 computed surface cover values is to change surface residue mass-cover input values in the residue description (i.e., values for α in equation 10.1). Changing this relationship directly changes surface cover without changing other residue variables that affect erosion.

RUSLE2 changes should be carefully thought out to avoid unintended consequences.

10.3.3.6. Dealing with multiple component residue descriptions

A single RUSLE2 residue description is assigned to each vegetation description. A residue description represents a composite of the residue components produced by the particular vegetation.

Residue produced by vegetation includes: (1) pieces having a wide range in geometry that affect decomposition (e.g., fine and coarse roots and stems); (2) multiple components (e.g. leaves, stems, seed pods, and chaff); (3) variation in composition within a component (e.g., corn stalks having decomposition resistant exterior shells and easily decomposed interior material); (4) components, especially stems, that decompose from the inside out without changing outside dimensions (e.g., wheat straw); (5) decomposition properties that vary with growth stage (e.g., tender young leaves that decompose much more rapidly than mature leaves); (6) differences between above ground and below ground plant components (e.g., leaves that decompose more rapidly than roots); and (7) multiple species within a plant community (e.g., multiple plant species on rangelands and multiple weed species on permanent, unimproved pasture lands and landfills). RUSLE2 uses a single mass-cover coefficient α and decomposition coefficient ϕ to represent residue even though residue is composed of multiple components, each having its own α and ϕ values.

Effective RUSLE2 mass-cover coefficient α and decomposition coefficient ϕ values vary temporally as the residue decomposes. Values for these coefficients are functions of the relative composition of residue components that decompose at different rates. Consequently, the assigned RUSLE2 mass-cover and decomposition coefficient values are a compromise. The result is that RUSLE2 computes decomposition rates that are too slow in the beginning and too fast at the end. However, a review of Figure 10.2 shows that a single value decomposition coefficient ϕ works satisfactorily for a year for residue produced by typical agricultural crops, especially considering the unexplained variability in residue data.

Priority was given to fitting RUSLE2 computed decomposition values to observed values within the first year after residue application. Thus, RUSLE2 most accurately estimates decomposition of the easily and rapidly decomposable portions of the residue and not the residue that remains after one year, as illustrated in Figure 10.7. Most RUSLE2 applications involve a substantial annual input of biomass from crop production or senescence by permanent vegetation, which minimizes errors in RUSLE2 decomposition estimates beyond one year after residue application.

An example of a multiple component residue is the residue produced by a cover crop bi-culture of hairy vetch and rye that is killed at corn planning time in central Illinois (Ruffo

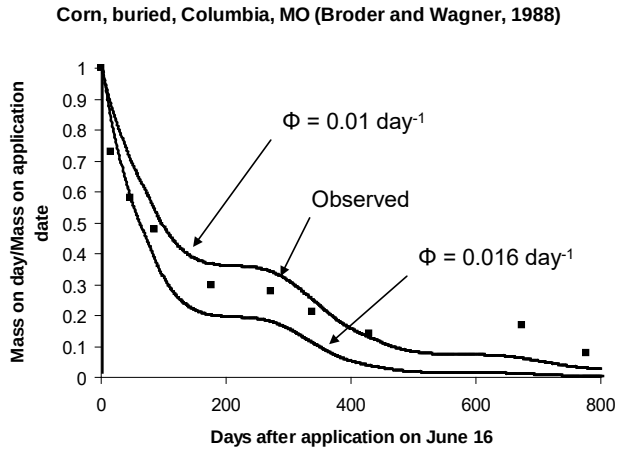

Figure 10.7. RUSLE2's estimate of residue decomposition over a 2-year period.

and Bollero, 2003). The hairy vetch cover crop residue component (ϕ = 0.032 day^{-1}) decomposes much more rapidly than does the rye cover crop component (ϕ = 0.017 day^{-1}).

Figure 10.8 shows RUSLE2 decomposition computations for hairy vetch and rye grown as mono-culture cover crops and a 1:1 bi-culture cover crop based on dry mass on the day that the cover crop is killed. The curve labeled "by-component" is the decomposition that should be computed for the bi-culture. The "by-component" values shown in Figure 10.8 were computed outside of RUSLE2.

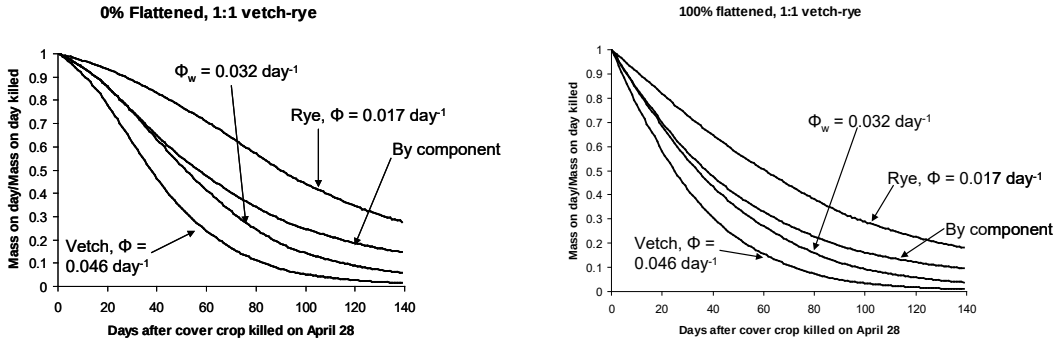

Figure 10.8. RUSLE2 computed decomposition of a 1:1 vetch-rye cover crop killed on April 28 in central Illinois. The Φ_w value is a weighted value based on dry mass on the date that the vegetation was killed.

A single value for the decomposition coefficient ϕ must be entered in the single composite RUSLE2 residue description that must be used to represent the combined residue produced by the hairy vetch and rye. One approach is to enter a weighted ϕ value based on dry mass of the hairy vetch and rye at the time that the cover crop vegetation is killed. As Figure 10.8 shows, initially RUSLE2 accurately computes decomposition but soon computes too much decomposition. The effective decomposition coefficient ϕ value should approach the ϕ value for rye over time as the hairy vetch decomposes much more rapidly than does the rye. An alternative input value for ϕ is an average of the weighted ϕ_w value at the time that the bi-culture cover crop is killed and the ϕ value for rye. RUSLE2 computes too little decomposition initially but computes much improved decomposition values after most of the vetch has decomposed.

Rather than developing a RUSLE2 procedure that adjusts the decomposition coefficient value as decomposition progresses, the best approach would be to modify RUSLE2 to accommodate multiple residue descriptions being assigned to a single vegetation description. In fact, the original RUSLE2 plan was to describe residue by its component parts. Using a residue description for each residue component would significantly improve RUSLE2's computations of residue decomposition and surface residue cover as a function of residue mass. Insufficient data existed for determining decomposition coefficient values for each plant residue component for the vast array of vegetations involved in RUSLE2 applications as a land use independent model.

The large decomposition coefficient ϕ values in Figure 10.8 for the hairy vetch and rye cover crops, 0.046 and 0.017 day^{-1}, respectively, illustrate how the decomposition coefficient ϕ is a function of crop stage. The ϕ value for mature hairy vetch residue is 0.020 day^{-1} while the ϕ value for mature rye is 0.0080 day^{-1}. The RUSLE2 decomposition coefficient values are about twice the values when the vegetation is killed as a cover crop when it is approximately half mature in comparison to the decomposition coefficient values for the vegetation after it reaches full maturity.

10.3.3.7. Effect of loading (application) rate

The decomposition coefficient ϕ seems to be a function of residue mass initially added to the soil surface as illustrated in Figures 10.9 and 10.10 (Steiner et al., 1999; Stott et al., 1990). **If initial surface residue mass affects the decomposition coefficient, the decomposition coefficient ϕ must also be a function of surface residue mass at any time after the residue is added to the soils surface.** The trend in both Figures 10.9 and 10.10 is that the decomposition coefficient ϕ decreases as surface residue mass increases. Therefore, Figure 10.9 and 10.10 imply that decomposition accelerates as surface residue mass decreases. However, this implication is inconsistent with the expectation that decomposition slows as the readily decomposable residue components disappear first, leaving the residue components that resist decomposition.

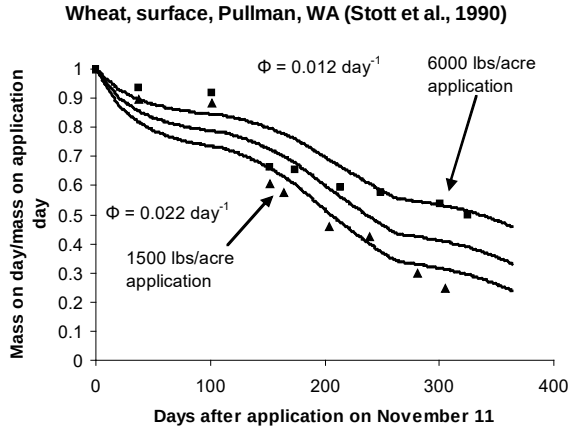

Figure 10.9. Effect of residue application rate on the decomposition coefficient ϕ.

Another concern is the great variability in decomposition coefficient values as illustrated in Figure 10.10. The RUSLE2 decomposition coefficient ϕ is proportional to the k decomposition coefficient in Figure 10.10. The comparable range in

ϕ for the range in k in Figure 10.10 for wheat straw is from 0.004 to 0.012 day^{-1}. RUSLE2 computes that 2100 and 600 lbs/acre of residue remain after 1 year for a 4000 lbs/ace wheat straw application at Columbia, Missouri for the ϕ values of 0.004 and 0.012 day^{-1}, respectively. The respective surface covers are 72 and 30 percent and the respective ground cover subfactor values, assuming **b** = 0.04 percent^{-1} in equation 6.6 (see **Section 6.3**), are 0.0561 and 0.301, which is a 5:1 erosion ratio. The uncertainty in decomposition coefficient ϕ values is much greater than the variation in ϕ as a function of application rate and surface residue mass as shown in Figure 10.10, especially for residue mass less than 6000 lbs/acre (600 g/m^2).

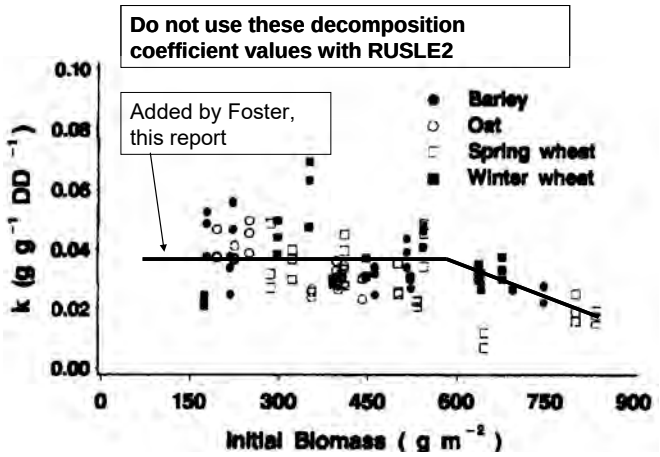

Figure 10.10. Variation of decomposition coefficient k (comparable to ϕ) values from another decomposition model with residue application rate. (Data source: Steiner et al., 1999; Line added by Foster, this report)

Furthermore, are the results illustrated in Figure 10.9 and 10.10 indicative of decomposition of the wide array of vegetation residue including vegetables, corn, wheat, hay, litter on rangelands, Eucalypt forest litter, and erosion control materials used on construction sites? Are the results illustrated in these figures indicative of application conditions that range from wheat straw being blown onto a construction site to wheat straw left in conventionally, reduced, and no-tilled fields?

The conclusion for RUSLE2 purposes is that the decomposition coefficient ϕ is not a function of residue application rate or surface residue mass. The uncertainty illustrated in Figure 10.10 reinforces the conclusion that RUSLE2 represents decomposition differences between major residue and erosion control material types, but not difference in small grain types, for example. An improvement in RUSLE2's decomposition computations can be gained by representing residue components such as legume and grasses and stems, leaves, seed pods, and chaff. Much more research is needed before the RUSLE2's decomposition coefficient ϕ can be made a function of application rate or surface residue mass. Furthermore, a standardized set of decomposition data for a wide range of materials are needed to determine RUSLE2 ϕ values.

10.3.3.8. Effect of irrigation on residue decomposition

RUSLE2's accuracy for estimating increased decomposition caused by irrigation was assessed using data reported by Schomberg et al. (1994) for decomposition of surface and buried alfalfa, wheat, and sorghum residue in mesh bags. Water varying in amounts from 5 to 336 mm was added by sprinkler irrigation during the study year in addition to 305

mm of natural precipitation. The long term average annual precipitation at Bushland, TX is 480 mm. The monthly precipitation and temperature distributions during the study are shown in Figure 10.11. Although monthly temperatures during the study were close to the long term values, the study's monthly precipitation distribution differed significantly from the long average distribution. The water added in each irrigation is given in Figure 10.12.

The objective of this analysis was to determine how well RUSLE2 computes the effect of added irrigation water on residue decomposition, not to determine decomposition coefficient ϕ values. The first step in the analysis was to adjust the decomposition coefficient ϕ value until a good fit was obtained between computed decomposition and

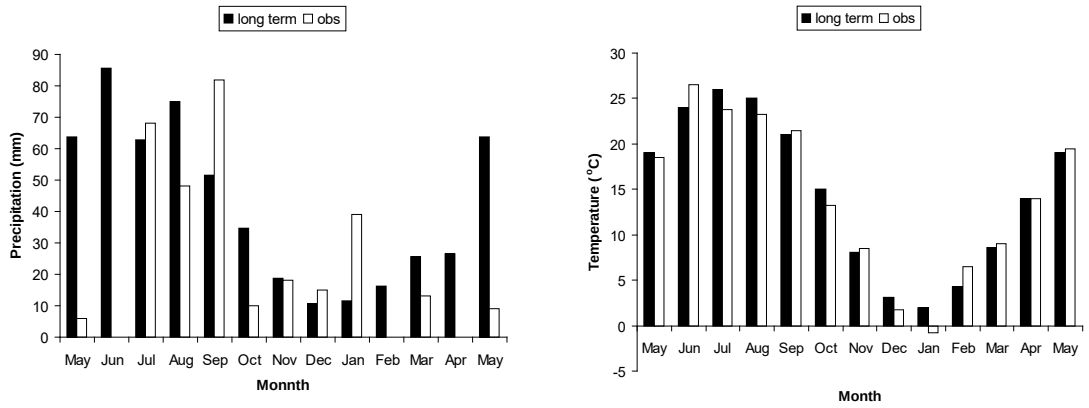

Figure 10.11. Long term average monthly precipitation (480 mm annual) and actual monthly precipitation (305 mm annual) and long term average monthly temperature and actual monthly temperature for Schomberg et al. (1994) study

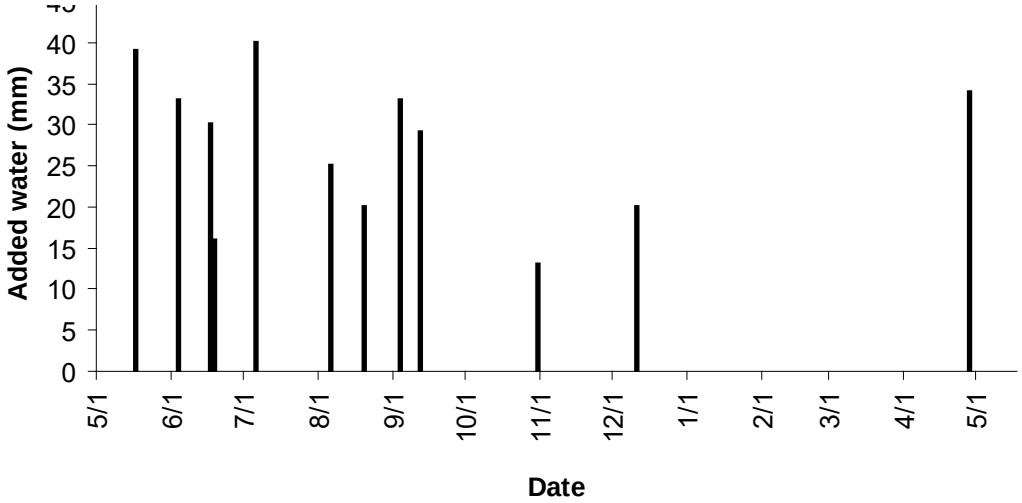

Figure 10.12. Water applied by sprinkler irrigation (total application of 336 mm) in Schomberg et al. (1994) study.

observed decomposition for the no-irrigation (only natural precipitation) condition.

Observed monthly precipitation and temperature values shown in Figure 10.11 were used in the analysis.

The decomposition coefficient ϕ value determined for natural precipitation alone was used to compute decomposition for the 305 mm natural precipitation plus 336 mm of added irrigation water distributed as shown in Figure 10.12. The results of those computations are shown in Figure 10.13.

Variability is a common problem in decomposition data. The data in Schomberg et al. (1994) study also was highly varied. For example, the fraction of surface sorghum residue remaining on December 10 was 53 percent while the fraction remaining on March 10 was 70 percent, which is an obvious error because residue mass does not increase over time. Another problem with these data is that the range in decomposition of surface residue as a function of added irrigation water is not consistent with the range in the observed data for surface sorghum and wheat residue.

As Figure 10.13 shows, the conclusion is that RUSLE2 described well how sprinkler irrigation affects decomposition of both surface and buried residue in the Schomberg et al. (1994) study. Furthermore, RUSLE2 described decomposition well for the natural

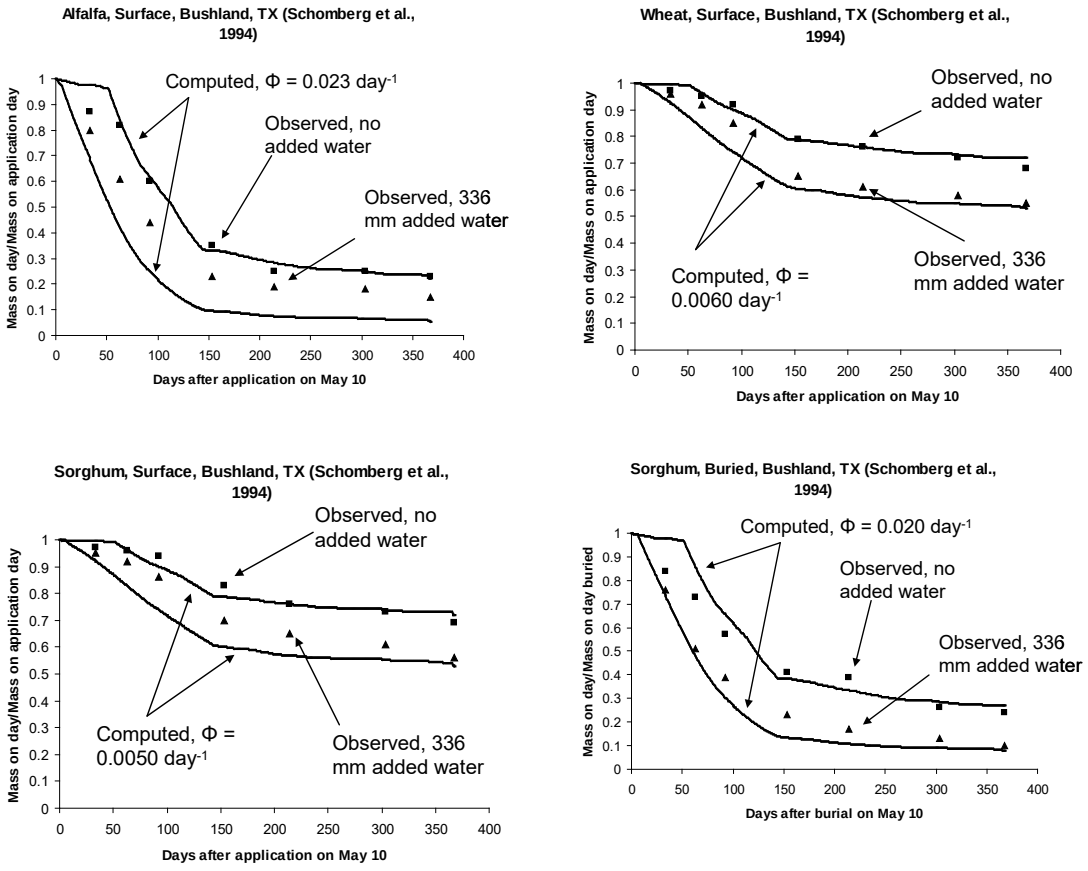

Figure 10.13. Effect of irrigation of buried and surface residue (data source: Schomberg et al., 1994)

precipitation without irrigation even though the actual monthly precipitation distribution did not vary smoothly month to month.

The Schomberg et al. (1994) data show major differences in decomposition rate between surface and buried residue. These differences seem to be a direct result of experimental procedures. That issue is discussed in detail in **Section 10.3.3.2**.

These results also show that decomposition of both surface and buried residue is a dampened process that does not react quickly to changes or irregularities in precipitation or temperature. Surface residue apparently continues to decompose longer after a water-application event that seems to have been assumed in some decomposition models (Schomberg and Steiner, 1997; Steiner et al., 1999). Decomposition of surface residue seems much more related to local soil moisture at the contact between the residue and soil than was previously considered.

An important question is whether residue decomposes the same per unit water added by irrigation as it does by unit water added by natural rainfall. Decomposition may be less per unit water applied by sprinkler irrigation than applied by natural rainfall. Water droplets in the irrigation-applied water have very low impact energy in comparison to natural rainfall. Thus, natural rainfall splashes many more soil particles that increase the contact between the soil and the residue (Foster et al., 1985a) than does sprinkler irrigation applied water. Irrigation-applied water may wash away soil particles previously bonded to the residue by rainfall. Also, deposition of sediment produced interrill-rill erosion (Brenneman and Laflen,1982) increases soil bonding between residue and soil at low residue application rates that does not occur with irrigation-applied water.

The type of irrigation should be considered in selecting irrigation inputs for RUSLE2. This decomposition analysis was based on sprinkler irrigation. The irrigation input values for sprinkler irrigation should be based on the water that actually reaches the soil. This amount can be significantly less than the amount discharged from the irrigation nozzles because of wind and evaporation losses.

Also, decomposition may be less on ridges when furrow irrigation is used than with flood irrigation on a smooth surface. Similarly, decomposition of surface residue may be reduced with drip irrigation. However, be careful in making adjustments to irrigation amounts because RUSLE2 uses the same amount in computing decomposition of both surface and buried residue. Also, RUSLE2 uses irrigation input values to compute temporal soil erodibility (see **Section 4.5**).

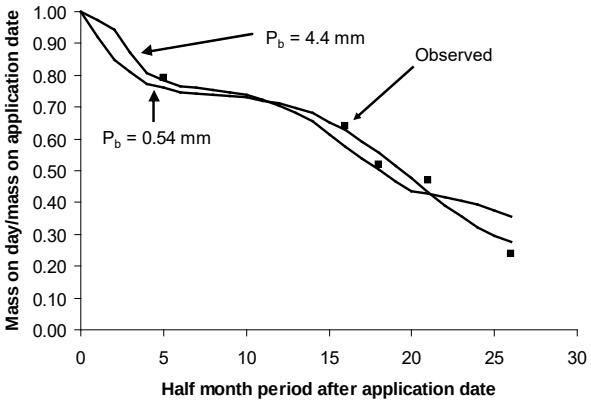

Figure 10.14. Effect of changing the base daily precipitation P_b value in the moisture function used to compute wheat straw residue decomposition at Pullman, Washington.

10.3.3.9. Special considerations for the NWRR and Req zones

The climate in the Northwest Wheat and Range Region

(NWRR), which is within the larger Req zone (see RUSLE2 User's Reference Guide), differs significantly from the climate in non-Req areas. An example is the relationship of monthly precipitation amount relative to number of precipitation events (see **Section 10.3.4.2**). Consequently, should the decomposition equations and coefficient values differ for the NWRR and the entire Req zone from those for other regions? To evaluate this possibility, the base moisture P_b value in the moisture function (W_f, equation 10.5) was determined by fitting the decomposition equations specifically to decomposition data collected at Pullman, Washington. A P_b value of 0.54 mm produced improvement for some data sets as illustrated in Figure 10.10, but not for all data sets. When 0.54 mm is used for P_b in equation10.5, RUSLE2 computes decomposition being controlled throughout the year by the temperature function (T_f, equation 10.6) at Pullman, Washington. When P_b = 4.4 mm, RUSLE2 computes that decomposition is controlled by the moisture function from May through October. Computing that decomposition is controlled by moisture when average monthly precipitation is as low as 0.45 inches (11 mm) in July and 0.64 inches (16 mm) in August seems more appropriate than the temperature function controlling decomposition during these dry months.

Decomposition coefficient ϕ values determined for wheat using P_b = 0.54 mm are essentially the same as decomposition coefficient values determined for wheat in other regions using P_b = 4.4 mm. Consequently, the difference in decomposition coefficient values in Table 10.2 between the NWRR and other regions may not be related to wheat varieties as implied in Table 10.2, but related to having an appropriate description of the moisture function W_f for the NWRR.

The recommendation is that 4.4 mm be used for P_b for the NWRR and Req zone along with the Req specific decomposition coefficient values given in Table 10.3 until additional research is conducted. This additional decomposition research for the Req zone, including the NWRR, can be conducted simultaneously with additional research needed on other RUSLE2 Req relationships throughout the Req zone, especially for locations outside of the central Washington to northern Idaho and Northeastern Oregon region.

10.3.4. Comparison of RUSLE2, RWEQ, WEPP, and WEPS decomposition

The RUSLE2 water erosion and RWEQ (Fryrear et al., 1998) wind erosion prediction technologies use comparable empirical structures involving long-term average monthly climate and management inputs and both were originally intended for conservation planning in USDA-Natural Resources Conservation Service (NRCS) field offices. The NRCS initially placed a high priority on RUSLE2 and RWEQ using the same equations and parameter values for computing residue mass values. Later the NRCS adopted WEPS (Hagan et al., 1996) instead of RWEQ for field office conservation planning. WEPS is a process-based simulation model that uses stochastic climate inputs. The comparable water erosion prediction model is WEPP (Flanagan and Nearing, 1995).

RUSLE2 and WEPS should compute comparable residue mass values because these models are being implemented by NRCS for routine conservation planning, and WEPP may be implemented in the future. Although erosion prediction clients may not know the residue mass values that these models should compute, clients readily recognize differences in values computed by the models and question differences when none should exist. Such differences reduce the creditability of the models and the conservation plans developed using them.

Decomposition estimates of surface applied residue were computed using RUSLE2, RWEQ, WEPP, and WEPS at the locations listed in Table 10.4.

Table 10.4. Locations for RWEQ, WEPP, and WEPS decomposition computations

Location	Annual precipitation (inches)	Model	Comments
Jefferson City, Missouri	37.8	All	Near Columbia, Missouri
Minneapolis, Minnesota	27.0	ALL	
W. Lafayette, Indiana	37.0	RWEQ	
Scottsbluff, Nebraska	15.1	WEPP/WEPS	
Jamestown, North Dakota	18.3	RWEQ	Used in Figure 10.19
Amarillo, Texas	20.1	RWEQ	Near Bushland, Texas
Borger, Texas	20.7	WEPP/WEPS	Near Bushland, Texas
Denton, Texas	33.1	WEPP/WEPS	
Dallas, Texas	36.0	WEPP/WEPS	
Houston, Texas	46.4	WEPP/WEPS	
Galveston, Texas	39.8	WEPP/WEPS	
Holly Springs, Mississippi	54.2	WEPP/WEPS	
Jackson, Mississippi	53.8	RWEQ	
Gulfport, Mississippi	60.0	WEPP/WEPS	
Mobile, Alabama	62.3	All	
Spokane, Washington	16.0	RWEQ	
Tucson, Arizona (Davis)	11.2	RWEQ	Davis-Monthan Air Force Base
Tucson, Arizona (Campbell)	12.4	WEPP/WEPS	University of Arizona Agricultural Experiment Station on Campbell Avenue
Albuquerque, New Mexico	9.3	RWEQ	Used in Figure 10.19

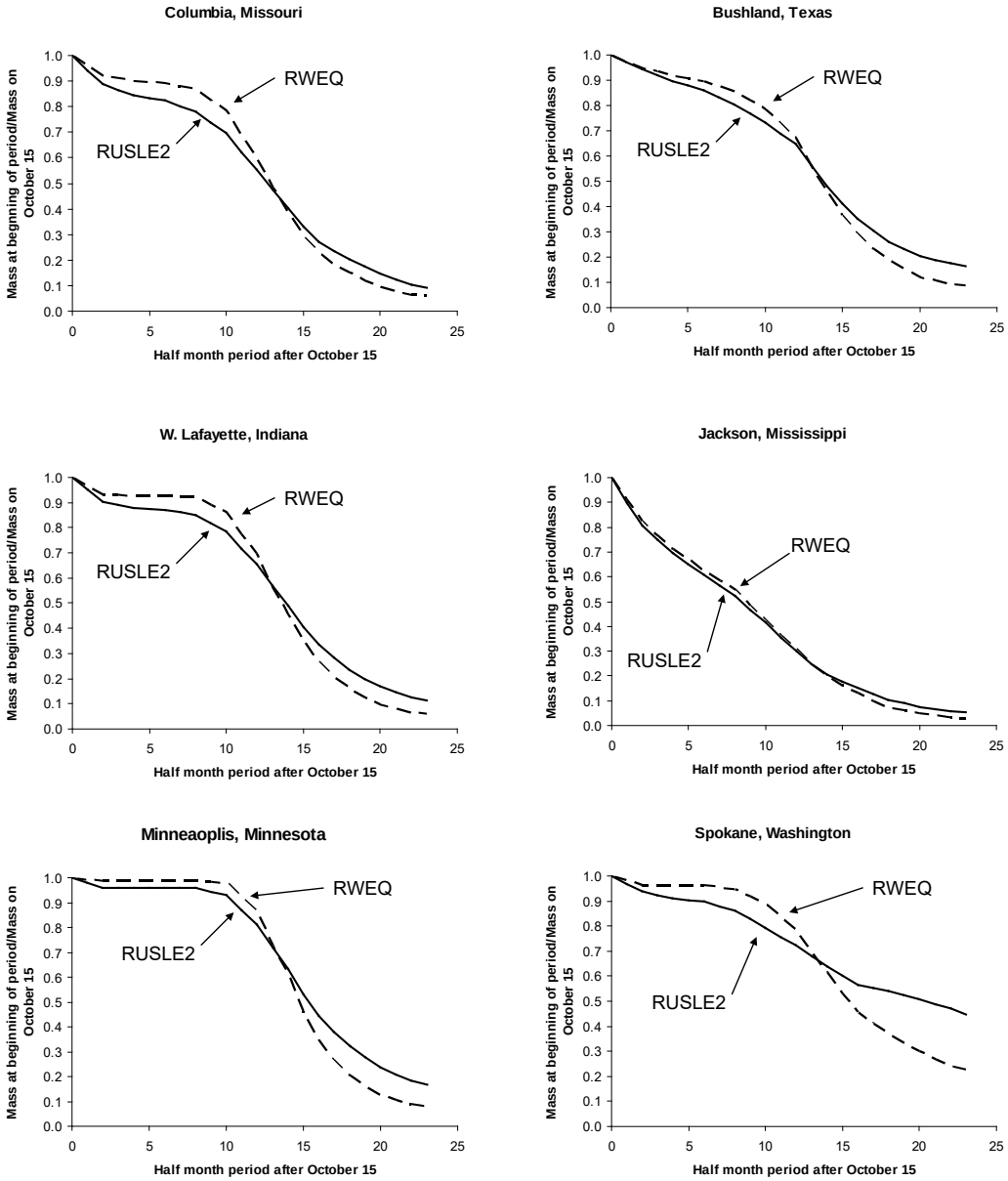

Figure 10.15. Residue decomposition computed with RUSLE2 and RWEQ

For the RWEQ computations, mulch was assumed to be surface applied on October 15 at 4500 lb/acre to a seedbed condition with no existing above ground or below ground biomass for all locations except Tucson, Arizona. The mulch was assumed to be applied on January 1 at Tucson.

The RWEQ decomposition coefficient value was adjusted to give the best fit of computed residue mass to RUSLE2 computed values at Columbia (Jefferson City), Missouri. This RWEQ decomposition coefficient value was used for all other locations, and the same RUSLE2 decomposition value was used for all locations.

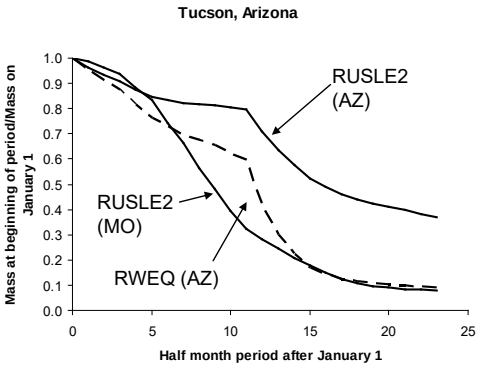

Figure 10.16. Residue decomposition computed with RUSLE2 and RWEQ at Tucson, Arizona

For the WEPP computations,[71] the same 4500 lbs/acre mulch rate was assumed to be applied on May 10, except for Tucson where the mulch was assumed to be applied on January 1. The mulch was applied to a soil that had not been tilled for a year. No above ground or below ground biomass was assumed. WEPP was run for 10 years with the same mulch amount applied each year with no soil disturbance throughout the 10 year simulation period.

WEPP computes daily residue mass for each annual mulch application. Daily computed surface residue mass for each mulch application was averaged for the 10 year simulation period. The WEPP computed residue mass values are equivalent to conducting annual experiments where the fate of mulch applied each year is determined. The WEPP computations represent each annual application placing new mulch on mulch remaining from previous years rather than mulch being applied each year to bare soil.

The RUSLE2 decomposition coefficient ϕ value was adjusted to give the best fit of RUSLE2 computed residue values to WEPP computed values for Columbia (Jefferson City), Missouri for a silt loam soil. This RUSLE2 decomposition coefficient value was used for all locations and the same WEPP decomposition coefficient value was used for the same silt loam soil for all locations.

Decomposition was computed with WEPP at the locations listed in Table 10.4. RUSLE2 computed decomposition values compared well with WEPP computed values for locations where temperature rather than moisture was the factor limiting decomposition. At locations where RUSLE2 computed that moisture limited decomposition, WEPP conputed decomposition amounts that were significantly greater than RUSLE2 computed, which was especially evident a Tucson, Arizona where the WEPP computed decomposition was essentially the same as decomposition computed at Columbia, Missouri even though average annual precipitation at Tucson as only 12 inches in comparison to 38 inches at Columbia, Missouri. Consequently, WEPP seems to be computing too much decomposition in dry locations.[72]

---

[71] The WEPP version used in these computations was dated May 18, 2006, which was downloaded from the USA-ARS WEPP Internet site in April 2008. This version is the most recent version available to the public.

[72] These results have been reported to Dennis Flanagan, lead WEPP developer, USDA-Agricultural Research Service, W. Lafayette, Indiana. WEPP developers are investigating whether WEPP may be

The WEPS compuations were made using the WEPS hydrology component rather than WEPS with the WEPP hydrology component.[73] The same 4000 lbs/acre mulch rate was assumed to be annually applied on October 15 at all locations. The management practice used to make the compuations represented a soil tilled with a moldplow plow and a tandem disk that buried all of the previous year's mulch and did not resurface any buried residue. WEPS was run for 15 years. Daily surface residue mass values were averaged

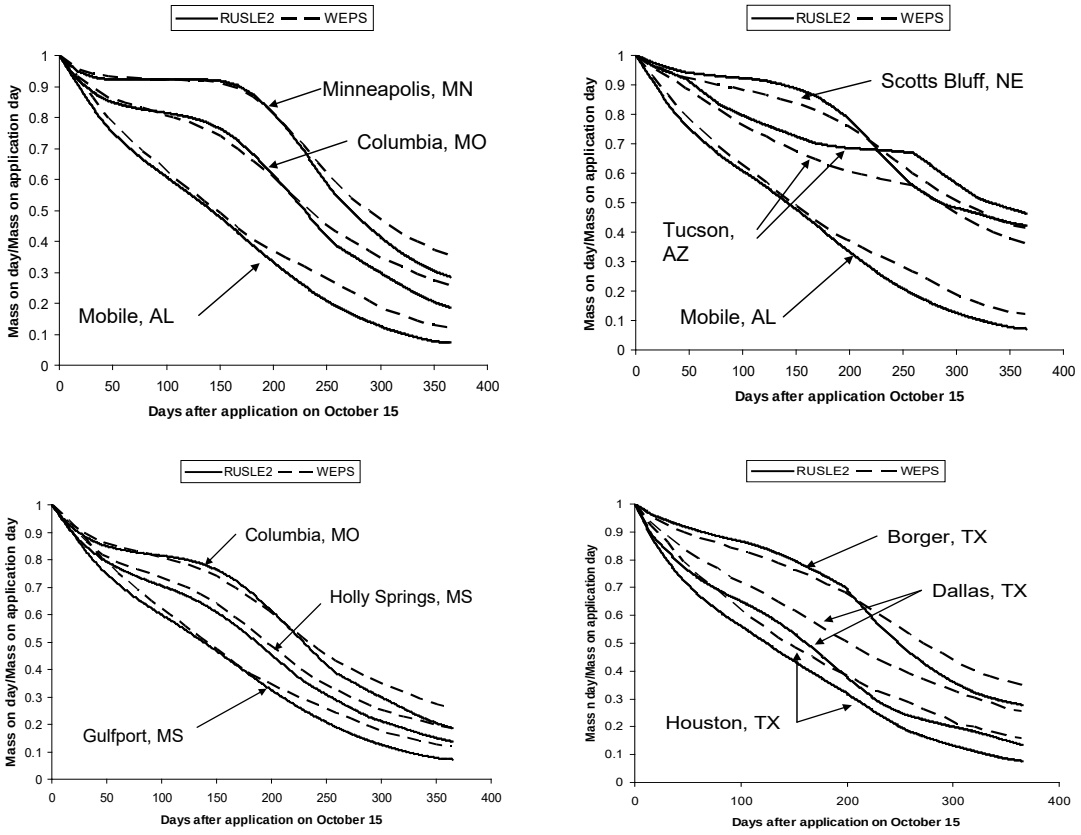

Figure 10.17. Residue decomposition computed with RUSLE2 and WEPS

for the 15 year simulation. The results are plotted in Figure 10.17.

The same WEPS decomposition coefficient value was used for all WEPS computations. The RUSLE2 decomposition coefficient ϕ value was adjusted to give the best fit of

---

computing too much decomposition at Tucson and other dry locations. Possible WEPP changes may made sometime soon (May 10, 2008).

[73] The WEPS version used in these computations was dated April 14, 2006, which was provided by Larry Wagner, lead WEPS developer, USDA-Agricultural Research Service, Manhattan, Kansas.

RUSLE2 computed residue values to WEPS computed values for Columbia (Jefferson City), Missouri for the Morley silty clay loam soil. This RUSLE2 decomposition coefficient value was used for all subsequent RUSLE2 computations.

10.3.4.1. Structure of decomposition computations

All four models (RUSLE2, RWEQ, WEPP, and WEPS) use moisture and temperature functions to compute decomposition. RUSLE2, WEPS, and WEPP use equation 10.4 that takes a minimum of the moisture and temperature functions instead of the product of these functions used in RWEQ. The differences in computed decomposition resulting from the RUSLE2 minimum structure and the RWEQ product structure are illustrated in Figures 10.15 and 10.16. With the exception of the Tucson location, the consistent trend is that the product structure computes reduced decomposition during cool periods and increased decomposition during warm periods.

Using a minimum of the moisture and temperature functions was judged to be better than the product of the functions based on an inspection of Figures 10.2 and 10.15.

The minimum of the moisture and temperature functions, which is equation 10.4, is also used in WEPP and WEPS. The Gregory et al. (1985) decomposition model was originally used in RUSLE1, but it was replaced with a modification of the WEPP decomposition model (Stott, 1991; Stott et al., 1995) because the Gregory et al. model also was judged to compute too little decomposition during cool periods and too much decomposition during warm periods.

10.3.4.2. Moisture function

10.3.4.2.1. Comparison with RWEQ

RUSLE2's moisture function used to compute decomposition is given by equation 10.5. The RWEQ moisture function is given by (Fryrear et al., 1998; Schomberg and Steiner, 1997):

$$W_{fwe} = 1.25 N_p / D_p \qquad [10.8]$$

where: W_{fwe} = the RWEQ moisture function used to compute decomposition, N_p = the number of precipitation events in the period D_p (days). The Schomberg and Steiner (1997) justification for using number of precipitation events is that surface residue does not remain moist long after a precipitation event, which conceptually implies that residue moisture content following a precipitation event is independent of the event's precipitation amount, which seems questionable. The moisture retained by residue depends greatly on residue type and mass and its contact with the soil mass. Similarly, the Schomberg-Steiner assumption seems questionable for mulch-till and no-till cropping systems where the soil-residue interface is not well defined and surface residue pieces are partially covered by soil. The assumption also seems questionable during fall and spring periods when evaporation is reduced. Dew may provide a significant moisture source, even on very hot days (Heilman et al, 1992).

Decomposition was computed with RUSLE2 and RWEQ at the locations identified in Table 10.4, and the computed values are shown in Figures 10.15 and 10.16. Except for the Tucson location, the RUSLE2 and RWEQ moisture functions performed similarly. The reason for the similar performance is that number of precipitation events in a given period in the RWEQ moisture function actually serves as a surrogate for precipitation amount used in the RUSLE2 moisture function. Precipitation amount in a given period is highly correlated with number of precipitation events in the period and the relationship is essentially the same across the eastern US as shown in Figure 10.18. However, a disadvantage of the RWEQ moisture function even in this region is that number of precipitation event is more spatially varied than precipitation amount. Also, data on number of precipitation events are much less available than long term monthly precipitation values, such as those that were easily found and used to compute decomposition in Canada (see Figure 10.2) and SW Australia (see Figure 10.3).

The RUSLE2 and RWEQ decomposition estimates differ greatly for Tucson, Arizona as shown in Figure 10.16. In this figure, decomposition was computed at Columbia, Missouri with RWEQ for mulch applied on January 1, the same as for Tucson. RWEQ computed the same decomposition for both Tucson and Columbia even though annual rainfall at Tucson (Davis) was only 11 inches in comparison to 38 inches at Columbia (see Table 10.4). The reason that RWEQ computes the same decomposition at the two locations is that the number of storms is comparable for the two locations even though annual precipitation differs significantly between the locations. Similarly, the number of storms per month in relation to monthly precipitation amount is high at Spokane Washington during the cool period, which is the reason for the difference between decomposition computed by RUSLE2 and RWEQ Spokane being greater than at the other locations in Figure 10.15.

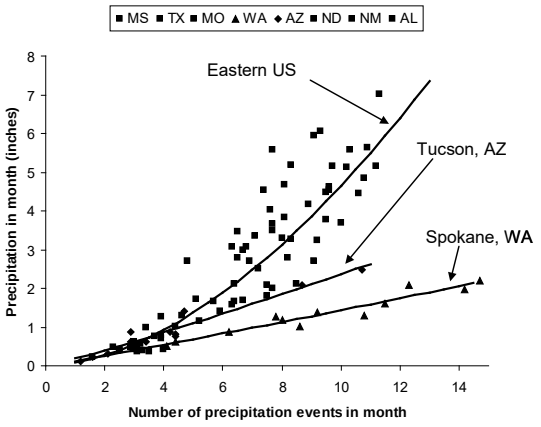

Figure 10.18. Relation of average monthly precipitation to number of precipitation events in a month.

Use of the RWEQ moisture function in RUSLE2 would require varying the decomposition coefficient value with location in the western US. This requirement is similar to the base precipitation value P_b in equation 10.5 needing to be changed so that the same RUSLE2 decomposition coefficient values can be used in the Palouse Region and in the eastern US (see **Sections 3.2.5 and 10.3.2**).

Overall, using precipitation in the RUSLE2 moisture function is judged superior to using number of precipitation events as in RWEQ. Using number of precipitation events would provide no fundamental improvement in RUSLE2's decomposition estimates. Precipitation amount appears to be superior in low precipitation regions in the western

US. Precipitation amounts are much more readily available and spatially stable than number of precipitation events in a given period.

10.3.4.2.2. Comparison with WEPP

The WEPP moisture function is given by (Stott et al., 1995):

$$W_{fwp} = \theta_t / \theta_o \qquad [10.9]$$

where: W_{fwp} = the WEPP moisture function used to compute decomposition of surface residue, θ_t = water content (volume of water/volume of bulk soil)[74] of the tilled soil layer and θ_o = the optimum water content (volume water/volume of bulk soil) for decomposition. The WEPP assumption is that the optimum moisture content for decomposition is 0.6 times the soil's pore space (volume pore space/volume of bulk soil). Consequently, the decomposition computed by WEPP should be a function of soil, tillage, and other factors that affect infiltration (e.g., precipitation, soil properties, and cover-management), soil water retention (e.g., soil properties), and soil water extraction (e.g., drainage and evapo-transpiration) (Alberts et al., 1995).

The present WEPP version does not computes the same decomposition amount at Tucson, Arizona as it does in Columba, Missouri, even average annuaj precipitation at Tucson is 12 inches in comparison to 38 inches at Columbia. These WEPP computations were judged tgo be erroneous, thus further computations were not made with WEPP. Changes are anticipated in WEPP to deal with this apparent problem (May 10, 2008).

10.3.4.2.3. Comparison with WEPS

The WEPP moisture function is given by (Hagan et al., 1996):

$$W_{fws} = \theta_s / \theta_f \qquad [10.10]$$

where: W_{fws} = the WEPP moisture function used to compute decomposition of surface residue, θ_s = water content (volume of water/volume of bulk soil) of the surface soil layer, which is thinner than the WEPP tilled soil layer, and θ_f = field capacity water content of the surface soil layer (volume water/volume of bulk soil), which is considered to be the optimum water content for decomposition. Soil water content in the surface soil layer is affected by precipitation, infiltration, drainage, and extraction. Consequently, WEPS decomposition should be a function of soil and cover-management.

As illustrated in Figure 10.17, RUSLE2 computed decomposition values compared well with WEPS computed values for locations where temperature rather than moisture was the factor limiting decomposition. However, a difference in trend between the RUSLE2 and WEPS compuated values was apparent at these locations where computed

---

[74] Bulk soil includes the volume of both soil particles and pore space.

decomposition rates were less for WEPS than for RUSLE2 during the maximum precipitation period. WEPS computed decomposition was significantly less than RUSLE2 computed decomposition at Tucson, Arizona. RUSLE2 computed less decomposition during the dry periods at Tucson than did WEPS. WEPS computed much less decomposition than did RUSLE2 at Dallas, Texas. The distinguishing feature at Dallas is a double peaked precipitation pattern. Precipitation (≈ 2.1 inches/month) in July and August is about half the precipitation in April and May (≈ 4.6 inches) and September and October (≈ 3.6 inches/month). In contrast to Tucson where RUSLE2 computed less decomposition than did WEPS, RUSLE2 computed more decomposition at Dallas than did WEPS.

Apparently the WEPS soil moisture values are dampened more than are the RUSLE2daily precipitation values used to compute decomposition, even at locations where precipitation is moderately high and greater such as Columbia, Missouri; Holly Springs and Gulfport, Mississippi; and Mobile, Alabama. This same dampening may be responsible for the differences at Tucson and Dallas.

These differences raise questions about the adequacy of the WEPS computed soil moisture values at all locations, but especially at locations where monthly precipitation changes greatly in a short time, and how well the RUSLE2 moisture function performs in dry regions. The decomposition data illustrated in Figure 10.2 are inadequate to definively make a determination about RUSLE2's moisture function used to compute decomposition or to show whether RUSLE2 or WEPS better computes decomposition.

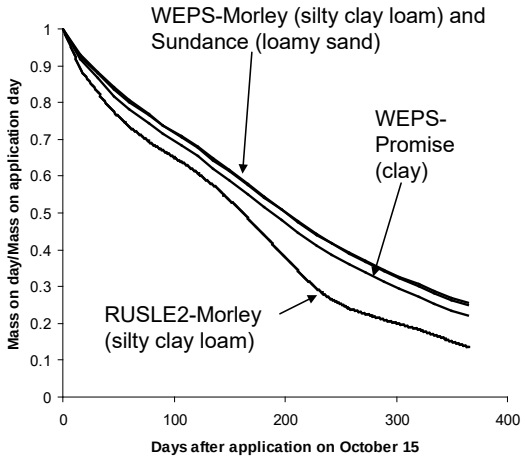

Figure 10.19. Effect of soil texture on WEPS computed decomposition at Dallas, Texas.

Figure 10.19 shows WEPS computed decomposition values for three soil textures at Dallas, Texas. The effect of soil texture on WEPS computed decomposition values are not great. RUSLE2 does not consider soil textue in its decomposition computations.

Figure 10.20 shows the effect of soil disturbance on WEPS computed decomposition. Whether the soil was only moldboard plowed or was moldboard plowed and disked had no effect on WEPS computed decomposition. However, WEPS computed increased decomposition for a soil not disturbed, which is the appropriate direction for computing decomposition for no-till farming practices.

10.3.4.3. Temperature function

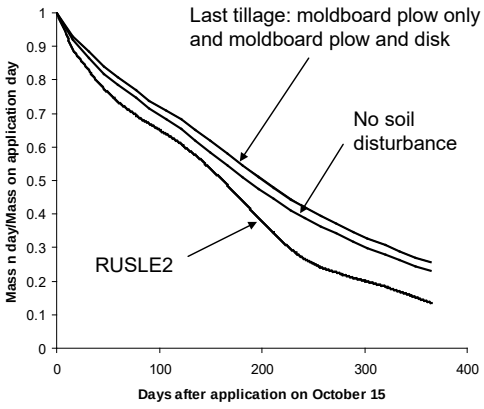

Figure 10.20. Effect of soil disturbance on WEPS computed decomposition

The same basic temperature function, equation 10.6, is used in RUSLE2, WEPP, WEPS, and RWEQ. Both RUSLE2 and WEPP compute a daily temperature function value using average daily temperature computed as the average of the maximum and minimum temperature for the day. RWEQ and WEPS compute a daily temperature function value by computing a temperature function value for both the daily maximum and minimum temperatures and averaging those two temperature function values. RUSLE2 and RWEQ use long term daily and monthly temperature values, respectively, whereas WEPP and WEPS uses stochastically generated daily temperature values.[75]

Each model uses slightly different values for the variables A and optimum temperature T_o in equation 10.6. For example, RWEQ and WEPS use A = 0 ^oC whereas RUSLE2 uses A = - 8 ^oC to compensate for using long-term average daily temperature in RUSLE2. RUSLE2 computes decomposition for a long term average daily temperature as low as -10 ^oC. In WEPP, A = -6.1 ^oC, which compensates for use of daily average temperature in computing a daily temperature function value. The optimum temperature value use in RUSLE2, RWEQ, and WEPS is 32 ^oC while 33 ^oC is used in WEPP.

RUSLE2 and WEPP compute almost identical long term average decomposition for conditions where the temperature function entirely controls rather than the moisture function. Little of the differences between RUSLE2 and WEPS in Figure 10.17 appear to be caused by differences in the temperature functions used to compute decomposition.

The RWEQ/WEPP temperature function approach is superior at high temperatures to the RUSLE2 approach. Flattening the temperature function around the optimum temperature, T_o in equation 10.6 would improve the RUSLE2 temperature function. The best approach would be to replace the RUSLE2 temperature function as described by Schomberg et al. (2002).

The end result is that RUSLE2 computed temperature function values at high temperatures were not a significant factor in fitting the measured decomposition data illustrated in Figure 10.2. In each case, the moisture function was limiting rather than the temperature function when temperatures were high. At low temperatures, the

[75] The RUSLE2 input is long term average monthly that RUSLE2 disaggreagtes into daily temperatures.

temperature function was limiting, where RUSLE2's temperature function is judged adequate.

Schomberg et al. (2002) found no improvement in the fit of RUSLE2 computed decomposition to measured data with their improved temperature function. However, their new temperature function required a decomposition coefficient ϕ value of 0.0048 day^{-1} in comparison to 0.0041 day^{-1} for the temperature function described by equation 10.6. Thus, decomposition coefficient values are moisture and temperature function dependent and model dependent in other ways including how soil moisture is computed for example.

10.3.4.4. Summary comments on RUSLE2 decomposition computations

For RUSLE2, WEPS, WEPP to give comparable long term surface residue cover estimates, decomposition data that best represents field conditions must be identified and used to calibrate all these models.

The RUSLE2 decomposition equations use simple inputs so that RUSLE2 is convenient for use in conservation and erosion control planning. The RUSLE2 purpose is not to accurately model residue decomposition processes in a research context. RUSLE2 users must be aware of RUSLE2 procedures and how to select RUSLE2 inputs to best represent residue for each particular application. Input values described in the RUSE2 User's Reference Guide and in the RUSLE2 Core Database were chosen to ensure that RUSLE2 is adequate for conservation and erosion control planning. RUSLE2 is a complex procedure that involves many mathematical relationships with numerous interactions. Input values must be carefully selected to avoid RUSLE2 computing erroneous erosion values when adjusting RUSLE2 inputs to obtain a desired value for a particular variable such as the portion of the soil surface covered by residue. Avoid changing a single variable such as the decomposition coefficient so that RUSLE2 computes an expected surface residue cover immediately before harvest.

The RUSLE2 decomposition procedures are better than those in RWEQ, a comparable model for wind erosion. Also, RUSLE2 computes decomposition values that are comparable to those computed by WEPS and WEPP, process-based models for wind and water erosion, respectively, when all three models are calibrated to the same data. The soil moisture computations in both WEPS and WEPP should be reveiwed for dry regions and regions when monthly precipitation is double peaked. Decomposition values computed by WEPS do not appear to vary much with soil texture or soil disturbance. Conquently, decomposition computed by RUSELE2 will not differ significantly from the values computed for WEPS when soil and cover-management vary at a location. Advantages of RUSLE2 are that it is robust, uses simple inputs, gives good results, and is easy to use, important attributes for its intended purpose of guiding conservation and erosion control in local field offices.

The RUSLE2 User's Reference Guide describes steps that should be observed in adjusting RUSLE2 input related to values computed for soil surface residue covered.

10.4. Standing residue

10.4.1. Decomposition

Certain operations convert live vegetation to standing residue (see **Section 8**). A portion of the standing residue is assumed to fall each day and become surface residue. Also, standing residue decomposes daily. This decomposition is computed using equations 10.3-10.6 but with a decomposition coefficient ϕ value that is 0.3 of that used to compute surface residue decomposition because reduced moisture is available for decomposition of standing residue.

RUSLE2 computes the decomposition of a unit stem mass assumed to represent decomposition at the base of standing residue stems. This decomposition is computed using equations 10.3 - 10.6 and the same decomposition coefficient ϕ value used to compute surface residue decomposition. That is, decomposition at the stem base is assumed to occur at the same rate as surface residue decomposition.

The portion of the standing residue mass that remains standing over time is assumed to be related to the portion of the remaining unit stem base mass. The RUSLE2 equation for this relationship is:

$$\gamma_t = -2.62\gamma_s^3 + 4.57\gamma_s^2 - 0.95\gamma_s \qquad [10.11]$$

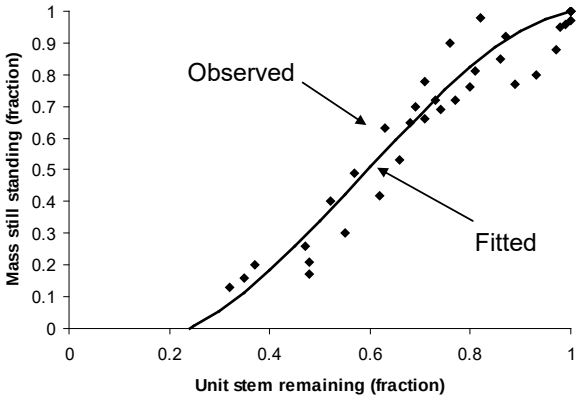

Figure 10.21. Relation of standing residue mass to computed unit stem base mass. (Data source: Steiner et al., 1994)

where: γ_t = portion (fraction) of original standing residue mass that remains and γ_s = portion (fraction) of the original unit stem base mass that remains at any given time. Equation 10.11 was derived by fitting to measured wheat data collected in Texas, Oregon, and North Dakota as illustrated in Figure 10.21 (Steiner et al., 1994). No similar data were found for other vegetation communities. However, equation 10.11 is

considered to be adequate for other plant types besides small grain.

10.4.2. Canopy cover-mass relationship

During the live period for a vegetation description, canopy cover is known directly from user input. These canopy cover values are used to estimate temporal values for live above ground biomass (see **Section 9.2.5**).

Once live above ground biomass is transferred to standing residue, the known variable is standing residue mass. This biomass is computed from standing live above ground biomass converted to standing residue on the conversion date, decomposition of standing residue over time, and the amount of the standing residue that has become surface residue computed with equation 10.11.

RUSLE2 computes canopy cover for standing residue using:

$$f_t = \mu B_t^{2/3} \qquad [10.12]$$

where: f_t = canopy cover provided by the standing residue and B_t = daily standing residue biomass (dry mass/area). The value for the coefficient μ is determined from:

$$\mu = f_{to} / B_{to}^{2/3} \qquad [10.13]$$

where: f_{to} and B_{to} = canopy cover and biomass (dry mass/area), respectively, when the standing residue is created from live above ground biomass.

10.4.3. Manning's n, effective vegetation ridge height, and effective fall height for standing residue

Values for the Manning's n and effective ridge height for standing residue are computed using:

$$n_t = n_{to}(B_t / B_{to}) \qquad [10.14]$$

$$H_t = H_{to}(B_t / B_{to}) \qquad [10.15]$$

where: n_t = the daily standing residue Manning's n, n_{to} = the live vegetation Manning's n on the day that the standing residue was created, H_t = daily effective standing residue ridge height (inches), and H_{to} = effective ridge height (inches) of the live vegetation on the day that the standing residue was created. The effective ridge height for standing residue is computed from:

$$h_f = h_{fo}(f_t / f_{to}) \qquad [10.16]$$

where: h_f = the daily effective fall height, h_{fo} = the effective fall height for the vegetation on the day that the standing residue was created, f_t = daily canopy cover, and f_{to} = the canopy cover of the vegetation on the day that the standing residue was created.

Although RUSLE2 uses a single vegetation description on any given day, RUSLE2 tracks multiple standing residue descriptions. RUSLE2 assumes that the overall Manning's n for standing residue and the overall effective ridge height for each standing residue description are the sums of the respective values for each standing residue description. The net effective fall height of the standing residue is weighted by the canopy cover for each standing residue description. These values are independent of corresponding values for live vegetation.

This approach for representing a composite of vegetation and multiple standing residue descriptions should involve interactions similar to those assumed for overlapping ground cover. However, the RUSLE2 procedure is judged to be satisfactory for conservation and erosion control planning. Only a few residue descriptions are used in most cover-management descriptions and most standing residue is removed by tillage or other operations.

10.5. List of symbols

A = a reference temperature in temperature function used to compute decomposition (-8 ^{o}C)

b = coefficient that desribes the effectiveness for a particular residue type for reducing erosion (percent^{-1})

B = mass (dry) in a particular residue/dead root pool (mass/area)

B_s = surface residue dry biomass (mass/area)

B_t = standing residue dry biomass (mass/area)

B_{to} = standing residue dry biomass on day when standing residue is created (mass/area)

c = daily cover-management factor

D = time in period over which decomposition is being computed (days)

D_p = period over which N_p precipitation events occur (days)

$D_{1/2}$ = residue half life (time)

f_g = ground (surface) residue cover (fraction)

f_{gm} = ground (surface) cover for crop residue or mulch assuming no other material is present (fraction)

f_{gn} = net ground (surface) cover provided by total surface residue mass (fraction)

f_{gr} = ground (surface) cover provided by the rock surface residue cover assuming no other surface residue is present (fraction)

f_t = canopy cover provided by the standing residue (fraction)

f_{to} = canopy cover provided by standing residue on day that standing residue is created (fraction)

g_c = daily ground cover subfactor

h_{fi} = effective fall height of standing residue (feet)

h_{fo} = effective fall height for the vegetation on day that the standing residue was created (feet)

H_t = effective standing residue ridge height (inches)

H_{to} = effective ridge height of live vegetation on day that the standing residue was created (inches)

n_t = standing residue Manning's n

n_{to} = live vegetation Manning's n on day that the standing residue was created

I = daily amount of water added by irrigation (inches)

N_p = Number of precipitation events in the period D_p

P = daily precipitation (inches)

P_b = base daily precipitation in moisture function used to compute decomposition (inches)

s_b = daily soil biomass subfactor

T = daily air temperature (^oC)

T_f = daily temperature function used to compute decomposition

T_o = optimum temperature for decomposition (^oC)

W_f = daily moisture function used to compute decomposition in RUSLE2

W_{fwe} = RWEQ moisture function used to compute decomposition

W_{fwp} = WEPP moisture function used to compute decomposition

W_{fws} = WEPS moisture function used to compute decomposition

α = coefficient in equation used to compute surface residue cover for a given residue mass [(mass/area^{-1})]

β = coefficient used to compute residue decomposition (day^{-1})

γ_s = portion of the unit stem base mass (dry basis) that remains

γ_t = portion of standing residue mass (dry basis) that remains

θ_f = field capacity moisture content (volume water/volume bulk soil)

θ_o = optimum soil moisture content for residue decomposition (volume water/volume bulk soil)

θ_s = soil moisture content for the surface soil layer (volume water/volume bulk soil)

θ_t = soil moisture content of the tilled soil layer (volume water/volume bulk soil)

μ = coefficient in equation used to compute canopy cover from standing biomass $(\text{mass/area})^{-2/3}$

ϕ = decomposition coefficient that is a function of biomass type (day^{-1})

ϕ_w = weighted decomposition coefficient for residue description composed of two or more distinct residue types (day^{-1})

Indices

i - day

11. SUMMARY

11.1. RUSLE2 overview

The Revised Universal Soil Loss Equation, Version 2, (RUSLE2) is a tool specifically developed to guide erosion control planning at the local field office. RUSLE2 computes estimates of soil erosion caused by rainfall and its associated overland flow. RUSLE2 computes soil erosion estimates based on site-specific conditions for climate, soil, topography, and land use. Typically, RUSLE2 is used to compute soil erosion estimates for alternative erosion control measures that might be applied at a specific site. The erosion control practices that result in erosion estimates less than the erosion control criteria are considered acceptable. Consequently, erosion control can be tailored to site-specific conditions and requirements by using RUSLE2.

RUSLE2 is land-use independent. It applies to all land conditions where mineral soil is exposed to the erosive forces of raindrop impact and surface runoff produced by Hortonian overland flow. This overland flow occurs when rainfall intensity exceeds the infiltration rate of rainwater into the soil. RUSLE2 applies to cropland; permanent pastureland; construction sites; military training grounds; landfills and similar waste disposal sites; rangelands; disturbed forestlands; right-away along highways, pipelines, and electric transmission lines; and other similar lands.

The basic spatial RUSLE2 computational unit is the overland flow path selected to represent the site. Surface runoff follows this path from its origin to where overland flow becomes collected in a channel. The overland flow path can be divided into segments so that RUSLE2 can capture the effects of soil, steepness, and land use conditions varying along the overland flow path. RUSLE2 computes net erosion or deposition (mass/area) for each segment, sediment load (mass/unit flow width) at the end of each segment and at the end of the overland flow path, and sediment characteristics at the detachment point and in the sediment load at the end of each segment.

RUSLE2 also computes deposition in terrace channels assuming uniform conditions along these channels and deposition in small impoundments used on overland flow areas. RUSLE2 does not compute erosion in concentrated flow areas, referred to as ephemeral gully erosion, that terminate the overland flow path.

The basic temporal RUSLE2 computational unit is the long-term average for each day during the computation period used to represent a site's land-use condition. RUSLE2 management descriptions used to represent land-use conditions can be rotations where land use conditions are repeated in cycles or non-rotations where land-use conditions exist only for a single duration. The rotation cycle duration is the computation period. Rotation-type management descriptions are typically used to represent cropland and similar land uses. Also, rotation-type management practices are used to represent permanent land-use conditions that do not change from year to year.

Non-rotation type management descriptions are used to represent one-time land use conditions, such as reclamation of construction sites and surface mines. The computation period for these examples is from final grading through the number of years required for the site to become stabilized.

RUSLE2 sums long-term average daily erosion values to compute average annual values for the computation period used in the management description, for each year, and other sub-periods within the overall computation period. The average annual erosion value for the overall computation period typically is used in erosion control planning. The RUSLE2 computed average annual erosion for the site is compared to the site's erosion control criteria, which is an allowable average annual erosion rate based on the on-site and off-site damages that soil erosion would cause.

RUSLE2 computes how temporal variability of climate, soil, and land-use conditions affects erosion. Soil erosion is greatest when periods of maximum erosivity coincide with periods when the soil is most susceptible to erosion. Climatic erosivity typically varies greatly during the year. Also, land-use conditions vary during the year, ranging from bare soil after a major mechanical disturbance to dense cover provided by mature vegetation. Even erosion susceptibility of a site in permanent vegetation can vary significantly during the year as above ground and below ground biomass grow and subside. Even if vegetative cover and soil biomass do not vary temporally, soil erodibility varies during the year. Soil erodibility is greatest during periods of high soil moisture.

11.2. RUSLE2 mathematical structure

RUSLE2 is hybrid soil erosion prediction (estimation) technology because it is a combination of the empirical, index-based Universal Soil Loss Equation (USLE) and process-based equations for the detachment, transport, and deposition of soil particles. RUSLE2 computes a long-term average daily sediment production value using the USLE factors for erosivity, soil erodibility, slope length, slope steepness, cover-management, and support practice. Each USLE factor, except the one for slope steepness, is modified in RUSLE2 to compute a daily value rather than the standard USLE average annual value.

The USLE mathematical structure is (Wischmeier and Smith, 1978):

$$A = RKLSCP$$

where: A = average annual erosion (mass/area·year), R = average annual erosivity factor (erosivity units/area·year), K = average annual soil erodibility factor (mass/erosivity unit), L = average annual slope length factor (dimensionless), S = average annual slope steepness factor (dimensionless), C = average annual cover-management factor (dimensionless), and P = average annual support practice factor (dimensionless) . Each USLE factor, except the erosivity factor, has the mathematical structure of:

$$F = \left(\sum_{i=1}^{I} f_i \phi_i \right) \Big/ N$$

where: F = average annual factor, f_i = factor value for the *ith* time period, ϕ_i = the fraction of the annual erosivity that occurs during the *ith* period, I = the number of sub-periods in the computationl period for the management description used to represent a site's land use conditions, N = number of years in the computation period. Thus, the USLE has the mathematical structure of:

$$A = R\left[\left(\sum_{i=1}^{I_k} k_i \phi_i \right) \Big/ N_k \right]\left[\left(\sum_{i=1}^{I_l} l_i \phi_i \right) \Big/ N_l \right]\left[\left(\sum_{i=1}^{I_s} s_i \phi_i \right) \Big/ N_s \right]\left[\left(\sum_{i=1}^{I_c} c_i \phi_i \right) \Big/ N_c \right]\left[\left(\sum_{i=1}^{I_p} p_i \phi_i \right) \Big/ N_p \right]$$

where: k_i = soil erodibility factor for the *ith* period (mass/erosivity unit), I_k = the number of periods in the N_k years used to determine an average annual soil erodibility factor value, l_i = slope length factor for the *ith* period (dimensionless), I_l = the number of periods in the N_l years used to determine an average annual slope length factor value, s_i = slope steepness factor for the *ith* period (dimensionless), I_s = the number of periods in the N_s years used to determine an average annual slope steepness factor value, c_i = cover-management factor for the *ith* period (dimensionless), I_c = the number of periods in the N_c years used to determine an average annual cover-management factor value, p_i = support practice factor for the *ith* period (dimensionless), and, I_p = the number of periods in the N_p years used to determine an average annual support practice factor value. In practice, the USLE mathematical structure is:

$$A = RKLS\left[\left(\sum_{i=1}^{I_c} c_i \phi_i \right) \Big/ N_c \right] P$$

where: temporally constant values for K, L, S, and P are used throughout the computation period.

The basic RUSLE1 mathematical structure is the same as the USLE structure except that a temporal soil erodibility factor is used as (Renard et al., 1997):

$$A = R\left[\left(\sum_{i=1}^{24} k_i \phi_i \right) \Big/ 24 \right] LS\left[\left(\sum_{i=1}^{24 N_c} c_i \phi_i \right) \Big/ 24\, N \right] P$$

where: each year is divided in 24 half month periods and N = years in the overall computation period. Additional sub-periods are added if an operation that disturbs the soil, vegetation, or residue occurs within a half month period.

The RUSLE2 mathematical structure is:

$$A = \left(\sum_{i=1}^{365N} r_i k_i l_i s_i c_i p_i \right) \Big/ N$$

where: r_i = daily erosivity factor (erosivity unit/year), k_i = daily soil erodibility factor (mass/area·erosivity unit), l_i = daily slope length factor (dimensionless), s_i = daily slope steepness factor (dimensionless), c_i = daily cover-management factor (dimensionless), and p_i = daily support practice factor (dimensionless), all long term averages for the *ith* day, and N = number of years in the overall computational period. In practice, a single time-invariant slope steepness S is used instead of a daily s_i slope steepness factor.

The difference in mathematical structure between the USLE, RUSLE1, and RUSLE2 results in the three methods giving different erosion estimates even when each method gives the same average annual values for each USLE factor. Also, RUSLE2 considers much more interdependence between the factors than either the USLE or RUSLE1 considers.

Fundamentally, the USLE applies to a uniform overland flow path where neither soil, steepness, cover-management, nor support practice vary along the flow path. A mathematical procedure is available to apply the USLE to non-uniform overland flow paths where deposition does not occur. The USLE can not be applied to overland flow paths where steepness along the flow path decreases sufficiently to cause deposition.

The same mathematical structure used in process-based erosion prediction technologies to compute deposition along non-uniform overland flow paths is used in RUSLE1 and RUSLE2. Deposition is computed at locations along the flow path where the sediment load exceeds surface runoff's sediment transport capacity. RUSLE2 computes deposition using the equation:

$$D_p = (\alpha V_f / q)(T_c - g)$$

where: D_p = deposition rate (mass/area·time), α = an empirically determined deposition coefficient (dimensionless), V_f = the sediment's fall velocity (length/time), q = surface runoff rate (volume/unit overland flow width·time), T_c = surface runoff's sediment transport capacity (mass/unit overflow width·time), and g =sediment load (mass/unit overflow width·time) being transported by surface runoff.

Five sediment classes (primary clay, primary silt, small aggregate, large aggregate, and primary sand) are used in RUSLE2 to represent sediment characteristics. RUSLE2 computes the distribution of the sediment among these classes and the diameters of the aggregate classes at the point of detachment as a function of soil texture. The specific gravity of the aggregate classes is about 65 percent of that for the primary particle classes. RUSLE2 computes how deposition changes sediment characteristics along the overland flow path by applying the deposition equation to each sediment class. RUSLE2 also computes an enrichment ratio based on the specific surface of the sediment load and the specific surface area of the surface soil.

Both the deposition and sediment transport capacity equations are functions of runoff rate. A daily runoff rate index is computed using the NRCS runoff curve number method and the 10 year-24 hour precipitation amount. RUSLE2 computes a daily curve number value as a function of daily cover-management variables.

RUSLE2 computes how soil surface conditions affect runoff's sediment transport capacity. The computation is based on a division of runoff shear stress between that acting on roughness elements, including live vegetation, standing residue, surface residue cover and soil surface roughness, and that acting on the soil grain roughness, which is the part responsible for sediment transport. A daily division of shear stress is computed using daily cover-management variables.

RUSLE2's erosivity and soil erodibility definitions and variables are the same as those used by the USLE, which are based on the unit-plot concept. Also, RUSLE2 can use the standard USLE soil erodibility nomograph to compute soil erodibility factor values for undisturbed soil profiles or a modified nomograph for highly disturbed soil conditions. RUSLE2 computes a daily erodibility factor value that is varied about the base soil erodibility factor values using daily precipitation and temperature values. Daily erosivity is computed as the product of average annual erosivity and the fraction of the annual erosivity that occurs on each day.

The RUSLE2 slope length factor, which is the same as the USLE and RUSLE1 slope length factor, is given by:

$$l_x = \left(x/\lambda_u\right)^m$$

where: l_x = slope length factor used to compute erosion at any location x along an overland flow path (dimensionless), λ_u = unit plot length, and m = a slope length factor exponent. Sediment is detached from the soil mass on overland flow area by impacting raindrops (interrill erosion) and surface runoff (rill erosion). Interrill erosion is uniform along a uniform overland flow path, in which case the exponent m = 0. Rill erosion increases along an overland flow path as runoff increases, in which case m = 1. RUSLE2 computes a daily exponent value (between 0 and 1) that depends on the ratio of rill-to-interrill erosion. This ratio is computed as a function of how soil texture, slope steepness, and surface cover affects rill erosion relative to interrill erosion. The rill-to-interrill erosion ratio changes daily as cover-management changes daily.

The RUSLE2 slope steepness factor is the same as the one used in RUSLE1. This factor is time invariant in RUSLE2.

11.3. Land use subfactors

11.3.1. Cover-management subfactors

The use of basic cover-management variables to compute daily cover-management factor and runoff curve number values gives RUSLE2's its land-use independence. Cover-management factor values are computed as the product of several subfactors. These subfactors are canopy, ground (surface) cover, soil surface roughness, soil ridging, soil consolidation, soil biomass, and ponding. An additional soil moisture subfactor is used when RUSLE2 is applied to cropland in certain areas of the northwestern US.

The canopy subfactor describes how above ground canopy (cover that does not touch the soil surface) affects rainfall erosivity. The variables used in this subfactor include fraction of the soil surface covered by canopy and effective fall height of water drops falling from the canopy. RUSLE2 includes equations that estimate effective fall height based on top and bottom canopy heights, canopy shape, and the vertical gradient of canopy mass.

In contrast to canopy cover, ground (surface) cover rests directly on the soil surface. The main component of the equation that computes ground cover subfactor is:

$$c_g = \exp(-bf_g)$$

where: c_g = the subfactor for ground cover. **b** = coefficient for effectiveness of ground cover for reducing erosion (percent^{-1}), and f_g = ground cover (percent). The **b** coefficient, which is a measure of the effectiveness of ground cover for reducing erosion, is a function of the rill-to-interrill erosion ratio. RUSLE2 computed **b** values vary from 0.025 when the erosion is entirely interrill erosion to 0.06 when the erosion is entirely rill erosion. An additional soil surface roughness term is added to this equation in RUSLE2 to account for surface cover having less effect as soil surface roughness increases.

The soil surface roughness subfactor represents how soil surface roughness influences erosion by reducing runoff's erosivity, by causing deposition in local depressions, and by ponding water that protects a portion of the soil surface from direct raindrop impact. Daily soil surface roughness subfactor values are computed as a function of the daily soil surface roughness index. Soil surface roughness decreases daily from the initial soil surface roughness left by a mechanical soil disturbance. RUSLE2 computes the daily decrease in the soil surface roughness index using values for daily precipitation and daily interrill erosion. The soil surface roughness index value left after a mechanical soil disturbance is computed as a function of the soil surface roughness index that exists at the time of the soil disturbance, the soil surface roughness index created by the mechanical soil disturbance applied to a standard soil condition, soil texture, soil biomass, and the degree that the mechanical soil disturbance obliterates existing soil surface roughness.

The soil ridging subfactor represents the effect of ridge side slope on interrill erosion. The soil ridging subfactor is a function of daily ridge height, which is a surrogate for ridge side slope. RUSLE2 decreases daily ridge height from an initial ridge height left by

a mechanical soil disturbance as a function of daily precipitation and daily interrill erosion.

The soil consolidation subfactor represents how a bare soil without soil biomass becomes less erodible over time as the soil experiences wetting and drying cycles. Soil consolidation in RUSLE2 refers to the re-bonding of soil particles after a mechanical soil disturbance. The RUSLE2 assumption is that mechanical soil compaction (increase in soil bulk density) does not decrease erosion. RUSLE2 computes soil consolidation subfactor values as a function of the time since the last mechanical soil disturbance. The RUSLE2 time to soil consolidation is seven years but increases to 20 years where average annual precipitation is less than 30 inches.

The soil biomass subfactor represents how soil biomass reduces erosion. RUSLE2 computes daily soil biomass subfactor values as a function of the daily amounts of live roots, dead roots, and buried biomass in the soil and the soil consolidation subfactor. Plant litter, crop residue, manure, and other types of biomass on the soil surface that is incorporated in the soil by mechanical soil disturbance adds to buried soil biomass. Also, injection of manure, sewage sludge, and other organic materials into the soil adds soil biomass. The runoff and erosion reduction computed by the soil biomass subfactor significantly increases as the soil becomes “consolidated” after a mechanical soil disturbance.

The ponding subfactor accounts for how a water layer on the soil surface decreases raindrop impact erosivity in high rainfall regions where land is nearly flat. The variables used to compute ponding subfactor values are land steepness and daily runoff depth, which in turn is a function of the 10 year-24 hour precipitation amount, soil properties, and cover-management.

The antecedent soil moisture subfactor, which is used only on cropland in the northwestern US, accounts for how previous cropping reduces soil moisture that in turn reduces erosion in subsequent cropping periods.

11.3.2. Support practice subfactors

The contouring subfactor computes how contour ridging affects rill erosion and sediment transport by redirecting surface runoff. Contouring subfactor values are computed as a function of daily runoff rate, overland flow path steepness, and ridge-furrow grade

RUSLE2 computes the location along an overland flow path (critical slope length) beyond which contour ridges fail. This computation is a function of the daily runoff rate, daily cover-management conditions, and land steepness.

RUSLE2 computes how profile shape(uniform, convex, concave, and complex) along the overland flow path affects erosion, deposition, and sediment yield from the overland flow path represented in a RUSLE2 computation. RUSLE2 computes the amount of deposition on concave portions of the overland flow path, how this deposition affects sediment characteristics by enriching the sediment in fine and less dense particles.

Strips of dense vegetation placed along overland flow paths can significantly reduce erosion and sediment yield. RUSLE2 computes the reduction in sediment production, the amount of deposition caused by the dense vegetation strips, and the change in sediment characteristics.

Terraces and diversions placed along an overland flow path reduce erosion by decreasing overland flow path length. RUSLE2 also computes deposition and its effect on sediment characteristics in low grade terraces assuming a uniform terrace grade. RUSLE2 does not compute erosion by flow in these channels.

RUSLE2 computes deposition in small impoundments such as small sediment basins used on construction sites and small impoundments created by parallel tile outlet terrace systems. A simple settling-type equation is used to compute deposition by sediment particle class.

The deposition computed by RUSLE2 depends on the characteristics of the sediment reaching the deposition area. Sediment characteristics at the point of detachment are computed as a function of soil texture, but deposition along the overland flow path enriches the sediment in fines and less dense particles that are deposited less readily. Consequently, less deposition is computed in dense grass strips, terrace channels, and in impoundments if upstream deposition has been computed.

RUSLE2 computes how irrigation affects erosion caused by rainfall and its associated overland flow. RUSLE2 takes into account increased yield and increased soil moisture, which increases biomass decomposition and soil erodibility, caused by the irrigation. RUSLE2 does not compute the erosion directly caused by irrigation itself.

The subsurface drainage subfactor represents how subsurface drainage reduces erosion by reducing surface runoff. This subfactor is based on how much subsurface drainage reduces a soil's runoff potential. The runoff potential (permeability) subfactor in RUSLE2's computation of unit-plot soil erodibility is used to adjust the soil erodibility value to account for the subsurface drainage effect.

11.4. Biomass accounting

Biomass on and in the soil has a great effect on soil erosion. The input value for production (yield) level provides the starting point for RUSLE2's biomass accounting. RUSLE2 tracks the conversion of live standing vegetation to dead standing residue by natural and mechanical processes. RUSLE2 accounts for soil surface biomass accumulation from standing residue becoming surface residue caused by standing residue falling by natural processes and mechanical events, by litter fall, and by events that add surface biomass such as straw mulch applications. RUSLE2 estimates the biomass in litter added to the soil surface by senescence based on the decrease in canopy cover.

The RUSLE2 sources of soil biomass are live and dead roots, soil surface biomass that is buried by mechanical soil disturbance, decomposed soil surface biomass that is added to soil, and biomass injected into the soil. RUSLE2 adds the daily decrease in live root

biomass to dead root biomass. Live roots decrease annually as a part of the growth cycle of perennial vegetation, and live roots become dead roots when vegetation is killed by a mechanical operation or a natural process such as frost.

RUSLE2 computes the daily decomposition loss of standing residue, surface residue, buried residue, and dead roots as a function of daily precipitation and temperature. The same decomposition coefficient value is used for all plant parts and whether the material is on the soil surface or buried in the soil. However, the decomposition coefficient for standing dead vegetation is assumed to be 30 percent of that for surface and buried material.

RUSLE2 uses a specific set of rules to transfer biomass between standing residue, surface residue, and buried residue pools. For example, live above ground biomass must be converted first to standing residue before live vegetation biomass can become surface residue. Next, standing residue must be converted to soil surface residue. Only surface residue can be buried. That is, standing residue can not be directly buried without first being converted to surface residue. A mechanical soil disturbing operation is required to bury or place residue in the soil, and a mechanical soil disturbing operation is required to resurface previously buried residue.

11.5. Cover-management descriptions

Users provide a cover-management description that RUSLE2 uses to compute how cultural practices affect erosion. A RUSLE2 cover-management description is a list of operations by date, vegetation descriptions and production levels (yields), and residue descriptions and amounts for material added to the soil surface or injected into the soil. A cover-management description is a rotation when the list of operations are repeated in a cycle with a particular duration, which is typical for cropland and permanent vegetation, or a non-rotation when each operation occurs only once over a particular duration, which is typical of construction sites.

11.6. Operation descriptions

Operations are events that affect the soil, vegetation, or residue. The user selects from several processes to describe the effects of an operation. **Begin growth** is the process that tells RUSLE2 to begin using data in a particular vegetation description on a particular date. **Add residue** is used to apply mulch. A residue description that describes the mulch characteristics is assigned in the cover-management description. **Kill vegetation** is the process used to convert live vegetation to standing residue and live roots to dead roots. It is used to describe harvest of an annual crop and to describe frost killing annual vegetation.

The **disturb soil** process describes a mechanical soil disturbance. For example, the operation description for a heavy offset disk includes a **disturb soil** process. The **disturb soil** process includes inputs for burial and resurfacing values for each of the five RUSLE2 residue types, the fraction of the standing residue that is converted to surface residue, the fraction of surface residue that is buried, and the fraction of the buried residue that is

resurfaced by the operation. The **disturb soil** process includes a designation for whether the operation buries residue by inverting the soil, by mixing the residue with the soil, by a combination of mixing and inversion, or by pressing the residue into the soil. The **disturb soil** process also includes values for soil disturbance depth, surface roughness left by the operation for a standard condition, and ridge height left by the operation, the degree that the operation obliterates existing soil roughness , and fraction of the soil surface disturbed by the operation.

An operation such as straw baling may include a **remove residue** process to describe reduction in surface residue cover after a small grain harvest, for example.

An operation description can include multiple processes. The sequence of the processes is critically important. For example, having an **add residue** process before a **disturb soil** process gives a very different surface residue cover than if the **add residue** process comes after the **disturb soil** process.

11.7. Vegetation descriptions

Computing the effects of vegetation on erosion is an important RUSLE2 feature. RUSLE2 uses values for vegetation variables including temporal canopy cover, effective fall height, live above ground biomass, and root biomass to compute cover-management subfactor and runoff values. Values for these variables are entered in vegetation descriptions.

RUSLE2 does not model vegetation growth as a function of environmental conditions. Instead RUSLE2 vegetation descriptions apply in particular ecological zones. Each vegetation description is for a particular base production (yield) level. The RUSLE2 user chooses the vegetation description for the site where RUSLE2 is being applied and a appropriate yield for the site is entered in the cover-management description. RUSLE2 adjusts the base vegetation description values according to the input yield value for the site.

11.8. Residue descriptions

A residue description is assigned to each vegetation description to describe the characteristics of residue produced by the vegetation. Also, a residue description is used to describe material added to the soil surface (e.g., straw mulch) and material (e.g., sewage sludge) injected into the soil. The residue description includes a decomposition coefficient value that describes how rapidly the residue decomposes under a standard condition, the fraction of the soil surface covered by a given residue mass, and designation of residue type that denotes the fragility of the residue and how well the residue conforms to the soil surface.

11.9. Climate descriptions

Climate descriptions contain the data on long term average monthly precipitation, temperature, and erosivity values that RUSLE2 uses to compute erosion. Each climate description is for a particular location, county, or rainfall zone.

11.10. Soil descriptions

Soil descriptions contain data on soil properties that RUSLE2 uses to compute erosion and deposition. These properties include soil texture, soil erodibility, runoff potential, rock cover, and time to soil consolidation, all for the reference unit plot condition. RUSLE2 includes soil erodibility nomographs that are used to estimate soil erodibility values from values for basic soil properties.

11.11. RUSLE2 databases

The user runs RUSLE2 by making menu selections from the RUSLE2 database. Each description in the database is stored by an identifier name. In a typical RUSLE2 application, the user selects a climate description by location, soil description by soil mapping unit or some other designator, cultural practice by a cover-management description identifier, and support practices by their identifiers, all appropriate for the site specific conditions. The user enters overland path steepness and length values based on the overland flow path chosen to represent the site.

A wide array of RUSLE2 descriptions, especially for cropland, is available from the USDA-Natural Resources Conservation Service (NRCS). Information can be downloaded and imported into your working RUSLE2 database from the NRCS National RUSLE2 Database and from the database of other RUSLE2 users.

Users can adjust values stored in their working RUSLE2 database to better match site conditions. Also, users can create new database entries. New user chosen values must be consistent with values in the RUSLE2 **Core Database**. RUSLE2 was calibrated using a particular set of **core values**. User input values must be consistent with these **core values** in order to obtain good results with RUSLE2 regardless of how much a user may disagree with the **core values**. If a **core value** were to be changed, other RUSLE2 internal or input values would have to be changed as well, because RUSLE2 has been calibrated to give desired erosion estimates with the **core value**. These core values are contained in the RUSLE2 **Core Database**.

11.12. RUSLE2 validation

The equations for the subfactors were primarily calibrated using data from Agriculture Handbook 537 (Wischmeier and Smith, 1978), which is a summary of more than 10,000 plot-years of data. Additional data from the literature were used to calibrate the equations for conditions not represented by the AH537 data. Erosion values were computed with RUSLE2 for a wide range of conditions, including conditions not represented by existing research data. These values were inspected to ensure that they

were consistent with the available research data and consistent with professional judgment.

Ground (surface) cover is perhaps the single most important RUSLE2 variable, at least for cropland conditions. The surface cover left by a cropping system immediately after planting in a key variable used by soil conservationists in judging the effectiveness of a particular cropping system. The adequacy of RUSLE2 for estimating surface cover was very carefully evaluated. An extensive array of literature was reviewed in this evaluation. Scientists have reported differences in RUSLE2 estimates with those made by other comparable erosion models. When RUSLE2 is fitted to the same data used to fit other methods, RUSLE2's estimates of surface cover are almost the same as those estimated by other methods for long term average conditions. The differences were primarily caused by variability in residue data and by differences in techniques used to measure residue mass as it decomposes.

11.13. List of symbols

A = average annual erosion (mass/area·year)

b = coefficient for effectiveness of ground cover for reducing erosion (percent^{-1})

c_g = the subfactor for ground cover (dimensionless)

c_i = cover-management factor for the *ith* period (dimensionless)

C = average annual cover-management factor (dimensionless)

D_p = deposition rate (mass/area·time)

f_g = ground cover (percent)

f_i = factor value for the *ith* time period

F = average annual factor

g =sediment load (mass/unit overflow width·time)

I = the number of sub-periods in the computation period for the management description used to represent a site's land use conditions

I_c = the number of periods in the N_c years used to determine an average annual cover-management factor value

I_k = the number of periods in the N_k years used to determine an average annual soil erodibility factor value

I_l = the number of periods in the N_l years used to determine an average annual slope length factor value

I_p = the number of periods in the N_p years used to determine an average annual support practice factor value

I_s = the number of periods in the N_s years used to determine an average annual slope steepness factor value,

k_i = soil erodibility factor for the *ith* period (mass/erosivity unit)

K = average annual soil erodibility factor (mass/erosivity unit)

l_i = slope length factor for the *ith* period (dimensionless)

l_x = slope length factor used to compute erosion at any location x along an overland flow path (dimensionless)

L = average annual slope length factor (dimensionless)

m = a slope length factor exponent

N = number of years in the computation period

N_c = number of years used to determine an average annual cover-management factor value

N_k = number of years used to determine an average annual soil erodibility factor value

N_l = number of years used to determine an average annual slope length factor value

N_s = number of years used to determine an average annual slope steepness factor value

p_i = support practice factor for the *ith* period (dimensionless)

P = average annual support practice factor (dimensionless)

q = surface runoff rate (volume/unit overland flow width·time)

r_i = erosivity factor for the *ith* period (erosivity unit/area·year)

R = average annual erosivity factor (erosivity unit/area·year)

s_i = slope steepness factor for the *ith* period (dimensionless)

S = average annual slope steepness factor (dimensionless)

T_c = surface runoff's sediment transport capacity (mass/unit overflow width·time)

V_f = the sediment's fall velocity (length/time)

x = distance along overland flow path (length)

α = an empirically determined deposition coefficient (dimensionless)

ϕ_i = the fraction of the annual erosivity that occurs during the *ith* period

λ_u = unit plot length (72.6 ft, 22.1 m)

Indices

i - time period (days)

12. REFERENCES

12.1. References cited

RUSLE2 User's Reference Guide (in publication)

Alberts, E.E. and W.D. Schrader. 1980.Cornstalk decomposition on a till-planted watershed. Agronomy Journal. 72:709-712.

Alberts, E.E., M.A. Nearing, M.A. Weltz, L.M. Risse, F.B. Pierson, X.C. Zhang, J.M. Laflen, and J.R. Simanton. 1995. Soil component. Capter 7. In: D.C. Flanagan and M.A. Nearing (editors). 1995. Technical Documentation, USDA-Water Erosion Prediction Project (WEPP). NSERL Report No. 10. National Soil Erosion Research Laboratory, Agricultural Research Service, U.S. Department of Agriculture. Washington, D.C.

Alonso, C.V., W.H. Neibling, and G.R. Foster. 1981. Estimating sediment transport capacity in watershed modeling. Transactions of the American Society of Agricultural Engineers 24:1211-1220, 1226.

Barfield, B.J., R.I. Barnhisel, M.C. Hirschi, and I.D. Moore. 1988. Compaction effects on erosion of mine spoil and reconstructed topsoil. Transactions of the American Society of Agricultural Engineers 31:447-452

Bengston, R.I. and G. Sabbage. 1988. USLE P-factor for subsurface drainage in a hot, humid climate. ASAE Paper 88-2122. American Society of Agricultural Engineers. St. Joseph, MI.

Birk, E.M. and R.W. Simpson. 1980. Steady state and the continuous input model of litter accumulation and decomposition in Australian Eucalypt forests. Ecology. 6:481-485.

Bonta, J.V. and W.R. Hamon. 1980. Preliminary evaluations of a sediment pond draining a surface mined watershed. Symposium on Surface Mining Hydrology, Sedimentology, and Reclamation. University of Kentucky. Lexington, KY. 371-381.

Borst, H.L.., A.G. McCall, and F.G. Bell. 1945. Investigations in erosion control and reclamation of eroded land at the Northwest Appalachian Conservation Experiment Station, Zanesville, Ohio, 1934-42. Technical Bulletin 888. U.S. Department of Agriculture, Washington, DC.

Box, J.E., Jr. 1981. The effects of slaty fragments on soil erosion by water. Soil Science Society of America Journal. 45:111-116.

Box, Jr, J.E. and E.N. Bui. 1993. Growing corn roots effects on interrill soil erosion. Soil Science Society of America Journal. 57:1066-1070.

Brenneman, L.G. and J.M. Laflen. 1982. Modeling sediment deposition behind corn residue. Transactions of the American Society of Agricultural Engineers. 25:1245-1250.

Broder, M.W. and G.H. Wagner. 1988. Microbial colonization and decomposition of corn, wheat, and soybean residue. Soil Science Society of America Journal. 52:112-117.

Brown, L.C., and G.R. Foster. 1987. Storm erosivity using idealized intensity distributions. Transactions of American Society of Agricultural Engineers 30(2):379-386.

Brown, L.C., G.R. Foster, and D.B. Beasley. 1989. Rill erosion as affected by incorporated crop residue and seasonal consolidation. Transactions of American Society of Agricultural Engineers 32:1967-1978, 1979.

Brown, L.C., R.K. Wood, and J.M. Smith. 1992. Residue management and demonstration and evaluation. Applied Engineering in Agriculture. 8:333-339.

Browning, F.M., R.A. Norton, A.G. McCall, and F.G. Bell. 1948. Investigations in erosion control and reclamation of eroded land at the Missouri Valley Loess Conservation Experiment Station, Clarinda, Iowa, 1931-42. Technical Bulletin 959. U.S. Department of Agriculture, Washington, DC.

Chapman, G. 1948of raindrops and their striking force at the soil surface in a red pine plantation. Transactions of the American Geophysical Union. 29:664-670.

Chow, V.T., 1959. Open-channel hydraulics. McGraw-Hill Book Co. New York, NY.

Cogo, N.C., W.C. Moldenhauer, and G. R. Foster. 1984. Soil loss reduction from conservation tillage practices. Soil Science Society of American Journal 48:368-373.

Colvin, T. S. and J. E. Gilley. 1987. Crop residue - soil erosion combatant. Crops and Soils 39:7-9.

Cooley, K.R. 1980. Erosivity values for individual design storms. Journal of Irrigation and Drainage Engineering Division. American Society of Civil Engineers 106:135-145.

Copley, T.L., L.A. Forrest, A.G. McCall, and F.G. Bell. 1944. Investigations in erosion control and reclamation of eroded land at the Central Piedmont Conservation Experiment Station, Statesville, North Carolina, 1930-40. Technical Bulletin 873. U.S. Department of Agriculture, Washington, DC.

Dabney, S.M., Meyer, L.D., Harmon, W.C., Alonso, C.V., and Foster, G.R. 1995. Runoff and soil loss from cotton plots with and without stiff-grass hedges. Transactions of the American Society of Agricultural Engineers. 38:1719-1729.

Dabney, S.M. 2005. Utility of mesh bag vs. grab sampling methods of measuring residue decomposition for calibrating RUSLE2 residue decomposition routines. Unpublished report. National Sedimentation Laboratory. Agricultural Research Service, U.S. Department of Agriculture. Oxford, Mississippi.

Daly, C., G. Taylor, and W. Gibson. 1997. The PRISM approach to mapping precipitation and temperature, 10th Conf. on Applied Climatology, American. Meteorological Society.

Daniel, H.A., H.M. Elwell, and M.B. Cox. 1943. Investigatins in erosion control and reclamation of eroded land at the Red Plains Cnservation Experiment Station, Guthrie, Oklahoma, 1930-40. Technical Bulletin 837. U.S. Department of Agriclture, Washington D.C.

Desmet, P.J.J. and G. Govers. 1996. A GIS procedure for automatically calculating the USLE LS factor on topographically complex landscape units. Journal of Soil and Water Conservation Service 51:427-433.

Dickey, E.C., C.R. Fenster, J.M. Lalen, an R.H. Mickelson. 1983. Effects of tillage on soil erosion in a wheat-fallow rotation. Transactions of the American Society of Agricultural Engineers. 26:814-820.

Dickey, E.C., D.P. Shelton, P.J. Jasa, and T.R. Peterson. 1985. Soil erosion from tillage systems used in soybean and corn residues. Transactions of the American Society of Agricultural Engineers. 28:1124-1129, 1140.

Dissmeyer, G.E. and G.R. Foster. 1981. Estimating the cover-management factor (C) in the universal soil-loss equation for forest conditions. Journal of Soil and Water Conservation 36:235-240.

Douglas, Jr., C.L., R.R. Allmaras, P.E. Rassmussen, R.E. Ramig, and N.C. Roager, Jr. 1980. Wheat straw composition and placement effects on decomposition in dryland agriculture of the Pacific Northwest. Soil Science Society of America Journal. 44:833-837.

Dubeux, Jr., J. C. B.; L. E. Sollenberger, J. M. B. Vendramini, R. L. Stewart, Jr. and S. M. Interrante. (2006). Litter Mass, Deposition Rate, and Chemical Composition in Bahiagrass Pastures Managed at Different Intensities. 46:1299-1304.

Elliot, W.J., J.M. Laflen, K.D. Kohl, K.D. 1989. Effect of soil properties on soil erodibility. ASAE Paper 89-2150. American Society of Agricultural Engineers. St. Joseph, MI.

Ellison, W.D. 1947. Soil erosion studies. Agricultural Engineering. 145-146, 197-201, 245-248, 297-300, 349-351, 402-405, 442-444.

El-Swaify, S.A. and E.W. Dangler. 1976. Erodibilities of selected tropical soils in relation to structural and hydrologic properties. In: Soil Erosion: Prediction and Control. Soil and Water Conservation Society of America. Ankeny, IA. pp. 105-114.

Fennessey, L.A.J. and A.R. Jarrett. 1997. Influence of principal spillway geometry and permanent pool depth on sediment retention of sedimentation basins. Transactions of the American Society of Agricultrual Engineers. 40:53-59.

Finkner, S.C., M.A. Nearing, G.R. Foster, and J.E. Gilley. 1989. A simplified equation for modeling sediment transport capacity. Transactions of American Society of Agricultural Engineers 32:1545-1550.

Flanagan, D.C., G.R. Foster, W.H. Neibling, and J.P. Burt. 1989. Simplified equations for filter strip design. Transactions of American Society of Agricultural Engineers 32(6):2001-2007.

Flanagan, D.C. and M.A. Nearing (editors). 1995. Technical Documentation, USDA-Water Erosion Prediction Project (WEPP). NSERL Report No. 10. National Soil Erosion Research Laboratory, Agricultural Research Service, U.S. Department of Agriculture. Washington, D.C.

Formanek, G.E, E. Ross, and J. Istok. 1987. Subsurface drainage for erosion reduction on croplands of northwestern Oregon. In: Irrigation Systems of the 21st Century. Proceeding Irrigation Division Specialty Conference. American Society of Civil Engineers. New York, NY. pp. 25-31.

Foster, G.R. and L.D. Meyer. 1972. Transport of soil particles by shallow flow. Transactions of the American Society of Agricultural Engineers 15:99-102.

Foster, G.R. and W.H. Wischmeier. 1974. Evaluating irregular slopes for soil loss prediction. Transactions of the American Society of Agricultural Engineers 17(2):305-307.

Foster, G.R. and L.D. Meyer. 1975. Mathematical simulation of upland erosion by fundamental erosion mechanics. *In:* Present and Prospective Technology for Predicting Sediment Yields and Sources. ARS-S-40 U.S. Department of Agriculture. pp. 190-204.

Foster, G.R., L.D. Meyer, and C.A. Onstad. 1977a. An erosion equation derived from basic erosion principles. Transactions of the American Society of Agricultural Engineers 20:678-682.

Foster, G.R., L.D. Meyer, and C.A. Onstad. 1977b. A runoff erosivity factor and variable slope length exponents for soil loss estimates. Transactions of the American Society of Agricultural Engineers 20:683-687.

Foster, G.R. L.J. Lane, J.D. Nowlin, J.M. Laflen, and R.A. Young. 1980a. A model to estimate sediment yield from field sized areas: Development of model. *In:* CREAMS - a field scale model for Chemicals, Runoff, and Erosion from Agricultural Management Systems. Vol. I: Model Documentation. Conservation Research Report No. 26. U.S. Department of Agriculture. pp. 36-64.

Foster, G.R., L.J. Lane, and J.D. Nowlin. 1980b. A model to estimate sediment yield from field sized areas: Selection of parameter values. *In:* CREAMS - a field scale model for Chemicals, Runoff, and Erosion from Agricultural Management Systems. Vol. II: User Manual. Conservation Research Report No. 26. U.S. Department of Agriculture. pp. 193-281

Foster, G.R., W.H. Neibling, S.S. Davis, and E.E. Alberts. 1980c. Modeling particle segregation during deposition by overland flow. *In:* Proceedings of Hydrologic Transport Modeling Symposium. American Society of Agricultural Engineers. St. Joseph, MI. pp. 184-195.

Foster, G.R. and V.A. Ferreira. 1981. Deposition in uniform grade terrace channels. *In:* Crop Production with Conservation in the 80's. American Society of Agricultural Engineers. St. Joseph, MI. pp. 185-197.

Foster, G.R., L.J. Lane, J.D. Nowlin, J.M. Laflen, and R.A. Young. 1981a. Estimating erosion and sediment yield on field sized areas. Transactions of the American Society of Agricultural Engineers 24:1253-1262.

Foster, G.R., D.K. McCool, K.G. Renard, and W.C. Moldenhauer. 1981b. Conversion of the universal soil loss equation to SI metric units. Journal of Soil and Water Conservation 36:355-359.

Foster, G.R. 1982. Modeling the erosion process. Chapter 8. *In:* Hydrologic Modeling of Small Watersheds. C.T. Haan, H.P. Johnson, D.L. Brakensiek, eds. American Society of Agricultural Engineers. St. Joseph, MI. pp. 297-382.

Foster, G.R., C.B. Johnson, and W.C. Moldenhauer. 1982a. Critical slope lengths of unanchored cornstalk and wheat straw residue. Transactions of the American Society of Agricultural Engineers 25:935-939, 947.

Foster, G.R. C.B. Johnson, and W.C. Moldenhauer. 1982b. Hydraulics of failure of unanchored cornstalk mulches for erosion control. Transactions of the American Society of Agricultural Engineers 25:940-947.

Foster, G.R., L.J. Lane, W.R. Osterkamp, and D.W. Hunt. 1982c. Effect of discharge on rill erosion. Paper No. 82-2572. American Society of Agricultural Engineers. St. Joseph. MI.

Foster, G.R., F. Lombardi, and W.C. Moldenhauer. 1982d. Evaluation of rainfall-runoff erosivity factors for individual storms. Transactions of the American Society of Agricultural Engineers 25:124-129.

Foster, G.R. and R.E. Highfill. 1983. Effect of terraces on soil loss: USLE P factor values for terraces. Journal of Soil and Water Conservation 38:48-51.

Foster, G.R. 1985. Understanding ephemeral gully erosion (concentrated flow erosion). *In:* Soil Conservation, Assessing the National Resources Inventory. National Academy Press. Washington, D.C. pp. 90-125.

Foster, G.R., G.C. White, T.E. Hakonson, and M. Dreicer. 1985a. A model for splash and retention of sediment and soil-borne contaminants on plants. Transactions of the American Society of Agricultural Engineers 28:1511-1520.

Foster, G.R., R.A. Young, and W.H. Neibling. 1985b. Sediment composition for nonpoint source pollution analyses. Transactions of the American Society of Agricultural Engineers 28:133-139, 146.

Foster, G.R., R.A. Young, M.J.M. Römkens, and C.A. Onstad. 1985c. Processes of soil erosion by water. *In:* Soil Erosion and Crop Productivity. American Society of Agronomy, Crop Science Society of America, Soil Science Society of America. R.F. Follett and B.A. Stewart, eds. Madison, WI. pp. 137-162.

Foster, G.R., G.A. Weesies, K.G. Renard, J.P. Porter, and D.C. Yoder. 1997. Support practice factor "P". *In:* A Guide to Conservation Planning with the Revised Soil Loss Equation (RUSLE). Agriculture Handbook 703. U.S. Department of Agriculture. Chapter 6.

Fournier, F. 1960. Climat et Erosion. Universitaries de France, Paris.

Fryrear, D.W., A. Saleh, J.D. Bilbro, H.M. Schomberg, J.E. Stout. and T. M. Zobeck. 1998. Revised Wind Erosion Equation. Technical Bulletin No. 1, Cropping Systems Research Laboratory, USDA-Agricultural research Service, Lubbock, Texas.

Ghidey, F. and E.E. Alberts. 1993. Residue type and placement effects on decomposition: Field study and model evaluation. Transactions of the American Society of Agricultural Engineers. 36:1611-1617.

Gilley, J.E., S.C. Finkner, R.G. Spomer, and L.N. Mielke. 1986. Runoff and erosion as affected by corn residue. I. Total losses. Transactions of the American Society of Agricultural Engineers. 29:157-160.

Gilley, J.E. and S.C. Finkner. 1991. Hydraulic roughness coefficients as affected by random roughness. Transactions of the American Society of Agricultural Engineers. 34:897-903.

Gilley, J.E. and E.R. Kottwitz. 1994. Darcy-Weisbach roughness coefficients for surfaces with residue and gravel cover. Transactions of the American Society of Agricultural Engineers. 38:539-544.

Gilley, J.E. and E.R. Kottwitz. 1995. Darcy-Weisbach roughness coefficients for selected crops. Transactions of the American Society of Agricultural Engineers. 37:467-471.

Govers, G. 1991. Rill erosion on arable land in central Belgium: Rates, control, and predictability. Catena. 18:133-135.

Graf, W.H. 1971. Hydraulic of Sediment Transport. McGraw Hill. New York, NY.

Gregory, J.M., T.R. McCarty, F. Ghidey, and E.E. Alberts. 1985. Derivation and evaluation of residue decay equation. Transactions of the American Society of Agricultrual Engineers. 28:98-101.

Ghidey, F. and E.E. Alberts. 1993. Residue type and placement effects on decomposition: Field study and model evaluation. Transactions of the American Society of Agricultural Engineers. 36:1611-1617.

Gunn , R. and Kinzer, G.D. 1949. The terminal velocity of fall for water droplets. Journal of Meteorology. 6:243-248.

Haan, C.T., B.J. Barfield and J.C. Hayes. 1994. Design hydrology and sedimentology for small catchments. Academic Press, New York, NY.

Hagan. L.J., L.E. Wagner, and J. Tatarko. 1996. Technical Documentation, Wind Erosion Prediction System (WEPS). Wind erosion Research Unit, USDA-Agricultural research Service, Manhattan, Kansas.

Hanna, H.M., S.W. Melvin, and R.O. Pope. 1995. Tillage implement operational effects on residue cover. Applied Engineering in Agriculture. 11:205-210.

Hayes, J.C., B.J. Barfield, and R.I. Barnhisel. 1984. Performance of grass filters under laboratory and field conditions. Transactions of the American Society of Agricultural Engineers 27:1321-1331.

Hays, O.E. and O.J. Attoe. 1957. Control of runoff and erosion on Almena silt loam in Wisconsin. ARS 41-16. U.S. Department of Agriculture, Washington, DC.

Hays, O.E., A.G. McCall, and F.G. Bell. 1949. Investigations in erosion control and reclamation of eroded land at the Upper Mississippi Valley Conservation Experiment Station near LaCrosse, Wisconsin, 1933-43. Technical Bulletin 973. U.S. Department of Agriculture, Washington, DC.

Heilman, J.L., K.J. McInnes, R.W. Gesch, and R.J. Lascano. 1992. Evaporation from ridge-tilled soil covered with herbicide-killed winter wheat. Soil Science Society of America Journal. 56:1278-1286.

Hill, H.O., W.J. Peevy, A.G. McCall, and F.G. Bell. 1944. Investigations in erosion control and reclamation of eroded land at the Blackland Conservation Experiment Station Temple, Texas, 1931-41. Technical Bulletin 859. U.S. Department of Agriculture, Washington, DC.

Hill, P.R. and D.E. Stott. 2000. Corn residue retention by a combination chisel plow. Soil Science Society of America Journal. 64:293-299.

Hollinger, S. E., J. R. Angel, and M. A. Palecki. 2002. Spatial Distribution, Variation, and Trends in Storm Precipitation Characteristics Associated with Soil Erosion in the United States. Contract report CR 2002-08. Illinois State Water Survey. Champaign, IL available at: www.isws.illinois.edu/pubdoc/CR/ISWSCR2002-08.pdf .

Hood, G.W. and R.P. Bartholomew. 1956. Soil and water conservation studies in the Ozark Highlands of Arkansas. Agricultural Experiment Station Bulletin 563. University of Arkansas.

Hunt, H.W. 1977. A simulation model for decomposition in grasslands. Ecology 58:469-484.

Jasa, P. J., E.C. Dickey, and D.P. Shelton. 1986. Soil erosion from tillage and planting systems used in soybean residue: Part II - influences of row direction. Transactions of the American Society of Agricultural Engineers. 29:761-766.

Johnson, R.R. 1988. Soil engaging tool effects on surface residue and roughness with chisel-type implements. Soil Science Society of America Journal.52:237-243.

Kay, B.D. and A.J. VanderBygaart. 2002. Conservation tillage and depth stratification of porosity and soil organic matter. Soil and Tillage Research. 66:107-118.

Knisel, W. G. (editor). 1980. CREAMS : a field scale model for Chemicals, Runoff, and Erosion from Agricultural Management Systems. Conservation Research Report 26. U.S. Department of Agriculture, Washington, DC.

Laflen, J.M., H.P. Johnson, and R.C. Reeve. 1972. Soil loss from tile outlet terraces. Journal of Soil and Water Conservation. 27:74-77.

Laflen, J. M., J. L. Baker, R. O. Hartwig, W. F. Buchele, and H. P. Johnson. 1978. Soil and water losses from conservation tillage systems. Transactions of the American Society of Agricultural Engineers. 21:881-885.

Laflen, J.M., W.C. Moldenhauer, and T.S. Colvin. 1980. Conservation tillage and soil erosion on continuously row-cropped land. In: Crop Production with Conservation in the 80's. American Society of Agricultural Engineers. St. Joseph, MI. pp. 121-133.

Laflen, J.M. and T.S. Colvin. 1981. Effect of crop residues on soil loss from continuous row cropping. Transaction of the American Society of Agricultural Engineers. 24:605-609.

Laflen, J.M., G.R. Foster, and C.A. Onstad. 1985. Simulation of individual-storm soil loss for modeling the impact of soil erosion on crop productivity. Individual-storm soil loss. Chapter 26. *In:* Soil Erosion and Conservation. S.A. El-Swaify, W.C. Moldenhauer, and Andrew Lo, eds. Soil Conservation Society of America. Ankeny, IA. pp. 285-295.

Laflen, J.M., W.J. Elliot, J.R. Simanton, C.S. Holzhey, and K.D. Kohl. 1991a. WEPP: soil erodibility experiments for rangeland and cropland soils. Journal of Soil and Water Conservation. 46:39-44.

Laflen, J.M., L.J. Lane, and G.R. Foster. 1991b. WEPP-A new generation of erosion prediction technology. Journal of Soil and Water Conservation 46(1):34-38.

Lattanzi, A.R., L.D. Meyer, and M.F. Baumgardner. 1974. Influence of mulch rate and slope steepness on interrill erosion. Soil Science Society of America Proceedings. 38:946-950.

Lindstrom, M. J. and C. A. Onstad. 1984. Influence of tillage systems on soil physical parameters and infiltration after planting. Journal of Soil and Water Conservation. 39:149-152.

Long, O.H. 1959. Root studies on some farm crops in Tennessee. Bulletin 301. Agricultural Experiment Station. University of Tennessee, Knoxville, TN. 42 pp.

Lu, J.Y., W.H. Neibling, G.R. Foster, and E.A. Cassol. 1988. Selective Transport and Deposition of Sediment Particles by Shallow Flow. Transactions of American Society of Agricultural Engineers 31(4):1141-1147.

Lyles, L. and J. Tatarko. 1987. Precipitation effects on ridges created by grain drills. Journal of Soil and Water Conservation. 42:269-271.

Mannering, J.V. and L.D. Meyer. 1963. Effects of various rates of surface mulch reduce soil erosion and runoff velocity. Soil Science Society of America Proceedings. 27:84-86.

Mannering, J.V., C.B. Johnson, and L.D. Meyer. 1968. Effect of cropping intensity on erosion and infiltration. Agronomy Journal. 60:206-209.

Mannering, J.V. 1981. The use of soil loss tolerance as a strategy for soil conservation. In: Soil Conservation: Problems and Prospects. R.P.C. Morgan (ed), John Wiley and Sons, Inc., NY. pp. 337-349.

McCool, D.K., L.C. Brown, G.R. Foster, C.K. Mutchler, and L.D. Meyer. 1987. Revised slope steepness factor for the Universal Soil Loss Equation. Transactions of the American Society of Agricultural Engineers 30:1387-1396.

McCool, D.K., G.R. Foster, C.K. Mutchler, and L.D. Meyer. 1989. Revised slope length factor for the Universal Soil Loss Equation. Transactions of American Society of Agricultural Engineers 32(5):1571-1576.

McCool, D.K., M.T. Walter, and L.G. King. 1995. Runoff index values for frozen soil areas of the Pacific Northwest. J. Soil and Water Conservation. 50: 466-469.

McCool, D.K., G.R. Foster, and G.A. Weesies. 1997. Slope length and steepness factors (LS). Chapter 4. *In:* Predicting Soil Erosion by Water: A Guide to Conservation Planning with the Revised Universal Soil Loss Equation (RUSLE). Agriculture Handbook 703. U.S. Department of Agriculture. Washington, DC.

McCool, D. K., G. R. Foster, A. H. Ingersoll, R. C. McClellan, and R. W. Rickman. 2002. Cover-Management Enhancements for RUSLE2 in the Pacific Northwest USA. Vol. II, p. 513-517. In: Proceedings of the 12th Conference of the International Soil Conservation Organization, Beijing, China. 2002.

McCormack, D.E. and K.K. Young. 1981. Technical and societal implications of soil loss tolerance. 364-376, In: Soil Conservation: Problems and Prospects. R.P.C. Morgan (ed), John Wiley and Sons, Inc., NY.

McGregor, K.C., J.D. Greer, G.E. Gurley, and G.C. Bolton. 1969. Runoff and sediment production from north Mississippi Loessial soil. Bulletin 777. Mississippi Agricultural Experiment Station. Mississippi State College, Mississippi.

McGregor, K.C., R.L. Bengtson, and C.K. Mutchler. 1988. Effects of surface straw on interrill runoff and erosion of Grenada silt loam soil. Transactions of the American Society of Agricultural Engineers. 31:111-116

McGregor, K.C., R.L. Bengston, and C.K. Mutchler. 1990. Surface and incorporated wheat straw effects on interrill runoff and soil erosion. Transaction of the American Society of Agricultural Engineers. 33:469-474.

McGregor, K.C., R.L. Bingner, A.J. Bowie, and G.R. Foster. 1995. Erosivity index values for northern Mississippi. Transactions of the American Society of Agricultural Engineers. 38:1039-1047.

McGregor, K.C., S.M. Dabney, and J.R. Johnson. 1999. Runoff and soil loss from cotton plots with and without stiff-grass hedges. Transactions of the American Society of Agricultural Engineers. 42:361-368.

McIsaac, G.F., Mitchell, J.K., and Hirschi, M.C. 1990. Contour and conservation tillage for corn and soybeans in the Tama Silt Loam Soil: hydraulics and sediment concentration. Transactions of the American Society of Agricultural Engineers. 33:1541-1550.

McIsaac, G.F., J.K. Mitchell, M.C. Hirschi, and L.K. Ewing. 1991. Conservation and contour tillage for corn and soybeans in the Tama silt loam soil: the hydrologic response. Soil and Tillage Research. 19:29-46.

Meyer, L.D., and J.V. Mannering. 1967. Tillage and land modification for water erosion control. In: Proceeding ASAE-ASA-SCSA Tillage Conference. American Society of Agricultural Engineers. St. Joseph, MI. 58-62.

Meyer, L.D. and W.H. Wischmeier. 1969. Mathematical simulation of the process of soil erosion by water. Transactions of the American Society of Agricultural Engineers 12:754-758, 762.

Meyer, L.D., W.H. Wischmeier, and G.R. Foster. 1970. Mulch rates required for erosion control on steep slopes. Soil Science Society of American Proceedings 34:928-931.

Meyer, L.D., W.H. Wischmeier, and W.H. Daniel. 1971. Erosion, runoff, and revegetation of denuded construction sites. Transactions of the American Society of Agricultural Engineers. 14:138-141.

Meyer, L.D., C.B. Johnson, and G.R. Foster. 1972. Stone and woodchip mulches for erosion control on construction sites. Journal Soil and Water Conservation 27:264-269.

Meyer, L.D., G.R. Foster, and M.J.M. Römkens. 1975a. Source of soil eroded by water from upland slopes. *In:* Present and Prospective Technology for Predicting Sediment Yields and Sources. ARS-S-40. U.S. Department of Agriculture. pp. 177-189.

Meyer, L.D., G.R. Foster, and S. Nikolov. 1975b. Effect of flow rate and canopy on rill erosion. Transactions of the American Society of Agricultural Engineers 18:905-911.

Meyer, L.D. and M. A. Ports.1976. Prediction and control urban erosion and sedimentation. Proceedings of National Symposium on Urban Hydrology, Hydraulics, and Sedimentation. Bulletin 111. University of Kentucky. Lexington, KY. pp. 323-331.

Meyer, L.D., W.C. Harmon, and L.L. McDowell. 1980. Sediment sizes eroded from crop row sideslopes. Transactions of the Society of Agricultural Engineers. 23: 891-898.

Meyer, L.D. and W. C. Harmon. 1985. Sediment losses from cropland furrows of different gradients. Trans. ASAE. 28: 448-453, 461.

Meyer, L.D. and W.C. Harmon. 1989. How row-sideslope length and steepness affect interrill erosion. Transactions of the Society of Agricultural Engineers. 32:639-644.

Moldenhauer, W.C. and W.H. Wischmeier. 1960. Soil and water losses and infiltration rates on Ida silt loam as influenced by cropping systems, tillage practices and rainfall characteristics. Soil Science Society of America Journal 24:409-413.

Mutchler, C.K., R.E. Burwell, and L.C. Staples. 1976. Runoff and Soil Losses from Barnes Soils in the Northwestern Corn Belt. ARS NC-36. U.S. Department of Agriculture.

Mutchler, C.K. 1970. Splash of a waterdrop at terminal velocity. Science 169:1311-1312.

Mutchler, C.K. and R.A. Young. 1975. Soil detachment by raindrops. 113-117, In: Present and Prospective Technology for Predicting Sediment Yields and Sources. ARS-S-40. U.S Dept of Agriculture, Science and Education Administration. Washington, DC.

Mutchler, C.K., C.E. Murphree, and K.C. McGregor. 1982. Subfactor method for computing C-factors for continuous cotton. Transactions of the American Society of Agricultural Engineers. 25:327-332.

Mutchler, C.K. and K.C. McGregor. 1983. Erosion from low slopes. Water Resources Research. 19:1323-1326.

Mutchler, C.K. and C.E. Carter. 1983. Soil erodibility variation during the year. Transactions of the American Society of Agricultural Engineers. 26:1102-1104, 1108.

Mutchler, C.K. and J.D. Greer.. 1984. Reduced tillage for soybeans. Transactions of the American Society of Agricultural Engineers. 27:1364-1369.

Mutchler, C.K. L.L. McDowell, and J.D. Greer. 1985. Soil loss cotton with conservation tillage. Transactions of the American Society of Agricultural Engineers. 28:160-163, 168.

Mutchler, C.K. and C.E. Murphree, Jr. 1985. Experimentally derived modifications of the USLE. In: Soil Erosion and Conservation. S.A. El-Swaify, W.C. Moldenhauer, and A. L (editors). Soil and Water Conservation Society, Ankeny , IA. pp. 523-527.

Mutchler, C.K. and L.L. McDowell. 1990. Soil loss cotton with winter cover crops. Transactions of the American Society of Agricultural Engineers. 33:432-436.

Nearing, M.A., G.R. Foster, L.J. Lane, and S.C. Finkner. 1989. A process-based soil erosion model for USDA Water Erosion Prediction Project technology. Transactions of American Society of Agricultural Engineers 32(5):1587-1593.

Neibling, W.H. and G.R. Foster. 1982. Transport and deposition of naturally eroded sediment by shallow flow. Paper No. 82-2088. American Society of Agricultural Engineers. St. Joseph, MI.

Parker, D.T. 1962. Decomposition in the field of buried and surface-applied cornstalk residue. Soil Science of America Proceeding 26:559-562.

Reeder, J.D., C.D. Franks, and D.G. Michunas. 2001. Root biomass and microbial processes. In: The Potential of U.S. Grazing Lands to Sequester Carbon and Mitigate the Greenhouse Effect. R.K. Follett, J.M. Kimble, and R. Lal (eds). Lewis Publisher, Boca Raton, FL.

Renard, K.G. and G. R. Foster. 1983. Soil conservation: Principles of erosion by water. Agronomy Monograph no. 23. *In:* Dryland Agriculture. American Society of Agronomy. Madison, WI. pp. 155-176.

Renard, K.G. and J.R. Freimund. 1994. Using monthly precipitation data to estimate the R-factor in the revised USLE. Journal of Hydrology 157:287-306.

Renard, K.G., G.R. Foster, G.A. Weesies, D.K. McCool, and D.C. Yoder (coordinators). 1997. Predicting Soil Erosion by Water: A Guide to Conservation Planning with the Revised Universal Soil Loss Equation (RUSLE). Agriculture Handbook 703. U.S. Department of Agriculture. Washington, DC.

Richardson, C.W., G.R. Foster, and D.A. Wright. 1983. Estimation of erosion index from daily rainfall amount. Transactions of the American Society of Agricultural Engineers 26:153-156, 160.

Römkens, M.J.M., D.W. Nelson, and C.B.Roth. 1975. Soil erosion on selected high clay subsoils. Journal of Soil and Water Conservation. 30:173-176.

Römkens, M.J.M., C.B. Roth, and D.W. Nelson. 1977. Erodibility of selected clay soubsoils in relation to physical and chemical properties. Soil Science Society of America Journal. 41:954-960.

Römkens, M.J.M., R.A. Young, J.W.A. Poesen, D.K.McCool, S.A. El-Swaify, and J.M. Bradford. 1997. Soil erodibility factor. In: Predicting Soil Erosion by Water: A Guide to Conservation Planning with the Revised Universal Soil Loss Equation (RUSLE). Agriculture Handbook 703. U.S. Department of Agriculture, Washington, DC.

Roth, C.B. and D.W. Nelson, and M.J.M. Römkens. 1974. Prediction of subsoil erodibility using chemical, mineralogical and physical parameters. EPA 660/2-74-043. U.S. Department of Environmental Protection, Washington, DC. 111 pp.

Ruffo, M.L. and G.A. Bollero. 2003. Modeling rye and hairy vetch residue decomposition as a function of degree-days and decomposition-days. Agronomy Journal. 95:900-907.

Schomberg, H.H., J.L. Steiner, and P.W. Unger. 1994. Decomposition and nitrogen dynamics of crop residues: Residue quality and water effects. Soil Science Society of America Journal. 58:372-381.

Schomberg, H.H. and J.L. Steiner. 1995. Comparison of residue decomposition models used in erosion prediction. Pre-publication copy. Agricultural Research Service. U.S. Department of Agriculture. Bushland, TX.

Schomberg, H.H., J.L. Steiner, S.R. Evett, and A.P. Moulin. 1996. Climatic influence on residue decomposition prediction in the Wind Erosion Prediction System. Theoretical and Applied Climatology. 54:5-16.

Schomberg, H.H. and J.L. Steiner. 1997. Comparison of residue decomposition models used in erosion prediction. Agronomy Journal 89:911-919.

Schomberg, H.H. G.R. Foster, J.L. Steiner, and D.E. Stott. 2002. An improved temperature function for modeling crop residue decomposition. Transactions of the American Society of Agricultural Engineers. 45:1415-1422.

Schwab, G.O., R.K. Frevert, T.W. Edminster, and K.K. Barnes. 1966. Soil and Water Conservation Engineering. John Wiley and Sons, New York, NY. pp. 542-559.

Schwab, G.O. and J.L. Fouss. 1967. Tile flow and surface runoff from drainage systems with corn and grass cover. Transactions of the American Society of Agricultural Engineers. 10:492-493, 496.

Schwab, G.O. 1976. Tile or surface drainage for Ohio's heavy soils? Ohio Report. March-April. Ohio Agricultural Experiment Station. Columbus, OH.

Shelton, C. H. and J. F. Bradley. 1987. Controlling erosion and sustaining production with no-till systems. Tennessee Farm and Home Science. Winter:18-23.

Shelton, D.P., P.J. Jasa, E.C. Dickey. 1986. Soil erosion from tillage and planting systems used in soybean residue: Part I - influences of row spacing. Transactions of the American Society of Agricultural Engineers. 29:756-760.

Siemens, J. C. and W. R. Oschwald. 1976. Erosion from corn tillage systems. Transactions of the American Society of Agricultural Engineers.19:69-72.

Simanton, J.R., E. Rawitz, and E.D. Shirley. 1984. The effects of rock fragments on erosion on semiarid rangeland soils. In: Erosion and Productivity of Soils Containing Rock Fragments. Chapter 7, Special Publication 13. Soil Science Society of American. Madison, WI. Pp. 65-72.

Simanton, J.R., M.A. Weltz, and H.D. Larson. 1991. Rangeland experiments to parameterize the water erosion prediction project model: vegetation canopy cover effects. Journal of Range Management. 44:276-282.

Skaggs, R.W., A Nassehzadeh-Tabrizi, and G.R. Foster. 1982. Subsurface drainage effects on erosion. Journal of Soil and Water Conservation 37:167-172.

Smith, J.H. and R.E. Peckenpaugh. 1986. Straw decomposition in irrigated soil: Comparison of twenty three cereal straws. Soil Science Society of America Journal. 50:928-932.

Smith, D.D., D.M. Whitt and A.W. Zingg. 1945. Investigations in erosion control and reclamation of eroded Shelby and related soils at the Conservation Experiment Station, Bethany, Missouri, 1932-42. Technical Bulletin 883. U.S. Department of Agriculture, Washington, DC.

Spaeth, Jr., K.E. F.B. Pierson, M.A. Weltz, and W.H. Blackburn. 2003. Evaluation of USLE and RUSLE estimated soil loss on rangeland. Journal of Range Management. 56:234-246.

Steiner, J.L. H.H. Schomberg, C.L. Douglas, Jr., and A.L. Black. 1994. Standing stem persistence in no-tillage small-grain fields. Agronomy Journal. 86:76-81.

Steiner, J.L., H.H. Schomberg, and P.W. Unger. 1995. Residue decomposition submodel. In: Wind Erosion Prediction System (WEPS), Technical Documentation, L.J. Hagan et al. (ed). Wind Erosion Research Unit, Agricultural Research Service, U.S. Department of Agriculture, Washington, DC. pp. D1-D12.

Steiner, J.L., H.H. Schomberg, P.W. Unger, and J. Cresap. 1999. Crop residue decomposition in no-tillage small-grain fields. Soil Science Society of America Journal 63:1817-1824.

Steiner, J.L., H.H. Schomberg, P.W. Unger, and J. Cresap. 2000. Biomass and residue cover relationships of fresh and decomposing small grain residue. Soil Science Society of America Journal. 64:2109-2114.

Stott, D.E., H.F. Stroo, L.F. Elliott, R.I. Papendick, and P.W. Unger. 1990. Wheat residue loss from fields under no-till management. Soil Science Society of America Journal. 54:92-98.

Stott, D.E. 1991. RSMAN: A tool for soil conservation education. Journal of Soil and Water Conservation. 46:332-333.

Stott, D.E. 1995. Analysis of RUSLE decomposition and mass-to-cover parameters. Unpublished report. National Soil Erosion Research Laboratory, U.S. Department of Agriculture, Agricultural Research Service, W. Lafayette, Indiana.

Stott, D.E., E.E. Alberts, and M.A. Weltz. 1995. Residue decomposition and management. Chapter 9. In: D.C. Flanagan and M.A. Nearing (editors). 1995. Technical Documentation, USDA-Water Erosion Prediction Project (WEPP). NSERL Report No. 10. National Soil Erosion Research Laboratory, Agricultural Research Service, U.S. Department of Agriculture. Washington, D.C.

Swanson, N. P., Dedrick, A. R., Weakley, H. E., Haise, H. R. 1965. Evaluation of mulches for water-erosion control. Transactions of the American Society of Agricultural Engineers. 8:438-440.

Swanson, N.P., A.R. Dedrick, and A.E. Dudeck. 1967. Protecting steep construction slopes against water erosion. Highway Research Record 206. Highway Research Board. Washington, DC. pp. 46-52.

Thomas, R.J. and N.M. Asakawa. 1993. Decomposition of leaf litter from tropical forage grasses and legumes. Soil Biology and Biochemistry. 25:1351-1361.

Toy, T.J. and G.R. Foster (coeditors). 1998. Guidelines for the use of the Revised Universal Soil Loss equation (RUSLE1.06) on mined lands, construction sites, and reclaimed lands. USDI-Office of Surface Mining. Denver. CO.

Toy, T.J. and G.R. Foster. 2000. Estimating Rill-interrill erosion on converging and diverging hillslopes. Unpublished report submitted to National Sedimentation Laboratory, Agricultural Research Service, U.S. Department of Agriculture. Oxford, Mississippi.

Toy, T.J., G.R. Foster, and K.G. Renard. 2002. Soil Erosion: Processes, Prediction, Measurement, and Control. John Wiley and Son, New York, NY.

U.S. Environmental Protection Agency (USEPA). 1976a. Effectiveness of surface mine sedimentation ponds. EPA-600/2-76-117. Environmental Protection Technology Series. Washington, D.C.

U.S. Environmental Protection Agency (USEPA). 1976b. Erosion and Sediment Control: Surface mingin in the Easter U.S. EPA-25/3-76-006. Environmental Protection Agency Technology Transfer Seminar Publication. Washington, D.C.

Van Doren, C.A., R.S. Stauffer, and E.H. Kidder. 1950. Effect of contour farming on soil loss and runoff. Soil Science of America Proceedings 15:413-417.

Van Klaveren, R.W. and D.K. McCool. 1998. Erodibility and critical shear stress of a previously frozen soil. Transactions of the American Society of Agricultural Engineers. 41:1315-1321.

Van Liew, M.W. and K.E. Saxton. 1983. Slope steepness and incorporated residue effects on rill erosion. Transactions of the American Society of Agricultural Engineers. 26: 1738-1743.

Vigil, M. F. and D. Sparks. 2004. Factors affecting the rate of crop residue decomposition under field conditions. Conservation tillage Fact Sheet #3-95. U.S. Department of Agriculture, Washington, DC.

Wagner, L.E. and R.G. Nelson. 1995. Mass reduction of standing and flat crop residue by selected tillage implements. Transactions of the American Society of Agricultural Engineers. 38:419-427.

Williams, J.R., C.A. Jones, J.R. Kiniry, and D.A. Spanel. 1989. The EPIC crop growth model. Transactions of the American Society of Agricultural Engineers. 32:497-511.

Wischmeier, W.H. and D.D. Smith. 1958. Rainfall energy and its relationship to soil loss. Transactions of American Geophysical Union. 39: 285-291.

Wischmeier, W.H. and D.D. Smith. 1965. Predicting rainfall-erosion losses from cropland east of the Rocky Mountains: A guide for selection of practices for soil and water conservation. Agriculture Handbook 282. U.S. Department of Agriculture, Washington, DC.

Wischmeier, W.H. and J.V. Mannering. 1969. Relation of soil properties to its erodibility. Soil Science Society of American Proceedings. 33:131-137.

Wischmeier, W.H., C.B. Johnson, and B.V. Cross. 1971. A soil erodibility monograph for farmland construction sites. Journal of Soil and Water Conservation. 26: 189-193.

Wischmeier, W.H. 1975. Estimating the soil loss equation's cover and management factor for undisturbed areas. In: Present and prospective technology for predicting sediment yields and sources. ARS-S40. U.S. Department of Agriculture. Washington, D.C. pp. 118-124.

Wischmeier, W. H. 1978. Conservation tillage to control water erosion. In: Conservation Tillage: The Proceedings of a National Conference. Soil and Water Conservation Society. Ankeny, IA. pp. 133-141.

Wischmeier, W.H. and D.D. Smith. 1978. Predicting rainfall-erosion losses: A guide to conservation planning. Agriculture Handbook 537. U.S. Dept. of Agriculture, Washington, DC.

Yoder, D.C., J.P. Porter, J.M. Laflen, J.R. Simanton, K.G. Renard, D.K. McCool, and G.R. Foster. 1997. Cover-management factor (C). In: A Guide to Conservation Planning with the Revised Soil Loss Equation (RUSLE). Agriculture Handbook 703. U.S. Department of Agriculture. Chapter 5.

Young, R.A. and C. K. Mutchler. 1969. Soil and water movement in small tillage channels. Transactions of the American Society of Agricultural Engineers. 12:543-545.

Young, R.A. and C.K. Mutchler. 1977. Erodibility of some Minnesota soils. Journal of Soil and Water Conservation. 32:180-182.

Zingg, A.W. 1940. Degree and length of land slope as it affects soil loss in runoff. Agricultural Engineering. 21:59-64.

12.2. References not cited

12.2.1. Contouring References

Diseker, E.G. and R.E. Yoder. 1936. Sheet erosion studies on Cecil clay. Bulletin 245. Alabama Agricultural Experiment Station. Auburn, University. Auburn, AL.

Jamison, V.C., D.D. Smith, and J.F. Thornton. 1968. Soil and water research on a claypan soil. Technical Bulletin 1379. U.S. Department of Agriculture. Washington, D.C.

Knoblauch, H.C. and J.L. Hayes. 1940. The effect of contour cultivation on runoff. Transactions of the American Geophysical Union. 21:499-504.

Lamb, Jr., J., J.S. Andrews, and A.F. Gustafson. 1944. Experiment in the control of soil erosion in southern New York. Bulletin 811. New York Agricultural Experiment Station. Cornell University, Ithaca, NY.

McIsaac, G, F., Mitchell, J. K., Siemans, J.C., Hummel, J. W. 1987. Row cultivation effects on runoff, soil loss and corn grain yield. Transactions of the American Society of Agricultural Engineers. 30:125-128,136.

Nichols, M.L. and H.D. Sexton. 1932. A method of studying soil erosion. Agricultural Engineering. 13:101-103.

Young, R.A., C.K. Mutchler, and W.H. Wischmeier. 1964. Influence of row direction and type of vegetal cover on the soil-loss relationship. Transactions of the American Society of Agricultural Engineers. 7:316-317, 320.

12.2.2. Decomposition References

Collins, H.P., L.F. Elliot, and R.I. Papendick. 1986. 1990. Wheat straw decomposition and changes in decomposition during field exposure. Soil Science Society of America Journal. 54:1013-1016.

Douglas, Jr., C.L. and R.W. Rickman. 1992. Estimating crop residue decomposition from air temperature, initial nitrogen content, and residue placement. Soil Science Society of America Journal. 56:272-278.

Ghidey, F., J. M. Gregory, T. R. McCarty, and E. E. Alberts. 1985. Residue decay evaluation and prediction. Transactions of the American Society of Agricultural Engineers. 28:102-105.

McGregor, K.C. and C.K. Mutchler 1983. C Factors for no-till and reduced-till corn. Transactions of the American Society of Agricultural Engineers. 26:785-788.

Murphree, C.E. and C.K. Mutchler. 1980. Cover and management factors for cotton. Transactions of the American Society of Agricultural Engineers. 23:585-588, 595.

Van Doren, Jr., D.M., W.C. Moldenhauer, and G.B. Triplett, Jr. 1984. Influence of long-term tillage and crop rotation on water erosion. Soil Society of America Journal 48:636-640.

Weaver, J.E. 1947. Rate of decomposition roots and rhizomes of certain range grasses in undisturbed prairie soils. Ecology. 28:221-240.

12.2.3. No-Till and other Conservation Tillage References

Adams, J. E. 1974. Residual effects of crop rotations on water intake, soil loss, and sorghum yield. Agronomy Journal 66:299-304.

Alberts, E. E., R. C. Wendt, and R. E. Burwell. 1985. Corn and soybean cropping effects on soil losses and C-factors. Soil Science Society of America Journal 49:721-728.

Andraski, B. J., D. H. Mueller, and T. C. Daniel. 1985. Effects of tillage and rainfall date on water and soil losses. Soil Science Society of America Journal 49:1512-1517.

Baker, J. L. and Laflen, J. M. 1983. Runoff losses of nutrients and soil from ground fall-fertilized after soybean harvest. Transactions of the American Society of Agricultural Engineers. 26:1122-1127

Blevins, R. L., W. W. Frye, P. L. Baldwin, S. D. Robertson. 1990. Tillage effects on sediment and soluble nutrient losses from a Maury Silt Loam Soil. Journal of Environmental. Quality. 19:683-686.

Blough, R. F., A. R. Jarrett, J. M. Hamlett, and M. D. Shaw. 1990. Runoff and erosion rates from slit, conventional, and chisel tillage. Transactions of the American Society of Agricultural Engineers. 33:1882-1888.

Burwell, R. E. and L. A. Kramer. 1983. Long-term annual runoff and soil loss from conventional and conservation tillage of corn. Journal of Soil and Water Conservation. 38:315-319.

Comis, D.L. 1984. Tennessee researchers find no-till, double-cropped soybeans cut erosion. Soil and Water Conservation News. 5:10.

Dabney, S. M., C. E. Murphree, and L. D. Meyer. 1993. Tillage, row spacing, and cultivation affect erosion from soybean cropland. Transactions of the American Society of Agricultural Engineers. 36:87-94.

Dick, W. A., McCoy, E. L., Edwards, W. M., and Lal, R. 1991. Continuous application of no-tillage to Ohio Soils. Agronomy Journal. 83:65-73.

Dickey, E. C., D. P. Shelton, P. J. Jasa, and T. R. Peterson. 1984. Tillage, residue and erosion on moderately sloping soils. Transactions of the American Society of Agricultural Engineers. 27:1093-1099.

Diezman, M. M., S. Mostaghimi, V. O. Shanholtz, J. K. Mitchell. 1987. Size distribution of eroded sediment from two tillage systems. Transactions of the American Society of Agricultural Engineers. 30:1642-1647.

Gilley, J. E., Finkner, S. C., Varvel, G. E. 1986. Runoff and erosion as affected by sorghum and soybean residue. Transactions of the American Society of Agricultural Engineers. 29:1605-1610.

Gilley, J. E., Finkner, S. C., and Varvel, G. E. 1987. Slope length and surface residue influences on runoff and erosions. Transactions of the American Society of Agricultural Engineers. 30:148-152.

Hairston, J. E., J. O. Sanford, H. C. Hayes, and L. L. Reinschmiedt. 1984. Crop yield, soil erosion, and net returns from five tillage systems in the Mississippi Blackland Prairie. Journal of Soil and Water Conservation. 39:391-395.

Hamlett, J. M., J. L. Baker, S. C. Kimes, H. P. Johnson. 1984. Runoff and sediment transport within and from small agricultural watersheds. Transactions of the American Society of Agricultural Engineers. 27:1355-1363, 1369.

Harrold, L. L., G. B. Triplett, Jr., and W. M. Edwards. 1970. No-tillage corn - characteristics of the system. Agricultural Engineering. 51:128-131.

Harrold, L. L., and W. M. Edwards. 1972. A severe rainstorm test of no-till corn. Journal of Soil and Water Conservation. 27:30.

Harrold, L. L. and W. M. Edwards. 1974. No-tillage system reduces erosion from continuous corn watersheds. Transactions of the American Society of Agricultural Engineers. 17:414-416.

Jasa, P.J., and E.C. Dickey. 1991. Subsoiling, contouring, and tillage effects on erosion and runoff. Applied Engineering in Agriculture. 7:81-85.

Jones, J.N., J. E. Moody, G. M. Shear, W. W. Moschler, and J. J. Lillard. 1968. The no-tillage system for corn. Agronomy Journal. 60:17-20.

Kramer, L. A. 1986. Runoff and soil loss by cropstage from conventional and conservation tilled corn. Transactions of the American Society of Agricultural Engineers. 29:774-779.

Laflen, J. M., Moldenhauer, .W. C., and Colvin, T. S. 1981. Conservation tillage and soil erosion on continuously row-cropped land. In Crop Production with Conservation in the 80's. American Society of Agricultural Engineers. St. Joseph, MI. pp. 121-133.

Laflen, J. M.and T. S. Colvin. 1982. Soil and water loss from no-till, narrow-row soybeans. Paper no. 82-2023. American Society of Agricultural Engineers. St Joseph, MI.

Langdale, G. W., A. P. Barnett, R. A. Leonard, and W. G. Fleming. 1979. Reduction of soil erosion by the no-till system in the Southern Piedmont. Transactions of the American Society of Agricultural Engineers. 21:82-86, 92.

Langdale, G. W., M. C. Mills, and A. W. Thomas. 1992. Use of conservation tillage to retard erosive effects of large storms. Journal of Soil and Water Conservation. 47:257-260.

Langdale, G. W., L. T. West, R. R. Bruce, W. P. Miller, and A. W. Thomas. 1992. Restoration of eroded soil with conservation tillage. Soil Technology. 5:81-90.

Mannering, J. V., L. D. Meyer, and Johnson, C.B. 1966. Infiltration and erosion as affected by minimum tillage for corn. Soil Science Society of America Proceedings. 30:101-105.

McGregor, K. C., J. D. Greer, and G. E. Gurley. 1975. Erosion control with no-till cropping practices. Transactions of the American Society of Agricultural Engineers. 18:918-920.

McGregor, K. C. and J. D. Greer. 1982. Erosion control with no-till and reduced-till corn for silage and grain. Transactions of the American Society of Agricultural Engineers. 25:154-159.

McGregor, K. C. 1983. C factors for no-till and conventional-till soybeans from plot data. Transactions of the American Society of Agricultural Engineers. 26:1119-1122.

McGregor, K. C. and C. K. Mutchler. 1983. C factors for no-till and reduced-till corn. Transactions of the American Society of Agricultural Engineers. 26:785-788, 794.

McGregor, K. C. and C. K. Mutchler. 1992. Soil loss from conservation tillage for sorghum. Transactions of the American Society of Agricultural Engineers. 35:1841-1845.

McIsaac, G, F., Mitchell, J. K., Siemans, J.C., Hummel, J. W. 1987. Row cultivation effects on runoff, soil loss and corn grain yield. Transactions of the American Society of Agricultural Engineers. 30:125-128,136.

McIsaac, G. F., Mitchell, J. K., and Hirschi, M. C. 1988. Runoff and sediment concentration from conservation tillage for corn and soybeans under simulated rainfall. Paper no. 88-2595. American Society of Agricultural Engineers. St. Joseph, MI.

McIsaac, G. F., M.C. Hirschi, and J. K. Mitchell. 1991. Nitrogen and phosphorus in eroded sediment from corn and soybean tillage systems. Journal of Environmental Quality 20:663-670.

McIsaac, G. F, and Mitchell, J. K. 1992. Annual variation in runoff and erosion from simulated rainfall on corn and soybean tillage systems. Paper no.91-2016. American Society of Agricultural Engineers. St. Joseph, MI.

McIsaac,G. F.,and Mitchell, J. K. 1992. Temporal variation in runoff and soil loss from simulated rainfall on corn and soybeans. Transactions of the American Society of Agricultural Engineers. 35:465-472.

Meyer, L. D. and J. V. Mannering. 1961. Minimum tillage for corn: its effect on infiltration and erosion. Transactions of the American Society of Agricultural Engineers. 42:72-75.

Mills, W. C., A. W. Thomas, and G. W. Langdale. 1986. Estimating soil loss probabilities for Southern Piedmont cropping-tillage systems. Transactions of the American Society of Agricultural Engineers. 29:948-955.

Mills, W. C., A. W. Thomas, and G. W. Langdale. 1992. Seasonal and crop effects on soil loss and rainfall retention probabilities: an example from the U.S. Southern Piedmont. Soil Technology. 5:67-79.

Moldenhauer, W. C., W. G. Lovely, N. P. Swanson, and H. D. Currence. 1971. Effect of row grades and tillage systems on soil and water losses. Journal of Soil and Water Conservation. 26:193-195.

Moldenhauer, W. C., G. W. Langdale, W. Frye, D. K. McCool, R. I. Papendick, D. E. Smika, and D. W. Fryrear. 1983. Conservation tillage for erosion control. Journal of Soil and Water Conservation. 38:144-151.

Mostaghimi, S., Dillaha, T. A., and Shanholtz, V. O. 1986. Influence of tillage systems and residue levels on runoff, sediment, and phosphorus losses. Transactions of the American Society of Agricultural Engineers. 31:128-132.

Mueller, D. H., R. C. Wendt, and T. C. Daniel. 1984. Soil and water losses as affected by tillage and manure application. Soil Science Society of America Journal. 48:896-900.

Mutchler, C. K., Murphree, C. E., and McGregor, K. C. 1982. Subfactor method for computing C factors for continuous cotton. Transactions of the American Society of Agricultural Engineers. 25:327-332.

Onstad, C. A. 1972. Soil and water losses as affected by tillage practices. Transactions of the American Society of Agricultural Engineers. 15:287-289.

Salehi, F., A. R. Pesant, and R. Lagace. 1991. Validation of the universal soil loss equation for three cropping systems under natural rainfall in Southeastern Quebeck. Canadian Agricultural Engineering. 33:11-16.

Seta, A.K., R.L. Blevins, W.W. Frye, and B.J. Barfield. 1993. Reducing soil erosion and agricultural chemical losses with conservation tillage. Journal of Environmental Quality. 22:661-665.

Shelton, C. H., F. D. Tomkins, and D. D. Tyler. 1983. Soil erosion from five soybean tillage systems. Journal of Soil and Water Conservation. 38:425-428.

Siemens, J. C. and W. R. Oschwald. 1978. Corn-soybean tillage systems: erosion control, effects on crop production, costs. Transactions of the American Society of Agricultural Engineers. 21:293-302.

Sloneker, L. L. and W. C. Moldenhauer. 1977. Measuring the amounts of crop residue remaining after tillage. Journal of Soil and Water Conservation. 32:231-236.

Stein, O. R., W. H. Neibling, T. J. Logan, and W. C. Moldenhauer. 1986. Runoff and soil loss as influenced by tillage and residue cover. Soil Science Society of America Journal. 50:1527-1531.

Sturgul, S. J., Daniel, T. C., and Mueller, H. D. 1990. Tillage and canopy cover effects on interill erosion from first-year alfalfa. Soil Science Society of America Journal. 54:1733-1739.

Van Doren, D. M., W. C. Moldenhauer, and G. B. Triplett. 1984. Influence of long-term tillage and crop rotation on water erosion. Soil Science Society of America Journal. 48:636-640.

Wendt, R. C. and R. E. Burwell. 1985. Runoff and soil losses for conventional, reduced, and no-till corn. Journal of Soil and Water Conservation. 40:450-454.

West, L. T., W. P. Miller, G. W. Langdale, R. R. Bruce, J. M. Laflen, A. W. Thomas. 1991. Cropping system effects on interrill soil loss in the Georgia Piedmont. Soil Science Society of America Journal. 55:460-466.

Wood, S. D. and A. D. Worsham. 1986. Reducing soil erosion in tobacco fields with no-tillage transplanting. Journal of Soil and Water Conservation 41:193-196.

Yoo, K. Y. and J. T. Touchton. 1988. Surface runoff and sediment yield from various tillage systems of cotton. Transactions of the American Society of Agricultural Engineers. 31:1154-1158.

Yoo, K. Y. and E. W. Rochester. 1989. Variation of runoff characteristics under conservation tillage systems. Transactions of the American Society of Agricultural Engineers. 32:1625-1630.

Yoo, K. Y. and J. T. Touchton. 1989. Runoff and soil loss by crop growth stage under three cotton tillage systems. Journal of Soil and Water Conservation. 44:225-228.

Zhu, J. C., C. J. Gantzer, S. H. Anderson, E. E. Alberts. 1989. Runoff, soil, and nutrient losses from no-till soybean with winter cover crops. Soil Science Society of America Journal. 53:1210-1214.

12.2.4. Redistribution of Material in Soil by Soil Disturbing Operations References

Allmaras R.R., S.M. Copeland, P.J. Copeland, and M. Oussible. 1996. Spatial relations between oat residue and ceramic spheres when incorporated sequentially by tillage. Soil Science Society of America Journal. 60:1209-1216.

Juzwik, J., D.L. Stenlund, R.R. Allmaras, S.M. Copeland, and R.E. McRoberts. 1997.Incorporation of tracers and dazomet by rotary tillers and a spading machine. Sol and Tillage Research. 41:237-248.

Staricka, J.A., P.M. Burford, R.R. Allmaras, and W.W. Nelson. 1990. Tracing the vertical distribution of simulated shattered seeds as related to tillage. Agronomy Journal. 82:1131-1134.

Staricka, J.A., R.R. Allmaras, and W.W. Nelson. 1991. Spatial variation of crop residue incorporated by tillage. Soil Science Society of America Journal. 53:1668-1674.

Staricka, J.A., R.R. Allmaras, W.W. Nelson, and W.E. Larson. 1992. Soil aggregate longevity as determined by the incorporation of ceramic spheres. Soil Science Society of America Journal. 56:1591-1597.

Stenlund, D.L., J. Juzwik, R.R. Allmaras, and S.M. Copeland. 1997. Incorporation of surface-applied materials by tillage implements. General Technical Report PNW 365. Forest Service. U.S. Department of Agriculture, Washington, D.C. pp 29-30.

12.2.5. Root and Root: Top Growth Ratios References

Arnon. I. 1975. Mineral Nutrition of Maize. International Potash Institute. Bern-Worblaufen, Switzerland.

Buyanovsky, G.A. and G.H. Wagner. 1986. Post-harvest residue input to cropland. Plant and Soil. 93:57-65.

Dalrymple, R.L. and D.D. Dwyer. 1967. Root and shoot growth of five range grasses. Journal of Range Management. 20:141-145.

Foth, H.D. 1962. Root and top growth of corn. Agronomy Journal. 54:49-52.

Kramer, J. and J.E. Weaver. 1936. Relative Efficiency of Roots and Tops of Plants in Protecting the Soil from Erosion. Bulletin 12. Conservation and Survery Division, University of Nebraska, Lincoln, NE.

Raper, Jr., C.D. and S.A. Barber. 1970. Rooting systems of soybeans. I. Difference in root morphology among varieties. Agronomy Journal. 62:581-584.

Taylor, R.S. Plant Root Systems: Their Function and Interaction with the Soil. Chapters 2 and 4. MCGraw-Hill Book Company. New York, NY.

Wallace, A., S.A. Bamburg, and J.W. Cha. 1974. Quantitative studies of roots of perennial plants in the Mojave Desert. Ecology. 55:1160-1162.

Weaver, J.E. and G.W. Harmon. 1935. Quantity of Living Plant Materials in Prairie Soils in Relation to Run-Off and Soil Erosion. Bulletin 8. Conservation and Survey Division. University of Nebraska. Lincoln, NE.

Assessment of erosion, sedimentation, and water quality impacts of the Mountain Valley Pipeline and Equitrans Expansion Project's proposed crossing of the Jefferson National Forest as it pertains to the U.S. Forest Service's Draft Supplemental Environmental Impact Statement dated December 2022

Prepared by Jonathan A. Czuba, Ph.D., Licensed Professional Engineer - February 9, 2023

REFERENCES
19

February 21, 2023

Journal of Hydrology 422–423 (2012) 17–29

Contents lists available at SciVerse ScienceDirect

Journal of Hydrology

journal homepage: www.elsevier.com/locate/jhydrol

A RUSLE approach to model suspended sediment load in the Lo river (Vietnam): Effects of reservoirs and land use changes

Roberto Ranzi [a,*], Thanh Hung Le [b], Maria Cristina Rulli [c]

[a] Department of Civil Engineering, Architecture, Land and Environment, University of Brescia, Brescia, Italy
[b] Faculty of Civil Engineering, Water Resources University, Hanoi, Viet Nam
[c] DIIAR, Politecnico di Milano, Milan, Italy

ARTICLE INFO

Article history:
Received 28 March 2011
Received in revised form 21 November 2011
Accepted 3 December 2011
Available online 22 December 2011
This manuscript was handled by Konstantine P. Georgakakos, Editor-in-Chief, with the assistance of Vincent S. Neary, Associate Editor

Keywords:
Soil erosion
Sediment load
Reservoirs
Lo river
RUSLE
Land use change

SUMMARY

This study addresses the problem of modelling sediment erosion at the catchment scale, in order to predict the possible impact of reservoirs and land use changes on sediment load in South East Asia. The investigated basin is the Lo river basin, (38,165 km^2 in Viet Tri), a left tributary of the Red River, where the Thac Ba and the recently built Tuyen Quang reservoirs have already been changing downstream sediment load since 1971 and 2005 when they were, respectively, in operations. The RUSLE equation is adopted in a distributed GIS framework to assess catchment erosion, and is coupled with a sediment accumulation and routing scheme to model suspended sediment load in the Lo basin at a monthly scale. Monthly precipitation were collected and used as input to the model. Suspended sediment load data, measured at eight gauging stations in Vietnam, from 1959 to 2007, were compared with the model's simulated sediment yield. Resulting average Nash–Sutcliffe efficiency is 0.45, ranging from 0.33 to 0.62 and bias is 5% at Vu Quang, close to the basin outlet, and results 1.4% by averaging biases at the eight stations, thus confirming that the model is adequate. Effects of reservoirs were analysed by modelling erosion and sediment yield passing from natural to impounded conditions and resulted in a suspended sediment load reduction of about 95% and 75% downstream, respectively, the Thac Ba reservoir in the Chay river and the Tuyen Quang reservoir in the Gam river. Land use change scenarios, parameterized on the basis of observed land use changes in the impounded basin and assuming that 20% of forest area is converted into rice and agricultural crops and 15% into bushes, shrubs and meadows, are expected to induce a 28% increase of suspended sediment load which can compensate, at least in part, sedimentation in reservoirs. Also agricultural and hillslope maintenance practices can modify sediment erosion in the basin.

1. Introduction

The dynamic equilibrium of sediment erosion, transport and deposition in a river basin can be modified by natural factors, as climate and vegetation changes, and anthropogenic factors, as reservoirs impoundment, agricultural and land use practices (Walling, 2011). In several countries with a fast developing economy, as Vietnam, the need of energy for national industrialisation and modernisation and of water demand for irrigation purposes in the dry season is leading to the construction of large reservoirs which trap sediments and change the sediment load in the downstream river network. This study addresses the problem of erosion at the catchment scale, and on a monthly time basis, in order to predict the possible impact of reservoirs and land use changes on sediment load in the Red River (Song Hong) basin, and specifically in the Lo river subcatchment, in Vietnam. Data and observations over 49 years show, in fact, that since the operation of reservoirs started, downstream sediment load and localised erosion phenomena have changed, thus rising some concern on the geomorphological equilibrium of the area. Similar dynamics are documented by Yang et al. (2006, 2007) and by Xu and Milliman (2009) about the impact, for instance, of the Three Gorges Dam on the Yangtze River in China after its impoundment.

Soil erosion prediction and assessment is a challenge to researchers and a wide range of models have been developed for erosion and sediment transport evaluation and they differ in terms of complexity, processes considered, and data required for model calibration and model use. In general there is no 'universal' model for all applications. The selection of the most suitable model is a logical process affected by numerous factors including the intended use, the characteristics of the catchment being considered and the data available.

* Corresponding author. Address: University of Brescia, DICATA – Department of Civil Engineering, Architecture, Land and Environment, Via Branze 43, 25123 Brescia, Italy. Tel.: +39 0303711291; fax: +39 0303711213.
E-mail address: ranzi@ing.unibs.it (R. Ranzi).

0022-1694/$ - see front matter © 2011 Elsevier B.V. All rights reserved.
doi:10.1016/j.jhydrol.2011.12.009

According to Merritt et al. (2003), erosion and sediment transport models are subdivided into three main categories, depending on the physical processes simulated, the model algorithms describing these processes and the data dependence of the model: (a) empirical or statistical, (b) conceptual, and (c) physics based. The distinction between models is not clear and therefore can be somewhat subjective. They are likely to contain a mix of modules from each of these categories.

Depending from the scientific environment where they are developed and apart from their different degree of sophistication, models proposed in the literature for assessing the river sediment load may be broadly classified in two categories: (a) models mainly oriented on the watershed-slopes' processes and (b) models mainly oriented on the river processes. Models of type (a) generally are developed in the agricultural and hydrologic engineering community and concentrate their attention on the rill and interril "surface erosion" especially on agricultural crops. They need, however, to be completed by a simplified, at least, sediment transfer model through the downstream river network (Moore, 1984). Models of (b) type, by contrast, represent the evolvement of theoretical and experimental research on sediment transport in rivers mainly performed by hydraulic engineers and are less focused on the processes on hillslopes which are one of the major sources of sediments to rivers.

In summary, models (a) and (b) are in principle correct, provided that both the sediment production from the watershed slopes and their routing along the river system are altogether accounted for with sufficient accuracy, no matter if most of the information is coming from the watershed or from the river.

In this paper, aiming at assessing the sediment transport at the basin scale, on a monthly time-scale, and in the lack of detailed information on stream geometry and sediment size distribution in rivers, a type (a) of modelling framework, completed with a conceptual sediment transport scheme, was adopted.

Focusing on the type (a) of hillslope models, empirical models accounting for sediment eroded from the catchment, like USLE (Wischmeier and Smith, 1978), MUSLE (Williams, 1975), RUSLE (Renard et al., 1997), are generally the simplest and most widely applied of the three model types, especially for large scale basins like the ones we investigated. They are based primarily on the analysis of observations and seek to characterise the basin response from these data (Wheater et al., 1993). A physical meaning is sometimes attributed to parameter values in empirical models obtained by calibration, without an appropriate conceptualisation of processes. Empirical models are often criticised for employing unrealistic assumptions about the physics of the catchment system, ignoring the heterogeneity of catchment inputs and characteristics, such as rainfall and soil types, as well as ignoring the inherent non-linearities in the catchment system (Wheater et al., 1993).

Conceptual models, like EMSS (Vertessey et al., 2001), HSPS (Johanson et al., 1980) are usually based on the representation of a catchment as a series or by a combination of known hydraulic structures like storages, channels etc. (see also Tyagi et al., 2008). They analyse mechanisms of sediment and runoff generation and propagation by representing each of them in the model structure. Conceptual models tend to include a general description of catchment processes, without including the specific details of process interactions, which would require detailed catchment information (Sorooshian, 1991). Parameter values for conceptual models have typically been obtained through calibration against observed data, such as stream discharge and sediment load measurements (Abbott et al., 1986). Due to the requirement that parameter values should be determined by comparing calibration with observed data, conceptual models tend to suffer from problems associated with the identifiability of their parameter values (Jakeman and Hornberger, 1993).

Physics-based models like WEPP (Laflen et al., 1991), TOPOG (CSIRO, 1991), AUGUSTO (Rulli and Rosso, 2005, 2007), are based on the solution of fundamental physical equations describing the processes involved in erosion and sediment transport. The equations used in such models are the equations of conservation of mass and momentum for flow and the equation of conservation of mass for sediment (Bennett, 1974; Pilotti and Menduni, 1997). The parameters used in physics-based models, as surface roughness, vegetation cover, soil particle size distribution, are measurable and have a physical meaning. However, a parameter calibration is unavoidable, because of the high spatial variability of some parameters involved in the processes, and the uncertainty in their measurements at some points. This poses severe problems in defining criteria for the acceptability of a model setup (Liu et al., 2009).

Each model type of hillslope erosion serves a purpose, and a particular model type may not categorically be considered more appropriate than others in all situations (Merritt et al., 2003).

In this paper a distributed Revised Universal Soil Loss Equation (RUSLE) formulation was coupled with a river network routing scheme to simulate suspended sediment load on a monthly basis at eight stream gauging stations, with the objective to assess the potential impact of reservoirs and land use changes on suspended sediment load in the Lo river basin. The study area is the Lo river basin, (38,165 km^2 in Viet Tri), a left tributary of the Red River (138,960 km^2 in Son Tay), where the Thac Ba reservoir (2.49×10^9 m^3 storage volume) and the new Tuyen Quang reservoir (2.245×10^9 m^3 storage volume) already changed sediment load after 1971 and 2005 when they were started to be regulated mainly for hydropower generation. Sediment load in this area was recently investigated by Le et al. (2007) who simulated runoff and suspended sediment on a daily basis for the year 2003 using a simple lumped modelling approach. In this paper the suspended sediment load was simulated over the 1959–2007 period, thus covering different climatic and land use conditions and including the effect of the construction of the two reservoirs mentioned above. Distributed information about topography, land use, and rainfall interpolated on a 1 km resolution grid was used to compute sediment erosion with a RUSLE formulation adapted to local conditions and a river network routing scheme to simulate suspended load on a monthly basis at several sites. Parameters of the RUSLE collected by Vezina et al. (2006) and by Pham (2007) in subbasins of the Lo basin were taken as a reference. In the second section, the physiographic characteristics of the Lo basin are described, together with the rainfall, runoff and suspended sediment regime. The third section describes the modelling approach adopted. Results are presented and discussed in the following section, where the effect of reservoirs is assessed and, finally, the potential impact of land use changes is investigated.

2. The Lo river basin

The Lo river is a main branch of the Red River (Song Hong), located on the eastern side of the basin (see Fig. 1). The river sources start from Ping Yuan of Yuanshan, in the Yunnan Province (China). The location of the river source is 105°37′E longitude, 23°35′N latitude, at an altitude of 1100 m above sea level. The location of the river mouth is 105°27′E longitude, 21°18′N latitude. The Lo river at the Viet Tri gauge, at an altitude of 16 m a.s.l., has a catchment area of 38,165 km^2 of which 22,600 km^2 are in Vietnam. The length of the Lo river is 470 km and 275 km are in Vietnam. It flows through the Cao Bang, Tuyen Quang and Yen Bai provinces in Vietnam and flows into the Thao river at Viet Tri, in the Phu Tho province, where the main stream takes the name of Red River (Song Hong). The average basin altitude is 880 m and the basin area above the

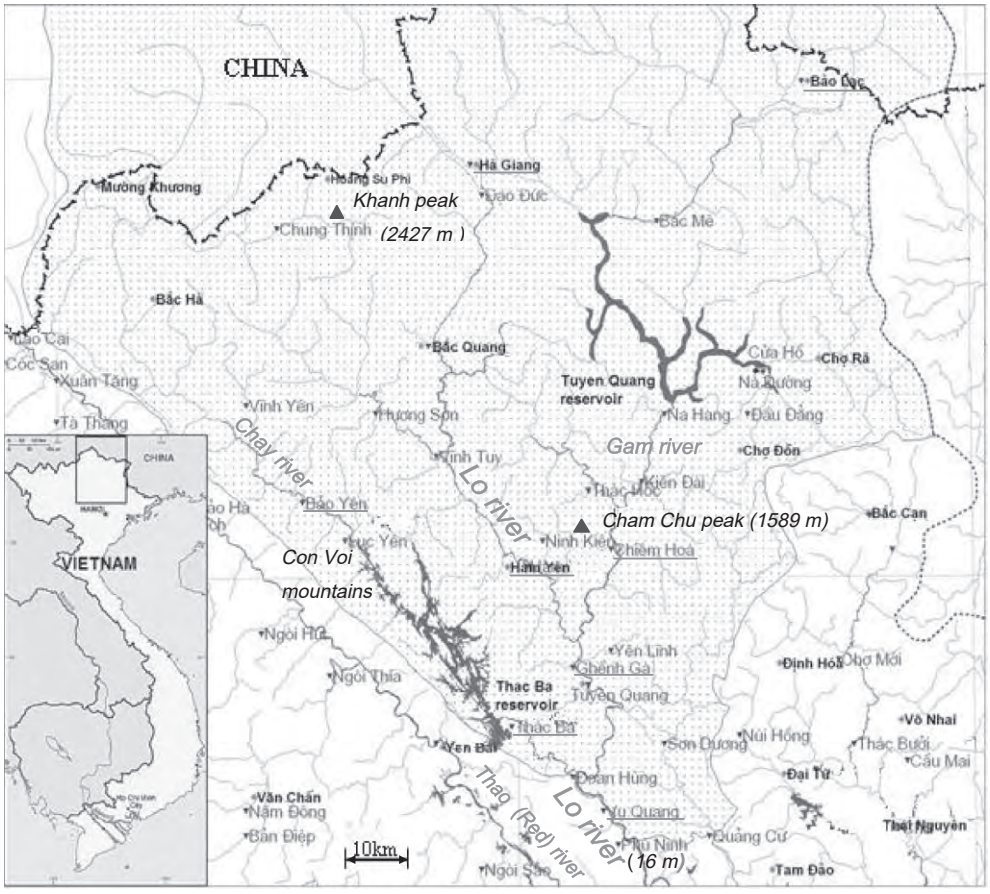

Fig. 1. The Lo river basin gauged at Phu Ninh (dotted area) with the hydrometric and, underlined, the eight suspended sediment load measurement stations considered in this study. The investigated area of the basin in Vietnam is zoomed here.

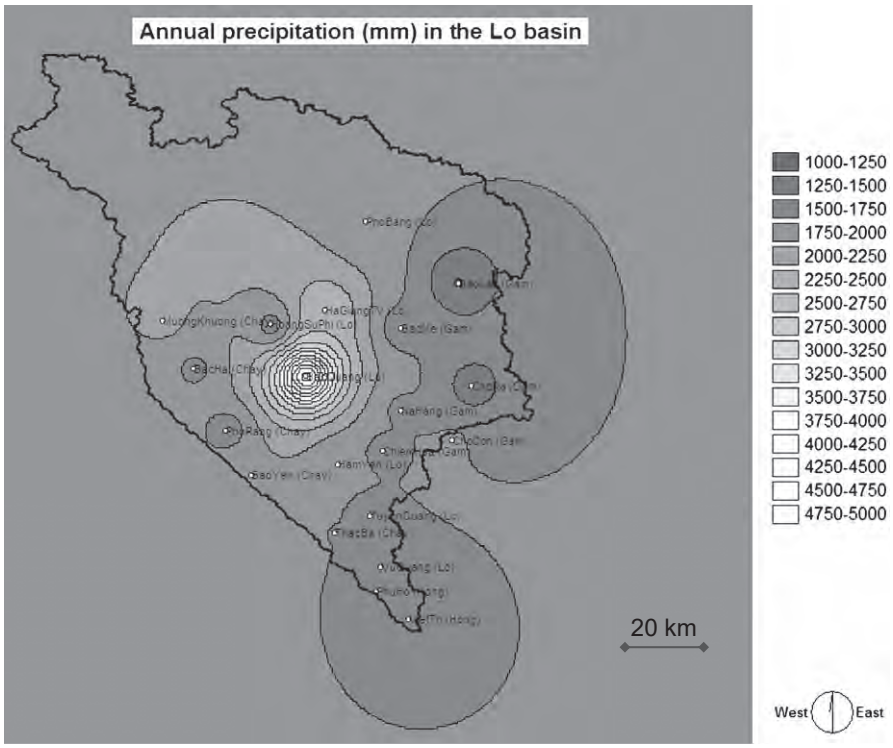

Fig. 2. Annual precipitation in the Lo basin, with the position of the rainguage stations (1959–2007).

altitude of 250 m covers more than 80% of the total basin area. The average slope of the Lo basin surface is 19.7%. The maximum elevation decreases from 2000 m altitude in China to 1000–1500 m altitude in Vietnam. The mountain topography is separated by four main rivers. The Thao and Chay rivers are separated by the Con Voi mountain range and Bac Ha plateau. The Khanh mountain ridge, reaching an altitude of 2427 m above sea level divides the Chay and the Lo rivers.

The drainage density is unevenly distributed in the basin. The western and the north-western parts of the basin are highlands where the rainfall amount is higher than in the south-eastern part (see Fig. 2). The river density ranges from 0.5 to 2.0 km/km^2, measured on 1:50,000 scale maps. Because of the lower rainfall amount, in the eastern and north-eastern part of the basin the drainage density is smaller, about 0.5 km/km^2. There are some major hydrometric stations in the Lo river, with runoff and suspended sediment load data records that go back more than 30 years, such as the Ha Giang station that gauges a 8300 km^2 basin drainage area, Ham Yen (11,900 km^2), Chiem Hoa (16,500 km^2), Ghenh Ga (29,600 km^2) and Vu Quang station with a basin 37,000 km^2 in size (see Fig. 1), for which 49 years of data were available for this study.

2.1. Terrain and geomorphology

Focusing on the Tuyen Quang province, which is representative for the Lo basin, where a new reservoir has been in operation since 2005, the terrain is dissected by a complex system of streams, rivers, heaps of mountains, hills, and deep valleys. Terrain height differentiation among areas in the province is large: the highest area is Cham Chu peak (Ham Yen District) with an altitude of 1589 m, the lowest place is the Southern Son Duong having an elevation of only 23 m above sea level.

From North to South, the basin can be divided into three altitudinal zones.

- *Terrain of high mountains:* it is mainly located in the northern part of the province and the terrain topography is very rough and difficult to access, with mountains up to the Cham Chu peak.
- *Terrain of low mountains:* includes about 40% of the area of the whole province, placed mainly in the southern part of the province including the southern part of Chiem Hoa, Ham Yen, Yen Son, and Son Duong district. The average elevation of this area is less than 500 m a.s.l. Peaks with an elevation over 500 m a.s.l. are the La mountain peak (550 m) and Lich mountain (933 m).
- The lower altitude zone includes fluvial plains and river valleys. Several fluvial fans develop at hills' foot and within main valleys originated from confluent rivers and they are very convenient for agricultural cultivation. Hills surrounding fluvial plains and fans show mild topography with residual hills of karst cones. This type of terrain is not very extended, only accounting for 10% of the area of the whole province, including the rest of Yen Son, the Son Duong District and Tuyen Quang.

The area surrounding Tuyen Quang shows the following geomorphologic features: river valley geomorphology develops along valleys of major rivers such as Lo, Gam, and Pho Day River. Karst geomorphology is a typical geomorphologic feature of limestone mountains, concentrated mainly in the Na Hang district, the mountainous area of Chiem Hoa, the Son Duong district. Mountains higher than 700 m a.s.l. are distributed mainly in the Na Hang district, north of Ham Yen, and Chiem Hoa district. Mountains ranging from 300 to 700 m a.s.l. include a large area, distributed mainly in Ham Yen, Yen Son, the Son Duong districts and part of the Chiem Hoa district. Low hills having an elevation less than 300 m a.s.l. are distributed mainly in the South of Yen Son, and in the Ham Yen district. Terrain's slope of Tuyen Quang is divided into four classes: areas with slope of less than 8% accounting for about 14% of the total province area, area with slope of 8–15% accounting for about 34%, area with slope of 15–25% accounting for about 26% and area with slope of more than 25% accounting for 21%. In the Lo basin, major land use classes correspond to agricultural land, forest, urban areas and water bodies.

2.2. Rainfall and runoff regime

Rainfall in the Lo basin is relevant, with a 1880 mm annual average, but uneven in distribution and highly variable in space and time, as shown in Figs. 2 and 3, depending on local terrain conditions and monsoon circulation in Northern Vietnam. The Ha Giang province is the rainiest, reaching an annual rainfall depth of 4815 mm measured, on average, at the Bac Quang station from 1961 to 2007. Similar to other areas in northern Vietnam, the climatic regime is divided into two seasons: the rainy season and the dry season. The rainy season is from May to October; the dry season is from November to April of the following year. Average annual rainfall on a climatic basis in the Tuyen Quang province fluctuates in the range from 1500 to 1800 mm. There are 150 rainy days per year on average. The rainy season occurs in summer with a total seasonal rainfall ranging, at different stations, in the 1310–2130 mm range, accounting for 85–94% of total annual rainfall; the dry season takes place in winter with a total seasonal rainfall ranging from 134 to 225 mm, only comprising 6–25% of the total annual rainfall. The most rainy months are July, August and September with rainfall of 250–320 mm/month, and up to 950 mm/month measured in September 2000 in Tuyen Quang town. The months with the lowest average rainfall are January and December with rainfall reaching only 16–25 mm/month. The fluctuations of monthly and annual rainfall in the 1959–2007 period in some stations of the Lo basin are reported more in detail in Le et al. (2010).

The runoff regime reflects the rainfall regime with mean annual runoff of 871 mm at the Vu Quang station, the runoff measurement station closer to the Lo basin outlet. More detailed information on interannual variability of runoff for eight stations are reported in Le et al. (2010).

2.3. Suspended sediment data

The runoff and suspended sediment load data used in the present analysis were measured at eight gauging stations in the Lo river

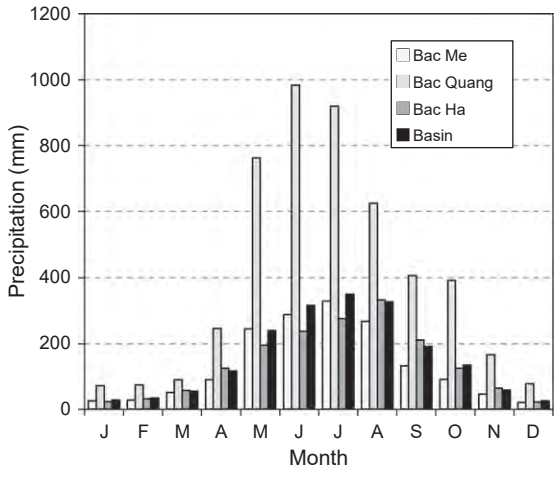

Fig. 3. Monthly precipitation regime in the Lo basin (1959–2007).

basin from 1959 to 2007. During that period two reservoirs, Thac Ba and Tuyen Quang, were put into operation. In Table 1, the mean suspended sediment load in the selected stations is reported, obtained by averaging daily sediment load data at the eight stations. Starting from 1971 the Thac Ba reservoir was in operation resulting, in the following years, in a dramatic drop in suspended sediment load. The average sediment concentration over the 1971–1975 period had fallen to 0.026 kg/m^3 from the 0.529 kg/m^3 average over the 1959–1963 and 1966–1970 period, prior to the dam construction with a resulting suspended sediment trap efficiency of 95%. In Fig. 4, the effect of the Thac Ba reservoir on suspended sediment impounds can be observed.

Starting with December 2004 the Tuyen Quang reservoir, draining an area of 13,454 km^2 computed from the digital river network was in operation. The average sediment concentration measured in the downstream Chiem Hoa (16,500 km^2) station over the 2005–2007 period dropped to 0.184 kg/m^3 from the 1965–2004 years period when it was 0.436 kg/m^3 with a resulting suspended sediment trap efficiency of 71% of the Tuyen Quang reservoir. Fig. 5 illustrates the effect of the Tuyen Quang reservoir on sediment load. These data are consistent with those by Nguyen et al. (2003) who reported that the suspended sediment load at the Son Tay station (138,960 km^2) decreased from 114×10^6 tons/year in the period 1958–1985 to 73×10^6 tons/year in the period 1986–1997, after the Hoa Binh reservoir, draining an area of 51,800 km^2, on the Da river has come into operation. Estimates of specific sediment load in the Da river at Hoa Binh are 1.200 kg/m^3 for the 1958–1985 period and 0.300 kg/m^3 for the 1986–1997 period, corresponding to a trap efficiency of 75%, as reported by Le et al. (2007). Such a significant decrease in suspended sediment load increases the flow capacity to erode the river channels and, indeed, erosion of riverbanks, bridge abutments and piers has been already

Table 1
Annual total suspended sediment load (10^6 tons/year) in the Lo river basin.

Year Area (km^2)	Bao Yen 5000	Thac Ba 6170	Ha Giang 8300	Ham Yen 11,900	Bao Lac 4060	Chiem Hoa 16,500	Ghenh Ga 29,600	Vu Quang 37,000
1959		2.53		3.12				9.61
1960		2.72		1.99			5.35	6.73
1961		3.23		3.58			9.10	9.82
1962		2.41		4.23			6.80	8.56
1963		3.28		1.80			4.84	4.69
1964				4.68	0.51		11.22	13.09
1965				2.75	0.39	2.21	7.44	7.90
1966		4.90		2.19	2.33	6.84	10.16	12.12
1967		2.71		2.52	0.66	2.43	5.33	7.22
1968		3.99		4.24	2.68	9.09	12.51	13.96
1969		2.99		4.40	1.36	4.08	9.38	10.13
1970		3.45		4.10	0.81	4.16	10.26	10.36
1971		0.48		6.78	2.26	7.61	16.55	15.60
1972		0.19		3.35	0.38	3.91	6.90	7.26
1973		0.09		5.74	0.98	2.98	10.88	9.25
1974		0.12	3.64	4.58	1.05	4.33	8.81	7.68
1975		0.05	4.15	4.67	1.16	5.14	8.59	10.79
1976			2.35	3.45	0.80	3.67	6.08	6.85
1977			2.02	2.77		2.23	3.86	4.91
1978			5.86	5.85		11.05	14.27	18.48
1979			9.71	12.47		9.26	17.77	15.97
1980			1.77	2.94		3.23	7.24	8.11
1981			3.72	3.67		4.94	10.10	8.92
1982			2.17	2.04		3.42	8.21	6.16
1983	3.51		2.04	2.83		3.38	5.96	3.69
1984	5.58		3.93	5.07		4.31	8.39	7.66
1985	3.36		4.95	5.01		5.28	9.16	8.64
1986	8.98		12.95	6.90		11.86	22.31	18.29
1987	3.29			5.33		2.87	8.64	8.80
1988	3.31		3.06			5.30	9.58	14.47
1989	3.58		3.09	13.09		4.28	9.77	12.05
1990	6.65		2.94	6.17		12.22	18.37	21.86
1991	5.38		3.68	4.93		4.11	9.98	12.88
1992	4.95		2.52	3.30		4.55	10.61	9.28
1993	3.20		3.31	2.34		7.43	12.70	8.59
1994	3.08		3.60	4.87		4.65	11.56	14.38
1995	6.75		3.69	9.35		4.41	11.88	22.42
1996	5.38		3.88	4.77		4.27	12.12	12.54
1997	3.95		3.43	4.00		5.79	12.75	11.55
1998	3.38		3.79	5.54		5.93	12.40	15.27
1999	3.18		3.04	4.62		4.59	9.58	11.82
2000	4.18		2.75	4.33		2.74	6.59	10.13
2001	5.00		3.06	3.91		6.61	10.65	12.57
2002	6.41		4.48	5.84		7.71	16.64	17.33
2003	4.21		2.90	3.37		3.17	9.06	8.03
2004	4.28		3.52	3.80		10.45	10.04	9.57
2005	3.39		1.52	2.54		3.13	5.87	5.45
2006	1.74		0.90	1.71		1.12	2.84	3.45
2007	2.58		1.33	1.18		1.35	3.04	3.66
Mean	4.37	2.21	3.63	4.43	1.18	5.16	9.84	10.58
Runoff (10^6 m^3/year)	4357	6292	4972	11,673	2168	11,923	24,401	32,220
Runoff (mm/year)	871	1020	599	981	534	723	824	871

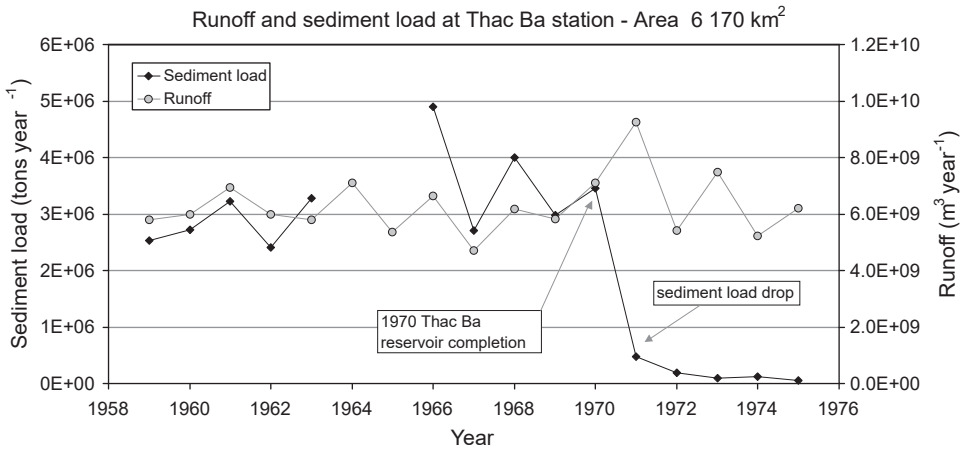

Fig. 4. Effect of the Thac Ba reservoir on suspended sediment load.

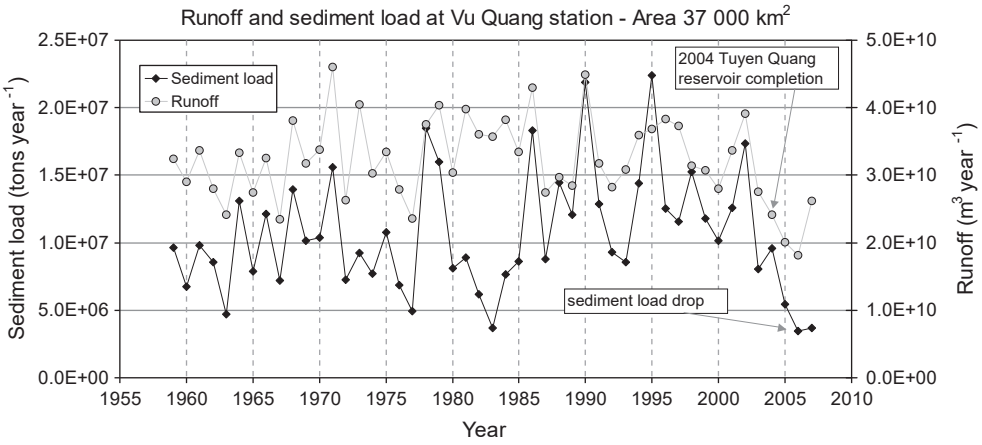

Fig. 5. Effect of Tuyen Quang reservoir on suspended sediment load.

observed downstream the Thac Ba and Tuyen Quang reservoirs, rising the concern of river management authorities. Riverbank erosion between the Vu Quang and Viet Tri hydrometric stations, in particular, is becoming a relevant problem.

3. RUSLE sediment erosion and transport modelling

3.1. The RUSLE modelling of sediment erosion

In our modelling approach, on the basis of the hydrological, the physiogeographic data available and their resolution and the research objectives, the sediment delivered from river bed erosion and landslides, which has a coarser grain size and mainly contributes to bed load (Patel and Ranga Raju, 1996) was not computed. Moreover, sediment deposition in reservoirs only, and not that along the river network, is considered in our conceptual modelling approach, thus balancing, at least in part, the underestimation of sediment supply.

As a result of these assumptions the RUSLE approach was adopted here for the computation of suspended sediment load at the catchment scale and an extended data set is used to test and verify our hypotheses. The Universal Soil Loss Equation (USLE, Wischmeier and Smith, 1978), and the revised version of it, named RUSLE (Renard and Freimund, 1994; Yoder and Lown, 1995; Renard et al., 1997), were developed to predict the long term average annual erosion, A, from field sized areas. Here the RUSLE approach was applied in a distributed manner, using a 1 km resolution GIS which makes spatial soil erosion assessment feasible with a reasonable cost and accuracy in larger areas. In particular, the RUSLE is a set of mathematical equations that estimate average annual soil loss and sediment yield resulting from interrill and rill erosion. RUSLE is one of the most popular and effective empirical models for the assessment and prediction of soil erosion due to water runoff. It was not originally intended to be valid for large study areas. However, satisfactory results on large-scale watersheds were also reported by many researchers.

The RUSLE basic equation includes six factors: R the rainfall-runoff erosivity factor, K the soil erodibility factor, L the slope length factor, S the slope gradient factor, C the crop and management factor and P the conservation support practice factor. The USLE/RUSLE model is often represented by the equation:

$$A = R \cdot K \cdot LS \cdot C \cdot P, \tag{1}$$

where A is average soil loss per unit of area during a unit period of time, usually one year (tons ha^{-1} year^{-1}).

R is average rainfall and runoff factor, the erosion potential of rainstorms (MJ ha^{-1} mm h^{-1}).

The conceptual framework to estimate the R factor in RUSLE has been significantly improved over that assumed in the original USLE approach. For this study, the threshold-type equation of Loureiro and Coutinho (2001) is adopted:

$$R = \frac{1}{N}\sum_{i=1}^{N}\sum_{m=1}^{12}(7.05 \cdot \text{rain}_{10} - 88.92 \cdot \text{days}_{10})_{m,i}, \quad (2)$$

where N is the number of observation years, rain_{10} is monthly rainfall, when $\geqslant 10$ mm, otherwise it is set to zero, day_{10} is monthly number of days with rainfall $\geqslant 10$ mm.

Eq. (2) gives a higher erosion potential of rainfall with higher monthly rainfall, rain_{10}. It also accounts for the fact that, for a given rainfall amount, the lower are the rainy days, days_{10}, the higher is the rainfall intensity and erosion potential, as expected. Using the above equation the monthly R factor value for rain gauges of the Lo river basin were computed and the resulting average annual R factor, interpolated with Thiessen polygons for the period 1959–2007, is shown in Fig. 6.

K is the average soil erodibility factor (tons MJ^{-1} h mm^{-1}). Some soil types are naturally more prone to soil erosion due to their physical structure. Erodibility is a function of soil texture, organic matter content and permeability.

In this study, the K factor is assumed equal to 0.022 according to literature data for watershed units in Vietnam's northern highlands (see Vezina et al., 2006; Pham, 2007), reported in Table 2 and Table 3. Such a value is also in agreement with literature data about China, (Zhang et al., 2004, 2008), which report a mean value of 0.038 in a 0.004–0.091 range and 0.0144 in a 0.0016–0.0381 range.

LS is the slope length and the slope gradient factor. Slope has a major effect on the rates of soil erosion. The higher the slope, the higher is the velocity of overland flow, thus increasing the shear stresses on the soil particles. As slope length increases, the overland flow and flow velocity also steadily increase, leading to greater erosion forces applied to the soil surface.

In this study, the equation of Moore and Burch (1986), adopted also, among others, by Pilotti and Bacchi (1997) for estimates of erosion at the catchment scale, was used.

$$LS = \left(\frac{A_s}{22.1}\right)^{m'} \cdot \left(\frac{\sin\beta}{0.0896}\right)^{n'}, \quad (3)$$

where A_s is the area of plot per unit width. Considering that crops are divided into small parcels in mountainous slopes of Vietnam, the standard reference value of 22.1 m was assumed. m', n' are coefficients set equal to 0.6 and 1.3, respectively and β is slope angle, computed from the DEM.

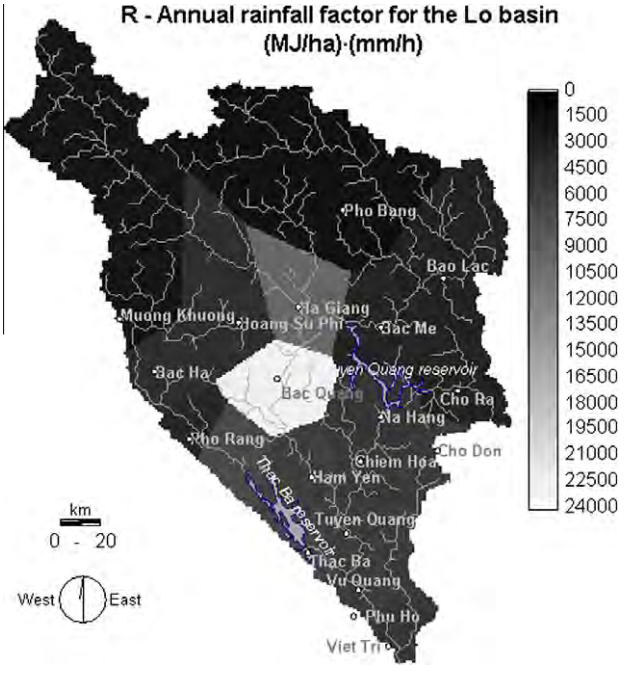

Fig. 6. The mean rainfall erosivity factor R (MJ ha^{-1} mm h^{-1}).

Table 2
Soil erodibility K factor (tons MJ^{-1} h mm^{-1}) after Vezina et al. (2006).

Soil type	K factor
Fluvisols	0.055
Regosols	0.025
Leptosols	0.028
Cambisols	0.050
Alisols	0.045
Phaozems	0.065

Table 3
Soil erodibility K factor (tons MJ^{-1} h mm^{-1}) after Pham (2007).

Soil type	D (mm)	K factor
Feralit humus from lime stone	0.082557	0.033
Feralit yellow-red from lime stone	0.180637	0.021
Feralit humus from acid stone	0.097749	0.030
Feralit humus yellow-red from granite stone	0.113501	0.028
Feralit yellow-red from acid stone	0.122138	0.027
Silt	0.14555	0.024
Feralit red-brown from gabrostone	0.117648	0.027
Feralit from typical limestone	0.130215	0.026

C is the cropping, vegetation and management factor and determines the relative effectiveness of soil and crop management systems in terms of preventing soil loss ($C = 1$ with bare soil, no vegetation and without management practices; $C < 1$ otherwise, with values close to zero in forested areas where surface erosion is mitigated by vegetation). The C factor plays a critical role in determining the rate of erosion. The leaves of plants protect the soil from raindrop impact and the roots hold the soil together. Plants also tend to increase infiltration of water, thus reducing the volume of overland flow running down the slope. The C factors of the Lo basin for individual crops in addition to mixed farming systems was selected from literature data as adopted for northern Vietnam (Vezina et al., 2006; Pham, 2007), as shown in Tables 4 and 5. These data were adapted to digital land use maps adopted by FAO, resulting in the cropping factor reported in Table 6 and shown in Fig. 7.

P is a supporting practice factor. It reflects the effects of practices that will reduce the amount and rate of the water runoff and thus reduces the amount of erosion, the higher the supporting practice, the lower the value of the P factor. The support practice factor expresses the effect of support practices such as contour cultivation, strip cropping around contours, arable land terrace and bench terrace and it cannot be assessed from coarse resolution land use map, as those available for this research. Table 7 reports the value of the P factor of the Lo basin adopted by Pham (2007), according to the International Soil Science Association, and Table 8 collects the values adopted by Vezina et al. (2006) for Vietnam's northern highlands. In this study, an average P factor is assumed and set to 0.2 because of the dominant soil conservation practices

Table 4
Cropping factor C (Pham, 2007).

Cropping system	C factor
Paddy rice and vegetable	0.60
Bush, shrub, grassland	0.18
Natural forest	0.003
Fallow, waste land	1.00

Table 5
Cropping factor *C* (Vezina et al., 2006).

Cropping system	*C* factor
Paddy rice (2 cycles)	0.55
Paddy rice (1 cycle)	0.40
Paddy rice (1 cycle) with corn	0.55
Cassava	0.22
Corn	0.12

Table 6
Cropping factor *C* adopted in this study.

Land use	*C* factor
Urban and built up land	0.0
Dryland Cropland and Pasture	0.5
Irrigated Cropland and Pasture	0.18
Mixed Dryland/Irrigated Cropland and Pasture	0.5
Cropland/Grassland Mosaic	0.5
Cropland/Woodland Mosaic	0.5
Grassland	0.18
Shrubland	0.18
Mixed Shrubland/Grassland	0.18
Savanna	0.18
Deciduous Broadleaf Forest	0.003
Deciduous Needleleaf Forest	0.003
Evergreen Broadleaf Forest	0.003
Evergreen Needleleaf Forest	0.003
Mixed Forest	0.003
Water Bodies	0.0
Herbaceous Wetland	0.18
Wooded Wetland	0.003
Barren or Sparsely Vegetated	0.18

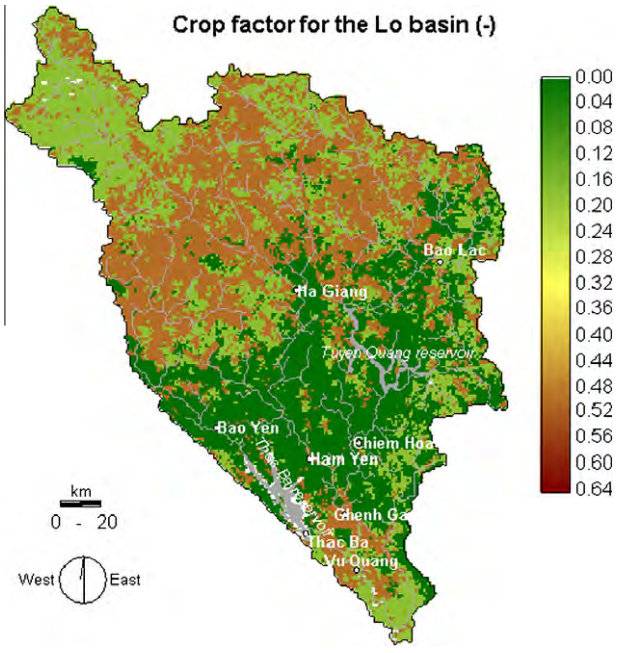

Fig. 7. The cropping, vegetation and management *C* factor.

in the basin, with extensive use of terraced crops and small crop parcels. With this value, which is one of the two calibration parameters of the model, the mean inter-basin bias of the simulated sediment production, compared with measurements was just 1.4%, as will be discussed later.

Table 7
Support practice factor *P* (Pham, 2007).

Slope (%)	Plant under the contour line and Plants with the bench	Plant under the furrow
1–2	0.3	0.12
3–8	0.25	0.1
9–12	0.3	0.12
13–16	0.35	0.14
17–20	0.4	0.16
21–25	0.45	0.18

Table 8
Support practice factor *P* (Vezina et al., 2006).

Cropping system	*P* factor
Paddy rice (2 cycles)	0.10
Paddy rice (1 cycle)	0.20
Paddy rice (1 cycle) with corn	0.10
Cassava	0.90
Corn	0.80

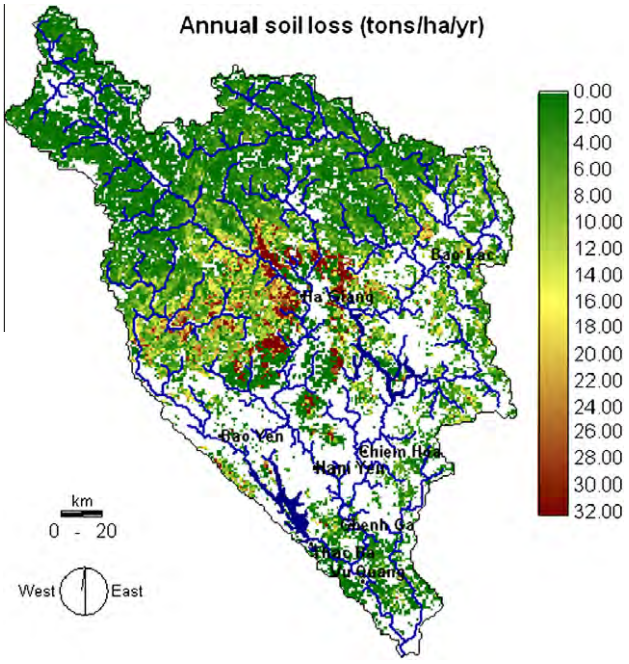

Fig. 8. Average soil loss (tons ha^{-1} $year^{-1}$) in the Lo river basin.

3.2. Sediment transport

The resulting mean annual soil losses evaluated with the RUSLE model are shown in Fig. 8. In particular, soil losses were computed on a monthly basis and then were accumulated across a channel network extracted from a 1-km resolution DEM using the standard D8 flow direction method (O'Callaghan and Mark, 1984). The resulting river network is in a good agreement with the observed 'blue lines', although a more accurate description of the drainage system could be achieved with more sophisticated methods (e.g. Orlandini and Moretti, 2009). The D8 scheme, already adopted by Ranzi et al. (2002), is part of the DIMOSHONG model (DIstributed hydrological MOdel for the Shong HONG) which was already applied for flood forecasting in the Red River basin (Ranzi et al., 2007; Ngo et al., 2010).

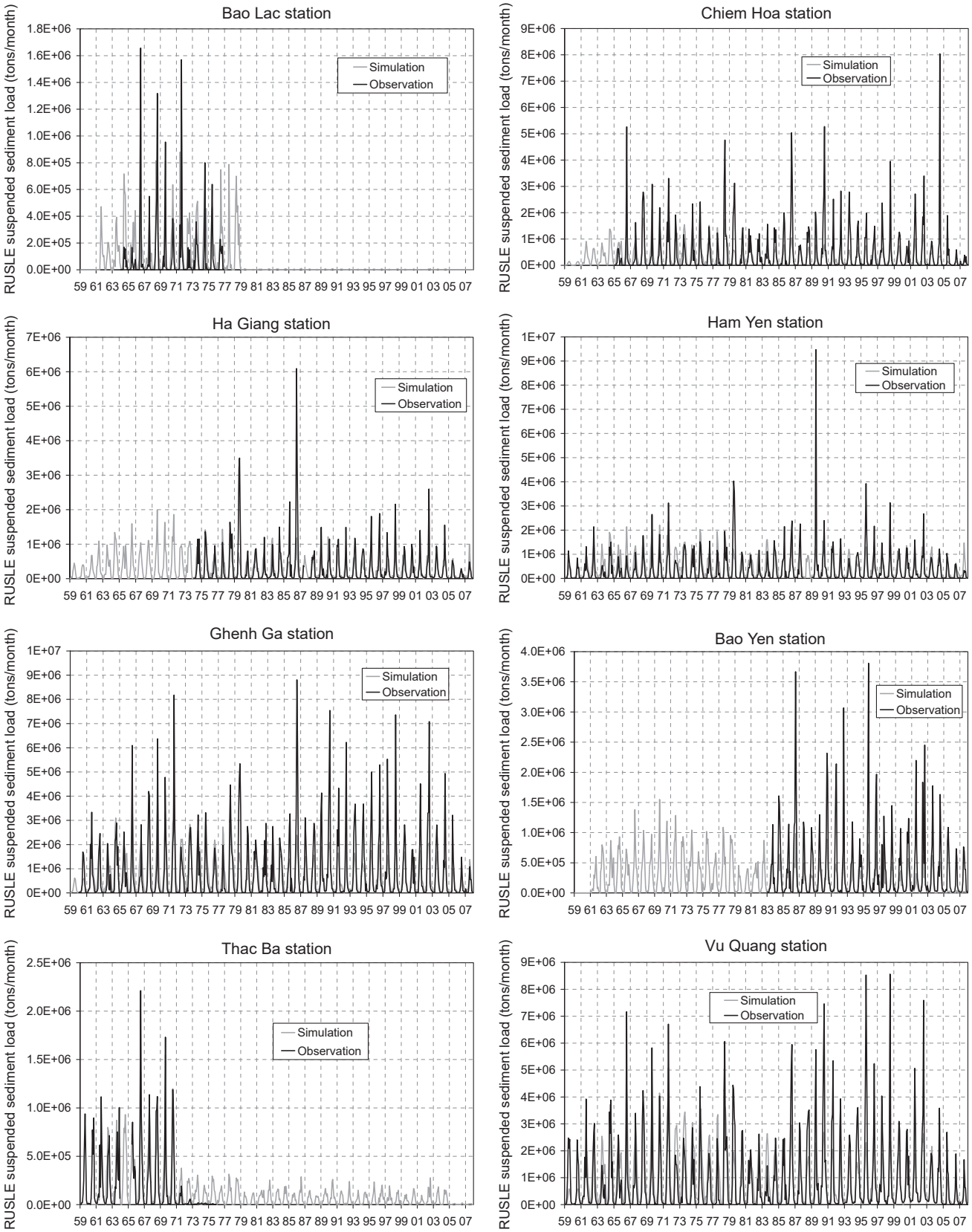

Fig. 9. Monthly sediment yield simulated and observed at eight hydrometric stations in the Lo river basin.

The accumulated monthly sediment production S_k, expressed in tons/day, in each of the basins upstream eight measurement stations ($k = 1,\ldots,K = 8$) is then routed through the channel network with a conceptual, lumped scheme, aiming at reproducing the dominant mode of behaviour of the sediment transport process (Moore, 1984). For the sediment translation function a plausible

assumption is that the travel time of sediments in the basin is a random variable with exponential distribution, with mean travel time θ_k, expressed in days and estimated as the ratio of a length scale, L_k, and of a velocity scale, V. The length scale is assumed as a power law function of each basin area, A_k, according to the Hack's law, $L = 1.4A^{0.6}$, with L being the mainstream length expressed in kilometres and the area A in km^2 (Hack, 1957; Rigon et al., 1996).

Assuming each kth basin as a storage, feeded by sediments detached from its hillslopes at a constant rate S_k during each month and releasing a sediment discharge $q_{s,k}(t)$ at its outlet, in the above assumption the sediment stored in the basin $W(t)$ is proportional to $q_{s,k}(t)$:

$$W_k(t) = \theta_k q_{s,k}(t), \tag{4}$$

and the equation of mass conservation for sediments at the basin scale becomes the differential equation of a linear reservoir:

$$dW_k(t)/dt = \theta_k dq_{s,k}(t)/dt = S_k - q_{s,k}(t), \tag{5}$$

which can be solved given the initial condition $q_{s,k}(t = 0) = q_{s,0,k}$.

In this conceptual and lumped modelling framework, the suspended sediment discharge $q_{s,i,k}$ (tons/day) at each kth basin's gauging station at the end of each ith month with duration of T days, results as:

$$q_{s,i,k} = q_{s,i-1,k}e^{-T/\theta_k} + S_{k,i}(1 - e^{-T/\theta_k}) \quad (\text{tons/day}), \tag{6}$$

and the monthly sediment yield is:

$$V_{s,i,k} = q_{s,i-1,k}\theta_k(1 - e^{-T/\theta_k}) + S_{k,i}T + S_{k,i}\theta_k(e^{-T/\theta_k} - 1) \quad (\text{tons}). \tag{7}$$

The optimal value for the spatio-temporal mean sediment transport velocity, which is the second model's parameter we calibrated, was estimated as $V = 0.5$ m/s by minimising, as objective function, the mean inter-basin Nash–Sutcliffe efficiency coefficient, NS, of the simulated vs. observed monthly sediment yield V_s, which resulted NS = 0.45.

4. Results and discussion

The soil loss computed on a monthly scale with the RUSLE approach and accumulated with the routing scheme described in the previous section was employed to evaluate the suspended sediment load at each of the eight sediment gauge stations in the Lo river. The modelling scheme with the parameters as described above was applied to the Lo river basin by using rainfall data from 20 rain gauges located in the basin. The resulting simulated monthly values are compared in Fig. 9 with measurements and in Fig. 10 the mean annual sediment load before the reservoirs impoundment is compared with data. The mean annual simulated soil losses in basins prior to reservoirs operation are in good agreement with observations, as reported in Table 9, with values ranging from 0.17 mm/year at Chiem Hoa to 0.34 mm/year at Thac Ba compared to the observed 0.19–0.35 mm/year range. The coefficient of determination results $R^2 = 0.89$, as Fig. 10 shows. Concerning the effect of reservoir impoundment on suspended sediment load, measured data indicate how the Thac Ba reservoir (2.49×10^9 m^3 storage) and the new Tuyen Quang reservoir (2.245×10^9 m^3 storage) have already changed sediment load since 1971 and 2005 when they were, respectively, in operation. Sediment impoundment in the reservoirs affects suspended sediment load in the river network downstream. The reservoir sedimentation efficiency was estimated 71% and 95% for the Tuyen Quang and Thac Ba reservoirs, respectively, by comparing the sediment yield after and before the dams construction. Assuming a 71% value for the sediment catch efficiency it was possible to reproduce quite well sediment load downstream these reservoirs also after their completion. A fairly good agreement between simulated and observed values for the stations downstream reservoirs is reported in the last two columns of Table 9.

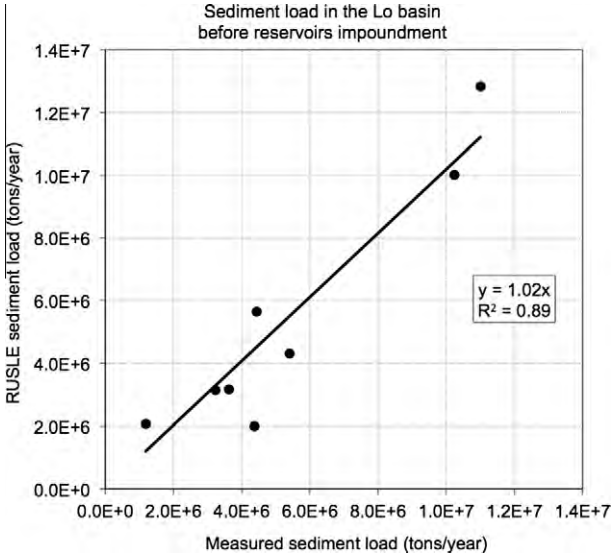

Fig. 10. The relationship between measured and RUSLE-modelled annual sediment load in the Lo basin.

In Fig. 9 and Table 10 statistics of the simulation over the entire 1959–2007 simulation period are reported, including the effect of reservoirs. The graphs show a satisfactory reproduction of the sediment load regime, both in the dry and wet season for all stations. Indicating that no systematic bias occurs, the mean inter-station relative error is 1.4%, being small, 4.7%, at the Vu Quang station, close to the basin outlet, but higher in the smaller basins, as Bao Lac where a 76% overestimation resulted from simulation. The linear correlation coefficient between simulated and observed data is in the 0.66–0.83 range, being 0.72 on average. The mean Nash–Sutcliffe efficiency results to be 0.45, ranging from 0.33 to 0.62. These data provide an indication of the overall predictive uncertainty of the model, which, considering the complexity of the process of sediment detachment and transport and the wide space and time scale investigated, can be considered satisfactory, in the author's expectations. Looking more in detail on the scatter-plot of the monthly simulations at Vu Quang over the entire 1959–2007 simulation period, in Fig. 11, some further considerations can be drawn. About one dozen of simulated values, out of 588 data, heavily underestimate high sediment load data. This occurs also at the Ham Yen station, not shown here, which is not influenced by upstream reservoirs. This underestimation in sediment load can be explained by considering that sediment delivered by landslides and debris flow and by erosion from stream channels are not taken into account in our modelling scheme. These processes occur mainly during high flow events and this can explain the observed biased data. We can argue, however, that sources of sediment other than surface erosion which should be separately evaluated and be better modelled with alternative approaches than RUSLE, as in Gavrilovic (1988, 1998), deliver the coarser fraction to the total sediment load, which does not contribute to the measured suspended sediment load and which deposits in the reservoirs. In addition, the neglected contribution to sediment delivery from landslides, debris flow and riverbed erosion is balanced, at least in part, by the effect of the assumption that no deposition is modelled along the river reach, with the exception of the reservoirs as described later. This can explain how, on one hand, no major systematic bias results from our modelling scheme and, on the other, the sediment load during some high flow events is underestimated.

Table 9
Annual total sediment load (tons/year) in the Lo river basin, measured and simulated with the model. Asterisk * indicate stations downstream reservoirs, for which measured sediment is computed also from the data in the observation period after they came into operation, in brackets in the fourth column.

Station	River	Area (km^2)	Observation period (with reservoirs)	Measured without reservoirs (tons/year)	RUSLE without reservoirs (tons/year)	Measured with reservoirs (tons/year)	RUSLE with reservoirs (tons/year)
Bao Yen	Chay	5000	1983–2007	4,370,884 (0.58 mm/year)	2,000,728 (0.27 mm/year)	4,370,884 (0.58 mm/year)	2,000,728 (0.27 mm/year)
Thac Ba*	Chay	6170	1959–1975 (1971–1975*)	3,221,854 (0.35 mm/year)	3,157,341 (0.34 mm/year)	186,249 (0.02 mm/year)	1,222,592 (0.13 mm/year)
Ha Giang	Lo	8300	1974–2007	3,628,797 (0.29 mm/year)	3,162,664 (0.25 mm/year)	3,628,797 (0.29 mm/year)	3,042,227 (0.24 mm/year)
Ham Yen	Lo	11,900	1959–2007	4,431,441 (0.25 mm/year)	5,652,585 (0.32 mm/year)	4,431,441 (0.25 mm/year)	5,514,879 (0.31 mm/year)
Bao Lac	Gam	4060	1964–1976	1,181,968 (0.19 mm/year)	2,079,477 (0.34 mm/year)	1,181,968 (0.19 mm/year)	2,079,477 (0.34 mm/year)
Chiem Hoa*	Gam	16,500	1965–2007 (2005–2007)	5,411,995 (0.22 mm/year)	4,326,636 (0.17 mm/year)	1,868,613 (0.08 mm/year)	639,120 (0.03 mm/year)
Ghenh Ga*	Lo	29,600	1960–2007 (2005–2007)	10,230,666 (0.23 mm/year)	10,018,721 (0.23 mm/year)	3,915,373 (0.09 mm/year)	4,087,866 (0.09 mm/year)
Vu Quang*	Lo	37,000	1959–2007 (2005–2007)	11,000,128 (0.20 mm/year)	12,825,106 (0.23 mm/year)	4,188,439 (0.08 mm/year)	4,225,354 (0.08 mm/year)

Table 10
Statistics of measurement vs. simulation errors of monthly suspended sediment yield (tons/month).

Mean travel time θ_s (days)	Bao Yen 5.4	Thac Ba 6.1	Ha Giang 7.3	Ham Yen 9.0	Bao Lac 4.7	Chiem Hoa 11.0	Ghenh Ga 15.6	Vu Quang 17.8
Observed mean	362,154	192,517	299,761	369,282	98,497	430,396	819,653	881,911
Simulated mean	166,648	207,883	251,969	411,309	173,327	332,305	749,969	923,371
Mean relative error	54.0%	8.0%	−15.9%	11.4%	76.0%	−22.8%	−8.5%	4.7%
Error standard deviation	425,626	211,363	432,784	507,636	190,886	662,213	894,525	918,045
Pearson correlation r (–)	0.83	0.79	0.66	0.66	0.68	0.66	0.77	0.74
Nash–Sutcliffe efficiency	0.34	0.62	0.41	0.42	0.33	0.44	0.55	0.55

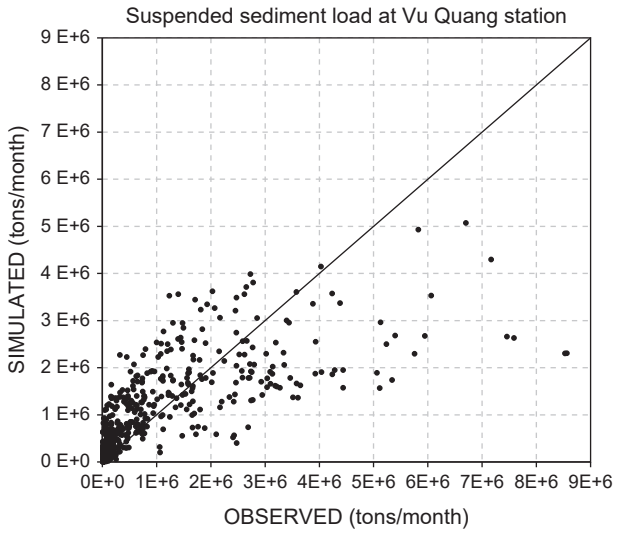

Fig. 11. Scatter plot of the monthly sediment load simulated and measured at the Vu Quang station (37,000 km^2) over the 1959–2007 simulation period.

Because of the complexity of the sediment erosion and deposition and sediment transport processes in large basins, the lack of data on input and parameters for detailed physics based models, the adoption of simplified conceptual schemes, as in our approach and also, for instance, in Le et al. (2007), Ali and De Boer (2009), Tyagi et al. (2008), Moore (1984) seems to be a plausible solution for sediment yield models in environments as that here investigated. We recognise, however, that our modelling approach could be improved by considering also, in a "hydraulic approach", streamflow data to assess localised erosion processes as those occurring in the river streams (see for instance Di Silvio and Nones, 2010). For the implementation of this type of models, however, more data are needed on the channel geometry and particle size distribution than those available, at the moment, to the authors for the rivers here investigated.

5. Land use change effect on suspended sediment load

Soil erosion assessment at the scale of large basins like that of the Lo river is necessary for sustainable land use and management. An assessment of the soil loss under land use changed conditions is valuable for understanding how the different land use classes can affect soil erosion and to predict the impact of anthropogenic influences and climate changes. The effect of land use changes on the hydrological response and the sediment load in the different regions is investigated by several authors (e.g. Le et al., 2007; Pham, 2007; Rosso and Rulli, 2002; Rulli and Rosso, 2005). Concerning the Lo basin, major land use classes correspond to agriculture, forest, urban areas and water respectively. Vegetation cover is changing in the last decades, due to deforestation for agriculture development and forest fires. In particular, Pham (2007) analyzed a small basin upstream the Ba Bê lake, draining an area of 420 km^2 upstream the Tuyen Quang dam and Bac Me, in the Lo basin. He observed a forested area decrease up to 35% in the last decades, with a 20% of forested area converted into rice fields and agricultural crop areas and 15% into bushes, shrubs and meadows. This land use change produced a severe impact on sediment production in that basin.

The effect of projected land use change to soil loss and sediment load over the whole Lo river basin was investigated by projecting a scenario of land use changes. It was obtained by a random

Table 11
Effect of land use changes on annual sedimentation load (tons/year) in the Lo river basin estimated over the 1990–2007 period.

Station	River	Area (km^2)	Measured (with reservoirs) (tons/year)	RUSLE (with reservoirs) (tons/year)	RUSLE (with reservoirs and land use changes) (tons/year)
Bao Yen	Chay	5000	4,315,193	1,851,864	2,114,557
Ha Giang	Lo	8300	3,018,363	2,630,838	2,859,101
Ham Yen	Lo	11,900	4,254,671	4,755,346	6,355,186
Chiem Hoa	Gam	16,500	1,868,613	639,120	833,979
Ghenh Ga	Lo	29,600	3,915,373	4,087,866	5,724,311
Vu Quang	Lo	37,000	4,188,439	4,225,354	5,968,811

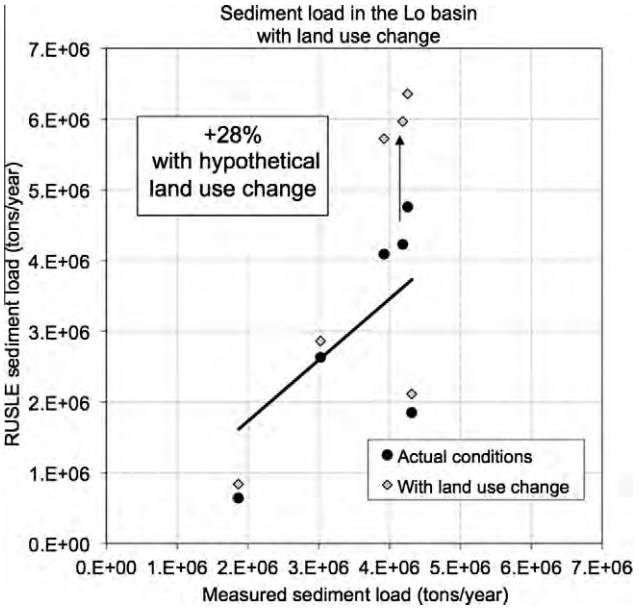

Fig. 12. The effect of hypothetical land use changes on suspended sediment load.

generation of land use change of forested areas using the same statistics of the Pham (2007) case study. The 1990–2007 period, when land use changes occurred was simulated under reference and land use change conditions. The results, summarised in Table 11 and Fig. 12, indicate that the land use change by forest area decreasing of 35% results in a soil loss erosion increase by 28%, compared to reference conditions.

6. Conclusions

Soil erosion is a serious problem in the Lo river basin as suspended sediment load data from stations downstream the Thac Ba and Tuyen Quang dams after their construction ad effect of land use change show. This study demonstrates that a conceptual modelling framework based on monthly precipitation data, distributed GIS information, RUSLE-based estimates of surface erosion and a conceptual sediment transfer scheme is a reasonable solution to model sediment load in the basin, also taking into account in a proper way land use management practices.

The analysis of daily rainfall shows that in the Lo river basin, about 83.3% of rainfall falls with intensity greater than 10 mm/day and enough energy for soil detachment according to the Loureiro and Coutinho (2001) equation, highlighting the major role of rainfall in soil erosion. The RUSLE model coupled with a river network routing scheme which assumes an exponential distribution of sediment travel time with a geomorphology derived time scale was employed to evaluate the soil loss. An extensive data set of monthly suspended sediment load measured at eight stations in the 1959–2007 period was used for model verification, with corresponding specific erosion rate ranging from 0.19 mm/year to 0.58 mm/year. Simulation results in a good agreement, with an $R^2 = 0.89$ statistic and no major bias, with average annual soil loss estimated at eight stations in the Lo river basin under natural basin conditions prior to the dams construction and operation.

The impoundment of two large reservoirs at Thac Ba and Tuyen Quang, in the Chay and Gam river basins has resulted in a considerable reduction of the measured total suspended load with a sediment load reduction of about 95% and 71%, respectively. Assuming the value of 0.71 for the sediment trap efficiency it was possible to simulate suspended sediment load on a monthly scale over the entire 1959–2007. By calibrating the supporting practice factor *P*, the mean inter-station simulation error results 1.4%, being small, 4.7%, at the Vu Quang station, close to the basin outlet, but higher in the smaller basins, as Bao Lac where a 76% overestimation resulted from simulation. The linear correlation coefficient between simulated and observed data is in the 0.66–0.83 range, being 0.72 on average. The mean Nash–Sutcliffe efficiency results to be 0.45, ranging from 0.33 to 0.62, by calibrating the mean sediment transport velocity. These data provide an indication of the overall predictive uncertainty of the model, which, considering the complexity of the process of sediment detachment and transport, including reservoirs sedimentation and the wide space and time scale investigated, can be considered satisfactory, in the author's expectations. A small percentage of simulated values underestimate high sediment load data. This model's limitation can be explained considering that sediment delivered by landslides and debris flow and by erosion from stream channels, processes occurring mainly during high flow events, are not taken into account in our modelling scheme. This balances, in part, the fact that no sedimentation is assumed along the river reach, with the exception of the reservoirs, and can explain how no major systematic bias results from our modelling scheme.

On the basis of observed land use changes in the basin, assuming that 20% of forest area is converted into rice and agricultural crops and 15% into bushes, shrubs and meadows, a 28% increase of sediment load is projected according to the model. This increase can compensate the sediment load decrease, in comparison with the past, observed downstream the dams, because of the reservoirs impoundment. A continuous monitoring of sediment yield, runoff, land use change and river channels is needed to manage soil conservation and the geomorphological equilibrium of the river network in the Lo river basin. Maintenance, at the basin scale, of traditional hillslope agricultural practices as in terraced crops and reforestation remain important but also the reduction of trap efficiency of reservoirs by management of spillways and outlet gates is fundamental to keep the equilibrium of sediments in the Lo river basin.

Acknowledgments

This research was supported by the Italian Ministry of Foreign affairs-Directorate for Development cooperation and Directorate

for Cultural Cooperation and the Vietnam's Ministry of Science and Technology. The data were provided with the help of Ngo Le An and Vu Minh Cat from the Water Resources University of Hanoi and they are thanked for their suggestions and advice. Giampaolo Di Silvio, Carlo Baroni, Stefano Barontini, Baldassare Bacchi are thanked, as well, for their comments and suggestions, together with the reviewers.

References

Abbott, M.B., Bathurst, J.C., Cunge, J.A., O'Connell, P.E., Rasmussen, J., 1986. An introduction to the European Hydrological System – Systeme Hydrologique Europeen, SHE. 1. History and philosophy of a physically-based, distributed modelling system. J. Hydrol. 87, 45–59.

Ali, K.F., De Boer, D.H., 2009. Spatially distributed erosion and sediment yield modeling in the upper Indus River basin. Water Resour. Res., WR00867.

Bennett, J.P., 1974. Concepts of mathematical modelling of sediment yield. Water Resour. Res. 10, 485–492.

CSIRO, 1991. TOPOG. <http://www.clw.csiro.au/topog/intro/intro.html>.

Di Silvio, G., Nones, M., 2010. Predicting the deviations from the curve of sediment transport vs. water flow. In: 11th International Symposium on River Sedimentation, 6–9 September 2010, Stellenbosch.

Gavrilovic, Z., 1988. The use of an empirical method (erosion potential method for calculating sediment production and transportation in unstudied or torrential streams. In: Proc. International Conference on RIVER REGIME: Wallingford, pp. 411–422.

Gavrilovic, Z., 1998. Methodology for Identification and Proclamation Erosion Zones. Institute for development of Water Resources "Jaroslav Černi", Belgrade.

Hack, J., 1957. Studies of Longitudinal Stream Profiles in Virginia and Maryland. US Geological Survey Professional Paper, 294-B.

Jakeman, A.J., Hornberger, G.M., 1993. How much complexity is warranted in a rainfall–runoff model? Water Resour. Res. 29 (8), 2637–2649.

Johanson, R.C., Imhoff, J.C., Davis, H.H., 1980. User's Manual for Hydrological Simulation Program – FORTRAN (HSPF). Research Grant No. R804971-01. Office of Research and Development, US Environmental Protection Agency, Athens, GA.

Laflen, J.M., Lane, L.J., Foster, G.R., 1991. WEPP: a new generation of erosion prediction technology. J. Soil Water Conserv. 46, 34–38.

Le, T.P.Q., Garnier, J., Gilles, B., Sylvain, T., Chau, V.M., 2007. The changing flow regime and sediment load of the Red River, Viet Nam. J. Hydrol. 334, 199–214.

Le, T.H., Rulli, M.C., Ranzi, R., 2010. Effect of reservoirs on sediment load in the Lo river basin (China-Vietnam). In: Proc. of the ICOLD – International Commission of Large Dams Symposium, Hanoi, 24–26 May 2010, 17 pp.

Liu, Y., Freer, J., Beven, K., Matgen, P., 2009. Towards a limit of acceptability approach to the calibration of hydrological models: extending observation error. J. Hydrol. 367, 93–103.

Loureiro, N.S., Coutinho, M.A., 2001. A new procedure to estimate the RUSLE EI30 index, based on monthly rainfall data and applied to the Algarve region, Portugal. J. Hydrol. 250, 12–18.

Merritt, W.S., Letcher, R.A., Jakeman, A.J., 2003. A review of erosion and sediment transport models. Environ. Modell. Software 18, 761–799.

Moore, R.J., 1984. A dynamic model of basin sediment yield. Water Resour. Res. 20 (1), 89–103.

Moore, I.D., Burch, F.J., 1986. Physical basic of the length–slope factor in the Universal Soil Loss Equation. Soil Sci. Soc. Am. J. 50, 1294–1298.

Ngo, L.A., Vu, M.C., Hoang, T.T., Buzzi, A., Drofa, O., Do, L.T., Barontini, S., Ranzi, R., 2010. A hydrometeorological flood forecasting system for the reservoir control in the Red River. In: Proc. of the ICOLD – International Commission of Large Dams Symposium, Hanoi, 24–26 May 2010, 11 pp.

Nguyen, V.P., Vu, V.T., Tran, T.X., 2003. Water Resources in Vietnam. Vietnamese Institute of Meteo-hydrology. Agricultural Edition (in Vietnamese).

O'Callaghan, J., Mark, D.M., 1984. The extraction of drainage networks from digital elevation data. Comput. Vision, Graphics, Image Process. 28 (3), 323–344.

Orlandini, S., Moretti, G., 2009. Determination of surface flow paths from gridded elegation data. Water Resour. Res. 45 (3), W03417.

Patel, P.L., Ranga Raju, K.G., 1996. Fractionwise calculation of bed load transport. J. Hydraul. Res. 34 (3), 363–378.

Pham, H., 2007. Evaluating Potential of Soil Loss Erosion in the Ba Be Lake Basin in Vietnam, Project, Hanoi-Vietnam (in Vietnamese).

Pilotti, M., Bacchi, B., 1997. Distributed evaluation of the contribution of soil erosion to the sediment yield from a watershed. Earth Surf. Proc. Land. 22 (13), 1239–1251.

Pilotti, M., Menduni, G., 1997. Application of lattice gas techniques to the study of sediment erosion and transport caused by laminar sheetflow. Earth Surf. Proc. Land. 22 (9), 885–893.

Ranzi, R., Bochicchio, M., Bacchi, B., 2002. Effects on floods of recent afforestation and urbanisation in the Mella River (Italian Alps). Hydrol. Earth Syst. Sci. 6 (2), 239–265.

Ranzi, R., Barontini, S., Ngo, L.A., Drofa, O., Buzzi, A., Tran, T.T., Vu, M.C., 2007. A hydrometeorological flood forecasting system for the Red River (China–Vietnam). In: Proc. of the AOGS – Asia Oceania Geosciences Society, 4th Annual Meeting, Bangkok, 30 July–4 August, 2007.

Renard, K.G., Freimund, J.R., 1994. Using monthly precipitation data to estimate the *R*-factor in the revised USLE. J. Hydrol. 157, 287–306.

Renard, K.G., Foster, G.A., Weesies, D.A., McCool, D.K., Yoder, D.C., 1997. Predicting Soil Erosion by Water: A Guide to Conservation Planning with the Revised Universal Soil Loss Equation (RUSLE). Agriculture Handbook No. 703, USDA, Washington, DC.

Rigon, R., Rodriguez-iturbe, I., Maritan, A., Giacometti, A., Tarboton, D.G., Rinaldo, A., 1996. On Hack's law. Water Resour. Res. 32 (11), 3367–3374.

Rosso, R., Rulli, M.C., 2002. An integrated simulation method for flash-flood risk assessment. 2. Effects of changes in land use under a historical perspective. Hydrol. Earth Syst. Sci. 6 (2), 285–294.

Rulli, M.C., Rosso, R., 2005. Modeling catchment erosion after wildfires in the San Gabriel Mountains of southern California. Geophys. Res. Lett. 32 (19), L19401.

Rulli, M.C., Rosso, R., 2007. Hydrologic response of upland catchments to wildfires. Adv. Water Res. 30 (10), 2072–2086.

Sorooshian, S., 1991. Parameter estimation, model identification, and model validation: conceptual type models. In: Bowles, D.S., O'Connell, P.E. (Eds.), Recent Advances in the Modelling of Hydrological Systems. Kluwer Academic, pp. 443–467.

Tyagi, J.V., Mishra, S.K., Singh, R., Singh, V.P., 2008. SCS-CN based time-distributed sediment yield model. J. Hydrol. 352 (3–4), 388–403.

Vertessey, R.A., Watson, F.G.R., Rahman, J.M., Cuddy, S.D., Seaton, S.P., Chiew, F.H., Scanlon, P.J., Marston, F.M., Lymbuner, L., Jeanelle, S., Verbunt, M., 2001. New software to aid water quality management in the catchments and waterways of the south-east Queensland region. In: Proceedings of the Third Australian Stream Management Conference, August 27–29, pp. 611–616.

Vezina, K., Bonn, F., Pham, V.C., 2006. Agricultural land-use patterns and soil erosion vulnerability of watershed units in Vietnam's northern highlands. Landscape Ecol. 21 (8), 1311–1325.

Walling, D.E., 2011. Human Impact on the Sediment Loads of Asian Rivers, Sediment Problems and Sediment Management in Asian River Basins. IAHS Publ. 349, Wallingford, pp. 37–51.

Wheater, H.S., Jakeman, A.J., Beven, K.J., 1993. Progress and directions in rainfall–runoff modelling. In: Jakeman, A.J., Beck, M.B., McAleer, M.J. (Eds.), Modelling Change in Environmental Systems. John Wiley and Sons, Chichester, pp. 101–132.

Williams, J.R., 1975. Sediment-yield Prediction with Universal Equation Using Runoff Energy Factor. Present and Prospective Technology for Predicting Sediment Yields and Sources, ARS-S-40, US Department of Agriculture, Agricultural Research Service, pp. 244–252.

Wischmeier, W.H., Smith, D.D., 1978. Predicting Rainfall Erosion Soil Losses, A Guide to Conservation Planning. Agriculture Handbook No. 282, No. 537, US Department of Agriculture, Washington, DC.

Xu, K.H., Milliman, J.D., 2009. Seasonal variations of sediment discharge from the Yangtze River before and after impoundment of the Three Gorges Dam. Geomorphology 104 (3–4), 276–283.

Yang, Z., Wang, H., Saito, Y., Milliman, J.D., Xu, K.H., Qiao, S., Shi, G., 2006. Dam impacts on the Changjiang (Yangtze) River sediment discharge to the sea: The past 55 years and after the Three Gorges Dam. Water Resour. Res. 42, W04407.

Yang, S.L., Zhang, J., Xu, X.J., 2007. Influence of the Three Gorges Dam on downstream delivery of sediment and its environmental implications, Yangtze River. Geophys. Res. Lett. 34, L10401.

Yoder, D.C., Lown, J.B., 1995. The future of RUSLE: inside the new revised universal soil loss equation. J. Soil Water Conserv. 50 (5), 484–489.

Zhang, K., Li, S., Peng, W., Yu, B., 2004. Erodibility of agricultural soils on the Loess Plateau of China. Soil Tillage Res. 76, 157–165.

Zhang, K.L., Shu, A.P., Xu, X.L., Yang, Q.K., Yu, B., 2008. Soil erodibility and its estimation for agricultural soils in China. J. Arid Environ. 72, 1002–1011.

Assessment of erosion, sedimentation, and water quality impacts of the Mountain Valley Pipeline and Equitrans Expansion Project's proposed crossing of the Jefferson National Forest as it pertains to the U.S. Forest Service's Draft Supplemental Environmental Impact Statement dated December 2022

Prepared by Jonathan A. Czuba, Ph.D., Licensed Professional Engineer - February 9, 2023

REFERENCES
20

February 21, 2023

Journal of Hydrology 594 (2021) 125963

Contents lists available at ScienceDirect

Journal of Hydrology

journal homepage: www.elsevier.com/locate/jhydrol

Research papers

Coupling the probability of connectivity and RUSLE reveals pathways of sediment transport and soil loss rates for forest and reclaimed mine landscapes

D. Mahoney [a,*], B. Blandford [b], J. Fox [a]

[a] Dept. of Civil Engineering, University of Kentucky, United States
[b] Kentucky Transportation Center, University of Kentucky, United States

ARTICLE INFO

This manuscript was handled by Jiri Simunek, Editor-in-Chief, with the assistance of Simon A. Mathias, Associate Editor

Keywords:
Sediment connectivity
Erosion modeling
Watershed model
Forest hydrology
Reclaimed mine hydrology

ABSTRACT

Coupling erosion formulae with sediment connectivity methods is one promising approach to better represent structural and functional variability of sediment processes. To advance this goal, the probability of connectivity approach is coupled with the revised universal soil loss equation (RUSLE) in a basin with forest and reclaimed mine landuses. Model evaluation showed unforeseen codependency between connectivity formulae and RUSLE. For example, the RUSLE *P* factor was codependent with the probability of downstream transport within the connectivity formula. Researchers should use feedback calibration schemes to resolve lack of model independence. Connectivity modelling advanced prediction of sediment processes because it simulated the unforeseen impact of legacy terracing on sediment connectivity and soil loss. Structural control dominates connectivity in this study, and soil loss and connectivity are self-similar. The structural control is contrary to recent suggestions that functional, dynamic processes control sediment connectivity in all landscapes. Self-similarity also remains an open topic because a number of studies show poor correlation between soil loss and connectivity. On average 12% of forested land and 47% of reclaimed mine land was connected for events studied. Predicted soil loss rates in the reclaimed mine were approximately 30 times greater than the forest land despite the fact that the reclamation is classified as phase 3. Spatially explicit results highlight pathways that should be targeted for remediation, and this study supports the idea of the Forestry Reclamation Approach for remediation of excess soil loss.

1. Introduction

Structural and functional watershed properties are now well known to control sediment yield and connectivity (Bracken et al., 2015; Wohl et al., 2017; Zingaro et al., 2019). Over the past six decades, watershed models have been widely implemented to simulate soil loss and understand controlling sediment processes at the watershed scale (USEPA, 2004), and now play an important role in measuring impacts of sediment on ecology, water supply, and water quality (Morris and Fan, 1998). We find, however, that watershed models currently are hindered for several reasons. Namely, seldom do watershed models represent structural and functional watershed variability at the fundamental spatial and temporal units at which sediment processes occur (Bracken et al., 2015; Nunes et al., 2017; Wohl et al., 2019; Batista et al., 2019). This results from spatial and temporal lumping of sediment processes across landscapes and hydrologic events, disassociating models from physical process and introducing empiricism. In years past, such lumping resulted from limited computing power and availability of spatially explicit data (Walling et al., 1983; Fryirs, 2013).

Coupling sediment models with connectivity theory (see Fryirs, 2013; Bracken et al., 2015; Wohl et al., 2019) and now widely available geospatial data (e.g., KYAPED, 2014) serves as one promising approach to better represent structural and functional variability of watershed properties. The ubiquity of high resolution geospatial data serves as one means to overcome data limitations that currently hinder sediment models, even in environments that have previously been considered "data sparse" (e.g., Fox, 2009).

Our motivation was to better understand structural and functional processes that control sediment yield and sediment connectivity by coupling watershed soil loss modeling with spatially explicit sediment

* Corresponding author. Current address: Oak Ridge Institute of Science and Education at US Environmental Protection Agency, Cincinnati, OH, USA.
E-mail address: tyler.mahoney@uky.edu (D. Mahoney).

https://doi.org/10.1016/j.jhydrol.2021.125963
Received 22 September 2020; Received in revised form 4 December 2020; Accepted 4 January 2021
Available online 12 January 2021

connectivity simulations. We applied the coupled model to a steep, forested watershed with reclaimed mine land in the Appalachian Region of Eastern Kentucky, USA. In this regard, this paper serves the motivations of: (1) advancing methods for coupling connectivity modelling with erosion rate modelling; (2) understanding spatially explicit soil loss in forested and reclaimed mine land uses; and (3) understanding and discussing controlling structural and functional watershed properties that limit sediment yield and sediment connectivity on forested and reclaimed mine hillslopes. Our intent was to improve process-based knowledge of active sediment pathways and assist with management of soil loss in steep, forested watersheds.

We couple the widely popular Revised Universal Soil Loss Equation (e.g., RUSLE, Renard et al., 1997) with connectivity theory (Bracken et al., 2015; Wohl et al., 2017) to better represent spatially explicit pathways that actively contribute sediment to the stream network. We chose to couple connectivity theory with RUSLE among other erosion models for a number of reasons. First, RUSLE has been widely applied across the United States and Europe (Batista et al., 2019), partially due to its success of implementation and relatively few input requirements (Fox and Martin, 2015). Second, the RUSLE formulation serves as the conceptual foundation for many popular non-point source sediment models, including (Ann)AGNPS (Bingner and Theurer, 2001) and the Soil and Water Assessment Tool (SWAT; Arnold et al., 1998). Third, the availability of high-resolution geospatial data, such as 1 m digital elevation models (DEMs), serves as a basis to improve the spatial resolution of hillslope erosion simulations. Fourth, RUSLE parameters have been incorporated in recent connectivity measures, such as the Index of Connectivity (see Borselli et al., 2008), suggesting that further coupling of the frameworks is possible.

While RUSLE has been widely applied, one underlying assumption of the model is that all soil generated on a hillslope or within a HRU reaches the stream network (Lenhart et al., 2005) and that deposition along hillslope pathways is negligible (de Vente et al., 2013; Zhao et al., 2020). Such assumptions limit the applicability of the model to predict sediment yield only on surfaces with known active erosion pathways (Renard et al., 1997).

To overcome limitations of current watershed models and simulate actively eroding pathways, we suggest coupling RUSLE simulations with connectivity theory. We define connectivity similarly to Heckmann et al., (2018) as an emergent system property that reflects the strength and continuity of sediment linkages between and within system compartments at a given point in time. Connectivity is an emerging field that aims to understand spatially and temporally explicit pathways that facilitate sediment transport (Fryirs, 2013; Bracken et al., 2015; Wohl et al., 2019). Theory and frameworks to understand sediment connectivity have been well developed within the geomorphology and engineering communities (e.g., Hooke, 2003; Borselli et al., 2008; Cavalli et al., 2013; Fryirs 2013; Heckmann et al., 2013; Bracken et al., 2015; Gran and Czuba, 2017; Mahoney et al., 2018, 2020a,b; Ali et al., 2018). Several promising advancements in coupling connectivity equations with soil loss formulae in recent years include studies from Vigiak et al., (2012), Jamshidi et al., (2014), Hamel et al., (2015), Mahoney et al., (2018, 2020a, b), Zhao et al., (2020), and Michalek et al. (2021) among others; the majority of whom have implemented the structurally-based Index of Connectivity from Borselli et al. (2008) to assess connectivity. We find that seldom in the literature have both structural and functional connectivity considerations been coupled with soil loss prediction, yet that structural and functional connectivity processes control sediment transport at both relatively short (event) timescales as well as relatively long (decadal) timescales (Bracken et al., 2015; Wohl et al., 2019; Mahoney et al., 2018; Mahoney et al., 2019; Ali et al., 2018).

In this study, we couple RUSLE with connectivity while seeking to advance methods to quantify the tenets of structural and functional connectivity that consider the magnitude of connections. It is now recognized that connectivity simulations should consider connectivity's magnitude, extent, timing, and continuity (Bracken et al., 2015; Grant et al., 2017; Ali et al., 2018; Wohl et al., 2019; Mahoney et al., 2020a,b). The model recently updated by Mahoney et al. (2020a,b) shows promise to serve this goal. We consider event variability of structural and functional watershed properties using the Probability of Connectivity $P(C)$ model from Mahoney et al., (2018, 2020a,b) and suggest that representing the magnitude of connectivity by coupling $P(C)$ with RUSLE serves as one approach to quantify connectivity's magnitude that is comparable across catchments.

Another motivation of this work is to better understand structural and functional processes that control sediment connectivity and transport in steep, forested catchments and on reclaimed mines, such as those found throughout the Appalachian Coal Belt region, USA (Taylor et al., 2009). Steep, forested catchments in the Appalachian region are well-known for soils with very high infiltration rates and limited runoff production (Hewlett and Hibbert, 1965; Khan and Ormsbee, 1989; Taylor et al., 2009; Fox and Martin, 2015), which is generally attributed to soil texture and macropore formations. Soil macropores efficiently transport subsurface interflow to stream networks (Gupta et al., 2016) and are formed from freeze-thaw processes, dissolution of limestone, and activity and decomposition of flora and fauna (Sloan et al., 1983; Guebert and Gardner, 2001; Warner et al., 2010) and we find the impact of macropores on sediment connectivity is understudied.

The Appalachian Coal Belt's namesake originates from the presence of coal seams located frequently throughout the mountainous region. Surface coal mining is one method commonly used to extract coal in the region and involves removing vegetation, timber, and topsoil from surfaces (Bonta, 2000) to access underlying coal seams which are subsequently excavated (Shrestha and Lal, 2006). During reclamation, land surfaces are regraded with mine spoils, crushed rock, and coal fragments (Wickham et al., 2007) and heavily compacted and reseeded to prevent mass wasting and landslides (Taylor et al., 2009; Warner et al., 2010). Generally, regraded hillslopes remain relatively steep post-reclamation, but are slightly flatter than the surrounding forest hillslopes (Fox and Martin, 2015). Notable difference in hydrology have been observed in reclaimed mine hillslopes compared to forested hillslopes in the region. Namely, compacted surfaces have much lower infiltration rates compared to forested hillslopes resulting in greater runoff production (Warner et al., 2010). We find that structural and functional controls on sediment connectivity in steep, forested hillslopes and reclaimed mine lands in the Appalachian Coal Belt region are understudied. The use of coupled models, such as the probability of connectivity and RUSLE, serves as one approach to better understand controls of sediment processes in these remote regions.

The objectives of this paper were to: (1) couple and evaluate the probability of connectivity model and RUSLE to advance spatially explicit watershed sediment modeling and (2) advance understanding of structural and functional variables that control connectivity and sediment yield in steep, forested watersheds and reclaimed mine land. We apply the model to a steep, forested watershed in Eastern Kentucky, USA with reclaimed mine land to fulfill these objectives.

2. Study site and materials

The study site is the Whitaker Branch watershed (2.63 km^2) located in Letcher County, Kentucky (see Fig. 1). Land use in the watershed is primarily second growth deciduous forest (2.47 km^2) and pastureland (0.16 km^2) which coincides with reclaimed surface mining. The deciduous forest consists primarily of maple beech, yellow poplar, oak, hickory, buckeye, and basswood. Soils in the watershed are primarily silt-loams with high infiltration capacity (Fox, 2009). In the late 19th century timber within the watershed was harvested and subsequently farmed, where contours were implemented for resource conservation purposes. The watershed was subsequently reforested and remained relatively undisturbed for approximately one hundred years, although some farming and residential areas existed in the lower part of the basin. Whitaker Branch watershed is located in the Appalachian Coal Belt and

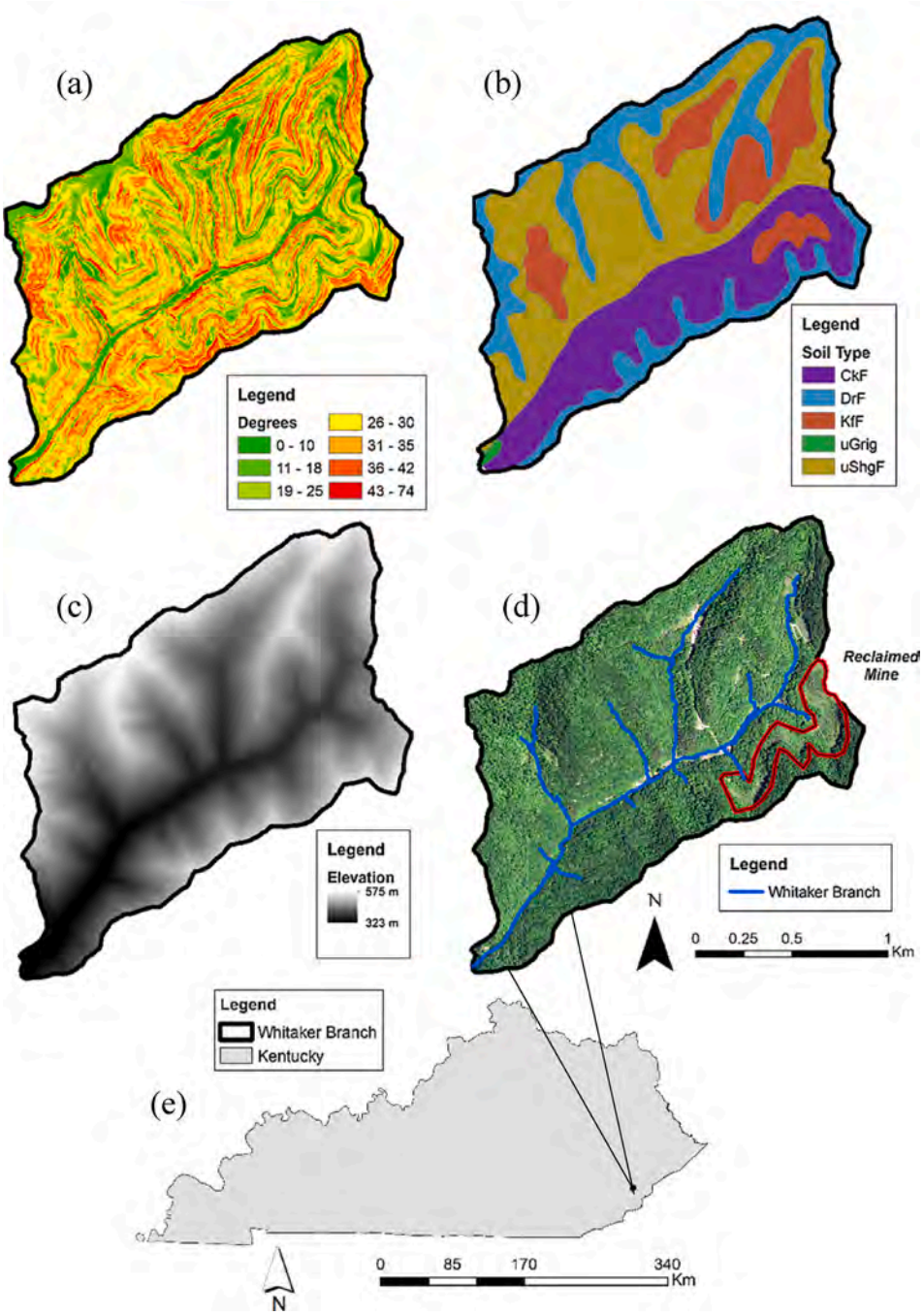

Fig. 1. Whitaker Branch watershed (2.63 km^2) maps in Letcher County, Kentucky including: (a) slope; (b) soil type; (c) elevation; (d) aerial imagery; and (e) location of Whitaker Branch in Kentucky, USA. Whitaker branch consists primarily of forested land (2.47 km^2) and reclaimed mine land (0.16 km^2). Reclaimed mine land is outlined in red in panel (d). (For interpretation of the references to colour in this figure legend, the reader is referred to the web version of this article.)

was subjected to surface mining between 1982 and 1988 and between 1998 and 2004 (Fox, 2009; Fox and Martin, 2015; see Fig. 1). Reclamation of the surface mining site began in 2004 and was completed according to regulations specified from the Surface Mine Reclamation Act (SMCRA). Notably, surfaces were regraded with mine spoils, crushed rock, and residual coal and were heavily compacted to prevent mass wasting (Fox, 2009). Limited regrowth from native trees has been observed as consequence from compaction procedures and due to reseeding with grasses (Fox, 2009; Fox and Martin, 2015).

Watershed morphology is considered to be very steep, with long, narrow ridgetops, and narrow valleys, with some variability due to the reclaimed mine. Average slope in the forested land is 0.51 m m^{-1} and 0.44 m m^{-1} on the reclaimed mine surfaces. Features that promote sediment connectivity include concentrated flow pathways, roads, and surfaces throughout the reclaimed mine (Bonta, 2000; Fox and Martin, 2015). Disconnecting morphology includes soil macropores that limit overland runoff production, and historic terracing, which dissects hillslopes (Fox and Martin, 2015).

Climate in Letcher County, Kentucky is temperate-humid with on average 102 cm of rainfall per year and average temperature of 1.7 °C during winter and 22.8 °C in summer. During the study period (2007), 12 storm events with rainfall that contributed to soil loss were identified. High infiltration rates on the order of 120 mm h^{-1} are common in steep, forested catchments throughout the Appalachian Coal Belt

(Harden and Scruggs, 2003), due to soil texture and the formation of macropores from flora and fauna, freeze–thaw cycling, and dissolution of limestone in the area (Sloan et al., 1983; Taylor et al., 2009; Guebert and Gardner et al., 2001; Warner et al., 2010; Fox and Martin, 2015). Observations throughout watersheds in the Appalachian Coal Belt region indicate that little overland flow is typically generated during storm events due to interception from the forest canopy and high infiltration rates due to the soil texture and macropore pathways (Taylor et al., 2009; Hewlett and Hibbert, 1965; Khan and Ormsbee, 1989; Sloan et al., 1983).

Rainfall-runoff response in the reclaimed surface mine varies from that of steep forested land uses. Reclamation of surface mines impacts infiltration rates of rainfall due to earthwork and compaction, and results in notable runoff production (Shukla et al., 2004; Guebert and Gardner et al., 2001; Warner et al., 2010). Researchers have observed decreases in infiltration from 120 mm h^{-1} to 10–20 mm h^{-1} from pre-mining conditions to post-reclamation (Warner et al., 2010; Taylor et al., 2009). Interception of rainfall is also impacted because of limited tree growth post-reclamation (Angel et al., 2005; Acton et al., 2011). A conceptual model highlighting differences in hydrology on steep, forested hillslopes and reclaimed mine hillslopes is shown in Fig. 2.

We used several materials to conduct probability of connectivity and RUSLE modeling including geospatial data, sediment field measurements, sediment fingerprinting results, previous sediment and hydrologic modeling, and field reconnaissance (see Table 1). Highly-resolved geospatial data used include 1.5 × 1.5 m DEMs, land use and land cover data, and soil data. All geospatial data are freely available across the Commonwealth of Kentucky. Precipitation data collected at the nearby USGS gage in Whitesburg, KY were used as an input to both the hydrologic model and the RUSLE model. Delineation of the reclaimed mine was completed using remote sensing, field reconnaissance, and spatial mapping of statewide mined out areas. We carried out hydrologic modeling using the Soil and Water Assessment Tool (SWAT) *via* ArcSWAT 2012.10.21 to predict event runoff generation and daily soil moisture content. Since the basin is ungauged, we verified hydrologic modeling by comparing annual water budget results generated from the modeling with results from similar catchments in the Appalachian Coal Belt, which improves our confidence in annual sediment yield modelling. We applied the probability of connectivity, $P(C)$, model developed by Mahoney et al. (2018, 2020a,b) to the Whitaker Branch watershed to determine the spatial extent of sediment connectivity during events. Connectivity modeling was carried out using ArcGIS 10.4.1 on a desktop PC (Intel® Core™ i7-6700 CPU at 3.40 GHz; 64-bit operating system, x64-based processor). RUSLE modeling and subsequent uncertainty analyses were performed in ArcGIS 10.4.1 and in Microsoft Excel on a desktop PC (Windows 10, Dell OptiPlex 9010, Intel i7-3770 3.40 GHz, 4 Cores). We utilized total suspended solids (TSS) samples and sediment fingerprinting results presented in Fox and Martin (2015) to determine soil loss rates on forest and reclaimed mine land uses in the watershed, which we used to evaluate the model. Sediment fingerprinting was conducted using stable carbon and nitrogen isotope tracers to identify contribution of sediment sources (Fox and Martin, 2015).

Table 1
Data inputs and model requirements.

Data Type	Source
1.5 m × 1.5 m DEM	KYAPED (2014)
Land Use/Land Cover Data	National Land Cover Database 2006
Precipitation	United States Geological Survey Station 03277300
Soil Type	USDA Web Soil Survey
Runoff	Hydrologic Simulation (SWAT)
Daily Curve Number	Hydrologic Simulation (SWAT)
Event *EI*	United States Geological Survey Station 03277300
Soil *K*	USDA Web Soil Survey
Landscape *LS*	KYAPED (2014)
Total Suspended Solids Samples	Fox and Martin (2015)
$\delta^{13}C\delta^{15}N$Sediment Samples	Fox and Martin (2015)
Sediment Fingerprinting	Fox (2009); Fox and Martin (2015)
Soil Loss	Fox and Martin (2015)
Watershed Slope	Fox (2009)

3. Methods

3.1. Sediment flux formulation via connectivity and erosion formulae

Simulation of sediment flux requires multiplication of connectivity formulae and an erosion generation function simulated using RUSLE. Connectivity is formulated using probability theory to reflect the stochastic nature of sediment transport and heterogeneity of hydrologic variables at the watershed scale (Wright and Webster, 1991; Papanicolaou et al., 2003; Borselli et al., 2008; Wohl et al., 2017; Mahoney et al., 2018). Formulation of sediment flux via connectivity theory is originally presented in Mahoney et al. (2020a,b) to reflect tenets of connectivity theory including connectivity's magnitude, extent, and timing (Bracken et al., 2015; Grant et al., 2017; Wohl, 2017; Ali et al., 2018; Wohl et al., 2019) as

$$\dot{m} = E[P(C) \cap P(\tau) \cap P(\gamma)] \quad (1)$$

where $\dot{m}$ is sediment flux generated from a spatial unit at an instant, E is a respective erosion rate, $P(C)$ is the probability of sediment connectivity representing the spatial extent of connectivity during an event, $P(\tau)$ is the probability of sediment timing representing the variability of connectivity and active erosion periods during an event, and $P(\gamma)$ is the

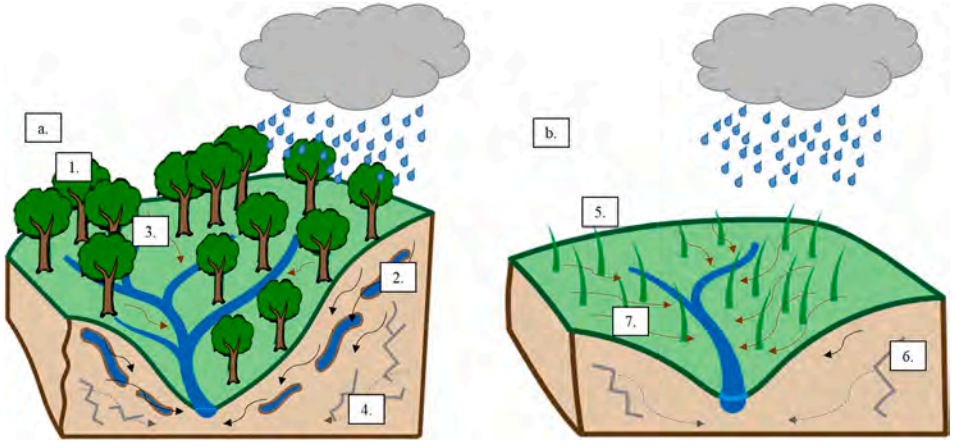

Fig. 2. Conceptual models of sediment connectivity on (a) steep, forested hillslopes and (b) on reclaimed mine land that has been converted to grassland. The following processes are highlighted for steep, forested hillslopes: (1) dense tree canopy increases rainfall interception; (2) frequent presence of subsurface macropores increases infiltration rates and creates preferential flow pathways; (3) sparse concentrated flowpaths transport water and sediment rapidly to stream networks; and (4) attenuated slowflow pathways contribute to baseflow following events. The following processes are highlighted for reclaimed mine lands: (5) conversion to grassland decreases interception rates; (6) compaction of earth during reclamation reduces macropore flow and decreases infiltration rates; and (7) prevalent overland flow pathways efficiently transport water and sediment.

probability of sediment (dis)continuity representing the continuity of sediment connectivity along the pathway. The bracketed probabilities represent aspects of connectivity while the erosion rate is used to represent the magnitude of flux (Mahoney et al., 2020a; Mahoney 2020).

The theoretical background of Eq. (1) is detailed in Mahoney et al., (2018) and Mahoney et al., (2020a) and we briefly summarize each concept below. $P(C)$ considers structural (e.g., slope, critical shear stress) and functional (e.g., runoff depth, soil moisture) watershed characteristics to predict active and inactive periods and locations of erosion entering a stream network (Borselli et al., 2008; Mahoney et al., 2018; Heckmann et al., 2018). $P(C)$ considers co-occurring sediment process to predict locations within a watershed that are likely connected during an event, as discussed in Sections 3.2 and 3.3 of this paper. $P(\tau)$ predicts temporal connectivity, i.e., temporal variability (Hoffmann, 2015) of sediment flux during an event due to sediment travel time from connected cells (Ali et al., 2018; Mahoney et al., 2020a). Mathematically, $P(\tau)$ represents the percent of landscape units within a watershed that likely contribute sediment to the stream network between two instances, determined via the integration of the frequency distribution of sediment travel time from connected landscape units between two instances of an event (Mahoney et al., 2020a,b; Mahoney, 2020). $P(\gamma)$ predicts (dis)continuity of sediment along a longitudinal pathway (e.g., Fryirs, 2013; Mahoney et al., 2020a), realized as the fraction of sediment lost along a pathway due to a morphologic barrier or a process such as deposition (Grant et al., 2017; Mahoney et al., 2020a). Intersecting probabilities are used to represent the connectivity components of Eq. (1) because detachment and transport must occur sequentially and coincidentally with some degree of sediment continuity for connectivity to be established (Bracken et al., 2015; Grant et al., 2017; Wohl et al., 2019; Mahoney et al., 2020a,b). Additionally, since the intersection probabilities of Eq. (1) simulate conditions necessary for sediment transport to be established, Mahoney et al., (2020a) introduce an erosion rate, E, to estimate the scalar magnitude of sediment flux at the fundamental unit scale.

During this analysis, we focus on estimating connectivity over the entire duration of storm events rather than inter-event variability, thus $P(\tau)$ becomes unity (see Mahoney et al., 2020a,b). Additionally, we find that very little instream deposition of fine fluvial sediment occurs due to the steep stream gradient (Fox, 2009; Fox and Martin, 2015), thus $P(\gamma)$ becomes unity. We note that $P(\gamma)$ has traditionally been formulated to represent instream (longitudinal) deposition rather than cumulative hillslope and stream network (lateral and longitudinal) deposition (e.g., Mahoney et al., 2020a,b; Mahoney, 2020) given recent sentiment to discretize connectivity into lateral, longitudinal, and vertical dimensions (e.g., Fryirs et al., 2007; Fryirs, 2013). In this formulation, hillslope deposition and disconnectivity are treated implicitly within $P(C)$ formula (see Sections 3.2 and 3.3 for justification), similarly to formulations presented in Mahoney et al. (2018) and Mahoney et al. (2020a,b). We emphasize that future work might focus on explicit treatment of deposition for both hillslopes and the stream network at the fundamental unit scale, which has been an area of research for our group. For example, Mahoney (2020) shows how $P(\gamma)$ in the connectivity formula (see Mahoney, 2020, pp. 241, Equation (7)) can also be parameterized to explicitly account for deposition.

Eq. (1) is discretized across the watershed to represent spatially distributed connectivity and flux in fundamental spatial units (e.g., geospatial cells) where erosion and transport processes occur during an event as:

$$\dot{m}_{ij} = E_{ij}[P(C)]_{ij} \tag{2}$$

where i is the event and j is the spatial unit. We utilize 1.5 × 1.5 m DEM cells to represent fundamental spatial units in this study because such resolution has been found to adequately capture morphologic features that influence sediment transport (Lopez-Vicente and Alvarez, 2018; Cantreul et al., 2018; Mahoney et al., 2018). Eq. (3) can be integrated in space and time over the watershed surface and over an event to determine sediment yield for the event as:

$$Y = E[P(C)] \tag{3}$$

where Y is sediment yield.

3.2. Formulation of the probability of sediment connectivity, $P(C)$

The probability of sediment connectivity $P(C)$ is defined as the probability that a landscape unit can detach and transport sediment laterally to the fluvial network (Borselli et al., 2008; Mahoney et al., 2018). $P(C)$ reflects the co-occurrence, or intersection, of several structural and functional (Wohl et al., 2019) sub-processes requisite of transport including sediment supply, sediment detachment, and sediment transport, as formulated by Mahoney et al., (2018) and Mahoney et al., (2020a). $P(C)$ is formulated as

$$P(C) = P(S) \cap P(G) \cap P(T) \cap \{1 - P(B)\} \tag{4}$$

where $P(S)$ is the probability of sediment supply, $P(G)$ is the probability of sediment generation, $P(T)$ is the probability of sediment transport, and $P(B)$ is the probability of a buffer that impedes lateral sediment transport (e.g., Fryirs, 2013). $P(B)$ is an implicit representation of hillslope deposition facilitated by morphologic features that impede lateral sediment transport and ultimately force deposition of upland sediment. Eq. (4) considers intersecting probabilities because each sub-process must occur coincidentally or sequentially for sediment originating in a spatial unit to reach the stream network (Leopold et al., 1964).

When considering that sediment generation and transport can occur via both hydrologic and non-hydrologic (e.g., mass wasting) processes, Eq. (4) is expanded as

$$P(C) = P(S) \cap P(D_H \cup D_{NH}) \cap P(T_H \cup T_{NH}) \cap \{1 - P(B)\} \tag{5}$$

where D_H and D_{NH} represent hydrologic and non-hydrologic detachment, respectively, and T_H and T_{NH} represent hydrologic, and non-hydrologic transport, respectively. Eq. (5) is expanded mathematically as

$$\begin{aligned} P(C) = P(S) \cdot \{P(D_H) + P(D_{NH}) - P(D_H)P(D_{NH})\} \cdot \{P(T_H) + P(T_{NH}) \\ - P(T_H)P(T_{NH})\} \cdot \{1 - P(B)\} \end{aligned} \tag{6}$$

We discretize Eq. (6) for all spatial units across the watershed surface during an event and integrate results to determine the percentage of the watershed that actively contributes sediment to the stream network.

3.3. Application of $P(C)$ for forest and reclaimed mine land

We make several simplifying assumptions regarding application of Eq. (6) to the Whitaker Branch watershed based on conceptual understanding of sediment processes observed during field reconnaissance. Herein we do not explicitly consider non-hydrologic detachment or transport processes based on field visits and previous studies in the watershed (Fox, 2009; Fox and Martin, 2015), which found that deep rooted trees generally stabilized surfaces in the watershed uplands limiting non-hydrologic transport. Additionally, we do not explicitly parameterize buffers $P(B)$ for the watershed because we did not observe the presence of morphologic features known to prohibit lateral sediment transport and connectivity during field reconnaissance and geospatial analysis (Fox, 2009; Fryirs, 2013; Fox and Martin, 2015). Similarly to Borselli et al., (2008), $P(T_H)$ is represented by upstream and downstream components, which conceptually reflects the likelihood for upstream sediment to transport to a cell and sediment generated within a cell to be transported downstream, respectively (Mahoney et al., 2018) as:

$$P(T_H) = P(T_{H-up}) \cap P(T_{H-dwn}) \tag{7}$$

where $P(T_{H-up})$ is the probability of upstream hydrologic transport and $P(T_{H-dwn})$ is the probability of downstream transport.

Thus, Eq. (6) is rewritten as:

$$P(C) = P(S) \cdot P(D_H) \cdot P(T_{H-up}) \cdot P(T_{H-dwn}) \quad (8)$$

Mahoney et al. (2018) explain in detail the parameterization of each subprocess, and we have parameterized Eq. (8) similarly for the Whitaker Branch watershed given our perception of sediment transport processes during field reconnaissance. We briefly discuss the parametrization of Eq. (8) as follows. Fig. 3 shows the probability of connectivity simulation structure adapted from Mahoney et al., (2018) and inputs used to parameterize sub-processes. We implement a Boolean approach similarly to Mahoney et al. (2018) to parameterize each geospatial cell across the Whitaker Branch watershed for each sub-process, where a value of 1 represents that a geospatial cell is connected with respect to the sub-process, and a value of 0 represents that a geospatial cell is disconnected with respect to the sub-process. $P(C)$ results were later integrated across the watershed surface to represent the percentage of the watershed area likely contributing sediment to the stream network.

The probability of sediment supply, $P(S)$ is parameterized as:

$$P(S)_{ij} = \begin{cases} 1, if\ \ sediment\ \ is\ \ present\ \ within\ \ the\ \ cell \\ 0, if\ \ sediment\ \ is\ \ absent\ \ within\ \ the\ \ cell \end{cases} \quad (9)$$

where as before, i is the temporal unit (i.e., a hydrologic event) and j is the spatial unit (i.e., a geospatial cell). We parameterized Eq. (9) by identifying geospatial cells with likely no erodible sediment via field reconnaissance and remote sensing of aerial imagery provided by NAIP during leaf-off time periods, for example, due to an impervious surface or rock outcrop being located within a cell.

The probability of hydrologic detachment is expressed using an excess shear stress approach as:

$$P(D_H)_{ij} = \begin{cases} 1, if\ \ \tau_{f\ \ ij} > \tau_{cr\ \ j} \\ 0, if\ \ \tau_{f\ \ ij} \le \tau_{cr\ \ j} \end{cases} \quad (10)$$

where τ_f is the fluid shear stress in cell j during event i and τ_{cr} is the critical shear stress of the soil. The fluid shear stress is parameterized in cells using the fluid momentum equation as:

$$\tau_{fij} = \gamma H_{ij} S_j \quad (11)$$

where γ is the specific weight of water, H is the depth of runoff in cell j during event i, and S is the slope of cell j. Runoff depth is estimated for

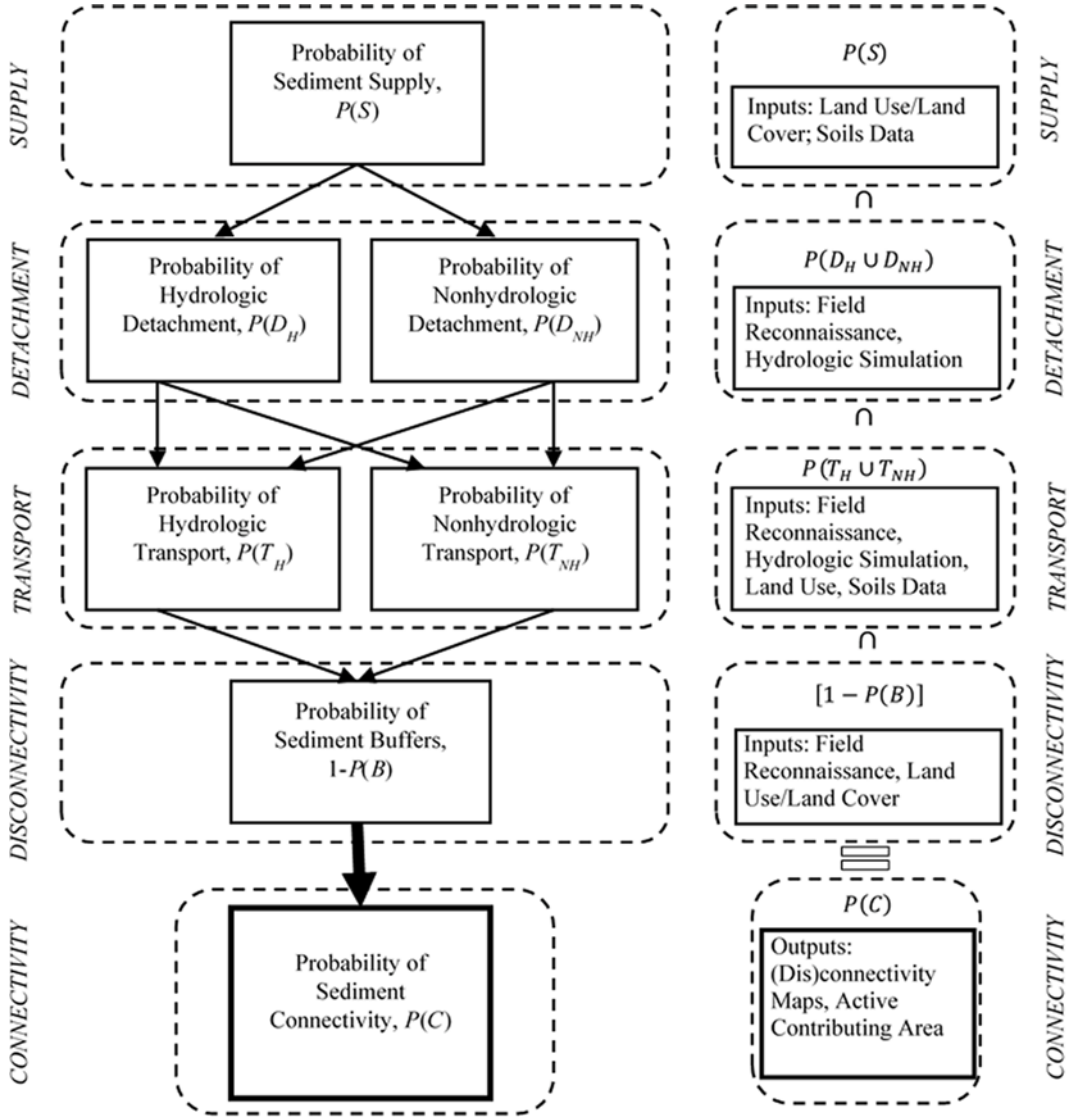

Fig. 3. Probability of connectivity parameterization, adapted from Mahoney et al., (2018).

geospatial cells for the 12 events analyzed during the study period using ArcSWAT 2012.10.21 (see Table 2). Slope is determined in ArcMap 10.4.1 via the Spatial Analyst toolbox. The critical shear stress parameter, τ_{cr}, is treated as a calibration parameter in this study, as will be explained in Section 3.5.

The probability of upstream hydrologic transport is parameterized as:

$$P(T_{H-up})_{ij} = \begin{cases} 1, if \ \ S_j > S_{cr\ ij} \\ 0, if \ \ S_j \le S_{cr\ ij} \end{cases} \quad (12)$$

where as before, S is the slope of cell j and S_{cr} represents a critical slope required to initiate sediment transport in cell j during event i, based on approaches similar to Torri and Poesen (2014). S_{cr} is parameterized similarly to Torri and Poesen (2014), and Mahoney et al., (2018) as:

$$S_{crij} = 0.73\eta_j e^{1.3RFC_j}\left(0.00124S_{0.05ij} - 0.37\right)UA_j^{-b} \quad (13)$$

where $S_{0.05}$ is a function of the daily curve number (taken as a proxy for daily soil moisture content) in cell j during event i, UA is the upstream contributing area of cell j, RFC is the rock fragment content of the soil in cell j as determined from USDA soil surveys, η is a connectivity rill/gully threshold coefficient representing processes that might stifle or promote connectivity (Torri and Poesen, 2014), and b is the runoff turbulence exponent representing the hydraulic regime of runoff facilitating transport (Torri and Poesen, 2014). Daily curve number is estimated for geospatial cells for the 12 events analyzed during the study period using ArcSWAT 2012.10.21 (see Table 2). Mahoney et al. (2018) envisaged that Eq. (12) represented requisites of upstream connectivity since the critical slope threshold is an inverse function of upstream contributing area. The connectivity η parameter and b exponent are treated as calibration parameters in this study, as discussed in Section 3.5. Connectivity parameter ranges are recorded in Table 3. Studies used to derive the parameter ranges are also recorded in Table 3.

The probability of downstream hydrologic transport is parameterized as:

Table 2
Event hydrologic parameters including precipitation, average simulated runoff and curve number across Whitaker Branch watershed, and *EI*, as calculated using Appendix B of Renard et al., (1997).

Event	Date Begin	Date End	Total Precip. (mm)	Avg. SWAT Runoff (mm)	Avg. SWAT Daily CN	EI (MJ·mm·[ha·h]$^{-1}$)
1	3/1/2007	3/1/2007	21.8	1.1	73.1	176.7
2	3/16/2007	3/16/2007	18.0	0.6	73.3	100.4
3	4/3/2007	4/4/2007	16.3	0.4	73.4	100.3
4	4/11/2007	4/11/2007	18.3	0.6	73.4	93.7
5	4/14/2007	4/15/2007	52.8	11.3	73.5	412.4
6	4/27/2007	4/27/2008	22.1	1.2	73.7	185.2
7	7/11/2007	7/11/2007	20.1	0.7	70.0	112.3
8	7/19/2007	7/19/2007	13.5	0.2	69.3	49.1
9	7/24/2007	7/24/2007	14.7	0.3	70.7	67.8
10	8/2/2007	8/2/2007	30.2	2.5	71.5	233.3
11	8/5/2007	8/5/2007	14.0	0.2	71.6	64.8
12	10/24/2007	10/24/2007	19.8	0.6	63.8	91.4

Table 3
Connectivity and RUSLE parameter ranges. b, c, τ_{cr}, C_{Mine}, and C_{Forest} are calibrated parameters. *EI*, *LS*, *K*, and *P* are inputs.

Parameter	Description	Range	Units	Source
b	Connectivity runoff turbulence exponent	0.1–0.5	Unitless	Torri and Poesen (2014)
η	Connectivity rill/gully threshold coefficient	0.1–1.0	Unitless	Torri and Poesen (2014)
τ_{cr}	Critical shear stress	0.5–20.0	Pascal	McCool et al., (1993); Hanson and Simon (2001)
EI	RUSLE storm erosivity parameter	Varies	MJ·mm·[ha·h]$^{-1}$	Renard et al., (1997)
C_{Mine}	RUSLE cropping and management factor for reclaimed mines	0.004–0.008	Unitless	Wischmeier and Smith (1978); Dissmeyer and Foster (1980)
C_{Forest}	RUSLE cropping and management factor for forest land	0.0004–0.0008	Unitless	Wischmeier and Smith (1978); Dissmeyer and Foster (1980)
LS	RUSLE slope length and steepness parameter	Varies	m·m^{-1}	Renard et al., (1997)
K	RUSLE soil erosivity parameter	0.0–0.37	tonne·ha·hr·[ha·MJ·mm]$^{-1}$	Renard et al., (1997)
P	RUSLE practice parameter	0.0–1.0	Unitless	Renard et al., (1997)

$$P(T_{H-dwn})_j = \begin{cases} 1, if \ \ S_j > \dfrac{\sum S_{up}}{N} \\ 0, if \ \ S_j \le \dfrac{\sum S_{up}}{N} \end{cases} \quad (14)$$

where S is the slope in the geospatial cell, $\frac{\sum S_{up}}{N}$ is the average slope of cells upstream of cell j calculated in ArcMap 10.4.1. Physically, Eq. (14) represents locations where the energy in a geospatial cell (represented by the slope) is sufficient for suspended sediments to transport through the geospatial cell to downstream cells (Mahoney, 2017; Mahoney et al., 2018). Hillslope deposition is also represented by the probability of hydrologic detachment $P(D_H)$ and the probability of downstream hydrologic transport $P(T_{H-dwn})$. These formula account for deposition because if the downstream slope of cell j is flatter than the average slope of upstream cells, then downstream transport of sediment is not possible, despite instances when detachment occurs (thus, detached sediment is assumed to deposit along the hillslope in these instances). Conceptually, the $P(T_{H-dwn})$ equation compares fluid energy to transport sediment in downstream cell j represented by the slope to incoming fluid energy represented by the average slope. We note, however, that disconnected cells downstream of upstream connected cells do not necessarily represent deposition from sediment in the connected cell. Rather, these cells are assumed to not contribute additional sediment to the sediment cascade during the hydrologic event (Mahoney, 2017; Mahoney et al., 2018; Mahoney et al., 2019).

Several variables in Eq. (9) through Eq. (14) represent structural and

functional attributes of the Whitaker Branch watershed. Structural connectivity, which represents morphometric properties (e.g., slope, soil texture) of watersheds with little variability from event to event over the course of the study period are represented with the probability of sediment supply $P(S)$ and probability of downstream hydrologic transport $P(T_{H-Dwn})$ (Mahoney et al., 2018; Wohl et al., 2019). We represent functional connectivity, defined as dynamic connectivity processes such as runoff generation and soil moisture flux, using the probability of detachment $P(D_H)$ and the probability of upstream hydrologic transport $P(T_{H-Up})$ (see Mahoney et al., 2018; Wohl et al., 2019). Hydrologic variables used to predict $P(D_H)$ and $P(T_H)$for the 12 events analyzed during the study period were estimated using ArcSWAT 2012.10.21 (see Table 2).

We conducted analyses of the estimated Rouse number for suspended sediments in this system which suggested that once sediment is detached and entrained at the hillslope scale, sediment likely remains suspended, justifying the implicit treatment of deposition in the $P(C)$ formulation for this system. We briefly detail this analysis below. The Rouse number is traditionally used in sediment transport to specify the dominant mode of sediment motion and provides a measure of the shear action of fluid on entrained particles comparatively to particle settling (Chang, 1998). The forest soils of the study watershed (see mapping in Fox, 2009 and Fig. 1) are silt-dominated and are generally classified as silt loam or silty clay loam (McIntosh, 2004). Based on our recent research, the crushed overburden making up the surface soils of reclaimed mining sites in this region also has a median particle size classified as silt (Fox et al., 2020).

Using this information, we analyzed the Rouse number for diameter, d, of 53 μm sediment. The Rouse number is defined as

$$z_* = \frac{\omega}{\kappa u_*} \tag{15}$$

where ω denotes the settling velocity, κ is defined as the von-Karman constant equal to 0.41, and u_* is the shear velocity of the flow. The settling velocity ω is calculated here via the Dietrich (1982) approach for nonspherical particles for $d = 53$ μm particles and is estimated to be 0.3 cm s^{-1}. The shear velocity of the flow is defined as:

$$u_* = (gRS)^{\frac{1}{2}} \tag{16}$$

where R is the hydraulic radius and is approximated as the flow depth H, S is the energy gradient approximated with the hillslope, and g is gravity. The average slope in the forested land is 0.51 m m^{-1} and 0. 44 m m^{-1} on the reclaimed mine surfaces and we assume a 1 cm flow depth in rills during erosion as a low bound on concentrated flow during fluvial erosion. These sediment and hydraulic conditions provide a Rouse number equal to approximately 1/30. Based on these conditions, we examine the possibility of sediment remaining suspended using the Rouse criteria. According to Vanoni (1941) (see Fig. 7.9 from Chang 1998, pp 149) the z_* value of 1/30 corresponds to highly suspended and nearly fully uniform sediment concentration profile. Therefore, it is estimated that sediment will remain suspended and not deposit once detached and entrained in this system.

3.4. RUSLE application to forested land and reclaimed mine

We apply the RUSLE model to represent erosion rates in geospatial cells to simulate sediment flux in Eq. (2). We assume that surface erosion occurs primarily *via* rill and sheet erosion in both the steep, forested hillslopes and the reclaimed mine sites, justifying our use of RUSLE to simulate erosion rates (Renard et al., 1997; Fox and Martin, 2015). The RUSLE model simulates soil loss on hillslopes at an event-basis (Renard et al., 1997) as

$$A = EI \cdot K \cdot LS \cdot C \cdot P \tag{17}$$

where A represents hillslope soil-loss (tonne ha^{-1}), EI is the storm erosivity factor (MJ • mm[ha • hr]$^{-1}$), K is the soil erodibility coefficient (tonne • ha • hr[ha • MJ • mm]$^{-1}$), LS is the slope length and steepness factor (m m^{-1}), C is the cover-management factor (unitless), and P is the supporting practice factor (unitless). We discretize Eq. (17) for geospatial cells to estimate annual soil loss throughout the Whitaker Branch watershed from both steep, forested hillslopes as well as slopes on the reclaimed mine. We modify Eq. (17) to account for connectivity by multiplying cells by $P(C)$ results, which represents the complete parameterization of Eq. (1). Additionally, we make the following assumptions: (1) the EI factor is uniform spatially across the watershed during an event; (2) the K, LS, C, and P factors remain constant temporally throughout the study period; (3) C factors vary between forest and reclaimed mine land uses; and (4) disconnected cells (i.e., $P(C) = 0$) do not yield sediment ($A = 0$). Eq. (17) is thus rewritten as

$$A_{ij} = EI_i \cdot K_j \cdot LS_j \cdot C_j \cdot P_j \cdot P(C)_{ij} \tag{18}$$

Average annual soil loss (tonne ha^{-1}) for steep, forested and reclaimed mine land uses is thus determined as

$$A_{forest} = \sum_{i=1}^{m} \frac{\sum_{j=1}^{n} A_{ij}}{n}, j \in [\text{steep, forest land}] \tag{19}$$

$$A_{mine} = \sum_{i=1}^{m} \frac{\sum_{j=1}^{k} A_{ij}}{k}, j \in [\text{reclaimed mine}] \tag{20}$$

where A_{forest} is the average annual soil loss (tonne ha^{-1}) across the entire steep, forested land use, i is an index representing the storm event, m is the total number of storm events during the study year, j is an index representing the geospatial cell, n is the total number of geospatial cells belonging to the forested land use, A_{mine} is the average annual soil loss (tonne ha^{-1}) across the entire reclaimed mine land use, and k is the total number of geospatial cells belonging to the reclaimed mine land use.

Since Eqs. (19) and (20) are divided by n and k, the total number of geospatial cells that belong to the land use, A_{forest} and A_{mine} represent soil loss rates from the entirety of each land use. Since sediment connectivity occurs on only a fraction of cells belonging to the varying land uses, we modify Eqs. (19) and (20) to represent normalized soil loss for only connected areas as

$$AC_{forest} = \sum_{i=1}^{m} \frac{\sum_{j=1}^{n} A_{ij}}{\alpha_i}, j \in [\text{steep, forest land}] \tag{21}$$

$$AC_{mine} = \sum_{i=1}^{m} \frac{\sum_{j=1}^{k} A_{ij}}{\beta_i}, j \in [\text{reclaimed mine}] \tag{22}$$

where AC_{forest} represents annual soil loss (tonne ha^{-1}) for connected forested land use, α_i is the total number of steep, forested geospatial cells connected during an event, AC_{mine} is the annual soil loss (tonne ha^{-1}) for the reclaimed mine land use, and β_i is the total number of reclaimed mine geospatial cells connected during an event. Also, $\alpha_i \leq n$ and $\beta_i \leq k$.

We parameterize RUSLE as follows: To parameterize the storm erosivity (EI) parameter, we focus only on rainfall events that produce more than 1.3 cm of rainfall and storms that produce at least 0.6 cm of rain in 15-min in accordance with Renard et al. (1997; p. 23). We utilize hourly rainfall data measured at the USGS gage in Whitesburg, Kentucky for 2007 to determine storms appropriate for analysis. 12 events during the study year were identified to produce sediment based on these requisites during 2007 (Renard et al., 1997). We determine EI (MJ • mm[ha • hr]$^{-1}$) values in accordance with Renard et al., (1997) as

$$EI = \sum_{r=1}^{p} 1099 \cdot \left[1 - 0.72 \cdot \exp\left(-1.27 \cdot \frac{\Delta V_r}{\Delta t_r}\right)\right] \cdot I_{30} \cdot 0.1702 \tag{23}$$

where r is a temporal index representing increments of a storm event, p is the total increments in the storm event, ΔV is the depth of rainfall during the increment r (in), Δt is the duration of the increment (h), and I_{30} is the 30-min rainfall intensity. We record EI values in Table 2.

We parameterize the soil erosivity (K) factor using USDA soils maps for the Whitaker Branch watershed and reported K values for each soil type (see Fig. 1 and Table 3). We parameterize the slope length and steepness (LS) factor by: (1) delineating slope lengths from the watershed boundary to the nearest downstream concentrated flow pathway, (2) defining slope along the slope length using the *Slope* tool in ArcGis 10.4.1, and (3) interpolating LS values reported in Table 4-1 from Renard et al., (1997). We parameterize the support practice (P) factor as being equal to 1.0. We justify this given that slopes are relatively steep in both forested hillslopes and reclaimed mine hillslopes (Renard et al., 1997). Additionally, we argue that this avoids overparameterization of the model given that disconnectivity due to terracing is already accounted for in $P(C)$ results (see Section 4.1). We treat the cover-management (C) factor as a calibration parameter in order to more accurately understand impacts of the reclaimed mine on soil loss, as discussed in Section 3.5. We justify using temporally-constant values for K, LS, C, and P given previous study in the watershed (Fox, 2009; Fox and Martin, 2015). RUSLE factor ranges are reported in Table 3.

3.5. Model calibration and evaluation

Data used to calibrate the coupled probability of connectivity and RUSLE models include geospatial analysis and field reconnaissance of sediment transport pathways, sediment fingerprinting analyses, and sediment concentration samples. Field reconnaissance of sediment transport pathways was conducted by Fox (2009) and geospatial analyses were conducted using DEMs (KYAPED, 2014) and orthophotographs. Samples to conduct sediment fingerprinting were collected from forest and reclaimed mine sources as described in Campbell et al. (2009), and instream samples were collected five times during 2007 as described in Fox (2009). TSS samples were collected using a Teledyne ISCO automated pump sampler as reported in Fox (2009) and Fox and Martin (2015). Observed soil loss estimates from forest and reclaimed mine land uses in 2007 were derived from TSS samples and fingerprinting results.

We completed evaluation of the model in two stages (see Fig. 4). In stage one, we calibrated results from the probability of connectivity model by qualitatively comparing spatially distributed connectivity

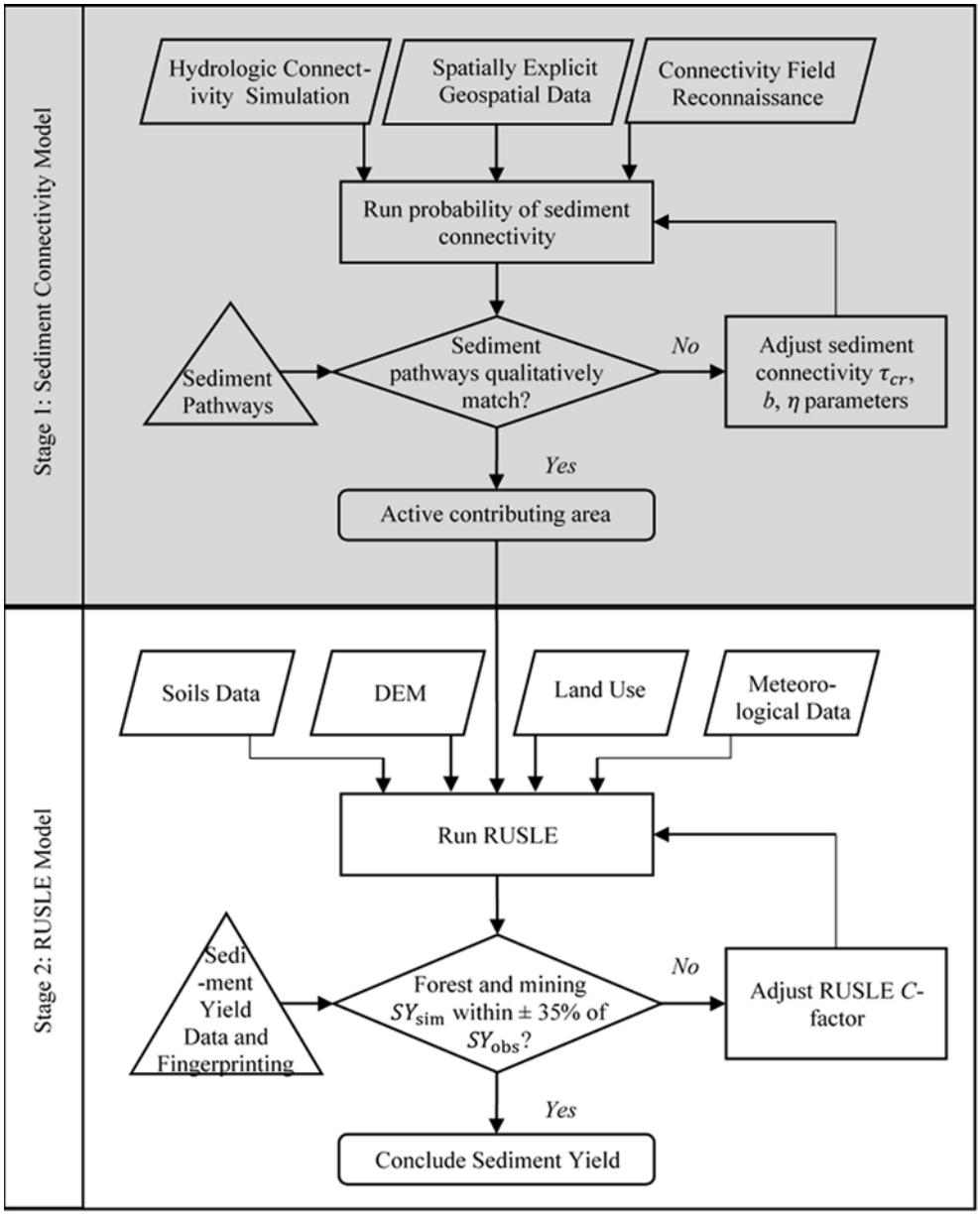

Fig. 4. Sediment flux evaluation flowchart that considers sediment connectivity and erosion simulated *via* RUSLE.

results with sediment pathways identified *via* field reconnaissance and remote sensing. If simulated sediment transport pathways were considered unacceptable, we adjusted connectivity parameters until the realization qualitatively matched known transport pathways. Connectivity parameters calibrated in this stage included: (1) b, the connectivity runoff turbulence exponent, (2) η the rill/gully threshold coefficient, and (3) τ_{cr} the critical shear stress of erodible surfaces. We used literature values to define ranges of parameter values (Torri and Poesen, 2014; McCool et al., 1993; Hanson and Simon, 2001). Since calibration is completed qualitatively, we defined wide parameter ranges to account for potential uncertainty (see Table 3). We justify the use of large parameter ranges given the difficulty of calibrating and validating spatially explicit sediment transport processes.

In stage two, we calibrated results from the combined connectivity and RULSE modeling by comparing simulated sediment yield to observed sediment yield for the forested land use and reclaimed mine (Fox, 2009; Fox and Martin, 2015). If simulated sediment yield was not within ±35% of observed sediment yield, we adjusted C factor for the forested and/or reclaimed mine land use until sediment yield results were acceptable. 35% uncertainty bounds surrounding modeling results considers error due to sediment fingerprinting (approx. 15%, Fox and Martin, 2015) and error due to sediment concentration measurements. Based on previous work, we estimate 20% error from sediment concentration measurements after empirical observations of the variability of ISCO sediment concentration samples. Upon calibrating the model initially, we recalibrated the model starting at stage one to account for landscape units with little or no soil loss that should be considered disconnected, thus we treat calibration of the coupled models as an iterative process.

We quantified model uncertainty by permuting realizations of parameter ranges and running the probability of connectivity and RUSLE model. We created over 200 permutations of the connectivity and RUSLE model to simulate sediment yield. We justify using a low number of model realizations due to restrictions related to model computing requirements and file size. We iteratively chose parameter ranges to reduce limitations related to the number of realizations (see Table 3). Realizations with simulated sediment yield within ±35% of the observed sediment yield were included in the solution space. We qualitatively validated RUSLE modeling by comparing spatially-explicit R, LS, K, and calibrated C parameters with separate RUSLE modeling that considered lumped R, LS, K, and calibrated C parameters. All lumped parameters were on the same order of magnitude as the zonal average of the spatially explicit analysis.

4. Results and discussion

4.1. Evaluation of coupled connectivity and RUSLE modelling: a need for iterative validation

We found that coupling the probability of connectivity model with RUSLE simulated both observed sediment yield and sediment fingerprinting results well. Optimal parameter values determined during model calibration are recorded in Table 4 and simulated and observed sediment yield results are recorded in Table 5. Uncertainty results suggest that relatively wide ranges of connectivity parameters adequately simulate sediment transport whereas the range for acceptable C factor values is much smaller (see Table 3). Approximately 55% of model realizations were included in the solution space, which we attribute to the tight parameter ranges associated with the C factor. We generally find that optimal parameters make physical sense, however some parameter values warrant further discussion, which is the focus below.

Optimal cropping and management (C) factor values are on the low end of proposed range, but still within the range suggested in research literature (see Table 3), for both the forest and reclaimed mine land surfaces. Low C factors have physical significance in the forested and reclaimed mine land use and likely reflect the presence of morphologic features that buffer sediment transport. In the forested land, subsurface macropore pathways increase rainfall infiltration rates and reduce the depth of runoff produced during storm events (Sloan et al., 1983), which is then manifested as the low C factors. Additionally, microtopography resulting from dense forest root mats and shielding from leaf detritus further reduce sediment transport and hence forest C factor values. Calibrated C factor values were an order of magnitude greater for the reclaimed mine site as compared to the forest, which is to be expected considering the increase in event runoff generation due to the high bulk density and low infiltration capacity of the soils on the reclaimed mine relative to the neighboring forests (Acton et al., 2011). The fact that the C factor was on the low end of suggested ranges for grassland reclaimed coal mine lands is reasonable because the land surface was classified as 'phase 3' of reclamation where final reclamation has been achieved (Fox, 2009). Erosion results in this region have shown erosion rates to reduce drastically once the land surface has entered phase 3 reclamation (Curtis, 1978; Bonta, 2000).

We parameterized the optimal RUSLE practice (P) factor as being equal to one, which indicates that no anthropogenic practices, such as associated with terracing, exist in the watershed to reduce soil loss (Renard et al., 1997). As will be shown in our connectivity results, we found that legacy-associated terracing occurred across the forest landscape of this system. Anthropogenic terracing existed from farming the mountains in the 19th century and early 20th century. This farming and terracing were common in this Appalachian forest region despite the steep slopes, and corn was grown for animal feeding, human consumption and illegally producing alcohol regionally known as 'moonshine' (Kalisz, 1986; Stewart and Bruce, 2003). The legacy terracing typically would warrant parameterization of a P factor less than one. However, our probability of connectivity model results causes these terraced areas to become disconnected. Therefore, the land surface area of the disconnected regions is not included in the calculation of mass flux because mass flux is the product of generation via RUSLE soil loss estimates and the probability of connectivity (see Eq. (1)). A P factor of less than one would over-account for terracing and erroneously reduce the estimated sediment mass flux estimate. For this reason, iterative calibration between RUSLE and connectivity modelling was important to account for unforeseen dependency between variables in Eq. (1). We set the P factor as equal to unity to avoid the dependency in this instance.

Our results suggest coupled connectivity-erosion rate modelling incorporate iterative, dual-calibration strategies where calibration of one model should feed-back or loop into calibration of the second model. Our results present evidence of the utility of such approach in two instances. First, as previously mentioned, we found that calibration of the P factor in RUSLE was unnecessary upon multiplication of the RUSLE results with $P(C)$. Specifically, we find that the probability of downstream hydrologic transport $P(T_{H-Dwn})$ causes terraced areas to be predicted as being disconnected. This is because $P(T_{H-Dwn})$ predicts that there is insufficient fluid energy to transport new sediment downstream due to the flat surfaces of the terraced landscapes (Mahoney et al., 2018). In this regard, care should be taken by the researcher to avoid unforeseen dependency between the coupled formula because, for example, parameterization of the $P(C)$ model may sometimes impact

Table 4
Optimal parameter values for connectivity and RUSLE models.

Parameter	Description	Value	Units
b	Connectivity runoff turbulence exponent	0.38	Unitless
η	Connectivity rill/gully threshold coefficient	0.5	Unitless
τ_{cr}	Critical shear stress (Average)	3.75	Pascal
C_{Mine}	RUSLE cropping and management factor for reclaimed mines	0.006	Unitless
C_{Forest}	RUSLE cropping and management factor for forest land	0.0006	Unitless

Table 5
Results of probability of connectivity, soil loss from connected surfaces (*AC*), soil loss rate (*A*) and sediment yield (*SY*) Observed sediment loss from forest and reclaimed mine land uses for 2007 are included.

Event		*P*(C)		*AC* (tonne ha^{-1})		*A* (tonne ha^{-1})		*SY* (tonne)	
		Forest	Mine	Forest	Mine	Forest	Mine	Forest	Mine
1		16.7%	52.60%	0.054	0.508	0.009	0.267	2.212	4.27
2		12.60%	49.60%	0.037	0.308	0.005	0.153	1.167	2.445
3		5.40%	37.90%	0.027	0.318	0.001	0.121	0.36	1.931
4		12.90%	50.30%	0.037	0.307	0.005	0.155	1.191	2.471
5		34.90%	57.10%	0.071	1.171	0.025	0.669	6.143	10.694
6		19.90%	52.70%	0.051	0.559	0.01	0.294	2.488	4.701
7		10.30%	50.50%	0.041	0.36	0.004	0.182	1.028	2.905
8		1.00%	34.40%	0.017	0.16	0	0.055	0.042	0.879
9		1.20%	35.40%	0.023	0.212	0	0.075	0.068	1.202
10		22.40%	54.80%	0.056	0.697	0.012	0.382	3.081	6.106
11		1.30%	35.10%	0.023	0.212	0	0.074	0.076	1.19
12		6.60%	50.50%	0.026	0.255	0.002	0.129	0.42	2.062
Sum	Avg.	12.10%	46.80%	0.462	5.068	0.074	2.557	18.28	40.86
Obs.						0.08	2.5		

RUSLE parameterization. Second, we noticed that upon completing RUSLE modeling that some landscape units in the forest were predicted to produce little to no sediment despite being predicted to be connected according to *P*(*C*). The lack of generation as predicted with RUSLE indicates the magnitude of connectivity is in fact weak on some landscape units such that sediment contribution from these areas is negligible and can be classified as disconnected following the criteria/definition of Heckmann et al., (2018); Wohl et al. (2019) and Ali et al. (2018). We present results from determining event *P*(*C*) with and without considering feedbacks between the models, referred to as initial calibration and final calibration in Table 6. Notably, considering the feedback between the models and iterative calibration caused a reduction in overall connectivity for all events. The result ranges from 0.1% to 13.8% reduction in connectivity, which is relatively high considering final connectivity ranges from 2.9% to 22.4%. This result and need for feedbacks between sediment generation and connectivity estimates is corroborated by recent sentiment in the literature and highlights the importance of considering not only the Boolean connectivity processes (e.g., Fryirs, 2013), but also the magnitude or continuity of connectivity (Grant et al., 2017; Wohl et al., 2019).

The model evaluation results of this study point out the researcher should use caution when coupling connectivity and erosion formula because parameters of the two model types are not necessarily independent. In the present study, the process of terracing impacts both erosion formula in the empirical RUSLE model and net connectivity estimates for predicting the erodible surface area of the basin. We may have under-predicted watershed erosion without this consideration, however, iterative calibration allowed us to account for dependence of the models on one another. As permeations of coupled connectivity and erosion models develop in future years, researchers should at the same time develop new evaluation procedures with qualitative and quantitative checks-and-balances to correct for unforeseen problems from model co-dependency.

Table 6
Probability of connectivity results using initial calibration and final calibration after considering the iterative feedback loop using RUSLE for the entire Whitaker Branch Watershed.

Event	P(C) – Initial calibration	P(C) – Final calibration
1	18.8%	13.7%
2	14.9%	12.3%
3	7.3%	5.5%
4	15.2%	12.5%
5	36.2%	22.4%
6	21.9%	14.0%
7	12.7%	10.2%
8	3.0%	2.9%
9	3.3%	3.2%
10	24.4%	13.9%
11	3.4%	3.3%
12	9.3%	7.5%

The efficacy of coupling connectivity theory and sediment modelling is corroborated by recent findings from Zhao et al. (2020), who, independently from this study, coupled RUSLE with the Index of Connectivity (*IC*) to predict sediment yield. Similar to Vigiak et al., (2012), Zhao et al. (2020) transformed the *IC* using a Boltzmann-type sigmoid function to represent potential sediment delivery ratios from landscape units. The formulation was evaluated to perform well and qualitatively validates the approach presented here.

We emphasize several important differences, however, between the study of Zhao et al., (2020) and the work presented herein. Namely, the *IC* used to represent connectivity is treated quasi-statically (*IC* is calculated once for a simulation in 1990 and once for a simulation in 2010), and thus only captures aspects of structural connectivity (e.g., Heckmann et al., 2018). The ability of the *IC* framework to rapidly assess connectivity elements is noteworthy given that recently developed geospatial toolboxes allow the *IC* to be calculated for a catchment on the order of several hours of simulation time (Crema and Cavalli, 2018). However, *IC* is recognized to only capture elements of structural connectivity due to the morphologic configuration of the watershed (Heckmann et al., 2018; Mahoney et al., 2020a,b). Consideration of functional connectivity is particularly meaningful when simulating sediment transport at relatively shorter timescales (e.g., event-daily) and for small, yet still important hydrologic events, as will be shown later in the results and as highlighted in Mahoney et al. (2018, 2020a,b). Incorporation of functional connectivity elements is one limitation of the current *IC* approach as emphasized by a number of researchers (e.g. Bracken et al., 2013; Heckmann et al., 2018; Mahoney et al., 2020a,b), however, recent developments from Gay et al. (2016), Kalantari et al. (2017) and several others present promise for coupling the *IC* with functional elements. Additionally, coupling elements of the Probability of Connectivity framework presented here and the *IC* may serve to better incorporate functional processes within the *IC*.

4.2. Event *P*(*C*) results: connectivity and disconnectivity in Appalachian forests and minelands

Results highlight behavior of event-based connectivity in the Whitaker Branch watershed. *P*(*C*) results vary between 2.9% connected (event 8) and 22.4% connected (event 5) at the watershed scale (see Table 6). This implies that 2.9% of the catchment and 22.4% of the catchment actively contribute sediment to the stream network during respective events (Ambroise, 2004; Mahoney et al., 2018). *P*(*C*) varied greatly between land uses throughout the 12 events. Namely, *P*(*C*) ranged from 34.4% to 57.1% in the reclaimed mine (μ = 46.8%, σ =

8.1%) and 1.0–34.9% in the forested land ($\mu = 12.1\%$, $\sigma = 9.8\%$) (see Table 5). We attribute the high percentages of connectivity in the reclaimed mine to increased runoff production and hence energy available to transport sediment caused by compaction of soils during reclamation processes.

Predicting the most connected pathways across the landscape was a notable result of this study, and our spatially explicit $P(C)$ results highlight morphologic pathways most sensitive to hydrologic activity in the Whitaker Branch watershed (Figs. 5 and 6). Specifically, our results indicate that landscape units within the reclaimed mine are connected during hydrologic events of low magnitude and remain connected during events of increased hydrologic magnitude (see Fig. 5a–d). Events shown in Fig. 5, Fig. 6, and Fig. 7 are approximately representative of minimum (event 8), 25% quartile (event 12), 75% quartile (event 1), and maximum (event 5) $P(C)$ results. Within the forest, we find that only areas with large upstream contributing area within close proximity to the stream network are connected during events with low hydrologic magnitude (see Fig. 5a and Table 2); and forest hillslopes only become connected during high magnitude events (Fig. 5d). Low connectivity on forested hillslopes in low and moderate events is attributed to the high infiltration rates in forest soils due to soil texture and macropores (Khan and Ormsbee, 1989). In contrast, connectivity occurs on both flat and steep reclaimed mine surfaces with variable upstream contributing areas during events with low hydrologic activity (see Fig. 5a). The connectivity of reclaimed mines is attributed to runoff generation during low and moderate events because of the high bulk density measured for the compacted reclaimed mine sites (Acton et al., 2011). We classify the landscape units within the reclaimed mine as highly sensitive, active pathways for this watershed since they are connected in much greater proportions and more frequently than forested hillslopes. Morphologic features promoting connectivity can be seen visually for both land cover types using orthophotos, gradient models and our connectivity results (Fig. 6). As shown, morphology causing connectivity in both the forest and reclaimed mine land include: (1) concentrated flow paths on steep surfaces in the forestland (Fig. 6a); (2) steep hillslopes between historic terracing (Fig. 6b); and (3) surfaces throughout the reclaimed mine (Fig. 6c).

Disconnectivity of the landscape was another important result of this study, and spatially explicit results also highlight morphologic buffers that disconnect sediments and impede sediment transport throughout the watershed (see Fig. 6a–c; Fryirs, 2013). We examine disconnectivity in Fig. 6 during the event with highest hydrologic activity (event 5),

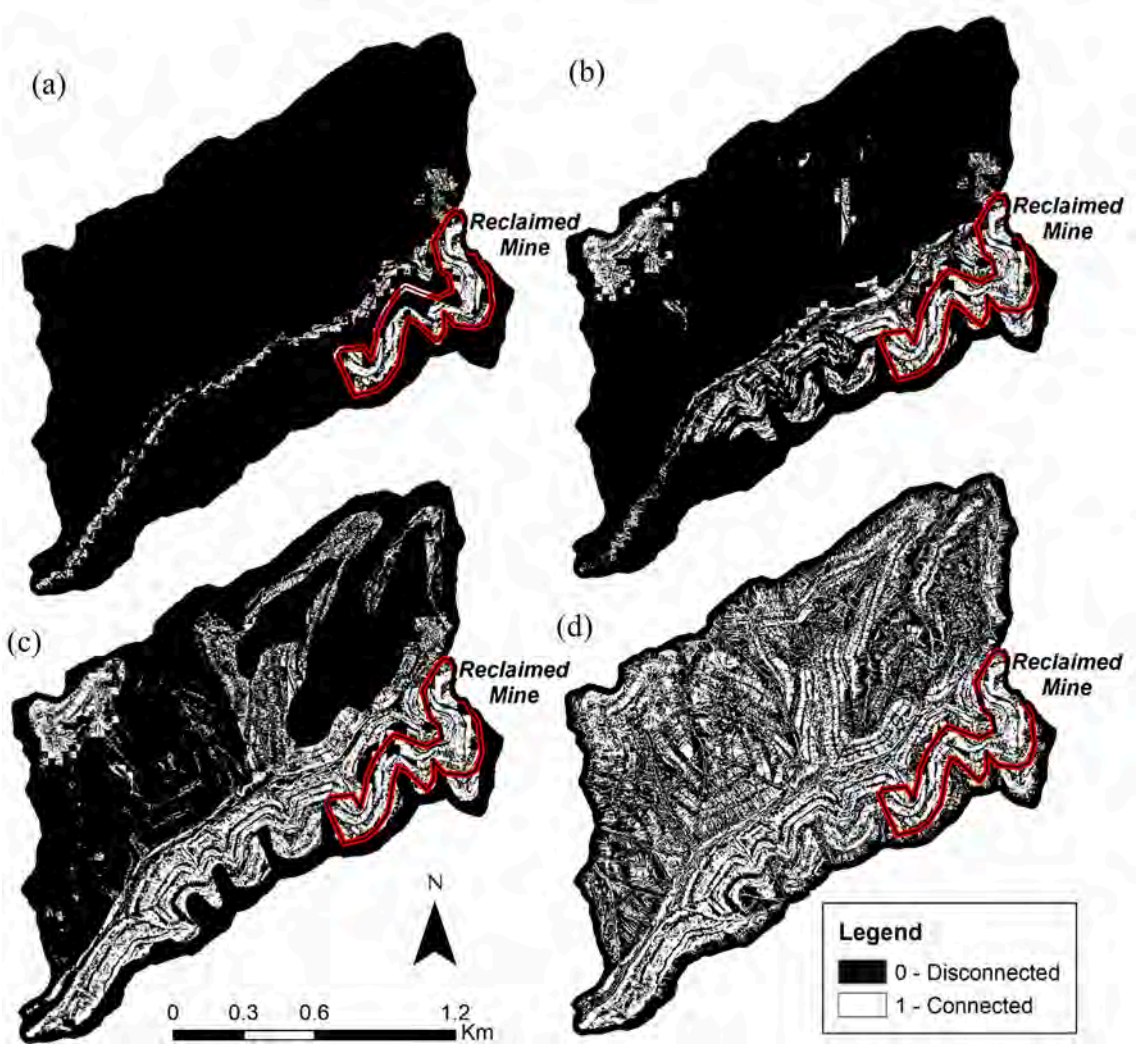

Fig. 5. Spatial probability of connectivity results for four events of increasing hydrologic magnitude in the Whitaker Branch watershed including: (a) 3.0% connectivity during event 8 (July 24, 2007); (b) 9.3% connectivity during event 12 (October 24, 2007); (c) 18.8% connectivity during event 1 (March 1, 2007); and (d) 36.2% connectivity during event 5 (April 14, 2007). These events approximately represent the minimum (event 8), 25% quartile (event 12), 75% quartile (event 1), and maximum (event 5) P(C) results. Note: cells within the watershed are predicted to be either connected (white cells) or disconnected (black cells). Any appearance of a gradient is artificial due to contrasting image/raster cell resolution.

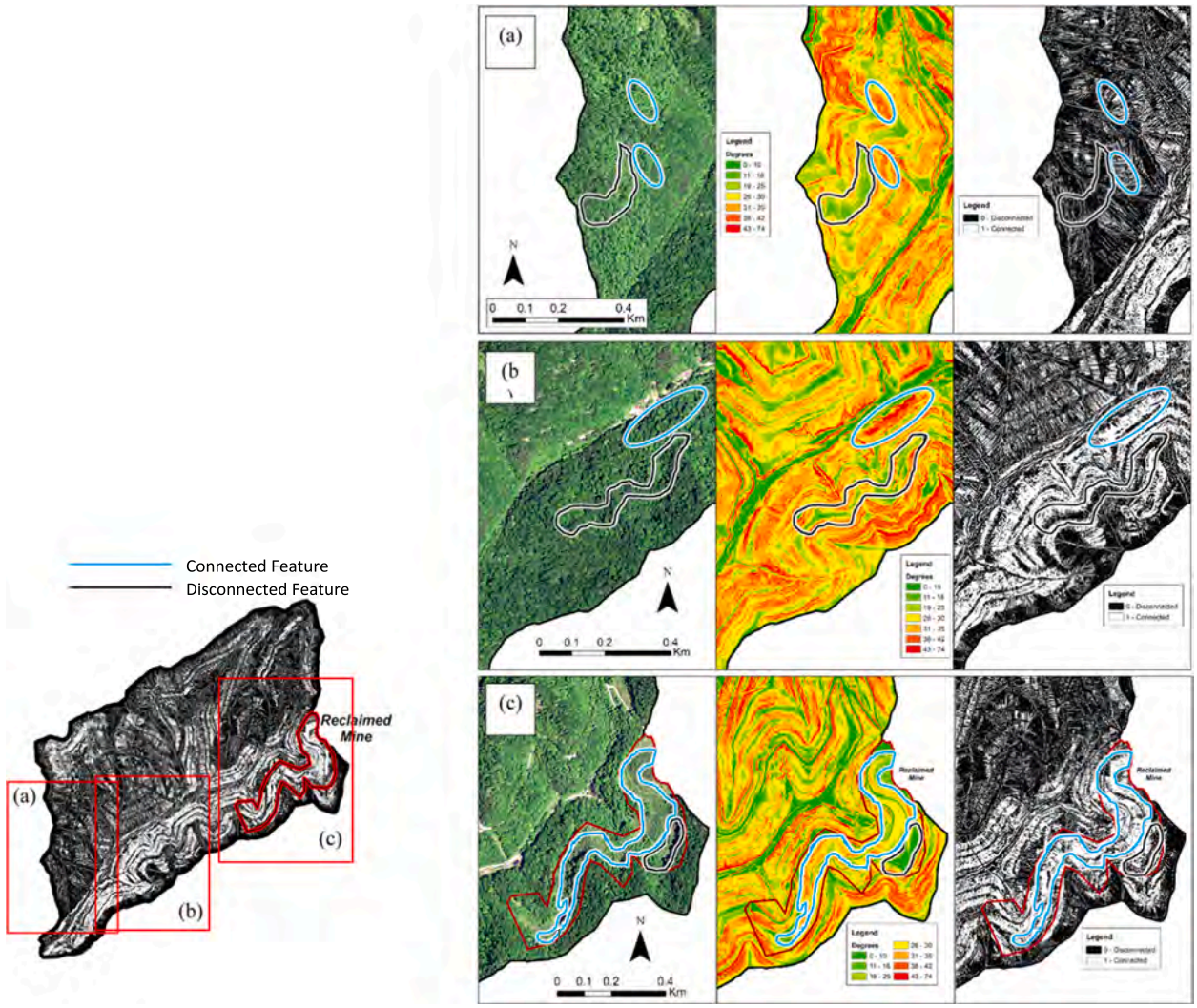

Fig. 6. Probability of connectivity results reveals connected and disconnected morphologic features. Imagery, slope, and probability of connectivity results are shown for three locations within the Whitaker Branch watershed. (a) Connectivity from concentrated forest pathways on steep slopes (circled in blue) and disconnectivity due to soil texture and fast drainage on flat swaths (circled in black). (b) Connectivity caused by steep slopes (circled in blue) and disconnectivity from historic terracing found throughout the watershed (circled in black). (c) Connectivity within the reclaimed mine (circled in blue) and disconnectivity on flat ridgelines created during reclamation (circled in black). The reclaimed mine is circled in red. (For interpretation of the references to colour in this figure legend, the reader is referred to the web version of this article.)

which highlights impedances due to structural watershed properties as opposed to impedances from functional hydrologic variability (e.g., runoff depth or soil moisture content), thus highlighting the upper limit of connectivity in the watershed. Fig. 6a indicates that even on the steepest surfaces, sediment connectivity seldom occurs in forested hillslopes. The prevalence of disconnectivity on these hillslopes is attributed to relatively high sand content of the soil texture and infiltration capacity of the soil. These soil drainage characteristics limit runoff generation and fluid energy to detach and transport sediment despite the steep hillslope gradient (i.e., average gradient = 0.51 m m^{-1}). Other morphologic features influencing disconnectivity on forested hillslopes include microtopography created from exposed tree roots and tree fall which promotes localized pockets of very flat slopes (e.g., 0–10°), decreasing fluid transport capacity. Also, Fig. 6b highlights disconnectivity due to historic terracing found throughout the watershed. Locally flat swaths (see Fig. 6b – slope) occur in contours throughout forested hillslopes and decrease overland fluid energy available to detach and transport sediment. We find that terraces particularly impacted the probability of downstream sediment transport ($P(T_{H-Down})$) and cause localized regions where deposition is likely. Disconnected landscape across the reclaimed mine was found to occur near ridgelines and locally flat areas created during reclamation (see Fig. 6c). Disconnectivity near ridgelines occurs because with very little upstream contributing area is available to accumulate water and produce shearing able to erode sediment. Disconnectivity of flat contours occurs because spoil is placed in lifts during surface mine reclamation (e.g., Skousen and Zipper, 2014). Each lift is constructed with near constant gradient with a slope length on the order of 50 m in this study, and the lifts are compacted in place. In between lifts, a near zero gradient berm of spoil is compacted across the contour and is between 5 and 10 m wide. These berms cause disconnectivity across the mining landscape.

4.3. Functional and structural controls on $P(C)$

Event variability of $P(C)$ sub-processes highlights structural and functional behavior that controls connectivity throughout the Whitaker Branch watershed. Sub-process connectivity probabilities for the Whitaker Branch watershed are shown in Fig. 7a.

We find that generally functional connectivity associated with the probability of hydrologic detachment $P(D_H)$ controls overall probability

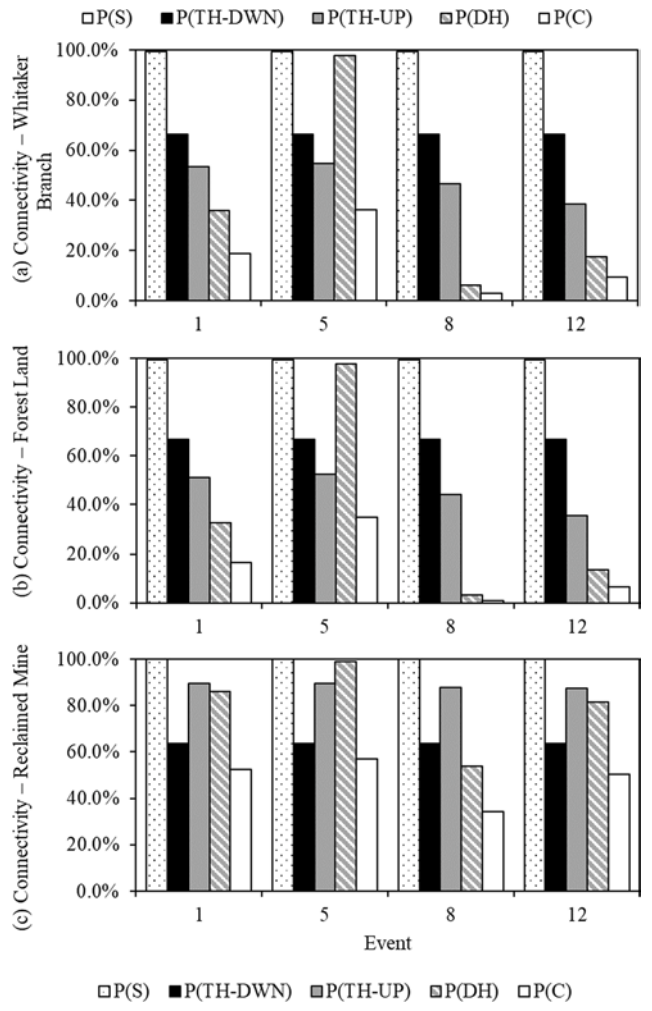

Fig. 7. Variability of sediment connectivity probabilities, including the probability of sediment supply, P(S), probability of downstream hydrologic transport, P(TH-DWN), probability of upstream hydrologic transport, P(TH-UP), probability of hydrologic detachment, P(DH) and probability of connectivity, P(C). Probabilities are shown for selected events in (a) Whitaker Branch, (b) forested land uses, and (c) reclaimed mine land. These events approximately represent the minimum (event 8), 25% quartile (event 12), 75% quartile (event 1), and maximum (event 5) $P(C)$ results.

of connectivity results in the forest and the Whitaker Branch watershed as a whole (see Fig. 7a and b). $P(D_H)$ limits $P(C)$ during all events at and below the 75% quartile (event 1, 8, 12), which indicates that detachment processes control sediment transport and connectivity across most surfaces in the Whitaker Branch watershed. Physically, this result is related to the very high infiltration rates in most soils in the Whitaker Branch watershed, which limits runoff production and hence sediment detachment. Only during the event with most extreme hydrologic activity (event 5) did $P(D_H)$ not limit overall connectivity. We notice similar trends in forest sub-process probabilities (see Fig. 7b), which is to be expected considering forest land covers 94% of the watershed.

Our results indicate notably different processes control the behavior of sediment connectivity in the reclaimed mine, and the structural control and to a lesser degree the functional control associated with the probability of hydrologic transport and detachment, respectively, play a role in the minelands (Fig. 7c). In nearly all events, the structurally dependent probability of downstream hydrologic transport $P(T_{H-Dwn})$ is the limiting connectivity sub-process, indicating that structural watershed variables (e.g., slope, stream density) limit connectivity in the reclaimed mine as opposed to functional variability (e.g., soil moisture content, runoff generation). One reason that this occurs is because soil texture disturbance reduces infiltration rates such that storms frequently produce relatively large runoff volumes compared to the surrounding forest. This results in elevated energy to detach and transport sediment manifested within the model by increased probability of functional sub-processes ($P(D_H)$ and $P(T_{H-Up})$), thus reducing functional control over $P(C)$ results.

Our findings add to an existing discussion of structural and functional control of connectivity in other watersheds, and specifically our results relax the notion that functional (dynamic) processes control sediment connectivity in all landscapes (Bracken et al., 2015; Mahoney et al., 2018). Rather, based on our review and experiences, structural connectivity shows the dominant control on connectivity for steep basins and/or during high magnitude hydrologic events when runoff production is high. Functional connectivity becomes more-and-more controlling on net connectivity for lower gradient basins, well-drained landscapes and/or low and moderate hydrologic events. For example, application of both the probability of connectivity and index of connectivity methods showed the importance of the dominant structural control for high magnitude events in the comparison by Mahoney et al. (2020a). Results of this basin show the importance of structural control for the steep Whitaker Branch catchment and structural control showing differences between land cover types (see Fig. 8). Functional control associated with $P(T_{H-Up})$ seldom limits $P(C)$ in the Whitaker Branch watershed likely because: (i) soil moisture is relatively high in the catchment promoting low critical slope thresholds to initiate erosion; and (ii) the steep slopes throughout the watershed easily overcome

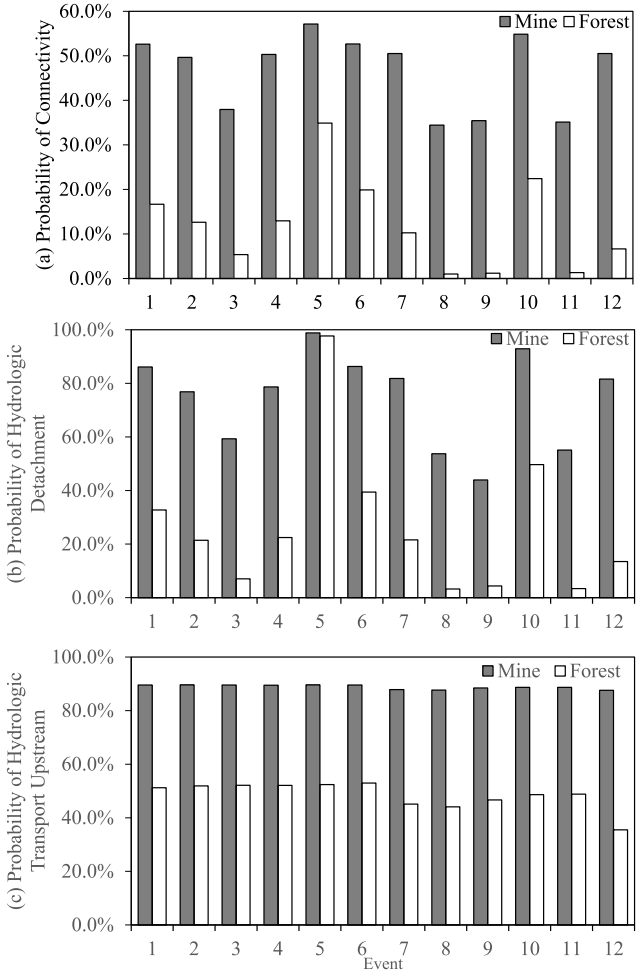

Fig. 8. Results of (a) probability of connectivity, (b) probability of hydrologic detachment and (c) probability of hydrologic upstream transport for each of the 12 hydrologic events for forest and reclaimed mining surface cover.

critical slope thresholds necessary to initiate rill or gully development. On the other hand, recent study has shown the importance of functional controls for lower gradient basins and lower magnitude events. Mahoney et al., (2018) found in the Upper South Elkhorn watershed (65.1 km^2), a gently rolling catchment (average slope 0.07 m m^{-1}) in central Kentucky, that sediment connectivity is generally controlled by the functional probability of upstream transport, $P(T_{H-Up})$, which is a function of soil moisture content, slope, and upstream contributing area. Soils within the Upper South Elkhorn are primarily silt loams and produce large runoff volumes during events, thus promoting detachment of sediment. The relatively flat slopes of the Upper South Elkhorn lack energy required to overcome critical slopes requisite of rill and gully development, explaining the control of $P(T_{H-Up})$on connectivity in the Upper South Elkhorn.

4.4. Coupled $P(C)$ and RUSLE model reveals connectivity and sediment loss rates

Our coupled $P(C)$ and RUSLE model indicates that sediment yield from the reclaimed mine is nearly two times the amount of sediment yield from the forest during the simulation period (see Table 5). This result is significant because the reclaimed mine makes up only 6.0% of the Whitaker Branch watershed. We find that soil loss rates (A) throughout the reclaimed mine are approximately 30 times greater than the forest land. We emphasize that this rate is normalized across the entire surface of the Whitaker Branch watershed (see Eqs. (19) and (20)) as opposed to surfaces where erosion actually occurs (see Eqs. (21) and (22)). When only considering soil loss on connected surfaces (AC), soil loss rates increase by nearly an order of magnitude in the forest land use and by a factor of two in the reclaimed mine (see Table 5). Increased simulated soil loss rates result from connected surfaces occurring, on average, on 12.1% of the forest land use and 46.8% of the reclaimed mine. We emphasize this result because AC soil loss rates are likely more

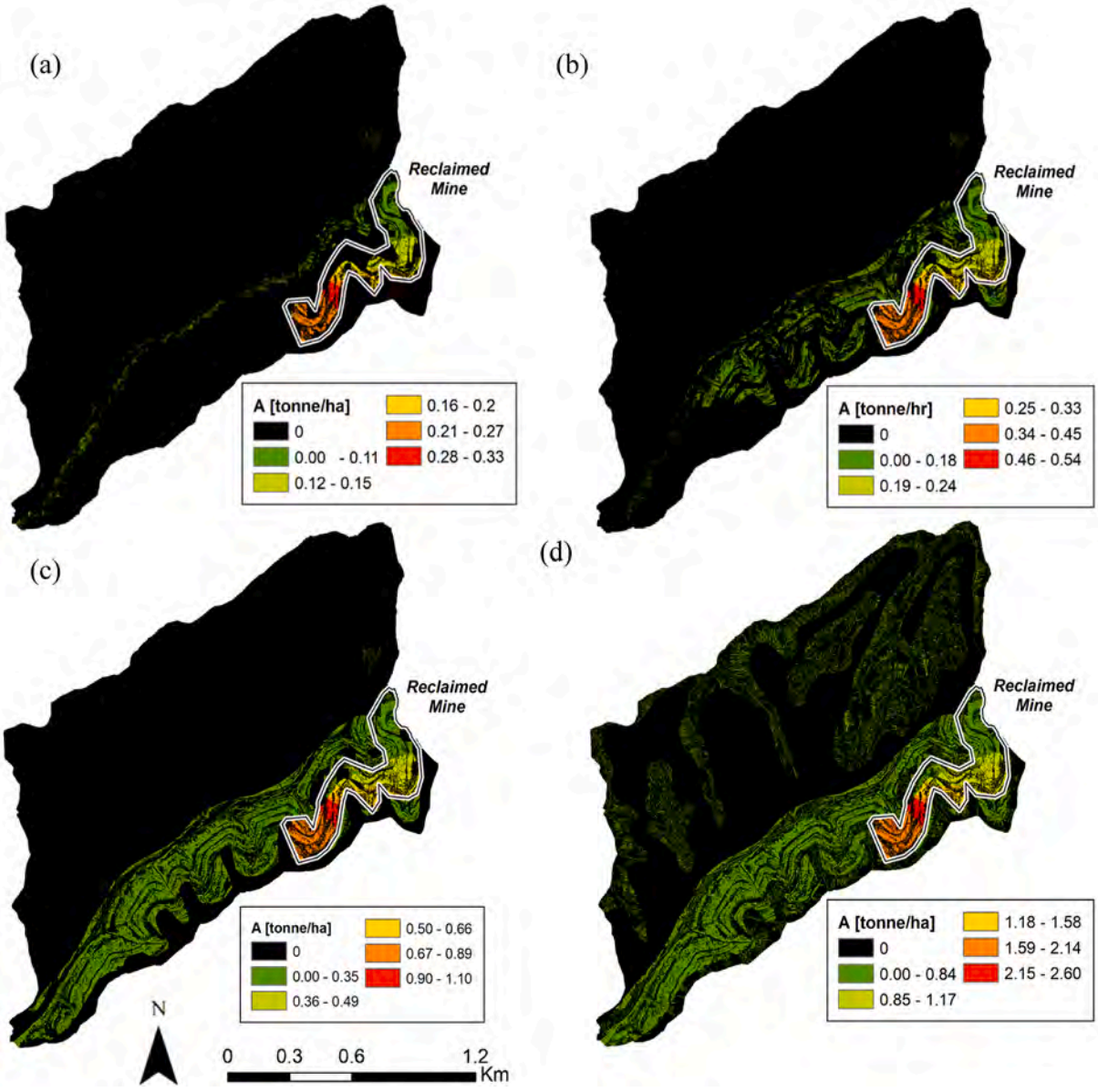

Fig. 9. Spatially-distributed erosion and connectivity results. Distributed connectivity and RUSLE results for four events of increasing probability of connectivity in the Whitaker Branch watershed including: (a) event 8 (July 24, 2007) with 3.0% connectivity; (b) event 12 (October 24, 2007) with 9.3% connectivity; (c) event 1 (March 1, 2007) with 18.8% connectivity; and (d) event 5 (April 14, 2007) with 36.2% connectivity.

realistic of soil loss occurring in the Whitaker Branch watershed. From a management standpoint, this result highlights pathways that should be targeted for remediation within the watershed. Mahoney et al., (2018) found that approximately 90% of sediment is transported in during events with greater than 3% connectivity, which gives us confidence that this analysis captures the majority of important sediment transport events during 2007.

Spatially explicit $P(C)$ and RUSLE modeling extends our view of sediment transport in the Whitaker Branch watershed and highlights connected pathways that produce the most sediment in the watershed (see. Fig. 9). In the four events presented in Fig. 9, soil loss rates within the reclaimed mine are greater than rates in the forest. This result highlights that the pathways most sensitive to connectivity are also pathways that contribute the greatest soil loss rates. Spatially explicit results of the coupled $P(C)$ and RUSLE model also highlight areas that are predicted to be connected but ultimately produce little sediment (see for example Fig. 5d and Fig. 9d). In particular, we find that forested regions of the watershed north of Whitaker Branch are predicted to be connected (Fig. 5d), yet produce zero or near zero soil loss, implying disconnectivity (Fig. 9d). We attribute this result to particularly rocky soils located throughout the forested hillslopes that increases effective critical shear stress of the soil and reduces potential for soil loss. This result highlights the importance of considering connectivity's magnitude in addition to the extent of connectivity during connectivity simulations (Fryirs, 2013; Bracken et al., 2015; Wohl et al., 2017).

Recent reclamation literature suggests that in addition to detrimentally impacting rainfall and runoff infiltration processes, excessive compaction of reclaimed soils reduces rates of native tree growth and promotes growth of short-rooted grasses (Acton et al., 2011). Our spatially explicit results highlight that connectivity occurs frequently and soil loss rates are greatest within the reclaimed mine. Angel et al. (2005) has suggested that one strategy to improve soil stabilization and regrowth of native trees on reclaimed mines is to compact soils and leave approximately 1 m of relatively loose spoil on top of compacted surface, now known as the Forestry Reclamation Approach (FRA; Williamson and Barton, 2020). This method limits mass wasting and recreates soil conditions akin to forested land uses. Related to the results herein, we suggest that this method likely decreases sediment connectivity and soil loss in the reclaimed mine because reestablishment of native trees and recreation of surface microtopography increases interception and infiltration of precipitation and runoff.

We plotted event soil loss against probability of connectivity results (see Fig. 10) and noticed a positive linear trend for both the forest ($R^2 = 0.95$) and reclaimed mine ($R^2 = 0.55$), implying a strong relationship exists between connectivity and soil loss. Relationships between soil loss and connectivity in the forest and reclaimed mine show trends of self-similarity, which implies that in steep watersheds, probability of connectivity might be a predictor of normalized soil loss based on land use.

Our results that *P(C)* is a good predictor of sediment yield agrees with findings from Vigiak et al., (2012) who found that calibrated hillslope sediment delivery ratio (HSDR), a function of the Index of Connectivity (Borselli et al., 2008), was well correlated with specific sediment yield. Vigiak et al., (2012) linked HSDR and IC and found HSDR predicted specific sediment yield well.

However, it is noteworthy that this result contrasts findings from Mahoney et al., (2018) and Mahoney et al., (2020a,b) where probability of connectivity was poorly related to soil loss and sediment yield ($R^2 = 0.26$ and $R^2 = 0.007$, respectively). This is because connectivity simulations presented in Mahoney et al., (2018, 2020a,b) were conducted in the much flatter Upper South Elkhorn watershed. We find that subprocesses controlling connectivity vary in the Whitaker Branch and Upper South Elkhorn watershed. Specifically, in the Whitaker Branch watershed, the probability of hydrologic detachment, $P(D_H)$, a function of runoff depth and slope, controls $P(C)$ results. Variability of soil loss (A), as determined by RUSLE, is also largely a function of event rainfall and runoff, which may explain the good relationship. This contrasts the Upper South Elkhorn where $P(C)$ is largely controlled by $P(T_{H-Up})$, which implies that such self-similarity is only realized in certain systems with very steep slopes where rill and gully development does not control sediment transport.

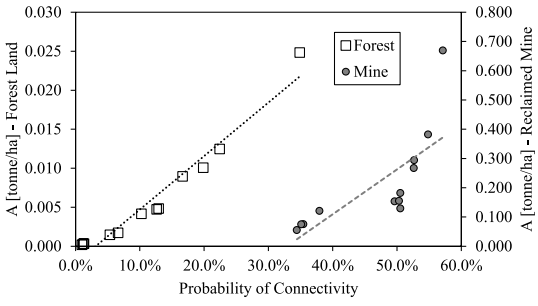

Fig. 10. Soil loss for land uses versus probability of connectivity results.

5. Conclusion

The conclusions of this study are as follows:

(1) The coupled probability of connectivity and RUSLE model simulates sediment transport on forested and reclaimed mine hillslopes well. However, unforeseen dependencies between connectivity formulae and RUSLE need to be accounted for. For example, the *P* factor in RUSLE was codependent with $P(C)$, and the *P* factor needed to be held at unity to account for dependence when coupling the models. We suggest future coupled models of connectivity and RUSLE should consider incorporating feedback calibration schemes, as was carried out in this study, to resolve potential overlap and discrepancies between connectivity modelling and RUSLE modelling.

(2) The coupled *P(C)* and RUSLE model tended to predict sediment transport well in this system. That being said, the *P(C)* model treats deposition in a rather implicit manner (i.e., parameterization of buffers through field assessment; a flatter downstream gradient classifying a given cell as disconnected), rather than an explicitly including a deposition formula in each cell of the upland model. Per our analyses of the Rouse number, this treatment is justified for the conditions of this study. However, explicit treatment of deposition could be improved upon in our sediment connectivity formula, and this has been an area of research for our group.

(3) Our understanding of sediment transport on steep hillslopes with forest and mining land uses was advanced because an unforeseen impact of legacy terracing controlled both sediment connectivity and soil loss. Legacy terracing following historic deforestation in forested land and subsequent surface mining activities in the reclaimed minelands created disconnectivity throughout the basin. Disconnectivity was also predicted to occur because of soil macropores and the high sand content of soils that increase infiltration rates in forested land, and because of constructed berms between compacted spoil lifts on reclaimed mine surfaces. Results show, on average, 12% of the drainage area of Appalachian forests was connected during hydrologic events and 47% of the drainage area of reclaimed minelands was connected. Connectivity was prevalent in concentrated flow paths in both land types.

(4) Structural control tended to dominate connectivity in this study, and soil loss and connectivity are self-similar. The structural control results are contrary to the notion that functional (dynamic) processes control sediment connectivity in all landscapes. Summarizing in the context of other published studies suggests structural control dominates connectivity for steep basins with

high runoff, and functional connectivity becomes more-and-more controlling for lower gradient basins, well-drained landscapes, or low to moderate hydrologic events. Self-similarity between soil loss and connectivity implies that in steep watersheds, probability of connectivity might be a predictor of normalized soil loss based on land use. This topic remains somewhat open because one recent study agrees with our findings but others suggest the probability of connectivity can be poorly correlated with soil loss and sediment yield in some basins.

(5) The soil loss rates of the reclaimed mine are approximately 30 times greater than the forest land despite the fact that the reclamation is classified as phase 3. Soil loss rates that consider spatially explicit connectivity are, on average, an order of magnitude higher in the forested land use and double in the reclaimed mine compared to analyses that assume lumped contributions from land uses. From a management perspective, spatially explicit results highlight pathways that should be targeted for remediation. Reforestation has been promoted in the region, and this study supports the idea that reforestation will likely decrease sediment connectivity and soil loss in the reclaimed mine because reestablishment of native trees and recreation of surface microtopography increases interception and infiltration of precipitation and runoff.

CRediT authorship contribution statement

T. Mahoney: Conceptualization, Data curation, Formal analysis, Investigation, Methodology, Software, Validation, Visualization, Writing - original draft, Writing - review & editing. **B. Blandford:** Formal analysis, Methodology, Software, Writing - review & editing. **J. Fox:** Conceptualization, Data curation, Funding acquisition, Investigation, Methodology, Project administration, Supervision, Writing - original draft, Writing - review & editing.

Declaration of Competing Interest

The authors declare that they have no known competing financial interests or personal relationships that could have appeared to influence the work reported in this paper.

Acknowledgement

We gratefully acknowledge the financial support of this research under National Science Foundation Award 163288. We thank LIF Creative (www.lif-creative.com) for illustration and graphic design assistance. We thank Chris Barton for sharing information regarding legacy farming and soil properties in the Appalachian region. We thank Editor Jiri Simunek and an anonymous reviewer, whose comments improved the quality of the manuscript.

References

Acton, P.M., Fox, J.F., Campbell, J.E., Jones, A.L., Rowe, H., Martin, D., Bryson, S., 2011. The role of soil health in maintaining environmental sustainability of surface coal mining. Environ. Sci. Technol. 45, 10265–10272.

Ali, G., Oswald, C., Spence, C., Wellen, C., 2018. The T-TEL method for assessing water, sediment, and chemical connectivity. Water Resour. Res. 54, 634–662. https://doi.org/10.1002/2017WR020707.

Ambroise, B., 2004. Variable'active' versus'contributing' areas or periods: a necessary distinction. Hydrol. Process. 18, 1149–1155. https://doi.org/10.1002/hyp.5536.

Angel, P., et al., 2005. The Appalachian Regional Reforestation Initiative. The Appalachian Regional Reforestation Initiative, Forest Reclamation Advisory No. 1.

Arnold, J.G., Srinivasan, R., Muttiah, R.S., Williams, J.R., 1998. Large area hydrologic modeling and assessment part I: model development 1. JAWRA J. Am. Water Resour. Assoc. 34 (1), 73–89.

Batista, P.V.G., Davies, J., Silva, M.L.N., Quinton, J.N., 2019. On the evaluation of soil erosion models: are we doing enough? Earth-Sci. Rev. 197, 102898 https://doi.org/10.1016/j.earscirev.2019.102898.

Bingner, R.L., Theurer, F.D., 2001. AGNPS 98: A Suite of water quality models for watershed use. In: Proceedings of the Sediment: Monitoring, Modeling, and Managing, 7th Federal Interagency Sedimentation Conference, Reno, NV, 25-29 March 2001: Subcommittee on Sedimentation of the Interagency Advisory Committee on Water Data, p. VII-1–VII-8.

Bonta, J.V., 2000. Impact of coal surface mining and reclamation on suspended sediment in three Ohio watersheds. J. Am. Water Resour. Assoc. 36 (4), 869–887.

Borselli, L., Cassi, P., Torri, D., 2008. Prolegomena to sediment and flow connectivity in the landscape: a GIS and field numerical assessment. Catena 75, 268–277. https://doi.org/10.1016/j.catena.2008.07.006.

Bracken, L.J., Wainwright, J., Ali, G.A., Tetzlaff, D., Smith, M.W., Reaney, S.M., Roy, A. G., 2013. Concepts of hydrological connectivity: research approaches, pathways and future agendas. Earth Sci. Rev. 119, 17–34.

Bracken, L.J., Turnbull, L., Wainwright, J., Bogaart, P., 2015. Sediment connectivity: a framework for understanding sediment transfer at multiple scales. Earth Surf. Process. Landforms 40, 177–188. https://doi.org/10.1002/esp.3635.

Campbell, J.E., Fox, J.F., Davis, C.M., Rowe, H.D., Thompson, N., 2009. Carbon and nitrogen isotopic measurements from southern Appalachian soils: assessing soil carbon sequestration under climate and land use variation. J. Environ. Eng., ASCE 135 (6), 439–448.

Cantreul, V., Bielders, C., Calsamiglia, A., Degré, A., 2018. How pixel size affects a sediment connectivity index in central Belgium. Earth Surf. Process. Landforms 43, 884–893. https://doi.org/10.1002/esp.4295.

Cavalli, M., Trevisani, S., Comiti, F., Marchi, L., 2013. Geomorphometric assessment of spatial sediment connectivity in small Alpine catchments. Geomorphology 188, 31–41. https://doi.org/10.1016/j.geomorph.2012.05.007.

Chang, H.H., 1998. Fluvial Processes in River Engineering. Krieger Publishing Company, Malabar, Florida.

Crema, S., Cavalli, M., 2018. SedInConnect: a stand-alone, free and open source tool for the assessment of sediment connectivity. Comput. Geosci. 111, 39–45.

Curtis, W.R., 1978. Effects of surface mining on hydrology, erosion, and sedimentation in eastern Kentucky. In: Fourth Kentucky Coal Refuse Disposal and Utilization Seminar, Lexington, KY, pp. 17–19.

De Vente, J., Poesen, J., Verstraeten, G., Govers, G., Vanmaercke, M., Van Rompaey, A., Arabkhedri, M., Boix-Fayos, C., 2013. Predicting soil erosion and sediment yield at regional scales: where do we stand? Earth-Sci. Rev. 127, 16–29. https://doi.org/10.1016/j.earscirev.2013.08.014.

Dietrich, W.E., 1982. Settling velocity of natural particles. Water Resour. Res. 18 (6), 1615–1626.

Dissmeyer, G.E., Foster, G.R., 1980. A guide for predicting sheet and rill erosion on forest land. Tech.. Publ. SA-TP-11, USDA-Forest Service-State and Private Forestry-Southeastern Area.

Fox, J.F., Campbell, J.E., Acton, P.M., 2020. Carbon sequestration by reforesting legacy grasslands on coal mining sites. Energies 13, 6340. https://doi.org/10.3390/en13236340.

Fox, J.F., 2009. Measurements of sediment transport processes in forested watersheds with surface coal mining disturbance using carbon and nitrogen isotopes. J. Am. Water Resour. Assoc. 45 (5), 1273–1289.

Fox, J.F., Martin, D.K., 2015. Sediment fingerprinting for calibrating a soil erosion and sediment-yield model in mixed land-use watersheds. J. Hydrol. Eng. 20 https://doi.org/10.1061/(ASCE)HE.1943-5584.0001011.

Fryirs, K., 2013. (Dis)Connectivity in catchment sediment cascades: a fresh look at the sediment delivery problem. Earth Surf. Process. Landforms 38, 30–46. https://doi.org/10.1002/esp.3242.

Fryirs, K.A., Brierley, G.J., Preston, N.J., Spencer, J., 2007. Catchment-scale (dis) connectivity in sediment flux in the upper Hunter catchment, New South Wales, Australia. Geomorphology 84, 297–316. https://doi.org/10.1016/j.geomorph.2006.01.044.

Gay, A., Cerdan, O., Mardhel, V., Desmet, M., 2016. Application of an index of sediment connectivity in a lowland area. J. Soils Sediments 16 (1), 280–293.

Gran, K.B., Czuba, J.A., 2017. Sediment pulse evolution and the role of network structure. Geomorphology 277, 17–30. https://doi.org/10.1016/j.geomorph.2015.12.015.

Grant, G.E., O'Connor, J., Safran, E., 2017. Excursions in fluvial (dis)continuity. Geomorphology 277, 145–153. https://doi.org/10.1016/j.geomorph.2016.08.033.

Guebert, M.D., Gardner, T.W., 2001. Macropore flow on a reclaimed surface mine: Infiltration and hillslope hydrology. Geomorphology 39, 151–169. https://doi.org/10.1016/S0169-555X(00)00107-0.

Gupta, R.S., 2016. Hydrology and Hydraulic Systems. Waveland Press, Long Grove, Illinois.

Hamel, P., Chaplin-Kramer, R., Sim, S., Mueller, C., 2015. A new approach to modeling the sediment retention service (InVEST 3.0): case study of the Cape Fear catchment, North Carolina, USA. Sci. Total Environ. 524, 166–177.

Hanson, G.J., Simon, A., 2001. Erodibility of cohesive streambeds in the loess area of the midwestern USA. Hydrol. Process. 15 (1), 23–38.

Harden, C.P., Scruggs, P.D., 2003. Infiltration on mountain slopes: a comparison of three environments. Geomorphology 55 (1–4), 5–24.

Heckmann, T., Cavalli, M., Cerdan, O., Foerster, S., Javaux, M., Lode, E., Smetanová, A., Vericat, D., Brardinoni, F., 2018. Indices of sediment connectivity: opportunities, challenges and limitations. Earth-Sci. Rev. 187, 77–108. https://doi.org/10.1016/j.earscirev.2018.08.004.

Heckmann, T., Schwanghart, W., 2013. Geomorphic coupling and sediment connectivity in an alpine catchment - exploring sediment cascades using graph theory. Geomorphology 182, 89–103. https://doi.org/10.1016/j.geomorph.2012.10.033.

Hewlett, J.D., Hibbert, A.R., 1965. Response of small watersheds to precipitation. In: International symposium on forest hydrology. Pergamon Press, New York.

Hoffmann, T, 2015. Sediment residence time and connectivity in non-equilibrium and transient geomorphic systems. Earth Sci. Rev. 150, 609–627.

Hooke, J., 2003. Coarse sediment connectivity in river channel systems: a conceptual framework and methodology. Geomorphology 56, 79–94. https://doi.org/10.1016/S0169-555X(03)00047-3.
Jamshidi, R., Dragovich, D., Webb, A.A., 2014. Distributed empirical algorithms to estimate catchment scale sediment connectivity and yield in a subtropical region. Hydrol. Process. 28 (4), 2671–2684.
Kalantari, Z., Cavalli, M., Cantone, C., Crema, S., Destouni, G., 2017. Flood probability quantification for road infrastructure: data-driven spatial-statistical approach and case study applications. Sci. Total Environ. 581, 386–398.
Kalisz, Paul J., 1986. Soil properties of steep Appalachian old fields, Ecology, Vol. 67, No. 4 (Aug., 1986), pp. 1011–1023.
Khan, A., Ormsbee, L., 1989. A comparison of two hydrologic models for steeply sloping forested watersheds. J. Hydrol. 109 (1989), 325–349.
KYAPED, 2014. Kentucky Aerial Photography and Elevation Data Program. Accessed: 01/30/19. http://kygeonet.ky.gov/kyfromabove/.
Lenhart, T., Van Rompaey, A., Steegen, A., Fohrer, N., Frede, H.-G., Govers, G., 2005. Considering spatial distribution anddeposition of sediment in lumped and semi-distributed models. Hydrol. Process. 19 (3), 785–794.
Leopold, L.B., Wolman, M.G., Miller, J.P., 1964. Fluvial Processes in Geomorphology. Freeman, New York, W.H.
López-Vicente, M., Álvarez, S., 2018. Influence of DEM resolution on modelling hydrological connectivity in a complex agricultural catchment with woody crops. Earth Surf. Process. Landforms 43, 1403–1415. https://doi.org/10.1002/esp.4321.
Mahoney, D.T., Fox, J.F., Al Aamery, N., 2018. Watershed erosion modeling using the probability of sediment connectivity in a gently rolling system. J. Hydrol. 561, 862–883. https://doi.org/10.1016/j.jhydrol.2018.04.034.
Mahoney, T., Fox, J., Al-Aamery, N., Clare, E., 2020a. Connectivity formula for watershed sediment modelling part I: model formulation and investigating the timing of sediment connectivity. Sci. Total Environ. in review.
Mahoney, T., Fox, J., Al-Aamery, N., Clare, E., 2020b. Connectivity formula for watershed sediment modelling part II: application and evaluating structural and functional connectivity. Sci. Total Environ. in review.
Mahoney, D.T., Al Aamery, N., Fox, J.F., Riddle, B., Ford, W., Wang, Y.T., 2019. Equilibrium sediment exchange in the earth's critical zone: evidence from sediment fingerprinting with stable isotopes and watershed modeling. J. Soils Sediments 19 (9), 3332–3356.
Mahoney, D.T., 2017. Sediment transport modelling using dynamic (dis)connectivity prediction for a bedrock controlled catchment. Theses and Dissertations–Civil Engineering. 55. https://uknowledge.uky.edu/ce_etds/55.
Mahoney, D.T., 2020. Probabilistic approach to water, sediment, and nutrient connectivity for advancing watershed modelling. Theses and Dissertations–Civil Engineering. 96. https://uknowledge.uky.edu/ce_etds/96.
McCool, D.K., Renard, K.G., Foster, G.R. 1993. The revised universal soil loss equation. In: Larionov, Nearing, (Eds.), Proc. Int'l. Workshop on Soil Erosion, Moscow, Russia. Center for Techn. Transfer and Pollution Prevention, Purdue Univ., USA, p. 45–59.
McIntosh, J.D., 2004. Soil Survey of Knott and Letcher Counties, Kentucky (2004), USDA NRCS.
Michalek, A., Zarnaghsh, A., Husic A. 2021. Modeling linkages between erosion and connectivity in an urbanizing landscape. Sci. Total Environ. In Press.
Morris, G.L., Fan, J., 1998. Reservoir sedimentation handbook: design and management of dams, reservoirs, and watersheds for sustainable use. McGraw Hill Professional.
Nunes, J.P., Wainwright, J., Bielders, C.L., Darboux, F., Fiener, P., Finger, D., Turnbull, L., 2017. Better models are more effectively connected models. Earth Surf. Process. Landforms 43, 1355–1360. https://doi.org/10.1002/esp.4323.
Papanicolaou, A.N., Fox, J.F., Marshall, J., 2003. Sediment source fingerprinting in the Palouse River Watershed, USA. Int. J. Sedim. Res. 18 (2), 278–284.
Renard, K., Foster, G., Weesies, G., McCool, D., Yoder, D., 1997. Predicting soil erosion by water: A guide to conservation planning with the Revised Universal Soil Loss Equation (RUSLE). United States Department of Agriculture, Washington D.C.
Shrestha, R.K., Lal, R., 2006. Ecosystem carbon budgeting and soil carbon sequestration in reclaimed mine soil. Environ. Int. 32, 781–796.
Shukla M.K., Lal, R., Ebinger, M., 2004. Soil quality indicators for reclaimed Minesoils in Southeastern Ohio, 0038-075X/04/16902-133–142 February 2004, Soil Science Vol. 169, No. 2.
Skousen, J., Zipper, C.E., 2014. Post-mining policies and practices in the Eastern USA coal region. Int. J. Coal Sci. Technol. 1, 135–151. https://doi.org/10.1007/s40789-014-0021-6.
Sloan, P.G., Moore, I.D., Coltharp, G.B., Eigel, J.D. 1983. Modeling surface and subsurface stormflow on steeply-sloping forested watersheds. Research Rep., Univ. of Kentucky, Lexington, KY.
Stewart, Bruce E., 2003. When Darkness Reigns Then is the Hour to Strike: Moonshining, Federal Liquor Taxation, and Klan Violence in Western North Carolina, 1868–1872. North Carolina Historical Review. 80 (4): 453–474. JSTOR 23522839.
Taylor, T.J., Agouridis, C.T., Warner, R.C., Barton, C.D., 2009. Runoff Curve Numbers for Losse-dumped Spoil in the Cumberland Plateau. Int. J. Min. Reclam. Environ. 23, 103–120.
Torri, D., Poesen, J., 2014. A review of topographic threshold conditions for gully head development in different environments. Earth Sci. Rev. 130, 73–85.
USEPA, 2004. The Incidence and Severity of Sediment Contamination in Surface Waters of the United States, EPA 823-R-04-007. http://www.epa.gov/waterscience/cs/report/2004/nsqs2ed-complete.pdf.
Vanoni, V.A., 1941. Some experiments on the transportation of suspended loads. Trans. Am. Geophys. Union 20 (3), 608–621.
Vigiak, O., Borselli, L., Newham, L.T.H., McInnes, J., Roberts, A.M., 2012. Comparison of conceptual landscape metrics to define hillslope-scale sediment delivery ratio. Geomorphology 138 (1), 74–88.
Walling, D.E., 1983. The sediment delivery problem. J. Hydrol. https://doi.org/10.1016/0022-1694(83)90217-2.
Warner, R.C., Agouridis, C.T., Vingralek, P.T., Fogle, A.W., 2010. Reclaimed Mineland curve number response to temporal distribution of rainfall. J. Am. Water Resour. Assoc. 46, 724–732.
Wickham, J.D., Riitters, K.H., Wade, T.G., Coan, M., Homer, C., 2007. The effect of Appalachian mountaintop mining on interior forest. Landscape Ecol. 22, 179–187.
Williamson, T.N., Barton, C.D., 2020. Hydrologic modeling to examine the influence of the forestry reclamation approach and climate change on mineland hydrology. Sci. Total Environ. 140605.
Wischmeier, W.H., Smith, D.D., 1978. Predicting rainfall erosion losses: a guide to conservation planning. Department of Agriculture No. 537.
Wohl, E., 2017. Connectivity in rivers. Prog. Phys. Geogr. 41, 345–362. https://doi.org/10.1177/0309133317714972.
Wohl, E., Brierley, G., Cadol, D., Coulthard, T.J., Covino, T., Fryirs, K.A., Grant, G., Hilton, R.G., Lane, S.N., Magilligan, F.J., Meitzen, K.M., Passalacqua, P., Poeppl, R. E., Rathburn, S.L., Sklar, L.S., 2019. Connectivity as an emergent property of geomorphic systems. Earth Surf. Process. Landforms 44, 4–26. https://doi.org/10.1002/esp.4434.
Wohl, E., Magilligan, F.J., Rathburn, S.L., 2017. Introduction to the special issue: connectivity in geomorphology. Geomorphology 277, 1–5. https://doi.org/10.1016/j.geomorph.2016.11.005.
Wright, A.C., Webster, R., 1991. A stochastic distributed model of soil erosion by overland flow. Earth Surf. Proc. Land. 16 (3), 207–226.
Zhao, G., Gao, P., Tian, P., Sun, W., Hu, J., Mu, X., 2020. Assessing sediment connectivity and soil erosion by water in a representative catchment on the Loess Plateau, China. Catena 185, 104284.
Zingaro, M., Refice, A., Giachetta, E., D'Addabbo, A., Lovergine, F., De Pasquale, V., Pepe, G., Brandolini, P., Cevasco, A., Capolongo, D., 2019. Sediment mobility and connectivity in a catchment: a new mapping approach. Sci. Total Environ. 672, 763–775. https://doi.org/10.1016/j.scitotenv.2019.03.461.

Assessment of erosion, sedimentation, and water quality impacts of the Mountain Valley Pipeline and Equitrans Expansion Project's proposed crossing of the Jefferson National Forest as it pertains to the U.S. Forest Service's Draft Supplemental Environmental Impact Statement dated December 2022

Prepared by Jonathan A. Czuba, Ph.D., Licensed Professional Engineer - February 9, 2023

REFERENCES
21

February 21, 2023

USGS
science for a changing world

Prepared in cooperation with the Nisqually Indian Tribe

Suspended Sediment Delivery to Puget Sound from the Lower Nisqually River, Western Washington, July 2010–November 2011

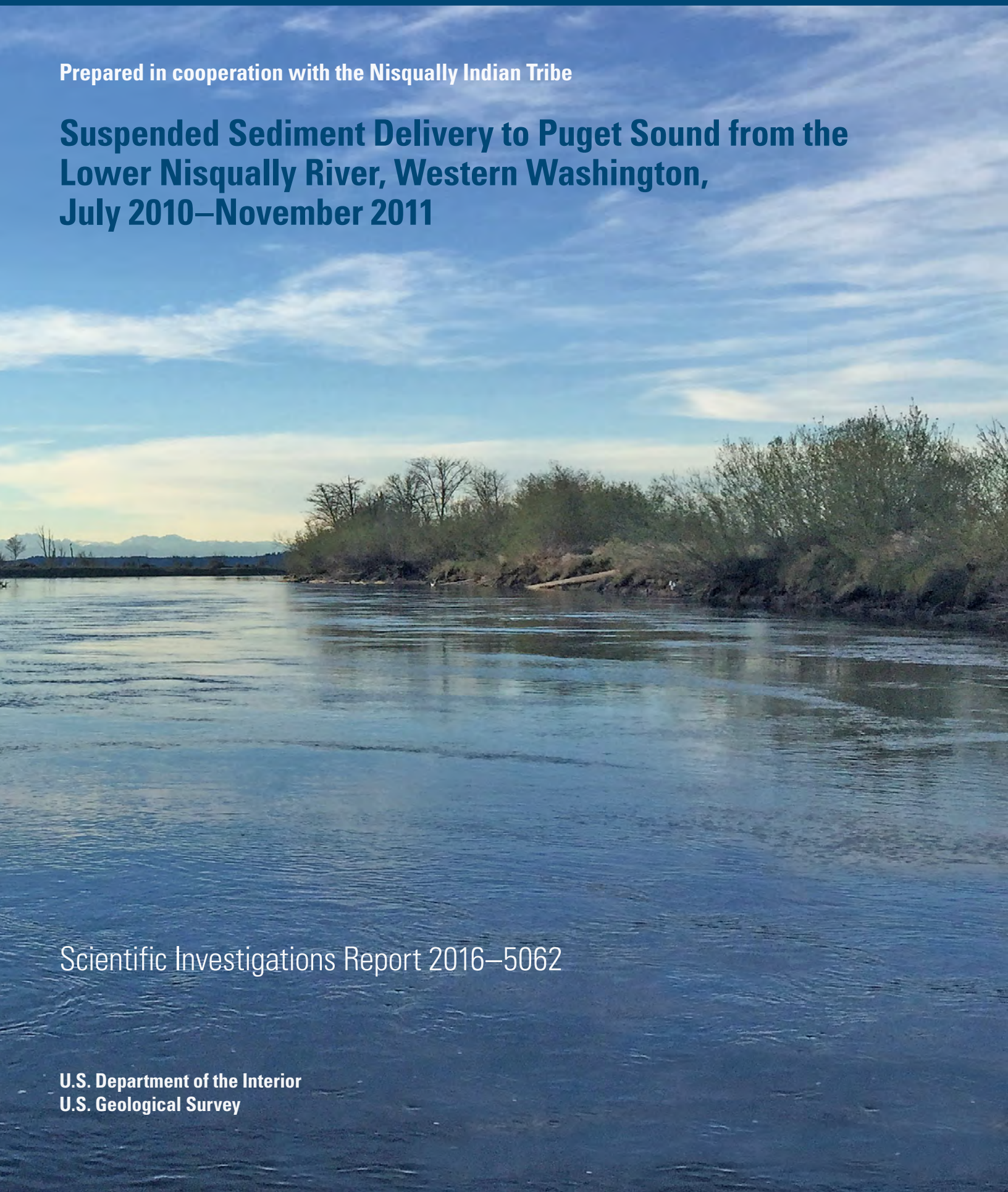

Scientific Investigations Report 2016–5062

U.S. Department of the Interior
U.S. Geological Survey

Cover: Downstream view of the lower Nisqually River, approximately 1 kilometer upstream of the river entrance into Puget Sound, Washington. Photograph by Christopher A. Curran, U.S. Geological Survey, March 29, 2016.

Suspended Sediment Delivery to Puget Sound from the Lower Nisqually River, Western Washington, July 2010–November 2011

By Christopher A. Curran, Eric E. Grossman, Christopher S. Magirl, and James R. Foreman

Prepared in cooperation with the Nisqually Indian Tribe

Scientific Investigations Report 2016–5062

U.S. Department of the Interior
U.S. Geological Survey

U.S. Department of the Interior
SALLY JEWELL, Secretary

U.S. Geological Survey
Suzette M. Kimball, Director

U.S. Geological Survey, Reston, Virginia: 2016

For more information on the USGS—the Federal source for science about the Earth, its natural and living resources, natural hazards, and the environment—visit http://www.usgs.gov or call 1–888–ASK–USGS.

For an overview of USGS information products, including maps, imagery, and publications, visit http://store.usgs.gov.

Suggested citation:
Curran, C.A., Grossman, E.E., Magirl, C.S., and Foreman, J.R., 2016, Suspended sediment delivery to Puget Sound from the lower Nisqually River, western Washington, July 2010–November 2011: U.S. Geological Survey Scientific Investigations Report 2016-5062, 17 p., http://dx.doi.org/10.3133/sir20165062.

ISSN 2328-0328 (online)

Contents

Figures

Tables

Conversion Factors

International System of Change not made Units to Inch/Pound

Multiply	By	To obtain
	Length	
meter (m)	3.281	foot (ft)
kilometer (km)	0.6214	mile (mi)
kilometer (km)	0.5400	mile, nautical (nmi)
meter (m)	1.094	yard (yd)
	Area	
square kilometer (km^2)	247.1	acre
square kilometer (km^2)	0.3861	square mile (mi^2)
	Volume	
milliliter (mL)	0.033814	ounce, fluid (fl. oz)
Liter (L)	0.2642	gallon (gal)
	Flow rate	
meter per second (m/s)	3.281	foot per second (ft/s)
cubic meter per second (m^3/s)	70.07	acre-foot per day (acre-ft/d)
cubic meter per second (m^3/s)	35.31	cubic foot per second (ft^3/s)
cubic meter per second (m^3/s)	22.83	million gallons per day (Mgal/d)
	Mass	
milligram (mg)	0.00003527	ounce, avoirdupois (oz)
metric ton per year (t/d)	1.102	ton per day (ton/d)
metric ton per year (t/yr)	1.102	ton per year (ton/yr)

Temperature in degrees Celsius (°C) may be converted to degrees Fahrenheit (°F) as

$$°F = (1.8 \times °C) + 32$$

Datums

Vertical coordinate information is referenced to the North American Vertical Datum of 1988 (NAVD 88).

Horizontal coordinate information is referenced to the North American Datum of 1983 (NAD 83).

Altitude, as used in this report, refers to distance above the vertical datum.

Abbreviations

EDI	Equal Discharge Increment
EWI	Equal-Width Increment
FNU	Formazin Nephelometric Unit
SSC	suspended-sediment concentration
USGS	U.S. Geological Survey
WY	water year (October 1–September 30)

Suspended Sediment Delivery to Puget Sound in the Lower Nisqually River, Western Washington, July 2010–November 2011

By Christopher A. Curran, Eric E. Grossman, Christopher S. Magirl, and James R. Foreman

Abstract

On average, the Nisqually River delivers about 100,000 metric tons per year (t/yr) of suspended sediment to Puget Sound, western Washington, a small proportion of the estimated 1,200,000 metric tons (t) of sediment reported to flow in the upper Nisqually River that drains the glaciated, recurrently active Mount Rainier stratovolcano. Most of the upper Nisqually River sediment load is trapped in Alder Lake, a reservoir completed in 1945. For water year 2011 (October 1, 2010–September 30, 2011), daily sediment and continuous turbidity data were used to determine that 106,000 t of suspended sediment were delivered to Puget Sound, and 36 percent of this load occurred in 2 days during a typical winter storm. Of the total suspended-sediment load delivered to Puget Sound in the water year 2011, 47 percent was sand (particle size >0.063 millimeters), and the remainder (53 percent) was silt and clay. A sediment-transport curve developed from suspended-sediment samples collected from July 2010 to November 2011 agreed closely with a curve derived in 1973 using similar data-collection methods, indicating that similar sediment-transport conditions exist. The median annual suspended-sediment load of 73,000 t (water years 1980–2014) is substantially less than the average load, and the correlation (Pearson's $r = 0.80$, $p = 8.1E\text{-}9$, $n=35$) between annual maximum 2-day sediment loads and normalized peak discharges for the period indicates the importance of wet years and associated peak discharges of the lower Nisqually River for sediment delivery to Puget Sound. The magnitude of peak discharges in the lower Nisqually River generally is suppressed by flow regulation, and relative to other free-flowing, glacier-influenced rivers entering Puget Sound, the Nisqually River delivers proportionally less sediment because of upstream sediment trapping from dams.

Introduction

Fluvial sediment delivery is fundamental to the formation of river deltas that support critical estuarine habitat for fish and ecosystem development and in Puget Sound can both benefit and threaten estuarine ecosystems (Czuba and others, 2011). Understanding the rate of sediment delivery in rivers entering Puget Sound is important in the assessment of the resiliency of nearshore ecosystems threatened by sea level rise and for predicting the efficacy of present and future nearshore restoration efforts (Cereghino and others, 2012).

The Nisqually River flows into southern Puget Sound providing important riverine and estuarine ecological function. Because of Tribal and Federal land holdings, much of the lower Nisqually River near Puget Sound contains a still-functioning riparian floodplain (Collins and others, 2012), and a major restoration project was completed in 2009 on the Nisqually River Delta to further improve the ecological health of the lower river corridor (U.S. Fish and Wildlife Service, 2010). Compared to other rivers entering Puget Sound (Czuba and others, 2011), the lower Nisqually River carries a relatively light sediment load because of substantial sediment accumulation in Alder Lake, a reservoir upstream of the 101-m-high Alder Dam, completed in 1945. Before 1945, the natural sediment load in the lower Nisqually River likely was suppressed by the predecessor to Alder Dam, the 11-m-high La Grande Dam completed in 1912 (Czuba and others, 2012a). In contrast, the sediment load in the Nisqually River upstream of Alder Lake is relatively large because of sediment generated from Mount Rainier (Czuba and others, 2012a).

Numerous geologic and sediment-transport studies have described the formative fluvial geomorphology of the Nisqually River or estimated the sediment load in the river and its tributaries. Nelson (1974) published a study of sediment measurements in the Nisqually and Deschutes River Basins, sampling suspended sediment from 1971 to 1972 at 16 sites. Downstream of Alder Lake, Nelson (1974) reported sediment loads of 95,000 t/yr for the Nisqually River at Nisqually and 91,000 t/yr for the Nisqually River above Powell Creek, near McKenna. Nelson (1974) also reported that mountainous catchments away from Mount Rainier produce a sediment yield at least one order of magnitude less than rivers directly draining Mount Rainier, and that catchments draining the Puget Lowland typically yield sediment at rates of about two orders of magnitude less than rivers draining Mount Rainier.

Based on bathymetric measurements of sediment accumulation in Alder Lake, Czuba and others (2012b) reported sediment yield similar to that of Nelson (1974) for the Nisqually River upstream of Alder Lake. Czuba and others (2012b) determined that from 1945 to 2011, the upper Nisqually River carried, on average, 1,200,000 ±180,000 t/yr of sediment and reported that 83–98 percent of this sediment load into Alder Lake originated from Mount Rainier. Czuba and others (2012b) also estimated that the trap efficiency of Alder Lake was 90 ±5 percent and that the long-term mean sediment load transported past Alder Dam was 120,000 ±18,000 t/yr. Using historical bathymetric surveys of Alder Lake, Czuba and others (2012b) reported that the average sediment load in the upper Nisqually River was just 860,000 ±300,000 t/yr from 1956 to 1985, indicating that sediment loads from Mount Rainier from 1956 to 1985 were less than the long-term average. This observation is notable because sediment sampled in 1971 and 1972 (Nelson, 1974) may have reflected sediment-transport conditions less in magnitude than the long-term mean.

Purpose and Scope

This report documents the timing and quantity of suspended-sediment load delivered by the Nisqually River to Puget Sound for July 25, 2010–November 30, 2011, which includes water year 2011 (October 1, 2010–September 30, 2011), for use in conjunction with nearshore circulation models to assess the sedimentation potential and efficacy of restoration efforts in the Nisqually River Delta. Sediment data collected in this study were used to develop sediment rating curves for estimating suspended-sediment load as a function of discharge and suspended-sediment concentration as a function of turbidity. Comparisons with a previous, similar study (Nelson, 1974) were made to assess differences in sediment-transport conditions and to estimate the mean annual suspended-sediment load delivered by the river to Puget Sound. Hydrology for the lower Nisqually River is examined from the long-term record of U.S. Geological Survey (USGS) streamgages in the basin and is used to provide a hydrologic context for the results of 2011 sediment loads. Turbidity is used as a surrogate measurement for suspended-sediment concentration (SSC) and, with sediment sample data, is used for assessing seasonal characteristics of sediment transport. This report includes the results of sediment-sample concentrations and particle size, and continuous turbidity data collected from July 2010 to November 2011.

Description of the Nisqually River Basin and Study Site

The Nisqually River is in the southeastern region of Puget Sound, a marine water body in western Washington formed as a result of Pleistocene glaciation (fig. 1; Booth, 1994; Porter and Swanson, 1998). The Nisqually River drains the Cascade Range, a part of the Puget Lowland, and the southwestern flank of Mount Rainier, a 4,392-m glaciated, recurrently active volcano (Crandell, 1971; Nelson, 1974; Sisson and Vallance, 2008; Czuba and others, 2012b). The Nisqually River formed after the retreat of the Puget Lobe of the Cordilleran Ice Sheet from the Puget Lowland about 16,000–17,000 years ago (Porter and Swanson, 1998). In establishing its late-Pleistocene course toward Puget Sound, the river incised into glacial till deposits (Collins and Montgomery, 2011) with a slope adequate to convey the large sediment loads originating from Mount Rainier. Active volcanism at Mount Rainier during the Holocene (Crandell, 1971; Scott and others, 1995; Sisson and Vallance, 2008) spawned multiple lahars, some large enough to travel to Puget Sound (Scott and others, 1995). Large-scale volcanism and associated increased sedimentation has not occurred on Mount Rainier in the past 150 years, but rainfall-induced debris flows from Mount Rainier and large floods have promoted ample sediment transport filling a portion of Alder Lake (Czuba and others, 2012b). The lower 5 km of the Nisqually River and its estuary occupy a former marine embayment of Puget Sound, acting as a Holocene sediment deposition zone; the river delta is the product of sediment deposition from the Nisqually River during the Holocene (Collins and Montgomery, 2011).

Discharge in the lower Nisqually River is regulated by the 100-m-high Alder Dam and smaller La Grande Dam, each owned and operated by Tacoma Power for flood control and hydroelectric power generation. The three primary tributaries draining Mount Rainier in the Nisqually River Basin are the mainstem Nisqually River, Kautz Creek, and Tahoma Creek. Major tributaries Mineral Creek and the Little Nisqually River enter upstream of Alder Dam and drain the Cascade Range away from Mount Rainier. Downstream of Alder Dam, the Mashel River is the only sizeable Nisqually River tributary draining mountainous terrain. Tributaries Ohop, Tanwax, and Muck Creeks all enter downstream of the Mashel River, but these tributaries drain predominantly the low-gradient Puget Lowland and sediment loads in these tributaries are relatively small (Nelson, 1974).

Figure 1. U.S. Geological Survey streamgages and sediment-monitoring site in the Nisqually River Basin, western Washington.

The climate of the Nisqually River Basin is predominantly wet and temperate (National Oceanic and Atmospheric Administration, 2010). The prevailing wind direction is from the south or southwest during the rainy season (October–June) and from the northwest during the relatively dry summer from July to September. During the winter, cold air from the Canadian interior occasionally flows southward, covering the region. The average January maximum temperature in the Puget Lowland is about 6 °C (43 °F) and the minimum temperature is about -1 °C (30 °F). During July, the average maximum temperature is about 24 °C (75 °F) and the average minimum temperature is about 10 °C (50 °F). Annual precipitation in the Puget Lowlands is about 1,000 mm (40 in.), and the winter season snowfall is about 380 mm (15 in.). Precipitation increases with altitude; annual rainfall in the Cascade Range in high-altitude catchments typically is 1,550–2,500 mm (60–100 in.), and total annual snowfall is between 10 and 15 m (400–600 in.) at altitudes of 1,200–1,600 m (4,000–5,500 ft) (National Oceanic and Atmospheric Administration, 2010).

Basin Hydrology

Mean annual discharge for the Nisqually River near National (USGS streamgage 12082500) is 22.0 m^3/s (777 ft^3/s) for the period of 1943–2014 (72 years), with dominant hydrologic inputs from rainfall in winter and snowmelt in spring and summer (table 1). Downstream of Alder Lake, the mean annual discharge for the Nisqually River at McKenna (USGS streamgage 12089500) is 36.9 m^3/s (1,301 ft^3/s). Late summer and autumn discharge is sustained by groundwater and glacial melt from Mount Rainier. The largest peak-flow events in the basin are caused by heavy autumn or winter precipitation associated with atmospheric rivers, strong synoptic systems from the Pacific Ocean that tap into tropical moisture sources (Neiman and others, 2011).

In the upper basin, the largest recorded peak discharge occurred in November 2006 during a large atmospheric river that caused widespread damage to Mount Rainier National Park (Czuba and others, 2012b). The peak discharge in the upper basin (Nisqually River near National, USGS streamgage 12082500) during the November 2006 event was 617 m^3/s (21,800 ft^3/s). Widespread flooding also affected the region in February 1996 when discharge peaked at 600 m^3/s (21,200 ft^3/s) on the Nisqually River near National. Smaller peak-flow events in the upper basin usually occur in late spring and early summer with the seasonal snowmelt. The lower basin is regulated by Alder Dam (constructed in 1945), which strongly affects the peak-flow hydrology. Although the February 1996 storm resulted in the peak discharge of record for the Nisqually River at McKenna (USGS streamgage 12089500) of 1,420 m^3/s (50,000 ft^3/s), the 2006 peak discharge was more tightly controlled by regulation at Alder Dam and resulted in a discharge of 436 m^3/s (15,400 ft^3/s). Hydrologic data at USGS streamgages typically are reported by water year, which is defined as the 12-month period October 1, for any given year through September 30, of the following year.

Sediment-Monitoring Site

The USGS sediment-monitoring site installed as part of this study, the Nisqually River near Yelm (site 12089970), is in the lower Nisqually River, 19.2 km upstream of the river mouth, 1.6 km downstream of the Centralia Power Canal outlet, and 15.8 km downstream of USGS streamgage Nisqually River at McKenna (12089500) (fig. 1). The lower Nisqually River is defined herein as the reach downstream of the outlet of the Centralia Power Canal about 20.8 km upstream of the mouth of the river at Puget Sound. The mixed-diurnal tidal influence in the lower river extends to about 5 km upstream of the mouth. The largest tributary in the lower river, Muck Creek, is 1.5 km downstream of the sediment-monitoring site, and remains a potential sediment source not included in this study. The drainage area of the basin at the sediment monitoring site is 1,520 km^2, and 50 percent of this area is upstream of the Alder and La Grande Dams.

Table 1. Summary of discharge at U.S. Geological Survey streamgages and a sediment-monitoring site in the Nisqually River Basin, western Washington.

[Mean annual discharge and discharge data for water years 1973 and 2011 are available at http://waterdata.usgs.gov/wa/nwis/sw. Water year is defined as the 12-month period October 1, for any given year through September 30, of the following year. **Abbreviations:** km^2, square kilometer; m^3/s, cubic meter per second]

Streamgage and No. or sediment-monitoring site and No.	Drainage area (km^2)	Period of discharge record (water year)	Mean annual discharge (m^3/s)	Discharge, water year 1973		Discharge, water year 2011	
				Mean (m^3/s)	Peak (m^3/s)	Mean (m^3/s)	Peak (m^3/s)
Nisqually River near National (12082500)	344	1943–2014	22.0	17.0	218	28.6	256
Nisqually River at La Grande (12086500)	756	1907–1910, 1920–1931, 1944–2014	40.8	34.5	[1]204	53.5	[1]309
Centralia Power Canal near McKenna (12089208)	–	1980–2014	[2]15.8	–	–	15.2	[1]20.6
Nisqually River near McKenna (12089500)	1,339	1948–1968, 1978–2014	36.9	–	–	52.3	[1]346
Nisqually River near Yelm (12089970)	1,520	1980–2014[3]	[3]52.7	–	–	[3]67.5	[3]356

[1]Discharge affected by regulation or diversion.

[2]Calculated from available discharge data.

[3]Estimated from the sum of discharge at streamgages 12089208 and 12089500 with consideration for time of travel.

Methods of Data Collection and Analysis

Discharge

A 15-minute time series of discharge, required for calculating suspended-sediment loads, was estimated for the sediment-monitoring site Nisqually River near Yelm (site 12089970) from the summation of instantaneous (15-minute) discharge records at Nisqually River at McKenna (streamgage 12089500; http://waterdata.usgs.gov/nwis/uv?site_no=12089500), 15.8 km upstream of the monitoring site, and Centralia Power Canal near McKenna (streamgage 12089208; http://waterdata.usgs.gov/wa/nwis/uv/?site_no=12089208), 23 km upstream of and where water is diverted from the main Nisqually River into the canal (fig. 1). To account for travel time in discharge between the upstream streamgages and the study site, a mean water velocity of 1.4 m/s was estimated between the streamgages and the study site, and 15-minute discharge records were lagged by 3.25 and 4.5 hours for the records at streamgages 12089500 and 12089208, respectively. To evaluate the accuracy of the estimated record, discharge was measured on site with a tethered boat equipped with an acoustic Doppler current profiler (usually in conjunction with suspended-sediment sample collection) over a range of flow conditions, following methods outlined by Mueller and others (2013). Discharge measurements made on site were compared with the estimated 15-minute discharge record to ensure consistency (table 2) and differences were less than 5 percent.

Suspended Sediment

Suspended-sediment samples were collected at various times over a range of flows at Nisqually River near Yelm (12089970) during water year 2011. The Equal Discharge Increment (EDI) and Equal-Width Increment (EWI) methods (Edwards and Glysson, 1999) were used to collect discrete, cross-section representative samples using depth-integrated, isokinetic samplers (fig. 2*A*) approved by the Federal Interagency Sedimentation Program and used routinely by USGS personnel (Davis, 2005). Additionally, an Isco automated-pump sampler was used to collect daily point samples of suspended sediment. The sampler intake was placed at the edge of the active channel (fig. 2*B*), and the sampler was programmed to collect 200-mL subsamples at 6-hour intervals, which were composited into a single daily 800 mL sample. A cross-section coefficient was used to account for potential bias in sample concentration due to the location of the sampler intake, and computed as the ratio of mean concentration in the cross section (from EDI or EWI samples) to the concentration of pumped samples (Edwards and Glysson, 1999). All samples were analyzed to determine the concentration of suspended sediment and the percentage of sand-size sediment (particles larger than 0.063 mm in size) at the USGS sediment laboratory at the Cascade Volcano Observatory in Vancouver, Washington.

Table 2. Instantaneous discharge measured at U.S. Geological Survey (USGS) sediment-monitoring site (Nisqually River near Yelm, 12089970) in 2010, compared with estimated discharge determined from summation of flows at upstream USGS streamgages (Nisqually River at McKenna, 12089500, and Centralia Power Canal near McKenna, 12089208), Nisqually River Basin, western Washington.

[**Estimated discharge:** Computed as the sum of discharges recorded at Nisqually River near McKenna (12089500) and Centralia Power Canal (12089208), adjusted for travel time. **Abbreviations:** m^3/s, cubic meter per second; m/s, meter per second]

Date	Local time	Discharge (m^3/s)		Percent difference	Measured mean water velocity (m/s)
		Measured	Estimated		
09-10-2010	1200	29.5	29.1	1.4	1.20
09-29-2010	1430	27.6	27.5	0.4	1.13
10-28-2010	1030	46.2	46.2	0.0	1.34
11-10-2010	1115	48.1	46.9	2.6	1.32
11-24-2010	0930	80.8	77.0	4.9	1.42
12-09-2010	0930	98.7	98.4	0.3	1.54
12-14-2010	1300	129	130	-0.8	1.8

Figure 2. Sediment sampling equipment (*A*), sample intake area at edge of active channel (*B*), and turbidity-monitoring installation (*C*), at the U.S. Geological Survey sediment-monitoring site Nisqually River near Yelm (12089970), Nisqually River Basin, western Washington, March 10, 2011. Photographs by Christopher A. Curran, U.S. Geological Survey.

Continuous Turbidity

River turbidity was continuously monitored during most of water year 2011 in which sediment sampling was conducted, with the exception of intermittent periods when instrument failure or excessive fouling occurred, and during a 6-week period in January–February when the instrument was lost during a high-flow event. Turbidity was measured using a YSI-6136 turbidity sensor with an optimal range of 0 to 1,000 Nephelometric Turbidity Units (YSI, Inc., 2007). This sensor was housed in a 2-inch steel pipe suspended over the thalweg of the river in a boom-type mount from the downstream bridge rail (fig. 2*C*). This mounting arrangement allowed turbidity measurements in an actively flowing part of the river channel and decreased the likelihood of debris build-up around the sensor face or on the mounting hardware, which could foul sensor readings. Turbidity data were recorded at 15-minute intervals and the sensor was serviced approximately once per month for downloading data and performing cleaning and calibration checks.

Sediment Load Computation

A daily record of suspended-sediment load at the monitoring site (12089970) was determined for water year 2011 based on the suspended-sediment concentration (SSC) of field samples and the discharge record following methods described by Porterfield (1972) and Koltun and others (2006). For periods when Isco samples were not available, turbidity was used as a surrogate for SSC. A regression was developed between SSC from cross-section samples and concurrently measured turbidity following methods outlined by Rasmussen and others (2009). A 15-minute time series of SSC was computed by applying the regression equation with 15-minute turbidity data and, for consistency with the daily time-step of the Isco sampler, daily mean suspended-sediment concentrations were determined. For periods when neither turbidity data nor pump sampler data were available, SSC was computed from discharge at the sediment-monitoring site (12089970) using a regression equation developed for this purpose.

Suspended Sediment Delivery

Discharge in Water Year 2011

Mean discharge at Nisqually River near National (streamgage 12082500) was 30 percent greater than average (28.6 m^3/s [1,010 ft^3/s]) in water year 2011, and at Nisqually River at La Grande (12086500), mean discharge was 31 percent greater than average (53.5 m^3/s [1,890 ft^3/s]). Farther downstream at Nisqually River at McKenna (streamgage 12089500), which includes discharge from Mashel and Ohop Creeks, mean discharge was 42 percent greater than average (52.3 m^3/s [1,850 ft^3/s]) in water year 2011 and, for water diverted around the McKenna streamgage through the Centralia Power Canal, it was near average (15.2 m^3/s [537 ft^3/s]). Seasonally, discharge in the Nisqually River upstream and downstream of reservoirs was greater than average for most months in water year 2011, except for February, when discharge was average. Discharge was substantially greater in January (+58–83 percent) and during the typical spring freshet period of April–June (+18–96 percent; fig. 3).

Examination of the hydrographs of daily mean discharge for all Nisqually River streamgages and the sediment-monitoring site in water year 2011, as shown in figure 4, indicates typical seasonal patterns of precipitation-induced discharge peaks and flow regulation (storage and release) from reservoir operations. Regulation of peak discharge was minimal during December and January storms, but for the rest of the year, peak discharges were moderated and did not occur downstream because of water storage behind dams. Discharge recorded at the McKenna streamgage (12089500) was greater than at the La Grande streamgage (12086500), particularly peak discharges, and represents contributions from Ohop and Mashel Creeks. The hydrograph for Nisqually River near Yelm (12089970) is estimated as the sum of daily mean discharges recorded at the McKenna and Centralia Canal streamgages.

In water year 2011, the instantaneous (15-minute) peak discharge at all streamgages in the Nisqually River Basin occurred on January 16, and at the McKenna streamgage (12089500), the instantaneous peak discharge was 346 m^3/s (12,200 ft^3/s) and the corresponding maximum daily mean discharge was 306 m^3/s (10,800 ft^3/s). Although affected by flow regulation, the peak discharge at the McKenna streamgage (12089500) in water year 2011 has occurred on average about once every 2.3 years, as determined from USGS software PEAKFQ (Veilleux and others, 2014) and based on 58 years of record (1948–68, 1978–2014). On average, daily mean discharge at the McKenna streamgage has equaled or exceeded 190 m^3/s (6,700 ft^3/s) three times per water year. In water year 2011, this discharge was exceeded for only 2 days (January17, 2011, for daily discharges of 306 m^3/s [10,800 ft^3/s] and 267 m^3/s [9,430 ft^3/s], respectively), suggesting that in terms of the frequency, the number of substantial discharge events was less than average in water year 2011 (fig. 5).

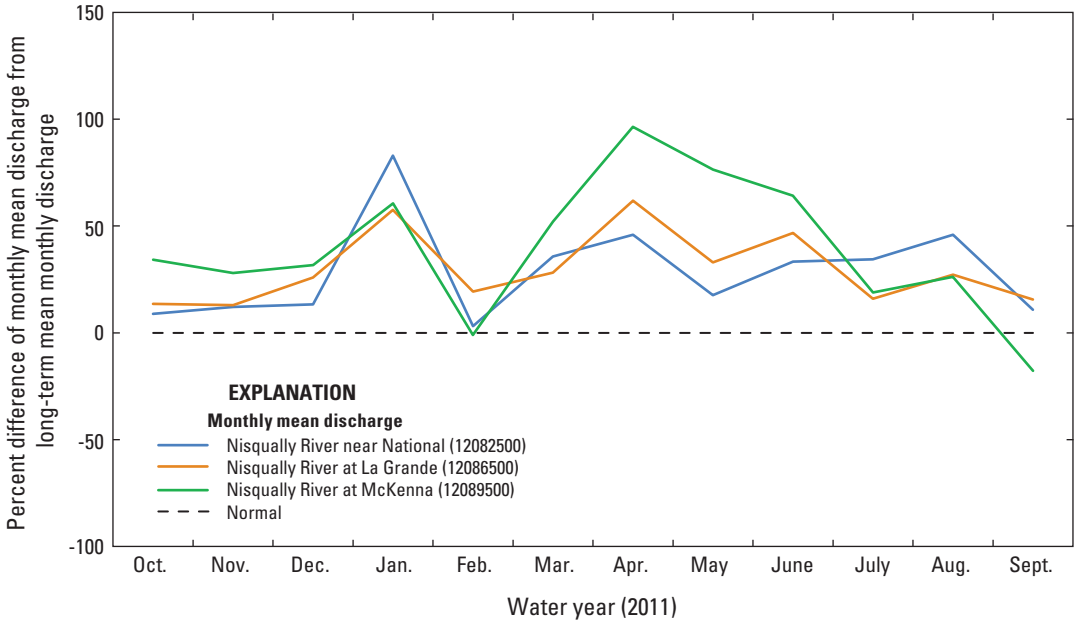

Figure 3. Monthly mean discharges at U.S. Geological Survey streamgages in water year 2011 relative to long-term mean monthly discharges for each streamgage, Nisqually River Basin, western Washington.

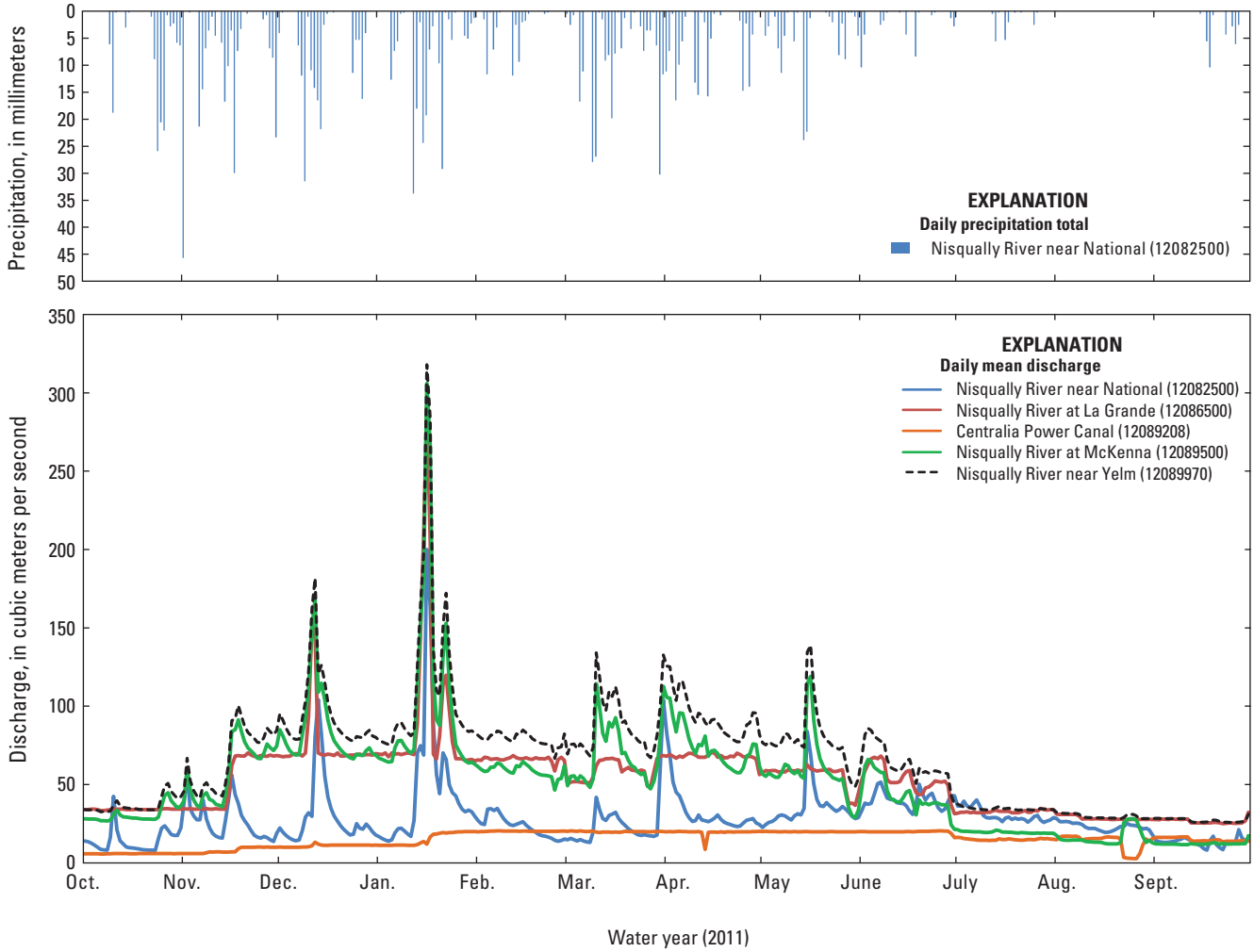

Figure 4. Daily precipitation at U.S. Geological Survey streamgage Nisqually River near National (12082500) and daily mean discharge of the Nisqually River at U.S. Geological Survey streamgages 12082500, 12086500, 12089208, and 12089500, and daily mean discharge estimated at sediment-monitoring site 12089970, Nisqually River Basin, western Washington, water year 2011.

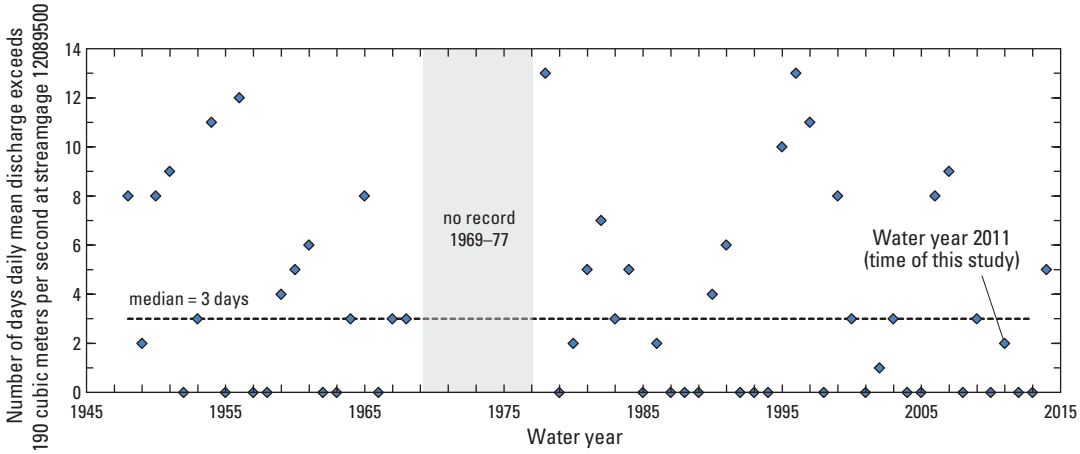

Figure 5. Number of times daily mean discharge exceeded 190 cubic meters per second in a water year (October 1–September 30) based on 57 years of discharge record (1943–68, 1978–2013) at U.S. Geological Survey streamgage Nisqually River at McKenna (12089500), Nisqually River Basin, western Washington.

Turbidity

Although continuous 15-minute turbidity data were recorded for more than 76 percent of the study period (36,175 of 47,448 times), extended time gaps (as much as 38 days) occurred because of sensor fouling, malfunction or power loss, and equipment loss. A tabulation of daily median turbidity data determined from 15-minute data, as well as periods of missing data, is shown in appendix A. A notable time gap in the turbidity record occurred during January 14–February 21, 2011, when the turbidity sensor was lost during a winter storm; this gap included the occurrence of the annual peak discharge on January 16, 2011. The recorded 15-minute turbidity data are tabulated in appendix B, the average turbidity was 14 Formazin Nephelometric Units (FNUs), and values ranged from 0.6 to 320 FNUs.

Suspended Sediment Load in Water Year 2011

From August 24, 2010, to September 30, 2011, suspended-sediment concentrations were obtained from 16 cross-section representative samples collected using EDI or EWI sampling methods and from 167 point samples using an Isco sampler. The EDI and EWI samples were paired with concurrently recorded turbidity (when available), and a regression model was developed for estimating suspended-sediment concentration from turbidity (fig. 6). Daily suspended-sediment concentrations were computed at USGS sediment-monitoring site Nisqually River near Yelm (12089970) during July 25, 2010–November 30, 2011 (fig. 7*C*) based on a combination of daily Isco samples (fig. 7*B*) and the continuous turbidity record when daily Isco samples were not available. Isco sample SSCs were 1.4 to 4.4 times higher than concurrent EDI/EWI samples and this bias, caused by the location of the sampler intake in the cross-section, decreased with increasing SSC and discharge. In lieu of a single cross-section correction factor, a linear regression (appendix C) relating the SSC of Isco samples to concurrent EWI samples was used to correct for bias in Isco sample SSC. For days when neither Isco sample data nor turbidity data were available, SSC was estimated from discharge (appendix D); during the water year 2011, this occurred on 29 days: October 1–8, 2010, February 8–9, March 6-7, June 26, 29, July 2, August 2–3 September 5, 2011.

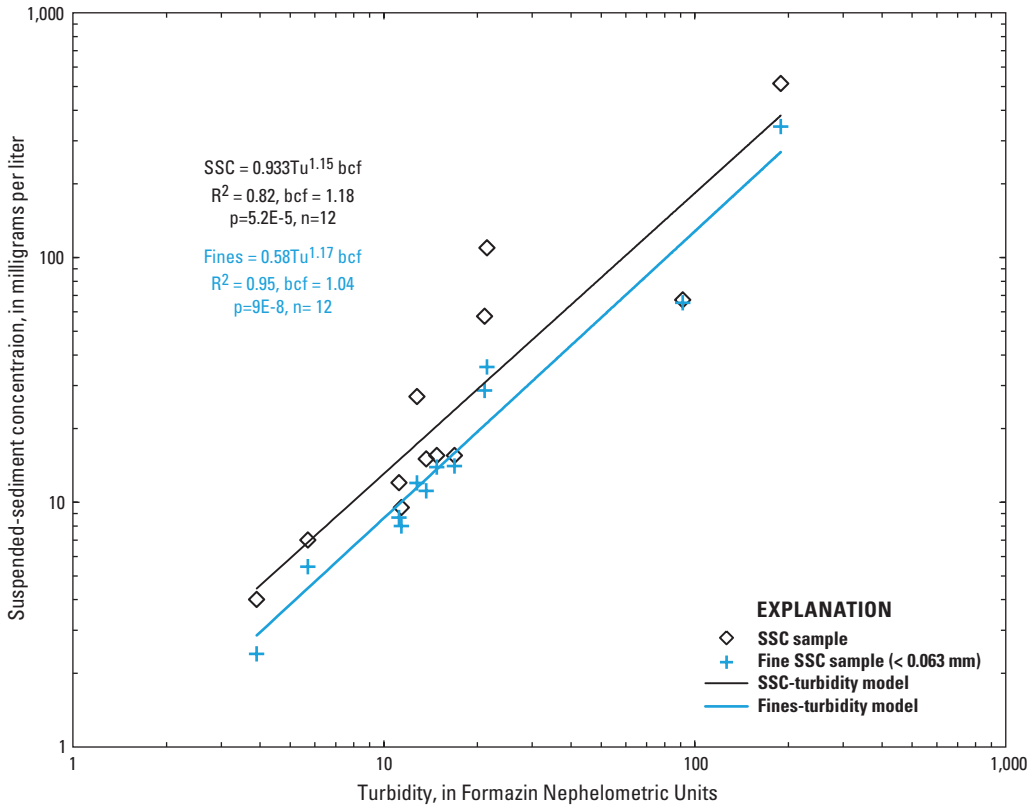

Figure 6. Regression models for estimating suspended-sediment concentration (SSC) and fine suspended-sediment concentration (fines, size less than 0.063 millimeters) from turbidity (YSI-6136 turbidity sensor) at the Nisqually River near Yelm (site 12089970), western Washington.

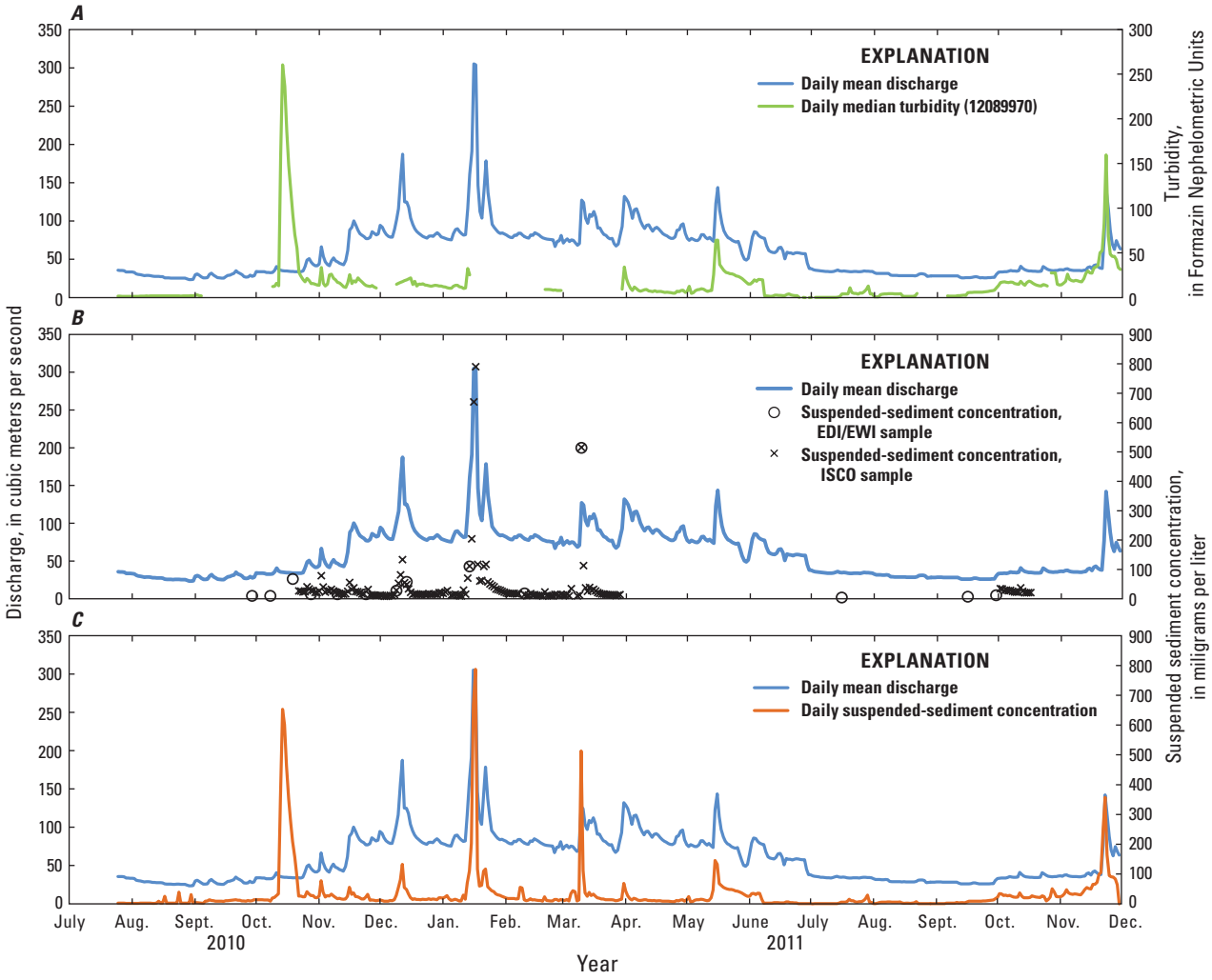

Figure 7. Daily suspended-sediment concentrations as determined from field samples and continuous turbidity, and discharge at Nisqually River near Yelm (site 12089970), western Washington, August 1, 2010–November 30, 2011.

The daily SSC for the monitoring period ranged from 1 to 787 mg/L; the average daily SSC was 33 mg/L and the median daily SSC was 13 mg/L. The maximum daily SSC was derived from Isco samples collected during a winter storm on January 17, 2011, for which the daily suspended-sediment load was 20,700 t. From October 13 to 19, 2010, a turbidity event occurred during seasonally low flows and is attributed to the release of turbid water from Alder Reservoir to maintain instream flows; the maximum daily SSC for this period was 651 mg/L on October 14, 2010. The suspended-sediment concentrations for discrete samples collected using the EDI or EWI methods are shown in table 3.

Daily suspended-sediment loads computed at sediment-monitoring site (Nisqually River near Yelm,12089970) for water year 2011 are shown in figure 8. The computed annual load of 104,000 t does not include the contribution from Muck Creek. Suspended-sediment load for Muck Creek is estimated at 2,000 t in water year 2011 based on the previous calculation by Nelson (1974) of 1,500 t/yr and a discharge weighting factor of 1.3 (to reflect the observed 30 percent greater than normal discharge) for the water year 2011. Thus, total suspended-sediment delivery from Nisqually River to Puget Sound for water year 2011 is 106,000 t. Of this suspended-sediment load, 36 percent (38,300 t) was generated in 2 days (January 16–17) during a typical winter storm. Of the total suspended-sediment load calculated for the water year 2011, 47 percent was sand (particle size >0.063 mm) and the remainder (53 percent) was silt and clay.

Table 3. Suspended-sediment sample data from cross-section representative samples collected at USGS sediment-monitoring site (Nisqually River near Yelm, 12089970), western Washington, 2010–11.

[**Discharge:** Computed as the sum of discharges recorded at Nisqually River at McKenna (12089500) and Centralia Power Canal (12089208), adjusted for travel time. **Abbreviations:** mg/L, milligram per liter; mm, millimeter; m^3/s, cubic meter per second; FNU, Formazin Nephelometric Unit; <less than; –, unavailable]

Date	Local time	Suspended-sediment concentration (mg/L)	Percentage of fines (<0.0625 mm)	Discharge (m^3/s)	Suspended-sediment load (metric tons per day)	Turbidity (FNU)
08-24-2010	1515	2	–	25.6	4	–
09-10-2010	0945	6	68	29.3	15	–
09-29-2010	1515	10	90	27.4	24	–
10-08-2010	1345	10	84	32.7	31	11.4
10-19-2010	1230	67	97	34.0	191	91.6
10-28-2010	1215	16	90	45.3	63	14.8
11-10-2010	1245	16	91	46.6	60	16.9
11-24-2010	1045	15	74	76.2	92	13.7
12-09-2010	1015	27	44	102	230	12.8
12-14-2010	1345	58	50	129	646	21.1
01-14-2011	1030	110	33	154	1,490	21.5
02-10-2011	1015	18	42	76.6	119	–
03-10-2011	1445	514	67	159	6,930	189
07-16-2011	1030	4	–	34.6	12	3.9
09-16-2011	0915	7	78	25.9	16	5.7
09-30-2011	1145	12	72	30.2	31	11.2

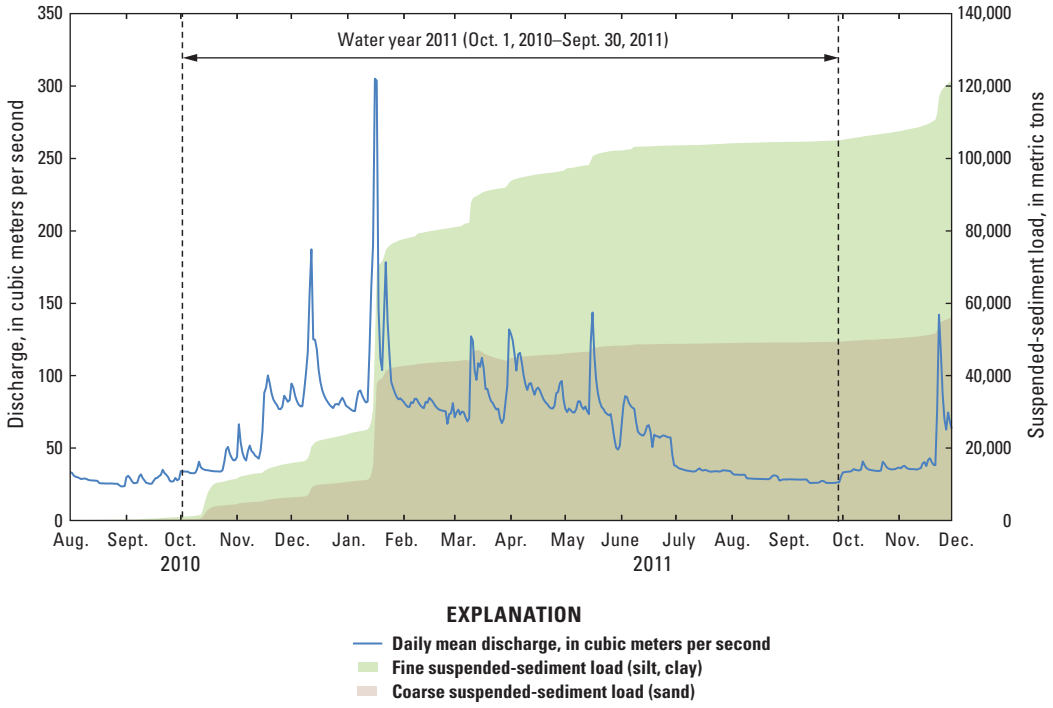

Figure 8. Discharge and cumulative suspended-sediment load calculated for sediment-monitoring site (Nisqually River near Yelm, 12089970), western Washington, water year 2011.

Comparison with Previous Estimates of Suspended-Sediment Load

The concentrations of EDI and EWI samples collected in this study (table 3) were used with concurrently measured or estimated discharge to develop by regression a sediment-rating curve for estimating suspended-sediment load as a function of discharge. A similar curve was developed using suspended-sediment concentrations and discharges reported graphically by Nelson (1974) and shown in table 4. Because regression models defining each curve were similar, the data were combined to develop a single sediment-rating curve (fig. 9) for the purpose of estimating suspended-sediment load at the sediment-monitoring site (Nisqually River near Yelm, 12089970). The model that defines the sediment-rating curve is:

$$L_s = 0.00199Q^{2.68}bcf \quad (1)$$

where

L_s is the suspended-sediment load in metric tons per day (t/d), and

Q is the discharge in cubic meters per second, and *bcf* is the bias correction factor equal to 1.17.

The coefficient of determination for the model (R^2) is 0.85, the p-value is 6.7E-13, and the number of observations is 30. Bias correction for the model output, required as a result of log-transforming regression variables and model uncertainty (Helsel and Hirsch, 1992; Rasmussen and others, 2009) was calculated using a parametric method (Ferguson, 1986) described in Helsel and Hirsch (1992).

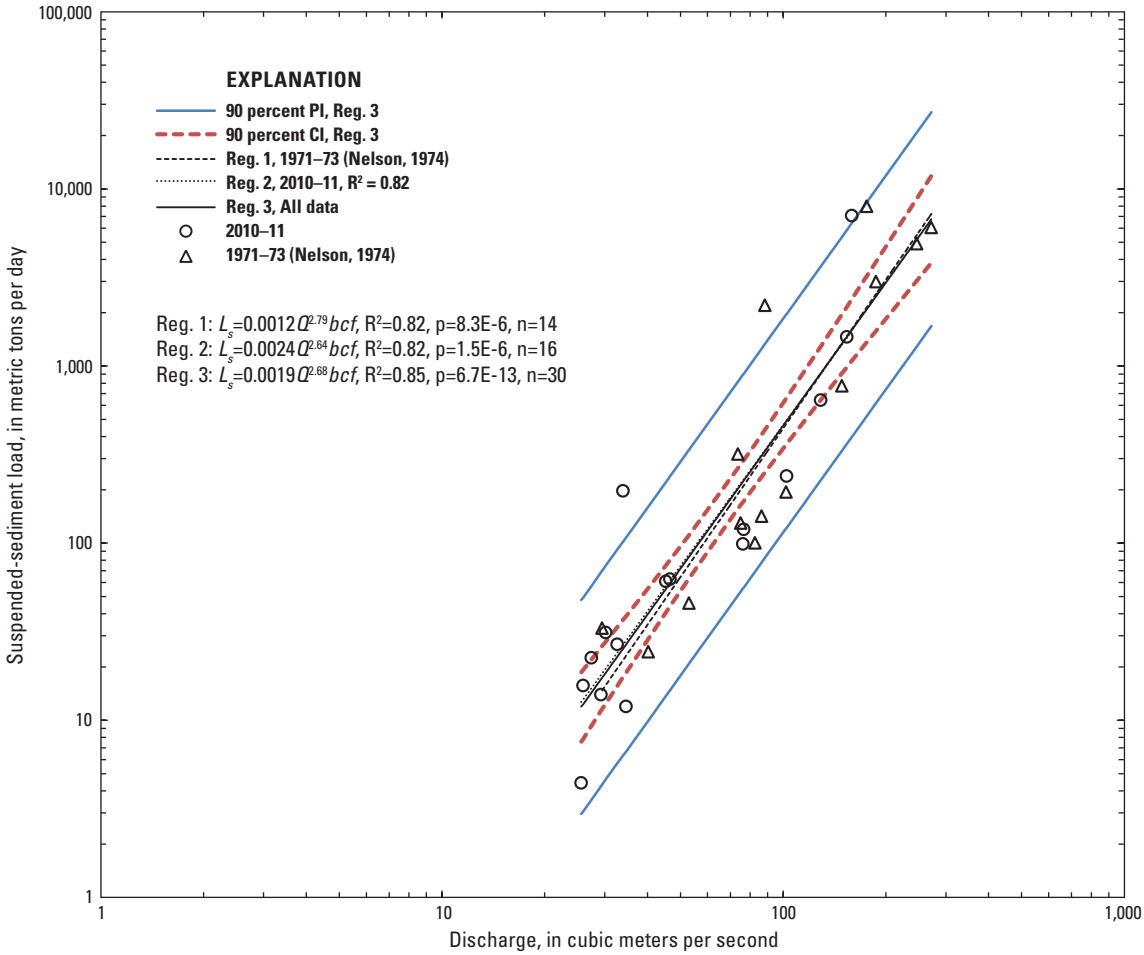

Figure 9. Regression model for estimating suspended-sediment load (L_s) from river discharge (Q) at sediment-monitoring site (Nisqually River near Yelm, 12089970), western Washington. Model was based on combined sediment data from this study and Nelson (1974) (Reg., regression model; PI, prediction interval for individual estimates; CI, confidence interval for the regression mean; *bcf*, bias-correction factor equal to 1.17; R^2, coefficient of determination; p, p-value; n, number of observations).

Table 4. Suspended-sediment concentrations and discharges reported by Nelson (1974) for samples collected at the Nisqually River near Nisqually, Washington, 1971–73, and computed suspended-sediment load used in developing a sediment-rating curve.

[**Abbreviations:** mg/L, milligram per liter; m^3/s, cubic meter per second; t, metric ton]

Sample No.	Suspended-sediment concentration (mg/L)	Water discharge (m^3/s)	Suspended-sediment load per day (t)
1	534	176	8,120
2	288	88.4	2,200
3	257	272	6,040
4	230	246	4,900
5	185	187	2,990
6	60	149	771
7	50	73.7	318
8	22	102	194
9	20	75.1	130
10	19	86.4	142
11	14	82.7	100
12	13	29.5	33
13	10	53.0	46
14	7	40.2	24

Using the combined sediment-rating curve (n=30) for the sediment-monitoring site (Nisqually River at Yelm, 12089970) and an estimated annual suspended-sediment contribution of 1,500 t from Muck Creek, average annual suspended-sediment load delivered by the lower Nisqually River to Puget Sound is estimated at 99,000 t/yr, with an uncertainty range of -37 to +54 percent (62,000–152,000 t/yr) at 90 percent confidence. This estimate is based on the combined record of daily discharges from water years 1980–2014 at McKenna (12089500) and the Centralia Power Canal (12089208) when discharges at both streamgages were reported (fig. 10; http://waterdata.usgs.gov/wa/nwis/sw). For comparison, the sediment-rating curve applied in water year 2011 resulted in an annual sediment load of 119,000 t, or 14 percent more than the load derived from the combined turbidity and Isco sample data in water year 2011.

The maximum annual suspended-sediment load for water years1980–2014 was estimated at 580,000 t for water year 1996, and the maximum 2-day total for this year was 250,000 t. The median annual load of 73,000 t is substantially less than the average (99,000 t), and the correlation (Pearson's $r = 0.80$, $p = 8.1E\text{-}9$, $n = 35$) between annual maximum 2-day sediment loads and normalized peak discharges for the period (water years 1980–2014; fig. 10) indicates the importance of wet years and associated peak discharges of the lower Nisqually River for sediment delivery to Puget Sound.

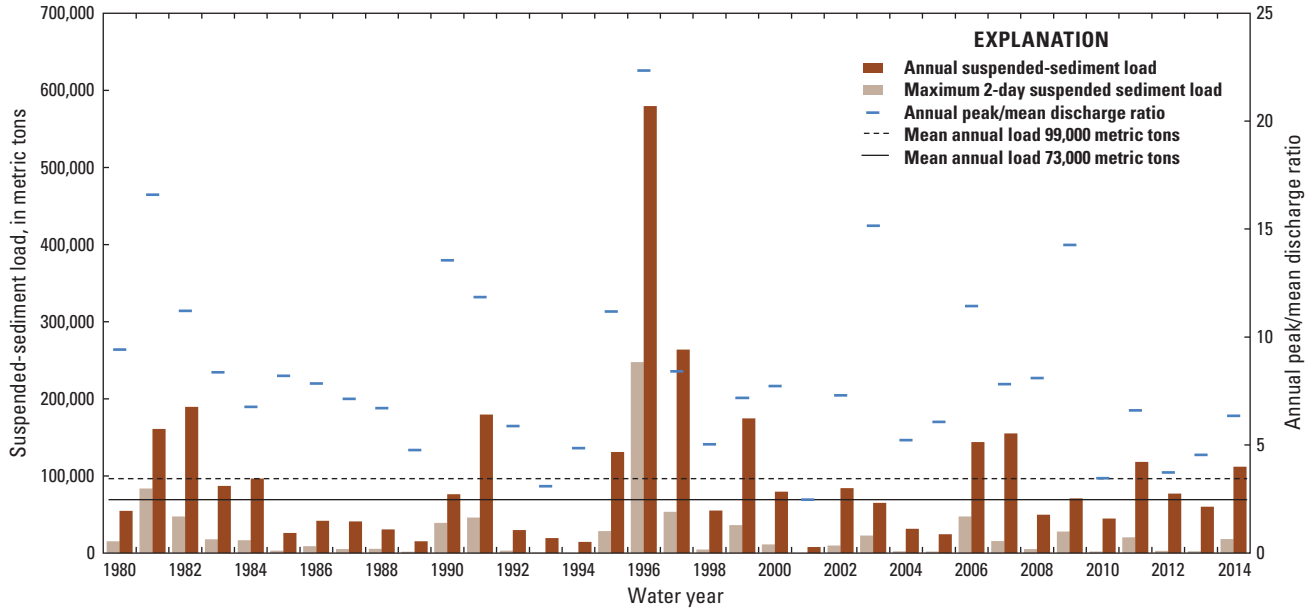

Figure 10. Annual and maximum 2-day totals of suspended-sediment load at sediment-monitoring site Nisqually River near Yelm (12089970), and the ratio of annual peak discharge to annual mean discharge at streamgage Nisqually River at McKenna (12089500), western Washington, water years 1980–2014.

Summary

This report documents the timing and quantity of suspended-sediment load delivered by the Nisqually River to Puget Sound in water year 2011 (October 1, 2010–September 30, 2011), for use in conjunction with nearshore circulation models to assess the sedimentation potential and efficacy of restoration efforts in the Nisqually River Delta. For water year 2011, daily sediment and continuous turbidity data were used to determine that 106,000 metric tons (t) of suspended sediment was delivered to Puget Sound (104,000 t at Nisqually River near Yelm, Washington, and an estimated 2,000 t from Muck Creek), and 36 percent of this load occurred in 2 days of a typical winter storm. Mean discharge in the Nisqually River upstream and downstream of reservoirs was about 30 percent greater than average, and monthly mean discharge was greater than average for all months except February, which was average. The magnitude of peak discharges in the lower Nisqually River generally is dampened by flow regulation and reservoirs, which trap sediment. Of the total suspended-sediment load delivered to Puget Sound in water year 2011, 47 percent was sand (particle size >0.063 millimeters), and the remainder (53 percent) was silt and clay. A sediment-transport curve developed from suspended-sediment samples collected during 2010–11 agreed closely with a curve derived in 1973 using similar data-collection methods, indicating that similar sediment-transport conditions exist. Using the transport curve, the mean annual suspended-sediment load delivered by the lower Nisqually River near Yelm to Puget Sound is estimated at 99,000 t/yr (-37 to +54 percent at 90 percent confidence) for water years 1980–2014. The sediment-transport curve applied to daily discharge in water year 2011 resulted in an annual suspended-sediment load that was 14 percent greater than the load determined using a combined turbidity and Isco sampler approach. The median annual suspended-sediment load of 73,000 t is substantially less than the average load (99,000 t), and the correlation (Pearson's $r = 0.80$, $p = 8.1E\text{-}9$, $n = 35$) between annual maximum 2-day sediment loads and normalized peak discharges for the period indicates the importance of wet years and associated peak discharges of the lower Nisqually River for sediment delivery to Puget Sound.

Acknowledgments

This study was supported by the USGS Coastal Habitats in Puget Sound Large River Deltas Project. We acknowledge the efforts of Steve Sumioka, Karen Payne, Greg Justin, Mathieu Marineau, and Mark Mastin of the USGS Washington Water Science Center for field assistance.

References Cited

Booth, D.B., 1994, Glaciofluvial infilling and scour of the Puget lowlands, Washington, during ice-sheet glaciation: Geology, v. 22, no. 8, p. 695–698.

Cereghino, P., Toft, J., Simenstad, C., Iverson, E., Campbell, S., Behrens, C., and Burke, J., 2012, Strategies for nearshore protection and restoration in Puget Sound: Washington Department of Fish and Wildlife, Olympia, Washington, and U.S. Army Corps of Engineers, Seattle, Washington, Puget Sound Nearshore Report No. 2012-01.

Collins, B.D., and Montgomery, D.R., 2011, The legacy of Pleistocene glaciation and the organization of lowland alluvial process domains in the Puget Sound region: Geomorphology, v. 126, nos. 1–2, p. 174–185, accessed June 4, 2013, at doi:10.1016/j.geomorph.2010.11.002.

Collins, B.D., Montgomery, D.R., Fetherston, K.L., and Abbe, T.B., 2012, The floodplain large-wood cycle hypothesis—A mechanism for the physical and biotic structuring of temperate forested alluvial valleys in the North Pacific coastal ecoregion: Geomorphology, v. 139–140, no. 0, p. 460–470, doi:10.1016/j.geomorph.2011.11.011.

Crandell, D.R., 1971, Postglacial lahars from Mount Rainier volcano, Washington: U.S. Geological Survey Professional Paper 677, 75 p. (Also available at http://pubs.er.usgs.gov/publication/pp677.)

Czuba, J.A., Magirl, C.S., Czuba, C.R., Grossman, E.E., Curran, C.A., Gendaszek, A.S., and Dinicola, R.S., 2011, Sediment load from major rivers into Puget Sound and its adjacent waters: U.S. Geological Survey Fact Sheet, 2011-3083, 4 p.

Czuba, J.A., Olsen, T.D., Czuba, C.R., Magirl, C.S., and Gish, C.C., 2012a. Changes in sediment volume in Alder Lake, Nisqually River Basin, Washington, 1945–2011: U.S. Geological Survey Open-File Report 2012-1068, 30 p.

Czuba, J.A., Magirl, C.S., Czuba, C.R., Curran, C.A., Johnson, K.H., Olsen, T.D., Kimball, H.K., and Gish, C.C., 2012b, Geomorphic analysis of the river response to sedimentation downstream of Mount Rainier, Washington: U.S. Geological Survey Open-File Report 2012-1242, 134 p. (Also available at http://pubs.usgs.gov/of/2012/1242/.)

Davis, B.E., 2005, A guide to the proper selection and use of federally approved sediment and water-quality samplers: U.S. Geological Survey Open-File Report 2005-1087, 26 p.

Edwards, T.K., and Glysson, D.G., 1999, Field methods for measurement of fluvial sediment: U.S. Geological Survey Techniques of Water-Resources Investigations, book 3, chap. C2, 89 p.

Ferguson, R.I., 1986, River loads underestimated by rating curves: Water Resources Research, v. 22, no. 1, p. 74–76.

Helsel, D.R., and Hirsch, R.M., 1992, Statistical methods in water resources: New York, Elsevier, 522 p.

Koltun, G.F., Eberle, M., Gray, J.R., and Glysson, D.G., 2006, User's manual for the Graphical Constituent Loading Analysis System (GCLAS): U.S. Geological Survey Techniques and Methods, book 4, chap. C1, 51 p.

Mueller, D.S., Wagner, C.R., Rehmel, M.S., Oberg, K.A., and Rainville, Francois, 2013, Measuring discharge with acoustic Doppler current profilers from a moving boat (ver. 2.0, December 2013): U.S. Geological Survey Techniques and Methods, book 3, chap. A22, 95 p., http://dx.doi.org/10.3133/tm3A22.

National Oceanic and Atmospheric Administration, 2010, Climate of Washington: National Oceanic and Atmospheric Administration Western Regional Climate Center Web site, accessed August 24, 2012, at http://www.wrcc.dri.edu/narratives/WASHINGTON.htm.

Neiman, P.J., Schick, L.J., Ralph, F.M., Hughes, M., and Wick, G.A., 2011, Flooding in western Washington—The connection to atmospheric rivers: Journal of Hydrometeorology v. 12, p. 1,337–1,358, doi:10.1175/2011JHM1358.1.

Nelson, L.M., 1974, Sediment transport by streams in the Deschutes and Nisqually River Basins, Washington, November 1971–June 1973: U.S. Geological Survey Open-File Report 74-1078, 33 p.

Porter, S.C., and Swanson, T.W., 1998, Radiocarbon age constraints on rates of advance and retreat of the Puget lobe of the Cordilleran Ice Sheet during the last glaciation: Quaternary Research, v. 50, no. 3, p. 205–213.

Porterfield, G., 1972, Computation of fluvial-sediment discharge: U.S. Geological Survey Techniques of Water-Resource Investigations, book 3, chap. C3, 66 p.

Rasmussen, P.P., Gray, J.R., Glysson, G.D., and Ziegler, A.C., 2009, Guidelines and procedures for computing time-series suspended-sediment concentrations and loads from in-stream turbidity-sensor and streamflow data: U.S. Geological Survey Techniques and Methods, book 3, chap. C4, 53 p.

Scott, K.M., Vallance, J.W., and Pringle, P.T., 1995, Sedimentology, behavior, and hazards of debris flows at Mount Rainier, Washington: U.S. Geological Survey Professional Paper 1547, 56 p. (Also available at http://pubs.er.usgs.gov/publication/pp1547.)

Sisson, T.W., and Vallance, J.W., 2008, Frequent eruptions of Mount Rainier over the last ~2,600 years: Bulletin of Volcanology, v. 71, no. 6, p. 595–681, doi:10.1007/s00445-008-0245-7.

U.S. Fish and Wildlife Service, 2010, Estuary restoration—The return of the Nisqually Delta: U.S. Fish and Wildlife Service brochure, 2 p., accessed May 10, 2013, at http://nisquallydeltarestoration.org/pdf/Est_Rest_BroOct.10.pdf.

Veilleux, A.G., Cohn, T.A., Flynn, K.M., Mason, R.R., Jr., and Hummel, P.R., 2014, Estimating magnitude and frequency of floods using the PeakFQ 7.0 program: U.S. Geological Survey Fact Sheet 2013–3108, 2 p., accessed March 10, 2014, at http://dx.doi.org/10.3133/fs20133108.

YSI Incorporated, 2007, E56-6136-Turbidity-sensor, technical specification sheet: YSI Incorporated Web site, accessed May 5, 2011, at http://www.ysi.com/accessoriesdetail.php?6136-Turbidity-Sensor-6-Series-94.

This page intentionally left blank.

Appendixes

Appendixes A–D are Microsoft® Excel files and are available for download at http://dx.doi.org/10.3133/sir20165062.

Appendix A. Daily Suspended-Sediment Concentrations and Loads at Nisqually River near Yelm, Washington (USGS Sediment Monitoring Site 12089970), July 25, 2010–November 30, 2011.

Appendix B. Continuous 15-Minute Turbidity Data at Nisqually River near Yelm, Washington (USGS Sediment Monitoring Site 12089970), July 25, 2010–November 30, 2011.

Appendix C. Data and Equations Used for Applying a Cross-Section Correction to Suspended-Sediment Concentrations of Isco Pump Samples.

Appendix D. Regression Model Used for Estimating Suspended-Sediment Concentration from Discharge.

Publishing support provided by the U.S. Geological Survey
Science Publishing Network, Tacoma Publishing Service Center

For more information concerning the research in this report, contact the
Director, Washington Water Science Center
U.S. Geological Survey
934 Broadway, Suite 300
Tacoma, Washington 98402
http://wa.water.usgs.gov

USGS

Curran and others—**Suspended Sediment Delivery to Puget Sound from the Lower Nisqually River, July 2010–November 2011**—Scientific Investigations Report 2016–5062

ISSN 2328-0328 (online)
http://dx.doi.org/10.3133/sir20165062

Assessment of erosion, sedimentation, and water quality impacts of the Mountain Valley Pipeline and Equitrans Expansion Project's proposed crossing of the Jefferson National Forest as it pertains to the U.S. Forest Service's Draft Supplemental Environmental Impact Statement dated December 2022

Prepared by Jonathan A. Czuba, Ph.D., Licensed Professional Engineer - February 9, 2023

REFERENCES
22

February 21, 2023

Major Groundwater Flow Directions in the Sinking Creek and Meadow Creek Drainage Basins of Giles and Craig Counties, Virginia, USA

Joseph W. Saunders, R. Keith Ortiz, and William F. Koerschner, III
3207 Melody Lane, Lansing, Michigan 48912

Abstract

Groundwater tracing with fluorescein dye has determined the resurgence points for underground drainage from ten sinking streams in a compound anticlinal carbonate valley in the Virginia mountains (eastern US). Springs of five of six underground drainage basins are involved in distributary flow patterns, with co-resurgences located from 100 to 2000 m apart and all but one co-resurgence pair operating only in higher flow stages. The fluorescein tracing indicated that the surface and subsurface drainage divides roughly coincided where the eastern continental divide crossed the valley, despite the headward growth of the Atlantic Ocean drainage at the expense of the Mexican Gulf drainage.

Zusammenfassung

Die mit Fluoresceinfarbstoff Grundwasserausspürung hat in einem zusammengesetzten kalksteinenen Anticlintal den Gebirgen Virginias (östliche US) den Brunnen der von zehn sinkenden Bächen unterirdischen Entwässerung versetzt. Aus die Brunnen sechs unterirdischen Einzugsgebieten schliessen sich fünf in Austeilungsfliessanlagen. Die Ko-austeilungsbrunnen stellen sich 100 bis zu 2000 m entfernt. Bis auf eins Ko-austeilungsbrunnenpaare verbinden such nur bei den höheren Fliess-ständen. Die Farbstoffausspürung deutet an, dass die oberflächlichen und unterirdischen Wasserscheide ungefähr zusammentreffen, wo die östliche Kontinental-wasserscheide das Tal durchschneidet. Wegen der von Atlantikentwässerung talaufwärts Erweiterung bewegen die Wasserscheide westlich auf Kosten vom Golf von Mexiko schon fort.

Introduction

In the central Appalachian mountains of the eastern United States, two of the major structural settings in which karst has developed are the long mountains and the anticlinal valleys. Both settings are characterized by topographic orientations along the trends of regional folding and faulting. Anticlinal valleys where narrow are typically floored with limestone or dolomite, whereas underlying clastic units commonly have been exposed in the wider anticlinal valleys, leaving the carbonates in strips on either side of the valley. Most of the anticlinal valleys maintain a relatively uniform width, and several terminate in distinct valley heads where the carbonates or underlying clastics on the floor plunge beneath the sandstones with typically form the rims of the valleys. Where faults are found on the valley floor, they are usually associated with crosssectional asymmetry of the valley.

The two anticlinal valleys studied here contain two major surface streams. Meadow Creek leaves the eastern valley head through a gap after rising at two large springs nearby. Westward flowing Sinking Creek heads at a spring complex 10 km from the end of the eastern valley, which has been made somewhat asymmetric by the Saltville Fault that enters the western end of the valley near Newport and runs the entire length of the valley. North of Newport, Sinking Creek crosses the fault complex and flows northward into a second valley. Clover Hollow at the eastern end of this second valley has a simple anticlinal structure. Westward to the New River the valley is wider with more complex structure.

Stratigraphically, both valleys are rimmed with Silurian sandstones. Cambro-Ordovician dolomites form the central floor of Clover Hollow and the eastern valley, with Ordovician limestones on the floor and lower slopes on either side of the dolomitic core. The dolomite is more resistant to weathering and tends to form a central ridge down the middle of Clover Hollow and the eastern valley, bordered on both sides by parallel talwegs on limestone. Westward from Clover Hollow both the valley and the limestone exposures on either side of the dolomitic core widen.

Surface drainage in the two valleys consists of small mountainside streams and the two master streams Sinking Creek and Meadow Creek. Most if not all mountainside streams heading near the rims of the valleys sink upon encountering the limestone. Flow from some of these sinking streams resurfaces at springs along Sinking Creek or Meadow Creek, with flow from the remainder resurging at either of the two rises of Meadow Creek or along the New River. Both Sinking Creek and Meadow Creek sink completely for much of the year.

Methodology

Sodium fluorescein in quantities of ½ to 8 kg was applied to sinking streams in the period 1974-1978. Fresh activated charcoal granules contained in 5 cm square staple-bound envelopes of nylon screening was used to absorb the fluorescein. Elution was accomplished with 10% KOH in 95% ethanol, with an ultraviolet lamp used to aid in visualization if necessary. With few exceptions, the charcoal traps were collected only once from each location for each test. Duplicate traps were usually placed in diferent spots at each spring to minimize risk of theft or chance contamination.

Results of Water Tracing and Descriptions of Major Groundwater Basins

Thirteen fluorescein dye tests were made from eleven locations in the two valleys to a total of ten springs from the New River in the west to the Meadow Creek Gap in the east. The sink-to-spring straight lines shown on the map (Figure 1) indicate that multiple outlets for groundwater are not unusual in the structural settings encountered there. Four of the six major groundwater systems studied discharge from more than one outlet.

Meadow Creek Drainage

Meadow Creek waters reach the Roanoke River and the Atlantic Ocean after leaving the anticlinal valley at Meadow Creek Gap. The eastern anticlinal valley is actually a hanging valley, surrounded on both sides by Atlantic-bound streams at 400-450 m elevation, which is at least 150 m below the lowest elevation in the anticlinal valley. Meadow Creek rises at two large springs near the gap through the sandstone rim. Local base level in the eastern end of the anticlinal valley, as well as the elevation of the springs, is determined by the elevation at which Meadow Creek spills over the lowest point of the rim. Meadow Creek has no doubt, grown immensely from a small mountainside stream on the outer rim wall of the anticlinal valley to a major karst-headed stream by the continuing process of headward drainage caputre to the west. Fractures in the valley head associated with the anticlinal plunge provided the weaknesses needed by the early mountainside predecessor of Meadow Creek to breach the sandstone rim and initiate piracy of the headwaters of the Gulf of Mexico bound Sinking Creek. Because of the steeper drainage gradient through the Meadow Creek Gap than westward along Sinking Creek to the New River, the Eastern Continental Divide (between the Atlantic Ocean and the Gulf of Mexico) has been moving westward.

Fluorescein dye tracing has established that there are two branches of Meadow Creek, with drainage being roughly divided by the central dolomitic core in the anticlinal valley. The northern branch is predominantly a surface stream fed by several small springs. After a surface route of four kilometers, it sinks in all flow stages into a large closed depression known as the Sinks of Meadow Creek. The north branch of Meadow Creek resurges at Dudding Spring 2 km from the Sinks. A portion of subterranean Meadow Creek can be seen at Cove Cave 500 m west of Dudding Spring. Cove Cave ends downstream in collapse, whereas upstream sumps. Most of the 60 m length of Cove Cave appears to be developed along or near the Saltville Fault. At high flow stages water discharges from the cave entrance. Thus the north branch of Meadow Creek has both a perennial and an intermittent rise.

The south branch of Meadow Creek rises from an im-

Major Groundwater Flow Directions in the Sinking Creek and Meadow Creek Drainage Basins of Giles and Craig Counties, Virginia, USA

Joseph W. Saunders, R. Keith Ortiz, and William F. Koerschner, III
3207 Melody Lane, Lansing, Michigan 48912

Abstract

Groundwater tracing with fluorescein dye has determined the resurgence points for underground drainage from ten sinking streams in a compound anticlinal carbonate valley in the Virginia mountains (eastern US). Springs of five of six underground drainage basins are involved in distributary flow patterns, with co-resurgences located from 100 to 2000 m apart and all hut one co-resurgence pair operating only in higher flow stages. The fluorescein tracing indicated that the surface and subsurface drainage divides roughly coincided where the eastern continental divide crossed the valley, despite the headward growth of the Atlantic Ocean drainage at the expense of the Mexican Gulf drainage.

Zusammenfassung

Die mit Fluoresceinfarbstoff Grundwasserausspürung hat in einem zusammengesetzten kalksteinenen Anticlintal den Gebirgen Virginias (östliche US) den Brunnen der von zehn sinkenden BÄchen unterirdischen Entwässerung versetzt. Aus die Brunnen sechs unterirdischen Einzugsgebieten schliessen sich fünf in Austeilungsfliessanlagen. Die Ko-austeilungsbrunnen stellen sich 100 bis zu 2000 m entfernt. Bis auf eins Ko-austeilungsbrunnenpaare verbinden such nur bei den höheren Fliess-ständen. Die Farbstoffausspürung deutet an, dass die oberflaÄchlichen und unterirdischen Wasserscheide ungefähr zusammentreffen, wo die östliche Kontinental-wasserscheide das Tal durchschneidet. Wegen der von Atlantikentwässerung talaufwärts Erweiterung bewegen die Wasserscheide westlich auf Kosten vom Golf von Mexiko schon fort.

Introduction

In the central Appalachian mountains of the eastern United States, two of the major structural settings in which karst has developed are the long mountains and the anticlinal valleys. Both settings are characterized by topographic orientations along the trends of regional folding and faulting. Anticlinal valleys where narrow are typically floored with limestone or dolomite, whereas underlying clastic units commonly have been exposed in the wider anticlinal valleys, leaving the carbonates in strips on either side of the valley. Most of the anticlinal valleys maintain a relatively uniform width, and several terminate in distinct valley heads where the carbonates or underlying clastics on the floor plunge beneath the sandstones with typically form the rims of the valleys. Where faults are found on the valley floor, they are usually associated with crosssectional asymmetry of the valley.

The two anticlinal valleys studied here contain two major surface streams. Meadow Creek leaves the eastern valley head through a gap after rising at two large springs nearby. Westward flowing Sinking Creek heads at a spring complex 10 km from the end of the eastern valley, which has been made somewhat asymmetric by the Saltville Fault that enters the western end of the valley near Newport and runs the entire length of the valley. North of Newport, Sinking Creek crosses the fault complex and flows northward into a second valley. Clover Hollow at the eastern end of this second valley has a simple anticlinal structure. Westward to the New River the valley is wider with more complex structure.

Stratigraphically, both valleys are rimmed with Silurian sandstones. Cambro-Ordovician dolomites form the central floor of Clover Hollow and the eastern valley, with Ordovician limestones on the floor and lower slopes on either side of the dolomitic core. The dolomite is more resistant to weathering and tends to form a central ridge down the middle of Clover Hollow and the eastern valley, bordered on both sides by parallel talwegs on limestone. Westward from Clover Hollow both the valley and the limestone exposures on either side of the dolomitic core widen.

Surface drainage in the two valleys consists of small mountainside streams and the two master streams Sinking Creek and Meadow Creek. Most if not all mountainside streams heading near the rims of the valleys sink upon encountering the limestone. Flow from some of these sinking streams resurfaces at springs along Sinking Creek or Meadow Creek, with flow from the remainder resurging at either of the two rises of Meadow Creek or along the New River. Both Sinking Creek and Meadow Creek sink completely for much of the year.

Methodology

Sodium fluorescein in quantities of ½ to 8 kg was applied to sinking streams in the period 1974-1978. Fresh activated charcoal granules contained in 5 cm square staple-bound envelopes of nylon screening was used to absorb the fluorescein. Elution was accomplished with 10% KOH in 95% ethanol, with an ultraviolet lamp used to aid in visualization if necessary. With few exceptions, the charcoal traps were collected only once from each location for each test. Duplicate traps were usually placed in different spots at each spring to minimize risk of theft or chance contamination.

Results of Water Tracing and Descriptions of Major Groundwater Basins

Thirteen fluorescein dye tests were made from eleven locations in the two valleys to a total of ten springs from the New River in the west to the Meadow Creek Gap in the east. The sink-to-spring straight lines shown on the map (Figure 1) indicate that multiple outlets for groundwater are not unusual in the structurd settings encountered there. Four of the six major groundwater systems studied discharge from more than one outlet.

Meadow Creek Drainage

Meadow Creek waters reach the Roanoke River and the Atlantic Ocean after leaving the anticlinal valley at Meadow Creek Gap. The eastern anticlinal valley is actually a hanging valley, surrounded on both sides by Atlantic-bound streams at 400-450 m elevation, which is at least 150 m below the lowest elevation in the anticlinal valley. Meadow Creek rises at two large springs near the gap through the sandstone rim. Local base level in the eastern end of the anticlinal valley, as well as the elevation of the springs, is determined by the elevation at which Meadow Creek spills over the lowest point of the rim. Meadow Creek has no doubt, grown immensely from a small mountainside stream on the outer rim wall of the anticlinal valley to a major karst-headed stream by the continuing process of headward drainage caputre to the west. Fractures in the valley head associated with the anticlinal plunge provided the weaknesses needed by the early mountainside predecessor of Meadow Creek to breach the sandstone rim and initiate piracy of the headwaters of the Gulf of Mexico bound Sinking Creek. Because of the steeper drainage gradient through the Meadow Creek Gap than westward along Sinking Creek to the New River, the Eastern Continental Divide (between the Atlantic Ocean and the Gulf of Mexico) has been moving westward.

Fluorescein dye tracing has established that there are two branches of Meadow Creek, with drainage being roughly divided by the central dolomitic core in the anticlinal valley. The northern branch is predominantly a surface stream fed by several small springs. After a surface route of four kilometers, it sinks in all flow stages into a large closed depression known as the Sinks of Meadow Creek. The north branch of Meadow Creek resurges at Dudding Spring 2 km from the Sinks. A portion of subterranean Meadow Creek can be seen at Cove Cave 500 m west of Dudding Spring. Cove Cave ends downstream in collapse, whereas upstream sumps. Most of the 60 m length of Cove Cave appears to be developed along or near the Saltville Fault. At high flow stages water discharges from the cave entrance. Thus the north branch of Meadow Creek has both a perennial and an intermittent rise.

The south branch of Meadow Creek rises from an impounded spring at the fish hatchery. In contrast to the north side of the anticlinal valley, drainage to the fish hatchery spring on the south side is entirely underground, excepting the sinking streams along 9 km of mountainside. Like the resurgences on the north side of the valley, the Fish Hatchery spring is developed in the limestone. It is the only major limestone spring in the study area that does not have a major associate distributary outlet, although there are two small flood outlets located within 30 m. It is likely that the difference in mass wasting which has kept drainage on the south side of the Meadow Creek valley well underground, whereas the surface of the north side of the valley is lower with predominantly surface drainage is due to the much higher dip and the Saltville Fault on the north side.

Head of Sinking Creek

Sinking Creek upstream from Newport is fed by numerous small to moderate sized springs in dolomite and limestone. The creek there is draining land with a low doline density. 1500 m west of the topographic divide with Meadow Creek, Sinking Creek rises at Early Spring on the south side of the valley. In higher flow stages an intermittent spring 100 m away becomes the surface head of Sinking Creek. A fluorescein trace in high flow from a mountainside sinking stream just west of the surface drainage divide tested positive in Early Spring and the intermittent spring, as well as at Slovensky Spring 300 m to the northwest. Considering that a sinking stream just east of the topographic divide had been traced to the fish hatchery spring, it would appear that the Eastern Continental Divide, known locally as "the Alleghenу", coincides approximately with the groundwater divide.

Travertine Spring on Sinking Creek at Saltville Fault Complex near Newport

There is a conspicous travertine deposit 2 m high, 10 m wide and 6 m long associated with a small spring along Sinking Creek where the Saltville Fault complex crosses the creek.

Subterranean Meander Cutoffs at Link's Bend

Dye dropped in Sinking Creek upstream of Link's Bend was detected in charcoal traps in Link Spring on the west (downstream) side of the bend the following day, and was thought to be visible in the spring at dusk forty minutes after the drop. No intake point is visible along the creek bank at the bend, so the waters that reappear at Link Spring after cutting under the neck of the meander must sink into the floor of the creek. There is a 30 m crawlway cave just above creek level on the upstream side of Link'a Bend almost directly upstrike from Link Spring. This small cave probably originated as a meander cutoff, and may still function as such during very high creek levels. To the south and out on the bend is Link's Cave, with about 300 m of passage and major trend along the strike. Link's Cave most likely is an abandoned subterranean meander cutoff route.

Clover Hollow Drainage

Most mountainside drainage in Clover Hollow sinks soon after encountering the limestone; only during very heavy runoff does surface drainage flow directly into Sinking Creek. Dye placed in Clover Hollow Cave and two sinking streams on the north side of Clover Hollow in separate traces was recovered in both Smokehole Spring and Tawney Spring on Sinking Creek, indicating a flow split. A careful examination of the main stream in Smokehole Cave behind the spring revealed a location where the cave stream split, with a major porportion entering a humanly impassable crevice while the remainder continued on out to Smokehole Spring. Subsequent in-cave dye drops from both just upstream and just downstream of the stream fork in Smokehole Cave, with traps at Smokehole Spring and the upstream reaches in Tawney's Cave behind Tawney Spring, indicated that all flow entering the crevice at the stream fork in Smokehole Cave resurged only at Tawney's Cave and Tawney Spring, whereas flow not entering the crevice resurged at Smokehole Spring. Together, these traces indicated that a single flow split existed.

Surveys of Tawney's Cave and Smokehole Cave indicate that the two caves are closely situated and represent major conduits for past and present drainage from Clover Hollow. It is clear that during the evolution of Smokehole Cave flow shifted direction from a westerly strike parallel trend to a southerly trend across the strike to the present Smokehole entrances, leaving large passage abondoned on the west side of the cave.

A dye trace from a sinking stream 1500 m north of the Smokehole-Tawney spring complex indicates that drainage from the far side of the dolomitic core is being transmitted across the strike and through the core rather than along the strike to a more distant spring. The next logical step in a study of the Clover Hollow karst hydrology would be the indentification of cave stream branches corresponding to the traced sinking streams in Clover Hollow, and subsequent analysis of waters from these tributaries of likely contrasting transmission routes.

The Rise of Sinking Creek

For about half the year the entire surface course of Sinking Creek down to the junction with the New River contains flowing water. At the lower flow stages the total flow of the creek is swallowed by several sink oints, the first visible one at a distance of 5 km from the New River. No passable openings are visible along the creek in the vinicity of the sinkpoints.

Despite being one of the largest springs in Virginia, the rise of Sinking Creek on the New River has a noticeably unimpressive appearance. Water discharges from a 30 m stretch of rubble forming part of a railroad embankment at the foot of a cliff.

Besides the trace of Sinking Creek to the rise on the New River, only one other sink point was traced to that rise. The stream sinking into Williams Cave 1500 m northwest of Tawney's Cave was traced in low flow stage to the rise of Sinking Creek only. Two traces in high flow stage, however, were detected both at the Sinking Creek to the New River is one of high doline density with very little flowing water, precluding an easy trace to define the low flow divide between Bell Spring and the rise of Sinking Creek.

Bell Spring Drainage

Doe Run was traced to Bell Spring from an upstream sink point, one of several along the stream course. A considerable portion of the doline field east and south of Doe Run probably drains to Bell Spring as well, aa do areas within a mile of Sinking Creek during high flow stages, as the traces from Williams Cave demonstrated.

Acknowledgements

The authors wish to gratefully acknowledge the financial support of the Resourses Advisory Committee of the National Speleological Society.

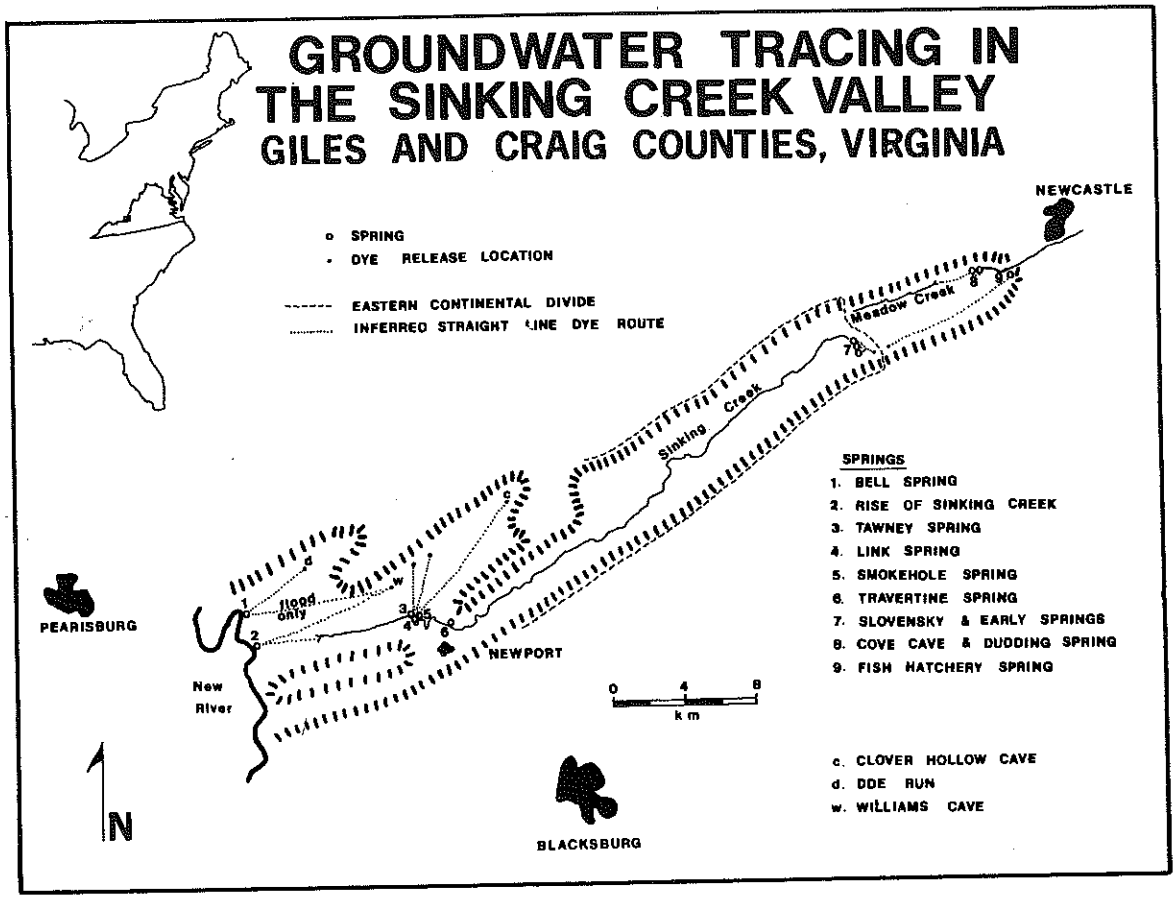
GROUNDWATER TRACING IN
THE SINKING CREEK VALLEY
GILES AND CRAIG COUNTIES, VIRGINIA
o SPRING
• DYE RELEASE LOCATION
EASTERN CONTINENTAL DIVIDE
INFERRED STRAIGHT LINE DYE ROUTE
NEWCASTLE
Meadow Creek
Sinking Creek
SPRINGS
1. BELL SPRING
2. RISE OF SINKING CREEK
3. TAWNEY SPRING
4. LINK SPRING
5. SMOKEHOLE SPRING
6. TRAVERTINE SPRING
7. SLOVENSKY & EARLY SPRINGS
8. COVE CAVE & DUDDING SPRING
9. FISH HATCHERY SPRING
c. CLOVER HOLLOW CAVE
d. DOE RUN
w. WILLIAMS CAVE
flood only
PEARISBURG
NEWPORT
New River
0 4 8
k m
N
BLACKSBURG

"Figure 1"

Assessment of erosion, sedimentation, and water quality impacts of the Mountain Valley Pipeline and Equitrans Expansion Project's proposed crossing of the Jefferson National Forest as it pertains to the U.S. Forest Service's Draft Supplemental Environmental Impact Statement dated December 2022

Prepared by Jonathan A. Czuba, Ph.D., Licensed Professional Engineer - February 9, 2023

REFERENCES
23

February 21, 2023

USGS
science for a changing world

Guidelines and Procedures for Computing Time-Series Suspended-Sediment Concentrations and Loads from In-Stream Turbidity-Sensor and Streamflow Data

Chapter 4 of
Book 3, Applications of Hydraulics
Section C, Sediment and Erosion Techniques

Techniques and Methods 3–C4

U.S. Department of the Interior
U.S. Geological Survey

Front cover. Background photograph shows Little Arkansas River near Sedgwick, Kansas. Inset photograph shows water-quality monitors suspended from bridge and lowered by USGS personnel into the Little Arkansas River near Sedgwick, Kansas (all photographs taken by Patrick Rasmussen, USGS) (*http://nrtwq.usgs.gov/*).

Back cover. Inset is screen capture from USGS Real Time Computed Water Quality for Kansas, Little Arkansas River near Sedgwick site (*http://nrtwq.usgs.gov/*).

Guidelines and Procedures for Computing Time-Series Suspended-Sediment Concentrations and Loads from In-Stream Turbidity-Sensor and Streamflow Data

By Patrick P. Rasmussen, John R. Gray, G. Douglas Glysson, and Andrew C. Ziegler

Chapter 4 of
Book 3, Applications of Hydraulics
Section C, Sediment and Erosion Techniques

Techniques and Methods 3–C4

U.S. Department of the Interior
U.S. Geological Survey

U.S. Department of the Interior
KEN SALAZAR, Secretary

U.S. Geological Survey
Marcia K. McNutt, Director

U.S. Geological Survey, Reston, Virginia: 2009
Revised: 2011

Suggested citation:
Rasmussen, P.P., Gray, J.R., Glysson, G.D., and Ziegler, A.C., 2009, Guidelines and procedures for computing time-series suspended-sediment concentrations and loads from in-stream turbidity-sensor and streamflow data: U.S. Geological Survey Techniques and Methods, book 3, chap. C4, 52 p.

ISBN 978-1–4113–2410–7

Contents

Figures

Tables

Conversion Factors

Multiply	By	To obtain
	Length	
micrometer (µm)	3.937×10^{-5}	inch (in.)
nanometer (nm)	3.937×10^{-5}	inch (in.)
	Area	
square mile (mi^2)	2.590	square kilometer (km^2)
	Rate	
cubic foot per second (ft^3/s)	0.02832	cubic meter per second (m^3/s)
ton per day (ton/d)	0.9072	metric ton per day
ton per second (ton/s)	0.9072	megagram per second (Mg/s)

Water-Quality Units

Chemical concentration is given in units of milligrams per liter (mg/L). Milligrams per liter are units expressing the mass of solute per unit volume (liter) of water. Milligrams per liter are equivalent to parts per million.

Acronymns and Abbreviations

≤	less than or equal to
>	greater than
ADAPS	Automated Data Processing System (U.S. Geological Survey)
ANCOVA	analysis of covariance
ASTM	American Society for Testing and Materials
AU	attenuation units
BCF	bias correction factor
BU	backscatter units
C_p	Mallow's C_p
DD	data descriptor
DECODES	Device Conversion and Delivery System (U.S. Geological Survey)
DV	daily value
e_i	residual error
FAU	formazin attenuation units
FBU	formazin backscatter units
FNMU	formazin nephelometric multibeam units
FNRU	formazin nephelometric ratio units
FNU	formazin nephelometric units
GCLAS	Graphical Constituent Loading Analysis System (U.S. Geological Survey)
ISO	International Organization for Standardization
$\log_{10}$	base-10 logarithm
MLR	multiple linear regression
MSPE	model standard percentage error

Acronymns and Abbreviations—Continued

MVUE	minimum variance unbiased estimator
NTMU	nephelometric turbidity multibeam units
NTRU	nephelometric turbidity ratio units
NTU	nephelometric turbidity units
NWIS	National Water Information System (U.S. Geological Survey)
OBS	optical backscatter
OLS	ordinary least squares
PPCC	probability plot correlation coefficient
PRESS	prediction error sum of squares
QWDATA	U.S. Geological Survey water-quality database
r	correlation coefficient
R^2	coefficient of determination
R^2_a	adjusted coefficient of determination
RDB	relational database
RMSE	root-mean-squared error
SLR	simple linear regression
SSC	suspended-sediment concentration
SSL	suspended-sediment load
TSS	total suspended solids
USEPA	U.S. Environmental Protection Agency
USGS	U.S. Geological Survey
UV	unit value
VIF	variance inflation factor
WSC	Water Science Center (U.S. Geological Survey)
YSI	YSI Inc. (Yellow Springs, Ohio)

Guidelines and Procedures for Computing Time-Series Suspended-Sediment Concentrations and Loads from In-Stream Turbidity-Sensor and Streamflow Data

By Patrick Rasmussen, John R. Gray, G. Douglas Glysson, and Andrew C. Ziegler

Abstract

In-stream continuous turbidity and streamflow data, calibrated with measured suspended-sediment concentration data, can be used to compute a time series of suspended-sediment concentration and load at a stream site. Development of a simple linear (ordinary least squares) regression model for computing suspended-sediment concentrations from instantaneous turbidity data is the first step in the computation process. If the model standard percentage error (*MSPE*) of the simple linear regression model meets a minimum criterion, this model should be used to compute a time series of suspended-sediment concentrations. Otherwise, a multiple linear regression model using paired instantaneous turbidity and streamflow data is developed and compared to the simple regression model. If the inclusion of the streamflow variable proves to be statistically significant and the uncertainty associated with the multiple regression model results in an improvement over that for the simple linear model, the turbidity-streamflow multiple linear regression model should be used to compute a suspended-sediment concentration time series. The computed concentration time series is subsequently used with its paired streamflow time series to compute suspended-sediment loads by standard U.S. Geological Survey techniques.

Once an acceptable regression model is developed, it can be used to compute suspended-sediment concentration beyond the period of record used in model development with proper ongoing collection and analysis of calibration samples. Regression models to compute suspended-sediment concentrations are generally site specific and should never be considered static, but they represent a set period in a continually dynamic system in which additional data will help verify any change in sediment load, type, and source.

Introduction

Collection, computation, storage, and publication of suspended-sediment concentrations (*SSC*s), suspend-sediment loads (*SSL*s), and related environmental data can be important parts of investigations to evaluate the effects of fluvial sediment on a water resource (Glysson, 1989a). Suspended sediment can adversely affect water supply, recreation, aquatic life, flood control, transportation, fisheries, reclamation, and navigation (Angino and O'Brien, 1968). The U.S. Environmental Protection Agency (2008) lists sediment and other solid-phase constituents to be the most prevalent source of impairment of the Nation's surface water.

Traditionally, *SSC* data have been derived from analytical results from physical samples collected by methods described by Edwards and Glysson (1999), Nolan and others (2005), and Gray and others (2008). *SSL* data have been computed from *SSC* and streamflow data by methods described by Porterfield (1972) and Koltun and others (1994, 2006). The traditional U.S. Geological Survey (USGS) computation technique presented by Porterfield (1972) is predicated on the availability of more frequent than daily (continuous) streamflow time-series data and a concurrent trace of *SSC* interpolated from physical samples, and where necessary, *SSC* estimates. Interpolated and estimated parts of a *SSC* trace for a stream site can include periods during which a substantial cumulative fraction of the annual *SSL* occurs. Hence, considerable hydrologic judgment often is required to compute sediment records by Porterfield's (1972) method.

Turbidity is an expression of the optical properties of a sample that causes light rays to be scattered and absorbed rather than transmitted in straight lines through the sample (Anderson, 2005; ASTM International, 2007). Turbid water results from the presence of suspended and dissolved matter such as clay, silt, finely divided organic matter, plankton, other microscopic organisms, organic acids, and dyes (ASTM International, 2007).

The magnitude of turbidity in streams, lakes, and estuaries is often proportional to *SSC*. When proportional, the turbidity-*SSC* relation can be quantified through linear regression analysis (Walling, 1977; Gilvear and Petts, 1985; Buchanan and Schoellhamer, 1995; Lewis, 1996; Christensen and others, 2000; Uhrich and Bragg, 2003; Lietz and Debiak, 2005; Rasmussen and others, 2005; Lee and others 2009). The turbidity-*SSC* regression model, in turn, can be used to compute *SSC* values from turbidity data within the turbidity

meter's measurement range. Continuously monitored turbidity data enable computation of a *SSC* time series that can be used with its paired streamflow time series to compute continuous *SSL* without the routine need for interpolation or estimation.

When the turbidity-*SSC* model is deemed adequate, regression-computed *SSC* can provide a more reliable and reproducible *SSC* time series with smaller uncertainty values than either a sediment-transport curve using streamflow as the sole independent variable for computations of *SSC* (Rasmussen and other, 2005; Lee and others, 2008) or arguably with *SSC* data produced by Porterfield's (1972) computational method (for which there is no quantitative method for deriving uncertainty). When the turbidity-*SSC* model is deemed inadequate, the addition of streamflow as a second model variable may result in an acceptable time series of *SSC*. The turbidity- or turbidity-and-streamflow-based computational scheme to produce *SSC* data has a number of advantages over that of Porterfield's (1972) method, as follows:

1. No subjective interpolation or estimation is required;
2. The computational procedure is precisely reproducible;
3. The scheme takes full advantage of the available database and computational resources; hence, it can substantially reduce the time and effort needed to compute *SSL* records; and
4. Estimates of uncertainty can be computed for the *SSC* time series.

The turbidity- or turbidity-and-streamflow-based computational scheme also has advantages over the traditional sediment-transport curve method (Glysson, 1987). The reliability of *SSL* computed from a transport curve depends on a number of factors, including the range of streamflow and *SSC* over which the data were collected to define the curve, the number and reliability of the concentration-discharge relations used to define the curve, and whether the data are representative of water and sediment loads for the computational period (Gray and Simões, 2008). Walling (1977) found that annual *SSL* computed using a sediment-transport curve could result in errors of as much as 280 percent, whereas errors in monthly *SSL* could range between +900 percent and -90 percent. Glysson and others (2001) compared *SSL* computed by the Porterfield (1972) method and a transport curve for 34 years of streamflow and suspended-sediment records at the USGS streamgage on the Rio Grande at Otowi Bridge, New Mexico. Daily *SSL* computed by these two techniques differed by as much as 4,000 percent, whereas the maximum difference in annual *SSL* computations was 526 percent. *SSL* for the 34-year period of record differed by 38 percent. Lee and others (2008) compared the uncertainty of annual *SSL* computed using a sediment-transport curve and a turbidity-*SSC* model at three sites near John Redmond reservoir, Kansas. The uncertainties associated with the annual *SSL* derived from sediment-transport curves ranged from 16–20 percent, whereas those derived from the turbidity-*SSC* model ranged from 1.1–3.2 percent.

Glysson and others (2001) observed that estimates of *SSL*s that are based on sediment-transport curves are subject to significant errors, in part because of the large range in *SSC* that can occur at any given water discharge. They concluded that, although a well-defined, carefully constructed and judiciously applied sediment-transport curve can be a useful tool for estimating *SSL*, *SSL* estimates derived from sediment-transport curves should not be considered a substitute for daily-sediment records computed by Porterfield's (1972) method. Lewis (1996) indicated that regression models using turbidity instead of streamflow improved the root-mean-squared errors of sediment rating curve estimates by 7 to 15 percent.

Hence, the use of a linear regression model to compute *SSC* from turbidity time-series data, and in some cases, turbidity and streamflow time-series data measured at a fixed location in a stream provide statistical estimates of uncertainty of *SSC* (Christensen and others, 2000). The use of a linear regression model, depending on the characteristics of the sediment in suspension, is likely a more accurate method for estimating a *SSC* time series than either the Porterfield (1972) method or traditional transport-curve method (Walling, 1977; Horowitz and others, 2003; Putnam and Pope, 2003).

SSC computed from regression models can be used for a variety of purposes, including use to describe variability in suspended-sediment conditions, to evaluate *SSC* relative to water-quality criteria and water-resource management goals, and to compare the *SSC* and *SSL* characteristics among watersheds. Computed *SSC* and streamflow data in riverine applications can be used to compute *SSL* to reservoirs, which in turn can be used to infer loss of reservoir capacity. Computed *SSC* and *SSL* also can be used in the study of channel morphology and basic process analysis of sediment sources. Also, by relating the continuous, time-series turbidity data to the sampled *SSC*, it may be possible to identify the sources and timing of sediment transport more accurately than on the basis of periodic sample collection. Subsequently, computed daily, monthly, seasonal, and annual *SSL* can be used to assess differences in fluvial-sediment characteristics between basins as a function of hydrologic conditions, contributing drainage area, land use, sediment sources, and (or) human activity. Turbidity time-series data also can be used to compute a variety of constituent concentrations—for example, total nitrogen and total phosphorus (Rasmussen and others, 2005) and indicator bacteria (Rasmussen and Ziegler, 2003) that correlate well with *SSC*, which in turn can be used to compute loads of those constituents.

Historically, most State agencies have collected samples for analyses of total suspended solids (*TSS*) in lieu of *SSC* samples (Pruitt, 2003). This is largely a consequence of the fact that the U.S. Environmental Protection Agency presently only recognizes the *TSS* analytical method (American Public Health Association, American Water Works Association, and Water Pollution Control Federation, 2005). *TSS* data tend to be biased low, particularly when sand constitutes more than about 20 percent of the mass of the water-sediment mixture (Gray and others, 2000; and Glysson and others, 2000, 2001). For

systems that convey primarily silt- and clay-sized sediment in suspension, Christensen and others (2000) and Rasmussen and others (2008) have used turbidity-*TSS* models to compute *TSS* values with acceptable uncertainties. However, *TSS* data are acceptable alternatives to *SSC* data only after being conclusively documented in a published report that the *TSS* data can adequately represent *SSC* data over the range of expected flows at a site (U.S. Geological Survey, 2000).

Purpose and Scope

This report provides guidelines and procedures for computing time series of *SSC* and *SSL* from time series of turbidity and streamflow data using a generally site-specific, simple or multiple regression model relating *SSC* from periodically collected in-stream water samples to in-stream turbidity measurements. Included is the requisite knowledge to:

1. Develop and evaluate an empirical statistical relation between turbidity and *SSC* measurements;
2. Compute time series of *SSC* and *SSL* from turbidity and streamflow time-series data; and
3. Maintain a long-term *SSC* record.

Examples of applications of the analytical and computational methods described herein are provided using data from USGS streamgages in California, Florida, Kansas, and Oregon. Although this guidance is for application in a riverine environment, selected aspects of the guidelines may be adapted for use in lacustrine or estuarine applications.

References to principles of sediment transport, sampling techniques, and related field procedures, along with quality-control procedures, are presented because an understanding of these principles and procedures is fundamental to the computation of time-series suspended-sediment records. Concepts, statistical procedures, and techniques are presented for computing *SSC* and *SSL* time series. Material in this report includes procedures and techniques to maintain a multiyear *SSC* time series and to prepare suspended-sediment data for public dissemination. Selected duplication of material contained in other publications and guidelines is necessary and intentional to provide guidance for computing *SSC* and *SSL* from turbidity and streamflow data. Specific USGS guidance on methods for computing and storing computed suspended-sediment data in the USGS National Water Information System (NWIS) database is presented.

Related Guidelines

Porterfield (1972) describes two basic types of sediment records—daily and periodic—calculated from sampled *SSC* and using gage height and (or) streamflow data to synthesize the *SSC* trace for unsampled periods. Daily records are prepared for sites where sufficient determinations of *SSC* and streamflow are obtained to enable computation of daily *SSL* (Porterfield, 1972). The end product is a tabulation of daily time-weighted mean *SSC*, *SSL*, and, in many cases, periodic determinations of particle-size distributions of suspended sediment and bed material. These are combined with other hydrologic data and released, usually by water year (October 1 through following September 30), by the USGS in stream-site data sheets for specific States or in the Open-File or Scientific Investigation Report series. Periodic records are prepared for sites where frequency of determination of *SSC* and (or) streamflow are insufficient to justify computation of daily *SSL* or where only miscellaneous samples are collected infrequently. In addition to publication of the records, the data and supporting documentation on computations are maintained on file in the USGS Water Science Centers and are available for examination or for use in interpretative reports and research.

Wagner and others (2006) provide basic guidelines and procedures used by USGS personnel for operating water-quality monitors, including site selection, field procedures, calibration of continuous water-quality monitors, record computation and review, and data reporting. In addition, Wagner and others (2006) present methods for servicing fixed-location water-quality monitors (including turbidity sensors) in freshwater environments and estuaries. Alternative methods for servicing monitors also are included. These basic guidelines are minimal requirements that may be modified to meet local environmental conditions or specific study objectives. Knowledge of monitoring-equipment operation and first-hand knowledge of the salient aspects of the watershed form the core of the data-evaluation process. Record-computation procedures presented in Wagner and others (2006) provide a uniform set of minimum requirements for computing water-quality records. Examples of the application of scientific judgment in the evaluation of data records are presented and are, by necessity, site specific. Other specific examples also are included to demonstrate the range of environmental conditions that affect the evaluation process.

Equipment and procedures for collection and measurement of fluvial sediment are described by Edwards and Glysson (1999), which contains two major sections regarding suspended-sediment equipment and techniques that are germane to developing turbidity/suspended-sediment relations. The “Sediment-Sampling Equipment” section includes information on the characteristics and limitations of various models of Federal Interagency Sedimentation Project (2008) isokinetic, depth- and point-integrating samplers (Davis, 2005), non-isokinetic single-stage samplers, automatic pumping samplers, and selected support equipment. The “Sediment-Sampling Techniques” section in Edwards and Glysson (1999) includes information on sediment-discharge measurements, including collection of representative samples, characteristics of sampling sites, equipment selection relative to the sampling conditions and needs, depth- and point-integration sampling techniques, surface and dip sampling, determination of sampler transit rates, sampling programs, and cold-weather sampling. The sediment-sampling equipment and techniques sections in Edwards and Glysson (1999), the subject matter of

which is also the focus of Nolan and others (2005) and Gray and others (2008), provide the fundamental information for collecting representative water-sediment samples. The derived *SSC* data, in turn, are used in correlations to turbidity. A more detailed description of suspended-sediment data-collection techniques is beyond the scope of this report.

Although streamflow computations can be accomplished by several techniques depending on site and equipment characteristics, they usually entail collection of stage records along with periodic streamflow measurements. Stage records are obtained from a water-stage recorder. Streamflow measurements usually are made with a current meter (Rantz and others, 1982; Kennedy, 1984) or acoustic Doppler current profiler (Lipscomb, 1995; U.S. Geological Survey, 2002). The methods are consistent with the American Society for Testing and Materials (ASTM) standards and generally follow the standards of the International Organization for Standardization (ISO). A more detailed description of streamflow time-series computation is beyond the scope of this report.

Helsel and Hirsch (2002) provide a stand-alone text of applied statistical methods for hydrology. Their chapters "Simple Linear Regression" and "Multiple Linear Regression" are cited throughout this guide and are essential for understanding and performing the statistical procedures presented.

Types of Turbidity Sensors

There are many methods for quantifying water clarity, including Secchi and black disks, laser diffraction (Gray and others, 2003; Gray and Gartner, 2009; Gray and Gartner, in press), digital-optic techniques (Gray and others, 2003; Gooding, in press) and optical light scattering and absorption techniques (table 1; Gray and others, 2003; Rasmussen and others, in press). The techniques in this report are predicated on use of either of two types of turbidity sensors that are based on nephelometric or optical-backscatter (OBS) principles and are commonly used to measure turbidity for the purposes of computing *SSC* (Gray and Gartner, 2006). These sensors are designed for extended in-situ deployment, are relatively inexpensive, and are either self recording or produce signals compatible with a data logger.

Table 1. Selected specifications for selected turbidity instruments (Anderson, 2005).

Light source	Multiple or single light sources	Detection angle	Single or multiple detectors	Designated units
White or broadband (400–680 nanometers)	Single	90-degree detection angle	Single	NTU (nephelometric turbidity unit)
White or broadband (400–680 nanometers)	Single	90-degree detection angle	Multiple detectors, ratio compensation	NTRU (nephelometric turbidity ratio unit)
White or broadband (400–680 nanometers)	Single	30- (plus or minus 15) degree detection angle (backscatter)	Single	BU (backscatter unit)
White or broadband (400–680 nanometers)	Single	180-degree detection angle (attenuation)	Single	AU (attenuation unit)
White or broadband (400–680 nanometers)	Multiple	Detectors at 90 degrees and possibly other angles to each beam	Multiple	NTMU (nephelometric turbidity multibeam unit)
Near infrared (780–900 nanometers) or monochrome	Single	90-degree detection angle	Single	FNU (formazin nephelometric unit)
Near infrared (780–900 nanometers) or monochrome.	Single	90-degree detection angle	Multiple detectors, ratio compensation	FNRU (formazin nephelometric ratio unit)
Near infrared (780–900 nanometers) or monochrome	Single	30- (plus or minus 15) degree detection angle (backscatter)	Single	FBU (formazin backscatter unit)
Near infrared or monochrome	Single	180-degree detection angle (attenuation)	Single	FAU (formazin attenuation unit)
Near infrared (780–900 nanometers) or monochrome (including Great Lakes Instruments, Inc., 1992—Method 2)	Multiple	Detectors at 90 degrees and possibly other angles to each beam	Multiple	FNMU (formazin nephelometric multibeam unit)

Unlike absolute measurements of selected physical properties of water, such as specific conductance, pH, temperature, or dissolved oxygen, turbidity is a relative index of scattering and absorption of light in water. Turbidity is not a direct measure of suspended particles in water but instead is a measure of the scattering and absorbing effect such particles have on light (Sadar, 1998). Anderson (2005) provides a review of available turbidity sensor technologies with a decision tree to select a suitable instrument for a specific site or application and guidelines for calibration, operation, quality-assurance procedures, and reporting of data. Several characteristics of the water and suspended-sediment mixture, such as particle size, shape, and color, can affect the optical measurement (Sadar, 1998; Davies-Colley and Smith, 2001; Ziegler, 2002a,b; Anderson, 2005; Downing, 2005, 2006). The effects of these characteristics are discussed in the section on "Factors Affecting Relation Between Turbidity and Suspended-Sediment Concentration."

Nephelometry

Nephelometry is the measurement of light scattering using a light detector 90 degrees from the incident light (U.S. Environmental Protection Agency, 1999). Nephelometric measurements reflect the collective optical properties of solution that cause light to be scattered or attenuated rather than transmitted in straight lines through the solution; the larger the amount of scatter or attenuation of light, the larger the value measured by the nephelometric turbidity meter. Nephelometric measurements typically are expressed in turbidity units defined by the light source, detection angle, and whether the sensor has single or multiple detectors (table 1). Approved methods (in 2008) for the measurement of turbidity include those that conform to at least three protocols. These are stated in: (1) U.S. Environmental Protection Agency (USEPA) Method 180.1 (U.S. Environmental Protection Agency, 1979), (2) ISO Method 7027 (International Organization for Standardization, 1999), and (3) standard methods recommended by the American Water Works Association and the Water Environment Federation (Clesceri and others, 1998).

Wagner and others (2006) describe methods for measuring turbidity with submersible-type (fig. 1) and nonsubmersible nephelometric sensors. The nephelometric measurements shown in the examples in this report were made with either an YSI 6026 or YSI 6136 turbidity probe (YSI Incorporated, 2003). These YSI sensors conform to the ISO Method 7027 and ASTM D-7315 measurement standards. Each has a light

Figure 1. Three self-cleaning nephelometric turbidity sensors—*A,* YSI Incorporated (Yellow Springs, Ohio) model 6136 turbidity sensor, *B,* Hydrolab (Loveland, Colorado) self-cleaning turbidity sensor, and *C,* Forest Technology Systems (Blaine, Washington) model DTS-12 turbidity sensor.

source of 860 ± 30 nanometers (nm) with a single detector oriented at 90 degrees from the incident light path. Nephelometric readings from the YSI 6026, YSI 6136, and other turbidity sensors can be different and not directly equivalent (Sadar, 1998; Davies-Colley and Smith, 2001; Landers, 2003; YSI Incorporated, 2003; Ziegler, 2003a; Rasmussen and others, 2005). Different turbidity values, therefore, can be measured for an individual sample by different turbidity sensors conforming to the same standard method. See the "Changes to Turbidity Sensor Model or Type" section of this report for a discussion of data processing from different turbidity sensors.

Optical Backscatter

OBS sensors measure the same properties as nephelometric sensors, but the angle between the light source and the detector is less than 90 degrees. An OBS sensor is typically a cylinder utilizing an optical window from which light is both emitted and received (fig. 2; Downing and others, 1981; Downing, 1983). A pulse of either white or near-infrared light is transmitted through the optical window and is scattered or reflected by particles in front of the window in a 165-degree conical zone within some distance. Some of this scattered or reflected light is returned to the optical window where a receiver converts the backscattered light to a proportional voltage output. The relation of OBS sensor voltage output to *SSC* varies depending on the size, shape, and optical properties of the suspended sediment (Levesque and Schoellhamer, 1995). Downing (2006) provides a thorough discussion of the history and use of OBS measurements to compute *SSC*. Typically, OBS sensors are used at locations where the nephelometric sensor maximum reporting level, ranging from 1,000 to 2,000 formazin nephelometric units (FNUs) or *SSC* values larger than 1,000 milligrams per liter (mg/L), are exceeded frequently.

A

B

Figure 2. Optical backscatter sensors—*A,* OBS 3+ (Campbell Scientific Inc., Logan, Utah) and *B,* Hach (Loveland, Colorado) Solitax.

Relation of Turbidity to Suspended-Sediment Concentration

A constituent concentration may be computed as a function of another measurement by means of linear regression models (Helsel and Hirsch, 2002). *SSC*, for example, can be computed from turbidity and (or) streamflow measurements by means of linear regression. The regression methods used in this guide are described in Helsel and Hirsch (2002) and are similar to those applied by Gilvear and Petts (1985), Lewis (1996), Christensen and others (2000), Uhrich and Bragg (2003), Lietz and Debiak (2005), and Rasmussen and others (2005).

To illustrate the techniques and methods discussed in these guidelines, turbidity, streamflow, and *SSC* data from USGS streamgage 07144100, Little Arkansas River near Sedgwick, Kansas, are used. A riverine example is presented because it is the most likely and common application of this method. Some of the methods discussed are not applicable to lacustrine or estuarine applications. Data sets and regression model examples of other riverine and estuarine data sets are provided in Appendix 1.

Steps in the procedure for computing time-series records of *SSC* and *SSL* are given in the checklist shown in figure 3. There are three major steps to completing the computation:

1. Compilation of a model-calibration data set of concurrent turbidity, streamflow, and *SSC* values;

2. Development of a linear regression model to compute instantaneous values of *SSC*; and

3. Computation and storage of instantaneous values of *SSC* and daily values of *SSL*.

Compilation, development, and computation methods are described in detail in the following sections.

Model-Calibration Data Set

Compilation of the model-calibration data set is the first step in the development of a linear regression model. The model-calibration data set consists of concurrent instantaneous in-stream measurements of turbidity and streamflow, and sampled *SSC* values that correspond to the paired turbidity-streamflow measurements. Appendix 2 discusses retrieval of these data types from the USGS National Water Information

[NWIS, U.S. Geological Survey National Water Information System; ADAPS, U.S. Geological Survey Automated Data Processing System; QWDATA, U.S. Geological Survey water-quality database; SSC, suspended-sediment concentration; SSL, suspended-sediment load, R^2, coefficient of determination; RMSE, root-mean-squared error; MSPE, model standard percentage error; PRESS, prediction error sum of squares; VIF, variance inflation factor; R^2a, adjusted coefficient of determination ; MVUE, minimum-variance unbiased estimator; ANCOVA, analysis of covariance]

Checklist for time-series suspended-sediment records

	Worked	Reviewed	Approved
1) Compile model calibration data set			
a) Retrieve data from NWIS	_____	_____	_____
i) Approved time-series data: turbidity and streamflow (from ADAPS)	_____	_____	_____
ii) Discrete sample data: SSC, sand-silt percentage (from QWDATA)	_____	_____	_____
b) Assign turbidity and streamflow values to be used in regression	_____	_____	_____
c) Plot raw data to identify potential outliers (turb against SSC)	_____	_____	_____
d) Plot samples on turbidity and streamflow duration curves	_____	_____	_____
e) Compile statistical summary of model calibration data set	_____	_____	_____
f) Write model-calibration data-set summary in station analysis	_____	_____	_____
2) Development of a regression model			
a) Correlations and scatter plots of all data	_____	_____	_____
b) Simple linear regression turbidity/SSC, untransformed and $\log_{10}$ transformed and regression diagnostics (R^2, R^2_a, RMSE, PRESS, MSPE)	_____	_____	_____
c) Determine proper transformation	_____	_____	_____
d) Model residual plots	_____	_____	_____
e) Plot model residual against streamflow, Julian day	_____	_____	_____
f) Evaluate simple and multiple linear regression models	_____	_____	_____
(residual plots, VIF, partial F-test, R^2_a, PRESS, MSPE)	_____	_____	_____
g) Bias correction factor (Duan or MVUE)			
h) 90-percent prediction interval	_____	_____	_____
i) Regression model summary in station analysis	_____	_____	_____
3) Computation and storage of time-series suspended-sediment concentration and load record in NWIS			
a) Set up data descriptors in ADAPS	_____	_____	_____
b) Enter bias adjusted equation	_____	_____	_____
c) Select period of suspended-sediment record for application of model	_____	_____	_____
d) Compute SSC unit value and SSL daily values	_____	_____	_____
e) Estimate missing SSC or SSL data	_____	_____	_____
f) Evaluate period of record graphs	_____	_____	_____
g) Update station analysis	_____	_____	_____
4) Annual model validation			
a) Plot calibration data set and recent annual data	_____	_____	_____
b) Compare original model to model with additional data (ANCOVA)	_____	_____	_____
c) Update model in ADAPS	_____	_____	_____
d) Determine start date and time of new model	_____	_____	_____

Figure 3. Checklist for development, verification, and approval of a regression model to compute suspended-sediment concentration and load time-series data.

System (NWIS) database. The sampled *SSC* must be representative of the mean cross-sectional *SSC* value at the time of collection. The rationale for examination and quality assurance of the data are presented in the following paragraphs. The computation of turbidity and streamflow time-series data are assumed to have been completed by means of established USGS guidelines and procedures (Wagner and others, 2006; U.S. Geological Survey, variously dated). The guidance that follows is intended only to supplement procedures presented in Wagner and others (2006).

Evaluation of Fixed-Location and Cross-Section Turbidity

Comparisons of fixed-location and cross-section in-stream turbidity measurements should be part of the turbidity record analysis (Wagner and others, 2006). Fixed-location, in-stream (hereinafter referred to as "fixed-location") turbidity measurements collected concomitant with cross-section turbidity measurements should be retrieved from the "approved" time-series data set (U.S. Geological Survey, 2006, p. 20, 188–195). The turbidity cross-section measurements should be made with a properly cleaned and calibrated field turbidity sensor of the same make and model as the fixed-location turbidity sensor. Cross-section turbidity measurements are collected at several points across the stream routinely near the surface and periodically at different depths (Anderson, 2005). Those points at suspended-sediment sampling verticals are used for either the equal-width increment or equal-discharge increment methods (Edwards and Glysson, 1999; Nolan and others, 2005; Gray and others, 2008). These measurements are averaged and used in evaluations of the representativeness of data produced from fixed-location turbidity time-series measurements (fig. 4).

Large turbidity values warrant special evaluation. Although the values may be valid, spurious data can occur, including those recorded when turbidity exceeds the sensor's maximum recording level. Sensor-measurement truncation produces constant-value artifacts when in-stream turbidity levels exceed the maximum recording level of the sensor (1,000–2,000 mg/L for most nephelometric sensors and 4,000–50,000 mg/L for most OBS). The maximum recording level is unique for each turbidity sensor and should be routinely quantified and documented for each sensor (Anderson, 2005). Because the maximum recording level of the sensor is reported for all turbidity values equal to or larger than the maximum recording level, truncation is manifested as a horizontal line or plateau in the temporal turbidity trace of plotted data (fig. 5). Routine calibration of the turbidity sensor can change the maximum recording level; therefore, turbidity measurements within about 10 percent of the maximum recording level should be evaluated to determine if those values are artifacts of truncation. Generally, these values should not be used as part of the model-calibration data set.

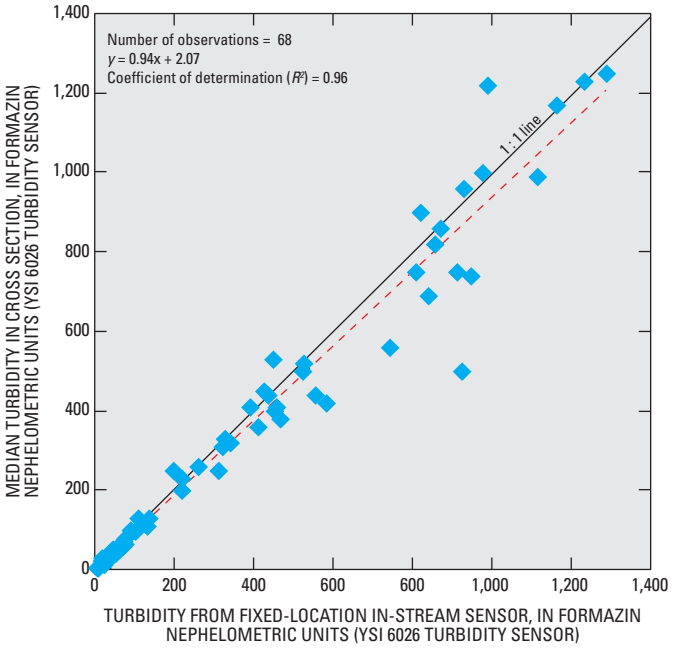

Figure 4. Comparison of fixed-location and median cross-section turbidity measurements for U.S. Geological Survey streamgage on Little Arkansas River near Sedgwick, Kansas, November 1998–June 2005.

Exceptions should be clearly noted and fully explained as part of the summary in the station analysis (Appendix 1 at the back of this report). The use of turbidity sensors to compute *SSC* at a site subject to frequent turbidity truncation may not be appropriate. OBS sensors should be used for streams where a significant percentage of *SSL* occurs at *SSC* values exceeding about 2,000 mg/L. However, currently (2009) most OBS sensors are not self cleaning and require more frequent routine maintenance.

Determination of Turbidity and Streamflow Associated with Suspended-Sediment Concentrations

Turbidity and streamflow corresponding to each *SSC* sample should be determined from the time-series data sets–preferably, time-weighted averages of turbidity and streamflow values recorded immediately before, immediately after, and during the *SSC* sample collection (fig. 5). The hydrographer should ensure that the turbidity and streamflow time-series data retrieved from the USGS time-series database, ADAPS, have a data-aging status of "approved" (U.S. Geological Survey, 2006, p. 20 and 188–195). Once turbidity and streamflow values have been determined for each *SSC* value, the hydrographer should compile a data set for statistical analyses.

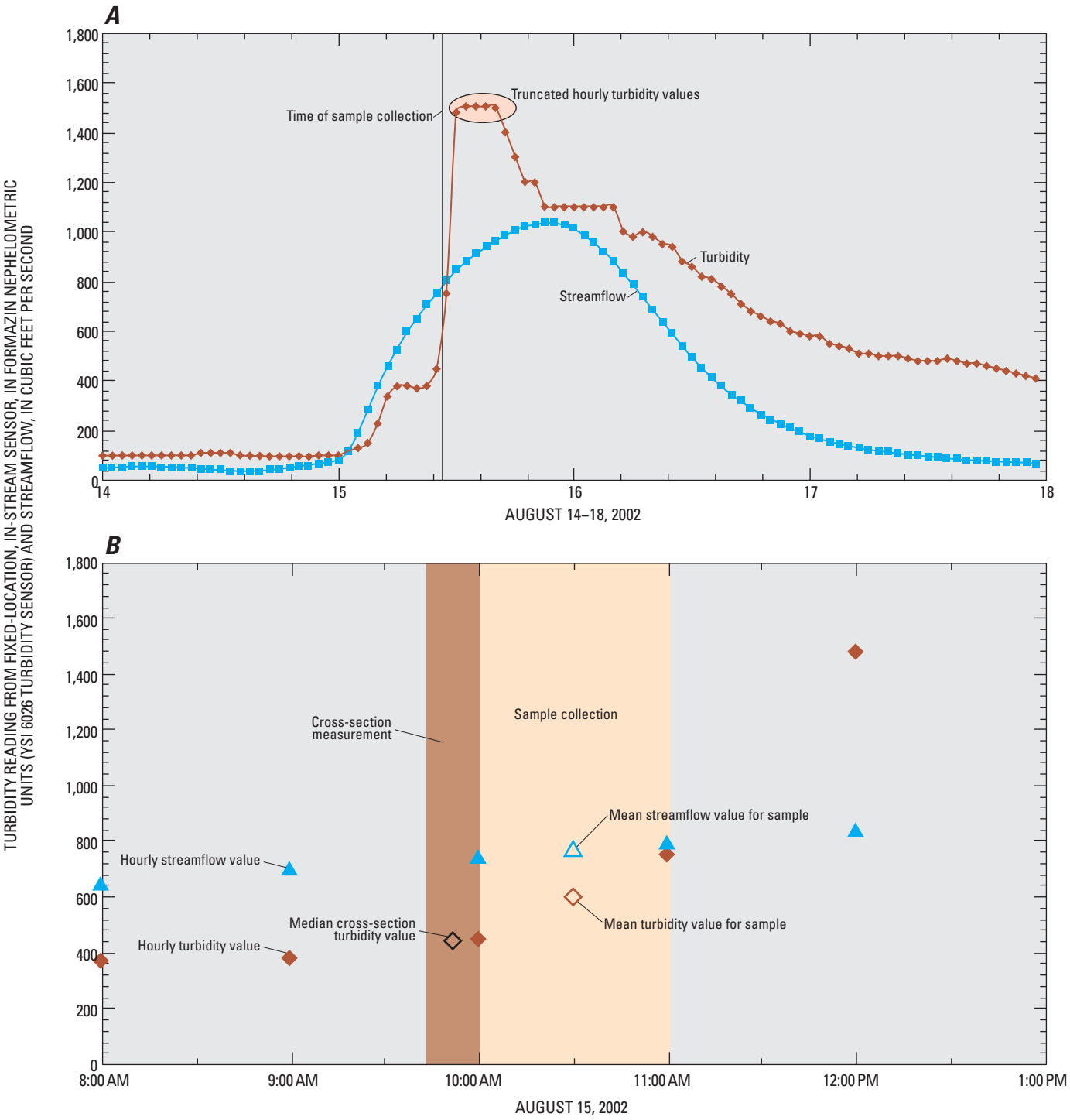

Figure 5. *A,* Time-series turbidity and streamflow data, August 14–18, 2002, and *B,* duration of cross-section turbidity and suspended-sediment sample collection, August 15, 2002, at U.S. Geological Survey streamgage on Little Arkansas River near Sedgwick, Kansas.

Identification of Outliers

The development of a *SSC* regression model should be preceded by evaluation of a scatterplot of the turbidity and *SSC* calibration data. The hydrographer can sometimes discern outliers on the basis of the scatter of the data. Helsel and Hirsch (2002, p. 11, 31–34, 246–248) provide additional guidance on the identification and treatment of outliers.

Once an outlier is identified, the hydrographer should use all technically supportable analytical tools and methods to attempt to discredit the value in question. This includes:

1. Confirmation that the correct value was entered into the database;
2. Evaluation of laboratory analytical results; and
3. Review of the field notes to ensure that proper collection techniques were used or to otherwise identify factors that might lend credit to or that might refute the outlier.

Remove outliers from the analysis that can be discredited with a high degree of confidence. Conversely, if an outlier cannot be discredited, the hydrographer must determine the type of adjustment and document the attempts to verify the value in the station analysis summary (Appendix 1). Outliers that cannot be discredited may affect the analysis and may help the hydrographer better understand the relations among site turbidity, *SSC*, and streamflow. Numerous outliers may be indicative of problems with the measuring apparatus and (or) monitoring site that may in turn warrant corrective measures.

In the comparison of Little Arkansas River fixed-location turbidity measurements to *SSC* (fig. 6), five data points plotted outside the scatter and pattern of the other 68 data points. Inspection of field and laboratory notes and results of particle-size analyses indicated that these outliers should be either corrected or removed. One of the five outliers was derived from a sample that arrived at the laboratory with a loose bottle lid and an abnormally small sample volume. On the basis of this information, it was surmised that some sample water had leaked while most if not all of the sediment remained at the container's bottom, resulting in a spuriously large *SSC*. The discredited outlier was removed from the data set.

Values for two *SSC* samples that plot as outliers on opposite sides of the data scatter (identified as "Database entry errors for *SSC* values" in figure 6) were evaluated. The field forms for these samples confirmed that turbidity values in the database matched the turbidity measurements made concomitant with *SSC* sample collection. However, a review of the analytical summaries for the *SSC* samples indicated that data-entry errors comprising misplaced decimal points resulted in one value appearing as 10-fold its true value and the other one-tenth of its true value. The two sample results were duly corrected in the database and replaced the erroneous values in the model-calibration data set.

Evaluation of the particle-size analyses performed on the suspended-sediment samples collected at relatively low streamflows indicated an abnormally large percentage of sand

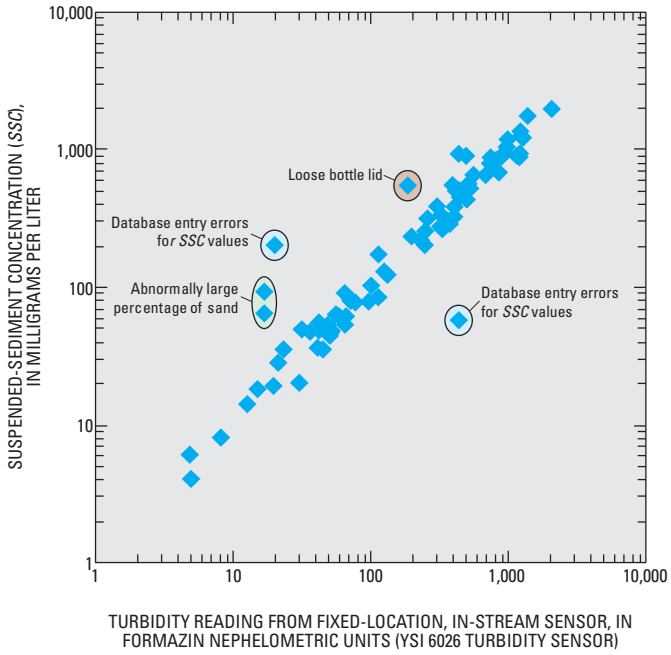

Figure 6. Comparison of turbidity to suspended-sediment concentration in water from U.S. Geological Survey streamgage on Little Arkansas near Sedgwick, Kansas, August 2000–June 2005.

(particle sizes exceeding 63 micrometers [µm]) for two other outliers. Typically, sand in samples collected at this site during similar low streamflow conditions constitutes no more than 2 percent of the sediment mass. Sand in these two samples constituted 10 and 30 percent of the dry sediment mass. Transport of sand at these low streamflows is unsupported by sedimentological theory and samples collected previously at this site. The outliers were deemed to be artifacts attributable to sampling error (inadvertently scooping sand-size bed material into the suspended-sediment sampler) and were removed from the data set.

A revised scatterplot identified no other data points that deviated sufficiently from the rest to justify further scrutiny.

Adequacy of Model-Calibration Data Set

An adequate model-calibration data set consists of an appropriate number of instantaneous, manual *SSC* samples and concurrent turbidity and streamflow measurements collected throughout the observed range of hydrologic conditions for the period of record (Glysson, 1989b; Rasmussen and others, 2002). The number of samples is often cited as the primary criterion for determining if a data set is adequate for computational purposes. Initially, approximately monthly samples collected over a 2- to 3-year period for the range of hydrologic conditions may be needed. Although the sample total is relevant, the distribution of the data over the range of observed turbidity, *SSC*, and streamflow values for the site is

of paramount importance. A regression model developed from 15 samples more or less evenly distributed throughout the seasons and range of turbidity and streamflow at a site might result in a more representative model than one developed using a 50-sample data set where distribution of values defines only a limited time or range of the sedimentological conditions over which the model will be applied. Defining turbidity-*SSC* relations during medium and high streamflow periods normally takes precedence over more equal spacing of data collection throughout the year, particularly if the purpose is to compute *SSL*. For example, where the number of site visits to collect manual samples is limited, sample collection should be skewed toward medium and higher flows. Regardless of the range of data values, the data points representing the extremes will have the greatest effect in determining the slope of the relation. For instance, erroneously large turbidity values during low streamflow and low *SSC* conditions can artificially increase the slope of the regression line.

Another factor to be considered when determining the adequacy of a data set is the amount of variability in the relation between turbidity and *SSC*. The larger the variability in the relation between turbidity and *SSC* at a site, the greater the need is to collect more samples. Often, the hydrographer's challenge is to adequately characterize this variability with the fewest number of samples.

Serial correlation (also called autocorrelation) occurs when data are collected close enough in time that the regression assumption of data independence is violated. For instance, multiple samples may be collected during the rising and falling limb of a single runoff period. The serial correlation between the multiple data points can cause underestimation of the regression uncertainty. Helsel and Hirsch (2002, p. 250–251) present methods for identifying the presence of serial correlation. If serial correlation is detected, the solution is to randomly select a single data point from each group of correlated data. The single point should be used in the model-calibration data set. Alternately, Glysson (1987) describes a procedure by which mean *SSC* values are computed for each of several contiguous, discrete *SSC* intervals for the data set. These mean values are used to develop the regression equation.

Duration curves represent another tool to evaluate the distribution of *SSC* data and adapt subsequent sample-collection strategies. Ideally, turbidity and streamflow associated with the *SSC* samples should span the ranges of the time-series turbidity and streamflow values for the site (Rasmussen and others, 2002). For example, turbidity and streamflow values associated with discrete *SSC* sample data are plotted on duration curves of turbidity and streamflow (fig. 7*A* and *B*). The turbidity duration curve in figure 7*A* was developed from hourly recorded turbidity measurements by the fixed-location sensor for the study period. The turbidity values associated with the *SSC* samples were plotted along the duration curve. Sample collection can be determined by closely monitoring the real-time turbidity and streamflow time-series data and optimizing sample-collection times to coincide with duration-curve segments undefined by sample values. As new *SSC* samples are collected, the hydrographer should add the corresponding turbidity and streamflow values to the duration-curve plots so that overall temporal distribution of samples can be assessed. Routine use of this tool will maximize the potential that the model-calibration data set optimally represents the range of turbidity and streamflow conditions.

Turbidity values for one or more years are sorted (or ranked) from smallest to largest to construct a turbidity duration curve from a turbidity time series. Then, exceedance probabilities are calculated for each turbidity value using Cunnane's plotting position (Cunnane, 1978; Helsel and Hirsch, 2002). The minimum turbidity-value duration percentage is 100 percent (all values within the data set are larger than or equal to this value). The maximum turbidity-value duration percentage is 0 percent (no values within the data set exceed this value). All the turbidity values within the data set are plotted according to calculated probabilities forming the turbidity duration curve. Symbols are plotted on the curve at the probability computed for turbidity values associated with each *SSC* sample. A streamflow duration curve can be constructed in a similar manner by substituting a streamflow time series for the turbidity time series. Streamflow duration curves representing the study period and, if different, the entire period of record provide study period and long-term comparisons.

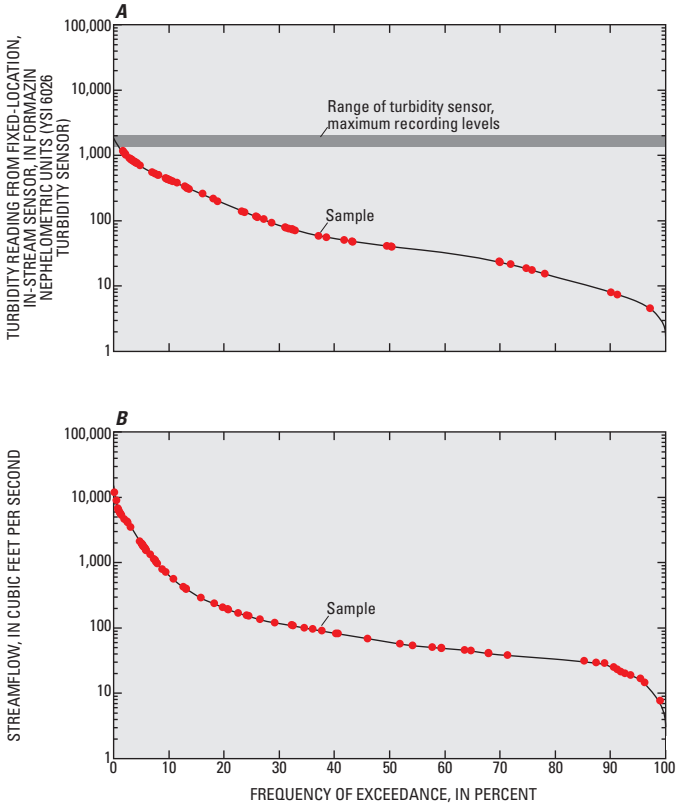

Figure 7. Duration curves for *A,* turbidity and *B,* streamflow and corresponding values associated with suspended-sediment concentration samples collected at U.S. Geological Survey streamgage on Little Arkansas River near Sedgwick, Kansas, 1999–2005.

Update of Station Analysis

The station analysis for a stream site should be updated to summarize the data analyses performed. This summary should include the rationale behind:

1. Determination of turbidity and streamflow values associated with each *SSC* value;
2. Acceptance or exclusion of turbidity values near the sensor-dependent turbidity maximum recording level;
3. Identification of outliers of turbidity, streamflow, and (or) *SSC* values; and
4. Determination of the adequacy of the model-calibration data set using turbidity and streamflow duration curves.

Other information necessary to complete the station analysis includes a table of summary statistics of the model-calibration data set. General statistics of the model-calibration data set and the time-series data set indicate the representativeness of the model-calibration data set (table 2). The minimum and maximum turbidity values for the model-calibration data set define the ideal limits for which the resulting regression model should be used to compute *SSC* values. An understanding of suspended-sediment transport processes and sound hydrologic judgment—ideally drawn from years of experience—is required when deciding if values outside these limits are appropriate.

The hydrographer should review data plots, duration curves, and data statistics to evaluate the sufficiency of the model-calibration data set for developing a reliable regression model. If any of these categories are insufficient, the hydrographer may opt to suspend the model analysis and focus on additional sample collection so that the model-calibration data set may better represent the range of the time-series data set. As new sample results are added to the model-calibration data set, these same steps can be used to evaluate how the new data enhance or otherwise alter the model.

Table 2. Statistical summary of model-calibration data set for U.S. Geological Survey streamgage on Little Arkansas River near Sedgwick, Kansas, November 1998–June 2005.

[mg/L, milligrams per liter; FNU, formazin nephelometric units; ft^3/s, cubic feet per second]

Summary statistic	Calibration data set (68 samples)			Time-series data set (61,200 hourly values)	
	Suspended-sediment concentration (mg/L)	Turbidity (FNU)	Streamflow (ft^3/s)	Turbidity (FNU)	Streamflow (ft^3/s)
Minimum	4	4	8	1	3
Maximum	1,250	1,300	12,000	2,000	15,000
Mean	350	370	1,500	140	380
Median	240	240	210	41	60
Standard deviation	350	380	2,500	260	1,200

Regression Model Development

The key elements for computing *SSC* time-series data from periodic instantaneous *SSC*, turbidity, and streamflow data are the type and goodness-of-fit of the regression model used in the computation. A number of quantifiable variables can be used to compute *SSC* in streams, including turbidity; hydrologic characteristics, including streamflow, stream stage, streamflow rise or fall, and rates of rise and fall; precipitation rate and intensity; and seasonality, sediment sources, and land use. The explanatory variables turbidity and streamflow generally are the most important in *SSC* regression analysis. Thus, these guidelines focus on turbidity and, to a lesser extent, streamflow as explanatory variables of *SSC*. A SLR model relating turbidity to *SSC* is often sufficient for reliable computations of *SSC*. Criteria are provided for determining the sufficiency of a SLR model and for determining when a multiple linear regression (MLR) model relating both turbidity and streamflow to *SSC* results in a significant improvement over the SLR model that is based on turbidity alone. Typically, addition of a streamflow variable is more likely to improve the turbidity-*SSC* regression as the percentage of the *SSC* that is sand-size or larger material (coarser than 63 μm) increases. Concepts for development and use of a SLR model to compute *SSC* and, when appropriate, a MLR model as a function of turbidity and streamflow to compute *SSC*, are explained in the following sections. The following regression analysis is site-specific and applies to a single model-calibration data set. A comparison between sites and model-calibration data sets is beyond the scope of this report. Specifically excluded from these guidelines is use of a SLR model for routine computation of *SSC* solely from streamflow due to varying degrees of hysteresis common in the *SSC*-streamflow relation. Currently (2009), ADAPS is limited to only SLR models using turbidity for computing a more frequent than daily *SSC* time series (U.S. Geological Survey, 2003). For example, ADAPS cannot compute more frequent than daily *SSC* using streamflow or more than one explanatory variable.

There are a variety of approaches to building an appropriate model, including SLR and MRL (Helsel and Hirsch, 2002) and Kendell-Theil robust line (Granato, 2006). The following sections provide some general guidance on develop a linear regression model using turbidity and streamflow as explanatory (x) variables and *SSC* as the response (y) variable. Linear regression is not only used to derive a final model to compute *SSC* but also is used in the intermediate steps to determine the final model form. The hydrographer may need to evaluate the performance of more than one intermediate regression model before determining the optimal model for computing *SSC*. Regression results are an effective means for

evaluating whether or not variables should be transformed and which variables are necessary to best estimate the variability in *SSC*. The following sections describe methods by Helsel and Hirsch (2002) for deriving the optimal regression model for computing *SSC*. A detailed summary of SLR development for turbidity-*SSC* and evaluation of MLR for turbidity and streamflow-*SSC* is presented in example 1 of Appendix 1. Complete and detailed presentations of these regression methods are not presented in these guidelines and procedures but can be found in Helsel and Hirsch (2002, p. 221–263 and 295–321). S-Plus (Insightful Corporation, 2001) is the USGS-supported statistics software package for performing SLR and MLR analyses. Microsoft® Excel®can be used, but results from Excel should always be verified with S-Plus derived results. Results from both software packages are provided in example 1 of Appendix 1.

Correlation

Correlation coefficients measure the strength of association between two variables (Helsel and Hirsch, 2002). The most commonly used measure of correlation is Pearson's *r*. This correlation also is called the linear correlation coefficient because *r* measures the linear association between two variables (Helsel and Hirsch, 2002, p. 218). Measures of correlation have the characteristic of being dimensionless and scaled to lie in the range $-1 \leq r \leq 1$. When there is no correlation between two variables, $r = 0$. When the increase or decrease in the variables is synchronous, *r* is positive. When the variables vary in opposite directions, *r* is negative. When one variable is a measure of time or location, correlation becomes a test for temporal or spatial trend, respectively.

Whenever a correlation coefficient is calculated, it should be presented with a scatter plot of the data. No single numerical measure can substitute for insights that can be gained from visual examination of such a plot. Scatter plots and correlations of turbidity, streamflow, and *SSC* values are simple and convenient ways of identifying which of the variables are statistically related and whether transformation of the data might improve the relation between the explanatory and response variables (fig. 8). The hydrographer can get a better idea from a simple analysis of which or both of two variables—turbidity and streamflow—are superior for computing *SSC*. Generally, the closer the correlation coefficient is to 1 (perfect positive correlation), the stronger the association between variables.

For MLR, multicollinearity—a case of MLR in which the explanatory variables are themselves highly correlated—can result in undesirable consequences for model results. Helsel and Hirsch (2002, p. 305) suggest computing a variance inflation factor (VIF) for measuring multicollinearity. The VIF for turbidity and streamflow is readily computed by using the coefficient of determination (R^2) from the regression of turbidity on streamflow (equation 11.6 in Helsel and Hirsch, 2002, p. 305). A VIF larger than 10 (or a Pearson's *r* larger than 0.95 between turbidity and streamflow) indicates multicollinearity between turbidity and streamflow, and suggests that the use of either variable would explain about the same amount of variability and that the two variables should not be used together as explanatory variables in a MLR (Helsel and Hirsch, 2002, p. 305–6). The scatter plot and VIF of data from the Little Arkansas River near Sedgwick, Kansas (fig. 9), suggest that turbidity and streamflow are not strongly multicollinear and could be used as explanatory variables in a MLR model to compute *SSC*.

Simple Linear Regression for Computation of Suspended-Sediment Concentrations

Values of a response variable can be expressed in terms of a single explanatory variable or many explanatory variables using linear regression models (Helsel and Hirsch, 2002). An explanatory variable such as turbidity can be used in a regression model to compute the response variable *SSC*. The most common estimation technique is SLR, as presented in chapter 9 of Helsel and Hirsch (2002). SLR models can be computed using many statistical software packages. SLR analysis of the Little Arkansas River model-calibration data set yields the plots shown in figure 10 using untransformed data and in figure 11 using $\log_{10}$-transformed data.

A list of diagnostics for linear regression can be used to evaluate various steps in the model- building process (Helsel and Hirsch, 2002, p. 226–7). The coefficient of determination adjusted (R^2_a) for the number of explanatory variables (or, equivalently, the degrees of freedom) in the model indicates the fraction of variability in the response variable that is explained by the model. The root-mean-squared error (*RMSE*) is a measure of the variance between regression-computed and observed values. The *RMSE* is approximately equal to one standard deviation (σ) or the 67-percent prediction interval and is expressed in the same units as the response variable. *RMSE* expressed in log units is not directly comparable with *RMSE* expressed in milligrams per liter. *RMSE* can be expressed as a percentage (Hardison, 1969), hereinafter referred to as the model standard percentage error (*MSPE*). *MSPE* can be used to compare any regression model. For *RMSE* expressed in $\log_{10}$ units, the *MSPE* interval is:

$$\text{Upper } MSPE = \left(10^{RMSE} - 1\right) \text{x } 100, \text{ and}$$
$$\text{Lower } MSPE = \left(1 - 10^{-RMSE}\right) \text{x } 100. \quad (1)$$

For *RMSE* expressed in milligrams per liter, the *MSPE* interval is:

$$MSPE = \pm \frac{RMSE}{\bar{y}} \text{x } 100, \quad (2)$$

where

$\bar{y}$ is the mean of the response variable.

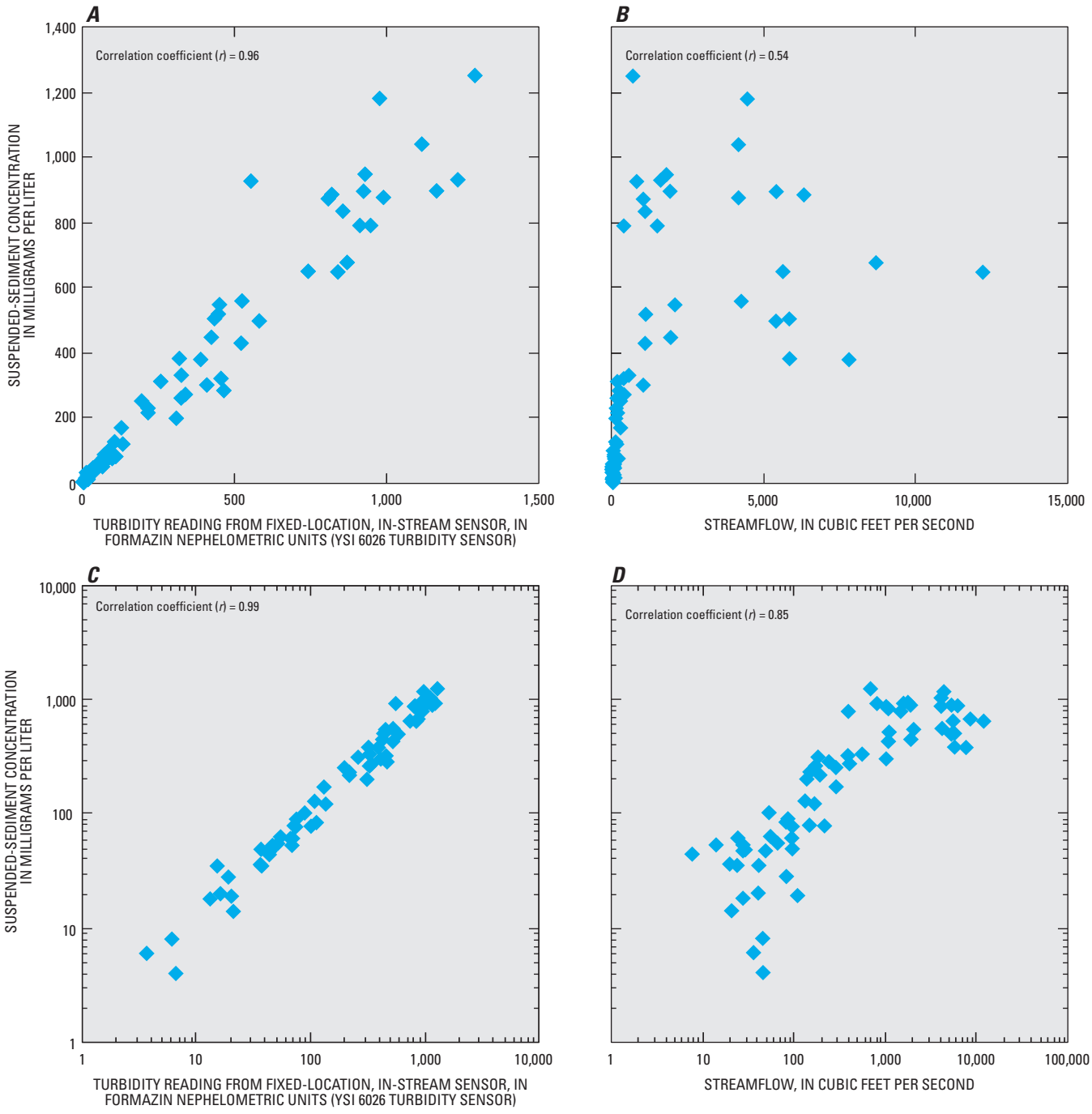

Figure 8. Relations between *A,* turbidity and suspended-sediment concentration, *B,* streamflow and suspended-sediment concentration in linear space, *C,* turbidity and suspended-sediment concentration, and *D,* streamflow and suspended-sediment concentration in $\log_{10}$ space for U.S. Geological Survey streamgage on Little Arkansas River near Sedgwick, Kansas, 1999–2005.

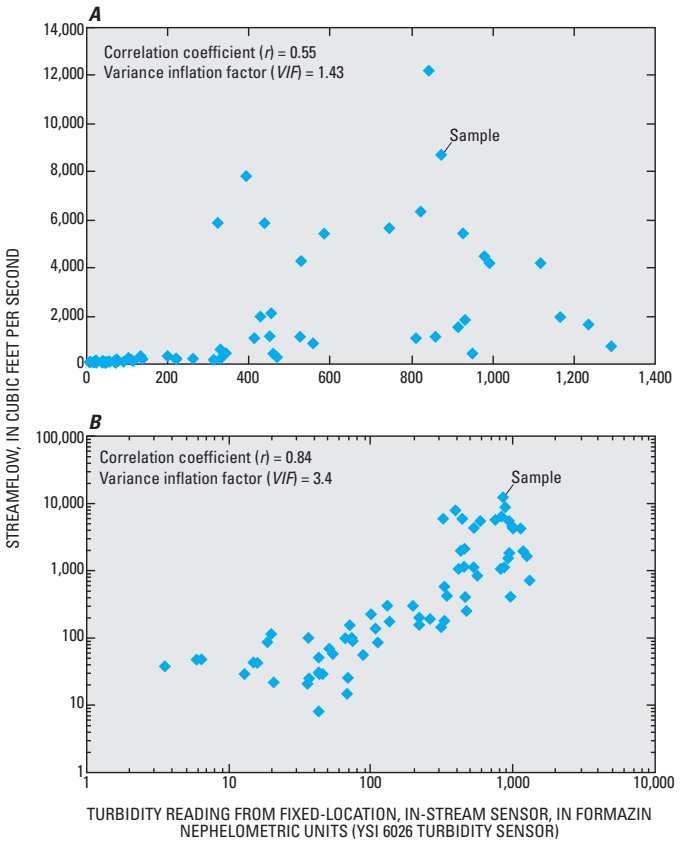

Figure 9. Comparison of turbidity and streamflow at the time of sample collection in *A*, linear space and in *B*, $\log_{10}$ space for U.S. Geological Survey streamgage on Little Arkansas River near Sedgwick, Kansas, 1999–2005.

The lowest *MSPE* corresponds to the model with the least uncertainty associated with regression-computed values. The PRESS (prediction error sum of squares) statistic is one of the best measures of the quality of a regression model and also can be computed using *RMSE* (Helsel and Hirsch, 2002, p. 247). Table 3 presents when and how a diagnostic statistic can be used for comparison among regression models. Note that none of these diagnostic statistics can be used to compare regression with different response variables units.

Transformation of Data

The purposes for transformation of data prior to an analysis are to make the residuals more symmetric, linear, and homoscedastic (associated with a constant variance). Helsel and Hirsch (2002, p. 252–4) describe the rationale for and the results of data-set transformations. Serious problems can occur when regression models are developed and residuals do not possess the assumed characteristics of symmetry, linearity, and homoscedasticity. Comparisons of transformed and untransformed data and regression results are presented throughout this section so that the hydrographer can better understand how data transformation improves the computation of *SSC*s.

Base-10 logarithmic transformation is one of several mathematical functions that sometimes can be used to transform data sets so that the assumptions for linear regression analysis are met. Helsel and Hirsch (2002, p. 12–14) discuss other transformation options and characteristics. Logarithmic base-10 transformation has been shown to be effective in normalizing residuals of turbidity-*SSC* regressions. Hydrographers should start with base-10 logarithm transformation but are encouraged to experiment with other transformation options to determine if a different transformation of the data-set results in a model that better satisfies the assumed residual characteristics for regression analysis. Other considerations should include the ease of retransforming the results from the model, the bias associated with the retransformation, and rationale for complex transformations. As Helsel and Hirsch (2002) point out, it is better to choose a single transformation for data from several sites than it is to have custom transformations for every data set. The examples presented here use a logarithmic base-10 transformation of both the response and explanatory variables, which is equivalent to the power function regression performed on untransformed variables and used for many streamflow-*SSC* transport curves (Glysson, 1987; Curtis and others, 2006). From Helsel and Hirsch (2002), page 315.

"Should *y* (*SSC*) be transformed? To decide whether to transform the *y* variable, plot residuals against predicted values for the untransformed data. Compare this to a residuals plot for the best-transformed model, looking for three things:

Table 3. Diagnostic statistics of linear regression for evaluation and comparison of regression models (Helsel and Hirsch, 2002).

[R^2, coefficient of determination; R^2_a, adjusted coefficient of determination; *RMSE*, root-mean-squared error; *MSPE*, model standard percentage error; ↑, maximize; ↓, minimize]

Type of models being compared	R^2	R^2_a	*RMSE*	PRESS	*MSPE*
Same response variable (*y*) units	↑	↑	↓	↓	↓
Differing response variable (*y*) units					↓
Same *y* and same number of *x* variables	↑	↑	↓	↓	↓
Same *y* and varying number of *x* variables		↑	↓	↓	↓
Should *y* be transformed?					↓
Should *x* ('s) be transformed?	↑	↑	↓	↓	↓

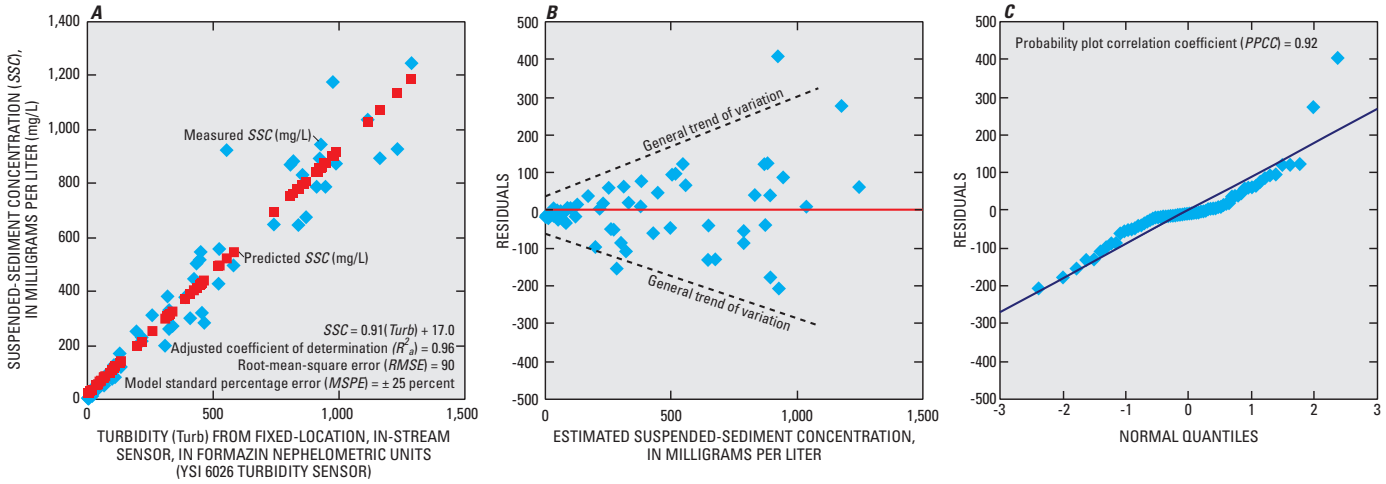

Figure 10. Results of simple linear regression analysis for *A,* turbidity and suspended-sediment concentration data, and a comparison of *B,* computed suspended-sediment concentrations and regression residuals, and *C,* probability plot of residuals for U.S. Geological Survey streamgage on Little Arkansas River near Sedgwick, Kansas, 1999–2005.

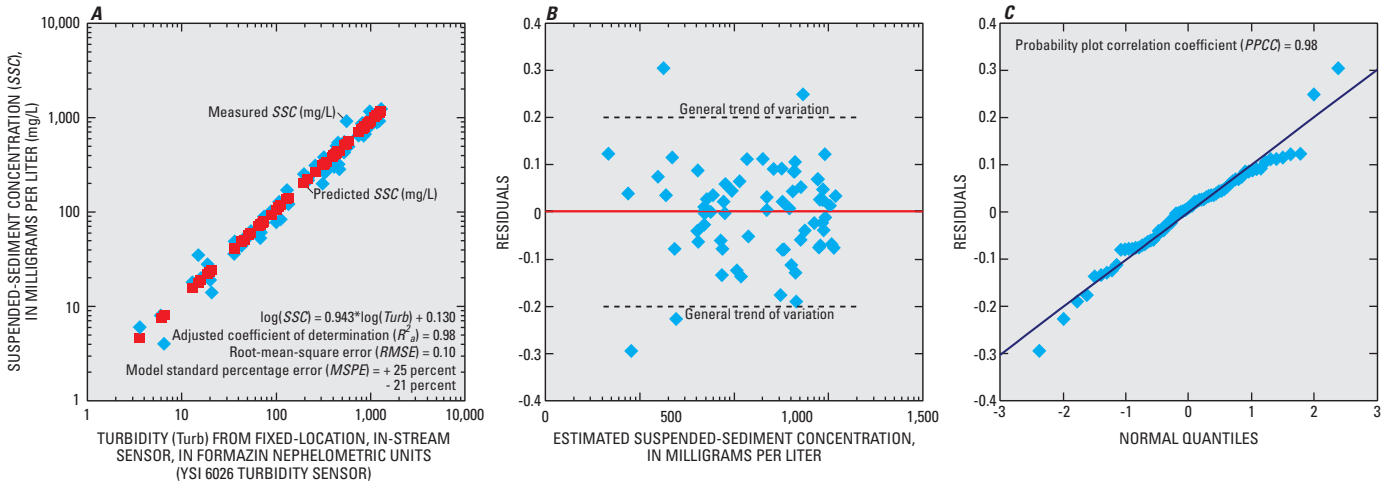

Figure 11. Results of simple linear regression analysis using log-transformed data for *A,* turbidity and suspended-sediment concentration data, and comparison of *B,* estimated $\log_{10}$ suspended-sediment concentration and regression residuals, and *C,* probability plot of residuals for U.S. Geological Survey streamgage on Little Arkansas River near Sedgwick, Kansas, 1999–2005.

1. Constant variance across the range of the *y* (*SSC*);
2. Normality of residuals; and
3. A linear pattern, not curvature, centered vertically around the zero residual line.

The statistics R^2, R^2_a, *RMSE*, and PRESS are not appropriate for comparison among models having different units of *y*.

Should *x* (or several *x*'s) be transformed? The decision about whether to transform an *x* variable should be made using partial-residual plots. Check for the same three patterns of constant variance, normality, and linearity. Considerable help can be obtained from statistics such as R^2_a (maximize it), or *RMSE* or PRESS (minimize it). Many transformations can be rapidly checked with such statistics, but a residuals plot should always be produced and inspected prior to accepting or rejecting a transformation scheme."

Model Residual Analysis

Regression models are evaluated by examining the model residuals. Ordinary residuals are defined as the difference between the observed values and the model estimates (the term "model estimate" is used here because the values are estimates of actual samples or observed values). The residual error (e_i) for the computed *SSC* values should be random and, in theory, should be normally distributed with a mean of zero and a constant variance (Helsel and Hirsch, 2002). The residuals from a regression of *SSC* on turbidity indicate how

the model-estimated *SSC* varies from the observed *SSC*. A residual value of 0 indicates that the model-estimated *SSC* is equal to the observed value. A positive residual indicates that the observed value was larger than the estimated value, and a negative residual indicates that the observed value was less than the estimated value.

The variance of the residuals can be evaluated by plotting them against the model estimated *SSC* (figs. 10*B* and 11*B*). The residuals plotted in figure 10*B* indicate a heteroscedastic pattern (nonconstant variance; as indicated by the dashed lines) where the variability of the residuals increases as estimated *SSC* values increase, which suggests the need for some sort of variance stabilizing transformation of the response variable. The residuals plot for the $\log_{10}$-transformed regression (fig. 11*B*) indicates a homoscedastic pattern (constant variance) and a more normal distribution. Normality of residuals can be evaluated by plotting residuals on a normal-probability plot (figs. 10*C* and 11*C*) and computing the probability plot correlation coefficient (PPCC; Helsel and Hirsch, 2002, p. 253). Non-normally distributed residuals will not be linear or equally distributed on a normal-probability plot and have a smaller PPCC. The probability plot for the $\log_{10}$-transformed regression provides a more linear, even distribution of residuals and a slightly larger PPCC than the residuals from the regression with untransformed variables (figs. 10*C* and 11*C*). The plots in figures 10*B* and 11*B* confirm that $\log_{10}$ transformation provides more homoscedastic, normally distributed residuals.

Simple Linear Regression Model and Bias Correction Factor

The SLR model for the Little Arkansas River near Sedgwick, Kansas, for data collected from November 1998 to June 2005 is shown below with basic model information, regression coefficients, model diagnostics, and Duan's bias correction factor (Duan, 1983):

$$\log_{10}(SSC) = 0.943\log_{10}(Turb) + 0.130, \quad (3)$$

where

SSC is suspended-sediment concentration, in milligrams per liter, and

Turb is turbidity, in formazin nephelometric units, measured with YSI model 6026.

Model information:

Number of measurements = **68**,
root-mean-squared error (*RMSE*) = **0.10**,
model standard percentage error (*MSPE*) = **+ 25.9 and -20.6 percent**,
90-percent prediction interval = **± 41 percent**,
adjusted coefficient of determination (R^2_a) = **0.98**,
PRESS = **0.663**.
Duan's bias correction factor = **1.03**.

Coefficients:

	Value	Standard error	t-statistic	p-value
Intercept	**0.130**	**0.041**	**3.02**	**0.0035**
$\log_{10}$(turbidity)	**0.943**	**0.018**	**50.9**	**1.13E-54**

Correlation matrix of coefficients:

	Intercept	$\log_{10}(Turb)$
Intercept	1	
$\log_{10}(Turb)$	-0.9588	1

Some of the regression statistics are useful in evaluating this regression model. For example, the *RMSE* (even though it is expressed in log units), the *MSPE*, and the 90-percent prediction interval indicate the range in uncertainty associated with each regression-computed *SSC* value. R^2_a indicates that the regression model explains 97 percent of the variability in sampled *SSC*. The PRESS is only relevant for comparisons to other regression models with the same response variable units. The t-statistics for the *y* intercept and coefficient (slope) of $\log_{10}$(turbidity) are larger than 2, and the p-values are less than 0.05, indicating that both are significant and should be included in the final model form. Helsel and Hirsch (2002, p. 239) discuss the option of omitting the *y* intercept (thus forcing the *y* intercept to equal zero). There are several tests the hydrographer can perform to help aid in the decision, but generally, omitting the *y* intercept is discouraged. Hydrographers are encouraged to develop a regression model by forcing the *y* intercept to equal zero as an iterative step in better understanding the data set and the effect of certain data points, specifically the smaller turbidity-*SSC* values.

Transformation of the response variable (*SSC*) has a consequence that must be considered when computing *SSC*: The regression estimates must be retransformed to the original units, a step that introduces a bias (usually negative) in computed *SSC* values (Miller, 1951; Koch and Smillie, 1986) unless the data are perfectly and positively correlated [as the R^2_a approaches 1.0, the bias correction factor (BCF) also approaches 1.0]. The bias arises because regression estimates are the mean of *y* given *x* in log units, and retransformation of these estimates is not equal to the mean of *y* given *x* in linear space. To correct for this retransformation bias, Duan (1983) introduced a nonparametric BCF called the "smearing" estimator (Helsel and Hirsch, 2002, p. 256). The equation to compute the smearing BCF for base-10 logarithmic transformation is:

$$BCF = \frac{\sum_{i=1}^{n} 10^{e_i}}{n}. \quad (4)$$

where

n is the number of samples, and

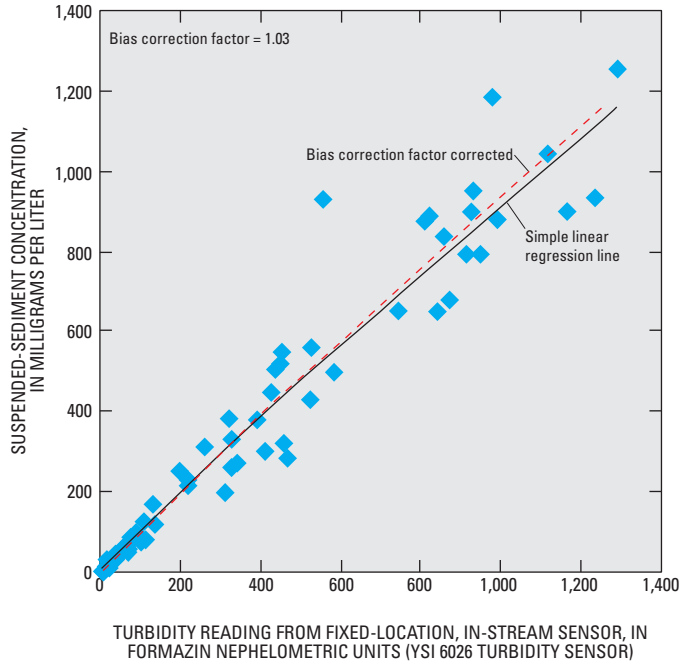

Figure 12. Comparison of turbidity and suspended-sediment concentration model-calibration data and uncorrected and bias-corrected simple linear regression lines for U.S. Geological Survey streamgage on Little Arkansas River near Sedgwick, Kansas, 1999–2005.

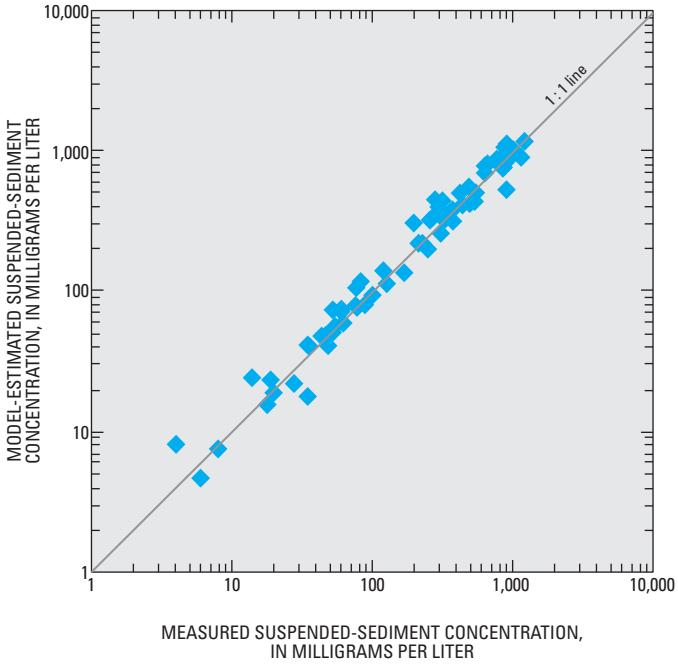

Figure 13. Comparison of measured and model-estimated suspended-sediment concentrations for U.S. Geological Survey streamgage on Little Arkansas River near Sedgwick, Kansas, 1999–2005.

e_i is the residual or the difference between each measured and estimated concentration, in log units.

Regression-computed *SSC* values for Little Arkansas River near Sedgwick, Kansas, are corrected for bias by multiplying the retransformed *SSC* value by the BCF.

Model-calibration data plotted concomitant with the bias-corrected model line may not always result in what appears to be the best fit of the data. For BCFs larger than 1.0, model values will plot on the high side (more data points are below the curve than above it; fig. 12); that is, when the results of the simple linear-regression line are multiplied by the BCF and plotted, the curve is shifted upward from the original position. This same effect of BCFs with sediment-transport equations has been shown to fit data on the high side in other sediment-transport studies (Bent, 2000). There also is an exact, minimum-variance unbiased estimator (MVUE; Cohn and others, 1989), but MVUE assumes a normal distribution of the residuals, which frequently is not the case.

A comparison of measured and model-estimated *SSC* indicates the accuracy of the regression model (fig. 13). The closer that points plot to the 1:1 line the more accurate the model predictions are.

Once the turbidity-*SSC* model is determined, the hydrographer needs to consider the potential benefits of adding streamflow as an explanatory variable. SLR analysis is preferred for sites where turbidity is the measure most strongly correlated with *SSC* or where *MSPE* is less than 20 percent. Sites with a homogeneous source of suspended sediment and more than about 80 percent of the suspended material finer than 63 µm are the best candidates for *SSC* computations using the SLR model. When turbidity is less correlated with *SSC* or when the MPSE is larger than 20 percent or sand (particle size coarser than 63 µm) constitutes an increasing percentage of the sediment in suspension as *SSC* increases, streamflow in addition to turbidity may better describe the variability in *SSC*. MLR model building is similar to SLR but should not precede SLR model development. Methods for building MLR models are discussed in a later section of this report titled "Multiple Linear Regression."

Prediction Intervals

Prediction intervals can be used to evaluate the uncertainty of *SSC* regression-computed values (Helsel and Hirsch, 2002). Prediction intervals define a range of values for the regression estimate associated with a known level of certainty. For a given turbidity value (explanatory variable), the 90-percent prediction interval represents a range of values within which there is a 90-percent certainty that the true *SSC* value occurs. The larger the 90-percent prediction interval, the more uncertainty there is associated with computed *SSC*. The prediction interval for a single response y_i is approximately:

$$E(y_i) \pm t \times s, \quad (5)$$

where

$E(y_i)$ is the regression-estimated value, at x_i;

t is the value of the student's t distribution having n-2 degrees of freedom (n is the number of observations) with the exceedance probability of $\alpha/2$ (alpha value obtained from t tables in the appendix of most statistics textbooks) for 90-percent prediction interval $\alpha = 0.10$; and

s is the standard error of regression or the *RMSE*.

Multiple Linear Regression

As previously stated, MLR represents an alternate tool for computing *SSC*s when the SLR *MSPE* is larger than 20 percent. However, MLR should only be considered for use when the p-value (probability value) of the partial F statistic (Helsel and Hirsch, 2002, p. 298) for streamflow is less than 0.025. Comparison plots of the residuals from the turbidity-*SSC* SLR to streamflow can indicate when an MLR model may decrease the amount of variability explained. The residual plots for the Little Arkansas River near Sedgwick, Kansas, indicate that there is little or no change in variability with streamflow (fig. 14*A* and *B*). Neither of these plots supports the addition of streamflow to the *SSC* model.

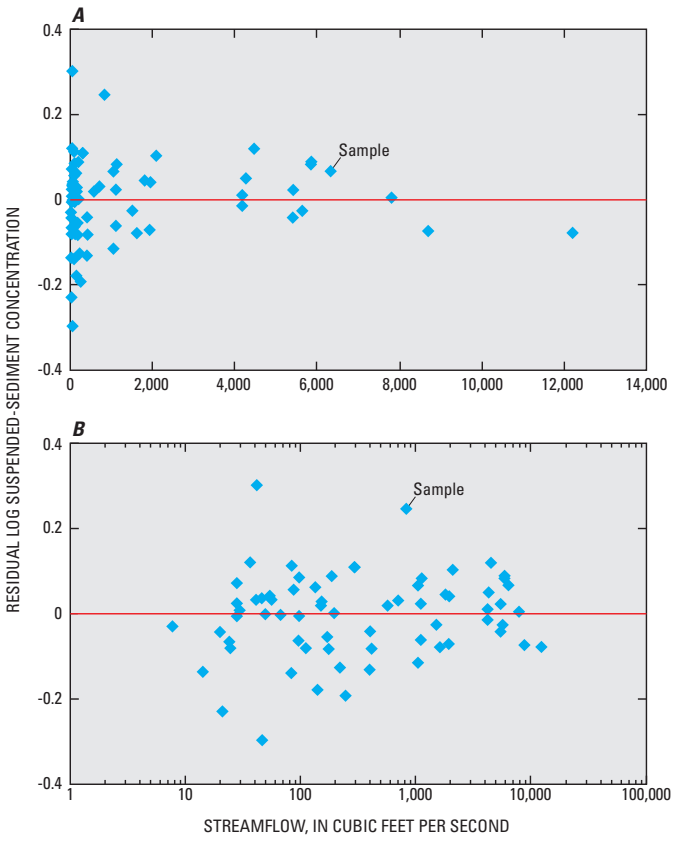

Figure 14. Comparison of streamflow in *A,* linear space and in *B,* $\log_{10}$ space to residuals from a simple linear regression analysis of turbidity and suspended-sediment concentrations for U.S. Geological Survey streamgage on Little Arkansas River near Sedgwick, Kansas, 1999–2005.

Other methods for evaluating which explanatory variables to include in the regression model are part of MLR model-building method described in Helsel and Hirsch (2002, p. 312–315). The possible explanatory variables in this case include turbidity and streamflow. Turbidity and streamflow are typically $\log_{10}$ transformed for a better regression model, but any combination of transformed or untransformed explanatory variables can be evaluated.

The *MSPE* for the SLR model of the Little Arkansas River near Sedgwick, Kansas, is larger than 20 percent, indicating that a MLR model with streamflow and turbidity should be considered. The streamflow variable is deemed significant in the regression model if the p-value of the partial F statistic is less than a predetermined alpha value (α) of 0.025. As shown in table 4, the p-value is larger than 0.025 for streamflow in the MLR model for the Little Arkansas River near Sedgwick, Kansas, indicating that the SLR model–and not a MLR model–should be used for computing *SSC*. The R^2_a should never be the sole criterion used to assess the appropriateness of a regression model because a large R^2_a can occur even though the linear fit is poor (see Helsel and Hirsch, 2002, p. 18 and 228, and Glysson, 1987, p. 39–43). The regression diagnostics are reported in the default regression model output from Microsoft Excel or the "Regression Subset Selection" option of the USGS library for S-Plus for Windows (Slack and others, 2003).

Comparison plots of measured and model-estimated *SSC* for the SLR and MLR models can indicate the regression model with the most accuracy (fig. 15*A* and *B*). The closer the points plot to the 1:1 line, the more accurate the model predictions are. The variance of the MLR residuals should be evaluated and compared to the SLR residuals (fig. 15*A* and *B*). The measured/estimated *SSC* and residual plots are nearly identical for the SLR and MLR models, suggesting that the models produce similar results.

Regression Model Summary

The regression model selected to compute *SSC* time-series values for the Little Arkansas River near Sedgwick, Kansas, is the turbidity-*SSC* SLR model. Comparisons with the MLR model indicate that the addition of the streamflow variable slightly improved the *SSC* prediction but not sufficiently so as to justify its inclusion. In general, the simplicity of a SLR model is preferred over a MLR model that imparts modest improvement in accuracy to the computational process. Currently (2009), ADAPS (U.S. Geological Survey, 2003) can compute *SSC* using a SLR model. The use of ADAPS for computing *SSC* is desired because of the documentation of the regression model and when it was used. Had the MLR model been chosen, *SSC* values would have to be

Table 4. Expressions for determining use of simple linear regression (SLR) or multiple linear regression (MLR) models for U.S. Geological Survey streamgage on Little Arkansas River near Sedgwick, Kansas.

[*n,* number of samples; R^2_a, adjusted coefficient of determination; *RMSE*, root-mean-squared error in log units; *MSPE*, model standard percentage error; n/a, not applicable]

Explanatory variables	*n*	R^2_a	*RMSE*	*MSPE*	p-value for streamflow	t-statistic for streamflow
Turbidity	68	0.975	0.101	+25.9, -20.6	n/a	n/a
Turbidity and streamflow	68	0.977	0.098	+25.3, -20.2	0.043314	2.06

computed outside of ADAPS and then loaded to ADAPS (see Appendix 2).

A summary of regression information and expressions should be recorded in the station analysis for "Suspended Sediment" (example 1 of Appendix 1). The summary contains information specific to the development of the regression model. The hydrographer should summarize the reasoning for selection of the model, the final regression model and associated statistics, and the dates for which the model was used to compute *SSC* and *SSL*. A senior hydrographer should review the summary to determine its adequacy.

Computation of Suspended-Sediment Concentration and Load Time-Series Record

SSC time series should be computed at the same time step as the measured in-stream turbidity and streamflow time series by means of an appropriate regression model. Depending on the model form and which explanatory variables are used, the regression model can be implemented as a turbidity-*SSC* rating in NWIS to calculate a *SSC* time series. Details for developing a *SSC* time series within NWIS are presented in Appendix 2.

Log_{10}-transformed SLR models can be expressed as a power function and used to compute instantaneous values of *SSC* in ADAPS. The "equation rating" in ADAPS computes instantaneous values for the output data description (DD) and *SSC* on the basis of instantaneous values of the input DD (turbidity; U.S. Geological Survey, 2003). Retransformation of the $\log_{10}$-transformed SLR model (equation 6) is shown in equation 7.

The $\log_{10}$-transformed SLR model follows:

$$\log_{10}(SSC) = b_1 \log_{10}(Turb) + b_0, \quad (6)$$

where

SSC is suspended-sediment concentration, in milligrams per liter;
b_1 is the slope;
Turb is turbidity; and
b_0 is the y intercept.

The $\log_{10}$-transformed SLR model (equation 6) can be retransformed and corrected for bias with a BCF resulting in equation 7:

$$SSC = 10^{b_0} Turb^{b_1} \times BCF. \quad (7)$$

For the Little Arkansas River near Sedgwick, Kansas, the model, $\log_{10}SSC = 0.943\log_{10}Turb + 0.130$, and *BCF*, 1.03, can be retransformed to $SSC = 10^{0.130}Turb^{0.943} \times 1.03$, or

$$SSC = 1.39Turb^{0.943}. \quad (8)$$

The hydrographer also should consider and perhaps limit computed values extrapolated beyond the range of explanatory variable values (minima and maxima of the explanatory variables). The veracity of extrapolated model values must be evaluated. Typically, the number of extrapolated values can be minimized if: (1) the range of the model-calibration data set is maximized by collecting samples at both extremes, and (2) the make and model of the fixed-location turbidity sensor are identical to the manually deployed field-turbidity sensor with similar maximum recording levels. Computed values that are substantially beyond the range of the calibration data should be withheld from public display until those values can be verified by new *SSC* data. If a replacement or supplemented sensor has a maximum recording level that is more than 10 percent larger than the maximum value of the calibration data set, the computed *SSC* values greater than the calibration data set maximum should be withheld from display until those values can be verified with samples collected in the range between the new sensor maximum recording level and the upper limit of the regression model.

Estimates for Periods of Missing Data

USGS policy (2009) precludes storage of estimated instantaneous values of turbidity in the NWIS database (Office of Water Quality Technical Memorandum 2005.03; U.S. Geological Survey, 2005). However, data collected from sources other than the fixed-location turbidity sensor can be used to supplement discrete periods of missing turbidity time-series record, which includes periods for which measured turbidity values are considered unreliable, such as from turbidity sensor

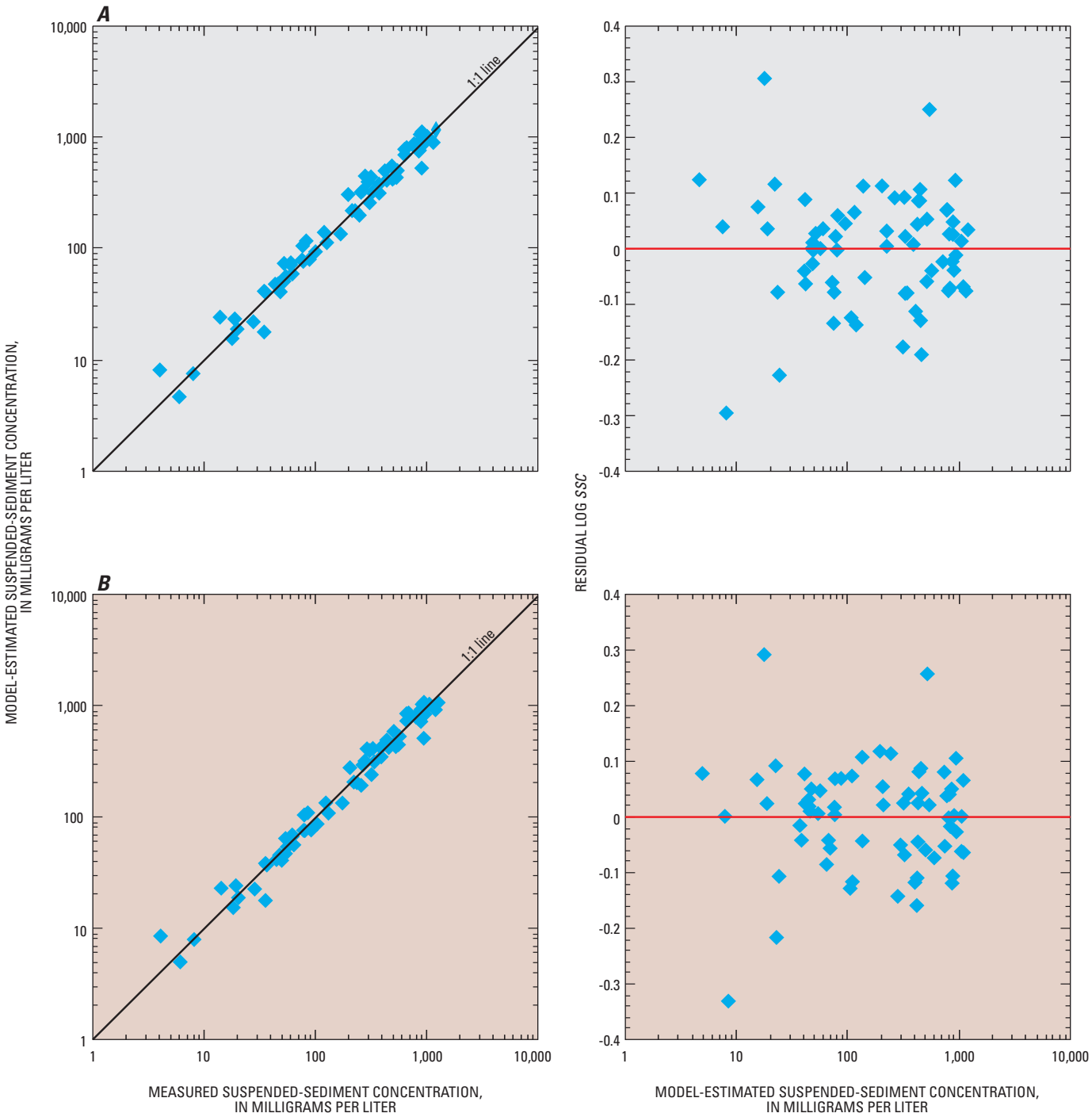

Figure 15. Comparison of measured and estimated suspended-sediment concentrations and residuals in log space from *A,* simple and *B,* multiple linear regression models for U.S. Geological Survey streamgage on Little Arkansas River near Sedgwick, Kansas.

truncation at large *SSC* values. For example, onsite measurements made using a cleaned and calibrated field sensor while the fixed-location sensor is being cleaned and calibrated can be used to fill in a part of the missing turbidity time-series record during the site visit.

The appropriateness of estimating mean daily turbidity values is governed by a number of factors, the most effectual of which are the duration of the missing record, availability of flow data for the missing-record period, and the availability of data describing historical relations among turbidity, streamflow, and *SSC*. Daily statistics for periods containing missing data should be calculated with an appropriate level of scrutiny and in accordance with Wagner and others (2006). Mean daily turbidity values should not be calculated solely for the purpose of calculating mean daily *SSC* values. Daily *SSC* values should be estimated by methods described by Porterfield (1972) or Koltun and others (2006). The hydrographer should note in the station analysis that the uncertainties associated with *SSC* estimates derived from estimated turbidity data are unknown. Rasmussen and Ziegler (2003), Bragg and others (2007), and Lee and others (2009) demonstrate different techniques for estimating missing or truncated instantaneous values of turbidity and *SSC*.

Estimation of missing or truncated instantaneous *SSC* values (without estimating turbidity values) in some instances can be performed outside of ADAPS to meet study objectives. The method(s) used in those instances to develop estimates should be well documented and peer reviewed.

Computation of Suspended-Sediment Load Time-Series Record

A time series of *SSL* is calculated from *SSC* and streamflow for the same site. Instantaneous *SSL* is calculated using the following equation:

$$SSL_i = SSC_i \times Q_i \times c, \tag{9}$$

where

SSL_i is the computed suspended-sediment load, in tons per second, or pounds per second;
SSC_i is the computed suspended-sediment concentration for the ith value, in milligrams per liter;
Q_i is the streamflow for the ith value, in cubic feet per second; and
c is a constant, 3.121×10^{-8}, for converting the units to tons per second, or 6.242×10^{-5} for pounds per second.

The instantaneous *SSC* and streamflow values also can be used to compute daily, monthly, or annual *SSL*s using the following equation:

$$SSL_n = \sum_{i=1}^{n} \frac{\left(C_1 + C_{i-1}\right) \times \left(Q_i + Q_{i-1}\right) \times \left(t_i - t_{i-1}\right)}{4} \times c, \tag{10}$$

where

SSL_n is the computed suspended-sediment load for the desired time period, in tons;
C_i is the suspended-sediment concentration for the ith time, in milligrams per liter;
C_{i-1} is the suspended-sediment concentration for the ith minus 1 time, in milligrams per liter;
Q_i is the streamflow for the ith value after midnight, in cubic feet per second;
Q_{i-1} is the streamflow for the ith minus 1 value after midnight, in cubic feet per second;
t_i is the time for the ith value after midnight;
t_{i-1} is the time for the (ith-1) value after midnight;
c is a constant, 0.0027, for converting the units to tons per day; and
n is the number of instantaneous values within the desired period (day, month, year).

The hydrographer should identify any periods of missing record and determine how to provide the best estimate of *SSL* for periods when computed *SSC* data, streamflow data, or both are missing. The options to estimate *SSL* include: (1) interpolate the missing values between known values, taking into consideration other available data, (2) estimate *SSL* on the basis of some other data, such as streamflow (a sediment-transport curve for the site) or *SSL* derived from a streamgage with similar sediment characteristics using appropriate scaling factors, or (3) another technically supportable method. Regardless of the method or combination of methods used to estimate missing *SSL* data, the rationale should be fully explained in the station analysis or associated report.

Uncertainty estimates of long-term suspended-sediment load computed by summing retransformed *SSC* from SLR or MLR models with transformed response variables can be computed. Estimates of the mean squares errors are discussed in Gilroy and others (1990).

Model Validation and Maintenance of a Long-Term Suspended-Sediment Concentration Record

Once an acceptable regression model is developed, it can be used to compute *SSC* beyond the period of record used in model development with proper sample collection and analysis. Maintenance of a long-term *SSC* record requires ongoing collection of turbidity and streamflow time-series data and sample collection for reanalysis and verification of the current *SSC* regression model. The method for validating the regression model is affected by the frequency of calibration-sample collection and the purpose of the study. Regression models can be validated annually (or at some other frequency as needed on the basis of the nature of the monitored hydrologic system and its watershed, and the needs and constraints of the monitoring program) after sufficient applicable new data have been collected or on the basis of other valid criteria. A fundamental

characteristic of hydrology is variability, with periods of floods and periods of droughts. Additionally, watershed conditions can change seasonally or from other factors such as through changes in land use, implementation of best management practices, or by wildfire. Therefore, regression models to compute *SSC* at a site should never be considered static but rather considered to represent a set period in a continually dynamic system in which additional data will help verify any change in *SSL*, type, and source.

Validation of Suspended-Sediment Concentration Model

One approach to updating the regression model is to plot new observations with the original model-calibration data set and recompute the regression coefficient(s) and *y*-intercept. Typically, at least 4 to 10 *SSC* samples and associated turbidity and streamflow values representing a wide range of streamflows are collected annually, depending on the site and monitoring program, to validate the existing regression model. More such data may be needed. The additional data plotted along with the model-calibration data set for comparison should indicate any significant change in the turbidity-*SSC* relation that would signal the need for a completely revised regression model or additional and more frequent sample collection. A review of the scatter plot for the Little Arkansas River near Sedgwick, Kansas, suggests that there has been no significant change in the turbidity-*SSC* relation (fig. 16).

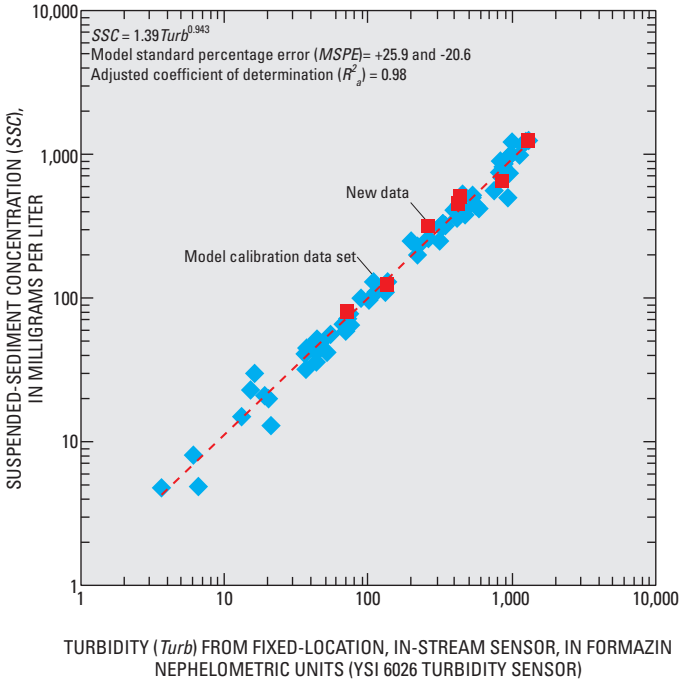

Figure 16. Model-calibration data set (water years 1999–2005) and new (water year 2006) turbidity and suspended-sediment concentration data for U.S. Geological Survey streamgage on Little Arkansas River near Sedgwick, Kansas.

A regression model developed from new measurements not used in previous model development should be compared to the existing regression model. Analysis of covariance (ANCOVA; see Helsel and Hirsch, 2002, p. 316) can be used to test (1) the regression model on the basis of the original model data and additional data, (2) the original regression model, and (3) the regression model solely on the basis of the additional data. ANCOVA will determine if the slope or *y* intercept of any of these models is significantly different, indicating a fundamental shift in the turbidity-*SSC* relation and the possible need to develop a new model. If a shift occurred, the hydrographer also will need to determine when it occurred and when to cease use of the existing model and begin use of a new model. A fundamental shift such as this should be accounted for by a major change in sediment source or transport processes in the watershed, such as those resulting from a substantial change in land use or land cover, construction or removal of an impoundment, wildfire, landslide, or a major flood. A more likely scenario is a gradual change over years that can be detected only by continued sample collection and analysis.

New data that do not significantly change the original regression should be added to the model-calibration data set to refine the regression model. The slope, *y* intercept, and the computed *SSC* values from the new model will not be significantly different from the old model, but the improved estimate of *RMSE* may reduce the prediction interval. The hydrographer has to determine when the refined model will take effect. If sample collection and analysis are considered on an annual basis, the new model should start at the beginning of the ensuing water year. An approved computed *SSC* time series should not be recomputed unless there is strong evidence that the turbidity-*SSC* relation changed during the approved period. The hydrographer in this case has determined that the revised model (fig. 16) will take effect at the beginning of water year 2006.

Sampling Plan

A sampling plan to obtain the requisite turbidity, streamflow, and *SSC* data should be devised to periodically validate and refine the existing regression model. Conditions or events that may cause variability in the turbidity-*SSC* relation also should be considered when devising a sampling plan for maintaining long-term *SSC* record. Sample values from the model-calibration data set may indicate periodic, seasonal, or other fluctuations that may induce variability in the current model. These fluctuations should be considered when collecting representative samples to facilitate adequate validation of an existing regression model. A prudent and affordable annual sampling plan for the Little Arkansas River near Sedgwick, Kansas, includes two to four spring stormwater runoff sample sets, two to four summer stormwater runoff or

base streamflow sample sets, and one to two winter base-flow sample sets.

Changes to Turbidity Sensor Model or Type

Different sensors can provide different turbidity readings for the same environmental sample (Landers, 2003). Manufacturers have made improvements and design changes to turbidity sensors over time. A change of sensor model or type most likely will require an adjustment to the historical values so that the equivalency of turbidity-sensor-response characteristics of historical and newly collected data is maximized. The hydrographer should compare turbidity measurements between differing sensors in a range of environmental samples. The difference between sensors cannot be identified in formazin standards (Hach; Loveland, Colo.) and may be reversed in polystyrene bead standards (APS Analytical Standards Inc.; Redwood City, Calif.; fig. 17).

Typically, turbidity data collected with an old sensor can be adjusted to an approximately equivalent reading for a new sensor by means of a conversion factor. The conversion factor is computed from a data set consisting of concurrent turbidity measurements collected by the old and new sensors arrayed adjacent to each other in the stream. Care should be taken to ensure that the range of the concurrent measurements spans the known range of turbidity values at the site. One way of achieving this is to operate both sensors in-stream, side-by-side, over a wide range of turbidity conditions. The resulting data set will provide a robust conversion factor for the monitoring site.

The site-specific turbidity conversion factor can be calculated several ways, such as from the mean or median of the instantaneous conversion factors or by means of an ordinary least squares (OLS) regression (if the relation is linear; fig. 18). The median conversion factor computed as the ratio, new sensor value/old sensor value, is the least likely to

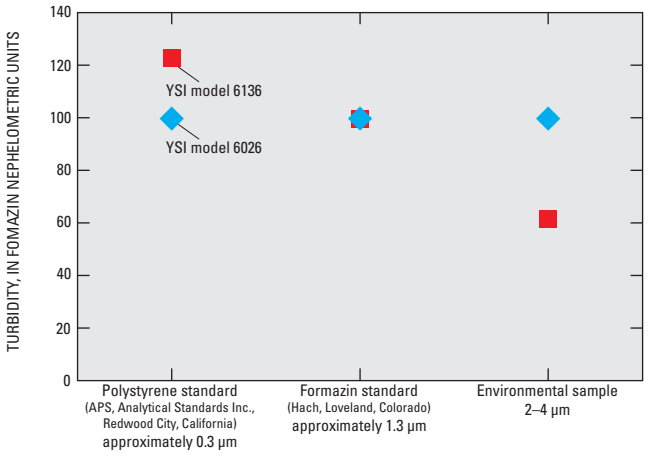

Figure 17. Comparison of turbidity measurements from YSI turbidity models 6026 and 6136 (YSI Incorporated, Yellow Springs, Ohio) in various solutions.

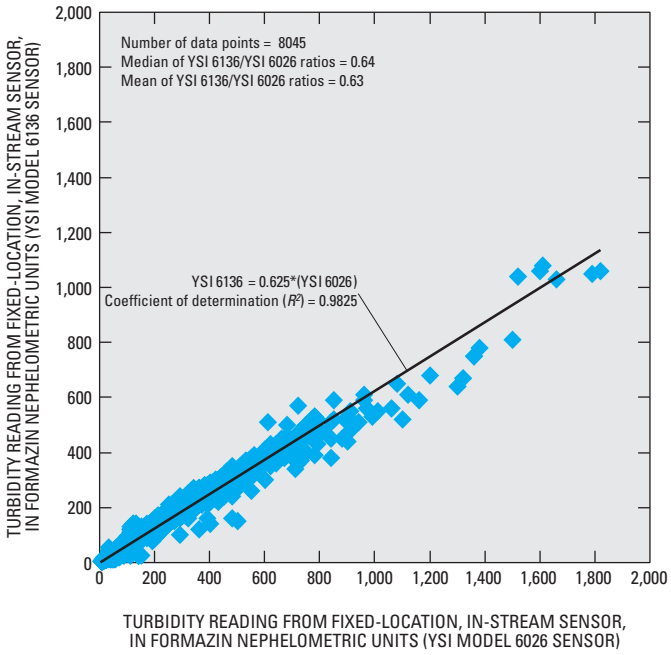

Figure 18. Relation between YSI 6026 and YSI 6136 turbidity sensor values, U.S. Geological Survey streamgage on Little Arkansas River near Sedgwick, Kansas, July 14, 2004, to August 26, 2005.

be affected by outliers and was selected for use. YSI Incorporated (2003) suggests a conversion factor of 0.65 for converting turbidity measurements made with sensor model 6026 to comparable measurements made with sensor model 6136. The conversion factor for the Little Arkansas River near Sedgwick, Kansas, was 0.64, which was obtained by taking the median of the instantaneous conversion factors from several months of concurrent in-stream turbidity measurements with both sensors (fig. 18).

The model-calibration data set can be adjusted using the conversion factor, and new regression model coefficients can be computed for the historical turbidity data. Each historical turbidity value in the model-calibration data set is multiplied by an empirically derived (or, lacking that, manufacturer-specified) conversion factor. Thus, the converted historical data are normalized with respect to the non-model data so that either sensor would provide the same value under identical environmental conditions. The adjusted model-calibration data then are used to recompute the regression model for computing *SSC* following the same steps used to develop the original model. The revised regression model then can be used to compute *SSC* on the basis of measurements from the new turbidity sensor. Historical *SSC* and turbidity time-series data with the ADAPS aging status of "approved" should not be recalculated or deleted. The hydrographer should plot the time series of historical *SSC* values that overlap with the time series from the new *SSC* regression model to ensure that the new and old equations are comparable.

Factors Affecting Relation Between Turbidity and Suspended-Sediment Concentration

The hydrographer should be mindful of factors other than *SSC* that can affect turbidity measurements. Particle size, shape, and color all affect the amount of light scattered, the important parameter for turbidity (Sutherland and others, 2000). Light is absorbed and scattered as it travels from a light source, to suspended particles, and is reflected back to a detector. When particle sizes larger than about 90 µm (very fine sand) are in suspension, the turbidity-*SSC* relation will be negatively biased, and that bias will increase as particle size increases (Anderson, 2005). Particle shape affects the scatter intensity. Darker or more black-colored (Munsell Color Co., 2000) particles also have been shown to substantially affect turbidity measurements by imparting a negative bias in measurements (Sutherland and others, 2000). Insights as to the potential effects of these and other factors might be gained from having particle-size and color analyses performed on selected water-sediment samples. Other factors affecting the turbidity-*SSC* relation are measurement error (including *SSC* sample collection and analysis) and natural variability caused by processes not evaluated in the regression model. Turbidity resulting from the presence of suspended microorganisms–principally phytoplankton–can result in increased uncertainty in the *SSC* determination. Hence, caution should be used when inferring *SSC* from turbidity or turbidity and streamflow values in water with substantial microbiological activity.

Summary

Collection, computation, and publication of suspended-sediment and related environmental data are a necessary part of investigations to evaluate effects of fluvial sediment and sediment-associated constituents on water resources. In-stream continuous turbidity data, or continuous turbidity and streamflow data, calibrated with measured suspended-sediment concentration (*SSC*) data, can be used to compute a time series of *SSC* and suspended-sediment load (*SSL*). Development of a simple linear regression model between turbidity and measured *SSC* data is the first step in computing a *SSC* time series. If the model standard percentage error (*MSPE*) simple linear regression model meets an established minimum criterion, this model can be used to compute a time series of *SSC*. If the simple regression model does not meet the acceptability criterion, a multiple linear regression model using paired instantaneous turbidity and streamflow data is developed. If the addition of streamflow is statistically significant and the uncertainty associated with the multiple regression model results in an improvement over that for the simple linear model and is ultimately acceptable, it is used as the basis for computing a time series of *SSC*. The computed *SSC* time series is subsequently used with its paired streamflow time series to compute a time series of *SSL* by standard U.S. Geological Survey techniques. Time-series *SSC* and *SSL* data can be used to better describe variability in suspended-sediment conditions, to evaluate *SSC* relative to numerical water-quality criteria and management goals, and to make watershed comparisons.

Once an acceptable regression model is developed, it can be used to compute *SSC* beyond the period of record used in model development with proper sample collection and analysis. Maintenance of a long-term *SSC* record requires ongoing collection of turbidity and streamflow time-series data and calibration-sample collection for reanalysis and verification of the current *SSC* regression model. The method for validating the regression model is affected by the frequency of sample collection and the purpose of the study. Regression models can be validated annually (or at some other frequency as needed on the basis of the nature of the monitored hydrologic system and its watershed, and the needs and constraints of the monitoring program) after sufficient new data have been collected or on the basis of other valid criteria. Regression models to compute *SSC* are generally site specific and should never be considered static but rather considered to represent a set period in a continually dynamic system in which additional data will help verify any change in *SSL*, type, and source.

Acknowledgments

This report was prepared by the USGS Kansas Water Science Center (WSC), Lawrence, Kansas, and the Offices of Surface Water and Water Quality, Reston, Virginia. USGS personnel in the California, Kansas, Oregon, and Pennsylvania WSCs provided astute technical advice and assistance. Information, discussion, comments, and suggestions from Teresa J. Rasmussen (Kansas WSC) and USGS colleague reviewers Paul A. Buchanan (California WSC), Elizabeth A. Hittle (Pennsylvania WSC), Gregory F. Koltun (Ohio WSC), David K. Mueller (Central Region), and Mark A. Uhrich (Oregon WSC) resulted in substantial improvements to this document. Trudy Bennett was responsible for oversight and data collection at the Little Arkansas River near Sedgwick, KS site.

Selected References

American Public Health Association, American Water Works Association, and Water Pollution Control Federation, 2005, Standard methods for the examination of water and wastewater (21st ed.): Washington, D.C., American Public Health Association, 1,368 p.

ASTM International, 2007, D4410, in terminology for fluvial sediment, annual book of standards, water and environmental technology: West Conshohocken, Pennsylvania, ASTM International, 7 p.

Anderson, C.W., 2005, Turbidity: U.S. Geological Survey Techniques of Water-Resources Investigations, book 9, chaps. A6.7, available on Web, accessed March 2008, at *http://pubs.water.usgs.gov/twri9A.*

Angino, E.E., and O'Brien, W.J., 1968, Effects of suspended material on water quality, *in* Proceedings of Symposium on Geochemistry, Precipitation, Evaporation, Soil Moisture, Hydrometry, General Assembly of Bern, September–October 1967: International Association of Science Hydrology, no. 78, p. 120–128.

Bent, G.C., 2000, Suspended-sediment characteristics in the Housatonic River Basin, western Massachusetts and parts of eastern New York and northwestern Connecticut, 1994–96: U.S. Geological Survey Water-Resources Investigations Report 00–4059, 121 p.

Bragg, H.M., Sobieszczyk, Steven., Uhrich, M.A., and Piatt, D.R., 2007, Suspended-sediment loads and yields in the North Santiam River Basin, Oregon, water years 1999–2004: U.S. Geological Survey Scientific Investigations Report 2007–5187, 26 p., available on Web, accessed March 2008, at *http://pubs.usgs.gov/sir/2007/5187/.*

Buchanan, P.A., and Ganju, N.K., 2004, Summary of suspended-sediment concentration data, San Francisco Bay, California, water year 2002: U.S. Geological Survey Open-File Report 2004–1219, 45 p., available on Web, accessed March 2008, at *http://pubs.usgs.gov/of/2004/1219/.*

Buchanan, P.A., and Schoellhamer, D.H., 1995, Summary of suspended-solids concentration data, Central and South San Francisco Bays, California, water years 1992 and 1993: U.S. Geological Survey Open-File Report 94–543, 15 p.

Christensen, V.G., Jian, Xiaodong, and Ziegler, A.C., 2000, Regression analysis and real-time water-quality monitoring to estimate constituent concentrations, loads, and yields in the Little Arkansas River, south-central Kansas, 1995–99: U.S. Geological Survey Water-Resources Investigations Report 00–4126, 36 p.

Clesceri, L.S., Greenberg, A.E., and Eaton, A.D., eds., 1998, Standard methods for the examination of water and wastewater (20th ed.): American Waterworks Association and Water Environment Federation, 1,200 p.

Cohn, T.A., DeLong, L.L., Gilroy, E.J., Hirsch, R.M., and Wells, D.K., 1989, Estimating constituent loads: Water Resources Research, v. 25, no. 5, p. 937–942.

Cunnane, C., 1978, Unbiased plotting positions—A review: Journal of Hydrology, v. 37, p. 205–222.

Curtis, J.A., Flint, L.E., Alpers, C.N., Wright, S.A., and Snyder, N.P., 2006, Use of sediment rating curves and optical backscatter data to characterize sediment transport in the upper Yuba River watershed, California, 2001–03: U.S. Geological Survey Scientific Investigations Report 2005–5246, 74 p.

Davies-Colley, R.J., and Smith, D.G., 2001, Turbidity, suspended sediment, and water clarity—A review: Journal of American Water Resources Association, v. 37, no. 55, p. 1,085–1,101.

Davis, B.E., 2005, A guide to the proper selection and use of Federally approved sediment and water-quality samplers: U.S. Geological Survey Open-File Report 2005–1087, 20 p.

Downing, J.P., 1983, An optical instrument for monitoring suspended particulates in ocean and laboratory: *in* OCEANS 1983, San Francisco, August 29–September 1, 1983, p. 199–202.

Downing, J.P., Sternberg, R.W., and Lister, C.R.B., 1981, New instrumentation for the investigation of sediment suspension processes in the shallow marine environment: Marine Geology, v. 42, p. 19–34.

Downing, John, 2005, Turbidity monitoring, chapt. 24, *in* Down, R.D., and Lehr, J.H., eds., Environmental instrumentation and analysis handbook: Hoboken, New Jersey, John Wiley and Sons, Inc., p. 511–546.

Downing, John, 2006, Twenty-five years with OBS sensors—The good, the bad, and the ugly: Continental Shelf Research, 20 p.

Duan, Naihua, 1983, Smearing estimate—A nonparametric retransformation method: Journal of the American Statistical Association, v. 78, no. 383, p. 605–610.

Edwards, T.K., and Glysson, G.D., 1999, Field methods for measurement of fluvial sediment: U.S. Geological Survey Techniques of Water-Resources Investigations, book 3, chap. C2, 89 p.

Federal Interagency Sedimentation Project, 2008, Home page available on Web, accessed January 21, 2009, at *http://fisp.wes.army.mil//.*

Gartner, J.W., and Gray, J.R., in press, Laser diffraction, *in* Gray, J.R., and Gartner, J.W., eds, Surrogate technologies for monitoring suspended-sediment and bed-load transport in rivers, *in* Charlesworth and Poleto, eds., Sedimentology in aqueous systems: London Wiley-Blackwell, Chapter 2.

Gilroy, E.J., Hirsch, R.M., and Cohn, T.A., 1990, Mean square error of regression-based constituent transport estimates: Water Resources Research, v. 26, no. 9, p. 2,069–2,077.

Gilvear, D.J., and Petts, G.E., 1985, Turbidity and suspended solids variations downstream of a regulating reservoir: Earth Surface Processes Landforms, v. 10, no. 4, p. 363–373.

Glysson, G.D., 1987, Sediment transport curves: U.S. Geological Survey Open-File Report 87–218, 53 p.

Glysson, G.D., 1989a, 100 Years of sedimentation study by the USGS, *in* Wang, Sam S.Y., ed., Proceedings of the International Symposium, Sediment Transport Modeling, August 14–18, 1989, New Orleans: New Orleans American Society of Civil Engineers, p. 260–265.

Glysson, G.D., 1989b, Criteria for a sediment dataset, *in* Proceedings of the International Symposium on Sediment Transport Modeling, August 14–18, 1989, New Orleans: New Orleans American Society of Civil Engineers, 7 p.

Glysson, G.D., Gray, J.R., and Conge, L.M., 2000, Adjustment of total suspended solids data for use in sediment studies, *in* Proceedings of the ASCE's 2000 Joint Conference on Water Resources Engineering and Water Resources Planning and Management, July 30–August 2, 2000, Minneapolis, Minnesota: Minneapolis, Minneapolis American Society of Civil Engineers, 10 p.

Glysson, G.D., Gray, J.R., and Schwarz, G.E., 2001, Comparison of load estimates using total suspended solids and suspended-sediment concentration data, *in* Proceedings of the ASCE World Water and Environmental Resources Congress, May 20–24, 2001, Orlando, Florida: American Society of Civil Engineers, 9 p.

Gooding, D.J., in press, Digital-optic imaging, *in* Gray, J.R., and Gartner, J.W., eds, Surrogate technologies for monitoring suspended-sediment and bed-load transport in rivers, *in* Charlesworth and Poleto, eds., Sedimentology in aqueous systems: London Wiley-Blackwell, Chapter 2.

Granato, G.E., 2006, Kendall-Theil Robust Line (KTRLine—ver. 1.0)—A visual basic program for calculating and graphing robust nonparametric estimates of linear-regression coefficients between two continuous variables: U.S. Geological Survey Techniques and Methods, book 4, chap. A7, 31 p.

Gray, J.R., and Gartner, J.W., 2006, Overview of selected surrogate technologies for continuous suspended-sediment monitoring, *in* Proceedings of the 8th Federal Interagency Sedimentation Conference, April 2–6, 2006, Reno, Nevada, p. 337-344, available on Web, accessed March 2008, at *http://pubs.usgs.gov/misc_reports/FISC_1947-2006/pdf/1st-7thFISCs-CD/8thFISC/Session%204C-1_Gray.pdf.*

Gray, J.R., and Gartner, J.W., 2009, Technological advances in suspended-sediment surrogate monitoring: Invited paper, Water Resources Research, v. 45, W00D29, doi:10.1029/2008WR007063, 20 p.

Gray, J.R., Glysson, G.D., and Edwards, T.E., 2008, Suspended-sediment samplers and sampling methods, *in* Garcia, Marcelo, ed., Sedimentation engineering—Processes, measurements, modeling, and practice: American Society of Civil Engineers Manual 110, chap. 5.3, p. 320–339.

Gray, J.R., Glysson, G.D., Turcios, L.M., and Schwarz, G.E., 2000, Comparability of total suspended solids and suspended-sediment concentration data: U.S. Geological Survey Water-Resources Investigations Report 00–4191, 14 p., available on Web, accessed March 2008, at *http://water.usgs.gov/osw/pubs/WRIR00-4191.pdf.*

Gray, J.R., Gooding D.J., Melis, T.S., Topping, D.J., and Rasmussen, P.P., 2003, U.S. Geological Survey suspended-sediment surrogate research, part II—Optic technologies: Proceedings of the Virginia Water Research Symposium 2003, Water Resource Management for the Commonwealth, Virginia Polytechnic Institute and State University, Blacksburg, October 8–10, 2003, p. 58–64, available on Web, accessed March 2008, at *http://water.usgs.gov/osw/techniques/sediment/sedsurrogate2003workshop/gray_melis.pdf.*

Gray, J.R., and Simões, F.J.M., 2008, Estimating sediment discharge, *in* Garcia, Marcelo, ed., Sedimentation engineering—processes, measurements, modeling, and practice: American Society of Civil Engineers Manual 110, Appendix D, p. 1,067–1,088.

Great Lakes Instruments, Inc., 1992, Turbidity measurement: Milwaukee, Wisconsin, Technical Bulletin Number T1 rev. 2–193, 7 p.

Hardison, C.H., 1969, Accuracy of streamflow characteristics, in Geological Survey Research, 1969: U.S. Geological Survey Professional Paper 650–D, p. D210–D214.

Helsel, D.R., and Hirsch, R.M., 2002, Statistical methods in water resources—hydrologic analysis and interpretation: U.S. Geological Survey Techniques of Water-Resources Investigations, book 4, chap. A3, 510 p., available on Web, accessed March 2008, at *http://pubs.usgs.gov/twri/twri4a3/.*

Horowitz, A.J., 2003, An evaluation of sediment rating curves for estimating suspended sediment concentrations for subsequent flux calculations: Hydrological Processes, v. 17, p. 3,387–3,409.

Insightful Corporation, 2001, S-PLUS 6 for Windows users guide: Seattle, Washington, Insightful Corporation, 688 p.

International Organization for Standardization, 1999, Water-quality determination of turbidity, method 7027: International Organization for Standardization, 10 p.

Kennedy, E.J., 1984, Discharge ratings at gaging stations: U.S. Geological Survey Techniques of Water-Resources Investigations, book 3, chap A10, 59 p.

Koch, R.W., and Smillie, G.M., 1986, Bias in hydrologic prediction using log-transformed regression models: American Water Resources Association, Water Resources Bulletin, v. 22, no. 5, p. 717–732.

Koltun, G.F., Eberle, Michael, Gray, J.R., and Glysson, G.D., 2006, User's manual for the Graphical Constituent Loading Analysis System (GCLAS): U.S. Geological Survey Techniques and Methods, book 4, chap. C1, 51 p.

Koltun, G.F., Gray, J.R., and McElhone, T.J., 1994, User's manual for SEDCALC, a computer program for computation of suspended-sediment discharge: U.S. Geological Survey Open-File Report 94–459, 46 p.

Landers, M.N., 2003, Summary of blind sediment reference sample measurement session, *in* Gray J.R., and Glysson, G.D., eds, Proceedings of the Federal Interagency Workshop on Turbidity and Other Sediment Surrogates, April 30–May 2, 2002, Reno, Nevada: U.S. Geological Survey Circular 1250, p. 29–30.

Lee, C.J., Rasmussen, P.P., and Ziegler, A.C., 2008, Characterization of suspended-sediment loading to and from John Redmond Reservoir, east-central Kansas, 2007–08: U.S. Geological Survey Scientific Investigations Report 2008–5123, 25 p.

Lee, C.J., Rasmussen, P.P., Ziegler, A.C., and Fuller, C.C., 2008, Transport and sources of suspended sediment in the Mill Creek watershed, Johnson County, northeast Kansas, 2006–07: U.S. Geological Survey Scientific Investigations Report 2009–5001, 52 p.

Levesque, V.A., and Schoellhamer, D.H., 1995, Summary of sediment resuspension monitoring, Old Tampa Bay and Hillsborough Bay, Florida, 1988–91: U.S. Geological Survey Water-Resources Investigations Report 94–4081, 31 p.

Lewis, Jack, 1996, Turbiditycontrolled suspended sediment sampling for runoff event load estimation: Water Resources Research, v. 32, no. 7, p. 2,299–2,310.

Lietz, A.C., and Debiak, E.A., 2005, Development of rating curve estimators for suspended-sediment concentration and transport in the C-51 canal based on surrogate technology, Palm Beach County, Florida, 2004–05: U.S. Geological Survey Open-File Report 2005–1394, 19 p., available on Web, accessed March 2008, at *http://pubs.usgs.gov/of/2005/1394/.*

Lipscomb, S.W., 1995, Quality assurance plan for discharge measurements using broadband acoustic doppler current profilers: U.S. Geological Survey Open-File Report 95–701, 12 p.

Miller, C.R., 1951, Analysis of flow-duration sediment rating curve method of computing sediment yield: U.S. Bureau of Reclamation, 55 p.

Munsell Color Co., 2000, Munsell soil color charts: Baltimore, Munsell Color Company, 22 p.

Nolan, K.M., Gray, J.R., and Glysson, G.D., 2005, Introduction to suspended-sediment sampling: U.S. Geological Survey Scientific Investigations Report 2005–5077, 1 CD-ROM, available on Web, accessed March 7, 2008, at *http://pubs.usgs.gov/sir/2005/5077/.*

Porterfield, George, 1972, Computation of fluvial-sediment discharge: U.S. Geological Survey Techniques of Water-Resources Investigations, book 3, chap. C3, 66 p.

Pruitt, B.A., 2003, Uses of turbidity by States and Tribes, *in* Gray, J.R., and Glysson, G.D., eds., Proceedings of the Federal Interagency Workshop on Turbidity and Other Sediment Surrogates, April 30–May 2, 2002, Reno, Nevada: U.S. Geological Survey Circular 1250, p. 31–43, available on Web, accessed February 23, 2009, at *http://pubs.usgs.gov/circ/2003/circ1250/pdf/circ1250.book_web.pdf.*

Putnam, J.E., and Pope, L.M., 2003, Trends in suspended-sediment concentration at selected stream sites in Kansas, 1970–2002: U.S. Geological Survey Water-Resources Investigations Report 03–4150, 36 p., available on Web, accessed March 2008, at *http://ks.water.usgs.gov/Kansas/pubs/reports/wrir.03-4150.html.*

Rantz, S.E., and others, 1982, Measurement and computation of streamflow, volumes 1 and 2: U.S. Geological Survey Water-Supply Paper 2175, 631 p.

Rasmussen, P.P., Bennett, Trudy, Lee, C.J., and Christensen, V.G., 2002, Continuous in-situ measurement of turbidity in Kansas, *in* Proceedings of Turbidity and Other Surrogates Workshop, April 30–May 2, 2002, Reno, Nevada: Subcommittee on Sedimentation, available on Web, accessed March 2008, at *http://water.usgs.gov/osw/techniques/TSS/rasmussen.pdf.*

Rasmussen, P.P., and Ziegler, A.C., 2003, Comparison and continuous estimates of fecal coliform and *Escherichia coli* bacteria in selected Kansas streams, May 1999 through April 2002: U.S. Geological Survey Water-Resources Investigations Report 03–4056, 80 p., available on Web, accessed March 2008, at *http://ks.water.usgs.gov/Kansas/pubs/abstracts/wrir.abstract.03-4056.html.*

Rasmussen, P.P., Gray, J.R., Ziegler, A.C., Glysson, G.D., and Anderson, Chauncy, in press, Turbidity (bulk optics), *in* Gray, J.R., and Gartner, J.W., eds, Surrogate technologies for monitoring suspended-sediment transport in rivers, *in* Charlesworth and Poleto, eds., Sedimentology in aqueous systems: London Wiley-Blackwell, Chapter 2.

Rasmussen, T.J., Ziegler, A.C., and Rasmussen P.P., 2005, Estimation of constituent concentrations, densities, loads, and yields on lower Kansas River, northeast Kansas, using regression models and continuous water-quality modeling, January 2000 through December 2003: U.S. Geological Survey Scientific Investigations Report 2005–5165, 117 p., available on Web, accessed March 2008, at *http://pubs.usgs.gov/sir/2005/5165/.*

Rasmussen, T.J., Lee, C.J., and Ziegler, A.C., 2008, Estimation of constituent concentrations, loads, and yields in streams of Johnson County, northeast Kansas, using continuous water-quality monitoring and regression models, October 2002 through December 2006: U.S. Geological Survey Scientific Investigatisons Report 2008–5014, 103 p., available on Web, accessed February 23, 2009, at *http://pubs.usgs.gov/sir/2008/5014/.*

Sadar, M.J., 1998, Turbidity science: HACH, Technical Information Series-Booklet No. 11, 26 p., available on Web, accessed March 2008, at *http://www.hach.com/fmmimghach?/CODE%3AL7061549%7C1.*

Slack, J.R., Lorenz, D.L., and others, 2003, USGS library for S-PLUS for Windows—Release 2.1: U.S. Geological Survey Open-File Report 03–357, 3 p., available on Web only, accessed February 18, 2009, at *http://water.usgs.gov/software/S-PLUS/.*

Sutherland, T.F., Lane, P.M., Amos, C.L., and Downing, J., 2000, The calibration of optical backscatter sensors for suspended sediment of varying darkness levels: Marine Geology, v. 162, p. 587–597.

Uhrich, M.A., and Bragg, H.M., 2003, Monitoring in-stream turbidity to estimate continuous suspended-sediment loads and yields and clay-water volumes in the Upper North Santiam River Basin, Oregon, 1998–2000: U.S. Geological Survey Water-Resources Investigations Report 03–4098, 43 p.

U.S. Environmental Protection Agency, 1979, Methods for chemical analysis of water and wastes: Cincinnati, Ohio, U.S. Environmental Monitoring Laboratory, Office of Research and Development 600/4/79/020, p. 180.1–1 to 180.1–3.

U.S. Environmental Protection Agency, 1999, Guidance manual for compliance with the interim enhanced surface water treatment rule—Turbidity provisions: Washington, D.C., U.S. Environmental Protection Agency, Office of Water, EPA 815-R-99-010, variously paged.

U.S. Environmental Protection Agency, 2001, Water quality standards: Office of Water, available on Web, accessed March 7, 2008, at *http://www.epa.gov/waterscience/standards/wqslibrary/.*

U.S. Environmental Protection Agency, 2008, Total maximum daily loads, causes of impairment for 303(d) listed waters, available on Web, accessed January 14, 2009, at *http://iaspub.epa.gov/waters10/attains_nation_cy.control?p_report_type=T#causes_303d.*

U.S. Geological Survey, variously dated, National field manual for the collection of water-quality data: U.S. Geological Survey Techniques of Water-Resources Investigations, book 9, chaps. A1–A9, available on Web, accessed February 18, 2009, at *http://pubs.water.usgs.gov/twri9A.*

U.S. Geological Survey, 2000, Collection and use of total suspended solids data—USGS policy on collection and use of total suspended solids data: Office of Surface Water, and Office of Water Quality Joint Technical Memorandum 2001.03 (*http://water.usgs.gov/admin/memo/SW/sw01.03.html*).

U.S. Geological Survey, 2002, Policy and technical guidance on discharge measurements using an acoustic doppler current profiler: Office of Surface Water Technical Memorandum 2002.02, available on Web, accessed January 21, 2009, at *http://water.usgs.gov/admin/memo/SW/OSW.2002.02.htm.*

U.S. Geological Survey, 2003, User's manual for the National Water Information System of the U.S. Geological Survey—automated data processing system (ADAPS), ver. 4.3: U.S. Geological Survey Open-File Report 03–123, 413 p., available on Web, accessed March 2008, at *http://pubs.usgs.gov/of/2003/ofr03123/.*

U.S. Geological Survey, 2005, Use of the program HYDRA to estimate or modify unit values in ADAPS: Office of Water Quality Technical Memorandum 2005.03, available on Web, accessed February 19, 2009, at *http://water.usgs.gov/admin/memo/QW/qw05.03.html.*

U.S. Geological Survey, 2006, User's manual for the National Water Information System of the U.S. Geological Survey, water-quality system (QWDATA), ver. 4.4: U.S. Geological Survey Open-File Report 2006–1145, 372 p., available on Web, accessed March 7, 2008, at *http://pubs.usgs.gov/of/2006/1145/.*

Wagner, R.J., Boulger, R.W., Jr., Oblinger, C.J., and Smith, B.A., 2006, Guidelines and standard procedures for continuous water-quality monitors—station operation, record computation, and data reporting: U.S. Geological Survey Techniques and Methods 1–D3, 51 p., 8 attachments, available on Web, accessed March 7, 2008, at *http://pubs.water.usgs.gov/tm1d3.*

Walling, D.E., 1977, Assessing the accuracy of suspended sediment rating curves for a small basin: Water Resources Research, v. 13, p. 531–538.

YSI, Incorporated, 2003, 6136 Technical document, available on Web, accessed March 2008, at *http://www.ysilifesciences.com/extranet/EPGKL.nsf/5992085488f9da9d85256a550047c2a2/f2c571cc22155adc85256b750076b4f5/$FILE/6136%20Turbidity%20Tech%20Doccomp.pdf.*

Ziegler, A.C., 2003a, Issues related to use of turbidity measurements as a surrogate for suspended sediment, *in* Gray, J.R., and Glysson, G.D., eds., Proceedings of the Federal Interagency Workshop on Turbidity and Other Sediment Surrogates, April 30–May 2, 2002, Reno, Nevada: U.S. Geological Survey Circular 1250, p. 16–18, on available on Web, accessed November 2008, at *http://water.usgs.gov/osw/techniques/TSS/ZieglerT.pdf.*

Ziegler, A.C., 2003b, Breakout session 1—definition of optical methods for turbidity and data reporting, *in* Gray, J.R., and Glysson, G.D., eds., Proceedings of the Federal Interagency Workshop on Turbidity and Other Sediment Surrogates, April 30–May 2, 2002, Reno, Nevada: U.S. Geological Survey Circular 1250, p. 16–18, available on Web, accessed November 2008, at *http://pubs.usgs.gov/circ/2003/circ1250/pdf/circ1250.book_web.pdf* .

Appendixes

Appendix 1. Examples of Suspended-Sediment Concentration Models from Kansas, Oregon, Florida, and California

Turbidity and *SSC* data and models from rivers in four States are presented to illustrate turbidity-*SSC* applications at a variety of geographic locations, drainage areas, and freshwater/saltwater conditions. Examples are courtesy of Heather Bragg and Mark Uhrich of the Oregon WSC (2007), Paul Buchanan of the California WSC (2004), A.C. Lietz (retired), and Elizabeth Hittle of the Pennsylvania WSC (2005).

U.S. Geological streamgages used for examples of turbidity and suspended-sediment concentration (SSC) data and regression models.

Example	Station number	Station name	Turbidity instrument make and model	Fresh- or saltwater	Drainage area (square miles)
1	07144100	Little Arkansas River near Sedgwick, Kansas	YSI model 6026	Freshwater	1,239
2	14178000	North Santiam River below Boulder Creek, Oregon	YSI model 6026	Freshwater	216
3	02279000	C-51 Canal, Palm Beach County, Florida	YSI model 6026	Freshwater	Not applicable
4	11458370	Mare Island Causeway, San Pablo Bay, California	D and A OBS	Saltwater	Not applicable

Example 1. Complete Review Package for Little Arkansas River near Sedgwick, Kansas

WATER-QUALITY MONITOR STATION ANALYSIS
2005 WATER YEAR
SUSPENDED-SEDIMENT RECORD
07144100
Little Arkansas River near Sedgwick, Kansas

MODEL-CALIBRATION DATA SET—All data were collected using USGS protocols and are stored in USGS NWIS databases. The regression model is based on 68 concurrent measurements of turbidity and streamflow and *SSC* samples collected from November 1998 through June 2005. Samples were collected throughout the range of continuously observed hydrologic and turbidity conditions. Turbidity and streamflow values are time-averaged approved unit values corresponding with the duration of sample collection. A comparison of cross-section mean and corresponding time-series monitor readings is provided. Water-quality data were collected using an YSI 6600 monitor with a 6026 turbidity sensor (FNU). Selected data values used to develop the regression models were removed on the basis of sample evaluation. Five *SSC* values were removed from the data set because of transcription errors, sampling errors, and a sample compromised during shipping. Three data values were affected by sensor limitations (within 10 percent of the sensor maxima) and, therefore, were removed from the data set. Summary statistics and the complete model-calibration data set are provided.

MODEL DEVELOPMENT—Initially, data plots of the response variable (*SSC*) and possible explanatory variables turbidity and streamflow indicate both are correlated to *SSC*. Regression analysis was done using S-Plus software, and the final output is provided. Turbidity and streamflow were examined together as explanatory variables for estimating *SSC*, but the p-values for streamflow were larger than 0.025. Different combinations of untransformed and $\log_{10}$-transformed data were evaluated. Log_{10}-transformed turbidity and *SSC* were selected as the best model on the basis of residual plots, *MSPE*, and p-value for streamflow. Residual plots for evaluating variance, normality, homoscedasticity, and curvature are provided. For $\log_{10}$-transformed models, estimated values were multiplied by a calculated retransformation bias correction factor (Duan, 1983). Ninety-percent prediction intervals are provided for evaluating uncertainty of the estimates.

MODEL SUMMARY—Summary of final regression analysis for suspended-sediment concentration at Little Arkansas River near Sedgwick, Kansas.

$$\log_{10}(SSC) = 0.943 \log_{10}(Turb) + 0.130,$$

where

SSC = Suspended-sediment concentration, in milligrams per liter; and
Turb = Turbidity (YSI 6026), in formazin nephelometric units.

Model information:

Number of measurements = **68**,
root-mean-squared error (*RMSE*) = **0.10**,
model standard percentage error (*MSPE*) = **+25.9 and -20.6 percent**
90-percent prediction intervals = **± 41 percent**,
adjusted coefficient of determination (R^2_a) = **0.98**,
PRESS = **0.663**.
Duan's bias correction factor = **1.03.**

Coefficients:

	Coefficient	Standard error	t-statistic	p-value
Intercept	0.130	0.041	3.02	0.0035
$\log_{10}(Turb)$	0.943	0.018	50.9	1.13E-54

Correlation matrix of coefficients:

	Intercept	$\log_{10}$(*Turb*)
Intercept	1	
$\log_{10}$(*Turb*)	-0.9588	1

***SSC* RECORD**—The record is computed using a regression model and ADAPS software. Data are computed at 15-minute intervals. The record is complete for the year except as noted. The turbidity monitor was removed for a short period in December-February to avoid ice damage.

Daily values for partial days were updated where data existed during the expected time for the occurrence of the maximum or minimum, if at least 12 hours of values were available for the day, and if values were present adjacent to the extreme for the day.

312 days of record out of 365 days (85 percent) will be published.

REMARKS—

- A new turbidity sensor, YSI model 6136, was installed to collected concurrent turbidity measurements. These measurements will be used to convert YSI model 6136 values to the YSI model 6026 to compute *SSC* with the new 6136 sensor.
- T.B. Bennett collected field data.
- Cross-section survey results can be retrieved from NWIS, database 02.
- The Excel® "Field Measurement Summary" spreadsheet for this site and water year summarizes the number of site visits, calibration results, and calculations of the magnitude of fouling and calibration drift.

Computed: P.P. Rasmussen, November 1, 2005
Checked: C.J. Lee, November 22, 2005
Reviewed: T.J. Rasmussen, November 26, 2005

Model-calibration data set for Little Arkansas River near Sedgwick, Kansas, November 1998–June 2005.

Date	Turbidity from fixed-location sensor, in formazin nephelometric units (YSI 6026 turbidity sensor)	Streamflow, in cubic feet per second	Suspended-sediment concentration, in milligrams per liter	Percentage of suspended sediment finer than 62 micrometers
November 5, 1998	390	7,800	381	92
December 4, 1998	100	219	78	99
February 1, 1999	977	4,460	1,180	95
February 19, 1999	20	111	19	89
April 7, 1999	912	1,500	791	98
April 16, 1999	924	5,410	896	93
May 24, 1999	1,233	1,610	931	99
June 18, 1999	457	396	323	100
June 21, 1999	452	2,080	549	97
August 3, 1999	1,115	4,170	1,040	97
September 28, 1999	1,164	1,920	897	99
February 9, 2000	19	84	28	86
March 7, 2000	448	1,120	520	98
May 19, 2000	74	87	90	99
May 31, 2000	326	175	263	100
June 28, 2000	856	1,100	835	99
July 20, 2000	107	134	129	99
August 16, 2000	37	24	35	97
September 8, 2000	36	20	36	96
September 25, 2000	21	21	14	78
October 26, 2000	582	5,400	499	78
November 8, 2000	112	83	84	97
December 4, 2000	6	46	8	81
April 13, 2001	947	400	791	100
April 26, 2001	36	97	49	85
May 8, 2001	217	152	232	100
June 4, 2001	808	1,040	873	99
June 6, 2001	870	8,690	678	92
June 23, 2001	525	4,260	560	94
July 11, 2001	51	67	55	97
August 2, 2001	69	25	61	98
August 28, 2001	44	28	47	97
August 28, 2001	46	28	53	95
September 20, 2001	989	4,170	877	98
October 31, 2001	13	28	18	89

Model-calibration data set for Little Arkansas River near Sedgwick, Kansas, November 1998–June 2005.—Continued

Date	Turbidity from fixed-location sensor, in formazin nephelometric units (YSI 6026 turbidity sensor)	Streamflow, in cubic feet per second	Suspended-sediment concentration, in milligrams per liter	Percentage of suspended sediment finer than 62 micrometers
January 10, 2002	4	37	6	96
February 21, 2002	15	42	35	97
April 9, 2002	66	96	61	99
May 13, 2002	340	412	274	100
May 22, 2002	310	140	201	100
June 6, 2002	466	245	286	100
June 13, 2002	743	5,630	651	100
July 9, 2002	43	30	48	98
August 15, 2002	555	823	927	100
September 19, 2002	68	14	53	100
December 18, 2002	16	41	20	100
March 20, 2003	820	6,320	886	91
April 23, 2003	196	292	254	100
May 29, 2003	218	195	218	100
June 11, 2003	73	97	77	100
June 24, 2003	54	56	63	99
July 30, 2003	43	8	44	100
September 3, 2003	327	567	333	99
October 14, 2003	523	1,100	431	97
December 11, 2003	7	46	4	95
March 9, 2004	929	1,800	948	98
March 30, 2004	130	294	172	99
May 26, 2004	43	49	47	100
June 16, 2004	88	54	102	99
June 22, 2004	410	1,040	303	93
July 27, 2004	320	5,850	384	99
January 27, 2005	135	170	122	99
March 23, 2005	435	5,840	506	89
March 31, 2005	71	150	79	--
May 10, 2005	259	186	314	--
May 27, 2005	1,290	700	1,250	--
June 6, 2005	425	1,940	449	98
June 9, 2005	840	12,200	649	99

Summary statistics of model-calibration data set for Little Arkansas River near Sedgwick, Kansas, November 1998–June 2005.

[FNU, formazin nephelometric unit; mg/L, milligrams per liter; ft^3/s, cubic feet per second; >, greater than; --, not applicable]

Statistical summary of data sets					
Summary statistic	Calibrated data set (68 samples)			Time-series data set (61,368 hourly values)	
	Turbidity, FNU	Suspended-sediment concentration, mg/L	Streamflow, ft^3/s	Turbidity, FNU	Streamflow, ft^3/s
Minimum	4	4	8	65	55
Maximum	1,300	1,200	12,000	>2,000	16,000
Mean	370	350	1,500	140	380
Median	250	240	210	41	60
Standard deviation	370	350	2,500	260	1,200
Missing turbidity values	--	--	--	1,264	643
Turbidity values greater than maximum sensor limit	--	--	--	254	--

S-Plus Output of Regression Model Development of Turbidity and *SSC* for Little Arkansas River near Sedgwick, Kansas

```
             *** Linear Model ***
Call: lm(formula = SSC ~ Turb, data = SDF5, na.action = na.exclude)
Residuals:
     Min       1Q   Median      3Q    Max
 -0.2943 -0.06414 0.009471 0.06104 0.3053

Coefficients:
              Value Std. Error t value Pr(>|t|)
(Intercept)  0.1298  0.0429     3.0256  0.0035
       Turb  0.9430  0.0185    50.8736  0.0000

Residual standard error: 0.1007 on 66 degrees of freedom
Multiple R-Squared: 0.9751
F-statistic: 2588 on 1 and 66 degrees of freedom, the p-value is 0

Correlation of Coefficients:
     (Intercept)
Turb -0.9586

Analysis of Variance Table

Response: SSC

Terms added sequentially (first to last)
          Df Sum of Sq  Mean Sq  F Value Pr(F)
     Turb  1  26.23809 26.23809 2588.118     0
Residuals 66   0.66910  0.01014
```

Example 2. Turbidity Computed Suspended-Sediment Concentrations from Oregon

From Bragg, H.M., Sobieszczyk, Steven, Uhrich, M.A., and Piatt, D.R., 2007, Suspended-sediment loads and yields in the North Santiam River Basin, Oregon, water years 1999–2004: U.S. Geological Survey Scientific Investigations Report 2007–5187, 26 p., available on Web, accessed March 2008, at *http://pubs.usgs.gov/sir/2007/5187/*.

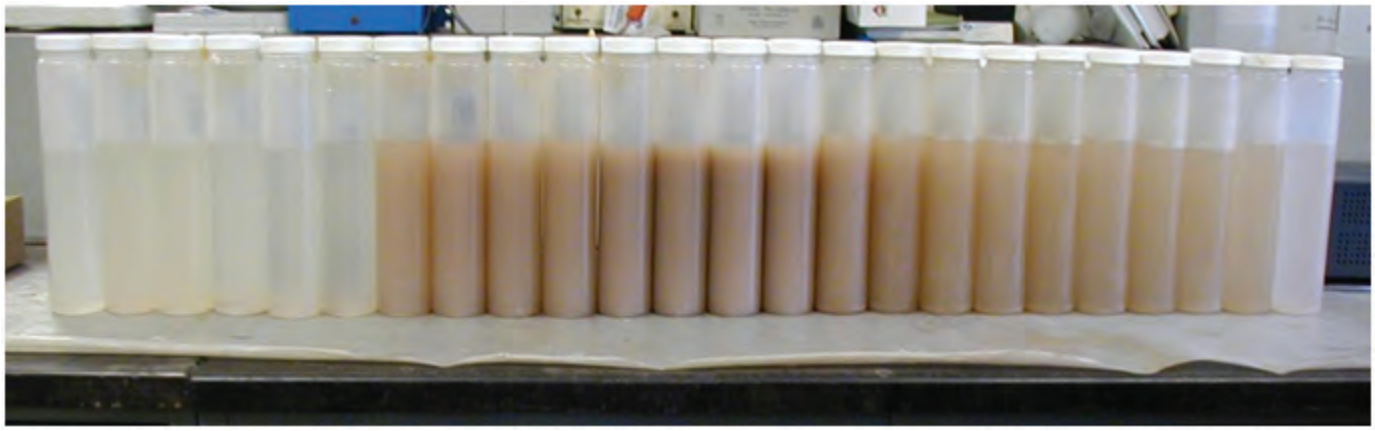

Samples collected every 15 minutes during a single period of runoff. (Photograph by Heather Bragg, U.S. Geological Survey, October 20–22, 2003.)

Model-calibration data set for North Santiam River below Boulder Creek, Oregon, October 1998–August 2004.

[*Q*, streamflow; ft^3/s, cubic feet per second; FNU, formazin nephelometric units; *SSC*, suspended-sediment concentration; mg/L, milligrams per liter]

Date and time	*Q* (ft^3/s)	Turbidity (FNU)	*SSC* (mg/L)
10/16/98 12:05	468	1	2
11/16/98 14:30	791	3	3
11/21/98 13:00	4,210	22	44
11/25/98 14:05	3,205	7	17
12/2/98 16:10	5,377	33	97
12/28/98 15:13	7,625	79	219
1/13/99 14:30	1,050	4	4
1/21/99 13:30	2,690	4	13
1/26/99 13:13	1,350	2	2
2/4/99 9:30	1,050	1	1
2/11/99 17:25	1,022	1	2
2/18/99 13:10	1,227	3	7
2/24/99 8:40	2,237	6	14
3/3/99 12:05	2,040	2	7
3/17/99 9:15	1,020	1	2
3/22/99 16:55	1,420	1	2
4/14/99 15:45	943	1	1
4/23/99 16:30	1,510	1	1
4/30/99 11:07	1,340	1	1
5/3/99 17:05	1,770	1	1
5/12/99 16:05	1,392	1	1
5/18/99 10:55	2,420	4	9
5/18/99 18:25	2,558	4	10
6/17/99 16:55	2,162	3	3
7/1/99 15:33	1,459	1	2
8/10/99 10:20	767	1	3
9/1/99 16:45	644	1	1
9/15/99 15:20	576	1	1
10/13/99 13:20	514	1	1
11/5/99 10:45	525	1	2
11/15/99 16:45	580	1	2
11/25/99 12:32	5,679	285	366
11/26/99 13:55	8,778	190	331
12/2/99 10:06	2,404	14	30
12/7/99 14:35	1,580	4	6
12/13/99 14:20	1,730	3	5
12/13/99 14:38	1,727	3	5
12/13/99 14:58	1,721	3	4
12/16/99 14:05	3,397	26	65
12/16/99 22:05	3,680	15	64
12/17/99 11:15	3,155	6	30
1/7/00 9:22	978	1	2
1/21/00 10:25	1,040	1	2

Model-calibration data set for North Santiam River below Boulder Creek, Oregon, October 1998–August 2004.—Continued

[*Q*, streamflow; ft³/s, cubic feet per second; FNU, formazin nephelometric units; *SSC*, suspended-sediment concentration; mg/L, milligrams per liter]

Date and time	*Q* (ft³/s)	Turbidity (FNU)	*SSC* (mg/L)
2/1/00 12:40	2,273	14	35
2/1/00 14:00	2,430	16	41
2/1/00 17:10	2,777	16	49
2/2/00 7:40	2,983	8	26
2/22/00 12:04	1,281	2	2
2/22/00 13:22	1,315	3	3
3/2/00 15:48	1,460	1	2
3/17/00 9:30	1,400	1	1
4/6/00 12:10	1,577	1	1
5/4/00 15:45	1,410	1	2
5/31/00 10:40	1,127	1	4
6/12/00 19:20	1,990	4	7
6/13/00 18:30	1,570	2	1
6/14/00 12:45	1,430	2	2
6/21/00 10:40	931	1	1
9/20/00 11:40	447	1	2
10/2/00 15:50	458	21	13
10/20/00 22:00	798	16	22
11/9/00 12:20	543	2	2
11/27/00 13:30	599	3	4
11/30/00 13:37	580	2	4
12/28/00 11:17	726	1	2
1/10/01 11:24	644	1	1
2/5/01 14:28	853	1	3
3/19/01 13:54	1,230	10	14
3/19/01 14:23	1,230	10	18
3/28/01 10:55	1,592	6	12
3/28/01 10:57	1,591	6	12
4/30/01 15:50	1,723	13	22
4/30/01 16:15	1,815	15	29
4/30/01 20:54	2,316	36	50
5/1/01 15:08	1,727	4	9
5/16/01 11:23	2,232	6	16
5/16/01 11:32	2,228	6	12
7/24/01 12:16	366	1	2
8/16/01 8:48	344	4	3
8/16/01 9:18	342	3	2
9/25/01 15:50	318	2	3
9/26/01 8:35	332	4	5
10/11/01 13:00	480	12	13
10/23/01 17:05	548	3	6
10/31/01 16:01	883	7	14
11/14/01 13:34	783	7	5

Model-calibration data set for North Santiam River below Boulder Creek, Oregon, October 1998–August 2004.—Continued

[*Q*, streamflow; ft^3/s, cubic feet per second; FNU, formazin nephelometric units; *SSC*, suspended-sediment concentration; mg/L, milligrams per liter]

Date and time	*Q* (ft^3/s)	Turbidity (FNU)	*SSC* (mg/L)
11/22/01 15:30	3,280	64	147
11/23/01 12:56	2,111	7	14
11/23/01 13:16	2,089	7	15
11/29/01 10:10	2,033	5	15
12/7/01 9:00	1,890	3	5
12/14/01 11:40	3,427	13	28
12/16/01 15:26	3,450	11	34
12/16/01 15:45	3,440	11	38
1/8/02 11:17	5,209	43	134
2/21/02 14:02	907	1	2
3/12/02 11:33	2,969	8	23
4/14/02 13:36	7,350	87	225
7/18/02 7:27	650	11	9
12/11/02 16:00	644	7	7
12/16/02 10:48	1,440	8	16
12/16/02 11:22	1,440	7	13
12/27/02 16:24	1,428	8	15
1/3/03 14:40	2,670	8	37
1/30/03 15:24	6,216	63	213
3/22/03 12:01	4,903	34	157
8/18/03 15:10	395	5	3
8/21/03 7:40	385	4	3
9/12/03 13:30	395	17	11
9/12/03 14:45	392	14	9
10/21/03 12:31	395	569	415
10/21/03 15:16	390	216	173
10/23/03 13:55	385	19	18
10/29/03 11:31	375	39	26
11/19/03 13:45	799	4	9
12/13/03 17:00	6,080	118	418
1/29/04 9:04	4,031	16	70
6/25/04 16:02	719	10	11
7/21/04 9:43	502	3	4
8/25/04 11:24	655	14	18
8/25/04 15:32	791	23	29

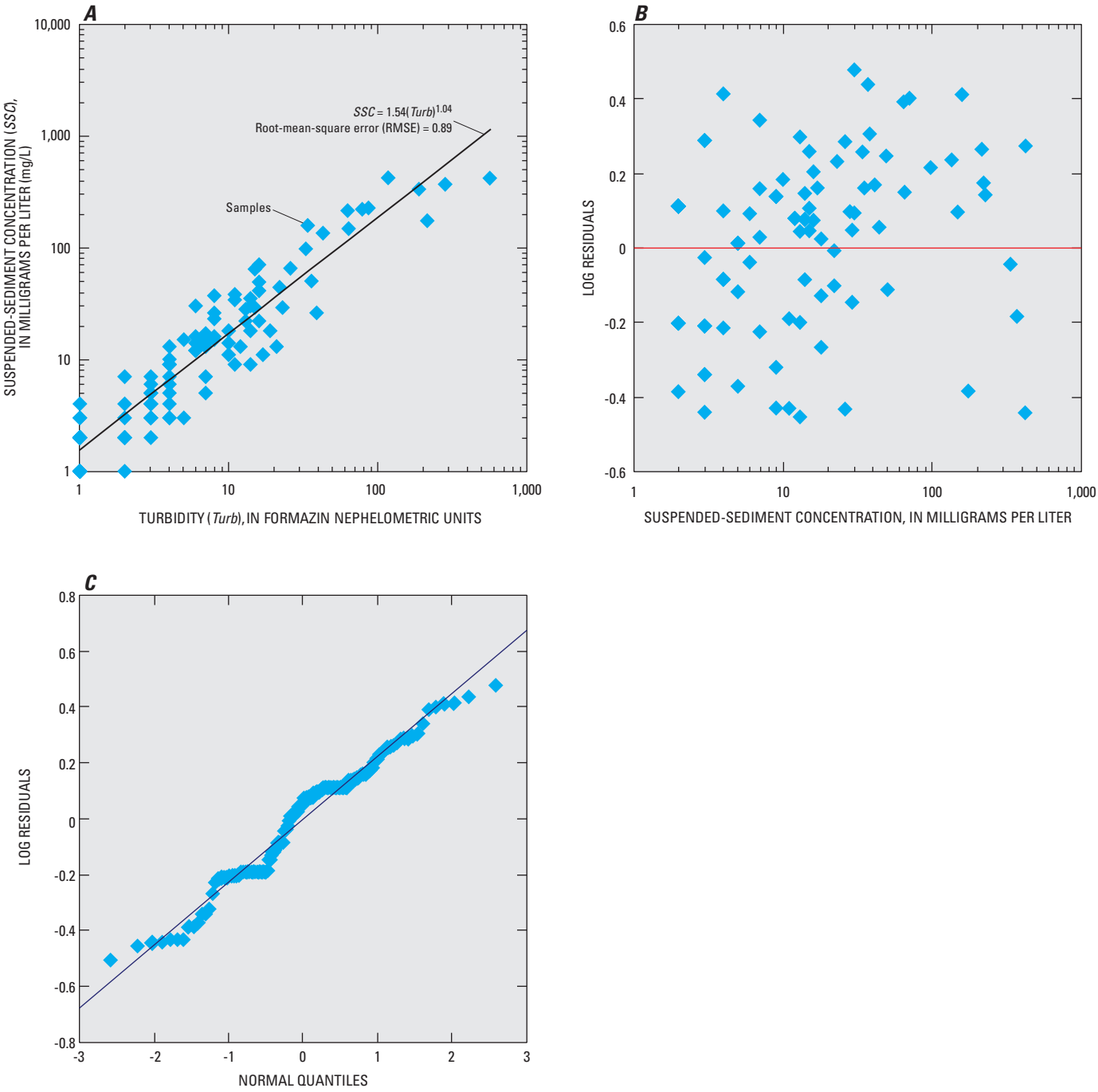

Results for simple linear regression analysis for *A*, turbidity and suspended-sediment concentration data, and comparison of *B*, computed suspended-sediment concentrations and regression residuals, and *C*, probability plot of residuals for U.S. Geological Survey streamgage on North Santiam River below Boulder Creek, Oregon, 1998–2004.

Example 3. Turbidity Computed Suspended-Sediment Concentrations from Florida

From Lietz, A.C., and Debiak, E.A., 2005, Development of rating curve estimators for suspended-sediment concentration and transport in the C-51 canal based on surrogate technology, Palm Beach County, Florida, 2004–05: U.S. Geological Survey Open-File Report 2005–1394, 19 p., available on Web, accessed March 2008, at *http://pubs.usgs.gov/of/2005/1394/.*

Model-calibration data set for C-51 Canal, Palm Beach County, Florida, November 2003–December 2004.

[*SSC*, suspended-sediment concentration, in milligrams per liter; *Turb*, turbidity, in formazin nephelometric units; *Q*, streamflow, in cubic feet per second; mm, millimeters; --, not determined]

Date (month/ day/year)	*SSC*	*Turb*	*Q*	Percentage finer than 0.063 mm
11/13/03	6	4.2	408	89
11/17/03	6	6.5	871	98
02/10/04	16	13.4	857	97
02/26/04	15	15.8	955	97
03/15/04	9	10.4	246	94
04/12/04	8	4.6	1,010	36
07/27/04	5	2.9	735	53
08/02/04	7	4.6	226	77
08/04/04	6	6.2	678	89
08/06/04	6	4.8	0	82
08/13/04	7	6.5	718	94
08/14/04	8	6.2	696	84
08/27/04	5	4.1	481	83
09/07/04	25	18.1	2,690	96
09/08/04	16	7.8	2,180	97
09/22/04	17	24.2	1,920	98
09/27/04	30	23.1	4,060	94
10/13/04	20	14.0	1,499	97
10/27/04	--	--	869	95
11/09/04	14	24.0	267	93
12/15/04	54	78.0	584	95

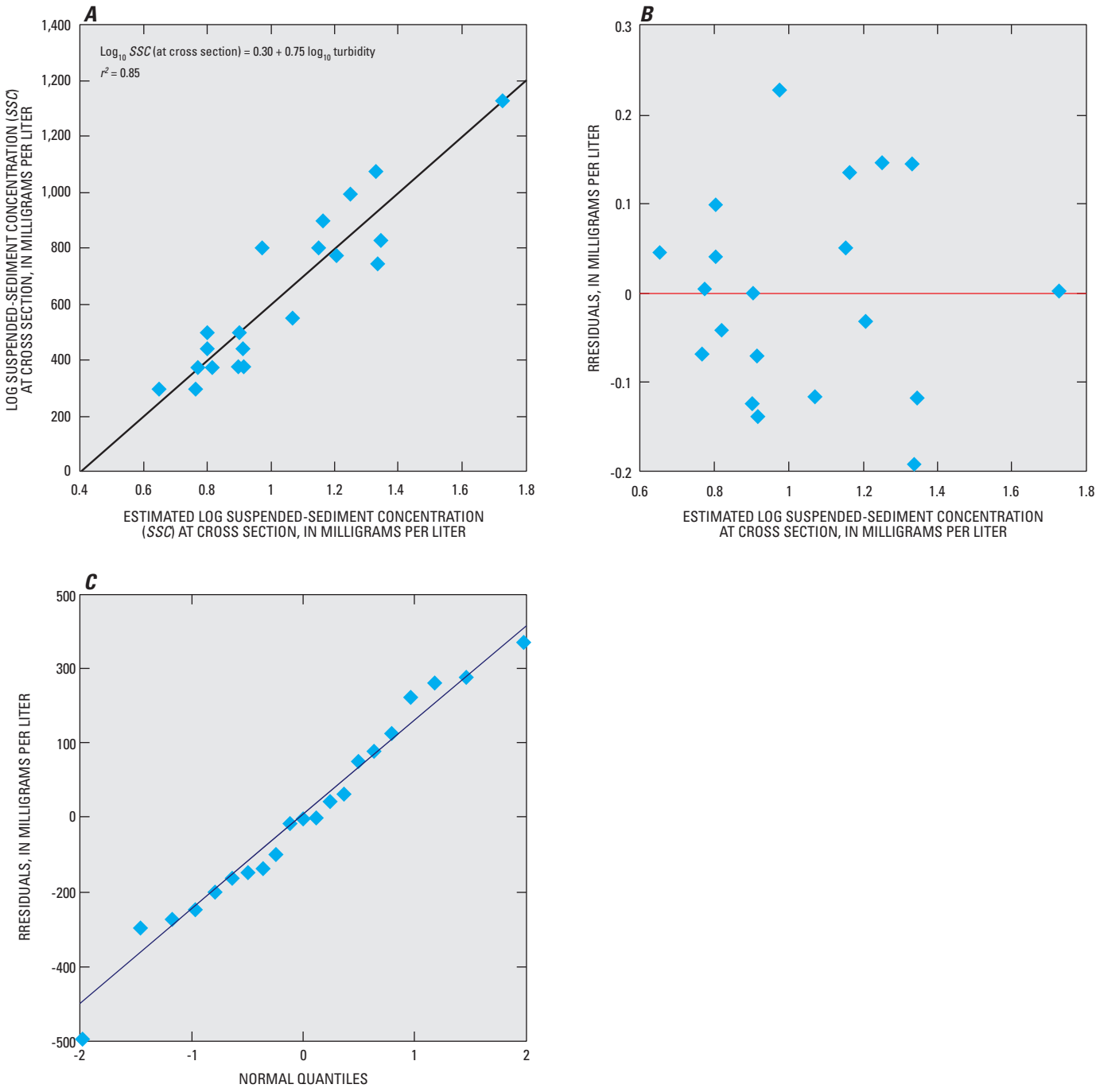

Results for simple linear regression analysis for *A*, turbidity and suspended-sediment concentration data, and comparison of *B*, computed suspended-sediment concentrations and regression residuals, and *C*, probability plot of residuals for U.S. Geological Survey streamgage on C-51 canal, Palm Beach County, Florida, 2003–4.

Example 4. Turbidity (Optical Backscatter) Computed Suspended-Sediment Concentrations Using Nonparametric Regression, California

From Buchanan, P.A., and Ganju, N.K., 2004, Summary of suspended-sediment concentration data, San Francisco Bay, California, water year 2002: U.S. Geological Survey Open-File Report 2004–1219, 45 p., available on Web, accessed March 2008, at *http://pubs.usgs.gov/of/2004/1219/*.

Model-calibration data set for Mare Island Causeway, San Pablo Bay, California, water years 2001–04.

[OBS, optical backscatter; *SSC*, suspended-sediment concentration; mg/L, milligrams per liter]

OBS sensor output (milliVolts)	*SSC* (mg/L)
22.3	11
45.9	31
100	74
94.7	55
166	88
138.6	77
283	186
272.5	161
77.9	36
77.5	26
254	156
49	17
110.55	61
203	118
220	141
144	76
135	91
60.4	20
71.6	28
37.8	18
47.7	24

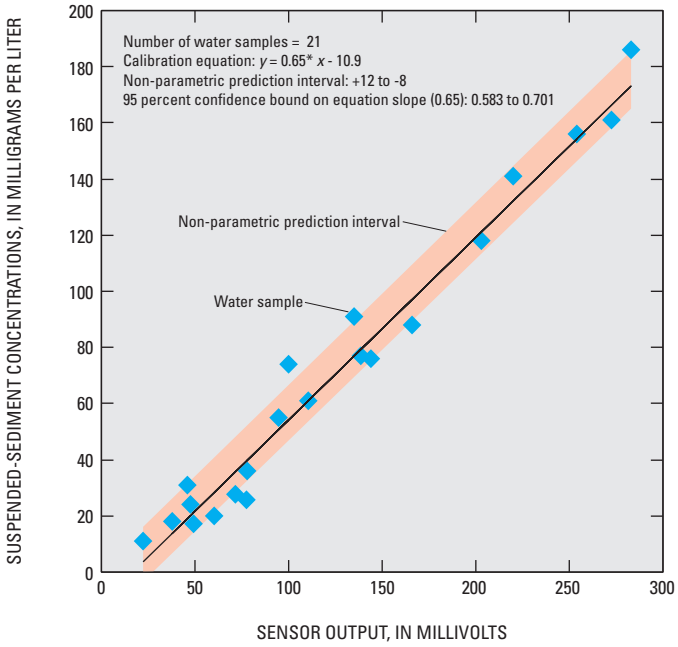

Calibration of mid-depth optical backscatter sensor at Mare Island Causeway, San Pablo Bay, California, water year 2004 (from Buchanan and Ganju, 2004).

Appendix 2. Computation, Storage, and Real-Time Display of Time-Series Suspended-Sediment Concentration and Load in National Water Information System

In some cases, ADAPS, a subsystem of NWIS, can compute *SSC* unit values (UVs) and *SSL* daily values (DVs). *SSC* UVs can only be computed in NWIS if turbidity is the sole explanatory variable in the regression model. Currently (2009), NWIS cannot compute *SSC* values if:

1. The model includes computed UVs, such as streamflow, for an explanatory variable, or
2. The model is a MLR model.

For *SSC* models that NWIS cannot compute, the hydrographer should refer to the Graphical Constituent Loading Analysis System (GCLAS; Koltun and others, 2006) or a spreadsheet application. The time series of computed *SSC* unit values then can be loaded to ADAPS using Device Conversion and Delivery System (DECODES) (U.S. Geological Survey, 2003).

SSL DVs are computed using mean daily *SSC* and streamflow. The resulting *SSL* DV is correct only if the *SSC* and streamflow are correlated in time. Typically, this is not the case and results in erroneous *SSL* DVs. Hydrographers should instead use GCLAS or a spreadsheet application to compute *SSL* UVs and DVs. The time series of computed *SSL* unit values then can be loaded to ADAPS using DECODES (U.S. Geological Survey, 2003).

The following presents the general methods for computation, storage, and real-time display of *SSC* unit values and *SSL* daily values using NWIS. For complete instructions, refer to U.S. Geological Survey (2003), *http://pubs.usgs.gov/of/2003/ofr03123/*. NOTE: The user must have a user class of "adba" or "syst" to have access to perform several of the following steps (U.S. Geological Survey, 2003).

In ADAPS, the site must have a data descriptor (DD) for computed:

- *SSC* unit values (NWIS parameter code 99409—suspended-sediment concentration, water, unfiltered, estimated by regression equation, milligrams per liter) and
- *SSL* unit values (NWIS parameter code 80295—sediment suspended sediment load, water, unfiltered, estimated by regression equation, pounds per second, 80296–sediment suspended sediment load, water, unfiltered, estimated by regression equation, tons per second, 80297–suspended sediment load, water, unfiltered, computed, the product of regression-computed suspended sediment concentration and streamflow, tons per day, or 80298–suspended sediment load, water, unfiltered, regression computed, turbidity and streamflow as regressors, tons per day).

The DD setup for *SSC* and *SSL* should include:

1. Adding a DD optional description (30 characters maximum).

   SSC—Add the SLR model (example, "*SSC* = 1.39*Turb*^0.943")
   SSL—example, "by regression using turbidity DD##," where DD## is the turbidity data descriptor number.
2. The processor for the *SSC* DD needs to be identified as a "standard rating computation" and have the turbidity DD identified as the input DD.
3. The rating values of measured turbidity and estimated *SSC* should be calculated outside of ADAPS using the SLR model and the BCF and entered as a "dependent, parameter" rating. The proper "rating expansion type" for Little Arkansas River near Sedgwick, Kansas example is "equation."

   - The rating "Remarks" (99 characters maximum) should include the SLR model, the BCF, and the turbidity sensor's manufacturer and model number and (or) the parameter and method codes. (example, *SSC* = 1.39*Turb*^0.943, *turb* = YSI 6026 = DD##, parameter 63680, method TS086).
   - The *SSC* values for Little Arkansas River near Sedgwick, Kansas, are computed using equation 7, where the BCF is incorporated into the model.
   - When *SSC* model coefficients change due to addition of samples, the rating, rating remarks, and start and end dates need to be updated.

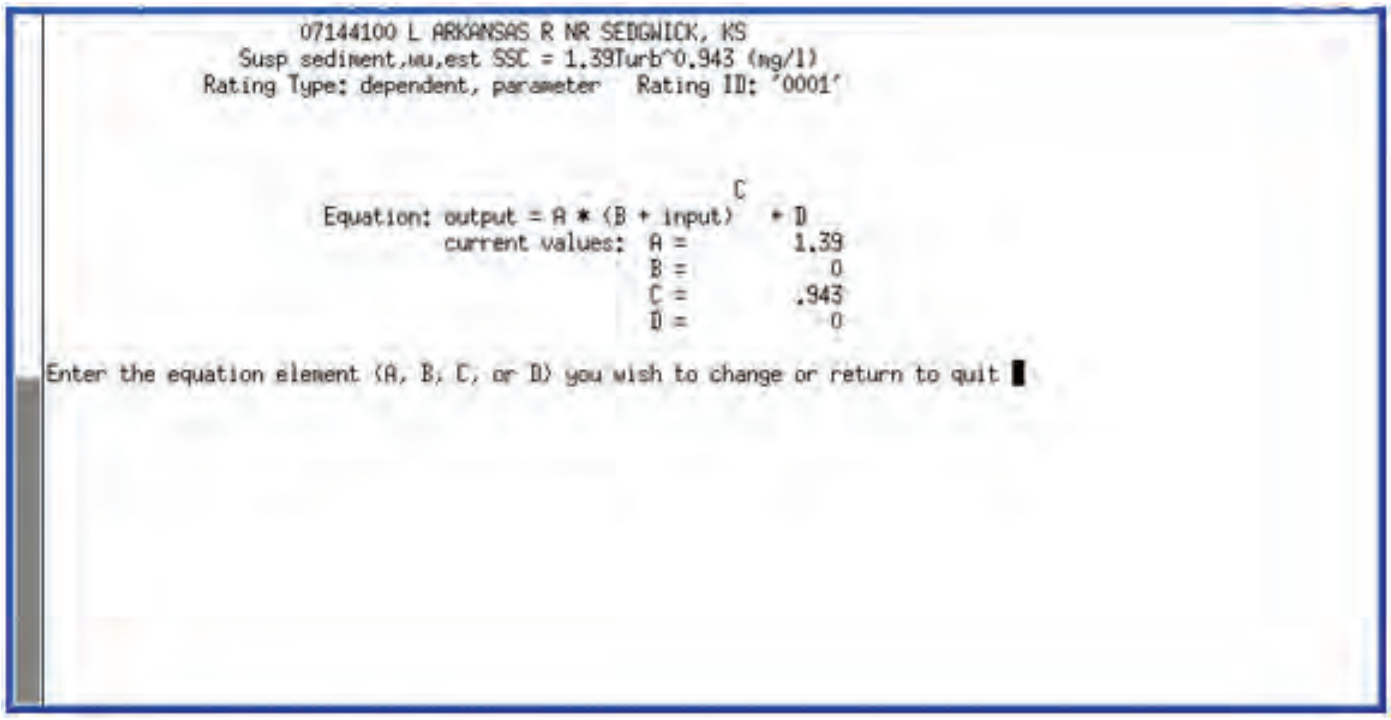

4. Primary computation must be performed on the *SSC* DD to compute the *SSC* UVs.

   - In ADAPS, select menu options:
     "PR—Primary Data Processing,"
     "7—Primary Computations,"
     select the desired site number, DD, and dates,
     <Enter>
     select the desired options, and
     <Enter> .
   - Enter Hydra to compare *SSC* UVs with turbidity UVs;
     select "PR—Primary Data Processing,"
     select "2—Edit Time-Series Data using Hydra,"
     select "3. COMPUTED UNIT VALUES,"
     select the desired site number, DD, and dates, and
     add a reference curve for the turbidity DD.
   - View the plot of the two curves and verify that the data look correct. For instance, for the Little Arkansas River near Sedgwick, Kansas, the *SSC* and turbidity are nearly identical at values less than 400. For *SSC* values larger than 400, the difference increases as *SSC* increases so that turbidity is larger than *SSC*.

5. Currently (2009), ADAPS computes mean daily *SSL* from mean daily *SSC* and streamflow and the appropriate conversion factor. The resulting *SSL* DV is only correct if *SSC* and streamflow are highly correlated ($r > 0.95$). In most cases, they are not highly correlated, and therefore, ADAPS should not be used to compute *SSL*. The hydrographer should use either GCLAS or a spreadsheet application for the computation of *SSL* UVs or DVs. If the hydrographer can verify that the *SSC* and streamflow for their site is highly correlated ($r > 0.95$), then the following instructions can be used to compute *SSL* DVs in ADAPS.

   Primary computations must be performed on the *SSL* DD to compute *SSL* DVs.

   - Compute *SSL* DVs using DV_MANIP in ADAPS. From the ADAPS prompt:
     type DV_MANIP (or "PR 9"),
     select "A" to write the DVs to ADAPS,
     select the desired site number, dates, and the *SSL* DD,
     <Enter>,
     select option (8) compute load from streamflow and concentration,
     select "A,"
     select the desired site number, dates, and the streamflow DD,
     <Enter>,
     select "A,"
     select the desired site number, dates, and the *SSC* DD,
     select "e" (edited or estimated) to set the DV remark code, and
     select "s" to store the data in ADAPS.

6. Plot to *SSL* DVs, *SSC* UVs, and streamflow UVs in either Hydra or Tkg2 for comparison.

7. NWISWeb can be configured to display up to 60 days of *SSC* unit values, all available daily values, daily, monthly, and annual statistics for turbidity, streamflow, *SSC*, and *SSL* and *SSC* values from discrete sample collection.

Appendix 3. Comparison of Computed Suspended-Sediment Concentrations with Water-Quality Criteria

Currently (2009), there are no State criteria for *SSC*. Five States (Hawaii, Nevada, New Jersey, South Dakota, and Utah) have numeric criteria for total suspended solids (*TSS*), which range from a minimum concentration of 35 milligrams per liter (mg/L) in Utah to a maximum of 158 mg/L in South Dakota (U.S. Environmental Protection Agency, 2001). The differences between values of *SSC* and *TSS* as metrics for the suspended solid-phase content of surface waters are discussed in Gray and others (2000). *SSC* remains one of the most cited water-quality impairments in the United States even with the lack of State criteria. The *SSC* values computed using SLR methods have a quantifiable uncertainty that allows for several methods of comparison with criteria. In the following examples, 100 mg/L is an assumed *SSC* water-quality criterion for comparison.

Continuous *SSC* can be used, for example, to construct cumulative frequency distribution (duration) curves to determine percentage of time that computed concentrations exceed water-quality criteria. Computed concentration duration curves can be used to evaluate current water-quality conditions and to estimate the duration and magnitude of potential water-quality degradation. Without *SSC* water-quality criteria, water-resource managers can use duration curves to assess how frequent a potential water-quality criterion may be exceeded. When OLS regression is used to generate estimates for which probability statements are made, such as with duration curves and probability of exceeding criteria, values at the upper end likely are underestimated, and values at the lower end may be overestimated (Helsel and Hirsch, 2002).

In the example below, 28 percent of the hourly computed *SSC* values exceeded 100 mg/L for the period October 1999 through September 2005. The 90-percent prediction interval indicates that 100 mg/L could be exceeded 22 to 36 percent of the time. Simple linear regression (SLR) was used to compute the values plotted in figure 20 after SLR was determined to be the most appropriate regression technique. Like all regression techniques, the true relation of the response and explanatory variables is unknown, and the regression model is only an estimate of this relation. Other regression techniques might yield different models and, therefore, different duration curves. The differences between regression techniques typically are within the 90-percent prediction interval of the SLR regression.

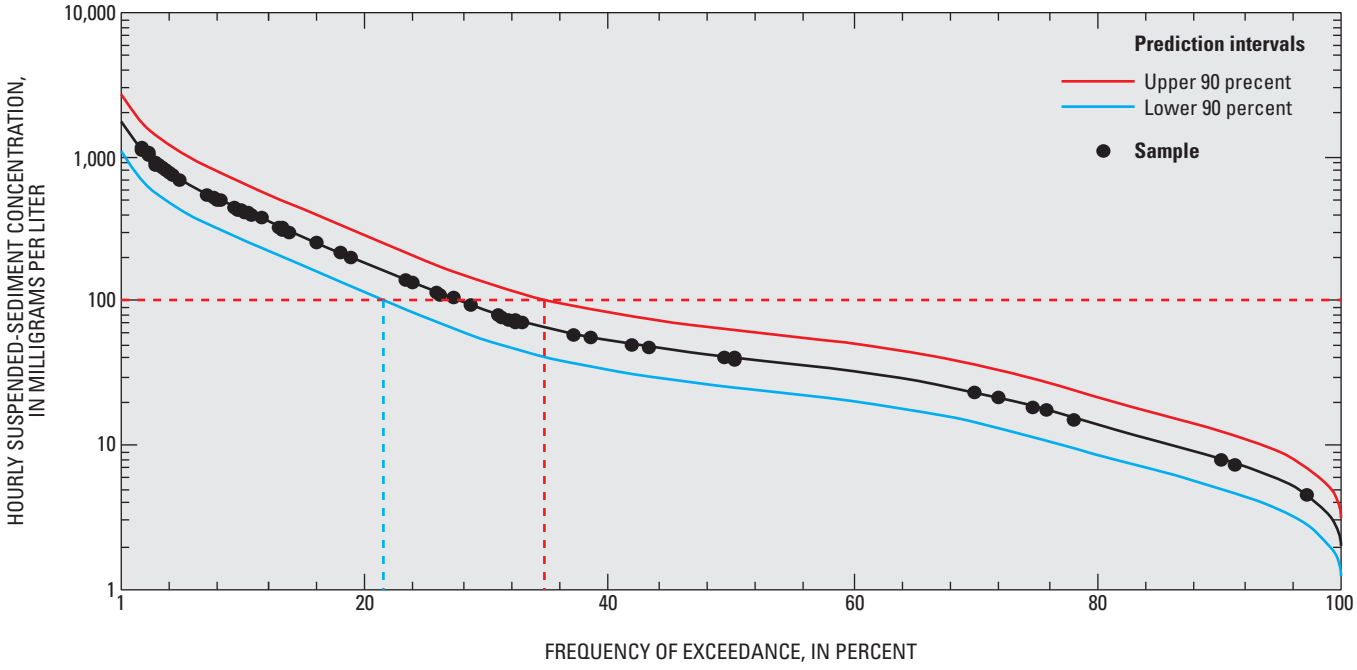

Duration curve and 90-percent prediction intervals for computed hourly suspended-sediment concentrations in Little Arkansas River near Sedgwick, Kansas, October 1999–September 2005.

Although prediction intervals are approximate indicators of uncertainty, a range of values is not very useful for comparing the water quality of a stream to water-quality criteria. Probability of exceedance provides water managers with a single hourly value for decisionmaking. Probabilities of exceeding designated water-quality criteria or other values of interest for a $\log_{10}$ transformed model can be determined as follows:

$$\Pr\left(SSC \le Criterion\right) = 1 - D\left[\frac{\log_{10}\left(SSC\right) - \log_{10}\left(Criterion\right)}{RMSE}\right]$$

where

Pr is the probability that the criterion has been exceeded ($0 < Pr < 1$),

D is the cumulative distribution function for the standard normal curve—values for it are obtained from tables in statistics textbooks or equations that approximate the exact values,

SC is the BCF-corrected, regression-computed *SSC* value;

Criterion assumed 100 mg/L [if *RMSE* is in $\log_{10}$ space, then criterion is $\log_{10}(100)$]; and

RMSE is root-mean-squared error, or standard error of the regression, or standard deviation of the residuals.

The probability of hourly *SSC* also can be displayed as probability curves. Each curve represents an *SSC* and is plotted using frequency of exceedance (x axis) and the probability that the actual *SSC* is equal to the given threshold (y axis). The figures can be used to estimate the frequency of exceedance for 5 values of *SSC*. For instance, 20 percent of all hourly values of *SSC* for Little Arkansas River at Sedgwick have a 99-percent chance of exceeding 100 mg/L. Two percent of all hourly *SSC* values have a 50-percent chance of exceeding 1,000 mg/L for Little Arkansas River at Sedgwick.

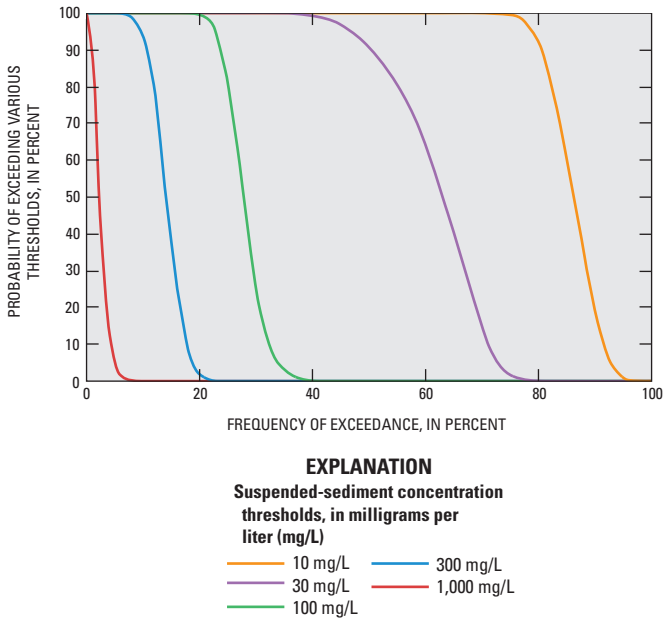

Cumulative frequency curves showing probability of exceedance of suspended-sediment concentration thresholds of 10, 30, 100, 300, and 1,000 milligrams per liter, Little Arkansas River near Sedgwick, Kansas, 1999–2005.

Publishing support provided by:
Rolla Publishing Service Center

For more information concerning this publication, contact:
Director, USGS Kansas Water Science Center
4821 Quail Crest Place
Lawrence, KS 66049
(785) 842–9909

Or visit the Kansas Water Science Center Web site at:
http://ks.water.usgs.gov

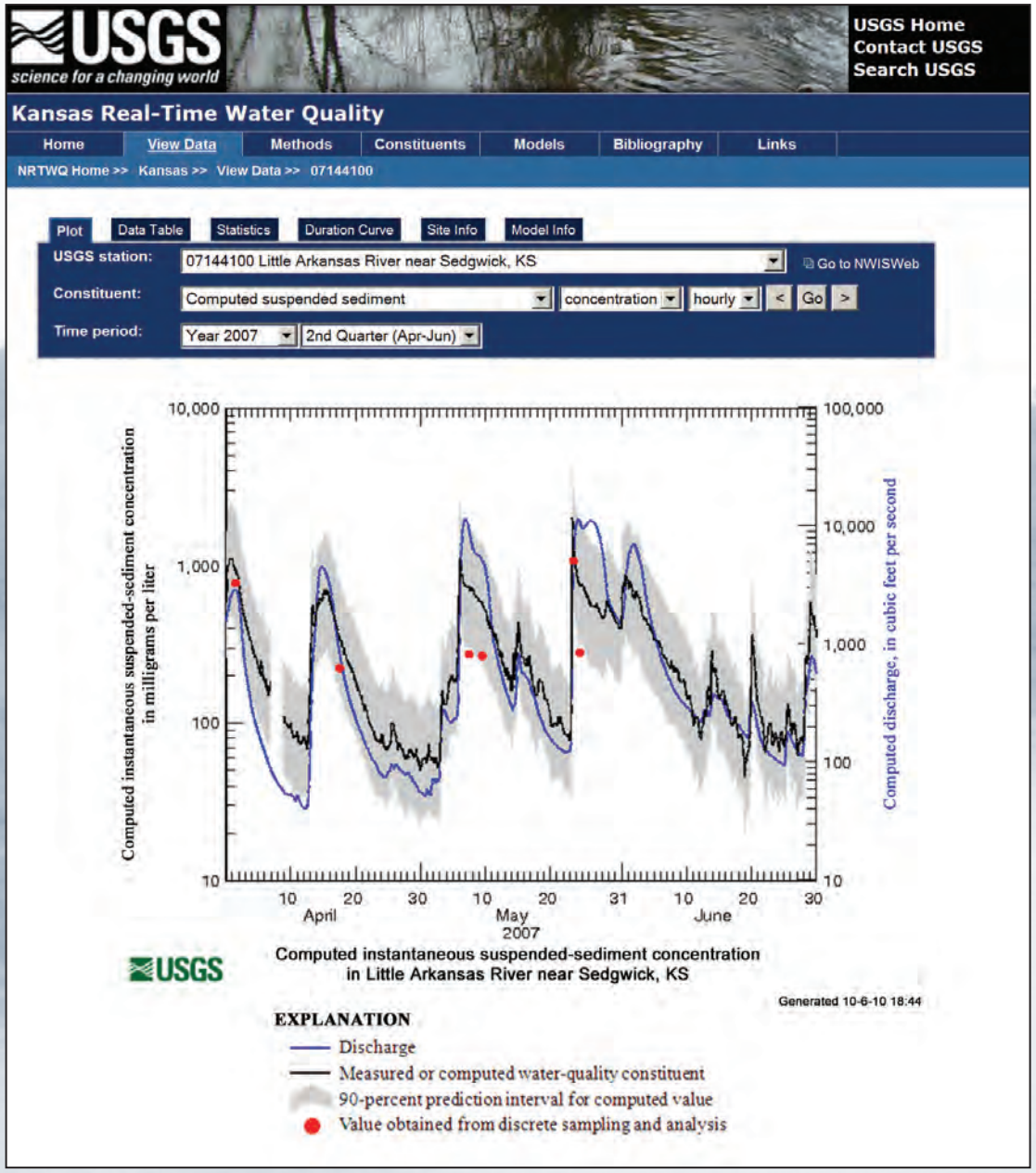

http://nrtwq.usgs.gov

ISBN 978-1-4113-2410-7

Assessment of erosion, sedimentation, and water quality impacts of the Mountain Valley Pipeline and Equitrans Expansion Project's proposed crossing of the Jefferson National Forest as it pertains to the U.S. Forest Service's Draft Supplemental Environmental Impact Statement dated December 2022

Prepared by Jonathan A. Czuba, Ph.D., Licensed Professional Engineer - February 9, 2023

REFERENCES
24

February 21, 2023

USGS
science for a changing world

Prepared in cooperation with the U.S. Army Corps of Engineers, Portland District

Correlations of Turbidity to Suspended-Sediment Concentration in the Toutle River Basin, near Mount St. Helens, Washington, 2010–11

Open-File Report 2014–1204

U.S. Department of the Interior
U.S. Geological Survey

Front cover: Mount St. Helens and North Fork Toutle River channel. (Photograph taken by Kurt R. Spicer, U.S. Geological Survey, December 11, 2013.)

Back cover: Sediment Retention Structure after spillway raise. (Photograph taken by Adam Mosbrucker, U.S. Geological Survey, November 27, 2012.)

Correlations of Turbidity to Suspended-Sediment Concentration in the Toutle River Basin, near Mount St. Helens, Washington, 2010–11

By Mark A. Uhrich, Jasna Kolasinac, Pamela L. Booth, Robert L. Fountain, Kurt R. Spicer, and Adam R. Mosbrucker

Prepared in cooperation with the U.S. Army Corps of Engineers, Portland District

Open-File Report 2014–1204

U.S. Department of the Interior
U.S. Geological Survey

U.S. Department of the Interior
SALLY JEWELL, Secretary

U.S. Geological Survey
Suzette M. Kimball, Acting Director

U.S. Geological Survey, Reston, Virginia: 2014

Suggested citation:
Uhrich, M.A., Kolasinac, Jasna, Booth, P.L., Fountain, R.L., Spicer, K.R., and Mosbrucker, A.R., 2014, Correlations of turbidity to suspended-sediment concentration in the Toutle River Basin, near Mount St. Helens, Washington, 2010–11: U.S. Geological Survey Open-File Report 2014-1204, 30 p., *http://dx.doi.org/10.3133/ofr20141204*.

ISSN 2331-1258 (online)

Contents

Figures

Tables

Conversion Factors and Datums

Conversion Factors

Inch/Pound to SI

Multiply	By	To obtain
	Length	
inch (in.)	2.54	centimeter (cm)
inch (in.)	25.4	millimeter (mm)
foot (ft)	0.3048	meter (m)
mile (mi)	1.609	kilometer (km)
	Area	
square mile (mi^2)	259.0	hectare (ha)
square mile (mi^2)	2.590	square kilometer (km^2)
	Volume	
cubic yard (yd^3)	0.7646	cubic meter (m^3)
	Flow rate	
cubic foot per second (ft^3/s)	0.02832	cubic meter per second (m^3/s)
	Mass	
ton, short (2,000 lb)	0.9072	megagram (Mg)

SI to Inch/Pound

Multiply	By	To obtain
	Length	
millimeter (mm)	0.03937	inch (in)

Concentrations of suspended sediment in water are given in milligrams per liter (mg/L)).

Datums

Horizontal coordinate information is referenced to the North American Datum of 1983 (NAD 83).
Vertical coordinate information is referenced to the North American Vertical Datum of 1929 (NAVD 29).
Elevation, as used in this report, refers to distance above the vertical datum.

Correlations of Turbidity to Suspended-Sediment Concentration in the Toutle River Basin, near Mount St. Helens, Washington, 2010–11

By Mark A. Uhrich, Jasna Kolasinac[2], Pamela L. Booth[3], Robert L. Fountain[2], Kurt R. Spicer[1], and Adam R. Mosbrucker[1]

Abstract

Researchers at the U.S. Geological Survey, Cascades Volcano Observatory, investigated alternative methods for the traditional sample-based sediment record procedure in determining suspended-sediment concentration (SSC) and discharge. One such sediment-surrogate technique was developed using turbidity and discharge to estimate SSC for two gaging stations in the Toutle River Basin near Mount St. Helens, Washington. To provide context for the study, methods for collecting sediment data and monitoring turbidity are discussed. Statistical methods used include the development of ordinary least squares regression models for each gaging station. Issues of time-related autocorrelation also are evaluated. Addition of lagged explanatory variables was used to account for autocorrelation in the turbidity, discharge, and SSC data. Final regression model equations and plots are presented for the two gaging stations. The regression models support near-real-time estimates of SSC and improved suspended-sediment discharge records by incorporating continuous instream turbidity. Future use of such models may potentially lower the costs of sediment monitoring by reducing time it takes to collect and process samples and to derive a sediment-discharge record.

Introduction

Suspended-sediment transport throughout the Toutle River Basin has been monitored and studied since 1980–81, following the eruption of Mount St. Helens on May 18, 1980. This study used standard U.S. Geological Survey (USGS) methods to compute sediment-discharge for gaging stations in the basin (Porterfield, 1977), along with standard laboratory and field procedures (Guy, 1977; Edwards and Glysson, 1999). Streamflow and suspended-sediment concentration (SSC) have been measured, and suspended-sediment discharge (SSQ) has been computed, in several drainages in the Toutle River Basin (Dinehart, 1998). SSC data are collected by pump sample most days and by depth-integrated methods on infrequent days. This report uses data from two long-term gaging stations on the North Forth Toutle River and main-stem Toutle River. Daily, monthly, and annual SSC and SSQ data are available online.

[1]U.S. Geological Survey.
[2]Portland State University.
[3]University of Rhode Island.

In recent years, technology improvements have spawned efforts to develop innovative and improved methods of generating time-series records of SSC and SSQ. Traditionally, sample-based methods require lengthy evaluation and review before sediment records are finalized, although interactive software referred to as Graphical Constituent Loading Analysis System (GCLAS) has improved this processing (Koltun and others, 2006). Using recently approved methods (Rasmussen and others, 2009); this study examines turbidity as an alternative or surrogate for SSC with the intention of better defining SSQ, streamlining record computations, and possibly lowering costs. Additionally, land, water, fish, and wildlife resource planners need real-time estimations of SSC and SSQ to more effectively respond to changes and disturbances in basins under their management. These techniques, which compute SSC from turbidity and streamflow, coupled with a gaging-station telemetry system, potentially would allow delivery of near real-time SSC and SSQ data. Because real-time SSQ estimates are considered provisional owing to sensor and sampling uncertainty, regression-based SSQ records would be finalized annually following approval of turbidity and streamflow data. Use of a regression model to compute sediment records may improve accuracy by incorporating high-frequency measurements of explanatory variables, and also may lower costs by reducing record processing time and the number of samples collected and analyzed. The sediment-sample collection, turbidity monitoring, and regression analysis for this study were conducted in cooperation with the U.S. Army Corps of Engineers, Portland District.

Purpose and Scope

- The primary objective of this study is to test the feasibility and application of instream turbidity sensors at two sites in the Toutle River Basin and to demonstrate the use of these sensors as a surrogate for SSC, and document the results.
- Turbidity and streamflow data from April 2010 to September 2011 are used to generate regression models for estimating SSC. Such models can be updated as new turbidity, streamflow, and sampled SSC data become available.
- Regression equations are provided for both streamgages and could be used to provide near-real-time estimates of SSC and SSQ. The proof of concept is shown and regression-based estimates for the time-series data could be finalized if they were deemed beneficial. Future projections of SSC also could be made available as an online data series.
- Finally, we make a preliminary assessment as to whether using such a regression approach would provide a better-quality SSQ estimate and would reduce effort and expense compared to previous methods.

Study Area

The number and location of streamflow-gaging and sediment-monitoring stations in the Toutle River Basin have evolved since their establishment in 1980–81. Current (2014) gaging stations shown in figure 1 include North Fork Toutle River below Sediment Retention Structure near Kid Valley, Washington (NF Toutle-SRS, 14240525); and Toutle River at Tower Road near Silver Lake, Washington (Toutle-Tower, 14242580). A third gaging station, South Fork Toutle River at Toutle, Washington (SF Toutle, 14241500), was discontinued in 2013. For the 6 water years (WYs 2007–12)

the reported NF Toutle-SRS total SSQ was more than 18 million tons (units in short tons), constituting more than 67 percent of the total SSQ of nearly 27 million tons computed for Toutle-Tower. For the 20-year period, WYs 1993–2012, the reported total SSQ for Toutle-Tower was more than 60 million tons, an annual average of 3 million tons. For the 1.5-year (April 2010–September 2011) period of data in this report, the Toutle-Tower SSQ totaled nearly 2.9 million tons, slightly less than the yearly average (*http://wdr.water.usgs.gov/*).

The Toutle-Tower gaging station, at 160-ft in elevation, is about 7 river miles (RMs) upstream of the confluence of the Toutle and Cowlitz Rivers and has a drainage area of 496 mi^2. The NF Toutle-SRS gaging station, at RM 12 of the North Fork Toutle River, drains 175 mi^2, and is about 30 RMs upstream of the Toutle-Tower gaging station (fig. 1). The NF Toutle-SRS station, at 700-ft elevation, is less than 2 RMs downstream of the Sediment Retention Structure (SRS). The SRS was completed in 1989 to retain and avert sediment eroded from the Mount St. Helens debris-avalanche deposit from being transported to the lower basin and eventually the Cowlitz and Columbia Rivers. Through 2012, the SRS has trapped about 115 million yd^3, representing about 3.5 percent of the total sand and gravel deposited after the 1980 eruption (Major and Spicer, 2003; Gibson and others, 2010). Nonetheless, a large volume of fluvial sediment passing the SRS is deposited downstream and is aggrading channel beds, thereby increasing the threat of flood inundation to the surrounding communities, as well as posing a hazard to river navigation and economically important commerce, drinking-water supplies, and migrating fish.

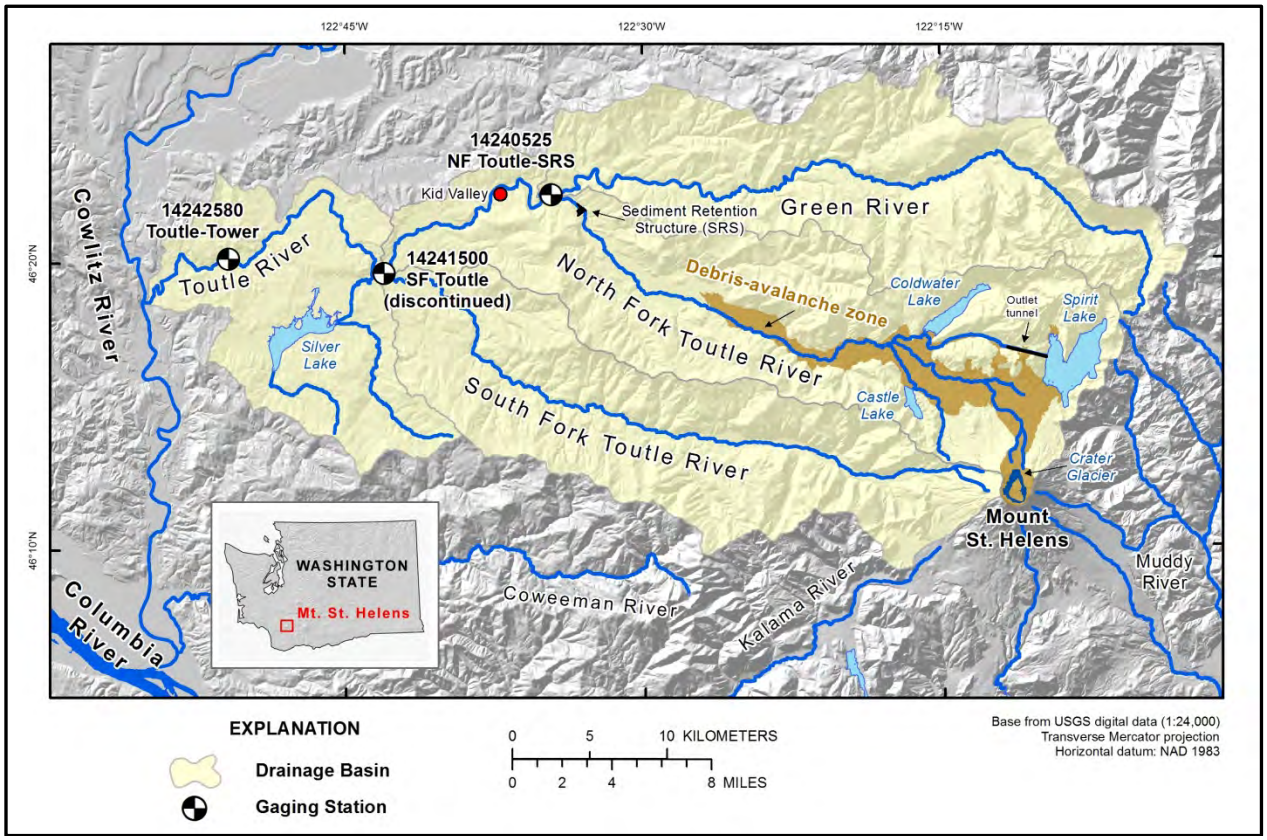

Figure 1. Map showing Toutle River Basin study area, drainage basins, and U.S. Geological Survey (USGS) gaging station locations, near Mount St. Helens, Washington.

Data Collection and Analysis Methods

To achieve the objectives in the section, "Purpose and Scope," we installed instream turbidity sensors at two gaging stations, NF Toutle-SRS and Toutle-Tower. Fifteen-minute unit-value turbidity and discharge data and periodic suspended-sediment samples were collected at both gaging stations (U.S. Geological Survey, 2010, 2011).

Matched pairs of turbidity and discharge with SSC were used as the explanatory and response variables, respectively, in a multi-linear regression using ordinary least squares (OLS) methods. Separate regression models were generated for each station. The resulting equations can be used to estimate 15-minute unit values of SSC from associated turbidity and water discharge unit values. Finally, the regression results, including accompanying uncertainty estimates, can be compared with previous sample-based sediment records computed for these stations in the Toutle River Basin in order to evaluate the relative utility of the traditional and surrogate methods.

Several established USGS methods were used to collect and process the suspended-sediment samples and to check, review, and publish the turbidity data.

Suspended-Sediment Sampling

This study started in April and May 2010 for the Toutle-Tower and NF Toutle-SRS streamgages, respectively, when turbidity calibrations and data collection began (figs. 2 and 3). Suspended-sediment samples were collected routinely in WYs 2010 and 2011, with an emphasis on storm, high-streamflow, and high-turbidity events.

Figure 2. Photographs showing suspended-sediment sampling, March 12, 2010 (large photograph), and servicing sensors, April 20, 2012 (inset), at North Fork Toutle River below Sediment Retention Structure near Kid Valley, Washington. Photographs taken by Kurt Spicer, USGS, Cascades Volcano Observatory.

Figure 3. Photographs showing suspended-sediment sampling at Toutle River at Tower Road near Silver Lake, Washington, December 13, 2012. Photographs taken by Kurt Spicer, USGS, Cascades Volcano Observatory.

Cross-Sectional, Depth-Integrated Sediment Samples

Manual suspended-sediment samples were collected at both gaging stations using standard USGS depth-integrated, equal-discharge-increment (EDI) and equal-width-increment (EWI) methods, (figs. 2 and 3; Edwards and Glysson, 1999). These sampling procedures have been used consistently at the NF Toutle-SRS and Toutle-Tower gaging stations since sampling began in the early 1980s. EDI and EWI sampling methods are the accepted procedures for providing representative cross-sectional SSCs.

Two sets of manual EDI/EWI samples (sets "A" and "B") usually were collected nearly simultaneously for each sampling visit and can be used independently or averaged to produce a single concentration and to better capture sample uncertainty (Topping and others, 2011). Manual data in this study used sample A and B sets so that each individual concentration could be used to better populate and define the regression model.

Point Samples

Automatic pumping samplers on the bank at each site were used to augment the EDI/EWI cross-sectional samples for periods between the manual collections. A single pump sample per day usually was collected in addition to multiple samples during high-flow events. Autosamplers draw water from a single point in depth and cross section, and, therefore, differ from the EDI/EWI methods that capture spatial variability throughout the stream width and water column. Autosampler concentrations nearest in

time to EDI/EWI samples were evaluated to determine if an adjustment or shift in the autosampler concentration was necessary. These point-sample correction adjustments or coefficients are used to shift autosampler concentrations to better reflect the mean cross-section concentration defined by manual EDI/EWI samples.

Autosampler concentrations typically are less than or equal to manual-sample concentrations (Glysson, 2008). To establish a correction coefficient, a pumping sample normally is manually triggered before and after an EDI/EWI cross-section sample set. Generally, if the pump and EDI/EWI sample concentrations agree to within 5 percent, no correction is applied and the coefficient is 1.0. If the difference is greater than 5 percent, the autosampler concentrations are adjusted to the manual concentration with a shift usually greater than 1.0. The shift is applied across time, either by relation to flow or by linear proration, until the next measured pumping sample coefficient. The corrections are defined by a manual cross-sectional sample or by a particular streamflow or turbidity event that may have altered the pumping efficiency or indicated a change in stream-channel dynamics (Guy, 1977; Guy, 1978; Porterfield, 1977; Bent and others, 2000). Finally, as in any sample collection program, there is a delay in acquiring the concentration data because of shipment time and laboratory processing, so that pump and manual sample results are not available in real time.

Turbidity Measurement and Data Processing

Turbidity data were collected and processed using established USGS procedures for continuous water-quality monitoring (Wagner and others, 2006). Continuous turbidity data were collected at NF Toutle-SRS and Toutle-Tower using a DTS-12 sensor™, manufactured by Forest Technology Systems, Victoria, Canada (*http://www.ftsenvironmental.com/products/sensors/dts12/*). The sensor has a large optical face that allows for a relatively wide water column area to be measured by the lens and detector. The probe has a large and durable wiper that virtually eliminates the need for cleaning corrections because debris buildup on the optics is removed at each reading. The head of the sensor is angled at 45 degrees to lessen the formation of air bubbles, which can interfere with the optics and cause false readings. The sensor head must be oriented facing down and into the main water body for correct turbidity readings. The DTS-12 sensor™ turbidity readings are reported in Formazin Nephelometric Units (FNU) (Anderson, 2005).

Suspended-sediment concentrations in the Toutle River Basin typically range from 10–50 milligrams per liter (mg/L) during extended periods of low flow, to 10,000–20,000 mg/L during storm runoff. Such sediment-laden waters can negatively affect instream electronic instrumentation. The DTS-12 sensors™ have worked consistently through these harsh conditions, requiring only routine cleanings with calibration checks every 3 to 6 months. The DTS-12 sensor™ takes 20 readings per second over 5 seconds and provides several parameters for those 100 readings. These parameters include mean, median, minimum, and maximum turbidity, and water temperature. Two variance parameters also are included to help with quality assurance for the other parameters. Near real-time median turbidity readings are reported on the USGS National Water Information System Web site (*http://waterdata.usgs.gov/wa/nwis/current/?type=flow*) in 15-minute intervals, and are used in the regression analyses. Daily median, minimum, and maximum turbidity for the two gaging stations are published in the Washington Annual Data Report (U.S. Geological Survey, 2010, 2011). Approved instantaneous turbidity and discharge data for NF-Toutle-SRS and Toutle-Tower used in this analysis are shown in figure 4.

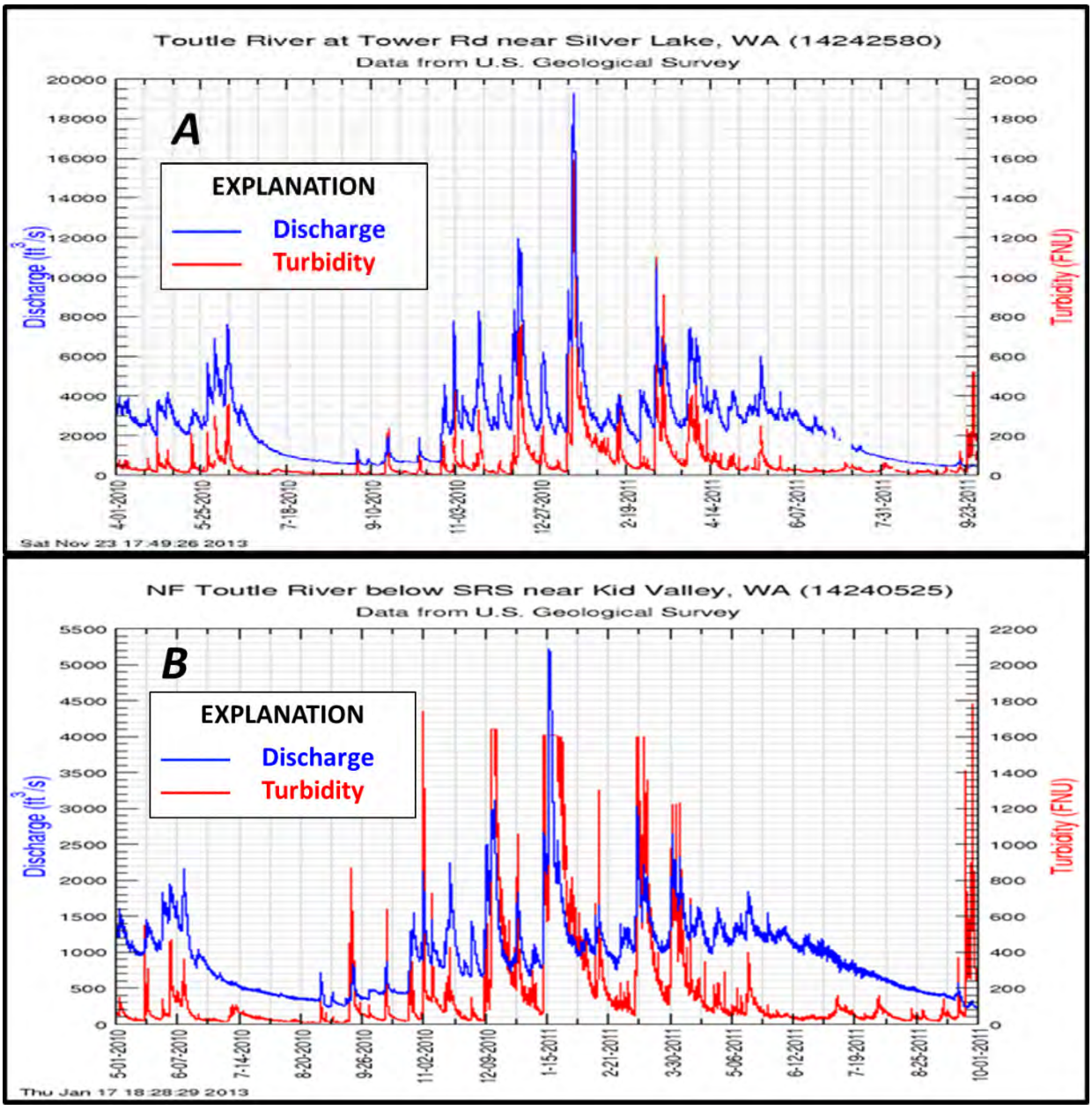

Figure 4. Graphs showing stream discharge and turbidity at two streamgages in Toutle River Basin, Washington, 2010–11. (*A*) April 1, 2010–September 30, 2011 and (*B*) May 1, 2010–September 30, 2011. (ft^3/s, cubic foot per second; FNU, Formazin Nephelometric Units.)

Turbidity Greater than Instrument Limits

All instream turbidity sensors have a maximum, instrument-specific reading. If turbidity surpasses that threshold, the sensor produces a false reading wherein the maximum value is reported repeatedly throughout the event. When graphed, this turbidity threshold displays as a horizontal line. After turbidity decreases to less than this threshold, the sensor again records valid measurements within the range of the probe.

The DTS-12 sensor™ threshold varies from sensor to sensor and ranges from about 1,600 to 2,100 FNU. Turbidity at NF Toutle-SRS reached the sensor threshold in December 2010, and in January and March 2011, with each threshold reading lasting from several hours to as long as 5 days. Turbidity at Toutle-Tower exceeded the sensor threshold on January 16, 2011, for 3 hours. Sediment samples collected during these turbidity sensor thresholds were not included in the regression models, as the true turbidity for the samples was unknown.

Existing alternative turbidity sensors suitable for instream monitoring that measure values greater than the DTS-12 sensor™ threshold potentially could provide a more consistent and complete turbidity record through peak events. Such a turbidity sensor was tested and routinely calibrated at NF Toutle-SRS, although the records for that sensor have not yet been approved. Data from this alternative sensor could be used to supplement periods when the DTS-12 sensor™ recorded threshold values and flat-lined. It then would be possible to run the regression models using these secondary values. The high-end turbidity values, if estimated or measured for missing or greater-than-threshold periods, also could be used to compute more complete and continuous model-generated SSC and SSQ values, which would be valuable given that these often are the periods of the greatest sediment transport. However, processing the high-end turbidity data would require further examination and review. Because the development of turbidity-surrogate regressions for this report was considered a proof of concept for the Toutle River gaging stations, processing high-end turbidity data was beyond the scope of this report; we, therefore, used only existing turbidity data that was approved and published. The potential utility of the high-turbidity data for refining the existing load estimates is considered in the section, "Discussion and Future Studies."

Selection of Turbidity and Sediment Concentration Data for Regression Analysis

Approved turbidity and SSC data were paired by matching the autosampler and EDI concentration to the closest-in-time turbidity value. If the EDI sample took more than 30 minutes to collect, the 15-minute turbidity values were averaged for the necessary time period in order to obtain a single value. Turbidity and sediment-sample data used for this report constitute roughly one-half of WY 2010 and the entire WY 2011 (April or May 2010–September 2011) for the Toutle-Tower and NF Toutle-SRS gaging stations, respectively. This provided a base dataset to begin construction of the regression models (appendix A). These relations can be evaluated from year to year, and can be compared with turbidity and SSC data collected in later years to determine any shift in turbidity-discharge to SSC relations and (or) transport regime.

To maintain consistency with the previously published sediment records for these periods (*http://wdr.water.usgs.gov/*), the identical sample concentrations (both EDIs and pumping samples) used in the sediment records were used in the regression analysis, except for turbidity and sample concentrations deleted from the analysis dataset when turbidity readings were at maximum threshold. The total number of EDI and pumping samples available for each gaging station collected from April or May 2010 through September 2011 are shown in table 1.

NF Toutle-SRS and Toutle-Tower discharge and turbidity with EDI samples collected from May 1 or April 1, 2010, through September 30, 2011, are shown in figure 5. Two EWI samples were collected, but neither sample was used because of contamination from the streambed.

Table 1. Number and type of sediment samples collected at North Fork Toutle River below Sediment Retention Structure near Kid Valley (NF Toutle-SRS) and Toutle River at Tower Road near Silver Lake (Toutle-Tower), Toutle River Basin, Washington, 2010–11.

Gaging station and sample dates	Equal-Discharge-Increment samples collected	Pumping samples collected
NF Toutle-SRS, May 2010–September 2011	48	605
Toutle-Tower, April 2010–September 2011	9	696

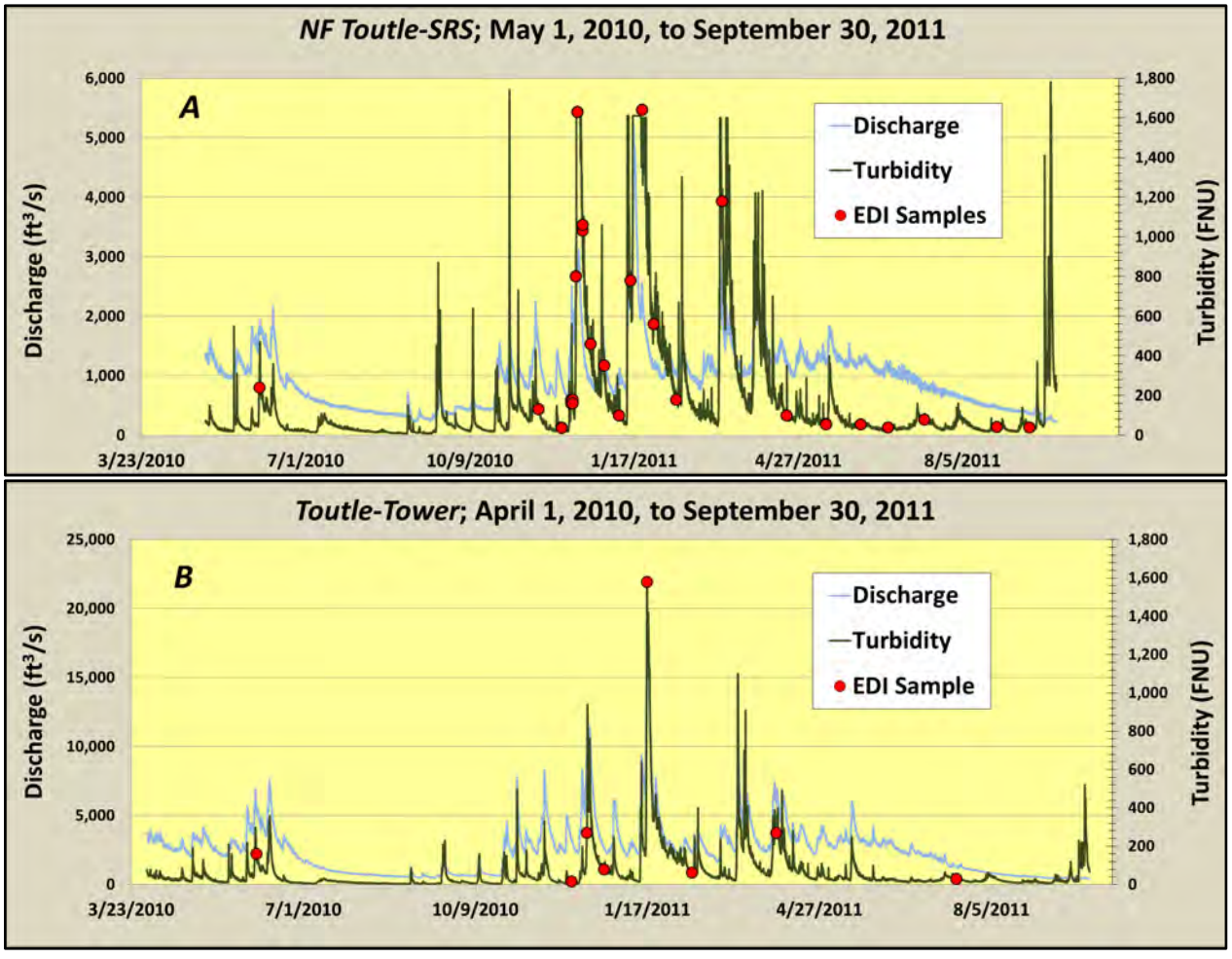

Figure 5. Graphs showing stream discharge and turbidity with time of equal-discharge-increment samples collected overlaid on turbidity, at (*A*) North Fork Toutle River below Sediment Retention Structure near Kid Valley (NF Toutle-SRS), May 1, 2010–September 30, 2011, and (*B*) Toutle River at Tower Road near Silver Lake (Toutle-Tower), April 1, 2010–September 30, 2011, Toutle River Basin, Washington. Discharge is measured in cubic feet per second (ft^3/s) and turbidity is measured in Formazin Nephelometric Units (FNU). Not all points are visible because of overlap of set A and B sample points collected close in time to each other.

These two sample sets indicate a strong reliance on autosamples, as is the normal routine in working a sample-based sediment-discharge record. As mentioned in the "Suspended-Sediment Sampling; Point Samples" section, autosamples, by nature of their position and orientation along the side of a channel cross section and as single-point samples, may not typically represent a concentration equal to the manual depth-integrated, cross-sectional samples. Therefore, a regression-based approach ideally would rely more on EDI/EWI samples than on pumping samples because of the differences in uncorrected concentrations between the two sample types.

Discharge Data

Water discharge values used for this analysis were computed from a stage-discharge rating developed from current-meter measurements and a 15-minute, time-series stage record, using established USGS techniques (Buchanan and Somers, 1976; Rantz and others, 1983). Streamflow measurements typically, but not always, accompanied cross-section EDI and EWI samples. Current-meter instruments were used exclusively for discharge data in this report. According to Sauer and Meyer (1992), the standard errors associated with individual discharge measurements can range from 2 to 20 percent, although most standard errors range from 3 to 6 percent. Discharge data for the Toutle River sites are available at *http://wdr.water.usgs.gov/*.

Statistical Methods

Regression Models Applied

We used OLS linear regression (Helsel and Hirsch, 2002) with turbidity and discharge as explanatory variables and the EDI/EWI and auto-sampled SSC data as the response variable. Regression model development for SSC is covered extensively in Rasmussen and others (2009), including various correlation and data transformation measures and use of available explanatory variables. We selected the best candidate model on the basis of supportive diagnostic statistics, the fit of the explanatory and response variables, and hydrographer knowledge of sediment dynamics and data collection at the individual sites.

Following visual and statistical analysis of the SSC, turbidity, and discharge datasets, as well as examination of the residuals from preliminary OLS models, we log-transformed the datasets of both streamgages to improve distributional normality. We also tried natural log, square, and cube root transformations. The log transformation worked best overall by compressing tailings and outliers, as well as addressing possible heteroscedasticity, thereby improving the fit of the regression (Helsel and Hirsch, 2002). We also tested using a univariate model with turbidity as the sole explanatory variable. Finally, the addition of discharge statistically improved the sum of squares error (SSE) and coefficient of determination (R^2) and, therefore, was used in a multiple linear regression (MLR). However, the log transformation and MLR did not alleviate time-related auto-correlation, as indicated by low Durban-Watson statistics (Helsel and Hirsch, 2002). Although this transformation improved overall model fit by decreasing the SSE and normalizing the residuals, autocorrelation was still a concern.

One method to address autocorrelation and to increase accuracy in the regression model was the inclusion of time lags of turbidity and discharge as additional explanatory variables. The final MLR used a single lag of turbidity as a third variable. The inclusion and importance of lagged turbidity is explained in the section, "Accounting for Autocorrelation."

Statistical Diagnostics and Analysis of Variance

Analysis of Variance (ANOVA) statistics generated for each gaging station regression are shown in tables 2 and 3. The structure of the ANOVA is written from left to right, with each column broadening the understanding and role that each "Source" statistic contributes to the development and significance of the final regression model. A base understanding of the terminology and structure of the statistics is necessary to better interpret the results.

The Sequential Sum of Squares (Seq. SS) consists of the decomposition of the sum of the squared difference between the individual observed value of the log of SSC and the mean of log of SSC into the "*Regression*" part and the "*Error*" part. The *Regression* part is the sum of the squared difference between the predicted value and the overall mean of log of SSC, whereas the *Error* part is the difference between the observed value and the predicted value. Because there are multiple values for each day, the *Error* is further decomposed into *Lack-of-Fit* (sum of square of difference between local average and fitted) and *Pure Error* (sum of square of difference between observed and local average). These SS values then are corrected for bias by their respective degrees of freedom (df) with the unbiased estimation value under Sequential Mean Square (Seq. MS). The Seq. MS functions as the value for the estimations of variance for the distributions of the *Regression* and the *Error*.

Table 2. Final Analysis of Variance (ANOVA) for logSSC compared to LogT, logT-lag, logQ, for North Fork Toutle River below Sediment Retention Structure near Kid Valley, Washington. [See text for explanation of statistical terms].

Source	Seq. SS	df	Seq. MS	F-statistic	P > F
Regression	145.62527	3	48.5419	929.71	0.000
Error	**33.8854**	649	0.05221		
Lack-of-Fit	33.798	624	0.0541635	15.48589	0.000
Pure Error	0.08744	25	0.0034976		
Total	179.5112	652			

$$\sqrt{MS_E} = 0.228499 \; R^2 = \mathbf{81.1}\% \; R^2_{adj} = 81.0\% \; PRESS = 34.4759 \; DW = 0.168913 \; Cp = 4$$

where

Seq. SS	*is Sequential Sum of Squares,*
Seq. MS	*is Sequential Mean Squares*,
df	*is degrees of freedom,*
Regression SS	*is Sum of Squares from Regression; Regression SS/Regression df*
Regression MS	*is Mean Squares from Regression (MS_E)*
Error SS	*is Sum of Squares Error (SSE)*; *Pure Error SS +Lack-of-Fit SS*
Error MS	*is Mean Squares Error (MS_E); SSE/Error df or Error SS/Error df*
Pure Error SS	*is True Error*
Lack-of-Fit SS	*is Error from poor estimation*
Total SS	*is Total Sum of Squares; Regression SS + SSE*

The *SSE* and R^2 values are important statistical and comparative diagnostics referred to in the "Accounting for Autocorrelation" section, hence appear bolded to emphasis.

Table 3. Final Analysis of Variance (ANOVA) for logSSC compared to LogT, logT-lag, logQ, for Toutle River at Tower Road near Silver Lake, Washington.

Source	Seq. SS	df	Seq. MS	F-statistic	P > F
Regression	428.1358	3	142.7112	2,968.57	0.000
Residual Error	**33.70**	701	0.04807		
Lack-of-Fit	33.55	693	0.0484127	2.5803	0.074
Pure Error	0.1501	8	0.0187625		
Total	461.8359	704			

$\sqrt{MS_E} = 0.219259\ R^2 = 92.7\%\ R^2_{adj} = 92.7\%\ PRESS = 34.3041\ DW = 0.686354\ Cp = 4$

In testing the significance or statistical fit of the regression equation for the NF Toutle-SRS and Toutle-Tower gaging stations, the ANOVA F-statistic from tables 2 and 3 indicates a significant relation between log of turbidity and log of SSC with a 1-percent probability of a type I error or the probability of incorrectly rejecting a true null hypothesis. The significance is determined by comparison to a critical F* value on the F-distribution with 3, and 649 or 701 df for the NF Toutle-SRS and Toutle-Tower sites, respectively, as determined by the numerator ($MS_{regression}$ = *Regression**SS***/*Regression**df***) and the denominator ($MS_E = Error\boldsymbol{SS}/Error\boldsymbol{df}$). This F-statistic is formed through the ratio of two probability distributions: the explained regression to the unexplained errors. The resulting ratio is an indicator of the overall fit of the regression model without involving units of measure or implying multiplicative effects.

The F-statistics for both regressions indicated that a significant proportion of the variation in log (SSC) was explained by the relation with log T (Turbidity) and log Q (Discharge) relative to the unexplained variation in log (SSC). Because the variance estimator Seq. ME (or MS_E from the ANOVA table) is expressed as *SSE* divided by df of the error, focusing on minimizing *SSE* was important for minimizing the estimate of the variance and standard deviation ($\sqrt{MS_E}$) of the model. The ANOVA tables 2 and 3 also included a "*Lack-of-Fit*" statistic that for both regressions was significant, indicating a poor overall fit. The discrepancy between the F and Lack-of-Fit statistics indicates a high variation within the data, including the possibility of autocorrelation of the errors observed through the distribution of the residuals, as reflected in the low Durban-Watson scores.

One of the best methods for determining the quality of a regression is the *PRESS* or prediction sum of squares. In general terms, the *PRESS* is a cross-validation calculation that provides a regression-fit summary that measures how well the model will perform in predicting new data. *PRESS* values were included and evaluated so that the best candidate model would have the lowest *PRESS*, and, thus, the best structure.

The Variance Inflation Factors (VIFs) in tables 4 and 5 also help determine the quality of a regression; VIFs measure the extent to which multicollinearity was present between the explanatory variables. Multicollinearity occurs when two or more variables are linear combinations of the other variables. A VIF greater than 5 is cause for concern, whereas a VIF greater than 10 is a major sign of colinearity, indicating that the predictors are highly correlated. Also provided in tables 2 and 3 are Mallow's Cp statistics, which are designed to minimize bias and standard error by keeping the number of coefficients low and in balance. Too few model variables cause bias, whereas too many predictors result in an imprecise model. Mallow's Cp is used so that the precision and bias of the full MLR is compared to the best subsets of predictors. The desired Mallow's Cp is a value that is close to the number of beta or explanatory variable coefficients plus the constant or y-intercept. This provides a model that is relatively precise and unbiased in estimating the correct regression coefficients, as well as predicting future responses or SSCs. Overall, the ANOVA results in tables 2 and 3 indicate that the final regressions between log SSC and the log transformed turbidity and discharge data are significant, with these variables explaining much of the variation in SSC. However, the strength of these relations is lessened because of the presence of significant autocorrelation.

Autocorrelation

The large number of daily and sub-daily pumping samples and paired EDI A and B sets, collected close in time to each other and available for this analysis, opened the dataset to potential problems associated with autocorrelation, or the serial correlation of a variable such as turbidity and (or) suspended-sediment concentration with itself over successive time intervals. When a variable indicates autocorrelation, one observation is related to another observation such that both observations will change together to some extent. In this case, the individual values of SSC, turbidity, or discharge are essentially similar to their previous value in the time series, such as during a storm event, and, therefore, do not represent random or independent occurrences. This presents a problem because statistically sound OLS regression models are assumed to have independent and normally distributed errors. When the errors, as observed through the residuals, show autocorrelation, the OLS method tends to underestimate the standard errors and coefficients of the model, thereby producing erroneously narrow confidence and prediction interval bands. These patterns typically can be identified through graphical analysis. For instance, if several samples are collected during a particular event, such as on the rising or falling limb of a hydrograph, the residuals may appear grouped together for that event in a non-random pattern.

Initial attempts to minimize the effects of autocorrelation led to averaging EDI-paired A and B sample sets, as well as randomly subsampling the autosamples. These smaller datasets then were tested by applying different regressions on the reduced number of autosamples and EDIs as suggested by Helsel and Hirsch (2002). Although these attempts reduced the potential for autocorrelation, the resulting graphical and statistical analysis showed minimal reduction. Therefore, additional methods were used to develop a model using all data (EDIs and autosamples), while also reducing the autocorrelation and *SSE*.

Evaluating Autocorrelation

The Durbin-Watson statistic (DW) (tables 2 and 3) essentially is the measure of the Sum of Error generated from the difference between a residual at index i and index i-1 taken over all residuals. A DW statistic between 0 and 1.6 generally indicates a positive auto-correlation for large sample sizes, especially when DW is less than 1. Because the DWs for both regressions were close to 0, there is a strong indication that positive autocorrelation was present. Because there was reason to be concerned about the variability of the residuals, a closer analysis of residual graphs for normality was warranted.

The normal probability graphs for the NF Toutle-SRS and Toutle-Tower gaging stations (figs. 6*A* and 7*A*) showed no strong deviation from a normal distribution of residuals. However, a comparison of the histogram (figs. 6*B* and 7*B*) and the "fitted values" against their residuals (figs. 6*C* and 7*C*) showed some abnormal grouping and tailing. Collectively, these three graphs show no reason for concern; for each station, the graphs of residuals against "observation order" (figs. 6*D* and 7*D*) showed that the residuals were related to each other across time, substantiating the DW statistic.

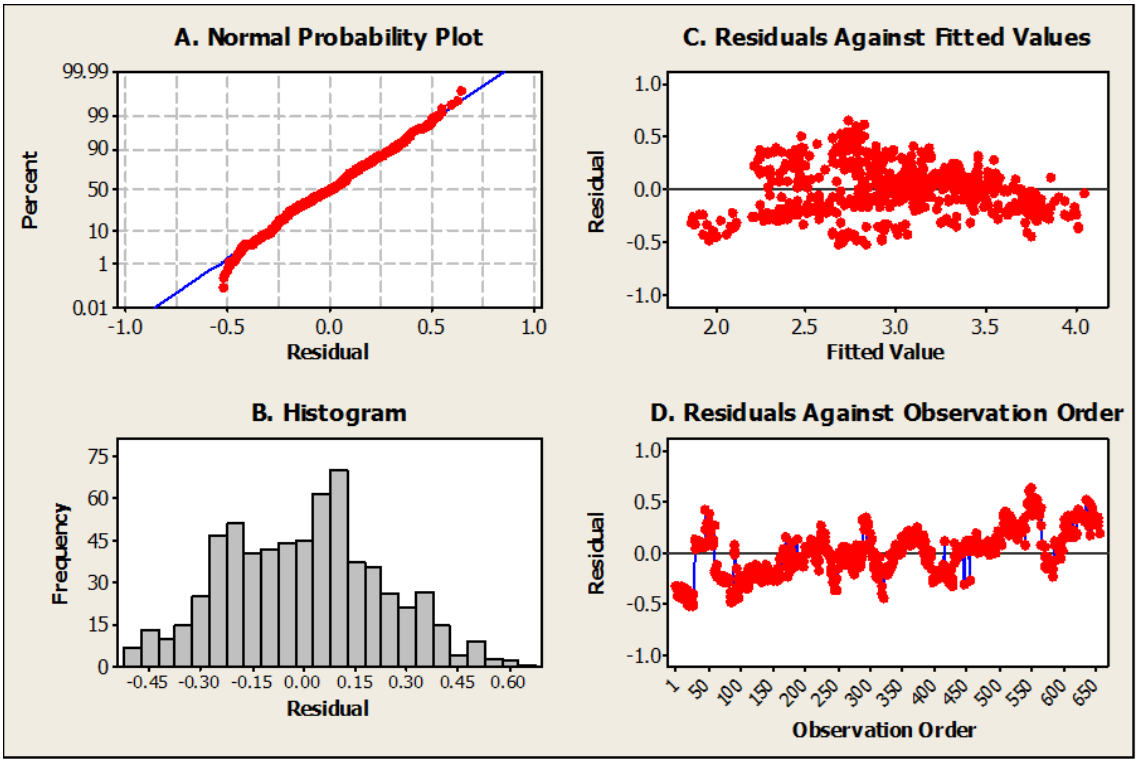

Figure 6. Graphs showing (*A*) normal probability distribution of residuals; (*B*) frequency distribution of residuals; (*C*) comparison of residuals with fitted values; and (*D*) comparison of residuals with observation order, for a multivariate regression of log(SSC) against log(T), log(Tlag), and log(Q), for North Fork Toutle River below Sediment Retention Structure near Kid Valley, Washington. Figure made from Minitab® software as 4-in-1 plots (*www.minitab.com*).

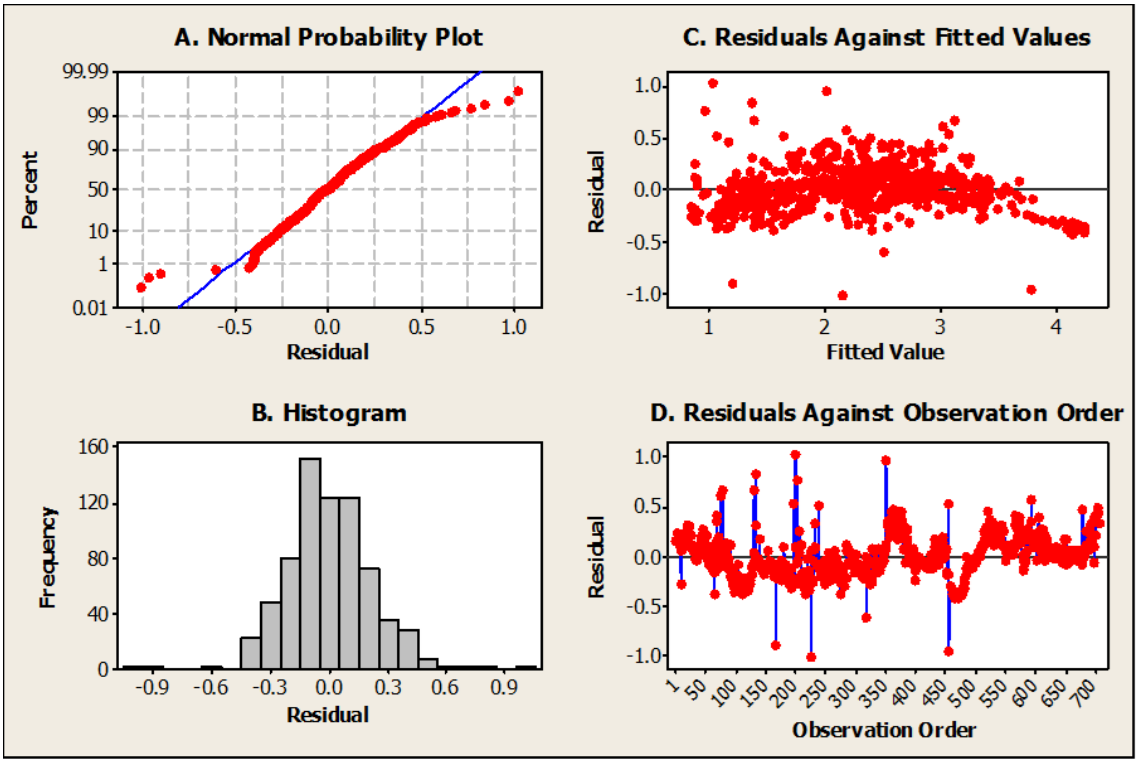

Figure 7. Graphs showing (*A*) normal probability distribution of residuals; (*B*) frequency distribution of residuals; (*C*) comparison of residuals with fitted values; and (*D*) comparison of residuals with observation order, for a multivariate regression of log(SSC) against log(T), log(Tlag), and log(Q), for Toutle River at Tower Road near Silver Lake, Washington. Figure made from Minitab® software as 4-in-1 plots (*www.minitab.com*).

Accounting for Autocorrelation

There are various options to account for time-related autocorrelation, including Auto-Regressive Moving Average (ARMA) modeling (Box and Jenkins, 1976); state-space modeling (SSM) using a Kalman filter (Harvey, 1989); and variable lagging, among others. Because this particular application was for real-time estimation and not for future forecasting, more extensive autocorrelation modeling techniques such as ARMA and SSM were not used. Additionally, the collection time difference between paired observations reduced the necessity for more extensive modeling as described in "Autocorrelations Die Out." Thus, regressions were run adding lag values of discharge and turbidity to account for some of the autocorrelation. The inclusion of lags increased R^2, lowered the standard error (*SSE*), and improved the DW statistic. The final R^2 and *SSE* are listed with tables 2 and 3.

Autocorrelations Die Out

Although this analysis indicated that autocorrelation was present in the datasets, use of more extensive time-series modeling was impractical for real-time application given that the correlation of logSSC with the most recent observed value of SSC died out after about 30 days. That is, the daily statistical dependence or strength of the relation between the 96 values of 15-minute logSSC variables decreases to near zero in about 1 month, such that the change in one 15-minute SSC will correspond to a change in another 15-minute SSC for only about 30 days. Because it normally takes more than 30 days for a sample concentration to become available from the laboratory and accessible for analysis, and because this dataset contained breaks in pump and manual sample collection that were longer than 30 days, this model used lagged values instead of a time-series component to increase accuracy in the regression model. Given these conditions, the regression developed using 2010–11 data worked adequately because the SSC correlations went to zero in such a relatively short time. In other words, the 30-day die out and the availability of new SSC sample data will almost never overlap, making the value of time-series models negligible in real-time estimation of SSC. If SSC were to be predicted into the future, a time-series model would be necessary.

Lagging Turbidity and Discharge

Regressions using lagged values of turbidity and discharge were tested for significance and improvement over the non-lagged MLR. A lag is a past value of the variable; a turbidity lag of 1would use the previous 15-minute value, a turbidity lag of 2 would use the previous 30-minute value, and so on. In our case, we evaluated using 1 lag of turbidity and 1 lag of water discharge by adding these values as third and fourth explanatory variables. On the basis of the regression diagnostics and ANOVA, we decided to use a single turbidity lag of 1, without using lags of discharge.

Robustness Checks

The term “robustness” here refers to statistics with good performance with the data, such that the coefficients are resistant to errors in the results and not unduly influenced by outliers. Robustness checks look for consistency of coefficient estimates by subsampling the original dataset and then estimating the model with out-of-sample data, along with other means of testing the validity of regression results.

The consistency of the OLS regression coefficient estimates for each streamgage was checked using the following methodology: Data for each streamgage first was condensed to a single matched pair per day. Days with only one value were automatically included. On days with multiple observations, one observation per day was randomly selected. For NF Toutle-SRS, the 653 observations came from 341 days, and for Toutle-Tower, the 705 observations came from 355 days.

This condensed dataset of 341 and 355 observations, respectively, was further subsampled. Each observation was given a random number and then sorted by that number from highest to lowest. The top 90 percent of the data with the highest random number were selected for use in generating the five potential OLS regression models. The five sets of explanatory variables included (1) logT; (2) logT and logT-lag; (3) LogT and logQ; (4) LogT, logT-lag, logQ; and (5) logT, logT-lag, logQ, logQ-lag. The remaining 10 percent of the data were used as out-of-sample or sequestered data and input to the 90-percent regression equation. That is, the turbidity, lagged turbidity, and discharge values from the 10-percent group were input to the 90-percent subsampled regression equation. The estimated SSC results and associated *SSE* were compared between the 90- and 10-percent datasets. For NF Toutle-SRS, 307 observations were used for the 90-percent regression and 34 observations were used for comparison. For Toutle-Tower, 320 observations were used for the 90-percent regression and 35 observations were used for the 10-percent comparison (appendix B).

OLS regressions were run on the 90-percent subsampled data for each of the five models for each gaging station. In using the 90-percent subsampled data for each model, two means of comparison were used. First, the coefficient estimates and standard errors were compared to their full data counterparts for consistency. Second, SSC was estimated and *SSE* was calculated using the 10-percent sequestered data. The model with the smallest *SSE* and most consistent estimates was considered the best model. If the 90-percent OLS estimates were grossly different and (or) had different signs from the full dataset OLS, then this model would not be the best to use.

Across models, although there was some deviation in the magnitude of the lagged turbidity estimate, the positive or negative sign remained the same and estimates for turbidity and discharge fluctuated within reason. Testing the subsample models on the 10-percent sequestered data showed that the ideal model using turbidity, lagged turbidity, and discharge (number 4 in the explanatory variable list) as explanatory variables had the lowest out-of-sample *SSE*. These results support the use of the final model and coefficient estimates.

Final Regression Models

Regression Model Coefficients

The log-log regression model analysis of SSC (response variable) with turbidity, turbidity-lag, and discharge (predictor variables) for the NF Toutle-SRS and Toutle-Tower gaging stations provided the output shown in tables 4 and 5. The coefficients are used to generate the regression equations listed as equations 1 and 2. The ANOVA statistics in tables 2 and 3 apply to these equations.

Table 4. Regression coefficients for North Fork Toutle River below Sediment Retention Structure near Kid Valley, Washington.

Parameter	Coefficient	SE	t-statistic	P-value	VIF
logT	0.1854	0.2882	0.64	0.52	322.304
logT lag	0.3545	0.2897	1.22	0.221	321.817
logQ	0.89518	0.04497	19.91	0	1.601
Constant	-0.8054	0.1135	-7.10	0	

$$\log_t SSC = -0.8054 + 0.1854 \log_t T + 0.3545 \log_t Tlag + 0.8952 \log_t Q \quad (1)$$

where

T	is turbidity,
Q	is discharge,
$Tlag$	is lag turbidity value for the previous 15-minute period, and
t	is the 15-minute interval time.

Table 5. Regression coefficients for Toutle River at Tower Road near Silver Lake, Washington..

Parameter	Coefficient	SE	t-statistic	P-value	VIF
logT	0.5676	0.1456	3.90	0	115.711
logT lag	0.1612	0.1449	1.11	0.266	112.942
logQ	0.9101	0.03587	25.37	0	3.149
Constant	-1.99049	0.09096	-21.88	0	

$$\log_t SSC = -1.9905 + 0.5676 \log_t T + 0.1612 \log_t Tlag + 0.9101 \log_t Q \quad (2)$$

Selecting the Predictor Variables for Model

Using the coefficients from the $\log_t SSC$ to $\log_t T$, $\log_t Tlag$, and $\log_t Q$ regression model, the unlogged or untransformed final equations became:

NF Toutle-SRS:
Equation (1) is converted to power form as equation 3,

$$SSC_t = 0.156531 * T_t^{0.1854} * Tlag_t^{0.3545} * Q_t^{0.8952} \quad (3)$$

Toutle-Tower:
Equation (2) is converted to power form as equation 4,

$$SSC_t = 0.010221 * T_t^{0.5676} * Tlag_t^{0.1612} * Q_t^{0.9101} \quad (4)$$

Applying the Bias Correction Factor

Because regressions were conducted on log-transformed variables, a bias was introduced that distorts the estimated SSC when the log values are converted back to their original linear form. Duan's smearing bias correction factor (BCF) was computed using the average of the unlogged residuals, as a best estimate of this introduced bias (Helsel and Hirsch, 2002; Rasmussen and others, 2009; Uhrich and Bragg, 2003). The BCF result for each station is computed as:

Bias Correction Factor (BCF): $\frac{\sum_i^n 10^{r_i}}{N} = 1.1491573\ and\ 1.14909$,

for **NF Toutle-SRS** and **Toutle-Tower**, respectively, and where r = logged residual values.

The right side of the regressions (equations 3 and 4) then are multiplied by the BCF to obtain the final equation:

NF Toutle-SRS:

$$SSC_t = 0.179879 * T_t^{0.1854} * Tlag_t^{0.3545} * Q_t^{0.8952} \quad (5)$$

Toutle-Tower:

$$SSC_t = 0.011745 * T_t^{0.5676} * Tlag_t^{0.1612} * Q_t^{0.9101} \quad (6)$$

Equations 5 and 6 are considered the general regression analysis (GRA) in this report and can be used normally to estimate SSC, with no further derivations.

The BCF accounts only for model error with no corrections for sample error, or error arising when estimating regression coefficients from a more finite dataset. That is, if one wanted to calculate the daily mean turbidity and averaged just three 15-minute values for that day, the sample error would be higher than if the mean turbidity was averaged using all ninety-six 15-minute values available for that day. Hence, larger sample sets, such as those used in this analysis, will tend to have a lower or negligible sample error. Although the BCF for model error increases SSC, the sample error correction has the inverse effect. Smaller sample sets without a sample error correction tend to overestimate the SSC. Because sample error was negligible in this analysis, no correction was applied.

Applying the Regression Models to Future Data

As new turbidity and discharge data are collected, they can be added to the original 15-minute turbidity and discharge datasets or kept separate as their own unique dataset. This distinction depends on the new GRA assembled from the additional SSC samples, which are paired with a turbidity and discharge value at the specific time of each sample. Analysis of covariance or ANCOVA can be used to test the significance of the original regression against future data added to the dataset. This would help determine if a change in the turbidity-SSC relation warrants developing a model for the new dataset (Helsel and Hirsch, 2002, p. 316). Rasmussen and others (2009) suggest that each water year be worked separately, and that the data from that water year then be compared to the data from the previous water year. If there is no significant difference in the slope and y-intercept between water years, the data could be joined together to refine the model and to generate a single multi-water year GRA. As a potential benefit, the refined model may have a lower *SSE* and reduced prediction interval. If the difference in regression models is significant, then a new GRA equation must be developed, using the methods described in this section, for the additional water year and (or) period of record. The new GRA equation then would be used until the analysis is reiterated using data from subsequent water years.

Final Regression Model Graphs

Graphs of the logSSC (measured) against logSSC (estimated) from final GRA equations for both gaging stations are shown in figures 8 and 9. The OLS lines in figures 8 and 9 represent the GRA relation defined by equations 5 and 6. The 95-percent prediction and confidence intervals are shown in figures 8 and 9, as provided by the statistical package used (*www.minitab.com*). A prediction interval is always wider than a confidence interval because it must account for both the uncertainty of the population mean and data scatter, also described as the model and sampling uncertainty. The distinction is that prediction intervals provide information on the distribution of values and not the uncertainty in determining the population mean, whereas confidence intervals provide information on how well the population mean was determined. The key point here is that confidence intervals provide information on the true population parameter, whereas prediction intervals represent ranges of values within which there is a 95-percent certainty (in this case) that the true population (SSC) occurs.

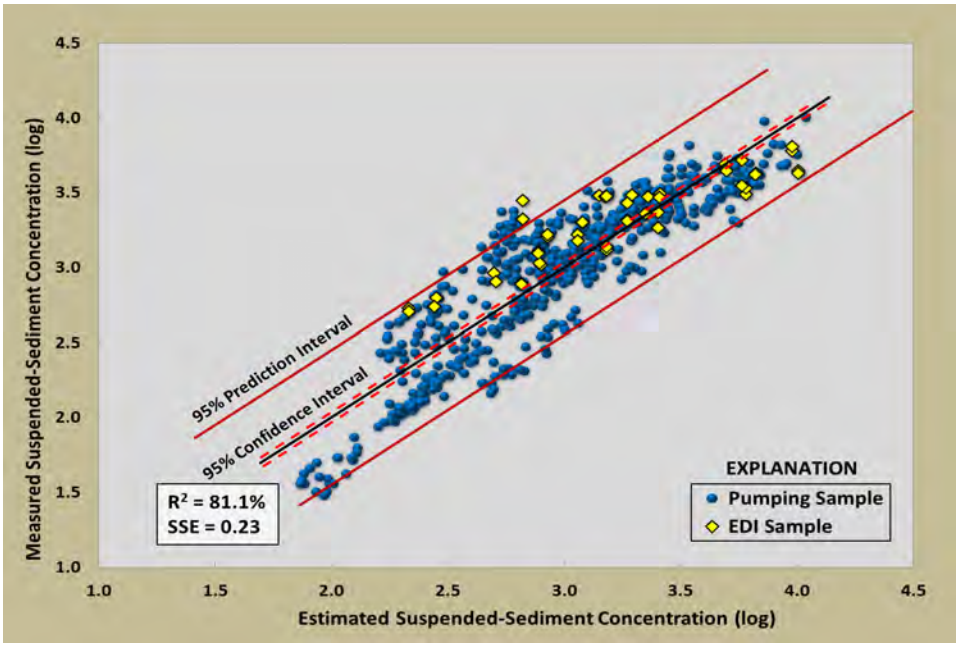

Figure 8. Final multiple linear regression model showing the general regression analysis line (equation 5) superimposed over measured and estimated suspended-sediment concentrations for pump and equal discharge increment samples, for North Fork Toutle River below Sediment Retention Structure near Kid Valley, Washington, water years 2010–11. Graph also shows 95-percent prediction and confidence intervals.

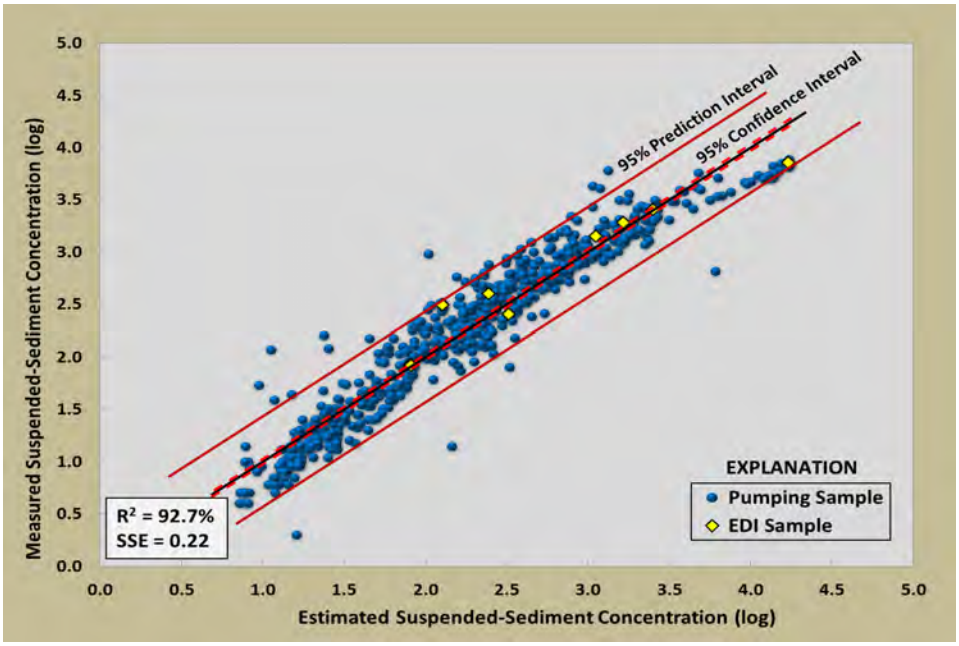

Figure 9. Final multiple linear regression model showing the general regression analysis line (equation 6) superimposed over measured and estimated suspended-sediment concentrations for pump and equal discharge increment samples, for Toutle River at Tower Road near Silver Lake, Washington, water years 2010–11. Graph also shows 95-percent prediction and confidence intervals.

Discussion and Future Studies

The use of surrogates for high-density measurements in real time offers many opportunities for improved understanding of hydrologic processes, along with well-characterized and reduced uncertainty, and ultimately better informed decision-making. In this study, we used turbidity as a surrogate for SSC in the sand-dominated Toutle River Basin; as a proof-of-concept approach to evaluate the feasibility of improving estimates of sediment loading and transport in the drainage basin; and possibly to reduce costs, compared to historical, manual techniques. The results of the study indicate that the potential for such improvements is high, with relatively robust regressions developed at both the NF-Toutle-SRS and Toutle-Tower sites. Although beyond the scope of this report, use of these regressions, together with discharge data from the two gaging stations, could be used to calculate 15-minute and daily concentrations and loads from the WYs 2010–11 dataset. The calculations also could be extended through WY 2012, with each computation being a relatively straightforward exercise. Future refinement and other uses of these regression techniques, beyond calculation of concentration and load, could provide additional information for understanding changes over time in sediment sources, transport, and deposition. Additionally, there remain some limitations and criteria to the regressions obtained in this report and to the overall use of surrogate technologies, which must be considered when using these results for decision-making.

Appropriate Uses of Turbidity-SSC Surrogate Regressions

Development of turbidity-SSC regressions are not conventionally universal across all water systems and riverine environments. The models developed herein can be used solely for the Toutle River Basin and cannot be transferred to other drainage basins. In addition, some waterways do not lend themselves to this type of analysis because of variability in the sediment-water matrix, as well as unacceptable monitoring conditions. From a monitoring standpoint, the turbidity-SSC surrogate regressions generally assume a consistent amount of light scattering by particles in transport over the range of the regression data. However, sediment grain-size distributions usually change during events or by season, based on the energy of the stream and the sediment sources, which can add uncertainty to the regression-based estimates of concentration or load. Based on past sediment events, it may be advantageous to subdivide the data by seasonal time frames or by increasing or decreasing streamflow and (or) turbidity components. This might produce a suite of regression models that could be used in conjunction with each other, each invoked by assessing in real time the sequential changes in turbidity and (or) discharge to determine which model to use, and thereby improve the estimates of sediment concentration.

By using these refined models, potential future work could compare results from the single regression model developed in this report to such a combined seasonal or event model approach. The combined approach likely would provide a tighter fit with a near-zero covariance between the residuals. The Toutle River Basin is a complex fluvial system that, upon further analysis, might lend itself to this type of event-based sediment-transport regime. Seasonal or event models may better estimate sediment-transport events that are unrelated to streamflow, which show up as tailings outside the confidence interval of the single regression line. Examples include volcanic- or glacial-influenced events from the Mount St. Helens crater, as well as landslides or localized streambank sloughing. These types of studies would provide insight into how the Mount St. Helens sediment-source terrain and depositional areas evolve over time, along with insight into management of sedimentation in the lower Toutle River Basin.

It also would be informative to test the comparability, cross-sectional representation, and cost effectiveness of a sampling regime that emphasizes more pump samples, as used for this study, compared to one composed of a greater number of manual EDIs. Such an evaluation could bolster the cost-effectiveness and usability of the data-collection program by assuring samples would be collected at the appropriate time and frequency. Additionally, the autosample sediment-size mixture of coarse and fine sediment can differ greatly from the EDIs and EWIs because of various pipe-hose lengths and configurations, hydraulic head required to pump and disperse the sample, and variable stream velocity and bed movement near the autosampler intake. Many of the pumping samples collected and used in this study were targeted to capture the full range of suspended sediment during peak discharge and turbidity events, when manual samples could not be collected. These samples provided valuable confirmation at critical sediment flux periods that otherwise would not have been possible. Regardless of this, if the surrogate-regression based approach is used, the number of pump samples collected and analyzed in the future could be decreased without significantly increasing manual EDI samples.

As a reasonable next step in processing these data, future work could include SSC as an online near-real-time parameter, using the regressions shown in this report with the ongoing continuous turbidity values. SSC could be added to the parameters of turbidity, stage, and discharge for each station, and also could be used as a comparison to the previous sample-based, sediment-record results.

As mentioned in the section, "Turbidity Greater than Instrument Limits," when the turbidity sensors are at their flat-line threshold, the data are not used in turbidity-discharge to SSC model development, as well as in any continuous SSC estimation. This is the most critical limitation to this study, as sediment transport is highest during these episodes and, therefore, is most vital in quantifying the sediment flux. Future work could include estimates through these peak periods or use alternative high-end turbidity sensors to provide a complete record of model-estimated SSC and SSQ. However, the high-end turbidity sensors would need to have their own instrument- and site-specific regressions generated. This prerequisite is owing to differences in light scattering and detection between a high-end sensor and the DTS-12 sensor™ used in this study (Rasmussen and others, 2009). One such high-end sensor initially was deployed at the NF Toutle-SRS site in 2011; therefore, a dataset with paired SSC sample results already is available, and can be used as the starting point from which to begin this work.

Finally, no inferences were drawn with respect to the sediment-size data. All manual samples and many of the autosamples include size-fraction data; however, none of these data were taken into account for this study. Regression models could be constructed for the individual sand/silt fraction, such that concentration and load for coarse- or fine-grain sizes could be determined separately. Additional work could use the size-fraction data to suggest source areas and to develop a synopsis of how specific areas have eroded and evolved over time, as well as to estimate the volumes of different size classes transported downstream past the NF Toutle-SRS gaging station to the main-stem Toutle and Cowlitz Rivers.

Updating Existing Regressions

The regression models in this report use data only from April 2010 to September 2011, as the time frame and scope for this work coincided with WYs 2010–11 approved and published turbidity and SSC records. The regression models and equations can easily be applied to or updated to include later water years. Inclusion of additional manual and pumping samples, the data for which already are available for WYs 2012–13, would better define the turbidity-discharge to SSC relation and improve the regression development and structure. By periodically evaluating the latest, finalized turbidity and discharge data, by water year, major changes in the sediment-transport system could be documented.

Trends and Use of State-Space Models

Sediment flux in the Toutle River Basin at both gaging stations responds to regional hydrology, but also responds to localized events and patterns. Specific erosional events from the Mount St. Helens crater and debris avalanche, and areas directly upstream of the SRS have all caused spikes and anomalies that are outside the typical sediment-transport pattern. These types of events can produce a hysteresis or differential pattern between sediment concentration and turbidity or discharge over varying parts of the event hydrograph. These patterns could reveal source or process information that, with closer evaluation, could be used to more effectively understand and manage sediment transport throughout the Toutle River Basin. The debris-avalanche deposit and braided channels formed through the entire valley, upstream and downstream of the SRS, also have implications for other environmental factors, such as fish survival and migration, along with the health and restoration of other aquatic species and habitats. Additional explanatory variables that weigh supplementary factors (such as seasonality, specific events, antecedent conditions, water temperature, and other water-quality parameters) could be incorporated in the model to help understand these wide-ranging ecological conditions.

In working within the 30-day autocorrelation die-off period, if SSC sample results, including laboratory analysis and database entry, could be routinely performed on a more real-time, continuous basis, such that SSC values were provided in less than 30 days, then autocorrelation modeling with a time-series component would be relevant to the results and should be applied. Realistically, however, most processing of sediment samples takes more than 30 days to generate an SSC value. One benefit of more real-time SSC data would be improved event-based estimation. Additionally, understanding and correcting for time-series properties of SSC would be most useful when interpolating between missing values of observed SSC. However, to apply these types of time-series corrections would require all SSC samples to be in an even time-step (Jones, 1986); although adjustments could be made using SSMs to alleviate this concern. Other time-series components, such as an ARMA model, also might be required, along with smoothing techniques to estimate intermediate values of SSC, such as using a Kalman filter in a SSM.

Such sophisticated techniques as ARMA processing and SSMs, if employed, would better simulate the trends in observed SSC by incorporating seasonality and rise/fall hysteresis variables. One possible parameter to better define rise/fall dynamics in fluvial constituent studies is use of the square of streamflow (Cohn and others, 1992). Particularly powerful are SSMs that use dynamic optimization techniques to define the best "path" through a deterministic or stochastic dataset. One such data-fusion procedure is a Kalman filter, which works by smoothing linear data and then estimating missing SSC in a feed-forward and feed-back manner by minimizing the mean square error of the estimated SSC (Maybeck, 1979). For instance, noisy, erratic data could be smoothed and estimates made in past, present, and future states. The Kalman filter works much like GCLAS by melding the observed sampled SSCs with estimated SSCs and interpolating missing values, although the two methods have their distinctions. GCLAS by its design is a human-based, more time-dependent interactive process, whereas SSM with a Kalman filter can be entirely automated. The distinct advantages of the SSM method are its reproducibility and reduced processing time, as well as the ability to estimate error metrics of the interpolated values. Thus, the more frequently samples are collected, the less the error estimate. After turbidity and discharge records are available, a sediment discharge record could be generated automatically with a defined uncertainty.

High-End Turbidity Sensor

As mentioned in the "Turbidity Greater Than Instrument Limits" section, a high-end turbidity sensor capable of monitoring suspended-sediment at levels at least one order of magnitude higher than the current turbidity sensor is in operation, on a trial basis, at NF Toutle-SRS. Future work could include this high-end sensor as part of the normal turbidity calibration and records-processing work, which could be published as a second turbidity parameter. Separate regressions for the high-end sensor also would need to be developed. See figure 10 for comparison of instream DTS-12 sensor™ and high-end sensor readings.

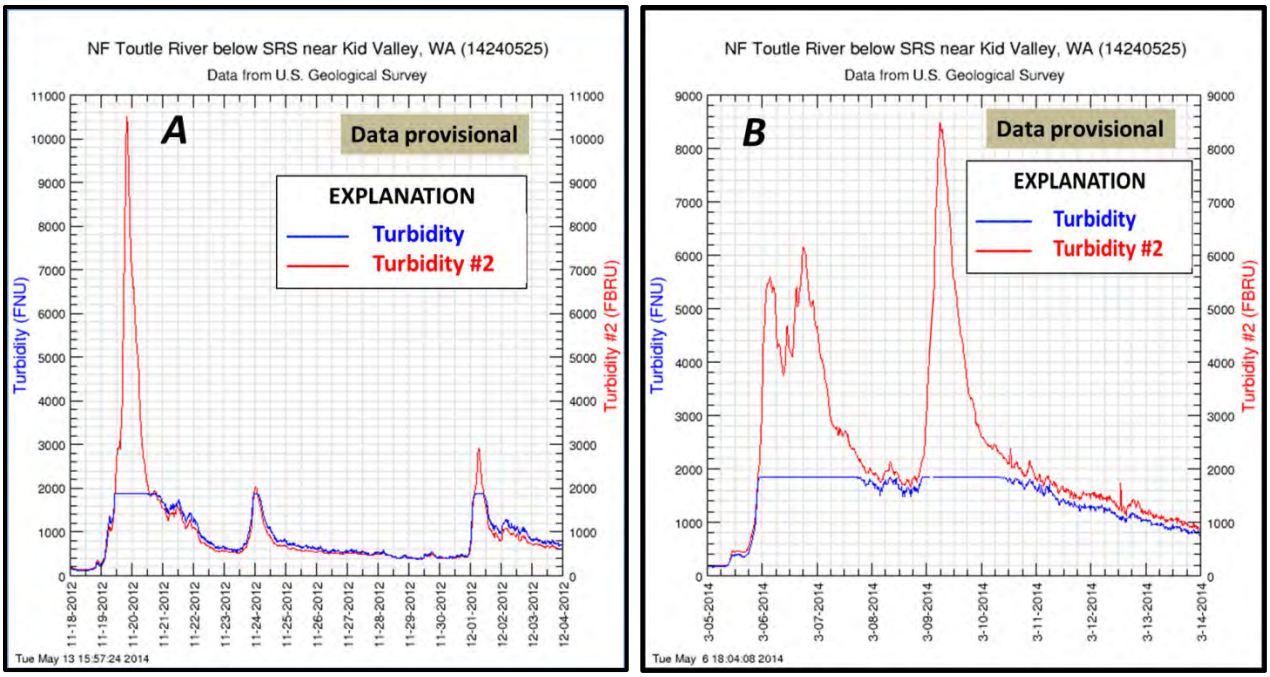

Figure 10. Graphs showing turbidity at North Fork Toutle River below Sediment Retention Structure near Kid Valley, Toutle River Basin, Washington, 2012 and 2014. Graph in blue shows how *NF Toutle-SRS* turbidity, for (*A*) November 18–December 4, 2012, and (*B*) March 5–March 14, 2014, reached the sensor maximum at near 2000 FNU. Graph in red shows, for the same time period and scale, how a high-end sensor (Turbidity #2) recorded turbidity (in formazin backscatter ratio units, FBRU) beyond the threshold level in blue.

Expected Effects of Raising SRS-Spillway

The SRS spillway was raised in elevation by 7 ft in September–October 2012, (back cover photograph; U.S. Army Corps of Engineers, 2012). The effects of this higher spillway on sediment transport and downstream channel morphology are not yet quantified. Additional analysis could integrate future turbidity and streamflow data into the established regression model, and also serve as a contrast to previous turbidity-discharge to SSC relations. For example, data directly preceding and following the spillway construction, such as data for WYs 2012 and 2013, could be compared. Any change in this relation would help to define and quantify new trends in sediment transport affected and (or) caused by this spillway raise. Similarly, future longer-term modifications to the SRS could be evaluated for any changes to the turbidity-SSC, turbidity-streamflow, and turbidity plus streamflow-SSC relation. Finally, the spillway raise may have affected the sediment-size fraction transported downstream past the SRS; one possible effect would be that relatively more coarse sediment is retained upstream of the SRS, with relatively more fine material transported downstream. Existing data on both size fractions and the nature of the turbidity-SSC regression could shed light on the degree to which these changes have occurred. The suspended-sediment loads could be computed with the percentage of certain size classes quantified by volume and compared year-to-year.

Conclusions

Despite the more than 30 years since the eruption of Mount St. Helens, sediment management in the Toutle River remains a daunting task. To help improve estimates of sediment transport and to reduce costs, the feasibility of instream turbidity measurement as a surrogate for suspended-sediment concentration (SSC) was tested in the Toutle River Basin. The results indicate that turbidity can be used reliably to augment the existing SSC sample collection, and possibly to improve the final estimates, as well as to reduce future data collection costs. The Toutle River at Tower Road (Toutle-Tower) near Silver Lake, Washington, and North Fork Toutle River below Sediment Retention Structure (NF Toutle-SRS) near Kid Valley, Washington, gaging stations each had sensors installed and data collected for the periods April 1 and May 1, 2010, through September 30, 2011, respectively. Multiple linear regression models using ordinary least square methods were generated and equations were provided for both gaging stations that use the instream turbidity and discharge data to enable prediction of real-time SSC. The equations to calculate SSC were corrected for bias using a smearing estimator.

The turbidity-SSC regressions were relatively successful, and could be improved in the future by employing sensors that have a higher maximum range. The use of pump samplers also could be optimized by finding a balance between cost savings from their unattended sampling capabilities, and the uncertainty they introduce. Uncertainty from pump samplers occurred because the sample represented a single point rather than a cross section, and the large number (as used herein) contributed to autocorrelation. Scheduling manual equal-discharge-increment sampling for times providing the most desirable and broadest range in streamflow and turbidity levels also could help to streamline the data-collection program.

In addition to the regression statistics, other tests and improvement measures were applied, such as the Durbin-Watson statistic to test for serial correlation and the use of lagged turbidity and discharge variables. The regression with the best supportive diagnostic statistics and best fit of the explanatory and response variables, along with minimal serial correlation, was selected as the final model and equation. The final regression equation used logged values of turbidity, discharge, and a single 15-minute lag of turbidity as explanatory variables in estimating SSC.

The dataset used in this study was confined to roughly 1.5 years of turbidity and SSC; however, additional years of data were made available after this data analysis was underway. Future water years could readily be added to better define and fine-tune these correlations. Sediment-size data were not used in this analysis, which prevented any inferences regarding sediment transport of various size fractions. Future models could be constructed for separate fine- or coarse-grain sediment transport.

Despite these limitations, the proof of concept described in the initial study objectives has shown that, even in a high sand-transport environment, rugged in-stream turbidity instrumentation, robust measuring technology, and appropriate statistical modeling methods may produce a more efficient and less costly alternative to conventional sample-based, sediment-record methods currently (2014) in use. More sophisticated statistical analysis would be useful for this dataset and future Toutle-Tower and NF Toutle-SRS datasets, as this would broaden the understanding of turbidity-discharge to SSC correlations by incorporating seasonality, trends, and rise/fall hysteresis terms. Future use of an Auto-Regressive Moving Average component and State-Space Models using a Kalman filter also would automate sediment-discharge computations, deliver reproducibility, and provide an error measurement of the load estimate.

Acknowledgments

We would like to recognize the scientific and financial support received from the U.S. Army Corps of Engineers (COE) in making this project possible. The COE Portland District personnel were staunch and consistent supporters of this research, particularly Chris Nygaard and Paul Sclafani of the Mount St. Helens Long-Term Sediment Management Team (*http://www.nwp.usace.army.mil/Missions/Currentprojects/MountStHelensEIS.aspx*).

We would like to extend our appreciation to Greg Schwarz of the USGS headquarters office in Reston, Virginia, for his statistical evaluation, suggestions, and insight which greatly enhanced the quality, usability, and extent of this work.

A special thanks to Tami Christianson, of the USGS Cascades Volcano Observatory, for her diligent work in collecting sediment samples, often under challenging conditions, and for checking and providing the turbidity and streamflow data. Finally, we would like to acknowledge Dennis Saunders, Arlene Sondergaard, and Katherine Norton, all from the USGS Cascades Volcano Observatory, for checking, processing, and disseminating our sediment concentration data.

References Cited

Anderson, C.W., 2005, Turbidity (ver. 2.1): U.S. Geological Survey Techniques of Water-Resources Investigations, book 9, chap. A6, section 6.7, 64 p., accessed May 6, 2014, at http://water.usgs.gov/owq/FieldManual/Chapter6/6.7_contents.html.

Bent, G.C., Gray, J.R., Smith, K.P., and Glysson, G.D., 2000, A synopsis of technical issues for monitoring sediment in highway and urban runoff: U.S. Geological Survey Open-File Report 00-497, accessed May 6, 2014, at *http://pubs.usgs.gov/of/2000/ofr00-497/*.

Box, G.E.P., and Jenkins, G.M., 1976, Time series analysis—forecasting and control (revised edition): San Francisco, California, Holden-Day, 575 p.

Buchanan, T.J., and Somers, W.P., 1976, Discharge measurements at gaging stations: U.S. Geological Survey Techniques of Water-Resources Investigations, book 3, chap. A8, 65 p., accessed May 6, 2014, at *http://pubs.usgs.gov/twri/twri3a8/*.

Cohn, T., Caulder, D.L., Gilroy, E.J., Zynjuk, L.D., and Summers, R.M., 1992, The validity of a simple statistical model for estimating fluvial constituent loads—An empirical study involving nutrient loads entering Chesapeake Bay: Water Resources Research, v. 28, no. 9, p. 2,353–2,364.

Dinehart, R.L., 1998, Sediment transport at gaging stations near Mount St. Helens, Washington, 1980–90—Data collection and analysis: U.S. Geological Survey Professional Paper 1573, 111 p., accessed May 6, 2014, at http://pubs.usgs.gov/pp/1573/.

Edwards, T.K., and Glysson, G.D., 1999, Field methods for measurement of fluvial sediment: U.S. Geological Survey Techniques of Water-Resources Investigations, book 3, chap. C2, 89 p., accessed May 6, 2014, at *http://pubs.usgs.gov/twri/twri3-c2/*.

Gibson, S., Nygaard, C., and Sclafani, P., 2010, Mobile bed modeling of the Cowlitz River using HEC-RAS—Assessing flooding risk and impact due to system sediment: U.S. Army Corps of Engineers, Portland District, 2nd Joint Federal Interagency Conference, Las Vegas, Nevada, June 27–July 1, 2010, accessed May 6, 2014, at *http://acwi.gov/sos/pubs/2ndJFIC/Contents/6C_Gibson_Nygaard_Modeling_of_Cowlitz_paper.pdf*.

Glysson, G.D., 2008, Guidelines and standards procedures for the use of automatic samplers for the collection of surface water-quality and sediment data: National Water Quality Monitoring Council, 6th National Monitoring Conference, Session C4, Atlantic City, New Jersey, May 18–22, 2008, accessed May 6, 2014, at *http://acwi.gov/monitoring/conference/2008/papers/C4-B.pdf*.

Guy, H.P., 1977, Laboratory theory and methods for sediment analysis: U.S. Geological Survey Techniques of Water-Resources Investigations, book 5, chap. C1, accessed May 6, 2014, at *http://pubs.usgs.gov/twri/twri5c1/html/pdf.html*.

Guy, H.P., 1978, Fluvial sediment concepts: U.S. Geological Survey Techniques of Water-Resources Investigations, book 3, chap. C1, p. accessed May 6, 2014, at *http://pubs.usgs.gov/twri/twri3-c1/*.

Harvey, A.C., 1989, Forecasting, structural time series models and the kalman filter: New York, Cambridge University Press, p. 554.

Helsel, D.R., and Hirsch, R.M., 2002, Statistical methods in water resources: U.S. Geological Survey Techniques of Water-Resources Investigations, book 4, chap. C3, p. 221–263, accessed May 6, 2014, at *http://pubs.usgs.gov/twri/twri4a3/*.

Jones, R.H., 1986, Time series regression with unequally spaced data: Journal of Applied Probability, v. 23A, Special Volume—Essays in Times Series and Allied Processes, p. 89–98.

Koltun, G.F., Eberle, Michael, Gray, J.R., and Glysson, G.D, 2006, User's manual for the Graphical Constituent Loading Analysis System (GCLAS): U.S. Geological Survey Techniques and Methods, book 4, chap. C1, 51 p., accessed May 6, 2014, at *http://pubs.usgs.gov/tm/2006/tm4C1/pdf/tm4C1.pdf*.

Major, J.J., and Spicer, K.R., 2003, Clearing Toutle River sediment issue—An op-ed opinion: The Columbian, August 9, accessed May 6, 2014, at *http://vulcan.wr.usgs.gov/Projects/JJMajor/Publications/TheColumbian/clearing_toutle_sediment_issue_aug9_03.html*.

Maybeck, P.S., 1979, Stochastic models, estimation and control—Volume 1, Chapter 1: New York, Academic Press, p. 3–16.

Porterfield, G., 1977, Computation of fluvial-sediment discharge: U.S. Geological Survey Techniques of Water-Resources Investigations, book 3, chap. C3; accessed May 6, 2014, at *http://pubs.usgs.gov/twri/twri3-c3/html/pdf.html*.

Rantz, S.E., and others, 1983, Measurement and computation of streamflow—Volume 1, Measurement of stage and discharge—Volume 2, Computation of discharge: U.S. Geological Survey Water Supply Paper 2175, 631 p., accessed May 6, 2014, at *http://pubs.usgs.gov/wsp/wsp2175*.

Rasmussen, P.P., Gray, J.R., Glysson, G.D., and Ziegler, A.C., 2009, Guidelines and procedures for computing time-series suspended-sediment concentrations and loads from in-stream turbidity-sensor and streamflow data: U.S. Geological Survey Techniques and Methods, book 3, chap. 4, 53 p., accessed May 6, 2014, at *http://pubs.usgs.gov/tm/tm3c4/*.

Sauer, V.B., and Meyer, R.W., 1992, Determination of error in individual discharge measurements: U.S. Geological Survey Open-File Report 92–144, 21 p., accessed May 6, 2014, at *http://pubs.usgs.gov/of/1992/ofr92-144/*.

Topping, D.J., Rubin, D.M., Wright, S.A., and Melis, T.S., 2011, Field evaluation of the error arising from inadequate time averaging in the standard use of depth-integrating suspended-sediment samplers: U.S. Geological Survey Professional Paper, 95 p., accessed May 6, 2014, at http://pubs.usgs.gov/pp/1774/.

Uhrich, M.A., and Bragg, H.M., 2003, Monitoring instream turbidity to estimate continuous suspended-sediment loads and yields and clay-water volumes in the upper North Santiam River Basin, Oregon, 1998–2000: U.S. Geological Survey Water-Resources Investigations Report 03-4098, accessed May 6, 2014, at, *http://pubs.usgs.gov/wri/WRI03-4098/*.

U.S. Army Corps of Engineers, 2012, Final environmental assessment—Sediment Retention Structure (SRS) spillway raise project, Mount St. Helens sediment management for flood risk reduction: U.S. Army Corps of Engineers, Portland District, accessed May 6, 2014, at *http://www.nwp.usace.army.mil/Portals/24/docs/locations/msh/Final_EA_SRS_Spillway_Raise.pdf*.

U.S. Geological Survey, 2010, Water-resources data for the United States, water year 2010: U.S. Geological Survey Water-Data Report WDR-US-2010, accessed May 6, 2014, at *http://wdr.water.usgs.gov/wy2010/pdfs/14240525.2010.pdf*, and *http://wdr.water.usgs.gov/wy2010/pdfs/14242580.2010.pdf*.

U.S. Geological Survey, 2011, Water-resources data for the United States, water year 2011: U.S. Geological Survey Water-Data Report WDR-US-2011, accessed May 6, 2014, at *http://wdr.water.usgs.gov/wy2011/pdfs/14240525.2011.pdf*, and *http://wdr.water.usgs.gov/wy2011/pdfs/14242580.2011.pdf*.

Wagner, R.J., Boulger, R.W., Jr., Oblinger, C.J., and Smith, B.A., 2006, Guidelines and standard procedure for continuous water-quality monitors—Station operation, record computation, and data reporting: U.S. Geological Survey Techniques and Methods, book 1, chap. D3, 51 p., plus 8 attachments, accessed May 6, 2014, at *http://pubs.water.usgs.gov/tm1d3*.

Appendix A. Suspended-Sediment Sample, Discharge, and Turbidity Data

Suspended-sediment sample data are presented for the discharge and turbidity monitoring gaging stations North Fork Toutle River below Sediment Retention Structure near Kid Valley, Washington (NF Toutle-SRS; U.S. Geological Survey [USGS] gaging station No. 14240525) and Toutle River at Tower Road near Silver Lake, Washington (Toutle-Tower; USGS gaging station No. 14242580). The data were used for regression model calibration and consist of the total suspended-sediment concentration and the corresponding discharge and turbidity recorded at the monitoring station during sample collection. When available, sample concentrations with fine suspended-sediment data are presented for particle sizes less than 0.0625 millimeters. Separate bar plot worksheets also are included that depict the number of samples collected at each gaging station. Each bar plot is differentiated by sample type as Equal-Discharge-Increment or pump sample, and by nine different ranges in turbidity that span the entire sensor measurement scale.

[Appendix A is a Microsoft© Excel file and can be downloaded at *http://pubs.usgs.gov/ofr/2014/1204/*.]

Appendix B. Robustness Check Data

Data used in checking for robustness is presented as two separate worksheets for each station in an Excel spreadsheet. Included are the sampled suspended-sediment concentration (SSC) data, and adjoining discharge (Q), turbidity (T) and lagged turbidity (T-lag) values for the 90- and 10-percent subsampled and sequestered out-of-sample data, respectively. Samples were randomly selected for the 90-percent group. One sample was randomly selected for days with more than one sample. The remaining samples were used for the 10-percent sequestered data. For NF Toutle-SRS, 653 samples were reduced to 307 and 34 samples for the 90- and 10-percent groups, respectively. For Toutle-Tower, 705 samples were reduced to 320 and 35 samples for the 90- and 10-percent groups, respectively.

[Appendix B is a Microsoft© Excel file and can be downloaded at *http://pubs.usgs.gov/ofr/2014/1204/*.]

Publishing support provided by the U.S. Geological Survey
Science Publishing Network, Tacoma Publishing Service Center

For more information concerning the research in this report, contact the
CVO, Volcano Science Center,
Cascades Volcano Observatory
U.S. Geological Survey
1300 SE Cardinal Court, Building 10, Suite 100
Vancouver, WA 98683-9589
http://vulcan.wr.usgs.gov/

USGS

Ulrich and others—**Correlations of Turbidity to Suspended-Sediment Concentration in the Toutle River Basin, Washington, 2010–11**—Open-File Report 2014–1204

ISSN 2331-1258 (online)
http://dx.doi.org/10.3133/ofr20141204

Assessment of erosion, sedimentation, and water quality impacts of the Mountain Valley Pipeline and Equitrans Expansion Project's proposed crossing of the Jefferson National Forest as it pertains to the U.S. Forest Service's Draft Supplemental Environmental Impact Statement dated December 2022

Prepared by Jonathan A. Czuba, Ph.D., Licensed Professional Engineer - February 9, 2023

REFERENCES
25

February 21, 2023

USGS
science for a changing world

Techniques of Water-Resources Investigations of the U.S. Geological Survey

Book 3, Applications of Hydraulics

Chapter C2

Field Methods for Measurement of Fluvial Sediment

By Thomas K. Edwards and G. Douglas Glysson

This manual is a revision of "Field Methods for Measurement of Fluvial Sediment," by Harold P. Guy and Vernon W. Norman, U.S. Geological Survey Techniques of Water-Resources Investigations, Book 3, Chapter C2, published in 1970.

U.S. DEPARTMENT OF THE INTERIOR

BRUCE BABBITT, Secretary

U.S. GEOLOGICAL SURVEY

Charles G. Groat, Director

Reston, Virginia 1999

ISBN 0-607-89738-4

For sale by the U.S. Geological Survey, Information Services
Box 25286, Federal Center
Denver CO 80225

TECHNIQUES OF WATER-RESOURCES INVESTIGATIONS OF THE U.S. GEOLOGICAL SURVEY

The U.S. Geological Survey publishes a series of manuals describing procedures for planning and conducting specialized work in water-resources investigations. The material is grouped under major subject headings called books and is further divided into sections and chapters. For example, Section A of Book 3 (Applications of Hydraulics) pertains to surface water. The chapter, the unit of publication, is limited to a narrow field of subject matter. This format permits flexibility in revision and publication as the need arises.

The reports listed below are for sale by the **U.S. Geological Survey, Information Services, Box 25286, Federal Center, Denver, Colorado 80225** (authorized agent of the Superintendent of Documents, Government Printing Office). Prepayment is required. Remittance should be sent by check or money order payable to the U.S. Geological Survey. Prices are not included because they are subject to change. **Current prices can be obtained by writing to the above address.** When ordering or inquiring about prices for any of these publications, please give the title, book number, chapter number, and "U.S. Geological Survey Techniques of Water-Resources Investigations."

TWRI 1-D1.	Water temperature—Influential factors, field measurement, and data presentation, by H.H. Stevens, Jr., J.F. Ficke, and G.F. Smoot. 1975. 65 pages.
TWRI 1-D2.	Guidelines for collection and field analysis of ground-water samples/for selected unstable constituents, by W.W. Wood. 1976. 24 pages. Reprint.
TWRI 2-D1.	Application of surface geophysics to ground-water investigations, by A.A.R. Zohdy, G.P. Eaton, and D.R. Mabey. 1974. 116 pages.
TWRI 2-D2.	Application of seismic-refraction techniques to hydrologic studies, by F.P. Haeni. 1988. 86 pages.
TWRI 2-E1.	Application of borehole geophysics to water-resources investigations, by W.S. Keys and L.M. MacCary. 1971. 126 pages.
TWRI 2-E2.	Borehole geophysics applied to ground-water investigations, by W.S. Keys. 1990. 150 pages.
TWRI 2-F1.	Application of drilling, coring, and sampling techniques to test holes and wells, by Eugene Shuter and Warren E. Teasdale. 1989. 97 pages.
TWRI 3-A1.	General field and office procedures for indirect discharge measurements, by M.A. Benson and Tate Dalrymple. 1967. 30 pages.
TWRI 3-A2.	Measurement of peak discharge by the slope-area method, by Tate Dalrymple and M.A. Benson. 1967. 12 pages.
TWRI 3-A3.	Measurement of peak discharge at culverts by indirect methods, by G.L. Bodhaine. 1968. 60 pages.
TWRI 3-A4.	Measurement of peak discharge at width contractions by indirect methods, by H.F. Matthai. 1967. 44 pages.
TWRI 3-A5.	Measurement of peak discharge at dams by indirect methods, by Harry Hulsing. 1967. 29 pages.
TWRI 3-A6.	General procedure for gaging streams, by R.W. Carter and Jacob Davidian. 1968. 13 pages.
TWRI 3-A7.	Stage measurements at gaging stations, by T.J. Buchanan and W.P. Somers. 1968. 28 pages.
TWRI 3-A8.	Discharge measurements at gaging stations, by T.J. Buchanan and W.P. Somers. 1969. 65 pages.
TWRI 3-A9.[1]	Measurement of time of travel and dispersion in streams by dye tracing, by E.P. Hubbard, F.A. Kilpatrick, L.A. Martens, and J.R. Wilson, Jr. 1982. 44 pages.
TWRI 3-A10.	Discharge ratings at gaging stations, by E.J. Kennedy. 1984. 59 pages.
TWRI 3-A11.	Measurement of discharge by moving-boat method, by G.F. Smoot and C.E. Novak. 22 pages.
TWRI 3-A12.	Fluorometric procedures for dye tracing, Revised, by J.F. Wilson, Jr., E.D. Cobb, and F.A. Kilpatrick. 1986. 41 pages.
TWRI 3-A13.	Computation of continuous records of streamflow, by E.J. Kennedy. 1983. 53 pages.
TWRI 3-A14.	Use of flumes in measuring discharge, by F.A. Kilpatrick and V.R. Schneider. 1983. 46 pages.
TWRI 3-A15.	Computation of water-surface profiles in open channels, by Jacob Davidian. 1984. 48 pages.
TWRI 3-A16.	Measurement of discharge using tracers, by F.A. Kilpatrick and E.D. Cobb. 1985. 52 pages.
TWRI 3-A17.	Acoustic velocity meter systems, by Antonius Laenen. 1985. 38 pages.
TWRI 3-A18.	Determination of stream reaeration coefficients by use of tracers, by F.A. Kilpatrick, R.E. Rathbun, Nobuhiro Yotsukura, G.W. Parker, and L.L. DeLong. 1989. 52 pages.
TWRI 3-A19.	Levels of streamflow gaging stations, by E.J. Kennedy. 1990. 27 pages.
TWRI 3-A20.	Simulation of soluble waste transport and buildup in surface waters using tracers, by F.A. Kilpatrick. 1993. 38 pages.
TWRI 3-A21.	Stream-gaging cableways, by C. Russell Wagner. 1995. 56 pages.
TWRI 3-B1.	Aquifer-test design, observation, and data analysis, by R.W. Stallman. 1971. 26 pages.
TWRI 3-B2.[2]	Introduction to ground-water hydraulics, a programmed text for self-instruction, by G.D. Bennett. 1976. 172 pages.
TWRI 3-B3.	Type curves for selected problems of flow to wells in confined aquifers, by J.E. Reed. 1980. 106 pages.

TWRI 3-B4.	Regression modeling of ground-water flow, by Richard L. Cooley and Richard L. Naff. 1990. 232 pages.
TWRI 3-B4. Supplement 1.	Regression modeling of ground-water flow—Modifications to the computer code for nonlinear regression solution of steady-state ground-water flow problems, by R.L. Cooley. 1993. 8 pages.
TWRI 3-B5.	Definition of boundary and initial conditions in the analysis of saturated ground-water flow systems—An introduction, by O. Lehn Franke, Thomas E. Reilly, and Gordon D. Bennett. 1987. 15 pages.
TWRI 3-B6.	The principle of superposition and its application in ground-water hydraulics, by Thomas E. Reilly, O. Lehn Franke, and Gordon D. Bennett. 1987. 28 pages.
TWRI 3-B7.	Analytical solutions for one-, two-, and three-dimensional solute transport in ground-water systems with uniform flow, by Eliezer J. Wexler. 1992. 190 pages.
TWRI 3-C1.	Fluvial sediment concepts, by H.P. Guy. 1970. 55 pages.
TWRI 3-C2.[3]	Field methods for measurement of fluvial sediment, by Thomas K. Edwards and G. Douglas Glysson. 1998. 89 pages.
TWRI 3-C3.	Computation of fluvial-sediment discharge, by George Porterfield. 1972. 66 pages.
TWRI 4-A1.	Some statistical tools in hydrology, by H.C. Riggs. 1968. 39 pages.
TWRI 4-A2.	Frequency curves, by H.C. Riggs. 1968. 15 pages.
TWRI 4-B1.	Low-flow investigations, by H.C. Riggs. 1972. 18 pages.
TWRI 4-B2.	Storage analyses for water supply, by H.C. Riggs and C.H. Hardison. 1973. 20 pages.
TWRI 4-B3.	Regional analyses of streamflow characteristics, by H.C. Riggs. 1973. 15 pages.
TWRI 4-D1.	Computation of rate and volume of stream depletion by wells, by C.T. Jenkins. 1970. 17 pages.
TWRI 5-A1.	Methods for determination of inorganic substances in water and fluvial sediments, by Marvin J. Fishman and Linda C. Friedman, editors. 1978. 545 pages.
TWRI 5-A2.	Determination of minor elements in water by emission spectroscopy, by P.R. Barnett and E.C. Mallory, Jr. 1971. 31 pages.
TWRI 5-A3.[4]	Methods for the determination of organic substances in water and fluvial sediments, edited by R.L. Wershaw, M.J. Fishman, R.R. Grabbe, and L.E. Lowe. 1987. 80 pages.
TWRI 5-A4.[5]	Methods for collection and analysis of aquatic biological and microbiological samples, by L.J. Britton and P.E. Greeson, editors. 1987. 363 pages.
TWRI 5-A5.	Methods for determination of radioactive substances in water and fluvial sediments, by L.L. Thatcher, V.J. Janzer, and K.W. Edwards. 1977. 95 pages.
TWRI 5-A6.	Quality assurance practices for the chemical and biological analyses of water and fluvial sediments, by L.C. Friedman and D.E. Erdmann. 1982. 181 pages.
TWRI 5-C1.	Laboratory theory and methods for sediment analysis, by H.P. Guy. 1969. 58 pages.
TWRI 6-A1.	A modular three-dimensional finite-difference ground-water flow model, by Michael G. McDonald and Arlen W. Harbaugh. 1988. 586 pages.
TWRI 6-A2.	Documentation of a computer program to simulate aquifer-system compaction using the modular finite-difference ground-water flow model, by S.A. Leake and D.E. Prudic. 1991. 68 pages.
TWRI 6-A3.	A modular finite-element model (MODFE) for areal and axisymmetric ground-water-flow problems, Part 1: Model description and user's manual, by L.J. Torak. 1993. 136 pages.
TWRI 6-A4.	A modular finite-element model (MODFE) for areal and axisymmetric ground-water-flow problems, Part 2: Derivation of finite-element equations and comparisons with analytical solutions, by R.L. Cooley. 1992. 108 pages.
TWRI 6-A5.	A modular finite-element model (MODFE) for areal and axisymmetric ground-water-flow problems, Part 3: Design philosophy and programming details, by L.J. Torak. 1993. 243 pages.
TWRI 7-C1.	Finite difference model for aquifer simulation in two dimensions with results of numerical experiments, by P.C. Trescott, G.F. Pinder, and S.P. Larson. 1976. 116 pages.
TWRI 7-C2.	Computer model of two-dimensional solute transport and dispersion in ground water, by L.F. Konikow and J.D. Bredehoeft. 1978. 90 pages.
TWRI 7-C3.	A model for simulation of flow in singular and interconnected channels, by R.W. Schaffranek, R.A. Baltzer, and D.E. Goldberg. 1981. 110 pages.
TWRI 8-A1.	Methods of measuring water levels in deep wells, by M.S. Garber and F.C. Koopman. 1968. 23 pages.
TWRI 8-A2.	Installation and service manual for U.S. Geological Survey manometers, by J.D. Craig. 1983. 57 pages.
TWRI 8-B2.	Calibration and maintenance of vertical-axis type current meters, by G.F. Smoot and C.E. Novak. 1968. 15 pages.

[1]This manual is a revision of "Measurement of Time of Travel and Dispersion in Streams by Dye Tracing," by E.F. Hubbard, F.A. Kilpatrick, L.A. Martens, and J.F. Wilson, Jr., Book 3, Chapter A9, published in 1982.

[2]Spanish translation also available.

[3]This manual is a revision of "Field Methods for Measurement of Fluvial Sediment," by Harold P. Guy and Vernon W. Norman, Book 3, Chapter C2, published in 1970.

[4]This manual is a revision of TWRI 5-A3, "Methods of Analysis of Organic Substances in Water," by Donald F. Goerlitz and Eugene Brown, published in 1972.

[5]This manual supersedes TWRI 5-A4, "Methods for Collection and Analysis of Aquatic Biological and Microbiological Samples," edited by P.E. Greeson and others, published in 1977.

CONTENTS

ILLUSTRATIONS

TABLES

UNIT CONVERSION

Multiply inch-pound unit	*By*	*To obtain SI unit*
	Length	
inch (in.)	25.40	millimeter (mm)
foot (ft)	0.3048	meter (m)
	Area	
square inch ($in.^2$)	6.452	square centimeter (cm^2)
square foot (ft^2)	929.0	square centimeter (cm^2)
	Volume	
U.S. liquid pint (pt)	0.4732	liter (L)
U.S. liquid quart (qt)	0.9464	liter (L)
U.S. liquid gallon (gal)	3.785	liter (L)
U.S. liquid gallon (gal)	3,785	milliliter (mL)
U.S. liquid gallon (gal)	0.003785	cubic meter (m^3)
cubic foot (ft^3)	28,317	cubic centimeter (cm^3)
	Flow rate	
foot per second (ft/s)	0.3048	meter per second (m/s)
cubic foot per second (ft^3/s)	0.02832	cubic meter per second (m^3/s)

Multiply inch-pound unit	*By*	*To obtain SI unit*
	Mass	
ounce, avoirdupois (oz)	28.35	gram (g)
ounce, avoirdupois (oz)	28,350	milligram (mg)
pound, avoirdupois (lb)	453.6	gram (g)
ton, short	0.9072	megagram (Mg)
	Temperature	
degree Fahrenheit (°F)	°C=5/9 (°F–32)	degree Celsius (°C)
	Pressure	
pound per square inch (lb/in.^{2})	6.895	kilopascal (kPa)
	Concentration (Mass/Volume)	
parts per million (ppm)[1]	1.0	milligrams per liter (mg/L)
ounces per quart (oz/qt)	29,955	milligrams per liter (mg/L)
pounds per cubic foot (lb/ft^3)	16,017	grams per cubic meter (g/m^3)

[1]This conversion is true for

mg/L = c(ppm) = c

when the ratio of weight of sediment to weight of water-sediment mixture is between 0 and 15,900. If this ratio is greater than 15,900, the investigator is referred to Guy (1969, table 1, p. 4) for the correct conversion factor to be used in the formula.

FIELD METHODS FOR MEASUREMENT OF FLUVIAL SEDIMENT

By Thomas K. Edwards and G. Douglas Glysson

Abstract

This chapter describes equipment and procedures for collection and measurement of fluvial sediment. The complexity of the hydrologic and physical environments and man's ever-increasing data needs make it essential for those responsible for the collection of sediment data to be aware of basic concepts involved in processes of erosion, transport, deposition of sediment, and equipment and procedures necessary to representatively collect sediment data.

In addition to an introduction, the chapter has two major sections. The "Sediment-Sampling Equipment" section encompasses discussions of characteristics and limitations of various models of depth- and point-integrating samplers, single-stage samplers, bed-material samplers, bedload samplers, automatic pumping samplers, and support equipment. The "Sediment-Sampling Techniques" section includes discussions of representative sampling criteria, characteristics of sampling sites, equipment selection relative to the sampling conditions and needs, depth- and point-integration techniques, surface and dip sampling, determination of transit rates, sampling programs and related data, cold-weather sampling, bed-material and bedload sampling, measuring total sediment discharge, and measuring reservoir sedimentation rates.

INTRODUCTION

Perspective

Knowledge of the erosion, transport, and deposition of sediment relative to land surface, streams, reservoirs, and other bodies of water is important to those involved directly or indirectly in the development and management of water and land resources. It also is becoming more important that such development and management be carried out in a manner that yields or conforms to a socially acceptable environment. The need for a clear understanding of hydrogeomorphologic processes associated with sediment requires the measurement of suspended and bed sediments for a wide range of hydrologic environments. The complex phenomena of fluvial sedimentation cause the required measurements and related analyses of sediment data to be relatively expensive in comparison with other kinds of hydrologic data. Accordingly, the purpose of this manual is to help standardize and improve efficiency in the techniques used to obtain sediment data, so the quantity and quality of the data can be maximized for a given investment of labor and resource.

Sediment data needs are of practical concern. Some of the general categories include:

1. The evaluation of sediment yield with respect to different natural environmental conditions—geology, soils, climate, runoff, topography, ground cover, and size of drainage area.
2. The evaluation of sediment yield with respect to different kinds of land use.
3. The time distribution of sediment concentration and transport rate in streams.
4. The evaluation of erosion and deposition in channel systems.
5. The amount and size characteristics of sediment delivered to a body of water.
6. The characteristics of sediment deposits as related to particle size and flow conditions.
7. The relations between sediment chemistry, water quality, and biota.

The scope of these requirements indicates that a wide variety of measurements are needed on streams and other bodies of water, ranging from large river basins to very small tributaries that drain areas such as parcels of land under urban development.

The equipment and methods discussed in this report for the collection of a suspended-sediment sample are designed to yield a representative sample of the water

sediment mixture. This representative sample may be analyzed for sediment concentration, particle-size distribution, or, if collected with the proper type sampler, any other dissolved, suspended, or total water-quality constituent. Therefore, the equipment and methods described in this report should be used to collect a representative sample for water-quality analysis.

Sediment Characteristics, Source, and Transport

Sediment is fragmental material transported by, suspended in, or deposited by water or air, or accumulated in beds by other natural agents. Sediment particles range in size from large boulders to colloidal-size fragments and vary in shape from rounded to angular. They also vary in mineral composition and specific gravity, the predominant mineral being quartz and the representative specific gravity being 2.65.

Sediment is derived from any parent material subjected to erosional processes by which particles are detached and transported by gravity, wind, water, or a combination of these agents. When the transporting agent is water, the sediment is termed "fluvial sediment." The U.S. Geological Survey (USGS) defines fluvial sediment as fragmentary material that originates mostly from weathering of rocks and is transported by, suspended in, or deposited from water (Federal Inter-Agency Sedimentation Project, 1963b); it includes chemical and biological precipitates and decomposed organic material, such as humus.

Erosion by water is classified as either sheet or channel erosion, with no distinct division between the two. Sheet erosion occurs when sediments are removed from a surface in a sheet of relatively uniform thickness by raindrop splash and sheet flow. Sediment-particle movement and the energy of the raindrops compact and partially seal the soil surface, effectively decreasing the infiltration rate and increasing the amount of flow available to erode and transport the sediment. The amount of material removed by sheet erosion is a function of surface slope, erodibility, and precipitation intensity and drop size.

Land-surface irregularities inhibit continuous sheet flow over large areas. This inhibition serves to concentrate the flow into small rills or channels and streams, which increase in size as they join together downstream. Within these channels, eroded material from the banks or bed of the stream is contributed to the flow until, in theory, the stream is transporting as much sediment as the energy of the stream will allow. Such channel erosion may be general or local along the stream but is primarily local in nature.

Some sediment is carried to streams by wind, but direct contribution to the stream channel by this conveyance usually accounts for only a small part of the total fluvial sediments. Aside from bank caving as a result of stream erosion or processes of mass wasting (Thornbury, 1969), gravitational transfer of sediments occurs toward and into streams. Conveyance by gravitational means ranges from slow creep to rapid landslide. Other significant sources of local sediments are glacial-melt outwash, volcanic activity, mining, earth movement, construction, or additional land-disturbance activities by man.

The stream usually transports sediment by maintaining the finer particles in suspension with turbulent currents and by rolling or skipping the coarser particles along the streambed. Generally, the finer sediments move downstream at about the same velocity as the water, whereas the coarsest sediments may move only occasionally and remain at rest much of the time.

Vertical distributions of suspended-sediment particle sizes may vary among streams and among cross sections within a stream. However, as a general rule, the finer particles are uniformly distributed throughout the vertical, and the coarser particles are concentrated near the streambed. Occasionally, coarse particles may reach the water surface, generally carried by turbulent flow or as a result of dispersive grain stress (Leopold and others, 1964). Thus, with use of the depth- or point-integrating suspended-sediment samplers described here, the sample obtained generally contains a range of particle sizes representative of the suspended-sediment discharge at the sampled vertical. The vertical is divided into two zones, as illustrated by figure 1. This separation is due to the design of the sampler, which limits the effective sampled depth. Sampling the entire depth is not possible because the physical location of the sampler nozzle relative to the bottom of the sampler prevents the nozzle from passing through the zone close to the bed. This portion of the depth is termed the unsampled zone and characteristically carries the higher concentration and coarser particles. The unsampled suspended sediment moving within this zone may or

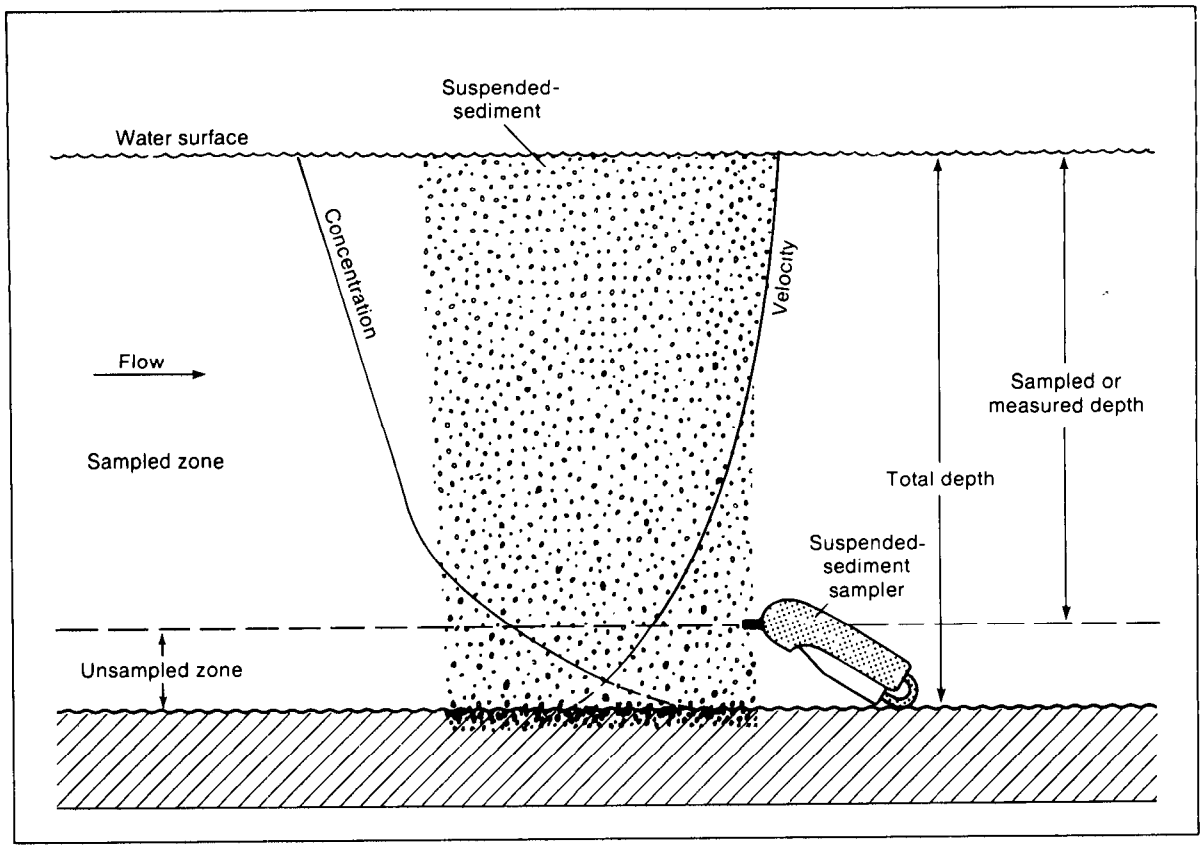

Figure 1. Sampled and unsampled zones in a stream sampling vertical, with respect to velocity of flow and sediment concentration.

may not account for a large part of the total suspended sediment, depending upon the depth, velocity, and turbulence of the flow through the vertical. The measured sediment discharge is nearly equal to the total sediment discharge if the velocity and turbulence conditions within the sampled vertical overcome the tractive force transporting the bedload in the unmeasured zone and effectively disperse all of the sediment being transported into suspension throughout the total depth.

The preceding discussion illustrates the complexity of the study of fluvial sediment transport and some of the many variables involved. The interested reader is directed to more detailed works concerning fluvial-sediment concepts and geomorphic processes, such as the contributions by Colby (1963), Leopold and others (1964), Guy (1970), and Vanoni (1975). The investigator also can obtain pertinent information on the subject by contacting the Federal Inter-Agency Sedimentation Project (F.I.S.P.), Waterways Experiment Station, Vicksburg, Mississippi.

Data Needs

No matter how precise the theoretical prediction of sedimentation processes becomes, it is inevitable that man's activities will continue to cause changes in the many variables affecting sediment erosion, transportation, and deposition; thus, there will be an increasing need for direct and indirect measurement of fluvial-sediment movement and its characteristics. Because of the rapid advances in technology, it seems of little value to list the many specific kinds of sediment problems and the kinds of sediment data required to solve such problems. However, some general areas of concern may be of interest. Sediment data are useful in coping with problems and goals related to water utilization. Many industries require sediment-free water in their processes. A knowledge of the amount and characteristics of sediment in the water resource is needed so that the sediment may be removed as economically as possible before the water is allowed to enter a distribution system. Information on sediment

movement and particle-size characteristics is needed in the design of hydraulic structures, such as dams, canals, and irrigation works. Streams and reservoirs that are free of sediment are highly regarded for recreation. Data on sediment movement and particle characteristics are needed to determine and understand how radionuclides, pesticides, and many organic materials are absorbed and concentrated by sediments, thus causing potential health hazards in some streams, estuaries, and water-storage areas. Knowledge concerning the effect of natural and man-made changes in drainage basins on the amount and characteristics of sediment yielded from the drainage basins is useful in helping to predict the stream environment when future basin changes are made. Knowledge about present fluvial-sediment conditions is being used to help establish criteria for water-quality standards and goals.

These data needs require sediment programs that will provide (1) comprehensive information on a national network basis, (2) special information about specific problem areas for water management, and (3) a description and understanding of the relations between water, sediment, and the environment (basic research). The reader is referred to Book 3, Chapter C1 of this series (Guy, 1970, p. 47) for a description of the kinds of sediment records commonly obtained at stream sites. Briefly, the records are of (1) the continuous or daily-record type, where sampling is sufficiently comprehensive to permit computation of daily loads, (2) the partial-record type, where a daily record is obtained for only a part of the year, and (3) the periodic-record type, where samples are taken periodically or intermittently. Usually a series of reconnaissance measurements is made prior to implementing any of these three programs. Even after a specific program is started, it is possible that adjustments may be necessary with respect to equipment, sample timing, or even measurement location. Realignment of efforts in this manner can be avoided in many instances by carefully applying design criteria to adequately meet the objectives of the project.

SEDIMENT-SAMPLING EQUIPMENT

General

In the early days of fluvial-sediment investigations, each investigator, or at least each agency concerned with sediment, developed methods and equipment individually as needed. It soon became apparent that consistent data could not be obtained unless equipment, data collection, and analytical methods were standardized. To overcome this difficulty, representatives of several Federal agencies (the Corps of Engineers of the Department of the Army, the Flood Control Coordinating Committee of the Department of Agriculture, the U.S. Geological Survey, the Bureau of Reclamation, the Office of Indian Affairs of the Department of the Interior, and the Tennessee Valley Authority) met in 1939 to form an interdepartmental committee, with the expressed purpose of standardizing sediment data-collection equipment, methods, and analytical techniques. The test facility for this work was initially located at the Iowa University Hydraulics Laboratory, in Iowa City, Iowa, and remained there for 9 years. In 1946, the committee became known as the Subcommittee on Sedimentation of the Federal Inter-Agency River Basin Committee. In 1948, the subcommittee moved the test facility to the St. Anthony Falls Hydraulic Laboratory, University of Minnesota, in Minneapolis, Minnesota. The subcommittee reorganized the project in 1956 to its present structure as the Federal Inter-Agency Sedimentation Project (F.I.S.P.). In 1992, F.I.S.P. was moved to its present location at the Waterways Experiment Station in Vicksburg, Mississippi. The project is sponsored by a technical committee composed of representatives of the U.S. Army Corps of Engineers, U.S. Geological Survey, Bureau of Reclamation, Agricultural Research Service, U.S. Forest Service, and Bureau of Land Management, working under a formal Guidance Memorandum describing the project's objectives and organization. The F.I.S.P. is overseen by the Technical Committee of the Subcommittee on Sedimentation of the Interagency Advisory Committee on Water Data.

Since its initiation in 1939, approximately 50 reports, dealing with nearly all aspects of measurement and analysis of fluvial sediment movement, have been published by F.I.S.P. The intent of this chapter is not to replace the Inter-Agency Project reports, but to condense and combine their information regarding sediment measurements. The interested reader should contact F.I.S.P. for a listing of individual reports presenting further background material and details on the standard samplers. Sampling equipment is available for purchase by any interested investigator from the F.I.S.P., 3909 Halls Ferry Road, Vicksburg, MS 39180-6199.

The samplers developed by the F.I.S.P. are designated by the following codes: US, United States standard sampler. (In the following discussions this code will appear in the initial reference but will be dropped from succeeding references to the sampler designations.)

D, depth integrating

P, point integrating

H, hand-held by rod or line. (This code is placed after the primary letter designation and is omitted when referring to cable- and reel-suspended samplers.)

BM, bed material

BP, battery pack

BL, bedload sampler

U or SS, single stage

PS or CS, pumping-type sampler

Year, last two digits of the year in which the sampler was developed.

Sediment samplers available from F.I.S.P. or Hydrologic Instrumentation Facility (HIF) include suites of depth-integrating suspended-sediment samplers, point-integrating suspended-sediment samplers, pumping samplers, bed-material samplers, and a bedload sampler. In addition, an array of instruments has been developed to fulfill the need for collecting samples during unpredictable high-flow events. One sampler of particular interest for use in the future is a suspended-sediment sampler that utilizes bags as sample containers to overcome the depth limits of standard samplers due to container size, nozzle diameter, and stream velocity (Federal Inter-Agency Sedimentation Project, 1982b).

Suspended-Sediment Samplers

The purpose of a suspended-sediment sampler is to obtain a representative sample of the water-sediment mixture moving in the stream in the vicinity of the sampler. The F.I.S.P. committee set up several criteria for the design and construction of suspended-sediment samplers:

1. To allow water to enter the nozzle isokinetically. (In isokinetic sampling, water approaching the nozzle undergoes no change in speed or direction as it enters the orifice.)
2. To permit the sampler nozzle to reach a point as close to the streambed as physically possible. (This varies from 3 to 7 inches, depending on the sampler.)
3. To minimize disturbance to the flow pattern of the stream, especially at the nozzle.
4. To be adaptable to support equipment already in use for streamflow measurement.
5. To be as simple and maintenance-free as possible.
6. To accommodate a standard bottle size [that is, 1-pint (473 mL) glass milk bottle, 1-quart (946 mL) glass, 1-liter (1,000 mL) plastic, 2-liter (2,000 mL) plastic, or 3-liter (3,000 mL) plastic, as listed in table 1].

When a suspended-sediment sampler is submerged with the nozzle pointing directly into the flow, a part of the streamflow enters the sampler container through the nozzle as air in the container exhausts under the combined effect of three forces:

1. The positive dynamic head at the nozzle entrance, due to the flow.
2. A negative head at the end of the air-exhaust tube, due to flow separation.
3. A positive pressure due to a difference in elevation between the nozzle entrance and the air-exhaust tube.

When the sample in the container reaches the level of the air exhaust, the flow rate drops, and circulation of the streamflow in through the nozzle and out through the air-exhaust tube occurs. Because the velocity of the water flowing through the bottle is less than the stream velocity, the coarser particles settle out, causing the concentration of coarse particles in the bottle to gradually increase.

Table 1. Sampler designations and characteristics

[Epoxy-coated versions of all samplers are available for collecting trace metal samples; US, United States; in., inches; lbs., pounds; ft/s, feet per second; cd, cadmium, do., ditto; X, type of sampler container size used; --, type of sampler container size not used]

Sampler designation (US)	Construction material	Sampler dimensions Length (in.)	Width (in.)	Weight (lbs.)	Nozzle distance from bottom (in.)	Suspension type	Maximum velocity (ft/s)	Maximum depth (ft)	Sampler container size Pint	Quart	Intake size (in.)	Nozzle color
DH-48	aluminum	13	3.2	4.5	3.5	rod	8.9	8.9	X	--	1/4	yellow
DH-75P[1]	cd-plated	9.25	4.25	1.5	3.27	do.	6.6	15	X	--	3/16	white
DH-75Q[1]	do.	9.25	4.25	1.5	4.49	do.	6.6	15	--	X	3/16	white
DH-75H[1]	do.	9.25	4.25	1.5	--	do.	6.6	15	(2 liter)		3/16	white
DH-59	bronze	15	3.5	22	4.49	handline	5.0	15	X	--	1/8	red
DH-59	do.	15	3.5	22	4.49	do.	5.0	15	X	--	3/16	red
DH-59	do.	15	3.5	22	4.49	do.	5.0	9	X	--	1/4	red
DH-76	do.	17	4.5	22	3.15	do.	6.6	15	--	X	1/8	red
DH-76	do.	17	4.5	22	3.15	do.	6.6	15	--	X	3/16	red
DH-76	do.	17	4.5	22	3.15	do.	6.6	15	--	X	1/4	red
DH-81	plastic	[1]7.5	4.0	.5	([2])	rod	8.9	9	([7])	--	3/16	white
DH-81	do.	[1]7.5	4.0	.5	([2])	do.	8.9	9	([7])	--	1/4	white
DH-81	do.	[1]7.5	4.0	.5	([2])	do.	8.9	9	([7])	--	5/16	white
D-49	bronze	24	5.25	62	4.00	cable reel	6.6	15	X	--	1/8	green
D-49	do.	24	5.25	62	4.00	do.	6.6	15	X	--	3/16	green
D-49	do.	24	5.25	62	4.00	do.	6.6	9	X	--	1/4	green
D-74	do.	24	5.25	62	4.06	do.	6.6	15	X[8]	X	1/8	green
D-74	do.	24	5.25	62	4.06	do.	6.6	15	X[8]	X	3/16	green
D-74	do.	24	5.25	62	4.06	do.	6.6	[3]9, [4]15	X[8]	X	1/4	green
D-74AL	aluminum	24	5.25	42	4.06	do.	5.9	15	X[8]	X	1/8	green
D-74AL	do.	24	5.25	42	4.06	do.	5.9	15	X[8]	X	3/16	green
D-74AL	do.	24	5.25	42	4.06	do.	5.9	[3]9, [4]15	X[8]	X	1/4	green
D-77	bronze	29	9.0	75	7.0	do.	8.0	15	(3 liter)		5/16	white
P-61	do.	28	7.34	105	4.29	do.	6.6	[5]180, [6]120	X[8]	X	3/16	blue
P-63	do.	37	9.0	200	5.91	do.	6.6	[5]180, [6]120	X[8]	X	3/16	blue
P-72	aluminum	28	7.34	41	4.29	do.	5.3	[5]72.2, [6]50.9	X[8]	X	3/16	blue

[1]Without sample bottle attached.
[2]Depends on bottle size used. Calibrated brass nozzles no longer available.
[3]Depth using pint sample container.
[4]Depth using quart sample container.
[5]Depth using pint sample container to transit in 15 to 30 foot increments until entire traverse is completed
[6]Depth using quart sample container to transit in 15 to 30 foot increments until entire traverse is completed.
[7]Any size bottle with standard mason jar treads.
[8]Pint milk bottle can be used with adapter sleeve.

Depth- and Point-Integrating Samplers

A depth-integrating sampler is designed to isokinetically and continuously accumulate a representative sample from a stream vertical while transiting the vertical at a uniform rate (Federal Inter-Agency Sedimentation Project, 1952, p. 22). The simple depth-integrating sampler collects and accumulates a velocity or discharge-weighted sample as it is lowered to the bottom of the stream and raised back to the surface.

The point-integrating sampler, on the other hand, uses an electrically activated valve, enabling the operator to isokinetically sample points or portions of a given vertical. For stream cross sections less than 30 feet deep, the full depth can be traversed in one direction at a time by opening the valve and depth integrating either from surface to bottom or vice versa. Stream cross sections deeper than 30 feet can be integrated in segments of 30 feet or less by collecting integrated-sample pairs consisting of a downward

integration and a corresponding upward integration in separate containers.

To eliminate confusion and more adequately differentiate between depth- and point-integrating samplers, a direct reference to Inter-Agency Report 14 (Federal Inter-Agency Sedimentation Project, 1963b, p. 60) is presented here to describe the characteristics of the point-integrating samplers that make them useful in conditions beyond the limits of the simpler depth-integrating samplers.

> Point-integrating samplers are more versatile than the simpler depth-integrating types. They can be used to collect a suspended-sediment sample representing the mean sediment concentration at any point from the surface of a stream to within a few inches of the bed, as well as to integrate over a range in depth. These samplers were designed for depth integration of streams too deep (or too swift) to be sampled in a continuous round-trip integration. When depth integrating, sampling can begin at any depth and proceed either upward or downward from that initial point through a maximum vertical distance of 30 feet.

A point-integrating sampler uses a 3/16-inch nozzle oriented parallel to the streamflow with the cross-sectional area exposed to approaching particles. The air is exhausted from the sample container and directed downstream away from the nozzle area as the sample enters. The intake and exhaust passages are controlled by a valve that can be activated on demand. When the valve is activated (opened to the sampling position), the sampling procedure is identical to that used for depth-integrating samplers. The increased effective depth to which a point-integrating sampler can be used, as compared to the maximum sampling depth to which a depth-integrating sampler is limited, is made possible by a pressure-equalizing chamber (diving-bell principle) enclosed in the sampler body. This chamber equalizes the air pressure in the sample container with the external hydrostatic head near the intake nozzle at all depths to alleviate the inrush of sample water, which would otherwise occur when the intake and air exhaust are opened at depth.

Hand-held samplers—US DH-81, US DH-75, US DH-48, US DH-59, and US DH-76

Where streams are wadable or access can be obtained from a low bridge span or cableway, a choice of five lightweight samplers can be used to obtain suspended-sediment samples via a wading rod or handline.

The DH-81 (fig. 2) consists of a DH-81A adapter and D-77 cap and nozzle. All parts are autoclavable. This construction enables the sampler to be used for collection of depth-integrated samples for bacterial analysis. The DH-81 can be used with 1/8-inch, 3/16-inch, or 1/4-inch nozzles and is suspended from a rod. Any bottle having standard mason jar threads can be used with this sampler. Obviously, the height of the unmeasured zone will vary depending on the size of

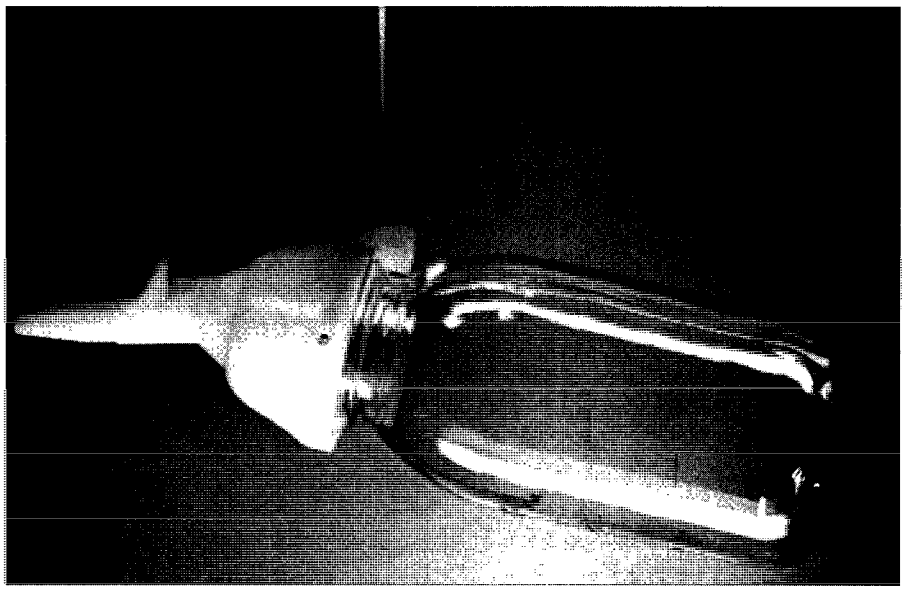

Figure 2. US DH-81 suspended-sediment sampler shown with a US DH-81A adapter, D-77 cap and nozzle, wading rod handle, and quart glass bottle.

bottle used. The DH-81 should be useful for sampling during cold weather because the plastic sampler head and nozzle attach directly to the bottle, eliminating a metal body (which would more rapidly conduct heat away from the nozzle, air exhaust, and bottle and create a more severe sampler-freezeup condition).

The DH-75 (fig. 3) weighs 0.9 pound and is available in two versions, the DH-75P and DH-75Q, which accept plastic containers of pint and quart volumes, respectively. The sampler consists of a cadmium-plated sheet-steel body 9 1/4 inches long, excluding the nozzle and sample container, with a retainer piece and shock cord assembly to hold the sample container against a cast silicone stopper through which the 3/16-inch nozzle and 180-degree air-exhaust tube pass to the mouth of the bottle. The DH-75 was developed as a freeze-resistant sampler. This sampler is not recommended for use as a general purpose depth-integrating suspended-sediment sampler.

The DH-48 sampler (fig. 4) features a streamlined aluminum casting 13 inches long that partly encloses the sample container. The container, usually a round pint glass milk bottle, is sealed against a gasket recessed in the head cavity of the sampler by a hand-operated spring-tensioned pull-rod assembly at the tail of the sampler. A modified version of this sampler is available to accommodate square pint milk bottles also. The sample enters the container through the intake nozzle as the air from the container is displaced and exhausted downstream through the air exhaust. The sampler, including container, weighs 4 1/2 pounds and can sample to within 3 1/2 inches of the streambed. This instrument is calibrated with an intake nozzle 1/4 inch in diameter, but may be used with a 3/16-inch nozzle in high-flow velocity situations (Federal Inter-Agency Sedimentation Project, 1963b, p. 57–60).

Two lightweight (24 and 25 pounds) handline samplers designated "DH-59" and "DH-76" (figs. 5 and 6) are designed for use in shallow unwadable streams with flow velocities up to 5 ft/s (feet per second). These samplers feature streamlined bronze castings 15 and 17 inches in length for the DH-59 and DH-76, respectively. The DH-59 accommodates a round pint sample bottle, while the DH-76, a more recent version of the sampler, is designed to take a quart container. The tail assembly extends below the body of the casting to ensure sampler alignment parallel to the flow direction with the intake nozzle entrance oriented upstream. Intake nozzles of 1/8-inch, 3/16-inch, and 1/4-inch diameters are calibrated for use with these samplers and may be interchanged as necessary when varying flow conditions are encountered from stream to stream. Suspended sediment can be collected to within 4 1/2 inches of the streambed with the DH-59, while the DH-76 can sample to within about 3 inches from the bottom.

These lightweight hand samplers are the most commonly used for sediment sampling during normal flow in small- and, perhaps, intermediate-sized streams. Because they are small, light, durable, and adaptable, they are preferred by hired observers and field people on routine or reconnaissance measurement trips. At many locations, a heavier sampler will be needed only for high-flow periods. It is often desirable, however, to require the observer to use a heavier sampler installed at a fixed location. The small size of the hand samplers also enables the person taking a sample in cold weather to warm the sampler readily if water freezes in the nozzle or air exhaust.

Cable-and-Reel Samplers—US D-74, US D-77, US P-61, US P-63, and US P-72

When streams cannot be waded, but are shallower than about 15 feet, depth-integrating samplers designated "D-74" and "D-77" can be used to obtain suspended-sediment samples. Forerunners of these samplers were the US D-43 and US D-49 samplers, both of which are no longer manufactured. These latter two are only mentioned here because many of these earlier designed instruments are still used at some locations. Sampling techniques for using the older samplers are identical to those presented later in this text relative to operation of the newer D-74 and D-77 samplers.

The D-74 (fig. 7) is a 62-pound sampler (approximately 40 pounds for the aluminum version) designed to be suspended from a bridge crane or cableway by means of a standard hanger bar and cable-and-reel system. This sampler replaces the earlier D-49, which replaced the D-43 for general use. The D-74 has a streamlined cast bronze (or aluminum) body 24 inches long that completely encloses the sample container. This sampler accommodates a round quart bottle, or with addition of an adapter sleeve, a standard pint milk bottle may be used. The sampler head is hinged at the bottom and swings downward to provide access to the sample-container chamber. In this manner, sample containers can be changed during the normal sampling

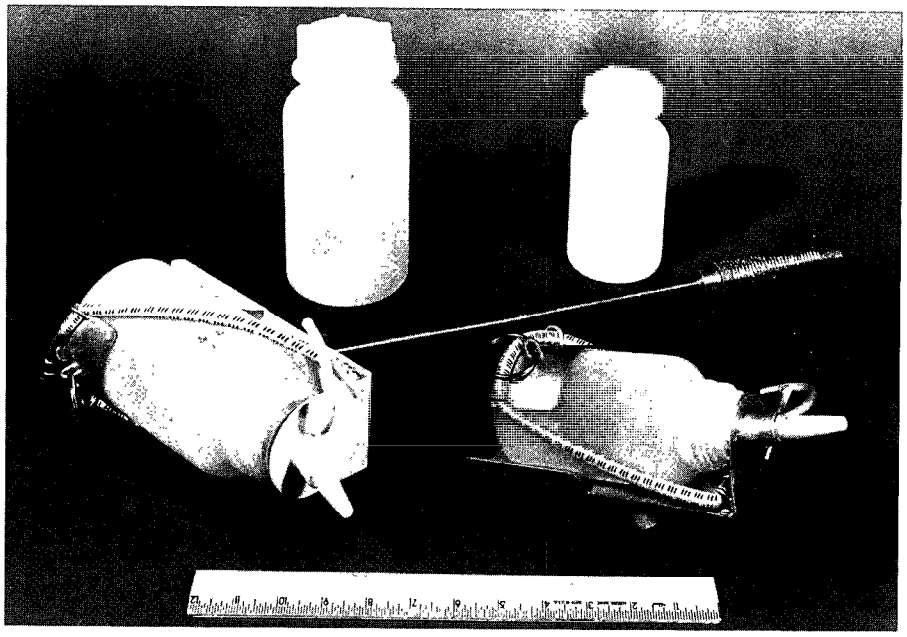

Figure 3. US DH-75 (P and Q) suspended-sediment samplers with sample containers and wading rod.

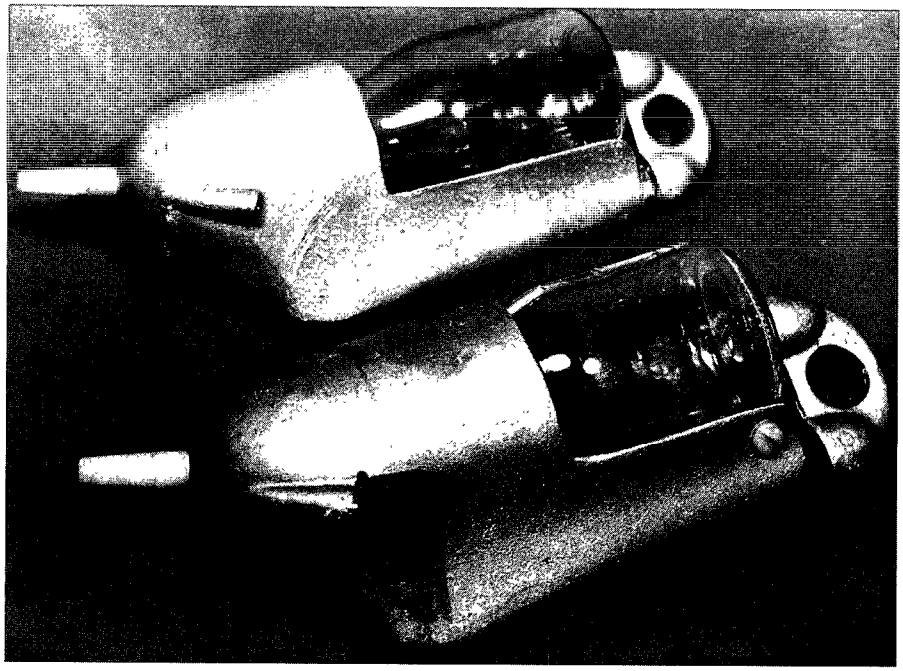

Figure 4. US DH-48 suspended-sediment sampler.

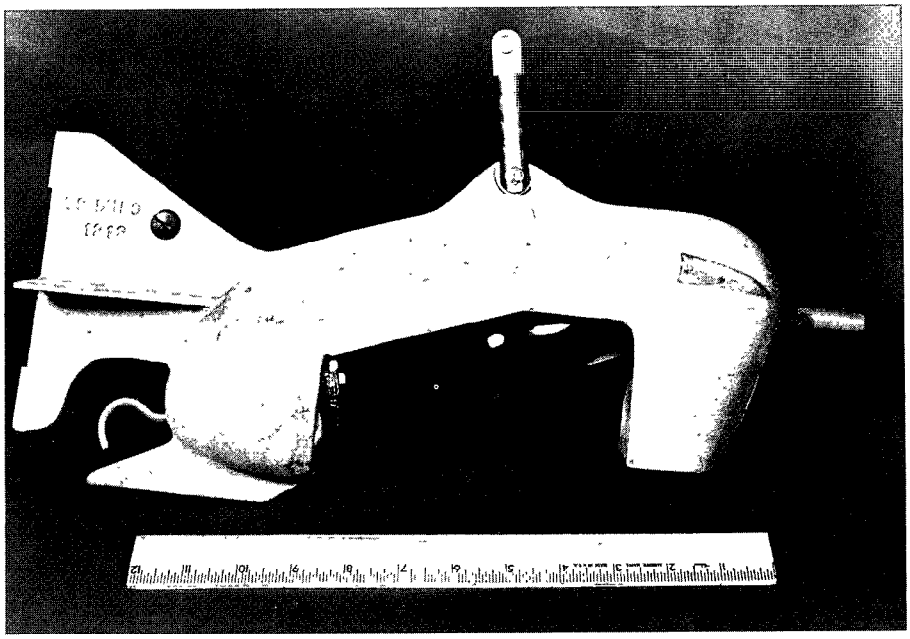

Figure 5. US DH-59 suspended-sediment sampler.

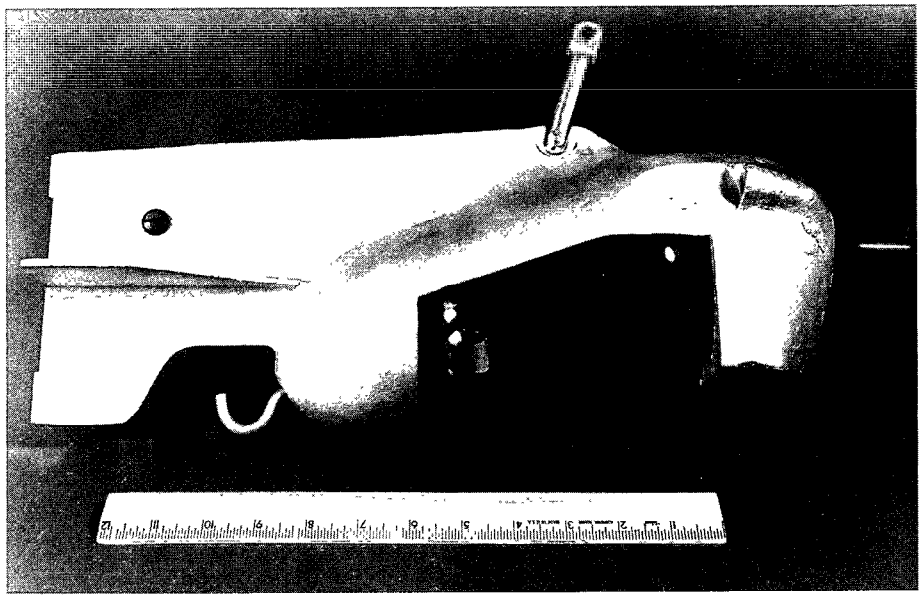

Figure 6. US DH-76 suspended-sediment sampler.

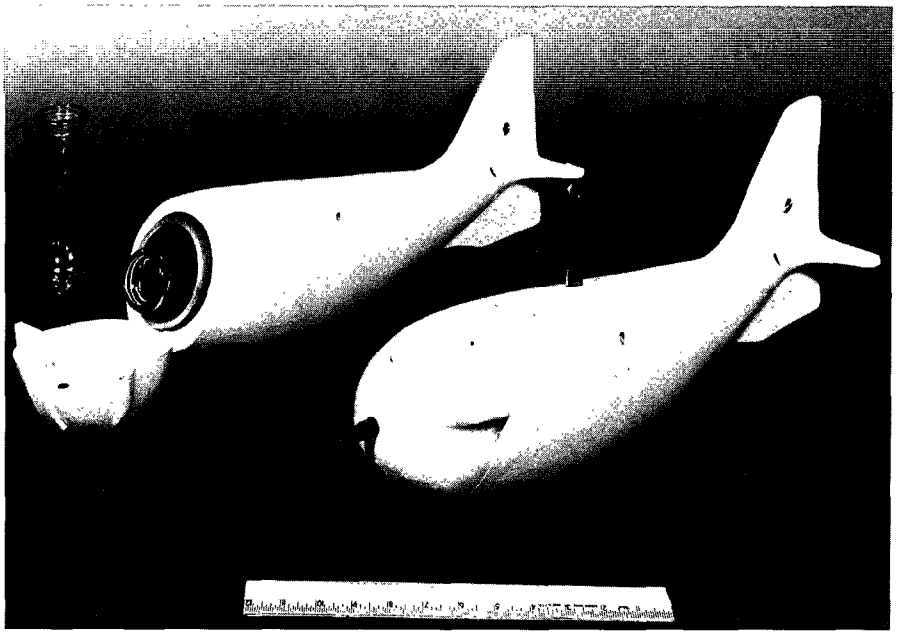

Figure 7. US D-74 suspended-sediment sampler.

routine. The body includes tail vanes that serve to align the sampler and the intake nozzle with the flow. Intake nozzles of 1/8-inch, 3/16-inch, and 1/4-inch diameters are available for use with the sampler and can be interchanged as varying flow conditions dictate. The sample container fills as a filament of water passes through the intake nozzle and displaces air from the container. The air is expelled in the downstream direction through an air-exhaust port in the side of the sampler head. The intake nozzle can be lowered to within about 4 inches of the streambed during sampling (approximately 4 1/3 inches for the aluminum version).

The D-77 is a dramatically different design (fig. 8) as compared to the design configuration of the D-74 and its predecessors. The sampler is 29 inches long and weighs 75 pounds; it has a bronze casting attached to a tail cone with four sheet-metal vanes welded in place to provide a means of orienting the intake nozzle into the flow. The casting is structured to accommodate a 3-liter autoclavable sample container that slides into the sample container chamber and is held in place by means of a spring clip on the bottom of the chamber. This sampler is constructed without a head assembly to cover the mouth of the container and facilitate attachment of the intake nozzle. Instead, a cap, nozzle, and air-exhaust assembly, constructed of autoclavable plastic, is screwed onto the mouth of the sample container, which is entirely exposed at the front of the sampler. This configuration was purposely chosen to allow collection of a large volume (2,700 mL), depth-integrated biological or chemical sample at near- or below-freezing temperatures. Although 1/8-inch, 1/4-inch, 3/16-inch, and 5/16-inch nozzles are available, only 5/16-inch nozzles are recommended for use with this sampler. The distance between the nozzle and sampler bottom is 7 inches.

A version of the D-77 sampler was tested by F.I.S.P. to eliminate the depth-range limit dictated by sample container size, nozzle size, and stream velocity (Federal Inter-Agency Sedimentation Project, 1982b). This version, commonly referred to as a "bag sampler," incorporates a sample bag inside a special rigid container. Information about this sampler and other bag samplers can be obtained from F.I.S.P.

Point-integrating samplers currently manufactured and widely used are the P-61, P-63, and P-72. Forerunners of these samplers were the P-46 and P-50 samplers, which are no longer manufactured but are mentioned here because several of these instruments are still used. The sampling techniques used for obtaining a sample with these older samplers are the same as for the newer samplers. The primary differences between these old and new versions are valve mechanisms and cost. The new versions have a simpler valve and are less expensive.

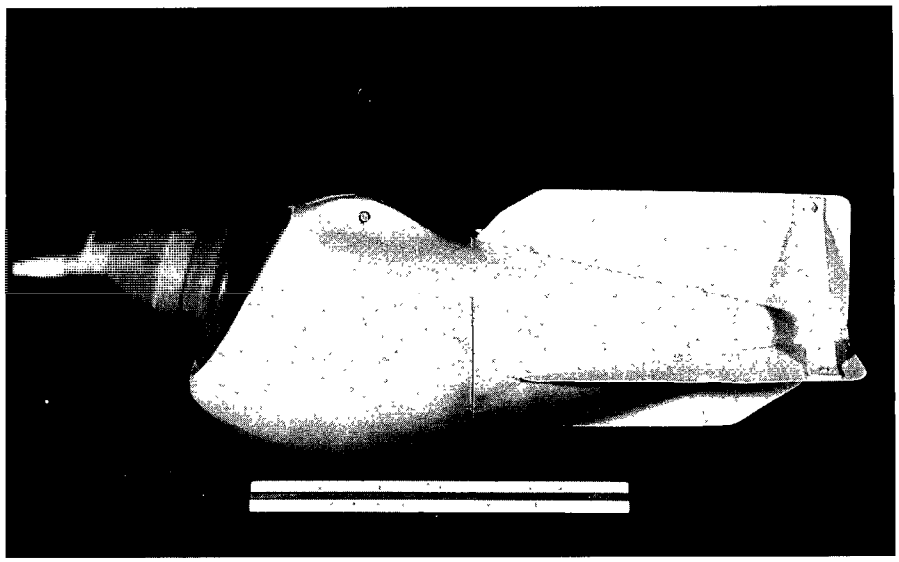

Figure 8. US D-77 suspended-sediment sampler.

The 105-pound P-61 (fig. 9) can be used for depth integration as well as for point integration to a maximum stream depth of 180 feet. The sampler valve for the P-61 has two positions. When the solenoid is not energized, the valve is in the nonsampling position, in which the intake and air-exhaust passages are closed, the air chamber in the body is connected to the cavity in the sampler head, and the head cavity is connected through the valve to the sample container. When the solenoid is energized, the valve is in the sampling position, in which the intake and air exhaust are open, and the connection from the sample container to the head cavity is closed. A P-61 sampler that has been modified to accommodate a quart bottle is illustrated in figure 9. When the ordinary pint bottle is used, the cylindrical adapter must be inserted into the bottle cavity. The maximum sampling depth is about 120 feet when the quart container is used.

The P-63 (fig. 10) is a 200-pound point-integrating suspended-sediment sampler and is better adapted to high velocities. The solenoid head is basically the same as that on the P-61. The P-63 differs from the P-61 mainly in size and weight. The P-63 is cast bronze, is 34 inches long, and has the capacity for a quart-sized round mayonnaise bottle. An adapter is furnished so that a round pint-sized milk bottle can be used. The maximum sampling depth is the same as for the P-61, about 180 feet with a pint sample container and about 120 feet with a quart container.

The 41-pound P-72 is a light-weight version of the P-61. It features a streamlined cast-aluminum shell rather than the bronze used to construct the P-61. The outward appearance of the P-72, the 3/16-inch intake nozzle, the solenoid head, and the accommodation for pint- and quart-sized containers are similar to the P-61. However, the listed maximum stream velocity at which the P-72 is recommended for use is 5.3 ft/s, as opposed to 6.6 ft/s for the P-61, and the depth limit to which this sampler should be used is about 72 feet using the pint container and 51 feet with the quart container. These depths are less than one-half of the maximum usable depths for the P-61 with the same container sizes.

All the point samplers are designed for suspension with a steel cable having an insulated inner conductor core. By pressing a switch located at the operator's station, the operating current may be supplied through the cable to the solenoid in the sampler head by storage batteries connected in series to produce 24 to 48 volts. If the suspension cable is longer than 100 feet, a higher voltage may be desirable. The US BP-76 battery pack has been designed as a portable power source for activating the P-61, P-63, and P-72 samplers and is available from the F.I.S.P. and HIF.

Because of the complex nature of point-integrating samplers, the user may find it necessary to seek additional information given in the Inter-Agency reports (Federal Inter-Agency Sedimentation Project, 1952, 1963b, and 1966).

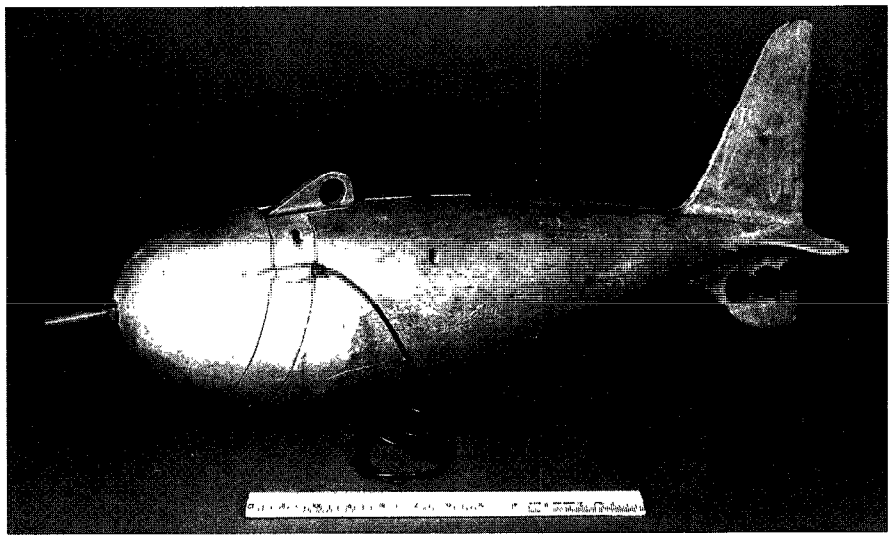

Figure 9. US P-61 point-integrating suspended-sediment sampler.

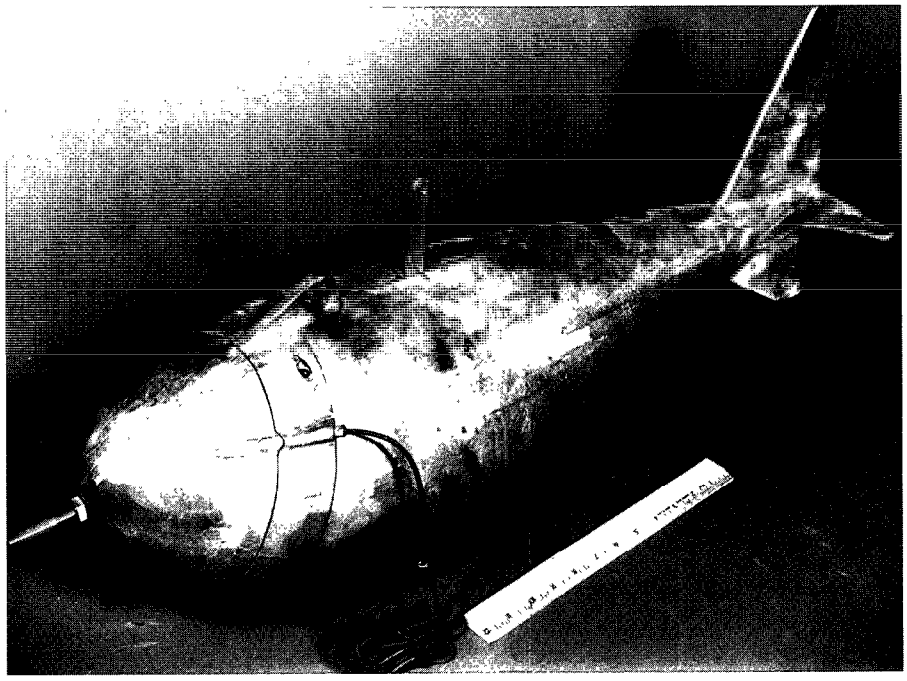

Figure 10. US P-63 point-integrating suspended-sediment sampler.

Sampler Accessories

Nozzles

Each suspended-sediment sampler is equipped with a set of nozzles specifically designed for the particular sampler. These nozzles are cut and shaped externally and internally to ensure that the velocity of water after entering the nozzle is within 8 percent of the ambient stream velocity when the stream velocity is greater than 1 ft/s. It has been found that a deviation in intake velocity from the stream velocity at the sampling point causes an error in the sediment concentration of the sample, especially for sand-sized particles. For example, a plus-10-percent error in sediment concentration is likely for particles of sediment 0.45 mm in diameter, when the intake velocity is 0.75 of the stream velocity (Federal Inter-Agency Sedimentation Project, 1941, p. 38–41). The relation between intake-velocity deviation and errors in concentration resulting from collecting a sample enriched or deficient in sand-size particles (greater than 0.062 mm) is illustrated by figure 11. When sand-size particles are entrained in

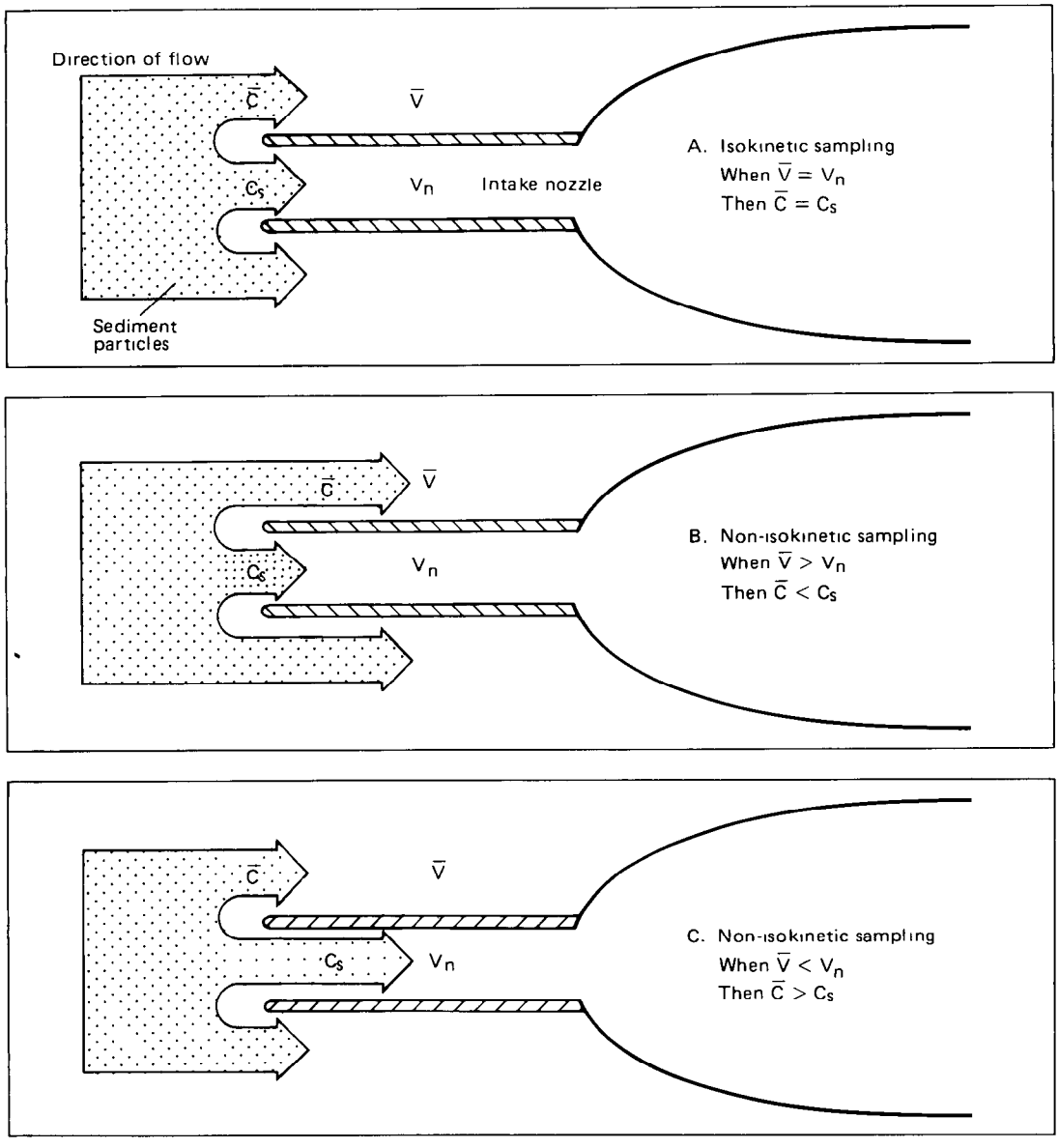

Figure 11. Relation between intake velocity and sample concentration for (*A*) isokinetic and (*B*, *C*) non-isokinetic sample collection of particles greater than 0.062 mm. When $\bar{V}$ = mean stream velocity, V_n = velocity in the sampler nozzle, $\bar{C}$ = mean sediment concentration in the stream, and C_s = sample sediment concentration.

the flow, the intake velocity within the sampler nozzle must be equal to the ambient stream velocity (isokinetic), in order to collect a sample representative of the mean discharge-weighted sediment concentration (fig. 11*A*). The resulting sediment concentration of the sample will be equal to the average discharge-weighted sediment concentration of the approaching flow. However, when the velocity in the nozzle is less than the stream velocity (non-isokinetic, fig. 11*B*), some water that should flow into the nozzle now curves to the side and flows around it. Inertia resists the curving flow and forces the approaching particles (greater than 0.062 mm) to follow straight-line paths into the nozzle. This combination of curved and straight-line movement increases the concentration of coarse particles in the sample. As a result, the sediment concentration in the sample is greater than the concentration in the approaching flow. Likewise, when the velocity in the nozzle is greater than the stream velocity (non-isokinetic, fig. 11*C*), some water that should flow past the nozzle curves to the side and flows into it. Again, inertia resists the curving flow and forces the particles (greater than 0.062 mm) to follow straight-line paths and flow past the nozzle. The result of this combination of curved and straight-line movement is a decrease in the sample concentration relative to the concentration of the approaching flow.

Because, in general, each sampler nozzle is designed for a particular series of samplers, it must be emphasized that a nozzle for one series of samplers should not be used in another series of samplers. However, there are two exceptions to this rule—the same nozzle can be used in the P-61, P-63, and P-72 series, and a nozzle can be interchanged between the D-49 and D-74. To ensure against incorrectly matching samplers and nozzles, all nozzles are color coded to specific sampler designs (table 1).

The reasons for the differences between the nozzles of different series are that (1) the length of flow paths for water and air are different, resulting in differences of flow resistance; and (2) the differential heads between the nozzle entrance and the air exhaust are different. Thus, interchanging nozzles among samplers of various series results generally in an incorrect intake velocity and, thus, incorrect sediment concentration and particle-size distribution in the sample. Therefore, when a nozzle is bent or broken, be certain to use a correct replacement nozzle.

If extra nozzles are needed for a sampler, they can be ordered from the F.I.S.P. at the address in the latest Inter-Agency report. The order must indicate the sampler series. If the exhaust tubes, tail fins, or any other part of a sampler are damaged, the entire sampler should be sent to the F.I.S.P. for repair and recalibration.

Three nozzle diameters—1/4 inch, 3/16 inch, and 1/8 inch—are available for use with all depth-integrating samplers, except for the DH-48, DH-75, D-77, and the point-integrating samplers. The D-77 sampler is the only depth-integrating sampler that uses a 5/16-inch nozzle. Although a nozzle may physically fit a sampler, the match may not be correct. For example, it is possible, but incorrect, to interchange any one of the 1/4-inch, 3/16-inch, and 1/8-inch nozzles listed in table 1 among the depth-integrating or point-integrating samplers. For instance, it is possible, but incorrect, to put DH-48 nozzles in DH-59 samplers. One exception is the D-77, which will not accept any nozzle other than the correct one. To help prevent the incorrect interchange of color-coded nozzles among samplers, new samplers ordered from F.I.S.P. are delivered with a color-coded plastic screw in the tail vane assembly, which indicates the correct color of nozzle to be used with the sampler (for example, DH-59 has a red screw and uses a red nozzle).

The reason for different size nozzles is that stream velocities and depths occur that will cause the sample bottle to overfill for a specific transit rate when using the largest nozzle. More specifically, for depth-integrating samplers with a pint bottle, the maximum theoretical sampling depths for round-trip integration are about 9 feet for the 1/4-inch, and 15 feet with both the 3/16-inch, and 1/8-inch nozzles. Therefore, to reduce the quantity of sample entering the bottle at depths over 9 feet, use a smaller bore nozzle in combination with a pint sample bottle. For a given situation, the largest nozzle should be used to reduce the chance of excluding large sand particles that may be in suspension.

Possible errors caused by using too small a nozzle are usually minor when dealing with fine material (less than 0.062 mm), but tend to increase in importance with increasing particle size. Small nozzles also are more likely than large ones to plug with organic material, sediment, and ice particles. This means that problems with nozzles can exist even when sampling streams transporting mostly fine material.

Point-integrating samplers are supplied only with a 3/16-inch nozzle to match the opening through the valve mechanism.

Gaskets

Of equal importance to using the correct nozzle in the instrument is the necessity for using the proper gasket to seal the bottle mouth sufficiently. Gaskets for this purpose are made of a sponge-like neoprene that deteriorates somewhat with use and time. When samples are being collected for water quality, such as for trace metal analysis, the gasket should be made of silicone rubber to avoid biasing the sample chemistry.

To check the gasket for adequate seal, insert a bottle in the proper position in the sampler; then block the air-exhaust port and force air into the sampler nozzle. **CAUTION**: A field person should never force air into the sampler by placing the mouth directly in contact with the nozzle—due to the possibility of questionable water quality at the site or the likelihood of receiving an electrical shock (if a brass nozzle is in use) upon activating the solenoid of a point-integrating sampler when opening the intake. A safe procedure to perform this check would be to block the air exhaust with a finger and place a short length of clean plastic or rubber tubing snugly over the nozzle and then apply air pressure by blowing into the tubing to force air through the nozzle. If air escapes around the bottle mouth, replace the gasket. If the problem persists, check the spring that pushes the bottle against the gasket. Each sampler series uses a different size or shape of gasket, so it is necessary to have spares for each series in use. Appropriate gaskets may be obtained from the F.I.S.P. (address can be obtained from the latest Inter-Agency report). Gaskets in the "P" series samplers also may be tested by lowering the sampler, with sample bottle in place, into the stream without opening the solenoid. After a minute or so, raise the sampler to the surface and inspect the sample bottle. If the gasket is sealing properly, less than a few milliliters of water should be present in the bottle.

Bottles

Depth- and point-integrating samplers accommodate different bottle sizes and types (fig. 12). Many field people still use pint glass milk bottles, which have been used for many years and can be adapted to every sampler series with the exception of the DH-81 and D-77. Quart-sized glass mayonnaise bottles (Owens-Illinois #6762) are increasing in general use because versions of all samplers, except the DH-48 and D-77, use this size sample container. The D-77

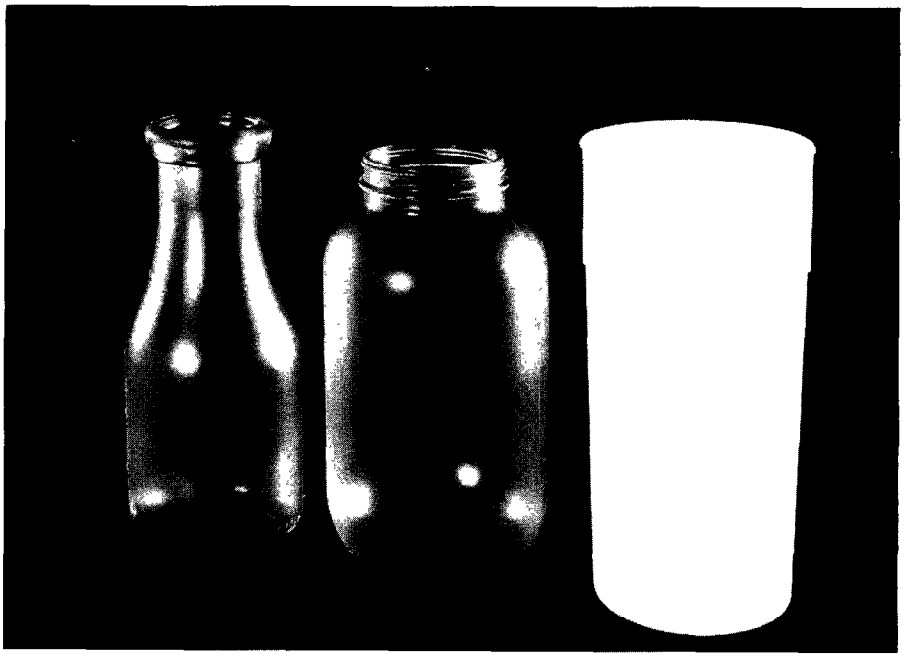

Figure 12. Sample containers to fit PS-69 pumping sampler (left to right): pint glass milk bottle, quart glass mayonnaise bottle, and quart plastic container to fit the PS-69 pumping sampler.

sampler holds a 3-liter plastic autoclavable bottle with standard mason jar threads (Nalge 2115-3000); the DH-81 holds any bottle with standard mason jar threads; and the DH-75 holds a plastic bottle (Bel-Art #F-10906, 1,000 mL) and a variety of other quart/liter bottles. Ideally, each type of glass bottle should have an etched surface to provide a labeling area to accommodate a record of pertinent information concerning each sample. Hydrofluoric acid has been used for this purpose, but care must be exercised when handling and storing this substance. In the past, commercial etching agents have been available for general use. However, the authors do not know of any such agent that is available at this time. This etched labeling surface should easily accept medium-soft blue or black pencil markings of sufficient durability to withstand handling and yet be easily removed during cleaning. Plastic bottles also require an area for labeling. However, this is less of a problem because a grease pencil or other marker that is not readily soluble in water, but that can be removed using a solvent, can be used to write on the side of the bottle.

The practice of using plain bottles with attached tags or marked caps for recording purposes should be avoided whenever possible. These labeling areas are generally small and provide little writing space. Additionally, the use of these labeling devices can result in tags being torn off during transport or in bottles being mislabeled by interchanging caps.

Plastic and teflon bottles are increasing in use throughout the Water Resources Division of the USGS. Several samplers have been designed to use plastic sample containers (the DH-75 series, the DH-81 and D-77 samplers). Compared to glass, these bottles are lightweight, strong, and useful when sampling for certain chemicals.

During depth integration, a collapsible bottle or bag would be the ideal arrangement to eliminate the problem of depth limitation due to the size of the sample container. Depth-integrating samplers incorporating this collapsible sample bag/bottle concept, are currently under development by F.I.S.P.

Bottles are usually stored and transported in wire, wooden, fiberboard, or plastic cases holding 12 to 30 bottles each. In the field, a small bottle carrier, which holds 6, 8, or 10 bottles, is more convenient; eliminates the need to handle the heavier 12- to 30-bottle cases while making a measurement; and provides a neat, convenient, and relatively safe place to set the bottles. When making wading measurements, both hands can be free to operate the sampler if the bottle carrier is suspended from the shoulder with a strap or rope.

Single-Stage Samplers

The single-stage samplers, US U-59 (fig. 13), also designated US SS-59, and US U-73, were designed and tested by the F.I.S.P. to meet the needs for instruments useful in obtaining sediment data on streams where remoteness of site location and rapid changes in stage make it impractical to use a conventional depth-integrating sampler.

The U-59 (SS-59) consists of a pint milk bottle or other sample container, a 3/16-inch inside diameter air exhaust, and 3/16-inch or 1/4-inch inside diameter intake constructed of copper tubing. Each tube is bent to an appropriate shape and inserted through a stopper

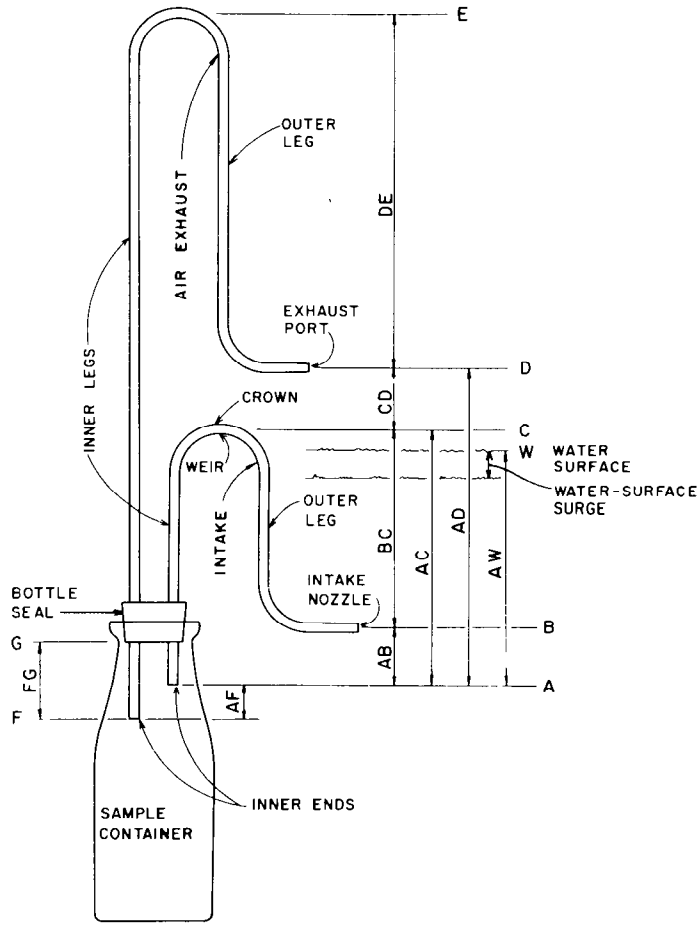

Figure 13. US U-59 single-stage suspended-sediment sampler. Sampling operation using designated letters is described in text (see also Federal Inter-Agency Sedimentation Project, 1961).

sized to fit and seal the mouth of the sample container. There are two general types of this sampler, one with a vertical intake and the other with a horizontal intake. The horizontal-intake type is further divided into three versions, each distinguished from the others by the height of the intake and air-exhaust tubes. Under some conditions either type could be used, but the two are not always interchangeable.

The vertical-intake sampler is used to sample streams carrying sediments finer than 0.062 mm. The vertical-intake sampler has the advantage of somewhat less tendency to fouling by debris and deposits of sediment in the intake nozzle than does the horizontal type of intake. Conversely, the horizontal-intake sampler should be used to sample streams carrying a considerable amount of sediment coarser than 0.062 mm.

The basic sampling operation of the instrument when velocities and turbulences are small is described by F.I.S.P. (1961, p. 17):

> When the stream surface rises to B, the elevation of the intake nozzle, the water-sediment mixture enters; and as the water surface continues to rise in the stream, it also rises in the intake. (The general elevation and dimensions are expressed without regard to the inside diameter of the tube or without distinction between the weir and the crown of the siphon.) When the water-surface elevation W reaches C, flow starts over the weir of the siphon, primes the siphon, and begins to fill the sample bottle under the head AC.
>
> Filling continues until the sample rises to F in the bottle, and water is forced up the air exhaust to the elevation W. Actually the momentum of flow in the tubes causes a momentary rise above W in the air exhaust. Water drains out of the inner leg of the intake. When the stream rises to D, air is trapped in the air exhaust. As long as sufficient air remains in the tubes, no flow can pass through to alter the original sample unless a differential head that exceeds the height of invert is built up. (If the legs of an invert are not symmetrical, the inverts have different effective air-trap heights resisting flow into and out of the bottle.) For conditions without significant surge and velocity effects at the intake nozzle or exhaust port, the heights BC and DE may be small.
>
> If, after the normal time of sampling, the depth of submergence over the sample bottle increases, the air in the bottle is compressed, and a small additional sample enters the bottle. This additional sample will enter through the tube having the smallest height of invert. Under variable submergence, the entrance of water will compress the air in the bottle on rising stages, and some expanding air will escape on falling stages; thus the quantity of air in the bottle becomes less and less, and the water rises in the bottle.

The sampling operation just described is somewhat idealistic because, in reality, the operation is affected by the flow velocity and turbulence, which alter the effective pressure at the nozzle entrance.

The U-59 has many limitations with respect to good sampling objectives. It must be considered a type of point sampler because it samples a single point in the stream at whatever stage the intake nozzle is positioned before a flow event occurs. Its primary purpose is to collect a sample automatically, and it is used at stations on flashy streams or other locations where extreme difficulty is encountered in trying to reach a station to manually collect samples. Besides being automatic, it is inexpensive; a "battery" of them can be used to obtain a sample at several elevations or times during the rising hydrograph. However, despite these seemingly important advantages, the U-59 has many limitations. Following are the most important:

1. Samples are collected at or near the stream surface, so that, in the analysis of the data, theoretical adjustments for vertical distribution of sediment concentration or size are necessary.
2. Samples are usually obtained near the edge of the stream or near a pier or abutment; therefore, theoretical adjustments for lateral variations in sediment distribution are required.
3. Even though several combinations of size, shape, and orientation of intake and air-exhaust tubes are available, the installed system may not result in intake ratios sufficiently close to unity to sample sands accurately for a specific runoff event.
4. Covers or other protection from trash, drift, and vandalism often create unnatural flow lines at the point of sampling.
5. Water from condensation may accumulate in the sample container prior to sampling.
6. Sometimes the sediment content of the sample changes during subsequent submergence.
7. The device is not adapted to sampling on falling stages or on secondary rises.
8. No specific sampler design is best for all stream conditions.
9. The time and gage height at which a sample was taken may be uncertain.
10. Under high velocities, circulation of flow into the intake nozzle and out the air exhaust can occur. This will increase the concentration of coarse material in the sample and can make the sample concentration several orders of magnitude higher than stream concentration.

To cover a wide range of operating conditions, four "standard" models of the U-59 are available. The many specific details of these are further described in F.I.S.P. (1961).

Before a bank of the U-59 samplers can be designed and installed, it is necessary to have some knowledge of the seasonal stage characteristics of the stream so that several samples can be obtained for a given storm event and throughout the season. The stream stage and flow-velocity characteristics not only affect the design with respect to the vertical spacing of the samplers, but also the support necessary for the bank of samplers.

The U-73 (fig. 14) is a more sophisticated single-stage sampling device. The sampler's design configuration solves several of the problems characteristic of the U-59. Specifically, this sampler (1) can be used to sample either a rising or falling stage, (2) has no problem of condensation in the sample container before the spring-loaded stoppers are tripped, and (3) features an exterior design that allows for a degree of protection from trash or drift without additional covers or deflection shields. Aside from these few advantages, the U-73 has the same limitations and should be used under the same conditions as the U-59.

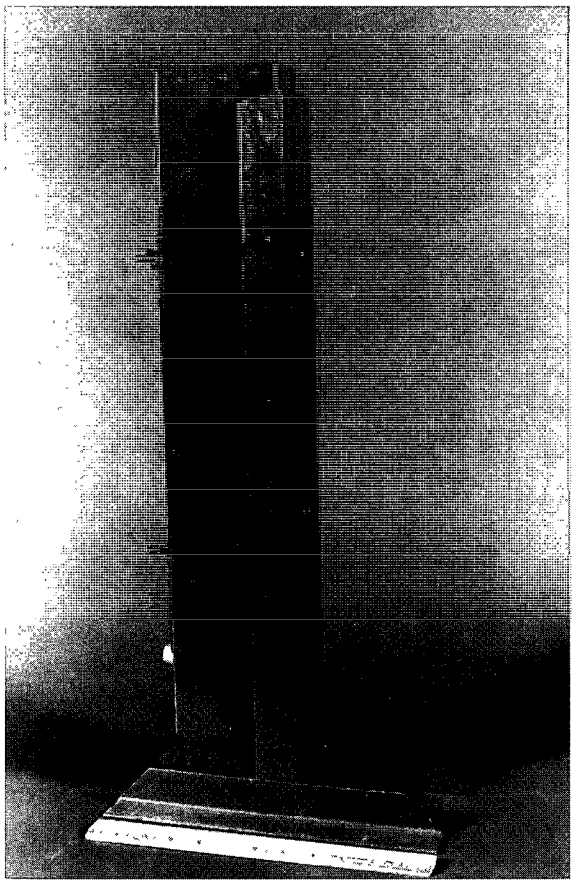

Figure 14. US U-73 single-stage suspended-sediment sampler.

The investigator using either the U-59 or U-73 may find protective measures necessary to avoid blockage of intakes or air exhausts due to nesting insects. In freezing climates, precaution may be warranted against sample-container breakage due to expansion of a freezing sample. Samples for water-quality analysis can be collected using the U-73-TM version of the U-73. However, do not use insecticides or antifreeze solutions if samples are to be analyzed for water quality because these will obviously contaminate the sample.

Bed-Material Samplers

Limitations

To properly sample bed material for interpretation, it is first necessary to establish what constitutes bed material and understand its relation to transported load, especially to bedload. Bedload is best defined as sediment that moves by sliding, rolling, or bouncing along on or near the streambed (Hubbell, 1964; Leopold and others, 1964; Emmett, 1980a). Bed material, on the other hand, is best defined in the Office of Water Data Coordination (1978) National Handbook, chapter 3, p. 3–5, which describes bed material as "the sediment mixture of which the bed is composed." In alluvial streams, bed-material particles are likely to be moved at any moment or during some future flow conditions. From the perspective of Leopold and others (1964), the streambed is composed of two elements, distinguished one from the other by particle size and their reaction to stream velocity. The first element consists of particles frequently transported as part of the suspended load or bedload, but considered as bed material when at rest. The second element consists of particles and aggregates of particles that compose definite structures on the streambed and reside there indefinitely or at least for long periods of time. The size fractions comprising the second element may only be moved by the most extreme flow events during which streambed erosion and scour occur.

The samplers described in this section can only accommodate bed material consisting of particles finer than about 30 or 40 mm in diameter. These bed-material samplers cannot accurately collect representative samples of particles larger than 16 mm, however. As noted in the description of individual samplers, there also may be limitations with respect to some very fine sediments because of poor sealing of the sampler after collection. This limits bed-material sampling, with standard US type samplers, to fine material that might be transported in suspension or as bedload at higher flows. The collection and analysis of material larger than coarse gravel are more difficult and costly because other techniques are required to handle heavy samples. Due to this difficulty in collecting large particle sizes, little information regarding bed-material size distribution is available for streams having gravel, cobble, and boulder beds. Therefore, much of the equipment for measurement of large bed material is of an experimental nature, and standard equipment for sampling large particles is unavailable. The interested investigator is directed to several references on direct and indirect methods of sampling and analysis of coarse bed materials, however, and is encouraged to contact Chief, Office of Surface Water, Reston, Virginia, or the F.I.S.P. for information (Lane and Carlson, 1953; Kellerhals, 1967; Wolman, 1954).

Hand-Held Samplers—US BMH-53, US BMH-60, and US BMH-80

Three types of instruments for hand sampling of bed material finer than medium gravel have been developed for general use. The BMH-53 (fig. 15) is designed to sample bed material in wadable streams. The instrument is 46 inches long and is made of corrosion-resistant materials. The sample container is a stainless-steel thin-walled cylinder 2 inches in diameter and 8 inches long with a tight-fitting brass piston. The piston is held in position by a rod that passes through the handle to the opposite end. The piston creates a partial vacuum above the material being sampled. This vacuum aids in overcoming the frictional resistance required to force the sampler into the bed. When sampling fine-grained material, this partial vacuum also aids in retaining the shallow core in the cylinder when the sampler is removed from the bed. The piston then serves to remove the sample from the cylinder by forcing it downward toward the bottom of the cylinder. In soft cohesive beds, this technique generally provides shallow cores with a minimum of distortion, from which sediment variations with depth and subsamples can be obtained. (See Federal Inter-Agency Sedimentation Project, 1963b and 1966, for more detailed information.) A version of this sampler, developed by the F.I.S.P. incorporates a "core catcher"

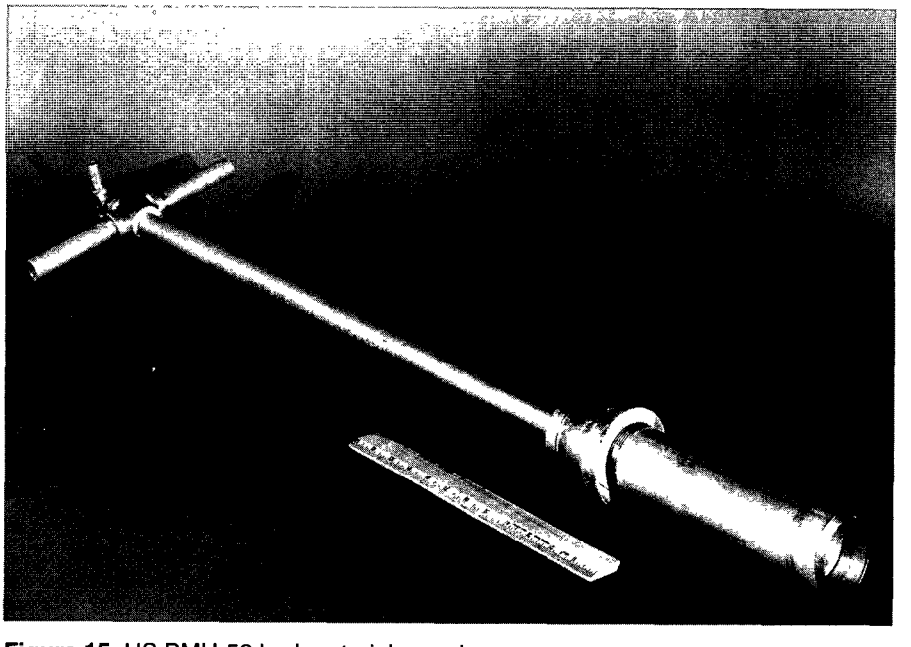

Figure 15. US BMH-53 bed-material sampler.

mechanism in the cylinder to retain samples containing a high percentage of sand.

The bed material of some wadable streams or lakes can be sampled with the US BMH-60 (fig. 16). This handline sampler is about 22 inches long, is made of cast aluminum, and weighs 30 pounds. Because of its light weight, it is useful only in streams of moderate depths and velocities. The bed material must be moderately firm and contain little or no gravel.

The sampler mechanism of the US BMH-60 consists of a scoop or bucket driven by a constant-torque spring that rotates the bucket from front to back. The scoop, when activated by release of tension on the hanger rod, can penetrate into the bed about 1.7 inches and can hold approximately 175 cubic centimeters of material. The scoop is aided in penetration of the bed by extra weight in the sampler nose. To cock the bucket into an open position for sampling (that is, retract it into the body), the sampler must first be supported by the handline, then the bucket can be rotated (back to front) with an allen wrench to an open cocked position.

The hanger rod to which the handline is attached is grooved so that a safety yoke can be placed in position to maintain tension on the hanger rod assembly. **CAUTION**: At no time should the hand or fingers be placed in the bucket opening because the bucket may accidentally close with sufficient force to cause permanent injury! A piece of wood or a brush can be used to remove any material adhering to the inside of the sample bucket. (See Federal Inter-Agency Sedimentation Project, 1963b and 1966, for more detailed information.)

After the safety yoke is removed, the bucket closes when tension on the handline is released, which occurs as the sampler strikes the streambed. A gasket on the closure plate prevents sampled material from being contaminated or being washed from the bucket.

Another bed-material hand-sampling instrument available for general use is designated BMH-80 (fig. 17). This sampler is 56 inches in total length and is used to sample the bed of wadable streams. The sampling mechanism is a semi-cylindrical bucket, resembling the BMH-60 bucket assembly, which is operated by positioning the lever on the handle to open or close the bucket. When the bucket is closed and a sample volume of approximately 175 cubic centimeters of bed material is captured, the closure is sufficiently sealed to prevent erosion of the sample while the instrument is lifted through the water column.

An additional handline sampler, used successfully for bed-material chemistry sampling on the Willamette and Columbia Rivers in Oregon, is the Ponar sampler.

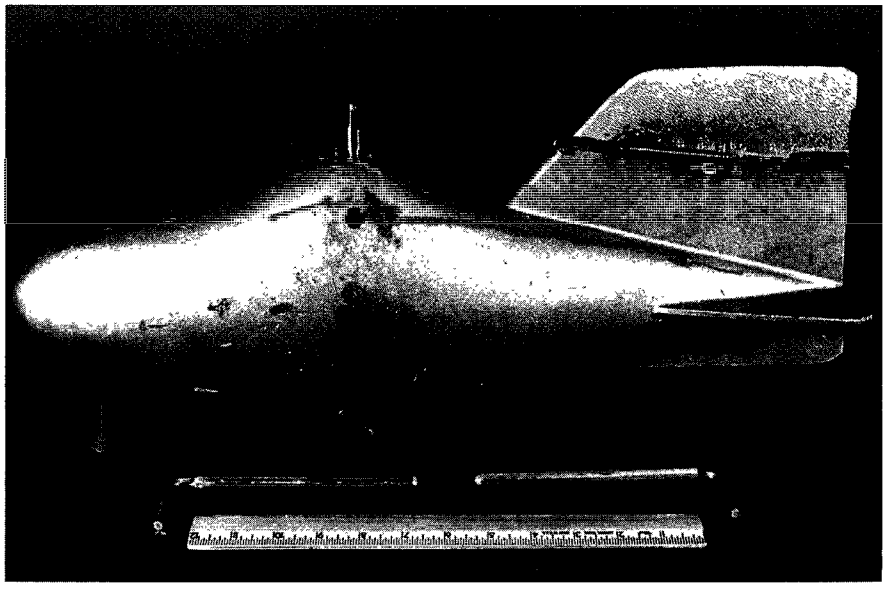

Figure 16. US BMH-60 bed-material sampler.

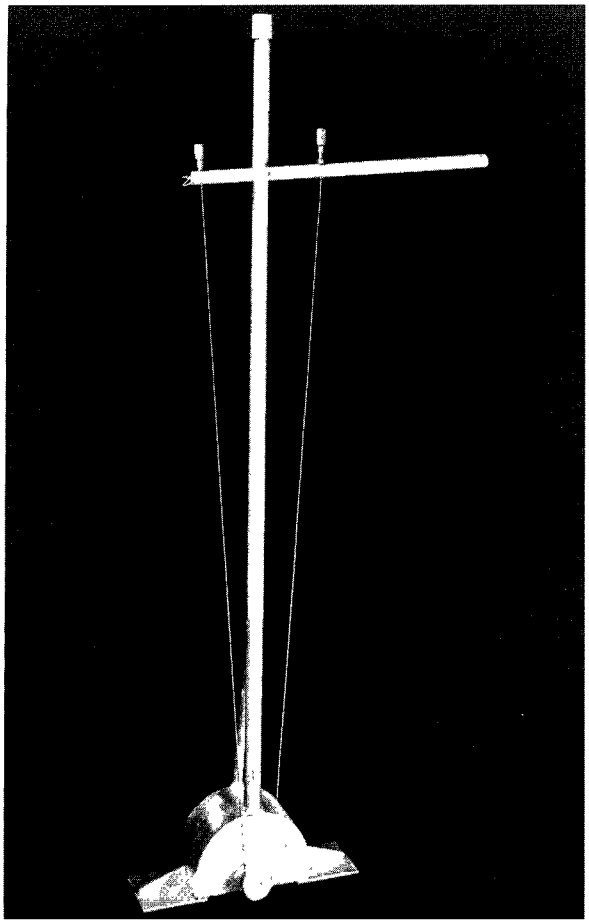

A

This is a clam-shell type sampler, consisting of two quarter-cylinder sections hinged together at the top. The sampler, which is constructed of galvanized or stainless steel, weighs about 25 pounds and can be suspended on a handline. The jaws of the instrument are held in the open position by a system of solid-notched bars and by the downward force created by the weight of the sampler on the suspension line. Gravity provides the necessary force for bottom penetration during sampling. The solid-notched bars holding the sampler jaws open are released when the downward force of the sampler's weight is released from the suspension line as the sampler strikes the bed. The sampler then closes as an upward force is applied to lift the sampler with the captured sediment. This sampler is particularly effective where bottom sediments consist of unconsolidated fines with no armoring present. Under these conditions, bottom penetration is 6 to 8 inches, resulting in a sample volume range of 8,000 cubic centimeters to 10,000 cubic centimeters of material. Some protection against erosion of the captured sediment is provided by an overlapping lip on the bottom and sides. However, a watertight seal does not exist, so care must be exercised when raising the sampler to the surface.

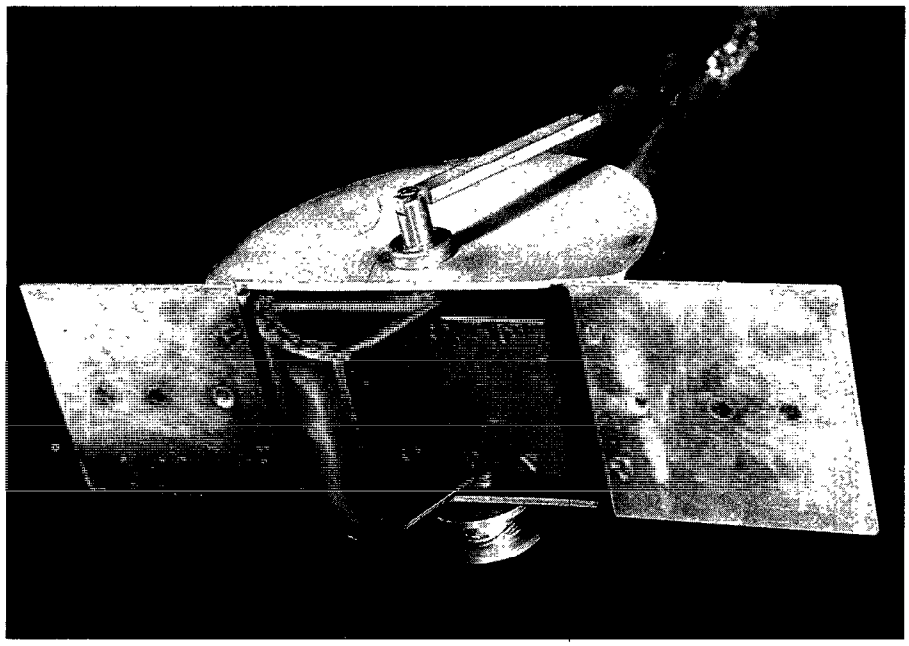

B

Figure 17. US BMH-80 rotary-scoop bed-material sampler. *A*, complete hand-sampling instrument (approximately 5 feet tall). *B*, Rotary-scoop assembly (approximately 12 inches long).

Cable-and-Reel Sampler—US BM-54

The 100-pound cable-and-reel suspended BM-54 sampler (fig. 18) can be used for sampling bed material of streams and lakes of any reasonable depth, except for streams with extremely high velocities. The body of the BM-54 is cast steel. Its physical configuration is similar to the cast aluminum BMH-60, 22 inches long and with tail vanes. Its operation also is similar to the BMH-60 in that it takes a sample when tension on the cable is released as the sampler touches the bed. The sampling mechanism externally looks similar to that of the BMH-60, but its operation is somewhat different.

The driving force of the bucket comes not from a constant-torque spring, but rather from a conventional coil-type spring. The tension on the spring is adjusted by the nut-and-bolt assembly protruding from the front of the sampler. The spring is powerful enough to obtain a sample from a bed of very compacted sand. It is suggested that the tension on the spring be released during extended periods of idleness even though the bucket is closed. Maximum tension need be used only when the streambed is very firm. Unlike the BMH-60, the spring and cable assembly rotates the bucket from the back to the front of the sampler. The trapped sample is kept from washing out by a rubber gasket. (See Federal Inter-Agency Sedimentation Project, 1963b, 1964, and 1966, for more complete description and details.)

BM-54 samplers obtained after 1956 are equipped with a safety mechanism similar to the safety yoke used on the BMH-60. This safety bar can be rotated over the cutting edge of the sample bucket when cocked into the open position. The bar keeps the bucket open when in the safety position, even if there is no tension on the hanger bar. As with the BMH-60, the cable tension on the catch mechanism holds the bucket open while the sampler is lowered. Safety bars can be obtained from F.I.S.P. and should be installed on any unit that does not have one. Again, personnel operating these samplers are cautioned to KEEP ONE'S HANDS AWAY FROM THE BUCKET CAVITY EVEN IF A SAFETY BAR IS IN USE. The power of the bucket is demonstrated by the fact that upon release, it has been observed to lift the 100-pound sampler from a hard surface.

A bed-material sampler incorporating the heavy streamlined body of the P-61 sampler and the spring-driven bucket of the BM-54 has been developed (C.W. O'Neal, Federal Inter-Agency Sedimentation Project, written commun., 1998). This sampler, the BM-84, is intended for use in large, swift rivers.

Prych and Hubbell (1966) developed a core sampler for use in deep flowing water in studies of the Columbia River estuary. This cable-suspended

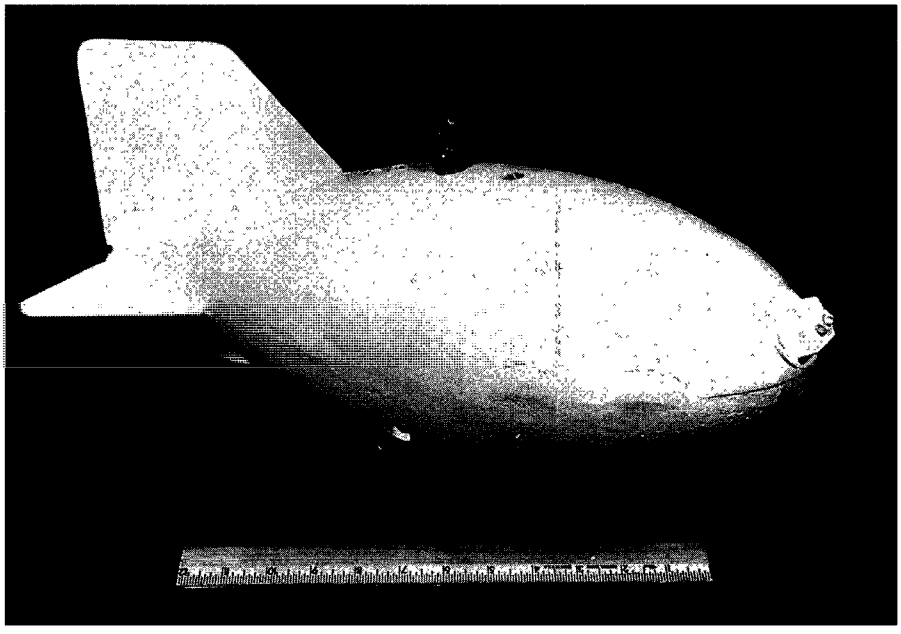

Figure 18. US BM-54 bed-material sampler.

sampler (fig. 19) is used to collect a 1 7/8-inch diameter by 6-foot-long core, by means of the combined action of vibration, suction, and an axial force derived through cables connected to a 250-pound streamlined stabilizing weight that rests on the streambed.

Smaller estuaries along the Oregon coast and other places have been successfully sampled using the Gravity Corer available from Benthos, Inc. This sampler is allowed to plunge to the bottom where, under the force of the gravitational pull on the sampler coupled with the momentum of its 250-pound total weight, it can penetrate up to 5 feet deep in soft bed material. However, much less penetration can be expected if the bed material consists of sand or gravel. The sampler is retrieved from the bed using a cable-reel boom assembly. The 2 5/8-inch diameter by 5-foot long core is retained in a core liner held in place by a core catcher at the bottom and protected against sample washout by a watertight valve at the top. The length of core and depth of penetration depend upon the degree of hardness of the bed being sampled. Other slightly more crude devices have been used with some success to sample bed material and thus deserve mention here. The two most notable of these devices are (1) the pipe dredge, which is lowered to the streambed and dragged a short distance to collect a sample; and (2) the "can on a stick" sampler, consisting of a rod with a scoop connected to the end, which can be used in wadable streams by lowering it to the streambed and scooping bed material from the bottom.

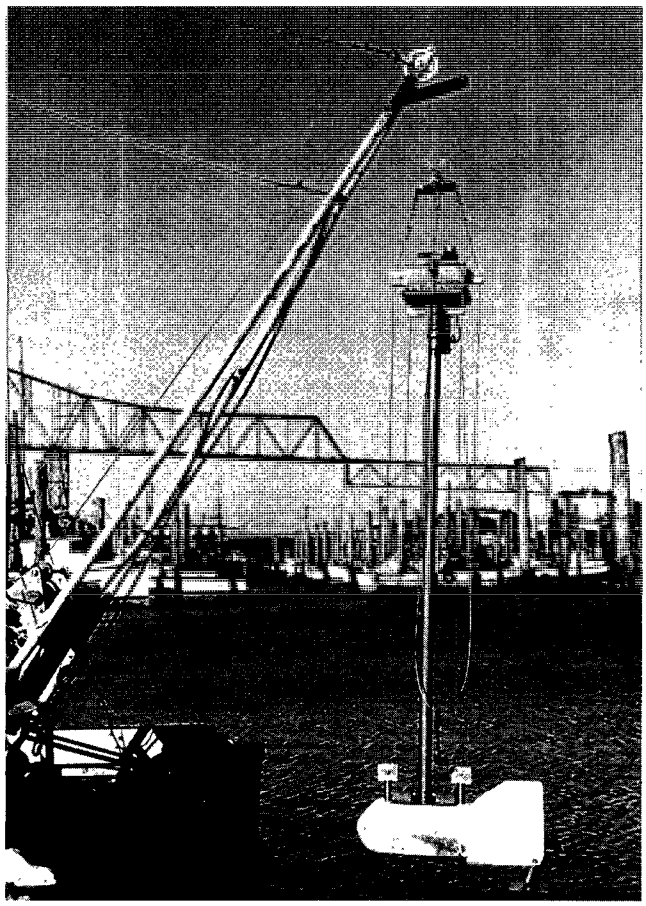

Figure 19. Vibra-core sampler prepared for coring (barrel approximately 5 feet long). From Prych and Hubbell (1966, plate 1).

Bedload Samplers

At this time, the reader should note the difference between bedload and unmeasured sediment. Remember from the bed-material section that bedload is the sediment that moves by sliding, rolling, or bouncing along on or very near the streambed. Unsampled sediment is comprised of bedload particles and particles in suspension in the flow below the sampling zone of the suspended-sediment samplers (fig. 1).

Bedload is difficult to measure for several reasons. Any device placed on or near the bed may disturb the flow and rate of bedload movement. More importantly, bedload transport rate and the velocity of water close to the bed vary considerably with respect to both space and time. Therefore, any sample obtained at a given point may not be representative of the mean transport rate for a reasonable interval of time because the bed particles move intermittently at a mean velocity much less than that of the water. Thus, a bedload sampler must be able to representatively sample, directly or indirectly, the mass or volume of particles moving along the bed through a given width in a specified period of time if bedload discharge is to be accurately determined.

Prior to 1940, most bedload was measured using some type of direct-collecting sampler. Bedload samplers developed during this era can be grouped into four categories: (1) box or basket, (2) pan or tray, (3) pressure difference, and (4) slot or pit samplers (Hubbell, 1964). Essentially, box or basket samplers consist of a heavy open-front box or basket apparatus, which is lowered to the streambed and positioned to allow collection of bedload particles as they migrate

downstream. The basket type, displaying various sampling efficiencies, has been used preferentially over box types. Pan or tray samplers consist of an entrance ramp leading to a slotted or partitioned box. These samplers also have varying sampling efficiencies. Pressure-difference samplers are designed to create a pressure drop at the sampler's exit and thus maintain entrance velocities approximately equal to the ambient stream velocity. Sampling efficiencies may be higher with this type of sampler than with others, and the deposition of sediments at the sampler entrance, inherent with basket or tray samplers, is eliminated. The best known early pressure-difference sampler is probably the Arnhem or Dutch sampler, after which the Helley-Smith bedload sampler is designed. Ideally, the best measurement of bedload would occur when all of the bedload moving through a given width during a specific time period was measured. The category of samplers that most closely meet this ideal is the slot or pit sampler. This type of sampler has efficiencies close to 100 percent. The slot openings of these pits are 100- to 200-grain diameters wide to ensure the high sampling efficiency. However, samples collected in the pits are removed only with great difficulty or by use of an elaborate conveyor device. A variation of this technique, consisting of a collection trough accessed by a series of hydraulically operated gates, extends from bank to bank at a site on the East Fork River, near Pinedale, Wyoming (Emmett, 1980a). Sediment trapped in the trough during sampling is removed by means of a continuous conveyor belt, which carries the sample to a weighing station on the stream bank.

The original Helley-Smith bedload sampler, introduced in 1971, was a variation of the Arnhem pressure-difference sampler. This sampler consists of an expanding nozzle, sample bag, and frame (fig. 20). The sampler design enables collection of particle sizes less than 76 mm at mean velocities to 9.8 ft/s. The sampler has a 3-inch by 3-inch square entrance nozzle, an area ratio (ratio of nozzle exit to entrance area) of 3.22, and a 295-square-inch polyester mesh sample bag that is 18 inches long with mesh openings of varying sizes (0.25 mm most commonly used), attached to the rear of the nozzle assembly with a rubber "O" ring. The total weight of the original sampler design is 66 pounds, requiring the use of a cable-reel suspension system. However, a lighter version incorporating a wading rod assembly also is available. Heavier versions weighing 99 pounds, 165 pounds, and 550 pounds (used on the Amazon River) have been used by USGS personnel (Emmett, 1980a). A scaled-up version of the sampler having a 6-inch by 6-inch square entrance has been used to sample streams with large particle sizes.

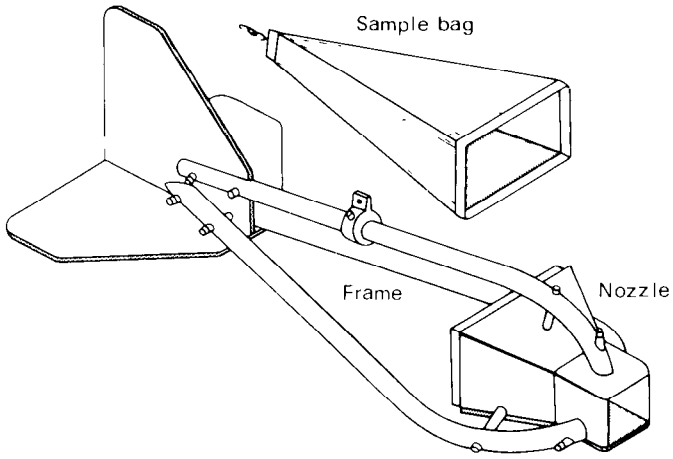

Figure 20. Helley-Smith bedload sampler. From Emmett (1980a, p. 2).

The standard 3-inch by 3-inch sampler has been calibrated in two different laboratory studies and in an extensive field study. Results of one laboratory study (Helley and Smith, 1971) indicated an average sampling efficiency of about 160 percent. Emmett (1980a) concluded from his field study that the overall sampling efficiency was close to 100 percent. A laboratory investigation (Hubbell and others, 1985) of varying bed materials and a range of transport rates indicates that the sampling efficiency of the standard 3-inch by 3-inch sampler varies with particle size and transport rate, displaying an approximate efficiency of 150 percent for sand and small gravel and close to 100 percent for coarse gravel. The standard 6-inch by 6-inch sampler had generally higher efficiencies. Tests of a Helley-Smith type sampler, which has a 3-inch by 3-inch nozzle with less expansion than the standard nozzle (an area ratio of 1.40), resulted in fairly constant efficiencies close to 100 percent for all transport rates and particle sizes. In May 1985, the 1.40 nozzle was approved by the Technical Committee on Sediment as a provisional standard sampler for use by U.S. Federal agencies. After some modifications to the frame, the 3-inch by 3-inch nozzle with 1.40-area-expansion ratio was designated the BL-84 sampler. The Water Resources Division of the USGS endorses the use of this new sampler with the 1.40-area-ratio nozzle; however, until additional testing is done, data obtained using the original 3.22-area-ratio Helley-Smith sampler will continue to be accepted.

Automatic Pumping-Type Samplers

Development and Design

Some sediment studies require frequent collection of suspended sediment at a site. Site location, flow conditions, frequency of collection, and operational costs frequently make collection of sediment data by manual methods impractical. For these reasons, F.I.S.P. and USGS personnel have developed and evaluated several models of automatic pumping-type samplers. The US PS-69 sampler is probably the best known of these samplers to be designed, tested, and used by USGS personnel. The US CS-77 (designed and tested by the Agricultural Research Service in Durant, Oklahoma) and the US PS-82 (Federal Inter-Agency Sedimentation Project, 1983) have been used. A number of automatic pumping-type samplers also have been designed by and are available through commercial sources. The Manning S-4050 and the ISCO 1680 are common commercially used samplers. (Manning Corp. is no longer in business.)

Automatic pumping-type samplers generally consist of (1) a pump to draw a suspended-sediment sample from the streamflow and, in some cases, to provide a back flush to clear the sampler plumbing before or after each sampling cycle; (2) a sample-container unit to hold sample bottles in position for filling; (3) a sample distribution system to divert a pumped sample to the correct bottle; (4) an activation system that starts and stops the sampling cycle, either at some regular time interval or in response to a rise or fall in streamflow (gage height); and (5) an intake system through which samples are drawn from a point in the sampled cross section. Ideally, this combination of components should be designed to meet the 17 optimum criteria as set forth by W.F. Curtis and C.A. Onions (U.S. Geological Survey, written commun., 1982).

1. Stream velocity and sampler intake velocity should be equal to allow for isokinetic sample collection if the intake is aligned with the approaching flow.
2. A suspended-sediment sample should be delivered from stream to sample container without a change in sediment concentration and particle-size distribution.
3. Cross contamination of sample caused by sediment carryover in the system between sample-collection periods should be prevented.
4. The sampler should be capable of sediment collection when concentrations approach 50,000 milligrams per liter and particle diameters reach 0.250 millimeter.
5. Sample-container volumes should be at least 350 milliliters.
6. The intake inside diameter should be 3/8 or 3/4 inch, depending upon the size of the sampler used.
7. The mean velocity within the sampler plumbing should be great enough to exceed the fall velocity of the largest particle sampled.
8. The sampler should be capable of vertical pumping lifts to 35 feet from intake to sample container.
9. The sampler should be capable of collecting a reasonable number of samples, dependent upon the purpose of sample collection and the flow conditions.
10. Some provision should be made for protection against freezing, evaporation, and dust contamination.
11. The sample-container unit should be constructed to facilitate removal and transport as a unit.
12. The sampling cycle should be initiated in response to a timing device or stage change.
13. The capability of recording the sample-collection date and time should exist.
14. The provision for operation using DC battery power or 110-volt AC power should exist.
15. The weight of the entire sampler or any one of its principal components should not exceed 100 pounds.
16. The maximum dimensions of the entire sampler or any one of its components should not exceed 35 inches in width or 79 inches in height.
17. The required floor area for the fully assembled sampler should not exceed 9 square feet (3 feet by 3 feet).

Installation and Use Criteria

The decision to use a pumping sampler for collection of sediment samples is usually based on both physical and fiscal criteria. These are real considerations; yet it should be understood that automatic

pumping samplers can be as labor intensive and costly as the manual sediment-data collection they were designed to supplement. Installation of an automatic pumping sampler requires intensive planning before installation, including careful selection of the sampler-site location and detailed background data, to ensure the collection of useful pumped sample data.

Before installation of an automatic pumping-type sampler, many of the problems associated with installing stream-gaging equipment must be dealt with. In addition, much data concerning the sediment-transport characteristics at the proposed sampling site must be obtained and evaluated prior to emplacement of the sampler and location of the intake within the streamflow. Logistically, the sample site must be evaluated as to ease of access, availability of electrical power, location of a bridge or cableway relative to the site, normal range of ambient air temperatures inherent with local weather conditions, and the availability of a local observer to collect periodic reference samples. The sediment-transport characteristics should include detailed information on the distribution of concentrations and particle sizes throughout the sampled cross section over a range of discharges.

Placement of Sampler Intake

The primary concept to consider when placing a sampler intake in the streamflow at a sample cross section is that only one point in the flow is being sampled. Therefore, to yield reliable and representative data, the intake should be placed at the point where the concentration approximates the mean sediment concentration for the cross section across the full range of flows. This idealistic concept has great merit, but the mean cross-section concentration almost never exists at the same point under varying streamflow conditions. It is even less likely that specific guidelines for locating an intake under given stream conditions at one stage would produce the same intake location relative to the flow conditions at a different stage. These guidelines would have even less transfer value from cross section to cross section and stream to stream. For these reasons, some very generalized guidelines presented by W.F. Curtis and C.A. Onions (written commun., 1982) are outlined here and should be considered on a case-by-case basis when placing a sampler intake in the streamflow at any given cross section.

1. Select a stable cross section of reasonably uniform depth and width to maximize the stability of the relation between sediment concentration at a point and the mean sediment concentration in the cross section. This guideline is of primary importance in the decision to use a pumping sampler in a given situation; if a reasonably stable relation between the sample-point concentration and mean cross-section concentration cannot be attained by the following outlined steps, the sampler should not be installed and an alternate location considered.
2. Consider only the part of the vertical that could be sampled using a standard US depth- or point-integrating suspended-sediment sampler, excluding the unsampled zone, because data collected with a depth- or point-integrating sampler will be used to calibrate the pumping sampler.
3. Determine, if possible, the depth of the point of mean sediment concentration in each vertical for each size class of particles finer than 0.250 mm, from a series of carefully collected point-integrated samples.
4. Determine, if possible, the mean depth of occurrence of the mean sediment concentration in each vertical for all particles finer than 0.250 mm.
5. Use the mean depth of occurrence of the mean sediment concentration in the cross section as a reference depth for placement of the intake.
6. Adjust the depth location of the intake to avoid interference by dune migration or contamination by bed material.
7. Adjust the depth location of the intake to ensure submergence at all times.
8. Locate the intake laterally in the flow at a distance far enough from the bank to eliminate any possible bank effects.
9. Place the intake in a zone of high velocity and turbulence to improve sediment distribution by mixing, reduce possible deposition on or near the intake, and provide for rapid removal of any particles disturbed during the purge cycle.

Because of the generalized nature of these guidelines, it will often be impossible to satisfy them all when placing a pumping sampler intake into naturally occurring streamflows. The investigator is encouraged, however, to try to satisfy these guidelines or, at the very least, to satisfy as many as possible and to minimize the effects of those not satisfied.

Sampler Advantages and Disadvantages

Automatic pumping-type samplers are very useful for collecting suspended-sediment samples during periods of rapid stage changes caused by storm-runoff events and in reducing the manpower necessary to carry out intensive sediment-collection programs (Federal Inter-Agency Sedimentation Project, 1981b). However, it should be noted that pumping samplers quite often require more man-hours and cost more to operate than a conventional, observer-sampled type of station. Pumping samplers, because of their mechanical complexity, power requirements, and limited sample capacity, quite often require more frequent site visits by the field personnel than would be required at the conventional observer station. In addition, problems associated with collecting high-flow, cross-section samples are still present.

In streams with significant amounts of suspended-sand loads, the problems associated with using a pumping sampler are so great that two records may have to be calculated, one for the silt-clay size fraction load and one for the sand-size fraction load. This requires that most of the samples collected with the pumping sampler, as well as the samples collected manually, be subjected to a full particle-size analysis. Extensive laboratory work of this type increases the cost of analysis and computation of the sediment-discharge record. Another disadvantage is that the pumping lift for most samplers is relatively small and may be less than the normal fluctuations in stage at some sites. This is especially true on western rivers, where stage ranges may exceed 50 feet, making it necessary to locate the pump outside of the sampler's shelter in order to maintain a manageable pumping lift.

Intake Orientation

The orientation of the pumping sampler intake nozzle can drastically affect sampling efficiency. There are five ways in which an intake could be oriented to the flow (fig. 21): (1) normal and pointing directly upstream (fig. 21*A*), (2) normal and horizontal to flow (fig. 21*B*), (3) normal and vertical with the orifice up (fig. 21*C*), (4) normal and vertical with the orifice down (fig. 21*D*), and (5) normal and pointing directly downstream (fig. 21*E*). Of these five orientations, 1, 3, and 4 should be avoided because of high sampling errors and trash collection problems. Orientation 2, with the nozzle positioned normal and horizontal to the flow, is the most common alternative used. The major problem with this orientation is that sand-size particles may not be adequately sampled (see the following section on pumped-sample data analysis). Orientation 5, pointing directly downstream, appears to have an advantage over orientation 2 (Winterstein and Stefan, 1983). When the intake is pointing downstream, a small eddy is formed at the intake, which envelops the sand particles and thus allows the sampler to collect a more representative sample of the coarse load. Winterstein and Stefan (1983) also have demonstrated that nozzle orientations at angles to the flow other than those illustrated in figure 21 do not improve the resultant sample and, therefore, do not represent any useful advantage.

Data Analysis

A major concern when evaluating sediment data collected by automatic pumping-type samplers is the relation between the data and the true mean suspended-sediment concentration in transport at the time of sample collection. In order to determine this relation, concentrations determined from the pumping sampler must be compared with the corresponding concentrations determined from a complete depth-integrated cross-section sample over the full range of flow. This relation then is used to adjust the pumped sample data.

It must be remembered that samples collected by pumping samplers are taken from a single point in the flow. Although attempts are made to ensure that cross-sectional mean sediment concentrations are obtained, in reality this rarely happens. However, if a stable relation between the concentration at the sample point and the mean concentration in the cross section exists, the sample can be considered as representative as possible. In addition, pumping samplers do not collect samples isokinetically (as do standard US depth- or point-integrating samplers), due to the pumping rate and the orientation of the intake orifice. Not sampling isokinetically introduces concentration errors, particularly for particles greater than 0.062 mm.

Pumping samplers rely on pump speed to create a velocity in the intake tube greater than the settling velocity of particles in suspension. This higher velocity is necessary to deliver the sample to the sample container without reducing the concentration of coarser particles by depositing them within the sampler's plumbing. The pumping action at the intake

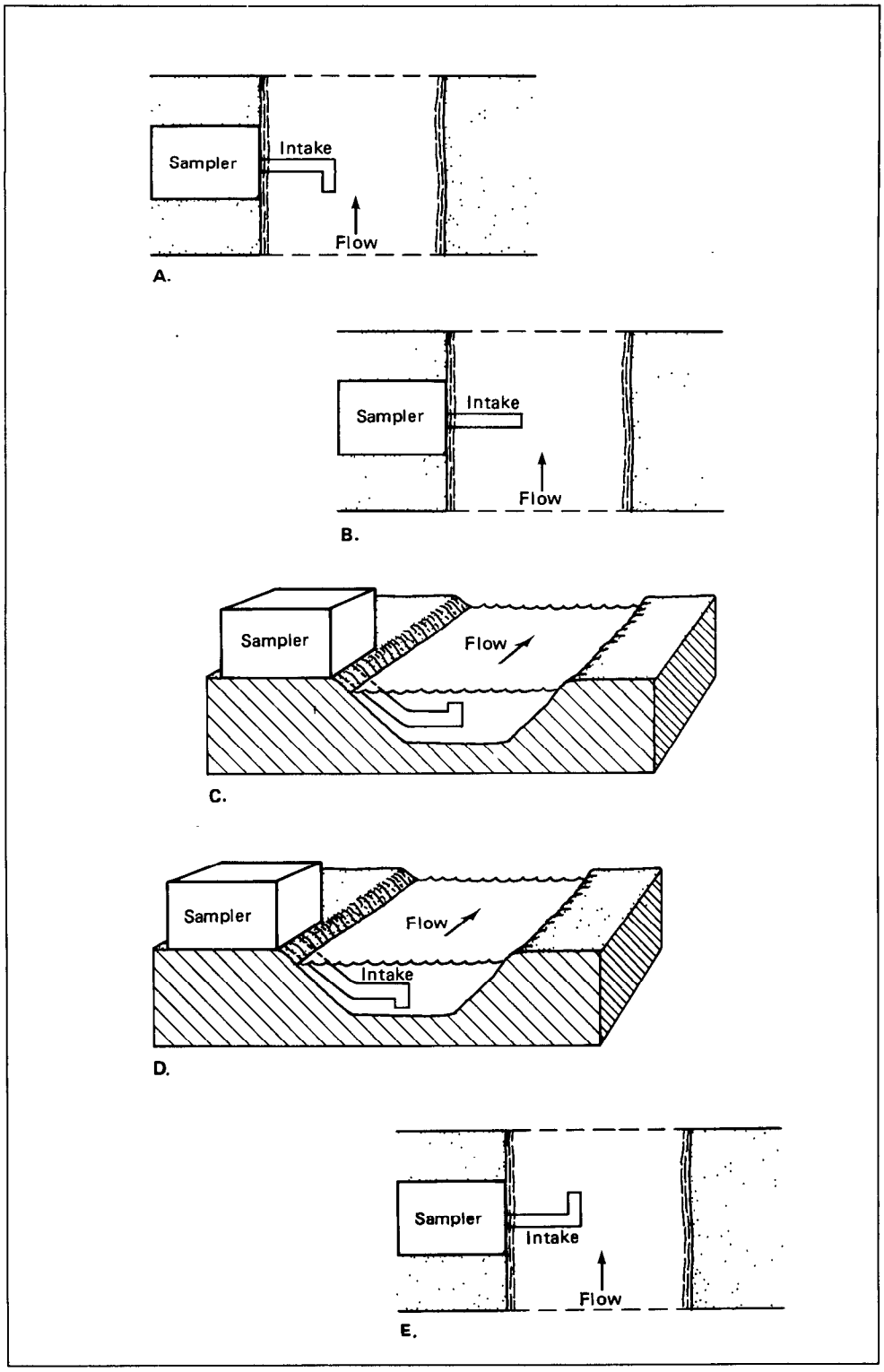

Figure 21. Examples of pumping-sampler intake orientations. *A*, Normal and pointing directly upstream. *B*, Normal and horizontal to flow. *C*, Normal and vertical with the orifice up. *D*, Normal and vertical with the orifice down. *E*, Normal and pointing directly downstream.

orifice bends the streamlines of sediment-laden flow as a sample is drawn into the intake and as particles are propelled through the sampler to the sample container. This force acts on particles carried past the orifice with varying results, dependent upon particle size and velocity (Federal Inter-Agency Sedimentation Project, 1941). That is, the pumping force attempts to pull particles laterally from their streamlines and accelerate them in the direction of the intake. At low stream velocities, when only fine silts and clays are being transported, this is not a problem. However, as stream velocity increases and particles larger than 0.062 mm begin to move in suspension, the pumping force must overcome the momentum of these larger particles, due to their mass and acceleration in the downstream direction, in order for a representative sample to be obtained. A decrease in sampling efficiency can result in a biased sample because fewer and fewer large particles are drawn into the intake as the distance from the intake increases (fig. 22). This figure shows that only those sediment particles passing directly in front of the intake, a short distance away, are greatly affected and subject to capture. It also should be realized that the zone (cone) of influence is an idealized concept, and pumping influence is much greater on sediments approaching the intake from upstream than on those sediments that have passed to the downstream side. As mentioned previously, this problem may be relieved somewhat by orienting the intake directly downstream.

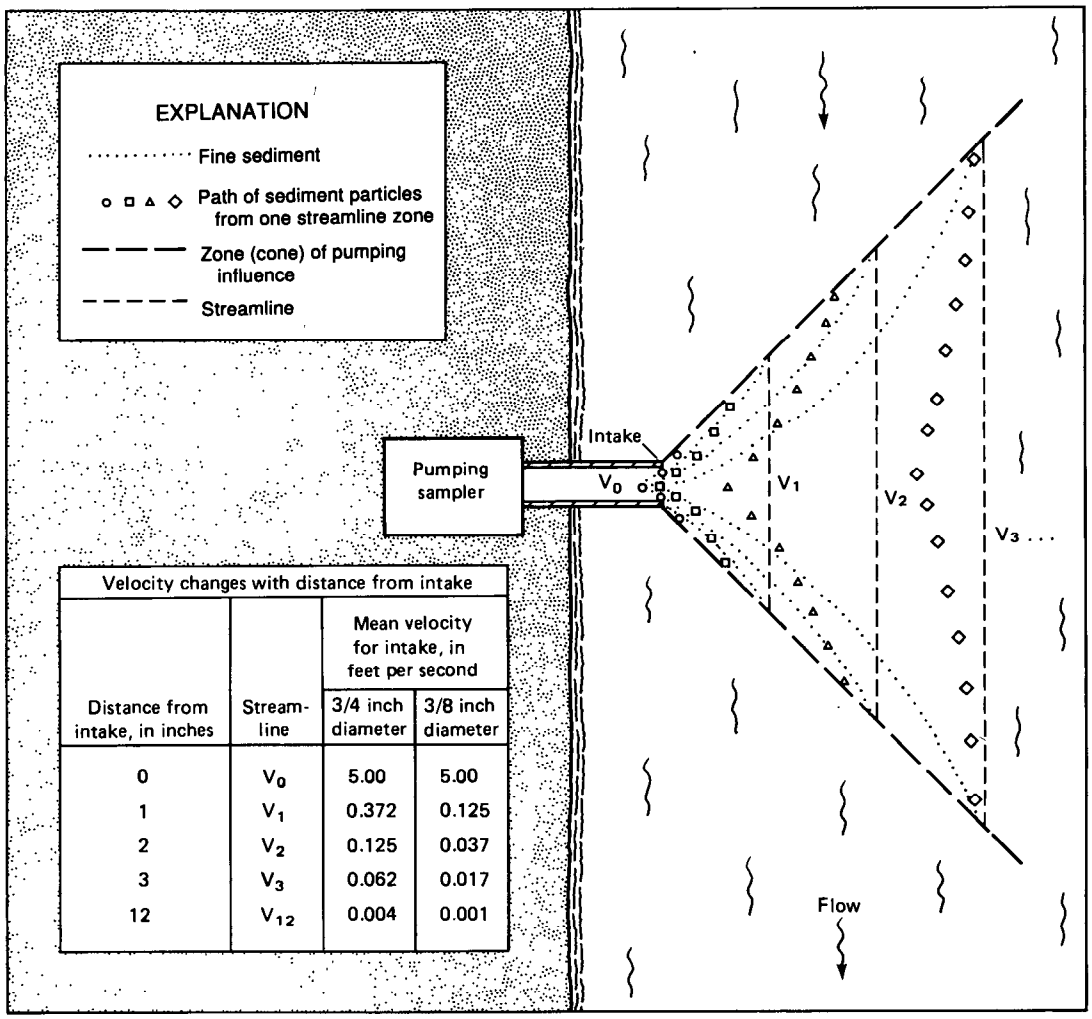

Velocity changes with distance from intake

Distance from intake, in inches	Stream-line	Mean velocity for intake, in feet per second	
		3/4 inch diameter	3/8 inch diameter
0	V_0	5.00	5.00
1	V_1	0.372	0.125
2	V_2	0.125	0.037
3	V_3	0.062	0.017
12	V_{12}	0.004	0.001

Figure 22. Pumping effect on sediment streamlines within the zone (cone) of influence and velocity changes with distance from intake (cone) of influence and velocity changes with distance from the intake oriented normal and horizontal to the flow for 3/4-inch and 3/8-inch diameter intakes with pumped velocity of 5 feet per second (from Federal Inter-Agency Sedimentation Project, 1966; W.F. Curtis and C.A. Onions, written commun., 1982).

Intake Efficiency

To facilitate accurate interpretation of data collected by automatic pumping-type samplers, some comparison between sediment concentration of the pumped sample (C_p) and mean sediment concentration of the streamflow (C_s) must be made. This comparison is made in terms of intake efficiency, which is the ratio of the pumped-sample sediment concentration to the mean concentration of the stream at the intake sampling point (Federal Inter-Agency Sedimentation Project, 1966), or:

$$\frac{C_p}{C_s}(100) = \text{intake efficiency.}$$

In reality, this relation is based on comparison of the pumped sample to sediment concentration of a point sample collected as close to the intake sampling point as possible, using a standard US depth- or point-integrating sampler.

Intake efficiencies should be determined for pumping samplers as soon as possible after installation-related sediment disturbances have stabilized. Additional efficiency values should be established over a broad range of flow conditions to determine actual effects of variations in particle sizes at a given sample site. These data then can be used to evaluate the sediment concentration of pumped samples and check their credibility.

Cross-Section Coefficient

Determining the degree of efficiency with which a pumping sampler obtains a representative sample is one step in the interpretation of suspended-sediment concentration data. These data should be further assessed relative to the cross-sectional mean suspended-sediment concentration. A coefficient should be determined based on how well the pumping sampler's data represents the cross-sectional mean, and this coefficient should be applied to the pumping sampler data.

From previous discussion, it should be evident that sediment samples taken at a single point of flow within a cross section seldom represent the mean sediment concentration. Therefore, cross-section coefficients must be determined to relate pumped-sample sediment concentration to the mean sediment concentration in the cross section. Because no theoretical relation exists between these parameters, an empirical comparison must be made between concentrations obtained from pumped samples and concentrations obtained from depth-integrated, cross-sectional samples collected at the same time. Obviously, it is impossible to collect an entire cross-sectional sample in the length of time it takes to cycle the pumping sampler to collect a single sample. Therefore, it is recommended that a sample collected with the pumping sampler be taken immediately before and after the cross-section sample. This procedure will help bracket any changes in concentration that might occur during the time period necessary to collect the cross-section sample. If it is suspected that the concentration is changing rapidly during the collection of the cross-section sample, try to collect one or more samples with the pumping sampler during the time that the cross-section sample is being collected. These data will help in the development of the cross-section coefficient. Collection and comparison of these check samples should be repeated during each station visit, as well as during rising and falling stages, and at peak flows for all seasonal periods (snowmelt runoff, thunderstorms, and so on). A more detailed discussion on development of cross-section coefficients is available to the interested reader in Guy (1970) and Porterfield (1972).

Description of Automatic Pumping-Type Samplers—US PS-69, US CS-77, US PS-82, Manning S-4050, and ISCO 1680

The US PS-69 pumping sampler (fig. 23) is a time- or stage-activated, electrically driven, suspended-sediment sampler capable of collecting up to 72 samples at volumes to 1,000 mL. Standard pumping lifts are to 17 feet vertically, but repositioning the pump or using multiple pumps in series can increase lift capabilities for extreme situations. This sampler must be placed in a shelter and protected against inclement weather and temperature extremes.

Particle sizes sampled range to 0.250 millimeter with some decrease in sampling efficiency for the larger particles. Sediment concentrations to 160,000 milligrams per liter have been sampled by USGS personnel in New Mexico, using an air-driven pump with the PS-69 (J.V. Skinner, written commun., 1985); extremely high concentrations also have been sampled in the vicinity of the Mount St. Helens volcano in Washington.

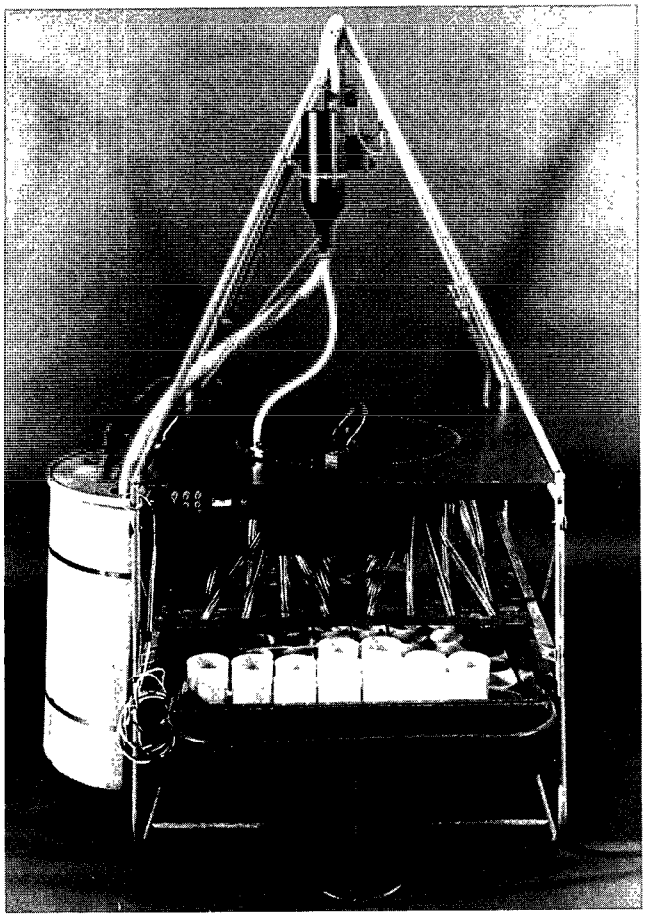

Figure 23. US PS-69 pumping sampler.

The PS-69 was evaluated by W.F. Curtis and C.A. Onions (written commun., 1982) by comparing the sampler's attributes to the 17 criteria previously listed. Results of this comparison are included in table 2.

The US CS-77, or Chickasha, sediment sampler (fig. 24) was designed and developed by the Agricultural Research Service, Durant, Oklahoma. This sampler was fashioned after an earlier design (US XPS-62, developed by F.I.S.P.) but has not been widely used by USGS personnel.

Like the PS-69, this sampler is time- or stage-activated to facilitate sampling on a predetermined schedule as well as during runoff events. Sampling times are recorded during the sampling procedure as part of the standard sampler's design of operation, in lieu of add-on modules and recording devices common to other samplers discussed here.

Table 2. Automatic pumping-type sampler evaluation

[A, US PS-69; B, US CS-77; C, US PS-82;D, Manning S-4050; E, ISCO 1680; mg/L, milligrams per liter; mL, milliliter; mm, millimeter; ≥, greater than or equal to; <, less than; >, greater than]

Evaluation criteria	Samplers meeting criteria
1. Sample collection isokinetic	None
2. Sediment concentration constant stream to sample container	A[1], B[2], C[2], D
3. Cross-contamination prevented	A, B, C, D
4. Collects concentrations to 50,000 mg/L and particles to 0.25 mm	A[1], B[2,1], C[1], D[1], E[2]
5. Sample volume >350 mL	A[3], B[3], C[3], D[3], E[3]
6. Intake diameter 3/4 inch	A
7. Mean velocity at intake and in internal plumbing great enough to ensure turbulent flow with a Reynolds number of 4,000	A[3], B[2], C[1], D[3], E[3]
8. Vertical pumping lift >35 feet	A[2], B[2], C[2]
9. Capable of collecting an adequate number of samples to accomplish the purpose of sampling	A[3], B[3], C[3], D, E
10. Sampler protected against freezing, evaporation, and dust	A[2], B[2], C, D[2], E[2]
11. Sample-container tray removable single unit	A, D, E
12. Sampling cycle activated by timer or stage change	A, B, C, D, E
13. Capable of recording sample date and time	A[2], B, C[2], D[2], E[2]
14. AC or DC power capability	A[2], B[2], C[2], D[2], E[2]
15. Sampler or principle components <100 pounds	A[2], B[2], C[3], D[3], E[3]
16. Sampler dimensions <35 inches wide by 79 inches high	A[2], B[2], C[3], D[3], E[3]
17. Required floor space <9 square feet (3 feet by 3 feet)	C[3], D[3], E[3]

[1]Sampler shows a reduction in capacity with particle sizes >0.250 mm.
[2]Sampler requires modification to meet criteria.
[3]Sampler exceeds criteria.

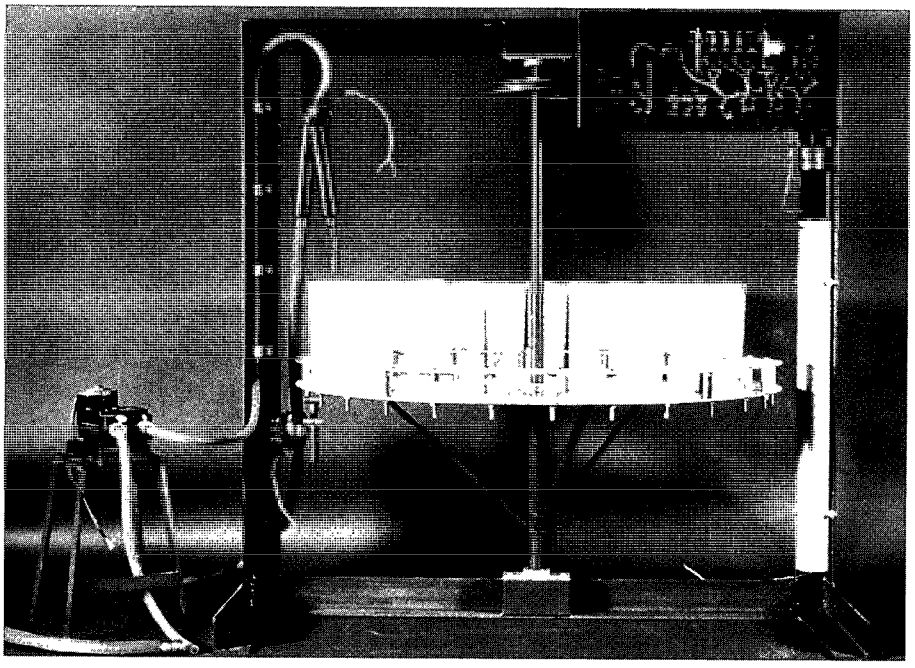

Figure 24. US CS-77 (Chickasha) pumping sampler.

Pumping lift attained by the standard CS-77 sampler configuration is 16 vertical feet; however, relocation of the pump unit to a lower elevation will establish a pull-push sequence, enabling greater sample lifts.

Further modification is necessary to improve the sampling efficiency for high concentration flows carrying greater than 10 percent sand-sized material. Additional information regarding this sampler may be obtained from the evaluation in table 2 and by contacting personnel at the F.I.S.P.

The US PS-82 automatic pumping-type sampler (fig. 25) was made available in March 1984 from F.I.S.P., but it is not widely used under field conditions. The Federal Inter-Agency Sedimentation Project (1983) describes the PS-82 as a lightweight portable pumping sampler, driven by 12-volt battery power, which is used to sample streamflows transporting particles ranging to fine sand size. These samplers weigh 35 pounds and can be housed under a 55-gallon oil drum. An evaluation of this sampler is included in table 2. For more specific information concerning the technical aspects of this sampler and its availability, the interested reader should contact the F.I.S.P.

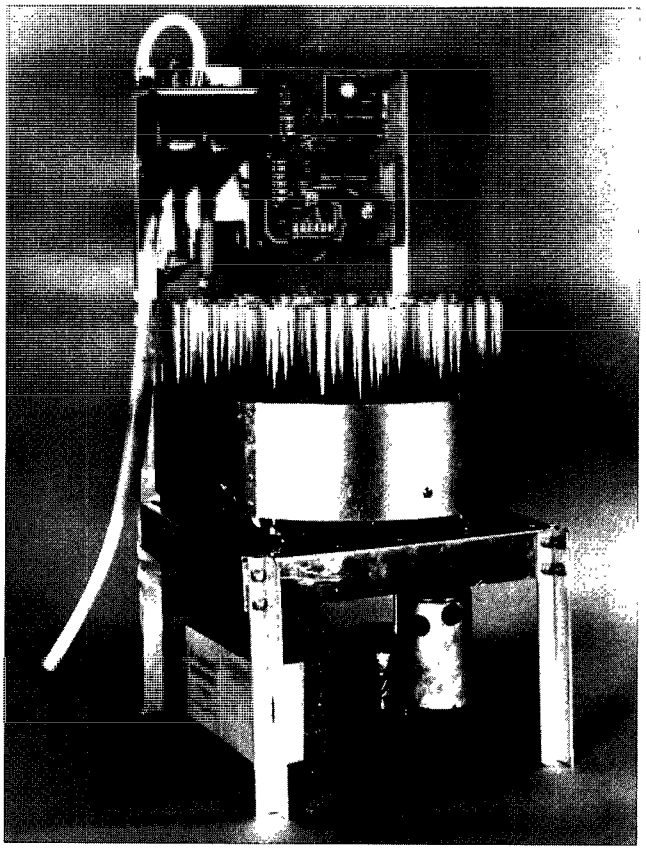

Figure 25. US PS-82 pumping sampler.

The aforementioned samplers were developed by Federal agencies concerned with the collection of suspended-sediment data in a timely, cost-effective manner and are available to the interested investigator from the F.I.S.P. at Waterways Experiment Station, 3909 Halls Ferry Road, Vicksburg, MS 39180-6199.

The following discussion is a description of the Manning S-4050 and ISCO 1680 automatic pumping-type samplers, which are not available through F.I.S.P., but may be obtained from the individual manufacturers. These samplers are described because they represent the types of samplers that are commonly available from commercial sources and used by the USGS.

The Manning S-4050 portable sampler was originally designed as a lightweight unit for sampling sewage. Modifications to this sampler have rendered it useful as a suspended-sediment sampler.

The sampler features a time- or stage-activated electric compressor, which purges the sample intake using the pressure side and draws a sample through the intake using the suction side to create a vacuum in the line, allowing atmospheric pressure to push the sample up to a maximum of 22 feet during the sampling mode. Particle suspension within the sampler is maintained by swirling action of the sample as it passes through the measuring chamber to the sample container.

Evaluation of this sampler in the same manner used for the previously discussed samplers indicates that this instrument is well suited to conditions where extreme pumping lifts are not necessary. Results of this evaluation are included in table 2.

The ISCO 1680, with a super-speed pump sampler, was originally developed as a sewage or wastewater sampler, like the Manning sampler. Normally, wastewater does not carry significant amounts of sediment. Therefore, representation of particle distribution was not a considered criteria during its design and testing stages. The sampler features an electrically driven peristaltic pump, which is activated on a predetermined schedule by an internal timer or in response to stage change. The intake tube is purged before and after each pumping period by automatic reversal of the pump.

The ISCO sampler demonstrates two major shortcomings regarding sediment collection: (1) continuity of sediment concentration from stream to sample container is not maintained efficiently, and (2) a possibility of cross contamination exists from sample to sample as a result of residue remaining in the system after the purge cycle. These problems can be minimized by the installation of a high output pump, available as an option with recent models. A sampler evaluation included in table 2 shows less than acceptable results for representative sediment-data collection.

Support Equipment

Sediment-sampling equipment has been designed by F.I.S.P. to facilitate the use of existing support equipment normally used in stream-gaging procedures. Other than wading rods and hand lines, support equipment is generally necessary for the proper operation of the heavier versions of sediment samplers. In general, support equipment consists of steel cable, hanger bars, reels, and cranes. However, specific conditions at a site may dictate modifications to these pieces of equipment to improve ease of handling in response to the local conditions. Modifications of support equipment necessary to facilitate the handling of samplers and improve safety are encouraged. Investigators are cautioned against alterations that might adversely affect sample collection, either by disturbing the streamflow in the cross section or by changing the sediment-trapping characteristics of the sampler. To ensure sample integrity, specialists should be consulted before any modifications of this type are made.

Commonly used support items include C-type hanger bars; type-A, type-B, and type-E reels; and portable cranes with 2-, 3-, and 4-wheel bases. The C-type hanger bars can be shortened to eliminate awkward and hazardous handling. Type-A reels can be used to suspend lightweight to medium-weight samplers and have been widely used at permanent single-vertical observer sites. Type-B and type-E reels are typically used with medium and heavy samplers. The type-B reel can be used manually or with an available power unit, allowing the sampler to be lowered by releasing the brake mechanism and letting it slip until the sampler reaches the water surface, then manually integrating the sampled vertical and raising the sampler, either manually or by activating the DC-powered motor to drive the reel. The type-E reel is a DC-powered reel that lends itself more readily to permanent installations where heavy sampling

equipment is required. Cranes are used to provide a mechanical advantage over hand-line or bridge-board suspended equipment, for more effective maneuvering of a sampler. The 2-, 3-, and 4-wheel base cranes are useful when sampling from a bridge deck; however, safety precautions should be taken to warn approaching traffic and to avoid blocking the roadway. Boom assemblies also are used in some instances, such as with truck- and boat-mounted installations. Reels, cranes, and powered hoists can be purchased from HIF. HIF can provide information on the availability, installation requirements, and operation of this equipment. Some additional information also may be obtained from the report "Discharge Measurements at Gaging Stations" (Buchanan and Somers, 1969).

SEDIMENT-SAMPLING TECHNIQUES

The sediment-sampling method and frequency of collection are dictated by the hydrologic and sediment characteristics of the stream, the required accuracy of the data, the funds available, and the proposed use of those data collected. When sampling sediment moving through a stream cross section, emphasis should be placed on the collection of a statistically representative population of the sediment particles in transit. To acquire a representative sample, one must first obtain a sample that adequately defines the concentration of particles over the full depth of the sampled vertical. Secondly, a sufficient number of verticals must be sampled to adequately define the horizontal variation in the cross section. The type of sampler used to collect the sample, the method of depth integration, the site at which the samples are collected, and the number of verticals needed to define the stream's concentration depend on the flow conditions at the time of sample collection, characteristics of the sediment being transported, the accuracy required of the data, and the objectives of the program for which the samples are being collected. The purpose of this section is to discuss site selection; equipment selection and maintenance; depth integration; sediment-discharge measurements; point integration; surface and dip sampling; transit rates; sample frequency, quantity, integrity, and identification; sediment-related data; cold-weather sampling; bed-material sampling; bedload sampling; total sediment discharge; and reservoir sedimentation. This section then deals with the decisions to be made and the instructions necessary to obtain the quantity and quality of samples required for computation and compilation of the desired sediment records.

Site Selection

The selection procedure for establishing a sampling location should emphasize the quest for a stream-data site. A stream-data site is best defined as a cross section displaying relatively stable hydrologic characteristics and uniform depths over a wide range of stream discharges, from which representative water-quality and sediment data can be obtained and related to a stage-discharge rating for the site. This is a rather idealized concept because the perfect site is rare at best. Therefore, it is necessary to note the limitations of the most suitable site available and build a program to minimize the disadvantages and maximize the advantages. Most often, sampling sites are located at or near existing gage sites, which may not always be well suited to water-quality and sediment-data collection. For this reason, future sites selected for stream gaging should be carefully assessed for suitability as a water-quality and sediment-sampling site.

As indicated, the site should be at or near a gaging station because of the obvious relation of sediment movement to the flow of the stream. If the sediment-measuring site is more than a few hundred feet from the water-stage recorder or at a site other than where the water-discharge measurement is made, it may be desirable to install a simple nonrecording stage indicator at the site so that a correlation of the flow conditions between the sediment and the distant water-measuring sites can be developed. The obvious difficulties with inflow between the sites from small tributaries also should be avoided where possible. Sites that may be affected by backwater conditions should be avoided whenever possible. Backwater affects both the stage-discharge and velocity-discharge relation at the site. Therefore, a given discharge may have varying stage and mean stream velocity and thus have varying sediment transport rates. If a site is affected by backwater, samples will have to be collected more frequently, and the cost in both man-hours and money will be significantly higher than for more "normal" sites.

A sediment-measuring site downstream from the confluence of two streams also may require extra sediment measurements. The downstream site may be adequate for water-discharge measurement, but could present problems if used as a sediment-measuring site due to incomplete mixing of the flows from the tributaries. Therefore, it might be desirable to move far enough downstream to ensure adequate mixing of the tributary flows. As indicated in Book 3, Chapter C1, "Fluvial Sediment Concepts" (Guy, 1970, p. 24), the distance downstream from a confluence that is required for complete mixing depends on the stream velocity, depth, and mixing width. If the flow at a sediment-measuring site is not mixed, extra samples will be required on a continuing basis because the relative flow quantity and sediment concentration from the two tributaries will change with time.

Aside from the confluence or tributary problem, the type of cross section for flow both in the channel and on the flood plain may affect the ease with which data can be obtained and the quality of the samples. The ratio of suspended load to total load and its variation with time can be greatly affected by the width-depth ratio, especially for sand-bed streams. For sites where the data are expected to be correlated with channel properties and the landforms of the region, a normal or average section should be used. When a fixed-routine sampling installation is used, a measuring section at a bend may provide a more stable thalweg and, hence, a more uniform adjustment coefficient with respect to time than one at a crossover. Sites in areas of active bank erosion should be avoided.

As a result of economic necessity, most sediment-measuring sites are located at highway bridges. These bridges are often constructed so that they restrict the flow width, or they may be located at a section where the channel is naturally restricted in width. Figure 26 (Culbertson and others, 1967) illustrates the conditions at several kinds of natural and artificially induced flow constrictions. As expected, the sand-bed type of stream causes the most serious flow problems with respect to scour in the vicinity of such constrictions. Even if the bridge abutments do not interfere with the natural width of the stream, the bridge may be supported by several midstream piers that can interfere with the streamflow lines and, thereby, reduce the effective cross-sectional area. As indicated in figure 26*F*, midstream piers can catch debris and, thereby, interfere with effective sediment sampling.

Because sediment samples must be obtained more frequently during floods, it is imperative that a site be selected where obtaining data during times of flooding is feasible. That is, particular attention should be given to the ease of access to the water-stage recorder and to a usable bridge or cable during a flood. Because of the need to collect samples frequently during floods, many of which occur at night, sites accessible only by poorly maintained backroads or trails should be avoided. Sometimes the choice of a sediment-measuring site also must be determined by the availability of a suitable observer to collect the routine samples.

In choosing a sediment-measurement site, it should be emphasized that samples need to be collected at the same cross-section location throughout the period of record. Different sampling cross sections can be used, if absolutely necessary, during the low-water wading stage and the higher stages requiring the use of a bridge or cableway. Although the total sediment transported through the different cross sections is probably equal at a given flow stage, the percentage of that total load represented by suspended-sediment load may be drastically different from one cross section to the other, due to differences in hydraulic and sediment-transport characteristics. When data computations are performed, these differences must be considered because the data may not be compatible, and the usefulness of the data in answering the objectives of the sampling program could be threatened. Sites where highway or channel realignment or other construction is anticipated during the period of record should be avoided. Good photographs of proposed or selected sediment-measuring sites are necessary to help document such features as channel alignment, water-surface conditions at various stages, composition of bed and bank material (at low flow), and natural or man-made features, which could affect the water-discharge and (or) sediment-discharge relations. Such pictures and extensive field notes are particularly useful when deciding on alternatives among sites and in later consideration of environmental changes at the site(s).

Equipment Selection and Maintenance

Before departing on a field trip where sediment data are to be collected, a field person should assemble and check all equipment needed to collect the best samples and related measurements. For example, if data are

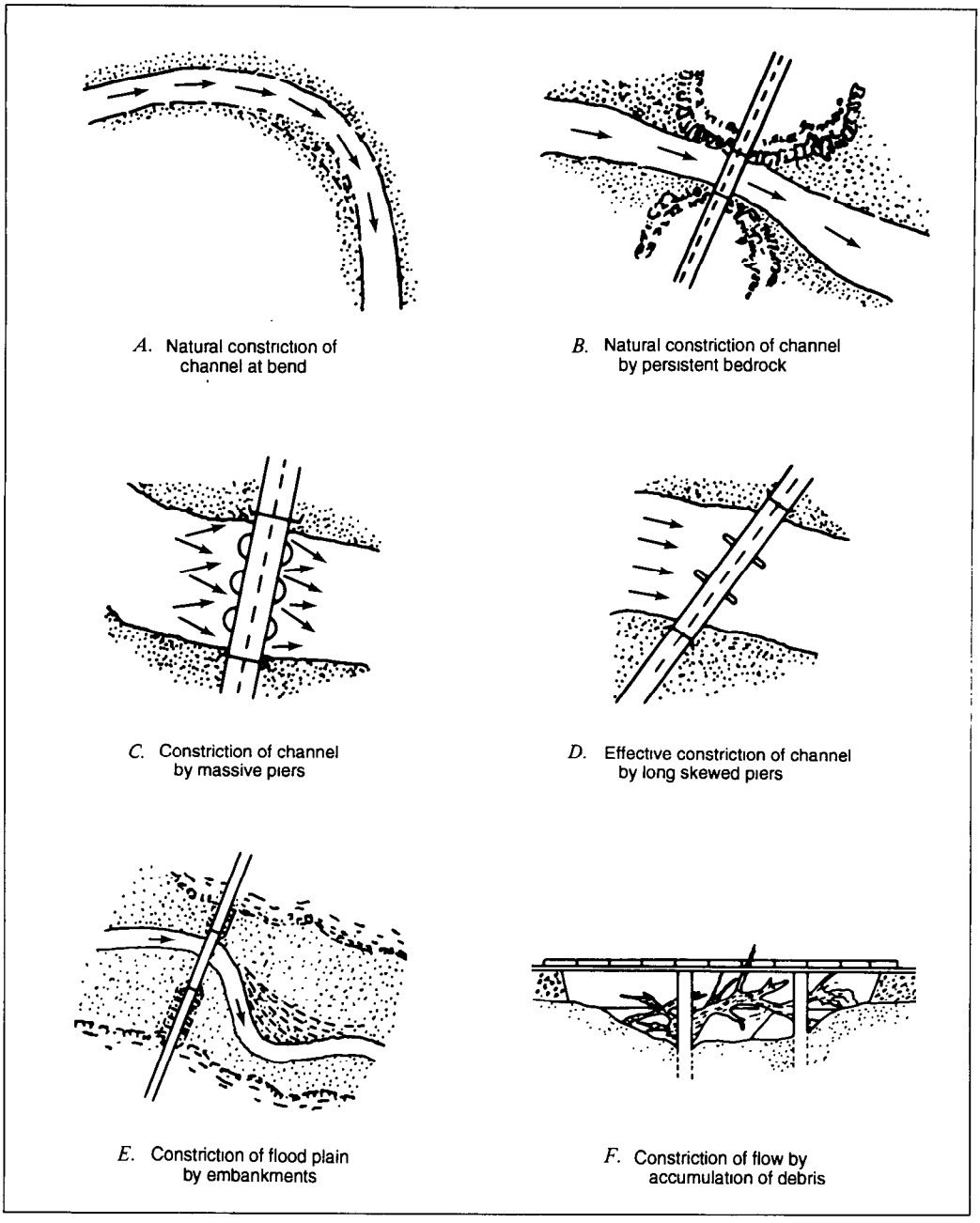

Figure 26. Examples of natural and artificially induced streamflow constrictions encountered at sediment-measurement sites. Modified from Culbertson and others (1967).

needed for total-load computation, equipment is needed for water-discharge measurement, suspended-sediment sampling, bedload sampling, and (or) bed-material sampling. If suspended-sediment concentration and particle-size profiles are required, point samplers and water-discharge-measuring equipment will be needed. Some of the special equipment used only at one location may be stored in the station gage house, with the observer, or in special storage shelters or boxes. However, a sampler or some support equipment could be damaged or stolen without the observer noticing or reporting the loss. Hence, it is necessary for field personnel to carry repair equipment, spare parts (including nozzles and gaskets), and perhaps even an extra sampler.

The streamflow conditions and sampling structures (bridge, cableway, or other) determine more specifically which sampler or samplers should be used at a

station. Stream depth determines whether hand samplers, such as the DH-48 or the BMH-53, or cable-suspended samplers, such as the D-74 or the P-61, should be used. Depths over 15 feet will require the use of point samplers as depth-integrating samplers to avoid overfilling or using too fast a transit rate. Stream velocity as well as depth are factors in determining whether or not a stream can be waded. A general rule is that when the product of depth in feet and velocity in feet per second equals 10 or greater, a stream's wadability is questionable. Application of this rule will vary considerably among field persons according to an individual's stature and the condition of the streambed. That is, if footing is good on the streambed, a heavier field person with a stocky build will generally wade more easily than will a lighter, thinner person when a stream depth-velocity product approaching 10 exists.

The depth-velocity product also affects the action of each sampler. The larger this product, the heavier and more stable the sampler must be to collect a good sample. At a new station or for inexperienced persons, considerable trial and error may be necessary to determine which sampler is best for a given stream condition.

All sampler nozzles, gaskets, and air exhausts, as well as the other necessary equipment, should be checked regularly and replaced or serviced if necessary. Sampler nozzles in particular should be checked to ensure that they are placed in the appropriate instrument or series. See the guidelines presented in table 1 to determine whether the nozzle is correct. The correct size of nozzle to use for a given situation must often be determined by trial. As mentioned in the previous section, it is best to use the largest nozzle possible that will permit depth integration without overfilling the sample bottle or exceeding the maximum transit rate (about 0.4 of the mean velocity in the sampled vertical for most samplers with pint containers).

If a sample bottle does not fill in the expected time, the nozzle or air-exhaust passages may be partly blocked. The flow system can be checked, as described in the section titled "Gaskets," by sliding a length of clean rubber or plastic tubing over the nozzle and blowing through the nozzle with a bottle in the sampler. This procedure should be performed carefully, avoiding direct contact with the nozzle, thus eliminating the possibility of ingesting any pollutant that might exist on the sampler. When air pressure is applied in this manner, circulation will occur freely through the nozzle, sample container, and out the air exhaust. Obstructions can be cleared by removing and cleaning the nozzle and (or) air exhaust, using a flexible piece of multistrand wire. This procedure should be adequate for most airway obstruction problems. However, if blockage results from accumulation of ice or from damage to the sampler, a heat source must be used to melt the ice or the sampler must be sent to the F.I.S.P. or HIF repair facility. Point samplers can be checked using the same technique, if the valve mechanism is placed in the sampling position while air is forced into the nozzle and through the air exhaust.

All support equipment required for sampling, such as cranes, waders, taglines, power sources, and current meters, should be examined periodically, and as used, to ensure an effective and safe working condition. For example, be certain that the supporting cable to the sampler or current meter is fastened securely in the connector; if worn or frayed places are noted, the cable should be replaced. Power equipment used with the heavier samplers and point samplers need a periodic operational check and battery charge. Point samplers should be checked immediately before use to determine, among other things, if the valve is opening and closing properly. By exercising such precautions, the field person will avoid unnecessary exposure to traffic on the bridge and will avoid lost sampling time should repairs and adjustments be required.

Maintenance of samplers and support equipment will be facilitated if a file of instructions for assembly, operation, and maintenance of equipment can be accumulated in the field office. Such a file could include F.I.S.P. reports as well as other pertinent information available from HIF.

Suspended-Sediment Sampling Methods

Sediment-Discharge Measurements

The usual purpose of sediment sampling is to determine the instantaneous mean discharge-weighted suspended-sediment concentration at a cross section. Such concentrations are combined with water discharge to compute the measured suspended-sediment discharge. A mean discharge-weighted suspended-sediment concentration for the entire cross

section is desired for this purpose and for the development of coefficients to adjust observer and automatic pumping-type sampler data.

Ideally, the best procedure for sampling any stream to determine the sediment discharge would be to collect the entire flow of the stream over a given time period, remove the water, and weigh the sediment. Obviously, this method is a physical impossibility in the majority of instances. Instead, the sediment concentration of the flow is determined by (1) collecting depth-integrated suspended-sediment samples that define the mean discharge-weighted concentration in the sample vertical and (2) collecting sufficient verticals to define the mean discharge-weighted concentration in the cross section.

Single Vertical

The objective of collecting a single-vertical sample is to obtain a sample that represents the mean discharge-weighted suspended-sediment concentration in the vertical being sampled at the time the sample was collected. The method used to do this depends on the flow conditions and particle size of the suspended sediment being transported. These conditions can be generalized to four types of situations: (1) low velocity ($v<2.0$ ft/s) when little or no sand is being transported in suspension; (2) high velocity ($2.0<v<12.0$ ft/s) when depths are less than 15 feet; (3) high velocity ($2.0<v<12.0$ ft/s) when depths are greater than 15 feet; and (4) very high velocities ($v>12.0$ ft/s).

First case.—In the first case, the velocity is low enough that no sand is being transported as suspended sediment. The distribution of sediment (silt and clay) is relatively uniform from the stream surface to bed (Guy, 1970, p. 15). The sampling error for this case, when only sediment particles less than 0.062 mm are in suspension, is small, even with intake velocities somewhat higher or lower than the ambient mean stream velocities. Therefore, it is not as important to collect the sample isokinetically with fines in suspension as it is when particles greater than 0.062 mm are in suspension. In shallow streams, a sample may be collected by submerging an open-mouthed bottle into the stream by hand. The mouth should be pointed upstream and the bottle held at approximately a 45-degree angle from the streambed. The bottle should be filled by moving it from the surface to the streambed and back. Care should be taken to avoid touching the mouth of the bottle to the streambed. An unsampled zone of about 3 inches should be maintained in order to obtain samples that are compatible with depth-integrated samples collected at higher velocities.

If the stream is not wadable, a weighted-bottle type sampler may be used. Remember that these samples are not discharge-weighted samples and that, if possible, their analytical results should be verified by or compared to data obtained using a standard sampler and sampling technique.

Second case.—In the second case, when $2.0<v<12.0$ ft/s and the depth is less than 15 feet, the standard depth-integrating samplers, such as DH-48, DH-75, DH-59, D-49, and D-74 may be used. The method of sample collection is basically the same for all these samplers, whether used while wading or from a bridge or cableway. Insert a clean sample bottle into the sampler and check to see that there are no obstructions in the nozzle or air-exhaust tube. Then lower the sampler to the water surface so that the nozzle is above the water, and the lower tail vane or back of the sampler is in the water for proper upstream-downstream orientation. After orientation of the sampler, depth integration is accomplished by traversing the full depth and returning to the surface with the sampler at a constant transit rate.

When the bottom of the sampler touches the streambed, immediately reverse the sampler direction and raise the sampler to clear the surface of the flow at a constant transit rate. The transit rate used in raising the sampler need not be the same as the one used in lowering, but both rates must be constant in order to obtain a velocity- or discharge-weighted sample. The rates should be such that the bottle fills to near its optimum level (approximately 3 inches below the top or 350 to 420 milliliters, for the pint milk bottle, or 2 inches below the top or 650 to 800 milliliters for the quart bottle).

For streams that transport heavy loads of sand, and perhaps for some other streams, at least two complete depth integrations of the sample vertical should be made as close together in time as possible, one bottle for each integration. Each bottle then constitutes a sample and can be analyzed separately or, for the purposes of computing the sediment record, concentrations from two or more bottles can be averaged, whereby they are called a set. This set then is a sample in time with respect to the record. Sample analyses from two or more individual bottles for a given

observation are useful for checking sediment variations among bottles—an obvious advantage in the event the sediment concentration in one bottle is quite different from the concentration in the other bottles for the same observation. Immediately after collection, every bottle or sample should be inspected visually by swirling the water in the bottle and observing the quantity of sand particles collected at the bottom. If there is an unusually large quantity or a difference in the quantity of sands between bottles, another sample from the same vertical should be taken immediately. The sample suspected of having too much sand should be discarded. If it is saved, an explanation such as "too much sand" should be clearly written on the bottle. If by chance, a bottle is overfilled or if a spurt of water is seen coming out of the nozzle when the sampler is raised past the water surface, the sample should be discarded. A clean bottle must be used to resample the vertical.

To help avoid the problem of striking the nozzle into a dune or settling the sampler too deeply into a soft bed, it is recommended that a slow downward integration be used, followed by a more rapid upward integration. Because most of the sand is transported near the bed, it is essential that the transit direction of the sampler be immediately reversed as the sampler touches the bed.

Pertinent information as shown in figure 27 must be available with each bottle for use in the laboratory and in compiling the record. Most districts provide bottles with an etched area on which a medium-soft lead (blue or black) or wax pencil can be used. Other districts use

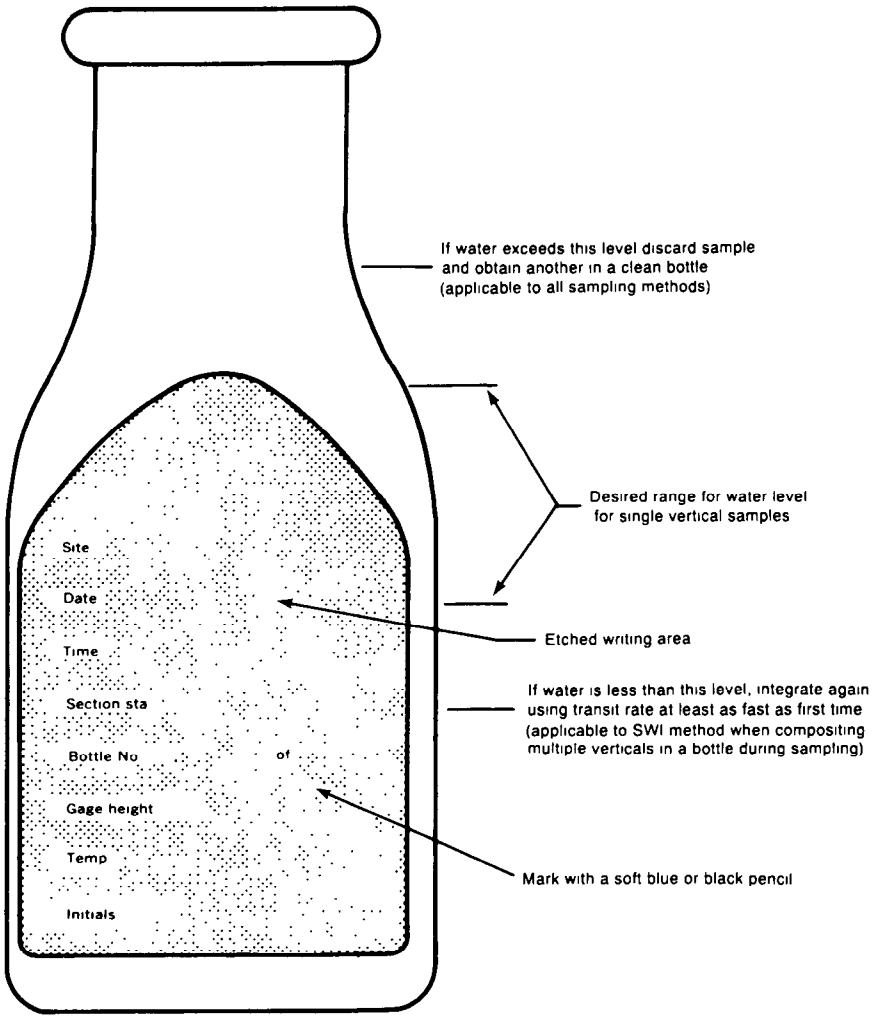

Figure 27. Sample bottle showing desired water levels for sampling methods indicated and essential record information applicable to all sampling methods.

plain bottles and attach tags for recording the required information. The required information may be recorded on the bottle cap if there are no other alternatives, but this should be avoided because of the small writing space and because of the possibility of putting the cap on the wrong bottle. Paper caps should not be used because they do not form as good a seal as do the plastic caps and may allow evaporation of the sample.

Third case.—In the third case, the depth-integrating samplers cannot be used because the depth exceeds the maximum allowable depth for these samplers. In this case, one of the point-integrating or bag-type samplers must be used. Because the bag sampler is still new and sufficient field data have not been collected to verify its sampling efficiency, USGS personnel who wish to use it must contact the Chief, Office of Surface Water, Reston, Virginia, and must set up a comparability sampling system to verify the sampler's efficiency under their specific conditions. The technique for collection of a sample using the bag-type sampler is similar to that used with the depth-integrating samplers.

The point samplers may be used to collect depth-integrated samples in verticals where the depth is greater than 15 feet. For streams with depths between 15 and 30 feet, the procedure is as follows:

1. Insert a clean bottle in the sampler and close the sampler head.
2. Lower the sampler to the streambed, keeping the solenoid closed and note the depth to the bed.
3. Start raising the sampler to the surface, using a constant transit rate. Open the solenoid at the same time the sampler begins the upward transit.
4. Keep the solenoid open until after the sampler has cleared the water surface. Close the solenoid.
5. Remove the bottle containing the sample, check the volume of the sample, and mark the appropriate information on the bottle. (If the sample volume exceeds allowable limits, discard the sample and repeat depth integration at a slightly higher transit rate.)
6. Insert another clean bottle into the sampler and close the sampler head.
7. Lower the sampler until the lower tail vane is touching the water, allowing the sampler to align itself with the flow.
8. Open the solenoid and lower the sampler at a constant transit rate until the sampler touches the bed.
9. Close the solenoid the instant the sampler touches the bed. (By noting the depth to the streambed in step 2 above, the operator will know when the sampler is approaching the bed.)

The transit rate used when collecting the sample in the upward direction need not be the same as that used in the downward direction, If the stream depth is greater than 30 feet, the process is similar, except that the upward and downward integrations are broken into segments no greater than 30 feet. Figure 28 illustrates the procedure for sampling a stream with a depth of 60 feet. Note the transit rate used in the upward direction (RT_3 and RT_4) is not equal to the transit rate in the downward direction (RT_1 and RT_2), but $RT_1 = RT_2$ and $RT_3 = RT_4$. Samples collected by this technique are composited for each vertical, and a single mean concentration is computed for the vertical. In addition to the usual information (fig. 27), the label on each bottle should indicate the segment or range of depth sampled and whether it was taken on a descending or ascending trip.

Samples **must** be obtained at a given vertical for both the downward and upward directions. Tests in the Colorado River (Federal Inter-Agency Sedimentation Project, 1951, p. 34) have shown an increase in the intake ratio of about 4 percent when descending versus a decrease in the intake ratio of about 4 percent on ascent.

Surface and Dip Sampling

Fourth case.—In the fourth case, circumstances are often such that surface or dip sampling is necessary. When the velocities are too high to use the depth- or point-integrating samplers or when debris makes normal sample collection dangerous or impossible, surface or dip samples may be collected.

A surface sample is one taken on or near the surface of the water, with or without a standard sampler. At some locations, stream velocities are so great that even the heaviest samplers will not reach the streambed while attempting to integrate the sampled vertical. Under such conditions, it can be expected that all, except the largest, particles of sediment will be thoroughly mixed within the flow; and, therefore, a sample near the surface is representative of the entire vertical. Extreme care should be used, however, because often such high velocities occur during floods when large debris is moving, especially on the rising part of the hydrograph. This debris may strike or

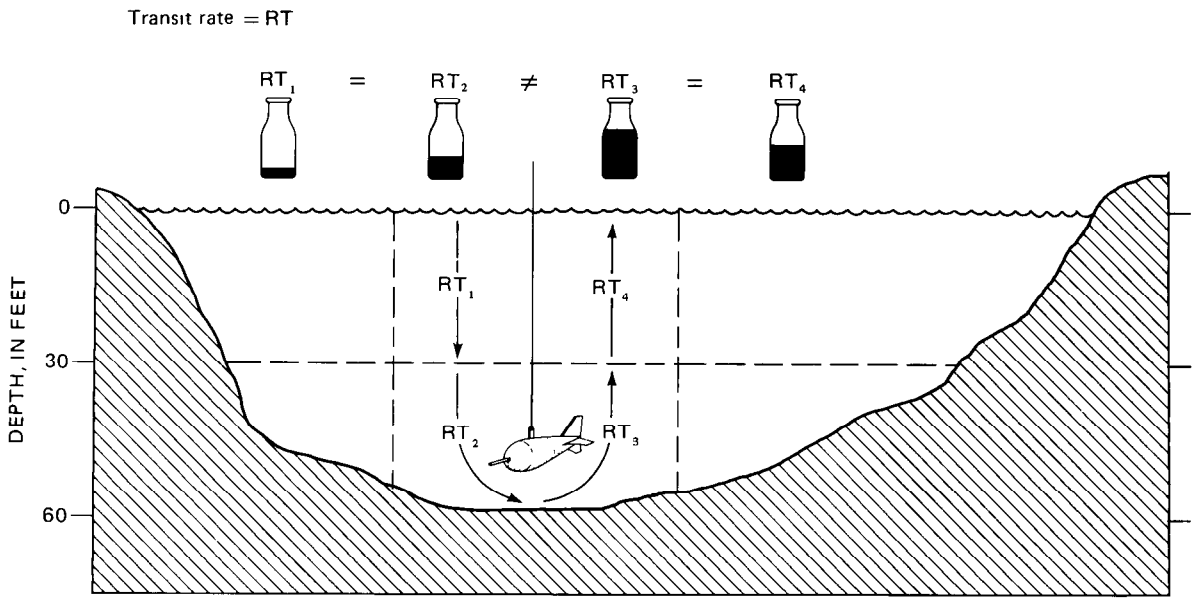

Figure 28. Uses of point-integrating sampler for depth integration of deep streams. RT, transit rate.

become entangled with the sampler and, thereby, damage the sampler, break the sampler cable, or injure the field person. Of course, a full explanation of sampling conditions should be noted on the bottle and in the field notes in order that special handling may be given the samples in the laboratory and in computing the records. The amount of debris in the flow may decrease considerably after the flood crest; even the velocity might decrease somewhat.

Because of the many problems associated with surface and dip sampling, these samples should be correlated to regular depth-integrated samples collected under more normal flow conditions, as soon as possible after the high flow recedes. Along with the depth-integrated sample, a sample should be collected in a manner duplicating the sampling procedure used to collect the surface or dip sample. These samples will be used to adjust the analytical results of the surface or dip sample collected during the higher flow, if necessary, to facilitate the use of these data in sediment-discharge computations and data analyses.

Multivertical

A depth-integrated sample collected using the procedures outlined in the previous section will accurately represent the discharge-weighted suspended-sediment concentration along the vertical at the time of the sample collection. As mentioned before, the purpose of collecting sediment samples is to determine the instantaneous sediment concentration at a cross section. The question now becomes, how do we locate the verticals in the cross section so that the end result will be a sample that is representative of the mean discharge-weighted sediment concentration?

The USGS uses two basic methods to define the location or spacing of the verticals. One is based on equal increments of water discharge; the second is based on equal increments of stream or channel width.

The Equal-Discharge-Increment Method

With the equal-discharge-increment method (EDI), samples are obtained from the centroids of equal-discharge increments (fig. 29). This method requires some knowledge of the distribution of streamflow in the cross section, based on a long period of discharge record or on a discharge measurement made immediately prior to selecting sampling verticals. If such knowledge can be obtained, the EDI method can save time and labor (compared to the equal-width-increment method, discussed in the next section), especially on the larger streams, because fewer verticals are required (Hubbell and others, 1956).

To use the EDI method without the benefit of previous knowledge of the flow distribution in the sampling cross section, first measure the discharge of the stream and determine the flow distribution across the channel at the sampling cross section prior to sampling. From the discharge measurement preceding the sampling (fig. 30) or from historic discharge-measurement records, equal-discharge increments can

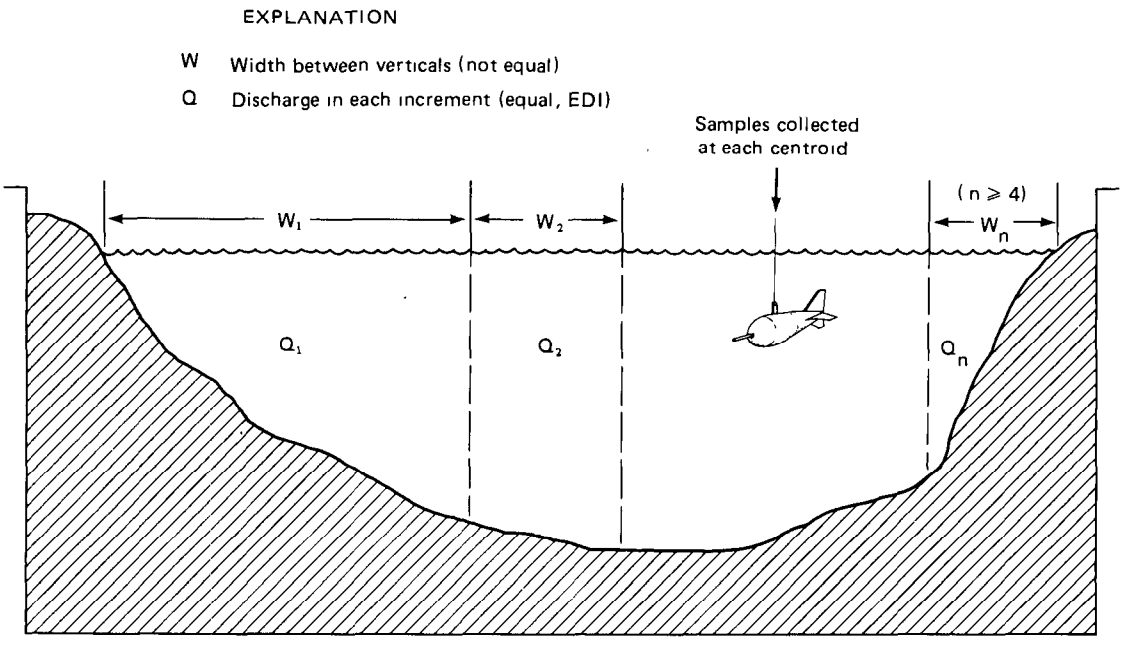

Figure 29. Example of equal-discharge-increment (EDI) sampling technique. Samples are collected at the centroids of flow of each increment.

be determined and centroids at which samples are to be collected can be located. In this example, the total discharge is equal to 166 ft^3/s (cubic feet per second). For illustration purposes, it was determined, by methods to be discussed later, that five verticals would be sampled. The equal increments of discharge (EDI's) then are computed by dividing the total discharge by the number of verticals (166 divided by 5 = 33.2 ft^3/s). The first vertical (A) is located at the centroid of the initial EDI or at a point where the cumulative discharge from the left edge of water (LEW) is one-half of the EDI, in this case 33.2 divided by 2 = 16.6 ft^3/s.

Subsequent centroids (B, C, and so on) are located by adding the increment discharge to the discharge at the previously sampled centroid; in this example, A = 16.6 ft^3/s, B = A + 33.2 ft^3/s, C = B + 33.2 ft^3/s, and so on. Samples are, therefore, collected at points where the cumulative discharge relative to the LEW is 16.6, 49.8, 83.0, 116.2, and 149.4 ft^3/s.

A minimum of four and a maximum of nine verticals should be used when using the EDI method. This method assumes that the sample collected at the centroid represents the mean concentration for the subsection.

To determine the stationing of the centroids, the field person must include a cumulative discharge column (ΣQ) on the discharge-measurement notes by adding the discharges shown in the "discharge" column and keeping a running total as shown in figure 31. The next step is to estimate the stationing of the above centroids. Each centroid is located at the station in the cross section corresponding to the occurrence of its computed cumulative discharge. As shown in figure 31, the cumulative discharge at station 26 equals 8.32 ft^3/s, while station 34 corresponds to 18.5 ft^3/s. Actually, the cumulative discharge is computed to the point midway between stations (far midpoint, fig. 31). Therefore, the point where the cumulative discharge equals 8.32 ft^3/s is located halfway between stations 26 and 34, at station 30. In like manner, the cumulative discharge of 18.5 ft^3/s occurs at the far mid-point between stations 34 and 42, at station 38. The first centroid then would be located between stations 30 and 38. Interpolating between these stations, the centroid discharge of 16.6 ft^3/s would be located at a station closer to station 38, where 18.5 ft^3/s occurs, in this case near station 37. Using the same procedure, estimates of centroid stationing yield stations 60, 83, 109, and 144 for the four remaining centroids.

If the cross section at the measurement site is stable and the control governing the stage at the measurement cross section also is stable, previous measure-

9-275-F
(May 1971)

UNITED STATES
DEPARTMENT OF THE INTERIOR
GEOLOGICAL SURVEY
WATER RESOURCES DIVISION

Meas. No. .....
Comp. by .....
Checked by .....

DISCHARGE MEASUREMENT NOTES

Sta. No. 14301000
Nehalem River near Foss, Oregon
Date JULY 12, 1982 Party Oster and Fuhrer
Width 160 Area 152 Vel. 1.10 G. H. 1.92 Disch. 166
Method 6 No. secs. 21 G. H. change 0 in 1.5 hrs. Susp. Rod
Method coef. 1 Hor. angle coef. 1 Susp. coef. 1 Meter No 1909
Type of meter Price
Date rated 5-16-64 for rod, other.
Meter ..... ft above bottom of weight
Spin before meas. ..... after .....
Meas plots .... % diff from rating .....
Wading, cable, ice, boat, upstr., downstr., side bridge ..... feet, mile, above, below gage, and above riffle
Check-bar, found .....
changed to ..... at .....
Correct .....
Levels obtained .....

GAGE READINGS

Time		Recorder	Inside	Outside
1048	1.91	1.92		1.89
1130	Start			
1200	Finish			
1220		1.92		
Weighted M G. H.				
G. H. correction				
Correct M G H.				

Measurement rated excellent (2%), good (5%), fair (8%), poor (over 8%), based on following conditions: Cross section gravel
Flow uniform Weather clear
Other ..... Air .....°F@.....
Gage ..... Water .....°F@.....
..... Record removed ..... Intake flushed (U) Yes
Observer .....

Control Gravel riffle 100 ft. downstream and clear
Remarks .....

G. H. of zero flow 1.9-1.0= 0.9 ft.

River at .....

Angle coef-ficient	Dist from initial point	Width	Depth	Observation depth	Revolutions	Time in seconds	VELOCITY At point	VELOCITY Mean in vertical	Adjusted for hor angle or ____	Area	Discharge
	10	4	0		LEW					0	0
	18	8	.6		15	47		.72		4.8	3.46
	26	8	.8		15	44		.76		6.4	4.86
	34	8	1.0		25	44		1.27		8.0	10 16
	42	8	1.0		30	45		1.48		8.0	11.84
	50	8	1.3		25	48		1.16		10.4	12.06
	58	8	1.25		20	44		1 01		10.0	10.10
	66	8	1.25		20	40		1.11		10.0	11 10
	74	8	1.3		20	39		1.14		10.4	11.86
	82	8	1 3		25	45		1.24		10.4	12.90
	90	8	1.2		25	45		1 24		9.6	11.90
	98	8	1 0		20	43		1 04		8.0	8.32
	106	8	.9		25	47		1.19		7 2	8.57
⊙	114	8	1 0		20	42		1 06		8.0	8.48
	122	8	1.0		20	40		1.11		8.0	8.88
	130	8	.9		15	43		.78		7.2	5.62
	138	8	8		20	40		1.11		6.4	7.10
	146	8	.7		25	44		1.27		5 6	7.11
	154	8	.9		25	44		1.27		7.2	9.14
	162	8	.8		10	54		.42		6.4	2 69
	170	4	0		REW					0	0
	160	160								152 0	166.15
											166

Figure 30. Record of discharge measurement for Nehalem River near Foss, Oregon.

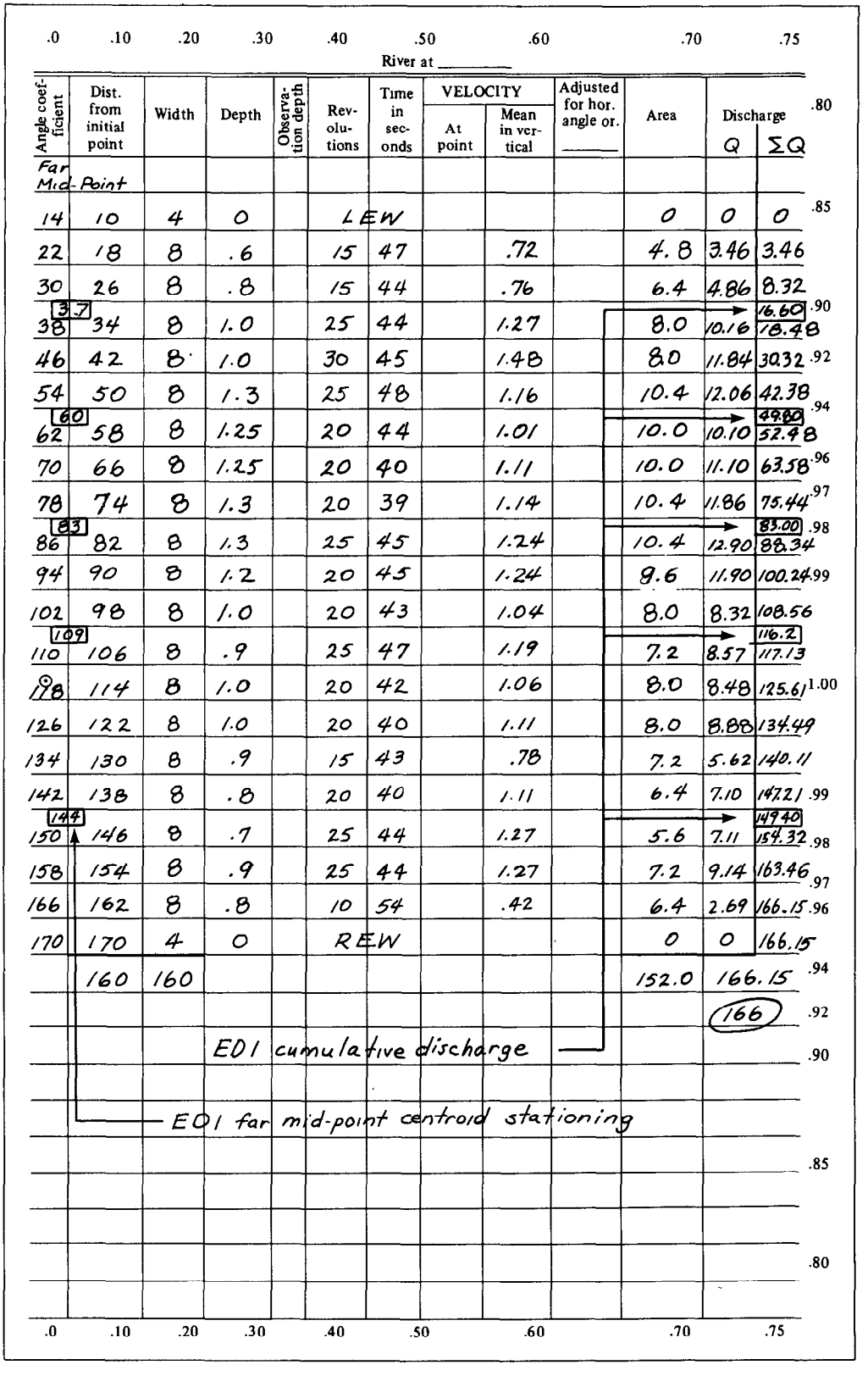

.0 .10 .20 .30 .40 .50 .60 .70 .75

River at _____

Angle coefficient	Dist. from initial point	Width	Depth	Observation depth	Revolutions	Time in seconds	VELOCITY At point	VELOCITY Mean in vertical	Adjusted for hor. angle or. _____	Area	Discharge Q	Discharge ΣQ	
Far Mid-Point													
14	10	4	0		LEW					0	0	0	.85
22	18	8	.6		15	47		.72		4.8	3.46	3.46	
30	26	8	.8		15	44		.76		6.4	4.86	8.32	
[37] 38	34	8	1.0		25	44		1.27		8.0	10.16	[16.60] 18.48	.90
46	42	8	1.0		30	45		1.48		8.0	11.84	30.32	.92
54	50	8	1.3		25	48		1.16		10.4	12.06	42.38	
[60] 62	58	8	1.25		20	44		1.01		10.0	10.10	[49.80] 52.48	.94
70	66	8	1.25		20	40		1.11		10.0	11.10	63.58	.96
78	74	8	1.3		20	39		1.14		10.4	11.86	75.44	.97
[83] 86	82	8	1.3		25	45		1.24		10.4	12.90	[83.00] 88.34	.98
94	90	8	1.2		20	45		1.24		9.6	11.90	100.24	.99
102	98	8	1.0		20	43		1.04		8.0	8.32	108.56	
[109] 110	106	8	.9		25	47		1.19		7.2	8.57	[116.2] 117.13	
⊙118	114	8	1.0		20	42		1.06		8.0	8.48	125.61	1.00
126	122	8	1.0		20	40		1.11		8.0	8.88	134.49	
134	130	8	.9		15	43		.78		7.2	5.62	140.11	
142	138	8	.8		20	40		1.11		6.4	7.10	147.21	.99
[144] 150	146	8	.7		25	44		1.27		5.6	7.11	[149.40] 154.32	.98
158	154	8	.9		25	44		1.27		7.2	9.14	163.46	.97
166	162	8	.8		10	54		.42		6.4	2.69	166.15	.96
170	170	4	0		REW					0	0	166.15	
	160	160								152.0	166.15		.94
											(166)		.92
			EOI cumulative discharge										.90
			EOI far mid-point centroid stationing										
													.85
													.80

.0 .10 .20 .30 .40 .50 .60 .70 .75

Figure 31. Discharge-measurement notes used to estimate the equal-discharge-increment centroid locations based on cumulative discharge and far-midpoint stationing.

ments may be used to determine centroids of equal increments of discharge.

By plotting the cumulative discharge versus stations for our example (fig. 32), the stations of the centroids may be read directly from the curve. Their values are 36, 59, 82, 110, and 146 ft^3/s, which correspond nicely with our previously estimated values.

A number of these measurements may be plotted on the same sheet (fig. 33) and carried into the field. For discharges that fall between those plotted, the field person can estimate the locations of the centroids by interpolating between the curves.

An alternate method of estimation is to plot cumulative percent of total discharge on the y-axis, instead of cumulative discharge (fig. 34). This method entails one additional step, in that the cumulative percent must be calculated; however, it does have the advantage of showing the variation in stations for the same percentage of flow for different discharges. For example, figure 34 shows that for discharges 86 to 200 ft^3/s, the 10-percent centroid (the centroid of the first 20 percent of flow) can range from station 20 to station 50.

The transit rate used in traversing the distance from water surface to streambed and back to water surface need not be the same in both directions and can vary among centroids. This technique should facilitate collection of approximately equal sample volumes from each centroid (fig. 35).

Individual bottles collected as part of an EDI sample set can be analyzed for concentration separately and their concentrations averaged to give the mean discharge-weighted concentration for the set. The advantage of this method is that data describing the cross-sectional variation in concentration are produced. Additionally, a bottle containing an abnormally high concentration compared to others in the set (due to recirculation or to digging the nozzle into the bed) could be excluded from the concentration calculation where it might seriously affect the results. If approximately equal volumes of sample are collected at each vertical, the samples may be composited prior to analysis.

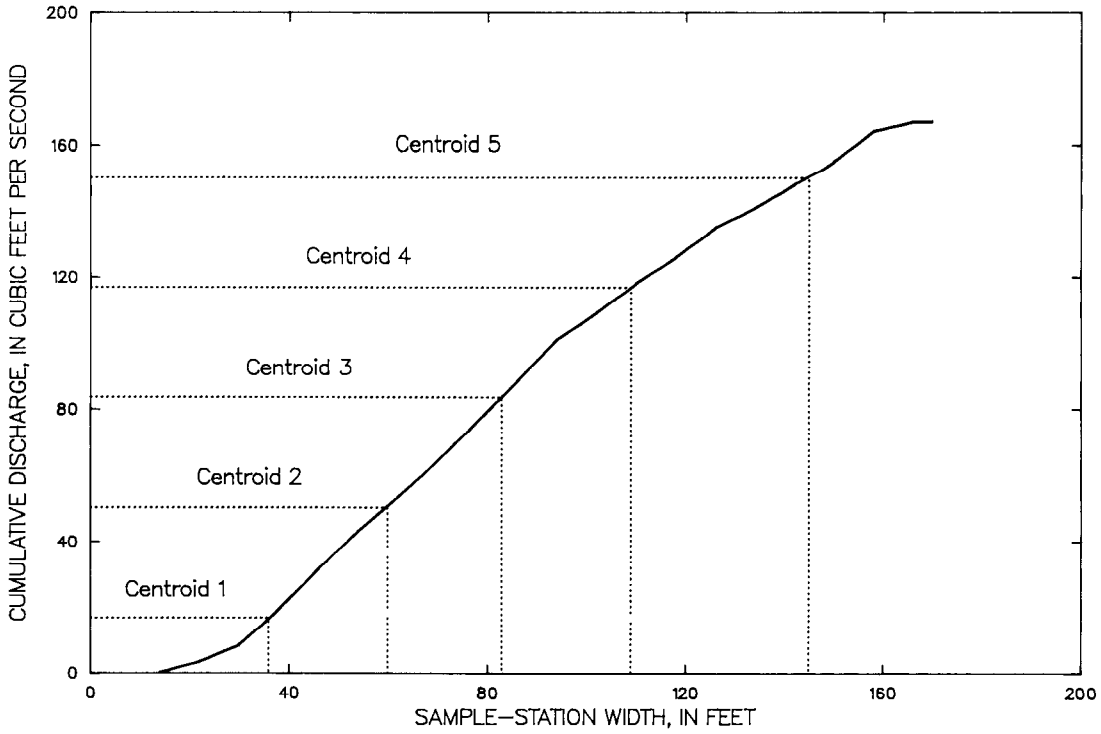

Figure 32. Cumulative discharge versus sample-station widths for determining equal-discharge-increment centroid locations.

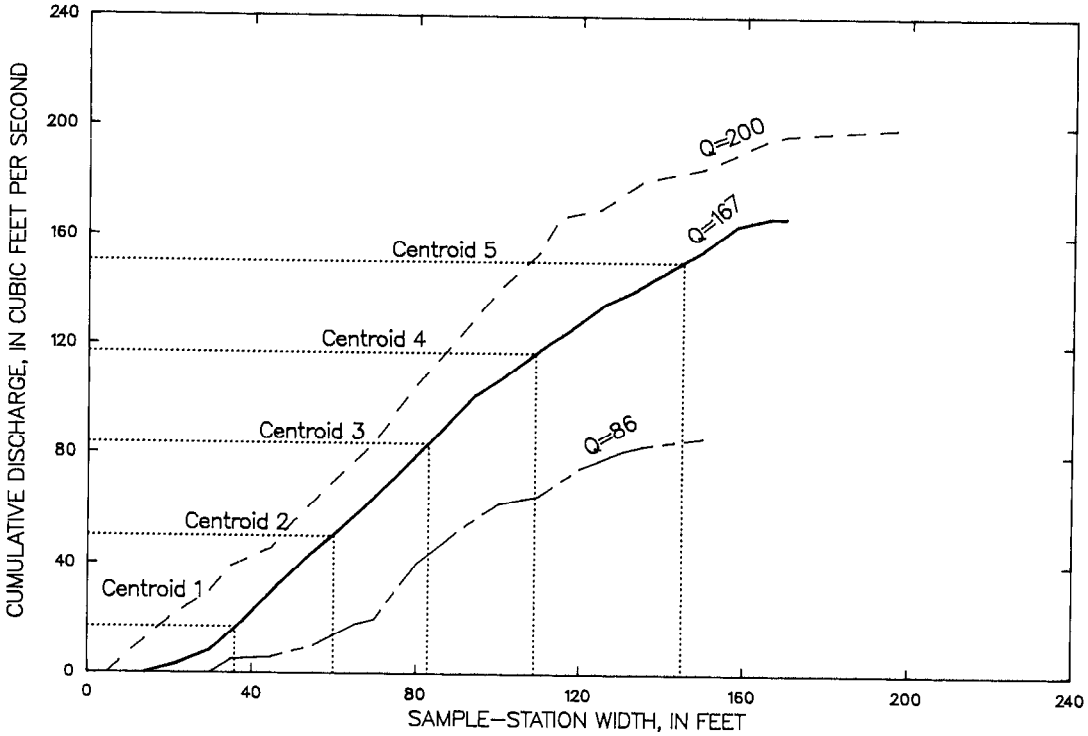

Figure 33. Cumulative discharge versus sample-station widths for determining equal-discharge-increment centroid locations. Multiple discharge-measurement plots allow users to estimate centroid locations by interpolating between curves.

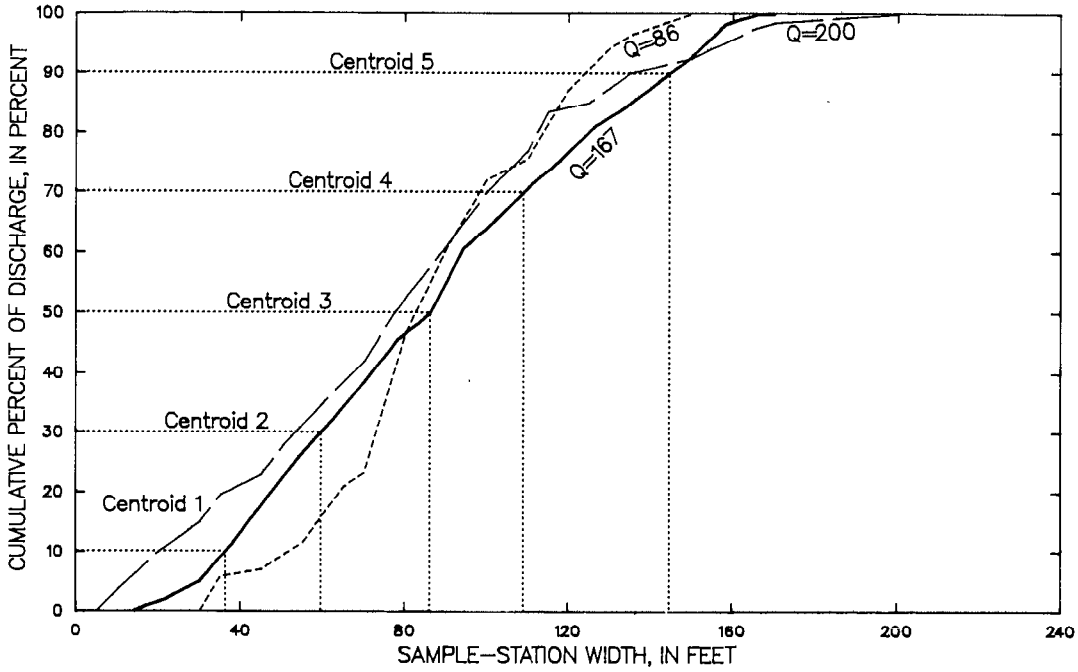

Figure 34. Cumulative percent of discharge versus sample-station widths for determining equal-discharge-increment centroid locations.

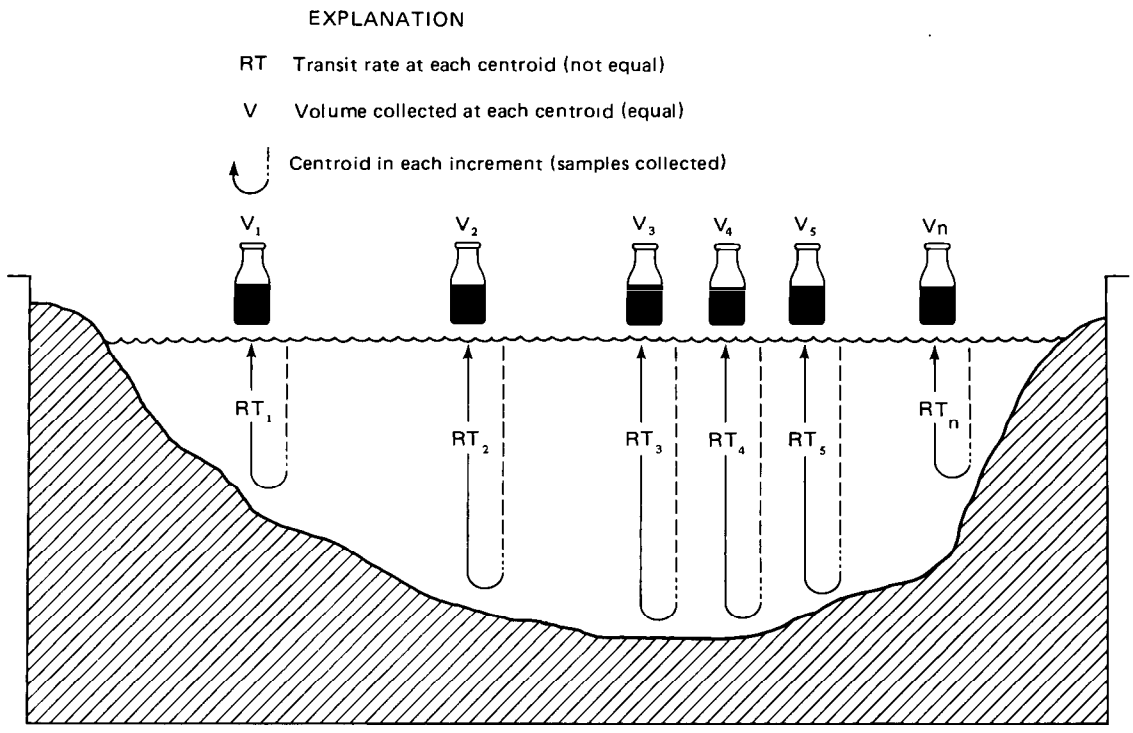

Figure 35. Vertical transit rate relative to sample volume collected at each equal-discharge-increment centroid.

The streambed of a sand-bed stream characteristically shifts radically, at single points and across segments of the width, over a period of weeks or in a matter of hours. This not only makes it impossible to establish cumulative discharge or cumulative percentage of discharge versus station curves applicable from one visit to the next, but also makes it impossible to be certain the discharge distribution does not change between the water-discharge measurement and the sediment sampling (see Guy, 1970, fig. 15).

The Equal-Width-Increment Method

A cross-sectional suspended-sediment sample obtained by the equal-width-increment (EWI) method requires a sample volume proportional to the amount of flow at each of several equally spaced verticals in the cross section. This equal spacing between the verticals (EWI) across the stream and sampling at an equal transit rate at all verticals yields a gross sample volume proportional to the total streamflow. It is important, obviously, to keep the same size nozzle in the sampler for a given measurement. This method was first used by B.C. Colby in 1946 (Federal Inter-Agency Sedimentation Project, 1963b, p. 41) and is used most often in shallow, wadable streams and (or) sand-bed streams where the distribution of water discharge in the cross section is not stable. It also is useful in streams where tributary flow has not completely mixed with the main-stem flow.

The number of verticals required for an EWI sediment-discharge measurement depends on the distribution of concentration and flow in the cross section at the time of sampling, as well as on the desired accuracy of the result. On many streams, both statistical approaches and experience are needed to determine the desirable number of verticals. Until such experience is gained, the number of verticals used should be greater than necessary. In all cases, a minimum of 10 verticals should be used for streams over 5 feet wide. For streams less than 5 feet wide, as many verticals as possible should be used, as long as they are spaced a minimum of 3 inches apart, to allow for discrete sampling of each vertical and to avoid overlaps. Through general experience with similar streams, field personnel can estimate the required minimum number of verticals to yield a desired level

of accuracy. For all but the very wide and shallow streams, a maximum of 20 verticals is usually ample.

The width of the increments to be sampled, or the distance between verticals, is determined by dividing the stream width by the number of verticals necessary to collect a discharge-weighted suspended-sediment sample representative of the sediment concentration of the flow in the cross section (fig 36). For example, if the stream width determined from the tagline, cableway, or bridge-rail markings at the sample cross section is 160 feet, and the number of verticals necessary is 10, then the width (W) of each sampled increment would be 16 feet. The sample station within each width increment is located at the center of the increment (W/2), beginning at a location of 8 feet from the bank nearest the initial point for width measurement. The verticals then are spaced 16 feet apart, resulting in sample stationing at 8, 24, 40, 56, 72, 88, 104, 120, 136, and 152 feet of width. However, in the event the width increment results in a fractional measurement, the width can be rounded to the nearest integer that will yield a whole numbered station for the initial sample vertical. That is, if the increment computation yields a width of 15.5 feet, the nearest integer width would be 16 feet, and the initial vertical would be located at 8 feet from the bank; the stationing would be similar to the previous example. Results of samples obtained using this nonideal stationing will not be measurably affected because alterations in width occur in the increments nearest the streambank, where flow velocity is low compared to midstream increments.

The EWI sampling method requires that all verticals be traversed using the transit rate (fig. 37) established at the deepest and fastest vertical in the cross section. The descending and ascending transit rates must be equal during the sampling traverse of each vertical, and they must be the same at all verticals. By using this equal-transit-rate technique with a standard depth- or point-integrating sampler at each vertical, a volume of water proportional to the flow in the vertical will be collected (fig. 37).

It is often difficult to maintain an equal transit rate when collecting samples while wading. The authors have found the following procedure to be effective in alleviating this difficulty. The field person should hold the sampler at a reference point on the body (for example, the hip), at which level the downward and upward integration is started and finished (even though part of the traverse is in air). The same reference point should be used at each vertical, allowing the same amount of time to elapse during the round trip traverse of the sampler (regardless of the stream depth encountered). In this manner, the transit rate will remain constant for the entire cross section. It should be remembered that the reference point at which the sampler traverse is started and stopped must be located above the water surface at the deepest vertical sampled and must be the same for each vertical.

Because the maximum transit rate must not exceed 0.4 v_m (v_m equals the mean ambient velocity in the sampled vertical) and because the minimum rate must be sufficiently fast to keep from overfilling any of the sample bottles, it is evident that the transit rate to be used for all verticals is limited by conditions at the vertical containing the largest discharge per foot of width (largest product of depth times velocity). A discharge measurement can be made to determine where this vertical is located, but generally, it is estimated by sounding for depth and acquiring a feel for the relative velocity with an empty sampler or wading rod. The transit rate required at the maximum discharge vertical then must be used at all other verticals in the cross section and is usually set to fill a bottle to the maximum sample volume in a round trip. It is possible to sample at two or more verticals using the same bottle if the bottle is not overfilled. If a bottle is overfilled, it must be discarded, and all verticals previously sampled using that bottle must be resampled, using a sufficient number of bottles to avoid overfilling. Note: a sample bottle is overfilled when the water surface in the bottle is above the nozzle or air exhaust with the sampler held level.

Advantages and Disadvantages of Equal-Discharge-Increment and Equal-Width-Increment Methods

Some advantages and disadvantages of both the EDI and EWI methods have been mentioned in the previous discussion. It must be remembered, however, that both methods, if properly used, yield the same results. The advantages of the EDI method are—

1. Fewer verticals are necessary, resulting in a shortened collection time.
2. Sampling during rapidly changing stages is facilitated by the shorter sampling time.
3. Bottles comprising a sample set may be composited for laboratory analysis when equal volumes of sample are collected from each vertical.

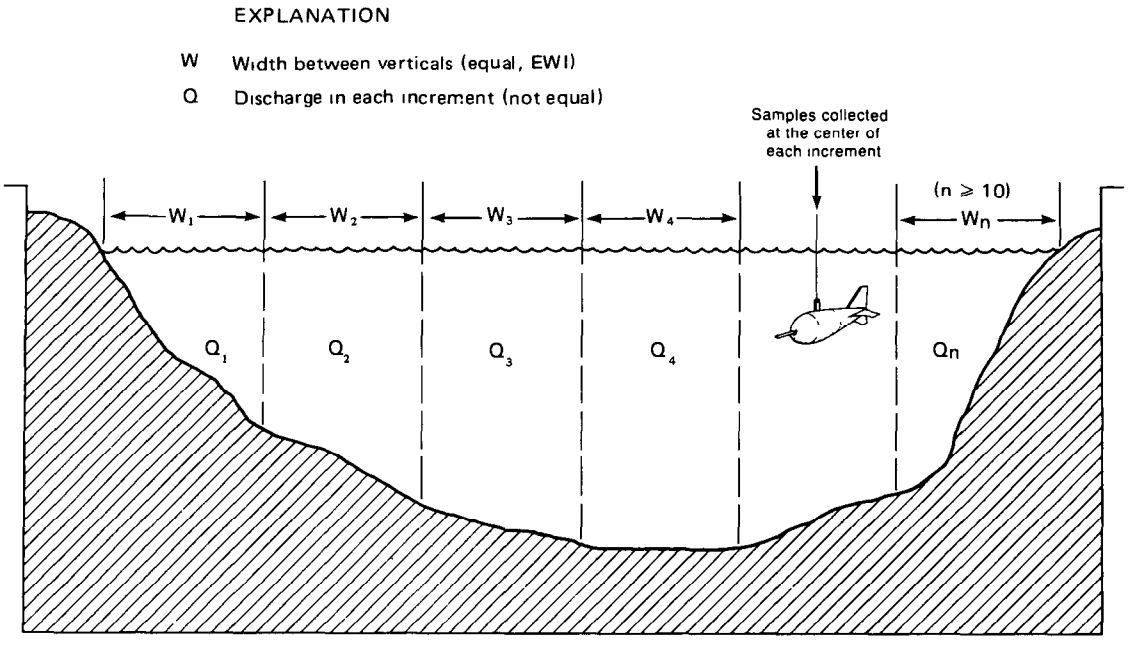

Figure 36. Equal-width-increment sampling technique.

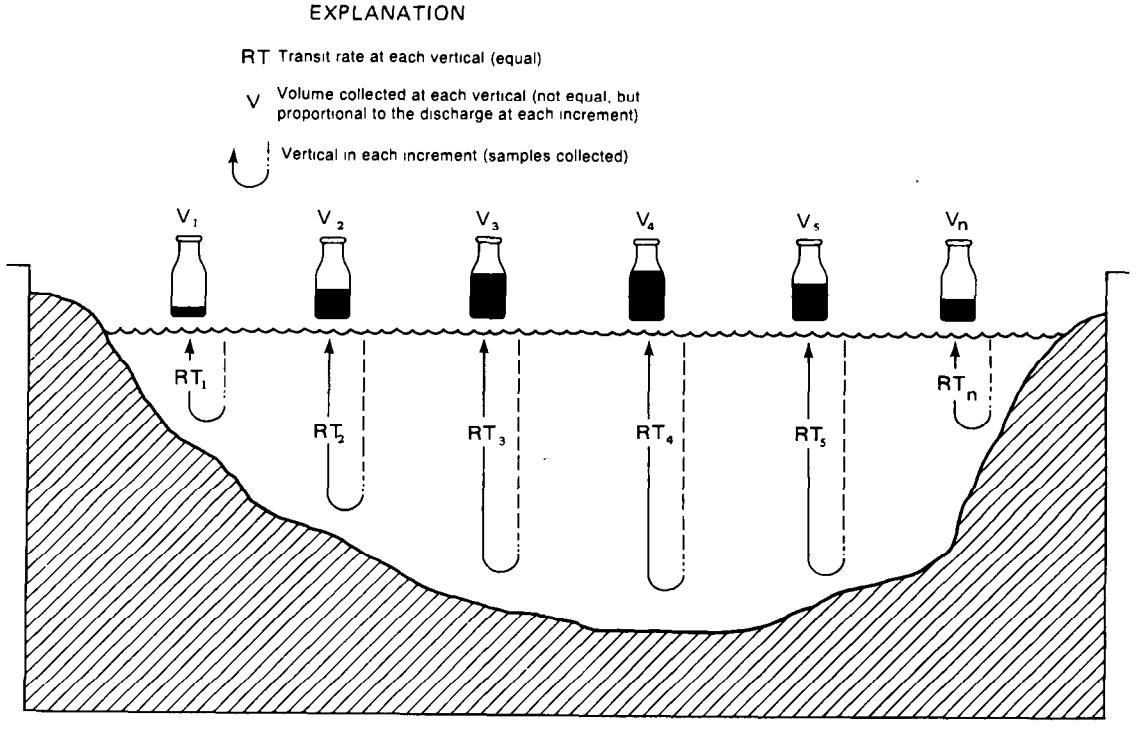

Figure 37. Equal-width-increment vertical transit rate relative to sample volume, which is proportional to water discharge at each vertical.

4. The cross-sectional variation in concentration can be determined if sample bottles are analyzed individually.
5. Duplicate cross-section samples can be collected simultaneously.
6. A variable transit rate can be used among verticals.

The advantages of the EWI method are—

1. Previous knowledge of flow distribution in the cross section is not required.
2. Variations in the distribution of concentration in the cross section may be better defined, due to the greater number of verticals sampled.
3. Analytical time is reduced as sample bottles are composited for laboratory analysis.
4. This method is easily taught to and used by observers because the spacing of sample verticals is based on the easily obtained stream width, instead of on discharge.
5. Generally less total time is required on site, if no discharge measurement is deemed necessary and the cross section is stable.

From the previous discussion it is obvious that, while both methods have definite advantages, the advantages of one method are, in many cases, the disadvantages of the other. One major disadvantage of the EWI method that should be noted is the inability to adequately distinguish obviously bad samples in the sample set, as illustrated by the following:

Example:

Vertical/bottle	1	2	3	4	5	6
Weight of sediment (g)	0.053	0.036	0.699	0.053	0.047	0.036
Weight of water sediment mixture (g)	350	300	325	330	360	355
Concentration (mg/L)	151	120	2,150	161	131	101

Mean concentration

EWI and EDI methods (composited) = 457 mg/L

EDI method (individual bottles analyzed, concentration averaged) = 469 mg/L

EDI method (individual bottles analyzed excluding bottle 3, concentration averaged) = 133 mg/L

As this example shows, if the sample were an EWI sample and composited for analysis, the computed mean concentration is 457 mg/L, which also is the mean concentration if the sample were considered as an EDI sample similarly composited for analysis. If, in the case of the EDI sample, the individual bottles were analyzed, normal computation would result in a mean concentration of 469 mg/L. From the data, bottle 3 appears to have been enriched and is not consistent with the other data points for this cross section. By exercising the flexibility of the EDI method and eliminating the number 3 bottle, the mean concentration of the remaining five bottles is computed to be 133 mg/L, which is probably more consistent with the actual mean concentration in the cross section.

Point Samples

A point sample is a sample of the water-sediment mixture collected from a single point in the cross section. It may be collected using a point-integrating sampler.

Point-integrated samples may be collected using one of the point-integrating samplers previously discussed. Data obtained in this manner may be used to define the distribution of sediment in a single vertical, such as the observer's fixed station, the vertical and horizontal distribution of sediment in a cross section, and the mean spatial sediment concentration.

The purpose for which point samples are to be collected determines the collection method to be used. If samples are collected for the purpose of defining the horizontal and vertical distribution of concentration and (or) particle size, samples collected at numerous points in the cross section, with any of the "P" type samplers, will be sufficient. Normally, 5 to 10 verticals are sufficient for horizontal definition. Vertical distribution can be adequately defined by obtaining samples from a number of points in each sample vertical. Specifically, samples should be taken at the surface, from 1 foot above the bed point, with the sampler touching the bed, and from 6 to 10 additional points in the vertical above the 1-foot-above-bed point. Each individual point sample should be analyzed separately. The results then can be plotted on a cross section relative to their instream location.

If point samples are collected to define the mean concentration in a vertical, 5 to 10 samples should be collected from the vertical. The sampling time for each sample (the time the nozzle is open) must be equal.

This will ensure that samples collected are proportional to the flow at the point of collection. These samples then are composited for laboratory analysis. If the EDI method is used to define the stationing of the verticals, the sampling time may be varied among verticals. If the EWI method is used to determine the location of verticals, a constant sampling time for samples from all verticals must be used.

Number of Verticals

The number of suspended-sediment sampling verticals at a measuring site may depend on the kind of information needed in relation to the physical aspects of the river. For example, to determine the distribution of sediment concentration or particle size across the stream, it is necessary to sample at several verticals. The number of verticals necessary to define such a cross-sectional distribution depends on the accuracy being sought and on the systematic variation of sediment concentration at different verticals across the stream.

As noted previously, suspended-sediment samplers are designed to accumulate a sample that is directly proportional to the stream discharge or velocity. The accumulated sample may be from a point in the stream cross section, a vertical line between the surface and streambed, or several such vertical lines across the entire stream cross section. Such a sample then can be considered to be representative of some element of cross-sectional flow, whether it be a few square feet adjacent to the point sample, a few square feet adjacent to both sides of a vertical line, or the area of the entire flow summed by several vertical lines. The number of verticals sampled must be adequate to represent the cross section in the sample. The number of sample bottles to be collected will depend on the kind of analysis to be made in the laboratory, and the location of the sampling verticals will depend on the concentration and size distribution of sediment moving through the stream cross section.

Both EDI and EWI methods of sediment-discharge measurement obtain a water-discharge weighted sample at each vertical. The volumetric sum from all verticals yields a sample volume proportional to the water discharge for the stream. Remember that all or nearly all of the concentration variations at different verticals across the stream may be the result of non-uniform distribution of sand-sized material and that finer sediments are generally more uniformly dispersed throughout the section. If the section is close to a tributary, mixing of main stream and tributary flows may not be complete. Therefore, locating sampling sections downstream from tributary inflows should be avoided.

Colby (1964) showed that the discharge of sand is approximately proportional to the third power of the mean velocity, with constant temperature and a given particle-size distribution for a range of velocity from about 2 to 5 ft/s and within some reasonable range of depths. Thus, $Q_s = k_1 v^3$, in which Q_s is the discharge of sand per unit width; k_1 is a constant for a given depth, particle size, and temperature; and v is the mean velocity. The sand discharge can be written as $Q_s = k_2 cvd$, in which k_2 is another constant, c is the mean discharge-weighted concentration in the sampled vertical, and d is the total sampled depth. Solving for c gives

$$c = \frac{k_1}{k_2} \frac{v^2}{d}$$

Thus, the variability of concentration at different sampling verticals should be closely related to the variability of v^2/d. In order to have a v^2/d index useful for comparison among all streams, the compound ratio

$$\frac{v^2 d_{(max)}}{v^2 d} \text{ is suggested,}$$

where $[v^2/d_{(max)}]$ is the ratio from the vertical having the maximum v^2/d, and v^2/d is the ratio of the mean velocity squared to the mean depth of the whole stream cross section. The mean velocity and mean depth are computed and available from water-discharge measurements.

Based on the v^2/d index concepts of variability, P.R. Jordan used data from Hubbell and others (1956) to prepare a nomograph (fig. 38) that indicates the number of sampling verticals required for a desired maximum acceptable relative standard error (sampling error) based on the percentage of sand and the v^2/d index. In the example illustrated by figure 38, the acceptable relative standard error is 15 percent, the sample is 100-percent sand, the v^2/d index is 2.0, and the required number of verticals is seven. Notice that if the sediment were 50-percent sand, the same results

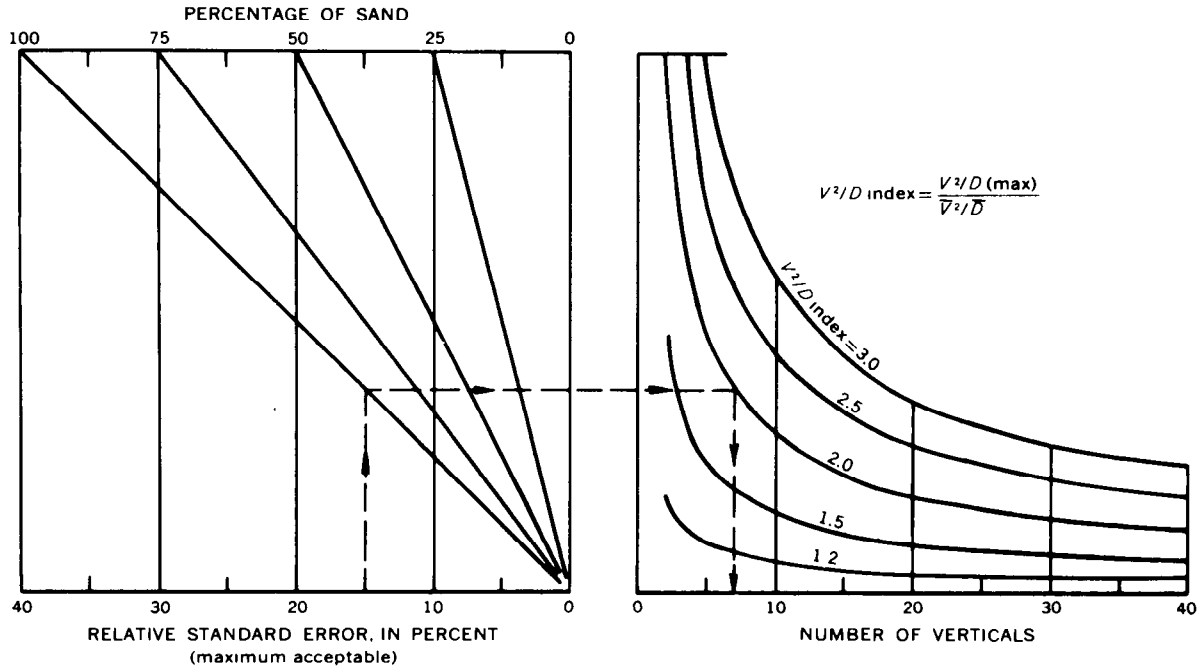

Figure 38. Nomograph to determine number of sampling verticals required to obtain results within an acceptable relative standard error.

could be obtained with three verticals; or, if seven verticals were used with 50-percent sand, the relative standard error would be about 8 percent. When the discharge of sand-sized particles is of primary interest, the 100-percent line should be used regardless of the amount of fines in the sample.

Transit Rates for Suspended-Sediment Sampling

The sample obtained by passing the sampler throughout the full depth of a stream is quantitatively weighted according to the velocity through which it passes. Therefore, if the sampling vertical represents a specific width of flow, the sample is considered to be discharge weighted because, with a uniform transit rate, suspended sediment carried by the discharge throughout the sampled vertical is given equal time to enter the sampler. In previous writings, the point was made to keep the transit rate of the samplers constant throughout at least a single direction of travel.

The maximum transit rate used with any depth-integrating sampler must be regulated to ensure the collection of representative samples. If the transit rate is too fast, the rate of air-volume reduction in the sample container is less than the rate of increase in hydrostatic pressure surrounding the sampler, and water may be forced into the intake or air exhaust. Additionally, an excessive transit rate can result in intake velocities less than the stream velocity at the intake, due to a large entrance angle between the nozzle and streamflow lines caused by the vertical movement of the sampler in the flow (Federal Inter-Agency Sedimentation Project, 1952). To alleviate these problems, transit rates should never exceed 0.4 of the mean velocity (0.4 v_m) in a vertical. Figures 39, 40, and 41 can be used to determine the appropriate transit rate to be used with a given nozzle-size/sample-container-size combination. These figures show that maximum transit rates vary from about 0.1 v_m to the approach angle limit of 0.4 v_m, previously noted. This variation is a function of both nozzle size and sample-container size. The smaller nozzle (1/8 inch) is greatly affected by approach angle intake velocity reductions; figures 39 and 40 show that the transit rate decreases directly with nozzle size. Also, by comparison of figures 39 and 40, it is obvious that transit rates are inversely affected by sample-container size because an increase in sampler container size produces a decrease in allowable transit rate due to the effects of hydrostatic pressure compressing the air within the container during the downward transit. Figures 39, 40, and 41 were constructed using procedures from F.I.S.P. (1952), Report 6, Section 8, as contained in the

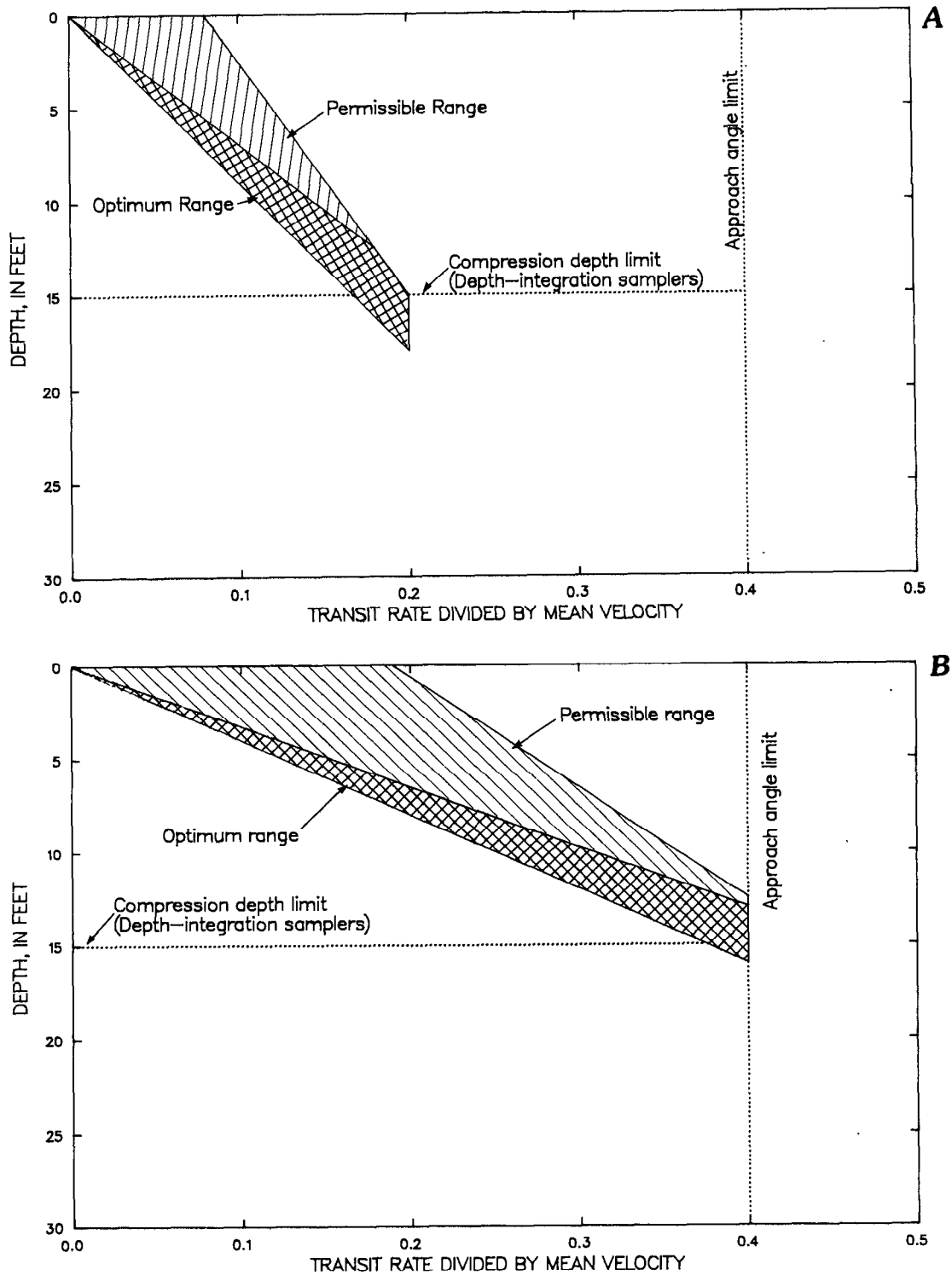

Figure 39. Variation of range of transit rate to mean velocity ratio versus depth relative to nozzle size for pint-size sample container. *A*, 1/8-inch nozzle. *B*, 3/16-inch nozzle. *C*, 1/4-inch nozzle.

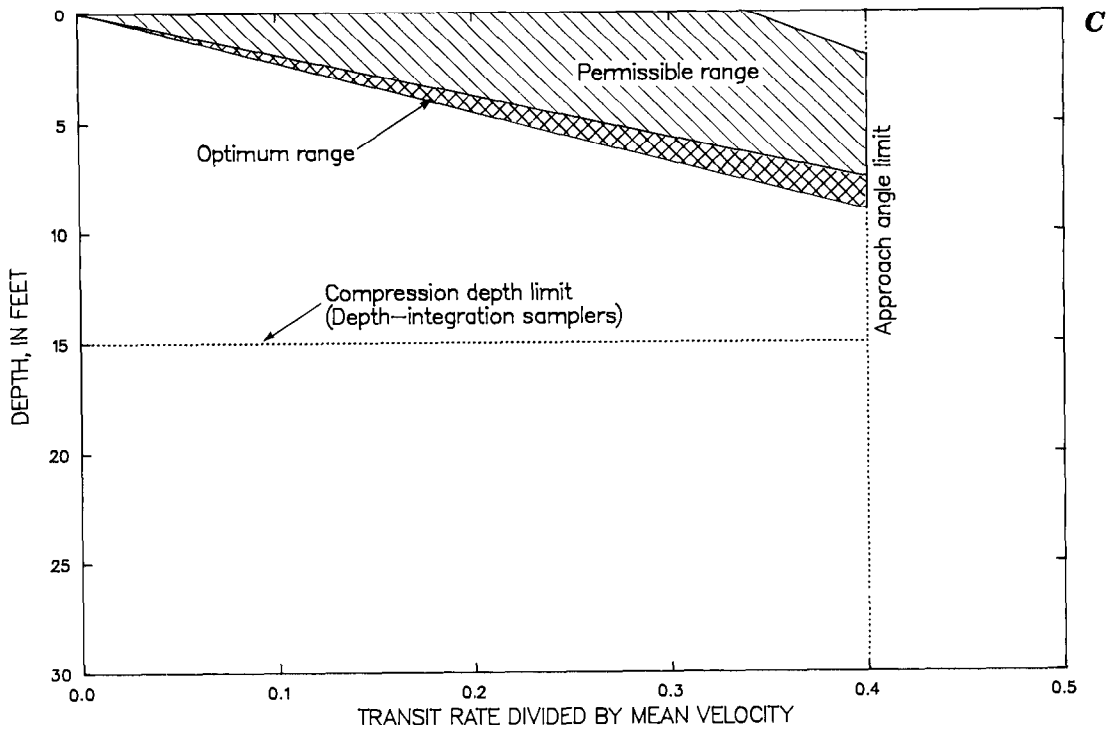

Figure 39. Variation of range of transit rate to mean velocity ratio versus depth relative to nozzle size for pint-size sample container. *A*, 1/8-inch nozzle. *B*, 3/16-inch nozzle. *C*, 1/4-inch nozzle—Continued.

sampling instructions for the D-74 depth-integrating sampler.

Figure 42 is a graphic presentation of the procedure to be followed when constructing transit-rate graphs similar to those presented in figures 39, 40, and 41, using the following nomenclature and equations:

A_n = Area of intake nozzle at entrance; square feet 1/8 inch = 8.52×10^{-5}, 3/16 inch = 19.2×10^{-5}, 1/4 inch = 34.1×10^{-5}, and 5/16 inch = 53.3×10^{-5}

d_c = Stream depth where bottom compression limit equals surface compression; feet

h_1 = Atmospheric pressure at water surface = 34 feet at sea level

Q_{max} = Maximum sample volume; cubic feet (pint bottle, 420 mL = 0.015 ft^3; quart bottle, 800 mL = 0.028 ft^3; 3-liter bottle, 2,700 mL = 0.095 ft^3)

Q_{min} = Minimum sample volume; cubic feet (pint bottle, 300 mL = 0.011 ft^3; quart bottle, 650 mL = 0.023 ft^3; 3-liter bottle, 2,000 mL = 0.071 ft^3)

r_b = Relative velocity near stream bottom; feet per second

RT = Transit rate of sampler; feet per second (rising rate equals lowering rate for EWI method)

r_s = Relative velocity at stream surface; feet per second

V_1 = Volume of container; cubic feet 1 pint = 0.01671 ft^3, 1 quart = 0.03342 ft^3, and 3-liter bottle = 0.105 ft^3

V_m = Mean stream velocity in vertical; feet per second

$$\text{Point 1}\quad \frac{RT}{V_m} = \frac{A_n r_b h_1}{V_1}$$

$$\text{Point 2}\quad \frac{RT}{V_m} = \frac{A_n h_s h_1}{V_1}$$

$$\text{Point 3}\quad d_c = \frac{h_1(r_s - r_b)}{r_{b+1}} =$$

15 feet, for assumed velocity profile in figure 42.

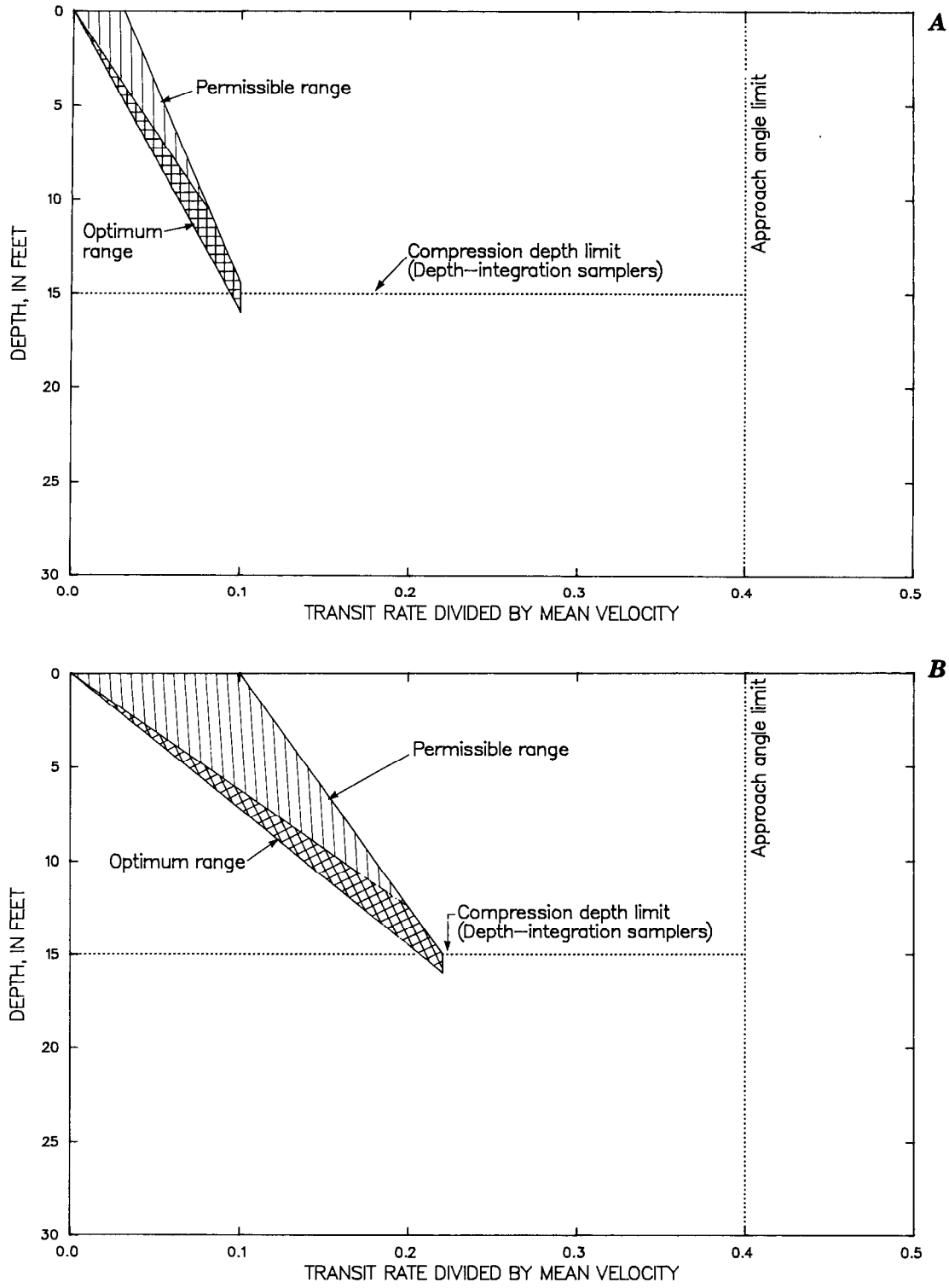

Figure 40. Variation of range of transit rate to mean velocity ratio versus depth relative to nozzle size for quart-size sample container. *A*, 1/8-inch nozzle. *B*, 3/16-inch nozzle. *C*, 1/4-inch nozzle.

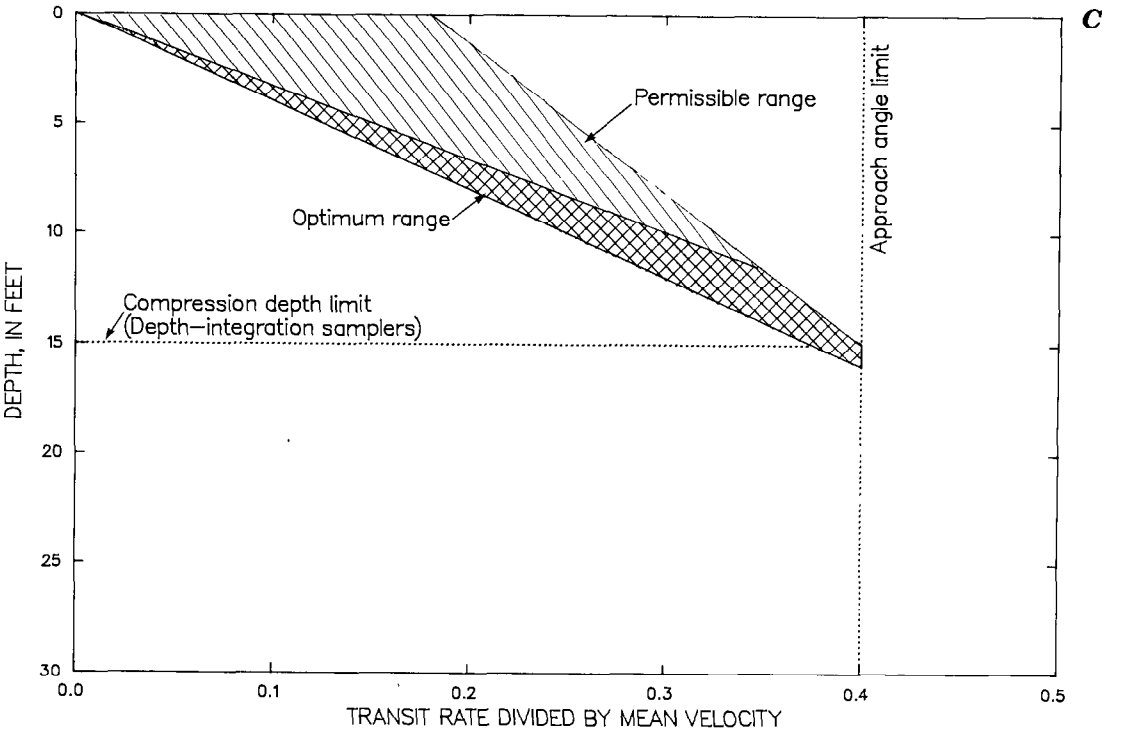

Figure 40. Variation of range of transit rate to mean velocity ratio versus depth relative to nozzle size for quart-size sample container. A, 1/8-inch nozzle B, 3/16-inch nozzle. C, 1/4-inch nozzle—Continued.

$$\text{Point 4}\ \frac{RT}{V_m} = \frac{20\ A_n}{Q_{max}}$$

$$\text{Point 5}\ \frac{RT}{V_m} = \frac{20\ A_n}{Q_{min}}$$

For points 4 and 5, the depth is arbitrarily taken at 10 feet to facilitate plotting. Also, the following sample vertical velocity profile is assumed:

Relative depth	*Velocity/ mean velocity in vertical*
surface	1.16
.1	1.17
.2	1.16
.3	1.15
.4	1.10
.5	1.05
.6	1.0
.7	.94
.8	.84
.9	.67
1.0 bottom	.5

The technique for use of figures 39, 40, and 41 to determine the transit rate to be used in a given situation depends upon (1) the depth of the sample vertical, (2) the mean velocity of the vertical, (3) the nozzle size being used, and (4) the sample-bottle size used in the sampler. An example of transit-rate determination is presented in figure 43. The nozzle size and sample-bottle size must be known so the proper figure can be selected. In this case, a 3 /16-inch nozzle and 1-pint bottle will be used. The depth and mean velocity of the sample vertical also must be known. For this example, a depth of 10 feet and mean velocity of 2 ft/s are assumed. To determine transit rate for this example (1) select the depth of the sample vertical (10 feet); (2) draw a line perpendicular to the depth on the vertical scale that terminates at the center of the optimum range; (3) read the value of RT/V_m from the horizontal scale corresponding to this point (0.28); and (4) multiply the RT/V_m value by the mean velocity (V_m = 2 ft/s) to determine the transit rate (RT = 0.56 ft/s). Note that, if the same nozzle, depth, and mean velocity were used with a quart sample container in lieu of the pint container (fig. 40*B*), an RT value of 0.30 ft/s would be used, reducing the transit rate by almost one-half.

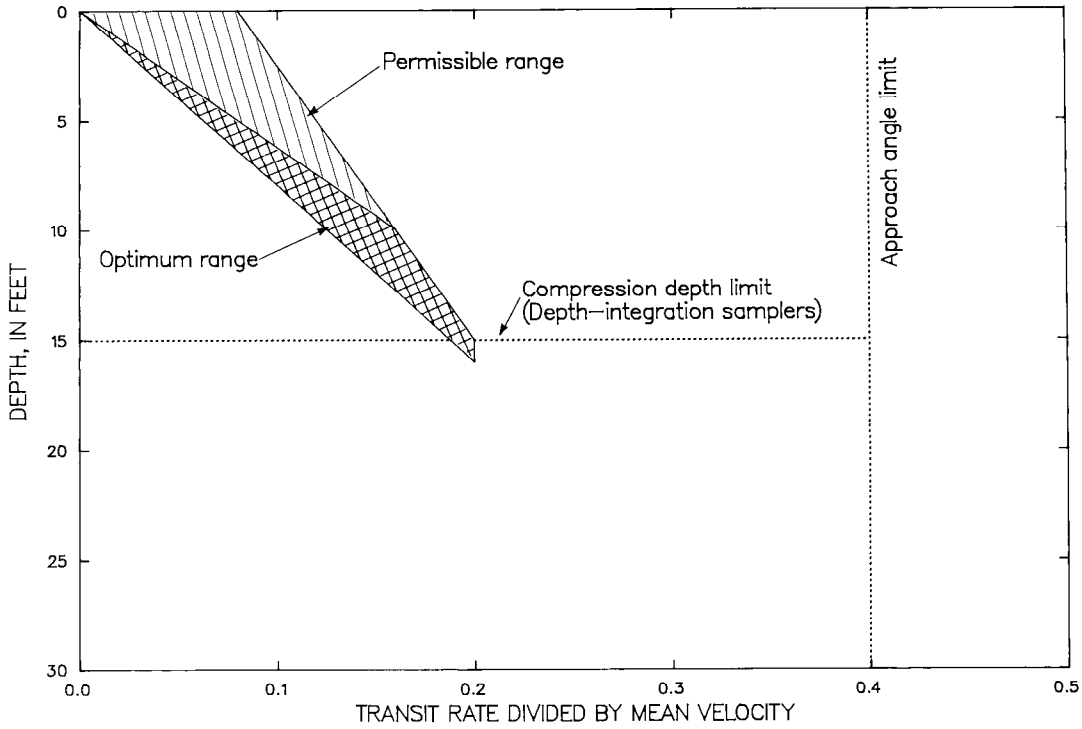

Figure 41. Range of transit rate to mean velocity ratio versus depth for 5/16-inch nozzle on a 3-liter sample bottle.

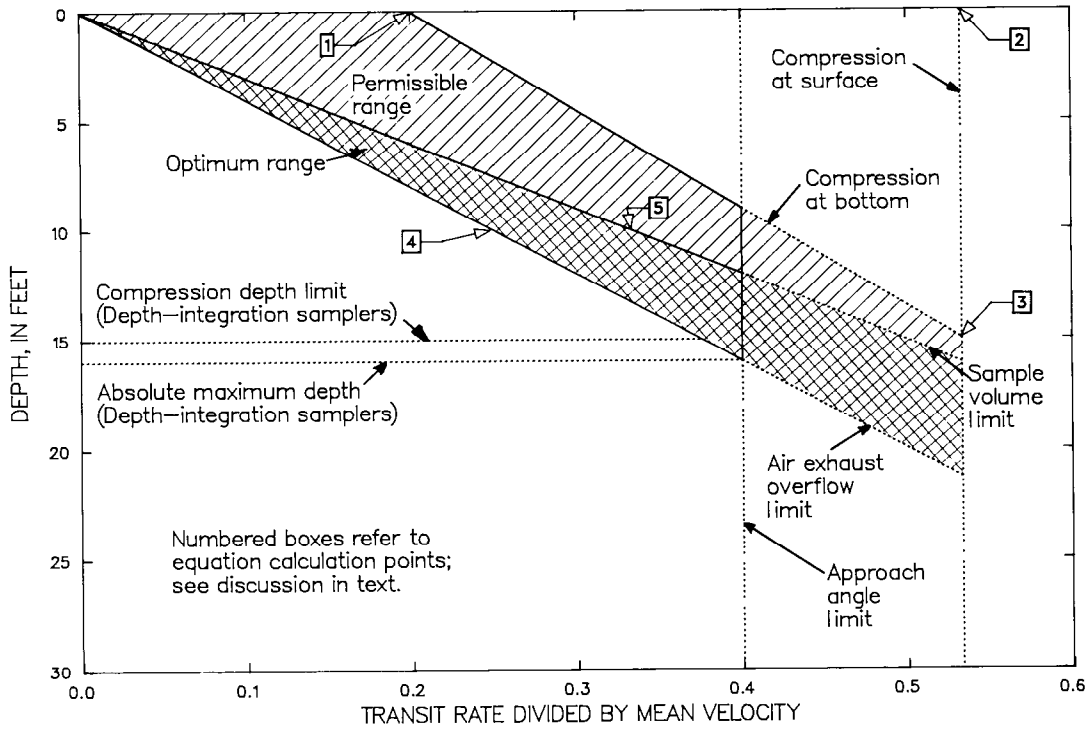

Figure 42. Construction of a transit-rate determination graph (see text for explanation of numbered points).

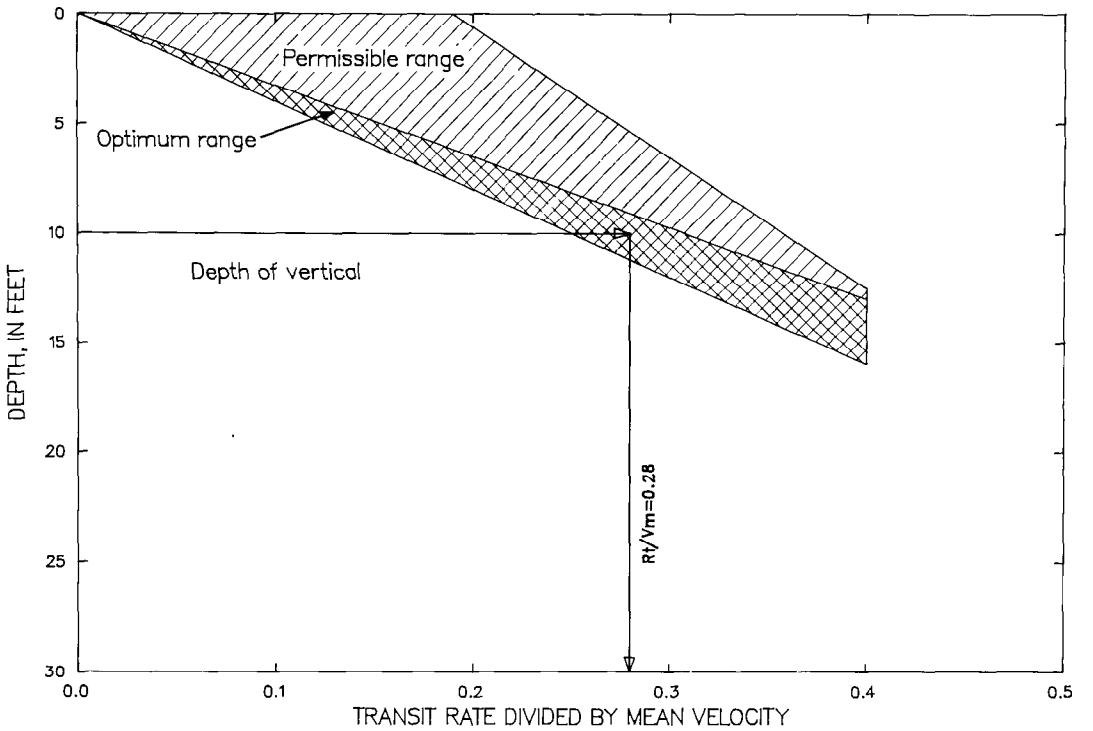

Figure 43. Example of transit rate determination using graph developed for 3/16-inch nozzle and a 1-pint sample container (see text for discussion).

Use of transit rates determined from the optimum range of figures 39, 40, or 41 will yield a representative sample of adequate volume to provide for laboratory analysis and avoid overfilling. In some instances, however, sampler operation within the optimum range is not possible. Under these conditions, operation using a transit rate determined from the permissible range is acceptable. In these cases, it should be realized that a representative sample can still be obtained, but the sample volume may be less than adequate for laboratory purposes and, therefore, more integrations may be required at each vertical to obtain the necessary volume of sample.

Additional explanation and qualifications with respect to the transit rate for depth-integrated suspended-sediment sampling include the following:

1. For cable-suspended samplers, the instantaneous actual transit rate, RT_a, may differ considerably from the computed rate, RT, if V_m exceeds about 6 ft/s and if the sampler is suspended from more than 20 feet above the water surface. Under such conditions, the sampler is dragged downstream, and the indicated depth is greater than the true depth. Corrections for indicated depth are given by Buchanan and Somers (1969, p. 50–56) for various angles and lengths of sounding line used for suspension of a weight in deep, swift water. The correct depth then would be used to enter in figures 39, 40, and 41 to determine the appropriate transit rate.

2. In theory, the allowable RT may be greater than 0.4 V_m, and sampling depth thereby increased if the sampler is cable suspended and capable of being tilted somewhat in the direction of vertical movement (that is, nozzle is slightly down when sampler is lowered and slightly up when sampler is raised, due to the effect of vertical forces on the horizontal tail-fin stabilizer). On the other hand, if the sampler cannot be tilted, the velocity at the bottom of the vertical is much less than V_m, and there is a heavy concentration of suspended sand near the bed, the use of an RT value near the 0.4 V_m limitation may cause RT to approach or even exceed the actual velocity near the bed and thus cause an excessive error in the collection of sand particles. The approach-angle theoretical depth limits will, of course, be less if either the downward or the upward transit rates, RT_d or RT_u, are different from RT. However, determining the attitude of the sampler during actual use is difficult at best and impossible under turbid flow conditions. For this reason, varying either RT or sampling beyond recommended limits is

not advisable and probably not necessary because small errors during descent will probably be cancelled during ascent.

3. The air-compression lower limit is based on the assumption that a uniform velocity distribution exists throughout the vertical. Actually, the velocity varies with the depth throughout the vertical. Therefore, where the velocity is considerably greater than the mean in the upper part of the vertical, the lower limit could be increased somewhat. In theory, the air-compression lower limit could be effectively increased by using a downward transit rate, RT_d, where RT_d is less than RT, and compensating for the extra filling of the bottle on the downward trip by using an upward transit rate, RT_u, where $RT_u = RT + (RT - RT_d)$. Note: this brief discussion is presented here as an interesting concept and should not be practiced in actual field conditions, where channel configuration and velocity profiles may not represent the ideal flow conditions found in a controlled flume environment.

4. Because of possible greater deviation from the ideal relation of intake velocity to stream velocity of 1.0, the 1/8-inch nozzle should not be used if there are significant quantities of sand larger than 0.25 mm in suspension. The 1/8-inch nozzle also is less reliable than the larger nozzles where small roots and other organic fibers are suspended in the flow.

5. In the event the sampler accommodates other than a pint-sized sample container, the RT should be carefully determined because RT for a quart container may be nearly one-half of that acceptable for a pint container with a given nozzle size. The use of a sample container larger than 1 pint does not, however, increase the sample depth range, due to the air-compression depth limit. Therefore, samples should not be taken from greater than about 15 feet with a depth-integrating sampler.

Observer Samples

At many sites, collection of suspended-sediment data is required on a frequent basis. To define the sediment-discharge trends, these data could be required once daily or more often (in the case of high-flow events). Frequent suspended-sediment data collection can put extreme pressure on a project's fiscal resources as well as on the personnel involved. In order to save money, travel time and, most importantly, to ensure timely collection of data on a regular basis and during extreme events, local residents are often contracted to work as observers.

Observers usually lack technical background, but can be trained to collect cross-section samples using either the EDI or EWI method. However, due to the complexities involved in computing centroids and a lack of expertise in obtaining the stream discharge for the EDI method, this technique is not recommended for observer-operated sites. Observers most often collect samples from an established single vertical in the cross section, as previously mentioned. The best location in the cross section for a single-vertical sediment sample is determined by data collection. Generally, each new sediment-record site is carefully investigated by means of several detailed sediment-discharge measurements to determine the concentration of sediment across the stream at different discharges. These sediment data can be collected using either the EDI or EWI method.

If the single vertical is used to obtain observer-collected samples, these data must be treated much the same as point-sample data collected with a pumping sampler. That is, cross-section samples must be taken occasionally for comparison with the observer samples in order to establish adjustment coefficients. Samples should be collected at the observer's single-vertical using the observer's equipment, both before and after each cross-section sample is taken. These samples then form the basis for a coefficient that can be used to adjust the concentration of the single-vertical samples. This adjustment coefficient, or comparison of the routine single vertical with the cross section, is determined by computing the ratio of the average concentration of cross-section samples to the average concentration of single-vertical samples. This ratio then can be applied to the daily samples taken between sediment-discharge measurements. If the coefficient is consistently above or below unity, it may be desirable to change the position of the fixed routine sampling installation to a location where the coefficient would be at or near unity. Generally, if the coefficients are within 5 percent of unity, a coefficient of 1.0 is applied, unless they are consistently high or low for long periods of time. Guy (1968) illustrated methods for determining the quality of the coefficient and the number of samples needed in a sample set. Porterfield (1972) gave further details on how coefficients are used in the computation of sediment records.

During high flows, when the depth of the single vertical exceeds the theoretical 15-foot compression

depth limit of the depth-integrating sampler, the observer should try to obtain a sample by altering the technique to collect the most representative sample possible. The best collection technique under these conditions would be to depth integrate 0.2 of the vertical depth (0.2*d*), or a 10-foot portion of the vertical. These samples then can be checked and verified by collecting a set of reference samples with a point-integrating sampler. By reducing the sampled depth during periods of high flow, the transit rate can be maintained at 0.4 V_m or less in the vertical, and a partial sample can be collected without overfilling the sample container, even under conditions of higher velocities that usually accompany increases in discharge.

Sampling Frequency, Sediment Quantity, Sample Integrity, and Identification

Sampling Frequency

When should suspended-sediment samples be taken? How close can samples be spaced in time and still be meaningful? How many extra samples are required during a flood period? These are some questions that must be answered because timing of sample observations is as important to record computations (see Porterfield, 1972) as is the technique for taking them. Answering such questions is relatively easy for those who compute and assemble the records because they have the historical record before them and can easily see what is needed. However, the field person frequently does not have this record and certainly cannot know what the conditions will be in the future.

Observers should be shown typical hydrographs or recorder charts of their stations or of nearby stations to help them understand the importance of timing their samples so that each sample yields maximum information. The desirable time distribution for samples depends on many factors, such as the season of the year, the runoff characteristics of the basin, the adequacy of coverage of previous events, and the accuracy of information desired or dictated by the purpose for which the data are collected.

For many streams, the largest concentrations and 70 to 90 percent of the annual sediment load occur during spring runoff; on other streams, the most important part of the sediment record may occur during the period of the summer thunderstorms or during winter storms. The frequency of suspended-sediment sampling should be much greater during these periods than during the low-flow periods. During some parts of these critical periods, hourly or more frequent sampling may be required to accurately define the trend of sediment concentration. During the remainder of the year, the sampling frequency can be stretched out to daily or even weekly sampling for adequate definition of concentration. Hurricane or thunderstorm events during the summer or fall require frequent samples during short periods of time. Streams having long periods of low or intermittent flow should be sampled frequently during each storm event because most of the annual sediment transport occurs during these few events.

During long periods of rather constant or gradually varying flow, most streams have concentrations and quantities of sediment that vary slowly and may, therefore, be adequately sampled every 2 or 3 days; in some streams, one sampling a week may be adequate. Several samplings a day may occasionally be needed to define the diurnal fluctuation in sediment concentration. Fluctuations in power generation and evapotranspiration can cause diurnal fluctuations. Sometimes diurnal temperature fluctuations result in a snow and ice freeze/thaw cycle causing an accompanying fall and rise in stage. Diurnal fluctuations also have been noted in sand-bed streams when water-temperature changes cause a change in flow regime and a drastic change in bed roughness (Simons and Richardson, 1965).

The temporal shape of the hydrograph is an indicator of how a stream should be sampled. Sampling twice a day may be sufficient on the rising stage if it takes a day or more for a stream to reach a peak rate of discharge. During the peak, samples every few hours may be needed. During the recession, sampling can be reduced gradually until normal sampling intervals are sufficient.

The sediment-concentration peak may occur at any time relative to the water discharge; it may coincide with the water-discharge peak or occur several days prior to or after it. Hydrographs for large rivers, especially in the Midwest, typically show water-discharge peaks occurring several days after a storm event. If the sediment concentration has its source locally, the sediment peak can occur a day or more prior to the water-discharge peak. In this case, the receding limb of the sediment-concentration curve will nearly coincide with the lagging water-discharge peak. In this event, intensive sampling logically should

be done prior to the water-discharge peak. Detailed sampling of hydrograph peaks during the initial stages of a monitoring program will help determine when the sediment-sampling frequency should be increased and decreased in order to optimize the sediment-sampling effort relative to peak-flow conditions.

Intermittent and ephemeral streams usually have hydrograph traces in which the stage goes from a base flow or zero flow to the maximum stage in a matter of a few minutes or hours, and the person responsible for obtaining the samples frequently does not know when such an event is to occur. A sampling scheme should be designed to define the sediment discharge by taking samples during the rising stage, then the peak stage and the recession. Generally, adequate coverage of the peak is obtained if samples on the rising limb are four times as frequent as samples collected during the recession. For example, if the recession is best sampled on a bi-hourly basis, the rising limb should be sampled every one-half hour.

Elaborate and intensive sampling schedules are not required for each and all events on small streams that drain basins of rather uniform geologic and soil conditions because similar runoff conditions will yield similar concentrations of sediment for the different runoff events. Once a concentration pattern is established, samples collected once or twice daily may suffice, even during a storm period (Porterfield, 1972).

Streams draining basins with a wide variety of soils and geologic conditions and receiving uneven distributions of precipitation cannot be adequately sampled by a rigid, predetermined schedule. Sediment concentration in the stream depends not only on the time of year, but also on the source of the runoff in the basin. Thus, each storm or changing flow event should be covered as thoroughly as possible, in a manner similar to that described for intermittent and ephemeral streams.

The accuracy needed in the sediment information also dictates how often a stream should be sampled. The greater the required accuracy and the more complicated the flow system, the more frequently it will be necessary to obtain samples. This increase in sampling frequency—with the added costs of laboratory analysis—greatly increases the cost of obtaining the desired sediment information. Often, however, the record may actually cost less when adequate samples are collected than when correlation and other synthetic means must be used to compute segments of a record because of inadequate sampling.

Stream-sediment stations may be operated or sampled on a daily, weekly, monthly, or on an intermittent or miscellaneous schedule. Usually, those operated on a daily basis are considered adequate to yield the continuous record. One should be mindful that each sample at a specific station costs about the same amount of money, but the amount of additional information obtained often decreases with each succeeding sample after the first few samples are taken. Sometimes samples obtained on a monthly basis yield more information for the money than those from a daily station, although there is a danger that too little information may be of no value or may even be misleading. For a given kind of record, the optimum number of samples should be a balance between the cost of collecting additional samples and the cost of a less precise record.

The frequency of collection of bed-material samples depends upon the stability of the streambed at the sample site. In many cases, seasonal samples may be adequate to characterize the distribution among particles comprising the bed. However, samples should be obtained whenever possible during high-flow events in order to describe the composition of bed material as compared to its composition during periods of normal or low flow. Particularly important is the collection of bed-material samples following high flows that have inundated the flood plain and greatly altered the streambed configuration.

Sediment Quantity

Previous sections discussed the number of sampling verticals required at a station to obtain a reliable sediment-discharge measurement or a sample of the cross-sectional concentration. The number of cross-sectional samples required to define the mean concentration within specific limits also has been discussed. The requirements in terms of quantity of sediment for use in the laboratory to determine particle-size gradation may at times exceed the other requirements for concentration. The size range and quantity of sediment needed for the several kinds of sediment analyses in the laboratory are given in table 3. The desirable minimum quantity of sediment for exchange capacity and mineralogical analyses is based on the requirements for radioactive cesium techniques described by Beetem and others (1962).

To estimate visually the quantity of sediment entrained in a sample or series of sample bottles

Table 3. The desired quantity of suspended sediment required for various sediment analyses

[mm, millimeter; g, gram]

Analysis	Size range (mm)	Desirable minimum quantity of sediment (g)
Size:		
Sieves:		
Fine	0.062–0.5	0.07
Medium	0.25–2	.5
Coarse	1.0–16	20
Visual accumulation tube:		
Smallest	0.062–0.5	.05
Largest	0.062–2	5
Pipette	0.002–0.062	[1].8
Bottom withdrawal tube	0.002–0.062	[1].5
Exchange capacity:		
Fine	0.002	1
Medium	0.002–0.062	2
Coarse	0.062–2	10
Mineralogical:		
Fine	0.002	1
Medium	0.002–0.062	2
Coarse	0.062–2	5

[1]Double the quantities shown if both native and dispersed media are required.

requires considerable experience. It also is difficult to determine what portion of the total sample is sands (greater than 0.062 mm) because the proportion can be different from stream to stream and from time to time in the same stream. To aid in estimating such sediment quantities, it is helpful to have, in the office or laboratory, reference bottles with various known quantities and concentrations for visual inspection. The number of bottles of sample, the amount of sand, and sample concentration needed for a given kind of analysis are shown in figure 44 (G. Porterfield, written commun., 1968).

Although it is possible to conduct the laboratory operation for particle-size analysis in a manner that also will give the sediment concentration, it is best to obtain separate samples for size analysis and concentration analysis. Such "special" samples should be plainly labeled. Generally, it is desirable to instruct the observer to collect additional samples for particle-size analysis.

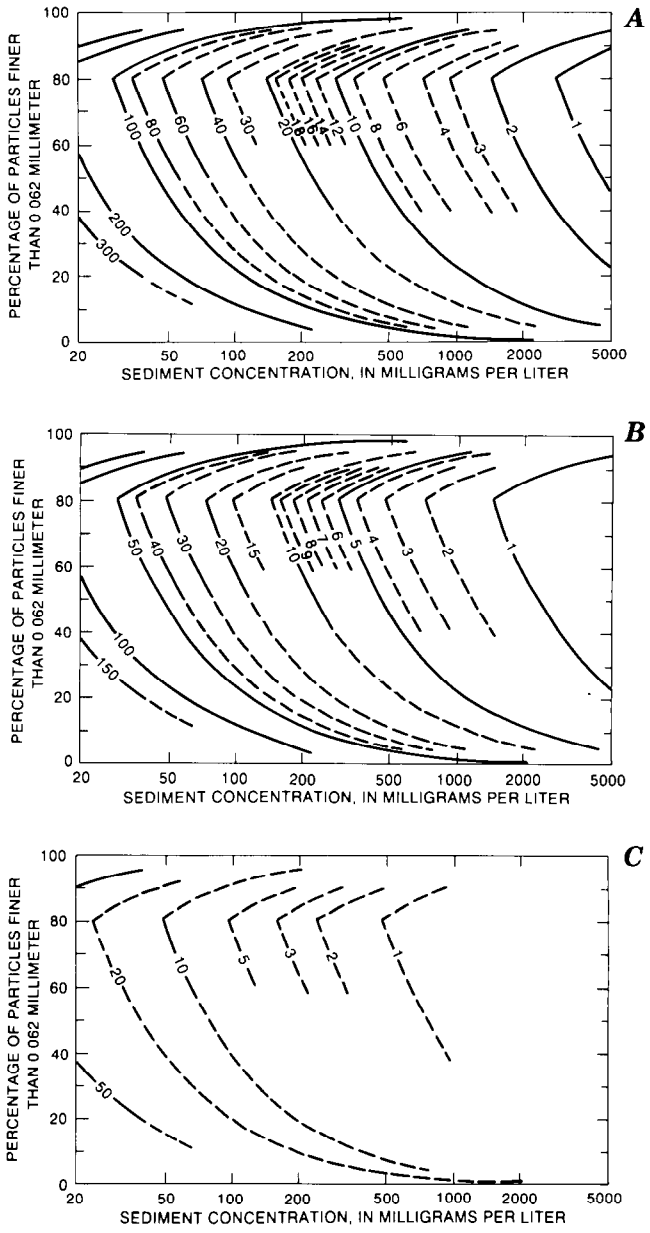

Figure 44. Minimum number of bottles containing optimum sample volume needed to yield sufficient sediment for size analysis (from Porterfield, 1972). *A*, Pint bottles each containing 400 milliliters with 1.0 gram of sediment. *B*, Quart bottles each containing 800 milliliters with 2.0 grams of sediment. *C*, Three-liter bottles each containing 2,400 milliliters with 3.0 grams of sediment.

Sample Integrity

Every sample taken by a field person should be, as previously indicated, the best sample possible considering the stream conditions, the available equipment, and the time available for sampling. Because sampling errors on sand-bed streams frequently occur in the dune regime where the nozzle of the sampler can

accidentally pick up sand from the downstream side of a dune, each sample bottle must be inspected in the field immediately after removing it from the sampler. The cost of the field and laboratory work, to say nothing of the embarrassment of a bad record, is sufficient incentive to make this simple check and, if necessary, to collect another sample.

After the first bottle is taken, it can be checked by swirling the contents of the bottle, then holding the bottle where the sand on the bottom can be seen moving. A mental note is made of the quantity of sand contained in the bottle. The second and remaining bottles then can be examined and compared with the previous bottles. Any vertical or verticals where a bottle or bottles contain a significantly different quantity of medium and coarse sand should be carefully resampled. If the check sample also contains a noticeably different amount of sand in comparison to others in the set, retain both bottles and note that the high or low concentration of sand is consistent at the vertical or verticals in question. If the check sample contains a smaller or more representative amount of sand, or if the quantity of sand is different from the first but still not normal, it may be desirable to wait several minutes to take a third bottle on the assumption that the dune face would move beyond the sample vertical. This procedure is qualitative, however, and it must be noted that the extremely high errors are more likely to be detected by this method than are small errors.

A more subtle error in sample concentration may occur when a bottle is overfilled. This error also results in too high a concentration, possibly caused by overfilling the sample bottle. Such a sample should be discarded and another sample obtained using an increased transit rate. If the transit rate or the nozzle must be changed to avoid overfilling during an EWI measurement, then it is best to discard any previous samples and resample in clean bottles. The computations required to make use of an EWI measurement having two transit rates are more costly and error prone than the minor expense of discarding samples.

Sample Identification

Although most of the information needed on sample bottles is indicated by figure 27, other information may be helpful in the laboratory and in records processing. The field person will need to keep the requirements for such processing in mind so that other explanatory notes can be recorded on the sample or inspection sheets (fig. 45). Such notes, some of which have been mentioned previously, may include:

1. Time—Sometimes operations cross zone boundaries or the use of daylight time may cause confusion.
2. Method or location—Routine vertical, EDI, or EWI cross-section sample.
3. Stationing—Is it one location or sampling vertical, or is the sample an accumulation of several verticals at different locations?
4. Unusual sample conditions—Consistent sampling of sand at this location: surface sample or dip sample.
5. Variation of desired technique—Such as change of transit rate, change of sampling vertical location, depth somewhat beyond capacity of instrument, or transit rate may have exceeded 0.4 V_m.
6. Condition of stream—Such as boils noted on water surface, soft dune bed, swift smooth water, braided stream, sandbar in cross section, or slush ice present.
7. Location in the vertical—If a point sampler is used for one-way integration, mention which direction the sampler was moving, the depth dividing the integrated portions, and the total depth.
8. Gage height—Note if the inside or outside gage was used. Note any unusual conditions that may affect the reading.
9. Collector's name.

Sediment-Related Data

Water Temperature

Water-temperature data may seem unimportant in comparison with the sediment data. However, it has a growing list of uses besides the need to help evaluate the sediment-transport characteristics of the stream. The temperature or viscosity of the flow affects sediment suspension and deposition and may affect the roughness of a sand-bed stream.

The best or preferred method to obtain the correct water temperature is to submerge the thermometer while wading some distance out in the stream. The thermometer is held beneath the water for sufficient time (about one-half minute) to allow the temperature of the thermometer to equalize with the water temperature. The stem or the scale of the thermometer is raised out of the water and held so that the etched scale

UNITED STATES
DEPARTMENT OF THE INTERIOR
GEOLOGICAL SURVEY
WATER RESOURCES DIVISION
INSPECTION SHEET

Sta No. 11-4810 Date JAN 14, 1969
Station MAD RIVER NEAR ARCATA, CALIF.
Party GAMBLE Disch 29,000
Width 191 Area 3000 Vel 9.70 Time 1000 G H 24.65 inside
G H _____ outside

SUSPENDED SEDIMENT SAMPLES Wading, (cable), ice, boat, upstr, downstr,
side bridge _____ feet, mile above, below gage and _____
Sampler D-43, (D-49), DH-48, DH-59, P-46, P-61, other _____

Method	Time	G H	No of Vert.	No of Bottles	Stations
CENT.	1030	24.67	4	8	50, 100, 150,
					200

Nozzle size 3/16 in.
Air 45° °F at 1045
Water 44 °F at 1045
Weather COOL RAINY
Flow TURBULENT
Turbidity _____

BED MATERIAL SAMPLES: Time 1210 G H 24.74 No samples 4
Sampler: DRAG Wading, cable, ice, boat, upstr, downstr, side
(bridge) 300 (feet) mile above, (below gage) and _____
Stations 50, 100, 150, 200

Stage: (Rising), falling, steady, peak Peak G H 24.77
Observer Contacted-yes ✓ no ____ Cases-in 3 out 3 res 6
INSTRUCTIONS: _____

REMARKS _____

Figure 45. Example of inspection sheet for use by field person to record the kinds of measurements made and the stream conditions observed during a visit to a sediment-measurement site.

on the stem is at right angles to the line of sight; the temperature then should be read to the nearest one-half degree. The bulb of the thermometer should always remain in the water until after the reading is obtained. The reading of a wet thermometer when exposed to the air may decrease several degrees in a matter of seconds because of evaporation, if the air is dry, or the wind is blowing. Be certain that the location in the stream where the temperature is taken is not affected by the inflow from a spring or tributary.

When it is not possible to wade out into a stream, the water temperature may be taken from a sample bottle. The thermometer should be inserted first into a bottle from near midstream to let the thermometer adjust to the approximate temperature. Then, immediately after removing the next bottle from the sampler, transfer the thermometer from the previous bottle and allow about 15 seconds for the temperature to stabilize. The thermometer should be read while the bulb of the thermometer is submerged. When removing the thermometer from a bottle, lift the thermometer about 2 inches from the bottom and shake slightly to remove sediment from the case of the thermometer. Most freshwaters freeze at 0°C; therefore, if a negative reading is obtained, an error is indicated. Brackish and brine waters freeze at temperatures somewhat less than 0°C, depending on the kind and concentration of ions present.

Stream Stage

As with temperature, stream-stage data may seem insignificant but in reality can be very important. The data may be used to construct missing gage-height records for periods of recorder failure or to verify time of sampling. Gage heights also may serve to indicate whether the observer actually obtained a sample at the time and in the manner indicated by available notes.

Remember that the gage height is defined as the water-surface elevation referred to some arbitrary gage datum. For the gage height to be considered correct, the observer or field person should always note which gage is read. The streamflow and sediment records are computed on the basis of the inside or recording gage. The observer is usually instructed to read only the outside or reference gage. Because of differences in location and the effect of velocity head, it is not expected that both gages will read the same at a given time, although some relation may exist between them as the stage changes (Buchanan and Somers, 1968; Carter and Davidian, 1968). The field person should record all stream-stage information on the inspection sheet (fig. 45).

The outside reference gage may be one of two types. The most common of those exposed continuously to the flowing stream are the staff gage and the slope gage. Under turbulent flow conditions, these exposed gages should be read by noting the average of several high and low readings made within a period of 10 or 15 seconds. It is necessary to make certain that the observers understand that the scale is divided into hundredths of a foot and not feet, inches, and fractions of an inch, and that they understand the divisions of the metric system if that is used. The other type of outside gage is the wire-weight gage or chain gage that is usually attached to a bridge railing. The weight from this type of gage is lowered so that its bottom breaks the water surface about one-half the time when there are water waves or ripples. For the wire-weight gage, the gage height is read on the scale of the drum at the pointer. For the chain gage, the reading is obtained by reference to the scale provided.

The inside gage height is usually referenced by tape from a float in a stilling well to a pointer. The stilling well is connected hydraulically to the flow of the stream. The inside reference gage should correspond to the gage height being recorded, but, as mentioned previously, it may vary somewhat from the outside gage. If the variance between inside and outside gages is unusually large and the inside gage is lagging the actual gage height of the stream, the intake should be flushed to remove any obstruction caused by sediment accumulation.

The field person should record the inside gage reading at least once each visit to ensure that the gage is working properly. Also, if the observer uses the outside gage, the field person should record the readings from both the outside and the inside gages.

Cold-Weather Sampling

Subfreezing temperatures can cause surface ice, frazil ice, and anchor ice to form on or in a stream and create many difficulties with regard to suspended-sediment sampling. The surface ice usually forms at the edges of the stream first and covers the midstream part last. If it is necessary to use surface ice for support to make holes for sampling, extreme caution should be exercised because the strength of such ice can be deceiving, especially if weakened during alternating

freezing and warm periods. If these auger holes are to be reused later, a cover of wood or some other low-cost insulating material can be used to protect them from refreezing. However, it should be realized that covers of this type may be lost if the weather warms sufficiently for the ice to break up. In some cases (to avoid walking out on the ice or if a warming trend is expected), it may be possible to prevent loss by attaching the cover to a line or to the sampler cable to allow its easy removal. If the sampler cable is used for this purpose, however, the sampler should be secured to or removed from the sampler shelter to avoid its loss by falling through the open bottom of the shelter. Suspended-sediment samplers should never be used to break through seemingly thin ice by dropping the sampler more than 3 or 4 inches because the sampler and nozzle can be damaged by the force of the drop. If the ice will not break by the sheer weight or very gentle drop of the sampler, a hole must be opened by some other means.

If the ice is too thin to safely support a person's weight, it is best not to obtain a sample for 1 or more days because winter samples are generally low in sediment concentration and are, therefore, most certainly not worth the chance of an accident. When the spring breakup occurs, the large slabs of floating ice can easily cause damage to the sampler or the support equipment or injure the operator. Under these conditions, a surface sample may be all that can be obtained between cakes of floating ice. Every effort should be made to obtain such a surface sample because the sediment concentration can, and usually does, change considerably under such conditions.

Frazil ice is composed of the small ice crystals formed at the surface in the turbulent part of the stream. The crystals are formed in a variety of shapes, from slender needles to flat flakes. They do not freeze together because of the swift current, but may bunch together to form a soft mass. This kind of ice may partly or completely clog the intake nozzle of the sampler. Sampling may be best accomplished by moving the sampler swiftly through the layer of frazil ice and then using a normal transit rate to sample the relatively ice-free region below. Often when such ice obstructs the nozzle, it will remove itself when the sampler is brought out of the water, and the only indication that the sample is in error would be that the quantity of water in the bottle is significantly less than would be expected under normal circumstances.

Anchor ice is formed on the bottom of shallow streams by radiation of heat during the colder nighttime hours. Incoming radiation and the warmer temperatures during the day allow this ice to break loose from the bottom and float to the top to mix with the frazil ice. Sometimes, when the nozzle contains frazil or small pieces of anchor ice as the sampler is brought out of the water, a subfreezing air temperature will cause the ice to freeze tight in the nozzle. If the ice freezes tight to the nozzle or if the sample bottle freezes to the sampler casing, it will be necessary to heat the sampler, by using the heater in the field vehicle, soaking the sampler in a container of warm water, or heating the nozzle and sampler head with a small propane torch. Care must be taken when employing the torch method because the gaskets in the sampler head and plastic nozzles can be damaged by the open flame. Some of these problems can be avoided by the use of two samplers; while one is thawing, the other can be used to sample.

If the sampler or samplers are kept beneath the heater in the field vehicle while the observer drives to the station or from one station to another, the first one or two verticals can be more easily sampled. The observer should be advised and encouraged to remove the nozzle from the sampler and leave the sampler head in the open position after completing the sampling. This will allow the gasket, nozzle, and air vent to dry more completely and may avoid a frozen sampler nozzle or sampler head frozen shut on the next visit.

Aside from the problems with plugged sampler nozzles, a very cold sampler may cause freezing of water between the sample bottle and the inside of the sampler. This problem can be minimized by removing the bottle as quickly as possible from the sampler after the integration is complete; otherwise, it may be necessary to heat the sampler as described above. It also should be obvious that samples in glass bottles must be protected from freezing after the measurement and during transport to the laboratory. Freezing itself does not harm a sample for sediment analysis, but a broken bottle will obviously result in loss of the sample.

If an extensive sampling program is to be carried out during the winter months in areas of extreme cold, it is advisable for the investigator to obtain DH-75 and D-77 samplers. These samplers are designed to be used in freezing conditions, as previously discussed. Several sample bottles and nozzle and cap assemblies can be taken to the site, where they can be easily changed if nozzle or air-exhaust freezeups occur during sampling.

Bed-Material Sampling

Data on the size of material making up the streambed (across the entire channel, including flood plains) are essential for the study of the long-range changes in channel conditions and for computations of unmeasured or total load.

Materials Finer Than Medium Gravel

Selection of a suitable bed-material sampler is dependent on the size of bed material to be sampled, and on stream depth and velocity. When a stream can be waded, the most practical of the standard samplers is the BMH-53 or BMH-80 (figs. 15 and 17). When sampling from a boat, these samplers can be used to depths of about 4 feet.

In use, the BMH-53 is placed in a vertical position on the streambed with the piston extended to the open end of the cylinder. The cylinder then is pushed a full 8 inches into the bed while the piston is held at the bed surface. Complete filling of the cylinder will help ensure a minimum of disturbance of the top 1 or 2 inches when the sampler is raised through the flow. When coarse sand or gravel material is being sampled, it is often necessary to pull on the piston rod while pushing on the cylinder. By pulling on the piston, a partial vacuum is created above the sample, which helps draw the sample into the cylinder. The sampler then is withdrawn from the bed and held in an inclined position above the water with the cylinder end highest. For most purposes, only the upper inch of material nearest the surface of the streambed is desired or needed in an analysis. This is obtained by pushing on the piston while the sampler is still inclined until only 1 inch of material remains in the tube. Any excess material is removed by smoothing off the end of the cylinder with a spatula or a straight pencil. The material left in the sampler is ejected into a container (usually a paper or plastic carton). An experienced field person can composite samples from the entire cross section into just a few cartons. The inexperienced field person would do well to use a separate container for each vertical. Before storing the sampler, it should be rinsed by stroking the piston a few times in the stream to remove sediment particles from the cylinder and piston seal.

The BMH-80 is used in a manner similar to that of the BMH-53. The sampler is extended to the streambed with the bucket in the open position. After the sampler contacts the bed material, the field person should keep a firm downward pressure on the sampler while closing the sample bucket, thus trapping a shallow sample of the streambed. This sampling procedure should be repeated until the streambed has been representatively sampled.

If the stream is too deep or swift for the BMH-53 or BMH-80, the BMH-60 or the BM-54 can be used. The 30-pound BMH-60 is easiest to use when stream velocities are under 2 or 3 ft/s and depths are less than about 10 feet. To use the BMH-60, suspend the entire weight of the sampler by the hanger rod and cock the bucket in the open position with the allen wrench provided. The energy thus imparted to the spring and the sharp edge of the bucket make it obvious that one must keep hands away from the bucket opening at all times. If necessary, the safety yoke may be fastened around the hanger bar while opening and cocking the bucket. After the safety yoke is removed and fastened to the tail, the sampler then can be lowered by hand or by cable and reel to the surface of the streambed. Any jerking motions made while lowering the sampler that would cause the cable to slack may release the catch and allow the bucket to close prematurely. This can happen if the water surface is struck too hard. After the cocked sampler touches the streambed and tension is released on the line, the sampler should be lifted slowly from the bed so the bucket will scoop a sample.

To remove the sample from the bucket, a carton or container is positioned under the sampler, and the bucket is opened with the allen wrench. The sampler need not be held by the hanger bar during sample removal unless considerable material is clinging to the flat plate within the bucket cavity. If removal of such material is required, the bucket should be cocked in the open position and the sample brushed into the container with a stick or small brush. When moving the sampler between verticals and when storing it in the vehicle, the bucket should be in the closed position to avoid an accidental closing and to reduce the tension on the spring. If the bucket is closed for transport as suggested, a stick, a piece of tire, or similar material should be used to cushion the force of the bucket when it is closed because the closing force is sometimes great enough to break welded joints in the mechanism (J.V. Skinner, Federal Inter-Agency Sedimentation Project, written commun., 1985).

The 100-pound BM-54 is used when velocities are greater than 2 or 3 ft/s and depths are greater than 10 feet. The BM-54 sampling action, described

previously, is similar to the BMH-60, except that the bucket opens front to back. It is used only with a cable-and-reel suspension and is rather awkward to handle when removing the sample. The techniques for taking a sample with the BM-54 are essentially the same as for the BMH-60. One important difference in operation is the use of a safety bar on the BM-54 to hold the bucket in an open position instead of the safety yoke as on the BMH-60. As noted earlier, the sampler should be stored with the bucket in a closed position and, if extended storage is anticipated, the tension on the spring should be further reduced.

A BM-54 can be used in extremely high velocities if a C-type weight is attached to the hanger bar above the sampler. If additional weights are required with the BM-54, extreme care should be taken to avoid bending and possibly breaking the hanger bar between the sampler and the C-type weight.

Personnel of F.I.S.P. have developed a heavy bed-material sampler (the BM-84, which weighs about 160 pounds). The P-61 point-integration sampler body is used to provide a large mass. The streamlined body configuration is fitted with a spring-driven sample scoop that is activated by a solenoid system similar to that used on point samplers. Otherwise, the sampler is similar to, and performs the same function as, the BM-54. The design is an attempt to cope with bed-material sampling problems encountered in the vicinity of Mount St. Helens volcano (J.V. Skinner, Federal Inter-Agency Sedimentation Project, oral commun., 1984). The weight of this configuration is increased by filling void space within the sampler body to increase the cross-sectional density of the sampler, thus increasing its stability in deep, high velocity conditions.

As previously discussed, other sampling equipment is available commercially—for example, the ponar sampler and core samplers, such as the vibra-core unit and gravity corer. These samplers can be very useful; however, careful planning of the proposed sampling project and analytical methods is essential to obtaining a representative sample and reliable data.

Materials Coarser Than Medium Gravel

Gravels in the 2- to 16-mm range can be analyzed by mechanical dry sieving; in order to obtain a representative particle-size distribution, the size of the sample to be collected must be increased with particle size. Large sediment sizes (>16 mm) are difficult both to collect and to analyze. The method now used for size determination of these very large particles involves a pebble count, in which at least 100 pebbles from a wadable streambed are manually collected and measured. A fixed grid pattern locating the sampling points can be paced, outlined by surveys, or designated by small floats. At the intersections of the fixed grid pattern, the pebble underlying the field person's toe is retrieved, and a measurement is made of the long, intermediate, or short diameters, or all three. The measurements are tabulated as to size interval, and the percentage of the total of each interval then is determined (Wolman, 1954).

Because the pebble-count method entails the measurement of the dimensions of randomly selected particles in the field, it is laborious and usually limits the number of particles counted. Too often this results in an inadequate sample of the population,

Another method for analyzing coarse particles involves the use of an instrument known as the Zeiss Particle Size Analyzer (Ritter and Helley, 1968). For the Zeiss technique, a photograph of the streambed is made during low flow with a 35-mm camera supported by a tripod about 2 meters above the streambed—the height depends on the size of the bed material. A reference scale, such as a steel tape or surveyor's rod, must appear near the center of the photograph to provide a size reference.

In the laboratory, particle diameters are registered cumulatively or individually on exponential or linear scales of size ranges (Guy, 1969). After the data are tabulated, the sizes registered on the counter of the particle-size analyzer must be multiplied by the reduction factor of the photograph, which is calculated from the reference scale in the photograph.

In nonwadable streams, a pipe dredge is useful in sampling these large particles. However, this method entails the use of equipment capable of handling extremely heavy loads and requires special attention to safety during operation.

Location and Number of Sampling Verticals

Bed-material samples are often collected in conjunction with a discharge measurement and (or) a set of suspended-sediment samples. If the discharge measurement and (or) the suspended samples are taken first, the bed-material samples should be collected at the same stations, but not necessarily from the same number of stations. By taking them at the same stationing points, any change in bed material or

radical change in discharge across the stream that would affect the sediment-discharge computations can be accounted for by subdividing the stream cross section at one or between two of the common verticals.

To avoid collection of bed-material samples from an excessively disturbed streambed, it is best to obtain the bed-material samples prior to making other measurements, especially in wadable streams. Also, by taking the bed material first, radical changes across the section in bed-material size and water discharge can be used as a basis for choosing desirable verticals for other measurements.

Most results from bed-material samples will not be noticeably affected, but it should be remembered that the sample taken with the BMH-53 or other core sampler is different from that taken with the BMH-60, BMH-80, and the BM-54. The cross section of the BMH-53 or other core sampler is constant with depth so that each increment of sample with depth is equally represented by volume. The curved buckets of the BMH-80, BMH-60, and BM-54 do not sample equal volumes of material with depth; instead, the bottom one-half inch of the 2-inch-deep bucket contains only 15 percent of the total sample, whereas the upper one-half inch contains 33 percent of the sample.

The number and location of bed-material samples required at a cross section must be adequate to provide a representative statistical population. This population should include samples collected from the entire cross section. To obtain this population, the logical procedure is to use the results from a rather detailed set of 10 to 20 uniformly spaced bed-material samples taken from the cross section. Some studies may require that flood-plain deposits be represented in the bed-material sampling scheme to get a representative population.

Sample Inspection and Labeling

As samples are obtained across the stream, the field person should visually check and compare each sample with the previous samples to see if the material varies considerably in size from one location to the next. Samples of different sizes and (or) weight should not be composited. If a given sample does contain considerable coarser or finer material, another sample should be obtained about a foot from the original location. If, after two or three tries in the vicinity of the first sample, no appreciable difference is noted, the first sample should be retained. Small deposits of material that are coarser or finer than most of the bed material are not considered representative of the bed-material size for the stream cross section.

Proper labeling of bed-material samples is not only necessary for future identification but also provides important information useful in the laboratory analysis and the preparation of records. Information desired on each bed-material sample carton should include:

Station Name
Date
Time
Gage height
Water temperature
Stationing number
Bed form and flow conditions
Carton number of the set
Kind of sampler used
Purpose of sample or special instructions for analysis and computations
Initials of field person

Bedload Sampling Technique

The sediment moving in the unsampled zone (see fig. 1) comprises suspended sediment and bedload. Bedload is the sediment that moves by sliding, rolling, or bouncing along on or within a few grain diameters of the streambed.

Although many investigations have provided extensive knowledge in the areas of how bedload moves in a channel and how pressure-differential bedload samplers operate, a great deal more work in these areas is needed. The following paragraph, taken from Hubbell (1964, p. 2), is still appropriate:

> In the past, attempts have been made to determine the bedload discharge in three general ways: by direct measurement with some type of apparatus, by definition of physical relations from which the bedload could be estimated, and by quantitative measurements of the results of some sedimentation process such as erosion or deposition. Unfortunately, direct-measuring apparatus have been useful for only a very limited range of sediment and hydraulic conditions; the definition of physical relations has not been complete enough to estimate precisely the bedload discharge; and the quantitative measurements have supplied information only on the characteristics of the reach that was studied. As a result, no single apparatus or procedure, whether theoretical or empirical, has been universally accepted as completely adequate for the determination of bedload discharge over the wide range of sediment and hydraulic conditions in nature.

Despite these difficulties, the hydrologist often is called upon to provide estimates of bedload transport from measurements. The purpose of this section is not only to outline instructions governing the collection of bedload samples, but also to present a discussion of variations in bedload-discharge rate, the problems involved in collecting samples, and considerations in the design and development of a sampling program to define bedload movement.

Bedload discharge can be extremely variable. Variations can occur both spatially and temporally during steady-flow conditions, as well as with changes in stream discharge. In order to collect a sample that represents the mean bedload-discharge rate, all variations must be taken into account.

Even for constant flow conditions, the temporal variation of bedload transport rates at a given point in a cross section is quite large. When dunes are present, bedload discharges are zero, or near zero, in the troughs, increase progressively along the upstream side of the dune, and are maximum at the crest. Even in streams with gravel beds, the bedload appears to move in cycles or slugs (Emmett, 1981). These variations have been measured in the laboratory flume by Hubbell and others (1981) and in the field by Emmett (1975) and Carey (1985) (fig. 46).

Temporal variation in sampled bedload rates collected at steady-flow conditions at a single vertical are primarily dependent on the ratio of sampling time to the time it takes one dune, cycle, or slug to pass by

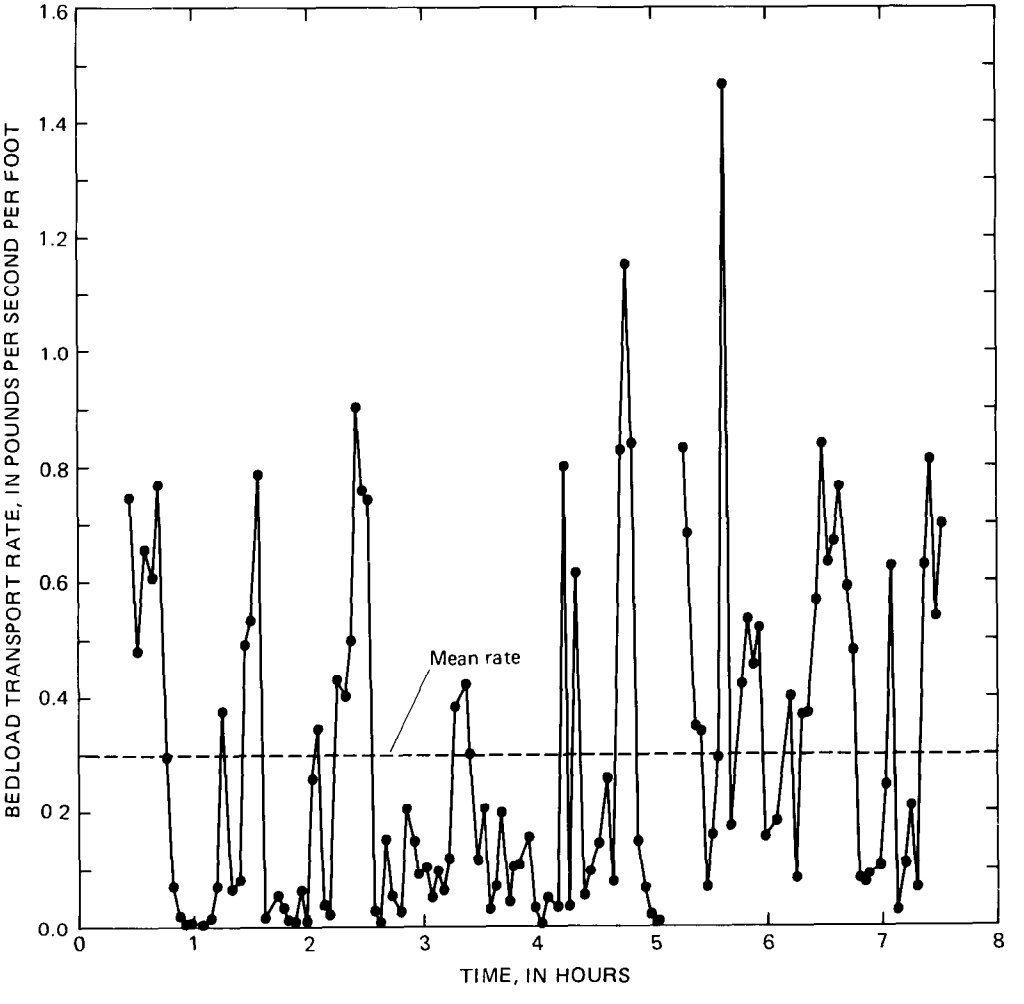

Figure 46. Temporal variation of bedload transport rates for 120 consecutive bedload samples from a stream with constant water discharge (Carey, 1985).

the sampling point. Obviously, if the sampling time were equal to the cycle period or several times greater than the cycle period, the temporal variation at a single sampling point would be small. However, as the sample time becomes less with respect to the cycle time, the temporal variation can become quite large.

Einstein (1937) and Hamamori (1962) both developed theoretical distributions to describe the temporal distribution of bedload transport rates at a vertical. Einstein based his distribution on the assumption that bedload particles move in a random series of steps and rests, with the particles generally resting a much longer period of time than they are moving. Hamamori's distribution was derived to define the temporal variation when dunes are present on the bed. Figure 47 shows a comparison of Einstein's and Hamamori's distributions. Einstein's T is defined as the nondimensional sampling time measured in terms of the average rest period. Einstein's T = 2 distribution (sample time equals the length of two average rest periods) and Hamamori's distribution are nearly identical. As T increases (sampling-time increases), the two theoretical distributions depart from one another, and Einstein's distribution indicates reduced variability.

The temporal variations in bedload transport rates measured by Carey (1985) at a single vertical in a sand-bed stream in Tennessee are shown in figure 46. The cumulative probability distribution of bedload discharges measured by Carey fit the theoretical distribution developed by Hamamori. As indicated in the figure, even for a constant flow condition, the rate determined from a sample taken from a single vertical at a point in time may differ considerably from the mean bedload discharge at that vertical. This extreme temporal variability in bedload transport rates has been known since at least 1931 (Hubbell, 1964).

The spatial or cross-channel variation in bedload discharge is usually significant. Typically, bedload transport rates vary from zero or small near banks through larger values toward midstream. The mean cross-channel distribution of bedload discharge may vary uniformly (fig. 48*A*), may be uniformly consistent (fig. 48*B*), may be erratic with varying tendencies (fig. 48*C*), or may be an unpredictable combination of varying tendencies (fig. 48*D*). Each river is likely to have a unique combination; adjacent reaches of the same river may have different configurations, and these configurations are likely to change

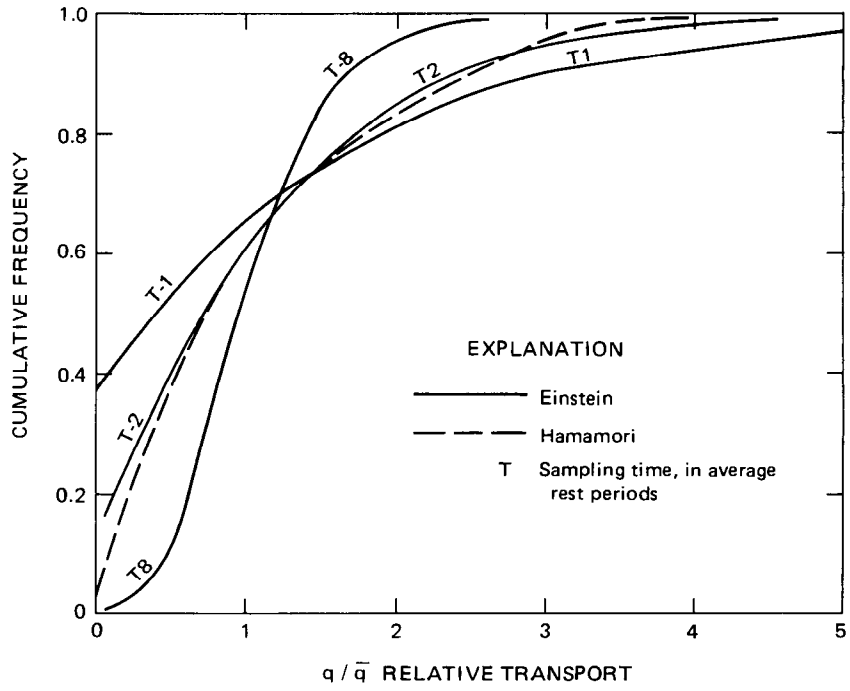

Figure 47. Comparison of cumulative probability distributions of bedload transport rates predicted by Einstein (1937) and Hamamori (1962) (D.G. McLean, University of British Columbia, written commun., 1986).

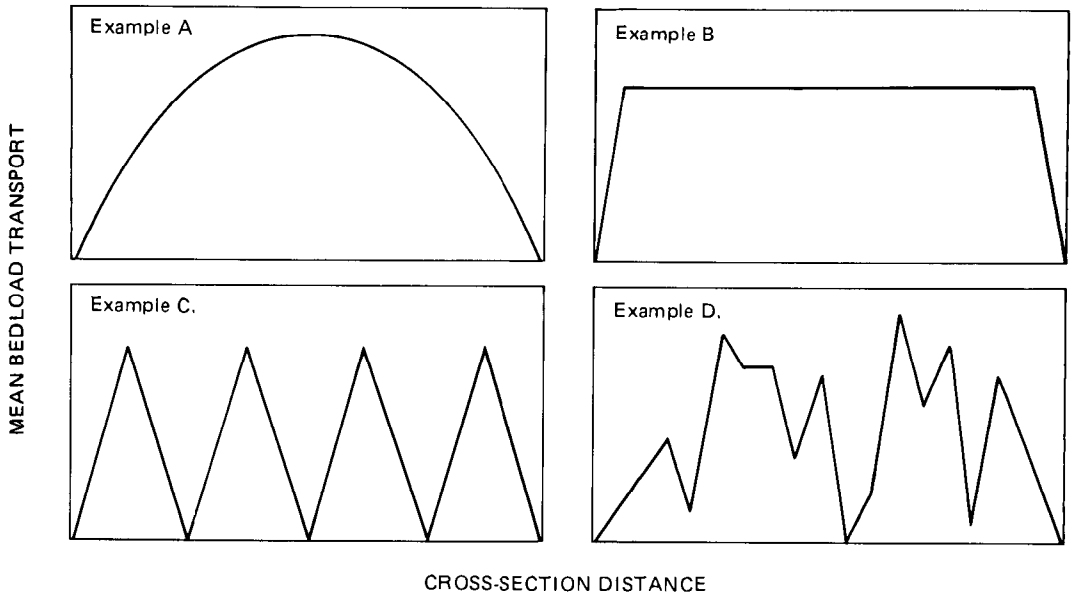

Figure 48. Examples of possible distribution of mean bedload transport rates in a cross section. *A*, Discharge varies uniformly. *B*, Discharge is uniformly consistent. *C*, Discharge is erratic with varying tendencies. *D*, Discharge is an unpredictable combination of varying tendencies.

with changing flow conditions (stages). There is little proven basis for predicting spatial variability.

The temporal and spatial variations in transport rates of bedload discharge that occur under steady-flow conditions are amplified when the stage changes rapidly. Because of these temporal and spatial variations, many samples have to be collected at many verticals in the cross section to ensure an accurate estimate of the mean bedload discharge. The samples also would have to be collected over a short enough period of time to avoid any change in transport rates due to changing stage. In most field sampling programs, the number of samples collected must represent and compromise between accuracy and economic or physical feasibility.

Another major problem encountered in bedload sampling is that of collecting a representative sample. To collect a representative sample, the sampler must (1) trap, during the sampling period, all bedload particles that would normally have passed through the width occupied by the sampler; and (2) reject all particles that normally would not have passed through the width during the same period. The degree to which this is accomplished is termed the "sampling efficiency," which is defined as the ratio of the mass of bedload collected to mass of bedload that would have passed through the sampler width in the same time period had the sampler not been there (Hubbell, 1964). For perfect representative sampling, the sampling efficiency should be 1.0 (or 100 percent) for all sizes of bedload particles in transport at the sampling point during the sampling period.

Currently, the most commonly used bedload sampler is the Helley-Smith sampler (see page 25 for discussion of recommended samplers). Over 3,000 of these samplers have been placed in use since the model was introduced in the early 1970's. It should be understood that the Helley-Smith is not a true bedload sampler because it collects some particles moving in suspension. As previously noted, bedload moves on or very near the streambed. Depending on the size of the unsampled zone, the Helley-Smith has the potential to collect a sample from the entire unsampled zone. Even if the Helley-Smith sampler has a sampling efficiency of 1.0, the total sediment discharge cannot necessarily be calculated by simply summing the measured suspended-sediment discharge and the measured bedload discharge. Figure 49 shows the percent error involved in computing total sediment discharge for a particular size range by summing the measured suspended-sediment discharge (Q_{sm}) and the bedload discharge measured with a Helley-Smith sampler (D) for that particular size range.

In order to make bedload sampling practical, methods must be used that minimize the number of samples required to obtain a reasonable estimate of the mean cross-sectional bedload discharge. Field

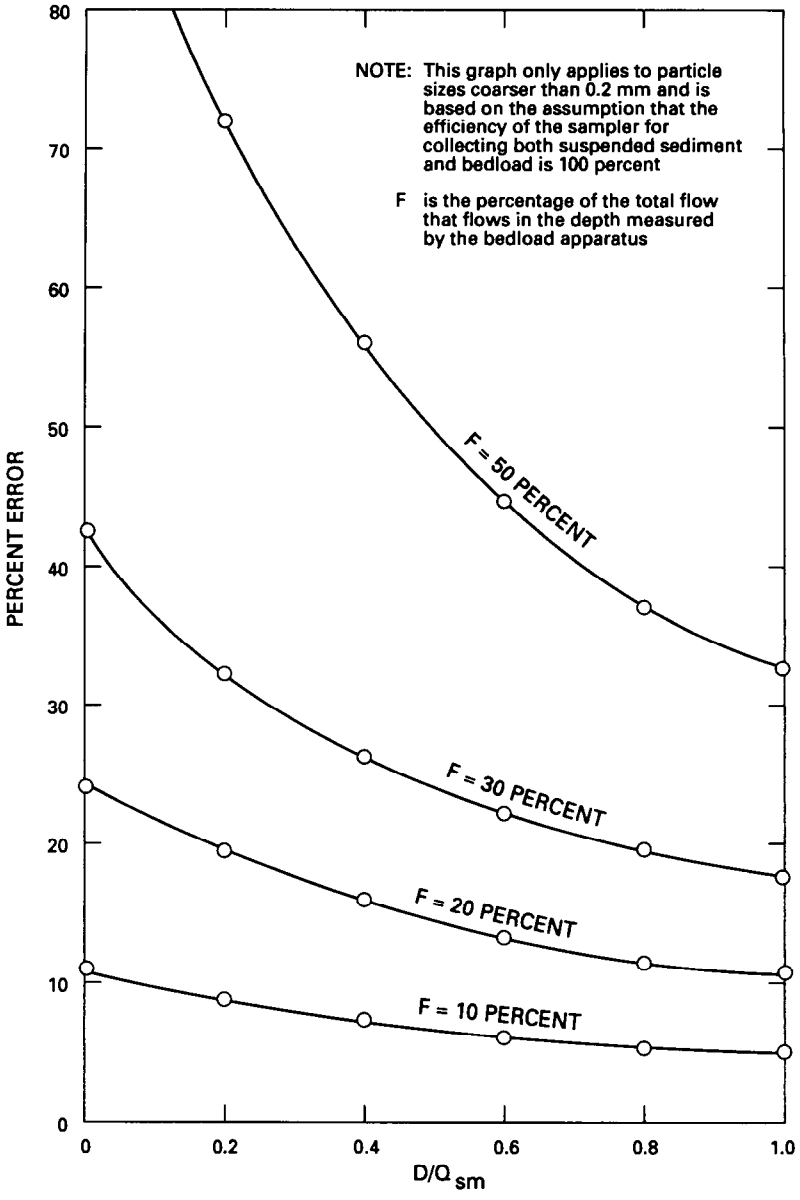

Figure 49. Percent error due to computing total sediment discharge of a size range by summing measured suspended-sediment discharge (Q_{sm}) and bedload discharge measured with a Helley-Smith sampler (D).

experience has shown that the collection of about 40 individual bedload transport rate measurements per cross-section sample is, in most cases, practical and economically feasible (Emmett, 1980a). The following general methods can be used to collect the samples.

(1) Starting at one bank and proceeding to the other, collect one sample per vertical at 20 evenly spaced verticals in the cross section, return to the bank, and repeat the process. We will refer to this method as the single equal-width-increment (SEWI) method (fig. 50). The time the sampler is left on the bottom should be equal for all verticals in a given cross section. The time the sampler is left on the bottom need not be the same for both cross sections collected. This procedure was first introduced by Emmett (1980a) and is widely used. The samples are collected at the midpoint of the evenly spaced increments. Samples collected in this manner can be composited for analytical purposes; however, a better understanding of the local bedload transport characteristics is gained if each vertical sample is analyzed individually.

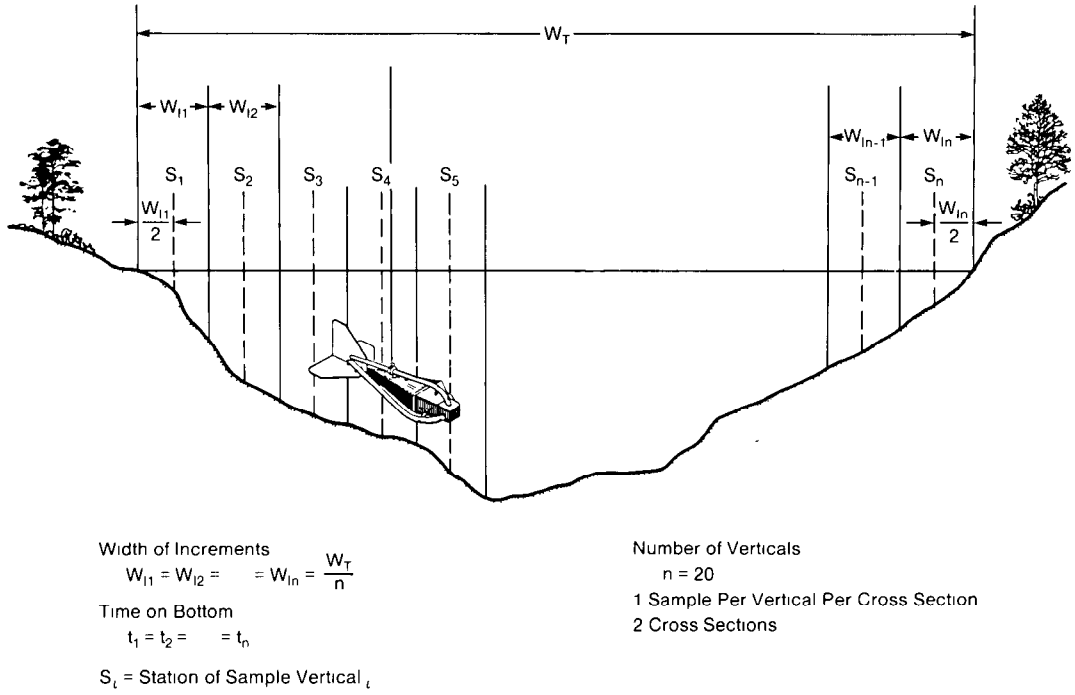

Figure 50. Single equal-width-increment bedload-sampling method.

(2) Starting at one bank and proceeding to the other, collect one sample at 4 or more evenly spaced verticals, return to the starting bank, and repeat the process multiple times until a total of 40 samples is collected. We will refer to this method as the multiple equal-width-increment (MEWI) method (fig. 51). If the sample collected at each vertical is bagged separately, the time the sampler is left on the bottom need not be equal at all verticals. If samples collected in a cross section are to be composited, sample times at each vertical in the cross section must be equal. As in the SEWI method, samples are collected at the midpoint of the evenly spaced increments.

(3) Starting at one bank and proceeding to the other, collect one sample from 4 or more unevenly spaced verticals, return to the starting bank, and repeat the process until a minimum of 40 samples is collected. We will refer to this method as the unequal-width-increment (UWI) method (fig. 52). This method requires some prior knowledge of the depths and velocities across the section. The selection of where to place the verticals in the UWI method depends, to a certain extent, on which method is to be used to calculate the bedload discharge. If the midsection method is used (see "Computation of Bedload-Discharge Measurements" section for explanation of calculation methods), the sampling verticals should be spaced unevenly in an attempt to delineate equal portions of the cross-section bedload discharge. To the extent possible, samples should be collected midway between breaks in the lateral bed slope and closer together in segments of high velocity and changing lateral bed slope. If the mean-section method is used to calculate the bedload discharge, sample verticals should be placed at the break points in the lateral cross-sectional distribution curve of mean bedload transport rate where the rate changes from one trend to another (that is, break in slope). At most sections, the lateral distribution in mean rates, once defined, can be related to velocity and lateral bed topography.

To quantify the approximate magnitude of sampling errors that could result from various sampling situations, Hubbell and Stevens (1986) developed a bedload transport simulation model. They used Hamamori's (1962) distribution to simulate temporal variations at the equally spaced sampling verticals and assumed that the sampler used had a 100-percent sampling efficiency. The results of test runs using two different spatial variations are shown in figure 53. In the first case, the lateral distribution of mean bedload transport rates is fairly uniform across the cross section and, in the second case, it is skewed. If these results were used to estimate maximum possible error for using the SEWI and MEWI methods, in the first

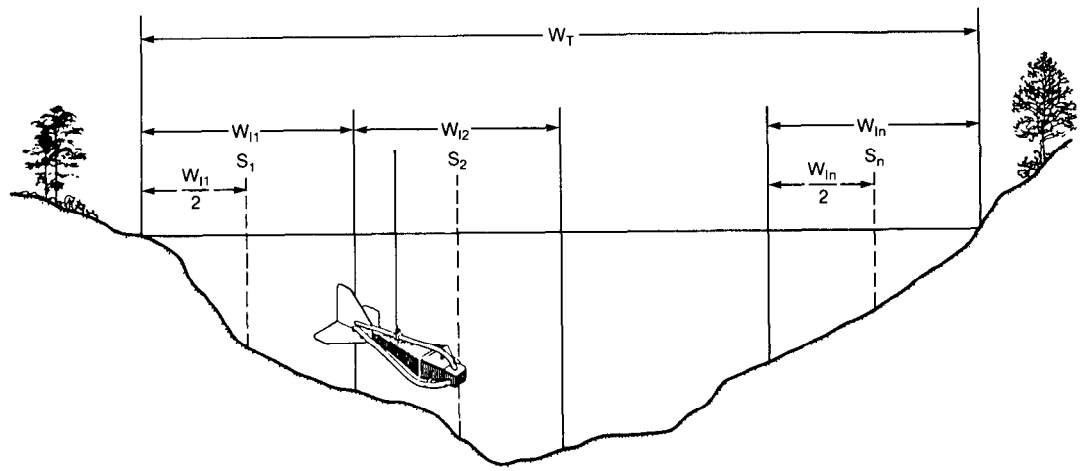

Width of Increments
$W_{I1} = W_{I2} = \quad = W_{In} = \frac{W_T}{n}$

Time on Bottom at $_i$
$t_1 \neq t_2 \neq \quad \neq t_n$

S_i = Station of Sample Vertical $_i$

Number of Verticals
n = 4-5
1 Sample Per Vertical Per Cross Section
8-10 Cross Sections

Figure 51. Multiple equal-width-increment bedload-sampling method.

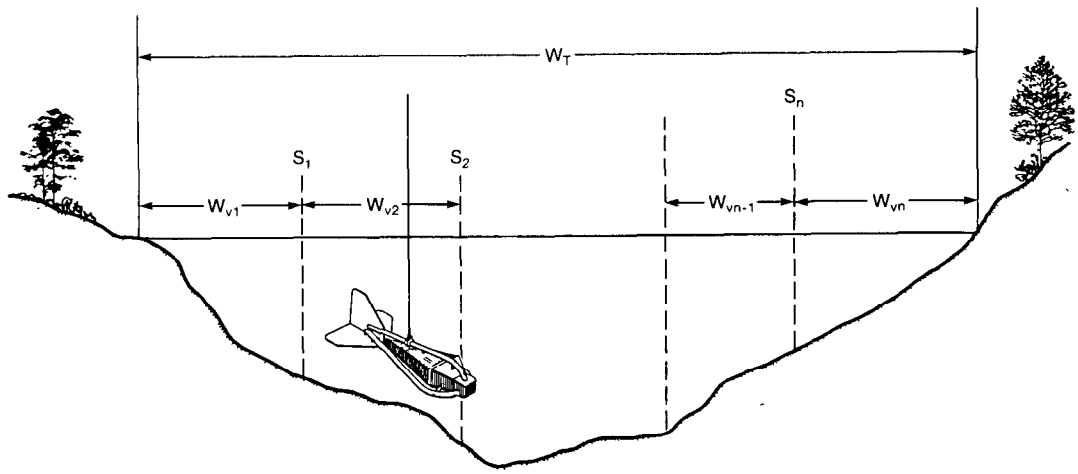

Width Between Sampled Verticals
$W_{v1} \neq W_{v2} \neq \quad \neq W_{vn}$

Time on Bottom
$t_1 \neq t_2 \neq \cdots \neq t_n$

S_i = Station of Sample Vertical $_i$

Number of Verticals
n = 4-10
1 Sample Per Vertical Per Cross Section
4-10 Cross Sections

Figure 52. Unequal-width-increment bedload-sampling method.

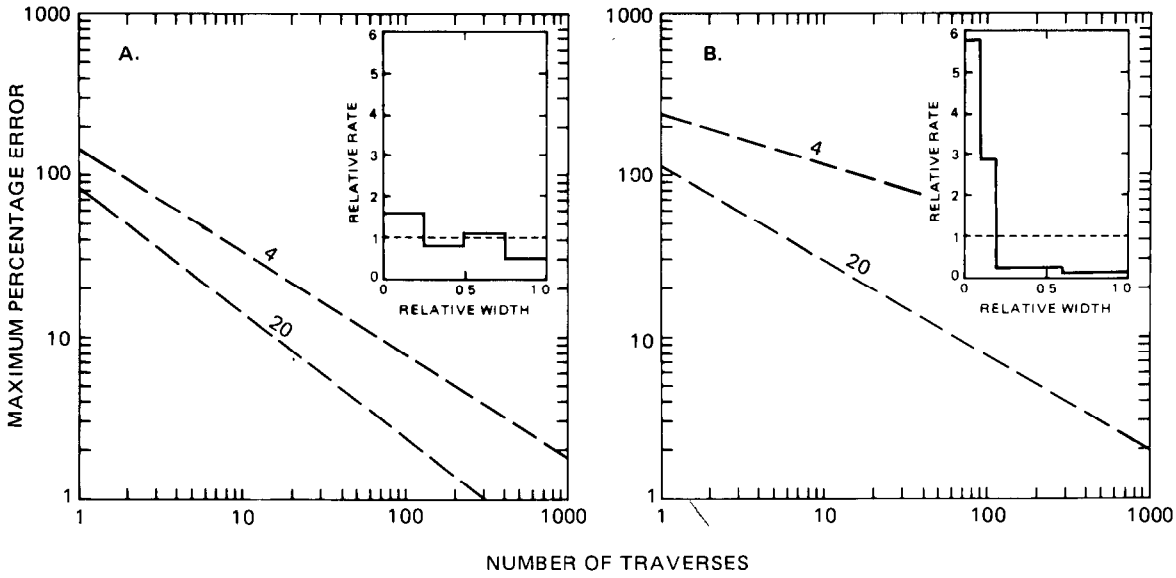

Figure 53. Variation in maximum probable errors with number of sampling traverses at 4 and 20 equally spaced verticals at cross sections with different bedload transport rates (modified from Hubbell and Stevens, 1986). *A*, Fairly uniform transport rates. *B*, Skewed transport rates.

case, the MEWI method would give a lower maximum possible error (35 percent) than would the SEWI method (50 percent). In the second case, however, using the SEWI method would result in a maximum error of 80 percent and using the MEWI method would result in a maximum error of 120 percent. The maximum probable error with the UWI method cannot be evaluated from figure 53.

From the previous discussion, it is obvious that no one method works best in all situations and that no one standard sampling protocol can be used at all stations. This should come as no surprise. There are two acceptable methods for collecting suspended-sediment samples (EWI and EDI). Both work equally as well as the other but are better suited to different stream conditions and cross-sectional sediment distributions. Likewise, a unique sampling protocol must be derived for each site at which bedload-discharge data are to be collected. Probably the best way to start sampling at a site is to do multiple sets of complete SEWI and MEWI or UWI measurements each time the site is visited and over as many flow ranges as possible. Unfortunately, human resources and budget restrictions, as well as hydrologic conditions, may prevent multiple or even single SEWI, MEWI, or UWI type cross-sectional measurements. If it is not possible or feasible to collect full SEWI, MEWI, and (or) UWI type samples, the approach listed below can be used as a minimum protocol to follow when first starting to collect bedload data at a site. Caution should be used, however, because the modified SEWI, MEWI, or UWI methods will not supply as much information as would the complete method. Therefore, more sets of samples may be needed to acquire sufficient knowledge of the cross section to design an efficient sampling protocol. (Note: The SEWI method helps define cross-sectional variations in bedload transport rates, whereas the MEWI and UWI methods are more effective in defining temporal variations at individual verticals.)

(1) Using the SEWI method, collect samples at approximately 20 equally spaced verticals in the cross section. The spacing and location of the verticals should be determined by the sampling procedure used in the EWI method. For very wide sections, where large variations in bedload rates are suspected, sampling stations should not be spaced more than 50 feet apart. For narrow cross sections, sampling stations need not be closer than 1 foot apart.

(2) Lower the sampler to the streambed and use a stopwatch to measure the time interval during which the sampler is on the streambed. The sampling-time interval should be the same for each vertical sampled

in the cross section. The time required to collect a proper sample can vary from 5 seconds or less to several hours or more. Generally, a sampling time that does not exceed 60 seconds is preferred. Because of the temporal variations in bedload transport rates, there is no easy way to determine the appropriate sampling time. Several test samples (as many as 10 or more collected sequentially at a vertical with a suspected high transport rate) may be needed in order to estimate the proper sampling-time interval to be used. The sample time should be short enough to allow for the collection of a sample from the section with the highest transport rate, without filling the sample bag more than about 40 percent full. The sample bag may be filled to 40 percent full with sediment coarser than the mesh size of the bag without reducing the hydraulic efficiency of the sampler (Druffel and others, 1976). Sediment that is approximately equal to the mesh size may clog the bag and cause a change in the sampling efficiency of the sampler.

(3) One sample should be collected at each vertical, starting at one bank and proceeding to the other. It is recommended that, during this initial data gathering stage, a minimum of one transect using the SEWI method be used. The samples should be placed in separate bags for individual analysis and labeled with the vertical's station number. They may be composited into one or several sample bags for a composite analysis, but if composited, no information on cross-sectional variability can be obtained from the data.

(4) A second sample should be collected using the UWI or MEWI methods. Four or five verticals should be sampled four or five times each, obtaining a total of 20 samples. Samples should be collected using the same procedure as described in number 2 above, except that the sample time for each sample need not be the same. All samples should be bagged and tagged for separate analysis.

(5) The following data must be recorded on a field note sheet for each cross-section sample:

- Station name/number
- Date
- Cross-section sample starting and ending times
- Gage height at the start and end of sample collection
- Total width of the cross section, including stations on both banks
- Width between verticals (SEWI method)
- Number of verticals sampled (SEWI method)
- Station of verticals sampled (UWI or MEWI method)
- Time sampler was on the bottom at each vertical
- Type sampler used
- Name of person collecting sample

In addition, the following information should be recorded on each sample container:

- Station name
- Date
- Designation of cross-section sample to which the container belongs (that is, if two cross-section samples were collected, one would be "A" and the other "B")
- Number of containers for that cross section (for example, "1 of 2" or "2 of 2")
- Stations(s) of the vertical(s) the sample was collected from
- Time sampler was on the bottom and at the vertical station
- Clock time the sample was collected (start and finish if composite)
- Collector's initials

Analysis of the first transect (SEWI method) will give some indication of the cross-sectional variability if individual verticals are analyzed separately. Analysis of the second set of transects (UWI or MEWI method) will give some indication of temporal variability. As stated before, the procedure described above should be considered the minimum to be followed when first collecting bedload data at a site. Additional samples and transects will help define the temporal and spatial variation at the site for all flow ranges. After a cross section has been sampled several times at different flow ranges using the above procedure, it should be possible to develop a sampling protocol that fits the site better.

Computation of Bedload-Discharge Measurements

The bedload transport rate at a sample vertical may be computed by the equation

$$R_i = \frac{KM_i}{t_i} \qquad (1)$$

where

R_i = bedload transport rate, as measured by bedload sampler, at vertical i, in tons per day per foot;

M_i = mass of the sample collected at vertical i, in grams;

t_i = time the sampler was on the bottom at vertical i, in seconds; and

K = a conversion factor used to convert grams per second per foot into tons per day per foot. It is computed as

$$K = (86{,}400 \text{ seconds/day}) \frac{1 \text{ ton}}{(907{,}200 \text{ grams})} \frac{1 \text{ foot}}{(N_w)} \quad (2)$$

where

N_w is the width of sampler nozzle in feet. (For a 3-inch nozzle, $K = 0.381$; for a 6-inch nozzle, $K = 0.190$.)

The cross-sectional bedload discharge measured by the Helley-Smith sampler may be computed using the total cross-section, midsection, or mean-section method. The simplest method of calculating bedload discharge from a sample collected with a Helley-Smith type bedload sampler is the total cross-section method (fig. 54). This method should only be used if the following three conditions are met:

1. The sample times (t_i) at each vertical are equal.
2. The verticals were evenly spaced across the cross section (that is, SEWI or MEWI method used).
3. The first sample was collected at one-half the sample width from the starting bank.

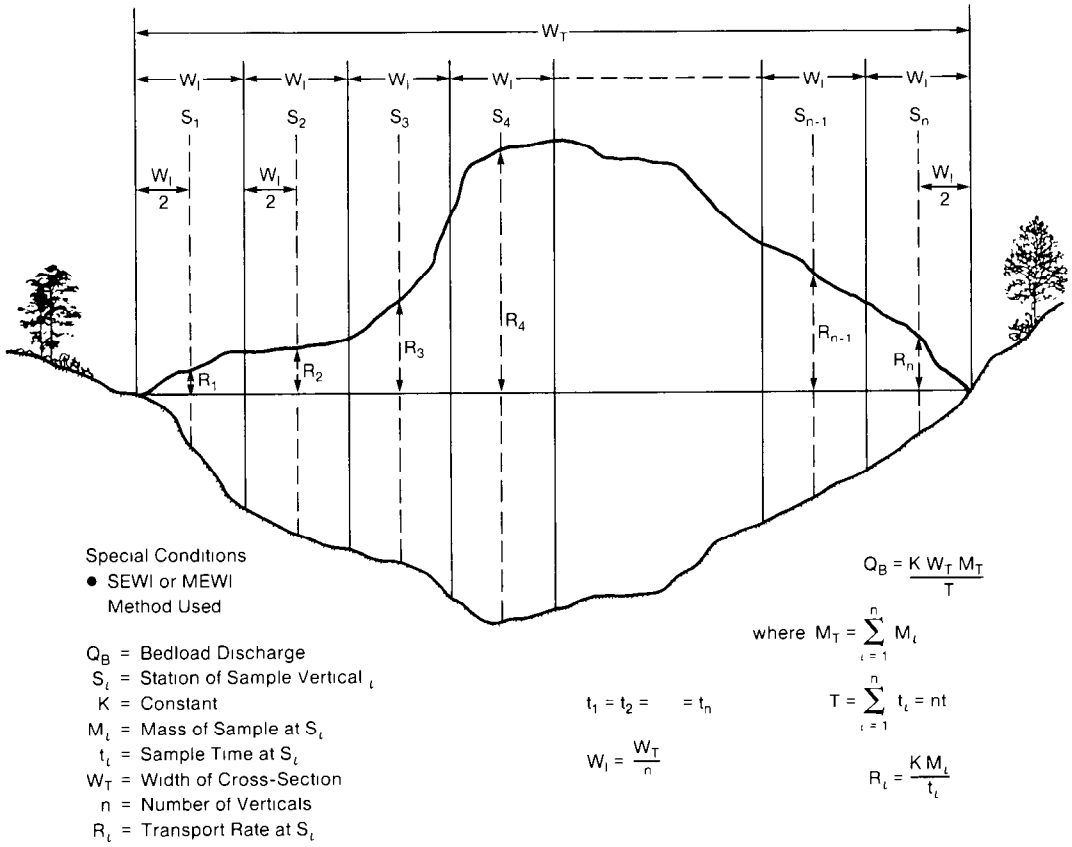

Figure 54. Total cross-section method for computing bedload discharge from samples collected with a Helley-Smith bedload sampler.

If these conditions are met, then

$$Q_B = K\frac{W_T}{t_T}M_T \qquad (3)$$

where

Q_B = bedload discharge, as measured by bedload sampler, in tons per day;

W_T = total width of steam from which samples were collected, in feet, and is equal to the increment width (W_i) times n (n = total number of vertical samples);

^tT = total time the sampler was on the bed, in seconds, computed by multiplying the individual sample time by n;

M_T = total mass of sample collected from all verticals sampled in the cross section, in grams; and

K = conversion factor as described in equation 2 above.

If any of the three conditions stated above are not met, then either the midsection or mean-section method should be used. Mathematically, the two methods, if used with no modifications, will produce identical answers. However, as indicated under the discussion of the UWI method, the placement of the sampling verticals with respect to breaks in the lateral cross-sectional distribution curve of mean bedload transport rate will somewhat dictate which method should be used. The midsection method (fig. 55) is computed using the following equation:

$$Q_B = \frac{R_1 W_1}{2} + \sum_{i=2}^{n-1} R_i\left[\frac{(S_i - S_{i-1})}{2} + \frac{(S_{i+1} - S_i)}{2}\right] + \frac{R_n W_{n-1}}{2} \qquad (4)$$

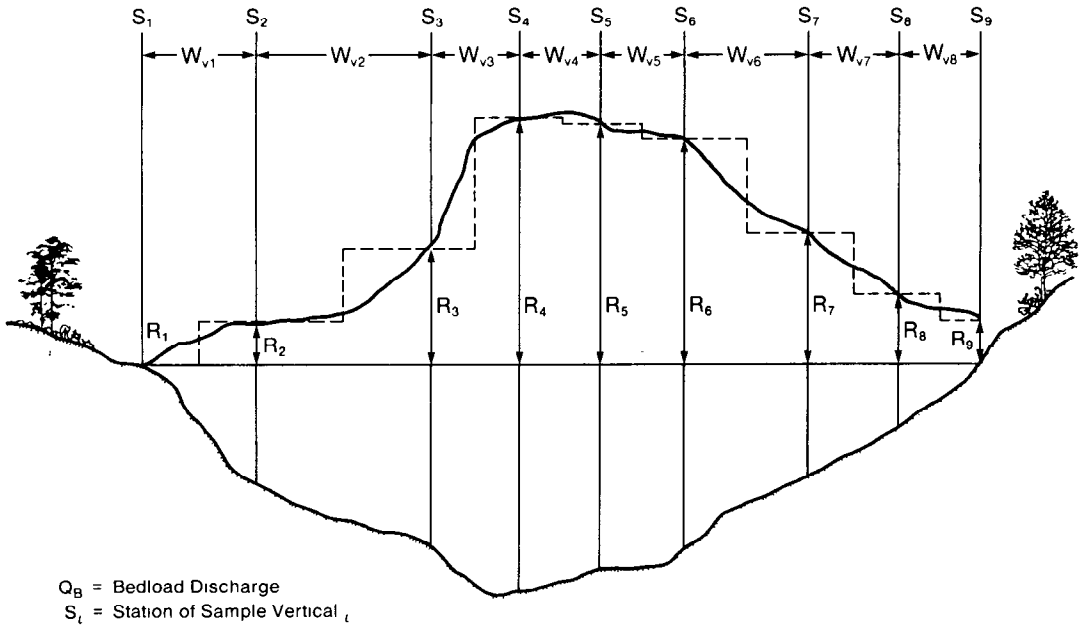

Q_B = Bedload Discharge
S_t = Station of Sample Vertical $_t$
R_t = Transport Rate at S_t
K = Constant
M_t = Mass of Sample Collected at S_t
t_t = Sample Time at S_t
n = Number of Verticals
W_{vt} = Width Between Verticals $_t$ and $_{t+1}$

$$Q_B = \frac{R_1 W_{v1}}{2} + \sum_{t=2}^{n-1} R_t\left[\frac{(S_t - S_{t-1})}{2} + \frac{(S_{t+1} - S_t)}{2}\right] + \frac{R_n W_{vn-1}}{2}$$

$$= \frac{K}{2}\left[\frac{M_1}{t_1}W_{v1} + \frac{M_n}{t_n}W_{vn-1} + \sum_{t=2}^{n-1}\frac{M_t}{t_t}(S_{t+1} - S_{t-1})\right]$$

Figure 55. Midsection method for computing bedload discharge from samples collected with a Helley-Smith bedload sampler.

where

W_i = width between sampling verticals i and $i+1$, in feet;

S_i = stations of the vertical (i) in the cross section measured from some arbitrary starting point, in feet; and

Q_B, n, R, and K have previously been defined,

You will note that equation 3 is very similar to the equation used to compute a surface-water discharge measurement. This method corresponds to the midpoint method currently used to compute surface-water discharge measurements (Buchanan and Somers, 1969). By combining equations 1 and 4 and rearranging terms:

$$Q_B = \frac{K}{2}\left[\frac{M_1 W_1}{t_1} + \frac{M_n W_{n-1}}{t_n} + \sum_{i=2}^{n-1} \frac{M_1}{t_i}(S_{i+1} - S_{i-1})\right] \quad (5)$$

One advantage to using the midsection method is that the distance W_1 need not necessarily be equal to the distance between sampling verticals. At times, it may become apparent, due to local conditions, that a particular R_1 should not be applied over a width equal to halfway back to the last station and halfway forward to the next, but applied to some other width. This width, sometimes referred to as the effective width, is decided on by the user. Bridge piers, large boulders, abrupt changes in velocity or lateral bed topography, or other conditions that may obstruct or cause sudden changes to bedload transport rate will affect the selection of the effective width.

The third method, the mean-section method (fig. 56), is computed using the following equation:

$$Q_B = \sum_{i=1}^{n-1} W_i \frac{(R_i + R_{i+1})}{2}, \quad (6)$$

which is equivalent to:

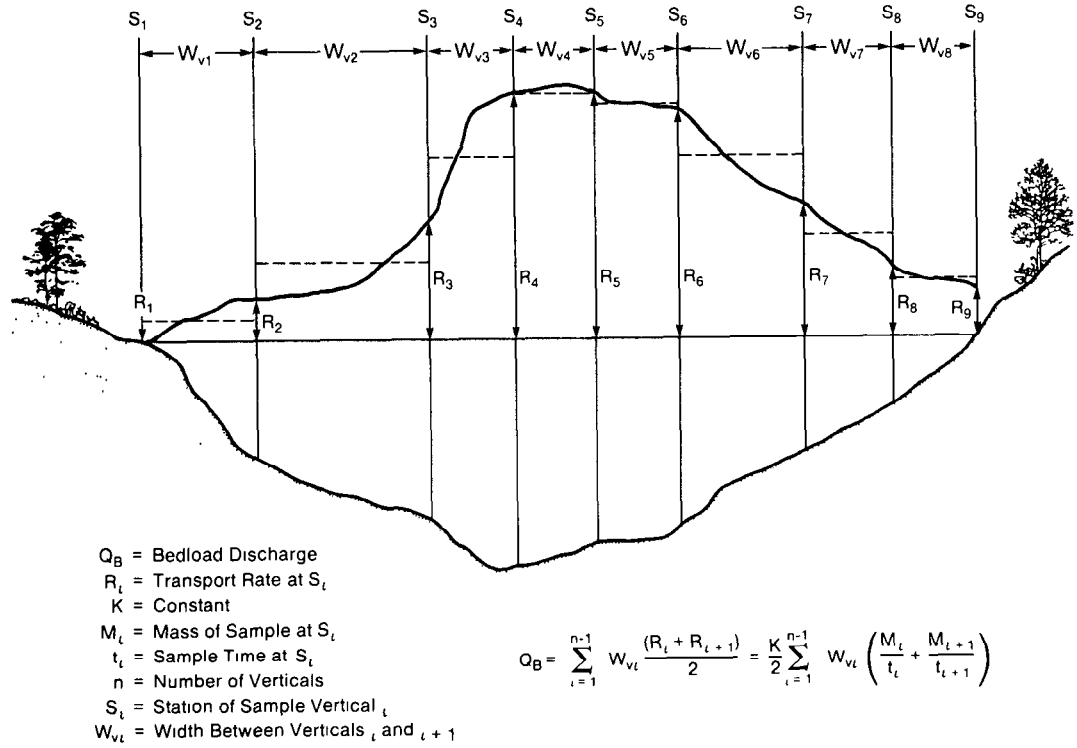

Figure 56. Mean-section method for computing bedload discharge from samples collected with a Helley-Smith bedload sampler.

$$Q_B = \frac{K}{2}\sum_{i=1}^{n-1} W_1\left(\frac{M_i}{t_i} + \frac{M_{i+1}}{t_{i+1}}\right) \quad (7)$$

All the above terms are the same as used in the midsection method. This method averages the two adjoining rates and applies the average rate over the distance between them. For this reason, it is important to try to place the sampling verticals at points where the trends in lateral mean bedload transport rate change. Under most field conditions, this might be difficult.

For situations where the total cross-section method cannot be used, it is recommended that the midsection method be used. This recommendation is made because of its similarity to the surface-water discharge-measurement method, which most field personnel are familiar with, and because of the flexibility in using the effective width concept.

Collecting bedload samples will generate 40 or more samples, creating a potential problem regarding transportation and analyses of so many samples. Carey (1984) adapted a procedure for measuring the submerged weight of bedload samples in the field and converting that measurement to dry weight from a laboratory procedure used by Hubbell and others (1981). The method uses the basic equation

$$W_{ds} = \frac{SG_s}{SG_s - 1} W_{ss} \quad (8)$$

where

W_{ds} = dry weight of the sediment;
SG_s = specific gravity of the sediment; and
W_{ss} = submerged weight of the sediment.

Measurements for Total Sediment Discharge

Total sediment discharge is the mass of all sediment moving past a given cross section in a unit of time. It can be defined as the sum of the (1) measured and unmeasured sediment discharges, (2) suspended-sediment discharge and bedload discharge, or (3) fine-material discharge (sometimes referred to as the washload) and coarse-material or bed-material discharge.

There are some sand-bed streams with sections so turbulent that nearly all sediment particles moving through the reach are in suspension. Sampling the suspended sediment in such sections with a standard suspended-sediment sampler represents very nearly the total load. Several streams with turbulent reaches are described in Benedict and Matejka (1953). Further discussion concerning total-load measurement also can be found in Inter-Agency Report 14 (Federal Inter-Agency Sedimentation Project, 1963b, p. 105–115). Turbulence flumes or special weirs can be used to bring the total load into suspension. Total load can usually be sampled with suspended-sediment samplers to a high degree of accuracy where the streambed consists of an erosion resisting material such as bedrock or a very cohesive clay. In such situations, most, if not all, the sediment being discharged is in suspension (or the bed would contain a deposit of sand).

Benedict and Matejka (1953) and Gonzales and others (1969) have described some structures used for artificial suspension of sediment to enable total-load sampling. However, most total-load sampling is usually accomplished at the crest of a small weir, dam, culvert outlet, or other place where the sampler nozzle integrates throughout the full depth of flow from the surface to the top of the weir.

Where such conditions or structures are not present, the unmeasured load must be computed by various formulas. The unmeasured load can be approximated by use of a bedload formula such as that of Meyer-Peter and Muller (1948), Einstein (1950), Colby and Hembree (1955), or Chang and others (1965). However, these computational procedures can give widely varying answers. The Colby and Hembree (1955) method [modified from Einstein (1950)] determines the total load in terms of the amount transported for different particle-size ranges. Colby and Hubbell (1961) later simplified the modified Einstein method to include the use of four nomographs in lieu of a major computational step. The essential data required for the Colby and Hubbell technique at a particular time and location are listed here:

1. Stream width, average depth, and mean velocity.
2. Average concentration of suspended sediment from depth-integrated samples.
3. Size analyses of the suspended sediment included in the average concentration.
4. Average depth of the verticals where the suspended-sediment samples were collected.

5. Size analyses of the bed material.
6. Water temperature.

Stevens (1985) has developed two computer programs for the computation of total sediment discharge by the modified Einstein procedure. One program is written in FORTRAN 77 for use on the PRIME computer; the other is in BASIC and can be used on most microcomputers.

Hubbell (1964) gives the following formula for determining the total sediment discharge of a given size range from the measured suspended-sediment discharge and the discharge measured with any type of bedload apparatus (see fig. 57).

$$Q_T = \frac{Q_D}{eff} + Q_{sm} + Q_{usm1} - FQ_{sm} + (1 - E/e)Q_{ts2} \quad (9)$$

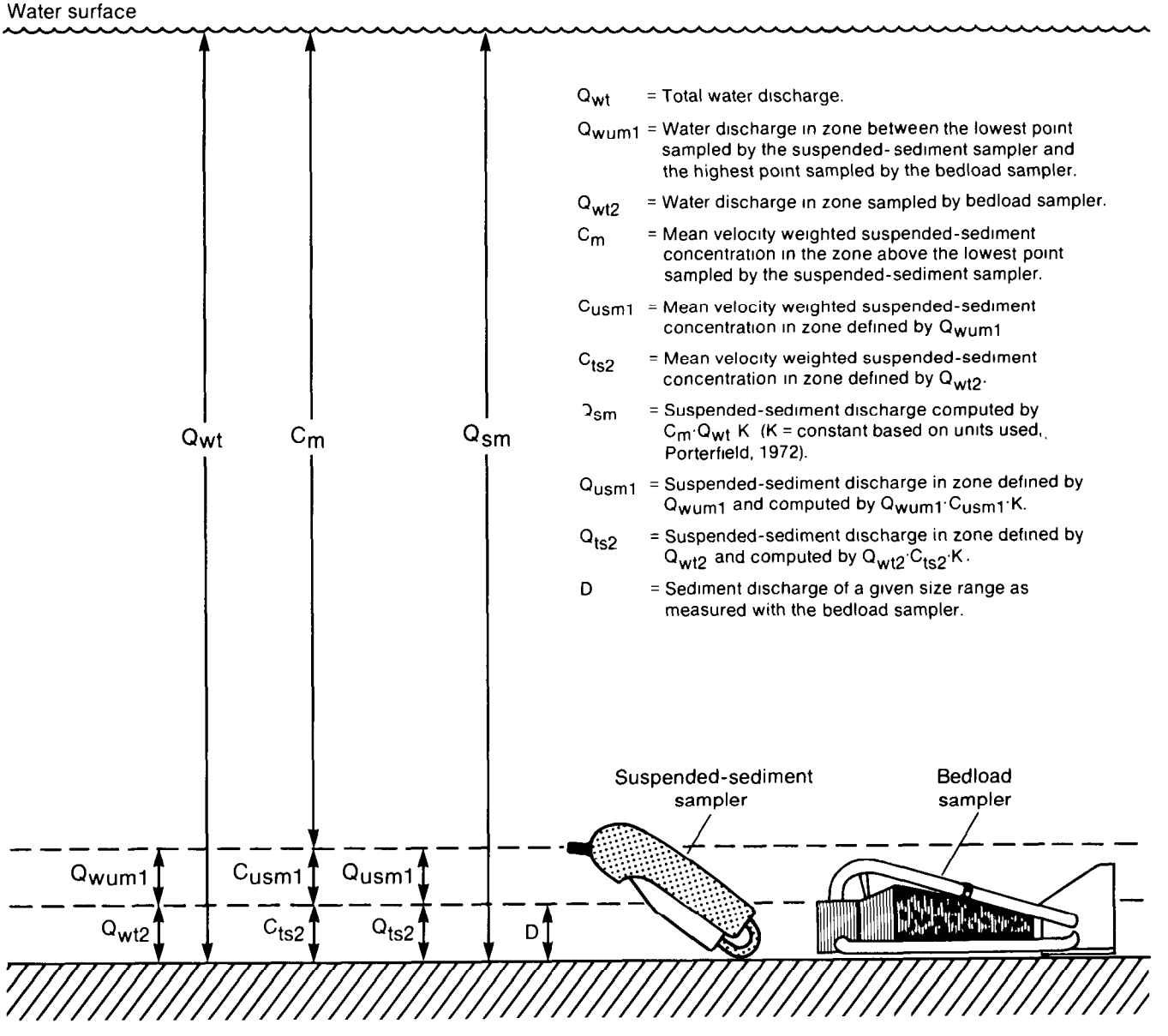

Figure 57. Zones sampled by suspended-sediment and bedload samplers and the unmeasured zone.

where

Q_T = total sediment discharge of the size range,

Q_D = discharge of the size range as measured with the bedload apparatus. If the apparatus measures more than the bedload discharge, as does the Helley-Smith, Q_D includes some of the suspended-sediment discharge,

e = efficiency of the bedload apparatus in measuring bedload discharge of the size range,

Q_{sm} = measured suspended-sediment discharge of the size range,

Q_{usm1} = unmeasured suspended-sediment discharge of the size range in the depth between the lowest point measured by the suspended-sediment sampler and the highest point measured by the bedload apparatus,

F = the fraction of the total depth represented by the flow in the depth measured by the bedload apparatus,

E = the efficiency of the bedload apparatus in measuring the suspended-sediment discharge of the size range transported through the vertical sampled by the apparatus, and

Q_{ts2} = total suspended-sediment discharge of the size range through the depth measured by the bedload apparatus.

A more detailed explanation of how to compute the total sediment discharge from measured suspended-sediment discharge and bedload discharge measured with a bedload measuring apparatus is given by Hubbell (1964, p. 7–9). If the efficiency of the bedload sampler is 100 percent for both bedload and suspended-sediment load and if the bedload sampler samples the entire unsampled zone, then the above equation is much simpler.

Reservoir-Trap Efficiency

The efficiency with which a reservoir traps sediment depends mostly on its size with respect to the rate of inflow. Other factors may include the reservoir shape, its operation, the water quality, and the size and kind of inflowing sediment. Except for small detentions with bottom outlets, all of the sand-sized and much of the silt-sized particles would be expected to be trapped. An evaluation of reservoir-trap efficiency must involve measurements of the quantity and size characteristics of the sediment entering and leaving the reservoir (Mundorff, 1964, 1966). Sometimes measurements of sediment accumulation in the reservoir plus the sediment output are used as a practical method of evaluating the sediment yield of the drainage basin.

Inflow Measurements

On many reservoirs, trap efficiency cannot be evaluated in sufficient detail from measurements of accumulation and sediment outflow. For such reservoirs, it is necessary to measure the sediment discharge and particle size entering the reservoirs. This measurement requires that stations be operated daily or continuously on streams feeding into the reservoir. Trap efficiency on a storm-event basis can be determined if several samples adequately define the concentration of the inflow and outflow hydrographs. For small detention reservoirs, it may be difficult or impractical to measure the inflow on a daily basis. If a continuous record is not possible, the objective should be to obtain observations sufficient to define the conditions for several inflow hydrographs so that a storm-event sediment rating curve can be constructed for use in estimating the sediment moved by the unsampled storms (Guy, 1965).

If it is impractical to obtain sufficient data to define the sediment content of several storm events, the least data for practical analysis should include 10 or 15 observations per year so that an instantaneous sediment rating curve can be constructed (Miller, 1951). It is expected that the instantaneous curve will yield less accurate results than the storm-event curve, which in turn will be less accurate than the continuous record. Each of the rating-curve methods may require data for a range of conditions so that adjustments can be determined for the effect of time of year, antecedent conditions, storm intensity, and possibly for the storm location in the basin (Colby, 1956; Jones, 1966).

As for most new sediment stations, particle-size analysis should be made on several of the inflow observations during the first year. These particle-size analyses will form a data base, which may make it possible to reduce the number of analyses required in future years.

Outflow Measurements

The outflow from a reservoir is drastically different from the inflow because of the attenuating effect of the

flow through the reservoir or because of possible willful control in the release of water (Carter and Godfrey, 1960; Mitchell, 1962). Logically, the smaller reservoirs, which are likely to have fixed outlets and the poorest trap efficiencies, require the most thorough outflow measurement schedules. If an inflow-outflow relation for sediment discharge can be constructed, such a relation may change considerably in the direction of greater sediment output (lower trap efficiency) as the reservoir fills with sediment.

Normally, the particle size of sediment outflow is expected to be finer than for the inflow; and, therefore, the concentration of outflowing sediment should not fluctuate as rapidly as that of the inflow. The normal slowly changing outflow concentration may not occur if the outflow is from the vicinity of the interface involving a density current.

A desirable sampling schedule for outflow may vary from once a week for the large reservoir to several observations during a storm event for a small reservoir. The need for outflow particle-size data also will depend on the scale of the stream and reservoir system, the trap efficiency, and how well the inflow is defined. With respect to quality control, if the trap efficiency of a reservoir is expected to be more than 95 percent and if the sediment inflow can only be measured to the nearest 10 or 15 percent of its expected true value, it is not necessary to measure the sediment outflow in great detail unless there is a need to accurately define the amount of sediment in the flow downstream from the reservoir.

Sediment Accumulation

The small reservoir or detention basin can be used—if trap efficiency can be estimated or measured—to provide a measure of the average annual sediment yield of a drainage basin. This method is useful in very small basins where the inflow is difficult to measure and where the amount of water-inflow and sediment-concentration data is not important.

For small catchment basins or reservoirs on ephemeral streams (those that are dry most of the time), the determination of sediment accumulation involves a detailed survey of the reservoir from which stage-capacity curves can be developed—usually 1-foot contours for the lower parts of the reservoirs and 2- to 5-foot contours for the upper parts, depending on the terrain and size of the reservoir (Peterson, 1962). The accretion of sediment then can be measured either by monumented range lines in the reservoir or by resurvey for a new stage-capacity curve.

For reservoirs not dry part of the time, the sediment accumulation is usually measured by sounding on several monumented range lines spaced to provide a representative indication of the sediment accumulation between measurements. Methods for reservoir surveys are described by Heinemann (1961), Porterfield and Dunnam (1964), and Vanoni (1975). A summary of reservoir sediment deposition surveys made in the United States through 1975 was compiled by Dendy and Champion (1978). The period from 1976 to 1980 has been covered by the Inter-Agency Advisory Committee on Water Data's Subcommittee on Sediment (1983).

In order to convert the measurements of sediment volume found in reservoirs to the usual expression of mass of sediment yield, it is necessary that the sedimentation surveys of reservoirs include information on the volume-mass of sediment. Heinemann (1964) reports that this was accomplished in Sebetha Lake, Kansas, using a gamma probe and a piston sampler. From his data, obtained at 41 locations, he found that the best equation for predicting volume-mass is

$$V_M = 1.688d - 0.888c + 98.8 \qquad (10)$$

where

V_M = the dry unit volume-mass, in pounds per cubic foot;

d = the depth of sample from the top of the deposit; and

c = the percentage of clay smaller than 0.002 mm.

On the basis of 1,316 reservoir deposit samples, Lara and Pemberton (1965) found the unit volume-mass to vary according to changes in reservoir operation and to the fraction of clay, silt, and sand. The Office of Water Data Coordination (1978) reported that refinements based on reservoir operation, sediment size, and compaction could be made to the estimates made by Lara and Pemberton (1965) and Lane and Koelzer (1943). The following formula, along with factors listed in table 4, may be used to estimate dry unit volume-mass:

$$V_M = V_{tc}P_c + V_{tm}P_m + V_{ts}P_s \qquad (11)$$

where

V_M = dry unit volume-mass, in pounds per cubic foot;
V_t = dry unit volume-mass as computed in equation 12, in pounds per cubic foot;
c = clay-size material;
m = silt-size material;
s = sand-size material;
P = percent of total sample, by weight, in size class (clay, silt, sand); and

$$V_t = V_i + 0.43K\left[\frac{T}{T-1}(\log T) - 1\right] \qquad (12)$$

where

V_i = initial unit volume-mass, in pounds per cubic foot from table 4;
K = Lane and Koelzer (1943) factors from table 4, in pounds per cubic foot; and
T = time after deposition, in years.

Table 4. Initial dry unit volume-mass (V_1) and K factors for computing dry unit volume-mass of sediment deposits in pounds per cubic foot (Office of Water Data Coordination, 1978)

Type of reservoir operation	V_1			K		
	Clay	Silt	Sand	Clay	Silt	Sand
1. Sediment submerged	26	70	97	16	5.7	0
2. Moderate to considerable annual drawdown	35	71	97	8.4	1.8	0
3. Normally empty	40	72	97	0	0	0
4. River sediment	60	73	97	0	0	0

OTHER SEDIMENT DATA-COLLECTION CONSIDERATIONS

In retrospect, it must be emphasized that field methods for fluvial-sediment measurements must be coordinated with methods for other hydrologic and environmental measurements. With the ever-increasing requirements of a thorough data-acquisition system, together with advances in technology, it must be expected that methods will continue to change in the future. For example, because there is a foreseeable need for increasing water-pollution surveillance studies with respect to stream-quality standards, it is apparent that a continuous recording of some indicator of sediment conditions is badly needed at a large number of sites. Consequently, the F.I.S.P. has undertaken the development of sensors and automatic pumping-type samplers with a view toward continuously recording the concentration of sediment that moves in streams. The development of such automatic equipment is likely to enhance rather than detract from the need for conventional manual observations.

The authors sincerely hope that the material regarding the equipment and techniques for sampling presented herein will stimulate the ongoing development of better equipment and techniques for the future and, at the same time, help to standardize and make more efficient the day-to-day operations.

The opportunity certainly exists at the field level for many innovations for improving the end product or the sediment record. Some field people, for example, may like to carry a copy of the station stage-discharge rating curve, on which all particle-size analyses are recorded, showing date and kind of sample for each measuring site. As communications and river forecasting become more sophisticated, it may be possible to have better dialogue between the office and the field people or local observers, who are trying to obtain the maximum information at many sampling sites. Such communication is especially critical during periods of flooding, when timely data are most important.

In addition to increasing coordination of sediment-data activities with other related measurements, it is important to stress that adequate notes be obtained (including pictures) so that those involved in the laboratory analysis of the samples, those responsible for preparing the record, and especially those responsible for interpreting the data can properly read what happened at the sample site. The amount of new information to be obtained from data interpretation is seriously affected by the quality of the information with respect to timing and representativeness of the sediment measurements.

The authors further emphasize the need for a concerted and continuing effort with respect to safety in the measurement program. Aside from the hazards of highway driving, the work usually involves the use of heavy equipment during floods or other unusual

natural events, often in darkness and under unpleasant weather conditions. Even though the hazards of working from highway bridges and cableways are mostly self-evident, there are many opportunities for the unusual to happen and, therefore, a great deal of effort must be expended to ensure safety. Such effort, of course, must be increased when it is necessary to accomplish the work in a limited amount of time and with a reduced work force.

SELECTED REFERENCES

American Society for Testing and Materials, 1987, Annual book of American Society for Testing and Materials Standards: Water and Environmental Technology, section 11, v. 11.02, 1,083 p.

Beetem, W.A., Janzer, V.J., and Wahlberg, J.S., 1962, Use of cesium-137 in the determination of cation exchange capacity: U.S. Geological Survey Bulletin 1140–B, 8 p.

Benedict, P.C., and Matejka, D.Q., 1953, The measurement of total sediment load in alluvial streams: Iowa City, Iowa, Iowa University, Proceedings of the Fifth Iowa Hydraulics Conference, Engineering Bulletin 34, p. 263–286.

Buchanan, T.J., and Somers, W.P., 1968, Stage measurements at gaging stations: U.S. Geological Survey Techniques of Water-Resources Investigations, chap. A7, book 3, 28 p.

——— 1969, Discharge measurements at gaging stations: U.S. Geological Survey Techniques of Water-Resources Investigations, chap. A8, book 3, 65 p.

Carey, W.P., 1984, A field technique for weighing bedload samples: Water Resources Bulletin, American Water Resources Association, v. 20, no. 2, p. 261–265.

———1985, Variability in measured bedload-transport rates: Water Resources Bulletin, American Water Resources Association, v. 21, no. 1, p. 39–48.

Carter, R.W., and Davidian, Jacob, 1968, General procedure for gaging streams: U.S. Geological Survey Techniques Water-Resources Investigations, chap. A6, book 3, 13 p.

Carter, R.W., and Godfrey, R.G., 1960, Storage and flood routing: U.S. Geological Survey Water-Supply Paper 1543–B, p. 102–104.

Chang, F.M., Simons, D.B., and Richardson, E.V., 1965, Total bed-material discharge in alluvial channels: U.S. Geological Survey Water-Supply Paper 1498–I, 23 p.

Colby, B.R., 1956, Relationship of sediment discharge to streamflow: U.S. Geological Survey Open-File Report, 170 p.

———1963, Fluvial sediments—A summary of source, transportation, deposition, and measurement of sediment discharge: U.S. Geological Survey Bulletin 1181–A, 47 p.

———1964, Discharge of sands and mean-velocity relationships in sand-bed streams: U.S. Geological Survey Professional Paper 462–A, 47 p.

Colby, B.R., and Hembree, C.H., 1955, Computations of total sediment discharge, Niobrara River near Cody, Nebraska: U.S. Geological Survey Water-Supply Paper 1357, 187 p.

Colby, B.R., and Hubbell, D.W., 1961, Simplified methods for computing total sediment discharge with the modified Einstein procedure: U.S. Geological Survey Water-Supply Paper 1593, 17 p.

Culbertson, D.M., Young, L.E., and Brice, J.C., 1967, Scour and fill in alluvial channels, with particular reference to bridge sites: U.S. Geological Survey Open-File Report, 58 p.

Dendy, F.E., and Champion, W.A., 1978, Sediment deposition in United States reservoirs, summary of data reported through 1975: U.S. Department of Agriculture, Agricultural Research Service, Miscellaneous Publication 1362, 84 p.

Druffel, Leroy, Emmett, W.W., Schneider, V.R., and Skinner, J.V., 1976, Laboratory hydraulic calibration of the Helley-Smith bedload sediment sampler: U.S. Geological Survey Open-File Report 76–752, 63 p.

Einstein, H.A., 1937, Die Eichung des im Rhein verwenderen Geschiebefangers [Calibrating the bedload trap as used in the Rhine]: Schweizer, Bauzeitung, v. 110, no. 12, p. 29–32.

———1950, The bedload function for sediment transportation in open channel flows: U.S. Department of Agriculture Technical Bulletin 1026, 70 p.

Emmett, W.W., 1975, The channels and waters of the upper Salmon River area, Idaho: U.S. Geological Survey Professional Paper 870–A, 116 p.

———1980a, A field calibration of the sediment-trapping characteristics of the Helley-Smith bed-load sampler: U.S. Geological Survey Professional Paper 1139, 44 p.

———1980b, Bedload sampling in rivers: International Symposium on River Sedimentation, Beijing, China, 1980, Proceedings, p. 991–1017.

———1981, Measurement of bed load in rivers, *in* Erosion and sediment transport measurement: Florence, International Association of Hydrological Sciences Association Proceedings 133, p. 3–5.

Emmett, W.W., Leopold, L.B., and Myrick, R.M., 1983, Some characteristics of fluvial processes in rivers: Second International Symposium on River Sedimentation, Nanjing, China, 1983, Proceedings, 29 p.

Emmett, W.W., and Seitz, H.R., 1974, Suspended and bedload sediment transport in the Snake and Clearwater Rivers in the vicinity of Lewiston, Idaho—July 1973 through July 1974: U.S. Geological Survey Basic-Data Report, 76 p.

Federal Inter-Agency Sedimentation Project, 1941, Laboratory investigation of suspended-sediment samplers: Iowa City, Iowa University Hydraulics Laboratory, Inter-Agency Report 5, 99 p.

———1951, Field tests on suspended-sediment samplers, Colorado River at Bright Angel Creek near Grand Canyon, Arizona: Iowa City, Iowa, University Hydraulics Laboratory, Inter-Agency Report F, 119 p.

———1952, The design of improved types of suspended-sediment samplers: Minneapolis, Minnesota, St. Anthony Falls Hydraulics Laboratory, Inter-Agency Report 6, 103 p.

———1958, Operating instructions for US DH–48 suspended-sediment hand sampler: Minneapolis, Minnesota, St. Anthony Falls Hydraulics Laboratory, Inter-Agency Report J, 5 p.

———1959, Sedimentation instruments and reports: Minneapolis, Minnesota, St. Anthony Falls Hydraulics Laboratory, Inter-Agency Report AA, 38 p.

———1961, The single-stage sampler for suspended-sediment: Minneapolis, Minnesota, St. Anthony Falls Hydraulics Laboratory, Inter-Agency Report 13, 105 p.

———1963a, A summary of the work of the Federal Inter-Agency Sedimentation Project: Minneapolis, Minnesota, St. Anthony Falls Hydraulics Laboratory, Inter-Agency Report S, 29 p.

———1963b, Determination of fluvial sediment discharge: Minneapolis, Minnesota, St. Anthony Falls Hydraulics Laboratory, Inter-Agency Report 14, 151 p.

———1964, Operation and maintenance of US BM–54 bed-material sampler: Minneapolis, Minnesota, St. Anthony Falls Hydraulics Laboratory, Inter-Agency Report M, 16 p.

———1965, Instructions for sampling with depth-integrating suspended-sediment samplers, US D–49 and DH–59: Minneapolis, Minnesota, St. Anthony Falls Hydraulics Laboratory, Inter-Agency Report O, 7 p.

———1966, Laboratory investigation of pumping-sampler intakes: Minneapolis, Minnesota, St. Anthony Falls Hydraulics Laboratory, Inter-Agency Report T, 59 p.

———1974, An investigation of a device for measuring the bulk density of water-sediment mixtures: Minneapolis, Minnesota, St. Anthony Falls Hydraulics Laboratory, Inter-Agency Report U, 35 p.

———1976, Instructions for sampling with depth-integrating, suspended-sediment samplers, D–74, D–74 AL, D–74 TM, and D–74 AL–TM: Minneapolis, Minnesota, St. Anthony Falls Hydraulics Laboratory, Inter-Agency Report, 13 p.

———1981a, Instruments and reports for fluvial sediments investigations: Minneapolis, Minnesota, St. Anthony Falls Hydraulics Laboratory, Inter-Agency Report Catalog, 134 p.

———1981b, Test and design of automatic fluvial suspended-sediment samplers: Minneapolis, Minnesota, St. Anthony Falls Hydraulics Laboratory, Inter-Agency Report W, 53 p.

———1982a, A fluid-density gage for measuring suspended-sediment concentration: Minneapolis, Minnesota, St. Anthony Falls Hydraulics Laboratory, Inter-Agency Report X, 125 p.

———1982b, Development of a bag-type suspended-sediment sampler: Minneapolis, Minnesota, St. Anthony Falls Hydraulics Laboratory, Inter-Agency Report Y, 32 p.

———1982c, Theory and operation manual for the autopipet semi-automatic pipet withdrawal apparatus: Minneapolis, Minnesota, St. Anthony Falls Hydraulics Laboratory, Inter-Agency Report Z, 71 p.

———1983, Operator's manual, PS–82 automatic pumping sampler: Minneapolis, Minnesota, St. Anthony Falls Hydraulics Laboratory, Inter-Agency Draft Report, 34 p.

Gonzales, D.D., Scott, C.H., and Culbertson, J.K., 1969, Stage-discharge characteristics of a weir in a sand-channel stream: U.S. Geological Survey Water-Supply Paper 1898–A, 29 p.

Guy, H.P., 1965, Residential construction and sedimentation at Kensington, Maryland—Proceedings of the Federal Inter-Agency Sedimentation Conference, Jackson, Mississippi, 1963: U.S. Department of Agriculture, Agriculture Research Service, Miscellaneous Publication 970, p. 30–37.

———1968, Quality control of adjustment coefficients, *in* Geological Survey Research 1968: U.S. Geological Survey Professional Paper 600–B, p. B165–B168.

———1969, Laboratory theory and methods for sediment analysis: U.S. Geological Survey Techniques of Water-Resources Investigations, chap. C1, book 5, 58 p.

———1970, Fluvial sediment concepts: U.S. Geological Survey Techniques of Water-Resources Investigations, chap. C1, book 3, 55 p.

Guy, H.P., and Simons, D.B., 1964, Dissimilarity between spatial and velocity-weighted sediment concentrations, *in* Short papers in geology and hydrology: U.S. Geological Survey Professional Paper 475–D, p. D134–D137.

Guy, H.P., Simons, D.B., and Richardson, E.V., 1966, Summary of alluvial channel data from flume experiments, 1956–61: U.S. Geological Survey Professional Paper 462–I, 96 p.

Hamamori, A., 1962, A theoretical investigation on the fluctuations of bedload transport: Delft Hydraulics Laboratory Report R4, 21 p.

Heinemann, H.G., 1961, Sediment distribution in small floodwater-retarding reservoirs in the Missouri Basin Loess Hills: U.S. Department of Agriculture Report, ARS 41–44, 37 p.

———1964, Volume-weight of reservoir sediment: American Society of Civil Engineers Transactions, v. 129, p. 64–66.

Helley, E.J., and Smith, Winchell, 1971, Development and calibration of a pressure-difference bedload sampler: U.S. Geological Survey Open-File Report 73–108, 38 p.

Hubbell, D.W., 1960, Progress report no. 2, Investigations of some sedimentation characteristics of sand-bed streams: U.S. Geological Survey Open-File Report, 54 p.

———1964, Apparatus and techniques for measuring bedload: U.S. Geological Survey Water-Supply Paper 1748, 74 p.

Hubbell, D.W., and others, 1956, Progress report no. 1, Investigations of some sedimentation characteristics of a sand-bed stream: U.S. Geological Survey Open-File Report, 78 p.

Hubbell, D.W., and Stevens, H.H., 1986, Factors affecting accuracy of bedload sampling: Proceedings of the Fourth Federal Interagency Sedimentation Conference, v. 1, p. 4–20–29.

Hubbell, D.W., Stevens, H.H., Skinner, J.V., and Beverage, J.P., 1981, Recent refinements in calibrating bedload samplers: Proceeding of the Specialty Conference, Water Forum 1981, American Society of Civil Engineers, San Francisco, California, v. 1, 13 p.

———1985, New approach to calibrating bedload samplers: American Society of Civil Engineers, Journal of Hydraulic Engineering, v. III, no. 4, p. 677–694.

Inter-Agency Advisory Committee on Water Data, Subcommittee on Sediment, 1983, Sediment deposition in U.S. reservoirs—Summary of data reported through 1976–80: U.S. Geological Survey, Office of Water Data Coordination, 32 p.

Jones, B.L., 1966, Effects of agricultural conservation practices on the hydrology of Corey Creek Basin, Pennsylvania, 1954–60: U.S. Geological Survey Water-Supply Paper 1532–C, 55 p.

Kellerhals, Rolf, 1967, Stable channels with gravel paved beds: Waterways and Harbors Division Journal, American Society of Civil Engineers, Proceedings, v. 93, no. WW1, p. 63.

Lane, E.W., and Carlson, E.J., 1953, Some factors affecting the stability of canals constructed in coarse granular materials: Minneapolis, Minnesota, International Association for Hydrologic Research, p. 76–81.

Lane, E.W., and Koelzer, V.A., 1943, Density of sediments deposited in reservoirs: Iowa City, Iowa University Hydraulics Laboratory, Federal Inter-Agency Sedimentation Project Report 9, 60 p.

Lara, J.M., and Pemberton, E.L., 1965, Initial unit weight of deposited sediments—Proceedings of the Federal Inter-Agency Sedimentation Conference, Jackson, Mississippi, 1963: U.S. Department of Agriculture, Agriculture Research Service, Miscellaneous Publication 970, p. 818–845.

Leopold, L.B., and Emmett, W.W., 1977, 1976 bedload measurement, East Fork River, Wyoming: Proceedings of the National Academy of Sciences, v. 74, no. 7, p. 2644–2648.

Leopold, L.B., Wolman, M.G., and Miller, J.P., 1964, Fluvial processes in geomorphology: San Francisco, California, W.H. Freeman and Company, 522 p.

Meyer-Peter, E., and Muller, R., 1948, Formulas for bedload transport: International Association of Hydraulic Structures Research, 2d meeting, Stockholm, Sweden, 1948, Proceedings, p. 39–64.

Miller, C.R., 1951, Analysis of flow-duration, sediment rating curve method of computing sediment yield: Bureau of Reclamation Report, 15 p.

Mitchell, W.D., 1962, Effect of reservoir storage on peak flow: U.S. Geological Survey Water-Supply Paper 1580–C, 25 p.

Mundorff, J.C., 1957, A handline suspended-sediment sampler: U.S. Geological Survey Open-File Report, 2 p.

———1964, Fluvial sediment in Kiowa Creek Basin, Colorado: U.S. Geological Survey Water-Supply Paper 1798–A, 70 p.

———1966, Sedimentation in Brownell Creek sub-watershed no. 1, Nebraska: U.S. Geological Survey Water-Supply Paper 1798–C, 49 p.

Office of Water Data Coordination, 1978, National handbook of recommended methods for water-data acquisition: U.S. Geological Survey, chap. 3—Sediment, 100 p.

Peterson, H.V., 1962, Hydrology of small watersheds in Western States: U.S. Geological Survey Water-Supply Paper 1475–I, p. 223–227.

Porterfield, George, 1972, Computation of fluvial sediment discharge: U.S. Geological Survey Techniques of Water-Resources Investigations, chap. C3, book 3, 66 p.

Porterfield, George, and Dunnam, C.A., 1964, Sedimentation of Lake Pillsbury, Lake County, California: U.S. Geological Survey Water-Supply Paper 1619–EE, 46 p.

Prych, E.A., and Hubbell, D.W., 1966, A sampler for coring sediments in rivers and estuaries: Geological Society of America Bulletin, v. 77, p. 549–556.

Randle, T.J., and Blanton, J.O., III, 1986, Underwater mapping river channels and reservoirs: Proceedings of the Fourth Federal Interagency Sedimentation Conference, v. 1, p. 1–79 to 1–88.

Ritter, J.R., and Helley, E.T., 1968, An optical method for determining particle sizes of coarse sediment: U.S. Geological Survey Open-File Report, 43 p.

Simons, D.B., and Richardson, E.V., 1965, A study of variables affecting flow characteristics and sediment transport in alluvial channels—Proceedings of the Federal Inter-Agency Sedimentation Conference, Jackson, Mississippi, 1963: U.S. Department of Agriculture, Agriculture Research Service, Miscellaneous Publication 970, p. 193–207.

———1966, Resistance to flow in alluvial channels: U.S. Geological Survey Professional Paper 422–J, 61 p.

Skinner, J.V., 1982, Proposed practice for sampling fluvial sediment in motion: American Society for Testing and Materials Standards, Annual Book, pt. 31, 24 p. [Published for information only].

Stevens, H.H., Jr., 1985, Computer program for the computation of total sediment discharge by the modified Einstein procedure: U.S. Geological Survey Water-Resources Investigations Report 85–4047, 76 p.

Thornbury, W.D., 1969, Principles of geomorphology (2d ed.): New York, Wiley, 594 p.

Vanoni, V.A., ed., 1975, Sedimentation engineering: American Society of Civil Engineers, Manuals and Reports on Engineering Practice, no. 54, 745 p.

Winterstein, T.A., and Stefan, H.E., 1983, Suspended-sediment sampling in flowing water—Laboratory study of the effects of nozzle orientation, withdrawal rate and particle size: Minneapolis, University of Minnesota, St. Anthony Falls Hydraulic Laboratory External Memorandum M–168, 97 p.

Wolman, M.G., 1954, A method of sampling coarse river bed material: American Geophysical Union Transcript, v. 35, no. 6, p. 951.

Assessment of erosion, sedimentation, and water quality impacts of the Mountain Valley Pipeline and Equitrans Expansion Project's proposed crossing of the Jefferson National Forest as it pertains to the U.S. Forest Service's Draft Supplemental Environmental Impact Statement dated December 2022

Prepared by Jonathan A. Czuba, Ph.D., Licensed Professional Engineer - February 9, 2023

REFERENCES
26

February 21, 2023

Measurement and Computation of Streamflow: Volume 1. Measurement of Stage and Discharge

By S. E. RANTZ *and others*

GEOLOGICAL SURVEY WATER-SUPPLY PAPER 2175

USGS
science for a changing world

UNITED STATES GOVERNMENT PRINTING OFFICE, WASHINGTON: 1982

UNITED STATES DEPARTMENT OF THE INTERIOR

JAMES G. WATT, *Secretary*

GEOLOGICAL SURVEY

Dallas L. Peck, ***Director***

First printing 1982
Second printing 1983

Library of Congress Cataloging in Publication Data

Measurement and computation of streamflow.

(Geological Survey Water-Supply Paper 2175)
Includes bibliographies.
Contents: v. 1. Measurement of stage and discharge.—
v. 2. Computation of discharge. 1. Stream
measurements.
I. Rantz, S. E. (Saul Edward), 1911– . II. Series.
TC175.M42 551.48'3'0287 81–607309
AACR2

For sale by the Superintendent of Documents, U.S. Government Printing Office
Washington, D.C. 20402

PREFACE

The science and, in part, art of stream gaging has evolved through the years, largely from the collective experiences and innovations of its practitioners. The earliest truly comprehensive manual on stream-gaging procedures and equipment, based on techniques developed up to that time, was published in 1943 by the Geological Survey as Water-Supply Paper 888, "Stream-Gaging Procedures," by D. M. Corbett and others. That report was an instant classic; it was received enthusiastically by the hydraulic-engineering profession throughout the world and became a major training document for at least two generations of stream gagers, hydrologists, and hydraulic engineers, both in the United States and abroad.

The need for updating Water-Supply Paper 888 has been obvious for some time as a result of later developments in stream-gaging techniques and equipment. Furthermore, it has been felt for some time that the scope of that report should be expanded to cover not only the newer field techniques but also the office procedures required to produce a published annual record of stream discharge. In recognition of those needs, the Geological Survey has sporadically produced supplementary reports that update the description of specific techniques and equipment or that describe specific field or office procedures not covered by Water-Supply Paper 888. These reports—some administrative, some open-file, and others in the published series titled "Techniques of Water-Resources Investigations"—are fragmentary in the sense that they deal only with selected aspects of the broad subject of stream gaging. Similar, but less detailed, reports on selected topics have also been produced by international agencies in the form of Technical Notes by the World Meteorological Organization and in the form of Recommendations and Standards by the International Standards Organization.

The present report evolved from that background. Its two volumes provide a comprehensive compilation of time-tested techniques presented as an up-to-date (1980) standardized manual of stream-gaging procedures.

Acknowledgments.—The material presented in the manual is based on the work of many hydraulic engineers and technicians, each of whom has contributed to the current state-of-the-art in the measurement and computation of streamflow. Many of those who contributed directly to the manual are listed in the references appended to each chapter. However, the authors wish to acknowledge a special group of colleagues who have made major contributions to this manual in the form of written (cited) methods and techniques, significant suggestions for correction and revision of the manuscript and illus-

trations, and all-out efforts to bring about development and publication of the material. These colleagues include:

Harry H. Barnes, Jr.	Thomas J. Buchanan
Rolland W. Carter	Frederick A. Kilpatrick
George F. Smoot	Ernest D. Cobb
Howard F. Matthai	Manual A. Benson
Alvin F. Pendleton, Jr.	Tate Dalrymple
Harry Hulsing	Carl E. Kindsvater
G. Lawrence Bodhaine	Hubert J. Tracy
Jacob Davidian	James F. Wilson

The authors also wish to acknowledge with thanks the suggestions of their many other colleagues, who are too numerous to mention.

CONTENTS

[Article headings are listed in the table of contents only in the volume of the manual in which they occur, but all chapter titles for the two volumes are listed in both volumes A complete index covering both volumes of the manual appears in each volume]

VOLUME 1. MEASUREMENT OF STAGE AND DISCHARGE

Chapter 5.—Measurement of Discharge by Conventional Current-Meter Method

Chapter 6.—Measurement of Discharge by the Moving-Boat Method

Chapter 7.—Measurement of Discharge by Tracer Dilution

Chapter 8.—Measurement of Discharge by Miscellaneous Methods

Chapter 9.—Indirect Determination of Peak Discharge

VOLUME 2. COMPUTATION OF DISCHARGE

ILLUSTRATIONS

TABLES

CONVERSION FACTORS

[Factors for converting inch-pound to metric units are shown to four significant figures However, in the text the metric equivalents, where shown, are carried only to the number of significant figures consistent with the values for the English units.]

Inch-pound	*Multiply by—*	*Metric*
acres	4.047×10^{3}	m^2 (square meters)
acre-ft (acre-feet)	1.233×10^{3}	m^3 (cubic meters)
acre-ft/yr (acre feet per year)	1.233×10^{3}	m^3/yr (cubic meters per year)
ft (feet)	3.048×10^{-1}	m (meters)
ft/hr (feet per hour)	3.048×10^{-1}	m/hr (meters per hour)
ft/s (feet per second)	3.048×10^{-1}	m/s (meters per second)
ft^3/s (cubic feet per second)	2.832×10^{-2}	m^3/s (cubic meters per second)
in (inches)	2.540×10	mm (millimeters)
lb (pounds)	4.536×10^{-1}	kg (kilograms)
mi (miles)	1.609	km (kilometers)
mi^2 (square miles)	2.590	km^2 (square kilometers)
oz (ounces)	2.835×10^{-2}	kg (kilograms)

MEASUREMENT AND COMPUTATION OF STREAMFLOW

VOLUME 1. MEASUREMENT OF STAGE AND DISCHARGE

By S. E. RANTZ and others

CHAPTER 1.—INTRODUCTION

PURPOSE OF THE MANUAL

The purpose of this manual is to provide a comprehensive description of state-of-the-art standardized stream-gaging procedures, within the scope described below. The manual is intended for use as a training guide and reference text, primarily for hydraulic engineers and technicians in the U.S. Geological Survey, but the manual is also appropriate for use by other stream-gaging practitioners, both in the United States and elsewhere.

SCOPE OF THE MANUAL

The technical work involved in obtaining systematic records of streamflow is discussed, in two volumes, in accordance with the following six major topics:

Volume 1. Measurement of stage and discharge
- a. Selection of gaging-station sites
- b. Measurement of stage
- c. Measurement of discharge

Volume 2. Computation of discharge
- d. Computation of the stage-discharge relation
- e. Computation of daily-discharge records
- f. Presentation and publication of stream-gaging data

In order to make the text as broadly usable as possible, discussions of instrumentation and measurement are aimed at the technician, and discussions of computational procedure are aimed at the junior engineer who has a background in basic hydraulics.

Many of the procedures for determining discharge that are discussed in volume 2 require specialized instrumentation to obtain field data that supplement the observation of stage. The descriptions of such specialized equipment and associated observational techniques

are given in appropriate chapters in volume 2 so that the reader may have unified discussions of the methodologies applicable to each type of problem in determining discharge.

In general the authors have attempted to prepare a manual that will stand independently—references are given to supplementary published material, but the reader should find relatively few occasions when there is pressing need to consult those references. There are three notable exceptions to that statement.

1. The subject of indirect determination of peak discharge (v. 1, chap. 9) is treated here only in brief because of space limitations; the subject is treated fully in five reports in the Geological Survey report series, "Techniques of Water-Resources Investigations." The five reports are named in the reference section of chapter 9.
2. Among the methods discussed in this manual for computing the discharge of tidal streams are four mathematical techniques for evaluating the differential equations of unsteady flow (v. 2, chap. 13). The four techniques are given only cursory treatment because a detailed description of the complex mathematical techniques is considered to be beyond the scope of the manual.
3. The processing of streamflow records by digital computer (v. 2, chap. 15) is a subject that is given only generalized treatment here. It was not practicable to include a detailed description of each step in the sequence of operation of an automated computing system because of space limitations, and also because the particulars of each step are somewhat in a state of flux in response to continual improvement in storage and access procedures.

STREAMFLOW RECORDS

Streamflow serves man in many ways. It supplies water for domestic, commercial, and industrial use; irrigation water for crops; dilution and transport for removal of wastes; energy for hydroelectric power generation; transport channels for commerce; and a medium for recreation. Records of streamflow are the basic data used in developing reliable surface-water supplies because the records provide information on the availability of streamflow and its variability in time and space. The records are therefore used in the planning and design of surface-water related projects, and they are also used in the management or operation of such projects after the projects have been built or activated.

Streamflow, when it occurs in excess, can create a hazard—floods cause extensive damage and hardship. Records of flood events obtained at gaging stations serve as the basis for the design of bridges, culverts, dams, and flood-control reservoirs, and for flood-plain delineation and flood-warning systems.

The streamflow records referred to above are primarily continuous records of discharge at stream-gaging stations, a gaging station being a stream-site installation so instrumented and operated that a continuous record of stage and discharge can be obtained. Networks of stream-gaging stations are designed to meet the various demands for streamflow information, including inventory of the total water resource. The networks of continuous-record stations, however, are often augmented by auxiliary networks of partial-record stations to fill a particular need for streamflow information at relatively low cost. For example, an auxiliary network of sites, instrumented and operated to provide only instantaneous peak-discharge data, is often established to obtain basic information for use in regional flood-frequency studies. An auxiliary network of uninstrumented sites for measuring low flow only is often established to provide basic data for use in regional studies of drought and of fish and wildlife maintenance or enhancement.

GENERAL STREAM-GAGING PROCEDURES

After the general location of a gaging station has been determined from a consideration of the need for streamflow data, its precise location is so selected as to take advantage of the best locally available conditions for stage and discharge measurement and for developing a stable stage-discharge relation.

A continuous record of stage is obtained by installing instruments that sense and record the water-surface elevation in the stream. Discharge measurements are initially made at various stages to define the relation between stage and discharge. Discharge measurements are then made at periodic intervals, usually monthly, to verify the stage-discharge relation or to define any change in the relation caused by changes in channel geometry and (or) channel roughness. At many sites the discharge is not a unique function of stage; variables other than stage must also be continuously measured to obtain a discharge record. For example, stream slope is measured by the installation of a downstream auxiliary stage gage at stations where variable backwater occurs. At other sites a continuous measure of stream velocity at a point in the cross section is obtained and used as an additional variable in the discharge rating. The rate of change of stage can be an important variable where flow is unsteady and channel slopes are flat.

Artificial controls such as low weirs or flumes are constructed at some stations to stabilize the stage-discharge relations in the low-flow range. These control structures are calibrated by stage and discharge measurements in the field.

The data obtained at the gaging station are reviewed and analyzed

by engineering personnel at the end of the water year. Discharge ratings are established, and the gage-height record is reduced to mean values for selected time periods. The mean discharge for each day and extremes of discharge for the year are computed. The data are then prepared for publication.

SELECTED REFERENCE

Carter, R. W., and Davidian, Jacob, 1968, General procedure for gaging streams: U.S. Geol. Survey Techniques Water-Resources Inv., book 3, chap. A6, p. 1–2.

CHAPTER 2.—SELECTION OF GAGING-STATION SITES

INTRODUCTION

The general location of a gaging station is dependent on the specific purpose of the streamflow record. If the streamflow record is needed for the design or operation of a water project, such as a dam and reservoir, the general location of the gaging station obviously will be in the vicinity of the water project. The selection of a gaging-station site becomes complicated, however, when the station is to be one of a network of stations whose records are required for study of the general hydrology of a region. Such studies are used to inventory the regional water resource and formulate long-range water-development plans. In that situation, attention to hydrologic principles is required in selecting the general locations of the individual stations in the network to ensure that optimum information is obtained for the money spent in data collection.

A discussion of the design of gaging-station networks is beyond the scope of this manual and for the purpose of this chapter we will assume that the general location of a proposed gaging station has been determined. The discussion that follows will be concerned with the hydraulic considerations that enter into the selection of the precise location of the gage to obtain the best locally available conditions for the measurement of stage and discharge and for the development of a stable discharge rating.

CONSIDERATIONS IN SPECIFIC SITE SELECTION

After the general location of a gaging station has been determined, a specific site for its installation must be selected. For example, if the outflow from a reservoir is to be gaged to provide the streamflow data needed for managing reservoir releases, the general location of the gaging station will be along the stretch of stream channel between the dam and the first stream confluence of significant size

downstream from the dam. From the standpoint of convenience alone, the station should be established close to the dam, but it should be far enough downstream from the outlet gates and spillway outlet to allow the flow to become uniformly established across the entire width of the stream. On the other hand the gage should not be located so far downstream that the stage of the gaged stream may be affected by the stage of the confluent stream. Between those upstream and downstream limits for locating the gage, the hydraulic features should be investigated to obtain a site that presents the best possible conditions for stage and discharge measurement and for developing a stable stage-discharge relation. If the proposed gaging station is to be established for purely hydrologic purposes, unconnected with the design or operation of a project, the general location for the gage will be the stretch of channel between two large tributary or confluent streams. The same consideration will apply in the sense that the gage should be far enough downstream from the upper tributary so that flow is fairly uniformly established across the entire width of stream, and far enough upstream from the lower stream confluence to avoid variable backwater effect. Those limits often provide a reach of channel of several miles whose hydraulic features must be considered in selecting a specific site for the gage installation.

The ideal gage site satisfies the following criteria:

1. The general course of the stream is straight for about 300 ft (approx. 100 m) upstream and downstream from the gage site.
2. The total flow is confined to one channel at all stages, and no flow bypasses the site as subsurface flow.
3. The streambed is not subject to scour and fill and is free of aquatic growth.
4. Banks are permanent, high enough to contain floods, and are free of brush.
5. Unchanging natural controls are present in the form of a bedrock outcrop or other stable riffle for low flow and a channel constriction for high flow—or a falls or cascade that is unsubmerged at all stages (chap. 3).
6. A pool is present upstream from the control at extremely low stages to ensure a recording of stage at extremely low flow, and to avoid high velocities at the streamward end of gaging-station intakes during periods of high flow.
7. The gage site is far enough upstream from the confluence with another stream or from tidal effect to avoid any variable influence the other stream or the tide may have on the stage at the gage site.
8. A satisfactory reach for measuring discharge at all stages is available within reasonable proximity of the gage site. (It is not nec-

essary that low and high flows be measured at the same stream cross section.)

9. The site is readily accessible for ease in installation and operation of the gaging station.

Rarely will an ideal site be found for a gaging station and judgment must be exercised in choosing between adequate sites, each of which has some shortcomings. Often, too, adverse conditions exist at all possible sites for installing a needed gaging station, and a poor site must be accepted. For example, all streams in a given region may have unstable beds and banks, which result in continually changing stage-discharge relations.

The reconnaissance for a gaging site properly starts in the office where the general area for the gage site is examined on topographic, geologic, and other maps. Reaches having the following pertinent characteristics should be noted: straight alinement, exposed consolidated rock as opposed to alluvium, banks subject to overflow, steep banks for confined flow, divided channels, possible variable backwater effect from a tributary or confluent stream or from a reservoir, and potential sites for discharge measurement by current meter. The more favorable sites will be given critical field examination; they should be marked on the map, access roads should be noted, and an overall route for field reconnaissance should be selected.

In the field reconnaissance the features discussed earlier are investigated. With regard to low flow, a stable well-defined low-water control section is sought. In the absence of such a control, the feasibility of building an artificial low-water control is investigated. If a site on a stream with a movable bed must be accepted—for example, a sand-channel stream—it is best to locate the gage in as uniform a reach as possible, away from obstructions in the channel, such as bridges, which tend to intensify scour and fill. (See page 377.) Possible backwater resulting from aquatic growth in the channel should also be investigated. If the gage is to be located at a canyon mouth where the stream leaves the mountains or foothills to flow onto an alluvial plain or fan, reconnaissance current-meter measurements of discharge should be made during a low-flow period to determine where the seepage of water into the alluvium becomes significant. The station should be located upstream from the area of water seepage in order to gage as much of the surface flow as possible; the subsurface flow or underflow that results from channel seepage is not "lost" water, but is part of the total water resource.

With regard to high stages, high-water marks from major floods of the past are sought and local residents are questioned concerning historic flood heights. Such information is used by the engineer in making a judgment decision on the elevation at which the stage-

recorder must be placed to be above any floods that are likely to occur in the future. The recorder shelter should be so located as to be sheltered from waterborne debris during major floods. Evidence is also sought concerning major channel changes, including scour and deposition at streambanks, that occurred during notable floods of the past. That evidence, if found, gives some indication of changes that might be expected from major floods of the future.

The availability of adequate cross sections for current-meter measurement of discharge should also be investigated. Ideally, the measurement cross section should be of fairly uniform depth, and flow lines should be parallel and fairly uniform in velocity throughout the cross section. The measurement section should be in reasonable proximity to the gage to avoid the need for adjusting measured discharge for change in storage, if the stage should change rapidly during a discharge measurement. However a distance of as much as 0.5 mi (approx. 1 km) between gage and measuring section is acceptable if such a distance is necessary to provide both a good stage-measurement site and a good discharge-measurement site. Low-flow discharge measurements of all but the very large streams are made by wading. For flows that cannot be safely waded, the current meter is operated from a bridge, cableway, or boat. It is most economical to use an existing bridge for that purpose, but in the absence of a bridge, or if the measuring section at a bridge site is poor, a suitable site should be selected for constructing a cableway. If construction of a cableway is not feasible because of excessive width of the river, high-water measurements will be made by boat when safe to do so. The cross section used for measuring high flows is rarely suitable for measuring low flows, and wading measurements are therefore made wherever measuring conditions are most favorable.

Consideration should be given to the possibility of variable backwater effect from a stream confluence or reservoir downstream from the general location of the required gaging station. Without knowledge of stage and discharge at a potential gage site and of concurrent stage at the stream confluence or reservoir, the engineer can only conjecture concerning the location on the stream where backwater effect disappears for various combinations of discharge and stage. A safe rule is the following: Given a choice of several acceptable gaging sites on a stream, the gaging site selected should be the one farthest upstream from the possible source of variable backwater. If it is necessary to accept a site where variable backwater occurs, a uniform reach for measurement of slope should be sought, along with a site for the installation of an auxiliary gage. If a gaging station must be placed in a tide-affected reach, the unsteady flow that must be gaged will also require an auxiliary gage, but in addition line

power must be available to insure the synchronized recording of stage at the two gages. The availability of line power or telephone lines is also a consideration, where needed for special instrumentation or for the telemetering units that are often used in flood-forecasting and flood-warning systems.

In cold regions the formation of ice always presents a problem in obtaining reliable winter records of streamflow. However in regions that are only moderately cold, and therefore subject to only moderate ice buildup, forethought in the selection of gage sites may result in streamflow records that are free of ice effect. Gage sites that are desirable from that standpoint are as follows:

1. Below an industrial plant, such as a paper mill, steel mill, thermal powerplant, or coal mine. "Waste" heat may warm the water sufficiently or impurities in the water may lower the freezing point to the extent that open-water conditions always prevail.
2. Immediately downstream from a dam with outlet gages. Because the density of water is maximum at a temperature of 4°C, the water at the bottom of a reservoir is commonly at or near that temperature in winter. Most outlet gates are placed near the bottom of the dam, and the water released is therefore approximately 4°C above freezing. It would take some time for that water to lose enough heat to freeze.
3. On a long fairly deep pool just upstream from a riffle. A deep pool will be a tranquil one. Sheet ice will form readily over a still pool, but the weather must be extremely cold to give complete cover on the riffle. At the first cold snap, ice will form over the pool and act as an insulating blanket between water and air. Under ice cover the temperature of the streambed is generally slightly above the freezing point and may, by conduction and convection, raise the water temperature slightly above freezing, even though water enters the pool at 0°C. That rise in temperature will often be sufficient to prevent ice formation on the riffle.

After the many considerations discussed on the preceding pages have been weighed, the precise sites for the recording stage gage and for the cableway for discharge measurements (if needed) are selected. Their locations in the field are clearly marked and referenced. The maximum stage at which the low-water control will be effective should be estimated; the intakes to the stage recorder should be located upstream from the low-water control, a distance equal to at least three times the depth of water on the control at that estimated maximum stage. If the intakes are located any closer than that to the control, they may lie in a region where the streamlines have vertical curvature; intake location in that region is hydraulically undesirable.

The gaging station on the Kaskaskia River at Bondville, Ill., shown

in figure 1, satisfies most of the requirements discussed in this chapter. Low-flow measurements are made by wading upstream from the control. The bridge site provides accessibility, convenience to power lines, and a good location for an outside reference gage, which is shown on the downstream parapet wall of the bridge.

Up to this point there has been no discussion of specific site location for crest-stage gages. Those gages provide peak-discharge data only. Where possible they should be installed upstream from road culverts, which act as high-water controls. The specific site for a gage is at a distance of one culvert width upstream from the culvert inlet. In the absence of such control structures, the crest-stage gage should be installed in a straight reach of channel that can be utilized in computing peak discharge by the slope-area method (chap. 9).

SELECTED REFERENCES

Carter, R. W., and Davidian, Jacob, 1968, General procedure for gaging streams: U.S. Geol. Survey Techniques Water-Resources Inv., book 3, chap. A6, p. 2–3.

World Meteorological Organization, 1974, Guide to hydrometeorological practices [3d ed.]: WMO-no. 168, p. 3.1–3.4, 3.13–3.16.

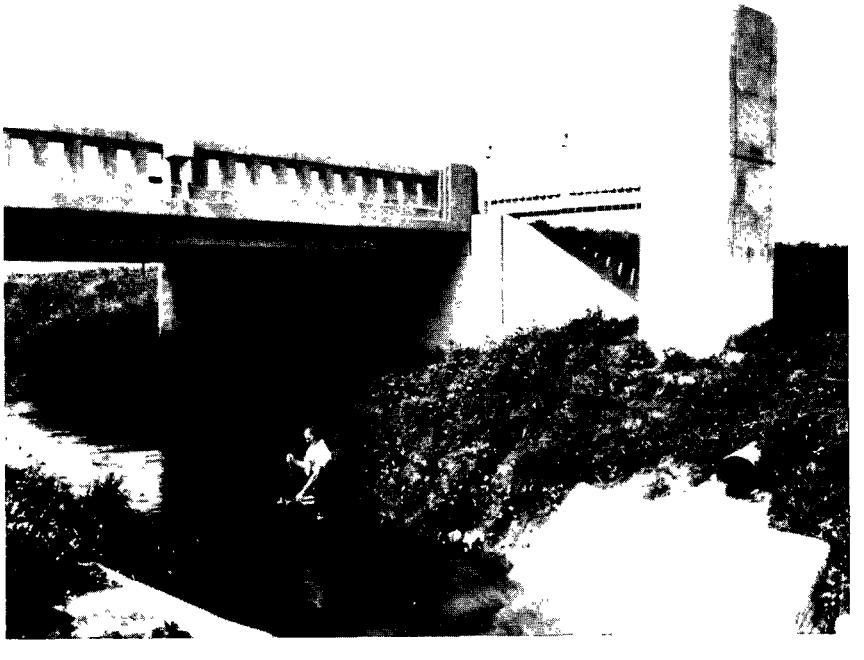

FIGURE 1.—Gage, concrete control, outside gage on bridge, and an engineer making a wading measurement, Kaskaskia River at Bondville, Ill.

CHAPTER 3.—GAGING-STATION CONTROLS

TYPES OF CONTROL

The conversion of a record of stage to a record of discharge is made by the use of a stage-discharge relation. The physical element or combination of elements that controls the relation is known as a control. The major classification of controls differentiates between section controls and channel controls. Another classification differentiates between natural and artificial controls. (Artificial controls are structures built for the specific purpose of controlling the stage-discharge relation; a highway bridge or paved floodway channel that serves incidentally as a control is not classed as an artificial control.) A third classification differentiates between complete, partial, and compound controls.

Section control exists when the geometry of a single cross section a short distance downstream from the gage is such as to constrict the channel, or when a downward break in bed slope occurs at the cross section. The constriction may result from a local rise in the streambed, as at a natural riffle or rock ledge outcrop, or at a constructed weir or dam; or it may result from a local constriction in width, which may occur naturally or be caused by some manmade channel encroachment, such as a bridge whose waterway opening is considerably narrower than the width of the natural channel. Examples of a downward break in bed slope are the head of a cascade or the brink of a falls.

Channel control exists when the geometry and roughness of a long reach of channel downstream from the gaging station are the elements that control the relation between stage and discharge. The length of channel that is effective as a control increases with discharge. Generally speaking, the flatter the stream gradient, the longer the reach of channel control.

A complete control is one that governs the stage-discharge relation throughout the entire range of stage experienced at the gaging station. More commonly, however, no single control is effective for the entire range of stage, and so the result is a compound control for the gaging station. A common example of a compound control is the situation where a section control is the control for low stages and channel control is effective at high stages. The compound control sometimes includes two section controls, as well as channel control. In that situation the upstream section control is effective for the very low stages, a section control farther downstream is effective for intermediate stages, and channel control is effective at the high stages.

With regard to complete controls, a section control may be a complete control if the section control is a weir, dam, cascade, or falls

of such height that it does not become submerged at high discharges. A channel control may be a complete control if a section control is absent, as in a sand channel that is free of riffles or bars, or in an artificial channel such as a concrete-lined floodway.

A partial control is a control that acts in concert with another control in governing the stage-discharge relation. That situation exists over a limited range in stage whenever a compound control is present. As an example consider the common situation where a section control is the sole control for low stages and channel control is solely operative at high stages. At intermediate stages there is a transition from one control to the other, during which time submergence is "drowning out" the section control. During that transition period the two controls act in concert, each as a partial control. In effect we have a dam (low-flow control) being submerged by tailwater; before complete submergence (channel control), the upstream stage for the particular discharge is dependent both on the elevation of the dam and on the tailwater elevation. Where the compound control includes two section controls, the degree of submergence of the upstream section control will be governed by the downstream section control, during a limited range in stage. When that occurs, each of the section controls is acting as a partial control. A constriction in channel width, unless unusually severe, usually acts as a partial control, the upstream stage being affected also by the stage downstream from the constriction.

ATTRIBUTES OF A SATISFACTORY CONTROL

The two attributes of a satisfactory control are permanence (stability) and sensitivity. If the control is stable, the stage-discharge relation will be stable. If the control is subject to change, the stage-discharge relation is likewise subject to change, and frequent discharge measurements are required for the continual recalibration of the stage-discharge relation. That not only increases the operating cost of a gaging station, but results in impairment of the accuracy of the streamflow record.

The primary cause of changes in natural controls is the high velocity associated with high discharge. Of the natural section controls, a rock ledge outcrop will be unaffected by high velocities, but boulder, gravel, and sand-bar riffles are likely to shift, boulder riffles being the most resistant to movement and sand bars the least resistant. Of the natural channel controls those with unstable bed and banks, as found in sand-channel streams, are the most likely to change as a result of velocity-induced scour and deposition.

Another cause of changes in natural controls is vegetal growth. The growth of aquatic vegetation on section controls increases the stage

for a given discharge, particularly in the low-flow range. Vegetal growth on the bed and banks of channel controls also affects the stage-discharge relation by reducing velocity and the effective waterway area. In the temperate climates, accumulations of water-logged fallen leaves on section controls each autumn clog the interstices of alluvial riffles and raise the effective elevation of all natural section controls. The first ensuing stream rise of any significance usually clears the control of fallen leaves.

Controls, particularly those for low flow, should be sensitive; that is, a small change in discharge should be reflected by a signficant change in stage. To meet that requirement it is necessary that the width of flow at the control be greatly constricted at low stages. In a natural low-water control such constriction occurs if the control is in effect notched, or if the controlling cross section roughly has a flat V-shape or a flat parabolic shape. Those shapes will ensure that the width of flow over the control decreases as discharge decreases. Generally speaking, a low-water control is considered to be sensitive if a change of no more than 2 percent of the total discharge is represented by a change of one unit of recorded stage. For example, in the U.S.A., stage is recorded in units of hundredths of a foot; therefore, for the low-water control to be regarded as sensitive, a change in stage of 0.01 ft (0.003 m) should represent a change of no more than about 2 percent of the total discharge.

In the interest of economy a gaging station should be located upstream from a suitable natural control (fig. 2). However, where natural conditions do not provide the stability or the sensitivity required, artificial controls should be considered. The artificial controls are all section controls; it is not feasible to pave or otherwise improve a long reach of channel solely for the purpose of stabilizing the stage-discharge relation.

ARTIFICIAL CONTROLS

An artificial control is a structure built in a stream channel to stabilize and constrict the channel at a section, and thereby simplify the procedure of obtaining accurate records of discharge. The artificial controls built in natural streams are usually broad-crested weirs that conform to the general shape and height of the streambed. (The term "broad-crested weir," as used in this manual, refers to any type of weir other than a thin-plate weir.) In canals and drains, where the range of discharge is limited, thin-plate weirs and flumes are the controls commonly built. Thin-plate weirs are built in those channels whose flow is sediment free and whose banks are high enough to accommodate the increase in stage (backwater) caused by the installation of a weir (fig. 3). Flumes are largely self cleaning and can

therefore be used in channels whose flow is sediment laden, but their principal advantage in canals and drains is that they cause relatively little backwater (head loss) and can therefore be used in channels whose banks are relatively low. Flumes are generally more costly to build than weirs.

Flumes may be categorized with respect to the flow regime that principally controls the measured stage; that is, a flume is classed as either a critical-flow flume or a supercritical-flow flume. The Parshall flume (fig. 4) is the type of critical-flow flume most widely used. Supercritical-flow flumes are used in streams that transport heavy loads of sediment that include rocks that are too large to pass through a critical-flow flume without being deposited in the structure. Of those flumes the trapezoidal supercritical-flow flume (fig. 5) is the most widely used by the U.S. Geological Survey.

Artificial controls eliminate or alleviate many of the undesirable characteristics of natural section controls. Not only are they physically stable, but they are not subject to the cyclic or progressive growth of aquatic vegetation other than algae. Algal slimes that sometimes form on artificial controls can be removed with a wire brush, and the controls are self cleaning with regard to fallen leaves. In moderately cold climates artificial controls are less likely to be affected by the formation of winter ice than are natural controls. The artificial control can, of course, be designed to attain the degree of sensitivity required for the gaging station. In addition, an artificial

FIGURE 2.—Gage and natural control, Little Spokane River at Elk, Wash.

control may often provide an improved discharge-measurement section upstream from the control by straightening the original angularity of flow lines in that cross section.

In canals or drains, where the range of discharge is limited, artificial controls are usually built to function as complete controls throughout the entire range in stage. In natural channels it is generally impractical to build the control high enough to avoid submergence at high discharges, and the broad-crested weirs that are usually built are effective only for low, or for low and medium, discharges. Figures 6 and 7 illustrate broad-crested weirs of two different shapes; the crests of both have a flat upward slope from the center of the stream to the banks, but in addition, the weir in figure 7 has a shallow V-notch in the center for greater sensitivity.

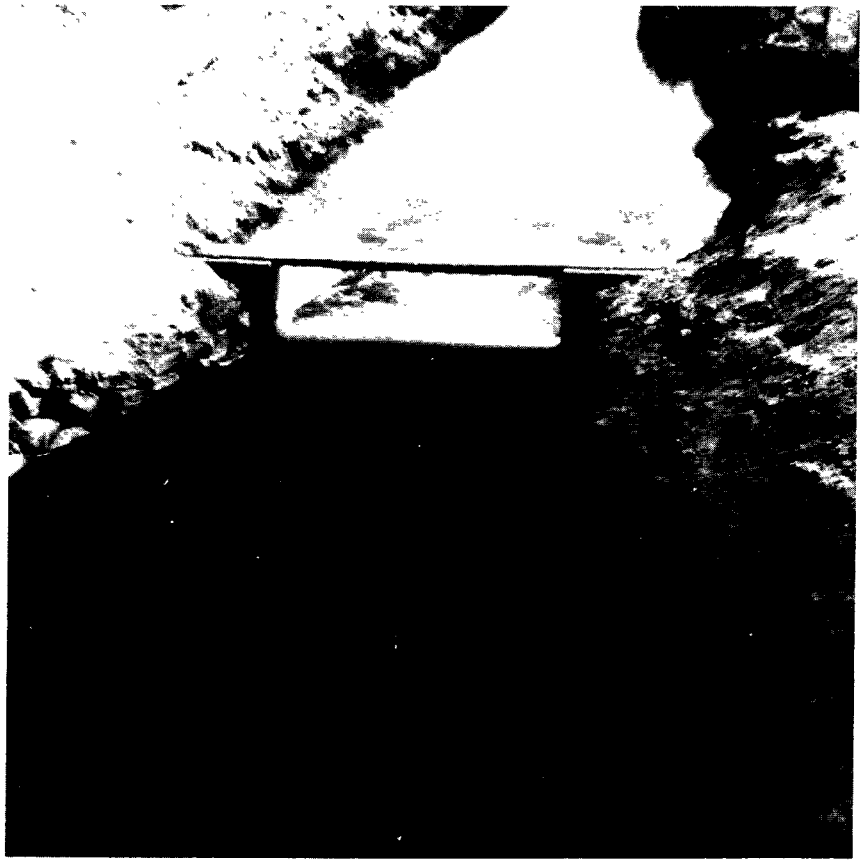

FIGURE 3.—Rectangular weir on Trifolium Drain 23 of Imperial Irrigation District, near Westmorland, Calif. (View looking downstream.)

The attributes desired in an artificial control include the following:

1. The control should have structural stability and should be permanent. The possibility of excessive seepage under and around the control should be considered, and the necessary precautions should be taken for the prevention of seepage by means of sheet piling or concrete cut-off walls and adequate abutments.
2. The crest of the control should be as high as practicable to possibly eliminate the effects of variable downstream conditions or to limit those effects to high stages only.
3. The profile of the crest of the control should be designed so that a small change in discharge at low stages will cause a measurable change in stage. If the control is intended to be effective at all stages, the profile of the crest should be designed to give a stage-discharge relation (rating curve) of such shape that it can be extrapolated to peak stages without serious error.
4. The shape of the control structure should be such that the passage of water creates no undesirable disturbances in the channel upstream or downstream from the control.

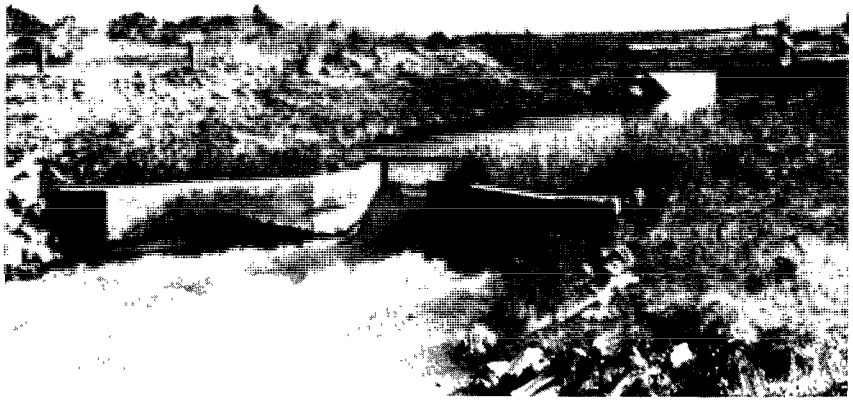

FIGURE 4.—Four-foot Parshall flume discharging 62 ft^3/s (1.76 m^3/s) under free-flow conditions. Scour protection is required with this height of fall. (Courtesy U.S. Bureau of Reclamation.)

5. If the stream carries a heavy sediment load, the artificial control should be designed to be self-cleaning. Flumes have that attribute; broad-crested weirs can often be made self-cleaning by a design modification in which the vertical upstream face of the weir is replaced by an upstream apron that slopes gently from the streambed to the weir crest.

Artificial controls are often built in conformance with the dimensions of laboratory-rated or field-rated weirs or flumes. The question arises whether to use the precalibrated rating or to calibrate in place each new installation. There are two schools of thought on the subject. In many countries, the precalibrated rating is accepted, and discharge measurements by current meter or by other means are made only periodically to determine if any statistically significant changes in the rating have occurred. If a change is detected, the new rating is defined by as many discharge measurements as are deemed neces-

FIGURE 5.—Flow through a 3-ft trapezoidal supercritical-flow flume showing transition from subcritical to supercritical flow.

sary. In other countries, including the U.S.A., the position is taken that it is seldom desirable to accept the rating curve prepared for the model structure without checking the entire rating of the prototype structure in the field by current-meter measurements, or by other methods of measuring discharge. The experience in the U.S.A. and elsewhere has been that differences between model and prototype invariably exist, if only in approach-channel conditions, and these differences are sufficient to require complete in place calibration of the prototype structure. In place calibration is sometimes dispensed with where the artificial control is a standard thin-plate weir having negligible velocity of approach.

CHOICE OF AN ARTIFICIAL CONTROL

Cost is usually the major factor in deciding whether or not an artificial control is to be built to replace an inferior natural control. The cost of the structure is affected most by the width of the stream and by the type or condition of bed and bank material. Stream width governs the size of the structure, and bed and bank material govern the type of construction that must be used to minimize leakage under and around the structure.

If an artificial control is to be used, the type and shape of the structure to be built is dependent upon channel characteristics, flow conditions, range of discharge to be gaged, sensitivity desired, and the maximum allowable head loss (backwater).

FIGURE 6.—Concrete artificial control on Mill Creek near Coshocton, Ohio.

CHOICE BETWEEN WEIR AND FLUME

As a general rule a weir is more advantageous for use as a control structure than a flume for the following reasons.

1. Weirs are usually cheaper to build than flumes.
2. A weir can be designed to have greater sensitivity at low flows with less sacrifice of range of discharge that can be accommodated, than is possible with a flume. Sensitivity is increased for a weir by notching the crest or by shaping the longitudinal profile of the crest in the form of a flat V or catenary. Sensitivity at low flow for a flume is usually attained by narrowing the effective width (converging sidewalls), or by using a trapezoidal cross section (narrower width at low stages), or by doing both; those measures significantly reduce the capacity of the flume.
3. The high water end of the stage-discharge relation for a weir can be extended beyond the stages at which the weir is effective as a control, with more confidence than can be done for a flume. In other words the stage-discharge relation for a flume becomes completely uncertain when any part of the structure upstream from the stage-measurement site is overtopped; the stage-discharge relation for a weir becomes completely uncertain only when the bank or abutment is overtopped and flow occurs around the end(s) of the weir.

If a flume is installed with the expectation that it will be overtop-

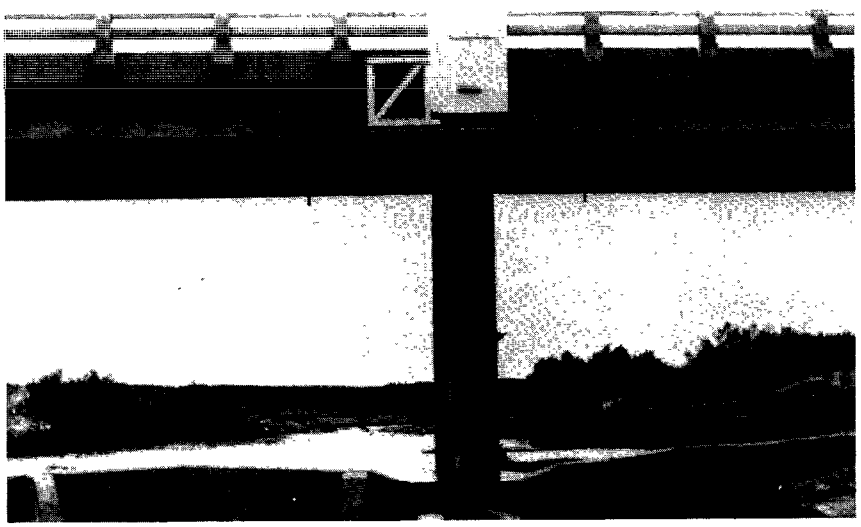

FIGURE 7.—Artificial control on Delaware River near Red Bluff, New Mex., with shallow V notch in the broad-crested weir.

ped by floodflows, it is advisable to install a nonrecording stage gage in a straight reach of channel, upstream or downstream from the flume but beyond the influence of the flume structure. Simultaneous observations of stage at the flume and in the unobstructed channel can be used to obtain a relation between the two stage gages. A stage-discharge relation for the site of the nonrecording gage can thus be derived from the flume rating, up to the discharge at which overflow starts at the flume. If for some reason, such as one of those discussed on page 273, high-flow discharge measurements are not available, the stage-discharge relation for the nonrecording gage can be extrapolated to flood stages; that extrapolation can then be used with the stage relation to define the overflow portion of the discharge rating for the flume.

However, in the following situations the use of a flume is more advantageous than the use of a weir.

1. If a heavy sediment load is carried by the stream, a weir will trap the sediment; accumulation of the sediment in the approach reach will alter the stage-discharge relation by changing the velocity of approach. Flumes however are usually self cleaning by virtue of their converging sidewalls and (or) steep floor. They therefore are more likely to maintain an unchanging stage-discharge relation. However, if the size of the sediment is not large, it is often possible to make a broad-crested weir self cleaning by including in its design an upstream apron that slopes downward from crest. An apron slope of 1 vertical to 5 horizontal will usually result in the transport of small sediment over the weir.
2. Weirs are usually not suitable for use in steep channels where the Froude number ($V/\sqrt{gd}$) is greater than about 0.75. Best results are obtained with weirs where the velocity head is a very minor part of the total head, and that is not the case in steep channels where the velocity head becomes excessively large. Furthermore, as explained above, weirs act as sediment traps on steep streams.
3. Flumes create less backwater for a given discharge than do weirs. Consequently it is more advantageous to use a flume if the channel has low banks. However for most natural streams it is impractical to design any type of structure to act solely as a metering device for the entire range of stage that may be experienced. In other words, for most natural streams sporadic overbank flooding is to be expected, with or without a control structure in the stream. Consequently the advantage of reduced backwater for a flume is usually realized only where the flow can be controlled to give some preassigned value of maximum dis-

charge. That situation occurs only in diversion canals or in natural streams having a bypass floodway.

CHOICE BETWEEN CRITICAL-FLOW FLUME AND SUPERCRITICAL-FLOW FLUME

After it has been decided for a particular site that the use of a flume is more desirable than the use of a weir, a decision must be made as to whether to use a critical-flow flume or a supercritical-flow flume.

Both types of flume will transport debris of considerable size without deposition in the structure, but if the transported rocks are excessively large, they may be deposited at or immediately upstream from the critical-depth section of a critical-flow flume. That will cause a change in the discharge rating of the flume. Therefore where that situation is likely to occur, a supercritical-flow flume should be selected for use.

If a critical-flow flume will pass the transported sediment load, that type of flume should be selected for use because the discharge rating for a critical-flow flume is more sensitive than that for a supercritical-flow flume.

SUMMARY

The artificial controls recommended for natural streams are as follows:

Sediment-transport characteristics	*Recommended structure*
Light load, small-size sediment	Weir.
Medium load, medium-size sediment	Parshall flume.
Heavy load, large-size sediment	Trapezoidal supercritical-flow flume.

The adjectives used above—light, medium, heavy, small, and large—are relative. Observation of both the study site and of the operation of control structures installed in an environment similar to that of the study site will provide the principle basis for the selection of the optimum type of control for use. In short, do not use a flume where a weir will do; if the use of a flume is indicated, do not use a supercritical-flow flume where a critical-flow flume (Parshall flume) will do.

The above recommendations also apply to canals or natural channels whose flow is controlled to limit the maximum discharge to some preassigned value. However, there is one exception; if the banks have little freeboard at the maximum discharge before the installation of an artificial control, a flume installation is generally preferable to a weir, in order to minimize the backwater caused by the structure.

DESIGN OF AN ARTIFICIAL CONTROL

Having decided on the type of artifical control to be used—weir, Parshall flume, or trapezoidal supercritical-flow flume—the next step is to design the structure. A standard design will usually be used, although channel conditions may make it necessary to make minor modification of the standard dimensions of the structure selected. The four factors—channel characteristics, range of discharge to be gaged, sensitivity desired, and maximum allowable head loss (backwater)—must be considered simultaneously in the precise determination of the shape, dimensions, and crest elevation of the control structure. However, two preliminary steps are necessary.

First, the head-discharge relations for various artificial controls of standard shape and of the type selected are assembled. Several such relations are to be found in hydraulics handbooks (King and Brater, 1963; World Meterological Organization, 1971). In addition, head-discharge relations for artificial controls that were field calibrated will usually be available in the files of water-resources agencies in the area—some are given in chapter 10. The head-discharge relations that are assembled need only be approximately correct, because channel conditions at the site of the proposed control will seldom match those for the model control.

The second preliminary step is to determine an approximate stage-discharge relation for the anticipated range in stage in the unobstructed channel at the site of the proposed control. That may be done by the use of an open-channel discharge equation, such as the Manning equation, in which uniform flow is assumed for the site and a value of the roughness coefficient is estimated. The reliability of the computed stage-discharge relation will be improved if one or more discharge measurements are made to verify the value of the roughness coefficient used in the computations. The purpose of the computations is to determine the tailwater elevation that is applicable to any given discharge after an artificial control is installed.

The next step is to consider the lower discharges that will be gaged. The tailwater elevations corresponding to those discharges are used to determine the minimum crest elevation permissible for the proposed artificial control at the lower discharges, under conditions of free flow or allowable percentage of submergence. If a flume is to be installed, the throat section should be narrow enough to ensure sensitivity at low discharges. If a weir is to be installed and the stream is of such width that a horizontal crest will be insensitive at low discharges, the use of a flat V crest is recommended—for example, one whose sides have a slope of 1 vertical to 10 horizontal. The sensitivity desired is usually such that the discharge changes no more than 2 percent for each change in stage of 0.01 ft (0.003 m). For a weir or

critical-flow flume (Parshall flume) it is also desirable that the minimum discharge to be gaged have a head of at least 0.2 ft (0.06 m) to eliminate the effects of surface tension and viscosity.

Stage-discharge relations for the several controls under consideration are next prepared for the anticipated range in discharge. A structure is then selected that best meets the demands of the site in acting as a control for as much of the range as possible, without exceeding the maximum allowable backwater (head loss) at the higher stages and with minor submergence effect and acceptable sensitivity at lower stages. In other words, a high crest elevation minimizes submergence but maximizes backwater effect which may cause or aggravate flooding; a low crest elevation maximizes submergence but minimizes backwater effect; and where flumes are concerned, the attainment of the desired range of discharge may require some sacrifice of sensitivity at extremely low discharges. The engineer must use judgment in selecting a control design that is optimum for the local conditions. For example, to design a flume whose throat is sufficiently wide to accommodate the desired range of discharge, it may be necessary to relax the 2-percent sensitivity criterion at extremely low flows; in that situation the engineer may accept a sensitivity such that a change in stage of 0.01 ft (0.003 m) results in as much as a 5-percent change in discharge.

From a practical viewpoint the use of artificial controls is limited to streams with stable channels. Artificial controls seldom operate satisfactorily in sand channels having highly mobile beds. The transport of sediment as bedload continually changes the characteristics of the approach channel, and the control itself may be buried or partially buried by the movement of sand dunes.

SELECTED REFERENCES

Carter, R. W., and Davidian, Jacob, 1968, General procedure for gaging streams: U.S. Geol. Survey Techniques Water-Resources Inv., book 3, chap. A6, p. 3–5.

Corbett, D. M., and others, 1943, Stream-gaging procedure: U.S. Geol. Survey Water-Supply Paper 888, p. 109–115.

King, H. W., and Brater, E. F., 1963, Handbook of hydraulics [5th ed.]: New York, McGraw-Hill, 1373 p.

World Meteorological Organization, 1971, Use of weirs and flumes in stream gaging: WMO-No. 280 Technical Note No. 117, Geneva, 57 p.

CHAPTER 4.—MEASUREMENT OF STAGE

GENERAL

The stage of a stream or lake is the height of the water surface above an established datum plane. The water-surface elevation re-

ferred to some arbitrary or predetermined gage datum is called the "gage height." Gage height is often used interchangeably with the more general term "stage," although gage height is more appropriate when used to indicate a reading on a gage. Stage or gage height is usually expressed in feet and hundredths of a foot, or in meters and hundredths or thousandths of a meter.

Records of gage height are used with a stage-discharge relation in computing records of stream discharge. The reliability of the discharge record is therefore dependent on the reliability of the gage-height record as well as on the accuracy of the stage-discharge relation. Records of stream stage are also useful in themselves for such purposes as the design of structures affected by stream elevation and the planning of flood-plain use. The gage-height record of a lake or reservoir provides, in addition to elevations, indexes of surface area and volume of the water body.

A record of stage may be obtained by systematic observations of a nonrecording gage or by means of a water-stage recorder. Special-purpose gages that do not give a complete record of stage are discussed on pages 74–78. The advantages of the nonrecording gage are the low initial cost and the ease of installation. The disadvantages are the need for an observer and the lack of accuracy of the estimated continuous-stage graph drawn through the plotted points of observed stage. For long-term operation the advantages of the recording gage far outweigh those of the nonrecording gage, and therefore the use of the nonrecording gage as a base gage is not recommended. However, at a recording-gage station, one or more nonrecording gages should be maintained as auxiliary gages for the operation of the station (p. 53–54). Telemetering systems are often used to transmit gage-height information to points distant from the gaging station (p. 54–59).

DATUM OF GAGE

The datum of the gage may be a recognized datum, such as mean sea level, or an arbitrary datum plane chosen for convenience. An arbitrary datum plane is selected for the convenience of using relatively low numbers for gage heights. To eliminate the possibility of minus values of gage height, the datum selected for operating purposes is below the elevation of zero flow on a natural control. Where an artificial control is used, the gage datum is usually set at the elevation of zero flow.

As a general rule a permanent datum should be maintained so that only one datum for the gage-height record is used for the life of the station. An exception occurs at gage sites where excessive streambed scour, after installation of the station, results in low-flow stages having a negative gage height. In that situation a change in gage datum

to eliminate the negative numbers is recommended, to avoid possible confusion involving the algebraic sign of the gage heights. Another exception occurs when channel changes at a station make it impractical to maintain the station at the existing site. It may then be necessary to move the station a distance, such that there is significant fall in the water-surface elevation between the old and new sites, even though discharges at the two sites are equivalent. In that situation there is generally little to be gained by establishing the datum at the new site at the same sea-level elevation as the datum at the original site. That is especially true if the station is moved downstream a distance such that negative gage heights would result from use of the original datum. When datum changes are made for whatever reason, a record of the change should be a part of the published station description.

In any event, when a station is established, it should be assumed that a permanent datum will be maintained at the site. To maintain a permanent datum, each gaging station requires at least two or three reference marks; that is, permanent points of known gage-height elevation that are independent of the gage structure. The datum at each gaging station is periodically checked by running levels from the reference marks to the gages at the station.

If an arbitrary datum plane is used, it is desirable that it be referred by levels to a bench mark of known elevation above mean sea level, so that the arbitrary datum may be recovered if the gage and reference marks are destroyed.

NONRECORDING STREAM-GAGING STATIONS

On page 23 it was mentioned that a record of stage could be obtained by systematic observation of a nonrecording gage. The advantages (low initial cost) and disadvantages (need for an observer, lack of accuracy) of a nonrecording gaging station were briefly discussed. On pages 53–54 the use of nonrecording gages as auxiliary and as reference (base) gages at recording-gaging stations will be discussed. Chapter 15 (p. 559–560) will describe the manner in which an observer's gage readings are used to compute a record of stage at a nonrecording gaging station. This section of the manual describes the various types of nonrecording gages.

Of the five types to be described, the two most generally used at nonrecording stations are either the staff or wire-weight gage. At such stations the nonrecording gage is usually read twice daily by an observer, and additional readings are made during periods of rapidly changing stage. The observer systematically records and reports his readings to headquarters. The record book and report cards shown in

figure 8 are used by the U.S. Geological Survey, the book being the permanent record of nonrecording-gage readings. The weekly report card serves as an interim report of the observations made. The weekly report cards are read promptly on their arrival at the headquarters office so that any problems or difficulties that arise can be handled without delay.

On each routine visit to a nonrecording stream-gaging station, the hydrographer also visits the observer to enter in the stage-record book the gage reading(s) that the hydrographer has made. At that time he also inspects the record book to check for discrepancies in the observer's readings. Such visits by the hydrographer are important; if they are not made the observer tends to feel that no one pays any attention to his work, and he may become less conscientious about his gage readings.

Descriptions of five types of nonrecording stage gages follow. The special-purpose crest-stage gage and its use as an adjunct to the nonrecording gaging station are described on pages 77–78.

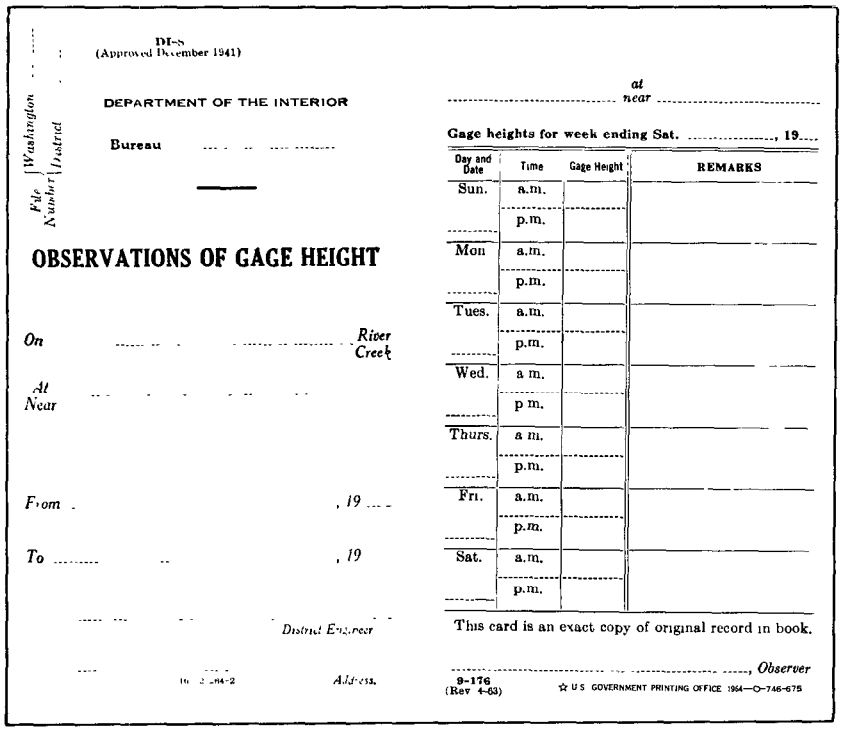

DI-S
(Approved December 1941)

DEPARTMENT OF THE INTERIOR

Bureau .....

File Number { Washington / District

OBSERVATIONS OF GAGE HEIGHT

On ..... *River / Creek*

At / Near .....

From ..... , *19* ....

To ..... , *19*

..... *District Engineer*

..... *Address.*

at ..... *near* .....

Gage heights for week ending Sat. ....., **19**....

Day and Date	Time	Gage Height	REMARKS
Sun.	a.m.		
	p.m.		
Mon	a.m.		
	p.m.		
Tues.	a.m.		
	p.m.		
Wed.	a m.		
	p m.		
Thurs.	a m.		
	p.m.		
Fri.	a.m.		
	p.m.		
Sat.	a.m.		
	p.m.		

This card is an exact copy of original record in book.

....., *Observer*

9-176
(Rev 4-63)

☆ U S GOVERNMENT PRINTING OFFICE 1964—O-746-675

FIGURE 8.—Cover of book and weekly report card for recording manual gage observations.

STAFF GAGE

Staff gages are either vertical or inclined. The standard Geological Survey vertical staff gage consists of porcelain-enameled iron sections, each 4 in (0.1 m) wide, 3.4 ft (1.04 m) long, and graduated every 0.02 ft (0.0067 m). (See fig. 9.) The vertical staff gage is used in stilling wells as an inside reference gage, or in the stream as an outside gage.

An inclined staff gage is usually a graduated heavy timber securely attached to permanent foundation piers. Inclined gages built flush with the streambank are less likely to be damaged by floods, floating ice, or drift than are projecting vertical staff gages. Copper barrelhoop staples and bronze numerals are generally used for the graduations. Inclined gages are used only as outside gages.

WIRE-WEIGHT GAGE

The wire-weight gage used in the U.S.A. is known as the type A wire-weight gage. It consists of a drum wound with a single layer of cable, a bronze weight attached to the end of the cable, a graduated disc, and a Veeder counter, all within a cast-aluminum box. (See fig. 10.) The disc is graduated in tenths and hundredths of a foot and is permanently connected to the counter and to the shaft of the drum. The cable is made of 0.045-in-diameter stainless-steel wire and is guided to its position on the drum by a threading sheave. The reel is equipped with a pawl and ratchet for holding the weight at any desired elevation. The diameter of the drum of the reel is such that each complete turn represents a 1-ft (0.305 m) movement of the weight. A horizontal checking bar is mounted at the lower edge of the instrument so that when it is moved to the forward position the bottom of the weight will rest on it. The gage is set so that when the bottom of the weight is at the water surface, the gage height is indicated by the combined readings of the counter and the graduated disc. The type A wire-weight gage is commonly mounted on a bridge handrail, parapet wall, or pier for use as an outside gage.

FLOAT-TAPE GAGE

A float-type gage consists of float, graduated steel tape, counterweight, and pulley. (See fig. 11.) The float pulley is usually 6 in (0.152 m) in diameter, grooved on the circumference to accommodate the tape, and mounted in a standard. An arm extends from the standard to a point slightly beyond the tape to carry an adjustable index. The tape is connected to the float by a clamp that also may be used for making adjustments to the tape reading if the adjustments necessary are too

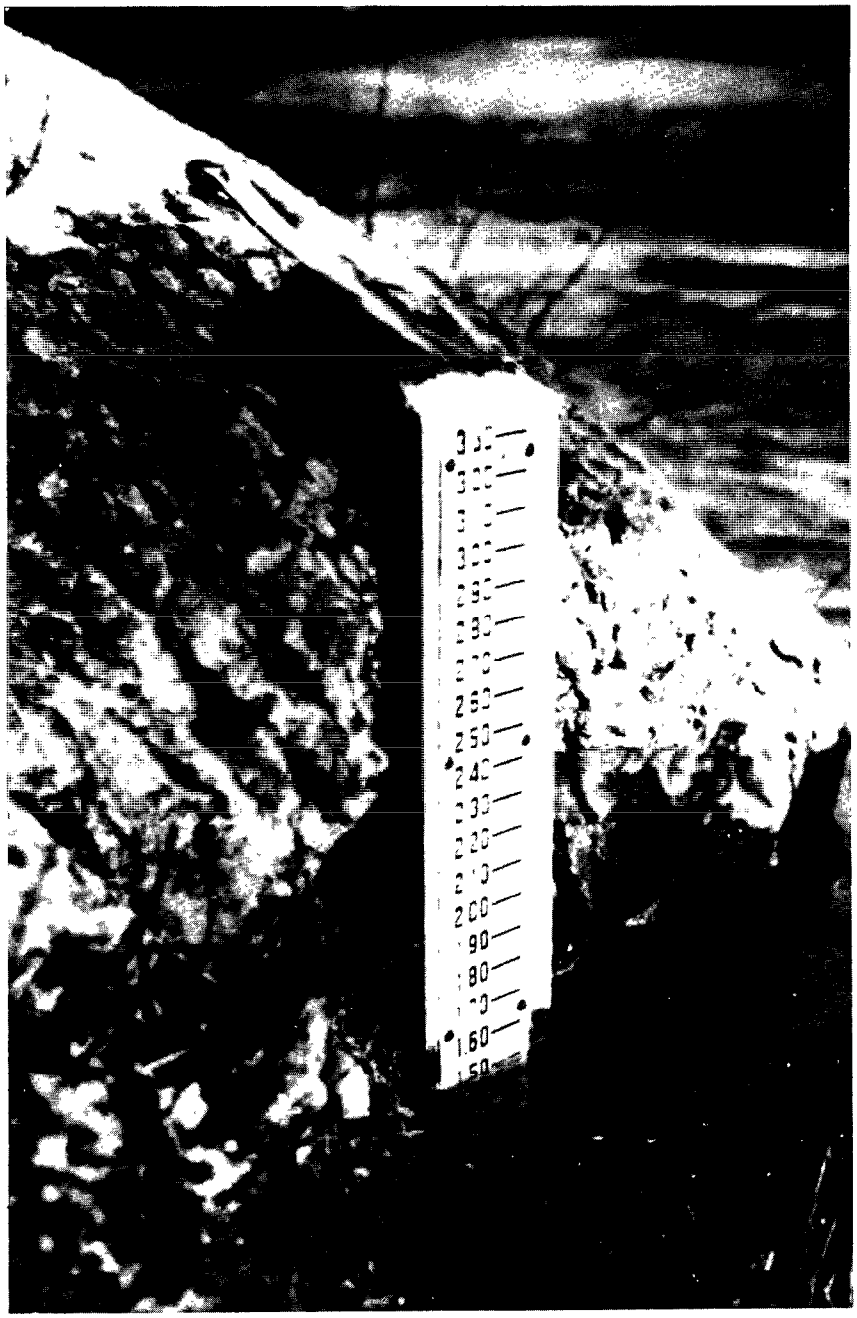

FIGURE 9.—Vertical staff gage.

large to be accommodated by the adjustable index. A 10-in (0.25 m)-diameter copper float and a 2-lb (0.9 kg) lead counterweight are normally used. The float-type gage is used chiefly in stilling wells as an inside reference or auxiliary gage.

ELECTRIC-TAPE GAGE

The electric-tape gage consists of a steel tape graduated in feet and hundredths of a foot, to which is fastened a cylindrical weight, a reel in a frame for the tape, a 4½-volt battery, and a voltmeter. (See fig. 12.) One terminal of the battery is attached to a ground connection, and the other to one terminal of the voltmeter. The other terminal of the voltmeter is connected through the frame, reel, and tape, to the weight. The weight is lowered until it contacts the water surface; this contact completes the electric circuit and produces a signal on the voltmeter. With the weight held in the position of first contact, the tape reading is observed at the index provided on the reel mounting. The electric-tape gage is used as an inside reference gage and occasionally as an outside gage. If oil is floating on the water surface, the gage will give the gage height of the interface, because oil is a dielectric. In some electric-tape gages a light or audible signal is substituted for the voltmeter.

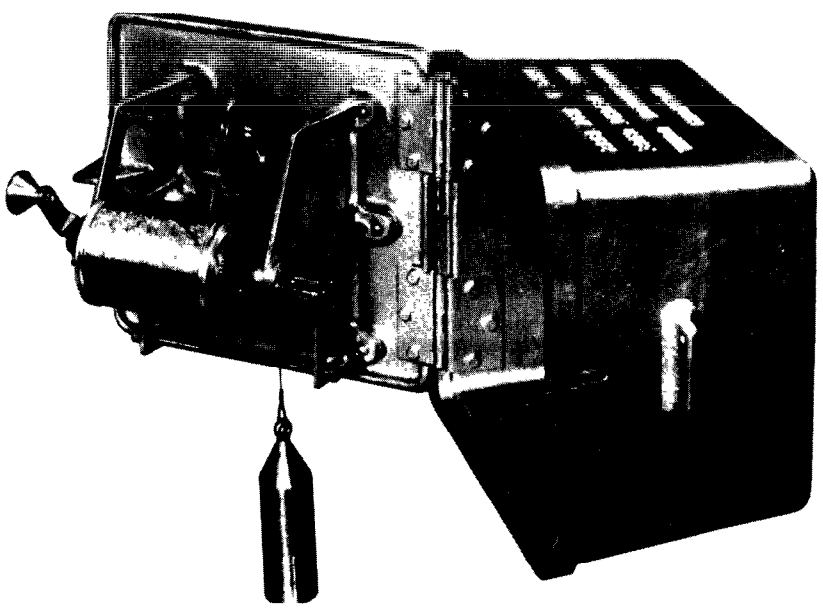

FIGURE 10.—Type A wire-weight gage.

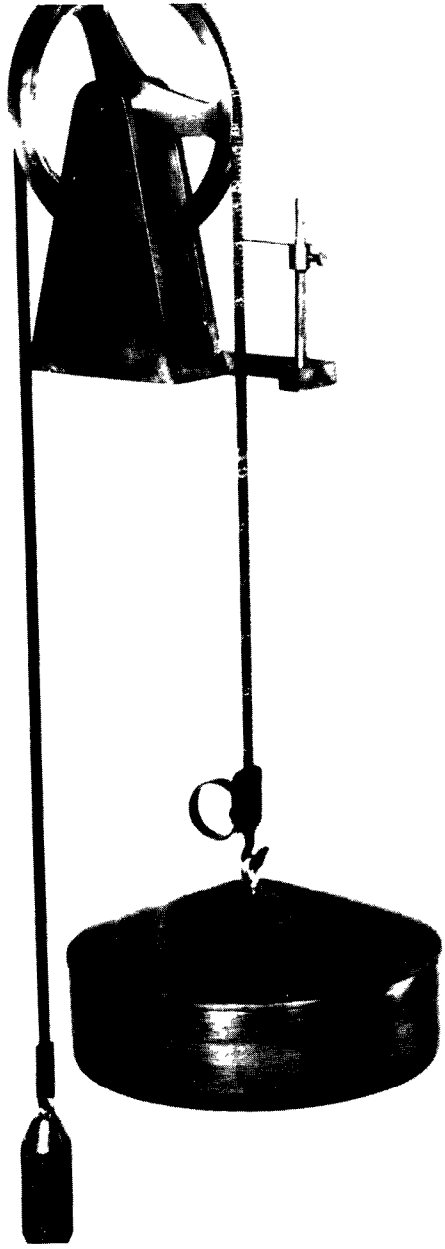

FIGURE 11.—Float-tape gage.

FIGURE 12.—Electric-tape gage.

CHAIN GAGE

A chain gage (fig. 13) is used where outside staff gages are difficult to maintain and where a bridge, dock, or other structure over the water is not available for the installation of a wire-weight gage. The chain gage can be mounted on a cantilevered arm which extends out over the stream, or which is made in such a way that it can be tilted to extend over the stream.

The chain gage consists of the cantilevered arm, one or more enamelled gage sections mounted horizontally on the cantilever, and a heavy sash chain that runs over a pulley on the streamward end of the cantilever. (See figure 13.) The chain is mounted so that it moves along the gage sections. A weight is attached to the streamward end of the chain, and an index marker (*M* in fig. 13) is attached near the other end at a distance from the weight that is appropriate for reading the gage height of low flows. Additional index markers can be attached to the chain at appropriate intervals to read gage heights greater than those directly obtainable from the mounted gage sections.

Stage is determined by lowering the weight until the bottom of the

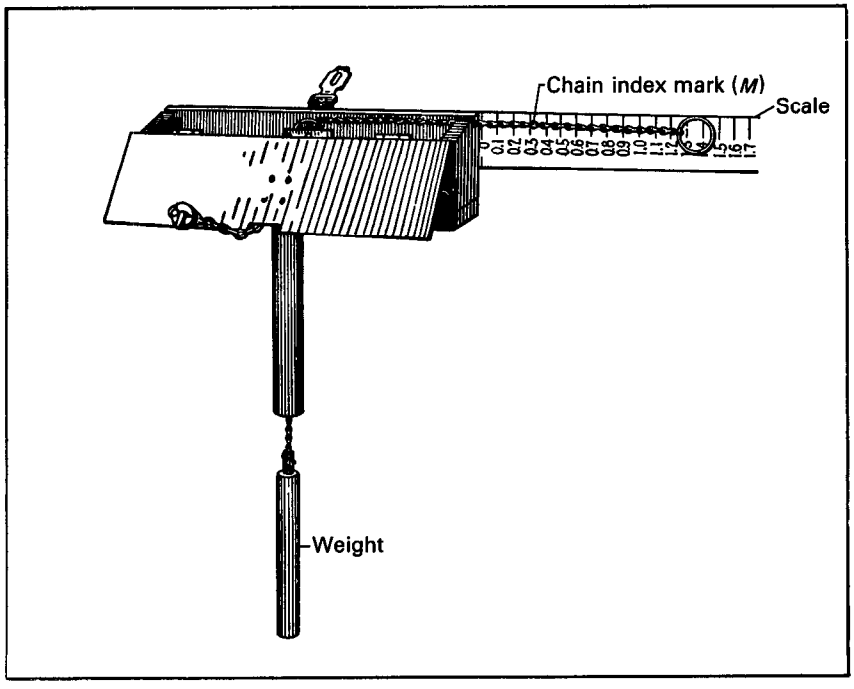

FIGURE 13.—Chain gage (cantilevered mount not shown).

weight just touches the water surface. The gage height then is read from the mounted gage plate at the location of the appropriate chain index marker.

RECORDING STREAM-GAGING STATIONS

METHODS OF SENSING STAGE FOR AUTOMATIC RECORDING

Stage is sensed for automatic recording by a float in a stilling well, or by a gas-purge system that transmits the pressure head of water in a stream to a manometer. The latter system, which does not require a stilling well, is known as a bubble gage.

FLOAT SENSOR

The float sensor consists of a tape or cable passing over a pulley, with a float in a stilling well attached to one end of the tape or cable and a counterweight attached to the other end. (See fig. 11.) The float follows the rise and fall of the water level, and the water level can be read by using an index and graduated tape, or the pulley can be attached to a water-stage recorder to transmit the water level to the recorder.

BUBBLE-GAGE SENSOR

The bubble-gage sensor (Barron, 1963) consists of a gas-purge system, a servomanometer assembly, and a servocontrol unit. (See fig. 14.) The gas-purge system transmits the pressure head of water in the stream to the manometer location. A gas, usually nitrogen, is fed through a tube and bubbled freely into the stream through an orifice at a fixed elevation in the stream. The gas pressure in the tube is equal to the piezometric head on the bubble orifice at any gage height.

The servomanometer converts the pressure in the gas-purge system to a shaft rotation for driving a water-stage recorder. Mercury is used as the manometer liquid to keep the overall manometer length to a minimum. The manometer has a sensitivity of 0.005 ft (0.0015 m) of water and can be built to record ranges in gage height in excess of 120 ft (36 m). The use of mercury in the manometer permits positioning of the pressure reservoir to maintain the float-switch contacts in null position. In this position, the vertical distance between mercury surfaces will be 1/13.6 times the head of water. A change in pressure at the reservoir displaces the mercury which in turn activates the float switch. This causes movement of the pressure reservoir until the distance of head of water divided by 13.6 is again maintained. This motion, in turn, is translated to the recorder.

The servocontrol unit provides the relay action necessary to permit the sensitive float switch to control the operation of the servomotor;

the unit also provides an appropriate time delay between the closing of the float switch and the starting of the motor.

Several bubble-gage sensors, differing in minor detail from that described above, are commercially available. Also commercially available is another type of bubble-gage sensor in which the nitrogen bubble tubing transmits the river-stage pressure to a bellows; the bellows, through a mechanical linkage, actuates a recording pen.

The proper placement of the orifice is essential for an accurate stage record. The orifice should be located where the weight of water above it represents the stage in the river. If the orifice is partly buried in sand or mud, the recorded stage will be greater than that in the river. An orifice preferably should not be installed in swift currents. If this is unavoidable, the orifice must be kept at right angles to the direction of flow. A recommended mounting for high-velocity flow is one in which the orifice is installed flush with the wall of the mounting structure. Care should also be taken to keep the orifice out of highly turbulent flow.

In unstable streambeds it is sometimes advantageous to place the bubble orifice in a vented well point driven into the unstable bottom.

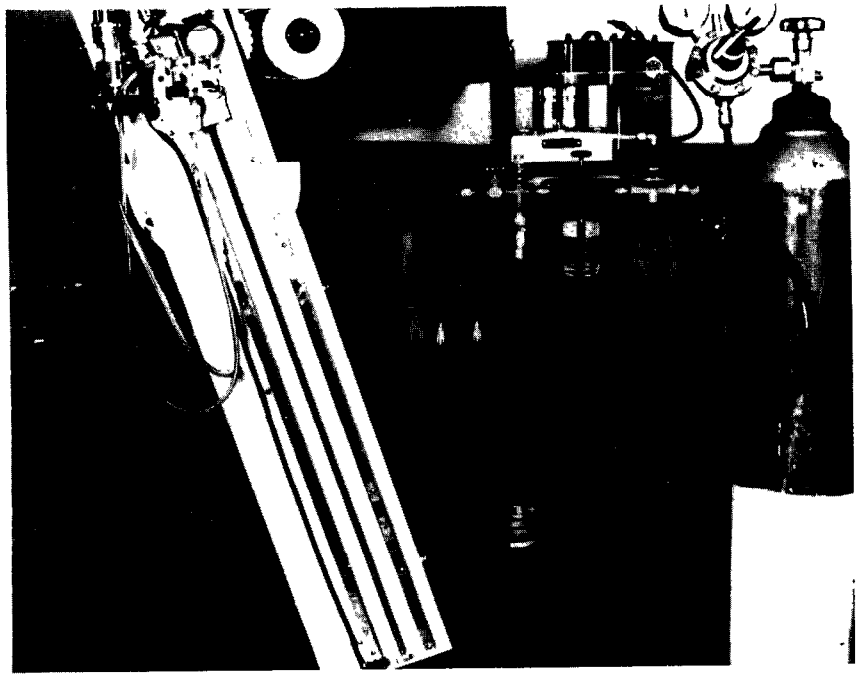

FIGURE 14.—Major units of the bubble gage.

If oil (generally kerosene) is to be added to prevent freezing in the vent pipe, the top of the well screen should be a sufficient distance below the minimum expected stream stage to retain the required depth of oil (fig. 15). To prevent variations in the depth of oil from affecting the manometer reading, the bubble orifice should be below the top of the screen so that the bubbles emerge into the water.

It is emphasized that for satisfactory operation of the well point the streambed material should not be so finely grained as to unduly impede the passage of river water to the well point and thereby cause lag in the recorded stage. To prevent clogging of the well-point screen, the screen should be made of material that will inhibit chemical reaction with substances in the water and (or) in the bed material. A stainless-steel screen set 1 to 3 ft (0.3 to 1.0 m) below the streambed is recommended.

The bubble gage is used primarily at sites where it would be expensive to install a stilling well. It is also used on sand-channel streams because the gas tends to keep the orifice from being covered with sand and the tube may be easily extended to follow a stream channel that shifts its location. However, the float stilling-well installation is cheaper to install at many sites, and its performance is usually more reliable than that of the bubble gage. The two systems have about the same accuracy—±0.01 ft (0.003 m). The choice of systems thus depends on the characteristics of the gage site.

WATER-STAGE RECORDERS

A water-stage recorder is an instrument for producing a graphic or punched-tape record of the rise and fall of a water surface with respect to time. It consists of a time element and a gage-height element which, when operating together, produce on a chart or on a tape a record of the fluctuations of the water surface. The time element is controlled by a clock that is driven by a spring, by a weight, or by electricity. The gage-height element is actuated by a float or a bubble gage.

If a float sensor is used, the float pulley is attached to the recorder. The float and counterweight are suspended on a perforated steel tape or on a plain or beaded cable. Cone-shaped protrusions on the circumference of the float-tape pulley match performations in the tape. As the float rises or falls the float pulley rotates in proportion to the change in stage; the rotation of the pulley is transmitted to the recorder and the appropriate gage height is thereby recorded. A copper float 10 in (0.25 m) in diameter is normally used, but other sizes are also used depending on the type of recorder, gage-height scale, and accuracy requirements.

If a bubble-gage sensor is used, the stage is translated to the recorder by a chain and sprocket arrangement. (See fig. 14.)

Stage recorders are either digital or graphic. Both types may be

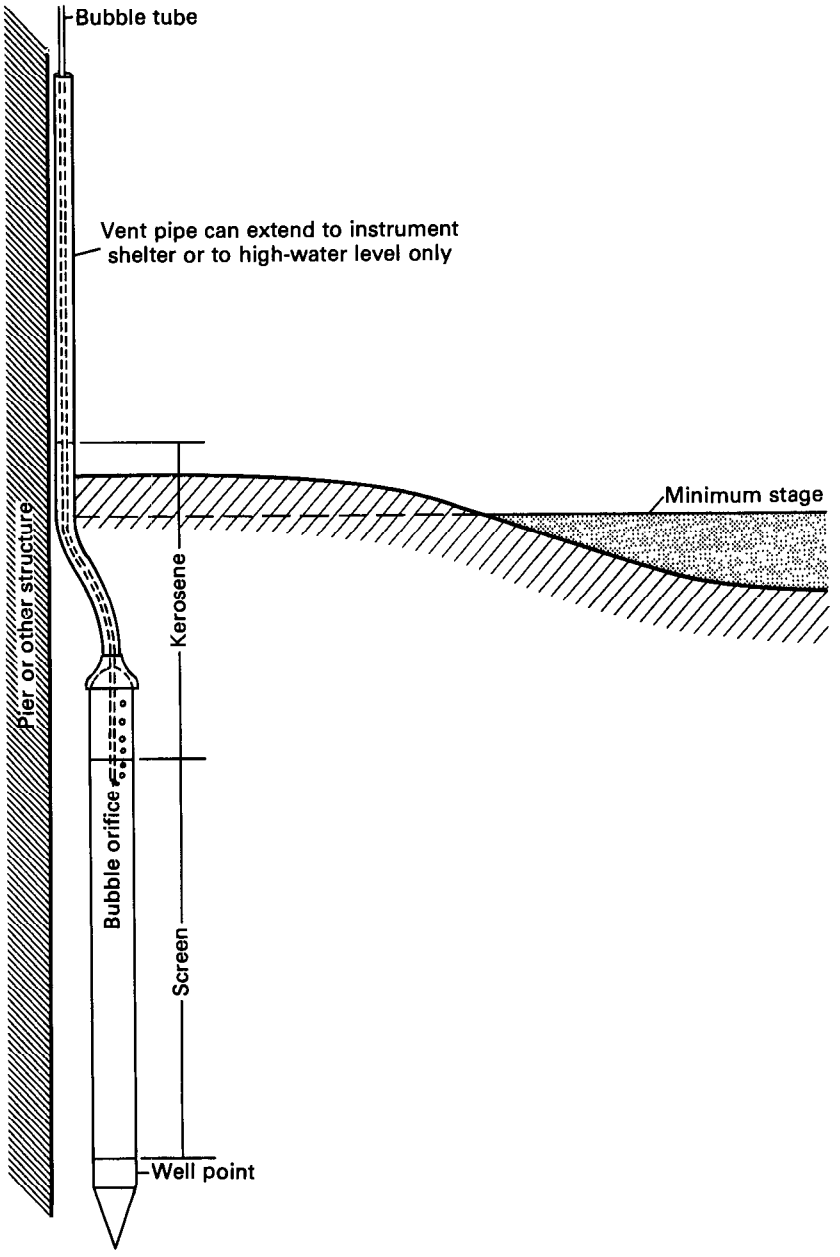

FIGURE 15.—Installation of bubble orifice in unstable streambed.

used with the float or bubble gage. Digital recorders are gradually replacing strip-chart (graphic) recorders at gaging stations in the United States. The two recorders are about equal in accuracy, reliability, and cost, but the digital recorder is compatible with the use of electronic computers in computing discharge records. This automated system offers greater economy and flexibility in the computation-publication process than do manual methods associated with graphic recording. However, the use of graphic recorders should be continued at those sites where a graphic record is necessary to detect ice effects, backwater, or frequent malfunctions of the recording system.

DIGITAL RECORDER

The digital recorder used by the U.S. Geological Survey (Isherwood, 1963) is a battery-operated slow-speed paper-tape punch which re-

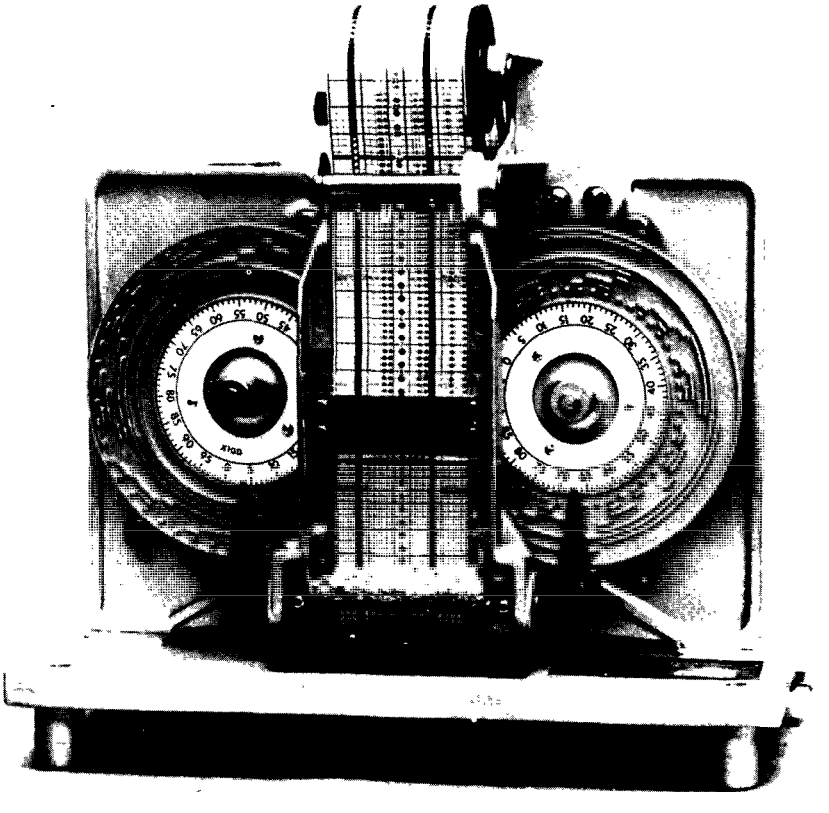

FIGURE 16.—Digital recorder.

cords a 4-digit number on a 16-channel paper tape at preselected time intervals. (See fig. 16.)

Stage is recorded by the instrument in increments of a hundredth of a foot from zero to 99.99 ft (30.5 m) and is transmitted to the instrument by rotation of the input shaft. Shaft rotation is converted by the instrument into a coded punch-tape record that is simple enough to be read directly from the tape. The code consists of four groups of four punches each. In each group, the first punch represents "1," the second "2," the third "4," and the fourth "8." Thus a combination of up to three punches in a group represents digits from 1 to 9, with a blank space for 0, and the four groups of punches represent all numbers from 1 to 9,999. (See fig. 17.)

Coding is done by means of two discs containing raised ridges in accordance with the punch code outlined above. One disc is mounted directly on the input shaft. The second code disc is connected to the first by a 100:1 worm gear so that one hundred revolutions of the input shaft rotate the second, or high-order disc, one complete revolution. A paper tape is moved upward through a punch block which is mounted on a movable arm hinged at the base of the recorder. The punch block contains a single row of 18 pins, 16 pins for the information punches and 2 for punching feed holes.

The tape is punched when the punch block with its protruding pins is forced against the code discs by spring action. Those pins, which strike the raised ridges of the discs, punch through the paper tape and record the position of the discs at that instant. The readout cycle begins with an impulse from the timer that causes a 6-volt motor to turn a sequencing camshaft. The sequence of operations for one reading includes punching the paper, advancing the paper, and compressing the punch spring for the next readout cycle.

The timers (fig. 18) used on the digital recorders are electromechanical timing devices that are powered by the same 7½-volt battery that operates the 6-volt motor. The timers provide contact closure for actuating the digital recorder at preselected time intervals of 5, 15, 30, or 60 minutes by using a different cam for each different time interval.

The cam on the timer corresponds to the minute hand on a clock; that is, it makes one revolution per hour in a clockwise direction. If the cam has one dropoff point, the recorder will punch hourly; if it has two dropoff points, it will punch every 30 minutes; and if it has four dropoff points, it will punch every 15 minutes. The timer in figure 18 has four dropoff points. The arm positioned by the cam operates a single-pole double-throw switch. When the cam dropoff point passes the arm, the switch initiates the major part of the readout cycle which includes punching of the tape. A preset action returns the switch to

the initial position prior to the next readout cycle. Alternating-current timers can be used with the digital recorders at places where

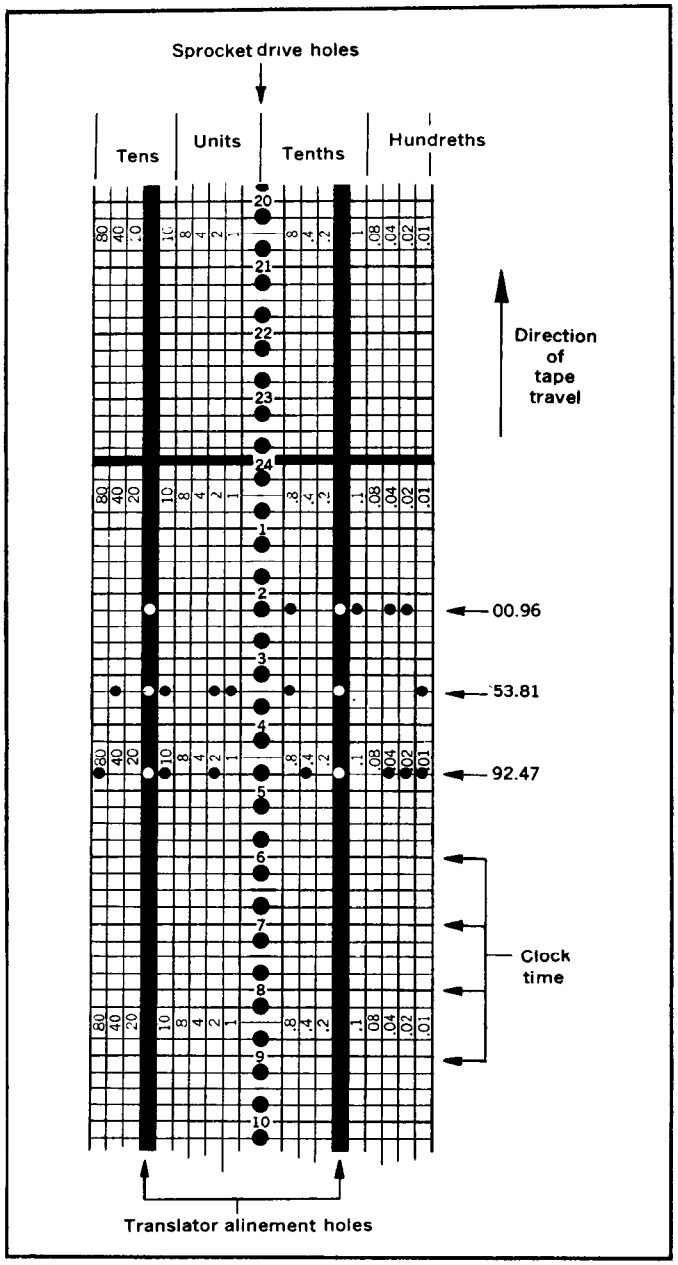

FIGURE 17.—Sample digital-recorder tape.

reliable alternating-current power is available.

Digital recorders may miss the absolute peak stage especially on flashy streams. However, a measure of the maximum peak that occurs between inspections of the recorder can be obtained by attaching a wire clip (similar to a paper clip) or small magnet to the float tape just below the instrument shelf in such a manner that it will slide along the tape as the stage rises but remain in a fixed position as the stage declines. (See p. 60–61).

Mechanically punched tape is the most practical for field use under widely varying conditions of temperature and moisture. Electronic translators are used to convert the 16-channel punch-tape records to a tape suitable for input into a digital computer for computation of a daily mean gage height and daily mean discharge.

In the metric version of the digital recorder, stage is recorded in increments of 1 millimeter from 0 to 9.999 m.

GRAPHIC RECORDER

The graphic, or analog, recorder furnishes a continuous trace of water stage, with respect to time, on a chart. Usually the gage-height element moves the pen or pencil stylus and the time element moves the chart, but in some recorders those actions are reversed. In the U.S.A. the common range of available gage-height scales is from 10 in=1 ft (10:12) to 10 in=20 ft (1:24). The width of strip charts is usually 10 in (0.25 m). The range of available time scales is from 0.3 to 9.6 in (0.0076 m to 0.244 m) per day. Normally the gage-height

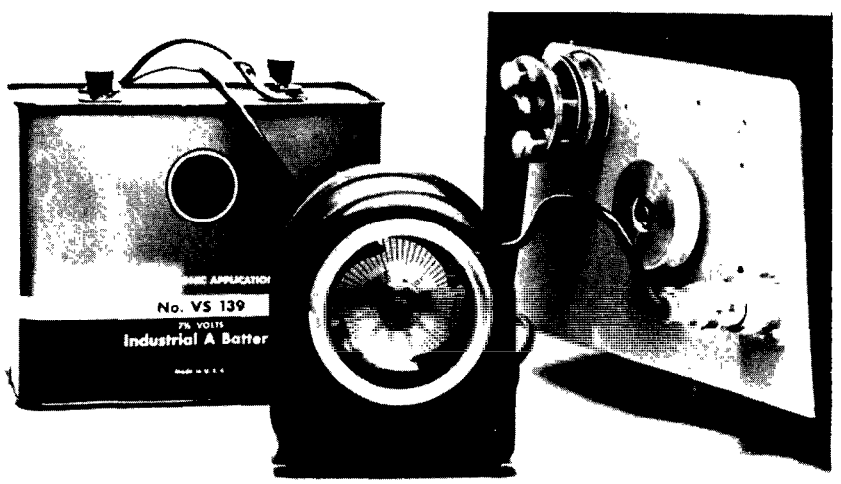

FIGURE 18.—Digital-recorder timer.

scale of 10 in=5 ft (1:6) or 10 in=10 ft (1:12) is used with a time scale of 1.2, 2.4, or 4.8 in per day.

Most graphic recorders can record an unlimited range in stage by a stylus-reversing device or by unlimited rotation of the drum.

Most strip-chart recorders will operate for several months without servicing. Drum recorders require attention at weekly intervals. Figure 19 shows a commonly used continuous strip-chart graphic recorder, and figure 20 a horizontal-drum recorder that must be serviced at weekly intervals. Attachments are available for the recorder

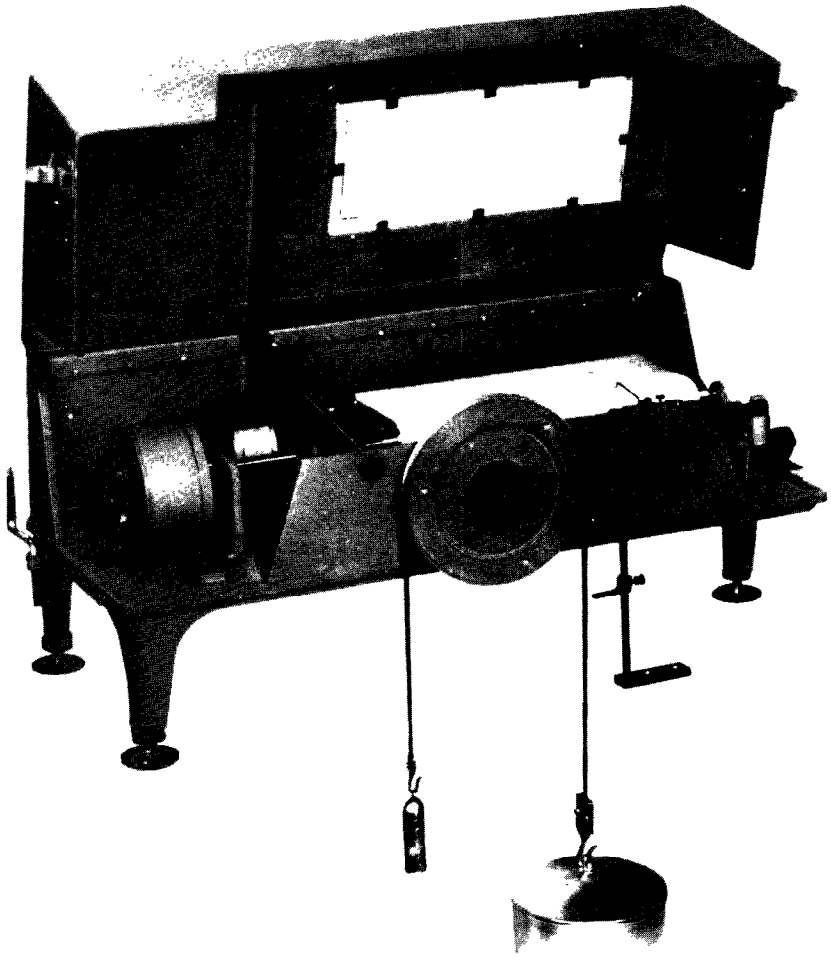

FIGURE 19.—Continuous strip-chart recorder.

shown in figure 19 to record water temperature or rainfall on the same chart with stage. Figure 21 is a section of a typical strip chart whose gage-height scale is 5:12 and whose time scale is 4.8 in per day.

STILLING WELLS

The stilling well protects the float and dampens the water-surface fluctuations in the stream caused by wind and turbulence. Stilling wells are made of concrete, reinforced concrete block, concrete pipe, steel pipe, and occasionally wood. They are usually placed in the bank of the stream (figs. 22–26), but often are placed directly in the stream and attached to bridge piers or abutments. (See figs. 27 and 28.) The

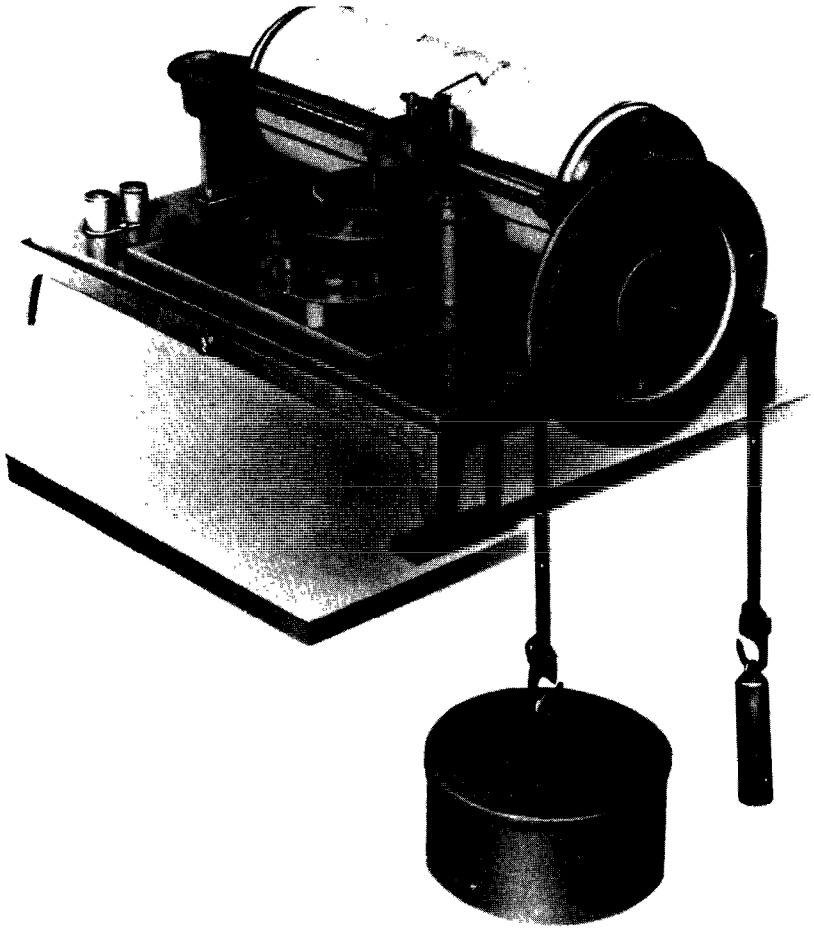

FIGURE 20.—Horizontal-drum recorder.

stilling well should be long enough for its bottom to be at least 1 ft (0.3 m) below the minimum stage anticipated, and its top preferably should be high enough so that the recording instrument will be above the level of the 100-year flood.

The inside of the well should be large enough to permit free operation of all the equipment to be installed. Usually a pipe 4 ft (1.2 m) in diameter or a well with inside dimensions 4 by 4 ft (1.2 by 1.2 m) is of satisfactory size, but pipes 1.5 ft (0.5 m) in diameter have been used for temporary installations where a conventional water-stage recorder was the only equipment to be installed. The 4 by 4 ft well provides ample space for the hydrographer to enter the well to clean it or to repair equipment. The smaller metal wells and the deep wells

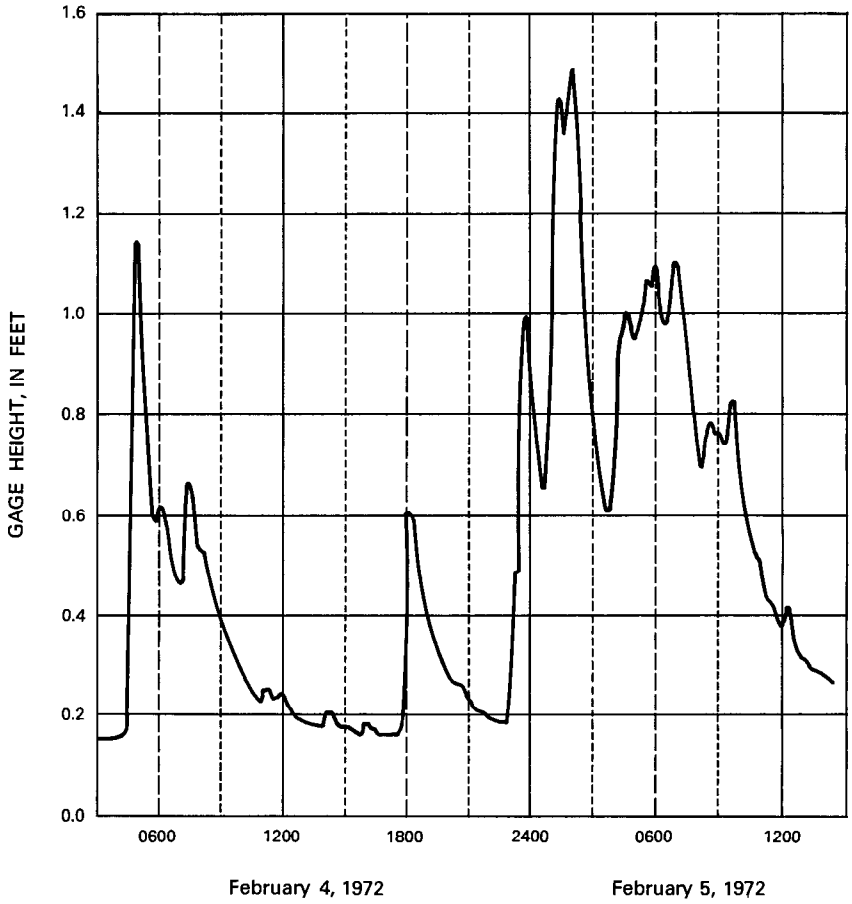

FIGURE 21.—Section of a typical strip chart.

should have doors at various elevations to facilitate cleaning and repairing. (See figs. 22 and 25.)

When placed in the bank of the stream the stilling well should have a sealed bottom so that ground water cannot seep into it nor stream water leak out.

Water from the stream enters and leaves the stilling well through the intake so that the water in the well is at the same elevation as the water in the stream. If the stilling well is in the bank of the stream, the intake consists of a length of pipe connecting the stilling well and the stream. The intake should be at an elevation at least 0.5 ft (0.15 m) lower than the lowest expected stage in the stream, and at least 0.5 ft above the bottom of the stilling well to prevent silt buildup from plugging the intake. In cold climates the intake should be below the

FIGURE 22.—Reinforced concrete well and shelter. (Note clean-out door.)

frostline. If the well is placed in the stream, holes drilled in the stilling well may act as an intake, taking the place of a length of pipe. Some wells placed in the stream have a cone-shaped hopper bottom that serves as an intake and is self cleaning.

Two or more pipe intakes are commonly installed at vertical intervals of about 1 ft (0.3 m). During high water, silt may cover the streamward end of the lower intakes while the higher ones will continue to operate. The intakes should be properly located and sized to minimize surge.

Most stations that have intakes subject to clogging are provided with flushing systems (see fig. 29) whereby water under several feet of head can be applied to the gage-well end of an intake. Ordinarily a pump raises water from the well to an elevated tank. The water is then released through the intake by the operation of a valve. Intakes without flushing systems may be cleaned with a plumber's snake or rod, or by building up a head of water in the well with a portable pump to force an obstruction out of the intakes.

The intakes for stations placed in the bank of the stream are usually galvanized-steel pipe. The most common size used is 2-in (0.05 m)-diameter pipe, but for some wells pipe diameters as large as 4 in (0.1 m) are used. After the size and location of the well have been decided upon, the size and number of intakes should be determined.

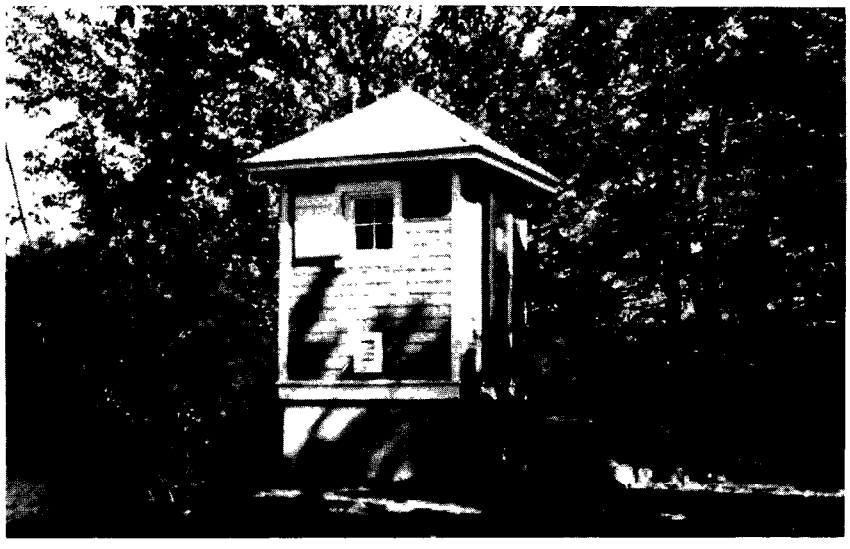

FIGURE 23.—Concrete well and wooden shelter with asphalt-shingle siding.

The intake pipe should be large enough for the water in the well to follow the rise and fall of stage without significant delay. The follow-

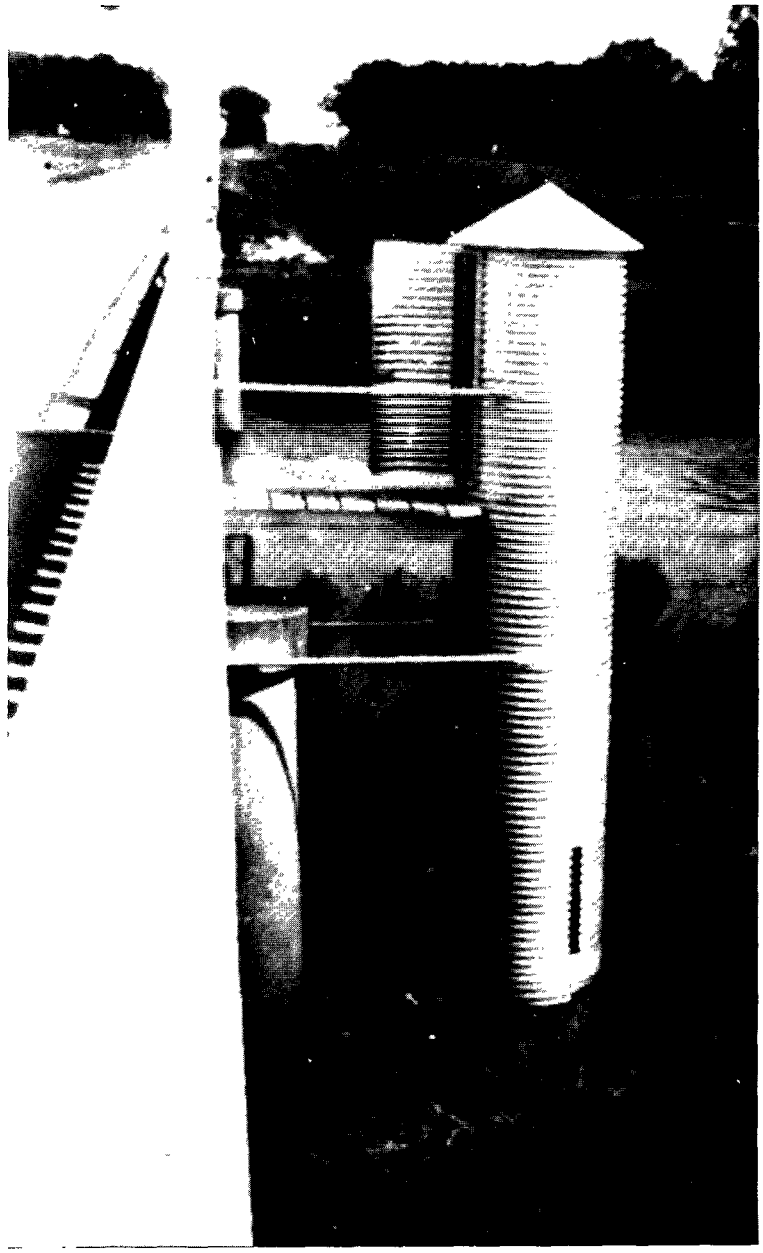

FIGURE 24.—Corrugated-galvanized-steel-pipe well and shelter.

ing relation may be used to predict the lag for an intake pipe for a given rate of change of stage:

$$\Delta h = \frac{0.01}{g} \frac{L}{D} \left(\frac{A_w}{A_p}\right)^2 \left(\frac{dh}{dt}\right)^2$$

in which

Δh = lag, in feet (or meters),

g = acceleration of gravity, in feet (or meters) per second per second,

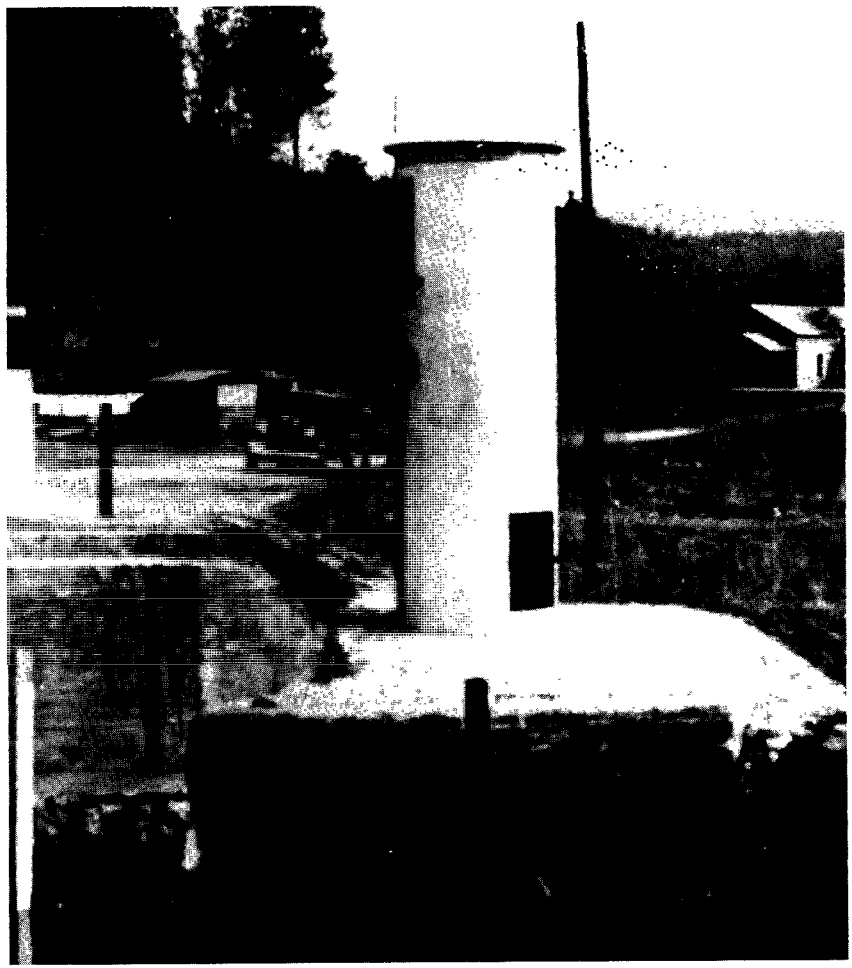

FIGURE 25.—Concrete-pipe well and shelter. (Note clean-out door, staff gage, and upper intake pipe.)

L = intake length in feet (or meters),
D = intake diameter, in feet (or meters),
A_w = area of stilling well, in square feet (or square meters),
A_p = area of intake pipe, in square feet (or square meters), and
$\frac{dh}{dt}$ = rate of change of stage, in feet (or meters) per second.

Smith, Hanson, and Cruff (1965) have studied intake lag in stilling-well systems, relating it to the rate of change of stage of the stream and to the various types and sizes of components used in the stilling-well intake system.

The intake pipe should be placed at right angles to the direction of flow, and it should be level. If the stream velocity at the end of the intake is high, either drawdown or pileup may affect the water level in the stilling well, depending on the angle of the flow at the intake opening. Drawdown causes the water level in the stilling well to be lower than that in the stream; pileup has the opposite effect. Drawdown commonly occurs at high velocities even when the intake pipe is at an angle of 90° with the flow. To reduce or possibly eliminate drawdown or pileup, a static tube should be attached to the streamward end of the intake pipe. A static tube is a short length of pipe attached to an elbow or tee on the end of the intake pipe and extending horizontally downstream. (See fig. 30.) The end of the static tube is capped, and water enters or leaves through holes drilled in the tube.

The usual means of preventing the formation of ice in the well

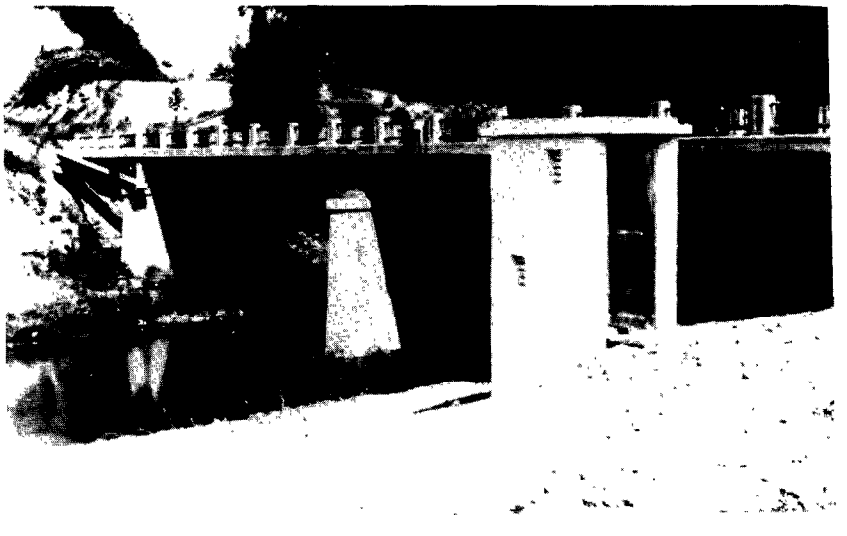

FIGURE 26.—Concrete-block shelter.

during cold weather are: (1) subfloors, (2) heaters, and (3) oil. Subfloors are effective if the station is placed in the bank and has plenty of fill around it. If the subfloor is built in the well below the frostline in the ground, ice will seldom form in the well as long as the stage remains below the subfloor. Holes are cut in the subfloor for the recorder float and weights to pass through, and removable covers are placed over the holes. Subfloors prevent air circulation in the well and the attendant heat loss.

An electric heater or heat lamps with reflectors may be used to keep the well free of ice. The cost of operation and the availability of electric service at the gaging station are governing factors. Heating cables are often placed in intake pipes to prevent ice from forming.

Oil is used in two ways: (1) Where the well is small and leakproof, the oil may be poured into the well; and (2) where the well is large or not leakproof, the oil—usually kerosene, fuel oil, or diesel oil—is poured into an oil tube. The oil tube, which is open ended and of sufficiently large diameter to accommodate the recorder float, is supported in the well in a vertical position with its lower end just above

FIGURE 27.—Steel-pipe well and look-in shelter attached to bridge abutment.

FIGURE 28.—Corrugated-steel-pipe well and wooden shelter attached to bridge pier.

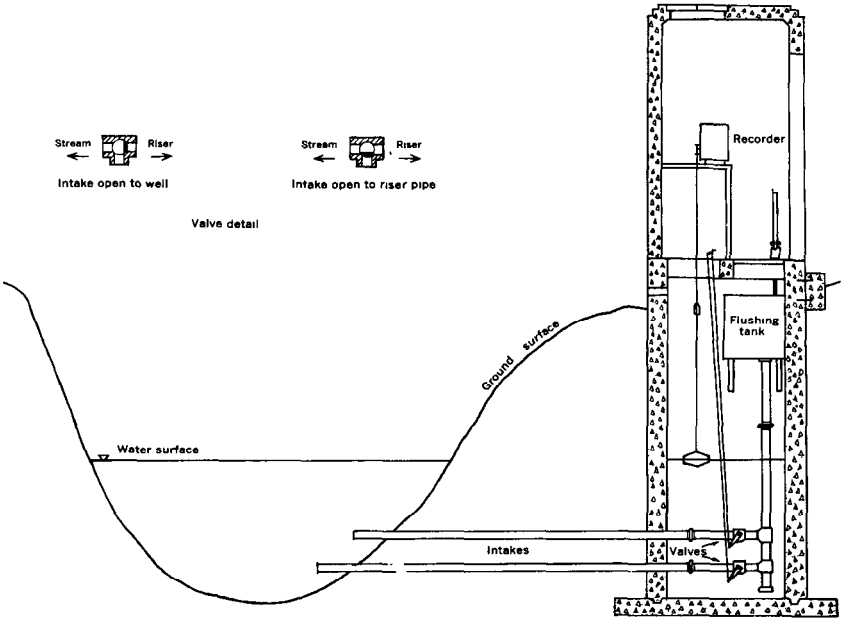

FIGURE 29.—Flushing system for intakes.

FIGURE 30.—Static tube for intakes. (Note outside reference gage.)

the floor of the well. The oil tube should be long enough to contain the oil throughout the range in stage expected during the winter. When oil is put in a well, the oil surface stands higher than the water surface in the stream. A correction must therefore be made to obtain the true river stage. The depth of oil required usually ranges from 0.5 to 2.0 ft (0.15 to 0.6 m) depending on the severity of the climate and the exposure of the well.

Stilling wells often fill with sediment, expecially those located in arid or semiarid regions. If a well is located on a stream carrying heavy sediment loads, it must be cleaned often to maintain a continuous record of stage. In those locations sediment traps are helpful in reducing the frequency and labor of sediment removal. A sediment trap is a large boxlike structure that occupies a gap in the lower intake line, streamward from the stilling well. The bottom of the sediment trap is usually about 3 ft (1.0 m) below the elevation of the intake. Inside the trap are one or more baffles to cause suspended sediment to settle in the trap, rather than pass into the well. A removable top to the trap provides access to the interior of the trap for the removal of trapped sediment.

The operation of type of recording stream-gaging station requires the installation of one or more nonrecording gages for use as auxiliary or reference gages. Reference gages are discussed on pages 53–54.

INSTRUMENT SHELTERS

Shelters are made of almost every building material available and in various sizes depending on local custom and conditions. (See figs. 22–28.) The most convenient type of shelter is one that the hydrographer can enter standing. A shelter with inside dimensions 4 by 4 ft (1.2 by 1.2 m) and with ceiling height 7 ft (2.2 m) above the floor is usually of adequate size, unless the shelter is also to be used to store sediment-sampling equipment and (or) house telemetry equipment (p. 54–59). Look-in shelters (fig. 27) are also used at sites where a limited amount of equipment is to be installed and a portable and inexpensive shelter is desired.

In humid climates, shelters are well ventilated and have a tight floor to prevent entry of water vapor from the well. Screening and other barriers are used over ventilators and other open places in the well or shelter to prevent the entry of insects, rodents, and reptiles.

The bubble gage does not require a stilling well. The instrument shelter for a bubble gage may be installed at any convenient location above the reach of floodwaters. This gage may be used to take advantage of existing natural or artificial features in a stream without costly excavation for well or intake and without need for any external

structural support. The bubble gage is especially well suited for short-term installations because the entire station is readily dismantled and relocated with practically no loss of investment.

A shelter with inside dimensions 4 by 4 by 7 ft (1.2 by 1.2 by 2.2m) is needed to accommodate the equipment for a bubble gage. Shelters similar to those in figures 22, 23, and 26 would be adequate. The shelter can be placed on a concrete slab or other suitable foundation. The bubble orifice is placed at least 0.5 ft (0.15 m) below the lowest expected stage in the stream. The plastic tube connecting the orifice and the instrument is encased in metal pipe or conduit, or buried to protect it from the elements, animals, and vandalism. A typical bubble-gage installation is shown in figure 31. The streamward end of the metal pipe should be flush with the streamward face of the pier shown in figure 31 to prevent disturbance of the streamlines of river flow in the vicinity of the orifice. The streamward end of the orifice line should also have a downward slope, as shown in the figure. It has been found that if the end of the orifice line is installed in a horizontal position, water tends to run up the bubble tube after each bubble is formed, and the induced surge is recorded by the stage recorder.

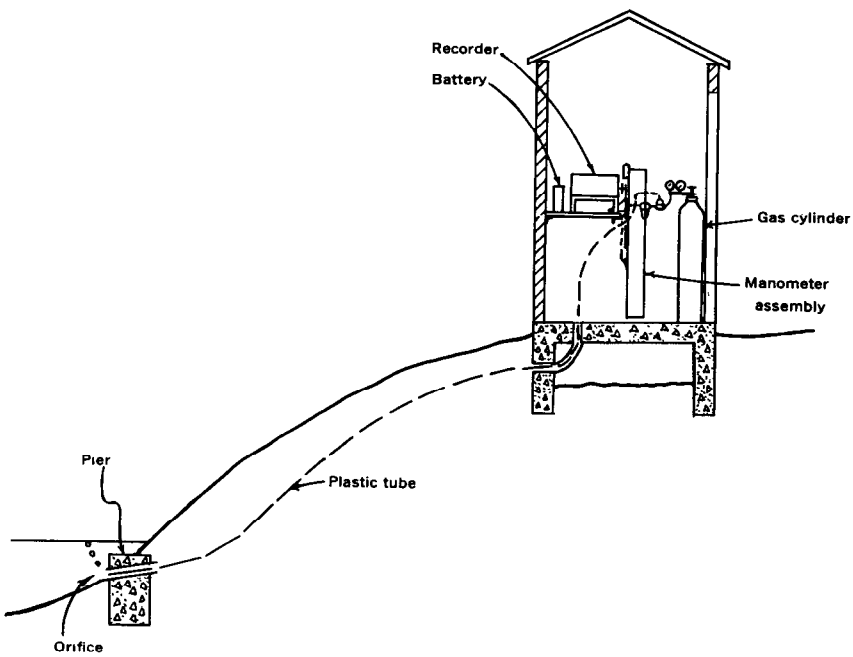

FIGURE 31.—Typical bubble-gage installation.

REFERENCE AND AUXILIARY GAGES AT RECORDING GAGING STATIONS

Nonrecording gages, which were discussed on pages 24–32, are used both as reference and auxiliary gages at recording stream-gaging stations. As used in this manual a reference gage is the gage to which the recording instrument is set; it is the base gage for the recording station. All other nonrecording gages at the recording station are considered to be auxiliary gages. A detailed discussion follows.

Outside gage—At bubble-gage stations a nonrecording gage, established in close proximity to the bubble orifice, acts as the base or reference gage for checking and resetting the gage height indicated by the water-stage recorder.

At stations equipped with a stilling well for the operation of a float-operated stage recorder, there is always the possibility that the stage in the stilling well may not be representative of the stage of the stream. For example, intakes can become plugged, floats can spring a leak, or oil can leak out of wells or oil tubes. Consequently, a nonrecording auxiliary gage is installed outside the stilling well so that the water level of the stream can be determined directly for comparison with the stage in the stilling well. It is not necessary that the two observed stages agree precisely; hydraulic conditions at the station may be such that precise agreement is not possible. If a reading of the outside auxiliary gage indicates that an unsatisfactory record is being obtained by the recording gage, the trouble is rectified immediately. If immediate repairs are not feasible, or if there has been an instrument failure, the outside auxiliary gage is used as a temporary substitute for the recording gage. The outside auxiliary gage can be read as needed by a local observer to continue the record of stage until the malfunction of the recording station is rectified.

Staff or wire-weight gages are usually used as outside auxiliary gages. Outside staff gages located in the pools near the gage structures are visible in figures 5, 6, 22, 25, and 30; a wire-weight auxiliary gage on the parapet wall of the bridge is visible in figure 1, and another is seen in figure 27.

Inside gage—At gaging stations equipped with a stilling well a nonrecording gage inside the structure is used to indicate the water-surface elevation in the stilling well. Readings on this inside gage are compared with readings on the outside auxiliary gage to assure that the stilling-well intakes are functioning properly. If the intakes are functioning properly, the inside gage is used for checking and resetting the gage height indicated by the water-stage recorder. In short, the inside gage is the base or reference gage for the station. Float- or electric-tape gages, or vertical staff gages, are the inside reference gages most commonly used in stilling wells.

On occasion a reference mark or reference point of known elevation, with respect to gage datum, is used in place of either a reference or auxiliary gage. The stage is then determined by measuring from the reference mark or point down to the water surface either in the stream or in the stilling well, as the case may be. While the practice of using a reference mark or point is acceptable, it is not nearly as convenient as the practice of using a standard nonrecording gage. (The distinction between a reference mark and reference point should be noted here: Both have elevations that are known, but a reference point is a point on the gage structure itself; a reference mark is a point that is not on the gage structure, and whose elevation is therefore unaffected by any movement of the gage structure.)

The practice described above of using the inside gage, rather than the outside gage, as the reference or base gage for a recorder equipped with a stilling well is followed in the U.S.A. and in many other countries. The reasoning behind that practice is that recorded (inside) gage heights will be used to determine discharge, and if differences exist between inside and outside stages, those differences will be known only for those times when both gages are read. If the outside gage is used as the base gage, corrections, known or assumed, must be applied to all recorded gage heights to convert them to outside stages. Furthermore, outside gages are often difficult to read with precision because of the action of wind and waves. In other countries the outside gage is used as the reference gage for the reasons that (1) river stage is often as important as discharge to the user of the record and (2) a stage-discharge relation is dependent on river stage, rather than on the stage inside a stilling well. The validity of both those reasons is recognized in the U.S.A. Therefore outside high-water marks are obtained for each flood event, and where the elevation of the marks differs significantly from the peak inside stage, both inside and outside stages are published. Also, where there is significant difference between inside and outside gage readings, the stage-discharge relation is first developed on the basis of outside-gage readings observed at the times when discharge is measured. The relation is then adjusted to correspond with inside-gage readings observed at the times of discharge measurement.

TELEMETERING SYSTEMS

Telemetering systems are used when current information on stream stage is needed at frequent intervals and it is impractical to visit the gaging station each time the current stage is needed. Current stage information is usually necessary for reservoir operation, flood forecasting, prediction of flows, and for current-data reporting. The types of telemetering systems are:

1. Those that continuously indicate or record stage at a distance from the gage site. Examples of this type are the position-motor and impulse telemetering systems.
2. Those that report instantaneous gage readings on call or at predetermined intervals. Examples of this type are the Telemark and resistance telemetering systems, and the experimental satellite data-collection systems.

POSITION-MOTOR SYSTEM

The position-motor system provides remote registering of water levels on graphic recorders or on counter or dial indicators over distances up to 15 mi (25 km). This system employs a pair of self-synchronizing motors—one on the transmitter, whose rotor is actuated by a float-tape gage or a bubble gage, and the other on the receiving unit, whose rotor follows the rotary motion of the transmitting motor to which it is electrically connected. Alternating current is used to operate the system, and a five-wire transmission line is required—two excitation wires and three line wires.

IMPULSE SYSTEM

The impulse system provides remote registering of water levels on graphic recorders or on counter and dial indicators over longer distances than does the position-motor system. This system will operate over leased telephone lines or other metallic circuits. The impulse sender at the gaging station is actuated by a float-tape gage or a bubble gage and sends electrical impulses over the line connecting it to the receiver. This system usually has a battery for the power source at the sender and alternating current at the receiver, though direct current or alternating current may be used at both ends. The advantage of this system over the position-motor system is that it will operate over long distances.

TELEMARK SYSTEM

The Telemark system codes instantaneous stage and signals this information either audibly over telephone circuits or by coded pulses for transmission by radio. The distance of transmission is unlimited because signals can be sent over long-distance telephone circuits or by radio. Telemark response to a telephone ring is automatic. When used in radio transmission, the signals are started by a timing device set for a predetermined broadcast schedule, or the Telemark may be interrogated by radio channel to start the signal.

The Telemark consists of (1) the positioning element which is actuated by a float-tape gage or a bubble gage (fig. 32) and (2) the signaling element which, when signaled, drives a contact across the

signaling drums that are positioned in correspondence with the stage. The Telemark may be operated by either alternating current or by batteries.

A Telemark that operates directly off a digital recorder is available and will probably be increasingly used. This Telemark does not need its own stage sensor; it uses that of the digital recorder. A memory system is used so that when the Telemark is signaled, the last gage height recorded on the digital recorder is transmitted.

Telemarks for radio reporting are equipped with an auxiliary switch and coding bar for transmitting identifying radio station call letters and numbers in international Morse code, in addition to transmitting the stage.

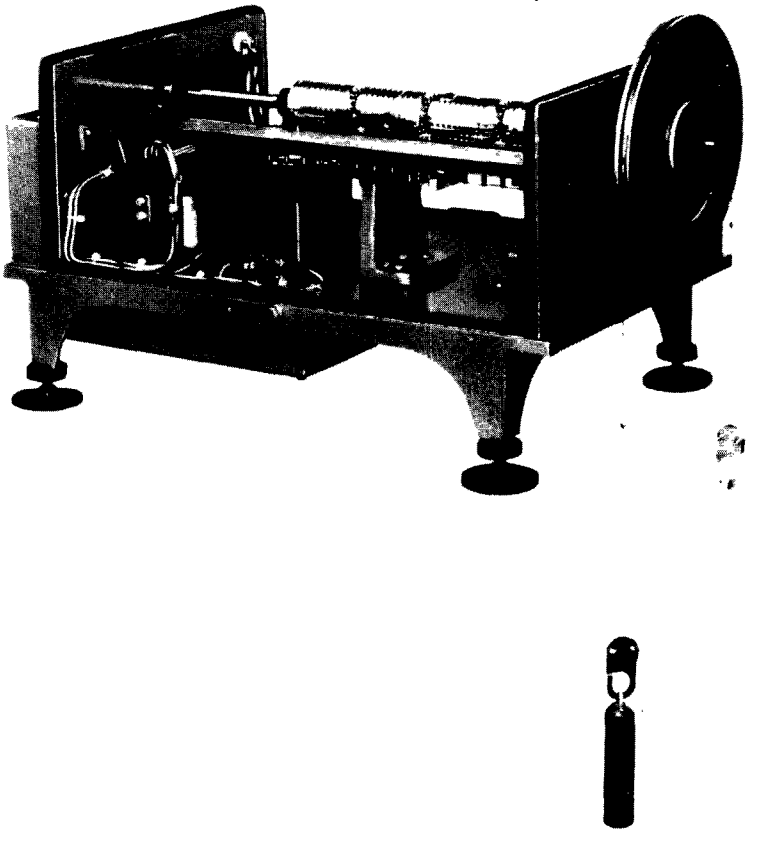

FIGURE 32.—Telemark gage.

RESISTANCE SYSTEM

The resistance system, as used in the U.S.A., was developed by the U.S. Weather Bureau. It provides remote indications of water level for distances up to about 40 mi (about 65 km). Two models are available, one for distances of about a mile (1.6 km) and the other for longer distances. The system consists of two potentiometers in a wheatstone-bridge circuit with a microammeter null indicator. One of the potentiometers is located in the gage house and is actuated by a float and pulley assembly. (See fig. 33.) The other potentiometer and the null indicator are housed at the observation site. (See fig. 34.) By adjusting this potentiometer for a null balance on the meter, the gage height can be read directly to tenths of a foot from a dial coupled to the potentiometer shaft. This system operates on batteries, and three wires connect the unit.

SATELLITE DATA-COLLECTION SYSTEM

The U.S. Geological Survey has been experimenting for several years with the collection of stream-stage data by use of an orbiting satellite which receives radio transmissions of stage and transmits

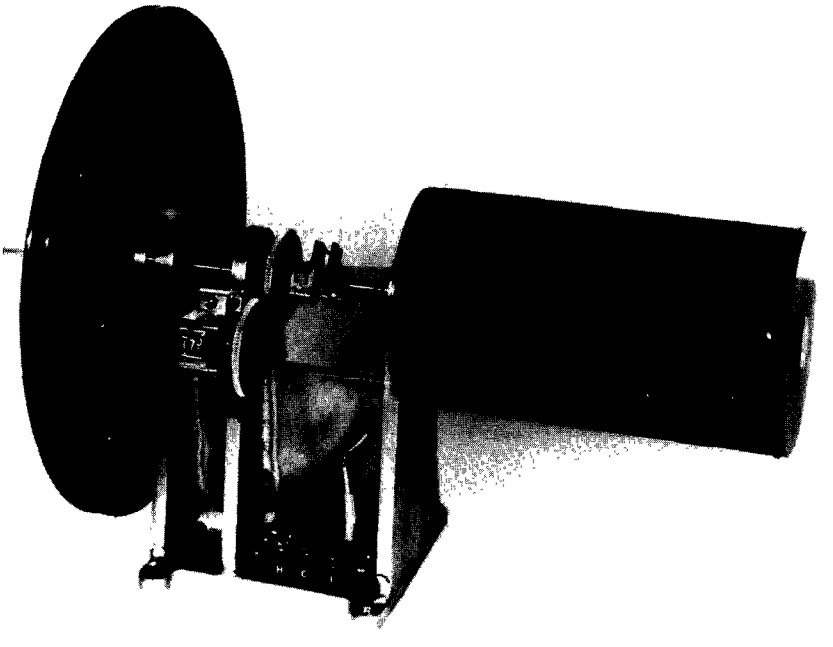

FIGURE 33.—Resistance system transmitter unit.

the data to central receiving stations. An operational system of that kind would make stage data continuously available for use by the managers of water projects who require current ("real time") information for project operation. Because the system is still in the experimental stage it will be described only briefly.

Experimental work on the system began soon after the launch of the Earth Resources Technology Satellite (ERTS) in July 1972. At numerous stream-gaging stations that are dispersed over a wide geographic area, inexpensive battery-operated radios, called data-collection platforms (DCP), are used to transmit stage data through ERTS to the National Aeronautics and Space Administration (NASA) receiving stations at Goldstone, California, and at Greenbelt, Maryland. The data are processed and distributed to experimenters from the ERTS Operations and Control Center in Greenbelt.

Data can be provided to a DCP either directly from a digital water-stage recorder or through an intermediate memory device. In the

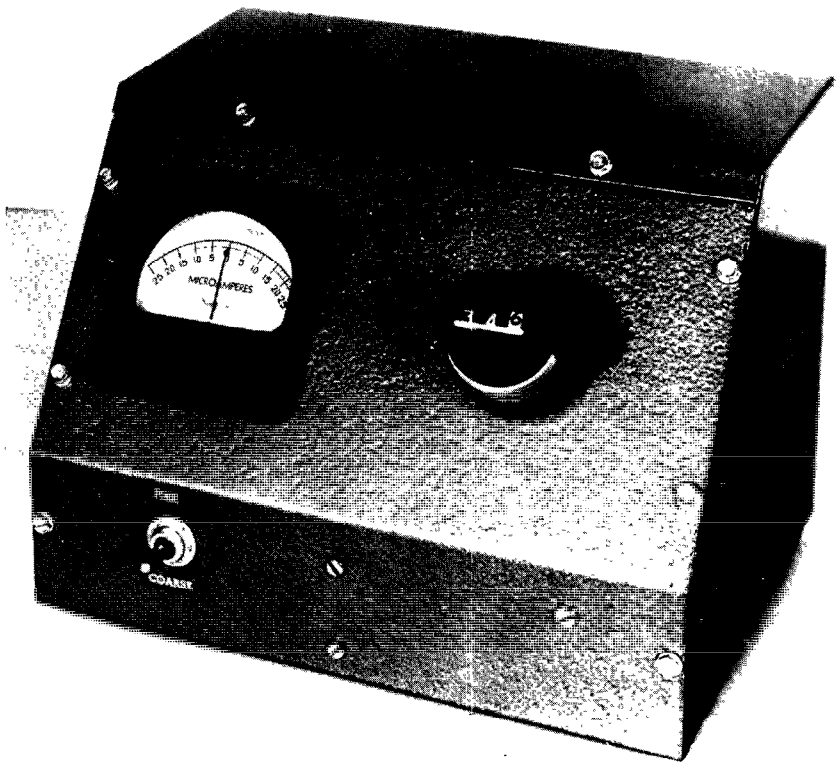

FIGURE 34.—Resistance system indicator unit.

direct communication the most recently recorded digital stream stage is continuously available to the DCP for inclusion in a 0.038-second radio message that is transmitted every 3 minutes. Several times daily the ERTS passes within 1,800 mi of the DCP, and the data are at that time relayed to the receiving stations. Where the intermediate memory device is used, the data are formatted efficiently in the device for inclusion in the periodic DCP message. By use of the memory device virtually all 24 of the hourly stream stages collected daily at North American stream-gaging stations can be accumulated and relayed, as opposed to the 5 or 6 hourly stages that are relayed daily when the DCP is directly connected to the digital-stage recorder. Tests of the satellite data-collection system have been successful to date (1980) and indicate that the satellite relay of environmental data from widely dispersed and remotely located gaging stations can be effectively and reliably performed.

OPERATION OF A RECORDING STREAM-GAGING STATION

Strip-chart or digital recorders are designed to give a continuous record of stage, but careful attention to details is necessary at each visit to the station to ensure a reliable and uninterrupted record during the period (commonly 4–6 weeks) that usually elapses between such visits. This section of the manual presents only general instructions for servicing recording stream-gaging stations. It is not practical to attempt to provide detailed instructions here for servicing stage-recorders because of the large numbers of such instruments of varying design that are available. For detailed instructions concerning any particular stage-recorder, it is necessary that the hydrographer consult the service manual prepared by the manufacturer of the instrument or prepared by the stream-gaging agencies that use the particular instrument.

The first thing done by the hydrographer on his visit to the recording station is to determine if the clock or timer is running. If it is a strip-chart recorder that is being serviced, the point at which the pen or pencil is resting is then circled; if it is a digital recorder that is being serviced, the instrument is caused to punch the digital tape and the set of punched holes is circled. The time by the hydrographer's watch is noted and the base nonrecording reference gage is read. Those observations are written on the chart or digital tape in proximity to the circled gage height. The hydrographer then reads all gages and notes the chart position or digital-tape position, with respect to time and gage height, of the circled pen mark or punched holes. All that information is also written on the chart or digital tape.

The various gage readings and the recorded gage heights are compared to determine if intakes are functioning properly or if there is a

malfunction in the gas-purge system of the bubble gage. The time indicated by the chart or digital tape is compared with the time indicated by the hydrographer's watch to determine if the instrument clock or timer is operating satisfactorily. The section of chart or digital tape bearing the gage-height record is next removed and is examined to determine if there has been any recorder malfunction since the previous servicing of the station.

The clock is then wound, or if the clock is battery driven, the battery voltage is checked and the chart or digital tape is rethreaded into the take-up roll. The pen or punch mechanism is next set to agree with the gage height indicated by the base reference gage, and the chart or digital tape is advanced to give agreement with the hydrographer's watch time. By resetting the recorder at this point, before completing his inspection of the station facilities, the hydrographer gives himself another opportunity to check the operation of the recorder after his work is completed and the instrument has been operating for a period of time.

If the station has a float-operated recorder, the hydrographer inspects the float to determine if it leaks and checks the float-clamp screw to make sure there can be no slippage of the float tape where it joins the float. He also checks the stilling well to be sure there is no unduly large accumulation of sediment in the well. If the well is equipped with an oil tube for winter operation he uses a point on the top of the tube to measure down to the oil surface within the tube and to the water surface outside the tube. The differential between the two measurements, when divided by a value equal to 1.0 minus the specific gravity of the oil, equals the depth of oil in the oil tube. The hydrographer can decide from that computation whether oil has leaked from the tube and the additional amount of oil, if any, to be added. If the stilling well is equipped with a flushing device, the intakes should be flushed as a matter of course. If no flushing device has been provided, and there are indications that the intakes are lagging, the intakes should be cleaned by forcing a plumber's snake through them.

If a high discharge has occurred since the previous visit to a stilling-well-equipped station, high-water marks should be sought both in the stilling well and outside the well, as a check on the peak stage shown by the stage recorder. After making that check, the high-water mark should be cleaned from the inside of the well to prevent confusion with high-water marks that will be left by subsequent peak discharges.

Another means of checking recorded peak stages is by having a wire clip (similar to a paper clip) or magnet attached to the float tape immediately below the shelf through which the tape passes. As the

stage rises, the wire clip or magnet, being too large to pass through the hole in the shelf, retains its position at the bottom of the shelf, and the moving float tape slides past it. When the stage recedes, the clip or magnet remains attached to the tape and moves downward as the float moves downward. Any one of several alternative methods may be used to determine the peak stage that had been attained. In one method the peak stage is obtained by subtracting a correction constant from the tape reading at the top of the wire clip. That correction constant is equal to the difference in elevation between the index pointer for the float gage and the bottom of the shelf. In a second method the visiting hydrographer computes the difference between readings on the float tape at the bottom of the shelf and at the top of the wire clip or magnet. He adds that difference to the current gage height to obtain the peak stage attained. A third method of determining the peak stage is to raise the float until the wire clip or magnet is at the bottom of the shelf; the corresponding tape-gage reading is the peak stage that had been attained. Regardless of the method used, after determining the peak stage the wire clip or magnet should be moved back to the bottom of the shelf for subsequent indication of peak stage.

If an indicator of minimum stage is desired, a similar device—wire clip or magnet—can be attached to the float tape immediately below the instrument shelf, but on the counterweight side of the float sheave. The operation of the minimum-stage indicator is similar to that described above for the peak-stage indicator.

If the station has a bubble-gage sensor, the bubble orifice should be inspected to make sure that it has not been buried by a deposit of sediment. A log of gas-feed rate, gas consumption, and gas-cylinder replacement (fig. 35) should be kept to insure a continuous supply of gas and to help in checking for leakage in the system. There can be no serious leak in the gas-purge system if (1) the manometer operates to indicate stage correctly and (2) the gas consumption based on the average bubble rate over a period of time corresponds with the gas consumption computed from the decrease in cylinder pressure. If a gas leak is evident, its location can be determined by isolating various parts of the gas-purge system by the sequential closing of valves in the system. If a high discharge has occurred since a previous visit to the station, a high-water mark should be sought in the vicinity of the base reference gage, as a check on the peak stage shown by the stage recorder.

After the hydrographer has completed his inspection of the station facilities, he returns to the stage recorder and repeats the first steps he had taken in servicing the recorder. He determines that the clock or timer is running; circles the point at which the pen is resting on the

BUBBLE GAGE LOG SHEET Station: Double Trouble Creek near Dry Bone, Ky.

Date	Time	Gage height			Air temp. °F	Pressure, psi		Bubbles per min.	Ft^3 of gas	Delay	Remarks
		Outside	Counter	Pen		Cylinder	Feed				
10-2-58	9:30a	1.31	1.32	1.32	75	1500	34	46	90	On	
11-1-58	1:00p	6.30	6.31	6.31	40	1275	36	44	88	On	Installed new batteries

FIGURE 35.—Sample log sheet for bubble gage.

strip chart; observes his watch time; reads all gages, and writes his observations on the strip chart or digital tape. He does not leave the station without assuring himself that: the recorded gage height and time agree with the gage height of the base reference gage and his watch time; the clock is running; all necessary valves are open; the float wheel (if any) is engaged; the pen (if any) is marking.

A few generalities may be stated concerning the maintenance of recording stream-gaging stations to increase the accuracy and improve the continuity of the stage record. Malfunctions of the recorder can be reduced by the periodic cleaning and oiling of the recorder and clock or timer. Each year intakes, stilling wells, and sediment traps should be thoroughly cleaned. Excessive humidity and temperatures in the gage house should be reduced to a minimum by proper ventilation, and if feasible, extremely cold temperatures in the gage house should be modified by the use of heating units or insulation. Humidity and temperature control reduce the errors associated with paper expansion and contraction. Experience in the U.S.A. has shown that a program of careful inspection and maintenance will result in a complete gage-height record about 98 percent of the time.

FACTORS AFFECTING THE ACCURACY OF THE STAGE RECORD

Continuous records of discharge at a gaging station are computed from the record of stage and the stage-discharge relation. For that purpose stage records having an accuracy of ±0.01 ft (±0.003 m) are generally required. That accuracy can usually be attained by use of the continuous stage-recording systems previously described. The record obtained by sketching a continuous-stage graph through the plotted points representing periodic observations of a nonrecording gage cannot attain such accuracy, of course, but with care the individual gage observations can usually have an accuracy within ±0.01 ft.

In the discussions that follow, nonrecording gages will be treated first and then recording gages will be discussed. A remark appropriate to a discussion of the accuracy of any gage concerns the maintenance of the gage datum to the accuracy criterion of 0.01 ft. That is achieved by running levels to reference marks for the gage (p. 24) and, if necessary, adjusting the gage to restore the original datum. Levels should be run at least once every 2–3 years, and oftener if conditions are known to be unstable. If a nonrecording gage is used only as an outside auxiliary gage for a stilling well, a larger error in gage datum may be tolerated, and adjustment to the gage need not be

made for datum discrepancies that do not exceed 0.02 ft (0.006 m). That is so because seldom will inside and outside gages agree exactly even when both are set precisely to the same datum. The inside reference gage, as explained earlier (p. 54) is the base gage for the station; the primary purpose of the outside gage at a station equipped with a stilling well is to indicate whether or not the intakes are operating properly. (As mentioned on page 54, in some countries the outside gage is used as the reference or base gage.)

NONRECORDING GAGES

STAFF GAGE

Settlement or uplift of the structure(s) supporting the staff gage may disturb the gage datum. Where levels from a reference mark show that the datum of an inclined staff gage (p. 26) has been disturbed, the gage is recalibrated by removing the staples used for the graduations and replacing them at the proper elevations. Vertical staff gages are usually made up of several porcelain-enameled iron sections, each about 3.4 ft (1.04 m) long and bearing permanent graduations. Where levels from a reference mark show disturbance of the datum of a vertical staff gage, it is necessary to reset the individual gage sections. The graduations of the manufactured gage plates often have minor discrepancies, and therefore if the gage plates must be reset, they should be reset so that a graduation near the center of each gage plate is at the proper datum.

It is often difficult to accurately detect the water line when making staff-gage observations under the conditions of poor light and (or) clear water. Under those conditions it is helpful to float a matchstick or some similar floatable material against the gage and thereby define the water line. When the water surface is surging rapidly as a result of wave action, the stage to be recorded is the mean of the elevations of the peak and trough of the waves.

WIRE-WEIGHT GAGE

Wire-weight gages (p. 26) are usually mounted on bridges, and changes in gage datum often result from the settlement of bridge abutments or piers, or from changes in the deflection of the bridges resulting either from differences in traffic loading at the times of observation or from seasonal changes in air temperature. In addition to errors attributable to datum changes, erroneous readings of the type A wire-weight gage may also be caused by slippage of the graduated disc of the gage; that slippage results from insecure tightening of the disc screws. The latter condition can be detected if a

reading of the gage height of the horizontal checking bar is always made prior to lowering the weight to the water surface.

In checking the datum of the type A wire-weight gage by levels from a reference mark, the elevation of the horizontal checking bar and that of the bottom of the weight at various heights above the water surface are compared with gage readings. When necessary, adjustment of the gage to give accurate readings is made by loosening the graduated disc, rotating the disc to the true gage height of the bottom of the weight as determined from levels, and then retightening the disc screws.

Reliable observations are difficult to obtain by wire-weight gage when the water surface is disturbed by waves; the stage sought under those circumstances is the mean of the elevations of the peak and trough of the waves. On the other hand, it is also difficult to sense the water surface from a high bridge when the water is quiescent. The ideal condition for sensing the water surface occurs when a slow-moving water current is present under the weight. When observations are made on a windy day, the wire that supports the weight will bow rather than hang vertically, thereby causing the gage to underregister. The error introduced will depend on the intensity of the wind and on the height of the gage above the water surface. The combination of a high wind and high bridge may cause appreciable underregistration of the gage.

Another source of error, and one that also increases with height above the water surface, is in the tendency of the weight to rotate about its vertical axis as the weight is being lowered. The rotation twists the wire, and sequences of untwisting and twisting of the wire follow. During each period of twisting the wire shortens and the weight ascends; during each period of untwisting the wire lengthens to its full length and the weight descends. Observation of the gage height of the water surface should not be made until the weight has ceased to rotate.

FLOAT-TAPE GAGE

Change in the datum of a float-tape gage (p. 26) may result from movement of the structure supporting the gage or from slippage of the adjustable index. A float-tape gage will also read incorrectly if the tape has slipped in the clamp connecting the tape and float (gage will overregister) or if the float has sprung a leak and has taken in water (gage will underregister). The first steps in checking a float-tape gage therefore are to make sure that the clamp screw bears tightly on the tape and to shake the float for indications of water sloshing within the float.

Where levels from a reference mark show the elevation of the adjustable index to be in error, the screw holding the index is loosened, the index is raised or lowered to its proper position, and the index screw is retightened. The elevation of the water surface in the stilling well is next obtained by measuring with a steel tape to the water surface from the index or other suitable point of known elevation. Any further adjustment that is needed to make the gage height agree with the water-surface elevation is made by adjusting the length of tape at the float clamp. After all adjustments are complete, a record should be made for future reference of the tape graduation at which the tape enters the tape clamp. If the stage of the stream is changing, the valves on the stilling-well intakes should be closed while adjustments to the float-tape gage are being made in order to maintain a constant water level in the stilling well.

ELECTRIC-TAPE GAGE

Change in the datum of an electric-tape gage (p. 28) can only result from movement of the structure supporting the gage, because the position of the index of the gage is permanent with respect to the instrument. An electric-tape gage may also read incorrectly (overregister) if the tape and weight are insecurely clamped together and slippage of the tape has occurred. Where levels from a reference mark show the gage index to be in error, nothing can be done about moving the index, but its new (and true) gage height is made a matter of record. The original datum of the gage can be maintained, however, by adjusting the effective length of the tape, that is, by changing the length of tape that is inserted and clamped in the gage weight (fig.12). In other words, when the tape is unreeled so that the bottom of the weight is, for example, 1.00 ft (0.3 m) below the index, the tape gage should read 1.00 ft (0.3 m) less than the gage height of the index. After the adjustment is completed, a record should be made, for future reference, of the tape graduation at which the tape enters the weight. If the stage of the stream is changing rapidly at the time a reading is to be taken in the stilling well, it is helpful to close the valves on the stilling-well intakes in order to obtain a constant water level in the stilling well.

Use of the electric-tape gage as the inside reference gage is practically a necessity where a small diameter stilling well is used in a cold climate. In that situation oil must be added to prevent freezing, and because the stilling well is too small to accommodate an oil tube (p. 48), the oil must be added in the well itself. Because the oil is lighter than water, the surface of the floating oil in the stilling well will be higher than the water level at the streamward end of the stilling-well

intakes. It is the gage height of the water level (*GH*) that is sought, and it may be computed by either of two equations:

$$GH = [\text{gage height of oil surface}] - [(1.0 - \text{specific gravity of oil}) \times (\text{depth of oil})] \quad (1)$$

or

$$GH = [\text{gage height of interface of oil and water}] + [(\text{specific gravity of oil}) \times (\text{depth of oil})]. \quad (2)$$

Use of an electric-tape gage makes it a simple matter to measure the distances needed in equation 2. That part of the tape above the weight is rubbed with carpenter's chalk for a distance of about 1.5 ft (0.5 m) above the weight, and the weight is then lowered until a signal is received on the voltmeter. At that point the electric-tape gage reading obtained will be that of the oil-water interface (p. 28). The tape is then reeled up and the lower end inspected. The oil will have wetted the chalk on the tape leaving a sharp demarcation between the wet and dry lengths of tape. The depth of oil is equal to the distance between the demarcation line and the bottom of the weight. If the depth of the oil is less than the length of the weight, the oil will not reach the tape. In that event, the weight is lowered a known distance below the oil-water interface—say, 1.0 ft (0.3 m)—and the apparent oil depth that is determined is reduced by 1.0 ft (0.3 m), the additional distance that the weight was lowered. The computed oil depth and the observed gage height of the oil-water interface are used in equation 2 to compute the true gage height.

CHAIN GAGE

Change in the datum of a chain gage (p. 31) can result from movement of the structure on which the gage is mounted, but there are many other sources of error. They include stretching of the chain, foreign material between chain links, wear of the chain links, and wear of the pulley wheel. For that reason the chain length between the bottom of the weight and the chain index markers should be measured at each visit by the hydrographer, using a 4-lb (2-kg) pull on the chain. A small spring balance is usually used to put the proper tension on the chain when measuring its length. If the chain length differs by more than 0.02 ft (0.006 m) from the "true" value established the last time the datum was checked by levels, the length of the chain is adjusted at the point where the chain is attached to the weight. The adjustment is easily made because the chain and weight are attached by means of a cotter pin through one of a series of holes

in the neck of the weight, the spacing between holes being about 0.02 ft (0.006 m).

In checking the gage datum by levels from a reference mark, the gage height of a point of known elevation on the supporting structure (reference point) is first checked. Next, the elevation of the bottom of the weight at one or more heights above the water surface, as determined by levels from a reference mark, is compared with gage readings. When necessary, adjustment of the chain length to give accurate gage readings is made in the manner indicated above. The length of the chain is measured and recorded before and after the adjustment.

The reliability of gage readings of the water surface is affected by wind, waves, and water current, in a manner similar to that discussed for the wire-weight gage (p. 65). There is no tendency, however, for the weight to rotate when lowered, as described in the discussion of the wire-weight gage.

ACCURACY OF FLOAT-OPERATED RECORDERS

This section of the report discusses the inaccuracies inherent in any float-operated instrument; the discussion is not concerned with such sources of error as datum changes, faulty intake operation, float leakage, float-tape slippage, and paper expansion, which were discussed in the preceding sections. The principal sources of error inherent in a float-operated instrument are float lag, line shift, and submergence of the counterweight (Stevens, 1921). With regard to the algebraic sign of the errors discussed below, a positive (+) sign indicates that the instrument shows a stage higher than the true stage, and a negative (−) sign indicates that the instrument underregisters.

Float lag.—If the float-operated recorder is set to the true water level while the water level is rising, it will thereafter show the correct water level, as far as float lag is concerned, for all rising stages. For falling stages, however, the recorded stage will be above the true water level (positive error) by the amount of float lag or change in flotation depth of the float. A reverse effect occurs if the original gage setting is made when the water level is falling. Float lag varies directly with the force (F) required to move the mechanism of the recorder and inversely as the square of the float diameter (D). F commonly ranges from 1 to 5 oz (0.03 to 0.15 kg) depending on the type and condition of the instrument.

The equation for maximum float-lag error ($MFLE$) is

$$MFLE = 0.37\, F/D^2 \text{ (English units)}, \qquad (3)$$

where $MFLE$ is expressed in feet, D is expressed in inches, and F is expressed in ounces. The equation is

$$MFLE = (0.00256)\, F/D^2 \text{ (metric units)}, \quad (4)$$

where $MFLE$ and D are expressed in meters, and F is expressed in kilograms.

If we assume a value of 3 oz (0.08 kg) for F and a value of 8 in (0.2 m) for D, $MFLE$ equals 0.017 ft (0.005 m). If the recorder was set to the true water level while the float was rising, the record on a falling stage will be in error by +0.017 ft. If however, the index were set at the true level at a stationary stage—that is, at the peak or trough of a changing stage, or when the valves in a stilling well were closed—then the error will be halved on a changing stage. The error will be +0.0085 ft for falling stages and −0.0085 for rising stages.

Line shift.—With every change of stage a part of the float tape passes from one side of the float pulley to the other, and the change in weight changes the depth of flotation of the float. The magnitude of change depends on the change in stage (ΔH) since the last correct setting of the recorder, the unit weight (U) of the tape, and the float diameter (D). The error will be positive (+) for a rising stage and a negative (−) for a falling stage.

The equation for line-shift error (LSE) is

$$LSE = 0.37 \left(\frac{U}{D^2}\right) \Delta H \text{ (English units)}, \quad (5)$$

where U is expressed in ounces per foot, D is in inches, and LSE and ΔH are in feet.

The equation is

$$LSE = (0.00256) \left(\frac{U}{D^2}\right) \Delta H \text{ (metric units)}, \quad (6)$$

where U is expressed in kilograms per meter, and LSE, D, and ΔH are expressed in meters.

If we assume a value of 0.14 oz/ft (0.013 kg/m) for U, a value of 50 ft (15 m) for ΔH, and a value of 8 in (0.2 m) for D, LSE equals 0.04 ft (0.012 m).

Submergence of the counterweight.—When the counterweight and any part of the float line become submerged as the stage rises, the pull on the float is reduced and its depth of flotation is increased. The converse is true when the submerged counterweight emerges from the water on a falling stage. Thus, the error caused by submergence or emergence is opposite to that of the line-shift error and tends to

compensate for the line-shift error. The submergence error is dependent on the weight of the counterweight (c) and the float diameter (D).

The equation for submergence error (SE) is

$$SE = 0.017 \frac{c}{D^2} \text{(English units)}, \tag{7}$$

where SE is expressed in feet, c is in ounces, and D is in inches.

The equation is

$$SE = (0.000118) \frac{c}{D^2} \text{(metric units)}, \tag{8}$$

where SE and D are expressed in meters and c is expressed in kilograms.

If we assume a value of 1.25 lb (0.57 kg) for c and a value of 8 in (0.2 m) for D, SE = 0.0053 ft (0.0016 m).

Although not related to errors inherent in a float-operated stage recorder, it might be mentioned here that error in recorded stage may be caused by expansion or contraction of the stilling well of a tall gage structure that is exposed to large temperature changes. For example, a steel well 80 ft (24 m) high, exposed to an increase in temperature of 40°C, will have its instrument shelf raised 0.04 ft (0.012 m), assuming, of course, that the instrument shelter is attached to the well.

Summary.—The errors inherent in a float-operated stage recorder will affect computed discharges. The effect of float lag can be reduced to any desired level by the use of an appropriately large float, and that accuracy level may then be maintained by keeping the instrument cleaned and oiled to reduce friction. The recorder should be set to the gage height in the stilling well when the stage in the well is constant, because the float-lag error in subsequent recorded gage-height will then be only half as large as it would be if the recorder setting were made during a period of changing stage in the stilling well. Even if the stage of the stream is changing, the stage in the well may be kept constant by keeping the intake valves closed while the recorder is being set.

The error resulting from counterweight submergence is a constant function of stage and becomes an integral part of the stage-discharge relation. The same would be true of line-shift error if the recorder settings were made only when the stage is low, but that practice is usually impractical. Line shift can be a significant source of error only at gaging stations that experience a wide range of stage.

ACCURACY OF BUBBLE-GAGE RECORDERS

This section of the report discusses the inaccuracies inherent in any bubble-gage system for sensing stage; the discussion is not concerned with such sources of error as datum corrections, sediment deposition on the bubble orifice, and leaks in the system, which were discussed in the preceding sections. The principal sources of error inherent in a bubble-gage recorder are variation in gas friction, variation in required bubble-feed rate with rate of increase in stage, and variation in weight of gas column with stage.

Variation in gas friction.—Friction created by the flow of gas through the bubble tubing results in the pressure at the manometer being slightly higher than that at the orifice. If the bubble-feed rate could be kept constant and temperature did not vary, the friction would remain constant and the accuracy of the gage would be unaffected, because the manometer is always set to agree with the water-surface elevation. However, changes in gas-feed rates cause variation in the friction of the gas flowing through the tube, and where long bubble tubes are used, the variation in friction can produce significant error in recorded gage height.

Inaccuracies due to variation in gas friction can be eliminated by using two gas tubes—one to feed gas to the bubble orifice, the other to act as a static pressure tube to transmit pressure from a point at or near the orifice back to the manometer.

As a conservative criterion for determining when the use of dual tubing is desirable, it is suggested that variations in gas friction be limited to 0.01 ft (0.003 m). If, for a given length of orifice line, an error no greater than 0.01 ft results from a 100 percent increase in bubble rate, a single bubble tube will be satisfactory. Figure 36, based on laboratory tests using the standard U.S. Geological Survey bubble gage shows the relation between the length of bubble tubing and a 100-percent variation in bubble rate for a gas-friction error of 0.01 ft. To illustrate the use of figure 36, assume that a 100-percent variation in bubble rate represents a change from 40 bubbles per minute to 80 bubbles per minute. The corresponding length of bubble tubing indicated by the diagram is 370 ft (113 m). Thus any length of single tubing up to 370 ft could be used in this particular case without introducing a friction error in excess of 0.01 ft. If more than 370 ft of tubing is required at this particular site, and a gage-height error greater than 0.01 ft cannot be tolerated, two gas tubes should be used. When two tubes are used, they should be joined at a T-connector, from whose vertical leg a single tube extends to the orifice. The T-connector should be located above the normal high-water elevation to prevent the entry of water into both legs of the system if pressure

loss occurs. Additional valves must also be provided so that the static pressure tube can be separately purged, if necessary.

Variation in required bubble-feed rate with rate of increase in stage.—During rapid rises in stage the instrument will lag if the

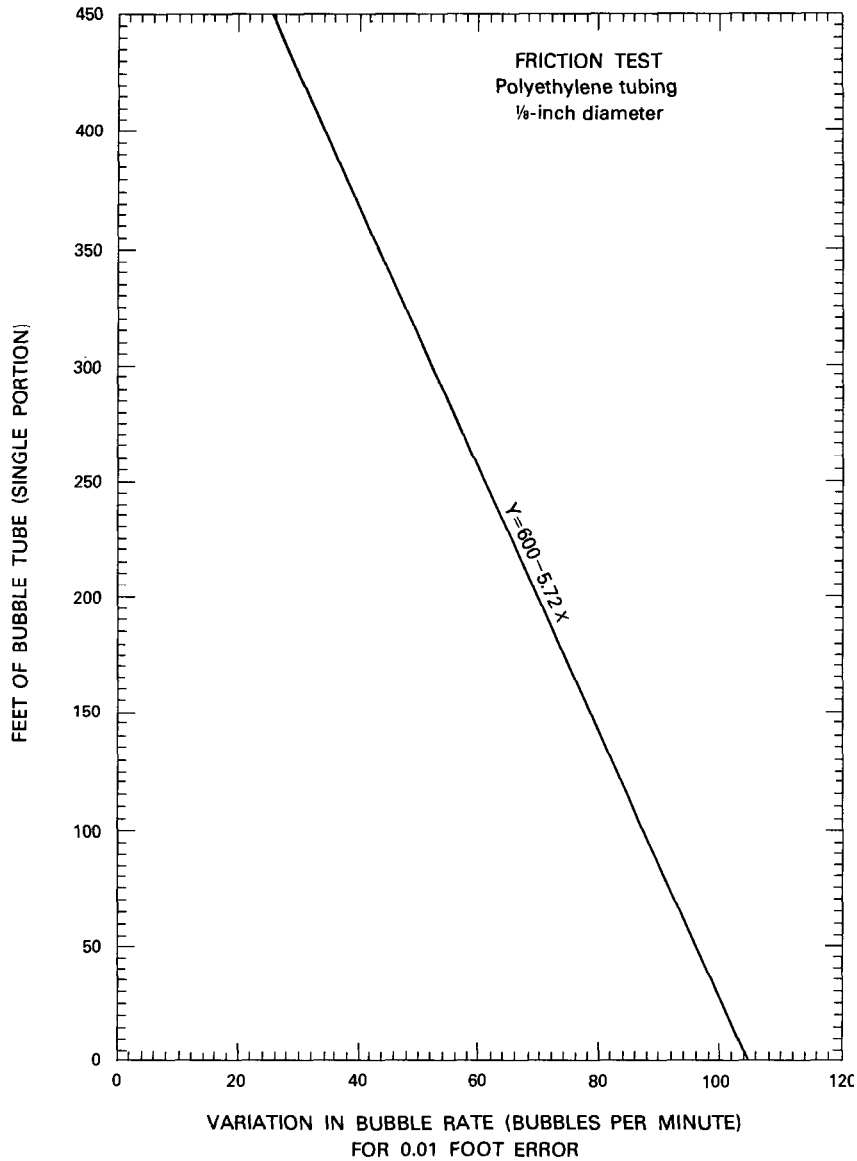

FIGURE 36.—Diagram for determining allowable length of bubble tubing for maximum friction error of 0.01 ft.

bubble-feed rate is too low. Laboratory tests on the standard U.S. Geological Survey bubble gage indicate that figure 37 may be used to

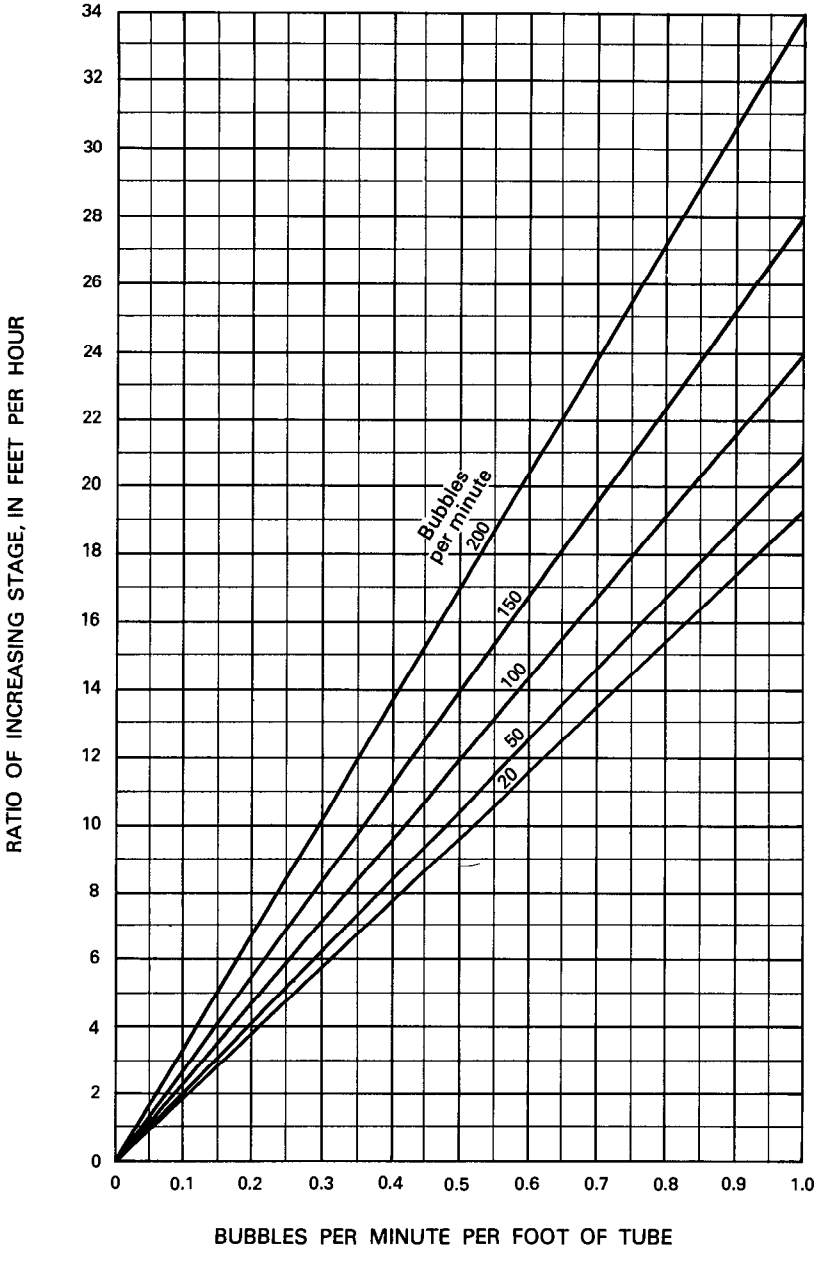

FIGURE 37.—Diagram for determining required bubble rate.

determine the bubble rate required for the maximum expected rate of increase of stage, where the minimum expected stage above the orifice will be less than 10 ft (3.0 m) for long periods of time. For periods when a minimum stage of more than 10 ft is expected to prevail, a lower bubble rate should be used to conserve gas, because the rate of increase of stage that a given bubble rate will support increases directly with stage. It was found that for installations where the minimum stage will continuously be higher than 10 ft, the maximum expected rate of increase of stage should be divided by $\frac{H_{(min)} + 33}{33}$ before entering figure 37. ($H_{(min)}$ is the minimum expected stage above the orifice.) For example, for a given expected rate of increasing stage, the adequate bubble rate for a minimum stage of 100 ft (30.0m) will be one-fourth of that for a minimum stage of 10 ft—the factor $\frac{100 + 33}{33}$ equals 4.

Variation in weight of gas column with stage.—At installations where the manometer is high above the bubble orifice, and large fluctuations in stage occur, the variation in weight of the gas column with stage will cause the manometer to read low (underregister) at high stages. The error varies almost linearly with stage and for that reason the manometer readout in that situation can be corrected without too much difficulty. Depending on the type of instrument used, either the inclination of the manometer is adjusted or a change is made in the gearing between the servosystem and the recording equipment.

As a matter of fact any source of error that varies linearly with stage—for example, the density of the water may increase with stage as a result of increased sediment load—may be compensated for by the adjustments mentioned above. Changes in temperature are usually a negligible source of error, except in high-head installations having large fluctuations in stage. In that situation it is recommended that the bubble-gage system be equipped with a temperature-compensated servomanometer to minimize the error attributable to temperature changes.

SPECIAL PURPOSE GAGES

MODEL T RECORDER

The model T recorder (fig. 38) is a graphic recorder that has a 1:6 gage-height scale and a time scale of 2.4 in. per day. Use of the recorder is limited to a 3-ft (0.9 m) range in stage and it should be serviced weekly, although it will record more than one trace on the 7-day chart. The model T recorder is operated by a motor-wound spring-

driven timer, and power is supplied to the timer by a 4½-volt battery. A timer is also available that operates on a 1½-volt battery. The housing of the recorder is designed to fit on the top of a vertical 3-in (0.076 m)-diameter pipe that can be used as the stilling well. This recorder is much cheaper and more compact than the conventional graphic recorders and is well suited for temporary installations for low-flow studies, particularly those concerned with diurnal fluctuation in discharge during low-flow periods. The model T recorder is not used at continuous-record gaging stations.

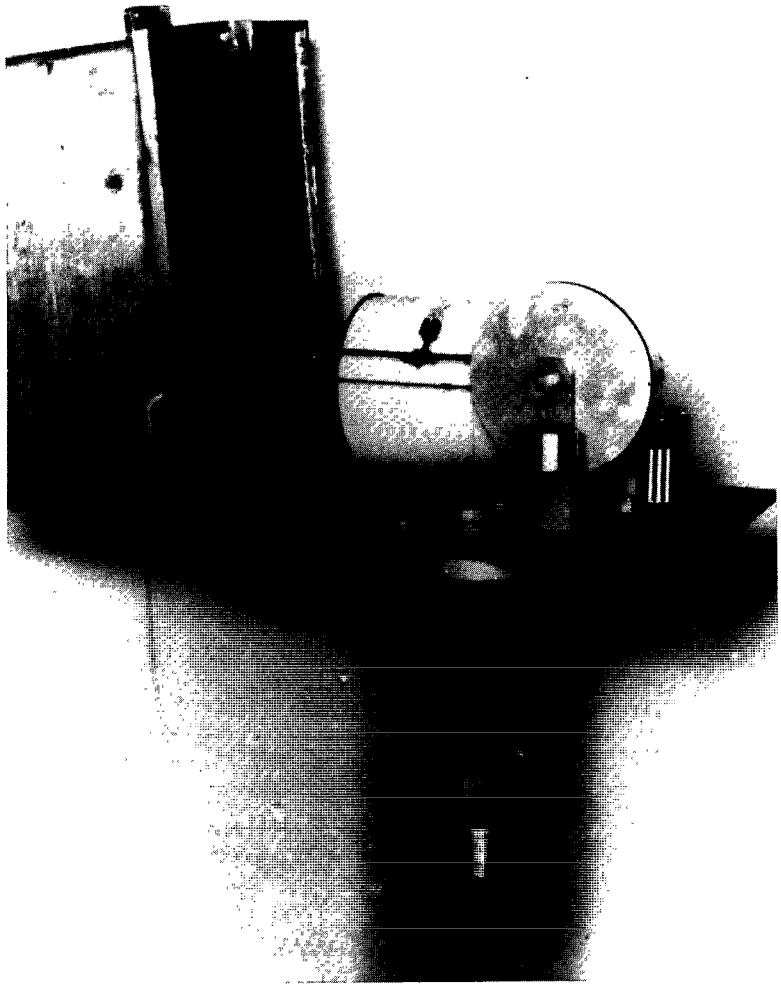

FIGURE 38.—Model T recorder.

SR RECORDER

The model SR recorder (fig. 39) is a graphic recorder that records flood stages and rainfall. A 5-in (0.127m)-diameter flat circular disc is rotated by a battery-wound clock. The power source is a 1½-volt battery. The chart is circular and turns one revolution in 24 hr. Three ranges in stage are available for the effective chart width of 2 in (0.05 m): 5, 10, or 20 ft. The recorder sits on a 2-in-diameter pipe that serves as the stilling well (similar to that for the model T). Five inches of rainfall can also be recorded on the effective width of the chart, but the rainfall reservoir can be equipped with a siphon that will allow an unlimited amount of rainfall to be recorded. The rainfall reservoir is a separate 2-in-diameter pipe that fills at the rate of 1 ft (0.3 m) for each 1 in (0.025 m) of rainfall. After the pipe has filled to a height of 5 ft (1.52 m), the siphon is tripped to empty the pipe.

The SR recorder is much cheaper and more compact than the conventional graphic recorders and is used for studying rainfall-runoff

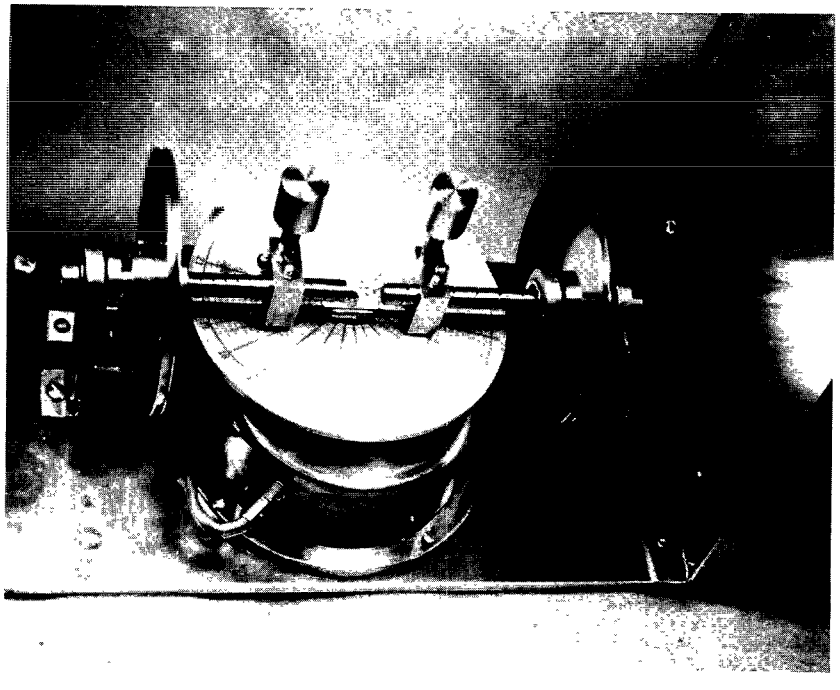

FIGURE 39.—Model SR recorder.

relations for isolated storms on small watersheds. The SR recorder is not used at continuous-record gaging stations.

A word of caution is in order at this point. The SR recorder has not proven to be an unqualified success, although it has performed satisfactorily at many installations. Its use is therefore recommended reservedly.

CREST-STAGE GAGE

The crest-stage gage is a device for obtaining the elevation of the flood crest of streams. The gage is widely used in the U.S.A. because it is simple, economical, reliable, and easily installed. Because of those attributes the crest-stage gage has become a basic instrument in regional studies of flood frequency. For such studies the network of standard gaging stations is augmented by a network of crest-stage gages, thereby providing flood-peak information at a great many sites in the region at reasonable cost.

A crest-stage gage is also a valuable adjunct to the nonrecording gage at nonrecording gaging stations. It provides a record of the peak stages of stream rises, and those stages can be used with the observer's routine readings when sketching the estimated continuous-stage graph through the plotted points of observed stage.

Many different types of crest-stage gages have been tested by the U.S. Geological Survey. (See, for example, Friday, 1965, and Carter and Gamble, 1963.) The one found most satisfactory is a vertical piece of 2-in (0.05 m) galvanized pipe containing a wood or aluminum staff held in a fixed position with relation to a datum reference. (See fig. 40.) The bottom cap has six intake holes located as shown in figure 40 to minimize nonhydrostatic drawdown or superelevation inside the pipe. Tests have shown this arrangement of intake holes to be effective with velocities up to 10 ft/s (3 m/s) and at angles up to 30 degrees with the direction of flow. The top cap contains one small vent hole.

The bottom cap, or a perforated tin cup or copper screening in cup shape attached to the lower end of the staff, contains regranulated cork. As the water rises inside the pipe the cork floats on the water surface. When the water reaches its peak and starts to recede the cork adheres to the staff inside the pipe, thereby retaining the crest stage of the flood. The gage height of a peak is obtained by measuring the interval on the staff between the reference point and the floodmark. Scaling can be simplified by graduating the staff. The cork should be cleaned from the staff before replacing the staff in the pipe to prevent confusion with high-water marks that will be left by subsequent peak discharges.

The datum of the gage should be checked by levels run from a reference mark to the top of the staff, the graduated staff being of

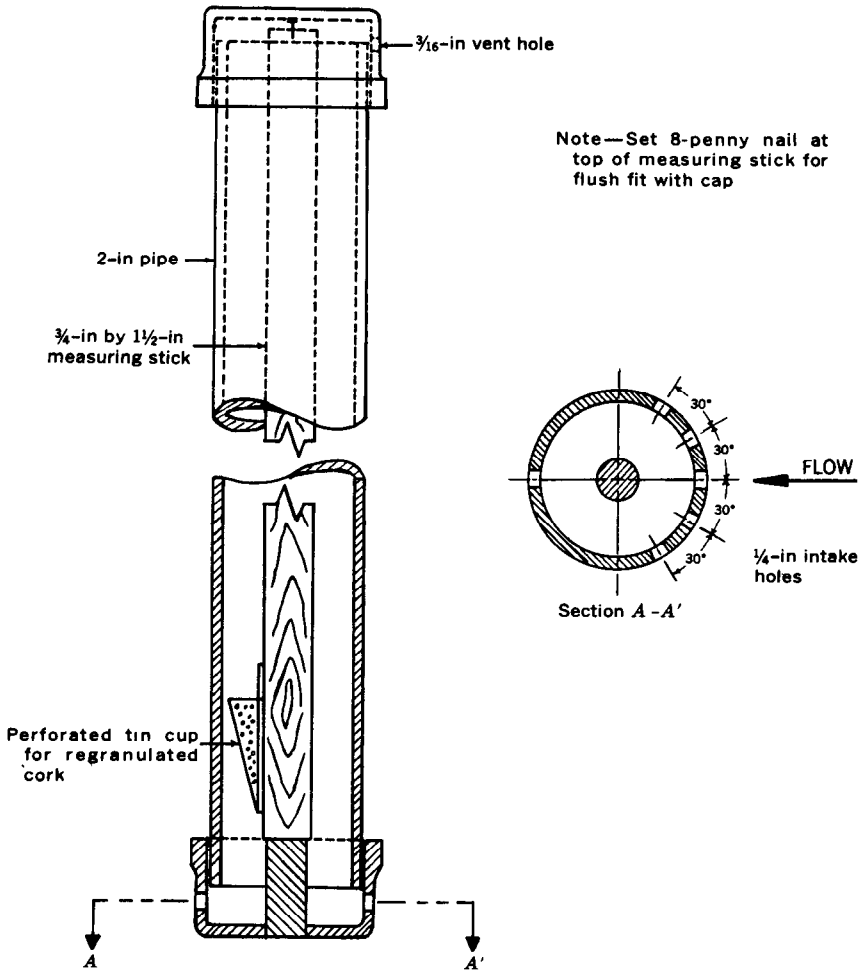

FIGURE 40.—Crest-stage gage.

known length. The gage itself should be serviced on a regular basis. However, the staff should not be removed from the pipe for any reason when the stage is high. If, after such removal, the staff is reinserted when water stands high in the pipe, the resulting surge of the water displaced by the staff will leave an artificial "high-water mark" on the staff.

SELECTED REFERENCES

Barron, E. G., 1963, New instruments for surface-water investigations, *in* Mesnier, G. N., and Iseri, K. T., Selected techniques in water-resources investigations: U.S. Geol. Survey Water-Supply Paper 1669–Z, 64 p.

Buchanan, T. J., and Somers, W. P., 1968, Stage measurement at gaging stations: U.S. Geol. Survey Techniques Water-Resources Investigations, Book 3, Chap. A–7, 28 p.
Carter, J. R., and Gamble, C. R., 1963, Tests of crest-stage gage intakes: U.S. Geol. Survey open-file report, Water-Resources Division, Washington, D.C.
Corbett, D. M., and others, 1943, Stream-gaging procedure: U.S. Geol. Survey Water-Supply Paper 888, p. 224–228.
Friday, John, 1965, Tests of crest-stage intake systems: U.S. Geol. Survey open-file report.
International Standards Organization, 1969, Liquid flow measurement in open channels—Establishment and operation of a gauging station and determination of the stage-discharge relation: ISO Recommendation R1100, Geneva, p. 9–11.
Isherwood, W. L., 1963, Digital water-stage recorder, *in* Mesnier, G. N., and Iseri, K. T., Selected techniques in water-resources investigations: U.S. Geol. Survey Water-Supply Paper 1669–Z, 64 p.
Mesnier, G. N., and Iseri, K. T., 1963, Selected techniques in water-resources investigations: U.S. Geol. Survey Water-Supply Paper 1669–Z, 64 p.
Smith, Winchell, Hanson, R. L., and Cruff, R. W., 1965, Study of intake lag in conventional stream-gaging stilling wells: U.S. Geol. Survey open-file report, Water-Resources Division, Menlo Park, Calif.
Stevens, J. C., 1921, The accuracy of water level recorders and indicators of the float type: American Society Civil Engineers Transactions, v. 83 (1919–20), p. 894–903.
World Meteorological Organization, 1962, Field methods and equipment used in hydrology and hydrometeorology: Flood Control Series no. 22, p. 18–24.

CHAPTER 5.—MEASUREMENT OF DISCHARGE BY CONVENTIONAL CURRENT-METER METHOD

INTRODUCTION

Streamflow, or discharge, is defined as the volume rate of flow of water, including any substances suspended or dissolved in the water. Discharge is usually expressed in cubic feet per second or cubic meters per second.

Discharge measurements are made at each gaging station to determine the discharge rating for the site. The discharge rating may be a simple relation between stage and discharge or a more complex relation in which discharge is a function of stage, slope, rate of change of stage, or other factors. Initially the discharge measurements are made with the frequency necessary to define the station rating, as early as possible, over a wide range of stage. Measurements are then made at periodic intervals, usually monthly, to verify the rating or to define any changes in the rating caused by changes in stream-channel conditions.

Discharge measurements may be made by any one of the methods discussed in chapters 5–8. However, the conventional current-meter method is most commonly used in gaging streams. When using this

method, observations of width, depth, and velocity are taken at intervals in a cross section of the stream, while the hydrographer is wading or supported by a cableway, bridge, ice cover, or boat. A current meter is used to measure velocity. This chapter describes the conventional current-meter method.

GENERAL DESCRIPTION OF A CONVENTIONAL CURRENT-METER MEASUREMENT OF DISCHARGE

A current-meter measurement is the summation of the products of the subsection areas of the stream cross section and their respective average velocities. The formula

$$Q = \Sigma(a\ v) \tag{9}$$

represents the computation, where Q is total discharge, a is an individual subsection area, and v is the corresponding mean velocity of the flow normal to the subsection.

In the midsection method of computing a current-meter measurement, it is assumed that the velocity sample at each vertical represents the mean velocity in a rectangular subsection. The subsection area extends laterally from half the distance from the preceding observation vertical to half the distance to the next, and vertically from the water surface to the sounded depth. (See fig. 41.)

The cross section is defined by depths at verticals 1, 2, 3, 4, . . . n. At each vertical the velocities are sampled by current meter to obtain the mean velocity for each subsection. The subsection discharge is then computed for any subsection at vertical x by use of the equation,

$$q_x = v_x \left[\frac{(b_x - b_{(x-1)})}{2} + \frac{(b_{(x+1)} - b_x)}{2}\right] d_x$$

$$= v_x \left[\frac{b_{(x+1)} - b_{(x-1)}}{2}\right] d_x \tag{10}$$

where

q_x = discharge through subsection x,
v_x = mean velocity at vertical x,
b_x = distance from initial point to vertical x,
$b_{(x-1)}$ = distance from initial point to preceding vertical,
$b_{(x+1)}$ = distance from initial point to next vertical, and
d_x = depth of water at vertical x.

Thus, for example, the discharge through subsection 4 (heavily outlined in fig. 41) is

$$q_4 = v_4 \left[\frac{b_5 - b_3}{2}\right] d_4.$$

The procedure is similar when x is at an end section. The "preceding vertical" at the beginning of the cross section is considered coincident with vertical 1; the "next vertical" at the end of the cross section is considered coincident with vertical n. Thus,

$$q_1 = v_1 \left[\frac{b_2 - b_1}{2}\right] d_1$$

and

$$q_n = v_n \left[\frac{b_n - b_{(n-1)}}{2}\right] d_n.$$

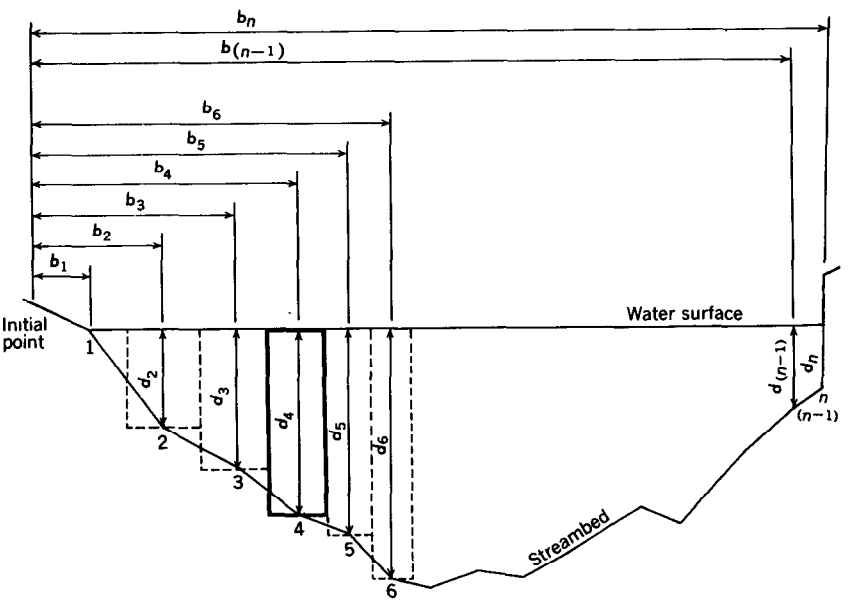

EXPLANATION

1, 2, 3 ..... n	Observation verticals
$b_1, b_2, b_3, \ldots . b_n$	Distance, in feet or meters, from the initial point to the observation vertical
$d_1, d_2, d_3, \ldots . d_n$	Depth of water, in feet or meters, at the observation vertical
Dashed lines	Boundaries of subsections; one heavily outlined is discussed in text

FIGURE 41.—Definition sketch of midsection method of computing cross-section area for discharge measurements.

For the example shown in figure 41, q_1 is zero because the depth at observation point 1 is zero. However, when the cross-section boundary is a vertical line at the edge of the water as at vertical n, the depth is not zero and velocity at the end vertical may or may not be zero. The formula for q_1 or q_n is used whenever there is water only on one side of an observation vertical such as at piers, abutments, and islands. It is necessary to estimate the velocity at an end vertical, usually as some percentage of the adjacent vertical, because it is impossible to measure the velocity accurately with the current meter close to a boundary. There is also the possibility of damage to the equipment if the flow is turbulent. Laboratory data suggest that the mean vertical velocity in the vicinity of a smooth sidewall of a rectangular channel can be related to the mean vertical velocity at a distance from the wall equal to the depth. The tabulation below gives values that define the relation.

Distance from wall, as a ratio of the depth	*Mean vertical velocity, as related to* V_n
0.00	$0.65V_n$
.25	$.90V_n$
.50	$.95V_n$
1.00	$1.00V_n$

NOTE—V_n is the mean vertical velocity at a distance from the vertical wall equal to the depth.

The summation of the discharges for all the subsections—usually 25 to 30 in number—is the total discharge of the stream. An example of the measurement notes used by the U.S. Geological Survey is shown in figure 42.

The mean-section method, used by the U.S. Geological Survey prior to 1950, differs from the midsection method, described above, in computation procedure. In the older method discharges are computed for subsections between successive observation verticals. The velocities and depths at successive verticals are each averaged, and each subsection extends laterally from one observation vertical to the next. Subsection discharge is the product of the average of two mean velocities, the average of two depths, and the distance between observation verticals. In both methods total discharge is the sum of the subsection discharges. A study by Young (1950) concluded that the midsection method is simpler to compute and is a slightly more accurate procedure than the mean-section method.

Current-meter meaurements are usually classified in terms of the means used to cross the stream during the measurement, such as wading, cableway, bridge, boat, or ice cover.

INSTRUMENTS AND EQUIPMENT

Current meters, timers, and a means of counting meter revolutions are needed for the measurement of discharge, along with additional

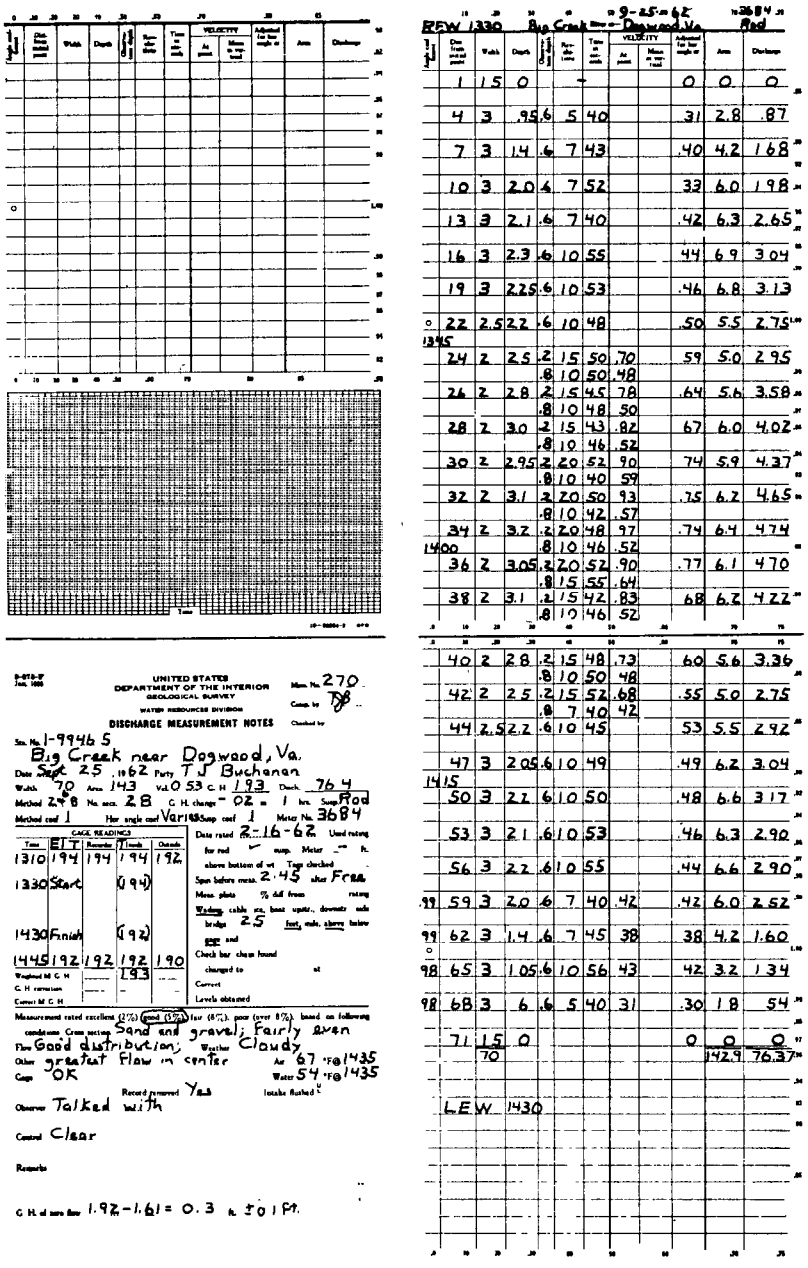

FIGURE 42.—Computation notes of a current-meter measurement by the midsection method.

equipment that depends on the manner in which the measurement is to be made—that is, whether by wading, cableway, bridge, boat, or from ice cover. Instruments and equipment used in making the current-meter measurements are described in this section of the manual under the following categories: current meters, sounding equipment, width-measuring equipment, equipment assemblies, and miscellaneous equipment.

CURRENT METERS

A current meter is an instrument used to measure the velocity of flowing water. The principle of operation is based on the proportionality between the velocity of the water and the resulting angular velocity of the meter rotor. By placing a current meter at a point in a stream and counting the number of revolutions of the rotor during a measured interval of time, the velocity of water at that point is determined.

The number of revolutions of the rotor is obtained by an electrical circuit through the contact chamber. Contact points in the chamber are designed to complete an electrical circuit at selected frequencies of revolution. Contact chambers can be selected having contact points that will complete the circuit twice per revolution, once per revolution, or once per five revolutions. The electrical impulse produces an audible click in a headphone or registers a unit on a counting device. The intervals during which meter revolutions are counted are timed with a stopwatch. A discussion of the required time interval follows.

Turbulent flow, which is ordinarily found in natural streams and in artificial channels, is always accompanied by local eddying, which results in pulsations in the velocity at any point. Figure 43, taken from a study by Pierce (1941), shows the pulsations observed in a laboratory flume for two different mean velocities. The greater magnitude of the pulsations, relative to the mean, at the lower velocity explains why current-meter observations at a point should cover a longer period when low velocities are being measured than when higher velocities are being measured. At high velocities, pulsations have only minor effect on the current-meter observations. In the U.S.A. it is customary to observe velocity at a point by current meter for a period that ranges from 40 to 70 s. It is recognized that the use of a period of from 40 to 70 s is not long enough to insure the accuracy of a single point-observation of velocity. However, because the pulsations are random and because velocity observations during a discharge measurement are made at 25 to 30 verticals, usually with two observations being made in each vertical, there is little likelihood that the pulsations will bias the total measured discharge of a stream. (See p. 181–182.) Longer periods of current-meter observation at a

point are not used, because it is desirable to complete a discharge measurement before the stage changes significantly and because the use of longer observation periods may add significantly to the operating cost of a large number of gaging stations.

Current meters generally can be classified with respect to two main types: those meters having vertical-axis rotors and those having horizontal-axis rotors. The comparative characteristics of these two types are summarized below:

1. Vertical-axis rotor with cups or vanes.
   a. Operates in lower velocities than do horizontal-axis meters.
   b. Bearings are well protected from silty water.
   c. Rotor is repairable in the field without adversely affecting the rating.
   d. Single rotor serves for the entire range of velocities.
2. Horizontal-axis rotor with vanes.
   a. Rotor disturbs flow less than do vertical-axis rotors because of axial symmetry with flow direction.
   b. Rotor is less likely to be entangled by debris than are vertical-axis rotors.
   c. Bearing friction is less than for vertical-axis rotors because bending moments on the rotor are eliminated.

VERTICAL-AXIS CURRENT METERS

A common type of vertical-axis current meter is the Price meter, type AA. (See fig. 44.) This meter is used extensively by the U.S. Geological Survey. The standard Price meter has a rotor 5 in (0.127

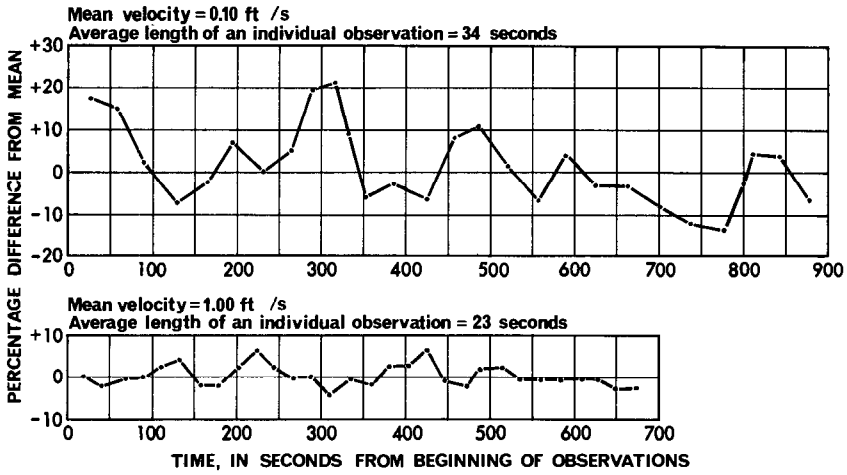

FIGURE 43.—Comparison of pulsations for two different mean velocities measured in a laboratory flume, 12 ft wide.

m) in diameter and 2 in (0.05 m) high with six cone-shaped cups mounted on a stainless-steel shaft. A pivot bearing supports the rotor shaft. The contact chamber houses both the upper part of the shaft and a slender bronze wire (cat's whisker) attached to a binding post. With each revolution an eccentric contact on the shaft makes contact with a bead of solder at the end of the cat's whisker. A separate reduction gear (pentagear), wire, and binding post provide a contact each time the rotor makes five revolutions. A tailpiece keeps the meter pointing into the current.

In addition to the standard type AA meter for general use there is a type AA meter for low velocities. No pentagear is provided. This modification reduces friction. The shaft usually has two eccentrics making two contacts per revolution. The low-velocity meter normally is rated from 0.2 to 2.5 ft/s (0.06 to 0.76 m/s) and is recommended for use when the mean velocity at a cross section is less than 1 ft/s (0.3 m/s).

In addition to the type AA meters, the U.S. Geological Survey uses a Price pygmy meter in shallow depths. (See fig. 44.) The pygmy meter is scaled two-fifths as large as the standard meter and has neither a tailpiece nor a pentagear. The contact chamber is an integral part of the yoke of the meter. The pygmy meter makes one contact per revolution and is used only with rod suspension.

The U.S. Geological Survey has recently developed a four-vane vertical-axis meter. (See fig. 45.) This meter is useful for measurements under ice cover because the vanes are less likely to fill with slush ice and because it requires a much smaller hole for passage through the ice. One yoke of the vane meter is made to be suspended at the end of a rod and will fit holes made by an ice drill. Another yoke

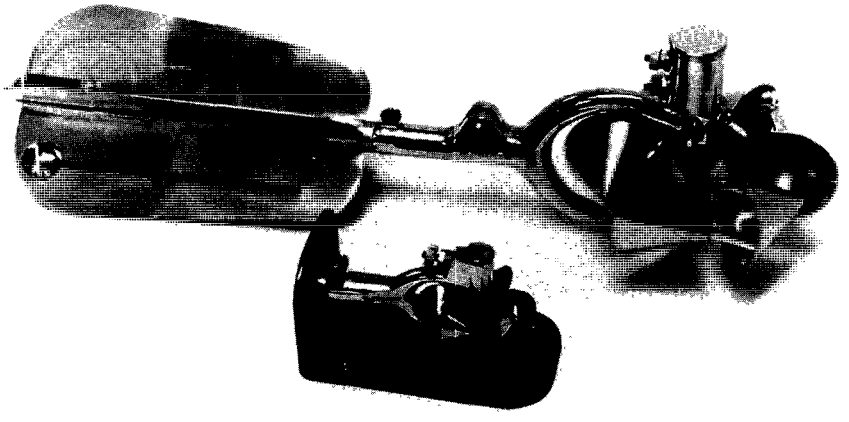

FIGURE 44.—Price type AA meter, top; Price pygmy meter, bottom.

is made for regular cable or rod suspension. (See fig. 45.) The vane meter has the disadvantage of not responding as well as the Price type AA meter at velocities less than 0.5 ft/s (0.15 m/s).

A new contact chamber has been designed by the U.S. Geological Survey to replace the wiper contact of the type AA and vane meters. The new contact chamber contains a magnetic switch, glass enclosed in a hydrogen atmosphere and hermetically sealed. The switch assembly is rigidly fixed in the top of the meter head just above the tip of the shaft. The switch is operated by a small permanent magnet rigidly fastened to the shaft. The switch quickly closes when the magnet is alined with it and then promptly opens when the magnet moves away. The magnet is properly balanced on the shaft. Any type AA meter can have a magnetic switch added by replacing the shaft and the contact chamber. The magnetic switch is placed in the special contact chamber through the tapped hole for the binding post. The rating of the meter is not altered by the change. An automatic counter (p. 130) is used with the magnetic-switch contact chamber. If a headphone is used, arcing may weld the contacts.

A Price meter accessory that indicates the direction of flow is described on page 129.

Vertical-axis current meters do not register velocities accurately when placed close to a vertical wall. A Price meter held close to a right-bank vertical wall will underregister because the slower water velocities near the wall strike the effective (concave) face of the cups. The converse is true at a left-bank vertical wall. (The terms "left bank" and "right bank" designate direction from the center of a stream for an observer facing downstream.) The Price meter also

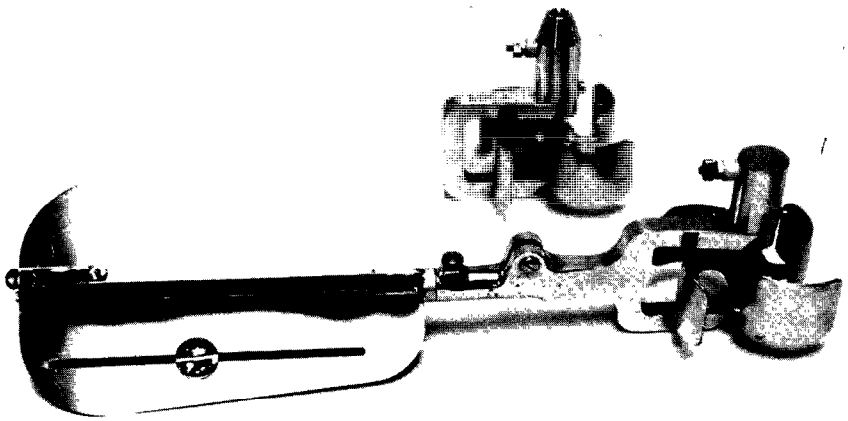

FIGURE 45.—Vane ice meter, top; vane meter with cable suspension yoke, bottom.

underregisters when positioned close to the water surface or close to the streambed.

HORIZONTAL-AXIS CURRENT METERS

The types of horizontal-axis meters most commonly used are the Ott, Neyrpic, Haskell, Hoff, and Braystoke. The Ott meter is made in Germany, the Neyrpic meter in France, and both are used extensively in Europe. The Haskell and Hoff meters were developed in the United States, where they are used to a limited extent. The Braystoke meter is used extensively in the United Kingdom. The Ott meter (fig. 46) is a precision instrument but is not widely used in the U.S.A. because it is not as durable as the Price meter under extreme conditions. The makers of the Ott meter have developed a component propeller that in oblique currents automatically registers the velocity component at right angles to the measuring section for angles as great as 45° and

FIGURE 46.—Ott current meter.

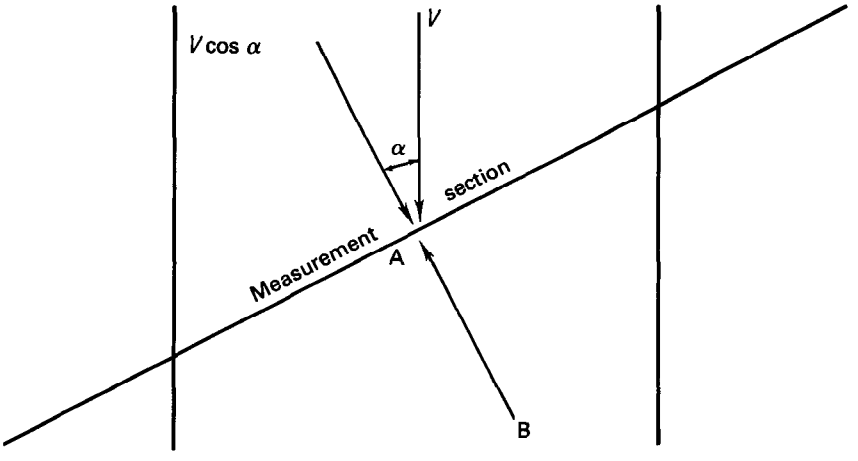

FIGURE 47.—Velocity components measured by Ott and Price current meters.

for velocities as great as 8 ft/s (2.4 m/s). For example, if this component propeller were held in the position AB in figure 47 it would register $V \cos \alpha$ rather than V, which the Price meter would register.

The Neyrpic meter is used rarely in the U.S.A. for the same reason that the Ott meter is rarely used there.

The Haskell meter has been used by the U.S. Lake Survey, Corps of Engineers, in streams that are deep, swift, and clear. By using propellers with a variety of screw pitches, a considerable range of velocity can be measured. The Haskell meter is more durable than most other horizontal-axis current meters.

The Hoff meter (fig. 48) is another current meter used in the U.S.A. The lightweight propeller has three or four vanes of hard rubber. The meter is suited for the measurement of low velocities but is not suited for rugged use.

COMPARISON OF PERFORMANCE OF VERTICAL-AXIS AND HORIZONTAL-AXIS CURRENT METERS

Comparative tests of the performance of vertical-axis and horizontal-axis current meters, under favorable measuring conditions, indicate virtually identical results from use of the two types of meter. That was the conclusion reached in 1958 by the U.S. Lake Survey, Corps of Engineers, after tests made with the Price, Ott, and Neyrpic current meters (Townsend and Blust, 1960). The results of one of their tests is shown in figure 49.

Between the years 1958 and 1960, the U.S. Geological Survey made 19 simultaneous discharge measurements on the Mississippi River using Price and Ott meters. The average difference in discharge between results from the two meters was -0.15 percent, using the measurements made with the Price meter as the standard for comparison. The maximum differences in discharge measured by the two meters was -2.76 and $+1.53$ percent.

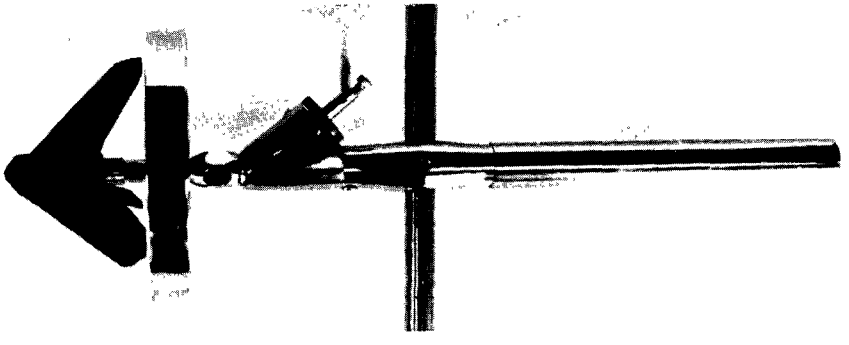

FIGURE 48.—Hoff current meter.

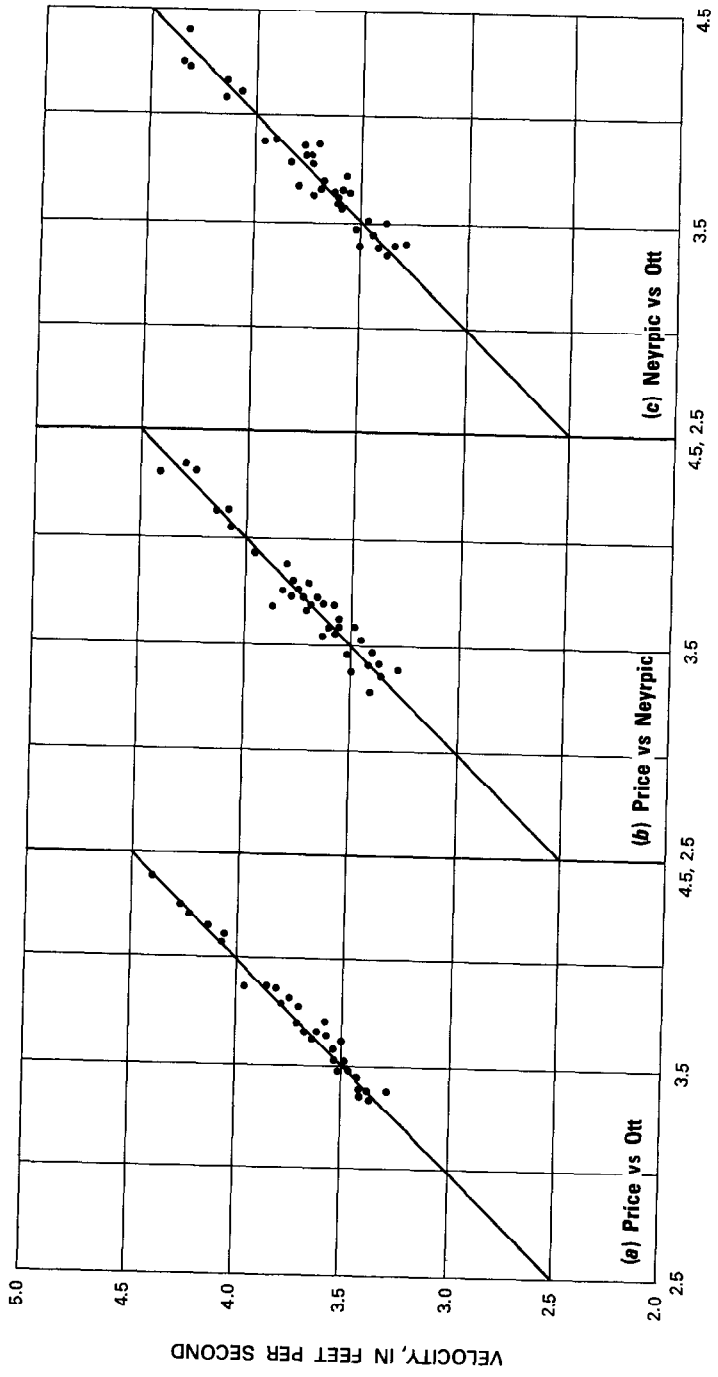

FIGURE 49.—*Comparison of mean velocities measured simultaneously by various current meters during 2-min periods, Stella Niagara section, Panel point 5.* (After Townsend and Blust, 1960.)

OPTICAL CURRENT METER

In recent years the U.S. Geological Survey has developed an optical current meter (fig. 50). The meter and its use have been described by Chandler and Smith (1971). The optical current meter is designed to measure surface velocities in open channels without immersing equipment in the stream. However, because it measures only surface velocity, the optical meter is not considered a substitute for conventional equipment in those situations where good measurements can be made by standard techniques. It is a device that has extended the capability of making discharge measurements to a range of situations under which standard current-meter techniques cannot be used. Those situations include flood velocities that are too high to be measured by conventional meter—for example, supercritical velocities in floodways—or the presence of a debris load during flood periods that makes it hazardous to immerse a current meter.

Basically, the meter is a stroboscopic device consisting of a low-power telescope, a single oscillating mirror driven by a cam, a variable-speed battery-operated motor, and a tachometer. The water surface is viewed from above through the meter, while gradually changing the speed of the motor to bring about synchronization of the

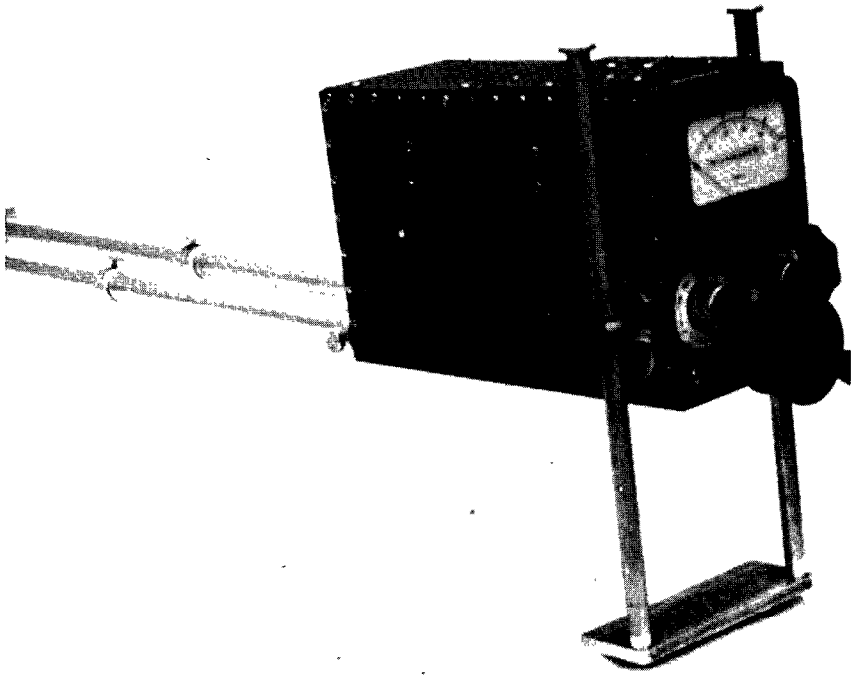

FIGURE 50.—Optical current meter.

angular velocity of the mirror and the surface velocity of the water. Synchronization is achieved when the motion of drift or disturbances on the water surface, as viewed through the meter, is stopped. A reading of the tachometer and height of the meter above the water surface are the only elements needed to compute the surface velocity.

The velocity measurement may be made from any bridge, walkway, or other structure that will support the optical meter. The vertical axis of the meter must be perpendicular to the water surface. Surface velocity (V_s) is computed from the equation

$$V_s = KRD,$$

where K is the constant for the meter, R is the readout from the tachometer, and D is the distance to the water surface in feet. The tachometer is scaled to produce a value of K equal to 1.00. The surface velocity computed from the above equation must be corrected by an appropriate coefficient to obtain the mean velocity in the vertical. The precise coefficient applicable is, of course, unique to the particular stream and to the location of the vertical in the stream cross section. However, data abstracted from conventional current-meter measurements show that application of a coefficient of 0.90 will not introduce errors of more than ±5 percent in concrete-lined channels. For natural channels a coefficient of 0.85 has been used.

A unique feature of the optical current meter is the automatic correction that is made for variations in the direction of the streamlines of flow. If the flow approaches the cross section at an angle other than the perpendicular, and if the axis of the oscillating mirror in the meter is parallel to the cross section, then at the null point of observation, the water will appear to move laterally across the field of view. The meter measures only the velocity vector normal to the cross section, and there is no need to apply horizontal angle corrections.

The range of velocities that can be measured with the optical current meter is limited at the lower end by the accuracy of the tachometer and at the upper end by the physical limitations of the human eye. Table 1 shows the range of velocities that can be meas-

TABLE 1.—*Range of velocities that can be measured with optical current meter*

Observation height (D)		Maximum velocity		Minimum velocity for ±5 percent resolution	
(ft)	(m)	(ft/s)	(m/s)	(ft/s)	(m/s)
5	1.52	25	7.62	1.6	0.49
10	3.05	50	15.2	3.2	.98
15	4.57	75	22.9	4.8	1.46
20	6.10	100	30.5	6.4	1.95

ured from various heights above the water surface with the U.S. Geological Survey model of the meter. The minimum velocities shown in column 3 of the table can be measured with an error of ±5 percent; the higher velocities at the various observation heights will be measured with lesser error.

CARE OF THE CURRENT METER

To insure reliable observations of velocity it is necessary that the current meter be kept in good condition. The care of conventional meters will be discussed first.

Before and after each discharge measurement the meter cups or vanes, pivot and bearing, and shaft should be examined for damage, wear, or faulty alinement. Before using the meter its balance on the cable-suspension hanger should be checked, the alinement of the rotor when the meter is on the hanger or wading rod should also be checked, and the conductor wire should be adjusted to prevent interference with meter balance and rotor spin. During measurements, the meter should periodically be observed when it is out of the water to be sure that the rotor spins freely.

Meters should be cleaned and oiled daily when in use. If measurements are made in sediment-laden water, the meter should be cleaned immediately after each measurement. For vertical-axis meters the surfaces to be cleaned and oiled are the pivot bearing, pentagear teeth and shaft, cylindrical shaft bearing, and thrust bearing at the cap.

After oiling, the rotor should be spun to make sure that it operates freely. If the rotor stops abruptly, the cause of the trouble should be sought and corrected before using the meter. The duration of spin should be recorded on the field notes for the discharge measurement. A significant decrease in the duration of spin indicates that the bearings require attention. In vertical-axis current meters the pivot requires replacement more often than other meter parts, and it therefore should be examined after each measurement. The pivot and pivot bearing should be kept separated, except during measurements, by use of the raising nut provided in the Price meter or by replacing the pivot with a brass plug in the pygmy meter. Fractured, worn, or rough pivots should be replaced.

Meter repairs by the hydrographer should be limited to minor damage only. That is particularly true of the rotor, where small changes in shape can significantly affect the meter rating. In vertical-axis meters, minor dents in the cups can often be straightened to restore the original shape of the cups, but in case of doubt, the entire rotor should be replaced with a new one. Badly sprung yokes, bent yoke stems, misalined bearings and tailpieces

should be reconditioned in shops equipped with the specialized facilities needed.

There are only few details connected with care of the optical current meter. The meter should be transported in a shock-proof carrying case and the battery should be checked periodically. Field performance of the tachometer should also be checked periodically. Three steps are involved in the checking process. First, a cam speed is measured by counting and timing mirror oscillations with a stopwatch, and the corresponding dial reading of the tachometer is observed. Next, a tachometer dial readout is computed from the measured cam speed and the known scale factor of the tachometer dial. In the final step the observed dial reading and the computed dial readout are compared.

RATING OF CURRENT METERS

To determine the velocity of the water from the revolutions of the rotor of a conventional current meter, a relation must be established between the angular velocity of the rotor and the velocity of the water that spins the rotor. That relation is known as the rating of the current meter. The rating is established by first towing the meter at a constant velocity through a long water-filled trough, and then relating the linear and rotational velocities of the current meter. The following paragraphs describe the rating of meters by the U.S. Geological Survey at the Hydrologic Instrumentation Facility in Mississippi.

The rating trough used is a sheltered concrete tank 450 ft (137 m) long, 12 ft (3.7 m) wide, and 12 ft (3.7 m) deep. An electrically driven car rides on rails extending the length of the tank. The car carries the current meter at a constant rate through the still water in the basin. Although the rate of travel can be accurately adjusted by means of an electronic regulating gear, the average velocity of the moving car is determined for each run by making an independent measurement of the distance it travels during the time that the revolutions of the rotor are electrically counted. Eight pairs of runs are usually made for each current meter. A pair of runs consists of two traverses of the basin, one in each direction, at the same speed. Practical considerations usually limit the ratings to velocities ranging from 0.1 to about 15 ft/s (0.03 to about 4.6 m/s), although the car can be operated at lower speeds. Unless a special request is made for a more extensive rating, the lowest velocity used in the rating is about 0.2 ft/s (0.06 m/s), and the highest is about 8.0 ft/s (2.5 m/s).

For convenience in field use, the data from the current-meter ratings are reproduced in tables, a sample of which is shown in figure 51.

UNITED STATES
DEPARTMENT OF THE INTERIOR
GEOLOGICAL SURVEY
Water Resources Division

RATING TABLE FOR TYPE AA CURRENT METER

EQUATIONS V=2 180R + 020 (2 200) 2 170R + 030 Std Rating No 1

Time in Seconds	VELOCITY IN FEET PER SECOND									Time in Seconds
	Revolutions									
	3	5	7	10	15	20	25	30	40	
40	183	292	401	565	.837	1.11	1 38	1 65	2 20	40
41	180	286	392	552	818	1 08	1.35	1 62	2 15	41
42	176	280	383	539	799	1 06	1 32	1 58	2 10	42
43	172	273	375	527	780	1 03	1 29	1 54	2 05	43
44	.169	268	367	515	.763	1 01	1 26	1 51	2 00	44
45	165	262	359	504	747	989	1.23	1 47	1 96	45
46	162	257	352	494	.731	968	1 20	1 44	1 92	46
47	159	252	345	484	716	948	1.18	1 41	1 88	47
48	156	247	338	474	701	928	1 16	1 38	1 84	48
49	153	242	331	.465	687	910	1 13	1 35	1 80	49
50	.151	238	325	.456	.674	892	1.11	1 33	1 76	50
51	148	234	319	447	661	875	1 09	1 30	1 73	51
52	146	230	313	.439	649	858	1 07	1 28	1 70	52
53	143	226	308	431	637	843	1 05	1 25	1 67	53
54	141	222	303	424	626	827	1 03	1 23	1 63	54
55	139	218	297	416	615	813	1 01	1 21	1 61	55
56	.137	215	292	409	604	.799	.993	1 19	1 58	56
57	135	211	288	402	594	785	976	1 17	1 55	57
58	133	208	283	396	584	.772	960	1 15	1 52	58
59	131	205	279	389	574	759	944	1 13	1 50	59
60	129	202	274	383	565	747	928	1 11	1 47	60
61	127	199	270	377	556	735	913	1 09	1 45	61
62	125	196	266	.372	547	723	899	1.07	1 43	62
63	.124	193	.262	366	539	712	885	1 06	1 40	63
64	122	190	258	.361	531	.701	.872	1 04	1 38	64
65	121	188	255	355	523	691	858	1 03	1 36	65
66	119	185	251	350	515	681	846	1 01	1 34	66
67	118	.183	248	345	508	.671	.833	996	1 32	67
68	116	180	.244	341	501	661	821	982	1 30	68
69	115	178	241	336	494	652	810	968	1 28	69
70	113	176	238	331	487	643	799	954	1 27	70
	3	5	7	10	15	20	25	30	40	

UNITED STATES
DEPARTMENT OF THE INTERIOR
GEOLOGICAL SURVEY
Water Resources Division

RATING TABLE FOR TYPE AA CURRENT METER

Actual Rating Limits 0 25 to 8 0 feet per second Date 03-05-70

Time in Seconds	VELOCITY IN FEET PER SECOND									Time in Seconds
	Revolutions									
	50	60	80	100	150	200	250	300	350	
40	2 74	3 28	4 37	5 45	8.17	10 88	13 59	16 30	19 02	40
41	2 68	3 21	4 26	5 32	7 97	10 62	13 26	15 91	18 55	41
42	2 61	3 13	4 16	5 20	7 78	10 36	12 95	15 53	18 11	42
43	2 55	3 06	4 07	5 08	7 60	10 12	12 65	15.17	17 69	43
44	2 50	2 99	3 98	4 96	7 43	9 89	12 36	14 83	17 29	44
45	2 44	2 92	3 89	4 85	7 26	9.67	12 09	14 50	16 91	45
46	2 39	2 86	3 80	4 75	7 11	9 46	11 82	14 18	16 54	46
47	2 34	2 80	3 72	4 65	6 96	9 26	11 57	13 88	16 19	47
48	2 29	2 74	3 65	4 55	6 81	9 07	11 33	13 59	15 85	48
49	2 24	2 69	3 57	4 46	6 67	8 89	11 10	13 32	15 53	49
50	2 20	2 63	3 50	4 37	6 54	8 71	10 88	13 05	15 22	50
51	2 16	2 58	3 43	4 28	6 41	8 54	10 67	12 79.	14 92	51
52	2 12	2 53	3 37	4 20	6 29	8 38	10 46	12 55	14 64	52
53	2 08	2 49	3 31	4 12	6 17	8 22	10 27	12 31	14 36	53
54	2 04	2 44	3 24	4 05	6 06	8 07	10 08	12 09	14 09	54
55	2 00	2 40	3 19	3 98	5 95	7 92	9 89	11 87	13 84	55
56	1 97	2 35	3 13	3 90	5 84	7 78	9 72	11 65	13 59	56
57	1 93	2 31	3 08	3 84	5 74	7 64	9 55	11 45	13 35	57
58	1 90	2 27	3 02	3 77	5 64	7 51	9 38	11 25	13 12	58
59	1 87	2 24	2 97	3 71	5 55	7 39	9 22	11 06	12 90	59
60	1 84	2 20	2 92	3 65	5 45	7 26	9 07	10 88	12 69	60
61	1 81	2 16	2 88	3 59	5 37	7 14	8 92	10 70	12 48	61
62	1 78	2 13	2 83	3 53	5 28	7 03	8 78	10 58	12 28	62
63	1 75	2 10	2 79	3 47	5 20	6 92	8 64	10 36	12 09	63
64	1 72	2 06	2 74	3 42	5 12	6 81	8 51	10 20	11 90	64
65	1 70	2 03	2 70	3 37	5 04	6 71	8 38	10 05	11 71	65
66	1 67	2 00	2 66	3 32	4 96	6 61	8 25	9 89	11 54	66
67	1 65	1 97	2 62	3 27	4 89	6 51	8 13	9 75	11 37	67
68	1 62	1 94	2 58	3 22	4 82	6 41	8 01	9 60	11 20	68
69	1 60	1 92	2 55	3 17	4 75	6 32	7 89	9 46	11 04	69
70	1 58	1 89	2 51	3 13	4 68	6 23	7 78	9 33	10 88	70
	50	60	80	100	150	200	250	300	350	

FIGURE 51.—Current-meter rating table.

The velocities corresponding to a range of 3 to 350 revolutions of the rotor within a period of 40 to 70 s are listed in the tables. This range in revolution and time has been found to cover general field requirements. To provide the necessary information for extending a table for the few instances where extensions are required, the equations of the rating table are shown in the spaces provided in the heading. The term, R, in the equations refers to revolutions of the rotor per second. The equation to the left of the figure in parentheses (2.20 in fig. 51) is the equation for velocities less than 2.20 ft/s (0.67 m/s), and the equation to the right is for velocities greater than 2.20 ft/s. The velocity 2.20 ft/s is common to both equations.

It should be noted that the equations given are those of the rating table and not necessarily those of the actual rating. If a rating table already on file matches a rating within close tolerances, that table is selected in preference to preparing a new one. The tolerances are listed below:

Revolutions of rotor per second (R)	*Tolerance, in percent*
Less than 1.0	1.0
1.0 and greater	.5

Because of the rigid control in the manufacture of the Price meter, virtually identical meters are now being produced, and their rating equations tend to be identical. Therefore, the U.S. Geological Survey now feels no need to calibrate the meters individually. Instead, an average standard rating is established by calibrating a large number of meters that have been constructed to U.S. Geological Survey specifications, and that rating is then supplied with each meter. To insure that all meters are virtually identical, the dies and fixtures for the construction of Price meters are supplied to the manufacturer.

Price meters that have been first rated using a wading-rod suspension, and then rated using a cable suspension with U.S. Geological Survey Columbus-type weights and hangers, have not shown significant differences in rating. Therefore, no suspension coefficients are needed, and none should be used, if Columbus-type weights and hangers are properly used. Tests that compared meters were discussed on pages 89–90. In those tests Columbus-type weights were used with all meters. The close agreement of results for all meters indicate that no suspension coefficients are required when horizontal-axis current meters are used with Columbus-type weights.

The rating of the optical current meter is relatively simple. Its operation is based on precise mathematical principles, and, given an accurate tachometer, meter accuracy is dependent only on the configuration of the cam that oscillates the mirror. A master cam is used in

the manufacture of the individual meter cams. The meter is rated by observation of a long endless belt driven at constant speed. That known belt speed is checked against the speed computed by multiplying the height of the meter above the belt by the tachometer reading. If the comparison of known and computed speeds shows a lack of agreement, the tachometer scaling is changed to bring about agreement.

SOUNDING EQUIPMENT

Sounding (determination of depth) is usually done mechanically, the equipment used being dependent on the type of measurement being made. Depth and position in the vertical are measured by a rigid rod or by use of a sounding weight suspended from a cable. The cable length is controlled either by a reel or by a handline. A sonic sounder is also available, but it is usually used in conjunction with a reel and a sounding weight.

Sounding equipment used by the U.S. Geological Survey is described in the following categories: wading rods, sounding weights, sounding reels, handlines, and sonic sounder.

WADING RODS

The two types of wading rods commonly used are the top-setting rod and the round rod. The top-setting rod is preferred because of the convenience in setting the meter at the proper depth and because the hydrographer can keep his hands dry in the process. The round rod can be used in making ice measurements as well as wading measurements and has the advantage that it can be disassembled to 1-ft (0.3-m) lengths for storing and transporting.

The top-setting wading rod has a 1/2-in (12.7-mm) hexagonal main rod for measuring depth and a 3/8-in (9.5-mm) diameter round rod for setting the position of the current meter (fig. 52).

The rod is placed in the stream so the base plate rests on the streambed, and the depth of water is read on the graduated main rod. When the setting rod is adjusted to read the depth of water, the meter is positioned automatically for the 0.6-depth method. (See p. 134.) The 0.6-depth setting might also be described as the 0.4-depth position measured up from the streambed. When the depth of water is divided by 2 and this new value is set, the meter will be at the 0.2 depth position measured up from the streambed. When the depth of water is multiplied by 2 and this value is set, the meter will be at the 0.8-depth position measured up from the streambed. These two positions represent the conventional 0.2- and 0.8-depth positions. (See p. 134.)

The round wading rod consists of a base plate, lower section, three or four intermediate sections, sliding support, and a rod end (not essential). The parts are assembled as shown in figure 53. The meter

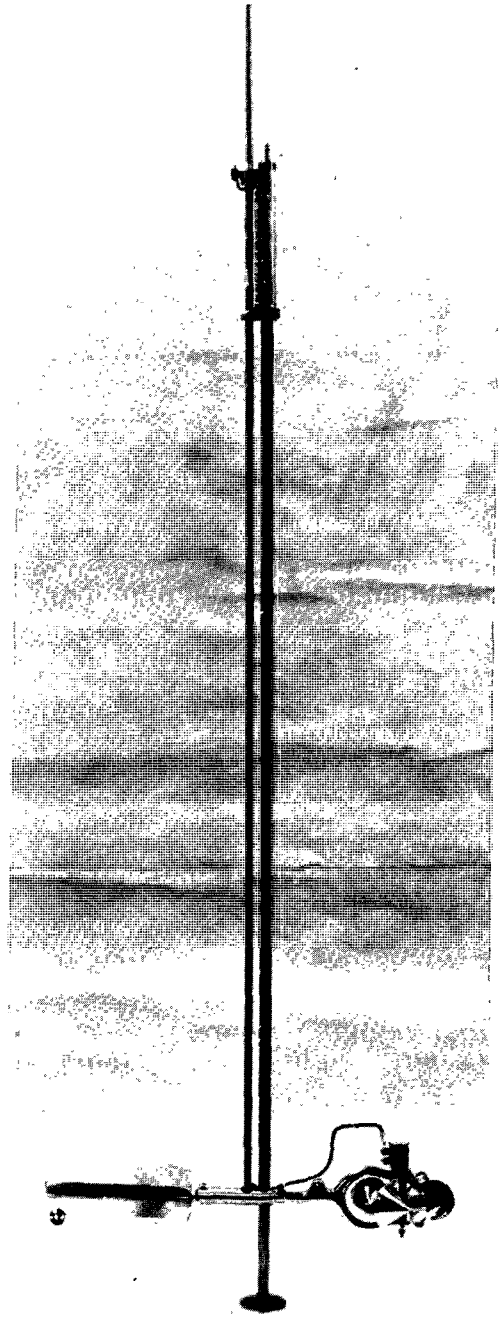

FIGURE 52.—Top-setting wading rod with meter attached.

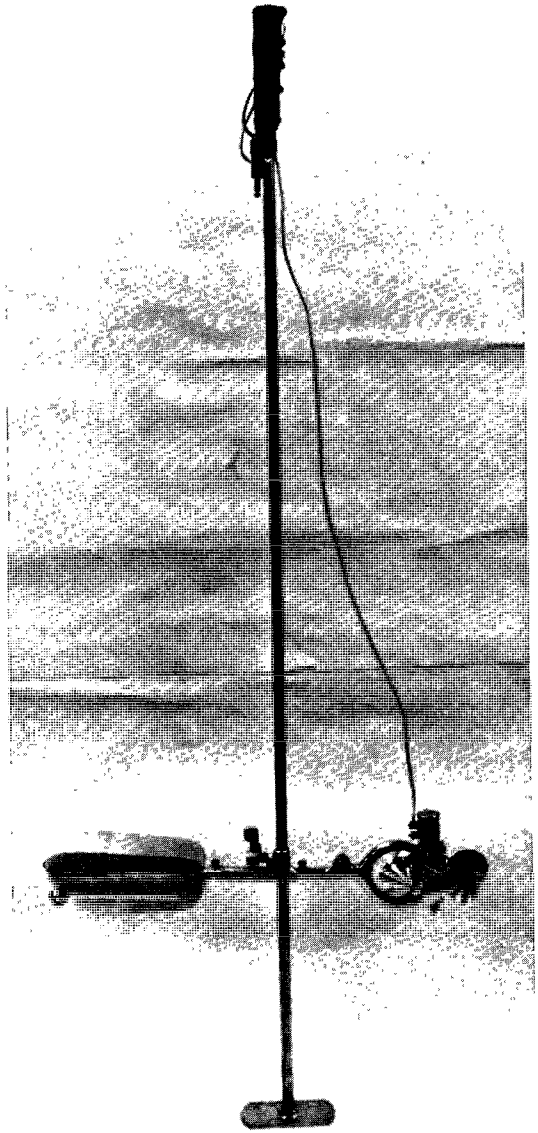

FIGURE 53.—Round wading rod with meter attached.

is mounted on the sliding support and is set at the desired position on the rod by sliding the support.

The round rod is also used in making ice measurements. Intermediate sections of the round rod are screwed together to make an ice

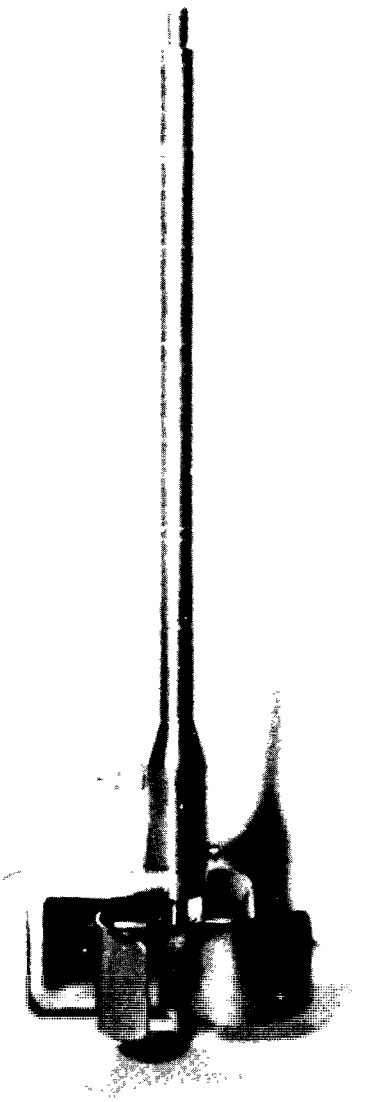

FIGURE 54.—Lower section of ice rod for use with vane ice meter.

rod of desired length (fig. 54). The most convenient length for an ice rod is about 3 ft (1 m) longer than the maximum depth of water to be found in a cross section. About 12 ft (4 m) is the maximum practical length for an ice rod; depths greater than 10 ft (3 m) are usually measured with a sounding weight and reel. The base plate, sliding support, and lower section are not used on an ice rod. Instead, a special lower section is screwed directly into the top of the contact chamber of the vane ice meter. (See fig. 54.) If a Price meter is used under ice cover, another special lower section is used to hold the meter by means of the hanger screw. (See fig. 55.) All lower sections for ice rods are now made so that the center of the vanes or cups is at the 0-ft point on the rod.

SOUNDING WEIGHTS AND ACCESSORIES

If a stream is too deep or too swift to wade, the current meter is suspended in the water by cable from a boat, bridge, or cableway. A sounding weight is suspended below the current meter to keep it

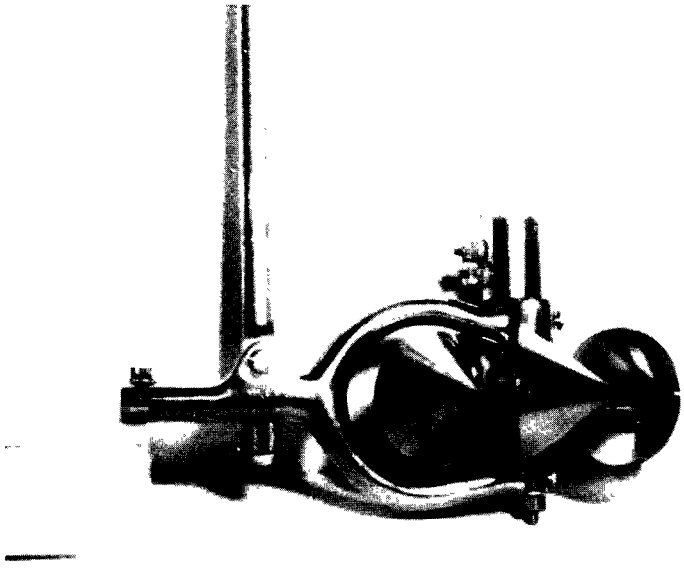

FIGURE 55.—Lower section of ice rod for use with Price meter.

stationary in the water. The weight also prevents damage to the meter when the assembly is lowered to the streambed.

The sounding weights now used in the U.S.A. are the Columbus weights, commonly called the C type. (See fig. 56.) The weights are streamlined to offer minimum resistance to flowing water. Each weight has a vertical slot and a drilled horizontal hole to accommodate a weight hanger and securing pin.

The weight hanger (fig. 57) is attached to the end of the sounding line by a connector. The current meter is attached beneath the connector, and the sounding weight is attached to the lower end of the hanger by means of the hanger pin.

In addition to the weights shown in figure 56, weights of 150, 200 and 300 lb (68, 91, and 136 kg) are used for measuring the discharge of deep, swift rivers. The sounding-weight hangers shown in figure 57 are designed to accommodate the weights of the various sizes. The height of the meter rotor above the bottom of the sounding weight must be considered in calculations to position the meter for velocity observations at various percentages of the stream depth.

SOUNDING REELS

A sounding reel has a drum for winding the sounding cable, a crank and ratchet assembly for raising and lowering the weight or holding it in any desired position, and a depth indicator. The U.S. Geological Survey has five types or sizes of sounding reel in common use, the choice of reel being dependent on the depth of water to be measured and on the weight required for sounding. The lightest of the reels, known as the Canfield reel (fig. 58), can be used with either single- or two-conductor cable; the other four reels use two-conductor cable, whose diameter ranges from 0.084 in to 0.125 in (2.13 to 3.18 mm),

FIGURE 56.—Columbus 15-, 30-, 50-, 75-, and 100-lb sounding weights.

depending on the weight to be handled. The three smaller reels have a hand crank for raising and lowering the meter and weight (fig. 58);

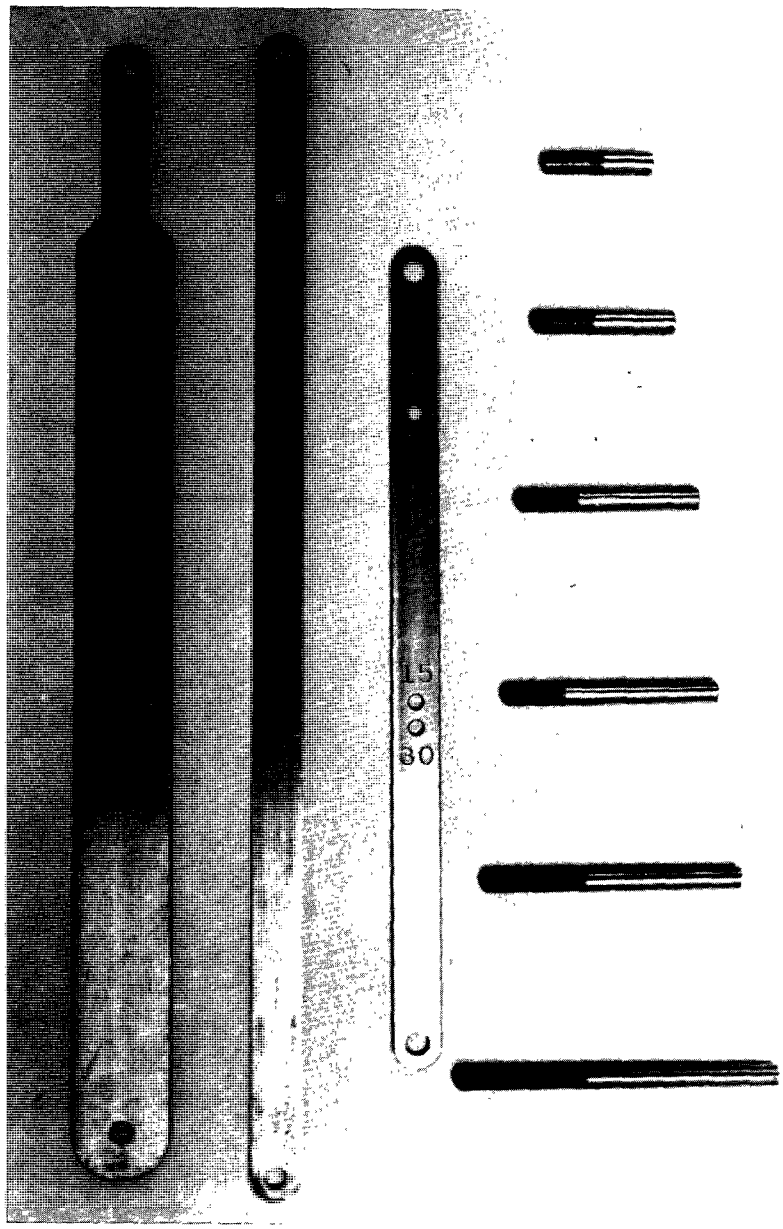

FIGURE 57.—Sounding-weight hangers and hanger pins.

the largest of the five reels is operated by a battery-powered unit but has a handcrank for emergency use; the second largest reel (fig. 59) may be operated either by a hand crank or a power unit. Specially designed connectors are used to join the end of the reel cable to the sounding-weight hanger.

The two smaller reels (Canfield and A-pack reels) are equipped with counters for indicating depth (fig. 58); the three larger reels are equipped with computing depth indicators (figs. 59 and 60). On the computing depth indicator, depth is indicated by a pointer. Tens of feet are read on a numbered dial through an aperture near the top of the main dial. The main dial also has a graduated spiral to indicate directly the 0.8-depth position (p. 134) for depths up to 30 ft (9.15 m).

HANDLINES

When discharge measurements that are to be made from a bridge require light sounding weights—15 or 30 lb (6.8 or 13.6 kg)—the weight and meter are often suspended on a handline (figs. 61 and 62). Handlines can also be used from cable cars, but they seldom are because a sounding reel mounted on the cable car is much more convenient to use.

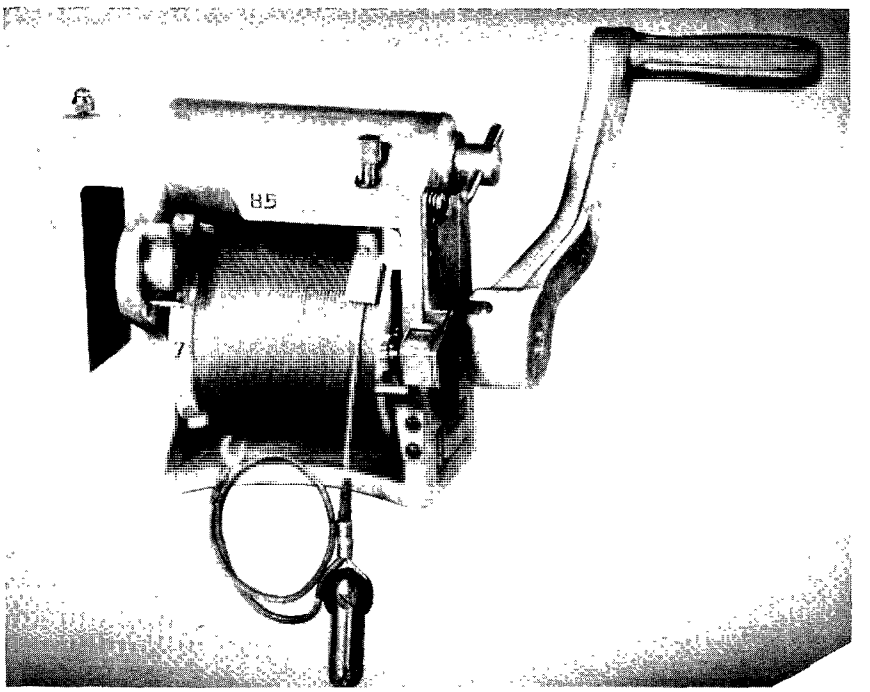

FIGURE 58.—Canfield reel.

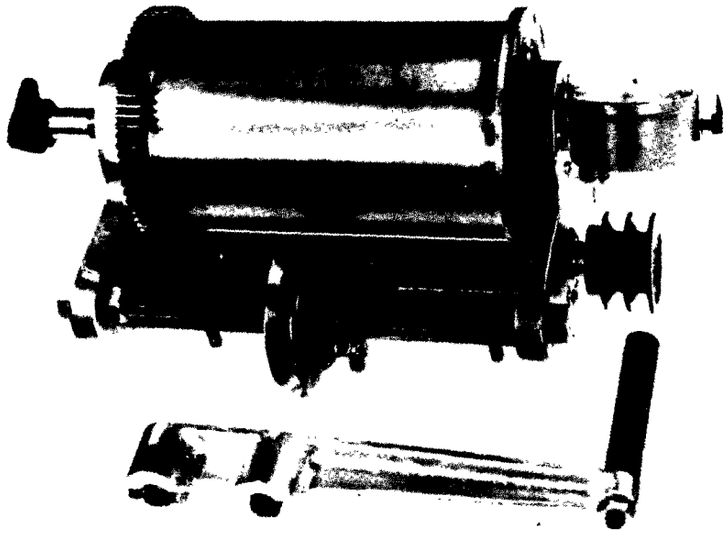

FIGURE 59.—B–56 reel.

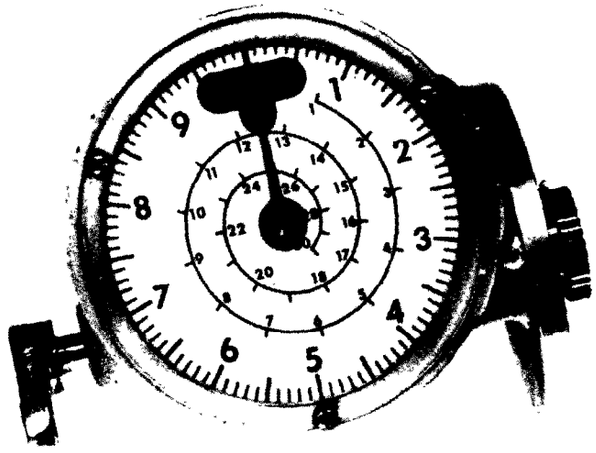

FIGURE 60.—Computing depth indicator.

The handline is made up of two separate cables that are electrically connected at a reel (fig. 63). The upper or hand cable is that part of the handline that is used above the water surface. It is a heavy-duty two-conductor electric cable, whose thick rubber protective covering makes the cable comfortable to handle. At its upper end is a connection for the headphone. The lower or sounding cable is a light reverse-lay steel cable with an insulated core. A connector joins the lower end of the sounding cable to the hanger that is used as a mount for the current meter and sounding weight. Sounding cable in excess of the length needed to sound the stream being measured is wound on

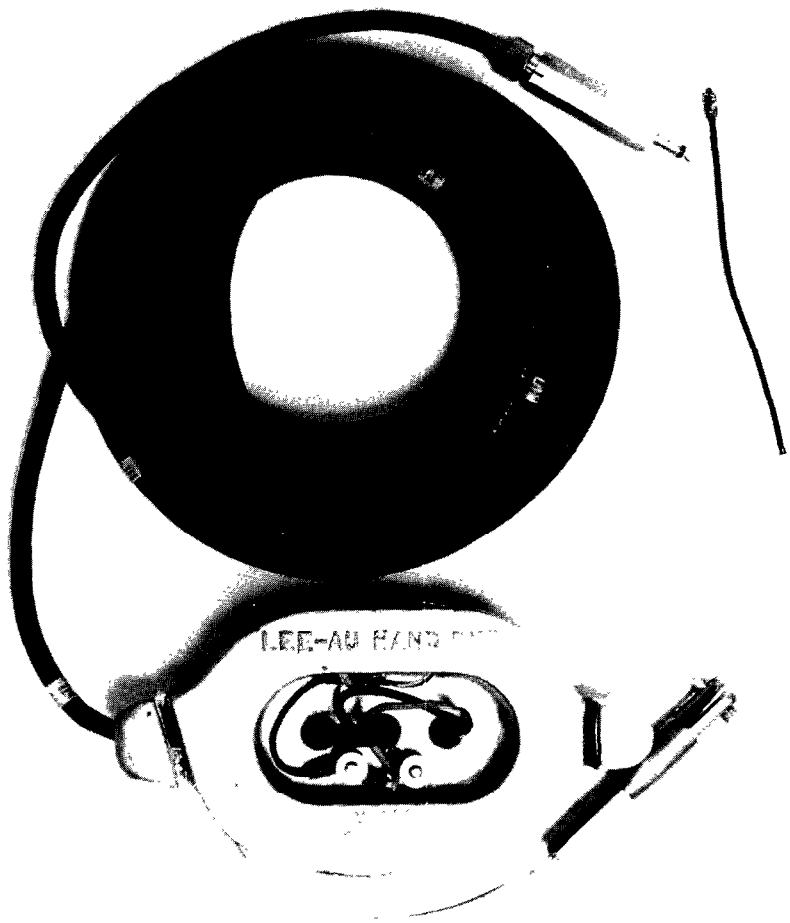

FIGURE 61.—Handline.

the reel. The sounding cable is tagged at convenient intervals with streamers of different colored binding tapes, each colored streamer being a known distance above the current-meter rotor. The use of these tags in determining depth is described on page 150.

The advantages of the handline are ease in assembling the equipment for a discharge measurement and relative ease in making discharge measurements from certain types of bridges, particularly truss bridges that do not have cantilevered sidewalks. The disadvantages of the handline are a lesser degree of accuracy in depth determination than that obtained with a sounding reel, more physical exertion is required in making the discharge measurement, and the handline can seldom be used for high-water measurements of large

FIGURE 62.—Handline in use from a bridge.

streams because of the heavy sounding weights needed for such measurements.

SONIC SOUNDER

A commercial, compact, portable sonic sounder has been adopted by the U.S. Geological Survey to measure stream depth. (See figs. 64 and 65.)

The sounder is powered by either a 6- or 12-volt storage battery and will operate continuously for 10 hr on a single battery charge. Three recording speeds are available, 36, 90, or 180 in (0.91, 2.29,4.57 m) per hr. Four operating ranges, 0–60, 60–120, 120–180, and 180–240 ft (0–18.3, 18.3–36.6, 36.6–54.9, and 54.9–73.2 m) allow intervals of 60 ft (18.3 m) of depth to be recorded. The sounder is portable, weighing only 46 lb (20.9 kg). The transducer has a narrow beam angle of 6° which minimizes errors on inclined streambeds and allows the hydrographer to work close to piers or other obstructions.

In swift debris-laden streams measurements can be made with this equipment without lowering the meter and weight to the streambed. As soon as the weight is in the water, the depth will be recorded. The meter can then be set at the 0.2 depth or just below the water surface for a velocity observation. The observed velocity can be converted to mean velocity in the vertical by applying an appropriate coefficient. (See p. 135–137.)

FIGURE 63.—Handline reels; Lee-Au (top) and Morgan (bottom).

Temperature change affects the sound-propagation velocity, but error from that source is limited to about ±2 percent in fresh water. That error can be eliminated completely by adjusting the sounder to

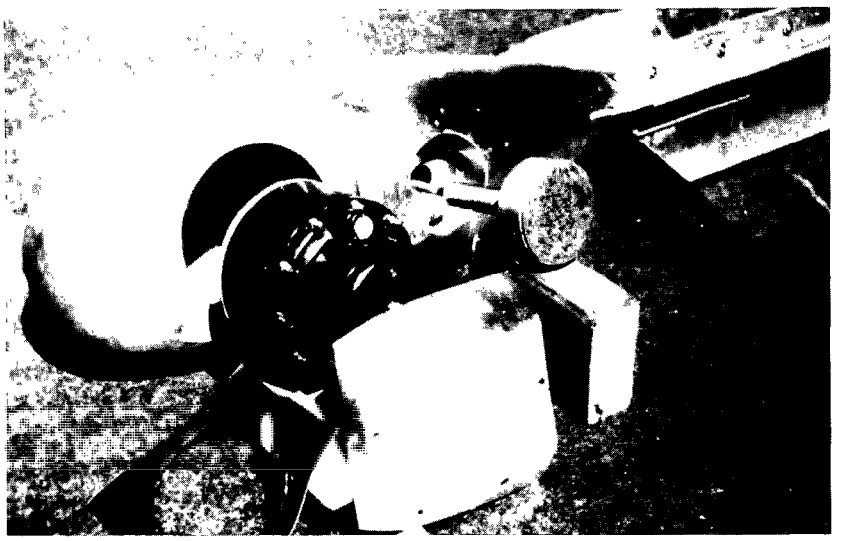

FIGURE 64.—Sounding weight with compass and sonic transducer ready for assembly.

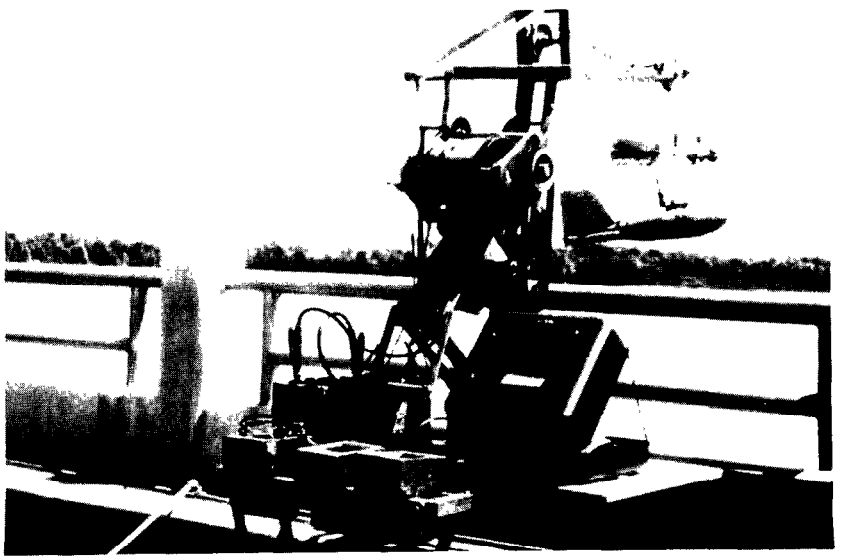

FIGURE 65.—Sonic measuring assembly.

read correctly at an appropriate average depth determined by other means.

WIDTH-MEASURING EQUIPMENT

The distance to any point in a cross section is measured from an initial point on the bank. Cableways and bridges used regularly for making discharge measurements are commonly marked at 2-, 5-, 10-, or 20-ft (0.61-, 1.52-, 3.05-, or 6.10-m) intervals by paint marks. Distance between markings is estimated, or measured with a rule or pocket tape.

For measurements made by wading, from boats, or from unmarked bridges, steel or metallic tapes or tag lines are used. Tag lines are made of 1/32-, 1/16-, 3/32-, or 1/8-in (0.79-, 1.59-, 2.38-, or 3.18-mm)-diameter galvanized steel aircraft cord having solder beads at measured intervals to indicate distances. The standard arrangement of solder beads or tags used by the U.S. Geological Survey is as follows:

one tag every 2 ft for the first 50 ft of tag line;
one tag every 5 ft for stations between 50 and 150 ft on the tag line;
one tag every 10 ft for stations between 150 ft and the end of the tag line.

For identifying the stationing of the tags, an additional tag (total of two tags) is used at stations 0, 10, 20, 30, 40, 50, 150, 250, 350, and 450 ft. Two additional tags (total of three tags) are used at stations 100, 200, 300, 400, and 500 ft.

The standard lengths of tag line are 300, 400 and 500 ft (91.4, 122, and 152m), but other sizes are available.

Three types of tag-line reels in use are Lee-Au, Pakron, and Columbus type A (fig. 66). Larger reels designed particularly for use with boats are described on page 120. It is practically impossible to string a tag line for discharge measurements from a boat when the width of the stream is greater than 2,500 ft (750 m). The methods used to determine width at such sites are described on pages 156–157.

EQUIPMENT ASSEMBLIES

Special equipment is necessary for each type of current-meter measurement. The meters, weights, and reels used have already been described. The additional equipment needed is described in this section.

The special equipment assemblies have been divided into five basic groups: cableway, bridge, boat, ice, and velocity-azimuth-depth assembly (VADA) equipment.

CABLEWAY EQUIPMENT

The cableway provides a track for the operation of a cable car from which the hydrographer makes a current-meter measurement. Cable

cars also support the sounding reel and other necessary equipment. Both sitdown and standup types of cable cars are used in stream gaging. (See figs. 67 and 68). Pierce (1947) describes plans for both types. Normally, sitdown cars are used for cableway spans less than 400 ft (122 m) and for those spans where the lighter sounding weights are used. The standup car is used on the longer spans and where heavy sounding weights are needed.

The cars are moved from one point to another on the cableway by means of cable-car pullers. (See fig. 69.) The standard car puller is a cast aluminum piece with a snub attached to act as a brake. The snub, usually four-ply belting, is placed between one of the car sheaves and the cable to prevent movement of the car along the cable. A second-type puller is used when a car is equipped with a follower brake (fig. 69). A third type, the Colorado River cable-car puller, is the same in principle as the puller used on cars equipped with a follower brake.

Power-operated cable cars are available for extremely long spans or other special situations. (See fig. 70.)

Sitdown cable cars have a variety of means of supporting the sounding reel. A-pack and Canfield reels are designed to clamp on the side of the car (fig. 71). Permanent or portable reel seats are attached to the cable cars for larger reels. (See figs. 67 and 72.)

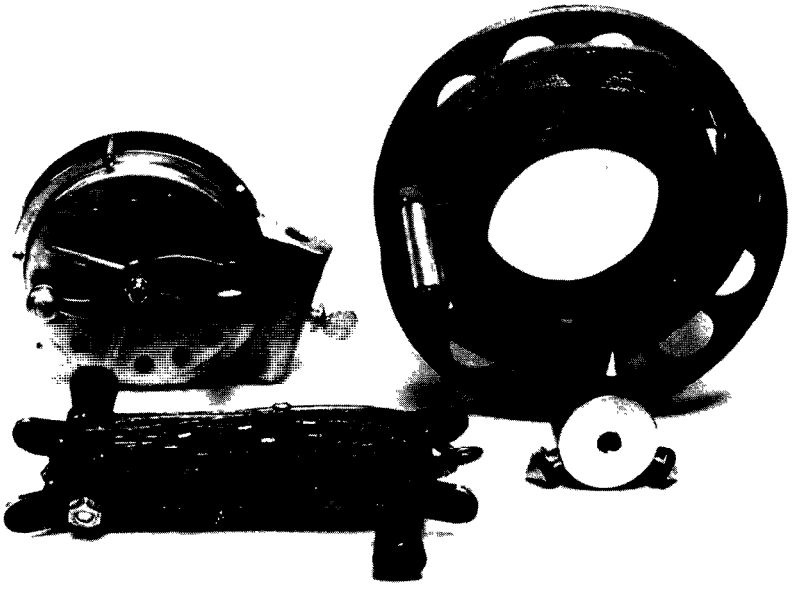

FIGURE 66 —Tag-line reels: top left, Pakron; top right, Lee-Au with removable hub in front; bottom, Columbus type A.

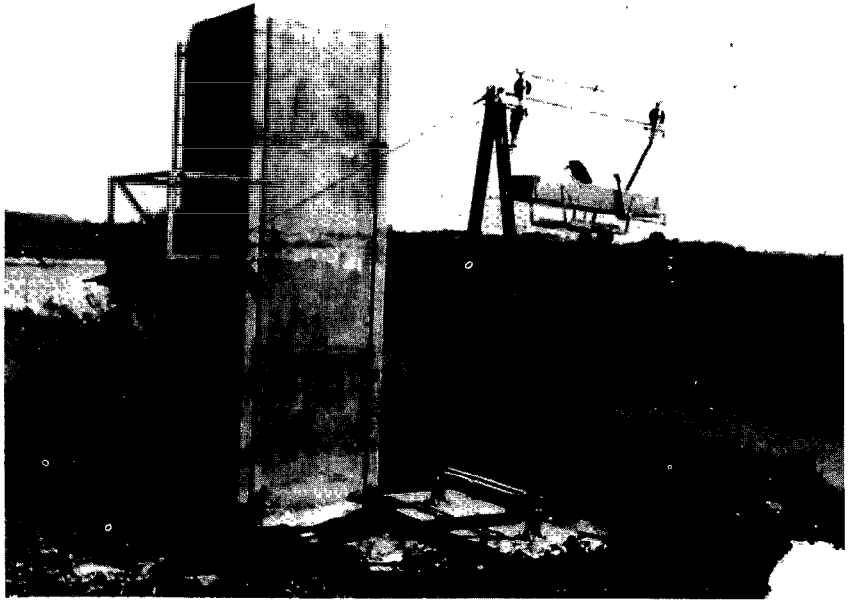

FIGURE 67.—Sitdown cable car.

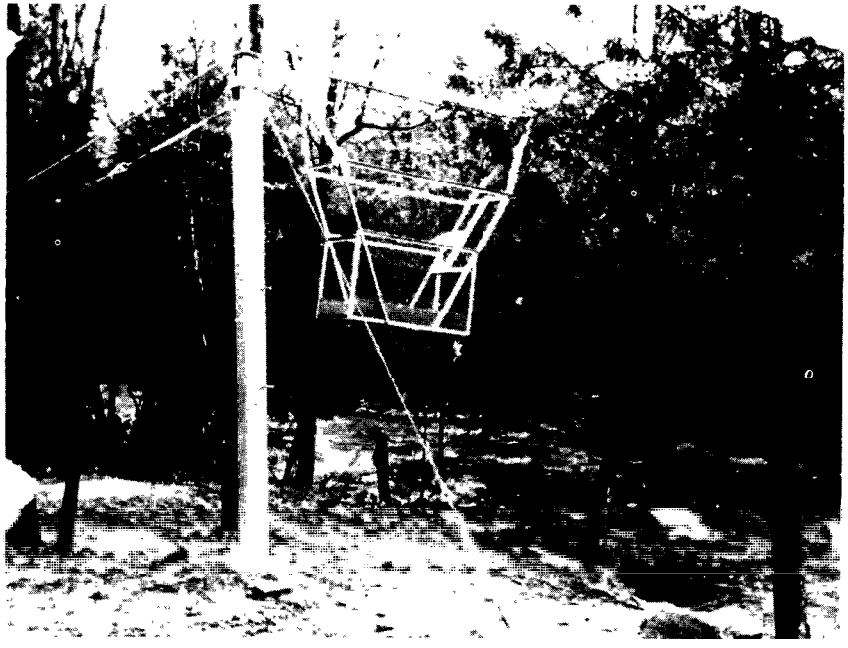

FIGURE 68.—Standup cable car.

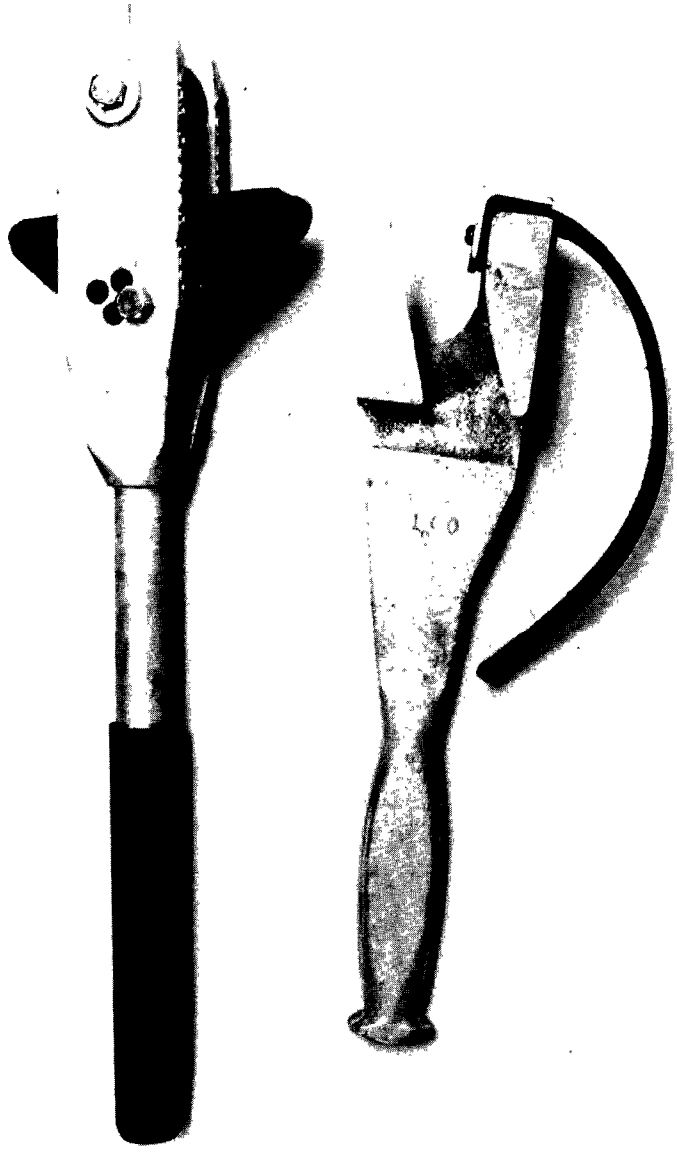

FIGURE 69.—Cable-car puller for follower-brake cable cars, left; for standard cars, right.

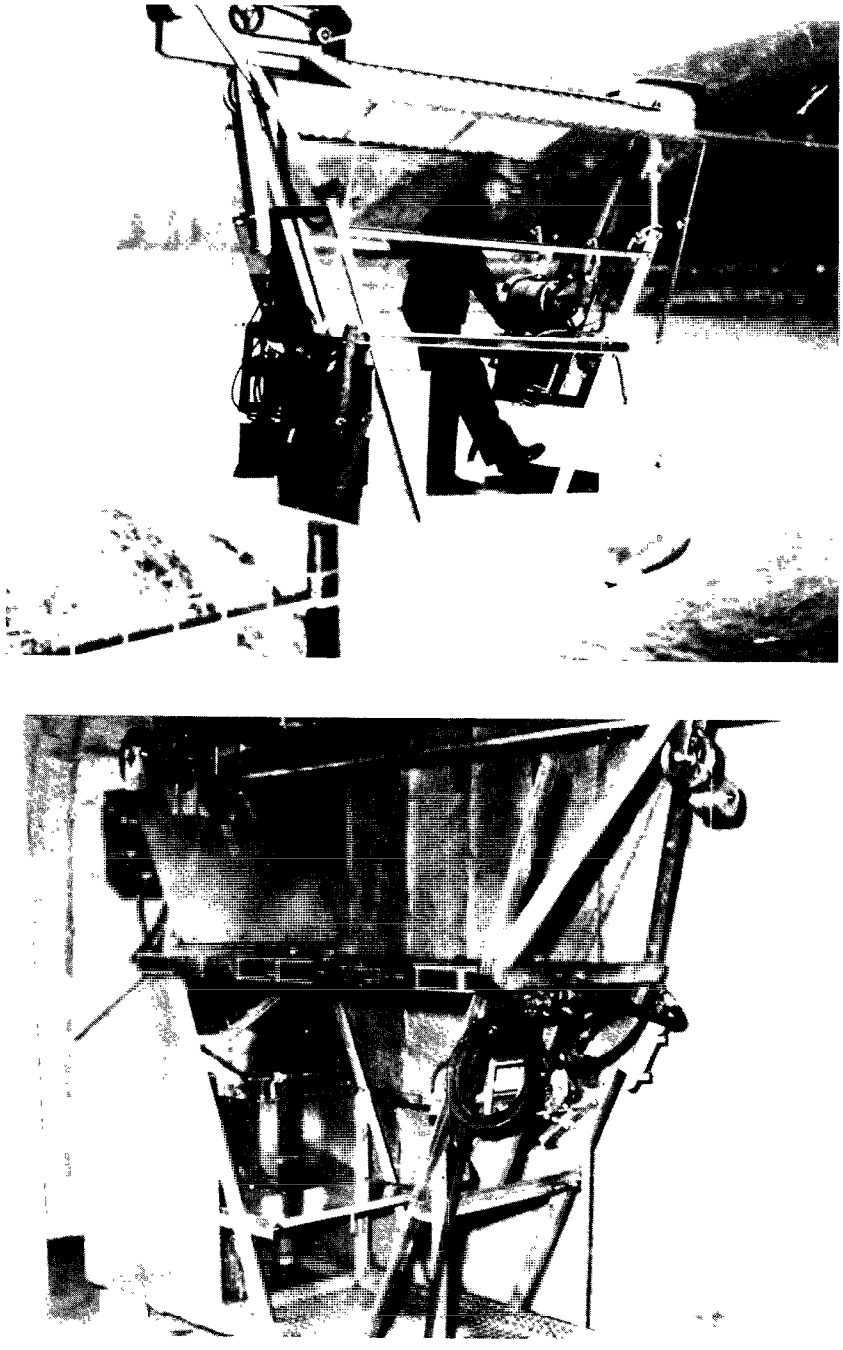

FIGURE 70.—Power-operated cable cars. (*A*) battery-powered car; (*B*) gasoline-powered car.

Standup cable cars have reel seats attached to the structural members of the car (fig. 68). A sheave attached to the structural members carries the sounding line so that the sounding weight and current meter will clear the bottom of the car. Power reels can also be used on standup cable cars.

Carrier cableways are sometimes used on the smaller streams for measuring discharge as well as for sediment sampling. They are used in areas where it is impossible to wade, where no bridges are avail-

FIGURE 71.—Sitdown cable car with Canfield reel clamped to side of car.

able, and where it has been impractical to build a complete cableway. The assembly is operated from the shore (fig. 73). Carrier cables are

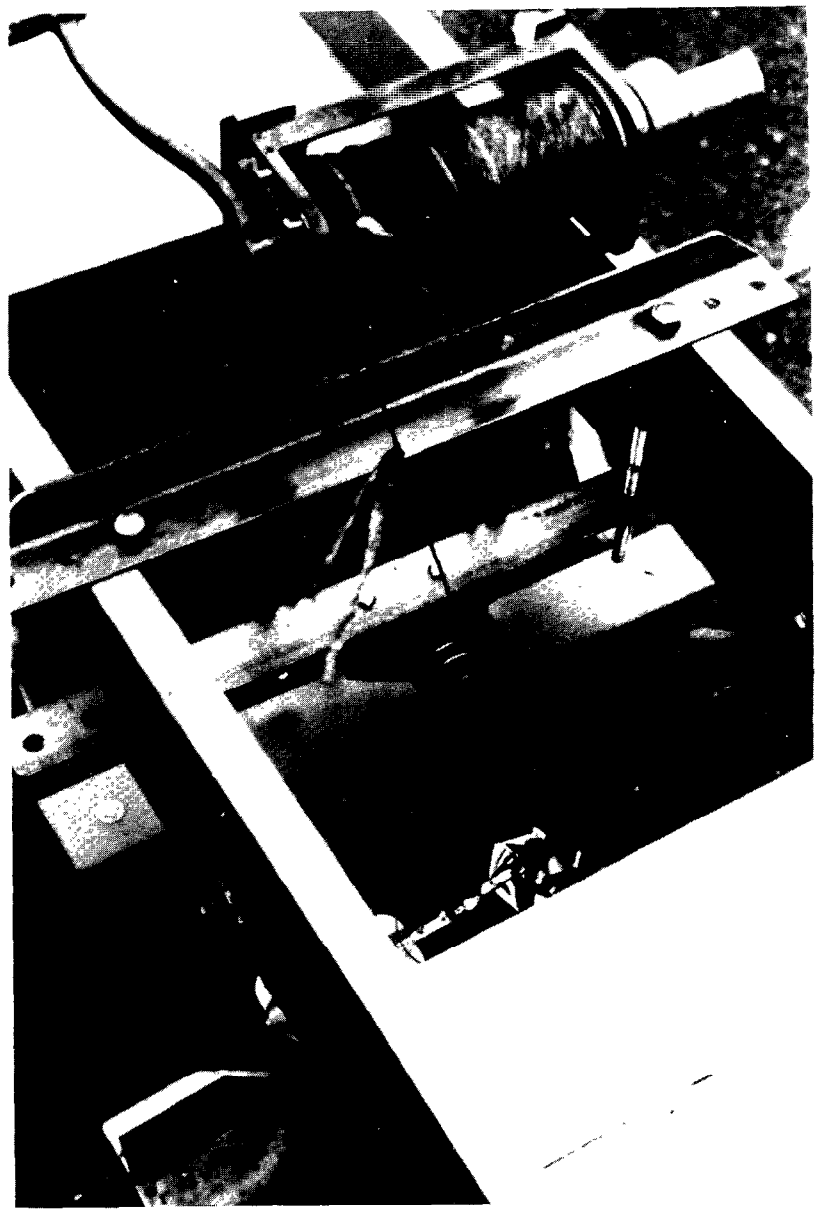

FIGURE 72.—Portable reel seat on sitdown-type cable car. (Note tags on sounding cable.)

more widely used in Europe, particularly in the United Kingdom, than they are in the U.S.A.

BRIDGE EQUIPMENT

When one measures from a bridge, the meter and sounding weight can be supported by a handline, or by a sounding reel mounted on a crane, or by a bridge board. The handline has been described on pages 104–108.

Two types of hand-operated portable cranes are the type A (figs. 74 and 75) for use with weights up to 100 lb (45.4 kg) and the type E for heavier weights.

All cranes are designed so that the superstructure can be tilted

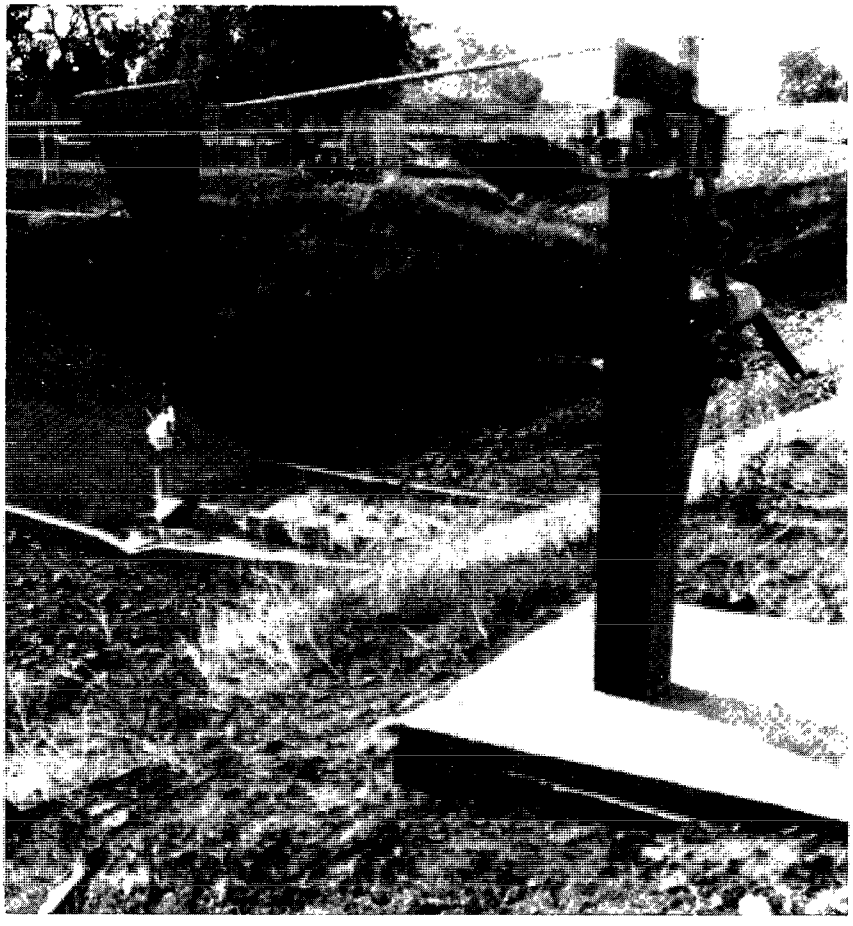

FIGURE 73.—Carrier (bank-operated) cableway. Two reels are used; one moves the meter assembly laterally, and the other moves the current meter vertically.

forward over the bridge rail far enough for the meter and weight to clear most rails. Where bridge members obstruct the movement of the crane from one vertical to the next, the weight and meter can be brought up, and the superstructure can be tilted back to pass by the obstruction. (See figs. 74 and 75.)

Cast-iron counterweights weighing 60 lb (27.2 kg) each are used with four-wheel-base cranes. (See fig. 75.) The number of such weights needed depends upon the size of the sounding weight being supported, the depth and velocity of the stream, and the amount of debris being carried by the stream.

A protractor is used on cranes to measure the angle the sounding line makes with the vertical when the weight and meter are dragged downstream by the water. The protractor is a graduated circle clamped to an aluminum plate. A plastic tube, partly filled with colored antifreeze, fitted in a groove between the graduated circle and

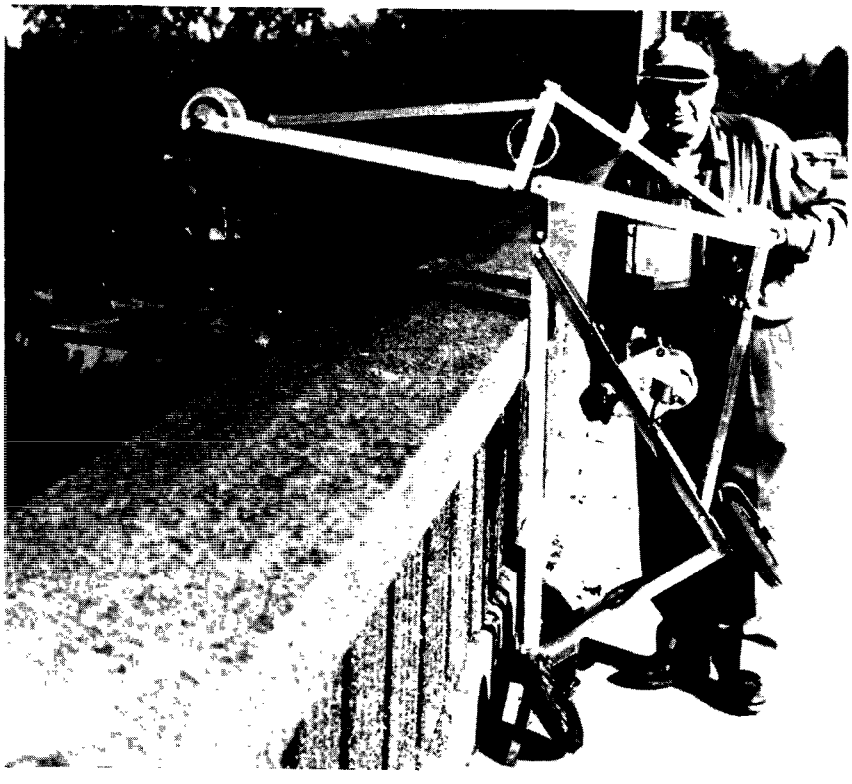

FIGURE 74.—Type-A crane with three-wheel base. (During soundings and velocity observations the crane is tilted against the bridge rail. An A–55 reel is mounted on the crane.)

the plate, is the protractor index. A stainless-steel rod is attached to the lower end of the plate to ride against the downstream side of the sounding cable. The protractor will measure vertical angles from −25° to +90°. The cranes in figures 74 and 75 are equipped with protractors at the outer end of the boom.

Bridge boards may be used with an A-pack or A-55 sounding reel and with weights up to 50 lb (22.7 kg). A bridge board is usually a plank about 6 to 8 ft (1.8 to 2.4 m) long with a sheave at one end over which the meter cable passes and a reel seat near the other end. The board is placed on the bridge rail so that the force exerted by the sounding weight suspended from the reel cable is counterbalanced by the weight of the sounding reel (fig. 76). The bridge board may be hinged near the middle to allow one end to be placed on the sidewalk or roadway.

Many special arrangements for measuring from bridges have been

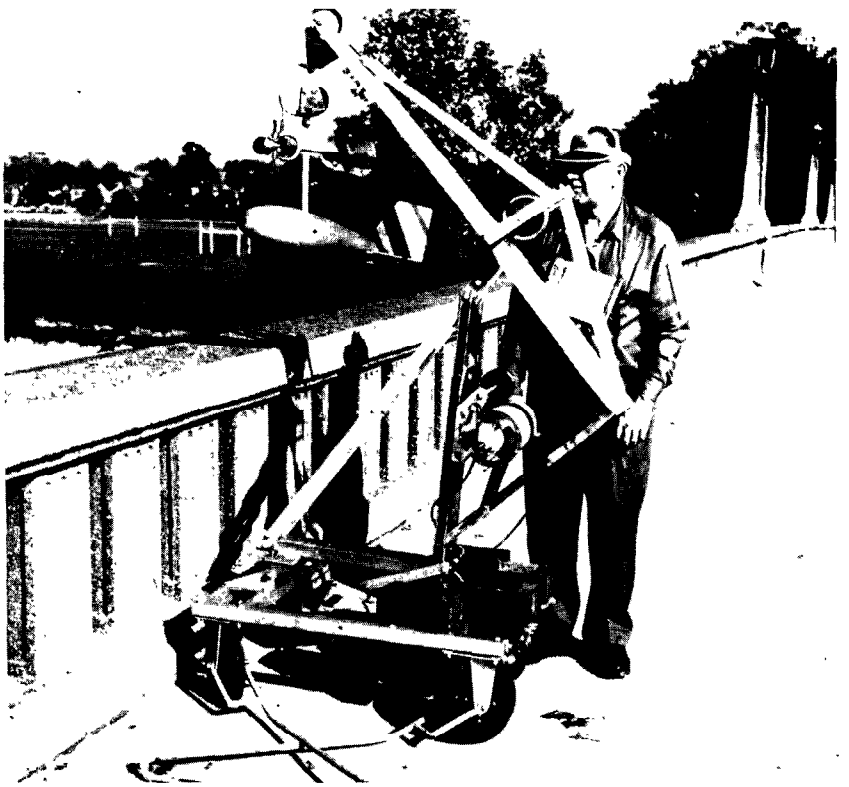

FIGURE 75.—Type-A crane with four-wheel base with boom in retracted position. (A B–56 reel is mounted on crane. Note fluid protractor on outer end of boom.)

devised to suit particular purposes. Truck-mounted cranes are often used for measuring from bridges over the larger rivers. (See fig. 77.) Monorail stream-gaging cars have been developed for large rivers. The car is suspended from the substructure of the bridge by means of an I-beam. The car is attached to the I-beam track by trolleys and is propelled by a forklift motor having a wheel in contact with the bottom of the beam. The drive mechanism and sounding equipment are powered by a 430-ampere-hour, 450-lb (204-kg), 12-volt battery.

BOAT EQUIPMENT

Measurements made from boats require special equipment not used for other types of measurement. Extra-large tag-line reels are used on wide streams. Three different tag-line reels are used by the U.S. Geological Survey for boat measurements:

1. A heavy duty horizontal-axis reel without a brake and with a capacity of 2,000 ft (610 m) of ⅛-in (3.18-mm)-diameter cable (fig. 78).

FIGURE 76.—Bridge board in use.

2. A heavy-duty horizontal-axis reel with a brake and with a capacity of 3,000 ft (914 m) of ⅛-in-diameter cable (fig. 79).
3. A vertical-axis reel without a brake and with a capacity of 800 ft (244 m) of ⅛-in-diameter cable (fig. 80).

A utility line of 30 ft (9 m) of 3/32-in (2.38-mm)-diameter cable with a harness snap at one end and a pelican hook at the other is connected to the free end of the boat tag line and fastened around a tree or post, thereby preventing damage to the tag line. After the tag line is strung across the stream, the reel is usually bolted to a plank and chained to a tree. The tag line has station markers at appropriate intervals.

Special equipment is necessary to suspend the meter from the boat when the depths are such that a rod suspension cannot be used. A crosspiece reaching across the boat is clamped to the sides of the boat and a boom attached to the center of the cross piece extends out over the bow. (See fig. 81.) The crosspiece is equipped with a guide sheave and clamp arrangement at each end to attach the boat to the tag line and make it possible to slide the boat along the tag line from one station to the next. A small rope can be attached to these clamps so

FIGURE 77.—Truck-mounted crane used on the Mississippi River.

that in an emergency a tug on the rope will release the boat from the tag line. The crosspiece also has a clamp that prevents lateral movement of the boat along the tag line when readings are being made. The boom consists of two structural aluminum channels, one telescoped within the other to permit adjustments in length. The boom is equipped with a reel plate on one end; on the other end is a sheave over which the meter cable passes. The sheave end of the boom is designed so that by adding a cable clip to the sounding cable, a short distance above the connector, the sheave end of the boom can be retracted when the meter is to be raised out of the water. The raised

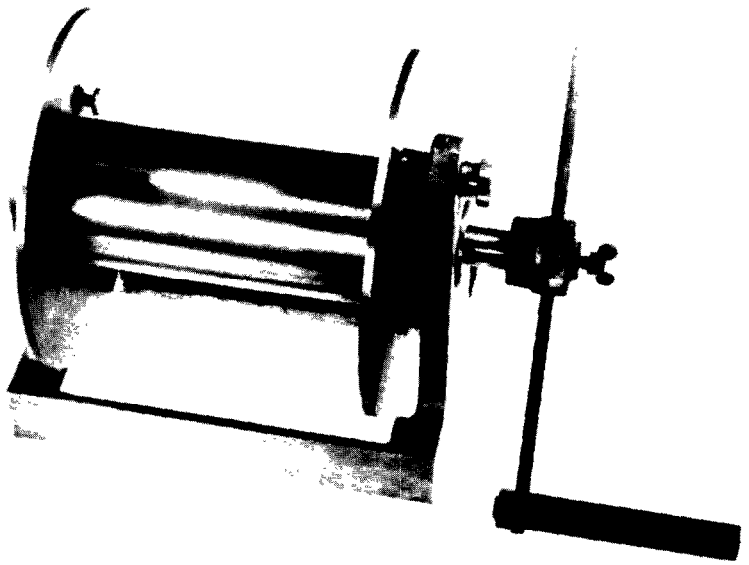

FIGURE 78.—Horizontal-axis boat tag-line reel without a brake.

meter is easy to clean and is in a convenient position when not being operated.

All sounding reels fit the boat boom except the A-pack and the Canfield reels, which can be made to fit by drilling additional holes in the reel plate on the boom.

In addition to the equipment already mentioned, the following items are needed when making boat measurements:

1. A stable boat big enough to support the hydrographers and equipment.
2. A motor that can move the boat with ease against the maximum current in the stream.
3. A pair of oars for standby use.
4. A life preserver for each hydrographer.
5. A bailing device.

Figure 82 shows the equipment assembled in a boat.

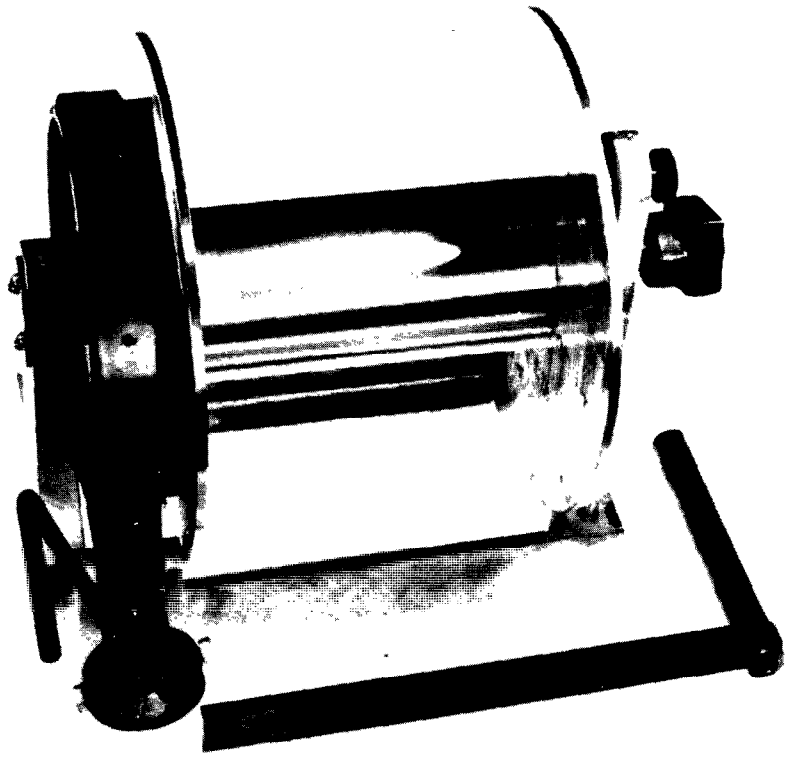

FIGURE 79.—Horizontal-axis boat tag-line reel with a brake.

ICE EQUIPMENT

Current-meter measurements made under ice cover require special equipment for cutting holes in the ice through which to suspend the meter.

Cutting holes through the ice on streams to make discharge measurements has long been a laborious and time-consuming job. The development of power ice drills, however, has eliminated many of the difficulties and has reduced considerably the time required to cut the holes. Holes are often cut with a commercial ice drill that cuts a 6-in (0.15-m) diameter hole (fig. 83). The drill weighs about 30 lb (13.6

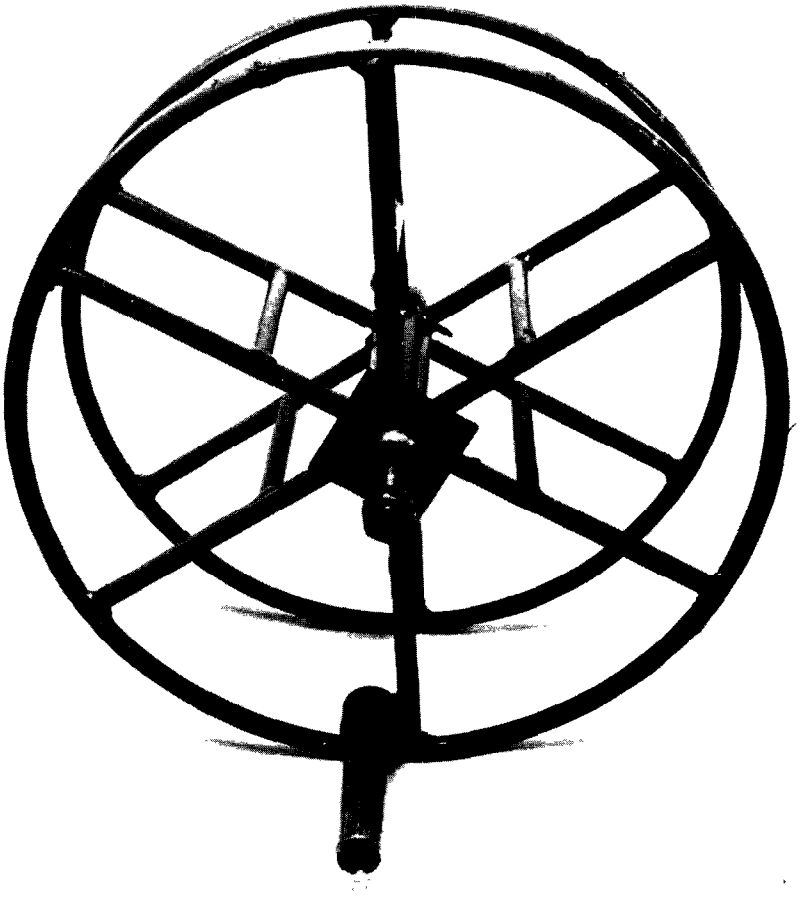

FIGURE 80.—Vertical-axis boat tag-line reel (when in use the axis of the reel is vertical).

kg) and under good conditions will cut through 2 ft (0.6 m) of ice in about a minute.

Where it is impractical to use the ice drill, ice chisels are used to cut the holes. Ice chisels used are usually 4 or 4½ ft (about 1.3 m) long and weigh about 12 lb (5.5 kg). The ice chisel is used when first crossing an ice-covered stream to determine whether the ice is strong enough to support the hydrographer. If a solid blow of the chisel blade does not penetrate the ice, it is safe to walk on the ice, providing the ice is in contact with the water.

Some hydrographers supplement the ice chisel with a Swedish ice auger. The cutting blade of this auger is a spadelike tool of hardened steel that cuts a hole 6–8 in (0.15–0.20 m) in diameter. The auger is operated by turning a bracelike arrangement on top of the shaft.

When holes are cut in the ice the water, which is usually under pressure because of the weight of the ice, rises in the hole. To determine the effective depth of the stream (p. 153–154), ice-measuring sticks are used to measure the distance from the water surface to the

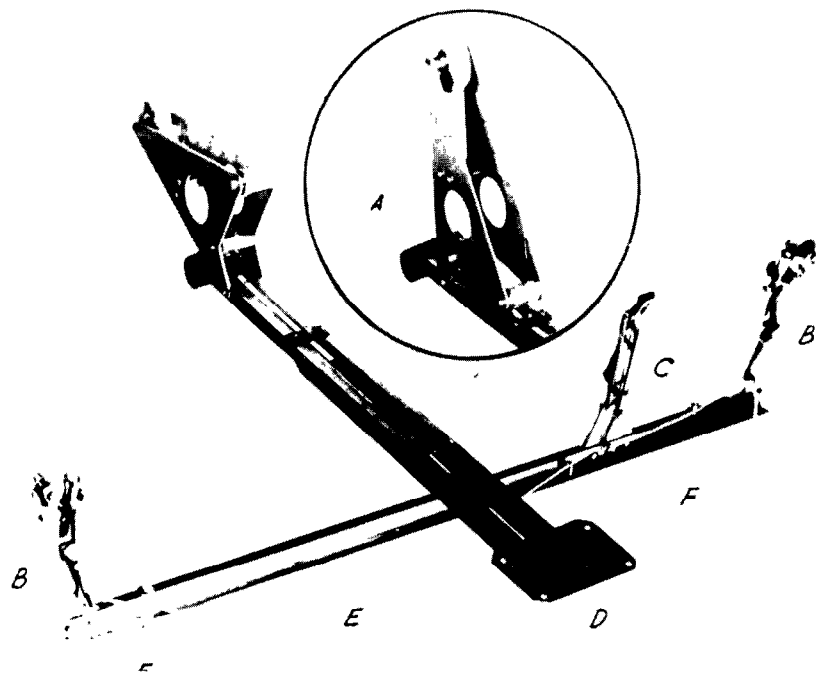

FIGURE 81.—Boom and crosspiece for use on boats. (*A*, retractable end of boom; *B*, guide sheave and clamp for attaching to tag line; *C*, clamp to prevent movement of the boat along the tag line; *D*, plate to accomodate reel; *E*, rope to release clamps (*B*) to free boat from tag line; and *F*, clamps to attach crosspiece to boat.)

bottom of the ice. This is done with a bar about 4 ft long (1.2 m), made of strap steel or wood, which is graduated in feet and tenths of a foot and has an L-shaped projection at the lower end. The horizontal part of the L is held on the underside of the ice, and the depth to that point

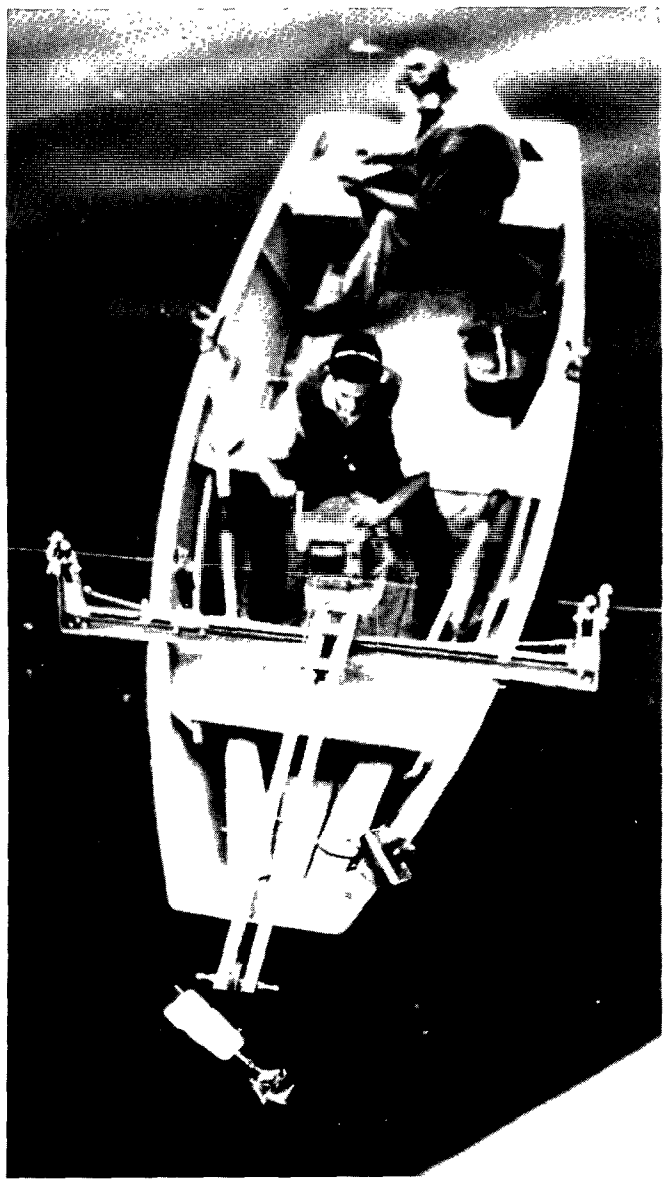

FIGURE 82.—Measuring equipment set up in a boat.

is read at the water surface on the graduated part of the stick. The horizontal part of the L is at least 4 in (0.1 m) long so that it may

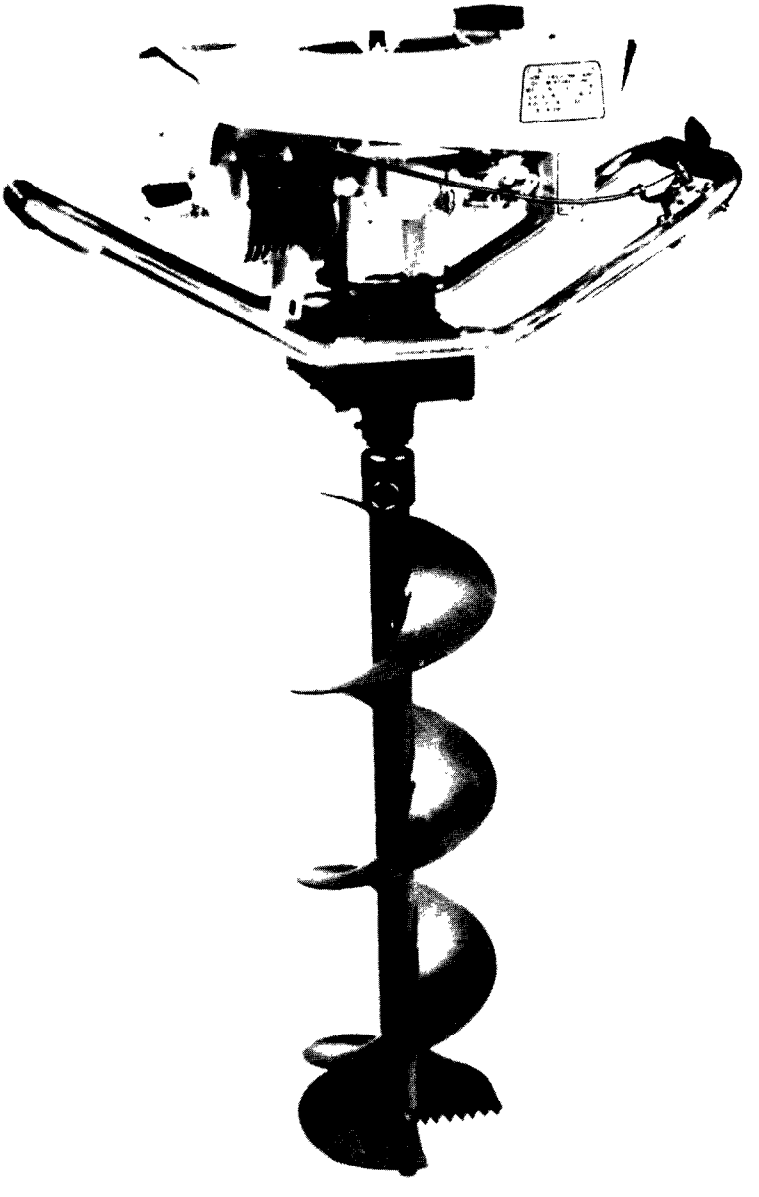

FIGURE 83.—Gasoline-powered ice drill. (Photograph by permission of General Equipment Co.)

extend beyond any irregularities on the underside of the ice.

When the total depth of water under ice cover is greater than 10 or 12 ft (3.0 or 3.6 m), a sounding reel or handline is usually used. The sounding reel is mounted on a collapsible support set on runners. (See fig. 84.)

A special ice-weight assembly is used for sounding under ice be-

FIGURE 84.—Collapsible reel support and ice-weight assembly.

cause a regular sounding weight will not fit through the hole cut by the ice drill (fig. 84). The weights and meter are placed in a framework that will pass through the drilled hole.

VELOCITY-AZIMUTH-DEPTH ASSEMBLY

The velocity-azimuth-depth assembly, commonly called VADA, combines a sonic sounder with a remote-indicating compass and Price current meter to record depth, indicate the direction of flow, and permit observations of velocity at any point.

In figure 85, the azimuth-indicating unit is shown mounted on a four-wheel crane. Incorporated within the remote-indicator box is the battery for the current-meter circuit, the headphone jacks, and the two-conductor jack for the sonic sounder. A switch allows the remote-indicating unit to be used separately or in conjunction with the sonic sounder. The sonic sounder is described on page 108. This assembly is useful in tidal investigations and in other special studies, as well as at regular gaging stations, where it is desirable to determine the

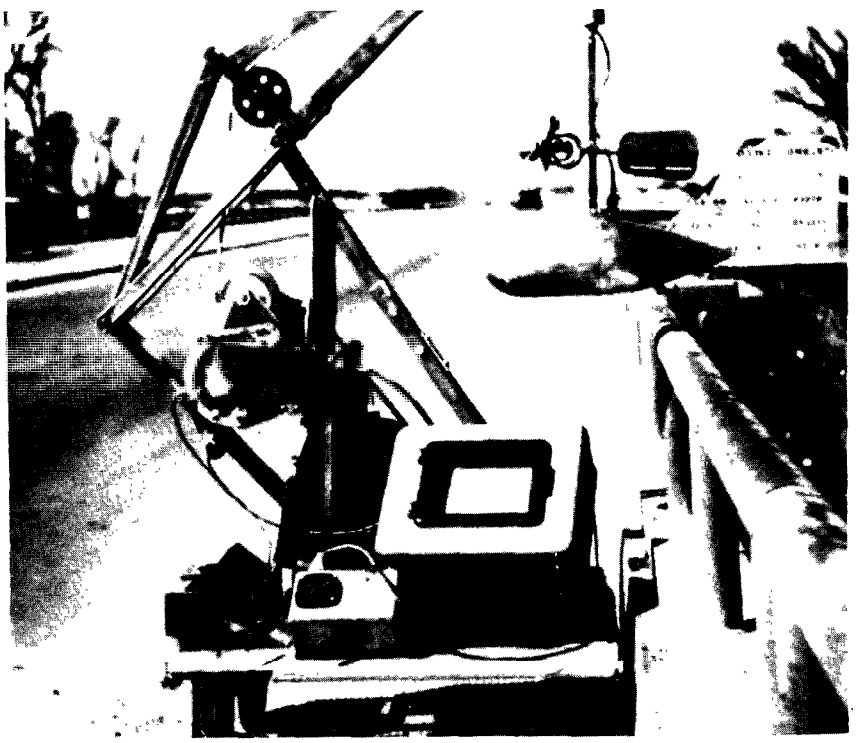

FIGURE 85.—Velocity-azimuth-depth assembly.

direction of flow beneath the water surface, because of the possibility that it may differ from that at the surface.

MISCELLANEOUS EQUIPMENT

Several miscellaneous items that have not been described are necessary when current-meter measurements are made. Three classifications of this equipment are timers, counting equipment, and waders and boots.

In order to determine the velocity at a point with a current meter, it is necessary to count the revolutions of the rotor in a measured interval of time, usually 40–70 s. The velocity is then obtained from the meter-rating table (fig. 51). The time interval is measured to the nearest second with a stopwatch.

The revolutions of the meter rotor during the observation of velocity are counted by an electric circuit that is closed each time the contact wire touches the single or penta eccentric of the current meter. A battery and headphone are part of the electrical circuit, and a click is heard in the headphone each time the contact wire touches. (See fig. 86.) Compact, comfortable hearing-aid phones have been adapted by some to replace the headphones.

A magnetic-switch contact chamber has been developed to replace the contact-wire chamber (p. 87). An automatic electric counter has also been developed for use with the magnetic contact chamber (fig. 86). The counter can register up to 999 and has a reset button. A metal clip is attached to the counter so that it may be easily carried on the hydrographer's belt. The electric counter should not be used with the contact-wire chamber, because at low velocities the contact wire wipes irregularly thereby sending several signals to the counter for each revolution.

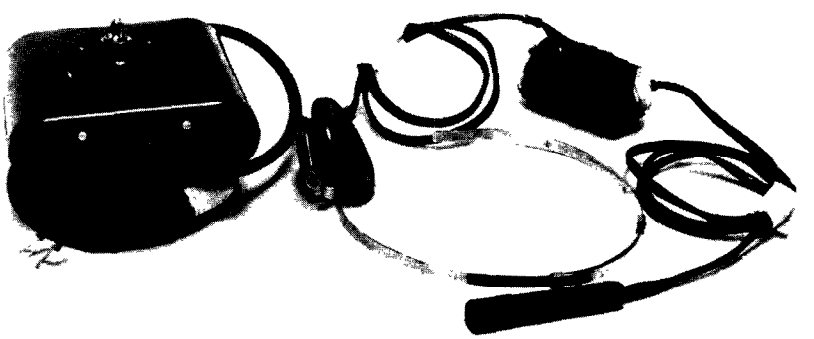

FIGURE 86.—Automatic counter (left) and headphone (right).

Waders or boots are needed when wading measurements are made. Waders should be loose fitting even after allowance has been made for heavy winter clothing. Ice creepers strapped on the shoe of boots or waders should be used on steep or icy streambanks and on rocky or smooth and slippery streambeds. (See fig. 87.)

MEASUREMENT OF VELOCITY

The current meter measures velocity at a point. The method of making discharge measurements at a cross section requires determination of the mean velocity in each of the selected verticals. The mean velocity in a vertical is obtained from velocity observations at many points in that vertical, but it can be approximated by making a few velocity observations and using a known relation between those velocities and the mean in the vertical. The more commonly used methods of determining mean vertical velocity are:

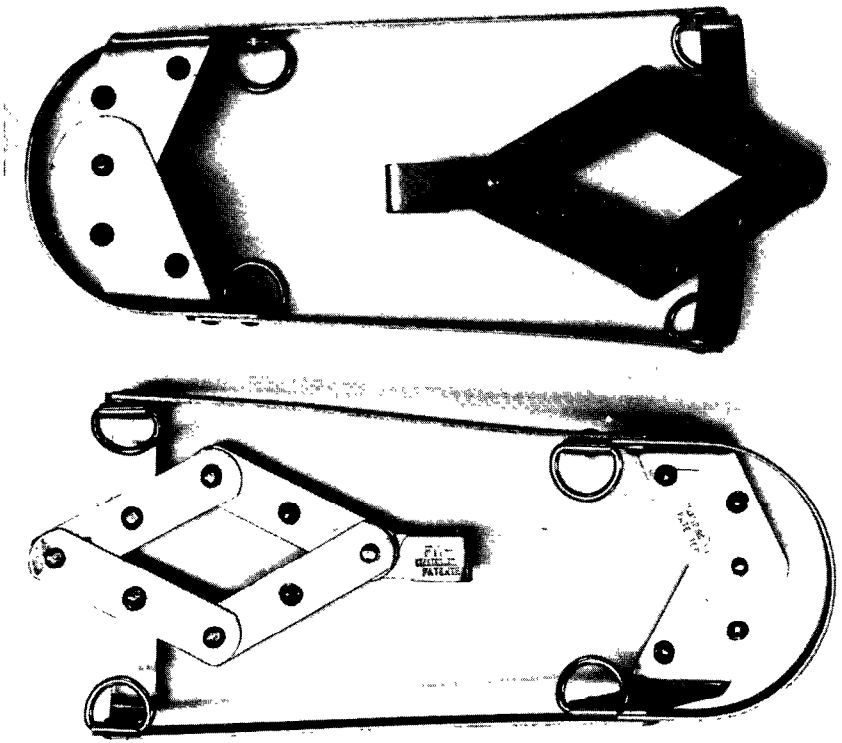

FIGURE 87.—Ice creepers for boots and waders.

1. Vertical-velocity curve.
2. Two-point.
3. Six-tenths-depth.
4. Three-point.
5. Two-tenths depth.
6. Subsurface-velocity.
7. Surface-velocity.
8. Integration.

Less commonly used are the following multipoint methods of determining mean vertical velocity:

9. Five-point.
10. Six-point.

VERTICAL-VELOCITY CURVE METHOD

In the vertical-velocity curve method a series of velocity observations at points well distributed between the water surface and the streambed are made at each of the verticals. If there is considerable curvature in the lower part of the vertical-velocity curve, it is advisable to space the observations more closely in that part of the depth. Normally, the observations are taken at 0.1-depth increments between 0.1 and 0.9 of the depth. Observations are always taken at 0.2, 0.6, and 0.8 of the depth so that the results obtained by the vertical-velocity curve method may be compared with those obtained by the more commonly used methods of velocity observation. Observations are made at least 0.5 ft (0.15m) below the water surface and above the streambed when the Price AA meter or the vane meter is used and are made at least 0.3 ft (0.09 m) from those boundaries when the Price pygmy meter is used; those meters underregister velocity when placed closer to the water surface or streambed.

The vertical-velocity curve for each vertical is based on observed velocities plotted against depth (fig. 88). In order that vertical-velocity curves at different verticals may be readily compared, it is customary to plot depths as proportional parts of the total depth. The mean velocity in the vertical is obtained by measuring the area between the curve and the ordinate axis with a planimeter, or by other means, and dividing the area by the length of the ordinate axis.

The vertical-velocity curve method is valuable in determining coefficients for application to the results obtained by other methods but is not generally adapted to routine discharge measurements because of the extra time required to collect field data and to compute the mean velocity.

Intensive investigation of vertical-velocity curves by Hulsing, Smith, and Cobb (1966) resulted in table 2 which shows average ordinates of the vertical-velocity curve.

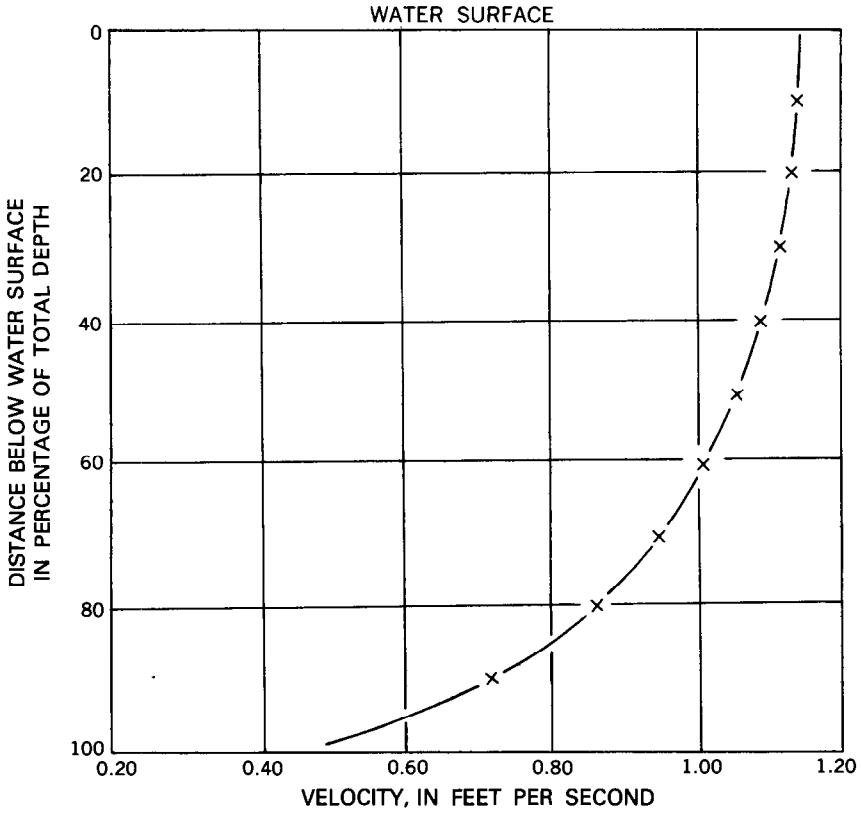

FIGURE 88.—Typical vertical-velocity curve.

TABLE 2.—*Coefficients for standard vertical-velocity curve*

Ratio of observation depth to depth of water	Ratio of point velocity to mean velocity in the vertical
0.05	1.160
.1	1.160
.2	1.149
.3	1.130
.4	1.108
.5	1.067
.6	1.020
.7	.953
.8	.871
.9	.746
.95	.648

TWO-POINT METHOD

In the two-point method of measuring velocities, observations are made in each vertical at 0.2 and 0.8 of the depth below the surface. The average of those two observations is taken as the mean velocity in the vertical. This method is based on many studies involving actual observation and mathematical theory. Experience has shown that this method gives more consistent and accurate results than any of the other methods listed, other than the five-point, six-point, and vertical-velocity curve methods. The two-point method is the one generally used by the U.S. Geological Survey. Table 2 indicates that the two-point method, on the average, gives results that are within 1 percent of the true mean velocity in the vertical.

The two-point method is not used at depths less than 2.5 ft (0.76 m) when measuring with a Price current meter, because the meter would then be too close to the water surface and to the streambed to give dependable results.

The vertical-velocity curve will be distorted by overhanging vegetation that is in contact with the water or by submerged objects, such as large rocks and aquatic growth, if those elements are in close proximity, either in the upstream or downstream direction, to the vertical in which velocity is being measured. Where that occurs the two-point method will not give a reliable value of the mean velocity in the vertical, and an additional velocity observation at 0.6 of the depth should be made. The three observed velocities should then be used in the three-point method (p. 135). A rough test of whether or not the velocities at the 0.2 and 0.8 depths are sufficient for determining mean vertical velocity is given in the following criterion: the 0.2-depth velocity should be greater than the 0.8-depth velocity but less than twice as great.

SIX-TENTHS DEPTH METHOD

In the 0.6-depth method, an observation of velocity made in the vertical at 0.6 of the depth below the surface is used as the mean velocity in the vertical. Actual observation and mathematical theory have shown that the 0.6-depth method gives reliable results. (See table 2.) The U.S. Geological Survey uses the 0.6-depth method under the following conditions:

1. Whenever the depth is between 0.3 ft (0.09 m) and 1.5 ft (0.46 m) and a Price pygmy meter is being used, or between 1.5 ft (0.46 m) and 2.5 ft (0.76 m) and a Price type AA (or type A) meter is being used. (See table 3 for depth and velocity limitations of each meter.)
2. When large amounts of slush ice or debris make it impossible to

observe the velocity accurately at the 0.2 depth. That condition prevents the use of the two-point method.

3. When the distance between the meter and the sounding weight is too great to permit placing the meter at the 0.8 depth. That circumstance prevents the use of the two-point method.
4. When the stage in a stream is changing rapidly and a measurement must be made quickly.

Although, the preceding paragraph states that the 0.6-depth method may be used with a pygmy meter when water depths are as shallow as 0.3 ft (0.09 m), strictly speaking, the 0.6-depth method should not be used when depths are less than 0.75 ft (0.23 m). This follows from the fact that the pygmy meter underregisters when set closer to the streambed than 0.3 ft (p. 132). From a practical standpoint, however, when it is necessary to measure velocities where water depths are as shallow as 0.3 ft, the 0.6-depth method is used. It is recognized, however, that the results obtained in that situation are only approximate values that underestimate the true velocity. Efforts made to date to define shallow-depth coefficients for natural streams have been unsuccessful.

THREE-POINT METHOD

In the three-point method velocities are observed at 0.2, 0.6, and 0.8 of the depth, thereby combining the two-point and 0.6-depth methods. The mean velocity is computed by averaging the 0.2- and 0.8-depth observations and then averaging that result with the 0.6-depth observation. When more weight to the 0.2- and 0.8-depth observations is desired, the arithmetical mean of the three observations may be used. The first procedure is usually followed, however.

The three-point method is used when the velocities in the vertical are abnormally distributed, as explained on page 134. When a Price type AA (or type A) current meter is used, the three-point method cannot be applied unless the depths are greater than 2.5 ft (0.76 m). (See table 3.)

TWO-TENTHS-DEPTH METHOD

In the 0.2-depth method the velocity is observed at 0.2 of the depth below the surface and a coefficient is applied to the observed velocity to obtain the mean in the vertical. The method is principally used for measuring flows of such high velocity that it is not possible to obtain depth soundings or to position the meter at the 0.8 or 0.6 depth.

A standard cross section or a general knowledge of the cross section at a site is used to compute the 0.2 depth when it is impossible to obtain soundings. A sizable error in an assumed 0.2 depth is not critical in the determination of velocity because the slope of the

vertical-velocity curve at this point is usually nearly vertical. (See fig. 88.) The 0.2 depth is also used in conjunction with the sonic sounder for flood measurements. (See p. 108.)

The measurement made by the 0.2-depth method is normally computed by using the 0.2-depth velocity observations without coefficients, as though each observation were a mean in the vertical. The approximate discharge thus obtained divided by the area of the measuring section gives the weighted mean value of the 0.2-depth velocity. Studies of many measurements made by the two-point method show that for a given measuring section the relation between the mean 0.2-depth velocity and the true mean velocity either remains constant or varies uniformly with stage. In either circumstance, this relation may be determined for a particular 0.2-depth measurement by recomputing measurements made at the site by the two-point method using only the 0.2-depth velocity observation as the mean in the vertical. The plotting of the true mean velocity versus the mean 0.2-depth velocity for each measurement will give a velocity-relation curve for use in adjusting the mean velocity for measurements made by the 0.2-depth method.

If at a site too few measurements have been made by the two-point method to establish a velocity-relation curve, vertical-velocity curves are needed to establish a relation between the mean velocity and the 0.2-depth velocity. The usual coefficient to adjust the 0.2-depth velocity to the mean velocity is about 0.87. (See table 2.)

The 0.2-depth method is not as reliable as either the two-point method or the 0.6-depth method when conditions are equally favorable for a current-meter measurement by any of the three methods.

SUBSURFACE-VELOCITY METHOD

In the subsurface-velocity method the velocity is observed at some arbitrary distance below the water surface. That distance should be at least 2 ft (0.6 m), and preferably more for deep swift streams to avoid the effect of surface disturbances. The subsurface-velocity method is used, in the absence of an optical current meter, when it is impossible to obtain soundings and the depths cannot be estimated with sufficient reliability to even approximate a 0.2-depth setting for a conventional current-meter measurement. Coefficients are necessary to convert the velocities observed by the subsurface-velocity method to the mean velocity in the vertical. A prerequisite in obtaining those coefficients is to determine the depths during the measurement from soundings made after the stage has receded enough for that purpose. Those depths are used with the known setting of the current meter below the water surface to compute ratios of depth of observation to total depth during the measurement. The coefficients

to be used with the subsurface-velocity observations can then be computed either by use of the data in table 2 or by obtaining vertical-velocity curves at the reduced stage of the stream.

SURFACE-VELOCITY METHOD

If an optical current meter (p. 91–93) is available, the surface-velocity method is used in preference to the subsurface-velocity method described above. In a natural channel a surface-velocity coefficient of 0.85 or 0.86 is used to compute mean velocity on the basis of the data in table 2. In a smooth artificial channel a surface-velocity coefficient of 0.90 is used. If the artificial channel has smooth vertical walls, the coefficients shown in figure 89 are used in the vicinity of the walls. Figure 89 is based on data obtained in a laboratory study. The fact that the coefficients close to the wall are greater than unity is explained by the fact that the secondary currents that form near

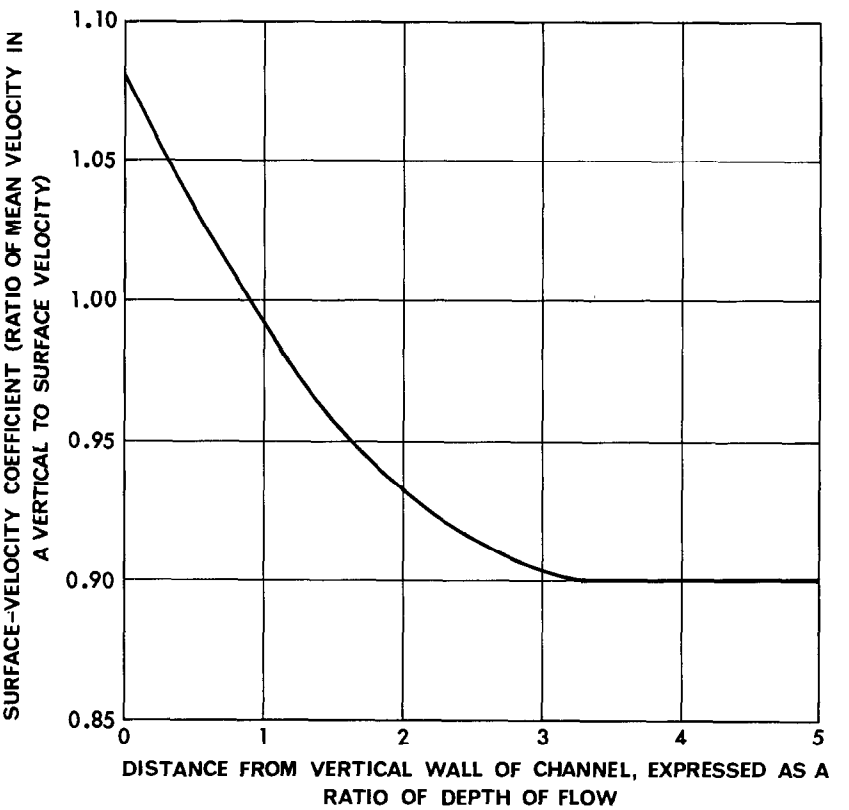

FIGURE 89.—Relation of surface-velocity coefficient to distance from vertical wall of a smooth rectangular channel.

the walls depress the position of the filaments of maximum velocity; that is, the maximum velocity in a vertical close to the wall does not occur at the water surface.

INTEGRATION METHOD

In the integration method the meter is lowered in the vertical to the bed of the stream and then raised to the surface at a uniform rate. During this passage of the meter the total number of revolutions and the total elapsed time are used with the current-meter rating table to obtain the mean velocity in the vertical. The integration method cannot be used with a vertical-axis current meter because the vertical movement of the meter affects the motion of the rotor; consequently, the method is not used in the U.S.A., where the Price meter is the standard current meter. However, the integration method is used to a degree in European countries where horizontal-axis meters are the standard current meters. The accuracy of the measurement is dependent on the skill of the hydrographer in maintaining a uniform rate of movement of the meter. A disadvantage of the method is the inability of the meter to measure streambed velocities because the meter cannot be placed that low. Coefficients smaller than unity are therefore required to correct the observed integrated velocity.

FIVE-POINT METHOD

The five-point method is rarely used in the U.S.A. Velocity observations are made in each vertical at 0.2, 0.6, and 0.8 of the depth below the surface, and as close to the surface and to the streambed as practical. The European criteria for surface and bottom observations state that the horizontal axis of the current meter should not be situated at a distance less than 1½ times the rotor height from the water surface, nor should it be situated at a distance less than 3 times the rotor height from the streambed. In addition, no part of the meter should break the surface of the water.

The velocity observations at the five meter positions are plotted in graphical form, and the mean velocity in the vertical is determined by the use of a planimeter, as explained on page 132. As an alternative, the mean velocity may be computed from the equation

$$V_{\text{mean}} = 0.1(V_{\text{surface}} + 3V_{0\,2} + 3V_{0.6} + 2V_{0.8} + V_{\text{bed}}).$$

SIX-POINT METHOD

The six-point method is rarely used in the U.S.A., but is sometimes used in European countries in situations where the existence of a distorted vertical-velocity distribution is known or suspected; for example, in the presence of aquatic growth or under ice cover. Veloc-

ity observations are made in each vertical at 0.2, 0.4, 0.6, and 0.8 of the depth below the surface, and also close to the surface and to the streambed. The criteria for surface and streambed observations are those given in the discussion above.

The velocity observations at the six meter positions are plotted in graphical form and the mean velocity in the vertical is determined by planimetering the area bounded by the vertical-velocity curve and the ordinate axis, as explained on page 132. The mean velocity may also be computed mathematically from the equation,

$$V_{mean} = 0.1(V_{surface} + 2V_{0.2} + 2V_{0.4} + 2V_{0.6} + 2V_{0.8} + V_{bed}).$$

PROCEDURE FOR CONVENTIONAL CURRENT-METER MEASUREMENT OF DISCHARGE

The first step in making a conventional current-meter measurement of discharge is to select a measurement cross section of desirable qualities. If the stream cannot be waded, and high-water measurements are made from a bridge or cableway, the hydrographer has no choice with regard to selection of a measurement cross section. If the stream can be waded, the hydrographer looks for a cross section of channel with the following qualities:

1. Cross section lies within a straight reach, and streamlines are parallel to each other.
2. Velocities are greater than 0.5 ft/s (0.15 m/s) and depths are greater than 0.5 ft (0.15 m).
3. Streambed is relatively uniform and free of numerous boulders and heavy aquatic growth.
4. Flow is relatively uniform and free of eddies, slack water, and excessive turbulence.
5. Measurement section is relatively close to the gaging-station control to avoid the effect of tributary inflow between the measurement section and control and to avoid the effect of storage between the measurement section and control during periods of rapidly changing stage.

It will often be impossible to meet all of the above criteria, and when that is the case, the hydrographer must exercise judgment in selecting the best of the sites available for making the discharge measurement.

If the stream cannot be waded and the measurement must be made from a boat, the measurement section selected should have the attributes listed above, except for those listed in item 2 concerning depth and velocity. Depth is no consideration in a boat measurement; if the stream is too shallow to float a boat, the stream can usually be waded. However, velocity in the measurement section is an important con-

sideration. If velocities are too slow, meter registration may be affected by an oscillatory movement of the boat, in which the boat, even though fastened to the tag line, moves upstream and downstream as a result of wind action; or, where a vertical-axis meter is used, meter registration may be affected by vertical movement of the boat as a result of wave action (p. 180–181). If velocities are too fast, it becomes difficult to string the tag line across the stream.

Regardless of the type of measurement that is to be made, if the gaging station is downstream from a hydroelectric powerplant, the stage will be changing too rapidly, most of the time, to assure a satisfactory discharge measurement. The hydrographer should obtain a schedule of operations from the powerplant operator, or determine the operating schedule from the gage-height chart, and plan to make his discharge measurements near the crest or trough of the stage hydrograph, or during periods of near-constant discharge from the powerplant.

After the cross section has been selected, the width of the stream is determined. A tag line or measuring tape is strung across the measurement section for measurements made by wading, from a boat, from ice cover, or from an unmarked bridge. Except where a bridge is used, the line is strung at right angles to the direction of flow to avoid horizontal angles in the cross section. For cableway or bridge measurements, use is made of the graduations painted on the cable or bridge rail as described on page 110. Next the spacing of the verticals is determined to provide about 25 to 30 subsections. If previous discharge measurements at the site have shown uniformity of both the cross section and the velocity distribution, fewer verticals may be used. The verticals should be so spaced that no subsection has more than 10 percent of the total discharge. The ideal measurement is one in which no subsection has more than 5 percent of the total discharge, but that is seldom achieved when 25 subsections are used. (The discharge measurement notes in figure 42 show that the subsection with the greatest discharge had 6.2 percent of the total discharge.) It is not recommended that all observation verticals be spaced equally unless the discharge is evenly distributed across the stream. The spacing between verticals should be closer in those parts of the cross section that have the greater depths and velocities.

After the stationing of the observation verticals has been determined, the appropriate equipment for the current-meter measurement is assembled and the measurement note sheets for recording observations are prepared. (See fig. 42.) The following information will be recorded for each discharge measurement:

1. Name of stream and location to correctly identify the established gaging station; or name of stream and exact location of site for a miscellaneous measurement.

2. Date, party, type of meter suspension, and meter number.
3. Time measurement was started using military time (24-hr clock system).
4. Bank of stream that was the starting point.
5. Control conditions.
6. Gage heights and corresponding times.
7. Water temperature.
8. Other pertinent information regarding the accuracy of the discharge measurement and conditions which might affect the stage-discharge relation.

The streambank is identified by the letters LEW or REW (left edge of water or right edge of water, respectively, when facing downstream). The time is recorded periodically in the notes during the course of the measurement. If the gaging station is equipped with a digital recorder it is advantageous to synchronize the time observations with the punch cycle of the recorder. (See fig. 42.) The time observations are important for computing the mean gage height of the discharge measurement, if the measurement is made during a period of appreciable change in stage. (See p. 170–173.) When the discharge measurement is completed, the time is recorded along with the streambank (LEW or REW) where the measurement ended.

We have digressed somewhat in discussing the measurement notes and now return to the details of the discharge measurement. After the note sheet is readied, the meter assembly is checked. The meter should balance on the hanger used and should spin freely; the electric circuit through the meter should operate satisfactorily; and the stopwatch should check satisfactorily in a comparison with the hydrographer's watch. After recording on the note sheet the station (distance from initial point) of the edge of water, the actual measurement is ready to be started.

Depth (if any) at the edge of water is measured and recorded. The depth determines the method of velocity measurement to be used, normally the two-point method (p. 134) or the 0.6-depth method (p. 134). The setting of the meter for the particular method to be used is then computed, and the meter position is recorded, using a designation such as 0.8 or 0.6 or 0.2, as the case may be. After the meter is placed at the proper depth and pointed into the current, the rotation of the rotor is permitted to become adjusted to the speed of the current before the velocity observation is started. The time required for such adjustment is usually only a few seconds if velocities are greater than 1 ft/s (0.3 m/s), but for slower velocities, particularly if the current meter is suspended on a cable, a longer period of adjustment is needed. After the meter has become adjusted to the current, the number of revolutions made by the rotor is counted for a period of 40 to 70 s. The stopwatch is started simultaneously with the first signal

or click, which is counted as "zero," and not "one." The count is ended on a convenient number coinciding with one of those given in the column headings of the meter rating table. The stopwatch is stopped on that count and is read to the nearest second or to the nearest even second if the hand of the stopwatch is on a half-second mark. That number of seconds and the number of revolutions are then recorded.

If the velocity is to be observed at more than one point in the vertical, the meter setting for the additional observation is determined, the revolutions are timed, and the data are recorded. The hydrographer moves to each of the observation verticals and repeats the above procedure until the entire cross section has been traversed. For each vertical he records distance from initial point, water depth, meter-position depth, revolutions of the meter, and the time interval associated with those revolutions (fig. 42).

Consideration must be given to the direction of flow, because it is the component of velocity normal to the measurement section that must be determined. The discussion that follows concerns currents that approach the measurement section obliquely, at angle α (fig. 47). If, in a wading measurement, the meter used is a horizontal-axis meter with a component propellor, such as the Ott meter, the propellor should be pointed upstream at right angles to the cross section, but only if α is less than 45°. Such a meter will register the desired component of velocity normal to the cross section, when α is less than 45°. If α is greater than 45°, the component meter should be pointed into the current. All other meters on a wading-rod suspension should likewise be pointed into the current. Any meter on a cable suspension, as is used for the higher stages, will automatically point into the current because of the effect of the meter vanes. When the meter is pointed into an oblique current the measured velocity must be multiplied by the cosine of the angle (α) between the current and a perpendicular to the measurement section in order to obtain the desired normal component of the velocity.

In the U.S.A., either of two methods is used to obtain cosine α (fig. 47). In the first method, use is made of the field notes which have a point of origin (o) printed on the left margin and cosine values on the right margin (fig. 42). The cosine of the angle of the current is measured by holding the note sheet in a horizontal position with the point of origin on the tag line, bridge rail, cable rail, or any other feature parallel to the cross section (fig. 90). With the long side of the note sheet parallel to the direction of flow, the tag line or bridge rail will intersect the value of cosine α on the top, bottom, or right edge of the note sheet. The direction of the current will be apparent from the direction of movement of floating particles. If the water is clear of floating material, small bits of floating material are thrown into the

stream and the edge of the note sheet is alined parallel to the direction of movement. If no such material is available, the inelegant, but time-honored method of spitting into the stream is used to obtain an indicator of the direction of flow. The measured velocity is multiplied by the cosine of the angle to determine the velocity component normal to the measurement section.

The second, and more reliable, method of obtaining cosine α involves the use of a folding foot-rule. These rules, which are either 3 or 6 ft long, are graduated in hundreths of a foot and are jointed every half foot. The first 2 ft of the rule is extended, the 2.00-ft marker is placed on the tag line or bridge rail (fig. 91), and the rule is alined with the direction of the current. The rule is folded at the 1-ft mark so that the first foot of the rule is normal to the tag line or bridge rail. That reading, subtracted from 1.00, is cosine α. For example, if the reading on the rule is 0.09 ft, cosine α equals 0.91.

Details peculiar to each of the various types of current-meter measurement are described in the sections of the manual that follow.

CURRENT-METER MEASUREMENT BY WADING

Current–meter measurements are best made by wading, if conditions permit. (See fig. 92.) Wading measurements have a distinct advantage over measurements made from cableways or bridges in that it is usually possible to select the best of several available cross sections for the measurement. The type AA or pygmy meter is used for wading measurements in the U.S.A. Table 3 lists the type of meter and velocity method to be used for wading measurements at various depths.

Some departure from table 3 is permissible. For example, if a type

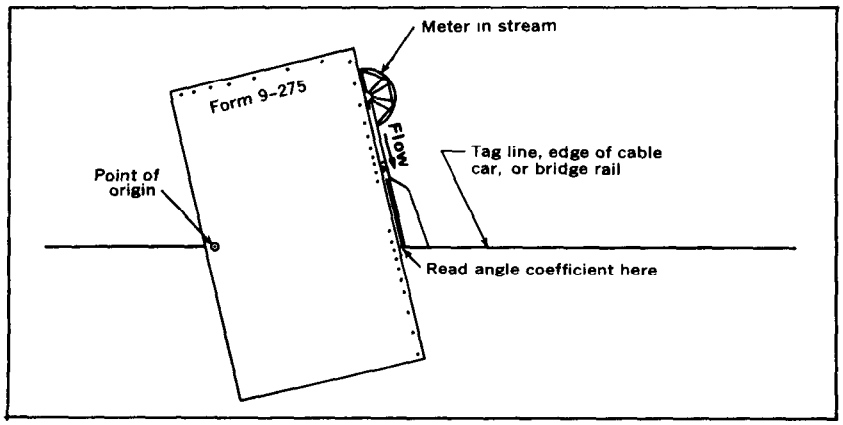

FIGURE 90.—Measurement of horizontal angle with measurement-note sheet.

AA meter is being used in a measurement section that has almost all its depths greater than 1.5 ft (0.46 m), the pygmy meter should not be substituted for the few depths that are less than 1.5 ft, or vice versa. With regard to the use of the type AA meter in depths less than 1.5 ft, strictly speaking, that meter should not be used in depths less than 1.25 ft (0.38 m). A depth of 1.25 ft will accommodate the 0.6-depth method without causing the meter to be set closer than 0.5 ft from the streambed; if the meter is set any closer to the streambed it will underregister the velocity (p. 132). However, if the hydrographer is using the type AA meter in a measurement section that has only few verticals shallower than 1.25 ft, he may use that meter for depths that are even as shallow as 0.5 ft (0.15 m) without changing to a pygmy meter. The hydrographer must make a judgment decision. He knows that his meter is underregistering the velocity by some unknown percentage in the depths shallower than 1.25 ft, but if that shallow-depth flow represents less than 10 percent of the total discharge, his total measured discharge should not be too greatly in error.

Neither the type AA meter nor the pygmy meter should be used for measuring velocities slower than 0.2 ft/s, unless absolutely necessary.

If depths or velocities under natural conditions are too low for a dependable current-meter measurement, the cross section should be modified, if practical, to provide acceptable conditions. It is often pos-

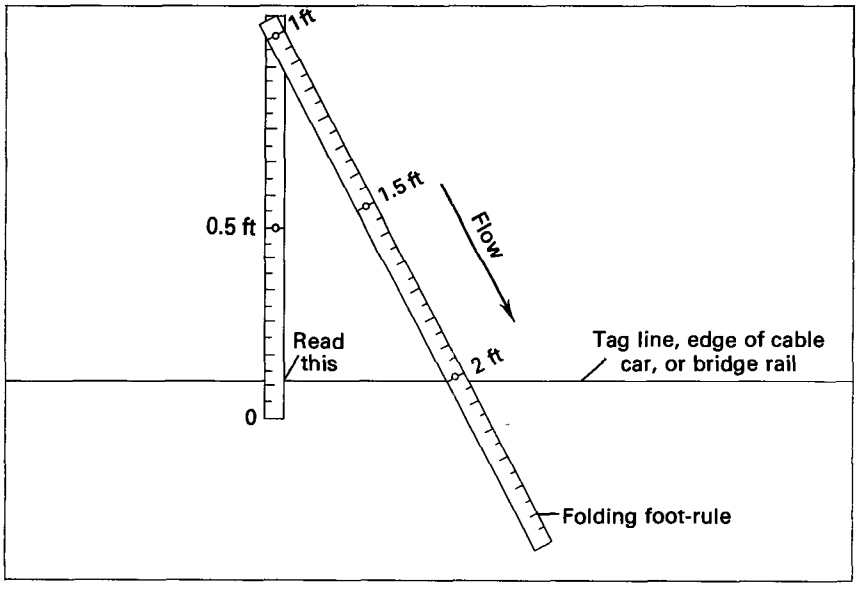

FIGURE 91.—Measurement of horizontal angle with folding foot-rule.

sible to build temporary dikes to eliminate slack water or shallow depths in a cross section, or to improve the cross section by removing rocks and debris within the section and in the reach of channel im-

FIGURE 92.—Wading measurement using top-setting rod.

TABLE 3.—*Current-meter and velocity-measurement method for various depths (wading measurement)*

Depth		Meter	Velocity method
(ft)	(m)		
2.5 or more	0.76 or more	Type AA (or type A)	0.2 and 0.8
1.5–2.5	0.46–0.76	---- do ----	.6
.3–1.5	.09– .46	Pygmy[1]	.6

[1]Used when velocities are less than 2 5 ft/s (0 76 m/s)

mediately upstream and downstream from the section. After the cross section has been modified, the flow should be allowed to stabilize before starting the discharge measurement.

The hydrographer should stand in a position that least affects the velocity of the water passing the current meter. That position is usually obtained by facing the bank so that the water flows against the side of the leg. The wading rod is held at the tag line by the hydrographer who stands about 3 in (0.07 m) downstream from the tag line and at least 1.5 ft (0.46 m) from the wading rod. He should avoid standing in the water if his feet and legs occupy a significantly large percentage of a narrow cross section. In small streams where the width permits, the hydrographer stands on an elevated plank or other support, rather than in the water.

The wading rod should be held in a vertical position with the meter parallel to the direction of flow while the velocity is being observed. If the flow is not at right angles to the tag line, the angle coefficient should be carefully measured (figs. 90 and 91).

When measuring streams having shifting beds, the soundings or velocities can be affected by the scoured depressions left by the hydrographer's feet. For such streams, the meter should be placed ahead of and upstream from the feet. For such streams, too, the hydrographer's notes should accurately describe the configuration of the streambed and water surface. (See p. 376–379.)

A measurement should be made of the depth of water over the lowest point of the control, either before or after the discharge measurement. The gage height corresponding to this lowest point (gage height of zero flow) is very useful in analyzing the stage-discharge relation for the gaging station. (See p. 333–334).

When the flow is too low for a reliable measurement of discharge by current meter, the discharge is determined by use of (1) a volumetric method of measurement, (2) a portable Parshall flume, or (3) a portable weir plate. Those three methods of discharge determination are discussed in chapter 8.

CURRENT-METER MEASUREMENTS FROM CABLEWAYS

The equipment assemblies for use on cableways are described on pages 110–117.

The size of the sounding weight used in current-meter measurements depends on the depth and velocity in the measurement cross section. A rule of thumb generally used is that the size of the weight (lb) should be greater than the maximum product of velocity (ft/s) and depth (ft) in the cross section. If insufficient weight is used, the meter assembly will be dragged downstream. If debris or ice is flowing or if the stream is shallow and swift, the weight used should

be appreciably heavier than that indicated by the above rule. The rule is not rigid, but it does provide a starting point for deciding on the size of weight required at various stages.

The Price type AA current meter is generally used in the U.S.A. when making discharge measurements from a cableway. The depth is measured by use of a sounding reel, and the velocity is measured by setting the meter at the proper position in the vertical. (See table 4.) Table 4 is designed so that no velocity observations will be made with the meter closer than 0.5 ft (0.15 m) to the water surface. In the zone from the water surface to a depth of 0.5 ft, the current meter is known to give erroneous results.

Some sounding reels are equipped with a computing depth indicator. To use the computing spiral, the indicator is set at zero when the center of the current-meter rotor is at the water surface. The sounding weight and meter are then lowered until the weight touches the streambed. If, for example, a 30 C .5 (see table 4) suspension is used and if the indicator reads 18.5 ft when the sounding weight touches the bottom, the depth would be 19.0 ft (18.5 ft + 0.5 ft). To move the meter to the 0.8-depth position (0.8×19.0 ft), the weight and meter are raised until the hand on the indicator is over the 19-ft mark on the graduated spiral (fig. 60); the hand will then be pointing to 15.2 on the main dial. To set the meter at the 0.2-depth position (0.2×19.0 ft), the weight and meter are raised until the hand on the indicator is pointing to 3.8 ft on the main dial.

One problem found in observing velocities from a cableway is that movement of the cable car from one station to the next causes the car to oscillate for a short time after coming to a stop. The hydrographer should wait until this oscillation has been dampened to the extent that it is negligible before counting meter revolutions.

Tags can be placed on the sounding line at known distances above the center of the meter cups as an aid in determining depths. Furthermore, the use of tags allows the meter to be kept submerged throughout the discharge measurement to prevent freezing in cold air during the winter measurements. The tags, which are usually streamers of different colored binding tape, are fastened to the sounding line by solder beads or by small cable clips. Tags are used for determining depth in either of two ways.

1. In the procedure that is usually preferred, a tag is set at the water surface, after which the depth indicator is set at the distance between that particular tag and the center of the meter cups. This is equivalent to setting the indicator at zero when the center of the meter rotor is at the water surface, and the hydrographer then proceeds with his depth settings as described in a preceding paragraph. If debris or ice is flowing, this method prevents damage to the meter.

TABLE 4.—*Velocity-measurement method for various meter suspensions and depths*

Suspension[1]	Minimum depth			
	0.6 method		0.2 and 0.8 method	
	(ft)	(m)	(ft)	(m)
15 C .5, 30 C .5	1.2	0.37	2.5	0.76
50 C .55	1.4	.43	2.8	.85
50 C .9	2.2	.67	4.5	1.37
75 C 1.0, 100 C 1.0, 150 C 1.0	2.5	.76	5.0	1.52
200 C 1.5, 300 C 1.5	[2]3.8	1.16	7.5	2.29

[1]Suspensions shown indicate the size of the sounding weight and the distance from the bottom of the weight to the current-meter axis. Thus "50 C .9" refers to a 50-pound Columbus-type weight, the suspension for which puts the meter 0.9 ft above the bottom of the weight.

[2]Use 0.2-depth method for depths between 2.5 and 3.7 ft, and apply appropriate coefficient (usually 0.87 from table 2).

2. In the second method the sounding weight is first lowered to the streambed, and the depth is then determined by raising the weight until the first tag below the water surface appears at the surface. The total depth is then sum of (a) the distance the weight was raised to bring the tag to the water surface, (b) the distance the tag is above the center of the meter cups, and (c) the distance from the bottom of the weight to the center of the cups. This method is usually used with handlines, and it is also used to simplify the measurement of deep, swift streams (p. 159–163).

If large quantities of debris are carried by the stream, the meter should be periodically raised to the cable car for inspection during the measurement to be certain that the pivot and rotor of the meter are free of debris. However, the meter should be kept in the water during the measurement if the air temperature is well below freezing. The hydrographer should carry a pair of lineman's side-cutter pliers when making measurements from a cableway. These can be used to cut the sounding line to insure safety if the weight and meter become caught on a submerged object or on heavy floating debris and it is impossible to release them. Sometimes the cable car can be pulled to the edge of the water where the entangling debris can be removed.

When a measurement of a deep, swift stream is made from a cableway, the meter and weight do not hang vertically but are dragged downstream. The vertical angle, that is, the angle between the meter-suspension cable and the vertical, should be measured by protractor in order to correct the soundings to give the actual vertical depth. The procedure used to correct soundings is described on pages 159–168.

If a handline is used to suspend the current meter and sounding weight, the measurement procedure to be followed is that described in the section on bridge measurements (p. 150–151).

CURRENT-METER MEASUREMENTS FROM BRIDGES

Bridges are often used for making discharge measurements of streams that cannot be waded. Measurement cross sections under bridges are often satisfactory for current-meter measurements, but cableway sections are usually superior.

No set rule can be given for choosing between the upstream or downstream side of the bridge for making a discharge measurement. The advantages of using the upstream side of the bridge are:

1. Hydraulic characteristics at the upstream side of bridge openings usually are more favorable.
2. Approaching drift can be seen and thus can be more easily avoided.
3. The streambed at the upstream side of the bridge is not likely to be scoured as badly as the downstream side.

The advantages of using the downstream side of the bridge are:

1. Vertical angles are more easily measured because the sounding line will move away from the bridge.
2. The flow lines of the stream may be straightened by passing through a bridge opening with piers.

Whether to use the upstream side or the downstream side of a bridge for a current-meter measurement should be decided individually for each bridge after considering the above factors. Other pertinent factors relate to physical conditions at the bridge, such as location of the walkway, traffic hazards, and accumulation of trash on pilings and piers.

In making the discharge measurement either a handline, or a sounding reel supported by a bridge board or by a portable crane, is used to suspend the current meter and sounding weight from the bridge. The velocity is measured by setting the meter at positions in the vertical as indicated in table 4. If velocities are high, the equipment is used no closer than several feet from piers and abutments. In that situation depths and velocities at the pier or abutments are estimated on the basis of observations in the vertical nearest the pier. (See p. 82.)

Where piers are in the measuring section, it is usually necessary to use more than 25–30 subsections to obtain results as reliable as those obtained with a similar measuring section that has no piers. Piers not only affect the horizontal distribution of velocities, but they frequently affect the direction of the current, causing horizontal angles that must be carefully measured.

Whether or not to exclude the area of a bridge pier from the area of the measurement cross section depends primarily on the relative locations of the measurement section and the end of the pier. If meas-

urements are made from the upstream side of the bridge, it is the relative location of the upstream end (nose) of the pier that is relevant; for measurements made from the downstream side it is the location of the downstream end (tail) of the pier that is relevant. If any part of the pier extends into the measurement cross section, the area of the pier is excluded. However, bridges quite commonly have cantilevered walkways from which discharge measurements are made. In that case the measurement cross section lies beyond the end of the pier—upstream from the nose or downstream from the tail, depending on which side of the bridge is used. In that situation it is the position and direction of the streamlines that determines whether or not the pier area is to be excluded. The hydrographer, if he had not previously noted the stationing of the sides of the pier when projected to the measurement cross section, does so now. If there is negligible or no downstream flow in that width interval (pier subsection)—that is, if only stagnation and (or) eddying exists upstream from the nose or downstream from the tail, whichever is relevant—the area of the pier is excluded. If there is significant downstream flow in the pier subsection, the area of the pier is included in the area of the measurement cross section. The horizontal angles of the streamlines in and near the pier subsection will usually be quite large in that circumstance.

Footbridges are sometimes used for measuring the discharge of canals, tailraces, and small streams. Often a rod suspension can be used for the meter when measuring from a footbridge. In low velocities the procedure for determining depth when using a rod suspension is the same as that used for wading measurements. For higher velocities depth is obtained from the difference in readings at an index point on the bridge when the base plate of the rod is at the water surface and when it is on the streambed. The measurement of depth by that method eliminates errors in reading the depth caused by the fast-moving water piling up on the upstream face of the rod. Handlines, bridge cranes, and bridge boards are also used from footbridges.

When using a sounding reel, depths and velocities are measured by the methods described in the preceding section of the manual on cableway measurements (p. 146–148). When using a handline, depth is determined by first lowering the sounding weight to the streambed and then raising the weight until one of the tags is at the water surface. The distance that the weight is raised is measured along the rubber-covered cable (p. 106) with either a steel or metallic tape, a folding foot-rule, or a graduated rod. The total depth of water is then the summation of (1) the distance the particular tag is above the meter cups, (2) the measured distance the meter and weight were raised, and (3) the distance from the bottom of the weight to the meter cups.

Another, less widely used, method of determining depth requires that the meter cups be set at the water surface, after which the sounding weight is lowered to the streambed while measuring, with tape or rule, the length of line that is let out. This measured distance, plus the distance from the bottom of the sounding weight to the meter cups, is the depth of water.

When using a handline, enough cable is unwound from the handline reel to keep the reel out of water when the sounding weight is on the streambed at the deepest part of the measuring section. That prevents submergence of the reel and thick rubber-covered cable and attendant drag on the equipment in high-velocity flow, and unless the bridge is relatively close to the water surface, it still permits the hydrographer to raise and lower the meter by means of the rubber-covered cable rather than the bare-steel cable. When the meter is set for a velocity observation, the hydrographer stands on the rubber-covered cable or ties it to the handrail to hold the meter in place. By doing so his hands are free to operate the stopwatch and record the data.

If the bridge has vertical truss members in the plane of the measurement cross section, the handline can be disconnected from the headphone wire and passed around the truss member with the sounding weight on the bottom. This eliminates the need for raising the weight and meter to the bridge each time a move is made from one vertical to another and is the principal advantage of a handline.

CURRENT-METER MEASUREMENTS FROM ICE-COVER

Discharge measurements under ice cover (fig. 93) are usually made under conditions that range from uncomfortable to severe, but it is extremely important that they be made, because the reliability of a large part of the computed discharge record for a winter period may depend on one such measurement.

Cross sections for possible use for measuring under ice cover should be selected during the open-water season when channel conditions can be observed and evaluated. Commonly the most desirable measurement section will be just upstream from a riffle because slush ice that collects under the ice cover is usually thickest at the upstream end of the pools created by riffles. The equipment used for cutting or drilling holes in the ice was described on pages 124–129.

The danger of working on ice-covered streams should never be underestimated. When crossing the stream, the hydrographer should test the strength of the ice with solid blows using a sharp ice chisel. Ice thickness may be irregular, especially late in the season when a thick snow cover may act as an insulator. Water just above freezing can slowly melt the underside of the ice, creating thin spots. Ice

FIGURE 93.—Ice rod being used to support current meter for a discharge measurement, top; ice drill being used to cut holes, bottom.

bridged above the water may be weak, even though relatively thick.

At the cross section selected for measurement three holes, one at each quarter point of the width, are cut to check on the possible presence of slush ice or possible maldistribution of flow. If poor conditions are found, other cross sections are similarly investigated to find one that is free of slush ice and has a favorable horizontal distribution of flow. After finding a favorable cross section, at least 20 holes are cut for the current-meter measurement of discharge. The holes should be spaced so that no subsection carries more than 10 percent of the total discharge. On narrow streams it may be simpler to remove all the ice in the cross section.

The effective depth of the water (fig. 94) is the total depth of water minus the distance from the water surface to the bottom of the ice. The vertical pulsation of water in the holes in the ice sometimes causes difficulty in determining the depths. The total depth of water is usually measured with an ice rod or with a sounding weight and reel, depending on the depth.

The distance from the water surface to the bottom of the ice is measured with an ice-measuring stick (p. 125), unless slush is present at the hole. In that situation the effective depth is the total depth

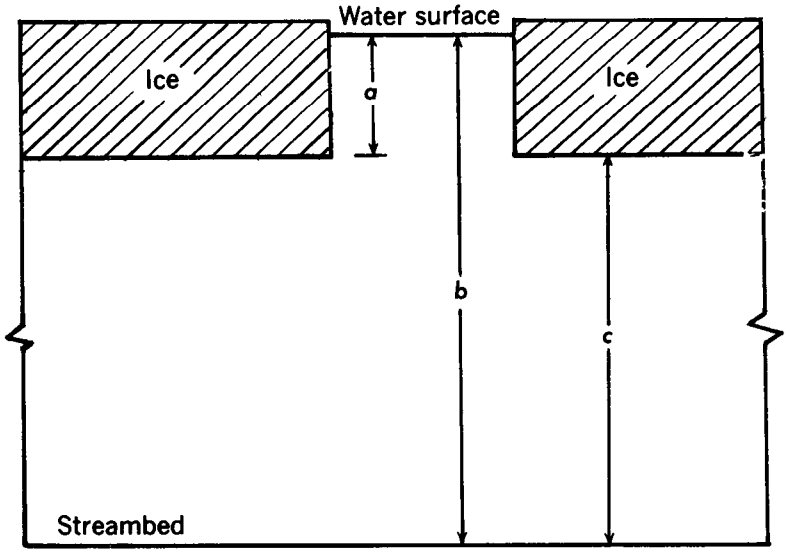

FIGURE 94.—Method of computing meter settings for measurements under ice cover.

minus the distance from the water surface to the interface between water and slush. To locate that interface, the current meter is suspended at a depth below the slush ice where the meter rotor turns freely. The meter is then slowly raised until the rotor stops; that point is considered the interface, and its depth below the water surface is measured for determining the effective depth. The effective depth is then used to compute the proper position of the meter in the vertical.

The vane ice meter is recommended for use under ice cover because (1) the vanes do not become filled with slush ice as the cups of the Price meter often do, (2) the yoke of the vane meter will fit in the hole made by the ice drill, and (3) the yoke and ice rod can serve as an ice-measuring stick. The contact chamber of the vane meter can be rotated to any position; its binding post is therefore placed perpendicular to the axis of the yoke to avoid interference when using the top of the yoke as the horizontal leg of an ice-measuring stick.

Because of the roughness of the underside of the ice cover, the location of the filament of maximum velocity is some distance below the underside of the ice. Figure 95 shows a typical vertical-velocity

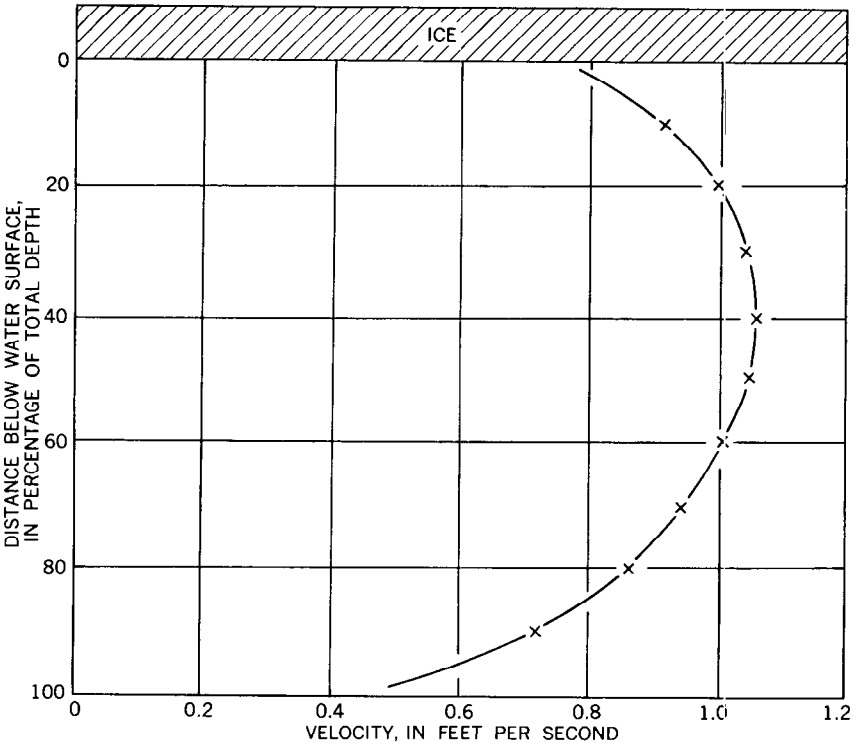

FIGURE 95.—Typical vertical-velocity curve under ice cover.

curve under ice cover. In making a discharge measurement the 0.2- and 0.8-depth method is recommended in the U.S.A. for effective depths equal to or greater than 2.5 ft, and the 0.6-depth method for effective depths less than 2.5 ft. It is also recommended that two vertical-velocity curves be defined when ice measurements are made to determine whether any coefficients are necessary to convert the velocity obtained by the 0.2- and 0.8-depth method, or by the 0.6-depth method, to the mean velocity. Normally the average of the velocities obtained by the 0.2- and 0.8-depth method gives the mean velocity, but a coefficient of about 0.92 usually is applicable to the velocity obtained by the 0.6-depth method. In Europe a three-point method is commonly used in which velocity observations are made at 0.15, 0.5, and 0.85 of the effective depth.

When measuring the velocity, the meter is kept as far upstream as possible to minimize any effect that the vertical pulsation of water in the hole might have on the meter registration. The meter is exposed as little as possible to the cold air so that its operation will not be impaired by the formation of ice on exposed parts.

If there is only partial ice cover on the measuring section, the procedure described above is used for the ice-covered observation verticals, and open-water methods are used for the open-water verticals.

A sample sheet of discharge-measurement notes for a measurement made under ice cover is shown in figure 96. Vertical-velocity curves that had been defined for that measurement had indicated that mean velocity in a vertical was given by the 0.2- and 0.8-depth method, and that the 0.6-depth method required a coefficient of 0.92.

CURRENT-METER MEASUREMENTS FROM BOATS

Discharge measurements are made from boats where no cableways or suitable bridges are available and where streams are too deep to wade. Personal safety is the limiting factor in the use of boats on streams having high velocities.

In making a boat measurement the tag line is first strung across the measurement section by unreeling the line as the boat moves across the stream. Some tag-line reels are equipped with brakes (fig. 79) to control the line tension during the unreeling. If a tag line whose reel is unequipped with a brake has been strung across a stream, the slack is taken up by means of a block and tackle attached to the reel and to an anchored support on the bank. If there is traffic on the river, one man must be stationed on the bank to lower and raise the tag line to allow river traffic to pass. Streamers should be attached to the tag line so that it may be seen by boat pilots. The method of positioning the boat for measuring depths and velocities, by sliding the boat along the tag line from one observation vertical to another, was described on page 121.

If the flow of traffic on the river is continual or if the width of the river is too great for a tag line to be used, other means are needed to position the boat. One method that dispenses with the tag line involves keeping the boat lined up with flags positioned on each end of

9-275a (September 1960)

UNITED STATES
DEPARTMENT OF THE INTERIOR
GEOLOGICAL SURVEY
WATER RESOURCES DIVISION

Meter V-378

Date March 18, 1962 Number of Meas. 36.5

DISCHARGE MEASUREMENT NOTES—ICE COVER

Frozen ~~River at~~ Creek, near Hot Springs, N.Y.

REW

	Dist. from initial point	Width	Total depth of water	W.S. to bot. ice	Effective depth	Depth of meter below water surface	Revolutions	Time in seconds	VELOCITY: At point	VELOCITY: Mean in vertical	Area	Discharge
	1315											
Veloc. coef.	24	3	0	-	-	-	-	-		0	0	0
.92	30	6	2.6	1.6	1.0	2.2	10	47	.50	.46	6.0	2.8
.92	36	6	3.6	1.8	1.8	2.9	15	49	.71	.65	10.8	7.0
.92	42	5	4.3	2.0	2.3	3.4	15	44	.79	.73	11.5	8.4
1.0	46	4	4.5	1.8	2.7	2.3	20	43	1.07	.87	10.8	9.4
						4.0	15	52	.67			
	50	4	4.7	1.7	3.0	2.3	20	40	1.15	.92	12.0	11.0
						4.1	15	50	.70			
	54	4	4.6	1.7	2.9	2.3	25	49	1.17	.96	11.6	11.1
	1325					4.0	15	46	.76			
	58	4	4.9	1.6	3.3	2.3	20	40	1.15	.92	13.2	12.1
						4.2	15	50	.70			
	62	4	4.8	1.6	3.2	2.2	25	48	1.20	.98	12.8	12.5
						4.2	15	46	.76			
	66	3.5	5.0	1.5	3.5	2.2	25	44	1.30	1.08	12.2	13.2
						4.3	15	41	.85			
	69	3	5.3	1.6	3.7	2.3	25	40	1.43	1.15	11.1	12.8
						4.6	15	40	.87			
	72	3	5.1	1.5	3.6	2.2	25	41	1.40	1.16	10.8	12.5
	1335					4.4	20	51	.91			
		49.5									122.8	112.8

No. 2 of 4 Sheets. Comp. by TDB Chk. by JRK

U. S. GOVERNMENT PRINTING OFFICE 16—63225-1

FIGURE 96.—Part of notes for discharge measurement under ice cover.

the measurement cross section. Flags on one bank would suffice, but it is better to have them on both banks. The position of the boat in the cross section can be determined by means of a transit on the shore and a stadia rod held in the boat (fig. 97). Another method of determining the position of the boat is by setting a transit on one bank at a convenient measured distance from, and at right angles to, the cross section. The position of the boat is computed by measuring the angle to the boat, as shown in figure 98. A third method of determining the position of the boat requires a sextant in the boat. The sextant is used to read the angle between a flag at the end of the cross section and another at a known distance perpendicular to the cross section (fig. 98). The boat position can be computed from the measured angle and the known distance between the flags on the shore. Unless anchoring is more convenient, the boat must be held stationary by its motor when readings are being taken.

Boat measurements are not recommended where velocities are

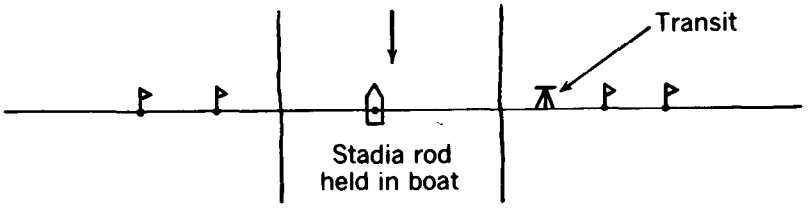

FIGURE 97.—Determining position in the cross section, stadia method.

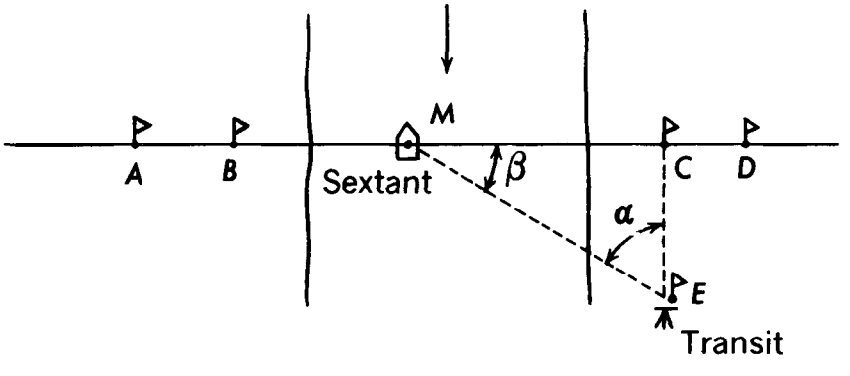

$$MC = CE \tan \alpha \text{ (transit)}$$

$$MC = \frac{CE}{\tan \beta} \text{ (sextant)}$$

FIGURE 98.—Determining position in the cross section, angular method.

slower than 1 ft/s (0.3 m/s) when the boat is subject to the action of wind and waves. (See p. 180–181.) If the maximum depth in the cross section is less than 10 ft (3 m) and the velocity is low, a rod is usually used for measuring the depth and supporting the current meter. For greater depths and velocities, a cable suspension with reel, boat boom, and sounding weight is used. The procedure for measuring discharge from a boat using the boat boom and crosspiece (p. 122–123) is the same as that for measuring from a bridge or cableway, once the special equipment has been set up and the method of positioning the boat has been established.

A special method of measuring discharge from a boat without stopping the boat at observation stations—the moving-boat method—is described in detail in chapter 6.

NETWORKS OF CURRENT METERS

Occasional special measurements require the simultaneous determination of velocities at several points in a cross section, distributed either laterally or vertically. For example, it may be necessary to measure a vertical-velocity profile quickly in unsteady flows and to check it frequently in order to determine the changes in shape of the vertical profile as well as the rates of those changes. Another example is the measurement of tide-affected streams where it is desirable to measure the total discharge continously during at least a full tidal cycle (approximately 13 hr). The need for so many simultaneous velocity determinations (one at each vertical in the cross section) for so long a period can be an expensive and laborious process using conventional techniques of discharge measurement.

A grouping of 21 current meters and special supplemental instrumentation has been used by the U.S. Geological Survey to facilitate measurements of the types just described. Only a few persons are required to operate the system. The 21 meters are connected so that the spacing between any two adjacent meters can be varied to distances as great as 200 ft (61 m). Furthermore, each meter has sufficient handline cable to be suspended vertically from a bridge for as much as 200 ft. The meters have a standard calibration. Revolutions of the rotors are recorded by electronic counters that are grouped compactly in one box at the center of the bank of meters. The operator, by flipping one switch, starts all 21 counters simultaneously and, after an interval of several minutes, stops all counters. The indicated number of revolutions for the elapsed time interval is converted to a velocity for each meter. The distance between meters is known; a record of stage is maintained to evaluate depth; prior information at the site is obtained to convert point velocities in the verticals to mean velocities in those verticals. All of the information necessary to compute discharge in the cross section is therefore available

and is tabulated for easy conversion to discharge.

Other countries have developed similar equipment; for example, a grouping of 40 meters is used in the United Kingdom.

SPECIAL PROBLEMS IN CONVENTIONAL CURRENT-METER MEASUREMENTS

MEASUREMENT OF DEEP, SWIFT STREAMS

The measurement of deep, swift streams by current meter usually presents no serious problems when adequate sounding weights are used and when floating ice or drift is not excessive. Normal procedures must sometimes be altered, however, when measuring streams under particularly adverse conditions, the four most common situations of that kind being represented by the following cases:

Case A. Possible to sound, but weight and meter drift downstream.

Case B. Not possible to sound, but a standard cross section is available.

Case C. Not possible to sound, and no standard cross section is available.

Case D. Not possible to submerge the meter in the water.

Procedures are described below for discharge measurements made under those adverse conditions. The procedures for cases B, C, and D are actually applicable only where channel conditions in the measurement cross section or reach are stable, meaning that no significant scour or deposition occurs.

CASE A. DEPTH CAN BE SOUNDED

Where it is possible to sound the depth but the weight and meter drift drownstream, the depths as measured by the usual methods will be in error, being too large (fig. 99). The correction for the error has two parts, the air correction and the wet-line correction. The air correction is shown in figure 99 as the distance *cd*. The wet-line correction in figure 99 is shown as the difference betwen the wet-line depth *de* and the vertical depth *dg*.

As shown in figure 99, the air correction depends on the vertical angle *P* and the distance *ab*. The correction is computed as follows:

$$ab=ac$$

$$\cos P=\frac{ab}{ad}=\frac{ab}{ac+cd}=\frac{ab}{ab+cd}$$

$$ab+cd=\frac{ab}{\cos P}$$

$$cd=\frac{ab}{\cos P}-ab=ab\left[\frac{1}{\cos P}-1\right]. \qquad (11)$$

The air correction for even-numbered angles between 4° and 36° and for vertical lengths between 10 and 100 ft is shown in table 5. The correction is applied to the nearest tenth of a foot; hundredths are given to aid in interpolation. Table 6 is a similar table in metric units.

The air correction may be nearly eliminated by using tags at

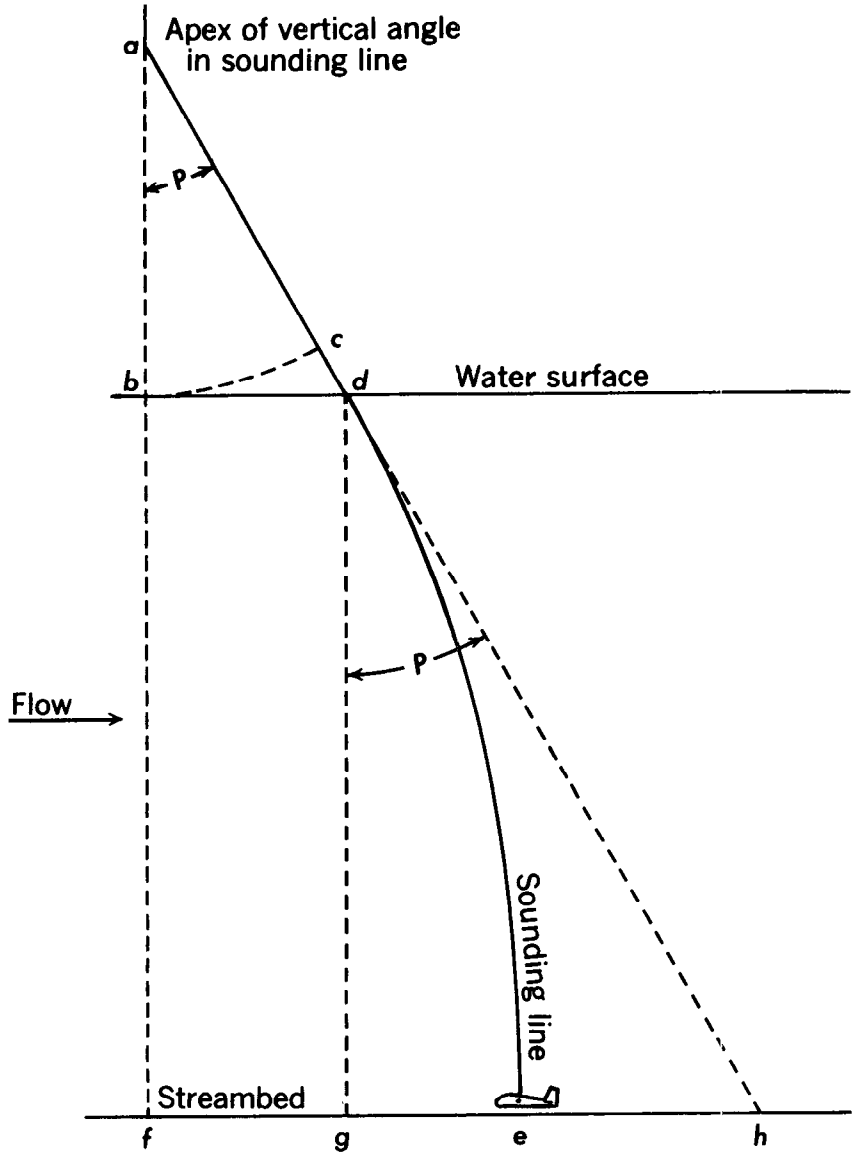

FIGURE 99.—Position of sounding weight and line in deep, swift water.

TABLE 5.—*Air-correction table, giving difference, in feet, between vertical length and slant length of sounding line above water surface for selected vertical angles*

Vertical length (ft)	Vertical angle of sounding line at protractor																	Vertical length (ft)
	4°	6°	8°	10°	12°	14°	16°	18°	20°	22°	24°	26°	28°	30°	32°	34°	36°	
10	0 02	0 06	0 10	0 15	0 22	0 31	0 40	0 51	0 64	0 79	0.95	1 13	1.33	1 55	1.79	2 06	2 36	10
12	.03	07	12	.19	27	37	48	62	77	94	1 14	1 35	1 59	1 86	2 15	2 47	2 83	12
14	03	08	14	22	.31	43	.56	72	90	1 10	1.32	1.58	1 86	2 17	2 51	2 89	3 30	14
16	04	09	16	25	.36	49	64	.82	1 03	1 26	1 51	1.80	2 12	2 48	2 87	3 30	3.78	16
18	04	.10	.18	28	.40	55	73	93	1.16	1.41	1 70	2 03	2 39	2.78	3.23	3.71	4.25	18
20	05	11	20	31	.45	61	81	1 03	1 28	1 57	1.89	2.25	2 65	3 09	3.58	4.12	4 72	20
22	05	12	22	34	49	67	89	1 13	1 41	1 73	2 08	2.48	2.92	3.40	3 94	4.54	5 19	22
24	06	13	24	37	54	.73	97	1 24	1.54	1 88	2 27	2 70	3 18	3.71	4.30	4.95	5 67	24
26	06	14	26	40	58	80	1 05	1.34	1.67	2 04	2 46	2.93	3 45	4 02	4 66	5.36	6 14	26
28	.07	15	28	43	63	.86	1.13	1 44	1 80	2 20	2 65	3 15	3 71	4 33	5 02	5 77	6 61	28
30	.07	17	29	46	.67	92	1 21	1 54	1 93	2 36	2 84	3.38	3 98	4 64	5 38	6 19	7.08	30
32	08	.18	31	49	.71	.98	1 29	1 65	2.05	2 51	3.03	3.60	4 24	4 95	5 73	6 60	7.55	32
34	08	.19	33	52	76	1 04	1 37	1 75	2 18	2 67	3.22	3 83	4.51	5.26	6 09	7 01	8 03	34
36	09	20	35	56	80	1 10	1 45	1.85	2.31	2.83	3 41	4 05	4.77	5.57	6.45	7.42	8 50	36
38	.09	21	.37	59	85	1.16	1.53	1 96	2 44	2 98	3 60	4 28	5.04	5 88	6.81	7.84	8 97	38
40	.10	22	39	62	.89	1 22	1 61	2 06	2 57	3 14	3 79	4.50	5.30	6 19	7 17	8.25	9 44	40
42	10	23	41	65	94	1 29	1.69	2 16	2 70	3.30	3 97	4.73	5.57	6 50	7 53	8 66	9 91	42
44	11	.24	.43	68	98	1 35	1 77	2 26	2 82	3.46	4.16	4 95	5.83	6 81	7 88	9.07	10 39	44
46	11	25	45	71	1 03	1 41	1 85	2 37	2.95	3.61	4.35	5 18	6 10	7 12	8 24	9.49	10 86	46
48	.12	26	.47	74	1.07	1.47	1.93	2 47	3 08	3.77	4 54	5 40	6.36	7.43	8 60	9.90	11 33	48
50	.12	28	49	77	1.12	1 53	2 02	2.57	3 21	3 93	4.73	5 63	6 63	7.74	8.96	10.31	11 80	50
52	13	29	51	80	1 16	1 59	2 10	2 68	3 34	4 08	4 92	5 86	6 89	8 04	9 32	10 72	12.28	52
54	13	.30	53	83	1 21	1 65	2 18	2 78	3 47	4.24	5 11	6.08	7.16	8 35	9.68	11 14	12 75	54
56	14	31	55	86	1 25	1 71	2 26	2 88	3.59	4 40	5.30	6.31	7 42	8.66	10 03	11.55	13 22	56
58	14	32	.57	89	1.30	1 78	2.34	2 98	3 72	4 55	5 49	6 53	7 69	8 97	10.39	11 96	13 69	58
60	.15	33	.59	93	1.34	1 84	2.42	3.09	3 85	4 71	5.68	6 76	7.95	9.28	10 75	12 37	14 16	60
62	15	34	61	96	1 39	1 90	2 50	3.19	3 98	4 87	5.87	6 98	8 22	9.59	11.11	12 79	14.64	62
64	16	.35	63	99	1.43	1 96	2 58	3 29	4 11	5 03	6.06	7.21	8 48	9.90	11.47	13.20	15 11	64
66	16	36	65	1 02	1 47	2 02	2.66	3 40	4 24	5 18	6.25	7.43	8 75	10.21	11 83	13.61	15 58	66
68	17	37	67	1 05	1.52	2 08	2.74	3 50	4 36	5.34	6 44	7.66	9 01	10 52	12 18	14 02	16 05	68
70	.17	39	69	1.08	1.56	2 14	2 82	3 60	4 49	5 50	6 62	7 88	9 28	10 83	12.54	14 44	16.52	70
72	18	40	71	1 11	1 61	2 20	2 90	3 71	4 62	5 65	6 81	8 11	9 55	11 14	12.90	14.85	17 00	72
74	.18	41	73	1 14	1 65	2 27	2 98	3 81	4 75	5 81	7 00	8 33	9 81	11.45	13.26	15.26	17 47	74
76	19	.42	.75	1 17	1 70	2 33	3 06	3 91	4 88	5 97	7.19	8.56	10 08	11 76	13.62	15.67	17.94	76
78	19	43	77	1 20	1.74	2 39	3.14	4.01	5.01	6 13	7 38	8.78	10 34	12 07	13.98	16.09	18 41	78
80	.20	44	.79	1 23	1 79	2 45	3 22	4 12	5 13	6 28	7.57	9.01	10 61	12 38	14 33	16.50	18.89	80
82	20	45	81	1 27	1 83	2 51	3 30	4 22	5 26	6 44	7 76	9.23	10 87	12 69	14 69	16 91	19 36	82
84	20	.46	83	1 30	1 88	2 57	3.39	4 32	5 39	6.60	7 95	9 46	11.14	12.99	15.05	17.32	19.83	84
86	21	47	85	1 33	1.92	2 63	3.47	4 43	5 52	6 75	8 14	9.68	11.40	13.30	15 41	17.73	20.30	86
88	21	48	.87	1 36	1 97	2 69	3.55	4.53	5.65	6.91	8.33	9.91	11 67	13 61	15.77	18.15	20 77	88
90	.22	50	.88	1 39	2 01	2 75	3 63	4 63	5 78	7 07	8.52	10.13	11 93	13 92	16 13	18.56	21 25	90
92	22	.51	90	1 42	2 06	2 82	3 71	4 73	5 90	7 22	8 71	10 36	12 20	14 23	16.48	18.97	21 72	92
94	.23	52	92	1.45	2.10	2 88	3.79	4 84	6 03	7.38	8 90	10 58	12.46	14 54	16 84	19 38	22.19	94
96	.23	53	.94	1 48	2 14	2 94	3.87	4 94	6 16	7.54	9 09	10 81	12 73	14.85	17 20	19 80	22.66	96
98	.24	54	.96	1 51	2 19	3.00	3 95	5.04	6.29	7 70	9.27	11.03	12 99	15.16	17 56	20.21	23 13	98
100	24	55	98	1 54	2 23	3.06	4 03	5 15	6.42	7 85	9.46	11 26	13 26	15 47	17 92	20.62	23.61	100

TABLE 6.—*Air-correction table, giving difference, in meters, between vertical length and slant length of sounding line above water surface for selected vertical angles*

Vertical length (m)	Vertical angle of sounding line at protractor (degrees)																												
	5	8	10	11	12	13	14	15	16	17	18	19	20	21	22	23	24	25	26	27	28	29	30	31	32	33	34	35
1	0 00	0 01	0 02	0 02	0 02	0 03	0 03	0 04	0 04	0 05	0 05	0.06	0 06	0 07	0 08	0 09	0.09	0 10	0 11	0.12	0 13	0.14	0 16	0 17	0 18	0.19	0 21	0.22
2	01	02	03	.04	04	05	06	07	08	09	.10	11	13	14	16	.17	.19	.21	22	24	26	29	.31	33	36	38	41	44
3	01	03	04	05	07	08	09	10	12	.14	16	17	19	21	.24	26	28	31	34	37	40	43	46	50	54	58	.62	.66
4	02	04	06	07	.09	.11	12	14	16	18	.21	23	26	28	.32	.34	.38	42	45	.49	.53	57	62	67	72	.77	82	88
5	02	05	08	09	11	14	16	18	20	23	26	29	32	35	40	43	47	.52	.56	61	66	72	78	.84	90	96	1 03	1 10
6	05	05	10	.10	15	.15	20	20	25	.30	30	35	40	45	.45	50	.55	60	.65	75	.80	.85	95	1.00	1.05	1.15	1 25	1 35
7	05	05	10	15	.15	20	20	25	30	30	35	40	45	50	.55	.60	65	.75	80	85	90	1 00	1 10	1 15	1 25	1 35	1 45	1 55
8	05	10	10	15	20	20	25	30	35	35	.40	45	50	55	65	.70	75	85	90	1.00	1 05	1.15	1 25	1.35	1.45	1.55	1 65	1.75
9	05	10	15	15	20	25	.30	30	35	40	45	50	60	65	70	.75	.85	95	1 00	1.10	1 20	1.30	1 40	1.50	1 60	1.75	1 85	2 00
10	.05	.10	15	20	20	25	30	35	.40	45	50	55	65	70	.80	85	95	1 05	1 10	1.20	1 30	1.45	1 55	1.65	1 80	1.90	2 05	2.20
11	1	.1	2	.2	2	3	3	4	4	.5	6	6	7	8	.9	1 0	1 0	1.1	1 2	1.3	1 4	1 6	1 7	1.8	2 0	2.1	2 3	2 4
12	1	1	2	2	3	3	4	4	5	6	6	7	8	8	1 0	1.0	1 1	1 2	1 3	1.5	1 6	1 7	1 9	2 0	2 2	2.3	2.5	2 6
13	1	1	.2	2	3	4	4	.5	5	6	7	7	9	9	1 0	1 1	1 2	1 4	1 5	1 6	1.7	1.9	2 0	2.2	2.3	2 5	2 7	2 9
14	1	1	2	2	3	4	4	5	.6	6	7	8	.9	1.0	1 1	1 2	1 3	1 5	1.6	1 7	1.8	2 0	2 2	2 3	2 5	2 7	2 9	3 1
15	.1	2	2	3	3	4	5	5	6	7	8	9	1 0	1.1	1.2	1 3	1.4	1 6	1.7	1.8	2.0	2 1	2 3	2.5	2 7	2 9	3.1	3.3
16	1	2	2	.3	.4	4	5	6	7	.7	8	9	1 0	1 1	1 3	1 4	1 5	1 7	1 8	2 0	2 1	2 3	2 5	2 7	2.8	3.1	3 3	3.5
17	1	2	3	.3	.4	.5	5	6	7	8	.9	1 0	1 1	1 2	1 3	1.5	1.6	1 8	1 9	2.1	2 2	2.4	2.6	2 8	3 0	3.3	3 5	3 8
18	1	2	3	.3	4	5	6	6	7	8	9	1 0	1.2	1.3	1 4	1 5	1 7	1 9	2 0	2 2	2 4	2 6	2 8	3 0	3 2	3 5	3 7	4.0
19	1	2	.3	3	4	5	6	.7	.8	9	1 0	1 1	1 2	1 4	1 5	1 6	1 8	2 0	2.1	2 3	2.5	2 7	2 9	3 2	3.4	3 6	3 9	4.2
20	1	2	.3	4	4	5	.6	7	.8	9	1 0	1 1	1 3	1 4	1.6	1 7	1 9	2.1	2.2	2 4	2.6	2 9	3.1	3 3	3.6	3.8	4 1	4.4

selected intervals on the sounding line, and then using the tags to reference the water surface. This practice is almost equivalent to moving the reel to a position just above the water surface.

The correction for excess length of line below the water surface is obtained by using an elementary principle of mechanics. If a known horizontal force is applied to a weight suspended on a cord, the cord takes a position of rest at some angle with the vertical, and the tangent of the vertical angle of the cord is equal to the horizontal force divided by the vertical force of the weight. If several additional horizontal and vertical forces are applied to the cord, the tangent of the angle in the cord above any point is equal to a summation of the horizontal forces below that point, divided by the summation of the vertical forces below the point.

The distribution of total horizontal drag on the sounding line is in accordance with the variation of velocity with depth. The excess in length of the curved line over the vertical depth is the sum of the products of each tenth of depth and the function $(1/\cos P)-1$ of the corresponding angles; the function is derived for each tenth of depth by means of the tangent relation of the forces acting below any point.

The wet-line correction for even-numbered angles between 4° and 36° and for wet-line depths between 10 and 100 ft is shown in table 7. (Table 8 is a similar table in metric units.) The correction is applied to the nearest tenth of a foot. The wet-line correction cannot be determined until the air correction has been deducted from the observed depth.

The following assumptions were used in deriving the wet-line correction tables:

1. The weight will go to the bottom despite the force of the current.
2. The sounding is made when the weight is at the bottom but entirely supported by the line.
3. Drag on the streamlined weight in the sounding position is neglected.
4. The table is general and can be used for any size sounding weight or line that is designed to offer little resistance to the current.

If the direction of flow is not perpendicular to the measuring section, the angle of the measuring line as indicated by the protractor will be less than the true angle of the line. The air correction and wet-line correction will then be too small. To correct for this it is necessary to either measure by protractor the horizontal angle between the direction of flow and a perpendicular to the measurement section, or determine the horizontal-angle coefficient by the methods described on pages 142–143.

If the horizontal angle of the direction of flow is called H, the measured vertical angle P, and the true vertical angle X, the relation

TABLE 7.—*Wet-line table, giving difference, in feet, between wet-line length and vertical depth for selected vertical angles*

Wet-line length (ft)	Vertical angle of sounding line at protractor																	Wet-line length (ft)
	4°	6°	8°	10°	12°	14°	16°	18°	20°	22°	24°	26°	28°	30°	32°	34°	36°	
10	0 01	0 02	0.03	0.05	0 07	0.10	0.13	0.16	0 20	0.25	0.30	0 35	0.41	0 47	0.54	0 62	0 70	10
12	01	.02	04	.06	09	.12	15	.20	24	.30	.36	.42	49	.57	.65	74	.84	12
14	01	02	.04	.07	.10	.14	18	23	29	.35	.41	.49	.57	66	76	.87	98	14
16	.01	03	05	08	12	.16	20	.26	.33	40	47	56	.65	.76	.87	.99	1.12	16
18	.01	.03	06	.09	13	.18	23	.30	.37	45	.53	63	73	.85	.98	1 12	1.26	18
20	.01	03	06	.10	14	20	26	33	41	50	.59	.70	.82	94	1 09	1.24	1.40	20
22	01	.04	07	.11	16	22	.28	.36	.45	55	65	.77	90	1.04	1.20	1 36	1.54	22
24	.01	04	.08	12	.17	24	31	39	49	60	.71	84	98	1 13	1 31	1 49	1 68	24
26	.02	04	08	.13	19	25	33	43	53	.64	77	91	1 06	1 23	1.41	1.61	1.81	26
28	.02	.04	09	.14	20	27	.36	.46	.57	69	83	98	1 14	1.32	1.52	1.74	1.95	28
30	02	.05	.10	.15	.22	29	38	.49	61	.74	.89	1 05	1 22	1.42	1.63	1 86	2.09	30
32	02	05	.10	.16	.23	31	41	52	65	.79	.95	1 12	1.31	1.51	1.74	1.98	2 23	32
34	.02	05	11	.17	24	.33	.44	56	.69	.84	1 01	1 19	1.39	1.60	1 85	2.11	2.37	34
36	.02	06	12	.18	26	35	46	59	73	.89	1.07	1 26	1.47	1.70	1.96	2.23	2.51	36
38	02	06	12	19	.27	.37	49	62	78	94	1.12	1 33	1 55	1.79	2.07	2.36	2.65	38
40	02	.06	.13	20	29	39	51	.66	.82	.99	1 18	1.40	1 63	1 89	2 18	2.48	2.79	40
42	03	07	13	.21	.30	41	54	69	.86	1 04	1 24	1.47	1.71	1.98	2.28	2 60	2.93	42
44	03	07	14	.22	.32	43	56	.72	90	1 09	1 30	1 54	1.80	2.08	2 39	2.73	3.07	44
46	03	07	.15	.23	33	.45	59	75	94	1.14	1.36	1 61	1.88	2.17	2.50	2.85	3.21	46
48	03	08	15	.24	.35	.47	61	79	98	1.19	1.42	1 68	1.96	2.27	2.61	2 98	3.35	48
50	03	08	16	25	36	.49	64	82	1 02	1 24	1.48	1 75	2.04	2.36	2 72	3.10	3 49	50
52	03	.08	17	26	.37	51	.67	.85	1 06	1 29	1 54	1.82	2 12	2 45	2.83	3 22	3 63	52
54	.03	.09	.17	.27	.39	.53	69	89	1.10	1 34	1.60	1 89	2 20	2 55	2 94	3 35	3 77	54
56	.03	09	18	.28	40	.55	72	92	1 14	1.39	1 66	1 96	2.28	2 64	3 05	3.47	3 91	56
58	03	09	19	29	.42	57	74	.95	1.18	1 44	1 72	2 03	2 37	2.74	3 16	3 60	4 05	58
60	04	10	19	.30	.43	59	.77	.98	1.22	1 49	1.78	2 10	2.45	2 83	3 26	3.72	4 19	60
62	04	.10	20	31	45	61	.79	1 02	1 26	1.54	1 84	2 17	2.53	2 93	3.37	3.84	4 33	62
64	.04	10	20	32	46	63	.82	1 05	1 31	1.59	1.89	2 24	2 61	3 02	3 48	3 97	4 47	64
66	04	11	21	33	.48	65	.84	1 08	1 35	1 64	1.95	2 31	2.69	3 12	3 59	4 09	4 61	66
68	04	11	.22	.34	49	.67	87	1 12	1 39	1.69	2 01	2 38	2 77	3.21	3 70	4.22	4 75	68
70	04	11	22	.35	50	69	90	1.15	1 43	1.74	2 07	2 45	2.86	3.30	3 81	4 34	4 89	70
72	04	.12	23	.36	52	71	92	1.18	1 47	1 79	2 13	2.52	2.94	3 40	3 92	4 46	5 03	72
74	.04	12	24	37	53	73	95	1.21	1 51	1.84	2 19	2.59	3.02	3.49	4 03	4 59	5 17	74
76	.05	12	.24	.38	55	.74	97	1 25	1.55	1.88	2.25	2 66	3.10	3 59	4 13	4 71	5.30	76
78	.05	12	25	.39	56	76	1 00	1 28	1.59	1.93	2.31	2 73	3.18	3 68	4.24	4 84	5 44	78
80	05	.13	25	40	58	78	1.02	1 31	1.63	1 98	2.37	2.80	3 26	3.78	4.35	4 96	5.58	80
82	.05	13	26	.41	59	80	1 05	1 34	1 67	2.03	2 43	2 87	3.35	3 87	4.46	5 08	5.72	82
84	05	13	27	42	60	82	1 08	1.38	1.71	2.08	2 49	2 94	3.43	3 96	4 57	5.21	5.86	84
86	.05	.13	.28	.43	.62	84	1.10	1 41	1.75	2 13	2.55	3 01	3.51	4 06	4 68	5.33	6 00	86
88	05	.14	28	.44	63	86	1 13	1 44	1.80	2 18	2.60	3 08	3.59	4 15	4 79	5.46	6.14	88
90	05	14	29	45	65	88	1.15	1 48	1 84	2.23	2 66	3 15	3.67	4.25	4.90	5 58	6 28	90
92	06	15	29	.46	66	90	1 18	1.51	1 88	2.28	2.72	3 22	3 75	4 34	5.00	5 70	6 42	92
94	06	15	30	.47	68	92	1.20	1 54	1 92	2.33	2.78	3 29	3.84	4 44	5.11	5 83	6.56	94
96	06	15	31	48	.69	.94	1 23	1 57	1 96	2 38	2.84	3 36	3.92	4.53	5 22	5 95	6.70	96
98	.06	16	31	49	71	96	1 25	1.61	2 00	2.43	2.90	3 43	4.00	4 63	5.33	6 08	6.84	98
100	.06	16	32	50	72	98	1 28	1 64	2 04	2.48	2 96	3.50	4 08	4 72	5.44	6.20	6 98	100

TABLE 8.—*Wet-line table, giving difference, in meters, between wet-line length and vertical depth for selected vertical angles*

Wet-line length (m)	Vertical angle of sounding line at protractor (degrees)																								
	10	11	12	13	14	15	16	17	18	19	20	21	22	23	24	25	26	27	28	29	30	31	32	33	34	35
1	0.01	0 01	0.02	0.02	0.02	0 03	0.03	0 03	0 03	0.04	0 04	0 04	0.05	0.05	0 06	0 06	0 07	0.07	0 08	0.08	0 09	0 10	0 10	0 11	0.12	0.12
2	02	02	03	03	04	.04	.05	.05	06	.06	07	.08	.08	.09	.09	.10	11	.11	.12	13	14	15	.16	17	18	.19
3	.03	04	.04	05	.05	.06	.06	07	.08	.08	09	10	11	.12	.13	.14	.15	16	.18	.19	20	.21	.23	.24	.26	27
4	.03	04	.04	.05	.06	07	.08	09	.10	.11	12	13	14	16	17	18	19	21	.22	.24	25	27	28	.30	32	.34
5	.04	.05	05	05	.07	08	.09	10	.11	.13	.14	15	17	.18	20	22	24	.26	27	29	31	33	35	.38	40	.42
6	.05	05	.05	.05	.10	10	.10	10	15	.15	15	.15	.20	.20	25	25	25	.30	.30	35	35	40	.40	45	45	.50
7	05	05	.05	.10	10	.10	.10	15	.15	15	20	20	25	.25	.25	.30	.30	35	35	.40	.40	45	.45	.50	.50	.55
8	.05	05	10	10	10	10	.15	.15	.15	.20	20	25	25	30	30	.35	.35	.40	.40	.45	.45	.50	55	.55	.55	65
9	05	10	.10	10	.10	.15	15	.20	20	.20	25	.25	.30	.30	35	35	.40	.45	45	50	55	.55	60	65	.70	.70
10	.05	10	10	10	.15	.15	.15	.20	20	.25	25	30	30	.35	35	.40	.45	.45	.50	.55	60	60	65	.70	75	.80
11	1	1	1	1	2	.2	.2	.2	.2	.3	.3	.3	3	4	4	.4	.5	.5	6	6	6	7	.7	8	.8	.9
12	.1	.1	.1	.1	.2	.2	.2	.2	.3	3	3	3	4	4	4	.5	.5	.6	.6	6	.7	.7	.8	.8	9	9
13	.1	1	1	1	.2	.2	.2	2	3	.3	3	.4	.4	4	5	.5	.6	6	7	.7	.8	8	.9	9	1.0	1 0
14	.1	.1	.1	1	.2	2	.2	3	.3	3	4	4	.4	.5	5	6	6	7	7	.8	.8	.9	.9	1.0	1 0	1 1
15	1	1	.1	2	.2	.2	2	3	3	3	.4	4	5	.5	.5	6	.6	7	7	.8	.8	9	1.0	1 0	1 1	1.2
16	.1	1	1	2	.2	.2	3	.3	3	.4	.4	.4	.5	.5	6	.6	.7	7	.8	.8	.9	1 0	1.0	1.1	1 2	1.2
17	.1	1	2	2	.2	2	.3	3	3	4	4	.5	.5	.6	6	.7	.7	8	.8	.9	1 0	1.0	1.1	1.2	1 2	1.3
18	1	1	.2	.2	2	.3	.3	.3	.4	4	5	5	6	6	.7	7	8	.8	.9	.9	1.0	1 1	1 2	1 2	1 3	1 4
19	1	.1	.2	2	.2	.3	.3	.3	.4	.4	.5	5	6	.6	.7	.7	.8	.8	.9	1 0	1.1	1 1	1.2	1 3	1.4	1 5
20	.1	.2	2	2	.2	.3	.3	4	4	5	5	.6	.6	7	.7	.8	.8	.9	1 0	1.1	1 1	1.2	1 3	1.4	1 5	1 6

between the angles is expressed by the equation

$$\tan X = \frac{\tan P}{\cos H} \text{ (fig. 100).} \qquad (12)$$

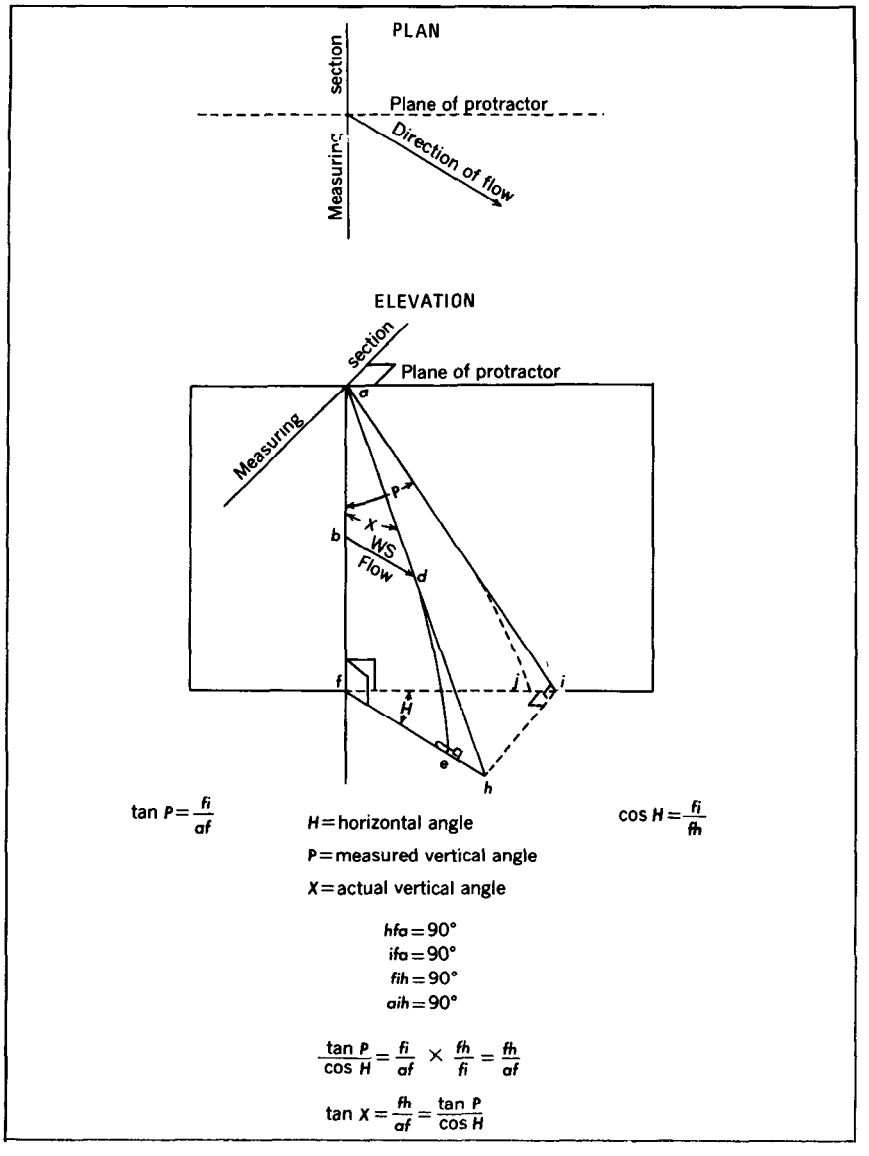

FIGURE 100.—Sketch of geometry of relation of actual to measured vertical angle when flow direction is not normal to measurement section.

Table 9 gives the quantities in tenths of degrees, to be added to observed vertical angles to obtain the true vertical angles for a range of horizontal angles between 8° and 28°.

The conditions that cause error in sounding the depth also cause error in setting the meter at selected depths. The correction tables are not strictly applicable to the problem of setting the meter for velocity observations because of the increased horizontal force on the sounding weight caused by higher velocities when the weight is raised from the streambed. A meter placed in deep, swift water by the ordinary methods for observations at selected percentages of the depth will be too high in the water. The use of tables 5–9 will tend to eliminate this error in the placement of the meter, and although not strictly applicable, their use for this purpose has become general.

For the 0.2-depth position, the curvature of the wet line is assumed to be negligible, and the length of sounding line from the apex of the vertical angle to the weight is considered a straight line. The method used to place the meter at the 0.2-depth position is as follows:

1. Compute the 0.2 value of the vertical depth.
2. Lower the meter this depth into the water and read the vertical angle.
3. Obtain the air correction from table 5 or 6. The vertical length used to obtain the air correction is the sum of (a) 0.2 of the vertical depth, (b) the distance from the water surface to the apex of the angle, and (c) the distance from the bottom of the weight to the meter.
4. Let out an additional amount of line equal to the air correction.
5. If the angle increases appreciably when the additional line is let out, let out more line until the total additional line, the angle, and the vertical distance are in agreement with figures in the air-correction table.

To set the meter at the 0.8-depth position, a correction to the amount of line reeled in must be made for the difference, if any, between the

TABLE 9.—*Degrees to be added to observed vertical angles to obtain actual vertical angles when flow direction is not normal to measurement section*

Observed vertical angle	Horizontal angle					
	8° cos=0.99	12° cos=0 98	16° cos=0 96	20° cos=0 94	24° cos=0 91	28° cos=0.88
8°	0.1	0.2	0.3	0.5	0.8	1.0
12°	.1	.3	.5	.8	1.1	1.5
16°	.1	.4	.6	1.0	1.4	2.0
20°	.2	.4	.7	1.2	1.7	2.4
24°	.2	.5	.8	1.4	2.0	2.8
28°	.2	.5	1.0	1.5	2.2	3.0
32°	.2	.6	1.0	1.6	2.4	3.3
36°	.2	.6	1.1	1.7	2.5	3.4

air correction for the sounding position and that for the 0.8-depth position. This difference is designated as m in table 10. If the angle increases for the 0.8-depth position, the meter must be lowered; if the angle decreases the meter must be raised.

In setting the 0.8-depth position of the meter, the wet-line correction may require consideration if the depths are more than 40 ft and if the change in vertical angle is more than 5 percent. If the vertical angle remains the same or decreases, the wet-line correction (table 7 or 8) for the 0.8-depth position is less than the wet-line correction for the sounding position by some difference designated as n in table 10. If the vertical angle increases, the difference in correction n deminishes until the increase in angle is about 10 percent; for greater increases in angle, the difference between corrections also increases. Table 10 summarizes the effect on air- and wet-line corrections caused by raising the meter from the sounding position to the 0.8-depth position.

For slight changes in the vertical angle, because of the differences m and n in the air- and wet-line corrections, the adjustments to the wet-line length of the 0.8-depth position are generally small and usually can be ignored. Table 10 indicates, however, that the meter may be placed a little too low if the adjustments are not made. Because of this possibility, the wet-line depth instead of the vertical depth is sometimes used as the basis for computing the 0.8-depth position, and no adjustments are made for the differences m and n.

CASE B. DEPTH CANNOT BE SOUNDED BUT STANDARD CROSS SECTION IS AVAILABLE

On occasion it is not possible to sound the bottom, but a standard measurement cross section at the bridge or cableway may be available from previous measurements that were made. Such a cross section

TABLE 10.—*Summary table for setting the meter at 0.8-depth position in deep, swift streams*

Change in vertical angle	Air correction		Wet-line correction	
	Direction of change	Correction to meter position	Direction of change	Correction to meter position
None	None	None	Decrease	Raise meter the distance n.
Decrease	Decrease	Raise meter the distance m.	do	Do.
Increase	Increase	Lower meter the distance m.	Decrease, then increase.	[1]

[1] Raise meter the distance n unless the increase in angle is greater than about 10 percent, then it is necessary to lower the meter the distance n.

will be useful only if all discharge measurements use the same permanent initial point for the stationing of verticals across the width of the stream, and if there is an outside reference gage or reference point on the bank or bridge to which the water-surface elevation at the measurement cross section may be referred. In the situation described above, the following procedure is used:

1. Determine depths at the observation verticals from the standard cross section and the known water-surface elevation at the measurement cross section.
2. Measure the velocity at 0.2 of the depth.
3. Compute the measurement in the normal manner using the measured velocities as though they were the mean velocities in the vertical, and using the depths from step 1.
4. Determine the coefficient to adjust the 0.2-depth velocity to mean velocity in the cross section, as explained on pages 135–136.
5. Apply the coefficient from step 4 to the computed discharge from step 3.

CASE C. DEPTH CANNOT BE SOUNDED AND NO STANDARD CROSS SECTION IS AVAILABLE

When it is not possible to sound the depth and a standard cross section is not available, the following procedure is used:

1. Refer the water-surface elevation before and after the measurement to an elevation reference point on a bridge, on a driven stake, or on a tree at the water's edge. (It is assumed here that no outside reference gage is available at the measurement cross section.)
2. Estimate the depth and observe the velocity at 0.2 of the estimated depth. The meter should be at least 2.0 ft (0.6 m) below the water surface. Record in the notes the actual depth the meter was placed below the water surface. If an estimate of the depth is impossible, place the meter 2.0 ft below the water surface and observe the velocity there.
3. Make a complete measurement at a lower stage and include some vertical-velocity curves.
4. Use the complete measurement and difference in stage between the two measurements to determine the cross section of the first measurement. To determine whether the streambed has shifted, the cross section should be compared with one obtained in a previous measurement at that site.
5. Use vertical-velocity curves, or the relationship between mean velocity and 0.2-depth velocity, to adjust the velocities observed in step 2 to mean velocity.
6. Compute the measurement in the normal manner using the depths from step 4 and the velocities from step 5.

CASE D. METER CANNOT BE SUBMERGED

If it is impossible to keep the meter and weight in the water because of high velocities and (or) floating drift, use the following procedure:

1. Obtain depths at the measurement verticals by the method explained for case B if a standard cross section is available, or by the method explained above for case C if no standard cross section is available.
2. Measure surface velocities with an optical current meter, as explained on pages 91–93, 137–138.
3. Compute the measurement in the normal manner using the surface velocities as though they were the mean velocities in the vertical, and using the depths from step 1.
4. Apply the appropriate velocity coefficient to the discharge computed in step 3; use a coefficient of 0.86 for a natural channel and 0.90 for an artificial channel.

If an optical current meter is not available, time floating drift over a measured course. (See p. 261–262.)

It should be noted here that the amount of floating drift or ice is usually greatly reduced just after the crest of a rise in stage. It may be possible at that time to obtain velocity observations with a standard current meter.

COMPUTATION OF MEAN GAGE HEIGHT OF A DISCHARGE MEASUREMENT

The mean gage height of a discharge measurement represents the mean stage of the stream during the measurement period. Because the mean gage height for a discharge measurement is one of the coordinates used in plotting the measurements to establish the stage-discharge relation, an accurate determination of the mean gage height is as important as an accurate measurement of the discharge. The computation of the mean gage height presents no problem when the change in stage is uniform and no greater than about 0.15 ft (0.05 m), for then the mean may be obtained by averaging the stage at the beginning and end of the measurement. However, measurements must often be made during periods when the change of stage is neither uniform nor slight.

As a prerequisite for obtaining an accurate mean gage height, the clock time at the beginning and end of the measurement should be recorded on the measurement notes, and additional readings of the clock time should be recorded on the notes at intervals of 15 to 20 min during the measurement. After the discharge measurement has been completed, the recorder chart should be read, and breaks in the slope of the gage-height graph that occurred during the measurement should be noted The breaks in slope are useful in themselves and are

also used to determine the gage height corresponding to the clock times noted during the measurement. If the station is equipped with a digital recorder, the gage-height readings punched during the measurement are to be read. At nonrecording stations the only way to obtain intermediate readings is for the stream gager to stop a few times during the measurement to read the gage, or to have someone else do this for him.

If the change in stage is greater than 0.15 ft (0.05 m) or if the change in stage has not been uniform, the mean gage height is obtained by weighting the gage heights corresponding to the clock-time observations. The weighting is done by using either partial discharge or time as the weighting factor. In the past the weighting in the U.S.A. was always done on the basis of partial discharges, but recent study indicates that discharge-weighting usually tends to overestimate the mean gage height, whereas time-weighting usually tends to underestimate the mean gage height. On the basis of the present state of our knowledge, it is suggested that the mean gage height for a discharge measurement be computed by both methods, after which the two results are averaged. A description of the two methods follows.

In the discharge-weighting process, the partial discharges measured between clock observations of gage height are used with the mean gage heights for the periods when the partial discharges were measured. The formula used to compute mean gage height is

$$H = \frac{q_1h_1 + q_2h_2 + q_3h_3 \ldots\ldots\ldots + q_nh_n}{Q}, \qquad (13)$$

in which

H = mean gage height (ft or m),

Q = total discharge measured (ft^3/s or m^3/s) = $q_1 + q_2 + q_3 \ldots . + q_n$,

where

$q_1, q_2, q_3, \ldots . q_n$ = discharge (ft^3/s or m^3/s) measured during time interval 1, 2, 3, ... n and

$h_1, h_2, h_3, \ldots . h_n$ = average gage height (ft or m) during time interval 1, 2, 3, ... n.

Figure 101 shows the computation of a discharge-weighted mean gage height. The graph at the bottom of figure 101 is a reproduction of the gage-height graph during the discharge measurement. The discharges are taken from the current-meter measurement notes shown in figure 42. The upper computation of the mean gage height in figure 101 shows the computation using equation 13. The lower computation has been made by a shortcut method to eliminate the multiplication

of large numbers. In that method, after the average gage height for each time interval has been computed, a base gage height, which is usually equal to the lowest average gage height, is chosen. Then, the

Angle coef. factor	Dist. from initial point (1)	Width (2)	Depth (3)	Observation depth	Revolutions (4)	Time in seconds	VELOCITY: At point	VELOCITY: Mean in vertical	Adjusted for hor. angle or	Area	Discharge
	Time	GHt.	Ave. GHt.		Q		(3)×(4)				
	1330	1.94	1.92		16.10		30.91				
	1345	1.90	1.70		24.31		41.33				
	1400	1.49	1.67		20.99		35.05				
	1415	1.85	1.88		14.97		28.14				
	1430	1.92									
			Total Q =		76.37	Total =	135.43				
0	M.G.H. =		Total (3)×(4) / Total Q		=	135.43 / 76.37	=	1.77			1.00

	Time (1)	G Ht. (2)	Ave. G Ht. (3)	Ave. G Ht. minus base (4)	Q (5)		(4)×(5)		
	1330	1.94	1.92	.25	16.10		4.02		
	1345	1.90	1.70	.03	24.31		.73		
	1400	1.49	1.67	.00	20.99		.00		
	1415	1.85	1.88	.21	14.97		3.14		
	1430	1.92							
	Base	1.67		Total Q =	76.37	Total =	7.89		
	MGH = Base +		Total (4)×(5) / Total Q		=	1.67 + 7.89/76.37	=	1.67+.10 = 1.77	

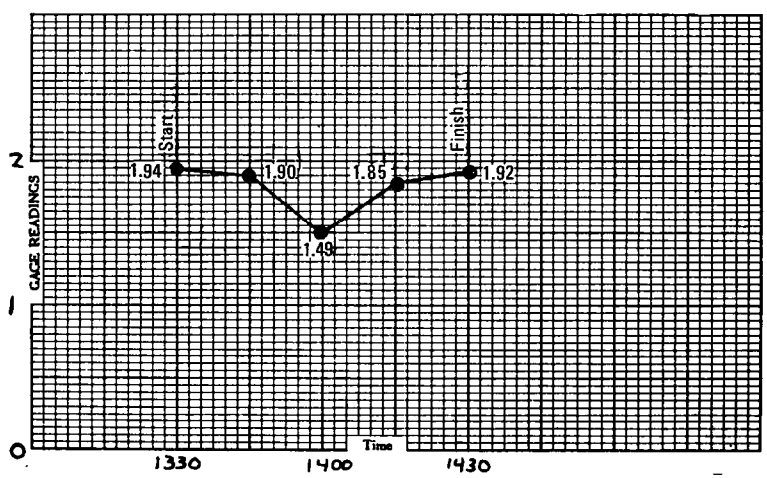

FIGURE 101.—Computation of discharge-weighted mean gage height.

differences between the base gage height and the average gage heights are used to weight the discharges. When the mean difference has been computed, the base gage height is added to it.

In the time-weighting process, the arithmetic mean gage height for time intervals between breaks in the slope of the gage-height graph are used with the duration of those time periods. The formula used to compute mean gage height is

$$H = \frac{t_1h_1 + t_2h_2 + t_3h_3 \ldots\ldots + t_nh_n}{T} \qquad (14)$$

in which

H = mean gage height, in feet or meters,

T = total time for the measurement, in minutes = $t_1 + t_2 + t_3 \ldots\ldots t_n$,

$t_1, t_2, t_3 \ldots\ldots t_n$ = duration of time intervals between breaks in slope of the gage-height graph, in minutes, and

$h_1, h_2, h_3 \ldots\ldots h_n$ = average gage height, in feet or meters, during time interval 1, 2, 3, ... n.

Using the data from figure 101, the computation of the time-weighted mean gage height is as follows:

Average gage height (*h*)	*Time interval* (*t*)	*h* × *t*
1.92	15	28.80
1.70	15	25.50
1.67	15	25.05
1.88	15	28.20
Total	60	107.55

Mean gage height = 107.55/60 = 1.79 ft

In the example used above there is little difference between the discharge-weighted mean gage height (1.77 ft) and the time-weighted mean gage height (1.79 ft); the average of the two values, 1.78 ft, is the preferred mean gage height for the discharge measurement.

When extremely rapid changes in stage occur during a measurement, the weighted mean gage height is not truly applicable to the discharge measured. To reduce the range in stage during the measurement, measurements under those conditions should be made more rapidly than those made under constant or slowly changing stage. It should be realized, however, that shortcuts in the measurement procedure usually reduce the accuracy of the measured discharge. Therefore measurement procedures during rapidly changing stage must be optimized to produce a minimal combined error in measured discharge and computed mean gage height.

MEASUREMENT PROCEDURES DURING RAPIDLY CHANGING STAGE

The preceding discussion on computing the mean gage height of discharge measurements demonstrated that under conditions of rapidly changing stage, measurement procedures must be streamlined, even at the expense of some accuracy. The reduction in measurement time makes it possible to obtain a gage-height value that is representative of the measured discharge. Where streams are uncontrolled, flood rises are more rapid on small streams than on large streams, because small streams are subject to flash floods that may rise and fall with sufficient rapidity to produce peak flows of almost momentary duration. Consequently the discussion that follows distinguishes between the procedures to be followed for measuring large streams and those for small streams, during periods of rapidly changing stage. The procedure to be followed for measuring streams whose flow is controlled by hydroelectric powerplants was discussed on page 140.

CASE A. LARGE STREAMS

During periods of rapidly changing stage on large streams, the time consumed in making a discharge measurement may be reduced by modifying the standard measurement procedure in the following manner:

1. Use the 0.6-depth method (p. 134). The 0.2-depth method (p. 135) or the subsurface method (p. 136) may be used if placing the meter at the 0.6-depth creates vertical angles requiring time-consuming corrections, or if the vertical angle increases because of drift collecting on the sounding line.
2. Reduce the velocity-observation time to about 20–30 s.
3. Reduce the number of sections taken to about 15–18.

By incorporating all three of the above practices a measurement can be made in 15–20 min. If the subsurface method of observing velocities is used, some vertical-velocity curves will be needed later to establish coefficients to convert observed velocity to mean velocity.

Carter and Anderson (1963) have shown that discharge measurements having 30 verticals, for which the two-point method of observation was used with a 45-s period of observation, will have a standard error of 2.2 percent (see p. 181–183). That means that two-thirds of the measurements made using standard procedures would be in error by 2.2 percent or less. They have also shown that the standard error for a 25-s period of observation, using the 0.6-depth method with depth and velocity observed at 16 verticals, is 4.2 percent. The error caused by using the shortcut method is generally less than the error to be expected as a result of the shifting flow patterns that commonly

occur during periods of rapidly changing stage, and in addition, uncertainty concerning the appropriate mean gage height for the measurement is eliminated.

CASE B. SMALL STREAMS

The discussion that follows deals with the measurement of flash floods on small streams. Flash floods begin and end with such abruptness that if the flow is to be measured, the hydrographer must have advance warning of the occurrence of such an event. The warning will enable him to reach the measuring site and make all necessary preparations for current-meter measurements before the stream starts to rise at the site. Once the rise begins it is essential that the many point observations required be made as rapidly as possible because of the rapidly changing discharge.

After arriving at the measuring site where the flash flood is expected, the hydrographer first marks the location of the observation verticals he intends to use. These marks are placed on the bridge rail or cableway that is used for discharge measurements. He then determines the elevation of the streambed, referred to gage datum, at those verticals. That is done both to save time during the actual discharge measurement and because he may be unable to sound the streambed when the flood is in progress. An auxiliary staff gage that can be read from the measuring bridge or cableway should be part of the gaging equipment.

In measuring the discharge during a flash flood, the procedure differs in the following ways from that used in making a conventional current-meter discharge measurement.

1. *Use 6 to 10 observation verticals in the measurement cross section.*—The actual number of verticals used will depend on the width and uniformity of the cross section. Current-meter observations are started when the stage starts to rise and are continued until the flow recedes to normal, or near-normal stage. After completing one traverse of the cross section, the next traverse is started immediately in the opposite direction, and observations continue to be made back and forth across the stream.

2. *Time is saved by making a single velocity observation at each observation vertical.*—If depths, velocities, and the absence of floating drift permit, the 0.6-depth method (p. 134) or 0.2-depth method (p. 135) is used. Otherwise, an optical current meter is used in the surface-velocity method (p. 137).

3. *Readings of the auxiliary staff gage are made at every third velocity observation and clock time is also recorded.*—That is done because the rapid change in stage will commonly make it impossible to later obtain accurate stages, corresponding to the time of each velocity

observation, from the automatic gaging-station record. Furthermore, during periods of rapidly changing stage, a staff-gage record is usually more reliable than an automatic-gage record because of "drawdown" at the intake or because of well or intake lag. Moreover if the gaging station is equipped with a digital recorder, the frequency of punches will seldom be adequate for a flash flood.

After the stream has receded, determinations of streambed elevation at the observation verticals are again made to learn if scour or fill has occurred. If there has been a change in streambed elevation, the change is prorated with time, or in accordance with the best judgment of the hydrographer, to provide the values of depth needed to compute discharge. The most reliable discharge results are obtained, of course, where the streambed is stable or relatively so, leaving no serious uncertainty about stream depths during the measurement.

4. *Computation procedure*—Normally, the discharge of a stream is computed for each current-meter traverse of the measurement cross section, using observed velocities, depths, and incremental channel widths. Because of the rapid change of stage that occurs during the course of a velocity-observation traverse, that conventional computation procedure should not be used when measuring the discharge of flash floods. If the conventional procedure is used there is great uncertainty as to the stage that applies to the computed discharge value. The recommended computation procedure for a flash flood is as follows.

The first step is to construct an individual relation of mean velocity to stage for each observation vertical. The mean velocity, it will be recalled, is obtained by applying an appropriate coefficient to each observed value of surface or subsurface velocity. For each vertical, mean velocity is plotted against stage, and each point is identified by clock time. A single smooth curve is usually fitted to the points, but the scatter of the points may indicate the need for two curves—one for the rising limb of the hydrograph and the other for the falling limb.

In either event, all the data needed are now available for constructing the stage-discharge relation for the entire cross section. The distance between observation verticals (incremental width) is known, and for any selected stage the corresponding depth and mean velocity at each observation vertical are likewise known. Those data are then used, in the conventional manner, to compute the total discharge corresponding to the selected stage. By repeating that operation for several stages, one obtains a stage-discharge relation for the entire range of stage, or, if necessary, two such relations—one for the rising limb of the hydrograph and one for the falling limb. As a final step, the stage-discharge relation(s) is applied to the stage hydrograph to compute the discharge hydrograph. In the absence of a reliable au-

tomatic stage record, the numerous visually observed values of stage provide the stage hydrograph.

CORRECTION OF DISCHARGE FOR STORAGE DURING MEASUREMENT

If a discharge measurement is made at a significant distance from the gage during a change in stage, the discharge passing the gage during the measurement will not be the same as the discharge at the measurement section because of the effect of channel storage between the measurement section and the gage.

Adjustment is made for channel storage by applying to the measured discharge a quantity obtained by multiplying the channel surface area by the average rate of change in stage in the reach. The equation used is

$$Q_G = Q_m \pm WL \frac{\Delta h}{\Delta t}, \tag{15}$$

where

Q_G = discharge passing the gage control (ft^3/s or m^3/s),
Q_m = measured discharge (ft^3/s or m^3/s),
W = average width of stream between measurement section and control (ft or m),
L = length of reach between measurement section and control (ft or m),
Δh = average change in stage in the reach L during the measurement (ft or m), and
Δt = elapsed time during measurement (s).

A reference point or a temporary gage is set at the measurement cross section if channel storage is likely to be significant. The water-surface elevations at the section and at the gage are determined before and after the measurement to compute Δh. If the measurement is made upstream from the control, the adjustment will be plus for falling stages and minus for rising stages; if made downstream from the control, the adjustment will be minus for falling stages and plus for rising stages.

Figure 102 shows the front sheet of a measurement that has been made 0.6 mi upstream from the control during a period of changing stage. The computation of the adjustment for storage for the measurement shown in figure 102 follows:

Measurement made 0.6 mi upstream, L = 3,170 ft.
Average width (W) between measurement section and control = 150 ft.
Change in stage at control, 5.84 to 6.74 ft = +0.90 ft.
Change in stage at measurement section, 12.72 to 13.74 = +1.02 ft. (Readings taken at measurement section from a reference point before and after measurement.)

Average change in stage (Δh) = (0.90 + 1.02) ÷ 2 = 0.96 ft.
Elapsed time during measurement = 1¼ hr = 4,500 s.
Measured discharge Q_m = 8,494 ft³/s.

$$Q_G = 8{,}494 - 150\,(3{,}170)\,\frac{0.96}{4{,}500} = 8{,}494 - 101 = 8{,}393 \text{ ft}^3/\text{s}.$$ Use 8,390 ft³/s.

9-0776-F
Jan. 1966

UNITED STATES
DEPARTMENT OF THE INTERIOR
GEOLOGICAL SURVEY
WATER RESOURCES DIVISION

Meas. No. 264
Comp. by TJB
Checked by

DISCHARGE MEASUREMENT NOTES

Sta. No. 1-9946.5
Big Creek near Dogwood, Va.
Date Mar. 26, 1962 Party T. J. Buchanan
Width 140 Area 1,040 Vel 8.07 G. H. 6.29 Disch. 8,390
Method 2-8 No. secs. 30 G. H. change +.90 in 1¼ hrs Susp 756
Method coef. 1 Hor. angle coef Varies Susp. coef. 1.00 Meter No. 3684

EST GAGE READINGS				
Time	El. T	Recorder	T Inside	Outside
1415	5.54	5.54	5.54	5.52
1440	Start	5.84		
1500		6.08		
1530		6.44		
1555	Finish	6.74		
1630	7.16	7.16	7.16	7.14
Weighted M G H				
G H correction				
Correct M G H				

Date rated 2-16-62 Used rating
for rod — susp Meter 1.0 ft
above bottom of wt Tags checked Yes
Spin before meas 2:55 after 2:50
Meas plots % diff from rating
Wading, cable, ice, boat, upstr., downstr., side bridge 0.6 feet, mile, above, below gage, and
Check-bar, chain found
changed to at
Correct
Levels obtained

Measurement rated excellent (2%), good (5%), fair (8%), poor (over 8%), based on following conditions Cross section Fairly even; stone and gravel bottom.
Flow Good distribution; some Weather Raining
Other debris flowing. Air 44 °F@ 1635
Gage OK Water 38 °F@ 1635
Record removed Yes Intake flushed
Observer Talked with
Control Clear
Remarks Discharge adjusted for storage effect
Qm = 8,494

G. H. of zero flow ft. Elev. RP = 30.00
RP to WS @ 1440 = 17.28; 30.00 - 17.28 = 12.72
RP to WS @ 1555 = 16.26; 30.00 - 16.26 = 13.74

16—76791-1

FIGURE 102.—Discharge-measurement notes with discharge adjusted for channel storage.

The adjusted discharge figure is the one used for defining the stage-discharge relation.

The adjustment of measured discharge for storage during a period of changing discharge is a separate and distinct problem from that of making adjustments for variable slope caused by changing discharge. (See p. 418–421.) Regardless of whether or not the discharge is to be adjusted later for variable slope, the storage adjustment to discharge is made immediately after completion of the discharge measurement.

SUMMARY OF FACTORS AFFECTING THE ACCURACY OF A DISCHARGE MEASUREMENT

The factors that affect the accuracy of a discharge measurement have been discussed in appropriate sections of the preceding text. This section provides a brief recapitulation of those factors.

1. *Equipment.*—Accurate measurement requires that measurement equipment be properly assembled and maintained in good condition. To avoid damage in transport, the equipment should be packed in appropriate containers or compartments of the vehicle used by the hydrographer. Current meters are especially susceptible to damage when in use, because measurements must often be made when drift or floating ice is present in a stream.

2. *Characteristics of the measurement section.*—The basic characteristics of the measurement section affect measurement accuracy. The attributes desired in a measurement section are those listed on page 139. If possible, the section should be deep enough to permit use of the two-point method of measuring velocity. The presence of bridge piers in or near the measurement section adversely affects the distribution of velocities. Piers also tend to induce local bed scour which affects the uniformity of depth. Those adverse effects are increased if the bridge piers tend to collect drift on their upstream faces.

3. *Spacing of observation verticals.*—The spacing of observation verticals in the measurement section can affect the accuracy of the measurement. Twenty-five to 30 verticals should normally be used, and the verticals should be spaced so that each subsection will have approximately equal discharge. However, a measurement vertical should be located fairly close to each bank and at "breaks" in depth. The spacing of the verticals should also be reduced in the vicinity of bridge piers. If many bridge piers are present in the section or if the streambed is nonuniform, more verticals than the recommended 25–30 should be used.

4. *Rapidly changing stage.*—When the stage changes rapidly during a discharge measurement, the computed discharge figure loses some of its significance, and there is uncertainty as to the appropriate gage height to apply to that discharge figure. Consequently, the standard procedure for making discharge measurements should be

shortened when the stage is changing rapidly, as explained on pages 174–177, even at the expense of some accuracy. The reduction in measurement time makes it possible to obtain a mean gage height that is representative of the measured discharge.

5. *Measurement of depth and velocity.*—Inaccuracies in sounding and in the placement of the current meter are most likely to occur in those sections having great depths and velocities. Heavy sounding weights should be used to reduce the vertical angle made by the sounding line, and where vertical angles exist, tags and (or) correction tables should be used in determining vertical distances. Where velocities are not perpendicular to the measurement section, the cosine of the angle between the perpendicular and the direction of the current must be determined. If a velocity-azimuth-depth assembly (p. 129–130) is not used, it is necessary to assume that the angle of the surface current prevails throughout the vertical; that assumption may be erroneous.

6. *Ice in the measuring section.*—Reliable measurements may usually be made when measuring from ice cover if the measurement verticals are free of slush ice. Slush ice interferes with the operation of the current-meter rotor and also causes difficulty in determining the effective depth of water. If the effective depth is considered to be that portion of the depth in which the current meter indicates velocity, the assumed effective depth may be too small if slush ice is interfering with free operation of the rotor. Collections of slush ice are generally thickest near the upstream end of ice-covered pools, and those areas should therefore be given little consideration as measurement sections. If the ice cover is layered so that there is water flowing between ice layers, it is almost impossible to obtain a reliable discharge measurement, particularly if the water layers are too thin to permit insertion of the meter between ice layers. The exposure of a wet current meter to subfreezing air temperatures may cause serious underregistration of the current meter as a result of ice forming in the meter bearings and contact chamber. Therefore, once the measurement is started, the current meter should be kept in the water as much as possible to avoid exposure to the cold air.

7. *Wind.*—Wind may affect the accuracy of a discharge measurement by obscuring the angle of the current, by creating waves that make it difficult to sense the water surface prior to sounding the depth, and by affecting the velocity at 0.2-depth in shallow streams, thereby distorting the vertical-velocity distribution. When making boat measurements, the wind-caused waves may induce vertical motion in a cable-suspended meter, or the wind may cause an oscillatory horizontal movement of the boat against the tag line; either movement may affect the operation of the current meter. Table 11 sum-

marizes the results of an investigation (Kallio, 1966) on the effect of vertical motion on the operation of Price, vane-type, and Ott (cosine rotor 8646–A) current meters. The plus signs in table 11 indicate overregistration by the meter; the minus signs indicate underregistration.

ACCURACY OF A DISCHARGE MEASUREMENT MADE UNDER AVERAGE CONDITIONS

Carter and Anderson (1963) made a statistical analysis of the error in discharge measurements made in natural streams under average measuring conditions. They tested the following four assumptions on which the computation of discharge measurements is based:

1. The rating of the current meter is applicable to the conditions of the measurement.
2. The velocity observed at a point is a true time-averaged velocity.
3. The ratio is known between the velocity of selected points in the vertical and the mean velocity in the vertical.

TABLE 11.—*Registration errors, in percentage of stream velocity, caused by vertical motion of current meter*

Stream velocity (ft/s)	Vertical motion (ft/s)						
	0 2	0.4	0.6	0.8	1 0	1.2	1 5
Price current meter (suspended by a cable)							
0 5	−2.0	+10	+36	+72	+120	+150	+210
1.0	−3 0	−1.0	+10	+24	+40	+50	+56
1 5	−6.7	−6 7	−4 0	+1.3	+8.0	+25	+27
2 0	−2.5	−2 5	−2.5	−2.0	0	+4.0	+14.0
2 5	0	0	0	0	0	+ 8	+4.0
3.0	0	0	0	0	−2.3	−2.0	0
4 0	0	0	0	0	−1 3	−1.3	0
5 0	+.4	+1 0	+.6	0	−.2	0	+.8
7 0	−.7	− 4	0	+ 1	−.4	−.7	− 4
10 0	− 5	− 3	0	0	− 3	− 7	−1.3
Vane-type current meter (suspended by a rod)							
0 5	+4.0	+6 0	+20	+44	+72	+100	+160
1 0	+5 0	+10	+12	+10	+11	+15	+26
1 5	+3 3	+8.7	+10	+6.7	+3.3	+3.3	+10
2 0	+2.0	+6.5	+9 0	+9.5	+8.5	+6 0	+7.5
2.5	+2.0	+4.4	+6.4	+7 6	+8.0	+7.2	+6 4
3.0	−1 7	+3.7	+5.3	+6.7	+7 3	+7 7	+6.7
4.0	+1 2	+ 8	+.3	+1 0	+2 5	+3.8	+3 3
5.0	−1.0	−2 6	−2 8	−2.0	−.4	− 2	−2.0
7 0	−.7	− 7	−.3	0	0	+.3	− 4
Ott current meter (cosine rotor 8646-A, standard tailpiece without vertical stabilizer, and two-pin attachment to cable hanger)							
0 5	0	+6.0	+10	+20	+30	+44	+70
1 0	0	0	0	+4.0	+9.0	+15	+30
1.5	0	0	0	+1 3	+4.0	+7 3	+17
2.0	0	0	0	+.5	+2 0	+4.5	+9 5
2.5	0	0	0	0	+1.6	+2 8	+6 4
3 0	0	0	0	+ 3	+1 0	+2.3	+6.0
4 0	0	0	+ 5	+1.0	+1 8	+2 5	+3.8
5.0	+ 4	+ 6	+ 4	+ 6	+1 0	+1 4	−2 0
7.0	0	0	0	0	+.3	+.7	+1.4

4. The depth measurements are correct, and the velocity and depth vary linearly with distance between verticals.

Assumption 1 was tested by comparing the ratings obtained for Price current meters when rated in flumes of different sizes. It was found that the ratings can be repeated within a fraction of 1 percent. When a Price meter was tested in a wind tunnel under differing degrees of turbulence, its performance was not affected by increased turbulence. The similarity of results using the Price, Ott, and Neyrpic current meters has already been discussed on page 89. It was therefore assumed that the standard deviation (S_{R_i}) of the error ratio between measurement results obtained with different current meters equals 1 percent.

Assumption 2 was tested in 23 different rivers where velocities for consecutive time periods of 15, 30, 45, 90, 120, and 240 s were observed for a 1-hr period at points corresponding to 0.2, 0.4, 0.6, and 0.8 depth. The measurement verticals ranged in depth from 2.4 to 26.7 ft (0.7 to 8.1 m), and velocities ranged from 0.43 to 7.9 ft/s (0.13 to 2.4 m/s). Statistical analysis showed that velocity fluctuations were randomly distributed in time and space and that if 45-s observations were taken at the 0.2- and 0.8-depth positions in 30 verticals, the standard deviation (S_{R_t}) of the error ratio between observed and true point velocity was 0.8 percent.

Assumption 3 was tested using more than 100 stream sites. The standard deviation (S_{R_s}) of the error ratio between the mean velocity obtained from 0.2- and 0.8-depth observations and the true vertical velocity, using 30 verticals for the discharge measurement, was 1.15 percent.

Assumption 4 was tested using discharge measurements made at 127 stream sites, in which more than 100 verticals were measured in each cross section. The discharge for each site was again computed using the data for 1/2, 1/4, 1/5, 1/7, and 1/10 of the total number of verticals in each cross section. Error ratios between those computed discharges and the discharges computed using all observation verticals were determined. When 30 observation verticals were used, the standard deviation (S_N) of the error ratios was 1.6 percent.

The standard error of a discharge measurement (S_T) was computed from the equation

$$S_T = \sqrt{(S_{R_i})^2 + (S_{R_t})^2 + (S_{R_s})^2 + (S_N)^2}. \quad (16)$$

For a measurement using velocity observations of 45 s at the 0.2- and 0.8-depth positions in each of 30 verticals, S_T equaled 2.2 percent. That means that if single discharge measurements were made at a number of gaging sites using the standard method recommended in

this manual, the errors of two-thirds of the measured discharges would be less than 2.2 percent.

SELECTED REFERENCES

Buchanan, T. J., and Somers, W. P., 1969, Discharge measurements at gaging stations: U.S. Geol. Survey Techniques Water-Resources Inv., book 3, chap. A8, 65 p.

Carter, R. W., and Anderson, I. E., 1963, Accuracy of current-meter measurements: Am. Soc. Civil Engineers Jour., v. 89, no. HY4, p. 105–115.

Chandler, T. S., and Smith, Winchell, 1971, Optical current meter use in southern California: Am. Soc. Civil Engineers Jour., v. 97, HY9, p. 1461–1469.

Corbett, D. M., and others, 1943, Stream-gaging procedure: U.S. Geol. Survey Water-Supply Paper 888, p. 65–76.

Hulsing, Harry, Smith, Winchell, and Cobb, E. D., 1966, Velocity-head coefficients in open channels: U.S. Geol. Survey Water-Supply Paper 1869–C, p.7.

International Standards Organization, 1968, Liquid flow measurement in open channels by velocity area methods: ISO Recommendation R748, Geneva, 34 p.

Kallio, N. A., 1966, Effect of vertical motion on current meters: U.S. Geol. Survey Water-Supply Paper 1869–B, 20 p.

Pierce, C. H., 1941, Investigations of methods and equipment used in stream gaging; Part 1, Performance of current meters in water of shallow depth: U.S. Geol. Survey Water-Supply Paper 868–A, 35 p.

Rouse, Hunter, 1950, Engineering Hydraulics: New York, John Wiley and Sons, p. 222, 223.

Schubauer, G. B., and Mason, M. A., 1937, Performance characteristics of a water current meter in water and air: Natl. Bur. Standards Research Paper RP 981.

Smoot, G. F., and Novak, C. E., 1968, Calibration and maintenance of vertical-axis type current meters: U.S. Geol. Survey Techniques Water-Resources Inv., book 8, chap. B2, 23 p.

Townsend, F. W., and Blust, F. A., 1960, A comparison of stream velocity meters: Am. Soc. Civil Engineers Jour., v. 86, no. HY4, p. 11–19.

World Meteorological Organization, 1962, Field methods and equipment used in hydrology and hydrometeorology: Flood Control Series no. 22, p. 38–47, 51–55.

Young, K. B., 1950, A comparative study of mean-section and mid-section methods for computation of discharge measurements: U.S. Geol. Survey open-file report, 52 p.

CHAPTER 6.—MEASUREMENT OF DISCHARGE BY THE MOVING-BOAT METHOD

INTRODUCTION

On large streams and estuaries the conventional methods of measuring discharge by current meter are frequently impractical and involve costly and tedious procedures. There may be no suitable facilities at remote sites. Where suitable facilities do exist, they may be inundated or inaccessible during floods. At some sites, unsteady flow conditions require that measurements be made as rapidly as possible. Measurements on tide-affected rivers must not only be made rapidly, but often continually, throughout a tidal cycle. The moving-

boat technique is a method of rapidly measuring the discharge of large streams. It requires no fixed facilities, and it lends itself to the use of alternate sites if conditions make this desirable.

The moving-boat technique is similar to the conventional current-meter measurement in that both use the velocity-area approach in determining discharge. (See chapter 5.) In each method, a measurement is the summation of the products of the subsections of the stream cross section and their respective average velocities. Both techniques require that the following information be obtained:

1. Location of sampling verticals 1, 2, 3,. . .n across the stream in reference to the distance from an initial point.
2. Stream depth, d, at each observation vertical.
3. Stream velocity, V, perpendicular to the cross section at each observation vertical.

During a traverse of the boat across the stream, a sonic sounder records the profile of the cross section, and a continuously operating current meter senses the combined stream and boat velocities. A vertical vane alines itself in a direction parallel to the movement of water past it, and an angle indicator attached to the vane assembly indicates the angle between the direction of the vane and the true course of the boat. The data from these instruments provide the information necessary for computing the discharge for the cross section. Normally, data are collected at 30 to 40 observation points in the cross section for each run. Experience has shown that discharges determined by the moving-boat technique match, within 5 percent, discharges determined by conventional means.

The principal difference between the conventional measurement and the moving-boat measurement lies in the method of data collection. The standard current-meter method of measurement uses what might be called a static approach in its manner of sampling; that is, the data are collected at each observation point in the cross section while the observer is in a stationary position. This is in contrast to the dynamic approach to data collection utilized in the moving-boat method. Here, data are collected at each observation point while the observer is aboard a boat that is rapidly traversing the cross section.

THEORY OF THE MOVING-BOAT METHOD

The moving-boat measurement is made by traversing the stream along a preselected path that is normal to the streamflow. The traverse is made without stopping, and data are collected at intervals along the path. During a traverse of the cross section, the boat operator maintains course by "crabbing" into the direction of the flow sufficiently to remain on line (fig. 103). The velocity, V_b, of the boat

with respect to the stream-bed along the selected cross-section path is the velocity at which the current meter is being pushed through the water by the boat. The force exerted on the current meter, then, is a combination of two forces acting simultaneously: one force resulting from the movement of the boat through the water along the cross-section path and the other a consequence of the natural streamflow normal to that path.

The velocity measurement taken at each of the sampling points in the cross section is a vector quantity that represents the relative velocity of water past the vane and meter. This velocity, V_V, is the vector sum of V, the component of stream velocity normal to the cross section at the sampling point, and V_b, the velocity of the boat with respect to the streambed along the selected path. The vector diagram in figure 104 depicts this relation.

The sampling data recorded at each observation point provide the necessary information to define V_V. The pulses-per-second reading from the rate-indicator unit is used in conjunction with a rating table to obtain the vector magnitude, V_V, while the angle reading, α, representing the angle the vane makes with the cross-section path, defines the direction of the vector.

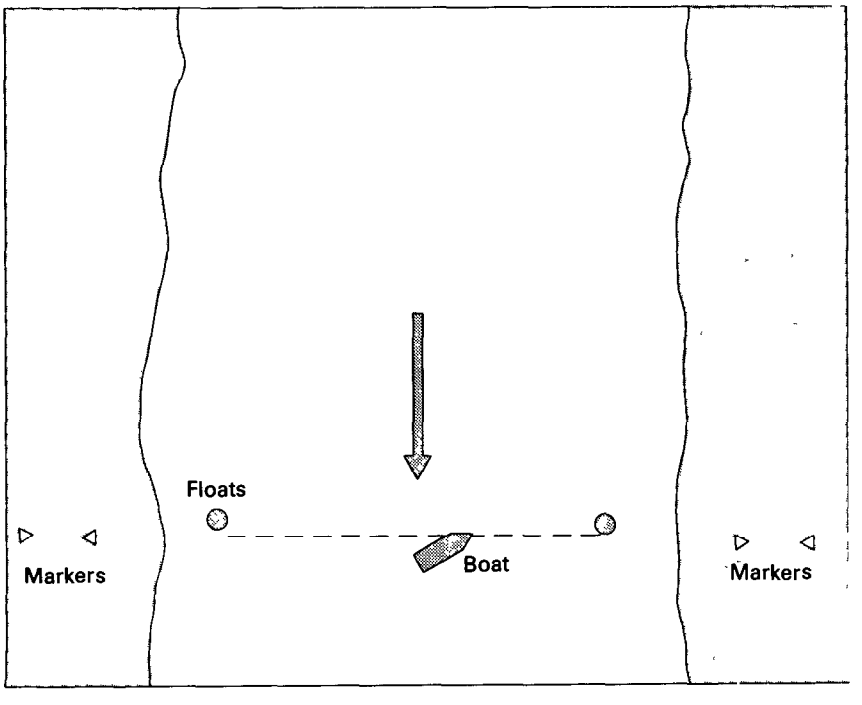

FIGURE 103.—Sketch of stream with markers.

Stream velocity, V, perpendicular to the boat path (true course) at each sampling point, 2, 3, 4, . . . $(n-1)$, can be determined from the relation

$$V = V_V \sin \alpha. \tag{17}$$

The solution of the above equation yields an answer which represents that component of the stream velocity that is perpendicular to the true course even though the direction of flow may not be perpendicular. This is the desired component.

From the same vector diagram, it can be seen that

$$L_b = \int V_V \cos \alpha \, dt, \tag{18}$$

where L_b is the distance that the boat has traveled along the true course between two consecutive observation points, provided the stream velocity is perpendicular to the path. Where the velocity is not perpendicular, an adjustment is required as explained on pages 207–208, where the adjustment of total width and area is discussed.

If one assumes that α is approximately uniform over the relatively short distance that makes up any one increment, then α may be treated as a constant. Therefore, equation 18 becomes

$$L_b \approx \cos \alpha \int V_V \, dt. \tag{19}$$

However,

$$\int V_V \, dt = L_V, \tag{20}$$

where L_V is the relative distance through the water between two consecutive observation points as represented by the output from the rate indicator and counter. Therefore,

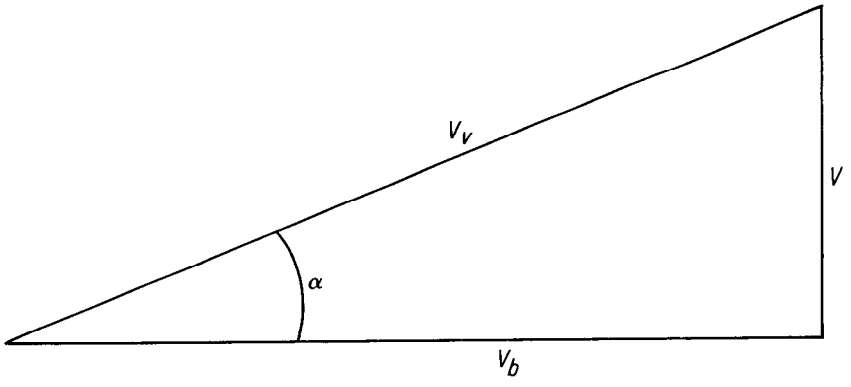

FIGURE 104.—Diagram of velocity vectors.

$$L_b \approx L_V \cos \alpha. \quad (21)$$

Finally, d, stream depth at each observation point, is obtained by adding the transducer depth to the depth obtained from the sonic-sounder chart. Upon determining V, L_b, and d for each vertical, the midsection method of computing a discharge measurement is used. (See p. 80–82.)

Much of the accuracy of a moving-boat discharge measurement depends upon the skill of the boat operator in maintaining a true course. Although even the most experienced pilot cannot be expected to keep the boat absolutely on course for an entire run, it is still extremely important that the measurement begin and end on line and that any deviations from the true course be kept as few in number and as small in magnitude as possible.

If velocity readings are taken while the boat is moving off course in an upstream direction, those readings will be greater than the true velocities; if the readings happen to be taken when the movement is toward the downstream direction, then the sampled velocity readings will be less than the true velocities. Thus, if one assumes the equal likelihood of overregistering or underregistering the stream velocities because of deviations from the true course, the errors can be considered compensating in nature. However, to further insure the reliability of the measurement, it is recommended that the results of at least six individual runs, each with from 30 to 40 observation points, be averaged to obtain the discharge when steady-flow conditions exist. This is practicable because of the ease and speed with which the extra runs can be made.

For unsteady-flow conditions on tidal streams, it will usually be desirable not to average the results from a series of runs but rather to keep them separate so as to better define the discharge cycle.

EQUIPMENT

Specialized instrumentation consisting of a sonic sounder, a vane with indicator, a special current meter with its associated electronic equipment, and an easily maneuverable small boat with some modifications, provide the capability needed for a moving-boat measurement.

VANE AND ANGLE INDICATOR

A vane with an indicating mechanism is mounted on the bow of the boat, with the vane centered approximately 3 to 4 ft (0.9 to 1.2 m) below the water surface (fig. 105). This assembly consists of a vertical, stainless-steel shaft with a pointer connected to its upper end and a thin vertical aluminum fin, 1-ft (0.3 m) high and 1½-ft (0.46m) long,

attached to its lower end. The shaft is housed in an aluminum bearing tube and is mounted with ball bearings at the upper end and a teflon bearing (no lubrication needed) in the lower end of the tube so that the assembly (vane, shaft, pointer) is free to rotate as a unit. The vertical vane alines itself in a direction parallel to the movement of the water past it. The pointer is attached to the shaft so that it will be in line with the vane, pointing directly into the flow past the vane. The angle between the direction of the vane and the true course of the boat (the line of the cross section) is indicated on a dial by the pointer. The circular dial, calibrated in degrees on either side of an index point, swivels freely about the upper end of the vertical shaft, just below the pointer. A sighting device attached to the dial provides a means of alining the index point on the dial with the true course. In positive (downstream) streamflow the pointer above the dial will always point to the upstream side of the true course. Because the upstream side may be to the left or right side, depending on the direction in which the boat is traveling, and also because of possible negative velocities, the dial is calibrated in degrees (from 0 to 90) on both sides of its index point.

CURRENT METER

The current meter used by the U.S. Geological Survey is a component propeller type with a custom body made for mounting on the leading edge of the vane (fig. 105). The component propeller is less susceptible than are other types of meters to vertical components of velocity and was chosen to minimize errors created by the bobbing of the boat.

A 24-toothed gear passing in the proximity of a magnetic field is

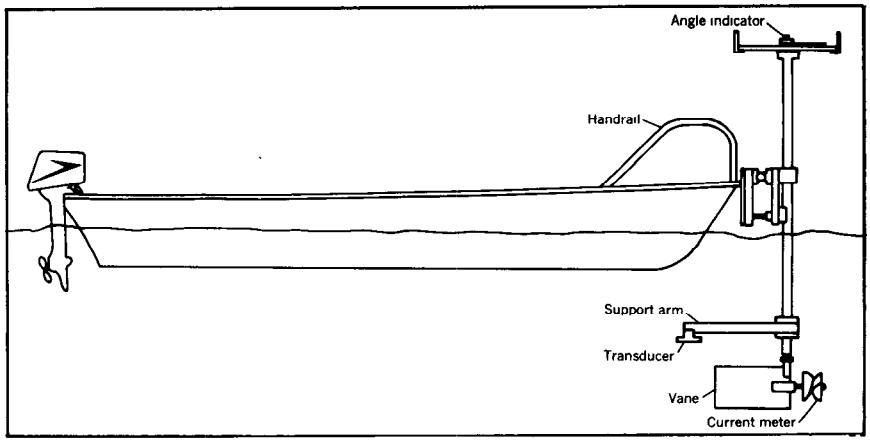

FIGURE 105.—Sketch of boat showing equipment.

used to generate 24 pulses per revolution of the propeller. The large number of pulses for each revolution facilitates the conversion of the pulse rate to an analog readout. An electronic pickup assembly registers these pulses and feeds them into a frequency-to-voltage converter, and they are then displayed as a reading on an electrical meter.

At one end of the meter cable is a metallic probe that is screwed into the meter body at the opening just behind the propeller nut (fig. 106). The probe is a permanent magnet that provides the magnetic field necessary for pulse generation. To function properly, the probe tip must be positioned within a few thousandths of an inch of the 24-toothed gear located within the meter. Adjustment of the probe position, which is seldom required, should be done with care to prevent damage to the probe tip.

Before the meter is used, the cup within the hub of the current-meter propeller should be filled with thin oil (Ott propeller oil) as shown in figure 106. The bearing assembly is then inserted into the hub, and the propeller nut is tightened. After the conclusion of a series of measurements, the cup should be emptied completely and cleaned before storage.

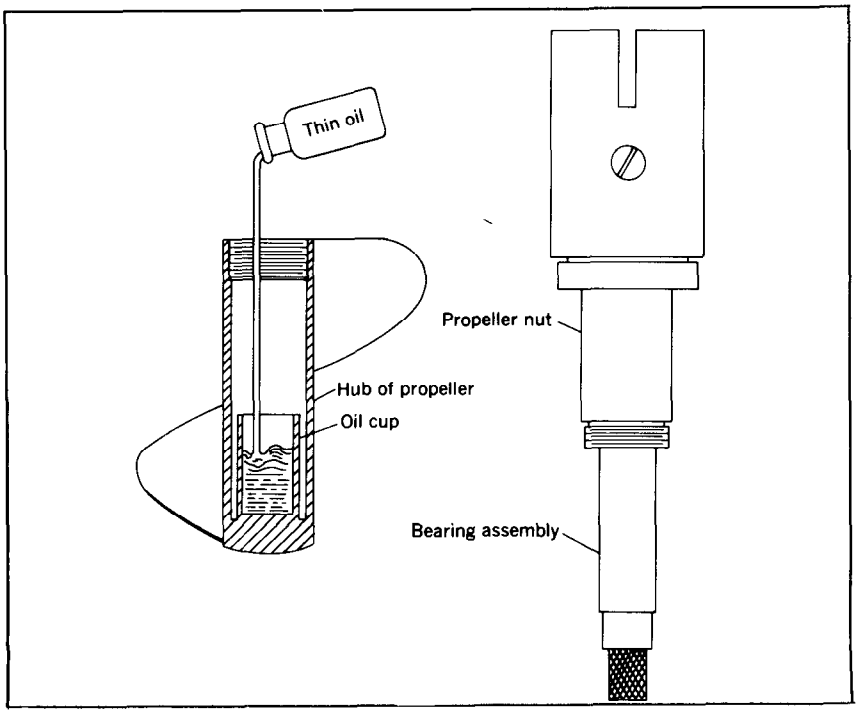

FIGURE 106.—Component propeller-type meter.

RATE INDICATOR AND COUNTER

One of the principal functions of the rate indicator and counter is to register the pulses received from the current meter, feed them into a frequency-to-voltage converter, and then display them as a reading on its electrical meter (fig. 107). These pulses are received through the current-meter cable which is plugged into the marked receptacle provided in the front panel of the unit. The current meter generating the pulses is calibrated so that the reading on the electrical meter in pulses per second can be converted to a particular velocity in feet per second through the use of a rating table (fig. 108). The value read from the electrical meter at any particular instant represents an instantaneous readout of velocity.

Two scale selections are available for the rate-indicator unit. If the switch is set at the "500" selection, the readout is taken from the lower scale of the panel meter; at the 1,000 setting, the upper scale is used. The 500 scale is the more sensitive of the two, and therefore its use is recommended during those measurements in which the velocity of the water past the meter is not great enough to give readings that exceed 500 pulses per second.

In addition to serving as a pulse-rate indicator from which velocity determinations can be made, this unit has also been designed to provide a method of automatically selecting measurement points in a section at regular intervals of travel distance. This design makes use of the fact that each revolution of the meter propeller generates 24

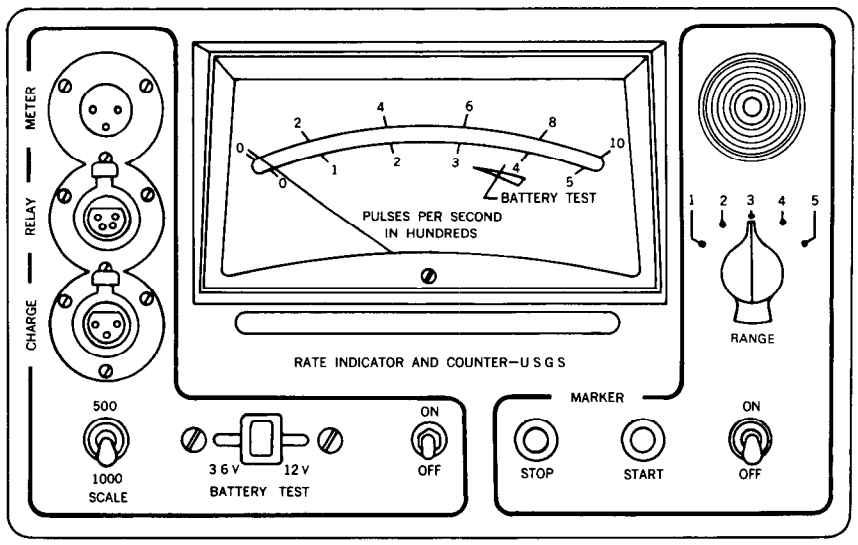

FIGURE 107.—Control panel of rate indicator and counter.

DEPARTMENT OF THE INTERIOR - GEOLOGICAL SURVEY
Water Resources Division
RATING TABLE FOR MOVING BOAT METER NO. 2-4
EQUATIONS: V = 0.01768N + 0.078 . . . . . Limits of actual rating . . 1.0 . . to . . 10 . . . feet per second. Rated JULY 5, 1967

Counts per Second	VELOCITY IN FEET PER SECOND																				Counts per Second
	0	5	10	15	20	25	30	35	40	45	50	55	60	65	70	75	80	85	90	95	
0 100	1.85	1.93	2.02	2.11	2.20	2.29	2.38	2.46	2.55	2.64	0.96 2.73	1.05 2.82	1.14 2.91	1.23 3.00	1.32 3.08	1.40 3.17	1.49 3.26	1.58 3.35	1.67 3.44	1.76 3.53	0 100
200 300	3.61 5.38	3.70 5.47	3.79 5.56	3.88 5.65	3.97 5.74	4.06 5.82	4.14 5.91	4.23 6.00	4.32 6.09	4.41 6.18	4.50 6.27	4.59 6.35	4.67 6.44	4.76 6.53	4.85 6.62	4.94 6.71	5.03 6.80	5.12 6.88	5.21 6.97	5.29 7.06	200 300
400 500	7.15 8.92	7.24 9.01	7.33 9.09	7.42 9.18	7.50 9.27	7.59 9.36	7.68 9.45	7.77 9.54	7.86 9.63	7.95 9.71	8.03 9.80	8.12 9.89	8.21 9.98	8.30 10.07	8.39 10.16	8.48 10.24	8.56 10.33	8.65 10.42	8.74 10.51	8.83 10.60	400 500
600 700	10.69 12.45	10.77 12.54	10.86 12.63	10.95 12.72	11.04 12.81	11.13 12.90	11.22 12.98	11.30 13.07	11.39 13.16	11.48 13.25	11.57 13.34	11.66 13.43	11.75 13.51	11.84 13.60	11.92 13.69	12.01 13.78	12.10 13.87	12.19 13.96	12.28 14.05	12.37 14.13	600 700
800 900	14.22 15.99	14.31 16.08	14.40 16.17	14.49 16.26	14.58 16.34	14.66 16.43	14.75 16.52	14.84 16.61	14.93 16.70	15.02 16.79	15.11 16.87	15.19	15.28	15.37	15.46	15.55	15.64	15.72	15.81	15.90	800 900

TABLES OF L_b, IN FEET

Range No.	Angle α in degrees	0	1	2	3	4	5	6	7	8	9
1	0	18.2	18.2	18.2	18.2	18.2	18.2	18.1	18.1	18.1	18.0
	10	18.0	17.9	17.9	17.8	17.7	17.6	17.5	17.5	17.4	17.3
	20	17.1	17.0	16.9	16.8	16.7	16.5	16.4	16.3	16.1	16.0
	30	15.8	15.6	15.5	15.3	15.1	14.9	14.8	14.6	14.4	14.2
	40	14.0	13.8	13.6	13.3	13.1	12.9	12.6	12.4	12.2	11.9
2	0	36.5	36.5	36.5	36.5	36.4	36.4	36.3	36.2	36.1	36.1
	10	35.9	35.8	35.7	35.6	35.4	35.3	35.1	34.9	34.7	34.5
	20	34.3	34.1	33.8	33.6	33.3	33.1	32.8	32.5	32.2	31.9
	30	31.6	31.3	31.0	30.6	30.3	29.9	29.5	29.2	28.8	28.4
	40	28.0	27.5	27.1	26.7	26.3	25.8	25.4	24.9	24.4	23.9
3	0	73.0	73.0	73.0	72.9	72.8	72.7	72.6	72.5	72.3	72.1
	10	71.9	71.6	71.4	71.1	70.8	70.5	70.2	69.8	69.4	69.0
	20	68.6	68.2	67.7	67.2	66.7	66.2	65.6	65.0	64.4	63.8
	30	63.2	62.6	61.9	61.2	60.5	59.8	59.0	58.3	57.5	56.7
	40	55.9	55.1	54.2	53.4	52.5	51.6	50.7	49.8	48.8	47.9
4	0	146	146	146	146	146	145	145	145	145	144
	10	144	143	143	142	142	141	140	140	139	138
	20	137	136	135	134	133	132	131	130	129	128
	30	126	125	124	122	121	120	118	117	115	114
	40	112	110	108	107	105	103	101	99.6	97.7	95.8
5	0	292	292	292	292	291	291	290	290	289	288
	10	288	287	286	284	283	282	281	279	278	276
	20	274	273	271	269	267	265	262	260	258	255
	30	253	250	248	245	242	239	236	233	230	227
	40	224	220	217	214	210	206	203	199	195	192

SIN of ANGLE α

Angle α	0	1	2	3	4	5	6	7	8	9
0	.000	.017	.035	.052	.070	.087	.105	.122	.139	.156
10	.174	.191	.208	.225	.242	.259	.276	.292	.309	.326
20	.342	.358	.375	.391	.407	.423	.438	.454	.469	.485
30	.500	.515	.530	.545	.559	.574	.588	.602	.616	.629
40	.643	.656	.669	.682	.695	.707	.719	.731	.743	.755
50	.766	.777	.788	.799	.809	.819	.829	.839	.848	.857

FIGURE 108.—Sample tables of meter rating, L_b, and sine α.

evenly spaced pulses, and that from the calibration of the meter it can be determined that one pulse is equal to some fraction of a foot of meter travel through the water, or of water travel past the meter. By using a set of frequency-dividing modules, provision is made for these pulses to be electronically counted to a preset number, at which time an audible signal is generated and the sounder chart is automatically marked. The counter then automatically resets itself, and the process is repeated. The purpose of the audible signal is to let the boat crew know when a sampling location is reached. At this point they will take an angle reading from the pointer and a readout from the electrical meter. The markings on the sounder chart are automatically triggered by an electrical impulse transmitted to the depth-sounder unit by a relay in the meter electronics. The relay cable from the counter to the sounder should be plugged into the appropriately marked receptacle on the front panel of both units. The markings on the sounder chart locate observation points in the cross section and thus show where depth readings should be taken.

Preset intervals that are available on each unit are as follows:

Range selection	*Pulse counts*	*Distance, in feet*
1	1,024	18.75
2	2,048	37.5
3	4,096	75
4	8,192	150
5	16,384	300

The distances listed above are typical; exact ones depend upon the calibration of the particular current meter used. If possible, the pulse-selector switch should be set for a distance that will divide the measured width between the two floats into from 30 to 40 increments. For example, if the distance between floats is 500 ft (150 m), range 1 should be selected; for a distance of 1,000 ft (300 m), range 2 should be used, and so on. Each distance listed in the table above represents L_V, the relative distance through the water, and it will be somewhat larger than the corresponding L_b value, the distance along the true course that the boat has traveled. L_b is the distance one should use to determine the number of observation points that will be taken in a given cross section. However, the listed L_V values can be used to estimate roughly the number of observation points—the estimated number will always be less than the actual number of observation points.

The rate indicator and counter has two internal power supply packs, each consisting of a set of nickel-cadmium rechargeable batteries. A battery test switch located on the front panel of the unit can be used to test the condition of either the 3.6-volt or the 12-volt power supply (fig. 107). Testing should be done with both the main

power and the marker switches off. A reading of the panel meter above the test switch will indicate the degree of charge. A needle deflection greater than the battery testline mark indicates a satisfactory charge level for most measurement requirements. A fully charged battery pack will operate satisfactorily from 12 to 16 hr. A marginal reading, with needle deflection just to the test mark, indicates approximately 4 to 8 hr of useful battery operation remaining. A reading below the mark serves as a warning that a battery charge is needed.

BATTERY CHARGER

The battery charger serves as a dual unit for charging either one of the two battery supply packs located within the rate indicator and counter unit. Its charge plug is inserted into the charge receptacle located on the panel of the rate indicator and counter. The other plug should be connected to a 115-volt, 60-cycle line power supply. With proper care the batteries should provide many years of service.

SONIC SOUNDER

A portable sonic sounder (fig. 109) is used to provide a continuous strip-chart record of the depth of the stream, that is, a profile of the cross section between the two floats. Its transducer releases bursts of ultrasonic energy at fixed intervals. The instrument measures the time required for these pulses of energy to travel to the streambed, to be reflected, and to return to the transducer. With a known propagation velocity of sound in water, the sounder computes and records the depth. Accuracy of the recording depth sounder is approximately ± 0.5 ft (0.15 m). The sounder used in this application is a commercially available model with a minor modification for automatically marking the chart at each observation point in response to an electrical pulse from the meter electronics. The sounder is powered by a standard lead-acid battery of 6 or 12 volts, depending on the model of the sounder.

One minor modification to the sonic sounder is the installation of a receptacle on its front panel into which is plugged the relay cable from the rate indicator and counter. The purpose of this relay connection is to transmit the electrical pulses from the counter unit that will automatically trigger the vertical-line markings on the sounder chart. This provision for automatically marking the sounder chart at regular intervals of distance traveled eliminates the need for the manually operated "mark" switch, except in the event that the relay cable is damaged or missing. Then, as an expedient measure, the chart is marked at each observation point by manually pulling the switch at each tone signal sounded by the counter unit.

Three paper-feed speeds are provided with the unit. The small lever

in the lower left-hand corner of the recorder chassis is the control. The set of speeds available will vary according to the model. Some models

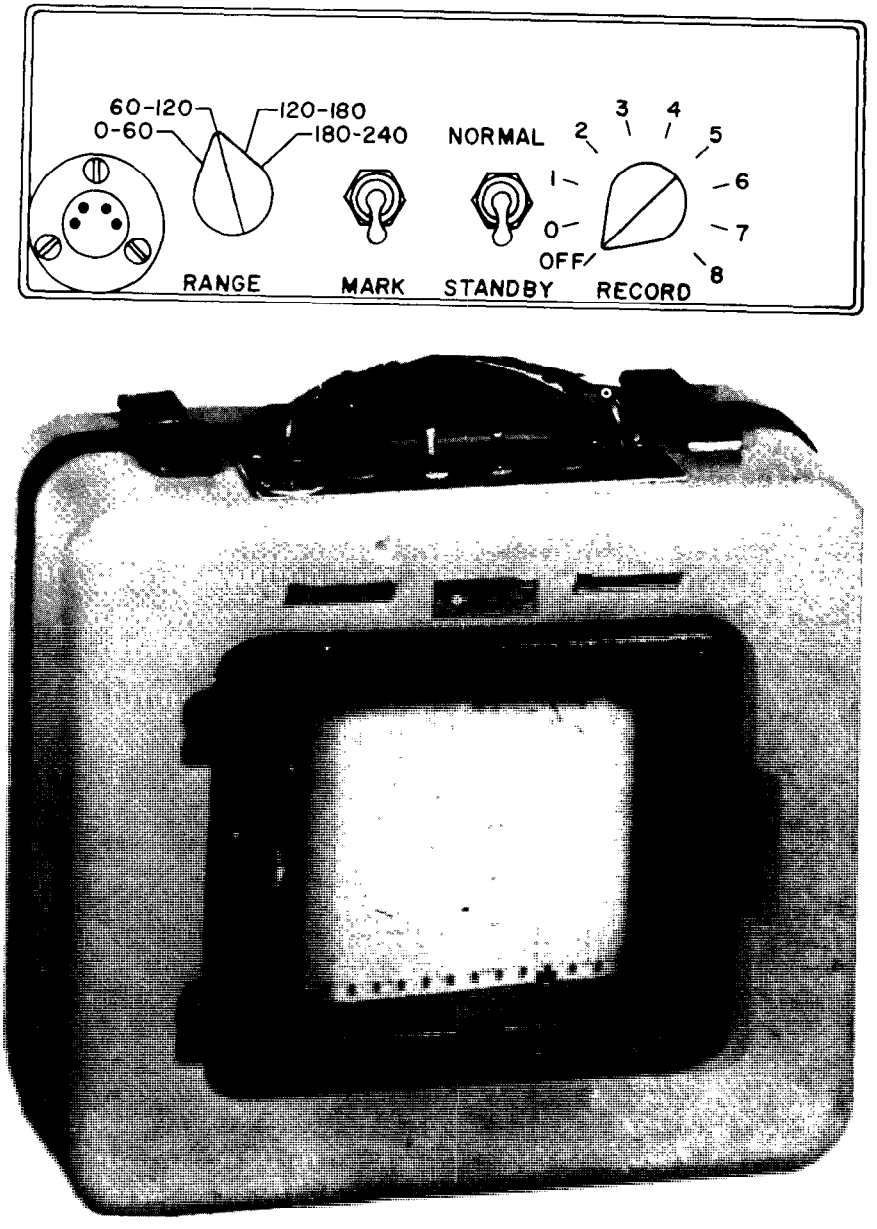

FIGURE 109.—Sonic sounder and control panel.

provide choices of 12, 30, and 60 in/hr (0.30, 0.76, and 1.52 m/hr), and others 36, 90, and 180 in/hr (0.91, 2.29, and 4.57 m/hr). A suitable chart speed is one that results in a spacing of approximately 0.25 in between the vertical-line markings that are set on the chart during the measurement. Spacing wider than that needlessly wastes chart paper, whereas much narrower spacing results in poor resolution of the streambed trace. Narrow spacing also causes difficulty in determining the fractional part of a full spacing that should be assigned to the final width increment. Width of spacing is dependent upon the range setting on the counter unit, the current-meter velocity, and the chart speed. Table 12, computed for a current-meter velocity of 5 ft/s (1.52m/s), provides an example of typical spacing distances expected for various combinations of chart speed and range distance.

BOAT

Any easily maneuverable small boat that is sufficiently stable for the stream on which it is to be used is adequate for a moving-boat measurement. A photograph of a boat with the vane assembly mounted is shown in figure 110.

Preparation of the boat.—A 12×12×¼-in steel plate should be so attached that it is centered on the bow of the boat, perpendicular to the centerline of the boat, and as nearly vertical as possible. This plate must be securely anchored because at high velocities great force will be exerted on it. It may be necessary, depending on the style of boat being used, to erect handrails on the forward part of the boat, similar to those shown in figure 105. This is done for the safety of the angle reader who must stand in the bow.

Mounting of the equipment.—The 12×12-in aluminum plate on the vane assembly is attached to the 12×12-in steel plate on the bow of the boat. It is necessary to clamp these two plates together and drill four holes for accepting bolts to permanently fasten the plates together. The general location of the bolt holes should be near the four corners, but exact placement is not critical.

The two cap screws in the depth adjustment clamp that hold the aluminum bearing tube of the assembly (fig. 111) can be loosened so

TABLE 12.—*Spacing of vertical-line markings, in inches, on the sonic-sounder chart for various combinations of chart speed and range distance*

[Computed for a current-meter velocity of 5 ft/s]

Chart speed	Range distance				
	18 75 ft	37.5 ft	75 ft	150 ft	300 ft
36 in/hr	0.04	0.08	0.16	0.32	0.64
90 in/hr	.10	.20	.40	.80	1.6
180 in/hr	.20	.40	.80	1.6	3.2

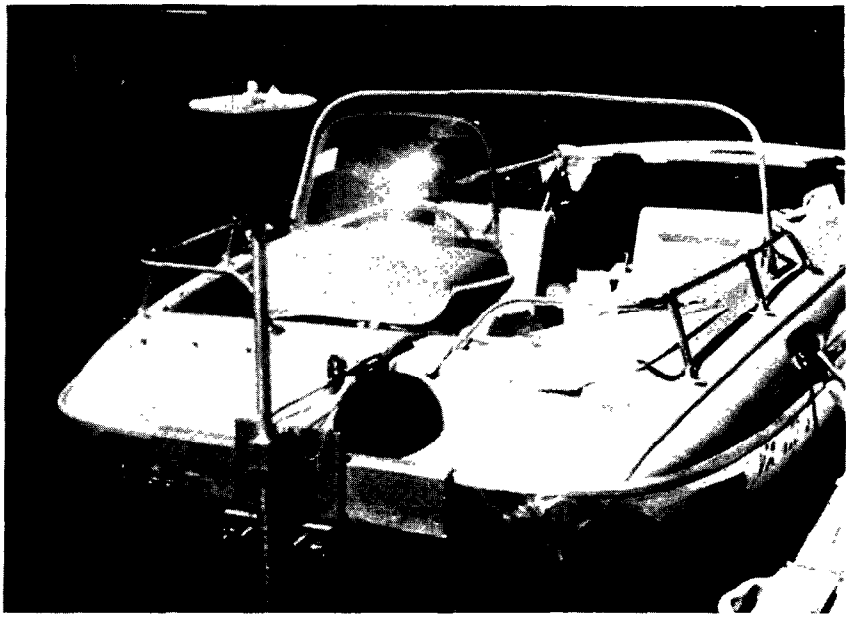

FIGURE 110.—Boat with mounted vane assembly.

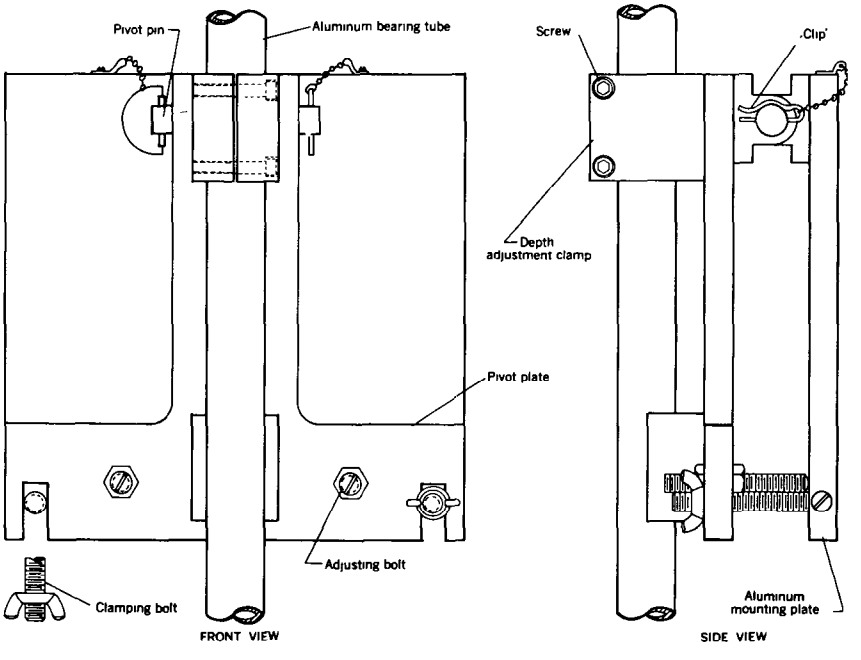

FIGURE 111.—Detailed view of vane-mounting assembly.

that the tube may be either raised or lowered in order to position the meter at the desired depth. This depth should preferably be at least 3 ft (0.91 m) to avoid the effect of surface disturbances and not greater than 4 ft (1.22 m) to avoid the danger of too great a torque being exerted at high velocities. Caution should be exercised to avoid high boat speeds, for the drag on the vane assembly is proportional to the square of the velocity of the water past the vane and therefore increases very rapidly with speed.

The sonic-sounder transducer is mounted on a support arm at a depth of either 2 or 3 ft (0.61 or 0.91m). It can be positioned by first loosening the two cap screws that secure the support arm to the aluminum bearing tube of the vane assembly and then moving the arm either up or down to the desired depth.

Because the vane assembly is mounted perpendicular to the centerline of the boat, it will change slightly from its original vertical position as a result of the raising of the bow of the boat during the moving-boat measurement. To offset this change and thus allow for vertical positioning of the assembly during normal boat operation, the mounting assembly provides for a compensating angle adjustment to be accomplished through the use of two adjusting bolts and a pivot plate (fig. 111). By screwing these bolts either inward or outward, the lower portion of the assembly can be pivoted toward or away from the boat. If the adjusting bolts are touching the aluminum plate when the assembly is in a vertical position, they must be screwed away from the plate so that the lower portion of the assembly can then be pivoted toward the boat and secured in position by use of two clamping bolts. The degree of adjustment would depend upon the operating velocity of the boat during the measurement.

Removal of the equipment.—After the measurements are completed, the vane assembly can be removed while leaving the aluminum plate bolted to the steel plate on the bow of the boat. This is accomplished by first loosening the wing nuts on the two clamping bolts of the plate and then removing the clip and sliding out the pivot pin that secures the assembly to the aluminum plate (fig. 111). Prior to doing this, the meter and the transducer cables should be disconnected from the rate indicator and the sonic sounder, respectively.

MEASUREMENT PROCEDURES

Procedures for a moving-boat measurement include selection and preparation of a suitable measuring site, preparation and assembly of the equipment used for the measurement, and a selection of settings for the instruments used to collect the data.

SELECTION AND PREPARATION OF THE MEASUREMENT SITE

Some preparation is required at the site prior to starting a series of

moving-boat measurements. First, a path for the boat to travel is selected, it being as nearly perpendicular to the flow direction as possible. Then, two clearly visible range markers are placed on each bank in line with this path. The color of these markers should contrast sharply with the background. Spacing between the markers is dependent upon the length of the path, the longer paths requiring greater spacing. Approximately 100 ft (30 m) of spacing is needed for each 1,000 ft (300 m) of path length. Next, anchored floats are placed in the stream 40 to 50 ft (12 to 15 m) from each shore along the selected path (fig. 103). In making a traverse, this distance is needed for maneuvering the boat when entering or leaving the path. The floats should be placed so that the depth of water in their vicinity is always greater than 3 to 4 ft (0.9 to 1.2 m), which is vane depth. Large plastic bleach containers are suitable for use as floats; styrofoam cubes can also be used. It is preferable not to place the floats directly in the boat path but rather 10 to 20 ft (3 to 6 m) upstream. Their purpose is to mark the beginning and ending points of the boat measurement, and by offsetting them upstream they can serve that purpose without being in the way as the boat approaches along the selected path. Finally, the width of the stream is measured by triangulation, stadia, or other methods, and the exact locations of the floats are determined. Because the floats are close to the bank, a tape measure can be used to determine the distance from edge of water to each float. These distances should be recorded in the spaces provided on the front page of the discharge-measurement notes, for they will be used in the computation of the measurement.

If a station is to serve as a site for moving-boat discharge measurements on a continuing basis, it will probably be desirable to construct permanent range markers. Such markers would serve two useful purposes. First, determination of stream width would become a relatively simple procedure because of the availability of the constant distance between the markers once this distance has been established. A tape measure could be used to obtain the horizontal distance from the nearest marker to the water's edge on each bank. Subtracting these two distances from the established distance between the two streamward markers would provide the width of the stream. A second advantage would be that if the need arose, the markers could serve as permanent initial points from which cross-section profiles of the measurement section could be constructed.

PREPARATION OF THE EQUIPMENT

The special equipment and instruments necessary for a moving-boat measurement have been described in some detail on pages 187–197 under the general heading "Equipment." The purpose of this

section of the manual is to summarize, for the convenience of the boat crew, the steps involved in the assembly of the equipment and in the selection of the instrument settings.

ASSEMBLY OF THE EQUIPMENT

The steps listed below should be followed in assembling the equipment:

1. Permanently mount a steel plate to the bow of the boat (p. 195) and then attach the aluminum plate of the vane assembly to it (p. 197). Both of these steps are "one time" operations that should be completed in advance of the trip.
2. Several days prior to the trip, check the batteries in the rate-indicator and counter unit and the storage battery for the sonic sounder to see that they are adequately charged. This will provide time to charge the batteries, if necessary, before the start of the trip.
3. Attach the sonic-sounder transducer to its support arm on the vane assembly (fig. 105).
4. Attach the current meter to the leading edge of the vane (fig. 105).
5. Use the pivot pin and clip and the two clamping bolts of the aluminum plate to secure the vane assembly to the plate (fig. 111).
6. Position the current meter at the desired depth (3 to 4 ft). This is done by loosening the two cap screws in the depth adjustment clamp and then raising or lowering the aluminum bearing tube to the proper position before retightening the screws. Measure the meter depth and record it in the measurement notes once positioning is completed.
7. Route the current-meter cable up the vane assembly and plug it into the marked receptacle on the rate indicator and counter unit. To prevent entanglement, the cable should be taped to the aluminum bearing tube in several places. It is necessary to provide some slack in the cable at its lower end to allow for the movement of the meter as the vane rotates during the measurement.
8. Position the sonic-sounder transducer at a depth of 2 or 3 ft. This is accomplished by first loosening the two cap screws that secure the support arm to the aluminum tube and then sliding the arm either up or down the tube to the proper position before tightening the screws. Measure the transducer depth and record it in the measurement notes at this time.
9. Route the transducer cable up the vane assembly, securing it by tape to the aluminum bearing tube; feed it through the hole

provided near the hinge of the sonic-sounder case; and then plug it into the marked receptacle at the back of the dividing plate.

10. Insert the battery cable of the sonic sounder into the marked receptacle at the back of the dividing plate of the unit. It can be fed through one of the holes provided near the hinge. A standard 6- or 12-volt storage battery, depending on the sonic-sounder model used, should be used as a power supply (p. 193).
11. Plug the relay cable from the counter unit to the sonic sounder into the marked receptacle on the front of each unit.
12. Use the two adjusting screws (fig. 111) to provide for the compensating angle adjustment of the vane assembly as described on page 197.

SELECTION OF THE INSTRUMENT SETTINGS

The notekeeper is responsible for the functioning of the rate indicator and counter and the recording depth sounder. To assure proper operation of the equipment, it is necessary that he make several preliminary instrument settings for each unit prior to the measurement. The following is a list of the steps involved in obtaining these settings:

Sonic sounder:

1. Check to see that the pulleys turn smoothly and that the stylus enters the track easily.
2. Set the operation switch to "stand by" position.
3. Turn on the unit by rotating the "record" switch clockwise to some low-numbered position and wait a few minutes for the tubes to warm up.
4. Set the depth-range selection at phase 1 (0–60 ft) and advance the gain control to obtain the "zero mark" near the top of the sounder chart.
5. Set the "zero mark" on the zero line of the recorder paper through use of the zero adjustment screw located behind the top pulley.
6. Continue to advance the gain until the "echo mark" appears somewhere below the "zero mark." If no echo appears when the gain is opened, switch the range control to the next phase (60–120 ft) and so on until the bottom is found.
7. Determine the optimum chart speed through use of table 12; then use the small lever in the lower left-hand corner of the recorder chassis to make this selection.
8. Change the operating switch from "stand by" to "normal" position several minutes before the measurement begins. This will start

the chart recording and provide an opportunity for a final check of instrument operation before the measurement begins.

Rate indicator and counter:

1. Select the desired scale for the rate-indicator meter located on the panel.
2. Check both battery packs with the battery test switch. This final check will have been preceded by a test several days before the measurement date in order to provide time to charge the batteries if needed (p. 199).
3. Set the rate-indicator switch to "on" position.
4. Set the marker switch to "on" position. (The actual marking will not begin until the "start" button is depressed.)
5. Select a range setting that will provide between 30 to 40 observation points. Because of the scale settings available, this may not always be possible, in which case choose that comprise setting that will come closest to meeting this provision.

After all the control settings are completed, the instruments are ready for use. The "start" and "stop" buttons on the panel of the counter unit are used to begin and end instrument operation at the precise moments the bow of the boat reaches the first and second floats, respectively. The operation of these button controls in regard to the starting and stopping procedure is described in the section of the manual that immediately follows.

FUNCTION OF THE CREW MEMBERS

Three crew members are necessary for making a moving-boat discharge measurement. They include a boat operator, an angle observer, and a notekeeper. Before crew members begin making discharge measurements by the moving-boat method, it is important that they develop a high degree of proficiency in all phases of the technique. This can be done by making practice measurements at a site where the discharge is known and then comparing the moving-boat discharge with the rated discharge. If there is no suitable site available for that purpose, the boat crew should make a series of moving-boat measurements at a single location and compare results for repeatability.

BOAT OPERATOR

Before the measurement begins, the boat operator should become thoroughly familiar with the sampling site. In tidal streams the operator should be familiar with conditions during all phases of the tidal cycle. This will help him avoid running the boat aground in shallow depths and damaging the submerged equipment. While man-

euvering the boat, it is necessary to avoid sudden sharp turns that might result in damage to the meter cable by causing it to be wrapped around the vane assembly.

The operator should select an approach path for the boat that will allow it to be properly maneuvered into position prior to passing the first float. The path should begin from a downstream position as close to the riverbank as depth considerations permit. From such a starting point the boat can be accelerated to near its normal operating speed and the turn into the measuring section can be completed before the measurement begins. By attaining both the proper speed and alinement prior to reaching the float, the instrument readings will have time to stabilize before the initial sample is taken.

During a traverse the only function of the boat operator is to pilot the boat. He maintains course by "crabbing" into the direction of flow sufficiently to remain on line throughout the run. As varying stream velocities are encountered in the cross section, he should rely more upon steering adjustments to keep the proper alinement than upon acceleration or deceleration of the boat. Alinement is determined by sighting on the shore which is being approached. Much of the accuracy of the measurement depends on the skill of the boat operator in maintaining a true course with the boat.

Because the stream velocity is calculated as a sine function of angle alpha (fig. 104, eq. 17), small angles should be avoided whenever possible. It is desirable to maintain angle alpha at approximately 45°. The reason for this is that an error of several degrees in reading angle alpha would be more significant at small angle readings than the same error at larger angle readings. In order to maintain an angle of 45°, the velocity of the boat must be equal to that of the stream. This can be done if the stream velocity is greater than 2.5 ft/s (0.75 m/s); however, control of the boat is difficult to maintain below that velocity. For example, in tidal streams the stream velocity will often vary from 0 to several feet per second; therefore, it is not always possible to maintain an angle as large as 45°, and the measurement must be made using smaller angles.

ANGLE OBSERVER

A second man alines the dial of the vane indicator through its sighting device and, upon receiving the audible signal from the pulse counter, he reads the angle formed by the vane with respect to the true course. He reports the angle to the notekeeper who then records it. If the boat has strayed from the true path, the angle reader should sight parallel to the cross-section markers rather than at the markers themselves.

NOTEKEEPER

The notekeeper has several functions to perform. Prior to the measurement it is his responsibility to see that the preparation of all equipment pertaining to the rate indicator and counter and to the sonic sounder is completed satisfactorily. That includes not only equipment assembly but also selection of appropriate instrument settings.

The accuracy of the sonic sounder varies with changes in the velocity of sound in water, which in turn varies slightly with temperature, dissolved solids, and other variables. Thus sounder output should be compared to a known depth. Any significant error detected in the comparison can be expressed as a percentage of the known depth, and this percentage would be applicable to all depths determined by the sonic sounder. Consequently, this percentage correction should be applied to the total area and total discharge.

A check to determine that the current meter and rate indicator are functioning properly is also desirable. Such a check can be made by comparing the indicated velocity to a velocity determined by the Price current meter. This test is intended to determine proper operation only and is not intended for calibration purposes.

It is the notekeeper's responsibility to operate the controls provided on the equipment for starting and stopping the counter. It is important to the accuracy of the measurement that this unit promptly begin and end its operation at the first and second floats, respectively. This is accomplished by operating the "start" and "stop" buttons on the panel of the counter in the following manner:

1. Approximately 1 s before the boat reaches the first float, the "start" button is depressed; then it is released at the moment of passing. This marks the sounder chart, resets the counter, and starts it.

Marking of the sounder chart and sounding of the beeper (tone signal) will be automatic during the measurement. This will occur at regular intervals as determined by the setting of the range switch on the panel of the counter unit.

2. At the moment the bow of the boat reaches the second float, the "stop" button is depressed for 1 s and then released. This marks the sounder chart, signifying the end of the measurement, and stops the counter.

During the measurement the notekeeper records the angle reading at each signal as it is called out by the angle reader. He also reads and records the instantaneous "velocity" from the rate indicator meter at the same time. Readings are taken at all observation points as defined by the tone signals, including the two float positions.

If the time between consecutive measurements is short, it is desira-

ble to leave the operating switch of the sonic sounder in the "normal" position until the measurement series is concluded. In this way the chart continues to advance between measurements, but there are no vertical line markings. This absence of vertical lines provides a gap on the chart that clearly sets off one measurement from another.

COMPUTATION OF THE DISCHARGE MEASUREMENT

COMPUTATION OF UNADJUSTED DISCHARGE

The method of computing discharge measured by the moving-boat technique is basically similar to the computation method used for conventional current-meter discharge measurements. (See p. 80–82). The discharge in a subsection, q, is the product of the subsection area of the stream cross section and the average velocity in the subsection. The midsection method of computation is used in which it is assumed that the average velocity at the observation vertical is the average velocity for a rectangular subsection. The rectangular subsection extends laterally from half the distance from the preceding observation vertical to half the distance to the following observation vertical and extends vertically from the water surface to the sounded depth (fig. 112). The summation of the discharges of the subsections, $q_1, q_2, q_3, \ldots q_n$, is the total unadjusted discharge of the stream. A step-by-step outline of the computation procedure, which refers to the sample measurement notes shown in figure 113, is given here as a guide to the hydrographer who computes the discharge from the field observations.

1. The data in the first column of figure 113 are the angle readings recorded by the notekeeper during the measurement. Because these readings begin and end at the float positions (there are no edge-of-water readings), they represent the values observed at locations 2, 3, 4, . . . $(n-1)$.

2. Each value in column 2 represents an incremental distance the boat has traveled along the cross-section path between two consecutive observation points. For example, α_x (col. 1) represents the angle reading at location x, and L_{b_x} (col. 2) is the incremental distance the boat has traveled along the true course, extending from the previous observation point, $x-1$, to the location x where the reading was taken.

The values in column 2 can be read directly from a table (fig. 108) by using the angle values recorded in column 1 and the range number as determined by the range selection on the counter unit. Two exceptions are the first and last values in the column, representing the distance to each float from its nearest edge of water. They are deter-

mined by direct measurement prior to the actual run. This is necessary because the actual boat run does not begin and end at the edge-of-water positions and thus is not set up to measure those distances. Therefore, the beginning angle reading, α_2, at the first float is not used for obtaining distance from the edge of water to that float. It should also be noted that L_{b_3} is always recorded as one-half of the value found in the table. This is necessary because the counter unit has been programed to signal at a "half-count" on its first count routine. All remaining values can be recorded directly from the table of L_b values, without any changes, with the possible exception of the one determined from the last angle reading which was made at the second float. This angle reading may or may not have been made at

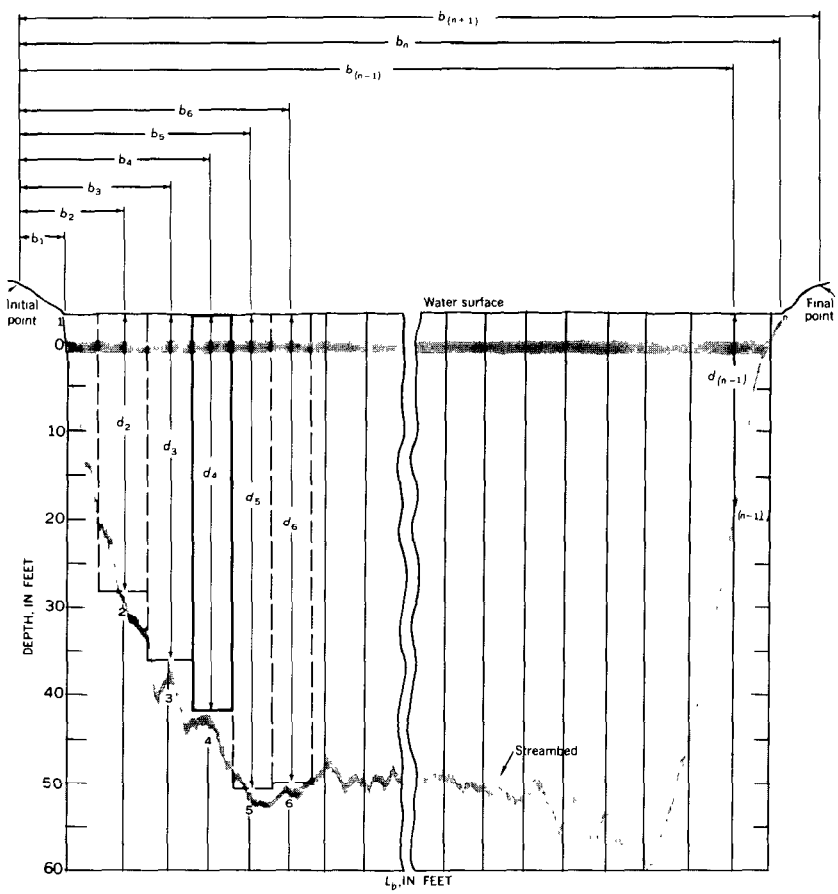

FIGURE 112.—Definition sketch of midsection method of computation superimposed on a facsimile of a sonic-sounder chart.

the end of a full count by the counter unit. In the sample measurement the value recorded was three-fourths of that in the table because the sounder chart distance between the last two vertical markings was approximately three-fourths of the normal spacing.

3. Each value recorded in column 3 represents the distance from the initial point (marker) to the observation point where the data were collected. The data in column 2, together with the "distance to float" and the "distance to marker" values recorded on the front sheet of the discharge measurement notes (fig. 113) are used to obtain these cumulative distances. For a moving-boat measurement, these distances are defined as follows:

b_1 = distance from initial point (marker) to edge of water

$b_2 = b_1$ + measured distance to float from edge of water

$b_3 = b_2 + L_{b_3}$

$b_4 = b_3 + L_{b_4}$

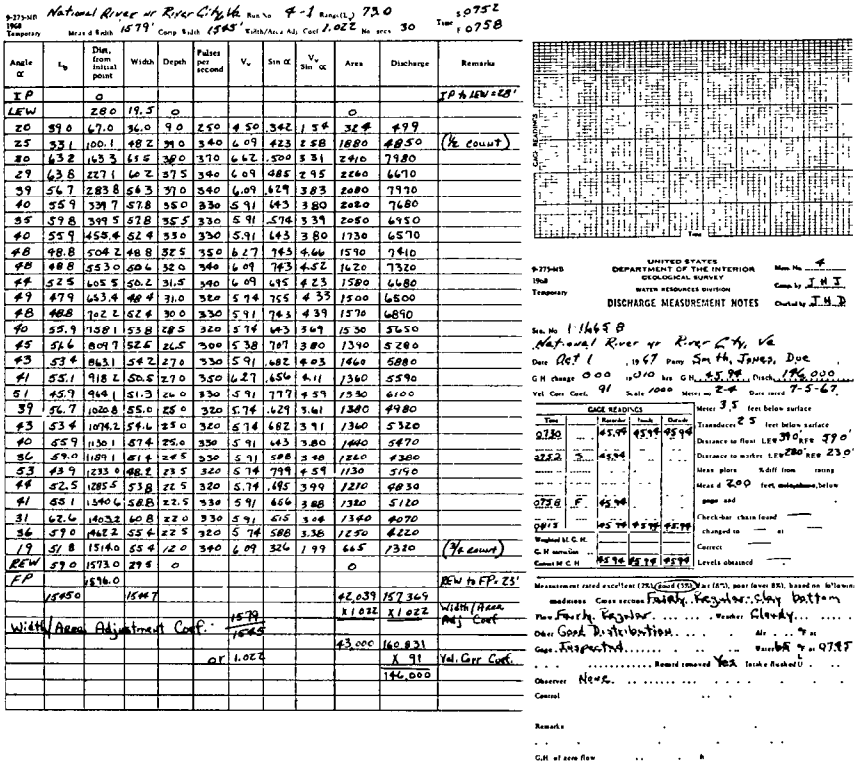

FIGURE 113.—Sample computation notes of a moving-boat measurement.

. . . . . .

$b_{(n-1)} = b_{(n-2)} + L_{b_{(n-1)}}$

$b_n = b_{(n-1)}$ + measured distance from float to edge of water

$b_{(n+1)} = b_n$ + distance to final point (marker).

4. Each of the incremental widths in column 4 represents the distance that extends laterally from half the distance from the preceding meter location $(x-1)$, to half the distance to the next, $(x+1)$. These values are obtained by using the distances in column 3.

5. Each of the values in column 5 represents the stream depth at a sampling point in the cross section. These values are obtained by adding the transducer depth to each of the depth readings recorded on the sounder chart at the sampling locations.

6. The data in column 6 are the pulses-per-second readings recorded by the notekeeper during the measurement.

7. The values recorded in column 7 represent the instantaneous velocity of the water past the vane at each observation point. They are read directly from the meter-rating table (fig. 108), using the pulses-per-second values of column 6.

8. The data in column 8 are the sine function values of the angle readings in column 1. These values may be obtained from the sine table in figure 108, using the angle readings of the first column.

9. Each of the values in column 9 represents the stream velocity normal to the cross section at that particular sampling point.. To obtain these values, it is necessary to multiply each V_V value in column 7 by the corresponding sin α value in column 8.

10. The values in column 10 represent the individual subsection areas for the measurement. They are obtained by multiplying the widths of column 4 by their corresponding depths in column 5. The incremental areas are then summed to provide the total unadjusted area for the measurement.

11. Each quantity in column 11 represents the unadjusted discharge through one of the subsections of the discharge measurement. These values are summed to provide the total unadjusted discharge of the measurement.

12. This column is used for recording any descriptive remarks pertaining to the measurement.

ADJUSTMENT OF TOTAL WIDTH AND AREA

As explained on page 186, the relation expressed by the equation $L_b \approx L_V \cos \alpha$ is used to obtain the incremental widths across the stream. This equation is based on the assumption that a right-triangle relationship exists among the velocity vectors involved. If the flow is not normal to the cross section, that assumed situation does not exist and the use of the equation can result in a computed width that is too

large or too small (fig. 114), depending on whether the vector quantity representing the oblique flow has a horizontal component that is opposed to, or in the direction of, that of the boat path. Thus in figure 114 the computed width would be AB' of the right triangle $AB'C$ rather than the true width AB of oblique triangle ABC. In this case the computed width is too large, whereas the computed width DE' of right triangle $DE'F$ is less than the actual width DE of oblique triangle DEF.

Ideally the correction for error in the computed width would be applied to that particular increment in the cross section where the error occurred. However, in practice only the overall width is directly measured, and thus only the total width is available for comparison with the computed quantities. Therefore, if the sum of the computed incremental widths does not equal the total measured width of the cross section, it is assumed that each increment requires a proportionate adjustment.

The moving-boat method uses the relation between the measured and computed widths of the cross section to determine a width/area adjustment factor. To obtain that coefficient, the measured width of the cross section is divided by its computed width, that is

$$k_B = \frac{B_m}{B_c} \tag{22}$$

where

k_B = width/area adjustment factor,
B_m = measured width of cross section, and
B_c = computed width of cross section.

The coefficient (k_B) is then used to adjust both total area and total discharge of the measurement, on the basis of the previously mentioned assumption that the error in width is evenly distributed, on a percentage basis, across each width increment of the cross section.

The computation notes in figure 113 provide an example of the application of a width/area adjustment coefficient.

ADJUSTMENT OF MEAN VELOCITY AND TOTAL DISCHARGE

During a moving-boat discharge measurement, the current meter is set at a predetermined fixed depth of from 3 to 4 ft (0.9 to 1.2 m) below the water surface. In other words, this technique uses the subsurface method of measuring velocity. (See page 136.) The measurement is computed by using constant-depth subsurface velocity observations without adjustment coefficients, as though each observed velocity were a mean in the vertical. In adjusting the computed discharge, each measured velocity should ideally be multiplied by a coefficient to adjust it to the mean velocity in its vertical. However, it

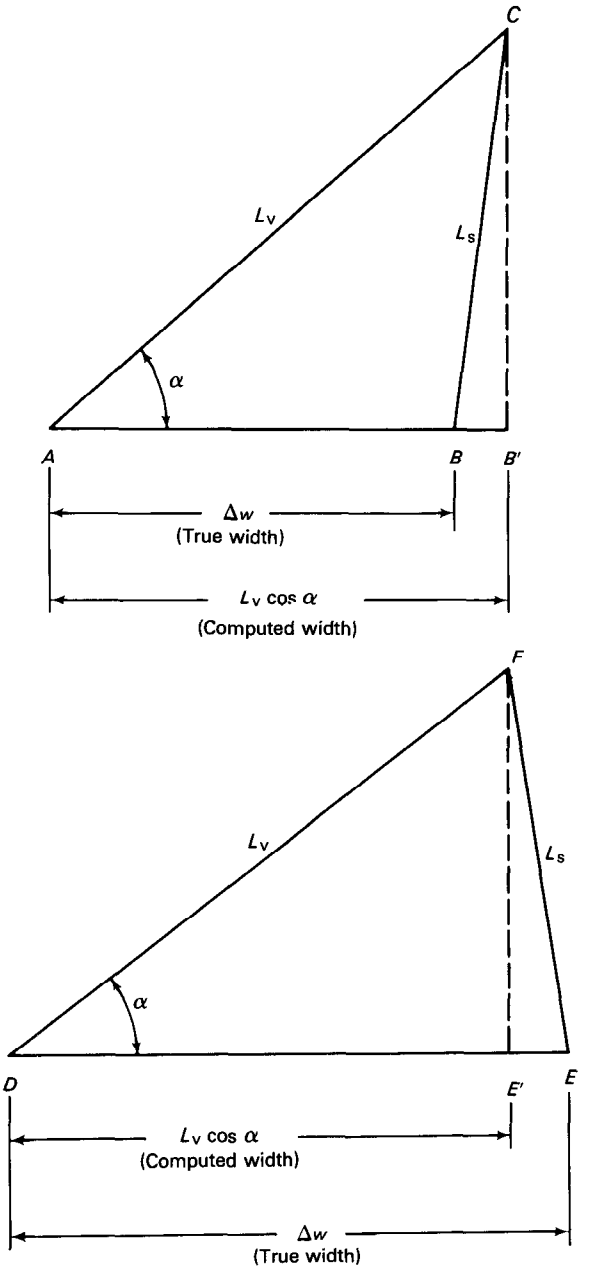

FIGURE 114.—Comparison of actual and computed values of incremental widths.

is assumed that in the larger streams where the moving-boat technique would be applicable, these coefficients would be fairly uniform across a section, thus permitting the application of an average velocity coefficient to the total discharge. Information obtained from several vertical-veolocity curves, well distributed across the measurement section, would be needed to determine a representative velocity coefficient for the total cross section.

DETERMINATION OF VERTICAL-VELOCITY ADJUSTMENT FACTOR

Vertical-velocity curves (p. 132–133) are constructed by plotting observed velocities against depth. The vertical-velocity curve method calls for a series of velocity observations (by conventional methods) at points well distributed between the water surface and the streambed. Normally these points are chosen at 0.1-depth increments between 0.1 and 0.9 of the depth. Observation should also be made at least 0.5 ft (0.15 m) from the water surface and 0.5 ft (0.15 m) from the streambed; for this particular application, a velocity reading should be made at the moving-boat sampling depth of from 3 to 4 ft (0.9 to 1.2 m) below the water surface. Once the velocity curve has been constructed, the mean velocity for the vertical can be obtained by measuring the area between the curve and the ordinate axis with a planimeter, or by other means, and then dividing this area by the length of the ordinate axis.

To obtain a velocity-correction coefficient at location x in the cross section, the mean velocity in the vertical is divided by the observed velocity at the measured depth, that is,

$$k_V = \frac{\overline{V}}{V}, \tag{23}$$

where

k_V = vertical-velocity adjustment factor,
$\overline{V}$ = mean velocity in the vertical, and
V = observed velocity (3- or 4-ft depth).

To arrive at a representative average coefficient, coefficients should be determined at several strategically located verticals that are representative of the main portion of the streamflow. Once an average coefficient has been determined, it should not be necessary to redetermine it each time when making future discharge measurements at the same site. However, it would be necessary to test its validity at several widely varying stages and, in estuaries, at widely different parts of the tidal cycle.

Investigations on the Mississippi River at both Vicksburg and St. Louis, on the Hudson River at Poughkeepsie, and on the Delaware

River at Delaware Memorial Bridge all indicated coefficients that lie in the narrow range of 0.90 to 0.92 for adjusting the subsurface velocity to the mean velocity. Carter and Anderson (1963) present a table of velocity ratios and standard deviations for various relative depths. That table indicates that for depths of 10 ft (3 m) or more, an average coefficient of 0.90 is satisfactory for adjusting velocities obtained 4 ft (1.2 m) below the surface to mean velocity. The sample from which the data in that table were obtained consisted of 100 stream sites at each of which 25 to 30 verticals had been used. Similar conclusions concerning subsurface velocity coefficients can be drawn from table 2 (p. 132).

APPLICATION OF VELOCITY ADJUSTMENT TO COMPUTED DISCHARGE

Application of the vertical-velocity adjustment factor is made immediately after the width-area adjustment has been applied to the computed discharge. In other words, after the computed discharge has been multiplied by the width-area adjustment factor, the resulting product is multiplied by the vertical-velocity adjustment factor. The final product is the adjusted, or "true," discharge for the measurement. (See fig. 113.)

SELECTED REFERENCES

Buchanan, T. J., and Somers, W. P., 1969, Discharge measurements at gaging stations: U.S. Geol. Survey Techniques Water Resources Inv., book 3, chap. A8, 65 p.

Carter, R. W., and Anderson, I. E., 1963, Accuracy of current-meter measurements: Am. Soc. Civil Engineers Jour., v. 89, no. HY4, p. 105–115.

Smoot, G. F., and Novak, C. E., 1969, Measurement of discharge by the moving-boat method: U.S. Geol. Survey Techniques Water Resources Inv., book 3, chap. A11, 22 p.

CHAPTER 7.—MEASUREMENT OF DISCHARGE BY TRACER DILUTION

GENERAL

The measurement of stream discharge by dilution methods depends on the determination of the degree to which an added tracer is diluted by the flowing water. Any substance can be used as a tracer if it meets the following criteria:

1. It dissolves readily in water at ordinary temperatures.
2. It is either absent in the water of the stream or present only in very low concentrations.
3. It is not decomposed in the water of the stream and is not retained or absorbed in significant quantity by sediments, plants, or other organisms.
4. It can be detected in extremely low concentrations by simple methods.

5. It is harmless to man and animals in the concentration it assumes in the stream.

Until recent years chemical salts, primarily common salt (NaCl), were usually used as the tracers injected into the streams. The use of salt tracers, on all but the smallest streams, was limited, however, to the sudden-injection method, because of the difficulty of handling the large quantities of salt solution required by the usually more accurate constant-rate-injection method. In recent years, and particularly in the U.S.A., the use of dye tracers in the constant-rate-injection method has become the most popular method of discharge measurement by tracer dilution. That has resulted from the development of fluorescent dyes and fluorometers that can detect those dyes at very low concentrations. The use of fluorescent dyes is not as popular in Europe as in the U.S.A. There, colorimetric analysis, using sodium dichromate as the tracer dye, is the most widely used means of measuring discharge by the constant-rate-injection method. However, where the sudden-injection method is to be used, the use of common salt as a tracer is still preferred, particularly on the smaller streams, because of the greater ease in handling salt and in determining concentrations. Radioactive elements, such as gold 198 and sodium 24, have also been used in recent years as the tracers in the sudden-injection method, but the use of such elements is still (1980) considered experimental.

The tracer-dilution methods of measuring discharge are more difficult to use than the conventional current-meter method, and under most conditions the results are less reliable. Dilution methods should therefore not be used when conditions are favorable for a current-meter measurement of discharge. Tracer-dilution methods of measuring discharge in open channels can be used advantageously in rough channels that carry highly turbulent flow.

THEORY OF TRACER-DILUTION METHODS

In the tracer-dilution methods of measuring discharge, a tracer solution is injected into the stream to be diluted by the discharge of the stream. From measurements of the rate of injection, the concentration of the tracer in the injected solution, and the concentrations of the tracer at a sampling cross section downstream from the injection site, the stream discharge can be computed.

Either of two methods may be used for determining the discharge of a stream by tracer dilution. The first method, the constant-rate-injection method, requires that the tracer solution be injected into the stream at a constant flow rate for a period sufficiently long to achieve a constant concentration of the tracer in the streamflow at the downstream sampling cross section. The second method, the sudden-

injection method, requires the instantaneous injection of a slug of tracer solution and an accounting of the total mass of tracer at the sampling cross section. Another use is often made of the sudden-injection method that is not concerned with degree of dilution. Where the cross-sectional area of the flow is constant, as in pressure conduit, the sudden-injection method may be used to determine the velocity of flow; discharge can then be computed by using that velocity and the known cross-sectional area. (See p. 533.)

THEORY OF THE CONSTANT-RATE-INJECTION METHOD

A constant-rate-injection system is shown schematically in figure 115. If the tracer is injected for a sufficiently long period, sampling of the stream at the downstream sampling cross section will produce a concentration-time curve similar to that shown in figure 116. The stream discharge is computed from the equation for the conservation of mass, which follows:

$$QC_b + qC_1 = (Q + q)C_2 \tag{24}$$

or

$$Q = \left[\frac{C_1 - C_2}{C_2 - C_b}\right] q,$$

where

q is the rate of flow of the injected tracer solution,
Q is the discharge of the stream,
C_b is the background concentration of the stream,
C_1 is the concentration of the tracer solution injected into the stream, and
C_2 is the measured concentration of the plateau of the concentration-time curve (fig. 116).

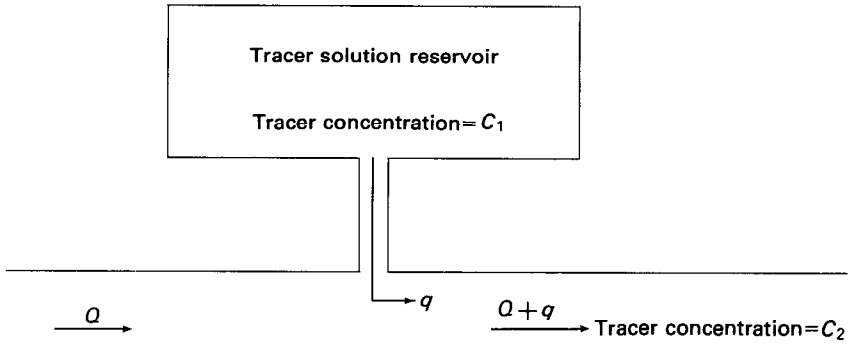

FIGURE 115.—Constant-rate-injection system.

THEORY OF THE SUDDEN-INJECTION METHOD

If a slug of tracer solution is instantaneously injected into a stream, sampling of the stream at the downstream sampling cross section will produce a concentration-time curve similar to that shown in figure 117. The equation for computing stream discharge, which is again based on the principle of the conservation of mass, is

$$Q = \frac{V_1 C_1}{\int_0^\infty (C - C_b) dt}, \tag{25}$$

where

Q is the discharge of the stream,
V_1 is the volume of the tracer solution introduced into the stream,
C_1 is the concentration of the tracer solution injected into the stream,
C is the measured tracer concentration at a given time at the downstream sampling site,
C_b is the background concentration of the stream, and
t is time.

The term $\int_0^\infty (C - C_b)\, dt$ is the total area under the concentration-time curve. In practice the term $\int_0^\infty (C - C_b) dt$ can be approximated by the term

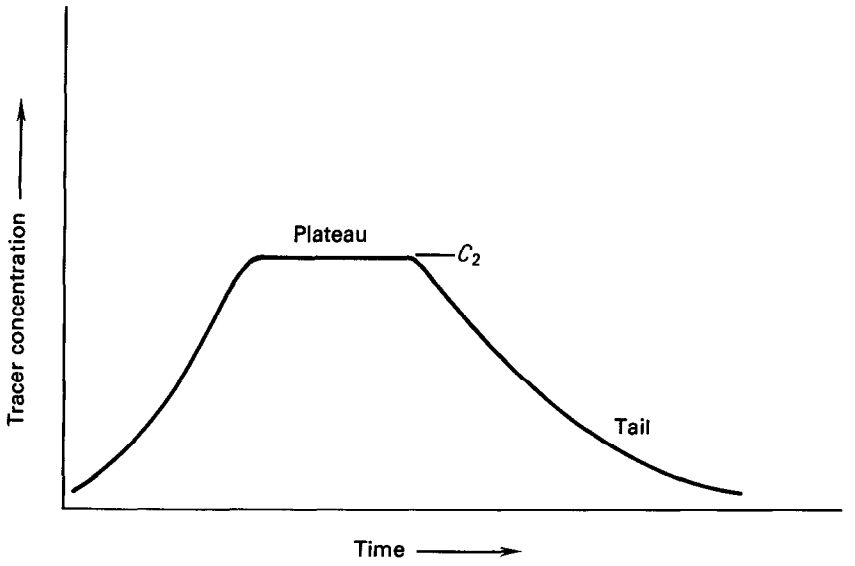

FIGURE 116.—Concentration-time curve at downstream sampling site for constant-rate injection.

$$\sum_{i=1}^{N} (C_i - C_b)(t_{i+1} - t_{i-1})/2,$$

where

i is the sequence number of a sample,
N is the total number of samples, and
t_i is time when a sample, C_i, is obtained.

FACTORS AFFECTING THE ACCURACY OF TRACER-DILUTION METHODS

Even if it is assumed that measurements of concentrations and of the injection rate are error free, there still remain three factors that affect the accuracy of tracer-dilution methods of measuring discharge. Those factors are stream turbidity, loss of tracer between the injection site and the downstream sampling site, and incomplete mixing throughout the stream cross section before the downstream sampling section is reached.

TURBIDITY

Turbidity may either increase or decrease the recorded tracer fluorescence depending upon the relative concentrations of tracer and turbidity (Feuerstein and Selleck, 1963). To minimize the effect of turbidity, samples should be permitted to stand long enough to allow

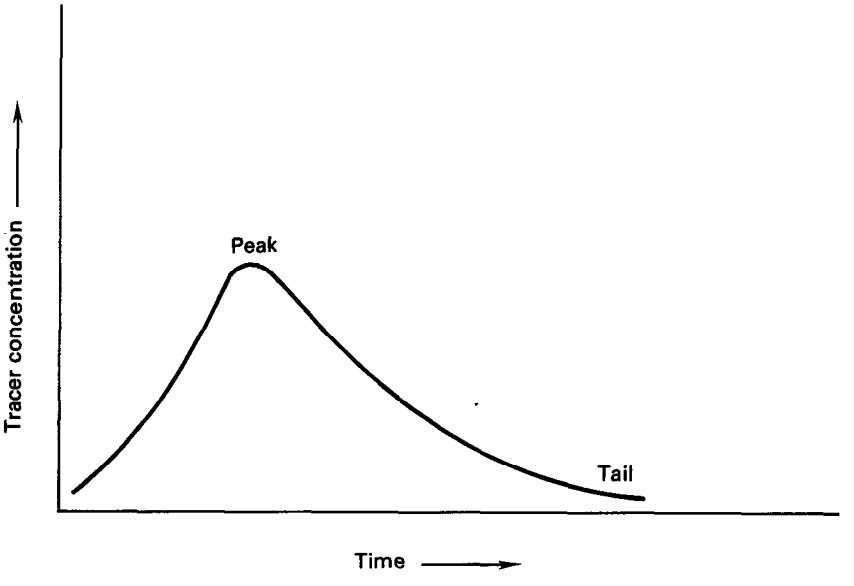

FIGURE 117.—Concentration-time curve at downstream sampling site for sudden injection.

suspended solids to settle prior to fluorometric analysis (p. 231, 240). Use of a centrifuge for the purpose of separating the suspended solids is even more effective, but a centrifuge is seldom used for that purpose in stream-gaging work.

LOSS OF TRACER

The computation of stream discharge, as mentioned earlier, is based on equations for the conservation of mass. Consequently, the accuracy of the computed discharge will be adversely affected if some of the tracer is lost in the reach of channel between the injection site and the downstream sampling site. Tracer losses are primarily due to sorption and chemical reaction between the tracer and one or more of the following: streambed material, suspended sediments, dissolved material in the river water, plants, and other organisms. For most of the tracers used, chemical reaction is a minor factor in comparison with sorption. The degree of tracer loss by sorption for a particular tracer varies primarily with the type and concentration of suspended and dissolved solids in the water. In routine stream gaging by the tracer-dilution method no attempt is made to quantify tracer loss by sorption; instead, the "best" tracer available from the standpoint of being least affected by sorption is used.

Photochemical decay is also a source of tracer loss which varies with the tracer material used and its residence time in direct sunlight. Loss from that source is usually negligible, even with fluorescent dyes, if the proper dye is used and if residence time in direct sunlight is limited to only a few hours, as it usually is in stream-gaging work.

Equations 24 and 25 show that loss of tracer will result in a computed discharge that exceeds the true stream discharge.

CRITERIA FOR SATISFACTORY MIXING

Tracer-dilution measurements require complete vertical and lateral mixing at the sampling site. Vertical mixing is usually accomplished very rapidly compared to lateral mixing; therefore, the distance required for lateral mixing is the primary consideration. Frequently, long reaches are needed for complete lateral mixing of the tracer. The mixing distance will vary with the hydraulic characteristics of the reach. Engmann and Kellerhals (1974) have demonstrated that ice cover significantly reduces the mixing capacity of a reach of river.

When the constant-rate-injection method is used, complete mixing is known to have occured when the concentration C_2, shown in figure 116, has the same value at all points in the downstream sampling cross section. When the sudden-injection method is used, complete

mixing is considered to have occurred when the area under the concentration-time curve, shown in figure 117, has the same value at all points in the downstream sampling section.

For a reach of channel of given geometry and stream discharge, the length of reach required for adequate mixing of the tracer is the same for either of the two methods of tracer injection. Several formulas are available for estimating the required mixing length for a particular set of conditions, but these formulas, while useful as guides, are too simplistic to give adequate consideration to the degree of mixing desired. Perfect mixing is seldom the optimum goal (see below) because perfect mixing usually requires an extremely long reach of channel, along with a correspondingly long period of injection in the constant-rate-injection (CRI) method and a correspondingly long period of sampling in the sudden-injection (SI) method.

Figures 116 and 117 are only rudimentary illustrations of the two methods. For either method to be successful an understanding is needed of the interrelations among mixing length and injection and sampling times. Figure 118 attempts to illustrate those interrelations for both types of injection. It is important to realize that unless adequate mixing is known to exist at a given sampling site, the tracer cloud in the SI method must be sampled for its entire time of passage at several locations laterally in the channel, such as at A, B, and C in figure 118. Similarly, in the CRI method the plateau concentration must be sampled at several locations laterally in the channel. Experience indicates that regardless of method or stream size, at least three lateral sampling points should be used at each sampling site.

Figure 118 indicates that there is an optimum mixing length for a given stream reach and discharge. Use of too short a distance will result in an inaccurate accounting of the tracer mass passing the sampling site. Use of too great a distance will yield excellent results, but only if it is feasible to inject the tracer for a long enough period (CRI method) or to sample for a long enough period (SI method). An optimum mixing length is one that produces mixing adequate for an accurate discharge measurement but does not require an excessively long duration of injection or sampling.

As mentioned earlier, figure 118 shows that the tracer cloud resulting from a sudden injection must be sampled at the sampling site from the time of its first appearance there until the time (T_t) of its disappearance at all points in the sampling cross section. For the same mixing reach and discharge, if the CRI method is used, a plateau will first be reached at all points in the sampling cross section at time T_t after injection starts at the injection site. Thus, it is seen that for the CRI method the duration of injection must at least be equal to T_t and injection should continue long enough thereafter to

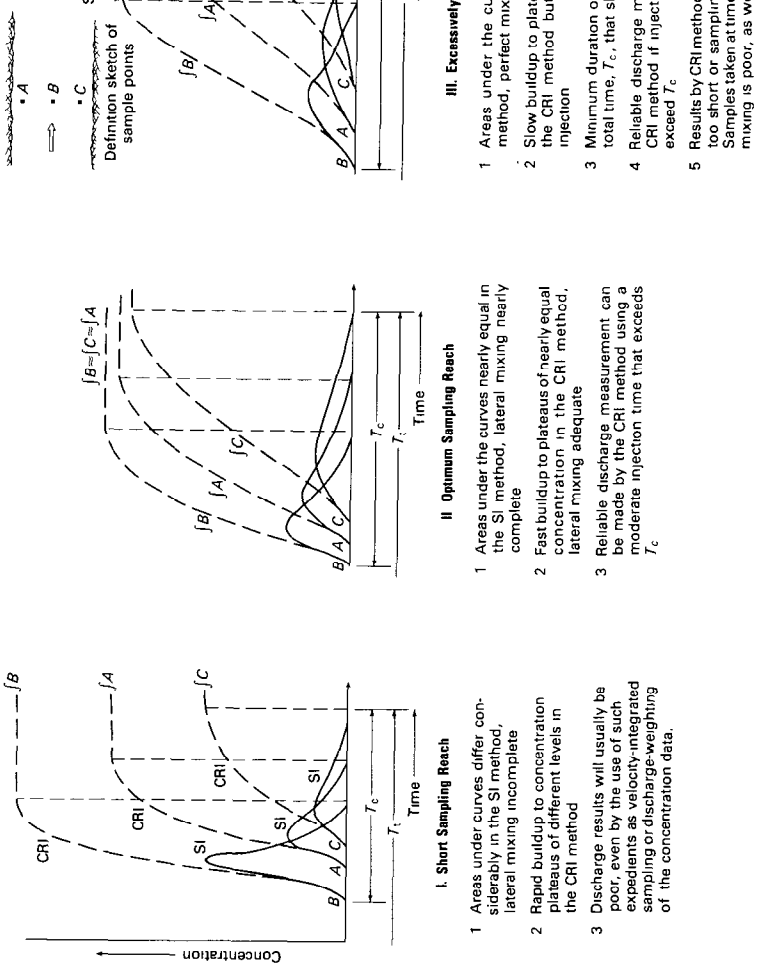

I. Short Sampling Reach

1. Areas under curves differ considerably in the SI method, lateral mixing incomplete
2. Rapid buildup to concentration plateaus of different levels in the CRI method
3. Discharge results will usually be poor, even by the use of such expedients as velocity-integrated sampling or discharge-weighting of the concentration data.

II Optimum Sampling Reach

1. Areas under the curves nearly equal in the SI method, lateral mixing nearly complete
2. Fast buildup to plateaus of nearly equal concentration in the CRI method, lateral mixing adequate
3. Reliable discharge measurement can be made by the CRI method using a moderate injection time that exceeds T_c

III. Excessively Long Sampling Reach

1. Areas under the curves are identical in the SI method, perfect mixing
2. Slow buildup to plateaus of equal concentration in the CRI method but only after a long period of injection
3. Minimum duration of constant injection is equal to total time, T_c, that slug dye cloud is present
4. Reliable discharge measurement can be made by CRI method if injection period is long enough to exceed T_c
5. Results by CRI method will be poor if injection time is too short or sampling is discontinued too soon Samples taken at time S would give impression that mixing is poor, as well as suggesting loss of dye

FIGURE 118.—Comparison of concentration-time curves obtained by SI and CRI methods, observed at three points in sampling cross section, for sampling reaches of three different lengths.

insure adequate sampling of the plateau. It should be noted that a stable condition of mixing is usually first attained in midchannel. Tracer lag along the streambanks will generally prolong the time required for complete lateral mixing.

The CRI method has become increasingly popular because reliable injection apparatus is available and the sampling process is relatively simple. If an injection period well in excess of T_c is used, the sampling can be done leisurely at several points in the sampling cross section. In the SI method the injection is simple, but the sampling process is much more demanding. More reliable results are usually obtained by the CRI method.

Figure 118 indicates that a satisfactory discharge measurement requires "nearly equal" areas under the concentration-time curves for the sampling points in the SI method and "nearly equal" concentration plateaus for the sampling points in the CRI method. A numerical criterion—P_m, the percentage of mixing—is often used as a quantitative index of the consistency of sampling results for the sampling cross section. A satisfactory discharge measurement can usually be obtained if the value of P_m is 95 percent or greater. The computation of P_m is discussed in the paragraphs that follow.

Percentage of mixing, P_m, is defined in this manual by the equation

$$P_m = 100 - \{|X_A - X_m|Q_A + |X_B - X_m|Q_B + |X_C - X_m|Q_C + \ldots\}\frac{50}{X_m Q}, \quad (26)$$

where

$X_A, X_B, X_C, \ldots$ are the areas under the concentration-time curves or, for constant-rate injection, the C_2 concentrations at the points A, B, C, . . . across the sampling section;

X_m is the mean area under the concentration-time curves or, for constant-rate injection, the mean C_2 concentration for points A, B, C, . . . across the sampling section;

$Q_A, Q_B, Q_C, \ldots$ are the subsection discharges applicable to the points, A, B, C, . . .;

Q is the total stream discharge.

If the distribution of discharge is unknown at the sampling section, the cross-sectional subareas applicable to each point should be used in place of Q_A, Q_B, Q_C; total cross-sectional area should be used in place of Q. If both discharge and area distribution are unknown, as will often be the case, the appropriate widths may be used. Terms $|X_A - X_m|$, $|X_B - X_m|$, $|X_C - X_m|$, . . . are absolute values.

The percentage of mixing can also be determined graphically, as shown in figure 119. Values of C_2 or $\int_0^\infty (C - C_b)dt$, depending on the

injection method used, are plotted for each sampling point against the distance from an initial point at water's edge. The mean value C_2 or $\int_0^\infty (C - C_b)dt$ is determined by dividing the area under the distribution curve for C_2 or $\int_0^\infty (C - C_b)dt$ by the total width of the section. The percentage of mixing, P_m, is then given as

$$P_m = \left(\frac{A}{A + B}\right) 100 \tag{27}$$

where

A is the area under the C_2 distribution and mean C_2 curves, or the area under the $\int_0^\infty (C - C_b)dt$ distribution and mean $\int_0^\infty (C - C_b)dt$ curves;

B is the area above the C_2 distribution and under the mean C_2 curves or the area above the $\int_0^\infty (C - C_b)dt$ distribution and under the mean $\int_0^\infty (C - C_b)dt$ curves.

The graphical technique illustrated in figure 119 can also be used if the distribution of discharge or area is known. The only change in the procedure that is required is a change in the abscissa of figure 119. In place of "distance from edge of water" either cumulative discharge or cumulative area from edge of water is substituted.

CALIBRATION OF MEASUREMENT REACH

Several theoretical studies have been made by the U.S. Geological Survey (for example, Yotsukura and Cobb, 1972) in which equations have been derived for determining the length of measurement reach required for satisfactory or complete mixing. However, the derived equations cannot be applied in the field without detailed information

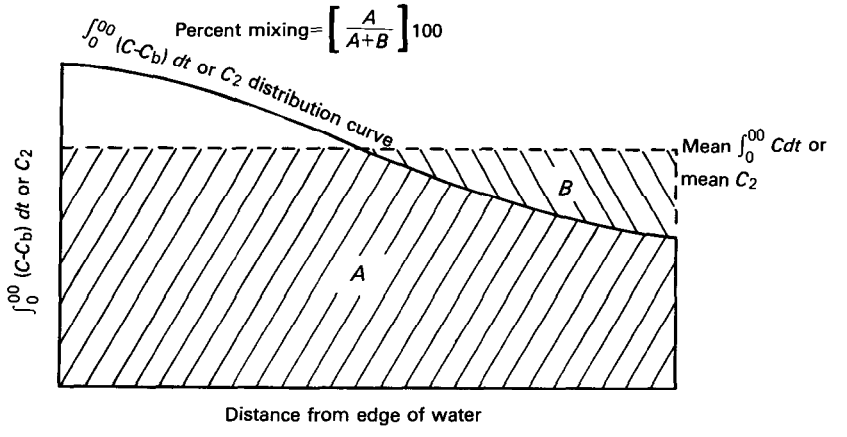

FIGURE 119.—Concentration-distribution curve illustrating the graphical method of determining the percentage of mixing.

on channel geometry and velocity distribution for the reach of channel. Consequently several gross formulas have been developed from the theoretical equations strictly for use as guides in determining a satisfactory length of measurement reach. Some of the simplified formulas follow:

a. Point injection at midchannel (English units)—

1. $$L=0.25\frac{V}{(gDS)^{1/2}}\frac{W^2}{D}, \tag{28}$$

where

L is distance downstream from the injection point,
V is mean velocity,
g is acceleration of gravity,
D is mean depth,
S is gradient of water surface or streambed, and
W is stream width.

2. $$L=0.6\frac{R^{1/6}}{ng^{1/2}}\frac{W^2}{D}, \tag{29}$$

where R is the hydraulic radius and n is the Manning roughness coefficient.

3. $$L=2V\ \frac{(W^2)}{D}\cdot \tag{30}$$

b. Point injection at bankside (English units)—

$$L=8V\frac{W^2}{D}. \tag{31}$$

Studies indicate that if more than one injection point is used, the mixing distance will vary inversely with the square of the number of injection points, provided that the injection points are located so that the dye will disperse equal distances both to the left and right of the injection points. This statement may seldom hold true for natural stream conditions, but it does indicate that the mixing length may be shortened considerably by using additional injection points.

In Europe the formula commonly used as a guide for determining the required length, L, between the injection site and sampling section is

$$L=0.13C\ \frac{(0.7C+6)}{g}\ \frac{b^2}{h}\text{(metric units)}, \tag{32}$$

where

b is the average width of the wetted cross section,
h is the average depth of flow,
C is the Chezy coefficient for the reach ($15<C<50$), and
g is acceleration of gravity.

Equation 32 is intended for use where injection is made at a single point in midstream.

Before making a discharge measurement by the tracer-dilution method, the proposed measurement reach should be calibrated to determine the length required for adequate mixing and the possibility of significant tracer loss. If repeated tracer-dilution measurements of the stream are to be made, it will be especially advantageous to make the calibration study comprehensive. One of the equations, 28 to 32, may be used as a guide in selecting a length of reach for the calibration tests; the quantity of tracer to be used for any given discharge is discussed later on pages 235–237. Instructions for calibration testing follow.

Select an injection site on the stream, and on the basis of one of the equations, 28 to 32, select several downstream sampling sites. Inject the tracer and then sample the water at three or more points in the cross section at each of the selected sampling sites. Take adequate samples at each point to define the plateau of the concentration-time curve if the constant-rate-injection method is used, or to define the entire concentration-time curve if the sudden-injection method is used. Analyze the samples and determine the percentage of mixing by use of equation 26. As mentioned earlier, for a satisfactory measurement of discharge the percentage of mixing should be at least 95. Mixing distances and losses may vary with discharge, and the reach may therefore have to be calibrated at more than one discharge. The quantity of tracer lost, if any, between successive sampling sites can be determined by a comparison of the values of C_2 (constant-rate-injection method) or of $\int_o^\infty (C - C_b)dt$ (sudden-injection method) obtained at each site. That determination provides a basis for the final selection of a sampling site from the several sites tested.

EFFECT OF INFLOW OR OUTFLOW BETWEEN INJECTION AND SAMPLING SITES

A satisfactory tracer-dilution measurement of discharge made in a reach that has no inflow or outflow between the injection and sampling sites will give the discharge occurring at all cross sections in the reach.

If tributary inflow enters the reach and if the tributary inflow is well mixed with the water in the main stream, the discharge measured will be that at the sampling site. If the tributary inflow is not well mixed, that fact may be evident from the difference in concentrations at the various sampling points in the sampling cross section; a low percentage of mixing would indicate that the particular sampling site could not be used for a satisfactory measurement of discharge.

If outflow occurs between the injection and sampling sites and if the tracer becomes completely mixed anywhere upstream from the outflow channel, the discharge measured at the sampling site will be that for the reach upstream from the outflow channel. If the tracer does not become completely mixed upstream from the outflow channel, the discharge measured at the sampling site will be indeterminate; the magnitude of the "measured" discharge will be dependent on the quantities of both tracer and water that are carried off in the outflow.

MEASUREMENT OF DISCHARGE BY FLUORESCENT DYE DILUTION

As mentioned earlier, the most popular type of tracer for the measurement of streamflow in the U.S.A. is fluorescent dye. The cost of the dye is relatively small because the quantity of dye needed for a discharge measurement is small; modern fluorometers are capable of accurately measuring dye concentrations of less than 1 μg/L (microgram per liter) and can detect concentrations as low as 0.02 μg/L.

FLUORESCENT DYES

Fluorescence occurs when a substance absorbs light at one wavelength and emits it at another, and usually longer, wavelength. The dyes commonly used as tracers are strongly fluorescent. They are organic dyes of the rhodamine family and are commercially available.

Dyes selected for use as tracers should (1) have a high detectability range, (2) have little effect on flora or fauna, (3) have a low sorption tendency, (4) have a low photochemical decay rate, (5) be soluble and disperse readily in water, (6) be chemically stable, (7) be inexpensive, (8) be easily separated from common background fluorescence, and (9) be easy to handle.

On the basis of recent studies in the U.S.A. on the adsorption potential and detectability of dyes, Rhodamine WT dye is recommended as the best dye available for use in dye-dilution measurements of discharge. Formerly used at times, but no longer recommended are Rhodamine B, BA, and Fluorescein.

FLUOROMETER

The fluorometer is an instrument that gives a measure of the strength of the light emitted by a fluorescent substance. Figure 120 is a schematic diagram of a fluorometer. The flurometer briefly described in this manual is the Turner model 111 fluorometer, and it is discussed because it is the instrument that is in general use by the U.S. Geological Survey. However, there are many satisfactory fluorometers that are commercially available, and for detailed in-

structions concerning any particular fluorometer it is necessary that the hydrographer consult the service manual prepared by the manufacturer of that instrument. The fluorometry techniques described in this manual are oriented toward use of the Turner fluorometer, but those techniques are applicable to most types of fluorometer. (Note.—The use of brand names in this manual is for identification purposes only and does not imply endorsement by the U.S. Geological Survey.)

DESCRIPTION OF FLUOROMETER

The principle of the operation of the Turner model 111 fluorometer is described in the operating manual (1963, p. 12) as follows:

This fluorometer is basically an optical bridge which is analogous to the accurate Wheatstone Bridge used in measuring electrical resistance. The optical bridge measures the difference between light emitted by the sample and that from a calibrated rear light path. A single photomultiplier surrounded by a mechanical light interrupter sees light alternately from the sample and the rear light path. Photomultiplier output is alternating current, permitting a drift-free A–C amplifier to be used for the first electronic stages. The second stage is a phase-sensitive detector whose output is either positive or negative, depending on whether there is an excess of light in the forward (sample) or rear light path, respectively. Output of the phase detector drives a servo amplifier which is in turn connected to a servo motor. The servo motor drives the light cam (and the "fluorescence" dial) until equal amounts of light reach the photomultiplier from the sample and from the rear light path. The quantity of light required in the rear path to balance that from the sample is indicated by the "fluorescence" dial. Each of this dial's 100 divisions add equal increments of light to the rear path by means of a light cam.

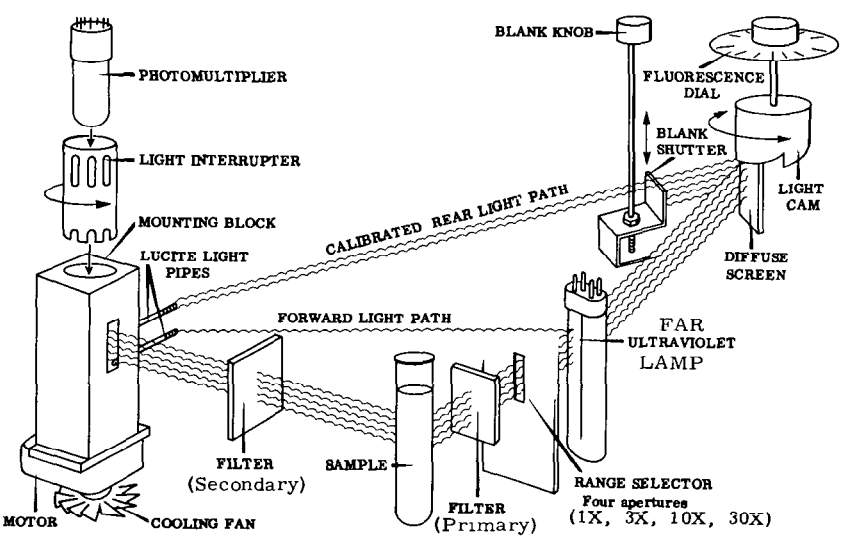

FIGURE 120.—Schematic diagram of the fluorometer (from G. K. Turner Associates, 1963, p.13).

Lamps.—At least three different lamps can be used as a light source for the fluorometer when the fluorescence of rhodamine dyes is tested. They are the general purpose ultraviolet lamp, the far ultraviolet lamp, and the green T–5 lamp. Although all three lamps work well, the far ultraviolet and green T–5 lamps are recommended as a light source because their outputs are compatible with the fluorescent properties of the dyes. Sensitivity of the fluorometer is increased approximately twofold to tenfold when the far ultraviolet and green T–5 lamps, respectively, are substituted for the general purpose ultraviolet lamp.

Filters.—The sensitivity of the fluorometer is directly related to the filter system employed. Light having undesirable wavelengths may be screened out by placing filters at two points in the fluorometer: (1) between the source light and the water sample and (2) between the water sample and the photomultiplier.

The filter (primary) recommended for use with rhodamine dyes for the absorbed light has a peak color specification of 546 mμ (millimicrons); that is, the greatest amount of light passed through the filter is at a wavelength of 546 mμ. Light at other wavelengths is subdued or eliminated. The recommended filter (secondary) for the emitted light has a peak color specification of 590 mμ. The peak color specifications for these filters are near the peak excitation and emittance wavelengths of the rhodamine dyes and will eliminate most natural background fluorescence. The filters may be used regardless of the type of lamp that is installed.

Doors.—Three main types of doors available for use with the fluorometer are the standard-cuvette (test tube) door, the temperature-stabilizing door, and flow-through door. All three doors are easily interchanged.

The standard-cuvette door is the easiest to use in the field for intermittent sampling and should be used with the green T–5 lamp. If the far ultraviolet lamp is used, a high-sensitivity kit should be installed on this door because it will increase the overall sensitivity of the fluorometer about tenfold. It is important to note that excessive sensitivity will be obtained if the high-sensitivity kit and green T–5 lamp are used together.

The temperature-stabilizing door is recommended for the final testing of samples. This door is similar to the standard-cuvette door with the high sensitivity kit but has, in addition, a water-cooled, copper block that surrounds the cuvette. Cooling water may be pumped or tap water of constant, or near-constant, temperature may be run through the door to stablize the sample temperature. Only round 12×75-mm cuvettes can be used with this door.

The flow through door permits continuous sampling which can be

recorded. A pump is used to circulate water from the stream through the cuvette in the door. The results may be recorded on any recorder with a 0 to 1 milliamp or 0 to 10 millivolt readout. The intake hose used with the flow-through door should be made of plastic or other nonabsorptive material. Different fittings and cuvette sizes are available for this door. The sensitivity of the flow-through door is about the same as that of the standard-cuvette door with the high sensitivity kit. That is so because of the larger cuvette used in the flow-through door.

Normally dye concentrations are not determined in the field because it is difficult to attain sufficient accuracy under such conditions. The flow-through door arrangement may be used for preliminary calibration of a reach, however. As a rule, bottle samples are collected and transferred to the laboratory for accurate fluorometric analysis.

EFFECT OF TEMPERATURE ON FLUOROMETRY

Accurate dilution discharge measurements require accurate fluorometry, and accurate fluorometry can only be attained in the laboratory where operating conditions are favorable. Temperature has a significant effect upon the fluorescence intensity of dyes. Fluorescence decreases with increasing temperature. This characteristic of the dyes has been investigated by several researchers, among them Feuerstein and Selleck (1963). For best results, all samples, including background and standard solutions, should be placed in a laboratory temperature bath and kept at constant temperature prior to fluorometric analysis. If the same temperature is used for all samples, no temperature corrections will be needed. If temperatures cannot be held constant, temperature corrections, as given in table 13 for Rhodamine WT dye, should be applied to dial readings or to concentrations.

Dunn and Vaupel (1965) point out the need for corrections to fluorometer dial readings as a result of changing compartment temperatures. However, tests by the U.S. Geological Survey showed that these corrections were needed only during the warmup period. A 1½-to 2-hr warmup will usually eliminate the need for this type of correction, although minor changes may still be observed thereafter. The warmup characteristics of each fluorometer should be determined. If possible, the fluorometer should not be operated where large temperature changes can occur rapidly.

CALIBRATION CHARACTERISTICS OF THE FLUOROMETER

Most fluorometers have a linear calibration ratio, meaning that dye concentration is directly proportional to the dial reading on the fluorometer and is related by the equation

TABLE 13.—*Temperature-correction coefficients for Rhodamine WT dye*

Temperature difference ($T_s - T$)[1]		Temperature-correction coefficient
F°	C°	
−20	−11.1	1.36
−15	−8.3	1.25
−10	−5.6	1.16
−8	−4.4	1.13
−6	−3.3	1.09
−5	−2.8	1.08
−4	−2.2	1.06
−3	−1.7	1.05
−2	−1.1	1.03
−1	−.6	1.02
0	0	1.00
+1	+.6	.99
2	1.1	.97
3	1.7	.96
4	2.2	.94
5	2.8	.93
6	3.3	.91
8	4.4	.89
10	5.6	.86
15	8.3	.80
20	11.1	.74

[1] T_s is the standard cuvette-sample temperature and T is the cuvette-sample temperature at the time the sample was tested in the fluorometer.

$$C = aD, \tag{33}$$

where

C is the dye concentration of the sample tested,

a is a coefficient, and

D is the fluorometer dial reading for the sample tested.

Solutions of known concentration are tested with the fluorometer, and the relation between concentration and dial reading is determined from equation 33.

Some fluorometers, however, do not have linear calibration ratios, and it is therefore necessary to determine the nature of the relation between concentration and dial reading by testing with standard solutions over a wide range of concentrations. A plot of concentration versus fluorometer-dial reading will give the shape of the calibration relation for the particular fluorometer. Experience to date indicates that nonlinear response occurs more frequently and to a greater degree at the low end of the curve; special effort should be made, therefore, to define that part of the curve.

If a fluorometer is found to have a nonlinear calibration relation, the instrument should be returned to the manufacturer for replace-

ment of parts or adjustment. Before an instrument is returned, one should be certain that the relation is truly nonlinear and not the result of an error in calibration. Inadequate instrument warmup is frequently the cause of a nonlinear calibration. If the instrument has to be used and the calibration is nonlinear, the derived nonlinear calibration curve should be used.

It is recommended that, if possible, dial readings of less than 10 be avoided, because the normal instrument error inherent in fluorometer operation can result in relatively large percentage errors for low dial readings. Low dial readings can be avoided by use of the proper fluorometer aperture. For example, the Turner fluorometer has four apertures, each designed to allow the passage of a different amount of light (fig. 120). The amount of light passed at each scale is approximately proportional to scale number; that is, the 30× scale will pass about 30 times as much light as the 1× scale. The relation between scales, for any fluorometer used, should be determined by testing each of several samples of different dye concentrations on more than one scale. A plot of dial readings for one scale against corresponding dial readings on another scale will give the desired relation. It should be mentioned here that low dial readings are unavoidable when testing the background (natural) fluorescence of river water. (See p. 231.)

PREPARATION OF STANDARD DYE SOLUTIONS FOR FLUOROMETER CALIBRATION

In calibrating the fluorometer it is necessary to first prepare samples of dye solution of known relative concentration, then test the samples in the fluorometer, and finally relate the readings on the fluorometer dial to the known relative concentrations. This matter of relative concentrations should be explained at this point. The accurate determination of stream discharge depends on the measurement of concentrations relative to each other; the absolute values of the concentrations are of no importance as long as the values of the concentrations are all determined in the same manner and all bear the same ratio to the absolute or true concentrations. Where the term "concentration" is used in this manual, it refers to "relative concentration"; the two terms are used here interchangeably. The calibration characteristics of the fluorometer were discussed in the preceding section of this manual. This section explains the preparation of standard dye solutions of various concentrations for use in the calibration process.

Standard dye solutions are prepared by diluting, with known amounts of water, the dye solution furnished by the manufacturer of the dye. The relative concentration of the furnished solution is the value given by the manufacturer. For example, if the manufacturer's

20-percent dye solution is used, its relative concentration is 200,000,000 $\mu g/l$. If the relative concentration of that solution differs from the true or absolute concentration by some small percentage, all diluted samples that are prepared from that batch of dye solution will have relative concentrations that differ from their absolute values by that same small percentage. Chlorinated tapwater should not be used in the dilution, because the chlorine present in the water quenches the fluorescence of rhodamine dyes.

The equipment and materials needed to make the dilutions are listed below. Where glass is specified for the equipment, other nonabsorptive materials may also be used.

1. Volumetric flasks (glass) of 100, 250, 500, 1,000, and 2,000 mL capacity.
2. Volumetric pipettes (glass) in an assortment of sizes.
3. Beakers (glass), or 1-gal (3.75 mL) glass jars.
4. Wash bottles (polyethylene).
5. Sample bottles (glass).
6. Masking tape and pen.
7. Distilled water. River or chlorinated tap water should not be used; however, tap water exposed to the air for 24 hr will lose its chlorine.

The dilution process is performed in steps, as illustrated in the example shown below. The relative concentration at each step is computed from the equation

$$C_n = \frac{C_i V_i}{V_a + V_i} , \tag{34}$$

where

C_n is the new concentration,
C_i is the initial concentration,
V_i is the volume of initial concentration, and
V_a is the added volume of water.

A flow chart similar to that shown in the example below is recommended when making the dilute solutions.

Example.—The original dye solution, as obtained from the manufacturer, is a 20-percent solution of Rhodamine WT. In making the solutions of known relative concentration, the process will be checked by duplicating the procedure for each of two samples. In other words, two samples of equal size of the original solution, are diluted in precisely the same manner. The resulting two dilute solutions are each diluted further in the same manner, and so on. As a result we will have two independent sets of standard solutions for use in calibrating the fluorometer.

To get back to the dilution process, 20 mL of the original 20-percent

solution is diluted to 2,000 mL with pure water. The concentration of the resulting solution is computed by use of equation 34. The process is repeated twice, each time using the solution last obtained, as indicated in the following flow chart:

$$C_n = \frac{\text{20 mL of } (200\times10^6)\ \mu\text{g/L dye solution}}{\text{2,000 mL total solution}} = \frac{1}{100}(200\times10^6) = 2\times10^6\ \mu\text{g/L}$$

$$\downarrow$$

$$\frac{\text{20 mL of } (2\times10^6)\ \mu\text{g/L solution}}{\text{2,000 mL total solution}} = \frac{1}{100}(2\times10^6) = 20{,}000\ \mu\text{g/L}$$

$$\downarrow$$

$$\frac{\text{20 mL of 20,000}\ \mu\text{g/L solution}}{\text{2,000 mL total solution}} = \frac{1}{100}(20{,}000) = 200\ \mu\text{g/L}$$

The solution obtained, with concentration equal to 200 μg/L, is referred to in this manual as a working standard solution because any lesser concentration that may be desired can be prepared from it by one additional serial dilution. For example, a dilution ratio of 1/200 will provide a solution with a concentration as low as 1 μg/L. No dilution ratios of less than 1/200 should ever be used. The working standard solution should be stored for future use. Experience has indicated that standard solutions of 200 or more μg/L when properly stored in hard glass dark bottles out of direct light will keep for periods of at least 6 months. There is evidence, though not conclusive, to indicate that very weak standard solutions tend to deteriorate or to adhere slightly to the bottles in which they are stored.

The stored working standard solution may be used for periodically checking the fluorometer calibration to determine if changes in the calibration have occurred, and enough of the standard solution should be retained for future use if the same dye lot from the manufacturer is to be used for discharge measurements. New sets of standard solutions should be prepared after 6 months to avoid the risk of decay of fluorescence in the stored standard solutions. In addition, new sets should also be prepared when new batches of dye are to be used for discharge measurements because the dyes received from the manufacturer may vary from batch to batch.

If the fluorometer calibration is known to be linear, from previous tests using standard solutions made with distilled or unchlorinated tap water, only a limited few concentrations need be prepared and tested for the discharge-measurement calibration of the fluorometer. The concentrations prepared should approximate the plateau concentration expected in stream samples that will be taken during the discharge measurement.

OPERATION OF THE FLUOROMETER

The U.S. Geological Survey uses the Turner model 111 fluorometer. The fluorometer is operated in accordance with the following instructions.

Allow a warmup period of 1½ to 2 hr before any tests are made. This warmup period will permit the instrument temperature to stabilize. If possible, have all samples, including standard and background solutions, at the same temperature. Establish the zero point on the fluorometer by inserting the dummy cuvette in the cuvette holder, after which the dial is adjusted to zero with the blank knob. To test a standard solution, fill the cuvette with that solution, but before putting the cuvette into the fluorometer, wipe the outside of the cuvette dry with laboratory-grade paper tissue. That prevents distortion from droplets on the glass or contamination of the fluorometer, and possible erroneous readings when testing other samples. After wiping, insert the cuvette in the holder and close the fluorometer door. After the fluorometer dial reaches a stable reading, record the reading. As mentioned earlier, test each pair of several standard solutions of different concentrations on more than one fluorometer scale for calibration of the instrument. An alternate, and perhaps more desirable, course of action is to first test all field samples on one fluorometer scale. If that scale accommodates all field samples, calibrate only that one scale in the range found pertinent.

If a water sample from a discharge measurement is being tested, first rinse the cuvette with tap water and then, after shaking out excess droplets, rinse the cuvette with the sample being tested. The cuvette may then be filled. It is important that any sediment in the sample be allowed to settle and that any oxygen bubbles be removed. (Cold samples taken from streams with a high dissolved-oxygen content will often have bubbles form on the sides of the cuvette.) If the samples have been allowed to sit in a temperature bath overnight, the sediment will have settled and the oxygen bubbles will usually have been released. If the oxygen bubbles have not been eliminated by allowing the samples to warm up before testing, they can usually be removed by tapping the cuvette before testing.

The blank and background samples should be tested at intervals during the fluorometer operation as a check against possible instrument malfunction or change in instrument calibration. Background samples are water samples used to define the natural fluorescence of the stream. Natural fluorescence should be determined for any dye-dilution measurement. Always correct water-sample concentrations for this background effect.

The frequency of testing known relative concentrations will depend primarily on the number of stream samples. Known relative concentrations are ordinarily tested before and after the stream samples, but more frequent testing is desirable where numerous samples are involved

Sample bottles made of polyethylene, glass, or similar nonabsorptive material can be used repeatedly for sampling. After each measurement all sample bottles should be thoroughly rinsed and drained. The bottles, if stored, should be well separated from any dye-contaminated equipment.

Whatever the equipment used, care should be taken at every step in the discharge determination to prevent contamination of stream samples, standard solutions, and the equipment used for measurement and analysis. A sample can be contaminated, from the standpoint of concentration, by the addition of pure water as well as by the addition of minute quantities of dye from the analyst's hands or other source.

DYE-INJECTION APPARATUS

Apparatus for the injection of dye solution at a constant rate is of three types: mariotte vessel, floating siphon, and pressure tank.

MARIOTTE VESSEL

The features of the mariotte vessel, shown in figure 121 are (1) an

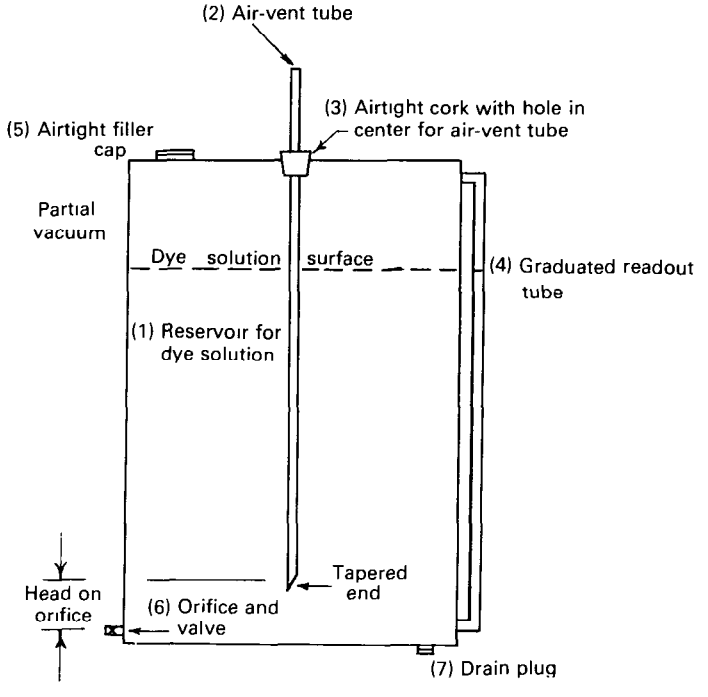

FIGURE 121.—Mariotte vessel (constant-head device).

airtight tank that holds the dye solution, (2) an air-vent pipe inserted into the tank through (3) a rubber stopper that will form an airtight seal both on the tank and the vent pipe, (4) a plastic or glass readout tube for determining the level of the liquid in the tank, (5) a filling plug that must be airtight, (6) a discharge orifice and valve, and (7) a flushing orifice and valve.

The lower tip of the air-vent pipe should be tapered to prevent the tip from being placed directly on the bottom of the tank and thereby obstructing the air flow. Discharge at more than one point may be obtained by installing the desired number of orifices in the tank.

The operation of the vessel is as follows. When the discharge valve (6) is opened, the level of the dye solution in the tank (1) will drop, creating a partial vacuum above the liquid (the top of the tank must be airtight). As the level of the liquid continues to drop, the vacuum increases causing the level of liquid in the air vent (2), which is open to the atmosphere, to drop until it reaches the bottom of the vent. As the solution continues to be discharged, air will enter the tank through the vent causing an equilibrium between the partial vacuum formed above the liquid surface and the weight of the liquid above the bottom of the air vent. When this equilibrium has been reached, a constant discharge will have been attained and will continue until the liquid in the tank drops to the bottom of the air vent. The acting head is the different in elevation between the bottom of the air vent and the orifice.

FLOATING SIPHON

Constant injection of a dye solution is possible through the use of the floating siphon device shown in figure 122. The device is designed to discharge at a constant rate by maintaining a fixed head on the orifice. The features of the floating siphon are (1) a tank that holds the solution, (2) a float with siphon tube and guide assembly, and (3) priming valves that can be used in activating the siphon. The discharge tube with orifice is permanently attached to the float in the position shown. Note that regardless of the position of the float within the reservoir, the operating head on the orifice remains the same. Stable, uniform movement of the float and siphon assembly is possible through the use of guides and a balance counterweight. When the siphon is effective, the float and assembly will drop with the water surface but at the same time maintain a constant discharge because of the steady head operating on the orifice.

The mariotte vessel and the floating siphon can both be equipped with readout gages that are used to calibrate the reservoirs volumetrically. These gages can be read at selected time intervals during the injection period to determine the constant-flow rate. The flow rate can

also be determined by volumetrically measuring the discharge from the orifice for a given period of time.

PRESSURE TANK

A constant-rate injection of dye solution may be obtained by use of a pressure tank in combination with a flow regulator (fig. 123). The flow regulator maintains a constant pressure differential across a valve in the regulator, thus giving a constant flow rate at any setting of the regulator. A pressure differential of a few pounds per square inch must be maintained for the flow regulator to function properly.

The solution to be injected is poured into the pressure tank, and the tank is sealed. Air is then pumped into the tank, providing the necessary pressure for the regulator. The solution is forced from the tank, by the pressure, through the regulator and to the injection lines.

Most commercially available flow regulators have a purge meter

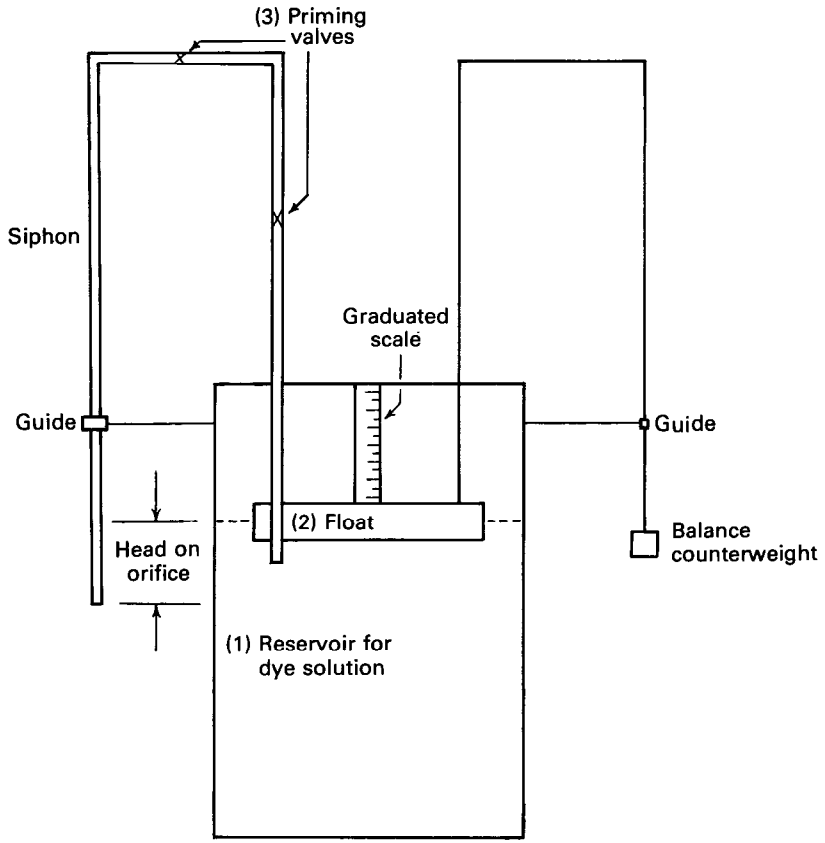

FIGURE 122.—Floating siphon (constant-head device).

attached to them. These meters may be used to obtain the approximate desired flow rate. The flow rate used in the computations should be determined from a volumetric measurement of the tank discharge.

Pressure tank and flow regulator systems are commercially available. These systems are as light as 8 lb (3.6 kg), when empty, for an operating-pressure tank capacity of about 2 gal (7.5 L). Flow regulators may be obtained for flow rates between 0.012 and 4 gal/hr or more. Flow rates once established will be maintained within ±2 percent.

DETERMINATION OF QUANTITIES OF FLUORESCENT DYE FOR MEASURING DISCHARGE

QUANTITY OF DYE NEEDED FOR MEASUREMENT BY THE CONSTANT-RATE-INJECTION METHOD

The volume of dye required to make a discharge measurement

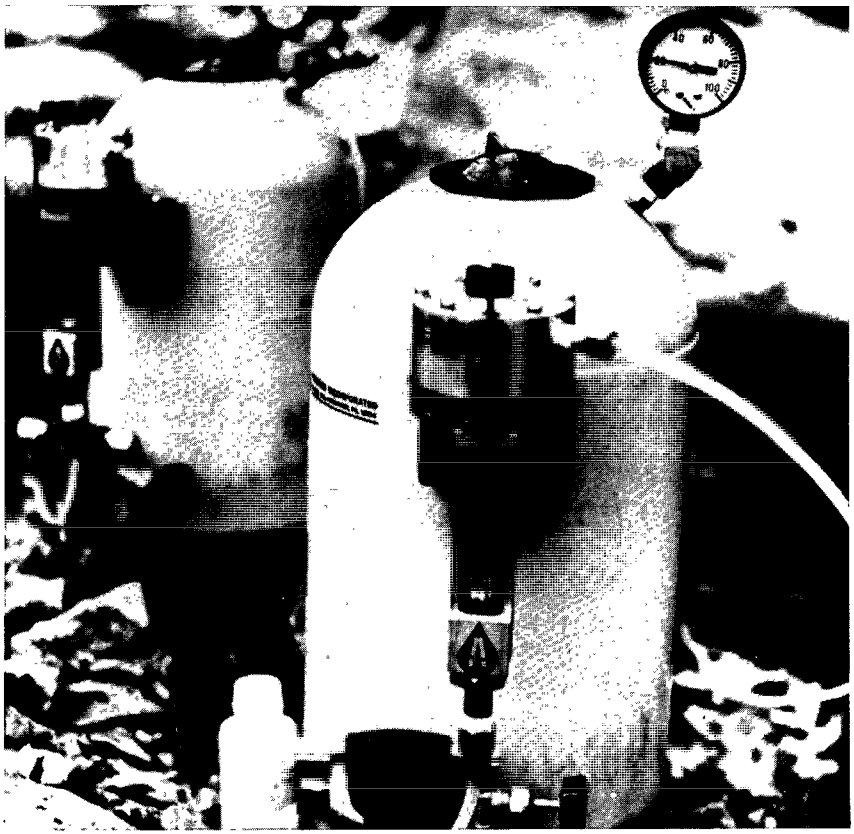

FIGURE 123.—Pressurized constant-rate injection tanks for injection of dye into streams.

using the constant-rate-injection method will depend on the discharge of the stream and on the total injection time. That volume can be estimated using the equation

$$V_d = 1.02 \times 10^8 \left(\frac{C_2}{C_d}\right) Q\, t_t, \tag{35}$$

where

V_d is the volume, in milliliters, of dye solution to be added to the water in the injection tank,

C_d is the concentration, in micrograms per liter, of the dye solution added to the water in the injection tank. If a 20 percent dye solution is added, the concentration of C_d is considered to be 200,000,000 μg/L. (See p. 228–229 for a discussion of relative and absolute concentration values.)

C_2 is the plateau concentration, in micrograms per liter, desired at the sampling site,

Q is the estimated stream discharge, in cubic feet per second, and

t_t is the total injection time, in hours.

The value of 1.02×10^8 is a combination of conversion factors. A concentration value for C_2 of 5 μg/L is recommended for Rhodamine WT.

The volume of tracer solution injected, which consists of the volume dye solution (V_d) plus added water, and the rate of injection are mutually dependent. Their limiting values are based on the size and characteristics of the dye-injection apparatus that is used. The capacity or volume of the apparatus divided by t_t gives the upper limiting value of the rate of injection, q. Any paired values of q and volume (qt_t) that are within the capability of the apparatus are satisfactory. However, it is recommended that no value of q less than 2×10^{-5} ft^3/s (0.57 mL/s) be used, because low injection rates are difficult to measure accurately. It is further recommended that V_d be diluted sufficiently to give the injection solution a concentration of no more than 25×10^6 μg/L, because more highly concentrated solutions tend to clog the injection apparatus.

QUANTITY OF DYE NEEDED FOR MEASUREMENT BY THE SUDDEN-INJECTION METHOD

If discharge is to be measured by the sudden-injection method, it is recommended that common salt be used as the tracer, rather than dye. (See p. 250–256.) However, as a matter of general interest, an equation is given here for computing the quantity of dye required for a discharge measurement of that type.

The volume of dye required to make a discharge measurement by the sudden-injection method can be estimated using the following

empirical equation:

$$V'_d = 3\times10^7 \left(\frac{C_p}{C'_d}\right) Qt_p, \tag{36}$$

where

V'_d is the volume, in milliliters, of dye solution of concentration C'_d to be introduced into the stream,

C_p is the peak dye concentration, in micrograms per liter desired at the sampling site,

Q is the estimated stream discharge, in cubic feet per second, and

t_p is the estimated time, in hours, for the dye peak to travel from the injection site to the sampling site.

The value of 3×10^7 is a combination of empirical equation constants and conversion factors. A concentration value for C_p of 10 μg/L is recommended for Rhodamine WT.

PROCEDURES FOR MEASURING DISCHARGE BY THE DYE-DILUTION METHOD

The only dye-dilution method that will be discussed here is the constant-rate-injection method. The sudden-injection method is not considered here because not only is it usually a less accurate method, but it is extremely laborious when dye is used and it can be applied with less effort by using common salt as a tracer. As mentioned earlier, the sudden-injection method requires that the entire concentration-time curve be defined, and for that purpose it is desirable to sample the stream concentration at intervals of less than a minute during periods of rapidly changing concentration. If the dye-dilution technique is used, it means that within a minute or so, grab samples must be obtained at all three sampling points in the sampling cross section. Furthermore, because it is recommended that at least 20 samples be taken at each sampling point to define the concentration-time curve, it means that a minimum of 60 stream samples must be analyzed by fluorometer, along with calibration and background samples. In short, it is not practical to use dye as a tracer in the sudden-injection method. Although recording fluorometers with flow-through doors are available, they seldom provide the precision required for a discharge measurement. When salt is used as the tracer, conductivity readings can be obtained at a point in a matter of a few seconds, by using a temperature-compensated probe and portable meter. (See p. 252–255.)

FIELD PROCEDURES

The following field procedures are recommended for determining

stream discharge by the dye-dilution method:

1. Select and calibrate the measurement reach (p. 220–222).

2. Select exact locations for the injection and sampling sites. Data obtained from the calibration tests are used in making the site selections, and consideration should be given to accessibility and convenience for conducting field operations. Bridges are often excellent for the purpose. The injection site for either single- or multiple-point injection should be one where the injection system can be readily observed and, if necessary, serviced. Select sampling sites where sampling is possible anywhere in the cross section. Locate a minimum of three sampling points in the cross section so that the section can be checked for lateral mixing.

The best location for a single-point injection is normally at the center of the cross section. A center injection generally produces the minimum possible mixing length if the dye is to be introduced at only one point. Space the injection points for a multiple-point injection so that each dye injection diffuses equal lateral distances.

3. Prepare the sample bottles. Show the following information on each bottle:

a. The sampling site (may be abbreviated).
b. Location of the sampling point in the cross section.
c. Sample number (if desired).
d. Sample time (use military time, that is, 24-hr clock system).
e. Date.

Make these notes with a ballpoint pen using masking tape for labels on the bottles. Note the time (sample time) when the sample is obtained.

4. Determine the amount of dye needed for injection from equation 35. The total injection time used in equation 35 includes the time required for the concentration plateau to have been reached at the sampling section and sufficient time to permit at least 15 min of sampling of the plateau.

5. Prepare the dye solution and injection equipment. Make certain that the solution is thoroughly mixed. Exercise caution in transporting the dye and do not carry excessive quantities of it on field trips. Dye in solution can be easily removed from containers by the use of pipettes. Adverse weather conditions, particularly high wind or rain, create serious problems in handling the dyes. Prepackaging of specific quantities of dye will facilitate operations in the field. River water taken at the site may be used in preparing the injection solution, but do not obtain river water immediately below a sewage outfall or at sites where chlorine is injected into the river system.

6. Obtain several background samples upstream from the injec-

tion site. Do this before handling the dye.

7. Obtain three samples of injection solution. These samples, each of about 2 oz (60 mL), may be taken immediately before or after the solution is injected into the stream.

8. Inject the diluted dye solution. Determine the actual rate of dye injection by timed observations of volume depletion in the injection tank. If a mariotte vessel is used for injection, check the fittings for air leakage before and during injection. Discharge will become constant within a few seconds after the orifice is opened if the tank is airtight. The sound of air bubbling from the air vent through the solution can be heard when the vessel is operating properly.

9. Do not inject the highly concentrated dye solution near the streambed; otherwise, the bed may be stained by the dye and excessive dye loss will result.

10. The time of arrival of the concentration plateau can be estimated from data obtained when the reach was calibrated. It is usually desirable to start sampling a little before the estimated time of arrival of the concentration plateau. Define the plateau with at least five samples at each of the three sampling points in the sampling cross section. If a fluorometer is available, the arrival and passage of the dye can be determined by using the flow-through door and recorder accessory, or by periodically testing individual samples using the standard door. Do not mistake a possible temporary leveling of the concentration-time curve as being the actual plateau. A short time should elapse between the taking of samples to minimize the effect of nonrepresentative surges of high or low concentration.

11. In obtaining stream samples at the sampling site, take samples just below the water surface and far enough from the banks to avoid areas of slack water. If possible, the sampling site should be at a contracted section of the stream or at one where velocities are fairly uniform across the entire section. The following equipment is needed for grab sampling:

a. Sampling device and line (for sampling from a structure).
b. Boots or waders (for sampling by wading).
c. Boat, motor, paddle, gasoline can, life jacket (for sampling by boat).
d. Bottles (glass or plastic, 4-oz, wide-mouth bottles are recommended).
e. Masking tape (for labeling samples).
f. Ballpoint pens (for making identifying notations on sample labels).
g. Watch.

12. Contamination of stream samples is always a possibility. When handling any dye, keep hands and clothes clean as a safeguard

against accidental contamination. Rinse bottles at least three times in stream water immediately before sampling. This precaution is necessary because bottles are used repeatedly and some may have had high concentrations of dye in them previously. Dye from stained hands can contaminate samples, resulting in erroneous concentration determinations; therefore, keep hands away from the uncapped mouths of bottles and out of the sample water.

13. Clean the injection and mixing equipment.

14. Store and carry sample bottles in an upright position to prevent leakage and to allow sediment to settle.

ANALYSIS AND COMPUTATIONS

Fluorometer analysis should not begin until the standard concentration solutions have been prepared. Place all samples, including background samples and standard concentration solutions, in a constant-temperature bath. By keeping the samples in the bath overnight, any sediment present will have an opportunity to settle, and any oxygen bubbles present will usually be released. After fluorometer warmup, all samples may be analyzed. Use of a constant-temperature bath will eliminate the need for temperature corrections. However, if for any reason a temperature bath was not used, the first step in the analysis procedure that follows is to make temperature corrections.

1. Correct each fluorometer reading for the effect of temperature by the following method. A standard cuvette-sample temperature is selected. This may be the mean, median, mode, or any other convenient cuvette-sample temperature recorded while testing the samples. The difference between each recorded cuvette-sample temperature and the standard temperature is used to select the appropriate coefficient from table 13. Temperature-correction coefficients are usually prorated with respect to time between temperature observations. Multiply the fluorometer dial-readings by the coefficients to obtain adjusted dial readings.

2. Next correct the dial readings, or temperature-adjusted dial readings if such adjustment had been necessary, for the effect of background fluorescence, as determined from the background samples. This background correction is applied to each water sample and to each sample of standard concentration.

Usually all fluorometer testing will be done using a single fluorometer aperture. If more than one aperature is used, obtain a background reading for each aperature and use a mean background value for correcting the dial readings. Do not use a mean background value if a definite change in background has been noted. A change in background fluorescence may result from a variety of causes such as

unstable fluorometer operation, increased suspended-sediment load, and the presence of sewage or industrial wastes. Enter the background readings in the notes. Subtract the background readings from the adjusted dial readings from step 1 above to obtain the final corrected dial readings.

3. Use the final corrected dial readings for the standard solution of known relative concentration to compute the fluorometer coefficient, a, in equation 33 (p. 227). When this standard solution is tested several times during a period of sample testing, the value of the coefficient is normally prorated, with respect to time, between testings.

4. Determine the relative concentrations of samples by multiplying the corrected dial readings, from step 2 above, by the coefficient, a.

5. Compute the stream discharge by use of equation 24. Because the background concentrations have already been subtracted from the stream sample concentrations, equation 24 becomes

$$Q = \left[\frac{C_1}{C_2} - 1 \right] q,$$

which can be simplified, without significant loss of precision, to

$$Q = \left(\frac{C_1}{C_2} \right) q. \tag{37}$$

An average value of C_2 is used in the computations. If the individual C_2 values show little variation among them, use the arithmetic mean. If the variation is significant, obtain the mean value of C_2 by weighting the mean plateau concentrations for each sampling point by the percentage of discharge associated with the sampling point. If the discharge distribution is unknown, but the area distribution is known, obtain the mean value of C_2 by weighting the plateau concentrations for each sampling point by the percentage of area associated with each sampling point. If both the discharge and area distributions are unknown, as will usually be the case, compute the mean value of C_2 by using percentage of width as the weighting factor.

6. Determine the percentage of mixing by using equation 26, or by use of the graphical procedure described on page 219–220. Reliable results are generally obtained when the percentage of mixing is 95 or more. Reliable results are also possible for flow conditions where the percentage of mixing is less than 95 if the discharge distribution at the sampling section is uniform or known.

SAMPLE COMPUTATION—CONSTANT-RATE-INJECTION METHOD

A sample computation of the constant-rate-injection method is

presented here based on data obtained on March 25, 1965, at Little Seneca Creek near Boyds, Md., in the course of a detailed investigation of dye-dilution methods of measuring discharge. The average width of Little Seneca Creek at the time of the measurement was 30–35 ft (9–10 m). Depths averaged between 1 and 2 ft (0.3 and 0.6 m). The streambed was composed mostly of gravel, with some rock outcrops. Flow in the measuring reach passed through several bends.

Calibration of the measurement reach at about the stage to be measured had indicated that a measuring reach of 1,800 ft (550 m) was satisfactory for adequate mixing when the dye was injected at three points across the stream. The calibration further indicated that the time required for the concentration plateau to arrive at the sampling site was about 45 min. Three sampling points, designated A, B, and C, respectively, were to be used at the sampling site. Grab-samples were taken immediately before and during the passage of the concentration plateau.

1. The required volume of dye (V_d), to be supplied from a mariotte vessel, was computed from equation 35,

$$V_d = (1.02\times10^8)\,\frac{C_2}{C_d}\,Qt_t\ .$$

The approximate value of the plateau concentration (C_2) desired at the sampling site was 5 μg/L. The estimated value of stream discharge (Q) was 50 ft^3/s. The total injection time (t_t) was estimated to be 80 min (1.33 hr)—45 min for traveltime and 35 min to insure a concentration plateau of adequate duration. The dye to be used was Rhodamine WT, 20-percent solution, and C_d was therefore equal to 2×10^8 μg/L. Consequently,

$$V_d = (1.02\times10^8)\quad\left(\frac{5}{2\times10^8}\right)(50)\,(1.33) = 170\text{ mL.}$$

2. The discharge rate of diluted dye solution (q) from the injection vessel that was selected was 1.50×10^{-4} ft^3/s. The volume of solution needed in the injection tank was equal to qt_t, where t_t was 1.33 hr, or 4,800 s. That volume was therefore

$$(1.50\times10^{-4})\,(4800) = 0.72\text{ ft}^3\text{, or approximately 20,000 mL.}$$

The 170 mL of dye solution was mixed with sufficient stream water to give an injection solution of 20,000 mL.

3. The concentration of the solution in the injection tank (C_n) was computed from equation 34,

$$C_n = \frac{C_i V_i}{V_a + V_i}$$

$$= \frac{(200{,}000{,}000)\ (170)}{20{,}000}$$

$$= 1{,}700{,}000\ \mu g/L.$$

4. Timed observations of the change in the level of the dye solution in the injection tank showed the actual rate of outflow to be 1.51×10^{-4} ft^3/s.

The steps that follow were taken in the office to complete the measurement.

1. A working standard solution of concentration 200 $\mu g/L$ had previously been prepared (p. 229–230). A dilution ratio of 1/40 was applied to that solution to obtain two standard sample solutions whose concentration was 5.00 $\mu g/L$.

Standard solutions of 5.00 $\mu g/L$ were used for calibration of the fluorometer because that was the expected value of the plateau concentration of the stream. (The concentration of the standard solutions should approximate the concentrations of the stream samples that will be used to compute stream discharge.)

2. A form for keeping notes was prepared as shown in figure 124. Column 1 of figure 124 shows the time when the sample was obtained in the field, and column 2 shows the time when the sample was tested in the fluorometer.

3. The samples had not been placed in a constant-temperature bath, and consequently temperature corrections were necessary. The samples, including those for background testing (stream water untouched by dye) and for fluorometer calibration (5.00 $\mu g/L$), were tested in the fluorometer. Columns 3 and 4 of figure 124 show dial readings on the fluorometer aperture that was used. Column 5 shows two temperature readings. The upper reading is the temperature of the water being circulated through the fluorometer door. The lower reading is the temperature of the fluorometer compartment. Obtain that temperature from a thermometer that can be taped to the compartment side at the left of the secondary filter. Column 6 shows the temperature of the cuvette sample. That temperature is taken immediately after the fluorometer dial is read by removing part of the water from the cuvette, inserting the thermometer in the cuvette, and replacing the cuvette in the door. Allow the thermometer to stabilize before reading. Compute temperature-correction coefficients from the observed cuvette-sample temperatures.

4. A standard cuvette sample temperature of 82°F (27.8°C) was selected for use. Temperature coefficients from table 13, correspond-

ing to the differences between 82°F and the observed cuvette-sample temperatures in column 6 of figure 124, were then obtained and recorded in column 7.

Little Seneca Creek near Boyds, Maryland, March 25, 1965

(1)	(2)	(3)	(4)	(5)	(6)	(7)	(8)	(9)	(10)	(11)	(12)	(13)
Time		Dial reading		Temperature		Temp coef.	Adj. dial reading	Background reading	corrected dial reading	C/D	Concentration (ppm)	Remarks
Sample	Fluor. test	30X	10X	circ./comp.	cuvette							
					Sample Point A							
Blank	1459	0										
1a	1500	65.8				1.02	67.1	1.2	65.9	.0759	5.00	*
1b	1501	67.7		79.5/93.5	83	1.02	69.1	1.2	67.9	.0736	5.00	*
										.0748		Mean
1250	1503	1.2				1.02	1.2	1.2	—	—	—	**
1313	1505	64.4				1.02	65.7	1.2	64.5	.0748	4.82	
1320	05	72.0				1.02	73.4	1.2	72.2	.0748	5.40	
1327	06	74.5				1.02	76.0	1.2	74.8	.0748	5.60	***
1335	07	75.8				1.02	77.3	1.2	76.1	.0748	5.69	***
1343	08	75.2				1.02	76.7	1.2	75.5	.0748	5.65	***
1350	08	75.2				1.01	76.0	1.2	74.8	.0748	5.60	***
1356	1509	74.6				1.01	75.3	1.2	74.1	.0748	5.54	***
					Sample Point B						5.62	Mean
Blank	1523	0										
1251	24	1.3				1.00	1.3	1.2	—	—	—	**
1322	27	71.0		80.9/93.5	81.5	1.00	71.0	1.2	69.8	.0747	5.21	
1328	27	74.6				1.00	74.6	1.2	73.4	.0747	5.48	***
1336	29	75.8				1.00	75.8	1.2	74.6	.0747	5.57	***
1344	30	76.2				1.00	76.2	1.2	75.0	.0747	5.60	***
1351	30	75.1				1.00	75.1	1.2	73.9	.0747	5.52	***
1357	1531	72.8				1.00	72.8	1.2	71.6	.0747	5.35	***
											5.50	Mean
					Sample Point C							
Blank	1546	0										
1252	1546	1.2				1.00	1.2	1.2	—	—	—	**
1315	48	65.8		80.0/94.0	82	1.00	65.8	1.2	64.6	.0746	4.82	
1321	50	73.3				1.00	73.3	1.2	72.1	.0746	5.38	***
1329	51	72.9				1.00	72.9	1.2	71.7	.0746	5.35	***
1337	52	72.0				1.00	72.0	1.2	70.8	.0746	5.28	***
1345	52	72.9				1.00	72.9	1.2	71.7	.0746	5.35	***
1352	53	72.0				1.00	72.0	1.2	70.8	.0746	5.28	***
											5.33	Mean
1a	1608	67.7				1.00	67.7	1.2	66.5	.0752	5.00	*
1b	1609	68.9				1.00	68.9	1.2	67.7	.0738	5.00	*
										.0745		Mean

Turner III Fluorometer Filters (546 mμ, 590mμ), Far ultraviolet lamp. Temperature-stabilized door. Standard cuvette-sample temperature, 82°F. Tested 3-29-65
* Standard solution of known relative concentration. ** Background sample.
*** Sample used to compute C_2.

FIGURE 124.—Sample analysis sheet used for computing discharge by the constant-rate-injection method of dye dilution.

5. The adjusted dial readings in column 8 were obtained by multiplying the values in either column 3 or column 4 by the temperature coefficients in column 7.

6. The average temperature-adjusted fluorometer reading for background fluorescence, obtained by testing the unaffected stream water, was recorded in column 9. Its value, 1.2 in this test, was then subtracted from all temperature-adjusted readings in column 8, and the corrected dial readings were recorded in column 10.

7. The fluorometer coefficient, a, in column 11, was obtained as the average of the ratios of the known concentration of the two background samples (5.00 μg/L) to their corrected dial readings. The background samples were tested at the beginning and end of the fluorometer analysis, and the fluorometer coefficients obtained were prorated with time for use in the analysis.

8. The concentrations of the samples listed in column 12 were obtained by multiplying the fluorometer coefficients in column 11 by the corrected dial readings in column 10.

9. The concentrations obtained for each sampling point are normally plotted against sampling time to determine the average concentration of the plateau C_2 at each of the three sampling points, A, B, and C. In this example, no plots were made; instead, C_2 for each sampling point was computed, in column 12 of figure 124, as the mean of the last five values obtained, it being evident that those values were plateau values.

10. Because the three sampling points, A, B, and C, were evenly spaced across the stream, each of the three values of C_2 from step 9 were given equal weight in computing the mean value of C_2 for the entire sampling section:

$$\text{mean } C_2 = \frac{5.62+5.50+5.33}{3} = 5.48 \ \mu\text{g/L}.$$

11. The discharge was computed from the simplified form of equation 24 that is shown as equation 37 on page 241.

$$Q = \frac{C_1}{C_2} q$$

$$= \left(\frac{170\times10^4}{5.48}\right)(1.51\times10^{-4}) = 46.8 \text{ ft}^3/\text{s}.$$

12. Mixing percentage (P_m) was computed, using appropriate widths in equation 26:

$$P_m = 100 - \frac{\left[|X_A - X_m|W_A + |X_B - X_m|W_B + |X_C - X_m|W_C\right]\times 50}{(W_{total})(X_m)}$$

Because the sampling points were evenly spaced, W_A, W_B, and W_C may each be replaced by 1, and W_{total} may be replaced by 3. Then

$$P_m = 100 - \frac{[|5.62-5.48| + |5.50-5.48| + |5.33-5.48|]\times 50}{3(5.48)}$$

$$= 100 - \frac{(0.31)\times 50}{16.44}$$

$$= 99 \text{ percent (satisfactory)}$$

In the original study of Little Seneca Creek, the discharge had been measured by current meter for a comparison with the discharge obtained by the dye-dilution method. The current-meter discharge was 47.3 ft^3/s, whereas the dye-dilution discharge was 46.8 ft^3/s. The two values differ by 1 percent.

SIMPLIFIED PROCEDURES FOR MAKING NUMEROUS DYE-DILUTION MEASUREMENTS OF DISCHARGE

The preceding description of the method of measuring discharge by the constant-rate-injection method was highly detailed to give complete understanding of the procedure. It should be apparent that there are many details to be considered in collecting and analyzing the samples. If only an occasional dye-dilution measurement is to be made, the procedures described above should be followed. If numerous dye-dilution measurements are to be made on a routine basis, "mass production" methods may be instituted to simplify and speed the procedure.

The first simplifying step is the laboratory production of two batches of solution, each of which represents a working standard concentration. Bulk production of the two concentrations will considerably reduce the amount of time that would otherwise be required later for serial dilutions and for calibrating the fluorometer. The standard concentration that is needed for fluorometer calibration is one that closely approximates the C_2 (plateau) concentrations that will be obtained in the discharge measurements. The value of C_2 will usually approximate 5 $\mu g/L$. Consequently one working standard solution of 200$\mu g/L$ should be produced in adequate quantity from the stock of 20-percent Rhodamine WT dye. The concentration of 200 $\mu g/L$ is high enough to permit storage of the solution for at least 6 months with little danger of deterioration and is still low enough to produce, with a single dilution, concentrations that approximate any C_2 values that may be obtained in a discharge measurement.

The other solution of working standard concentration that should be produced in bulk is one that can be used as the injection solution in a discharge measurement without further dilution. By way of background explanation we examine figure 125, the basis of which is equation 37. Figure 125 shows the relation among Q, q, and C_1 for a constant value of C_2. The constant value of C_2 that is used is 5 μg/L, which is the optimum value of the plateau concentration in the constant-rate-injection method. Concentration values of C_1 ranging from 0.05 percent (0.5×10^6 μg/L) to 2.5 percent (25×10^6 μg/L) are shown in the diagonal lines of figure 125. To produce a C_1 solution of, say 0.4 percent, 8 L of water is added to the parenthetical quantity of 137.2 mL of 20-percent Rhodamine WT dye. Examination of figure 125 shows that with a given injection concentration (C_1) a wide range of discharges may be measured by merely changing the injection rate (q). For example, a C_1 concentration of 0.4 percent (4×10^6 μg/L) permits the measurement of stream discharges from 15 ft^3/s to almost 300 ft^3/s, while still creating a plateau concentration (C_2) of 5 μg/L. Even those discharge limits may be exceeded by allowing C_2 to vary from its value of 5 μg/L. By using figure 125 with a knowledge of the range of discharges to be measured, a suitable value of C_1 can be selected for use as a working standard concentration.

To recapitulate what has been said up to this point, two working standard concentrations should be used for laboratory production of bulk solutions.

1. A concentration (C_1) of 4×10^6 μg/L, or one more suitable for the range of discharges to be measured, should be used for one solution. That solution will be used, without further dilution, as the injection solution for discharge measurements.

2. A concentration of 200 μg/L should be used for the second solution. A single dilution of that solution will provide standard solutions for calibrating the fluorometer at concentration C_2 (usually about 5 μg/L). Both solutions must be made from the same batch of 20-percent Rhodamine WT dye that is received from the manufacturer.

The discharge measurements will be made in the manner described in the earlier sections of this chapter, but before analysis by fluorometer, all samples and standard solutions should be allowed to sit overnight in a laboratory temperature bath. That will eliminate the need for temperature corrections to fluorometer dial readings.

As the hydrographer gains experience with the dye-dilution method, he will find that he can dispense with the computation of percentage of mixing (P_m) at the conclusion of his fluorometer analysis. By visual inspection of the computed individual plateau concentrations, he will be able to judge whether or not satisfactory mixing had been attained at the site of his sampling

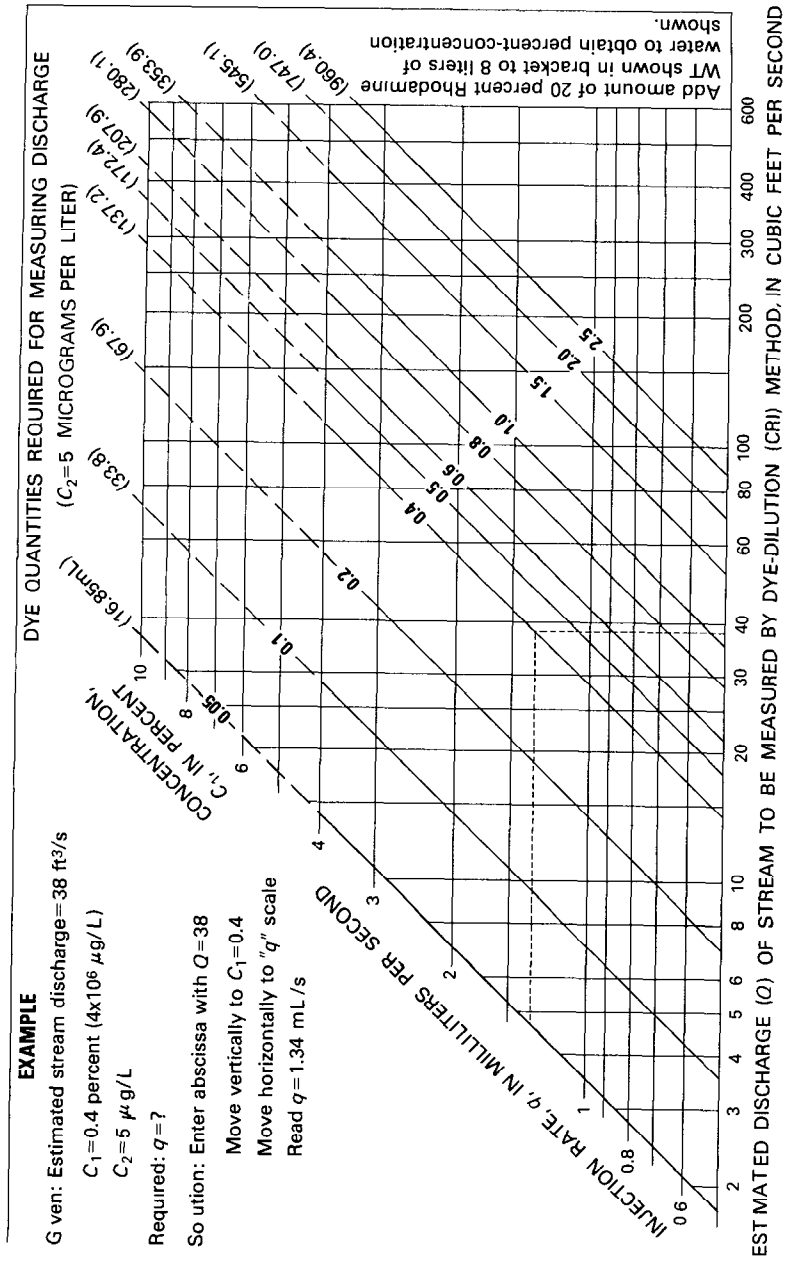

FIGURE 125.—Dye-injection rate of various stock dye concentrations related to estimated stream discharge.

MEASUREMENT OF DISCHARGE BY SODIUM DICHROMATE DILUTION

GENERAL

In Europe colorimetric analysis, using sodium dichromate ($Na_2Cr_2O_7 \cdot 2H_2O$) as the tracer, is the most widely used means of measuring discharge by the constant-rate-injection method. Because colorimetric analysis is rarely used in the U.S.A., the method will be described here only in brief; detailed descriptions are available in a report by the International Standards Organization (1973) and in a paper by Hosegood, Sanderson, and Bridle (1969).

The solubility of sodium dichromate is relatively high—the stock solution commonly used has a concentration of 600 g/L—and the salt satisfies most of the requirements for a tracer that are listed on page 211. Complications resulting from the presence of chromium ions in the water being gaged seldom occur, because natural waters generally contain few such ions. However, the nature and quantity of suspended sediment in the natural water can seriously affect the accuracy of analysis because of the possibility of sorption of sodium dichromate by the sediment. Another consideration in the use of sodium dichromate as a tracer is its potential toxicity to aquatic life, particularly in localized areas of high concentration; drinking-water standards in the U.S.A., for example, recommend a limiting concentration of 0.05 mg/L for chromium ions (Environmental Protection Agency, Environmental Studies Board, 1972, p. 62).

The factors that enter into the selection of a reach of channel for a measurement of discharge by sodium dichromate dilution are identical with those discussed earlier on pages 215–223. The types of apparatus for constant-rate-injection—mariotte vessel, floating siphon, and pressure tank—were described on pages 232–235.

The method of sampling for a discharge measurement by the constant-rate-injection method is similar to that described for fluorescent dyes (p. 237–240).

PRINCIPLE OF COLORIMETRIC ANALYSIS

Colorimetric analysis permits the measurement of extremely low concentrations of sodium dichromate. In that type of analysis a colorimeter is used to compare (1) the natural dilution of stream samples after tracer injection with (2) the known dilution of a stock solution of the salt. The comparison is based on differences in the absorption of light by the solutions after a reagent has been added to each of them.

The colorimeter is calibrated by the use of standard solutions, and it is recommended that the colorimeter used be one that gives a linear

relation between color intensity (concentration) and meter reading. The colorimeter coefficient is then equal to the known concentration of the standard solutions divided by the average of the colorimeter readings.

METHOD OF ANALYSIS BY COLORIMETER

As mentioned earlier, the stock solution commonly used for discharge measurements contains 600 g of sodium dichromate in each liter of solution. The injection rate of this stock solution depends on the estimated river discharge and the desired increase or rise in concentration of chromium ions (Cr^6) corresponding to the plateau concentration. That rise in concentration, $(C_2 - C_b)$ in the equation that follows, is generally in the range of 0.04 to 0.08 mg/L.

Discharge is computed by use of the equation

$$Q = \left[\frac{C_1}{C_2 - C_b}\right] q, \tag{38}$$

where

Q is stream discharge (m^3/s),
q is rate of flow of injected solution (m^3/s or $mL/s \times 10^{-6}$),
C_1 is concentration of the injected solution (mg/L),
C_2 is concentration of the plateau of the concentration-time curve shown in fig. 116 (mg/L), and
C_b is background concentration of the stream (mg/L).

MEASUREMENT OF DISCHARGE BY SALT DILUTION

GENERAL

As mentioned earlier, when salt is the tracer used in measuring discharge by the tracer-dilution technique, the sudden-injection method is generally used. Although the sudden-injection method is usually less accurate than the constant-rate-injection method, the difficulty of handling the large quantities of salt solution required by the constant-rate-injection method make the method impractical. Common salt (NaCl) is the salt tracer generally used because it is relatively cheap and it meets all the criteria for a tracer that are listed on page 211.

The basic principles behind the salt-dilution method are as follows. The ion concentration of a dilute salt solution, such as natural river water, increases as the salt content increases. Consequently, the easily measured electrical conductivity (conductance) of the solution is an index of the salt concentration. Furthermore, over a wide range of concentrations the conductance is directly proportional to salt concentration. Therefore, after injection of a concentrated salt solution

into a stream, the discharge can be computed by use of the ratios of the conductances of the injected and sampled salt solutions, instead of the ratios of the salt concentrations themselves. The procedure followed in the salt-dilution method is analogous to that used in the dye-dilution method in that relative conductance values are used rather than absolute values.

The factors that enter into the selection of the reach of channel for a salt-dilution measurement of discharge are identical with those discussed earlier on pages 215–223. Although loss of salt in the measurement reach by sorption is a negligible concern, reaches that have areas of slack water should be avoided, if possible, because the storage and slow release of tracer from those areas greatly prolongs the time required for the entire salt cloud to pass the sampling site. The sampling site should be free of excessive turbulence because the operation of the electrode cell that is placed in the stream to measure relative conductance is adversely affected by the presence of air bubbles.

The salt-dilution method of measuring discharge in open channels is littled used in the U.S.A. but is popular elsewhere, as in the U.S.S.R. The description of the salt-dilution technique that follows, and the sample computation that concludes the discussion, have been taken from a description of salt-dilution technique that follows, and the sample computation that concludes the discussion, have been taken from a description of salt-dilution stream gaging in the U.S.S.R. (World Meteorological Organization, 1962, p. 47–49). The subject is discussed under the following three headings:

1. Preparation and injection of the concentrated salt solution.
2. Measurement of relative conductance at the sampling site.
3. Computation of discharge.

PREPARATION AND INJECTION OF THE CONCENTRATED SALT SOLUTION

The following equipment is needed for the preparation and injection of the concentrated salt solution at the injection site:

1. Two tanks, each having a capacity of 60–70 L; one tank is used for preparation of the solution and the other for injection of the solution.
2. A measuring vessel of 10-L capacity, having a mark showing the exact level for 10 L of liquid.
3. A wooden or aluminum paddle for mixing the solution.
4. A vessel having a capacity of 0.3–0.5 L for adding small volumes of solution to the 10-L measuring tank.
5. A glass flask with a ground glass stopper, having a capacity of 20–30 mL, in which a sample of the solution is retained.

The quantity of salt (NaCl) required for injection depends on the

discharge to be measured; 1–2 kg of salt is needed for each cubic meter per second of stream discharge. The smaller unit quantity of salt is used for streams having a low natural concentration of dissolved material. In estimating the quantity of salt to be brought to the injection site, consideration should also be given to the possibility that the discharge measurement will have to be repeated.

The preparation and measurement of the injection solution takes place at the injection site, but at a distance from the river to avoid any accidental spill of salt or salt solution into the river. An accident of that kind could affect the results of the discharge measurement. To prepare the injection solution, the quantity of salt needed is first determined from an estimate of the discharge and the natural concentration of dissolved materials in the stream. The computed quantity of salt is then placed in one of the large tanks, and river water is added to the tank at the rate of 10 L to each 3 kg of salt. The mixture is then stirred to obtain a saturated salt solution. After the larger undissolved crystals have settled to the bottom of the tank, the solution is transferred to the second large tank, and its volume is carefully measured in the process, the transfer being made by means of the 10-L measuring vessel. An additional amount of river water sufficient to fill the small glass flask (20–30 mL) to its brim is then added to the measured solution in the second large tank. The flask and stopper are carefully rinsed in that tank, after which the contents of the tank are thoroughly stirred once more. The small glass flask is then filled with the solution, tightly stoppered, and is delivered to the sampling site downstream for later use there. The large tank now holds the volume of salt solution that was originally measured into it. The large tank is then moved to the river, and at a signal from the sampling site that all is in readiness there, the tank is overturned to spill its contents almost instantaneously into midstream. That act completes the work to be done at the injection site.

MEASUREMENT OF RELATIVE CONDUCTANCE AT THE SAMPLING SITE

A conductance meter (fig. 126) that is a modification of a Wheatstone bridge is set up at the sampling site. The principal elements of the meter are a rheochord, a 10,000-ohm resistance chamber, and an electrode cell immersed in the stream, well away from the bank. The resistance chamber is used to compensate for the natural conductance of the water in the stream so that the needle of the galvanometer reads zero. The indicator on the rheochord is also set at zero. When this has been done, the signal to inject the salt solution is sent to the injection site.

After the solution has been poured into the stream at the injection

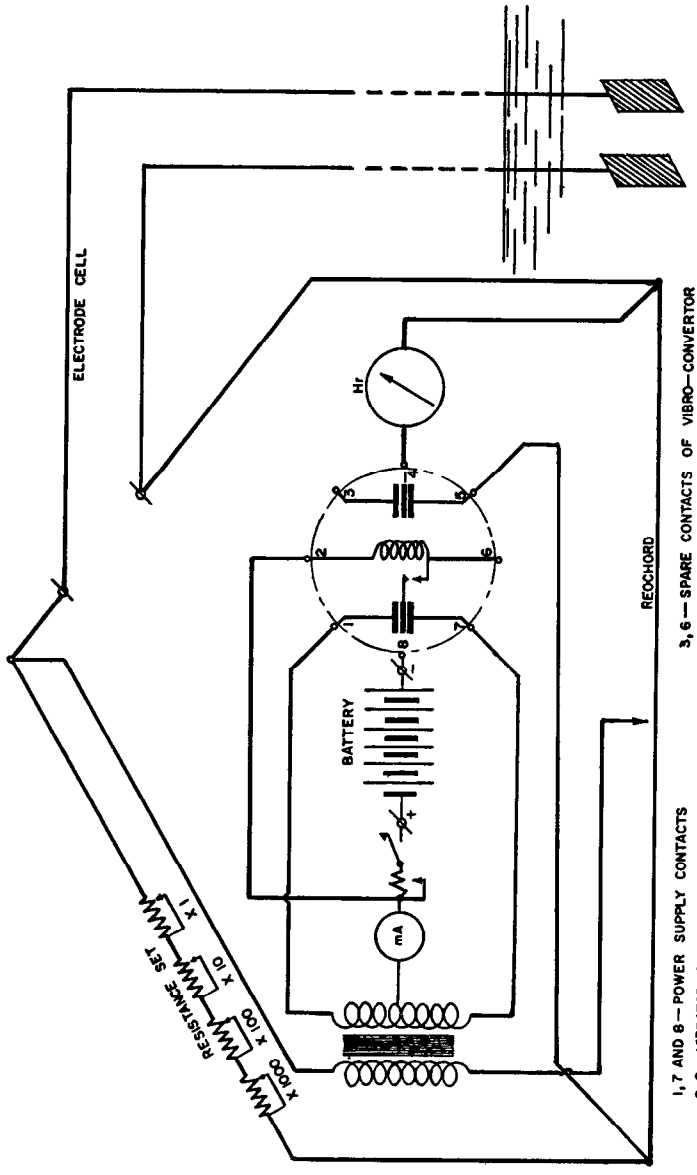

FIGURE 126.—Schematic diagram of conductance meter used in salt-dilution method of measuring discharge. (From World Meteorological Organization, 1962, p. 47.)

site, the current is switched on in the conductance meter, and the stability of the compensation for natural conductance is checked. If the galvanometer needle has deviated from zero, it is returned to zero by changing the resistance. Constant observation of the needle then begins. When the needle begins a perceptible movement to the right, it is a sign that the solution, or ionic wave, is approaching, and the stopwatch is started. From that time on, the galvanometer needle is maintained in a position approximating the zero reading by turning the rheochord handle. Every 15 s the needle is returned exactly to zero and the indicator position on the rheochord scale is read. That reading represents relative conductance (P) expressed in tenths of a percent (0/00):

$$P_W = 1{,}000 \left[\frac{(EC)_W - (EC)_o}{(EC)_o} \right], \tag{39}$$

where EC is conductance (electrical conductivity), subscript W refers to the ionic wave, and subscript o refers to the natural water in the stream. (Note.—Conductance is the reciprocal of resistance.)

As the ionic wave passes the sampling site, relative conductance increases rapidly at first, reaches a peak, and then recedes slowly to zero or to a constant value slightly above or below zero. When the rheochord readings remain constant for 5 or 6 readings (1½ min) near the zero value, the measurement is terminated. Immediately thereafter the determination of the relative conductance of the injection solution begins, using the sample in the small flask obtained at the injection site just before the measurement began. For this determination the following equipment is needed:

1. A 10-L measuring vessel.
2. A jug for adding water to the measuring vessel.
3. A wooden or aluminum paddle for mixing the solution.
4. A 1-mL glass pipette.

The measuring vessel is rinsed three or four times with river water. It is then filled with river water to the 10-L mark, and the electrode cell of the conductance meter is immersed in it. The rheochord needle is set to zero, the current is switched on, and the resistance is adjusted to set the galvanometer needle to zero. The pipette is next rinsed in the injection solution that had been delivered in the small flask, and the pipette is used to add 1 mL of that solution to the 10 L of river water in the measuring vessel. The pipette is then rinsed three times in the vessel to insure that all of the extremely small volume of salt in the 1 mL of solution is introduced into the vessel. The contents of the vessel are then thoroughly mixed, and the relative conductance of the greatly diluted injection solution is measured with the meter, using the technique described for measuring relative conductance in the

ionic wave. The ratio of dilution for the sample of injection solution is 1:10,000, because 1 mL of injection solution was mixed with 10 L of river water.

COMPUTATION OF DISCHARGE

The simplest way to describe the computation of discharge from salt-dilution data is by means of an example. Assume that in the preceding discussion of methodology, the stream discharge had been estimated to be about 4.5 m^3/s. The unit quantity of salt to be used was 2 $kg/m^3/s$ of discharge; consequently about 9 kg of salt was prepared. Water was added to the salt at the rate of 10 L per 3 kg of salt. As a result, 30 L (0.03 m^3) of injection solution was prepared. This value is shown on line 1 on the left-hand side of the computation sheet in figure 127. At the sampling site, 10 L of river water (line 2) was mixed with 1 mL of injection solution (line 3), giving a dilution ratio of 10,000 (line 4). The resistance of the river water was found to be 969 ohms (lines 5 and 6), and the resistance of the sample of diluted (1:10,000) injection solution was found to be 691 ohms (line 7). The relative conductance of that sample, as read on the rheochord in tenths of a percent, was 402 (line 8). On line 9, the rheochord reading for the dilute sample of injection solution is checked mathematically by use of the measured resistances. The equation used on line 9 is identical with equation 39. On line 10 the relative conductance of the injected solution is computed by multiplying the relative conductance of the diluted injection sample by the dilution ratio.

On the right-hand side of figure 127 are shown the relative conductance values read on the rheochord scale at 15-s intervals during the 15-min passage of the ionic wave. Subtotals are shown for the three columns of relative conductance values; the grand total is 1,933. The data are presented graphically in figure 128, where relative conductance is plotted against time.

Discharge is computed from equation 40, the denominator of which is the area under the curve of relative conductance versus time:

$$Q = \frac{V_1 P_p}{F \pm \Delta F}, \tag{40}$$

where

- Q is discharge, in cubic meters per second,
- V_1 is volume of the injected solution, in cubic meters,
- P_p is relative conductance of the injected solution, in tenths of a percent,
- F is the product of the sampling interval, in seconds, multiplied by the sum of the observed values of relative conductance, and
- ΔF is a correction factor for any change in reading of the rela-

tive conductance of the natural river water between the start and end of the measurement:

$$\Delta F = \frac{P_{start} - P_{end}}{2}(t_n - t_1),$$ where $t_n - t_1$ is the time, in seconds, that elapsed during the measurement.

The discharge is computed in lines 11–16 on the left-hand side of figure 127. Line 11 shows the sampling interval—15 s; line 12 shows the sum of the observed relative conductances of the ionic wave—1,933; line 13 shows the computation of F—28,995; line 14 shows the computation of ΔF—there was no change in natural relative conductance during the 900 s that elapsed during the measurement. The value of the denominator of equation 40 is shown on line 15. The discharge, computed in accordance with equation 40, is shown on line 16.

MEASUREMENT OF DISCHARGE BY DILUTION OF RADIOACTIVE TRACERS

GENERAL

The use of radioactive material for measuring discharge by tracer

Basic measurements data				Observations of ionic wave					
Item	Symbol	Value	Units	Time t	‰ I	Time t	‰ P	Time t	‰ P
1 Volume of initial solution	V_1	0,0300	m^3						
2 Volume of river water for dilution	Wo	10000	ml	0 00″	0	6 15″	52	12 30″	3
				15″	1	30″	48	45″	2
3 Volume of initial solution for dilution	W_1	1	ml	30″	3	45″	44	13'00″	2
				45″	7	7'00″	40	15″	1
4 Dilution ratio $\frac{Wo}{W_1}$	n	10000	—	1'00″	13	15″	37	30″	1
				15″	20	30″	33	45″	1
5 Resistance of river water flow	R_n	969	ohms	30″	32	45″	29	14'00″	1
				45″	44	8'00″	26	15″	1
6 Resistance of river water in tank	R	969	ohms	2'00″	56	15″	24	30″	1
				15″	66	30″	21	45″	1
7 Resistance of mixture	R_t	691	ohms	30″	75	45″	19	15'00″	0
				45″	81	9'00″	18	15″	0
8 Relative electrical conductivity of mixture on rheochord	P_t	402	‰	3'00″	85	15″	15	30″	0
				15″	88	30″	13	45″	0
9 Or from formula $P_t = \left(\frac{R}{R_t} - 1\right) 1000$ ‰	P_t	402	‰	30″	90	45″	12	16'00″	0
				45″	91	10 00″	10	15″	0
				4'00″	90	15″	9	30″	0
10 Relative electrical conductivity of initial solution $P_p = P_t \cdot n$	P_p	4020000	‰	15″	88	30″	8	45″	0
				30″	85	45″	7	17'00″	0
Discharge calculation				45″	81	11'00″	6	15″	
11 Time between observations	$\triangle t$	15	sec	5'00″	77	15″	5	30″	
12 Sum of ordinates of ionic wave graph	ΣP	1933	‰	15″	72	30″	5	45″	
				30″	66	45″	4	18 00″	
13 Product $F = \triangle t(\Sigma P)$	F	28,995	‰ sec	45″	61	12 00″	3		
				0'00	56	15″	3		
14 Correction $\triangle F = \frac{P_1 - P_n}{2}(t_n - t_1) = 0$			‰ sec	$\Sigma P =$	1428	$\Sigma P =$	491	$\Sigma P =$	14
15 Area of ionic wave graph $F \pm \triangle F$		28995	‰ sec						
16 Water discharge $Q = \frac{V_1 \cdot P_p}{F \pm \triangle F} = \frac{(0,0300)(4020000)}{28995}$			4 16 m^3/sec						

FIGURE 127.—Sample computation of discharge using salt dilution in the sudden injection method. (From World Meteorological Organization, 1962, p. 49.)

dilution will not be described in detail, because the method is still (1980) considered to be in the experimental stage. Radioactive tracers should be ideal for the dilution method because concentrations as low as 10^{-9} ci/L may be accurately determined with a counter or count-rate meter whose sensing probe is immersed in the stream.

The radioactive element that has been most commonly used is gold 198, which has a half-life of 2.7 d. Tests have also been made using sodium 24, which has a half-life of 14.9 hr. It is necessary that the radioactive tracer have a short half-life so that the radioactivity introduced into the stream will decay to an insignificant level in a short

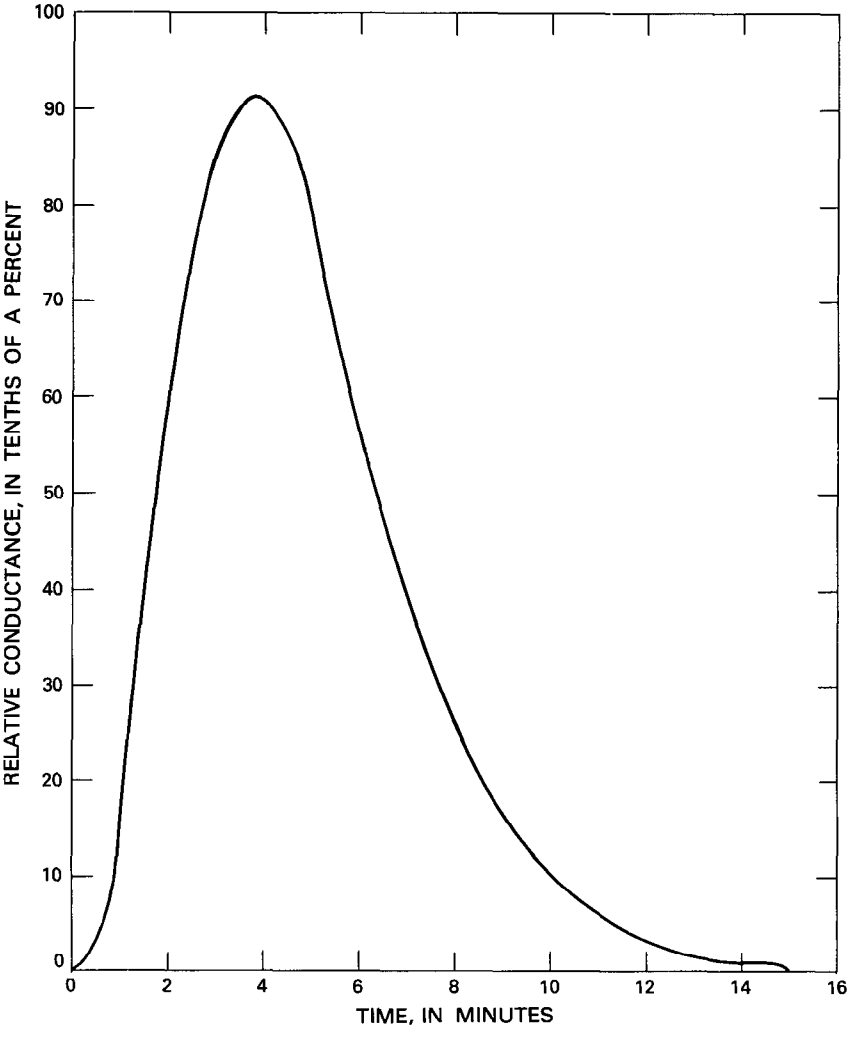

FIGURE 128.—Curve of relative conductance versus time for the ionic wave in the sample problem. (From World Meteorological Organization, 1962, p. 48.)

time. That requirement introduces a problem in logistics, in that the radioactive element must arrive from the nuclear plant and be used at the measurement site at the scheduled time, so that excessive decay of the radiation does not occur before the discharge measurement is made. Another factor that tends to discourage the use of radioactive tracers is the requirement of a government license merely to handle the material; radiation shielding must be provided while shipping and handling the material because of the potential threat to public health. In addition, approval must usually be obtained at all government levels, including the local level, before the radioisotope can be used in a stream, and local fear of radioactive pollution is often difficult to overcome.

METHODOLOGY

A measurement reach of channel is selected, using one of the equations, 28 to 32 (p. 221–222), as a guide in determining the length of reach needed for satisfactory mixing. Before the measurement is started, the instrument for counting gamma-ray emissions—Geiger or scintillation counter—is calibrated, taking into account the exact conditions under which the counter will be used.

A measured quantity of the radioisotope is introduced into the stream at the injection site by being quickly poured out of a bottle; or more frequently, a glass bottle containing the radioisotope is placed in a wire-screen container that is then lowered into the stream, after which the glass bottle is shattered to release the isotope for mixing in the streamflow. At the sampling site downstream, where the probe of the Geiger or scintillation counter is immersed in the stream, gamma-ray emissions are continuously counted. The counters are started well before the arrival of the isotope-stream mixture so that the counts received from natural (background) radiation sources may be measured. The counters continue to count throughout the passage of the isotope-stream mixture until the count returns to the background level. The total net count (N) is equal to the gross count obtained minus the background count accumulated during the period of the gross count.

The discharge is computed from the equation

$$Q = \frac{FA}{N}, \tag{41}$$

where

Q = stream discharge (volume per unit time),
F = a calibration factor for the probe and counting system,
A = total quantity of radioactivity introduced into the stream, and
N = total net count recorded by the counter.

SELECTED REFERENCES

Barnes, H. H., and Kilpatrick, F. A., 1973, Techniques for measurement of discharge by dye dilution, *in* Koblenz, 1970, Symposium on hydrometry: Internat. Assoc. Sci. Hydrology, Pub. 99, p. 251–259.

Cobb, E. D., and Bailey, J. F., 1965, Measurement of discharge by dye-dilution methods: U.S. Geol. Survey Surface-Water Techniques, book 1, chap. 14, 27 p.

Dunn, Bernard, and Vaupel, D. E., 1965, Effects of sample and fluorometer-compartment temperatures on fluorometer readings: U.S. Geol. Survey Prof. Paper 525–D, p. D225–D227.

Engmann, J. E. O., and Kellerhals, Rolf, 1974, Transverse mixing in an ice-covered river: Water Resources Research, v. 10, no. 4, p. 775–784.

Environmental Protection Agency, Environmental Studies Board, 1972, Water quality criteria 1972—a report of the Committee on Water Quality Criteria: Washington, U.S. Govt. Printing Office, 594 p.

Feuerstein, D. L., and Selleck, R. E., 1963, Tracers for dispersion measurements in surface waters: California Univ., Berkeley Sanitary Eng. Research Lab., Report no. 63–1, 69 p.

Frederick, B. J., Reck, C. W., and Carter, R. W., 1962, Use of a radioisotope to measure water discharge: U.S. Geol. Survey Prof. Paper 450–D, p. 185–186.

Glover, R. E., 1964, Dispersion of dissolved or suspended materials in flowing streams: U.S. Geol. Survey Prof. Paper 433–B, 32 p.

Godfrey, R. G., and Frederick, B. J., 1963, Dispersion in natural streams: U.S. Geol. Survey open-file report, 75 p.

Hosegood, P. H., Sanderson, P. R., and Bridle, M. K., 1969, Manual of dilution gaging with sodium dichromate: Water Research Assoc. ILR no. 34, Medmenham, Marlow, Buckinghamshire, England, 36 p.

International Standards Organization, 1973, Liquid flow measurement in open channels—Dilution methods for measurement of steady flow—Constant-rate-injection method: International Standard 555, Geneva, 18 p.

Kilpatrick, F. A., 1968, Flow calibration by dye-dilution measurement: Civil Eng., v. 38, no. 2, p. 74–76.

Pritchard, D. W., and Carpenter, J. H., 1960, Measurements of turbulent diffusion in estuarine and inshore waters: Internat. Assoc. Sci. Hydrology, Bull. no. 20, p. 37–50.

Schuster, J. C., 1965, Canal discharge measurements with radioisotopes: Am. Soc. Civil Engineers Trans., v. 91, no. HY2, part 1, p. 101–124.

Spencer, E. A., and Tudhope, J. S., 1958, A literature survey of the salt-dilution method of flow measurement: Inst. Water Engineers Jour., v. 12, no. 2, p. 127–138.

Turner, G. K. Associates, 1963, Operating and service manual, model 111 fluorometer: Palo Alto, Calif., 28 p.

U.S. Bureau of Reclamation, 1971, Water measurement manual [2d ed.]: Water Resources Tech. Pub., p. 166–168.

World Meteorological Organization, 1962, Field methods and equipment used in hydrology and hydrometeorology: Flood Control Series no. 22, p. 47–49.

Wright, R. R., and Collings, M. R., 1964, Application of fluorescent tracing techniques to hydrologic studies: Am. Water Works Assoc. Jour., v. 56, no. 6, p. 748–754.

Yotsukura, Nobuhiro, and Cobb, E. D., 1972, Transverse diffusion of solutes in natural streams: U.S. Geol. Survey Prof. Paper 582–C, 19 p.

CHAPTER 8. MEASUREMENT OF DISCHARGE BY MISCELLANEOUS METHODS

GENERAL

This chapter deals with the measurement of discharge when conditions are such that it is not feasible to use either a velocity meter or tracer-dilution equipment. The situations and methodologies discussed include the following:

A. High flow
   1. Timed observation of floats
B. Low flow
   1. Volumetric measurement
   2. Use of a calibrated portable weir plate
   3. Use of a calibrated portable Parshall flume
C. Unstable flow—roll waves or slug flow
   1. Use of photographic techniques

Not discussed here is the practice followed in many countries, other than the U.S.A., in which discharge is measured by observing the head on gaging-station controls that are built in conformity with laboratory-rated weirs or flumes. The transfer of a laboratory discharge rating to a structure in the field requires the existence, and maintenance, of similitude between laboratory model and prototype, not only with regard to the structure, but also with regard to the approach channel. For example, scour and (or) fill in the approach channel will change the head-discharge relation, as will algal growth on the control structure. Both the structure and the approach channel must be kept free from accumulations of debris, sediment, and vegetal growth. Flow conditions downstream from the structure are significant only to the extent that they control the tailwater elevation, which may influence the operation of structures designed for free-flow conditions.

The existence or development of conditions that differ from laboratory conditions will necessitate in place calibration of the control to establish the extent of departure from the laboratory discharge ratings. In place calibration requires the measurement of discharge by current meter or by other means, as described in chapters 5 through 9. Because experience in the U.S.A. has indicated that departure from laboratory conditions is the norm, rather than the exception, gaging-station controls are always calibrated in place by the U.S. Geological Survey.

The reader who is interested in the measurement of discharge by the use of precalibrated controls is referred to publications by the World Meteorological Organization (1971) and the International Standards Organization (1969).

FLOATS

Floats are seldom used in stream gaging but are useful in an emergency for measuring high discharges under the following circumstances:

1. No conventional or optical current meter is available.
2. A current meter is available but the measurement structure—bridge or cableway—has been destroyed, and equipment for measuring from a boat is unavailable.
3. A conventional current meter is available, but floating ice or drift make it impossible to use the meter.

Surface floats are used in those situations, and they may be almost any distinguishable article that floats, such as wooden disks; bottles partly filled with either water, soil, or stones; or oranges. Floating ice cakes or distinguishable pieces of drift may be used if they are present in the stream.

Two cross sections are selected along a reach of straight channel for a float measurement. The cross sections should be far enough apart so that the time the float takes to pass from one cross section to the other can be measured accurately. A traveltime of at least 20 s is recommended, but a shorter time may be used for streams with such high velocities that it is not possible to find a straight reach of channel having adequate length. The water-surface elevation should be referenced to stakes along the bank at each cross section and at one or more intermediate sites. Those elevations will be used at a later date, when conditions permit, to survey cross sections of the measurement reach, and the end stakes will be used to obtain the length of the reach. The surveyed cross sections will then be used to derive an average cross section for the reach.

In making a float measurement a number of floats are distributed uniformly across the stream width, and the position of each with respect to distance from the bank is noted. The floats should be introduced a short distance upstream from the upstream cross section so that they will be traveling at the speed of the current when they reach the upstream section. A stopwatch is used to time their travel between the end cross sections of the reach. The estimated position of each float with respect to the bank is also noted at the downstream cross section.

If there is no bridge or cableway from which to introduce the floats in the stream, the floats will have to be tossed in from the streambank. If that is the situation that exists at a wide stream, it may be impossible to position any floats in the central core of the stream where most of the flow occurs. A float measurement of discharge made under those conditions would be meaningless. However, the difficulty of introducing floats at intervals across the entire width

of a wide stream can be overcome if a boat can be obtained for the purpose.

The velocity of a float is equal to the distance between the end cross sections divided by the time of travel. The mean velocity in the vertical is equal to the float velocity multiplied by a coefficient whose value is dependent on the shape of the vertical-velocity profile of the stream and on the depth of immersion of the float with respect to stream depth. A coefficient of 0.85 is commonly used to convert the velocity of a surface float to mean velocity in the vertical.

The procedure for computing the discharge is similar to that used in computing the discharge for a conventional current-meter measurement. (See chapter 5.) The discharge in each subsection of the average cross section is computed by multiplying the area of the subsection by the mean vertical velocity for that subsection. The total discharge is equal to the sum of the discharges for all subsections.

Float measurements of discharge that are carefully made under favorable conditions may be accurate to within ±10 percent. Wind may adversely affect the accuracy of the computed discharge by its effect on the velocity of the floats. If a nonuniform reach is selected and few floats are used in the cross section, measurement results may be in error by as much as 25 percent.

VOLUMETRIC MEASUREMENT

The volumetric measurement of discharge is only applicable to small discharges, but it is the most accurate method of measuring such flows. In that method the hydrographer observes the time required to fill a container of known capacity, or the time required to partly fill a calibrated container to a known volume. The only equipment required, other than the calibrated container, is a stopwatch.

The container is calibrated in either of two ways. In the first method, water is added to the container by known increments of volume, and the depth of water in the container is noted after the addition of each increment. In the second method, the empty container is placed on a weighing scales, and its weight is noted. Water is added to the container in increments, and after each addition the total weight of container and water is noted, along with the depth of water in the container. The equation used to determine the volume corresponding to a depth that was read is

$$V = \frac{W_2 - W_1}{w}, \tag{42}$$

where

V = volume of water in container, in cubic feet or cubic meters,

W_2 = weight of water and container, in pounds or kilograms,

W_1 = weight of empty container, in pounds or kilograms, and
w = unit weight of water, 62.4 lb/ft^3 or 1,000 kg/m^3.

Volumetric measurements are usually made where the flow is concentrated in a narrow stream, or can be so concentrated, so that all the flow may be diverted into a container. Examples of sites presenting the opportunity for volumetric measurement of discharge are a V-notch weir; an artificial control where all the flow is confined to a notch or to a narrow width of catenary-shaped weir crest; and a cross section of natural channel where a temporary earth dam can be built over a pipe of small diameter, through which the entire flow is directed. Sometimes it is necessary to place a trough against the artificial control to carry the water from the control to the calibrated container. If a small temporary dam is built, the stage behind the dam should be allowed to stabilize before the measurement is begun. The measurement is made three or four times to be certain no errors have been made and to be sure the results are consistent.

Volumetric measurements have also been made under particular circumstances when no other type of measurement was feasible. One such circumstance involved a small stream that was in actuality a series of deep pools behind broad-crested weirs that acted as drop structures to dissipate the energy of the stream. At low flows the depth of water on the weir crest was too shallow to be measured by current meter, and the velocity in the pools was too slow for such measurement. To measure the discharge a large container of known volume was placed on a raft held close to the downstream weir face by ropes operated from the banks. A sharp-edged rectangular spout of known width was held so that one end butted tightly against the downstream face of the weir, the base of the spout being held just below the weir crest. The other end of the spout led to the container of known volume. Timed samples of the flow, sufficient to fill the container, were taken at a number of locations along the downstream face of the weir, the raft being moved laterally across the stream, from location to location, by the ropes. The procedure was analogous to making a conventional current-meter discharge measurement. Instead of measuring depth and velocity at a series of observation sites in the cross section, as is done in a current-meter measurement, the discharge per width of spout opening was measured at a series of observation sites. The discharge measured at each site was multiplied by the ratio of subsection width to spout width to obtain the discharge for the subsection. The total discharge of the stream was the summation of the discharges computed for each subsection.

PORTABLE WEIR PLATE

A portable weir plate is a useful device for determining discharge

when depths are too shallow and velocities too low for a reliable current-meter measurement of discharge. A 90° V-notch weir is particularly suitable because of its sensitivity at low flows. Three different sizes of weir plate are commonly used by the U.S. Geological Survey; their recommended dimensions are given in figure 129.

The weir plate is made of galvanized sheet iron, using 10- to 16-gauge metal. The 90° V-notch that is cut in the plate is not beveled but is left with flat, even edges. The larger weir plates are made of thinner material than the smaller weir plates, but the medium and large plates are given additional rigidity by being framed with small angle irons fastened to the downstream face. A staff gage, attached to the upstream side of the weir plate with its zero at the elevation of the bottom of the notch, is used to read the head on the weir. The staff gage should be installed far enough from the notch to be outside the region of drawdown of water going through the notch. Drawdown becomes negligible at a distance from the vertex of the notch that is equal to twice the head on the notch. Consequently, if the weir plate has the dimensions recommended in figure 129, the staff gage should be installed near one end of the plate.

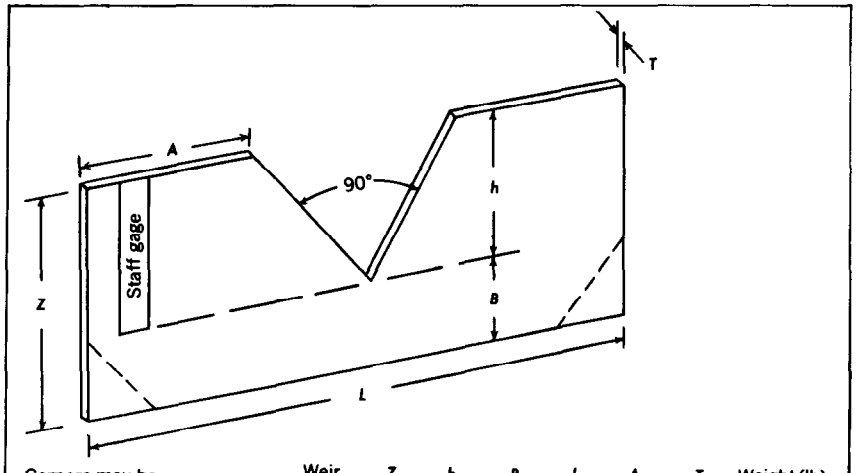

Corners may be trimmed if desired

Weir	Z	h	B	L	A	T	Weight (lb)
Large	1.75	1.00	0.75	4.0	1.0	16 ga.	24
Medium	1.25	.80	.45	3.0	.7	14 ga.	17
Small	.75	.47	.28	2.0	.53	10 ga.	8

All dimensions, other than T, are in feet

FIGURE 129.—Portable weir-plate sizes.

To install the weir, the weir plate is pushed into the streambed. A pick or shovel may be necessary to remove stones or rocks that prevent even penetration of the plate. A carpenter's level is usually used to insure that the top of the plate is horizontal and that the face of the plate is vertical. Another means of leveling the weir plate is by the use of a staff gage or level bubble attached at each end of the plate. The weir plate is then leveled by adjusting it until both staff gages give identical readings of the water surface or until the level bubbles are centered. Through eyebolts that are attached to the plate, rods are driven into the streambed to maintain the weir in a vertical position. Soil or streambed material is packed around the weir plate to prevent leakage under and around it. Canvas is placed immediately downstream from the weir to prevent undercutting of the bed by the falling jet. It ordinarily requires only one man to make the installation.

A large weir plate of the dimensions shown in figure 129 can measure discharges in the range from 0.02 to 2.0 ft^3/s (0.00057 to 0.057 m^3/s) with an accuracy of ±3 percent, if the weir is not submerged. A weir is not submerged when there is free circulation of air on all sides of the nappe. The general equation for flow over a sharp-edged 90° V-notch weir is

$$Q = Ch^{5/2}, \tag{43}$$

where

Q = discharge, in cubic feet per second or cubic meters per second,
h = static head above the bottom of the notch, in feet or meters, and
C = coefficient of discharge.

Each weir should be rated by volumetrically measuring the discharge corresponding to various values of head. In the absence of such a rating, a value of 2.47 may be used for C in equation 43 when English units are used, or 1.36 when metric units are used.

When the weir is installed it will cause a pool to form on the upstream side of the plate. No readings of head on the notch should be recorded until the pool has risen to a stable elevation. The head should then be read at half-minute intervals for about 3 min, and the mean value of those readings should be the head used in equation 43 to compute discharge. After the completion of the measurement the weir plate is removed.

PORTABLE PARSHALL FLUME

A portable Parshall flume is another device for determining discharge when depths are too shallow and velocities too low for a current-meter measurement of discharge. The portable flume used by the U.S. Geological Survey is a modified form of the standard Par-

shall flume (p.314–319) having a 3-in (0.076 m) throat. The modification consists, primarily, of the removal of the downstream diverging section of the standard flume. The purpose of the modification is to reduce the weight of the flume and to make it easier to install. Because the portable Parshall flume has no downstream diverging section, it cannot be used for measuring flows when the submergence ratio exceeds 0.6. The submergence ratio is the ratio of the downstream head on the throat to the upstream head on the throat. Although a submergence ratio of 0.6 can be tolerated without affecting the rating of the portable flume, in practice the flume is usually installed so that the flow passing the throat has virtually free fall. That is usually accomplished by building up the streambed a couple of inches under the level converging floor of the flume. (See fig. 130.)

Figure 130 shows the plan and elevation of the portable Parshall flume. The gage height or upstream head on the throat is read in the small stilling well that is hydraulically connected to the flow by a ⅜-in hole. The rating for the flume is given in table 14.

When the flume is installed in the channel, the floor of the converging section is set in a level position by using the level bubble that is attached to one of the braces (fig. 130). A carpenter's level can be used for that purpose if the flume is not equipped with a level bubble. Soil or streambed material is then packed around the flume to prevent leakage under and around it. Figure 131 shows a typical field installation. After the flume is installed, water will pool upstream from structure. No gage-height readings should be recorded until the pool has risen to a stable level. As with the portable weir, after stabilization of the pool level, gage-height readings should be taken at half-

TABLE 14.—*Rating table for 3-in modified Parshall flume*

Gage height (ft)	Discharge (ft^3/s)	Gage height (ft)	Discharge (ft^3/s)	Gage height (ft)	Discharge (ft^3/s)
0.01	0.0008	0.21	0.097	0.41	0.280
.02	.0024	.22	.104	.42	.290
.03	.0045	.23	.111	.43	.301
.04	.0070	.24	.119	.44	.312
.05	.010	.25	.127	.45	.323
.06	.013	.26	.135	.46	.334
.07	.017	.27	.144	.47	.345
.08	.021	.28	.153	.48	.357
.09	.025	.29	.162	.49	.368
.10	.030	.30	.170	.50	.380
.11	.035	.31	.179	.51	.392
.12	.040	.32	.188	.52	.404
.13	.045	.33	.198	.53	.417
.14	.051	.34	.208	.54	.430
.15	.057	.35	.218	.55	.443
.16	.063	.36	.228	.56	.456
.17	.069	.37	.238	.57	.470
.18	.076	.38	.248	.58	.483
.19	.083	.39	.259	.59	.497
.20	.090	.40	.269		

minute intervals for about 3 min. The mean value of those readings is the stage used in table 14 to obtain the discharge. A carefully made measurement should have an accuracy of ±2 or 3 percent. After completion of the measurement, the portable flume is removed.

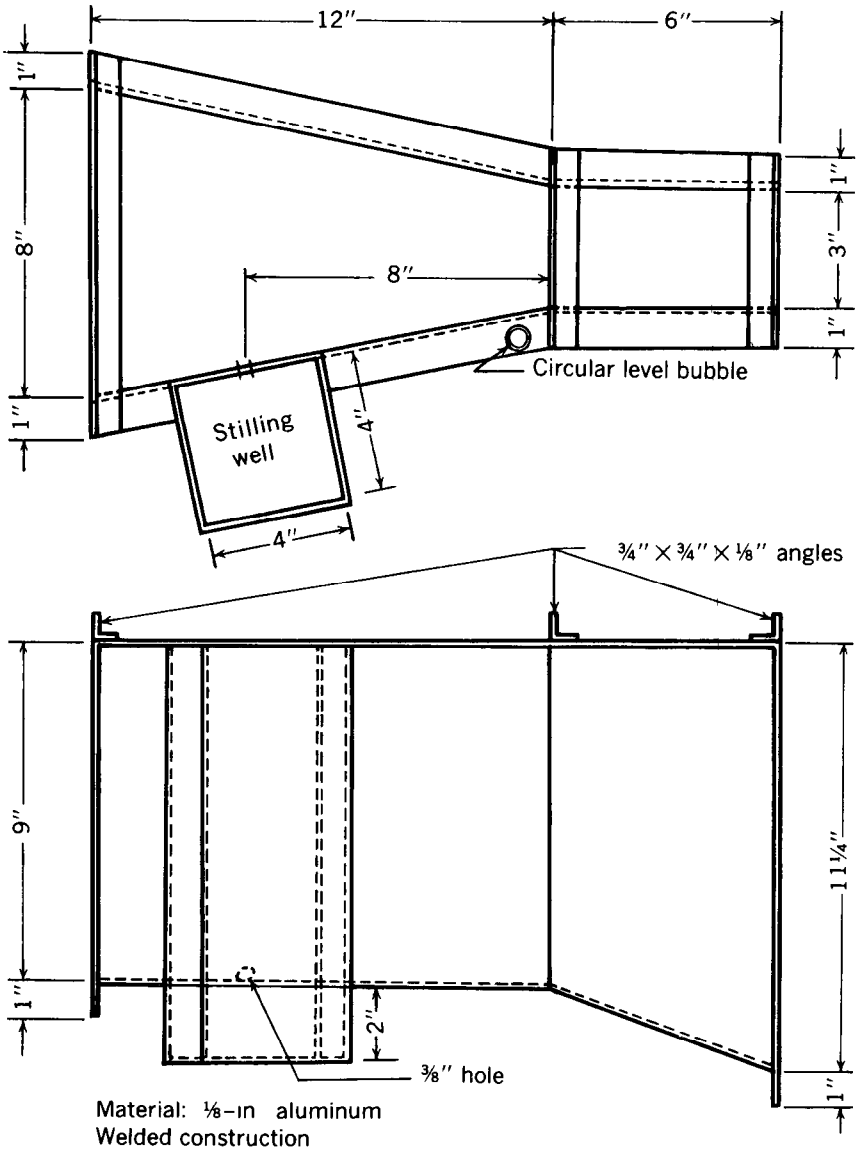

FIGURE 130.—Working drawing of modified 3-in Parshall flume.

MEASUREMENT OF UNSTABLE FLOW—ROLL WAVES OR SLUG FLOW

CHARACTERISTICS OF UNSTABLE FLOW

Unstable or pulsating flow often occurs during flash floods in arid areas. In pulsating flow the longitudinal profile is marked by a series of abrupt translatory waves (fig. 132) that rapidly move downstream. Translatory waves, commonly called roll waves or slug flow, can only develop in steep channels of supercritical slope and, therefore, are a matter of concern to the designer of steep-gradient channels. Channels are usually designed for stable flow. Should pulsating flow occur at high stages in a channel so designed, the channel capacity may be inadequate at a discharge much smaller than the design flow. Furthermore, if the overriding translatory wave carries an appreciable part of the total flow, conventional stream-gaging methods cannot be used to determine the discharge. Conventional water-stage recorders

FIGURE 131.—Modified 3-in Parshall flume installed for measuring discharge.

of either the float or pressure-sensing type do not react quickly enough to record the rapidly fluctuating stage; depths and velocities change too rapidly to permit discharge measurement by current meter; no stage-discharge relation exists for pulsating flow; and the commonly used formulas for computing stable open-channel discharge are not applicable.

DETERMINATION OF DISCHARGE

In brief, the method of determining the discharge of pulsating flow requires (1) computation of the discharge (Q_w) in the overriding waves and (2) computation of the discharge (Q_1) in the shallow-depth, or overrun, part of the flow. The sum of the two discharges is the total discharge at the time of observation.

To compute the discharge (Q_w) in an overriding wave, which is usually wedge shaped (fig. 132), the dimensions of the wave are observed, and the volume of the wave is divided by the elapsed time between the arrival of waves. For example, if the wedge-shaped wave in a train of waves has a volume of 200 ft^3 (5.67 m^3) and a wave arrives every 10 s, the discharge in the overriding wave is 200/10, or 20 ft^3/s (0.57 m^3/s). Average values are usually used in the computation—for example, the average volumes of five consecutive waves and the average time interval between the arrival of those consecutive waves. It should be mentioned at this point that the longitudinal profile of the wave is actually slightly concave upward and the wave front, while extremely steep, is not vertical. However, to simplify the computation of discharge, the waves are assumed to have a simple wedge shape.

To compute the discharge (Q_1) in the shallow-depth, or overrun, part of the flow, the cross-sectional area of the shallow-depth flow is

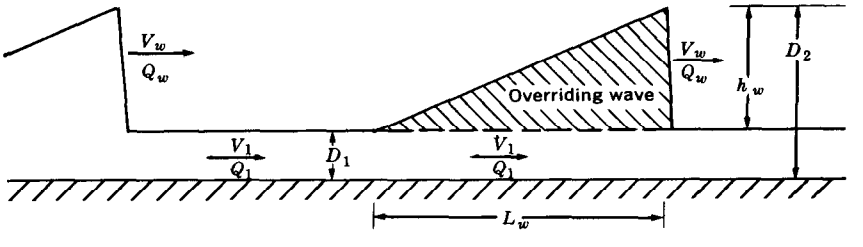

FIGURE 132.—Schematic sketch of longitudinal water-surface profile during pulsating flow.

observed (D_1 × channel width), and that area is multiplied by its velocity, V_1. Seldom will there be time enough between waves to obtain velocity observations of V_1 with a conventional current meter. V_1 may be computed by some stable-flow equation, such as the Manning equation, but preferably the surface velocity of shallow-depth flow should be measured by optical current meter. (See p. 91–93.) The surface velocity can then be multiplied by an appropriate coefficient—0.9 or 0.85, for example—to give the mean velocity, V_1. The final step is to compute the total discharge at the time of observation by adding Q_w and Q_1.

EXAMPLES OF DISCHARGE DETERMINATION

This section briefly describes two examples of discharge determinations made under conditions of pulsating flow in southern California.

Holmes (1936) obtained photographic documentation of a train of translatory waves in a steep stormflow channel. The rectangular channel was 43 ft (13.10 m) wide, 8 ft (2.44 m) high, and had a slope of 0.02. The waves themselves lapped at the top of the manmade channel giving them a height (D_2) of 8 ft, and their length (L_w) was about 600 ft (180 m). The average distance between wave crests was about 1,200 ft (360 m), and the average time interval between arrival of the waves (T_p) was 51 s. The channel between waves was dry or nearly so ($D_1=0$), meaning that the entire discharge was transported in the waves. The average discharge over the time T_p, computed from the equation

$$Q = (\text{volume})/T_p = \tfrac{1}{2}\,(W)\,(h_w)\,(L_w)/(T_p), \tag{44}$$

was therefore about 2,000 ft^3/s (56 m^3/s). The channel had been designed for stable-flow conditions and, according to the Manning equation, had a capacity of about 16,000 ft^3/s (405 m^3/s). We see then, that under the observed conditions of unstable flow the channel could accommodate only one-eighth of the design discharge.

Thompson (1968) described the experimental measurement of pulsating flow in the rectangular stormflow channel of Santa Anita Wash in Arcadia, California. The concrete channel was 28 ft (8.5 m) wide and had a slope of 0.0251. On the infrequent occasions when the channel had carried storm runoff in the past, the flow had been observed to be pulsating. For the test, water was released into the channel from an upstream reservoir at controlled rates of approximately 100 ft^3/s (2.8 m^3/s), 200 ft^3/s (5.6 m^3/s), 300 ft^3/s (8.5 m^3/s). Unstable flow did not develop until the flow came out of a bend in the steep storm channel and entered a straight reach of the channel. In other words, the released flow was stable upstream from the bend and pulsating downstream from the bend. During the release of water, dis-

charge measurements were made continuously by current meter in the stable flow upstream from the bend. The discharge hydrograph based on those measurements is shown by solid line in figure 133. Downstream from the bend a simultaneous attempt was made to measure the unstable flow by the method described in this paper, for the purpose of verifying the method.

At the test site, about 3,300 ft (1,000 m) downstream from the bend, the equivalent of a series of staff gages, in the form of a grid, was painted on one of the vertical channel walls so that water-surface

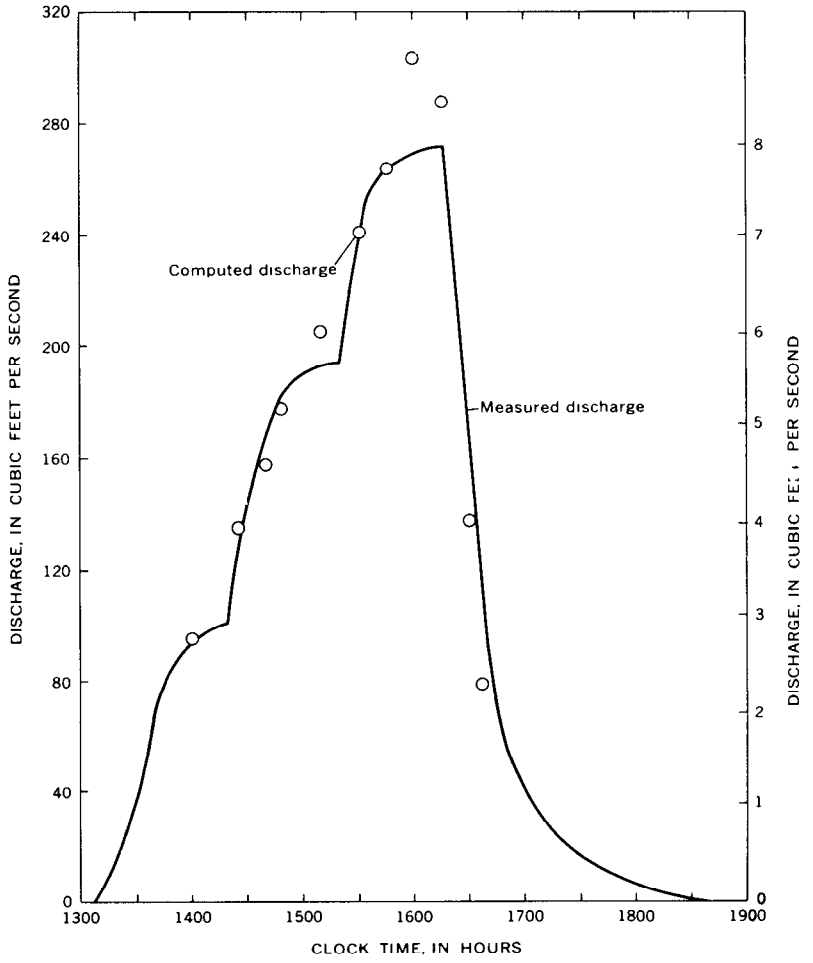

FIGURE 133.—Discharge hydrograph at Santa Anita Wash above Sierra Madre Wash, Calif., April 16, 1965, and plot of discharges computed from observations of flow.

elevations could easily be read by a crew of observers. Some of the observers were equipped with both still- and motion-picture cameras to document the observations; others were equipped with stopwatches to time wave velocity over a measured course of 102 ft (31 m) and to obtain the elapsed time between the arrival of waves. The waves were not evenly spaced and occasionally one wave would overtake another, but in general the waves were fairly uniform in size, maintained their spacing, and underwent little attenuation in the 3,300-ft reach above the test site. For computation purposes the average volumes of five consecutive waves and their average elapsed time between arrivals (T_p) were used, and discharges were computed at 15 min intervals using the procedure described earlier. For example, at the time of greatest discharge, the average value of T_p was 9.6 s, and the average wave dimensions were $D_1 = 0.42$ ft (0.13 m), $h_w = 0.66$ ft (0.20 m), and $L_w = 158$ ft (48.2 m). The computed value of Q_w equaled 152 ft^3/s (4.30 m^3/s). No optical current meter was available at the time, and Q_1 was therefore computed by the Manning equation. The computed value of Q_1 also equaled 152 ft^3/s (4.30 m^3/s), giving a computed total discharge 304 ft^3/s (8.60 m^3/s) at the time of observation. The values of discharge that were computed at 15-min intervals are plotted as open circles in figure 133 and show satisfactory agreement with the "true" discharge hydrograph. The field test of the method was therefore considered a success.

PROPOSED INSTRUMENTATION

There is as yet no instrumentation that is operational for automatically recording the data required to compute discharge under conditions of pulsating flow. Thompson concluded the above-cited report (1968) by describing three types of automatic instrumentation—photographic, depth sensing, and dye dilution—that might be developed for that purpose.

SELECTED REFERENCES

Buchanan, T. J., and Somers, W. P., 1969, Discharge measurements at gaging stations: U.S. Geol. Survey Techniques Water-Resources Inv., book 3, chap. A8, p. 57–63.

Holmes, W. H., 1936, Traveling waves in steep channels: Civil Eng., v. 6, no. 7, p. 467–468.

International Standards Organization, 1969, Liquid flow measurement in open channels—Establishment and operation of a gauging station and determination of the stage-discharge relation: ISO Recommendation R1100, Geneva, 44 p.

Thompson, T. H., 1968, Determination of discharge during pulsating flow: U.S. Geol. Survey Water-Supply Paper 1869–D, 22 p.

U.S. Bureau of Reclamation, 1971, Water measurement manual [2d ed.]: Water Resources Tech. Pub., p. 157–159.

World Meteorological Organization, 1962, Field methods and equipment used in hydrology and hydrometeorology: Flood Control Ser. no. 22, p. 50–51.

———1971, Use of weirs and flumes in stream gauging:WMO-no. 280, Tech. Note no. 117, Geneva, 57 p.

CHAPTER 9.—INDIRECT DETERMINATION OF PEAK DISCHARGE

INTRODUCTION

During floods, it is frequently impossible or impractical to measure the peak discharges when they occur because of conditions beyond control. Roads may be impassable; structures from which current-meter measurements might have been made may be nonexistent, not suitably located, or destroyed; knowledge of the flood rise may not be available sufficiently in advance to permit reaching the site near the time of the peak; the peak may be so sharp that a satisfactory current-meter measurement could not be made even with an engineer present at the time; the flow of debris or ice may be such as to prevent use of a current meter; or limitations of personnel might make it impossible to obtain direct measurements of high-stage discharge at numerous locations during a short flood period. Consequently, many peak discharges must be determined after the passage of the flood by indirect methods such as slope-area, contracted opening, flow-over-dam, or flow-through-culvert.

Indirect determinations of discharge make use of the energy equation for computing streamflow. The specific equations differ for different types of flow, such as unobstructed open-channel flow, flow over dams, and flow through culverts. However, all the methods involve these general factors:

1. Physical characteristics of the channel; that is dimensions and conformation of the channel within the reach used and boundary conditions.
2. Water-surface elevations at time of peak stage to define the upper limit of the cross-sectional areas and the difference in elevation between two or more significant cross sections.
3. Hydraulic factors based on physical characteristics, water-surface elevations, and discharge, such as roughness coefficients and discharge coefficients.

This chapter provides only a brief general discussion of the procedures used in collecting field data and in computing discharge by the various indirect methods. That highly specialized subject is treated in detail in the several manuals of the series "Techniques of Water-Resources Investigations of the United States Geological Survey" that are listed as references at the end of this chapter.

It should be remembered that the discharge that is determined by either direct measurement or by indirect methods includes not only the water but also any substances suspended or dissolved in the water (p. 79).

COLLECTION OF FIELD DATA

The data required for the computation of discharge by indirect methods are obtained in a field survey of a reach of channel. The survey includes the elevation and location of high-water marks corresponding to the peak stage; cross sections of the channel along the reach; selection of a roughness coefficient; and description of the geometry of dams, culverts, or bridges, depending on the type of peak-discharge determination to be made. The selection of a suitable site is a most important element in the application of the indirect method of discharge determination.

It is recommended that a transit be used to make a "transit-stadia" survey of the selected site. That method combines vertical and horizontal control surveys in one operation and is accurate, simple, and speedy.

Selection of a roughness coefficient remains essentially an "art" that is developed through experience. The factors that exert the greatest influence on the coefficient of roughness are the character of the streambed material, cross section irregularity, the presence of vegetation, and the alinement of the channel. In the Manning equation the roughness coefficient, n, ranges from as low as 0.012 for a concrete-lined channel in excellent condition or for a smooth sand channel of regular geometry to more than 0.1 for overbank areas having a heavy cover of brush.

SLOPE-AREA METHOD

The slope-area method is the most commonly used technique of indirect discharge determination. In the slope-area method, discharge is computed on the basis of a uniform-flow equation involving channel characteristics, water-surface profiles, and a roughness or retardation coefficient. The drop in water-surface profile for a uniform reach of channel represents energy losses caused by bed and bank roughness.

In applying the slope-area method, any one of the well-known variations of the Chezy equation may be used. However the Manning equation is preferred in most countries, including the U.S.A., because it is simple to apply, and the many years of experience in its use have shown that it produces reliable results.

The Manning equation, written in terms of discharge, is

$$Q = \frac{1.486}{n} AR^{2/3}S^{1/2}, \quad \text{(in English units), or} \qquad (45)$$

$$Q = \frac{AR^{2/3}S^{1/2}}{n} \quad \text{(in metric units),} \qquad (45a)$$

where

Q = discharge,
A = cross-sectional area,
R = hydraulic radius,
S = friction slope, and
n = roughness coefficient.

The Manning equation was developed for conditions of uniform flow in which the water-surface profile and energy gradient are parallel to the streambed and the area, hydraulic radius, and depth remain constant throughout the reach. For lack of a better solution, it is assumed that the equation is also valid for the nonuniform reaches that are invariably encountered in natural channels, if the water-surface gradient is modified by the difference in velocity-head between cross sections. The energy equation for a reach of nonuniform channel between cross section 1 and cross section 2 shown in figure 134 is

$$(h_1 + h_{v_1}) = (h_2 + h_{v_2}) + (h_f)_{1-2} + k(\Delta h_v)_{1-2}, \qquad (46)$$

where

h = elevation of the water surface at the respective cross sections above a common datum,
h_v = velocity head at the respective cross sections = $\alpha V^2/2g$, where α = velocity-head coefficient,
h_f = energy loss due to boundary friction in the reach,
Δh_v = upstream velocity head minus the downstream velocity head, used as a criterion for expansion or contraction of reach, and
$k(\Delta h_v)$ = energy loss due to acceleration or deceleration in a contracting or expanding reach, where
k = energy loss coefficient.

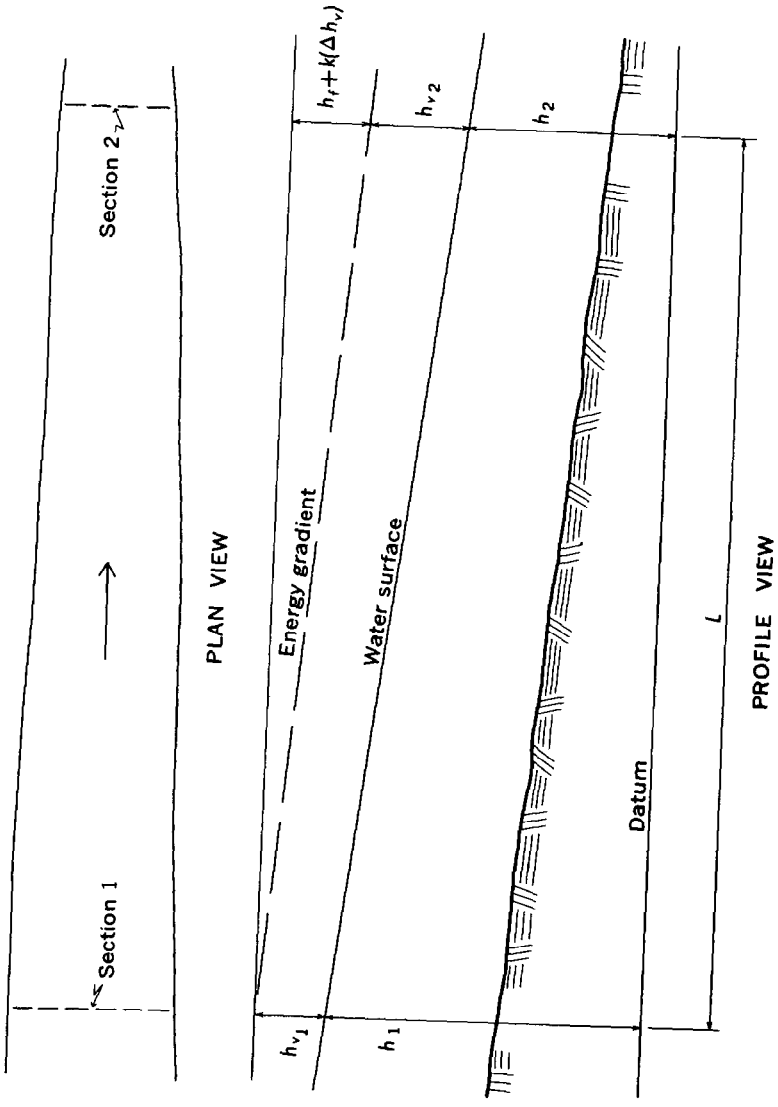

FIGURE 134.—Definition sketch of a slope-area reach.

The friction slope (S) to be used in the Manning equation is thus defined as

$$S = \frac{h_f}{L} = \frac{\Delta h + \Delta h_v - k(\Delta h_v)}{L}, \tag{47}$$

where Δh is the difference in water-surface elevation at the two sections and L is the length of the reach.

In using the Manning equation the conveyance, K, is computed for each cross section as $(1.486/n)AR^{2/3}$ in English units, or $(1/n)AR^{2/3}$ in metric units. The mean conveyance in the reach is then computed as the geometric mean of the conveyance at the two sections. This procedure is based on the assumption that the conveyance varies uniformly between sections. The discharge is computed by use of the equation

$$Q = \sqrt{K_1 K_2 S}, \tag{48}$$

where S is the friction slope as previously defined.

CONTRACTED-OPENING METHOD

The contraction of a stream channel by a roadway crossing creates an abrupt drop in water-surface elevation between an approach section and the contracted section under the bridge. The contracted section framed by the bridge abutments and the channel bed is in a sense a discharge meter that can be utilized to compute floodflows. The head on the contracted section is defined by high-water marks, and the geometry of the channel and bridge is defined by field surveys.

In computations of peak discharge at a contraction, the drop in water-surface level between an upstream section and a contracted section is related to the corresponding change in velocity. The discharge equation results from writing the energy and continuity equations for the reach between these two sections, designated as sections 1 and 3 in figure 135.

The discharge equation is

$$Q = CA_3\sqrt{2g\left(\Delta h + \alpha_1 \frac{V_1^2}{2g} - h_f\right)}, \tag{49}$$

in which

Q = discharge,
g = acceleration of gravity,
C = coefficient of discharge based on the geometry of the bridge and embankment,
A_3 = gross area of section 3; this is the minimum section parallel to the constriction between the abutments, and it is not

necessarily located at the downstream side of the bridge,

Δh = difference in elevation of the water surface between sections 1 and 3,

$\alpha_1 \frac{V_1^2}{2g}$ = weighted average velocity head at section 1, where V_1 is the average velocity, Q/A_1, and α_1 is coefficient that takes into account the variation in velocity in that section, and

h_f = the head loss caused by friction between sections 1 and 3.

The friction loss, h_f, as computed by the Manning equation, is only

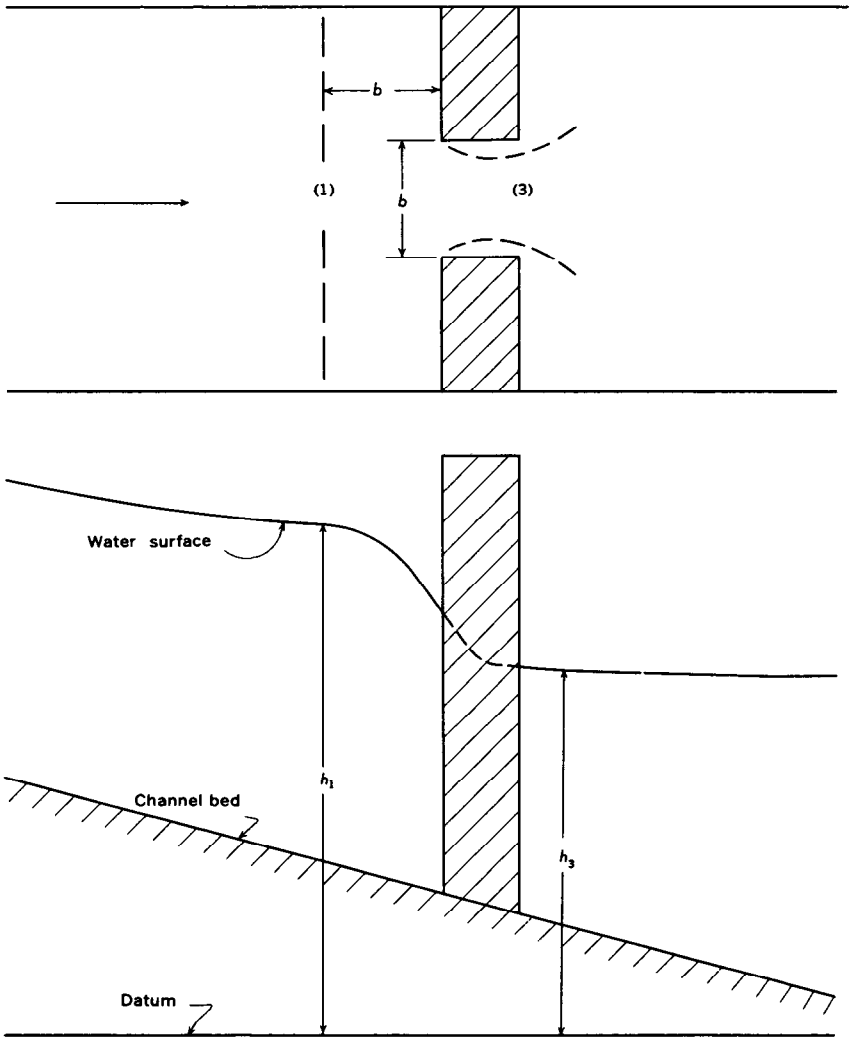

FIGURE 135.—Definition sketch of an open-channel contraction.

an approximation of the actual loss because of the rapid change in velocity from section 1 to section 3. Therefore, satisfactory results are attainable only if the term "h_f" is small relative to the difference in head, Δh.

FLOW OVER DAMS AND WEIRS

The term "dams," as used here, also includes highway and railway embankments that act as broad-crested dams during floods. The peak discharge over a dam or weir can be determined on the basis of a field survey of high-water marks and the geometry of the particular structure. (The terms "dam" and "weir" are used interchangeably.)

The basic equation for flow over a dam is

$$Q = CbH^{3/2}, \tag{50}$$

where

Q = discharge,
C = a coefficient of discharge having the dimensions of the square root of the acceleration of gravity,
b = width of the dam normal to the flow, excluding the width of piers, if any, and
H = total energy head ($h + V_a^2/2g$) referred to the crest of the dam, where h = static head, and V_a = mean velocity at the approach section to the dam.

It is apparent from equation 50 that the reliability of a computation of flow over a dam is dependent primarily on using the correct dam coefficient, C. Values of C vary with the geometry of the dam and with the degree of submergence of the dam crest by tailwater. One of the manuals referred to on page 273 (Hulsing, 1967) treats in detail the coefficients associated with sharp-crested (thin-plate) weirs, broad-crested weirs, round-crested weirs, and weirs of unusual shape. Because the technical details in that manual cannot be readily summarized here, the reader is referred to the Hulsing report.

FLOW THROUGH CULVERTS

The peak discharge through culverts can be determined from high-water marks that define the headwater and tailwater elevations. This indirect method is used extensively to measure flood discharges from small drainage areas.

The placement of a roadway fill and culvert in a stream channel causes an abrupt change in the character of flow. This channel transition results in rapidly varied flow in which acceleration, rather than boundary friction, plays the primary role. The flow in the approach channel to the culvert is usually tranquil and fairly uniform. However, within the culvert the flow may be tranquil, critical, or rapid if the culvert is partially filled, or the culvert may flow full under pressure.

The physical features associated with culvert flow are illustrated in figure 136. They are the cross section in the approach channel located upstream from the culvert entrance at a distance that is equivalent to the width of the culvert opening; the culvert entrance; the culvert barrel; the culvert outlet; the farthest downstream section of the barrel; and the tailwater downstream from the culvert barrel.

The change in the water-surface profile in the approach channel reflects the effect of acceleration that results from the contraction of cross sectional area. Loss of energy near the entrance is related to the sudden contraction and subsequent expansion of the live stream within the barrel, and entrance geometry has an important influence on this loss. The important features that control the stage-discharge relation at the approach section can be the occurrence of critical depth in the culvert, the elevation of the tailwater, the entrance or barrel geometry, or a combination of these elements.

The peak discharge through a culvert is determined by application of the continuity equation and the energy equation between the approach section and a section within the culvert barrel. The location of the downstream section depends on the state of flow in the culvert barrel. For example, if critical flow occurs at the culvert entrance, the headwater elevation is not a function of either the barrel friction loss or the tailwater elevation, and the terminal section is located at the upstream end of the culvert.

Information obtained in the field survey includes the peak elevation of the water surface upstream and downstream from the culvert and the geometry of the culvert and approach channel. Reliable high-water marks can rarely be found in the culvert barrel; therefore, the type of flow that occurred during the peak flow cannot always be determined directly from field data, and classification becomes a trial-and-error procedure.

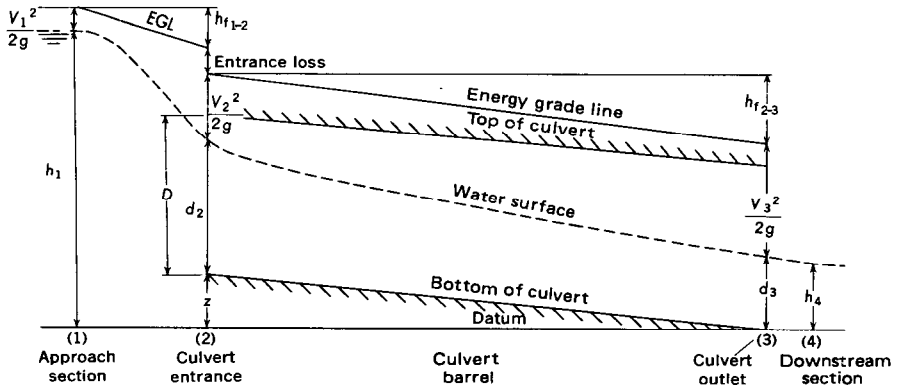

FIGURE 136.—Graphical presentation of the Bernoulli equation in culvert flow.

GENERAL CLASSIFICATION OF FLOW

For convenience in computation, culvert flow has been classified into six types on the basis of the location of the control section and the relative heights of the headwater and tailwater elevations. The six types of flow are illustrated in figure 137, and pertinent characteristics of each type are given in table 15. From that information the general classification of types of flow can be made.

1. If h_4/D is equal to or less than 1.0 and $(h_1 - z)/D$ is less than 1.5, only types I, II, and III flow are possible.
2. If h_4/D is greater than 1.0, only type IV flow is possible.
3. If h_4/D is equal to or less than 1.0 and $(h_1 - z)/D$ is equal to or greater than 1.5, only types V and VI flow are possible.

A manual by Bodhaine (1968) discusses trial-and-error procedures for further identification of the type of culvert flow and for the computation of discharge.

ESTIMATING DISCHARGE FROM SUPERELEVATION IN BENDS

Situations exist where none of the four methods previously described for determining peak discharge can be reliably applied. For example, in a highly sinuous, steep canyon stream, there may be no straight reaches of sufficient length for reliable application of the slope-area method; no abrupt area contractions may exist; and no manmade structures, such as dams or culverts, may have been built. In the above situation the peak discharge may sometimes be estimated from the superelevation in a bend of the stream (Apmann, 1973). The discharge should be estimated at each of several bends, after which the several estimated discharges are averaged.

A fundamental characteristic of open channel flow is the deformation of the free surface in a bend because of the action of centrifugal force. The water surface rises on the concave or outside bank of the

TABLE 15.—*Characteristics of types of culvert flow*

[D = maximum vertical height of barrel and diameter of circular culverts]

Flow type	Barrel flow	Location of terminal section	Kind of control	Culvert slope	$\frac{h_1-z}{D}$	$\frac{h_4}{h_c}$	$\frac{h_4}{D}$
I	Partly full	Inlet	Critical depth.	Steep	<1.5	<1.0	≤1.0
II	do	Outlet	do	Mild	<1.5	<1.0	≤1.0
III	do	do	Backwater	do	<1.5	>1.0	≤1.0
IV	Full	do	do	Any	>1.0	–	>1.0
V	Partly full	Inlet	Entrance geometry.	do	≥1.5	–	≤1.0
VI	Full	Outlet	Entrance and barrel geometry.	do	≥1.5	–	≤1.0

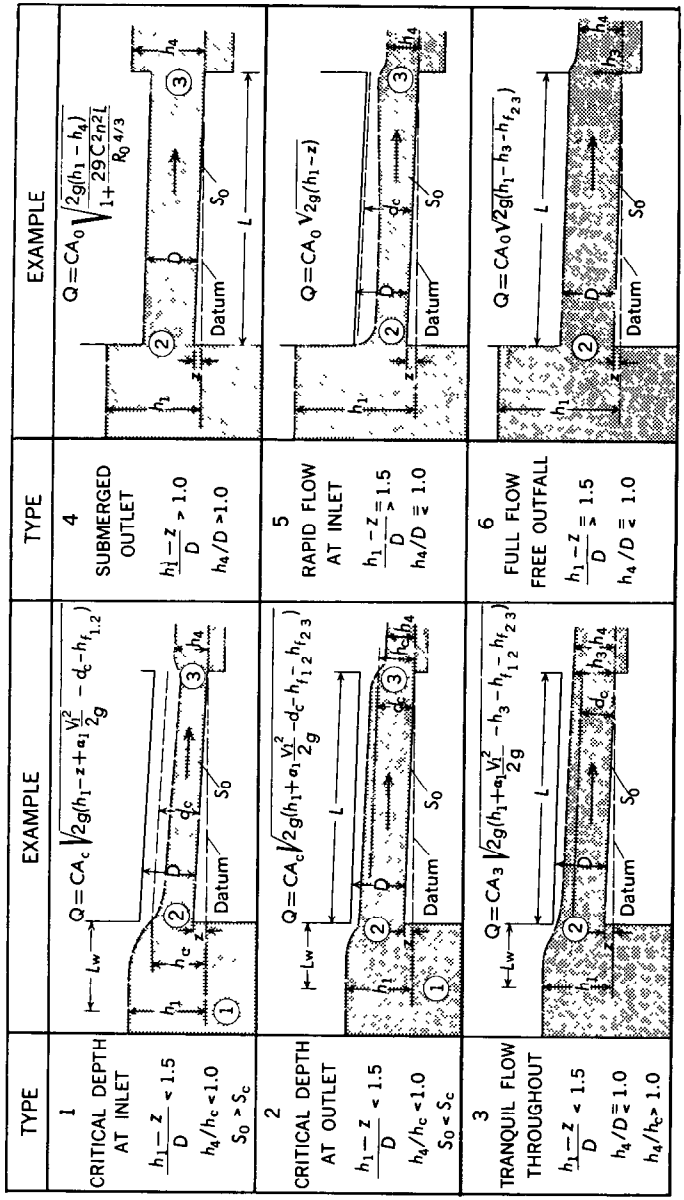

FIGURE 137.—Classification of culvert flow.

bend and lowers along the convex or inside bank of the bend. The difference in water-surface elevation between the banks is the superelevation. Superelevation varies with angular distance in the bend because of acceleration of the fluid entering and leaving the curve and because of the varying curvature of streamlines within the bend.

The discharge equation given by Apmann (1973) is

$$Q = A\sqrt{\frac{gh}{K}} \tag{51}$$

where

Q = discharge,
A = average radial cross section in the bend,
g = acceleration of gravity,
h = superelevation, that is, the maximum difference in water-surface elevation, measured along a radius of the bend, between inner and outer banks of the bend, and
K = superelevation coefficient.

The value of K is determined from the equation

$$K = \frac{5}{4}\tanh\left(\frac{r_c\Theta}{b}\right)\ln\left(\frac{r_o}{r_i}\right). \tag{52}$$

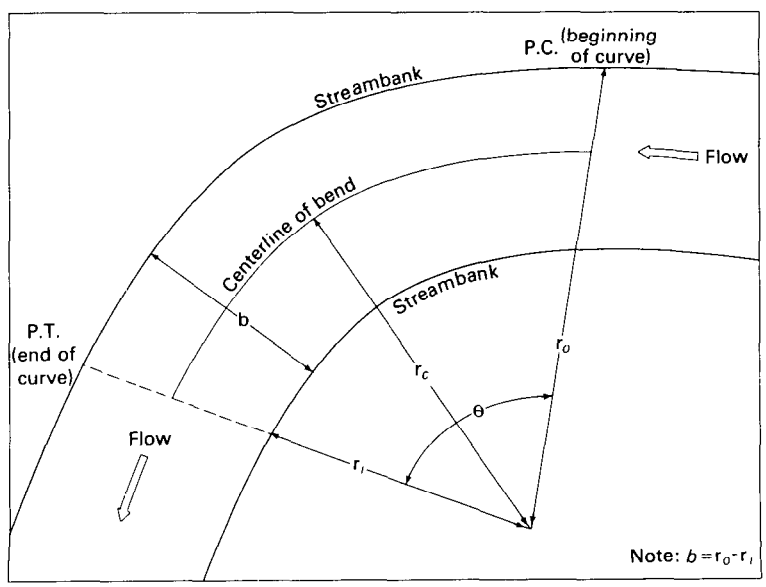

FIGURE 138.—Idealized sketch of a bend (plan view).

(NOTE.—tanh is the hyperbolic tangent)

The symbols in equation 52 are shown in the sketch in figure 138.

The method described applies only to bends having no overbank flow. The limited amount of work that has been done with the method indicates that it should not be applied where superelevations are less than 0.25 ft (0.076 m) because of uncertainties regarding the elevations of high-water marks at the banks. These uncertainties result from wave action and from the thickness of the bank-deposited debris that is often used as a high-water mark.

SELECTED REFERENCES

American Society of Civil Engineers, 1975, Sedimentation engineering· A S.C.E. Manuals and Reports on Engineering Practice no. 54, 745 p.

Apmann, R. P., 1973, Estimating discharge from superelevation in bends: Am. Soc Civil Engineers, Hydraulics Div. Jour., v. 99, no. HY1, p. 65–79.

Benson, M. A., and Dalrymple, Tate, 1967, General field and office procedures for indirect discharge measurements: U.S. Geol. Survey Techniques Water-Resources Inv., book 3, chap. A1, 30 p.

Bodhaine, G. L., 1968, Measurement of peak discharge at culverts by indirect methods: U.S. Geol. Survey Techniques Water-Resources Inv., book 3, chap A3, 60 p

Dalrymple, Tate, and Benson, M. A., 1967, Measurement of peak discharge by the slope-area method: U.S. Geol. Survey Techniques Water-Resources Inv., book 3, chap. A2, 12 p.

Hulsing, Harry, 1967, Measurement of peak discharge at dams by indirect methods: U.S. Geol. Survey Techniques Water-Resources Inv., book 3, chap. A5, 29 p.

Matthai, H. F., 1967, Measurement of peak discharge at width contractions: U.S. Geol. Survey Techniques Water-Resources Inv., book 3, chap A4, 44 p.

INDEX

The index covers the two volumes of this manual. Volume I contains pages 1-284 and Volume II contains pages 285-631

E

S

W

Z

Water Supply Paper 2175, Vol. I, Table 8 on page 165 should be replaced by the following table:

TABLE 8.—*Wet-line table, giving difference, in meters, between wet-line length and vertical depth for selected vertical angles*

Wet-line length (m)	Vertical angle of sounding line at protractor (degrees)																									
	10	11	12	13	14	15	16	17	18	19	20	21	22	23	24	25	26	27	28	29	30	31	32	33	34	35
1	.00	.01	.01	.01	.01	.01	.01	.01	.02	.02	.02	.02	.02	.03	.03	.03	.03	.04	.04	.04	.05	.05	.05	.06	.06	.07
2	.01	.01	.01	.02	.02	.02	.03	.03	.03	.04	.04	.05	.05	.05	.06	.06	.07	.08	.08	.09	.09	.10	.11	.12	.12	.13
3	.01	.02	.02	.03	.03	.03	.04	.04	.05	.06	.06	.07	.07	.08	.09	.10	.10	.11	.12	.13	.14	.15	.16	.17	.19	.20
4	.02	.03	.03	.03	.04	.05	.05	.06	.07	.07	.08	.09	.10	.11	.12	.13	.14	.15	.16	.18	.19	.20	.22	.23	.25	.26
5	.02	.03	.04	.04	.05	.06	.06	.07	.08	.09	.10	.11	.12	.14	.15	.16	.17	.19	.20	.22	.24	.25	.27	.29	.31	.33
6	.03	.04	.04	.05	.06	.07	.08	.09	.10	.11	.12	.14	.15	.16	.18	.19	.21	.23	.24	.26	.28	.30	.33	.35	.37	.40
7	.04	.05	.05	.06	.07	.08	.09	.10	.11	.13	.14	.16	.17	.19	.21	.23	.24	.27	.29	.31	.33	.36	.38	.41	.43	.46
8	.04	.05	.06	.07	.08	.09	.10	.12	.13	.15	.16	.18	.20	.22	.24	.26	.28	.30	.33	.35	.38	.41	.44	.47	.50	.53
9	.05	.06	.06	.08	.09	.10	.12	.13	.15	.17	.18	.20	.22	.24	.27	.29	.31	.34	.37	.40	.42	.46	.49	.52	.56	.59
10	.05	.06	.07	.08	.10	.11	.13	.15	.16	.18	.20	.23	.25	.27	.30	.32	.35	.38	.41	.44	.47	.51	.54	.58	.62	.66
11	.06	.07	.08	.09	.11	.12	.14	.16	.18	.20	.22	.25	.27	.30	.33	.36	.38	.42	.45	.48	.52	.56	.60	.64	.68	.72
12	.06	.08	.09	.10	.12	.14	.15	.18	.20	.22	.24	.27	.30	.32	.36	.39	.42	.45	.49	.53	.57	.61	.65	.70	.74	.79
13	.07	.08	.09	.11	.13	.15	.17	.19	.21	.24	.26	.29	.32	.35	.38	.42	.45	.49	.53	.57	.61	.66	.71	.76	.81	.86
14	.07	.09	.10	.12	.14	.16	.18	.20	.23	.26	.28	.31	.34	.37	.41	.45	.48	.53	.57	.62	.66	.71	.76	.81	.87	.92
15	.08	.09	.11	.13	.15	.17	.19	.22	.25	.28	.31	.34	.37	.40	.44	.48	.52	.57	.61	.66	.71	.76	.82	.87	.93	.99
16	.08	.10	.12	.14	.16	.18	.20	.23	.26	.29	.33	.36	.40	.44	.47	.52	.56	.61	.65	.70	.76	.81	.87	.93	.99	1.05
17	.08	.10	.12	.14	.17	.19	.22	.25	.28	.31	.35	.38	.42	.46	.50	.55	.59	.64	.69	.75	.80	.86	.92	.99	1.05	1.12
18	.09	.11	.13	.15	.18	.20	.23	.26	.30	.33	.37	.41	.45	.49	.53	.58	.63	.68	.73	.79	.85	.91	.98	1.05	1.12	1.19
19	.09	.12	.14	.16	.19	.21	.24	.28	.31	.35	.39	.43	.47	.52	.56	.61	.66	.72	.78	.84	.90	.97	1.03	1.11	1.18	1.25
20	.10	.12	.14	.17	.20	.23	.26	.29	.33	.37	.41	.45	.50	.54	.59	.65	.70	.76	.82	.88	.94	1.02	1.09	1.16	1.24	1.32

Water Supply Paper 2175, Vol. I, Table 6 on page 162 should be replaced by the following table:

TABLE 6.—*Air-correction table, giving difference, in meters, between vertical length and slant length of sounding line above water surface for selected vertical angles*

Vertical length (m)	Vertical angle of sounding line at protractor (degrees)																														
	5	8	10	11	12	13	14	15	16	17	18	19	20	21	22	23	24	25	26	27	28	29	30	31	32	33	34	35			
1	.00	.01	.02	.02	.02	.03	.03	.04	.04	.05	.05	.06	.06	.07	.08	.09	.09	.10	.11	.12	.13	.14	.15	.17	.18	.19	.21	.22			
2	.01	.02	.03	.04	.04	.05	.06	.07	.08	.09	.10	.12	.13	.14	.16	.17	.19	.21	.23	.24	.27	.29	.31	.33	.36	.38	.41	.44			
3	.01	.03	.05	.06	.07	.08	.09	.11	.12	.14	.15	.17	.19	.21	.24	.26	.28	.31	.34	.37	.40	.43	.46	.50	.54	.58	.62	.66			
4	.02	.04	.06	.07	.09	.11	.12	.14	.16	.18	.21	.23	.26	.28	.31	.35	.38	.41	.45	.49	.53	.57	.62	.67	.72	.77	.82	.88			
5	.02	.05	.08	.09	.11	.13	.15	.18	.20	.23	.26	.29	.32	.36	.39	.43	.47	.52	.56	.61	.66	.72	.77	.83	.90	.96	1.03	1.10			
6	.02	.06	.09	.11	.13	.16	.18	.21	.24	.27	.31	.35	.39	.43	.47	.52	.57	.62	.68	.73	.80	.86	.93	1.00	1.08	1.15	1.24	1.32			
7	.03	.07	.11	.13	.16	.18	.21	.25	.28	.32	.36	.40	.45	.50	.55	.60	.66	.72	.79	.86	.93	1.00	1.08	1.17	1.25	1.35	1.44	1.55			
8	.03	.08	.12	.15	.18	.21	.24	.28	.32	.37	.41	.46	.51	.57	.63	.69	.76	.83	.90	.98	1.06	1.15	1.24	1.33	1.43	1.54	1.65	1.77			
9	.03	.09	.14	.17	.20	.24	.28	.32	.36	.41	.46	.52	.58	.64	.71	.78	.85	.93	1.01	1.10	1.19	1.29	1.39	1.50	1.61	1.73	1.86	1.99			
10	.04	.10	.15	.19	.22	.26	.31	.35	.40	.46	.51	.58	.64	.71	.79	.86	.95	1.03	1.13	1.22	1.33	1.43	1.55	1.67	1.79	1.92	2.06	2.21			
11	.04	.11	.17	.21	.25	.29	.34	.39	.44	.50	.57	.63	.71	.78	.86	.95	1.04	1.14	1.24	1.35	1.46	1.58	1.70	1.83	1.97	2.12	2.27	2.43			
12	.05	.12	.19	.22	.27	.32	.37	.42	.48	.55	.62	.69	.77	.85	.94	1.04	1.14	1.24	1.35	1.47	1.59	1.72	1.86	2.00	2.15	2.31	2.47	2.65			
13	.05	.13	.20	.24	.29	.34	.40	.46	.52	.59	.67	.75	.83	.92	1.02	1.12	1.23	1.34	1.46	1.59	1.72	1.86	2.01	2.17	2.33	2.50	2.68	2.87			
14	.05	.14	.22	.26	.31	.37	.43	.49	.56	.64	.72	.81	.90	1.00	1.10	1.21	1.32	1.45	1.58	1.71	1.86	2.01	2.17	2.33	2.51	2.69	2.89	3.09			
15	.06	.15	.23	.28	.34	.39	.46	.53	.60	.69	.77	.86	.96	1.07	1.18	1.30	1.42	1.55	1.69	1.83	1.99	2.15	2.32	2.50	2.69	2.89	3.09	3.31			
16	.06	.16	.25	.30	.36	.42	.49	.56	.64	.73	.82	.92	1.03	1.14	1.26	1.38	1.51	1.65	1.80	1.96	2.12	2.29	2.48	2.67	2.87	3.08	3.30	3.53			
17	.06	.17	.26	.32	.38	.45	.52	.60	.69	.78	.87	.98	1.09	1.21	1.34	1.47	1.61	1.76	1.91	2.08	2.25	2.44	2.63	2.83	3.05	3.27	3.51	3.75			
18	.07	.18	.28	.34	.40	.47	.55	.63	.73	.82	.93	1.04	1.16	1.28	1.41	1.55	1.70	1.86	2.03	2.20	2.39	2.58	2.78	3.00	3.23	3.46	3.71	3.97			
19	.07	.19	.29	.36	.42	.50	.58	.67	.77	.87	.98	1.09	1.22	1.35	1.49	1.64	1.80	1.96	2.14	2.32	2.52	2.72	2.94	3.17	3.40	3.65	3.92	4.19			
20	.08	.20	.31	.37	.45	.53	.61	.71	.81	.91	1.03	1.15	1.28	1.42	1.57	1.73	1.89	2.07	2.25	2.45	2.65	2.87	3.09	3.33	3.58	3.85	4.12	4.42			

Measurement and Computation of Streamflow: Volume 2. Computation of Discharge

By S. E. RANTZ *and others*

GEOLOGICAL SURVEY WATER-SUPPLY PAPER 2175

USGS
science for a changing world

UNITED STATES GOVERNMENT PRINTING OFFICE, WASHINGTON: 1982

UNITED STATES DEPARTMENT OF THE INTERIOR

JAMES G. WATT, *Secretary*

GEOLOGICAL SURVEY

Dallas L. Peck, *Director*

First printing 1982
Second printing 1983

Library of Congress Cataloging in Publication Data

Measurement and computation of streamflow.

(Geological Survey Water-Supply Paper 2175)
Includes bibliographies.
Contents: v. 1. Measurement of stage and discharge.—
v. 2. Computation of discharge. 1. Stream
measurements.
I. Rantz, S. E. (Saul Edward), 1911– . II. Series.
TC175.M42 551.48'3'0287 81-607309
AACR2

For sale by the Superintendent of Documents, U.S. Government Printing Office
Washington, D.C. 20402

CONTENTS

[Article headings are listed in the table of contents only in the volume of the manual in which they occur, but all chapter titles for the two volumes are listed in each volume A complete index covering both volumes of the manual appears in each volume]

VOLUME 1. MEASUREMENT OF STAGE AND DISCHARGE

VOLUME 2. COMPUTATION OF DISCHARGE

Chapter 10—Discharge Ratings Using Simple Stage-Discharge Relations

Chapter 10—Discharge Ratings Using Simple Stage-Discharge Relations—Continued

Chapter 11—Discharge Ratings Using Slope as a Parameter

Chapter 11—Discharge Ratings Using Slope as a Parameter—Continued

Chapter 12—Discharge Ratings Using a Velocity Index as a Parameter

Chapter 13—Discharge Ratings for Tidal Streams

Chapter 13—Discharge Ratings for Tidal Streams—Continued

Chapter 14—Discharge Ratings for Miscellaneous Hydraulic Facilities

Chapter 15—Computation of Discharge Records

Chapter 15—Computation of Discharge Records—Continued

Chapter 16—Presentation and Publication of Stream-Gaging Data

ILLUSTRATIONS

TABLES

CONVERSION FACTORS

[Factors for converting inch-pound to metric units are shown to four significant figures However, in the text the metric equivalents, where shown, are carried only to the number of significant figures consistent with the values for the English units]

Inch-pound	*Multiply by—*	*Metric*
acres	4.047×10^{3}	m^2 (square meters)
acre-ft (acre-feet)	1.233×10^{3}	m^3 (cubic meters)
acre-ft/yr (acre feet per year)	1.233×10^{3}	m^3/yr (cubic meters per year)
ft (feet)	3.048×10^{-1}	m (meters)
ft/hr (feet per hour)	3.048×10^{-1}	m/hr (meters per hour)
ft/s (feet per second)	3.048×10^{-1}	m/s (meters per second)
ft^3/s (cubic feet per second)	2.832×10^{-2}	m^3/s (cubic meters per second)
in (inches)	2.540×10	mm (millimeters)
lb (pounds)	4.536×10^{-1}	kg (kilograms)
mi (miles)	1.609	km (kilometers)
mi^2 (square miles)	2.590	km^2 (square kilometers)
oz (ounces)	2.835×10^{-2}	kg (kilograms)

MEASUREMENT AND COMPUTATION OF STREAMFLOW

VOLUME 2. COMPUTATION OF DISCHARGE

By S. E. RANTZ and others

CHAPTER 10.—DISCHARGE RATINGS USING SIMPLE STAGE-DISCHARGE RELATIONS

INTRODUCTION

Continuous records of discharge at gaging stations are computed by applying the discharge rating for the stream to records of stage. Discharge ratings may be simple or complex, depending on the number of variables needed to define the stage-discharge relation. This chapter is concerned with ratings in which the discharge can be related to stage alone. (The terms "rating," "rating curve," "stage rating," and "stage-discharge relation" are synonymous and are used here interchangeably.)

Discharge ratings for gaging stations are usually determined empirically by means of periodic measurements of discharge and stage. The discharge measurements are usually made by current meter. Measured discharge is then plotted against concurrent stage on graph paper to define the rating curve. At a new station many discharge measurements are needed to define the stage-discharge relation throughout the entire range of stage. Periodic measurements are needed thereafter to either confirm the permanence of the rating or to follow changes (shifts) in the rating. A minimum of 10 discharge measurements per year is recommended, unless it has been demonstrated that the stage-discharge relation is unvarying with time. In that event the frequency of measurements may be reduced. It is of prime importance that the stage-discharge relation be defined for flood conditions and for periods when the rating is subject to shifts as a result of ice formation (see section titled, "Effect of Ice Formation on Discharge Ratings") or as a result of the variable channel and control conditions discussed in the section titled, "Shifts in the Discharge Rating." It is essential that the stream-gaging program have sufficient flexibility to provide for the nonroutine scheduling of additional measurements of discharge at those times.

If the discharge measurements cover the entire range of stage experienced during a period of time when the stage-discharge relation is stable, there is little problem in defining the discharge rating for that

period. On the other hand, if, as is usually the case, discharge measurements are lacking to define the upper end of the rating, the defined lower part of the rating curve must be extrapolated to the highest stage experienced. Such extrapolations are always subject to error, but the error may be reduced if the analyst has a knowledge of the principles that govern the shape of rating curves. Much of the material in this chapter is directed toward a discussion of those principles, so that when the hydrographer is faced with the problem of extending the high-water end of a rating curve he can decide whether the extrapolation should be a straight line, or whether it should be concave upward or concave downward.

The problem of extrapolation can be circumvented, of course, if the unmeasured peak discharge is determined by use of the indirect methods discussed in chapter 9. In the absence of such peak-discharge determinations, some of the uncertainty in extrapolating the rating may be reduced by the use of one or more of several methods of estimating the discharge corresponding to high values of stage. Four such methods are discussed in the section titled "High-flow Extrapolation."

In the discussions that follow it was generally impractical to use both English and metric units, except where basic equations are given. Consequently English units are used throughout, unless otherwise noted.

STAGE-DISCHARGE CONTROLS

The subject of stage-discharge controls was discussed in detail in chapter 3, but a brief summary at this point is appropriate.

The relation of stage to discharge is usually controlled by a section or reach of channel downstream from the gage that is known as the station control. A section control may be natural or manmade; it may be a ledge of rock across the channel, a boulder-covered riffle, an overflow dam, or any other physical feature capable of maintaining a fairly stable relation between stage and discharge. Section controls are often effective only at low discharges and are completely submerged by channel control at medium and high discharges. Channel control consists of all the physical features of the channel that determine the stage of the river at a given point for a given rate of flow. These features include the size, slope, roughness, alinement, constrictions and expansions, and shape of the channel. The reach of channel that acts as the control may lengthen as the discharge increases, introducing new features that affect the stage-discharge relation.

Knowledge of the channel features that control the stage-discharge relation is important. The development of stage-discharge curves where more than one control is effective, and where the number of

measurements is limited, usually requires judgment in interpolating between measurements and in extrapolating beyond the highest measurements. That is particularly true where the controls are not permanent and the various discharge measurements are representative of changes in the positioning of segments of the stage-discharge curve.

GRAPHICAL PLOTTING OF RATING CURVES

Stage-discharge relations are usually developed from a graphical analysis of the discharge measurements plotted on either rectangular-coordinate or logarithmic plotting paper. In a preliminary step the discharge measurements available for analysis are tabulated and summarized on a form such as that shown in figure 139. Discharge is then plotted as the abscissa, corresponding gage height is plotted as the ordinate, and a curve or line is fitted by eye to the plotted points. The plotted points carry the identifying measurement numbers given in figure 139; the discharge measurements are numbered consecutively in chronological order so that time trends can be identified.

At recording-gage stations that use stilling wells, systematic and significantly large differences between inside (recorded) gage heights and outside gage heights often occur during periods of high stage, usually as a result of intake drawdown (see section in chapter 4 titled, "Stilling Wells"). For stations where such differences occur, both inside and outside gage heights for high-water discharge measurements are recorded on the form shown in figure 139, and in plotting the measurements for rating analysis, the outside gage readings are used first. The stage-discharge relation is drawn through the outside gage readings of the high-water discharge measurements and is extended to the stage of the outside high-water marks that are observed for each flood event. The stage-discharge relation is next transposed to correspond with the inside gage heights obtained from the stage-recorder at the times of discharge measurement and at flood peaks. It is this transposed stage-discharge relation that is used with recorded stages to compute the discharge.

The rationale behind the above procedure is as follows. The outside gage readings are used for developing the rating because the hydraulic principles on which the rating is based require the use of the true stage of the stream. The transposition of the rating to inside (recorded) stages is then made because the recorded stages will be used with the rating to determine discharge. The recorded stages are used for discharge determination because if differences exist between inside and outside gage readings, those differences will be known only for those times when the two gages are read concurrently. If the

FORM 9-207
(Rev. 11-59)

UNITED STATES DEPARTMENT OF THE INTERIOR
GEOLOGICAL SURVEY (WATER RESOURCES DIVISION)
DISCHARGE MEASUREMENT SUMMARY SHEET

Station No 11-4770

Discharge measurements of Eel River at Scotia, Calif. during the year ending Sept 30, 1966

No	Date	Made by—	Width	Area	Mean velocity	Gage height	Discharge	Rating: Shift adj	Rating: Percent diff	Method	Number meas sections	Gage height change	Time	Meas rated	Water temp °C	Outside gage	REMARKS
	1965	Hammond	Feet	W Sq ft	Fps	Feet	Cfs	Feet				Feet	Hr				
495	Aug. 31	McGuire	153	199	0.78	8.92	155			0.6	34	-.01	1.2	G	74	8.78	
496	Oct. 5	La Rue	155	W 148	0.82	8.79	121			.6	28	0	.5	G	61	8.87	Zero flow = 8.5 ± 0.05
497	Nov 2	do	154	W 158	0.85	8.88	135			.6	29	0	.5	G	60	8.89	Zero flow = 8.5 ± 0.05
498	30	La Rue Crumrine	454	2,030	2.47	12.52	5,010			.6; .2/.8	33	-.01	1.1	G	46	12.55	
499	1966 Jan. 3	La Rue	553	6,790	7.19	21.03	48,800			.2/.8	29	+0.52	1.75	G/c	46	21.05	
500	25	Hammond Crumrine	512	2350	1.73	12.74	4,050			.6; .2/.8	25	-.02	1.3	P	45	12.80	(Jan 5) peak 45.84
501	25	do	506	2270	1.71	12.73	3,880			.6; .2/.8	29	0	2	F	—	12.80	
502	31	La Rue	543	3960	4.18	16.08	16,500			.6; .2/.8	32	-.07	1.25	G	—	16.13	
503	Feb. 21	do	533	3000	2.70	13.85	8,100			.2/.8	36	-.03	1.4	G	48	13.86	
504	Mar. 31	do	2-Channels	—	—	13.59	7,420			.2/.8	37	.00	1.6	G	57	13.59	
505	Apr 28	do	454	1890	1.90	12.13	3,600			.6; .2/.8	36	-.01	1.3	G	58	12.18	
506	June 1	Palmer	434	1200	0.83	10.62	1,000			.6; .2/.8	40	0	1.7	G	62	10.64	
507	July 6	do	196	193	1.56	9.82	302			.6	39	0	.9	G	70	9.83	
508	Aug. 8	do	184	W 126	1.11	9.40	140			.6	38	0	.75	F/p	67	—	Zero Flow = 9.05 ± 0.05
509	Sept. 12	Hammond	77	W 74.1	1.48	9.26	110			.6	31	0	.8	F	66	9.3±	.02 Zero Flow = 9.0 ± 0.0
510	Oct. 4	Palmer	184	116	1.01	9.30	117			.6	34	0	.7	F	64	9.3±	.01

Copied by Computed by W-Wading Checked by

U S GOVERNMENT PRINTING OFFICE 1963 O

FIGURE 139.—Example of form used for tabulating and summarizing current-meter discharge measurements.

outside gage heights were used with the rating to determine discharge, variable corrections, either known or assumed, would have to be applied to recorded gage heights to convert them to outside stages. We have digressed here to discuss differences between inside and outside gage heights, because in the discussions that follow no distinction between the two gages will be made.

The use of logarithmic plotting paper is usually preferred for graphical analysis of the rating because in the usual situation of compound controls, changes in the slope of the logarithmically plotted rating identify the range in stage for which the individual controls are effective. Furthermore, the portion of the rating curve that is applicable to any particular control may be linearized for rational extrapolation or interpolation. A discussion of the characteristics of logarithmic plotting follows.

The measured distance between any two ordinates or abscissas on logarithmic graph paper, whose values are printed or indicated on the sheet by the manufacturer of the paper, represents the difference between the logarithms of those values. Consequently, the measured distance is related to the ratio of the two values. Therefore, the distance between pairs of numbers such as 1 and 2, 2 and 4, 3 and 6, 5 and 10, are all equal because the ratios of the various pairs are identical. Thus the logarithmic scale of either the ordinates or the abscissas is maintained if all printed numbers on the scale are multiplied or divided by a constant. This property of the paper has practical value. For example, assume that the logarithmic plotting paper available has two cycles (fig. 140), and that ordinates ranging from 0.3 to 15.0 are to be plotted. If the printed scale of ordinates is used and the bottom line is called 0.1, the top line of the paper becomes 10.0, and values between 10.0 and 15.0 cannot be accommodated. However, the logarithmic scale will not be distorted if all values are multiplied by a constant. For this particular problem, 2 is the constant used in figure 140, and now the desired range of 0.3 to 15.0 can be accommodated. Examination of figure 140 shows that the change in scale has not changed the distance between any given pair of ordinates; the position of the ordinate scale has merely been transposed.

We turn now to a theoretical discussion of rating curves plotted on logarithmic graph paper. A rating curve, or a segment of a rating curve, that plots as a straight line of logarithmic paper has the equation,

$$Q = p(G - e)^{\backslash}, \tag{53}$$

where

Q is discharge;

$(G - e)$ is head or depth of water on the control—this value is indicated by the ordinate scale printed by the manufacturer or

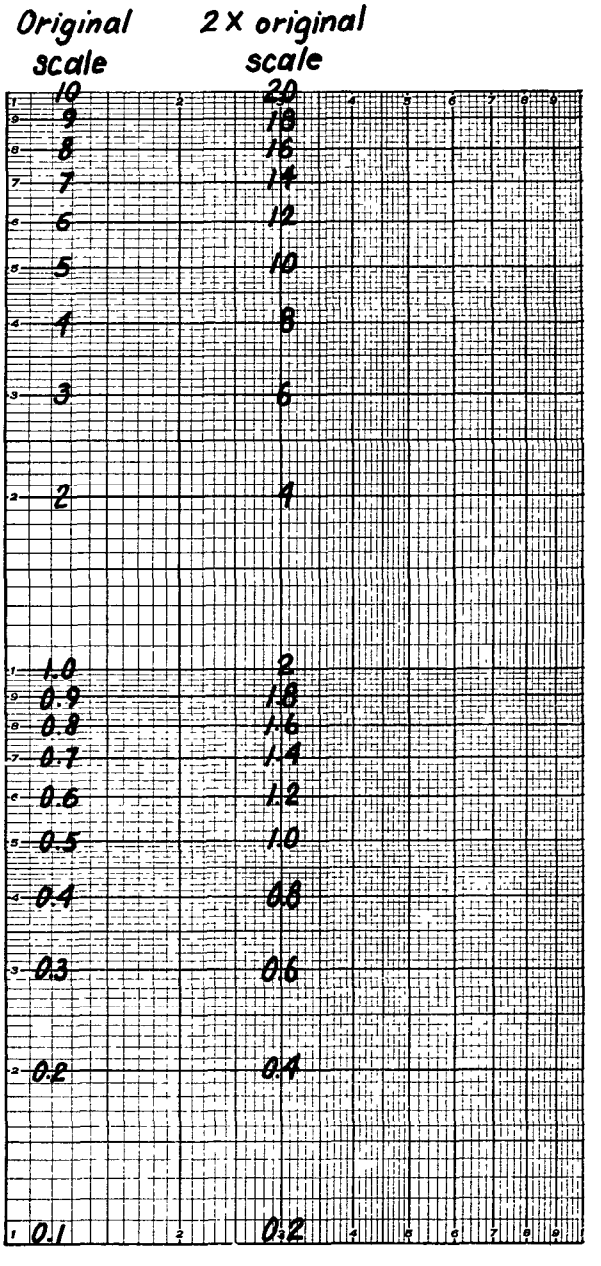

FIGURE 140.—Example showing how the logarithmic scale of graph paper may be transposed.

by the ordinate scale that has been transposed, as explained in the preceding paragraph;

G is gage height of the water surface;

e is gage height of zero flow for a section control of regular shape, or the gage height of effective zero flow for a channel control or a section control of irregular shape;

p is a constant that is numerically equal to the discharge when the head $(G - e)$ equals 1.0 ft or 1.0 m, depending on whether English or metric units are used; and

N is slope of the rating curve. (Slope in equation 53 is the ratio of the horizontal distance to the vertical distance. This unconventional way of measuring slope is necessary because the dependent variable Q is always plotted as the abscissa.)

We assume now that a segment of an established logarithmic rating is linear, and we examine the effect on the rating of changes to the control. If the width of the control increases, p increases and the new rating will be parallel to and to the right of the original rating. If the width of the control decreases, the opposite effect occurs; p decreases and the new rating will be parallel to and to the left of the original rating. If the control scours, e decreases and the depth $(G - e)$ for a given gage height increases; the new rating moves to the right and will no longer be a straight line but will be a curve that is concave downward. If the control becomes built up by deposition, e increases and the depth $(G - e)$ for a given gage height decreases; the new rating moves to the left and is no longer linear but is a curve that is concave upward.

When discharge measurements are originally plotted on logarithmic paper, no consideration is given to values of e. The gage height of each measurement is plotted using the ordinate scale provided by the manufacturer or, if necessary, an ordinate scale that has been transposed as illustrated in figure 140. We refer now to figure 141. The inside scale $(e = 0)$ is the scale printed by the paper manufacturer. Assume that the discharge measurements have been plotted to that scale and that they define the curvilinear relation between gage height (G) and discharge (Q) that is shown in the topmost curve. For the purpose of extrapolating the relation, a value of e is sought, which when applied to G, will result in a linear relation between $(G - e)$ and Q. If we are dealing with a section control of regular shape, the value of e will be known; it will be the gage height of the lowest point of the control (point of zero flow). If we are dealing with a channel control or section control of irregular shape, the value of e is the gage height of *effective* zero flow. The gage height of effective zero flow is not the gage height of some identifiable feature on the irregular section control or in the channel but is actually a mathematical constant

that is considered as a gage height to preserve the concept of a logarithmically linear head-discharge relation. Effective zero flow is usually determined by a method of successive approximations.

In successive trials, the ordinate scale in figure 141 is varied for e values of 1, 2 and 3 ft, each of which results in a different curve, but each new curve still represents the same rating as the top curve. For example, a discharge of 30 ft^3/s corresponds to a gage height (G) of 5.5 ft on all four curves. The true value of e is 2 ft, and thus the rating plots as a straight line if the ordinate scale numbers are increased by that value. In other words, while even on the new scale a discharge of 30 ft^3/s corresponds to a gage height (G) of 5.5 ft, the head or depth on the control for a discharge of 30 ft^3/s is $(G-e)$, or 3.5 ft; the linear rating marked $e = 2$ crosses the ordinate for 30 ft^3/s at 5.5 ft on the new scale and at 3.5 ft on the manufacturer's, or inside, scale. If values of e smaller than the true value of 2 ft are used, the rating curve will be concave upward, if values of e greater than 2 ft are used, the curve will be concave downward. The value of e to be used for a rating curve, or for a segment of a rating curve, can thus be determined by adding or subtracting trial values of e to the numbered scales on the logarithmic plotting paper until a value is found that results in a straight-line plot of the rating. It is important to note that if the logarithmic ordinate scale must be transposed by multiplication or division to accommodate the range of stage to be plotted, that transposition must be made before the ordinate scale is manipulated for values of e.

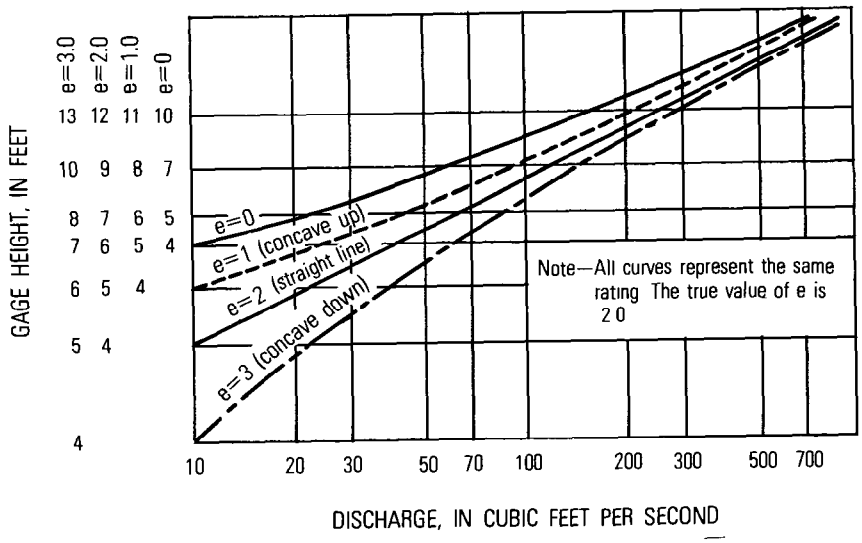

FIGURE 141.—Rating-curve shapes resulting from the use of differing values of effective zero flow.

A more direct solution for e, as described by Johnson (1952) is illustrated in figure 142. A plot of G versus Q has resulted in the solid-line curve which is to be linearized by subtracting a value of e from each value of G. The part of the rating between points 1 and 2 is chosen, and values of G_1, G_2, Q_1 and Q_2 are picked from the coordinate scales. A value of Q_3 is next computed, such that

$$Q^2_3 = Q_1 Q_2.$$

From the solid-line curve, the value of G_3 that corresponds to Q_3 is picked. In accordance with the properties of a straight line on logarithmic plotting paper,

$$(G_3 - e)^2 = (G_1 - e)(G_2 - e). \tag{54}$$

Expansion of terms in equation 54 leads to equation 55 which provides a direct solution for e.

$$e = \frac{G_1 G_2 - G_3^2}{G_1 + G_2 - 2G_3} \tag{55}$$

A logarithmic rating curve is seldom a straight line or a gentle curve for the entire range in stage. Even where a single cross section of the channel is the control for all stages, a sharp break in the

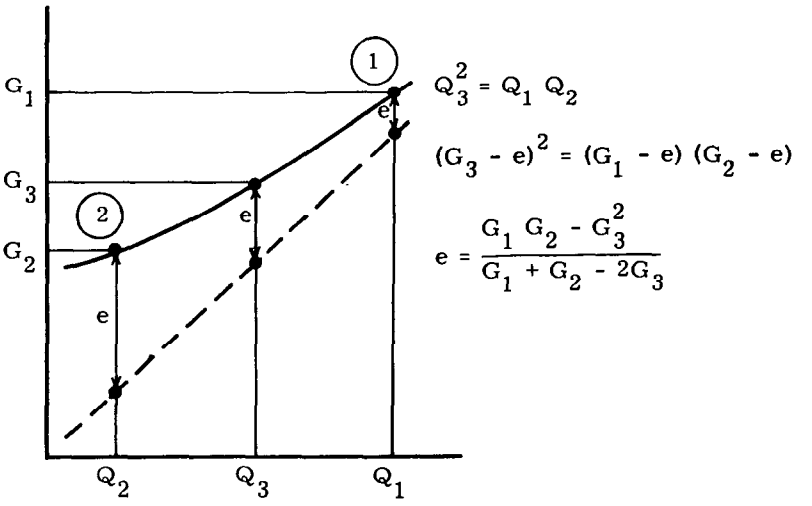

FIGURE 142.—Schematic representation of the linearization of a curve on logarithmic graph paper.

contour of the cross section, such as an overflow plain, will cause a break in the slope of the rating curve. Commonly, however, a break in slope is due to the low-water control being drowned out by a downstream section control becoming effective or by channel control becoming effective.

The use of rectangular-coordinate paper for rating analysis has certain advantages, particularly in the study of the pattern of shifts in the lower part of the rating. A change in the low-flow rating at many sites results from a change in the elevation of effective zero flow (e), which means a constant shift in gage height. A shift of that kind is more easily visualized on rectangular-coordinate paper because on that paper the shift curve is parallel to the original rating curve, the two curves being separated by a vertical distance equal to the change in the value of e. On logarithmic paper the two curves will be separated by a variable distance which decreases as stage increases. A further advantage of rectangular-coordinate paper is the fact that the point of zero flow can be plotted directly on rectangular-coordinate paper, thereby facilitating extrapolation of the low-water end of the rating curve. That cannot be done on logarithmic paper because zero values cannot be shown on that type of paper.

As a general rule logarithmic plotting should be used initially in developing the general shape of the rating. The final curve may be displayed on either type of graph paper and used as a base curve for the analysis of shifts. A combination of the two types of graph paper is frequently used with the lower part of the rating plotted on an inset of rectangular-coordinate paper or on a separate sheet of rectangular-coordinate paper.

SECTION CONTROLS

ARTIFICIAL CONTROLS

At this point we digress from the subject of logarithmic rating curves to discuss the ratings for artificial section controls. A knowledge of the rating characteristics of controls of standard shape is necessary for an understanding of the rating characteristics of natural controls, almost all of which have irregular shapes. On pages that follow we first discuss thin-plate weirs, then broad-crested weirs, and finally flumes.

Thin-plate weirs are generally used in small clear-flowing streams, particularly where high accuracy is desired and adequate maintenance can be provided, as in small research watersheds. Flumes are preferred for use in small streams and canals that carry sediment and debris, and in other situations where the head loss (backwater) associated with a thin-plate weir is unacceptable. Most types of flume may also be used under conditions of submergence, as opposed to free-flow

conditions, thereby permitting them to operate with even smaller head loss but with some loss of accuracy of the stage-discharge relation. The broad-crested weirs are commonly used in the larger streams.

TRANSFERABILITY OF LABORATORY RATINGS

Standard shapes or dimensions are commonly used in building artificial controls, and many of these standard structures have been rated in laboratory model studies (World Meteorological Organization, 1971). The transfer of a laboratory discharge rating to a structure in the field requires the existence, and maintenance, of similitude between laboratory model and prototype, not only with regard to the structure, but also with regard to the approach channel. For example, scour and (or) fill in the approach channel will change the head-discharge relation, as will algal growth on the control structure. Both the structure and the approach channel must be kept free from accumulations of debris, sediment, and vegetal growth. Flow conditions downstream from the structure are significant only to the extent that they control the tailwater elevation, which may influence the operation of structures designed for free-flow conditions.

Because of the likelihood of the existence or development of conditions that differ from those specified in a laboratory model study, the policy of the Geological Survey is to calibrate the prototype control in the field by discharge measurements for the entire range of stage that is experienced. (See section in chapter 3 titled, "Artificial Controls.") In-place calibration is sometimes dispensed with where the artificial control is a standard thin-plate weir having negligible velocity of approach.

THIN-PLATE WEIRS

The surface of the weir over which the water flows is the crest of the weir. A thin-plate weir has its crest beveled to a chisel edge and is always installed with the beveled face on the downstream side. The crest of a thin-plate weir is highly susceptible to damage from floating debris, and therefore such weirs are used as control structures almost solely in canals whose flow is free of floating debris. Thin-plate weirs are not satisfactory for use in canals carrying sediment-laden water because they trap sediment and thereby cause the gage pool to fill with sediment, sometimes to a level above the weir crest. The banks of the canal must also be high enough to accommodate the increase in stage (backwater) caused by the installation of the weir, the weir plate being an impedance to flow in the canal. The commonly used shapes for thin-plate weirs are rectangular, trapezoidal, and triangular or V-notch.

The information needed to compute the discharge over a thin-plate weir is as follows:

1. Static head (h), which is the difference in elevation between the weir crest and the water surface at the approach section; the approach section is located upstream from the weir face a distance equal to about $3h$ or more. (See section in chapter 2 titled, "Considerations in Specific Site Selection" for discussion of location of gage intakes.)
2. Length of crest of weir (b) if weir is rectangular or trapezoidal.
3. Width of channel in the plane of the weir face (B).
4. Angle of side slopes if weir is triangular or trapezoidal.
5. Average depth of streambed below elevation of weir crest (P). P is measured in the approach section.

RECTANGULAR THIN-PLATE WEIR

Flow over a rectangular thin-plate weir is illustrated in figure 143. The discharge equation for this type of weir is:

$$Q = Cbh^{3/2}, \tag{56}$$

where

Q = discharge,
C = discharge coefficient,
b = length of weir crest normal to flow, and
h = static or piezometric head on a weir, referred to the weir crest.

Information on discharge coefficients for rectangular thin-plate weirs is available from the investigations of Kindsvater and Carter (1959) and others, and is given in the previously cited WMO Technical Note No. 117 (1971). Those investigations show that the coefficient for free discharge is a function of certain dimensionless ratios which describe the geometry of the channel and the weir;

$$C = f\left(\frac{h}{P}, \frac{b}{B}, E\right), \tag{57}$$

where E is the slope of the weir face; the other variables are depicted in figure 143.

The relation between C, h/P and E for weirs with no side contraction ($b/B = 1.0$) is shown in figure 144, where each of the four curves corresponds to a particular value of E. The coefficient is defined in the range of h/P from 0 to 5. The value of the coefficient becomes uncertain at high values of h/P. The greater the value of h/P, the greater the velocity of approach, and therefore the greater the coefficient. The coefficients in figure 144 are for use with English units, where all

linear measurements are expressed in feet and discharge is in cubic feet per second. If linear measurements are expressed in meters and discharge is in cubic meters per second, all values of C must be multiplied by the factor 0.552.

Side contractions reduce the effective length of the weir crest. That effect is accounted for by multiplying the value of C from figure 144 by a correction factor that is a function of b/B, h/P, and the degree of rounding of the upstream vertical edge of the weir-notch abutments. Rounding is a factor only in the situation where the horizontal weir crest is set between vertical abutments. For a rectangular thin-plate weir with sharp-edged entry, the correction factor is k_c; appropriate values of k_c are obtained from the curves in figure 145. For a

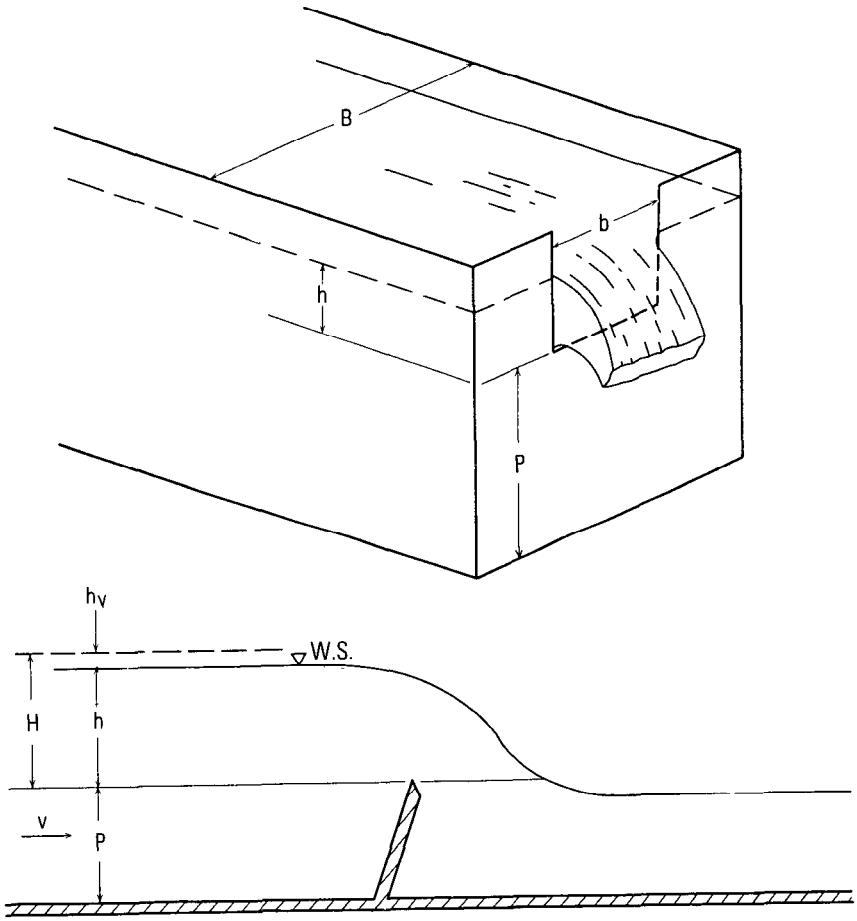

FIGURE 143.—Definition sketch of a rectangular thin-plate weir.

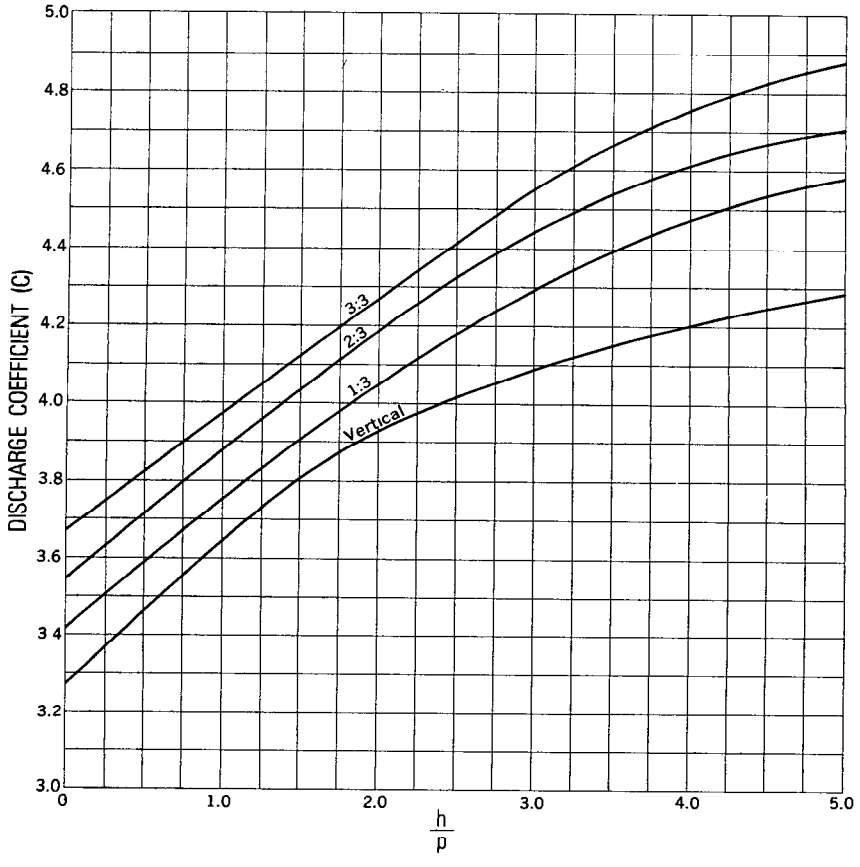

FIGURE 144.—Discharge coefficients for full-width, vertical and inclined, rectangular thin-plate weirs.

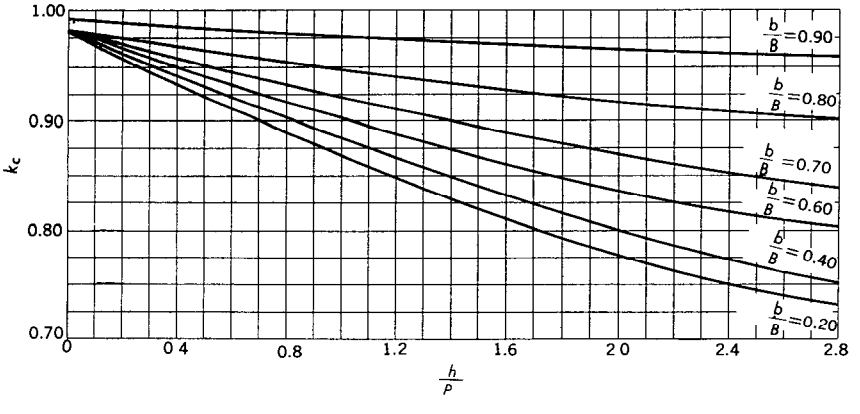

FIGURE 145.—Definition of adjustment factor, k_c, for contracted rectangular thin-plate weirs.

rectangular thin-plate weir having vertical abutments rounded with radius r, the correction factor, when $r/b \geq 0.12$, is assumed to equal $(1 + k_c)/2$, where again k_c is read from figure 145. For rounded abutments having a lesser value of r/b, the correction factor is obtained by interpolating between the appropriate k_c value from figure 145 and the value $(1 + k_c)/2$. In other words, for given values of b/B, h/P, and r/b between 0 and 0.12, we interpolate linearly between the value of k_c (corresponds to $r/b=0$) and the value of $(1 + k_c)/2$ (corresponds to $r/b = 0.12$).

We will now prepare the rating for a hypothetical rectangular thin-plate weir for the purpose of examining the implications of a logarithmic plot of the rating. The discharges corresponding to various stages will be computed by use of the theoretical equation for a rectangular weir, using figures 144 and 145 to obtain the constant in the equation. We will assume that the computed discharges represent the results of carefully made discharge measurements.

Assume that we have a rectangular thin-plate weir, with vertical face, and that discharge measurements (computations) have been made at heads ranging from 0.1 ft to 7.0 ft. The dimensions of the weir using the symbols in figure 142 are given in table 16. The data and computations are also shown in table 16 and should be self-explanatory. The weir constant is actually equal to $C(k_c)$. The stages and corresponding discharges are plotted on logarithmic graph paper and fitted with a curve by eye in figure 146.

Figure 146 shows that a tangent can be fitted to the plotted points at heads greater than 0.3 ft ($G=1.3$ ft). The intercept (p) of the tangent at $G - e=1.0$ ft is 67 ft^3/s and the measured slope of the tangent is 1.55. (Note that the slope of the rating curve Q/h is the ratio of the horizontal distance to the vertical distance.) In accordance with equation 53, the equation of the tangent is therefore $Q=67h^{1.55}$ However, the equation for discharge over a rectangular weir is $Q=(Ck_cb)h^{1.50}$. Therefore (Ck_cb) must vary with stage, as we know it does, and $Ck_cb=67h^{0.05}$; the exponent 0.05 is obtained by subtracting the theoretical exponent 1.50 from the empirical exponent 1.55. Because b has a constant value of 20 ft, $Ck_c=3.35h^{0.05}$; the coefficient 3.35 is obtained by dividing the original coefficient (67) by the value of b (20 ft). We can extrapolate the tangent in figure 146 with some confidence. If we wish to determine the discharge from the curve for a gage height of 11 ft ($h=10$ ft), the extrapolated value of Q is 2,380 ft^3/s; that is, if a value of 10 ft is substituted in the equation $Q=67h^{1.55}$, Q will equal 2,380 ft^3/s. That value matches the true value computed on the bottom line of table 16 for a gage height of 11 ft.

TRAPEZOIDAL THIN-PLATE WEIR

Few experimental data are available for determining the discharge

TABLE 16.—*Computation of discharge rating for a hypothetical rectangular thin-plate weir*

[*Given* P=2.0 ft, b=20 ft, B=25 ft, b/B=0.8 Gage height of weir crest (e)=1.0 ft, h=Gage height (G) minus e]

G (ft)	$h=G-e$ (ft)	h/P	C (from fig. 144)	k_c (from fig. 145)	Ck_c	Ck_cb	$h^{3/2}$	$Q=Ck_cbh^{3/2}$ (ft^3/s)
1.0	0	----	----	----	----	----	----	0
1.1	0.1	0.05	3.29	0.980	3.224	64.48	0.0316	2.04
1.3	.3	.15	3.33	.977	3.253	65.06	.1643	10.7
1.5	.5	.25	3.37	.973	3.279	65.58	.3536	23.2
2.0	1.0	.50	3.46	.965	3.339	66.78	1.000	66.8
2.5	1.5	.75	3.56	.955	3.400	68.00	1.837	125
3.0	2.0	1.0	3.65	.947	3.456	69.12	2.828	195
4.0	3.0	1.5	3.81	.930	3.543	70.86	5.196	368
5.0	4.0	2.0	3.93	.920	3.616	72.32	8.000	579
6.0	5.0	2.5	4.02	.905	3.638	72.76	11.18	813
7.0	6.0	3.0	4.08	.900	3.672	73.44	14.70	1,080
Computation to check extrapolation obtained from figure 146								
11.0	10.0	5.0	4.28	.88	3.766	75.32	31.62	2,380

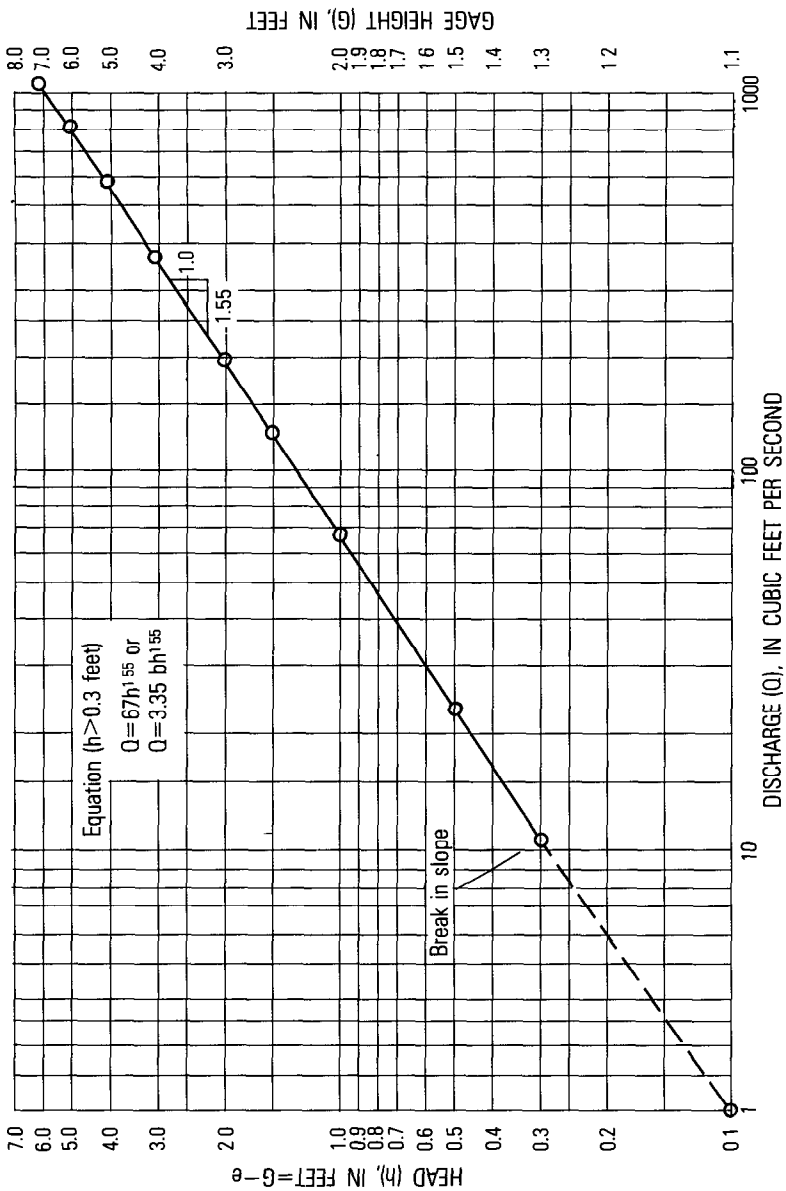

FIGURE 146.—Rating curve for hypothetical rectangular thin-plate weir.

coefficients of trapezoidal weirs (fig. 147). One exception is the vertical Cippoletti weir, which is a sharp-crested trapezoidal weir whose sides have a slope of 1 horizontal (x) to 4 vertical (y). The slope of the sides is approximately that required to obtain a discharge through the two triangular parts of the weir opening that equals the decrease in discharge resulting from end contractions. In other words, the Cippoletti weir acts as a rectangular thin-plate weir whose crest length is equal to b and whose contraction coefficient, k_c, is equal to 1.0. The dimension B (fig. 147) for a Cippoletti weir has little bearing on the discharge. The equation used to compute discharge is again

$$Q=Cbh^{3/2}, \tag{56}$$

and close approximations of values of C are obtained from figure 144. The head, h, and height of notch, P, are both measured in the approach section.

If we compute the discharge for a vertical thin-plate Cippoletti weir whose value of b is 20 ft and whose value of P is 2.0 ft, similar to the dimensions used in computing the hypothetical rating shown in table 16, the rating will approximate that obtained for the thin-plate rectangular weir of table 16. The only difference in discharge will be that attributable to the fact that the value of k_c is 1.00 for all values of head for the Cippoletti weir. A logarithmic plot of the rating (not shown here) indicates that the equation for all but the very small values of head is

$$Q=69h^{1.58}, \text{ (English units)}$$

meaning that $C=3.45h^{0.08}$.

For trapezoidal weirs other than Cippoletti weirs, the general empirical equation for discharge is

$$Q=Cb(h+h_v)^{\gamma}, \tag{58}$$

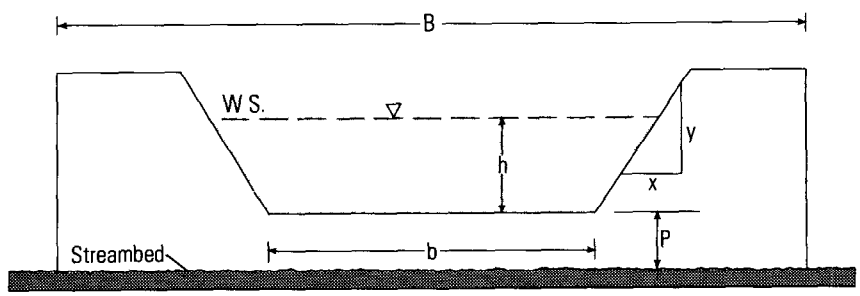

FIGURE 147.—Sketch of upstream face of a trapezoidal weir.

where h_v, the velocity head at the approach section, is equal to $V_a^2/2g$, V_a being the mean velocity in the approach section and g being the acceleration of gravity. The coefficient C and exponent N must be determined from current-meter discharge measurements that cover the entire range of stage that is experienced. If discharge measurements are not available for the highest stage experienced, a rating curve is obtained by plotting on logarithmic paper the head $(G-e)$ against discharge (Q) for the measurements that have been obtained, and then fitting a curve to the plotted points. The upper end of that curve should be a tangent, or possibly an extremely flat curve, that can be extrapolated to the highest stage experienced. Because the limiting shapes of a trapezoid are a rectangle at one extreme and a triangle at the other, the slope of the tangent will lie somewhere between 1.5, which is the theoretical slope for a rectangular weir, and 2.5 which is the theoretical slope for a triangular weir. The closer the shape is to a rectangle, the closer the slope will be to 1.5; the closer the shape is to a triangle, the closer the slope will be to 2.5.

The reader will note the difference in form between equations 56 and 58. Equation 56 uses static head (h), whereas equation 58 uses total head $(h+h_v)$. Velocity head is a factor in any discharge equation for a weir. In the more modern laboratory studies of weir discharge, the static-head term is used in the discharge equation, and velocity head, as indicated by a term h/P, is used directly as a variable in the determination of C. (See equation 57.) In older laboratory investigations, a more empirical approach for determining C was followed in that the total-head term was used in the discharge equation and the values of C that were determined do not vary directly with change in velocity head. Both forms of the weir-discharge equations will be found in this manual; the older type of equation is shown wherever it has not been superseded by later laboratory studies.

TRIANGULAR OR V-NOTCH THIN-PLATE WEIR

Triangular or V-notch thin-plate weirs (fig. 148) are installed at sites where low discharges occur; they are highly sensitive to low flows but have less capacity than rectangular or trapezoidal weirs. Because the area of the notch is invariably small compared to the cross-sectional area of the channel, water is pooled upstream from the weir and the approach velocity is necessarily low. The approach velocity head can usually be neglected in computing the discharge for a 90° V-notch weir ($\Theta=90°$ in fig. 148). Actually, for values of Θ equal to or less than 90°, it has been specified that velocity of approach is negligible if h/P is less than 0.4 and h/B is less than 0.2 (WMO Tech. Note 117, 1971). Whether or not the velocity head can be ignored in computing discharges for V-notch weirs having central angles greater

than 90° depends on the relative size of the areas occupied by the water in the notch and the water in the approach section. Virtually no experimental work has been done with triangular weirs having significant velocity of approach, and all equations discussed below are for installations where the velocity of approach can be neglected. Furthermore the equations are applicable only for thin-plate V-notch weirs whose faces are vertical.

Both the cross-sectional area of the flow in the notch and its velocity in the notch are functions of the head (h). Consequently, the general equation for a triangular thin-plate weir is $Q=Ch^{\backprime}$, and the constants in that equation do not vary greatly from those in the following equations:

$$Q=2.5(\tan \Theta/2)h^{5/2},$$

where h is in feet and Q is in cubic feet per second; or

$$Q=1.38(\tan \Theta/2)h^{5/2},$$

where h is in meters and Q is in cubic meters per second.
The head is measured in the approach section, a distance about $3h$ upstream from the weir face. From an earlier discussion it is apparent that the above equations will plot as straight lines on logarithmic graph paper. The slope of the ratings will be 2.5, and the intercept, where $h=1$, will be either 2.5 tan $\Theta/2$ or 1.38 tan $\Theta/2$, depending on whether English or metric units are used.

V-notch weirs are most commonly built with a central angle of 90°. Much experimental work has been done with thin-plate 90°

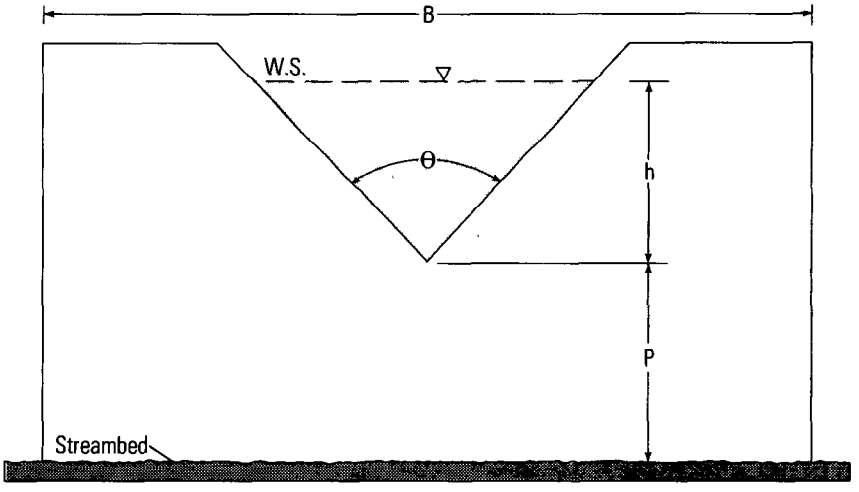

FIGURE 148.—Sketch of upstream face of a triangular or V-notch weir.

V-notches, and the discharge equation usually recommended in the U.S.A. is

$$Q=2.47h^{2.50} \text{ (English units).}$$

More precise values of the weir coefficient, which vary with h, are given for use with metric units in WMO Technical Note No. 117.

The only other central angle that is commonly used in the U.S.A. for V-notch weirs is 120°. The recommended discharge equation is

$$Q=4.35h^{2.50} \text{ (English units).}$$

SUBMERGED THIN-PLATE WEIRS

Submergence occurs at a weir when the elevation of the downstream water surface (tailwater) exceeds the elevation of the weir crest (fig. 149). The tailwater elevation is measured downstream from the turbulence that occurs in the immediate vicinity of the downstream face of the weir. The degree of submergence is expressed by the ratio h_t/h. For any given head h, submergence has the effect of reducing the discharge that would occur under the condition of free flow; the greater the submergence ratio h_t/h, the greater the reduction in discharge. Villemonte (1947) combined the results of his tests with those of several other investigators to produce the generalized relation shown in figure 150. Figure 150 is applicable to all shapes of vertical thin-plate weirs. In that figure, the abscissa is the submergence ratio raised to a power N, where N is the exponent in the free-flow discharge equation; for example, $N=1.5$ for a rectangular weir and $N=2.5$ for a triangular weir. The ordinate in figure 150 is the ratio of discharge under the submerged condition (Q_s) to free-flow discharge (Q). The relation shown in figure 150 agrees reasonably with the individual results obtained by the various investigators of submerged-weir discharge. However, if great accuracy is essential, it

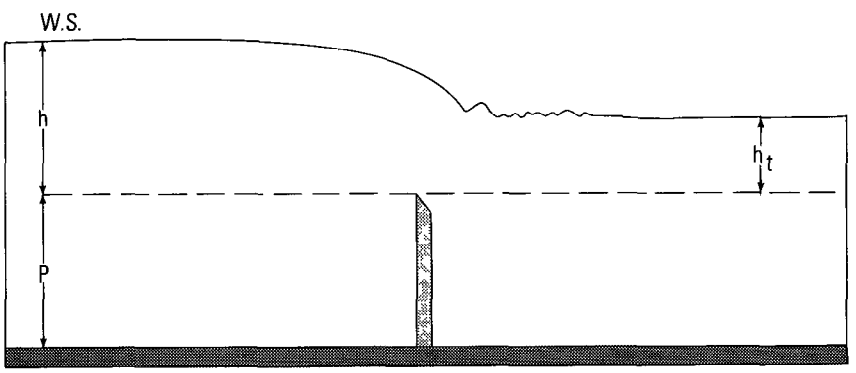

FIGURE 149.—Sketch showing submergence of a weir.

is recommended that the particular weir be calibrated in the field or in a laboratory under conditions similar to field conditions.

BROAD-CRESTED WEIRS

The term "broad-crested weir", as used here, refers to any weir that is not of the thin-plate type. The most common type of artificial control built in natural channels is the broad-crested weir. A structure of that type has the necessary strength and durability to withstand possible damage by floating debris. When installed in a stream channel that carries sediment-laden water, the weir is often built with a gently sloping upstream apron (slope: 1 vertical to 5 horizontal) so that there is no abrupt impedance to the flow and sediment is carried over the weir and not deposited in the gage pool. Because the

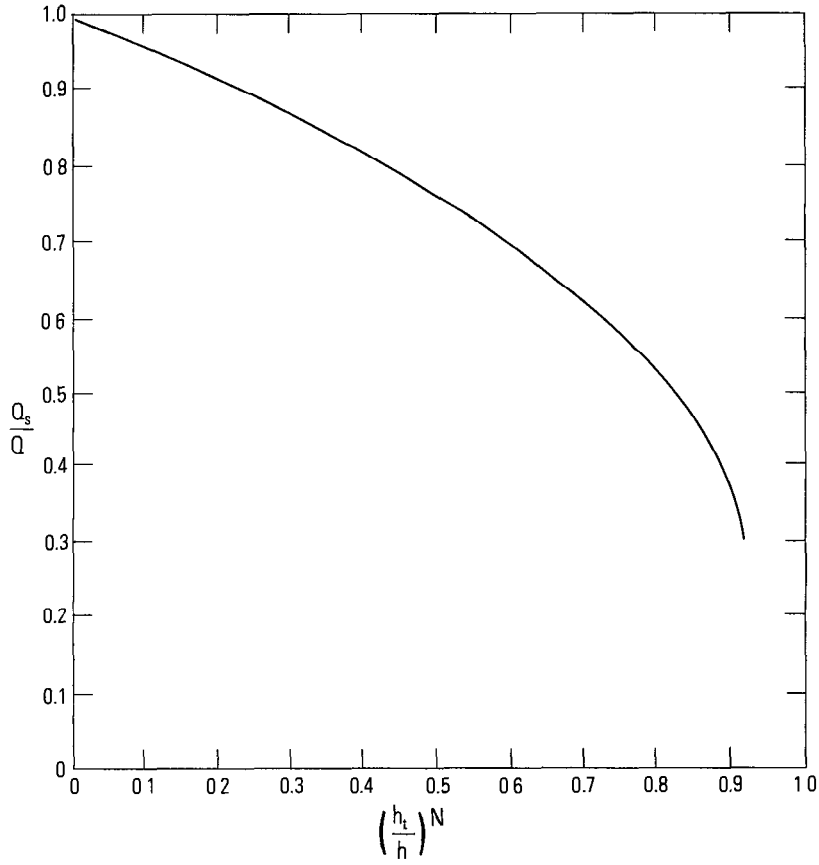

FIGURE 150.—Generalized relation of discharge ratio to submergence ratio for vertical thin-plate weirs. (After Villemonte, 1947.)

backwater caused by a high weir can aggravate flood problems along a stream, broad-crested weirs are usually built low to act as low-water controls and they become submerged at intermediate and high stages.

There are a myriad of crest shapes that can be used for broad-crested weirs, and there will be no attempt to describe the characteristics of the rating curve for each. Much of the material for such a discussion can be found in WMO Technical Note No. 117 (1971), in a report by Hulsing (1967), and in a textbook by King and Brater (1963). Instead, this section of the report will present a discussion of general principles as they apply to the definition of the discharge rating and will present the approximate ratings for broad-crested weirs commonly used as gaging-station controls in the U.S.A. The weirs are all intended to be field calibrated by current-meter discharge measurements.

Before proceeding to the discussion of broad-crested weirs commonly used in the U.S.A., it might be mentioned in passing that perhaps the most popular weir for use as a gaging-station control in Europe, and particularly in the United Kingdom, is the Crump weir (World Meteorological Organization, 1971). The Crump weir is triangular in cross section; the *upstream* face has a slope of 1 (vertical) to 2 (horizontal) and the *downstream* face has a slope of 1 (vertical) to 5 (horizontal). The crest, or apex of the triangular cross section, is usually horizontal over its entire length (b), but for greater sensitivity the crest may be given the shape of a flat Vee, the sides of which often have a slope of 1 (vertical) to 10 (horizontal). The basic equation for the Crump weir with horizontal crest is,

$$Q = Cb\,(h + h_v)^{3/2},$$

where C equals about 3.55 when English units are used and 1.96 when metric units are used.

FLAT-CRESTED RECTANGULAR WEIR

The simplest type of broad-crested weir is one that is rectangular in cross section and whose crest is horizontal over its entire length, b. The basic discharge equation for that weir is $Q = Cb(h + h_v)^{1.5}$, where h_v is the head attributable to velocity of approach. The coefficient C will increase with stage in the manner shown in figure 151, and h_v will also increase with stage as a result of the velocity of approach increasing with stage. (Figure 151 also shows the relation of C to stage for flat-crested weirs with sloping faces.) The rating curve for a flat-crested rectangular weir, when plotted on logarithmic graph paper, will be a straight line except for extremely low stages. The equation

of the line will be of the form $Q=p(G-e)^N$, where the slope of the line, N, will have a value greater than 1.5 because both the weir coefficient and the velocity head increase with stage.

Most flat-crested rectangular weirs are not sufficiently sensitive at low flows. To increase the low-flow sensitivity, the crest is often modified as shown in figure 152. Instead of the crest being horizontal over its entire length, b, the crest is given a gentle slope from one streambank to the other, or the crest is given the shape of an extremely flat Vee or catenary. As a result of this modification, the area of flow over the weir is triangular, or nearly so, at low flows and approximately rectangular at high flows. In other words, the length of weir crest that is utilized by the flow varies with stage until the stage rises high enough to flow over the entire length of the crest (b in fig. 152). In the general equation for the weir discharge, $Q=Cb(h+h_v)^{1.5}$, not only do C and h_v increase with stage, but length of weir crest, b, also increases with stage, as stated in the preceding sentence. Consequently if the weir rating plots as a straight line on logarithmic graph paper in accordance with equation, $Q=p(G-e)^N$, the slope of the line, N, will be considerably greater than 1.5, and invariably will be greater than 2.0.

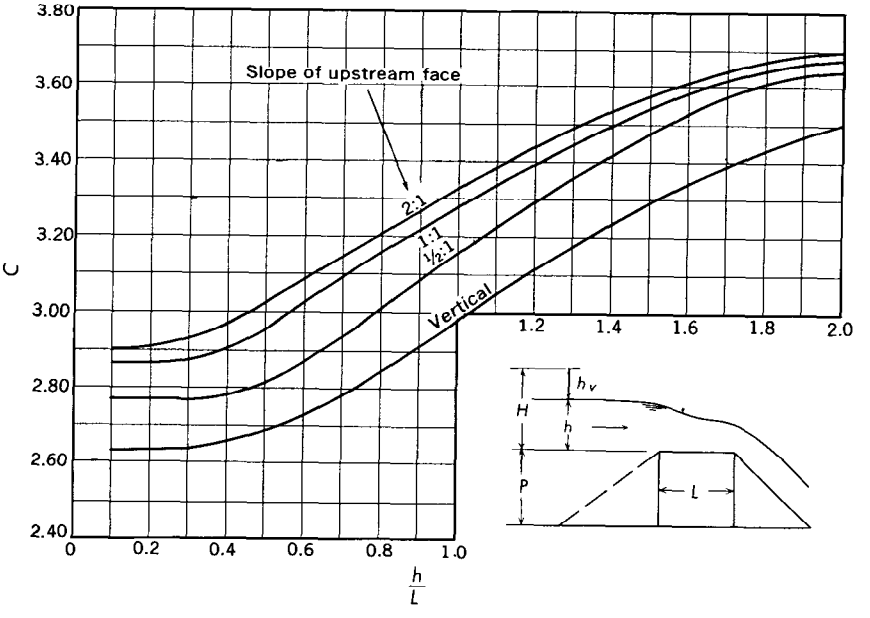

FIGURE 151.—Coefficients of discharge for full-width, broad-crested weirs with downstream slope ≤ 1:1 and various upstream slopes. (Slope is the ratio of horizontal to vertical distance.)

NOTCHED FLAT-CRESTED RECTANGULAR WEIR

Figure 153 shows the notched flat-crested rectangular weir that is the control for a gaging station on Great Trough Creek near Markles-burg, Pa.

Because there is a sharp break in the cross section at gage height 1.4 ft, a break occurs in the slope of the rating curve at that stage. The gage-height of zero flow for stages between 0.0 and 1.4 ft is 0.0 ft; for stages above 1.4 ft, the effective zero flow is at some gage height between 0.0 and 1.4 ft. If the low end of the rating is made a tangent, the gage height of zero flow (e) is 0.0 ft, and the slope of this tangent turns out to be 2.5, which, as now expected, is greater than the theoretical slope of 1.5. The upper part of this rating curve is concave upward because the value of e used (0.0 ft) is lower than the effective value of zero flow for high stages.

If the upper end of the rating is made a tangent, it is found that the value of e, or effective zero flow, must be increased to 0.6 foot. Because we have raised the value of e, the low-water end of the curve will be concave downward. The high-water tangent of the curve, principally because of increased rate of change of velocity of approach, will have a

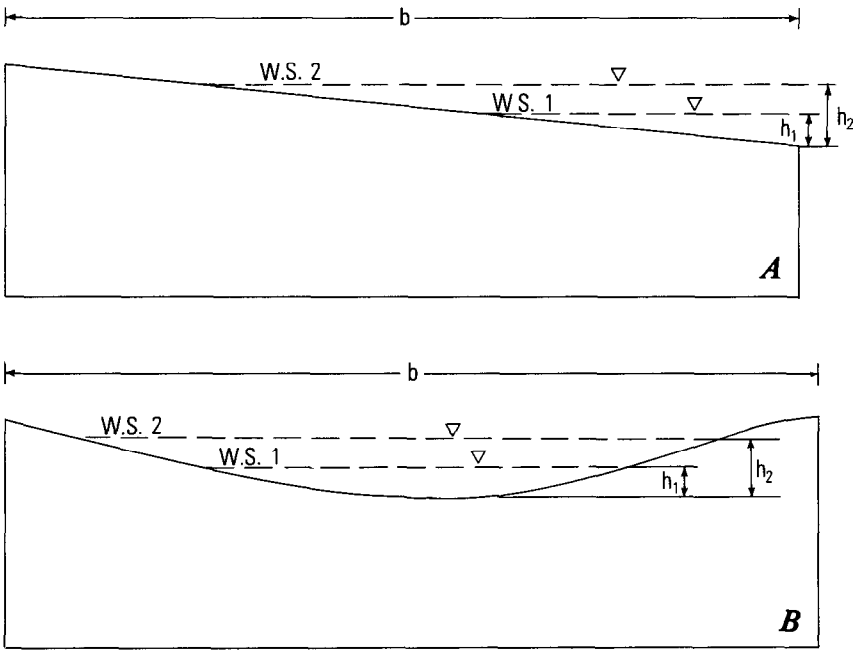

FIGURE 152.—Sketch of upstream face of flat-crested weir with (A) sloping crest and (B) catenary crest.

slope that is greater than that of the low-water tangent of the curve previously described; its slope is found to have a value of 3.0.

The low-water tangent for the notched control, which is defined by discharge measurements, warrants further discussion. Its slope of 2.5 is higher than one would normally expect for a simple flat-crested rectangular notch. One reason for the steep slope is the fact that the range of stage involved, 0.0 ft to 1.4 ft, is one in which the theoretical weir coefficient C increases very rapidly with stage. A more important reason is the geometric complexity of the notch which is not indicated in figure 153. At the downstream edge of the notch is a sharp-edged plate; its elevation is at 0.0 ft, but the sharp edge is about 0.1 ft higher than the concrete base of the notch. The details of the notch are not important to this discussion; they are mentioned here only to warn the reader not to expect a slope as great as 2.5 in the rating for a simple flat-crested rectangular notch. In fact, the sole purpose here of discussing the low-water tangent of the rating curve is to demonstrate the effect exerted on the curve by varying the applied values of e. The low-water end of a rating curve is usually well defined by discharge measurements, and if it is necessary to

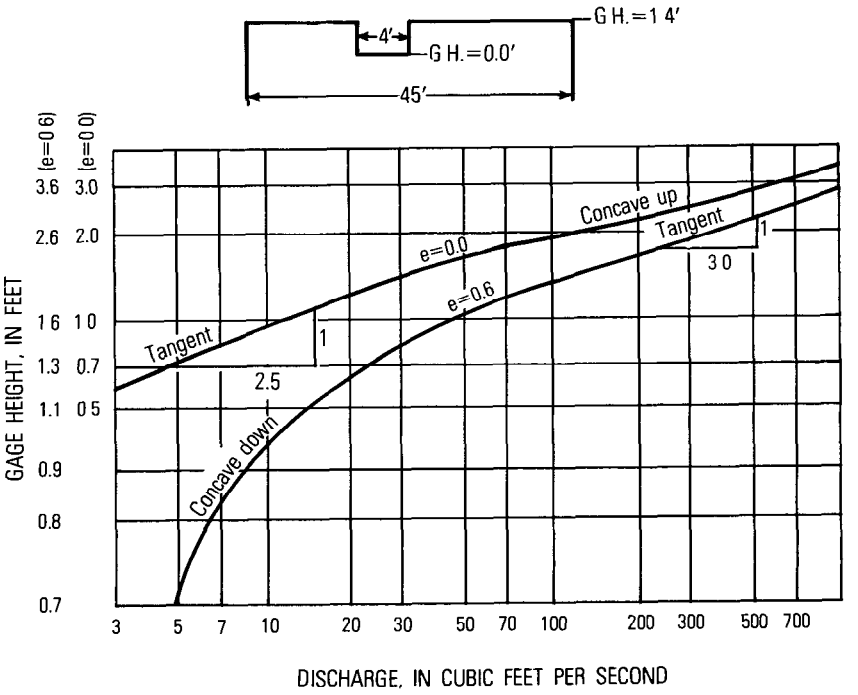

FIGURE 153.—Rating curve for a notched broad-crested control at Great Trough Creek near Marklesburg, Pa.

extrapolate the rating downward, it is best done by replotting the low-water end of the curve on rectangular-coordinate graph paper, and extrapolating the curve down to the point of zero discharge. (See section titled, "Low-Flow Extrapolation.")

TRENTON-TYPE CONTROL

The so-called Trenton-type control is a concrete weir that is frequently used in the U.S.A. The dimensions of the cross section of the crest are shown in figure 154. The crest may be constructed so as to be horizontal for its entire length across the stream, or for increased low-flow sensitivity the crest may be given the shape of an extremely flat Vee. For a horizontal crest, the equation of the stage-discharge relation, as obtained from a logarithmic plot of the discharge measurements, is commonly on the order of $Q=3.5bh^{1.65}$(English units). The precise values of the constants will vary with the height of the weir above the streambed, because that height affects the velocity of approach. The constants of the equation are greater than those for a flat-crested rectangular weir (see section titled, "Flat-crested Rectangular Weir") because the cross-sectional shape of the Trenton-type control is more efficient than a rectangle with regard to the flow of water.

When the Trenton-type control is built with its crest in the shape of a flat Vee, the exponent of h in the discharge equation is usually 2.5 or more, as expected for a triangular notch where velocity of approach

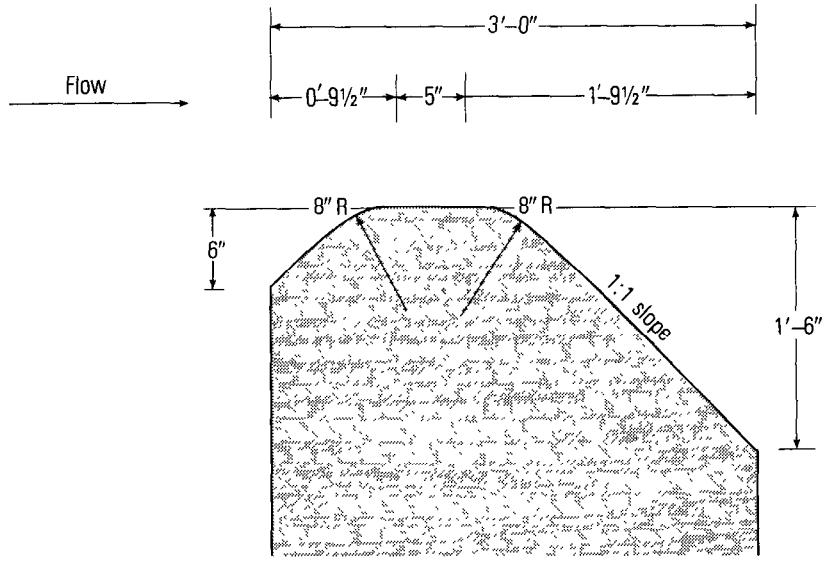

FIGURE 154.—Cross section of Trenton-type control.

is significant. Again, the precise values of the constants in the discharge equation are dependent on the geometry of the installation.

COLUMBUS-TYPE CONTROL

One of the most widely used controls in the U.S.A. is the Columbus-type control. This control is a concrete weir with a parabolic notch that is designed to give accurate measurement of a wide range of flows (fig. 155). The notch accommodates low flows; the main section, whose crest has a flat upward slope away from the notch, accommodates higher flows. The throat of the notch is convex along the axis of flow to permit the passage of debris. For stages above a head of 0.7 ft, which is the elevation of the top of the notch, the elevation of effective zero flow is 0.2 ft, and the equation of discharge is approximately,

$$Q = 8.5(h - 0.2)^{3.3} \text{ (English units)}$$

The precise values of the constants in the equation will vary with conditions for each installation. The shape of the crest above a stage of 0.7 ft is essentially a flat Vee for which the theoretical exponent of head is 2.5 in the discharge equation. However, the actual value of the exponent is greater than 2.5 principally because of the increase of velocity of approach with stage.

SUBMERGED BROAD-CRESTED WEIRS

Weir submergence was defined earlier in the section titled, "Submerged Thin-Plate Weirs." As in the case of thin-plate weirs, for a given static head (h) the discharge decreases as the submergence ratio (h_t/h) increases. Little quantitative data are available to define the relation of discharge ratio to submergence ratio for the many types of broad-crested weir. However, it is known that for horizontal crests the submergence ratio must be appreciable before any significant reduction in discharge occurs. This threshold value of the submergence ratio at which the discharge is first affected ranges from about 0.65 to 0.85, depending on the cross-sectional shape of the weir crest.

FLUMES

Flumes commonly utilize a contraction in channel width and free fall or a steepening of bed slope to produce critical or supercritical flow in the throat of the flume. The relation between stage measured at some standard cross section and discharge is thus a function only of the characteristics of the flume and can be determined, on an interim basis at least, prior to installation.

In the section in chapter 3 titled, "Artificial Controls," it was mentioned that flumes may be categorized with respect to the flow regime

that principally controls the measured stage; that is, a flume may be classed as either a critical-flow flume or a supercritical-flow flume. The most commonly used critical-flow flume is the Parshall flume, and it is the only one of that type that will be described here. The

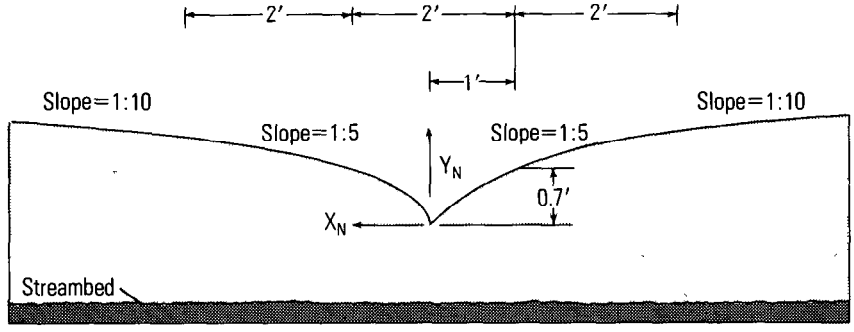

Profile of weir crest and notch

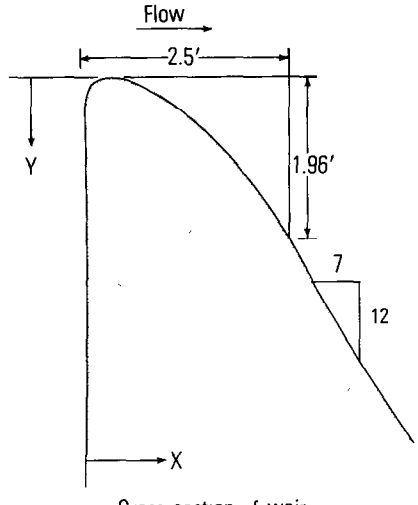

Cross section of weir

Coordinates of notch profile, in feet

X_N	Y_N
0.00	0.00
.046	.1
.108	.2
.192	.3
.302	.4
.452	.5
.665	6
1.00	7

Coordinates of cross section of weir crest, in feet

X	Y
0.0	0.126
.1	.036
2	.007
.3	.000
.4	.007
.6	.060
8	.142
1.0	.257
1.2	.397
1.4	565
1.7	.870
2.0	1.22
2 5	1.96

FIGURE 155.—Dimensions of Columbus-type control.

supercritical-flow flume is less widely used, but fills a definite need. (See section in chapter 3 titled "Choice of an Artificial Control.") Of that type of flume, the trapezoidal supercritical-flow is preferred by the Geological Survey; it too will be described here.

PARSHALL FLUME

The principal feature of the Parshall flume is an approach reach having converging sidewalls and a level floor, the downstream end of which is a critical-depth cross section. Critical flow is established in the vicinity of that cross section by having a sharp downward break in the bed slope of the flume. In other words, the bed slope downstream from the level approach section is supercritical. The primary stage measurement is made in the approach reach at some standard distance upstream from the critical-depth cross section.

The general design of the Parshall flume is shown in figure 156. Table 17 gives the dimensions corresponding to the letters in figure 156 for various sizes of flumes. The flumes are designated by the width (W) of the throat. Flumes having throat widths from 3 in. to 8 ft have a rounded entrance whose floor slope is 25 percent. The smaller

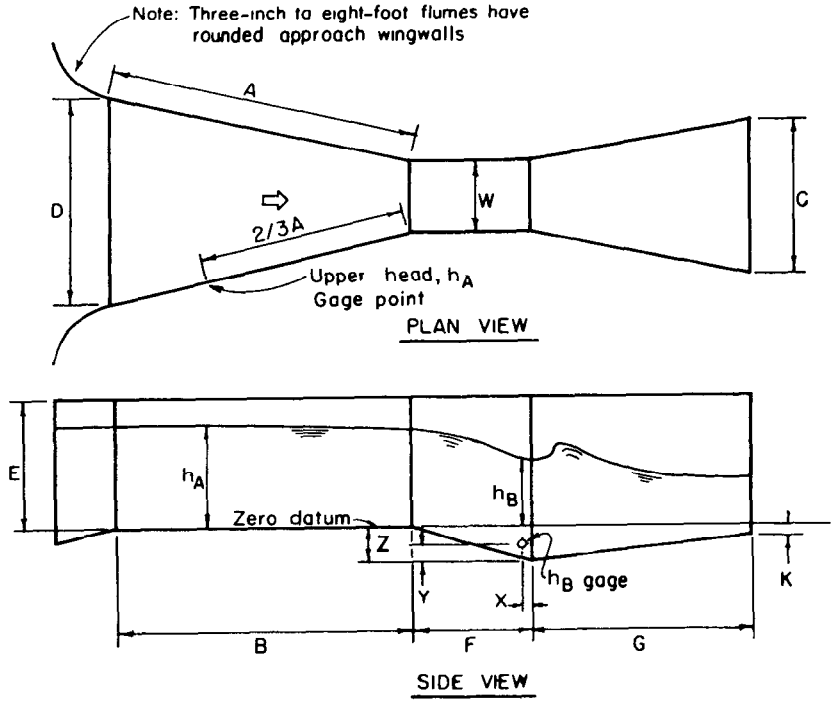

FIGURE 156.—Configuration and descriptive nomenclature for Parshall flumes.

TABLE 17.—*Dimensions and capacities of all sizes of standard Parshall flumes*

[For sizes 1 ft to 8 ft, $A=W/2+4$. For all sizes, h_4 is located a distance of 2/3 A from crest, distance is converging wall length, not axial]

Widths			Axial Lengths			Wall Depth in	Vertical distance below crest		Converging wall length	Gage Points			Free Flow Capacities	
Size, Throat width W	Upstream end D	Downstream end C	Converging Section B	Throat Section F	Diverging Section G	Converging Section E	Dip at Throat Z	Lower end of flume K	A	h_4, dist. upstream from crest	h_B X	h_B Y	Min.	Max.
inches	feet	feet	feet	feet	feet	feet	feet	feet	feet	feet	feet	feet	ft ^{3}/s	ft ^{3}/5s
1	0.549	0.305	1.17	0.250	0.67	0.5-0.75	0 094	0.062	1.19	0.79	0.026	0.042	0.005	0.15
2	.700	.443	1.33	.375	.83	0.50-0.83	.141	.073	1.36	.91	.052	.083	.01	.30
3	.849	.583	1.50	.500	1.00	1.00-2.00	.188	.083	1.53	1.02	.083	.125	.03	1.90
6	1.30	1.29	2.00	1.00	2.00	2.0	.375	.25	2.36	1.36	.167	.25	.05	3.90
9	1.88	1.25	2.83	1.00	1.50	2.5	.375	.25	2.88	1.93	.167	.25	.09	8.90
feet														
1.0	2.77	2.00	4.41	2.0	3.0	3.0	.75	.25	4.50	3.00	.167	.25	.11	16.1
1.5	3.36	2.50	4.66	2.0	3.0	3.0	.75	.25	4.75	3.17	.167	.25	.15	24.6
2.0	3.96	3.00	4.91	2.0	3.0	3.0	.75	.25	5.00	3.33	.167	.25	.42	33.1
3.0	5.16	4.00	5.40	2.0	3.0	3.0	.75	.25	5.50	3.67	.167	.25	.61	50.4
4.0	6.35	5.00	5.88	2.0	3.0	3.0	.75	.25	6.00	4.00	.167	.25	1.30	67.9
5.0	7.55	6.00	6.38	2.0	3.0	3.0	.75	.25	6.50	4.33	.167	.25	1.60	85.6
6.0	8.75	7.00	6.86	2.0	3.0	3.0	.75	.25	7.0	4.67	.167	.25	2.60	103.5
7.0	9.95	8.00	7.35	2.0	3.0	3.0	.75	.25	7.5	5.00	.167	.25	3.00	121.4
8.0	11.15	9.00	7.84	2.0	3.0	3.0	.75	.25	8.0	5.33	.167	.25	3.50	139.5
10	15.60	12.00	14.0	3.0	6.0	4.0	1.12	.50	9.0	6.00			6	300
12	18.40	14.67	16.0	3.0	8.0	5.0	1.12	.50	10.0	6.67			8	520
15	25.0	18.33	25.0	4.0	10.0	6.0	1.50	.75	11.5	7.67			8	900
20	30.0	24.00	25.0	6.0	12.0	7.0	2.25	1.00	14.0	9.33			10	1340
25	35.0	29.33	25.0	6.0	13.0	7.0	2.25	1.00	16.5	11.00			15	1660
30	40.4	34.67	26.0	6.0	14.0	7.0	2.25	1.00	19.0	12.67			15	1990
40	50.8	45.33	27.0	6.0	16.0	7.0	2.25	1.00	24.0	16.00			20.	2640
50	60.8	56.67	27.0	6.0	20.0	7.0	2.25	1.00	29.0	19.33			25	3280

Note: Flume sizes 3 inches through 8 feet have approach aprons rising at a 1:4 slope and the following entrance roundings: 3 through 9 inches, radius =1.33 feet; 1 through 3 feet, radius=1 67 feet, 4 through 8 feet, radius=2 00 feet

and larger flumes do not have that feature, but it is doubtful whether the performance of any of the flumes is significantly affected by the presence or absence of the entrance feature as long as approach conditions are satisfactory.

Parshall flumes have provision for stage measurements both in the approach reach and in the throat reach, but the downstream gage is required only when submerged-flow conditions exist. The datum for both gages is the level floor in the approach. The raised floor, length G in figure 156, in the downstream diverging reach is designed to reduce scour downstream and to produce more consistent stage-discharge relations under conditions of submergence. The percentage of submergence for Parshall flumes is computed by the formula,

$$\frac{h_B}{h_A} \times 100.$$

Where free-flow conditions exist for all flows, the downstream gage, h_B, may be omitted and the entire diverging reach may be dispensed with if desired. That simplification has been used in the design of small portable Parshall measuring flumes. (See section in chapter 8 titled, "Portable Parshall Flume.")

Tables 18 and 19 summarize the relation of discharge to stage at h_A under conditions of free flow (low stage at h_B) for flumes of the various sizes. Although the free-flow stage-discharge relations for the various flumes were derived experimentally, all relations can be expressed closely by the following equation, (Davis, 1963),

$$Y_0 + \frac{Q_0^2}{2Y_0^2\,(1 + 0.4X_0)^2} = 1.351\,Q_0^{\,0.645} \text{ (English units)} \qquad (59)$$

in which

Y_0 = nondimensional depth, y_1/b
Q_0 = nondimensional discharge, $Q/g^{1/2}b^{5/2}$
X_0 = nondimensional distance, x/b
y_1 = depth at measuring section
b = channel width at throat
Q = discharge
g = acceleration of gravity
x = distance from throat crest to measuring section.

For flumes with throat widths no greater than 6 ft, the following simplified form of the above equation (Dodge, 1963) can be used:

$$Y_0 = 1.19 Q_0^{\,0.645} X_0^{\,0.0494} \qquad (60)$$

When the stage h_B is relatively high, the free-flow discharge corresponding to any given value of h_A is reduced. The percentage of submergence, or value of $[(h_B/h_A)\times 100]$, at which the free-flow discharge is first affected, varies with the size of flume. For flumes whose throat width is less than 1 ft, the submergence must exceed 50 percent before there is any backwater effect; for flumes with throat width from 1 to 8 ft, the threshold submergence is 70 percent; for flumes with throat width greater than 10 ft, the threshold submergence is 80 percent. Figure 157 shows the discharge ratings for Parshall flumes, from 2 inches to 9 inches, under both free-flow and submergence conditions. Figure 158 shows the correction in discharge, which is always negative, that is to be applied to free-flow discharges for various percentages of submergence and various values of h_A, for flumes having throat widths between 1 and 50 feet. The appropriate correction factor (k_s) for flume size is applied to the corrections read from the graphs. In other words,

$$Q_s = Q_f - k_s Q_c,$$

where

Q_s = discharge under submergence conditions,
Q_f = discharge under free-flow conditions, and
Q_c = discharge correction unadjusted for flume size.

The stage-discharge relations, both for free-flow and submergence conditions, given in the preceding tables and graphs, should be used only as guides or as preliminary ratings for Parshall flumes built in the field. Those installations should be field-calibrated because the structural differences that invariably occur between model and prototype flume usually cause the discharge rating for the field structure to differ from the experimental ratings given in this manual.

TABLE 18.—*Discharge table for Parshall flumes, sizes 2 inches to 9 inches, for free-flow conditions*

[Discharges for standard 3-inch Parshall flumes are slightly less than those for the modified 3-inch Parshall flume discussed in chapter 8; see table 14]

h_A (feet)	2 inches (ft^3/s)	3 inches (ft^3/s)	6 inches (ft^3/s)	9 inches (ft^3/s)
0.1	0.02	0.03	0.05	0.09
.2	.06	.08	.16	.26
.3	.11	.15	.31	.49
.4	.17	.24	.48	.76
.5	.24	.34	.69	1.06
.6	.31	.45	.92	1.40
.7	.40	.57	1.17	1.78
.8		.70	1.45	2.18
.9		.84	1.74	2.61
1.0		.89	2.06	3.07
1.1			2.40	3.55
1.2			2.75	4.06
1.3			3.12	4.59
1.4			3.51	5.14
1.5				5.71
1.6				6.31
1.7				6.92
1.8				7.54
1.9				8.20

TABLE 19.—*Discharge table for Parshall flumes, sizes 1 foot to 50 feet for free-flow conditions*

h_A (feet)	1 foot (ft^3/s)	1 5 feet (ft^3/s)	2 feet (ft^3/s)	3 feet (ft^3/s)	4 feet (ft^3/s)	5 feet (ft^3/s)	6 feet (ft^3/s)	7 feet (ft^3/s)	8 feet (ft^3/s)
0 10	0 11	0.15							
15	20	30	0 42	0 61					
20	35	51	66	97	1 26	1 55			
25	49	.71	93	1 37	1 80	2 22	2.63	3 02	3 46
30	.64	94	1 24	1.82	2.39	2.96	3 52	4.08	4 62
4	99	1.47	1 93	2 86	3 77	4 68	5 57	6 46	7 34
5	1 39	2 06	2 73	4 05	5.36	6 66	7 94	9.23	10.5
6	1 84	2 73	3 62	5 39	7 15	8 89	10.6	12.4	14.1
7	2 33	3 46	4.60	6 86	9.11	11 4	13.6	15.8	18 0
.8	2.85	4 26	5.66	8 46	11 3	14.0	16.8	19 6	22 4
9	3 41	5 10	6 80	10 2	13.6	16 9	20 3	23.7	27.0
10	4 00	6 00	8 00	12 0	16 0	20 0	24.0	28 0	32.0
12	5 28	7.94	10 6	16.0	21 3	26 7	32.1	37 5	42.9
14	6 68	10 1	13 5	20 3	27 2	34 1	41 1	48 0	55.0
16	8 18	12 4	16 6	25 1	33.6	42 2	50 8	59.4	68 1
18	9 79	14.8	19 9	30 1	40 5	50 8	61 3	71.8	82.3
20	11 5	17 4	23 4	35 5	47.8	60 1	72 5	84.9	97.5
22	13 3	20 2	27 2	41 3	55.5	69.9	84.4	98.9	113.6
24	15 2	23 0	31.1	47 3	63 7	80 3	97.0	113 7	130 7

h_A (feet)	10 feet (ft^3/s)	12 feet (ft^3/s)	15 feet (ft^3/s)	20 feet (ft^3/s)	25 feet (ft^3/s)	30 feet (ft^3/s)	40 feet (ft^3/s)	50 feet (ft^3/s)
0 30	5.75	6 75	8 4	11.1	13 8	16 5	21 8	27.3
04	9 05	10 85	13 3	17 7	21.8	26 1	34 6	43 2
0 5	13.0	15 4	19 1	25 1	31 2	37 2	49.5	61 8
0 6	17 4	20 6	25 5	33 7	41.8	50 0	66 2	82 6
0 7	22 2	26.2	32 7	43 1	53.4	64 0	84 8	105.5
0 8	27 5	32.7	40.4	53 4	66.3	79 2	105	131
0 9	33 3	39.4	48 9	64 3	80 1	95 5	127	158
1 0	39 4	46 8	57 9	76 3	94 8	113 2	150	187
1 2	52.7	62 6	77 3	102 0	127 0	152	201	250
1.4	67 4	80 1	99 0	130 5	162	194	257	320
1.6	83 5	99 1	122.8	162	201	240	318	396
1.8	100 9	119 8	148 0	195	243	290	384	479
2 0	119 4	141 8	175 3	232	287	343	454	567
2 2	139 0	165 0	204	269	334	400	530	660
2 4	159.9	189 8	235	310	384	459	609	758
2.6	181.7	215 7	267	352	437	522	692	864
3 0	228.4	271 2	335	442	549	656	870	1084
3.5	294	347	429	566	703	840	1113	1387
4 0	363	430	531	700	870	1040	1379	1717
4.5	437	518	641	846	1051	1255	1664	2073
5.0	517	614	759	1002	1244	1486	1970	2453
5 5			885	1166	1448	1730	2295	2860
6 0			1016	1340	1664	1988	2638	3285

Note· Available data indicates that extension of the above ratings to greater heads is reliable

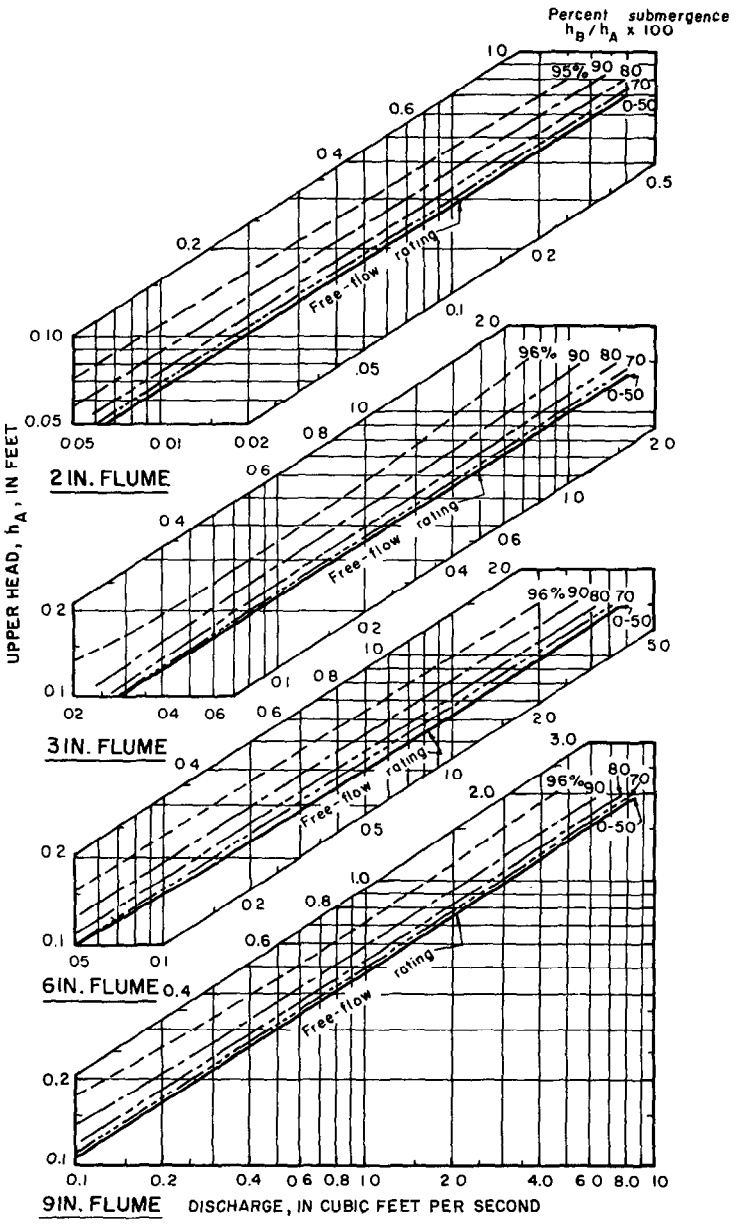

FIGURE 157.—Discharge ratings for "inch" Parshall flumes for both free-flow and submergence conditions.

TRAPEZOIDAL SUPERCRITICAL-FLOW FLUME

The principal feature of the trapezoidal supercritical-flow flume is a reach of flume (throat) whose bed has supercritical slope, upstream from which is a critical-depth cross section. The general design of the flume and the dimensions for the flumes of three throat widths that have been installed by the Geological Survey are shown in figure 159. The purpose of having the flume trapezoidal in cross section is to increase the sensitivity of the stage-discharge relation, particularly at low flows. Wide latitude exists with regard to the height (E) of the

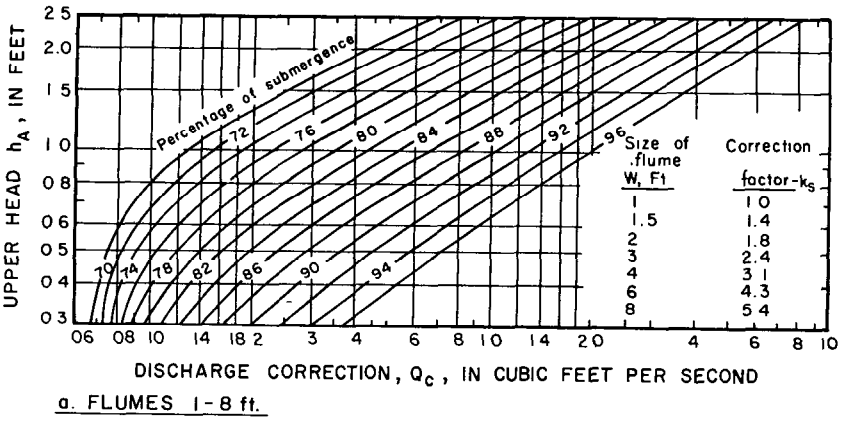

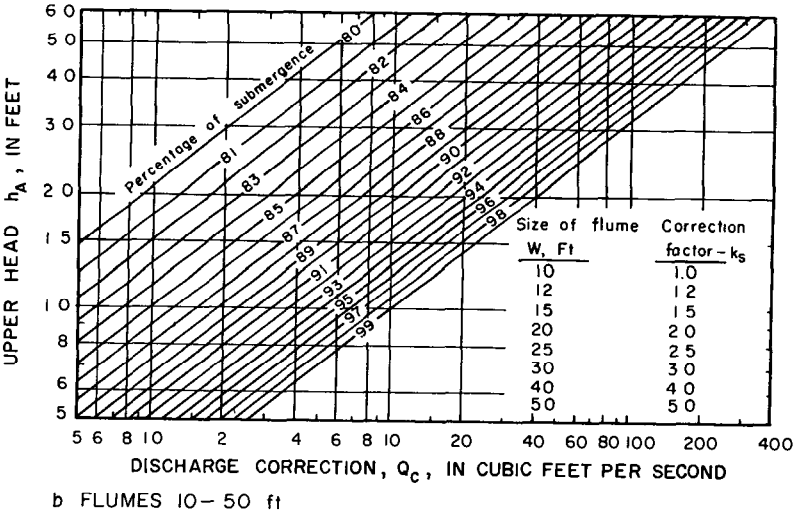

FIGURE 158.—Correction factors for submerged flow through 1- to 50-ft Parshall flumes.

sidewalls that can be used, and thus the range of discharge that can be accommodated by a supercritical-flow flume of any particular throat width is quite flexible. Stage (vertical depth of flow) is measured at a cross section at midlength of the throat reach, gage datum being the floor of the flume at the stage-measurement site. The measurement of stage must be precise because the stage-discharge relation for supercritical flow is extremely insensitive—a small change in stage corresponds to a large change in discharge.

Were it not for the severe width constriction at the downstream end of the converging reach, critical flow would occur at the break in floor slope at the downstream end of the approach reach and flow would be supercritical at all cross sections downstream from the approach reach. However for all but extremely low flows, the sharp constriction in width resulting from the use of a convergence angle (ϕ) of 21.8° (fig.159) causes backwater that extends upstream into the approach

Dimensions of trapezoidal supercritical-flow flume

Flume size, W_T feet	Width of approach reach, W_A feet	Angles		Lengths			Minimum capacity, ft^3/s	Floor slopes	
		Sloping walls θ	Converging walls ϕ	Approach reach, L_A feet	Converging reach, L_C feet	Throat reach, L_T feet		Approach reach, percent	Converging and throat reaches, %
1	5	30°	21.8°	5.0	5.0	5.0	0.7	0	5
3	9	30°	21.8°	variable	7.5	10.0	2.0	0	5
8	14	30°	21.8°	variable	7.5	12.0	6.0	0	5

Note—Height of wall (E) is dependent on magnitude of maximum discharge to be gaged

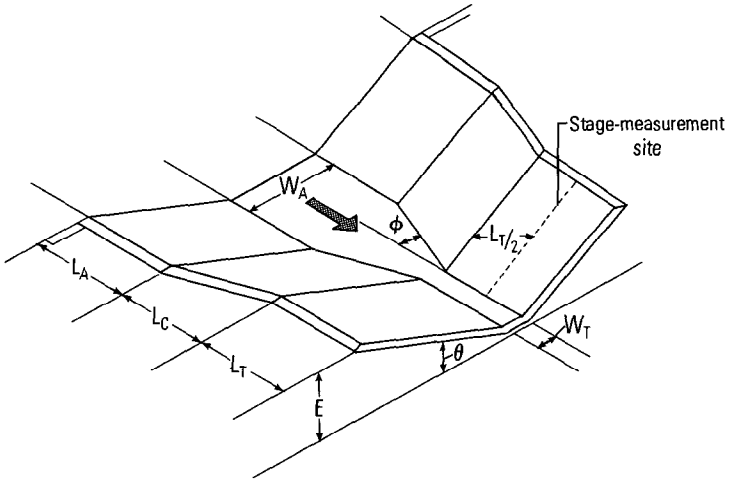

FIGURE 159.—Configuration and dimensions of trapezoidal supercritical-flow flumes of three throat widths.

reach. As a result critical depth occurs at the most constricted cross section in the converging reach, the flow being subcritical in the approach and converging reaches and supercritical in the throat reach. That is seen in figure 5 (chap. 3) which is a photograph of a 3-foot trapezoidal flume in Owl Creek in Wyoming. The purpose of the converging reach is to obtain an increased velocity at the critical-depth cross section and thereby reduce the likelihood of debris deposition at that cross section; such deposition could affect the stage-discharge relation in the throat of the flume.

The measured stage corresponding to any discharge is a function of the stage of critical depth at the head of the throat reach and the geometry of the throat reach upstream from the stage-measurement cross section. Consequently a theoretical rating for all but the smallest discharges can be computed by use of the Bernoulli or total-energy equation for the length of throat reach upstream from the stage-measurement site (fig. 160). By equating total energy at the critical-depth cross section (c) at the head of the throat reach to total energy at the stage-measurement cross section (m), we have,

$$\frac{V_c^2}{2g} + h_c + z_c = \frac{V_m^2}{2g} + h_m + z_m + h_f, \tag{61}$$

where

V is mean velocity,
g is acceleration of gravity,
h is vertical depth,
z is elevation of flume floor above any arbitrary datum plane, and
h_f is friction loss.

We make the assumption that the friction loss h_f in the short reach is negligible and may be ignored. Then by substituting, in equation 61 values from the two equations

$$Q = A_c V_c = A_m V_m \quad \text{and} \quad \Delta Z = Z_c - Z_m,$$

we obtain

$$\frac{Q^2}{2gA^2_c} + h_c + \Delta z = \frac{Q^2}{2gA^2_m} + h_m. \tag{62}$$

From the properties of critical-depth flow (Chow, 1959, p. 64), the critical-section factor (J) is computed by the formula

$$J = A_c \sqrt{\frac{A_c}{T_c}} \tag{63}$$

where A_c is the area and T_c is the top width at the critical-depth cross section. The discharge (Q) at the critical-depth cross section is

$$Q = J\sqrt{g} \tag{64}$$

By assuming a depth (h_c) at the critical-depth cross section, we can compute Q and A_c, and thus the values of all terms on the left side of equation 62 will be known for any chosen value of h_c. Because h_m is uniquely related to A_m, equation 62 can be solved by trial and error to obtain the depth (stage) at the measurement cross section corresponding to the value of Q that was computed earlier.

The entire procedure is repeated for other selected values of h_c to provide a discharge rating curve for the entire range of discharge. The value of h_c corresponding to the maximum discharge to be gaged represents the height to which the sidewalls of the throat section must be built to contain that discharge. An additional height of at least 0.5 ft should be added for freeboard to accommodate surge and wave action.

The computed discharge rating should be used only until the rating can be checked by current-meter discharge measurements. The sources of error in the computed rating are uncertainty as to the exact location of the critical-depth cross section for any given discharge and neglect of the small friction loss (h_f). However, the general shape of the discharge rating curve will have been defined by the computed values, and relatively few discharge measurements should be required for any needed modification of the rating.

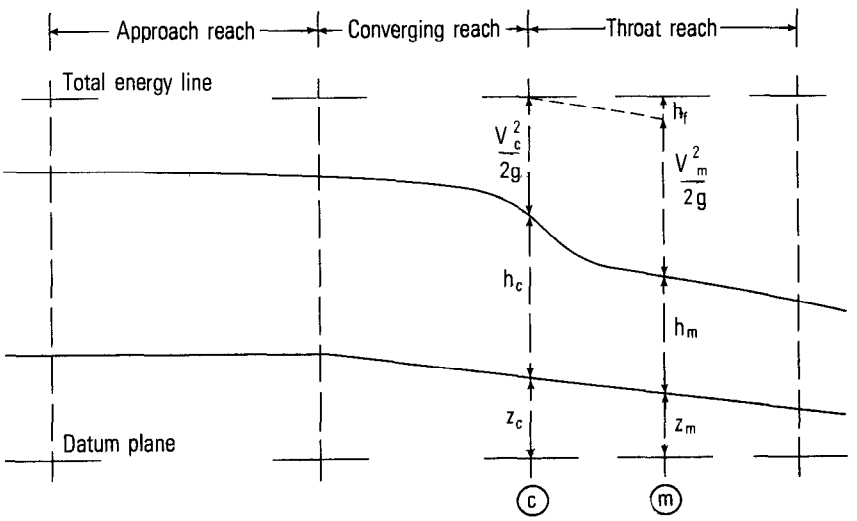

FIGURE 160.—Sketch illustrating use of the total-energy (Bernoulli) equation.

The total-energy equation (eq. 61) should also be applied to the converging reach to obtain the required height of the sidewalls at the upper end of the converging reach. The height plus an additional freeboard height of at least 0.5 ft should be used for the sidewalls in the approach reach. In applying equation 61 to the converging reach, the value of discharge used is the maximum discharge that is to be gaged, and the depth used at the lower end of the converging reach is the corresponding critical depth (h_c) that was computed earlier for the throat reach.

The solid-line curves on figures 161–163 are the theoretical discharge rating curves for the flumes of the three throat widths that have been field tested. The agreement between measured and theoretical discharges has generally been good except at extremely low stages. Nevertheless the theoretical curves should be considered as interim rating curves for newly built flumes until later measurements either corroborate the ratings or show the need for modification of the ratings. It is expected that the stage-discharge relation will not be affected by submergence, as long as submergence percentages do not exceed 80 percent. (Percentage of submergence for a given discharge is defined as the ratio, expressed as a percentage, of the stage in the natural channel immediately downstream from the throat reach to the stage at the stage-measurement site, both stages being referred to the floor elevation of the flume at the stage-measurement site.)

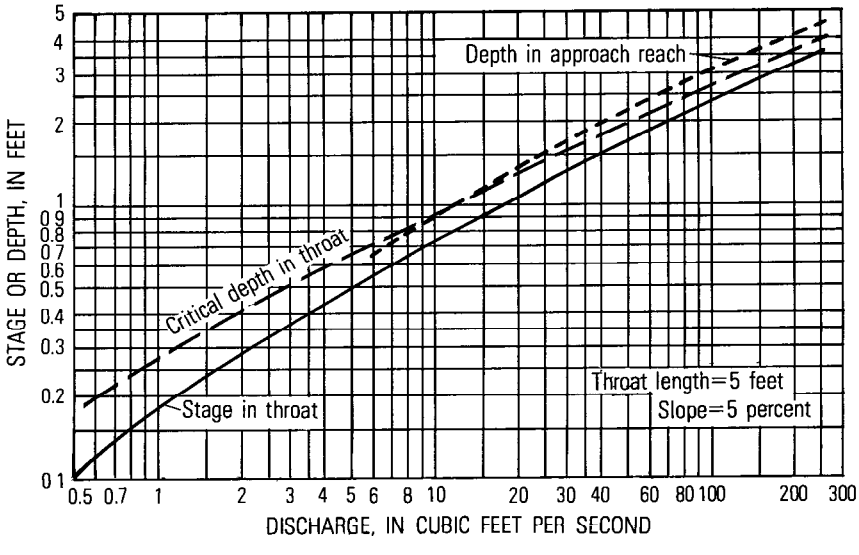

FIGURE 161.—Stage-discharge relation and significant depth-discharge relations for 1-ft trapezoidal supercritical-flow flume.

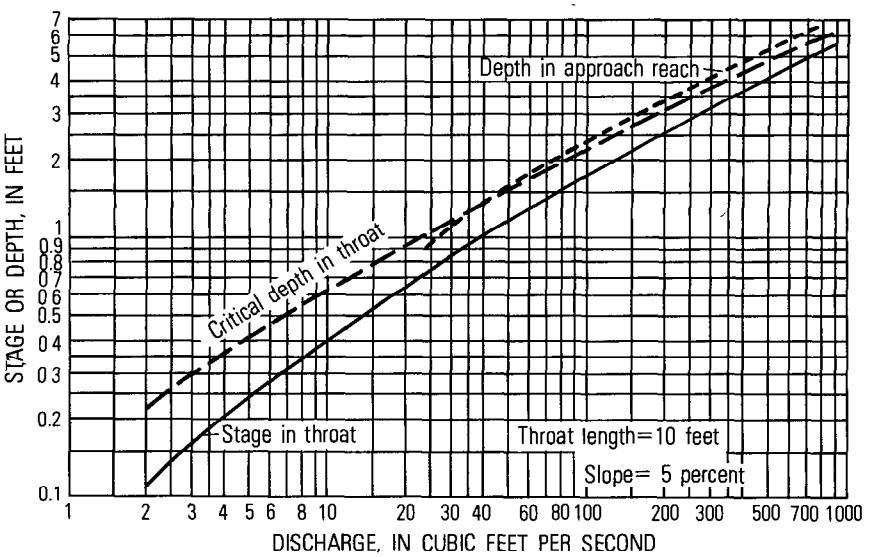

FIGURE 162.—Stage-discharge relation and significant depth-discharge relations for 3-ft trapezoidal supercritical-flow flume.

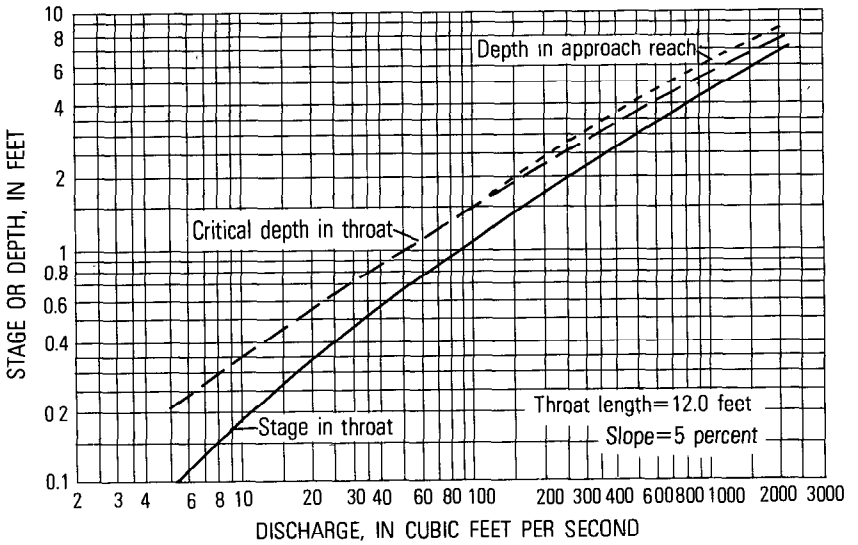

FIGURE 163.—Stage-discharge relation and significant depth-discharge relations for 8-ft trapezoidal supercritical-flow flume.

Also shown on each of the three rating-curve graphs are curves labeled "critical depth in throat" and "depth in approach reach." These curves are used to obtain the heights of sidewalls required to

contain the maximum discharge for which the flume is designed. For example, let us assume that an 8-ft flume is to be built to gage a range of discharges whose maximum value is 1200 ft^3/s. Figure 163 shows that the theoretical stage for that discharge is 5.2 ft; the height of the throat sidewall (critical depth) is shown to be 6.0 ft and the height of the approach sidewall is 6.8 ft. To those sidewall heights will be added at least 0.5 ft of freeboard, and the top of the sidewalls in the converging reach will be sloped uniformly to join the tops of the sidewalls of the approach and throat reaches.

Up to this point little has been said concerning the approach reach. Its sidewalls are extended upstream from the converging reach by means of rock fill or concrete to meet the natural channel banks. As long as the approach reach provides a smooth transition from the natural channel to the converging reach, its actual geometry will have no effect on the theoretical rating. The level floor of the approach reach will provide a site for current-meter measurements of discharge and will also induce the deposition of large debris, thereby helping to keep the more vital parts of the flume structure free of sediment deposition.

NATURAL SECTION CONTROLS

Natural section controls, listed in order of permanence, are usually a rock ledge outcrop across the channel, or a riffle composed of loose rock, cobbles, and gravel, or a gravel bar. Less commonly, the section control is a natural constriction in width of the channel, or is a sharp break in channel slope, as at the head of a cascade or brink of a falls.

Where the control is a rock outcrop, riffle, or gravel bar, the stage-discharge relation, when plotted on logarithmic paper, conforms to the general principles discussed for broad-crested artificial controls. If the natural control is essentially horizontal for the entire width of the control, the head on the control is the difference between the gage heights of the water surface and the crest of the control. The exponent (N) of the head in the equation of discharge,

$$Q = p(G - e)^N \tag{53}$$

will be greater than the theoretical value 1.5, primarily because of the increase in velocity of approach with stage. If the crest of the control has a roughly parabolic profile, as most natural controls have (greater depths on the control near midstream), the exponent N will be even larger because of the increase in width of the stream with stage, as well as the increase in velocity of approach with stage. The value of N will almost always exceed 2.0. If the control is irregularly

notched, as is often the case, the gage height of effective zero flow (e) for all but the lowest stages, will be somewhat greater than that for the lowest point in the notch. (The method of determining values of e was explained in the section titled, "Graphical Plotting of Rating Curves.")

The above principles are also roughly applicable to the discharge equations for an abrupt width contraction or an abrupt steepening of bed slope. The exponent N and the gage height of effective zero flow are influenced, as described above, by the transverse profile of the streambed at the control cross section.

An example of natural section control is treated in the following discussion.

COMPOUND SECTION CONTROLS

Where the control section is a local rise in the streambed, as at a rock outcrop, riffle, or gravel bar, that cross section is invariably a control only for low flows. The gaging station in that circumstance has a compound control, the high flows being subject to channel control. Occasionally there is a second outcrop or riffle, downstream from the low-water riffle, that acts as a section control for flows of intermediate magnitude. When the control for intermediate stages is effective it causes submergence of the low-water control. At high flows the section control for intermediate stages is in turn submerged when channel control becomes effective. An example of a compound control involving two section controls follows; an example of a compound control involving a section control that is submerged when channel control becomes effective is described in the section titled, "Compound Controls Involving Channel Control."

Figure 164 shows the rating for the compound section control at the gaging station on Muncy Creek near Sonestown, Pa. The control consists of two rock-ledge riffles, effective zero flow (e) for very low stages being at gage height 1.3 feet and for higher stages at gage height 1.2 feet. If the low end of the rating is made a tangent, it means that too large a value of e is used for the high end of the rating (1.3 ft vs 1.2 ft), and the high-water end of the curve becomes concave downward. Conversely, if the high end of the curve is made a tangent, the low-water end of the curve becomes concave upward. The high-water tangent of the curve has a greater value of exponent N than the low-water tangent of the other curve. This difference in the values of N reflects the effect of differences in the geometries of the two controls as well as the effect of increased rate of change of approach velocities at the higher stages. The slopes of the two tangents are 2.9 and 2.2, both values being greater than the theoretical slope of 1.5.

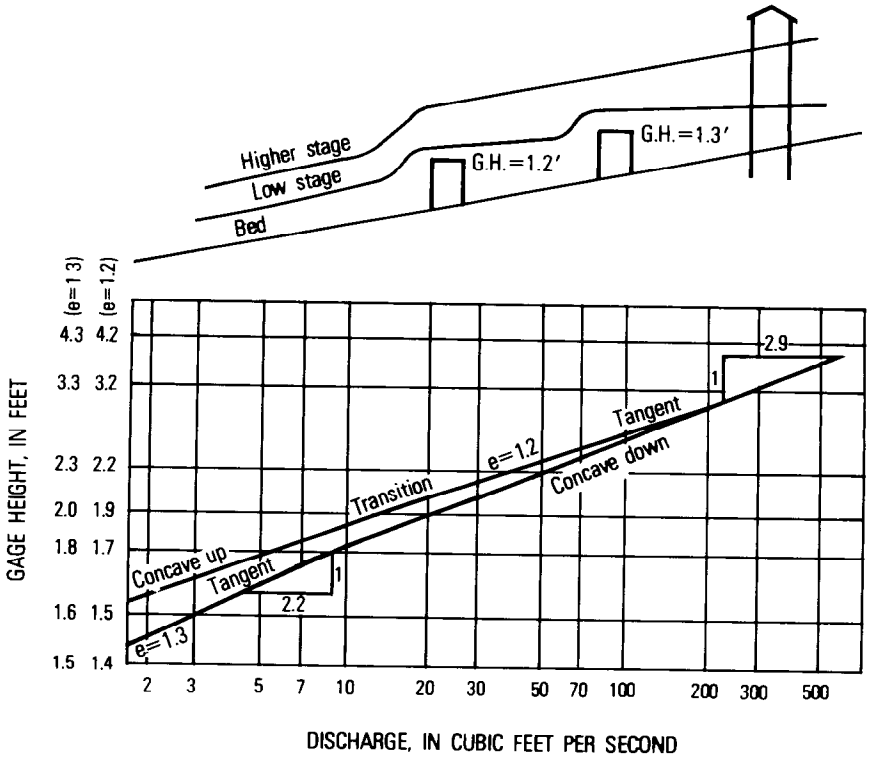

FIGURE 164.—Rating curve for a compound section control at Muncy Creek near Sonestown, Pa.

CHANNEL CONTROL

CHANNEL CONTROL FOR STABLE CHANNELS

The term "stable channels," as used in this report, is a relative term. Virtually all natural channels are subject to at least occasional change as a result of scour, deposition, or the growth of vegetation, but some alluvial channels, notably those whose bed and banks are composed of sand, have movable boundaries that change almost continuously, as do their stage-discharge relations. For the purpose of this manual, stable channels include all but sand channels. Sand channels are discussed in the section titled, "Sand-Channel Streams."

Almost all streams that are unregulated by man have channel control at the higher stages, and among those with stable channels, all but the largest rivers have section control at low stages. Because this section of the manual discusses only stable channels that have channel control for the entire range of stage experienced, the discussion is limited to the natural channels of extremely large rivers and

to artificial channels constructed without section controls. The artificial channels may be concrete-lined, partly lined or rip-rapped, or unlined. Streams that have compound controls involving channel control are discussed in the section titled, "Compound Controls Involving Channel Control."

The Manning discharge equation for the condition of channel control, as discussed in chapter 9, under the heading, "Slope-Area Method," is

$$Q = \frac{1.486}{n} AR^{2/3}S^{1/2} \text{ (English units)}, \tag{65}$$

or

$$Q = \frac{1}{n} AR^{2/3}S^{1/2} \text{ (metric units)} \tag{66}$$

In analyzing an artificial channel of regular shape, whose dimensions are fixed, flow at the gage is first assumed to be at uniform depth. Consequently, for any stage all dimensions on the right side of the equations are known except n. A value of n can be computed from a single discharge measurement, or an average value of n can be computed from a pair of discharge measurements, and thus a preliminary rating curve for the artificial channel can be computed for the entire range of stage from the results of a pair of discharge measurements. If subsequent discharge measurements depart from the computed rating curve, it is likely that the original assumption of flow at uniform depth was erroneous. That means that the energy slope, S, is not parallel to the bed slope, but varies with stage, and that the value of n, which was computed on the basis of bed slope, is also in error. The rating curve must be revised to fit the plotted discharge measurements, but the preliminary rating curve may be used as a guide in shaping the required extrapolation of the rating curve. The extrapolation should also be checked by application of the conveyance-slope method of rating extrapolation, which is described in the section titled, "Conveyance-Slope Method."

To understand the principles that underlie the stage-discharge relation for channel control in a natural channel of irregular shape we return to the Manning equation and make some simplifying assumptions in that equation. We assume, not unreasonably, that at the higher stages n is a constant and that the energy slope (S) tends to become constant. Furthermore, area (A) is approximately equal to depth (D) times width (W). We make the substitution for A in equation 65 or 66, and by expressing $S^{1/2}/n$ as a constant, C_1, we obtain

$$Q = C_1 (D) (W) R^{2/3}. \text{ (approx.)}$$

If the hydraulic radius (R) is considered equal to D, and W is considered a constant, the equation becomes

$$Q = CD^{1.67} = C(G-e)^{1.67} \text{ (approx.)} \quad (67)$$

However, unless the stream is exceptionally wide, R is appreciably smaller than D. This has the effect of reducing the exponent in the last equation although this reduction may be offset by an increase of S or W with discharge. Changes in roughness with stage will also affect the value of the exponent. The net result of all these factors is a discharge equation of the form

$$Q = C\,(G-e)^N$$

where N will commonly vary between 1.3 and 1.8 and practically never reach a value as high as 2.0.

An example of a discharge rating for channel control in a natural stream is given in the following section, where compound controls that involve channel control are discussed.

COMPOUND CONTROLS INVOLVING CHANNEL CONTROL

In the preceding section mention was made of the fact that compound control of the stage-discharge relation usually exists in natural channels, section control being effective for the lower stages and channel control being effective for the higher stages. An example of that situation is shown in figure 165, the rating curve for the Susquehanna River at Harrisburg, Pa. The low-water control is a low weir with zero flow at gage height 2.2 feet. At a stage of 3.9 feet this control starts to drown out and channel control becomes effective. If the low end of the rating is made a tangent, a value of $e = 2.2$ ft must be used. Because the value of e for the upper end of the rating is something less than 2.2 feet, the high end becomes concave downward. If the high end of the curve is made a tangent, the effective value of e is found to be 0.0 ft. This being too low a value of e for the lower end of the curve, the low end becomes concave upward.

If the rating for a section control (low end of the curve) is a tangent, the value of the exponent N is expected to be greater than 2.0. In this example, $N = 2.3$. If the rating for a channel control (high end of the curve) is a tangent, the value of N is expected to be less than 2.0, and probably between 1.3 and 1.8. In this example $N = 1.3$. Should overbank flow occur the rating curve will bend to the right.

It can be demonstrated, nonrigorously, that straight-line rating curves for section control almost always have a slope greater than 2.0 and that those for channel control have a slope less than 2.0. It has

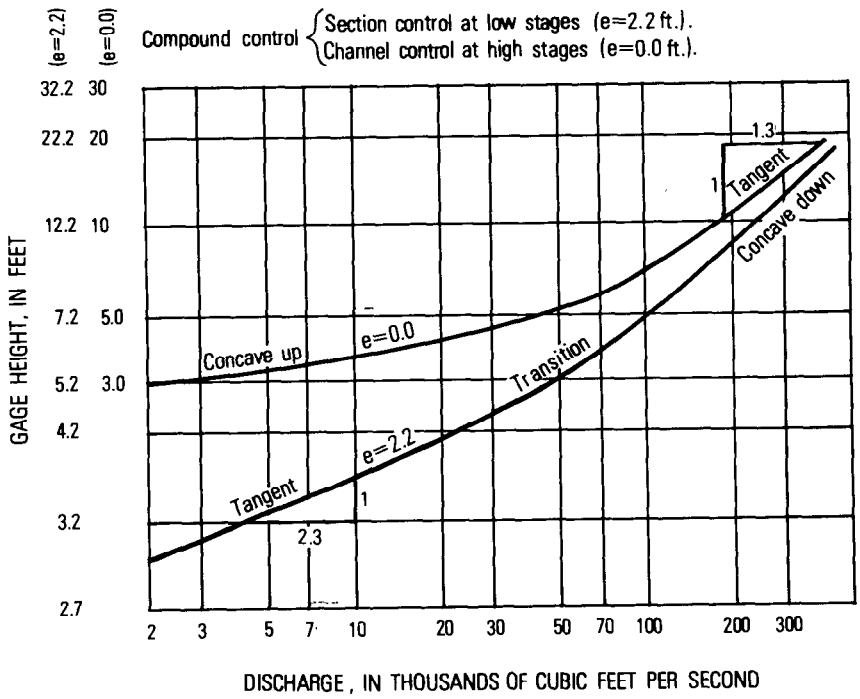

FIGURE 165.—Rating curve for a compound control at Susquehanna River at Harrisburg, Pa.

been shown that the equation for a straight-line rating on log paper is $Q = CH^N$, where N is the slope of the line. The first derivative of this equation is a measure of the change in discharge per tenth of a foot change in stage. The first derivative is:

$$\frac{dQ}{dH} = CNH^{N-1}.$$

Second differences are obtained by differentiating again. The second derivative is:

$$\frac{d^2Q}{dH^2} = CN\ (N-1)H^{N-2}.$$

Examination of the second derivative shows that second differences increase with stage when N is greater than 2.0 and decrease with stage when N is less than 2.0.

The hypothetical rating for a compound control is shown in table 20. This rating represents the condition of section control at the lower

TABLE 20.—*Hypothetical stage-discharge rating for a compound control*

[The higher values of discharge are rounded as normally used in a rating table; the precise values that required rounding are in parentheses]

Gage height (ft)	Discharge (ft ^{3}/s)	Difference per tenth of a foot	Second difference
1.0	100		
		20	
1.1	120		1
		21	
1.2	141		1
		22	
1.3	163		2
		24	
1.4	187		2
		26	
1.5	213		3
		29	
1.6	242		3
		32	
1.7	274		4
		36	
1.8	310		3
		40 (39)	
1.9	350 (349)		2
		40 (41)	
2.0	390		2
		45 (43)	
2.1	435 (433)		2
		45 (45)	
2.2	480 (478)		2
		45 (47)	
2.3	525		1
		50 (48)	
2.4	575 (573)		1
		50 (49)	
2.5	625 (622)		1
		50 (50)	
2.6	675 (672)		1
		50 (51)	
2.7	725 (723)		1
		50 (52)	

stages and channel control at the higher stages. If two values of discharge are shown for an item in the rating table, the figure in parenthesis is the exact value and the figure without a parenthesis is the "rounded" value that normally would be used in the rating table. Experienced hydrographers will recognize the progression of discharge values in this table as being typical. Inspection of the second difference column shows the second differences to be increasing at the low-water end (section control, $N > 2$) and decreasing at the high-water end (channel control, $N < 2$). These are the results that one would predict from the discussion in the preceding paragraph.

EXTRAPOLATION OF RATING CURVES

Rating curves, more often than not, must be extrapolated beyond the range of measured discharges. The preceding material in this

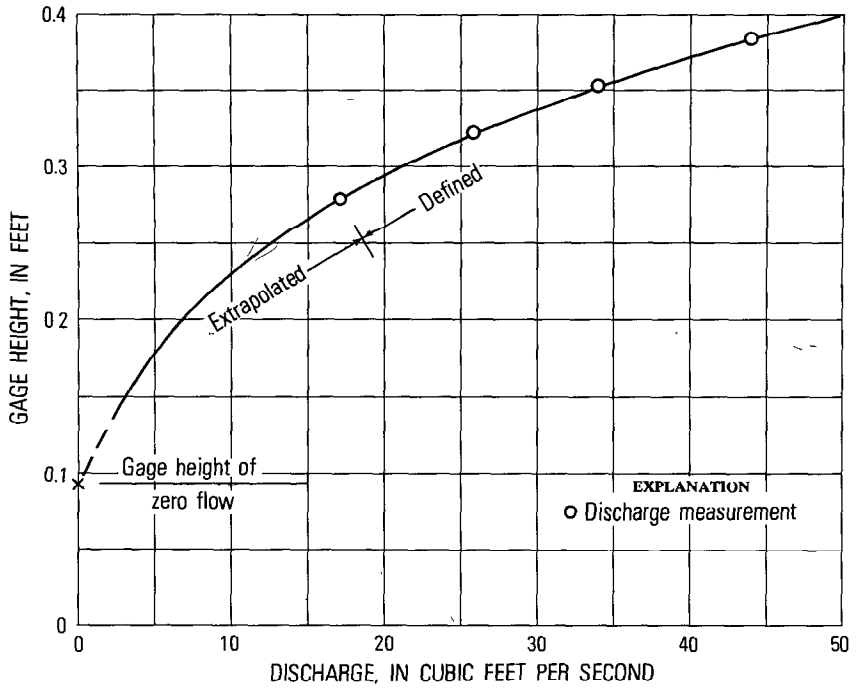

FIGURE 166.—Example of low-flow extrapolation on rectangular-coordinate graph paper.

chapter explained the principles governing the shape of logarithmic rating curves to guide the hydrographer in shaping the extrapolated segment of a rating. However, even with a knowledge of those principles, a large element of uncertainty exists in the extrapolation process. The purpose of this section of the manual is to describe methods of analysis that will reduce the degree of uncertainty.

LOW-FLOW EXTRAPOLATION

Low-flow extrapolation is best performed on rectangular-coordinate graph paper because the coordinates of zero flow can be plotted on such paper. (Zero discharge cannot be plotted on logarithmic graph paper.) An example of such an extrapolation is shown in figure 166, where the circled points represent discharge measurements plotted on the coordinate scales of gage height versus discharge. The rating in the example is defined by the measurements down to a gage height of 0.28 ft, but an extrapolation to a gage height of 0.14 ft is required. Field observation has shown the low point on the control (point of zero flow) to be at gage height 0.09 ft.

The method of extrapolation in figure 166 is self-evident. A curve

has been drawn between the plotted points at gage heights 0.09 ft and 0.28 ft to merge smoothly with the rating curve above 0.28 ft. There is no assurance that the extrapolation is precise—low-flow discharge measurements are required for that assurance—but the extrapolation shown is a reasonable one.

HIGH-FLOW EXTRAPOLATION

As mentioned in the "Introduction" of this chapter, the problem of high-flow extrapolation can be avoided if the unmeasured peak discharge for the rating is determined by the use of the indirect methods discussed in chapter 9. In the absence of such peak-discharge determinations, estimates of the discharges corresponding to high values of stage may be made by using one or more of the following four techniques:

1. conveyance-slope method,
2. areal comparison of peak-runoff rates,
3. step-backwater method, and
4. flood routing.

As a matter of fact, only as a last resort should the rating curve be extrapolated beyond a discharge value equal to twice the greatest measured discharge. If a greater extrapolation is required, the hydrologist should first try to define the upper end of the rating by use of one of the indirect peak-discharge determination methods of chapter 9. If for some reason, that course of action is not feasible, he should then use at least one of the four techniques listed above.

The knowledgeable reader of this manual may notice the absence from the above list of two techniques that used to be standard practice—the velocity-area method and the Q vs $Ad^{1/2}$ method. The Q vs $Ad^{1/2}$ method was superior to the velocity-area method and largely supplanted it; similarly, the conveyance-slope method, because of its superiority, has, in the last two decades, largely supplanted the Q vs $Ad^{1/2}$ method. Of the three somewhat similar methods, only the conveyance-slope method is described here, because a description of the two earlier methods (Corbett and others, 1943, p. 91–92) would have only academic, rather than practical, value.

CONVEYANCE-SLOPE METHOD

The conveyance-slope method is based on equations of steady flow, such as the Manning equation. In the Manning equation,

$$Q = KS^{1/2}. \tag{68}$$

The conveyance, K, equals $\frac{1.486}{n} AR^{2/3}$ when English units are used,

and $K=\frac{1}{n}AR^{2/3}$ when metric units are used. Values of A and R corresponding to any stage can be obtained from a field survey of the discharge-measurement cross section, and values of the coefficient n can be estimated in the field. Thus, the value of K, embodying all the elements that can be measured or estimated, can be computed for any given stage. (We shall soon see that errors in estimating n are usually not critical.) Values of gage height vs K, covering the complete range of stage up to the required peak gage height, are computed and plotted on rectangular graph paper. A smooth curve is fitted to the plotted points.

Values of slope, S, which is actually the energy gradient, are usually not available even for measured discharges. However, for the measured discharges, $S^{1/2}$ can be computed by dividing each measured discharge by its corresponding K value; S is then obtained by squaring the resulting value of $S^{1/2}$. Values of gage height vs S for the measured discharges are plotted on rectangular graph paper, a curve is fitted to the plotted points, and the curve is extrapolated to the required peak gage height. The extrapolation is guided by the knowledge that S tends to become constant at the higher stages. That constant slope is the "normal" slope, or slope of the streambed. If the upper end of the defined part of the curve of gage height vs S indicates that a constant or near-constant value of S has been attained, the extrapolation of the curve can be made with confidence. The discharge for any particular gage height will be obtained by multiplying the corresponding value of K from the K curve by the square root of the corresponding value of S from the S curve. We see that errors in estimating n will have minor effect because the resulting percentage error in computing K is compensated by a similar percentage error in the opposite direction in computing $S^{1/2}$. In other words, the constancy of S is unaffected, but if K is, say, 10 percent high, $S^{1/2}$ will be 10 percent low, and the two discrepancies are canceled when multiplication is performed. However, if the upper end of the defined part of the curve of gage height vs S has not reached the stage where S has a near-constant value, the extrapolation of the curve will be subject to uncertainty. In that situation the general slope of the streambed, as determined from a topographic map, provides a guide to the probable constant value of S that should be attained at high stages.

As mentioned in the preceding paragraph, the discharge for any particular gage height is obtained by the multiplication of appropriate values of K and $S^{1/2}$, and in that manner the upper end of the stage-discharge relation is constructed.

Figure 167 provides an example of the conveyance-slope method, as used for rating-curve extrapolation at the gaging station on Klamath River at Somes Bar, Calif. The conveyance curve is based on

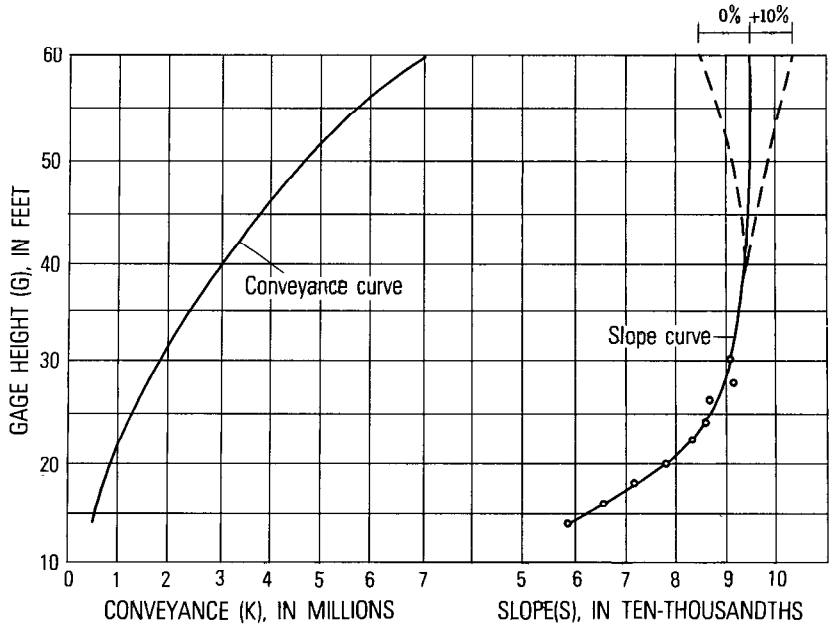

FIGURE 167.—High-flow extrapolation by use of conveyance-slope method—Klamath River at Somes Bar, Calif.

values of K computed from the geometry of the measurement cross section. The slope curve is defined to a gage height of 30 ft by discharge measurements (circled points), and extrapolated as the solid line to the peak gage height of 60 ft. It appears highly unlikely that the slope curve at a gage height of 60 ft will fall outside the limiting dashed curves shown in figure 167; in other words, it appears unlikely that the value of S at 60 ft (0.00095) is in error by more than ± 10 percent. If that is true, when the square root of S is computed and then used in a computation of peak discharge, the error for both $S^{1/2}$ and Q reduces to ± 5 percent. Although the attainment of so high an accuracy is highly improbable, the fact remains that one can place considerable confidence in the discharge computed for a gage height of 60 ft in this example. It should be mentioned here that the likelihood of a decrease in slope at high stages, as shown by the dashed curve on the left of the slope curve, is greatest when overbank flows occur.

In the above example conditions were ideal for application of the conveyance-slope method, and the example in figure 167 may therefore be misleading with regard to the general accuracy of the method. The conveyance-slope method assumes first that the geometry of the cross-section used for discharge measurements is fairly representa-

tive of that of a long reach of downstream channel. The need to meet this assumption immediately eliminates from consideration those gaging stations where discharge measurements are made at constricted cross sections, such as occur at many bridge- and cableway-measurement sections.

The conveyance-slope method also assumes that slope tends to become constant (uniform flow) at the higher stages. That is strictly true only for long, straight channels of uniform cross section, but natural channels that meet that description are virtually nonexistent. Consequently, the slope-stage relation may be anything but a vertical line at the upper stages. In the example in figure 167, a judgment decision, based on a knowledge of the channel characteristics, was made concerning the "probable" limiting positions of the stage-slope relation—the dashed lines on the graph—to give some idea of the "probable" error of the discharge computation. However, even given that knowledge of channel characteristics, if the two highest discharge measurements (two highest circles on the slope curve) had not been available it would have been impossible to position the upper end of the slope curve with any confidence. Fortunately there is a mitigating factor; an error of even as much as 40 percent in the value of slope at the upper end of the slope curve would give an error in discharge of either +18 percent ($\sqrt{1.40}-1.0=0.18$) or −23 percent ($1.0-\sqrt{0.60}=0.23$), depending on whether the estimate of slope was high or low.

In summary, the conveyance-slope method is a helpful adjunct in extrapolating rating curves, but its limitations must be understood so that it is not misused.

AREAL COMPARISON OF PEAK-RUNOFF RATES

When flood stages are produced over a large area by an intense general storm, the peak discharges can often be estimated, at gaging stations where they are lacking, from the known peak discharges at surrounding stations. Usually each known peak discharge is converted to peak discharge per unit of drainage area before making the analysis. In other words, peak discharge is expressed in terms of cubic feet per second per square mile or cubic meters per second per square kilometer.

If there has been relatively little difference in storm intensity over the area affected, peak discharge per unit area may be correlated with drainage area alone. If storm intensity has been variable, as in mountainous terrain, the correlation will require the use of some index of storm intensity as a third variable. Figure 168 illustrates a multiple correlation of that type where the independent variables

used were drainage area and maximum 24-hour basinwide precipitation during the storm of December 1964 in north coastal California.

The peak discharges estimated by the above method should be used only as a guide in extrapolating the rating curve at a gaging station. The basic principles underlying the extrapolation of logarithmic rating curves are not to be violated to accommodate peak-discharge values that are relatively gross estimates, but the estimated discharges should properly be given consideration in the extrapolation process.

STEP-BACKWATER METHOD

The step-backwater method is a technique in which water-surface profiles for selected discharges are computed by successive approximations. The computations start at a cross section where the stage-discharge relation is known or assumed, and they proceed to the gage site whose rating requires extrapolation. If flow is in the subcritical regime, as it usually is in natural streams, the computations must proceed in the upstream direction; computations proceed in the downstream direction if flow is in the supercritical regime. In the discussion that follows, the usual situation of subcritical flow will be assumed.

Under conditions of subcritical flow, water-surface profiles converge upstream to a common profile. For example, the stage for a given discharge at a gated dam may have a wide range of values depending on the position of the gates. At a gaging station far enough upstream to be beyond the influence of the dam, the stage for that discharge will be unaffected by the gate operations. Consequently, when the water-surface profile is computed for a given discharge in the reach between the dam and the gaging station, the segment of the computed profile in the vicinity of the gage will be unaffected by the value of stage that exists at the dam. However, it will be necessary that the computations start at the dam and proceed upstream, subreach by subreach (in "steps"). It follows, therefore, that if an initial cross section for the computation of the water-surface profile is selected far enough downstream from the gage, the computed water-surface elevation at the gage, corresponding to any given discharge, will have a single value regardless of the stage selected for the initial site.

A guide for determining the required distance (L) between gaging station and initial section is found in the dimensionless graph in figure 169. The graph, (Bailey and Ray, 1966), has for its equation,

---

FIGURE 168.—Relation of peak discharge to drainage area and maximum 24-hour basinwide precipitation in north coastal California, December 1964.

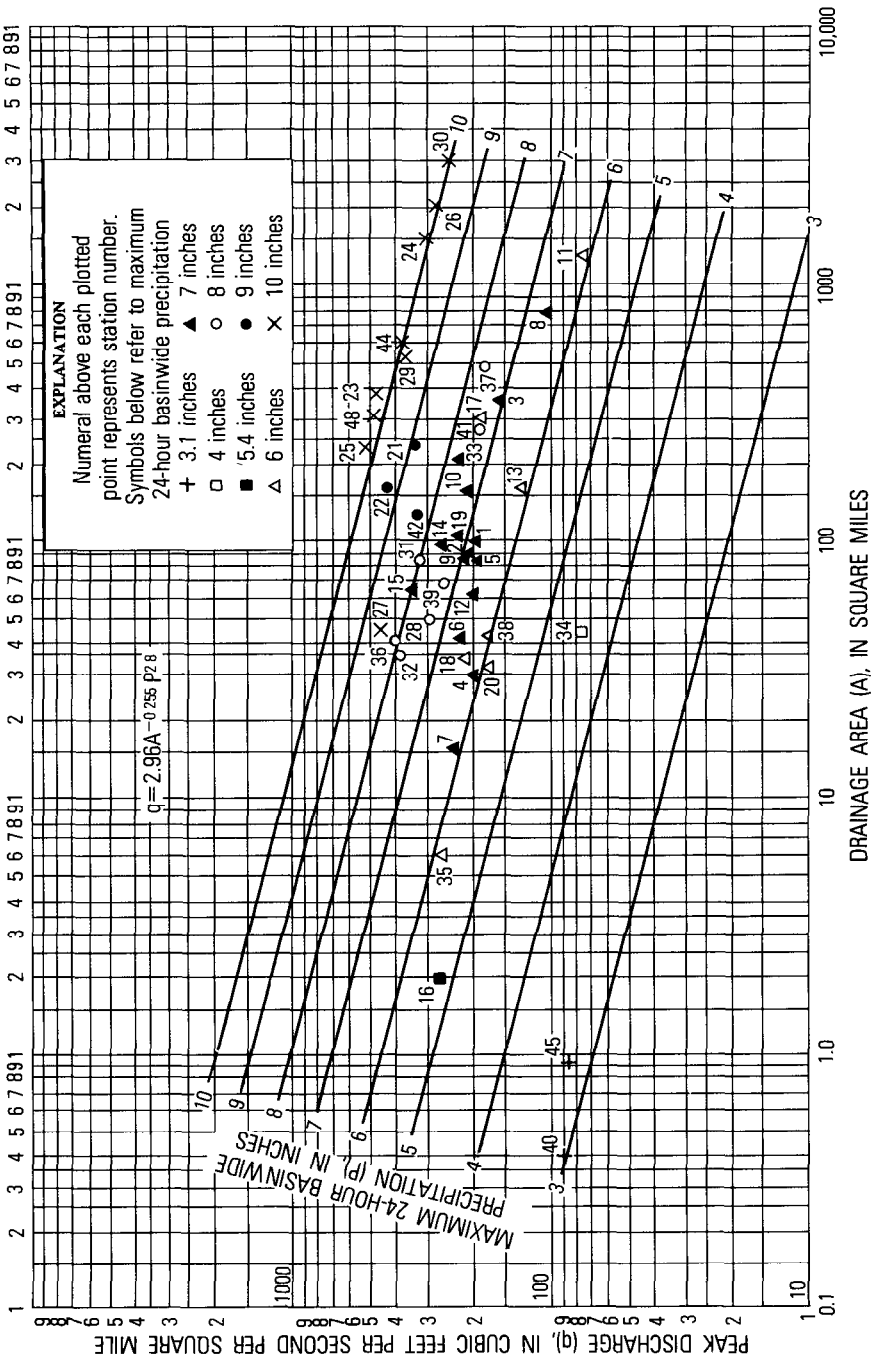
EXPLANATION
Numeral above each plotted point represents station number.
Symbols below refer to maximum 24-hour basinwide precipitation
+ 3.1 inches
▲ 7 inches
□ 4 inches
○ 8 inches
■ 5.4 inches
● 9 inches
△ 6 inches
× 10 inches
$q = 2.96A^{-0.255}P2.8$
MAXIMUM 24-HOUR BASINWIDE PRECIPITATION (P_t), IN INCHES
PEAK DISCHARGE (q_p), IN CUBIC FEET PER SECOND PER SQUARE MILE
DRAINAGE AREA (A), IN SQUARE MILES

$$\frac{LS_o}{\bar{d}} = 0.86 - 0.64\left(\frac{S_o C^2}{g}\right) \tag{69}$$

where

L is the distance required for convergence,
S_o is bed slope,
$\bar{d}$ is mean depth for the smallest discharge to be considered,
g is the acceleration of gravity, and
C is the Chezy coefficient.

If a rated cross section is available downstream from the gage, that cross section would be used as the initial section, of course, and there would be no need to be concerned with the above computation of L.

After the initial site is selected, the next step is to divide the study reach, that is, the reach between the initial section and the gaging station, into subreaches. That is done by selecting cross sections where major breaks in the high-water profile would be expected to occur because of changes in channel geometry or roughness. Those cross sections are the end sections of the subreaches. The cross sections are surveyed and roughness coefficients are selected for each subreach. That completes the field work for the study.

The first step in the computations is to select a discharge, Q, for study, and obtain a stage at the initial section for use with that value of discharge. If the initial section is a rated cross section, that stage will be known. If the initial section is not a rated cross section, an estimated stage there is computed from the estimated mean depth ($\bar{d}$) for discharge Q; $\bar{d}$ in turn is estimated by cut-and-try computations from a variation of the Chezy equation,

$$\bar{d} = \frac{Q^2}{(CA)^2 S_o} \tag{70}$$

where

C is the Chezy coefficient,
A is the cross-sectional area corresponding to $\bar{d}$, and
S_o is the bed slope (or water-surface slope).

Step-backwater computations are then applied to the subreach farthest downstream. We have a known or estimated stage at the downstream cross section for the value of Q being considered; the object of the computations is to determine the stage at the upstream end of the subreach that is compatible with that value of Q. The computation for each subreach is based on a steady-flow equation, such as the Chezy or Manning equation, after the equation has been modified for nonuniformity in the subreach by use of the difference in velocity head at the end cross sections. (See section in chapter 9 titled,

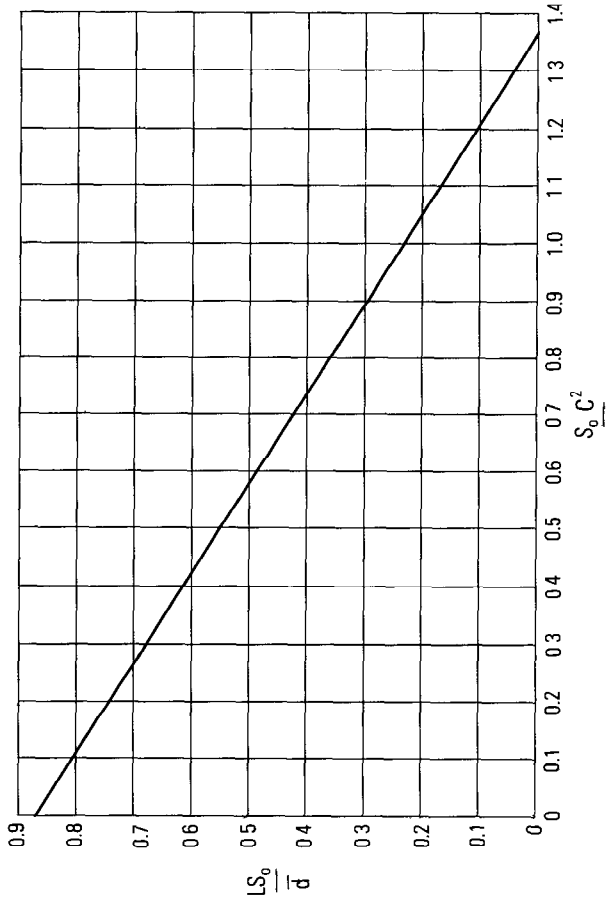

FIGURE 169.—Dimensionless relation for determining distance required for backwater profiles to converge.

"Slope-Area Method.") It will be recalled that the Chezy equation is related to the Manning equation by the formulas,

$$C = \frac{1.486}{n} R^{1/6} \text{ (English units)} \tag{71}$$

or

$$C = \frac{1}{n} R^{1/6} \text{ (metric units)} \tag{71a}$$

where n is the Manning roughness coefficient and R is the hydraulic radius.

By shifting terms in the modified Chezy equation, the following equation is obtained for the difference in water-surface elevation (Δh) between the upstream (subscript 1) and downstream (subscript 2) cross sections.

$$\Delta h = h_1 - h_2 = \frac{(\Delta L) V_1 V_2}{C^2 R_1^{1/2} R_2^{1/2}} + \frac{(\alpha_2 V_2^2 - \alpha_1 V_1^2)}{2g} (1+k), \tag{72}$$

where

h is stage;

ΔL is the length of the subreach;

V is average velocity in the cross section;

g is the acceleration of gravity;

k is a constant whose value is zero when $\alpha_2 V_2^2 > \alpha_1 V_1^2$; and whose value is 0.5 when $\alpha_2 V_2^2 < \alpha_1 V_1^2$; and

α is the velocity-head coefficient whose value is dependent on the velocity distribution in the cross section.

As for α, in many countries its value is assumed to be 1.1; in the U.S.A. its value is assumed to be 1.0 for cross sections of simple shape, but its value is computed for cross sections of complex shape that require subdivision. The equation used for that purpose is

$$\alpha = \frac{\Sigma (K_i^3/a_i^2)}{K_T^3/A_T^2}, \tag{73}$$

where the subscript i refers to the conveyance (K) or area (a) of the individual subsections, and the subscript T refers to the conveyance (K) or area (A) of the entire cross section. With regard to conveyance, K,

$$K_i = C a_i R_i^{1/2}, \text{ and } K_T = \Sigma K_i$$

We return to our computations for the downstream subreach. A trial value of stage for discharge Q is selected for the upstream cross

section, and values of A, V, and R are computed for the upstream and downstream cross sections. Those values are substituted in equations 72 and 73 and after solving for Δh, the computed value of Δh is compared with the difference between the trial value of stage at the upstream cross section and the known or assumed stage at the downstream cross section. Seldom will the two values agree after a single trial computation; if they do not agree, a second trial value of stage is selected for the upstream cross section. The computational procedure is repeated and the newly computed value of Δh is compared with its corresponding trial value. The computations are repeated as many times as are necessary to obtain agreement between the computed Δh and the difference between the trial stage at the upstream cross section and the known or assumed stage at the downstream cross section.

After a satisfactory value of stage has been determined for the upstream cross section, that cross section becomes the downstream cross section for the next subreach upstream. Computations similar to those described in the preceding paragraph are repeated for that subreach, and for each succeeding subreach, to provide a water-surface profile extending to the gaging station that is applicable to the discharge value (Q) being studied.

If the stage corresponding to discharge Q at the initial cross section was known, the stage computed for the gage is satisfactory. If the stage at the initial cross section was estimated from equation 70, it is necessary to repeat the above computations twice using other values of stage at the initial cross section for the same discharge Q. That is done to assure convergence of the water-surface profiles at the gage. The computations are repeated, first using an initial stage about 0.5 to 1.0 ft (0.15 to 0.30 m) higher than that originally used, and then using an initial stage about 0.5 to 1.0 ft lower than that originally used. All three sets of computations for discharge should result in almost identical values of stage at the gaging station for discharge Q. If they do not, the initial cross section for the step-backwater computation should be moved farther downstream, and all computations previously described must be repeated. If the three sets of computations give water-surface profiles that converge at a common stage at the gage, the entire procedure is repeated for other discharges until enough data are obtained to define the high-water rating for the gaging station.

From the preceding discussion it should be evident that the computations will be expedited if, in a preliminary step, the three relations of stage versus area (A), hydraulic radius (R), and conveyance (K), are computed for each cross section. Even then, the computations will be laborious and the use of a digital computer is therefore recommended.

The step-backwater method can be used to prepare a preliminary rating for a gaging station before a single discharge measurement is made. A smooth curve is fitted to the logarithmic plot of the discharge values that are studied. The preliminary rating can be revised, as necessary, when subsequent discharge measurements indicate the need for such revision. If the step-backwater method is used to define the high-water end of an existing rating curve, the discharge values investigated should include one or more of the highest discharges previously measured. By doing so, selected roughness coefficients can be verified, or can be modified so that step-backwater computations for the measured discharges provide stages at the gaging station that are in agreement with those observed. The computations for the high-water end of the rating can then be made with more confidence, in the knowledge that reasonable values of the roughness coefficients are being used. There will also be assurance of continuity between the defined lower part of the rating and the computed upper part.

FLOOD ROUTING

Flood-routing techniques may be used to test and improve the overall consistency of records of discharge during major floods in a river basin. The number of direct observations of discharge during such flood periods is generally limited by the short duration of the flood and the inaccessibility of certain stream sites. Through the use of flood-routing techniques, all observations of discharge and other hydrologic events in a river basin may be combined and used to evaluate the discharge hydrograph at a single site. The resulting discharge hydrograph can then be used with the stage hydrograph for that gage site to construct the stage-discharge relation for the site; or, if only a peak stage is available at the site, the peak stage may be used with the peak discharge computed for the hydrograph to provide the end point for a rating-curve extrapolation.

Flood-routing techniques, of which there are many, are based on the principle of the conservation of mass—inflow plus or minus change in storage equals outflow. It is beyond the scope of a stream-gaging manual to treat the subject of flood routing; it is discussed in most standard hydrology texts (for example, Linsley, Kohler, and Paulhus, 1949, p. 485–541).

SHIFTS IN THE DISCHARGE RATING

Shifts in the discharge rating reflect the fact that stage-discharge relations are not permanent but vary from time to time, either gradually or abruptly, because of changes in the physical features that form the control for the station. If a specific change in the rating

stabilizes to the extent of lasting for more than a month or two, a new rating curve is usually prepared for the period of time during which the new stage-discharge relation is effective. If the effective period of a specific rating change is of shorter duration, the original rating curve is usually kept in effect, but during that period shifts or adjustments are applied to the recorded stage, so that the "new" discharge corresponding to a recorded stage is equal to the discharge from the original rating that corresponds to the adjusted stage. For example, assume that vegetal growth on the control has shifted the rating curve to the left (minus shift), so that in a particular range of discharge, stages are 0.05 ft higher than they originally had been. To obtain the discharge corresponding to a recorded stage of, say, 1.30 ft, the original rating is entered with a stage of 1.25 ft (1.30−0.05) and the corresponding discharge is read. The period of time during which such stage adjustments are used is known as a period of shifting control.

Frequent discharge measurements should be made during a period of shifting control to define the stage-discharge relation, or magnitude(s) of shifts, during that period. However, even with infrequent discharge measurements the stage-discharge relation can be estimated during the period of shifting control if the few available measurements are supplemented with a knowledge of shifting-control behavior. This section of the report discusses such behavior. That part of the discussion that deals with channel-control shifts does not include alluvial channels, such as sand channels, whose boundaries change almost continuously; sand channels are discussed in the section titled, "Sand-Channel Streams."

The formation of ice in the stream and on section controls causes shifts in the discharge rating, but ice effect is not discussed here; it is discussed separately in the section titled. "Effect of Ice Formation on Discharge Ratings."

DETECTION OF SHIFTS IN THE RATING

Stage-discharge relations are usually subject to minor random fluctuations resulting from the dynamic force of moving water, and because it is virtually impossible to sort out those minor fluctuations, a rating curve that averages the measured discharges within close limits is considered adequate. Furthermore, it is recognized that discharge measurements are not error-free, and consequently an average curve drawn to fit a group of measurements is probably more accurate than any single measurement that is used to define the average curve. If a group of consecutive measurements subsequently plot to the right or left of the average rating curve, it is usually clearly evident that a shift in the rating has occurred. (An exception to that

statement occurs where the rating curve is poorly defined or undefined in the range of discharge covered by the subsequent measurements; in that circumstance the indication is that the original rating curve was in error and requires revision.) If, however, only one or two measurements depart significantly from a defined segment of the rating curve, there may be no unanimity of opinion on whether a shift in the rating has actually occurred, or whether the departure of the measurement (s) results from random error that is to be expected occasionally in measurements.

Two schools of thought exist with regard to identifying periods of shifting control. In the U.S.A. and many other countries, a pragmatic approach is taken that is based on certain guidelines and on the judgment of the analyst. In other countries, notably the United Kingdom, the approach used is based on statistical theory. (It is reiterated that the discussion that follows excludes the constantly shifting alluvial channels that are discussed in the section on "Sand-Channel Streams.")

In the U.S.A., if the random departure of a discharge measurement from a defined segment of the rating curve is within ±5 percent of the discharge value indicated by the rating, the measurement is considered to be a verification of the rating curve. If several consecutive measurements meet the 5-percent criterion, but they all plot on the same side of the defined segment of the rating curve, they may be considered to define a period of shifting control. It should be mentioned that when a discharge measurement is made, the measurement is computed before the hydrographer leaves the gaging station and the result is plotted on a rating curve that shows all previous discharge measurements. If the discharge measurement does not check a defined segment of the rating curve by 5 percent or less, or if the discharge measurement does not check the trend of departures shown by recent measurements, the hydrographer is normally expected to make a second discharge measurement to check his original measurement. However, at many stations the 5-percent criterion may be too stringent for low-flow measurements because of control insensitivity. At those installations departures in excess of 5 percent are generally acceptable if the indicated shift does not exceed 0.02 ft.

In making a check measurement, the possibility of systematic error is eliminated by changing the measurement conditions as much as possible. The meter and stopwatch are changed, or the stopwatch is checked against the movement of the second hand of a standard watch. If the measurements are being made from a bridge, boat, or cableway, the measurement verticals are changed by measuring at verticals between those originally used; if wading measurements are being made, a new measurement section is sought, or the meas-

urement verticals in the original section are changed. If the check measurement checks the original rating curve or current rating trend by 5 percent or less, the original discharge measurement will be given no consideration in the rating although it is still entered in the records. If the check measurement checks, by 5 percent or less, the original discharge measurement or the trend of that measurement if the stage has changed, the two measurements are considered to be reliable evidence of a new shift in the stage-discharge relation. If the check measurement fails to check anything that has gone before, a second check measurement is made and the most consistent two of the three measurements are used for rating analysis. The need for a second check measurement is a rarity, but it may possibly occur.

Thus, in the U.S.A., a single discharge measurement and its check measurement, even if unsupported by later measurements, may mark a period of shifting control. The engineer who analyzes the rating does have the responsibility of explaining the reason for the short-lived shift—it can often be explained as having started as a result of fill (or scour) on a preceding stream rise and as having ended as a result of scour (or fill) on the recession or on a following rise.

In the United Kingdom, the analysis of the rating starts in the usual way; the chronologically numbered discharge measurements are plotted on logarithmic graph paper and are fitted by eye with a smooth curve. Where compound controls exist, there may be one or more points of inflection in the curve. In the statistical analysis that follows, each segment of the rating curve between inflection points is treated separately. The standard deviation ($S_{//}$) of the plotted points, in percent, is computed for each segment, using the standard statistical equation,

$$S_{//} = \sqrt{\frac{\Sigma d^2}{N-1}} \quad , \tag{74}$$

where

d is the departure of a discharge measurement from the rating curve, in percent, and

N is the number of measurements used to define the segment of the rating curve.

Use of the standard deviation ($S_{//}$) in detecting rating shifts is explained as follows in ISO Recommendation R 1100 (1969, p. 15). On the average, 19 out of 20 measurements should depart from the particular segment of the rating curve by no more than $2S_{//}$ percent. Any subsequent discharge measurement that departs by a much greater percentage—say, $3S_{//}$ percent—can be regarded as the result of faulty measurement, except in those cases where two or more consecutive measurements, either chronologically or over a range of stage, appear to be well on one side of the $\pm 2S_{//}$ limit. Where that occurs, a change

in the stage-discharge relation is required—either in the form of a reconstruction of the original relation using the additional discharge measurements, or in the form of a new stage-discharge relation because a shift in the control is indicated.

In the United Kingdom, additional statistical tests are given the rating to assure that : (1) the discharge measurements show no preponderance of either plus or minus departures from the rating curve; (2) the number of "runs" of successive plus or minus departures from the rating, examined in ascending order of stage, are neither excessively large nor excessively small, and (3) the average percentage departure of all measurements from the rating curve does not differ significantly from zero.

In the U.S.A. the above statistical approach is not favored for several reasons. First, it is felt that the limiting criteria of $2S_p$ percent will usually exceed the 5 percent criteria preferred in the U.S.A. Second, any statistical approach gives equal weight to all discharge measurements used in the analysis. In the U.S.A. hydrographers rate the probable accuracy of the measurements they make on the basis of measuring conditions at the time, without reference to how closely the measurements plot on the rating curve. The feeling in the U.S.A. is that more weight in the analysis should be given to measurements rated good to excellent than to measurements rated fair to poor. Third, while it is agreed that in general an average curve drawn to fit a group of measurements is probably more accurate than any single measurement that is used to define the average curve, it is also felt in the U.S.A. that any subsequent measurement that is verified by a check measurement is more accurate than the rating-curve value of discharge, particularly at a station that is historically known to have rating-curve shifts.

RATING SHIFTS FOR ARTIFICIAL CONTROLS

Weirs.—Artificial controls are not subject to scour and fill by high flows, but the streambed immediately upstream from the weir may be so affected. If scour occurs in the pool formed by the weir, the pool is deepened and velocity of approach decreases. The net result is a smaller discharge for a given stage than under pre-scour conditions; that is, the rating curve for the period of scour will shift to the left of the rating curve for pre-scour conditions. The converse occurs if the weir pool has been subjected to deposition or fill.

The effect of such scour and fill on the stage-discharge relation is usually relatively minor, and usually can be expressed by a parallel shift of most of the section-control portion of the rating curve that is plotted as a straight line on logarithmic graph paper. If only a single discharge measurement is available for defining the parallel shift

curve, the shift curve is drawn to pass through that measurement. If more than one discharge measurement is available, and there is no evidence of a progressive rating shift with time, the parallel shift curve is drawn to average the discharge measurements. If the discharge measurements indicate a progressive rating shift with time, shifts are prorated with time. However, what may appear to be a gradually progressive shift, may in fact be several discrete shifts caused by individual peak flows whose occurrences are not widely separated in time. The shift in stage to be applied to recorded gage heights during the period of shifting control is determined from the vertical spacing between the original rating curve and the shift curve.

The shift, if attributable to fill, is considered to start after the peak discharge of a stream rise that preceded the first of the variant discharge measurements. Shift adjustments are therefore started on the recession of that rise. The shift, if attributable to scour, is considered to start during the high stages of a stream rise that preceded the first of the variant discharge measurements. Because those high stages generally occur when the section control is "drowned out" by channel control, the shift in the section-control segment of the rating is again commonly first applied after the peak discharge of the rise. The shifts are ended on a stream rise that follows the last variant discharge measurement, using the general principle that scour in the gage pool usually occurs during high stages and fill usually occurs during the recession of a stream rise.

The parallel shift discussed in a preceding paragraph requires some elaboration. A parallel shift of the rating curve on logarithmic graph paper indicates that for all stages the discharge changes by a fixed percentage, and that the difference in stage between the two lines increases with stage. However, it is not quite true that the discharge changes by a fixed percentage when the weir pool has scoured or filled. At extremely low flows there will be no effect because velocity of approach is negligible; that section of the original rating has a break in slope (see fig. 146; $G = 1.3$ ft), and the lower end of the parallel shift curve above the break in slope should be warped to join the extreme low-water curve. The effect of scour or fill on the percentage change in discharge increases rapidly with stage to a maximum value and then slowly decreases to a percent change that does not differ greatly from the maximum percentage. The parallel shift drawn through the available discharge measurement(s) will adequately fit those relatively large percentage changes in discharge at the higher stages; the warped section of the shift curve at the lower stages will adequately fit the rapidly increasing percentage change in discharge at those lower stages. Figure 170 illustrates the above discussion; the

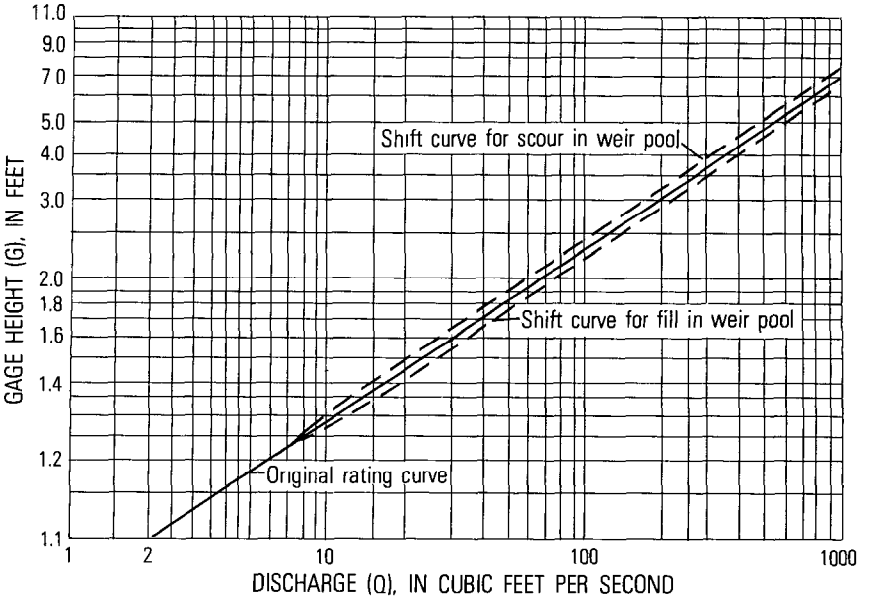

FIGURE 170.—Rating curve for hypothetical rectangular thin-plate weir, with shift curves for scour and fill in the weir pool.

original rating curve shown is a reproduction of that given in figure 146.

It has been mentioned frequently in this manual that section controls are usually submerged at high stages as a result of channel control becoming effective. The parallel shift curve described above should be extended to the stage where it either intersects the actual rating for channel control (in the case of scour in the weir pool) or can be warped into the rating for channel control (in the case of fill in the weir pool). If a shift has occurred simultaneously in the channel control (see section titled, "Rating Shifts for Channel Control"), the shift curves for the section-control and channel-control segments of the rating are drawn to form a continuous curve.

Up to now we have discussed changes in the velocity of approach that are caused only by scour and fill in the weir pool. The velocity of approach may also be affected by aquatic vegetation growing in the weir pool. Usually such an occurrence will reduce the velocity of approach by greatly increasing the friction loss, and the rating curve will shift to the left. However, the shift will not be abrupt, but will gradually increase as the growing season progresses. The aquatic growth in the pool may also encroach on the weir to the extent that the effective length (b) of the weir is reduced. The effect of a reduction in effective length of the weir is a parallel shift of the rating to the left

when plotted on logarithmic graph paper. At all stages the discharge will be reduced by a percentage that is equal to the percentage change in effective length of the weir. The shift will either decrease gradually as the vegetation dies in the dormant season, or the shift may terminate abruptly if the vegetation is washed out by a stream rise.

Moss or algal growth may sometimes attach itself to a weir crest and thereby reduce the head on the weir for any given gage height (G). The head will be reduced by a constant value that is equal to the thickness of the growth. In other words, in the equation, head$=G-e$, the value of e is increased by the thickness of the growth. The reduction in head causes the rating to shift to the left, it being displaced vertically by an amount equal to the thickness of the growth. If the shift rating is plotted on rectangular-coordinate graph paper, it will be parallel to the original rating. If the shift rating is plotted on logarithmic graph paper, it will be a curve that is concave upward and asymptotic to the original linear rating curve at the higher stages. The growth of algae or moss on the weir should be removed with a wire brush before it becomes heavy enough to affect the stage-discharge relation. The effect of the shift caused by the algal growth disappears during stages when channel control becomes effective.

Flumes.—Shifts in the stage-discharge relation for flumes are most commonly caused by changes in the approach section—either in the channel immediately upstream from the flume or in the contracting section of the flume upstream from the throat. In either event the change is caused by the deposition of rocks and cobbles that are too large to pass through the flume; the flume is self-cleaning with regard to sediment of smaller size. Manual removal of the large debris should restore the original discharge rating of the flume.

The deposition of rocks and debris upstream from the flume may divert most of the flow to the gage-side of the flume and the build-up of water at the gage will result in a shift of the discharge rating to the left. Conversely, if most of the flow is diverted to the side of the flume opposite the gage, the discharge rating will shift to the right. In the above situation, the shift curve is usually drawn parallel to the original rating curve on logarithmic graph paper in much the same manner as was described earlier for shifts resulting from scour and fill in the pool behind the weir.

If rocks and cobbles are deposited at the entrance to the throat of the flume, they will cause the discharge rating to shift to the left because the stage at the gage will be raised higher than normal for any given discharge. A similar backwater effect will result from the growth of algae at the entrance to the throat.

The backwater effect, or decrease in head for a given gage height

caused by deposition or algal growth at the entrance to the throat of the flume, has the effect of increasing the value of e in a linear logarithmic plot of the rating. The shift rating on logarithmic graph paper will be a curve that is concave upward and asymptotic to the original linear rating curve at the higher stages. The deposition of rocks and debris will be associated with a high-water event; the growth of algae will increase gradually with time.

Large rocks driven by high-velocity flow through the flume may erode the walls and floor of a concrete flume. The resulting increase in roughness and decrease in elevation of the concrete may cause shifts in the stage-discharge relation. The two effects tend to be compensating; an increase in roughness will shift the discharge rating to the left, and a decrease in elevation of the concrete surface will shift the discharge rating to the right. However, the latter effect usually predominates, particularly in supercritical-flow flumes.

RATING SHIFTS FOR NATURAL SECTION CONTROLS

The primary cause of changes in natural section controls is the high velocity associated with high discharge. Of those controls, a rock ledge outcrop will be unaffected by high velocities, but boulder, gravel, and sand-bar riffles are likely to shift, boulder riffles being the most resistant to movement and sand bars the least resistant. After a flood the riffles are often altered so drastically as to bear no resemblance to their pre-flood state, and a new stage-discharge relation must be defined. Minor stream rises usually move and sort the materials composing the riffle, and from the standpoint of the rating curve, the greatest effect is usually a change in the gage height of effective zero flow (e). The shift curve ideally should be defined by current-meter discharge measurements. However, if only one or two measurements are available for the purpose, they are examined and the gage-height shift that they indicate is applied to the section-control segment of the original rating curve. If the shift rating is plotted on rectangular paper, it will tend to be parallel to the original rating. The extreme low-water end of the curve can be extrapolated to the actual point of zero flow, as determined in the field when low-water discharge measurements are made. If the shift rating is plotted on logarithmic graph paper, it will be a curve that is either concave upward or downward, depending on whether the shift is to the left (increase in e) or the right (decrease in e). The shift curve will tend to be asymptotic to the linear rating at the higher stages of section control, but its precise slope in the range of stage where channel control is beginning to exert an effect, will depend on whether or not a shift has occurred in the channel-control segment of the rating curve.

(See section titled, "Rating Shifts for Channel Control.")

Vegetal growth in the approach channel of the control or on the control itself will affect the stage-discharge relation in the manner described on preceding pages, where rating shifts for weirs were discussed. Aquatic vegetation in the approach channel will affect the velocity of approach, and if the channel growth encroaches on the control, it may reduce the effective length of the control. Aquatic growth on the control itself will reduce the discharge corresponding to any given stage by reducing the head on the control and increasing the resistance to flow, and (or) by reducing the effective length of the control. The shifts associated with vegetal growth are cyclic and therefore change with time. The growth increases as the growing season progresses and declines during the dormant season, but shifts may terminate abruptly if the vegetation is washed out by a stream rise.

In temperate climates, accumulations of water-logged fallen leaves on section controls each autumn clog the interstices and raise the effective elevation of all section controls. The effect of an increase in the gage height of effective zero flow (e) is explained on a preceding page in the discussion of moss and algal growth on weirs. The build-up of water-logged leaves is progressive starting with the first killing frost (usually in October in the Northern Hemisphere) and reaching a maximum when the trees are bare of leaves. The first ensuing stream rise of any significance usually clears the control of fallen leaves.

Two other causes of backwater (increased gage height for a given discharge), unassociated with hydrologic events, also warrant discussion. Vacationers in the summer often use the gage pool for swimming, and they will often pile rocks on the control to create a deeper pool. This change in the height of the control manifests itself in the record of stage as an abrupt increase in gage height, usually during a rainless period, without any corresponding decline in stage that would be associated with the passage of a stream rise. The abrupt rise in stage fixes the time when the shift in the rating occurred; the magnitude of the change in stage is a measure of the change in the value of e. In some regions another cause of backwater is the construction of dams by beavers. These dams are built of boughs, logs, stones, and mud to create a pool that is part of the beavers' habitats. Again, the time of occurrence and the effect on the stage of the stream can be detected in the gage-height record which will show a gradual rise, usually over a period of a few days as the dam is being built, without the corresponding decline in stage that would be associated with a stream rise. The beaver dams usually remain in place until washed out by a high discharge.

RATING SHIFTS FOR CHANNEL CONTROL

As mentioned earlier, most natural streams have compound controls—section control for low-stages and channel control for high stages. The shifts in section control that were described on the preceding pages are commonly accompanied by shifts in channel control.

The most common cause of a shifting channel control, in a relatively stable channel, is scour or fill of the streambed caused by high-velocity flow. The scour usually occurs during a stream rise and fill usually occurs on the recession, but that statement is an oversimplification of the highly complex process of sediment transport. The degree of scour in a reach is dependent not only on the magnitude of the discharge and velocity, but also on the sediment load coming into the reach. On some streams it has been found that when scour is occurring in a pool at a meander bend there is simultaneous filling on the bar or riffle at the crossover, or point of inflection between successive meander bends; on other streams scour has been found to take place simultaneously through relatively long reaches of channel, both in pools and over bars. A further complication is the fact that the length of channel that is effective as a control is not constant, but increases with discharge.

From the preceding discussion it should be apparent that there is no really satisfactory substitute for discharge measurements in defining shifts in the channel-control segment of the rating; of particular importance are measurements made at or near the peak stage that occurs during periods of shifting control. However, in the usual situation a few (or less) measurements made at medium stages are the only ones available for analyzing channel-control shifts, and the shifts must be extrapolated to peak stages. The assumptions usually made in the rating analysis are those discussed below. The results are accepted unless they are shown to be invalid by a determination of peak discharge as described in chapter 9, or are shown to be invalid by use of one or more of the methods of rating-curve extrapolation as described in the section on "High-flow Extrapolation."

If a single predominantly large stream rise occurred shortly before the first measurement that indicated a shift, the shifts are assumed to have been caused solely by that rise. If more than one large stream rise occurred shortly before the first shift measurement, the shift curve may be prorated between rises. For example, if two rises of almost equal magnitude occurred just before the first shift measurement, and if the shift curve indicates a shift of 0.30 ft at a given stage, the shift to be used during the period between the two rises would be 0.15 ft at the given stage. It is often helpful to plot the shifts indicated by the discharge measurements against the observed stage of those measurements to obtain the trend of the shifts.

The pattern of scour and fill in the control channel determines whether the shift will increase with stage, decrease with stage, or be relatively constant at all stages. Figure 171 (graph *A*) illustrates a common situation where the shifts, either plus in the case of scour or minus in the case of fill, increase in absolute value as stage decreases. The highest value of the shift is assumed to be only slightly greater than the maximum value observed in order to avoid "overcorrecting" the original rating. Graph *B* of figure 171 shows the shift ratings corresponding to measurements nos. 1 and 2. The ratings have been plotted on rectangular-coordinate graph paper because the shifts are more easily visualized, at least by the inexperienced hydrographer, on that type of plotting paper. The stage-shift curve is usually plotted on rectangular-coordinate paper, but the rating curves are usually plotted on logarithmic graph paper. On logarithmic paper the shift curves in this example would converge more rapidly toward the original rating curve at high stages. The shift curves at low stages would be shaped to join smoothly with the shift curve for section control. The period for applying the shifts would be terminated on the stream rise following the last shift measurement; the original rating would be used on the recession from that rise.

In analyzing shifts there is no substitute for experience with a given stream because the shift pattern can often be interpreted logically in more than one way. For example, refer to the shift curve for channel fill in graph *B* of figure 171. Assume that measurements nos. 1 and 2 were made on a stream recession, and the measurement no. 1 was made a few days before measurement no. 2. Measurement no. 2 shows the effect of greater fill than measurement no. 1; fill usually occurs on a recession; therefore it is possible that the shifts should have been made to vary with time or to vary with time and stage, rather than with stage alone as shown in figure 171*A*. In the absence of additional knowledge the simplest interpretation is generally made, as was done here. Given more discharge measurements or a better knowledge of the behavior of the particular stream, a more accurate analysis can be made.

Figure 172 (graph *A*) illustrates a less common situation where the shifts increase as stage increases. Again the highest value of shift is assumed to be only slightly greater than the maximum value observed in order to prevent "overcorrecting" the original rating. Graph *B* of figure 172 shows the shift ratings corresponding to measurements nos. 1 and 2. The period for applying shifting-control corrections would be terminated on the stream rise following the last shift measurement; the original rating would be used on the rising limb of that rise. As in the case of figure 171, in the absence of additional knowledge, more than one interpretation can be given to

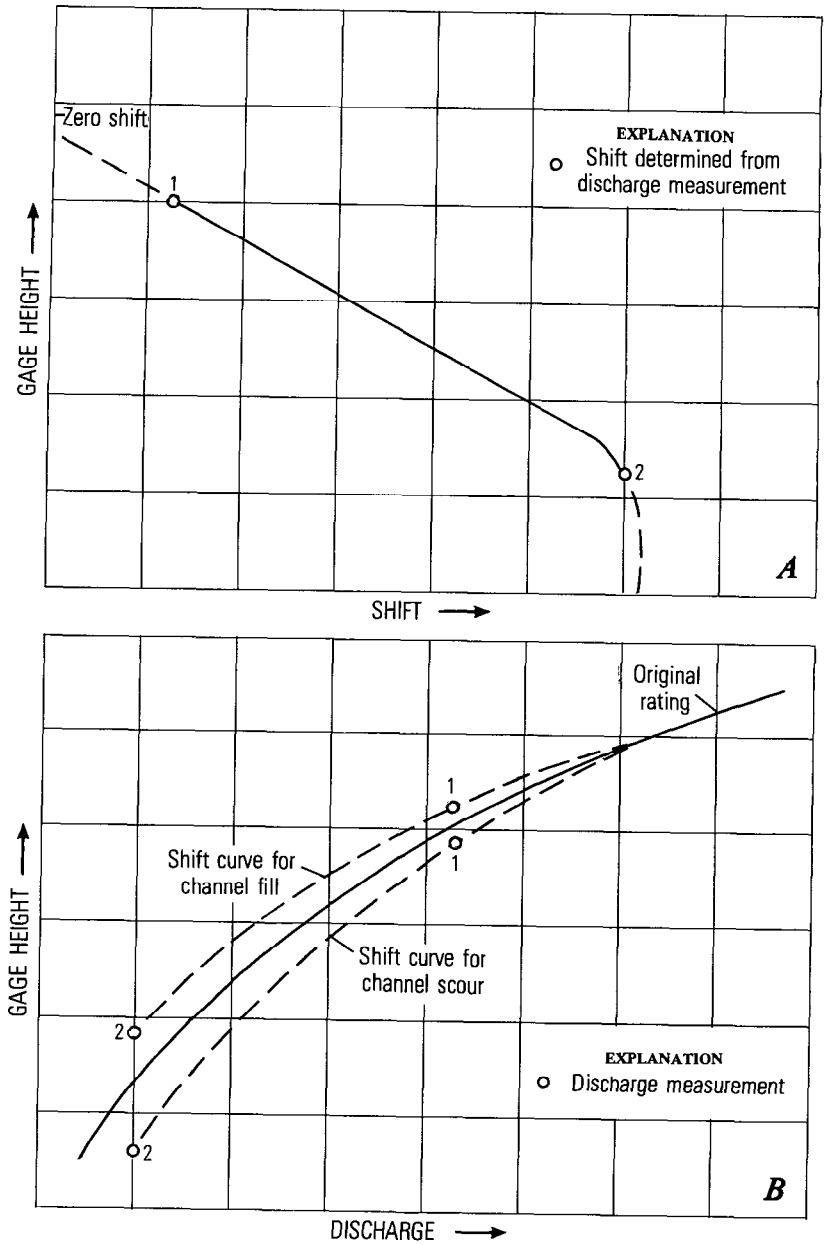

FIGURE 171.—First example of a stage-shift relation and the corresponding stage-discharge relation caused by scour or fill in the control channel.

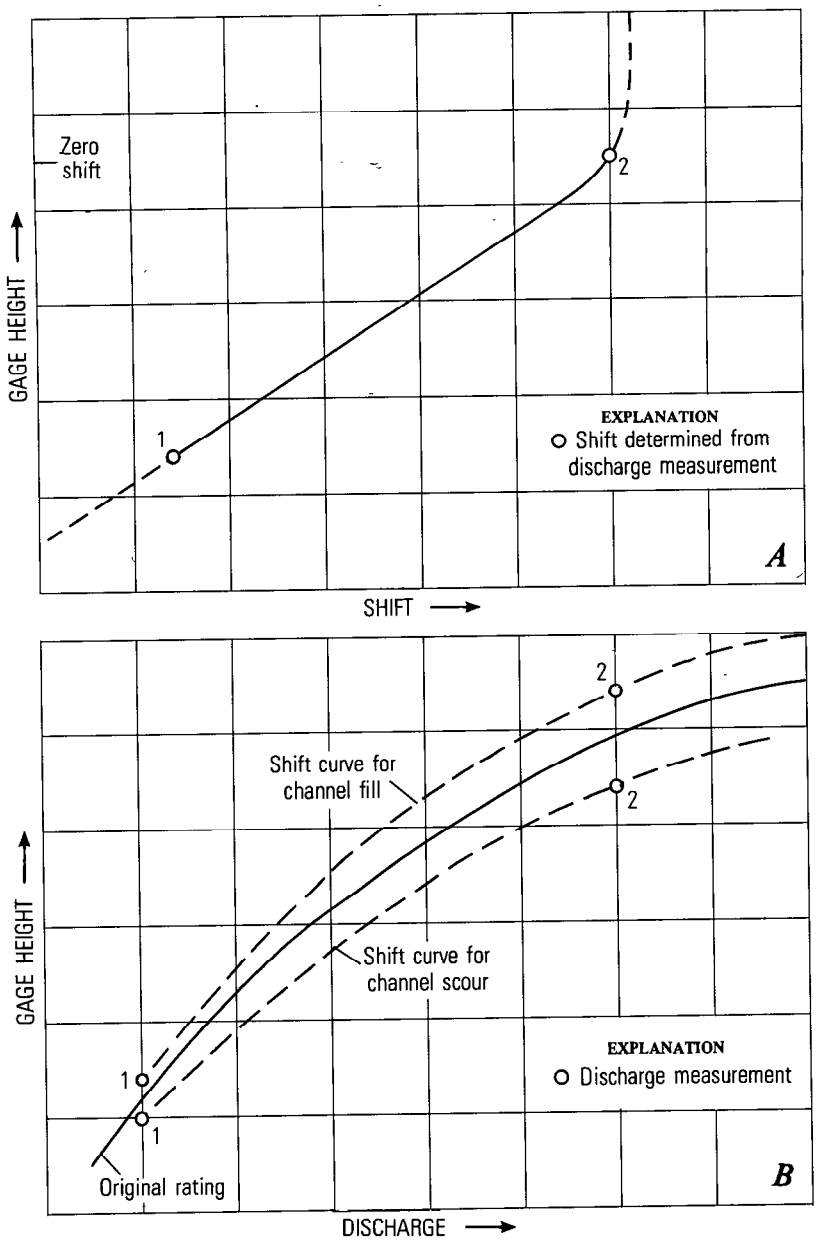

FIGURE 172.—Second example of a stage-shift relation and the corresponding stage-discharge relation caused by scour or fill in the control channel.

shifts shown by measurements nos. 1 and 2, depending on the relative times when the measurements were made and the fact that scour generally occurs on stream rises and fill generally occurs on stream recessions.

If there had been an additional major rise, one that occurred between the pairs of measurements shown in figures 171 and 172, other courses of action would be available. If the analyst had no additional data on which to base a judgment, he could assume that two separate shift events occurred, each attributable to the rise that preceded a discharge measurement. For each shift period, he could use a constant shift, equal to that shown by the discharge measurement made during that shift period. If, however, the analyst has had experience in the past with shifting control at the station caused by scour and fill in the control channel and if that experience had shown that shifts tend to vary with stage, another course of action would suggest itself. For each of the stage periods, the analyst could use a stage-shift relation of average shape that passed through the shift value shown by the appropriate discharge measurement. The above discussion would also apply to the situation of a single shift period and the availability of only a single discharge measurement made during that period. (It is assumed that the single discharge measurement would be accompanied by a check measurement to verify its accuracy, as discussed in the section on "Detection of Shifts in the Rating.")

If, during a period of shifting control, several measurements had been made but few of them could be fitted with a smooth shift curve, it would then be necessary to prorate the shifts with both time and stage, or possibly with time alone, based on the average shape of a stage-shift relation.

As mentioned earlier, scour in the control channel causes a plus shift because depth, and therefore discharge, is increased for a given gage height. Deposition or fill in the control channel causes a minus shift, because depth, and therefore discharge, is decreased for a given gage height. Thus the effect on the discharge of scour or fill in a channel control is opposite to that of scour and fill in a weir pool, which affects only the velocity of approach. Therefore, if a permanent weir is part of a compound control, scour in both the weir pool and in the channel control will cause a minus shift in the rating for section control and a plus shift in the rating for channel control. The converse is true when fill occurs in both the weir pool and the channel control. That situation is compatible with the stage-shift relation shown in figure 172, where a further decrease in stage would change the sign of the shifts. If the section control is a natural riffle, that riffle is likely to scour when the channel scours and fill when the channel fills, a situation that is compatible with the stage-shift relation shown in

figure 171. In any event, the shift curves for low stages of channel control should be shaped to join smoothly with the shift curves for high stages of section control where a compound control exists.

Up to now the discussion of channel-control shifts has been confined to shifts caused by streambed scour and deposition. Shifts may also be caused by changes in the width of the channel. Even in a relatively stable channel the width of the channel may be increased during intense floods by widespread bank-cutting, and in some areas (for example, north coastal California) channel widths may be constricted by widespread landslides that occur when steep streambanks are undercut. In meandering streams changes in channel width occur as point bars are built up by deposition and later eroded by flood flows. The effect of a change in channel width on the stage-discharge relation, unaccompanied by a change in streambed elevation, is to change the discharge, for a given gage height, by a fixed percentage. When the original rating curve for channel control is plotted linearly on logarithmic graph paper, in accordance with the equation,

$$Q = p(G-e)^{\backslash}, \tag{53}$$

the value of p increases with an increase in width and decreases with a decrease in width. The shift curve for a change in width alone will therefore plot on logarithmic graph paper as a straight line that is parallel to the original linear rating curve. Under those conditions a single discharge measurement is sufficient for constructing a shift curve for channel control.

When a change in channel width occurs concurrently with a change in streambed elevation, the effects of the two changes are compounded. The resulting shift curve is complex and requires at least several discharge measurements for its definition.

The growth of vegetation in a stream channel will affect the stage-discharge relation by reducing the discharge for a given gage height. The shift rating will therefore plot to the left (minus shift) of the original rating. The vegetation will increase the roughness coefficient of the channel and will tend to constrict the effective or unobstructed width of the channel. Both those factors reduce the value of p in equation 53, and if the changes in roughness coefficient and effective width are unvarying with stage, the shift curve will be parallel to, and to the left of, the original rating curve that has been plotted linearly on logarithmic graph paper. Usually, however the changes are not independent of stage. If the growth consists of aquatic weeds, the weeds will be overtopped and bent over by high water; if the growth consists of alders and willows, the backwater effect will be greater at higher stages when the tree crowns as well as when the tree trunks are submerged. The rating shift caused by channel vege-

tation is, of course, variable with time as the growth spreads and increases in size.

EFFECT OF ICE FORMATION ON DISCHARGE RATINGS

GENERAL

The formation of ice in stream channels or on section controls affects the stage-discharge relation by causing backwater that varies in effect with the quantity and nature of the ice, as well as with the discharge. Because of the variability of the backwater effect, discharge measurements should be made as frequently as is feasible when the stream is under ice cover, particularly during periods of freeze-up and thaw when flow is highly variable. (Procedures for making measurements under ice cover are described in the section in chapter 5 titled, "Current-Meter Measurements from Ice Cover.") In midwinter the frequency of measurements will depend on climate, accessibility, size of stream, winter runoff characteristics, and required accuracy of the discharge record. As a general rule, two measurements per month is the recommended frequency. At stations below powerplants that carry a variable load, it may be necessary to make two measurements during each winter visit—one at the high stage of the regulated flow and the other at the low stage. The backwater effects may be markedly different at the two stages. In very cold climates where winter ice-cover persists and winter discharge shows a relatively smooth recession, fewer winter measurements are needed than in a climate that promotes the alternate freezing and thawing of river ice.

Knowledge of the three types of ice formation—frazil, anchor, and surface ice—and their possible effects, is helpful in analyzing streamflow records for ice-affected periods. With regard to the type of stage recorder that is preferred for use at ice-affected stations, the graphic recorder, described under that heading in Chapter 4, is by far the best because the recorder graph generally provides dependable evidence of the presence and type of ice formation.

FRAZIL

Frazil is ice in the form of fine elongated needles, thin sheets, or cubical crystals, formed at the surface of turbulent water, as at riffles. The turbulence prevents the ice crystals from coalescing to form sheet ice. The crystals may form in sufficient numbers to give the water a milky appearance. When the crystals float into slower water they come together to coalesce into masses of floating slush. When the current carries slush ice under a sheet of downstream surface ice, the slush may become attached to the underside of the surface ice, thereby increasing the effective depth of the surface ice. Most of the slush that adheres to the surface ice does so near the upstream end of the ice sheet.

Frazil or floating slush has no effect on the stage-discharge relation, but it may interfere with the operation of a current meter. It is particularly troublesome to operators of hydroelectric plants; by adhering and building up on trash racks the ice may effectively reduce the flow to the turbines.

ANCHOR ICE

Anchor ice is an accumulation of spongy ice or slush adhering to the rocks of a streambed. In former years the theory was held that the ice resulted from loss of heat by longwave radiation from streambed to outer space, because anchor ice generally formed on clear cold nights on the streambeds of open reaches of river. This theory has been shown to be invalid, because all of the long-wave radiation that can be lost from the bed of a stream at 0°C would be absorbed in less than 1 cm of water. Anchor ice is now commonly believed to be either (1) frazil that turbulent currents have carried to the streambed where the ice adhered to the rocks, or (2) ice that formed as the result of supercooled water finding nucleating agents on the streambed on which to crystallize. The ice crystals first formed on the rocks act as a nucleating agents for the continued growth of the ice mass.

Regardless of how anchor ice forms, it cannot form or exist when the rocks are warmed by shortwave radiation from the sun which penetrates the water. When the morning sun strikes anchor ice that had formed the night before and the streambed is warmed by the incoming solar radiation, the anchor ice is released and floats to the surface, often carrying small stones that it has picked up from the bed. For the next few hours the stream will be full of floating slush released in a similar manner upstream.

Anchor ice on the streambed or on the section control may build up the bed and (or) control to the extent that a higher than normal stage results from a given discharge. The solid-line graph in figure 173 shows a typical effect of anchor ice on a water-stage recorder graph. The rise starts in late evening or early morning, many hours after the sun has set, when ice begins to adhere to the rocks and raise the water level. By 10 a.m. the sun has warmed the streambed sufficiently to release the ice and the stage starts to fall. The distinguishing feature of the "anchor-ice hump" is that the rise is slow compared to the fall, whereas an actual increase in streamflow would occur in the opposite sequence, or at least the rise would be as rapid as the fall.

The small rises in actual discharge in the late afternoon, shown by the short-dashed lines in figure 173, probably result from water being released from channel storage when anchor ice upstream goes out. There may also be some runoff from the melting of snow and ice during the warmer part of the day.

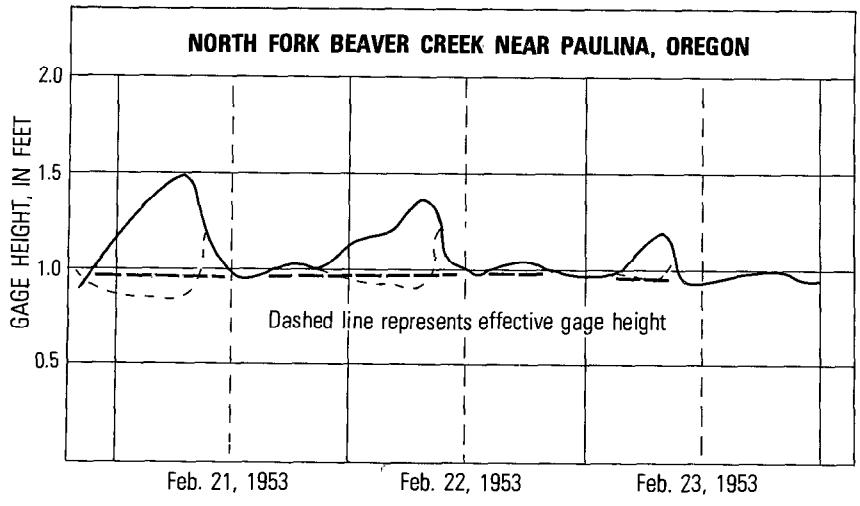

FIGURE 173.—Typical anchor-ice rises. (After Moore, 1957.)

SURFACE ICE

FORMATION OF ICE COVER

As the name implies, surface ice forms on the surface, first as a fringe of shore ice, which then, if the stream is not too turbulent, spreads to form a continuous ice cover spanning the stream from bank to bank. A description of the formation of surface ice follows.

With the onset of cold weather, the water in a stream is gradually cooled. Along the banks where the water is quiescent, temperature stratification occurs as in a lake. Because depths near the bank are usually very shallow, temperatures reach the freezing point more quickly there; ice crystals form and adhere to the banks, twigs, and projecting rocks, and a thin ice sheet forms. In the open part of the channel, temperature stratification is generally absent because of turbulent mixing, and the entire water body must reach 0°C before any freezing will occur. In the absence of nuclei or foreign material on which the ice crystals may form, there may be slight supercooling of the surface layer before any ice crystals are produced.

The ice sheet builds out from the shore as supercooled water, or water carrying ice crystals, impinges on the already-formed shore ice, and the transported or newly formed ice crystals adhere to the sheet. In the center of the stream, turbulence prevents coalescence of the ice crystals (frazil) that form. In the less turbulent areas, groups of crystals coalesce to form small pans of floating slush. These pans and (or) individual ice crystals are carried by the currents until they too impinge and adhere to existing ice sheets. In this manner an ice sheet finally forms across the entire stream. The ensuing increase in thick-

ness of the ice sheet occurs almost entirely at the interface of ice and water.

On a fairly wide stream there is no great buildup of pressure as a result of the ice cover because the ice is, to a large degree, in floatation. Ice is weak in tension. If the stage rises or if the ice thickens considerably, the increased upward force of the water causes tension cracks to appear at the banks. The ice floats up to a position in equilibrium with the water, and water fills the tension cracks and freezes. The result is again a solid sheet in equilibrium with the river. If the stage drops, the unsupported weight of the ice again causes tension cracks, especially at the banks, and the ice drops to an equilibrium position with respect to the water. Water again fills the tension cracks, freezes, and again a solid sheet of ice results.

On narrow streams the ice may be in floatation, bridged, or under pressure. If the stream is so narrow or the ice so thick that the ice can resist the tensile stress placed on it by changes in stage, the ice will not change position regardless of change in stage. At high stages the stream, in effect, will be flowing in a pressure conduit; at low stages the ice sheet will be bridged so that it makes no contact with the water. This is particularly true when there are large boulders in the stream to which the ice is frozen, thereby reducing the length of the unsupported free span.

EFFECT OF SURFACE ICE ON STREAM HYDRAULICS

Surface ice when in contact with the stream may, in effect, change streamflow from open-channel flow to closed-conduit flow. Frictional resistance is increased because a water-ice interface replaces the water-air interface, hydraulic radius is decreased because of the additional wetted perimeter of the ice, and the cross-sectional area is decreased to a degree by the thickness of the ice. The stage will therefore increase for a given discharge. Figure 174 shows the water-stage recorder graph for a gaging station as the formation of surface ice begins to cause backwater effect. In this example, daily mean discharge remained about the same as before the freezeup, although the discharge undoubtedly fluctuated somewhat during each day. It can be seen from figure 174 that surface ice can cause much uncertainty regarding the discharge because the stage-discharge relation becomes indeterminate. It is evident in figure 174 that backwater effect exists and is increasing, because the rise looks very unnatural, but the amount of backwater effect cannot be determined directly from the recorder chart.

Surface ice can also cause siphon action when it forms on a section control, but that effect is not very common. In figure 175 when water filled the entire space between control and ice, siphon action began

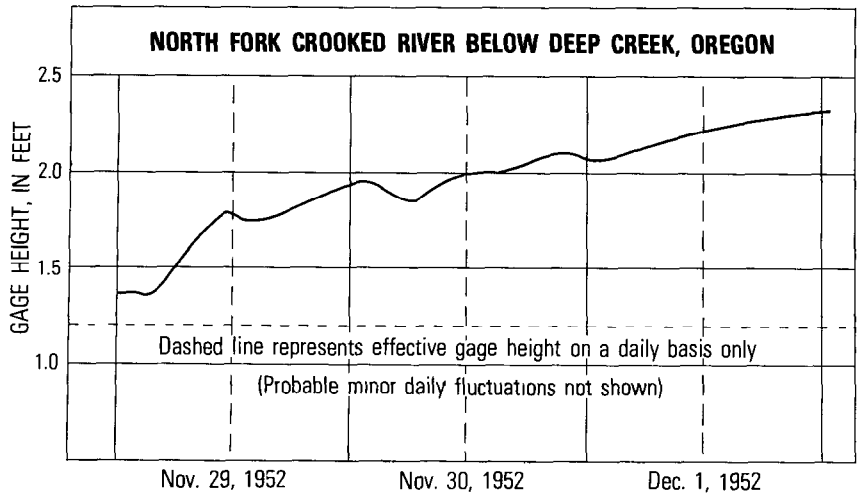

FIGURE 174.—Typical rise as complete ice cover forms. (After Moore, 1957.)

and water flowed over the control faster than it entered the gage pool. The gage pool was pulled down 0.3 ft below the point of zero flow before air entered the system and broke up the siphon action. Discharge ceased and then became a trickle while the inflow again filled the gage pool. When the entire space between control and ice was filled once more, siphon action began again. Siphon action is easily recognizable from the rapid fluctuations of the stage record. If the gaging station is visited at that time, the discharge measurement should be made far enough upstream from the gage pool to be beyond the effect of the fluctuating pool level.

If the section control is open and the gage is not too far removed from the control, there will probably be no backwater effect even though the entire pool is ice covered. The only effect of the ice cover will be to slow up the velocity of approach, and this effect will probably be minor. If the gage, however, is a considerable distance upstream from the riffle, surface ice on the pool may cause backwater as the covered reach of pool becomes a partial channel control.

Ice forming below an open-section control may jam and raise the water level sufficiently to introduce backwater effect at the control.

COMPUTATION OF DISCHARGE DURING PERIODS OF BACKWATER FROM ANCHOR ICE

Discharge measurements are usually not made when anchor ice is present for the following reasons. First, adjustment of the stage record for the effect of anchor ice can be made quickly and reliably. Second, a discharge measurement made at that time is of little help in

the analysis because discharge is highly variable with time as a result of water entering or leaving channel storage.

Anchor-ice rises are clearly recognizable on the recorder chart. In computing discharge for periods of anchor-ice effect, adjustments to gage-height are made directly on the gage-height graph. In figure 173 the long-dashed line connecting the low points of the "anchor-ice hump" is the effective gage height to use during the hours when the hump was recorded. Actually, the true effective gage height is shown by the short-dashed line. As the anchor ice builds up, the flow decreases faster than the normal recession shown by the long-dashed line, because some of the flow is going into storage as a result of the increased stage.

When the anchor ice goes out at about 9 or 10 a.m., a slug of water is released from storage and the true effective gage height rises. It can be seen however, that the areas formed by the short-dashed lines

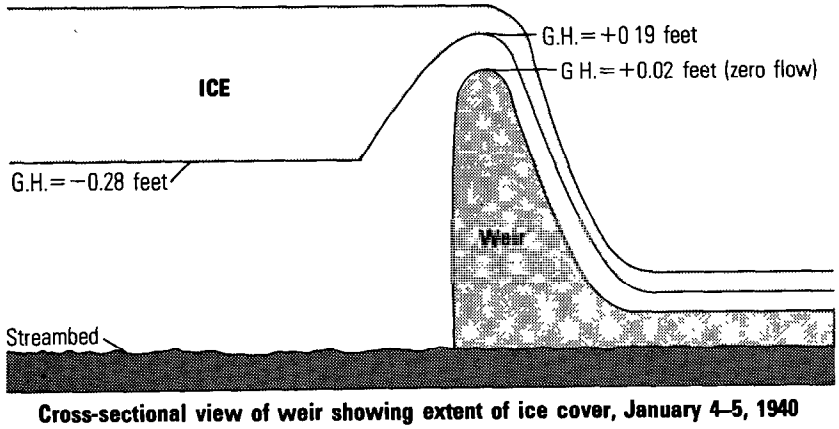

Cross-sectional view of weir showing extent of ice cover, January 4–5, 1940

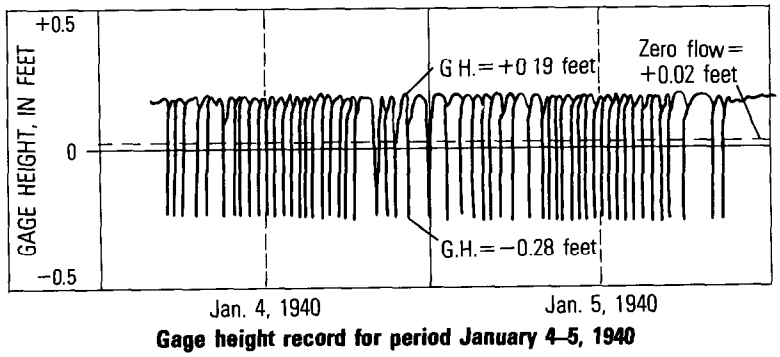

Gage height record for period January 4–5, 1940

FIGURE 175.—Effect of siphon action at artificial control in Sugar Run at Pymatuning, Pa., January 4–5, 1940.

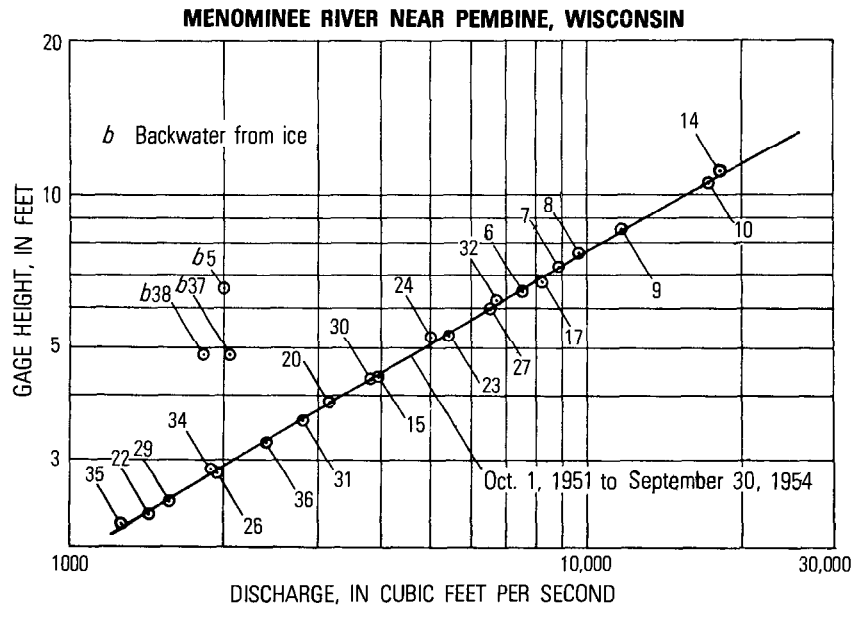

FIGURE 176.—Rating curve for Menominee River near Pembine, Wis. (After Moore, 1957.)

above and below the long-dashed line balance, and we would get identical daily mean values from use of either of the dashed lines. The rule then for obtaining effective gage height during anchor-ice periods is to cut off the hump with a straight line connecting the low points of the gage-height graph.

COMPUTATION OF DISCHARGE DURING PERIODS OF BACKWATER FROM SURFACE ICE

Figure 176 is an example of how discharge measurements (nos. 5, 37, 38), made during periods of ice effect, plot on a rating curve. Figure 174 is an example of a gage-height graph as complete ice cover forms. It is apparent from figure 174 that the backwater effect from surface ice cannot be determined directly from the recorder chart. The recorder chart is very helpful, however, in determining which periods during the winter are affected by ice. Complete notes describing ice conditions at the times the station was visited are also very valuable. Most important of all are discharge measurements made during ice-affected periods. A discharge measurement gives a definite point on a hydrograph plot of daily mean discharge versus date (fig. 177) through which the graph of estimated true daily discharge must pass. If little change in stage occurred during the day the discharge measurement was made, the measured discharge is considered to be the daily mean discharge. If a significant change in stage occurred that

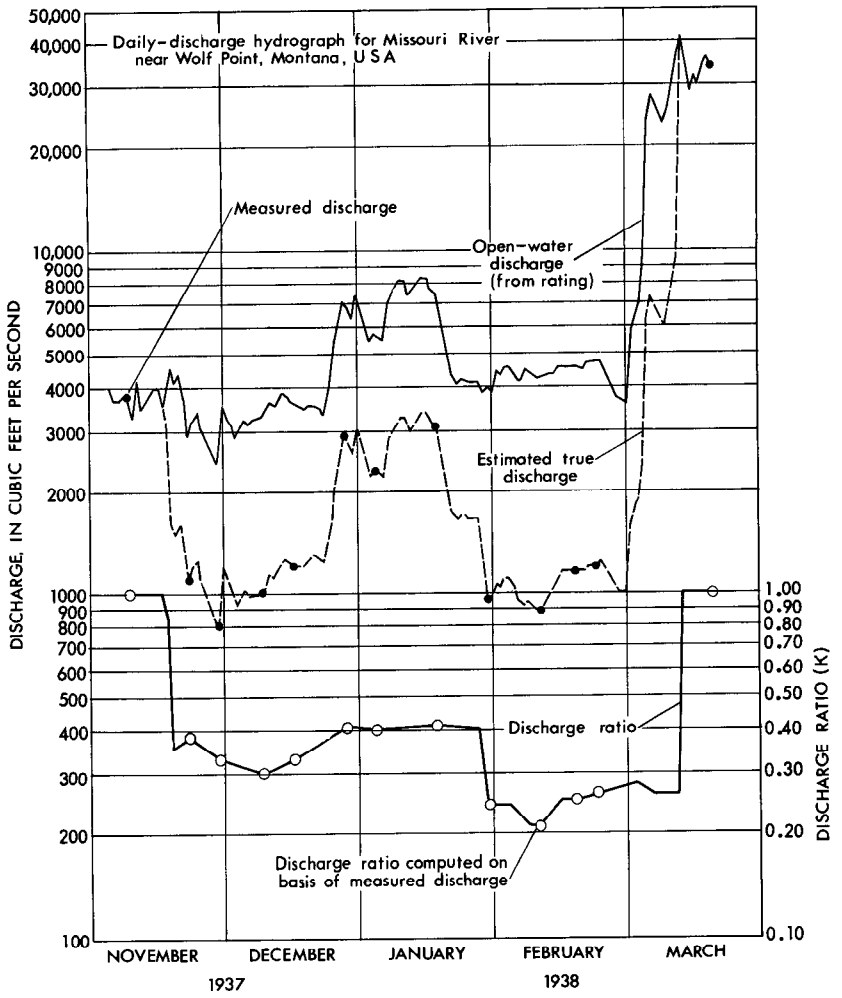

FIGURE 177.—Example of discharge-ratio method for correcting discharge record for ice effect.

day, the daily mean discharge (Q) is computed from the formula,

$$Q = Q_a \left(\frac{Q_m}{Q_r} \right), \tag{75}$$

where

Q_a is the discharge from the open-water (ice-free) rating curve corresponding to the daily mean gage height,

Q_m is the measured discharge and

Q_r is the discharge from the open-water rating curve corresponding to the gage height of the discharge measurement.

Three methods of correcting open-water discharge for ice effect are in use. (The term "open-water discharge", as used in this section of the manual, refers to the discharge for ice-free conditions obtained by applying the gage height record to the rating or shift curve that was in use immediately before the start of the ice-affected period.) The three methods are:

1. discharge-ratio method (sometimes known in the U.S.A. as the Lithuanian method),
2. shifting-control method or Stout method, and
3. hydrographic-and climatic-comparison method.

The reliability of each of the methods varies almost directly with the number of discharge measurements that were made during the ice-affected period that is being studied. Regardless of the method used, the corrected hydrograph of daily discharge, if possible, should be checked for consistency with other records. If the station being studied is on a stream that carries natural flow (flow not significantly affected by manmade development), its corrected record is compared with those for nearby streams that likewise carry natural flow. Particularly useful for that purpose are the hydrographs of streams that are unaffected by ice. If the station being studied is on a regulated stream, its corrected hydrograph is compared with the record of upstream reservoir releases or upstream hydroelectric generation, expressed either in units of discharge or in units of power output.

DISCHARGE-RATIO METHOD

In the discharge-ratio method which is used in many European countries, the open-water daily mean discharge is multiplied by a variable factor K to give the corrected discharge during periods of ice cover. A value of K is computed for each discharge measurement as the ratio of measured discharge (Q_m) to the open-water discharge (Q_i). Because K varies during the winter with time, as changes occur in the ice cover, the value of K for use on any given day is obtained by interpolation, on the basis of time, between K values computed for consecutive discharge measurements. Meteorological data are generally used to modify the simple interpolation between K values for consecutive discharge measurements; for example, during a period of extremely low temperatures the values of K indicated by simple interpolation would be reduced because the discharge usually decreases sharply at such times. The dates on which ice effect begins and ends are based on the observed or deduced beginning and end of ice cover.

An example of the discharge-ratio method is shown in figure 177. Note that discharge is plotted on a logarithmic scale. The upper daily hydrograph shows open-water discharges and the solid circles are

discharge measurements; the lower graph shows the K values obtained from discharge measurements (open circles) and the interpolation between those values; the middle graph is the hydrograph of estimated true daily discharges, obtained by multiplying concurrent values from the upper and lower graphs. The nonlinear interpolations for K values during the periods November 9–23, January 18 to February 19, and February 24 to March 20, were based on the observer's notes concerning ice conditions and on temperature and precipitation records (not shown in fig. 177).

SHIFTING-CONTROL METHOD

The shifting-control method, at one time the standard method used in the U.S.A., is seldom used here now, but it is still used in other countries. In the shifting-control method, recorded gage heights are reduced by a variable backwater value to obtain the effective daily gage heights. The effective gage heights are then applied to the open-water rating to obtain estimated true daily discharges. The backwater correction on days when discharge measurements are made is computed as the difference between the actual gage height and the effective gage height—effective gage height being the gage height from the open-water rating that corresponds to the measured discharge. The backwater correction for use on any given day is obtained by interpolation, on the basis of time, between the backwater corrections computed for consecutive discharge measurements. As in the discharge-ratio method, the interpolation is subject to modification on the basis of meteorological records, and the dates on which ice effect begins and ends are based on the observed or deduced beginning and end of ice cover.

An example of the shifting-control method is shown in figure 178. The method is applied to the same gaging station used in the example in figure 177. Note that a natural (not logarithmic) scale is used in figure 178. The upper daily hydrograph in figure 178 shows recorded gage heights and the solid circles are the effective gage heights for discharge measurements; the lower graph shows the backwater corrections obtained from discharge measurements (open circles) and the interpolation between those values; the middle graph is the hydrograph of effective gage height, obtained by subtracting values on the lower graph from concurrent values on the upper graph. The nonlinear interpolations for backwater corrections during various periods were based on the observer's notes concerning ice conditions and on temperature and precipitation records (not shown in fig. 178). As mentioned in the preceding paragraph, the effective gage heights (middle graph) are applied to the rating curve to obtain estimated true daily discharges.

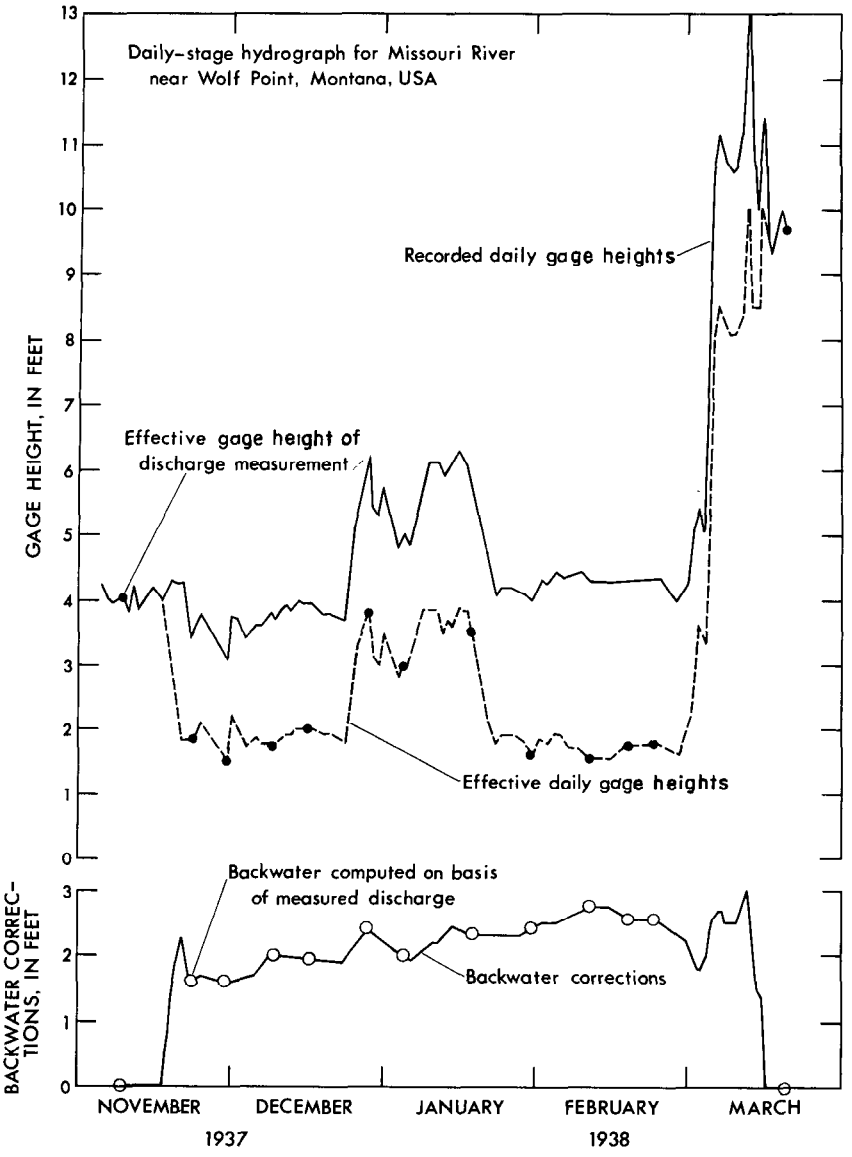

FIGURE 178.—Example of shifting-control method for adjusting stage record for ice effect.

HYDROGRAPHIC- AND CLIMATIC-COMPARISON METHOD

The method of hydrographic and climatic comparison has been favored in the U.S.A. for the last 30 years. The mechanics of the method differ from those of the discharge-ratio method, but both methods

basically correct the daily open-water discharge by a variable percentage.

The first step is to compute the station discharge record for the entire year as though there were no ice effect at any time. The daily hydrograph of open-water discharge and the discharge measurements are then plotted, using a logarithmic discharge scale, and notes concerning ice conditions are entered on the graph. At this point the hydrograph sheet resembles the upper graph in figure 177. If a measurement of ice-affected discharge is not representative of the daily mean discharge because of changing stage during the day, the daily mean discharge, as computed by equation 75, is also plotted. All is then in readiness for estimating the true daily discharge directly on the hydrograph sheet, and that is done on the basis of three comparisons:

1. comparison with records for nearby gaging stations,
2. comparison with weather records, and
3. comparison with the base-flow recession curve for the gaging station that is being studied.

Comparison with records for nearby gaging stations

Comparison with other discharge records is the most important basis for determining the probable discharge for periods between discharge measurements. Even though the record used for comparison may also have been corrected for ice effect, its use provides an additional independent set of basic data—another stage record and another set of current-meter measurements. Without a nearby record that compares well with the record being studied, the accuracy of the daily discharges estimated between the dates of discharge measurements may be greatly reduced. However, hydrographic comparisons are not infallible because the relation between the flow of two streams may vary significantly during the year; hence the importance of making many discharge measurements during ice-affected periods.

In making the hydrographic comparison, the nearby station with the most reliable winter streamflow record is selected for use as a reference station. The reliability of the reference station may have been established by the fact that its discharge is unaffected by ice or is affected by ice for only a relatively short period, or by the fact that many winter measurements have been made at the station and the true discharge between the dates of measurement can be estimated from weather records. (See discussion below on use of weather records.) A hydrograph of daily discharge, corrected for ice effect if necessary, is prepared for the reference station on a separate sheet of

graph paper, similar to that used for plotting the daily hydrograph for the station being studied.

A light table is used in comparing the two hydrographs. A light table is a glass-topped table that is illuminated by light from below the glass top, so that when one hydrograph is superposed on the other on the table top, both hydrographs can be viewed simultaneously. The hydrograph for the reference station is taped to the top of the light table. The hydrograph for the study station is then superposed on that of the reference station and positioned laterally so that the date lines of the two hydrographs coincide. The period preceding the first measurement (no. 1) that showed ice effect at the study station is the period first selected for consideration. The hydrograph for the study station is positioned vertically so that hydrographs for the two stations roughly coincide for the period immediately preceding the day or days when the start of ice effect is suspected. A comparison of the hydrographs and an inspection of the weather records should fix the date when ice effect started. That date will be preceded by a period of subfreezing weather, and on that date—usually a rainless day—the hydrograph for the study station will start a gradual rise not shown by the hydrograph for the reference station. For an appreciable period thereafter the hydrograph for the study station will remain above that of the reference station.

After the starting date (*A*) of ice-effect at the study station has been selected, the vertical position of the hydrograph for the study station is changed slightly, if necessary, to make the two hydrographs coincide on that date. If that positioning causes measurement no. 1 to fall directly on the hydrograph for the reference station, the hydrograph for the reference station between date *A* and measurement no. 1 is traced with dashed lines on the hydrograph sheet for the study station. The daily discharges indicated by the dashed lines are the estimated true discharges at the study station during the period between date *A* and measurement no. 1.

However, only rarely does measurement no. 1 coincide with the reference hydrograph when discharges at the two stations are made to coincide on date *A*; measurement no. 1 will usually lie above or below the hydrograph for the reference station. In that situation, as discharges from the reference hydrograph are being transferred to the sheet bearing the study hydrograph, the study sheet will in effect be moved up or down, as the case may be, so that when the transfer of discharge points reaches measurement no. 1, measurement no. 1 will coincide exactly with the reference hydrograph. If the temperature record shows no great fluctuation from day to day during the period between date *A* and measurement no. 1, the vertical displacement of the sheet bearing the study hydrograph will be made uniformly dur-

ing the transfer process. If the temperature record does fluctuate from day to day during the period, the vertical displacement will be made at a variable rate to reflect the fact that the ratio of true discharge to open-water discharge usually decreases during sharp drops in temperature; the ratio increases during sharp rises in temperature. In other words, the vertical distance between open-water discharge and true discharge increases on the study-hydrograph sheet during sharp drops in temperature; the vertical distance decreases during sharp rises in temperature. Observer's notes concerning major changes in the ice cover, particularly where complete cover is intermittent during the winter, are also very helpful in estimating the degree of ice effect.

After correcting the discharge between date *A* and measurement no. 1, the process is repeated for the period between discharge measurement no. 1 and the next successive discharge measurement (no. 2). The two hydrographs are made to coincide at measurement no. 1 and the transfer of discharge points to the study hydrograph proceeds to measurement no. 2. In that manner the open-water discharge for the study station is corrected until the date is reached when ice effect ceases.

Comparison with weather records

Records of air temperature and precipitation are a most valuable aid in making corrections for ice effect. The temperature record helps the engineer decide whether the precipitation is rain or snow—snow will have no immediate effect on the runoff. The temperature record also helps the engineer decide whether ice cover is forming, increasing, or dissipating. For stations for which there are no nearby discharge records for comparison and for which the recorder chart does not provide dependable clues to the fluctuation of discharge, it may be necessary to correct open-water discharges for ice effect almost solely on the basis of weather records and available measurements of discharge. Discharge usually follows closely the "ups-and-downs" of the air temperature record, and the discharge measurements help fix, within reasonable limits, the estimated rises and falls of the "true" discharge hydrograph. An exception to that statement is found in regions of extreme cold, such as the Arctic, that become blanketed with a heavy snow cover. The snow acts as an insulator for the underlying ground, and it then requires a prolonged change in temperature to significantly change the slow uniform recession of streamflow during the winter.

It should be mentioned here that a water-temperature recorder is a helpful adjunct to a gaging station. When the water temperature is above the freezing level, there is little likelihood of ice effect.

Comparison with base-flow recession curves

During periods of subfreezing weather, virtually all the flow in a stream is base flow; that is, water that comes out of ground-water storage to sustain the flow of the stream during periods when there is no surface runoff. It will often be found that during cold ice-affected periods, the flow of the stream will be declining at a rate similar to the rate of recession shown by that stream during ice-free periods. Thus if we have a known discharge of say, 20 ft^3/s, on some day during the ice-affected period and we wish to estimate daily discharge during the next 10 days, all of which were free of rain or snowmelt, we look for an ice-free period elsewhere in the record for the study station when there was no surface runoff, and choose a day whose discharge is 20 ft^3/s. We then note the receding values of discharge for the following 10 days, and use those same discharges for the 10 days to be estimated. The ice-free period that is used for an index should preferably be in the nongrowing season because the use of water by vegetation affects the rate of base-flow recession.

It is possible that daily discharges estimated from the base-flow recession for a warmer period may be somewhat high because extremely cold weather reduces the rate at which water percolates through the ground, and because some of the water that does reach the stream may go into storage behind ice dams. Nevertheless a standard base-flow recession curve provides a valuable guide to the probable flow during recession periods when the stream is ice-covered. Because the discharge during periods of base flow originates as ground water, a record of the fluctuations of ground-water levels of wells in the area can be useful as an index for estimating the true discharge during those periods.

An example of the application of the hydrographic- and climatic-comparisons method is illustrated in figures 179 and 180. Figure 179 shows a portion of a plotted hydrograph of daily mean discharge for the gaging station on North Fork John Day River at Monument, Oreg. The solid line represents open-water discharge obtained by applying recorded gage heights to the rating curve, and the X on January 26 represents the open-water discharge corresponding to the gage height of discharge measurement C made on that date. The open-water discharge is almost 10 times as great as the measured discharge on January 26. The dashed line on figure 179 represents the estimated true daily discharge obtained by comparison with the hydrograph of daily mean discharge for John Day River at Service Creek, Oreg. and by comparison with the record of daily maximum and minimum temperature at Dayville, Oreg. The reference hydrograph and temperature record used for the comparison are shown in figure 180. Actually the precipitation record at Dayville was also

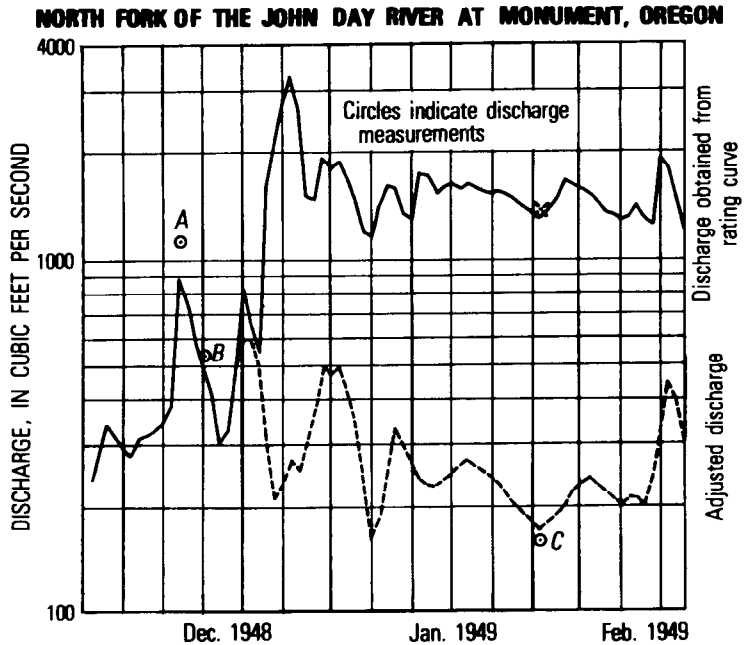

FIGURE 179.—Daily hydrographs for open-water discharge and for discharge corrected for ice effect. (After Moore, 1957.)

considered, but because all precipitation during the study period occurred as snow and therefore had no immediate effect on the runoff, the precipitation record is not shown in figure 180.

Also shown on figure 180 is the corrected hydrograph for the study station on North Fork John Day River at Monument; the hydrograph of open-water discharge at that station has been omitted to reduce clutter in the illustration. The discharge for the reference station on John Day River at Service Creek was unaffected by ice. The shapes of the two hydrographs are not identical, but useful comparison between the hydrographs for two stations does not require that their shapes be identical, as long as their discharge trends are similar. It can be seen on figure 180 that both hydrographs respond to the effect of air-temperature fluctuations during the winter period.

In applying the method of hydrographic and climatic comparison, the hydrograph of "true" daily discharge, plotted on a logarithmic scale, was displaced from the open-water hydrograph by a variable vertical distance. That means, in effect, that discharge ratios, variable with time, were applied to the open-water discharges, and there-

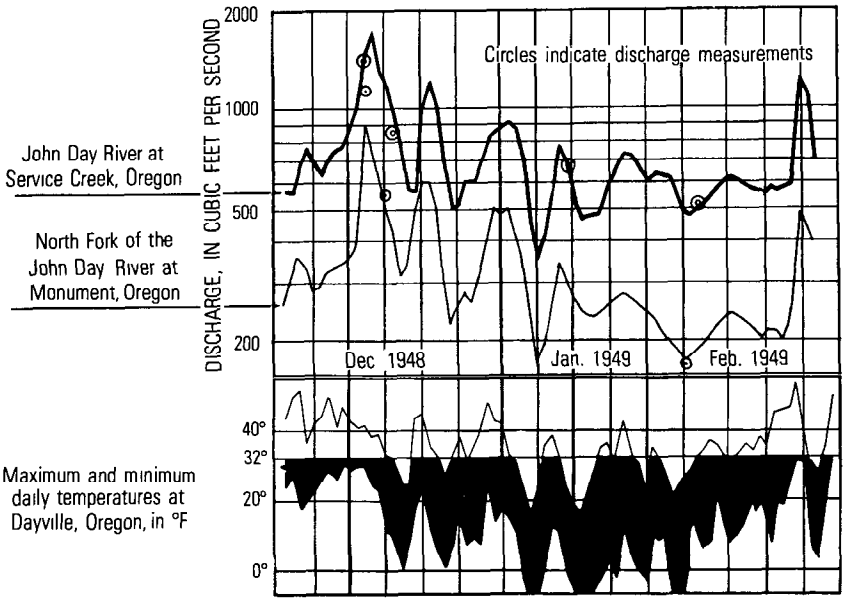

FIGURE 180.—Comparison of daily winter discharge at two gaging stations showing their response to air-temperature fluctuations. (After Moore, 1957.)

fore a basic similarity exists between the hydrographic-comparison method and the discharge-ratio method. It appears to the author that application of the hydrographic-comparison method would be greatly facilitated if the hydrograph of open-water discharge for the study station were first adjusted by the discharge-ratio method because application of that method is relatively simple. The adjusted hydrograph would then be refined by using it, rather than the open-water hydrograph, in the hydrographic-comparison method. It is much simpler to apply the hydrographic-comparison method for refining discharge estimates than it is to apply that method for making original discharge estimates.

SAND-CHANNEL STREAMS

In fixed channels, well-defined stage-discharge relations can usually be developed that show only minor shifting at low flow. In sand-channel streams, however, stage-discharge relations are continually changing with time because of scour and fill and because of changes in the configuration of the channel bed. These changes cause the shape and position of the stage-discharge relation to vary from time to time and from flood to flood, and it becomes very difficult to explain the apparent haphazard scatter of discharge measurements available to define the rating. Familiarity with the results of research

studies as reported by Colby (1960), Dawdy (1961), Simons and Richardson (1962), Beckman and Furness (1962), and Culbertson and Dawdy (1964) will greatly assist the analyst in defining the discharge rating.

For a stream with rigid boundaries, the best site for a stream-gaging station is upstream from a constriction because the constriction will provide a stable and sensitive control. An opposite effect occurs, however, at a constriction on a sand-channel stream; the rating will be unstable there because the constricted section will experience maximum streambed scour and fill. In fact, any contracting reach on a sand-channel stream is undesirable for use as a gaging-station site, and a straight uniform reach should be sought. Preferably both the gage and the cableway site for high-water discharge measurements should be located in a reach suitable for the determination of peak discharge by the slope-area method (chap. 9). This will permit the use of high-water current-meter measurements to verify computed peak discharges as well as develop the hydraulics of the stage-discharge relation. The fieldwork for a sand-channel stream should also include the collection of samples of bed materials at the stream-gaging site.

BED CONFIGURATION

On the basis of laboratory investigation, Simons and Richardson (1962) described the bed configuration of sand-channel streams as ripples, dunes, plane bed, standing waves, and antidunes. This sequence of bed configurations occurs with increasing discharge. When the dunes wash out, and the sand is rearranged to form a plane bed, there is a marked decrease in resistance to flow which may result in an abrupt discontinuity in the stage-discharge relation. The forms of bed roughness, as shown in figure 181 and described in table 21, are grouped according to the two separate conditions of depth-discharge relationship that are evident in a given channel. The sequence of configurations described in table 21 is developed by continually increasing discharge. The lower regime occurs with lower discharges; the upper regime with higher discharges; an unstable discontinuity in the depth-discharge relationship appears between these two more stable regimes.

The presence of fine sediment in the flow influences the configuration of the sand bed and thus the resistance to flow. It has been found by Simons and Richardson (1962, p. 4) that with concentrations on the order of 40,000 milligrams per liter of fine material, resistance to flow in the dune range is reduced as much as 40 percent. The effect is less pronounced in the upper regime, but fine sediment may change a standing-wave condition into a breaking antidune which will increase the resistance to flow. Thus the stage-discharge relation for a

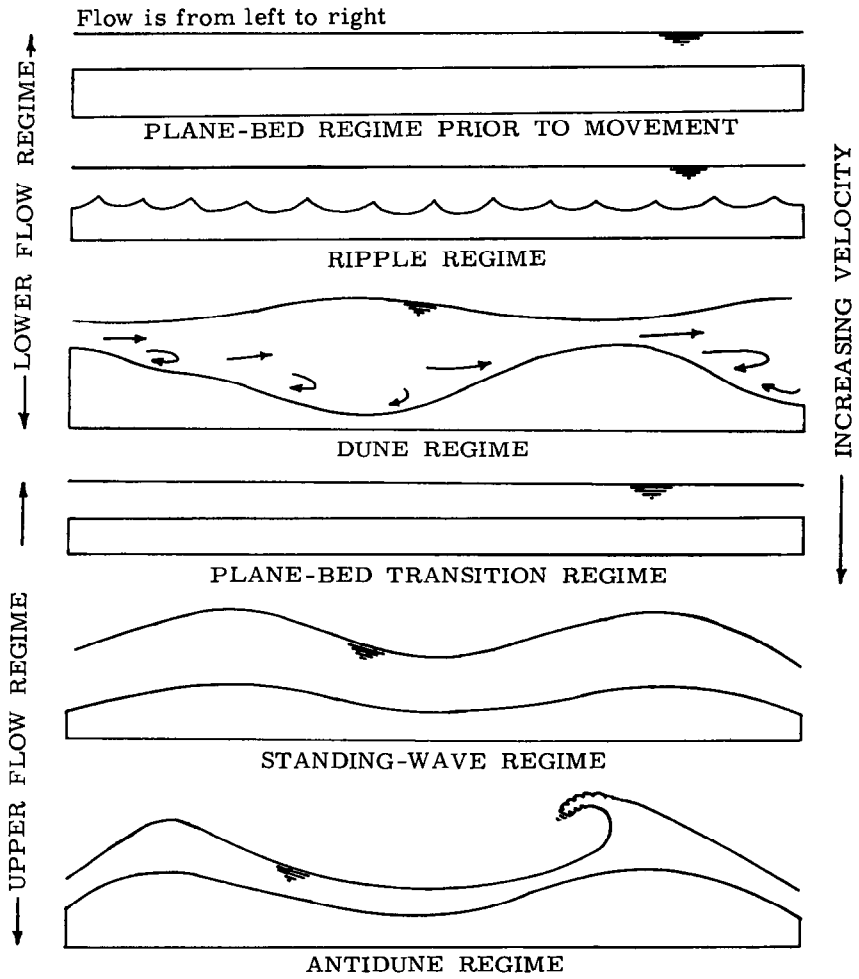

FIGURE 181.—Idealized diagram of bed and water-surface configuration of alluvial streams for various regimes of flow.

stream may vary with sediment concentration if the flow is heavily laden with fine sediment.

Changes in temperature can also alter the form of bed roughness, and, hence, the resistance to flow. Lowering the temperature increases the viscosity of the water and increases the mobility of the sand. If, for example, the form of bed roughness is in transition or nearly so, and if there is a reduction in the temperature of the water, the increased mobility of the sand may cause the dunes to wash out and the bed to become plane. This phenomenon is reversible.

Changes in bed forms do not occur instantaneously with increasing or decreasing discharge. The time lag between change in bed form

TABLE 21.—*Surface and bed descriptions for the various flow regimes*

Type of configuration	Description	
	Bed	Flow
Lower regime flow:		
Plane bed	Plane; no sediment movement.	Plane surface; little turbulence.
Ripples	Small uniform waves; no sediment movement.	Plane surface; little turbulence.
Dunes	Large, irregular, saw-toothed waves formed by sediment moving downstream; waves move slowly downstream.	Very turbulent; large boils.
Upper regime of flow:		
Plane bed	Dunes smoothed out to plane bed.	Plane surface; little turbulence.
Standing waves	Smooth sinusoidal waves in fixed position.	Standing sinusoidal waves in phase with bed waves; termed "sand waves."
Antidunes	Symmetrical sinusoidal waves progressing upstream and increasing in amplitude; suddenly collapse into suspension then gradually reform.	Symmetrical sand waves progressing upstream in phase with bed waves; amplitude increases until wave breaks, whole system collapses then gradually reforms.

and change in discharge may result in loop rating curves. For example, if bed configuration is initially dunes, the dunes will persist on rising stages to a discharge that is greater than the discharge at which the dunes will reform on falling stages. Thus at a given stage, the discharge may be greater when the stage is falling. Because the form of each loop curve depends on the initial condition of bed configuration and the rate of change of discharge, an infinite number of different loop curves, and even multiple-loop curves, may occur for a given reach of channel across the transition from dunes to plane bed. The stage-discharge relation within the transition band may be indeterminate. An example of a loop curve, typical of some channels, is shown in figure 182.

RELATION OF MEAN DEPTH TO DISCHARGE

A plot of stage against discharge in sand-channel streams often obscures any underlying hydraulic relationship because neither the bottom nor sides of these streams are fixed. Figure 183 shows as an extreme example the stage-discharge plot for Huerfano River near Undercliffe, Colo., for 1941 and 1942. The relation between stage and discharge is indeterminate. However, the underlying hydraulic relation may be revealed by a change in variables. The effect of variation in bottom elevation is eliminated by replacing stage by mean depth or hydraulic radius. The effect of variation in width is eliminated by

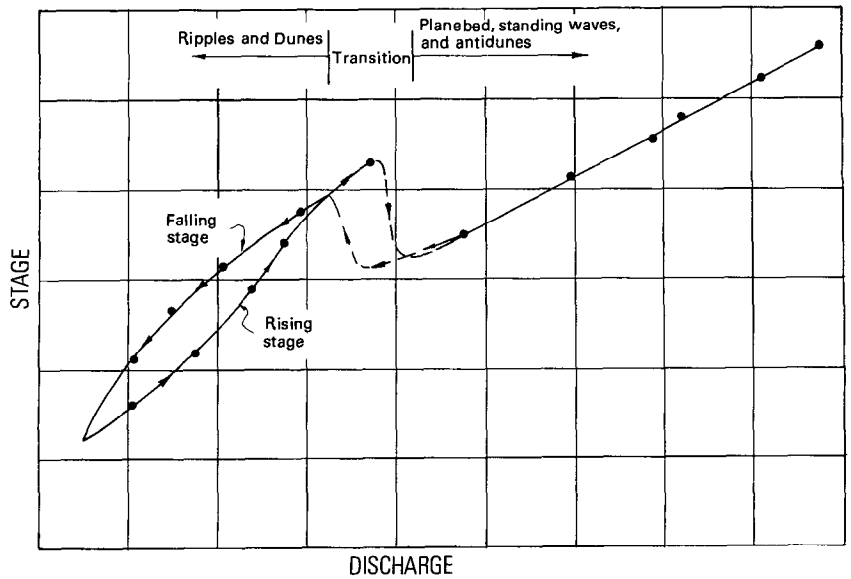

FIGURE 182.—Typical loop curve of stage versus discharge for a single flood event in a sand channel. (After Stepanich, Simons, and Richardson, 1964.)

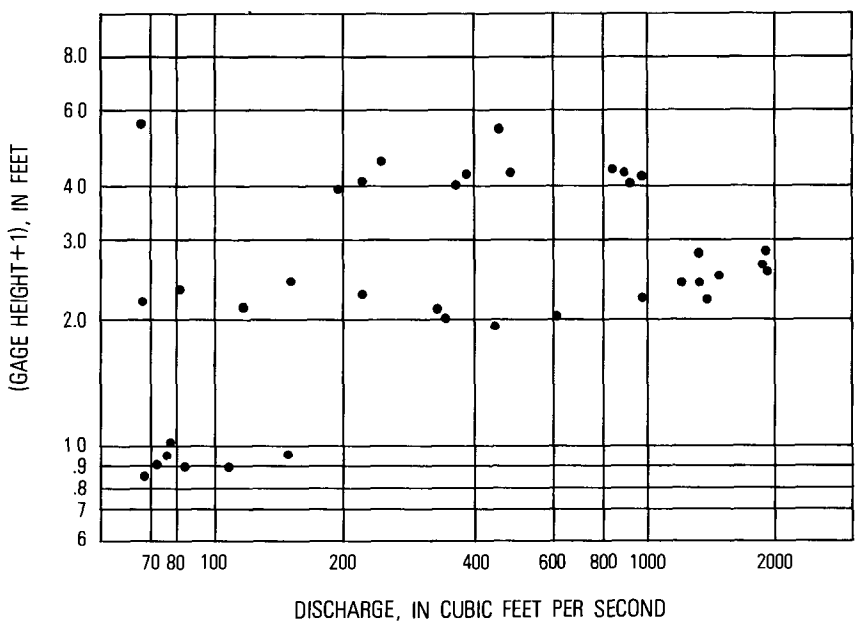

FIGURE 183.—Stage-discharge relation for Huerfano River near Undercliffe, Colo.

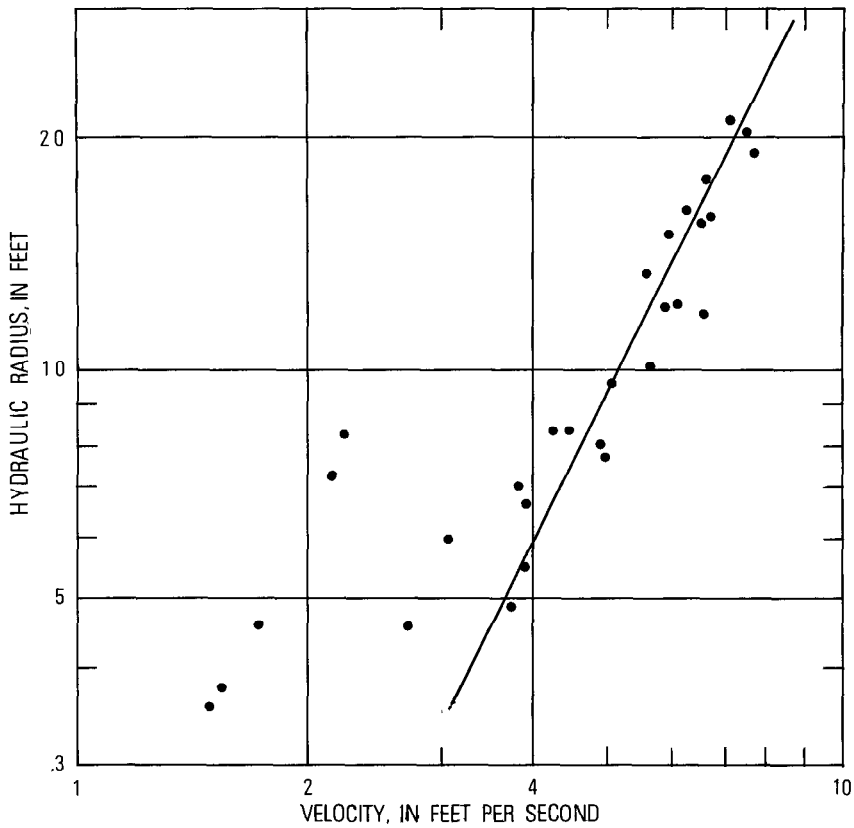

FIGURE 184.—Relation of velocity to hydraulic radius for Huerfano River near Undercliffe, Colo.

using mean velocity. Figure 184 shows most of the same measurements for Huerfano River that were plotted in figure 183, now replotted on the basis of velocity and hydraulic radius. Measurements for this stream with a hydraulic radius greater than one foot define a single curve with bed forms corresponding to the upper regime. Measurements in the transition range from dunes to plane bed scatter wildly as would be expected from the previous discussion.

The discontinuity in the depth-discharge relation is further illustrated in figure 185 which shows a plot of hydraulic radius against velocity for Rio Grande near Bernalillo, N. Mex. The measurements plotted on the left represent bed configurations of ripples and dunes and the curve on the right represents bed configurations of plane bed, standing waves, or antidunes.

According to Dawdy (1961), the curve representing the upper regime in a true sand-bed stream usually fits the following relation,

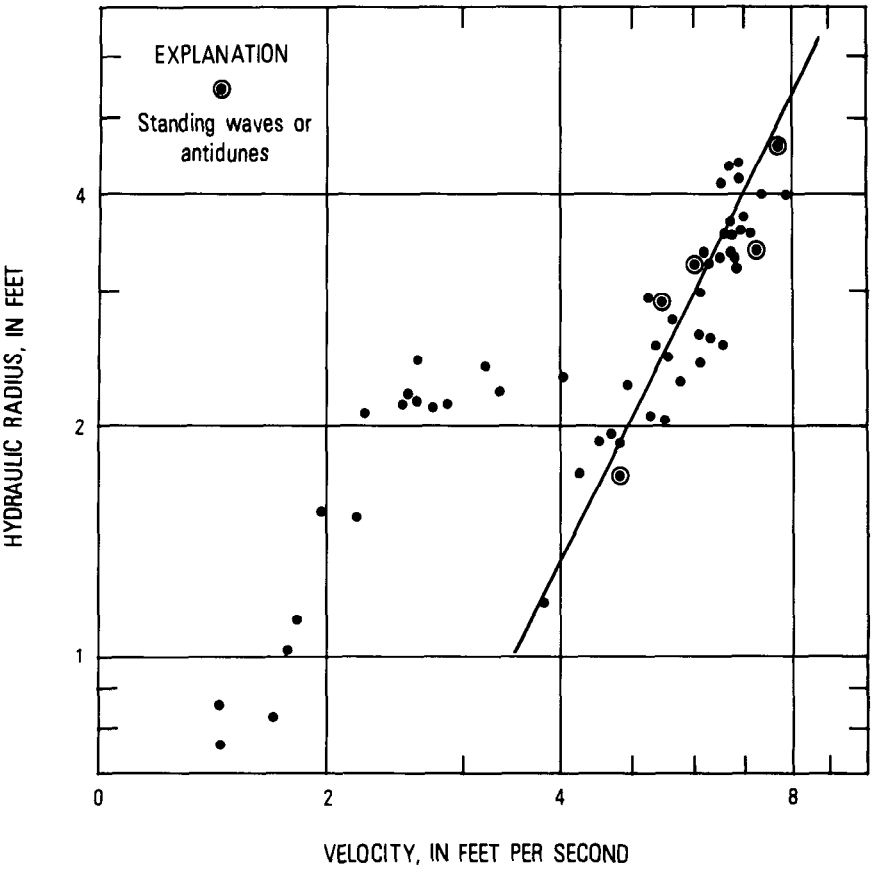

FIGURE 185.—Relation of velocity to hydraulic radius for Rio Grande near Bernalillo, N. Mex.

$$V = kR^{1/2},$$

where V is the mean velocity, k is a constant, and R is the hydraulic radius. He found this relation to be applicable for 26 of the 27 streams used in his study. More recent study has shown that the exponent of R ranges from ⅔, as in the Manning equation, to ½, the larger exponents being associated with the coarser grain sizes.

DEVELOPMENT OF DISCHARGE RATING

Plots of mean depth or hydraulic radius against mean velocity or discharge per foot of width are valuable in the analysis of stage-discharge relations. These plots clearly identify the regimes of bed configuration and assist in the identification of the conditions represented by individual discharge measurements. For example, only

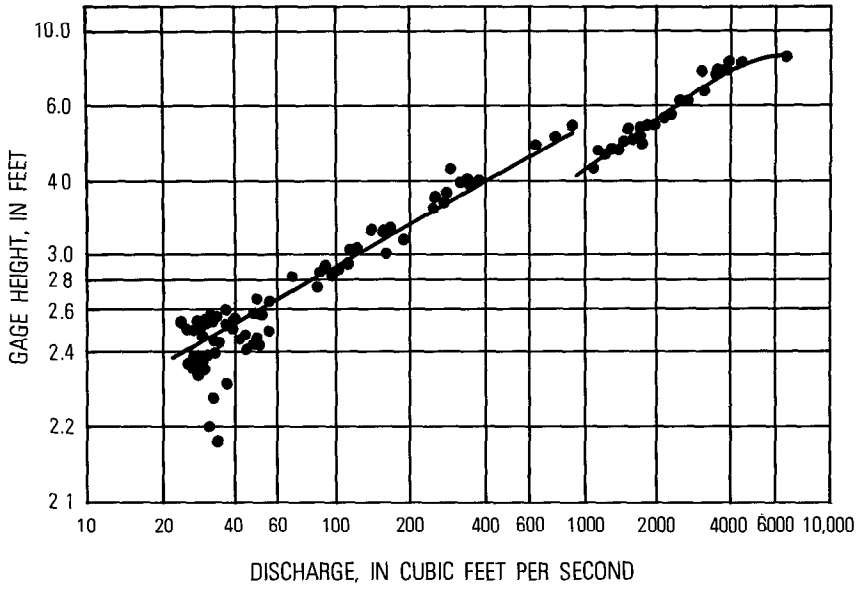

FIGURE 186.—Stage-discharge relation for station 34 on Pigeon Roost Creek, Miss. (After Colby, 1960.)

those measurements identified with the upper regime should be used to define the position and slope of the upper portion of the stage-discharge curve; similarly, only those measurements identified with the lower regime should be used to define the lower portion of the stage-discharge curve. Measurements made in the transition zone may be expected to scatter widely but do not necessarily represent shifts in more stable portions of the rating.

Plots of stage against mean depth and stage against width are also helpful in developing a mean stage-discharge relation and in analyzing the cause of shifts from the mean relation. In the upper regime the use of these plots in conjunction with the plot of velocity versus mean depth or hydraulic radius raised to the ½ to ⅔ power, depending on grain size, may be useful in establishing a reasonable slope to the upper part of the stage-discharge relation.

The stage-discharge relation developed by Colby (1960) for Pigeon Roost Creek, Miss., is shown in figure 186. This stream is about 75 ft wide, the banks are relatively stable, and the median size of the bed material is 0.4 mm. The mean elevation of the channel bed does not change appreciably with time or discharge. The discontinuity in the stage-discharge relation is very abrupt. Discharges from 900 to 1,800 ft^3/s may occur at a stage of 5.3 ft.

According to Colby (1960, p. 19, 20), stage-discharge relations may

be expected to have a discontinuity if the reach has all of the following characteristics:

1. a bed of uniform and readily shifting sediment that does not form distinct pools and riffles,
2. at some flows almost all of the stream-bed is covered with loose sand dunes,
3. at higher flows the bed of the stream is mostly plane or has antidunes,
4. the depth of flow at the point of discontinuity is sufficiently great so that changes in the stage-discharge relation at the discontinuity can be distinguished from changes caused by small local shifts of the channel bottom, and
5. the lateral distribution of depths and velocities is sufficiently uniform for the bed configuration to change across most of the streambed in a relatively short time.

The above conditions are very restrictive. Many streams with sand beds have well developed pools and riffles at the stage where the discontinuity might otherwise occur. Streams do not generally have uniform sediment sizes; many have large sorting coefficients. A few streams having suitable bed material may never show the discontinuity because dunes exist even at the highest flow rates. Others may have such high slopes that the lower regime cannot be defined by discharge measurements because of the shallow depths at which the discontinuity occurs. Winding streams seldom have uniform lateral distribution of velocity and depths. Some streams have such gradual or inconsistent transitions between dunes and plane bed that the discontinuity may be difficult, if not impossible, to define. Dunes may exist near the banks at the same time that a plane bed exists near the center of the stream. The transition in this case may occur so gradually with increasing stage that the discontinuity in rating is eliminated. However, at any station where dunes exist at low flows and a plane bed exists at higher flows, there is a major change in bed roughness. Knowledge of the bed forms that exist at each stage or discharge can be very helpful in developing the discharge rating.

EVIDENCES OF BED FORMS

Evidence of the bed forms that exist at a given time at a particular station can be obtained in several ways, a listing of which follows.

1. Visual observation of the water surface will reveal one of several conditions: large boils or eddies, which indicate dunes; a very smooth water surface, which indicates a plane bed; standing waves, which indicate smooth bed waves in phase with the surface waves; or breaking waves, which indicate antidunes. Visual observations of the water surface should be recorded on each discharge measurement.

2. Noting whether the sand in the bed is soft or firm. A soft bed often indicates lower regime conditions. The streambed during upper regime flow will usually be firm.

3. Measurements of bed elevations in a cross section will usually indicate the type of bed forms. A large variation in depth indicates dunes, and a small variation in depth a plane bed. The small variation in depths for a plane-bed (upper-regime) configuration should not be confused with small variations caused by ripples or by small dunes, both of which are definitely lower-regime configurations. A large variation in bed elevation at a particular point in the cross section during a series of discharge measurements indicates the movement of dunes.

4. The amount of surge on a recorder chart may also indicate the configuration of the channel bed. Medium surge may indicate dunes, little or no surge may indicate a plane bed, and violent surge may indicate standing waves or antidunes. The transition from plane bed to dunes during a discharge recession may cause a secondary hump on the gage-height trace if the transition occurs over a short time period.

5. Relations that define the occurrence of bed forms as a function of hydraulic radius (R), slope (S), mean velocity (V), and grain size (d), are useful in developing discharge ratings. A relation of that type, presented by Simons and Richardson (1962), is shown in figure 187. In that figure the dimension of R is feet; that of V is feet per second. Recent studies suggest that: the lower regime of bed forms will occur when the ratio,

$$\frac{V^4}{g^2 D^{1/2} d_{50}^{3/2}} , \tag{76}$$

is less than 1×10^3; the upper regime of bed forms will occur when the ratio is greater than 4×10^3; the bed will be in transition if the ratio is between those values. In the above ratio, V is the mean velocity in feet per second, g is the acceleration of gravity in feet per second per second, D is the mean depth in feet, and d_{50} is the median grain size of bed material in feet.

SHIFTING CONTROLS

The upper part of the stage-discharge relation is relatively stable if it represents the upper regime of bed forms. Rating shifts that occur in upper-regime flow can be analyzed in accordance with the methods or principles discussed in the section titled, "Rating Shifts for Channel Control." However, the shift ratings after minor stream rises will generally have a strong tendency to parallel the base rating when plotted on rectangular-coordinate graph paper; that is, the equation

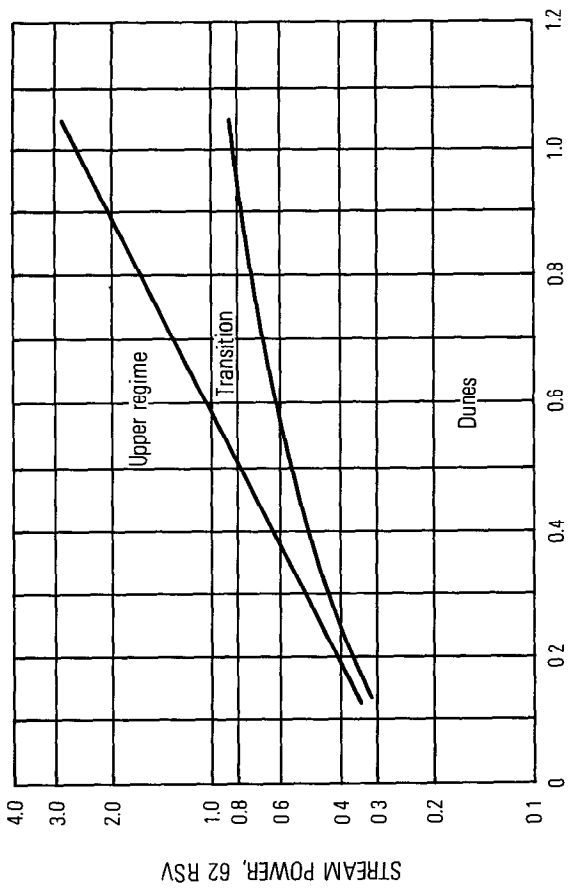

FIGURE 187.—Relation of stream power and median grain size to form of bed roughness.

for each shift curve will differ from that of the base rating by a change in the value of e in the basic equation,

$$Q=p(G-e)^N. \tag{53}$$

The shifts will change on stream rises and will often vary with time between rises. Major stream rises may also change the value of p in equation 53.

The lower part of the rating is usually in the dune regime and the stage-discharge relation varies almost randomly with time. Frequent discharge measurements are necessary to define the stage-discharge relation, and for some streams they are necessary to determine the variation of discharge with time in the absence of any usable relation between stage and discharge. In the U.S.A. a frequency of three discharge measurements per week is often recommended, but for some streams, even daily measurements barely suffice.

A mean curve for the lower regime is frequently used with shifts as defined by discharge measurements. In some instances the shift defined by a single discharge measurement represents only the temporary position of a dune moving over a partial section control. A series of discharge measurements made at short time intervals over the period of a day may define a pattern of shifts caused by dune movement. When discharge is constant but the stage fluctuates, the changing gage-height trace generally reflects dune movement.

Continuous definition of the stage-discharge relation in a sand channel stream at low flow is a very difficult problem. The installation of a control structure should be considered if at all feasible.

ARTIFICIAL CONTROLS FOR SAND CHANNELS

When conventional controls are installed in sand channels, they are seldom satisfactory, even those designed to be self-cleaning. The principal difficulty is that for such controls in a sand channel, discharge is dependent not only on water-surface elevation, but also on the bed elevation and flow regime upstream from the structure. A satisfactory control is one whose stage-discharge relation is unaffected by bed configuration. A few successful low-water controls have been designed for use in sand channels; one example is the weir designed for the gaging station on the Rio Grande conveyance channel near Bernardo, N. Mex. (Richardson and Harris, 1962). That structure will not be described here because generalizations concerning control shape are meaningless; each control structure must be individually designed for compatibility with channel and flow conditions that exist at the proposed site for the control. A laboratory model study involving a reach of channel is therefore needed for each

site investigated. Efforts continue to design low-water controls that are both relatively cheap and that have satisfactory operating characteristics when installed in sand channels (Stepanich and others, 1964).

SELECTED REFERENCES

Bailey, J.F., and Ray, H.A., 1966, Definition of stage-discharge relation in natural channels by step-backwater analysis: U.S. Geol. Survey Water-Supply Paper 1869–A, 24 p.

Beckman, E.W., and Furness, L.W., 1962, Flow characteristics of Elkhorn River near Waterloo, Nebr.: U.S. Geol. Survey Water-Supply Paper 1498–B, 34 p.

Carter, R.W., and Davidian, Jacob, 1965, Discharge ratings at gaging stations: U.S. Geol. Survey Surface-Water Techniques, book 1, chap. 12, p. 1–15.

Chow, V.T., 1959, Open-channel hydraulics: New York, McGraw-Hill, 680 p.

Colby, B.R., 1960, Discontinuous rating curves for Pigeon Roost and Cuffawa Creeks in northern Mississippi: U.S. Dept. Agr. ARS 41–36, 31 p.

Corbett, D.M., and others, 1943, Stream-gaging procedure: U.S. Geol. Survey Water-Supply Paper 888, 245 p.

Culbertson, J.K., and Dawdy, D.R., 1964, A study of fluvial characteristics and hydraulic variables, Middle Rio Grande, N. Mex.: U.S. Geol. Survey Water-Supply Paper 1498-F, 74 p.

Dawdy, D.R., 1961, Depth-discharge relations of alluvial streams—discontinuous rating curves: U.S. Geol. Survey Water-Suppy Paper 1498–C, 16 p.

Hulsing, Harry, 1967, Measurement of peak discharge at dams by indirect methods: U.S. Geol. Survey Techniques, Water Resources Inv., book 3, chap. A5, 29 p.

International Standards Organization, 1969, Liquid flow measurement in open channels—Establishment and operation of a gauging station and determination of the stage-discharge relation: ISO Recommendation R1100, Geneva, 44 p.

Kilpatrick, F.A., 1965, Use of flumes in measuring discharge at gaging stations: U.S. Geol. Survey Surface-Water Techniques, book 1, chap. 16, 27 p.

Kindsvater, C.E., and Carter, R.W., 1959, Discharge characteristics of rectangular thin-plate weirs: Am. Soc. Civil Engineers Trans., v. 124, p. 772–801.

King, H.W., and Brater, E.F., 1963, Handbook of hydraulics (5th ed.): New York, McGraw-Hill, 1373 p.

Linsley, R.K., Kohler, M.A., and Paulhus, J.L.H., 1949, Applied hydrology: New York, McGraw Hill, 689 p.

Moore, A.M., 1957, Measuring streamflow under ice conditions: Am. Soc. Civil Engineers Proc., Paper 1162, Hydraulics Div. Jour., v. 83, no. HY1, p. 1–12.

Reinhart, K.G., and Pierce, R.S., 1964, Stream-gaging stations for research on small watersheds: U.S. Forest Service, Agr. Handb. no. 268, 37 p.

Richardson, E.V., and Harris, D.D., 1962, A control structure for measuring water discharge and sediment load: U.S. Geol. Prof. Paper 450–D, p. D182–D184.

Simons, D.B., and Richardson, E.V., 1962, The effect of bed roughness on depth-discharge relations in alluvial channels: U.S. Geol. Survey Water-Supply Paper 1498–E, 26 p.

Stepanich, F.C., Simons, D.B., and Richardson, E.V., 1964, Control structures for sand-bed channels: Am. Soc. Civil Engineers Proc. Paper 3895, Waterways and Harbors Div. Jour., v. 90, no. WW2, p. 1–18.

Villemonte, J.R., 1947, Submerged-weir discharge studies: Eng. News-Record, v. 139, no. 26, p. 54–56.

World Meteorological Organization, 1968, Measurement of peak discharge by indirect methods: WMO-no. 225, TP. 119, Technical Note no. 90, Geneva, p. 129–157.
———1971, Use of weirs and flumes in stream gaging: WMO–no. 280, Technical Note no. 117, Geneva, 57 p.

CHAPTER 11—DISCHARGE RATINGS USING SLOPE AS A PARAMETER

GENERAL CONSIDERATIONS

If variable backwater or highly unsteady flow exists at a gaging station, the energy slope is variable at a given stage and the discharge rating cannot be defined by stage alone.

Variable backwater is most commonly caused by variable stage at a downstream confluence for a given discharge upstream or by the manipulation of gates at a downstream dam. The discharge under those conditions is a function of both stage and slope of the energy gradient. If the rate of change of stage is sufficiently great, the acceleration head must also be considered, but this chapter deals only with situations where the acceleration head has insignificant effect and can be neglected.

The unsteady-flow situation treated in this chapter is that of a natural flood wave, in which the flow maintains a stable wave profile as it moves down the channel. That type of wave is known as a uniformly progressive wave, and it often produces a loop rating at the gaging station; that is, for a given stage the discharge is greater when the stream is rising than it is when the stream is falling. The difference between the two discharges is significant only when the flow is highly unsteady. The term "highly unsteady", when associated only with the property of producing loop ratings, is a relative term, because channel slope is of equal importance in determining whether or not loop ratings will occur. A flood wave in a steep mountain channel will have a simple stage-discharge relation; that same flood wave in a flat valley channel may have a loop rating. The sections of this chapter that deal with unsteady flow are concerned only with loop ratings whose definition requires the use of slope, as well as stage, in a relation with discharge.

When a new gaging station is established, the need for a slope parameter in the rating can often be anticipated from the rating procedures used for existing stations nearby in a similar hydrologic and hydraulic environment. At other times the need for a slope parameter is not as evident. However, a plot of a series of discharge measurements made at medium and high stages will indicate the type of rating required for the station and will dictate whether or not an auxiliary gage is necessary to continuously measure water-surface slope.

If a pair of gages is needed, the locations of the base and auxiliary gage are based on the characteristics of the slope reach. The length of the reach should be such that ordinary errors that occur in the deter-

mination of gage heights at stage stations will cause no more than minor error in computing the fall in the reach. A fall of about 0.5 ft (0.15 m) is desirable but satisfactory records can often be obtained in reaches where the minimum fall is considerably less than 0.5 ft. Channel slope in the reach should be as uniform as possible. The reach should be as far upstream from the source of backwater as is practicable, and inflow between the two gages should be negligible. If possible, reaches with frequent or appreciable overbank flow should be avoided, as should reaches with sharp bends or unstable channel conditions. If the reach includes a natural control for low stages, the upstream (base) gage should be located just upstream from that control so that a simple stage-discharge relation will apply at low stages. Rarely will a slope reach be found that has all of the above attributes, but they should be considered in making a selection from the reaches that are available for slope measurement.

THEORETICAL CONSIDERATIONS

Variable slopes that affect flow in open channels are caused by variable backwater, by changing discharge, or by variable backwater in conjunction with changing discharge. The pair of differential equations given below provides a general solution to both gradually varied and unsteady flow.

$$\frac{Q^2}{K^2} = -\frac{\partial H}{\partial x} - \frac{1}{g}\frac{\partial V}{\partial t} \tag{77}$$

$$\frac{\partial Q}{\partial x} = -B\frac{\partial h}{\partial t} \tag{77a}$$

In the equations Q is the discharge, K is the conveyance of the cross section, H is the total energy head, x the distance along the channel, g the acceleration of gravity, V the mean velocity, t the time, B the top width of the channel, and h is the water-surface elevation. A solution to these equations in uniform channels may be obtained by approximate step methods after the conveyance term has been evaluated by discharge measurements.

In those practical problems of determining flow in open channels that require application of equation 77 the increment of slope due to the acceleration head $\frac{1}{g}\frac{\partial V}{\partial t}$ is, in general, so small with respect to the other two terms that its effect may be neglected. Thus, in equation 77 the terms that remain in addition to discharge (Q), are conveyance (K) which is a function of stage, and energy gradient ($\partial H/\partial x$) which is related to water-surface slope. At those sites where tidal action or

variation in power production cause the acceleration head to be large, approximate methods of integration of equations 77 and 77a are used in conjunction with an electronic computer. Those methods are described briefly in chapter 13 of this manual.

The discussion of stage-fall-discharge ratings presented in the present chapter draws heavily on previously published reports. The three primary references used are Corbett and others (1945), Eisenlohr (1964), and Mitchell (1954).

VARIABLE SLOPE CAUSED BY VARIABLE BACKWATER

The stage at a gaging station for a given discharge, under the usual subcritical flow conditions, is influenced by downstream control elements. A brief discussion of those elements is now in order.

Previous discussions of controls in this manual have dealt primarily with such elements as natural riffles, weirs and dams, flumes, and the physical properties of the stream channel. It had also been explained that a control may act independently for some range of stage or it may act in concert with one or more other controls. However, it had also been mentioned in appropriate places in this manual that the stage at downstream stream confluences may affect the stage-discharge relation at a gaging station. Where that occurs, the confluent stream must be classed as a control element that acts in concert (partial control) with the control(s) in the gaged stream. Furthermore, when a confluent stream acts as a control element, it usually does so as a variable element. That is, the stage at the gaging station will no longer be related solely to the discharge of the main stream, but will also vary with variation of the discharge in the confluent stream.

At gaging stations on tide-affected streams, the tide itself must be considered as a variable control element because of its effect on the stage-discharge relation at the gaging station. As mentioned earlier tide-affected stage-discharge relations are treated in chapter 13.

A less clear-cut situation with regard to control elements exists in many streams in southeastern United States. These streams have extremely wide flood plains that are crossed in places by highway embankments whose bridge openings locally constrict the flow severely. At high flow if water occupies the flood plain, the stage-discharge relation at the bridge is affected; for a given discharge through the bridge the corresponding stage will vary, depending on whether streamflow is entering the overbank areas as on a rising stage, or whether water is returning to the main channel from the overbank areas as on a falling stage. In that situation the overbank flow itself is acting as a variable control element in concert with the "more conventional" and more stable control elements, such the

geometry of the bridge opening and the geometry and roughness of the downstream main channel and overbank areas. The streamflow that is entering the overbank areas acts, in effect, as an extremely wide downstream distributary; the overbank flow that is returning to the stream acts, in effect, as an extremely wide downstream tributary. The streams usually have extremely flat gradients and the rating may possibly be complicated by the effect of changing discharge on streams of flat slope. However, as explained in the section titled, "Variable Slope Caused by a Combination of Variable Backwater and Changing Discharge," streams affected by both variable backwater and changing discharge are treated as though they were affected by variable backwater alone.

The control elements that affect the stage-discharge relation for a stream have now been identified and their descriptions have been amplified for the discussion of backwater that follows. At any given discharge the effect on the stage at the gaging station that is attributable to the operative control element(s) is known as backwater. As long as the control elements are unvarying, the backwater for a given discharge is unvarying, and the discharge is a function of stage only; the slope of the water surface at that stage is also unvarying. If some of the control elements are variable—for example, movable gates at a downstream dam or the varying stage at a downstream stream confluence—for any given discharge the stage at the station and the slope are likewise variable. In a preceeding discussion titled "Theoretical Considerations," it was demonstrated that for the above variable conditions, discharge can be related to stage and slope. Because the slope between two fixed points is measured by the fall between those points, it is more convenient to express discharge as a function of stage and fall.

Stage-fall-discharge ratings are usually determined empirically for observations of (1) discharge, (2) stage at the base gage, which is usually the upstream gage, and (3) the fall of the water surface between the base gage and an auxiliary gage. The general procedure used in developing the ratings is as follows:

1. A base relation between stage and discharge for uniform flow or for a fixed backwater condition is developed from the observations. The discharge from that relation is termed Q_r.
2. The corresponding relation between stages and the falls for conditions of uniform flow or fixed backwater is developed. Those falls are termed rating falls, F_r. Figure 188 shows schematically three forms the stage-fall relation may have.
3. The ratios of discharges Q_m, measured under conditions of variable backwater, to Q_r, are correlated with the ratios of the measured falls F_m to the rating falls F_r. Thus,

$$\frac{Q_m}{Q_r} = f\left(\frac{F_m}{F_r}\right). \tag{78}$$

The form of the relation depends primarily on the channel features that control the stage-discharge relation. The relation commonly takes the form,

$$\frac{Q_m}{Q_r} = \left(\frac{F_m}{F_r}\right)^N, \tag{78a}$$

where N varies from 0.4 to 0.6, the theoretical value of N being 0.5. Generally speaking, the stage-fall-discharge rating can be extrapolated with more confidence when the data are such that they fit equation 78a best when an N value of 0.5 is used.

The fall between the base and auxiliary gage sites, as determined from recorded stages at the two gages, may not provide a true representation of the slope of the water surface between the two sites. That situation may result from the channel and gaging conditions that are described below.

First, the water surface in any reach affected by backwater is not a plane surface between points in the reach, as sinuosity of the channel

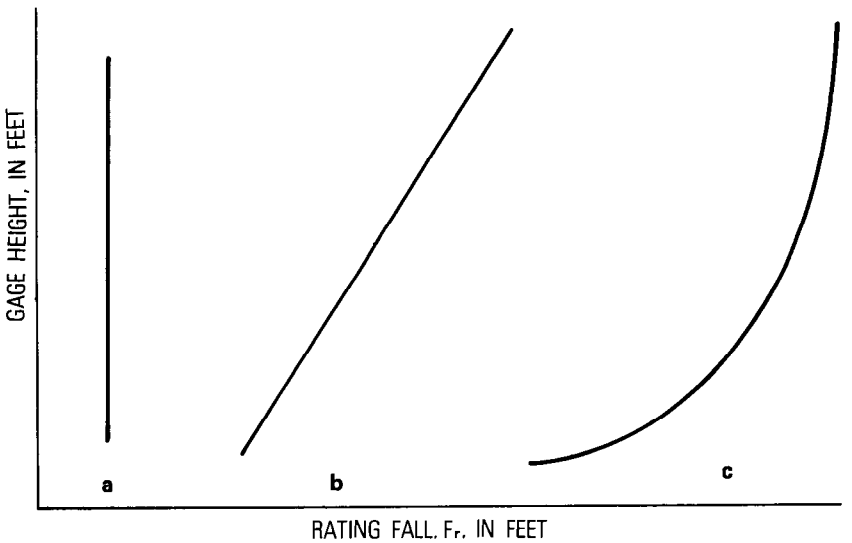

FIGURE 188.—Schematic representation of typical stage-fall relations. Curve (a), rating fall constant; curve (b), rating fall a linear function of stage; curve (c), rating fall a curvilinear function of stage.

will produce variations in the height of the water surface, both across and along the reach; variations in channel cross section and the effects of backwater also tend to produce curvature of the water surface. The slope determined from observed differences in stages is that of a chord connecting the water-surface elevations at points at the ends of a reach. It may not represent the slope of the water surface at either end of the reach but may be parallel to a line that is tangent to the water surface at some point in the reach.

Second, no reach of a natural stream selected for the determination of slope is completely uniform. The area of the cross section may vary considerably from point to point in the reach, but more important is the effect that shoals, riffles, rapids, or bends in the stream channel within the reach may have on the slope of the water surface, as well as on the energy gradient.

Third, the positions of the gages at the ends of the reach with respect to the physical features of the channel may have a material effect on the recorded gage heights and hence on the indicated slope. For example, if one gage is on the inside of a rather sharp bend and the other on the outside of a similar bend, the slope computed from records of stages at those gages may be widely different from the average slope of the water surface. Also, if differing drawdown effects exist at the intakes of the two gages, the two stage records obtained may not provide a true index of the water-surface slope.

Fourth, both gages may not be set to exactly the same datum, the difference in datum possibly being a large percentage of the total fall if the fall is small. The slope determined from gages not set to the same datum would not indicate the true water-surface slope because the computed slope would include the quantity y/L, where y is the difference in datum and L is the length of the reach.

Because of those conditions, theoretical relations between stage, fall, and discharge cannot be directly applied, and the relations must be empirically defined by discharge measurements made throughout the range of backwater conditions. Thus, the "best" value of the exponent of F_m/F_r in equation 78a will often be found to be in the range from 0.4 to 0.6, rather than having the theoretical value of 0.5; or, it may even be necessary to depart from a pure exponential curve in order to fit the plotted points satisfactorily. At other times the substitution of a term, $F+y$, for F values in equation 78a will improve the discharge relation. The use of a constant, y, whose best value is determined by trial computations, compensates in part for the inaccuracies in the value of F that were discussed above.

It is convenient to classify stage-fall-discharge ratings according to the types of relation that may be developed between stage and rating fall. The two types are:

1. *Rating fall constant.*—This type of relation (curve *a* in fig. 188) may be developed for channels that tend to be uniform in nature and for which the water-surface profile between gages does not have appreciable curvature.

2. *Rating fall a function of stage.*—This type of relation (curves *b* and *c* in fig. 188) may be developed if any of the following conditions exist:

   a. appreciable curvature occurs in the water-surface profile between gages;
   b. the reach is nonuniform;
   c. a submerged section control exists in the reach between gages, but the control does not become completely drowned by channel control even at high discharges; and
   d. a combination of some of the conditions listed above.

It is not uncommon for variable backwater to be effective for only part of the time. That follows from the two general principles that apply to backwater effect. The first states that for a given stage at the variable control element, backwater decreases at the base gage as discharge increases. For example, in a long gage reach of fairly steep slope, a given stage at the variable control element may cause significant backwater at the base gage when the discharge in the gaged stream is low but cause no backwater during periods when the discharge is high. The second principle states that for a given discharge, backwater decreases at the base gage as stage decreases at the variable control element. For example, at a given discharge in the gaged stream a high stage at the variable control element may cause significant backwater at the base gage, but a low stage at the variable control element may cause no backwater.

Other basic principles and detailed procedures used in defining stage-fall-discharge ratings are discussed on the pages that follow. The discussions are arranged in accordance with the preceding classification of stage-rating fall relations. A knowledge of the hydraulic principles applicable to a given slope reach is essential as a guide to the empirical analysis of the data.

RATING FALL CONSTANT

GENERAL DISCUSSION OF RATING PRINCIPLES

In uniform channels the water-surface profile is parallel to the bed; the slope, and therefore the fall, is the same for all discharges. The rating fall, F_r, for the condition of no variable backwater (uniform-flow conditions) would be the same at any stage. The stage-discharge relation with no backwater could be described by the Chezy equation,

$$Q_0 = CA_0\sqrt{R_0 S_0},$$

where the subscripts denote uniform flow; or by the equation,

$$Q_r = CA\sqrt{RF_r/L}, \tag{79}$$

where the subscripts denote the base rating conditions.

If variable backwater is imposed on the reach by a downstream tributary, the measured fall, F_m, and measured discharge, Q_m, would be less at a given stage than indicated by the uniform-flow rating. If the slope or fall as measured truly represents the slope at the base gage, those measurements would define, as shown in figure 189, a family of stage-discharge curves, each for a constant but different value of fall. The relation of each curve in the family to the curve for base rating conditions according to equation 79, is expressed by the equation,

$$\frac{Q}{Q_r} = \sqrt{\frac{F}{F_r}} \tag{80}$$

The discharge under variable backwater conditions may be computed as the product of (*a*) the discharge Q_r from the base rating and (*b*) the

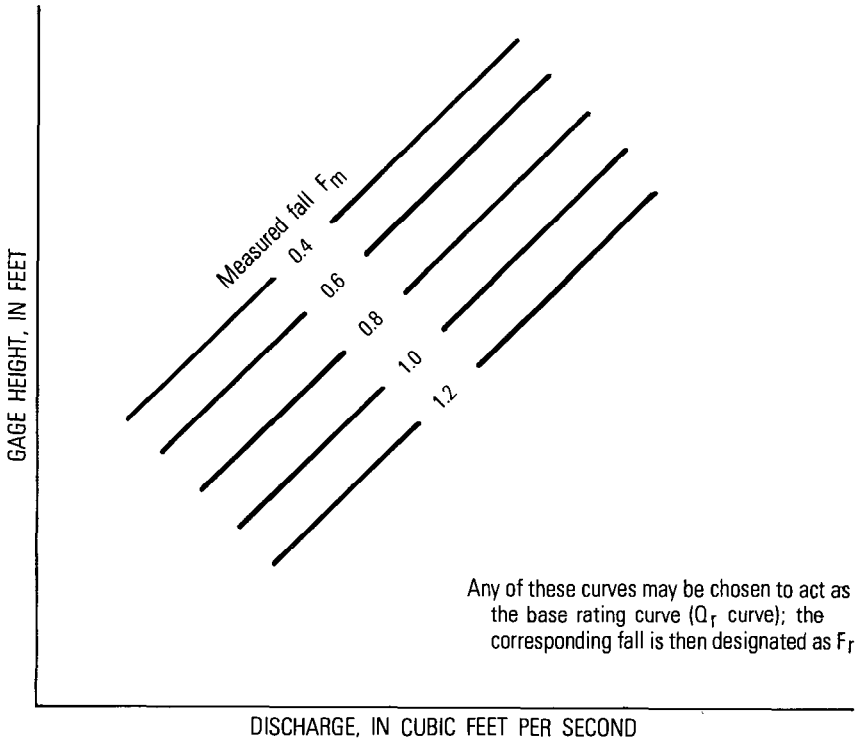

FIGURE 189.—Schematic representation of family of stage-discharge curves, each for a constant but different value of fall.

square root of the ratio of the measured fall to the constant-value rating fall.

A constant rating fall may also exist at sites where the base rating is controlled by a dam downstream from the reach in which fall is measured. If the curvature in the backwater profile is not significant, and if the channel is uniform, the water-surface profile will approximately parallel the channel-bed profile at all discharges. For example, the curve in figure 189 for a constant fall of 1.2 ft may be taken to represent the base stage-discharge relation for a fixed or stable control element. The curve for lesser falls that might result from variable submergence of the dam, are theoretically related to this base curve by the square root of the fall ratios, as described above. Quite commonly a constant value of 1.0 ft is used for F_r in equation 80. That special case of the constant rating-fall method, usually referred to as the unit-fall method, simplifies the computations because equation 80 then reduces to

$$Q_r = Q/\sqrt{F.} \tag{81}$$

A constant rating fall is not the usual case encountered in natural streams. However, if discharge measurements cover the entire range of flow conditions and if such measurements conform to a constant rating fall, there is no need to use a more complicated technique. If profile curvature and velocity-head increments are truly negligible, the relation between the discharge ratio and fall ratio should resolve into a single curve; otherwise the relation may be a family of curves with stage as a third variable.

PROCEDURE FOR ESTABLISHING THE RATING

The general procedure used in establishing a stage-fall-discharge rating with constant rating fall is outlined as follows:

1. Plot all discharge measurements using stages at the base gage as ordinates and discharges as abscissas, and note the measured fall (F_m) beside each plotted point. If the information on this plot indicates a family of curves, each corresponding to a constant value of fall (fig. 189), the use of a constant rating fall should be investigated.

2. The most satisfactory type of constant-fall rating, from the standpoint of high-water extrapolation, is one whose discharge ratio-fall ratio relation is a pure parabolic relation, as in equation 80, with the exponent equal to, or nearly equal to, 0.5. If such a relation fits the measured discharges, the results are unaffected by whatever value of constant fall (F_r) is used. For convenience, unit fall is used, as in equation 81.

3. For each discharge measurement (Q_m), compute Q_r by use of the equation $Q_r = Q_m/(F_m)^{0.5}$.

4. Plot values of gage height versus Q_r for each discharge measurement and fit a curve to the plotted points to obtain the Q_r discharges from the Q_r rating curve.

5. Compute and tabulate the percentage departures of the plotted Q_r discharges from the Q_r rating curve.

6. Repeat steps 3–5, using exponents of F_m other than, but close to, 0.5. Try exponents equal to 0.40, 0.45, 0.55, and 0.60.

7. Compare the five Q_r rating curves and select the curve that best fits the plotted points used to define it. In steps 8 and 9 that follow, the discharges from that "best" rating curve will be referred to as Q_{rd}, and the corresponding exponent of F_m will be referred to as d.

8. If the plotted discharges closely fit the Q_{rd} rating curve, that curve and the relation of (Q_m/Q_{rd}) to F_m are accepted for use.

9. If the plotted discharges do not closely fit the Q_{rd} rating curve repeat steps 3–5, using the exponent d but substituting the term (F_m+y) for F_m. Several values of y, a small quantity that may be either positive or negative, are tried to obtain a Q_r rating curve that closely fits the plotted discharge.

10. Compare the various Q_r rating curves obtained from step 9 and select the curve that best fits the plotted points used to define it. If the plotted discharges closely fit that Q_r rating curve, that rating curve and the corresponding relation of (Q_m/Q_r) to (F_m+y) are accepted for use. If the fit is not considered to be sufficiently close, the use of a pure parabolic relation, such as equation 81, is abandoned and the strictly empirical approach described in the following steps is used.

11. From the family of stage-discharge curves discussed in step 1, select one as the base Q_r curve and use the constant fall for this curve as F_r.

12. Compute the ratios Q_m/Q_r and F_m/F_r, plot the discharge ratios as ordinates and the fall ratios as abscissas, and draw an average curve through the plotted points that passes through the point whose coordinates are 1.0, 1.0.

13. Adjust each measured discharge by dividing it by the discharge ratio corresponding to the fall ratio on the above curve. Plot these computed values of Q_r against stage, and draw an average curve (Q_r curve) through the plotted points.

14. Repeat steps 11–13 using alternative constant values of F_r until the best relation between stage, fall, and discharge is established.

15. If the best relation derived from the application of steps 11–14 is still unsatisfactory, use the more flexible method described in the section titled, "Rating Fall a Function of Stage."

EXAMPLE OF RATING PROCEDURE

The stage-fall-discharge rating for Tennessee River at Guntersville, Ala. is presented in figure 190 as an example of a rating with constant rating fall. The upper gage is a water-stage recorder installed in a well attached to a pier of a highway bridge. The lower gage is a water-stage recorder installed on the right bank 43,700 ft below the upper gage and 3,300 ft above Guntersville Dam. The channel conditions in this reach are reasonably uniform. Variable backwater is caused by the operations at Guntersville Dam.

A satisfactory relation between stage, fall, and discharge could not be established for the upper (base) gage by use of the procedures for a pure parabolic fall-ratio curve that are described in steps 1–10. The empirical approach described in steps 11–14 was therefore used. The best rating was obtained by using a value of F_r equal to 1.5 ft. The fall-ratio curve in figure 190 approximately fits equation 80 for all fall ratios no greater than 1.0; for fall ratios greater than 1.0 the curve is flatter than a parabola defined by equation 80.

To plot, on the Q_i rating curve, a subsequent discharge measurement (Q_m) having a fall F_m, the fall ratio, F_m/F_r or $F_m/1.5$, is first computed. The fall-ratio curve is then entered with the computed fall ratio, and the discharge ratio, Q_m/Q_r, is read. Q_m is then divided by that value of the discharge ratio to give the value of Q_i to be plotted.

The method of obtaining the discharge corresponding to a given gage height and a given fall (F_m) is explained in the section titled, "Determination of Discharge from Relations for Variable Backwater."

RATING FALL A FUNCTION OF STAGE

GENERAL DISCUSSION OF RATING PRINCIPLES

Where variable backwater is a factor in the discharge rating, it will generally be found that fall is a function of stage. The average relation between fall and discharge may be linear, or fall may be a complex function of stage. Rating principles are best discussed by reference to examples.

The right-hand graph in figure 191 for the Columbia River at The Dalles, Oreg., is an example of a linear relation between stage and fall. The stage-discharge relation at the base gage is affected by reservoir operations at Bonneville Dam, more than 80 miles downstream. The auxiliary gage is located at Hood River bridge, 19 miles downstream from the base gage. Within the range of measured discharges, fall increases linearly with stage.

A much more complex stage-fall relation is shown in the right-hand graph in figure 192 for the Ohio River at Metropolis, Ill. At the downstream (auxiliary) gage, the stage-discharge relation is affected only at the lower stages by a constriction, the backwater from which causes fall to decrease with stage in the slope reach. At the higher

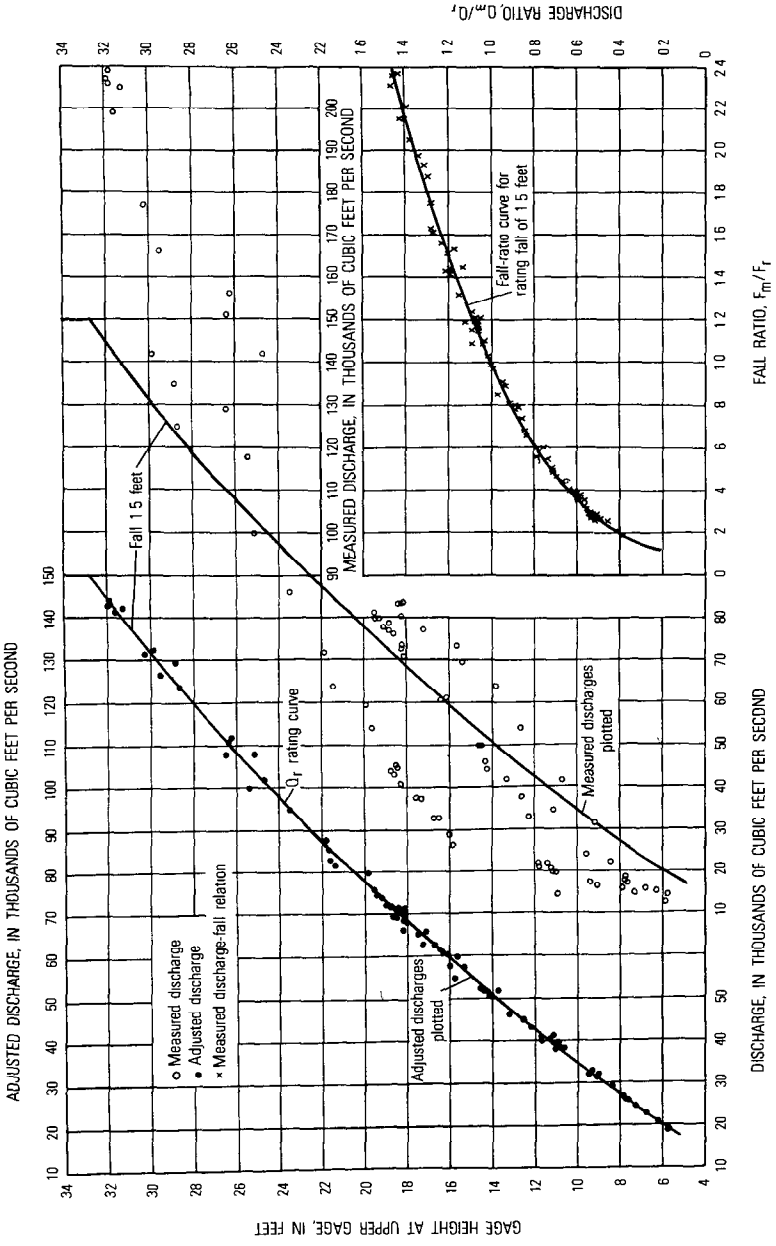

FIGURE 190.—Stage-fall-discharge relations for Tennessee River at Guntersville, Ala.

stages the constriction has little effect and fall increases with stage.

Another example of a complex stage-fall relation is shown in the right-hand graph in figure 193 for Kelly Bayou near Hosston, La. The base gage for this rating is about 2.7 miles upstream from the mouth of Kelly Bayou. The auxiliary gage is on Black Bayou, 4.2 miles downstream from the base gage. At low stages, fall increases with stage; at medium and high stages the backwater effect from Black Bayou is more pronounced and fall tends to assume a constant value.

Where a section control exists just downstream from the base gage, it is necessary to identify those situations when backwater effect is absent at the base gage. Obviously there will be no backwater when the tailwater at the section control is below the crest of the control. Most artificial controls are broad-crested, and submergence is generally effective only when tailwater rises to a height above the crest that is equal to or greater than 0.7 times the head on the control. Looked at another way, submergence is effective only when the fall between the upstream and downstream stages is equal to or less than 0.3 times the head on the control. Thus a straight line of initial submergence may be drawn on the curve of stage versus fall; the line passes through the coordinates representing the elevation of the control crest and zero fall, with a slope of 3 ft of stage per foot of fall.

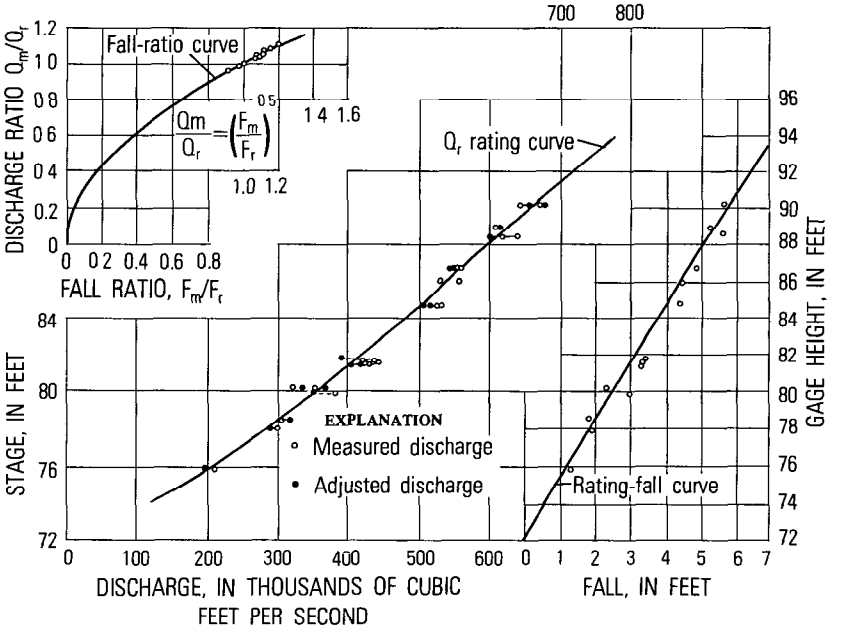

FIGURE 191.—Stage-fall-discharge relations for Columbia River at The Dalles, Oreg.

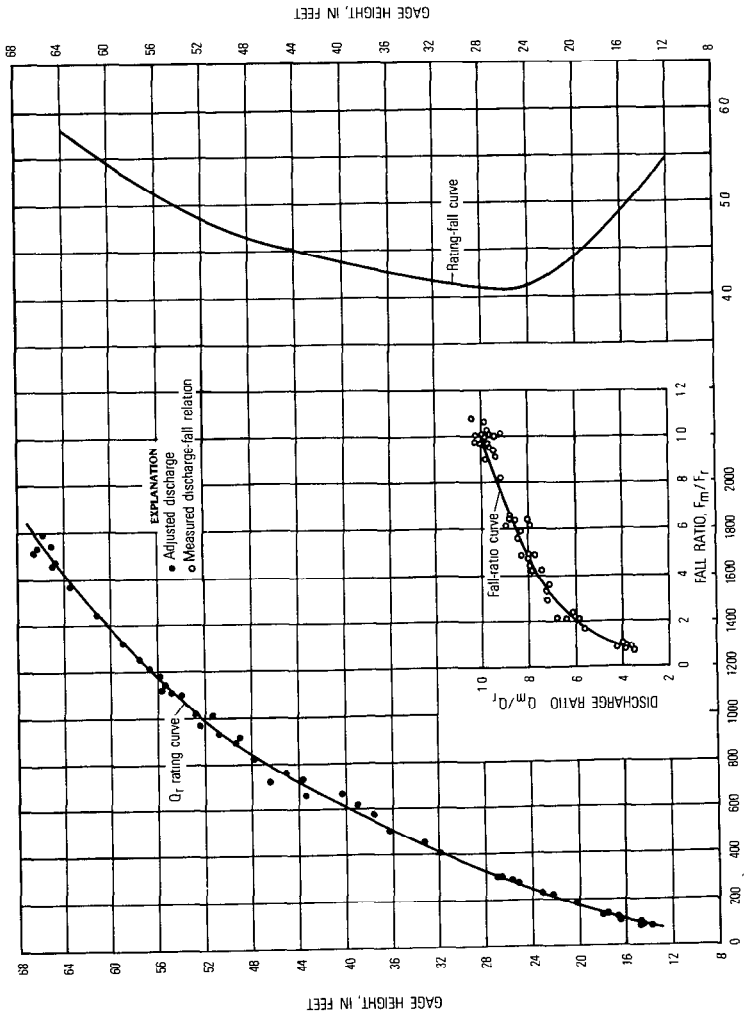

FIGURE 192.—Stage-fall-discharge relations for Ohio River at Metropolis, Ill.

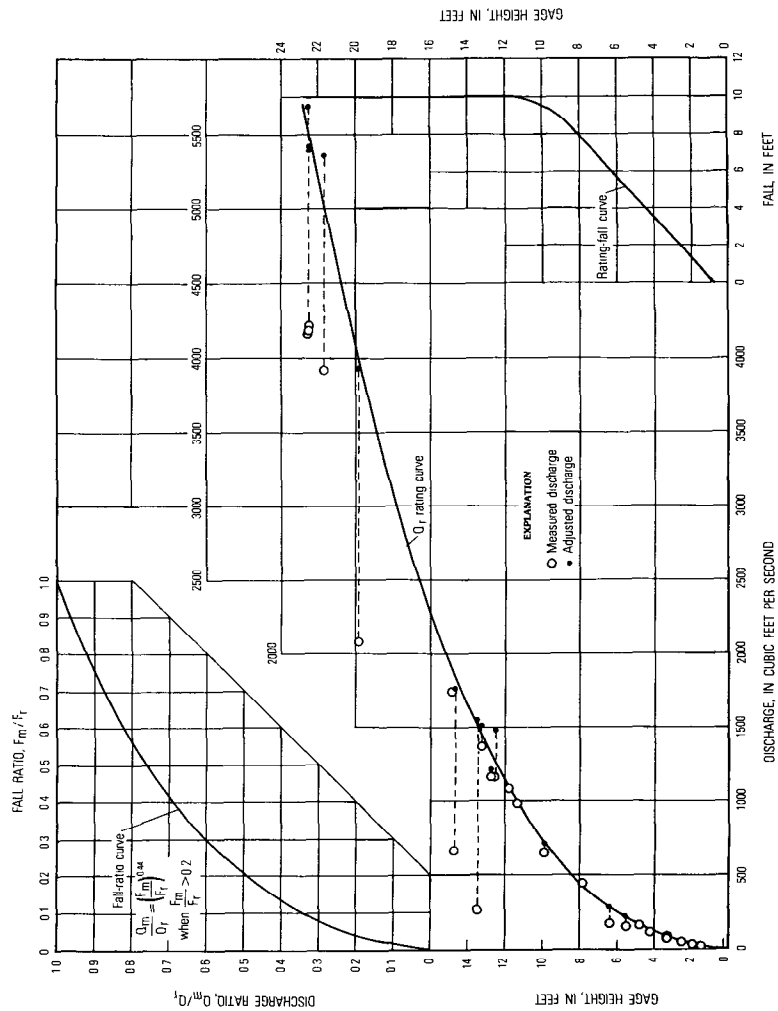

FIGURE 193.—Stage-fall-discharge relations for Kelly Bayou near Hosston, La.

The precise position and slope of the line will depend on the location of the downstream auxiliary gage with respect to the section control. If the auxiliary gage is immediately downstream from the control, the line of initial submergence will have the position and slope stated above. If the auxiliary gage is far downstream from the control, the line on the stage-fall graph will intersect the elevation of the control crest at a value of fall greater than zero, and the slope of the line will depend on the hydraulic features of the station; field observation will be necessary to define the graph coordinates of the line of initial submergence. All observed or recorded values of fall that lie below the line of initial submergence indicate free-fall discharge (discharge unaffected by the tailwater elevation); all observed or recorded values of fall that lie above the line of initial submergence indicate discharge affected by variable backwater. Furthermore, if the auxiliary (tailwater) gage is close to the control, the fall-ratio curve for discharges affected by backwater should closely fit the theoretical equation,

$$(Q_m/Q_r) = (F_m/F_r)^{0.5}.$$

If the auxiliary (tailwater) gage is distant from the control, the fall-ratio curve will depart from the theoretical equation.

The right-hand graph in figure 194 shows the stage-fall relation for Colusa Weir near Colusa, Calif. The base gage for the station is a short distance upstream from an ungated weir which acts as a section control, and the auxiliary gage is a short distance downstream from the control. There is no pool immediately upstream from Colusa Weir, the streambed being at the elevation of the weir crest; there is a drop of about 2 ft immediately downstream from the weir. The line of initial submergence shown crossing the lower part of the stage-fall relation has the theoretical position and slope discussed above. Colusa Weir is at the downstream end of a large natural detention basin along the left bank of the Sacramento River, and water that passes over the weir immediately enters the river. Because the river stage rises faster than the stage of the detention pool, fall decreases with stage at the base gage, as shown by the rating-fall curve.

The right-hand graph in figure 195 is a plot of stage versus fall for the Kootenay River at Grohman, B.C., Canada. The base gage for this station is on the west arm of Kootenay Lake about 2 miles upstream from Grohman Narrows. Downstream from the narrows is the forebay of the Corra Linn powerplant, and in the forebay is the auxiliary gage, about 8 miles downstream from the base gage. Grohman Narrows is the control for the base gage, but operations of Corra Linn Dam cause variable submergence of the control when the stage of the

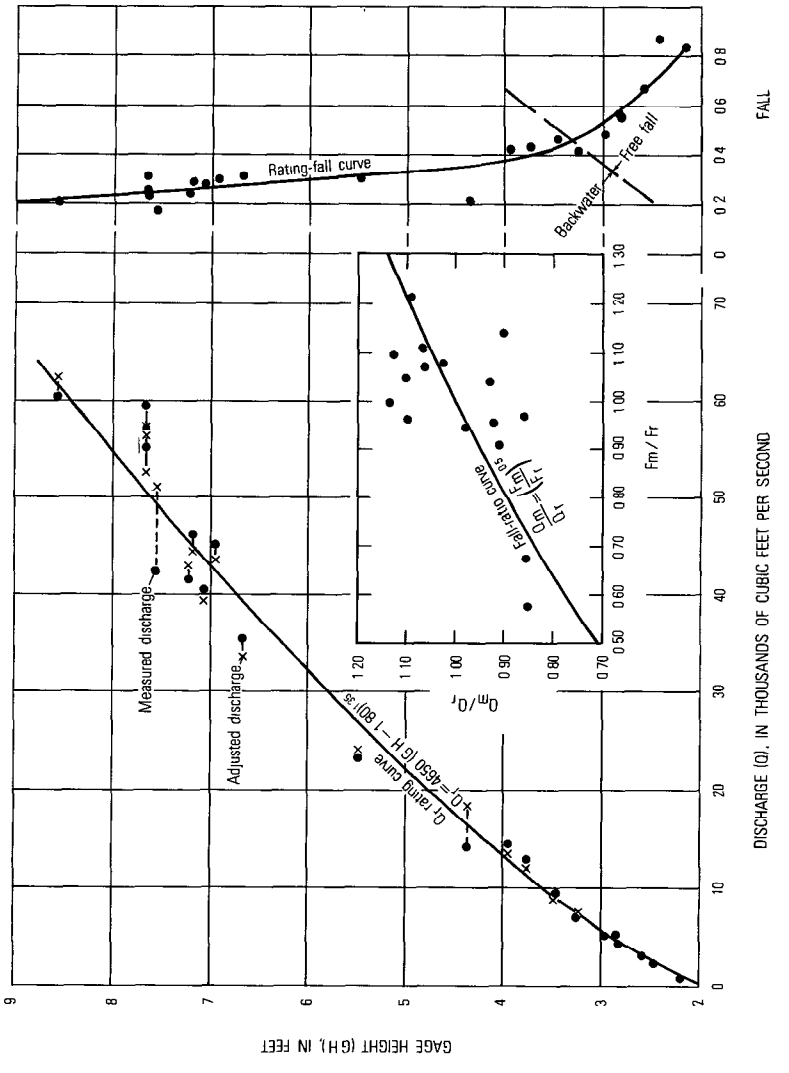

FIGURE 194.—Stage-fall-discharge relations for Colusa Weir near Colusa, Calif

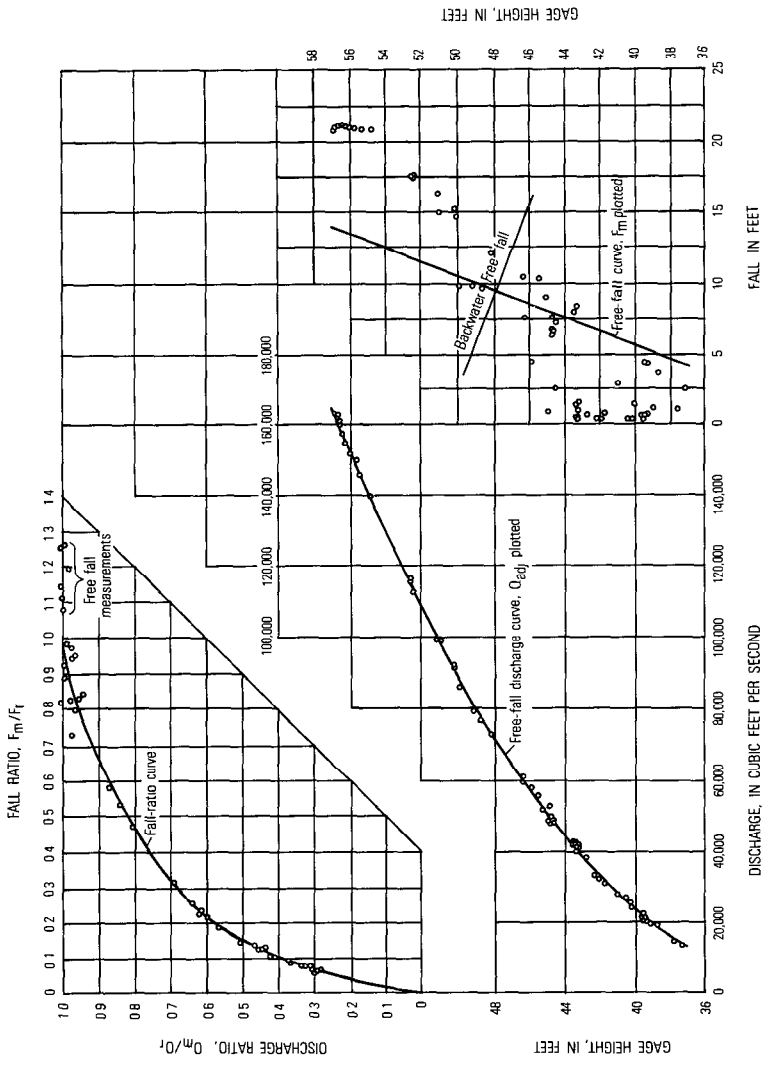

FIGURE 195.—Stage-fall-discharge relations for Kootenay River at Grohman, British Columbia, Canada. Measurements with falls less than 0.4 feet not plotted.

forebay is sufficiently high. The line of initial submergence, shown as the free-fall curve in figure 195, was determined from observation and discharge measurements. Discharge measurements whose values of fall plot below, or to the right of, the free-fall curve are unaffected by backwater and those discharges are therefore independent of fall. Discharge measurements whose values of fall plot above, or to the left of, the free-fall curve are affected by variable backwater. For those measurements the graph shows no apparent relation between stage and fall, and the free-fall curve (line of initial submergence) was used as the rating-fall curve for the measurements affected by variable backwater.

The rating for a gaging station whose base gage has no section control is analyzed in a manner similar to that previously described in the section on "Rating Fall Constant—Procedure for Establishing the Rating," the principal difference being that instead of using a constant value of rating fall, the rating fall for any stage is obtained from the rating-fall curve. The rating for a gaging station whose base gage has a section control is analyzed in two separate steps. The free-fall part of the rating (no variable backwater) is analyzed as explained in chapter 10, where simple stage-discharge relations are discussed. That part of the rating that is affected by variable backwater is analyzed as though no section control existed. It is not necessary to use the free-fall rating curve as the basis for establishing that part of the rating that is affected by variable backwater although that course of action is commonly followed.

Summary.—In view of the many different and complex situations that exist in natural channels, it is difficult to give general guidelines for establishing stage-fall-discharge relations. The analyst should make every effort to acquaint himself with the physical characteristics of the channel and the source of variable backwater. The best position of the relation curves that comprise the discharge rating must be determined by trial and error. The complexity of those relations determines, to a large degree, the number of discharge measurements necessary to define the discharge rating. Although the methods are empirical, experience has shown that there may be found a stage-discharge relation (the Q_r curve) which, taken in conjunction with its associated stage-fall relation (the rating-fall curve), will give close approximation to the true discharge under all possible combinations of stage and fall, by the application of a single-curve relation, Q_m/Q_r versus F_m/F_r. It is desirable, but not always possible, to have that relation take the theoretical form,

$$Q_m/Q_r = (F_m/F_r)^{0.5} \tag{80}$$

PROCEDURE FOR ESTABLISHING THE RATING

The general procedure used in establishing a stage-fall-discharge rating with variable fall is outlined as follows:

1. Plot all discharge measurements using stages at the base gage as ordinates and discharges (Q_m) as abscissas, and note the measured fall (F_m) beside each plotted point.

2. On another graph plot the measured fall (F_m) for each discharge measurement against stage at the base gage, using stage as the ordinate.

3. If the base gage has a section control, determine the position of the line of initial submergence on the plot of stage versus measured fall. Its position is based on discharge measurements known to have been made under conditions of free fall. Those measurements, plotted against stage on logarithmic graph paper, are fitted with a free-fall rating curve which is extrapolated in accordance with the principles discussed in chapter 10. The remaining measurements are added to the logarithmic rating plot; those measurements that plot to the left of the extrapolation are considered to be affected by backwater. That knowledge, along with a knowledge of the probable degree of submergence required to cause backwater effect, enables the analyst to fix the position of the line of initial submergence. Only those measurements that plot above, or to the left of, the line of initial submergence are used in the analysis of the rating for variable backwater that is discussed in the steps that follow.

4. Fit a curve, Q_r rating curve, to the stage-discharge plot in step 1, and another curve, F_r, or rating-fall curve, to the stage-fall plot in step 2.

5. From the curves in step 4 obtain values of Q_r and F_r corresponding to the stage of each discharge measurement.

6. Compute the ratios Q_m/Q_r and F_m/F_r for each discharge measurement.

7. Plot Q_m/Q_r as ordinate against F_m/F_r as abscissa, and on that graph draw the curve $Q_m/Q_r=(F_m/F_r)^{0.5}$.

8. On the basis of the scatter of the plotted points about the curve in step 7, adjust the Q_r and F_r curves (step 4) to obtain revised values of Q_r and F_r (step 5), such that the new ratios of Q_m/Q_r and F_m/F_r fit the curve in step 7 as closely as possible. The adjustments to the Q_r and F_r curve should not be so drastic that the adjusted curves are no longer smooth curves.

9. Repeat steps 4–8, using exponents of (F_m/F_r) other than, but close to 0.5. Try exponents equal to 0.40, 0.45, 0.55, and 0.60.

10. Compare the five plots of Q_m/Q_r versus F_m/F_r and select the one which shows the best fit between curve and plotted points. (The ratio of plotted values of Q_m/Q_r to curve values of Q_m/Q_r is identical with

the ratio of measured discharge to discharge obtained from the stage-fall-discharge relations.) In steps 11 and 12 that follow, the exponent of that best fall-ratio curve will be referred to as d.

11. If the plotted ratios closely fit the curve $(Q_m/Q_r) = (F_m/F_r)^d$, that curve and the corresponding Q_r and F_r curves are accepted for use.

12. If the plotted ratios do not closely fit the curve $(Q_m/Q_r) = (F_m/F_r)^d$, repeat steps 4–8, using the exponent d but substituting the terms $(F_m + y)$ for F_m and $(F_r + y)$ for F_r. Several values of y, a small quantity that may be either positive or negative, are tried to obtain a close fit between plotted points and the curve $(Q_m/Q_r) = \left[(F_m+y)/(F_r+y)\right]^d$.

13. Compare the various plots of the fall-ratio graph obtained from step 12 and select the one showing the best fit between curve and plotted points. If the fit is satisfactory, that curve and the corresponding Q_r and F_r curves are selected for use. If the fit is not considered to be sufficiently close, the use of a pure parabolic relation, such as

$$Q_m/Q_r = (F_m/F_r)^d \tag{82}$$

or

$$Q_m/Q_r = \left[(F_m+y)/(F_r+y)\right]^d \tag{83}$$

is abandoned and the strictly empirical approach described in the following steps is used.

14. Select one of the trial Q_r and F_r curves, such as were constructed in step 4, along with the corresponding values of Q_r, F_r, Q_m/Q_r, and F_m/F_r, such as were obtained in steps 5 and 6.

15. Plot the discharge ratios as ordinates and the fall ratios as abscissas, and draw an average curve through the plotted points that passes through the point whose coordinates are (1.0, 1.0).

16. On the basis of the scatter of the plotted points about the curve in step 15, adjust the Q_r and F_r curves (step 14), as well as the fall-ratio curve. Again, the reminder that the adjusted curves must remain smooth curves.

17. Repeat steps 14–16, using other trial curves of Q_r, F_r, and fall ratio versus discharge ratio, until the best relation is established between stage, fall, and discharge; in other words, until a close fit is obtained between plotted points and the fall-ratio curve.

18. After having obtained acceptable Q_r, F_r, and fall-ratio curves, plot adjusted values of the discharge measurements on the Q_r rating curve. The adjusted values are computed as follows: Given a measured discharge (Q_m) and a measured fall (F_m). Enter the F_r curve (stage-fall relation) with the gage height of the discharge measurement and read F_r. Next, compute the fall ratio, F_m/F_r, and enter

the fall-ratio curve to obtain the discharge ratio, Q_m/Q_r. Obtain the value Q_r to be plotted by dividing Q_m by (Q_m/Q_r).

The method of obtaining the discharge corresponding to a given gage height and a given fall (F_m) will be explained in the section titled, "Determination of Discharge from Relations for Variable Backwater."

EXAMPLES OF RATING PROCEDURE

Figures 191–195 are examples of stage-fall-discharge relations for slope stations where fall is a function of stage.

Figure 191 for a Columbia River station shows that excellent results were achieved in the range of discharge that was measured. The linear trend of fall increasing with stage is clearly evident, and the fall-ratio curve not only is represented by the theoretical equation 80, but is closely fitted by the plotted points. Where the rating-fall curve (stage versus fall) is so well defined, the first estimate of the Q_r curve is usually made by the use of equation 80, in which Q would represent the measured discharges. The computed Q_r values for the discharge measurements would then be plotted against stage, and a curve fitted to the plotted points would represent the first trial Q_r curve.

Figure 192 for an Ohio River station is an extremely complex example, as can be seen from the shape of the rating-fall curve. It is not surprising that the fall-ratio curve could not be expressed by a simple parabolic equation such as equation 82 or 83.

Figure 193 for a station on Kelly Bayou shows that there is relatively minor effect from variable backwater at low stages. At medium and high stages, the variable stage of Black Bayou causes variable backwater at the base gage. The rating-fall used during high-water periods has the constant value of 10.0 ft. The fall-ratio curve, for values of F_m/F_r greater than 0.2, has the equation

$$Q_m/Q_r = (F_m/F_r)^{0.44}.$$

Because the exponent 0.44 does not differ greatly from its theoretical value of 0.5, the Q_r rating curve can be extrapolated with some confidence.

Figure 194 for Colusa Weir is an example of the stage-fall-discharge relation for a station whose base gage has a section control. There is no variable backwater at low flow, as shown by the 6 discharge measurements that plot below the line of initial submergence on the graph of stage versus fall. The remaining 16 discharge measurements show the effect of variable backwater. While the fit of adjusted measured discharges to the Q_r rating curve is not completely satisfactory, there is some satisfaction to be derived from the facts that

the equation of the fall-ratio curve is theoretically correct and the fall-ratio curve balances the plotted points.

Figure 195 for a station on the Kootenay River is an example of the stage-fall-discharge relation for a station whose base gage has a control that is unsubmerged at high stages. Of the 59 discharge measurements shown, 23 were made under free-fall conditions; they plot below, or to the right of, the line of initial submergence on the graph of stage versus fall. The remaining 36 discharge measurements are affected by variable backwater and were used in the stage-fall-discharge analysis. Because the line of initial submergence was used as F_r in the analysis, the value of F_m for any measurement affected by backwater is less than F_r. Consequently the fall-ratio curve was fitted empirically to the plotted points and is not expressed by a simple parabolic equation such as equation 82 or 83.

DETERMINATION OF DISCHARGE FROM RELATIONS FOR VARIABLE BACKWATER

After the three necessary graphical relations are available—stage versus rating fall (F_r), stage versus rating discharge (Q_r), and Q_m/Q_r versus F_m/F_r—the graphs are converted to tables. The determination of discharge (Q_m) corresponding to a given stage and a given fall (F_m) proceeds as follows:

1) From the stage-fall table determine the rating fall, F_r, for the known stage.
2) Compute the ratio F_m/F_r.
3) From the table of discharge ratios, (Q_m/Q_r) and fall ratios (F_m/F_r), determine the value of the ratio Q_m/Q_r.
4) From the stage-discharge table, determine the rating discharge, Q_r, for the known stage.
5) Compute Q_m by multiplying the ratio Q_m/Q_r by the value of Q_r.

Much emphasis has been placed on obtaining a purely parabolic function, such as equation 82 or 83, for the relation between fall ratio and discharge ratio. Such a relation not only permits the analyst to extrapolate the Q_r curve with more confidence, but it also expedites the computation of discharge. For example equation 82 may be transposed to

$$Q_m = \left(\frac{Q_r}{F_r^{\alpha}}\right)\left(F_m^{\alpha}\right). \tag{82a}$$

Two tables can be prepared, one giving the values of the quantity (Q_r/F_r^{α}) corresponding to stage, and the other giving values of (F_m^{α}) corresponding to values of F_m. The discharge is then computed as the

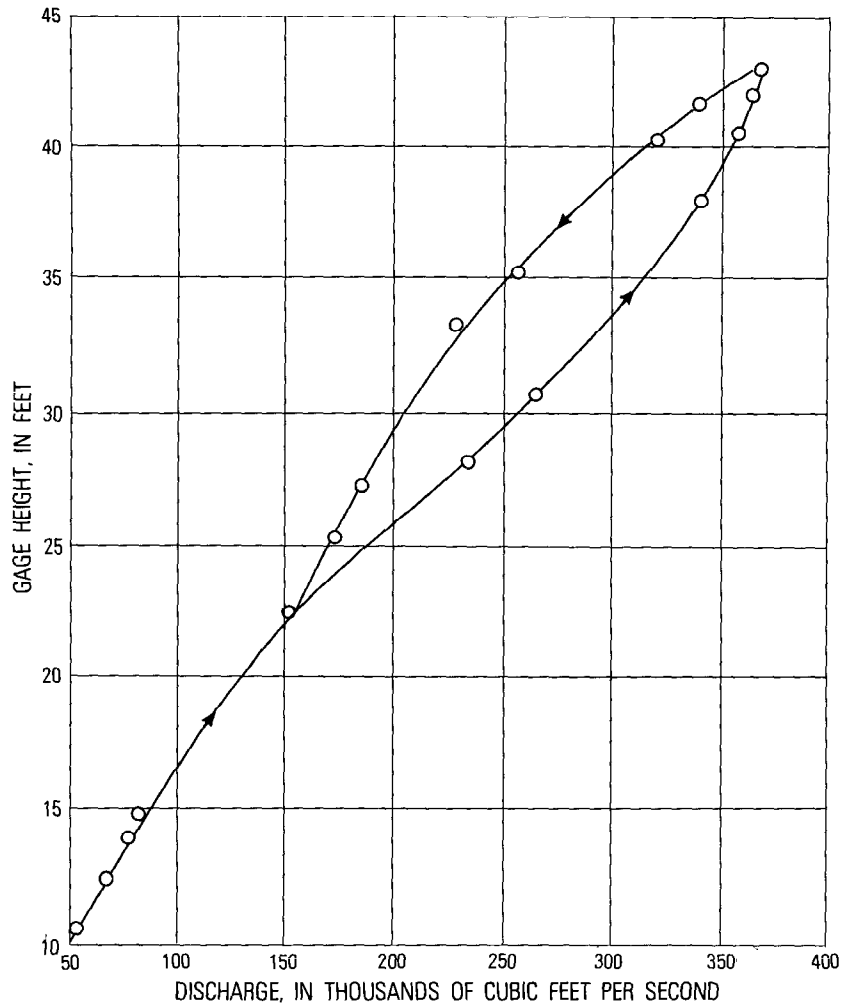

FIGURE 196.—Stage-discharge loop for the Ohio River at Wheeling, W. Va., during the flood of March 14–27, 1905.

product of the two values picked from the tables. Equation 83 may be transposed in a similar way.

VARIABLE SLOPE CAUSED BY CHANGING DISCHARGE

THEORETICAL CONSIDERATIONS

Where channel control is effective, the effect of changing discharge on a graph of the stage-discharge relation is such as to produce a loop curve (fig. 196), on which the discharge for a given stage is greater

when the stream is rising than it is when the stream is falling. In other words, given a simple stage-discharge relation for steady flow—that is, a rating that averages all discharge measurements—it will be found that the measurements made on a rising stage plot to the right of the curve and those made on a falling stage plot to the left. The discharge measurements for individual flood waves will commonly describe individual loops in the rating. The departure of measurements from the rating curve for steady flow is of significant magnitude only if the slope of the stream is relatively flat and the rate of change of discharge is rapid. For gaging stations where this scatter of discharge measurements does occur, the discharge rating must be developed by the application of adjustment factors that relate steady flow to unsteady flow. (Unsteady flow refers to discharge at a site that changes appreciably with time, as in the passage of a flood wave.)

The relation between the discharges for steady and unsteady conditions at the same stage can be derived from the general equations for unsteady flow (Rouse, 1950). A simplified equation shown below may also be derived by neglecting all terms representing change of velocity head or acceleration.

$$\frac{Q_m}{Q_c} = \sqrt{1 + \frac{1}{S_c\, v_w}\,\frac{dh}{dt}} \tag{84}$$

where Q_m is the discharge for unsteady flow, Q_c and S_c are the discharge and energy slope for steady flow at the same stage, v_w is the wave velocity, and dh/dt is the rate of change of stage with respect to time (dh is positive for rising stages).

Because equation 84 is basic to the methods commonly used for adjusting discharge ratings for the effect of changing discharge, it is appropriate to elaborate on its derivation. The ratio of the magnitudes of two discharges that occur at a given stage is equal to the ratio of the square roots of their energy slopes. That principle can be expressed in the following basic equation, which is similar to equation 80 that was used in preceding sections of the manual.

$$\frac{Q_m}{Q_c} = \frac{\sqrt{S_m}}{\sqrt{S_c}} \tag{85}$$

where S_m is the energy slope for unsteady flow at the time of Q_m; the remaining terms are defined above for equation 84.

During changing discharge, the slope of the water surface increases or decreases by an increment of slope (ΔS), where

$$\Delta S = \frac{1}{v_w} \frac{dh}{dt} \cdot \tag{86}$$

If we assume that the increment of slope by which the energy gradient changes is likewise equal to ΔS, then

$$S_m = S_c + \Delta S = S_c + \frac{1}{v_w} \frac{dh}{dt} \cdot \tag{87}$$

By combining equations 85 and 87,

$$\frac{Q_m}{Q_c} = \left(\frac{S_c + \frac{1}{v_w} \frac{dh}{dt}}{S_c} \right)^{1/2}, \tag{88}$$

or

$$\frac{Q_m}{Q_c} = \left(1 + \frac{1}{S_c v_w} \frac{dh}{dt} \right)^{1/2} \cdot \tag{84}$$

The wave velocity v_w in the above equations may be evaluated by the Seddon principle (Seddon, J. E., 1900).

$$v_w = \frac{1}{B} \frac{dQ}{dh},$$

where B is the width of the channel at the water surface, and dQ/dh is the slope of the stage-discharge curve for constant-flow conditions. From examination of formulas for mean velocity (V_m) in open channels, the ratio of wave velocity to mean velocity may be shown to vary as follows,

	Ratio v_w/V_m	
Channel Type	*Manning*	*Chezy*
Triangular	1.33	1.25
Wide rectangular	1.67	1.50
Wide parabolic	1.44	1.33

Experience seems to indicate that the most probable value of the ratio in natural channels is 1.3.

Equation 84 explains why the effect of changing discharge is significant only on flat streams during rapid changes in discharge; that combination is necessary to make the right-hand side of the

equation differ significantly from unity. During rapid changes in discharge, absolute values of dh/dt are large. On flat streams both energy slope (S_e) and wave velocity (v_w) are small. The combination of a large value of dh/dt and small values of S_e and v_w gives the right-hand side of the equation a value that is significantly larger than unity during a rising stage (dh/dt is positive) and significantly smaller than unity during a falling stage (dh/dt is negative).

METHODS OF RATING ADJUSTMENT FOR CHANGING DISCHARGE

The two methods used to adjust discharge for the effect of changing slope attributable to changing discharge are the Boyer method and the Wiggins method. Both methods are based on equation 84. The knowledgeable reader of this manual may notice that the Jones and Lewis methods are not included among the techniques for adjusting discharge. Those two methods have been supplanted by the somewhat similar Boyer method and therefore are not described here. For a description of the Jones and Lewis methods the interested reader is referred to the manual by Corbett (1943, p. 159–165).

BOYER METHOD

The Boyer method provides a solution of equation 84 without the necessity for individual evaluation of v_u and S_e. The method requires numerous discharge measurements made under the conditions of rising and falling stage. Measured discharge (Q_m) is plotted against stage in the usual manner, and beside each plotted point is noted the value of dh/dt for the measurement. For convenience dh/dt is expressed in feet or meters per hour and the algebraic sign of dh/dt is included in the notation—plus for a rising stage and minus for a falling stage. A trial Q_e rating curve, representing the steady-flow condition where dh/dt equals zero, is fitted to the plotted discharge measurements, its position being influenced by the values of dh/dt noted for the plotted points. Values of Q_e from the curve corresponding to the stage of each discharge measurement, are used in equation 84, along with the measured discharge (Q_m) and observed change in stage (dh/dt), to compute corresponding values of the adjustment factor, $1/S_e v_u$. The computed values of $1/S_e v_w$ are then plotted against stage and a smooth curve is fitted to the plotted points. If the plotted values of $1/S_e v_w$ scatter widely about the curve, the Q_e curve is modified to produce some new values of $1/S_e v_u$ that can be better fitted by a smooth curve. The modifications of the curves of Q_e and $1/S_e v_u$ should not be so drastic that the modified curves are no longer smooth curves, nor should the modified shape of the Q_e rating curve violate the principles underlying rating curves, as discussed in chap-

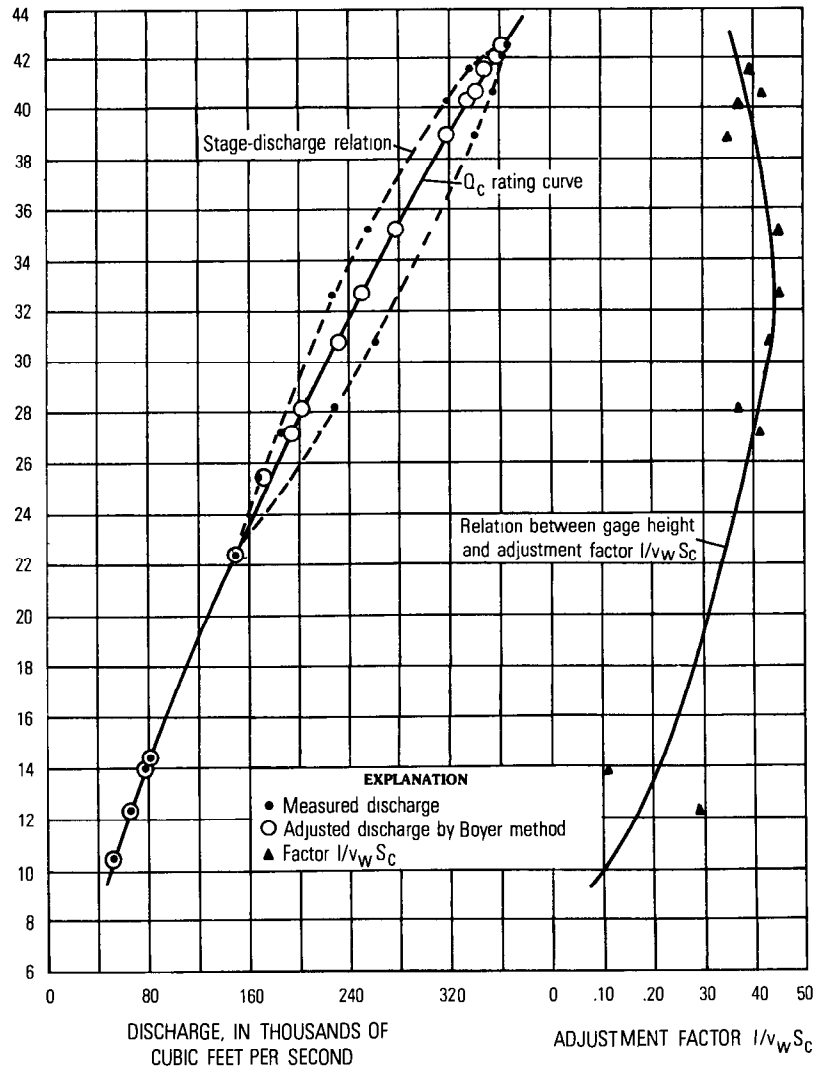

FIGURE 197.—Adjustment of discharge measurements for changing discharge, Ohio River at Wheeling, W. Va., during the period March 14–27, 1905.

ter 10. Construction of the two curves completes the rating analysis. Figure 197 is an example of such an analysis.

To adjust the value of subsequent discharge measurements for plotting on the Q_c rating curve, the adjustment-factor curve is first entered with the stage of the measurement to obtain the appropriate value of the factor, $1/S_c v_w$. Next, the observed value of dh/dt is used

with that factor to compute the term, $\left(1+\frac{1}{S_c v_w}\frac{dh}{dt}\right)^{0.5}$. That term is then divided into the measured discharge (Q_m) to obtain the required value of Q_c.

To determine discharge from the Q_c rating curve and adjustment-factor curve, during a period when the stage and rate of change of stage are known, the procedure described above is used to obtain the value of the term $\left(1+\frac{1}{S_c v_w}\frac{dh}{dt}\right)^{1/2}$. That term is then multiplied by Q_c, which is obtained by entering the Q_c rating curve with the known stage. The product is the required discharge (Q_m).

WIGGINS METHOD

The Wiggins method is convenient for adjusting measured discharge (Q_m) for the effect of changing discharge to obtain the corresponding steady-flow discharge (Q_c). However, the reverse procedure of computing discharge for unsteady flow (Q_m) from the steady-flow discharge rating is rather complicated. Consequently, the Wiggins method is used only for those stations where only occasional adjustment of measured discharge at high stages is required. If the discharge is affected by changing stage on numerous days each year, the more accurate Boyer method of discharge adjustment should be used. Unlike the Boyer method, application of the Wiggins method does not require numerous discharge measurements that have been made under conditions of both rising and falling stage.

The discharge measurement adjusted by the Wiggins method are used to define the steady-flow rating, and that rating is used directly with the gage-height record to obtain daily values of discharge. That course of action is justifiable for those streams whose discharge is affected by changing discharge on only a few days each year. For that type of stream, it will generally be found that the discharge adjustment is less than 10 percent. On the affected days, the discharge obtained from the steady flow rating will be underestimated by a small percentage when the discharge is rising rapidly, and overestimated by a small percentage when the discharge is falling rapidly. The discrepancies are compensating, and if only few days are involved, the streamflow record is not significantly impaired. The advantage of applying the adjustment to discharge measurements made under unsteady-flow conditions is that the scatter of discharge measurements on the rating curve is reduced, and the rating curve can therefore be more precisely defined.

Application of the Wiggins method has been simplified by the preparation of diagrams that eliminate much of the computational labor. Figures 198*A-D* are used to determine the value of the energy slope

(S_m) at the time of the discharge measurement (Q_m), for combinations of values of mean velocity (V_m) and hydraulic radius (R). The Manning equation was used in preparing the graphs, and each of the four sheets is applicable for a particular value of Mannings n, as shown in the following tabulation:

Figure 198A—n=0.025 Smooth bed and banks.
198B—n=0.035 Fairly smooth.
198C—n=0.050 Rough.
198D—n=0.080 Very rough.

Figure 199 is used to determine the increment of energy slope $\left(\frac{1}{v_w}\frac{dh}{dt}\right)$ attributable to changing discharge, for combinations of values of flood-wave velocity (v_w) and rate of change of stage (dh/dt). Flood-wave velocity is assumed to equal $1.3V_m$.

Figures 200*A* and *B* are used to determine the factor to apply to the measured discharge (Q_m) to obtain the steady-flow discharge (Q_c). The factor, which is equal to

$$\left[\frac{S_m-\left(\frac{1}{\bar{v}_u}\right)\left(\frac{dh}{dt}\right)}{S_m}\right]^{0.5},$$

is given for combinations of values of S_m from figure 198 and of $\left(\frac{1}{v_w}\frac{dh}{dt}\right)$ from figure 199. (Note that the factor differs from that given in equation 88, because S_m is used here as the base slope, rather than S_c as in equation 88.) Figure 200*A* is used for rising stages and figure 200*B* is used for falling stages.

An example of the use of the Wiggins diagrams follows.

Given: a discharge measurement with the following data for a stream with fairly smooth bed (n=0.035);

Q_m=23,000 ft^3/s
Area=53,900 ft^2
Width= 2,700 ft
V_m=4.27 ft/s
Change in stage=0.87 ft in 1.5 hours (rising)

Compute adjusted discharge to be plotted on rating curve.

First compute:

$$R = \frac{\text{Area}}{\text{Width}} = \frac{53{,}900}{2{,}700} = 20 \text{ ft}$$

$$v_u = 1.3\ V_m = 1.3 \times 4.27 = 5.55 \text{ ft/s}$$

$$\frac{dh}{dt} = \text{change in stage per hour} = \frac{0.87}{1.5} = 0.58 \text{ ft/hr}$$

Then: (a) Enter figure 198*B* with $V_m = 4.27$ and $R = 20$ and read $S_m = 0.00018$

(b) Enter figure 199 with $\frac{dh}{dt} = 0.58$ and $v_w = 5.55$ and read slope increment $(\frac{1}{v_w}\frac{dh}{dt}) = 0.000029$

(c) Enter figure 200*A* (rising stage) with $S_m = 0.00018$ and slope increment = 0.000029 and read factor = 0.915.

Adjusted discharge = 0.915 × 230,000 = 210,000 ft³/s.

Because the stage was rising, the unadjusted discharge would plot to the right of the rating curve. The computed adjustment moves the measurement to the left.

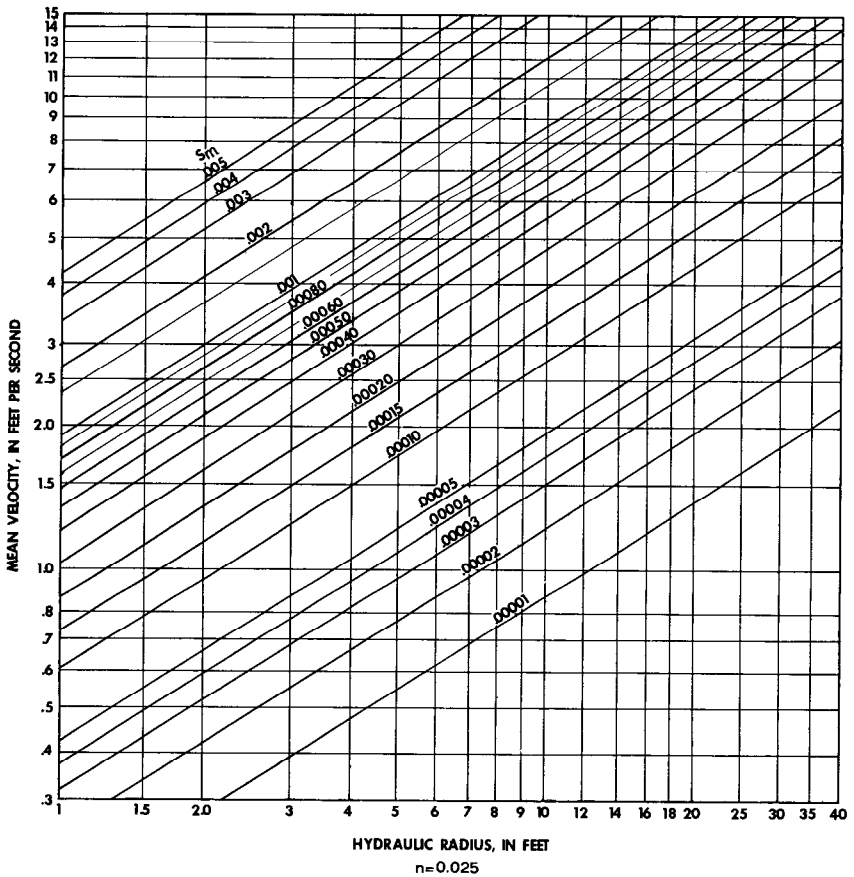

FIGURE 198*A*.—Diagram for solution of the Manning equation to determine S_m. Smooth bed and banks (n=0.025).

Both the measured (Q_m) and adjusted (Q_c) discharges are entered in the list of discharge measurements and both are plotted on the rating curve. Suitable symbols are used, however, to differentiate between the measured and adjusted discharges.

VARIABLE SLOPE CAUSED BY A COMBINATION OF VARIABLE BACKWATER AND CHANGING DISCHARGE

Where the rating for a gaging station is affected by a combination of variable backwater and changing discharge, the rating should be analyzed as though it were affected by variable backwater only, using the fall-rating methods described in the section titled, "Rating Fall a Function of Stage." The basic equation for variable-backwater adjustments (eq. 80) and that for changing-discharge adjustments (eq.

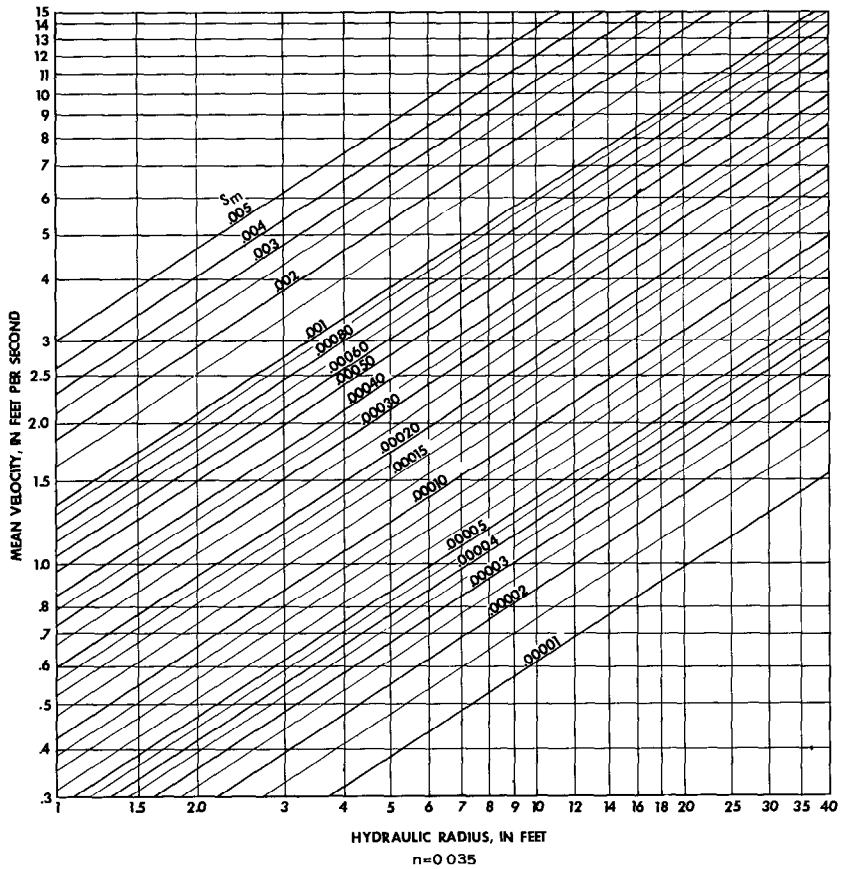

FIGURE 198*B*.—Diagram for solution of the Manning equation to determine S_m. Fairly smooth bed (n=0.035).

85) are similar, but only the fall-rating methods are versatile enough to handle the combined effect of the two factors.

SHIFTS IN DISCHARGE RATINGS WHERE SLOPE IS A FACTOR

Changes in channel geometry (scour or fill) and (or) changes in flow conditions (vegetal growth) will cause shifts in the discharge rating where slope is a factor, just as they cause shifts in simple stage-discharge relations. When discharge measurements indicate a shift in the rating for a slope station, the shifts should be applied to the Q_r rating curve if the station is affected by variable backwater, or to the Q_c rating curve if the station is affected by changing discharge. Extrapolation of the shift curves should be performed in accordance with the principles discussed in chapter 10 for shifts in simple stage-

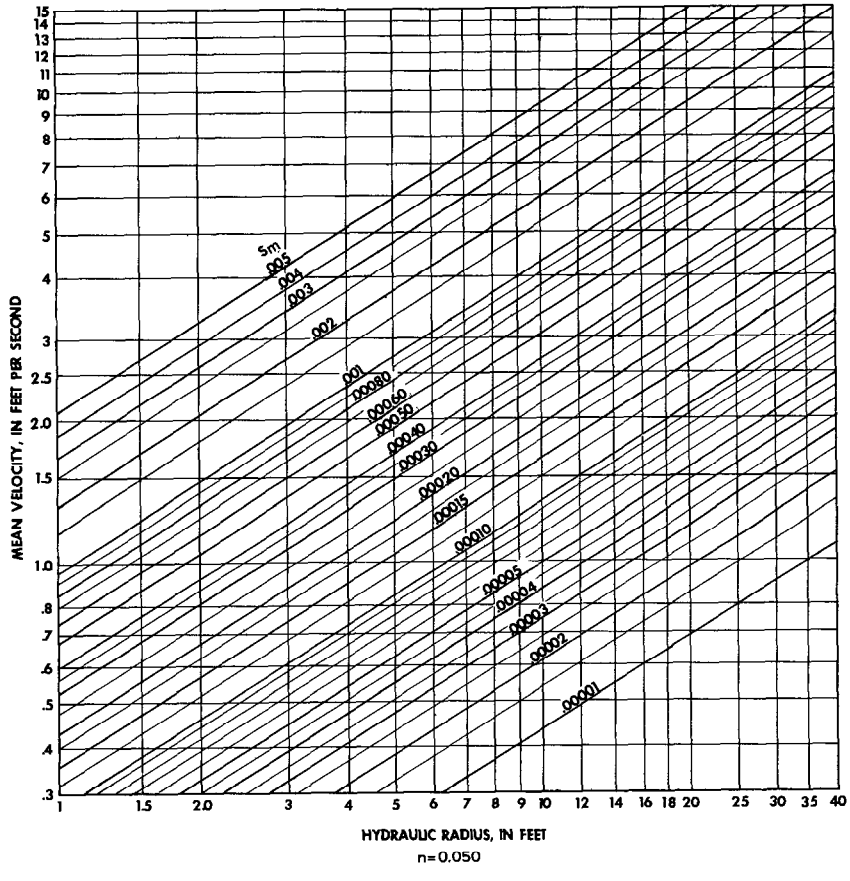

FIGURE 198*C*.—Diagram for solution of the Manning equation to determine S_m. Rough bed (n=0.050).

discharge relations. (See section in chapter 10 titled, "Shifts in the Discharge Rating.")

A SUGGESTED NEW APPROACH FOR COMPUTING DISCHARGE RECORDS FOR SLOPE STATIONS

Now that the use of electronic computers has become commonplace, it appears that a fresh approach might be tried with regard to computing streamflow records for gaging stations equipped with a stage-recorder at each end of a slope reach. Instead of using the various graphical empiricisms that were described in this chapter, a computer program could be written to compute discharge for the reach by the Manning equation or by some similar equation for open-channel flow. (It is assumed that acceleration head can be neglected.) Dis-

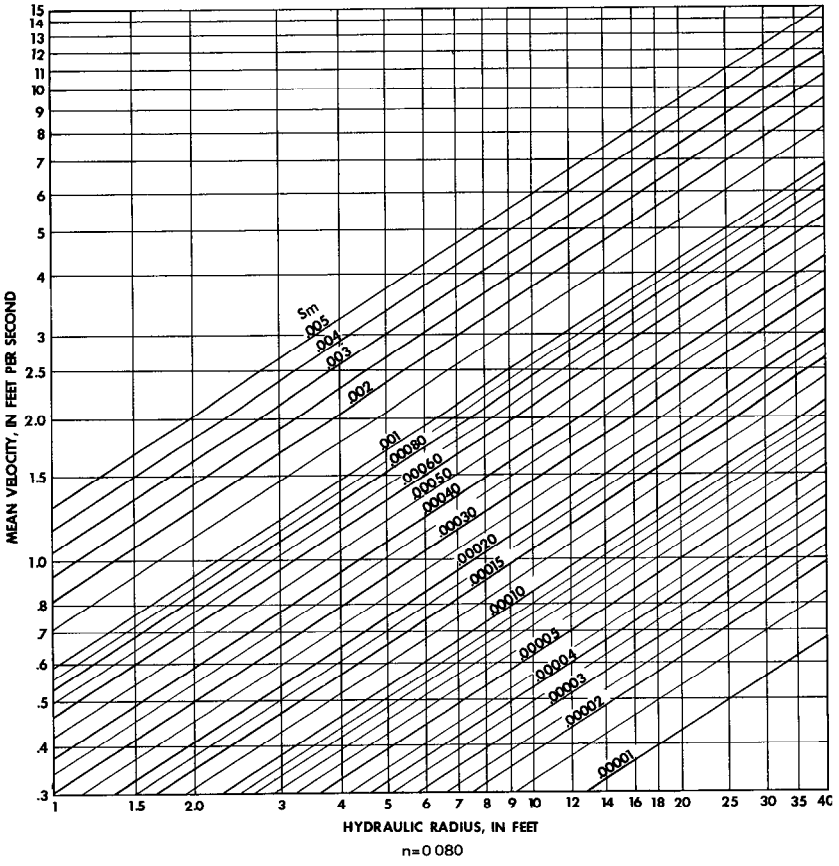

FIGURE 198*D*.—Diagram for solution of the Manning equation to determine S_m. Very rough bed (n=0.080).

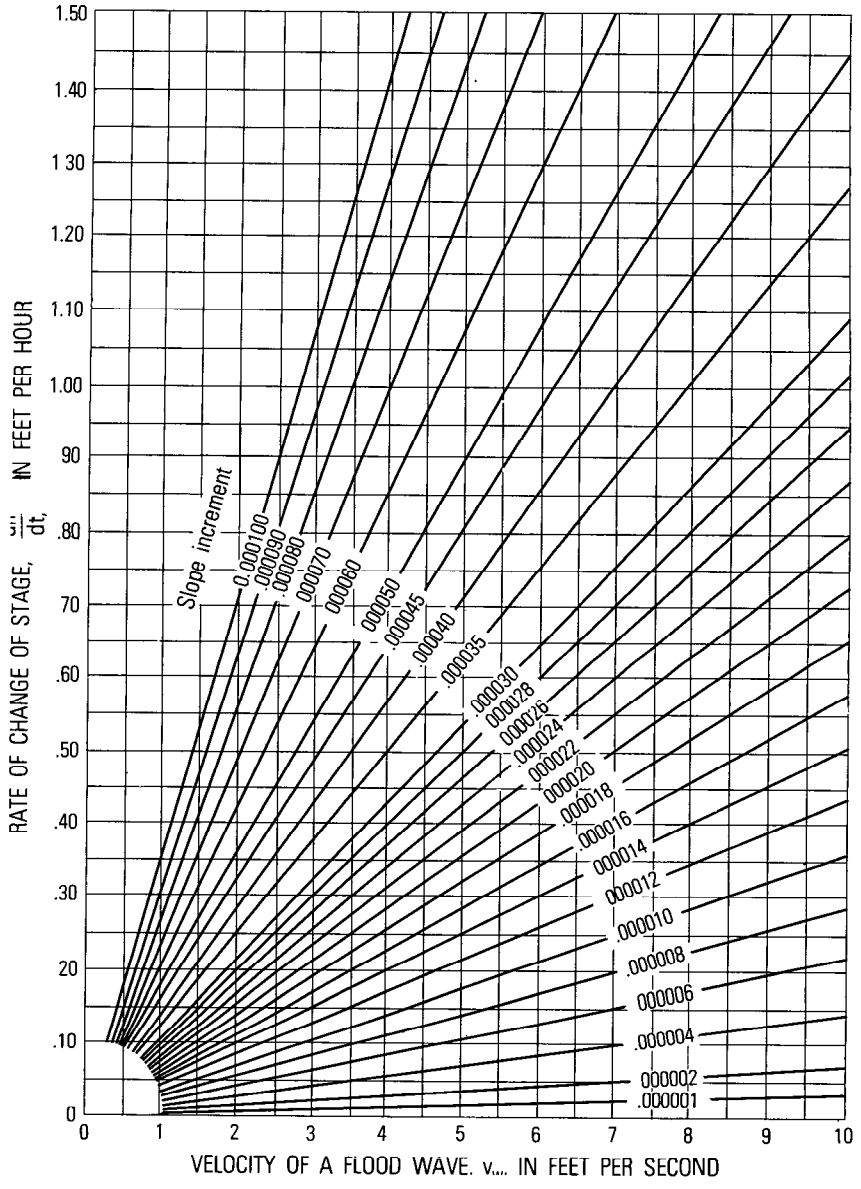

FIGURE 199.—Diagram for determining slope increment resulting from changing discharge.

charge measurements would be made solely for the purpose of determining the Manning roughness coefficient (n) from the measured discharge, thereby obtaining the only unkown factor needed to compute the conveyance (K) at each end of the slope reach.

The value of n computed from a discharge measurement usually would not represent the true value of the roughness coefficent but would actually be a "catchall" value that included the effect of error in the computed value of the energy slope in the reach. The computed values of n would likely vary with stage.

The discharge computations would proceed along the following lines. The basic form of the Manning equation is

$$Q = KS^{1/2} \tag{89}$$

where

Q is discharge;
K is conveyance, which is equal to $\frac{1.49}{n} AR^{2/3}$ (A is cross-sectional area and R is hydraulic radius); and
S is the energy gradient.

Equation 89 can be expanded to

$$Q = K_2 \sqrt{\frac{F}{\frac{K_2}{K_1} L + \frac{K_2^2}{2gA_2^2}\left[-\alpha_1\left(\frac{A_2}{A_1}\right)^2(1-k)+\alpha_2(1-k)\right]}} \tag{90}$$

where

F is fall in the reach,
L is length of reach,
g is the acceleration of gravity,
α is the velocity-head coefficient whose value is dependent on the velocity distribution in the cross section,
k is a coefficient of energy loss whose value is considered to be zero for contracting reaches and 0.5 for expanding reaches;
subscript 1 refers to the upstream cross section, and
subscript 2 refers to the downstream cross section.

For the cross section at each end of the slope reach, relations would be prepared between stage and each of the following three elements: K, A, and α. A computer program would be written to solve equation 90. Then, given the stage at each end of the reach, the computer would compute F, A, K, α, and finally, Q.

For those slope stations where the change in velocity head in the reach is so minor an item that it can be neglected, the conventional constant-fall method (see section titled, "Rating Fall Constant") could be continued in use; computer computation would be optional.

It is emphasized that the above method of computing discharge records is as yet untried, but it is suggested that it be tested.

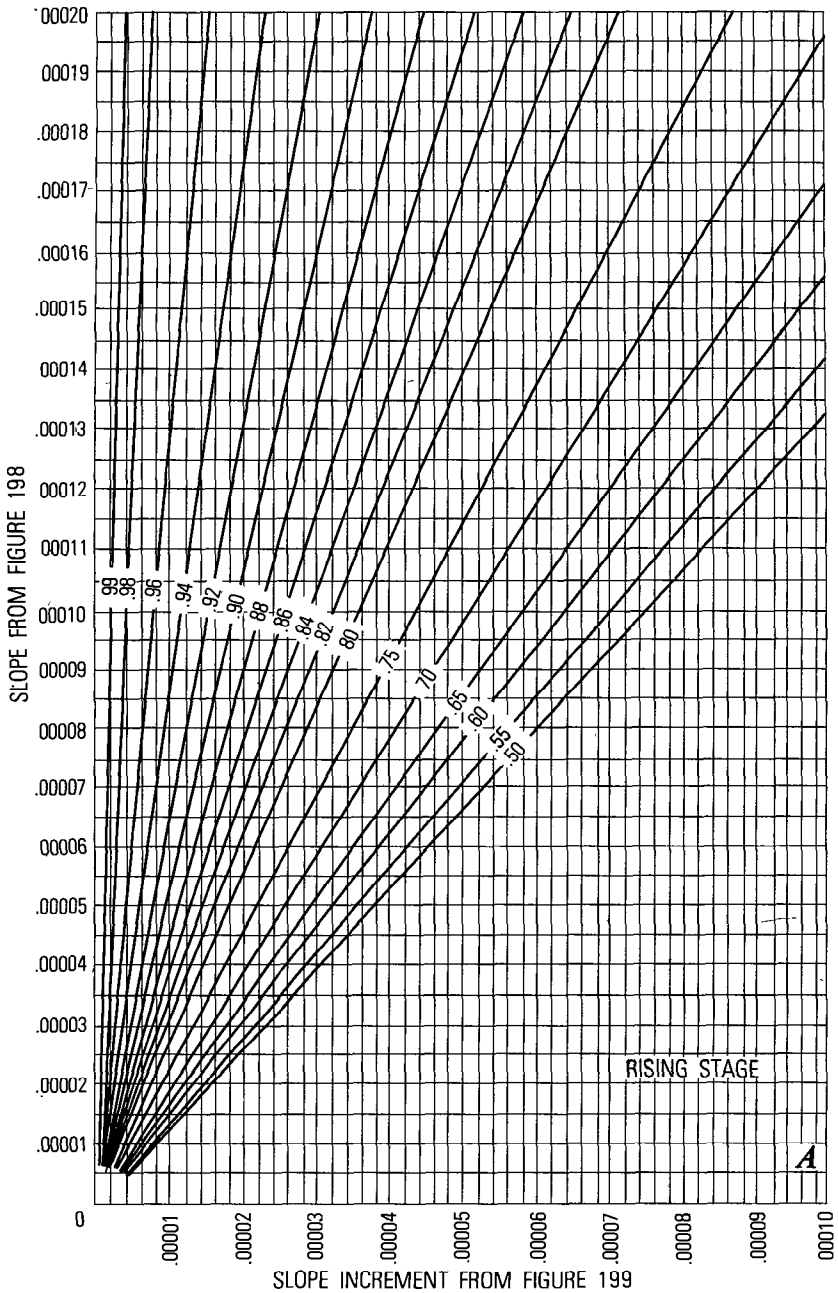

FIGURE 200A.—Diagram for determining factor to apply to measured discharge—rising stage.

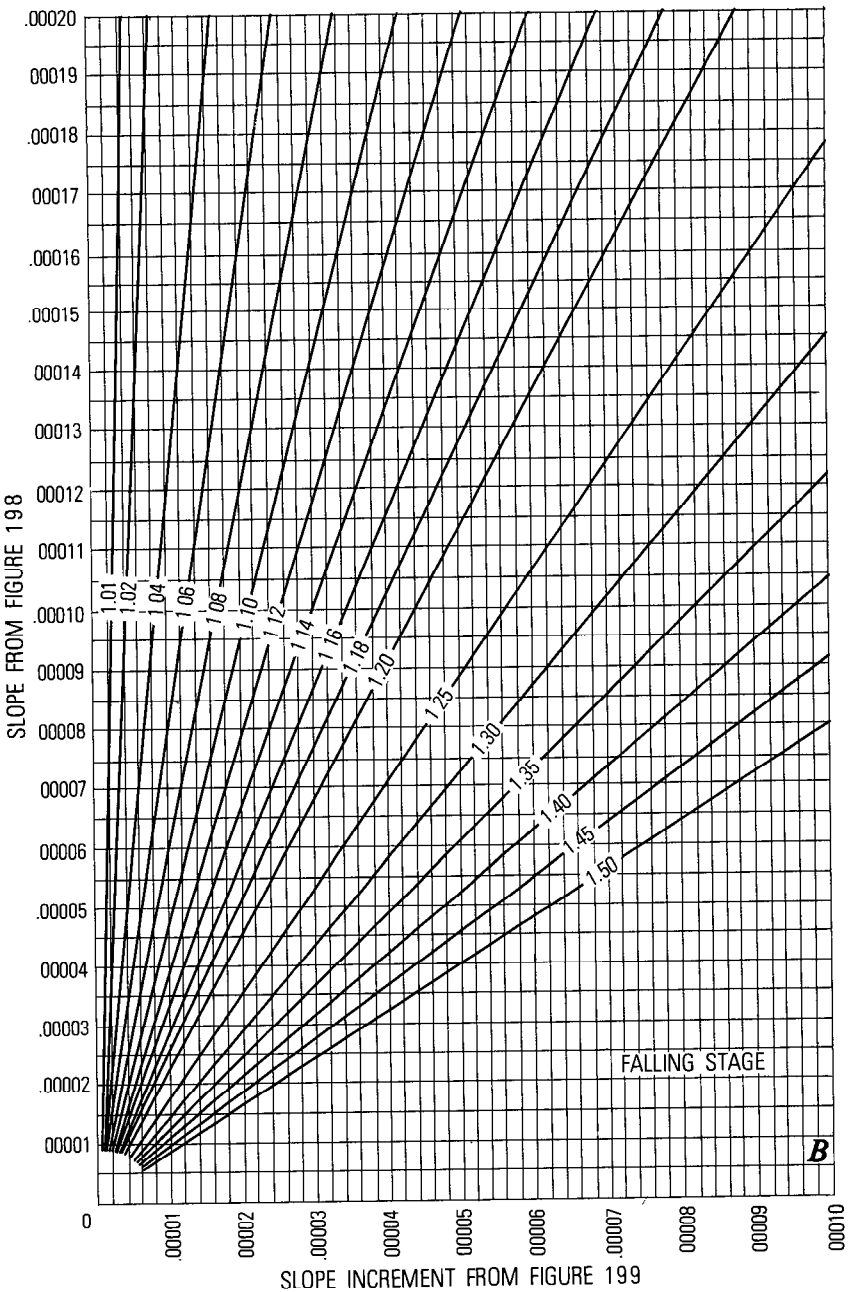

FIGURE 200*B*.—Diagram for determining factor to apply to measured discharge—falling stage.

SELECTED REFERENCES

Carter, R. W., and Davidian, Jacob, 1965, Discharge ratings at gaging stations: U.S. Geol. Survey Surface-Water Techniques, book 1, chap. 12, p. 15–36.

Corbett, D. M., and others, 1943, Stream gaging procedure: U.S. Geol. Survey Water-Supply Paper 888, p. 130–167.

Eisenlohr, W. S., Jr., 1964, Discharge ratings for streams at submerged section controls: U.S. Geol. Survey Water-Supply Paper 1779–L, 32 p.

Jones, B. E., 1916, A method for correcting river discharge for a changing stage: U.S. Geol. Survey Water-Supply Paper 375, p. 117–130.

Mitchell, W. D., 1954, Stage-fall-discharge relations for steady flow in prismatic channels: U.S. Geol. Survey- Water-Supply Paper 1164, 162 p.

Rouse, Hunter, 1950, Engineering hydraulics: New York, John Wiley, p. 638–661.

Seddon, J. E., 1900, River hydraulics: Am. Soc. Civil Eng. Trans, v. 43, p. 179–243.

CHAPTER 12—DISCHARGE RATINGS USING A VELOCITY INDEX AS A PARAMETER

INTRODUCTION

Chapter 11 discussed the use of a slope parameter for developing discharge ratings at gaging stations where the use of stage alone was inadequate for rating purposes. However, it is not feasible to use a slope parameter for all stations for which no simple stage-discharge relation can be developed. Often slopes are so flat that the available reach of channel for developing slope is too short to give sufficiently accurate values of fall in the reach. At other sites, as on tidal streams or on some streams used for hydroelectric power generation, the acceleration head (p. 391) in the equations of unsteady flow is of such magnitude that it cannot be ignored as was done in chapter 11. In those situations it is often possible to develop a discharge rating by using a velocity index in a stage-velocity-discharge relation.

The principle behind a stage-velocity-discharge relation is simple enough. A continuous stage record provides a means of obtaining a continuous record of cross-sectional area from a relation of area to stage. If a continuously recorded velocity index, at a point or in a transverse line, can be related to stage and mean velocity in the cross section, the product of cross sectional area and mean velocity gives the discharge at any time. The calibration of the velocity relation—that is, the relation of recorded index velocity to stage and mean velocity—requires discharge measurements for the determination of mean velocity. The discharge measurements also furnish the values of cross-sectional area to be used in the stage-area relation.

Four types of instrumentation have been used to provide an index of mean velocity in a measurement cross section. They are:

1. standard current meter,
2. deflection meter,
3. acoustic velocity meter, and
4. electromagnetic velocity meter.

The simplest instruments for recording velocity at a fixed point in the cross section are the standard current meter and the deflection meter. Their use is limited to the smaller streams and canals where the hazard of damage by boats or debris is minimal. The acoustic velocity meter integrates the velocity along a transverse line in the stream. It has been used in large rivers to provide an index to mean velocity in the measurement cross section. The use of an electromagnetic velocity meter is still (1980) in the experimental stage, and its use has been limited mostly to the smaller streams. Experimental work in the U.S.A. with the electromagnetic current meter has been largely in the use of the meter to obtain a continuous record of velocity at a point; in several European countries the experimental

work has been largely in the use of the meter to obtain a continuous record of an index value of integrated mean velocity in the entire measurement cross section.

STANDARD CURRENT-METER METHOD

The use of an unattended standard current meter, securely anchored in a fixed position in the stream below the minimum expected stage, is attractive because of the simplicity of the device. The most desirable location for the meter will be in the central core of the flow, away from the influence of the banks or any other impediment to flow, where streamlines are parallel and at right angles to the measurement cross section. For streams of irregular alignment or cross section, it may be necessary to experiment with meter location to determine the most suitable site for the meter.

Any of several schemes may be used for recording revolutions of the current meter. For example, one might use a modification of the system for recording velocity that was described earlier for the moving-boat method of measuring discharge (see section in chapter 6 titled, "Rate Indicator and Counter"). In that system a clock-activated moving chart is automatically marked after each occurrence of a predetermined number of meter revolutions. In another system that might be used, the current meter would be connected to a digital recorder and at predetermined time intervals—say, 15 minutes—the number of revolutions that occurred in the preceding 15 minutes would be punched. In either system the current-meter rating equation would be used to convert revolutions per time interval to average velocity during the time interval.

As mentioned earlier, discharge measurements would be used to calibrate the stage-velocity-discharge relation. The cross-sectional areas shown by the discharge measurements would be used with stage to define the stage-area relation, which could be extrapolated by the use of data obtained in a field survey. The mean velocities shown by the discharge measurements would be used in a graphical relation of mean velocity to stage and to the index velocities indicated by the fixed current meter. Extrapolation of that relation would be aided if a vertical-velocity curve were obtained at the site of the index current meter at the time of each discharge measurement, and if the mean velocity in the vertical at the index meter site, as computed from each vertical velocity curve, were related to mean velocity in the measurement cross section. The use of such relations is illustrated in the hypothetical example that follows where, for simplicity, it is assumed that the relations can be expressed mathematically.

Assume that the vertical-velocity curves at the index site can consistently be defined by the equation,

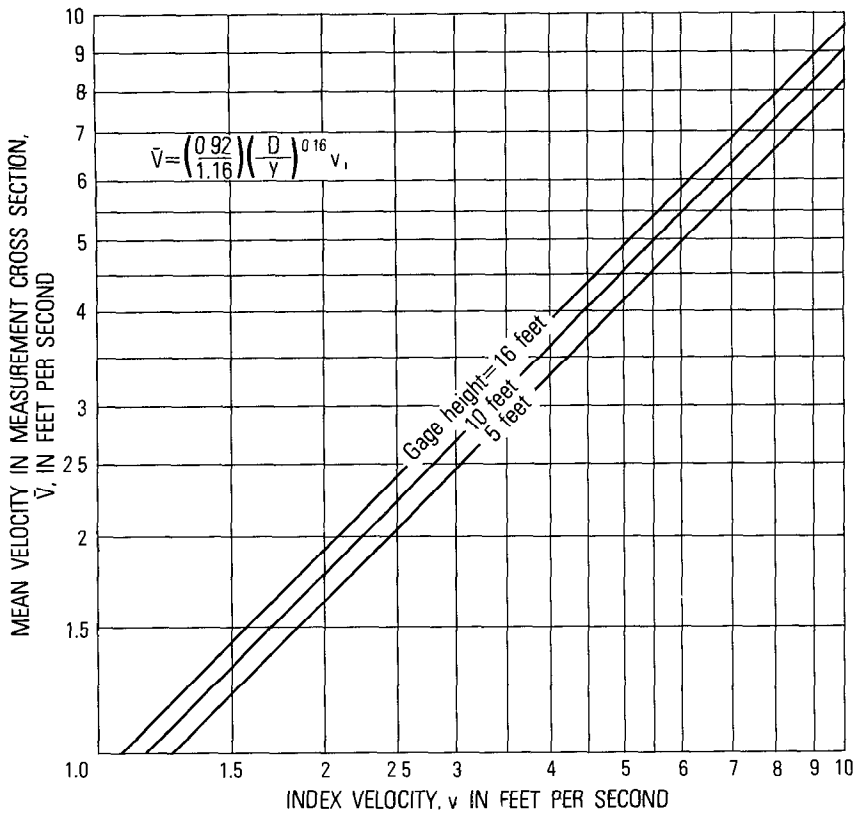

FIGURE 201.—Hypothetical relation of mean velocity in measurement cross section to stage and index velocity.

$$v_i = 1.16\ V_m\ (y/D)^{0.16},$$

where

V_m is the mean velocity in the vertical,

D is the depth, and

v_i is the velocity at a height, y, above the streambed.

Assume further that the ratio of mean velocity in the measurement cross section to mean velocity in the vertical at the index-meter site is consistently 0.92. It is also assumed that gage height and depth are equivalent, that stage is expected to range from 6 to 16 ft, and that the index meter is set at an elevation 5 ft above the streambed. Under those assumptions, the relation of mean velocity in the cross section to stage and index velocity would be that shown in figure 201. The mean velocity obtained by the use of figure 201 would be multiplied by the appropriate cross-sectional area to obtain the required discharge.

The utilization of a standard current meter to obtain an index of mean velocity has certain disadvantages that inhibit its use. The meter is susceptible to damage or impairment by submerged drift, but even where that hazard is negligible, there is a strong tendency for the meter to become fouled, after long immersion, by algae and other aquatic growth that becomes attached to the meter. Stoppage or impaired operation of the meter invariably results from the attachment of such growth, and constant servicing of the meter is usually a necessity. Suspended sediment in the stream also adversely affects the operation of an unattended current meter.

DEFLECTION-METER METHOD

GENERAL

Deflection meters are used to provide a velocity index in small canals and streams where no simple stage-discharge relation can be developed. The inability to develop a simple stage-discharge relation usually results from tide effect or from downstream gate operations to regulate the flow. At such gaging stations a recording stage-gage is operated in conjunction with the deflection meter.

The deflection meter has a submerged vane that is deflected by the force of the current. The amount of deflection, which is roughly proportional to the velocity of the current impinging on the vane, is transmitted either mechanically or electrically to a recorder. Values of the mean velocity of the stream are determined from discharge measurements, and mean velocity is then related to deflection and stage.

The ideal location for a deflection meter is in midchannel of a straight reach. However, it seldom is feasible to install the meter in midchannel; a site close to the bank of a straight reach is usually used.

Through the years, two basic types of deflection vane have evolved—the vertical-axis and the horizontal-axis types. The vertical-axis type has been most commonly used. Both types are described in the sections that follow.

VERTICAL-AXIS DEFLECTION VANE

The vertical-axis deflection vane is attached to a vertical shaft that is free to pivot about its vertical axis. Figure 202 shows two variations of the vertical-axis deflection vane. Vane A on the left is designed to sample a "point" or local velocity; vane B on the right is designed to integrate velocities throughout the greater part of a vertical. Vane B is used particularly in tidal streams where at times during a tidal cycle, stratification and density currents occur. At those times the denser salt water at the bottom of the channel flows upstream while fresh water in the upper zone starts to flow seaward.

Vane B extends from about 6 inches above the streambed to an elevation just below the water surface at low tide. While vane B is used in other circumstances, it cannot be used in a narrow channel where velocities are high, because a hydraulic jump may occur on the downstream side of the vane and affect the meter rating.

The force of the current acting on a vertical-axis vane turns the vertical shaft and the motion is transmitted to a graphic or digital

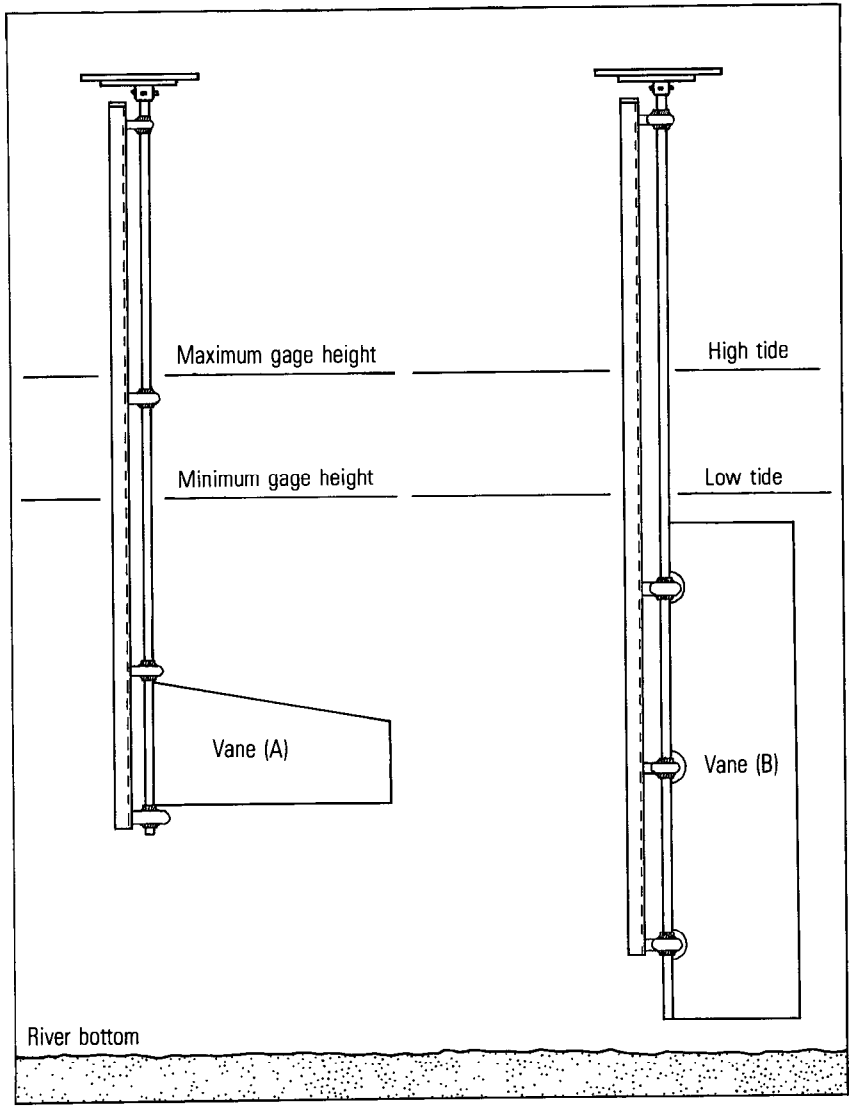

FIGURE 202.—Sketch of two types of vertical-axis deflection vanes.

recorder. A graphic recorder is shown in the system in figure 203. The vertical shaft also has an index plate fastened to it, and to the index plate is attached a counterweighted cable. When the velocity is zero, no lateral force is exerted on the vane and the counterweight will hold the vane in a position that is perpendicular to the direction of flow. A 15- to 20-pound counterweight is generally used with most vanes, but high velocities and (or) the use of a large vane may necessitate the use of a heavier counterweight in order to provide the counter-torque necessary to resist the rotary movement of the vane.

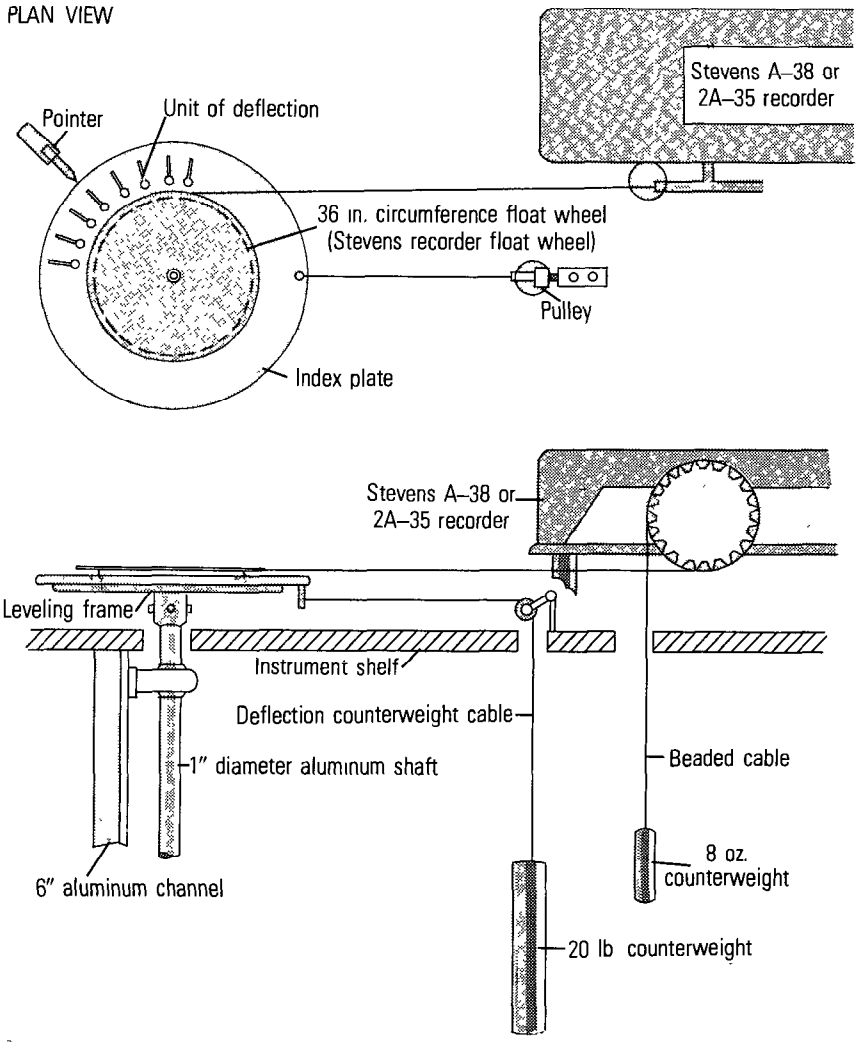

FIGURE 203.—Plan and front elevation views of a vertical-axis deflection meter attached to a graphic recorder.

A pointer for indicating the units of deflection on the index plate is attached to the instrument shelf. The index plate is calibrated by placing the recorder pen at zero position on the recorder and locking it there. The index plate is then scribed with a mark opposite the pointer. The index plate is rotated until the pen moves 1 inch on the recorder chart and another mark is scribed opposite the pointer. This process is repeated until marks for the full range of deflection have been scribed on the index plate and numbered. These units of deflection on the calibrated index plate are the reference marks for checking and resetting the recorder pen on future inspections of the deflection meter.

The vertical-axis deflection vane does have several drawbacks, the most serious of which is its tendency to collect floating debris which, in turn, affects the calibration of the vane. Another problem is the high degree of bearing friction resulting from the weight and bearing system of the vane assembly; the friction causes insensitivity at low velocities. In addition, removal of the vane for service and repair is difficult because of the weight involved. Furthermore, the projection of the vane assembly above the water surface makes it susceptible to damage by ice.

HORIZONTAL-AXIS DEFLECTION VANE

A recent development is the horizontal-axis or pendulum type deflection vane. This type is designed to overcome many of the difficulties mentioned in connection with the vertical-axis vane. For example, the pendulum vane can be installed with the mount totally submerged, thus reducing the possibility of collecting debris at or near the water surface where such debris is usually found. Its light weight and simplified bearing design greatly reduce the bearing friction, thus improving its low-velocity characteristics. Because no parts protrude from the water, there is little danger of damage by ice.

The pendulum-type vane consists of a flat triangular plate, suspended from above, that pivots about a horizontal axis located at the apex of the triangle (fig. 204). Interchangeable weights are available for attachment to the base of the triangular plate, thereby providing for optimum adjustment to the desired veolcity range. The location and design of the weights serve the additional purpose of reducing fluctuations caused by eddy shedding.

The force of the current acting on the horizontal-axis vane causes it to deflect. The angle formed by the vane itself and a small reference pendulum sealed within the pivot chamber is the angle of deflection. A potentiometer is positioned to generate an electrical signal that is proportional to the angle of deflection. The voltage that is generated is converted to a proportional shaft position for recording by a digital or graphic recorder.

It can be demonstrated that when the horizontal-axis vane is deflected by flowing water and the system is in mechanical equilibrium, the following relation exists between velocity of the water, angle of deflection, and the physical properties of the vane:

$$V^2 = \left(\frac{2WL_M}{\rho A L_A}\right)\left(\frac{\sin\Theta}{C_D\cos^2\Theta + C_L\sin^2\Theta}\right),$$

where V is horizontal velocity of the water,
W is weight of the pendulum in water,

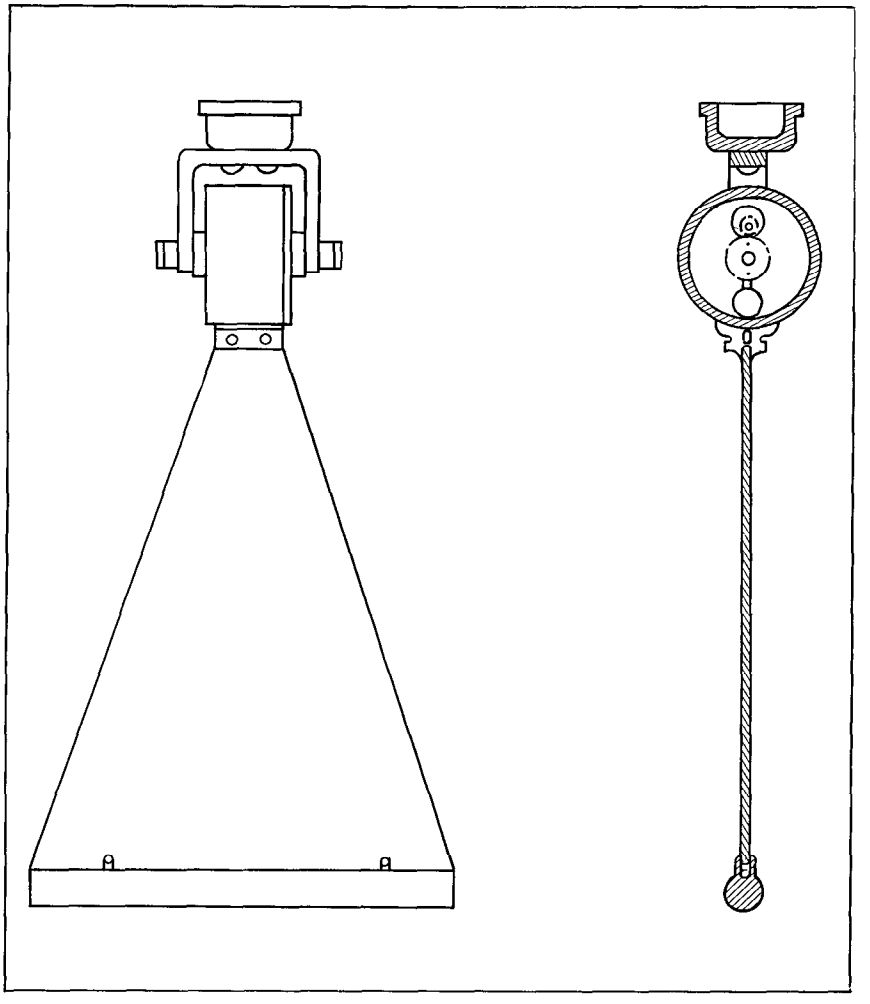

FIGURE 204.—Sketch of a pendulum-type deflection vane.

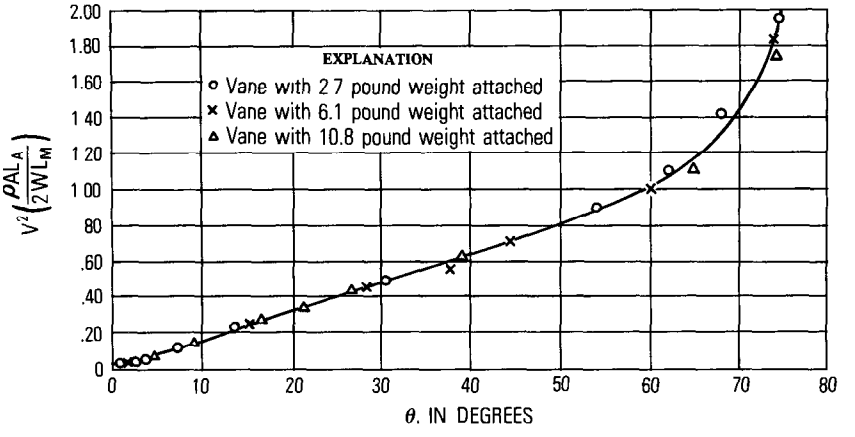

FIGURE 205.—Calibration curve for pendulum-type deflection vane.

ρ is the density of water,
A is the area of the vane,
L_M is the distance from the pivot point to the center of mass,
L_A is the distance from the pivot point to the center of the area,
Θ is the angle of deflection,
C_D is the coefficient of drag, and
C_L is the coefficient of lift.

Figure 205 is a graphical presentation of the above relation that can be used for selecting the weight needed for a given velocity range.

EXAMPLES OF STAGE-VELOCITY-DISCHARGE RELATIONS BASED ON DEFLECTION-METER OBSERVATIONS

Figure 206 shows a graphic-recorder chart for a gaging station in Florida where tidal flow reverses direction. The upper pen trace shows the stage at various times during the tide cycle for the period May 4–6, 1962. The lower pen trace shows the deflection units recorded during the same period. Zero flow is represented by a reading of four units on the deflection scale. Flow is in the seaward direction when the deflection is less than 4 units (hachured part of deflection graph in fig. 206); flow is in the inland direction when the deflection is greater than four units.

The rating curves shown in figure 207 were derived from discharge measurements. The units of deflection are indicative of velocity in a single vertical in the channel, having been obtained from a vertical-axis deflection meter equipped with vane B (fig. 202). The velocity curve shows the relation of deflection units to measured mean velocity in the channel; stage was not a factor in the relation because of the limited range (2 ft) in stage. For deflections of less than four units, velocity is negative, meaning that flow is in the seaward direction.

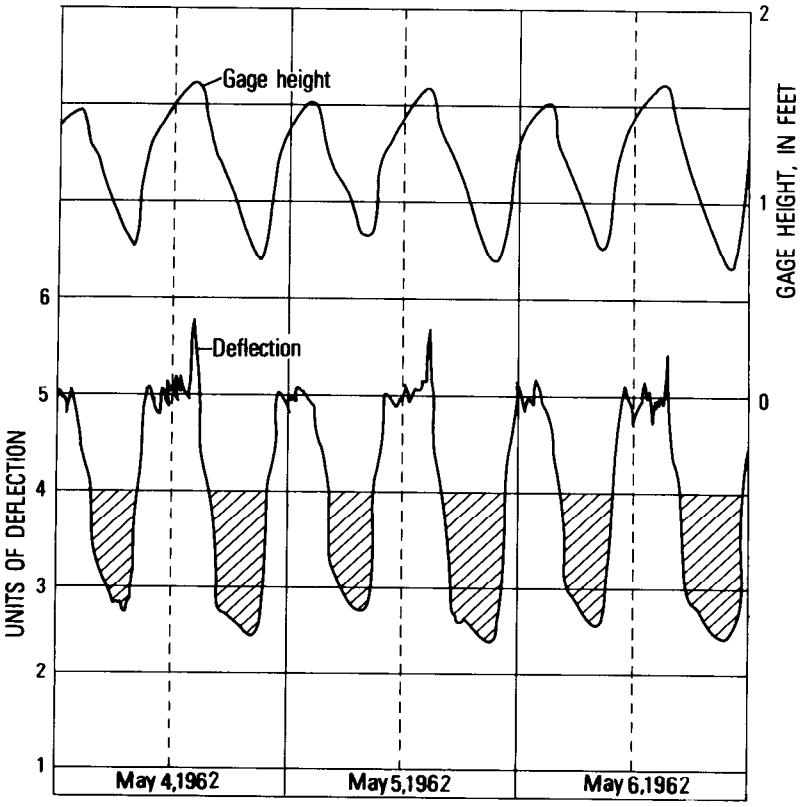

FIGURE 206.—Recorder chart for a deflection-meter gaging station on a tidal stream.

The stage at the time of discharge measurements was used to construct the area curve, which relates stage to cross-sectional area. Discharge is computed by multiplying area by mean velocity; negative values of discharge indicate seaward flow and positive values indicate inland flow.

Figure 208 shows the rating for a gaging station at the outlet of a large natural lake, immediately downstream from which are gates that regulate the flow for hydroelectric-power generation farther downstream. The deflection meter at the station is of the vertical-axis type and is equipped with vane A (fig. 202) to measure deflection at a "point" in the rectangular channel. Instead of deriving separate relations of stage versus cross-sectional area and deflection versus mean velocity, a single graphical relation, in the form of a family of curves, was derived for discharge versus stage and deflection. A preliminary study had shown that mean velocity was related to a combination of deflection and stage. The ratings for values of deflection other than

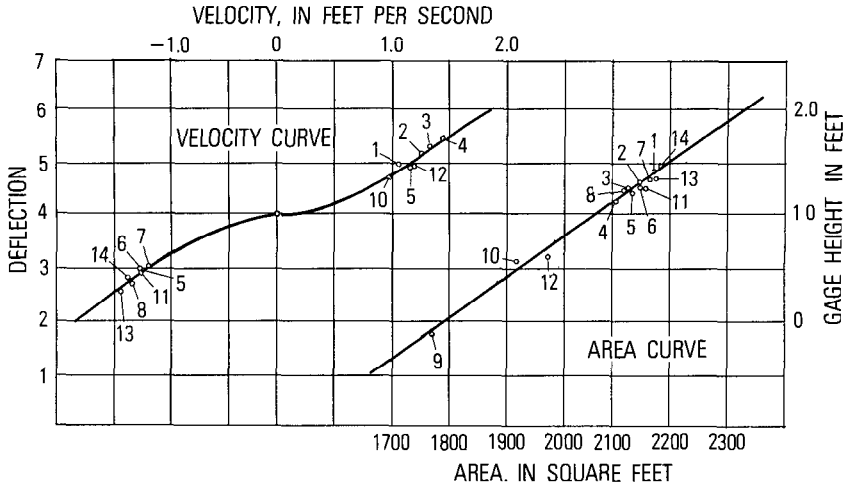

FIGURE 207.—Rating curves for a deflection-meter gaging station on a tidal stream.

those shown by the individual curves in figures 208 were obtained by interpolation between curves. Most of the 40 discharge measurements, which are shown by the small circles in figure 208, depart from the interpolated ratings by no more than 2 percent.

The use of separate relations for area and mean velocity is considered preferable to the use of a single compound relation for discharge, as was done in figure 208, because separate analysis of two components of discharge is simpler. Shifts in the discharge rating—that is, differences between measured and computed discharge—are also more easily analyzed when separate relations for area and mean velocity are prepared.

ACOUSTIC VELOCITY-METER METHOD

DESCRIPTION

Acoustic velocity meters are particularly advantageous in obtaining a continuous record of the discharge of large rivers in those situations where neither a simple stage-discharge relation nor a stage-fall-discharge relation can be applied satisfactorily. Those situations, as mentioned in the first section of this chapter, usually involve tidal flow or flow affected by hydroelectric-power generation, where the acceleration head in the equations of unsteady flow (p. 391) cannot be ignored. Acoustic velocity meters operate on the principle that the velocity of sound propagation through a fluid in motion is the algebraic sum of the fluid velocity and the acoustic propagation rate through the fluid. Thus acoustic pulses transmitted in the direction of flow will traverse a given path in shorter time than will acoustic pulses transmitted in opposition to the flow. The difference in transit

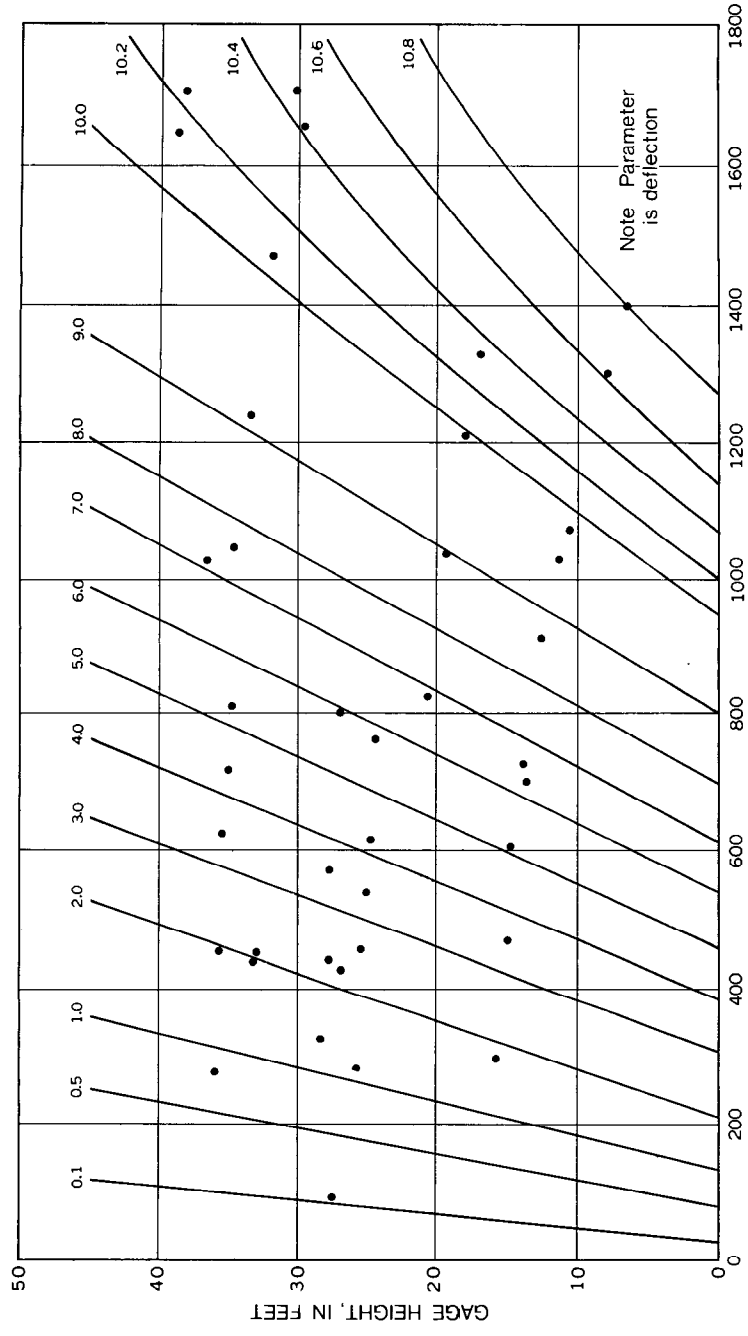

FIGURE 208.—Rating curves for a deflection-meter gaging station on Lake Winnipesaukee outlet at Lakeport, N.H.

times provides a measure of the line velocity—that is, the average value of the water velocity at the elevation of the acoustic path—and the line velocity is a satisfactory index of mean velocity in the channel. Because the transducers that transmit and receive the acoustic pulses are installed in the stream at a fixed elevation, the relation of line velocity to mean velocity varies with stage. The stage data required for the velocity relation are obtained from the stage recorder, which also provides an index of cross-sectional area.

Differences exist among the various acoustic-velocity metering systems that are commercially available, but the differences are not vital, and only one system will be briefly described. The major components of the acoustic monitoring system are two submerged transducers (fig. 209) and a console (fig. 210) housed on the streambank and electrically connected to both transducers. The two transducers, one on each side of the channel, are installed at the same elevation—an elevation that is below the lowest expected stage of the stream—on a diagonal path across the stream. The transducers convert electrical impulses generated in the console into sound pulses that travel through the water. They also convert the received sound pulses back into electrical signals. The console contains: the operating controls, the signal-generating and -receiving circuits (acoustic unit), the system clock that provides the basic timing pulses for the system and also furnishes the time-of-day readout, the digital processor (digital unit) that controls the transmission of acoustic pulses and performs the computations of the velocity index, and the velocity-index display. The velocity index is a measure of the line velocity. In the U.S.A., power for the system is usually furnished by a 110-volt alternating-current power supply.

Although acoustic-velocity meter systems are currently (1980) operational, the techniques and instrumentation are relatively new and are continually being improved. The cost of an acoustic-velocity meter installation is roughly 10 times that of a conventional gaging station. For that reason the acoustic-velocity method is limited to those sites where an accurate record of discharge is unattainable by the more conventional methods, but is of great value for water-management purposes.

THEORY

Measurement of the water velocity is possible because the velocity of a sound pulse in moving water is the algebraic sum of the acoustic propagation rate and the component of velocity parallel to the acoustic path. Reference is made to figure 211 in the following derivation of the mathematical relations of the system.

The traveltime of an acoustic pulse originating from a transducer at A and traveling in opposition to the flow of water along the path

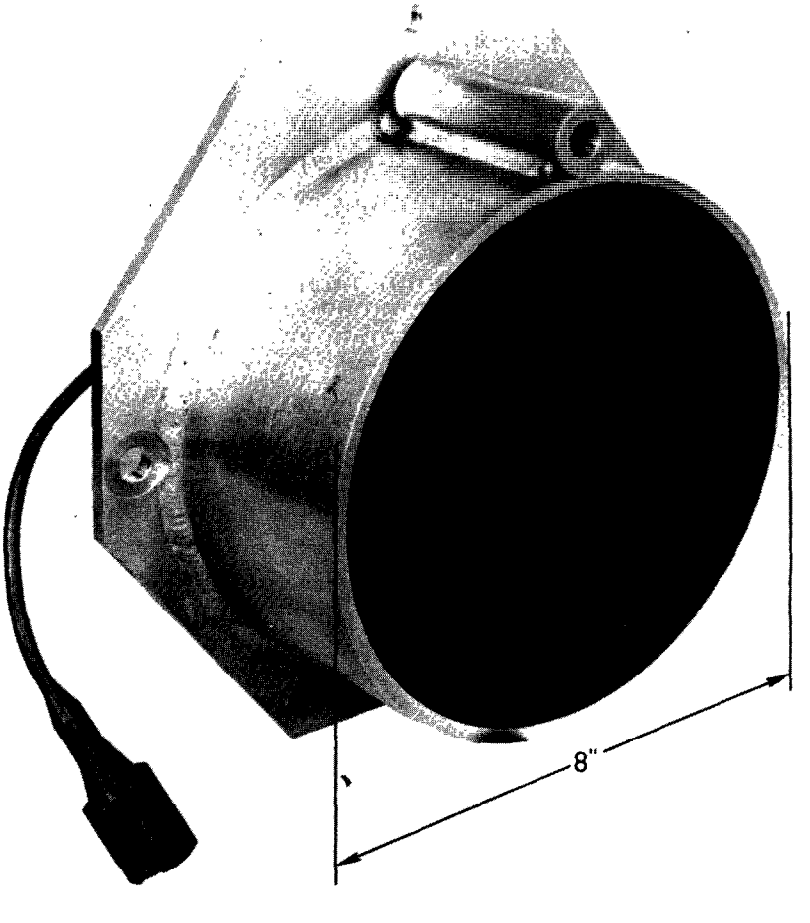

FIGURE 209.—Transducer.

A–C can be expressed as

$$T_{AC} = \frac{B}{c - V_P} \quad , \tag{91}$$

where

c is the propagation rate of sound in still water,
B is the length of the acoustic path from A to C,
T_{AC} is traveltime from A to C, and
V_P is average component of water velocity parallel to the acoustic path.

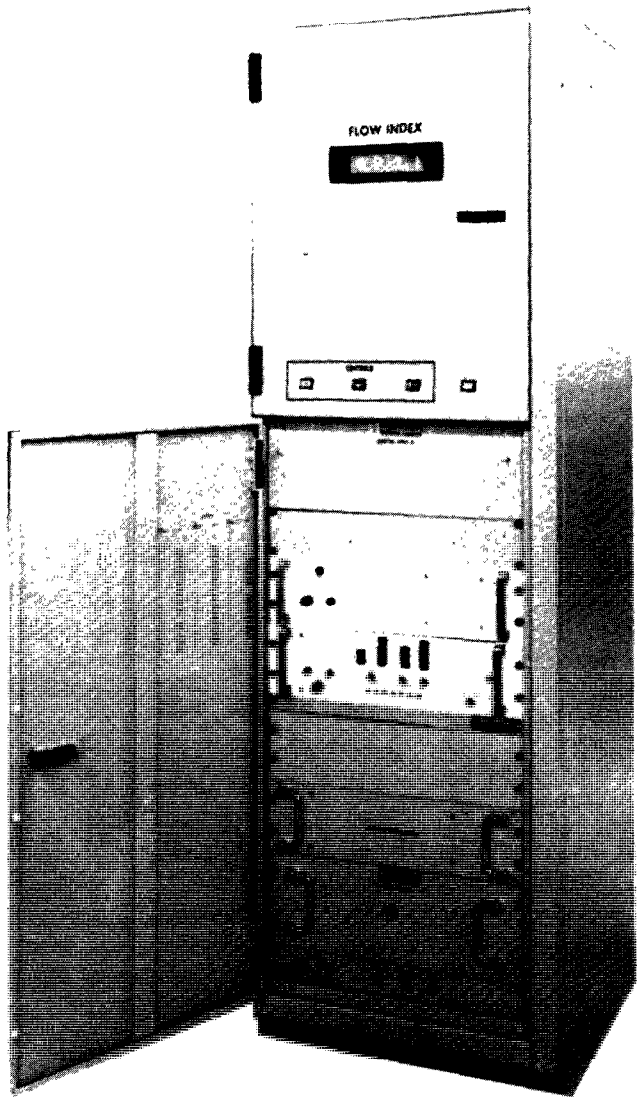

FIGURE 210.—Console.

Similarly, the traveltime for a pulse traveling with the current from C to A is

$$T_{CA} = \frac{B}{c + V_P} , \tag{92}$$

where T_{CA} is traveltime from C to A.

ΔT is the difference between T_{AC} and T_{CA}; therefore,

$$\Delta T = \frac{B}{c - V_P} - \frac{B}{c + V_P} = \frac{2BV_P}{c^2 - V_P{}^2} \quad ; \tag{93}$$

and since $V_P{}^2 <<< c^2$,

$$\Delta T \cong \frac{2BV_P}{c^2} \quad , \tag{94}$$

or

$$V_P \cong \frac{\Delta T c^2}{2B} \quad . \tag{95}$$

Both ΔT and c in equation 95 can be defined by measurement of the traveltimes of acoustic signals transmitted in each direction between transducers, c being computed by solving equations 91 and 92 simultaneously. The digital processor in the console can be scaled to produce a velocity index (I) that is equal to V_P. In some of the older systems used in the U.S.A. the velocity index was not scaled to equal V_P, but instead the velocity index was directly proportional to V_P, so that

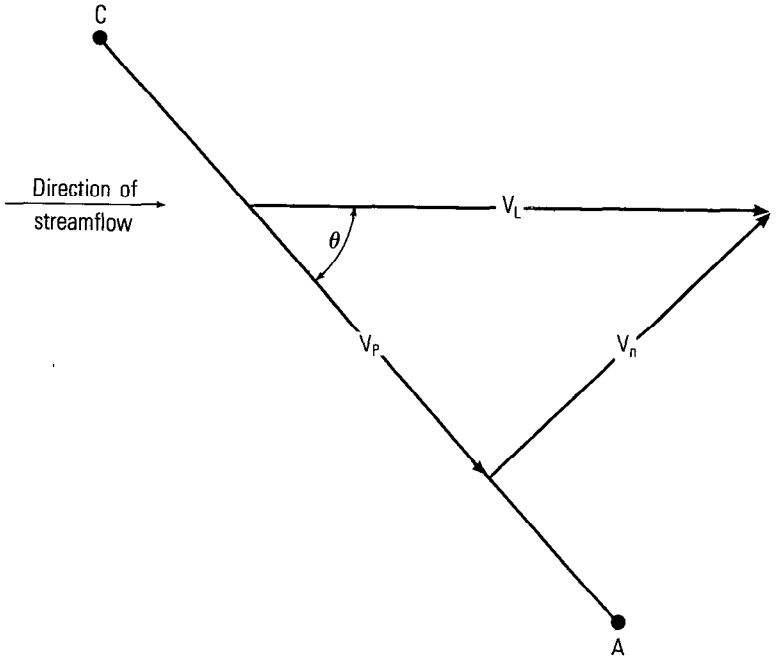

FIGURE 211.—Sketch to illustrate operating principles of the acoustic velocity meter.

$$V_P = C_1 I, \tag{96}$$

where C_1 is a constant of proportionality.
In the continuing discussion of "Theory", equation 96 will be used with the understanding that $C_1 = 1.00$ in some of the acoustic-velocity meter systems.

Figure 211 shows that

$$V_L = \frac{V_P}{\cos \Theta}, \tag{97}$$

where V_L is the average water velocity at the elevation of the acoustic path, and Θ is the acute angle between the streamline of flow and the acoustic path, AC.

By combining equations 96 and 97,

$$V_L = \left(\frac{C_1}{\cos\Theta}\right) I \tag{98}$$

Experimentation has shown V_L to be a stable index of $\overline{V}$, the mean velocity in the cross section at right angles to the streamlines of flow. The relation between V_L and $\overline{V}$ can be expected to vary with stage because V_L is a measure of the mean velocity along a line at a fixed elevation in the cross section. As the stage rises, the position of this line is moved downward in the cross section relative to the total depth, and resultant changes in the velocity distribution in the vertical column cause a change in the ratio between V_L and $\overline{V}$. Correlation of the ratio $V_L/\overline{V}$ with stage is accordingly necessary, and $\overline{V}$ can be expressed as follows:

$$\overline{V} = C_2 V_L, \tag{99}$$

where C_2 is a function of stage.

The basic equation for discharge (Q) is

$$Q = \overline{V} A, \tag{100}$$

where A is area of the cross section.

By substituting in equation 100, terms given in equations 98 and 99, the following equation is obtained:

$$Q = I\left(\frac{C_1 C_2}{\cos \Theta}\right) A. \tag{101}$$

When the symbol K is substituted for $\frac{(C_1 C_2)}{\cos \Theta}$ in equation 101, the result is

$$Q = KIA. \tag{102}$$

K varies with stage including, as it does, C_2 which is a function of stage.

To calibrate the system, discharge measurements are made to obtain measured values of A and $\overline{V}$. The measured values of A are correlated with stage to obtain a graphical stage-area relation. Measured values of $\overline{V}$ are divided by concurrent values of I, recorded by the console digital processor, to obtain concurrent values of K. Those values of K are correlated with stage to obtain an empirical graphical relation of K to stage. Such a relation is shown in figure 212.

To compute the discharge for any given value of I, the concurrent value of stage is first read. That value of stage is then used in the above graphical relations to obtain the corresponding values of A and K. In a final step the values of K, I, and A are multiplied together, in accordance with equation 102, to obtain the required value of discharge.

Newer acoustic-meter velocity systems that have been designed provide a readout of discharge after the calibration coefficients have been determined. The additional calibration coefficients needed are provided by substituting mathematical relations of A to stage and K to stage, in place of the graphical relations discussed above. The computation of discharge is based on the following two assumptions:

1. The relation between area (A) and stage (H) is stable and can be adequately defined by the second-order equation,

$$A = C_1 + C_2H + C_3H^2, \tag{103}$$

   where C_1, C_2, and C_3 are constants.

2. The ratio (K) between mean stream velocity ($\overline{V}$) and the velocity index (I), which is equal to, or linearly related to, the line velocity (V_p), can be defined by the second-order equation,

$$K = \overline{V}/I = C_4 + C_5H + C_6H^2, \tag{104}$$

   where C_4, C_5, and C_6 are constants.

If sufficient data from discharge measurements are available, the "best" values of C in equations 103 and 104 can be computed from a least-squares solution of each of the equations. Usually, however, the C values in the two equations are obtained from the graphical relations of A versus H and K versus H. That is done by first selecting the coordinates of three significant points on one of the graphical relations, and then substituting those values in the appropriate equation—equation 103 when the area relation is used. The three resulting simultaneous equations are solved to produce the required C values. The process is then repeated, using equation 104 for the K relation. The six C values so obtained are then entered in the program for computing discharge. Discharge is computed as before, in

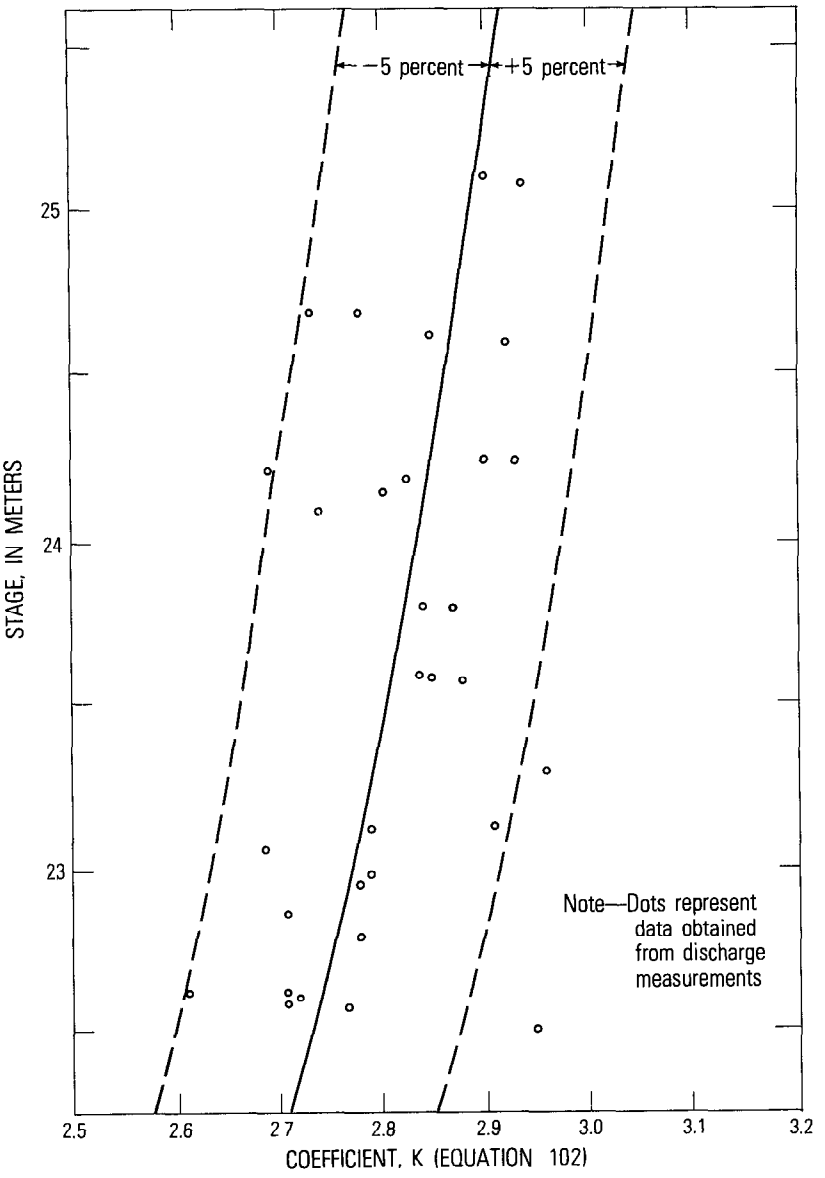

FIGURE 212.—Relation between stage and mean-velocity coefficient, K, for the acoustic-velocity meter (AVM) system, Columbia River at The Dalles, Oreg.

accordance with equation 102, except that the computations are performed in the console digital processor. The digital processor uses the C values, along with concurrent values of I and H, to make the required computations and provide a readout of K, I, A, H, and Q.

It would be simple, of course, to multiply I by the product of equations 103 and 104 and thereby obtain a single equation for Q. The result would be a fourth order equation of the form,

$$Q = I(k_1+k_2H+k_3H^2+k_4H^3+k_5H^4), \quad (105)$$

in which the k constants represented combinations of the C constants from equations 103 and 104. The "best" values of the constants could be obtained by a least-squares solution of equation 105, using measured values of Q and concurrent values of I and H. The use of equation 105 would simplify the computation of discharge, but the analyst would then lose much of his ability to analyze error sources in the calibration of shifts in the basic relations. It is therefore recommended that equations 103 and 104 be used rather than equation 105.

EFFECT OF TIDAL FLOW REVERSAL ON RELATION OF MEAN VELOCITY TO LINE VELOCITY

The value of C_2 in equation 99, $\overline{V} = C_2V_l$, varies only with stage in unidirectional flow. In streams where the direction of flow reverses in response to tide, the value of C_2 may vary not only with stage, but also with the four phases of the tide cycle. For such streams numerous discharge measurements, preferably by the moving-boat method (chap. 6), are required to evaluate C_2 for each of the tide phases. In using the moving-boat method of discharge measurement, it is necessary to determine a velocity coefficient for each individual discharge measurement and that is done by continuously defining the vertical-velocity distribution at several strategically located verticals that are representative of the main portion of streamflow. (See section in chapter 6 titled, "Adjustment of Mean Velocity and Total Discharge.")

The results of an evaluation of C_2 for a particular cross section in the Sacramento River in California are given in table 22 (Smith, 1969, p. 11–18). Column heading, $\overline{C_2}$, in table 22 refers to the mean values of C_2; column heading, s, refers to the standard deviations of C_2 values. Figure 213 is a plot of the data from columns headed, $\overline{V}$ and $\overline{C_2}$, in table 22.

ORIENTATION EFFECTS AT ACOUSTIC-VELOCITY METER INSTALLATIONS

EFFECT OF ACOUSTIC-PATH ORIENTATION ON ACCURACY OF COMPUTED LINE VELOCITY (V_l)

The basic accuracy or resolution of a given acoustic-velocity meter (*AVM*) system is controlled principally by the accuracy with which the arrival times of the acoustic pulses can be discriminated and by the accuracy of the timing circuitry used to measure elapsed times. A related factor that affects the accuracy of results obtained with a par-

TABLE 22.—*Variation of C_2 with tidal phase*
[$\overline{C}_2$ are mean values of C_2; s are standard deviations of C_2 values]

Velocity range (ft/s)	Increasing ebb			Decreasing ebb			Increasing flood			Decreasing flood		
	$\overline{V}$ (ft/s)	$\overline{C}_2$	s	$\overline{V}$ (ft/s)	$\overline{C}_2$	s	$\overline{V}$ (ft/s)	$\overline{C}_2$	s	$\overline{V}$ (ft/s)	$\overline{C}_2$	s
<1.00	0.90	0.961	(1)	0.84	1.030	0.031	0.87	1.005	0.030	----	----	----
1.00–1.40	1.16	.957	0.035	----	----	----	1.21	1.006	(1)	1.11	0.983	(1)
1.41–1.80	1.52	.965	(1)	1.41	1.040	(1)	1.75	.982	(1)	1.58	.997	0.022
1.81–2.20	1.96	.981	.011	2.02	1.019	.017	2.09	.970	(1)	2.08	.991	.020
2.21–2.60	2.44	.978	.014	2.46	1.019	.018	2.43	.985	.011	2.43	.992	.009
>2.60	2.75	.985	.009	2.76	.990	.014	2.92	.982	.007	2.84	.982	.009

[1]Not computed, only one or two values of C_2 available for determining $\overline{C}_2$

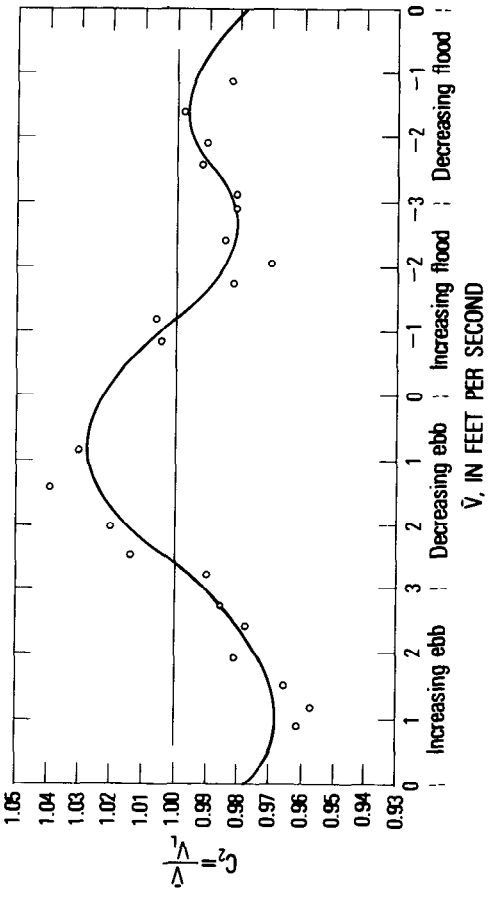

FIGURE 213.—Relation between C_2 and velocity and tide phase.

ticular *AVM* system is the orientation of the acoustic path with respect to the streamlines of flow. The effect of path orientation will now be examined for one of the *AVM* systems used in the U.S.A. It is assumed that no changes in the basic circuitry are made for operations over acoustic paths of various orientations, that the streamlines at all times and stages are parallel and their direction is invariant, and that acoustic performance is thoroughly reliable.

From figure 211

$$V_P = V_L \cos \Theta \tag{97a}$$

Insertion of the resolution error (R_e) for the system in equation 97a yields

$$V_P = V_L \cos \Theta \pm R_e$$

or,

$$V_L = \frac{V_p}{\cos \Theta} \pm \frac{R_e}{\cos \Theta} \cdot \tag{106}$$

The last term in equation 106 represents the error (E) in computed values of V_L, meaning that

$$E = \pm \frac{R_e}{\cos \Theta} \tag{107}$$

In other words, for a given *AVM* system, the error in computed values of V_L decreases as Θ decreases.

According to the claim of the manufacturer of the *AVM* system under discussion, inaccuracy (E) attributable to the resolution error is ± 0.05 ft/s when angle Θ is 45°. From equation 107, the implication is that the resolution error (R_e) equals $\pm 0.05 \cos \Theta$, or ± 0.035 ft/s. Table 23 was computed from equation 107 using the above value of R_e. Because the error in computed values of V_L is independent of the magnitude of V_L, the greatest percentage errors in computed velocity occur at low velocities for any given orientation of the acoustic path.

EFFECT OF VARIATION IN STREAMLINE ORIENTATION

If an *AVM* system were located a short distance downstream from the confluence of two streams, as shown in figure 214, the direction of

TABLE 23.—*Error in computed* V_L, *attributable to resolution error, for various acoustic-path orientations, for a given* AVM *system*

Path-orientation angle Θ, in degrees	Error in V_L, in ft/s
30	±0.04
45	± .05
60	± .07
70	± .10
80	± .20

the streamlines of flow at the gage site could be expected to vary with the proportion of total discharge contributed by the tributary stream. When the tributary flow is low, the angle between streamlines and acoustic path is Θ, V_L is the velocity normal to the cross section whose area is A, and a value of V_p is recorded by the AVM;

$$V_L = \frac{V_p}{\cos \Theta} \quad , \tag{108}$$

and

$$Q_{AVM} = AV_L \tag{109}$$

If stage and discharge remain constant, but the proportion of flow from the tributary increases significantly, the angle Θ between the streamlines of flow and the acoustic path will increase by an increment ϕ, but V_L will remain constant because the discharge and stage remain constant. A value of V'_p will now be recorded by the AVM, where

$$V'_p = V' \cos(\Theta+\phi) \tag{110}$$

But,

$$V' = \frac{V_L}{\cos \phi} \tag{111}$$

Therefore,

$$V'_p = \frac{V_L \cos (\Theta+\phi)}{\cos \phi} \tag{112}$$

However the discharge has not changed. If the AVM system had been calibrated under conditions where, for the given discharge and given stage, the angle between streamlines and acoustic path was Θ, the AVM system will be unaware of the increase in angle from Θ to $(\Theta+\phi)$, and the discharge will be computed as

$$Q'_{AVM} = \frac{AV'_p}{\cos \Theta} = \frac{AV_L \cos(\Theta+\phi)}{\cos \Theta \cos \phi} \tag{113}$$

But the true AVM discharge (line velocity times area) is that shown by equation 109. Therefore the ratio between computed AVM discharge for the condition of the angle being $(\Theta+\phi)$ and the true AVM discharge is,

$$\frac{Q'_{AVM}}{Q_{AVM}} = \frac{\left(\frac{AV_L \cos (\Theta+\phi)}{\cos \Theta \cos \phi}\right)}{AV_L} \tag{114}$$

$$= \frac{\cos (\Theta+\phi)}{\cos \Theta \cos \phi}$$

$$= 1 - \tan\Theta \tan\phi \tag{115}$$

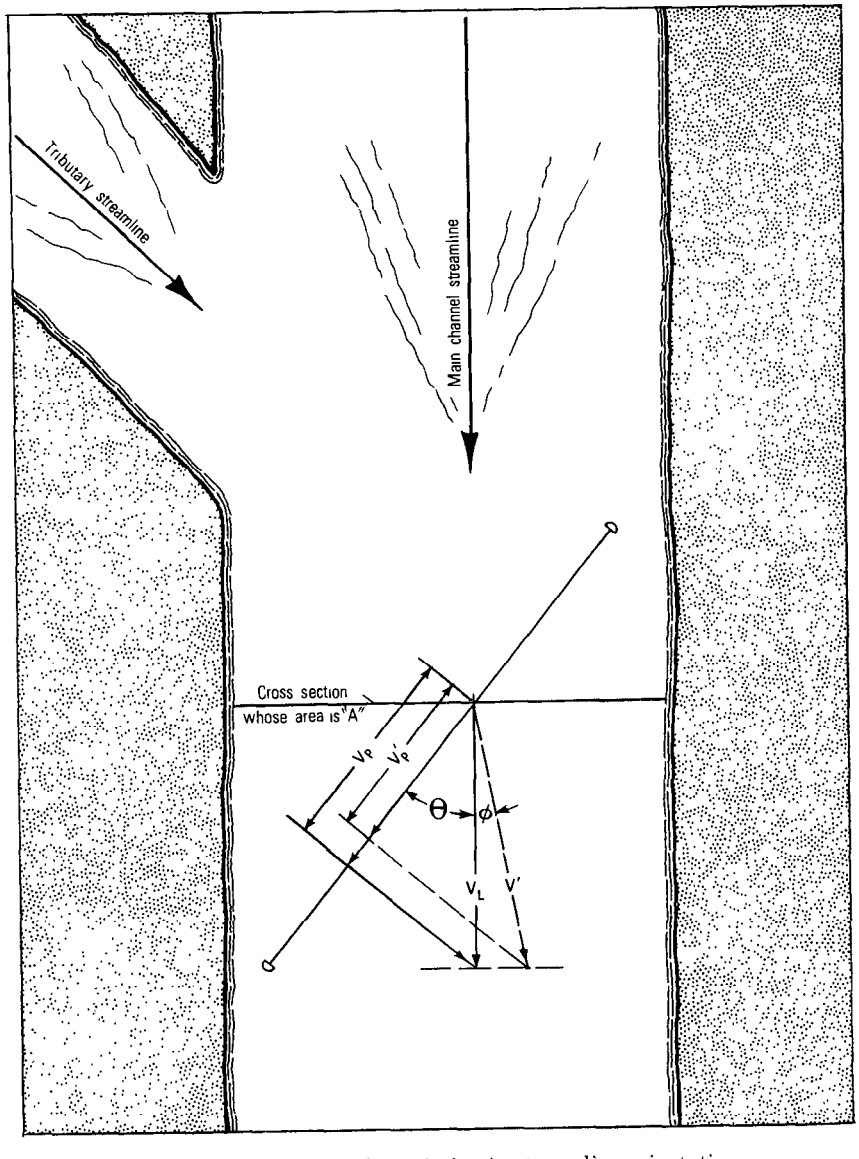

FIGURE 214.—Possible variation in streamline orientation.

Equation 115 is evaluated in table 24 for acoustic path orientations (Θ) ranging from 30° to 60°, and for streamline variations (ϕ) ranging from −4° to +4°.

As a general rule one should avoid installing an *AVM* system immediately downstream from the confluence of two streams. It is true

TABLE 24.—*Ratio of computed discharge to true discharge for various combinations of* Θ *and* ϕ

Θ	Ratios for the values of ϕ indicated below								
	−4°	−3°	−2°	−1°	0°	+1°	+2°	+3°	+4°
30°	1.040	1.030	1.020	1.010	1.000	0.990	0.980	0.970	0.960
45°	1.070	1.052	1.035	1.017	1.000	.983	.965	.948	.930
50°	1.083	1.062	1.042	1.021	1.000	.979	.958	.938	.917
60°	1.121	1.091	1.060	1.030	1.000	.970	.940	.909	.879

that calibration of the system will be unaffected if, for each value of total discharge, there exists a particular ratio of tributary discharge to mainstream discharge. However, if that ratio is not constant for a given total discharge, error will be introduced in the calibration of the system, and therefore, in the computation of discharge.

FACTORS AFFECTING ACOUSTIC-SIGNAL PROPAGATION

In the installation of an *AVM* system, consideration must be given to the factors that affect the propagation of the acoustic signal through the water. Refraction or reflection of the acoustic beam away from the selected path or attenuation of the acoustic signal may result from:

1. temperature gradients in the stream,
2. boundary proximity,
3. air entrainment,
4. sediment concentration, and
5. aquatic vegetation.

TEMPERATURE GRADIENTS

Periodic loss of signal at some *AVM* installations where the transducers were relatively close to the water surface of a deep stream have led engineers to theorize that the development of even extremely small temperature gradients in the water column may cause refraction of the acoustic signal. In streams where mixing is poor, changes in solar radiation and air temperature could conceivably cause such gradients to develop. It has been reasoned that location of the acoustic path near mid-depth of the stream should minimize temperature gradients caused by variations in temperature or possibly by heat exchange between the water and channel perimeter.

BOUNDARY PROXIMITY

When the acoustic path is located near the water surface or near the streambed, part of the acoustic signal will be reflected from the boundary (air-water interface or streambed). The reflected component may arrive at the receiving transducer almost simultaneously with, but out of phase with, the primary pulse. In extreme cases, signals may be almost completely blanked out. This phenomenon is related to

the ratio of path length to distance to a boundary and to the frequency of the transmitted signal.

The above considerations, combined with the possibility of the thermal effects discussed above, have led the designers of some *AVM* systems to develop the criteria curves for *AVM* site selection shown in figure 215. The curves indicate the performance that can probably be expected from some systems in a given channel geometry when the transducer elevation is set at mid-depth. The terms "excellent" and "acceptable" are relative, and their significance is dependent upon the reliability requirements at the site. The curves show that the depth of water required increases as the path length increases. For example, for a path length of 500 ft, excellent acoustic performance would be expected for depths greater than 18 ft and acceptable performance would be anticipated for depths between 10 and 18 ft, but for depths less than 10 ft, on-site investigation of the characteristics of acoustic transmission would be necessary. For a path length of 1,000 ft, these depth ranges change to 34 ft or more for excellent transmission and from 19 to 34 ft for acceptable transmission. On-site studies would be required for depths less than 19 ft. The curves in figure 215 should not be construed as providing all the information

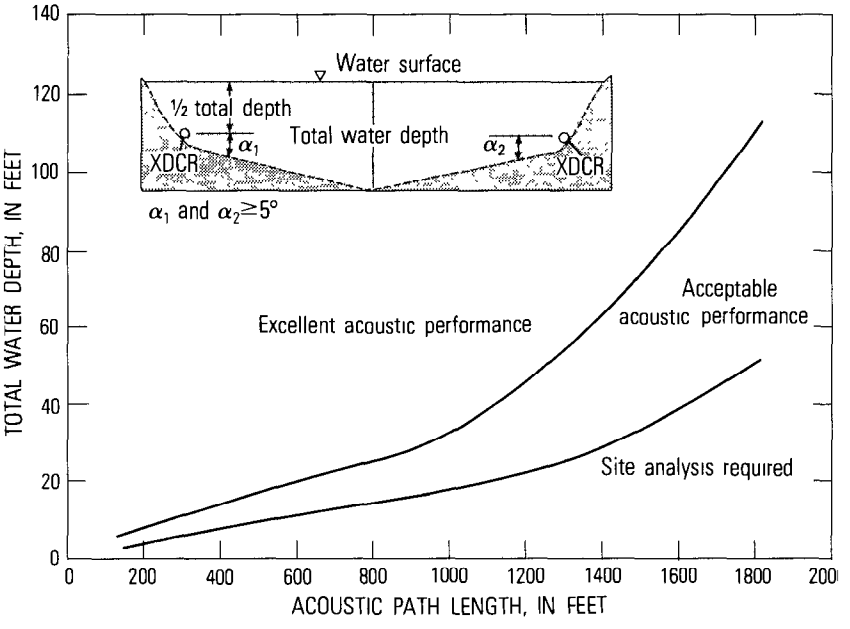

FIGURE 215 —Curves used as a preliminary guide for AVM site selection, based solely on consideration of channel geometry.

required for assessment of the potential for utilizing an *AVM* system. By these criteria, broad, shallow channels would seem to be questionable sites, but it is possible that further developments in transducer design and system characteristics may provide reliable performance in such channels also.

AIR ENTRAINMENT

Little quantitative information is available concerning the attenuation of acoustic signals by air bubbles entrained in the water, but the effect of air entrainment has been observed downstream from dams where the falling water becomes highly aerated. Bubbles formed at such sites may remain entrained in the water for a considerable distance downstream, and they absorb and reflect the acoustic signal much as fog absorbs and reflects a beam of light. The highly absorptive characteristics of water with entrained air precludes satisfactory operation of *AVM* systems, and locations close to spillways or other sources of air entrainment should consequently be avoided.

SEDIMENT CONCENTRATION

The degree of attenuation of signal strength caused by the reflection and scatter of the acoustic signals from sediment particles suspended in the stream has not been fully documented. The attenuation is influenced not only by suspended-sediment concentration, but also by the size of the sediment particles, water temperature, and length of the acoustic path. Equations given by Flammer (1962) for the evaluation of energy loss are:

$$E = E_0 10^{-0.1\alpha x}, \tag{116}$$

where

E = sound energy flux at a given point, if sediment is suspended in the transmitting fluid;

E_0 = sound-energy flux at the same point, if no sediment were present;

α = attenuation coefficient that is due to sediment alone, measured in decibels per inch; and

x = distance from the point of measurement to the sound source.

The attenuation coefficient α can be evaluated as

$$\alpha = C\left[\frac{K(\gamma-1)^2 S}{S^2+(\gamma+\tau)^2}+\frac{K^4 r^3}{6}\right]\frac{22.05}{2}, \tag{117}$$

where

C = concentration (1,000 mg/L = 0.001),

$K = 2\pi/\lambda$,

$\gamma = \rho_1/\rho_2$,

$S = [9/(4\beta r)]\,[1+1/(\beta r)]$,

$\tau = \frac{1}{2}+9/(4\beta\tau)$, and

r=particle radius, in centimeters;

in which

λ=wave length of sound in water, in centimeters; ρ_1 and ρ_2=densities of particle and fluid, respectively;

$\beta=\left[\omega/2\upsilon\right]^{1/2}$

$\omega=2\pi f$;

υ=kinematic viscosity of water, in stokes; and

f=frequency of sound wave.

An example of the evaluation of equations 116 and 117 for an *AVM* site investigated in central California is shown in figure 216. Pertinent site and *AVM* characteristics were as follows:

Particle size—0.004 mm
Sediment concentration—20-100 mg/L
Water temperature—60°F(15.6°C)
Sonic-path length—4,000 ft (1219 m)
Sound frequency—20 kc

Figure 216*A* illustrates the general problem and shows the reduction in signal strength resulting from sediment concentrations ranging from 50 mg/L to 400 mg/L over acoustic paths as long as 4,000 ft. Figure 216*B* shows the signal loss for a given concentration and path length, as affected by particle size, and relates signal loss, for a path length of 4,000 ft, to sediment size when the sediment concentration is held constant at 100 mg/L. Figure 216*C* relates signal loss, for a path length of 4,000 ft, to sediment concentration when the sediment size is held constant at 0.004 mm. Figure 216*C* is of particular significance; it indicates that for the probable range in suspended-sediment concentrations at the site under consideration (20–100 mg/L), signal strength will vary from 90 to 56 percent of the levels possible in clear water. One of the requirements of an *AVM* designed for use at this site would be that no calibration changes should result from signal strength variations of that magnitude.

AQUATIC VEGETATION

The effect of aquatic weeds in the acoustic path is variable, depending on the location and density of the weed growth. Dense growth may cause complete blockage of the signal. It has been found, in experiments in the United Kingdom, that the removal of only a small amount of weeds will increase the amplitude of the received signal. Further experimentation (Green and Ellis, 1974) has shown that weeds growing close to the transducer may actually cause the *AVM* system to overregister the velocity; the weeds reflect and scatter the wave train and the extra scattered signals are detected by the transducer. On the other hand, weeds in the midchannel result in a widely variable registration of velocity, in which the velocity is underestimated. In short, aquatic weeds in the acoustic path interfere with

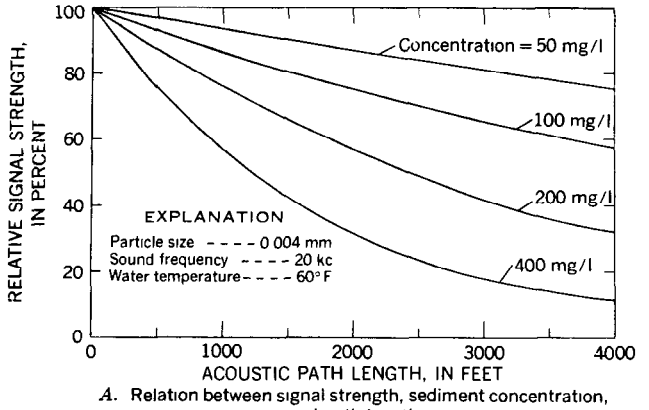

A. Relation between signal strength, sediment concentration, and path length

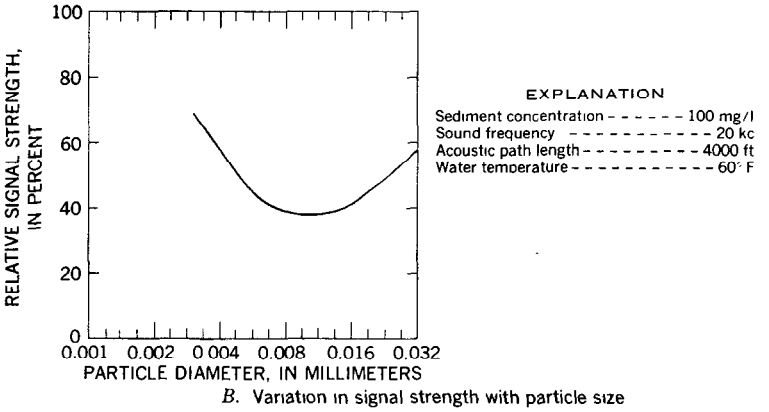

B. Variation in signal strength with particle size

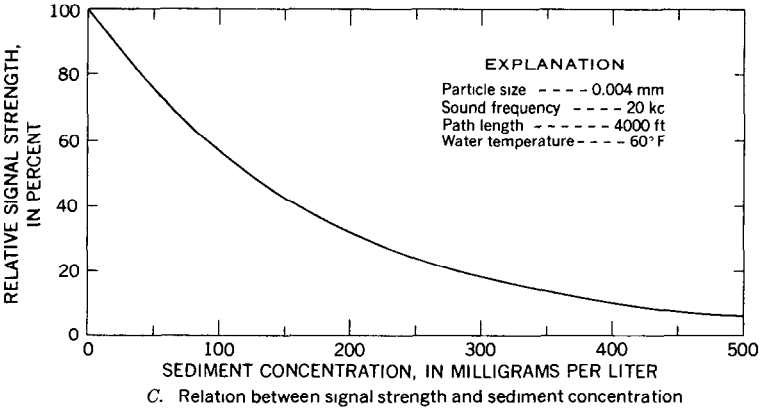

C. Relation between signal strength and sediment concentration

FIGURE 216.—Interrelation between signal strength, sediment concentration, particle size, and acoustic-path length.

the operation of an *AVM* system, but the quantitative results of experimentation with weed growths are not transferable from the experimental sites to other *AVM* sites.

It should also be noted that there has been no experimentation to relate attenuation caused by weed growth to sonic frequency. It appears probable that operation at a low frequency might reduce the attenuation; however, that would also reduce the basic accuracy of the *AVM* system.

SUMMARY OF CONSIDERATIONS FOR ACOUSTIC-VELOCITY METER INSTALLATIONS

The foregoing discussions of factors that influence *AVM* operation demonstrate that the interrelation of those factors must be considered in site selection of the acoustic path of an *AVM* system in a given stream. The most important consideration is to ensure reliable acoustic transmission and reception, and from that standpoint the acoustic path should be as short as possible to minimize acoustic refraction and attenuation losses. On the other hand, consideration of the hydraulic aspects of the system suggests use of a long path at a small angle of incidence (Θ in fig. 211) to the streamlines to achieve the best resolution of velocity and to reduce the effect of variations in streamline direction. These are opposing restraints on the system configuration, therefore compromise is often required. For most installations, the desired resolution can be attained by utilizing a path at the mid-depth position and at an angle of 45° to the streamlines. Narrow deep sections of a river are to be preferred over broad shallow sections, and locations influenced by tributary inflow should be avoided. On-site investigation of acoustic-propagation characteristics will be desirable at sites where the depth-to-path length criteria of figure 215 indicate possible problems.

Weed-covered sites and sites where air bubbles are entrained in the water should be avoided in selecting an acoustic path because of the likelihood of signal attenuation. For that same reason, the use of *AVM* systems may not be practical in streams that frequently carry large sediment loads.

ELECTROMAGNETIC VELOCITY-METER METHOD

GENERAL

The electromagnetic method of measuring velocity in streamgaging operations will be discussed only briefly because it is still (1980) in the experimental stage. Experimental work in the U.S.A. has been largely in the use of the electromagnetic meter to obtain a continuous record of velocity at a point. The observed point velocities

are then used as indexes of mean velocity in the stream, precisely as explained in earlier sections of this chapter, where the standard current meter and the deflection meter were the instruments used for continuously measuring point velocities. In several European countries, notably the United Kingdom, experimental work in electromagnetic stream-gaging has been largely in the use of an electromagnetic meter to obtain a continuous record of an index value of integrated mean velocity in the entire measurement cross section.

The operation of an electromagnetic velocity meter is based on the principle that an electromotive force, or voltage, is induced in an electrical conductor moving through a magnetic field. For a given field strength the magnitude of the induced voltage is proportional to the velocity of the conductor. In the electromagnetic velocity meter, the conductor is the flowing water whose velocity is to be measured. Although all devices for measuring water velocity electromagnetically are based on the above principle, the actual instrumentation for measuring point velocities differs greatly from that used for integrating the mean velocity in a cross section.

POINT-VELOCITY INDEX

INSTRUMENTATION

A variety of electromagnetic meters for measuring point velocity are available commercially. The meters differ in details of construction and performance, but essentially there are two general types.

One type of meter consists of the following elements: a nonmagnetic tube or pipe through which the water flows; two magnetic coils, one on each side of the pipe; electrodes in the walls of the pipe between the magnetic coils; and suitable electrical circuits to transform the induced voltage into a velocity indication on a meter dial. The other type of meter consists of a probe, or cylinder, containing an electromagnet internally and two pairs of external electrodes in contact with the water. Flow around the cylindrical probe intersects magnetic flux lines causing voltages to be generated that are detected by the electrodes. Electrical circuitry is provided to transform the induced voltage into a velocity indication on a meter dial.

For either type of meter, a source of electrical power is needed to activate the magnetic field and a transmitter is used to record the velocity signals on digital tape or to send the signals to desired stations. The meters used in the U.S.A. generally require an alternating-current source of 110 volts, but many are battery powered. The meters cause negligible head loss; accuracy claimed by the manufacturers is generally in the range of ± 2 to ± 3 percent or ± 0.005 to ± 0.007 ft/sec, whichever is larger. In other words, from a standpoint of percentage error, the higher velocities are more accu-

rately measured than low velocities.

At the gage site the unattended electromagnetic velocity meter is securely anchored in a fixed position in the stream below the minimum expected stage. The considerations governing the precise location of the meter in the stream are identical with those discussed for the standard current meter when it is used to provide a point-velocity index (see section titled "Standard Current-Meter Method"). A recording stage-gage is operated in conjunction with the velocity meter. Velocity and stage are usually recorded on digital tape.

ANALYSIS OF POINT-VELOCITY DATA

The point-velocity data from the electromagnetic meter are analyzed in the same manner as discussed earlier in this chapter for the fixed standard current meter. Mean velocity for the measurement cross section, as obtained from discharge measurements, is correlated with concurrent stage and point velocity. Cross-sectional area is related to stage. The product of mean velocity and cross-sectional area gives the required discharge. Experimentation in the U.S.A. in the use of an unattended electromagnetic meter as a point-velocity index for gaging open-channel flow had lagged, primarily because of problems in suppressing electrical noise and in preventing the contamination of electrodes, but experimentation has recently been renewed. A description of a gaging-station operation in which point-velocity data are being obtained from an electromagnetic probe follows.

The gaging site on the Alabama River near Montgomery, Ala. is at a pool formed by a dam 43 miles downstream. The river is 600 ft wide and 40 ft deep, and the flow is largely controlled by the operation of hydroelectric-power dams upstream. The flow of the river is thus highly unsteady and in addition the water-surface slope varies because of operations at the downstream dam. The discharge of the river could not be related to stage or to stage and slope. Consequently, an electromagnetic meter was installed to provide point-index velocities.

The meter is of the portable probe type, is battery powered, and features solid-state electronics in a durable field housing. The form and size of the probe are shown in figure 217. The electromagnetic probe is mounted on a structure attached to the upstream end of a bridge pier in the center of the stream. The probe was positioned to sense the velocity at a point 6 ft upstream from the nose of the pier and 6 ft below the minimum stage of the water surface. The recorder and electronic package are installed in the gage house on the pier, about 35 feet above the mean high-water stage. The Geological Survey developed the electronics necessary to average the continuously generated velocity signal over 30-minute intervals and to record this average velocity on a digital recorder.

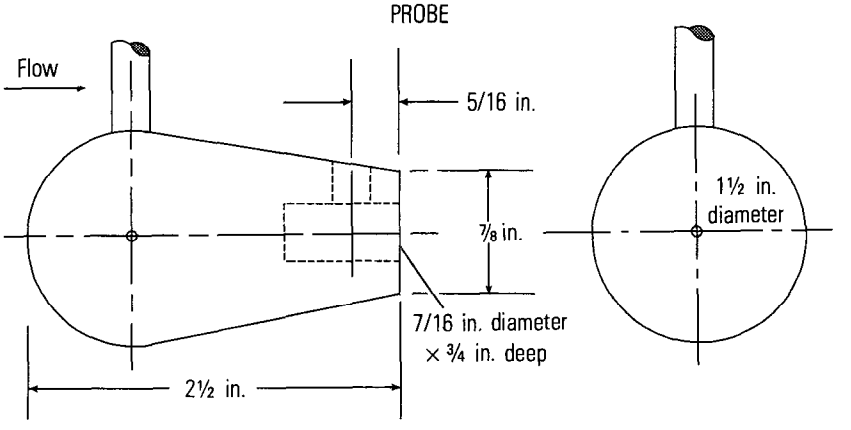

FIGURE 217.—Electromagnetic probe, model 201, Marsh-McBirney.

A series of current-meter discharge measurements was made to calibrate the relation of point velocity, as indicated by the probe, to the average velocity of the stream, as determined from the discharge measurements. Because of the unsteady flow, it was necessary that the discharge measurements be completed as quickly as possible. For that reason the measurements were made by defining the variation of velocity with time at a number of verticals in the stream-measurement cross section, as described in the section in chapter 5 titled, "Measurement Procedures During Rapidly Changing Stage—Case B. Small Streams." The relation between recorded point-index velocity and mean stream velocity determined from the discharge measurements is shown in figure 218. Although several of the plotted points scatter widely, the relation appears to be adequately defined over the range of velocity that was experienced. An attempt to improve the relation by the use of stage as an additional parameter, as in figure 201, was unsuccessful. A continuous record of discharge is computed at the gaging station by using the records of stage and point velocity, stage being an index of the cross-sectional area and point velocity an index of mean stream velocity.

Experience with the electromagnetic probe at the Alabama River gaging station has been very encouraging. The instrumentation appears to have wide application for gaging streams at sites where simpler rating methods such as stage-discharge or stage-slope-discharge are not adequate. The system has the sensitivity and accuracy required even at low velocities, is relatively inexpensive, has flexibility with regard to location because it is powered by dry-cell batteries, and can probably be used even at sites where the direction of flow reverses. The use of the system for gaging streams is consid-

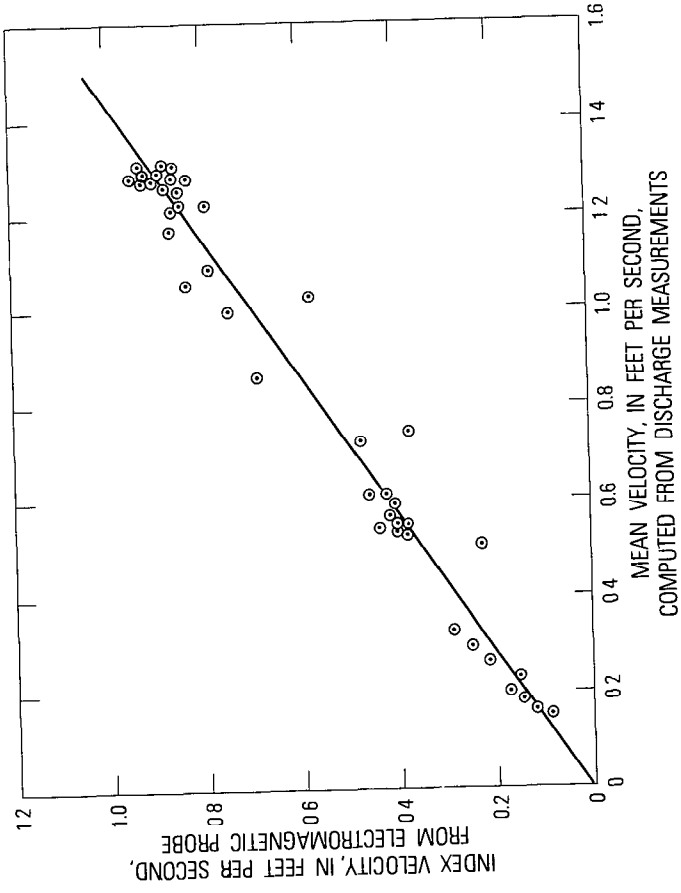

FIGURE 218.—Relation between point-index velocity and mean stream velocity for Alabama River near Montgomery, Ala.

ered to be in the experimental stage (1980), but it is hoped that further testing and development will result in the perfection of a reliable tool for gaging streams.

INTEGRATED-VELOCITY INDEX

THEORY

The discussions that follow have been extracted from British publications (Herschy and Newman, 1974; Newman, 1974; Plessey Radar, 1974).

If a conductor moves through a magnetic field, an electromotive force (voltage) is generated in the conductor. That principle can be applied to stream gaging. An electric current, flowing through a coil placed on a streambed at right angles to the flow, generates a magnetic field in the vertical direction. The flowing water is the conductor moving through the field, and the electromotive force (emf) generated in the water is at right angles to the flow. In accordance with Faraday's law of electromagnetic induction, the equation relating the length of the conductor moving in the magnetic field to the emf that is generated, is

$$E = HVb, \tag{118}$$

where

E is emf generated, in volts;
H is magnetic field intensity, in Tesla;
V is average velocity of the river water, in meters per second, and
b is river width, in meters.

In practice most streambeds will have some significant electrical conductivity that will allow electric currents to flow in the bed. The electric currents have the effect of attenuating the signal, predicted from equation 118, by a theoretically predictable factor called the conductivity-attenuation factor δ,

$$\delta = \frac{1}{1 + \left(\frac{b\sigma_0}{2h\sigma_1}\right)} \tag{119}$$

where

b is stream width,
h is stream depth,
σ_0 is streambed conductivity, and
σ_1 is river-water conductivity.

Equation 118 then becomes

$$E = HVb\delta \tag{120}$$

In an operational electromagnetic gaging station, the river and streambed conductivity should be continuously monitored and the output signal corrected accordingly.

When an electromagnetic gaging station uses an artificially produced magnetic field, that is, a magnetic field produced by a current-carrying coil, the field must, from practical considerations, be spatially limited. This means that electric currents flow in the areas outside the magnetic field, thereby reducing the output potential by a factor β, the end-shorting factor. That factor is a constant for a given coil size and configuration. Equation 120 now becomes

$$E = HVb\delta\beta. \tag{121}$$

For a given electromagnetic gaging station the magnetic-field intensity H, and the end-shorting factor β, are constants. The streambed resistivity attenuation factor, δ, is a function of the river-aspect ratio (the stage, if the river width is constant) and of the river-to-streambed conductivity ratio, σ_0/σ_1. Therefore, to insert the correct value of δ in equation 121 it is necessary to have measurements of the stage and the river-to-streambed conductivity ratio. The mean velocity of the river can then be computed. To obtain the discharge, the velocity is multiplied by the river cross-sectional area.

INSTRUMENTATION

An electromagnetic system for integrating stream velocity can be installed anywhere in a river or canal where the conductivity of the water is uniform but not necessarily constant. At present, installations have been confined to small streams. Measuring sections that are bounded by heavily reinforced concrete or by steel pilings are not suitable because of the relatively high electrical conductivity of those boundary elements. Although the signal-recovery techniques that are used make the system immune to ambient electrical noise, sites close to overhead or buried powerlines should be avoided if possible.

A description of one of the operational systems for integrating the stream velocity electromagnetically follows. In that system a large coil (fig. 219) is buried under the streambed and banks to a depth of about 0.5 m (1.5 ft, approx.). The trench in which the coil is laid roughly follows the contours of the bed and banks to minimize the effect of variation in the velocity profile. A magnetic field is produced by an electric current flowing through the coil.

Two signal probes placed in the magnetic field are fixed against the banks (fig. 219) or are driven vertically into the banks (fig. 220). The probes are used to detect the electromotive force induced in the moving water and to define precisely the cross section of the measurement area. The purpose of driving the signal probes vertically into the bank, as in figure 220, is to define a cross section whose area is rectangular. Such materials as aquatic vegetation and bed and bank sediments streamward from the probes are included in the size of the

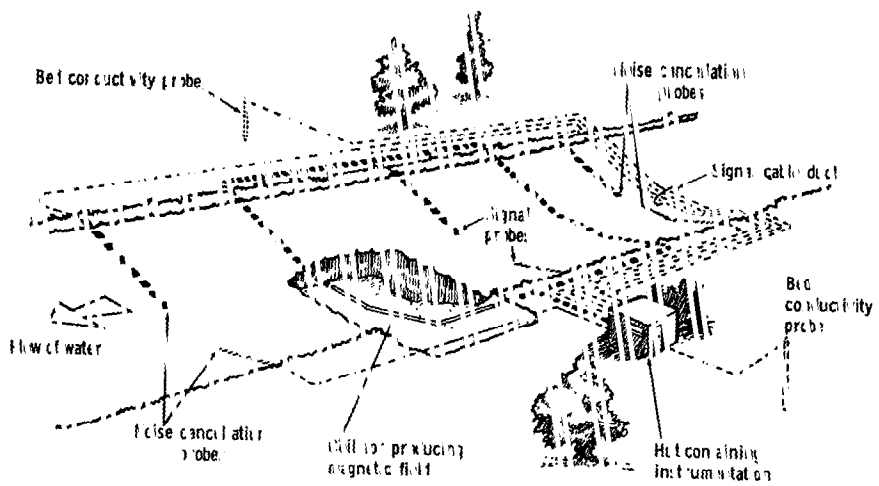

FIGURE 219.—Instrumentation for an electromagnetic stream-gaging station. (After Hershy and Newman, 1974.)

cross-sectional area the velocity of the extraneous material is zero and its effect on the system is therefore as innocuous as that of stagnant water.

Four noise-cancelation probes (fig. 219) outside the influence of the induced magnetic field are used to detect the ambient electrical noise which is later subtracted from the signal induced by the coil. These probes are mounted in a manner similar to the signal probes, with one pair upstream and one pair downstream from the measurement area.

Two bed-conductivity probes (fig. 219) are placed on each side of the stream, at a distance back from the bank that is approximately equal to the width of the stream. The probes and their cables may be buried sufficiently deep to avoid damage by agricultural work or other ground-disturbing activities. By the use of the bed-conductivity probes and the signal probes, the conductivity of the streambed is measured.

The power-supply unit provides a direct-current source that is connected to the coil through a switching unit. The switching unit in response to timing pulses from the data-processor unit described below reverses the direction of the current flowing through the coil at half-second intervals. This causes a synchronous change in the polarity of the electrical potential induced in the moving water by the magnetic field with the result that the signal can be detected by the signal probes in the presence of electrical noise. At the signal-recovery unit, the probe voltage is amplified, and after filtering and conversion, a digital signal is provided to the data-processor unit.

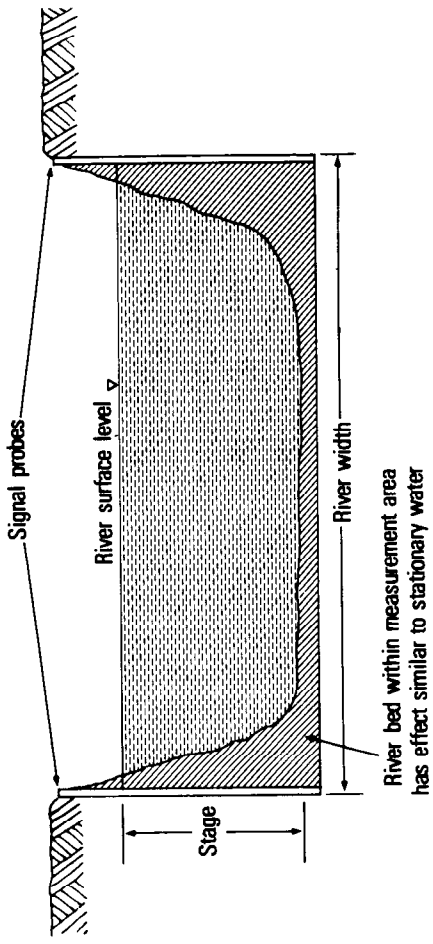

FIGURE 220.—Schematic diagram showing inclusion of bed and bank material in stream cross section. (After Herschy and Newman, 1974)

Additional instrumentation in the system includes a stage sensor and a power-operated pump that delivers continuous samples of water to a conventional conductivity sensor. The stage sensor, usually operating in a stilling well, provides a digital signal of stage to the data processor.

The block diagram in figure 221 shows the function of the data processor. In the data processor, the information from the probes is combined with that from the sensors for conductivities and stage. The latest information received is combined with similar prior information to provide a weighted average value. The weighted average value is then scaled, using preprogramed constants, to give an output of discharge in conventional units. The principles underlying the computation of discharge have been discussed in the subsection on theory of the integrated-velocity index. However, in the system described here, no separate computations of area and mean velocity are made. The two computations are easily combined because the cross-sectional area is a simple function of stage, the area bounded by the signal probes being a simple rectangle (fig. 220) or a trapezoid. The time constant in the process of averaging values is normally 15 minutes, which is also the time interval used in logging the data.

Information relating to discharge, stage, and water and streambed conductivities may be recorded locally on computer-compatible punched paper tape or on magnetic tape. Alternatively, the data may be transmitted to a control center over telephone lines or by a radio link. The transmission can be incorporated in a wider telemetry system for flood or pollution warning.

An initial field calibration, using discharge measurements, is required for the system. However, because the relation of electromagnetic output to discharge is linear, few discharge measurements are required to define the relation.

APPRAISAL OF METHOD

Studies to date (1980) indicate that the technique of electromagnetic stream gaging is feasible although there are still problems to be resolved. The method would probably have its principal use in gaging those streams that are not amenable to the more conventional methods of stream gaging—sand-channel streams with movable beds (see section in chapter 10 titled "Sand-Channel Streams,") and streams with profuse growths of aquatic weeds.

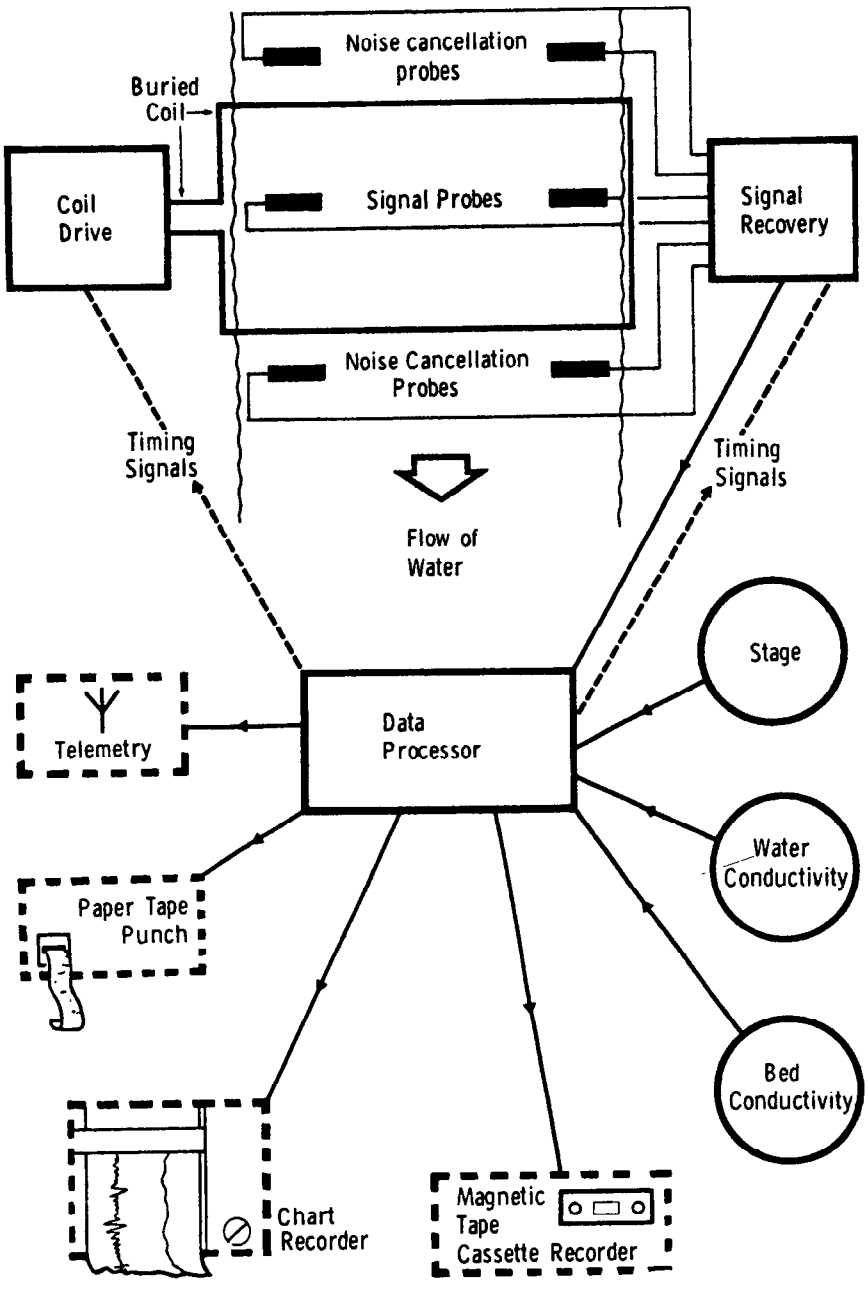

FIGURE 221.—Block diagram showing the function of the data processor. (After Plessey Radar, 1974. Reprinted by permission of the Plessey Company, Ltd.)

SELECTED REFERENCES

Flammer, G. H., 1962, Ultrasonic measurement of suspended sediment: U.S. Geol. Survey Bull. 1141–A, 48 p.

Green, M. H., and Ellis, J. C., 1974 Knapp Mill ultrasonic gauging station on the River Avon, Christchurch, Dorset, art. 2 *in* Analysis of Gauging Results: Water Research Centre symposium on river gauging by ultrasonic and electromagnetic methods, Sess. 2, Reading, England, Dec. 1974, p. 28–65.

Herschy, R. W., and Newman, J. D., 1974. Electromagnetic river gauging: Water Research Centre symposium on river gauging by ultrasonic and electromagnetic methods, Sess. 2, Reading, England, Dec. 1974, 23 p.

Newman, J. D., 1974, Princes Marsh electromagnetic gauging station on the River Rother, Liss, Hants, art. 1 *in* Analysis of Gauging Results: Water Research Centre symposium on river gauging by ultrasonic and electromagnetic methods, Sess. 2, Reading, England, Dec. 1974, p. 1–27.

Plessey Radar, 1974, The electromagnetic flow gauge, advance information: Addlestone, Weybridge, Surrey, England, 5 p.

Smith, Winchell, 1969, Feasibility study of the use of the acoustic velocity meter for measurement of net outflow from the Sacramento-San Joaquin Delta in California: U.S. Geol. Water-Supply Paper 1877, 54 p

——— 1971, Techniques and equipment required for precise stream gaging in tide-affected fresh-water reaches of the Sacramento River, California: U.S. Geol. Water-Supply Paper 1869–G, 46 p.

——— 1974. Experience in the United States of America with acoustic flowmeters: Water Research Centre symposium on river gauging by ultrasonic and electromagnetic methods, Sess. 3, Reading, England, Dec. 1974, 13 p.

Smith, Winchell, Hubbard, L L., and Laenen, Antonious, 1971, The acoustic streamflow-measuring system on the Columbia River at The Dalles, Oreg.: U.S. Geol. Survey open-file report, 59 p.

U.S. Bureau of Reclamation, 1971, Water measurement manual (2d ed): Water Resources Tech. Pub., p. 208–209.

CHAPTER 13—DISCHARGE RATINGS FOR TIDAL STREAMS

GENERAL

A discharge rating can be obtained for a tidal or tide-affected stream if a velocity index is used as a parameter in the rating along with stage. If the stream is quite small, a deflection meter is a satisfactory device for obtaining a continuous record of velocity; the electromagnetic method of stream-gaging is still in the experimental stage. For the larger streams the acoustic velocity meter is a satisfactory device for obtaining an index of velocity. (The instrumentation and methodologies involved in the use of deflection meters, electromagnetic velocity meters, and acoustic velocity meters were described in Chapter 12.) In the absence of such devices, there are two general approaches for obtaining a continuous discharge record—the theoretical approach involving evaluation of the equations of unsteady flow for a tide-affected reach of channel, and the empirical approach involving empirical relations whose effectiveness generally varies inversely with the degree of importance of the acceleration head (see section in chapter 11, titled "Theoretical Considerations"). The theoretical approach is much preferred.

Either approach requires a recording stage gage at each end of a long reach of channel. The two gages must be synchronized so that simultaneous stages at the two sites can be obtained from the stage records. Either approach requires discharge measurements for calibrating the discharge model; the moving-boat method of measuring discharge (chap. 6) is recommended for the larger streams.

EVALUATION OF UNSTEADY-FLOW EQUATIONS

It is beyond the scope of this manual to treat in detail the various methods of evaluating the equations of unsteady flow. Basic to all methods is the solution, by approximate step procedures, of the following pair of differential equations:

$$\frac{Q^2}{K^2} = -\frac{\partial H}{\partial x} - \frac{1}{g}\frac{\partial V}{\partial t} \tag{122}$$

$$\frac{\partial Q}{\partial x} = -B\frac{\partial h}{\partial t}, \tag{122a}$$

where Q is the discharge, K is the conveyance of the cross section, H is the total energy head, x the distance along the channel, g the acceleration of gravity, V the mean velocity, t the time, B the top width of the

channel, and h is the water-surface elevation. Solution of the equations requires the use of a digital computer.

The four methods of equation evaluation that will be briefly discussed are:

1. power series,
2. method of characteristics,
3. implicit method, and
4. Fourier series.

For any of the four methods, it is necessary that a series of current-meter discharge measurements be made over several tidal cycles at either end of the reach. The measurements are needed to compute the resistance and conveyance properties of the reach and to serve as checks on the computed discharges. The series of measurements should include one series made at a time of low freshwater discharge and large tidal range, and another made when the freshwater discharge is high. These two series of measurements may be sufficient if the channel is stable with regard to scour and fill, but for an unstable alluvial channel, it is necessary that several additional series of discharge measurements be made. For meaningful results it is necessary that the channel either be stable (unchanging) or if subject to change, the channel changes must occur in the same way for each change in discharge during rises and subsequent recessions.

During a series of discharge measurements over a tidal cycle, enough measurements must be made to define the discharge hydrograph to an accuracy that will permit momentary discharges to be determined at 15-minute intervals for the duration of the cycle. The discharge measurements are commonly made at about hourly intervals and cover a few hours more than the duration of the tidal cycle.

The exact procedure used to measure the discharge in a tidal reach will vary with size of channel and flow conditions. For a small tide-affected stream, one or two field crews measuring continuously across the stream may be adequate for obtaining the data for an accurate definition of the discharge hydrograph. For a large tide-affected river, several measuring crews may be required, and it may be necessary to compute the hydrograph in the manner described for flash floods on small streams (see section in chapter 5 titled, "Measurement Procedures During Rapidly Changing Stage—Case B. Small Streams"). In that method a stage-mean velocity relation is first determined for each measurement vertical, and total stream discharge is then computed for selected stages. The preferred method of measuring discharge in a large tide-affected stream is, of course, the moving-boat method (chap. 6).

One of the basic assumptions of the methods to be presented is that the water in the tidal reach is substantially of homogeneous density,

thereby eliminating the possibility of density currents. Therefore, consideration should be limited to those portions of tidal reaches that are affected by the propagation of long, low-amplitude, translatory waves but in which salinity intrusion does not cause a saline wedge to form or cause distinct stratification of flow.

An important consideration in the choice of a reach is the availability of a 110-volt power supply at both ends to drive the digital stage recorders synchronously. Although standby DC units, equipped with DC to AC inverters, are available to take over immediately in the event of a power failure, standby units should be used for periods no longer than absolutely necessary; the use of standby units for long periods of time invariably results in loss of synchronization. Any loss of synchronization between the two clocks, even fractions of a minute, may cause significant error in the computation of discharge. Recent (1976) tests indicate that battery-operated electronic clocks may have the required accuracy and reliability, and if so, the availability of a 110-volt power supply will no longer be a requirement.

POWER SERIES

In solving the equations of unsteady flow by use of a power series—commonly a Taylor series—finite differences are used. Velocity and stage and all orders of their derivatives are continuous functions with respect to x and t. The value of Δx, or length of reach to be used, is generally 3 to 7 miles—there is a theoretical maximum length that depends on tidal wave length (hours) and mean channel depth. The value of Δt to be used is usually 15 minutes.

In the power-series method, tidal flow is considered to be one-dimensional unsteady flow in a prismatic channel. However, a natural reach of channel usually differs greatly from an idealized tidal reach that has an unvarying prismatic cross-section and a constant bottom slope. Consequently, it is necessary to determine a mean cross-section that is representative of the reach and whose dimensions are variable with stage. From such a representation, the geometric parameters required for the discharge computations can be obtained. The number of cross sections to be surveyed in the field in order to compute a representative mean cross-section depends on the length and degree of uniformity of the tidal reach. Usually ten or more cross sections, somewhat evenly spaced in the reach, are required.

Local inflow or outflow (diversions) to or from the tidal reach is considered in the solution, but the quantity of such flow must be small in comparison with the flow in the main channel. The local inflow or outflow is often assumed to be constant throughout a complete tidal cycle and is considered to enter or leave the main channel uniformly

along the entire length of reach; thus large concentrations of flow at a single point cannot be accommodated by the method.

A mathematical description of the mechanics of computing discharge in tidal reaches, by the use of a power series for solving the equations of unsteady flow, is beyond the scope of this manual. For such information the reader is referred to papers by Baltzer and Shen (1961, 1964) and by Davidian (1964).

METHOD OF CHARACTERISTICS

The method of characteristics is well adapted to the solution of partial differential equations in two variables, such as equations 122 and 122a. (All terms in those equations are related to velocity and (or) stage.) In the method, the basic partial differential equations are first transformed to characteristic equations and then to corresponding difference equations.

As in the power-series method, tidal flow is considered to be one-dimensional unsteady flow in a prismatic channel. In the finite-difference solution of the equations, computations are made at equal time intervals Δt (usually 15 minutes, or less) and at equal increments of distance x along the channel. The selected value of Δx must meet the criterion,

$$\Delta x \geq \Delta t \, (V + \sqrt{gd}), \tag{123}$$

where

V is mean velocity of flow at the starting cross section of increment Δx,

g is the acceleration of gravity, and

d is depth.

Both velocity and stage, as well as discharge, which is the product of velocity and area, can be obtained explicitly for each new step of Δt. Unlike the power-series method which provides the desired information for only one variable at a time—for example, the discharge at one end of the reach—the method of characteristics provides the desired information simultaneously for any selected points in the reach that lie at multiples of Δx from the end of the reach. However, it is possible to change the values of Δx and Δt during the computation, if that is desired, as long as the relation of Δt to Δx meets the criterion given in equation 123.

A single representative cross section is normally used for the entire reach, as in the power-series method. However, a multiple reach may also be used (Lai, 1967a). A long reach is divided into several subreaches, each with its own individual geometry and roughness coefficient. The basic method of characteristics is applied to each subreach, and additional boundary conditions are imposed at each junction be-

tween subreaches. Furthermore, the method of characteristics will accommodate the entrance of a large gaged tributary into the reach; the boundary conditions are then more involved, but there is no complication in principle.

The mathematical details of the method of characteristics are described by Lai (1965a, 1967a), Lister (1960), and Stoker (1953).

IMPLICIT METHOD

The implicit method is yet another finite-difference procedure for solving the basic partial differential equations for flows of homogeneous density in tidal reaches. The implicit method has one advantage over the method of characteristics in that the choice of Δt is less restricted; the stability of the solution is not limited by the criterion of equation 123.

The mathematical details of the implicit method are described by Lai (1965b, 1967b, 1968) and by O'Brien, Hyman, and Kaplan (1951).

FOURIER SERIES

The equations of unsteady flow have also been solved by a method of harmonics in which a Fourier series is used. The distinctive characteristic of a Fourier series is the periodicity of the trigonometric terms of which it is composed. The Fourier series lends itself well to the expression of periodic phenomena that are represented by linear differential functions; the equations of unsteady flow, however, are quasi-linear hyperbolic differential functions. Consequently, it is necessary to linearize the equation system when using a Fourier series. That distorts the equation system. An even more significant consideration is whether or not tidal flow can be described as a truly periodic phenomenon. The long translatory wave motion introduced into a tidal reach by the astronomical tide is periodic, but its periodicity is disturbed when the natural upland flow of a river system is superimposed on the tidal wave motion or when storm surges from the ocean occur.

Despite these drawbacks, Fourier series evaluation techniques for determining flow in tidal reaches have been developed (Dronkers, 1947, p. 127–137; Dronkers and Schönfeld, 1955, p.11–24; Schonfeld, 1951, p. 70–87 and 143–152). However this type of solution is the least suitable of the four methods that have been briefly described here for solving the differential equations of unsteady flow in tidal reaches.

EMPIRICAL METHODS

Four empirical methods of rating tidal reaches have been in use, all but one of which were developed before the use of digital computers became commonplace. Those techniques are:

1. method of cubatures,
2. rating-fall method,
3. tide-correction method, and
4. coaxial graphical-correlation method.

All the above methods have their shortcomings which are discussed, where appropriate, in the sections of the manual that follow.

METHOD OF CUBATURES

One of the oldest methods of computing discharge in tidal estuaries is the method of cubatures (Pillsbury, 1956). The method, still in use, is based on the equation of the conservation of mass;

Outflow at the study station = inflow ± change in storage.

The inflow term in the above equation is the freshwater discharge measured at a gaging station at or upstream from the head of tide—that is, a gaging station having a simple stage-discharge relation. The storage term refers to volume of water in the reach between the inflow gaging station and the study station on the estuary. Intermediate stage gages are usually needed for evaluating the storage term. The gages are spaced at such distances that no significant error is introduced in the computations by considering the water surfaces between gages as planes. That requirement ordinarily is met by stations some miles apart but suitably placed with regard to marked changes in the cross section of the waterway. The differences in the tidal ranges on the opposite shores of a wide estuary may usually be disregarded, but it may be necessary to establish tidal stations on any long tidal tributaries of the main waterway. For convenience in the computations, the tides at all stations should be reduced to the same horizontal datum, preferably taken low enough to make all stages positive.

If existing surveys do not afford reliable data on the areas of the water surfaces between the selected tidal stations, a survey to establish these surfaces is required. Usually such surface areas may be taken as increasing uniformly from low water to high water, but if there are any considerable tide flats that are exposed at the lower tidal stages, the area at the stage at which such flats are covered also should be found.

Freshwater inflow to the reach from tributary streams is estimated if the tributary flow is relatively small. If the tributary streams are large, they are gaged upstream from the head of tide to provide a continuous record of freshwater inflow, just as is done with the principal inflow stream.

A sample computation is shown in figure 222 for a 5.8 mile reach of the Delaware River between Trenton and Fieldsboro, N.J. This is the second reach in the estuary; the first reach extends upstream from

Time	Tidal stage			Mean stage during time interval	Water-surface area (A) at mean stage	Change in stage (Δy) during time interval	Change in storage			Outflow Q
	Upper station	Lower station	Mean (y)				In study reach $\Delta Q = A(\Delta y/\Delta t)$	In upstream reach	Total (upstream plus study reaches)	
(hr)	(ft)	(ft)	(ft)	(ft)	(1000's of ft^2)	(ft)	(ft^3/sec)	(ft^3/sec)	(ft^3/sec)	(ft^3/sec)
1	2	3	4	5	6	7	8	9	10	11
0500	2.78	2.52	2.65							
				2.48	39,703	- 0.35	-7,720	-500	- 8,220	-20,420
0530	2.43	2.16	2.30							
				2.12	38,880	- .35	- 7,560	- 490	- 8,050	-20,250
0600	2.09	1.81	1.95							
				1.80	38,206	- .31	- 6,580	- 430	- 7,010	-19,210
0630	1.79	1.50	1.64							
				1.52	37,656	- .25	- 5,230	- 410	- 5,640	-17,340
0700	1.51	1.27	1.39							
				1.59	37,800	.40	8,400	20	8,420	- 3,780
0730	1.52	2.06	1.79							
				2.52	39,686	1.47	32,410	2,840	35,250	23,050
0800	3.48	3.04	3.26							
				3.77	42,247	1.02	23,940	1,350	25,290	13,090
0830	4.41	4.16	4.78							
				4.66	44,053	.76	18,600	1,090	19,690	7,490
0900	5.16	4.93	5.04							
				5.36	45,478	.64	16,170	920	17,090	4,890
0930	5.79	5.58	5.68							
				5.96	46,702	.55	14,270	770	15,040	2,840
1000	6.32	6.14	6.23							
				6.48	47,755	.49	13,000	690	13,690	1,490
1030	6.80	6.64	6.72							

FIGURE 222.—Sample computation of tide-affected discharge by method of cubatures, using 30-minute time intervals. (After Pillsbury, 1956.)

Trenton to the Delaware River gaging station that is upstream from head of tide. Total freshwater inflow to the second reach is −12,200 ft^3/s, flow in the downstream (ebb) direction being considered negative in the computations. That inflow consists of 12,000 ft^3/s for the Delaware River mainstream and 200 ft^3/s for tributary inflow. The time interval (Δt) used in the computations is 30 minutes, or 1,800 seconds. The computations in the table in figure 222 are largely self-explanatory. The figures in column 9 were obtained from similar computations (not shown) for the reach upstream from the study reach. Column 10 is the sum of columns 8 and 9; column 11, the outflow from the study reach, is the sum of the total storage change (column 10) and the total freshwater inflow (−12,200 ft^3/s).

Figure 223 is the discharge hydrograph obtained by first plotting the outflow histogram (values from column 11 of fig. 222), and then drawing a smooth hydrograph to give balance between areas above and below the horizontal bars of the histogram.

The method of cubatures is not only cumbersome, but the discharge figures obtained are only rough approximations of the true values

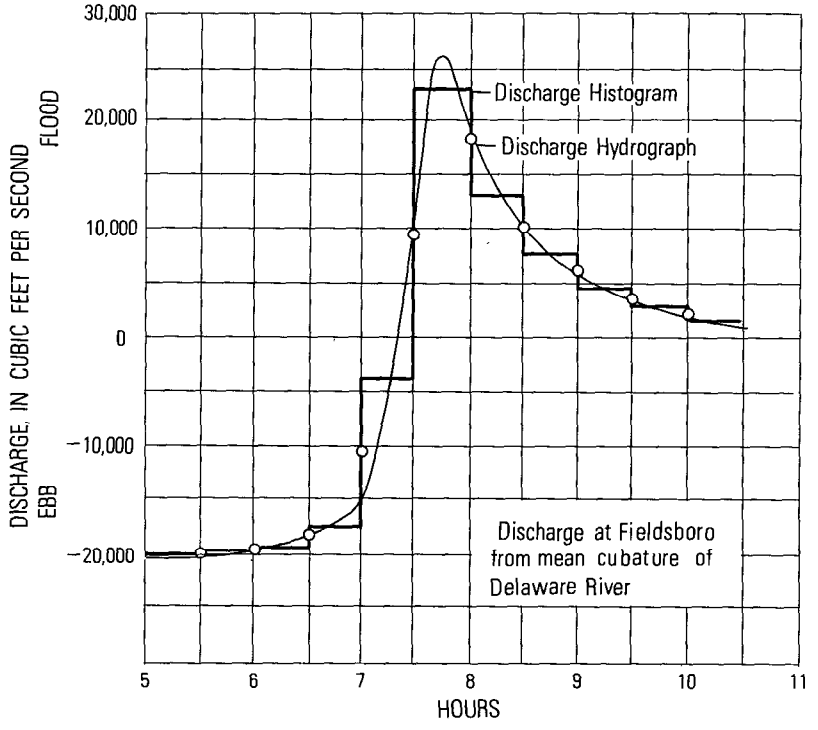

FIGURE 223.—Discharge hydrograph obtained for sample problem by method of cubatures. (After Pillsbury, 1956.)

because of the large errors inherent in computing the storage component of the continuity equation. When the method is used, the results, although approximate, should be checked for consistency—total computed outflow should approximate total inflow over some long-term period whose net change in storage is negligible.

RATING-FALL METHOD

Stage-fall-discharge relations have been used successfully for rating tide-affected streams where acceleration head is a minor factor. The rating-fall method that is discussed in detail in the section in chapter 11 titled, "Variable Slope Caused by Variable Backwater," is used for that purpose. Acceleration head is often a minor factor where the slope reach is located at the upper end of an estuary near the head of tide. Consequently, it is usually only at or near such locations that the rating-fall method can be used successfully.

TIDE-CORRECTION METHOD

The tide-correction method assumes that a direct proportionality exists between the cyclic range in stage observed at any two points within a tidal reach. On the basis of that assumption, a relation of mean discharge for a tidal cycle to mean stage for a tidal cycle is developed for the base-gage site. In calibrating that relation, the mean discharge for a tidal cycle, obtained by averaging several individual measurements made 1–2 hours apart throughout the cycle, is plotted against adjusted mean stage at the base gage. The adjustment applied to the mean stage at the base gage is determined from the difference, at the secondary gage, between observed mean stage and the stage that is presumed to exist under conditions of least tide fluctuation. That difference (D) is multiplied by the ratio of the stage range at the base gage to the stage range at the secondary gage; the product is the stage adjustment required at the base gage. In practice, the secondary stage observations are frequently made at a nearby ocean inlet. Mean sea level is assumed to represent the condition of least tidal fluctuation, and therefore, if all gages have their datums set to mean sea level, D is always equal to the mean stage for a tidal cycle at the secondary gage. Essentially the tide-correction method attempts to approximate the stage that would occur for a particular steady-flow discharge under a fixed backwater condition. An example of the tide-correction method (Parker and others, 1955) follows.

At Hialeah, Fla., the base gage is on the Miami Canal, 7.6 miles upstream from the ocean. A tide gage on the ocean is used as the secondary gage. Both gages have their datum at mean sea level. On a given date the following tidal-cycle data were obtained from the stage gages:

	Base gage	*Secondary gage*
Mean stage (ft)	2.64	1.61 = D
Maximum stage (ft)	3 18	2.74
Minimum stage (ft)	2.10	.48
Stage range (ft)	1.08	2.26

$$\text{Stage correction (base gage)} = D\left(\frac{\text{stage range at base gage}}{\text{stage range at secondary gage}}\right)$$

$$= 1.61\left(\frac{1.08}{2.26}\right)$$

$$= 0.77 \text{ ft}$$

The stage correction is always negative and therefore the stage at the base gage, to be applied to the mean discharge for the tidal cycle on that date, is

$$\text{Gage height} = 2.64 - 0.77 = 1.87 \text{ ft.}$$

The mean-cycle discharge, as determined from 20 sets of discharge measurements, was plotted against the actual mean-cycle gage height and also against the tide-corrected gage height, as indicated on figure 224. The rating curve shows the relation between the tide-corrected gage height and the mean tide-cycle discharge for the upper gage. The discharge, when plotted against actual mean-cycle gage height, shows a considerable scatter of the plotted points, but the discharge plotted against tide-corrected gage height shows a very

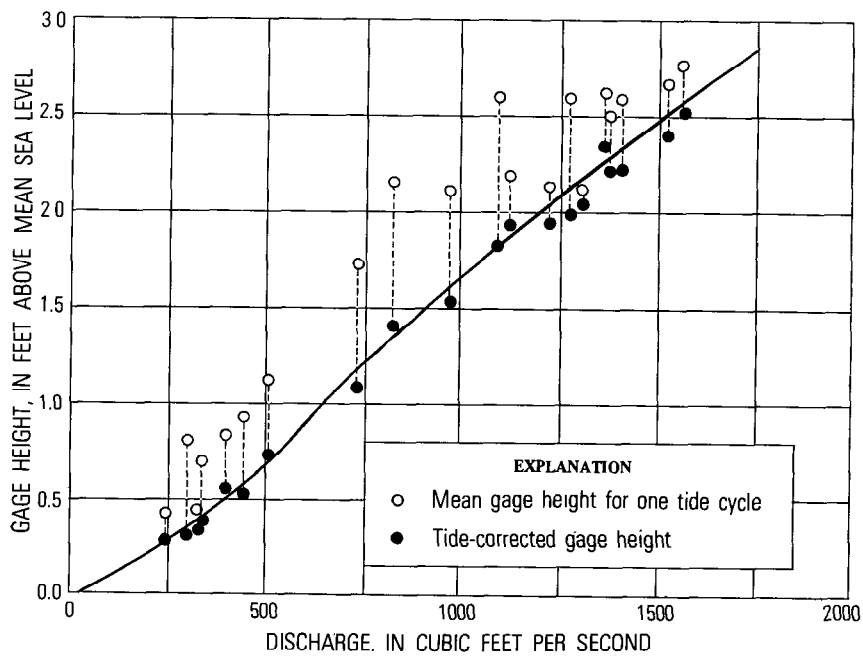

FIGURE 224.—Graph of relation between tide-corrected gage height and discharge for Miami Canal at Water Plant, Hialeah, Fla.

close agreement for the numerous measurements. The shape of the rating curve is characteristic of that for a stream having a large initial cross-sectional area at the point of zero flow.

The tide-correction method of rating a tide-affected stream may be used where reverse flows occur during a part of each tide cycle because the mean discharge for the cycle is the value used in the computation. It is also applicable to a reach of tidal waterway, on which both observation stations are upstream from the mouth of the waterway. Mean-cycle discharge obtained from the rating curve can be plotted against mean-cycle time on a hydrograph sheet, and after connecting the points by straight lines, the daily mean discharges can be determined.

The tide-correction method has been satisfactory, though cumbersome, for computing the daily discharge of tide-affected canals in Florida, but efforts to adopt the method for use elsewhere in the U.S.A. have generally been unsuccessful.

COAXIAL RATING-CURVE METHOD

The coaxial method of graphical correlation to determine discharge in a tidal reach was developed to fill the need for a simple method of making reasonably accurate "on-the-spot" determinations of streamflow. A method of this kind is required, for example, in the operation of a sewage plant discharging its effluent into a tide-affected stream. The method that was developed fills this need in that readings from a pair of stage gages can be used to determine momentary discharge directly from a set of rating curves.

The coaxial method is best described by an example. Coaxial rating curves were developed for the Sacramento River at Sacramento, Calif., on the basis of 302 discharge measurements made during the years 1957–60 (Rantz, 1963). Actually only 52 of the measurements were used to develop the curves; the remaining 250 discharge measurements were used to test the rating curves and refine them slightly. Measured discharges ranged from 4,060 ft^3/s (115 m^3/s) to 19,300 ft^3/s (547 m^3/s).

The streamflow-measurement section is at the site of the stage recorder in the city of Sacramento; the auxiliary stage recorder is 10.8 mi (17.4 km) downstream near the town of Freeport. Local inflow into the 10.8-mile reach of channel is negligible. The reach itself is located far enough upstream on the Sacramento River estuary so that no reversal of flow occurs. When upland flow (streamflow) into the estuary is less than about 30,000 ft^3/s (850 m^3/s), however, the discharge is affected by tidal action, and the flow in the reach is unsteady. The relative magnitude of the tidal effect in the reach increases with decrease in the upland flow and with increase in the range of elevation between high and low tides. The stages at Sacramento and

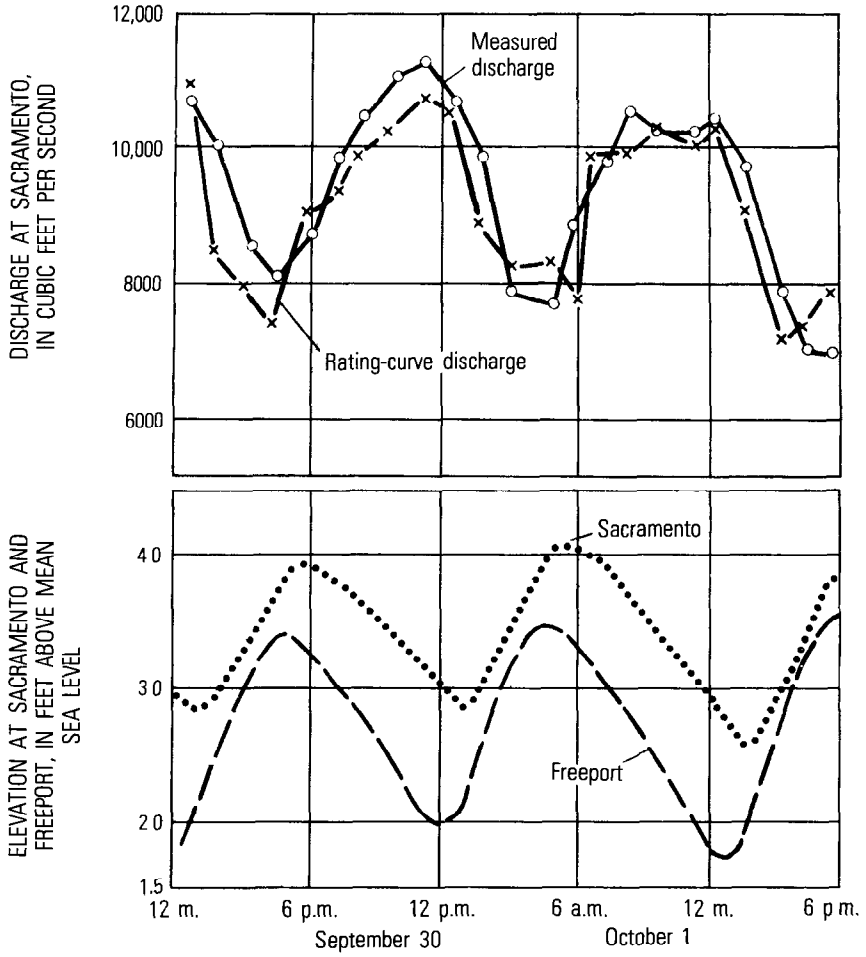

FIGURE 225.—Stage and discharge of the Sacramento River at Sacramento, Calif., Sept. 30 to Oct. 1, 1959.

Freeport during a 36-hour period and the fluctuation of discharge at Sacramento illustrate a typical low-flow condition (fig. 225). The upland flow above Sacramento was 9,300 ft/s (263 m^3/s). As a result of tidal effect, the discharge at Sacramento varied from 6,800 ft^3/s (193 m^3/s) to 11,300 ft^3/s (320 m^3/s).

The differential equations of unsteady flow were used to devise a graphical technique for determining discharge. The following parameters serve as indices of the terms that appear in these differential equations:

Dependent variable.—Measured discharge at Sacramento.

Independent variables.—(1) Stage at Sacramento, (2) fall in the

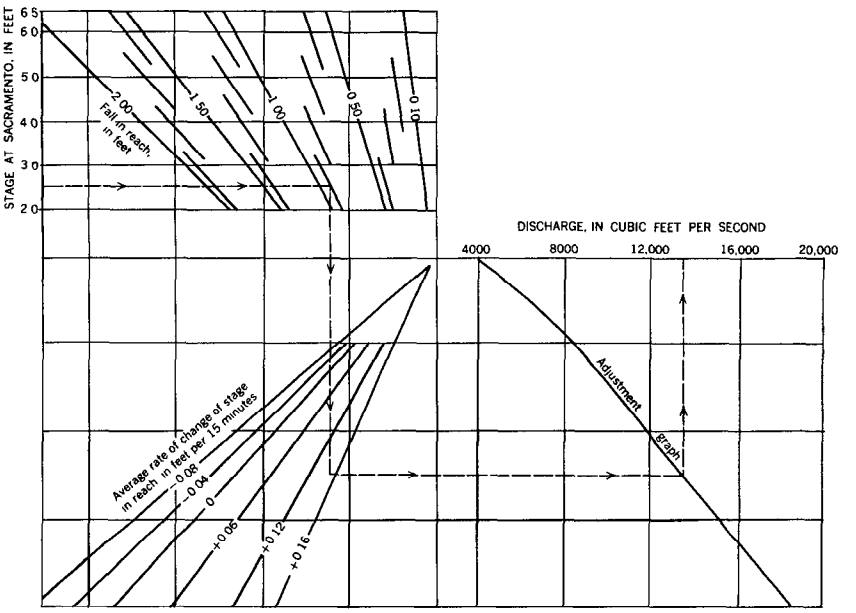

FIGURE 226.—Coaxial rating curves for the Sacramento River at Sacramento, Calif. (Dashed lines and arrows illustrate use of the curves.)

reach between Sacramento and Freeport, and (3) the algebraic average of the change in stage observed at Sacramento and Freeport during a 15-minute interval.

Because of the differential form of the equations of unsteady flow, there is no statistical model on which to base the relationship of these variables. A further complication arises from the fact that joint functions are involved, for interrelations among the independent variables affect the flow at Sacramento. The versatile statistical technique known as the coaxial method of graphical multiple correlation (Linsley and others, 1949, p. 650–655) was adopted for developing the rating curves for the Sacramento River.

The coaxial graphical correlation that was the end product of this study is shown in figure 226. In the interest of simplicity, only a few lines are shown in each family of curves. To use the graph, first, the curves in the upper left-hand group are entered with the stage at Sacramento and the fall in the reach; next, the curves in the lower left-hand group are entered with the average rate of change of stage in the reach; finally, the adjustment graph to the right is entered and the discharge is read. The adjustment graph was added to the correlation to introduce a necessary curvilinearity to the relationship. This curve may also serve another purpose—if the relation should change, as a result of channel dredging, for example, only the adjustment

graph need be revised, thereby eliminating the laborious task of revising the two families of curves.

Of the 305 discharge measurements, 268, or 89 percent of them, checked the rating within ±10%; 286 measurements, or 95 percent of the measurements, checked the rating within ±15%. The rating was weakest during periods of low upland flow, but for only a few hours of any day during those periods. Those hours coincided with times when the acceleration head in the equations of unsteady flow was of relatively major importance.

The coaxial rating-curve method fulfills its purpose of being useful for making "on-the-spot" estimates of tidal flow at Sacramento, but the method is too cumbersome for use in computing a continuous record of discharge for a gaging station. Solution of the theoretical equations of unsteady flow (see section on "Evaluation of Unsteady-Flow Equations") is much better for the latter purpose.

SELECTED REFERENCES

Baltzer, R. A., and Shen, J., 1961, Flows of homogeneous density in tidal reaches: U.S. Geol. Survey open-file report, 107 p.

——— 1964, Computation of homogeneous flows in tidal reaches by finite-difference method: U.S. Geol. Survey Prof. Paper 424–C, p. C39–C43.

Davidian, Jacob, 1964, Computation of discharge in tidal reaches: U.S. Geol. Survey Surface-Water Techniques, book 1, chap. 2, 49 p.

Dronkers, J. J., 1947, Methoden van getijberekening (Methods of tidal calculation): De Ingenieur Netherlands, v. 40, p. 121–137.

Dronkers, J. J., and Schonfeld, J. C., 1955, Tidal computations in shallow water: Am. Soc. Civil Engineers Proc., Hydraulics Div., v. 81, sep. no. 714, 49 p.

Lai, Chintu, 1965a, Flows of homogeneous density in tidal reaches—solution by the method of characterisitics: U.S. Geol. Survey open-file rept , 58 p.

——— 1965b, Flows of homogeneous density in tidal reaches—solution by the implicit method: U.S. Geol. Survey open-file rept., 43 p.

——— 1967a, Computation of transient flows in rivers and estuaries by the multiple-reach method of characteristics: U.S. Geol. Survey Prof. Paper 575–D, p. D273–D280.

——— 1967b, Computation of transient flows in rivers and estuaries by the multiple-reach implicit method: U.S. Geol. Survey Prof. Paper 575–B, p. B228–B232.

——— 1968, The boundary conditions in the implicit solution of river transients: U.S. Geol. Survey Prof. Paper 600–C, p. C204–C210.

Linsley, R. K , Kohler, M. A., and Paulhus, J. J. H., 1949, Applied hydrology: New York, McGraw-Hill Book Co., 689 p.

Lister, M., 1960, The numerical solutions of hyperbolic partial differential equations by the method of characteristics, *in* Mathematical methods for digital computers, A. Ralston and H. S. Wilf, eds.; New York, John Wiley, p. 165–179.

O'Brien, G. G., Hyman, M. A., and Kaplan, S., 1951, A study of the numerical solution of partial differential equations. Jour. of Mathematics and Physics, Massachusetts Inst. of Technology, v. 24, no 4, p. 223–251.

Parker, G.G., Ferguson, G.E., Love, S. K., and others, 1955, Water resources of southeastern Florida: U.S. Geol. Survey Water–Supply Paper 1255, p. 471–475 .

Pillsbury, G. B., 1956, Tidal hydraulics: U.S. Army Corps of Engineers, Waterways Experiment Station, Vicksburg, Mississippi, p. 220–228.

Rantz, S. E., 1963, An empirical method of determining momentary discharge of tide-affected streams: U.S. Geol. Survey Water-Supply Paper 1586–D, 28 p.

Stocker, J. J., 1953, Numerical solution of flood prediction and river regulation problems—derivation of basic theory and formulation of numerical method of attack: New York Univ., Institute of Mathematical Sci., Rept. no. IMM–200, 36 p.

Schonfeld, J. C., 1951, Propagation of tides and similar waves: Gravenhage, Netherlands, Staatsdrukkerij-en-Vitgevenijbedijf, 233 p.

CHAPTER 14—DISCHARGE RATINGS FOR MISCELLANEOUS HYDRAULIC FACILITIES

INTRODUCTION

This chapter is a "catchall" for specialized problems in establishing discharge ratings for various hydraulic facilities, using techniques that are not specifically described in chapters 10–13. The hydraulic facilities are discussed under the following principal headings:

1. dams with movable gates,
2. navigation locks,
3. pressure conduits, and
4. urban storm drains.

DAMS WITH MOVABLE GATES

GENERAL

Dams are commonly equipped with movable gates for better control of pool stage and outflow. As a general rule the movable gates, as such, are not rated; instead, the channel downstream is rated by the most practicable method—simple stage-discharge relation (chap. 10), or stage-fall-discharge relation (chap. 11), or by use of a velocity index furnished, for example, by an acoustic velocity meter (chap. 12). However, in some situations none of those rating methods may be satisfactory. For example, consider a river controlled by a series of low navigation dams. In that situation, the river profile resembles a huge staircase—successive pools separated by dams. The movable dam crests negate the use of a simple stage-discharge relation; the slope of the water surface in the pools may be too flat for a stage-fall-discharge relation; and velocities may be too slow for accurate evaluation by an acoustic velocity meter. In that situation, the most practicable method of obtaining a continuous record of discharge is to calibrate the flow through or over the movable gates. If boat traffic is heavy and natural inflow is light, a significant part of the discharge may be the flow released through the navigation locks and the lockages must likewise be calibrated (see section on "Navigation Locks").

Calibration of the gates by discharge measurements during periods of light releases of water may be extremely difficult. If boat lockages are infrequent, standard current-meter measurements made downstream by boat, using a low-velocity meter, may be adequate. If boat lockages are frequent, the surges in discharge attributable to the lockages may cause unsteady and nonuniform flow conditions downstream; discharge measurements must then be made as rapidly as possible under conditions that are not conducive to accurate

results. A rapid discharge measurement may be made by the moving-boat method (chap. 6) or by use of a bank of current meters operated from a bridge (see section in chapter 5 titled, "Networks of Current Meters"). If velocities are too slow for accurate measurement by either of those two methods, and if only small quantities of water are being released under the dam-crest gates, the best course of action might be to use the volumetric method for measuring flow over a dam crest that is described in the section in chapter 8 titled, "Volumetric Measurement." In using the volumetric method, the barge carrying the calibration tank is kept in place not only by lines operated from the banks, but also by an outboard motor on the barge to keep the barge from drifting downstream. The difficulty of measuring low flow under the conditions described above is apparent. At those times it may also be difficult to determine the actual head on the gates because lockages often cause longitudinal seiche-like waves to traverse the gage pool, and those waves travel back and forth over the length of the pool for a considerable period of time.

The flow at movable dam-crest gates may be placed in two general categories—weir flow over the gate or dam crest and orifice flow under the gate. Each of those types of flow may be either free or submerged, depending on the relative elevations of headwater, tailwater, and pertinent elements of the dam crest or gate. Listed below are the crest gates that will be discussed.

1. Drum gates
2. Radial or Tainter gates
3. Vertical lift gates
4. Roller gates
5. Movable dams
    a. Bear-trap gates
    b. Hinged-leaf gates
    c. Wickets
    d. Inflatable dams
6. Flashboards
7. Stop logs and needles

A gated dam usually has several gates along its crest. The gates are installed in bays that are separated by piers. All other conditions being equal, the discharge through a single gate, when adjacent gates are open, will be about 5 percent greater than the discharge through that same gate when adjacent gates are closed. The various types of gates should be calibrated by discharge measurements, but as an aid to shaping the calibration curves, experimental ratings where available are given in the text that follows.

Discharge measurements for the purpose of determining gate coefficients will almost always be made in the downstream channel and

will include the flow for all the gates that are open. Furthermore, for given stages upstream and downstream from the gates, the gate coefficient will commonly vary with the gate position or opening. Consequently, if discharge is to be measured with more than one gate open, arrangements should be made, if possible, for all gates to be positioned identically. If the difference in the positioning of the gates are minor, and if the gate coefficient does not vary significantly with its positioning, a discharge measurement may be made; in the computation of the gate coefficient, an average gate position will be assumed for each of the bays carrying flow.

DRUM GATES

A drum gate consists of a segment of a cylinder which, in the open or lowered position, fits in a recess in the top of the spillway. When water is admitted to the recess, the hollow drum gate is forced upward to a closed position. One type of drum gate (fig. 227*A*) is a completely enclosed gate hinged at the upstream edge; buoyant forces aid in its lifting. That type of gate is adapted to automatic operation and also conforms closely to the shape of the ogee crest when lowered. A second type (fig. 227*B*) has no bottom plate and is raised by water pressure alone. Because of the large recess required by drum gates in the lowered position, they are not adapted to small dams.

With regard to its calibration, the drum gate resembles a thin-plate weir with a curved upstream face over the greater part of its travel. Given an adequate positioning indicator, the drum gate can serve as a satisfactory stream-gaging control. Its use for that purpose has been investigated by Bradley (1953), and the discussion that follows is taken almost verbatim from Bradley's paper dealing with a drum gate of the type shown in figure 227*A*.

When the drum gate simulates a thin-plate weir—that is, when a line drawn tangent to the downstream lip of the gate makes a positive angle with the horizontal, as shown in figure 228*A*—four principal factors are involved. These factors are H, the total head above the high point of the gate; Θ, the angle between the horizontal and a line

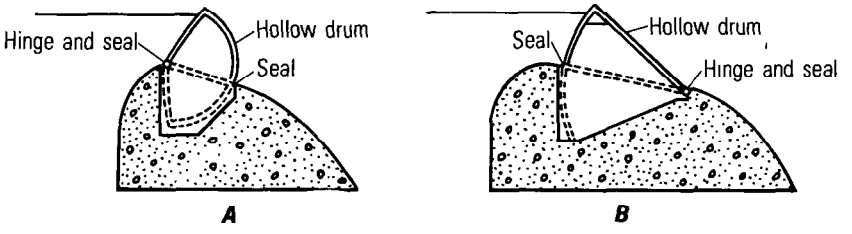

FIGURE 227.—Two types of drum gate.

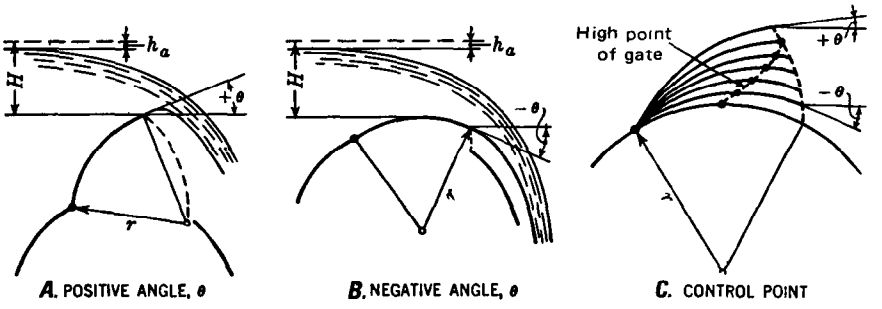

FIGURE 228.—Drum-gate positions. (After Bradley, 1953.)

drawn tangent to the downstream lip of the gate; r, the radius of the gate, or an equivalent radius if the shape of the gate is parabolic; and C_u, the coefficient of discharge in equation,

$$Q = C_u b H^{3/2}, \tag{124}$$

where

Q is discharge (ft^3/s), and

b is length of the gate (ft) normal to the discharge.

The velocity in the approach section was not included as a variable because the drum-gate installations studied were on high dams where approach effects were negligible. It has been shown that when the approach depth measured below the high point of the gate is equal to or greater than twice the head on the gate, a further increase in the approach depth produces little change in the coefficient of discharge. Most drum-gate installations are on dams that meet the above depth criterion, particularly when the gate is in a raised position. Therefore, in the usual case of adequate approach depth, the four variables, H, Θ, r, and C_u completely define the flow over this type of gate when angle Θ is positive (fig. 228*A*).

For negative values of Θ (fig. 228*B*), the downstream lip of the gate no longer controls the flow. In that situation the control point shifts upstream to the vicinity of the high point of the gate for each setting, as illustrated in figure 228*C*, and flow conditions gradually approach those of the free crest as the gate is lowered. Although other factors enter the problem, similitude in the computation exists down to an angle of about $-15°$.

Experimentation with eleven drum gates produced the family of curves for C_u shown in figure 229. The discharge coefficients in the region between $\Theta = -15°$ and the gate completely down are determined by graphical interpolation, a method that will be explained in the example that follows. The effect of submergence of the drum gate on C_u was not investigated because drum gates are invariably used on high dams, and the probability of submergence is negligible. The data

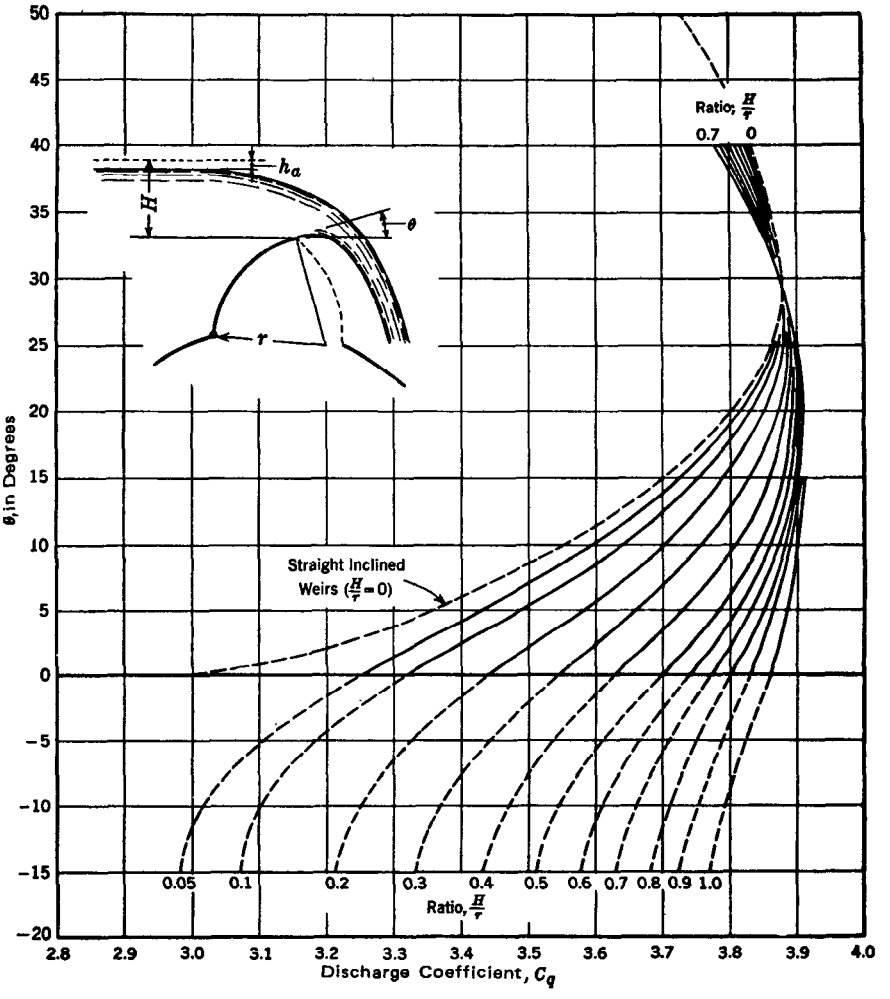

FIGURE 229.—General curves for the determination of discharge coefficients. (After Bradley, 1953.)

to be continuously recorded for computing discharge over rated drum gates are reservoir stage and the indication of drum-gate position for each gate.

The method of rating a drum gate on a round-crested weir will now be demonstrated using as an example the plan and spillway cross section of Black Canyon diversion dam in Idaho (figs. 230 and 231). The first step is the determination of the design head of the dam and the corresponding discharge coefficient for the free crest. That is done in accordance with the technique described under the heading "Nappe-fitting method" in the U.S.G.S. manual on computing peak

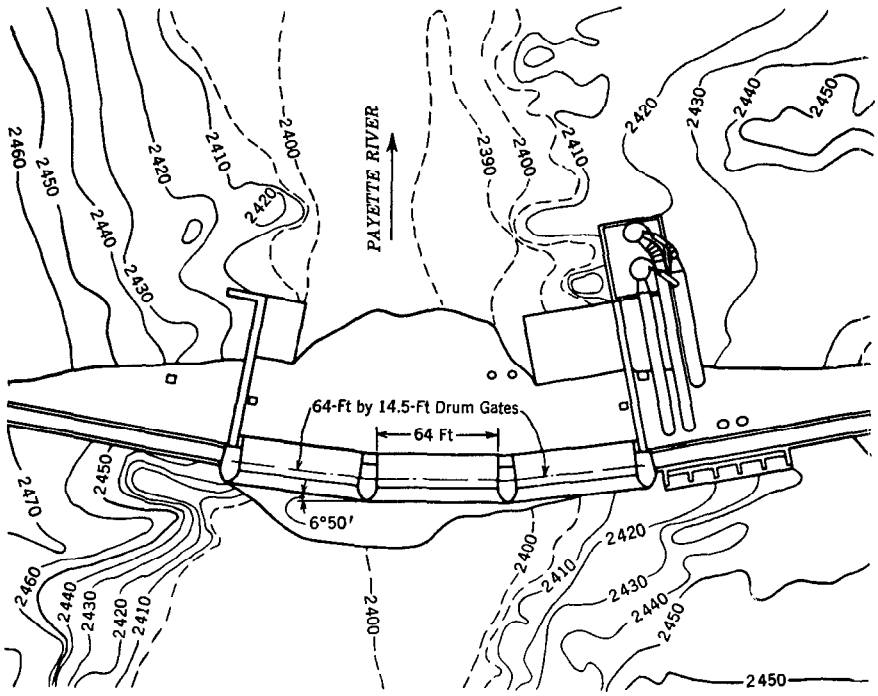

FIGURE 230.—Plan of Black Canyon Dam in Idaho. (After Bradley, 1953.)

discharge at dams (Hulsing, 1967, p. 13–23). If a discharge measurement has been made under the condition of flow over a free crest, the results of the measurement are used to check the value of design head and design-head coefficient, using the technique described under the heading "Index-measurement method" in the previously cited manual by Hulsing (1967, p. 23–24). The design head (H_0) of Black Canyon diversion dam was found to be 14.5 ft and the corresponding coefficient of discharge (C_0) was found to be 3.48.

With the coefficient of discharge known for free flow at the design head, the entire free-flow coefficient curve can be established by use of figure 232. The free-flow coefficient curve for the spillway of Black Canyon diversion dam (H_0 = 14.5 ft; C_0 = 3.48) is constructed by arbitrarily assuming several values of H/H_0 and reading the corresponding values of C/C_0 in figure 232. The method of computation is illustrated in table 25, and the head-coefficient curve for free flow (gate down) obtained in that manner is shown in figure 233.

Before considering the rating of the spillway with gates in raised positions, it is necessary to construct a diagram, such as that shown in figure 234, to relate gate elevation to the angle Θ for the Black

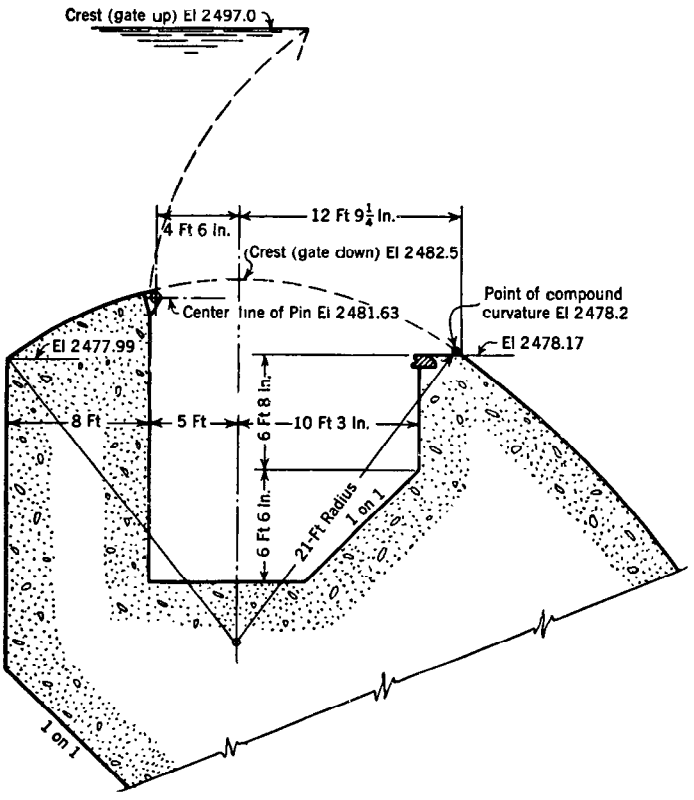

FIGURE 231.—Spillway crest detail, Black Canyon Dam, Idaho. (After Bradley, 1953.)

Canyon Dam gate. The tabulation in figure 234 shows the angle Θ for corresponding elevations of the downstream lip of the gate at intervals of 2 ft.

Beginning with the maximum positive angle of the gate, which is 34.883°, the computation may be started by choosing a representative number of reservoir elevations as indicated in column 2 of table 26. The difference between the reservoir elevation and the high point of the gate constitutes the total head on the gate, and values of head are recorded in column 3. Column 4 shows these same heads divided by the radius of the gate, which is 21.0 ft.

The discharge coefficients listed in column 5 (table 26) of the set of computations designated "A", are obtained by entering the curves in figure 229 with the values in column 4 for $\Theta = +34.883°$. The remainder of the procedure outlined in columns 6 and 7 of table 26, consists of computing the discharge for one gate from the equation,

$$Q = C_a\, bH^{3/2}. \tag{124}$$

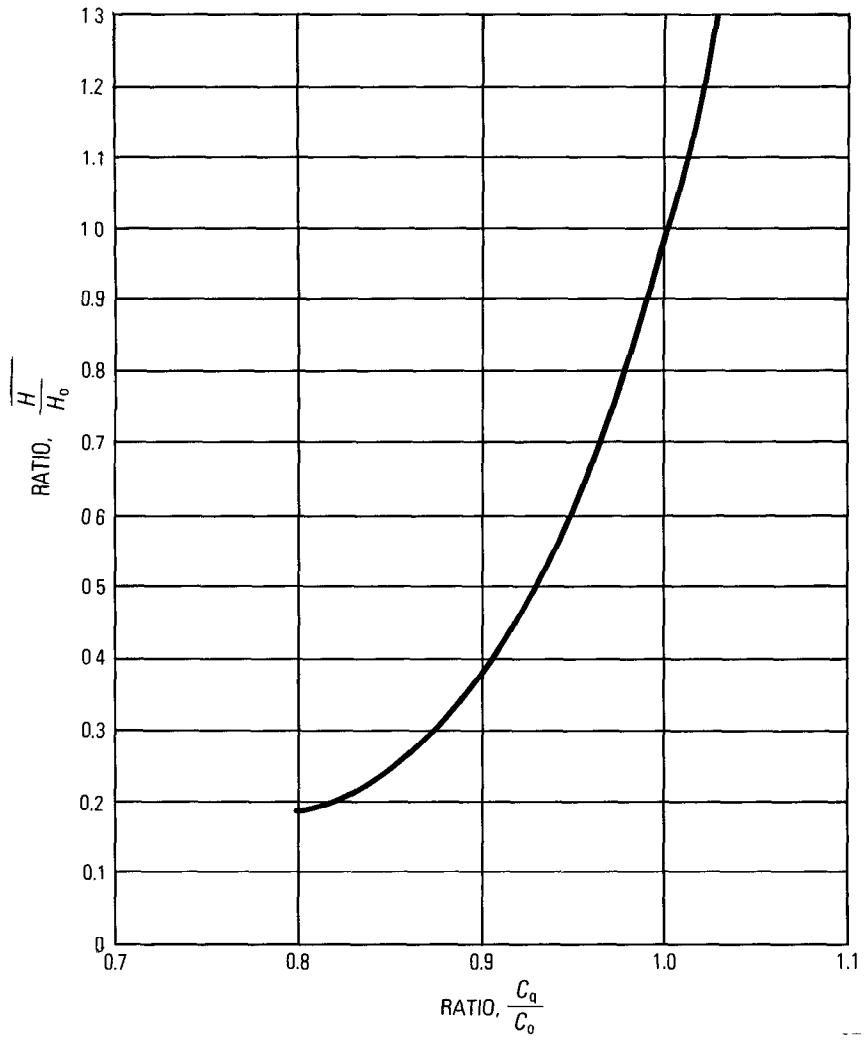

FIGURE 232.—Diagram for determining coefficients of discharge for heads other than the design head (After Bradley, 1953.)

A similar computation procedure is repeated for other positive angles of Θ, as in sets B, C, and D of table 26.

For positive values of angle Θ the high point of the gate is the downstream lip of the gate. As the angle Θ decreases to negative values, the high point of the gate is no longer the downstream lip. In determining the discharge for negative values of Θ between 0° and −15°, the procedure remains the same as was used for positive values

TABLE 25.—*Head and Discharge Computations for a Free Crest (Black Canyon Dam in Idaho)*

[After Bradley, 1953]

Total head, H, in ft	Reservoir elevation, in ft	Ratio,[1] H/H_o	Ratio,[2] C_u/C_o	Coefficient, C_u	Q, in ft^3/s [3]
(1)	(2)	(3)	(4)	(5)	(6)
17	2499.5	1.172	1.020	3.55	15,950
16	2498.5	1.104	1.012	3.52	14,420
14.5	2497.0	1.0	1.0	3.48	12,296
12	2494.5	0.827	0.980	3.41	9,072
10	2492.5	0.690	0 960	3.34	6,759
8	2490.5	0.552	0.940	3.27	4,736
6	2488.5	0.414	0.905	3.135	2,949
4	2486.5	0.276	0.850	2.957	1,514
3	2485.5	0.207	0.815	2.835	943
2	2484.5	0.138	0.760	2.642	478

[1] H_o = 14.5 ft. [2] C_o = 3.48. [3] The discharge for one gate: $Q = C_u b H^{3/2}$, in which b = 64.0 ft.

of Θ, but as mentioned above, the controlling difference between reservoir elevation and high point of the gate is no longer the head above the downstream lip. (See fig. 234.) Discharge computation for negative angles down to $-15.017°$ are tabulated in sets E, F, and G of table 26.

The plotting of values of discharge, reservoir elevation, and gate elevation from table 26, results in the seven curves in figure 235 that bear the plotted points, shown by closed circles. An eighth curve, the extreme lower curve, which bears plotted points shown by X's, represents the discharge of the free crest with the gate completely down; the plotted points represent values obtained from table 25.

The discharge values shown in figure 235 are for one gate only. When more than one gate is in operation, the discharges from the separate gates may be totaled, providing the gates are each raised the same amount. The experimental models used in this study had from one to eleven gates operating, so that a reasonable allowance for pier effect on the discharge is already present in the results.

The intervals between the eight curves in figure 235 that are identified by plotted points are too great for rating purposes, particularly the gap between gate elevations 2485.75 and 2482.5 ft. That deficiency is remedied by cross-plotting the eight curves for various constant values of discharge as shown in figure 236. Fortunately the result is a straight-line variation for any constant value of discharge. The lines in figure 236 are not quite parallel, and there is no assurance that they will be straight for every drum gate. Nevertheless, this uncertainty will not detract appreciably from the accuracy obtained. Interpolated information from figure 236 is then utilized to construct the additional curves in figure 235. Figure 235 now shows the rating

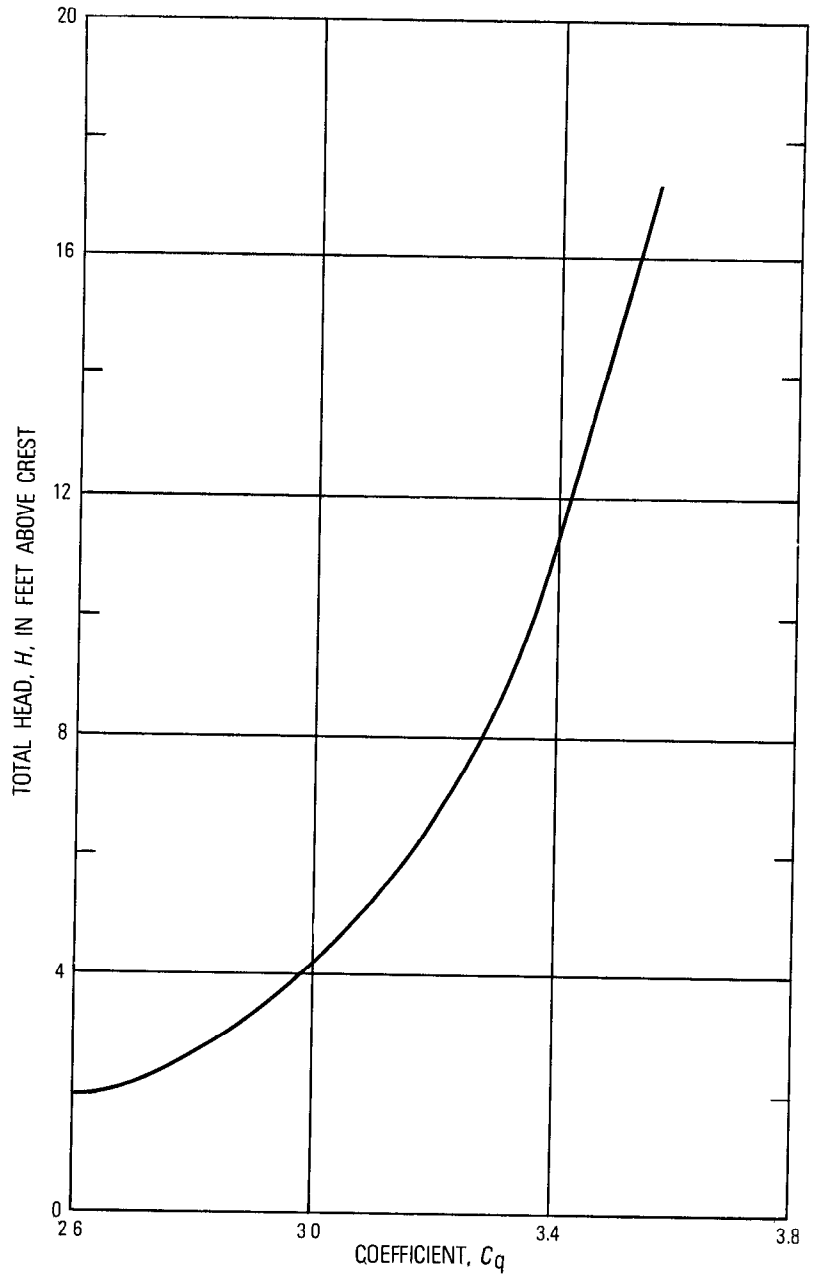

FIGURE 233.—Head-coefficient curve, Black Canyon Dam, Idaho. (After Bradley, 1953.)

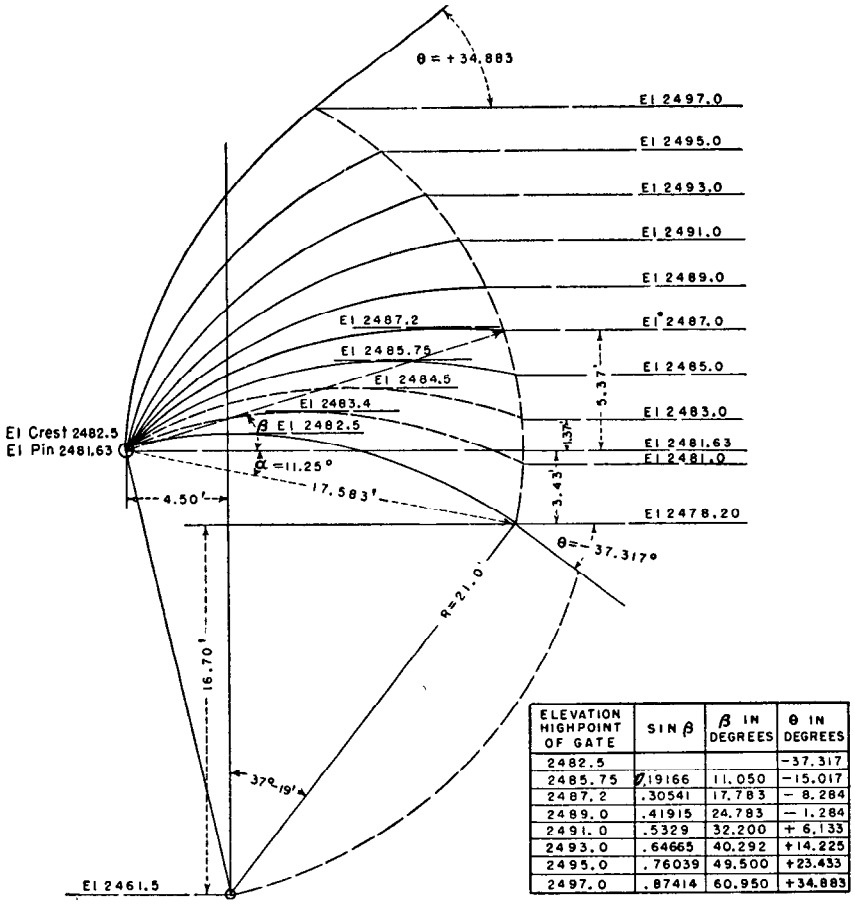

ELEVATION HIGHPOINT OF GATE	SIN β	β IN DEGREES	θ IN DEGREES
2482.5			-37.317
2485.75	.19166	11.050	-15.017
2487.2	.30541	17.783	- 8.284
2489.0	.41915	24.783	- 1.284
2491.0	.5329	32.200	+ 6.133
2493.0	.64665	40.292	+14.225
2495.0	.76039	49.500	+23.433
2497.0	.87414	60.950	+34.883

FIGURE 234.—Relation of gate elevation to angle θ. (After Bradley, 1953.)

for the Black Canyon Dam spillway for gate intervals of 0.5 ft. For intermediate values, straight-line interpolation is permissible.

RADIAL OR TAINTER GATES

The damming face of a radial or Tainter gate is essentially a segment of a hollow steel cylinder spanning between piers on the dam crest. The cylindrical segment is supported on a steel framework that pivots on trunnions embedded in the downstream part of the piers. The gate is raised or lowered by hoisting cables that are attached to each end of the gate; the cables lead to winches on a platform above the gate. In its closed position, the lower lip of the gate rests on the dam crest.

TABLE 26.—*Head and discharge computations for drum gates in raised positions*

[After Bradley, 1953]

Set (1)	Reservoir elevation, in ft (2)	H, in ft (3)	Ratio, $\frac{H}{r}$ (4)	Coefficients, C_d (5)	$H^{1/2}$ (6)	Q, in ft^3/s[b] (7)
	Gate Elevation 2497 0, θ = + 34 88°					
A	2498 0	1	0 048	3 86	1	247
	2499 0	2	0 095	3 86	2 828	699
	2500 0	3	0 143	3 86	5 196	1 283
	Gate Elevation 2495 0, θ = + 23 43°					
B	2496 0	1	0 048	3 85	1	246
	2497 0	2	0 095	3 86	2 828	698
	2498 0	3	0 143	3 87	5 196	1,281
	2499 0	4	0 190	3 87	8 00	1,979
	2500 0	5	0 238	3 88	11 18	2,770
	Gate Elevation 2493 0, θ = +14 22°					
C	2494 0	1	0 048	3 69	1	236
	2495 0	2	0 095	3 73	2 828	675
	2496 0	3	0 143	3 75	5 196	1,247
	2498 0	5	0 238	3 80	11 18	2,719
	2500 0	7	0 333	3 84	18 52	4,552
	Gate Elevation 2491 0, θ = + 6 13°					
D	2492 0	1	0 048	3 47	1	222
	2493 0	2	0 095	3 51	2 828	635
	2494 0	3	0 143	3 57	5 196	1,187
	2496 0	5	0 238	3 63	11 18	2,597
	2498.0	7	0 333	3 70	18 52	4,386
	2500 0	9	0 429	3 77	27 00	6,515
	Gate Elevation 2489 0, θ = − 1 28°					
E	2490 0	1	0 048	3 21	1	205
	2491 0	2	0 095	3 28	2 828	594
	2492 0	3	0 143	3.34	5.196	1,111
	2494 0	5	0 238	3 45	11 18	2,469
	2496 0	7	0 333	3 545	18 52	4,202
	2498 0	9	0 429	3.63	27 00	6,273
	2500 0	11	0.524	3 695	36 48	8,627
	Gate Elevation 2487 2, θ = − 8 28°					
F	2488 0	0 8	0 038	3 02	0 716	138
	2489 0	1 8	0 086	3 10	2 415	479
	2490 0	2 8	0 133	3 17	4 685	950
	2492 0	4 8	0 229	3 31	10 52	2,229
	2494 0	6 8	0 324	3 43	17 73	3,892
	2496 0	8 8	0 419	3 51	26 10	5,863
	2498 0	10 8	0 515	3 58	35 49	8,131
	2500 0	12 8	0 610	3 635	45 79	10,653
	Gate Elevation 2485 75, θ = − 15 02°					
G	2487 0	1 25	0 060	3 00	1 398	268
	2488 0	2 25	0 107	3 07	3 375	663
	2489 0	3 25	0 155	3 15	5 859	1,181
	2491.0	5 25	0 250	3 275	12 03	2,522
	2493 0	7 25	0 315	3 375	19 52	4,216
	2495 0	9 25	0 440	3 465	28 13	6,238
	2497 0	11 25	0 536	3 51	37 73	8 548
	2499 0	13 25	0 631	3 595	48 23	11,097

[a]H is the total head on the gate. [b]The discharge for one gate: $Q = C_d b H^{3/2}$.

RADIAL GATES ON A HORIZONTAL SURFACE

Experimental work has been performed to determine discharge coefficients for radial gates that control flow along a horizontal surface (Toch, 1953). The results of those experiments are shown in figures 237 to 240. Figure 237 is a definition sketch for a radial gate on a horizontal surface. The discharge coefficient, C_d, is defined as

$$C_d = \frac{q}{b(2gh_v)^{1/2}} \tag{125}$$

where q is discharge per unit width of gate, g is acceleration of gravity, and h_v and b are elements shown in the definition sketch (fig. 237).

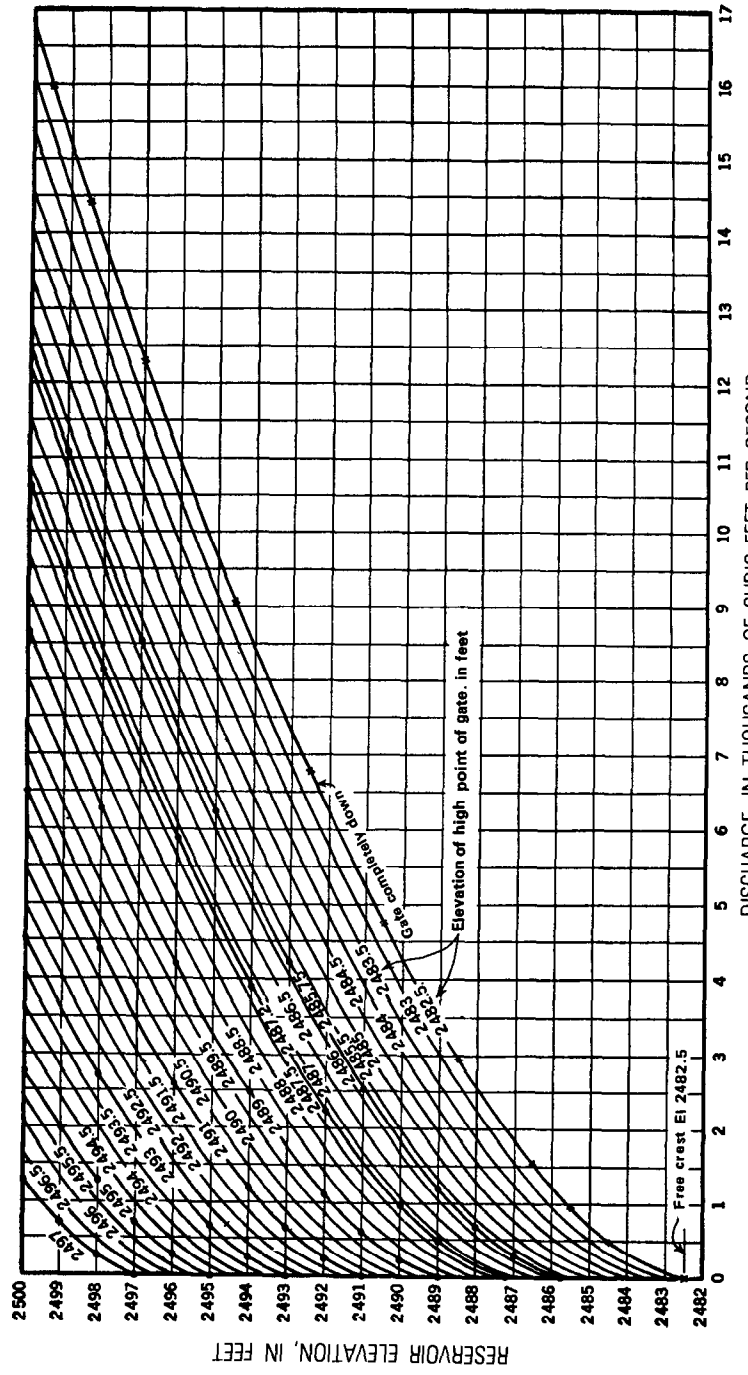

FIGURE 235.—Rating curves for drum-gate spillway of Black Canyon Dam, Idaho. (After Bradley, 1953.)

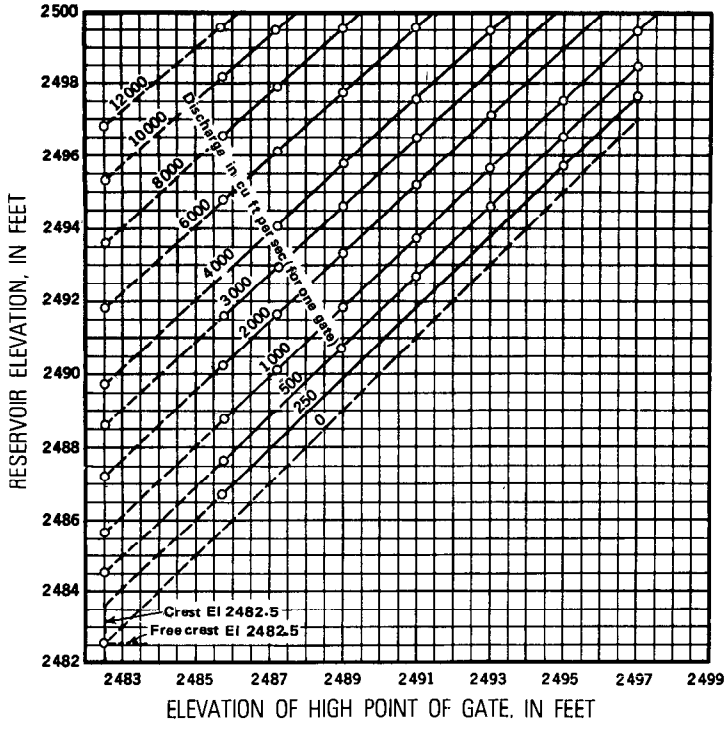

FIGURE 236.—Cross-plotting of values from initial rating curves, Black Canyon Dam, Idaho. (After Bradley, 1953.)

Figures 238 to 240 show values of C_d for three values of the ratio a/r, where a is trunnion elevation and r is gate radius. In the relations shown in the three figures, all pertinent elements have been made dimensionless by using gate radius, r, as a reference. Thus the relative headwater depth is h_1/r, the relative tailwater depth is h_2/r, the relative height of opening is b/r, and the relative trunnion height is a/r. Free efflux (flow) occurs when $h_2 < b$; submerged efflux occurs when $h_2 \geq b$. Each of the three graphs shows values of the coefficient of discharge for:

a. Free efflux for three values of b/r,
b. Submerged efflux for two values of b/r, when $h_2/r = 0.5$, and
c. Submerged efflux for three values of b/r, when $h_2/r = 0.7$.

RADIAL GATES ON A CURVED DAM CREST OR SILL

More commonly radial gates are used to control the flow over a curved dam crest or over a sill. The discharge coefficients determined for a radial gate on a horizontal surface cannot be transferred to a

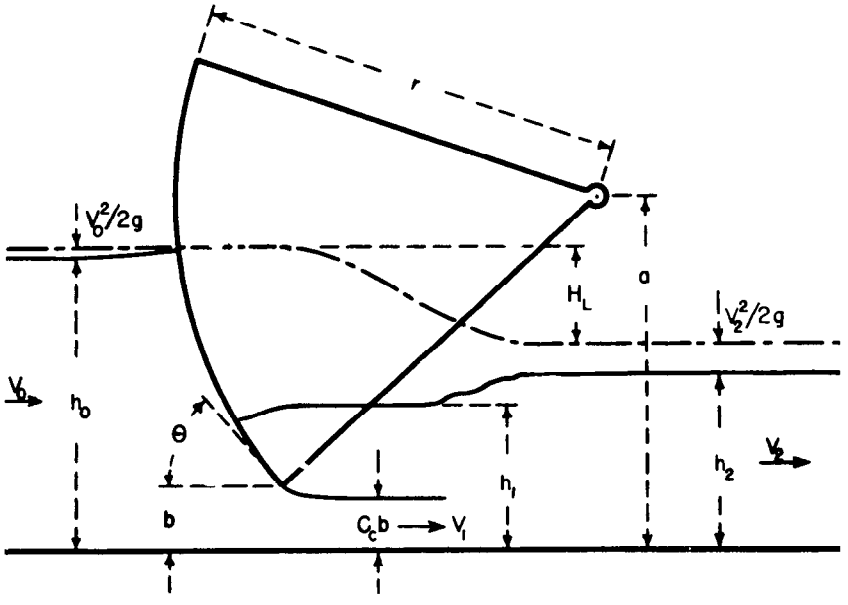

FIGURE 237.—Definition sketch of a radial gate on a horizontal surface. (After Toch, 1953.)

radial gate on a curved dam crest or sill because of differences in the pressure distribution. The flow under radial gates on a curved crest or sill is controlled by the geometry of three interrelated variables—the crest shape, the gate, and the gate setting. Major factors that influence the discharge relations are the position of the gate-seal point with respect to the highest point of the spillway crest and the curvature of the upstream face of the gate. Therefore, experimentally derived discharge coefficients for various prototype dams cannot be transferred to other installations unless the several variables involved are similar. Consequently, radial gates will invariably require rating by current-meter discharge measurements.

When radial gates control the flow over a sill or a curved dam crest, six flow regimes may occur, namely,

1. free orifice flow,
2. submerged orifice flow,
3. free weir flow,
4. submerged weir flow,
5. free flow over closed radial gate, and
6. submerged flow over closed radial gate.

Figure 241 is a definition sketch for the discussions that follow, all of which are concerned with only a single gate. As mentioned earlier in this discussion of movable gates, when discharge measurements for

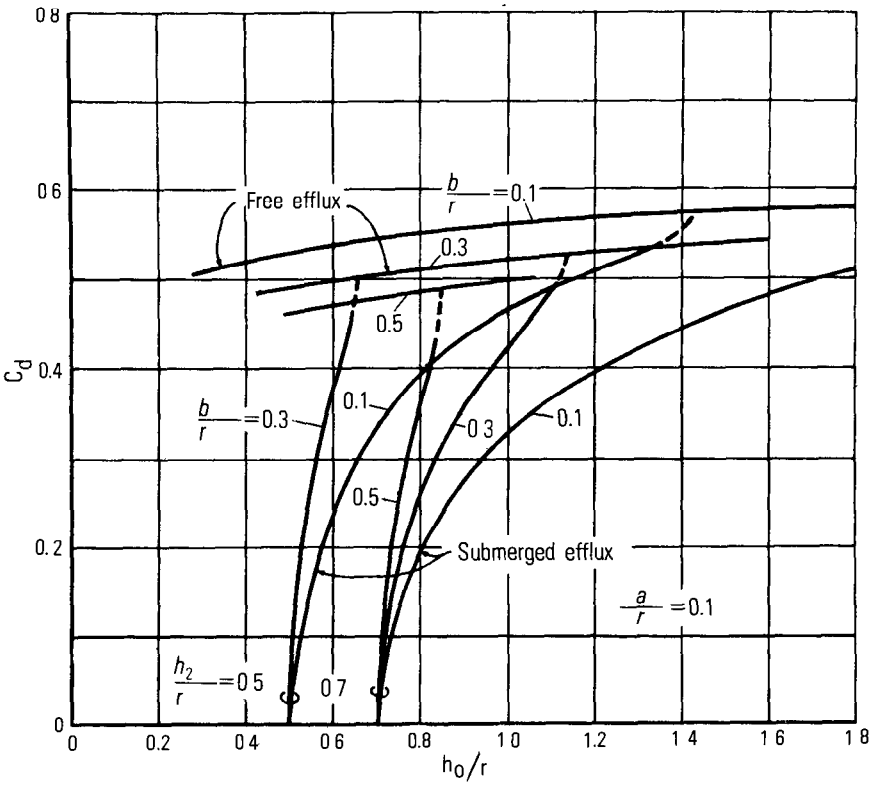

FIGURE 238.—Coefficient of discharge for free and submerged efflux, a/r = 0.1. (After Toch, 1953.)

calibration purposes are made with several gates open, it is highly desirable that all gate openings be identical, unless of course the gates are all raised sufficiently for their lower lips to be clear of the water. If gate openings are variable under the condition of orifice flow, it will be necessary to use an average gate opening in computing discharge coefficients for the gates from the measured discharge.

Free orifice flow.—Free orifice flow occurs when the lower lip of the raised gate is submerged by headwater but is above the elevation of tailwater. When the radial gate is on a sill, as in figure 241, free orifice flow occurs under the gate when h_g is less than $(2/3)h_1$, and h_3 is less than h_g. Discharge for that condition is computed from the equation,

$$Q = Ch_g b\ (2gh_1)^{1/2}, \tag{126}$$

where

Q = discharge for one gate,
c = discharge coefficient,

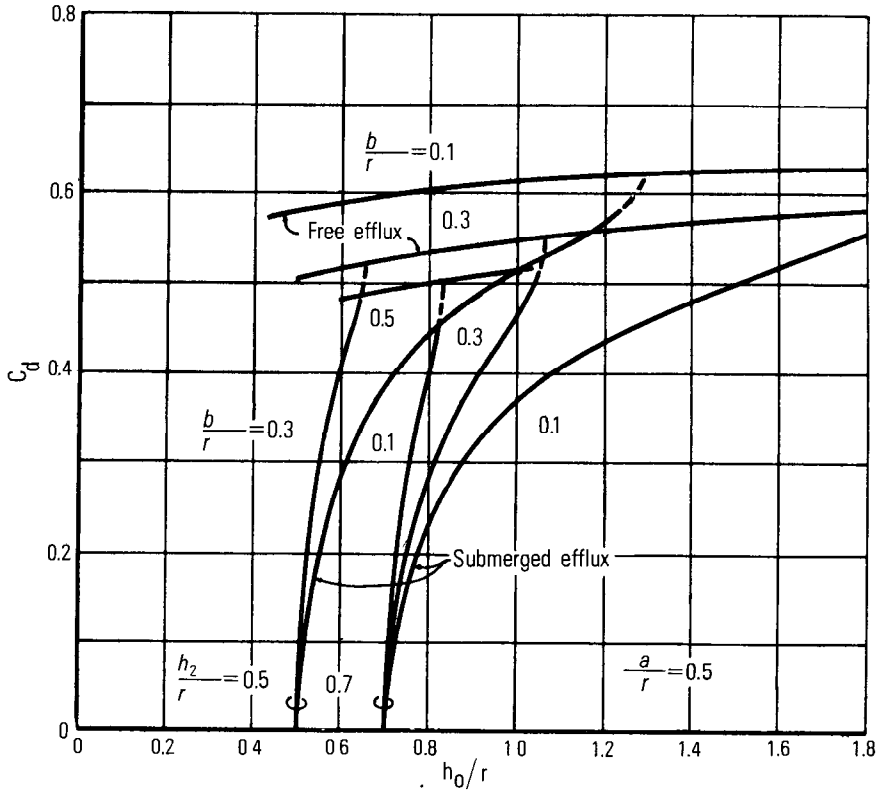

FIGURE 239.—Coefficient of discharge for free and submerged efflux, a/r = 0.5 (After Toch, 1953.)

b = lateral gate length (normal to flow), and
g = acceleration of gravity.

The remaining symbols in equation 126 are defined in figure 241. Values of C will vary inversely with h_a because the change in slope of the lower lip of the gate, as the gate is raised, progressively decreases the hydraulic efficiency of the orifice. There is also a tendency for C to increase with h_1, particularly at low stages, but that effect is usually minor compared to the effect of h_a. Consequently C can usually be related to h_a alone. In developing the relation, discharge measurements should be made throughout the expected range of h_a and h_1. Values of C are then plotted against h_g and the plotted points are fitted with a smooth curve. For convenience in later computations of discharge, the ordinates of the curve are put in tabular form.

The vertical gate opening, h_a, is computed from the following equation based on gate geometry and the position of the reference point at various gate settings:

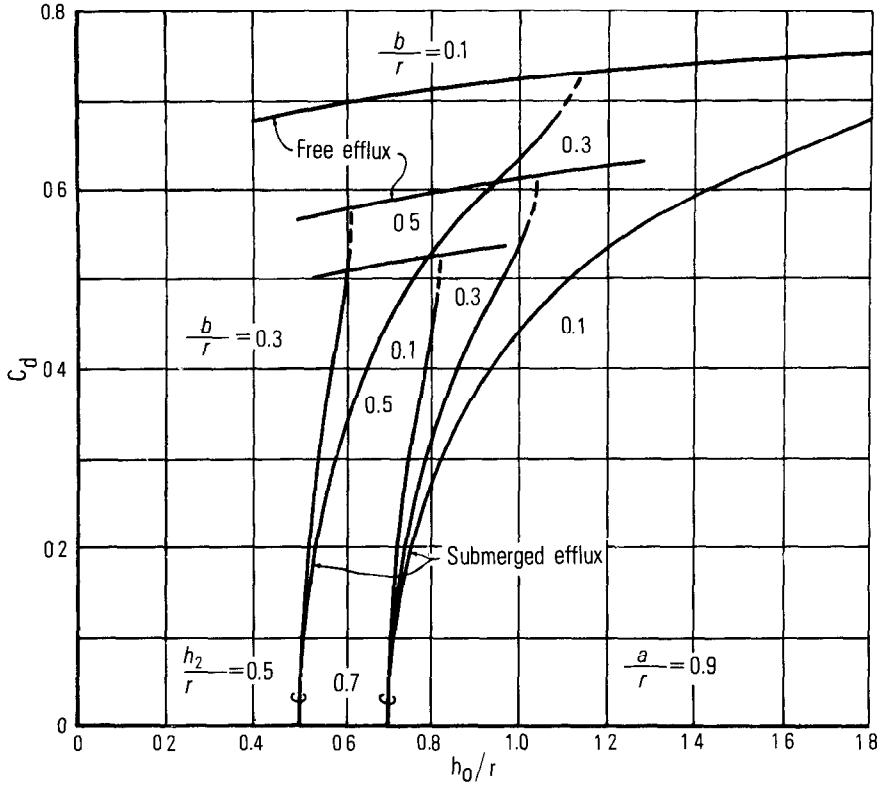

FIGURE 240.—Coefficient of discharge for free and submerged efflux, $a/r = 0.9$. (After Toch, 1953.)

$$h_u = R\cos\Theta\left(\frac{c-a}{r}\right) + a - R\sin\Theta\sqrt{1-\left(\frac{c-a}{r}\right)^2},$$

where

$$\Theta = \Phi_1 - \Phi_2 = \sin^{-1}\left(\frac{a}{R}\right) - \sin^{-1}\left(\frac{a-d}{r}\right).$$

Because C does not vary linearly with h_u it is highly desirable, and often necessary, that all gates be positioned identically during a discharge measurement to avoid the necessity of using an average value of h_u in the computation of C.

Submerged orifice flow.—Submerged orifice flow occurs when the lower lip of the raised gate is submerged by both headwater and tailwater. When the radial gate is on a sill, as in figure 241, submerged orifice flow occurs when h_3 is greater than h_u, and h_u is less than $(2/3)h_1$. The basic equation for computing discharge is

$$Q = C_u h_u b(2g\Delta h)^{1/2}, \qquad (127)$$

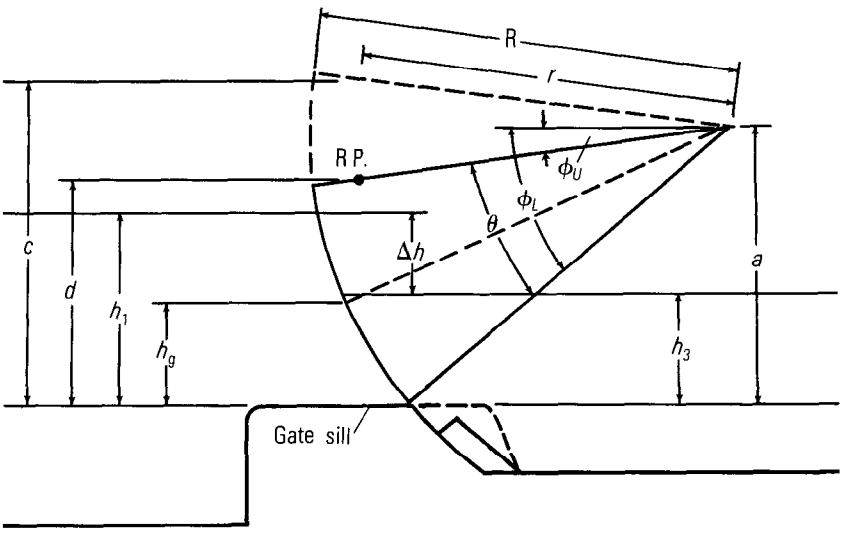

Definitions of symbols used in sketch are:

a = elevation difference, trunnion centerline to sill;
c = elevation difference, gate reference point (R.P.) to sill,
d = elevation difference, gate R.P to sill with the gate in a closed position;
h_1 = static headwater referenced to gate sill;
h_3 = static tailwater referenced to gate sill;
h_g = vertical gate opening,
r = radius from trunnion centerline to gate R.P.,
R = radius from trunnion centerline to upstream face of a Tainter gate;
R P = reference point used as indicator of gate position,
$\Delta h = h_1 - h_3$ = static head loss through structure;
θ = included angle between radial lines from the trunnion centerline through the R P. and through the lower lip of the gate,
ϕ_L = the angle measured from horizontal to the radial line from the trunnion centerline through the lower lip of the gate with the gate in a closed position, and
ϕ_U = the angle measured from horizontal to the radial line from the trunnion centerline through the gate R.P

FIGURE 241.—Definition sketch of a radial or Tainter gate on a sill

where C_{qs} is the coefficient of discharge for a submerged gate. The remaining symbols in equation 127 are defined either in figure 241 or in the preceding discussion of equation 126. Values of C_{qs} are determined from discharge measurements, and in addition, values of h_3/h_g and h_3/h_1 are computed for each measurement. For calibration purposes it is desirable to have measurements that cover the range of 1 to 100 for the ratio h_3/h_g, with several in the range of 1 to 2. The value of C_{qs} is a function of h_g, h_1, and h_3, and the complexity of that function

depends on the geometry of the hydraulic structure. The geometry may be such that all computed values of C_{gs} show little variation from a mean value, and when that occurs the mean value of C_{gs} is used in equation 127.

However, computed values of C_{gs} will often vary, particularly in the range of 1 to 2 for the ratio h_3/h_g. If that occurs, three relations involving C_{gs} are plotted graphically, and the one that best fits the plotted points is selected for use. The three relations are:

C_{gs} versus h_g,
C_{gs} versus h_3/h_1, and
C_{gs} versus h_3/h_g.

Quite often the last of the three relations will show the best fit. It will plot as a straight line on logarithmic graph paper and have the general equation,

$$C_{gs} = K(h_3/h_g)^B. \tag{128}$$

When equation 128 is substituted in equation 127, the result is

$$Q = K(h_3/h_g)^B h_g b(2g\Delta h)^{1/2}. \tag{129}$$

Ordinates of the relation indicated by equation 128 are put in tabular form for convenience in later computations of discharge. Because C_{gs} does not vary linearly with h_g, it is highly desirable, and often necessary, that all open gates be positioned identically during a discharge measurement to avoid the necessity of using an average value of h_g in the computation of C_{gs} from measured discharge.

Free weir flow.—Weir flow will occur when the lower lip of the gate is above the water surface. When the radial gate is on a sill, as in figure 241, weir flow will occur when h_g is greater than $(2/3)h_1$, because of drawdown of the water surface at the dam crest; the lower lip of the gate will then be above the water surface. Whether the weir flow is free or submerged will depend on the relative elevations of h_3 and h_1. Free weir flow will occur when the submergence ratio, h_3/h_1, is less than about 0.5–0.7, depending on the geometry of the weir crest. The discharge equation is,

$$Q = C_w b h_1^{3/2}, \tag{130}$$

where C_w is the coefficient of discharge for free weir flow. Values of C_w, which are dependent on the shape of the dam crest, are determined from discharge measurements, and the computed values are then plotted against h_1. Approach velocity head is usually negligible, but even where it is not, its effect is included in the variable coefficient, C_w. Measurements should be made at headwater (h_1) intervals of 1 to 2 feet throughout the expected headwater range to establish the functional relation between C_w and h_1. Information contained in a

previously cited report by Hulsing (1967) will usually be helpful as a guide to the probable shape of that relation.

Submerged weir flow.—As mentioned above, weir flow is submerged when the submergence ratio h_3/h_1 is greater than about 0.5–0.7, depending on the geometry of the weir crest. The discharge equation for that condition is

$$Q = C_w C_{ws} b h_1^{3/2}, \tag{131}$$

where C_w is the coefficient previously determined from equation 130. Values of C_{ws}, which is a submergence coefficient, must be determined from discharge measurements and expressed as a function of h_3/h_1. Satisfactory definition of the functional relation will probably require 10–12 discharge measurements well distributed over the range of h_3/h_1. Information contained in the Hulsing report (1967) will often be helpful in the analysis. If the submergence is greater than 0.95 for much of the time, it may be advisable to attempt to develop a relation of discharge to tailwater stage for use during periods of excessive submergence.

Flow over closed radial gate.—At extremely high flows, the closed radial gate may be overtopped, at which time the discharge over the gate is computed from the general weir equation,

$$Q = C b h^{3/2}, \tag{132}$$

where h is the head on the upper lip of the gate. The gate itself will act as a thin-plate weir. Values of the discharge coefficient C will vary primarily with the geometry of the gate and with h; the geometry of the dam crest or sill will have a lesser effect on the value of C. Discharge measurements will be required to define the rating for flow over the gate, both for unsubmerged flow (tailwater below the upper lip of the gate) and for submerged flow (tailwater above the upper lip of the gate).

Flow over a radial gate can also occur at low stages if the gate is of the submersible type. A submersible gate is designed to be lowered to allow flushing of upstream debris over the top of the gate. When so lowered, the bottom lip of the gate drops below the normal sill elevation. The upper surface of a submersible gate usually has an ogee or rounded crest.

Automated digital recording of elements for computing discharge.—To facilitate the computation of discharge, the Geological Survey has developed an automated digital system for the multiple recording of those elements that are required for discharge computation. The elements monitored are headwater, tailwater, and individual crest-gate positions. At navigation dams additional elements recorded include the number of lockages and, where supple-

mental hydroelectric power is produced, turbine pressure drops or commercial turbine monitor outputs. All of these elements are recorded on a digital recorder at preselected time intervals, usually hourly or bihourly. The recorded values of headwater, tailwater, and gate settings are the instantaneous values of those elements at the time of recording. The lockage count recorded is the number of lockages between the recordings. The turbine monitor integrates turbine pressure drops over the time interval between recordings.

All data at a site are recorded on paper punch tape in a preselected sequence by a master control console that queries the individual monitors in sequence. The punched tape is removed, usually once a month, and information from that tape is transferred to a magnetic tape. The magnetic tape is then used as input to a computer program for the computation of the streamflow record.

VERTICAL LIFT GATES

Vertical lift gates are simple rectangular gates of wood or steel spanning between piers on the dam crest. The gates move vertically in slots in the piers, and all but the smallest gates are mounted on rollers to reduce the friction caused by the hydrostatic force on the gate. The vertical lift gate, like the radial gate, must be hoisted at both ends, and the entire weight is suspended from the hoisting cables or chains (U.S. Army Corps of Engineers, 1952.) Piers must be extended to a considerable height above high water to provide guide slots for the gate in the fully raised position. To reduce the height of the piers required for operating large vertical lift gates, the large gates are often built in two horizontal sections, so that the upper section may be lifted and placed in another gate slot before raising the lower section. This design also reduces the load on the hoisting mechanism. Discharge may occur over either one or both sections of the gate or over the spillway crest. Discharge over the spillway crest may occur as weir flow if the gate is raised above the water surface, or as orifice flow if the raised gate does not clear the water surface.

The principles that govern the rating of radial gates likewise apply to vertical-lift gates. When the elevation of the lower edge of the raised gate is less than two-thirds of the upstream head, orifice flow occurs. The orifice flow is free if the tailwater is below the lower edge of the raised gate; the orifice flow is submerged if the tailwater is above the lower edge. General equations 126 and 127 apply to the discharge, and values of C and C_{qs} in those equations must be determined from discharge measurements.

If the elevation of the lower edge of a raised gate is greater than two-thirds of the upstream head, weir flow over the dam occurs. If the weir flow is free, equation 130 applies; if the elevation of the tailwater

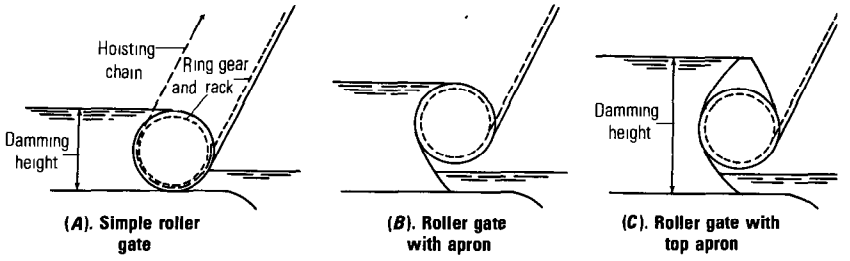

FIGURE 242.—Schematic sketches of roller gates. (U.S. Army Corps of Engineers, 1952.)

causes submergence effect, equation 131 applies. The coefficients in the two weir equations are primarily dependent on the shape of the weir crest. Values of the coefficients are determined from discharge measurements, but helpful information concerning them is found in a report by Hulsing (1967).

When a closed gate is overtopped by headwater, the upper edge of the gate acts as a weir and general equation 132 is applicable. The upper edge of a vertical-lift gate commonly has the shape of a modified horizontal broad-crested weir. Coefficients of discharge are determined from discharge measurements, but again, helpful information is to be found in the Hulsing report (1967).

ROLLER GATES

A roller (or rolling) gate (fig. 242) is a horizontal, internally braced, metal cylinder spanning between piers. Rings of gear teeth at the ends of the cylinder mesh with inclined metal racks supported by the piers, and when a pull is exerted on the hoisting cable or chain, the gate rolls up the rack (fig. 242*A*). The effective damming height of the cylinder can be increased by means of a projecting apron (fig. 242*B*) which rotates into contact with the dam crest as the gate rolls down the inclined racks (U.S. Army Corps of Engineers, 1952). A similar apron or rounded lip may be added to the top of the gate (fig. 242*C*).

As in the case of radial and vertical-lift gates, orifice flow will occur under partly raised rolling gates; weir flow over the dam will occur when the gates are raised sufficiently (⅔ or more of the headwater elevation) to be clear of the water surface, and weir flow over the gates will occur when the closed gates are overtopped by headwater. The principles of rating roller gates are similar to those discussed for radial gates and vertical-lift gates.

MOVABLE DAMS

A movable dam consists of a low concrete sill and a damming surface that can be raised above the water surface to maintain a desired

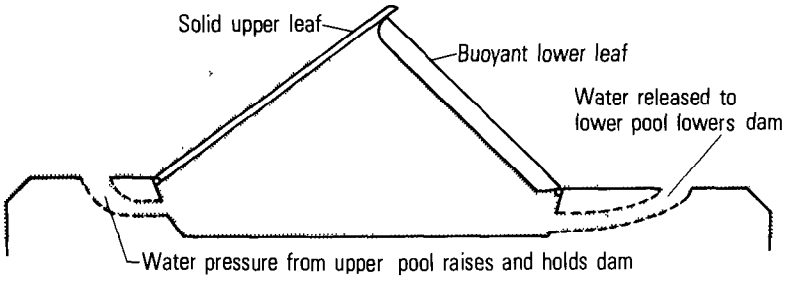

FIGURE 243.—Bear-trap gate. (U.S. Army Corps of Engineers, 1952.)

pool level, or lowered to the sill at higher discharges so as to offer no interference to the flow. The most commonly used gates or damming surfaces are bear-trap gates, hinged-leaf gates, wickets, and inflatable dams.

Bear-trap gate.—A bear-trap gate (fig. 243) consists of two leaves of timber or steel hinged and sealed to the dam or sill. When water is admitted to the space under the leaves, they are forced upward. The downstream leaf is hollow so that its buoyancy aids the lifting operation. When the dam is collapsed by the release of water from under the leaves, the leaves lie flat. (U.S. Army Corps of Engineers, 1952).

Hinged-leaf gate.—A hinged-leaf gate (fig. 244) is a rigid flat leaf hinged at bearings along its lower edge. In its raised position, the leaf slopes upward and downstream at an angle of between 20° and 30° from the vertical. When lowered, it lies approximately in a horizontal position. The position of the leaf is controlled by a mechanical hoist or by a counterweight device that causes the leaf to rise or fall automatically with slight incremental changes in headwater level.

Wickets.—A wicket is a shutter held in position against the water load by a metal prop (fig. 245*A*). It is not intended that water flow over the wicket at an appreciable depth, because the resultant water load will shift to a point above the prop and cause the wicket to overturn or vibrate violently (U.S. Army Corps of Engineers, 1952). The metal prop, hinged at midlength of the wicket, seats against a shoulder on a metal fixture ("hurter") embedded in the foundation. The wicket is raised by an upstream pull on a hoisting line attached to the bottom of the wicket. This causes the prop to fall into its seat after which the wicket is rotated into position against the sill (fig. 245*B*). The wicket is lowered by pulling upstream on a line attached to the top of the wicket; the base of the prop is pulled away from its seat and falls to one side into a groove in the hurter in which it can slide freely downstream. Wickets are raised and lowered by use of a boat operating on the upstream side of the dam. Figures 245*C* and

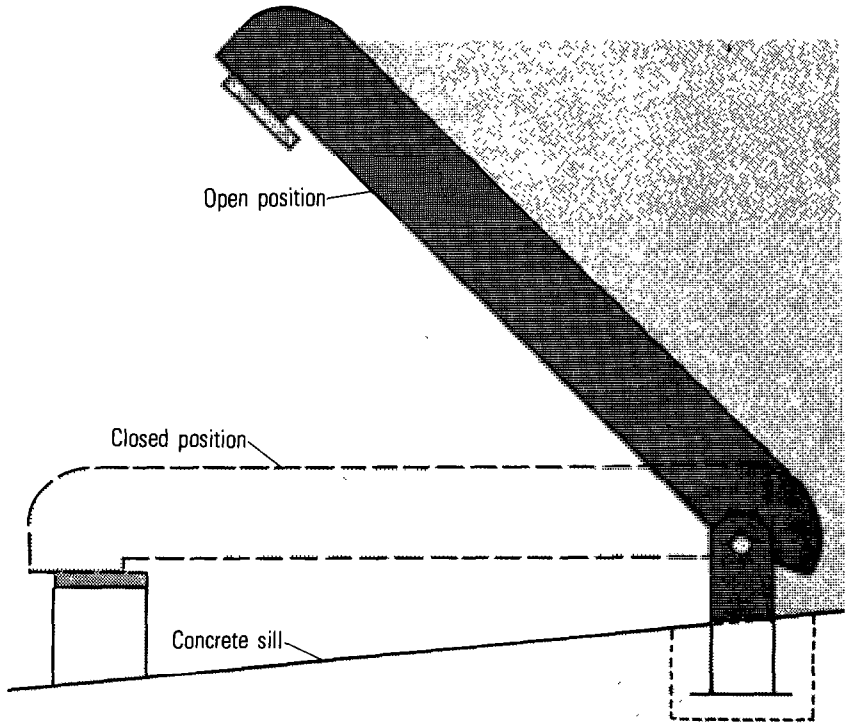

FIGURE 244.—Hinged-leaf gate.

245*D* show improved types of wickets. The Bebout wicket (fig. 245*D*) trips automatically to permit the passage of high flows.

Inflatable dams.—An inflatable dam, before activation, is a collapsed nylon-rubber bladder that occupies the full width of the stream and is attached to a concrete sill on the channel bottom. The dam is activated by pumping water into the bladder, thereby inflating it to form a barrier across the channel. The dam is deactivated by releasing water from inside the bladder. Inflatable dams are usually used on shallow streams to maintain a water level in the stream that is sufficiently high to submerge the intake of a diversion works. When the river stage is high, the dam is deflated. The inflation and deflation are often automatically controlled in response to the changing stage of the stream. Although it would probably be feasible to determine the rating for an inflatable dam by monitoring both the stream stage and the pressure within the dam bladder, inflatable dams have not been used as gaging-station controls. It is invariably simpler to operate a conventional gaging station on the stream either downstream from the inflatable dam or far enough upstream to be beyond the

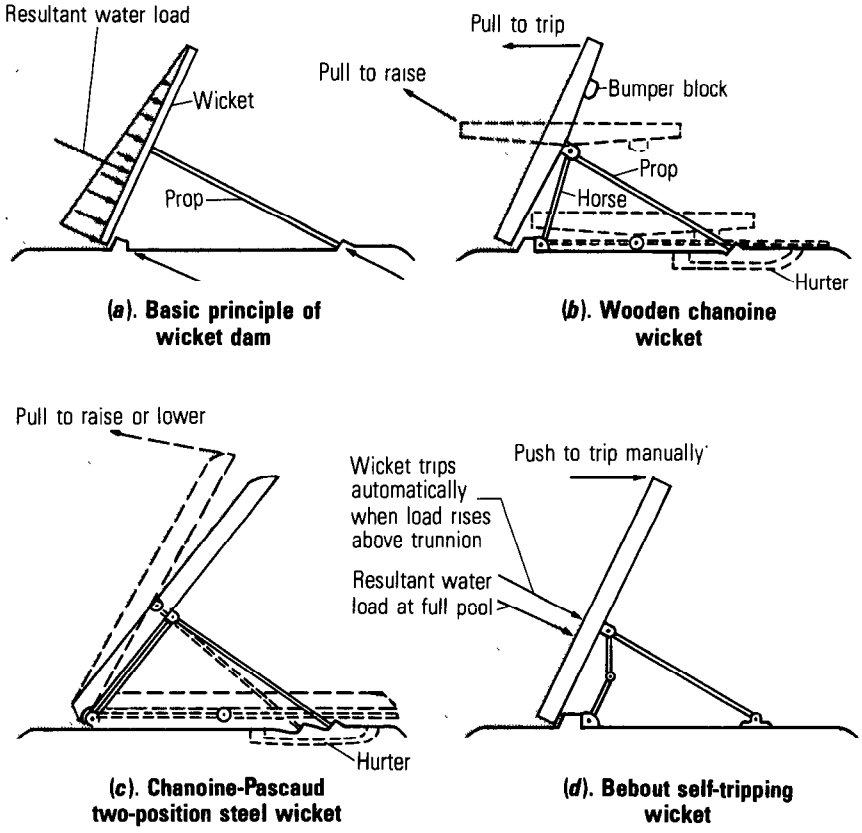

FIGURE 245.—Wickets. (U.S. Army Corp of Engineers, 1952.)

influence of backwater from the dam.

Discharge characteristics.—The discharge characteristics of bear-trap gates, hinged-leaf gates, and wickets are similar. In their lowered position they act as broad-crested weirs that control the stage-discharge relation over a limited range of low-water stage. The stage at which they become submerged depends primarily on the height of the sill on which they rest. Their discharge ratings in the lowered position will resemble that for a highway embankment (Hulsing, 1967, p. 26–27) whose general equation is

$$Q = CbH^{3/2}, \tag{133}$$

where

Q is discharge,
C is the coefficient of discharge,
b is the width normal to the flow, and
H is the total head.

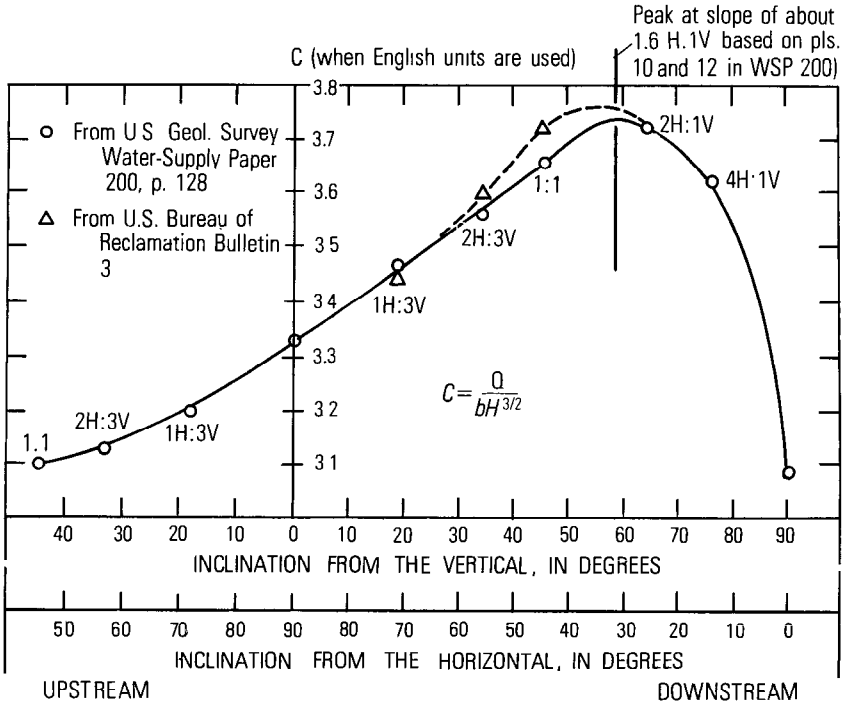

FIGURE 246.—Discharge coefficients for an inclined rectangular thin-plate weir.

The value of C will be dependent on the elevations of headwater and tailwater, the length of the crest in the direction of flow, and the geometry of the crest. For unsubmerged flow (tailwater $\leq$ 0.7 times headwater) C, when English units are used, can be expected to range from about 2.6 to 3.1, depending primarily on the ratio of static head (h) to length of sill in the direction of flow (L). For submerged flow, the free-flow value of C will be multiplied by a factor that ranges from almost zero to almost 1.00, depending on the degree of submergence.

When overtopped in their raised position by headwater, the three types of movable dam—bear-trap gate, hinged-leaf gate, and wickets—act as inclined thin-plate rectangular weirs. Figure 246 gives values of the discharge coefficient C in the general weir equation (eq. 133) for various angles of inclination of such weirs. If the upstream edge of the crest is rounded, the value of C may increase by 5–10 percent.

FLASHBOARDS

The usual flashboard installation consists of horizontal wooden panels supported by vertical pins placed on the crest of a spillway (fig. 247*A*). Such installations are temporary and are designed to fail

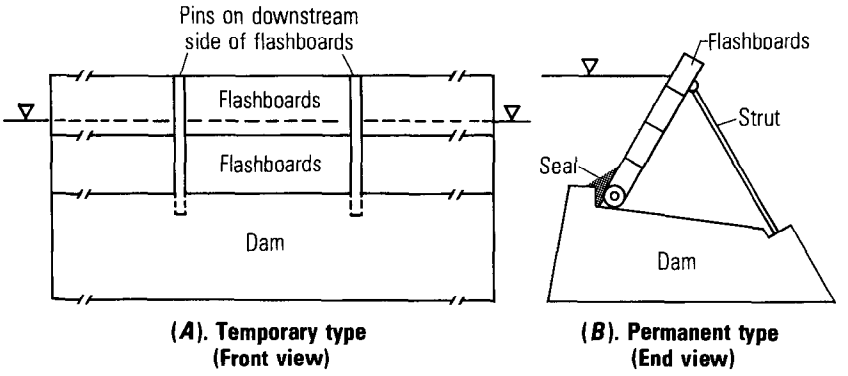

FIGURE 247.—Flashboards.

when the water surface in the reservoir reaches a predetermined level. A common design uses steel pipe or rod set loosely in sockets in the crest of the dam and designed to bend and release the flashboards at the desired water level. Temporary flashboards of this type have been used in heights up to 4 or 5 ft. Because temporary flashboards are lost each time the supports fail, permanent flashboards are more economical for large installations. Permanent flashboards usually consist of horizontal wooden panels that can be raised or lowered from an overhead cableway or bridge. The bottom edge of the panels is placed in a seat or hinge on the spillway crest, and the panels are supported in the raised position by struts (fig. 247*B*) or by attaching the top edge of the panels to the bridge.

To rate the vertical flashboards shown on figure 247*A*, a value of $C = 3.33$ (English units) is usually used in the general weir equation,

$$Q = CbH^{3/2} \tag{133}$$

As for the permanent flashboards in figure 247*B*, when the flashboards are lowered, the value of C that should be used is that for the free dam crest (no flashboards). The value of C to use when the flashboards are raised and supported by struts is determined from figure 248, which shows C values for various angles of inclination. If the raised flashboards are supported in an inclined position by a bridge so that the top edge of the flashboards is flush with the upstream edge of the bridge floor, we have in effect a flat-crested rectangular weir with inclined upstream face. The bridge floor acts as the flat weir crest and the flashboards act as the inclined upstream face of the weir. Discharge is computed by the use of equation 133; the value of C to be used in that equation can be obtained from figure 151 (chap. 10).

STOP LOGS AND NEEDLES

Stop logs consist of horizontal timbers, similar to flashboards, spanning between vertically slotted piers on the dam crest. The timbers may be inserted into, or removed, from the vertical slots by hand or with a hoist. There is usually considerable leakage between the timbers and considerable time may be required for their removal if they become jammed in the slots. Stop logs are ordinarily used only for small installations where the cost of more elaborate devices is not warranted or in situations where the removal or replacement of the stop logs is expected only at infrequent intervals.

Needles consist of timbers standing on end with their lower ends resting in a keyway in the spillway and their upper ends supported against the upstream edge of a bridge floor. Needles are easier to remove than stop logs but are difficult to place in flowing water. Consequently, they are used mainly for emergency bulkheads that are installed during periods of low flow.

The simple crest shape of stop logs and needles makes it easy to determine the theoretical value of the discharge coefficient C in the general weir equation 133. (See report by Hulsing (1967) on computing discharge over dams.) However, it is usually futile to rate stop logs or needles theoretically because of the appreciable leakage between them.

NAVIGATION LOCKS

Navigation locks are required for boat traffic to overcome the difference between headwater and tailwater elevations at a dam. The boat enters the open gate of the lock; the lock is closed behind the boat; valves are used for filling or emptying the locks, as the case may be, to bring the water level in the lock to that of the pool ahead of the boat; the other lock gate is opened and the boat proceeds on its journey. Various lock-filling and lock-emptying systems have been devised as a compromise between two conflicting demands: (1) that the filling time be short so as not to delay traffic, and (2) that the disturbances in the lock chamber not cause stresses in mooring hawsers which might cause the boat or barges to break loose and thereby damage either the boat or lock structure.

The flow through navigation locks is computed as the total volume of water released during a finite time interval, usually 1 day. The volume of water discharged for any one lockage is the product of the plan or water-surface area of the lock and the difference between headwater and tailwater at the time of lockage. These volumes are summed for the day and divided by 86,400, which is the number of seconds in a day, to obtain the average lockage flow in cubic feet per second or cubic meters per second. Usually it will be sufficiently accu-

rate to compute the daily average lockage discharge (Q_L) by use of the equation,

$$Q_L = \frac{N}{86{,}400} A(h_h - h_t), \tag{134}$$

where

N is the number of lockages in a day,
A is the plan or surface area of the lock,
h_h is the daily mean headwater elevation, and
h_t is the daily mean tailwater elevation.

If appreciable leakage through the lock occurs between boat lockages, the daily average leakage must be added to the daily average lockage discharge.

MEASUREMENT OF LEAKAGE THROUGH NAVIGATION LOCKS

If the leakage through the closed lock gates is great, it can be measured in the forebay with a low-velocity current meter. The leakage will seldom be that great, however, and it usually will have to be computed by a volumetric method.

If, for considerable periods of time between lockages, the lockmaster keeps the valves and lower gates closed and the upper gates open, leakage will occur through the lower gates, and it is that leakage (Q_{Lm}) that must be determined. If, instead, it is the valves and upper gates that are kept closed and the lower gates that are kept open, leakage will occur through the upper gates, and it is that leakage ($Q_{t\,m}$) that must be determined. If all valves and gates are kept closed, it is the equilibrium leakage (Q_{Le}) through the lower gate that must be determined.

Instructions for determining Q_{Lm}, $Q_{t\,m}$, and Q_{Le} follow. Figure 248 is a definition sketch of a lock.

FIELD WORK

1. Close upper and lower lock gates and open the valve to fill the lock chamber. When the lock chamber is filled, close the valve and open one upper gate slightly.

2. Attach the zero end of a steel tape by a small staple to the middle of a long plank. Float the plank in a lock chamber against the lock wall after first setting a reference mark on top of the wall for use as an index for reading the tape. A portable electric-tape gage (see section in chapter 4 titled, "Electric-Tape Gage") is even more satisfactory for reading stages in the lock chamber.

3. Record gage heights in the upper pool and lower pool and the tape reading in the lock chamber.

4. Close the upper gate. Read the tape immediately after the gate is fully closed and seated, and start a stop watch. Thereafter, read the

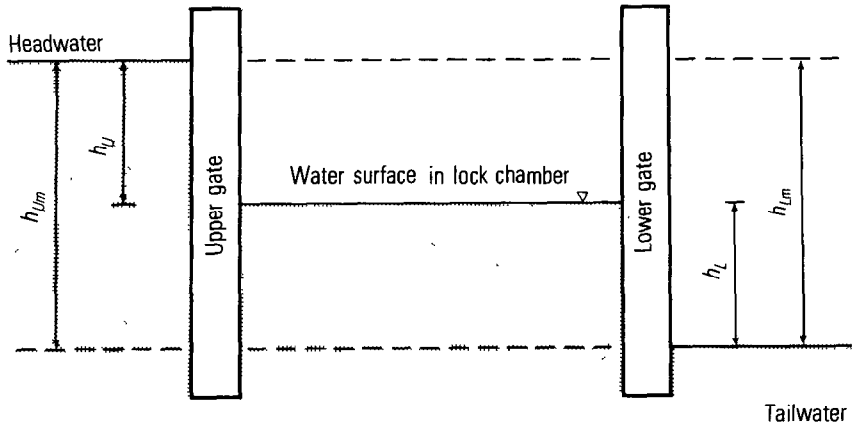

Definitions

$h_{Um}=h_{Lm}$	Maximum head on upper or lower gates for given headwater and tailwater stages
h_U	Head on upper gate
h_L	Head on lower gate
Q_U	Leakage through upper gate produced by h_U
Q_{Um}	Leakage through upper gate produced by h_{Um}
Q_L	Leakage through lower gate produced by h_L
Q_{Lm}	Leakage through lower gate produced by h_{Lm}
Q_n	Rate of storage in lock with both gates closed=Q_L-Q_U. (When Q_n is negative, the water level rises in lock chamber, when Q_n *is positive, the water level falls in lock chamber.)*
h_{Ue}	Equilibrium head on upper gate when $Q_U=Q_L$
h_{Le}	Equilibrium head on lower gate when $Q_U=Q_L$
Q_{Le}	Leakage through lower gate produced by h_{Le}

$$h_U+h_L=h_{Um}=h_{Lm}$$
$$h_{Ue}+h_{Le}=h_{Um}=h_{Lm}$$

FIGURE 248.—Definition sketch of a lock.

tape and stop watch at intervals of about 0.5 ft as stage decreases in the chamber, or at 1-minute intervals, whichever comes first. Continue for about 10 minutes.

5. Empty the lock chamber by opening the lower gate, and then partly close the lower gate; that is, leave one lower gate slighty open.

6. Record gage heights in the upper pool and lower pool, and the tape reading in the lock chamber.

7. Close the lower gate. Read the tape immediately after the gate is fully closed and seated and start a stopwatch. Thereafter read the tape and stopwatch at intervals of about 0.5 foot as stage increases in the chamber, or at 1-minute intervals, whichever comes first. Continue for about 10 minutes.

8. Obtain dimensions of the lock chamber for use in computing

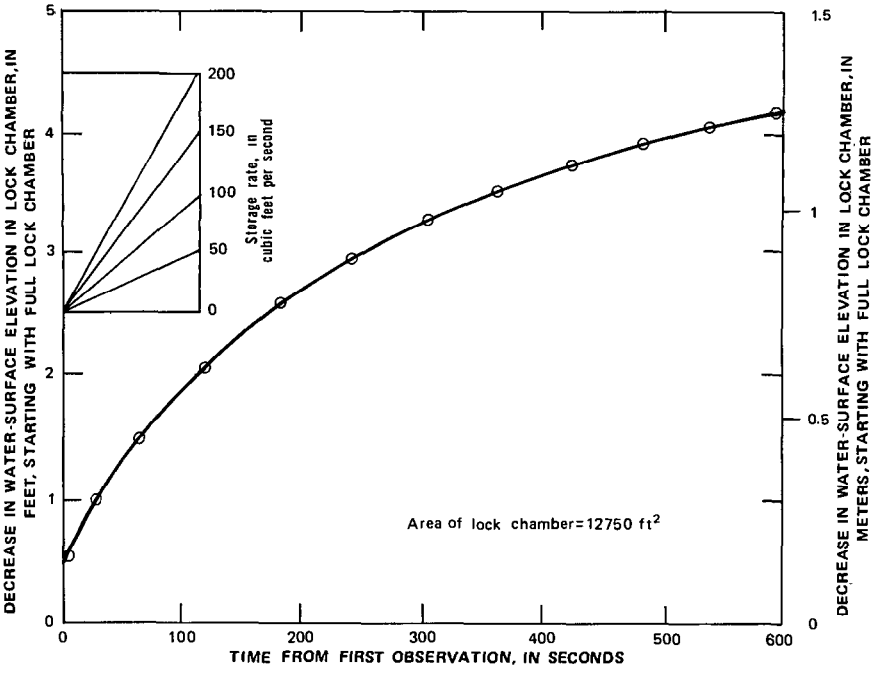

FIGURE 249.—Storage diagram starting with lock chamber full.

volumes of water involved in the leakage. That completes the field work.

COMPUTATIONS FOR Q_{Lm}

1. Use readings obtained when observations were started with a full lock chamber. Subtract initial tape reading (made with upper gate open slightly) from all tape readings.

2. Plot adjusted tape readings from step 1 against time in seconds. The first reading made after the upper gate was fully closed is plotted at zero seconds. Too much uncertainty usually exists as to when the gate actually seated to use the closure of the gate as the starting time for the graph. See figure 249. The plot should be made on a large sheet of graph paper.

3. Connect the plotted points with a smooth curve. A tangent to the curve at any value of the abscissa represents the rate of change of water-surface elevation at that instant. The rate of change multiplied by the surface area of the lock chamber gives the instantaneous rate of storage in the lock chamber; that is, the difference in rate of leakage out of the chamber through the lower gate and rate of leakage into the chamber through the upper gate.

At the instant the upper gate is closed, the leakage out of the chamber is at its maximum, Q_{Lm} (full head on the lower gate), and the

leakage into the chamber is zero (zero head on the upper gate). As the stage in the chamber falls, the leakage out of the chamber decreases because of the decreased head on the lower gate, and leakage into the chamber increases because of the increased head on the upper gate. Eventually leakage into the lock would equal the leakage out of the lock (Q_{Le}), and the stage in the chamber would remain constant.

4. In order to obtain the rate of storage at any instant from the tangent of the curve showing the decrease in lock stage with time, construct a diagram showing the storage rate (Q_n) for various tangential slopes.

The method of constructing the diagram is demonstrated in figure 249. The area of the lock chamber is 12,750 ft^2. If the stage in the chamber dropped 2 feet, the change in volume would be 2 × 12,750 or 25,500 ft^3. If Q_n were 200 ft^3/s, the time required for a 2 ft drop would be 127.5 seconds. A vertical line is drawn at 127.5 seconds on figure 249 and a diagonal line having a drop of 2 ft is drawn between the abscissa values of 0 and 127.5 seconds. A tangent to the storage curve having a similar slope would have a Q_n value of 200 ft^3/s. Diagonals representing other values of Q_n are added as shown.

5. Select two points on the storage curve, one near the origin (0 seconds) and the other no more than 1 ft lower in stage. Draw tangents to those points and use the slopes of those tangents with the tangential rate diagram to obtain the two values of Q_n. To obtain the tangential slope at a point on the curve, use a pair of dividers to lay off short equal distances on the curve on each side of the selected point. A chord connecting the equidistance points will have a slope approximately equal to that of the tangent.

6. The two values of Q_n obtained in the preceding step will be used to compute Q_{Lm}. No further use will be made of the leakage curve, except that it has value for making a rough check on the basic assumption that will be made in the computations that follow. That assumption is that the leakage through a gate can be treated as though it all occurred at an orifice at the bottom of the gate. In other words,

$$\frac{Q_L}{Q_{Lm}} = \left(\frac{h_L}{h_{Lm}}\right)^{1/2} \quad \text{and} \quad \frac{Q_{L'}}{Q_{L'm}} = \left(\frac{h_{L'}}{h_{L'm}}\right)^{1/2}$$

or

$$Q_L = Q_{Lm}\left(\frac{h_L}{h_{Lm}}\right)^{1/2} \quad \text{and} \quad Q_{L'} = Q_{L'm}\left(\frac{h_{L'}}{h_{L'm}}\right)^{1/2} \tag{135}$$

7. From figure 248 and equation 135.

$Q_n = Q_L - Q_l$

or
$$Q_n = Q_{Lm}\left(\frac{h_L}{h_{Lm}}\right)^{1/2} - Q_{Um}\left(\frac{h_U}{h_{Um}}\right)^{1/2} \tag{136}$$

For each of the two values of Q_n, all values in equation 136 are known, except for the values of Q_{Lm} and Q_{Um}. The known values can be substituted in equation 136 to give two simultaneous equations, which can then be solved for the desired value of Q_{Lm}.

8. In the preceding step, it would be a simple matter to solve for Q_{tm}, but we do not do so. Our basic assumption of orifice flow may not be strictly correct, and experience has shown that the desired value of Q_{tm} can be computed with much more accuracy by using the field data obtained when observations of leakage were started with an empty lock chamber.

9. Obtain values of leakage through the lower gate when the upper gate is open, for other values of total head. Use the following equation:
$$Q'_{Lm} = Q_{Lm}\left(\frac{h'_{Lm}}{h_{Lm}}\right)^{1/2} \tag{137}$$

where Q_{Lm} and h_{Lm} are values obtained from a leakage test as described above, and Q'_{Lm} is the leakage through the lower gate corresponding to any other value of total head, h'_{Lm}.

10. Prepare a rating table of Q_{Lm} versus h_{Lm}.

COMPUTATIONS FOR Q_{tm}

1. Use readings obtained when observations were started with an empty lock chamber. Subtract initial tape reading (made with lower gate slightly open) from all tape readings.

2. Plot adjusted tape readings from step 1 against time in seconds.

3. Proceed with computations in a manner analogous to that used in the computation of Q_{Lm}.

4. Obtain Q_n for two points on the leakage curve, one near the origin (0 seconds) and the other no more than 1 ft higher in stage.

5. Use equation 136 to solve for the desired value of Q_{tm}.

6. Obtain values of leakage through the upper gate when the lower gate is open, for other values of total head. Use the following equation:
$$Q'_{Um} = Q_{Um}\left(\frac{h'_{Um}}{h_{Um}}\right)^{1/2}, \tag{138}$$

where Q_{tm} and h_{tm} are values obtained from a leakage test as described above, and Q'_{tm} is the leakage through the upper gate corresponding to any other value of total head h'_{tm}.

7. Prepare a rating table of Q_{Um} versus h_{Um}.

COMPUTATIONS FOR Q_{Le}

1. Q_{Le} is the leakage through the lower gate when equilibrium exists; that is, the stage in the lock chamber is constant because $Q_U = Q_L$.

2. Starting with the equation, $Q_{Ue} = Q_{Le}$, it is a simple matter to transform the equation to

$$h_{Le} = h_{Lm} \Big/ \left[(Q^2_{Lm} / Q^2_{Um}) + 1 \right] \tag{139}$$

All values on the right-hand side of equation 139 are known because in preceding steps Q_{Lm} and Q_{Um} had been computed. Solve for h_{Le}.

3. Obtain the desired value of Q_{Le} from the equation

$$Q_{Le} = Q_{Lm} \left(\frac{h_{Le}}{h_{Lm}} \right)^{1/2}. \tag{140}$$

4. Use the rating tables for Q_{Lm} and Q_{Um} with equations 139 and 140, to prepare a rating table of Q_{Le} versus h_{Lm}.

PRESSURE CONDUITS

GENERAL

In one respect, the gaging of a pressure conduit is simple in that the cross-sectional area is constant for all discharges. The calibration of the metering device offers difficulty, however, because the discharge measurements require special instrumentation unless they can be made by current meter in the forebay or afterbay of the conduit where open-channel conditions exist.

The following are the metering devices used for pressure conduits:

1. Mechanical meters
   - a. Displacement meter
   - b. Inferential meter
   - c. Variable-area meter
2. Differential-head meters
   - a. Constriction meters
     - (1) Venturi meter
     - (2) Flow nozzle
     - (3) Orifice meter
   - b. Bend meter
   - c. Pressure differential in a reach of unaltered conduit
3. Electromagnetic velocity meter
4. Acoustic velocity meter
5. Laser flowmeter.

Changes in the rating of mechanical meters occur only as a result of wear on the moving parts of the meter. Changes in the rating of differential-head meters that are kept clean occur only as a result of changes in perimeter roughness of the conduit with time. The electromagnetic, acoustic, and laser velocity meters are complex electronic devices, and as such, they are subject to the occasional calibration drift that for various reasons affect such devices.

The various meters must be calibrated when first installed, and the calibration must be periodically checked thereafter. Methods of measuring discharge for that purpose include:

1. pitot-static tubes and pitometers,
2. salt-velocity method, and
3. Gibson method.

This section of the manual closes with a brief discussion of discharge ratings for turbines, pumps, gates, and valves, all of which are associated with pressure conduits.

METERING DEVICES FOR PRESSURE-CONDUIT FLOW

MECHANICAL METERS

Mechanical meters are widely used in water-distribution systems because of their low cost and small size, but they can only be used to measure a relatively narrow range of discharge. They are not suited for the measurement of very low flow rates because the liquid may pass the meter without moving the mechanical elements; they are seldom used to measure discharges greater than 10 ft^3/s (0.28 m^3/s) because of high head loss. A large variety of mechanical meters are commercially available, but only the three general types—displacement, inferential, and variable-area—will be described here (Howe, 1950, p. 210–212).

Displacement meters.—An elementary form of displacement meter consists of a single or multiple piston arrangement in which fluid passing through the meter moves a piston back and forth. The movement of the piston is readily registered upon a counting device calibrated in any desired units to give total volume of flow. Such meters can have a fairly large capacity and are accurate if no slippage occurs.

Another commonly used displacement meter is the disk meter which oscillates in a measuring chamber; for each oscillation a known volume of water passes the meter. The motion of the disk operates a gear train which in turn activates a counting mechanism, thereby furnishing a measure of the total volume of flow. When the disk is new, the meter is accurate to within 1 percent, but the meter may underregister significantly as the disk becomes worn.

Inferential meters.—Inferential meters are in effect small turbines and are called "inferential" because the rate of flow is inferred from

the speed of rotation of the propeller. An essential element of such meters is a set of guide vanes which may be adjusted to change the calibration of the meter. However, the calibration may inadvertently change if the surface of the propellor blades becomes worn or coated. Although inferential meters normally register only volume of flow, equipment may be added to the meter to indicate instantaneous rate of discharge.

Variable-area meter.—The variable-area meter consists of a vertical tapered tube containing a small plunger "float." In some instruments the plunger is completely immersed in a transparent, graduated tube; in others, a stem projects through the end of the conical tube and traverses a scale. In both types the plunger rises as the rate of flow increases, thereby increasing the area around it. By calibration, the position of the plunger can be related to the rate of flow. These instruments are restricted to the measurement of rather small discharges and will not accommodate any great change in viscosity without recalibration. Accuracy within 1 percent is possible.

DIFFERENTIAL-HEAD METERS

The flow of fluid through a constriction in a pressure conduit results in a lowering of pressure at the constriction. The drop in piezometric head in the reach between the undisturbed flow and the constriction is a function of the flow rate. The venturi meter, flow nozzle, and orifice meter (fig. 250) are constriction meters that make use of this principle. The difference in piezometric head may be measured with a differential manometer or pressure gages. In order that such an installation may function properly, a straight length of pipe at least 10 diameters long should precede the meter. Straightening vanes may also be installed in the conduit just upstream from the meter to suppress disturbances in the flow.

Venturi meters.—Venturi meters (fig. 250*A*) are highly accurate and efficient flow meters; they have no moving parts, require little maintenance, and cause little head loss (U.S. Bureau of Reclamation, 1971). They operate on the principle that flow in a given closed-conduit system moves more rapidly through areas of small cross section (D_2 in fig. 250*A*) than through areas of large cross section (D_1 in fig. 250*A*). The total energy in the flow, consisting primarily of velocity head and pressure head, is virtually the same at D_1 and D_2 within the meter. Thus the pressure must decrease in the constricted throat, D_2, where the velocity is higher; and conversely the pressure must be greater at D_1, upstream from the throat, where the velocity is lower. This reduction in pressure from the meter entrance to the meter throat is directly related to the rate of flow passing through the meter and is the measurement used to determine flow rate. Tables or dia-

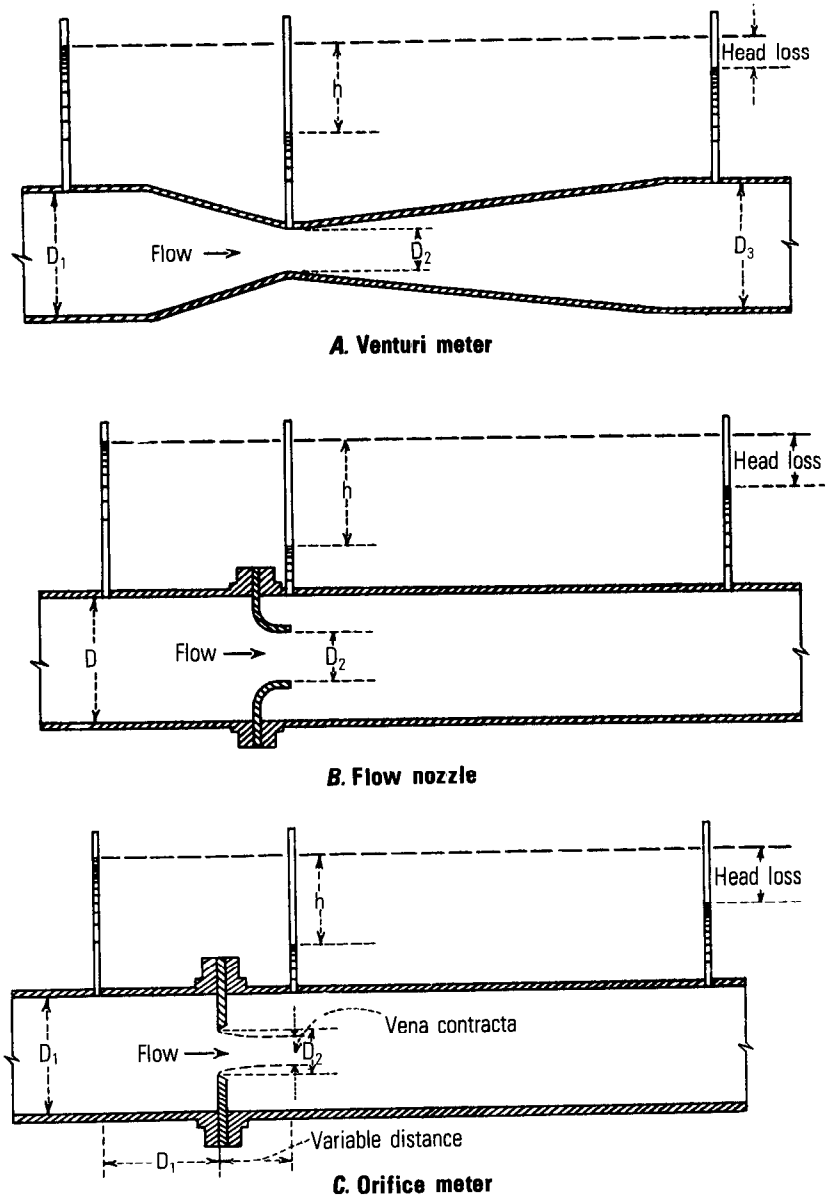

FIGURE 250.—Three types of constriction meter for pipe flow. (Courtesy of U.S. Bureau of Reclamation.)

grams of this head differential versus rate of flow may be prepared, and flow indicators or flow recorders may be used to display the differential or the rate of flow.

The relation of rate of flow, or discharge, to the head and dimensions of the meter is

$$Q = \frac{CA_2\sqrt{2gh}}{\sqrt{1 - r^4}}, \tag{141}$$

where

A_2 = cross-sectional area of the throat, in square feet,
h = difference in pressure head between upstream pressure-measurement section and the downstream pressure-measurement section, in feet,
g = 32.2 feet per second per second,
r = ratio of the throat diameter to pipe diameter = D_2/D_1, and
C = coefficient of discharge for the venturi meter.

The coefficient of discharge for the venturi meter varies with a Reynolds number that is based on the diameter and velocity at the throat and on the kinematic viscosity of the water; the kinematic viscosity of the water is in turn a function of the water temperature. The formula for computing the Reynolds number is

$$R = \frac{V_2 D_2}{\nu}, \tag{142}$$

where

R = Reynolds number (dimensionless),
V_2 = mean velocity in the throat (ft/s),
D_2 = throat diameter (ft), and
ν = kinematic viscosity (ft^2/s).

Table 27 gives values of kinematic viscosity corresponding to selected

TABLE 27.—*Values of kinematic viscosity corresponding to selected water temperatures*

[From American Society of Civil Engineers (1942, p 60)]

Water temperature (°F)	Kinematic viscosity ($\nu \times 10^5$) (ft^2/s)
32	1.931
40	1.664
50	1.410
60	1.217
70	1.059
80	.930
90	.826
100	.739
110	.667
120	.609
130	.558
140	.514
150	.476
160	.442
170	.413
180	.385
190	.362
200	.341
212	319

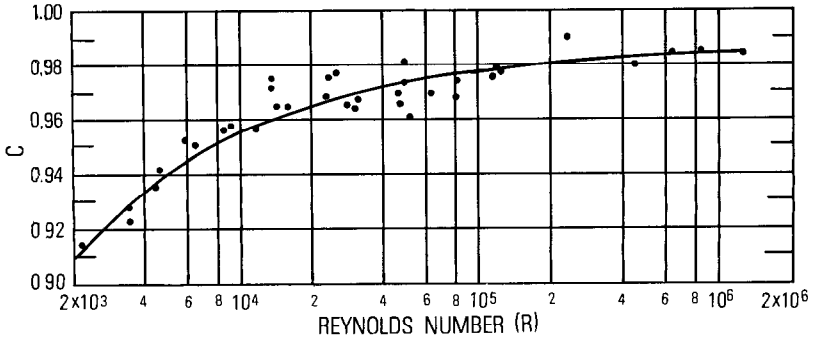

FIGURE 251.—Discharge coefficients for venturi meters as related to Reynolds number. (After Howe, 1950. Reprinted by permission of John Wiley & Sons, Inc.)

water temperatures. Figure 251 shows values of the discharge coefficient for venturi meters as related to the Reynolds number. Figure 251 is based on discharge data for meters having a diameter ratio (r) equal to 0.5, and although the discharge coefficient will vary slightly with the geometry of the venturi meter, the relation shown in the figure is considered accurate to within 1 percent for meters that are carefully maintained.

Flow nozzles.—Flow nozzles operate on the same basic principle as venturi meters. In effect, the flow nozzle is a venturi meter that has been simplified and shortened by omitting the long diffuser on the outlet side (fig. 250*B*). The streamlined entrance of the nozzle provides a straight cylindrical jet without contraction, so that the coefficient is similar, in considerable degree, to that for the venturi meter. In the flow nozzle, the jet is allowed to expand of its own accord, and the high degree of turbulence created downstream from the nozzle causes a greater loss of head than occurs in the venturi meter where the long diffuser suppresses turbulence.

The relation of rate of flow to the head and dimensions of the flow nozzle is

$$Q = \frac{CA_2\sqrt{2gh}}{\sqrt{1 - r^4}}, \tag{141a}$$

which is identical with equation (141) given above for the venturi meter. The symbols have the same meaning in both equations, except that C in equation 141a is the coefficient of discharge for the flow nozzle.

Specifications for the manufacture and installation of flow nozzles vary, and extensive research on the various types has resulted in the accumulation of a large body of data on discharge coefficients. Space limitations preclude detailed discussion of those coefficients, but it

may be stated that for the more popular types of design and in the usual range of operation the coefficients generally range from 0.96 to 0.99; for any type of flow nozzle, the discharge coefficients increase with Reynolds number and tend to become constant at Reynolds numbers greater than 10^6. A recommended source of data on discharge coefficients is a report of the American Society of Mechanical Engineers (1937).

The upstream pressure connection for measuring head is frequently made through a hole in the wall of the conduit at a distance of about 1 pipe diameter upstream from the starting point of the flare of the nozzle. The pressure observed is that of the stream before it has begun to turn inward in response to the inlet curvature of the nozzle. The downstream pressure connection may be made through the pipe wall opposite the end of the nozzle throat.

Orifice meters.—A thin-plate orifice inserted across a pipeline can be used for measuring flow in much the same manner as a flow nozzle (fig. 250*C*). The upstream pressure connection is often located at a distance of about 1 pipe diameter upstream from the orifice plate. The pressure of the jet ranges from a minimum at the vena contracta—the smallest cross section of the jet—to a maximum at about 4 or 5 conduit diameters downstream from the orifice plate. The downstream pressure connection—the center connection shown in figure 250*C*—is usually made at the vena contracta to obtain a large pressure differential across the orifice. The location of the vena contracta may be determined from data provided in standard hydraulic handbooks.

The relation of rate of flow to the head and dimensions of the metering section is

$$Q = \frac{CA_2\sqrt{2gh}}{\sqrt{1 - r^4}}, \tag{141b}$$

which is identical with equations 141 and 141a except that C in equation 141b is the coefficient of discharge for the orifice meter.

For pressure taps located 1 pipe diameter upstream from the orifice plate and at the vena contracta, the coefficient of discharge ranges from 0.599 for an r value of 0.20 to 0.620 for an r of 0.71, when the Reynolds number exceeds 2×10^5. The principal disadvantage of orifice meters, as compared to venturi meters or flow nozzles, is their greater loss of head. On the other hand, they are inexpensive and are capable of producing accurate flow measurements.

Bend meters.—Another type of differential head meter is the bend meter, which utilizes the pressure difference between the inside and outside of a pipe bend. The meter is simple and inexpensive. An elbow already in the line may be used without causing added head loss. For

best results a bend meter should be calibrated in place. The meter equation is

$$Q = CA\sqrt{2gh}\,, \tag{143}$$

where C is the coefficient of discharge, h is the difference in piezometric head between the outside and inside of the bend at the midsection, and A is the cross-sectional area of the pipe. For best results it is recommended that the lengths of straight pipe upstream and downstream from the bend be equal to at least 25 pipe diameters and 10 pipe diameters, respectively.

Lansford (1936) experimented with 90° bends, and he concluded that if calibration of a 90° bend is not feasible, results at moderate to high Reynolds numbers that are accurate to within 10 percent can be obtained from a simple formula for C, in which

$$C = \sqrt{r/(2D)}\,. \tag{143a}$$

In equation 143a, D is the pipe diameter and r is the centerline radius of the bend.

Pressure differential in a reach of unaltered conduit.—If a pressure-conduit system has high velocities and low pressures, it may not be practical to install a venturi meter in the line because cavitation will occur in the throat along with excessive vibration. In that situation the installation of a manometer between two piezometer taps in the conduit, several hundred feet apart, may be the most feasible method of metering the flow. One but preferably two discharge measurements would suffice to rate the manometer, and a third measurement could be made to check the rating equation which is,

$$Q = K\sqrt{\Delta h}\,, \tag{144}$$

where

Q = discharge,
K = a constant, and
Δh = head differential.

If two discharge measurements are used in the initial calibration, the two computed K values, which should agree closely, are averaged.

In the case of reaction turbines, the discharge may be metered by a manometer that measures the pressure drop in the scroll case. The scroll case of a reaction turbine has a decreasing diameter, being largest at its upstream end where it is joined to the penstock. A set of piezometer taps is installed at each end of the scroll case forming, in effect, a type of venturi section. Discharge is computed by use of equation 144, K being determined from discharge measurements, preferably made over the complete range of output, and simultaneous observations of the pressure drop. The calibration should remain constant as long as the turbine efficiency does not change.

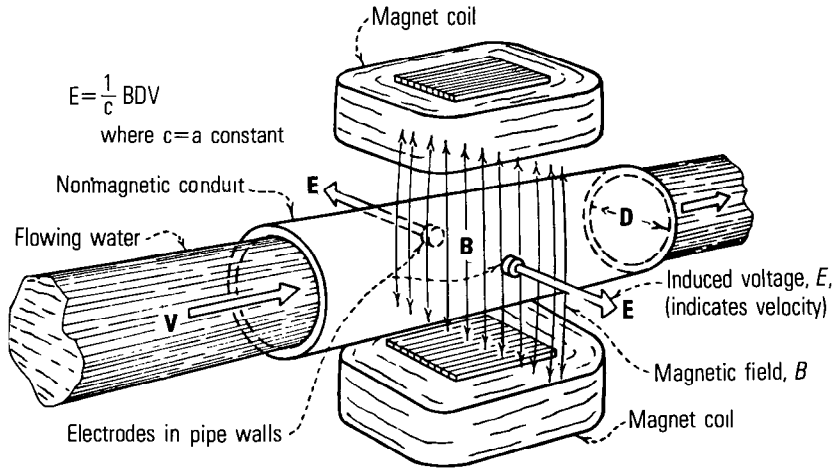

FIGURE 252.—Schematic view of one type of electromagnetic velocity meter. (Courtesy of U.S. Bureau of Reclamation.)

Summary.—Differential-head meters are very satisfactory metering devices as long as they are kept clean and the velocities in the conduit are high enough to give significant pressure differentials between the two piezometer taps.

ELECTROMAGNETIC VELOCITY METER

Electromagnetic velocity meters for measuring flow in pressure conduits are commercially available. The principle of the electromagnetic velocity meter was explained in the section in chapter 12 titled, "Electromagnetic Velocity-Meter Method"; but to repeat briefly, when a fluid which is an electric conductor moves across a magnetic field at 90°, as shown in figure 252, an electromotive force is produced in the fluid at right angles to both the flux of the magnetic field and the velocity of the fluid. The induced voltage is proportional to the average velocity of the fluid, V. If the pipe is a conductor, as it usually will be, an insulating liner must be installed in the metering section and the probes must contact the water. Two or more discharge measurements are required to calibrate the meter.

ACOUSTIC VELOCITY METER

Acoustic velocity meters for measuring flow in pressure conduits are commercially available. The principle of the acoustic velocity meter was explained in the section in Chapter 12 titled, "Acoustic Velocity-Meter Method," and will not be discussed further other than to state that better results are obtained with the transducers of the meter in direct contact with the fluid stream than are obtained with the transducers mounted on the outside of the conduit walls

(Schuster, 1975). The acoustic velocity meter should be calibrated by discharge measurements.

LASER FLOWMETER

Laser (light amplification by stimulated emission radiation) beams have been used for studying the turbulent characteristics of flowing liquids and for determining the velocity of fluid flow (Schuster, 1970). The Doppler principle, which involves a measurable shift in the frequency of the light rays under the influence of an external velocity imposed on the system, underlies the operation of the laser flowmeter. The flowing water scatters part of a beam of light (laser) directed through it. By comparing the frequencies of the scattered and unscattered rays, collected in receiving lenses on the opposite side of the stream, the velocity of the water (hence the discharge) can be calculated. In laboratory experiments, the instrument has measured fluid flows as slow as a fraction of an inch per second and as fast as 1,000 or more feet per second. The device is a valuable research tool, but it should also be considered a possible future device for measuring discharge in both open channels and pressure conduits.

DISCHARGE-MEASUREMENT METHODS FOR METER CALIBRATION

MEASUREMENT OF DISCHARGE BY PITOT-STATIC TUBES AND PITOMETERS

Pitot-static tubes and pitometers may be classed as differential-head meters, but they are seldom used for continuous-flow measurement. Instead, they are usually used for calibrating other metering devices in place and for intermittent measurements. Pitot tubes and pitometers indicate the velocity head at a point in the conduit cross section.

The operation of pitot-static tubes or pitometers is based on the principle that the increase in head at the mouth of a bent tube facing upstream is a measure of the velocity head of the oncoming flow. The most commonly used type of pitot-static tube (fig. 253*A*) consists of two separate parallel tubes, one for indicating total head, P_t (sum of static and velocity heads), and the other for indicating only static (pressure) head, P_s. Manometers are commonly used to measure these heads, the velocity head being the difference between the static head and the total head. A pressure transducer may also be used instead of the manometer for measuring the differential head. Where pitot-static tubes are used for continuous-flow measurement, oscillograph or digital recording of the electrical signal from the transducer provides a continuous record of the changes in head.

The general equation for pitot-static tubes and pitometers is

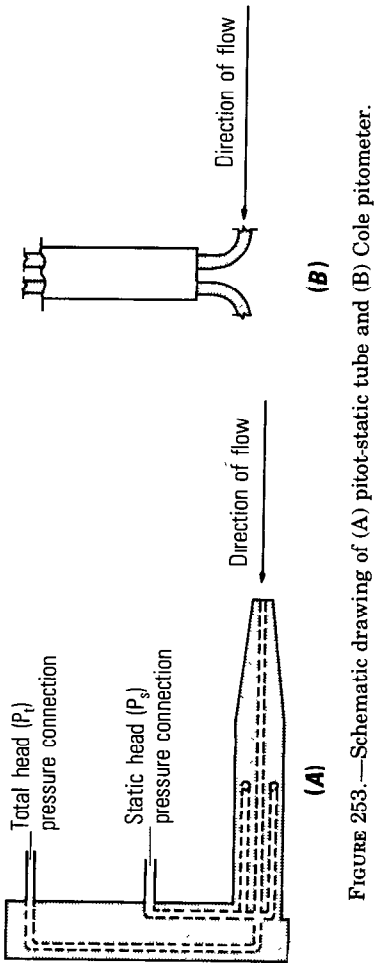

FIGURE 253.—Schematic drawing of (A) pitot-static tube and (B) Cole pitometer.

$$V = C_1\sqrt{2g\Delta h}, \tag{145}$$

where

V = velocity,
C_1 = coefficient,
g = acceleration of gravity, and
Δh = observed velocity-head differential.

The coefficient C_1 will vary with the dimensions and geometry of the meter, but the instruments are usually individually rated by the manufacturer in the manner that current meters are rated, and the value of C_1 is therefore known. For the pitot-static tube shown in figure 253*A* the value of C_1 usually ranges from 0.98 to 1.00.

Another commonly used type of pitot device is the Cole pitometer (fig. 253*B*), which consists of two tubes headed in opposite directions. The tubes can be rotated so that the instrument may be inserted through a small bushing in a pipe. When in operating position, the downstream tube registers a negative pressure because its opening is in the wake of the instrument. The differential of the water columns is therefore considerably greater than $V^2/2g$. The value of C_1 in equation 145 usually ranges from 0.84 to 0.87.

Reinforced pitot tubes and pitometers have been used successfully in pipes up to five feet in diameter having flow velocities of 5–20 ft/s (U.S. Bureau of Reclamation, 1971). Even larger pipes can be traversed by pitometer by having access ports on both sides of the pipe and by probing to or past the conduit centerline from each side. The principal disadvantage encountered is that relatively large forces push on the tube when flow velocities are high, making positioning and securing of the instrument difficult. Dynamic instability may also occur, causing the tube to vibrate and produce erroneous readings. At moderate flow velocities the measurements are accurate.

The most common pressure conduit is the circular pipe. For a constant rate of flow, the velocity varies from point to point across the stream, gradually increasing from the walls to the center of the pipe. The mean velocity is obtained by dividing the cross-sectional area of the pipe into a number of concentric equal-area rings and a central circle. The standard 10-point system is shown in figure 254*A*. More divisions may be used if large flow distortions or other unusual flow conditions exist. Observations are made at specific locations in these subareas (fig. 254*A*) and mean velocity is computed from the equation,

$$V_{\text{mean}} = C_1(\sqrt{2g})(\sqrt{\Delta h})_{\text{average}}. \tag{146}$$

The mean velocity in rectangular ducts can be determined by first dividing the cross section into an even number—at least 16—of equal

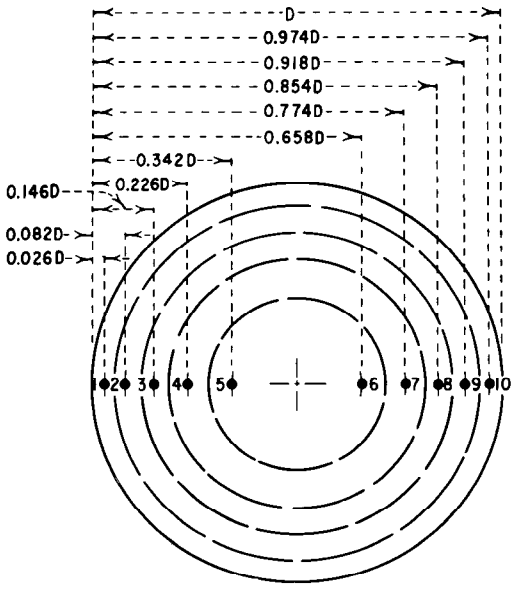

(A). Ten-point system for circular conduits

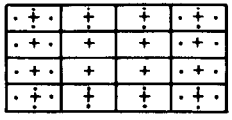

(B). System for rectangular conduits, where at least 16 divisions must be used

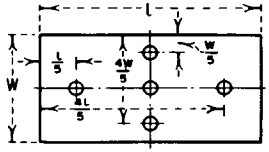

(C). Additional points for data in areas around periphery of the rectangular conduit

FIGURE 254.—Locations for pitot-tube measurements in circular and rectangular conduits. (Reproduced from B.S. 1042, Flow Measurement (1943), by permission of the British Standards Institution.)

rectangles geometrically similar to the duct cross section, and then making a pitot-tube observation at the center of each subarea (fig. 254*B*). Additional readings should be taken in the areas along the periphery of the cross section in accordance with the diagram in figure 254*C*. Mean velocity is then computed from equation 146.

When using pitot-static tubes or pitometers, it must be remembered that at low velocities, head differentials are small and errors in reading head differentials will seriously affect the results. Also the openings in the tubes are small and foreign material in the water, such as sediment or trash, can plug the tubes.

MEASUREMENT OF DISCHARGE BY SALT-VELOCITY METHOD

Discharges in conduits flowing full may be determined from the known dimensions of the conduit and velocity observations made by the salt-velocity method. Basically, the method uses the increased conductivity of salt water as a means of timing the travel of a salt solution through a length of conduit. A concentrated solution of sodium chloride is suddenly injected into the conduit at an injection station. At two downstream stations, electrodes are connected to a recording ammeter. An increase in the recorded electric current occurs when the prism of water containing the salt passes the electrodes (fig. 255). The difference in time (t) between the centers of gravity of the recorded salt passage is obtained from the recorder chart as shown in figure 255. The discharge is equal to the volume of the conduit between the two electrodes—it is not necessary that the conduit be uniform—divided by time, t, in seconds.

The brine-injection system that is used is quite complex (figs. 256 and 257). A turbulence-creating device (turbulator) is also sometimes used to insure adequate mixing of the brine and water by the time the upstream electrode station is reached. The required equipment and techniques have been described in detail by Thomas and Dexter (1955).

MEASUREMENT OF DISCHARGE BY THE GIBSON METHOD

The Gibson method was developed for computing the discharge of a conduit or penstock controlled by a valve, turbine, or regulating device located at the downstream end. The pressure conduit must extend at least 25 feet, and preferably much more, upstream from the valve or regulating device, but the conduit need not be of uniform

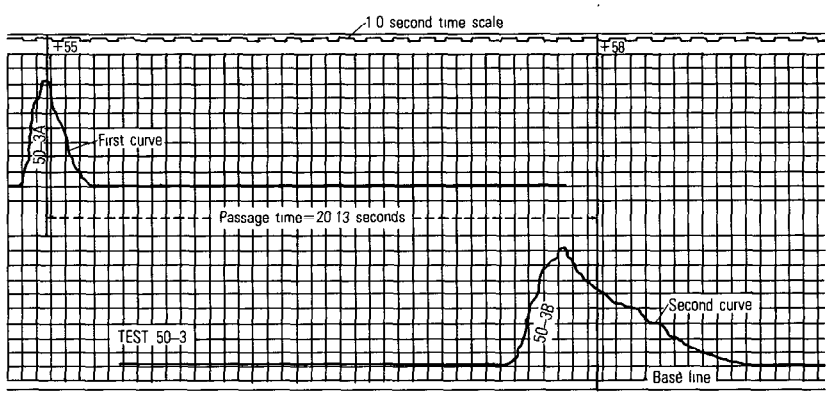

FIGURE 255.—Sample record of a salt cloud passing upstream and downstream electrodes in the salt-velocity method of measuring flows in pipelines. (Courtesy of U.S. Bureau of Reclamation.)

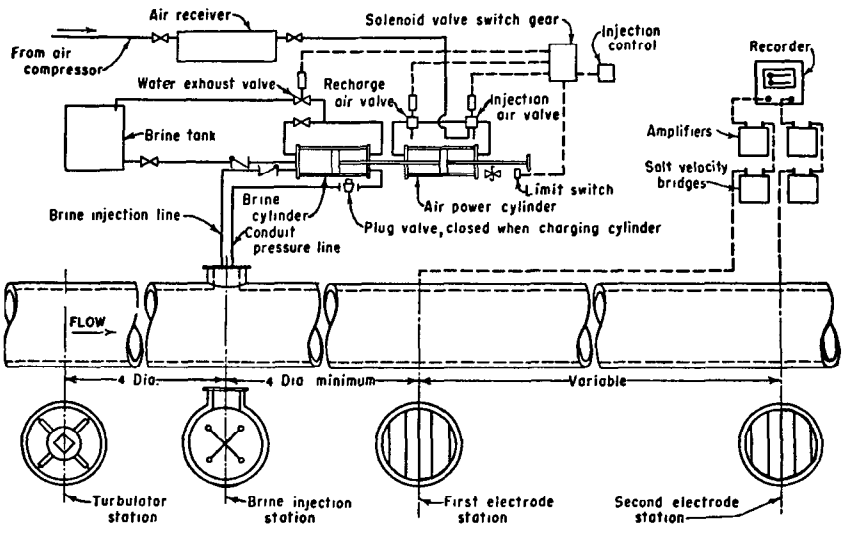

FIGURE 256.—General arrangement of salt-velocity equipment for pressure conduits. (Courtesy of U.S. Bureau of Reclamation.)

cross-sectional area. The underlying principle of the method is that the pressure rise that results from gradually shutting off the flow in a conduit is an indication of the original velocity of the water (Howe, 1950, p. 209–210).

The Gibson apparatus (fig. 258*A*) consists of: a mercury U-tube connected to the penstock just upstream from a gate; a light source behind the U-tube and a pendulum that swings in front of the box; and a narrow slit in the box directly behind the U-tube. Light shines through the U-tube and exposes a film on a rotating drum unless blocked by the pendulum or the mercury in the tube. During a test, the film therefore registers the fluctuation of the mercury column and the time intervals indicated by the pendulum (fig. 258*B*). The period of deceleration, T, terminates when the oscillations become symmetrical (point B, fig. 258*B*, where $t_1 = t_0$). An integration of the area $ABCA$ leads directly to the discharge through application of the equation,

$$Q = \left(\frac{\pi D^2}{4}\right)\left(\frac{g}{L}\right)(\text{area } ABCA), \tag{147}$$

in which Q is the discharge, D and L the diameter and length of conduit, and g the gravitational constant. The lower boundary of the area AC (practically a straight line) must be located by a trial-and-error process which is somewhat time-consuming but which nevertheless gives an accurate location of the line.

Equation 147 is applicable for a conduit of uniform cross section. If

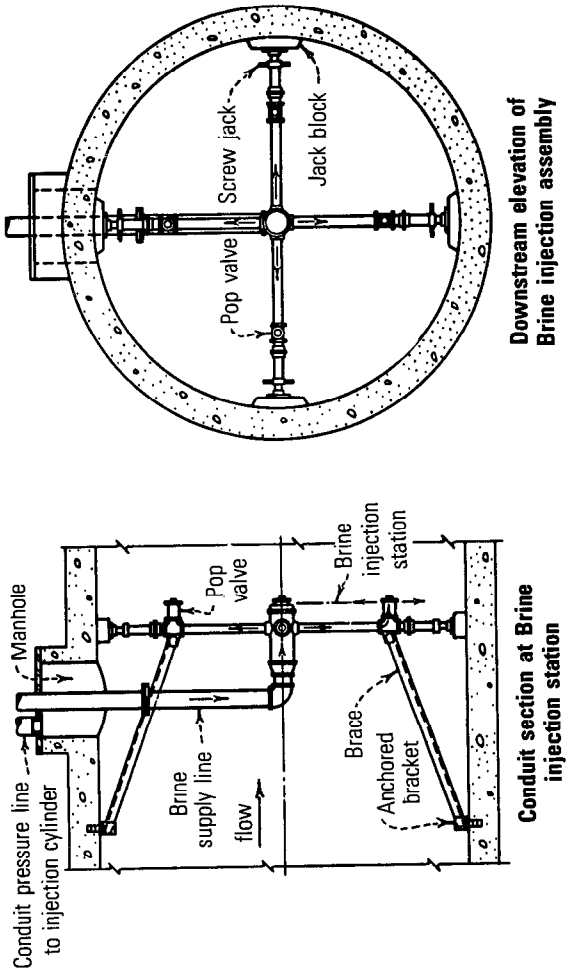

FIGURE 257.—Brine injection equipment in conduit. (Courtesy of U.S. Bureau of Reclamation.)

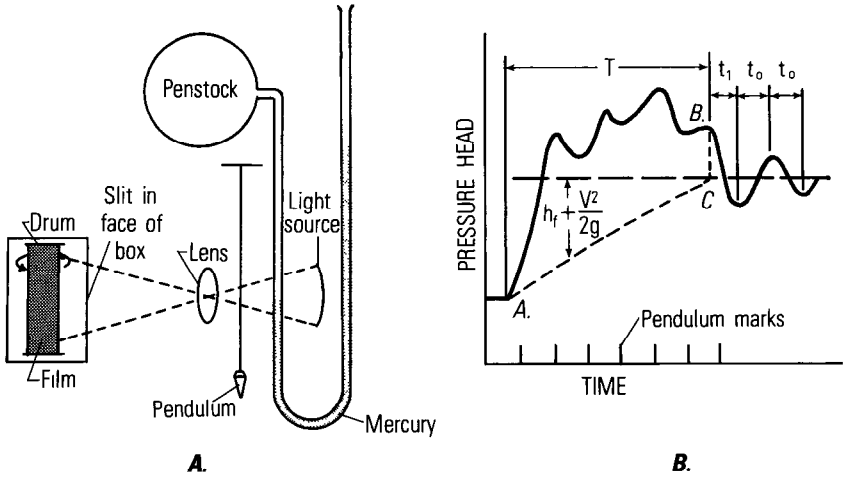

FIGURE 258.—Gibson apparatus and pressure-variation chart. (After Howe, 1950. Reprinted by permission of John Wiley & Sons, Inc.)

the conduit is not of uniform cross section throughout its length but is made up of a series of different sections of length l_1, l_2, l_3, etc. having cross-sectional areas a_1, a_2, a_3, etc., equation 147 must be modified. In that modification, we substitute the value $\Sigma(a/l)$ for the composite term $\left(\frac{\pi D^2}{4}\right)/L$; the value $\Sigma(a/l)$ is the sum of the quotients obtained by dividing the cross-sectional area of each conduit section by its respective length. The modified equation is therefore,

$$Q = g[\Sigma(a/l)]\ [\text{area } ABCA] \qquad (147a)$$

It is generally agreed that the Gibson method is very accurate. As an application of the momentum principle, this might be expected. The personnel requirements are not great, since only one operator is required to run the instrument. Neither is cost of the equipment excessive. A series of tests consumes a considerable time, however, because of the necessity for alternately shutting down the flow and bringing it back to a steady rate. Nevertheless, it must be concluded that the Gibson method offers a fairly simple and accurate approach to certain measurement problems that might otherwise be difficult.

CALIBRATION OF TURBINES, PUMPS, GATES, AND VALVES

The calibration of a reaction turbine by the measurement of pressure drop in the scroll case was discussed at the end of the section titled, "Differential-Head Meters." However, in some hydraulic systems it may be desirable, or perhaps necessary, to consider the turbine, pumps, gates, or valves themselves as flowmeters for the sys-

tem. To do that, it is required that the pertinent hydraulic element be calibrated. The calibration is often done in the laboratory using hydraulic models, but it is preferable that the hydraulic element be calibrated in place, or at least have its laboratory-derived calibration checked by field measurements of discharge. For field calibration, discharge measurements are made by one of the three methods discussed in the section on "Discharge-Measurement Methods for Meter Calibration," if they cannot be made by current meter in the forebay or afterbay of the system where open-channel conditions exist.

In the case of turbines or pumps, relations of discharge versus power are generally desired. They may be defined by observing the metered power output or input during periods when discharge measurements are made for various load conditions. Suitable curves or tables may be developed from these test data to show the discharge (Q) that occurs for specific types of operation. Curves or tables may also be prepared from model test data if the test data can be verified by a few discharge measurements. The calibration will change with time if there is a change in the efficiency of the turbine or pump resulting from long service or from other factors that cause deterioration.

If the range of operating conditions for a pump or turbine is narrow, the calibration is simplified. In such a situation—for example, where power input or output is metered—a simple relation of discharge versus power divided by head may be adequate. For a pump operated by an internal-combustion engine, where power was not metered but rotational speed was automatically recorded, the following calibration scheme has been used. For the most commonly used rotational speed, $(RPM)_r$, a base rating of discharge (Q_r) versus head was defined by current-meter discharge measurements. To obtain the discharge (Q_m) for other rotational speeds, $(RPM)_m$, an empirical adjustment relation of Q_m/Q_r versus $(RPM)_m/(RPM)_r$ was defined by the discharge measurements. (The method of defining the two relations is similar to that used in the constant-fall method of rating open-channel discharges, discussed in the section in chapter 11 titled, "Rating-Fall Constant." The use of head in the pump rating is analogous to the use of stage in the open-channel method; the use of rotational speed of the pump is analogous to the use of fall in the open-channel method.) After the two relations have been defined, to obtain the discharge (Q_m) for a given head and a given rotational speed, $(RPM)_m$, the ratio $(RPM)_m$ to $(RPM)_r$ is first computed. That ratio is then used in the adjustment relation to obtain the ratio Q_m/Q_r. The value Q_r is the discharge corresponding to the given head in the base rating. The desired discharge (Q_m) is then computed by multiplying Q_r by the ratio Q_m/Q_r.

For gates and valves, relations of discharge versus gate opening for various appropriate heads are desired. They may be defined by observing the gate or valve openings during periods when discharge measurements are made for various operating heads. Measurements made over the full range of gate openings and heads will provide the data for establishing the required curves or tables. Generally the relations are in the form of discharge (Q) for gate openings expressed as a percentage of full opening for pertinent operating heads. Curves or tables may also be prepared from model test data if the test data can be verified by a few discharge measurements. As with turbines and pumps, the calibrations for gates and valves are subject to change with time as wear or deterioration occurs.

URBAN STORM DRAINS

Quantitative studies of urban storm runoff have been handicapped by a lack of proper instrumentation for metering the flow in sewers. An ideal sewer flowmeter should have the following characteristics: (1) capability to operate under both open-channel and full-flow conditions, (2) a known accuracy throughout the range of measurement, (3) a minimum disturbance to the flow or reduction in pipe capacity, (4) a minimum requirement of field maintenance, (5) compatibility with real-time remote data-transmission, and (6) reasonable construction and installation costs.

Over the years many devices have been tested for use as sewer flowmeters. Wenzel (1968) has reviewed the methods and devices tested—weirs, depth measurement, depth and point-velocity measurements, dilution methods, and venturi flumes—and found that all have disadvantages of one kind or another. Of those devices, one of the most favorable was the flat-bottom venturi flume specifically designed for flow measurements in conduits by Palmer and Bowlus (1936). That flume has a throat of trapezoidal cross section, a flat bottom, and upstream and downstream side and bottom transitions. The flat bottom permits debris to flow smoothly through the throat and the transitions reduce the head loss substantially below that which would be caused by a weir, for example.

Wenzel (1968), in his study, concluded that further effort in designing some new modifications of a venturi flume offered the greatest promise of success in developing a more satisfactory flowmetering device for urban storm drains. Accordingly three new variations of a venturi section have been designed and laboratory tested in the U.S.A. The U.S.G.S. sewer flowmeter is now (1976) being field tested; the Wenzel asymmetrical and symmetrical sewer flowmeters are still awaiting installation in the field. The three types are briefly described below.

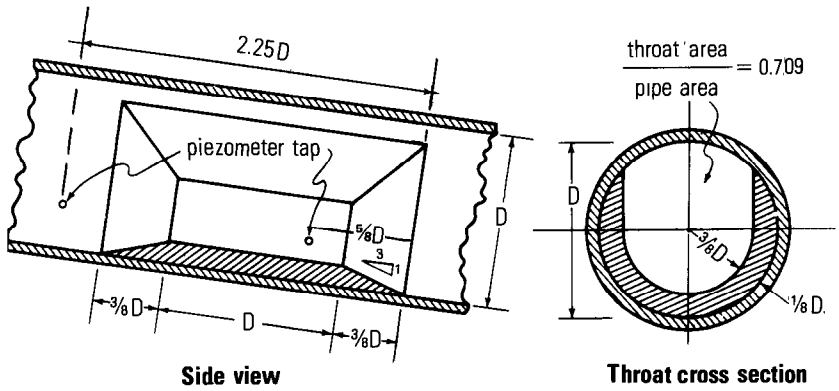

FIGURE 259.—Sketch of USGS flowmeter in a sewer.

U.S.G.S. sewer flowmeter.—The U.S.G.S. meter is a U-shaped constriction made to be inserted in a circular pipe (fig. 259). The symmetry of the design permits fabrication in two half sections for easy transportation and installation. Molds are available for fiberglass prototypes in standard pipe sizes from 24 to 60 in. (0.61 to 1.52 m).

The overall length from toe to heel is 1.75 pipe diameters. The throat length, equal to one pipe diameter, and the approach and getaway apron slopes of 1 on 3, resemble venturi meter specifications. The constriction, in fact, is a venturi flume for open channel flows; for pressure flows it may be considered to be a modified venturi meter.

For subcritical open-channel flows, the constriction dams up the flow, which then passes through critical depth as it spills through the throat. If the oncoming flow is supercritical, two conditions are possible: a hydraulic jump may be forced to form, which then spills through the throat and continues downstream as supercritical flow, or, on steeper slopes, the oncoming flow may remain supercritical throughout the entire constriction. As discharge increases, the water surface on the upstream side rises, touches the top of the pipe, and fills the upstream pipe, while the downstream side continues to flow part full. A discharge rating is available for each of these open-channel conditions.

Further increases in discharge trigger full-pipe conditions, which also are well rated. It is for these pressure-flow conditions that the question of head loss becomes of interest. Head loss, or backwater, is taken to be the increase in the upstream piezometric grade line caused by the presence of the constriction in the sewer line. For this constriction shape, the head loss is expressed as a function of the throat velocity head:

$$H_L = 0.04\frac{V^2_t}{2g}.$$

The constriction is considered to be self-cleaning. Inasmuch as sewers are generally laid to a self-scouring slope, any silting upstream from the constriction is expected to flush out on the next rise. The deposition of silt would have a negligible effect on the rating for small discharges, and no effect for high discharges.

The curved floor in the throat, parallel to the circumference of the pipe rather than being horizontal, retains some self-cleaning ability. It is a compromise between a V-notch base which would have great rating sensitivity for small discharges but a tendency to clog with small debris, and the other extreme, a horizontal floor as in a Palmer-Bowlus trapezoidal constriction. The floor thickness, one eighth of the pipe diameter, provides enough height to produce and maintain a stable hydraulic jump, and it also provides enough constriction (throat area is 0.709 of pipe area) to produce an adequate pressure drop for full-pipe flows. Yet, it is low enough to maintain open-channel flow for a larger range of discharge than would be maintained by a thicker constriction. By leaving the upper part of the pipe unconstricted, a quick transition from open-channel to full-pipe flow conditions is assured, and pressure build-up upstream from the constriction and head loss are minimized.

The pressures in the approach and in the throat of the constriction are measured remotely by pressure transducers. Dry nitrogen gas is bubbled at a constant rate through tubes to the two piezometer openings. The pressure at each opening is reflected to the head of the gas column where the transducer is located.

Data from the flowmeter are entered into the system and converted to two digital numbers proportional to the two pressures measured. The two transducer outputs are applied to a dual analog input amplifier that transforms them to analog voltage levels, which are then applied to analog-to-digital converters. Provisions are made so that one may compress, expand, or shift the range at the analog section.

The format under which data are recorded is dependent upon the conditions indicated by the system data inputs. The system logic inhibits data recordings during dry-weather, no-flow conditions. When flow begins in the sewer to be monitored by the system, the pressure at the approach tap will increase. During the period when this pressure exceeds a preset value, as indicated by the corresponding analog voltage exceeding a programed level, recordings will be continuous on a 1-minute cycle. The recordings are usually on on-site digital-punched paper tape, but variations have provided for analog recording as well as telemetry.

One or more recording precipitation gages and an automatic water sampler are included in the instrumentation for studying urban storm runoff.

It is desirable that the meter be calibrated in place by current-meter discharge measurements. However, as a guide to the probable meter rating and for use until field calibration is completed, the following laboratory discharge equations are presented. The coefficients shown are for use with English units.

A. *Pipe flowing full*

$$Q/D^{5/2} = 5.74\left(\frac{\Delta h}{D}\right)^{0.52}, \tag{148}$$

where

Q is discharge,

D is pipe diameter, and

Δh is the head differential between piezometer readings.

The constant 5.74 includes the constant for the acceleration of gravity. The exponent 0.52 fits the laboratory data better than the theoretical exponent 0.5.

B. *Open-channel flow*

1. *Supercritical regime*

$$Q/D^{5/2} = 5.58\,(h_1/D)^{1.58}, \tag{149}$$

where h_1 is the depth above pipe invert at the upstream piezometer.

2. *Subcritical regime—slope of culvert <0.020*

a. *For $h_1/D \geq 0.30$*

$$Q/D^{5/2} = 2.85\,(h_1/D - 0.191)^{1.76} \tag{150}$$

b. *For $h_1/D < 0.30$*

$$Q/D^{5/2} = 1.15\,(h_1/D - 0.177)^{1.38} \tag{151}$$

3. *Subcritical regime—slope of culvert ≥ 0.020*

$$Q/aD^{5/2} = 1.07\,(h_1/D)^{2.71} \tag{152}$$

where $a = 2.15 + \left[(9.49)(10)^{11}\,(\text{Slope} - 0.008)^{6.76}\right]$. (153)

C. *Transitional flow between open-channel flow and full-pipe flow*

$$Q/D^{5/2} = 2.6 \pm\left(\frac{|0.590 - h_2/D|}{0.164}\right)^{1/2}, \tag{154}$$

where h_2 is the depth above the flowmeter invert at the downstream piezometer.

Wenzel asymmetrical and symmetrical flowmeters.—A generalized drawing of the asymmetrical venturi section devised by Wenzel (1975) is shown in figure 260. The symmetrical venturi section differs from the asymmetrical type shown by having identical constrictions on either side of the vertical centerline of the pipe. The constriction

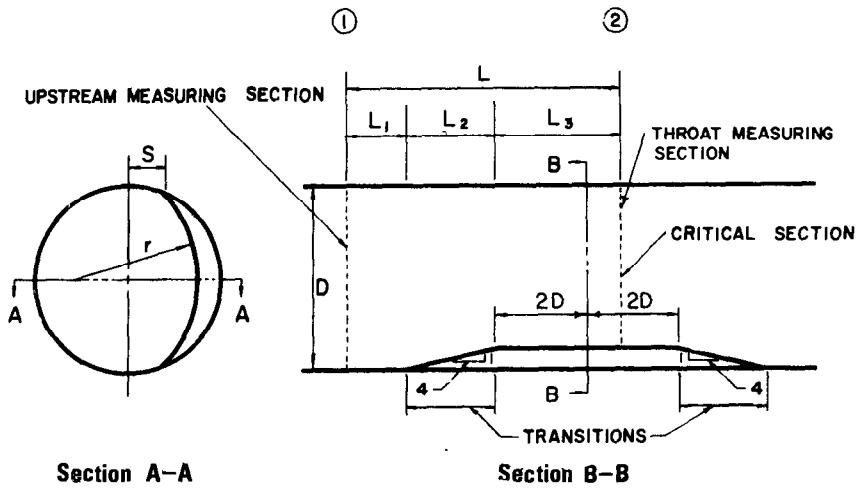

FIGURE 260.—Sketch of Wenzel asymmetrical flowmeter in a sewer. (After Wenzel, 1975.)

consists of a cylindrical section, whose radius is greater than that of the pipe, with entrance and exit transitions having a slope of 1 on 4. The cylindrical section intersects the pipe wall a distance S from the centerline, thereby maintaining the invert region free of obstruction so that self-cleaning is facilitated. In all laboratory tests, a constant value of 0.1 was maintained for S/D, but the ratio r/D was varied to provide various ratios of throat area to pipe area for testing. A throat length between $2.25D$ and $4.0D$ is recommended. The upstream piezometer tap is located approximately $D/3$ upstream from the beginning of the entrance transition; the downstream piezometer tap is located approximately at the center of the throat. As mentioned earlier, no information on the field performance of the Wenzel flowmeters is as yet available.

SELECTED REFERENCES

American Society of Civil Engineers, 1942, Hydraulic models: Am. Soc. Civil Eng. Manual of Eng. Practice No. 25, 110 p.

American Society of Mechanical Engineers, 1937, Part 1, Fluid meters, their theory and application (4th ed.): New York, Am. Soc. Mech. Eng.

Bradley, J. N., 1952, Discharge coefficients for irregular overfall spillways: Engineering Mon. 9, U.S. Bur. Reclamation, 53 p.

———1953, Rating curves for flow over drum gates: Am. Soc. Civil Engineering Proc., Hydraulics Div., v. 79, sep. no. 169, 18 p.

Davis, C. V., 1952, Handbook of applied hydraulics: New York, McGraw-Hill, p. 291–334.

Horton, R. E., 1907, Weir experiments coefficients and formulas: U.S. Geol. Survey Water-Supply Paper 200, 195 p.

Howe, J. W., 1950, Flow measurement, *in* Rouse, Hunter, Engineering hydraulics: New York, John Wiley and Sons, p. 177–228.

Hulsing, Harry, 1967, Measurement of peak discharge at dams by indirect methods: U.S. Geol. Survey Tech. Water-Resources Inv., book 3, chap. A5, 29 p.

King, H. W., and Brater, E. F., 1963, Handbook of hydraulics: New York, McGraw-Hill, p. 12–1 to 12–32.

Kirkpatrick, K. W., 1955, Discharge coefficients for spillways at TVA dams: Am. Soc. Civil Engineers Proc., Hydraulics Div., v. 81, sep. no. 626, 27 p.

Lansford, W. M., 1936, The use of an elbow in a pipe line for determining the rate of flow in a pipe: Univ. Illinois Eng. Exp. Sta. Bull. 289, 36 p.

Linsley, R. K., and Franzini, J. B., 1972, Water-resources engineering: New York, McGraw-Hill, p. 243–247, 499–506, 309–312.

Palmer, H. K., and Bowlus, F. D., 1936, Adaption of venturi flumes to flow measurements in conduits: Am. Soc. Civil Engineers Trans., v. 101, p. 1195–1239.

Schuster, J. C., 1970, Water measurement procedures—irrigation operators workshop: U.S. Bureau of Reclamation REC–OCE–70–38, 49 p.

———1975, Measuring water velocity by ultrasonic flowmeter: Am. Soc. Civil Engineers, Hydraulics Div. Jour., v. 101, no. HY12, p. 1503–1518.

Smoot, G. F., Davidian, Jacob, and Billings, R. H., 1974, Urban storm rainfall-runoff-quality instrumentation, *in* Symposium—Flash floods, Paris, September 1974, Proceedings: Internat. Assoc. Hydrol. Sci. Pub. no. 112, p. 44–47.

Thomas, C. W., and Dexter, R. B., 1955, Modern equipment for application of salt-velocity method of discharge measurement for performance tests: Proc. of Sixth Gen. Mtg, Internat. Assoc. Hydraulic Research, v. 2, The Hague, Netherlands, 1955, p. 1–10.

Toch, Arthur, 1953, Discharge characteristics of Tainter gates: Am. Soc. Civil Engineering Proc., Hydraulics Div., v. 79, sep. no. 295, 20 p.

U.S. Army Corps of Engineers, 1952, Navigation lock and dam design—navigation dams: Eng. Manual 1110–2–2606, 22 p.

U.S. Bureau of Reclamation, 1948, Studies of crests for overfall dams: Bull. 3, Part VI (Hydraulic Investigations), Boulder Canyon Proj. Final Repts, 186 p.

——— 1971, Water measurement manual (2d ed): Water Resources Tech. Pub., p. 185–212.

Wenzel, H. G., 1968, A critical review of methods of measuring discharge within a sewer pipe: Am. Soc. Civil Engineers Urban Water Resources Research Tech. Memo. no. 4, 20 p.

———1975, Meter for sewer flow measurement: Am. Soc. Civil Engineers, Hydraulics Div. Jour., v. 101, no. HY1, p. 115–133.

CHAPTER 15—COMPUTATION OF DISCHARGE RECORDS

GENERAL

Streamflow records for each gaging station are computed and published annually. The 12-month period used, which is known as the water year, usually does not coincide with the calendar year. In the U.S.A. the water year runs from October 1 to September 30 and is designated by the calendar year of the last 9 months—for example, the 1975 water year runs from October 1, 1974 to September 30, 1975. The following considerations govern the choice of the 12 months that will constitute the water year. The 12-month record is essentially an inventory of the water supply. As with any inventory, it should be made when the stock on hand (available water resource) is at a minimum. That is the case in most of the U.S.A. on September 30, at which time the growing season is at an end. Not only are groundwater, soil-moisture, and surface storage at or near a minimum on that date as a result of heavy water use during the preceding summer, but the replenishing rains of autumn have not yet begun and streamflow is also near minimal. In short, the 12-month period to be used as the water year is determined by the climatic regime of the region.

A daily record of discharge, along with momentary values of peak discharge and minimum flow, is computed for the water year from the record of stage and the discharge rating for the gaging station. The type of stage recorder used determines whether the computations are performed manually or by an electronic computer. In either system, the engineer must study the data and prepare what is termed a station analysis before the actual computation of discharge is begun.

STATION ANALYSIS

A station analysis, which documents the results of the study of the data, is prepared for each station for each water year. The study includes the following items, all of which are needed as a preliminary to computing the discharge record.

1. A review of field surveys of gage datum and a determination of the datum corrections, if any, to be applied to stage observations or recordings during the year.
2. A listing and review of discharge-measurement notes
3. An analysis of the discharge rating and the determination of the rating (or shift) applicable during each period of the year.
4. The preparation of tables that express the discharge rating, using the rating curves derived in the above item 3.

Documentation of items in the station analysis is made as the various steps in the analysis and computation of the discharge record are completed. The station-analysis document is described in detail later in this chapter after all items in the analysis and computation of discharge have been discussed. Examples of the methods of analysis and computation are interspersed in the discussions of methodology for illustrative purposes.

DATUM CORRECTIONS

The datum of the gaging station is the elevation of the zero point of the base or reference gage, preferably referred to mean sea level. (For a discussion of reference and auxiliary gages see the section so-titled in chapter 4. The base gage or reference gage is the gage to which the recording instrument is set; at a nonrecording station it is the gage whose daily readings are recorded by the observer.) Levels are run periodically to all bench marks, reference marks, reference points, and gages at each station for the purpose of determining if any datum changes have occurred as a result of settlement or other movement of any of the gages or of the bubble orifice. If significant movement is indicated by the levels, the gage or bubble orifice is reset to its original datum.

Figure 261 is a typical set of level notes obtained in checking the datum of a recording stage-gage of the float-sensor type; the base gage is a vertical staff gage in the stilling well immediately below a reference point (RP1). Where a vertical staff gage consists of a number of standard USGS porcelain-enameled gage plates, each 3.4 ft long, the elevation of one of the central graduations on each plate should be checked. This is usually done by measuring to each plate with a steel tape whose zero end is held at a reference point of known elevation; the reference point, as mentioned, is established directly above the staff gage. The level notes in figure 261 for the inside staff gage (IG) show that the above procedure was followed.

The level notes are checked in the field for mathematical errors before the field party leaves the gaging station.

If a change in datum has occurred, it is necessary to determine the effective date of the change. In the absence of any evidence indicating the date when the datum change occurred, the change is assumed to have occurred gradually from the time the last levels were run, and the change is prorated with time. On the station-analysis document there would be entered the date(s) when levels were run, the period(s) and magnitude(s) of the datum correction(s) required, and the date and time when the original datum was restored to eliminate the need for corrections. If no datum corrections were required, as indicated, for example, in the level notes of figure 261, that fact would be entered in the station–analysis document.

File No. 10-2450

LEVEL NOTES
(First sheet, to be completed in the field)

Station Clear Creek near Utopia, Calif.

Date Oct 6, 1965 Party Patch & Sweet ϕ

Date level adjusted: Oct 6, 1965

Object of these levels:

To check gage datum

Conclusions

Elevations of RM's and RP checked within 0.002 ft.
Outside staff-gage datum checked within 0.01 ft.
Inside staff-gage datum checked within 0.003 ft.

Changes made:
To inside staff gage, out staff gage, tape gage, or R.M.'s.
No changes required; none made.

Remarks

Data to be added to, or changed on, Station Description (9-197) as a result of these levels.
No changes or additions to be made.

Sheet No. 1 of 2 sheets. S.F. 2-45

9-276 (Rev. 7-67)
UNITED STATES
DEPARTMENT OF THE INTERIOR
GEOLOGICAL SURVEY
WATER RESOURCES DIVISION

Station Number 10-2450

LEVEL NOTES

Stream Clear Creek
Locality near Utopia, Calif
Party Patch & Sweet ϕ Date Oct 6 1965

STATION	B S	HT INST	F S.	ELEVATION	REMARKS
RM 1				11.142	Given
RM 2				20.142	Given
RP 1				19.870	Given
RM 2	1.510	21 652		20 142	Bronze tablet, 40' DS
RP 1			1.781	19.871	Head of brass screw
RM 1	10.746	21.889	10.509	11 143	Bronze tablet, 20' DS
RP 1			2 017	19 872	
RM 2			1 746	20.143	
	Levels to outside staff				
RM 1	0 657	11 799		11 142	
OG			10.19	1 61	1.60 ft graduation
OG			3 79	8 01	8.00 ft. "
OG			-3 20	15.00	15.00 ft "
Levels to inside staff - measured by steel tape from RP					
RP 1	0.000	19.870		19 870	
IG			18 268	1 602	1.60 ft. graduation
IG			14 869	5 001	5.00 " "
IG			11.572	8.298	8.30 " "
IG			8.271	11 599	11.60 " "
IG			4.873	14.997	15.00 " "
W.S. in well			18.850	1 020	Gage read 1.02

No. 2 of 2 sheets Comp. by MAP Chk. by GS

U.S. GOVERNMENT PRINTING OFFICE 1958 O—514178 895.172

FIGURE 261.—Level notes for check of gage datum.

REVIEW OF DISCHARGE MEASUREMENTS

The first step in the review of discharge measurements is to check the mathematics of the measurements. It is usually considered expedient, however, to accept, without checking, the results of a discharge measurement made by an experienced hydrographer if the measurement checks the rating curve within ±5 percent and if the measured discharge does not exceed all previously measured discharges. The discharge measurements (fig. 42), including indirect determinations of discharge (chap. 9), are then arranged in chronological order and numbered consecutively. The measurements are next compared with the gage-height record to ensure that all discharge measurements are at hand—the inspection notes on the stage record should indicate whether or not a discharge measurement had been made—and also to check the gage heights shown on the measurement sheet. If a datum correction is applicable, it is applied to the mean gage height for the measurement.

The measurements are then tabulated on a special form (USGS form 9-207 in fig. 262). Most of the column headings in figure 262 are self-explanatory. Those on the right half of the table supply information that is helpful to the analyst in appraising the comparative accuracy of the discharge measurements, in case he should find it necessary to give more weight to one measurement than to another in developing the discharge rating. The hydrographer's field appraisal of the probable accuracy of his measurement is shown in the column headed "Meas. rated," where E is excellent, G is good, F is fair, and P is poor. For example, measurements nos. 31, 32, 34–35A, and 44 are rated "poor" because the depths were too shallow or the velocities too low to obtain reliable discharges. In addition, only a few sections (verticals) were used for measurement nos. 32, 34, and 44. The gage-height change during the time required for the measurement is also listed because a rapidly changing stage would adversely affect the adequacy of the measurement. The outside gage reading is listed to provide the analyst with information as to whether or not the gage-well intakes were functioning properly. (Small differences between the readings of the base gage and of the outside auxiliary gage are often the norm because of the difference in location between intakes and outside gage.) The two columns headed "Rating. . . ." are discussed in the section titled, "Rating-Curve Analysis."

The "Remarks" column is most important to the analyst. If a measurement was made by any means other than wading, the method and the sounding weight used are indicated. Measurements made from a bridge or cableway are directly comparable for studying changes in the measurement cross section because the same cross section is used for all discharge measurements. With regard to noting the

FORM 9-207
(Rev. 11-69)

UNITED STATES DEPARTMENT OF THE INTERIOR

GEOLOGICAL SURVEY (WATER RESOURCES DIVISION)
DISCHARGE MEASUREMENT SUMMARY SHEET

Station No 10-2450

Discharge measurements of Clear Creek near Utopia, Calif. during the year ending Sept 30, 1966.

No	Date 1965	Made by—	Width (Feet)	Area (Sq ft)	Mean velocity (Fps)	Gage height (Feet)	Discharge (Cfs)	Rating 3: Shift adj (Feet)	Rating 3: Percent diff	Method	Number meas sections	Gage height change (Feet)	Time (Hr)	Meas rated	Time / Water temp °C	Out side gage	REMARKS
30	Aug. 27	A L Barnes E C King	10	5.76	0.72	2.56	4.18	—	+3	.6	20	0	.7	G	0840 14	2.57	Zero flow = 1.95 ± .05 Control clear.
31	Sept. 29	H B Rend	4.5	1.26	.65	2.18	.82	—	0	.6	16	0	.3	P	1050 10	2.18	Zero flow = 1.95 ± .05 Control clear.
32	1965-66 Oct. 9	A. N. Dunn	3.1	.33	.91	2.08 2.06	.30	-.02 0	0 0	.6	6	0	.4	P	1510 8	2.07	Removed tree limb from control. *F = 1.95
33	27	E.C.K.	8.7	4.17	.72	2.48	3.00	—	-2	.6	17	0	.5	G	1600 4	2.49	Zero flow = 2.00 ± .05 Control clear.
34	Nov. 20	S.K. Steen.	3.2	.35	.60	2.04	21	—	0	.6	4	0	.2	P	1120 2	2.05	No ice in stream.
35	Dec. 16	E. C. K	15	16.1	.13	*3.12	2.15	Ice -.75	—	.6	18	-.02	.6	P	0930 1	3.12	Complete ice cover *OG
35A	1966 Jan. 18	S K S	9.2	10.2	.32	*3.26	1.76	Ice -.84	—	.6	15	0	.6	P	1430 1	3.26	Complete ice cover *OG
36	Feb. 25	R L B H.B.R	10	6.05	.76	2.68	4.60	Rating 4 —	-1	.6	20	+.01	.5	G	1550 1	2.68	Control clear Intakes thawed.
37	Mar. 29	H.B.R.	3	channels		6.60	210	—	-1	.2-.8	26	0	.8	G	1310 3	6.62	No ice in stream Control clear.
38	Apr. 25	E.C.K.	52	344	2.38	10.90	820	—	+3	.2-.8	30	+.02	1.1	G	1000 4	10.92	Cable - 50#
39	May 27	H B R	—	—	—	32.51	9,310	—	0	Slope Area	—	—	—	F	—	*32.61	*From HWM F = 0.68, n = 0.035
40	June 28	H B R	31	75.9	1.41	5.26	107	—	+1	.2-.8	24	0	.9	G	1240 10	5.26	Control clear
41	July 26	E C K	18	20.5	1.00	3.45	20.5	—	-2	.6	21	0	.8	G	1420 14	3.46	Gravel bar below gage. Zero flow 2.05 ± .05
42	Aug. 25	A N D	15	17.2	.89	3.22	15.3	—	+3	.6	22	+.01	.7	G	1350 16	3.24	Gravel bar moved out. Zero flow 2.00 ± .05
43	Sept. 28	S K S	12	8.76	.82	2.84	7.20	—	+2	.6	18	0	.5	G	0910 14	2.84	Control clear Zero flow 2.00 ± .05
44	1966-67 Oct 10	E C K	3.6	.65	.65	2.21	.42	—	-5	.6	7	0	.3	P	1740 13	2.22	Control clear Zero flow 2.05 ± .05

Copied by R B C Computed by LRG Checked by R.H.H

U.S. GOVERNMENT PRINTING OFFICE

FIGURE 262.—List of discharge measurements.

sounding-weight size, the measured discharge tends to be greater than the true discharge if too light a weight is used in high-velocity flow because depth soundings tend to be erroneously high and the meter also tends to rise to a higher (and faster) level than intended when positioned at the desired depth for a velocity observation.

The condition of the control—whether clear, ice-covered, or debris-covered—is also noted in the "Remarks" column, along with the gage height of zero flow on the control at the time of low-flow measurements. (Zero flow equals gage-height minus depth of water over the lowest point on the control.) The stability of the rating is dependent on control conditions; the elevation of zero flow is highly important for extrapolating the low-water end of the rating.

In the case of an indirect discharge determination (no. 39), the gage-height of the outside high-water mark is noted in the "Remarks" column, along with the Froude number and roughness coefficient. The equation for computing the Froude number (F) is $F=V/\sqrt{gd}$, where V is mean velocity in the measurement section, g is the acceleration of gravity, and d is mean depth in the measurement section; d is computed by dividing the area of the measurement section by its width. A Froude number close to unity casts some doubt on the indirect determination because it indicates the probability of unstable flow conditions. As for the roughness coefficient, more reliability is generally attached to indirect determinations for smooth channels (low roughness coefficient) than to such measurements for rough channels (high roughness coefficient).

If the gaging station is on an intermittent stream—one that goes dry for periods during the year—the list of discharge measurements should also list chronologically the dates when the hydrographer actually observed that there was no flow in the stream.

STATION RATING—SIMPLE STAGE-DISCHARGE RELATION

The rating curve for a gaging station is a graphical depiction of the relation between stage and discharge. Additional parameters such as fall or velocity index may be required in the rating (see section titled, "Stage Rating—Three-Parameter Discharge Relation"), but this section of the manual deals only with simple stage-discharge relations. Each station rating curve presents individual problems based on the control characteristics for the station, a knowledge of which is a prerequisite for the rating analysis. The principles underlying simple stage-discharge relations were discussed in chapter 10; this section deals only with the mechanics of computing and preparing the station rating.

PLOTTING OF DISCHARGE MEASUREMENTS

Rating curves and discharge measurements should be plotted on

logarithmic graph paper, and it is often advantageous to have an additional plot of the low-flow data on rectangular-coordinate graph paper so that the point of zero flow may be plotted. If a new station is being analyzed, the scales selected should be such as to accommodate the ranges of stage and discharge that are expected. If the station is not new, all measurements made since the analysis of the preceding year should be plotted on the prints of the last-used rating curve. Each plotted measurement is tagged with its identifying number, and if the "Remarks" column of the list of measurements indicates that a measurement was made under altered control conditions, that fact should be temporarily indicated alongside the measurement number. Measurements that are affected by ice (nos. 35 and 35A in fig. 262) are not plotted because they serve no purpose in defining the rating. (The use of ice-affected discharge measurements is discussed in the section titled "Rating-Curve Analysis" that follows.) The measurements listed in figure 262 are plotted on the logarithmic rating-curve sheet used during the preceding year (fig. 263). In actual practice, the rating-curve sheet that is used is large enough to accommodate both parts of the plot shown in figure 263. In figure 264, the low-water discharge measurements have been replotted on rectangular-coordinate graph paper that bears a copy of the last-used discharge rating. Logarithmic rating-curve sheets have been designed with a rectangular-coordinate scale in one corner, thereby permitting both logarithmic and rectangular plotting on the same sheet.

RATING-CURVE ANALYSIS

The principles involved in simple stage-discharge relations (chap. 10) are used in analyzing the rating. After reviewing and plotting the discharge measurements, the analyst must determine whether the last-used rating is applicable for part or all of the water year. To do that, he computes percentage departures of his measured discharges from the discharges for the measurement stages, as indicated by the last-used rating table (rating no. 3 on figs. 263 and 264). The percentages are tabulated on the list of discharge measurements (fig. 262). As long as the departures are random in sign (plus and minus) and within ±5 percent, the last-used rating is kept in effect. Aside from the two ice-affected measurements, nos. 35 and 35A, all measurements above a stage of 3.00 ft closely check rating no. 3. Sometime between measurements no. 35A (January 18) and no. 36 (February 25), the ice in Clear Creek went out. When the ice went out, it apparently moved bed material which built up the lower part of the low-water control by about 0.06 ft; the build-up is evident from the change in zero-flow elevation (see "Remarks" column of fig. 262) and from the plotting of the measurements on the low-water curves of figures 263 and 264. Inspection of the gage-height chart indicates that the ice

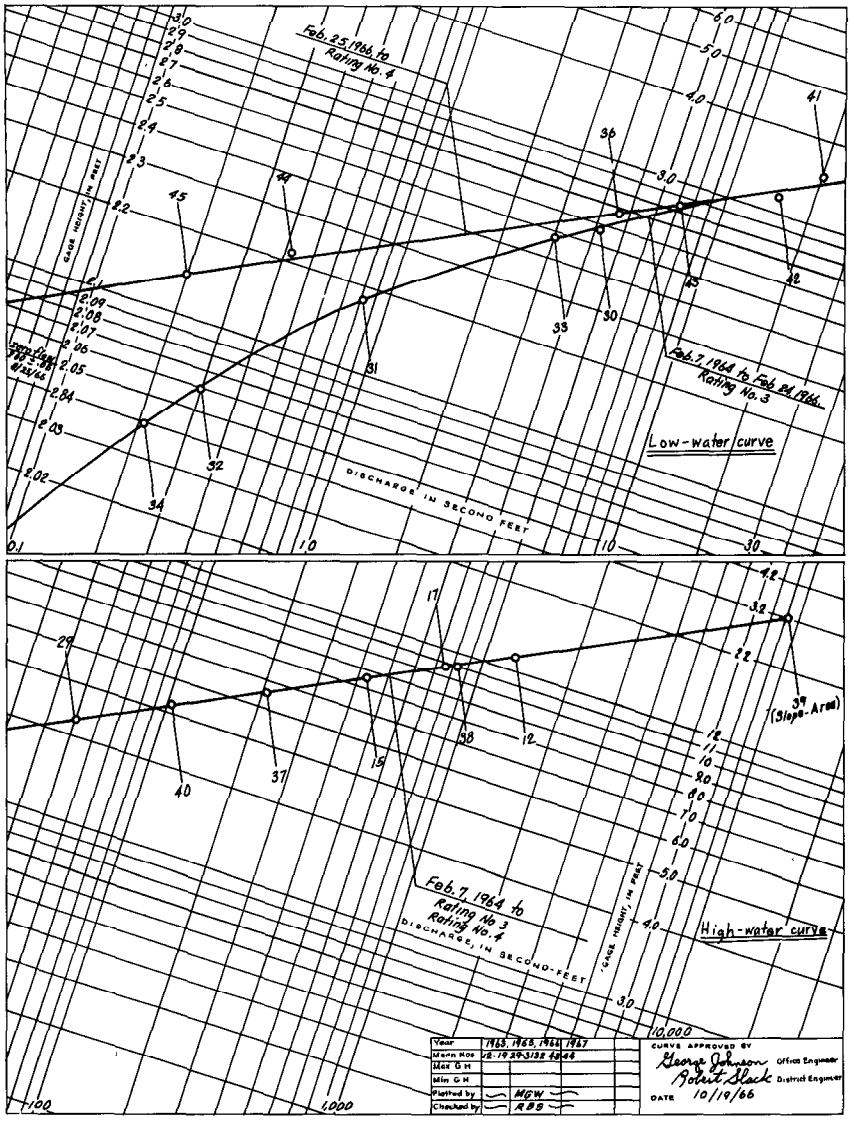

FIGURE 263.—Logarithmic plot of rating curve.

probably went out on a small rise in stage on February 24. Consequently a new rating curve (rating no. 4), based on measurements made after February 24, was developed for use starting February 25. Rating no. 4 is identical with rating no. 3 above a stage of 3.00 ft. One would expect the rating to change as a result of the major peak of May 27 (meas. no. 39), but no such change was evident from subsequent discharge measurements.

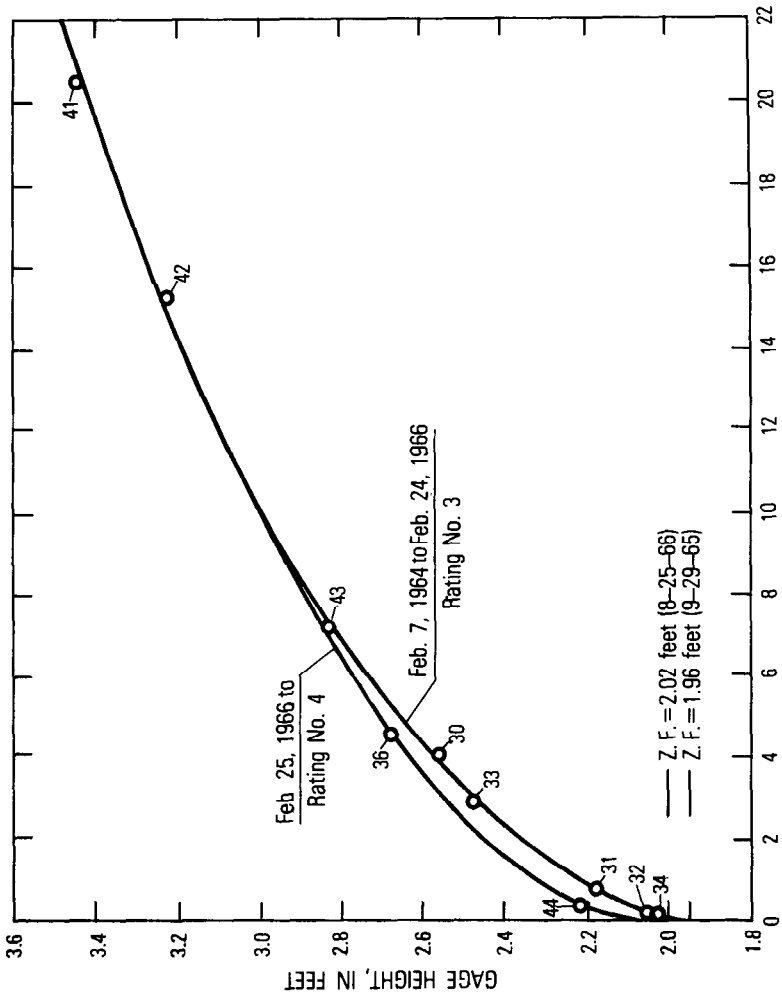

FIGURE 264.—Rectangular plot of low-water rating curve.

When discharge measurements depart from the rating curve by more than 5 percent, but the indicated change in rating is short-lived—less than a month or two—it is common practice not to establish a new rating curve, as such, for the short period. Instead, gage-height shifts (adjustments) are applied either to the rating in use prior to the period of shifting control or to a new rating, if one is later needed, that is established for use starting with the period of shifting control. (Shifts are discussed in detail in the section in chapter 10 titled, "Shifts in the Discharge Rating.") In our example for Clear Creek, aside from the period of ice effect shown by measurements nos. 35 and 35A, only one period of shifting control is in evidence. When the hydrographer visited the station on October 9, he found a heavy tree limb lodged on part of the control. He made his discharge measurement (no. 32) and then removed the limb. That is the proper sequence; had he removed the tree limb before the measurement, his results would be misleading unless he waited long enough for the surcharge storage to drain from the pool so that the stage and discharge became stabilized at the lower stage. That may take an hour or more, but if the measurement is made first, the drop in stage after removing the obstruction can be read later from the stage graph or punched tape. To get back to measurement no. 32, the stage dropped 0.02 ft after removal of the tree limb, and the measured discharge checked the rating curve at the lower gage height. The limb is believed to have lodged on the control on the recession following the minor rise of September 30. Consequently a shift of −0.02 ft is applied to all stages from October 1 to 1300h October 9 when the limb was removed. During that period 0.02 ft is subtracted from all recorded gage heights before obtaining the corresponding discharge from the rating table.

The period of rating shift that occurs as a result of ice effect is not classed as a period of shifting control because discharges are usually not computed by applying shifts to the gage-height record during an ice-affected period. The method of computing discharge for periods of ice effect is discussed in detail in chapter 10.

The basic rating curves to be used during the water year have now been defined and the next step is to transfer the ordinates of the rating curve to a rating table. That is done to refine the rating curve and to provide a more convenient way of obtaining the discharge corresponding to any given stage. The mechanics of preparing the rating table are described in the next section on "Rating Tables." At this point, we will assume that the rating table for rating no. 4 has been prepared, and the next task is to complete the forms that have been used up to now.

The first items to be considered are the two columns headed "Rat-

ing . . . ." in figure 262. A heavy line is drawn across the columns between the last measurement (no. 35A) for which rating no. 3 was used and the first measurement (no. 36) for which rating no. 4 was used, and above the latter measurement is inserted the heading "Rating 4." For measurement no. 32, the shift of −0.02 is inserted, as shown by the change in stage when the tree limb was removed from the control. Percentage differences are recomputed for measurements nos. 36–44, using discharges from rating table no. 4 as a base. The originally computed percentage differences for those measurements made at a stage greater than 3.00 ft will remain unchanged because the rating above the stage is unchanged. Shifts are computed and entered for the ice-affected measurements (nos. 35 and 35A), but no percentage differences are computed for ice-affected measurements because as mentioned earlier, shifting-control adjustments, as such, are not applied during the ice-affected periods. The shifts computed for ice-affected discharge measurements, therefore, are not an absolute requirement; they are shown solely for the purpose of giving the rating analyst a quick view of the magnitude of the backwater effect caused by ice. As an example of how shifts are computed, we consider measurement no. 35. The measured discharge of 2.15 ft^3/s corresponds to a gage height of 2.37 ft in rating table no. 3. The observed stage was 3.12 ft. The shift adjustment is −0.75 ft because that is the adjustment that must be applied to the observed stage (2.37 − 3.12) to obtain the stage corresponding to a discharge of 2.15 ft^3/s in rating table no. 3.

On figures 263 and 264 a closing date is added to rating curve no. 3. Rating curve no. 4 is replotted from the refined table for that rating—departures from the original plot of the rating should be very minor—and the new curve is tagged with its identifying number and the date on which it became effective.

To return to generalities about plotting discharge measurements and rating curves, the number of measurements and curves that have accumulated on a rating-curve sheet may in time be sufficient to clutter the sheet to the extent that the data are confusing. In that event a new rating curve should be drawn on a fresh sheet. Old high-water and extreme low-water measurements that are needed as supporting data for the new rating curve are transferred to the new curve sheet.

In the Clear Creek example that has been discussed, there was no need to extrapolate the rating curve. A slope-area determination of discharge had been made at the peak stage to define the high-water end of the curve, and current-meter discharge measurements defined the low-water end of the curve. Had extrapolation been required for either end of the curve, it would have been done by use of the methods

discussed in the section in chapter 10 titled, "Extrapolation of Rating Curves."

RATING TABLES

The rating table is a tabular expression of the information that is graphically presented by the rating curve. A part of rating table no. 4 for the Clear Creek example is given in figures 265 and 266.

In preparing the rating table from the rating curve, it is important to transfer to the table the identifying number of the rating and its starting date or period of application. Then starting with the low-water curve, the discharge is read and tabulated at intervals of 0.1 ft of stage on the standard rating-table form (fig. 265). On reaching the stage where the rating curve is no longer strongly curvilinear, the discharge may be tabulated at intervals of 0.5 ft of stage, and when the curve becomes more linear, the discharge is tabulated at intervals of 1.0 ft or more. For those parts of the rating that are truly linear on a logarithmic plot, the discharge may be computed from the equation of the rating (chap. 10). The blank spaces in the discharge column of the rating curve are then filled with values that are interpolated between the discharges that were entered in the table.

Differences in discharge for each 0.1 foot of gage height are then computed and entered in the appropriate column of the rating table (fig. 265). The differences should increase uniformly with stage, but this will seldom result from the discharges first entered from the rating curve. It will be necessary to adjust the differences so that they do vary uniformly, which in turn will necessitate a recomputation of the discharge figures, starting with the lowest value whose difference has been adjusted. The adjustment of the rating table must be done judiciously so that the recomputed discharges do not depart significantly from the original rating curve values, particularly in the vicinity of the plotted discharge measurements. Because the rating curve usually has changes in slope, the variation of the difference values can seldom be perfectly uniform. The aim of the smoothing process is to eliminate abrupt changes in the progression of differences, because those abrupt changes would indicate sharp bends in the rating curve. The differences should never decrease with increasing stage unless there is an actual reversal in the shape of the rating curve. Such reversals can only occur where some impeding effect on the discharge (increased backwater) comes into play; for example, where an arch bridge is the high-water control, the increase in waterway area with stage slows and finally ceases at the stages where the archway becomes submerged.

If difficulty is encountered in smoothing the progression of difference values while still adhering to the rating curve, it is helpful to compute second differences, that is, the differences between the dif-

9-210
(Rev. 2-67)

UNITED STATES DEPARTMENT OF THE INTERIOR
GEOLOGICAL SURVEY (WATER RESOURCES DIVISION)

Sta. No. 11224500
Table No. 04
Begin 66 02 25 00 (YR MO DA HR)

Rating table for Clear Creek near Utopia, Calif.
from Feb. 25, 1966 to ..... from ..... to ..... from ..... to .....

Gage height	Discharge	Difference	Gage height	Discharge	Difference	Gage height	Discharge	Difference	Gage height	Discharge	Difference	Gage height	Discharge	Difference	Gage height	Discharge	Difference	Gage height	Discharge	Difference
feet	cfs	cfs	feet	cfs	cfs	feet	cfs	cfs	feet	cfs	cfs	feet	cfs	cfs	feet	cfs	cfs	feet	cfs	cfs
2.00	0		4.00	40	4	6.00	160	8	8.00	360	12	10.00	640	16	12.00	1,000	20	14.00	1430	25
.10	.10	curvilinear	.10	44		.10	168		.10	372		.10	656		.10	1,020		.10	1455	
.20	.40		.20	48	4	.20	176	8	.20	384	12	.20	672	16	.20	1,040		.20	1480	
.30	.90		.30	52		.30	185		.30	396		.30	689		.30	1,060		.30	1505	
.40	1.6		.40	57	5	.40	194	9	.40	409	13	.40	706	17	.40	1,080		.40	1530	
.50	2.5	1.1	.50	62		.50	203		.50	422		.50	723		.50	1,100		.50	1555	
.60	3.6	1.3	.60	67	5	.60	212		.60	435		.60	740		.60	1,120		.60	1580	
.70	4.9	1.5	.70	72	6	.70	221	9	.70	448	13	.70	757	17	.70	1,140		.70	1605	
.80	6.4	1.7	.80	78		.80	230	10	.80	462	14	.80	774	18	.80	1,160		.80	1630	
.90	8.1	1.9	.90	84		.90	240		.90	476		.90	792		.90	1,180		.90	1655	
3.00	10.0	2.1	5.00	90		7.00	250		9.00	490		11.00	810		13.00	1,200		15.00	1680	
.10	12.1	2.3	.10	96		.10	260		.10	504		.10	828		.10	1,220		.10	1705	
.20	14.4	2.5	.20	102	6	.20	270	10	.20	518	14	.20	846	18	.20	1,240		.20	1730	
.30	16.9	2.7	.30	108	7	.30	280	11	.30	532	15	.30	864	19	.30	1,260	20	.30	1755	25
.40	19.6	2.9	.40	115		.40	291		.40	547		.40	883		.40	1,280	25	.40	1780	30
.50	22.5	3.1	.50	122		.50	302		.50	562		.50	902		.50	1,305		.50	1810	
.60	25.6	3.3	.60	129	7	.60	313	11	.60	577	15	.60	921	19	.60	1,330		.60	1840	
.70	28.9	3.5	.70	136	8	.70	324	12	.70	592	16	.70	940	20	.70	1,355		.70	1870	
.80	32.4	3.7	.80	144		.80	336		.80	608		.80	960		.80	1,380		.80	1900	
.90	36.1	3.9	.90	152	8	.90	348	12	.90	624	16	.90	980	20	.90	1,405	25	.90	1930	30

This table is applicable for open channel conditions. It is based on 20 discharge measurements made during 1963, 65 and 66 water years and is ..... well defined between 0 cfs and 1,500 cfs and extended to slope-area meas. at 9,300 cfs. Same as rating no. 3 above

Comp by LRG date 10/18/67
Ckd by RHH date 10/18/67

gage height 3.00 ft.

U.S. GOVERNMENT PRINTING OFFICE 1967 O—249-765

FIGURE 265.—Standard rating table.

P-210 b
(2-67)

UNITED STATES DEPARTMENT OF THE INTERIOR
GEOLOGICAL SURVEY (WATER RESOURCES DIVISION)

Sta No 10245000
Table No 04
Begin 66 YR 02 MO 25 D 00 HR

Rating table for Clear Creek near Utopia, Calif

from Feb. 25, 1966 *to* — , *from* — *to* — , *from* — *to* —

Gage height	Discharge	Gage height	Discharge	Gage height	Discharge	Gage height	Discharge	Gage height	Discharge	Gage height	Discharge	Gage height	Discharge	Gage height	Discharge	Gage height	Discharge	Gage height	Discharge
Feet	Cfs	Feet	Cfs	Feet	Cfs	Feet	Cfs	Feet	Cfs	Feet	Cfs	Feet	Cfs	Feet	Cfs	Feet	Cfs	Feet	Cfs
2.00	0	2.20	0.90	40	1.60	60		80		00		20		40		60		80	
01	0	21	.94	41	1.68	61		81		01		21		41		61		81	
02	0	22	.98	42	1.76	62		82		02		22		42		62		82	
03	.01	23	.52	43	1.84	63		83		03		23		43		63		83	
04	.02	24	.56	44	1.92	64		84		04		24		44		64		84	
05	.03	25	.60	45	2.00	65		85		05		25		45		65		85	
06	.04	26	.66	46	2.10	66		86		06		26		46		66		86	
07	.05	27	.72	47	2.20	67		87		07		27		47		67		87	
08	.06	28	.78	48	2.30	68		88		08		28		48		68		88	
09	.08	29	.84	49	2.40	69		89		09		29		49		69		89	
2.10	.10	30	.90	50	2.50	70		90		10		30		50		70		90	
11	.12	31	.96	51		71		91		11		31		51		71		91	
12	.14	32	1.02	52		72		92		12		32		52		72		92	
13	.16	33	1.08	53		73		93		13		33		53		73		93	
14	.19	34	1.15	54		74		94		14		34		54		74		94	
15	.22	35	1.22	55		75		95		15		35		55		75		95	
16	.25	36	1.29	56		76		96		16		36		56		76		96	
17	.28	37	1.36	57		77		97		17		37		57		77		97	
18	.32	38	1.44	58		78		98		18		38		58		78		98	
19	.36	39	1.52	59		79		99		19		39		59		79		99	
	.40		1.60																

This table is applicable for open-channel conditions. It is based on 20 discharge measurements made during 1963, 65 and 66 water years and is well defined between 0 cfs and 9,300 cfs.

Comp by LRG date 10/18/67
Ckd by RHH date 10/18/67

GPO 1967 O—265-764

FIGURE 266.—Expanded rating table.

ferences per tenth of a foot of stage. The second differences are then adjusted so that they form a uniform progression; second differences usually change quite slowly. After adjusting the second differences, the first differences are recomputed and finally the discharges are recomputed. As an aid in smoothing the second differences, it is often helpful to plot second differences against stage and then fit a smooth curve to the plotted points. It is highly desirable that a smooth rating table be obtained, but too great an effort to attain the ultimate in smoothness is unwarranted.

To obtain discharges from the rating table for gage heights that are expressed in hundredths of a foot, the discharges are computed by linear interpolation between the values shown for tenths of a foot of stage. Where sharp curvature occurs at the low-water end of the rating curve, such interpolation may be too crude. In that case the discharge for each hundredth of a foot of stage is picked from a large-scale plot of the low-water rating curve, and the discharge values are transferred to an expanded rating table (fig. 266).

Each rating table should be complete within itself for the entire range of stage through which it will be used so that it will not be necessary to refer to some other table that may be identical in part. For example, rating no.4 for Clear Creek is identical with the preceding rating no. 3 at stages above 3.0 feet. Nevertheless, rating no. 4 is completed in figure 265 for all stages above 3.0 ft so that there will be no shuffling back and forth between rating table sheets when applying discharges to recorded stages. By having each rating table complete in itself, the probability of error is reduced. If, as in the case of rating no. 4, the rating is identical with some former rating for some particular range of stage, that fact should be noted at the bottom of the rating table. The blank spaces below the rating table should also be filled to indicate the data on which the rating is based, the range of discharge that has actually been measured by current meter, and the basis of rating-curve extrapolation. As mentioned earlier, the completed rating table is used as the basis for computing the percentage differences for discharge measurements in figure 262, and it is also used to replot the rating curves in final form in figures 263 and 264. As a general rule, no more than three significant figures are used for discharge in the rating table.

STATION RATING—THREE-PARAMETER DISCHARGE RELATION

When a station rating involves three parameters—stage, discharge, and a third parameter such as fall or velocity index—the instructions given in the preceding sections will require some amending. The list of discharge measurements (fig. 262) will require an additional column for the third parameter. The additional column can

be provided by reducing the width of the "Remarks" column or by using the column normally reserved for outside gage height.

The general principles concerning the plotting of the discharge measurements and rating curves remain unchanged, but additional curves are required as shown, for example, in figures 190–195. The curves may be plotted on rectangular-coordinate graph paper, as shown in figures 190–195, but logarithmic graph paper may be preferable because then the principles of rating analysis are more easily followed. It may also be advantageous to use more than one sheet of graph paper for the curves to avoid clutter and attendant confusion in working with the graphs.

Because a 3-parameter discharge relation requires more than one relation curve—for example; a rating-fall curve, a fall-ratio curve, and a Q_r rating curve—more than one rating or relation table is required. The general principles discussed on the preceding pages for transferring curve ordinates to a table are applicable for any table.

COMPUTATION OF DISCHARGE RECORDS FOR A NONRECORDING GAGING STATION

The computation of discharge records for a nonrecording gaging station is identical with that for a recording station equipped with a graphic recorder, except for the early steps in computing the gage-height record. Consequently only those early steps will be discussed in this section of the manual. The remaining steps in the computation of the discharge record are discussed on those pages of this chapter that deal with stations equipped with graphic stage recorders.

COMPUTATION OF GAGE-HEIGHT RECORD

The first step in computing the record for a nonrecording gage is to compare the readings on the weekly gage cards mailed in by the observer with those he has entered in his quarterly book of gage height observations. (See introductory pages of the section in chapter 4 titled, "Nonrecording Stream-Gaging Stations.") The observer's readings should also be compared with readings made by the hydrographer on his regular visits. After reconciling any differences, the next step is to apply datum corrections, if any, to the observed gage heights. Both the corrections applied and the corrected gage-height values are entered in the book of gage observations (fig. 8). The corrected gage-heights are plotted at the appropriate time ordinates on fragments of unused recorder chart that are excess when a new roll of recorder paper is installed in a graphic stage-recorder. It is not necessary to plot gage heights for the long periods of gradually receding flows that follow stream rises. For the days during such periods, the

daily mean gage heights are computed as the mean of the two observed readings for each day.

A stage hydrograph is sketched through the plotted gage heights, using the graphic stage record from a nearby recording gaging station as a guide to the probable shape of the stage hydrograph. Observed high-water marks, for each of which the gage-height has been determined, and crest-stage gage readings are used where available, to give the peak stage of major rises. (Crest-stage gages are discussed in the last section of chapter 4.) The result is a stage hydrograph which, from the standpoint of discharge-computation methodology, is equivalent to the stage record from a graphic recorder after the recorder chart has had time and gage-height corrections applied to it.

Consequently, the remaining steps in computing the discharge record are, in effect, continued on the pages that follow the discussion of time and gage-height corrections for graphic-recorder charts. As mentioned above, from that point on the computation procedures are identical for nonrecording and graphic stage-recorder stations.

COMPUTATION OF DISCHARGE RECORDS FOR A RECORDING STATION EQUIPPED WITH A GRAPHIC RECORDER

COMPUTATION OF GAGE-HEIGHT RECORD

At a station visit when the recorded segment of the gage-height chart is removed and a fresh segment of chart is started, the hydrographer makes note of all information that will be needed in computing daily gage heights. His notations are made both on the end of the recorded chart and on the beginning of the fresh segment of chart. Those notations include name of the station, date, readings on all gages and the time of those readings, the instrument stage ratio, and notes explaining any unusual appearance of the pen trace. In addition to making a pen "tick" at the point where the pen rests at the time of chart removal and again at the time the fresh segment of chart is started, the hydrographer also rotates the float wheel to indicate the pen-reversal points on the chart. If the float wheel of the recorder is equipped with a tape, the step method of checking pen reversal is used. (See fig. 267.) The step method is used in making gage-height corrections to the pen trace and is explained in the section on "Determination of Gage-Height Corrections."

DETERMINATION OF TIME CORRECTIONS

Before determining the time corrections to be applied to the gage-height record, the chart should be dated. Each day is numbered on

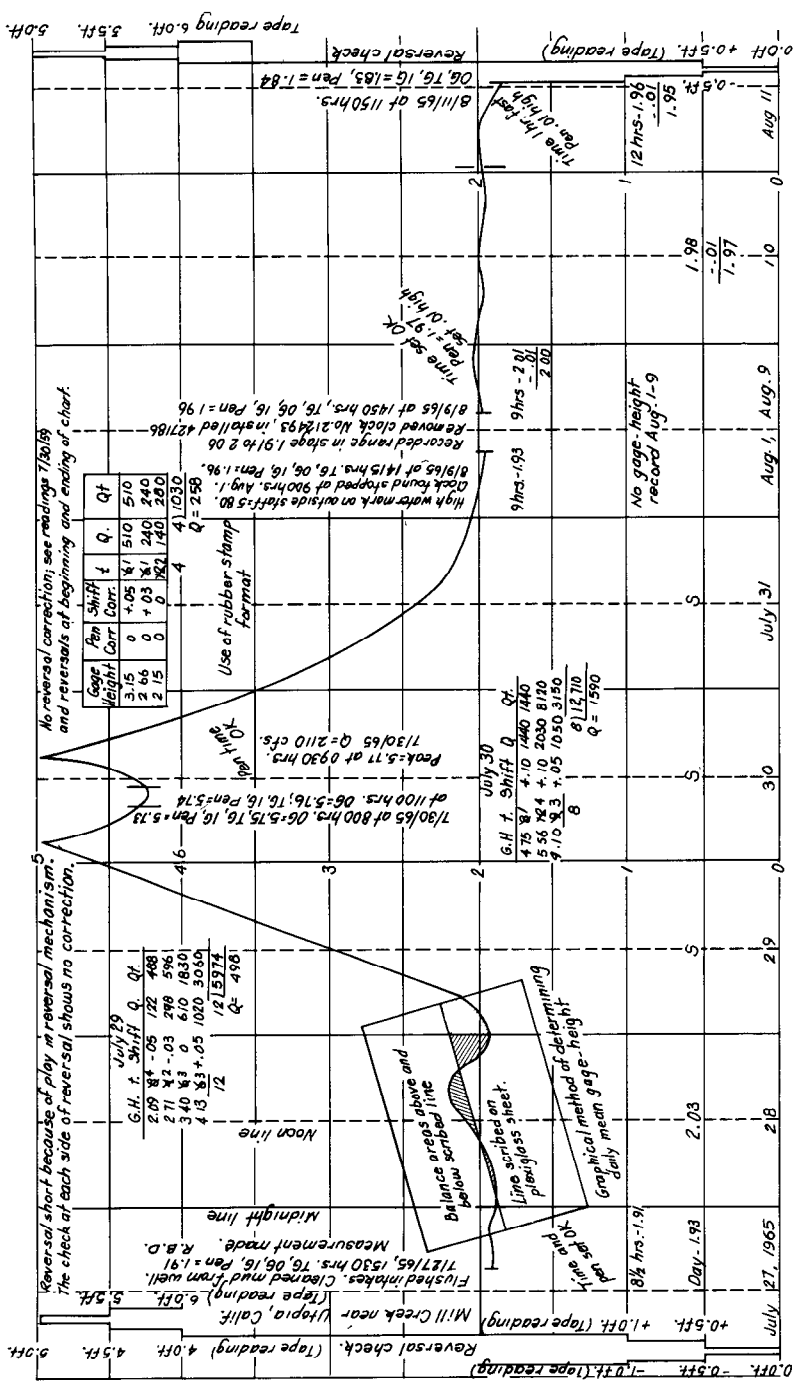

FIGURE 267.—Computation of daily mean gage height on graphic-recorder chart.

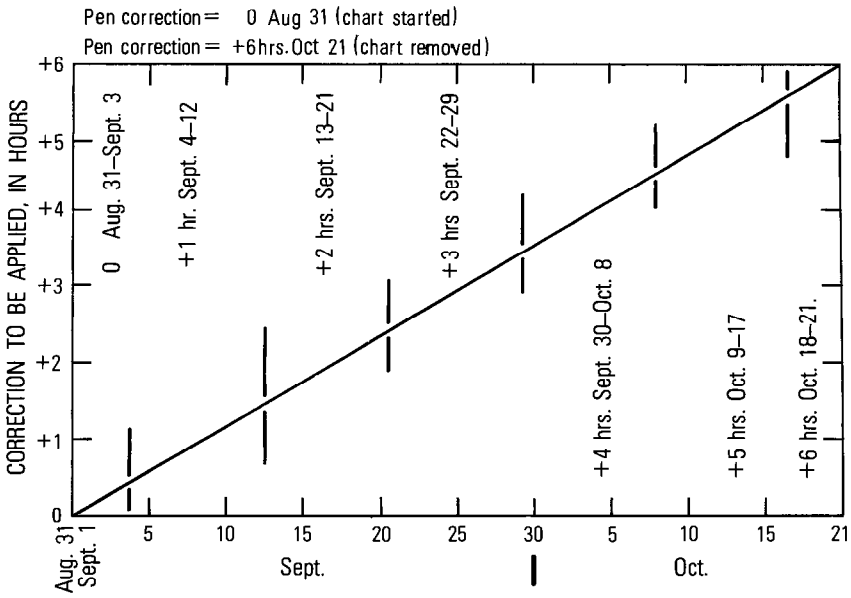

FIGURE 268.—Example of graphical interpolation to determine time corrections.

the lower base line at the noon line. The month is shown about every fifth day, and the year is shown about once a month.

The first step in computing time corrections for a segment of chart is to list the time corrections needed at each of the two or more days when the chart was field inspected. If the time correction at the end of the chart is large, the record should be inspected for evidence of large abrupt timing error—for example, clocks have been known to stop and then restart some hours later. If no abrupt timing errors are found, the time corrections are prorated by straight-line interpolation in which corrections are determined to the nearest hour. Figure 268 is an example of such an interpolation. The graph in figure 268, which is self-explanatory, would normally be drawn on the recorder chart near the beginning of the chart segment being studied. If the total time correction for the chart segment is small, the interpolated distribution of time corrections may be computed arithmetically without the use of a graph.

The computed time corrections are applied by changing the positions of the midnight lines for the affected days. Heavy vertical lines are drawn to indicate the new midnight lines, using care to ensure that the time adjustments are applied in the correct direction. It is advisable to make all interpretive notes, figures, and time corrections in colored pencil on the gage-height chart to differentiate them from the original notes.

DETERMINATION OF GAGE-HEIGHT CORRECTIONS

Gage-height corrections to the recorder trace are next determined. They are based on differences in readings of the recorder pen and the base gage, usually the inside staff, at station inspections. These corrections are also prorated with time unless there is evidence of abrupt instrumental error, such as would occur as a result of float-wheel slippage, or unless a systematic error with stage is shown to exist when the reversal points are checked by the step method at station inspections. An error in setting the pen at the start of a segment of strip chart will be carried throughout the length of that segment, but the original error may be increased or decreased by the above-mentioned errors. Gage-height corrections should be noted on the chart in such a manner that they can be easily applied to the gage-height values that are determined later.

Reversal errors, that is, errors that occur when the pen reverses direction at or near the upper or lower base lines, and systematic errors that vary with stage are usually caused by expansion or contraction of the chart, but they may also be caused by skewed travel of the chart. Reversal errors may also result from wear or maladjustment of the reversal mechanism of the stage recorder.

The step method of checking reversal points when changing the chart in the field provides a means of determining the gage-height corrections that vary with stage. The method requires that the recorder float wheel be equipped with a tape. The procedure used by the hydrographer is as follows:

1. Before removing the chart, raise the float tape to a value that is exactly 1 foot less than the foot mark at which the pen reverses; pull the chart forward a short distance to put an identifying "step" on the chart at that stage (fig. 267). Enter the tape reading on the chart.
2. Raise the float tape an additional half-foot and repeat the procedure.
3. Raise the float tape to the reversal point and repeat the procedure.
4. Repeat the above procedure, first with the tape reading 0.5 ft more than the foot mark at which the pen reverses, and again with the tape reading 1.00 ft more than the reversal foot mark.
5. Continue to raise the float tape and repeat steps 1 to 4 for the other base line reversal.
6. After the recorded segment of chart has been removed and the fresh segment of chart has been engaged, the pen is set to the correct gage height and steps 1 to 5 are repeated.

An example of the step method of checking reversal points is shown in figure 267. The step method in figure 267 actually indicates the need for a correction of +0.01 foot at a recorded stage of 4.99 ft and a

correction of −0.01 foot at a recorded stage of 5.01 ft. In other words a true stage of 5.00 ft is recorded as 4.99 ft on one side of the reversal and 5.01 ft on the other side. However, the gage inspections at 5.73 ft and 5.74 ft indicate that no corrections are needed and none were applied.

As a final step, datum corrections (see section on "Datum Corrections"), if required, are noted for each affected day. The recorder chart is now ready for the determination of daily gage heights.

DETERMINATION OF DAILY MEAN GAGE HEIGHT

Daily mean gage heights are usually determined graphically by the use of a thin rectangular piece of clear plastic whose dimensions are approximately 2 by 4 inches; a centerline is scribed on the plastic parallel to the long edge. The plastic is placed over a 24-hour segment of the recorder chart with the scribed line approximately over the pen trace. The plastic is then maneuvered into a position where the areas bounded by the midnight lines and lying above the scribed line but below the pen trace are equal in size to the areas lying below the scribed line but above the pen trace. When the areas above and below the scribed line are so balanced, the gage height of the point at which the scribed line intersects the noon line is the uncorrected mean gage height for the day. An example of the graphical method of determining daily mean gage height is shown for July 28 in figure 267.

A gage-height correction and (or) a datum correction, if applicable, will have been entered on the chart at about the noon line and about 1½ inches above the base line. The uncorrected daily mean gage height determined by the graphical method is then entered above the correction(s), the required addition or subtraction is performed to obtain the corrected daily mean gage height, and the corrected value is written below the correction as shown for August 10 in figure 267.

SUBDIVISION OF DAILY GAGE HEIGHTS

When there is large variation in stage during the day, it is necessary to: subdivide the day into smaller increments of time, determine the mean gage height for each time increment, apply the corresponding discharge from the rating table to each incremental mean gage height, and compute a time-weighted mean discharge for the day. That procedure is necessary because the stage-discharge relation is curvilinear; consequently the discharge corresponding to the mean gage height for a segment of stage of large range will differ significantly from the true discharge, which is the discharge integrated over that range of stage. The allowable range of stage, for which the use of a mean gage height introduces no significant error in

discharge, depends on the curvature of the stage-discharge relation; the more nearly linear the rating is, the larger the allowable range in stage.

The rule generally followed in the U.S.A. is to subdivide the gage-height graph for the day if the discharge corresponding to the daily mean gage height differs by 4 percent or more from the average of the two discharges corresponding to the maximum and minimum gage heights in the day. For any normal rating table, the average of the two discharges will be the larger figure. A simple method of computing a table of allowable range of stage for a rating is outlined below, using the rating table in figures 265 and 266 as an example.

First, a gage height G is selected near the lower end of the rating. Because the allowable difference in discharge is 4 percent, the average of the two extreme discharges in the allowable range of stage is $1.04\ Q_G$ where Q_G is the discharge from the rating table corresponding to gage height G. That means that $2.08\ Q_G$ equals the sum of the two extreme discharges in the allowable range of stage. (A definition sketch is given in fig. 269.) The analyst using the rating table moves small equal distances in stage up and down from gage height G until he obtains a pair of stages whose discharges total $2.08\ Q_G$. The range,

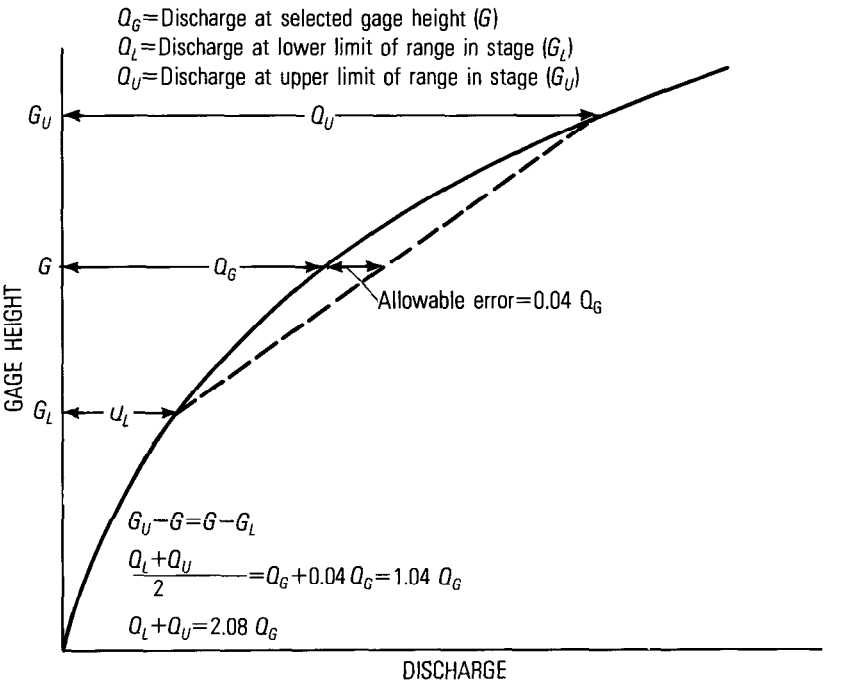

FIGURE 269.—Definition sketch illustrating computation of stage limits for application of discharge.

Mean gage height (ft)	Q (ft^3/s)	Q x 2.08 (ft^3/s)	Allowable limits of stage (ft) / Corresponding discharge (ft^3/s)	Allowable range of stage (ft)
2.2	0 4	0.83	2.15–2.25 (0.22+0.60=0.82)	0.10
2.4	1.6	3.30	2.32–2.48 (1.02+2.30=3.32)	.16
2.8	6.4	13 3	2.65–2.95 (4 25+9.05=13.3)	.30
3.4	19.6	40.8	3.1–3.7 (12.1+28.9=41.0)	.6
4.0	40	83.2	3.6–4.4 (25.6+57.0=82.6)	.8
4.8	78	162	4.2–5.4 (48+115=163)	1.2
6.0	160	333	5.2–6.8 (122+203=325)	1.6
7.5	302	628	6.4–8.6 (194+435=629)	2.2
9.0	490	1020	7.6–10.4 (313+706=1019)	2.8

FIGURE 270.—Results of computation of allowable limits of stage for Rating No. 4, Clear Creek near Utopia, Calif.

in feet, between the pair of stages is the allowable range in stage for a mean gage height of G. The procedure just described is then used to obtain the allowable range in stage for other values of gage height. The results of such computations for the rating table in figures 265 and 266 are shown in figure 270. The information given by the table in figure 270 is reorganized to provide the table of allowable rise shown in figure 271, which is more convenient for use in subdividing days. For days that are subdivided it is not necessary to compute the daily mean gage height.

The table of allowable ranges for subdivision may require some revision for periods when shifting-control adjustments are used.

Gage height (ft)	Allowable rise (ft)	Gage height (ft)	Allowable rise (ft)
2.15	0.10	4.2	1.2
2 32	.16	5.2	1.6
2.65	.3	6.4	2.2
3.1	.6	7.6	2.8
3.6	.8		

FIGURE 271.—Table of allowable rise for use with Rating No. 4, Clear Creek near Utopia, Calif.

However, revision will usually be necessary only in the unusual situation where the shifts to be applied are so extreme that they radically change the shape of the stage-discharge relation.

Either of two methods are used for computing discharge for subdivided days, and the procedure for subdividing the day varies with the method used. The first method is the increment-mean method. In that method the mean gage height is determined for each increment of the day by using the graphical process of balancing areas that was described earlier. Shifts, if appropriate, are applied to the mean gage heights, corresponding values of incremental mean discharge are obtained from the rating table, and a time-weighted daily mean discharge is computed. The time-weighting is done by first multiplying each incremental mean discharge by the number of hours in the increment, then adding the products, and finally dividing the sum of the products by 24 (number of hours in the day). The arithmetic is simplified if the increments of the day are all multiples of either 2, 3, 4, 6, 8, or 12 hours, because then the numerical values of the hours used can be reduced by factoring. For example, if the day had been subdivided into three increments of 6, 6, and 12 hours, those time periods could be expressed as multiples of 6. For weighting purposes, the hour values would be factored to give 1, 1, and 2, and the sum of the products would be divided by 4 rather than 24. (See subdivision for July 31 in fig. 267.)

The procedure for subdividing a day by the increment-mean method is as follows. The analyst starts at the lowest point of the pen trace and moves upward as far as the table of allowable rises will permit. That upper value of stage then becomes the starting point for the next increment of the day, whose upper limit is also determined from the table of allowable rises. The process is continued until the entire day has been subdivided. The ends of the time increments are adjusted to coincide with the nearest hour lines, but the adjustment should, if anything, decrease the range in stage for an increment from that indicated by the table of allowable rises. If feasible, the time increments are further adjusted to permit the factoring discussed in the preceding paragraph.

The second method of computing discharge for subdivided days is the point-intercept method. In that method, gage heights are noted along with the clock hour of occurrence, at the beginning of the day, the end of the day, and at all "breaks" in slope of the stage hydrograph during the 24 hours. It is important, however, not to permit the difference in stage between consecutive recorded gage heights to exceed values given by the table of allowable rises. If the stage difference for a time increment does exceed the allowable rise, one or more additional intermediate points on the hydrograph must be selected

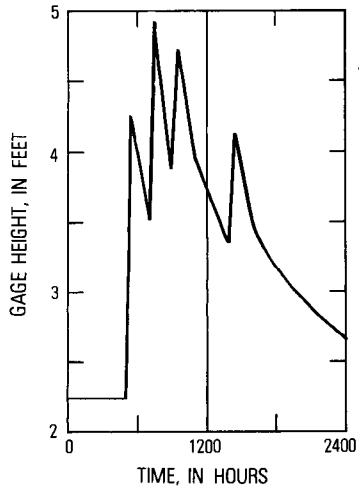

JULY 1

(1) Time	(2) Corrected gate height	(3) Shift	(4) Time increase (hrs)	(5) Discharge (ft^3/s)
0000	2 25	0	2½	24
0500	2.22	0	2¾	22
0530	4 28	0	½	464
0600	4.04	0	¾	392
0700	3.50	0	¾	250
0730	4.94	0	½	716
0800	4 55	0	¾	560
0900	3 87	0	¾	342
0930	4 77	0	½	648
1000	4.49	0	¾	536
1100	3.97	0	2	371
1400	3 34	0	1¾	213
1430	4.16	0	½	428
1500	3 88	0	¾	345
1600	3.48	0	2½	245
2000	2 94	0	4	133
2400	2 66	0	2	79
			24	*5484 5

229.0=Mean Q

*Summation of individual products of column 4 times column 5

FIGURE 272.—Sample computation of daily mean discharge for a subdivided day by point-intercept method.

for use. The end result is a tabulation such as that shown in the example in figure 272 where the gage heights are tabulated at the nonuniform hours associated with breaks in slope of the stage hydrograph.

Computation of the daily mean discharge by the point-intercept method is similar to that for the increment-mean method except for the manner of determining the number of hours (col. 4 of fig. 272) associated with each tabulated gage height. Each of the gage heights is assumed to represent the mean gage height for a time interval that extends from (a) the clock time midway to the preceding tabulated gage height to (b) the clock time midway to the following tabulated gage height. The discharges in column 5 of figure 272 correspond to the tabulated gage heights in column 2 after those gage heights have been adjusted for the shifts, if any, shown in column 3. The time-weighting of the discharge is then done by first multiplying each discharge (col. 5) by the correspnding number of incremental hours (col. 4). The individual products, which are not shown in figure 272, are then added, and finally the sum of the products is divided by 24 (number of hours in the day).

The advantage of the point-intercept method over the increment-mean method of computing daily mean discharge for subdivided days lies in the fact that the point-intercept method provides the data for reproducing the stage or discharge hydrograph for storm runoff. Con-

sequently, the point-intercept method is always used in flood reports. Because daily mean discharges computed by the two methods will seldom agree exactly, it is best to use the point-intercept method, at least for major runoff events. Then if the major runoff event is made the subject of a later flood report, daily mean discharge in the flood report and in the routine annual streamflow report will agree. For complex flood events, such as that shown in figure 272, the point-intercept method will usually give somewhat more accurate daily mean discharges than will the increment-mean method, but only because more gage heights per day are usually used in the point-intercept method for such events. Subdivision is really a crude form of mathematical integration of the hydrograph. Mathematical integration gives the only truly accurate value of mean discharge, and the more points that are used in the subdivision, the more closely the subdivision will resemble integration. The difference in results between mathematical integration and subdivision rapidly dwindles to insignificance when sufficient points are used in the subdivision. Mechanical integrators, now largely superseded by digital recording and computation, are available to compute daily mean discharge for stations having large and frequent stage fluctuations, such as those that occur downstream from hydroelectric power plants.

COMPUTATION OF DAILY DISCHARGE

PREPARATION OF FORM FOR COMPUTING AND TABULATING DISCHARGE

The first step in the computation of daily discharge for a nonrecording station or a recording station equipped with a graphic recorder is to prepare a form, such as USGS form 9–192a which is shown in figure 273, to receive the computed values. The form in figure 273 provides columns for daily mean gage height and discharge for the 12 months in the water year, as well as spaces for monthly and annual summaries which will be discussed in the section on "Completion of the Discharge Form." The analyst fills in the blanks at the top of the form that supply general information such as name of station, drainage area, type of recorder, water-year date, numbers of the rating tables used, and so on. It is important that the form be prepared carefully because the data are copied from this form on to offset sheets used for publication of the data. In addition, prints of the form are often furnished to water users as preliminary data in advance of the published data.

Daily mean gage heights from the original water-stage recorder chart are copied in the columns headed "Gage height." In addition, the maximum and minimum gage heights that occurred during the year are listed in the spaces provided at the left margin. For those days that are subdivided for the computation of daily discharge, no

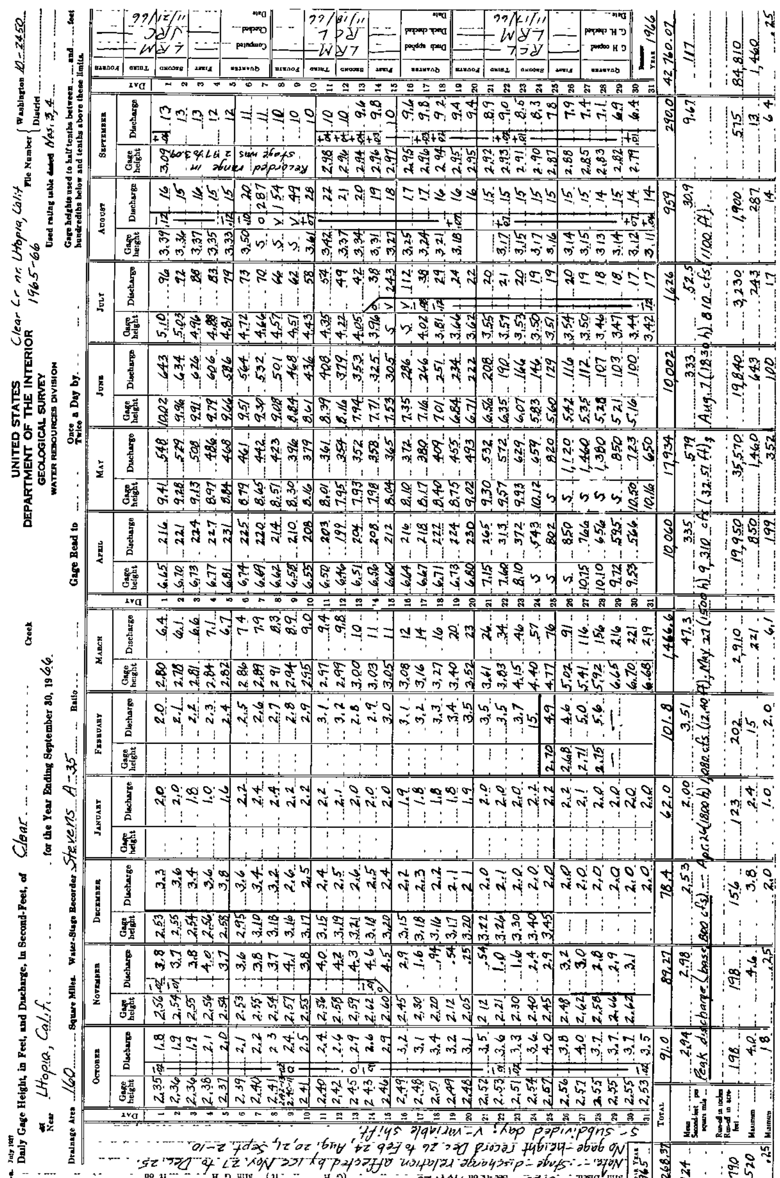

FIGURE 273.—Computation of daily discharge.

figures of daily mean gage height will be computed; for those days an uppercase letter "*S*" is entered in the gage-height columns. That symbol, as well as any others that are used, is explained by a footnote in the left margin; for example "*S*—subdivided day." For days of recorder malfunction, if the daily mean gage height is computed from a graph based on the observer's gage readings, the symbol "*g*" is added to the left of the gage-height value.

In a last step before applying discharges from the rating table to the gage heights, values of shifts to be applied are entered in columns constructed on the left side of the wide columns headed "Discharge" in figure 273. Little has been said about shifts in this chapter of the manual because they have been discussed in detail in the section in chapter 10 titled, "Shifts in the Discharge Rating." Shifts, it will be recalled, may vary with stage. If, during a subdivided day, shifts of varying magnitude are to be used because of the varying stage during the day, the symbol "v" is used in place of a numerical value in the shift column. The application of discharges to gage heights for subdivided days has been discussed in the section on "Subdivision of Daily Gage Heights." The reader is warned at this point that the shifts shown in figure 273 have no relation to the rating-curve analysis discussed in the section on "Rating-Curve Analysis." That analysis for Clear Creek indicated only a short period of shifting control in early October. Shifts have been scattered throughout figure 273 for the purpose of illustrating various conditions in applying discharge.

DETERMINATION OF DISCHARGE FROM THE GAGE-HEIGHT RECORD

Discharges are determined by applying the appropriate rating tables to the gage heights tabulated in figure 273. The rating analysis indicated a change in the rating after February 24, rating no. 3 being used up to and including that date and rating no. 4 thereafter. Consequently, before applying discharges a heavy horizontal line is drawn in the discharge column of figure 273 between February 24 and February 25 to warn the analyst of the change in rating on February 25. The daily mean discharges, in cubic feet per second, are entered in the discharge columns of figure 273. Daily discharges are shown to the nearest hundredth from 0.01 to 0.99 ft^3/s, to the nearest tenth from 1.0 to 9.99 ft^3/s, to the nearest unit from 10 to 999 ft^3/s, and to three significant figures above 1,000 ft^3/s. Where shifts are indicated, the amount of the shift is added algebraically to the tabulated gage height, and the discharge corresponding to the shift-adjusted gage height is determined from the appropriate rating table. It is important that there be no discontinuity between the discharge on the last day of the preceding water year and the first day of the

current water year. That can easily occur if a new rating table is placed in effect on the first day of the current water year, or if shift adjustments to the gage height are used on either or both the first and last days of the two water years. Consequently the discharge for the last day of the preceding water year should be examined to ensure consistency.

To facilitate the determination of discharges from the rating table, it is advisable to expand the rating table to show the discharge for each one-hundredth of a foot of stage, as in figure 266, to cover the frequently occurring stages. For example, if the rating table were expanded to a stage of 7.0 ft, it would cover most of the gage heights tabulated in figure 273, thereby reducing the probability of error in mentally interpolating discharge values between the tenths of a foot of stage given in the standard rating table (fig. 265).

At this point all boxes for daily mean discharge in figure 273 will have been filled, except those opposite gage-height boxes that are blank for lack of record because of instrument malfunction, or those opposite gage-height boxes that carry the symbol "S" for subdivided day. The discharges for subdivided days are next computed. The method of computation was explained in the section on "Subdivision of Daily Gage Heights." The daily mean discharges are computed on the gage-height chart, as shown in figure 267, where the increment-mean method of computation was used. The computed discharges are then transferred to the discharge columns in figure 273.

ESTIMATION OF DAILY DISCHARGE FOR PERIODS OF INDETERMINATE STAGE-DISCHARGE RELATION

After the mean discharge has been computed for each day of the water year for which there is a gage-height record, a hydrograph of daily mean discharge is prepared on a form that has a logarithmic discharge scale. Discharge measurements are also plotted on the hydrograph sheet. The hydrograph is used for comparison with similar hydrographs of daily discharge for nearby stations as a test for consistency of the computed record. Obviously such comparison is only valid for streams whose daily flow is essentially natural, that is, not controlled significantly by the works of man. Hydrographic comparison usually brings to light any serious errors in the basic data computations and interpretations; it also provides a means of estimating discharge for days of no gage-height record and for days of indeterminate stage-discharge relation. A period of indeterminate stage-discharge relation does not refer to one in which the gage-height record is faulty; if the recorded gage-heights do not reflect the true stage of the stream, the period affected is considered to be one of no gage-height record. A period of indeterminate stage-discharge relation is one for

which a satisfactory gage-height record is available, but one for which no stage-discharge relation can be determined. The most common situation of that kind occurs during an ice-affected period, and it may also occur during the passage of sand waves in an alluvial channel. Sometimes ephemeral backwater effect occurs when a channel is choked by debris for a few days, but in that situation the stage-discharge relation is not really indeterminate but is merely undefined because of the limited opportunity to define it by discharge measurements.

A period of indeterminate or undefined stage-discharge relation is indicated on the discharge tabulation form (fig. 273) by a heavy vertical line drawn between the gage-height and discharge columns. Such a line appears in November and December in figure 273 to indicate that the ice-affected discharges during those months bear no relation to the recorded stages. Where preliminary discharge values from the rating table have been entered for such days in figure 273 and are then shown by hydrographic comparison to be in error, they are replaced in figure 273 by the revised discharge figures.

Periods of ice effect.—The method of estimating discharge during periods of ice effect was discussed in detail in chapter 10 and will not be repeated here. Measurements nos. 35 and 35A (fig. 262) clearly indicated, by the magnitude of the backwater effect (shift values), that ice affected the stage-discharge relation.

Other periods of indeterminate stage-discharge relation.—For periods of indeterminate stage-discharge relation other than ice effect, discharges are estimated as though they occurred during periods of no gage-height record. Methods of treating periods of no gage-height record are described on the pages that follow; hydrographic comparison is one of those methods.

ESTIMATION OF DAILY DISCHARGE FOR PERIODS OF NO GAGE-HEIGHT RECORD

The analyst is often required to estimate discharge for periods of no gage-height record resulting from recorder malfunction, or a frozen well, or a plugged intake. Such periods are shown in figure 273 for periods December 26 to February 24, August 20–21, and September 2–10. The task of the analyst is greatly facilitated if the fieldman who finds the gage-height record incomplete makes an effort to collect as much supplementary information as possible. An attempt should be made to get the range in stage during the period of no gage-height record because that information indicates the limits of discharge within which any estimates made may vary. If the clock has stopped but the pen continues to function, the vertical line recorded on the chart will give the range in stage. Because of the possibility of the pen

reversing during the period of no record, when the pen was scribing a vertical line, there may be some doubt as to the maximum gage-height reached during that period. If the tape gage is equipped with either a magnet or wire clip for indicating peak stage (see the section in chapter 10 titled, "Operation of a Recording Stream-Gaging Station"), the peak indicated by either of those devices should be noted. High-water marks should be sought both in the well and outside the gage structure. If the intakes have been plugged or the well frozen and a high stage had occurred during the period of no record, again an outside high-water mark should be sought. Local residents should be interviewed in an attempt to determine the time the peak occurred.

The previously mentioned annual hydrograph of daily mean discharge, with gaps left for periods of no gage-height record, along with the annual hydrograph of daily discharge for nearby stations, are prerequisites for estimating the discharges sought. Each of the station hydrographs should be plotted on a separate graph sheet, but the logarithmic discharge scales and time scales on the individual sheets should be identical. It is particularly helpful if one or more of the stations used is on the same stream as the station being studied. The hydrographs for uncontrolled streams in the same vicinity will usually have similar patterns of discharge.

In the discussion that follows, the procedure for estimating discharge for periods of no gage-height record is described under the following subheadings:

1. No gage-height record during a low- or medium-flow recession on an uncontrolled stream.
2. No gage-height record during periods of fluctuating discharge on an uncontrolled stream.
3. No gage-height record for a station on a hydroelectric powerplant canal.
4. No gage-height record for a station immediately downstream from a reservoir.
5. No gage-height record for a station on a controlled stream where the station is far downstream from the known controlled release.

CASE A. NO GAGE-HEIGHT RECORD DURING A LOW- OR MEDIUM-FLOW RECESSION ON AN UNCONTROLLED STREAM

If the vertical trace left by the inoperative recorder indicates no stages higher than that when the clock stopped nor any stages lower than that when the stoppage was discovered, there may well have

been an unbroken recession from the time the clock first stopped. The hydrographs plotted for other nearby stations, particularly those on the stream being studied, should then be examined. If there is no evidence of anything but an unbroken recession, the discharge should be estimated by semilogarithmic interpolation. That is, the gap in the logarithmically plotted hydrograph for the station being studied should be filled by either a straight line or a smooth flat curve, depending on which best merges with the graph on either side of the dates of no gage-height record. The daily discharges that are estimated on the hydrograph are then transferred to the discharge-tabulation form with appropriate notation. (See record for September 2–10 in fig. 273.) If the period of no gage-height record involves only a few days, it is permissible to interpolate gage heights graphically on the recorder chart and then obtain the corresponding discharges from the rating table. That was actually done for August 20, 21 in figure 273.

CASE B. NO GAGE-HEIGHT RECORD DURING PERIODS OF FLUCTUATING DISCHARGE ON AN UNCONTROLLED STREAM

If a short period of recorder stoppage occurred near the peak of a stream rise, such as might occur if the float could not operate freely, knowing the peak stage of a stream makes it possible to sketch in the missing portion of gage-height record on the recorder chart. An even better estimate can be made on the recorder chart if the time of the peak is also known.

If long periods of no gage-height record are involved, the best method of making discharge estimates is by hydrographic comparison. A "light table" is used for the purpose in the manner described in the section in chapter 10 titled, "Hydrographic- and Climatic-Comparison Method." The logarithmic hydrograph of daily discharge for the study station is superposed on the logarithmic hydrograph for the reference station, and the date lines for the two sheets are matched. If the two stations are comparable, the two hydrographs should show similar runoff patterns. The study hydrograph is moved vertically until the hydrographs on either side of the period of no gage-height record match closely, making sure that the date lines match perfectly. An exception, to the perfect matching of date lines occurs, for example, where the two stations are on the same stream, but so distant from each other that the travel time between stations is approximately 24 hours. It would then be necessary to lag the hydrographs by a day. After matching the hydrographs, the missing portion of the study hydrograph is sketched by tracing the underlying reference hydrograph.

The hydrographic comparison also provides a simple means of comparing the runoff yield per square mile (unit yield) for the two stream basins. To make that comparison a short horizontal line, showing drainage-area size is marked on the logarithmic ordinate of each hydrograph. If, when the two hydrographs are matched vertically, the drainage-area lines also match, the two basins have equal unit yield. If the drainage area lines do not match, the basin whose drainage-area line is the lower of the two has the greater unit yield.

More often than not, it will be found that when the low-water part of the study hydrograph is matched with the low-water part of the reference hyrograph, the high-water parts of the two hydrographs do not match, and vice versa. When that occurs, the low-water parts of the two hydrographs are matched for sketching the low-water estimates, and the high-water parts of the two hydrographs are matched for sketching the high-water estimates of discharge. The discharge estimates for the medium-flow part of the study hydrograph is sketched while gradually sliding that hydrograph up or down, as required. Any discharge measurements made at the study station during the period of no gage-height record are especially valuable in positioning the two hydrographs, and unless it is known that the discharge measurement was made at a time of rapidly changing stage and is not representative of daily mean discharge, the sketched discharge on the study hydrograph should pass through the discharge measurement. If the range of stage for the period of no gage-height record is known, no estimated daily mean discharge should be smaller than the discharge corresponding to the minimum gage height for the period; no estimated daily mean discharge should equal or be greater than the discharge corresponding to the maximum gage height for the period, because the maximum daily discharge is seldom as great as the maximum momentary peak discharge. In figure 273 the daily mean discharges for the period of no gage-height record, December 26 to February 24, were estimated by hydrographic comparison with discharges for a nearby station.

It is desirable that hydrographic comparisons be made with more than a single reference station. The different comparisons will give estimates of daily discharge that differ from each other to some degree. In averaging the estimates, the greatest weight should be given to the results obtained from: reference hydrographs that show the closest fit with the study hydrograph; reference hydrographs on the same stream as the study station; and reference hydrographs for stations whose drainage areas approximate that of the study station.

If the period of no gage-height record involves a snowmelt period and the maximum stage is known, the maximum daily mean discharge can often be estimated fairly closely. Discharge has a diurnal

fluctuation during snowmelt periods, and the ratio of maximum daily mean to maximum momentary discharge will vary with such factors as air temperature and date. However, examination of discharge records for the study station and for a snowmelt reference station may show how concurrent ratios vary at the two stations, and thereby give a strong clue to the ratio to be used to estimate maximum daily mean discharge during the period of no gage-height record.

On occasion, the station that has a period of no gage-height record may be located immediately upstream from a reservoir for the purpose of measuring inflow to the reservoir. If reliable records are available showing daily change in reservoir contents and daily spill and release from the reservoir, it is then a simple matter to compute the daily discharge (Q) at the gaging station from the formula:

Q = Daily spill + daily release ± daily change in reservoir contents.

There may be times when record for a flood period is lacking and there is no nearby gaging station with which to compare runoff records. Under those circumstances, daily discharges for the flood period may be estimated from a model study of rainfall-runoff relations. It is beyond the scope of this manual to detail the development of such hydrologic models. A simpler task is to estimate the total volume of storm runoff from precipitation records. For general storms in the past at the study station, tabulate the total storm precipitation, its duration in days, and the total volume of storm runoff in inches or millimeters. Compute the value (infiltration index) that must be subtracted from each daily increment of precipitation during a storm to give the total volume of runoff from that storm. The infiltration index will vary with storms, but it can often be related to antecedent precipitation and month of the year. Apply the appropriate infiltration index to the storm precipitation during the period of no gage-height record to obtain the total volume of storm runoff during that period. This simple method provides only an approximate result; it should be used sparingly for general storms, and not at all for thunderstorms, which usually occur over limited areas.

CASE C. NO GAGE-HEIGHT RECORD FOR A STATION ON A HYDROELECTRIC-POWERPLANT CANAL

For a period of no gage-height record for a station on a powerplant canal, it is generally possible to use the powerplant record of daily kilowatt output to estimate reliably the daily mean discharges. That is done by means of a relation of daily discharge to daily power output that is developed for periods preceding and following the period of no gage-height record.

CASE D. NO GAGE-HEIGHT RECORD FOR A STATION IMMEDIATELY DOWNSTREAM FROM A RESERVOIR

Ratings are often available, or may be computed, for a reservoir spillway, gates, valves, and turbines (see the section in chapter 14 titled, "Pressure Conduits"). Ratings of those types will enable the engineer to estimate the discharge for a period of no gage-height record at a station immediately downstream from a reservoir.

Another method may be used if the reservoir itself is equipped with a stage gage so that a reliable record of daily change in reservoir contents is available. Daily changes in reservoir contents may be added algebraically to the daily mean discharge at the study station downstream from the reservoir to provide daily mean values of reservoir inflow during periods of record at the study station. An annual hydrograph of daily mean reservoir inflow is prepared and is compared with the hydrograph for a nearby natural-flow station. Using the technique described for Case B, the daily mean values of reservoir inflow are estimated for the period of no gage-height record at the study station. The known daily changes of reservoir contents are then subtracted algebraically from those estimated daily values of reservoir inflow to give the required daily discharge at the study station.

CASE E. NO GAGE-HEIGHT RECORD FOR A STATION ON A CONTROLLED STREAM WHERE THE STATION IS FAR DOWNSTREAM FROM THE KNOWN CONTROLLED RELEASE

Case E is a situation somewhat similar to Case D, except that the study station is so far downstream from the reservoir that tributary inflow between the reservoir and the study station cannot be ignored. Outflow from the reservoir cannot be compared directly with the discharge at the study station because the reservoir outflow is completely controlled and the discharge at the study station is partially controlled. The method of attacking the problem is to estimate daily tributary inflow during the period of no gage-height record at the study station, and then to add the estimated daily tributary inflow to the known upstream reservoir releases to obtain the required daily discharges at the study station. What is needed, therefore, is a means of estimating tributary inflow.

Daily releases from the reservoir are subtracted from the daily mean discharge at the study station to provide daily mean values of tributary inflow during periods of record at the study station. An annual hydrograph of daily mean tributary inflow is prepared and is compared with the hydrograph for a nearby natural-flow station. Using the technique described for Case B, the daily mean values of tributary inflow are estimated for the period of no gage-height record

at the study station. As mentioned above, those estimated values of tributary inflow, when added to the concurrent reservoir releases, give the required discharges at the study station.

The above computational procedure may also be used for study reaches of channel that have diversions as well as tributary inflow, provided that the diverted discharges are measured. In that situation, the diversions must be subtracted from the reservoir releases. In other words, for reservoir release or outflow in the above description, we substitute reservoir outflow minus diverted flow.

COMPLETION OF THE DISCHARGE FORM

After all daily mean discharges have been entered on the discharge form (fig. 273), little is required to complete the form. Discharges from the appropriate rating table are entered in the left margin for the maximum and minimum stages of the water year that were previously recorded there. The summary discharge values at the bottom of figure 273 for each month, the water year, and the calendar year, are next computed. The mechanics of computing those total and average values are self-evident. The remaining entry in figure 273—peak discharges above a stated base—requires some explanation.

For stations whose high flows are not significantly regulated, peak discharges are shown for all peaks whose discharge equals or exceeds a chosen peak discharge, regardless of the number of peaks that occur in any given water year. A properly chosen base discharge is one that is exceeded, on the average, three times a year. The following suggestions are offered for selecting the base discharge:

1. For stations having records of more than 5 years, list the annual flood peaks, compute their recurrence intervals (R) in years by the formula, $R = (N + 1)/M$, and select as a base the discharge (rounded upward to two significant figures) whose value of R is 1.15 years. (In the formula, N is the number of years of record; M is the order number of the peak discharge after the peaks have been ranked in order of magnitude starting with 1 for the greatest peak.)
2. For stations having records of 5 years or less, select a base discharge, guided by judgment and by comparison with nearby stations having records of longer duration. The selected base can be modified as more data become available. It is, therefore, better to select a base discharge originally that is on the low side; if the base is later raised, it is a simple matter to drop originally selected peak discharges that do not exceed the new base value. If it is desirable later to lower the base discharge, it becomes necessary to search the earlier re-

corder charts for peak discharges that are smaller than the original base discharge but greater than the new base.

If two peak discharges that exceed the base discharge occur within 48 hours of each other, it is likely that the two peaks are not independent; only the larger of the two, or the earlier of the two if they are both equal, should be listed. If two adjacent peak discharges, both larger than the base, are separated by more than 48 hours, the lower of the two peaks is shown only if it is at least 1.33 times as large as the discharge of the trough between the adjacent peaks. For periods of diurnal peak discharges caused by snowmelt, only the highest peak that occurred during each distinct period of melting is shown regardless of the fact that other peaks may meet the criterion stated in the preceding sentence.

RECORD OF PROGRESS OF DISCHARGE COMPUTATIONS

Completion of the discharge form (fig. 273) marks the end of the actual computation of discharge for the water year. It is necessary, of course, that all computations be checked before the discharge figures are considered final. Furthermore, it is customary for the checker to initial and date any graphs or computation forms that he checks.

In the interest of efficiency it is advantageous to have a progress check list (fig. 274) attached to the folder in which the station computation forms are kept. The items on the check list are shown in the order in which they should be completed for maximum efficiency. Each item on the list has two boxes on the left margin. A checkmark is placed in the box at the extreme left when the item is completed; a checkmark is placed in the other box when the item has been checked. The supervisor of the discharge computations need only glance at the set of boxes to inform himself of the progress of the computations at a station.

STATION-ANALYSIS DOCUMENT

A complete analysis of data collected, procedures used in processing the data, and the logic upon which the computations were based must be recorded for each year of record to provide a basis for review and to serve as a reference in the event that questions arise about the records at some future date. Such a report is called the "Station Analysis." A record of any changes in: records collected, equipment, location, or other physical features should be included. The document should be written clearly and concisely and should contain sufficient information so that those who are totally unfamiliar with the station will be able to follow the reasoning used in computing the records. A

PROGRESS CHECK LIST
COMPUTATION OF GRAPHIC RECORDER RECORD

Station_____ Water Year_____

Index Number_____

Check work done. Complete in order. Initial when finished.

☐ Review chart for continuity, errors, peaks, faulty record.
☐ Check level notes. Apply datum corrections to chart and measurements.
☐ Check measurements, field notes, level notes for peak data. Enter on chart.
☐ Check mean gage heights of measurements. Compare with chart.
☐ List measurements and observations of no flow chronologically on 9-207 (fig. 262).
☐ Plot measurements on rating curve. Develop new curve and table, if necessary.
☐ Copy gage heights on 9-192 (fig. 273).
☐ Compute shifts, percentage differences on 9-207 (fig. 262).
☐ Enter shift corrections on 9-192 (fig. 273). "S" days on chart.
☐ Write station analysis.

Computed_____ Checked_____

.....

☐ Apply discharge to 9-192 (fig. 273) and "S" days.

Computed_____ Checked_____

.....

☐ Plot hydrograph. Enter measurements. Show drainage area size and discharge from rating tables.

.....

☐ Estimate discharge for ice, missing, doubtful or backwater periods.
☐ Revise and complete daily discharges on 9-192 (fig. 273).
☐ Review and complete station analysis.

Computed_____ Checked_____

.....

☐ Make monthly and yearly computations on 9-192 (fig. 273).
☐ Enter notes, maximum, minimum and peaks on 9-192 (fig. 273).
☐ Revise manuscript from previous year.

Computed_____ Checked_____

.....

Final Review_____

FIGURE 274.—Form showing progress of computation of graphic-recorder record.

station analysis should be prepared for each station, including those for which records are furnished by other agencies.

The introductory paragraphs of the station analysis describe the equipment installed and the hydrologic characteristics of the drainage basin above the station. The remaining sections of the analysis outline the quality of the base data collected and the methods used to convert those data into the final discharge figures. The discussions are organized under the headings that follow.

(Station name and number)
STATION ANALYSIS
(WATER YEAR)

Equipment.—
Hydrologic conditions.—
Gage-height record.—
Datum corrections.—
Rating.—
Discharge.—
Special computations.—
Remarks.—
Recommendations.—

The following detailed discussion of each of the above items describes the type of information to be presented. As mentioned in the introductory pages of this chapter, documentation of that information is made as the various steps in the analysis and computation of the discharge record are completed.

STATION ANALYSIS

Equipment.—Provide a short statement that describes the equipment at the site. Designate the type of gage (float sensor or bubble-gage sensor); type of recorder; measurement facilities; artificial control, if any. Report any changes in equipment that may affect the accuracy of the record. Review the station description, revise it if necessary and include the statement, "Equipment conforms to station description dated. . . ."

Hydrologic conditions.—A brief description of the hydrologic characteristics of the basin should be carried forward in the station analysis from year to year. Review this paragraph and briefly describe any changes that might affect the runoff regime. These changes may result from fire (give date and percentage of basin area affected), or urban development (describe type and extent of development and give approximate dates), or from logging or road building operations. Usually several years elapse before the effects of these hydrologic changes become stabilized. Therefore, even if no changes occur in the current year, this paragraph should carry a statement referring to changes in the recent past such as: "No changes since the fire of August 21, 1961, which burned 6,000 acres of woodland;" or "No increase in urban development since September 1962."

Gage-height record.—Tabulate periods of faulty or no gage-height record and reasons for those problems. Discuss briefly any large instrument errors that affect the accuracy of the gage-height record. If portions of the gage-height record have been synthesized or adjusted on the basis of observers' readings and other data, this should be explained. Do *not* discuss in this paragraph how discharge was computed during periods of no gage-height record. That should be explained in the "Special Computations" paragraph.

Datum corrections.—Confusion frequently exists as to what should be included in this paragraph. Datum errors result from settlement of the base or reference gage to which the recording instrument is set or from movement of the bubble-gage orifice. Care should be taken, particularly with manometer and digital recorder combinations to differentiate between datum corrections and shift corrections. If datum corrections are necessary, the reasons should be explained and corrections listed in tabular form such as:

Period	*Correction applied*
Oct. 1–Jan. 15	+0.04
Jan. 16–Apr. 15	+0.05
Apr. 16–Aug. 3	+0.06
Aug. 4–Sept. 30	0

If applicable use a simple statement such as "None applied, last levels run on (date) ."

Rating.—Start this section with a description of the channel and the control, and provide sufficient detail to give anyone unfamiliar with the site a fairly good picture of the dominant features. Items discussed should include the size of the channel, composition of the bed (sand, gravel, boulders, or bedrock), location of the gage relative to the control, and the approximate elevation of any overflow areas.

Example: "The controlling reach of channel is sharply incised in the flood plain. Bed material is predominantly sand and gravel. The low-water control is generally a gravel riffle which moves up and down the channel in response to flood flows. At bankfull stage (about 21 feet), the channel is about 150 feet wide. At higher stages, it spreads out rapidly to a width of about 300 feet at a stage of 25 feet."

The remainder of the rating paragraph should be a chronological narrative of what occurred, hydraulically, during the year. Begin with a statement as to the number of measurements made and how they plot in relation to the rating curve in use at the end of the previous year. If new ratings are required, explain how this conclusion was reached and what caused the shift from one rating to the

other. State exact time and date when rating changes were made. If ratings are modified during periods of significant flow by use of the shifting-control method, document these rating changes with shift tables or shift curves. These are rating changes too, and require the same explanations that a new table does. Because the reviewer does not always have access to the basic data, it is most important that the distribution of shifts be explained in detail, particularly if any unusual methods were used.

The statement "Shifts were distributed on basis of stage and (or) time" does not constitute a detailed explanation. The reviewer needs sufficient detail so that he can at least determine if a shift must be applied to the maximum and secondary peak stages and know its magnitude. For example, discharge measurements were obtained before and after a peak of 12.55 ft; the measurement preceding the peak shows a shift of −0.26 ft at gage height 2.56 ft, and the one following the peak shows a shift of + 0.06 ft at gage height 9.63 ft. One might reason that the rise scoured out the channel gradually, and the shift was zero at the peak. In the analysis, one might state "It was assumed that the shift of −0.26 ft indicated by measurement No. xx was gradually reduced during rise, and there was no shift at the peak; therefore, the shift between measurements No. xx and xxx was distributed on basis of stage." Or, one might have basis for this statement: "On the basis of shifts indicated by measurements No. xx and xxx and succeeding measurements, shift distribution was made on the assumption that the shift varied during the rise from −0.26 ft at gage height 2.50 ft to +0.06 ft at the peak and remained at +0.06 ft through the date of measurement No. xxx." Those two statements would indicate to the reviewer the shift needed for the peak stage and would give him a better idea of the distribution of shifts that was made. If a shift distribution were made on the basis of time, the statement "Shifts were distributed on the basis of time" is sufficient. However, if a peak discharge occurred during that shifting-control period, a statement should be added giving the shift used for the peak.

Discuss also the adequacy of the high-water rating. Is it defined to within 50 percent of the maximum discharge for the current year on the basis of measurements made during the year? (The 50 percent criterion is discussed early in the section in chapter 10 titled, "High-Flow Extrapolation.") If the extension has been made on the basis of older measurements or on the basis of a slope-area determination (chap. 9), give the date of those measurements or of the slope-area determination and state whether or not significant channel changes might have occurred within the intervening period.

Discharge.—This paragraph is a summary explaining how the stage

records and rating data were combined to produce the discharge record. The information can best be presented in tabular form; an example for a station equipped with a graphic stage-recorder follows. (The table would be more complex for a station equipped with a digital stage-recorder; see page 599.)

Period	*Rating table used*	*Periods of shifting control*
Oct. 1 to Feb. 24	No. 3	Oct. 1–9, Oct. 14 to Nov. 14
Feb. 25 to Sept. 30	No. 4	July 15 to Sept. 1, Sept. 11–30

Special computations.—Describe the methods used for determining discharges during the periods of no gage-height record, ice effect, backwater, or other special conditions. Explain any unusual method for determining shifts. If daily discharges were estimated on the basis of hydrographic comparison with records for nearby stations, state the name of the stations used and how closely the station records compared. If weather records were used in the analysis, give the name or names of the weather stations used.

Remarks.—A statement should be made concerning the general accuracy of the daily records along with special accuracy statements regarding periods of ice effect, no gage-height record, high water, low water, backwater, shifting control, or other unusual conditions. A statement should be made here indicating that a hydrographic comparison was made. Identify station or stations used for comparison and state how well the hydrographs compared. Although the statement concerning hydrographic comparison duplicates some of the material given above under the heading "Special computations," the duplication is warranted because it will expedite the preparation of the "Remarks" paragraph of the manuscript station description. (See figs. 286*H* and 289.) It is helpful if all statements to be included in that manuscript paragraph can be drawn from material in the "Remarks" section of the station-analysis document. The "Remarks" section of the station-analysis document should also include any additional comments pertinent to the analysis of the record.

Recommendations.—A sample recommendation might read, "Flood schedule for next year should place high priority on high water measurements at this site. No measurements greater than 8,000 ft^3/s have been made since 1967. There have been several major peaks since that date."

(Authors) W. W. Smith (date)
A. R. Brown (date)

COMPUTATION OF DISCHARGE RECORDS WHEN A THREE-PARAMETER DISCHARGE RELATION IS USED

The section of this chapter titled, "Station Analysis," ended with a brief discussion of the preparation of the station rating when three parameters are involved—stage, discharge, and a third parameter such as fall or velocity index.

The first step that follows completion of the station rating is the computation of the gage-height record for the base-gage recorder, and for the auxiliary-gage recorder if fall is the third parameter. The daily mean gage heights are determined by the procedures explained for the graphic recorder in the section titled, "Computation of Gage–Height Record." Where subdivision of the day is required, the same time increments are used for both recorder charts. The daily mean fall, or mean fall for a time increment in a subdivided day, is computed by subtracting the downstream stage from the upstream stage. If a velocity index is the third parameter, as for example, where a deflection meter is used, the velocity-index record is used to determine daily mean values of the index or mean values for the time increments used in subdivided days. Gage-heights and velocity-index values are entered on a form similar to, but larger than, the form shown in figure 273. The expansion of the form is to accommodate an additional column each month for recording daily values of the third parameter; the additional column lies between the gage-height and discharge columns that are shown in figure 273.

The mechanics of computing discharge from stage and concurrent values of the third parameter were discussed in chapters 11 and 12. In chapter 11 slope (fall) is the third parameter; in chapter 12 a velocity index is the third parameter. Computed values of daily discharge are entered on the form bearing the daily values of stage and the third parameter. The daily discharges for periods of no record or of indeterminate discharge rating, such as ice-affected periods, are computed precisely as explained in a preceding section titled, "Computation of Daily Discharge;" hydrographic comparison is the principal method used. After all boxes for daily mean discharge on the discharge form are filled, the form is completed as shown in figure 273 and explained in the section on "Completion of the Discharge Form."

Throughout the computation procedure, a record of progress is kept, similar to that shown in figure 274 but modified to accommodate the additional steps needed to compute discharge when a 3-parameter discharge relation is used. A station-analysis document is prepared, similar to that described in the section immediately preceding this discussion of 3-parameter relations; the various items that are in-

cluded are documented as corresponding steps in the analysis and computation of the discharge record are completed.

COMPUTATION OF DISCHARGE RECORDS FOR A RECORDING STATION EQUIPPED WITH A DIGITAL RECORDER

GENERAL

The fact that a gaging station is equipped with a digital stage-recorder does not affect the preparation of the station analysis (see the section on "Station Analysis"). Datum corrections are determined, discharge measurements are listed and reviewed, and graphical ratings are prepared and then converted to rating tables. The computations that follow the station analysis are similar to those described for a station equipped with a graphic stage-recorder, but instead of being performed manually they are performed by an electronic computer; the principal output forms are machine adaptations of the manual computation forms. The field offices generally send their input data to a central computer center where the computations are performed. The processing between field office and computer center may be accomplished by a combination of two or more of the following: mail, 16-channel paper-tape reader-transmitter, telephone line, and computer terminal.

The sequence and operation of an automated computing system is described in general terms in the last section of this chapter. It is not practicable to include a more detailed description of each step in the sequence because although the system of automated computation is well established, the particulars of each step are somewhat in a state of flux in response to continual improvement in storage and access procedures. Space limitations in this manual are also a factor in the treatment given to the subject. Additional pertinent information for the interested reader can be found in the following references that are listed at the end of this chapter: Carter and others, 1963; Edwards and others, 1974; WMO Technical Note No. 115, 1971 (contains a noteworthy bibliography).

The automated computation of discharge records from digital stage records is now (1980) more common in the U.S.A. than the manual computation of discharge records from graphic stage records. It may therefore seem incongruous to devote more space in this manual to manual computation than to automated computation. The two types of computation, however, are essentially similar, and a description of the manual method provides a far superior vehicle for explaining the computational technique.

INPUT TO COMPUTER

The input to the computer for a routine gaging station consists of: (1) the digital record of stage, accompanied by a list of corrections, if needed, for instrumental error in recording time and (or) gage height (any necessary datum corrections are included with the gage-height corrections); and (2) the discharge ratings accompanied by a list of any necessary shift adjustments. (See USGS form 9–1536 in fig. 275.) Stations for which the stage-fall-discharge type of rating is applicable require that the digital-tape records of stage for both the primary and auxiliary gages be furnished to the computer. Also required are the stage-discharge relation and such supplementary information as the stage-fall relation and the relation of fall ratio to discharge ratio. For stations at which velocity index is a third parameter—for example, a station equipped with a deflection meter—input requirements include the digital stage record, the digital record of deflection units, the stage-area relation, and the relation of deflection units to mean velocity, along with any necessary shift adjustments to those two relations.

OUTPUT FROM COMPUTER

The principal output from the computer consists of two forms—the primary computation sheet and the print-out of daily discharge. The primary computation sheet presents the initial or preliminary discharge computations. Normally, the computation sheet is edited, discharges are corrected or revised where necessary, and the corrections are fed back to the computer before the print-out of daily discharge is produced. Computer-produced hydrographs of daily mean discharge may be obtained for both preliminary and final discharge values. The discharge hydrograph of daily mean discharge based on preliminary values of discharge is very helpful for correcting the preliminary values; the method used is that of hydrographic comparison with final records for a nearby station, as explained in the section titled, "Computation of Daily Discharge." (Hydrographic comparison of discharge records is discussed in the two subsections that deal with the estimation of daily discharge.)

The primary computation sheet for a routine gaging station includes a listing for each day of: the maximum, minimum, hourly, and mean gage heights; mean discharge; the gage height equivalent to the mean discharge; the shift adjustment; and the datum correction. Figure 276 is an example of a primary computation sheet for a routine gaging station. The primary computation sheet for a slope station, shown in figure 277, differs somewhat. Listed for each day are: the maximum, minimum, and mean gage heights, mean fall, and mean and hourly discharge. For a deflection-meter station, the primary computation sheet (fig. 278) lists for each day maximum,

Form 9-1536
(Rev 10-69)

UNITED STATES DEPARTMENT OF THE INTERIOR—GEOLOGICAL SURVEY—WATER RESOURCES DIVISION

Correction Sheet For Water Data

Sta No .....

3 Shift 6 Discharge
4 Datum 7 Gage Height
5 Aux Datum 8 Sediment Conc
9 Susp Sediment

Corrections for _____ for year ending Sept 30, 19.....

DAY	OCT (10)	NOV (11)	DEC (12)	JAN (01)	FEB (02)	MAR (03)	DAY	APR (04)	MAY (05)	JUNE (06)	JULY (07)	AUG (08)	SEPT (09)	DAY
1							1							1
2							2							2
3							3							3
4							4							4
5							5							5
6							6							6
7							7							7
8							8							8
9							9							9
10							10							10
11							11							11
12							12							12
13							13							13
14							14							14
15							15							15
16							16							16
17							17							17
18							18							18
19							19							19
20							20							20
21							21							21
22							22							22
23							23							23
24							24							24
25							25							25
26							26							26
27							27							27
28							28							28
29							29							29
30							30							30
31							31							31

Remarks *Return to Boise, Idaho*

O.C.R. PROCESSING

U. S. Geological Survey
Water Resources Division
Room 365, Federal Building
550 West Fort Street
Boise, Idaho 83702

Monthly Summary Code .....
Gage Height Code .....
Drainage Area .....
Cfs-Day Total (Jan-Sept) .....
Max Daily (Jan-Sept) .....
Min Daily (Jan-Sept) .....
Skip Code .....

U.S. GOVERNMENT PRINTING OFFICE 1969 O—349-378

FIGURE 275.—Correction and update form for daily values of discharge.

UNITED STATES DEPARTMENT OF INTERIOR - GEOLOGICAL SURVEY - WATER RESOURCES DIVISION
PRIMARY COMPUTATION OF GAGE HEIGHTS AND DISCHARGE
DIST 25

01103500 DATA PROCESSED 01-14-74
CHARLES RIVER AT CHARLES RIVER VILLAGE, MASS. USE RT 32

PROVISIONAL DATA FOR WATER YEAR ENDING SEPT. 30, 1973 TEST DIFF 0.2 PUNCH INT 15 MIN STORE PARM 00060, STATISTIC 00003
PARM 00065, STATISTIC 00003

DATE	MAX GH (TIME)	MIN GH (TIME)	MEAN GH	EQUIV GH	MEAN DISCH	SHIFT AT ADJ HR	DATUM AT CORR HR		STAGE, IN HUNDREDTHS OF FEET, AT INDICATED HOURS 1	2	3	4	5	6	7	8	9	10	11	12
9-18	1.07 (16301)	0.92 (0715)	0.98	.98	113			AM	93	93	93	93	93	93	93	93	92	93	93	93
								PM	96	99	104	106	107	106	105	104	104	103	102	102
9-19	1.02 (0015)	1.00 (0315)	1.00	1.01	122			AM	101	101	101	100	100	100	100	100	100	101	101	101
								PM	101	101	101	101	101	101	101	102	101	101	101	101
9-20	1.04 (1215)	1.01 (0015)	1.02	1.03	131			AM	101	102	102	102	102	103	103	103	103	103	103	103
								PM	104	104	104	104	104	104	104	103	104	104	104	104
9-21	1.04 (0015)	1.00 (2230)	1.02	1.02	127			AM	103	103	103	103	103	103	103	102	103	102	102	102
								PM	102	102	102	101	101	101	101	101	101	101	100	100
9-22	1.00 (0015)	0.98 (1200)	0.98	.99	116			AM	100	100	100	100	100	100	100	99	99	99	99	98
								PM	98	98	98	98	98	98	98	98	98	98	98	98
9-23	0.98 (0100)	0.96 (1315)	0.97	.97	110			AM	98	98	98	97	97	97	97	97	97	97	97	97
								PM	97	97	97	97	97	97	97	97	97	98	98	98
9-24	1.06 (2230)	0.98 (0015)	1.01	1.02	125			AM	98	99	99	99	99	100	100	100	101	101	101	101
								PM	101	101	102	102	103	103	104	105	105	105	106	106
9-25	1.14 (2030)	1.06 (0015)	1.09	1.10	155			AM	106	106	107	107	107	107	108	108	109	110	110	110
								PM	110	110	111	111	112	112	113	113	114	114	114	114
9-26	1.17 (0845)	1.14 (0015)	1.16	1.16	177			AM	115	115	115	115	116	116	116	116	117	117	117	117
								PM	117	117	117	117	117	117	117	117	117	117	117	117
9-27	1.17 (0015)	1.14 (1945)	1.16	1.16	175			AM	117	117	117	117	117	117	117	117	117	117	116	116
								PM	116	116	116	116	115	115	115	114	114	114	114	114
9-28	1.14 (0015)	1.07 (2015)	1.10	1.10	156			AM	113	113	113	113	113	112	112	112	112	111	111	111
								PM	110	110	109	109	108	108	108	108	107	107	107	107
9-29	1.07 (0015)	1.00 (2030)	1.03	1.04	133			AM	107	105	106	106	105	105	105	105	105	104	104	105
								PM	104	104	103	103	102	102	101	101	100	100	100	100
9-30	1.00 (0015)	0.94 (1945)	0.96	.97	109			AM	99	99	99	99	98	98	98	98	98	98	98	98
								PM	97	95	96	96	95	95	95	94	94	94	94	94
MONTH					116															
PERIOD	1.17	0.83																		

RECORDER CLOCK RUNNING 3.1 MINUTES PER DAY FAST. RECORD ADJUSTED.

NOTE. SYSBOLS USED ABOVE HAVE THE FOLLOWING MEANINGS
A - SUCCESSIVE ADJUSTED PUNCH READINGS DIFFER BY MORE THAN THE SPECIFIED ALLOWABLE TEST DIFFERENCE
P - DAILY SUMMARY IS FOR AN INCOMPLETE DAY
R - ONE OR MORE INPUT VALUE IS OUTSIDE THE RANGE OF THE RATING IN USE
W - SHIFT IS A VALUE WEIGHTED BY DISCHARGE WHERE SHIFT VARYS WITH STAGE DUPING THE DAY

FIGURE 276.—Primary computation sheet for routine gaging station.

UNITED STATES DEPARTMENT OF INTERIOR - GEOLOGICAL SURVEY - WATER RESOURCES DIVISION DIST 36
PRIMARY COMPUTATION OF DISCHARGE WHERE SLOPE OF THE WATER SURFACE IS A FACTOR

04246500 DATA PROCESSED 02-11-74
ONEIDA RIVER AT CAUGHDENOY NY DISCH RT 3 FALL RT 2 RATIO RT 1

PROVISIONAL DATA FOR WATER YEAR ENDING SEPT. 30, 1974
BASE GAGE IS UPSTREAM DATUM DIFFERENCE BETWEEN GAGES 0.00 TEST DIFF 0.1 STORE PARM 00060, STATISTIC 00003
SLOPE IS NOT A FACTOR BELOW OR ABOVE PUNCH INTERVAL 60 MIN

S	DATE	MAX GH (TIME)	MIN GH (TIME)	MAX DISCH (TIME)	MEAN GH	MEAN FALL	MEAN DISCH	DISCHARGE AT INDICATED HOURS (1ST LINE A.M., 2ND LINE P.M.) 1	2	3	4	5	6	7	8	9	10	11	12
	12-25	8.22	7.98	4560	8.06	3.08	4310	4180	4180	4230	4230	4260	4250	4260	4260	4220	4220	4230	4280
		(2300)	(0100)	(2300)				4310	4310	4330	4310	4340	4330	4390	4410	4420	4500	4560	4450
B	12-27	8.62	8.19	5220	8.40	3.42	4850	4920	4850	4660	4640	4710	4630	4710	4630	4820	4740	4870	4750
		(2400)	(0100)	(2400)				4930	4830	4970	4930	5050	5000	5080	5030	5150	5140	5200	5220
	12-28	9.00	8.50	5860	8.82	3.84	5550	5190	5240	5300	5400	5350	5460	5390	5420	5390	5460	5520	5590
		(2400)	(0100)	(2400)				5620	5610	5640	5660	5690	5740	5740	5780	5790	5810	5840	5860
	12-29	9.17	9.00	6150	9.09	4.11	6010	5860	5910	5860	5940	5930	5940	5940	5960	6000	5980	6030	6000
		(2100)	(0100)	(2100)				6050	6010	6050	6060	6080	6060	6130	6100	6150	6100	6130	6090
	12-30	9.23	9.05	6250	9.17	4.21	6150	6110	6080	6000	5940	6050	6080	6230	6080	6210	6130	6180	6100
		(1700)	(0400)	(1700)				6160	6110	6230	6150	6250	6200	6230	6210	6210	6210	6230	6250
	12-31	9.27	9.21	6320	9.24	4.23	6260	6270	6250	6270	6230	6280	6230	6300	6280	6320	6270	6300	6270
		(0900)	(2100)	(0900)				6300	6250	6270	6250	6280	6270	6250	6270	6210	6270	6210	6210
	MONTH						4927												
	1-01	9.24	9.11	6270	9.19	4.16	6170	6230	6230	6250	6270	6200	6210	6200	6200	6230	6210	6210	6200
		(0400)	(1400)	(0400)				6160	6050	6180	6100	6160	6080	6180	6080	6150	6100	6130	6100
	1-02	9.15	9.07	6110	9.12	4.10	6060	6100	6110	6100	6110	6100	6100	6100	6100	6100	6080	6060	6100
		(0200)	(2300)	(0200)				6060	6050	6050	6050	6050	6030	6010	6010	6030	6010	5980	6030
	1-03	9.08	8.97	6000	9.03	4.02	5920	5980	6000	5960	6000	5940	5980	5980	5980	5930	5950	5890	5940
		(0200)	(2200)	(0200)				5890	5910	5860	5890	5890	5840	5880	5830	5880	5810	5880	5830
	1-04	8.99	8.93	5840	8.95	3.91	5780	5840	5790	5810	5780	5760	5760	5790	5760	5740			
		(0100)	(0900)	(0100)															

PERIOD MAX GH 9.27 (0900) 12-31 MIN GH 7.76 (0700) 12-21 MAX DISCH 6320 (0900) 12-31 MIN DISCH 1470.00 ON 11-16

NOTE.- SYMBOLS USED ABOVE HAVE THE FOLLOWING MEANINGS
A - SUCCESSIVE RECORDED GAGE HEIGHTS AT AUXILIARY GAGE DIFFER BY MORE THAN THE SPECIFIED ALLOWABLE TEST DIFFERENCE
B - SUCCESSIVE RECORDED GAGE HEIGHTS AT BASE GAGE DIFFER BY MORE THAN THE SPECIFIED ALLOWABLE TEST DIFFERENCE
R - ONE OR MORE INPUT VALUE IS OUTSIDE THE RANGE OF THE RATING TABLE
* - OBSERVED FALL IS ZERO OR NEGATIVE FOR ONE OR MORE SETS OF OBSERVATIONS

FIGURE 277.—Primary computation sheet for slope station.

minimum, and mean gage heights; maximum, minimum, hourly, and mean discharges; maximum and minimum velocities; volume and direction of flow (for a tidal stream whose flow reverses direction); and shift adjustments to the area and velocity relations.

The printout of daily discharge is virtually the same for all types of gaging stations. In addition to daily mean discharges, the printout includes monthly and yearly summaries in the same format that is used for publication (fig. 279). Besides being published, the figures on the printout are stored on a magnetic tape or disk. If, for some reason, it is found necessary to revise the computed records at some later date, corrections are made on the stored tape or disk.

SEQUENCE OF OPERATION OF AN AUTOMATED COMPUTING SYSTEM

The sequence of operation of the automated computing system used by the Geological Survey is as follows:

1. River stage is punched on 16-channel tape by the digital recorder in the gage house. When a segment of the tape is started by the hydrographer, he leaves a fresh inspection form (USGS form 9–176D in fig. 280) in the instrument shelter. On that form he fills out the box headed "Started by".
2. Tape is removed by field personnel at intervals of 30 to 60 days. Upon removal, the tape is checked for continuity and quality of record, and appropriate notes concerning identity of the station and quality of the record are made on the tape. The boxes headed "Removed by" and "Battery voltage" on inspection form 9–176D (fig. 280) are also filled out by the hydrographer, and the form accompanies the segment of 16-channel tape to the field office. If the hydrographer merely inspects the recorder without removing the punched segment of tape, he fills out the box headed "Insp'd by" on the inspection form and leaves the inspection form in the instrument shelter.
3. The tape, rating table, datum correction, and table of shifts are forwarded from the field office to the Automatic Data Processing Unit. Ratings may be submitted in one of three alternate forms. Discharge may be tabulated for each 0.01 foot of gage height for the part where curvilinear expansion between tenths of feet is necessary; it may be tabulated for each 0.1 foot; or, preferably, it may be defined by a series of coordinate values at the ends of straight-line segments on a logarithmic plot of the rating curve. The entry of ratings directly from the logarithmic plot eliminates the preparation of a rating table in the usual form. Shift adjustments are prorated with time to give a shift for each day between the days for which values of shift are submitted. A new rating may be put in use at any

UNITED STATES DEPARTMENT OF THE INTERIOR - GEOLOGICAL SURVEY - WATER RESOURCES DIVISION DIST 21
COMPUTATION OF DISCHARGE AT DEFLECTION METER STATION

03438192 DATA PROCESSED 02-26-74

BARKLEY-KENTUCKY CANAL NEAR GRAND RIVERS, KY. STANDARD DATUM CORR 0.00 FEET

PROVISIONAL DATA FOR WATER YEAR ENDING SEPT. 30, 1974 PUNCH INTERVAL 15 MIN STORE PARM 00060, STATISTIC 00003

DATE	GAGE HEIGHT IN FEET		DISCHARGE IN CFS		TIME	VELOCITY IN FT/SEC		VOLUMES IN MCF		HOURLY DISCHARGE (6 HOURS PER LINE, BEGINNING AT 1 A.M.) 1	2	3	4	5	6
1-23	MAX	62.87	MAX	35000.00	AT 0600	MAX 2.90	DOWN	1299.45	AM	10900.00	9840.00	8730.00	16200.00	24800.00	35000.00
	MIN	62.29	MIN	729.00	AT 0130	MIN .06	UP		AM	26100.00	2420.00	15900.00	7280.00	12200.00	6440.00
	MEAN	62.54	MEAN	15000.00					PM	11800.00	3170.00	21900.00	1590.00	18400.00	5640.00
	(DATUM	0.00)	(SHIFT TO AREA	0.00)		(SHIFT TO VEL	0.00)		PM	22500.00	21300.00	22000.00	11300.00	22600.00	21100.00
1-24	MAX	63.17	MAX	23400.00	AT 0030	MAX 1.90	DOWN	1115.41	AM	19100.00	6530.00	13000.00	21700.00	21700.00	10300.00
	MIN	62.83	MIN	1620.00	AT 1430	MIN .13	UP		AM	17200.00	12400.00	22800.00	17200.00	15600.00	18200.00
	MEAN	62.99	MEAN	13000.00					PM	11300.00	11100.00	8490.00	8960.00	10700.00	8560.00
	(DATUM	0.00)	(SHIFT TO AREA	0.00)		(SHIFT TO VEL	0.00)		PM	7470.00	10700.00	6510.00	9720.00	9350.00	4990.00
1-25	MAX	63.44	MAX	12500.00	AT 0545	MAX 1.00	DOWN	370.17	AM	6620.00	5000.00	12100.00	8370.00	12100.00	9010.00
	MIN	63.16	MIN		AT 0930	MIN	UP		AM	3250.00	8640.00	4130.00	2510.00		4140.00
	MEAN	63.31	MEAN	4310.00					PM	10300.00	4150.00	3270.00	3270.00	4150.00	2520.00
	(DATUM	0.00)	(SHIFT TO AREA	0.00)		(SHIFT TO VEL	0.00)		PM	735.00	756.00			1640.00	756.00
1-26	MAX	63.84	MAX	31900.00	AT 1545	MAX 2.50	DOW	475.20	AM	756.00	7550.00	1640.00	758.00		758.00
	MIN	63.40	MIN		AT 0030	MIN	UP		AM	1640.00	758.00	759.00	760.00	760.00	760.00
	MEAN	63.61	MEAN	5500.00					PM	6720.00	8520.00	14800.00	28000.00	13400.00	14100.00
	(DATUM	0.00)	(SHIFT TO AREA	0.00)		(SHIFT TO VEL	0.00)		PM	15100.00	5110.00	4200.00	1660.00	3320.00	1660.00
1-27	MAX	63.78	MAX	10500.00	AT 2145	MAX 1.47	DOWN	578.32	AM	6750.00		2550.00	2550.00	764.00	764.00
	MIN	63.39	MIN		AT 0015	MIN	UP		AM	764.00	763.00	764.00	1660.00	763.00	10900.00
	MEAN	63.62	MEAN	6640.00					PM	762.00	762.00	2540.00	9510.00	15700.00	10900.00
	(DATUM	0.00)	(SHIFT TO AREA	0.00)		(SHIFT TO VEL	0.00)		PM	10380.00	16300.00	12600.00	9070.00	17200.00	13600.00
1-28	MAX	63.41	MAX	28700.00	AT 1100	MAX 2.29	DOWN	971.55	AM	16360.00	17500.00	16800.00	10200.00	12500.00	10100.00
	MIN	62.97	MIN	4090.00	AT 2300	MIN .33	UP		AM	18800.00	13600.00	28100.00	17400.00	28700.00	16400.00
	MEAN	63.20	MEAN	11300.00					PM	13500.00	10100.00	6600.00	5730.00	4110.00	4100.00
	(DATUM	0.00)	(SHIFT TO AREA	0.00)		(SHIFT TO VEL	0.00)		PM	4100.00	4100.00	4090.00	4090.00	4090.00	5700.00
1-29	MAX	62.97	MAX	20700.00	AT 1445	MAX 1.68	DOWN	819.42	AM	5640.00	5690.00	5590.00	5690.00	4940.00	4940.00
	MIN	62.80	MIN	4940.00	AT 0600	MIN .40	UP		AM	5540.00	5580.00	5670.00	5670.00	5570.00	5670.00
	MEAN	62.87	MEAN	9440.00					PM	8500.00	16200.00	11400.00	17100.00	15900.00	9960.00
	(DATUM	0.00)	(SHIFT TO AREA	0.00)		(SHIFT TO VEL	0.00)		PM	12000.00	11700.00	8510.00	15900.00	13900.00	15900.00
1-30	MAX	63.37	MAX	20600.00	AT 1215	MAX 1.66	DOWN	9[illegible].41	AM	18440.00	15300.00	15300.00	14900.00	10600.00	8510.00
	MIN	62.84	MIN	5680.00	AT 0900	MIN .46	UP		AM	8810.00	8270.00	5680.00	18900.00	16200.00	10600.00
	MEAN	63.03	MEAN	10600.00					PM	11400.00	6580.00	6600.00	8350.00	6620.00	7560.00
	(DATUM	0.00)	(SHIFT TO AREA	0.00)		(SHIFT TO VEL	0.00)		PM	6520.00	5760.00	6760.00	5780.00	5780.00	8420.00
PERIOD	MAX	64.16	MAX	60973.47		MAX 5.43									
	MIN	57.28	MIN			MIN									

FIGURE 278.—Primary computation sheet for deflection-meter station.

PROCESS DATE IS 02-27-7

UNITED STATES DEPARTMENT OF INTERIOR • GEOLOGICAL SURVEY

STATION NUMBER 11183600 WALNUT CREEK AT CONCORD, CALIF. STREAM SOURCE AGENCY USGS
LATITUDE 375643 LONGITUDE 1220255 DRAINAGE AREA 85.10 DATUM 35.44 STATE 06 COUNTY 013

DISCHARGE, IN CUBIC FEET PER SECOND, WATER YEAR OCTOBER 1974 TO SEPTEMBER 1975
MEAN VALUES

DAY	OCT	NOV	DEC	JAN	FEB	MAR	APR	MAY	JUN	JUL	AUG	SEP
1	12	16	9.2	9.7	116	27	45	30	18	13	12	9.8
2	12	17	23	10	170	32	40	29	19	12	13	9.8
3	11	9.2	98	9.7	121	25	44	31	20	13	13	9.9
4	9.7	17	44	10	170	24	184	30	21	13	13	11
5	9.7	8.6	14	10	32	38	272	26	19	14	13	11
6	9.2	8.1	12	86	23	42	130	26	19	13	11	11
7	9.2	20	11	23	61	177	170	24	18	14	13	10
8	9.7	18	10	90	55	127	354	24	18	13	13	11
9	9.7	10	11	19	293	44	110	23	17	13	13	11
10	9.2	17	10	15	201	133	81	23	17	13	12	10
11	10	9.7	11	14	48	52	71	22	16	13	13	11
12	10	10	11	12	71	35	65	23	16	12	13	9.3
13	9.2	9.7	11	12	574	439	59	23	16	13	13	9.3
14	9.2	8.1	11	12	84	157	57	22	15	12	13	10
15	9.7	8.1	10	12	45	142	71	23	14	17	13	9.6
16	10	8.1	11	12	34	227	59	23	17	14	12	9.9
17	10	8.1	10	12	27	81	50	21	16	14	12	10
18	27	8.6	9.2	12	25	63	45	22	15	14	15	9.6
19	11	8.6	9.2	12	47	55	44	22	14	13	14	9.5
20	14	8.1	9.2	12	48	50	42	19	14	13	13	12
21	19	32	9.2	12	25	1370	42	18	14	13	12	12
22	11	14	9.2	13	23	486	39	19	16	14	12	10
23	10	9.7	9.2	12	21	145	36	19	15	13	12	9.5
24	10	8.6	9.2	13	21	119	71	19	16	14	11	9.6
25	11	12	9.2	13	21	733	81	18	16	14	11	9.0
26	10	9.2	9.2	12	22	145	36	17	14	14	11	8.3
27	15	9.2	79	10	24	90	31	18	14	12	11	7.8
28	69	9.2	88	12	25	70	36	18	13	12	11	7.9
29	18	9.2	17	12	---	60	39	19	13	12	11	8.0
30	14	9.2	12	11	---	55	31	20	13	12	10	7.8
31	30	---	10	139	---	50	---	20	---	12	10	---
TOTAL	438.5	350.3	606.0	663.4	2427	5293	2435	691	483	408	381	294.6
MEAN	14.1	11.7	19.5	21.4	86.7	171	81.2	22.3	16.1	13.2	12.3	9.82
MAX	69	32	98	139	574	1370	354	31	21	17	15	12
MIN	9.2	8.1	9.2	9.7	21	24	31	17	13	12	10	7.8
AC-FT	870	695	1200	1320	4810	10500	4830	1370	958	809	756	584

CAL YR 1974 TOTAL 17259.8 MEAN 47.3 MAX 1450 MIN 8.1 AC-FT 34230
WTR YR 1975 TOTAL 14470.8 MEAN 39.6 MAX 1370 MIN 7.8 AC-FT 28700

FIGURE 279.—Printout of daily discharge.

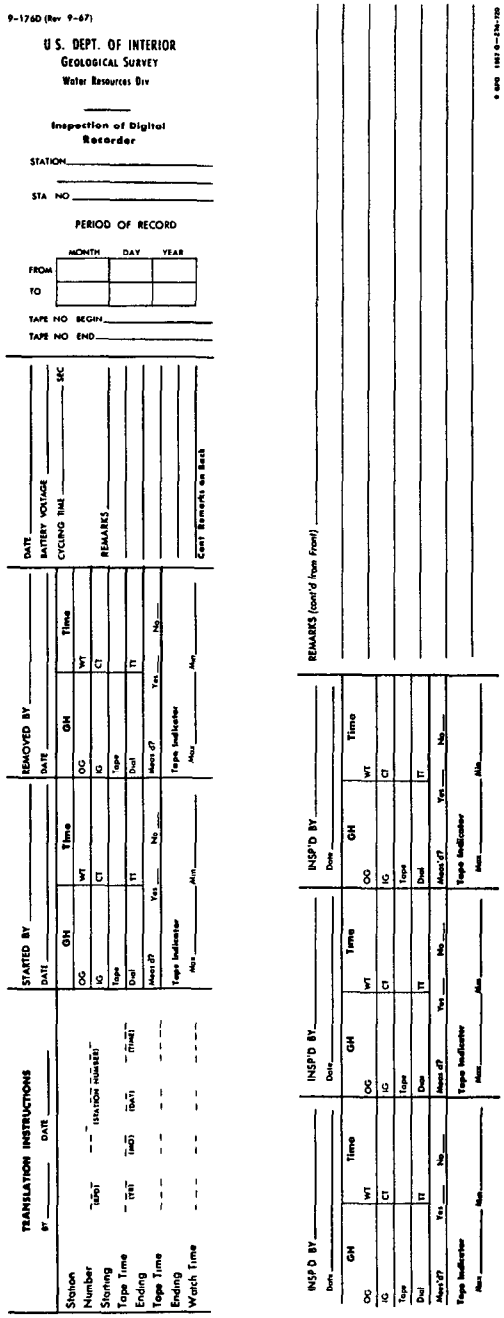

FIGURE 280.—Digital-recorder inspection form.

time during a day, and any shift applicable to the old rating on the same day will be dropped when the new rating takes effect.

The refinement considered in ratings for the initial run through the computer depends upon the complexity of the rating problem and the completeness of the data available. Sometimes final ratings can be prepared at the outset, at other times the output from the first run will be needed to complete the analysis. In the latter situation, only base ratings and approximate shift corrections are supplied.

Data from the 16-channel tape are translated by the central processing unit onto magnetic tape. The information on ratings is manually punched on cards. The magnetic tape and punch cards comprise the input to the digital computer. The rating table is stored on magnetic disk or tape at the computer center after the initial run.

4. The computer converts each instantaneous reading of river stage into a discharge value. Both daily mean discharge and daily mean gage height are computed as an average of instantaneous values. An equivalent daily mean gage height (the gage height corresponding to the daily mean discharge) is computed for each day so that recomputation, if necessary, can be made at a later date without reference to the individual items of the original base data. Daily mean values of gage height, discharge, and equivalent gage height are stored on a magnetic tape or disk. The printed output from the first computer pass consists of two items; a primary computation sheet, which is standard, and a daily discharge sheet, which is optional.

   The primary computation sheet (fig. 276) gives for each day the maximum, minimum, and mean gage heights, equivalent mean gage height, the datum and shift corrections applied, and the daily mean discharge. In addition, hourly gage heights and the time when maximums occurred are printed out.

   The printout of daily discharges (fig. 279), which is suitable for outside distribution, lists daily mean discharges for the period from the beginning of the water year to the end of the record being computed.

5. The field offices use the primary computation sheet in quality checks of the original and computed data, in further analysis of the stage-discharge relation, and in selecting instantaneous peak discharges to be published. Daily discharges from this sheet can be plotted for comparison with adjacent streams, and the usual studies can be made for periods of ice effect, no gage-height record, or backwater from various sources. Estimates can be made for all anomalous periods, and ratings can be revised, if

necessary, so that daily discharge can be recomputed from the effective mean gage heights on the second pass through the computer. The information necessary for revision or recomputation is forwarded to the Automatic Data Processing Unit.

6. The final tabulation is the same as figure 279 except that it is complete for the year and is produced on the second pass (update) through the computer. Where rating changes have been made as a result of the quality control analysis or where individual discharge figures have been estimated, the recomputation will involve substituting the estimated figures on the magnetic storage record, recomputing other discharge figures from revised ratings and the equivalent daily mean gage height, and printing out of the final discharge figures. (A printout from the subprogram for updating the primary computation sheet is shown in figure 281.) The printout from the final computer update is for the complete year. The format of the output is suitable for direct offset reproduction. The data on this form are also stored on magnetic tape for permanent storage.
7. A tabulation of daily mean gage heights may also be printed out during the second computer pass for stations designated by the field offices. That tabulation is prepared only for those stations for which there is a specific need.
8. The documentation file in the field offices consists of the original measurement notes, the 16-channel tapes, a station analysis, a list of discharge measurements, a rating curve, the primary computation sheet, a table of daily mean discharges from the final computer run, and possibly a rating table.

A record of progress of the discharge computations is kept in the field office on a check list such as that shown in figure 282. That form or perhaps a more detailed one, such as figure 283, is especially necessary because of the complication caused by records being shuttled back and forth between the field office and the computer center.

It is also necessary that a station-analysis document be prepared in the field office, as described for the graphic recorder in the section titled, "Station-Analysis Document." In that description it was mentioned that the "Discharge" paragraph showing the ratings used during the water year would be more complex for a digital-recorder station than for a graphic-recorder station. For a digital-recorder station, it is necessary to explain the origin of figures shown on the primary computation sheet as well as those on the final print-out. Documentation received on updating computer runs should therefore be referred to in the "Discharge" paragraph. A sample table of ratings used for a digital-recorder station having a somewhat complicated rating problem follows:

```
                UNITED STATES DEPARTMENT OF INTERIOR - GEOLOGICAL SURVEY - WATER RESOURCES DIVISION          DIST 17
                          UPDATE BY SUBSTITUTION OR RECOMPUTATION OF DAILY VALUES
03337000                                  DATA PROCESSED 02-11-74
BONEYARD CREEK AT URBANA, ILL
PROVISIONAL DATA FOR WATER YEAR ENDING SEPT. 30, 1973                    STORE PARM 00065, STATISTIC 00003

                    DAILY GAGE HEIGHTS SUBSTITUTED(EQUIV GH SET THE SAME)
                                  9-20-73 TO  9-22-73
                                  9-25-73 TO  9-27-73

                              STAGE-SHIFT VARIATION DIAGRAM
                          HIGH POINT     2.00 SHIFT AT GH  5.00
                          BASE           1.00 SHIFT AT GH  2.00
                          LOW POINT      0.10 SHIFT AT GH  0.20

                                   SHIFT ADJUSTMENTS
                                     ADJ      DATE
                                      .09  09-13-73  AT GH   .55 PROJECTED TO   0.33 AT BASE GH
                                     -.02  10-01-73  AT GH   .65 PROJECTED TO  -0.06 AT BASE GH

                                DAILY DISCHARGE RECOMPUTED
                                      USE RT 07
                                  09-18-73 TO 09-30-73
                                (SHIFTS VARIED WITH STAGE)
```

FIGURE 281.—Printout from subprogram for updating primary computation sheet.

PROGRESS CHECK LIST
COMPUTATION OF DIGITAL RECORDER RECORD

Station_____ Water Year_____.

Index Number_____

Check work done. Complete in order. Initial when finished.

1 2 3 4

Examine and prepare tapes for transmittal.
List measurements on 9-207 (fig. 262).
Plot measurements on rating curve. Develop new curve and table, if needed.
Compute shift corrections, percentage difference on 9-207 (fig. 262).
Enter shift or datum corrections on 9-1536 (fig. 275).
Write preliminary rating analysis.

Computed_____ Checked_____

.....

Tape transmitted.
Ratings transmitted.
9-1536 transmitted (fig. 275)

.....

Inspect primary computation sheet.
Check measurements and field notes for peak data. Enter on PC sheets.
Revise shifts and recompute daily discharges on primary computation sheet.
Plot hydrograph.
Estimate discharge for ice, missing, doubtful or backwater periods.
Complete daily discharges monthly totals on primary computation sheets.
Complete station analysis.

Computed_____ Checked_____

.....

☐ Transmit updating corrections.

.....

Enter notes, maximum, minimum and peaks on 9-211m (fig. 279).
Revise manuscript from previous year.

Computed_____ Checked_____

FIGURE 282.—Form showing progress of computation of digital-recorder record (sample 1).

"*Discharge.*—Computed as follows:

Ratings Used

Period	*Primary*	*Final*	*Update*
Oct. 1 to Jan. 4	No. 4	No change	None
Jan. 5 to Jan. 20	———	Special	May 12, 1973
Jan. 21 to Jan. 29	No. 4	No. 5	May 12, 1973
Jan. 30 to Feb 20	No. 4	Special	May 12, 1973
Feb. 21 to Aug. 10	No. 5	No. 5	None
Aug. 11 to Sept. 30	———	Special	Oct. 20, 1973"

All other instructions on the preparation of the station-analysis documents (p. 580–585) are applicable for a digital-recorder station.

SELECTED REFERENCES

Carter, R. W., and Davidian, Jacob, 1968, General procedure for gaging streams: U.S. Geol. Survey Techniques Water Resources Inv., book 3, chap. A6, p. 12–13.

WRD-ID-11
Jan 76

19__ water year A.D.P. check list

Station No._____
Station Name_____

List of measurements:
- Gage-heights . . . . . checked (_____)
- Original list of measurements. . checked (_____)
- List of measurements . . . . . checked (_____)
- Shifts O.K. as submitted . . . . yes ( ) no ( )
- Shifts . . . . . updated (_____ checked (_____)

Rating curve:
- Measurements . . . . . plotted (_____) checked (_____)
- New curve needed . . . . . yes ( ) no ( )
- Measurements . . . . . plotted (_____) checked (_____)
- Curve. . . . . drawn (_____) checked (_____)
- Rating table . . . . . computed (_____) checked (_____)

Primary sheets:
- Record complete. . . . . yes ( ) no ( )
- Primary shifts O.K. . . . . yes ( ) no ( )
- Primary datum corr. O.K. . . . . yes ( ) no ( )
- Correct rating in use. . . . . yes ( ) no ( )
- Rating changed during year . . . yes ( ) no ( )
- Missing record . . . . . estimated (_____) checked (_____)
- Ice period . . . . . estimated (_____) checked (_____)
- Shift. . . . . update (_____) checked (_____)
- Datum. . . . . update (_____) checked (_____)
- Discharge. . . . . update (_____) checked (_____)
- Re-update. . . . . yes ( ) checked (_____)
- Re-update. . . . . yes ( ) checked (_____)

Station analysis:
- Written by_____ checked by_____
- Reviewed by_____

Discharge table:
- Two copies . . . . . yes ( ) no ( )
- Left margin attached . . . . . yes ( ) no ( )
- Extremes . . . . . computed (_____) checked (_____)
- Supplemental peaks . . . . . (_____) checked (_____)
- Footnotes. . . . . (_____) checked (_____)
- Table annotated. . . . . (_____) checked (_____)

Manuscript:
- Mean flow. . . . . computed (_____) checked (_____)
- Sheet updated with current data. (_____) checked (_____)
- Historical data changed. . . . . yes ( ) no ( )
- Footnotes. . . . . updated (_____) checked (_____)
- Skeleton rating. . . . . (_____) checked (_____)

FIGURE 283.—Form showing progress of computation of digital-recorder record (sample 2).

Carter, R. W., and others, 1963, Automation of streamflow records: U.S. Geol. Survey Circular 474, 18 p.

Corbett, D. M., and others, 1943, Stream-gaging procedure: U.S. Geol. Survey Water-Supply Paper 888, 245 p.

Edwards, M. D., and others, 1974, National water data storage and retrieval system; processing digital recorder records: U.S. Geol. Survey open-file report, 139 p.

World Meteorological Organization, 1971, Machine processing of hydrometeorological data: WMO–no. 275, Technical Note no. 115, 79 p.

CHAPTER 16—PRESENTATION AND PUBLICATION OF STREAM-GAGING DATA

GENERAL

After the computations of the discharge records for a water year are completed, the records are reviewed by designated engineering personnel and are prepared for publication. The publication process in the U.S.A. usually involves photo-offset printing, and copy must therefore be put in final form for photographing. From the photographic copy, a plate is made for use in the offset printing process.

FORMAT

The published annual report consists of an introductory text, stream-gaging and reservoir station records, tabulations of discharge at partial-record stations and at miscellaneous sites, and an index. The publication format used by the Geological Survey is illustrated in the example pages in figures 284–303 at the end of this chapter. The items that are included in the annual publication are listed in figure 284, which is an example of the table of contents of the report.

In general, most of the figures are self-explanatory, but some require additional explanation. The 9 pages of figure 286 include the 12 items in the table of contents (fig. 284) that start with "Introduction" and end with "Selected references." The 12 items are shown as part of a single figure because they constitute the introductory text that is printed on continuing pages; that is, each item is not started on a fresh page. The map in figure 287 is optional; if the map scale required to show the State or region on a single page is so small that the stations plot in a confusing clutter, the map may be omitted in the annual discharge report. However, any summary reports that cover a period of years of record for the stations should include a map of suitable scale that is folded and placed in a pocket attached to the back cover of the report. The graph in figure 288 is associated with the section titled "Hydrologic Conditions," near the end of the introductory text.

Figures 289–294 show samples of streamflow and reservoir tabulations for the water year that would appear in the main body of the annual report. Figure 289 is a sample page for a routine gaging station. Figure 290 is a sample page for a gaging station whose flow is regulated by a reservoir. Because the flow is controlled, no tabulation is made of supplementary peak discharges (those greater than a given base discharge). In the monthly and annual summaries at the bottom of figure 290, additional figures are given for the mean discharge adjusted for change in reservoir contents. Figure 291 is a sample page

for a reservoir showing daily contents along with a monthly tabulation of change in contents. Daily contents are published only for major reservoirs. More commonly only the month end contents and the monthly change in contents are published, as in figure 292. Where the river basin contains several large reservoirs for which only month end contents and monthly change in contents are to be published, a table, such as that shown in figure 293*A* is published for the entire group. A table of that kind would usually be the last table for the river basin. Figure 293*B* is a continuation sheet for a group of such reservoirs. If all the reservoirs in the basin were relatively small, the data for the group of reservoirs would be abridged to take the form shown in figure 294.

In figure 295, tables *A* and *B* illustrate the way in which the records would be published if the gaging station were originally established a short time before October 1, the starting date of the water year. Table *A* is for a station that was established on Sept. 10. The data for the last 20 days in September would be published with the data for the complete year that followed. The short table shown as Table *A* would precede the daily table for the complete year. Table *B* is for a station that was established on August 1. The short table for August and September would precede the daily table for the complete year. Table *C* in figure 295 is a sample of the daily table for a station on an ephemeral stream that has few days of flow during the water year.

Figure 296 shows a sample "Revisions" paragraph for a gaging station whose past records require extensive revision. The revisions paragraph is always the last paragraph of the station description, as in figure 292. (The symbols used in the revisions paragraph in figure 292 are explained in figure 286*F*.)

If a highly developed river basin has a system of storage and diversion facilities that is too complex to be adequately described in the "Remarks" paragraph of the individual gaging stations, a schematic diagram is provided showing the locations of the reservoirs and canals with respect to the gaging stations. Such a diagram is found in figure 297; the diagram usually precedes the first discharge record for the basin.

Figures 298 and 299 show sample discharge records for partial-record stations. Figure 298 lists low-flow discharge measurements at sites where one or more such measurements are systematically made each year. Figure 299 lists peak discharges for the year, and occasionally one or more smaller peak discharges at sites equipped with a crest-stage gage (see last section in chapter 4). The discharges corresponding to observed peak stages are obtained from a rating table based on indirect determinations of discharge, such as slope-area determinations (chap. 9). Figure 300 shows the results of discharge

measurements made at miscellaneous sites for special studies of various types. Miscellaneous sites are sites other than those where complete records or partial records are obtained each water year.

Figures 301 and 302 show the results of discharge measurements made at miscellaneous sites for two types of studies that are common enough to be identified by a general title. Figure 301 gives the results of a seepage investigation where base flow is measured at intervals in a reach of stream channel; the contribution of intervening tributary flow and the depletion of flow in intervening diversion canals are also measured. The purpose of the study is to investigate water gains and losses resulting from seepage through the streambed and banks. Figure 302 shows the results of low-flow discharge measurements made at miscellaneous sites during a drought period for the purpose of appraising the regional availability of surface flow during periods of critically low runoff.

The last section of the annual discharge report is an alphabetical index; figure 303 is a sample of the first page of such an index. Entries are made in the index for each station or measurement site for which figures of discharge or reservoir storage are given. For each station equipped with a continuous-recording gage, the entry is made under both the stream name and the place name. In addition, entries in the index are made for each section of the introductory text, for each of the terms listed under "Definitions of terms and abbreviations," for each illustration, and for each station plotted on the graph of hydrologic conditions (fig. 288).

In the past, basic groundwater and water-quality data were published under separate covers. At present (1980) the reports incorporate, in a single volume, those data with the surface-water discharge information that was described on the preceding pages. A discussion of ground-water and water-quality data is, however, beyond the scope of this manual.

SELECTED REFERENCE

Hodges, E. B., Ham, C. B., and Anderson, B. A., 1973, Preparation of surface-water data reports: U.S. Geol. Survey Surface-Water Techniques, book 9, chap. 1, 145 p.

CONTENTS

ILLUSTRATIONS

FIGURE 284.—Table of contents for annual published report.

GAGING STATIONS, IN DOWNSTREAM ORDER,
FOR WHICH RECORDS ARE PUBLISHED

FIGURE 285.—List of surface-water stations.

WATER RESOURCES DATA FOR INDIANA. 19XX

PART 1. SURFACE-WATER RECORDS

INTRODUCTION

Surface-water records for the 19XX water year for Indiana, including records of streamflow or reservoir storage at gaging stations, partial-record stations, and miscellaneous sites, are given in this report and their locations shown in figures ___, ___. Records for a few pertinent gaging stations in bordering States also are included. The records were collected and computed by the Water Resources Division of the U.S. Geological Survey under the direction of M. D. Hale, district chief. These data represent that portion of the National Water Data System collected by the U.S. Geological Survey and cooperating State and Federal agencies in Indiana.

Through September 30, 1960, the records of discharge and stage of streams and canals and contents and stage of lakes or reservoirs were published in an annual series of U.S. Geological Survey water-supply papers entitled "Surface Water Supply of the United States."

Beginning with the 1961 water year, surface-water records have been released by the Geological Survey in annual reports on a State-boundary basis. Distribution of these reports is limited; they are designed primarily for rapid release of data shortly after the end of the water year to meet local needs. The discharge and reservoir storage records for 1961-65 also will be published in a Geological Survey water-supply paper series entitled "Surface Water Supply of the United States 1961-65."

COOPERATION

The U.S. Geological Survey and organizations of the State of Indiana have had cooperative agreements for the systematic collection of surface-water records since 1930. Organizations that supplied data are acknowledged in station descriptions. Organizations that assisted in collecting data through cooperative agreement with the Survey are:

State Department of Natural Resources, J. E. Mitchell, director, through Bureau of Water and Mineral Resources, W. J. Andrews, deputy director.

State Highway Commission, R. F. Whitehead, chairman, M. L. Hayes, executive director, and F. L. Ashbaucher, chief engineer.

State Board of Health, A. C. Offutt, commissioner, and B. A. Pool, director and chief engineer.

Assistance in the form of funds or services was given by the Corps of Engineers, U.S. Army, in collecting records for 67 gaging stations published in this report.

FIGURE 286A.—Introductory text.

WATER RESOURCES DATA FOR INDIANA, 19XX

The following organizations aided in collecting records:

The city of Indianapolis, through its Board of Public Works and Sanitation and its Flood Control Board; cities of Anderson, Bloomington, Muncie, North Vernon, Richmond, and Jasper; Indianapolis Water Co.; Indianapolis Power and Light Co.; Public Service Co. of Indiana; * * *.

DEFINITION OF TERMS

Definition of terms related to streamflow and other hydrologic data, as used in this report, are defined as follows:

Acre-foot (AC-FT, acre-ft) is the quantity of water required to cover 1 acre to a depth of 1 foot and is equivalent to 43,560 cubic feet or 325,851 gallons.

Cfs-day is the volume of water represented by a flow of 1 cubic foot per second for 24 hours. It is equivalent to 86,400 cubic feet, 1.9835 acre-feet, or 646,317 gallons, and represents a runoff of 0.0372 inch from 1 square mile.

Contents is the volume of water in a reservoir or lake. Unless otherwise indicated, volume is computed on the basis of a level pool and does not include bank storage.

Control designates a feature downstream from the gage that determines the stage-discharge relation at the gage. This feature may be a natural constriction of the channel, an artificial structure, or a uniform cross section over a long reach of the channel.

Cubic feet per second per square mile (CFSM) is the average number of cubic feet of water flowing per second from each square mile of area drained, assuming that the runoff is distributed uniformly in time and area.

Cubic foot per second (cfs) is the rate of discharge representing a volume of 1 cubic foot passing a given point during 1 second, and is equivalent to 7.48 gallons per second or 448.8 gallons per minute.

Discharge is the volume of water (or more broadly, total fluids), that passes a given point within a given period of time.

Drainage area of a stream at a specified location is that area, measured in a horizontal plane, enclosed by a topographic divide from which direct surface runoff from precipitation normally drains by gravity into the stream above the specified point. Figures of drainage area given herein include all closed basins, or noncontributing areas, within the area unless otherwise noted.

Gage height (G.H.) is the water-surface elevation referred to some arbitrary gage datum. Gage height is often used interchangeably with the more general term "stage," although gage height is more appropriate when used with a reading on a gage.

Gaging station is a particular site on a stream, canal, lake, or reservoir where systematic observations of gage height or discharge are obtained. When used in connection with a discharge record, the term is applied only to those gaging stations where a continuous record of discharge is obtained.

FIGURE 286*B*.—Introductory text—Continued.

WATER RESOURCES DATA FOR INDIANA, 19XX

Partial-record station is a particular site where limited streamflow data are collected systematically over a period of years for use in hydrologic analyses.

Runoff in inches (IN.) shows the depth to which the drainage area would be covered if all the runoff for a given time period were uniformly distributed on it.

Stage-discharge relation is the relation between gage height and the amount of water flowing in a channel, expressed as volume per unit of time.

WRD is used as an abbreviation for "Water-Resources Data" in the summary REVISIONS paragraph to refer to previously published State annual basic-data reports.

WSP is used as an abbreviation for "Water-Supply Paper" in references to previously published reports.

SPECIAL NETWORKS AND PROGRAMS

Hydrologic bench-mark station is one that provides hydrologic data for a basin in which the hydrologic regimen will likely be governed solely by natural conditions. Data collected at a bench-mark station may be used to separate effects of natural from man-made changes in other basins which have been developed and in which the physiography, climate, and geology are similar to those in the undeveloped bench-mark basin.

International Hydrological Decade (IHD) River Stations provide a general index of runoff and materials in the water balance (discharge of water, and dissolved and transported solids) of the world. In the United States, IHD Stations provide indices of runoff and of the general distribution of water in the principal river basins of the conterminous United States and Alaska.

DOWNSTREAM ORDER AND STATION NUMBERS

Records are listed in a downstream direction along the main stream, and stations on tributaries are listed between stations on the main stream in the order in which those tributaries enter the main stream. Stations on tributaries entering above all mainstream stations are listed before the first mainstream station. Stations on tributaries to tributaries are listed in a similar manner. In the list of gaging stations in the front of this report the rank of tributaries is indicated by indention, each indention representing one rank.

As an added means of identification, each gaging station and partial-record station has been assigned a station number. These are in the same downstream order used in this report. In assigning station numbers, no distinction is made between partial-record stations and continuous-record gaging stations; therefore, the station number for a partial-record station indicates downstream order position in a list made up of both types of stations. Gaps are left in the numbers to allow for new stations that may be established; hence the numbers are not consecutive. The complete 8-digit number for each station, such as 03-3355.00, includes the part number "03" and a 6-digit station number. In this report, the nonessential zeros are not shown. For example, the complete number 03-3355.00 would appear as 3-3355, just to the left of the station name. In this report,

FIGURE 286C.—Introductory text—Continued.

the records are listed in downstream order by parts. All records for a drainage basin encompassing more than one State could be arranged in downstream order by assembling pages from the various State reports by station number to include all records in the basin.

EXPLANATION OF SURFACE-WATER DATA

Collection and Computation of Data

The base data collected at gaging stations consists of records of stage and measurements of discharge of streams or canals, and stage, surface area, and contents of lakes or reservoirs. In addition, observations of factors affecting the stage-discharge relation or the stage-capacity relation, weather records, and other information are used to supplement base data in determining the daily flow or volume of water in storage. Records of stage are obtained from a water-stage recorder that gives a continuous graph of the fluctuations (for digital recorders, a tape punched at 15-, 30-, or 60-minute intervals) or from direct readings on a nonrecording gage. Measurements of discharge are made with a current meter, using the general methods adopted by the Geological Survey on the basis of experience in stream gaging since 1888. These methods are described in standard textbooks on the measurement of stream discharge. (See also SELECTED REFERENCES.) Surface areas of lakes or reservoirs are determined from instrument surveys using standard methods. The configuration of the reservoir bottom is determined by sounding at many points.

For a stream-gaging station rating tables giving the discharge for any stage are prepared from stage-discharge relation curves defined by discharge measurements. If extensions to the rating curves are necessary to define the extremes of discharge, they are made on the basis of indirect measurements of peak discharge (such as slope-area or contracted-opening measurements, computation of flow over dams or weirs), velocity-area studies, and logarithmic plotting. The application of the daily mean gage heights to the rating table gives the daily mean discharge, from which the monthly and the yearly mean discharge are computed. If the stage-discharge relation is subject to change because of frequent or continual change in the physical features that form the control, the daily mean discharge is determined by the shifting-control method, in which correction factors based on individual discharge measurements and notes by engineers and observers are used in applying the gage heights to the rating tables. If the stage-discharge relation for a station is temporarily changed by the presence of aquatic growth or debris on the control, the daily mean discharge is computed by what is basically the shifting-control method.

At some stream-gaging stations the stage-discharge relation is affected by backwater from reservoirs, tributary streams, or other sources. This necessitates the use of the slope method in which the slope or fall in a reach of the stream is a factor in determining discharge. Information required for determining the slope or fall is obtained by means of an auxiliary gage set at some distance from the base gage. At some stations the stage-discharge relation is affected by changing stage; at these stations the rate of change in stage is used as a factor in determining discharge.

At some stream-gaging stations the stage-discharge relation is affected by ice in the winter, and it becomes impossible to compute the discharge in the usual manner. Discharge for periods of ice effect is computed on the basis of the gage-height record and

FIGURE 286*D*.—Introductory text—Continued.

WATER RESOURCES DATA FOR INDIANA, 19XX

occasional winter discharge measurements, consideration being given to the available information on temperature and precipitation, notes by gage observers and hydrologists, and comparable records of discharge for other stations in the same or nearby basins.

For a lake or reservoir station, capacity tables giving the contents for any stage are prepared from stage-area relation curves defined by surveys. Discharge over spillways is computed from a stage-discharge relation curve defined by discharge measurements. The application of the stage to the capacity table gives the contents, from which the daily, monthly, or yearly change in contents is computed.

If the stage-capacity curve is subject to changes because of deposition of sediment in the reservoir, periodic resurveys of the reservoir are necessary to define new stage-capacity curves. During the period between reservoir surveys the computed contents may be increasingly in error due to the gradual accumulation of sediment.

For some gaging stations there are periods when no gage-height record is obtained or the recorded gage height is so faulty that it cannot be used to compute daily discharge or contents. This happens when the recorder stops or otherwise fails to operate properly, intakes are plugged, the float is frozen in the well, or for various other reasons. For such periods the daily discharges are estimated on the basis of recorded range in stage, adjoining good record, discharge measurements, weather records, and comparison with other station records from the same or nearby basins. Likewise daily contents may be estimated on the basis of operator's log, adjoining good record, inflow-outflow studies, and other information.

The data in this report generally comprise a description of the station and tabulations of basic data. For gaging stations on streams or canals a table showing the daily discharge and monthly and yearly discharge is given. For gaging stations on lakes and reservoirs a monthly summary table of stage and contents or a table showing the daily contents is given. Tables of daily mean gage heights are included for some streamflow stations and for some reservoir stations. Records are published for the water year, which begins on October 1 and ends on September 30. A calendar for the 19XX water year is shown on the reverse side of the front cover to facilitate finding the day of the week for any date.

The description of the gaging station gives the location, drainage area, period of record, type and history of gages, average discharge, extremes of discharge or contents, and general remarks. The location of the gaging station and the drainage area are obtained from the most accurate maps available. River mileage, given under "LOCATION" for some stations, is that determined and used by the Corps of Engineers or other agencies. Periods for which there are published records for the present station or for stations generally equivalent to the present one are given under "PERIOD OF RECORD." The type of gage currently in use, the datum of the present gage above mean sea level, and a condensed history of the types, locations, and datums of previous gages used during the period of record are given under "GAGE." In references to datum of gage, the phrase "mean sea level" denotes "Sea Level Datum of 1929" as used by the Topographic Division of the Geological Survey, unless otherwise qualified. The average discharge for the number of years indicated is given under "AVERAGE DISCHARGE"; it is not given for stations having fewer than 5 complete years of record or for stations where changes in water development during the period of record cause the figure to have little significance. In addition, the median of yearly mean discharges is given for stream-gaging stations having 10 or more complete years of record if the median differs from the average by more than 10 percent. The maximum discharge (or contents) and the maximum gage height, the minimum discharge if there is little or no regulation (or the minimum contents), and the

FIGURE 286*E*.—Introductory text—Continued.

WATER RESOURCES DATA FOR INDIANA, 19XX

minimum gage height if it is significant are given under "EXTREMES." The minimum daily discharge is given if there is extensive regulation (also the minimum discharge and gage height if they are abnormally low). In the first paragraph headed "Current year:" the data given are for the complete current water year unless otherwise specified. In the second paragraph under "EXTREMES" headed "Period of record:" the data given are for the period of record given in the PERIOD OF RECORD paragraph. Reliable information concerning major floods that occurred outside the period of record is given in the third or last paragraph under "EXTREMES." Unless otherwise qualified, the maximum discharge (or contents) corresponds to the crest stage obtained by use of a water-stage recorder (graphic or digital), a crest-stage gage, or a nonrecording gage read at the time of the crest. If the maximum gage height did not occur at the same time as the maximum discharge or contents, it is given separately. Information pertaining to the accuracy of the discharge records, to conditions that affect the natural flow at the gaging station, and availability of Water Quality records, is given under "REMARKS"; for reservoir stations information on the dam forming the reservoir, the capacity, outlet works and spillway, and purpose and use of the reservoir, is also given under "REMARKS."

Previously published records of some stations have been found to be in error on the basis of data or information later obtained. Revisions of such records are usually published along with the current records in one of the annual or compilation reports. In order to make it easier to find such revised records, a paragraph headed "REVISIONS (WATER YEARS)" has been added to the description of all stations for which revised records have been published. Listed therein are all the reports in which revisions have been published, each followed by the water years for which figures are revised in that report. In listing the water years only one number is given; for instance, 1933 stands for the water year October 1, 1932, to September 30, 1933. If no daily, monthly, or annual figures of discharge were revised, that fact is brought out by notations after the year dates as follows: "(M)" means that only the instantaneous maximum discharge was revised; "(m)" that only the instantaneous minimum was revised; and "(P)" that only peak discharges were revised. If the drainage area has been revised, the report in which the revised figure was first published is given. It should be noted that for all stations for which cubic feet per second per square mile and runoff in inches are published, a revision of the drainage area necessitates corresponding revision of all figures based on the drainage area. Revised figures of cubic feet per second per square mile and runoff in inches resulting from a revision of the drainage area only are usually not published in the annual series of reports.

Skeleton rating tables are published for stream-gaging stations where they serve a useful purpose and the dates of applicability can be easily identified.

Skeleton capacity tables are published for all reservoirs for which records of contents are published on a daily basis.

The daily tables for stream-gaging stations give the discharge corresponding to the daily mean gage height unless there are large or rapid changes in the discharge during a day. For days having large or rapid changes, discharge for the day is computed by averaging the mean discharge for several parts of a day. For digital recorders, the daily mean discharge is always the average of the discharges at each punched reading. For stations equipped with nonrecording gages, the daily discharge corresponds to once-daily readings of the gage or to the mean of twice-daily readings; but for periods of rapidly changing stage the discharge is determined from a gage-height graph based on gage readings.

FIGURE 286*F*.—Introductory text—Continued.

WATER RESOURCES DATA FOR INDIANA, 19XX

The daily tables for reservoir stations give the contents corresponding to the water-surface elevation at a given time, usually at 2400 each day. For some reservoirs the elevation at a given time is given in the daily table.

The monthly summary is given below the daily table. For stream-gaging stations the line headed "TOTAL" gives the sum of the daily figures; it is the total cubic feet per second per day for the month. The line headed "MEAN" gives the average flow in cubic feet per second during the month. The lines headed "MAX" and "MIN" give the maximum and minimum daily discharges, respectively, for the month. Discharge for the month also may be expressed in cubic feet per second per square mile (line headed "CFSM"), or in inches (line headed "IN.") or in acre-feet (line headed "AC-FT"). Figures of cubic feet per second per square mile and runoff in inches are omitted if there is extensive regulation or diversion, if the drainage area includes large noncontributing areas, or if the average rainfall on the drainage basin is usually less than 20 inches.

For reservoir stations the monthly summary gives the elevation (or gage height) at the end of the month and the change in contents during the month. If elevation or gage height is given in the daily table, the monthly summary gives the contents at the end of the month, rather than the elevation or gage height. For some reservoirs a tabulation of monthly evaporation from the water surface also is included.

In the yearly summary below the monthly summary, the figures of maximum are the maximum daily discharges for the calendar and water years; likewise, the minimums in this summary are the minimum daily discharges.

For reservoir stations the yearly summary gives the change in contents for the calendar year and for the water year. For some reservoirs the yearly evaporation also is included.

Peak discharges and their times of occurrence and corresponding gage heights for many stations are listed below the yearly summary. All independent peaks above the selected base are given. The base discharge, which is given in parentheses, is selected so that an average of about three peaks a year can be presented. Peak discharges are not published for any canals, ditches, drains, or for any stream for which the peaks are subject to substantial control by man. Time of day is expressed in 24-hour local standard time; for example, 12:30 a. m. is 0030 and 1:30 p. m. is 1330.

In a general footnote, introduced by the word "NOTE" certain periods are indicated for which the discharge is computed or estimated by special methods because of no gage-height record, backwater from various sources, or other unusual conditions. Periods of no gage-height record are indicated if the period is continuous for a month or more or includes the maximum discharge for the year. Periods of backwater from an unusual source, of indefinite stage-discharge relation, or of any other unusual condition at the gage are indicated only if they are a month or more in length and the accuracy of the records is affected. Days on which the stage-discharge relation is affected by ice are not indicated. The methods used in computing discharge for various unusual conditions have been explained in preceding paragraphs. Footnotes to reservoir tables may be used to explain the use of new capacity tables or for other special conditions.

FIGURE 286*G*.—Introductory text—Continued.

WATER RESOURCES DATA FOR INDIANA, 19XX

Accuracy of Data

The accuracy of discharge data depends primarily on (1) the stability of the stage-discharge relation or, if the control is unstable, the frequency of discharge measurements, and (2) the accuracy of observations of stage, measurements of discharge, and interpretation of records.

The station description under "REMARKS" states the degree of accuracy of the records. "Excellent" means that about 95 percent of the daily discharges is within 5 percent; "good" within 10 percent; and "fair" within 15 percent. "Poor" means that daily discharges have less than "fair" accuracy.

Figures of daily mean discharge in this report are shown to the nearest hundredth of a cubic foot per second for discharges of less than 1 cfs; to tenths between 1.0 and 10 cfs; to whole numbers between 10 and 1,000 cfs; and to 3 significant figures above 1,000 cfs. The number of significant figures used is based solely on the magnitude of the figure. The same rounding rules apply to discharge figures listed for partial-record stations and miscellaneous sites.

Discharge at many stations, as indicated by the monthly mean, may not reflect natural runoff due to the effects of diversion, consumptive use, regulation, evaporation, or other factors. For such stations, discharge in cubic feet per second per square mile and runoff in inches are not published unless satisfactory adjustments can be made for such effects. Evaporation from a reservoir is not included in the adjustments for changes in reservoir contents, unless it is so stated. Even at those stations where adjustments are made, large errors in computed runoff may occur if adjustments or unadjusted losses (consumptive use, evaporation, seepage, etc.) are large in comparison with the observed discharge.

Publications

Each volume of the 1960 series of U.S. Geological Survey water-supply papers entitled "Surface Water Supply of the United States" contains a listing of the numbers of all water-supply papers in which records of surface-water data were published for the area covered by the individual volumes. Each volume also contains a list of water-supply papers that give detailed information on major floods for the area. A new series of water-supply papers containing surface-water records for the 5-year period October 1, 1960, to September 30, 1965, also will include lists of annual and special reports published as water-supply papers.

Records through September 1950 for the area covered by this report have been compiled and published in Water-Supply Papers 1305(3A), 1307(4), and 1308(5); records for October 1950 to September 1960 have been compiled and published in Water-Supply Papers 1725(3A), 1727(4), and 1728(5). These reports contain summaries of monthly and annual discharge and monthend storage for all previously published records, as well as some records not contained in the annual series of water-supply papers. All records were reexamined and revised where warranted. Estimates of discharge were made to fill short gaps whenever practical. The yearly summary table for each gaging station lists the numbers of the water-supply papers in which daily records were published for that station.

Special reports on major floods or droughts or of other hydrologic studies for the area have been issued in publications other than water-supply papers. Information relative to these reports may be obtained from the district office.

FIGURE 286*H*.—Introductory text—Continued.

WATER RESOURCES DATA FOR INDIANA, 19XX

Other Data Available

Data collected at partial-record stations and at miscellaneous sites are given in three tables at the end of the surface-water records in this report. The first is a table of discharge measurements at low-flow partial-record stations, the second is a table of annual maximum stage and discharge at crest-stage stations, and the third is a table of discharge measurements at miscellaneous sites.

More detailed information than that published for most of the gaging stations, such as discharge measurements, gage-height records, and rating tables, is on file in the district office. Many gaging-station records in (State) through (1966) have been analyzed to give several statistical summaries: (1) the number of days in each year that the daily discharge was between selected limits (duration tables); (2) the lowest mean discharge for selected numbers of consecutive days in each year; and (3) the highest mean discharge for selected numbers of consecutive days in each year.

At or near some gaging stations, water-quality records also are collected. Data are obtained on the chemical quality of the stream water, on water temperature, on suspended-sediment concentration, and on the particle-size distribution of suspended sediment and bed material. These data are given in Part 2 of this report. Under the "REMARKS" paragraph of the gaging-station description, reference is made to water-quality records collected on a regular basis.

HYDROLOGIC CONDITIONS

Precipitation was scattered throughout the year by area and time. Heavy rains the first half of December caused minor flooding in the Wabash and Maumee River basins. Lack of late summer showers left the central and southern parts 3 to 9 inches below average rainfall.

Deficient streamflow in October was relieved in the south by mid-November and in the north by the end of the month. Excessive to near excessive streamflow existed in the first part of December with near record streamflow in the upper Wabash River and Maumee River basins. Near normal streamflow existed from January to May with generally bankfull stages in March and May. Deficient * * *. *(to be completed)*

SELECTED REFERENCES

Carter, R. W., and Davidian, Jacob, 1968, General procedure for gaging streams: U.S. Geol. Survey Techniques Water-Resources Inv., book 3, chap. A6, 13 p.

Corbett, D. M., and others, 1943, Stream-gaging procedure, a manual describing methods and practices of the Geological Survey: U.S. Geol. Survey Water-Supply Paper 888, 245 p.

Langbein, W. B., and Iseri, K. T., 1960, General introduction and hydrologic definitions: U.S. Geol. Survey Water-Supply Paper 1541-A, 29 p.

FIGURE 286 *I*.—Introductory text—Continued.

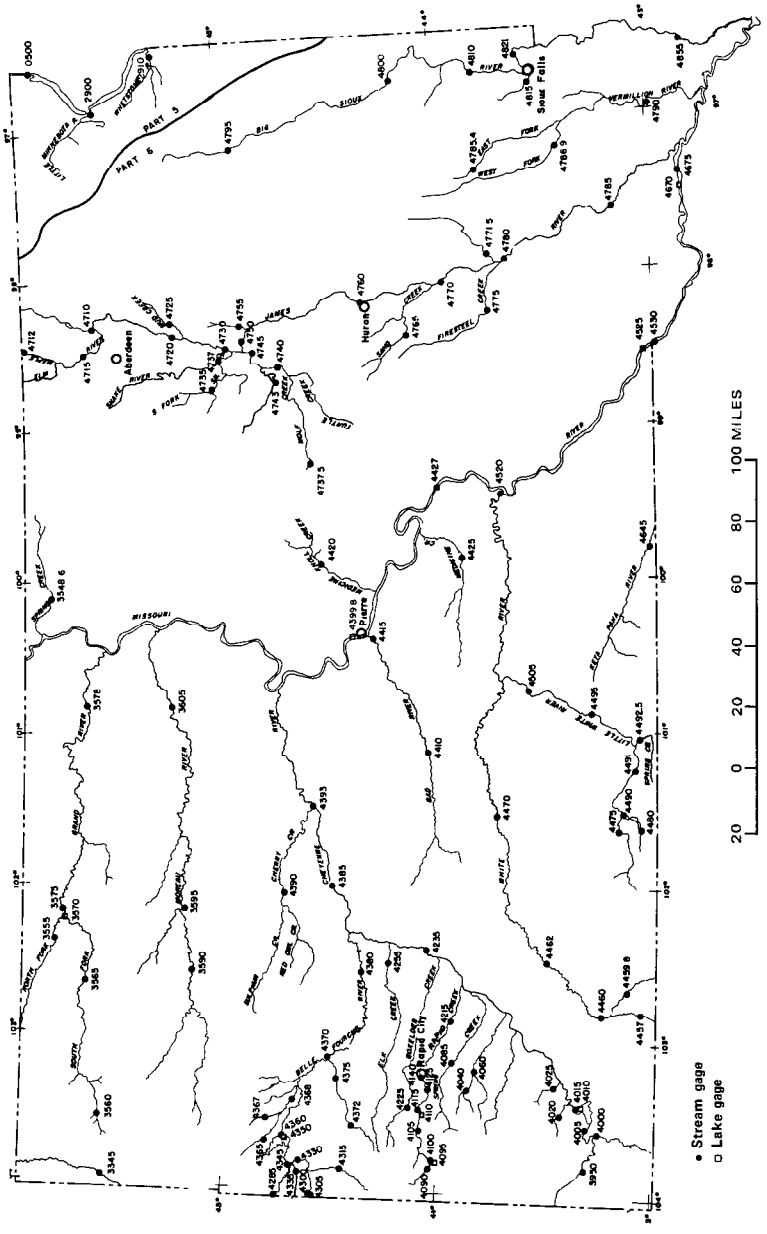

FIGURE 287.—Map of gaging-station locations.

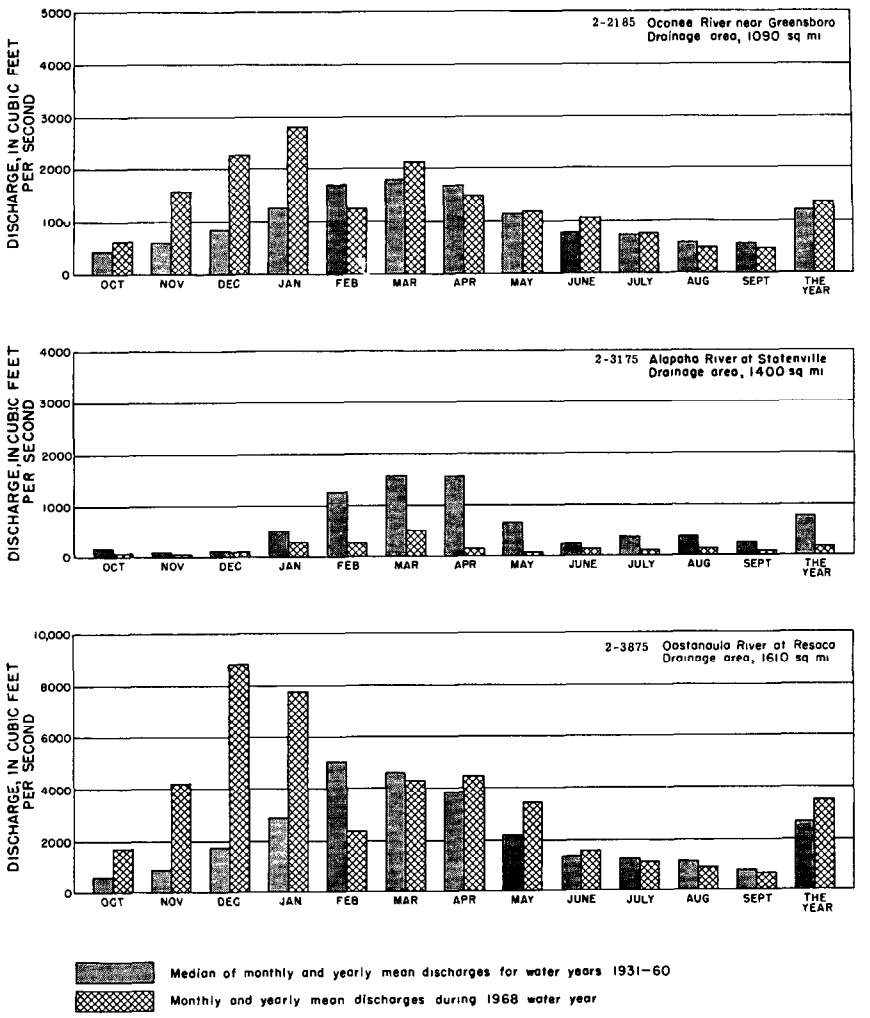

FIGURE 288.—Bar graph of hydrologic conditions.

SKUNK RIVER BASIN

5-4710. South Skunk River below Squaw Creek, near Ames, Iowa

LOCATION.--Lat 42°00'31", long 93°35'38", in NE¼NW¼ sec.13, T.83 N., R.24 W., Story County, on right bank 15 ft downstream from county highway bridge, 0.2 mile downstream from Squaw Creek, 0.3 mile upstream from bridge on U.S. Highway 30, 2 miles southeast of Ames, and at mile 222.6.

DRAINAGE AREA.--556 sq mi.

PERIOD OF RECORD.--October 1952 to current year. Prior to October 1966, published as Skunk River below Squaw Creek, near Ames.

GAGE.--Water-stage recorder and concrete control. Datum of gage is 867.10 ft above mean sea level.

AVERAGE DISCHARGE.--16 years, 226 cfs (5.52 inches per year, 163,600 acre-ft per year).

EXTREMES.--Current year: Maximum discharge, 7,310 cfs June 25 (gage height, 12.07 ft); no flow for many days.
Period of record: Maximum discharge, 9,260 cfs Mar. 30, 1960 (gage height, 13.20 ft); no flow for many days during 1953-57, 1964-65, 1967-68.
Flood of May 19, 1944, reached a stage of 13 ft, from floodmarks (discharge, 10,000 cfs).

REMARKS.--Records good except those for winter periods and period of no gage-height record, which are poor.

DISCHARGE, IN CFS, WATER YEAR OCTOBER 1967 TO SEPTEMBER 1968

DAY	OCT	NOV	DEC	JAN	FEB	MAR	APR	MAY	JUN	JUL	AUG	SEP
1	16	17	2.3	0	10	0	52	68	48	847	64	13
2	17	12	2.5	0	8.6	0	52	62	40	592	56	11
3	19	9.8	2.7	0	7.4	0	35	58	35	449	50	18
4	18	7.2	2.9	0	6.2	0	29	52	26	352	50	118
5	17	6.2	3.1	0	6.2	0	17	48	22	284	52	83
6	15	5.2	3.2	0	7.2	0	12	44	19	252	48	58
7	24	3.6	6.2	0	39	0	11	48	17	271	44	56
8	5.4	3.6	5.7	0	6.2	7.8	9.2	48	16	216	95	40
9	5.2	3.2	6.7	0	2.2	76	7.8	44	26	182	103	28
10	4.8	3.6	7.8	0	2.0	62	7.8	40	94	135	92	23
11	4.3	3.9	7.2	0	1.8	52	6.7	38	493	114	70	19
12	4.0	3.6	7.8	0	1.6	52	5.7	36	129	101	60	16
13	4.6	3.6	4.3	0	.58	38	6.7	38	52	98	54	14
14	4.0	3.2	3.6	0	.22	26	23	48	519	90	46	11
15	3.4	3.2	3.2	0	0	19	11	44	272	79	42	9.2
16	28	2.8	2.8	0	0	18	9.2	46	111	75	38	8.5
17	2.4	2.8	3.6	0	0	19	11	46	60	77	33	17
18	2.1	2.6	3.2	0	0	17	26	42	48	353	40	14
19	1.8	2.8	2.8	0	0	18	30	44	42	424	35	14
20	1.6	2.8	3.6	0	0	15	70	42	36	241	28	12
21	2.2	2.8	2.0	0	0	13	62	38	31	173	24	10
22	2.2	2.6	1.0	0	0	9.2	60	36	26	128	19	9.2
23	2.2	2.0	.54	0	0	6.2	233	36	52	181	17	8.5
24	5.7	2.6	.28	0	0	6.2	480	33	735	158	14	7.8
25	6.7	2.8	.15	0	0	5.7	324	36	5,910	107	15	6.2
26	6.7	2.6	0	0	0	5.2	216	52	3,600	90	21	5.7
27	6.2	2.5	0	0	0	6.2	153	52	2,000	157	16	4.7
28	5.7	2.4	0	2.0	0	57	107	65	1,330	161	13	4.7
29	10	2.3	0	18	0	5.7	85	92	1,980	103	12	47
30	12	2.2	0	7.2	------	57	75	54	1,440	83	15	38
31	15	------	0	6.7	------	14	------	54	------	72	15	------
TOTAL	133.6	127.5	89.17	33.9	64.10	502.6	2,123.3	1,484	19,209	6,645	1,281	724.3
MEAN	4.31	4.25	2.88	1.09	2.21	16.2	70.8	47.9	640	214	41.3	24.2
MAX	15	17	7.8	18	10	76	480	92	5,910	847	103	118
MIN	1.5	2.0	0	0	0	0	5.2	33	16	72	12	4.7
CFSM	.008	.008	.005	.002	.004	.03	.13	.09	1.15	.38	.07	.04
IN.	.009	.009	.006	.002	.004	.03	.14	.10	1.28	.44	.09	.05
AC-FT	265	253	177	67	127	997	4,210	2,940	38,100	13,180	2,540	1,440

CAL YR 1967: TOTAL 47,968.01 MEAN 131 MAX 4,070 MIN 0 CFSM .24 IN. 3.21 AC-FT 95,140
WTR YR 1968: TOTAL 32,417.87 MEAN 88.6 MAX 5,910 MIN 0 CFSM .16 IN. 2.17 AC-FT 64,300

PEAK DISCHARGE (BASE, 2,500 CFS)

DATE	TIME	G.H.	DISCHARGE	DATE	TIME	G.H.	DISCHARGE
6-25	1700	12.07	7,310	6-29	1500	6.71	2,550

NOTE.--No gage-height record Oct. 6 to Nov. 20.

FIGURE 289.—Daily discharge record.

MOBILE RIVER BASIN

2-3940. Etowah River at Allatoona Dam, above Cartersville, Ga.

LOCATION.--Lat 34°09'48", long 84°44'30", Bartow County, on right bank 0.8 mile downstream from Allatoona Dam, 2.0 miles upstream from Nashville, Chattahoogo and St. Louis Railway bridge, and 3.0 miles east of Cartersville.

DRAINAGE AREA.--1,110 sq mi, approximately.

PERIOD OF RECORD.--September 1938 to current year. Prior to October 1949, published as Etowah River above Cartersville.

GAGE.--Water-stage recorder. Datum of gage is 686.92 ft above sea level (levels by Corps of Engineers). Prior to Dec. 19, 1938, nonrecording gage at same site and datum.

AVERAGE DISCHARGE.--30 years, 1,800 cfs (22.02 inches per year), adjusted for storage since 1950.

EXTREMES.--Current year: Maximum discharge, 9,340 cfs Jan. 18 (gage height, 7.65 ft); minimum daily, 213 cfs Jan. 27, 28, Feb. 3, 4. Period of record: Maximum discharge, 40,400 cfs Jan. 8, 1946 (gage height, 20.8 ft), from rating curve extended above 26,000 cfs; minimum daily, 152 cfs Oct. 15, 1966.

REMARKS.--Flow regulated by Allatoona Reservoir since December 1949 (See sta 2-3935.)

COOPERATION.--Gage-height record, 19 discharge measurements, and computations of daily discharge furnished by Corps of Engineers; records reviewed by Geological Survey.

DISCHARGE, IN CFS, WATER YEAR OCTOBER 1967 TO SEPTEMBER 1968

DAY	OCT	NOV	DEC	JAN	FEB	MAR	APR	MAY	JUN	JUL	AUG	SEP
1	220	3,630	5,430	5,200	5,190	855	1,510	3,820	227	2,130	992	289
2	2,650	3,580	280	5,240	5,230	227	1,160	3,820	227	2,140	939	289
3	2,650	3,570	220	5,250	213	234	1,500	3,820	2,540	2,140	256	950
4	2,650	264	5,300	5,250	213	1,480	1,500	272	2,540	234	248	950
5	2,650	264	5,490	5,240	1,860	1,470	1,500	272	2,560	2,140	1,600	950
6	2,650	5,330	5,540	220	1,840	1,480	3,810	2,440	2,550	234	1,600	950
7	234	3,020	5,570	220	1,840	1,480	272	2,440	2,550	227	1,630	280
8	234	2,850	5,570	4,980	1,840	1,480	5,120	2,440	234	1,220	1,630	289
9	1,390	2,860	234	4,980	1,840	234	5,180	2,440	234	1,220	1,630	1,680
10	1,390	2,910	227	2,590	220	234	5,180	2,440	1,780	1,220	272	1,660
11	1,390	2,590	5,180	1,340	220	1,270	5,230	256	2,910	1,220	280	1,660
12	1,390	1,120	5,540	1,340	2,430	1,270	5,230	264	2,910	1,220	1,470	1,660
13	1,390	5,280	5,580	1,510	2,430	2,710	272	1,480	2,910	234	1,480	1,660
14	248	5,310	5,600	1,500	2,490	2,710	272	1,490	2,910	234	1,480	289
15	248	5,330	5,580	5,600	2,460	2,710	4,040	1,490	241	1,510	1,480	289
16	1,780	5,380	220	5,940	2,460	5,170	4,040	5,460	234	1,510	1,480	1,680
17	1,780	5,400	220	7,140	220	1,860	4,040	5,460	1,710	1,510	280	1,700
18	1,780	241	5,020	7,370	220	5,820	4,040	248	1,700	1,510	280	1,660
19	1,820	234	5,050	7,530	1,290	5,530	4,040	241	1,700	1,510	1,470	1,660
20	1,860	4,580	5,050	5,390	1,290	5,530	280	3,890	1,710	241	1,480	1,660
21	256	4,620	5,560	1,890	1,290	5,530	280	3,890	1,700	241	1,470	289
22	256	4,640	1,500	5,730	1,290	5,590	1,030	3,910	227	1,640	1,780	289
23	2,190	241	794	5,750	1,290	256	1,030	3,890	227	1,640	1,470	1,780
24	2,190	4,620	1,690	5,780	227	248	1,030	3,890	1,030	1,640	280	1,810
25	2,210	241	2,380	5,780	220	4,900	1,030	241	1,030	1,640	280	1,810
26	2,210	234	4,970	5,780	842	4,930	1,030	248	1,030	1,640	879	1,810
27	2,190	5,280	5,610	213	842	4,930	280	929	1,030	248	867	1,810
28	256	5,340	5,610	213	849	4,930	280	2,710	1,030	248	574	272
29	248	5,360	5,610	5,100	855	5,010	1,680	2,730	227	992	867	272
30	3,580	5,400	4,880	5,120	------	256	2,820	2,730	227	932	886	1,610
31	3,600	------	1,750	5,140	------	256	------	2,730	------	932	289	------
TOTAL	49,590	99,719	117,255	130,326	43,501	80,590	68,706	72,381	42,135	35,397	31,619	33,957
MEAN	1,600	3,324	3,782	4,204	1,500	2,600	2,290	2,335	1,405	1,142	1,020	1,132
MAX	3,600	5,400	5,610	7,530	5,230	5,820	5,230	5,460	2,910	2,140	1,780	1,810
MIN	220	234	220	213	213	227	272	241	227	227	248	272
MEAN†	1,197	2,524	3,327	4,362	2,169	3,317	3,198	2,366	1,415	1,079	680	840
CFSM†	1.08	2.27	3.00	3.93	1.95	2.99	2.88	2.13	1.27	.97	.61	.76
IN.†	1.24	2.53	3.46	4.53	2.10	3.45	3.21	2.46	1.42	1.12	.70	.85

CAL YR 1967: TOTAL 799,710 MAX 7,930 MIN 192 MEAN 2,191 MEAN† 2,230 CFSM† 2.01 IN.† 27.28
WTR YR 1968: TOTAL 805,176 MAX 7,530 MIN 213 MEAN 2,200 MEAN† 2,209 CFSM† 1.99 IN.† 27.09

† Adjusted for change in contents in Allatoona Reservoir.

FIGURE 290.—Daily discharge record (adjusted).

ARKANSAS RIVER BASIN

7-2590. Blue Mountain Reservoir near Waveland, Ark.

LOCATION.--Lat 35°06'06", long 93°39'02", in NE¼ sec.15, T 5 N., R 25 W., Yell County, at control tower for outlet works of dam on Petit Jean Creek, 1.3 miles southwest of Waveland

DRAINAGE AREA.--488 sq mi.

PERIOD OF RECORD.--March 1947 to current year.

GAGE --Water-stage recorder Datum of gage is at mean sea level (levels by Corps of Engineers)

EXTREMES --Current year. Maximum contents, 130,940 acre-ft May 23 (elevation, 405 37 ft); minimum, 2,150 acre-ft Oct 2, 3 (elevation, 370.68 ft).
Period of record: Maximum contents, 298,560 acre-ft May 26, 19XX (elevation, 422.54 ft), including 40,560 acre-ft of uncontrolled storage above spillway crest; minimum since initial filling to conservation pool level, 2,150 acre-ft Oct. 2, 3, 19XX (elevation, 370.68 ft).

REMARKS.--Reservoir is formed by earthfill dam, storage began Mar 13, 1947. Total capacity, 258,000 acre-ft at elevation 419.0 ft (crest of uncontrolled spillway), including 25,000 acre-ft at elevation 384.0 ft (conservation pool level), and 1,940 acre-ft of dead storage at elevation 370.00 ft (invert of gate sills of outlet tunnel). Under normal operating conditions reservoir water surface will be maintained at approximately conservation pool level for purposes of conservation and recreation, storage above this level is used for flood control. Figures given herein represent total contents.

COOPERATION.--Records furnished by Corps of Engineers.

Capacity table (elevation, in feet, and contents, in acre-feet)

370	1,940	390	44,810
371	2,250	395	66,370
372	2,920	400	93,620
375	5,680	405	128,140
380	14,400	406	135,700
385	27,700		

CONTENTS, IN ACRE-FEET, AT 2400, WATER YEAR OCTOBER 19XX TO SEPTEMBER 19XX

DAY	OCT	NOV	DEC	JAN	FEB	MAR	APR	MAY	JUN	JUL	AUG	SEP
1	2,160	2,380	2,460	15,000	3,250	26,810	29,480	29,940	104,570	28,620	26,230	23,220
2	2,150	2,380	2,450	12,440	3,250	26,810	29,320	29,910	101,410	28,470	25,930	23,110
3	2,920	2,450	2,430	10,020	3,310	26,750	29,200	29,850	97,420	28,250	25,650	23,050
4	5,580	13,190	2,420	7,340	5,050	26,660	29,320	29,970	92,740	28,560	25,560	23,020
5	6,400	15,780	2,420	5,950	8,780	26,320	29,510	33,560	88,610	28,680	25,440	22,970
6	5,750	14,140	2,420	5,120	11,620	25,860	29,720	51,800	84,600	28,430	25,280	22,890
7	4,580	11,340	2,420	4,680	13,300	25,310	29,910	57,390	80,830	28,130	25,220	22,830
8	3,450	8,740	2,440	4,740	14,730	25,310	30,030	57,780	77,100	27,910	25,160	22,750
9	3,080	6,400	2,450	5,160	16,140	26,110	29,910	56,340	72,680	27,790	25,100	22,800
10	2,850	4,940	2,580	5,420	17,020	26,600	29,850	53,850	68,350	27,610	25,040	22,720
11	2,580	3,680	5,310	5,420	17,680	26,690	29,850	51,040	64,010	27,490	24,950	22,670
12	2,420	3,050	8,290	5,310	18,230	26,320	29,750	47,680	59,750	27,360	24,790	22,480
13	2,850	2,750	9,290	5,450	18,710	26,050	29,720	44,190	55,940	27,700	24,730	22,370
14	2,990	2,580	8,430	9,620	19,090	28,190	29,720	40,860	51,840	27,790	24,590	22,200
15	2,880	2,620	6,760	21,070	19,760	34,630	29,720	37,420	48,000	27,580	24,500	22,170
16	2,650	2,750	8,170	11,670	20,310	37,090	29,820	34,060	44,550	27,330	24,450	22,060
17	2,480	2,780	16,280	18,230	21,900	36,920	29,910	31,680	41,550	27,090	24,340	22,010
18	2,400	2,780	26,690	21,160	23,960	36,110	29,750	32,920	38,660	27,090	24,370	21,950
19	2,340	2,780	30,490	20,640	25,250	34,940	29,540	56,470	35,810	26,940	24,310	21,870
20	2,360	2,740	29,750	18,660	25,890	33,460	29,690	100,700	33,390	26,840	24,310	21,870
21	2,380	2,670	27,700	16,140	26,480	31,810	29,380	127,160	31,850	27,030	24,340	22,310
22	2,380	2,550	25,130	13,450	26,780	30,490	29,290	130,180	30,800	27,090	24,260	22,280
23	2,360	2,480	22,450	11,330	27,120	29,880	29,320	130,410	30,000	28,560	24,090	22,170
24	2,340	2,410	19,210	9,420	27,000	29,450	29,410	128,520	29,600	32,350	23,980	22,230
25	2,320	2,340	16,210	7,770	26,540	30,120	29,410	126,260	29,230	33,120	23,820	22,370
26	2,320	2,320	12,990	5,900	25,890	30,940	29,480	124,520	29,690	32,750	23,740	22,170
27	2,320	2,330	19,210	4,840	25,310	31,240	29,480	121,350	29,850	31,440	23,630	21,950
28	2,320	2,440	23,270	3,900	25,930	31,110	29,510	118,060	29,540	30,000	23,540	21,680
29	2,320	2,480	22,830	3,410	26,900	31,170	29,820	114,810	29,200	28,560	23,460	21,430
30	2,320	2,480	20,800	3,280	------	30,280	29,850	111,360	29,170	27,640	23,380	21,240
31	2,370	------	17,950	3,250	------	29,820	------	107,630	------	26,940	23,300	------
(†)	371.18	371.35	381.49	372.50	384.74	385 69	385.70	402.16	385.48	384.75	383.51	382.76
(#)	+210	+110	+15,470	-14,700	+23,650	+2,920	+30	+77,780	-78,460	-2,230	-3,640	-2,060
MAX	6,400	15,780	30,490	21,160	27,120	37,090	30,030	130,410	104,570	33,120	26,230	23,220
MIN	2,150	2,320	2,420	3,250	3,250	25,310	29,200	29,850	29,170	26,840	23,300	21,240

CAL YR 19XX..... . . .. # -7,240
WTR YR 19XX. . . .. # +19,080

† Elevation, in feet, at end of month.
# Change in contents, in acre-feet.

FIGURE 291.—Daily reservoir record.

MISSISSIPPI RIVER MAIN STEM

5-2010. Winnibigoshish Lake near Deer River, Minn.

LOCATION.--Lat 47°25'42", long 94°03'00", in XX¼ sec.25, T 146 N., R.27 W., Itasca County, at dam on Mississippi River, 1 mile northwest of Little Winnibigoshish Lake and 14 miles northwest of town of Deer River.

DRAINAGE AREA --1,442 sq mi

PERIOD OF RECORD.--April 1884 to current year (monthend contents only). Prior to October 1941 monthend contents published in WSP 1308. Published as Winnibigoshish Reservoir near Deer River October 1941 to September 1956.

GAGE --Water-stage recorder. Datum of gage is 1,289.47 ft above mean sea level. Prior to July 8, 1949, nonrecording gage at same site and datum

EXTREMES.--Current year: Maximum contents, 561,880 acre-ft July 29 (gage height, 9.95 ft); minimum, 466,570 acre-ft Apr. 1 (gage height, 8.50 ft).
Period of record: Maximum contents observed, 996,500 acre-ft July 30, 1905 (gage height, 14.45 ft), minimum observed, 33,680 acre-ft below zero of capacity table Oct. 20, 1931 (gage height, -0.69 ft).

REMARKS --Reservoir is formed by concrete and timber dam controlling Winnibigoshish Lake and several other natural lakes; dam completed and storage began in 1884. Capacity, 967,930 acre-ft between gage height 0.00 and 14.2 ft (maximum operating level), of which 653,580 acre-ft is usable storage above 6.00 ft (minimum allowable level). Figures given herein represent contents above gage height 0.00 ft. Water is used to benefit navigation on Mississippi River below Minneapolis.

COOPERATION.--Records furnished by Corps of Engineers in cfs-days and converted to acre-feet by Geological Survey.

REVISIONS (WATER YEARS).--WSP 1308: 1905(M).

MONTHEND GAGE HEIGHT AND CONTENTS AT 2400, WATER YEAR OCTOBER 19XX TO SEPTEMBER 19XX

Date	Gage height (feet)	Contents (acre-feet)	Change in contents (acre-feet)
Sept.30	9.63	540,740	-
Oct. 31	9.51	532,880	-7,860
Nov. 30	9 31	519,750	-13,130
Dec. 31	9.28	517,780	-1,970
CAL YR 19XX	-	-	+106,510
Jan. 31	9.22	513,840	-3,940
Feb. 29	8.94	495,460	-18,380
Mar. 31	8.51	467,230	-28,230
Apr. 30	9 05	502.680	+35,450
May 31	9.37	523,690	+21,010
June 30	9.63	540,740	+17,050
July 31	9.80	551,900	+11,160
Aug. 31	9.21	513,190	-38,710
Sept 30	8.82	487,580	-25,610
WTR YR 19XX	-	-	-53,160

FIGURE 292.—Monthly reservoir record.

YAKIMA RIVER BASIN

Reservoirs in Yakima River basin

12-4740. KEECHELUS LAKE.--Lat 47°19'XX", long 121°20'XX", Kittitas County, at dam on Yakima River at outlet of Keechelus Lake, 3.X miles northwest of Martin and 10 miles northwest of Easton. Drainage area, 55.8 sq mi. Period of record, January 1906 to current year. Nonrecording gage read twice daily. Datum of gage is at mean sea level (Bureau of Reclamation bench mark). Extremes for current year: Maximum contents observed, 159,930 acre-ft June 17 (elevation, 2,517.84 ft); minimum observed, 33,560 acre-ft Sept. 30 (elevation, 2,450.97 ft). Extremes for period of record: Maximum contents observed, 160,570 acre-ft May 16, 1925 (elevation, 2,518.09 ft); minimum observed, 448 acre-ft Sept. 6, 12, 13, 1906 (original crib dam); minimum elevation observed, 2,428.30 ft Sept. 20, 1926.

Reservoir is formed on natural lake by earth- and gravel-fill dam completed in 1917; storage above crib dam began Jan. 12, 1906; above present dam Aug. 19, 1914. Initial filling of present reservoir June 15, 1920. Usable capacity, 157,800 acre-ft between elevation 2,425 00 (invert of gate sill) and 2,517.00 ft (spillway crest). Dead storage below elevation 2,425.00 ft, XXX acre-ft. Spillway raised 2 ft Sept. 12, 1952. Figures given herein represent usable contents. Water is used for irrigation.

12-4755. KACHESS LAKE.-- * * *. (Format similar to the above)

12-4785. CLE ELUM LAKE.-- * * *. (Format similar to the above)

12-4875. BUMPING LAKE.--Lat 46°52'XX", long 121°18'XX", in SW¼ sec.23, T.16 N., R.12 E. (unsurveyed), Yakima County, at dam on Bumping River at outlet of Bumping Lake, 12 miles upstream from American River and 19 miles west of Nile. Drainage area, 68.6 sq mi. Period of record, June to July 1906, April 1909 to current year. Nonrecording gage read twice daily. Datum of gage is at mean sea level (Bureau of Reclamation bench mark). Extremes for current year: Maximum contents observed, 36,160 acre-ft June 16 (elevation, 3,427.85 ft); minimum observed, 4,980 acre-ft Sept. 30 (elevation, 3,396.67 ft). Extremes for period of record: Maximum contents observed, 39,840 acre-ft June 21, 22, 1925 (elevation, 3,430.55 ft); minimum obeerved, 1,130 acre-ft Feb. 5-9, 1949 (elevation, 3,390.80 ft).

Reservoir is formed on natural lake by earthfill dam completed in 1910; storage begun Nov 3, 1910. Usable capacity, 33,700 acre-ft between elevation 3,389.00 (invert of gate sill) and 3,426.00 ft (spillway crest). No dead storage Figures given herein represent usable contents Water is used for irrigation.

MONTHEND ELEVATION AND CONTENTS AT 2400, WATER YEAR OCTOBER 19XX TO SEPTEMBER 19XX

Date	Elevation (feet)	Contents (acre-feet)	Change in contents (acre-feet)	Elevation (feet)	Contents (acre-feet)	Change in contents (acre-feet
	12-4740. Keechelus Lake			12-4755. Kachess Lake		
Sept.30	2,486.95	90,120	-	2,246.60	172,150	-
Oct. 31	2,493.45	103,090	+12,970	2,252 57	197,330	+25,180
Nov. 30	2,505.50	129,580	+26,490	2,259.10	225,930	+28,600
Dec 31	2,495.52	107,420	-22,160	2,252.02	194,970	-30,960
CAL YR 19XX	-	-	-15,540	-	-	+5,890
Jan. 31	2,482.77	82,300	-25,120	2,248.11	178,420	-16,550
Feb. 29	2,486.84	93,800	+11,500	2,250.63	189,030	+10,610
Mar. 31	2,496 23	108,920	+15,120	2,254.11	203,980	+14,950
Apr. 30	2,509.21	138,380	+29,460	2,260.20	230,860	+26,880
May 31	2,514.95	152,560	+14,180	2,260.39	231,710	+850
June 30	2,517.38	158,750	+6,190	2,261.88	238,440	+6,730
July 31	2,502.09	121,750	-37,000	2,250.93	190,310	-48,130
Aug. 31	2,473.38	66,130	-55,620	2,242 39	155,110	-35,200
Sept.30	2,450 79	33,320	-32,810	2,237.37	135,660	-19,450
WTR YR 19XX	-	-	-56,800	-	-	-36,490
	12-4785. Cle Elum Lake			12-4875. Bumping Lake		
Sept.30	2,181.55	192,540	-	3,404.42	10,700	-
Oct. 31	2,199.96	262,020	+69,480	3,400.70	7,820	-2,880
Nov. 30	2,226.81	375,470	+113,450	3,412.50	18,060	+10,240
Dec. 31	2,217 13	332,920	-42,550	3,403.55	10,000	-8,060
CAL YR 19XX	-	-	+102,930	-	-	-4,110
Jan. 31	2,202.74	273,140	-59,780	3,397.77	5,730	-4,270
Feb. 29	2,207.24	291,440	+18,300	3,400.18	7,440	+1,710
Mar. 31	2,215.62	326,460	+35,020	3,408.68	14,370	+6,930
Apr. 30	2,229.42	387,310	+60,850	3,413.32	18,900	+4,530
May 31	2,233.11	404,330	+17,020	3,421.87	30,980	+12,080
June 30	2,237.95	427,130	+22,800	3,427.31	35,430	+4,450
July 31	2,216.17	328,800	-98,330	3,410.90	16,470	-18,960
Aug. 31	2,187.53	214,330	-114,470	3,403.30	9,810	-6,660
Sept.30	2,158.33	115,360	-98,970	3,396.60	4,930	-4,880
WTR YR 19XX	-	-	-77,180	-	-	-5,770

FIGURE 293A.—Group reservoir records (large reservoirs).

RIO GRANDE BASIN

Reservoirs in Rio Grande basin--Continued

MONTHEND ELEVATION OR GAGE HEIGHT AND CONTENTS, WATER YEAR OCTOBER 19XX TO SEPTEMBER 19XX

Date	Gage height (feet)	Contents (acre-feet)	Change in contents (acre-feet)	Elevation or gage height (feet)	Contents (acre-feet)	Change in contents (acre-feet)	Elevation or gage height (feet)	Contents (acre-feet)	Change in contents (acre-feet)
	8-3165. Nichols Reservoir†			8-3285. Jemez Canyon Reservoir†			8-3414. Bluewater Lake‡		
Sept. 30	142.3	168	-	0	0	-	7,371.2	5,510	-
Oct. 31	139.0	129	-39	5,143.2	753	+753	7,370.4	5,170	-340
Nov. 30	143.1	178	+49	0	0	-753	7,370.0	5,000	-170
Dec. 31	143.8	187	+9	0	0	0	7,369.7	4,880	-120
CAL YR 19XX	-	-	-349	-	-	0	-	-	-2,500
Jan 31	-	a228	+41	0	0	0	7,369.5	4,800	-80
Feb. 29	150.0	279	+51	0	0	0	7,369.4	4,760	-40
Mar. 31	157.7	438	+159	5,146.40	1,090	+1,090	7,381.4	12,020	+7,260
Apr. 30	167.5	701	+263	5,142.70	480	-610	7,381.0	11,700	-320
May 31	167.5	701	0	5,128.80	0	-480	7,380.4	11,240	-460
June 30	165 1	628	-73	0	0	0	7,379.5	10,560	-680
July 31	159.4	477	-151	0	0	0	7,378.5	9,820	-740
Aug. 31	154.2	360	-117	0	0	0	7,377.5	9,120	-700
Sept. 30	139.0	129	-231	0	0	0	7,376.7	8,580	-540
WTR YR 19XX	-	-	-39	-	-	0	-	-	+3,070
	8-3605. Elephant Butte Res.††			8-3620. Caballo Reservoir‡			8-3840. Alamogordo Reservoir‡		
Sept. 30	4,334.46	532,800	-	4,140.42	41,690	-	4,269.90	100,600	-
Oct. 31	4,333.30	517,500	-15,300	4,144.95	58,170	+16,480	4,269.80	100,200	-400
Nov. 30	4,335.70	549,300	+31,800	4,145.20	59,200	+1,030	4,270.40	102,600	+2,400
Dec. 31	4,338.40	586,400	+37,100	4,145.55	60,640	+1,440	4,271.90	108,600	+6,000
CAL YR 19XX	-	-	-402,400	-	-	-85,360	-	-	-15,100
Jan 31	4,338.50	587,800	+1,400	4,152.53	92,290	+31,650	4,273 20	114,100	+5,500
Feb. 29	4,338 50	587,800	0	4,157 71	125,850	+33,560	4,274.15	118,200	+4,100
Mar. 31	4,336.07	554,300	-33,500	4,152.24	92,340	-33,510	4,269.15	97,710	-20,490
Apr. 30	4,338 98	594,500	+40,200	4,156.60	118,400	+26,060	4,271.10	105,400	+7,690
May 31	4,336.90	565,700	-28,800	4,159.16	135,700	+17,300	4,264.10	79,540	-25,860
June 30	4,335.53	547,100	-18,600	4,157.49	124,300	-11,400	4,267.70	92,270	+12,730
July 31	4,330.10	476,400	-70,700	4,152.30	92,670	-31,630	4,274.90	121,600	+29,330
Aug. 31	4,324.61	410,100	-66,300	4,136.24	29,260	-63,410	4,274.65	120,500	-1,100
Sept. 30	4,322.42	385,100	-25,000	4,123 48	4,900	-24,360	4,273.95	117,400	-3,100
WTR YR 19XX	-	-	-147,700	-	-	-36,790	-	-	+16,800
	8-4005. Lake McMillan‡			8-4038. Lake Avalon‡			8-4100. Red Bluff Reservoir††		
Sept. 30	19 10	9,620	-	15.70	1,560	-	2,807.9	63,150	-
Oct. 31	18.30	7,330	-2,290	16.30	1,920	+360	-	a65,100	+1,950
Nov. 30	18.75	8,580	+1,250	17.40	2,620	+700	-	a69,100	+4,000
Dec 31	19.50	10,850	+2,270	18.20	3,200	+580	2,809.7	70,300	+1,200
CAL YR 19XX	-	-	-26,890	-	-	-2,060	-	-	-35,900
Jan 31	19 75	11,650	+800	15.75	1,590	-1,610	2,810.6	73,900	+3,600
Feb. 29	19.65	11,330	-320	16.10	1,800	+210	2,810.8	74,700	+800
Mar. 31	22.30	20,940	+9,610	14.75	1,070	-730	2,811.0	75,500	+800
Apr. 30	17.60	5,510	-15,430	15.40	1,400	+330	2,807.4	61,400	-14,100
May 31	19.75	11,650	+6,140	15.55	1,480	+80	2,805.5	54,750	-6,650
June 30	21.05	16,150	+4,500	14.75	1,070	-410	2,804.3	50,900	-3,850
July 31	25.95	38,580	+22,430	19.15	3,960	+2,890	2,815.4	96,000	+45,100
Aug. 31	24.15	29,140	-9,440	16.00	1,740	-2,220	-	a93,000	-3,000
Sept. 30	21.15	16,520	-12,620	15.70	1,560	-180	-	a85,400	-7,600
WTR YR 19XX	-	-	+6,900	-	-	0	-	-	+22,250

† Elevation or gage height at 2400.
‡ Elevation or gage height at 0800.
†† Daily mean gage height.
a Interpolated.

FIGURE 293 *B*. Group reservoir records (large reservoirs)—Continued.

ANDROSCOGGIN RIVER BASIN

Reservoirs in Androscoggin River basin

1-0505. RANGELEY LAKE on Rangeley Stream, at Oquossoc, Maine, used for power and log driving, has usable capacity of 1,339,200,000 cu ft in top 4 ft of lake (top of flashboards). Gage-height record furnished by Union Water Power Co.

1-0510. MOOSELOOKMEGUNTIC LAKE at Upper Dam, in Richardson Township, Maine, used for power and log driving, has usable capacity of 8,370,000,000 cu ft between gage heights 8.3 and 20.5 ft. Gage-height record furnished by Union Water Power Co.

1-0515. UPPER AND LOWER RICHARDSON LAKES on Rapid River, at Middle Dam, Maine, used for power and log driving, has usable capacity of 5,691,500,000 cu ft between gage heights 3.0 and 20.5 ft. Gage-height record furnished by Union Water Power Co.

1-0520. AZISCOHOS LAKE on Magalloway River, in Lincoln Township, 3 miles east of village of Wilsons Mills, Maine, completed in 1911 for power, has usable capacity of 9,593,000,000 cu ft between elevations 1,490.0 and 1,535.0 ft. Elevation record furnished by Union Water Power Co.

1-0530. UMBAGOG LAKE on Androscoggin River, at Errol Dam, 0.8 mile northeast of Errol, N.H., used for power and log driving, has usable capacity of 3,080,160,000 cu ft between gage heights 5.5 and 15.0 ft. Gage-height record furnished by Union Water Power C

1-0560. GULF ISLAND POND on Androscoggin River, 3 miles upstream from Lewiston, Maine, completed in 1928 for power, has capacity of 1,100,000,000 cu ft in top 10 ft of pond below elevation 262 ft. Elevation record furnished by Central Maine Power Co.

1-0565. LAKE AUBURN on outlet stream to Androscoggin River, at East Auburn, Maine, used for storing water supply of Auburn and Lewiston, has usable capacity of 580,000,000 cu ft between elevations 254.7 and 260.7 ft. .Elevation record furnished by Auburn Water District.

1-0575. PENNESSEEWASSEE LAKE on short outlet stream to Little Androscoggin River, at Norway, Maine, used for recreation, has usable capacity of 192,000,000 cu ft between gage heights 95.0 and 100.0 ft. Gage-height record furnished by Town of Norway.

1-0580. THOMPSON LAKE on short outlet stream to Little Androscoggin River, at Oxford, Maine, used for power and process water, has usable capacity of 950,000,000 cu ft between gage heights 95.0 and 100.0 ft. Gage-height record furnished by Robinson Manufacturing Co.

MONTHEND CONTENTS, IN MILLIONS OF CUBIC FEET, WATER YEAR OCTOBER 1967 TO SEPTEMBER 1968

Date	Rangeley Lake†	Mooselookmeguntic Lake†	Upper and Lower Richardson Lakes†	Aziscohos Lake†	Umbagog Lake†
Sept. 30, 1967	754	4,470	4,047	6,492	1,434
Oct. 31	837	3,076	3,862	6,926	1,668
Nov. 30	194	1,266	4,084	6,576	1,848
Dec. 31	84	534	4,047	6,688	1,920
Jan. 31, 1968	0	124	3,233	5,098	1,506
Feb. 29	0	0	2,540	3,938	850
Mar. 31	265	1,033	2,339	4,410	1,794
Apr. 30	1,366	6,474	4,918	8,830	3,138
May 31	1,366	8,154	5,691	9,702	2,300
June 30	1,366	8,370	5,691	9,872	3,119
July 31	1,185	7,724	5,350	9,253	1,958
Aug. 31	920	5,799	4,269	7,587	1,884
Sept. 30	656	4,368	3,270	6,394	1,578

Date	Gulf Island Pond‡	Lake Auburn†	Pennesseewassee Lake††	Thompson Lake‡‡
Sept. 30, 1967	2,316	386	98	1,913
Oct. 31	2,416	408	107	1,799
Nov. 30	2,195	386	111	1,742
Dec. 31	2,296	408	116	1,780
Jan. 31, 1968	2,199	430	111	1,723
Feb. 29	2,080	430	111	1,685
Mar. 31	2,500	604	111	1,970
Apr. 30	2,495	664	116	2,065
May 31	2,487	640	98	2,046
June 30	2,497	640	78	2,046
July 31	2,199	556	59	1,932
Aug. 31	2,211	474	66	1,818
Sept. 30	2,370	419	74	1,742

† Contents at 0700 on first day of following month.
‡ Contents at 2400.
†† Contents as of last day of month, by interpolation.
‡‡ Contents at 0800.

FIGURE 294.—Group reservoir records (small reservoirs).

"A"

DISCHARGE, IN CUBIC FEET PER SECOND, 19XX

Sept 10	4.6	Sept.21	5.3
11	4.4	22	6.5
12	4.6	23	6.7
13	4.7	24	6.7
14	4.9	25	6.8
15	4.7	26	7.1
16	4.4	27	10
17	4.4	28	11
18	4.4	29	11
19	4.4	30	11
20	4.7		

[Daily table for complete year follows.]

"B"

DISCHARGE, IN CUBIC FEET PER SECOND, 19XX

DAY	AUG	SEP	DAY	AUG	SEP	DAY	AUG	SEP	DAY	AUG	SEP	DAY	AUG	SEP
1	6.9	5.4	7	9.3	5.4	13	6.9	4.1	19	6.4	3.1	25	4.9	3.4
2	6.4	4.9	8	12	5.4	14	6.4	3.8	20	5.9	3.8	26	4.1	3.8
3	6.4	4.9	9	12	6.4	15	8.6	3.4	21	5.9	3.4	27	4.5	3.8
4	6.4	4.9	10	10	4.5	16	11	2.8	22	6.4	3.4	28	4.5	3.8
5	7.4	4.9	11	17	4.1	17	6.9	2.3	23	6.4	3.1	29	4.5	3.8
6	9.3	4.9	12	8.0	4.1	18	6.9	2.8	24	5.4	3.4	30	4.5	3.4
												31	5.4	
Total													226.6	121.2
Max													17	6.4
Min													4 1	2.3
Mean													7.31	4.04
Runoff in acre-feet													449	240

PEAK DISCHARGE (BASE, 50 CFS).--No peak above base.

[Daily table for complete year follows.]

"C"

DISCHARGE, IN CUBIC FEET PER SECOND, FEBRUARY 1961 TO SEPTEMBER 1965

July 3, 1961	1.9	Nov. 7, 1963	0
July 30, 1961	1.5	Nov. 21, 1963	2
Aug. 18, 1961	3.4	Aug. 12, 1964	
Nov. 21, 1961	6	Sept.14, 1964	1
Aug. 17, 1963	8	Aug. 17, 1965	
Oct. 19, 1963	.3		

Month	Cfs-days	Maximum	Minimum	Mean	Runoff acre-fe
July 1961	3.4	1.9	0	0.11	6.7
August	3.4	3.4	0	.11	6.7
November	.6	.6	0	.02	1.2
WTR YR 1962	.6	.6	0	.002	1.2
CAL YR 1962	0	0	0	0	0
August 1963	.8	.8	0	.03	1.6
WTR YR 1963	.8	.8	0	.002	1.6
October 1963	.3	.3	0	.01	.6
November	2.9	2.6	0	.10	5.8
CAL YR 1963	4.0	2.6	0	.01	8 0
August 1964	.5	.5	0	.02	1 0
September	1.0	1.0	0	.03	2.0
WTR YR 1964	4.7	2.6	0	.01	9.4
CAL YR 1964	1.5	1.0	0	.004	3.0
August 1965	.1	.1	0	.003	.2
WTR YR 1965	.1	.1	0	.0003	.2

PEAK DISCHARGE (BASE, 20 CFS).--July 3, 1961 (2130) 113 cfs (3.36 ft); July 30, 1961 (1500) 90 cfs (3.02 ft); Aug. 18, 1961 (2000) 179 cfs (4.28 ft); Nov. 21, 1961 (1030) 39 cfs (2.16 ft); Aug. 17, 1963 (1030) 46 cfs (2.28 ft); Oct. 19, 1963 (0700) 25 cfs (1.93 ft); Nov. 7, 1963 (1430) 24 cfs (1.91 ft); Nov. 21, 1963 (1300) 61 cfs (2.53 ft); Sept. 14, 1964 (about 2000) 74 cfs (2.75 ft).

NOTE.--Flow occurred only on days listed above.

FIGURE 295.—Discharge tables for short periods.

REVISIONS (WATER YEARS) --WSP 1277: 1939-42. Revised figures of discharge, in cubic feet per second, for the water years 1963-65, superseding those published in WRD XXXX, 1963-65, are given herewith

Date	Discharge	Date	Discharge	Date	Discharge
1962		1963-Con.		1965	
Dec. 28	137	July 22	157	Feb. 15	164
29	137	29	505	16	239
30	267			22	464
31	122	1964		26	228
1963		Mar. 6	276	Mar. 3	408
Mar. 11	137	7	256	6	227
*	*	23	184	20	552
20	323	* *	*	*	*
		Apr. 12	206	June 18	676

Month	Cfs-days	Maximum	Minimum	Mean	Per square mile	Runoff in inches
December 1962.....	1,676	267	13	54.1	1.45	1.67
CAL YR 1962.....	X,XXX.X	XXX	X.X	XX.X	.XX	XX.XX
March 1963.....	3,137	891	16	101	2 71	3.12
* *	*	*	*	*	*	*
CAL YR 1965.... ..	14,970 6	1,150	5 9	41 0	1.10	14.95

FIGURE 296.—Revisions of published records.

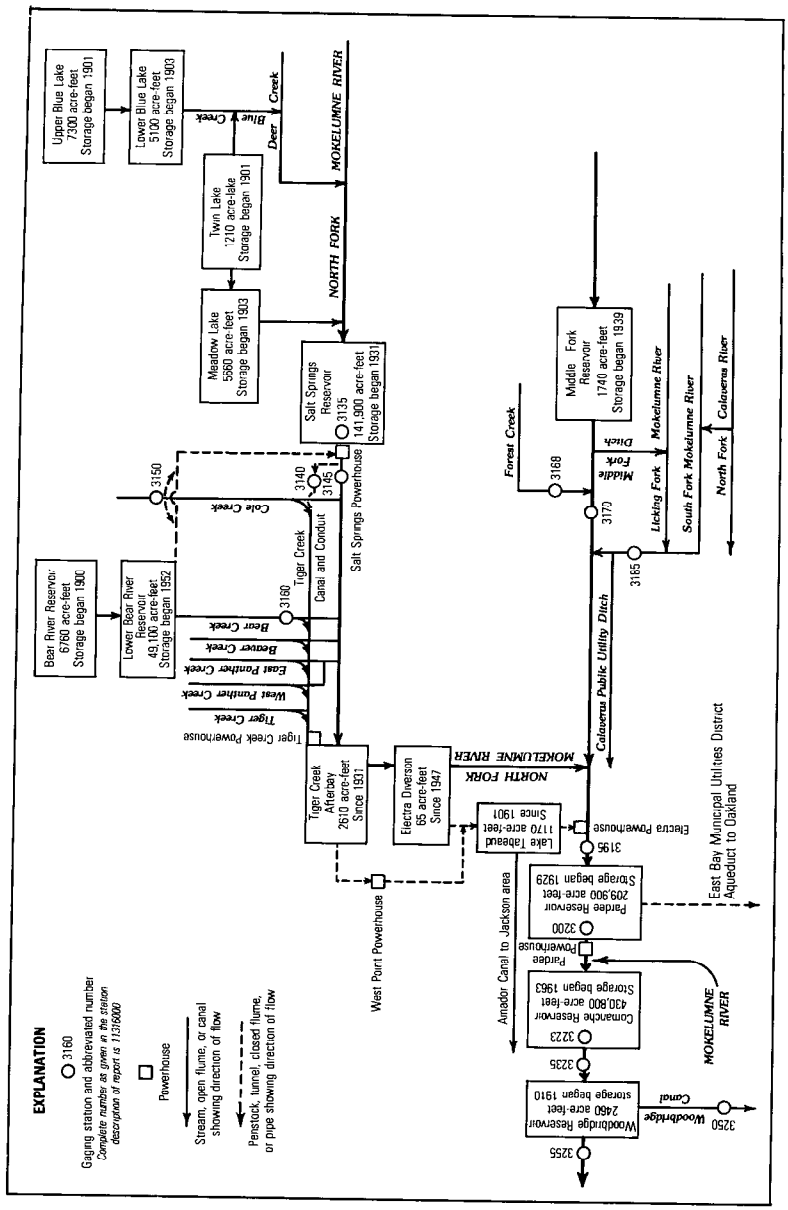

FIGURE 297.—Schematic diagram showing reservoirs, canals, and gaging stations.

DISCHARGE AT PARTIAL-RECORD STATIONS AND MISCELLANEOUS SITES

As the number of streams on which streamflow information is likely to be desired far exceeds the number of stream-gaging stations *feasible to operate at one time, the Geological Survey collects limited streamflow data at sites other than stream-gaging* stations. When limited streamflow data are collected on a systematic basis over a period of years for use in hydrologic analyses, the site at which the data are collected is called a partial-record station. Data collected at these partial-record stations are usable in low-flow or floodflow analyses, depending on the type of data collected. In addition, discharge measurements are made at other sites not included in the partial-record program. These measurements are generally made in times of drought or flood to give better areal coverage to those events. Those measurements and others collected for some special reason are called measurements at miscellaneous sites.

Records collected at partial-record stations are presented in two tables. The first is a table of discharge measurements at low-flow partial-record stations, and the second is a table of annual maximum stage and discharge at crest-stage stations. Discharge measurements made at miscellaneous sites for both low flow and high flow are given in a third table.

Low-flow partial-record stations

Measurements of streamflow in the area covered by this report made at low-flow partial-record stations are given in the following table. *Most of these measurements were made during periods of base flow when streamflow is primarily from ground-water* storage. These measurements, when correlated with the simultaneous discharge of a nearby stream where continuous records are available, will give a picture of the low-flow potentiality of a stream. The column headed "Period of record" shows the water years in which measurements were made at the same, or practically the same, site.

Discharge measurements made at low-flow partial-record stations during water year 1968

Station No.	*Station name*	*Location*	Drainage *area* (sq mi)	Period *of* record	Measurements	
					Date	Discharg (cfs)
		Savannah River basin				
2-1804	Tiger Creek at Lakemont, Ga.	Lat 34°47'03", long 83°24'58", Rabun County, at county highway bridge, at Lakemont.	a26	1951, 1959-60, 1962-68	7- 2-68 8-28-68	34 17
*2-1913	Broad River above Carlton, Ga.	Lat 34°04'37", long 83°00'22", Madison County, at State Highway 72, 2.8 miles northeast of Carlton.	760	1897-1913‡, 1943, 1953-54, 1959, 1962-68	7-22-68 9-13-68	532 396
* 2-1975.3	* Sweetwater Creek near Bonesville, Ga.	* Lat 33°26'16", long 82°27'00", McDuffie County, at State Highway 10, 0.8 mile northwest of Bonesville.	* 7.46	* 1953, 1955, 1959-61, 1963, 1965-68	* 8-30-68	* .30

* Also a crest-stage partial-record station.
‡ Operated as a continuous-record gaging station.
a Approximately.

FIGURE 298.—Low-flow partial records.

DISCHARGE AT PARTIAL-RECORD STATIONS AND MISCELLANEOUS SITES

The following table contains annual maximum discharge for crest-stage stations. A crest-stage is a device which will register the peak stage occurring between inspections of the gage. A stage-discharge relation for each gage is developed from discharge measurements made by indirect measurements of peak flow or by current meter. The date of the maximum discharge is not always certain but is usually determined by comparison with nearby continuous-record stations, weather records, or local inquiry. Only the maximum discharge for each water year is given. Information on some lower floods may have been obtained, and discharge measurements may have been made for purposes of establishing the stage-discharge relation, but these are not published herein. The years given in the period of record represent water years for which the annual maximum has been determined.

Annual maximum discharge at crest-stage partial-record stations during water year 1968

Station No.	Station name	Location	Drainage area (sq mi)	Period of record	Annual maximum		
					Date	Gage height (feet)	Discharge (cfs)
Virgin River basin							
9-4151	Pulsipher Wash near Mesquite, Nev.	Lat 36°48'04", long 114°06'35", in NW¼SW¼ sec.18, T.13 S., R.71 E., Clark County, at culvert on U.S. Highway 91, 2.4 miles west of Mesquite.	4.58	1963-68	11-21-67	a5.85	b150
Walker Lake basin							
10-2952	West Walker River at Leavitt Meadows, near Coleville, Calif.	Lat 38°19'XX", long 119°33'XX", in NW¼NW¼ sec.34, T.6 N., R.22 E., Mono County, at Leavitt Meadows Lodge, 16 miles south of Coleville.	73.0	1946-64, 1967-68	7- -67 6- -68	5.95 4.71	c1,600 940
Owyhee River basin							
13-1759	Reed Creek near Owyhee, Nev.	Lat 41°53'46", long 116°03'39", in SW¼SE¼ sec.7, T.46 N., R.53 E., Elko County, at culvert on State Highway 11-A, 3.X miles southeast of Owyhee.	6.51	1962-68	2-20-68	2.58	d5
13-1766	Taylor Canyon tributary near Tuscarora, Nev.	Lat 41°14'XX", long 116°02'XX", in S½ sec.29, T.39 N., R.53 E., Elko County, at culvert on State Highway 11, 11 miles southeast of Tuscarora.	e1.2	1967-68	1967 2-20-68	(f) 2.99	d7 (f)

See footnotes at end of table, p._____.

FIGURE 299.—Crest-stage partial records.

DISCHARGE AT PARTIAL-RECORD STATIONS AND MISCELLANEOUS SITES

Discharge measurements at miscellaneous sites

Measurements of streamflow at points other than gaging stations are given in the following table. Those that are measurements base flow are designated by an asterisk (*), measurements of peak flow by a dagger (†)

Discharge measurements made at miscellaneous sites during water year 19XX

Stream	Tributary to	Location	Drainage area (sq mi)	Measured previously (water years)	Measurements	
					Date	Discharge (cfs)
Part 6A		Yellowstone River basin				
Little Wind River a/	Wind River	Lat 42°57'37", long 108°29'54", in NE¼SE¼ sec 22, T 1 S , R 3 E , Fremont County, at bridge on county road, 1.2 miles upstream from Popo Agie River, 0.5 mile west of Arapahoe, Wyo	b650	1966-67	10-26-XX 2- 1-XX 3-30-XX 6-23-XX 8- 1-XX	137 91 53 †3,760 *7 8
Bighorn River	Yellowstone River	Lat 44°12'XX", long 107°55'XX", in sec.28, T 49 N , R 92 W , Big Horn County, at bridge on county road, 0 2 mile west of Fairden, 1.2 miles downstream from Fivemile Creek, 5.8 miles southeast of Manderson, Wyo.	11,020	1949-55*, 1955-56*	10- 3-XX 2-11-XX 5-17-XX	*437 *c980 7,430
Do	.. do	Lat * * *.	-	-	6- 7-XX	†d17,300
Part 9		Green River basin				
Bitter Creek	Green River	Lat 41°31'25", long 109°25'41", in NE¼SE¼ sec.24, T.18 N , R 107 W , Sweetwater County, 1.7 miles east of town of Green River, Wyo., and 1.9 miles upstream from mouth.	-	1958, 1966-67	10- 6-XX 3-19-XX 7-13-XX	*5.6 15 * 91
Part 10		Bear River basin				
Bear River	Great Salt Lake	Lat 41°19'XX", long 111°01'XX", in NE¼ sec.1, T 15 N , R.121 W , Uinta County, at bridge on county road, 3.5 miles northwest of Evanston, Wyo.	715	1913-56*	9-12-XX	*8 3
Part 13		Salt River basin				
Stump Creek	Salt River	Lat 42°47'00", long 111°03'10", in NE¼SW¼ sec 27, T.7 S., R 46 E , Lincoln County, at bridge on county road, 1.2 miles upstream from Wyoming-Idaho State line, 3.3 miles west of Auburn, Wyo.	102	1946-49*, 1962-65	11- 3-XX 1-16-XX 5-21-XX 8-28-XX	*24 *11 †375 *26

* Operated as a continuous-record gaging station
a Formerly published as Popo Agie River.
b Approximately.
c Not previously published.
d Revised

FIGURE 300.—Discharge measurements at miscellaneous sites.

RIO GRANDE BASIN

Pecos River seepage investigations—Acme to Artesia, N Mex.

Two series of discharge measurements were made during the 19XX water year, on Jan. 20 and Mar. 31, on the Pecos River and tributaries and diversions in New Mexico, to study channel gains and losses. The reach is 81 6 miles in length and extends from the gaging station Pecos River near Acme (8-3860) to the gaging station Pecos River near Artesia (8-3965). The measurements were made during periods of constant base flow of the streams, for 10 days before the investigations no measurable precipitation had fallen Tributary flow was considered a contribution and not a gain; diversion was considered a deduction and not a loss Indicated gains or losses may be substantially in error as affected by small inaccuracies in open-channel measurements Records of chemical analyses and water temperatures obtained at the time of this investigation are published in Part 2 of this report. Previous seepage investigations of this reach were made at least once each water year 1953-60, 1962-66

Pecos River mile	Stream	Location	Discharge, in cubic feet per second			
			Meas. disch.	Gain or loss	Meas disch.	Gain or loss
			Jan 20, 19XX		Mar. 31, 19XX	
94 0	Pecos River	Gaging station near Acme (8-3860).	4.83	-	40 9	-
89 1	.. do ..	SE¼SW¼NE¼ sec.27, T.9 S , R 25 E., above Bitter Lakes.	2 33	-2 50	28 3	-12 6
78 4	. do. .	NE¼NE¼NE¼ sec.33, T 10 S , R 25 E , at mouth of Bitter Creek..	4.25	+1 92	33 8	+5.5
78 4	Bitter Creek	NE¼NE¼NE¼ sec 33, T 10 S , R 25 E , at mouth....	2 96	-	5 76	-
74.7	Pecos River	SE¼SE¼NE¼ sec.9, T.11 S., R.25 E., above Rio Hondo..	8.79	+1 58	43 8	+4.2
74 6	Rio Hondo	NE¼NE¼SE¼ sec 9, T.11 S., R 25 E., at mouth	7 14	-	7.23	-
74 5	Pecos River	SE¼NE¼SE¼ sec 9, T.11 S , R 25 E., below Rio Hondo.	15.8 *	-.13 *	49.4 *	-1.6
46 7	Pecos River	SE¼NE¼NE¼ sec 12, T.14 S., R 26 E., at Hagerman bridge.	31 8	+9 7	70 9	+15.4
46 5	Diversion	* * *	9 42	-	15.7	-
44 2	Pecos River	SW¼SW¼NE¼ sec 13, T.14 S , R 26 E.... .... * * *	22 5 *	+ 1 *	58 6 *	+3 4
30 6	Pecos River	Gaging station near Lake Arthur (8-3955) .... * * * *	25.7 *	+3 05 *	54.5 *	-2.9
12 4	Pecos River	Gaging station near Artesia (8-3965).	34.0	+2 78	54.1	-4.2
		Overall net gain or loss		+14.8		+1.4

[NOTE.--In the above example many lines have been omitted as indicated by asterisks, but the figures of "gain or loss" are based on complete data.]

FIGURE 301.—Seepage investigation.

STREAMS TRIBUTARY TO LAKE ST. CLAIR

North Branch Clinton River basin low-flow investigations

Two series of base-flow discharge measurements were made in the North Branch Clinton River basin as part of a comprehensive program now being carried on in cooperation with the Macomb County Board of Supervisors and the Macomb County Road Commission to investigate the surface water resources of the county The first series was made on June 9, as soon as conditions were suitable for high base flow The second series was made on Aug. 18, under conditions of low base flow. The data collected in these series of measurements, along with that already collected and to be collected in the future, will provide the basis for determining the base-flow yields of various parts of the basin.

Weather records at Mount Clemens near the southern part of the area and at Romeo near the west-central part show that no precipitation occurred for five days prior to June 9 and four days prior to Aug. 18. Therefore, the measurements are considered to represent base flow

The measurements on each stream are listed in order proceeding downstream, and each tributary is inserted in the order in which it enters the main stream. Drainage areas shown were determined from recent U.S Geological Survey topographic maps of a scale of 1:24,000 and contour interval of 5 to 10 ft Previous series of measurements were made in water years 1959-64

Discharge measurements of North Branch Clinton River and tributaries near Mount Clemens, Mich

Stream	Location	Drainage area (sq mi)	Discharge, in cubic feet per second			
			Measured discharge	Cfs per square mile	Measured discharge	Cfs per square mile
			June 9, 19XX		Aug. 18, 19XX	
North Branch Clinton River.	NW¼ sec 27, T 6 N , R 12 E , at State Highway 53, in Almont	9 56	2.42	0 253	1.19	0.124
Do	NW¼ sec.1, T 5 N , R.12 E., at Macomb-Lapeer County line, 2.8 miles southeast of Almont	17.1	3 34	195	1 26	.074
Apel drain	NW¼ sec.13, T 5 N , R.12 E , at McKay Rd., 0 5 mile above mouth and 3 8 miles north of Romeo	4 04	93	.230	.48	.119
Newland drain	SW¼ sec 19, T 5 N , R 13 E , at mouth, 2.8 miles northeast of Romeo.	9 39	2.11	.225	60	.064
Mahaffy drain	NW¼ sec.25, T 5 N , R 12 E , at Mack Rd. (34-Mile), 0.6 mile above mouth and 2 1 miles northeast of Romeo	2.64	.52	197	05	019
North Branch Clinton River	SW¼ sec.30, T 5 N , R 13 E , at 33-Mile Rd , 2 2 miles northeast of Romeo	49 7	11.0	.221	4 00	.080
East Pond Creek	SW¼ sec 7, T.5 N., R 12 E., at Dewey Rd (36-Mile), 3.8 miles northeast of Lakeville.	9.49	1.87	197	.06	.006
Do	SW¼ sec.29, T 5 N , R 12 E , at Schooley Rd. (33-Mile), 3.1 miles northwest of Romeo.	14 2	4 24	.299	1.47	.104
Do	Gaging station near Romeo (4-1641).	21.8	8.13	373	3.10	142
Do	NW¼ sec.6, T 4 N , R.13 E , at Powell Rd , 0.5 mile above mouth and 1.6 miles east of Romeo	24.5	8.52	348	3.43	.140
North Branch Clinton River	NW¼ sec 16, T 4 N , R 13 E , at 30-Mile Rd , 2 0 miles northwest of Ray Center.	80 5	18 2	.226	5 77	.072
Coon Creek	NE¼ sec.21, T 5 N., R 13 E , at Armada Center Rd., 2 1 miles west of Armada	3.98	75	188	33	083
Do	SW¼ sec.1, T 4 N , R 13 E , at North Rd , 3.4 miles south of Armada.	10 0	1.35	135	.34	.034
Do	SW¼ sec 25, T 4 N , R 13 E , at North Rd , 1.4 miles north of Meade.	15.2	1 26	083	05	003
Tupper Brook	NW¼ sec 11, T.4 N , R 13 E , at 31-Mile Rd., 3.7 miles south of Armada	4.21	0	0	0	0
Do	NW¼ sec.23, T 4 N., R.13 E , at 29-Mile Rd , at Ray Center.	8 62	0	0	0	0
East Branch Coon Creek	SE¼ sec 2, T 5 N , R.13 E , at Pratt Rd , 3 0 miles north of Armada.	8.34	50	.060	.04	005
Do	Gaging station at Armada (4-1643)	13.0	.71	.055	06	005
Middle Branch Clinton River.	Private Claim 546, T 2 N., R.13 E., at Heydereich Rd., near mouth, just above Miller drain, 1 0 mile west of Mount Clemens	74 7	8.88	119	2 71	.036

FIGURE 302.—Low-flow investigation.

INDEX

FIGURE 303.–Index for annual published report (only first page).

INDEX

The index covers the two volumes of this manual. Volume I contains pages 1-284 and Volume II contains pages 285-631

A

B

E

S

T

U

W

Z

Assessment of erosion, sedimentation, and water quality impacts of the Mountain Valley Pipeline and Equitrans Expansion Project's proposed crossing of the Jefferson National Forest as it pertains to the U.S. Forest Service's Draft Supplemental Environmental Impact Statement dated December 2022

Prepared by Jonathan A. Czuba, Ph.D., Licensed Professional Engineer - February 9, 2023

REFERENCES
27

February 21, 2023

USGS
science for a changing world

Discharge Measurements at Gaging Stations

Chapter 8 of Book 3, Section A

Techniques and Methods 3–A8

U.S. Department of the Interior
U.S. Geological Survey

Front cover: On the left, photograph of a USGS hydrographer making a FlowTracker acoustic Doppler velocimeter discharge measurement at Little Eagle Creek at Speedway, Ind. (USGS station no. 03353600); on the right, photograph of a USGS hydrographer making a tethered boat acoustic Doppler current profiler discharge measurement from a cableway at the Snake River near Moran, Wyo. (USGS station no. 13011000).

Back cover: In the background, 1890 black and white photograph of USGS hydrographers making a mechanical current meter discharge measurement from a cableway at the Arkansas River near Canyon City, Colo. (USGS station no. 07096000); and on the right, 1958 black and white photograph of a USGS hydrographer making a mechanical current meter discharge measurement at the Cedar River at Belgrade, Nev. (USGS station no. 06791800).

Discharge Measurements at Gaging Stations

By D. Phil Turnipseed and Vernon B. Sauer

Techniques and Methods 3–A8

U.S. Department of the Interior
U.S. Geological Survey

U.S. Department of the Interior
KEN SALAZAR, Secretary

U.S. Geological Survey
Marcia K. McNutt, Director

U.S. Geological Survey, Reston, Virginia: 2010

For more information on the USGS—the Federal source for science about the Earth, its natural and living resources, natural hazards, and the environment—visit *http://www.usgs.gov* or call 1–888–ASK–USGS.

For an overview of USGS information products, including maps, imagery, and publications, visit *http://www.usgs.gov/pubprod*.

To order this and other USGS information products, visit *http://store.usgs.gov*.

Suggested citation:
Turnipseed, D.P., and Sauer, V.B., 2010, Discharge measurements at gaging stations: U.S. Geological Survey Techniques and Methods book 3, chap. A8, 87 p. (Also available at *http://pubs.usgs.gov/tm/tm3-a8/*.)

ISBN 978–1–4113–2969–0

Preface

This series of manuals on techniques and methods (TM) describes approved scientific and data-collection procedures and standard methods for planning and executing studies and laboratory analyses. The material is grouped under major subject headings called "books" and further subdivided into sections and chapters. Section A of book 3 is on surface-water techniques.

The unit of publication, the chapter, is limited to a narrow field of subject matter. These publications are subject to revision because of experience in use or because of advancement in knowledge, techniques, or equipment, and this format permits flexibility in revision and publication as the need arises. Chapter A8 of book 3 (TM 3–A8) deals with discharge measurements at gaging stations. The original version of this chapter was published in 1969 as U.S. Geological Survey (USGS) Techniques for Water-Resources Investigations, chapter A8 of book 3. New and improved equipment, as well as some procedural changes, have resulted in this revised second edition of "Discharge measurements at gaging stations."

This edition supersedes USGS Techniques of Water-Resources Investigations 3A–8, 1969, "Discharge measurements at gaging stations," by T.J. Buchanan and W.P. Somers, available at *http://pubs.usgs.gov/twri/twri3a8/*, and supplements USGS Water-Supply Paper 2175, volume 1, 1982, "Measurement and computation of streamflow: Measurement of stage and discharge," by S.E. Rantz and others, available at *http://pubs.usgs.gov/wsp/wsp2175/html/WSP2175_vol1.html*.

This revised second edition of "Discharge measurements at gaging stations" is published online at *http://pubs.usgs.gov/tm/tm3-a8/* and is for sale by the U.S. Geological Survey, Science Information Delivery, Box 25286, Federal Center, Denver, CO 80225.

This page left blank intentionally.

Contents

Figures

Tables

Conversion Factors

Multiply	By	To obtain
	Length	
inch (in.)	2.54	centimeter (cm)
inch (in.)	25.4	millimeter (mm)
foot (ft)	0.3048	meter (m)
mile (mi)	1.609	kilometer (km)
	Area	
acre	4,047	square meter (m^2)
acre	0.4047	hectare (ha)
acre	0.4047	square hectometer (hm^2)
acre	0.004047	square kilometer (km^2)
square foot (ft^2)	929.0	square centimeter (cm^2)
square foot (ft^2)	0.09290	square meter (m^2)
	Volume	
gallon (gal)	3.785	liter (L)
gallon (gal)	0.003785	cubic meter (m^3)
gallon (gal)	3.785	cubic decimeter (dm^3)
million gallons (Mgal)	3,785	cubic meter (m^3)
cubic foot (ft^3)	28.32	cubic decimeter (dm^3)
cubic foot (ft^3)	0.02832	cubic meter (m^3)
acre-foot (acre-ft)	1,233	cubic meter (m^3)
acre-foot (acre-ft)	0.001233	cubic hectometer (hm^3)
	Flow rate	
acre-foot per day (acre-ft/d)	0.01427	cubic meter per second (m^3/s)
acre-foot per year (acre-ft/yr)	1,233	cubic meter per year (m^3/yr)
acre-foot per year (acre-ft/yr)	0.001233	cubic hectometer per year (hm^3/yr)
foot per second (ft/s)	0.3048	meter per second (m/s)
cubic foot per second (ft^3/s)	0.02832	cubic meter per second (m^3/s)
cubic foot per second per square mile [$(ft^3/s)/mi^2$]	0.01093	cubic meter per second per square kilometer [$(m^3/s)/km^2$]
cubic foot per day (ft^3/d)	0.02832	cubic meter per day (m^3/d)
gallon per minute (gal/min)	0.06309	liter per second (L/s)
gallon per day (gal/d)	0.003785	cubic meter per day (m^3/d)
gallon per day per square mile [$(gal/d)/mi^2$]	0.001461	cubic meter per day per square kilometer [$(m^3/d)/km^2$]
million gallons per day (Mgal/d)	0.04381	cubic meter per second (m^3/s)
million gallons per day per square mile [$(Mgal/d)/mi^2$]	1,461	cubic meter per day per square kilometer [$(m^3/d)/km^2$]
	Mass	
pound, avoirdupois (lb)	0.4536	kilogram (kg)

Multiply	By	To obtain
	Pressure	
atmosphere, standard (atm)	101.3	kilopascal (kPa)
pound-force per square inch (lbf/in^2)	6.895	kilopascal (kPa)
pound per square foot (lb/ft^2)	0.04788	kilopascal (kPa)
pound per square inch (lb/in^2)	6.895	kilopascal (kPa)
	Density	
pound per cubic foot (lb/ft^3)	16.02	kilogram per cubic meter (kg/m^3)
pound per cubic foot (lb/ft^3)	0.01602	gram per cubic centimeter (g/cm^3)

Temperature in degrees Celsius (°C) may be converted to degrees Fahrenheit (°F) as follows:

$$°F=(1.8×°C)+32$$

Temperature in degrees Fahrenheit (°F) may be converted to degrees Celsius (°C) as follows:

$$°C=(°F-32)/1.8$$

Vertical coordinate information is referenced to the insert datum name (and abbreviation) here for instance, "North American Vertical Datum of 1988 (NAVD 88)."

Horizontal coordinate information is referenced to the insert datum name (and abbreviation) here for instance, "North American Datum of 1983 (NAD 83)."

Elevation, as used in this report, refers to distance above sea level. Because this report is based on a large number of previously published scientific investigations, "sea level" is not referenced to a single vertical datum. "Mean sea level" also is not used with reference to a single datum; where used, the phrase means the average surface of the ocean as determined by calibration of measurements at tidal stations.

Abbreviations and Acronyms

AA	Price AA current meter
ADCP	acoustic Doppler current profiler
ADC	acoustic digital current meter
ADV	acoustic Doppler velocimeters
Aquacalc	JBS Instruments Aquacalc Pro Discharge Measurement Computer
C1	C1 connector
CMD	current meter digitizer
CMCsp	Hydrological Services Current Meter Counter signal processor
CSG	crest stage gage
CST	Central Standard Time
C type	Columbus type
DCP	Data Collection Platform
DGPS	global positioning system with differential corrections
dB	decibels
EDT	Eastern Daylight Time

EFN	electronic field notebook
EST	Eastern Standard Time
FlowTracker	SonTek/YSI FlowTracker Handheld acoustic Doppler velocimeter
GPS	global positioning system
HIF	U.S. Geological Survey Hydrologic Instrumentation Facility
HWM	high water mark
Hz	hertz
ISO	International Organization for Standardization
kHz	kilohertz
LEW	left edge of water
MHz	megahertz
NAD 83	North American Datum of 1983
NAVD 88	North American Vertical Datum of 1988
NWIS	U.S. Geological Survey National Water Information System
OFR	U.S. Geological Survey Open-File Report
PDA	portable digital assistant
PFD	personal flotation device
QA/QC	quality assurance and quality control
RD	Teledyne RD Instruments
REW	right edge of water
RP	reference point
RTK	real-time kinematic
RTK-GPS	real-time kinematic global positioning system
SNR	signal-to-noise ratio
SWAMI	surface water measurement and inspection
TM	U.S. Geological Survey Techniques and Methods
TRDI	Teledyne RD Instruments
TWRI	U.S. Geological Survey Techniques of Water-Resources Investigations
USGS	U.S. Geological Survey
WAAS	Wide Area Augmentation System
WRD	Water Resources Division/Discipline
WSC	Water Science Center
WSCan	Environment Canada Ministry Water Survey of Canada Agency

Definitions of Symbols

a_i	cross-section area for the *i*th segment of the *n* segments into which the cross section is divided
arctan	arctangent
b	width of the throat section (in units of distance)
b_i	distance from initial point to location i
$b_{(i-1)}$	distance from initial point to preceding location
$b_{(i+1)}$	distance from initial point to next location
d_i	depth of water at location *i*
C	coefficient of discharge

c	speed of sound (in distance per unit time)
$\cos \alpha$	cosine of the angle alpha
°C	temperature in degrees Celsius
$CORR_{wl}$	correction (in units of distance) to subtract from the wet-line depth to obtain the vertical depth
D_{wl}	wet-line depth (in units of distance)
D_v	vertical depth (in units of distance)
Δs	average change in stage in the reach *L* during the measurement (in units of distance)
Δt	elapsed time during measurement
$\Delta \alpha$	computed phase difference
°F	temperature in degrees Farenheit
H	weighted mean gage height (in units of distance)
h	static head, head, elevation, or gage height (in units of distance)
IQR	interquartile range
L	length of reach between measuring section and control (in units of distance)
m	difference (in feet) between the air-line correction for the sounding position and that for the 0.8 position
n	difference (in feet) between the wet-line correction for the sounding position and that for the 0.8 position, if the depths are greater than 40 feet and the change in vertical angle is more than 5 percent
P	vertical angle (in degrees)
α	ratio of the circumference to the diameter of a circle; approximately equal to 3.14159
Q	discharge (in volume per unit time)
$Q1$	25 percent of samples are less than this value
$Q3$	75 percent of samples are less than this value
q_i	discharge through partial section i, (in volume per unit time)
R	number of rotor revolutions per second
T	total time for the measurement
t_1	duration of time intervals between breaks in the slop of the gage height graph
tan	tangent
α	time lag between pulses
V	velocity (in distance per unit time)
Vx	velocity (in distance per unit time) in the x direction (perpendicular to the tag line)
Vy	velocity (in distance per unit time) in the y direction (parallel to the tag line)
V	volume of water in container
v_i	mean velocity (in units of distance per unit time) of the flow normal to the ith segment, or vertical
W	average width of stream between measuring section and control (in units of distance)
W_1	weight of empty container (in units of mass)
W_2	weight of container with water (in units of mass)
w	unit weight of water (in units of mass per volume)
x	x-direction (perpendicular to the tag line) or x-component of velocity

Discharge Measurements at Gaging Stations

By D. Phil Turnipseed and Vernon B. Sauer

Abstract

The techniques and standards for making discharge measurements at streamflow gaging stations are described in this publication. The vertical axis rotating-element current meter, principally the Price current meter, has been traditionally used for most measurements of discharge; however, advancements in acoustic technology have led to important developments in the use of acoustic Doppler current profilers, acoustic Doppler velocimeters, and other emerging technologies for the measurement of discharge. These new instruments, based on acoustic Doppler theory, have the advantage of no moving parts, and in the case of the acoustic Doppler current profiler, quickly and easily provide three-dimensional stream-velocity profile data through much of the vertical water column. For much of the discussion of acoustic Doppler current profiler moving-boat methodology, the reader is referred to U.S. Geological Survey Techniques and Methods 3–A22 (Mueller and Wagner, 2009).

Personal digital assistants (PDAs), electronic field notebooks, and other personal computers provide fast and efficient data-collection methods that are more error-free than traditional hand methods. The use of portable weirs and flumes, floats, volumetric tanks, indirect methods, and tracers in measuring discharge are briefly described.

Purpose and Scope

The U.S. Geological Survey (USGS) makes tens of thousands of streamflow measurements each year across the United States and its territories. Measured discharges range from a trickle in a small ditch or stream [less than 0.01 cubic foot per second (ft^3/s)], to a flood on the Mississippi River (greater than 1,800,000 ft^3/s). Several methods are used by the USGS to make streamflow measurements. Principally, the USGS uses mechanical current meters and hydroacoustic meters [for example, acoustic Doppler current profilers (ADCPs) and acoustic Doppler velocimeters (ADVs)]. The purpose of this report is to describe the equipment and procedures used by the USGS and others for making discharge measurements, and to describe new developments in equipment and procedures. Other traditional methods of measuring streamflow include portable weirs and flumes, and volumetric, float, indirect, and tracer measurements. Relatively new developments include the use of a moving boat with the ADCP (Mueller and Wagner, 2009), the wading rod mounted ADV, electromagnetic current meters, electronic field notebooks, personal digital assistants (PDAs), and various procedural changes.

The original version of USGS Techniques of Water-Resources Investigations book 3, chapter A8 (TWRI 3–A8), by Buchanan and Somers (1969), was used as an extensive resource in the preparation of this publication because much of the equipment and techniques described by Buchanan and Somers are still applicable to current streamgaging methods. The USGS publications "Measurement and Computation of Streamflow, volumes 1 and 2," by Rantz and others (1982); "Discharge measurements using a broad-band acoustic Doppler current profiler," by Simpson (2002); "Quality-assurance plan for discharge measurements using acoustic Doppler current profiler," by Oberg and others (2005); and "Measuring discharge with acoustic Doppler current profilers from a moving boat," by Mueller and Wagner (2009), were also used extensively in the preparation of this publication. Numerous parts of this chapter were taken verbatim from Buchanan and Somers (1969), Rantz (1982), Simpson (2002), Oberg and others (2005), and Mueller and Wagner (2009), and even though some of these parts are not specifically denoted, credit is hereby given to these authors.

Definition of Streamflow

Streamflow, or discharge, is defined as the volumetric rate of flow of water (volume per unit time) in an open channel, including any sediment or other solids that may be dissolved or mixed with it that adhere to the Newtonian physics of open-channel hydraulics of water. The definition of streamflow in this chapter does not include non-Newtonian flow events such as debris flows and lahars (an avalanche of volcanic mud and water down the slopes of a volcano). Streamflow in the USGS is usually expressed in English dimensions of cubic feet per second (ft^3/s). Other common units are million gallons per day (Mgal/d) and acre-feet per day (ac-ft/d). Streamflow cannot be measured directly but must be computed from variables that can be measured directly, such as stream width, stream depth, and streamflow velocity. Even though streamflow is computed from measurements of other variables, the term "streamflow measurement" or "discharge measurement" is generally applied to the final result of the calculations.

Discharge Measurements at Gaging Stations

Procedures for making most types of current-meter [mechanical meters, electromagnetic meters, ADV meters, acoustic digital current meters (ADCs), and so forth)], moving-boat ADCP, and ADCP midsection measurements are described in the following sections. For much of the discussion of moving-boat ADCP, the reader is referenced to Mueller and Wagoner (2009). The chapter includes discussions on the selection of a measuring section, laying out the stationing for subsection verticals, width measurements, depth measurements, velocity measurements, direction of flow measurements, and recording of field notes. Additional details that pertain to instrumentation and specific types of measurements, such as wading, cableway, bridge, boat, and ice, are described in subsequent sections. Special procedures such as networks of current meters, measurement of deep, swift streams, and measurements during rapidly changing stage are also described.

Velocity-Area Method

The most practical method of measuring the discharge of a stream is the velocity-area method. Discharge is computed as the product of the area and velocity. The measurement is made by subdividing a stream cross section into segments (sometimes referred to as partial areas, sections, subareas, verticals, stations, profiles, panels, or ensembles), and by measuring the depth and velocity in a vertical within each segment. The total discharge is the summation of the products of the partial areas of the stream cross section and their respective average velocities. This computation is classically expressed by the equation

$$Q = \sum_{i=1}^{n} a_i v_i, \tag{1}$$

where Q total discharge, in cubic feet per second,
a_i cross-section area, in square feet, for the ith segment of the n segments into which the cross section is divided, and
v_i the corresponding mean velocity, in feet per second of the flow normal to the ith segment, or vertical.

Midsection Method

The current-meter midsection method of making a current-meter discharge measurement is used by the USGS and others. The method assumes that the mean velocity in each vertical represents the mean velocity in a partial rectangular area (segment). The mean velocity in each vertical is determined by measuring the velocity at one or more selected points in that vertical, as described in a later section of this chapter. The cross-section area for a segment extends laterally from half the distance from the preceding vertical to half the distance to the next vertical, and vertically, from the water surface to the sounded depth as shown in figure 1.

The cross section in figure 1 is defined by depths at locations 1, 2, 3, 4, . . . , n. At each location, the velocities are sampled by current meter to obtain the mean of the vertical distribution of velocity. The partial discharge is now computed for any partial section (segment) at location i as

$$q_i = v_i \left[\frac{\left(b_i - b_{(i-1)}\right)}{2} + \frac{\left(b_{(i+1)} - b_i\right)}{2} \right] d_i, \text{ or} \tag{2}$$

$$= v_i \left[\frac{b_{(i+1)} - b_{(i-1)}}{2} \right] d_i, \tag{3}$$

where q_i discharge through partial section i,
v_i mean velocity at location i,
b_i distance from initial point to location i,
$b_{(i-1)}$ distance from initial point to preceding location,
$b_{(i+1)}$ distance from initial point to next location, and
d_i depth of water at location i.

Thus, for example, the discharge through partial section 4 (heavily outlined in figure 1) is

$$q_4 = v_4 \left[\frac{b_5 - b_3}{2} \right] d_4. \tag{4}$$

The procedure is similar when i is at an end section. The "preceding location" at the beginning of the cross section is considered coincident with location 1; the "next location" at the end of the cross section is considered coincident with location n. Thus,

$$q_1 = v_1 \left[\frac{b_2 - b_1}{2} \right] d_1, \text{ and} \tag{5}$$

$$q_n = v_n \left[\frac{b_n - b_{(n-1)}}{2} \right] d_n. \tag{6}$$

For the example shown in figure 1, q_1 is zero because the depth at observation point 1 is zero. However, when the cross-section boundary is a vertical line at the edge of the water as at location n, the depth is not zero and velocity at the end section may or may not be zero. Equations 5 and 6 are used whenever there is water only on one side of an observation point, such as at the edge of the stream, piers, abutments, and islands. It usually is necessary to estimate the velocity at an end section because it normally is impossible to measure the velocity accurately with the current meter close to a boundary. There also is the possibility of damage to the equipment if the flow is turbulent. The estimated velocity is usually made as a percentage of the adjacent section.

The summation of the discharges for all the partial sections is the total discharge of the stream. An example of the measurement notes is shown in figure 2*A*. In the hydraulic properties reported, the summation of discharges from an ADV discharge

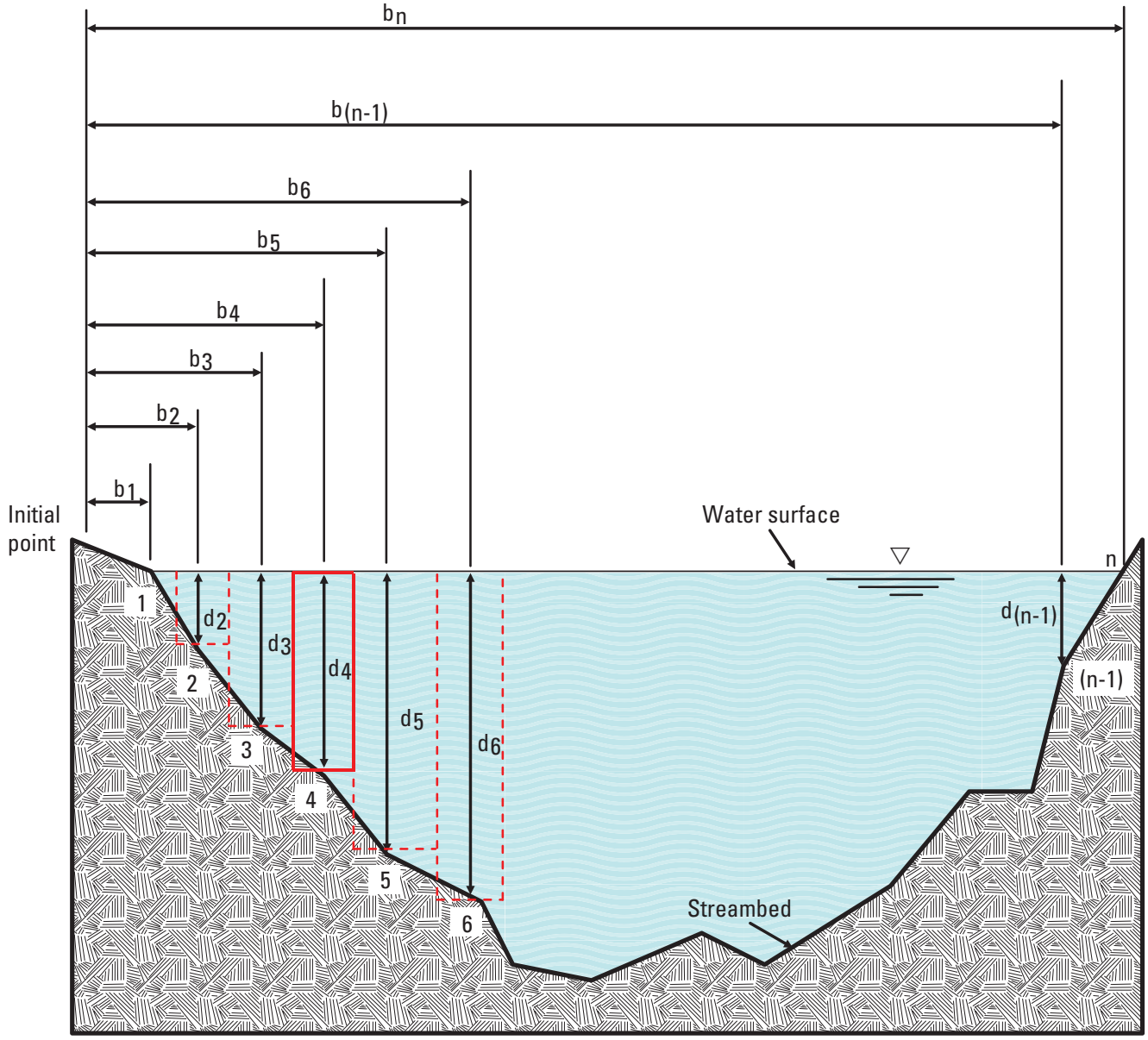

Figure 1. Definition sketch of the current-meter *midsection* method of computing cross-section area for discharge measurements.

measurement (fig. 2*B*) is similar to that of a current meter; however, it is designed to report the properties inherent to the ADV software and signal processing necessary to compute discharge using acoustic Doppler technology. A program written by staff in the USGS Maine Water Science Center entitled Surface Water Measurements and Inspections (SWAMI) has become common in use in the USGS with a PDA, and may be used to record discharge measurements, inspections, differential level surveys, and other field measurements (fig. 2*C*).

Included here for convenience is a typical, well-documented ADCP discharge measurement (fig. 2*D*). This measurement serves as an example of how an ADCP measurement note should be kept in the field. Further discussion of ADCP measurements can be found in subsequent sections of this chapter.

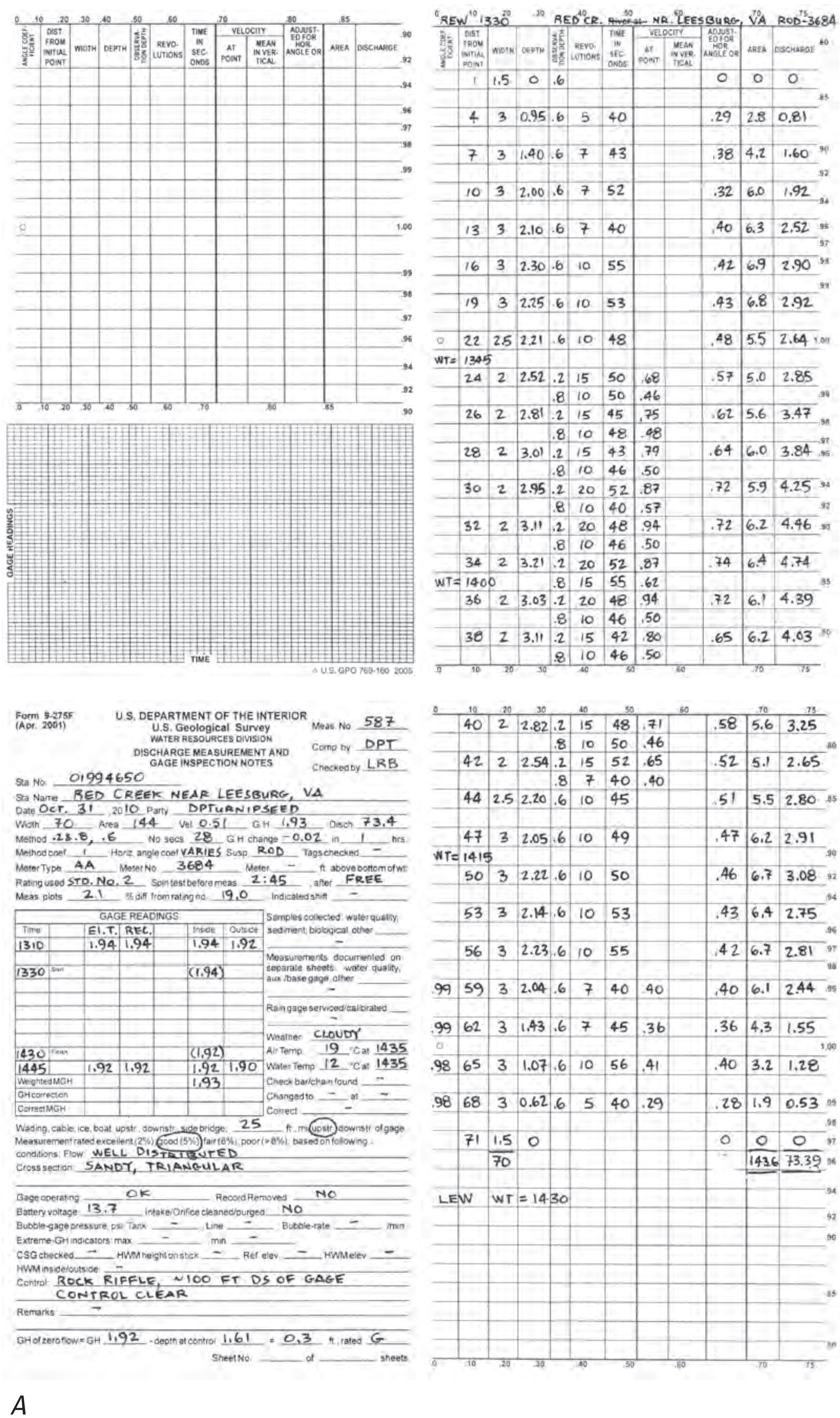

Form 9-275F (Apr. 2001)

U.S. DEPARTMENT OF THE INTERIOR
U.S. Geological Survey
WATER RESOURCES DIVISION
DISCHARGE MEASUREMENT AND GAGE INSPECTION NOTES

Meas. No. 587
Comp. by DPT
Checked by LRB

Sta. No. 01994650
Sta. Name RED CREEK NEAR LEESBURG, VA
Date OCT. 31, 2010 Party DPTURNIPSEED
Width 70 Area 144 Vel. 0.51 G.H. 1.93 Disch. 73.4
Method .2&.8, .6 No. secs. 28 G.H. change −0.02 in 1 hrs.
Method coef. 1 Horiz. angle coef. VARIES Susp. ROD Tags checked —
Meter Type AA Meter No. 3684 Meter — ft. above bottom of wt.
Rating used STD. NO. 2 Spin test before meas. 2:45 after FREE
Meas. plots 2.1 % diff. from rating no. 19.0 Indicated shift —

GAGE READINGS				
Time	El. T.	Rec.	Inside	Outside
1310	1.94	1.94	1.94	1.92
1330 Start			(1.94)	
1430 Finish			(1.92)	
1445	1.92	1.92	1.92	1.90
Weighted MGH			1.93	
GH correction				
Correct MGH				

Samples collected: water quality, sediment, biological, other —
Measurements documented on separate sheets: water quality, aux./base gage, other —
Rain gage serviced/calibrated —
Weather CLOUDY
Air Temp. 19 °C at 1435
Water Temp. 12 °C at 1435
Check bar/chain found —
Changed to — at —
Correct —

Wading, cable, ice, boat, upstr., downstr., side bridge 25 ft., mi. (upstr.) downstr. of gage
Measurement rated excellent (2%), (good (5%)), fair (8%), poor (>8%), based on following conditions: Flow WELL DISTRIBUTED
Cross section SANDY, TRIANGULAR

Gage operating OK Record Removed NO
Battery voltage 13.7 Intake/Orifice cleaned/purged NO
Bubble-gage pressure, psi: Tank — Line — Bubble-rate — /min
Extreme-GH indicators: max — min —
CSG checked — HWM height on stick — Ref. elev. — HWM elev. —
HWM inside/outside —
Control ROCK RIFFLE, ~100 FT DS OF GAGE
CONTROL CLEAR
Remarks —

GH of zero flow = GH 1.92 − depth at control 1.61 = 0.3 ft., rated G
Sheet No. ___ of ___ sheets

REW 1330 RED CR. ~~River at~~ NR. LEESBURG, VA ROD-3684

Angle coef.	Dist. from initial point	Width	Depth	Observation depth	Revolutions	Time in seconds	Velocity at point	Mean in vertical	Adjusted for hor. angle or	Area	Discharge
	1	1.5	0	.6					0	0	0
	4	3	0.95	.6	5	40			.29	2.8	0.81
	7	3	1.40	.6	7	43			.38	4.2	1.60
	10	3	2.00	.6	7	52			.32	6.0	1.92
	13	3	2.10	.6	7	40			.40	6.3	2.52
	16	3	2.30	.6	10	55			.42	6.9	2.90
	19	3	2.25	.6	10	53			.43	6.8	2.92
	22	2.5	2.21	.6	10	48			.48	5.5	2.64
WT= 1345											
	24	2	2.52	.2	15	50	.68		.57	5.0	2.85
				.8	10	50	.46				
	26	2	2.81	.2	15	45	.75		.62	5.6	3.47
				.8	10	48	.48				
	28	2	3.01	.2	15	43	.79		.64	6.0	3.84
				.8	10	46	.50				
	30	2	2.95	.2	20	52	.87		.72	5.9	4.25
				.8	10	40	.57				
	32	2	3.11	.2	20	48	.94		.72	6.2	4.46
				.8	10	46	.50				
	34	2	3.21	.2	20	52	.87		.74	6.4	4.74
WT= 1400				.8	15	55	.62				
	36	2	3.03	.2	20	48	.94		.72	6.1	4.39
				.8	10	46	.50				
	38	2	3.11	.2	15	42	.80		.65	6.2	4.03
				.8	10	46	.50				
	40	2	2.82	.2	15	48	.71		.58	5.6	3.25
				.8	10	50	.46				
	42	2	2.54	.2	15	52	.65		.52	5.1	2.65
				.8	7	40	.40				
	44	2.5	2.20	.6	10	45			.51	5.5	2.80
	47	3	2.05	.6	10	49			.47	6.2	2.91
WT= 1415											
	50	3	2.22	.6	10	50			.46	6.7	3.08
	53	3	2.14	.6	10	53			.43	6.4	2.75
	56	3	2.23	.6	10	55			.42	6.7	2.81
.99	59	3	2.04	.6	7	40	.40		.40	6.1	2.44
.99	62	3	1.43	.6	7	45	.36		.36	4.3	1.55
.98	65	3	1.07	.6	10	56	.41		.40	3.2	1.28
.98	68	3	0.62	.6	5	40	.29		.28	1.9	0.53
	71	1.5	0						0	0	0
		70								143.6	73.39
LEW		WT = 1430									

A

Figure 2. Computation notes of: *A*, a current-meter measurement by the *midsection* method; *B*, an ADV discharge measurement; *C*, from the Surface Water Measurement and Inspection (SWAMI) form; and *D*, an ADCP discharge measurement.

9-275-x	01/24/2007	U.S. DEPARTMENT OF THE INTERIOR	Meas. No.	625
Station Number		*U.S. Geological Survey*	Comp. by	SEM
03329700		**ADV Discharge Measurement Notes**	Checked by	RGK

Station Name	Deer Creek nr Delphi, IN				
Date	8/18/2009	Party	SEMorlock		
Width	Area	Velocity	SNR	Gage Height	Discharge
63	51.6	1.16	32	2.08	59.8
Method		# Sections	Gage Height Change		
.6		30	-.01 in .52 hrs.		
Diagnostic Test File		Std Velocity Profile	Measured Water Temp		Weather
P156.080509.bmc		(Y) or N or Uncertain	24.5 °F / C at 1100		Cloudy
Raw Data File		ADV Sync'd to WT	ADV Water Temp		Wind Speed / Dir.
03329700.WAD		(Y) at 1120 or N	73.1 °F / at 1140		0-5/SW
Manufacturer	Model	Serial No.	Firmware	Software	
Sontek	Flowtracker	P156A	3.3	2.20	

EST Time	Gage Readings	DCP	ETG Inside	STAFF Outside	
1052		2.09	2.08	2.08	Rating number 30
					Percent from rating 3.5
1123	S				Indicated shift Ø
1155	F				
					Rain gage serviced/calibrated
					n/a
1207		2.08	2.07	2.07	Salinity
					— ppt at —

Weighted MGH		Checkbar found	na
GH corrections		Checkbar Changed to	
Correct MGH		— at —	

Wading ~~cable, ice, boat, upstr., downstr., side bridge~~ at ~~ft, mi upstr., downstr.~~ of gage

Measurement rated excellent (2%), (good (5%)), fair (8%), poor (>8%) based on following conditions

Flow	Steady and Even
Cross section	Sand and gravel, fairly even
Control	Sand, gravel and cobbles 100'ds clear

Gage operating	(Y) or N	Record removed	(Y) or N	Filename	03329700.log
Battery voltage	12.8 V	Intakes/~~Orifice~~ cleaned/~~purged~~		Yes	
Bubble-gage psi	Tank na	Line na	Bubble rate na		/ min
Extreme-GH indicators:	Max 2.45	Min 1.87	CSG Checked	(Y) or N	
HWM on stick	no	Ref elev. 4.32	HWM elevation	na	
GH of zero flow = GH	2.08	- depth at control 1.20	= .88 ft.	Rated	Fair
Remarks					

Sheet No. 1 of 2 sheets

SEM

Discharge Measurement Summary

Date Generated: Tue Nov 17 2009

File Information

File Name	03329700.WAD
Start Date and Time	2009/08/18 11:23:50

Site Details

Site Name	
Operator(s)	HTM

System Information

Sensor Type	FlowTracker
Serial #	P156A
CPU Firmware Version	3.3
Software Ver	2.20

Units (English Units)

Distance	ft
Velocity	ft/s
Area	ft^2
Discharge	cfs

Discharge Uncertainty

Category	ISO	Stats
Accuracy	1.0%	1.0%
Depth	0.2%	1.0%
Velocity	0.6%	3.1%
Width	0.1%	0.1%
Method	1.5%	-
# Stations	1.7%	-
Overall	**2.6%**	**3.4%**

Summary

Averaging Int.	40	# Stations	30
Start Edge	LEW	Total Width	63.000
Mean SNR	32.0 dB	Total Area	51.550
Mean Temp	73.12 °F	Mean Depth	0.818
Disch. Equation	Mid-Section	Mean Velocity	1.1593
		Total Discharge	**59.7613**

Measurement Results

St	Clock	Loc	Method	Depth	%Dep	MeasD	Vel	CorrFact	MeanV	Area	Flow	%Q
0	11:23	0.00	None	0.000	0.0	0.0	0.0000	1.00	0.0000	0.000	0.0000	0.0
1	*11:23*	*4.00*	*0.6*	*0.400*	*0.6*	*0.160*	*0.2966*	*1.00*	*0.2966*	*1.200*	*0.3558*	*0.6*
2	11:25	6.00	0.6	0.500	0.6	0.200	0.4426	1.00	0.4426	1.000	0.4426	0.7
3	*11:26*	*8.00*	*0.6*	*0.600*	*0.6*	*0.240*	*0.6266*	*1.00*	*0.6266*	*1.200*	*0.7521*	*1.3*
4	*11:27*	*10.00*	*0.6*	*0.800*	*0.6*	*0.320*	*0.7802*	*1.00*	*0.7802*	*1.600*	*1.2481*	*2.1*
5	11:28	12.00	0.6	1.100	0.6	0.440	0.9803	1.00	0.9803	2.200	2.1568	3.6
6	11:29	14.00	0.6	1.300	0.6	0.520	0.8986	1.00	0.8986	2.600	2.3362	3.9
7	11:30	16.00	0.6	1.300	0.6	0.520	0.9829	1.00	0.9829	2.600	2.5554	4.3
8	11:32	18.00	0.6	1.300	0.6	0.520	1.1299	1.00	1.1299	2.600	2.9375	4.9
9	11:33	20.00	0.6	1.300	0.6	0.520	1.2979	1.00	1.2979	2.600	3.3742	5.6
10	*11:34*	*22.00*	*0.6*	*1.100*	*0.6*	*0.440*	*0.9744*	*1.00*	*0.9744*	*2.200*	*2.1438*	*3.6*
11	11:36	24.00	0.6	1.100	0.6	0.440	1.4452	1.00	1.4452	2.200	3.1797	5.3
12	11:37	26.00	0.6	1.200	0.6	0.480	0.9862	1.00	0.9862	2.400	2.3672	4.0
13	11:38	28.00	0.6	1.200	0.6	0.480	1.0472	1.00	1.0472	2.400	2.5137	4.2
14	*11:39*	*30.00*	*0.6*	*1.000*	*0.6*	*0.400*	*0.9636*	*1.00*	*0.9636*	*2.000*	*1.9272*	*3.2*
15	11:40	32.00	0.6	1.000	0.6	0.400	0.9551	1.00	0.9551	2.000	1.9101	3.2
16	11:41	34.00	0.6	1.000	0.6	0.400	1.5469	1.00	1.5469	2.000	3.0938	5.2
17	11:42	36.00	0.6	1.000	0.6	0.400	1.4954	1.00	1.4954	2.000	2.9908	5.0
18	11:44	38.00	0.6	1.000	0.6	0.400	1.4741	1.00	1.4741	2.000	2.9482	4.9
19	11:45	40.00	0.6	0.900	0.6	0.360	1.5633	1.00	1.5633	1.800	2.8138	4.7
20	*11:46*	*42.00*	*0.6*	*0.900*	*0.6*	*0.360*	*1.3133*	*1.00*	*1.3133*	*1.800*	*2.3638*	*4.0*
21	11:47	44.00	0.6	0.800	0.6	0.320	1.6240	1.00	1.6240	1.600	2.5980	4.3
22	11:48	46.00	0.6	0.800	0.6	0.320	1.2562	1.00	1.2562	1.600	2.0096	3.4
23	11:49	48.00	0.6	0.700	0.6	0.280	1.6437	1.00	1.6437	1.400	2.3016	3.9
24	11:51	50.00	0.6	0.700	0.6	0.280	1.4249	1.00	1.4249	1.400	1.9952	3.3
25	11:52	52.00	0.6	0.600	0.6	0.240	1.2969	1.00	1.2969	1.200	1.5565	2.6
26	11:53	54.00	0.6	0.600	0.6	0.240	1.4646	1.00	1.4646	1.200	1.7577	2.9
27	11:54	56.00	0.6	0.500	0.6	0.200	1.4452	1.00	1.4452	1.000	1.4452	2.4
28	11:55	58.00	0.6	0.500	0.6	0.200	0.9639	1.00	0.9639	1.750	1.6868	2.8
29	11:55	63.00	None	0.000	0.0	0.0	0.0000	1.00	0.0000	0.000	0.0000	0.0

Rows in italics indicate a QC warning. See the Quality Control page of this report for more information.

B

01031500 - Site Visit Summary - 2009-05-20

SWAMI ver. 0.1.5

Site Visit Summary

Site Number: 01031500 **Site Name:** Piscataquis River near Dover-Foxcroft, Maine
Date: 2009-05-20 **StartTime:** 09:13:07 **EndTime:** 10:48:46
Party: LEF **Weather:** Sunny
Comment:

Discharge Measurement

Meas #: 872 **Meas Flow:** 440 cfs **Time:** 10:05:48
Stage: 3.02 ft. **Stage Change:** -.01 ft. **Change Duration:** 1.4 hrs.
Qm Rated: Fair (8%) **Base Flow:** Unspecified
Comment: Rated fair due to boulders encountered during QM.// This was a good/fair QM.

Channel 0 Summary

Name: Main **Meas Flow:** 440.013 cfs () **Qm Type:** Wading
Qm Method: Midsection **Condition:** firm, uneven, cobbles-boulders **Vel Method:** Price AA
Horiz Flow: Even **Vel Desc:** Steady **Sect Loc.:** Downstream 600ft. to gage
Start Point: Left edge of water **Mtr Type:** Price AA **Mtr S/N:** ME_P450
Mtr Susp: Top-setting wading rod **Mtr Insp B4:** true **Mtr Insp Aft:** true
Dist to Mtr: **Wt. Used:** **Summary Only:** false
Total Area: 272 **Total Width:** 133 **Mean Vel:** 1.62

Stn. #	Time	Point/Int	Cond%	Dist (ft)	Width (ft)	TotDepth (ft)	Ice (ft)	IceDepth (ft)	Velocity Observations				Adj Vel	Area (ft^2)	Discharge (ft^3/s)	Com
									%Depth	Rev	Time	Adj% Vel				
1	09:22:56	Est/N	75	3.0	0.5	.91							0.578	0.46	0.266	**
2	09:25:36		.98	4.0	1.75	.80			.6	14	41	0.771	0.756	1.4	1.058	
3	09:28:31		1.00	6.5	2	1.20			.6	19	41	1.04	1.04	2.4	2.496	
4	09:31:07		1.00	8.0	2.75	1.32			.6	25	40	1.4	1.4	3.63	5.082	
5	09:33:27		1.00	12	4	1.63			.6	25	40	1.4	1.4	6.52	9.128	**
6	09:35:08		1.00	16	4	1.85			.6	23	41	1.25	1.25	7.4	9.25	
7	09:37:05		1.00	20	4	1.65			.6	27	41	1.47	1.47	6.6	9.702	**
8	09:39:54		1.00	24	3	2.92			.2	33	40	1.84	1.575	8.76	13.797	
									.8	24	41	1.31				
9	09:43:15		1.00	26	3	3.06			.2	38	40	2.11	1.78	9.18	16.340	
									.8	26	40	1.45				
10	09:46:30		1.00	30	3	3.14			.2	38	40	2.11	1.63	9.42	15.355	
									.8	21	41	1.15				
11	09:49:36		1.00	32	3	3.28			.2	37	40	2.06	1.755	9.84	17.269	
									.8	26	40	1.45				
12	09:52:34		1.00	36	3	3.42			.2	43	41	2.33	1.92	10.26	19.699	
									.8	27	40	1.51				
13	09:55:30		1.00	38	3	3.32			.2	42	40	2.33	1.975	9.96	19.671	
									.8	29	40	1.62				
14	09:58:34		1.00	42	3	3.24			.2	46	40	2.55	2.17	9.72	21.092	
									.8	33	41	1.79				
15	10:01:18		1.00	44	3	3.02			.2	45	40	2.50	2.195	9.06	19.887	
									.8	34	40	1.89				
16	10:04:29		1.00	48	3	3.05			.2	49	41	2.65	2.3	9.15	21.045	
									.8	35	40	1.95				
17	10:07:32		1.00	50	3	3.20			.2	51	40	2.83	2.39	9.6	22.944	
									.8	35	40	1.95				
18	10:10:30		1.00	54	3	3.12			.2	49	40	2.72	2.39	9.36	22.370	
									.8	37	40	2.06				
19	10:13:59		1.00	56	3	2.65			.2	48	40	2.66	2.28	7.95	18.126	
									.8	35	41	1.90				
20	10:17:20		1.00	60	3	2.86			.2	46	40	2.55	2.09	8.58	17.932	
									.8	30	41	1.63				
21	10:21:21		1.00	62	3	2.91			.2	46	40	2.55	2.085	8.73	18.202	
									.8	29	40	1.62				
22	10:24:08		1.00	66	4	2.62			.2	44	40	2.44	2.14	10.48	22.427	
									.8	33	40	1.84				
23	10:26:11		1.00	70	4	2.46			.6	38	40	2.11	2.11	9.84	20.762	
24	10:27:43		1.00	74	4	2.42			.6	31	42	1.65	1.65	9.68	15.972	
25	10:29:32		1.00	78	4	1.82			.6	30	41	1.63	1.63	7.28	11.866	
26	10:31:20		1.00	82	5	1.84			.6	22	44	1.12	1.12	9.2	10.304	
27	10:33:20		1.00	88	6	1.72			.6	25	40	1.4	1.4	10.32	14.448	
28	10:35:16		1.00	94	6	1.58			.6	22	41	1.2	1.2	9.48	11.376	
29	10:36:50		1.00	100	6	1.50			.6	19	40	1.07	1.07	9	9.63	
30	10:38:22		1.00	106	6	1.32			.6	18	40	1.01	1.01	7.92	7.999	
31	10:40:12		1.00	112	6	1.18			.6	15	41	0.824	0.824	7.08	5.834	
32	10:45:50		1.00	118	7	1.02			.6	8	42	0.438	0.438	7.14	3.127	**
33	10:45:26		1.00	126	5	1.58			.6	8	45	0.41	0.41	7.9	3.239	**
34	10:47:38		1.00	128	5	1.73			.6	5	44	0.268	0.268	8.65	2.318	
35	10:48:40		1.00	136	4	0			.6	0	40	0	0	0	0	**

Midsection Comments

Stn #	Comment
1	LEW
5	Behind rock
7	Top of rock
32	Left edge of sand bar.
33	Right edge of sand bar.
35	REW

C

Acoustic Profiler Discharge Measurement Notes							**Filename Prefix:** foxmon_ds1200_
Left Bank: (Sloping) Vertical Other:_____					Right Bank:	(Sloping) Vertical Other:_____	
Transect No.	Starting			Ending		Total Discharge	Notes
	Bank	Time	Distance	Distance	Time		
0	L R						Moving bed test in center of channel
1	L (R)	1249	16	69	1255	1,321	Simultaneous comparison discharge measurements
2	(L) R	1256	69	16	1301	1,358	upstream of dam
3	L (R)	1301	69	———	———	———	Transect aborted due to debris in river
4	L (R)	1303	69	16	1308	1,327	
5	(L) R	1309	16	69	1315	1,356	
	L R						
	L R						
	L R						
	L R						
	L R						
	L R						
	L R						
Notes	All times are in CST. Measurement was made using a temporary rope-and-pulley cableway. Edge distances were measured with laser rangefinder by marking the start and ending positions on the rope and measuring the distance from edge of water to the center of the tethered boat.						

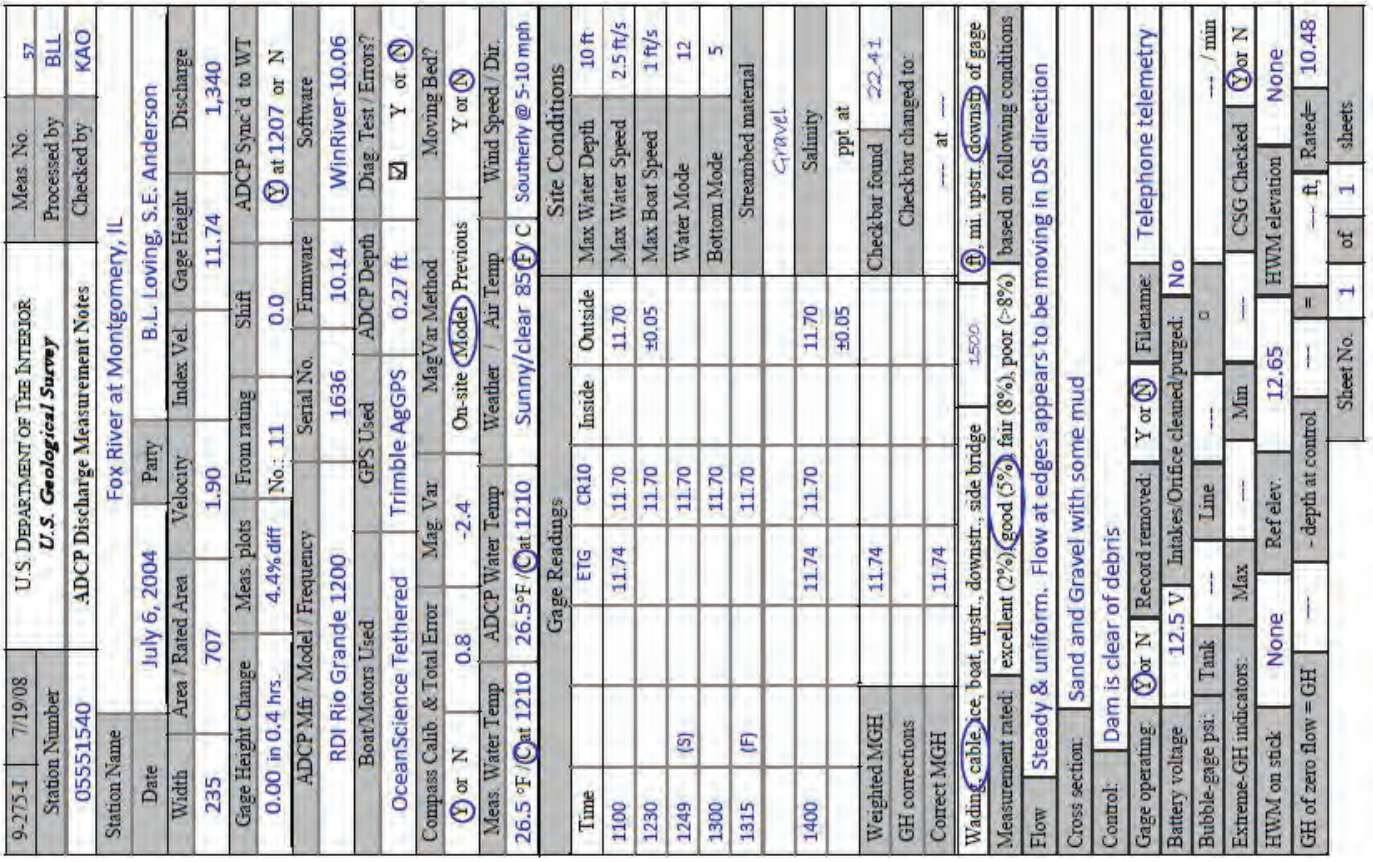

D

The mean-section method used by the USGS prior to 1950 differs from the midsection method in computation procedure. Partial discharges are computed for partial sections between successive verticals. The velocities and depths at successive verticals are each averaged, and each partial section extends laterally from one vertical to the next. Discharge is the product of the average of two mean velocities, the average of two depths, and the distance between verticals. A study by Young (1950) concluded that the midsection method is simpler to compute and is a slightly more accurate procedure than the mean-section method.

Site Selection

The first and most critical step in making a midsection current-meter or ADV measurement, or an ADCP measurement is to select a measurement cross section of desirable qualities. If the stream cannot be waded, nor high-water measurements made from a bridge, moving or tethered boat, or cableway, the hydrographer may have little or no choice in selecting a measurement cross section. If the stream can be waded or the measurement can be made from a boat, the hydrographer should look for a cross section with the following characteristics:

- There is a reasonably straight channel with streamlines parallel to each other; a stable streambed free of large rocks, weeds, and obstructions that would create eddies, slack water, and turbulence; and desirable measurement sections that are roughly parabolic, trapezoidal, or rectangular. These conditions are obviously not always possible, but remember that most current meters are rated in a still water tank by towing them through the tank at a known speed. With that in mind, these are conditions a hydrographer should seek in the field: a smooth, mirror-like water surface with steady, uniform, nonvarying flow conditions in the stream reach where the discharge measurement will be taken.
- The velocities are, for the most part, greater than 0.5 ft/s, and depths that are greater than about 0.5 ft. These conditions are not always possible to find in the field.
- The measurement section is relatively close to the gaging station control to avoid the effect of tributary and (or) intervening drainage area inflows between the measurement section and the control, and to avoid the effect of channel storage between the measurement section and the control during periods of changing stage.

It is usually not possible to satisfy all of these conditions. Select the best possible reach using these criteria and then select a cross section. For a further discussion regarding site selection when using a mechanical or other point-velocity current meter refer to Rantz and others (1982).

For convenience, special site-selection considerations for an ADCP discharge measurement are presented as follows, and further discussion of ADCP methods and instruments is presented in subsequent sections of this chapter:

- The minimum depth near the left and right edges of water at the measurement site should allow for the measurement of velocity in two or more depth cells while being close enough to minimize the estimated edge discharges.
- Make sure velocities are, for the most part, greater than 0.5 ft/s, and depths are greater than the minimum depth required by the ADCP. Although measurements can be made in low velocities, keep boat speeds extremely slow (if possible, less than or equal to the average water velocity), which requires special techniques for boat control (Simpson, 2002).
- Avoid measurement sections having local magnetic fields, especially if a moving bed is present and a Global Positioning System with differential corrections (DGPS) or the Loop Method (Mueller and Wagoner, 2006) is used. For example, during measuring, avoid overhead truss bridges, low steel-beam spans, power lines, and other sources of magnetic fields. Just as with ADCP mounts and boats, the presence of ferrous metals will result in ADCP compass errors.
- If possible, avoid asymmetric channel geometries (for example, deep on one side and shallow on the other; Simpson, 2002) and avoid cross sections with abrupt changes in channel-bottom slope. The streambed cross section should be as uniform as possible and free from debris and vegetation or plant growth.
- When using DGPS with an ADCP, avoid cross-section locations where multipath interference, such as riparian vegetation (low-hanging trees and large bushes on river or stream banks), buildings at or near the river banks, bridges, and other flow-control structures, could impede or block signals from GPS satellites.

It is usually not possible to attain all of these conditions, but site selection cannot be understated as a critical part of a discharge measurement. Select the best possible reach using these criteria and then select a cross section. For more discussion regarding site selection when using an ADCP, refer to Mueller and Wagner (2009).

Layout and Stationing of Partial Sections and Verticals in a Midsection Current-Meter Discharge Measurement

After the cross section has been selected, determine the width of the stream. For a mechanical current-meter or other point-velocity measurement, string a tag line or measuring tape for measurements made by wading, from a boat, from ice cover, or from an unmarked bridge. Except for bridges, string the line

at right angles to the direction of flow to avoid horizontal angles in the cross section. For cableway or bridge measurements, use the graduations painted on the cable or bridge rail. Next, determine the spacing of the verticals, generally using about 25 to 30 partial sections. With a smooth cross section and even velocity distribution, fewer partial sections may be used. Space the partial sections so that no partial section has more than 10 percent of the total discharge in it. The ideal measurement is one in which no partial section has more than 5 percent of the total discharge in it; this can be challenging when only 25 partial sections are used. For example, the discharge measurement shown in figure 2*A* had 6.5 percent of the total discharge in the partial section with the greatest discharge. Equal widths of partial sections across the entire cross section are not recommended unless the discharge is evenly distributed. Lessen the width of the partial sections as depths and velocities become greater. Usually an approximate or expected total discharge can be obtained from the stage-discharge curve. Space the verticals so the discharge in each partial section is about 5 percent of the expected total discharge from the rating curve. When using an electronic field notebook [such as the JBS Instruments Aquacalc Pro Discharge Measurement Computer (Aquacalc), a PDA with the Hydrological Services Current Meter Counter signal processor (CMCsp), or the SonTek FlowTracker], the expected total discharge can be entered prior to starting the discharge measurement. During the measurement, a warning message will be displayed if a partial discharge exceeds 10 percent of the expected total discharge. When using an ADV or other acoustic point-velocity instrument, make sure the instrument is appropriately aligned and plumbed to the tag line because slight variations in the alignment of the instrument can result in large errors in the measurement of point velocity. See further discussion of the use of acoustic point-velocity instruments in this chapter.

For a standard mechanical current-meter discharge measurement, the usual procedure, after selecting and laying out the section, is to measure and record at each vertical (1) the distance from the initial point, (2) the depth, (3) the meter position, (4) the number of revolutions, (5) the time interval, and (6) the horizontal angle of flow. The starting point can be either bank. The edge of water, which may have a depth of zero, is considered to be the first vertical. The hydrographer should move to each of the verticals in succession and repeat the procedure until the measurement is completed at the opposite bank.

Measurement of Width

The first measurement made in a discharge measurement is usually the determination of horizontal stationing (width) in the cross section being measured. Width needs to be measured using the proper equipment and procedures that apply to the type of measurement being made (that is, wading, bridge, cableway, boat, or ice). Details of measuring width using a variety of equipment, and under different flow conditions, are described in subsequent sections of this chapter.

The horizontal distance to any vertical in a cross section is measured from an initial point on the bank. Cableways and bridges used regularly for making discharge measurements are commonly marked at 2-, 5-, 10-, and (or) 20-ft intervals by paint marks. Distance between markings is interpolated, or measured with a rule or pocket tape. Steel or Kevlar tag lines and metallic tapes are used for measurements made by wading, from boats, or from unmarked bridges. For wide streams of about 2,500 ft or more, where conventional measuring methods cannot be used, surveying methods and Global Positioning Systems (GPS) can be used.

Tapes and Tag Lines

Tag lines used for wading measurements are usually made of either galvanized steel aircraft cord with solder beads at measured intervals, or Kevlar, which is marked with black ink and waxed to resist abrasion. A Kevlar tag line consists of a Kevlar core with a nylon jacket.

The standard arrangement of solder beads on steel tag lines is shown in table 1. The standard markings for Kevlar tag lines is one mark every 2 ft, two marks every 10 ft, and three marks every 100 ft. The standard lengths of tag lines are 300, 400, and 500 ft, but other sizes are available.

Four types of tag-line reels typically used for the steel tag lines are the Lee-Au, Pakron, Columbus type A, and the USGS Stainless Steel Tag line as shown in figure 3. The reel used for the Kevlar tag line is shown in figure 4.

Larger reels, used for boat measurements, are designed to hold up to 3,000 ft of ⅛-inch (in.) diameter steel tag line. These reels and boat measurement methods have largely been replaced by the ADCP technology. Two different types of reels still available are as follows:

- A heavy-duty, horizontal-axis reel without a brake, and with a capacity of 5,000 ft of ⅛-in. beaded tag line or 3,000 ft of $^{3}/_{16}$-in. Kevlar boat tag line, as shown in figure 5.
- A vertical-axis reel without a brake (fig. 6), and with a capacity of 1,500 ft of ⅛-in diameter steel tag line (800 ft tag lines are standard) or up to 900 ft of 3/16-in. Kevlar boat tag-line cable.

Table 1. Standard markings for steel tag lines.

Distance from initial point (zero mark), in feet	Distance between marks, in feet	Number of solder beads, or tags
0 to 50	2	1 (single bead)
50 to 100	5	1
150 to 500	10	1
0 to 50	10	2 (double bead)
50 to 450	100	2
0 to 500	100	3 (triple bead)

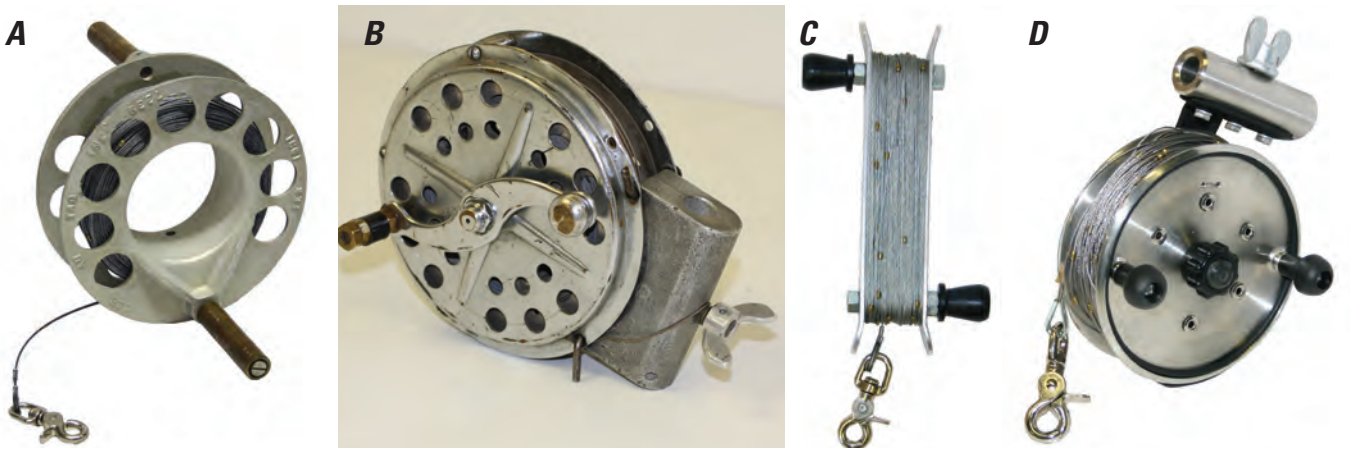

Figure 3. Type-A reels: *A*, Lee-Au; *B*, Pakron; *C*, Columbus; and *D*, USGS stainless steel tag line.

Figure 4. Kevlar tag-line reel.

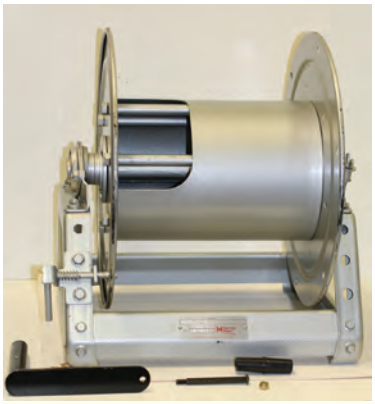

Figure 5. Horizontal-axis boat tag-line reel without a brake.

Figure 6. Vertical-axis boat tag-line reel.

Surveying Methods of Width Measurement, Surveying Level, and Electronic Total Station

For wide streams where it is not practical to string a tag line for discharge measurements from a boat, surveying methods can be used to measure stream width and stationing for measurement points. Surveying methods require the use of a surveying level, as shown in figure 7, or electronic total station instrumentation, as shown in figure 8. The procedure to determine width with a transit is used less frequently, but is described in the section of this chapter on boat measurements.

With the advent of electronic total station surveying instruments and digital surveying levels, a direct reading of the distance can be made from the digital surveying level or from the total station instrument setup point to the boat. One example of a commercially available total station instrument is shown in figure 8. Most of these instruments require a reflector target at the point where a measurement is desired (in this case the boat); however, total station instruments are also available that provide accurate measurements of distance without a reflector target. Accurate distance measurements can be made with total station instruments over distances of 1 mi or more, provided the boat can be seen and not obstructed by intervening objects.

Figure 7. Surveying level and tripod.

Figure 8. Total station surveying equipment: A, instrument and tripod and B, instrument reflector targets and surveying tape.

Global Positioning System With Differential Corrections

Measurement points can be stationed for wide streams, such as flood plains that may be several miles wide, or large tidal estuaries, with a global positioning system with differential corrections (DGPS) instrument, such as that shown in figure 9, which is a real-time kinematic (RTK) GPS base station with radio transmitter. RTK-GPS and other DGPS instruments utilize satellite telemetry from an array of satellites, and use radio triangulation to compute positions for any point on the Earth. In order to obtain the accuracy necessary for a discharge measurement, the raw GPS positions must have differential corrections applied on the basis of simultaneous readings at a base station. Most DGPS units contain built-in differential correction receivers that make automatic and instantaneous corrections. Other GPS units may use a separate receiver that attaches to the GPS unit with a cable. In either case, base station data are received by radio signal from nearby ground base stations or via communications satellites from a network of ground stations, such as the Wide Area Augmentation System (WAAS).

A surveying grade DGPS unit with capability of storing and recalling data is preferred. These units may or may not have built-in or attached differential correction receivers. If instantaneous differential corrections are not made, then use correction data obtained after the fact from a separate GPS base station to postprocess coordinate data. Various agencies collect and provide the base station data via the Internet. Coordinate data for the measurement points are downloaded from the GPS unit to a computer for postprocessing. Software is available to make the differential corrections, to compute corrected coordinates of the measurement points, and to automatically compute distances between and to plot a map of the measurement points.

Figure 9. Global positioning system with real-time kinematic (RTK–GPS) base station and radio transmitter.

Accuracy of GPS coordinates will vary depending on the type of GPS unit used and whether or not differential corrections are made. Coordinates without differential corrections can be in error by as much as ±300 ft because of various errors in the system. Obviously, this is not acceptable for discharge measurements. However, if care is taken in making observations, and then making differential corrections, errors can be reduced to as little as ±3 ft, and even less in ideal conditions. This method is acceptable for wide flood plains and inaccessible estuaries with open skies and minimal reflective surfaces, which can result in multipath errors.

Measurement of Depth

The second measurement normally made at a vertical is the stream depth. Depth should be measured using the proper equipment and procedures that apply to the type of measurement being made (that is, wading, bridge, cableway, boat, or ice). Details of measuring depth using various equipment and under different flow conditions are described in the following sections of this chapter. The water depth of a stream at a selected vertical can be measured in several ways, depending on the type of measurement being made, the total depth of the stream, and the velocity of the stream. Stream depth is usually measured by use of a wading rod, sounding lines and weights, acoustic Doppler sensor, or another sonic sounder, as described in the following sections of this chapter.

Use of Wading Rod

Use a wading rod for measuring stream depth when depth is shallow enough, or when measuring from a low footbridge or other supportive structure over the stream. Likewise, use the wading rod for measuring from ice cover for shallow depths. Wading rods can even be used from a boat if depths are not too great. The top-setting wading rod can be used for depths up to 4 ft, but greater depths can be measured with 6-, 8-, and 10-ft top-setting wading rods. The round wading rod, which is assembled with 1-ft sections, can be made up into any length, but generally is not used for depths greater than about 10 ft. Velocity of flow is also a consideration because high velocity may not allow for keeping a long wading rod in place.

Wading rods have a small foot on the bottom to allow the rod to be placed firmly on the streambed, and yet not sink into the streambed under most conditions. In sand-bottom streams, or in soft muck, it is sometimes difficult to keep the wading rod from sinking into the streambed as the weight of the rod and meter and the eroding power of the flowing water cause the foot of the wading rod to sink. The hydrographer must use care in these conditions to be sure the measured water depth, as well as the depth of the current-meter placements, are accurately based on the surface of the streambed. In some cases, the wading rod may need to be supported in some manner other than resting on the streambed.

When using a wading rod in streams with moderate-to-high velocity, there will be a velocity-head build-up of water on the wading rod. The stream depth should be based on where the surface of the stream intersects the wading rod, and not on the top of the velocity-head build-up. Wading rods are graduated in tenths-of-a-foot, and stream depths are generally measured or estimated and recorded to the nearest 0.01 ft.

Use of Sounding Lines and Weights

Water depth is measured with sounding lines and weights when the depth is too great to use a wading rod, and when measuring conditions require measuring from a bridge, cableway, or boat. This section will describe the measurement of depth when using sounding reels and handlines. It also discusses the procedures used to correct observed depths when high velocity causes the weight and meter to drift downstream.

Use of Sounding Reels

When using one of the sounding reels described in a subsequent section of this chapter, a counter or dial is used to determine the length of cable that has been dispensed. Depths are measured to the nearest 0.1 ft when using a sounding line and weight.

The size of the sounding weight used in current-meter measurements depends on the maximum depth and velocity in a cross section. A rule of thumb is that the size of the weight in pounds should be greater than the maximum product of velocity and depth in the cross section. If insufficient weight is used, the sounding line will be dragged at an angle downstream. If debris or ice is flowing or if the stream is shallow and swift, a heavier weight can be used than the rule designates. The rule is not rigid but it does provide a starting point for deciding on the size of the weight that is needed. If available, notes can be examined of previous measurements at a site to help determine the size of the weight needed at various stages.

Some sounding reels are equipped with a computing depth indicator, or spiral. To use the computing spiral, the dial pointer must be set at zero when the center of the current-meter rotor is at the water surface. After the sounding weight and meter are lowered until the weight touches the streambed, and the indicated depth should be read. The distance that the meter is mounted above the bottom of the weight should be added. For example, if a 30 C .5 (that is, a 30-pound Columbus weight is being used and the center of the meter cups is 0.5 ft above the bottom of the weight) suspension is used and the dial pointer reads 18.5 ft when the sounding weight touches the streambed, the depth would be 19.0 ft (18.5 + 0.5). To move the meter to the 0.8-depth position, merely raise the weight and the meter until the pointer is at the 19-ft mark on the graduated spiral, which will correspond to 15.2 ft on the main dial (0.8 × 19.0). To set the meter at the 0.2-depth position, raise the weight and meter until the pointer is at 3.8 ft on the main dial (0.2 × 19.0).

Tags can be placed on the sounding line a known distance above the center of the meter cups as an aid in determining depth. The tags, which are usually streamers of

different-colored binding tape, are fastened to the sounding line by solder beads or by small cable clips. Tags are used for determining depth in two ways; the following is the preferred procedure:

1. Set the tag at the water surface and then set the depth indicator to read the distance of that tag above the center of the meter cups.
2. Continue as if the meter cups themselves have been set at the water surface.
3. When the weight touches the streambed, read the depth indicator and add the distance that the meter is above the bottom of the weight to obtain the total depth.
4. Use the spiral indicator, as described above, for setting the 0.8-depth meter position. If debris or ice is flowing, this method keeps the meter below the water surface and helps to prevent damage to the meter.

This is an alternate method that is sometimes used with handlines and sounding reels: With the sounding weight on the streambed, raise the weight until the first tag below the water surface appears at the surface. If using a reel, determine the distance the weight was raised by subtracting before and after readings of the depth indicator; if using a handline, use a tape or measuring stick. The total stream depth is the sum of (a) the distance the weight was raised to bring the tag to the water surface, (b) the distance the tag is above the center of the meter cups, and (c) the distance from the bottom of the weight to the center of the cups.

Use of a Handline

Although rarely used in the USGS, handlines still provide a viable means of measuring discharge from bridges. When using a handline, unwind enough cable from the handline reel to keep the reel out of water when the sounding weight is on the streambed at the deepest part of the cross section. If the bridge is high enough above the water surface, raise and lower the weight and meter by the rubber-covered cable rather than by the bare cable.

The usual procedure for determining depths is to set the meter cups at the water surface and then lower the sounding weight to the streambed while measuring the amount of line needed to reach the streambed. Measure along the rubber-covered service cord with a steel or metallic tape or a graduated rod to determine the distance the weight is lowered. This measured distance, plus the distance from the bottom of the sounding weight to the meter cups, is the depth of water. When the meter is set for the velocity observation, stand on the rubber-covered cable or tie it to the handrail to hold the meter in place. This arrangement frees the hands to record the data.

Another method of determining depth when using a handline includes the use of tags set at a known distance above the meter. Lower the sounding weight to the streambed, and then raise the weight until one of the tags is at the water surface. Measure along the rubber-covered service cord with a steel or metallic tape or a graduated rod to determine the distance the weight is raised. The total depth of water is then the summation of (1) the distance the particular tag is above the meter cups, (2) the measured distance the meter and weight was raised, and (3) the distance from the bottom of the weight to the meter cups.

Depth Corrections for Downstream Drift of Current Meter and Weight

Where it is possible to sound but the weight and meter drift downstream, the depths measured by the usual methods are too great. Figure 10 graphically illustrates this condition. The correction for this error has two parts, the air correction and the wet-line correction. The air correction is shown in figure 10 as the distance *cd*. The wet-line correction in figure 10 is shown as the difference between the wet-line depth *de* and the vertical depth *dg*.

As shown in figure 10, the air correction depends on the vertical angle *P* and the distance *ab*. The correction is computed as follows:

$$\cos P = \frac{ab}{ad} = \frac{ab}{ac+cd} = \frac{ab}{ab+cd} \Rightarrow$$
$$ab + cb = \frac{ab}{\cos P} \Rightarrow \quad , \qquad (7)$$
$$cd = \frac{ab}{\cos P} - ab = ab\left[\frac{1}{\cos P} - 1\right]$$

where $ab = ac$

The air correction for even-numbered angles between 4 degrees and 36 degrees and vertical lengths between 10 and 100 ft is shown in table 2. The correction is applied to the nearest tenth of a foot; hundredths are given to aid in interpolation.

Use of an air correction table may be nearly eliminated by using tags at selected intervals on the sounding line and using the tags to refer to the water surface. This practice is almost equivalent to moving the reel to a position just above the water surface.

The correction for excess length of line below the water surface is obtained by using an elementary principle of mechanics. If a known horizontal force is applied to a weight suspended on a cord, the cord takes a position of rest at some angle with the vertical. The tangent of the vertical angle of the cord is equal to the horizontal force divided by the vertical force owing to the weight. If several additional horizontal and vertical forces are applied to the cord, the tangent of the angle in the cord above any point is equal to a summation of the horizontal forces below that point, divided by the summation of the vertical forces below the point.

The distribution of total horizontal drag on the sounding line is in accordance with the variation of velocity with depth. The excess in length of the curved line over the vertical depth is the sum of the products of each tenth of depth and the function $[(1/\cos P) - 1]$ of the corresponding angles. The function is derived for each tenth of depth by means of the tangent relation of the forces acting below any point.

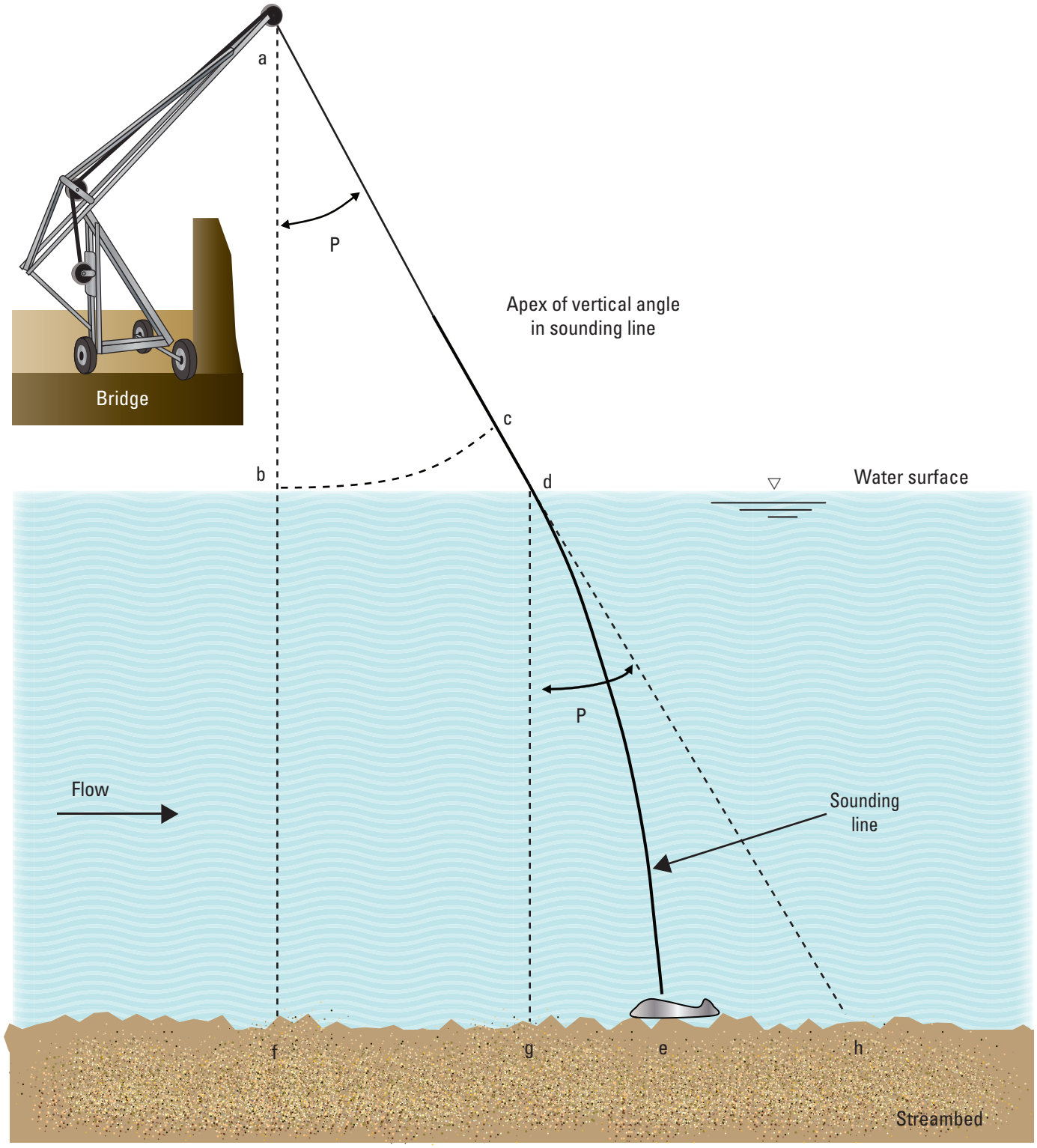

Figure 10. Position of sounding weight and line in deep, swift water.

The wet-line correction for even-numbered angles between 4 degrees and 36 degrees and wet-line depths between 10 and 100 ft is shown in table 3. The correction is applied to the nearest tenth of a foot. The wet-line correction cannot be determined until the air correction has been deducted from the observed depth.

The following assumptions were used in deriving the wet-line correction table:

1. The weight will go to the bottom despite the force of the current.
2. The sounding is made when the weight is at the bottom but entirely supported by the line.
3. Drag on the streamlined weight in the sounding position is neglected.
4. The air-line/wet-line table is generic and can be used for any size sounding weight or line, provided they are designed to offer little resistance to the current.

Wet-line corrections can also be computed with the equation below. This polynomial equation was derived by Kenneth L. Wahl (U.S. Geological Survey [ret.], Regional Surface Water Specialist, written commun., 2000) from the data in table 3, and reproduces the table values to within a few hundredths of a foot. It can be used in a field computer to quickly and easily compute wet-line corrections. With additional programming, depths and depth settings can also be computed.

$$CORR_{wl} = D_{wl} - D_v = \left(0.0004081 - 0.0001471 \times P + 0.00005731 \times P^2\right) \times D_{wl}, \quad (8)$$

where $CORR_{wl}$ the correction, in feet, to subtract from the wet-line depth to obtain the vertical depth,
D_{wl} the wet-line depth, in feet,
D_v the vertical depth, in feet, and
P the vertical angle, in degrees.

If the direction of flow is not perpendicular to the measuring section, the observed angle in the measuring line as indicated by a protractor will be less than the true angle of the line. The air correction and wet-line correction will then be too small. To correct for this, measure the horizontal angle between the direction of flow and a perpendicular to the measuring section with a protractor, or determine the horizontal angle coefficient as described in a subsequent section of this publication. The geometry of this condition is illustrated in figure 11.

If the horizontal angle of the direction of flow is called H, the observed vertical angle P, and the true vertical angle X, the relation between the angles is expressed by the equation

$$\tan X = \frac{\tan P}{\cos H}. \quad (9)$$

Table 4 gives the amounts in tenths of degrees. Add these to observed vertical angles to obtain the true vertical angles for a range of horizontal angles between 8 degrees and 28 degrees.

The conditions that cause error in sounding the depth also cause error in the placement of the meter at selected depths. The correction tables are not strictly applicable to the problem of placing the meter because of the increased pressure placed on the sounding weight by higher velocities when it is raised from the streambed. A meter placed in deep, swift water by the ordinary methods for observations at selected percentages of the depth will be too high in the water. The use of tables 2 and 3 will tend to eliminate this error in placement of the meter, and although not strictly applicable, their use for this purpose has become general.

For the 0.2-depth position, the curvature of the wet line is assumed to be negligible and the length of sounding line from the apex of the vertical angle to the weight is considered to be a straight line. The method used to place the meter at the 0.2-depth position is as follows:

1. Compute the 0.2 value of the vertical depth.
2. Lower the meter to this depth into the water and read the vertical angle.
3. Obtain the air correction from table 2. The vertical length used to obtain the air correction is the sum of (a) 0.2 of the vertical depth, (b) the distance from the water surface to the apex of the angle, and (c) the distance from the bottom of the weight to the meter.
4. Let out an additional amount of line equal to the air correction.

Table 2. Air correction table (in feet), giving differences between vertical length and slant length of sounding line above water surface for selected vertical angles.

Vertical length (feet)	Vertical angle of sounding line at protractor																	Vertical length (feet)
	4°	6°	8°	10°	12°	14°	16°	18°	20°	22°	24°	26°	28°	30°	32°	34°	36°	
10	0.02	0.06	0.10	0.15	0.22	0.31	0.40	0.51	0.64	0.79	0.95	1.13	1.33	1.55	1.79	2.06	2.36	10
12	0.03	0.07	0.12	0.19	0.27	0.37	0.48	0.62	0.77	0.94	1.14	1.35	1.59	1.86	2.15	2.47	2.83	12
14	0.03	0.08	0.14	0.22	0.31	0.43	0.56	0.72	0.90	1.10	1.32	1.58	1.86	2.17	2.51	2.89	3.30	14
16	0.04	0.09	0.16	0.25	0.36	0.49	0.64	0.82	1.03	1.26	1.51	1.80	2.12	2.48	2.87	3.30	3.78	16
18	0.04	0.10	0.18	0.28	0.40	0.55	0.73	0.93	1.16	1.41	1.70	2.03	2.39	2.78	3.23	3.71	4.25	18
20	0.05	0.11	0.20	0.31	0.45	0.61	0.81	1.03	1.28	1.57	1.89	2.25	2.65	3.09	3.58	4.12	4.72	20
22	0.05	0.12	0.22	0.34	0.49	0.67	0.89	1.13	1.41	1.73	2.08	2.48	2.92	3.40	3.94	4.54	5.19	22
24	0.06	0.13	0.24	0.37	0.54	0.73	0.97	1.24	1.54	1.88	2.27	2.70	3.18	3.71	4.30	4.95	5.67	24
26	0.06	0.14	0.26	0.40	0.58	0.80	1.05	1.34	1.67	2.04	2.46	2.93	3.45	4.02	4.66	5.36	6.14	26
28	0.07	0.15	0.28	0.43	0.63	0.86	1.13	1.44	1.80	2.20	2.65	3.15	3.71	4.33	5.02	5.77	6.61	28
30	0.07	0.17	0.29	0.46	0.67	0.92	1.21	1.54	1.93	2.36	2.84	3.38	3.98	4.64	5.38	6.19	7.08	30
32	0.08	0.18	0.31	0.49	0.71	0.98	1.29	1.65	2.05	2.51	3.03	3.60	4.24	4.95	5.73	6.60	7.55	32
34	0.08	0.19	0.33	0.52	0.76	1.04	1.37	1.75	2.18	2.67	3.22	3.83	4.51	5.26	6.09	7.01	8.03	34
36	0.09	0.20	0.35	0.56	0.80	1.10	1.45	1.85	2.31	2.83	3.41	4.05	4.77	5.57	6.45	7.42	8.50	36
38	0.09	0.21	0.37	0.59	0.85	1.16	1.53	1.96	2.44	2.98	3.60	4.28	5.04	5.88	6.81	7.84	8.97	38
40	0.10	0.22	0.39	0.62	0.89	1.22	1.61	2.06	2.57	3.14	3.79	4.50	5.30	6.19	7.17	8.25	9.44	40
42	0.10	0.23	0.41	0.65	0.94	1.29	1.69	2.16	2.70	3.30	3.97	4.73	5.57	6.50	7.53	8.66	9.91	42
44	0.11	0.24	0.43	0.68	0.98	1.35	1.77	2.26	2.82	3.46	4.16	4.95	5.83	6.81	7.88	9.07	10.39	44
46	0.11	0.25	0.45	0.71	1.03	1.41	1.85	2.37	2.95	3.61	4.35	5.18	6.10	7.12	8.24	9.49	10.86	46
48	0.12	0.26	0.47	0.74	1.07	1.47	1.93	2.47	3.08	3.77	4.54	5.40	6.36	7.43	8.60	9.90	11.33	48
50	0.12	0.28	0.49	0.77	1.12	1.53	2.02	2.57	3.21	3.93	4.73	5.63	6.63	7.74	8.96	10.31	11.80	50
52	0.13	0.29	0.51	0.80	1.16	1.59	2.10	2.68	3.34	4.08	4.92	5.86	6.89	8.04	9.32	10.72	12.28	52
54	0.13	0.30	0.53	0.83	1.21	1.65	2.18	2.78	3.47	4.24	5.11	6.08	7.16	8.35	9.68	11.14	12.75	54
56	0.14	0.31	0.55	0.86	1.25	1.71	2.26	2.88	3.59	4.40	5.30	6.31	7.42	8.66	10.03	11.55	13.22	56
58	0.14	0.32	0.57	0.89	1.30	1.78	2.34	2.98	3.72	4.55	5.49	6.53	7.69	8.97	10.39	11.96	13.69	58
60	0.15	0.33	0.59	0.93	1.34	1.84	2.42	3.09	3.85	4.71	5.68	6.76	7.95	9.28	10.75	12.37	14.16	60
62	0.15	0.34	0.61	0.96	1.39	1.90	2.50	3.19	3.98	4.87	5.87	6.98	8.22	9.59	11.11	12.79	14.64	62
64	0.16	0.35	0.63	0.99	1.43	1.96	2.58	3.29	4.11	5.03	6.06	7.21	8.48	9.90	11.47	13.20	15.11	64
66	0.16	0.36	0.65	1.02	1.47	2.02	2.66	3.40	4.24	5.18	6.25	7.43	8.75	10.21	11.83	13.61	15.58	66
68	0.17	0.37	0.67	1.05	1.52	2.08	2.74	3.50	4.36	5.34	6.44	7.66	9.01	10.52	12.18	14.02	16.05	68
70	0.17	0.39	0.69	1.08	1.56	2.14	2.82	3.60	4.49	5.50	6.62	7.88	9.28	10.83	12.54	14.44	16.52	70
72	0.18	0.40	0.71	1.11	1.61	2.20	2.90	3.71	4.62	5.65	6.81	8.11	9.55	11.14	12.90	14.85	17.00	72
74	0.18	0.41	0.73	1.14	1.65	2.27	2.98	3.81	4.75	5.81	7.00	8.33	9.81	11.45	13.26	15.26	17.47	74
76	0.19	0.42	0.75	1.17	1.70	2.33	3.06	3.91	4.88	5.97	7.19	8.56	10.08	11.76	13.62	15.67	17.94	76
78	0.19	0.43	0.77	1.20	1.74	2.39	3.14	4.01	5.01	6.13	7.38	8.78	10.34	12.07	13.98	16.09	18.41	78
80	0.20	0.44	0.79	1.23	1.79	2.45	3.22	4.12	5.13	6.28	7.57	9.01	10.61	12.38	14.33	16.50	18.89	80
82	0.20	0.45	0.81	1.27	1.83	2.51	3.30	4.22	5.26	6.44	7.76	9.23	10.87	12.69	14.69	16.91	19.36	82
84	0.20	0.46	0.83	1.30	1.88	2.57	3.39	4.32	5.39	6.60	7.95	9.46	11.14	12.99	15.05	17.32	19.83	84
86	0.21	0.47	0.85	1.33	1.92	2.63	3.47	4.43	5.52	6.75	8.14	9.68	11.40	13.30	15.41	17.73	20.30	86
88	0.21	0.48	0.87	1.36	1.97	2.69	3.55	4.53	5.65	6.91	8.33	9.91	11.67	13.61	15.77	18.15	20.77	88
90	0.22	0.50	0.88	1.39	2.01	2.75	3.63	4.63	5.78	7.07	8.52	10.13	11.93	13.92	16.13	18.56	21.25	90
92	0.22	0.51	0.90	1.42	2.06	2.82	3.71	4.73	5.90	7.22	8.71	10.36	12.20	14.23	16.48	18.97	21.72	92
94	0.23	0.52	0.92	1.45	2.10	2.88	3.79	4.84	6.03	7.38	8.90	10.58	12.46	14.54	16.84	19.38	22.19	94
96	0.23	0.53	0.94	1.48	2.14	2.94	3.87	4.94	6.16	7.54	9.09	10.81	12.73	14.85	17.20	19.80	22.66	96
98	0.24	0.54	0.96	1.51	2.19	3.00	3.95	5.04	6.29	7.70	9.27	11.03	12.99	15.16	17.56	20.21	23.13	98
100	0.24	0.55	0.98	1.54	2.23	3.06	4.03	5.15	6.42	7.85	9.46	11.26	13.26	15.47	17.92	20.62	23.61	100

Table 3. Wet-line table (in feet) giving differences between wet-line length and vertical depth for selected vertical angles.

Wet-line length (feet)	Vertical angle of sounding line at protractor																	Wet-line length (feet)
	4°	6°	8°	10°	12°	14°	16°	18°	20°	22°	24°	26°	28°	30°	32°	34°	36°	
10	0.01	0.02	0.03	0.05	0.07	0.10	0.13	0.16	0.20	0.25	0.30	0.35	0.41	0.47	0.54	0.62	0.70	10
12	0.01	0.02	0.04	0.06	0.09	0.12	0.15	0.20	0.24	0.30	0.36	0.42	0.49	0.57	0.65	0.74	0.84	12
14	0.01	0.02	0.04	0.07	0.10	0.14	0.18	0.23	0.29	0.35	0.41	0.49	0.57	0.66	0.76	0.87	0.98	14
16	0.01	0.03	0.05	0.08	0.12	0.16	0.20	0.26	0.33	0.40	0.47	0.56	0.65	0.76	0.87	0.99	1.12	16
18	0.01	0.03	0.06	0.09	0.13	0.18	0.23	0.30	0.37	0.45	0.53	0.63	0.73	0.85	0.98	1.12	1.26	18
20	0.01	0.03	0.06	0.10	0.14	0.20	0.26	0.33	0.41	0.50	0.59	0.70	0.82	0.94	1.09	1.24	1.40	20
22	0.01	0.04	0.07	0.11	0.16	0.22	0.28	0.36	0.45	0.55	0.65	0.77	0.90	1.04	1.20	1.36	1.54	22
24	0.01	0.04	0.08	0.12	0.17	0.24	0.31	0.39	0.49	0.60	0.71	0.84	0.98	1.13	1.31	1.49	1.68	24
26	0.02	0.04	0.08	0.13	0.19	0.25	0.33	0.43	0.53	0.64	0.77	0.91	1.06	1.23	1.41	1.61	1.81	26
28	0.02	0.04	0.09	0.14	0.20	0.27	0.36	0.46	0.57	0.69	0.83	0.98	1.14	1.32	1.52	1.74	1.95	28
30	0.02	0.05	0.10	0.15	0.22	0.29	0.38	0.49	0.61	0.74	0.89	1.05	1.22	1.42	1.63	1.86	2.09	30
32	0.02	0.05	0.10	0.16	0.23	0.31	0.41	0.52	0.65	0.79	0.95	1.12	1.31	1.51	1.74	1.98	2.23	32
34	0.02	0.05	0.11	0.17	0.24	0.33	0.44	0.56	0.69	0.84	1.01	1.19	1.39	1.60	1.85	2.11	2.37	34
36	0.02	0.06	0.12	0.18	0.26	0.35	0.46	0.59	0.73	0.89	1.07	1.26	1.47	1.70	1.96	2.23	2.51	36
38	0.02	0.06	0.12	0.19	0.27	0.37	0.49	0.62	0.78	0.94	1.12	1.33	1.55	1.79	2.07	2.36	2.65	38
40	0.02	0.06	0.13	0.20	0.29	0.39	0.51	0.66	0.82	0.99	1.18	1.40	1.63	1.89	2.18	2.48	2.79	40
42	0.03	0.07	0.13	0.21	0.30	0.41	0.54	0.69	0.86	1.04	1.24	1.47	1.71	1.98	2.28	2.60	2.93	42
44	0.03	0.07	0.14	0.22	0.32	0.43	0.56	0.72	0.90	1.09	1.30	1.54	1.80	2.08	2.39	2.73	3.07	44
46	0.03	0.07	0.15	0.23	0.33	0.45	0.59	0.75	0.94	1.14	1.36	1.61	1.88	2.17	2.50	2.85	3.21	46
48	0.03	0.08	0.15	0.24	0.35	0.47	0.61	0.79	0.98	1.19	1.42	1.68	1.96	2.27	2.61	2.98	3.35	48
50	0.03	0.08	0.16	0.25	0.36	0.49	0.64	0.82	1.02	1.24	1.48	1.75	2.04	2.36	2.72	3.10	3.49	50
52	0.03	0.08	0.17	0.26	0.37	0.51	0.67	0.85	1.06	1.29	1.54	1.82	2.12	2.45	2.83	3.22	3.63	52
54	0.03	0.09	0.17	0.27	0.39	0.53	0.69	0.89	1.10	1.34	1.60	1.89	2.20	2.55	2.94	3.35	3.77	54
56	0.03	0.09	0.18	0.28	0.40	0.55	0.72	0.92	1.14	1.39	1.66	1.96	2.28	2.64	3.05	3.47	3.91	56
58	0.03	0.09	0.19	0.29	0.42	0.57	0.74	0.95	1.18	1.44	1.72	2.03	2.37	2.74	3.16	3.60	4.05	58
60	0.04	0.10	0.19	0.30	0.43	0.59	0.77	0.98	1.22	1.49	1.78	2.10	2.45	2.83	3.26	3.72	4.19	60
62	0.04	0.10	0.20	0.31	0.45	0.61	0.79	1.02	1.26	1.54	1.84	2.17	2.53	2.93	3.37	3.84	4.33	62
64	0.04	0.10	0.20	0.32	0.46	0.63	0.82	1.05	1.31	1.59	1.89	2.24	2.61	3.02	3.48	3.97	4.47	64
66	0.04	0.11	0.21	0.33	0.48	0.65	0.84	1.08	1.35	1.64	1.95	2.31	2.69	3.12	3.59	4.09	4.61	66
68	0.04	0.11	0.22	0.34	0.49	0.67	0.87	1.12	1.39	1.69	2.01	2.38	2.77	3.21	3.70	4.22	4.75	68
70	0.04	0.11	0.22	0.35	0.50	0.69	0.90	1.15	1.43	1.74	2.07	2.45	2.86	3.30	3.81	4.34	4.89	70
72	0.04	0.12	0.23	0.36	0.52	0.71	0.92	1.18	1.47	1.79	2.13	2.52	2.94	3.40	3.92	4.46	5.03	72
74	0.04	0.12	0.24	0.37	0.53	0.73	0.95	1.21	1.51	1.84	2.19	2.59	3.02	3.49	4.03	4.59	5.17	74
76	0.05	0.12	0.24	0.38	0.55	0.74	0.97	1.25	1.55	1.88	2.25	2.66	3.10	3.59	4.13	4.71	5.30	76
78	0.05	0.12	0.25	0.39	0.56	0.76	1.00	1.28	1.59	1.93	2.31	2.73	3.18	3.68	4.24	4.84	5.44	78
80	0.05	0.13	0.25	0.40	0.58	0.78	1.02	1.31	1.63	1.98	2.37	2.80	3.26	3.78	4.35	4.96	5.58	80
82	0.05	0.13	0.26	0.41	0.59	0.80	1.05	1.34	1.67	2.03	2.43	2.87	3.35	3.87	4.46	5.08	5.72	82
84	0.05	0.13	0.27	0.42	0.60	0.82	1.08	1.38	1.71	2.08	2.49	2.94	3.43	3.96	4.57	5.21	5.86	84
86	0.05	0.14	0.28	0.43	0.62	0.84	1.10	1.41	1.75	2.13	2.55	3.01	3.51	4.06	4.68	5.33	6.00	86
88	0.05	0.14	0.28	0.44	0.63	0.86	1.13	1.44	1.80	2.18	2.60	3.08	3.59	4.15	4.79	5.46	6.14	88
90	0.05	0.14	0.29	0.45	0.65	0.88	1.15	1.48	1.84	2.23	2.66	3.15	3.67	4.25	4.90	5.58	6.28	90
92	0.06	0.15	0.29	0.46	0.66	0.90	1.18	1.51	1.88	2.28	2.72	3.22	3.75	4.34	5.00	5.70	6.42	92
94	0.06	0.15	0.30	0.47	0.68	0.92	1.20	1.54	1.92	2.33	2.78	3.29	3.84	4.44	5.11	5.83	6.56	94
96	0.06	0.15	0.31	0.48	0.69	0.94	1.23	1.57	1.96	2.38	2.84	3.36	3.92	4.53	5.22	5.95	6.70	96
98	0.06	0.16	0.31	0.49	0.71	0.96	1.25	1.61	2.00	2.43	2.90	3.43	4.00	4.63	5.33	6.08	6.84	98
100	0.06	0.16	0.32	0.50	0.72	0.98	1.28	1.64	2.04	2.48	2.96	3.50	4.08	4.72	5.44	6.20	6.98	100

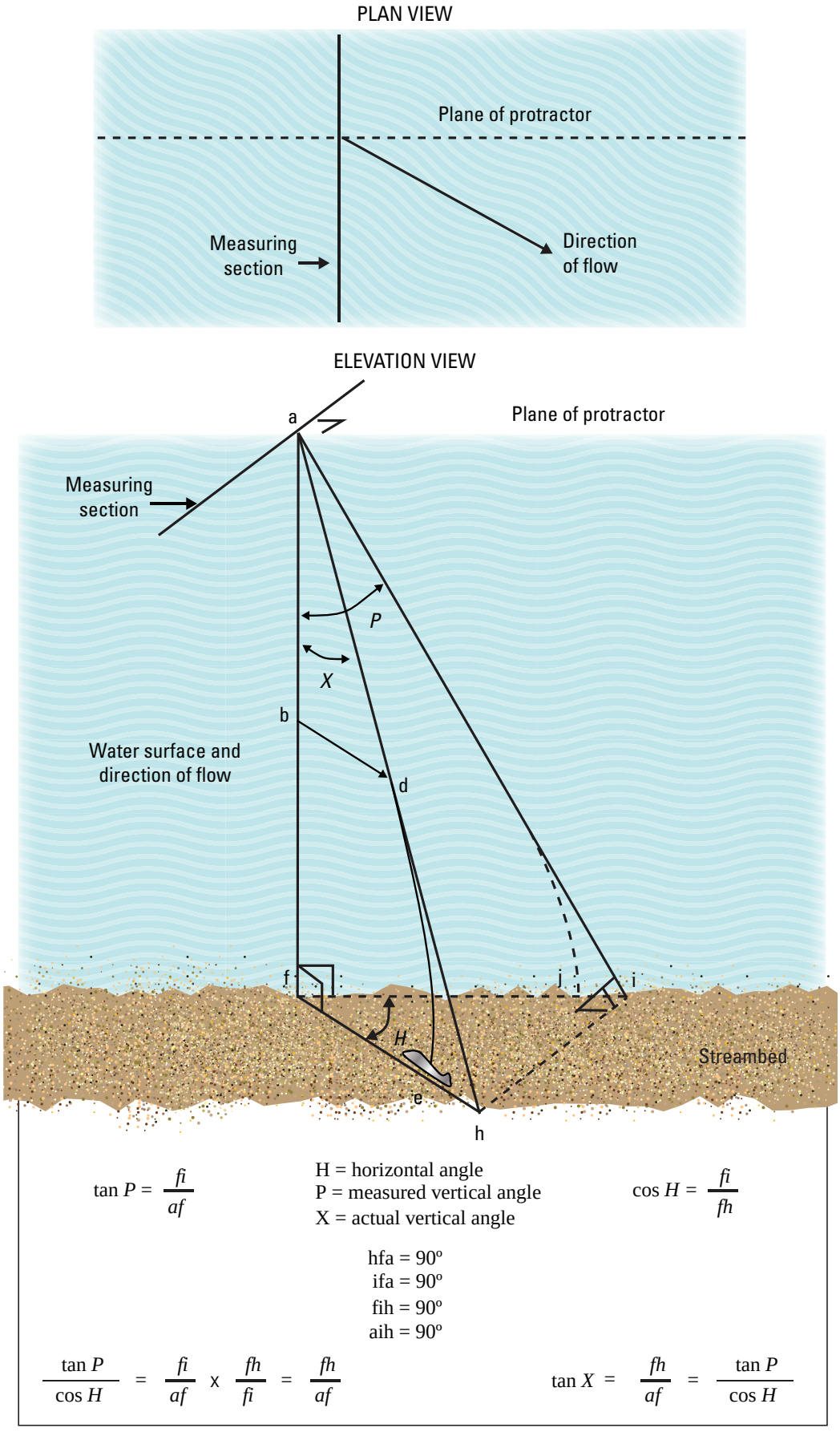

Figure 11. Sketch of geometric relationship of actual to measured vertical angle when flow direction is not normal to the measuring section.

5. If the angle increases appreciably when the additional line is let out, let out more line until the total additional line, the angle, and the vertical distance are in agreement with values presented in the air-correction table.

To place the meter at the 0.8-depth position, a correction to the amount of line reeled in must be made for the difference, if any, between the air correction for the sounding position and that for the 0.8-depth position. This difference is designated as *m* in table 5. If the angle increases for the 0.8-depth position, the meter must be lowered; if it decreases, the meter must be raised.

For the 0.8-depth position of the meter, the wet-line correction may require consideration if the depths are more than 40 ft and if the change in vertical angle is more than 5 percent. If the vertical angle remains the same or decreases, the wet-line correction (table 3) for the 0.8-depth position is less than the wet-line correction for the sounding position by some difference, designated as *n* in table 5. If the vertical angle increases, the difference in correction *n* diminishes until the increase in angle is about 10 percent; for greater increases in angle, the difference between corrections increases also. Table 5 summarizes the effect on air and wet-line corrections caused by raising the meter from the sounding position to the 0.8-depth position.

For slight changes in the vertical angle, because of the differences *m* and *n* in the air and wet-line corrections, the adjustments to the wet-line length of the 0.8-depth position are small and usually can be ignored. Table 5 indicates that the meter may be placed a little too deep if the adjustments are not made. Because of this possibility, the wet-line depth instead of the vertical depth is sometimes used as the basis for computing the 0.8-depth position with no adjustments for the differences *m* and *n*.

Use of Sonic Sounder

The sonic sounder has been used primarily for measuring depth when making a moving boat measurement and in ADCP discharge measurements, and is generally not utilized for measurements where sounding weights are used. However, it can be used in swift, debris-laden streams, where it is difficult or dangerous to lower the sounding weight and meter into the water. The sonic sounder will record the depth when the weight is just below the water surface. For moving boat measurements, the sonic sounder records a continuous trace of the streambed on a digital or analog chart. Details of the setup and use can be found in Smoot and Novak (1969). Relevant information on the use of acoustic sounders in a riverine environment is discussed in detail in Mueller and Landers (1999) and by the International Organization for Standardization (2003). For use of a sonic sounder in ADCP measurements, consult Mueller and Wagner (2009).

Table 4. Degrees to be added to observed vertical angle, *P*, to obtain true vertical angle when flow direction is not normal to measurement section.

Observed vertical angle, *P*, in degrees	Horizontal angle, *H*, in degrees					
	8 cos = 0.99	12 cos = 0.98	16 cos = 0.96	20 cos = 0.94	24 cos = 0.91	28 cos = 0.88
8	0.1	0.2	0.3	0.5	0.8	1.0
12	0.1	0.3	0.5	0.8	1.1	1.5
16	0.1	0.4	0.6	1.0	1.4	2.0
20	0.2	0.4	0.7	1.2	1.7	2.4
24	0.2	0.5	0.8	1.4	2.0	2.8
28	0.2	0.5	1.0	1.5	2.2	3.0
32	0.2	0.6	1.0	1.6	2.4	3.3
36	0.2	0.6	1.1	1.7	2.5	3.4

Table 5. Summary table for setting the meter at 0.8-depth position in deep, swift streams.

Change in vertical angle	Air correction		Wet-line correction	
	Direction of change	Correction to meter position	Direction of change	Correction to meter position
None	None	None	Decrease	Raise meter the distance *n*
Decrease	Decrease	Raise meter the distance *m*	Decrease	Raise meter the distance *n*
Increase	Increase	Lower meter the distance *m*	Decrease, then increase	[1]

[1]Raise meter the distance *n* unless the increase in angle is greater than about 10 percent, then it is necessary to lower the meter the distance *n*.

Measurement of Velocity

With point-velocity meters, after the width and depth at a vertical are measured and recorded, determine the method of velocity measurement. Normally the two-point method or the 0.6-depth method is used. Details of velocity measurement methods using various equipment and under different flow conditions are described in subsequent sections of this chapter.

Compute the setting of the meter for the particular method that will be used at that depth. For the top-setting wading rod, or the spiral-computing dial, some meter settings are self-computing. Record the meter position as 0.8, 0.6, 0.2, or another setting. After the meter is placed at the proper depth, let it adjust to the current before starting the velocity observation. With an ADV, make sure the instrument is located perpendicular to the tag line and the wading rod is plumbed (that is, vertical to the channel bed) before beginning measurement. The time required for adjustment to the undisturbed stream velocity is usually only a few seconds if the velocities are greater than 1 ft/s; however, for lower velocities, particularly if the current meter is suspended by a cable, a longer period of adjustment is needed. After the meter has become adjusted to the current, count the number of revolutions made by the rotor for a period of 40 to 70 seconds; for an ADV, this time period is typically programmed into the instrument's discharge measurement software.

If using a stopwatch to time the revolutions of a mechanical current meter, start the stopwatch simultaneously with the first signal or click, counting "zero," not "one." End the count on a convenient number given in the mechanical current meter rating table column heading. Stop the stopwatch on that count and read the time to the nearest second. Record the number of revolutions and the time interval. If the velocity is to be observed at more than one point in the vertical, determine the meter setting for the additional observation, set the meter to that depth, time the revolutions, and record the data.

When using a current meter digitizer (CMD), a personal digital assistant (PDA), or an electronic notebook such as the Aquacalc or an ADV, observe the same basic procedure for setting the meter, and for providing time for the meter to stabilize. With these instruments, however, the counting and timing of the rotor revolutions or the acoustic pulse measurement are performed automatically. The number of revolutions, time, and velocity displayed by the CMD must be transferred manually to paper field notes, whereas, these data are electronically recorded by the Aquacalc, a PDA, or an ADV. When using any of these automatic meter counting devices and a mechanical current meter, make sure that multiple counts are not occurring during measurement of slow velocity. This can sometimes be determined by visually observing the rotation of the rotor while simultaneously listening to the audible clicks or beeps from the counting device. With the ADV, instead of audible clicks, acoustic Doppler theory is applied. The ADV can sense and measure velocities much smaller than those rated and measured by mechanical meters and are not prone to the multiple count errors of the mechanical current meter.

Current meters, in general, measure stream velocity at a point. One notable exception is the ADCP. This method will be discussed in a subsequent section of this chapter; a thorough discussion of a moving boat discharge measurement using an ADCP is documented in Mueller and Wagner (2009).

The method of making discharge measurements at a cross section by using a current meter that measures point velocities requires determination of the mean velocity in each of the selected verticals. The mean velocity in a vertical is obtained from velocity observations at several points in that vertical. The mean velocity can be approximated by making a few velocity observations and using a known relation between those velocities and the mean in the vertical. The various methods of measuring velocity are: vertical-velocity curve, two-point, 0.6-depth, 0.2-depth, three-point, and surface and subsurface.

Vertical-Velocity Curve Method

In the vertical-velocity curve method, a series of velocity observations at points well distributed between the water surface and the streambed are made at each of the verticals. If there is considerable curvature in the lower part of the vertical-velocity curve, then it is advisable to space the observations more closely together in that part of the depth. Normally, the observations are taken at 0.1-depth increments between 0.1 and 0.9 of the depth. Observations are always taken at 0.2, 0.6, and 0.8 of the depth so that the results obtained by the vertical-velocity curve method may be compared with the commonly used methods of velocity observation. Observations are made at least 0.5 ft from the water surface and from the streambed with the Price AA meter, at least 0.3 ft from these boundaries with the Price pygmy meter, or at least 0.2 ft from these boundaries with the FlowTracker ADV.

The vertical-velocity curve for each vertical is based on observed velocities plotted against depth, as shown in figure 12. In order that vertical-velocity curves at different verticals may be readily compared, it is customary to plot depths as proportional parts of the total depth. The mean velocity in the vertical is obtained by measuring the area between the curve and the ordinate axis with a planimeter, or by other means, and dividing the area by the length of the ordinate axis.

The vertical-velocity curve method is valuable in determining coefficients for application to the results obtained by other methods, but is not generally adapted to routine discharge measurements because of the extra time required to collect field data and to compute the mean velocity. A typical vertical-velocity curve for the cross section should be measured and evaluated at all new measurement sites, and perhaps at new measurement sections if the new section is significantly different in hydraulic characteristics than the section normally used at a regular measurement site.

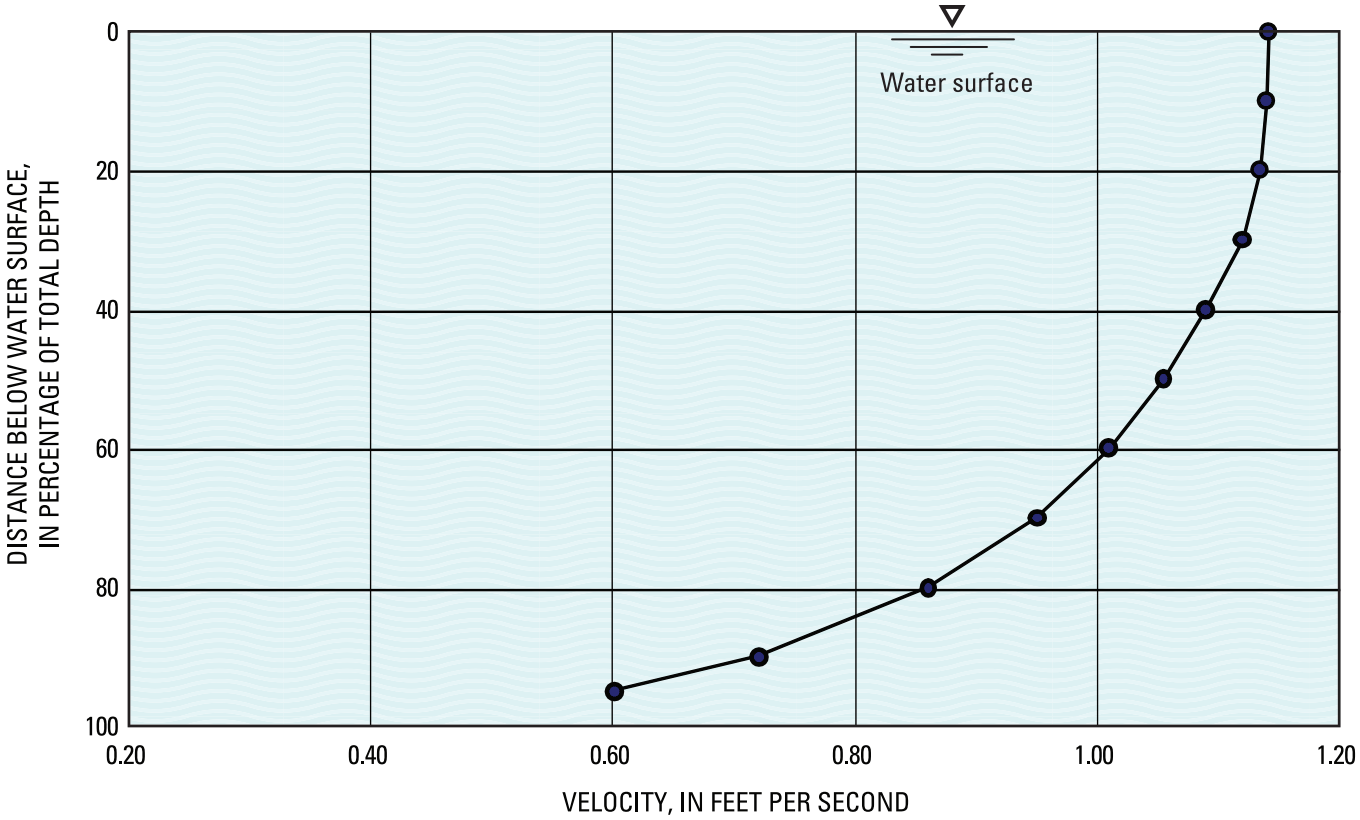

Figure 12. Typical vertical-velocity curve.

Two-Point Method

This is the preferred method for making midsection discharge measurements with point velocity meters. In the two-point method of measuring velocities, observations are made in each vertical at 0.2 and 0.8 of the depth below the surface. The average of these two observations is used as the mean velocity in the vertical. This method is based on many studies of actual observation and on mathematical theory. Experience has shown that this method gives more consistent and accurate results than any of the other methods, except for the vertical-velocity curve method. Use the two-point method for depths of 2.5 ft or greater, unless using a pygmy current meter or an ADV, in which case, this method is used in depths of 1.5 ft or greater.

With an ADV, the actual instrument has much less drag or resistance to the flow as compared to a mechanical current meter. To prevent boundary interference, avoid placing the ADV sample volume [typically 10 centimeters (about 4 in.) from the center transmitting transducer] within 2 in. from any solid boundary. This boundary condition with the ADV allows for measurement of velocity closer to the water surface and channel bed than a Price AA or to the pygmy (fig. 13). With the Price AA current meter, the two-point method is not used at depths less than 2.5 ft because the current meter would be too close to the water surface and to the streambed to give dependable results.

Six-Tenths-Depth Method

In the 0.6-depth method, an observation of velocity made at 0.6 of the depth below the water surface in the vertical is used as the mean velocity in the vertical. Actual observation and mathematical theory have shown that the 0.6-depth method gives reliable results and is used by the USGS under the following conditions:

Price AA Current Meter

1. Whenever the depth is between 0.3 ft and 2.5 ft.
2. When large amounts of slush ice or debris make it impossible to observe the velocity accurately at the 0.2 depth. (This condition prevents the use of the two-point method.)
3. When the meter is placed a distance above the sounding weight, which makes it impossible to place the meter at the 0.8 depth. (This condition prevents the use of the two-point method.)
4. When the stage in a stream is changing rapidly and you must make a quick measurement.

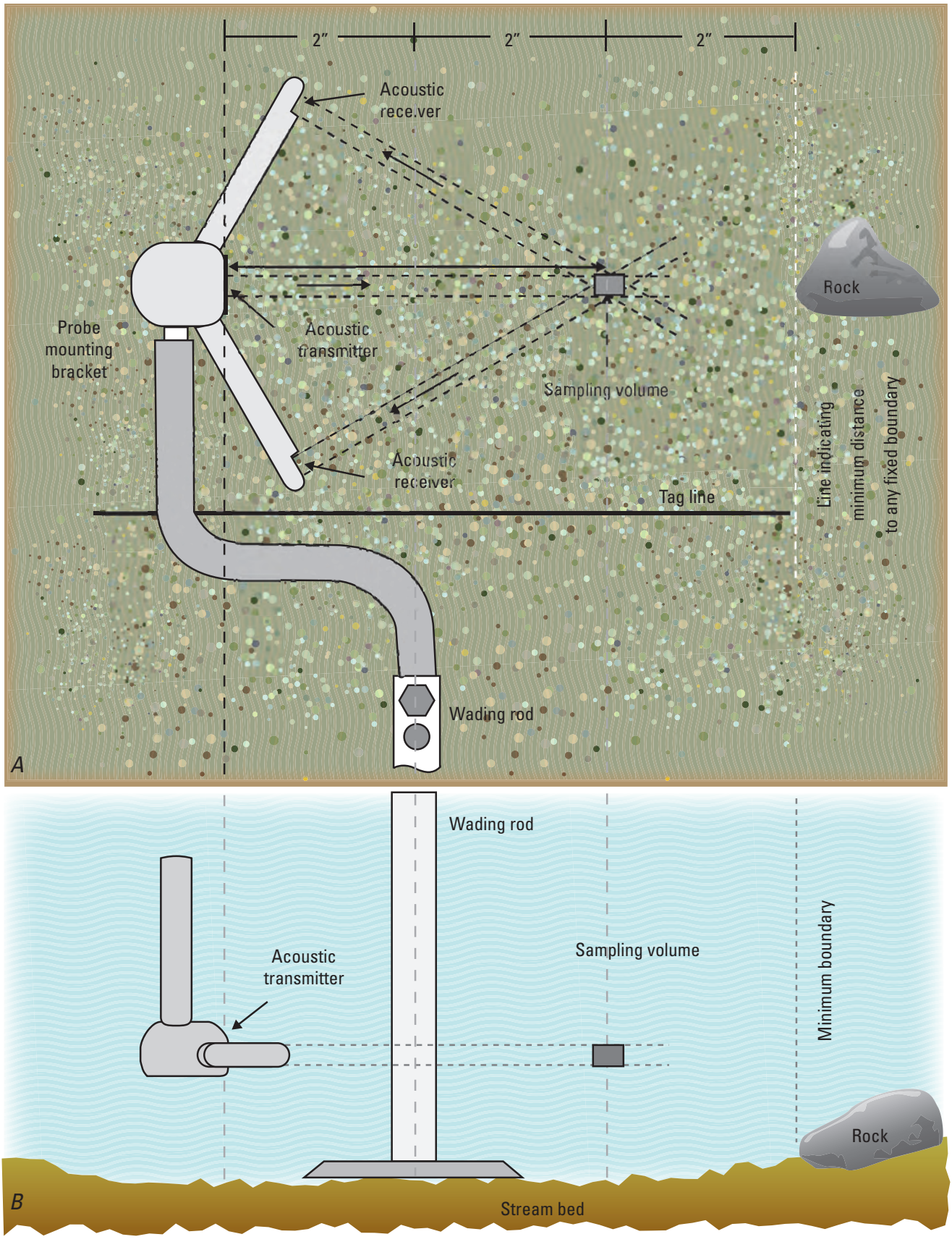

Figure 13. Schematic showing A, plan vie and B, cross section of the FlowTracker sampling volume and the proximity to a fixed boundary in the stream. (Note: Probe mounting bracket not shown.)

Pygmy Current Meter

1. Whenever the depth is between 0.3 ft and 1.5 ft.
2. When large amounts of slush ice or debris make it impossible to observe the velocity accurately at the 0.2 depth. (This condition prevents the use of the two-point method.)
3. When the stage in a stream is changing rapidly and a measurement must be made quickly.

Acoustic Doppler Velocimeter

1. Whenever the depth is between 0.25 ft and 1.5 ft.
2. When large amounts of slush ice or debris make it impossible to observe the velocity accurately at the 0.2 depth. (This condition prevents the use of the two-point method.)
3. When the stage in a stream is changing rapidly and a measurement must be made quickly.

Two-Tenths-Depth Method

The 0.2-depth method consists of observing the velocity at 0.2 of the depth below the surface and applying a coefficient to this observed velocity to obtain the mean in the vertical. It is used mainly during times of high water when the velocities are great, making it impossible to obtain soundings or to place the meter at the 0.8 or the 0.6 depth.

Use a standard cross section or a general knowledge of the cross section at a site to compute the 0.2 depth when it is impossible to obtain depth soundings. A sizeable error in an assumed 0.2 depth is not critical because the slope of the vertical-velocity curve at this point is usually nearly vertical. The 0.2 depth is also used in conjunction with the sonic sounder for flood measurements. The two-point method and the 0.6-depth method are preferred over the 0.2-depth method because of their greater accuracy.

The discharge measurement is normally computed by using the 0.2-depth velocity observations without coefficients as though each were a mean in the vertical. The approximate discharge thus obtained divided by the area of the measuring section gives the weighted mean value of the 0.2-depth velocity. Studies of many measurements made by the two-point method show that for a given measuring section, the relation between the mean 0.2-depth velocity and the true mean velocity either remains constant or varies uniformly with stage. In either circumstance, this relation may be determined for a particular 0.2-depth measurement by recomputing measurements made at the site by the two-point method using only the 0.2-depth velocity observation as the mean in the vertical. The plotting of the true mean velocity versus the mean 0.2-depth velocity for each measurement will give a velocity-relation curve for use in adjusting the mean velocity for measurements made by the 0.2-depth method.

If not enough measurements by the two-point method are available at a site to establish a velocity-relation curve, vertical-velocity curves are needed to establish a relation between the mean velocity and the 0.2-depth velocity. The usual coefficient to adjust the 0.2-depth velocity to the mean velocity is about 0.88.

Three-Point Method

The three-point method consists of observing the velocity at 0.2, 0.6, and 0.8 of the depth, thereby combining the two-point and 0.6-depth methods. The preferred method of computing the mean velocity is to average the 0.2- and 0.8-depth observations and then average this result with the 0.6-depth observation. However, when more weight to the 0.2- and 0.8-depth observations is desired, the arithmetic mean of the three observations may be used.

The three-point method is used when the velocities in the vertical are abnormally distributed [for example, the 0.2 (top) velocity is more than twice the 0.8 (bottom) velocity, or the 0.8 (bottom) velocity is greater than the 0.2 (top) velocity]. It is also used when the 0.8-depth observation is made where the velocity is seriously affected by friction or by turbulence produced by the streambed or an obstruction in the stream. If using a Price AA, the depths must be greater than 2.5 ft to use this method. If using a Price pygmy or ADV, the depths must be greater than 1.5 ft to use this method.

Surface and Subsurface Methods

Surface and subsurface methods consist of observing the velocity at the water surface or some distance below the water surface. Surface measurements may be made with the optical current meter, or by observing and timing surface floats. Subsurface measurements are made with a current meter at a distance of at least 2 ft below the surface to avoid the effect of surface disturbances. Surface and subsurface measurements are used primarily for deep swift streams where it is impossible or dangerous to obtain depth and velocity soundings at the regular 0.2, 0.6, and 0.8 depths.

Coefficients are necessary to convert the surface or subsurface velocities to the mean velocity in the vertical. Vertical-velocity curves obtained at the particular site are the best method to compute these coefficients. However, the coefficients are generally difficult to determine reliably because they may vary with stage, depth, and position in the measuring cross section. Experience has shown that the coefficients generally range from about 0.84 to about 0.90, depending on the shape of the vertical-velocity curve. The higher values are usually associated with smooth streambeds and normally shaped vertical-velocity curves, whereas the lower values are associated with irregular streambeds and irregular vertical-velocity curves.

Direction of Flow Measurements

Consider the direction of flow because the component of velocity normal to the measurement section is that which must be determined by both mechanical and acoustic Doppler point-velocity current meters. Generally, for the mechanical meter, the relation for velocity components not normal to the measuring section can be visualized in figure 14, and should be corrected using the cosine of alpha.

Flow direction is also critical with respect to an ADV, since the ADV assumes a horizontal and perpendicular plane to the flow. The hydrographer must pay close attention to the flow angle reported by the FlowTracker. Always hold the wading rod (with FlowTracker attached) perpendicular to the tag line so that the pulse generated by the transmitter is parallel to the tag line. Ideally, the tag line should be set up in the cross section to be measured so that flow is perpendicular to the tag line. Flow angle, as calculated by the FlowTracker, is defined as the direction of flow relative to the x-direction of flow, so that:

$$FlowAngle = \arctan(Vy / Vx), \quad (10)$$

where Vy is the velocity in the y direction (parallel to the tag line), and

Vx is the velocity in the x direction (perpendicular to the tag line) used to calculate discharge.

The flow angle calculated by the FlowTracker can result from two sources: (1) the flow is not perpendicular to the tag line, and (2) the flow is perpendicular to the tag line but the wading rod is not held correctly relative to the tag line, as described above. Regarding source (1), some small angles and variation in the flow angle at a site is not unusual. However, if large fluctuations of flow angles are reported, make measurements at another section with more uniform flow. Regarding source (2), holding the FlowTracker so that it is skewed at any angle relative to the tag line will result in a measurement of velocity that is biased low. Small angles do not result in significant biases, but because of these biases, users should be careful to minimize this error. If the FlowTracker is held so that it is skewed at an angle of approximately 8 degrees from the tag line, the measured velocity may be in error by as much as 1 percent (assuming that flow is perpendicular to the tag line). Large variations in flow angles may be indicative of poor or inconsistent alignment of the wading rod or poor site selection for the measurement.

In a wading measurement, if the meter used is a horizontal-axis meter with a component propeller, such as the Ott meter, the propeller should be pointed upstream at right angles to the cross section, but only if alpha is less than 45 degrees. Such a meter will register the desired component of velocity normal to the cross section when alpha is less than 45 degrees. The same procedure should be used if an electromagnetic component meter is used. These meters also measure the component of velocity normal to the measuring section. Generally, for either type of meter, if alpha is greater than 45 degrees, the component meter should be pointed directly into the current,

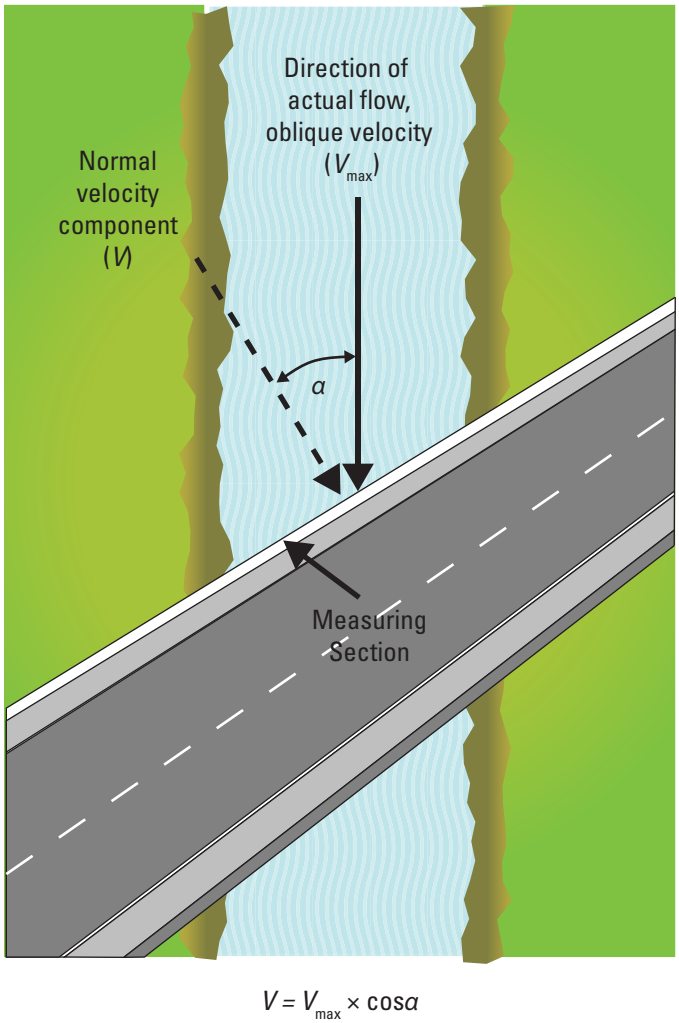

Figure 14. Velocity components when flow is not normal to measuring section.

and the horizontal angle correction should be applied as described in the following paragraphs.

Other meters on a wading-rod suspension, such as the vertical-axis Price current meter, should be pointed into the current. Any meter on a cable suspension will automatically point into the current because of the effect of the meter vanes. When the meter is pointed into an oblique current, the measured velocity must be multiplied by the cosine of the angle (alpha) between the current and a perpendicular to the measurement section in order to obtain the desired normal component of the velocity.

Either of two methods may be used to obtain the cosine of the angle alpha. In the first method, use the field note sheet that has a point of origin (o) printed on the left margin and cosine values on the right margin (see figure 2A). Measure the cosine of the angle of the current by holding the note sheet in a horizontal position with the point of origin on the tag line, bridge rail, cable rail, or any other feature parallel to the cross section, as shown in figure 15. With the long side of the note sheet parallel to the direction of flow, the tag line or bridge rail

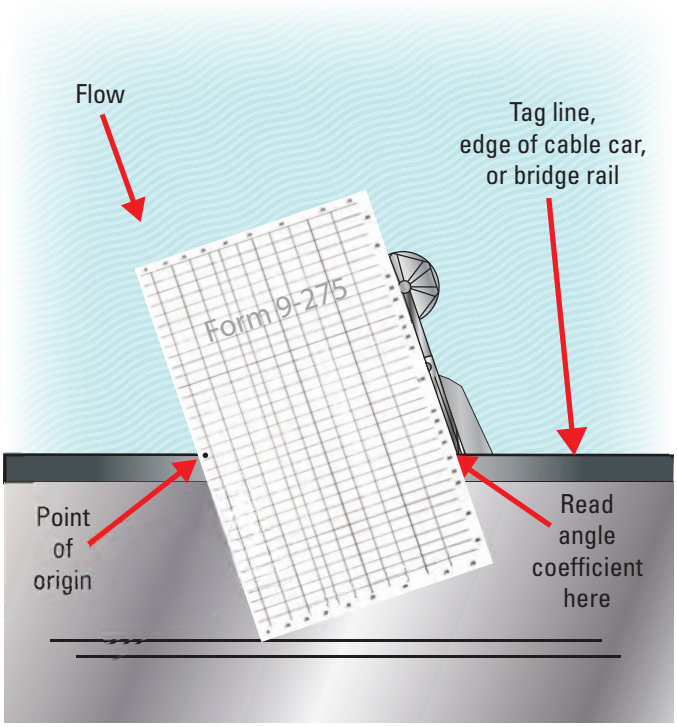

Figure 15. Measurement of horizontal angle with measurement note sheet.

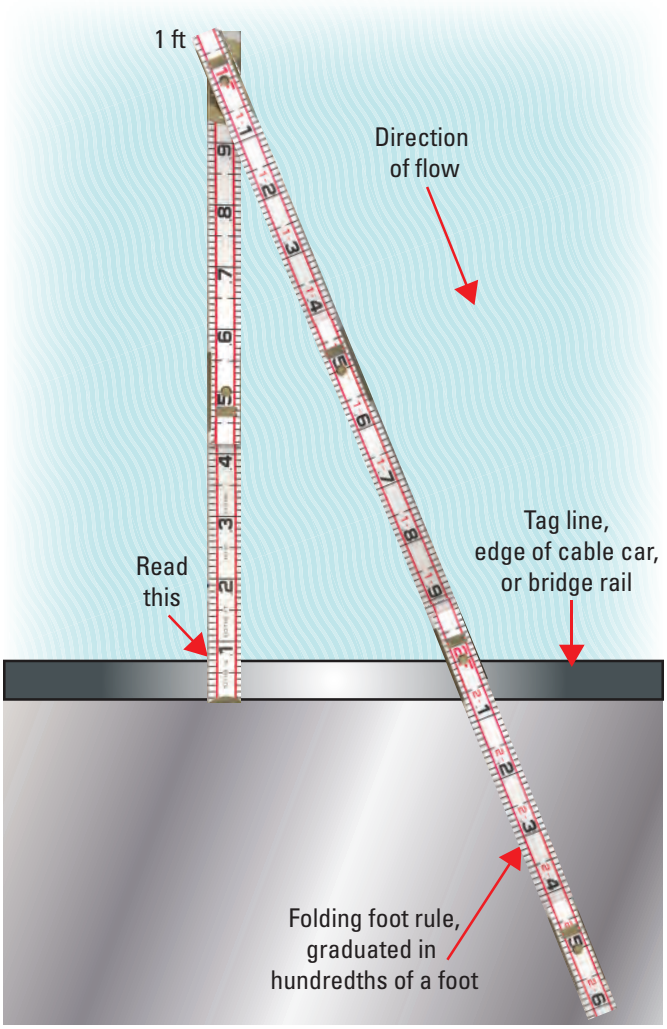

Figure 16. Measurement of horizontal angle with a folding rule.

will intersect the value of cosine alpha on the top, bottom, or right edge of the note sheet. The direction of the current will be apparent from the direction of movement of floating particles. If the water is clear of floating material, the edge of the note sheet is aligned parallel to the direction of movement. If no such material is available, the rather inelegant, but time-honored method of spitting into the stream can be used to discern the direction of flow. The position of the current meter may also be used if it can be seen below the water surface. Multiply the measured velocity by the cosine of the angle to determine the velocity component normal to the measurement section.

The second method of obtaining the cosine of the angle alpha involves the use of a folding rule that folds at 0.5-ft or 1-ft intervals. The rule must be graduated in hundredths of a foot and jointed every 0.5 ft or 1 ft. Extend the first 2 ft of the rule and place the 2.00-ft marker on the tag line or bridge rail, as shown in figure 16, with the rule aligned with the direction of flow. Fold the rule at the 1-ft mark so that the first foot of the rule is normal to the tag line or bridge rail. Make a reading where the 1-ft section intersects the tag line or bridge rail. That reading, subtracted from 1.00, is the cosine of the angle alpha. For example, if the reading on the rule is 0.07 ft (fig. 16), the cosine of alpha equals 0.93.

The direction of flow, as observed on the surface of the stream, may not always be a reliable indication of the direction of flow at some distance below the surface. For instance, when measuring a stream influenced by tidal fluctuations, it is possible to have flow moving downstream near the surface of the stream, and flow moving upstream near the bottom of the stream. Therefore, whenever it is suspected that the direction of flow is variable at different depths, other means than those already mentioned must be used to determine the direction of flow. One such method is to use a rigid rod or pole, with a vane attached to the bottom, and an indicator parallel to the vane attached to the top. Another method is to use a sounding weight with a compass and remote readout, as described in the equipment section of this chapter. If the variation of the direction of flow in the vertical is not great, then an average value of the cosine of the angle may be used for computing the component mean velocity for the vertical. However, if the variation is considerable, then you may need to subdivide the vertical and make separate computations for each subdivision. This may require additional measurements of velocity in the vertical.

If available, an ADCP from a moving boat can be used to quickly discern multidirectional flow in the vertical and across the selected cross-section. In a tidal affected reach, an ADCP is the preferred method of measuring discharge because of its use in the measurement of three dimensional velocity through most of the water column.

Current-Meter Measurements by Wading

Current-meter measurements by wading are preferred, if conditions permit. Wading measurements offer the advantage over measurements from bridges and cableways because the hydrographer can usually chose the best of several available cross sections for the measurement. Figure 17 shows a wading measurement being made with a top-setting rod.

Use the type AA, pygmy, or ADV meter for wading measurements. Table 6 lists the type of meter and velocity method to use for wading measurements at various depths.

If a type AA meter is being used in a cross section where most of the depths are greater than 1.5 ft, do not change to the pygmy meter for a few depths less than 1.5 ft or vice versa. The Price AA meter is not recommended for depths of 1.0 ft or less because the registration of the meter is affected by its proximity to the water surface and to the streambed. However, it can be used at depths as shallow as 0.5 ft to avoid changing meters if only a few verticals of this depth are required. The type AA meter or the pygmy meter should not be used in velocities less than 0.2 ft/s unless it is absolutely necessary.

Figure 17. Wading measurement using a top-setting rod.

Table 6. Current meter and velocity-measurement method for various depths.

Depth, in feet	Current meter	Velocity method
2.5 and greater	Price Type AA	0.2 and 0.8
1.5 - 2.5	Price Type AA	0.6
0.3 - 1.5	Price Pygmy	0.6
1.5 and greater	Price Pygmy	0.2 and 0.8
0.3 - 1.5	ADV	0.6
1.5 and greater	ADV	0.2 and 0.8

It is no longer recommended to use coefficients given by Pierce (1941) for the performance of current meters in water of shallow depth and low velocities.

When natural conditions for measuring are in the range considered undependable, modify the measuring cross section, if practical, to provide acceptable conditions. Often it is possible in small streams to build dikes to cut off dead water and shallow flows in a cross section, or to improve the cross section by removing the rocks and debris within the section and from the reach of stream immediately upstream from it. After modifying a cross section, allow the flow to stabilize before starting the discharge measurement.

Stand in a position that least affects the velocity of the water passing the current meter by facing the bank, with the water flowing against the side of the leg. Holding the wading rod at the tag line, stand from 1 to 3 in. downstream from the tag line and 18 in. or more from the wading rod. Avoid standing in the water if feet and legs would occupy a considerable percentage of the cross section of a narrow stream. In small streams where the width permits, stand on a plank or other support above the water rather than in the water. Velocity bias caused by effects of the hydrographer's position can be significant. Observance of these conditions is important while using mechanical meters, ADVs, and any wading measurement where an obstacle could interfere with the natural flow conditions of the stream.

When using a Price meter, keep the wading rod in a vertical position and the meter parallel to the direction of flow while observing the velocity. If the flow is not at right angles to the tag line, measure the angle coefficient carefully. When using an ADV or other instrument that can measure the x component velocity, the instrument should be aligned more precisely with the tag line. See the discussion of FlowTracker use and flow angles in the "Measurement of Velocity" section of this chapter.

During measurements of streams with shifting beds, the scoured depressions left by the hydrographer's feet can affect soundings or velocities. Generally, place the meter ahead of and upstream from the hydrographer's body and feet. Record an accurate description of streambed and water-surface configuration each time a discharge measurement is made in a sand-channel stream.

For discharge measurements of flow too small to measure with a current meter, use a volumetric method, Parshall flume, or weir plate. Those methods are described in subsequent sections of this chapter.

Current-Meter Measurements From Cableways

The Price type-AA current meter is generally used in conjunction with sounding weights and a sounding reel when measuring discharge from a cableway, although in recent years, using an ADCP mounted to a tethered craft has become much more widespread. Stationing (for width measurements) is usually determined from marks painted on the cableway. The velocity is measured by setting the meter at the proper position in the vertical, as indicated in table 7. Table 7 is designed so that no velocity observations will be made with the meter closer than 0.5 ft to the water surface. In the zone from the water surface to a depth of 0.5 ft, the current meter is known to give erratic results.

One problem found while measuring velocities from a cableway is that the movement of the cable car from one station to the next causes the car to oscillate for a short time after coming to a stop. Wait until this oscillation has decreased to a negligible amount before counting the revolutions.

By using a method of tagging the sounding cable at convenient intervals with streamers of different-colored binding tapes, each colored streamer being a known distance above the current-meter rotor (known as using tags), the meter can be kept under water at all times to prevent it from freezing in cold air. Tags are also used in measurements of deep, swift streams. See the section of this chapter on "Measurement of depth."

If large amounts of debris are flowing in the stream, raise the meter up to the cable car several times during the measurement to be certain the pivot and rotor of the meter are free of debris. However, keep the meter in the water during the measurement if the air temperature is considerably below freezing.

During floods, there is always a danger of catching a submerged or floating object, such as a tree or log, which can endanger the sounding equipment, meter, and most importantly, the hydrographer. Always be sure that the sounding cable has been installed on the sounding reel, according to the breaking loads specified in table 8. This assures that the sounding cable will break when it reaches its end, thereby preventing a potentially serious accident where the cable car and hydrographer could be spilled into the stream. Also, for added safety, always carry a pair of lineman's side-cutter pliers while making measurements from a cableway. If the sounding cable becomes hopelessly hung and does not break, as it should, cut the sounding line to ensure safety. Sometimes the cable car can be pulled to the edge of the water and the debris can be released.

When measurements are made from cableways where the stream is deep and swift, measure the angle that the meter suspension cable makes with the vertical due to the drag. The vertical angle, measured by protractor, is needed to correct the soundings to obtain the actual vertical depth, as described in the section on "Depth corrections for downstream drift of current meter and weight."

Table 7. Velocity-measurement method for various suspensions and depths.

Suspension	Minimum depth, in feet	
	0.6 method	0.2 and 0.8 method
15 C .5[1], 30 C .5	1.2	2.5
50 C .55	1.4	2.8
50 C .9	2.2	4.5
75 C 1.0, 100 C 1.0, 150 C 1.0	2.5	5.0
200 C 1.5, 300 C 1.5	3.8[2]	7.5

[1]15 pound Columbus-type weight, 0.5 above channel bed.

[2]Use 0.2 method for depths 2.5 to 3.7 feet with appropriate coefficient (for example, 0.87 or 0.88).

Table 8. Breaking loads for Ellsworth stranded cable.

Sounding cable	Diameter, in inches	Total number of strands	Rated total breaking load, in pounds	Recommended breaking load, in pounds	Number of strands to cut	Number of strands to remain
Ellsworth 0.084	0.084	36	500	250	15	21
Ellsworth 0.100	0.100	30	1,000	500	15	15
Ellsworth 0.125	0.125	30	1,500	500	20	10

Current-Meter Measurements From Bridges

When a stream cannot be waded, a bridge may be used to obtain current-meter measurements. Many measuring sections under bridges are satisfactory for current-meter measurements, but cableway sections are usually better because they provide an unobstructed reach of the channel. In addition, cableways usually have no bridges constricting the free flow of the stream in the measuring reach.

No set rule can be given for choosing between the upstream or downstream side of the bridge while making a discharge measurement. The advantages of using the upstream side of the bridge are the following:

- Hydraulic characteristics at the upstream side of bridge openings usually are more favorable. Flow is usually smoother and there is less turbulence than at the downstream side of the bridge.
- Approaching drift can be seen and be more easily avoided.
- The streambed at the upstream side of the bridge is not likely to scour as much as at the downstream side.

The advantages of using the downstream side of the bridge are:

- Vertical angles are more easily measured because the sounding line will move away from the bridge.
- The flow lines of the stream may be straightened out by passing through a bridge opening with piers.

Using the upstream side or the downstream side of a bridge for a current-meter or ADCP measurement should be decided based on circumstances for each bridge. Consider the factors mentioned above and the physical conditions at the bridge, such as location of the walkway, traffic hazards, and accumulation of trash on piles and piers.

For an ADCP measurement with a tethered craft, unless a special rigid support for deployment or bank-operated cableway has been developed for the upstream side of the bridge, the downstream side of the bridge is usually where the ADCP is most conveniently deployed. Bridge piers can cause excessive turbulence during high streamflow, especially if debris accumulates on the piers and(or) the piers are skewed to the flow. The effect of bridge-pier-induced turbulence may be reduced when deploying an ADCP from the downstream side of the bridge by lengthening the tether to increase the distance between the bridge and the tethered boat. Close attention should be paid to the cross section to ensure that no large eddies that could cause flow to be nonhomogeneous are present. Possible alternatives to measuring off the downstream side of the bridges include using a bank-operated cableway, a rigid extension that allows the hydrographer to deploy from the upstream side of the bridge, or having personnel on each bank hold a rope or cord attached to the platform to pull the tethered boat back and forth across the river.

For a mechanical current meter measurement, use either a handline, or a sounding reel supported by a bridge board or a portable crane, to suspend the current meter and sounding weight from bridges. Depth measurements should be made as described in the section entitled “Measurement of depth.” Measure the velocity by setting the meter at the position in the vertical as indicated in table 7. Keep equipment several feet from piers and abutments if velocities are high. Estimate the depth and velocity next to the pier or abutment on the basis of the observations at the nearest vertical.

If there are piers in the cross section, it is usually necessary to use more than 25 to 30 partial sections to get results as reliable as those from a similar section without piers. Piers will often cause horizontal angles that must be carefully measured. Piers also cause rapid changes in the horizontal-velocity distribution in the section.

Whether or not to exclude the area of a bridge pier from the area of the measurement cross section depends primarily on the relative locations of the measurement section and the end of the pier. If measurements are made from the upstream side of the bridge, it is the relative location of the upstream end (nose) of the pier that is relevant; for measurements made from the downstream side, it is the location of the downstream end (tail) of the pier that is relevant. If any part of the pier extends into the measurement cross section, the area of the pier is excluded. Bridges quite commonly have cantilevered walkways from which discharge measurements are made. In these cases, the measurement cross section lies beyond the end of the pier (upstream from the pier nose or downstream from the pier tail, depending on which side of the bridge is used). In that situation, it is the position and direction of the streamlines that determines whether or not the pier area is to be excluded. If the stationing of the sides of the pier when projected to the measurement cross section was not already done, the hydrographer does it at this point. If there is negligible or no downstream flow in that width interval (pier subsection), then the pier is excluded. That is, if only stagnation and (or) eddying exists upstream from the pier nose or downstream from the pier tail, whichever is relevant, the area of the pier is excluded. If there is substantial downstream flow in the pier subsection, the area of the pier is included in the area of the measurement cross section. In that circumstance, the horizontal angles of the streamlines in and near the pier subsection will usually be quite large.

Footbridges are sometimes used for measuring canals, tailraces, and small streams. Rod suspension can be used from many footbridges. The procedure for determining depth in low velocities is the same as for wading measurements. For higher velocities, obtain the depth by the difference in readings at an index point on the bridge when the base plate of the rod is at the water surface and on the streambed. Measuring the depth in this manner will eliminate errors caused by the water piling up on the upstream face of the rod. ADCP tethered boats, handlines, bridge cranes, and bridge boards are also used from footbridges.

The handline can be disconnected from the headphone wire and passed around a truss member with the sounding

weight on the bottom. This eliminates the need for raising the weight and meter to the bridge each time a move is made from one vertical to another; it is the principal advantage of a handline.

Safety is a primary consideration when measuring discharge from bridges. High-speed traffic can present a major safety hazard; in fact, it is no longer permissible to make discharge measurements from some Interstate route bridges without special permission. Observe all safety precautions, such as the use of traffic cones, traffic signs, and flag persons, that are prescribed in the USGS Water Science Center's flood plan and safety plan.

Observe the same safety precautions regarding the snagging of debris, such as floating or submerged trees or logs, as described above for cableways.

Current-Meter Measurements From Ice Cover

Discharge measurements under ice cover, as shown in figure 18, are made under the most severe conditions, but are extremely important because a large part of the discharge record during a winter period may depend on one measurement. In recent years ADCPs and ADVs have increasingly been used to make measurements from ice cover.

Select the possible locations of the cross section to be used for measurement from ice cover during the open-water season when channel conditions can be evaluated. Commonly, the most desirable measurement section will be just upstream from a riffle because slush ice that collects under the ice cover is usually thickest at the upstream end of the pools created by riffles.

The equipment used for cutting or drilling the holes in the ice is described in a previous section of this chapter.

Never underestimate the danger of working on ice-covered streams. When crossing, test the strength of the ice with solid blows using a sharp ice chisel. Ice thickness may be irregular, especially late in the season when a thick snow cover may act as an insulator. Water just above freezing can slowly melt the underside of the ice, creating thin spots. Ice that is bridged above the water may be thick but still be weak.

Cut the first three holes in the selected cross section at the quarter points to detect the presence of slush ice or poor distribution of the flow in the measuring section. If poor conditions are found, investigate other sections to find one that is free of slush ice and that has good distribution of flow. After finding a suitable cross section, make at least 20 holes in the ice for a current-meter measurement. Space the holes so that no partial section contains more than 10 percent of the total discharge. On narrow streams, it may be simpler to remove all of the ice in the cross section.

The effective depth of the water, as shown in figure 19, is the total depth of water minus the distance from the water surface to the bottom of the ice. The vertical pulsation of water

Figure 18. *A*, Ice drill being used to cut holes and *B*, ice rod being used to support current meter for a discharge measurement.

in the holes in the ice sometimes causes difficulty in determining the depths. The total depth of water is usually measured with an ice rod or with a sounding weight and reel, depending on the depth.

Measure the distance from the water surface to the bottom of the ice with an ice-measuring stick. Do not use the ice-measuring stick if there is slush under the solid ice at a hole. In order to find the depth at which the slush ice ends, suspend the current meter below the slush ice with the meter rotor turning freely. Raise the meter slowly until the rotor stops. This point is used as the depth of the interface between water and slush. After the effective depth of the water has been determined, compute the proper position of the meter in the vertical as shown in figure 19.

Use the Price winter Water Survey of Canada (WSCan) current meter yoke, with a polymer rotor, under ice cover when slush ice is present because the cups are solid and cannot become filled with slush ice; this is what happens with the cups of the regular Price meter. For situations where slush ice is not present, use the Price winter WSCan current meter yoke

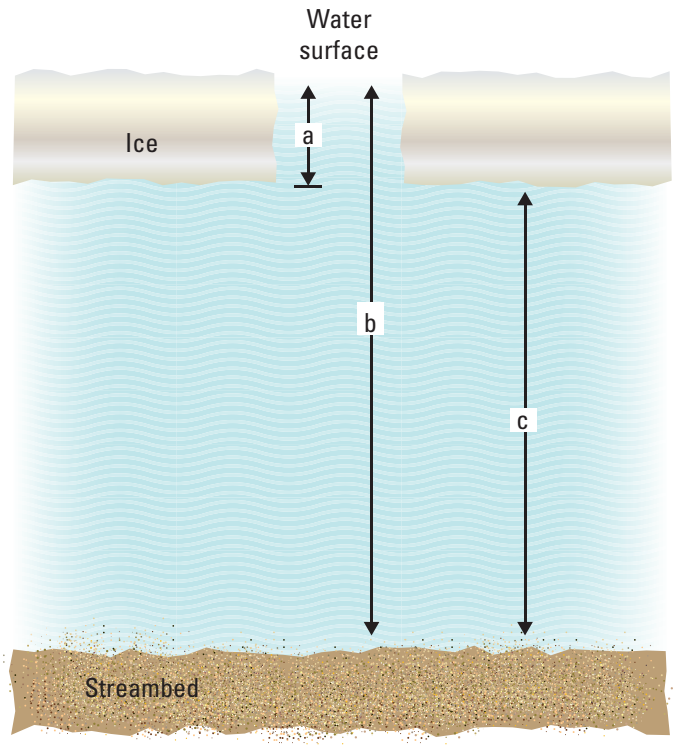

a = Water surface to bottom of ice
b = Total depth of water
c = Effective depth (c=b-a)

0.2-depth setting = a + 0.2c
0.8-depth setting = b - 0.2c
0.6-depth setting = b - 0.4c

Figure 19. Method of computing meter settings for measurements under ice cover.

with regular Price metal cups. The old-style vane ice meter is no longer recommended, primarily because of its poor performance in slow velocities.

The velocity distribution under ice cover, when the water is in contact with the underside of the ice, is similar to that in a pipe, with a lower velocity nearer the underside of the ice. This is illustrated in figure 20. Use the 0.2- and 0.8-depth method for effective depths of 2.5 ft or greater, and the 0.6-depth method for effective depths of less than 2.5 ft. Define two vertical-velocity curves while making ice measurements to determine whether any coefficients are necessary to convert the velocity (obtained by the 0.2- and 0.8-depth method or the 0.6-depth method) to the mean velocity. Normally, the average of the velocities obtained by the 0.2- and 0.8-depth method gives the mean velocity, but a coefficient of about 0.92 usually is applicable to the velocity obtained by the 0.6-depth method.

When measuring the velocity, keep the meter as far upstream as possible to avoid any effect that the vertical pulsation of water in the hole might have on the meter. Eliminate as much as possible the exposure of the meter to the cold air during the measurement. The meter must be free of ice when the velocity is being measured.

If there is partial ice cover at a cross section, use the procedure described above where there is ice cover, and use open-water methods elsewhere.

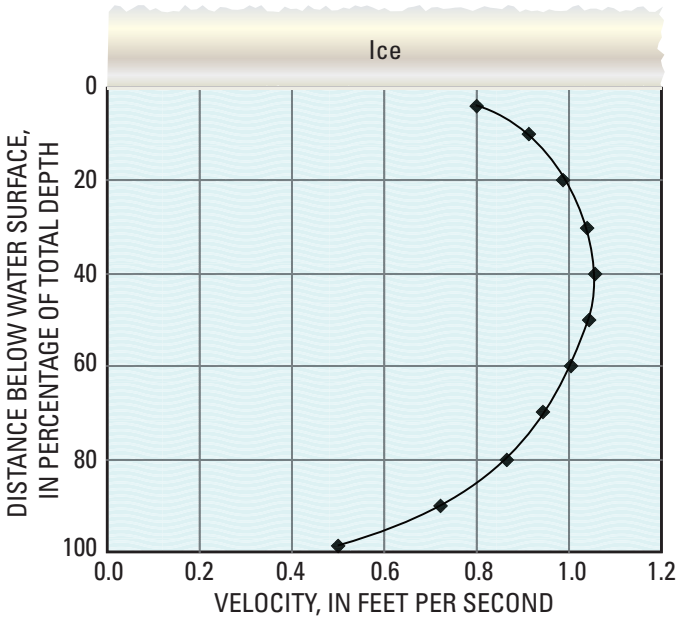

Figure 20. Typical vertical-velocity curve under ice cover.

DISCHARGE MEASUREMENT NOTES—ICE COVER

FRIO River, at / Creek, near COLD HARBOR, ME

METER = V-587

REW Dist. from initial point	Width	Total depth of water	W.S. to bot. ice	Effective depth	Depth of meter below water surface	Rev-olu-tions	Time in seconds	VELOCITY At point	VELOCITY Mean in vertical	Area	Discharge
1315											
24	3	0							0	0	0
30	6	2.6	1.6	1.0	2.2	10	47	.49	.45	6.0	2.7
36	6	3.6	1.8	1.8	2.9	15	49	.69	.63	10.8	6.8
42	5	4.3	2.0	2.3	3.4	15	44	.77	.71	11.5	8.2
46	4	4.5	1.8	2.7	2.3	20	43	1.04	.84	10.8	9.1
					4.0	15	52	.65			
50	4	4.7	1.7	3.0	2.3	20	40	1.12	.90	12.0	10.8
					4.1	15	50	.68			
54	4	4.6	1.7	2.9	2.3	25	49	1.14	.94	11.6	10.9
1325					4.0	15	46	.74			
58	4	4.9	1.6	3.3	2.3	20	40	1.12	.90	13.2	11.9
					4.2	15	50	.68			
62	4	4.8	1.6	3.2	2.2	25	48	1.17	.96	12.8	12.3
					4.2	15	46	.74			
66	3.5	5.0	1.5	3.5	2.2	25	44	1.27	1.04	12.2	12.7
					4.3	15	41	.82			
69	3	5.3	1.6	3.7	2.3	25	40	1.40	1.12	11.1	12.4
					4.6	15	40	.84			
72	3	5.1	1.5	3.6	2.2	25	41	1.36	1.12	10.8	12.1
1335					4.4	20	51	.88			
	49.5									122.8	109.9

Figure 21. Part of note sheet for discharge measurement under ice cover.

A sample sheet of discharge-measurement notes under ice cover is shown in figure 21. In this measurement, the vertical-velocity curves indicate that the 0.2- and 0.8-depth method gives the mean velocity and that the 0.6-depth method requires a coefficient of 0.92.

Current-meter measurements under ice cover are frequently made with a special winter-style sounding rod, ADV or ADCP, as described in this chapter. When depths are too deep for rod suspension, use an equipment assembly mounted on runners, such as shown in figure 22. For winter conditions, the 30-pound C-type weights should be used with a special, collapsible hanger assembly (shown in figure 22) that can be passed through an 8-in. hole in the ice. A handline can also be used for making ice measurements.

Where it is impractical to use a powered ice drill, use ice chisels to cut the holes. Ice chisels are usually 4- or 4.5-ft long and weigh about 12 pounds. Use the ice chisel when first crossing an ice-covered stream to determine whether the ice is strong enough to support the hydrographer. If a solid blow of the chisel blade does not penetrate the ice, it is safe to walk on, providing the ice is in contact with the water.

Some hydrographers supplement the ice chisel with a Swedish ice auger. The cutting blade of this auger is a spade-like tool of hardened steel that can cut a hole 6 to 8 in. in diameter by turning a brace-like arrangement on top of the shaft.

After the hole is made in the ice, water will be forced up, owing to the water being under pressure from the weight of the ice. In order to determine the effective depth of the stream, use ice-measuring sticks to measure the distance from the water surface to the bottom of the ice. Measuring this distance is done using a bar about 4 ft long, made of strap steel or wood, graduated in feet and tenths of a foot and having an L-shaped projection at the lower end. Hold the horizontal part of the L on the underside of the ice and read the depth to that point at the water surface on the graduated part of the stick. The horizontal part of the L is at least 4 in. long so that it may extend beyond any irregularities on the underside of the ice.

Figure 22. Collapsible hanger assembly for used with 30- and 50-pound C-type weights, for measurements under ice (*A*, in measurement position and *B*, collapsed).

Current-Meter Measurements From Stationary Boats

Discharge measurements are made from boats where no cableways or suitable bridges are available and where the stream is too deep to wade, although ADCP discharge measurements from a moving boat, now a USGS standard operating procedure, have largely replaced this method. Personal safety is the limiting factor in the use of boats on streams having high velocity of flow.

For boat measurements whether using a mechanical meter or an ADCP, select a cross section that has attributes similar to those described in the previous section "Site selection," except for those listed in items concerning depth and velocity. There is no need to consider depth in a boat measurement because if the stream is too shallow to float a boat, the stream can usually be waded. Velocity, however, is an important concern. If velocities are too slow, mechanical current meter registration may be affected by an oscillatory movement of the boat, in which the boat (even though fastened to a tag line) moves upstream and downstream as a result of wind action. Vertical movement of the boat as a result of wave action may also affect a vertical-axis current meter. If velocities are too fast, it becomes difficult to string a tag line across the stream.

If it is feasible to use a tag line in making a boat measurement, string it at the measuring section by unreeling the line as the boat moves across the stream. After a tag line without a brake has been stretched across the stream, take up the slack by means of a block and tackle attached to the reel and to an anchored support on the bank. If there is traffic on the river, one person must be stationed on the bank to lower and raise the tag line to allow the river traffic to pass. Place streamers on the tag line so that it is visible to boat pilots. If there is a continual flow of traffic on the river, or if the width of the river is too great to stretch a tag line, other means will be needed to position the boat. Night measurements by boat are not recommended because of the safety concerns.

When no tag line is used, the boat can be kept in the cross section by lining it up with flags positioned on each end of the cross section, as illustrated in figure 23. Flags on one bank would suffice but it is better to have them on both banks. Determine the position of the boat in the cross section by using a transit or total station on the shore and a stadia rod held in the boat. Another method of determining the position of the boat is by setting a transit or total station on one bank a convenient, known distance from and at right angles to the cross-section line. The position of the boat is determined by measuring the angle α to the boat, measuring the distance CE, and computing the distance MC as shown in figure 24. A third method of determining the position of the boat is done with a sextant read from the boat. Position a flag on the cross-section line and another at a known distance perpendicular to the line. The boat position can be computed by measuring the angle β with the sextant, as shown in figure 24. Boat position can also be determined by using a global positioning system with differential corrections (DGPS). This method is especially useful on wide streams and in flood plains where other methods of determining boat position are not applicable. Unless anchoring is more convenient, the motor must hold the boat stationary while readings are being taken.

Do not take boat measurements at velocities less than 1 ft/s when the boat is subject to wave action. The up-and-down movement of the boat (and the meter) seriously affects the velocity observations. If the maximum depth in the cross section is less than 10 ft and the velocity is low, the hydrographer can use a rod for measuring the depth and for supporting the current meter. For greater depths and velocities, use a cable suspension with a reel and sounding weight. The procedure for measuring from a stationary boat using the boat boom and crosspiece is the same as that for measuring from a bridge or a cableway, as described in previous sections of this chapter.

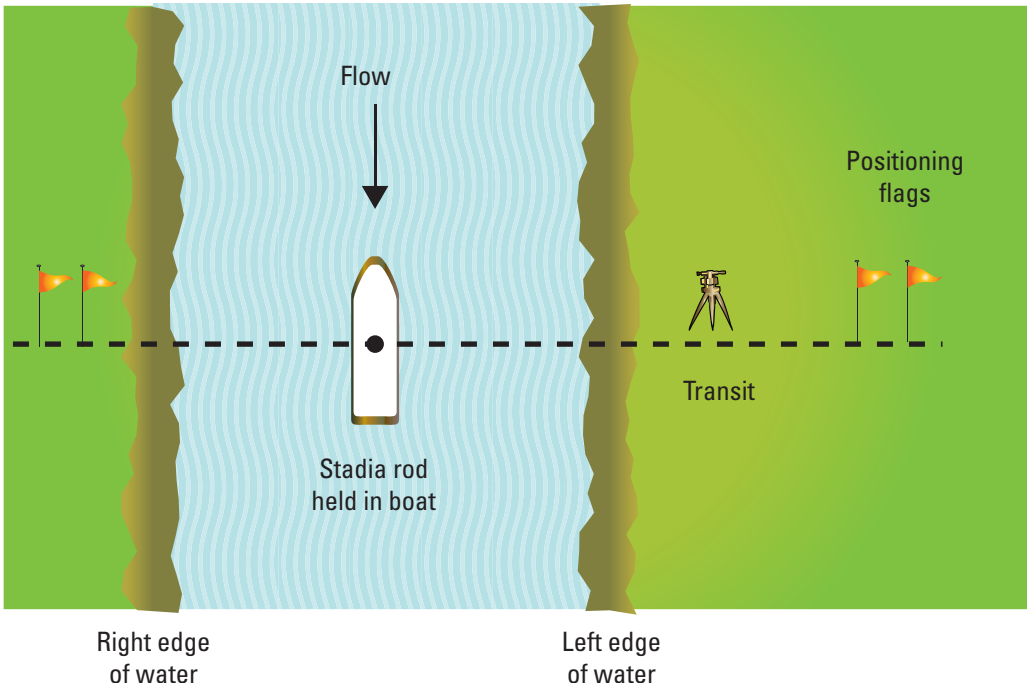

Figure 23. Determining the position in a cross section using the stadia method.

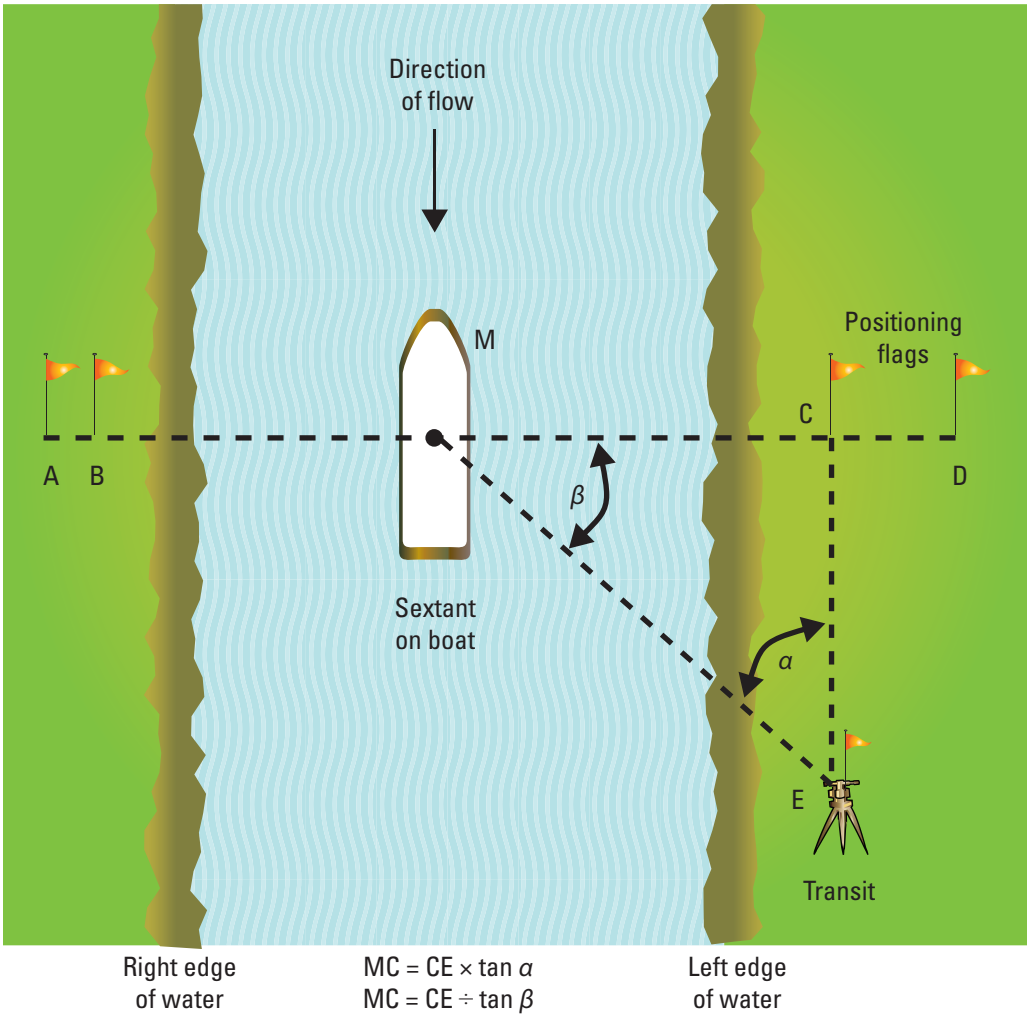

Figure 24. Determining the position in a cross section using the angular method.

Moving-Boat Measurements of Discharge

On large streams and estuaries, the midsection methods of measuring discharge are frequently impractical and involve costly and tedious procedures. There may be no facilities at remote sites. Where facilities do exist, they may be inundated or inaccessible during floods. At some sites, unsteady flow conditions require that measurements be made as rapidly as possible. Measurements on tide-affected rivers must not only be made frequently, but continually, throughout a tidal cycle. The moving-boat technique is a method of quickly measuring a large stream. It requires no fixed facilities, and it lends itself to the use of alternate sites if conditions make this applicable. Brief descriptions of three moving-boat methods are given in the following sections. It must be stated here that these methods have been almost entirely replaced by the use of ADCP discharge measurements. Details of ADCP setup and use can be found in Mueller and Wagner (2009) and subsequent section of this chapter discussing the moving boat method using an ADCP.

Manual Method, Using a Mechanical Current Meter

Smoot and Novak (1968) describe the manual moving-boat technique in detail. It is similar to the mechanical current-meter measurement in that the velocity-area approach is used to determine the discharge. The total discharge is the summation of the products of the partial areas of the stream cross section and their respective average velocities. During the traverse of a stream by boat, a sonic sounder records the geometry of the cross section, and a continuously operating current meter senses the combined stream and boat velocities.

The current meter used for a moving-boat measurement is a component propeller type, such as the Ott current meter, with a custom body made for mounting on the leading edge of a vane. The current meter and vane assembly are attached to a vertical rod and bearing assembly that allows them to rotate freely. An angle indicator is located at the top of the rod, which indicates the crab angle.

It usually takes three people to make a moving-boat measurement: one to operate the boat, one to make crab-angle observations, and one to take notes. The note keeper is responsible for recording the crab-angle observations and the current-meter pulses. Depths are recorded automatically on the sonic-sounder chart. Special computations and conversions, which are somewhat tedious, are required to determine stationing and normal mean velocities for each vertical. Discharge can then be computed similar to a standard velocity-area discharge measurement. Experience has shown that measurements obtained by the moving-boat technique compare within 5 percent of measurements obtained by conventional means.

Automatic Computerized Method, Using a Mechanical Current Meter

The automatic computerized moving-boat method is the same basic procedure as the manual moving-boat method described above, except that all readings of depth, velocity, crab angles, and boat position are automatically fed into an onboard computer. A substantial difference is that the automated moving-boat method requires only two crew members—a boat operator and an instrument operator. The manual method requires three crew members.

The automated method requires an electronic compass that provides automatic input of the crab angle. The current meter and depth sounder likewise provide automatic input of pulse rates and depth, respectively. The computer is programmed to make the conversions and computations that would normally be made manually, thereby speeding up the computation process and virtually eliminating arithmetic errors. A computed measurement is available immediately after completion of the data collection.

Moving-Boat Method, Using an ADCP

ADCPs can be used to measure unsteady, bidirectional, and other flows with nonlogarithmic velocity distributions—problems hydrologists have faced for decades. ADCPs are called profilers because they provide measurements of velocity throughout the water column. The ADCP divides the water column into depth cells (also referred to by some software and references as “bins”) and reports a velocity for each depth cell; however, an ADCP cannot measure velocities near the water surface or near the bed. The length of the unmeasured zone at the water surface is a function of the draft of the instrument deployment, the effect of the transducer mechanics, and the flow disturbance around the instrument. The length of the unmeasured zone near the streambed is due to side-lobe interference, which is a function of the mechanics of transducers and the slant angle of the beams. The ADCP must be deployed below the water surface; therefore, it cannot measure the water velocity above the transducers.

Although ADCPs have no moving parts and typically require no calibration, the instruments and associated software and firmware are complex. Using quality-assurance procedures defined by Oberg and others (2005) and Mueller and Wagner (2009) will help identify potential instrument problems.

ADCPs can be mounted on either side of manned boats, off the bow, or in a well through the hull. A tethered boat can be defined as a small boat (usually less than 6.5 ft long) attached to a rope, or tether, that can be deployed from a bridge, a fixed cableway, a moving boat, or a temporary or permanent bank-operated cableway. The tethered boat should be equipped with an ADCP mount that meets all of the specifications for manned boats. Unmanned, remote-control ADCP boats are also used and allow the deployment of ADCPs where deployment with a manned boat or tethered boat may not be feasible or ideal. Similar to (but smaller than) a manned boat,

a remote-control boat has self-contained motors and a remote-control system for maneuvering the boat across the river.

The procedures for predeployment preparation, field data collection, and processing of collected data are discussed in detail by Mueller and Wagner (2009). A detailed description of how an ADCP measures velocity and computes discharge and additional details on selected topics are presented in the appendices (Mueller and Wagner, 2009).

Networks of Current Meters

In the past, occasional special measurements made by USGS hydrographers have required simultaneous velocities at several points in a cross section, distributed either laterally or vertically. For example, it may be necessary to measure a vertical-velocity profile quickly in unsteady flows and to check it frequently in order to determine the changes in shape of the vertical profile, as well as the rates of these changes. In another example, for the measurement of tide-affected streams, it is desirable to measure the total discharge continuously during at least a full tidal cycle (approximately 13 hours). The need for so many simultaneous velocity determinations (one at each vertical in the cross section) for so long a period could be an expensive and laborious process using conventional techniques of discharge measurement.

A grouping of 21 current meters and special instrumentation has been devised in the past by the USGS to facilitate measurements of the types just described. The 21 meters are connected together so that the spacing between any two adjacent meters can vary up to 200 ft. In using this method, each meter should be uniformly calibrated and have sufficient handline cable to be suspended vertically from a bridge as much as 200 ft. Revolutions of the rotors are recorded by electronic counters that are grouped compactly in one box at the center of the bank of meters. The operator, by flipping one switch, starts all 21 counters simultaneously, and after an interval of several minutes, stops all counters. The indicated number of revolutions for the elapsed time interval is converted to a velocity for each meter. The distance between meters is known, and a record of stage is maintained to evaluate depth. Prior information at the site is obtained to convert point velocities in the verticals to mean velocities in those verticals. All of the information necessary to compute discharge in the cross section is available, and is tabulated for easy conversion to discharge. If possible a concurrent ADCP discharge measurement should be completed in close proximity and time to this measurement to corroborate the results.

Discharge Measurement of Deep, Swift Streams With a Mechanical Current Meter

Discharge measurements of deep, swift streams with a mechanical current meter usually present no serious problems when adequate sounding weights are used and when floating drift or ice is not excessive. Normal procedures must sometimes be altered, however, when measuring these streams. The four most common circumstances are the following:

1. It is possible to sound, but the weight and meter drift downstream.
2. It is not possible to sound, but a standard cross section is available.
3. It is not possible to sound, and a standard cross section is not available.
4. It is not possible to put the weight and meter in the water.

Procedures are described below for use during measurements made under each of these conditions. Use procedures for items 2, 3, and 4 where there is a stable cross section. The procedure for unstable channels must be determined by conditions at each location.

Possible To Sound, but Weight and Meter Drift Downstream

For some streams, it may be possible to sound the streambed, but because of the force of high velocities, the weight and meter are carried downstream. This may be a condition for only a few verticals near the center of the stream, or it may affect many of the verticals. Make corrections to the observed depths and meter settings to account for the downstream drift. These corrections are commonly referred to as “vertical angle corrections.” The procedure for computing vertical angle corrections is described in a previous section of this chapter entitled “Depth corrections for downstream drift of current meter and weight.” The corrections can be computed manually, or they may be computed automatically through the use of an electronic notebook or a PDA.

Not Possible To Sound, but Standard Cross Section Available

When it is not possible to sound the streambed, use a standard cross section from previous measurements at the bridge or cableway for determining depth. Such a cross section is useful only if all discharge measurements use the same permanent initial point for the stationing of verticals across the width of the stream. There should also be an outside reference gage or reference point on the bank or bridge to which the water-surface elevation at the measurement cross section

may be referred. If these conditions are met, use the following procedure to make a discharge measurement:

1. Determine the depths from the standard cross section, based on the water-surface elevation.
2. Measure the velocity at 0.2 of the depth at each vertical.
3. Compute the measurement in the normal manner using the measured 0.2-depth velocities as though they were the mean velocities in the vertical. Apply horizontal-angle corrections, if necessary. Use depths as determined in step 1 above.
4. Determine the coefficient to adjust the 0.2-depth velocity to the mean velocity on the basis of previous measurements at the site by the two-point method. See a previous section of this chapter entitled "Two-tenths-depth method."
5. Apply the coefficient from step 4 to the computed discharge from step 3.

Not Possible To Sound, and Standard Cross Section Not Available

When it is not possible to sound the streambed and a standard cross section is not available, use the following procedure:

1. Reference the water-surface elevation before and after the measurement to an elevation reference point on a bridge, on a driven stake, or on a tree at the water's edge. It is assumed here that no outside reference gage is available at the measurement cross section.
2. Estimate the depth and observe the velocity at 0.2 of the estimated depth. The meter should be at least 2.0 ft below the water surface. In the notes, record the actual depth the meter was placed below the water surface. If an estimate of the depth is impossible, place the meter 2.0 ft below the water surface and observe the velocity at that point.
3. Make a complete measurement, including some vertical-velocity curves, at a lower stage when you can sound the streambed.
4. Use the complete measurement and difference in stage between the two measurements to determine the cross section of the first measurement. To determine whether the streambed has shifted, compare the cross section with one taken for a previous measurement at that site.
5. Use vertical-velocity curves, or the relation between mean velocity and 0.2-depth velocity, to adjust the velocities observed in step 2 to mean velocity. Apply horizontal-angle corrections as necessary.
6. Compute the measurement in the normal manner using the depths from step 4 and the velocities from step 5.

Not Possible To Put the Weight and Meter in Water

If it is impossible to put the sounding weight and mechanical current meter in the water because of high velocities and (or) floating drift, use the following procedure:

1. Obtain depths at the measurement verticals from a standard cross section, if one is available. If a standard cross section is not available, determine depths by the method explained above in the section "Not possible to sound, and standard cross section not available."
2. Measure velocities and compute discharge using an ADCP.
3. Measure surface velocities by timing floating drift, or by using an optical or other approved noncontact flowmeter.
4. Compute the measurement in the normal manner, using the surface velocities as though they were the mean velocities in the vertical, and using the depths from step 1.
5. Apply the appropriate velocity coefficient to the discharge computed in step 3. Use a coefficient of 0.86 for a natural channel and 0.90 for an artificial channel.

The optical current-meter and ADCP measurement procedures are described in previous sections of this chapter and by Mueller and Wagner (2009). The optical current meter is portable, battery operated, and requires no great skill for quick and accurate readings of the surface rate of flow. The meter is not immersed, so it does not disturb the flow, and it is in no danger of damage from floating debris or ice. In many cases, the ADCP has become the most efficient alternative to the mechanical current meter where velocities are too great; however, the ADCP also has limitations. See the previous sections of this chapter for information on velocity, depth, turbidity, and other site-condition limitations of the ADCP.

Keep in mind that just after the crest, the amount of floating drift or ice is usually greatly reduced, and it may be possible to obtain velocity observations with a current meter. These observations can help define the velocity coefficient mentioned in step 5 above.

Recording Field Notes

Field notes for a discharge measurement may be recorded on standard paper note sheets (for example, USGS Forms 9-275-F, 9-275-I, and other special field forms). With the ADCP discharge measurement, the software attached to each instrument contains digital forms for the recording of some of the field data. The USGS has developed a paper form for recording field data observed during an ADCP discharge measurement (fig. 2*D*). With a current-meter discharge measurement, field forms can be recorded using an electronic notebook, such as the Aquacalc or a Personal Digital Assistant (PDA). With an ADV measurement, there are special field forms to accommodate its specifications and details. These methods are described in more detail in subsequent paragraphs in this section. The SWAMI program with a PDA (commonly used by the USGS) can be used to record discharge measurements, inspections, differential level surveys, and other field measurements. SWAMI has an interface with the National Water Information System (NWIS), so measurements are easily uploaded to NWIS (fig. 2*C*).

Standard Paper Note Keeping for a Mechanical Current-Meter Discharge Measurement

Paper note sheets, as shown in figure 2*A*, are the traditional way to record the field observations for a mechanical current meter, ADV, or ADCP discharge measurement. Generally, for each discharge measurement, the hydrographer should record the following information, at a minimum, on the front sheet of the measurement notes (the information may vary, depending on the meter and method being used):

- Measurement number, who computed, and who checked the measurement;
- Downstream station identification number and station name (station name includes stream name and location, to correctly identify an established gaging station). For a miscellaneous measurement, record the stream name and exact location of site;
- Date of measurement and members of measurement party (initials and last name);
- Measured channel width, area, average velocity (computed as a ratio of the measured discharge/measured area), average gage height, and discharge;
- Vertical velocity method(s) of measurement, number of sections, and change in gage height during the discharge measurement;
- Measurement method coefficient, horizontal-angle coefficient, type of meter suspension (for example, rod, 100#C, and so forth) and whether tags were checked;
- Type of meter (for example, AA or pygmy), the current meter's serial number; and the elevation of the meter above the channel bottom;
- Meter rating used (for example, Standard Rating No. 2) and the most recent spin test results;
- Measurement percentage (after computed) from the existing stage-discharge rating, and the indicated shift in feet from that rating;
- GAGE READINGS: Do not erase inside this block on the front sheet. If an error is made, cross through the error and write the correct reading.
  - Start time measurement using 24-hour clock time, and record the time zone (that is, EST, CST, EDT, and so forth).
  - Record inside and outside gage, and also readings from recording devices (for example, data logger, graphic, and so forth).
  - Compute weighted mean gage height either by averaging readings, or if sufficient change in gage height occurred, by using methods for weighting gage height discussed in this chapter.
  - Compute gage-height correction caused by difference in true gage height (reference gage) and recorder or other gage that is reading incorrectly.
  - Record the correct mean gage height.
- Samples collected: Indicate type of water-quality measurements and samples [that is, water-quality, sediment, and (or) biological], and indicate if the measurements are documented on separate sheets (that is, water quality, aux./base gage, other);
- Indicate whether the rain gage (if applicable) was serviced/calibrated;
- Briefly describe the weather (for example, sunny, cloudy, rainy, cold, or other);
- Record the air temperature in degrees Celsius and the time of the reading;
- Record the water temperature in degrees Celsius and the time of the reading;
- Record the check bar reading (if a wire weight is present), time of the reading, and any adjustments in elevation made to the check bar.
- Indicate the type of measurement (wading, cable, ice boat, and so forth) and location of measurement relative to the gage (upstream, downstream, and so forth).
- Rate the measurement based on the hydrologic/hydraulic conditions in which the measurement was made [that is, excellent (2 percent), good (5 percent), fair (8 percent), or poor (more than 8 percent)].
- Flow: Document the hydraulic condition of the flow (steady, unsteady, where the flow was within the cross section, and so forth).
- Cross section: Geomorphologically describe the cross section (that is, sand, clay, cobble, and so forth), shape, presence of vegetation, and any other roughness affecting flow.

- Document if the gage is operating and whether the record was removed during this visit;
- Note the battery voltage and the cleaning of the orifice or intakes;
- If appropriate, indicate pressure readings of the nonsubmersible pressure transducer (that is tank, line, bubble-rate (bubbles/minute);
- Indicate if appropriate, readings of extreme indicators of high flow.
- Document the condition of the crest stage gage (CSG) and record the high water mark (HWM) if a reading is available on the CSG and the reference elevation.
- Record any other HWM obtained at the gage, if appropriate.
- Control conditions: Describe what and where the control of flow is for the gage pool (that is, gravel riffle about 80 ft downstream of the gage, and so forth).
- REMARKS: Use this space to document any unusual conditions in the gage reach that might affect the measurement, record, or other pertinent information regarding the accuracy of the discharge measurement and conditions that might affect the stage-discharge relation and document any observer reading or results of discussions with an observer.
- Measure the gage height of zero flow as many times a year as possible; record to the nearest 0.1 ft. Do this by recording the gage height at the gage at the time the gage height at zero flow is measured. Subtract the gage height from the depth of flow at the point the gage height at zero flow is measured and rate this measurement as good, fair, or poor.
- Fill in all items on the front sheet or mark with a dash after the measurement is completed and computed.

Mechanical Current-Meter Inside Notes

In the inside notes of a mechanical current-meter discharge measurement, identify the measurement starting point by either left edge of water or right edge of water (LEW or REW, respectively), when facing downstream, and record the time you started the measurement. If a significant change in stage is expected during the measurement, periodically record the time for intermediate verticals during the course of the measurement. If possible, synchronize this time with the recording interval of the digital recorder or data logger. Intermediate times are important because if there is any appreciable change in stage during the measurement, these recorded times are used to determine intermediate gage heights, which are then used to compute a weighted mean gage height for the measurement, as described in a subsequent section of this chapter. When the measurement is completed, record the time and the bank of the stream (LEW or REW) where the section ends.

Begin the measurement by recording the distance from the initial point to the edge of the water. Measure and record the depth, and velocity (if any), at the edge of water. Compute the width using the midsection method described in a previous section of this chapter. Proceed across the measurement section by measuring and recording the distance of each vertical from the initial point; the depth at the vertical; the observation depths as 0.6, 0.2, 0.8, and so forth; the revolutions and time for each velocity observation; and the horizontal angle coefficient if different than 1.00.

Complete all computations required for the inside notes to determine the total width, area, and discharge. Transfer these values to the front sheet and complete other items on the measurement front sheet. The measurement computations should be made, and the note sheets completed, before the hydrographer leaves the gaging station.

Erasures of original field data are not allowed. This includes items such as gage readings, distances, depths, meter revolutions, times, horizontal-angle coefficients, and other field measurements that cannot be repeated. If a variable is remeasured, and it is necessary to change the originally recorded value of that variable, cross it out and record the new measurement above or adjacent to the original. The original measurement should remain legible, even though it is crossed out. On the other hand, it is permissible to erase computed values, such as velocities, areas, widths, and discharges.

Standard Paper Note Keeping for an ADV Discharge Measurement

Paper note sheets, as shown in figure 2*B*, are the traditional method to record the field observations for an ADV discharge measurement. If using paper note keeping with an ADV for each measurement, the hydrographer should record the information, at a minimum, as if it were a mechanical velocity-meter discharge measurement, with a few variations. Indicate the filename of the infield diagnostic test performed on the ADV during the discharge measurement. Fill in all items on the front sheet or mark with a dash after the measurement is completed and computed.

ADV Inside Notes

An electronic summation of an ADV discharge measurement is produced by the ADV software. This information contains much of the information on the front sheet of the standard discharge measurement form, plus depths, widths, velocities, angles, area, and discharge. Typically ADV software does all the computations for an ADV discharge measurement. Print this output and attach it to the discharge measurement form for archival. Recent programming with personal digital assistants (PDAs) has further facilitated the collection, processing, and entry of discharge measurements into digital databases. See the sections entitled Electronic counters" and "Other electronic counters, electronic field notebooks, and personal digital assistants" for further discussion of the use of PDAs for field measurements.

Mean Gage Height of Discharge Measurements

The mean gage height of a discharge measurement represents the mean height of the stream during the period the measurement was made and is referenced to the datum of the gaging station. Just as an accurate determination of the discharge is important, so is an accurate determination of the mean gage height because it is one of the coordinates used in plotting the discharge measurement to establish the stage-discharge relation. The computation of the mean gage height presents no problem when the change in stage is small (0.1 ft or less). At gage-height changes of less than 0.1 ft, the mean gage height for the discharge measurement can be obtained by averaging the gage heights at the beginning and end of the measurement, without significant error. Measurements, however, must sometimes be made during floods or regulation when the stage significantly changes more than 0.1 ft.

To compute an accurate mean gage height for a discharge measurement, read the gage at the beginning and end of the discharge measurement, and several times during the measurement if there are significant changes. If the station is equipped with an electronic data logger or DCP that automatically records at intervals of 15 minutes or less, you can take the intermediate gage-height readings from those instruments after the measurement is completed. The hydrographer should accurately synchronize watch time and recorder time, and should record watch time for selected verticals at intervals during the discharge measurement. If the recording interval is greater than 15 minutes (that is, 30 minutes or 1 hour), intermediate gage- height readings should be obtained by reading the gage once or twice during the discharge measurement.

If the change in stage during the measurement is greater than about 0.1 ft (Rantz, 1982, suggests a change of 0.15 ft), the mean gage height should be computed by weighting the gage-height readings. In the past, the mean gage height was computed by weighting the gage readings with partial discharges from the discharge measurement. Later studies show, however, that this method tends to overestimate the mean gage height. Time weighting has also been used to compute a weighted mean gage height, but this method tends to underestimate the mean gage height. Therefore, it is recommended that both methods of weighting be used for discharge measurements having stage changes of 0.10 or more, and that an average of the two results be used for the mean gage height.

Plot the gage-height readings so that intermediate readings can be interpolated where necessary. Pay particular attention to breaks in the slope of the gage-height graph. Figure 25 illustrates a plot of gage heights for a discharge measurement. Gage heights for this measurement were determined from the stage recorder at 15-minute intervals.

In the discharge-weighting procedure, the partial discharges measured between recorded watch times are used with the mean gage height for that same time period. The equation used to compute the weighted mean gage height is:

$$H = \frac{q_1h_1 + q_2h_2 + q_3h_3 + \ldots + q_nh_n}{Q}, \quad (11)$$

where H weighted mean gage height, in feet,
Q total discharge measured, in cubic feet per second = $q_1 + q_2 + q_3 + \ldots + q_n$,
$q_1, q_2, q_3 \ldots q_n$ amount of discharge measured during time interval 1, 2, 3...n, in cubic feet per second,
$h_1, h_2, h_3 \ldots h_n$ average gage height during time interval 1, 2, 3...n, in feet.

Figure 25 shows the computation of a discharge-weighted mean gage height. The graph at the bottom is a reproduction of the gage-height graph during the discharge measurement. To help explain the method, the discharges are taken from the current-meter measurement shown in figure 2*A*. The upper computation of the mean gage height in figure 25 shows the computation using the given formula. The lower computation was calculated using a shortcut method to eliminate the multiplication of large numbers. In this method, after the average gage height for each time interval has been computed, a base gage height, which is usually equal to the lowest average gage height, is chosen. Then, the difference between the base gage height and the average gage heights is used to weight the discharges. When the mean difference has been computed, the base gage height is added to it.

In the time-weighting procedure, the arithmetic mean gage height for time intervals between breaks in the slope of the gage-height graph is used with the duration of those time periods. The equation used to compute mean gage height is

$$H = \frac{t_1h_1 + t_2h_2 + t_3h_3 + \ldots + t_nh_n}{T}, \quad (12)$$

where H weighted mean gage height, in feet,
T total time for the measurement, in minutes ($t_1 + t_2 + t_3 + \ldots + t_n$),
$t_1, t_2, t_3, \ldots, t_n$ duration of time intervals between breaks in the slope of the gage height graph, in minutes, and
$h_1, h_2, h_3, \ldots, h_n$ average gage height, in feet, during time interval 1, 2, 3, ..., n.

Using the data from figure 25, the computation of the time-weighted mean gage height is as follows:

Average gage height (*h*) in ft	Time interval (*t*) in minutes	*h* x *t*
1.92	15	28.80
1.70	15	25.50
1.67	15	25.05
1.88	15	28.20
Totals	60	107.55

The mean gage height is computed as $H = 107.55/60 = 1.79$ ft.

In this example, there is little difference between the discharge-weighted mean gage height (1.77 ft) and the time-weighted mean gage height (1.79 ft). The average of the

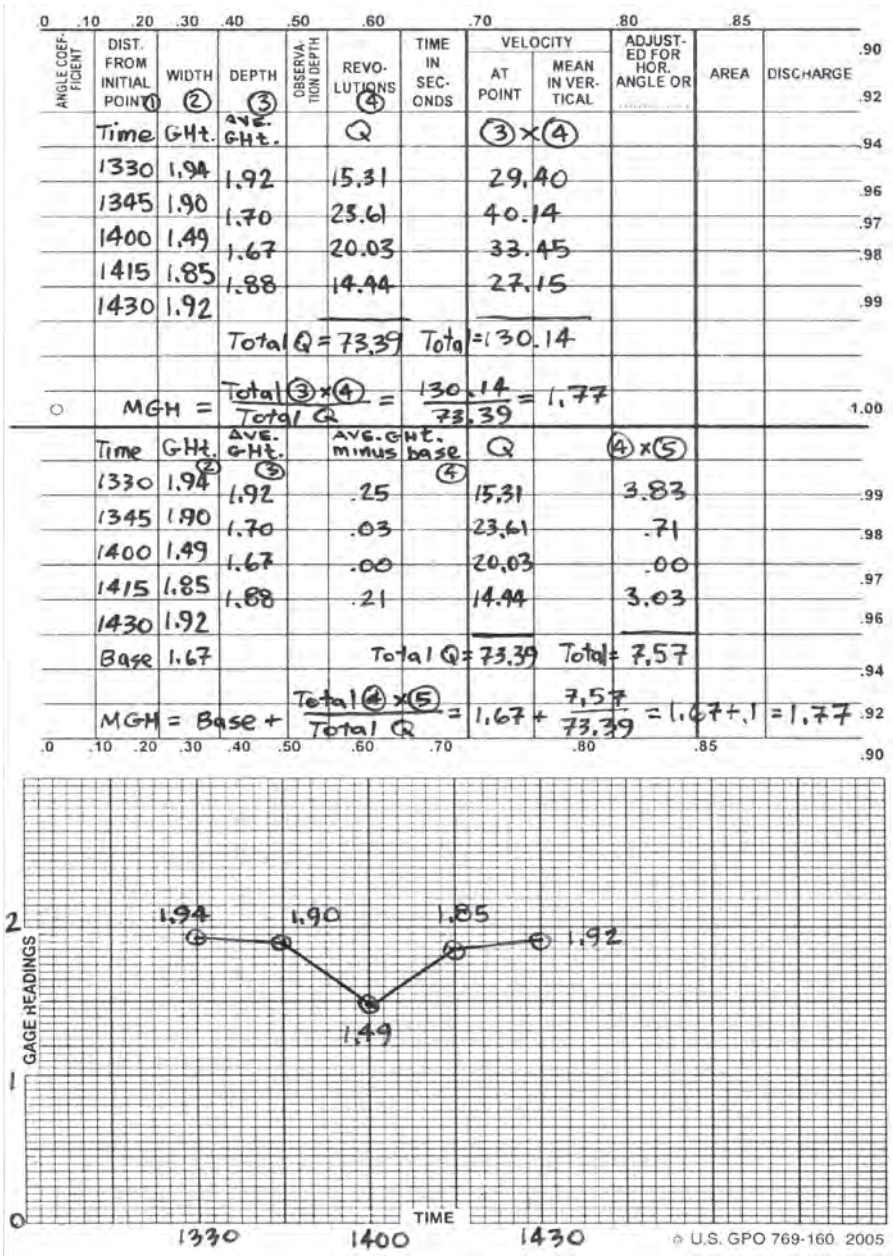

Figure 25. Graph of readings used to compute a weighted mean gage height.

two values, 1.78 ft, is the preferred mean gage height for the discharge measurement.

When extremely rapid changes in stage occur during a measurement, the weighted mean gage height is not truly applicable to the discharge measured. To reduce the range in stage during the measurement, try to reduce the time required for making the discharge measurement; however, keep in mind that shortcuts in the measurement procedure usually reduce the accuracy of the measured discharge. Therefore, measurement procedures during rapidly changing stage must be optimized to produce a minimal combined error in measured discharge and computed mean gage height. The following section of this chapter describes procedures for making discharge measurements during periods of rapidly changing stage.

Discharge Measurements During Rapidly Changing Stage

Discharge measurements during periods of rapidly changing stage are more difficult to obtain, and accuracy is often not as good as for measurements made when the stage is fairly constant. The computation of total discharge and the corresponding stage are both subject to more uncertainty when the stage significantly changes during the period of the measurement. Two procedures are suggested for shortening the time required for a discharge measurement. The first procedure is applicable more for large streams where the stage changes are usually not as great as for small streams. The second procedure is designed more for the flash-flood conditions experienced with small streams, where peaks can be of momentary duration, and where the rising and falling stage is rapid. Keep in mind that the moving-boat ADCP discharge measurement can be used during these conditions. For a more detailed discussion of procedures for using an ADCP moving-boat during rapidly changing stage, see Mueller and Wagoner (2009).

Measurements of Large Streams With Rapidly Changing Stage

During periods of rapidly changing stage in a large stream, make measurements as quickly as possible to keep the change in stage to a minimum. This will minimize discharge errors caused by the shifting of flow patterns and other variables as the stage changes, and will provide a more accurate stage computation for the measurement. To reduce the time required for making a discharge measurement, make fewer than the usual number of observations and shorten the time to make them. This is sometimes referred to as a shortcut method. Following is a list of some of the things that can be done to reduce the time:

1. Use the 0.6-depth method rather than the 0.2 and 0.8 method. If the 0.6 method cannot be used because the flow is too swift, or if debris makes it too hazardous, then use the 0.2-depth method or the subsurface method. If an optical meter is available, use surface-velocity measurements.
2. Reduce the velocity observation time to about 20 to 30 seconds. This is referred to as half-counts.
3. Only measure about 15 to 18 sections. For some conditions, even use less than 15 sections may be used.
4. Observe and record the watch time at about every third vertical. If possible, observe and record the stage once or twice during the measurement.

By incorporating the above practices, a measurement can usually be made in 15 to 20 minutes. The surface or subsurface method for observing velocities is used, then some vertical-velocity curves will be needed later to establish coefficients to convert observed velocity to mean velocity. Compute a weighted mean gage height for the discharge measurement, as described in a previous section of this chapter.

Use the determination of error in discharge measurements, as described by Sauer and Meyer (1992), to illustrate the difference in errors between the standard measurement procedure and the shortcut procedure. The results shown in table 9 are based on a firm and smooth streambed. The additional uncertainty caused by using the shortcut method is generally less than the error that can be expected from the shifting of flow patterns and other variables that may occur during periods of rapidly changing stage.

Measurements of Small Streams With Rapidly Changing Stage

A series of "instantaneous" discharge measurements can be made during flash flood conditions on small streams by rating individual subsections, or verticals. This method requires repeated observations of gage height, depth, and velocity at selected verticals during the rise and fall of the flood wave. Two procedures are described below, with the primary difference being the method of determining depth at each vertical. In the first procedure, the streambed elevation referenced to gage datum is predetermined for each selected vertical. Depth is then determined as the difference between the gage height and the streambed elevation. In the second procedure, depth is measured at the selected verticals by sounding each time velocity is observed. The first procedure is faster; however, it may not be suitable if the streambed is unstable.

The method of computing the discharge measurements is also slightly different for the two procedures. For both procedures, a rating of gage height versus mean velocity is required

Table 9. Comparison of discharge measurement error for standard and shortcut methods.

[No., number; s, seconds; ft/s, feet per second; ft, feet]

Measurement	Meter type	No. of verticals	Points in vertical	Suspension	Observation time, s	Mean velocity, ft/s	Mean depth, ft	Uncertainty percent	Measurement rated
Standard	AA	30	2	cable	50	2.50	10.0	2.3	Excellent/good.
Shortcut	AA	15	1	cable	25	2.50	10.0	5.1	Good/fair.

for each subsection, or vertical. For the second procedure, a rating of gage height versus depth is required for each vertical. The two procedures are described below.

Procedure 1—Depth Is Computed From Predetermined Streambed Elevations at Each Vertical

1. Select about 10 verticals, or subsections. For very small streams, you may use fewer verticals. Mark the selected verticals in some way so that repeated observations can be made at the same vertical each time.
2. Determine the streambed elevation referenced to gage datum for each selected vertical prior to making the series of discharge measurements. After the flood recedes, determine the streambed elevations at each vertical again to see if changes occurred during the flood. If the streambed is not stable, it will be necessary to interpolate the changes based on time and the best judgment of the hydrographer. Depth is determined at each vertical as the difference between this elevation and the gage height.
3. Take velocity observations at each vertical using the 0.6-depth method. Full counts of 40 seconds or more are recommended, but half-counts may be used if the stream is rising or falling extremely fast. If the 0.6 method cannot be used, then take velocity observations at the 0.2 depth or the subsurface depth. If an optical or other approve noncontact flowmeter is available, use it to take surface-velocity readings. For surface- and subsurface-velocity readings, it will be necessary to determine the coefficient required for converting the readings to a mean velocity. Meter positions should be based on the depth, as computed in item 2 above.
4. Make observations of other factors that would affect the computation of discharge, such as horizontal-angle coefficients.
5. Repeat the velocity and other observations at each of the selected verticals several times over the duration of the flood wave.
6. Record the watch time of each vertical measurement, and make corresponding gage- height observations frequently during the period of the flood wave.
7. Develop a rating of gage height versus mean velocity for each of the selected verticals. If surface- or subsurface-velocity observations were made, apply adjustments so that the rating represents mean velocity in the vertical. In some cases, it may be necessary to develop more than one rating for each vertical. For instance, a rating for the rising side of the flood wave, and a separate rating for the falling side of the flood wave, may be necessary.
8. Select a gage height for which a discharge measurement is to be computed. Use a standard discharge measurement note sheet for computing the discharge measurement. Enter the stationing for the edge of water and for each of the selected verticals. Enter the depths at each vertical, computed on the basis of the selected gage height minus the streambed elevation. Enter the mean velocity at each vertical on the basis of the gage height versus mean velocity ratings. Enter other adjustments, such as horizontal-angle coefficients, as observed during the observation of velocities. Compute the discharge measurement similar to a regular discharge measurement.
9. Repeat the process described in item 8 above for other selected gage heights. If the ratings of gage height versus mean velocity change, such as for rising and falling stage, then compute separate discharge measurements for the rising and falling limbs of the flood wave.

Procedure 2—Depth Is Measured by Sounding at Each Vertical

1. Select about 10 verticals, or subsections, as described in the first procedure above. For very small streams, fewer verticals may be used. Mark the selected verticals in some way so that repeated observations can be made at the same vertical each time.
2. Determine the depth for each selected vertical by sounding the streambed each time you measure a vertical. Use this method when it is possible to easily make soundings, and when there is a likelihood of streambed elevation changes caused by scour or fill during the course of the measurement.
3. Take velocity observations at each vertical using the 0.6-depth method. Full counts of 40 seconds or more are recommended, but half-counts may be used if the stream is rising or falling extremely fast. It is not likely that you will need to make surface or subsurface observations because depth soundings are possible with this procedure. Meter positions should be based on the sounded depth.
4. Make observations of other factors that would affect the computation of discharge, such as horizontal-angle coefficients.
5. Repeat the observations of depth, velocity, and other variables at each of the selected verticals several times over the duration of the flood wave.
6. Record the watch time of each vertical measurement, and make frequent, corresponding gage-height observations during the period of the flood wave.
7. Develop a rating of gage height versus mean velocity for each of the selected verticals. As described in the first procedure, it may be necessary to develop more than one rating, such as for the rising and falling sides of the flood wave.
8. Develop a rating of gage height versus depth for each of the selected verticals. If streambed changes occur during the measurements, it will be necessary to take these into account by making appropriate corrections.

9. Select a gage height for which a discharge measurement is to be computed. Using a standard discharge-measurement note sheet, enter the stationing for the edge of water and for each of the selected verticals. Enter the depths at each vertical, based on the selected gage height and the ratings of gage height versus depth. Enter the mean velocity at each vertical on the basis of the gage height versus mean velocity ratings. Enter other adjustments, such as horizontal-angle coefficients, as observed during the observation of depths and velocities. Compute the discharge measurement similar to a regular discharge measurement.
10. Repeat the process described in item 9 above for other selected gage heights. If the depth and (or) mean velocity ratings change, such as for rising and falling stage, or for streambed scour or fill, then compute separate discharge measurements for conditions before and after the changes.

Correction of Discharge for Storage During Measurement

Most discharge measurements are made at or near the gaging station and the gage control. However, at some gages, it may be necessary to make discharge measurements at a substantial distance away from the gage and (or) control. For instance, during a flood, the only place to measure may be at a bridge located some distance from the gage. Or for some sites, the low-water section control may be located at a substantial distance downstream from the gage. If a discharge measurement is made at a substantial distance from the gage control during a change in stage, the discharge passing the control during the measurement will not be the same as the discharge at the measurement section. In these situations, an adjustment must be applied to the measured discharge to account for the change in channel storage that occurs between the measurement section and the control during the period of the measurement. The adjustment for channel storage is computed by multiplying the channel surface area by the average rate of change in stage in the reach between the measurement section and the control. The equation is

$$Q_G = Q_m \pm WL\frac{\Delta h}{\Delta t}, \quad (13)$$

where Q_G discharge going over the control, in cubic feet per second,
Q_m measured discharge, in cubic feet per second,
W average width of stream between measuring section and control, in feet,
L length of reach between measuring section and control, in feet,
Δh average change in stage in the reach L during the measurement, in feet, and
Δt elapsed time during measurement, in seconds.

Determine the change in stage at each end of the reach (that is, at the control and at the measuring section) and use an average of these two values. Generally, the gage height at the gage is used at one end of the reach, and a reference point (RP) or a temporary gage is set at the other end of the reach. The water-surface elevation at each end of the reach is determined before and after the measurement to compute Δh. If the measurement is made upstream from the control, the adjustment will be plus for falling stages and minus for rising stages; if it is made downstream from the control, it will be minus for falling stages and plus for rising stages.

An example computation for a flood measurement that was made 0.6 mile upstream from the gage (and control) during a period of changing stage is shown below:

- Measurement made 0.6 mile upstream, L = 3,170 feet. Average width between measuring section and control, W = 150 ft.
- Gage height at beginning of measurement, at the gage (and control) = 5.84 ft.
  Gage height at end of measurement, at the gage (and control) = 6.74 ft.
  Change in stage at gage (and control), 6.74 – 5.84 = +0.90 ft.
- Gage height at beginning of measurement, at measuring section, = 12.72 ft.
  Gage height at end of measurement, at measuring section = 13.74 ft.
  Change in stage at measuring section, 13.74 – 12.72 = +1.02 ft.

Readings taken at measuring section from a reference point before and after measurement.

- Average change in stage in the reach, Dh = (0.90+1.02)/2 = 0.96 ft.
  Elapsed time during measurement, Dt = l.25 hours = 4,500 seconds.
  Measured discharge, Q_m = 8,494 ft^3/s.

$$Q_G = 8,494 - \left(150 \times 3,170 \times \frac{0.96}{4,500}\right) = 8,494 - 101 = 8,393\ \frac{ft^3}{s}, \quad (14)$$

This discharge should then be rounded to 8,390 ft^3/s, which represents the discharge at the gage, or control.

The adjustment of the measured discharge for storage between the gage (or control) and measuring site, as described above, is a separate and distinct problem from that of making adjustments owing to variable water-surface slopes caused by changing discharge. Those adjustments are related to stage-discharge rating analysis, and are described by Kennedy (1984), and by Rantz (1982). The storage adjustment they described should be made immediately following the completion of the discharge measurement, and the resulting adjusted discharge is later used for rating analysis.

Instruments and Equipment

Point-velocity current-meter and profiler measurements are usually classified in terms of the method used to cross the stream during the measurement (that is, wading, bridge, cableway, or ice), the method used to compute the discharge, such as midsection, ADCP, flume, or volumetric, and the method used to compute the velocity (if applicable to the discharge method), such as Price AA meter, ADCP, or ADV. Instruments and equipment used in making current-meter measurements will vary, depending upon which of these measurement types are being used. Current meters, timers, and electronic and other counting equipment are generally common to all types of current-meter and profiler measurements. This section describes equipment currently used by USGS field offices.

Current Meters

A point-velocity current meter, in the context of this report, is a precision instrument calibrated to measure the velocity of flowing water in a single point or fixed volume. Several types of current meters are available for use, including rotating-element mechanical meters, electromagnetic meters, acoustic Doppler velocimeters (ADVs or FlowTrackers), acoustic digital current meters (ADCs), and optical meters.

The principle of operation for a mechanical meter is based on the proportionality between the velocity of the water and the resulting angular velocity of the meter rotor. By placing a mechanical current meter at a point in a stream and counting the number of revolutions of the rotor during a measured interval of time, the velocity of water at that point can be determined from the meter rating.

An electromagnetic current meter is based on the principle that a conductor (water) moving through a magnetic field will produce an electrical current. By measuring this current and the resultant distortion in the magnetic field, the instrument can be calibrated to determine point velocities of flowing water.

The acoustic meter or profiler (for example, ADV or ADCP) uses the Doppler principle to determine velocities of flowing water. Acoustic meters and profilers have been developed to measure point velocities in the vertical profile of an open-channel flow, as well as multicell vertical-velocity profiles. The ADCP has been adapted for use with the moving-boat method of measuring discharge, as described by Mueller and Wagner (2009). The ADV has been developed and adapted to mount on the standard USGS wading rod to measure point velocities in a manner similar to the method for measuring velocity with a vertical-axis rotating-element mechanical meter. ADVs will be described in a later section of this chapter.

The following sections describe the various types of current meters and profilers in more detail, give advantages and disadvantages of each, and provide guidance on care and maintenance.

Current Meters—Mechanical and Vertical Axis

Historically, the most commonly used meter by the USGS to measure open-channel velocities in rivers and streams has been the vertical-axis, mechanical current meter. The original prototype for this kind of current meter was designed and built in 1882 by W.G. Price, while he was working with the Mississippi River Commission. The Price current meter has evolved through a number of different models and refinements since 1882, but the basic theory and concepts remain the same. The Price AA meter is the most commonly used mechanical current meter for discharge measurements made by the USGS; however there are other variations of this meter, such as the Price AA slow velocity, the Price pygmy, and the Price AA winter meter. The following sections describe the various Price meters in more detail, and table 10 summarizes the various configurations and recommendations for the Price current meter, Price AA low velocity, the Price pygmy, the Price AA winter yoke with polymer and metal cups, and the SonTek FlowTracker ADV.

Price AA Meter

Historically, most current-meter measurements made by the USGS have been made with the vertical-axis Price AA and the Price pygmy current meters, as shown in figures 26 and 27. The basic components of the Price AA meter include the shaft and rotor (bucket wheel) assembly, the contact chamber, the yoke, and the tailpiece. The rotor, or bucket wheel, is 5 in. in diameter and 2 in. high with six cone-shaped cups mounted on a stainless-steel shaft. A vertical pivot supports the vertical shaft of the rotor, hence the name vertical-axis current meter. The contact chamber houses the upper part of the shaft and provides a method of counting the number of revolutions the rotor makes. A reduction gear (commonly referred to as the penta gear) on the lower part of the shaft allows counting every fifth revolution of the rotor when it is activated. The penta gear is used in discharge measurements with very high velocities. Contact chambers that can be used on the Price AA meter are described in a later section of this chapter. The yoke is the framework that holds the other components of the meter. A tailpiece is used for balance and keeps the meter pointing into the current.

When placed in flowing water, the rotors of the Price current meters turn at a speed proportional to the speed of the water. For practical purposes, these current meters are considered nondirectional because they register the maximum velocity of the water, even though they may be placed at an angle to the direction of flow. Advantages of the vertical-axis current meter are:

1. They operate in lower velocities than do horizontal-axis meters.
2. Bearings are well protected from silt-laden water.
3. The rotor is easily repairable in the field without adversely affecting the rating.
4. USGS standard ratings apply to the Price AA and Price pygmy meters.
5. A single rotor serves for the entire range of velocities.

Table 10. Price current meter and SonTek ADV configurations, usages, and recommended ranges of depth (without boundary interference) and velocity.

Meter	Contact chamber	Counting method	Rating	Velocity range, feet per second[1]	Depth range, feet	Remarks
Price AA	Standard, cat'swhisker and penta gear	Headphones, CMD[2], or EFN[3]	Standard	0.2 to 12	1.25 or greater	The Price AA meter can be used as a low-velocity meter if equipped with an optic contact chamber.
			Individual	0.1 to 12		
	Magnetic	CMD[2] or EFN[3]	Standard	0.2 to 12		
			Individual	0.1 to 12		
	Optic		Standard or individual	0.1 to 12		
Price AA, low velocity	Cat's-whisker with double contact lobe on shaft. No penta gear.	Headphones, CMD[2], or EFN[3]	Individual	0.1 to 12	1.25 or greater	This is the traditional Price AA low velocity meter. An individual rating is recommended; however, a standard rating can be used if less accuracy is acceptable.
Price pygmy	Cat's whisker	Headphones, CMD[2], or EFN[3]	Standard or individual	0.2 to 4.0	0.3 to 1.5	--
Price, winter WSC[4] yoke, polymer cups	Cat's whisker	Headphones, CMD[2], or EFN[3]	Individual, with suspension device	0.1 to 12	1.25 or greater	This meter is recommended for conditions where slush ice is present.
	Magnetic or Optic	CMD[2] or EFN[3]				
Price, winter WSC[4] yoke, metal cups	Cat's whisker	Headphones, CMD[2], or EFN[3]	Individual, with suspension device	0.1 to 12	1.25 or greater	This meter is recommended for conditions where slush ice is not present.
	Magnetic or Optic	CMD[2] or EFN[3]				
SonTek FlowTracker ADV	N/A	N/A	Individual	0.003 to 13[5]	0.25 or greater	The FlowTracker has been documented by the USGS to provide velocities comparable to mechanical vertical axis current meters.

[1]Low- and high-velocity limits shown in the table are based on a small-to-moderate extrapolation of the lower and upper meter calibration limits. It is not recommended that the meters be used for velocities less than the lower limit. The velocity rating for the Price meter may allow additional extrapolation in the upper range to about 20 feet per second. The upper range of the Price pygmy meter rating may be extrapolated to about 5 feet per second. Standard errors within the meter calibration limits are less than ±5% in all cases. Standard errors in the extrapolated range of velocities are unknown, but are probably within ± 5%.

[2]Current-meter digitizer. Observe cautions for low velocities. See text.

[3]Electronic field notebook, such as Aquacalc or DMX. Observe cautions for low velocities. See text.

[4]Water Survey of Canada.

[5]Manufacturer's specification.

Price AA Meter (Slow Velocity)

In addition to the Price AA meter described above, there is a Price AA meter modified slightly for use in measuring low velocities. To reduce friction, the penta gear has been removed from this meter, and the shaft has two eccentrics making two contacts with the cat's whisker per revolution. The low-velocity meter normally is rated from 0.2 to 2.5 ft/s and is recommended when the mean velocity at a cross section is less than 1 ft/s.

Price Pygmy Meter

A miniature version of the Price AA meter is the Price pygmy meter, as shown in figures 26 and 27, which is used for measuring velocities in shallow depths. The Price pygmy meter is scaled two-fifths the size of the standard meter and has neither a tailpiece nor a penta gear. The contact chamber is an integral part of the yoke of the meter. The Price pygmy meter makes one contact for each revolution and is used only for rod suspension.

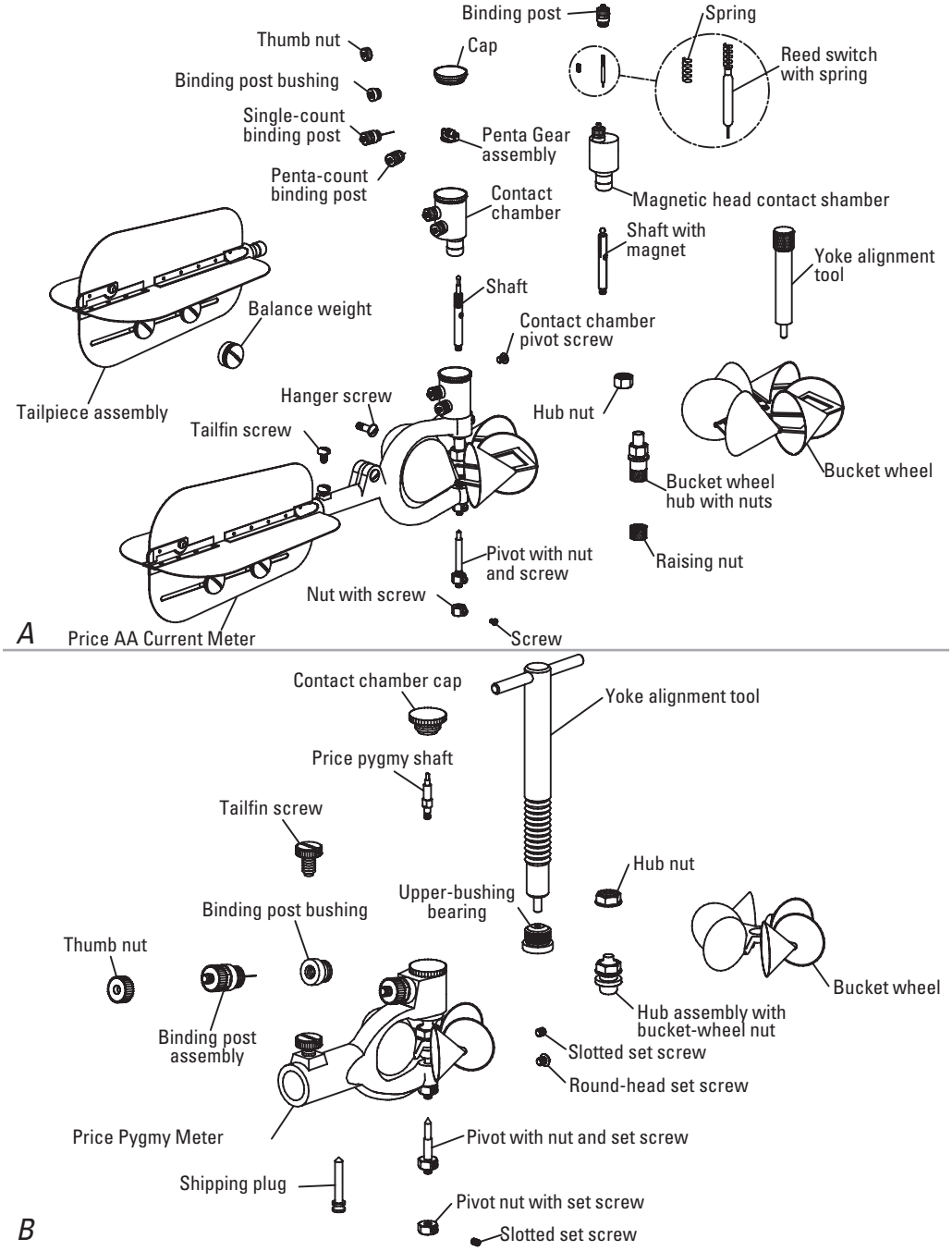

Figure 26. Assembly drawing of the *A*, Price AA current meter and *B*, Price pygmy current meter.

Figure 27. *A*, Price AA and *B*, Price pygmy current meters.

Price AA Winter Meter

In streams where slush ice is present, use a modified Price AA meter, as shown in figure 28. This meter is built with a WSCan winter-style yoke, and uses a polymer rotor (bucket wheel) in place of the standard metal-cup rotor. The WSCan winter-style yoke meters require an individual rating due to increased tolerances in manufacturing. The solid polymer rotor has the advantage that it does not fill with slush ice during a measurement, and the slush ice does not easily adhere to it. If slush ice is not present, alternative methods can be used, including replacing the polymer rotors with metal cups or using a pygmy meter. Regular Price AA meters with metal-cup rotors are also acceptable for slush-free conditions, if there are no problems with cutting the required larger holes through the ice. In recent years, the USGS has increasingly used ADCPs and ADVs as alternatives to the Price AA for making discharge measurements in streams where ice is present.

Figure 28. Price AA meter with winter-style yoke and polymer rotor.

Current Meters—Mechanical and Horizontal Axis

A number of mechanical current meters are available that have a propeller-, or vane-, type of rotor mounted on a horizontal shaft. These meters are used extensively in Europe and some Asian countries, but very little in the United States, and are generally not recommended by the USGS because they are not as durable as the Price current meter. Horizontal-axis current meters include the Ott (Germany), Neyrpic (France), Haskell (U.S.), Hoff (U.S.), Braystoke (United Kingdom), and Valeport. Various models of each of these are also available. As a group, horizontal-axis current meters have the following advantages:

1. The rotor, or propeller, disturbs flow less than vertical-axis rotors because of axial symmetry with flow direction.
2. The rotor is less likely to be entangled by debris than vertical-axis rotors.
3. Bearing friction is less than for vertical-axis rotors because bending moments on the rotor are eliminated.
4. In oblique currents, some of these meters (for example, the Ott meter) measure the velocity normal to the measuring section when the meter is held normal to the measuring section.
5. Rotors with propellers of different pitches are available for some of the meters, allowing measurement of a considerable range of velocity.

See figures 29, 30, and 31, respectively, for examples of the Ott, Hoff, and Valeport current meters.

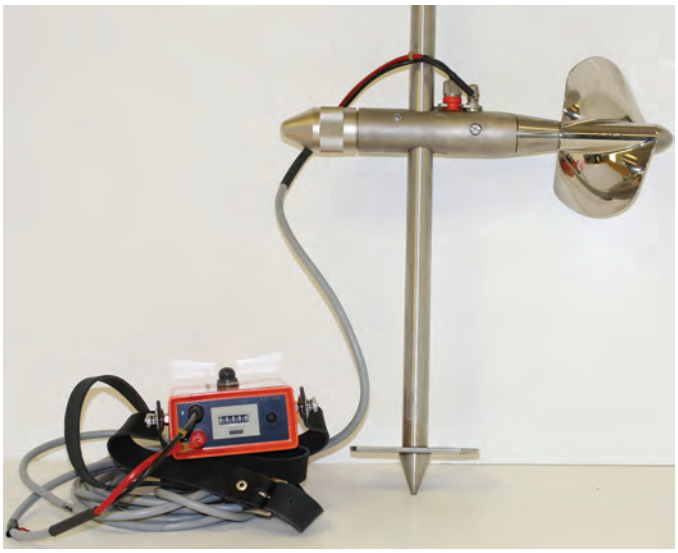

Figure 29. Ott current meter.

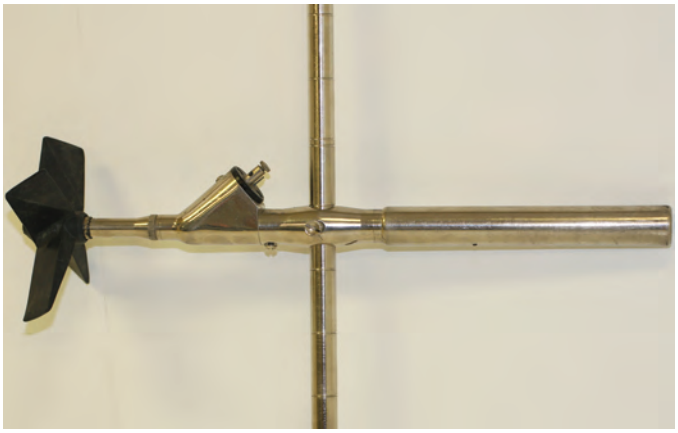

Figure 30. Hoff current meter.

Figure 31. Valeport current meter.

Current-Meter Contact Heads (Vertical Axis)

The Price current meter is normally fitted with a contact chamber that has a cat's-whisker type of circuitry used for counting the number of revolutions of the rotor. Two other types of contact chambers—the magnetic switch type and the optical type—can be fitted to the Price AA meter.

Cat's Whisker

When placed in flowing water, the rotor of the current meter turns at a speed proportional to the speed of the water. The number of revolutions of the rotor is obtained by counting electrical impulses generated in the contact chamber. An eccentric contact on the upper end of the rotor shaft wipes a slender alloy wire (cat's whisker) attached to the binding post, which closes an electrical circuit. This electrical impulse produces an audible click in a headphone or registers a unit on a counting device. Contact points in the chamber are designed to complete the electrical circuit at selected frequencies of revolution, such as twice per revolution, once per revolution, or once per five revolutions (by use of the penta gear). The penta gear, wire, and binding post provide a contact each time the rotor makes five revolutions. Figure 32 shows the contact chamber and shaft for the cat's-whisker-type chamber, with a single-count binding post.

Two types of cat's-whisker wires have been used: one is the simple bronze wire, and the other is the old type of wire with a small solder bead on the end of it. Adjust the cat's whisker for the penta gear so that it always touches the penta eccentric, even when the penta counter is not in use. Otherwise, the meter rating may be affected.

Magnetic Switch

A contact chamber housing a magnetic-type switch, as shown in figure 32, is available to replace the cat's-whisker-contact chamber. The magnetic switch is composed of glass that is enclosed in a hydrogen atmosphere and hermetically sealed. The switch assembly is rigidly fixed in the top of the meter head just above the tip of the shaft. The switch is operated by a small permanent magnet rigidly fastened to the shaft. Two types of magnets used: (1) a bar magnet and (2) a circular magnet. If the contact chamber uses the bar magnet, it should be identified with an "A" stamped on the top surface of the chamber to indicate it has been modified. Older, unmodified contact chambers with the bar magnet were found to under-register for velocities greater than about 2 ft/s. The chambers that utilize the circular magnets fit the standard rating throughout its range.

The magnetic switch quickly closes when the magnet is aligned with it, and then promptly opens when the magnet moves away. The magnet is properly balanced on the shaft. Any type of AA meter can have a magnetic switch added by replacing the shaft and the contact chamber. The magnetic switch is placed in the contact chamber through the tapped hole for the binding post. The rating of the meter is not altered by the change.

An automatic counter, as described in a later section of this chapter, is used with the magnetic-switch contact chamber. Do not use a headphone with the magnetic head because arcing can weld the contacts.

Figure 32. *A*, Price AA magnetic head current meter contact chamber; *B*, single count binding post; and *C*, shaft with magnet for magnetic heads.

Optical Head

A contact head utilizing fiber-optics technology is available for reading the pulse rate of the Price AA current meter. A special rotor containing two fiber-optic bundles is attached to the upper end of the bucket-wheel shaft. The rotation of these fiber-optic bundles gates infrared light from a photo diode to a photo transistor, creating a pulse rate that is proportional to the rotor's revolutions. The pulses are counted, stored, and then compared with a quartz crystal oscillator. This information is processed to display stream velocity on a liquid crystal readout. The display has three averaging periods selected by a rotary switch. The averaging periods range from a minimum of about 5 seconds to a maximum of about 90 seconds. The unit is powered by a 9-volt battery.

Output of pulses from the optical sensing unit can be counted by the current-meter digitizer and the electronic field notebooks described in subsequent sections of this chapter. A standard rating table based on tow-tank calibration tests at the USGS Hydrologic Instrumentation Facility (HIF) is used to convert pulse rate to stream velocity.

A special tail-fin assembly is required for the optical meter so it will balance properly when submerged. The vertical section of this tail fin is marked with the letters OAA, and the horizontal section is marked PAA.

Vertical-Axis Current-Meter Timers and Counters

The determination of velocity using a mechanical current meter requires that the number of revolutions of the rotor be counted during a specified time interval, usually 40 to 70 seconds. Several methods are available for timing and counting the revolutions, as described in the following paragraphs.

Stopwatch and Headset

For current meters having a cat's-whisker-type contact chamber, an electrical circuit is closed each time the contact wire touches the single or penta eccentric of the current meter. A battery and headphone, as shown in figure 33, are parts of the electrical circuit, and an audible click can be heard in the headphone at each electrical closure. Some hydrographers have adapted compact, comfortable hearing-aid-type phones to replace headphones. Beepers that can be heard without the headset are also sometimes used. Do not use a headset, or similar device, with the magnetic contact chamber because arcing can weld the contacts.

Measure the time interval to the nearest second with a stopwatch. Figure 33 shows the standard analog stopwatch; however, a digital wrist watch can also be used.

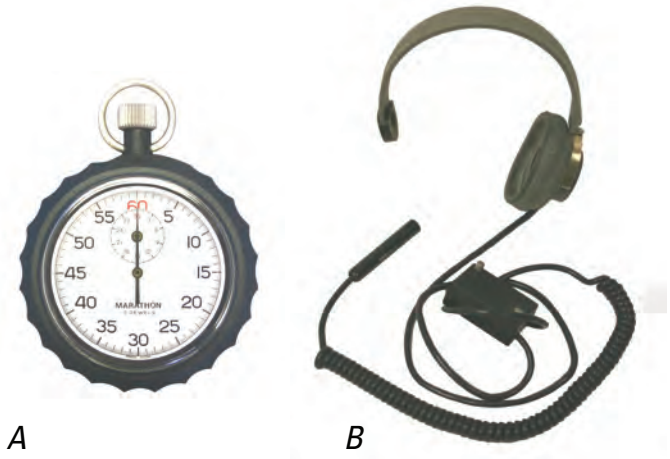

Figure 33. *A*, Analog stopwatch and *B*, current-meter headset.

Electronic Counters

Current-Meter Digitizer (CMD)

A current-meter digitizer (CMD), or automatic electronic counter, as shown in figure 34, was developed for use with the cat's-whisker-, optic-, and magnetic-contact chambers. It can be used with any of the mechanical, vertical-axis current meters, but be careful to avoid false counts when using it for low velocities when the cat's-whisker-contact chamber is used. The CMD automatically counts and displays the number of revolutions of the current-meter rotor and the elapsed time. A buzzer produces an audible signal at each contact closure, and the total counts and elapsed time are shown in the display at the completion of the velocity measurement. A coded chip can be installed in the CMD that will compute and display the velocity from the standard rating table for the particular meter being used. The CMD is powered with five rechargeable batteries, and has an adapter that can be used to attach it to the top of a wading rod.

Figure 34. Current-meter digitizer.

Other Electronic Counters, Electronic Field Notebooks, and Personal Digital Assistants

Electronic counters and timers for mechanical current meters are also available in some commercially available devices. Electronic field notebooks (EFNs), such as the JBS Instruments Aquacalc Pro Discharge Measurement Computer, are designed for electronic recording of discharge-measurement data. These will be described in more detail in a later section of this chapter. Both the Aquacalc and the Hydrological Services Current Meter Counter signal processor (CMCsp) contain built-in digitizers that count and time the current-meter rotor revolutions. Built-in ratings convert the revolutions and elapsed time to velocity. Just as with the CMD described above, the EFNs should be used with caution to avoid false counts when measuring low velocities with meters equipped with a cat's-whisker-contact chamber.

The USGS is increasing development and use of personal digital assistants (PDAs) for primary data collection and processing of discharge measurements and surface-water field data. Software programs such as the Surface WAter Measurement and Inspection application (SWAMI) continue to streamline field activities by reducing the need for paper forms in the field through the development of electronic field forms written for the PDA. SWAMI, as described in previous sections of this chapter, is used in many USGS Water Science Centers, and other PDA applications and programs are continually being developed.

Care of the Vertical-Axis Mechanical Current Meter

There are a number of documents describing the care and maintenance of the vertical-axis current meters. Among these, the most important originated from the USGS and are by Smoot and Novak (1968) and by Rantz (1982), and Office of Surface Water Technical Memorandum No. 89.07 (1989) and Office of Surface Water Technical Memorandum No. 99.06 (1999). These instructions represent a long history of experience based on field use of the meters, as well as from individuals in the Office of Surface Water Hydraulic Laboratory who have repaired and adjusted current meters to calibrate them within close tolerances. A brief description of the recommended procedure for checking the condition of a current meter, and for its care and cleaning during daily field use, is presented in the next few paragraphs. For complete details, consult the above-mentioned documents.

Recommended Procedure Before, During, and After Each Discharge Measurement

1. Before each discharge measurement, make a visual examination of the meter cups or vanes, pivot, bearing, and shaft for damage, wear, or faulty alignment. Inspect the bearing surface for water. This will usually appear as a milky emulsification of oil and water on the lower bearing and pivot, and in the contact chamber. If water is found, dry the meter parts and re-oil because the presence of water will affect the performance of the meter. The lower bearing is probably the most susceptible to the entrance of water.
2. Spin the rotor to make certain it operates freely, and allow it to slowly return to a resting position. If the rotor does not turn smoothly, or if it stops abruptly, then it is a sign of some problem and it should be corrected before using the meter. Check the balance and alignment of the meter on the hanger or wading rod. Be sure that the conductor wire does not interfere with meter balance and rotor spin.
3. During measurements, check the meter periodically when it is out of the water to be sure that the rotor spins freely, and that there is no debris or other substance obstructing it.
4. After a measurement is completed, make another visual inspection as described above to ensure that nothing was damaged or caused the meter to malfunction during the measurement. If there is a problem, you may have to make another discharge measurement.
5. Timed spin tests (described later in this chapter) are not required for each discharge measurement. The visual inspection described above is preferred over timed spin tests made in the field.

Recommended Procedure After a Day of Use in the Field

1. Examine the pivot and bearing surfaces for wear and damage, especially the pivot point. The pivot should feel sharp, not rounded or dull. It should not have a burr detectable visually or with the fingernail. A magnifying glass is helpful in making this examination. If the pivot is dull or burred, replace it with a new one.
2. Clean and lightly oil the pivot, bearing, and upper shaft with current-meter oil. Do not use regular machine oil, such as “3-in-1,” because it tends to become gummy when exposed to water.
3. Check and carefully adjust cat’s-whisker contacts, if necessary. Cat’s whiskers should be made of simple bronze wire, not beaded wire.
4. After replacing the contact-chamber cap, spin the meter to see if it is operating correctly, as previously described. A timed spin test is not required.

Recommended Procedure After Each Field Trip

After each field trip, completely disassemble, inspect, and clean current meters. Make any necessary repairs. Detailed instructions for the disassembly, inspection, and adjustment of Price AA (both standard and magnetic head) and pygmy current meters are contained in the attachments to Office of Surface Water Technical Memorandum No. 99.06 (1999). A timed spin test may also be performed after each field trip, and after meter repairs.

Inactive Current Meters

Disassemble, inspect, and clean current meters as described above, prior to storing them. If the period of storage is less than 1 year, the meter may be used without further maintenance if an inspection and a spin test indicate it is operating properly. If the meter has been in storage longer than 1 year, or an indeterminate period, complete inspection, cleaning, and adjustment before using the meter.

Spin Tests

A timed spin test, made in the field before and after each discharge measurement, is no longer a requirement as it was in the past. The visual tests as described above are adequate for checking the meter in the field. Note “OK” or “free” in the spaces on the front sheet of the discharge measurement for spin test information to indicate that the visual check of the meter was acceptable.

Perform the full-timed spin test under controlled conditions between field trips, when the meter is suspect, and before and after repairs. Place the meter on a stable, level surface to perform the spin test. There should be no wind currents or drafts that can affect the rotor spin. Sharply spin the rotor while starting a stopwatch. Stop the stopwatch when the rotor comes to a complete stop. The minimum, acceptable spin times are as follows:

All types of Price pygmy meters	0:45 seconds
All types of Price AA meters	2:00 minutes

These are considered to be absolute minimum spin times. Meters in good condition will perform substantially better.

Recordkeeping

Maintain a current-meter log to record the results of the timed spin tests for each current meter. In addition, the log should contain information that identifies the meter and rotor, a history of repairs to the meter, as well as the name of the person who checked the meter, and dates of occurrences. Figure 35 shows a recommended format for the current meter log. The current-meter log should become a permanent record and archived with other water-resources data.

CURRENT METER LOG				
Meter Type: AA Pygmy Other_____ (Circle one)		Meter No.________________		Rotor No._______________
Date	Meter User	Entry made by	Spin Time	Description of repairs, notation of disassembly, inspections, and remarks
			:	
			:	
			:	
			:	
			:	
			:	
			:	
			:	
			:	
			:	
			:	
			:	
			:	
			:	
			:	
			:	
			:	
			:	
			:	
			:	
			:	
			:	
			:	
			:	
			:	
			:	
			:	
			:	
			:	
			:	
			:	
			:	
			:	
			:	
			:	
			:	
			:	
			:	
			:	
			:	
			:	
			:	
			:	

Figure 35. Example of a current-meter log (suggested format).

Rating of Mechanical Current Meters

In order to determine the velocity of the water from the revolutions of the rotor of a mechanical current meter, a relation must be established between the angular velocity of the rotor and the velocity of the water turning it. This relation is referred to as the current-meter rating, and is expressed in an equation or in tabular format.

The current-meter rating facility is operated by the USGS, and is located at the Hydraulics Laboratory of the HIF at Stennis Space Center, Miss. The rating facility consists of a sheltered, reinforced concrete basin 400 ft long, 6 ft wide, and 6 ft deep, commonly called the tow tank. An electrically driven car rides on rails alongside and extending the length of the water-filled basin, and carries the current meter at a constant rate through the still water. Although the rate of travel can be accurately adjusted by means of a hydraulic regulating gear, the average velocity of the moving car is determined for each run by making an independent measurement of the distance it travels during the time that the revolutions of the rotor are electrically counted. A scale graduated in feet and tenths of a foot is used for this purpose. Eight pairs of runs are usually made for each current meter. A pair of runs consists of two traverses of the basin, one in each direction, at approximately the same speed. Practical considerations usually limit the ratings to velocities ranging from 0.1 ft/s to about 15 ft/s, although the rating car can be operated at lower speeds. Unless a special request is made for a more extensive rating, the lowest velocity used in the rating is about 0.2 ft/s, and the highest is about 8.0 ft/s.

Because there is rigid control in the manufacture of the Price meter, virtually identical meters are produced and, for practical purposes, their rating equations are identical. Therefore, there is no need to calibrate the meters individually, which is a major advantage and time saver. Instead, a standard rating is established by calibrating a group of meters that have been constructed according to USGS specifications. This standard rating is essentially an average rating for the calibration group, and it is then supplied with all meters manufactured according to USGS specifications. Identicalness of meters is ensured by supplying the dies and fixtures for the construction of Price current meters to the manufacturer who makes the successful bid. Another advantage of the standard rating is that field repairs can be made to a meter without requiring that it be recalibrated. On the other hand, there are somewhat larger errors associated with the standard ratings, as opposed to the individual meter ratings. For additional details see Office of Surface Water Technical Memoranda Nos. 91.01 (1991) and 99.05 (1999).

Standard current-meter ratings are not mandatory for use with the Price meters. For some applications, it may be appropriate to use individually rated meters to avoid the additional uncertainty of the standard ratings. All winter-style meters must be individually rated with the suspension device that will be used with it.

Standard current-meter ratings, as of 1999, have been defined for the Price AA with the cat's-whisker- and magnetic-contact chambers, and the Price pygmy with the cat's-whisker-contact chamber. The standard rating for the Price AA with the fiber-optic-contact chamber was defined in 1991. These ratings are as follows:

- Price AA with cat's-whisker- and magnetic-contact chambers (Standard rating No. 2)

$$V = 2.2048R + 0.0178 \quad (15)$$

- Price pygmy with cat's-whisker-contact chamber (Standard rating No. 2)

$$V = 0.9604R + 0.0312 \quad (16)$$

- Price AA with fiber-optic-contact chamber

$$V = 2.194R + 0.014 \ (R<0.856) \quad (17)$$

$$V = 2.162R + 0.041 \ (R>0.856) \quad (18)$$

where V velocity, in feet per second (ft/s), and
R the number of rotor revolutions per second.

For convenience in field use, the data from the current-meter ratings are reproduced in tables, samples of which are shown in figures 36 and 37. In figure 36, the velocities corresponding to a range of 3 to 200 revolutions of the rotor within a period of 40 to 70 seconds are listed in the tables.

In figure 37, the velocities corresponding to a range of 3 to 350 revolutions of the rotor within a period of 40 to 70 seconds are listed in the tables. This range in revolution and time has been found to cover general field requirements. To provide the necessary information for extending a table for the few instances where extensions are required, the equation of the rating table is shown in the heading.

Meters that have been rated by means of rod suspension, and then by means of cable suspension using Columbus-type weights and hangers, have not shown significant differences in their ratings. Therefore, no suspension coefficients are needed if weights and hangers are properly used.

The preceding discussion relates primarily to the Price current meters. Other types of meters, such as the horizontal-axis meters and the electromagnetic meters, can also be calibrated in the tow tank in a similar manner as the Price meters. The HIF designed and constructed a special tow tank for testing and calibrating the acoustic Doppler point-velocity FlowTracker velocimeter. In the near future, there are HIF plans to build and operate a tow tank designed to test and calibrate ADCPs.

STANDARD RATING TABLE NO. 2 FOR PYGMY CURRENT METER (6/99)
EQUATION: V = 0.9604 R+ 0.0312 (R=revolutions per second)

Seconds	VELOCITY IN FEET PER SECOND Revolutions														
	3	5	7	10	15	20	25	30	40	50	60	80	100	150	200
40	0.103	0.151	0.199	0.271	0.391	0.511	0.631	0.752	0.992	1.23	1.47	1.95	2.43	3.63	4.83
41	0.101	0.148	0.195	0.265	0.383	0.500	0.617	0.734	0.968	1.20	1.44	1.91	2.37	3.54	4.72
42	0.100	0.146	0.191	0.260	0.374	0.489	0.603	0.717	0.946	1.17	1.40	1.86	2.32	3.46	4.60
43	0.098	0.143	0.188	0.255	0.366	0.478	0.590	0.701	0.925	1.15	1.37	1.82	2.26	3.38	4.50
44	0.097	0.140	0.184	0.249	0.359	0.468	0.577	0.686	0.904	1.12	1.34	1.78	2.21	3.31	4.40
45	0.095	0.138	0.181	0.245	0.351	0.458	0.565	0.671	0.885	1.10	1.31	1.74	2.17	3.23	4.30
46	0.094	0.136	0.177	0.240	0.344	0.449	0.553	0.658	0.866	1.08	1.28	1.70	2.12	3.16	4.21
47	0.093	0.133	0.174	0.236	0.338	0.440	0.542	0.644	0.849	1.05	1.26	1.67	2.07	3.10	4.12
48	0.091	0.131	0.171	0.231	0.331	0.431	0.531	0.631	0.832	1.03	1.23	1.63	2.03	3.03	4.03
49	0.090	0.129	0.168	0.227	0.325	0.423	0.521	0.619	0.815	1.01	1.21	1.60	1.99	2.97	3.95
50	0.089	0.127	0.166	0.223	0.319	0.415	0.511	0.607	0.800	0.992	1.18	1.57	1.95	2.91	3.87
51	0.088	0.125	0.163	0.220	0.314	0.408	0.502	0.596	0.784	0.973	1.16	1.54	1.91	2.86	3.80
52	0.087	0.124	0.160	0.216	0.308	0.401	0.493	0.585	0.770	0.955	1.14	1.51	1.88	2.80	3.73
53	0.086	0.122	0.158	0.212	0.303	0.394	0.484	0.575	0.756	0.937	1.12	1.48	1.84	2.75	3.66
54	0.085	0.120	0.156	0.209	0.298	0.387	0.476	0.565	0.743	0.920	1.10	1.45	1.81	2.70	3.59
55	0.084	0.119	0.153	0.206	0.293	0.380	0.468	0.555	0.730	0.904	1.08	1.43	1.78	2.65	3.52
56	0.083	0.117	0.151	0.203	0.288	0.374	0.460	0.546	0.717	0.889	1.06	1.40	1.75	2.60	3.46
57	0.082	0.115	0.149	0.200	0.284	0.368	0.452	0.537	0.705	0.874	1.04	1.38	1.72	2.56	3.40
58	0.081	0.114	0.147	0.197	0.280	0.362	0.445	0.528	0.694	0.859	1.02	1.36	1.69	2.51	3.34
59	0.080	0.113	0.145	0.194	0.275	0.357	0.438	0.520	0.682	0.845	1.01	1.33	1.66	2.47	3.29
60	0.079	0.111	0.143	0.191	0.271	0.351	0.431	0.511	0.671	0.832	0.992	1.31	1.63	2.43	3.23
61	0.078	0.110	0.141	0.189	0.267	0.346	0.425	0.504	0.661	0.818	0.976	1.29	1.61	2.39	3.18
62	0.078	0.109	0.140	0.186	0.264	0.341	0.418	0.496	0.651	0.806	0.961	1.27	1.58	2.35	3.13
63	0.077	0.107	0.138	0.184	0.260	0.336	0.412	0.489	0.641	0.793	0.946	1.25	1.56	2.32	3.08
64	0.076	0.106	0.136	0.181	0.256	0.331	0.406	0.481	0.631	0.782	0.932	1.23	1.53	2.28	3.03
65	0.076	0.105	0.135	0.179	0.253	0.327	0.401	0.474	0.622	0.770	0.918	1.21	1.51	2.25	2.99
66	0.075	0.104	0.133	0.177	0.249	0.322	0.395	0.468	0.613	0.759	0.904	1.20	1.49	2.21	2.94
67	0.074	0.103	0.132	0.175	0.246	0.318	0.390	0.461	0.605	0.748	0.891	1.18	1.46	2.18	2.90
68	0.074	0.102	0.130	0.172	0.243	0.314	0.384	0.455	0.596	0.737	0.879	1.16	1.44	2.15	2.86
69	0.073	0.101	0.129	0.170	0.240	0.310	0.379	0.449	0.588	0.727	0.866	1.14	1.42	2.12	2.81
70	0.072	0.100	0.127	0.168	0.237	0.306	0.374	0.443	0.580	0.717	0.854	1.13	1.40	2.09	2.78
	3	5	7	10	15	20	25	30	40	50	60	80	100	150	200

Figure 36. Example of a standard current-meter rating table No. 2 for Price pygmy current meters with cat's-whisker contact chamber.

STANDARD RATING TABLE NO. 2 FOR AA CURRENT METERS (6/99)
EQUATION: V = 2.2048 R + 0.0178 (R=revolutions per second)

Seconds	VELOCITY IN FEET PER SECOND Revolutions									Seconds
	3	5	7	10	15	20	25	30	40	
40	0.183	0.293	0.404	0.569	0.845	1.12	1.40	1.67	2.22	40
41	0.179	0.287	0.394	0.556	0.824	1.09	1.36	1.63	2.17	41
42	0.175	0.280	0.385	0.543	0.805	1.07	1.33	1.59	2.12	42
43	0.172	0.274	0.377	0.531	0.787	1.04	1.30	1.56	2.07	43
44	0.168	0.268	0.369	0.519	0.769	1.02	1.27	1.52	2.02	44
45	0.165	0.263	0.361	0.508	0.753	0.998	1.24	1.49	1.98	45
46	0.162	0.257	0.353	0.497	0.737	0.976	1.22	1.46	1.94	46
47	0.159	0.252	0.346	0.487	0.721	0.956	1.19	1.43	1.89	47
48	0.156	0.247	0.339	0.477	0.707	0.936	1.17	1.40	1.86	48
49	0.153	0.243	0.333	0.468	0.693	0.918	1.14	1.37	1.82	49
50	0.150	0.238	0.326	0.459	0.679	0.900	1.12	1.34	1.78	50
51	0.147	0.234	0.320	0.450	0.666	0.882	1.10	1.31	1.75	51
52	0.145	0.230	0.315	0.442	0.654	0.866	1.08	1.29	1.71	52
53	0.143	0.226	0.309	0.434	0.642	0.850	1.06	1.27	1.68	53
54	0.140	0.222	0.304	0.426	0.630	0.834	1.04	1.24	1.65	54
55	0.138	0.218	0.298	0.419	0.619	0.820	1.02	1.22	1.62	55
56	0.136	0.215	0.293	0.412	0.608	0.805	1.00	1.20	1.59	56
57	0.134	0.211	0.289	0.405	0.598	0.791	0.985	1.18	1.57	57
58	0.132	0.208	0.284	0.398	0.588	0.778	0.968	1.16	1.54	58
59	0.130	0.205	0.279	0.391	0.578	0.765	0.952	1.14	1.51	59
60	0.128	0.202	0.275	0.385	0.569	0.753	0.936	1.12	1.49	60
61	0.126	0.199	0.271	0.379	0.560	0.741	0.921	1.10	1.46	61
62	0.124	0.196	0.267	0.373	0.551	0.729	0.907	1.08	1.44	62
63	0.123	0.193	0.263	0.368	0.543	0.718	0.893	1.07	1.42	63
64	0.121	0.190	0.259	0.362	0.535	0.707	0.879	1.05	1.40	64
65	0.120	0.187	0.255	0.357	0.527	0.696	0.866	1.04	1.37	65
66	0.118	0.185	0.252	0.352	0.519	0.686	0.853	1.02	1.35	66
67	0.117	0.182	0.248	0.347	0.511	0.676	0.840	1.01	1.33	67
68	0.115	0.180	0.245	0.342	0.504	0.666	0.828	0.991	1.31	68
69	0.114	0.178	0.241	0.337	0.497	0.657	0.817	0.976	1.30	69
70	0.112	0.175	0.238	0.333	0.490	0.648	0.805	0.963	1.28	70
	3	5	7	10	15	20	25	30	40	

STANDARD RATING TABLE NO. 2 FOR AA CURRENT METERS (6/99)
EQUATION: V = 2.2048 R + 0.0178 (R=revolutions per second)

Seconds	VELOCITY IN FEET PER SECOND Revolutions									Seconds
	50	60	80	100	150	200	250	300	350	
40	2.77	3.33	4.43	5.53	8.29	11.04	13.80	16.55	19.31	40
41	2.71	3.24	4.32	5.40	8.08	10.77	13.46	16.15	18.84	41
42	2.64	3.17	4.22	5.27	7.89	10.52	13.14	15.77	18.39	42
43	2.58	3.09	4.12	5.15	7.71	10.27	12.84	15.40	17.96	43
44	2.52	3.02	4.03	5.03	7.53	10.04	12.55	15.05	17.56	44
45	2.47	2.96	3.94	4.92	7.37	9.82	12.27	14.72	17.17	45
46	2.41	2.89	3.85	4.81	7.21	9.60	12.00	14.40	16.79	46
47	2.36	2.83	3.77	4.71	7.05	9.40	11.75	14.09	16.44	47
48	2.31	2.77	3.69	4.61	6.91	9.20	11.50	13.80	16.09	48
49	2.27	2.72	3.62	4.52	6.77	9.02	11.27	13.52	15.77	49
50	2.22	2.66	3.55	4.43	6.63	8.84	11.04	13.25	15.45	50
51	2.18	2.61	3.48	4.34	6.50	8.66	10.83	12.99	15.15	51
52	2.14	2.56	3.41	4.26	6.38	8.50	10.62	12.74	14.86	52
53	2.10	2.51	3.35	4.18	6.26	8.34	10.42	12.50	14.58	53
54	2.06	2.47	3.28	4.10	6.14	8.18	10.23	12.27	14.31	54
55	2.02	2.42	3.22	4.03	6.03	8.04	10.04	12.04	14.05	55
56	1.99	2.38	3.17	3.95	5.92	7.89	9.86	11.83	13.80	56
57	1.95	2.34	3.11	3.89	5.82	7.75	9.69	11.62	13.56	57
58	1.92	2.30	3.06	3.82	5.72	7.62	9.52	11.42	13.32	58
59	1.89	2.26	3.01	3.75	5.62	7.49	9.36	11.23	13.10	59
60	1.86	2.22	2.96	3.69	5.53	7.37	9.20	11.04	12.88	60
61	1.83	2.19	2.91	3.63	5.44	7.25	9.05	10.86	12.67	61
62	1.80	2.15	2.86	3.57	5.35	7.13	8.91	10.69	12.46	62
63	1.77	2.12	2.82	3.52	5.27	7.02	8.77	10.52	12.27	63
64	1.74	2.08	2.77	3.46	5.19	6.91	8.63	10.35	12.08	64
65	1.71	2.05	2.73	3.41	5.11	6.80	8.50	10.19	11.89	65
66	1.69	2.02	2.69	3.36	5.03	6.70	8.37	10.04	11.71	66
67	1.66	1.99	2.65	3.31	4.95	6.60	8.24	9.89	11.54	67
68	1.64	1.96	2.61	3.26	4.88	6.50	8.12	9.74	11.37	68
69	1.62	1.94	2.57	3.21	4.81	6.41	8.01	9.60	11.20	69
70	1.59	1.91	2.54	3.17	4.74	6.32	7.89	9.47	11.04	70
	50	60	80	100	150	200	250	300	350	

Figure 37. Example of a standard current-meter rating table No. 2 for Price AA current meters with cat's-whisker and magnetic contact chambers.

Electromagnetic Current Meters

Electromagnetic current meters, with no moving parts, are commercially available for measuring point velocities. These meters are based on the principle that a conductor (in this case, water) moving through a magnetic field will produce an electric current. The velocity of the moving water can be related to the electric current produced, and the distortion created in the magnetic field. The electromagnetic meters can be accurately calibrated in a tow tank, similar to the calibration of mechanical meters; however, tests have shown that the electromagnetic meters are less accurate than the Price AA meters, especially at low velocities (less than about 0.5 ft/s). The Price AA meters also have less variance than the electromagnetic meters at all velocities. Advantages of the electromagnetic current meter are as follows: no moving parts; direct readout of velocity; and, in oblique flow, the velocity measured is normal to the measuring section when the meter is held normal to it.

Marsh-McBirney 2000

An electromagnetic current meter successfully used by the USGS for making discharge measurements is the Model 2000, produced by Marsh-McBirney. This meter, as shown in figure 38, is designed to mount on a standard round or top-setting wading rod. The meter is not designed for cable suspension.

A display meter, also shown in figure 38, shows a direct readout of the velocity. No conversion equation or table is necessary. The meter must be kept clean for accurate readings, and it is recommended that the rating be occasionally spot checked to verify that it is still accurate. This can be done in two ways. First, submerge the meter in a bucket of still water to verify the zero point of the rating. Second, place the meter in close proximity to a Price AA meter, in flowing water, to verify that it gives the same velocity reading. If there are differences, rate the electromagnetic meter again in the tow tank.

Figure 38. Marsh-McBirney Model 2000 electromagnetic flowmeter and display meter.

Ott Electromagnetic Current Meter

An Ott electromagnetic current meter is available; however, it has not been used extensively in the United States. The Ott meter, shown in figure 39, works in a manner similar to the Marsh-McBirney meter.

Figure 39. Ott electromagnetic current meter.

Acoustic Current Meters

Acoustic Doppler current meters, with no moving parts, are commercially available for measuring point velocities. These meters are based on the Doppler principle. The velocity of the moving water is measured using the transmitted and received signals from sound pulses reflecting off particles in the moving water column. These acoustic meters can be accurately calibrated in a tow tank, similar to the calibration of mechanical meters. Advantages of an acoustic Doppler current meter are as follows: no moving parts; direct readout of velocity; and ability to sense very low velocities less than the rated velocities in standard mechanical current meters.

Acoustic Doppler Velocimeter (ADV)

The SonTek/YSI FlowTracker handheld ADV ("FlowTracker" and "ADV" are used interchangeably in this chapter) is designed as an alternative to the Price AA and pygmy meters for wading discharge measurements. The FlowTracker operates at an acoustic frequency of 10 MHz and measures the phase change caused by the Doppler shift in acoustic frequency that occurs when a transmitted acoustic signal reflects off particles in the flow. The magnitude of the phase change is proportional to the flow velocity. The phase difference can be positive or negative, allowing ADVs to measure positive and negative velocities. The FlowTracker measures the velocity at a rate of approximately 10 MHz, averages the data, and records 1-second velocity-vector data.

The maximum velocity the FlowTracker can measure is reduced when measuring flow that is not perpendicular to the transmitting transducer. The receiving transducers can measure a velocity range of only ±1.15 m/s (3.77 ft/s). A velocity component placed directly toward or away from the receiving transducers larger than 1.15 m/s (3.77 ft/s) will result in erroneous velocities. Because of the geometric arrangement of the transmitting and receiving transducers, a velocity of 4.5 m/s flowing perpendicular to the transmitting transducer face will result in the maximum velocity towards a receiving transducer of 1.15 m/s (3.77 ft/s).

The FlowTracker probe is mounted to a standard top-setting wading rod with a special offset-mounting bracket (fig. 40). This bracket is designed to locate the FlowTracker probe at the front of the wading rod, with the sampling volume

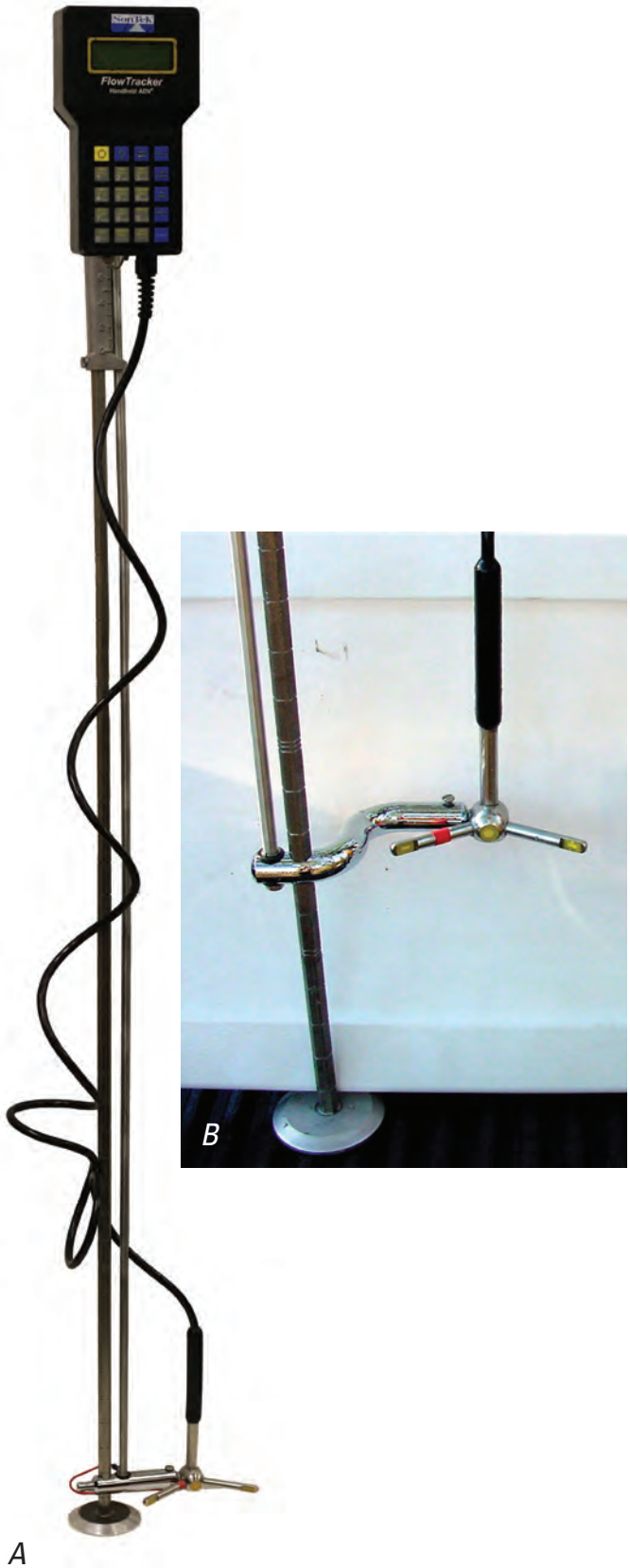

Figure 40. *A*, SonTek/YSI FlowTracker acoustic Doppler velocimeter (ADV) mounted on a standard top-setting wading rod and *B*, closer view of transmitting and receiving transducers and offset-mounting bracket.

about 2 in. (5 cm) to the right of the wading rod. Although the probe is inserted into the flow, the sampling volume is about 4 in. (10 cm) away from all physical parts of the probe, to minimize flow disturbance in the sampling volume.

FlowTrackers have several unique data-processing requirements because of their method of operation and some of the inherent limitations of the acoustic Doppler measurement technique. Unlike mechanical meters that use the momentum of the water to turn a propeller and directly measure the velocity of the water, the FlowTracker does not measure the velocity of the water. The FlowTracker measures the velocity of particles (sediment, small organisms, and bubbles) suspended in the flow, assuming that these particles travel at the same velocity as the water. Therefore, the quality of the measurement is dependent on the presence of particles within the sampling volume that reflect a transmitted signal. The FlowTracker records the signal-to-noise ratio (SNR), standard error of velocity (based on 1-second data), angle of the measured flow (relative to the x-axis of the FlowTracker probe), number of filtered velocity spikes, and a boundary quality-control flag. These velocity and quality-assurance data may be used to evaluate the measurement conditions. Few similar quality-assurance data are available for Price current-meter measurements.

Although a FlowTracker can measure within about 1.2 in. (3 cm) of a boundary, the velocity measurement might be affected by acoustic interference when the sampling volume is close to boundaries or underwater objects, even when the sampling volume is not directly on or past the boundary. At the start of each velocity measurement, if the probe detects nearby acoustic boundaries that could cause interference with the velocity measurement, a boundary adjustment is automatically made. The boundary adjustment attempts to overcome the possible interference by reducing the lag times of the acoustic signals transmitted by the FlowTracker, causing a reduction of the velocity range that can be measured. Any changes are noted in the boundary quality-control flag. Because the sampling volume is located about 4 in. (10 cm) from the transmitting transducer it can be difficult to ascertain the precise location of the sampling volume. If the sampling volume is on or past a boundary, the velocity data will be erroneous. Be careful to avoid boundaries while making measurements in depths less than 3.54 in. (9 cm), especially in channels with irregular bottoms.

Spikes in velocity data occur with any acoustic Doppler velocity sensor such as the FlowTracker. Spikes may have a variety of causes (for example, large particles in the flow, air bubbles, or acoustic anomalies). Velocity data from each FlowTracker measurement are evaluated to look for spikes. The FlowTracker spike filter is a variation on a method called "Tukey's Outlier." In this method, a histogram of each velocity component is calculated. The FlowTracker determines the lower quartile (*Q1*; 25 percent of samples are less than this value), the upper quartile (*Q3*; 75 percent of samples are less than this value), and the interquartile range ($IQR = Q3-Q1$). If the *IQR* is less than 0.015 m/s (0.049 ft/s), *IQR* is set to

0.015 m/s (0.049 ft/s). Any value less than (*Q1–2*IQR*) or greater than (*Q3+2*IQR*) is considered a spike and is not used for mean-velocity calculations.

The FlowTracker measures magnitude and direction of velocity. The operator must keep the wading rod perpendicular to the tag line so that the pulse generated by the transmitter is parallel to the tag line, regardless of flow direction. To compute discharge, the FlowTracker uses the component of velocity perpendicular to the transmitting transducer and reports the flow angle from the FlowTracker's x-axis as a quality-control value. A flow angle measured by the FlowTracker may be the result of flow that is not perpendicular to the tag line, or a wading rod that is not being held perpendicular to the tag line (operator error). Flow angles of less than 20 degrees with small variations between verticals are not unusual. Large fluctuations of flow angles between verticals, however, may indicate a poorly measured cross section. If there is angular flow, and the wading rod is oriented with the flow, the velocity used and resulting discharge would be biased high. If the flow is truly perpendicular to the cross section, but the wading rod is erroneously held at an angle, the velocity and resulting discharge would be biased low. To avoid possible errors in the measured velocities, it is important that the operator always carefully and accurately aligns the wading rod.

Signal-to-Noise Ratio (SNR)

Adequate signal-to-noise ratio is needed to obtain an accurate measurement of the flow velocity. SNR is a measure of the strength of the reflected acoustic signal relative to the ambient noise level of the instrument. SNR is a function of the concentration and size distribution of the particles that reflect the acoustic signal. SNR is recorded for each beam with each 1-second sample. The manufacturer states that optimal SNR is 10 decibels (dB) or above (SonTek/YSI, 2002). USGS policy is that FlowTrackers should not be used for measuring discharge if the SNR for any single beam is less than 4 dB.

Speed of Sound

The accuracy of hydroacoustics instruments like the FlowTracker is dependent on an accurate speed of sound. The speed of sound is primarily a function of the temperature and salinity of the water. The FlowTracker has a built-in temperature sensor. To verify that the temperature sensor is working correctly, take an independent water-temperature measurement prior to each discharge measurement. If the FlowTracker has been stored in an environment with a different ambient temperature from the water, the probe may need to be placed in the water for a period of time, allowing it to equilibrate with the water temperature. A 5°F error in temperature will result in approximately a 1-percent bias in the measured velocity. The speed of sound is also sensitive to salinity. A 5-part-per-thousand error in salinity would result in an approximate velocity bias of 1 percent, when used in saline environments like estuaries; therefore, the operator needs to measure the salinity and input the value into the FlowTracker.

Maintenance and Care

Although the built-in QCTest is reliable for detecting issues, a BeamCheck stores more system performance data and still may be needed to evaluate the unit in more detail when there is a potential issue.

QCTests and BeamChecks

- Perform a QCTest and store it with each measurement. When a QCTest is completed as part of a measurement, it will print out on the measurement summary.
- Complete a QCTest in flowing water with the sample volume away from any boundaries.
- Perform a BeamCheck if you notice any anomalies in the QCTest. Any failures in a QCTest require a BeamCheck.
- Perform a BeamCheck after any possible physical damage (drop, and so forth), firmware upgrade, or repair.

As stated previously, the FlowTracker is an acoustic Doppler velocimeter (ADV) that has been adapted to fit on a typical USGS streamgaging wading rod, developed by the USGS in cooperation with the SonTek/YSI Inc., and is widely used by the USGS. The FlowTracker has undergone extensive testing to evaluate differences between the FlowTracker performance and vertical-axis current meters (that is, Price AA, pygmy, and so forth).

The USGS Office of Surface Water, through the HIF, has put into place a process that will check and recalibrate each FlowTracker approximately every 3 years to ensure the quality assurance/quality control of this instrument in the measurement of the Nation's surface-water resources. For additional details, see Office of Surface Water Memorandum 2010.02 (2010).

Acoustic Digital Current Meter (ADC)

Another development that is a potential alternative to the Price AA and pygmy meters for wading discharge measurements is the Ott acoustic digital current meter (ADC) (fig. 41). The Ott ADC operates with two transducers at an acoustic frequency of 6 MHz, and measures the phase change caused by the Doppler shift in acoustic frequency that occurs when a transmitted acoustic signal reflects off particles in the flow. The phase measurement is restricted to ±180 degrees and uses a pulse scheme with two different time delays to resolve the phase ambiguity.

The velocity (V) is computed using the following formula:

$$V = \frac{c \times \Delta\Phi}{4 \times \Pi \times \tau}, \quad (19)$$

where V velocity (in distance per unit time),
c speed of sound in water (in distance per unit time),
$\Delta\Phi$ computed phase difference, and
τ time lag between pulses.

The Ott ADC uses a pulse-coherent technique. Transmitted pulses have a known lag time (τ). Backscatter echoes are amplified in the sensor head and then sent to the handheld display where they are digitized. A stable quartz oscillator controls the measurement sequence.

The Ott ADC has several unique data-processing requirements because of its method of operation and some of the inherent limitations of the acoustic Doppler measurement technique. Unlike mechanical meters that use the momentum of the water to turn a propeller and directly measure the velocity of the water, the Ott ADC, as with other acoustic Doppler current meters in use in the USGS and elsewhere, does not measure the velocity of the water. The Ott ADC measures the velocity of particles (sediment, small organisms, and bubbles) suspended in the flow, assuming that these particles travel at the same velocity as the

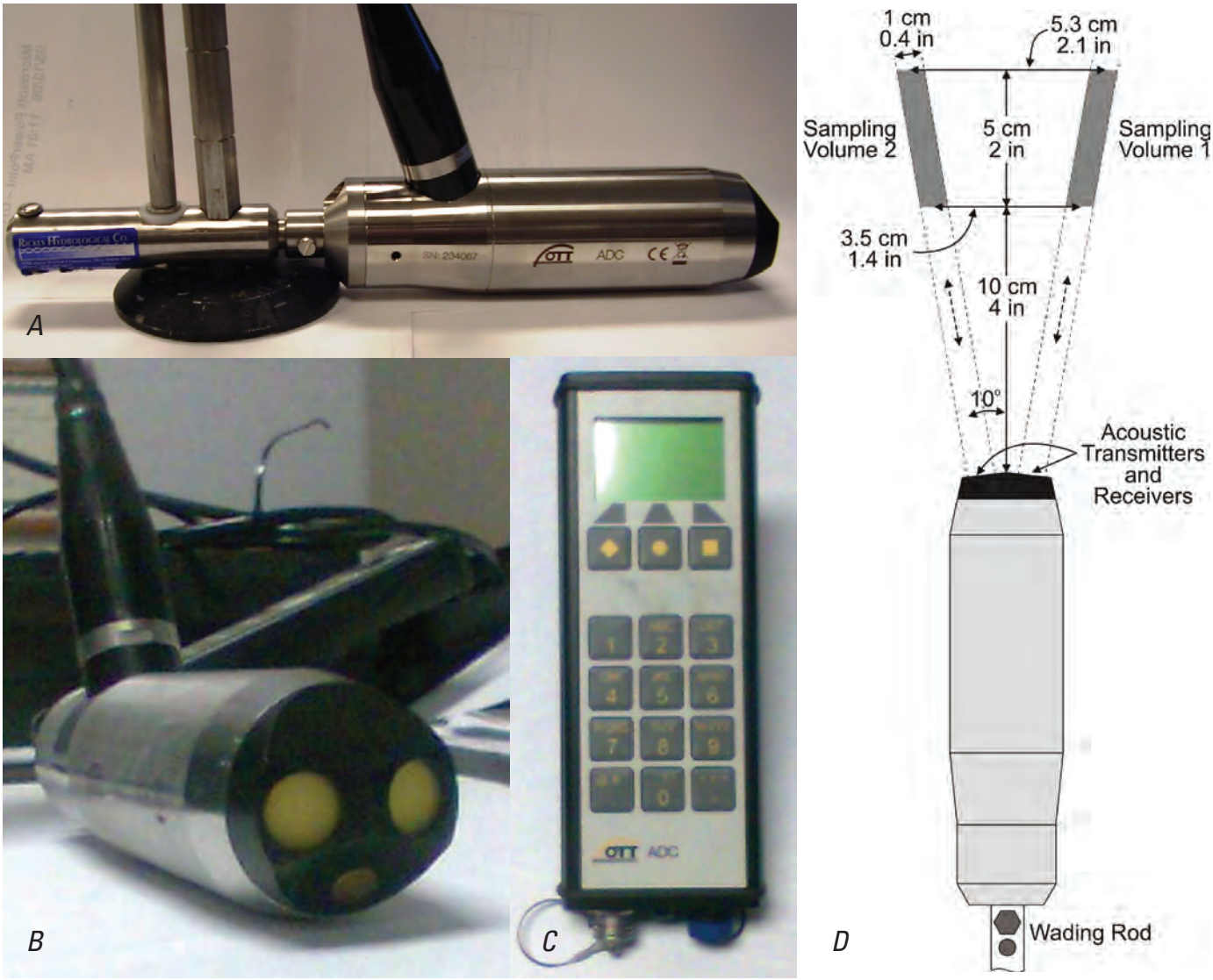

Figure 41. *A*, Ott acoustic digital current meter (ADC) mounted on a standard top-setting wading rod; *B*, closer view of transmitting and receiving transducers; *C*, ADC datalogger; and *D*, schematic of the sampling volume and transducers.

water. Therefore, the quality of the measurement is dependent on the presence of particles within the sampling volume that reflect a transmitted signal. In addition, the Ott ADC measures depth by using an absolute piezoresistive pressure cell with a range of 0 to about 16.4 ft (0–5 m). The pressure cell is located inside the probe and protected by the wading rod adapter, which is securely fastened with two screws. The hydrographer can estimate a depth without reading the top-setting rod.

Preliminary testing of the Ott ADC at the HIF indicates this technology has a lot of potential for use as an alternative to mechanical current meters.

Acoustic Doppler Current Profiler (ADCP)

The ADCP measures velocity magnitude and direction using the Doppler shift of acoustic energy reflected by material suspended in the water column, providing essentially a complete vertical profile of velocity.

Broadband, narrowband, and other pulse-to-pulse coherent ADCPs transmit pairs of acoustic pulses along a narrow beam from each of multiple transducers. As the pulses travel through the water column, they strike suspended sediment and organic particles (referred to as "scatterers") that reflect some of the acoustic energy back to the ADCP. The ADCP receives and records the reflected pulses. The reflected pulses are separated by time differences (range gating) into successive volumes called "depth cells." The frequency shift (known as the Doppler effect) is proportional to the velocity of the scatterers relative to the ADCP. The ADCP computes a velocity component along each beam, because the beams are positioned at a known angle from the vertical (usually 20 or 30 degrees) and in known horizontal orientations so that trigonometric relations can be used to compute three-dimensional water-velocity vectors for each depth cell. Therefore, the ADCP produces vertical profiles of velocity composed of water speeds and directions at regularly spaced intervals, vertical profiles of velocity, discharge profiles, and a wealth of information for a discharge measurement (fig. 42).

The Broadband ADCPs (such as the Teledyne RD Instruments Rio Grande ADCPs) use phase-coded pulses, such that many independent measurements of velocity can be made by a single Broadband pulse of the same length as a narrow-band pulse. These independent measurements are averaged to produce a velocity with a lower uncertainty than would be possible with a single measurement. Narrow-band systems (such as the SonTek/YSI RiverSurveyor S5 and M9) typically compensate for this characteristic by pinging faster (sending more pulses per second, up to 20 Hz) and reporting a velocity based on the average of many pulses with a typical velocity output of 1 Hz.

Currently, the most common main external components of an ADCP are a transducer assembly and a pressure case. Commonly, the transducer assembly consists of three to nine transducers that operate at a fixed, ultrasonic frequency, typically 300 to 3,000 kilohertz (kHz). The transducers are horizontally spaced around the transducer assembly; all transducers have the same fixed angle from the vertical, referred to as a "beam angle," that is typically between 20 and 30 degrees. The transducer assembly may have a convex or concave configuration or, in the case of the phased array, an essentially flat surface. The pressure case is attached to the transducer assembly. Examples of several different ADCPs used in the USGS are shown in figure 43.

When an ADCP is deployed from a moving boat, it is connected by cable to a power source and by cable or radio modem to a portable microcomputer. The computer is used to program the instrument, monitor its operation, and collect and store the data. For a detailed description of how an ADCP measures velocity and computes discharge, and detailed instruction in the use of ADCP technology with reference to moving boats, see Mueller and Wagner (2009).

Midsection Method With an ADCP

When an ADCP is deployed to perform a midsection method discharge measurement, most best practices used for mechanical-meter discharge measurements still apply. These practices, including site selection, are well documented in Rantz and others (1982). The midsection method with an ADCP is similar to the midsection method used for mechanical-meter discharge measurements and involves measuring the channel area and water velocities of a stream at a cross section; however, instead of point measurements of velocity, with this method, the average velocity is obtained by profiling the velocity in the water column at each section. The channel is divided into a number of vertical subsections. Most natural channels must be divided into 20 or 30 subsections to adequately characterize their irregular geometry. The depth and average velocity are measured at each subsection and are applied to a subarea whose width extends halfway to the preceding and following observation points. The area of each subsection is determined by directly measuring width and depth. The average water velocity in each subsection is estimated using the measured velocity at elected locations in the vertical. The total discharge within the stream is the sum of the individual subsection discharges.

Additional details and in-depth discussion of ADCP technology, methodology, and quality assurance and quality control can be found in USGS publications by Simpson and Oltmann (1993), in Lipscomb (1995), Morlock (1996), Oberg and others (2005), and Mueller and Wagner (2009). The ADCP method is a relatively new and evolving technology, and as a result, there are ongoing changes to the hardware, software, and firmware.

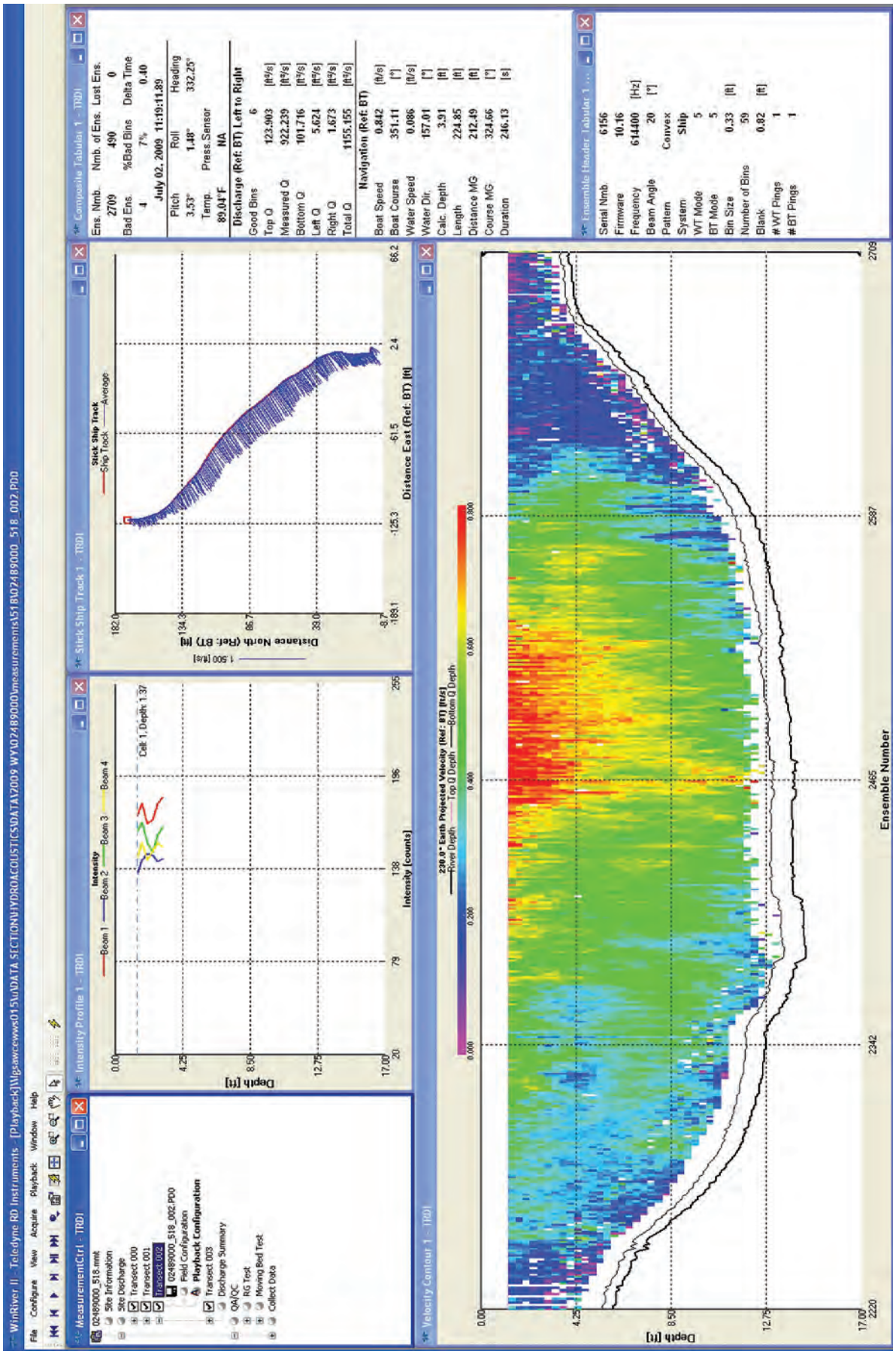

Figure 42. Screen capture of an ADCP measurement of discharge for the Pearl River near Columbia, MS (02489000).

Figure 43. Examples of acoustic Doppler current profilers (ADCPs) used to measure discharge at gaging stations; *A*, Teledyne RD Instruments 600 kHz Rio Grande ADCP; *B*, Teledyne RD Instruments 600 kHz RiverRay phased array ADCP, and *C*, closeup view of phased array transducer; *D*, SonTek/YSI RiverSurveyor S5; *E*, SonTek/YSI RiverSurveyor M9; and *F*, Teledyne RD Instruments StreamPro ADCP.

Optical Current Meters

An optical current meter, as shown in figure 44, is a stroboscopic device designed to measure surface velocities in open channels without immersing equipment in the stream. The optical current meter is used principally in measurements of surface velocity during floods when it is impossible to use streamgaging equipment that requires placement in the water, because of extremely high velocities and high-debris content in the stream. Use of this technology and other technologies, such as radar, deserves further investigation in the measurement of discharge using surface velocities.

Figure 44. Hydrographer using an optical current meter to measure surface velocity.

Sounding Equipment

Sounding (determination of depth) is commonly done mechanically; the equipment used depends upon the type of measurement being made. Measure depth and position in the vertical with a rigid rod or by a sounding weight suspended from a cable. The cable is controlled either by a reel or by a handline. A sonic sounder is also available, but it is usually used in conjunction with a reel and a sounding weight. The various equipment that can be used for sounding is described in the following paragraphs. In addition, ADCPs can sound depths using sophisticated algorithms that may have global positioning features and capabilities. Mueller and Wagner (2009) discuss ADCP sounding in more detail.

Top-Setting Wading Rods

The two types of wading rods commonly used are the top-setting rod and the round rod. The top-setting rod is preferred because of the convenience in setting the meter at the proper depth and because the hydrographer can keep his hands dry.

The top-setting wading rod, as shown in figure 45, has a ½-in. hexagonal main rod for measuring depth and a ⅜-in. diameter round rod for setting the position of the current meter.

The rod is placed in the stream so the base plate rests on the streambed, and the depth of water is read on the graduated main rod. When the setting rod is adjusted to read the depth of water, the meter is positioned automatically for the 0.6-depth method, as shown in figure 46. The 0.6-depth setting is the setting measured down from the water surface. This setting is the same as the 0.4-depth position when measured up from the streambed. When the depth of water is divided by 2, and this value is set on the setting rod, the meter will be at the 0.8-depth position from the water surface. When the depth of water is multiplied by 2, and this value is set, the meter will be at the 0.2-depth position from the water surface.

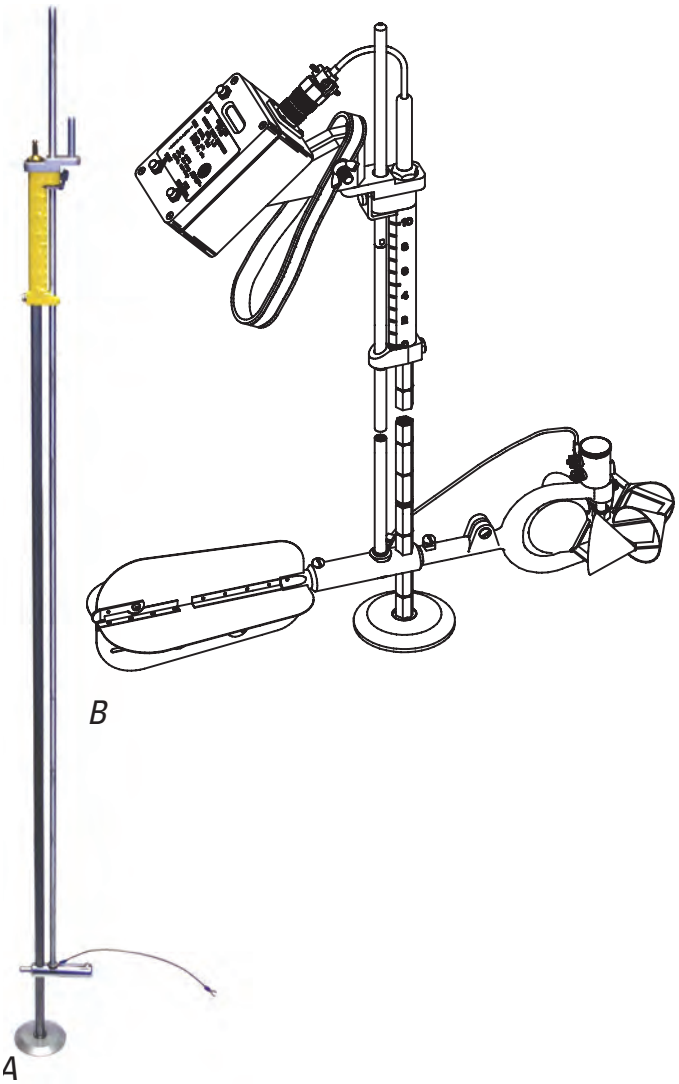

Figure 45. *A*, Top-setting wading rod and *B*, schematic of a top-setting wading rod with Price AA current meter and current-meter digitizer (CMD) attached.

Figure 46. Closeup view of setting scale on handle of top-setting wading rod.

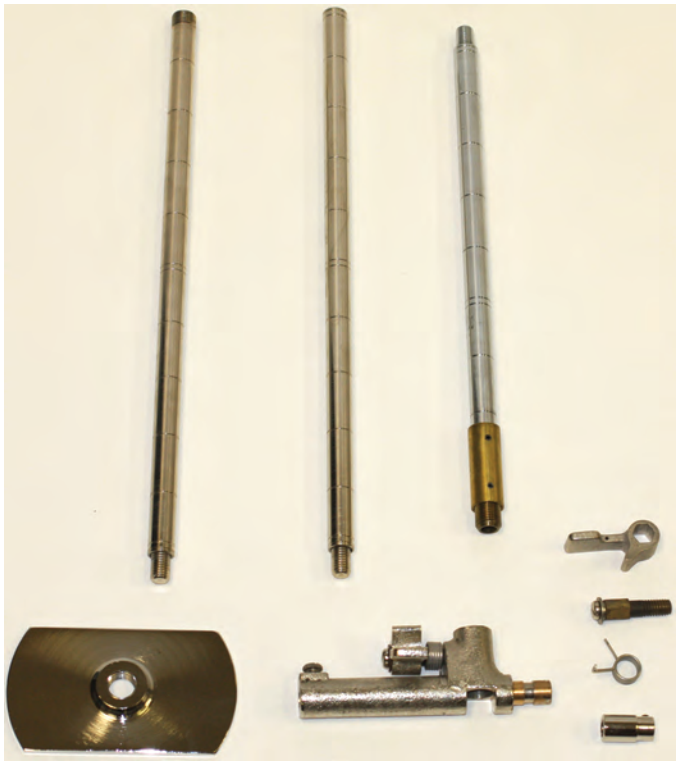

Figure 47. Parts for the round wading rod.

Round Wading Rods

The round wading rod, as shown in figure 47, consists of a base plate, lower section, sliding support, three or four intermediate sections, and a rod end (not essential). The parts are assembled as shown in figure 48. The meter is mounted on the sliding support and is set at the desired position on the rod by sliding the support. The round rod can be assembled into various lengths using the 1-ft sections, and it is easy to store and transport when disassembled.

Figure 48. Round wading rod with Price AA current meter attached.

Winter-Style Suspension Wading Rods

Measurements made under ice cover should use the WSCan winter sounding rods, either in the ½- or 1-in.-diameter versions. These rods are available in sections so that the desired length can be assembled. A special foot fits the lower section, and the rods will accommodate the winter-style current-meter yoke, as shown in figure 49.

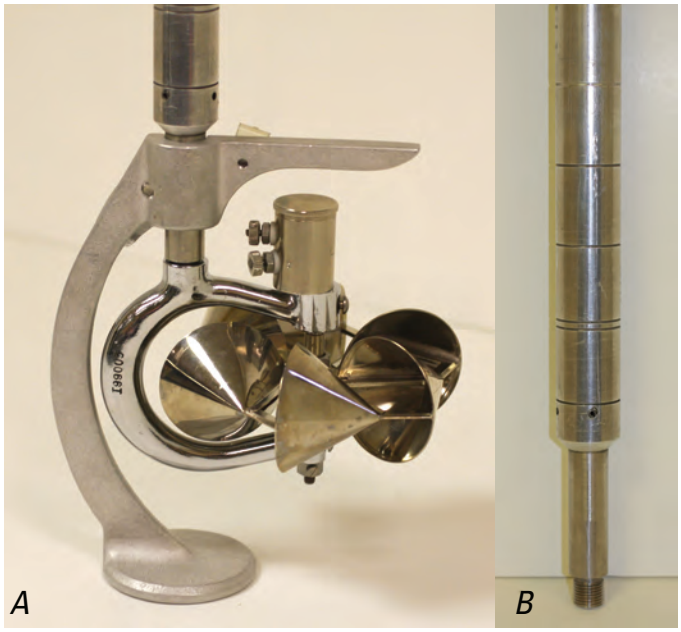

Figure 49. Water Survey Canada winter-style round 1-inch suspension rod and meter: *A*, with Price AA meter in a winter-style yoke attached and *B*, closer view of round 1-inch diameter suspension rod.

Figure 50. Columbus C-type sounding weights (15 through 300 pounds).

Sounding Weights

If a stream is too deep or too swift to wade, the current meter is suspended in the water from a boat, bridge, or cableway. A sounding weight is suspended below the current meter to keep it stationary in the water. The weight also prevents damage to the meter when the assembly is lowered to the streambed.

The sounding weights currently used are the Columbus weights, commonly called the C type, and are shown in figure 50. The weights are streamlined to offer minimum resistance to flowing water. The weights are available in 15-, 30-, 50-, 75-, 100-, 150-, 200-, and 300-pound sizes. Each weight has a vertical slot and a drilled horizontal hole to accommodate a weight hanger and securing pin.

Hanger Bars

The weight hanger is attached to the end of the sounding line by a connector. The current meter is attached to the hanger bar beneath the connector, and the sounding weight is attached to the lower end of the hanger bar.

There are three types of weight hanger bars, as shown in figure 51:

1. The Columbus or C type, ⅛ × ¾ × 12 in. (for weights up to 150 pounds);
2. Heavy weight, ⅛ × ¾ × 18 in. (for 200- and 300-pound weights);
3. Heavy weight, ⅛ × 1 ½ ×18 in. (for 200- and 300-pound sounding weights that have the slots properly extended to accommodate a l½-in. wide hanger bar).

Figure 51. Sounding weight hanger bars and hanger pins.

The Columbus hanger bar contains three holes in order to properly position the meter. The hanger screw of the current-meter yoke is placed through the bottom hole to support the meter when a 30-pound sounding weight is used. The center of the meter cups is then 0.5 ft above the bottom of the weight. This arrangement is designated as 30 C .5, which means that a 30-pound Columbus weight is being used and the center of the meter cups is 0.5 ft above the bottom of the weight. The hanger screw goes through the middle hole when 15- or 50-pound weights are used. The designations for these arrangements are 15 C .5 and 50 C .55. The hanger screw goes through the upper hole when 50-, 75-, 100-, and 150-pound weights are used. The designations for these arrangements are 50 C .9, 75 C 1.0, 100 C 1.0, and 150 C 1.0. Each of the two heavy-weight hangers has only one hole for the hanger screw of the meter. The designations for these arrangements are 200 C 1.5 and 300 C 1.5.

Weight-hanger pins of various lengths, as shown in figure 51, are available for attaching the sounding weight to the hanger bar. The stainless steel pins are threaded on one end to screw into the hanger bar and slotted on the other.

Sounding Reels

Several different types of sounding reels are available for use with the Columbus C-type weights. In general, a sounding reel has a drum for winding the sounding cable, a crank-and-ratchet assembly for raising and lowering the weight or holding it in any desired position, and a depth indicator. Table 11 contains detailed information on each of the five most commonly used reels.

The A-pack reel, as shown in figure 52, is light, compact, and ideal for use at cableway sites a considerable distance from the highway. It can also be used on cranes, bridge boards, and boat booms.

Figure 52. A-pack reel.

Table 11. Sounding reel data.

Reel	Sounding cable	Cable diameter, in inches	Drum circumference, in feet	Cable capacity, in feet	Maximum weight, in pounds	Depth indicator	Brake	Type of operation
A-pack	Ellsworth	0.084	1	45	50	Counter	No	Hand.
Canfield	Single conductor[1]	.0625	1	45	50	Counter	No	Hand.
A-55	Ellsworth	.084 .10	1	95 80	50 100	Self computing	No	Hand.
B-56	Ellsworth	.10 .125	1.5	144 115	150 200	Self computing	Yes	Hand or power.
E-53	Ellsworth	.10 .125	2	206 165	150 300	Self computing	Yes	Power.

[1]Some Canfield reels have been converted to double-conductor cable but most of them are still used as single-conductor reels.

The Canfield reel, as shown in figure 53, is also compact with uses similar to that of the A-pack reel. The Canfield reel is not available from the HIF, and must be obtained from Leupold and Stevens Instruments, Inc.

The A–55 reel is for general purpose use with the lighter sounding weights, as shown in figure 54.

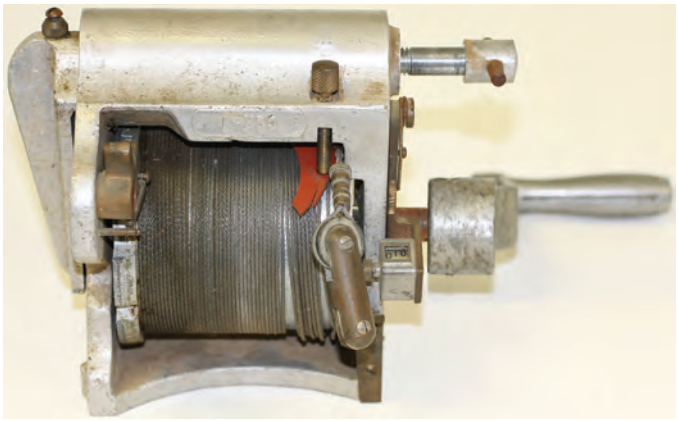

Figure 53. Canfield reel.

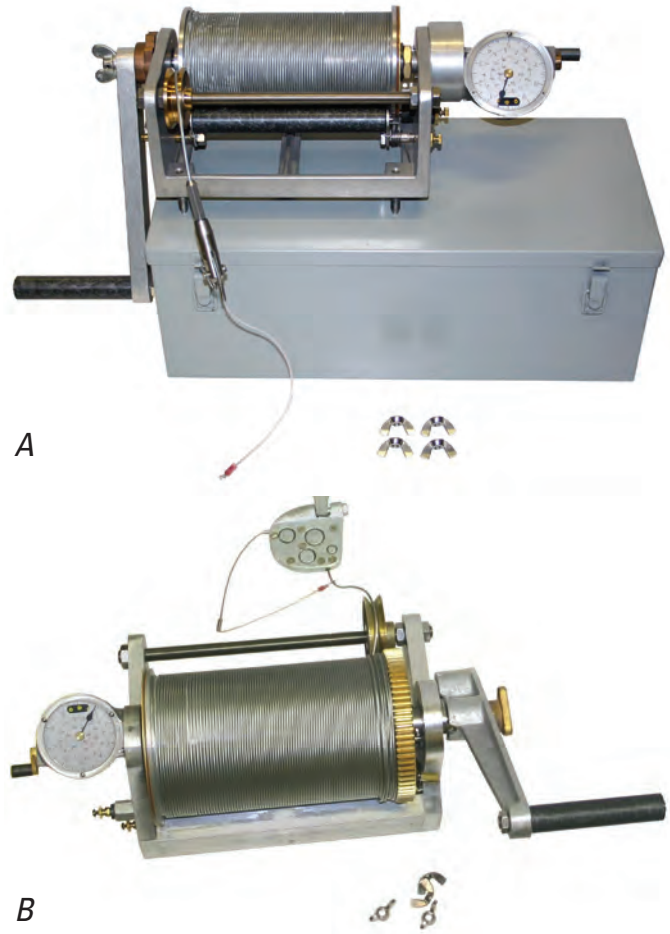

Figure 54. *A*, A–55 reel and *B*, B–56 reel.

The B–56 reel (a major modification of the B–50 reel) can handle all but the heaviest sounding weights and has the advantage that it can be used with a hand crank or power equipment, as shown in figure 54.

The E–53 reel is the largest reel commonly used for current-meter measurements. This reel will handle the heaviest sounding weights and is designed exclusively for use with power equipment. It has a hand crank for emergency use, as shown in figure 55.

Figure 55. E–53 reel.

Sounding Cable

Ellsworth reverse-lay two-conductor stranded cable is normally used on all sounding reels, except the single-conductor Canfield reel, which uses galvanized steel aircraft cord. Ellsworth cables are normally available in 0.084-, 0.100-, and 0.125-in. diameters. It is important to use the appropriate size cable-laying sheave on the reels.

For safety purposes, when measuring floods, it is important to connect the sounding cable to the sounding reel in such a way that the cable will break in the event that heavy debris is caught and cannot be released. The cable will usually unwind (pay out) from the sounding reel until it reaches its end, at which point there is danger to the equipment and the hydrographer unless the cable is cut or breaks. Precut some of the cable strands when installing the cable on the reel so that the remaining strands will break when the load reaches a specified limit. Table 8 provides information about cable strength and number of strands to cut to provide the necessary safety margin. Complete instructions for making the cable installation are given in a HIF technical information sheet dated April 1999.

Connectors

A connector is used to join the end of the sounding cable to the sounding-weight hanger. The three types of connectors generally used are types B, C1, and pressed sleeve, as shown in figure 56. The type B connector is used with A–55, B–56, and E–53 reels. The C1 connector is used with the A-pack and Canfield reels, although the pressed-sleeve connector can be used on these reels. The pressed-sleeve connector is also used on handlines.

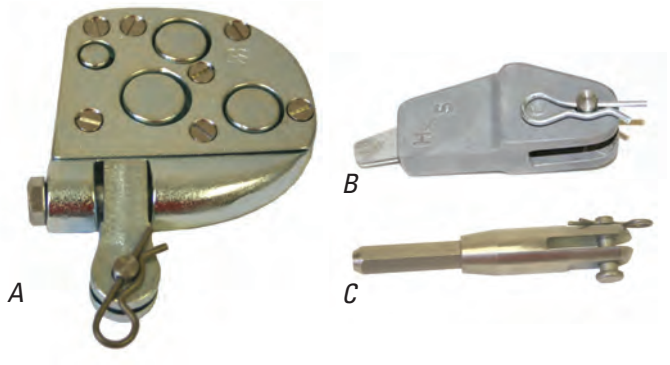

Figure 56. Connectors for attaching sounding cable to sounding-weight hanger; *A*, Type B; *B*, Type C1; and *C*, pressed sleeve.

Depth Indicators

A computing depth indicator, as shown in figure 57, is used on the A–55, B–56, and E–53 reels. The stainless-steel indicator is less than 3 in. in diameter and has nylon bushings that do not require oil. The main dial is graduated in feet and tenths of a foot from 0 to 10 ft. The depth is indicated by a pointer. Tens of feet are read on a numbered inner dial through an aperture near the top of the main dial.

The main dial has a graduated spiral to indicate directly the 0.8-depth position for depths up to 30 ft.

The A-pack and Canfield reels, shown in figures 52 and 53, are equipped with counters for indicating depths.

Figure 57. Computing depth indicator.

Handlines

A handline, shown in figure 58, is a device used for making discharge measurements from bridges using a 15- or 30-pound sounding weight. The advantages of using the handline are that it is easy to set up, it eliminates the use of a sounding reel and supporting equipment, and it reduces the difficulty in making measurements from bridges, which have interfering members, such as trusses. The disadvantages of using the handline are that there is a greater possibility of making errors in determining depth because of slippage of the handline, measuring scale, or tape, and it requires great physical exertion, especially in deep streams. Handlines can be used from cable cars, but this is not recommended because of the disadvantages mentioned above.

Ellsworth cable is recommended for handlines because of its flexibility and durability. Two-conductor electrical service cord is used between the headset connector and the handline reel.

The pressed-sleeve connector or the C1 connector is used on handlines because they are lighter in weight than the type B connector, yet strong enough for the sounding weights used with handlines.

Figure 58. Handline.

Power Unit

Power units, as shown in figure 59, are available for the B–56 and E–53 reels to raise and lower the sounding weight and meter. The power unit can be used with 6-, 12-, 18-, or 24-volt batteries.

Figure 59. Power units for sounding reels; *A*, J & H Single Speed Power Drive and *B*, USGS Variable Speed Reel Drive System.

Sonic Sounder

A commercial, compact, portable sonic sounder has been adapted to measure stream depth. The sounder is powered by either a 6- or 12-volt storage battery and will operate continuously for 10 hours on a single battery charge. Three recording speeds are available—36, 90, and 180 in. per hour. Four operating ranges—0 to 60 ft, 60 to 120 ft, 120 to 180 ft, and 180 to 240 ft—allow intervals of 60 ft of depth. The sounder is portable, weighing only 46 pounds. The depth recorded is from the water surface to the streambed. The transducer has a narrow beam angle of 6 degrees, which minimizes errors on inclined streambeds and allows the hydrographer to work close to piers or other obstructions.

Measurements can be made with this equipment without lowering the meter and weight to the streambed. As soon as the weight is in the water, the depth will be recorded. The meter can then be set at the 0.2 depth, or just below the water surface where a velocity reading is obtained. Then a coefficient is applied to convert measured velocity to the mean in the vertical.

Temperature change affects the sound propagation velocity, but this error is limited to about plus or minus 2 percent in freshwater. This error can be eliminated completely by adjusting the sounder to read correctly at a particular average depth determined by other means.

Cableway Equipment

The USGS cableway provides a track for the operation of a manned cable car from which the hydrographer makes a current-meter measurement. Most cableways have a clear span of 1,000 ft or less, although a few structures have been built with clear spans approaching 2,000 ft. The design and construction of cableways are described in detail by Wagner (1995).

Cable cars provide a movable platform from which the hydrographer, sounding reel, and other necessary equipment are supported. The newer versions of these cable cars are fabricated from aluminum, and have a standard follower brake and integral-reel mounts, which will accept all standard sounding reels, including battery-powered reels. Cable cars can also be equipped with the Sandpoint type cable-car brake, which allows the cable car to be slowed or stopped. Both sitdown and standup types of manually propelled cable cars are used in streamgaging, as shown in figures 60 and 61, and have space for two people to work. Some older cable cars still in use are fabricated partially from wood, may or may not have permanent reel mounts, and may have space for only one person.

Manned cable cars are moved from one point to another on the cableway by means of cable-car pullers, as shown in figure 62. The standard car puller is an aluminum-cast handle with a snub attached. The snub, usually four-ply belting, is placed between one of the car sheaves and the cable to prevent movement of the car along the cable. A second type of puller, also shown in figure 62, is used when a car is equipped with a follower brake. A third type, the Colorado River cable-car

Figure 60. Sit-down cable car.

Figure 61. Stand-up cable car.

Figure 62. Cable-car pullers: *A*, with belt and *B*, with follower brake.

puller, is the same in principle as the puller used on cars equipped with a follower brake.

Power-operated cable cars, such as the battery-powered car shown in figure 63, are available for extremely long spans or other special situations where extensive streamgaging and monitoring is required. The power assist on these cable cars is also utilized to operate a type E sounding reel.

Unmanned, remotely operated cable carriages, such as the Hydrological Services Hornet, are used for discharge measurements as well as for sediment sampling. The cable carriage and sounding equipment can be remotely operated from the stream bank, as shown in figure 64. They are used in areas where it is impossible to wade, where no bridges are available, and where it is not practical to build or maintain a manned cableway.

Unmanned cableways are used more in Europe than in the United States, but are becoming more common in the United States. These bank-operated cableways have obvious benefits in safety and convenience (fig. 65). Both permanent and portable bank-operated cableways are becoming more useful in the measurement of discharge, especially for more narrow streams, generally 300 ft or less in top-bank width.

Figure 63. Battery-powered cable car.

Figure 64. Remotely operated Hydrological Services Hornet cable carriage with ADCP and trimaran used by the USGS.

Figure 65. Bank-operated cableway.

Bridge Equipment

Streamflow measurements are frequently made from a bridge. The meter and sounding weight can be supported by a handline, a bridge board, or by a sounding reel mounted on a crane. An ADCP mounted on a tethered craft can also be deployed from a bridge. Tethered ADCP craft are rapidly becoming the prevalent means of measuring discharge from a bridge.

Handlines and Bridge Boards

A handline, as described in a previous section of this chapter, is the simplest form of bridge-measuring equipment. Used extensively in the 20th century, it does not require any separate reels or handling equipment; however, it can only be used with light sounding weights, such as the 15- and 30-pound size. It also requires that depth be measured with tags, and a tape or measuring stick.

A bridge board is a portable platform made from wood or metal upon which a small reel can be mounted. Bridge boards may be used with an A-pack, A–55, or B–56 sounding reel and weights up to 75 pounds. A bridge board is usually about 6 to 8 ft long, with a sheave at one end over which the meter cable passes, and a reel seat near the other end. The board is placed on the bridge rail so that the force exerted by the sounding weight suspended from the reel cable is counterbalanced by the weight of the sounding reel. The bridge board may be hinged near the middle to allow one end to be placed on the sidewalk or roadway. Figure 66 shows a bridge board in use.

Figure 66. Measuring from a bridge with a bridge board.

Portable Cranes

Two types of hand-operated portable cranes are the type A for weights up to 100 pounds, and the type E for weights greater than 100 pounds. The type A crane mounts on a three-wheel or four-wheel base or truck, and the type E crane mounts on a four-wheel base or truck. Cranes can be easily moved by hand along the sidewalk or floor of the bridge. Figure 67 shows a type A crane mounted on a three-wheel base, and figure 68 shows a type E crane mounted on a four-wheel base.

Any of the reels described in table 11 may be used on either of the portable cranes; however, the power-driven reels (B–56 and E–53) are used only with the Type E crane. Various combinations of cranes, bases (trucks), and reels are possible.

Figure 67. Type A crane mounted on a three-wheel base.

Figure 68. Type E crane mounted on a four-wheel base.

All cranes are designed so that the crane can be tilted forward over the bridge rail far enough for the meter and weight to clear most rails and be lowered to the water. Where bridge members obstruct passage of the crane along the bridge, the weight and meter can be raised and the crane can be tilted back to pass by the obstruction.

Use cast-iron counterweights weighing 60 pounds with four-wheel-base cranes. The number of such weights needed depends upon the size of sounding weight being supported, the depth and velocity of the stream, and the amount of debris being carried by the stream.

Use a protractor on the outer end of cranes to measure the angle the sounding line makes with the vertical when the weight and meter are dragged downstream by high-velocity water. The protractor is a graduated circle clamped to an aluminum plate. A plastic tube, partly filled with colored antifreeze (ethylene glycol), is the protractor index. This tube is fitted in a groove between the graduated circle and the aluminum plate. A stainless-steel rod is attached to the lower end of the plate to ride against the downstream side of the sounding cable. The protractor will measure vertical angles from -25 degrees to +90 degrees. Figure 69 is a close-up view of a protractor mounted at the outer end of the boom.

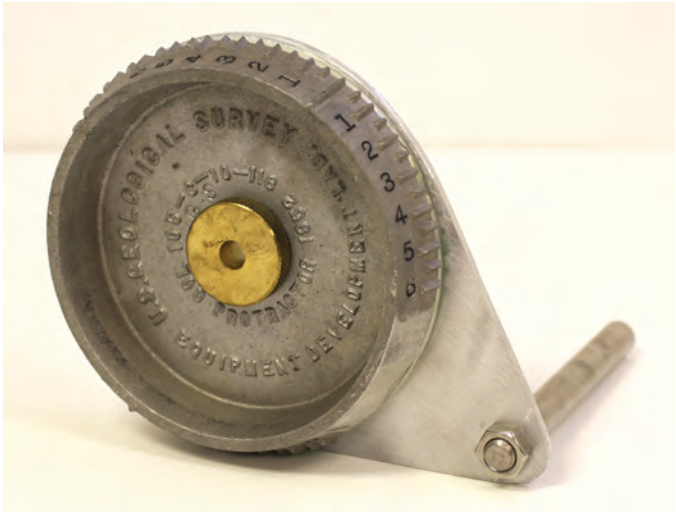

Figure 69. Protractor used for measuring vertical angles.

Power-Driven Cranes

Many special arrangements for measuring from bridges have been devised to suit a particular purpose. Vehicle-mounted cranes are often used for measuring from bridges over larger rivers, as shown in figure 70. Monorail streamgaging cars have also been developed for large rivers. The car is suspended from the substructure of bridges by means of I-beams.

Tethered Craft

The USGS, in cooperation with manufacturers, continues to test and refine tethered-platform designs for measuring streamflow. Platform specifications have been developed for

Figure 70. Vehicle-mounted, power-driven crane.

radio-modem telemetry of acoustic Doppler current profiler (ADCP) data, potential platform-hull sources have been investigated, and many hull configurations have been tested and evaluated.

Platforms, which included a variety of hull configurations, were tested for drag and stability at the USGS Hydraulic Laboratory tow tank and at a field site below a reservoir. The testing indicated that trimaran designs provided the best all-around performance under a range of conditions. The trimaran designs house the ADCP in the center hull. Waterproof radio modems that operate at 900 MHz are used to communicate wirelessly with instruments at high-baud rates.

A tethered-platform design with a trimaran hull, and 900-MHz radio modems, are commercially available from several vendors. Continued field use has resulted in USGS procedures for making tethered-platform discharge measurements, including methods for tethered-boat deployment, moving-bed tests, and measurement of edge distances. Figure 71 shows a tethered craft ADCP in wide usage in the USGS (Mueller and Wagner, 2009; Rehmel and others, 2003).

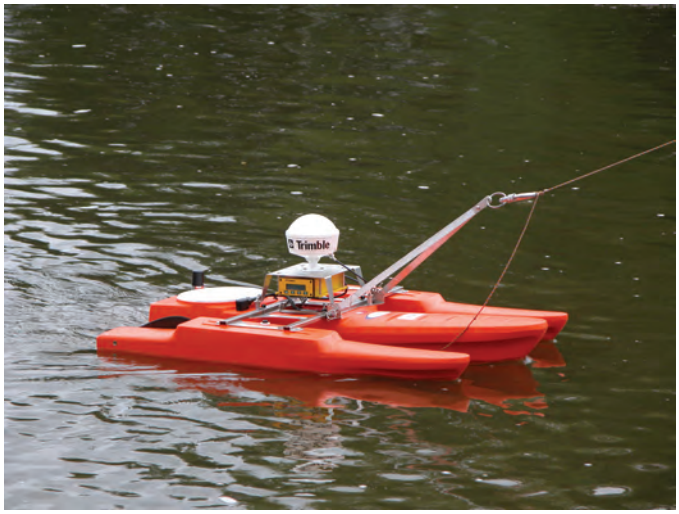

Figure 71. Measuring with a tethered ADCP, DGPS, and trimaran.

Boat Equipment

There are five basic types of boat measurements: the manual stationary boat, the manual moving boat, the automatic moving boat, the ADCP moving boat, and the remote-controlled ADCP moving boat. Equipment requirements for each of these boat measurement types are described in the following paragraphs.

Manual Stationary Boat

The manual stationary boat method uses a boat as a platform for the hydrographer and the sounding equipment. The boat is attached to a tag line or cable to stabilize it at each vertical where soundings are made. The heavy-duty tag lines required for boat measurements are described in a previous section of this chapter.

Special equipment assemblies, as shown in figure 72, are necessary to suspend the meter from the boat if the depths do not allow using rod suspension. A crosspiece spanning the boat is clamped to its sides, and a boom attached to the center of the crosspiece extends out over the bow. The crosspiece is equipped with a guide sheave and clamp arrangement at each end to attach the boat to the tag line, and makes it possible to slide the boat along the tag line from one station to the next. A small rope can be attached to these clamps so that in an emergency a tug on the rope will release the boat from the tag line. The crosspiece also has a clamp that prevents lateral movement of the boat along the tag line during readings. The boom consists of two structural aluminum channels, one telescoped within the other to permit adjustments in length. The boom is equipped with a reel plate on one end and a sheave over which the meter cable passes. The sheave end of the boom is designed so that by adding a cable clip to the sounding cable a short distance above the connector, the sheave end of the boom can be retracted when the meter is raised out of the water. The raised meter is easy to clean and is in a convenient position when not being operated.

Figure 72. Manual stationary-boat equipment assembly.

All sounding reels fit the boat boom, except the A-pack and the Canfield, which can be made to fit by drilling additional holes in the reel plate on the boom.

In addition to the equipment already mentioned, the following items are needed for making boat measurements:

1. A stable boat big enough to support the hydrographers and equipment;
2. A motor that can easily move the boat against the maximum current in the stream;
3. A pair of oars for standby use;
4. A personal floatation device (PFD) for each hydrographer; and
5. A bailing device.

Manual Moving Boat

Equipment requirements for the manual moving boat method of making a discharge measurement are described in detail by Smoot and Novak (1969); they are not described in this chapter. In summary, the manual moving-boat method requires a sonic sounder, a vane with indicator, a special current meter, and an easily maneuverable small boat. The manual moving-boat method is seldom used since the advent of the ADCP moving-boat method, which is described below.

Automatic Moving Boat

The automatic moving-boat method is similar to the manual moving-boat method, except that all readings of depth, velocity, angles, and distance are recorded automatically by onboard computer equipment. Equipment requirements are more complex in order to enable the automatic sensing and recording.

Like the manual moving-boat method, the automatic moving-boat method is seldom used since the advent of the ADCP moving-boat method.

ADCP Moving Boat

Currently, the ADCP moving-boat method is the most common moving-boat method in the USGS. All readings of depth, velocity, angles, and distance are recorded to a laptop or PDA and the discharge measurement is computed using ADCP software and input from the hydrographer.

As shown in figure 73, described in other sections of this chapter, and in depth by Mueller and Wagoner (2009), ADCP moving-boat measurement techniques have almost entirely superseded the automatic moving method.

Remote-Controlled ADCP Moving Boat

There are commercially available unmanned, remote-controlled craft with ADCPs used by the USGS and others for the measurement of discharge where a manned boat or tethered boat may not be feasible. Similar to but smaller than the ADCP moving-boat, these remote-controlled craft typically come with self-contained motors and a remote-controlled system for driving the boat across a stream or river. See Mueller and Wagner (2009) for an in depth discussion of remote-controlled ADCP moving boat discharge measurements.

Figure 73. ADCP equipment mounted and operated on *A*, a moving boat and *B*, a tethered platform.

Electronic Field Notebooks and Personal Digital Assistants (PDAs)

Recent developments in electronics have produced commercially available electronic field notebooks (EFNs) and personal digital assistants (PDAs), designed specifically for the purpose of recording field notes while making a discharge measurement (fig. 74) . The PDAs are also designed for other field procedures, including discharge-measurement data collection and processing, station inspection, differential-level survey notes, and water-quality data collection and equipment calibration. The USGS commonly uses the Surface Water Measurements and Inspections (SWAMI) program with a PDA. The program can be used to record discharge measurements, inspections, differential-level surveys, and other field measurements. This software provides an efficient means of collecting field data (fig. 2*C*) and has been specifically designed to interface with the USGS NWIS.

The recording process is semiautomatic. Basic information and data still must be entered manually for measurements of stream depth, stationing, horizontal angle of flow, equipment, and other basic data.

EFNs automatically count meter revolutions and elapsed times, and make the conversion to stream velocity. They also assist the hydrographer with certain tasks, such as locating each subsection so that no more than 10 percent of the total flow will be included in each subsection. The notebook makes all of the measurement calculations to obtain the final discharge, and to summarize all pertinent items of the measurement.

The EFNs and PDAs can store many discharge-measurement reports. The EFN and (or) PDA reports for a discharge measurement are similar to the paper note sheets used for manual note keeping. A header, similar to the paper "front sheet," contains site information, equipment information, and a summary of measurement data. The report also contains

Figure 74. Personal digital assistants (PDAs) and electronic field notebooks (EFNs), clockwise from the top: *A*, the Trimble Juno SB PDA with GPS, Bluetooth, and Parani Serial Adapter; *B*, the Trimble Nomad 800 GL PDA with GPS and Bluetooth; *C*, the Trimble Recon PDA without GPS; *D*, the JBS Instruments Aquacalc Pro Discharge Measurement Computer; and *E*, the Hydrological Services Current Meter Counter Signal Processor with Bluetooth (CMCsp).

complete measurement data, similar to the paper "inside notes," for all of the individual subsections. In addition, the report contains various warning flags and quality-control information. Complete reports for each discharge measurement can be downloaded to a computer for viewing, printing, and other analysis.

One EFN widely used within the USGS is the Aquacalc Pro Discharge Measurement Computer (Aquacalc) by JBS Instruments. The Current Meter Counter Signal Processor (CMCsp) by Hydrological Services is used in concert with a PDA to measure discharge with a mechanical current meter, as shown in figure 74. The Aquacalc and the CMCsp will work with the cat's-whisker-, magnetic-, and optic-contact chambers on the Price current meters. As with all EFNs, care should be taken to avoid false counting of meter revolutions when measuring low velocities with mechanical meters that have a cat's-whisker-contact chamber.

PDAs are manufactured by many computer companies in the United States and abroad. Several are considered reliable and have been successfully field tested. At this writing, the PDA can interface with most of the ADCPs and electronic data loggers used by the USGS.

Miscellaneous Equipment and Personal Items

Other personal equipment and items will be needed while making discharge measurements, or when working in and around rivers, creeks, and streams. Waders or boots should be worn while making wading measurements. Waders should be loose fitting, even when allowing for heavy winter clothing.

Ice chains, as shown in figure 75, should be strapped onto the soles of boots or waders for use on steep or icy stream banks, and on rocky or smooth and slippery streambeds.

A properly fitted personal-floatation device (PFD) must be worn when working near, in, or over water. This includes while wading streams, and working on a cableway, bridge, or water retention or control structure, on ice, or in a boat.

Figure 75. *A*, Ice chains for boots and waders and *B*, Sure Grip Ice Treads for boots and waders.

Accuracy of Current-Meter Discharge Measurements

The accuracy of a discharge measurement is dependent on many factors, including the equipment used, the location and characteristics of the measuring section, the number and spacing of verticals, the rate of change in stage, the measurement of depth and velocity, presence of ice and (or) debris in the measuring section, wind, experience of the hydrographer, carefulness (or carelessness) of the hydrographer, and various conditions that can occur during the process of making the measurement. The evaluation of the accuracy of a measurement has long been a qualitative assessment that takes some or all of these factors into account. A quantitative measure of the accuracy for some discharge measurements can also be made. The following two sections of this chapter describe these methods.

Qualitative Evaluation

Every discharge measurement should be evaluated for accuracy using the qualitative method. Historically, this has been the preferred method, and the hydrographer should make this evaluation immediately after making the measurement. The evaluation should be based on the hydrographer's opinion of the accuracy of the measurement—not on how well, or how poorly, the measurement plots on the stage-discharge relation. It is difficult to provide written guidelines for making a qualitative evaluation of accuracy. A good qualitative evaluation depends mostly on the experience and training of the hydrographer. Several of the factors that should be considered by the hydrographer are as follows:

Measuring section.—Consider factors such as the uniformity of depths, the smoothness of the streambed, the streambed material (that is, smooth sand; small, firm gravel; large rocks; soft muck; and so forth), the ability to accurately measure the depth, the approach conditions, presence of bridge piers, and other conditions that would affect measurement accuracy.

Velocity conditions.—Consider smoothness of velocity, uniformity of velocity, very slow velocity, very high velocity, turbulence, obstructions that may affect the vertical velocity distribution, use of one-point or two-point method, length of counting (40 or more seconds versus half-counts), and other factors that affect accuracy of velocity measurements.

Equipment.—Consider the type of current meter used (Price AA, Price pygmy, acoustic, or electromagnetic), the type of depth-sounding equipment, and the condition of the equipment.

Spacing of observation verticals.—Use about 25 to 30 verticals for a discharge measurement, spaced so that no more than 5 percent of the total discharge is contained in each subsection. Although this is frequently difficult to attain, except in unusual cases, no more than 10 percent of the total discharge should be in a subsection. Otherwise, the accuracy will be negatively affected.

Rapidly changing stage.—Although discussed in previous sections of this chapter, this condition should also be considered when assessing the accuracy of the measurement. Using the shortcut methods previously described will result in less accurate measurements of discharge.

Ice measurements.—Making discharge measurements under ice cover is usually more difficult, and sometimes less accurate, than making open-water discharge measurements. Presence of slush ice, layered ice, and anchor ice will have adverse affects on accurate measurement of depth and velocity. Velocity distribution will be affected if the water surface is in contact with the ice. Freezing of water in the meter cups and pivot chamber may affect performance of the equipment.

Wind.—Wind can affect the accuracy of a discharge measurement by obscuring the angle of the current, or by creating waves that make it difficult to sense the water surface prior to making depth soundings. Wind can also affect the vertical-velocity distribution, particularly near the surface, and can cause vertical and (or) horizontal movement of the current meter while making a boat measurement, introducing possible error in velocity measurements.

The qualitative method of assessing the accuracy of a discharge measurement requires that the hydrographer consider all of the above items and their cumulative effect on the measurement accuracy. The front page of the discharge measurement note sheet (see figure 2) has space for describing (1) the cross section, (2) the flow, (3) the weather, and (4) any other flow conditions that relate to the accuracy. These descriptions, along with the type of equipment, number of verticals, velocity measurement method, and other measurement conditions, should provide the basis for rating the measurement as excellent (2 percent), good (5 percent), fair (8 percent), or poor (more than 8 percent).

For instance, a measurement might be rated as excellent (2 percent) if (1) the cross section is smooth, firm, and uniform; (2) the velocity is smooth and evenly distributed; (3) the equipment is in good condition; (4) the two-point velocity measurement method was used; and (5) weather conditions are good (no wind or ice). On the other hand, if several of these factors make it difficult to accurately measure depth and (or) velocity, the measurement might be rated fair (8 percent), or even poor (more than 8 percent).

As stated previously, it is not possible to provide absolute guidelines for making the qualitative evaluation of accuracy. As a general rule, the accuracy of most discharge measurements will be about 5 percent, or qualitatively a "good" measurement. This is sometimes used as the base-line accuracy, with accuracy upgraded to "excellent" when measuring conditions are substantially better than average, and accuracy downgraded to "fair" or "poor" when conditions are substantially worse than average. The qualitative-accuracy evaluation is based on the hydrographer's judgment. For more detailed qualitative-evaluation information on discharge measurements using ADCPs, see Oberg and others (2005) and Mueller and Wagner (2009).

Quantitative Evaluation

A quantitative-accuracy evaluation can be made for some current-meter discharge measurements by using the procedure described by Sauer and Meyer (1992), Herschy (1994), and the International Organization for Standardization (1997). These procedures compute the uncertainty, or standard error, using a root-mean-square error analysis of individual component errors. The component errors include errors in the measurement of width, depth, and velocity, and in computation procedures. These procedures can be used to compute the standard error for most discharge measurements made with the vertical-axis, cup-type current meter. These procedures do not apply to measurements made with other types of current meters, or other methods of making discharge measurements. Likewise, they do not apply to discharge measurements where wind, ice, boundary effects, flow obstructions, improper equipment, incorrect measuring procedures, and hydrographer carelessness are factors in the measurement.

The details of the Sauer and Meyer (1992) method are described in USGS Open-File Report 92–144, and therefore are not included in this chapter. A computer program is available to compute the standard error for individual discharge measurements, and it is recommended that this quantitative evaluation be made for each discharge measurement for which it applies. Computations using this method show that the standard error of individual discharge measurements can range from about 2 percent for ideal conditions, to about 20 percent for very poor measuring conditions. Standard errors range from about 3 percent to 6 percent for measurements having generally normal measuring conditions. The standard errors computed by this method are in close agreement with qualitative evaluations.

ADCP Discharge-Measurement Accuracy

There are many sources of error in an ADCP discharge measurement. A complete measurement is composed of the ADCP-measured channel subsection, extrapolated top subsection, extrapolated bottom subsection, and edge-estimated subsections.

The largest and most substantial subsection is the ADCP-measured channel subsection. Most errors can be greatly reduced if factors, such as moving bed, water temperature, salinity, cross-section choice, instrument configuration, and boat speed, are carefully considered and accounted for, as described in previous sections of this chapter. Software is usually provided by the manufacturer that can be used to compute the ADCP instrument error for the measured subsection.

Errors for the extrapolated top, bottom, and edge subsections will vary, depending upon the extrapolation methods and relative proportion of the total discharge represented in these subsections. Again, these errors can be kept to a minimum through proper choice of cross section and careful measurement of variables, such as ADCP transducer depth and distances from each shore to the nearest ADCP section.

Studies by Morlock (1996) and Oberg and Mueller (2007) concluded that ADCP discharge measurements can be used successfully for streamflow data collection under a variety of field conditions. In Morlock (1996), 31 ADCP discharge measurements were compared to discharge ratings defined by conventional methods for the period over which the ADCP measurements were made. These comparisons showed that 25 ADCP measurements were within 5 percent of the conventional measurements. Six of the ADCP measurements differed by more than 5 percent, the maximum departure being 7.6 percent.

The study by Morlock (1996) stated that ADCP discharge measurement error was indicated by the standard deviations of the ADCP discharge measurements. The standard deviations ranged from about 1 to 7 percent of the measurement discharges. The estimated error of each ADCP discharge measurement also was computed from formulas derived by the manufacturer of ADCPs. The computations of estimated measurement error assume that ADCP instrument- and unmeasured-subsection extrapolation errors are the main source of measurement error. The standard deviations for most ADCP discharge measurements were higher than the estimated measurement errors, indicating that significant components of measurement error were not related to the instruments; errors of this nature include temporal variations of flow. It was concluded that measurement precision can be positively affected by selection of a measurement location with minimal flow variations, and negatively affected by instrument- and boat-operation factors.

Uncertainties in Discharge Measurements

All discharge measurements, no matter how carefully made, are subject to uncertainty. The measurement uncertainty can be thought of as a quantitative measure of the dispersion of the measured discharge about the true discharge. This uncertainty arises because each measurement is subject to errors of unknown magnitude. The total uncertainty in a discharge measurement may arise from several sources, including:

- uncertainty in the measurement of the cross-sectional area, which in turn arises from the following:
  - uncertainty in measurements of width; and
  - uncertainty in measurements of depth;
- uncertainty in the measurement of the water-velocity profile, which in turn arises from the following:
  - instrument uncertainty;
  - pulsation and turbulence in open-channel flow;
  - deviation from our assumptions about the vertical-velocity distribution; and
  - uncertainty due to oblique angles in the flow velocity;
- uncertainty due to deviation from assumptions used in the computation procedures; and
- other random or systematic errors.

These component uncertainties can be combined to estimate the total uncertainty of a single discharge measurement. Where feasible, values for these component uncertainties should be estimated independently for each site.

The uncertainty is often expressed as a standard deviation. If we assume that measurement errors are normally distributed, then this uncertainty can be used to construct confidence intervals for the measured discharge value. For example, the true discharge can be expected to be within one standard deviation of the measured value at the 68-percent confidence level. At the 95-percent confidence level, the true discharge can be expected to be within two standard deviations of a single measured value.

Quality Assurance and Quality Control

It should be the goal of each hydrographer to make discharge measurements of the highest quality and with as little error as possible. As explained in other sections of this chapter there are many actions that must be performed before, during, and after the actual measuring process. In the many implicit decisions that must be made during the course of a discharge measurement, the hydrographer, through training and experience, must develop a keen sense of what is correct and incorrect through hydrologic/engineering judgment, and strive to continually take the correct course of action in making a discharge measurement. This is commonly known as quality assurance and quality control, sometimes referred to as QA/QC. Some of the QA/QC functions are implicit; that is, they are generally understood, performed automatically, and are not specifically defined in the measurement notes and sometimes must be accomplished through hydrologic/engineering judgement. Careful regard for safety, good hydrologic/engineering judgment, and observance of proper procedure are implicit functions that cannot be overstressed in making a precise and accurate discharge measurement. On the other hand, some actions are explicit, such as performing regular spin tests of current meters, or making check measurements when the first measurement may be suspect. Following are some of the QA/QC actions that should be observed for making high-quality discharge measurements. These are not all inclusive, and each hydrographer should always include and document any other actions that relate to the quality of the measurement. Additional QA/QC requirements are given in the QA/QC plan for each USGS Water Science Center.

- *Care of current meters, current profilers, and sounding equipment.*—Previous sections of this chapter describe the proper care of current meters, current profilers, and sounding equipment. Current meters are especially susceptible to damage and misalignment while in use, as well as in transit, if they are not properly protected. The hydrographer should follow all established guidelines to ensure that the streamgaging equipment, especially the current meter and (or) profiler, are in good working condition. While making a discharge measurement, the current meter should be periodically observed and checked to be sure it is operating smoothly and has not become fouled by debris, ice, or other obstructions.
- *Spin tests of current meters.*—One of the requirements for maintaining and checking current meters is a periodic, timed spin test under controlled conditions. The procedure for making a timed spin test is described in a previous section of this chapter. In addition, before, during, and after a discharge measurement, check that the rotor is turning smoothly and does not come to an abrupt stop.
- *Carefulness, good judgment, and proper procedure.*—It is the hydrographer's responsibility to apply proper procedures with care and good judgment while making streamflow measurements. These implicit functions of QA/QC should be observed at all times.
- *Computing and plotting the measurement on site.*—Compute a discharge measurement as soon as possible after it is completed. Do this at the site before leaving. If the measurement does not plot within 5 percent (or other specified percentage) of the rating curve in use, or if it is not in line with the previous trend of measurements, try to find an explanation. For instance, there may be an obvious change of the control that would explain the deviation. All such explanations should be documented in the measurement notes. If a satisfactory explanation cannot be found, then make a check measurement.
- *Making check measurements.*—If possible, while making a check measurement, select a different cross section from the original section and use a different current meter. Make the check measurement as close in time and gage height to the original measurement as possible.
- *Checking discharge measurements.*—In general, hand-computed discharge measurements are not checked for mathematical errors. Nevertheless, check measurements that do not plot within an acceptable percentage of the rating curve, or within the previous trend of measurements. Likewise, check measurements that define a significant extrapolation of the low end or high end of a rating curve. Discharge measurements recorded in an electronic notebook, such as the Aquacalc, are automatically computed and do not require checking.
- *Documentation of QA/QC.*—Document in the measurement notes, if possible, all measures taken to ensure that discharge measurements are accurate and of high quality. Some QA/QC measures require specific documentation independent of the measurement notes. For example, current-meter spin tests have specific forms that document the spin-test results and all repairs to the meter.

Safety Requirements

Practicing personal and overall safety is of utmost importance when working near, in, and above water. It is not the purpose of this chapter to describe all of the safety requirements; however, each hydrographer should be familiar with, and should observe, those requirements. Other documents provide the details of specific safety requirements for making wading measurements, and for working on ice, bridges, cableways, and boats. For instance, each USGS Water Science Center flood plan addresses such things as one-person versus multiple-person field parties, use of an approved PFD, and traffic control while making discharge measurements from bridges, cableway safety, and boat safety. USGS WRD Memorandum No. 99.32 (1999) provides safety guidance as it is related to discharge measurements, sampling, and other related streamgaging activities. Each Water Science Center has a safety officer and a safety plan; both should be consulted for specific safety issues.

Portable Weir-Plate Measurements

Current-meter measurements made in shallow depths and low velocities are usually inaccurate, if not impossible, to obtain. Under these conditions, a portable weir plate is a useful device for measuring the discharge.

A 90-degree V-notch weir is suitable because of its favorable accuracy at low flows. A weir made of 10- to 16-gage galvanized sheet iron will produce a free-flowing nappe, having the effect of a sharp-crested weir, and will give satisfactory performance. The thickness of the plate should vary with the size of the weir. Refer to figure 76 for recommended proportions. Decreasing the plate thickness on larger weirs will help maintain portability. The notch is cut, without sharpening, leaving a flat, even edge. Framing, in the form of small-angle irons, is required for medium and large sizes. Canvas attached on the downstream or upstream side prevents leakage under or around the weir. Eyebolts, properly placed, will secure rods driven in earth channels to stabilize the plate.

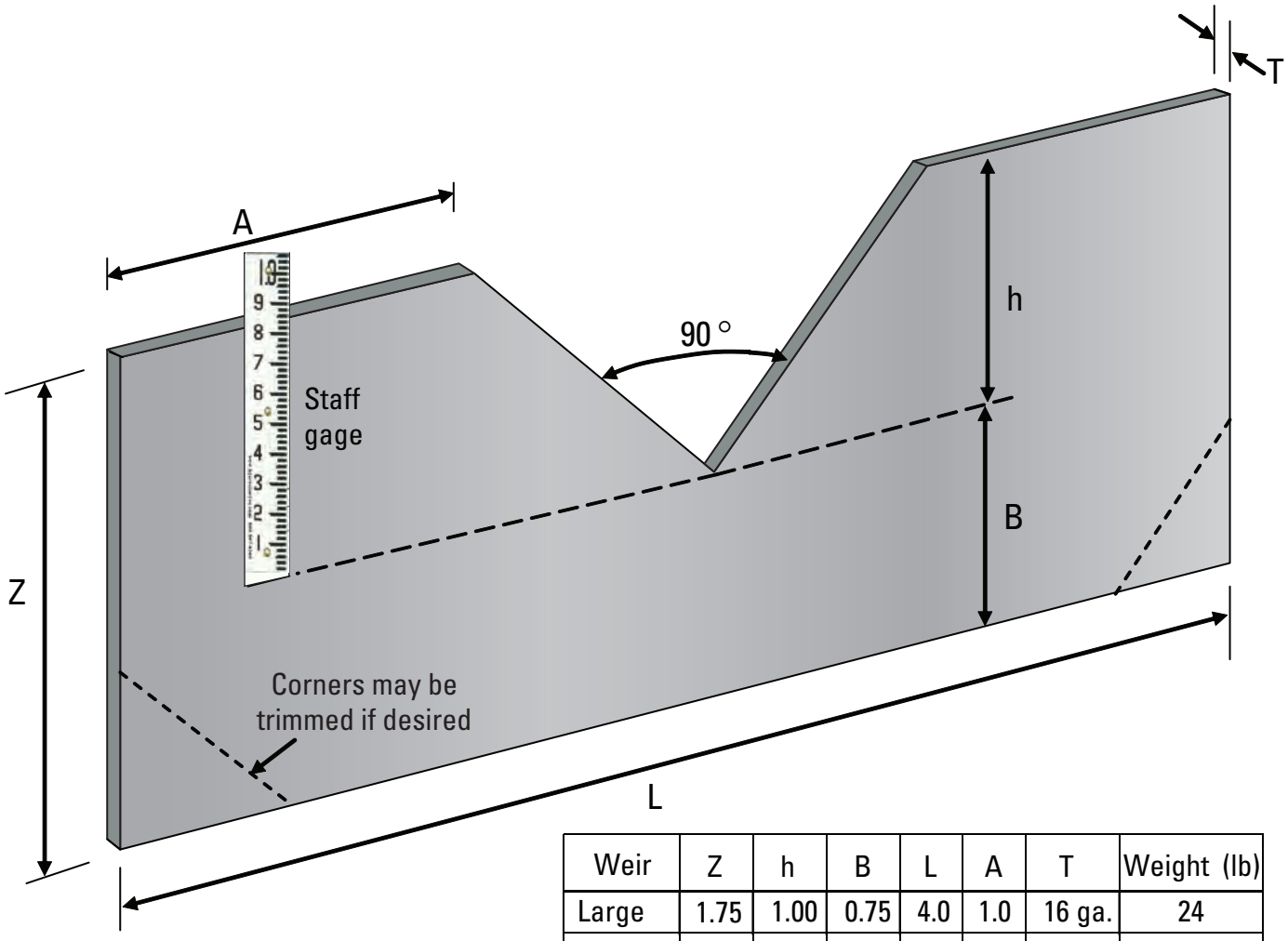

Weir	Z	h	B	L	A	T	Weight (lb)
Large	1.75	1.00	0.75	4.0	1.0	16 ga.	24
Medium	1.25	0.80	0.45	3.0	0.7	14 ga.	17
Small	0.75	0.47	0.28	2.0	0.53	10 ga.	8

Figure 76. Portable weir plate.

Attach a staff gage to the upstream face of the weir plate, with the zero point at the same elevation as the bottom of the weir notch. The staff should be far enough from the notch to be outside of the zone of drawdown, which is a distance greater than twice the head on the notch. The staff gage is used to obtain head on the weir.

The general equation for flow over a sharp-edged triangular weir with a 90-degree notch is

$$Q = Ch^{\frac{5}{2}}, \tag{20}$$

where Q discharge, in ft³/sec,
h static head, in ft, and
C the coefficient of discharge.

The weir should be rated by determining the flow volumetrically for various values of head, or by having it rated in the HIF laboratory. In the absence of a rating, a value of C of 2.47 may be used.

Flows from 0.02 to 2.0 ft³/s are measured with the large weir of figure 76. Discharges can be measured within 3-percent accuracy if the weir is not submerged. A weir is not submerged when there is free circulation of air on all sides of the nappe.

To place the plate in a sand or silt channel, only a carpenter's level and a shovel are needed. Push the weir into the streambed, and drive the rods through the eyebolts on each end to stabilize the weir. Use the level to make the top of the plate horizontal and the plate plumb. Another way to level the plate is by fastening a staff gage or level bubble to each end of the weir, where the staff gages are set at the same elevation. The plate is leveled by making the staff-gage readings identical or by using the level bubbles. Pack soil and streambed material around the ends and bottom of the weir to prevent leakage. Place canvas immediately downstream from the weir to prevent the falling jet from undercutting the streambed. Let the flow stabilize before making a measurement. Read the gage height at half-minute intervals for a period of about 3 minutes, and use a mean value in the above equation to compute the discharge. Ordinarily, one person can measure with a weir of this type. Remove the weir after you have completed the measurement.

Portable Parshall-Flume Measurements

A portable Parshall measuring flume is useful for measuring discharge when the depths are shallow and the velocities are low. The standard Parshall flume has a converging section, a throat, and a diverging section. The floor of the converging (or upstream) section is level both longitudinally and transversely when in place. The floor of the throat section slopes downward and the floor of the diverging or downstream section slopes upward. The standard Parshall flume can be used to measure discharge under free-flow conditions, as well as submerged conditions.

The flume used by the USGS is a modified version of the standard Parshall flume. The modification consists primarily of the removal of the downstream section, which reduces the weight of the flume and makes it easier to install. Because it has no downstream section, however, it can only be used to measure free-flow conditions (that is, where the submergence ratio is 0.6 or less). This can usually be accomplished by building up the streambed by a couple of inches under the level, converging floor of the flume when the flume is installed.

Free flow occurs when the ratio of the lower head to the upper head is less than 0.6. The discharge under this condition depends only on the length of crest (width of throat section) and depth of water at the upper gage. A flume that is properly constructed has an accuracy of 2 to 3 percent under free-flow conditions.

Install the flume by placing it in the channel; fill in with available channel bed or bank material around it to prevent any water from bypassing it. Use a carpenter's level to set the floor of the converging section level. Some flumes are equipped with levels attached to the braces on the flume. After the flume is in place, the streamflow is allowed to stabilize before reading the gage. After the flow stabilizes, take gage readings at about half-minute intervals for about 3 minutes. Use an average of the gage readings with the flume rating to determine the discharge. Remove the flume after the measurement is complete.

A modified 3-in. Parshall flume is shown in figure 77. This modified version is virtually the same as the standard Parshall flume except that it does not have a diverging section. The gage height, or upstream head on the throat, is read in the small stilling well that is hydraulically connected to the flow by a ⅜-in. hole.

The basic rating equation for a flume is

$$Q = Cbh^{\frac{3}{2}}, \tag{21}$$

where Q discharge, in cubic feet per second (ft³/s),
C a dimensionless coefficient of discharge that can vary with head and other factors,
b width of the throat section, in feet, and
h head, or gage height, in the converging section, in feet.

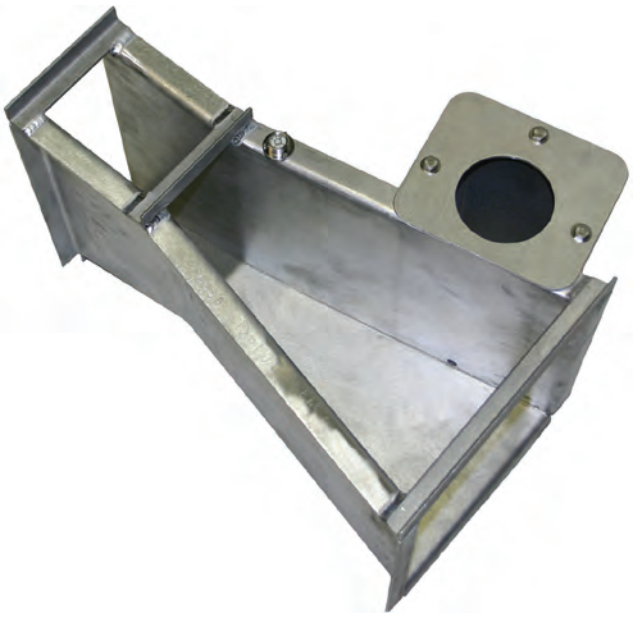

Figure 77. Modified 3-inch Parshall flume.

The rating for the 3-in. modified Parshall flume described in this section is given in table 12, and was taken from Buchanan and Somers (1969). An identical table is published by Kilpatrick and Schneider (1983), and also by Rantz (1982). The original source of this rating is unknown, but was probably based on laboratory tests. The rating in table 12 plots as a straight line on logarithmic plotting paper, and the equation for this rating was computed by regression analysis as follows:

$$Q = 1.1392h^{1.5797}. \quad (22)$$

This equation is close to one that can be derived for the 3-in. modified Parshall flume, based on the procedures given by Kilpatrick and Schneider (1983). The above equation will reproduce values of discharge precisely as shown in table 12, except for a few instances where the computed discharge deviates by 0.001 to 0.005 ft^3/s. This equation should not be used for values of gage height less than 0.01 ft or greater than 0.59 ft.

Table 12. Rating table for 3-inch modified Parshall flume.

[ft, feet; ft^3/s, cubic foot per second]

Gage height (ft)	Discharge (ft^3/s)	Gage height (ft)	Discharge (ft^3/s)	Gage height (ft)	Discharge (ft^3/s)
0.01	0.0008	0.21	0.097	0.41	0.280
0.02	0.0024	0.22	0.104	0.42	0.290
0.03	0.0045	0.23	0.111	0.43	0.301
0.04	0.0070	0.24	0.119	0.44	0.312
0.05	0.010	0.25	0.127	0.45	0.323
0.06	0.013	0.26	0.135	0.46	0.334
0.07	0.017	0.27	0.144	0.47	0.345
0.08	0.021	0.28	0.153	0.48	0.357
0.09	0.025	0.29	0.162	0.49	0.368
0.10	0.030	0.30	0.170	0.50	0.380
0.11	0.035	0.31	0.179	0.51	0.392
0.12	0.040	0.32	0.188	0.52	0.404
0.13	0.045	0.33	0.198	0.53	0.417
0.14	0.051	0.34	0.208	0.54	0.430
0.15	0.057	0.35	0.218	0.55	0.443
0.16	0.063	0.36	0.228	0.56	0.456
0.17	0.069	0.37	0.238	0.57	0.470
0.18	0.076	0.38	0.248	0.58	0.483
0.19	0.083	0.39	0.259	0.59	0.497
0.20	0.090	0.40	0.269		

Volumetric Measurements

The most accurate way of measuring small discharges is the volumetric method. This method is performed by observing the time it takes to fill a container of known capacity, or the time required to partly fill a calibrated container to a known volume. The basic equipment needed for this method is a calibrated container and a stopwatch.

Two methods can be used to calibrate the container. The first method is to add known volumes of water by increments and note the depth of water in the container. The second method is to first weigh the empty container and then add varying amounts of water to it, each time weighing the container with water, and noting the depth of water in the container. The following equation can then be used to compute the volume of water corresponding to the depth that was read:

$$V = \frac{W_2 - W_1}{w}, \tag{23}$$

where V volume of water in container, in cubic feet,
W_2 weight of container with water, in pounds,
W_1 weight of empty container, in pounds,
w unit weight of water, 62.4 lb/ft^3.

Volumetric measurements of discharge are made with two types of conditions:

- When the flow is or can be concentrated so that all of it may be diverted into a calibrated container.
- When the depth of water flowing over broad-crested weirs and dams is small and volumetric-increment samples can be obtained.

Under the first condition, measurements are made at V-notch weirs at artificial controls where all the flow is in a notch or catenary, and at places where a small earth dam can be built and all the water diverted through a pipe of small diameter. Sometimes it is necessary to place a trough against the artificial control to carry the water from the control to the calibrated container. If a small dam is built, the stage behind the dam must be allowed to stabilize before the measurement is begun. The measurement is made three or four times to ensure error-free and consistent results.

Volumetric measurements are made under the second condition by catching a segment of the streamflow with a container having a known width of opening. Samples are taken at a number of locations across the dam or weir similar to procedures used for current-meter measurements. The flow rate of each sample is increased by the ratio of the subsection width to the sampled width to obtain a discharge rate for each subsection. The total discharge of the stream is the summation of the discharge rates of each subsection.

Float Measurements

Floats have limited use in streamgaging, but they can be used where the velocity is too low to obtain reliable measurements with the current meter, or where flood measurements are needed and the measuring structure has been destroyed or it is impossible to use a meter. Both surface floats and rod floats can be used. Surface floats may be almost anything that floats, such as wooden disks, partly filled bottles, oranges, or pumpkins. Floating debris or ice cakes may serve as natural floats. Rod floats are usually made of wood and weighted on one end so they will float upright in the stream. Rod floats are sometimes made in sections so their length can be adjusted to fit the stream depth; however, they should not touch the streambed.

Two cross sections are selected along a reach of straight channel for a float measurement. The cross sections should be far enough apart so that the time the float takes to pass from one cross section to the other can be measured accurately. A travel time of at least 20 seconds is recommended, but a shorter time can be used on small streams with high velocities, where it is impossible to select an adequate length of straight channel. The edge of water for both cross sections should be referenced to stakes (or other marker) on each bank. Those points will be used at a later date, when conditions permit, to survey cross sections of the measurement reach, and to obtain the distance between cross sections. The surveyed cross sections will be used to determine the average cross section for the reach.

Float measurements may sometimes be made through a reach extending from the upstream to the downstream side of a bridge. This kind of reach may be useful where velocity is very slow and velocity observations by current meter are not reliable.

The procedure for a float measurement is to distribute a number of floats uniformly over the stream width, noting the position of each with respect to the bank. They should be placed far enough upstream from the first cross section so they attain the velocity of the stream before they reach the first cross section. Use a stopwatch to time their travel between the two cross sections. As each float passes the second cross section, note its distance.

The velocity of the float is equal to the distance between the cross sections divided by the time of travel. The mean velocity of flow in the vertical is equal to the float velocity multiplied by a coefficient that is based on the shape of the vertical-velocity profile and relative depth of immersion of the float. A coefficient of about 0.85 to 0.88 is commonly used to convert surface velocity to mean velocity. The coefficient for rod floats varies from 0.85 to 1.00, depending upon the shape of the cross section, the length of the rod, and the velocity distribution.

The procedure for computing discharge is similar to that for a mechanical current-meter measurement. The discharge in each partial section is computed by multiplying the average area of the partial section by the mean velocity in the vertical for that partial section. The total discharge is equal to the sum of the discharges for all the partial sections.

Discharge measurements made with floats under favorable conditions may be accurate to within ±10 percent. Wind may adversely affect the accuracy of the computed discharge by its effect on the velocity of the floats, especially if velocity is very slow. If a poor reach is selected and not enough float runs are made, the results can be as much as 25 percent in error.

Indirect Discharge Measurements

During floods, it is frequently impossible or impractical to measure peak discharges when they occur. Roads may be impassable; structures from which current-meter measurements might have been made may be nonexistent, not suitably located, or destroyed; knowledge of the flood rise may not be available enough in advance to allow reaching the site near the time of the peak; the peak may be so sharp that a satisfactory current-meter measurement could not be made, even with a hydrographer present at the time; the flow of debris or ice can prevent use of a current meter; or personnel limitations might make it impossible to obtain direct measurements of high-stage discharge at numerous locations during a short flood period. Consequently, many peak discharges must be determined after the passage of the flood by indirect methods, such as slope-area, contracted-opening, flow-over-dam, or flow-through-culvert, rather than by direct current-meter measurement. Detailed descriptions of the procedures used in collecting field data and in computing the discharge are given by Benson and Dalrymple (1967), Dalrymple and Benson (1967), Bodhaine (1968), Matthai (1967), and Hulsing (1967), which are in book 3, chapters Al–A5, of the USGS Techniques and Methods series. Various computer programs are available for computing the discharge for indirect measurements.

Tracer Discharge Measurements

Measurement of discharge by this method depends on determination of the degree of dilution of an added tracer solution by the flowing water. A solution of a stable tracer, such as a fluorescent dye or a radioactive chemical, is injected into the stream at either a constant rate or all at once. The solution becomes diluted by the discharge of the stream. Measurement of the rate of injection, the concentration of the tracer in the injected solution, and the concentration of the tracer at a cross section downstream from the injection point permits the computation of stream discharge. The accuracy of the method critically depends upon complete mixing of the injected solution through the stream cross section before the sampling station is reached and upon no adsorption of the tracer on stream-bottom materials. The method is recommended only for those sites where conventional methods cannot be employed owing to shallow depths, extremely high velocities, or excessive turbulence. A detailed description of the procedures and equipment used in measuring discharge by a dye-dilution method is given by Kilpatrick and Cobb (1985).

References Cited

Benson, M.A., and Dalrymple, Tate, 1967, General field and office procedures for indirect measurements: U.S. Geological Survey Techniques of Water-Resources Investigations, book 3, chap. Al, 30 p. (Also available at *http://pubs.usgs.gov/twri/twri3-a1/*.)

Bodhaine, G.L., 1968, Measurement of peak discharge at culverts by indirect methods: U.S. Geological Survey Techniques of Water-Resources Investigations, book 3, chap. A3, 60 p. (Also available at *http://pubs.usgs.gov/twri/twri3-a3/*.)

Buchanan, T.J., and Somers, W.P., 1969, Discharge measurements at gaging stations: U.S. Geological Survey Techniques of Water-Resources Investigations, book 3, chap A8, 65 p. (Also available at *http://pubs.usgs.gov/twri/twri3a8/*.)

Dalrymple, Tate, and Benson, M.A., 1967, Measurement of peak discharge by the slope-area method: U.S. Geological Survey Techniques of Water-Resources Investigations, book 3, chap. A2, 12 p. (Also available at *http://pubs.usgs.gov/twri/twri3-a2/*.)

Fulford, J.M., and Sauer, V.B., 1986: Comparison of velocity interpolation methods for computing open-channel discharge, *in* Subitsky, S.Y. , ed., Selected papers in the hydrologic sciences: U.S. Geological Survey Water-Supply Paper 2290, p. 139–44. (Also available at *http://pubs.usgs.gov/wsp/wsp2290/*.)

Herschy, Reg, 1994, The analysis of uncertainty in the stage-discharge relation: Flow Measurement and instrumentation, v. 5, no. 3, p. 188–190.

Hulsing, Harry, 1967, Measurement of peak discharge at dams by indirect methods: U.S. Geological Survey Techniques of Water-Resources Investigations, book 3, chap. A5, 29 p. (Also available at *http://pubs.usgs.gov/twri/twri3-a5/*.)

International Organization for Standardization, 1997, Measurement of liquid flow in open channels—Velocity-area methods, ISO 748:1997E, 41 p.

International Organization for Standardization, 2003, Hydrometry—Echo sounders for water depth measurements: International Organization for Standardization ISO–CD_4366_ (E revised), 15 p.

Kennedy, E.J., 1984, Discharge ratings at gaging stations: U.S. Geological Survey Techniques of Water-Resources Investigations, book 3, chap. A10, 59 p. (Also available at *http://pubs.usgs.gov/twri/twri3-a10/*.)

Kilpatrick, F.A., and Cobb, E.D., 1985, Measurement of discharge using tracers: U.S. Geological Survey Techniques of Water-Resources Investigations, book 3, chap. A16, 52 p. (Also available at *http://pubs.usgs.gov/twri/twri3-a16/*.)

Kilpatrick, F.A., and Schneider, V.R., 1983, Use of flumes in measuring discharge: U.S. Geological Survey Techniques

of Water-Resources Investigations, book 3, chap. A14, 46 p. (Also available at *http://pubs.usgs.gov/twri/twri3-a14/*.)

Lipscomb, S.W., 1995, Quality assurance plan for discharge measurements using broadband acoustic Doppler current profilers: U.S. Geological Survey Open-File Report 95–701, 7 p. (Also available at *http://pubs.usgs.gov/of/1995/ofr95-701/*.)

Matthai, H.F., 1967, Measurement of peak discharge at width contractions by indirect methods: U.S. Geological Survey Techniques of Water-Resources Investigations, book 3, chap. A4, 44p. (Also available at *http://pubs.usgs.gov/twri/twri3-a4/*.)

Morlock, Scott, E., 1996, Evaluation of acoustic Doppler current profiler measurements of river discharge: U.S. Geological Survey Water-Resources Investigations Report 95–4218, 37 p. (Also available at *http://pubs.usgs.gov/wri/wri95-4218/*.)

Mueller, D.S., and Wagner, C.R., 2009, Measuring discharge with acoustic Doppler current profilers from a moving boat: U.S. Geological Survey Techniques and Methods 3–A22, 72 p. (Also available at *http://pubs.water.usgs.gov/tm3a22*.)

Mueller, D.S., and Wagner, C.R., 2006, Application of the Loop method for correcting acoustic Doppler current profiler discharge measurements biased by sediment transport: U.S. Geological Survey Scientific Investigations Report 2006–5079, 18 p. (Also available at *http://pubs.usgs.gov/sir/2006/5079/*.)

Oberg, K.A., Morlock S.E., and Caldwell, W.S., 2005, Quality assurance plan for discharge measurements using acoustic Doppler current profilers: U.S. Geological Survey Scientific Investigations report 2005–5183, 35 p. (Also available at *http://pubs.usgs.gov/sir/2005/5183/*.)

Oberg, K.A., and Mueller, D.S., 2007, Validation of streamflow measurements made with acoustic Doppler current profilers: Journal of Hydraulic Engineers, v. 133, no. 12, p. 1421–1432.

Pierce, C.H., 1941, Investigations of methods and equipment used in stream gaging, part 1, Performance of current meters in water of shallow depth: U.S. Geological Survey Water-Supply Paper 868–A, 35 p. (Also available at *http://pubs.usgs.gov/wsp/wsp868-a/*.)

Pierce, C.H., 1947, Equipment for river measurements—Structures for cableways: U.S. Geological Survey Circular 17, 38 p., 25 pl. (Also available at *http://pubs.usgs.gov/circ/circ17/*.)

R.D. Instruments, Inc., 1989, Acoustic Doppler current profilers, principles of operation—A practical primer: San Diego, Calif., R.D. Instruments, Inc., 52 p.

R.D. Instruments, Inc., 1995, Direct reading and self contained broadband acoustic Doppler current profiler technical manual for Firmware version 5.XX: San Diego, Calif., R.D. Instruments, Inc., 460 p.

R.D. Instruments, 1996, Principals of operation. A practical primer for broadband acoustic Doppler current profilers (2d ed.): San Diego, Calif., R.D. Instruments, Inc., 52 p.

Rantz, S.E., and others, 1982, Measurement and computation of streamflow: U.S. Geological Survey Water-Supply Paper 2175, v. 2, 631 p. (Also available at *http://pubs.usgs.gov/wsp/wsp2175/html/wsp2175_vol2.html*.)

Rehmel, M.S., Stewart, J.A., and Morlock, S.E., 2003, Tethered acoustic Doppler current profiler platforms for measuring streamflow: U.S. Geological Survey Open-File Report 03–237, 15 p. (Also available at *http://pubs.usgs.gov/of/2003/ofr03-237/*.)

Sauer, V.B., and Meyer, R.W., 1992, Determination of error in individual discharge measurements: U.S. Geological Survey Open-File Report 92–144, 21 p. (Also available at *http://pubs.usgs.gov/of/1992/ofr92-144/*.)

Simpson, M.R., 2002, Discharge measurements using a Broad-Band Acoustic Doppler Current Profiler: U.S. Geological Survey Open-File Report 01–01, 123 p. (Also available at *http://pubs.usgs.gov/of/2001/ofr0101/*.).

Simpson, M.R., and Oltmann, R.N., 1993, Discharge measurement system using an acoustic Doppler current profiler with applications to large rivers and estuaries: U.S. Geological Survey Water-Supply Paper 2395, 32 p. (Also available at *http://pubs.usgs.gov/wsp/wsp2395/*.)

Smoot, G.F., and Novak, C.E., 1968, Calibration and maintenance of vertical-axis type current meters: U.S. Geological Survey Techniques of Water-Resources Investigations, book 8, chap. B2, 23 p. (Also available at *http://pubs.usgs.gov/twri/twri8b2/*.)

Smoot, G.F., and Novak, C.E., 1969, Measurement of discharge by the moving-boat method: U.S. Geological Survey Techniques of Water-Resources Investigations, book 3, chap. A11, 22 p. (Also available at *http://pubs.usgs.gov/twri/twri3-a11/*.)

SonTek/YSI Corporation, 2002, SonTek/YSI FlowTracker Handheld ADV technical documentation: San Diego, Calif., SonTek/YSI Corporation, 2 p.

Wagner, C.R., 1995, Stream-gaging cableways: U.S. Geological Survey Techniques of Water-Resources Investigations, book 3, chap. A21, 56 p. (Also available at *http://pubs.usgs.gov/twri/twri3-a21/*.)

Young, K.B., 1950, A comparative study of mean-section and midsection methods for computation of discharge measurements: U.S. Geological Survey Open-File Report 53–277, 52 p.

This page left blank intentionally.

Manuscript approved for publication June 1, 2010.
Prepared by the Reston Publishing Service Center.
Edited by Marilyn A. Billone.
Graphics by Annette L. Goode.
Design and typography by Anna N. Glover.

For more information, please contact:
D. Phil Turnipseed
U.S. Geological Survey
415 National Center
Reston, VA 20192
E-mail: pturnip@usgs.gov

USGS

Turnipseed and Sauer—**Discahrge Measurements at Gaging Stations**—Techniques and Methods 3–A8

ISBN 978-1-4113-2969-0

Printed on recycled paper

Assessment of erosion, sedimentation, and water quality impacts of the Mountain Valley Pipeline and Equitrans Expansion Project's proposed crossing of the Jefferson National Forest as it pertains to the U.S. Forest Service's Draft Supplemental Environmental Impact Statement dated December 2022

Prepared by Jonathan A. Czuba, Ph.D., Licensed Professional Engineer - February 9, 2023

REFERENCES
28

February 21, 2023

19 Southeast

Federal Coordinating Lead Author
Adam Terando
U.S. Geological Survey,
Southeast Climate Adaptation Science Center

Chapter Lead
Lynne Carter
Louisiana State University

Chapter Authors
Kirstin Dow
University of South Carolina

Kevin Hiers
Tall Timbers Research Station

Kenneth E. Kunkel
North Carolina State University

Aranzazu Lascurain
North Carolina State University

Doug Marcy
National Oceanic and Atmospheric Administration

Michael Osland
U.S. Geological Survey

Paul Schramm
Centers for Disease Control and Prevention

Review Editor
Alessandra Jerolleman
Jacksonville State University

Technical Contributors are listed at the end of the chapter.

Recommended Citation for Chapter
Carter, L., A. Terando, K. Dow, K. Hiers, K.E. Kunkel, A. Lascurain, D. Marcy, M. Osland, and P. Schramm, 2018: Southeast. In *Impacts, Risks, and Adaptation in the United States: Fourth National Climate Assessment, Volume II* [Reidmiller, D.R., C.W. Avery, D.R. Easterling, K.E. Kunkel, K.L.M. Lewis, T.K. Maycock, and B.C. Stewart (eds.)]. U.S. Global Change Research Program, Washington, DC, USA, pp. 743–808. doi: 10.7930/NCA4.2018.CH19

On the Web: https://nca2018.globalchange.gov/chapter/southeast

19 Southeast

Red mangrove in Titusville, Florida

Key Message 1

Urban Infrastructure and Health Risks

Many southeastern cities are particularly vulnerable to climate change compared to cities in other regions, with expected impacts to infrastructure and human health. The vibrancy and viability of these metropolitan areas, including the people and critical regional resources located in them, are increasingly at risk due to heat, flooding, and vector-borne disease brought about by a changing climate. Many of these urban areas are rapidly growing and offer opportunities to adopt effective adaptation efforts to prevent future negative impacts of climate change.

Key Message 2

Increasing Flood Risks in Coastal and Low-Lying Regions

The Southeast's coastal plain and inland low-lying regions support a rapidly growing population, a tourism economy, critical industries, and important cultural resources that are highly vulnerable to climate change impacts. The combined effects of changing extreme rainfall events and sea level rise are already increasing flood frequencies, which impacts property values and infrastructure viability, particularly in coastal cities. Without significant adaptation measures, these regions are projected to experience daily high tide flooding by the end of the century.

Key Message 3

Natural Ecosystems Will Be Transformed

The Southeast's diverse natural systems, which provide many benefits to society, will be transformed by climate change. Changing winter temperature extremes, wildfire patterns, sea levels, hurricanes, floods, droughts, and warming ocean temperatures are expected to redistribute species and greatly modify ecosystems. As a result, the ecological resources that people depend on for livelihood, protection, and well-being are increasingly at risk, and future generations can expect to experience and interact with natural systems that are much different than those that we see today.

Key Message 4

Economic and Health Risks for Rural Communities

Rural communities are integral to the Southeast's cultural heritage and to the strong agricultural and forest products industries across the region. More frequent extreme heat episodes and changing seasonal climates are projected to increase exposure-linked health impacts and economic vulnerabilities in the agricultural, timber, and manufacturing sectors. By the end of the century, over one-half billion labor hours could be lost from extreme heat-related impacts. Such changes would negatively impact the region's labor-intensive agricultural industry and compound existing social stresses in rural areas related to limited local community capabilities and associated with rural demography, occupations, earnings, literacy, and poverty incidence. Reduction of existing stresses can increase resilience.

Executive Summary

The Southeast includes vast expanses of coastal and inland low-lying areas, the southern portion of the Appalachian Mountains, numerous high-growth metropolitan areas, and large rural expanses. These beaches and bayous, fields and forests, and cities and small towns are all at risk from a changing climate. While some climate change impacts, such as sea level rise and extreme downpours, are being acutely felt now, others, like increasing exposure to dangerous high temperatures, humidity, and new local diseases, are expected to become more significant in the coming decades. While all regional residents and communities are potentially at risk for some impacts, some communities or populations are at greater risk due to their locations, services available to them, and economic situations.

Observed warming since the mid-20th century has been uneven in the Southeast region, with average daily minimum temperatures increasing three times faster than average daily maximum temperatures. The number of extreme rainfall events is increasing. Climate model simulations of future conditions project increases in both temperature and extreme precipitation.

Trends towards a more urbanized and denser Southeast are expected to continue, creating new climate vulnerabilities. Cities across the Southeast are experiencing more and longer summer heat waves. Vector-borne diseases pose a greater risk in cities than in rural areas because of higher population densities and other human factors, and the major urban centers in the Southeast are already impacted by poor air quality during warmer months. Increasing precipitation and extreme weather events will likely impact roads, freight rail, and passenger rail, which will likely have cascading effects across the region. Infrastructure related to drinking water and wastewater treatment also has the potential to be compromised by climate-related events. Increases in extreme rainfall events and high tide coastal floods due to future climate change will impact the quality of life of permanent residents as well as tourists visiting the low-lying and coastal regions of the Southeast. Sea level rise is contributing to increased coastal flooding in the Southeast, and high tide flooding already poses daily risks to businesses, neighborhoods, infrastructure, transportation, and ecosystems in the region.[1,2] There have been numerous instances of intense rainfall events that have had devastating impacts on inland communities in recent years.

The ecological resources that people depend on for livelihoods, protection, and well-being are increasingly at risk from the impacts of climate change. Sea level rise will result in the rapid conversion of coastal, terrestrial, and freshwater ecosystems to tidal saline habitats. Reductions in the frequency and intensity of cold winter temperature extremes are already allowing tropical and subtropical species to move northward and replace more temperate species. Warmer winter temperatures are also expected to facilitate the northward movement of problematic invasive species, which could transform natural systems north of their current distribution. In the future, rising temperatures and increases in the duration and intensity of drought are expected to increase wildfire occurrence and also reduce the effectiveness of prescribed fire practices.[3,4,5,6]

Many in rural communities are maintaining connections to traditional livelihoods and relying on natural resources that are inherently vulnerable to climate changes. Climate trends and possible climate futures show patterns that are already impacting—and are projected to further impact—rural sectors, from agriculture and forestry to human health and labor productivity. Future temperature increases are projected to pose challenges to human health. Increases in temperatures, water stress, freeze-free days, drought, and wildfire risks, together with changing conditions for invasive species and the movement of diseases, create a number of potential risks for existing agricultural systems.[7] Rural communities tend to be more vulnerable to these changes due to factors such as demography, occupations, earnings, literacy, and poverty incidence.[8,9,10] In fact, a recent economic study using a higher scenario (RCP8.5)[11] suggests that the southern and midwestern populations are likely to suffer the largest losses from future climate changes in the United States. Climate change tends to compound existing vulnerabilities and exacerbate existing inequities. Already poor regions, including those found in the Southeast, are expected to continue incurring greater losses than elsewhere in the United States.

Historical Changes in Hot Days and Warm Nights

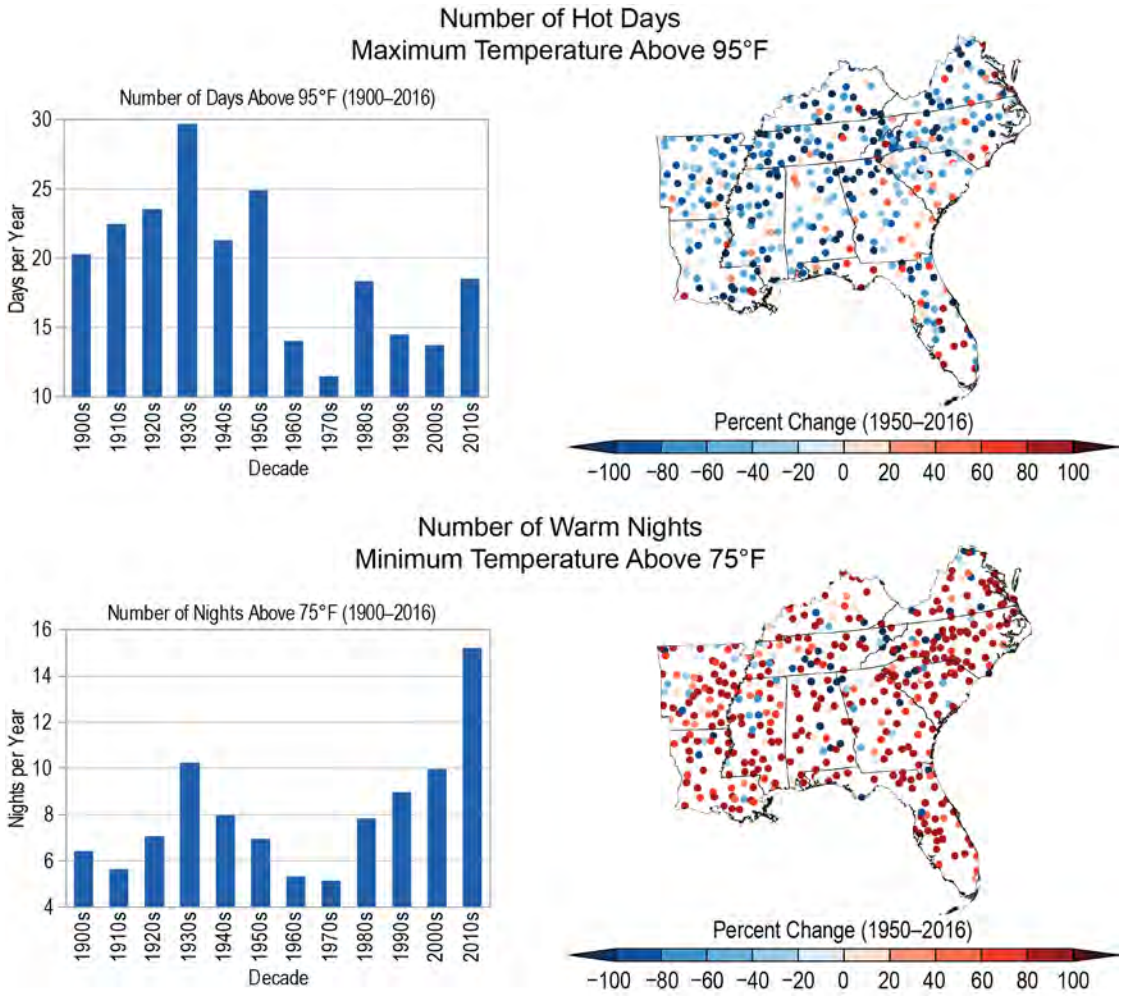

Sixty-one percent of major Southeast cities are exhibiting some aspects of worsening heat waves, which is a higher percentage than any other region of the country.[12] Hot days and warm nights together impact human comfort and health and result in the need for increased cooling efforts. Agriculture is also impacted by a lack of nighttime cooling. Variability and change in (top) the annual number of hot days and (bottom) warm nights are shown. The bar charts show averages over the region by decade for 1900–2016, while the maps show the trends for 1950–2016 for individual weather stations. Average summer temperatures during the most recent 10 years have been the warmest on record, with very large increases in nighttime temperatures and more modest increases in daytime temperatures, as indicated by contrasting changes in hot days and warm nights. (top left) The annual number of hot days (maximum temperature above 95°F) has been lower since 1960 than the average during the first half of the 20th century; (top right) trends in hot days since 1950 are generally downward except along the south Atlantic coast and in Florida due to high numbers during the 1950s but have been slightly upward since 1960, following a gradual increase in average daytime maximum temperatures during that time. (bottom left) Conversely, the number of warm nights (minimum temperature above 75°F) has doubled on average compared to the first half of the 20th century and (bottom right) locally has increased at most stations. *From Figure 19.1 (Sources: NOAA NCEI and CICS-NC)*.

Historical Change in Heavy Precipitation

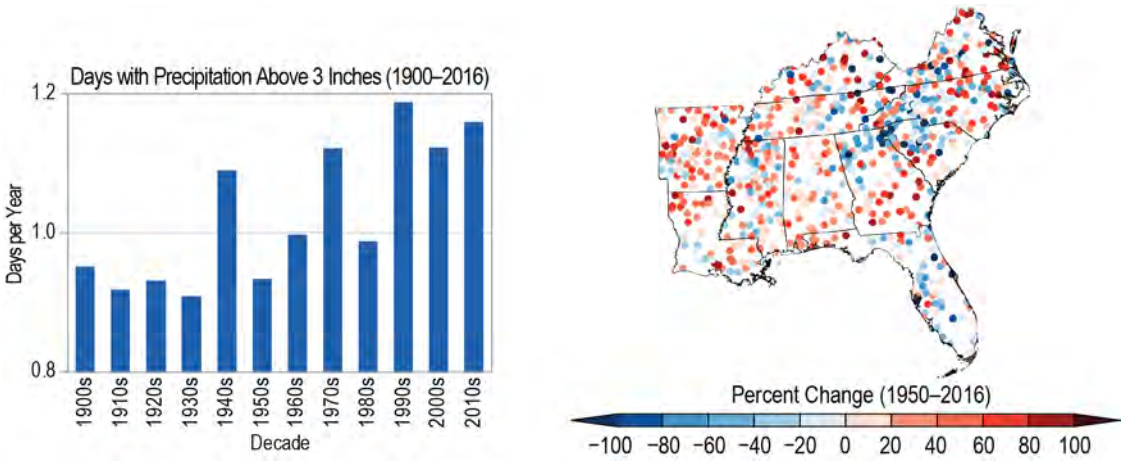

The figure shows variability and change in (left) the annual number of days with precipitation greater than 3 inches (1900–2016) averaged over the Southeast by decade and (right) individual station trends (1950–2016). The number of days with heavy precipitation has increased at most stations, particularly since the 1980s. *From Figure 19.3 (Sources: NOAA NCEI and CICS-NC)*

Background

Throughout the southeastern United States, the impacts of sea level rise, increasing temperatures, extreme heat events, heavy precipitation, and decreased water availability continue to have numerous consequences for human health, the built environment, and the natural world. This assessment builds on the above concerns described in the Third National Climate Assessment (NCA3) and includes impacts to urban and rural landscapes as well as natural systems. The impacts from these changes are becoming visible as 1) flooding increases stress on infrastructure, ecosystems, and populations; 2) warming temperatures affect human health and bring about temporal and geographic shifts in the natural environment and landscapes; and 3) wildfires and growing wildfire risk create challenges for natural resource managers and impacted communities.

The Southeast includes vast expanses of coastal and inland low-lying areas, the southern (and highest) portion of the Appalachian Mountains, numerous high-growth metropolitan areas, and large rural expanses. Embedded in these land- and seascapes is a rich cultural history developed over generations by the many communities that call this region home. However, these beaches and bayous, fields and forests, and cities and small towns are all at risk from a changing climate. These risks vary in type and magnitude from place to place, and while some climate change impacts, such as sea level rise and extreme downpours, are being acutely felt now, others, like increasing exposure to dangerously high temperatures—often accompanied by high humidity—and new local diseases, are expected to become more significant in the coming decades. While all regional residents and communities are potentially at risk for some impacts, some communities or populations are at greater risk due to their locations, services available, and economic situations. In fact, a recent economic study using a higher scenario (RCP8.5)[11] suggests that the southern and midwestern populations are likely to suffer the largest losses from projected climate changes in the United States. According to the article, "[b]ecause losses are largest in regions that are already poorer on average, climate change tends to increase preexisting inequality in the United States."[11] Understanding the demographic and socioeconomic composition of racial and ethnic groups in the region is important, because these characteristics are associated with health risk factors, disease prevalence, and access to care, which in turn may influence the degree of impact from climate-related threats.

Historical Climate and Possible Future Climates

The Southeast region experienced high annual average temperatures in the 1920s and 1930s, followed by cooler temperatures until the 1970s. Since then, annual average temperatures have warmed to levels above the 1930s; the decade of the 2010s through 2017 has been warmer than any previous decade (App 5: FAQs, Figure A5.14), both for average daily maximum and average daily minimum temperature. Seasonal warming has varied. The decade of the 2010s through 2017 is the warmest in all seasons for average daily minimum temperature and in winter and spring for average daily maximum temperature. However, for average daily maximum temperature, the summers of the 1930s and 1950s and the falls of the 1930s were warmer on average. The southeastern United States is one of the few regions in the world that has experienced little overall warming of daily maximum temperatures since 1900. The reasons for this have been the subject of much research, and hypothesized causes include both human and natural influences.[13,14,15,16,17] However, since the early 1960s, the Southeast has been warming at a similar rate as the rest of the United States (Ch.

2: Climate, Figure 2.4). During the 2010s, the number of nights with minimum temperatures greater than 75°F was nearly double the long-term average for 1901–1960 (Figure 19.1), while the length of the freeze-free season was nearly 1.5 weeks greater than any other period in the historical record (Figure 19.2). These increases were widespread across the region and can have important effects on both humans and the natural environment.[18] By contrast, the number of days above 95°F has been lower since 1960 compared to the pre-1960 period, with the highest numbers occurring in the 1930s and 1950s, both periods of severe drought (Figure 19.1). The differing trends in hot days and warm nights reflect the seasonal differences in average daily maximum and average daily minimum temperature trends.

Historical Changes in Hot Days and Warm Nights

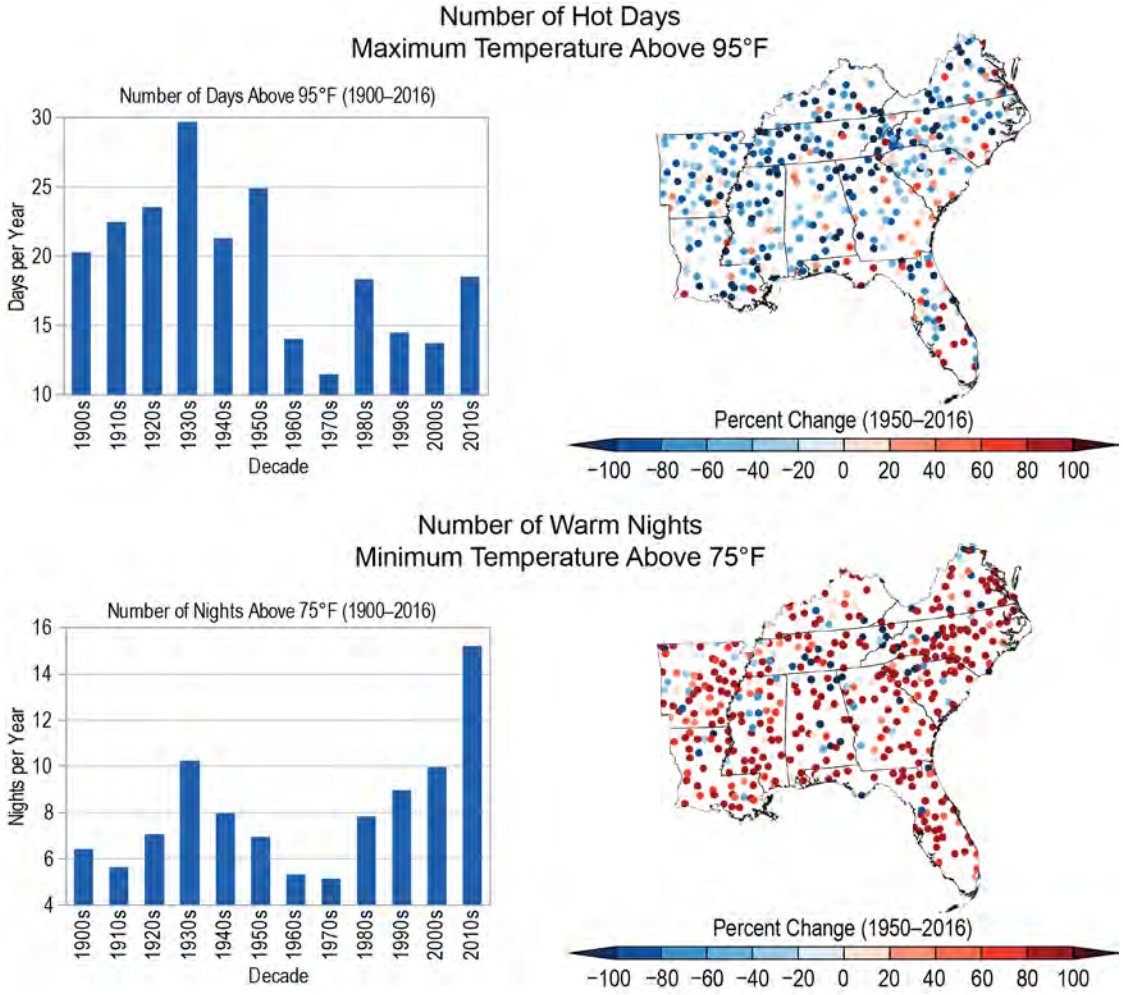

Figure 19.1: Sixty-one percent of major Southeast cities are exhibiting some aspects of worsening heat waves, which is a higher percentage than any other region of the country.[12] Hot days and warm nights together impact human comfort and health and result in the need for increased cooling efforts. Agriculture is also impacted by a lack of nighttime cooling. Variability and change in (top) the annual number of hot days and (bottom) warm nights are shown. The bar charts show averages over the region by decade for 1900–2016, while the maps show the trends for 1950–2016 for individual weather stations. Average summer temperatures during the most recent 10 years have been the warmest on record, with very large increases in nighttime temperatures and more modest increases in daytime temperatures, as indicated by contrasting changes in hot days and warm nights. (top left) The annual number of hot days (maximum temperature above 95°F) has been lower since 1960 than the average during the first half of the 20th century; (top right) trends in hot days since 1950 are generally downward except along the south Atlantic coast and in Florida due to high numbers during the 1950s but have been slightly upward since 1960, following a gradual increase in average daytime maximum temperatures during that time. (bottom left) Conversely, the number of warm nights (minimum temperature above 75°F) has doubled on average compared to the first half of the 20th century and (bottom right) locally has increased at most stations. Sources: NOAA NCEI and CICS-NC.

Historical Change in Freeze-Free Season Length

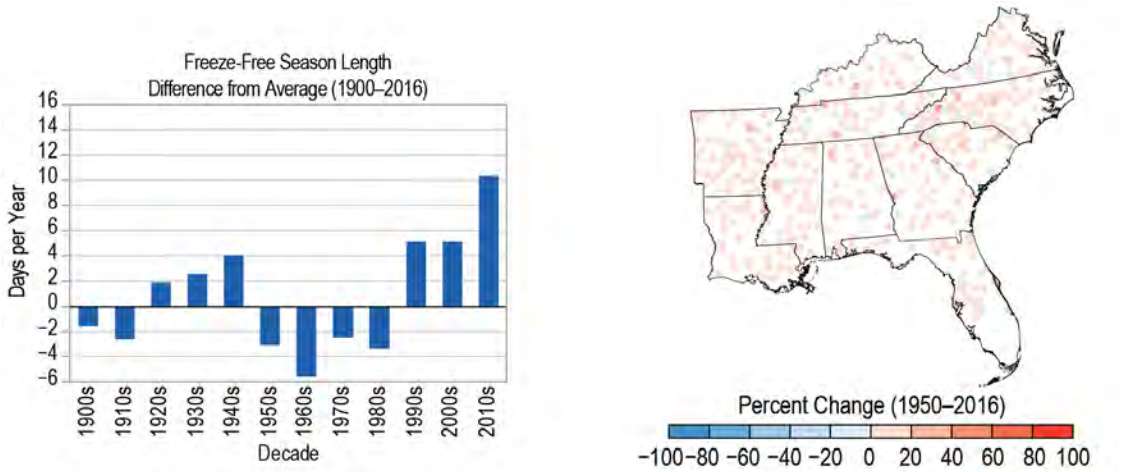

Figure 19.2: The figure shows the variability and change in the length of the freeze-free season. (left) The bar chart shows differences in the length of the freeze-free season by decade (1900–2016) as compared to the long-term average for the Southeast. (right) The map shows trends over 1950–2016 for individual weather stations. The length of the freeze-free season has increased at most stations, particularly since the 1980s. Sources: NOAA NCEI and CICS-NC.

Historical Change in Heavy Precipitation

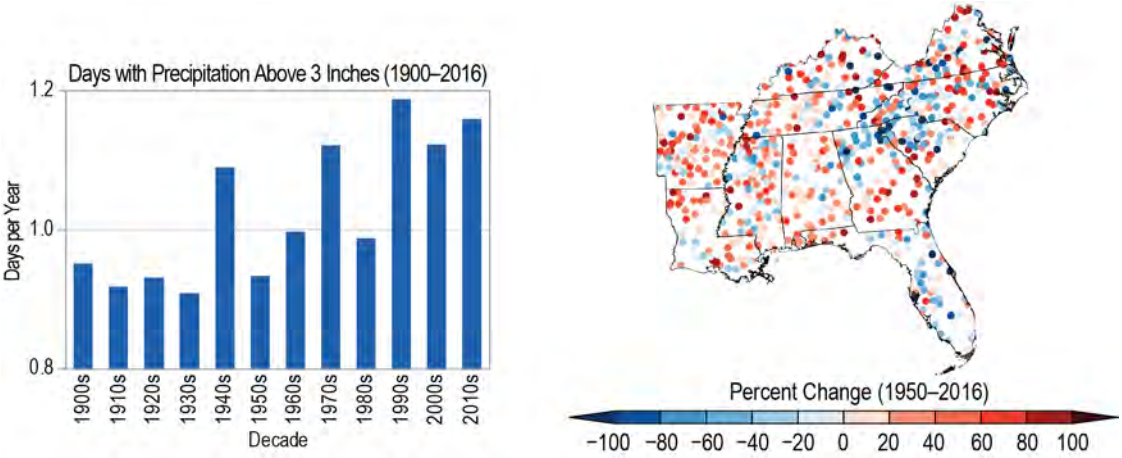

Figure 19.3: The figure shows variability and change in (left) the annual number of days with precipitation greater than 3 inches (1900–2016) averaged over the Southeast by decade and (right) individual station trends (1950–2016). The numbers of days with heavy precipitation has increased at most stations, particularly since the 1980s. Sources: NOAA NCEI and CICS-NC.

The number of extreme rainfall events is increasing. For example, the number of days with 3 or more inches of precipitation has been historically high over the past 25 years, with the 1990s, 2000s, and 2010s ranking as the decades with the 1st, 3rd, and 2nd highest number of events, respectively (Figure 19.3). More than 70% of precipitation recording locations show upward trends since 1950, although there are downward trends at many stations along and southeast of the Appalachian Mountains and in Florida (Figure 19.3).

Climate model simulations of future conditions project increases in temperature and extreme precipitation for both lower and higher scenarios (RCP4.5 and RCP8.5; see Figure 19.5).[13,19] After the middle of the 21st century, however, the projected increases are lower for the lower scenario (RCP4.5). Much larger changes are simulated by the late 21st century under the higher scenario (RCP8.5), which most closely tracks with our current consumption of fossil fuels. Under the higher scenario, nighttime

minimum temperatures above 75°F and daytime maximum temperatures above 95°F become the summer norm and nights above 80°F and days above 100°F, now relatively rare occurrences, become commonplace. Cooling degree days (a measure of the need for air conditioning [cooling] based on daily average temperatures rising above a standard temperature—often 65°F) nearly double, while heating degree days (a measure of the need for heating) decrease by over a third (Figure 19.22). The freeze-free season lengthens by more than a month, and the frequency of freezing temperatures decreases substantially.[20,21]

Key Message 1

Urban Infrastructure and Health Risks

Many southeastern cities are particularly vulnerable to climate change compared to cities in other regions, with expected impacts to infrastructure and human health. The vibrancy and viability of these metropolitan areas, including the people and critical regional resources located in them, are increasingly at risk due to heat, flooding, and vector-borne disease brought about by a changing climate. Many of these urban areas are rapidly growing and offer opportunities to adopt effective adaptation efforts to prevent future negative impacts of climate change.

Rapid Population Shifts and Climate Impacts on Urban Areas

While the Southeast is historically known for having a rural nature, a drastic shift toward a more urbanized region is underway. The Southeast contains many of the fastest-growing urban areas in the country, including a dozen of the top 20 fastest-growing metropolitan areas (by percentage) in 2016.[22] Metropolitan Atlanta has been swiftly growing, adding 69,200 residents in just one year.[23] At the same time, many rural counties in the South are losing population.[24] These trends towards a more urbanized and dense Southeast are expected to continue, creating new climate vulnerabilities but also opportunities to adapt as capacity and resources increase in cities (Ch. 17: Complex Systems). In particular, coastal cities in the Southeast face multiple climate risks, and many planning efforts are underway in these cities. Adaptation, mitigation, and planning efforts are emphasizing "co-benefits" (positive benefits related to the reduction of greenhouse gases or implementation of adaptation efforts) to help boost the economy while protecting people and infrastructure.

Increasing Heat

Cities across the Southeast are experiencing more and longer summer heat waves. Nationally, there are only five large cities that have increasing trends exceeding the national average for all aspects of heat waves (timing, frequency, intensity, and duration), and three of these cities are in the Southeast region—Birmingham, New Orleans, and Raleigh. Sixty-one percent of major Southeast cities are exhibiting some aspects of worsening heat waves, which is a higher percentage than any other region of the country.[12] The urban heat island effect (cities that are warmer than surrounding rural areas, especially at night) adds to the impact of heat waves in cities (Ch. 5: Land Changes, KM 1). Southeastern cities including Memphis and Raleigh have a particularly high future heat risk.[25]

The number of days with high minimum temperatures (nighttime temperatures that stay above 75°F) has been increasing across the Southeast (Figure 19.1), and this trend is projected to intensify, with some areas experiencing more than 100 additional warm nights per year by the end of the century (Figures 19.4 and 19.5). Exposure to high nighttime minimum temperatures reduces the ability of some people to recover from high daytime temperatures, resulting in heat-related illness and death.[26] This effect is particularly pronounced in cities, many of which have urban heat islands that already cause elevated nighttime temperatures.[27] Cities are taking steps to prevent negative health impacts from heat. For example, the Louisville, Kentucky, metro government conducted an urban heat management study and installed 145,000 square feet of cool roofs as part of their goal to lessen the risk of climate change impacts.[28]

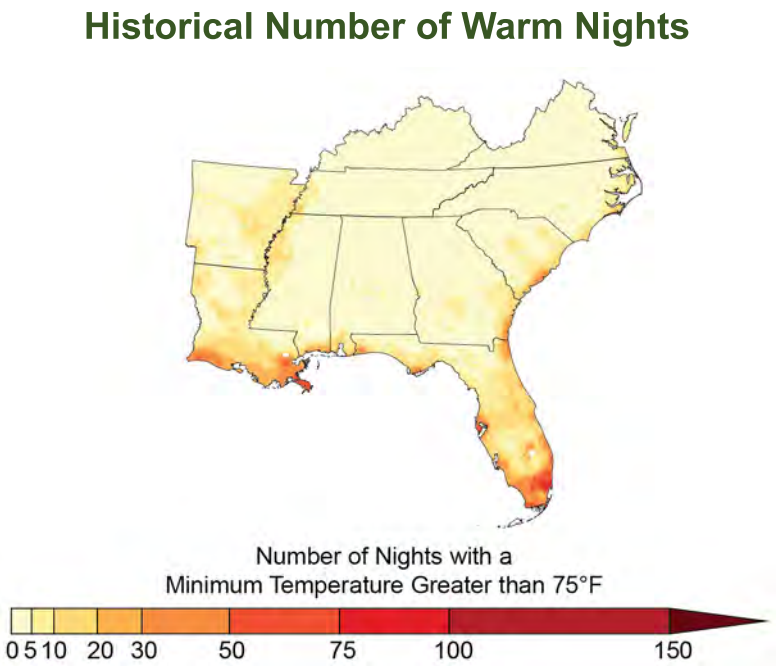

Figure 19.4: The map shows the historical number of warm nights (days with minimum temperatures above 75°F) per year in the Southeast, based on model simulations averaged over the period 1976–2005. Sources: NOAA NCEI and CICS-NC.

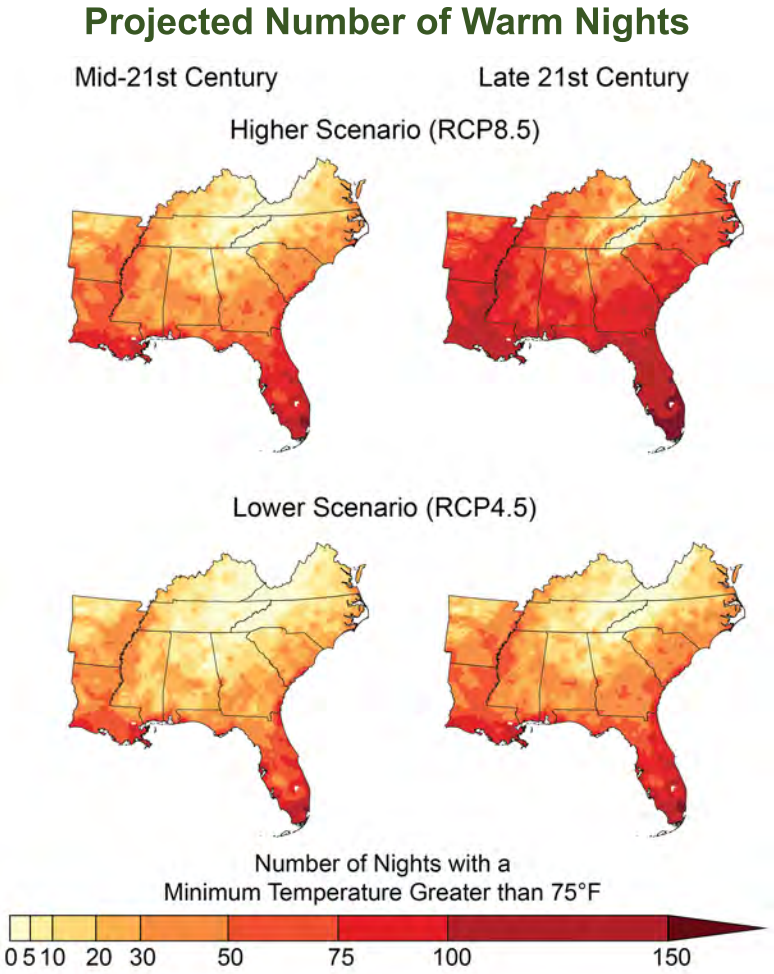

Figure 19.5: The maps show the projected number of warm nights (days with minimum temperatures above 75°F) per year in the Southeast for the mid-21st century (left; 2036–2065) and the late 21st century (right; 2070–2099) under a higher scenario (RCP8.5; top row) and a lower scenario (RCP4.5; bottom row). These warm nights currently occur only a few times per year across most of the region (Figure 19.4) but are expected to become common events across much of the Southeast under a higher scenario. Increases in the number of warm nights adversely affect agriculture and reduce the ability of some people to recover from high daytime temperatures. With more heat waves expected, there will likely be a higher risk for more heat-related illness and deaths. Sources: NOAA NCEI and CICS-NC.

Vector-Borne Disease

The transmission of vector-borne diseases, which are spread by the bite of an animal such as a mosquito or tick, is complex and depends on a number of factors, including weather and climate, vegetation, animal host populations, and human activities (Ch. 14: Human Health, KM 1). Climate change is likely to modify the seasonality, distribution, and prevalence of vector-borne diseases in the Southeast.[29] Vector-borne diseases pose a greater risk in cities than in rural areas because of higher population densities and other human factors (for example, pools of standing water in man-made structures, such as tires or buckets, are breeding grounds for some species of mosquitoes). Climatic conditions are currently suitable for adult mosquitoes of the species *Aedes aegypti*, which can spread dengue, chikungunya, and Zika viruses, across most of the Southeast from July through September (Figure 19.6), and cities in South Florida already have suitable conditions for year-round mosquito activity. The Southeast is the region of the country with the most favorable conditions for this mosquito and thus faces the greatest threat from diseases the mosquito carries.[30] Climate change is expected to make conditions more suitable for transmission of certain vector-borne diseases, including year-round transmission in southern

Florida. Summer increases in dengue cases are expected across every state in the Southeast. Despite warming, low winter temperatures may prevent permanent year-round establishment of the virus across the region.[31] Strategies such as management of urban wetlands have resulted in lower dengue fever risk in Puerto Rico.[32] Similar adaptation strategies have the potential to limit vector-borne disease in southeastern cities, particularly those cities with characteristics similar to Caribbean cities that have already implemented vector control strategies (Ch. 20: U.S. Caribbean).[33,34] The Southeast is also the region with the greatest projected increase in cases of West Nile neuroinvasive disease under both a lower and higher scenario (RCP4.5 and RCP8.5).[35,36]

Air Quality and Human Health

Poor air quality directly impacts human health, resulting in respiratory disease and other ailments. In the Southeast, poor air quality can result from emissions (mostly from vehicles and power plants), wildfires, and allergens such as pollen. The major urban centers in the Southeast are already impacted by poor air quality during warmer months. The Southeast has more days with stagnant air masses than other regions of the country (40% of summer days) and higher levels of fine (small) particulate matter ($PM_{2.5}$), which cause heart and lung disease.[37] There is mixed evidence on the future health impacts of these pollutants. Ozone concentrations would be expected to increase under higher temperatures; however, a variety of factors complicate projections (Ch. 13: Air Quality, KM 1). There are many possible future wind and cloud cover conditions for the Southeast as well as the potential for continued shifts in land-use patterns, demographics and population geography, and vehicle and power plant emissions standards. Increases in precipitation and shifts in wind trajectories may reduce future health impacts of ground level ozone in the Southeast,[35] but warmer and drier autumns are expected to result in a lengthening of the period of ozone exposure.[38] Warmer August temperatures in the Southeast from 1988 to 2011 were associated with increased human sensitivity to ground-level ozone.[39]

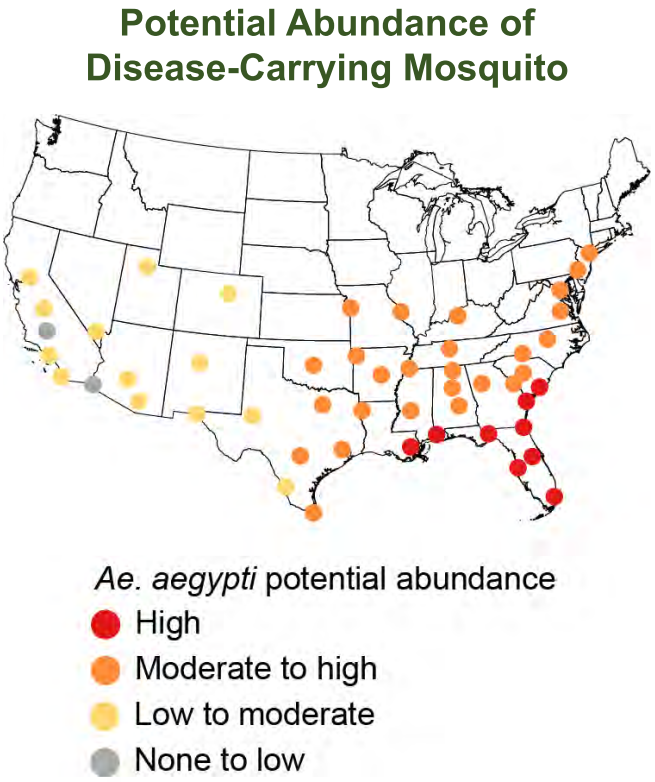

Figure 19.6: The map shows current suitability for the *Aedes aegypti* mosquito in July in 50 different cities. *Aedes aegypti* mosquitoes can spread several important diseases, including dengue fever, chikungunya, and Zika fever. The Southeast is the region of the country with the greatest potential mosquito activity. Warming temperatures have the potential to expand mosquito habitat and disease risk. Source: adapted from Monaghan et al. 2016.[30]

The fast growth rate of urban areas in the Southeast contributes to aeroallergens, which are known to cause and exacerbate respiratory diseases such as asthma. Urban areas have higher concentrations of CO_2, which causes allergenic plants, such as ragweed, to grow faster and produce more pollen than in rural areas.[40] Continued rising temperatures and atmospheric CO_2 levels are projected to further contribute to aeroallergens in cities (Ch. 13: Air Quality, KM 3).

Infrastructure

Infrastructure, particularly roads, bridges, coastal properties, and urban drainage, is vulnerable to climate change and climate-related events (see Key Message 2) (see also Ch. 3: Water, KM 2; Ch. 11: Urban, KM 2; Ch. 12: Transportation, KM 1).[41] By 2050, the Southeast is the region expected to have the most vulnerable bridges.[35] An extreme weather vulnerability assessment conducted by the Tennessee Department of Transportation found that the urban areas of Memphis and Nashville had the most at-risk transportation infrastructure in the state.[42] Increasing precipitation and extreme weather events will likely impact roads, freight rail, and passenger rail, especially in Memphis, which will likely have cascading effects across the region.[43] Transit infrastructure, such as the rail lines of the Metropolitan Atlanta Rapid Transit Authority (MARTA), are also at risk. As a result, MARTA has begun to identify vulnerable assets and prioritize improvements to develop a more resilient system.[44]

Many cities across the Southeast are planning for the impacts sea level rise is likely to have on their infrastructure (see Case Study "Charleston, South Carolina, Begins Planning and Reinvesting" and Key Message 2). Flood events in Charleston, South Carolina, have been increasing, and by 2045 the city is projected to face nearly 180 tidal floods (flooding in coastal areas at high tide) per year, as compared to 11 floods per year in 2014.[45] These floods affect tourism, transportation, and the economy as a whole. The city has responded by making physical modifications, developing a more robust disaster response plan, and improving planning and monitoring prior to flood events.

Infrastructure related to drinking water treatment and wastewater treatment may be compromised by climate-related events (Ch. 3: Water, KM 2). Water utilities across the Southeast are preparing for these impacts. Tampa Bay Water, the largest wholesale water utility in the Southeast, is coordinating with groups including the Florida Water and Climate Alliance to study the impact of climate change on its ability to provide clean water in the future.[46,47] Spartanburg Water, in South Carolina, is reinforcing the ability of the utility to "cope with, and recover from disruption, trends and variability in order to maintain services."[48] Similarly, the Seminole Tribe of Florida, which provides drinking and wastewater services, assessed flooding and sea level rise threats to their water infrastructure and developed potential adaptation measures.[49] The development of "green" water infrastructure (using natural hydrologic features to manage water and provide environmental and community benefits), such as the strategies promoted in the City of Atlanta Climate Action Plan, is one way to adapt to future water management needs. Implementation of these strategies has already resulted in a reduction in water consumption in the city of Atlanta, relieving strain on the water utility and increasing resilience.[50]

There are still gaps in knowledge regarding the potential effects of climate change on cities across the Southeast. Cross-disciplinary groups such as the Georgia Climate Project (http://www.georgiaclimateproject.org) are developing research roadmaps that can help to prioritize research and action with relevance to policymakers, practitioners, and scientists.

Key Message 2

Increasing Flood Risks in Coastal and Low-Lying Regions

The Southeast's coastal plain and inland low-lying regions support a rapidly growing population, a tourism economy, critical industries, and important cultural resources that are highly vulnerable to climate change impacts. The combined effects of changing extreme rainfall events and sea level rise are already increasing flood frequencies, which impacts property values and infrastructure viability, particularly in coastal cities. Without significant adaptation measures, these regions are projected to experience daily high tide flooding by the end of the century.

Sea Level Rise Is Contributing to Increased Coastal Flooding in the Southeast

Average global sea level (or global mean sea level; GMSL) has risen about 8–9 inches since 1880, with about 3 inches of that rise occurring since 1990.[51,52] This recent increase in the rate of rise is projected to accelerate in the future due to continuing temperature increases and additional melting of land ice.[51] This recent global rate increase, combined with the local effects of vertical land motion (sinking) and oceanographic effects such as changing ocean currents, has caused some areas in the Southeast to experience even higher local rates of sea level rise than the global average.[53,54,55,56,57,58,59] Analyses at National Oceanic and Atmospheric Administration (NOAA) tide gauges show as much as 1 to 3 feet of local relative sea level rise in the past 100 years in low-lying areas of the Southeast.[54,59] This recent rise in local relative sea level has caused normal high tides to reach critical levels that result in flooding in many coastal areas in the region.

Monthly and seasonal fluctuations in high tide levels are caused by a combination of astronomical factors (sun and moon gravitational attraction) and non-astronomical factors such as geomorphology (landscape of the area), as well as meteorological (weather) conditions. The highest tides of the year are generally the perigean, or spring, tides, which occur when the moon is full or new and is closest to the Earth. These perigean tides, also known as "king tides," occur twice a year and in many cities are causing what has been called "nuisance" or "recurrent" flooding (referred to herein as high tide flooding). These floods can cause problems ranging from inconvenient to life changing. While the challenges brought on by rising perigean tides are diverse, important examples include increasingly frequent road closures, excessive water in storm water management systems, and deterioration of infrastructure such as roads and rail from saltwater. NOAA's National Weather Service (NWS) issues coastal flood advisories and warnings when water levels at tide gauges are expected to exceed flood thresholds. These thresholds correspond to discrete water levels relative to NOAA tide gauges.

Recent analyses of historical water levels at many NOAA tide gauges has shown an increase in the number of times that these warning thresholds were exceeded compared to the past. Annual occurrences of high tide coastal flooding have increased 5- to 10-fold since the 1960s in several low-lying coastal cities in the Southeast (Figure 19.7).[51,60] In 2015, several Southeast coastal cities experienced all-time records of coastal flooding occurrences, including Wilmington, NC (90 days), Charleston, SC (38 days), Mayport, FL (19 days), Miami, FL (18 days), Key West, FL (14 days), and Fernandina Beach, FL (7 days). These flooding occurrences increased more than 50% in 2015 compared to 2014.[58] In 2016, three all-time records were either tied (14 days at Key West,

FL) or broken (50 days at Charleston, SC, and 38 days at Savannah, GA). The Miami area nearly matched the 2015 record of 18 days.[61] This increase in high tide flooding frequency is directly tied to sea level rise. For example, in Norfolk, Virginia, local relative sea level rise has led to a fourfold increase in the probability of exceeding NWS thresholds compared to the 1960s (Figure 19.8). High tide flooding is now posing daily risks to businesses, neighborhoods, infrastructure, transportation, and ecosystems in the Southeast.[1,2]

Global sea level is very likely to rise by 0.3–0.6 feet by 2030, 0.5–1.2 feet by 2050, and 1.0–4.3 feet by 2100 under a range of scenarios from very low (RCP2.6) to high (RCP8.5),[51,52,62] which would result in increases in both the depth and frequency of coastal flooding (Figure 19.7).[51] Under higher emissions scenarios (RCP8.5), global sea level rise exceeding 8 feet (and even higher in the Southeast) by 2100 cannot be ruled out.[51] By 2050, many Southeast cities are projected to experience more than 30 days of high tide flooding regardless of scenario.[63] In addition, more extreme coastal flood events are also projected to increase in frequency and duration.[60] For example, water levels that currently have a 1% chance of occurring each year (known as a 100-year event) will be more frequent with sea level rise. This increase in flood frequency suggests the need to consider revising flood study techniques and standards that are currently used to design and build coastal infrastructure.

Higher sea levels will cause the storm surges from tropical storms to travel farther inland than in the past, impacting more coastal properties. The combined impacts of sea level rise and storm surge in the Southeast have the potential to cost up to $60 billion each year in 2050 and up to $99 billion in 2090 under a higher scenario (RCP8.5).[35] Even under a lower scenario (RCP4.5), projected damages are $56 and $79 billion in 2050 and 2090, respectively (in 2015 dollars, undiscounted).[35] Florida alone is estimated to have a 1-in-20 chance of having more than $346 billion (in 2011 dollars) in property value (8.7%) below average sea level by 2100 under a higher scenario (RCP8.5).[64] An assessment by the Florida Department of Health determined that 590,000 people in South Florida face “extreme” or “high” risk from sea level rise, with 125,000 people living in these areas identified as socially vulnerable and 55,000 classified as medically vulnerable.[65] In addition to causing direct injury, storm surge and related flooding can impact transportation infrastructure by blocking or flooding roads and affecting access to healthcare facilities (Ch. 12: Transportation, KM 1). Marine transportation can be impacted as well. Large ports in the Southeast, such as Charleston, Savannah, and Jacksonville, and the rails and roads that link to them, are particularly vulnerable to both coastal flooding and sea level rise (Ch. 12: Transportation, KM 1; Ch. 8: Coastal, KM 1). The Port of Jacksonville provides raw material for industries, food, clothes, and essential goods to Puerto Rico, thus impacting the U.S. Caribbean region, as well (Ch. 20: U.S. Caribbean, KM 3). It is estimated that with a meter (about 3.3 feet) of sea level rise, the Southeast would lose over 13,000 recorded historic and prehistoric archaeological sites and more than 1,000 locations currently eligible for inclusion on the National Register of Historic Places.[66] This includes many historic buildings and forts in cities like Charleston, Savannah, and St. Augustine.

Annual Number of High Tide Flooding Days

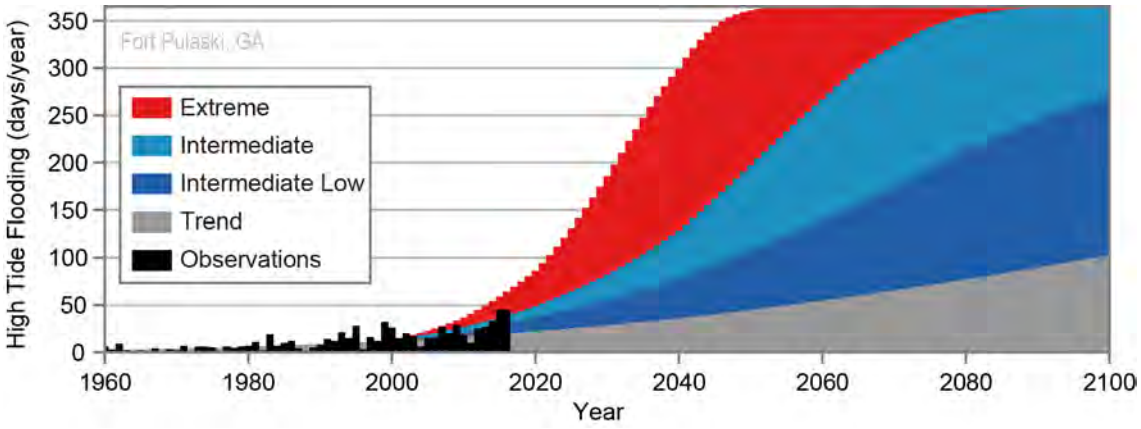

Figure 19.7: The figure shows the annual number of days experiencing high tide floods based on observations for 1960–2016 for Fort Pulaski, near Savannah, Georgia (black), and projected increases in the number of annual flood events based on four future scenarios: a continuation of the current relative sea level trend (gray) and the Intermediate-Low (dark blue), Intermediate (light blue), and Extreme (red) sea level rise scenarios. See Sweet et al. (2017)[51] and Appendix 3: Data & Scenarios for additional information on projection and trend data. Source: adapted from Sweet and Park 2014.[63]

Range of Daily Highest Water Levels in Norfolk, Virginia

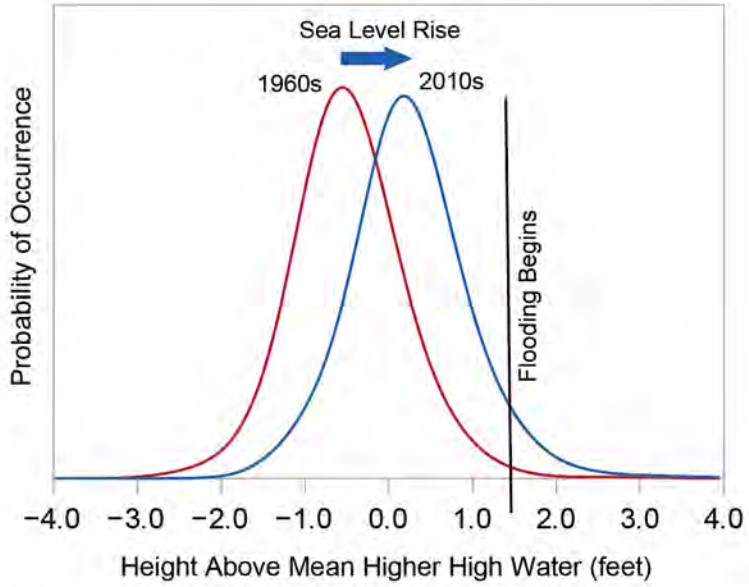

Figure 19.8: The curves in this figure show a range of daily Mean Higher High Water (MHHW) levels in Norfolk, Virginia (Sewells Point), for the 1960s and 2010s. Local sea level rise has shifted the curve closer to the point where high tide flooding begins (based on warning thresholds established by the National Weather Service). This shows why many more high tide flood events occur now than they did in the past (increase of 6 flood days per year). Source: adapted from Sweet et al. 2017.[52] *This figure was revised in June 2019. See Errata for details: https://nca2018.globalchange.gov/downloads*

Case Study: Charleston, South Carolina, Begins Planning and Reinvesting for Sea Level Rise

The main crosstown traffic artery in Charleston, South Carolina (U.S. 17 Septima Clark Parkway–crosstown), has historically been susceptible to flooding events (Figure 19.9). Charleston experienced all-time record high tide flood occurrences in 2015 (38 days) and 2016 (50 days).[52,58] By 2045, Charleston is projected to experience up to 180 high tide flood events a year.[1] The City of Charleston estimated that each flood event that affects the crosstown costs $12.4 million (in 2009 dollars). Over the past 50 years, the resultant gross damage and lost wages have totaled more than $1.53 billion (dollar year not specified). As a result, Charleston has developed a Sea Level Rise Strategy that plans for 50 years out based on moderate sea level rise scenarios (Figure 19.10) and that reinvests in infrastructure, develops a response plan, and increases readiness.[45] As of 2016, the City of Charleston has spent or set aside $235 million (in 2015 dollars) to complete ongoing drainage improvement projects (Figure 19.9) to prevent current and future flooding.

Figure 19.9: (left) U.S. Highway 17 (Septima Clark Parkway—crosstown) in Charleston, South Carolina, during a flood event. Floodwaters can get deep enough to stall vehicles. (right) Market Street drainage tunnel being constructed in Charleston, South Carolina, as part of a drainage improvement project to prevent current and future flooding. This tunnel crosses a portion of downtown Charleston 140 feet underground and is designed to rapidly convey storm water to the nearby Ashley River. Photo credit: City of Charleston 2015.[45]

Projected Sea Level Rise for Charleston, South Carolina

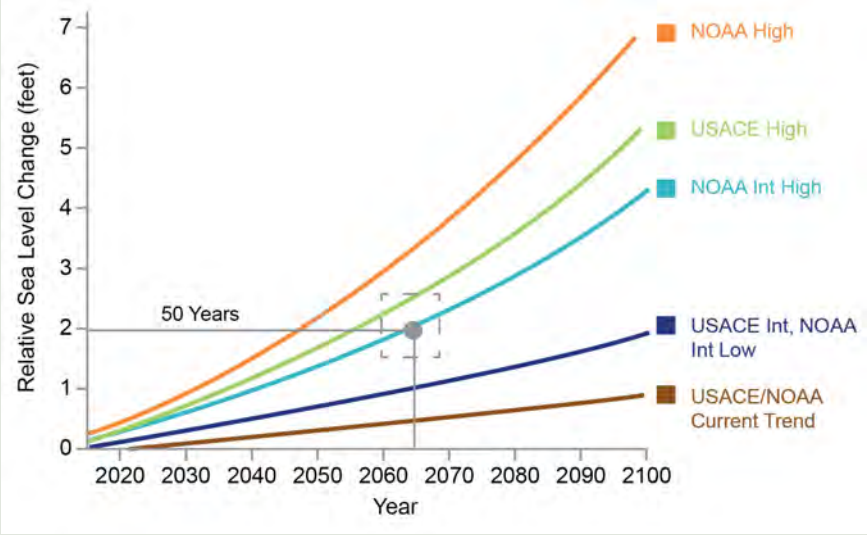

Figure 19.10: The City of Charleston Sea Level Rise Strategy calls for a 50-year outlook, based on existing federal sea level change projections in 2015 (colored curves), and calls for using a range of 1.5–2.5 feet of sea level rise (dashed box). A 1.5-foot increase will be used for short-term, less vulnerable investments, such as a parking lot. A 2.5-foot increase will be used for critical, longer-term investments, such as emergency routes and public buildings. This 1-foot range was chosen to approximate the average of these projections in 2065. Source: City of Charleston 2015.[45]

Many of the older historical coastal cities in the Southeast were built just above the current Mean Higher High Water (MHHW) level (the average height of the higher of the two daily high tides at a given location), with a gravity-driven drainage system designed to drain rainwater into the tidal estuaries. As sea levels have risen locally in the last one hundred years, the storm water systems in these areas are no longer able to perform as designed. When these cities experience high tide coastal flooding due to perigean tides, the tidewater enters the storm water system, which prevents rainwater from entering storm drains and causes increased impacts from flooding. In the future, the gravity-driven nature of many of these systems may cease to function as designed, causing rainwater to flood streets and neighborhoods until the tide lowers and water can drain normally. Cities such as Charleston and Miami have already begun to improve storm water infrastructure and explore natural and nature-based infrastructure design to reduce future flood risk.

Much of the Southeast region's coast is bordered by large expanses of salt marsh and barrier islands. Long causeways with intermittent bridges to connect the mainland to these popular tourism destinations were built decades ago at only a few feet above MHHW. Sea level rise has put these transportation connection points at risk. High tide coastal flooding has started to inundate these low-lying roads, restricting access during certain times of the day and causing public safety concerns. The U.S. East Coast, for example, already has 7,508 miles of roadways, including over 400 miles of interstate roadways, currently threatened by high tide coastal flooding (Ch. 12: Transportation, KM 1 and Figure 12.2).

Sea level rise is already causing an increase in high tide flood events in the Southeast region and is adding to the impact of more extreme coastal flooding events. In the future, this flooding is projected to become more serious, disruptive, and costly as its frequency, depth, and inland extent grow with time (Ch. 12: Transportation, KM 1).[52,63,67,68]

Case Study: A Lesson Learned for Community Resettlement: Isle de Jean Charles Band of Biloxi-Chitimacha-Choctaw Tribe

Coastal communities in the Southeast are already experiencing impacts from higher temperatures, sea level rise, increased flooding, and extreme weather events.[69,70,71,72] Several communities in the United States are already discussing the complexities of relocation; most are tribal and Indigenous communities.[73] Some have chosen to stay in their homelands, while others have few options but to relocate (Ch. 15: Tribes, KM 3).

Isle de Jean Charles is a narrow island in the bayous of South Terrebonne Parish, Louisiana, and home to the Isle de Jean Charles Band of Biloxi-Chitimacha-Choctaw, a tribal community already living the day-to-day impacts of land loss, sea level rise, and coastal flooding. The island has lost 98% of its landmass since 1955 and has only approximately 320 acres (approximately 1/2 square mile) remaining. The population living on the Island has fallen from 400 to 85 people. The decline is due in large part to land loss and flooding driven by climate change, extreme weather, and unsustainable development practices, which stem from oil and gas production, extraction, and water-management practices.[74] This process has resulted in family separation, spreading them across southern Louisiana.[75] In addition, the Tribe continues to lose parts of its livelihood and culture, including sacred places, cultural sites and practices, healing plants, traditional foods, and lifeways.[76]

Case Study: A Lesson Learned for Community Resettlement: Isle de Jean Charles Band of Biloxi-Chitimacha-Choctaw Tribe, *continued*

The Third National Climate Assessment[77] discussed the initial plans for resettlement of the Isle de Jean Charles community. Recently, after nearly 20 years of tribal persistence and two previous efforts, the U.S. Department of Housing and Urban Development (HUD) through the National Disaster Resilience Competition,[78] along with technical assistance from The Rockefeller Foundation, awarded the State of Louisiana $48 million (in 2016 dollars) to implement the Tribe's resettlement plan: a community-driven, culturally appropriate, sustainable development-based plan. It was developed in partnership with the Lowlander Center, a local nongovernmental organization with a long-standing relationship with the Tribe and other scientists, researchers, and planners. The award provides the Tribe with a historic opportunity to reunite a community.[79] While the application to relocate was initiated by the Tribe, the relocation funds now are for all residents of Isle de Jean Charles, according to the Louisiana State Office of Community Development.[75]

Figure 19.11: Chantel Comardelle, Isle de Jean Charles Tribe's Executive Secretary, leads a discussion at a community meeting for the Tribe's resettlement planning process in Pointe-aux-Chenes, Louisiana, on January 18, 2016. The meeting was supported by the Lowlander Center. Photo credit: The Lowlander Center Team.

The resettlement plan is expected to be implemented by 2022 with the inclusion of many facilities in the new location to revitalize the tribal community, including a tribal center and a healthcare facility. The Tribe's experience highlights how success can be achieved when at-risk communities are engaged in the resettlement planning process from the beginning to ensure long-term successful relocation and maintain community integrity.[80] It also highlights an opportunity for institutions to evolve in more flexible ways to accommodate the growing number of communities that may need to relocate.

Extreme Rainfall Events Are Contributing to Increased Inland and Coastal Flooding

Extreme rainfall events have increased in frequency and intensity in the Southeast, and there is *high confidence* they will continue to increase in the future (Figure 19.3).[19] The region, as a whole, has experienced increases in the number of days with more than 3 inches of precipitation (Figure 19.3) and a 16% increase in observed 5-year maximum daily precipitation (the amount falling in an event expected to occur only once every 5 years).[19] Both the frequency and severity of extreme precipitation events are projected to continue increasing in the region under both lower and higher scenarios (RCP4.5 and RCP8.5). By the end of the century under a higher scenario (RCP8.5), projections indicate approximately double the number of heavy rainfall events (2-day precipitation events with a 5-year return period) and a 21% increase in the amount of rain falling on the heaviest precipitation days (days with a 20-year return period).[19,81] These projected increases would directly affect the vulnerability of the Southeast's coastal and low-lying areas. Natural resources (see Key Message 3),

industry, the local economy, and the population of the region are at increasing risk to these extreme events.

Across the Southeast since 2014, there have been numerous examples of intense rainfall events—many approaching levels that would be expected to occur only once every 500 years[82,83]—that have made state or national news due to the devastating impact they had on inland communities. Of these events, four major inland flood events have occurred in just three years (2014–2016) in the Southeast, causing billions of dollars in damages and loss of life (see Table 19.1 and Case Study "Coastal and Inland Impacts of Extreme Rainfall").[84]

A closer look at the August 2016 event in Louisiana provides an example of how vulnerable inland communities in the Southeast region are to these extreme rainfall events. Between August 11–15 2016, nearly half of southern Louisiana received at least 12–14 inches of rainfall. While urban areas such as Baton Rouge and Lafayette were hit the hardest, receiving upwards of 30 inches in a few days, coastal locations were also inundated with up to 20 inches of rain. Rainfall totals across the region exceeded amounts that would be expected to occur once every 1,000 years (or a less than 0.1% annual probability of occurrence), causing the Amite and Comite Rivers to surge past their banks and resulting in some 50,000 homes across the region filling with more than 18 inches of water.[85] Nearly 10 times the number of homes received major flooding (18 inches or more) during this event compared to a historic 1983 flood in Baton Rouge, and the damage resulted in more than 2 million cubic yards of curbside debris from cleaning up homes (enough to fill over 600 Olympic-sized pools).[86] A preceding event in northern Louisiana on March 8–12, 2016, caused $2.4 billion in damages (in 2017 dollars; $2.3 billion in 2015 dollars) and five casualties,[84] illustrating that inland low-lying areas in the Southeast region are also vulnerable to flooding impacts. Events of such magnitudes are projected to become more likely in the future due to a changing climate,[19,87] putting more people in peril from future floods. Existing flood map boundaries do not account for future flood risk due to the increasing frequency of more intense precipitation events, as well as new development that would reduce the floodplain's ability to manage storm water. As building and rebuilding in flood-prone areas continue, the risks of the kinds of major losses seen in these events will continue to grow.

The growing number of extreme rainfall events is stressing the deteriorating infrastructure in the Southeast. Many transportation and storm water systems have not been designed to withstand these events. The combined effects of rising numbers of high tide flooding and extreme rainfall events, along with deteriorating storm water infrastructure, are increasing the frequency and magnitude of coastal and lowland flood events.[45,88,89,90]

Billion-Dollar Flood Events in the Southeast, 2014–2016

Event	Date	Damages	Casualties
Southeast tornadoes and flooding (FL, AL, AR)	April 27–28, 2014	$1.8 Billion	33
South Carolina record flooding	October 1–5, 2015	$2.1 Billion	25
Hurricane Matthew	October 7–9, 2016	$10.1 Billion	49
Louisiana flooding (Baton Rouge)	August 11–15, 2016	$10.1 Billion	13

Table 19.1: Values are Consumer Price Index adjusted and are in 2017 dollars. Source: NOAA NCEI 2017.[84]

The recent increases in flood risk have led many cities and counties to take adaptive actions to reduce these effects. Four counties in Southeast Florida formed a climate compact in 2010 to address climate change impacts, including sea level rise and high tide flooding.[91] Recently updated in 2017, their climate action plan was one of the first intergovernmental collaborations to address climate change, adaptation, and mitigation in the country. Since then, cities like Charleston, South Carolina, have started to invest in flood management activities (see Case Study "Charleston, South Carolina, Begins Planning and Reinvesting"). Other examples include Miami Beach, Florida, which has a multiyear, $500-million program to raise public roads and seawalls and improve storm water drainage.[92] Norfolk, Virginia, has begun comprehensive planning to fix its high tide flooding issues.[93] Biloxi, Mississippi, has put in place several adaptation strategies to lessen the future impacts, including enacting a new building code that requires elevating structures an additional one foot above the base flood elevation.[94] Tybee Island, Georgia, has developed a sea level rise adaptation plan with recommendations to flood-proof a 5.5-mile stretch of their sole access causeway, replace two vulnerable bridges, and retrofit their existing storm water infrastructure to improve drainage.[95] In response to the 2016 flooding, eight parishes in the Acadiana region of Louisiana came together to collaborate at a watershed level, pooling their federal hazard mitigation grant funding to support projects across the Teche-Vermilion watershed. This is the only watershed-level hazard mitigation collaboration of this kind happening in the state and has the support of the Federal Emergency Management Agency (FEMA), the Governor's Office of Homeland Security and Emergency Preparedness, and the Louisiana Office of Community Development.[96]

Many communities in the Southeast also participate in FEMA's Community Rating System (CRS) program, which provides reduced flood insurance premiums to communities that go above and beyond the minimum National Flood Insurance Program regulation standards.[97] Many communities require a safety factor, also known as freeboard, expressed as feet above the base flood elevation, for construction in special flood hazard areas. Several Southeast communities—such as Hillsborough and Pinellas Counties, Florida; Biloxi, Mississippi; Chatham County, Georgia; and Myrtle Beach, South Carolina—have earned low CRS classes (5 on a scale of 1–10, with 1 being the best or most insurance premium discount) by implementing freeboard and other regulations that exceed the minimum standards.[97]

Case Study: Coastal and Inland Impacts of Extreme Rainfall

In October 2015, an extreme rainfall event impacted both inland and coastal South Carolina, leading to the largest flood-related disaster in the state since Hurricane Hugo struck in 1989. The October 2015 event is among a series of devastating precipitation events that have occurred across the Southeast in recent years. From October 1–5, 2015, deep tropical moisture combined with a slow-moving (stalled) upper-level low pressure system to pump moisture into South Carolina's coastal and interior regions. Much of the affected region received between 10 and 26 inches of rain over the 4-day event, breaking many all-time precipitation records (Figure 19.12). Mount Pleasant, located on South Carolina's coast, received 26.88 inches of rain, which is an extremely rare event. The rainfall sparked inland flooding that led to three dam breaches and the destruction of countless roads and homes (see Figure 19.13 showing flash flooding impacts to inland roads). Roughly 52,000 residents applied for disaster relief, and 160,000 homes sustained some type of damage. At the coast, a combination of high tide and heavy rain caused significant flooding in downtown Charleston. A high tide of 2.38 feet above Mean Higher High Water (MHHW) occurred in the afternoon of October 3. This was the seventh highest tide ever recorded in Charleston Harbor and the highest since Hurricane Hugo in 1989. Under future climate scenarios, the combination of extreme precipitation and higher tides due to local sea level rise will likely cause more frequent events of this intensity and magnitude.[98]

Case Study: Coastal and Inland Impacts of Extreme Rainfall, *continued*

October 2015 Extreme Rainfall Event

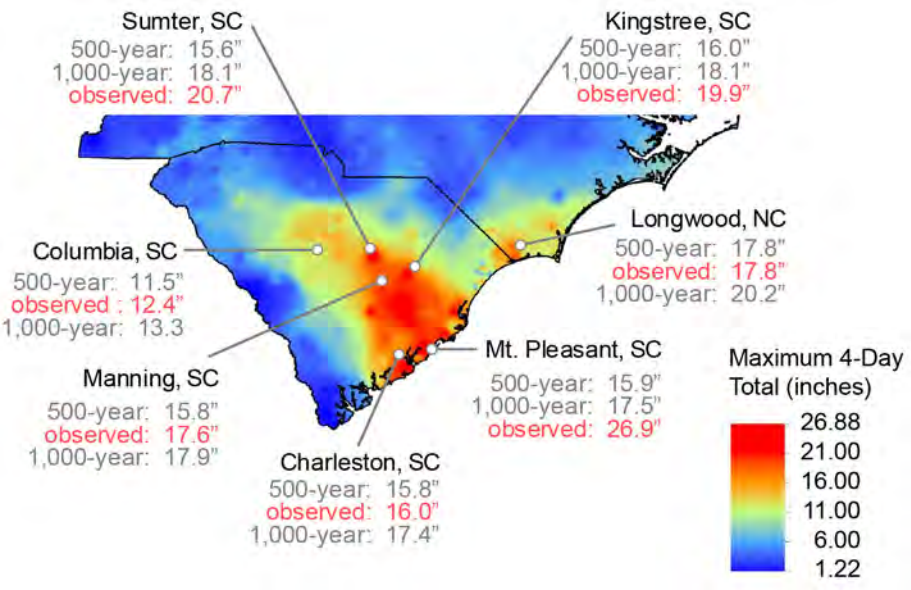

Figure 19.12: The map shows rainfall totals from the October 2015 South Carolina flood event. Red colors in the map indicate areas that received excessive rainfall totals that broke all-time records. Some of these totals exceeded the 500-year and 1,000-year return period amounts (rainfall amounts that would be expected to have only a 0.2% or 0.1% chance of occurring in a given year). Extreme precipitation events will likely increase in frequency in the Southeast. Source: CISA 2015.[98]

Figure 19.13: Many roads became impassable in the inland areas of South Carolina as a result of the October 2015 extreme rainfall event. This photo shows a neighborhood in North Charleston after the event with knee-deep flooding. Photo credit: Ryan Johnson (CC BY-SA 2.0).

Increases in extreme rainfall events and high tide coastal floods due to future climate change could impact the quality of life of permanent residents as well as tourists visiting the low-lying and coastal regions of the Southeast. Recent social science studies have indicated that people may migrate from many coastal communities that are vulnerable to the impacts of sea level rise, high tide flooding, saltwater intrusion, and storm surge.[71] Even though many communities are starting to develop adaptation strategies to address current flooding issues, many adaptation strategies are not being designed for longer time horizons and more extreme worst-case climate scenarios.[1,67]

The 2017 Hurricane Season

For the United States, 2017 was a historic year for weather and climate disasters, with widespread impacts and lingering costs. While 2017 tied the previous record year of 2011 for the total number of billion-dollar weather and climate disasters—16—the year broke the all-time previous record high costs by reaching $306.2 billion in damages (in 2017 dollars; $297 billion in 2015 dollars). The previous record year was 2005 with a total of $214.8 billion (in 2017 dollars; $208.4 billion in 2015 dollars), which included the impacts of Hurricanes Dennis, Katrina, Rita, and Wilma.[99]

In 2017, Hurricane Irma was one of three major hurricanes to make landfall in the United States and territories, with the most significant impacts occurring in the Southeast region. Irma was a Category 4 storm with 130 mph wind speeds when it made landfall at Cudjoe Key, Florida (20 miles north of Key West). Storm surge inundations at Cudjoe and the surrounding Keys were between 5 and 8 feet.[100] Prior to landfall in Florida, Irma caused significant damage in the U.S. Virgin Islands and parts of Puerto Rico as a Category 5 hurricane with 185 mph wind speeds (see Ch. 20: U.S. Caribbean, Box 20.1 and KM 5).[84]

Irma's intensity was impressive by any measure. According to the National Weather Service, Hurricane Irma was only the fifth hurricane with winds of 185 mph or higher in the whole of the Atlantic Basin since reliable record keeping began, and it was the strongest observed hurricane in the open Atlantic Ocean.[101] For three days, the storm maintained maximum sustained winds of 185 miles per hour, the longest observed duration in the satellite era.[101,102] Not only was Irma extremely strong, it was also very large with tropical storm force winds reaching as far away as 400 miles from the hurricane's center and driving hurricane force winds up to 80 miles away.[101] Two factors supported Irma's strength: the very warm waters it passed over, which exceeded 86°F,[102] and the light winds Irma encountered in the upper atmosphere (Figure 19.14).[101] High-intensity hurricanes such as Irma are expected to become more common in the future due to climate change.[103] Rapid intensification of storms is also more likely as the climate warms,[104] even though there is also some historical evidence that the same conditions that lead to this intensification also act to weaken hurricane intensity near the U.S. coast, but it is unclear whether this relationship will continue as the climate warms further (see Kossin et al. 2017,[103] Box 9.1).

The storm tracked up the west coast of Florida, impacting both coasts of the Florida peninsula with 3–5 feet of inundation from Cape Canaveral north to the Florida–Georgia border and even further, impacting coastal areas of Georgia and South Carolina with high tides and storm surge that reached 3–5 feet. Inland areas were also impacted by winds and heavy rains with river gauges and high-water marks showing upwards of 2–6 feet above ground level.[100] The winds eventually fell below tropical storm strength near Columbus, Georgia. Even though the wind speed fell below tropical storm strength, many communities along the coasts of Florida, Georgia,

North and South Carolina, and Virginia experienced severe wind and storm surge damage with some near-historic levels of coastal flooding. A state of emergency was declared in four states from Florida north to Virginia and in Puerto Rico and the U.S. Virgin Islands, and, for the first time ever, Atlanta was placed under a tropical storm warning.[105,106,107,108] In Florida, a record 6.8 million people were ordered to evacuate, as were 540,000 coastal residents in Georgia and untold numbers in other coastal locations.[102,109,110] Nearly 192,000 evacuees were housed in approximately 700 emergency shelters in Florida alone.[109] According to NOAA's National Centers for Environmental Information (NCEI),[84] Irma significantly damaged 65% of the buildings in the Keys and destroyed 25% of them.

Warm Waters Contribute to the Formation of Hurricane Irma

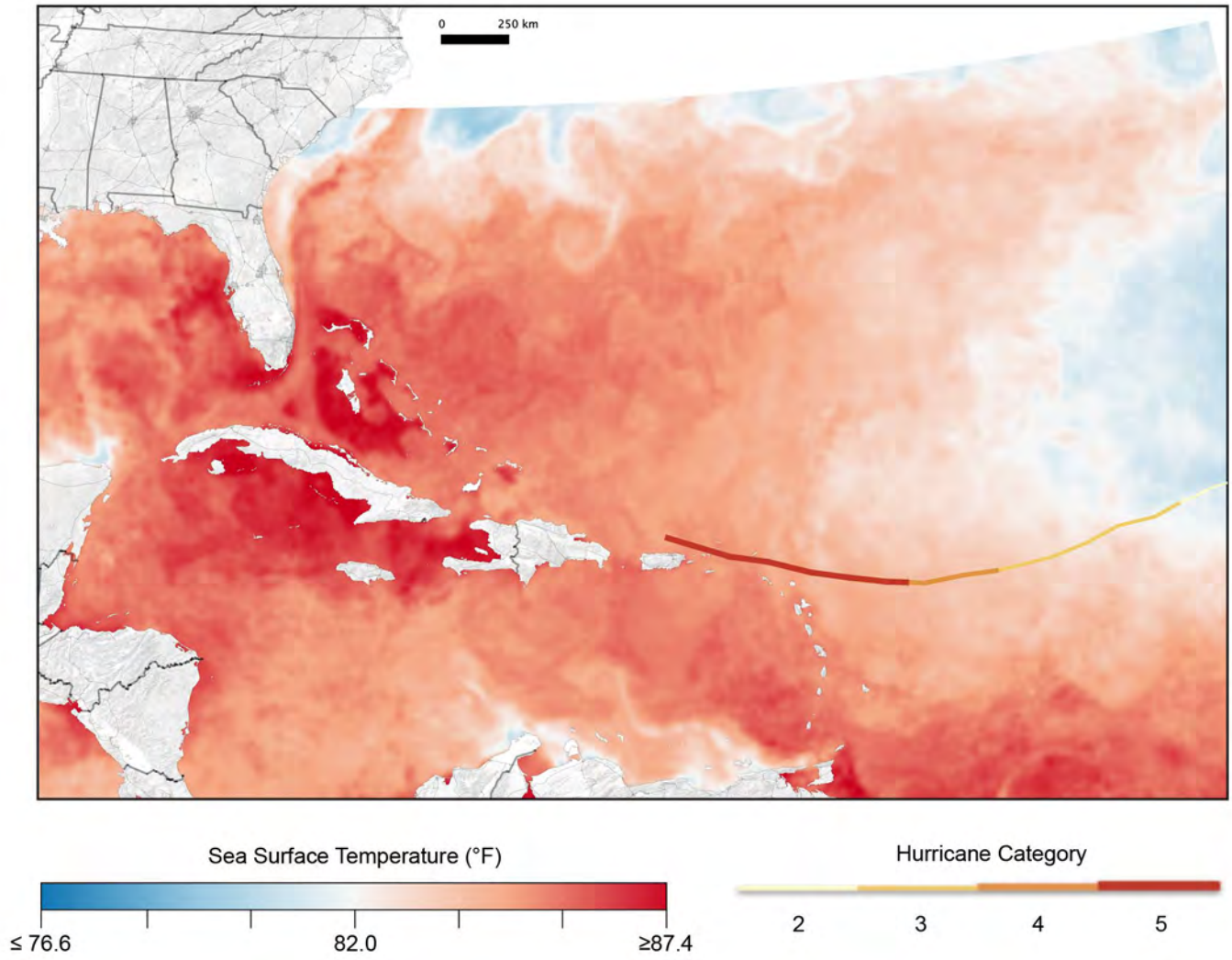

Figure 19.14: Two factors supported Hurricane Irma's strength as it reached the Southeast region: the very warm waters it passed over, depicted in this figure, and the light winds Irma encountered in the upper atmosphere.[101] High-intensity hurricanes such as Irma are expected to become more common in the future due to climate change.[103] Source: NASA 2017.[102]

High rainfall totals were experienced in many impacted areas, with Fort Pierce, Florida, receiving the highest rainfall of more than 21.5 inches[100] and the Florida Keys receiving 12 inches of rain.[84,102] Flooding occurred on most rivers in northern Florida and in many rivers in both Georgia and South Carolina to the point that rescues were required. In Jacksonville, Florida, heavy rains were the major issue causing rivers to reach major or record flood stage and flooded some city streets up to 5 feet deep in water. The heavy rainfall was noted even in Alabama, at 5 inches, and near 6 inches in the mountains of western North Carolina.[100] Twenty-five tornadoes were confirmed from Hurricane Irma, and many of them occurred along the east coast of central and northern Florida.[100] Even as Irma headed north, continuing to lose force, there were still 6.7 million people without electricity.[109]

According to NCEI,[84] the U.S. direct cost from Hurricane Irma is approximately $50 billion (in 2017 dollars), and the non-U.S. territory Caribbean Islands could add another $10–$15 billion to that total. Of the $50 billion, approximately $30–$35 billion accounts for wind and flood damage to a combination of residential and commercial properties, automobiles, and boats—with 80%–90% of this cost felt in Florida. The remainder of the costs include $5 billion for infrastructure repairs and $1.5–$2.0 billion for damage to the agricultural sector, also mainly in Florida. The remaining costs would address losses in the U.S. Virgin Islands and Puerto Rico.[84] The losses could have been worse except for the fact that Florida has implemented one of the strictest building codes in the country after the destruction caused by Hurricane Andrew in 1992.[111] Recent estimates using insured loss data show that implementing the Florida Building Code resulted in a 72% reduction of windstorm losses, and for every $1 in added cost to implement the building code, there is a savings of $6 in reduced losses, with the return or payback period being roughly 8 years (in 2010 dollars).[111]

Indirect impacts and costs are difficult to calculate and would add to the totals. In Central and South Florida, such things would include the closing of schools, colleges, and universities; the closing of tourist attractions and the cancellation of thousands of flights into and out of region; and the closing or restricting of the use of seaports including Canaveral, Key West, Miami, and Jacksonville, among others.[109,112] The Select Committee on Hurricane Response and Preparedness: Final Report[109] estimates that there were 84 U.S. deaths attributable to Hurricane Irma and other untold damage and human suffering. While the hurricane directly damaged portions of the Southeast, the impacts could be felt around the country in the form of business interruptions (such as tourism), transportation and infrastructure damages (such as ports, roadways, and airports), increases in fuel costs, and $2.5 billion (in 2018 dollars) in total estimated crop losses,[109] which had the potential to impact the cost of food and other products for all Americans.

Key Message 3

Natural Ecosystems Will Be Transformed

The Southeast's diverse natural systems, which provide many benefits to society, will be transformed by climate change. Changing winter temperature extremes, wildfire patterns, sea levels, hurricanes, floods, droughts, and warming ocean temperatures are expected to redistribute species and greatly modify ecosystems. As a result, the ecological resources that people depend on for livelihood, protection, and well-being are increasingly at risk, and future generations can expect to experience and interact with natural systems that are much different than those that we see today.

Ecosystems in the Southeast span the transition zone between tropical and temperate climates. The region's more temperate ecosystems include hardwood forests, spruce-fir forests, pine-dominated forests, and salt marshes. The region's more tropical ecosystems include mangrove forests, coral reefs, pine savannas, and the tropical freshwater wetlands of the Everglades. Ecological diversity in the Southeast is high,[113,114,115,116,117] and southeastern ecosystems and landscapes provide many benefits to society. In addition to providing habitat for fish and wildlife species, ecosystems in the Southeast provide recreational opportunities, improve water quality, provide seafood, reduce erosion, provide timber, support food webs, minimize flooding impacts, and support high rates of carbon sequestration (or storage).[118,119,120] These ecological resources that people depend on for livelihoods, protection, and well-being are increasingly at risk from the impacts of climate change.

Climate greatly influences the structure and functioning of all natural systems (Ch. 7: Ecosystems). An analysis of ecological changes that have occurred in the past can help provide some context for anticipating and preparing for future ecological changes. In response to past climatic changes, many ecosystems in the Southeast were much different than those present today. For example, since the end of the last glacial maximum (about 19,000 years ago—the most recent period of maximum ice extent),[121] forests in the region have been transformed by warming temperatures, sea level rise, and glacial retreat.[122,123] Spruce species that were once present in the region's forests have moved northward and have been replaced by oaks and other less cold-tolerant tree species that have expanded from the south.[124] And along the coast, freeze-sensitive mangrove forests and other tropical coastal species have been expanding northward and upslope since the last glacial maximum.[125,126,127,128,129]

In the coming decades and centuries, climate change will continue to transform many ecosystems throughout the Southeast,[6,130,131,132,133,134,135] which would affect many of the societal benefits these ecosystems provide. As a result, future generations can expect to experience, interact with, and potentially benefit from natural systems that are much different than those that we see today (Ch. 7: Ecosystems).[136,137]

Warming Winter Temperature Extremes

Changes in winter air temperature patterns are one aspect of climate change that will play an especially important role in the Southeast. By the late 21st century under the higher scenario (RCP8.5), the freeze-free season is expected to lengthen by more than a month. Winter air temperature extremes (for example, freezing and chilling events) constrain the northern limit of many tropical and subtropical species.[138,139,140,141,142,143,144] Certain ecosystems in the region are located near thresholds where small changes in winter air temperature regimes can trigger comparatively large and abrupt landscape-scale ecological changes (in other words, ecological regime shifts).[135,145] Reductions in the frequency and intensity of cold winter air temperature extremes can allow tropical and subtropical species to move northward and replace more temperate species. Where climatic thresholds are crossed, certain ecosystem and landscapes will be transformed by changing winter air temperatures.

Plant hardiness zone maps help convey the importance of winter air temperature extremes for species and natural systems in the Southeast. To help gardeners and farmers, the U.S. Department of Agriculture has produced plant hardiness zone maps that can be used to determine which species are most likely to survive and thrive in a given location. The plant hardiness zones are reflective of the frequency and intensity of winter air temperature

extremes in a specific region. Already, in response to climate change, plant hardiness zones in certain areas are moving northward and are expected to continue their northward and upslope progression.[139,142,146,147] Continued reductions in the frequency and intensity of winter air temperature extremes are expected to change which species are able to survive and thrive in a given location (Figure 19.15). For example, citrus species are sensitive to freezing and chilling temperatures.[148] However, in the future, climate change is expected to enable the survival of citrus in areas that are north of the current tolerance zone.[142]

The effects of changing winters reach far beyond just agricultural and garden plants. Along the coast, for example, warmer winter temperatures are expected to allow mangrove forests to move northward and replace salt marshes (Figures 19.16 and 19.17).[135,149,150,151,152] Coastal wetlands, like mangrove forests and salt marshes, are abundant in the Southeast.[153,154] The societal benefits provided by coastal wetlands are numerous.[119] Hence, where coastal wetlands are abundant (for example, the Mississippi River Delta), their cumulative value can be worth billions of dollars each year and trillions of dollars over a 100-year period.[155] Coastal wetlands provide seafood, improve water quality, provide recreational opportunities, reduce erosion, support food webs, minimize flooding impacts, and support high rates of carbon sequestration.[118] Foundation species are species that create habitat and support entire ecological communities.[156,157] In coastal wetlands and many other ecosystems, foundation plant species play an especially important role. Hence, the loss and/or replacement of foundation plant species, like salt marsh grasses, will have ecological and societal consequences in certain areas.[135,145,157,158,159,160,161,162,163,164]

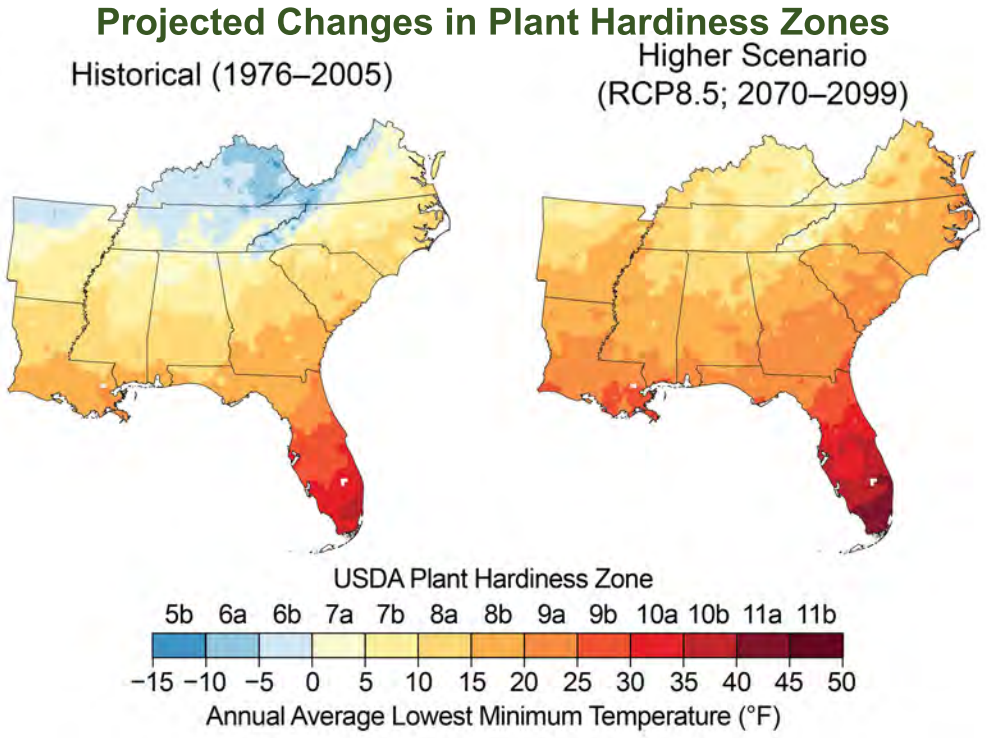

Figure 19.15: Increasing winter temperatures are expected to result in a northward shift of the zones conducive to growing various types of plants, known as plant hardiness zones. These maps show the mean projected changes in the plant hardiness zones, as defined by the U.S. Department of Agriculture (USDA), by the late 21st century (2070–2099) under a higher scenario (RCP8.5). The USDA plant hardiness zones are based on the average lowest minimum temperature for the year, divided into increments of 5°F. Based on these projected changes, freeze-sensitive plants, like oranges, papayas, and mangoes, would be able to survive in new areas.[142] Note that large changes are projected across the region, but especially in Kentucky, Tennessee, and northern Arkansas. Sources: NOAA NCEI and CICS-NC.

While salt marsh and mangrove wetlands both contain valuable foundation species, some of the habitat and societal benefits provided by existing salt marsh habitats will be affected by the northward expansion of mangrove forests.[145,158,160,161,164,165]

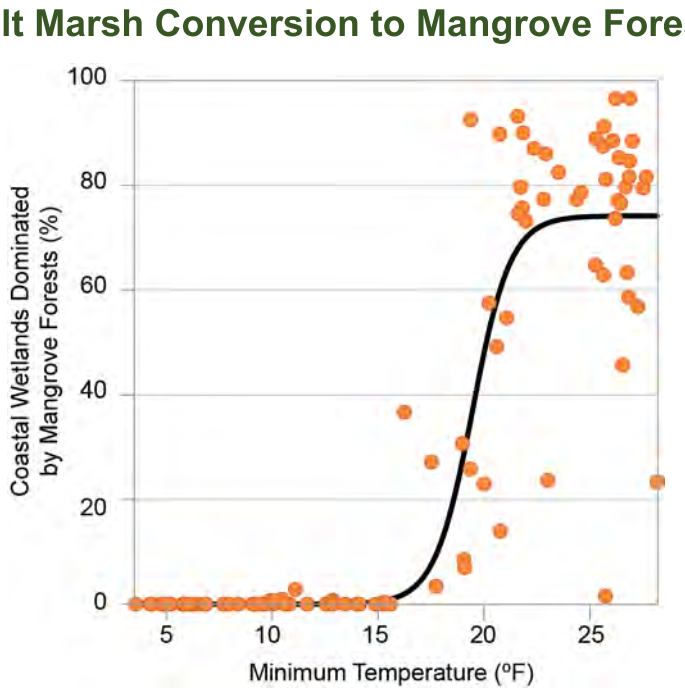

Figure 19.16: Where tropical and temperate ecosystems meet, warmer winter temperatures can lead to large ecological changes such as mangrove forest replacement of salt marshes along the Gulf and Atlantic Coasts. Mangrove forests are sensitive to freezing temperatures and are expected to expand northward at the expense of salt marshes. The figure shows the relationship between temperature and the percentage area dominated by mangrove forests. Mangrove expansion would entail a grassland-to-forest conversion, which would affect fish and wildlife habitat and many societal benefits. Source: adapted from Osland et al. 2013.[135] ©2012 Blackwell Publishing Ltd.

Transitioning Coastal Ecosystems

Figure 19.17: In Louisiana and parts of northern Florida, future coastal wetlands are expected to look and function more like the mangrove-dominated systems currently present in South Florida and the Caribbean. Like salt marshes (left), mangrove forests (right) provide coastal protection against wind and waves (Ch. 20: U.S. Caribbean, KM 2). Photo credit: Michael Osland.

In addition to plants, warmer winter air temperatures will also affect the movement and interactions between many different kinds of organisms. For example, certain insect species, including mosquitoes and tree-damaging beetles, are expected to move northward in response to climate change, which could affect human health and timber supplies.[30,144,166,167,168,169,170,171,172] And some bird species, including certain ducks, are not expected to migrate as far south in response to milder winters,[173] which could affect birding and hunting recreational opportunities. Many recreational fishery populations in tropical coastal areas are freeze-sensitive[138,174,175,176,177,178] and are, therefore, expected to move northward in response to warmer water and air temperatures. Although the appearance of tropical recreational fish, like snook for example, may be favorable for some anglers, the movement of tropical marine species is expected to greatly modify existing food webs and ecosystems (Ch. 7: Ecosystems, Figure 7.4).[179] Some problematic invasive species are expected to be favored by changing winters. For example, in South Florida, the Burmese python and the Brazilian pepper tree are two freeze-sensitive, nonnative species that have, respectively, decimated mammal populations and transformed native plant communities within Everglades National Park.[180,181,182,183,184,185,186,187,188] In the future, warmer winter temperatures are expected to facilitate the northward movement of these problematic invasive species, which would transform natural systems north of their current distribution.

Warm Winters Favor Invasive Species

Figure 19.18: Burmese pythons are apex predators (not preyed upon by other animals) that are sensitive to cold temperatures and are expected to be favored by warming winters. This photo is from Everglades National Park, where unintentionally introduced pythons have expanded and reduced native mammal populations. Photo credit: U.S. Geological Survey.

Changing Patterns of Fire

In the Southeast region, changing fire regimes (defined by factors including frequency, intensity, size, pattern, season, and severity) are expected to have a large impact on natural systems. Fire has historically played an important role in the region, and ecological diversity in many southeastern natural systems is dependent upon fire.[115,116,134,189] Although the total area burned by wildfire is greatest in the western United States, the Southeast has the largest area burned by prescribed fire (see Case Study "Prescribed Fire") and the highest number of wildfires.[134,190] In the future, rising temperatures and increases in the duration and intensity of drought are expected to increase wildfire occurrence and also reduce the effectiveness of prescribed fire.[3,4,5,6] Moreover, rapid urban expansion near managed forests has the potential to reduce opportunities to use prescribed fire, which could lead to native species declines, increased wildfire occurrence, and economic and health impacts.[134,191]

A recent example of the importance of fire lies in the forests of the southern Appalachians. Over the last century, invasive insects, logging, and pathogens have transformed forests in the region.[192] Warmer temperatures and insects have led to the loss of cold-adapted boreal communities, and flammable, fire-adapted tree species have been replaced by less flammable, fire-sensitive species—a process known as mesophication.[193,194] However, intense fires, like those observed in 2016, can halt the mesophication process. High temperatures, increases in accumulated plant material on the forest floor, and a four-month seasonal drought in the fall of 2016 collectively produced the worst wildfires the region has seen in a century. Intra-annual droughts, like the one in 2016, are expected to become more frequent in the future.[6] Thus, drought and greater fire activity[134] are expected to continue to transform forest ecosystems in the region (see Ch. 6: Forests, KM 1).

Case Study: Prescribed Fire

With wildfire projected to increase in the Southeast,[6,191] prescribed fire (the purposeful ignition of low-intensity fires in a controlled setting), remains the most effective tool for reducing wildfire risk.[4,195] Department of Defense (DoD) lands represent the largest reservoirs of biodiversity and native ecosystems in the region.[117] Military activities are a frequent source of wildfires, but increases in prescribed fire acres (Figure 19.19) show a corresponding decrease in wildfire ignitions for DoD.[4] Climate resilience by DoD is further achieved through restoration of native longleaf pine forests that occupy a wide range of site types, including wetland and well-drained soils—the latter leading many to characterize this forest as being drought resistant.[196,197,198,199] In addition to proactive adaptation through prescribed fire, DoD has been a leader in climate strategies that include regional conservation planning, ecosystem management, endangered species recovery, and research funding.

Wildlife and Prescribed Fire

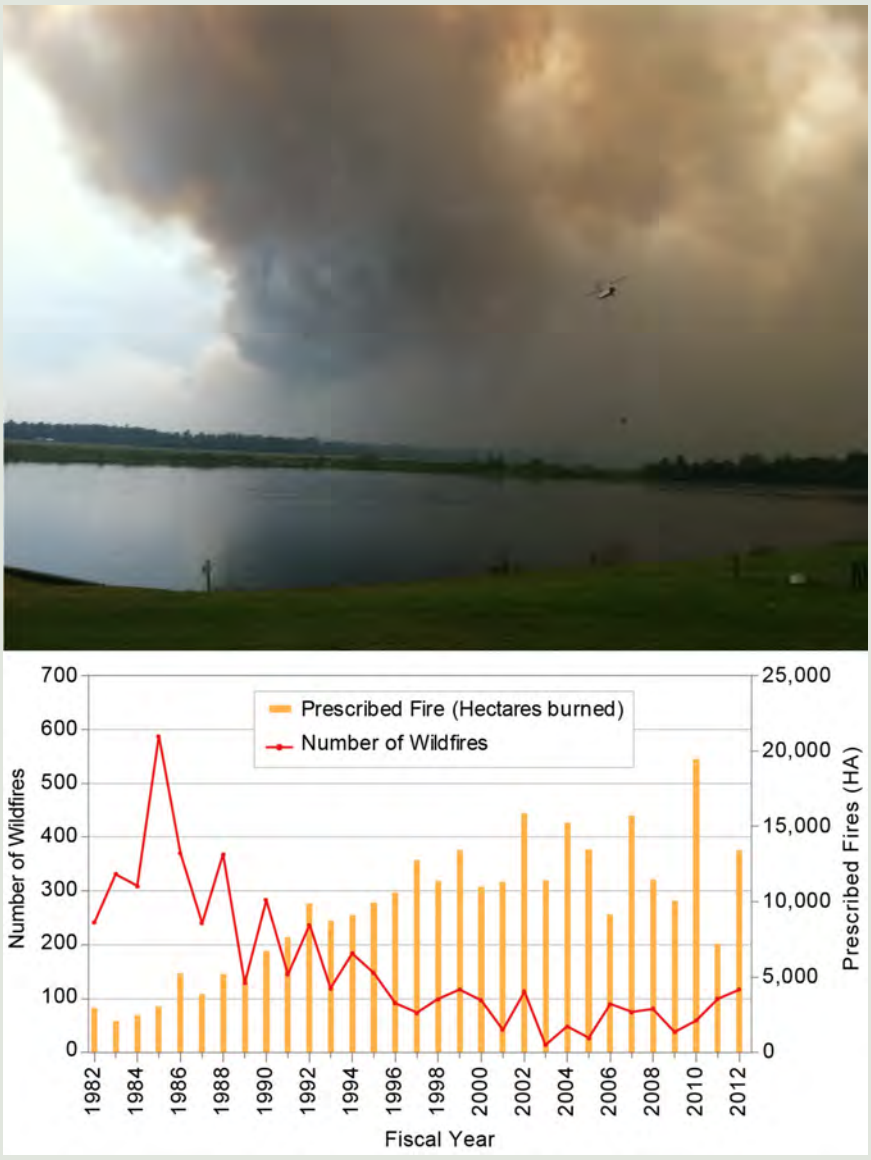

Figure 19.19: (top) A helicopter drops water on a 1,500-hectare wildfire on Hurlburt Field (Eglin Air Force Base) in Florida in June of 2012. (bottom) The increased use of prescribed fire at Ft. Benning, Georgia, led to a decrease in wildfire occurrence from 1982 to 2012. Photo credit: Kevin Hiers, Tall Timbers. Figure source: adapted from Addington et al. 2015.[4] Reprinted by permission of CSIRO Australia, ©CSIRO.

Rising Sea Levels and Hurricanes

Rising sea levels and potential changes in hurricane intensity are aspects of climate change that are expected to have a tremendous effect on coastal ecosystems in the Southeast (Ch. 8: Coastal, KM 2; Ch. 9: Oceans, KM 1). Since coastal terrestrial and freshwater ecosystems are highly sensitive to increases in inundation and salinity, sea level rise will result in the rapid conversion of these systems to tidal saline habitats. Historically, coastal ecosystems in the region have adjusted to sea level rise by vertical and horizontal movement across the landscape.[125,129,200,201] As sea levels rise in the future, some coastal ecosystems will be submerged and converted to open water, and saltwater intrusion will allow salt-tolerant coastal ecosystems to move inland at the expense of upslope and upriver ecosystems.[128,202,203,204,205,206,207,208] Where barriers are present (for example, levees and other coastal infrastructure), the potential for landward migration of natural systems will be reduced and certain coastal habitats will be lost (Ch. 20: U.S. Caribbean, KM 3).[204] With higher sea levels and increasing saltwater intrusion, the high winds, high precipitation rates, storm surges, and salts that accompany hurricanes will have large ecological impacts to terrestrial and freshwater ecosystems.[209,210]

An example of the effects of rising sea levels can be found in Louisiana, which faces some of the highest land loss rates in the world. The ecosystems of the Mississippi River Delta provide at least $12–$47 billion (in 2017 dollars) in benefits to people each year.[155] These benefits include hurricane storm protection, water supply, furs, habitat, climate stability, and waste treatment. However, between 1932 and 2016, Louisiana lost 2,006 square miles of land area (see Case Study "A Lesson Learned for Community Resettlement"),[211] due in part to high rates of relative sea level rise.[212,213,214,215] The rate of wetland loss during this period equates to Louisiana losing an area the size of one football field every 34 to 100 minutes.[211] To protect and restore the Louisiana coast, the Louisiana Coastal Protection and Restoration Authority (CPRA) has worked with local, state, and federal partners to iteratively develop a 2017 Coastal Master Plan that identifies investments that can provide direct restoration and risk reduction benefits.[216] The aim of the 50-year, $50-billion strategy is to sustain Louisiana's coastal ecosystems, safeguard coastal populations, and protect vital economic and cultural resources.[216]

Drought and Extreme Rainfall

Climate change is expected to intensify the hydrologic cycle and increase the frequency and severity of extreme events like drought and heavy rainfall. Drought and extreme heat can result in tree mortality and transform the region's forested ecosystems (Ch. 6: Forests, KM 1).[217,218,219,220,221,222,223] Drought can also affect aquatic and wetland ecosystems,[224] for example by contributing to mortality and ecological transformations in salt marshes,[225,226] mangrove forests,[227,228,229,230,231] and tidal freshwater forests.[232] In addition to drought, extreme rainfall events are also expected to become more frequent and severe in the future. The prolonged inundation and lack of oxygen that results from extreme rainfall can also result in mortality, such as the dieback of critical foundation plant species, and other large impacts to natural systems.[233] In combination, future increases in the frequency and severity of both extreme drought and extreme rainfall are expected to transform many ecosystems in the Southeast region. Natural systems in the region will have to become resistant and resilient to both too little water and too much water. The ecological transformations induced by these extreme events will affect many of the benefits that natural systems provide to society.

Warming Ocean Temperatures

Warming ocean temperatures due to climate change are expected to have a large effect on marine and coastal ecosystems (Ch. 9: Oceans, KM 3).[234,235,236] Many species are sensitive to small changes in ocean temperature; hence, the distribution and abundance of marine organisms are expected to be greatly altered by increasing ocean temperatures. For example, the distribution of tropical herbivorous fish has been expanding in response to warmer waters, which has resulted in the tropicalization of some temperate marine ecosystems and decreases in the cover of valuable macroalgal plant communities.[179] A decrease in the growth of sea turtles in the West Atlantic has been linked to higher ocean temperatures.[237] Due to climate change, warming ocean temperatures in the coming decades are expected to transform many marine and coastal ecosystems across the Southeast. However, the impacts to coral reef ecosystems in the region have been and are expected to be particularly dire. Coral reefs are biologically diverse ecosystems that provide many societal benefits, including coastal protection from waves, habitat for fish, and recreational and tourism opportunities.[238,239] However, coral reef mortality in the Florida Keys and across the globe has been very high in recent decades, due in part to warming ocean temperatures, nutrient enrichment, overfishing, and coastal development.[240,241,242,243,244] Small increases in ocean temperature can cause corals to expel the symbiotic algae upon which they depend for nourishment. When this happens, corals lose their color and die in a process known as coral bleaching (Ch. 9: Oceans, KM 1). Coral elevation and volume in the Florida Keys have been declining in recent decades,[245] and present-day temperatures in the region are already close to bleaching thresholds; hence, it is likely that many of the remaining coral reefs in the Southeast region will be lost in the coming decades.[246,247] In addition to warming temperatures, accelerated ocean acidification is also expected to contribute to coral reef mortality and decline.[248,249] When coral reefs are lost, coastal communities lose the many benefits provided by these valuable ecosystems, including lost tourism opportunities, a decline in fisheries, and a decrease in wave protection.[246,247]

Key Message 4

Economic and Health Risks for Rural Communities

Rural communities are integral to the Southeast's cultural heritage and to the strong agricultural and forest products industries across the region. More frequent extreme heat episodes and changing seasonal climates are projected to increase exposure-linked health impacts and economic vulnerabilities in the agricultural, timber, and manufacturing sectors. By the end of the century, over one-half billion labor hours could be lost from extreme heat-related impacts. Such changes would negatively impact the region's labor-intensive agricultural industry and compound existing social stresses in rural areas related to limited local community capabilities and associated with rural demography, occupations, earnings, literacy, and poverty incidence. Reduction of existing stresses can increase resilience.

In the Southeast, over 56% of land remains rural (nonmetropolitan) and home to approximately 16 million people, or about 17% percent of the region's population.[250] These rural areas are important to the social and economic well-being of the Southeast. Many in rural communities are maintaining connections to traditional livelihoods and relying on natural

resources that are inherently vulnerable to climate change. The Southeast has the second highest number of farmworkers hired per year compared to other National Climate Assessment (NCA) regions.[251] Climate trends and possible climate futures show patterns that are already impacting—and are expected to further impact—rural sectors, from agriculture and forestry to human health and labor productivity (Ch. 10: Ag & Rural, KM 3). For example, shrimping, oystering, and fishing along the coast are long-standing traditions in the coastal economy that are expected to face substantial challenges. For example, by the end of the century, annual oyster harvests in the Southeast are projected to decline between 20% (19%–22%) under a lower scenario (RCP4.5) and 46% (44%–48%) under a higher scenario (RCP8.5), leading to projected price increases of 48% (RCP4.5) to 140% (RCP8.5).[35] Projected warming ocean temperatures, sea level rise, and ocean and coastal acidification are raising concern over future harvests (Ch. 9: Oceans, KM 2).[35,252] While adaptation and resilience can moderate climate change impacts, rural areas generally face other stressors, such as poverty and limited access to healthcare, which will make coping to these climate-related challenges more difficult.

Heat-related stresses are presently a major concern in the Southeast. Future temperature increases are projected to pose challenges for human health. While recent regional temperature trends have not shown the same consistent rate of daytime maximum temperature increase as observed in other parts of the United States, climate model simulations strongly suggest that daytime maximum temperatures are likely to increase as humans continue to emit greenhouse gases into the atmosphere.[13] The resulting temperature increases are expected to add to the heat health burden in rural, as well as urban, areas.[35] Projected temperature increases also pose challenges for crop production dependent on periods of lower temperatures to reach full productivity. Drought has been a recurrent issue in the Southeast affecting agriculture, forestry, and water resources.[253] With rapid growth in population and overall demand, drought is increasingly a concern for water resource management sectors such as cities, ecosystems, and energy production.

Diverse Rural Regions

Urban and rural areas exist along a continuum from major metro areas to suburbs, small towns, and lightly populated places. These areas are linked through many processes, commuting patterns, and shared central services, such as airports and hospitals, that connect the risks. Rapid population growth with associated urbanization and suburbanization over the last several decades has resulted in a more fine-grained forest landscape with smaller and more numerous forest patches.[254] Agriculture, manufacturing, tourism, and other major economic sectors are spread across the Southeast region. Rural counties in the region generally have a diversified economy with a relatively low percentage being heavily dependent on one sector. While well known for agriculture and forestry, rural areas also support manufacturing and tourism.[250]

In 2013, approximately 34% of the U.S. manufacturing output, or about $700 billion (dollar year not reported), came from the Southeast and Texas, including rural areas.[255] While manufacturing growth has been particularly strong in the Southeast in recent years, future climate changes would pose challenges for economic competitiveness. For companies involved in food processing, there are additional secondary economic risks associated with climate impacts on crops and livestock that could alter price or availability.[64,255] Facilities that are energy- or water-intensive are more likely to face increases in the costs and

decreases in the availability of these resources, with potential impacts to their economic competitiveness.[246,255]

Energy production, and its dependence on water availability, is a key concern in the Southeast, given the region's growing population and large, diversified economy. An increasing number of high heat and dry days as the climate warms poses a risk to efficient power generation, particularly under conditions where the mode of primary generation moves towards natural gas and water-intensive nuclear power.[256]

Risks to Agriculture and Forestry

Agriculture, livestock rearing, and forestry activities are widespread and varied through the Southeast region.[7] Climate change is expected to have an overall negative impact on agricultural productivity in the United States,[35] although some crops could also become newly viable alternatives (Key Message 3, Figure 19.15). Increases in temperatures, water stress, freeze-free days, drought, and wildfire risks, together with changing conditions for invasive species and the movement of diseases, create a number of potential risks for existing agricultural systems (Ch. 10: Ag & Rural, KM 1).[7] In particular, precipitation trends for the Southeast region show an inclination towards slightly drier summers, which could reduce productivity, and wetter fall seasons, which can make it difficult to harvest the full crop. Multimodel averages of climate model simulations (CMIP3 [SRES A2] and CMIP5 [RCP8.5] higher scenarios) show that there is a greater risk of drier summers by the middle of the century in the western portion of the Southeast and in southern Florida, while wetter fall seasons are more likely in the eastern portion of the region.[257]

The conditions for raising and harvesting crops and livestock are projected to change. Higher temperatures can result in decreasing productivity of some cultivated crops, including cotton, corn, soybeans, and rice.[7] Livestock, which includes hogs and pigs, horses, ponies, mules, burros, and donkeys as well as poultry and processed poultry for consumption (for example, chicken nuggets), is a large component of the agricultural sector for these states and the Nation.[258] Livestock are all vulnerable to heat stress, and their care under projected future conditions would require new or enhanced adaptive strategies (Ch. 10: Ag & Rural, KM 3).

Recent changes in seasonal temperatures that are critical for plant development will continue to impact regionally important crops. Plants collected from the wild may become less available as the ideal conditions for their growth shift to other areas (see Case Study "Mountain Ramps"). Peaches—an important crop in the Southeast—require an adequate period of cool temperatures, called the chill period, to produce yields that are economically viable. Peaches also require warm temperatures at specific times during their development.[259] If the warm temperatures come too early, the chill periods could be too short or the peach blossoms can flower too soon and be in danger of late freeze impacts. A late freeze in March 2017 caused over a billion dollars of damages to peaches and other fruit crops.[84] To assist peach growers in adapting to such changes, researchers are working to develop peach varieties that can produce quality fruits in warmer winters and are developing winter chill models that can assist in adaptation planning efforts.[260,261]

Forests, both natural and plantation, in the Southeast are vulnerable to climate variability and change. Southeastern forests represent almost 27% of the U.S. total[262] and are the highest-valued crop in the region.[7] The vast majority of forest is held in private hands, primarily corporate. Forest cover ranges from almost 50% to 80% in these states, creating

large areas of interface between populations and forests.[262] Jobs in timber, logging, and support for agriculture and forestry totaled approximately 458,000.[263] (See Ch. 6: Forests, KM 3 for additional discussion on forest change impacts on rural landscapes.)

The Southeast is one of the most dynamic regions for forest change on the globe,[269] though much of the change owes to intensive rotations of pine production and economic forces that drive frequent conversion between forest and agricultural uses in rural areas.[270,271] Climate is expected to have an impact on the region's forests primarily through changes in moisture regimes.[272] Species migration westward across the eastern United States in response to changing precipitation patterns has already been noted.[273] Drought is likely to alter fire regimes and further interact with species distributions (see Key Message 3). The interactions of altered precipitation and natural disturbances will be important in understanding impacts to the forests not dominated by industrial forestry (Ch. 6: Forests, KM 1 and KM 3).[274]

Wildfire is a well-known risk in the Southeast region, where it occurs with greater frequency than any other U.S. region.[275] However, mitigation strategies, particularly the use of prescribed fire, can significantly reduce wildfire risk and have been widely adopted across rural communities in the Southeast.[190] A doubling of prescribed fire at the landscape scale has been found to reduce wildfire ignitions by a factor of four,[4] while it is well documented that prescribed fire reduces the potential for crown fire in treated forest stands.[276] With greater projected fire risks,[191,277] more attention on how to foster fire-adapted communities offers opportunities for risk reduction (see Case Study "Prescribed Fire" and Key Message 3).[278,279]

Case Study: Mountain Ramps

The Cherokee have been harvesting ramps, a wild onion (*Allium tricoccum*), in the southern Appalachians, their ancestral homelands, for thousands of years.[264,265] Collecting ramps for food sustenance is only one aspect of this cultural tradition. The family-bound harvesting techniques are equally as important and make up part of the deeply held tribal lifeways (Ch. 15: Tribes, KM 2). Ramps emerge in springtime and provide important nutrients after a long winter with a dearth of fresh vegetables. These plants grow in moist forest understory areas that are sensitive to temperature and soil moisture.[266]

Figure 19.20: This up-close image of a ramp (*Allium tricoccum*), harvested from the wild, shows leaves and the bulb/corm of the plant. Photo credit: Gary Kaufman, USDA Forest Service Southern Research Station.

In the southern Appalachians, ramps are threatened by two major processes: overharvesting pressures and a changing climate that could expose these plants to higher temperatures and lower soil moisture conditions during sensitive growth periods (Ch. 10: Ag & Rural, KM 1).[267,268] Although ramps are found all along the Appalachian mountain range, on Cherokee ancestral lands, they are already in their southernmost range. Climate change thus acts to increase the vulnerability of this plant to the existing stressors.

Heat, Health, and Livelihoods

Heat-related health threats are already a risk in outdoor jobs and activities. While heat illness is more often associated with urban settings, rural populations are also at risk. For example, higher rates of heat-related illness have been reported in rural North Carolina compared to urban locations.[280] However, strategies to reduce health impacts on hot days, such as staying indoors or altering times outdoors, are already contributing to reducing heat-related illness in the Southeast.[281]

Workers in the agriculture, forestry, hunting, and fishing sectors together with construction and support, waste, and remediation services work are the most highly vulnerable to heat-related deaths in the United States, representing almost 68% of heat-related deaths nationally.[282] Six of the ten states with the highest occupational heat-related deaths in these sectors are in the Southeast region, accounting for 28.6% of occupational heat-related deaths between 2000 and 2010.[282] By 2090, under a higher scenario (RCP8.5), the Southeast is projected to have the largest heat-related impacts on labor productivity in the country, resulting in average annual losses of 570 million labor hours, or $47 billion (in 2015 dollars, undiscounted), a cost representing a third of total national projected losses, although these figures do not include adaptations by workers or industries (Figure 19.21).[35]

Investing in increased cooling is one likely form of adaptation. Among U.S. regions, the Southeast is projected to experience the highest costs associated with meeting increased electricity demands in a warmer world.[35]

Compounding Stresses and Constraints to Adaptation

The people of the rural Southeast confront a number of social stresses likely to add to the challenges posed by increases in climate stresses.[283] Rural communities tend to be more vulnerable due to factors such as demography, occupations, earnings, literacy, poverty incidence, and community capacities (Ch. 10: Ag & Rural, KM 4).[8,9,10] Reducing stress associated with these factors can increase household and community resilience.[9,284]

Projected Changes in Hours Worked

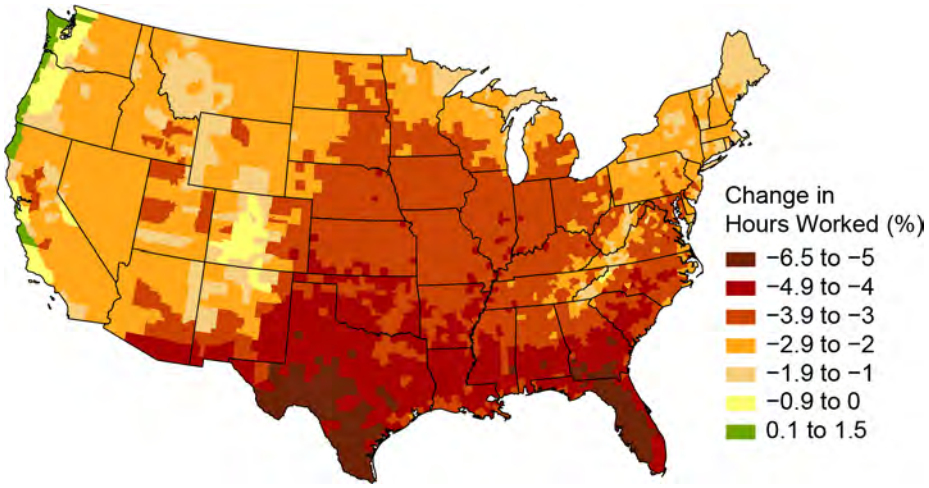

Figure 19.21: This map shows the estimated percent change in hours worked in 2090 under a higher scenario (RCP8.5). Projections indicate an annual average of 570 million labor hours lost per year in the Southeast by 2090 (with models ranging from 340 million to 820 million labor hours).[35] Estimates represent a change in hours worked as compared to a 2003–2007 average baseline for high-risk industries only. These industries are defined as agriculture, forestry, and fishing; hunting, mining, and construction; manufacturing, transportation, and utilities. Source: adapted from EPA 2017.[35]

Persistent rural poverty stands out in the Southeast (Figure 19.22). The rural counties in the region are experiencing higher levels of population loss (13% of rural counties lost population) and low educational attainment (38% of rural counties), with 35% of rural counties experiencing poverty rates of more than 20% persisting over approximately 30 years.[10] The Southeast is expected to experience the highest costs associated with meeting increased energy demands; an estimated $3.3 billion each year under a higher scenario (RCP8.5) and $1.2 billion annually under a lower scenario (RCP4.5) by the end of the century.[35] Energy poverty is a situation "where individuals or households are not able to adequately heat or provide other required energy services in their homes at affordable cost."[285] A case study from rural eastern North Carolina further explains energy poverty as a function of the energy efficiency of the home, energy provision infrastructure, physical health, low incomes, and support of social networks, which collectively influence households' choices about the amount of heating and cooling they can afford.[286] The National Weather Service (NWS) calculates degree days,[287] a way of tracking energy use. NWS starts with the assumption that when the average outside temperature is 65°F, heating or cooling is not needed in order to be comfortable. The difference between the average daily temperature and 65°F is the number of cooling or heating degrees for that day. These days can be added up over time—a month or a year—to give a combined estimate of energy needed for heating or cooling. Although heating costs are expected to decrease as the climate warms in the Southeast, the number of cooling degree days is expected to increase and the length of the cooling season expected to expand, increasing energy demand and exacerbating rural energy poverty (Figure 19.22).

The ability to cope with current and potential impacts, such as flooding, is further reduced by limited county resources. A study of hazard management plans (2004–2008) in 84 selected rural southeastern counties found these plans scored low across various criteria.[288] The rural, geographically remote locations contributed to more difficult logistics in reaching people. Interviewees also identified low-income and minority communities, substandard housing, lack of access to vehicles for evacuation, limited modes of communication, and limited local government capacity as contributing factors to difficulties in emergency planning.[288]

The healthcare system in the Southeast is already overburdened and may be further stressed by climate change. Between 2010 and 2016, more rural hospitals closed in the Southeast than any other region, with Alabama, Georgia, Mississippi, and Tennessee being among the top five states for hospital closures.[289] This strain, when combined with negative health impacts from climate change stressors (such as additional patient demand due to extreme heat and vector-borne diseases and greater flood risk from extreme precipitation events), increases the potential for disruptions of health services in the future. The Green River District Health Department recently did an assessment of ways to reduce vulnerability to negative health impacts of climate change in a mostly rural region of western Kentucky.[290] As a result, the local health department plans to enhance existing epidemiology, public health preparedness, and community health assessment services.[290]

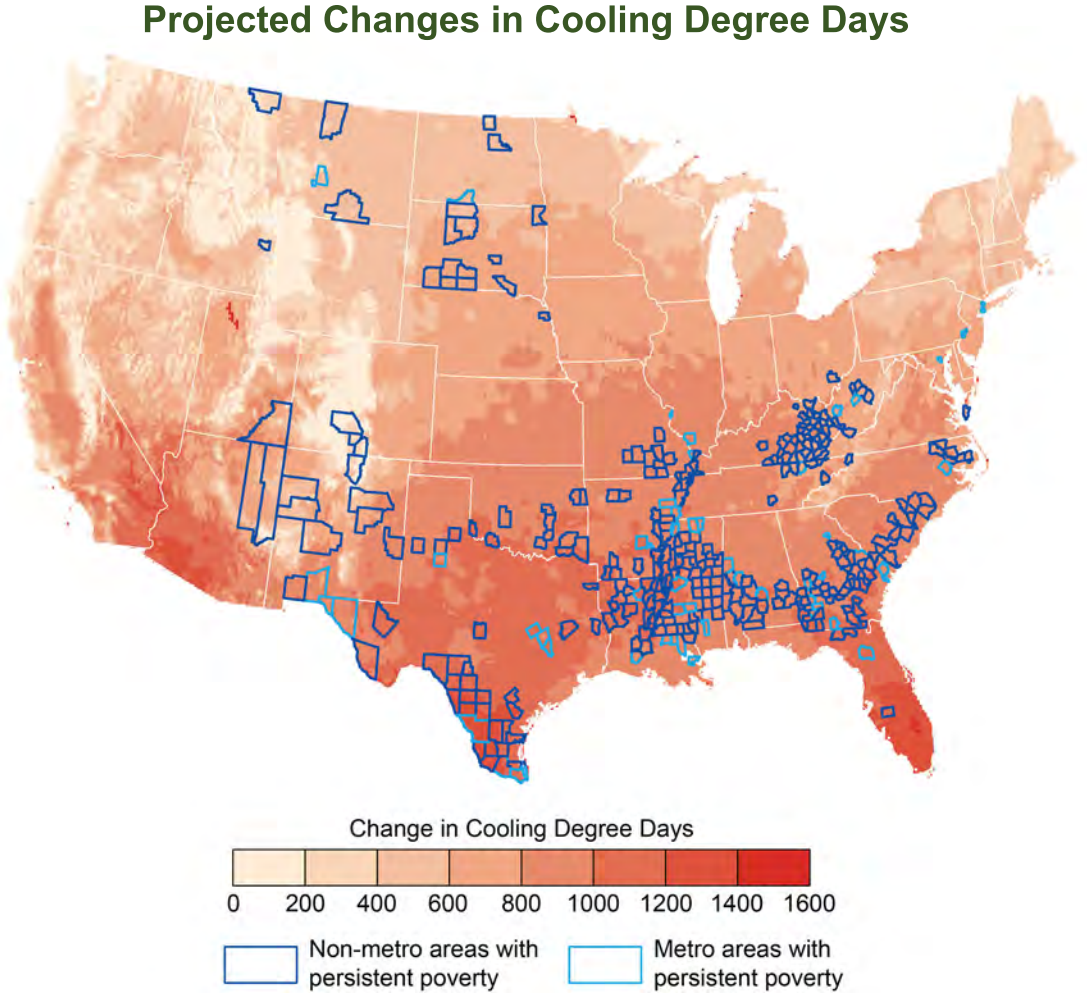

Figure 19.22: The map shows projected changes in cooling degree days by the mid-21st century (2036–2065) under the higher scenario (RCP8.5) based on model simulations. Rural counties experiencing persistent poverty are concentrated in the Southeast, where the need for additional cooling is expected to increase at higher rates than other areas of the country by mid-century. Sources: NOAA NCEI, CICS-NC, and ERT, Inc.

Acknowledgments

Technical Contributors

Vincent Brown
Louisiana State University

Barry Keim
Louisiana State University

Julie K. Maldonado
Livelihoods Knowledge Exchange Network

Colin Polsky
Florida Atlantic University

April Taylor
Chickasaw Nation

USGCRP Coordinators

Allyza Lustig
Program Coordinator

Matthew Dzaugis
Program Coordinator

Natalie Bennett
Adaptation and Assessment Analyst

Opening Image Credit

Red mangrove: © Katja Schulz/Flickr (CC BY 2.0). Adaptation: cropped top and bottom to conform to the size needed for publication.

Traceable Accounts

Process Description

Prior to identifying critical issues for the Southeast assessment focuses for the Fourth National Climate Assessment (NCA4), the Chapter Lead (CL) contacted numerous professional colleagues representing various geographic areas (e.g., Florida, Louisiana, and South Carolina) for expert opinions on critical climate change related issues impacting the region, with a particular emphasis on emerging issues since the Third National Climate Assessment (NCA3) effort.[77] Following those interviews, the CL concluded that the most pressing climate change issues to focus on for the NCA4 effort were extreme events, flooding (both from rainfall and sea level rise), wildfire, health issues, ecosystems, and adaptation actions. Authors with specific expertise in each of these areas were sought, and a draft outline built around these issues was developed. Further refinement of these focal areas occurred in conjunction with the public Regional Engagement Workshop, held on the campus of North Carolina State University in March 2017 and in six satellite locations across the Southeast region. The participants agreed that the identified issues were important and suggested the inclusion of several other topics, including impacts on coastal and rural areas and people, forests, and agriculture. Based on the subsequent authors' meeting and input from NCA staff, the chapter outline and Key Messages were updated to reflect a risk-based framing in the context of a new set of Key Messages. The depth of discussion for any particular topic and Key Message is dependent on the availability of supporting literature and chapter length limitations.

Key Message 1

Urban Infrastructure and Health Risks

Many southeastern cities are particularly vulnerable to climate change compared to cities in other regions, with expected impacts to infrastructure and human health (*very likely, very high confidence*). The vibrancy and viability of these metropolitan areas, including the people and critical regional resources located in them, are increasingly at risk due to heat, flooding, and vector-borne disease brought about by a changing climate (*likely, high confidence*). Many of these urban areas are rapidly growing and offer opportunities to adopt effective adaptation efforts to prevent future negative impacts of climate change (*very likely, high confidence*).

Description of evidence base

Multiple studies have projected that urban areas, including those in the Southeast, will be adversely affected by climate change in a variety of ways. This includes impacts on infrastructure[41,42,43,291,292,293] and human health.[30,31,38,294] Increases in climate-related impacts have already been observed in some Southeast metropolitan areas (e.g., Habeeb et al. 2015, Tzung-May Fu et al. 2015[12,39]).

Southeastern cities may be more vulnerable than cities in other regions of the United States due to the climate being more conducive to some vector-borne diseases, the presence of multiple large coastal cities at low elevation that are vulnerable to flooding and storms, and a rapidly growing urban and coastal population.[22,295,296]

Many city and county governments, utilities, and other government and service organizations have already begun to plan and prepare for the impacts of climate change (e.g., Gregg et al. 2017; FTA 2013; City of Fayetteville 2017; City of Charleston 2015; City of New Orleans 2015; Tampa Bay Water 2014; EPA 2015; City of Atlanta 2015, 2017; Southeast Florida Regional Climate Change Compact 2017[44,45,46,50,91,246,297,298,299]). A wide variety of adaptation options are available, offering opportunities to improve the climate resilience, quality of life, and economy of urban areas.[77,300,301,302,303,304]

Major uncertainties

Population projections are inherently uncertain over long time periods, and shifts in immigration or migration rates and shifting demographics will influence urban vulnerabilities to climate change. The precise impacts on cities are difficult to project. The scope and scale of adaptation efforts, which are already underway, will affect future vulnerability and risk. Technological developments (such as a potential shift in transportation modes) will also affect the scope and location of risk within cities. Newly emerging pathogens could increase risk of disease in the future, while successful adaptations could reduce public health risk.

Description of confidence and likelihood

There is *very high confidence* that southeastern cities will *likely* be impacted by climate change, especially in the areas of infrastructure and human health.

Key Message 2

Increasing Flood Risks in Coastal and Low-Lying Regions

The Southeast's coastal plain and inland low-lying regions support a rapidly growing population, a tourism economy, critical industries, and important cultural resources that are highly vulnerable to climate change impacts (*very likely, very high confidence*). The combined effects of changing extreme rainfall events and sea level rise are already increasing flood frequencies, which impacts property values and infrastructure viability, particularly in coastal cities. Without significant adaptation measures, these regions are projected to experience daily high tide flooding by the end of the century (*likely, high confidence*).

Description of evidence base

Multiple lines of research have shown that global sea levels have increased in the past and are projected to continue to accelerate in the future due to increased global temperature and that higher local sea level rise rates in the Mid-Atlantic and Gulf Coasts have occurred.[51,52,53,54,55,56,57,59,61,62]

Annual occurrences of high tide flooding have increased, causing several Southeast coastal cities to experience all-time records of occurrences that are posing daily risks.[1,52,58,60,61,63,67,68]

There is scientific consensus that sea level rise will continue to cause increases in high tide flooding in the Southeast as well as impact the frequency and duration of extreme water level events, causing an increase in the vulnerability of coastal populations and property.[1,60,63,67,68]

In the future, coastal flooding is projected to become more serious, disruptive, and costly as the frequency, depth, and inland extent grow with time.[1,2,35,64,65,67,68]

Many analyses have determined that extreme rainfall events have increased in the Southeast, and under higher scenarios, the frequency and intensity of these events are projected to increase.[19,21,88]

Rainfall records have shown that since NCA3, many intense rainfall events (approaching 500-year events) have occurred in the Southeast, with some causing billions of dollars in damage and many deaths.[68,82,84]

The flood events in Baton Rouge, Louisiana, in 2016 and in South Carolina in 2015 provide real examples of how vulnerable inland and coastal communities are to extreme rainfall events.[81,85,86]

The socioeconomic impacts of climate change on the Southeast is a developing research field.[65,71]

Major uncertainties

The amount of confidence associated with the historical rate of global sea level rise is impacted by the sparsity of tide gauge records and historical proxies as well as different statistical approaches for estimating sea level change. The amount of unpredictability in future projected rates of sea level rise is likely caused by a range of future climate scenarios projections and rate of ice sheet mass changes. Flooding events are highly variable in both space and time. Detection and attribution of flood events are difficult due to multiple variables that cause flooding.

Description of confidence and likelihood

There is *high confidence* that flood risks will *very likely* increase in coastal and low-lying regions of the Southeast due to rising sea level and an increase in extreme rainfall events. There is *high confidence* that Southeast coastal cities are already experiencing record numbers of high tide flooding events, and without significant adaptation measures, it is *likely* they will be impacted by daily high tide flooding.

Key Message 3

Natural Ecosystems Will Be Transformed

The Southeast's diverse natural systems, which provide many benefits to society, will be transformed by climate change (*very likely, high confidence*). Changing winter temperature extremes, wildfire patterns, sea levels, hurricanes, floods, droughts, and warming ocean temperatures are expected to redistribute species and greatly modify ecosystems (*very likely, high confidence*). As a result, the ecological resources that people depend on for livelihood, protection, and well-being are increasingly at risk, and future generations can expect to experience and interact with natural systems that are much different than those that we see today (*very likely, high confidence*).

Description of evidence base

Winter temperature extremes, fire regimes, sea levels, hurricanes, rainfall extremes, drought extremes, and warming ocean temperatures greatly influence the distribution, abundance, and performance of species and ecosystems.

Winter air temperature extremes (for example, freezing and chilling events) constrain the northern limit of many tropical and subtropical species.[30,48,127,132,135,138,139,140,141,142,143,144,145,148,149,150,152,166,167,168,169,170,172,173,174,175,176,177,178] In the future, warmer winter temperatures are expected to facilitate the northward movement of cold-sensitive species, often at the expense of cold-tolerant species.[132,135,142,145,149,150,152,166,169,173,179] Certain ecosystems are located near thresholds where small changes in winter air temperature regimes can trigger comparatively large and abrupt landscape-scale ecological changes (i.e., ecological regime shifts).[135,145,152]

Changing fire regimes are expected to have a large impact on natural systems. Fire has historically played an important role in the region, and ecological diversity in many southeastern natural systems is dependent upon fire.[115,116,134,189] In the future, rising temperatures and increases in the duration and intensity of drought are expected to increase wildfire occurrence and also reduce the effectiveness of prescribed fire.[3,4,5,6]

Hurricanes and rising sea levels are aspects of climate change that will have a tremendous effect on coastal ecosystems in the Southeast. Historically, coastal ecosystems in the region have adjusted to sea level rise via vertical and/or horizontal movement across the landscape.[125,129,200,201] As sea levels rise in the future, some coastal ecosystems will be submerged and converted to open water, and some coastal ecosystems will move inland at the expense of upslope and upriver ecosystems.[203,204] Since coastal terrestrial and freshwater ecosystems are highly sensitive to increases in inundation and/or salinity, sea level rise will result in the comparatively rapid conversion of these systems to tidal saline habitats. In addition to sea level rise, climate change is expected to increase the impacts of hurricanes; the high winds, storm surges, inundation, and salts that accompany hurricanes will have large ecological impacts to terrestrial and freshwater ecosystems.[209,210]

Climate change is expected to intensify the hydrologic cycle and increase the frequency and severity of extreme events. Extreme drought events are expected to become more frequent and severe. Drought and extreme heat can result in tree mortality and transform southeastern forested ecosystems.[217,218,219,220,221,222,223] Drought can also affect aquatic and wetland ecosystems.[224,225,226,227,228,229,232] Extreme rainfall events are also expected to become more frequent and severe in the future. The prolonged inundation and lack of oxygen that result from extreme rainfall events can also result in mortality and large impacts to natural systems.[233] In combination, future increases in both extreme drought and extreme rainfall are expected to transform many southeastern ecosystems.

Warming ocean temperatures due to climate change are expected to have a large effect on marine and coastal ecosystems.[234,235,236] Many species are sensitive to small changes in ocean temperature; hence, the distribution and abundance of marine organisms are expected to be greatly altered by increasing ocean temperatures. For example, the distribution of tropical herbivorous fish has been expanding in response to warmer waters, which has resulted in the tropicalization of some temperate marine ecosystems and decreases in the cover of valuable macroalgal plant communities.[179] A decrease in the growth of sea turtles in the West Atlantic has been linked to higher ocean temperatures.[237] The impacts to coral reef ecosystems have been and are expected to be particularly dire. Coral reef mortality in the Florida Keys and across the globe has been very high in recent decades, due in part to warming ocean temperatures, nutrient enrichment, overfishing, and coastal development.[240,241,242,243,244] Coral elevation and volume in the Florida Keys have been

declining in recent decades,[245] and present-day temperatures in the region are already close to bleaching thresholds; hence, it is likely that many of the remaining coral reefs in the Southeast will be lost in the coming decades.[246,247] In addition to warming temperatures, accelerated ocean acidification is also expected to contribute to coral reef mortality and decline.[248,249]

Major uncertainties

In the Southeast, winter temperature extremes, fire regimes, sea level fluctuations, hurricanes, extreme rainfall, and extreme drought all play critical roles and greatly influence the distribution, structure, and function of species and ecosystems. Changing climatic conditions (particularly, changes in the frequency and severity of climate extremes) are, however, difficult to replicate via experimental manipulations; hence, ecological responses to future climate regimes have not been fully quantified for all species and ecosystems. Natural ecosystems are complex and governed by many interacting biotic and abiotic processes. Although it is possible to make general predictions of climate change effects, specific future ecological transformations can be difficult to predict, especially given the number of interacting and changing biotic and abiotic factors in any specific location. Uncertainties in the range of potential future changes in multiple and concurrent facets of climate and land-use change also affect our ability to predict changes to natural systems.

Description of confidence and likelihood

There is *high confidence* that climate change (e.g., changing winter temperatures extremes, changing fire regimes, rising sea levels and hurricanes, warming ocean temperatures, and more extreme rainfall and drought) will *very likely* affect natural systems in the Southeast region. These climatic drivers play critical roles and greatly influence the distribution, structure, and functioning of ecosystems; hence, changes in these climatic drivers will transform ecosystems in the region and greatly alter the distribution and abundance of species.

Key Message 4

Economic and Health Risks for Rural Communities

Rural communities are integral to the Southeast's cultural heritage and to the strong agricultural and forest products industries across the region. More frequent extreme heat episodes and changing seasonal climates are projected to increase exposure-linked health impacts and economic vulnerabilities in the agricultural, timber, and manufacturing sectors (*very likely, high confidence*). By the end of the century, over one-half billion labor hours could be lost from extreme heat-related impacts (*likely, medium confidence*). Such changes would negatively impact the region's labor-intensive agricultural industry and compound existing social stresses in rural areas related to limited local community capabilities and associated with rural demography, occupations, earnings, literacy, and poverty incidence (*very likely, high confidence*). Reduction of existing stresses can increase resilience (*very likely, high confidence*).

Description of evidence base

Analysis of the sensitivity of some manufacturing sectors to climate changes anticipates secondary risks associated with crop and livestock productivity.[64,255]

Multiple analyses anticipate that energy- or water-intensive industries could face water stress and increased energy costs.[8,64,255,256]

A large body of evidence addresses the sensitivity of many crops grown in the Southeast to changing climate conditions including increased temperatures, decreased summer rainfall, drought, and change in the timing and duration of chill periods.[7,35] Extensive research documents livestock sensitivity to heat stress.[7]

Multiple lines of evidence indicate that forests are likely to be impacted by changing climate, particularly moisture regimes and potential changes in wildfire activity.[191,195,272,274] There is extensive research on heat-related illness and mortality among those living and working in the Southeast. While there is more evidence focused on urban areas, limited research has identified higher levels of heat-related illness in rural areas.[280,281] Research on occupational heat-related mortality identifies some of the Nation's highest levels in southeastern states.[282] Computer model simulations of heat-related reductions in labor productivity anticipate the greatest losses will occur in the Southeast. However, these models do not account for adaptations that may reduce estimated losses.[35,64] By the end of the century, mean annual electricity costs are estimated at $3.3 billion each year under RCP8.5 (model range: $2.4 to $4.2 billion; in 2015 dollars, undiscounted) and mean $1.2 billion each year under RCP4.5 (model range $0.9 to $1.9 billion; in 2015 dollars, undiscounted).[35]

Rural communities tend to be vulnerable due to factors such as demography, occupations, earnings, literacy, and poverty incidence.[8,9,10,250,283,284,305] Reducing the stress created by such factors can improve resilience.[9,284] The availability and accessibility of planning and health services to support coping with climate-related stresses are limited in the rural Southeast.[288,289]

Major uncertainties

There are limited studies documenting direct connections between climate changes and economic impacts. Models are limited in their ability to incorporate adaptation that may reduce losses. These factors restrict the potential to strongly associate declines in agricultural and forest productivity with the level of potential economic impact.

Projections of potential change in the frequency and extent of wildfires depend in part on models of future population growth and human behavior, which are limited, adding to the uncertainty associated with climate and forest modeling.

Many indicators of vulnerability are dynamic, so that adaptation and other changes can affect the patterns of vulnerability to heat and other climate stressors over time. Limited studies indicate concerns over the planning and preparedness of capacity at local levels; however, information is limited.

Projected labor hours lost vary by global climate model, time frame, and scenario, with a mean of 0.57 and a model range of 0.34–0.82 billion labor hours lost each year for RCP8.5 by 2090. The annual mean projected losses are roughly halved (0.28 billion labor hours) and with a model range from 0.19 to 0.43 billion labor hours lost under RCP4.5 by 2090.[35]

Description of confidence and likelihood

There is *high confidence* that climate change (e.g., rising temperatures, changing fire regimes, rising sea levels, and more extreme rainfall and drought) will *very likely* affect agricultural and forest products industries, potentially resulting in economic impacts. There is *high confidence* that increases in temperature are *very likely* to increase heat-related illness, deaths, and loss of labor productivity without greater adaptation efforts.

References

1. Spanger-Siegfried, E., M. Fitzpatrick, and K. Dahl, 2014: Encroaching Tides: How Sea Level Rise and Tidal Flooding Threaten U.S. East and Gulf Coast Communities over the Next 30 Year. Union of Concerned Scientists, Cambridge, MA, 64 pp. http://www.ucsusa.org/global_warming/impacts/effects-of-tidal-flooding-and-sea-level-rise-east-coast-gulf-of-mexico

2. McNeill, R., D.J. Nelson, and D. Wilson, 2014: Water's Edge: The Crisis of Rising Sea Levels. Reuters Investigates. Thomson Reuters. https://www.reuters.com/investigates/special-report/waters-edge-the-crisis-of-rising-sea-levels/

3. Abatzoglou, J.T. and A.P. Williams, 2016: Impact of anthropogenic climate change on wildfire across western US forests. *Proceedings of the National Academy of Sciences of the United States of America*, **113** (42), 11770-11775. http://dx.doi.org/10.1073/pnas.1607171113

4. Addington, R.N., S.J. Hudson, J.K. Hiers, M.D. Hurteau, T.F. Hutcherson, G. Matusick, and J.M. Parker, 2015: Relationships among wildfire, prescribed fire, and drought in a fire-prone landscape in the south-eastern United States. *International Journal of Wildland Fire*, **24** (6), 778-783. http://dx.doi.org/10.1071/WF14187

5. Littell, J.S., D.L. Peterson, K.L. Riley, Y. Liu, and C.H. Luce, 2016: A review of the relationships between drought and forest fire in the United States. *Global Change Biology*, **22** (7), 2353-2369. http://dx.doi.org/10.1111/gcb.13275

6. Liu, Y., J. Stanturf, and S. Goodrick, 2010: Trends in global wildfire potential in a changing climate. *Forest Ecology and Management*, **259** (4), 685-697. http://dx.doi.org/10.1016/j.foreco.2009.09.002

7. McNulty, S., S. Weiner, J. Moore Myers, H. Farahani, L. Fouladbash, D. Marshall, and R.F. Steele, 2015: Southeast Regional Climate Hub Assessment of Climate Change Vulnerability and Adaptation and Mitigation Strategies. Anderson, T., Ed. USDA Agricultural Research Service, Washington, DC, 61 pp. https://www.srs.fs.usda.gov/pubs/50521

8. Lal, P., J.R.R. Alavalapati, and E.D. Mercer, 2011: Socio-economic impacts of climate change on rural United States. *Mitigation and Adaptation Strategies for Global Change*, **16** (7), 819-844. http://dx.doi.org/10.1007/s11027-011-9295-9

9. Jurjonas, M. and E. Seekamp, 2018: Rural coastal community resilience: Assessing a framework in eastern North Carolina. *Ocean & Coastal Management*, **162**, 137-150. http://dx.doi.org/10.1016/j.ocecoaman.2017.10.010

10. ERS, 2018: Rural Poverty & Well-Being: Geography of Poverty. USDA, Economic Research Service (ERS), Washington, DC, accessed March 14. https://www.ers.usda.gov/topics/rural-economy-population/rural-poverty-well-being/#geography

11. Hsiang, S., R. Kopp, A. Jina, J. Rising, M. Delgado, S. Mohan, D.J. Rasmussen, R. Muir-Wood, P. Wilson, M. Oppenheimer, K. Larsen, and T. Houser, 2017: Estimating economic damage from climate change in the United States. *Science*, **356** (6345), 1362-1369. http://dx.doi.org/10.1126/science.aal4369

12. Habeeb, D., J. Vargo, and B. Stone, 2015: Rising heat wave trends in large US cities. *Natural Hazards*, **76** (3), 1651-1665. http://dx.doi.org/10.1007/s11069-014-1563-z

13. Vose, R.S., D.R. Easterling, K.E. Kunkel, A.N. LeGrande, and M.F. Wehner, 2017: Temperature changes in the United States. *Climate Science Special Report: Fourth National Climate Assessment, Volume I*. Wuebbles, D.J., D.W. Fahey, K.A. Hibbard, D.J. Dokken, B.C. Stewart, and T.K. Maycock, Eds. U.S. Global Change Research Program, Washington, DC, USA, 185-206. http://dx.doi.org/10.7930/J0N29V45

14. Meehl, G.A., J.M. Arblaster, and G. Branstator, 2012: Mechanisms contributing to the warming hole and the consequent US east–west differential of heat extremes. *Journal of Climate*, **25** (2012), 6394-6408. http://dx.doi.org/10.1175/JCLI-D-11-00655.1

15. Walsh, J., D. Wuebbles, K. Hayhoe, J. Kossin, K. Kunkel, G. Stephens, P. Thorne, R. Vose, M. Wehner, J. Willis, D. Anderson, S. Doney, R. Feely, P. Hennon, V. Kharin, T. Knutson, F. Landerer, T. Lenton, J. Kennedy, and R. Somerville, 2014: Ch. 2: Our changing climate. *Climate Change Impacts in the United States: The Third National Climate Assessment*. Melillo, J.M., T.C. Richmond, and G.W. Yohe, Eds. U.S. Global Change Research Program, Washington, DC, 19-67. http://dx.doi.org/10.7930/J0KW5CXT

16. Pan, Z., R.W. Arritt, E.S. Takle, W.J. Gutowski, Jr., C.J. Anderson, and M. Segal, 2004: Altered hydrologic feedback in a warming climate introduces a "warming hole." *Geophysical Research Letters*, **31** (17), L17109. http://dx.doi.org/10.1029/2004GL020528

17. Partridge, T.F., J.M. Winter, E.C. Osterberg, D.W. Hyndman, A.D. Kendall, and F.J. Magilligan, 2018: Spatially distinct seasonal patterns and forcings of the U.S. warming hole. *Geophysical Research Letters*, **45** (4), 2055-2063. http://dx.doi.org/10.1002/2017GL076463

18. Kunkel, K., R. Frankson, J. Runkle, S. Champion, L. Stevens, D. Easterling, and B. Stewart, 2017: State Climate Summaries for the United States. NOAA Technical Report NESDIS 149. National Oceanic and Atmospheric Administration, National Centers for Environmental Information, Asheville, NC, [various] pp. https://statesummaries.ncics.org/

19. Easterling, D.R., K.E. Kunkel, J.R. Arnold, T. Knutson, A.N. LeGrande, L.R. Leung, R.S. Vose, D.E. Waliser, and M.F. Wehner, 2017: Precipitation change in the United States. *Climate Science Special Report: Fourth National Climate Assessment, Volume I*. Wuebbles, D.J., D.W. Fahey, K.A. Hibbard, D.J. Dokken, B.C. Stewart, and T.K. Maycock, Eds. U.S. Global Change Research Program, Washington, DC, USA, 207-230. http://dx.doi.org/10.7930/J0H993CC

20. Pierce, D.W., D.R. Cayan, and B.L. Thrasher, 2014: Statistical downscaling using Localized Constructed Analogs (LOCA). *Journal of Hydrometeorology*, **15** (6), 2558-2585. http://dx.doi.org/10.1175/jhm-d-14-0082.1

21. USGCRP, 2017: Scenarios for Climate Assessment and Adaptation: LOCA Viewer [web tool]. U.S. Global Change Research Program, Washington, DC. https://scenarios.globalchange.gov/loca-viewer/

22. Census Bureau, 2017: Press kit: County and Metro Area Population. *Census Newsroom*, March 23. U.S. Census Bureau. https://www.census.gov/newsroom/press-kits/2017/20170323_popestimates.html

23. ARC 33°N, 2016: Regional Snapshot: 2016 Population Estimates. Atlanta Regional Commission (ARC), Atlanta, GA. http://33n.atlantaregional.com/regional-snapshot/regional-snapshot-2016-population-estimates

24. Census Bureau, 2017: County Population Totals and Components of Change: 2010-2016. U.S. Census Bureau. https://www.census.gov/data/datasets/2016/demo/popest/counties-total.html

25. Diem, J.E., C.E. Stauber, and R. Rothenberg, 2017: Heat in the southeastern United States: Characteristics, trends, and potential health impact. *PLOS ONE*, **12** (5), e0177937. http://dx.doi.org/10.1371/journal.pone.0177937

26. Sarofim, M.C., S. Saha, M.D. Hawkins, D.M. Mills, J. Hess, R. Horton, P. Kinney, J. Schwartz, and A. St. Juliana, 2016: Ch. 2: Temperature-related death and illness. *The Impacts of Climate Change on Human Health in the United States: A Scientific Assessment*. U.S. Global Change Research Program, Washington, DC, 43–68. http://dx.doi.org/10.7930/J0MG7MDX

27. Zhou, Y. and J.M. Shepherd, 2010: Atlanta's urban heat island under extreme heat conditions and potential mitigation strategies. *Natural Hazards*, **52** (3), 639-668. http://dx.doi.org/10.1007/s11069-009-9406-z

28. Sustain Louisville, 2017: 2016 Progress Report. Office of Sustainability, Louisville, KY, 24 pp. https://louisvilleky.gov/sites/default/files/sustainability/sustain_louisville_2016_progress_report.pdf

29. Beard, C.B., R.J. Eisen, C.M. Barker, J.F. Garofalo, M. Hahn, M. Hayden, A.J. Monaghan, N.H. Ogden, and P.J. Schramm, 2016: Ch. 5: Vector-borne diseases. *The Impacts of Climate Change on Human Health in the United States: A Scientific Assessment*. U.S. Global Change Research Program, Washington, DC, 129–156. http://dx.doi.org/10.7930/J0765C7V

30. Monaghan, A.J., C.W. Morin, D.F. Steinhoff, O. Wilhelmi, M. Hayden, D.A. Quattrochi, M. Reiskind, A.L. Lloyd, K. Smith, C.A. Schmidt, P.E. Scalf, and K. Ernst, 2016: On the seasonal occurrence and abundance of the Zika virus vector mosquito *Aedes aegypti* in the contiguous United States. *Plos Currents: Outbreaks*. http://dx.doi.org/10.1371/currents.outbreaks.50dfc7f46798675fc63e7d7da563da76

31. Butterworth, M.K., C.W. Morin, and A.C. Comrie, 2017: An analysis of the potential impact of climate change on dengue transmission in the southeastern United States. *Environmental Health Perspectives*, **125**, 579-585. http://dx.doi.org/10.1289/EHP218

32. De Jesús Crespo, R., P. Méndez Lázaro, and S.H. Yee, 2018: Linking wetland ecosystem services to vector-borne disease: Dengue fever in the San Juan Bay Estuary, Puerto Rico. *Wetlands*. http://dx.doi.org/10.1007/s13157-017-0990-5

33. Wong, G.K.L. and C.Y. Jim, 2018: Abundance of urban male mosquitoes by green infrastructure types: Implications for landscape design and vector management. *Landscape Ecology*, **33** (3), 475-489. http://dx.doi.org/10.1007/s10980-018-0616-1

34. Lindsay, S.W., A. Wilson, N. Golding, T.W. Scott, and W. Takken, 2017: Improving the built environment in urban areas to control *Aedes aegypti*-borne diseases. *Bulletin of the World Health Organization*, **95** (8), 607-608. http://dx.doi.org/10.2471/BLT.16.189688

35. EPA, 2017: Multi-model Framework for Quantitative Sectoral Impacts Analysis: A Technical Report for the Fourth National Climate Assessment. EPA 430-R-17-001. U.S. Environmental Protection Agency (EPA), Washington, DC, 271 pp. https://cfpub.epa.gov/si/si_public_record_Report.cfm?dirEntryId=335095

36. Harrigan, R.J., H.A. Thomassen, W. Buermann, and T.B. Smith, 2014: A continental risk assessment of West Nile virus under climate change. *Global Change Biology*, **20** (8), 2417-2425. http://dx.doi.org/10.1111/gcb.12534

37. Schnell, J.L. and M.J. Prather, 2017: Co-occurrence of extremes in surface ozone, particulate matter, and temperature over eastern North America. *Proceedings of the National Academy of Sciences of the United States of America*, **114** (11), 2854-2859. http://dx.doi.org/10.1073/pnas.1614453114

38. Zhang, Y. and Y. Wang, 2016: Climate-driven ground-level ozone extreme in the fall over the Southeast United States. *Proceedings of the National Academy of Sciences of the United States of America*, **113** (36), 10025-10030. http://dx.doi.org/10.1073/pnas.1602563113

39. Fu, T.-M., Y. Zheng, F. Paulot, J. Mao, and R.M. Yantosca, 2015: Positive but variable sensitivity of August surface ozone to large-scale warming in the southeast United States. *Nature Climate Change*, **5**, 454-458. http://dx.doi.org/10.1038/nclimate2567

40. Ziska, L.H., D.E. Gebhard, D.A. Frenz, S. Faulkner, B.D. Singer, and J.G. Straka, 2003: Cities as harbingers of climate change: Common ragweed, urbanization, and public health. *Journal of Allergy and Clinical Immunology*, **111** (2), 290-295. http://dx.doi.org/10.1067/mai.2003.53

41. Neumann, J.E., J. Price, P. Chinowsky, L. Wright, L. Ludwig, R. Streeter, R. Jones, J.B. Smith, W. Perkins, L. Jantarasami, and J. Martinich, 2015: Climate change risks to US infrastructure: Impacts on roads, bridges, coastal development, and urban drainage. *Climatic Change*, **131** (1), 97-109. http://dx.doi.org/10.1007/s10584-013-1037-4

42. FHWA, 2017: FHWA Climate Resilience Pilot Program: Tennessee Department of Transportation. FHWA-HEP-16-076. Federal Highway Administration's (FHWA), Climate Resilience Pilot Program, Washington, DC, 4 pp. https://www.fhwa.dot.gov/environment/sustainability/resilience/pilots/2013-2015_pilots/tennessee/index.cfm

43. Abkowitz, M., J. Camp, and L. Dundon, 2015: Assessing the Vulnerability of Tennessee Transportation Assets to Extreme Weather. 3 Sigma Consultants for Tennessee Department of Transportation, Nashville, TN, 49 pp. https://www.fhwa.dot.gov/environment/sustainability/resilience/pilots/2013-2015_pilots/tennessee/final_report/tdot.pdf

44. Amekudzi, A., M. Crane, D. Springstead, D. Rose, and T. Batac, 2013: Transit Climate Change Adaptation Assessment for the Metropolitan Atlanta Rapid Transit Authority. FTA Report No. 0076 Federal Transit Administration, Washington, DC, 49 pp. https://www.transit.dot.gov/research-innovation/transit-climate-change-adaptation-assessment-metropolitan-atlanta-rapid-transit

45. City of Charleston, 2015: Sea Level Rise Strategy. Mayor's Office, Charleston, SC, 17 pp. http://www.charleston-sc.gov/DocumentCenter/View/10089

46. Tampa Bay Water, 2014: Tampa Bay Water Hosts Florida Water and Climate Alliance Workshop. November 4. https://www.tampabaywater.org/newsroom/agency-news/tampa-bay-water-hosts-florida-water-and-climate-alliance-workshop

47. WUCA Strategic Planning Committee, 2016: Water Utility Climate Alliance 2017–2021 Strategic Plan. Water Utility Climate Alliance (WUCA), Las Vegas, NV, 6 pp. https://www.wucaonline.org/assets/pdf/about-strategic-plan-2021.pdf

48. Ross Strategic, 2016: International Water and Climate Forum, 2015. Synthesis Report. Association of Metropolitan Water Agencies, Washington, DC, 19 pp. https://bit.ly/2P2NL8t

49. EPA, 2015: Case Study: Water and Wastewater Utilities Planning for Climate Change. Seminole Tribe of Florida. EPA 800-Q-15-004. U.S. Environmental Protection Agency (EPA), Washington, DC, 2 pp. https://nepis.epa.gov/Exe/ZyPURL.cgi?Dockey=P100SHVY.txt

50. City of Atlanta, 2015: Climate Action Plan. Mayor's Office of Sustainability, Atlanta, GA, 48 pp. http://p2catl.com/wp-content/uploads/Atlanta-Climate-Action-Plan-07-23-2015.pdf

51. Sweet, W.V., R. Horton, R.E. Kopp, A.N. LeGrande, and A. Romanou, 2017: Sea level rise. *Climate Science Special Report: Fourth National Climate Assessment, Volume I*. Wuebbles, D.J., D.W. Fahey, K.A. Hibbard, D.J. Dokken, B.C. Stewart, and T.K. Maycock, Eds. U.S. Global Change Research Program, Washington, DC, USA, 333-363. http://dx.doi.org/10.7930/J0VM49F2

52. Sweet, W.V., R.E. Kopp, C.P. Weaver, J. Obeysekera, R.M. Horton, E.R. Thieler, and C. Zervas, 2017: Global and Regional Sea Level Rise Scenarios for the United States. NOAA Tech. Rep. NOS CO-OPS 083. National Oceanic and Atmospheric Administration, National Ocean Service, Silver Spring, MD, 75 pp. https://tidesandcurrents.noaa.gov/publications/techrpt83_Global_and_Regional_SLR_Scenarios_for_the_US_final.pdf

53. Sallenger, A.H., K.S. Doran, and P.A. Howd, 2012: Hotspot of accelerated sea-level rise on the Atlantic coast of North America. *Nature Climate Change*, **2**, 884-888. http://dx.doi.org/10.1038/nclimate1597

54. Zervas, C., 2009: Sea Level Variations of the United States 1854–2006. NOAA Technical Report NOS CO-OPS 053. National Oceanic and Atmospheric Administration, National Ocean Service, Silver Spring, MD, various pp. https://tidesandcurrents.noaa.gov/publications/Tech_rpt_53.pdf

55. Mitchum, G.T., 2011: Sea Level Changes in the Southeastern United States: Past, Present and Future. Florida Climate Institute, Gainesville, FL, 20 pp. http://www.FloridaClimateInstitute.org/images/reports/201108mitchum_sealevel.pdf

56. Boon, J.D., 2012: Evidence of sea level acceleration at U.S. and Canadian tide stations, Atlantic Coast, North America. *Journal of Coastal Research*, **28**, 1437-1445. http://dx.doi.org/10.2112/JCOASTRES-D-12-00102.1

57. Hall, J.A., S. Gill, J. Obeysekera, W. Sweet, K. Knuuti, and J. Marburger, 2016: Regional Sea Level Scenarios for Coastal Risk Management: Managing the Uncertainty of Future Sea Level Change and Extreme Water Levels for Department of Defense Coastal Sites Worldwide. U.S. Department of Defense, Strategic Environmental Research and Development Program, Alexandria VA, 224 pp. https://www.usfsp.edu/icar/files/2015/08/CARSWG-SLR-FINAL-April-2016.pdf

58. Sweet, W.V. and J.J. Marra, 2016: 2015 State of U.S. Nuisance Tidal Flooding. Supplement to State of the Climate: National Overview for May 2016. National Oceanic and Atmospheric Administration, National Centers for Environmental Information, 5 pp. http://www.ncdc.noaa.gov/monitoring-content/sotc/national/2016/may/sweet-marra-nuisance-flooding-2015.pdf

59. Kopp, R.E., A.C. Kemp, K. Bittermann, B.P. Horton, J.P. Donnelly, W.R. Gehrels, C.C. Hay, J.X. Mitrovica, E.D. Morrow, and S. Rahmstorf, 2016: Temperature-driven global sea-level variability in the Common Era. *Proceedings of the National Academy of Sciences of the United States of America*, **113** (11), E1434-E1441. http://dx.doi.org/10.1073/pnas.1517056113

60. Sweet, W., J. Park, J. Marra, C. Zervas, and S. Gill, 2014: Sea Level Rise and Nuisance Flood Frequency Changes Around the United States. NOAA Technical Report NOS CO-OPS 073. National Oceanic and Atmospheric Administration, National Ocean Service, Silver Spring, MD, 58 pp. https://bit.ly/1niTPQK

61. Sweet, W.V., J.J. Marra, and Gregory Dusek, 2017: 2016 State of U.S. High Tide Flooding and a 2017 Outlook. Supplement to State of the Climate: National Overview for June 2017. National Oceanic and Atmospheric Administration, National Centers for Environmental Information, 8 pp. https://bit.ly/2svZ9O2

62. Parris, A., P. Bromirski, V. Burkett, D. Cayan, M. Culver, J. Hall, R. Horton, K. Knuuti, R. Moss, J. Obeysekera, A. Sallenger, and J. Weiss, 2012: Global Sea Level Rise Scenarios for the United States National Climate Assessment. NOAA Tech Memo OAR CPO-1. National Oceanic and Atmospheric Administration, Silver Spring, MD, 37 pp. http://scenarios.globalchange.gov/sites/default/files/NOAA_SLR_r3_0.pdf

63. Sweet, W.V. and J. Park, 2014: From the extreme to the mean: Acceleration and tipping points of coastal inundation from sea level rise. *Earth's Future*, **2** (12), 579-600. http://dx.doi.org/10.1002/2014EF000272

64. Houser, T., S. Hsiang, R. Kopp, K. Larsen, M. Delgado, A. Jina, M. Mastrandrea, S. Mohan, R. Muir-Wood, D.J. Rasmussen, J. Rising, and P. Wilson, 2015: *Economic Risks of Climate Change: An American Prospectus*. Columbia University Press, New York, 384 pp.

65. Emrich, C.T., D.P. Morath, G.C. Bowser, and R. Reeves, 2014: Climate-Sensitive Hazards in Florida: Identifying and Prioritizing Threats to Build Resilience Against Climate Effects. Florida Department of Health, Tallahassee, FL, various pp. http://www.floridahealth.gov/environmental-health/climate-and-health/_documents/climate-sensitive-hazards-in-florida-final-report.pdf

66. Anderson, D.G., T.G. Bissett, S.J. Yerka, J.J. Wells, E.C. Kansa, S.W. Kansa, K.N. Myers, R.C. DeMuth, and D.A. White, 2017: Sea-level rise and archaeological site destruction: An example from the southeastern United States using DINAA (Digital Index of North American Archaeology). *PLOS ONE*, **12** (11), e0188142. http://dx.doi.org/10.1371/journal.pone.0188142

67. Dahl, K.A., E. Spanger-Siegfried, A. Caldas, and S. Udvardy, 2017: Effective inundation of continental United States communities with 21st century sea level rise. *Elementa: Science of the Anthropocene*, **5**, Article 37. http://dx.doi.org/10.1525/elementa.234

68. Moftakhari, H.R., A. AghaKouchak, B.F. Sanders, D.L. Feldman, W. Sweet, R.A. Matthew, and A. Luke, 2015: Increased nuisance flooding along the coasts of the United States due to sea level rise: Past and future. *Geophysical Research Letters*, **42** (22), 9846-9852. http://dx.doi.org/10.1002/2015GL066072

69. USGCRP, 2016: *The Impacts of Climate Change on Human Health in the United States: A Scientific Assessment*. U.S. Global Change Research Program, Washington, DC, 312 pp. http://dx.doi.org/10.7930/J0R49NQX

70. Hauer, M.E., J.M. Evans, and D.R. Mishra, 2016: Millions projected to be at risk from sea-level rise in the continental United States. *Nature Climate Change*, **6** (7), 691-695. http://dx.doi.org/10.1038/nclimate2961

71. Hauer, M.E., 2017: Migration induced by sea-level rise could reshape the US population landscape. *Nature Climate Change*, **7** (5), 321-325. http://dx.doi.org/10.1038/nclimate3271

72. Strauss, B.H., R. Ziemlinski, J.L. Weiss, and J.T. Overpeck, 2012: Tidally adjusted estimates of topographic vulnerability to sea level rise and flooding for the contiguous United States. *Environmental Research Letters*, **7** (1), 014033. http://dx.doi.org/10.1088/1748-9326/7/1/014033

73. Burkett, M., R.R.M. Verchick, and D. Flores, 2017: Reaching Higher Ground: Avenues to Secure and Manage New Land for Communities Displaced by Climate Change. Center for Progressive Reform, Washington, DC, 43 pp. http://progressivereform.org/articles/ReachingHigherGround_1703.pdf

74. Isle de Jean Charles Tribe, 2017: Bienvenue, Aiokpanchi, Welcome to Isle de Jean Charles [web site], Isle de Jean Charles, LA, accessed October 17. http://www.isledejeancharles.com/

75. Office of Community Development, 2018: Isle de Jean Charles Resettlement Project. State of Louisiana. http://isledejeancharles.la.gov/

76. Maldonado, J.K. and K. Peterson, 2018: A community-based model for resettlement: Lessons from coastal Louisiana *Routledge Handbook of Environmental Displacement and Migration*. McLeman, R. and F. Gemenne, Eds. Routledge, 289-299.

77. Carter, L.M., J.W. Jones, L. Berry, V. Burkett, J.F. Murley, J. Obeysekera, P.J. Schramm, and D. Wear, 2014: Ch. 17: Southeast and the Caribbean. *Climate Change Impacts in the United States: The Third National Climate Assessment*. Melillo, J.M., T.C. Richmond, and G.W. Yohe, Eds. U.S. Global Change Research Program, Washington, DC, 396-417. http://dx.doi.org/10.7930/J0NP22CB

78. NDRC, 2016: National Disaster Resilience Competition (NDRC): Grantee Profiles. U.S. Department of Housing and Urban Development, Washington, DC, 23 pp. https://www.hud.gov/sites/documents/NDRCGRANTPROF.PDF

79. NDRC, 2016: State of Louisiana. *National Disaster Resilience Competition (NDRC): Grantee Profiles*. U.S. Department of Housing and Urban Development, Washington, DC, 7-8. https://www.hud.gov/sites/documents/NDRCGRANTPROF.PDF

80. Gonzalez, C.G., A. Kaswan, R. Verchick, Y. Huang, N. Jamhour, and S. Bowen, 2016: Climate Change, Resilience, and Fairness: How Nonstructural Adaptation Can Protect and Empower Socially Vulnerable Communities on the Gulf Coast. Center for Progressive Reform White Paper. Center for Progressive Reform, Washington, DC, 97 pp. https://works.bepress.com/carmen_gonzalez/42/

81. Allan, R.P. and B.J. Soden, 2008: Atmospheric warming and the amplification of precipitation extremes. *Science*, **321** (5895), 1481-1484. http://dx.doi.org/10.1126/science.1160787

82. Perica, S., D. Martin, S. Pavlovic, I. Roy, M.S. Laurent, C. Trypaluk, D. Unruh, M. Yekta, and G. Bonnin, 2013: Precipitation-Frequency Atlas of the United States. Volume 9 Version 2.0: Southeastern States (Alabama, Arkansas, Florida, Georgia, Louisiana, Mississippi) NOAA Atlas 14 Volume 9. NOAA National Weather Service, Silver Spring, MD, various pp. http://www.nws.noaa.gov/oh/hdsc/PF_documents/Atlas14_Volume9.pdf

83. NOAA RCC, 2017: xmACIS2 [Applied Climate Information System online tool]. National Oceanic and Atmospheric Administration (NOAA), Regional Climate Centers (RCC). http://xmacis.rcc-acis.org/

84. NOAA NCEI, 2018: Billion-Dollar Weather and Climate Disasters [web page]. NOAA National Centers for Environmental Information, Asheville, NC. https://www.ncdc.noaa.gov/billions/events/US/1980-2017

85. Gallo, A., 2016: "Which Baton Rouge ZIP codes were hit hardest? New data lends scope to flooding devastation." *The Advocate*, Sep 2. http://www.theadvocate.com/louisiana_flood_2016/article_e8832d38-714d-11e6-b2c7-ab4b6ed62f15.html

86. Colten, C., 2017: Floods collide with sprawl in Louisiana's Amite River Basin. *Focus on Geography*, **60**. http://dx.doi.org/10.21690/foge/2017.60.2f

87. van der Wiel, K., S.B. Kapnick, G.J. van Oldenborgh, K. Whan, S. Philip, G.A. Vecchi, R.K. Singh, J. Arrighi, and H. Cullen, 2017: Rapid attribution of the August 2016 flood-inducing extreme precipitation in south Louisiana to climate change. *Hydrology and Earth System Sciences*, **21** (2), 897-921. http://dx.doi.org/10.5194/hess-21-897-2017

88. NWS, 2016: The Historic South Carolina Floods of October 1–5, 2015. Service Assessment. NOAA National Weather Service (NWS), Silver Spring, MD, various pp. https://www.weather.gov/media/publications/assessments/SCFlooding_072216_Signed_Final.pdf

89. Wahl, T., S. Jain, J. Bender, S.D. Meyers, and M.E. Luther, 2015: Increasing risk of compound flooding from storm surge and rainfall for major US cities. *Nature Climate Change*, **5** (12), 1093-1097. http://dx.doi.org/10.1038/nclimate2736

90. Wdowinski, S., R. Bray, B.P. Kirtman, and Z. Wu, 2016: Increasing flooding hazard in coastal communities due to rising sea level: Case study of Miami Beach, Florida. *Ocean & Coastal Management*, **126**, 1-8. http://dx.doi.org/10.1016/j.ocecoaman.2016.03.002

91. SFRCCC, 2017: Regional Climate Action Plan 2.0 [web tool]. South Florida Regional Climate Change Compact (SFRCCC), Broward, Miami-Dade, Monroe, and Palm Beach Counties, FL. http://www.southeastfloridaclimatecompact.org/regional-climate-action-plan/

92. Morales, J., 2016: Miami Beach coastal flooding forum. In *Forum on Indicators of Coastal Flooding and Flood Impacts*, West Palm Beach, FL, May 26. South Flordia Water Management District, 3-25. ftp://ftp.sfwmd.gov/pub/jabarne/Coastal_Flooding_25May2016.pdf

93. Behr, J.G., R. Diaz, and M. Mitchell, 2016: Building resiliency in response to sea level rise and recurrent flooding: Comprehensive planning in Hampton Roads. *The Virginia News Letter*, **92** (1), 1-6. https://vig.coopercenter.org/sites/vig/files/VirginiaNewsLetter_2016_V92-N1.pdf

94. Biloxi Mississippi Code of Ordinances, 2017: Flood damage prevention: Specific standards. Chapter 8, Art. III, Sec. 8-3-2. https://library.municode.com/ms/biloxi/codes/code_of_ordinances?nodeId=COOR_CH8FLDAPR_ARTIIIFLHAPRST_S8-3-2SPST

95. Evans, J.M., J. Gambill, R.J. McDowell, P.W. Prichard, and C.S. Hopkinson, 2016: Tybee Island: Sea Level Rise Adaptation Plan. NOAA, Georgia Sea Grant, Athens, GA, 82 pp. http://dx.doi.org/10.13140/RG.2.1.3825.9604/1

96. Acadiana Planning Commission, 2018: APC Board allocates $25 million in HMGP funding to regional flood mitigation projects. Lafayette, LA. February 20. http://planacadiana.org/uncategorized/apc-board-allocates-25-million-in-hmgp-funding-to-regional-flood-mitigation-projects/

97. FEMA, 2016: Community Rating System (CRS) Communities and Their Classes. Federal Emergency Management Agency (FEMA), National Flood Insurance Program. https://www.fema.gov/media-library/assets/documents/15846

98. CISA, 2016: The South Carolina Floods of October 2015. Carolinas Integrated Sciences & Assessments (CISA), Columbia, SC, 4 pp. http://www.cisa.sc.edu/PDFs/October%202015%20Flood%20Event%204%20Pager.pdf

99. Smith, A.B., 2018: 2017 U.S. billion-dollar weather and climate disasters: A historic year in context. Climate.gov. https://www.climate.gov/news-features/blogs/beyond-data/2017-us-billion-dollar-weather-and-climate-disasters-historic-year

100. Cangialosi, J.P., A.S. Latto, and R. Berg, 2018: Tropical Cyclone Report: Hurricane Irma (AL112017), 30 August-12 September 2017. National Hurricane Center, 111 pp. https://www.nhc.noaa.gov/data/tcr/AL112017_Irma.pdf

101. NWS, 2017: Detailed Meteorological Summary on Hurricane Irma [web page]. NOAA National Weather Service (NWS), Tallahassee, FL. https://www.weather.gov/tae/Irma_technical_summary

102. Voiland, A., 2017: Hot water ahead for Hurricane Irma. NASA *Earth Observatory*, September 6. NASA. https://earthobservatory.nasa.gov/images/90912/hot-water-ahead-for-hurricane-irma

103. Kossin, J.P., T. Hall, T. Knutson, K.E. Kunkel, R.J. Trapp, D.E. Waliser, and M.F. Wehner, 2017: Extreme storms. *Climate Science Special Report: Fourth National Climate Assessment, Volume I*. Wuebbles, D.J., D.W. Fahey, K.A. Hibbard, D.J. Dokken, B.C. Stewart, and T.K. Maycock, Eds. U.S. Global Change Research Program, Washington, DC, USA, 257-276. http://dx.doi.org/10.7930/J07S7KXX

104. Emanuel, K., 2017: Will global warming make hurricane forecasting more difficult? *Bulletin of the American Meteorological Society*, **98** (3), 495-501. http://dx.doi.org/10.1175/bams-d-16-0134.1

105. AJC Staff, 2017: "Gov. Deal: 'Virtually the entire state' to be impacted by Irma." *The Atlanta Journal-Constitution*, September 10. https://www.ajc.com/news/gov-deal-virtually-the-entire-state-impacted-irma/pm6pW2vlt4GQpM34a7s4TO/

106. Shaffer, J., A. Bennett, and A. Bylythe, 2017: "NC governor declares state of emergency ahead of 'powerful' Hurricane Irma: 'Get ready.'" *The News & Observer*, September 6. https://www.newsobserver.com/news/weather/article171616057.html

107. Townsend, E. and M. Tomasic, 2017: "S.C. Governor declares state of emergency as Hurricane Irma's forecast path shifts." *The Sun News*, September 6. https://www.myrtlebeachonline.com/news/local/article171519002.html

108. Wise, S., 2017: "Virginia Governor declares state of emergency ahead of Hurricane Irma." WTVR (*CBS Affiliate*), September 8. https://wtvr.com/2017/09/08/hurricane-irma-virginia-state-of-emergency/

109. Florida House of Representatives, 2018: Select Committee on Hurricane Response and Preparedness Final Report. Tallahassee, FL, 113 pp. https://bit.ly/2mRD7Rw

110. Deal, N., 2017: Deal declares state of emergency ahead of Hurricane Irma. Office of the Governor, Atlanta, GA. September 6. https://gov.georgia.gov/press-releases/2017-09-06/deal-declares-state-emergency-ahead-hurricane-irma

111. Simmons, K.M., J. Czajkowski, and J. Done, 2017: Economic Effectiveness of Implementing a Statewide Building Code: The Case of Florida. SSRN, 64 pp. http://dx.doi.org/10.2139/ssrn.2963244

112. Scott, R., 2017: Gov. Scott issues updates on Hurricane Irma preparedness. Tallahassee, FL. September 9. https://www.flgov.com/2017/09/09/gov-scott-issues-updates-on-hurricane-irma-preparedness-10/

113. Cartwright, J.M. and W.J. Wolfe, 2016: Insular Ecosystems of the Southeastern United States: A Regional Synthesis to Support Biodiversity Conservation in a Changing Climate. USGS Professional Paper 1828. U.S. Geological Survey, Reston, VA, 162 pp. http://dx.doi.org/10.3133/pp1828

114. Jenkins, C.N., K.S. Van Houtan, S.L. Pimm, and J.O. Sexton, 2015: US protected lands mismatch biodiversity priorities. *Proceedings of the National Academy of Sciences of the United States of America*, **112** (16), 5081-5086. http://dx.doi.org/10.1073/pnas.1418034112

115. Noss, R.F., 2012: *Forgotten Grasslands of the South: Natural History and Conservation*. Island Press, Washington, DC, 320 pp.

116. Noss, R.F., W.J. Platt, B.A. Sorrie, A.S. Weakley, D.B. Means, J. Costanza, and R.K. Peet, 2015: How global biodiversity hotspots may go unrecognized: Lessons from the North American Coastal Plain. *Diversity and Distributions*, **21** (2), 236-244. http://dx.doi.org/10.1111/ddi.12278

117. Stein, B.A., L.S. Kutner, and J.S. Adams, Eds., 2000: *Precious Heritage: The Status of Biodiversity in the United States*. Oxford University Press, Oxford; New York, 432 pp.

118. Barbier, E.B., S.D. Hacker, C. Kennedy, E.W. Koch, A.C. Stier, and B.R. Silliman, 2011: The value of estuarine and coastal ecosystem services. *Ecological Monographs*, **81** (2), 169-193. http://dx.doi.org/10.1890/10-1510.1

119. Costanza, R., R. de Groot, P. Sutton, S. van der Ploeg, S.J. Anderson, I. Kubiszewski, S. Farber, and R.K. Turner, 2014: Changes in the global value of ecosystem services. *Global Environmental Change*, **26**, 152-158. http://dx.doi.org/10.1016/j.gloenvcha.2014.04.002

120. Millennium Ecosystem Assessment, 2005: *Ecosystems and Human Well-Being: Synthesis*. Sarukhán, J., A. Whyte, and MA Board of Review Editors, Eds. Island Press, Washington, DC, 137 pp. https://www.millenniumassessment.org/documents/document.356.aspx.pdf

121. Clark, P.U., A.S. Dyke, J.D. Shakun, A.E. Carlson, J. Clark, B. Wohlfarth, J.X. Mitrovica, S.W. Hostetler, and A.M. McCabe, 2009: The last glacial maximum. *Science*, **325** (5941), 710-714. http://dx.doi.org/10.1126/science.1172873

122. Jackson, S.T., R.S. Webb, K.H. Anderson, J.T. Overpeck, T. Webb III, J.W. Williams, and B.C.S. Hansen, 2000: Vegetation and environment in Eastern North America during the Last Glacial Maximum. *Quaternary Science Reviews*, **19** (6), 489-508. http://dx.doi.org/10.1016/S0277-3791(99)00093-1

123. Williams, J.W., B.N. Shuman, T. Webb, P.J. Bartlein, and P.L. Leduc, 2004: Late-quaternary vegetation dynamics in North America: Scaling from taxa to biomes. *Ecological Monographs*, **74** (2), 309-334. http://dx.doi.org/10.1890/02-4045

124. Davis, M.B. and R.G. Shaw, 2001: Range shifts and adaptive responses to quaternary climate change. *Science*, **292** (5517), 673-679. http://dx.doi.org/10.1126/science.292.5517.673

125. Doyle, T.W., B. Chivoiu, and N.M. Enwright, 2015: Sea-Level Rise Modeling Handbook: Resource Guide for Coastal Land Managers, Engineers, and Scientists. USGS Professional Paper 1815. U.S. Geological Survey, Reston, VA, 76 pp. http://dx.doi.org/10.3133/pp1815

126. Kennedy, J.P., M.W. Pil, C.E. Proffitt, W.A. Boeger, A.M. Stanford, and D.J. Devlin, 2016: Postglacial expansion pathways of red mangrove, *Rhizophora mangle*, in the Caribbean Basin and Florida. *American Journal of Botany*, **103** (2), 260-276. http://dx.doi.org/10.3732/ajb.1500183

127. Sherrod, C.L. and C. McMillan, 1985: The distributional history and ecology of mangrove vegetation along the northern Gulf of Mexico coastal region. *Contributions in Marine Science*, **28** (9), 129-140. http://hdl.handle.net/1969.3/19073

128. Williams, K., Z.S. Pinzon, R.P. Stumpf, and E.A. Raabe, 1999: Sea-Level Rise and Coastal Forests on the Gulf of Mexico. Open-File Report 99-441. U.S. Geological Survey, Center for Coastal Geology, St. Petersburg, FL, various pp. http://pubs.er.usgs.gov/publication/ofr99441

129. Woodroffe, C.D. and J. Grindrod, 1991: Mangrove biogeography: The role of quaternary environmental and sea-level change. *Journal of Biogeography*, **18** (5), 479-492. http://dx.doi.org/10.2307/2845685

130. Costanza, J., S. Beck, M. Pyne, A. Terando, M.J. Rubino, R. White, and J. Collazo, 2016: Assessing Climate-Sensitive Ecosystems in the Southeastern United States. USGS Open-File Report 2016-1073. US Geological Survey, Reston, VA, 278 pp. http://dx.doi.org/10.3133/ofr20161073

131. Dale, V.H., L.A. Joyce, S. McNulty, R.P. Neilson, M.P. Ayres, M.D. Flannigan, P.J. Hanson, L.C. Irland, A.E. Lugo, C.J. Peterson, D. Simberloff, F.J. Swanson, B.J. Stocks, and B.M. Wotton, 2001: Climate change and forest disturbances: Climate change can affect forests by altering the frequency, intensity, duration, and timing of fire, drought, introduced species, insect and pathogen outbreaks, hurricanes, windstorms, ice storms, or landslides. *BioScience*, **51** (9), 723-734. http://dx.doi.org/10.1641/0006-3568(2001)051[0723:ccafd]2.0.co;2

132. Gabler, C.A., M.J. Osland, J.B. Grace, C.L. Stagg, R.H. Day, S.B. Hartley, N.M. Enwright, A.S. From, M.L. McCoy, and J.L. McLeod, 2017: Macroclimatic change expected to transform coastal wetland ecosystems this century. *Nature Climate Change*, **7**, 142-147. http://dx.doi.org/10.1038/nclimate3203

133. IPCC, 2013: *Climate Change 2013: The Physical Science Basis. Contribution of Working Group I to the Fifth Assessment Report of the Intergovernmental Panel on Climate Change*. Stocker, T.F., D. Qin, G.-K. Plattner, M. Tignor, S.K. Allen, J. Boschung, A. Nauels, Y. Xia, V. Bex, and P.M. Midgley, Eds. Cambridge University Press, Cambridge, UK and New York, NY, 1535 pp. http://www.climatechange2013.org/report/

134. Mitchell, R.J., Y. Liu, J.J. O'Brien, K.J. Elliott, G. Starr, C.F. Miniat, and J.K. Hiers, 2014: Future climate and fire interactions in the southeastern region of the United States. *Forest Ecology and Management*, **327**, 316-326. http://dx.doi.org/10.1016/j.foreco.2013.12.003

135. Osland, M.J., N. Enwright, R.H. Day, and T.W. Doyle, 2013: Winter climate change and coastal wetland foundation species: Salt marshes vs. mangrove forests in the southeastern United States. *Global Change Biology*, **19** (5), 1482-1494. http://dx.doi.org/10.1111/gcb.12126

136. Jackson, S.T. and J.T. Overpeck, 2000: Responses of plant populations and communities to environmental changes of the late Quaternary. *Paleobiology*, **26** (sp4), 194-220. http://dx.doi.org/10.1666/0094-8373(2000)26[194:ROPPAC]2.0.CO;2

137. Williams, J.W. and S.T. Jackson, 2007: Novel climates, no-analog communities, and ecological surprises. *Frontiers in Ecology and the Environment*, **5** (9), 475-482. http://dx.doi.org/10.1890/070037

138. Boucek, R.E., E.E. Gaiser, H. Liu, and J.S. Rehage, 2016: A review of subtropical community resistance and resilience to extreme cold spells. *Ecosphere*, **7** (10), e01455. http://dx.doi.org/10.1002/ecs2.1455

139. Daly, C., M.P. Widrlechner, M.D. Halbleib, J.I. Smith, and W.P. Gibson, 2012: Development of a new USDA plant hardiness zone map for the United States. *Journal of Applied Meteorology and Climatology*, **51**, 242-264. http://dx.doi.org/10.1175/2010JAMC2536.1

140. Kozlowski, T.T. and S.G. Pallardy, 1997: *Growth Control in Woody Plants*. Roy, J., Ed. Academic Press, San Diego, 641 pp.

141. Larcher, W., 2003: *Physiological Plant Ecology: Ecophysiology and Stress Physiology of Functional Groups*, 4th ed. Springer, Berlin, 514 pp.

142. Parker, L.E. and J.T. Abatzoglou, 2016: Projected changes in cold hardiness zones and suitable overwinter ranges of perennial crops over the United States. *Environmental Research Letters*, **11** (3), 034001. http://dx.doi.org/10.1088/1748-9326/11/3/034001

143. Sakai, A. and W. Larcher, 1987: *Frost Survival of Plants: Responses and Adaptation to Freezing Stress*. 321 pp. http://dx.doi.org/10.1007/978-3-642-71745-1

144. Williams, C.M., H.A.L. Henry, and B.J. Sinclair, 2015: Cold truths: How winter drives responses of terrestrial organisms to climate change. *Biological Reviews*, **90** (1), 214-235. http://dx.doi.org/10.1111/brv.12105

145. Osland, M.J., N.M. Enwright, R.H. Day, C.A. Gabler, C.L. Stagg, and J.B. Grace, 2016: Beyond just sea-level rise: Considering macroclimatic drivers within coastal wetland vulnerability assessments to climate change. *Global Change Biology*, **22** (1), 1-11. http://dx.doi.org/10.1111/gcb.13084

146. Krakauer, N.Y., 2012: Estimating climate trends: Application to United States plant hardiness zones. *Advances in Meteorology*, **2012**, Article ID 404876. http://dx.doi.org/10.1155/2012/404876

147. McKenney, D.W., J.H. Pedlar, K. Lawrence, P. Papadopol, K. Campbell, and M.F. Hutchinson, 2014: Change and evolution in the plant hardiness zones of Canada. *BioScience*, **64** (4), 341-350. http://dx.doi.org/10.1093/biosci/biu016

148. Attaway, J.A., 1997: *A History of Florida Citrus Freezes*. Flordia Science Source, Ocala, FL, 368 pp.

149. Cavanaugh, K.C., J.D. Parker, S.C. Cook-Patton, I.C. Feller, A.P. Williams, and J.R. Kellner, 2015: Integrating physiological threshold experiments with climate modeling to project mangrove species' range expansion. *Global Change Biology*, **21** (5), 1928-1938. http://dx.doi.org/10.1111/gcb.12843

150. Cavanaugh, K.C., J.R. Kellner, A.J. Forde, D.S. Gruner, J.D. Parker, W. Rodriguez, and I.C. Feller, 2014: Poleward expansion of mangroves is a threshold response to decreased frequency of extreme cold events. *Proceedings of the National Academy of Sciences of the United States of America*, **111** (2), 723-727. http://dx.doi.org/10.1073/pnas.1315800111

151. Osland, M.J., R.H. Day, C.T. Hall, M.D. Brumfield, J.L. Dugas, and W.R. Jones, 2017: Mangrove expansion and contraction at a poleward range limit: Climate extremes and land-ocean temperature gradients. *Ecology*, **98** (1), 125-137. http://dx.doi.org/10.1002/ecy.1625

152. Osland, M.J., L.C. Feher, K.T. Griffith, K.C. Cavanaugh, N.M. Enwright, R.H. Day, C.L. Stagg, K.W. Krauss, R.J. Howard, J.B. Grace, and K. Rogers, 2017: Climatic controls on the global distribution, abundance, and species richness of mangrove forests. *Ecological Monographs*, **87** (2), 341-359. http://dx.doi.org/10.1002/ecm.1248

153. Engle, V.D., 2011: Estimating the provision of ecosystem services by Gulf of Mexico coastal wetlands. *Wetlands*, **31** (1), 179-193. http://dx.doi.org/10.1007/s13157-010-0132-9

154. Field, D.W., A.J. Reyer, P.V. Genovese, and B.D. Shearer, 1991: Coastal Wetlands of the United States: An Accounting of a Valuable National Resource. A Special NOAA 20th Anniversary Report. National Oceanic and Atmospheric Administration, Washington, DC, 59 pp. https://catalog.hathitrust.org/Record/002499265

155. Batker, D., I. de la Torre, R. Costanza, P. Swedeen, J. Day, R. Boumans, and K. Bagstad, 2010: Gaining Ground: Wetlands, Hurricanes and the Economy: The Value of Restoring the Mississippi River Delta. Earth Economics, Tacoma, WA, 98 pp. http://pdxscholar.library.pdx.edu/cgi/viewcontent.cgi?article=1038&context=iss_pub

156. Dayton, P.K., 1972: Toward an understanding of community resilience and the potential effects of enrichments to the benthos at McMurdo Sound, Antarctica. In *Proceedings of the Colloquium on Conservation Problems in Antarctica*, Blacksburg, VA. Allen Press. Parker, B.C., Ed., 81-96. http://daytonlab.ucsd.edu/Publications/Dayton72_Understanding.pdf

157. Ellison, A.M., M.S. Bank, B.D. Clinton, E.A. Colburn, K. Elliott, C.R. Ford, D.R. Foster, B.D. Kloeppel, J.D. Knoepp, G.M. Lovett, J. Mohan, D.A. Orwig, N.L. Rodenhouse, W.V. Sobczak, K.A. Stinson, J.K. Stone, C.M. Swan, J. Thompson, B. Von Holle, and J.R. Webster, 2005: Loss of foundation species: Consequences for the structure and dynamics of forested ecosystems. *Frontiers in Ecology and the Environment*, **3** (9), 479-486. http://dx.doi.org/10.1890/1540-9295(2005)003[0479:LOFSCF]2.0.CO;2

158. Bianchi, T.S., M.A. Allison, J. Zhao, X. Li, R.S. Comeaux, R.A. Feagin, and R.W. Kulawardhana, 2013: Historical reconstruction of mangrove expansion in the Gulf of Mexico: Linking climate change with carbon sequestration in coastal wetlands. *Estuarine, Coastal and Shelf Science*, **119**, 7-16. http://dx.doi.org/10.1016/j.ecss.2012.12.007

159. Chavez-Ramirez, F. and W. Wehtje, 2012: Potential impact of climate change scenarios on whooping crane life history. *Wetlands*, **32** (1), 11-20. http://dx.doi.org/10.1007/s13157-011-0250-z

160. Comeaux, R.S., M.A. Allison, and T.S. Bianchi, 2012: Mangrove expansion in the Gulf of Mexico with climate change: Implications for wetland health and resistance to rising sea levels. *Estuarine, Coastal and Shelf Science*, **96**, 81-95. http://dx.doi.org/10.1016/j.ecss.2011.10.003

161. Doughty, C.L., J.A. Langley, W.S. Walker, I.C. Feller, R. Schaub, and S.K. Chapman, 2016: Mangrove range expansion rapidly increases coastal wetland carbon storage. *Estuaries and Coasts*, **39** (2), 385-396. http://dx.doi.org/10.1007/s12237-015-9993-8

162. Guo, H., C. Weaver, S.P. Charles, A. Whitt, S. Dastidar, P. D'Odorico, J.D. Fuentes, J.S. Kominoski, A.R. Armitage, and S.C. Pennings, 2017: Coastal regime shifts: Rapid responses of coastal wetlands to changes in mangrove cover. *Ecology*, **98** (3), 762-772. http://dx.doi.org/10.1002/ecy.1698

163. Smee, D.L., J.A. Sanchez, M. Diskin, and C. Trettin, 2017: Mangrove expansion into salt marshes alters associated faunal communities. *Estuarine, Coastal and Shelf Science*, **187**, 306-313. http://dx.doi.org/10.1016/j.ecss.2017.02.005

164. Yando, E.S., M.J. Osland, J.M. Willis, R.H. Day, K.W. Krauss, and M.W. Hester, 2016: Salt marsh–mangrove ecotones: Using structural gradients to investigate the effects of woody plant encroachment on plant–soil interactions and ecosystem carbon pools. *Journal of Ecology*, **104** (4), 1020-1031. http://dx.doi.org/10.1111/1365-2745.12571

165. Kelleway, J.J., K. Cavanaugh, K. Rogers, I.C. Feller, E. Ens, C. Doughty, and N. Saintilan, 2017: Review of the ecosystem service implications of mangrove encroachment into salt marshes. *Global Change Biology*, **23** (10), 3967-3983. http://dx.doi.org/10.1111/gcb.13727

166. Ayres, M.P. and M.a.J. Lombardero, 2000: Assessing the consequences of global change for forest disturbance from herbivores and pathogens. *Science of the Total Environment*, **262** (3), 263-286. http://dx.doi.org/10.1016/S0048-9697(00)00528-3

167. Bentz, B.J. and A.M. Jönsson, 2015: Chapter 13: Modeling bark beetle responses to climate change. *Bark Beetles: Biology and Ecology of Native and Invasive Species*. Hofstetter, R.W., Ed. Academic Press, San Diego, 533-553. http://dx.doi.org/10.1016/B978-0-12-417156-5.00013-7

168. Duehl, A.J., F.H. Koch, and F.P. Hain, 2011: Southern pine beetle regional outbreaks modeled on landscape, climate and infestation history. *Forest Ecology and Management*, **261** (3), 473-479. http://dx.doi.org/10.1016/j.foreco.2010.10.032

169. Ebi, K.L. and J. Nealon, 2016: Dengue in a changing climate. *Environmental Research*, **151**, 115-123. http://dx.doi.org/10.1016/j.envres.2016.07.026

170. Morin, C.W., A.C. Comrie, and K. Ernst, 2013: Climate and dengue transmission: Evidence and implications. *Environmental Health Perspectives*, **121**, 1264-1277. http://dx.doi.org/10.1289/ehp.1306556

171. Robinet, C. and A. Roques, 2010: Direct impacts of recent climate warming on insect populations. *Integrative Zoology*, **5** (2), 132-142. http://dx.doi.org/10.1111/j.1749-4877.2010.00196.x

172. Ungerer, M.J., M.P. Ayres, and M.J. Lombardero, 1999: Climate and the northern distribution limits of *Dendroctonus frontalis* Zimmermann (Coleoptera: Scolytidae). *Journal of Biogeography*, **26** (6), 1133-1145. http://dx.doi.org/10.1046/j.1365-2699.1999.00363.x

173. Notaro, M., M. Schummer, Y. Zhong, S. Vavrus, L. Van Den Elsen, J. Coluccy, and C. Hoving, 2016: Projected influences of changes in weather severity on autumn-winter distributions of dabbling ducks in the Mississippi and Atlantic flyways during the twenty-first century. *PLOS ONE*, **11** (12), e0167506. http://dx.doi.org/10.1371/journal.pone.0167506

174. Boucek, R.E. and J.S. Rehage, 2014: Climate extremes drive changes in functional community structure. *Global Change Biology*, **20** (6), 1821-1831. http://dx.doi.org/10.1111/gcb.12574

175. Martin, J.H. and L.W. McEachron, 1996: Historical Annotated Review of Winter Kills of Marine Organisms in Texas Bays. Management Data Series No. 118. Texas Parks and Wildlife Department, Coastal Fisheries Division, Austin, TX, 20 pp. https://tpwd.texas.gov/publications/pwdpubs/media/mds_coastal/Series%202_MDS118.pdf

176. Rehage, J.S., J.R. Blanchard, R.E. Boucek, J.J. Lorenz, and M. Robinson, 2016: Knocking back invasions: Variable resistance and resilience to multiple cold spells in native vs. nonnative fishes. *Ecosphere*, **7** (6), e01268. http://dx.doi.org/10.1002/ecs2.1268

177. Stevens, P.W., D.A. Blewett, R.E. Boucek, J.S. Rehage, B.L. Winner, J.M. Young, J.A. Whittington, and R. Paperno, 2016: Resilience of a tropical sport fish population to a severe cold event varies across five estuaries in southern Florida. *Ecosphere*, **7** (8), e01400. http://dx.doi.org/10.1002/ecs2.1400

178. Storey, M. and E.W. Gudger, 1936: Mortality of fishes due to cold at Sanibel Island, Florida, 1886-1936. *Ecology*, **17** (4), 640-648. http://dx.doi.org/10.2307/1932762

179. Vergés, A., P.D. Steinberg, M.E. Hay, A.G.B. Poore, A.H. Campbell, E. Ballesteros, K.L. Heck, D.J. Booth, M.A. Coleman, D.A. Feary, W. Figueira, T. Langlois, E.M. Marzinelli, T. Mizerek, P.J. Mumby, Y. Nakamura, M. Roughan, E. van Sebille, A.S. Gupta, D.A. Smale, F. Tomas, T. Wernberg, and S.K. Wilson, 2014: The tropicalization of temperate marine ecosystems: Climate-mediated changes in herbivory and community phase shifts. *Proceedings of the Royal Society B: Biological Sciences*, **281** (1789). http://dx.doi.org/10.1098/rspb.2014.0846

180. Avery, M.L., R.M. Engeman, K.L. Keacher, J.S. Humphrey, W.E. Bruce, T.C. Mathies, and R.E. Mauldin, 2010: Cold weather and the potential range of invasive Burmese pythons. *Biological Invasions*, **12** (11), 3649-3652. http://dx.doi.org/10.1007/s10530-010-9761-4

181. Dorcas, M.E., J.D. Willson, R.N. Reed, R.W. Snow, M.R. Rochford, M.A. Miller, W.E. Meshaka, P.T. Andreadis, F.J. Mazzotti, C.M. Romagosa, and K.M. Hart, 2012: Severe mammal declines coincide with proliferation of invasive Burmese pythons in Everglades National Park. *Proceedings of the National Academy of Sciences of the United States of America*, **109** (7), 2418-2422. http://dx.doi.org/10.1073/pnas.1115226109

182. Ferriter, A., Ed. 1997: *Brazilian Pepper Management Plan for Florida*. Florida Exotic Pest Plant Council, Gainesville, FL, 26 pp. http://www.fleppc.org/Manage_Plans/schinus.pdf

183. Jacobson, E.R., D.G. Barker, T.M. Barker, R. Mauldin, M.L. Avery, R. Engeman, and S. Secor, 2012: Environmental temperatures, physiology and behavior limit the range expansion of invasive Burmese pythons in southeastern USA. *Integrative Zoology*, **7** (3), 271-285. http://dx.doi.org/10.1111/j.1749-4877.2012.00306.x

184. Jones, W.D., 1979: Effects of the 1978 freeze on native plants of Sonora, Mexico. *Desert Plants*, **1**, 33-36. http://hdl.handle.net/10150/528203

185. Mazzotti, F.J., M.S. Cherkiss, K.M. Hart, R.W. Snow, M.R. Rochford, M.E. Dorcas, and R.N. Reed, 2011: Cold-induced mortality of invasive Burmese pythons in south Florida. *Biological Invasions*, **13** (1), 143-151. http://dx.doi.org/10.1007/s10530-010-9797-5

186. Mazzotti, F.J., M.S. Cherkiss, M. Parry, J. Beauchamp, M. Rochford, B. Smith, K. Hart, and L.A. Brandt, 2016: Large reptiles and cold temperatures: Do extreme cold spells set distributional limits for tropical reptiles in Florida? *Ecosphere*, **7** (8), e01439. http://dx.doi.org/10.1002/ecs2.1439

187. Morton, J.F., 1978: Brazilian pepper—Its impact on people, animals and the environment. *Economic Botany*, **32** (4), 353-359. http://dx.doi.org/10.1007/bf02907927

188. Provancha, M.J., P.A. Schmalzer, and C.R. Hall, 1986: Effects of the December 1983 and January 1985 freezing air temperatures on select aquatic poikilotherms and plant species of Merritt Island, Florida. *Florida Scientist*, **49** (4), 199-212. http://www.jstor.org/stable/24320159

189. Christensen, N.L., 1981: Fire regimes in southeastern ecosystems. In *Fire Regimes and Ecosystem Properties*, Honolulu, HI. Mooney, H.A., T.M. Bonnicksen, N.L. Christensen, J.E. Lotan, and W.A. Reiners, Eds., 112-136. https://archive.org/stream/CAT83781017#page/112/mode/2up/search/christensen

190. Melvin, M.A., 2015: 2015 National Prescribed Fire Use Survey Report. Technical Report 02-15. Coalition of Prescribed Fire Councils, 17 pp. https://stateforesters.org/sites/default/files/publication-documents/2015%20Prescribed%20Fire%20Use%20Survey%20Report.pdf

191. Prestemon, J.P., U. Shankar, A. Xiu, K. Talgo, D. Yang, E. Dixon, D. McKenzie, and K.L. Abt, 2016: Projecting wildfire area burned in the south-eastern United States, 2011–60. *International Journal of Wildland Fire*, **25** (7), 715-729. http://dx.doi.org/10.1071/WF15124

192. Gandhi, K.J.K. and D.A. Herms, 2010: Direct and indirect effects of alien insect herbivores on ecological processes and interactions in forests of eastern North America. *Biological Invasions*, **12** (2), 389-405. http://dx.doi.org/10.1007/s10530-009-9627-9

193. Kreye, J.K., J.M. Varner, J.K. Hiers, and J. Mola, 2013: Toward a mechanism for eastern North American forest mesophication: Differential litter drying across 17 species. *Ecological Applications*, **23** (8), 1976-1986. http://dx.doi.org/10.1890/13-0503.1

194. Nowacki, G.J. and M.D. Abrams, 2008: The demise of fire and "mesophication" of forests in the eastern United States. *BioScience*, **58** (2), 123-138. http://dx.doi.org/10.1641/B580207

195. Mercer, D.E., J.P. Prestemon, D.T. Butry, and J.M. Pye, 2007: Evaluating alternative prescribed burning policies to reduce net economic damages from wildfire. *American Journal of Agricultural Economics*, **89** (1), 63-77. http://dx.doi.org/10.1111/j.1467-8276.2007.00963.x

196. Swanteson-Franz, R.J., D.J. Krofcheck, and M.D. Hurteau, 2018: Quantifying forest carbon dynamics as a function of tree species composition and management under projected climate. *Ecosphere*, **9** (4), e02191. http://dx.doi.org/10.1002/ecs2.2191

197. Mitchell, R.J., L.K. Kirkman, S.D. Pecot, C.A. Wilson, B.J. Palik, and L.R. Boring, 1999: Patterns and controls of ecosystem function in longleaf pine-wiregrass savannas. I. Aboveground net primary productivity. *Canadian Journal of Forest Research*, **29** (6), 743-751. http://dx.doi.org/10.1139/x99-051

198. Kirkman, L.K., R.J. Mitchell, R.C. Helton, and M.B. Drew, 2001: Productivity and species richness across an environmental gradient in a fire-dependent ecosystem. *American Journal of Botany*, **88** (11), 2119-2128. http://dx.doi.org/10.2307/3558437

199. Starr, G., C.L. Staudhammer, H.W. Loescher, R. Mitchell, A. Whelan, J.K. Hiers, and J.J. O'Brien, 2015: Time series analysis of forest carbon dynamics: Recovery of *Pinus palustris* physiology following a prescribed fire. *New Forests*, **46** (1), 63-90. http://dx.doi.org/10.1007/s11056-014-9447-3

200. Doyle, T.W., G.F. Girod, and M.A. Books, 2003: Modeling mangrove forest migration along the southwest coast of Florida under climate change. *Integrated Assessment of the Climate Change Impacts on the Gulf Coast Region*. Ning, Z.H., R.E. Turner, T. Doyle, and K.K. Abdollahi, Eds. Gulf Coast Climate Change Assessment Council (GCRCC) and Louisiana State University (LSU) Graphic Services, Baton Rouge, LA, 211-222. http://www.climateimpacts.org/us-climate-assess-2000/regions/gulf-coast/gulfcoast-chapter12.pdf

201. Woodroffe, C.D., K. Rogers, K.L. McKee, C.E. Lovelock, I.A. Mendelssohn, and N. Saintilan, 2016: Mangrove sedimentation and response to relative sea-level rise. *Annual Review of Marine Science*, **8** (1), 243-266. http://dx.doi.org/10.1146/annurev-marine-122414-034025

202. Conner, W.H., T.W. Doyle, and K.W. Krauss, Eds., 2007: *Ecology of Tidal Freshwater Forested Wetlands of the Southeastern United States*. Springer, Dordrecht, The Netherlands, 518 pp.

203. Doyle, T.W., K.W. Krauss, W.H. Conner, and A.S. From, 2010: Predicting the retreat and migration of tidal forests along the northern Gulf of Mexico under sea-level rise. *Forest Ecology and Management*, **259** (4), 770-777. http://dx.doi.org/10.1016/j.foreco.2009.10.023

204. Enwright, N.M., K.T. Griffith, and M.J. Osland, 2016: Barriers to and opportunities for landward migration of coastal wetlands with sea-level rise. *Frontiers in Ecology and the Environment*, **14** (6), 307-316. http://dx.doi.org/10.1002/fee.1282

205. Howard, R.J., R.H. Day, K.W. Krauss, A.S. From, L. Allain, and N. Cormier, 2017: Hydrologic restoration in a dynamic subtropical mangrove-to-marsh ecotone. *Restoration Ecology*, **25** (3), 471-482. http://dx.doi.org/10.1111/rec.12452

206. Neubauer, S.C., 2013: Ecosystem responses of a tidal freshwater marsh experiencing saltwater intrusion and altered hydrology. *Estuaries and Coasts*, **36** (3), 491-507. http://dx.doi.org/10.1007/s12237-011-9455-x

207. Saha, A.K., S. Saha, J. Sadle, J. Jiang, M.S. Ross, R.M. Price, L.S.L.O. Sternberg, and K.S. Wendelberger, 2011: Sea level rise and South Florida coastal forests. *Climatic Change*, **107** (1), 81-108. http://dx.doi.org/10.1007/s10584-011-0082-0

208. Williams, K., K.C. Ewel, R.P. Stumpf, F.E. Putz, and T.W. Workman, 1999: Sea-level rise and coastal forest retreat on the West Coast of Florida, USA. *Ecology*, **80** (6), 2045-2063. http://dx.doi.org/10.1890/0012-9658(1999)080[2045:SLRACF]2.0.CO;2

209. Doyle, T.W., T.J. Smith, III, and M.B. Robblee, 1995: Wind damage effects of Hurricane Andrew on mangrove communities along the southwest coast of Florida, USA. *Journal of Coastal Research*, **SI 21**, 159-168. http://www.jstor.org/stable/25736006

210. Smith, T.J., III, M.B. Robblee, H.R. Wanless, and T.W. Doyle, 1994: Mangroves, hurricanes, and lightning strikes: Assessment of Hurricane Andrew suggests an interaction across two differing scales of disturbance. *BioScience*, **44** (4), 256-262. http://dx.doi.org/10.2307/1312230

211. Couvillion, B.R., H. Beck, D. Schoolmaster, and M. Fischer, 2017: Land Area Change in Coastal Louisiana (1932 to 2016). Scientific Investigations Map 3381. U.S. Geological Survey, Reston, VA, 16 pp. http://dx.doi.org/10.3133/sim3381

212. Blum, M.D. and H.H. Roberts, 2009: Drowning of the Mississippi Delta due to insufficient sediment supply and global sea-level rise. *Nature Geoscience*, **2** (7), 488-491. http://dx.doi.org/10.1038/ngeo553

213. Day, J.W., Jr., D.F. Boesch, E.J. Clairain, G.P. Kemp, S.B. Laska, W.J. Mitsch, K. Orth, H. Mashriqui, D.J. Reed, L. Shabman, C.A. Simenstad, B.J. Streever, R.R. Twilley, C.C. Watson, J.T. Wells, and D.F. Whigham, 2007: Restoration of the Mississippi Delta: Lessons from Hurricanes Katrina and Rita. *Science*, **315** (5819), 1679-1684. http://dx.doi.org/10.1126/science.1137030

214. Jankowski, K.L., T.E. Törnqvist, and A.M. Fernandes, 2017: Vulnerability of Louisiana's coastal wetlands to present-day rates of relative sea-level rise. *Nature Communications*, **8**, Article 14792. http://dx.doi.org/10.1038/ncomms14792

215. Twilley, R.R., S.J. Bentley, Q. Chen, D.A. Edmonds, S.C. Hagen, N.S.-N. Lam, C.S. Willson, K. Xu, D. Braud, R. Hampton Peele, and A. McCall, 2016: Co-evolution of wetland landscapes, flooding, and human settlement in the Mississippi River Delta Plain. *Sustainability Science*, **11** (4), 711-731. http://dx.doi.org/10.1007/s11625-016-0374-4

216. Coastal Protection and Restoration Authority of Louisiana, 2017: Louisiana's Comprehensive Master Plan for a Sustainable Coast. Coastal Protection and Restoration Authority of Louisiana, Baton Rouge, LA, 171 pp. http://coastal.la.gov/our-plan/2017-coastal-master-plan/

217. Allen, C.D., D.D. Breshears, and N.G. McDowell, 2015: On underestimation of global vulnerability to tree mortality and forest die-off from hotter drought in the Anthropocene. *Ecosphere*, **6** (8), 1-55. http://dx.doi.org/10.1890/ES15-00203.1

218. Allen, C.D., A.K. Macalady, H. Chenchouni, D. Bachelet, N. McDowell, M. Vennetier, T. Kitzberger, A. Rigling, D.D. Breshears, E.H. Hogg, P. Gonzalez, R. Fensham, Z. Zhang, J. Castro, N. Demidova, J.-H. Lim, G. Allard, S.W. Running, A. Semerci, and N. Cobb, 2010: A global overview of drought and heat-induced tree mortality reveals emerging climate change risks for forests. *Forest Ecology and Management*, **259** (4), 660-684. http://dx.doi.org/10.1016/j.foreco.2009.09.001

219. Berdanier, A.B. and J.S. Clark, 2016: Multiyear drought-induced morbidity preceding tree death in southeastern U.S. forests. *Ecological Applications*, **26** (1), 17-23. http://dx.doi.org/10.1890/15-0274

220. Clark, J.S., L. Iverson, C.W. Woodall, C.D. Allen, D.M. Bell, D.C. Bragg, A.W. D'Amato, F.W. Davis, M.H. Hersh, I. Ibanez, S.T. Jackson, S. Matthews, N. Pederson, M. Peters, M.W. Schwartz, K.M. Waring, and N.E. Zimmermann, 2016: The impacts of increasing drought on forest dynamics, structure, and biodiversity in the United States. *Global Change Biology*, **22** (7), 2329-2352. http://dx.doi.org/10.1111/gcb.13160

221. Luce, C.H., J.M. Vose, N. Pederson, J. Campbell, C. Millar, P. Kormos, and R. Woods, 2016: Contributing factors for drought in United States forest ecosystems under projected future climates and their uncertainty. *Forest Ecology and Management*, **380**, 299-308. http://dx.doi.org/10.1016/j.foreco.2016.05.020

222. Moore, G.W., C.B. Edgar, J.G. Vogel, R.A. Washington-Allen, Rosaleen G. March, and R. Zehnder, 2016: Tree mortality from an exceptional drought spanning mesic to semiarid ecoregions. *Ecological Applications*, **26** (2), 602-611. http://dx.doi.org/10.1890/15-0330

223. Williams, A.P., C.D. Allen, A.K. Macalady, D. Griffin, C.A. Woodhouse, D.M. Meko, T.W. Swetnam, S.A. Rauscher, R. Seager, H.D. Grissino-Mayer, J.S. Dean, E.R. Cook, C. Gangodagamage, M. Cai, and N.G. McDowell, 2013: Temperature as a potent driver of regional forest drought stress and tree mortality. *Nature Climate Change*, **3** (3), 292-297. http://dx.doi.org/10.1038/nclimate1693

224. Brock, M.A., D.L. Nielsen, R.J. Shiel, J.D. Green, and J.D. Langley, 2003: Drought and aquatic community resilience: The role of eggs and seeds in sediments of temporary wetlands. *Freshwater Biology*, **48** (7), 1207-1218. http://dx.doi.org/10.1046/j.1365-2427.2003.01083.x

225. McKee, K.L., I.A. Mendelssohn, and M. D. Materne, 2004: Acute salt marsh dieback in the Mississippi River deltaic plain: A drought-induced phenomenon? *Global Ecology and Biogeography*, **13** (1), 65-73. http://dx.doi.org/10.1111/j.1466-882X.2004.00075.x

226. Silliman, B.R., J. van de Koppel, M.D. Bertness, L.E. Stanton, and I.A. Mendelssohn, 2005: Drought, snails, and large-scale die-off of southern U.S. salt marshes. *Science*, **310** (5755), 1803-1806. http://dx.doi.org/10.1126/science.1118229

227. Diop, E.S., A. Soumare, N. Diallo, and A. Guisse, 1997: Recent changes of the mangroves of the Saloum River Estuary, Senegal. *Mangroves and Salt Marshes*, **1** (3), 163-172. http://dx.doi.org/10.1023/a:1009900724172

228. Duke, N.C., J.M. Kovacs, A.D. Griffiths, L. Preece, D.J.E. Hill, P. van Oosterzee, J. Mackenzie, H.S. Morning, and D. Burrows, 2017: Large-scale dieback of mangroves in Australia's Gulf of Carpentaria: A severe ecosystem response, coincidental with an unusually extreme weather event. *Marine & Freshwater Research*, **68** (10), 1816-1829. http://dx.doi.org/10.1071/MF16322

229. Lovelock, C.E., K.W. Krauss, M.J. Osland, R. Reef, and M.C. Ball, 2016: The physiology of mangrove trees with changing climate. *Tropical Tree Physiology: Adaptations and Responses in a Changing Environment*. Goldstein, G. and L.S. Santiago, Eds. Springer, Switzerland, 149-179.

230. Lovelock, C.E., I.C. Feller, R. Reef, S. Hickey, and M.C. Ball, 2017: Mangrove dieback during fluctuating sea levels. *Scientific Reports*, **7** (1), Article 1680. http://dx.doi.org/10.1038/s41598-017-01927-6

231. Reef, R. and C.E. Lovelock, 2015: Regulation of water balance in mangroves. *Annals of Botany*, **115** (3), 385-395. http://dx.doi.org/10.1093/aob/mcu174

232. Desantis, L.R.G., S. Bhotika, K. Williams, and F.E. Putz, 2007: Sea-level rise and drought interactions accelerate forest decline on the Gulf Coast of Florida, USA. *Global Change Biology*, **13** (11), 2349-2360. http://dx.doi.org/10.1111/j.1365-2486.2007.01440.x

233. Mitsch, W.J. and J.G. Gosselink, 2007: *Wetlands*, 4th ed. Wiley, New York, 600 pp.

234. Doney, S.C., M. Ruckelshaus, J.E. Duffy, J.P. Barry, F. Chan, C.A. English, H.M. Galindo, J.M. Grebmeier, A.B. Hollowed, N. Knowlton, J. Polovina, N.N. Rabalais, W.J. Sydeman, and L.D. Talley, 2012: Climate change impacts on marine ecosystems. *Annual Review of Marine Science*, **4**, 11-37. http://dx.doi.org/10.1146/annurev-marine-041911-111611

235. Hoegh-Guldberg, O. and J.F. Bruno, 2010: The impact of climate change on the world's marine ecosystems. *Science*, **328** (5985), 1523-1528. http://dx.doi.org/10.1126/science.1189930

236. Poloczanska, E.S., C.J. Brown, W.J. Sydeman, W. Kiessling, D.S. Schoeman, P.J. Moore, K. Brander, J.F. Bruno, L.B. Buckley, M.T. Burrows, C.M. Duarte, B.S. Halpern, J. Holding, C.V. Kappel, M.I. O'Connor, J.M. Pandolfi, C. Parmesan, F. Schwing, S.A. Thompson, and A.J. Richardson, 2013: Global imprint of climate change on marine life. *Nature Climate Change*, **3**, 919-925. http://dx.doi.org/10.1038/nclimate1958

237. Bjorndal, K.A., A.B. Bolten, M. Chaloupka, V.S. Saba, C. Bellini, M.A.G. Marcovaldi, A.J.B. Santos, L.F.W. Bortolon, A.B. Meylan, P.A. Meylan, J. Gray, R. Hardy, B. Brost, M. Bresette, J.C. Gorham, S. Connett, B.V.S. Crouchley, M. Dawson, D. Hayes, C.E. Diez, R.P. van Dam, S. Willis, M. Nava, K.M. Hart, M.S. Cherkiss, A.G. Crowder, C. Pollock, Z. Hillis-Starr, F.A. Muñoz Tenería, R. Herrera-Pavón, V. Labrada-Martagón, A. Lorences, A. Negrete-Philippe, M.M. Lamont, A.M. Foley, R. Bailey, R.R. Carthy, R. Scarpino, E. McMichael, J.A. Provancha, A. Brooks, A. Jardim, M. López-Mendilaharsu, D. González-Paredes, A. Estrades, A. Fallabrino, G. Martínez-Souza, G.M. Vélez-Rubio, R.H. Boulon, J.A. Collazo, R. Wershoven, V. Guzmán Hernández, T.B. Stringell, A. Sanghera, P.B. Richardson, A.C. Broderick, Q. Phillips, M. Calosso, J.A.B. Claydon, T.L. Metz, A.L. Gordon, A.M. Landry, D.J. Shaver, J. Blumenthal, L. Collyer, B.J. Godley, A. McGowan, M.J. Witt, C.L. Campbell, C.J. Lagueux, T.L. Bethel, and L. Kenyon, 2017: Ecological regime shift drives declining growth rates of sea turtles throughout the West Atlantic. *Global Change Biology*, **23** (11), 4556-4568. http://dx.doi.org/10.1111/gcb.13712

238. Ferrario, F., M.W. Beck, C.D. Storlazzi, F. Micheli, C.C. Shepard, and L. Airoldi, 2014: The effectiveness of coral reefs for coastal hazard risk reduction and adaptation. *Nature Communications*, **5**, 3794. http://dx.doi.org/10.1038/ncomms4794

239. Moberg, F. and C. Folke, 1999: Ecological goods and services of coral reef ecosystems. *Ecological Economics*, **29** (2), 215-233. http://dx.doi.org/10.1016/S0921-8009(99)00009-9

240. Hoegh-Guldberg, O., P.J. Mumby, A.J. Hooten, R.S. Steneck, P. Greenfield, E. Gomez, C.D. Harvell, P.F. Sale, A.J. Edwards, K. Caldeira, N. Knowlton, C.M. Eakin, R. Iglesias-Prieto, N. Muthiga, R.H. Bradbury, A. Dubi, and M.E. Hatziolos, 2007: Coral reefs under rapid climate change and ocean acidification. *Science*, **318** (5857), 1737-1742. http://dx.doi.org/10.1126/science.1152509

241. Hughes, T.P., A.H. Baird, D.R. Bellwood, M. Card, S.R. Connolly, C. Folke, R. Grosberg, O. Hoegh-Guldberg, J.B.C. Jackson, J. Kleypas, J.M. Lough, P. Marshall, M. Nyström, S.R. Palumbi, J.M. Pandolfi, B. Rosen, and J. Roughgarden, 2003: Climate change, human impacts, and the resilience of coral reefs. *Science*, **301** (5635), 929-933. http://dx.doi.org/10.1126/science.1085046

242. Kuffner, I.B., B.H. Lidz, J.H. Hudson, and J.S. Anderson, 2015: A century of ocean warming on Florida Keys coral reefs: Historic in situ observations. *Estuaries and Coasts*, **38** (3), 1085-1096. http://dx.doi.org/10.1007/s12237-014-9875-5

243. Manzello, D.P., 2015: Rapid recent warming of coral reefs in the Florida Keys. *Scientific Reports*, **5**, Article 16762. http://dx.doi.org/10.1038/srep16762

244. McClenachan, L., G. O'Connor, B.P. Neal, J.M. Pandolfi, and J.B.C. Jackson, 2017: Ghost reefs: Nautical charts document large spatial scale of coral reef loss over 240 years. *Science Advances*, **3** (9), e1603155. http://dx.doi.org/10.1126/sciadv.1603155

245. Yates, K.K., D.G. Zawada, N.A. Smiley, and G. Tiling-Range, 2017: Divergence of seafloor elevation and sea level rise in coral reef ecosystems. *Biogeosciences*, **14** (6), 1739-1772. http://dx.doi.org/10.5194/bg-14-1739-2017

246. EPA, 2015: Climate Change in the United States: Benefits of Global Action. EPA 430-R-15-001. U.S. Environmental Protection Agency (EPA), Office of Atmospheric Programs, Washington, DC, 93 pp. https://www.epa.gov/cira/downloads-cira-report

247. Lane, D.R., R.C. Ready, R.W. Buddemeier, J.A. Martinich, K.C. Shouse, and C.W. Wobus, 2013: Quantifying and valuing potential climate change impacts on coral reefs in the United States: Comparison of two scenarios. *PLOS ONE*, **8** (12), e82579. http://dx.doi.org/10.1371/journal.pone.0082579

248. Anthony, K.R.N., J.A. Maynard, G. Diaz-Pulido, P.J. Mumby, P.A. Marshall, L. Cao, and O.V.E. Hoegh-Guldberg, 2011: Ocean acidification and warming will lower coral reef resilience. *Global Change Biology*, **17** (5), 1798-1808. http://dx.doi.org/10.1111/j.1365-2486.2010.02364.x

249. Doney, S.C., V.J. Fabry, R.A. Feely, and J.A. Kleypas, 2009: Ocean acidification: The other CO_2 problem. *Annual Review of Marine Science*, **1** (1), 169-192. http://dx.doi.org/10.1146/annurev.marine.010908.163834

250. ERS, 2017: Atlas of Rural and Small-Town America [web tool]. USDA, Economic Research Service (ERS), Washington, DC, accessed April 25. https://www.ers.usda.gov/data-products/atlas-of-rural-and-small-town-america/

251. NASS, 2017: Farm Labor Methodology and Quality Measures. USDA National Agricultural Statistics Service (NASS), Washington, DC, 11 pp. https://www.nass.usda.gov/Publications/Methodology_and_Data_Quality/Farm_Labor/11_2017/Quality%20Measures%20and%20Methodology

252. Lovett, H.B., S.B. Snider, K.K. Gore, and R.C. Muñoz, Eds., 2016: *Gulf of Mexico Regional Action Plan to Implement the NOAA Fisheries Climate Science Strategy*. NOAA Technical Memorandum NMFS-SEFSC-699. NOAA Southeast Fisheries Science Center, Miami, FL, 40 pp. http://dx.doi.org/10.7289/V5/TM-SEFSC-699

253. C3P, 2017: Carolinas Precipitation Patterns & Probabilities (C3P): An Atlas of Hydroclimate Extremes [web page]. Drought Indexes. Carolinas Integrated Sciences and Assessments, Columbia, SC, accessed June 4. https://www.cisa.sc.edu/atlas/carolinas-drought.html

254. Griffith, J.A., S.V. Stehman, and T.R. Loveland, 2003: Landscape trends in mid-Atlantic and southeastern United States ecoregions. *Environmental Management*, **32** (5), 572-588. http://dx.doi.org/10.1007/s00267-003-0078-2

255. Kinniburgh, F., M.G. Simonton, and C. Allouch, 2015: Come Heat and High Water: Climate Risk in the Southeastern U.S. and Texas. Gordon, K., Ed. Risky Business Project, New York, 109 pp. https://riskybusiness.org/site/assets/uploads/2015/09/Climate-Risk-in-Southeast-and-Texas.pdf

256. Ernst, K.M. and B.L. Preston, 2017: Adaptation opportunities and constraints in coupled systems: Evidence from the U.S. energy-water nexus. *Environmental Science & Policy*, **70**, 38-45. http://dx.doi.org/10.1016/j.envsci.2017.01.001

257. Sun, L., K.E. Kunkel, L.E. Stevens, A. Buddenberg, J.G. Dobson, and D.R. Easterling, 2015: Regional Surface Climate Conditions in CMIP3 and CMIP5 for the United States: Differences, Similarities, and Implications for the U.S. National Climate Assessment. NOAA Technical Report NESDIS 144. National Oceanic and Atmospheric Administration, National Environmental Satellite, Data, and Information Service, 111 pp. http://dx.doi.org/10.7289/V5RB72KG

258. USDA-NASS, 2017: Statistics by State [web site]. USDA, National Agricultural Statistical Service (NASS), Washington, DC, accessed July 18, 2017. https://www.nass.usda.gov/Statistics_by_State/

259. Clemson Cooperative Extension, 2018: About Peaches. Clemson University, Clemson, SC. https://www.clemson.edu/extension/peach/index.html

260. Luedeling, E., E.H. Girvetz, M.A. Semenov, and P.H. Brown, 2011: Climate change affects winter chill for temperate fruit and nut trees. *PLOS ONE*, **6** (5), e20155. http://dx.doi.org/10.1371/journal.pone.0020155

261. Luedeling, E., 2012: Climate change impacts on winter chill for temperate fruit and nut production: A review. *Scientia Horticulturae*, **144** (0), 218-229. http://dx.doi.org/10.1016/j.scienta.2012.07.011

262. Oswalt, S.N., W.B. Smith, P.D. Miles, and S.A. Pugh, 2014: Forest Resources of the United States, 2012: A Technical Document Supporting the Forest Service 2010 Update of the RPA Assessment. Gen. Tech. Rep. WO-91. USDA, Forest Service, Washington Office, Washington, DC, 218 pp. https://srs.fs.usda.gov/pubs/47322

263. Census Bureau, 2017: Annual Survey of Manufactures (ASM) [web site]. U.S. Census Bureau, accessed May 17. https://www.census.gov/programs-surveys/asm.html

264. Howell, B.J., 2002: Appalachian culture and environmental planning: Expanding the role of cultural sciences. *Culture, Environment, and Conservation in the Appalachian South*. Howell, B.J., Ed. University of Illinois Press, Urbana and Chicago (IL), 1-16.

265. Lewis, C., 2012: The case of the wild onions: The impact of ramps on Cherokee rights. *Southern Cultures*, **18** (2), 104-117. http://dx.doi.org/10.1353/scu.2012.0019

266. Bernatchez, A. and L. Lapointe, 2012: Cooler temperatures favour growth of wild leek (*Allium tricoccum*), a deciduous forest spring ephemeral. *Botany*, **90** (11), 1125-1132. http://dx.doi.org/10.1139/b2012-089

267. Leopold, S., 2017: Ramps now on the "to-watch" list: Time to ramp up conservation efforts. *United Plant Savers*. https://unitedplantsavers.org/ramps-now-on-the-to-watch-list/

268. NRCS, 2017: Plant profile: *Allium tricoccum* Aiton ramp. USDA Natural Resources Conservation Service (NRCS). https://plants.usda.gov/core/profile?symbol=ALTR3

269. Hansen, M.C., P.V. Potapov, R. Moore, M. Hancher, S.A. Turubanova, A. Tyukavina, D. Thau, S.V. Stehman, S.J. Goetz, T.R. Loveland, A. Kommareddy, A. Egorov, L. Chini, C.O. Justice, and J.R.G. Townshend, 2013: High-resolution global maps of 21st-century forest cover change. *Science*, **342** (6160), 850-853. http://dx.doi.org/10.1126/science.1244693

270. Brown, D.G., K.M. Johnson, T.R. Loveland, and D.M. Theobald, 2005: Rural land-use trends in the conterminous United States, 1950-2000. *Ecological Applications*, **15** (6), 1851-1863. http://dx.doi.org/10.1890/03-5220

271. Drummond, M.A. and T.R. Loveland, 2010: Land-use pressure and a transition to forest-cover loss in the eastern United States. *BioScience*, **60** (4), 286-298. http://dx.doi.org/10.1525/bio.2010.60.4.7

272. Pederson, N., A.W. D'Amato, J.M. Dyer, D.R. Foster, D. Goldblum, J.L. Hart, A.E. Hessl, L.R. Iverson, S.T. Jackson, D. Martin-Benito, B.C. McCarthy, R.W. McEwan, D.J. Mladenoff, A.J. Parker, B. Shuman, and J.W. Williams, 2015: Climate remains an important driver of post-European vegetation change in the eastern United States. *Global Change Biology*, **21** (6), 2105-2110. http://dx.doi.org/10.1111/gcb.12779

273. Fei, S., J.M. Desprez, K.M. Potter, I. Jo, J.A. Knott, and C.M. Oswalt, 2017: Divergence of species responses to climate change. *Science Advances*, **3** (5), e1603055. http://dx.doi.org/10.1126/sciadv.1603055

274. McEwan, R.W., J.M. Dyer, and N. Pederson, 2011: Multiple interacting ecosystem drivers: Toward an encompassing hypothesis of oak forest dynamics across eastern North America. *Ecography*, **34** (2), 244-256. http://dx.doi.org/10.1111/j.1600-0587.2010.06390.x

275. Balch, J.K., B.A. Bradley, J.T. Abatzoglou, R.C. Nagy, E.J. Fusco, and A.L. Mahood, 2017: Human-started wildfires expand the fire niche across the United States. *Proceedings of the National Academy of Sciences of the United States of America*, **114** (11), 2946-2951. http://dx.doi.org/10.1073/pnas.1617394114

276. Stephens, S.L., J.J. Moghaddas, C. Edminster, C.E. Fiedler, S. Haase, M. Harrington, J.E. Keeley, E.E. Knapp, J.D. McIver, K. Metlen, C.N. Skinner, and A. Youngblood, 2009: Fire treatment effects on vegetation structure, fuels, and potential fire severity in western U.S. forests. *Ecological Applications*, **19** (2), 305-320. http://dx.doi.org/10.1890/07-1755.1

277. Terando, A.J., B. Reich, K. Pacifici, J. Costanza, A. McKerrow, and J.A. Collazo, 2016: Uncertainty quantification and propagation for projections of extremes in monthly area burned under climate change: A case study in the coastal plain of Georgia, USA. *Natural Hazard Uncertainty Assessment: Modeling and Decision Support*. Riley, K., P. Webley, and M. Thompson, Eds. American Geophysical Union, 245-256. http://dx.doi.org/10.1002/9781119028116.ch16

278. Newman, S., M. Carroll, P. Jakes, and L. Higgins, 2014: Hurricanes and wildfires: Generic characteristics of community adaptive capacity. *Environmental Hazards*, **13** (1), 21-37. http://dx.doi.org/10.1080/17477891.2013.841090

279. Wyman, M., S. Malone, T. Stein, and C. Johnson, 2012: Race and wildfire risk perceptions among rural forestland owners in north-central Florida. *Society & Natural Resources*, **25** (12), 1293-1307. http://dx.doi.org/10.1080/08941920.2012.681752

280. Kovach, M.M., C.E. Konrad, and C.M. Fuhrmann, 2015: Area-level risk factors for heat-related illness in rural and urban locations across North Carolina, USA. *Applied Geography*, **60**, 175-183. http://dx.doi.org/10.1016/j.apgeog.2015.03.012

281. Sugg, M.M., C.E. Konrad, and C.M. Fuhrmann, 2016: Relationships between maximum temperature and heat-related illness across North Carolina, USA. *International Journal of Biometeorology*, **60** (5), 663-675. http://dx.doi.org/10.1007/s00484-015-1060-4

282. Gubernot, D.M., G.B. Anderson, and K.L. Hunting, 2015: Characterizing occupational heat-related mortality in the United States, 2000–2010: An analysis using the census of fatal occupational injuries database. *American Journal of Industrial Medicine*, **58** (2), 203-211. http://dx.doi.org/10.1002/ajim.22381

283. Gutierrez, K. and C. LePrevost, 2016: Climate justice in rural southeastern United States: A review of climate change impacts and effects on human health. *International Journal of Environmental Research and Public Health*, **13** (2), 189. http://dx.doi.org/10.3390/ijerph13020189

284. Morss, R.E., O.V. Wilhelmi, G.A. Meehl, and L. Dilling, 2011: Improving societal outcomes of extreme weather in a changing climate: An integrated perspective. *Annual Review of Environment and Resources*, **36** (1), 1-25. http://dx.doi.org/10.1146/annurev-environ-060809-100145

285. Pye, S., A. Dobbins, C. Baffert, J. Brajković, I. Grgurev, R. De Miglio, and P. Deane, 2015: Energy Poverty and Vulnerable Consumers in the Energy Sector Across the EU: Analysis of Policies and Measures. Policy Report 2. European Commission, Insight_E, Stockholm, Sweden, 77 pp. https://ec.europa.eu/energy/en/studies/energy-poverty-and-vulnerable-consumers-energy-sector-across-eu-analysis-policies-and

286. Harrison, C. and J. Popke, 2011: "Because you got to have heat": The networked assemblage of energy poverty in eastern North Carolina. *Annals of the Association of American Geographers*, **101** (4), 949-961. http://dx.doi.org/10.1080/00045608.2011.569659

287. NWS, [2018]: What Are Heating and Cooling Degree Days [web page]. NOAA National Weather Service (NWS), Key West, FL, accessed February 27. https://www.weather.gov/key/climate_heat_cool

288. Horney, J., M. Nguyen, D. Salvesen, C. Dwyer, J. Cooper, and P. Berke, 2017: Assessing the quality of rural hazard mitigation plans in the southeastern United States. *Journal of Planning Education and Research*, **37** (1), 56-65. http://dx.doi.org/10.1177/0739456x16628605

289. NC Rural Health Research Program, 2017: Rural Hospital Closures: January 2010–Present. UNC, Cecil G. Sheps Center for Health Services Research, Chapel Hill, NC. http://www.shepscenter.unc.edu/programs-projects/rural-health/rural-hospital-closures/

290. Houghton, A., J. Austin, A. Beerman, and C. Horton, 2017: An approach to developing local climate change environmental public health indicators in a rural district. *Journal of Environmental and Public Health*, **2017**, 16. http://dx.doi.org/10.1155/2017/3407325

291. Douglas, E., J. Jacobs, K. Hayhoe, L. Silka, J. Daniel, M. Collins, A. Alipour, B. Anderson, C. Hebson, E. Mecray, R. Mallick, Q. Zou, P. Kirshen, H. Miller, J. Kartez, L. Friess, A. Stoner, E. Bell, C. Schwartz, N. Thomas, S. Miller, B. Eckstrom, and C. Wake, 2017: Progress and challenges in incorporating climate change information into transportation research and design. *Journal of Infrastructure Systems*, **23** (4), 04017018. http://dx.doi.org/10.1061/(ASCE)IS.1943-555X.0000377

292. Miller, R., D. Arthur, B. Barami, A. Breck, S. Costa, K. Lewis, K. McCoy, and E. Morrison, 2016: Hampton Roads Climate Impact Quantification Initiative: Baseline Assessment of the Transportation Assets & Overview of Economic Analyses Useful in Quantifying Impacts. DOT-VNTSC-OSTR-17-01. Volpe National Transportation Systems Center, Cambridge, MA, 167 pp. https://trid.trb.org/view/1428258

293. Arnbjerg-Nielsen, K., P. Willems, J. Olsson, S. Beecham, A. Pathirana, I. Bülow Gregersen, H. Madsen, and V.-T.-V. Nguyen, 2013: Impacts of climate change on rainfall extremes and urban drainage systems: A review. *Water Science and Technology*, **68** (1), 16-28. http://dx.doi.org/10.2166/wst.2013.251

294. Bell, M.L., R. Goldberg, C. Hogrefe, P.L. Kinney, K. Knowlton, B. Lynn, J. Rosenthal, C. Rosenzweig, and J.A. Patz, 2007: Climate change, ambient ozone, and health in 50 US cities. *Climatic Change*, **82** (1-2), 61-76. http://dx.doi.org/10.1007/s10584-006-9166-7

295. Census Bureau, 2015: Press release: New Census Bureau Population Estimates Reveal Metro Areas and Counties That Propelled Growth in Florida and the Nation. *Census Newsroom*, March 26. U.S. Census Brueau. https://www.census.gov/newsroom/press-releases/2015/cb15-56.html

296. ARC, 2017: Population & Employment Forecasts. Atlanta Regional Commission (ARC), Atlanta, GA. http://www.atlantaregional.com/info-center/forecasts

297. Gregg, R.M., W.A. Reynier, A. Score, and L. Hilberg, 2017: State of Climate Adaptation in Water Resources Management: Southeastern United States and U.S. Caribbean. EcoAdapt, Bainbridge Island, WA, 214 pp. https://www.cakex.org/sites/default/files/documents/EcoAdapt_State%20of%20Adaptation_U.S.%20Southeast%20and%20Caribbean_December%202017.pdf

298. City of Fayetteville, 2017: Arkansans Can Take Steps to Respond to Climate Change. Fayetteville, AR. http://www.fayetteville-ar.gov/DocumentCenter/View/14890/Commentary_Climate-Change?bidId=

299. City of Atlanta, 2017: Resilient Atlanta: Actions to Build a More Equitable Future. 100 Resilient Cities, 150 pp. http://100resilientcities.org/wp-content/uploads/2017/11/Atlanta-Resilience-Strategy-PDF-v2.pdf

300. Stone, B., J. Vargo, P. Liu, Y.T. Hu, and A. Russell, 2013: Climate change adaptation through urban heat management in Atlanta, Georgia. *Environmental Science & Technology*, **47** (14), 7780-7786. http://dx.doi.org/10.1021/es304352e

301. Rosenzweig, C., W. Solecki, P. Romero-Lankao, S. Mehrotra, S. Dhakal, T. Bowman, and S. Ali Ibrahim, 2015: ARC3.2 Summary for City Leaders. Urban Climate Change Research Network, Columbia University, New York. http://uccrn.org/arc3-2/

302. Demuzere, M., K. Orru, O. Heidrich, E. Olazabal, D. Geneletti, H. Orru, A.G. Bhave, N. Mittal, E. Feliu, and M. Faehnle, 2014: Mitigating and adapting to climate change: Multi-functional and multi-scale assessment of green urban infrastructure. *Journal of Environmental Management*, **146**, 107-115. http://dx.doi.org/10.1016/j.jenvman.2014.07.025

303. Masson, V., C. Marchadier, L. Adolphe, R. Aguejdad, P. Avner, M. Bonhomme, G. Bretagne, X. Briottet, B. Bueno, C. de Munck, O. Doukari, S. Hallegatte, J. Hidalgo, T. Houet, J. Le Bras, A. Lemonsu, N. Long, M.P. Moine, T. Morel, L. Nolorgues, G. Pigeon, J.L. Salagnac, V. Viguié, and K. Zibouche, 2014: Adapting cities to climate change: A systemic modelling approach. *Urban Climate*, **10**, 407-429. http://dx.doi.org/10.1016/j.uclim.2014.03.004

304. Gill, S.E., J.F. Handley, A.R. Ennos, and S. Pauleit, 2007: Adapting cities for climate change: The role of the green infrastructure. *Built Environment*, **33** (1), 115-133. http://dx.doi.org/10.2148/benv.33.1.115

305. Binita, K.-C., J.M. Shepherd, and C.J. Gaither, 2015: Climate change vulnerability assessment in Georgia. *Applied Geography*, **62**, 62-74. http://dx.doi.org/10.1016/j.apgeog.2015.04.007

Assessment of erosion, sedimentation, and water quality impacts of the Mountain Valley Pipeline and Equitrans Expansion Project's proposed crossing of the Jefferson National Forest as it pertains to the U.S. Forest Service's Draft Supplemental Environmental Impact Statement dated December 2022

Prepared by Jonathan A. Czuba, Ph.D., Licensed Professional Engineer - February 9, 2023

REFERENCES
29

February 21, 2023

7 Precipitation Change in the United States

KEY FINDINGS

1. Annual precipitation has decreased in much of the West, Southwest, and Southeast and increased in most of the Northern and Southern Plains, Midwest, and Northeast. A national average increase of 4% in annual precipitation since 1901 is mostly a result of large increases in the fall season. (*Medium confidence*)

2. Heavy precipitation events in most parts of the United States have increased in both intensity and frequency since 1901 (*high confidence*). There are important regional differences in trends, with the largest increases occurring in the northeastern United States (*high confidence*). In particular, mesoscale convective systems (organized clusters of thunderstorms)—the main mechanism for warm season precipitation in the central part of the United States—have increased in occurrence and precipitation amounts since 1979 (*medium confidence*).

3. The frequency and intensity of heavy precipitation events are projected to continue to increase over the 21st century (*high confidence*). Mesoscale convective systems in the central United States are expected to continue to increase in number and intensity in the future (*medium confidence*). There are, however, important regional and seasonal differences in projected changes in total precipitation: the northern United States, including Alaska, is projected to receive more precipitation in the winter and spring, and parts of the southwestern United States are projected to receive less precipitation in the winter and spring (*medium confidence*).

4. Northern Hemisphere spring snow cover extent, North America maximum snow depth, snow water equivalent in the western United States, and extreme snowfall years in the southern and western United States have all declined, while extreme snowfall years in parts of the northern United States have increased (*medium confidence*). Projections indicate large declines in snowpack in the western United States and shifts to more precipitation falling as rain than snow in the cold season in many parts of the central and eastern United States (*high confidence*).

Recommended Citation for Chapter

Easterling, D.R., K.E. Kunkel, J.R. Arnold, T. Knutson, A.N. LeGrande, L.R. Leung, R.S. Vose, D.E. Waliser, and M.F. Wehner, 2017: Precipitation change in the United States. In: *Climate Science Special Report: Fourth National Climate Assessment, Volume I* [Wuebbles, D.J., D.W. Fahey, K.A. Hibbard, D.J. Dokken, B.C. Stewart, and T.K. Maycock (eds.)]. U.S. Global Change Research Program, Washington, DC, USA, pp. 207-230, doi: 10.7930/J0H993CC.

Introduction

Changes in precipitation are one of the most important potential outcomes of a warming world because precipitation is integral to the very nature of society and ecosystems. These systems have developed and adapted to the past envelope of precipitation variations. Any large changes beyond the historical envelope may have profound societal and ecological impacts.

Historical variations in precipitation, as observed from both instrumental and proxy records, establish the context around which future projected changes can be interpreted, because it is within that context that systems have evolved. Long-term station observations from core climate networks serve as a primary source to establish observed changes in both means and extremes. Proxy records, which are used to reconstruct past climate conditions, are varied and include sources such as tree ring and ice core data. Projected changes are examined using the Coupled Model Intercomparison Project Phase 5 (CMIP5) suite of model simulations. They establish the likelihood of distinct regional and seasonal patterns of change.

7.1 Historical Changes

7.1.1 Mean Changes

Annual precipitation averaged across the United States has increased approximately 4% over the 1901–2015 period, slightly less than the 5% increase reported in the Third National Climate Assessment (NCA3) over the 1901–2012 period.[1] There continue to be important regional and seasonal differences in precipitation changes (Figure 7.1). Seasonally, national increases are largest in the fall, while little change is observed for winter. Regional differences are apparent, as the Northeast, Midwest, and Great Plains have had increases while parts of the Southwest and Southeast have had decreases. The slight decrease in the change in annual precipitation across the United States since NCA3 appears to be the result of the recent lingering droughts in the western and southwestern United States.[2,3] However, the recent meteorological drought in California that began in late 2011[4,5] now appears to be largely over, due to the substantial precipitation and snowpack the state received in the winter of 2016–2017. The year 2015 was the third wettest on record, just behind 1973 and 1983 (all of which were years marked by El Niño events). Interannual variability is substantial, as evidenced by large multiyear meteorological and agricultural droughts in the 1930s and 1950s.

Changes in precipitation differ markedly across the seasons, as do regional patterns of increases and decreases. For the contiguous United States, fall exhibits the largest (10%) and most widespread increase, exceeding 15% in much of the Northern Great Plains, Southeast, and Northeast. Winter average for the United States has the smallest increase (2%), with drying over most of the western United States as well as parts of the Southeast. In particular, a reduction in streamflow in the northwestern United States has been linked to a decrease in orographic enhancement of precipitation since 1950.[6] Spring and summer have comparable increases (about 3.5%) but substantially different patterns. In spring, the northern half of the contiguous United States has become wetter, and the southern half has become drier. In summer, there is a mixture of increases and decreases across the Nation. Alaska shows little change in annual precipitation (+1.5%); however, in all seasons, central Alaska shows declines and the panhandle shows increases. Hawai'i shows a decline of more than 15% in annual precipitation.

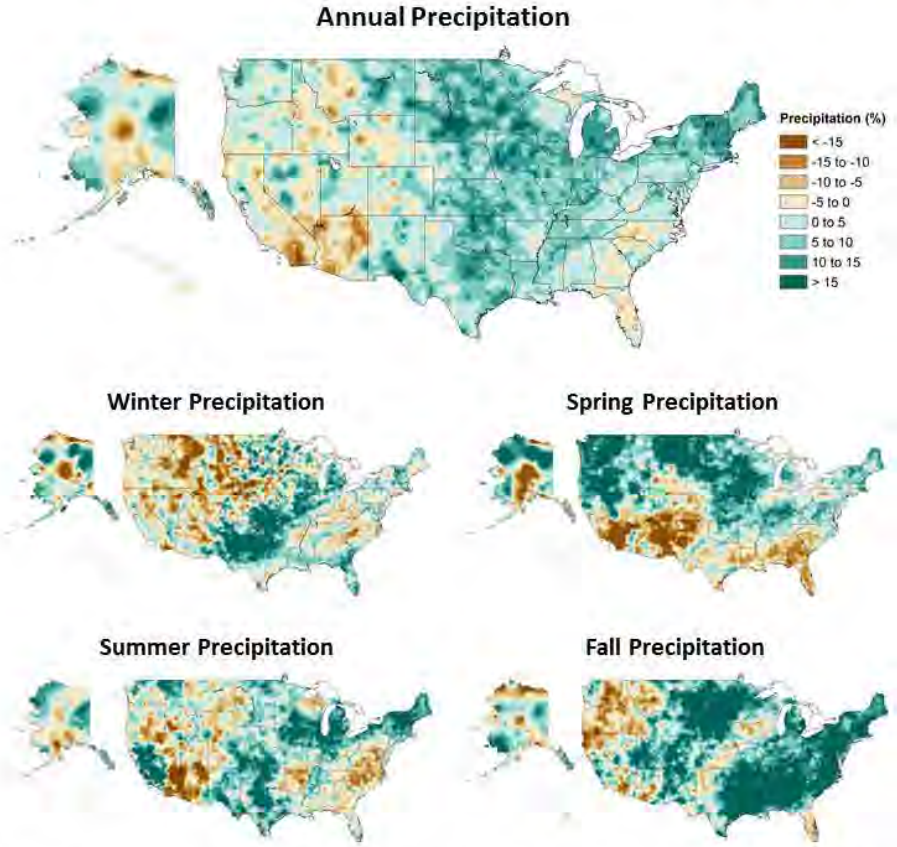

Figure 7.1: Annual and seasonal changes in precipitation over the United States. Changes are the average for present-day (1986–2015) minus the average for the first half of the last century (1901–1960 for the contiguous United States, 1925–1960 for Alaska and Hawai'i) divided by the average for the first half of the century. (Figure source: [top panel] adapted from Peterson et al. 2013,[78] © American Meteorological Society. Used with permission; [bottom four panels] NOAA NCEI, data source: nCLIMDiv].

7.1.2 Snow

Changes in snow cover extent (SCE) in the Northern Hemisphere exhibit a strong seasonal dependence.[7] There has been little change in winter SCE since the 1960s (when the first satellite records became available), while fall SCE has increased. However, the decline in spring SCE is larger than the increase in fall and is due in part to higher temperatures that shorten the time snow spends on the ground in the spring. This tendency is highlighted by the recent occurrences of both unusually high and unusually low monthly (October–June) SCE values, including the top 5 highest and top 5 lowest values in the 48 years of data. From 2010 onward, 7 of the 45 highest monthly SCE values occurred, all in the fall or winter (mostly in November and December), while 9 of the 10 lowest May and June values occurred. This reflects the trend toward earlier spring snowmelt, particularly at high latitudes.[8] An analysis of seasonal maximum snow depth for 1961–2015 over North America indicates a statistically significant downward trend of 0.11 standardized anomalies per decade and a trend toward the seasonal maximum snow depth occurring earlier—approximately one week earlier on average since the 1960s.[8] There has been a statistically significant decrease over the period of 1930–2007 in the frequency of years with a large number of snowfall days (years exceeding the 90th percentile) in the southern United States and the U.S. Pacific Northwest and an increase in the northern United States.[9] In the snow belts of the Great Lakes, lake effect snowfall has increased overall since the early 20th century for Lakes Superior, Michigan-Huron, and Erie.[10] However, individual studies for

Lakes Michigan[11] and Ontario[12] indicate that this increase has not been continuous. In both cases, upward trends were observed until the 1970s/early 1980s. Since then, however, lake effect snowfall has decreased in these regions. Lake effect snows along the Great Lakes are affected greatly by ice cover extent and lake water temperatures. As ice cover diminishes in winter, the expectation is for more lake effect snow until temperatures increase enough such that much of what now falls as snow instead falls as rain.[13, 14]

End-of-season snow water equivalent (SWE)—especially important where water supply is dominated by spring snow melt (for example, in much of the American West)—has declined since 1980 in the western United States, based on analysis of in situ observations, and is associated with springtime warming.[15] Satellite measurements of SWE based on brightness temperature also show a decrease over this period.[16] The variability of western United States SWE is largely driven by the most extreme events, with the top decile of events explaining 69% of the variability.[17] The recent drought in the western United States was highlighted by the extremely dry 2014–2015 winter that followed three previous dry winters. At Donner Summit, CA, (approximate elevation of 2,100 meters) in the Sierra Nevada Mountains, end-of-season SWE on April 1, 2015, was the lowest on record, based on survey measurements back to 1910, at only 0.51 inches (1.3 cm), or less than 2% of the long-term average. This followed the previous record low in 2014. The estimated return period of this drought is at least 500 years based on paleoclimatic reconstructions.[18]

7.1.3 Observed changes in U.S. seasonal extreme precipitation.

Extreme precipitation events occur when the air is nearly completely saturated. Hence, extreme precipitation events are generally observed to increase in intensity by about 6% to 7% for each degree Celsius of temperature increase, as dictated by the Clausius–Clapeyron relation. Figure 7.2 shows the observed change in the 20-year return value of the seasonal maximum 1-day precipitation totals over the period 1948–2015. A mix of increases and decreases is shown, with the Northwest showing very small changes in all seasons, the southern Great Plains showing a large increase in winter, and the Southeast showing a large increase in the fall.

A U.S. index of extreme precipitation from NCA3 was updated (Figure 7.3) through 2016. This is the number of 2-day precipitation events exceeding the threshold for a 5-year recurrence. The values were calculated by first arithmetically averaging the station data for all stations within each 1° by 1° latitude/longitude grid for each year and then averaging over the grid values across the contiguous United States for each year during the period of 1896–2015. The number of events has been well above average for the last three decades. The slight drop from 2006–2010 to 2011–2016 reflects a below-average number during the widespread severe meteorological drought year of 2012, while the other years in this pentad were well above average. The index value for 2015 was 80% above the 1901–1960 reference period average and the third highest value in the 120 years of record (after 1998 and 2008).

Maximum daily precipitation totals were calculated for consecutive 5-year blocks from 1901 (1901–1905, 1906–1910, 1911–1915, …, 2011–2016) for individual long-term stations. For each 5-year block, these values were aggregated to the regional scale by first arithmetically averaging the station 5-year maximum for all stations within each 2° by 2° latitude/longitude grid and then averaging across all grids within each region to

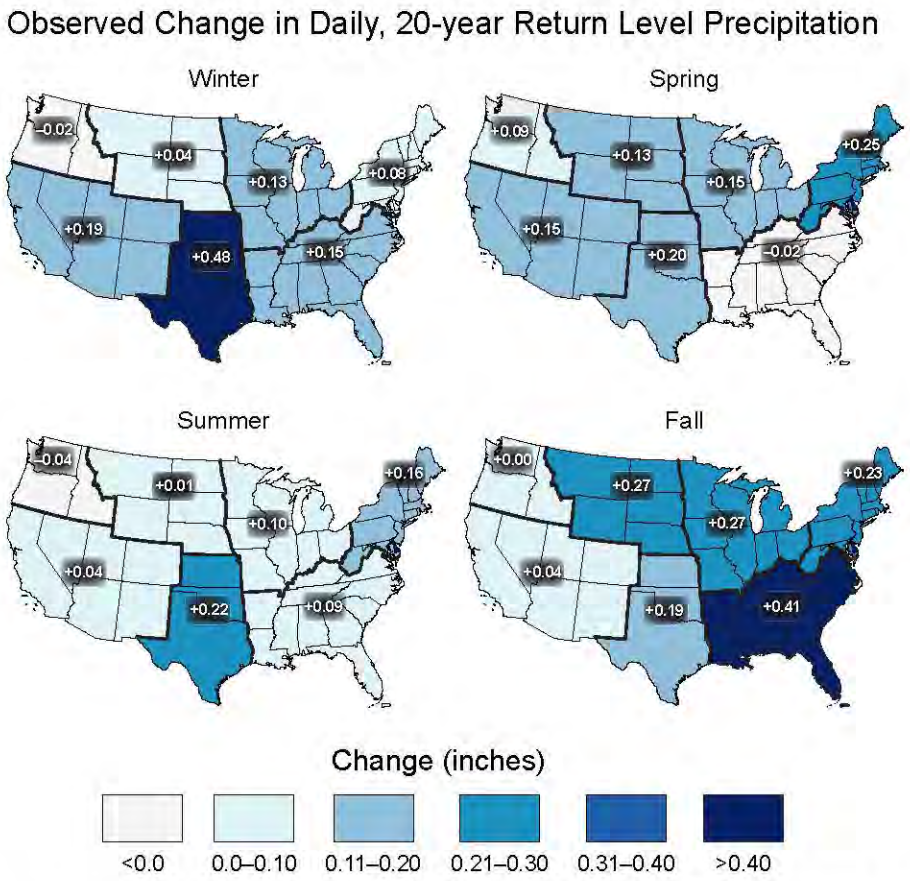

Figure 7.2: Observed changes in the 20-year return value of the seasonal daily precipitation totals for the contiguous United States over the period 1948 to 2015 using data from the Global Historical Climatology Network (GHCN) dataset. (Figure source: adapted from Kunkel et al. 2013;[61] © American Meteorological Society. Used with permission.)

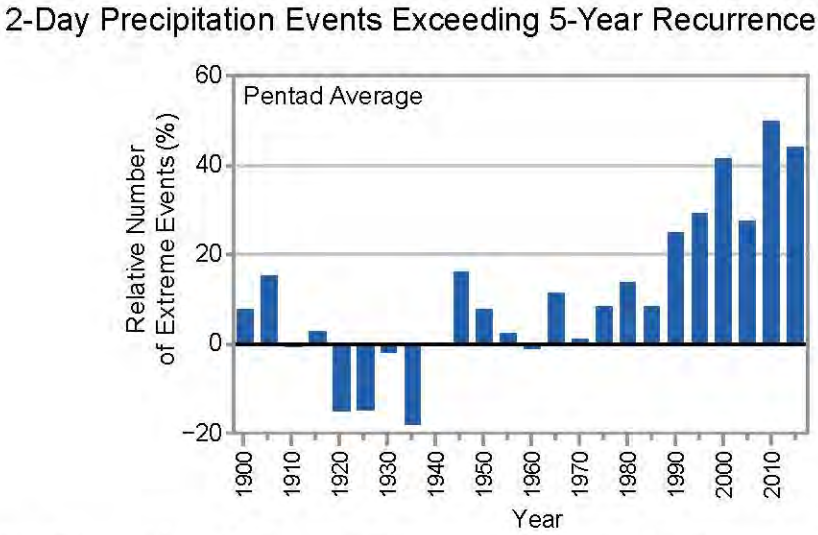

Figure 7.3: Index of the number of 2-day precipitation events exceeding the station-specific threshold for a 5-year recurrence interval in the contiguous United States, expressed as a percentage difference from the 1901–1960 mean. The annual values are averaged over 5-year periods, with the pentad label indicating the ending year of the period. Annual time series of the number of events are first calculated at individual stations. Next, the grid box time series are calculated as the average of all stations in the grid box. Finally, a national time series is calculated as the average of the grid box time series. Data source: GHCN-Daily. (Figure source: CICS-NC and NOAA NCEI).

create a regional time series. Finally, a trend was computed for the resulting regional time series. The difference between these two periods (Figure 7.4, upper left panel) indicates substantial increases over the eastern United States, particularly the northeastern United States with an increase of 27% since 1901. The increases are much smaller over the western United States, with the southwestern and northwestern United States showing little increase.

Another index of extreme precipitation from NCA3 (the total precipitation falling in the top 1% of all days with precipitation) was updated through 2016 (Figure 7.4, upper right panel). This analysis is for 1958–2016. There are increases in all regions, with the largest increases again in the northeastern United States. There are some changes in the values compared to NCA3, with small increases in some regions such as the Midwest and Southwest and small decreases in others such as the Northeast, but the overall picture of changes is the same.

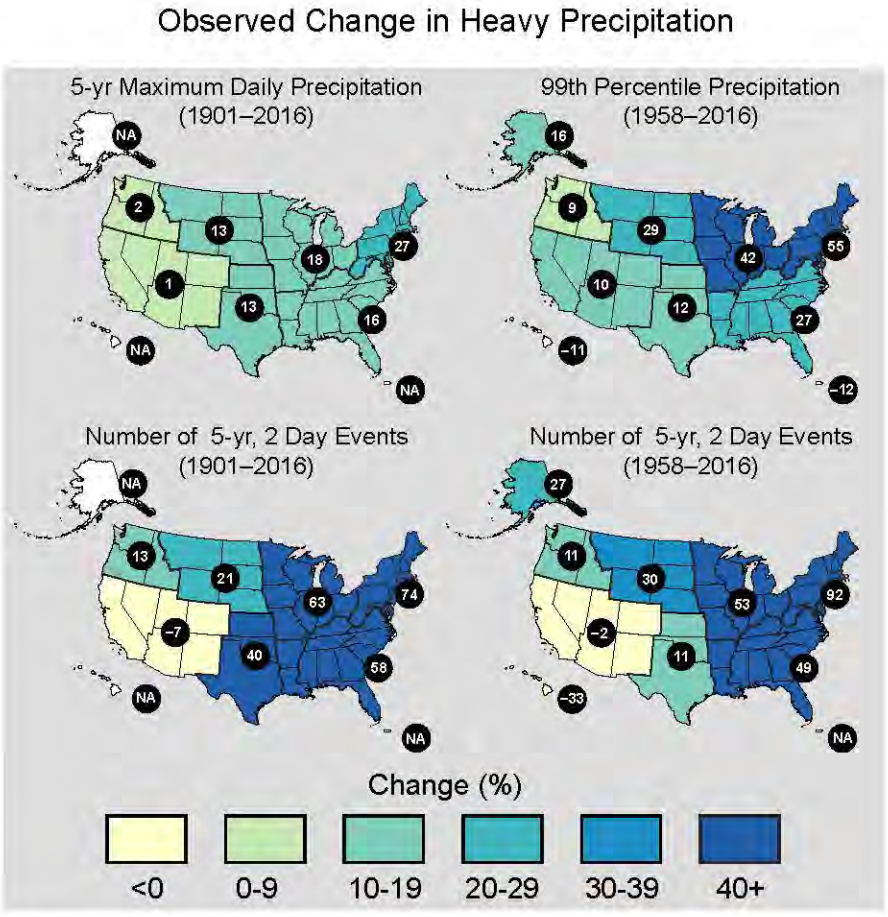

Figure 7.4: These maps show the change in several metrics of extreme precipitation by NCA4 region, including (upper left) the maximum daily precipitation in consecutive 5-year blocks, (upper right) the amount of precipitation falling in daily events that exceed the 99th percentile of all non-zero precipitation days, (lower left) the number of 2-day events with a precipitation total exceeding the largest 2-day amount that is expected to occur, on average, only once every 5 years, as calculated over 1901–2016, and (lower right) the number of 2-day events with a precipitation total exceeding the largest 2-day amount that is expected to occur, on average, only once every 5 years, as calculated over 1958–2016. The numerical value is the percent change over the entire period, either 1901–2016 or 1958–2016. The percentages are first calculated for individual stations, then averaged over 2° latitude by 2° longitude grid boxes, and finally averaged over each NCA4 region. Note that Alaska and Hawai'i are not included in the 1901–2016 maps owing to a lack of observations in the earlier part of the 20th century. (Figure source: CICS-NC and NOAA NCEI).

The national results shown in Figure 7.3 were disaggregated into regional values for two periods: 1901–2016 (Figure 7.4, lower left panel) and 1958–2016 (Figure 7.4, lower right panel) for comparison with Figure 7.4, upper right panel. As with the other metrics, there are large increases over the eastern half of the United States while the increases in the western United States are smaller and there are actually small decreases in the Southwest.

There are differences in the magnitude of changes among the four different regional metrics in Figure 7.4, but the overall picture is the same: large increases in the eastern half of the United States and smaller increases, or slight decreases, in the western United States.

7.1.4 Extratropical Cyclones and Mesoscale Convective Systems

As described in Chapter 9: Extreme Storms, there is uncertainty about future changes in winter extratropical cyclones (ETCs).[19] Thus, the potential effects on winter extreme precipitation events is also uncertain. Summertime ETC activity across North America has decreased since 1979, with a reduction of more than 35% in the number of strong summertime ETCs.[20] Most climate models simulate little change over this same historical period, but they project a decrease in summer ETC activity during the remainder of the 21st century.[20] This is potentially relevant to extreme precipitation in the northeastern quadrant of the United States because a large percentage of the extreme precipitation events in this region are caused by ETCs and their associated fronts.[21] This suggests that in the future there may be fewer opportunities in the summer for extreme precipitation, although increases in water vapor are likely to overcompensate for any decreases in ETCs by increasing the likelihood that an ETC will produce excessive rainfall amounts. A very idealized set of climate simulations[22] suggests that substantial projected warming will lead to a decrease in the number of ETCs but an increase in the intensity of the strongest ETCs. One factor potentially causing this model ETC intensification is an increase in latent heat release in these storms related to a moister atmosphere. Because of the idealized nature of these simulations, the implications of these results for the real earth–atmosphere system is uncertain. However, the increased latent heat mechanism is likely to occur given the high confidence in a future moister atmosphere. For eastern North America, CMIP5 simulations of the future indicate an increase in strong ETCs.[19] Thus, it is possible that the most extreme precipitation events associated with ETCs may increase in the future.

Mesoscale convective systems (MCSs), which contribute substantially to warm season precipitation in the tropics and subtropics,[23] account for about half of rainfall in the central United States.[24] Schumacher and Johnson[25] reported that 74% of all warm season extreme rain events over the eastern two-thirds of the United States during the period 1999–2003 were associated with an MCS. Feng et al.[26] found that large regions of the central United States experienced statistically significant upward trends in April–June MCS rainfall of 0.4–0.8 mm per day (approximately 20%–40%) per decade from 1979 to 2014. They further found upward trends in MCS frequency of occurrence, lifetime, and precipitation amount, which they attribute to an enhanced west-to-east pressure gradient (enhanced Great Plains low-level jet) and enhanced specific humidity throughout the eastern Great Plains.

7.1.5 Detection and Attribution

Trends

Detectability of trends (compared to internal variability) for a number of precipitation metrics over the continental United States has been examined; however, trends identified for the U.S. regions have not been clearly attribut-

ed to anthropogenic forcing.[27, 28] One study concluded that increasing precipitation trends in some north-central U.S. regions and the extreme annual anomalies there in 2013 were at least partly attributable to the combination of anthropogenic and natural forcing.[29]

There is *medium confidence* that anthropogenic forcing has contributed to global-scale intensification of heavy precipitation over land regions with sufficient data coverage.[30] Global changes in extreme precipitation have been attributed to anthropogenically forced climate change,[31, 32] including annual maximum 1-day and 5-day accumulated precipitation over Northern Hemisphere land regions and (relevant to this report) over the North American continent.[33] Although the United States was not separately assessed, the parts of North America with sufficient data for analysis included the continental United States and parts of southern Canada, Mexico, and Central America. Since the covered region was predominantly over the United States, these detection/attribution findings are applicable to the continental United States.

Analyses of precipitation extreme changes over the United States by region (20-year return values of seasonal daily precipitation over 1948–2015, Figure 7.2) show statistically significant increases consistent with theoretical expectations and previous analyses.[34] Further, a significant increase in the area affected by precipitation extremes over North America has also been detected.[35] There is likely an anthropogenic influence on the upward trend in heavy precipitation,[36] although models underestimate the magnitude of the trend. Extreme rainfall from U.S. landfalling tropical cyclones has been higher in recent years (1994–2008) than the long-term historical average, even accounting for temporal changes in storm frequency.[10]

Based on current evidence, it is concluded that detectable but not attributable increases in mean precipitation have occurred over parts of the central United States. Formal detection-attribution studies indicate a human contribution to extreme precipitation increases over the continental United States, but confidence is *low* based on those studies alone due to the short observational period, high natural variability, and model uncertainty.

In summary, based on available studies, it is concluded that for the continental United States there is *high confidence* in the detection of extreme precipitation increases, while there is *low confidence* in attributing the extreme precipitation changes purely to anthropogenic forcing. There is stronger evidence for a human contribution (*medium confidence*) when taking into account process-based understanding (increased water vapor in a warmer atmosphere), evidence from weather and climate models, and trends in other parts of the world.

Event Attribution

A number of recent heavy precipitation events have been examined to determine the degree to which their occurrence and severity can be attributed to human-induced climate change. Table 7.1 summarizes available attribution statements for recent extreme U.S. precipitation events. Seasonal and annual precipitation extremes occurring in the north-central and eastern U.S. regions in 2013 were examined for evidence of an anthropogenic influence on their occurrence.[29] Increasing trends in annual precipitation were detected in the northern tier of states, March–May precipitation in the upper Midwest, and June–August precipitation in the eastern United States since 1900. These trends are attributed to external forcing (anthropogenic and natural) but could not be directly attributed to anthropogenic forcing alone. However, based on this analysis, it is

Table 7.1. A list of U.S. extreme precipitation events for which attribution statements have been made. In the far right column, "+" indicates that an attributable human-induced increase in frequency and/or magnitude was found, "–" indicates that an attributable human-induced decrease in frequency and/or magnitude was found, "0" indicates no attributable human contribution was identified. As in Tables 6.1 and 8.2, several of the events were originally examined in the *Bulletin of the American Meteorological Society's* (BAMS) State of the Climate Reports and reexamined by Angélil et al.[76] In these cases, both attribution statements are listed with the original authors first. Source: M. Wehner.

Authors	Event year and duration	Region	Type	Attribution statement
Knutson et al. 2014[29] / Angélil et al. 2017[76]	ANN 2013	U.S. Northern Tier	Wet	+/0
Knutson et al. 2014[29] / Angélil et al. 2017[76]	MAM 2013	U.S. Upper Midwest	Wet	+/+
Knutson et al. 2014[29] / Angélil et al. 2017[76]	JJA 2013	Eastern U.S. Region	Wet	+/–
Edwards et al. 2014[77]	October 4–5, 2013	South Dakota	Blizzard	0
Hoerling et al. 2014[37]	September 10–14, 2013	Colorado	Wet	0
Pall et al. 2017[38]	September 10–14, 2013	Colorado	Wet	+
Northwest	3.66°F	4.67°F	4.99°F	8.51°F

concluded that the probability of these kinds of extremes has increased due to anthropogenic forcing.

The human influence on individual storms has been investigated with conflicting results. For example, in examining the attribution of the 2013 Colorado floods, one study finds that despite the expected human-induced increase in available moisture, the GEOS-5 model produces fewer extreme storms in the 1983–2012 period compared to the 1871–1900 period in Colorado during the fall season; the study attributes that behavior to changes in the large-scale circulation.[37] However, another study finds that such coarse models cannot produce the observed magnitude of precipitation due to resolution constraints.[38] Based on a highly conditional set of hindcast simulations imposing the large-scale meteorology and a substantial increase in both the probability and magnitude of the observed precipitation accumulation magnitudes in that particular meteorological situation, the study could not address the question of whether such situations have become more or less probable. Extreme precipitation event attribution is inherently limited by the rarity of the necessary meteorological conditions and the limited number of model simulations that can be performed to examine rare events. This remains an open and active area of research. However, based on these two studies, the anthropogenic contribution to the 2013 Colorado heavy rainfall-flood event is unclear.

An event attribution study of the potential influence of anthropogenic climate change on

the extreme 3-day rainfall event associated with flooding in Louisiana in August 2016[39] finds that such extreme rainfall events have become more likely since 1900. Model simulations of extreme rainfall suggest that anthropogenic forcing has increased the odds of such a 3-day extreme precipitation event by 40% or more.

7.2 Projections

Changes in precipitation in a warmer climate are governed by many factors. Although energy constraints can be used to understand global changes in precipitation, projecting regional changes is much more difficult because of uncertainty in projecting changes in the large-scale circulation that plays an important role in the formation of clouds and precipitation.[40] For the contiguous United States (CONUS), future changes in seasonal average precipitation will include a mix of increases, decreases, or little change, depending on location and season (Figure 7.5). High-latitude regions are generally projected to become wetter while the subtropical zone is projected to become drier. As the CONUS lies between these two regions, there is significant uncertainty about the sign and magnitude of future anthropogenic changes to seasonal precipitation in much of the region, particularly in the middle latitudes of the Nation. However, because the physical mechanisms controlling extreme precipitation differ from those controlling seasonal average precipitation (Section 7.1.4), in particular atmospheric water vapor will increase with increasing temperatures, confidence is *high* that precipitation extremes will increase in frequency and intensity in the future throughout the CONUS.

Global climate models used to project precipitation changes exhibit varying degrees of fidelity in capturing the observed climatology and seasonal variations of precipitation across the United States. Global or regional climate models with higher horizontal resolution generally achieve better skill than the CMIP5 models in capturing the spatial patterns and magnitude of winter precipitation in the western and southeastern United States (e.g., Mearns et al. 2012;[41] Wehner 2013;[42] Bacmeister et al. 2014;[43] Wehner et al. 2014[44]), leading to improved simulations of snowpack and runoff (e.g., Rauscher et al. 2008;[45] Rasmussen et al. 2011[46]). Simulation of present and future summer precipitation remains a significant challenge, as current convective parameterizations fail to properly represent the statistics of mesoscale convective systems.[47] As a result, high-resolution models that still require the parameterization of deep convection exhibit mixed results.[44, 48] Advances in computing technology are beginning to enable regional climate modeling at the higher resolutions (1–4 km), permitting the direct simulation of convective clouds systems (e.g., Ban et al. 2014[49]) and eliminating the need for this class of parameterization. However, projections from such models are not yet ready for inclusion in this report.

Important progress has been made by the climate modeling community in providing multimodel ensembles such as CMIP5[50] and NARCCAP[41] to characterize projection uncertainty arising from model differences and large ensemble simulations such as CESM-LE[51] to characterize uncertainty inherent in the climate system due to internal variability. These ensembles provide an important resource for examining the uncertainties in future precipitation projections.

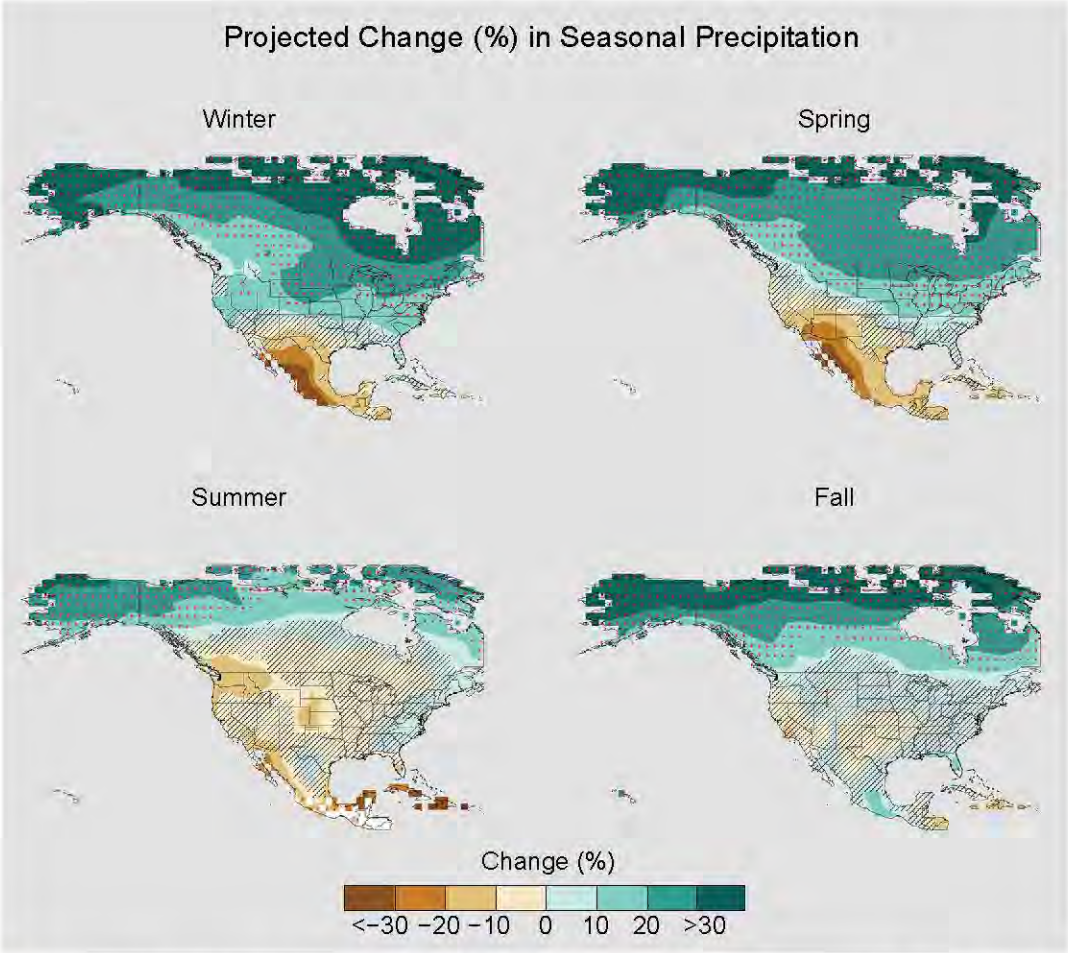

Figure 7.5: Projected change (%) in total seasonal precipitation from CMIP5 simulations for 2070–2099. The values are weighted multimodel means and expressed as the percent change relative to the 1976–2005 average. These are results for the higher scenario (RCP8.5). Stippling indicates that changes are assessed to be large compared to natural variations. Hatching indicates that changes are assessed to be small compared to natural variations. Blank regions (if any) are where projections are assessed to be inconclusive. Data source: World Climate Research Program's (WCRP's) Coupled Model Intercomparison Project. (Figure source: NOAA NCEI).

7.2.1 Future Changes in U.S. Seasonal Mean Precipitation

In the United States, projected changes in seasonal mean precipitation span the range from profound decreases to profound increases. In many regions and seasons, projected changes in precipitation are not large compared to natural variations. The general pattern of change is clear and consistent with theoretical expectations. Figure 7.5 shows the weighted CMIP5 multimodel average seasonal change at the end of the century compared to the present under the higher scenario (RCP8.5; see Ch. 4: Projections for discussion of RCPs). In this figure, changes projected with high confidence to be larger than natural variations are stippled. Regions where future changes are projected with high confidence to be smaller than natural variations are hatched. In winter and spring, the northern part of the country is projected to become wetter as the global climate warms. In the early to middle parts of this century, this will likely be manifested as increases in snowfall.[52] By the latter half of the century, as temperature continues to increase, it will be too warm to snow in many current snow-producing situations, and precipitation will mostly be rainfall. In the southwestern

United States, precipitation will decrease in the spring but the changes are only a little larger than natural variations. Many other regions of the country will not experience significant changes in average precipitation. This is also the case over most of the country in the summer and fall.

This pattern of projected precipitation change arises because of changes in locally available water vapor and weather system shifts. In the northern part of the continent, increases in water vapor, together with changes in circulation that are the result of expansion of the Hadley cell, bring more moisture to these latitudes while maintaining or increasing the frequency of precipitation-producing weather systems. This change in the Hadley circulation (see Ch. 5: Circulation and Variability for discussion of circulation changes) also causes the subtropics, the region between the northern and southern edges of the tropics and the midlatitudes (about 35° of latitude), to be drier in warmer climates as well as moving the mean storm track northward and away from the subtropics, decreasing the frequency of precipitation-producing systems. The combination of these two factors results in precipitation decreases in the southwestern United States, Mexico, and the Caribbean.[53]

Projected Changes In Snow

The Third National Climate Assessment[54] projected reductions in annual snowpack of up to 40% in the western United States based on the SRES A2 emissions scenario in the CMIP3 suite of climate model projections. Recent research using the CMIP5 suite of climate model projections forced with a higher scenario (RCP8.5) and statistically downscaled for the western United States continues to show the expected declines in various snow metrics, including snow water equivalent, the number of extreme snowfall events, and number of snowfall days.[55] A northward shift in the rain–snow transition zone in the central and eastern United States was found using statistically downscaled CMIP5 simulations forced with RCP8.5. By the end of the 21st century, large areas that are currently snow dominated in the cold season are expected to be rainfall dominated.[56]

The Variable Infiltration Capacity (VIC) model has been used to investigate the potential effects of climate change on SWE. Declines in SWE are projected in all western U.S. mountain ranges during the 21st century with the virtual disappearance of snowpack in the southernmost mountains by the end of the 21st century under both the lower (RCP4.5) and higher (RCP8.5) scenarios.[57] The projected decreases are most robust at the lower elevations of areas where snowpack accumulation is now reliable (for example, the Cascades and northern Sierra Nevada ranges). In these areas, future decreases in SWE are largely driven by increases in temperature. At higher (colder) elevations, projections are driven more by precipitation changes and are thus more uncertain.

7.2.2 Extremes

Heavy Precipitation Events

Studies project that the observed increase in heavy precipitation events will continue in the future (e.g. Janssen et al. 2014,[58] 2016[59]). Similar to observed changes, increases are expected in all regions, even those regions where total precipitation is projected to decline, such as the southwestern United States. Under the higher scenario (RCP8.5) the number of extreme events (exceeding a 5-year return period) increases by two to three times the historical average in every region (Figure 7.6) by the end of the 21st century, with the largest increases in the Northeast. Under the lower scenario (RCP4.5), increases are 50%–100%. Research shows that there is strong evidence, both from the observed record and modeling studies, that increased water vapor resulting from high-

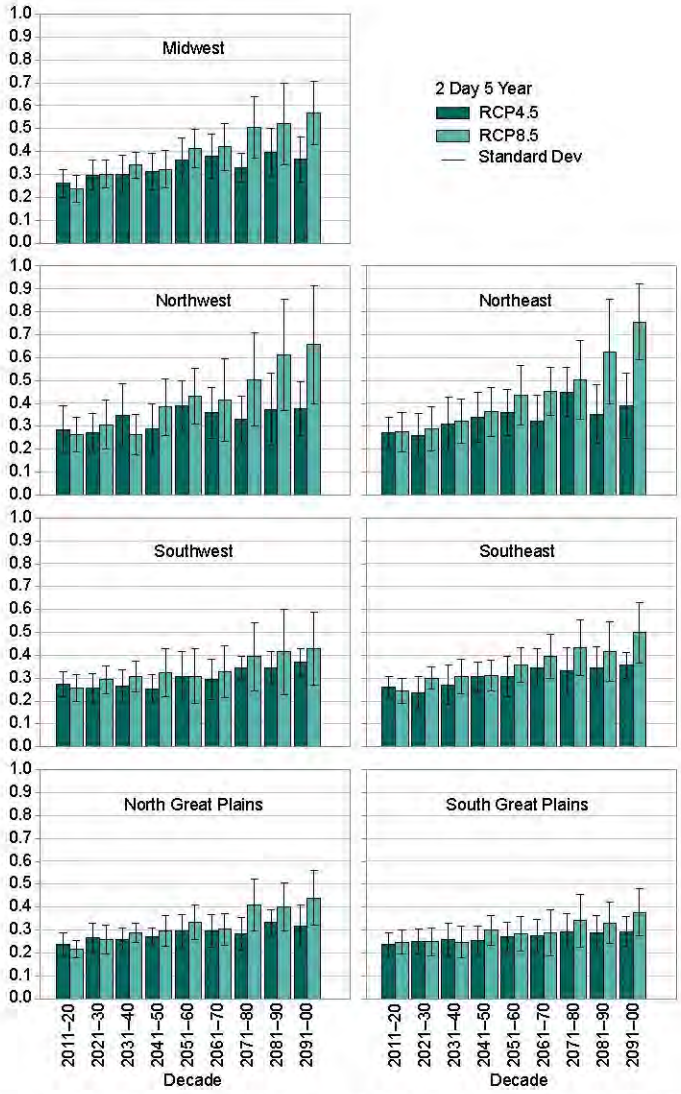

Figure 7.6: Regional extreme precipitation event frequency for a lower scenario (RCP4.5) (green; 16 CMIP5 models) and the higher scenario (RCP8.5) (blue; 14 CMIP5 models) for a 2-day duration and 5-year return. Calculated for 2006–2100 but decadal anomalies begin in 2011. Error bars are ±1 standard deviation; standard deviation is calculated from the 14 or 16 model values that represent the aggregated average over the regions, over the decades, and over the ensemble members of each model. The average frequency for the historical reference period is 0.2 by definition and the values in this graph should be interpreted with respect to a comparison with this historical average value. (Figure source: Janssen et al. 2014[58]).

er temperatures is the primary cause of the increases.[42, 60, 61] Additional effects on extreme precipitation due to changes in dynamical processes are poorly understood. However, atmospheric rivers (ARs), especially along the West Coast of the United States, are projected to increase in number and water vapor transport[62] and experience landfall at lower latitudes[63] by the end of the 21st century.

Projections of changes in the 20-year return period amount for daily precipitation (Figure 7.7) using LOcally Constructed Analogs (LOCA) downscaled data also show large percentage increases for both the middle and late 21st century. A lower scenario (RCP4.5) show increases of around 10% for mid-century and up to 14% for the late century projections. A higher scenario (RCP8.5) shows even larger increases for both mid- and late-century

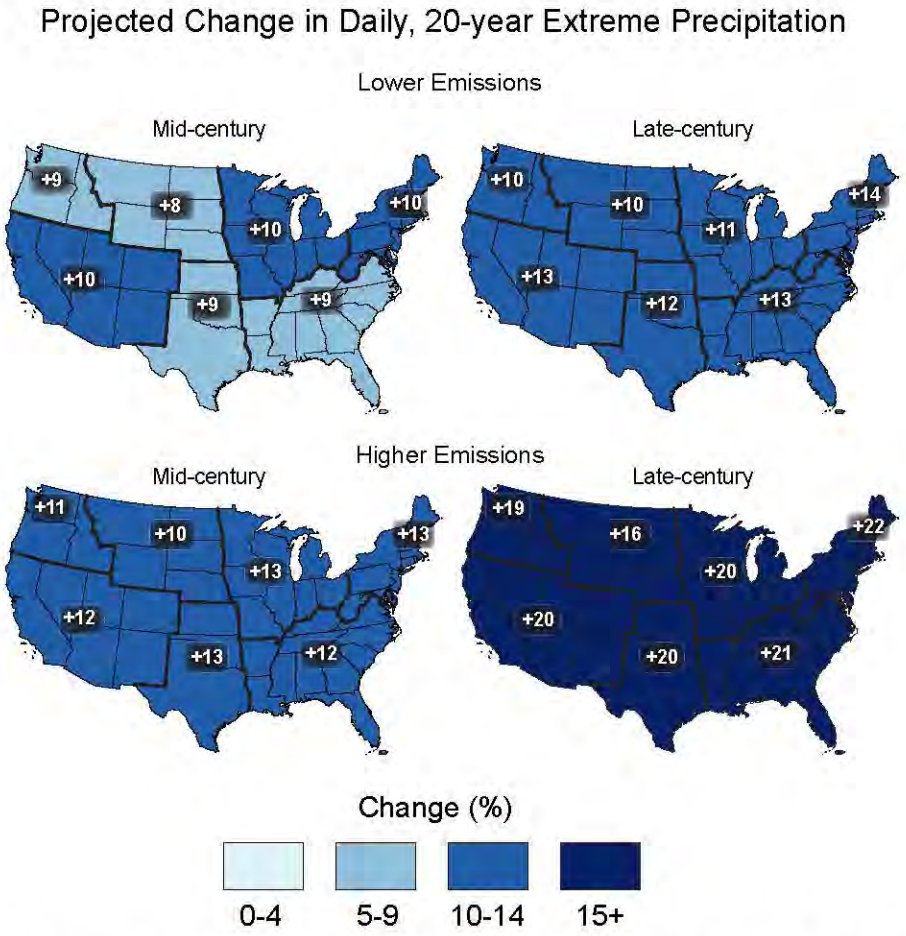

Figure 7.7: Projected change in the 20-year return period amount for daily precipitation for mid- (left maps) and late-21st century (right maps). Results are shown for a lower scenario (top maps; RCP4.5) and for a higher scenario (bottom maps, RCP8.5). These results are calculated from the LOCA downscaled data. (Figure source: CICS-NC and NOAA NCEI).

projections, with increases of around 20% by late 21st century. No region in either scenario shows a decline in heavy precipitation. The increases in extreme precipitation tend to increase with return level, such that increases for the 100-year return level are about 30% by the end of the century under a higher scenario (RCP8.5).

Projections of changes in the distribution of daily precipitation amounts (Figure 7.8) indicate an overall more extreme precipitation climate. Specifically, the projections indicate a slight increase in the numbers of dry days and the very lightest precipitation days and a large increase in the heaviest days. The number of days with precipitation amounts greater than the 95th percentile of all non-zero precipitation days increases by more than 25%. At the same time, the number of days with precipitation amounts in the 10th–80th percentile range decreases.

Most global climate models lack sufficient resolution to project changes in mesoscale convective systems (MCSs) in a changing climate.[64] However, research by Cook et al.[65] attempted to identify clues to changes in dynamical forcing that create MCSs. To do this, they examined the ability of 18 coupled ocean–atmosphere global climate models (GCMs) to simulate potential 21st century changes in warm-season flow and the associated U.S. Midwest hydrology resulting from increases in greenhouse gases. They selected a subset of six models that best captured the

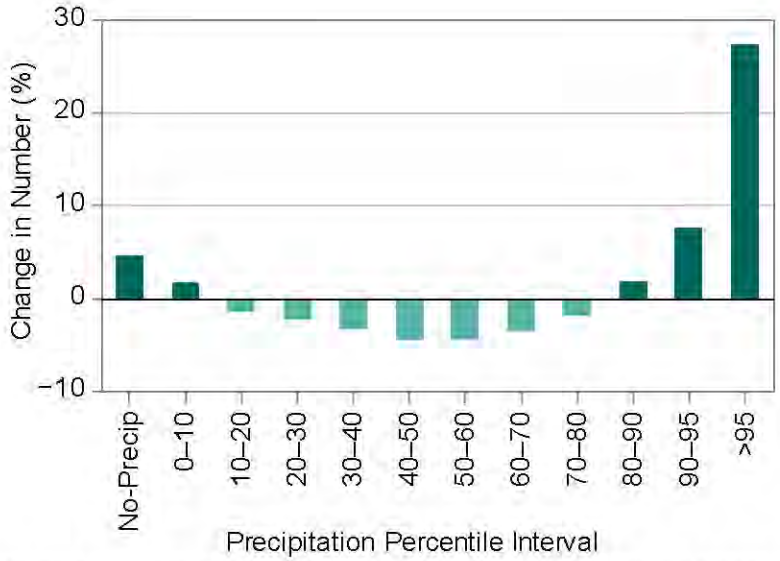

Figure 7.8: Projected change (percentage change relative to the 1976–2005 reference period average) in the number of daily zero ("No-Precip") and non-zero precipitation days (by percentile bins) for late-21st century under a higher scenario (RCP8.5). The precipitation percentile bin thresholds are based on daily non-zero precipitation amounts from the 1976–2005 reference period that have been ranked from low to high. These results are calculated from the LOCA downscaled data. (Figure source: CICS-NC and NOAA NCEI).

low-level flow and associated dynamics of the present-day climate of the central United States and then analyzed these models for changes due to enhanced greenhouse gas forcing. In each of these models, springtime precipitation increases significantly (by 20%–40%) in the upper Mississippi Valley and decreases to the south. The enhanced moisture convergence leading to modeled future climate rainfall increases in the U.S. Midwest is caused by meridional convergence at 850 hPa, connecting the rainfall changes with the Great Plains Low-Level Jet intensification.[66] This is consistent with findings from Feng et al.[26] in the observational record for the period 1979–2014 and by Pan et al.[67] by use of a regional climate model.

Changes in intense hourly precipitation events were simulated by Prein et al.[68] where they found the most intense hourly events (99.9 percentile) in the central United States increase at the expense of moderately intense (97.5 percentile) hourly events in the warm season. They also found the frequency of seasonal hourly precipitation extremes is expected to increase in all regions by up to five times in the same areas that show the highest increases in extreme precipitation rates.

Hurricane Precipitation

Regional model projections of precipitation from landfalling tropical cyclones over the United States, based on downscaling of CMIP5 model climate changes, suggest that the occurrence frequency of post-landfall tropical cyclones over the United States will change little compared to present day during the 21st century, as the reduced frequency of tropical cyclones over the Atlantic domain is mostly offset by a greater landfalling fraction. However, when downscaling from CMIP3 model climate changes, projections show a reduced occurrence frequency over U.S. land, indicating uncertainty about future outcomes. The average tropical cyclone rainfall rates within 500 km (about 311 miles) of the storm center increased by 8% to 17% in the simulations, which was at least as much as expected from the water vapor content increase factor alone.

Several studies have projected increases of precipitation rates within hurricanes over ocean regions,[69] particularly for the Atlantic basin.[70] The primary physical mechanism for this increase is the enhanced water vapor content in the warmer atmosphere, which enhances moisture convergence into the storm for a given circulation strength, although a more intense circulation can also contribute.[71] Since hurricanes are responsible for many of the most extreme precipitation events in the southeastern United States,[10, 21] such events are likely to be even heavier in the future. In a set of idealized forcing experiments, this effect was partly offset by differences in warming rates at the surface and at altitude.[72]

TRACEABLE ACCOUNTS

Key Finding 1

Annual precipitation has decreased in much of the West, Southwest, and Southeast and increased in most of the Northern and Southern Plains, Midwest, and Northeast. A national average increase of 4% in annual precipitation since 1901 is mostly a result of large increases in the fall season. (*Medium confidence*)

Description of evidence base

The key finding and supporting text summarizes extensive evidence documented in the climate science peer-reviewed literature. Evidence of long-term changes in precipitation is based on analysis of daily precipitation observations from the U.S. Cooperative Observer Network (http://www.nws.noaa.gov/om/coop/) and shown in Figure 7.1. Published work, such as the Third National Climate Assessment,[73] and Figure 7.1 show important regional and seasonal differences in U.S. precipitation change since 1901.

Major uncertainties

The main source of uncertainty is the sensitivity of observed precipitation trends to the spatial distribution of observing stations and to historical changes in station location, rain gauges, the local landscape, and observing practices. These issues are mitigated somewhat by new methods to produce spatial grids through time.[74]

Assessment of confidence based on evidence and agreement, including short description of nature of evidence and level of agreement

Based on the evidence and understanding of the issues leading to uncertainties, confidence is *medium* that average annual precipitation has increased in the United States. Furthermore, confidence is also *medium* that the important regional and seasonal differences in changes documented in the text and in Figure 7.1 are robust.

Summary sentence or paragraph that integrates the above information

Based on the patterns shown in Figure 7.1 and numerous additional studies of precipitation changes in the United States, there is *medium confidence* in the observed changes in annual and seasonal precipitation over the various regions and the United States as a whole.

Key Finding 2

Heavy precipitation events in most parts of the United States have increased in both intensity and frequency since 1901 (*high confidence*). There are important regional differences in trends, with the largest increases occurring in the northeastern United States (*high confidence*). In particular, mesoscale convective systems (organized clusters of thunderstorms)—the main mechanism for warm season precipitation in the central part of the United States—have increased in occurrence and precipitation amounts since 1979 (*medium confidence*).

Description of evidence base

The key finding and supporting text summarize extensive evidence documented in the climate science peer-reviewed literature. Numerous papers have been written documenting observed changes in heavy precipitation events in the United States, including those cited in the Third National Climate Assessment and in this assessment. Although station-based analyses (e.g., Westra et al. 2013[34]) do not show large numbers of statistically significant station-based trends, area averaging reduces the noise inherent in station-based data and produces robust increasing signals (see Figures 7.2 and 7.3). Evidence of long-term changes in precipitation is based on analysis of daily precipitation observations from the U.S. Cooperative Observer Network (http://www.nws.noaa.gov/om/coop/) and shown in Figures 7.2, 7.3, and 7.4.

Major uncertainties

The main source of uncertainty is the sensitivity of observed precipitation trends to the spatial distribution of observing stations and to historical changes in station location, rain gauges, and observing practices. These issues are mitigated somewhat by methods used to produce spatial grids through gridbox averaging.

Assessment of confidence based on evidence and agreement, including short description of nature of evidence and level of agreement

Based on the evidence and understanding of the issues leading to uncertainties, confidence is *high* that heavy precipitation events have increased in the United States. Furthermore, confidence is also *high* that the important regional and seasonal differences in changes documented in the text and in Figures 7.2, 7.3, and 7.4 are robust.

Summary sentence or paragraph that integrates the above information

Based on numerous analyses of the observed record in the United States there is *high confidence* in the observed changes in heavy precipitation events, and *medium confidence* in observed changes in mesoscale convective systems.

Key Finding 3

The frequency and intensity of heavy precipitation events are projected to continue to increase over the 21st century (*high confidence*). Mesoscale convective systems in the central United States are expected to continue to increase in number and intensity in the future (*medium confidence*). There are, however, important regional and seasonal differences in projected changes in total precipitation: the northern United States, including Alaska, is projected to receive more precipitation in the winter and spring, and parts of the southwestern United States are projected to receive less precipitation in the winter and spring (*medium confidence*).

Description of evidence base

Evidence for future changes in precipitation is based on climate model projections and our understanding of the climate system's response to increasing greenhouse gases and of regional mechanisms behind the projected changes. In particular, Figure 7.7 documents projected changes in the 20-year return period amount using the LOCA data, and Figure 7.6 shows changes in 2 day totals for the 5-year return period using the CMIP5 suite of models. Each figure shows robust changes in extreme precipitation events as they are defined in the figure. However, Figure 7.5, which shows changes in seasonal and annual precipitation, indicates where confidence in the changes is higher based on consistency between the models and that there are large areas where the projected change is uncertain.

Major uncertainties

A key issue is how well climate models simulate precipitation, which is one of the more challenging aspects of weather and climate simulation. In particular, comparisons of model projections for total precipitation (from both CMIP3 and CMIP5, see Sun et al. 2015[75]) by NCA3 region show a spread of responses in some regions (for example, the Southwest) such that they are opposite from the ensemble average response. The continental United States is positioned in the transition zone between expected drying in the subtropics and wetting in the mid- and higher-latitudes. There are some differences in the location of this transition between CMIP3 and CMIP5 models and thus there remains uncertainty in the exact location of the transition zone.

Assessment of confidence based on evidence and agreement, including short description of nature of evidence and level of agreement

Based on evidence from climate model simulations and our fundamental understanding of the relationship of water vapor to temperature, confidence is *high* that extreme precipitation will increase in all regions of the United States. However, based on the evidence and understanding of the issues leading to uncertainties, confidence is *medium* that that more total precipitation is projected for the northern U.S. and less for the Southwest.

Summary sentence or paragraph that integrates the above information

Based on numerous analyses of model simulations and our understanding of the climate system there is *high confidence* in the projected changes in precipitation extremes and *medium confidence* in projected changes in total precipitation over the United States.

Key Finding 4

Northern Hemisphere spring snow cover extent, North America maximum snow depth, snow water equivalent in the western United States, and extreme snowfall years in the southern and western United States have all declined, while extreme snowfall years in parts of the northern United States have increased (*medium confidence*). Projections indicate large declines in snowpack in the western United States and shifts to more precipitation falling as rain than snow in the cold season in many parts of the central and eastern United States (*high confidence*).

Description of evidence base

Evidence of historical changes in snow cover extent and a reduction in extreme snowfall years is consistent with our understanding of the climate system's response to increasing greenhouse gases. Furthermore, climate models continue to consistently show future declines in snowpack in the western United States. Recent model projections for the eastern United States also confirm a future shift from snowfall to rainfall during the cold season in colder portions of the central and eastern United States. Each of these changes is documented in the peer-reviewed literature and are cited in the main text of this chapter.

Major uncertainties

The main source of uncertainty is the sensitivity of observed snow changes to the spatial distribution of observing stations and to historical changes in station location, rain gauges, and observing practices, particularly for snow. Another key issue is the ability of climate models to simulate precipitation, particularly snow. Future changes in the frequency and intensity of meteorological systems causing heavy snow are less certain than temperature changes.

Assessment of confidence based on evidence and agreement, including short description of nature of evidence and level of agreement

Given the evidence base and uncertainties, confidence is *medium* that snow cover extent has declined in the United States and *medium* that extreme snowfall years have declined in recent years. Confidence is *high* that western United States snowpack will decline in the future, and confidence is *medium* that a shift from snow domination to rain domination will occur in the parts of the central and eastern United States cited in the text.

Summary sentence or paragraph that integrates the above information

Based on observational analyses of snow cover, depth, and water equivalent there is *medium confidence* in the observed changes, and based on model simulations for the future there is *high confidence* in snowpack declines in the western United States and *medium confidence* in the shift to rain from snow in the eastern United States.

REFERENCES

1. Walsh, J., D. Wuebbles, K. Hayhoe, J. Kossin, K. Kunkel, G. Stephens, P. Thorne, R. Vose, M. Wehner, J. Willis, D. Anderson, S. Doney, R. Feely, P. Hennon, V. Kharin, T. Knutson, F. Landerer, T. Lenton, J. Kennedy, and R. Somerville, 2014: Ch. 2: Our changing climate. *Climate Change Impacts in the United States: The Third National Climate Assessment*. Melillo, J.M., T.C. Richmond, and G.W. Yohe, Eds. U.S. Global Change Research Program, Washington, D.C., 19-67. http://dx.doi.org/10.7930/J0KW5CXT

2. NOAA, 2016: Climate at a Glance: Southwest PDSI. http://www.ncdc.noaa.gov/cag/time-series/us/107/0/pdsi/12/12/1895-2016?base_prd=true&firstbaseyear=1901&lastbaseyear=2000

3. Barnston, A.G. and B. Lyon, 2016: Does the NMME capture a recent decadal shift toward increasing drought occurrence in the southwestern United States? *Journal of Climate*, **29**, 561-581. http://dx.doi.org/10.1175/JCLI-D-15-0311.1

4. Seager, R., M. Hoerling, S. Schubert, H. Wang, B. Lyon, A. Kumar, J. Nakamura, and N. Henderson, 2015: Causes of the 2011–14 California drought. *Journal of Climate*, **28**, 6997-7024. http://dx.doi.org/10.1175/JCLI-D-14-00860.1

5. NOAA, 2016: Climate at a Glance: California PDSI. http://www.ncdc.noaa.gov/cag/time-series/us/4/0/pdsi/12/9/1895-2016?base_prd=true&firstbaseyear=1901&lastbaseyear=2000

6. Luce, C.H., J.T. Abatzoglou, and Z.A. Holden, 2013: The missing mountain water: Slower westerlies decrease orographic enhancement in the Pacific Northwest USA. *Science*, **342**, 1360-1364. http://dx.doi.org/10.1126/science.1242335

7. Vaughan, D.G., J.C. Comiso, I. Allison, J. Carrasco, G. Kaser, R. Kwok, P. Mote, T. Murray, F. Paul, J. Ren, E. Rignot, O. Solomina, K. Steffen, and T. Zhang, 2013: Observations: Cryosphere. *Climate Change 2013: The Physical Science Basis. Contribution of Working Group I to the Fifth Assessment Report of the Intergovernmental Panel on Climate Change*. Stocker, T.F., D. Qin, G.-K. Plattner, M. Tignor, S.K. Allen, J. Boschung, A. Nauels, Y. Xia, V. Bex, and P.M. Midgley, Eds. Cambridge University Press, Cambridge, United Kingdom and New York, NY, USA, 317–382. http://www.climatechange2013.org/report/full-report/

8. Kunkel, K.E., D.A. Robinson, S. Champion, X. Yin, T. Estilow, and R.M. Frankson, 2016: Trends and extremes in Northern Hemisphere snow characteristics. *Current Climate Change Reports*, **2**, 65-73. http://dx.doi.org/10.1007/s40641-016-0036-8

9. Kluver, D. and D. Leathers, 2015: Regionalization of snowfall frequency and trends over the contiguous United States. *International Journal of Climatology*, **35**, 4348-4358. http://dx.doi.org/10.1002/joc.4292

10. Kunkel, K.E., D.R. Easterling, D.A.R. Kristovich, B. Gleason, L. Stoecker, and R. Smith, 2010: Recent increases in U.S. heavy precipitation associated with tropical cyclones. *Geophysical Research Letters*, **37**, L24706. http://dx.doi.org/10.1029/2010GL045164

11. Bard, L. and D.A.R. Kristovich, 2012: Trend reversal in Lake Michigan contribution to snowfall. *Journal of Applied Meteorology and Climatology*, **51**, 2038-2046. http://dx.doi.org/10.1175/jamc-d-12-064.1

12. Hartnett, J.J., J.M. Collins, M.A. Baxter, and D.P. Chambers, 2014: Spatiotemporal snowfall trends in central New York. *Journal of Applied Meteorology and Climatology*, **53**, 2685-2697. http://dx.doi.org/10.1175/jamc-d-14-0084.1

13. Wright, D.M., D.J. Posselt, and A.L. Steiner, 2013: Sensitivity of lake-effect snowfall to lake ice cover and temperature in the Great Lakes region. *Monthly Weather Review*, **141**, 670-689. http://dx.doi.org/10.1175/mwr-d-12-00038.1

14. Vavrus, S., M. Notaro, and A. Zarrin, 2013: The role of ice cover in heavy lake-effect snowstorms over the Great Lakes Basin as simulated by RegCM4. *Monthly Weather Review*, **141**, 148-165. http://dx.doi.org/10.1175/mwr-d-12-00107.1

15. Pederson, G.T., J.L. Betancourt, and G.J. McCabe, 2013: Regional patterns and proximal causes of the recent snowpack decline in the Rocky Mountains, U.S. *Geophysical Research Letters*, **40**, 1811-1816. http://dx.doi.org/10.1002/grl.50424

16. Gan, T.Y., R.G. Barry, M. Gizaw, A. Gobena, and R. Balaji, 2013: Changes in North American snowpacks for 1979–2007 detected from the snow water equivalent data of SMMR and SSM/I passive microwave and related climatic factors. *Journal of Geophysical Research Atmospheres*, **118**, 7682–7697. http://dx.doi.org/10.1002/jgrd.50507

17. Lute, A.C. and J.T. Abatzoglou, 2014: Role of extreme snowfall events in interannual variability of snowfall accumulation in the western United States. *Water Resources Research*, **50**, 2874-2888. http://dx.doi.org/10.1002/2013WR014465

18. Belmecheri, S., F. Babst, E.R. Wahl, D.W. Stahle, and V. Trouet, 2016: Multi-century evaluation of Sierra Nevada snowpack. *Nature Climate Change*, **6**, 2-3. http://dx.doi.org/10.1038/nclimate2809

19. Colle, B.A., Z. Zhang, K.A. Lombardo, E. Chang, P. Liu, and M. Zhang, 2013: Historical evaluation and future prediction of eastern North American and western Atlantic extratropical cyclones in the CMIP5 models during the cool season. *Journal of Climate*, **26**, 6882-6903. http://dx.doi.org/10.1175/JCLI-D-12-00498.1

20. Chang, E.K.M., C.-G. Ma, C. Zheng, and A.M.W. Yau, 2016: Observed and projected decrease in Northern Hemisphere extratropical cyclone activity in summer and its impacts on maximum temperature. *Geophysical Research Letters*, **43**, 2200-2208. http://dx.doi.org/10.1002/2016GL068172

21. Kunkel, K.E., D.R. Easterling, D.A. Kristovich, B. Gleason, L. Stoecker, and R. Smith, 2012: Meteorological causes of the secular variations in observed extreme precipitation events for the conterminous United States. *Journal of Hydrometeorology*, **13**, 1131-1141. http://dx.doi.org/10.1175/JHM-D-11-0108.1

22. Pfahl, S., P.A. O'Gorman, and M.S. Singh, 2015: Extratropical cyclones in idealized simulations of changed climates. *Journal of Climate*, **28**, 9373-9392. http://dx.doi.org/10.1175/JCLI-D-14-00816.1

23. Nesbitt, S.W., R. Cifelli, and S.A. Rutledge, 2006: Storm morphology and rainfall characteristics of TRMM precipitation features. *Monthly Weather Review*, **134**, 2702-2721. http://dx.doi.org/10.1175/mwr3200.1

24. Fritsch, J.M., R.J. Kane, and C.R. Chelius, 1986: The contribution of mesoscale convective weather systems to the warm-season precipitation in the United States. *Journal of Climate and Applied Meteorology*, **25**, 1333-1345. http://dx.doi.org/10.1175/1520-0450(1986)025<1333:tcomcw>2.0.co;2

25. Schumacher, R.S. and R.H. Johnson, 2006: Characteristics of U.S. extreme rain events during 1999–2003. *Weather and Forecasting*, **21**, 69-85. http://dx.doi.org/10.1175/waf900.1

26. Feng, Z., L.R. Leung, S. Hagos, R.A. Houze, C.D. Burleyson, and K. Balaguru, 2016: More frequent intense and long-lived storms dominate the springtime trend in central US rainfall. *Nature Communications*, **7**, 13429. http://dx.doi.org/10.1038/ncomms13429

27. Anderson, B.T., D.J. Gianotti, and G.D. Salvucci, 2015: Detectability of historical trends in station-based precipitation characteristics over the continental United States. *Journal of Geophysical Research Atmospheres*, **120**, 4842-4859. http://dx.doi.org/10.1002/2014JD022960

28. Easterling, D.R., K.E. Kunkel, M.F. Wehner, and L. Sun, 2016: Detection and attribution of climate extremes in the observed record. *Weather and Climate Extremes*, **11**, 17-27. http://dx.doi.org/10.1016/j.wace.2016.01.001

29. Knutson, T.R., F. Zeng, and A.T. Wittenberg, 2014: Seasonal and annual mean precipitation extremes occurring during 2013: A U.S. focused analysis [in "Explaining Extreme Events of 2013 from a Climate Perspective"]. *Bulletin of the American Meteorological Society*, **95 (9)**, S19-S23. http://dx.doi.org/10.1175/1520-0477-95.9.S1.1

30. Bindoff, N.L., P.A. Stott, K.M. AchutaRao, M.R. Allen, N. Gillett, D. Gutzler, K. Hansingo, G. Hegerl, Y. Hu, S. Jain, I.I. Mokhov, J. Overland, J. Perlwitz, R. Sebbari, and X. Zhang, 2013: Detection and attribution of climate change: From global to regional. *Climate Change 2013: The Physical Science Basis. Contribution of Working Group I to the Fifth Assessment Report of the Intergovernmental Panel on Climate Change*. Stocker, T.F., D. Qin, G.-K. Plattner, M. Tignor, S.K. Allen, J. Boschung, A. Nauels, Y. Xia, V. Bex, and P.M. Midgley, Eds. Cambridge University Press, Cambridge, United Kingdom and New York, NY, USA, 867–952. http://www.climatechange2013.org/report/full-report/

31. Min, S.K., X. Zhang, F.W. Zwiers, and G.C. Hegerl, 2011: Human contribution to more-intense precipitation extremes. *Nature*, **470**, 378-381. http://dx.doi.org/10.1038/nature09763

32. Min, S.-K., X. Zhang, F. Zwiers, H. Shiogama, Y.-S. Tung, and M. Wehner, 2013: Multimodel detection and attribution of extreme temperature changes. *Journal of Climate*, **26**, 7430-7451. http://dx.doi.org/10.1175/JCLI-D-12-00551.1

33. Zhang, X., H. Wan, F.W. Zwiers, G.C. Hegerl, and S.-K. Min, 2013: Attributing intensification of precipitation extremes to human influence. *Geophysical Research Letters*, **40**, 5252-5257. http://dx.doi.org/10.1002/grl.51010

34. Westra, S., L.V. Alexander, and F.W. Zwiers, 2013: Global increasing trends in annual maximum daily precipitation. *Journal of Climate*, **26**, 3904-3918. http://dx.doi.org/10.1175/JCLI-D-12-00502.1

35. Dittus, A.J., D.J. Karoly, S.C. Lewis, and L.V. Alexander, 2015: A multiregion assessment of observed changes in the areal extent of temperature and precipitation extremes. *Journal of Climate*, **28**, 9206-9220. http://dx.doi.org/10.1175/JCLI-D-14-00753.1

36. Dittus, A.J., D.J. Karoly, S.C. Lewis, L.V. Alexander, and M.G. Donat, 2016: A multiregion model evaluation and attribution study of historical changes in the area affected by temperature and precipitation extremes. *Journal of Climate*, **29**, 8285-8299. http://dx.doi.org/10.1175/jcli-d-16-0164.1

37. Hoerling, M., K. Wolter, J. Perlwitz, X. Quan, J. Eischeid, H. Want, S. Schubert, H. Diaz, and R. Dole, 2014: Northeast Colorado extreme rains interpreted in a climate change context [in "Explaining Extreme Events of 2013 from a Climate Perspective"]. *Bulletin of the American Meteorological Society*, **95 (9)**, S15-S18. http://dx.doi.org/10.1175/1520-0477-95.9.S1.1

38. Pall, P.C.M.P., M.F. Wehner, D.A. Stone, C.J. Paciorek, and W.D. Collins, 2017: Diagnosing anthropogenic contributions to heavy Colorado rainfall in September 2013. *Weather and Climate Extremes*, **17**, 1-6. http://dx.doi.org/10.1016/j.wace.2017.03.004

39. van der Wiel, K., S.B. Kapnick, G.J. van Oldenborgh, K. Whan, S. Philip, G.A. Vecchi, R.K. Singh, J. Arrighi, and H. Cullen, 2017: Rapid attribution of the August 2016 flood-inducing extreme precipitation in south Louisiana to climate change. *Hydrology and Earth System Sciences*, **21**, 897-921. http://dx.doi.org/10.5194/hess-21-897-2017

40. Shepherd, T.G., 2014: Atmospheric circulation as a source of uncertainty in climate change projections. *Nature Geoscience*, **7**, 703-708. http://dx.doi.org/10.1038/ngeo2253

41. Mearns, L.O., R. Arritt, S. Biner, M.S. Bukovsky, S. Stain, S. Sain, D. Caya, J. Correia, Jr., D. Flory, W. Gutowski, E.S. Takle, R. Jones, R. Leung, W. Moufouma-Okia, L. McDaniel, A.M.B. Nunes, Y. Qian, J. Roads, L. Sloan, and M. Snyder, 2012: The North American regional climate change assessment program: Overview of phase I results. *Bulletin of the American Meteorological Society*, **93**, 1337-1362. http://dx.doi.org/10.1175/BAMS-D-11-00223.1

42. Wehner, M.F., 2013: Very extreme seasonal precipitation in the NARCCAP ensemble: Model performance and projections. *Climate Dynamics*, **40**, 59-80. http://dx.doi.org/10.1007/s00382-012-1393-1

43. Bacmeister, J.T., M.F. Wehner, R.B. Neale, A. Gettelman, C. Hannay, P.H. Lauritzen, J.M. Caron, and J.E. Truesdale, 2014: Exploratory high-resolution climate simulations using the Community Atmosphere Model (CAM). *Journal of Climate*, **27**, 3073-3099. http://dx.doi.org/10.1175/JCLI-D-13-00387.1

44. Wehner, M.F., K.A. Reed, F. Li, Prabhat, J. Bacmeister, C.-T. Chen, C. Paciorek, P.J. Gleckler, K.R. Sperber, W.D. Collins, A. Gettelman, and C. Jablonowski, 2014: The effect of horizontal resolution on simulation quality in the Community Atmospheric Model, CAM5.1. *Journal of Advances in Modeling Earth Systems*, **6**, 980-997. http://dx.doi.org/10.1002/2013MS000276

45. Rauscher, S.A., J.S. Pal, N.S. Diffenbaugh, and M.M. Benedetti, 2008: Future changes in snowmelt-driven runoff timing over the western US. *Geophysical Research Letters*, **35**, L16703. http://dx.doi.org/10.1029/2008GL034424

46. Rasmussen, R., C. Liu, K. Ikeda, D. Gochis, D. Yates, F. Chen, M. Tewari, M. Barlage, J. Dudhia, W. Yu, K. Miller, K. Arsenault, V. Grubišić, G. Thompson, and E. Gutmann, 2011: High-resolution coupled climate runoff simulations of seasonal snowfall over Colorado: A process study of current and warmer climate. *Journal of Climate*, **24**, 3015-3048. http://dx.doi.org/10.1175/2010JCLI3985.1

47. Boyle, J. and S.A. Klein, 2010: Impact of horizontal resolution on climate model forecasts of tropical precipitation and diabatic heating for the TWP-ICE period. *Journal of Geophysical Research*, **115**, D23113. http://dx.doi.org/10.1029/2010JD014262

48. Sakaguchi, K., L.R. Leung, C. Zhao, Q. Yang, J. Lu, S. Hagos, S.A. Rauscher, L. Dong, T.D. Ringler, and P.H. Lauritzen, 2015: Exploring a multiresolution approach using AMIP simulations. *Journal of Climate*, **28**, 5549-5574. http://dx.doi.org/10.1175/JCLI-D-14-00729.1

49. Ban, N., J. Schmidli, and C. Schär, 2014: Evaluation of the convection-resolving regional climate modeling approach in decade-long simulations. *Journal of Geophysical Research Atmospheres*, **119**, 7889-7907. http://dx.doi.org/10.1002/2014JD021478

50. Taylor, K.E., R.J. Stouffer, and G.A. Meehl, 2012: An overview of CMIP5 and the experiment design. *Bulletin of the American Meteorological Society*, **93**, 485-498. http://dx.doi.org/10.1175/BAMS-D-11-00094.1

51. Kay, J.E., C. Deser, A. Phillips, A. Mai, C. Hannay, G. Strand, J.M. Arblaster, S.C. Bates, G. Danabasoglu, J. Edwards, M. Holland, P. Kushner, J.-F. Lamarque, D. Lawrence, K. Lindsay, A. Middleton, E. Munoz, R. Neale, K. Oleson, L. Polvani, and M. Vertenstein, 2015: The Community Earth System Model (CESM) large ensemble project: A community resource for studying climate change in the presence of internal climate variability. *Bulletin of the American Meteorological Society*, **96 (12)**, 1333-1349. http://dx.doi.org/10.1175/BAMS-D-13-00255.1

52. O'Gorman, P.A., 2014: Contrasting responses of mean and extreme snowfall to climate change. *Nature*, **512**, 416-418. http://dx.doi.org/10.1038/nature13625

53. Collins, M., R. Knutti, J. Arblaster, J.-L. Dufresne, T. Fichefet, P. Friedlingstein, X. Gao, W.J. Gutowski, T. Johns, G. Krinner, M. Shongwe, C. Tebaldi, A.J. Weaver, and M. Wehner, 2013: Long-term climate change: Projections, commitments and irreversibility. *Climate Change 2013: The Physical Science Basis. Contribution of Working Group I to the Fifth Assessment Report of the Intergovernmental Panel on Climate Change*. Stocker, T.F., D. Qin, G.-K. Plattner, M. Tignor, S.K. Allen, J. Boschung, A. Nauels, Y. Xia, V. Bex, and P.M. Midgley, Eds. Cambridge University Press, Cambridge, United Kingdom and New York, NY, USA, 1029–1136. http://www.climatechange2013.org/report/full-report/

54. Georgakakos, A., P. Fleming, M. Dettinger, C. Peters-Lidard, T.C. Richmond, K. Reckhow, K. White, and D. Yates, 2014: Ch. 3: Water resources. *Climate Change Impacts in the United States: The Third National Climate Assessment*. Melillo, J.M., T.C. Richmond, and G.W. Yohe, Eds. U.S. Global Change Research Program, Washington, D.C., 69-112. http://dx.doi.org/10.7930/J0G44N6T

55. Lute, A.C., J.T. Abatzoglou, and K.C. Hegewisch, 2015: Projected changes in snowfall extremes and interannual variability of snowfall in the western United States. *Water Resources Research*, **51**, 960-972. http://dx.doi.org/10.1002/2014WR016267

56. Ning, L. and R.S. Bradley, 2015: Snow occurrence changes over the central and eastern United States under future warming scenarios. *Scientific Reports*, **5**, 17073. http://dx.doi.org/10.1038/srep17073

57. Gergel, D.R., B. Nijssen, J.T. Abatzoglou, D.P. Lettenmaier, and M.R. Stumbaugh, 2017: Effects of climate change on snowpack and fire potential in the western USA. *Climatic Change*, **141**, 287-299. http://dx.doi.org/10.1007/s10584-017-1899-y

58. Janssen, E., D.J. Wuebbles, K.E. Kunkel, S.C. Olsen, and A. Goodman, 2014: Observational- and model-based trends and projections of extreme precipitation over the contiguous United States. *Earth's Future*, **2**, 99-113. http://dx.doi.org/10.1002/2013EF000185

59. Janssen, E., R.L. Sriver, D.J. Wuebbles, and K.E. Kunkel, 2016: Seasonal and regional variations in extreme precipitation event frequency using CMIP5. *Geophysical Research Letters*, **43**, 5385-5393. http://dx.doi.org/10.1002/2016GL069151

60. Kunkel, K.E., T.R. Karl, H. Brooks, J. Kossin, J. Lawrimore, D. Arndt, L. Bosart, D. Changnon, S.L. Cutter, N. Doesken, K. Emanuel, P.Y. Groisman, R.W. Katz, T. Knutson, J. O'Brien, C.J. Paciorek, T.C. Peterson, K. Redmond, D. Robinson, J. Trapp, R. Vose, S. Weaver, M. Wehner, K. Wolter, and D. Wuebbles, 2013: Monitoring and understanding trends in extreme storms: State of knowledge. *Bulletin of the American Meteorological Society*, **94**, 499–514. http://dx.doi.org/10.1175/BAMS-D-11-00262.1

61. Kunkel, K.E., T.R. Karl, D.R. Easterling, K. Redmond, J. Young, X. Yin, and P. Hennon, 2013: Probable maximum precipitation and climate change. *Geophysical Research Letters*, **40**, 1402-1408. http://dx.doi.org/10.1002/grl.50334

62. Dettinger, M., 2011: Climate change, atmospheric rivers, and floods in California–a multimodel analysis of storm frequency and magnitude changes. *Journal of the American Water Resources Association*, **47**, 514-523. http://dx.doi.org/10.1111/j.1752-1688.2011.00546.x

63. Shields, C.A. and J.T. Kiehl, 2016: Atmospheric river landfall-latitude changes in future climate simulations. *Geophysical Research Letters*, **43**, 8775-8782. http://dx.doi.org/10.1002/2016GL070470

64. Kooperman, G.J., M.S. Pritchard, and R.C.J. Somerville, 2013: Robustness and sensitivities of central U.S. summer convection in the super-parameterized CAM: Multi-model intercomparison with a new regional EOF index. *Geophysical Research Letters*, **40**, 3287-3291. http://dx.doi.org/10.1002/grl.50597

65. Cook, K.H., E.K. Vizy, Z.S. Launer, and C.M. Patricola, 2008: Springtime intensification of the Great Plains low-level jet and midwest precipitation in GCM simulations of the twenty-first century. *Journal of Climate*, **21**, 6321-6340. http://dx.doi.org/10.1175/2008jcli2355.1

66. Higgins, R.W., Y. Yao, E.S. Yarosh, J.E. Janowiak, and K.C. Mo, 1997: Influence of the Great Plains low-level jet on summertime precipitation and moisture transport over the central United States. *Journal of Climate*, **10**, 481-507. http://dx.doi.org/10.1175/1520-0442(1997)010<0481:iotgpl>2.0.co;2

67. Pan, Z., R.W. Arritt, E.S. Takle, W.J. Gutowski, Jr., C.J. Anderson, and M. Segal, 2004: Altered hydrologic feedback in a warming climate introduces a "warming hole". *Geophysical Research Letters*, **31**, L17109. http://dx.doi.org/10.1029/2004GL020528

68. Prein, A.F., R.M. Rasmussen, K. Ikeda, C. Liu, M.P. Clark, and G.J. Holland, 2017: The future intensification of hourly precipitation extremes. *Nature Climate Change*, **7**, 48-52. http://dx.doi.org/10.1038/nclimate3168

69. Knutson, T.R., J.L. McBride, J. Chan, K. Emanuel, G. Holland, C. Landsea, I. Held, J.P. Kossin, A.K. Srivastava, and M. Sugi, 2010: Tropical cyclones and climate change. *Nature Geoscience*, **3**, 157-163. http://dx.doi.org/10.1038/ngeo779

70. Knutson, T.R., J.J. Sirutis, G.A. Vecchi, S. Garner, M. Zhao, H.-S. Kim, M. Bender, R.E. Tuleya, I.M. Held, and G. Villarini, 2013: Dynamical downscaling projections of twenty-first-century Atlantic hurricane activity: CMIP3 and CMIP5 model-based scenarios. *Journal of Climate*, **27**, 6591-6617. http://dx.doi.org/10.1175/jcli-d-12-00539.1

71. Wang, C.-C., B.-X. Lin, C.-T. Chen, and S.-H. Lo, 2015: Quantifying the effects of long-term climate change on tropical cyclone rainfall using a cloud-resolving model: Examples of two landfall typhoons in Taiwan. *Journal of Climate*, **28**, 66-85. http://dx.doi.org/10.1175/JCLI-D-14-00044.1

72. Villarini, G., D.A. Lavers, E. Scoccimarro, M. Zhao, M.F. Wehner, G.A. Vecchi, T.R. Knutson, and K.A. Reed, 2014: Sensitivity of tropical cyclone rainfall to idealized global-scale forcings. *Journal of Climate*, **27**, 4622-4641. http://dx.doi.org/10.1175/JCLI-D-13-00780.1

73. Melillo, J.M., T.C. Richmond, and G.W. Yohe, eds., 2014: *Climate Change Impacts in the United States: The Third National Climate Assessment*. U.S. Global Change Research Program: Washington, D.C., 841 pp. http://dx.doi.org/10.7930/J0Z31WJ2

74. Vose, R.S., S. Applequist, M. Squires, I. Durre, M.J. Menne, C.N. Williams, Jr., C. Fenimore, K. Gleason, and D. Arndt, 2014: Improved historical temperature and precipitation time series for U.S. climate divisions. *Journal of Applied Meteorology and Climatology*, **53**, 1232-1251. http://dx.doi.org/10.1175/JAMC-D-13-0248.1

75. Sun, L., K.E. Kunkel, L.E. Stevens, A. Buddenberg, J.G. Dobson, and D.R. Easterling, 2015: Regional Surface Climate Conditions in CMIP3 and CMIP5 for the United States: Differences, Similarities, and Implications for the U.S. National Climate Assessment. NOAA Technical Report NESDIS 144. National Oceanic and Atmospheric Administration, National Environmental Satellite, Data, and Information Service, 111 pp. http://dx.doi.org/10.7289/V5RB72KG

76. Angélil, O., D. Stone, M. Wehner, C.J. Paciorek, H. Krishnan, and W. Collins, 2017: An independent assessment of anthropogenic attribution statements for recent extreme temperature and rainfall events. *Journal of Climate*, **30**, 5-16. http://dx.doi.org/10.1175/JCLI-D-16-0077.1

77. Edwards, L.M., M. Bunkers, J.T. Abatzoglou, D.P. Todey, and L.E. Parker, 2014: October 2013 blizzard in western South Dakota [in "Explaining Extreme Events of 2013 from a Climate Perspective"]. *Bulletin of the American Meteorological Society*, **95 (9)**, S23-S26. http://dx.doi.org/10.1175/1520-0477-95.9.S1.1

78. Peterson, T.C., R.R. Heim, R. Hirsch, D.P. Kaiser, H. Brooks, N.S. Diffenbaugh, R.M. Dole, J.P. Giovannettone, K. Guirguis, T.R. Karl, R.W. Katz, K. Kunkel, D. Lettenmaier, G.J. McCabe, C.J. Paciorek, K.R. Ryberg, S. Schubert, V.B.S. Silva, B.C. Stewart, A.V. Vecchia, G. Villarini, R.S. Vose, J. Walsh, M. Wehner, D. Wolock, K. Wolter, C.A. Woodhouse, and D. Wuebbles, 2013: Monitoring and understanding changes in heat waves, cold waves, floods and droughts in the United States: State of knowledge. *Bulletin of the American Meteorological Society*, **94**, 821-834. http://dx.doi.org/10.1175/BAMS-D-12-00066.1

Assessment of erosion, sedimentation, and water quality impacts of the Mountain Valley Pipeline and Equitrans Expansion Project's proposed crossing of the Jefferson National Forest as it pertains to the U.S. Forest Service's Draft Supplemental Environmental Impact Statement dated December 2022

Prepared by Jonathan A. Czuba, Ph.D., Licensed Professional Engineer - February 9, 2023

REFERENCES
30

February 21, 2023

Town of Blacksburg

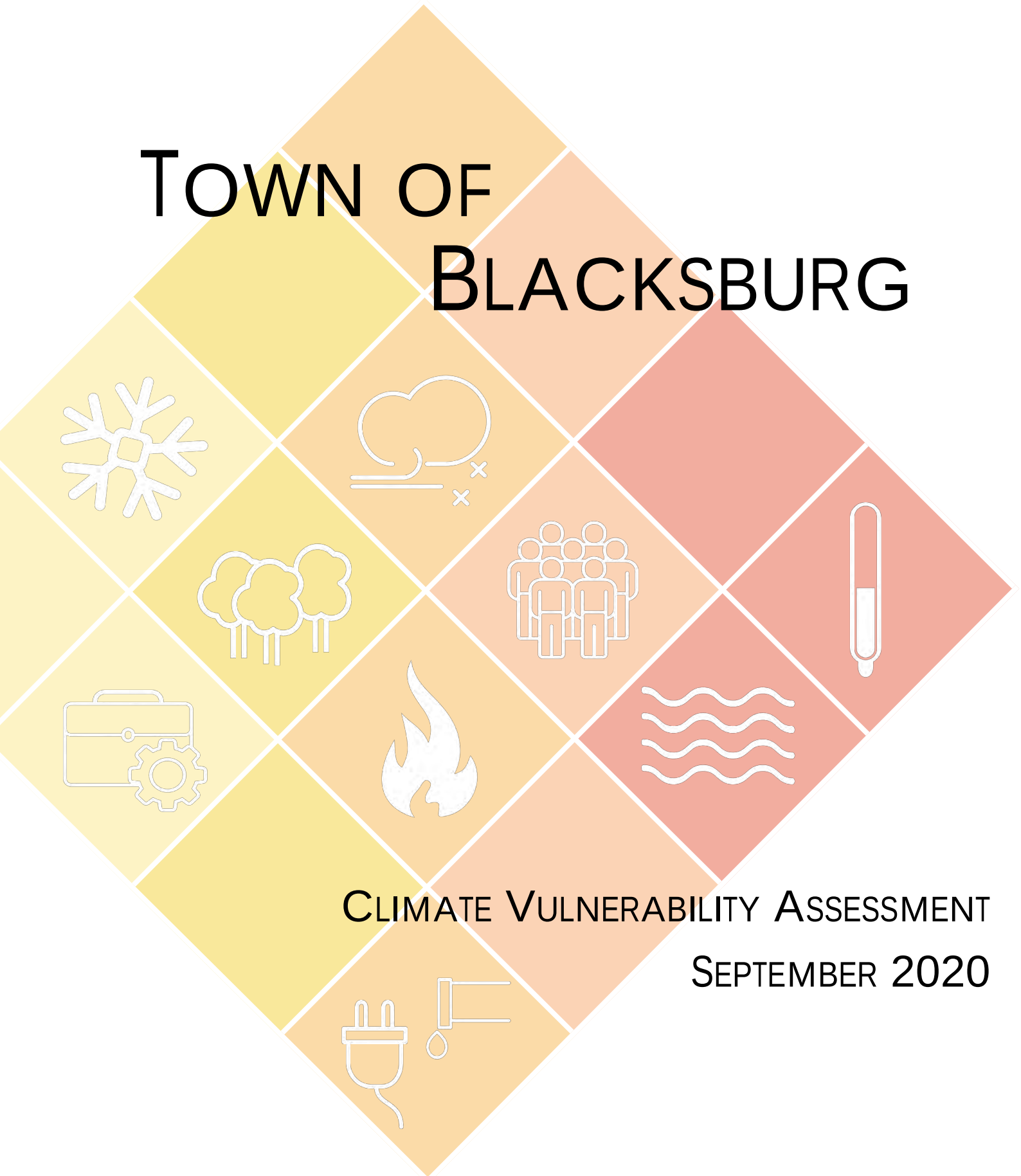

Climate Vulnerability Assessment

September 2020

Table of Contents

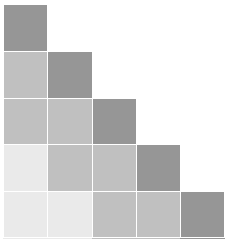

Introduction & Background

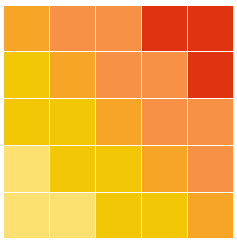

Hotter Summers

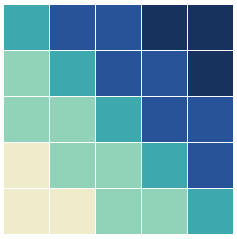

Warmer Winters

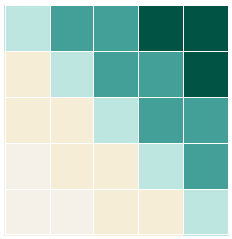

Changing Precipitation Patterns

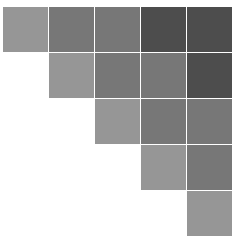

Sources, Conclusion & Next Steps

Message from Mayor Leslie Hager-Smith

Blacksburg is proud to be counted among the hundreds of local governments across America that are taking action to address climate change, while making their communities healthier and more resilient. We have long recognized our fundamental responsibility to take stock of our share of the planet's greenhouse gas emissions and hold up our end of the bargain to ensure a stable climate for future generations. One key way we are doing that is by integrating goals from Blacksburg's 2016 Climate Action Plan into its Comprehensive Plan, which will elevate climate priorities into future land-use, infrastructure, and transportation decision.

We also know that reducing emissions, while critically important, will not be enough. As a global community, we have been burning fossil fuels at an ever-accelerating pace since the advent of the industrial revolution. Those emissions are already in our atmosphere and we will have to contend with a certain amount of climate change that is already baked in.

Stressors like poverty, inequality, public health challenges, economic volatility, and environmental degradation will almost certainly be made worse by a changing climate. These changes have the potential to disrupt our lives and livelihoods in numerous ways, and we know we will need to adapt. For Blacksburg to do that, we need to first assess which community systems might be at risk. We also recognize that the needs of people who are likely to be hurt first and worst by climate change should be prioritized in our future plans for climate adaptation.

To become a truly climate-resilient community, Blacksburg has to do three things: continue to act boldly to reduce our greenhouse gas emissions; begin adapting to changes that cannot be avoided under a low-emissions scenario; and, pro-actively plan for how we might respond to the challenges of a high-emissions scenario. The good news is, climate mitigation and adaptation strategies can work in concert, providing benefits that align with community goals around affordable housing, resilient natural systems, expanded transportation options, and thriving civic spaces.

As I reflect on the ways in which Blacksburg has come together so many times in the past to overcome daunting challenges, I know we are equal to the task ahead of us.

Leslie Hager-Smith

Mayor of Blacksburg, VA

Centering Equity

Centering Equity in Climate Adaptation and Resiliency Planning & Implementation

Climate change does not affect everyone equally. In evaluating potential impacts a key consideration is to recognize that some people will be disproportionately worse off than others. These groups are commonly referred to as "vulnerable populations" or "marginalized groups." For the purposes of this report, they will be identified as **FRONTLINE COMMUNITIES**, because it is they who will be on the front lines of the unfolding climate emergency. Factors that increase the potential impact of climate hazards on individuals include:

- Age factors (very young and very old people are more vulnerable to heat stress)
- Complex health challenges -or- mobility, sensory or cognitive impairments
- Limited social connections or support networks
- Limited financial resources
- Working outdoors or in unconditioned spaces
- Inadequate, unstable or unaffordable housing options
- Insecure or unaffordable transportation options
- Language or cultural barriers

With the exception of age, the factors listed above are disproportionately found among people of color, indigenous peoples, immigrant communities, and in rural areas. The following excerpt from "Making Equity Real in Climate Adaptation and Community Resilience Guidebook", emphasizes the historical context and clear need to place equity at the center of climate adaptation work:

> *"Decades of underinvestment and unjust systems have left frontline communities with high levels of poverty and pollution, poorer health outcomes, a lack of quality jobs and education opportunities, outdated and weak critical infrastructure, disproportionately high costs for energy, transportation and basic necessities, and limited access to public services. Moreover, frontline communities have long been excluded from policy and funding decision-making processes that can be used to address the injustices they experience and support a transition to healthy communities. Exclusion from the decision-making table is one reason the needs of frontline communities have not been prioritized. As a result of these injustices, frontline communities have fewer resources to deal with the risks from climate change. These communities are often hit first and worst by climate impacts, which only exacerbate the environmental and socioeconomic inequities they already face."*

To make equity real in its climate adaptation and resilience work, the Town of Blacksburg commits to:

1. Embedding equity in the mission, vision and values for Blacksburg's adaptation and resilience plan.
2. Building equity and deep engagement into the planning and implementation process.
3. Ensuring equity outcomes by responding to community needs in policy-making and implementation.
4. Measuring and analyzing for equity outcomes over time with an eye toward continual improvement.

How hot is too hot and when does it become a problem?

How wet is too wet and when does it become a problem?

How do these and other changes to the climate intersect?

How should localities like Blacksburg plan and adapt?

The answers to these questions are challenging to navigate. We can explore the question through some comparative examples. Take for instance, a midsummer day in Anchorage, Alaska where a temperature above 80°F would be considered extremely hot, since the average daily highs in July are usually in the mid to high 60s. Yet this same temperature would be considered unseasonably cool for Phoenix, Arizona, where July average daily highs topping 105°F are the norm. In these two places, as in all places, both the natural systems and the built environment have emerged, were cultivated, or were constructed to accommodate a predictable range of climatic conditions.

Blacksburg falls between these two extremes, with an average high temperature in July in the low to mid 80s. Occasional hotter days are not unheard of in our region. The historic record shows that between 1950 and 2013, Blacksburg had around 4-5 days per year where the temperatures got above 90°F, with far fewer days that topped 95°F. (source: NOAA Climate Explorer, Blacksburg, VA in Montgomery County—Days with max >90°F, >95°F, Historical Observed).

Communities are built over a long time. Buildings and infrastructure are constructed to perform within a predictable range of conditions and are expected to be around for many decades, if not centuries. Similarly, natural systems, which contribute diverse and incalculable value to the surrounding community, are highly tied to a predictable set of climatic conditions for that region. Whole economies like agriculture and tourism revolve around predictability of the seasons. All of these systems become vulnerable and potentially unstable if climatic conditions change substantially.

Communities like Blacksburg will be well served by taking an honest look at the climate vulnerabilities they will be facing in the coming years and decades. Decisions we make now around infrastructure, land use, transportation investments, buildings, and public health can prepare us, not just to survive in a changing climate, but to thrive.

Introduction, Background & Process

Climate Action: Mitigation *and* Adaptation

Climate Change will be the defining challenge of the 21st century. Evidence continues to mount that continued inaction on greenhouse gas emissions could lead to catastrophic changes, destabilizing the very systems that support and sustain human civilizations. Billions of people will experience these changes through threats to public health, disruption of national and local economies, and food and water insecurity. Buildings and infrastructure will be increasingly impacted by the severity and frequency of weather events. For certain coastal communities, these threats will be amplified by rising sea levels.

A business-as-usual pattern of carbon emissions is likely to create 4°C of warming, and could lock in enough sea level rise to submerge land currently home to 470 to 760 million people, with unstoppable rise unfolding over centuries. By contrast, significant cuts to global carbon emissions limiting warming to 2°C could bring the number as low as 130 million people. Foreign policy experts increasingly warn that people internally displaced from sea level rise, droughts, wildfires, food insecurity, and super storms are considered a risk to domestic stability within their own countries and international security more broadly.

While a worldwide policy response to climate change is urgently required, a great deal of the action and implementation will have to take place at the local level. Back in 2007, Blacksburg was proud to join a growing list of U.S. cities that stepped forward to make a formal commitment to reduce their community's greenhouse gas emissions. In 2016, Blacksburg took a major step toward operationalizing that commitment by adopting a Climate Action Plan.

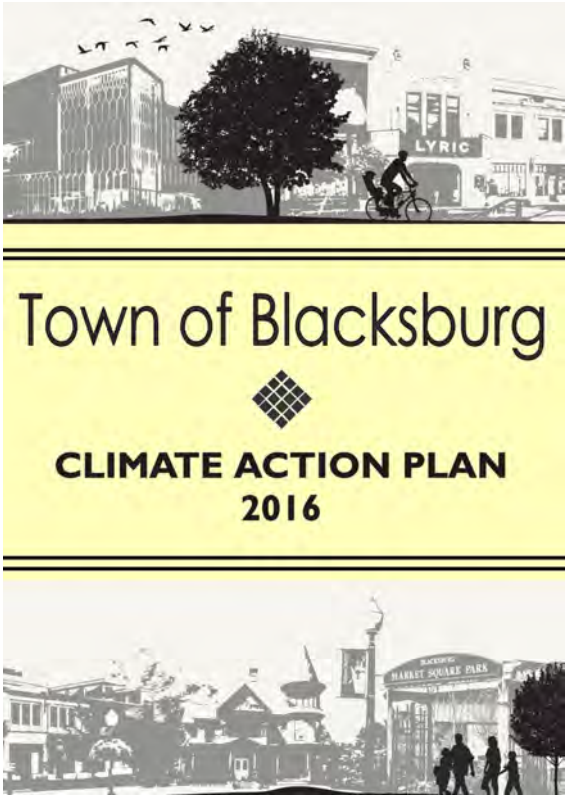

Blacksburg's Climate Action Plan (CAP) is solely focused on mitigation, and establishes a set of strategies that will enable Blacksburg to significantly reduce community-wide greenhouse gas emissions. While recognizing the seriousness of the climate crisis, the CAP does not attempt to evaluate ***how Blacksburg might be specifically vulnerable*** in a changing climate, or what we, as a community can do to prepare and adapt. Mitigation and adaptation measures are both clearly needed if we intend transition to a thriving, resilient future.

In the pages that follow, this Climate Vulnerability Assessment will demonstrate these area of heightened vulnerability for Blacksburg and will point toward a set of objectives for how Blacksburg can adapt.

Planning for the Unavoidable...and More

Climate change is already here. We can see the evidence in temperature records being broken year after year along with other accelerating indicators like sea level rise, melting glaciers, and more frequent and intense storms. Blacksburg has committed to doing its part to reduce its share of greenhouse gas emissions. At the same time, we also recognize that there is a certain amount of climate change that is unavoidable, even under a best-case scenario. Even if we are successful, not just locally, but as a global community in sharply reducing greenhouse gas emissions over the next decade, there is a certain amount of climate change that is simply "baked in" at this point. At a minimum, all communities should start planning now for how they will address the changes that are anticipated under this best case/low-emissions scenario. Despite near unanimity among climate scientists that this is a problem requiring urgent, bold, and coordinated action, it is increasingly unclear if the needed political leadership will emerge on the national and world stages to put us on a path to that lower-emission scenario. Therefore, common sense dictates that it would be wise to plan for higher-emissions scenarios as well.

Climate Metrics Considered

To evaluate the climate hazards Blacksburg may need to start planning for, thirteen key temperature and precipitation metrics were analyzed. Each of these metrics point to potential areas of vulnerability: to people, to natural systems, to the economy, and to infrastructure and basic services.

The climate metrics evaluated for this report include:

- **Cooling Degree Days** (indicator of energy required to cool buildings in warmer months)
- **Growing Degree Days** (indicator of agricultural production potential, as well as plant heat stress)
- **Modified Growing Degree Days** (indicator of heat-related plant stress for key agricultural staple crops)
- **Heating Degree Days** (indicator of energy required to heat buildings in cold months)
- **Days with Maximum Temperature > 90 degrees** (hot days—risk of heat stress)
- **Days with Maximum Temperature > 95 degrees** (very hot days—high risk of heat stress)
- **Days with Minimum Temperature < 32 degrees** (cold days)
- **Days with Maximum Temperature < 32 degrees** (very cold days)
- **Average Daily Minimum Temperature** (overnight temperatures)
- **Total Annual Precipitation** (indicator of changes to overall hydrological cycle)
- **Total Monthly Precipitation** (indicator of changes in seasonal precipitation)
- **Days with > 1" precipitation** (indicator of potential flooding events)
- **Dry Days, days with < .01" precipitation** (indicator of drought or change of precipitation frequency)

Introduction, Background & Process

Temporal, Emissions, and Geographic Scopes Evaluated

While it might seem intuitive that only local changes to the climate would be relevant, changes at the national level may prove to be just as impactful. At the local level, we can anticipate vulnerabilities for individuals, private property, natural systems, and infrastructure. At the national level, we may see complex, interdependent systems like the electric grid or networks of food production stressed, possibly to the breaking point. Extreme changes to the climate may even make some parts of the country less livable to its residents prompting populations to voluntarily displace.

With an eye toward development of an adaptation and resiliency plan, it is also useful to explore different time scales. For some adaptation strategies, a shorter time horizon is most appropriate (e.g. a public engagement campaign on mitigating heat stress for outdoor workers). For others, particularly those that involve investments in infrastructure or buildings, a focus on climate realities nearer the end of this century are more salient.

For these reasons, mid-century and end-of-century time scales, low- and high- emissions scenarios, and local and national geographic scopes were evaluated for each of the thirteen climate metrics under consideration in order to identify and prioritize the top climate hazards of concern for Blacksburg.

Temporal Scopes & Emissions Scenarios

Historical Averages:

Local Observed Historical Average (1950-2013)

Local Modeled Historical Average (1950-2006)

National Observed Historical Average (1961-1990)

Mid-Century Projections/Modeling

Local Modeled Low-Emissions Scenario (avg. 2036-2065)

Local Modeled High-Emissions Scenario (avg. 2035-2065)

National Model Low-Emission Scenario (avg. 2050s)

National Modeled High-Emissions Scenario (avg. 2050s)

End-of-Century Projections/Modeling

Modeled Low-Emissions Scenario (avg. 2065-2095)

Modeled High-Emissions Scenario (avg. 2065-2095)

National Model Low-Emission Scenario (avg. 2090s)

National Modeled High-Emissions Scenario (avg. 2090s)

Geographic Scopes

Local/Regional (Montgomery County, VA)

Low-Emissions Scenario

High-Emissions Scenario

Continental United States

Low-Emissions Scenario

High-Emissions Scenario

Identifying Top Climate Hazards

Evaluating each climate metric in this way indicates the primary climate hazards of concern for Blacksburg:

- **HOTTER SUMMERS** (Blacksburg and U.S.)
- **WARMER WINTERS** (Blacksburg and U.S.)
- **INCREASED PRECIPITATION** (Blacksburg) & **CHANGING PRECIPITATION PATTERNS** (U.S.)

Now that we have a sense of the degree of change (frequency, intensity) of each of the key climate metrics, we can turn our attention to what that might mean for Blacksburg. Specifically, what community systems might be most impacted?

Community Systems at Risk

Changes to the climate are expected to impact most aspects of our lives and livelihoods. Significant shifts in precipitation patterns and seasonal temperatures within and even beyond Blacksburg's borders have the potential to result in an array of local impacts that we can and should begin planning for today. However, in order to determine where the Town should focus its efforts, the critical community systems that may be at risk should first be identified. The table below organizes these community systems into four broad categories: people & community, natural systems, economy & employment, and infrastructure & basic services. Elements and systems that are critical to the functioning of our community and the well being of residents are listed below each heading.

Climate Hazards and Critical Community Systems: Potential Areas of Vulnerability

People & Community	Natural Systems	Economy & Employment	Infrastructure & Basic Services
A. Financial Wellbeing (HH)	G. Agriculture/Farming	L. Business Continuity	P. Emergency Services/Management
B. Food Security	H. Ecosystem Services	M. Employment Continuity	Q. Energy Access & Delivery
C. Homes & Buildings	I. Forests/Tree Cover	N. Industrial Operations	R. Internet & Communications
D. Human Health & Wellbeing	J. Hydrology/Watershed	O. Tourism	S. Law & Order
E. Population Displacement	K. Invasives/Species Shift		T. Stormwater Infrastructure
F. Public Safety			U. Transportation System
			V. Water Supply
			W. Water/Wastewater Infrastructure

Introduction, Background & Process

Prioritizing Risks

To be sure, not all community systems are created equal, nor will they be equally impacted by hotter summers, warmer winters, and changing precipitation patterns. For each of the thirteen climate metrics the following questions were used to evaluate the relative vulnerability of each community system:

What is the **POTENTIAL IMPACT** of a given climate metric on this community system? (low to high)

- Probability, frequency, and intensity of change
- Community systems that could be adversely impacted
- Types and degree of anticipated impact on each community system
- Geographic scope of impact (narrow to broad)
- Demographic scope + equity lens: likelihood of disproportionate impacts on frontline communities

How much **ADAPTIVE CAPACITY** exists to mitigate these anticipated impacts? (high to low)

- Practical or technological feasibility of adaptation measures
- Degree of local control to enact adaptation measures
- Available resources to pursue adaptation measures

Within each chapter, a **CRITICAL COMMUNITY SYSTEMS TABLE** and **RISK PRIORITIZATION MATRIX** offer a snapshot of the community systems most at risk from each climate hazard. The Critical Community Systems Table is broken up into four groupings: People & Community, Natural Systems, Economy & Employment, and Infrastructure & Basic Services.

PEOPLE AND COMMUNITY

NATURAL SYSTEMS

ECONOMY AND EMPLOYMENT

INFRASTRUCTURE AND BASIC SERVICES

Note that the letters A-W in both the table and matrix correspond with one another. For both, the darker squares indicate the community systems that may be the most vulnerable in a changing climate. It is these areas of heightened potential vulnerability that will warrant special attention and focus for climate adaptation policy-making.

Critical Community Systems: Potential Areas of Vulnerability (Sample)			
People & Community	**Natural Systems**	**Economy & Employment**	**Infrastructure & Basic Services**
A. Financial Wellbeing (HH)	G. Agriculture/Farming	L. Business Continuity	P. Emergency Services/Management
B. Food Security	H. Ecosystem Services	M. Employment Continuity	Q. Energy Access & Delivery
C. Homes & Buildings	I. Forests/Tree Cover	N. Industrial Operations	R. Internet & Communications
D. Human Health & Wellbeing	J. Hydrology/Watershed	O. Tourism	S. Law & Order
E. Population Displacement	K. Invasives/Species Shift		T. Stormwater Infrastructure
F. Public Safety			U. Transportation System
			V. Water Supply
			W. Water/Wastewater Infrastructure

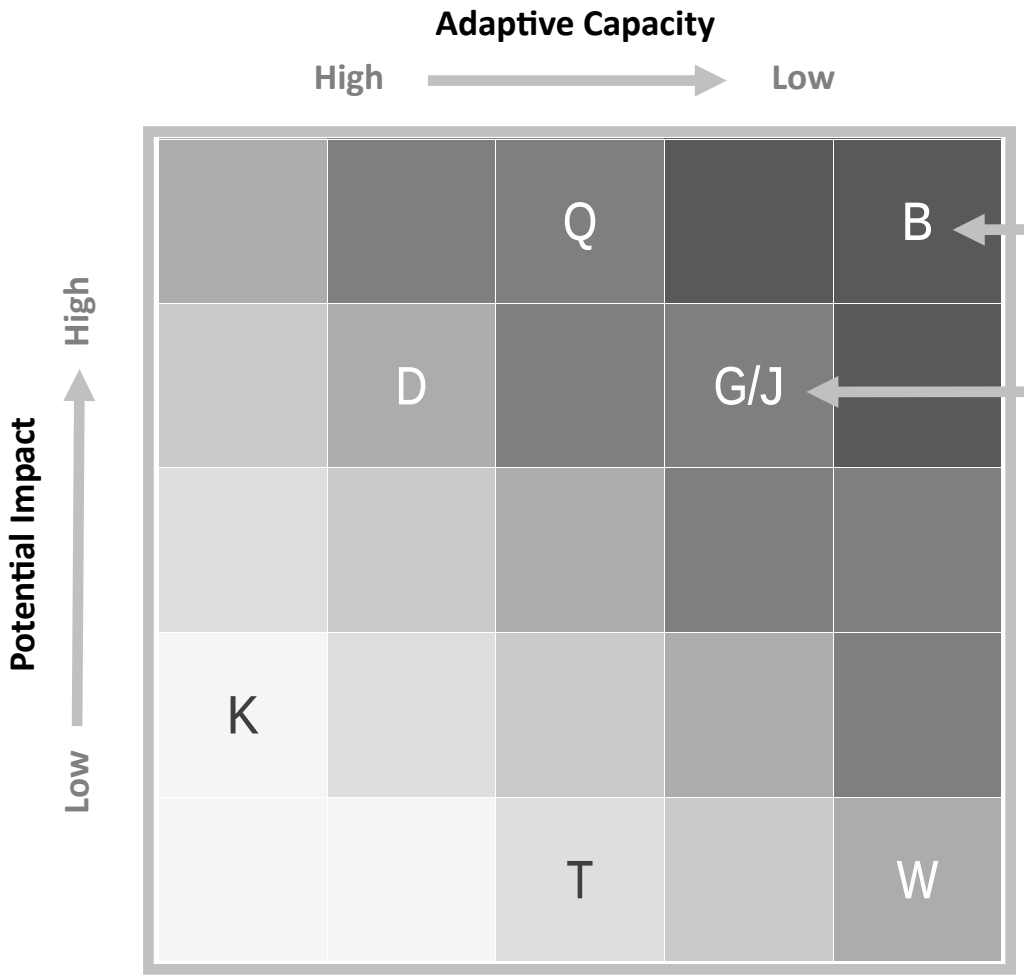

In the chapters that follow, you will find a paired community systems table (above) with a risk matrix (left) similar to the samples shown here.

These show the anticipated degree of risk for each community system relative to Blacksburg's primary climate hazards:

Hotter Summers
Warmer Winters
Changing Precipitation

Proposed adaptation strategies will center around areas of highest anticipated risk (darker squares).


HOTTER SUMMERS

Hazard: Hotter Summers in Blacksburg

In Blacksburg, the average temperature in July is usually in the low to mid 80s, but hotter days are not unheard of in our region. Between 1950 and 2013, the historic record shows that Blacksburg had around 4-5 days per year where the temperatures got above 90°F, with far fewer days that topped 95°F. Looking ahead, the weighted mean of climate models indicate that summer highs will be increasing in our area. By 2050, we are likely to see more than a six-fold increase in the number of days that top 90°F even under a low-emissions scenario. This is the amount of climate change that appears unavoidable based on greenhouse gas emissions already in the atmosphere. We can expect even more high-heat days under a higher emissions scenario by midcentury. Nearer to the end of this century, a much sharper divergence in the number of very hot days is anticipated under the low– and high-emissions scenarios. (sources: NOAA Climate Explorer, Blacksburg, VA in Montgomery County—Days with max >90°F, >95°F, Historical Observed, Projected Modeled Data; Impacts, Risks, and Adaptation in the United States: Fourth National Climate Assessment, Volume II, Chapter 19, Southeast United States.)

Outdoor workers and people who lack air conditioning may experience extreme discomfort or heat illness on hot days, especially if humidity is high and wind is light. Hot days also stress plants, animals, and infrastructure such as electric lines, roads, and rails. Increased demand for electricity to cool homes and businesses also stresses energy infrastructure on hot days.

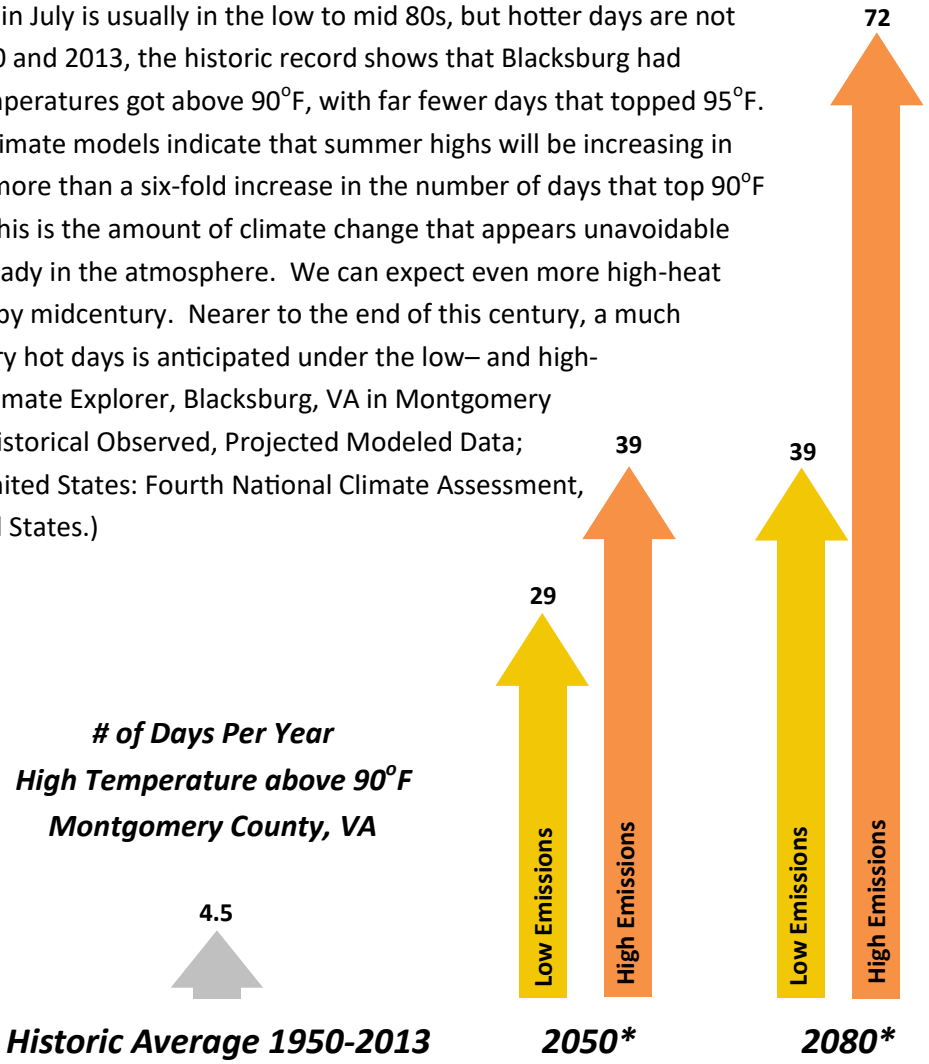

**30 year averages around each target year for low– and high-emissions scenarios; 2035-2065 and 2065-2095, respectively*

Climate modeling for our area also indicate other measures of heat increasing over the next century, with a range of potential impacts to people & community, natural systems, economy & employment, and infrastructure & basic services.

Frontline Communities & Hotter Summers

Frontline communities are likely to be disproportionately impacted by hotter summers. For instance, if someone is suffering from asthma that is exacerbated by an extended heat wave, and they don't have health insurance...how would they get the medical help they need? As we evaluate the range of possible adaptation strategies to hotter summers in Blacksburg, frontline communities should be at the decision-making table to guide the process of identifying and developing the policies and programs that will best align with their needs.

- Age factors (very young and very old)
- Complex health challenges
- Mobility, sensory or cognitive impairments
- Limited social connection or support networks
- Limited financial resources
- Working outdoors or in unconditioned spaces
- Inadequate, unstable or unaffordable housing
- Insecure or unaffordable transportation
- Language or cultural barriers

Hazard: Hotter Summers across the United States

Increasing heat beyond Blacksburg's borders also has the potential to create local impacts. The maps below compare different scenarios for # of days with a maximum temperature above 90°F. The top map shows the historical average, while the middle and bottom maps show the anticipated # of high-heat days across the continental United States by midcentury under low–emissions and end of century under a high-emissions scenarios, respectively. While an overall warming trend is indicated, note that greater relative warming that is expected for the South and Midwest. What might this mean for agricultural productivity and overall food security? Or for population migration due to water scarcity or wildfire risk? Or the range of certain disease-vector insects? In addition to the local heat-related hazards identified on the previous page, increasing summer heat at the national scale has the potential to create local impacts that should also be considered as we evaluate Blacksburg's vulnerabilities to climate change.

United States: # of Days Per Year with Maximum Temperature > 90°F

Historical Average 1961-1990

Low-Emissions Scenario 2050s

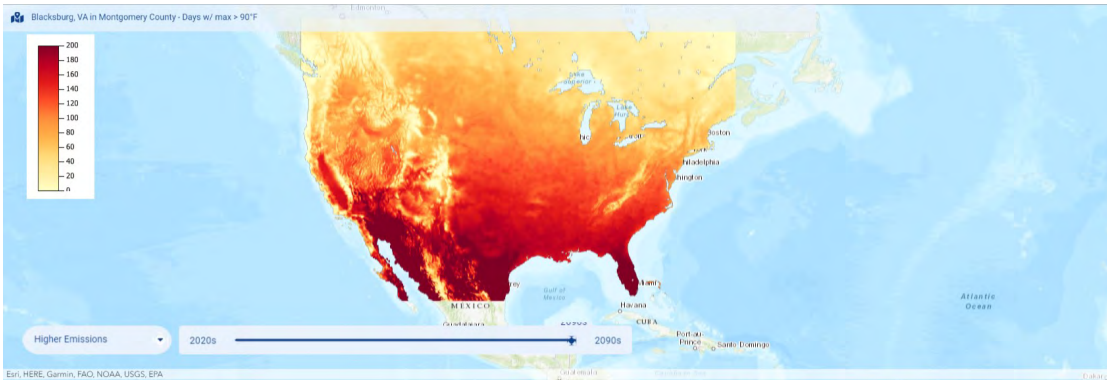

High-Emissions Scenario 2090s

Climate Metrics: Hotter Summers in Blacksburg & the U.S.

Hotter Summers: Key Climate Metrics & Findings

Of the thirteen climate metrics evaluated, these six point to an array of potential vulnerabilities for Blacksburg.

Cooling Degree Days (CDDs)

- The number of cooling degree days reflects the amount of energy typically used to cool a building when it is warm outside. At the household level, increasing cooling degree days will disproportionately impact low-income households, and people without air-conditioning or who live in older less energy-efficient homes. At the regional and national level, increasing cooling degree days points to the potential for energy infrastructure to become stressed beyond its capacity.

Modified Growing Degree Days

- Corn growers use the number of modified growing degree days to monitor the development of corn crops. As corn development occurs only when temperature is above 50°F but below 86°F, the standard calculation for growing-degree days is modified to omit conditions outside this range. In future decades, regions where temperatures regularly exceed 86°F may be less successful in growing corn and potentially other staple crops that form the backbone of our food system.

Days with Max Temp > 90 degrees and **Days w/Max Temp > 95 degrees** (hot and very hot days)

- Outdoor workers and people who lack air conditioning may experience extreme discomfort or heat illness on hot days, especially if humidity is high and wind is light. Hot days also stress plants, animals, and infrastructure such as electric lines, roads, and rails. A significant anticipated increase in hot and very hot days will lead to higher and more frequent peak demand for electric power, further stressing the electricity grid and increasing the risk of power interruptions.

Average Daily Minimum Temperature and **Days with Minimum Temperature > 80 degrees**

- A day's lowest (minimum) temperature usually occurs in the early morning, just before sunrise. Averaging the daily low temperatures for any period results in a mean minimum temperature for that period. These daily periods of low temperature give plants, animals, and people a chance to recover from daytime heat. When daily minimum temperatures aren't sufficiently cool, plant and animal responses can trigger ecosystem changes. The # of warm nights associated with rising average daily minimum temperatures, especially # of days with minimum temperature above 80 degrees can also increase the demand for energy in a 24-hour period and can stress energy infrastructure.

Prioritized Areas of Risk: Hotter Summers

Prioritized Areas of Risk

To identify areas of heightened potential vulnerability, climate metrics for hotter summers were evaluated relative to critical community systems for Blacksburg. In addition to evaluating the direction of anticipated change for these climate metrics, the following factors were explored to evaluate overall risk:

What is the **POTENTIAL IMPACT** of **HOTTER SUMMERS** on our critical community system? (low to high)

- Probability, frequency, and intensity of change
- Community systems that could be impacted
- Types and degree of anticipated impact on each community system
- Geographic scope of impact (narrow to broad)
- Demographic scope + equity lens: likelihood of disproportionate impacts on frontline communities

How much **ADAPTIVE CAPACITY** exists to mitigate these anticipated impacts? (high to low)

- Practical or technological feasibility of adaptation measures
- Degree of local control to enact adaptation measures
- Available resources to effectively pursue adaptation measures

The **COMMUNITY SYSTEMS TABLE** and **RISK PRIORITIZATION MATRIX** on the following page offer a snapshot of the community systems most at risk from hotter summers. At a glance, it is apparent that hotter summers have the potential to disrupt most of our community's critical systems to some degree. Note that the letters A-W in the risk matrix correspond to the community systems listed in the community systems table above it. The darker squares indicate the systems that may be the most vulnerable to increasing heat in our community. It is these areas of heightened potential vulnerability that will warrant special attention and focus for climate adaptation policy-making.

To be sure, the task before us is daunting. For some of the community systems most at risk (ecosystem services), the scale of the challenge and our capacity to implement effective adaptation strategies seem quite limited. For others, (public health) a path forward to address heat stress and heat illness for vulnerable segments of the population may be more straightforward.

The following pages list out some recommended adaptation paths for community systems most at risk from hotter summers. Translating these recommendations into actionable policies and programs will require further collaboration with frontline communities, decision-makers and other stakeholders to ensure the resulting adaptation and resilience strategies are realistic, effective, and equitable.

Hotter Summers and Critical Community Systems: Potential Areas of Vulnerability

People & Community	Natural Systems	Economy & Employment	Infrastructure & Basic Services
A. Financial Wellbeing (HH)	G. Agriculture/Farming	L. Business Continuity	P. Emergency Services/Management
B. Food Security	H. Ecosystem Services	M. Employment Continuity	Q. Energy Access & Delivery
C. Homes & Buildings	I. Forests/Tree Cover	N. Industrial Operations	R. Internet & Communications
D. Human Health & Wellbeing	J. Hydrology/Watershed	O. Tourism	S. Law & Order
E. Population Displacement	K. Invasives/Species Shift		T. Stormwater Infrastructure
F. Public Safety			U. Transportation System
			V. Water Supply
			W. Water/Wastewater Infrastructure

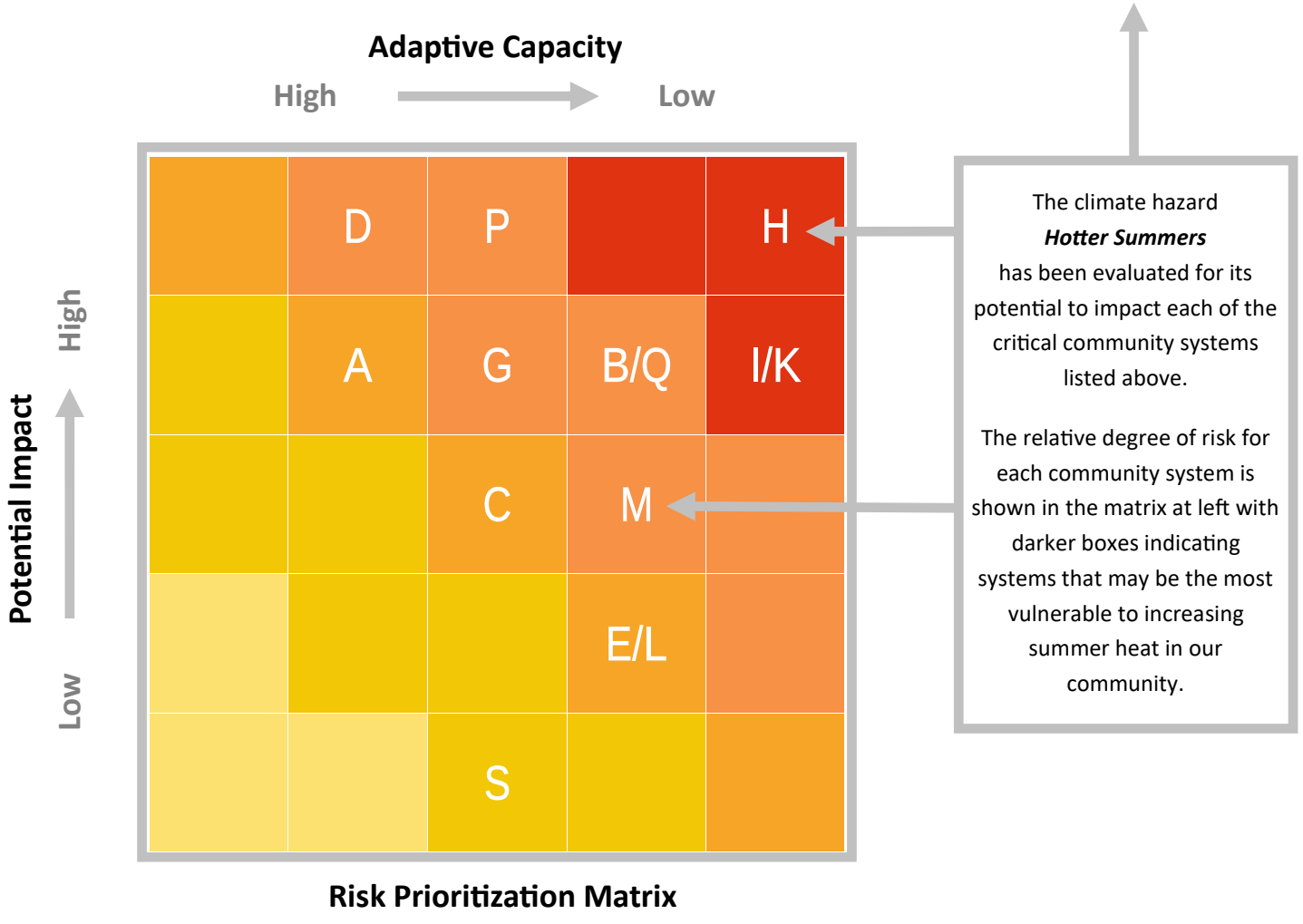

Adaptation & Resilience Strategies: Hotter Summers

People and Community

Community System at Risk	Anticipated Impacts	Sources
Food Security	>> reduced ag output, rising food prices	21,22,23,25
Human Health & Wellbeing	>> heat related illness, quality of life	8,9,11,12

Natural Systems

Community System at Risk	Anticipated Impacts	Sources
Agriculture/Farming	>> reduced ag output and quality	18, 19, 20
Ecosystem Services	>> loss of biodiversity	6
Forests/Tree Cover	>> loss of heat intolerant tree species	6
Invasive Species	>> shift of invasive plants, insects	6

Economy and Employment

Community System at Risk	Anticipated Impacts	Sources
Employment Continuity	>> reduced productivity, outdoor workers	10, 13, 16

Infrastructure and Basic Services

Community System at Risk	Anticipated Impacts	Sources
Emergency Services/Mgmt	>> increase demand for EMS, urgent care	14
Energy Access & Delivery	>> critical stress on electrical grid	15

Adaptation & Resilience Strategies: Hotter Summers

Recommendations: Hotter Summers + People and Community

- Convene a climate food resiliency and security stakeholder team for the region; develop a food resiliency plan.
- Develop a community heat action plan strategy >> advocate for adoption into regional heat action plan.

Recommendations: Hotter Summers + Natural Systems

- Identify and foster agricultural climate adaptation best practices (collaboration with ag extension).
- Protect open and natural spaces to serve a reservoir for biodiversity.
- Offer incentives/establish policies to plan tree species on private and public lands that are more heat tolerant.
- Develop invasive species management plans for public lands; encourage private landowners to adopt practices.

Recommendations: Hotter Summers + Economy & Employment

- Develop a hot weather employment safety and continuity plan (integrate into regional heat action plan)

Recommendations: Infrastructure & Basic Services

- Develop a hot weather response plan for EMS and healthcare facilities (integrate into regional heat action plan)
- Provide accessible/cost-effective options for individuals to be safe in their homes and at work from heat illness

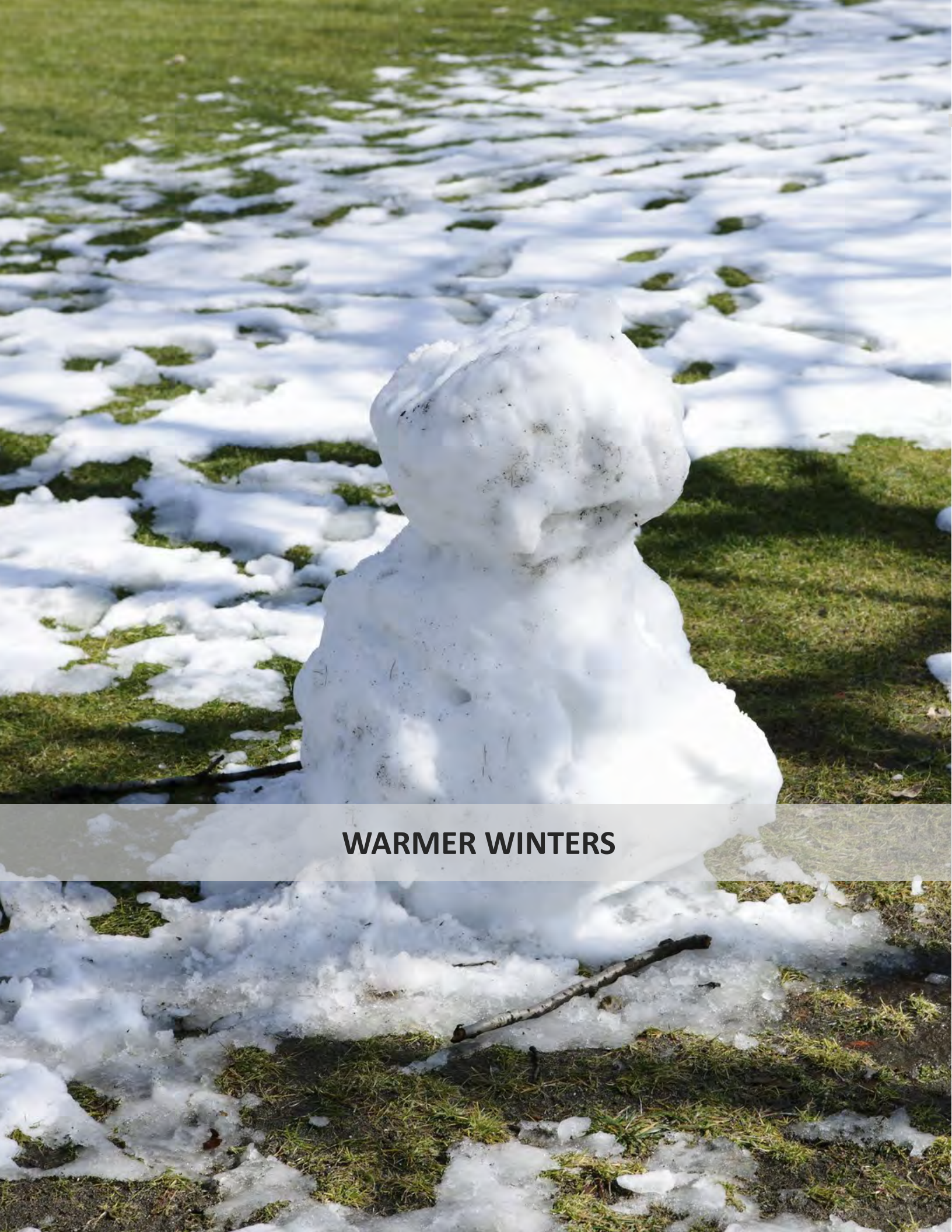

WARMER WINTERS

Hazard: Warmer Winters in Blacksburg

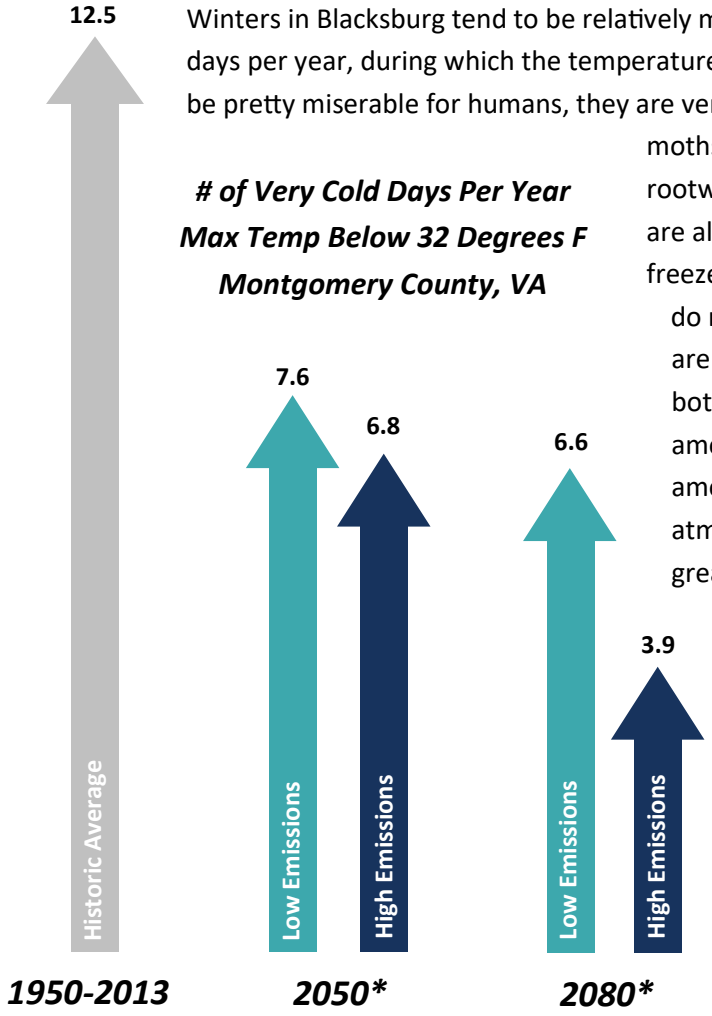

# of Very Cold Days Per Year
Max Temp Below 32 Degrees F
Montgomery County, VA

Winters in Blacksburg tend to be relatively mild. Traditionally, we have around a dozen deep freeze days per year, during which the temperature never gets above 32 degrees F. Although these days can be pretty miserable for humans, they are very important for the health of farms and forests. Gypsy moths, hemlock woolly adelgids, emerald ash borers, corn rootworm, southern pine beetles, and marmorated stink bugs are all susceptible to very cold temperatures. With fewer deep freeze events, populations of these pest insects may flourish and do major damage to our local forests and farms. By 2050, we are likely to see the number of very cold days cut in half under both the low-emissions and high-emissions scenarios. This amount of climate change appears unavoidable based on the amount of greenhouse gas emissions already in the atmosphere. Nearer to the end of this century, there is greater anticipated divergence between the low– and high-emissions scenarios, and the number of very cold days could fall to less than a third of the historic average. In addition to a reduction in the number of very cold days and deep freeze events, average daily temperatures in the winter months are expected to rise. This may bring about an additional agricultural challenge due to a reduction in "chill hours", periods when the temperature hovers just above freezing. Many fruit-bearing trees require a certain number of chill hours in order to produce fruit the following year.

**30 year averages around each target year for low– and high-emissions scenarios; 2035-2065 and 2065-2095, respectively*

Climate modeling for our area also indicate other measures of winter warming over the next century, with a range of potential impacts to people & community, natural systems, economy & employment, and infrastructure & basic services.

Frontline Communities & Warmer Winters

At the local geographic scale, warmer winters may not seem to pose much of a disproportionate risk to frontline communities, in fact, there is likely to be reduced energy cost burden in the winter months, a challenge for many low-income households. At a national geographic scale, however, warmer winters are anticipated to be very disruptive to ecological cycles and agricultural productivity. Warmer winters may also extend the range of disease-carrying insects farther north. As a result, vector-borne diseases and food insecurity may both rise.

- Age factors (very young and very old)
- Complex health challenges
- Mobility, sensory or cognitive impairments
- Limited social connection or support networks
- Limited financial resources
- Working outdoors or in unconditioned spaces
- Inadequate, unstable or unaffordable housing
- Insecure or unaffordable transportation
- Language or cultural barriers

Hazard: Warmer Winters in the United States

In addition to concerns about the affect of warmer winters on farms and forests there are also public health implications to consider, namely that warmer winters across much of the U.S. are likely to expand the territory of human disease vector insects carrying tropical illnesses like malaria, yellow fever, Zika, dengue, and Chagas disease. Of these tropical diseases, dengue is probably the most concerning for Blacksburg and the surrounding region, as the northernmost bound of this virus is just to the south of us and may reach our area by 2085. For tick– and mosquito-borne diseases that are already here such as Lyme disease, Rocky Mountain Spotted Fever, and West Nile Virus, warmer winters will likely increase the number of ticks and mosquitoes that are able to survive the winter and expand the number of months per year when they are active.

United States: # of Days Per Year with Minimum Temperature Below 32°F

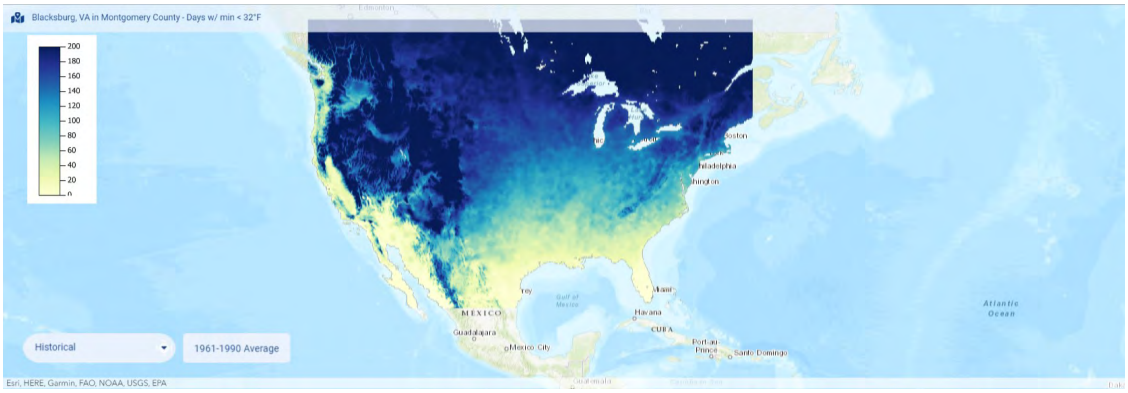

Historical Average 1961-1990

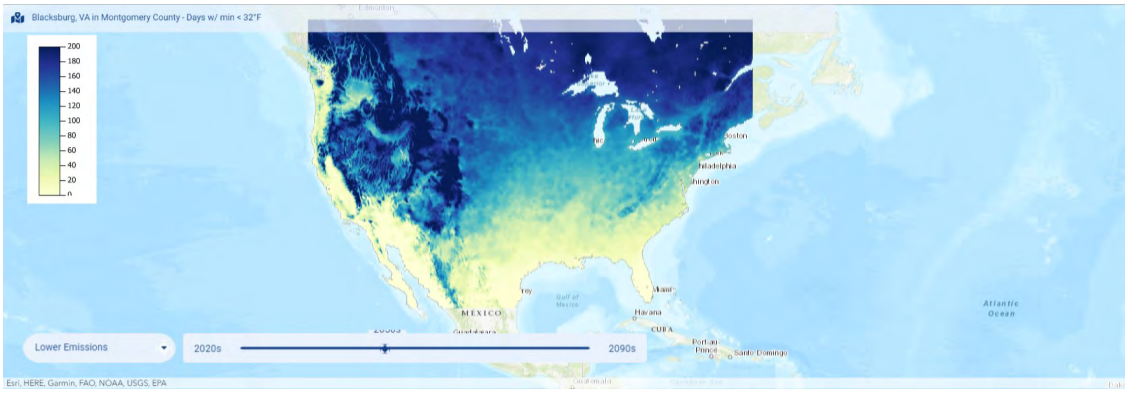

Low-Emissions Scenario 2050s

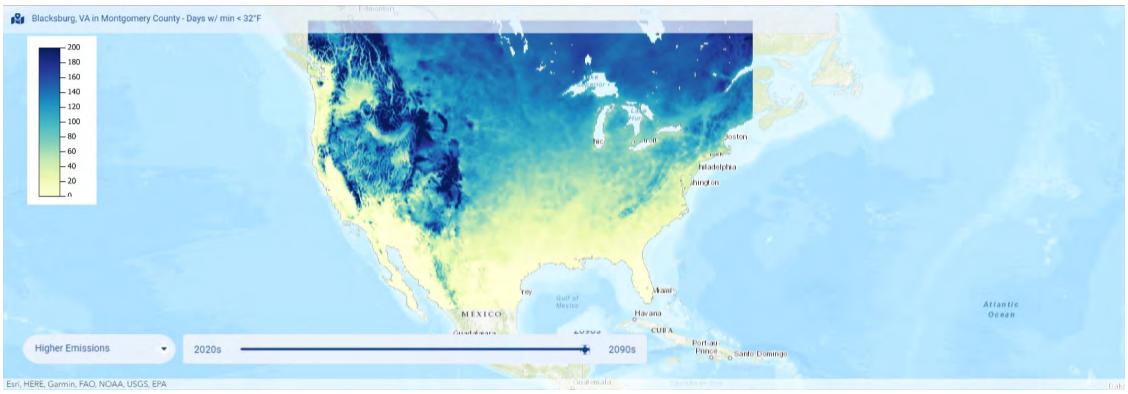

High-Emissions Scenario 2090s

Climate Metrics: Warmer Winters in Blacksburg & the U.S.

Warmer Winters: Key Climate Metrics & Findings

Of the thirteen climate metrics evaluated, these three point to a mix of vulnerabilities and other outcomes for Blacksburg.

Heating Degree Days (HDDs)

- The number of heating degree days at any location reflects the amount of energy people use to heat a building when it is cool outside. Lower numbers of heating degree days indicate lower demand for energy. Heating degree days measure how much (in degrees), and for how long (in days), outside air temperature is below 65°F. Engineers and utility companies use a location's annual number of heating degree days as one input when estimating demand for energy in the cold season.

Days with Minimum Temperature < 32 degrees (cold days)

- The total number of days per year when the temperature dips below 32°F (0°C) is an indicator of how often cold days occur. A decrease in the number of days temperature drops below freezing promotes earlier spring snowmelt and runoff, with important consequences for managing water resources. Below-freezing temperatures can cause driving hazards, aircraft icing, and damage to infrastructure, yet ski resorts and other winter recreation businesses depend on sufficiently cold days to maintain snowpack. Some plants require a cumulative number of days below freezing before they can begin budding or blooming in the spring.

Days with Maximum Temperature < 32 degrees (very cold days)

- The total number of days per year when the highest temperature is less than 32°F (0°C) is an indicator of how often very cold days occur. Days when the highest temperature doesn't rise above the freezing point of water are called "icing days." The annual number of icing days tells us how much rest plants get from growing. With too few icing days, some plants do not perceive a "reset" signal to begin budding or blooming in the spring. The annual number of icing days can also help predict how populations of pest and disease-vector insects will grow or shrink in response to changing seasonal patterns.

Prioritized Areas of Risk: Warmer Winters

Prioritized Areas of Risk

To identify areas of heightened potential vulnerability, climate metrics for warmer winters were evaluated relative to critical community systems for Blacksburg. In addition to evaluating the direction of anticipated change for these climate metrics, the following factors were explored to evaluate overall risk:

What is the **POTENTIAL IMPACT** of **WARMER WINTERS** on our critical community systems? (low to high)

- Probability, frequency, and intensity of change
- Community systems that could be impacted
- Types and degree of anticipated impact on each community system
- Geographic scope of impact (narrow to broad)
- Demographic scope + equity lens: likelihood of disproportionate impacts on frontline communities

How much **ADAPTIVE CAPACITY** exists to mitigate these anticipated impacts? (high to low)

- Practical or technological feasibility of adaptation measures
- Degree of local control to enact adaptation measures
- Available resources to effectively pursue adaptation measures
- Available resources to effectively pursue adaptation measures

The **COMMUNITY SYSTEMS TABLE** and **RISK PRIORITIZATION MATRIX** on the following page offer a snapshot of the community systems most at risk from warmer winters. At a glance, it is apparent that warmer winters have the greatest potential to disrupt our natural systems with additional worrying impacts to food security and human health. Note that the letters A-W in the risk matrix correspond to the community systems listed in the community systems table above it. The darker squares indicate the systems that may be the most vulnerable to warmer winters in our community and beyond. It is these areas of heightened potential vulnerability that will warrant special attention and focus for climate adaptation policy-making.

As with hotter summers, warmer winters' potential to affect agricultural productivity at the national and international scale is worrying. Similarly, northward spread of disease vector insects, invasive species, and agricultural pests is likely. Local forestlands, with tree species that are accustomed to a certain climatic range may become stressed. All of these risks are very challenging to adapt to at the local level.

The following pages list out some recommended adaptation paths for community systems most at risk from warmer winters. Translating these recommendations into actionable policies and programs will require further collaboration with frontline communities, decision-makers, and other stakeholders to ensure the resulting adaptation and resilience strategies are realistic, effective, and equitable.

Prioritized Areas of Risk: Warmer Winters

Warmer Winters and Critical Community Systems: Potential Areas of Vulnerability			
People & Community	**Natural Systems**	**Economy & Employment**	**Infrastructure & Basic Services**
A. Financial Wellbeing (HH)	**G. Agriculture/Farming**	L. Business Continuity	P. Emergency Services/Management
B. Food Security	**H. Ecosystem Services**	M. Employment Continuity	Q. Energy Access & Delivery
C. Homes & Buildings	**I. Forests/Tree Cover**	N. Industrial Operations	R. Internet & Communications
D. Human Health & Wellbeing	J. Hydrology/Watershed	O. Tourism	S. Law & Order
E. Population Displacement	**K. Invasives/Species Shift**		T. Stormwater Infrastructure
F. Public Safety			U. Transportation System
			V. Water Supply
			W. Water/Wastewater Infrastructure

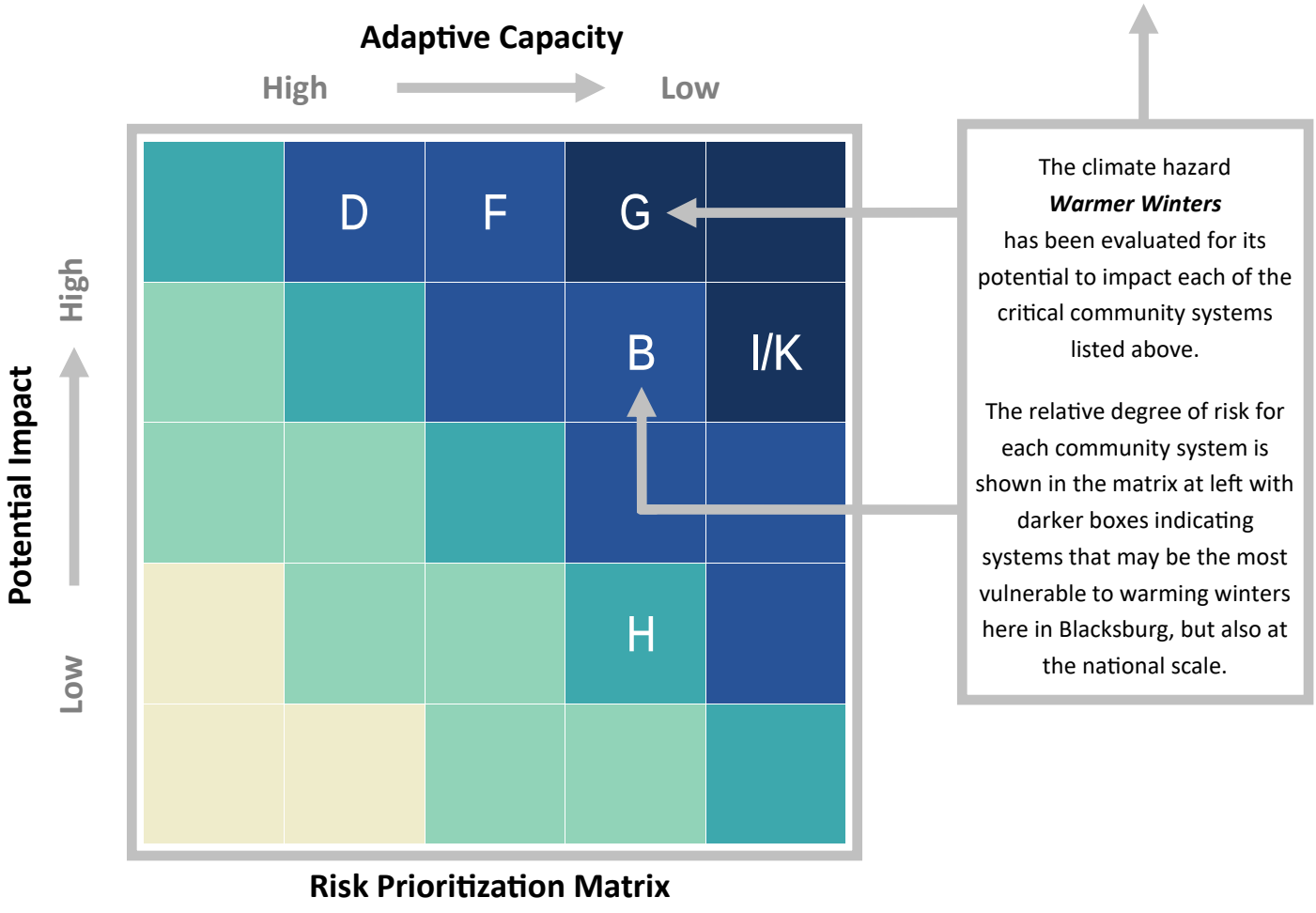

The climate hazard ***Warmer Winters*** has been evaluated for its potential to impact each of the critical community systems listed above.

The relative degree of risk for each community system is shown in the matrix at left with darker boxes indicating systems that may be the most vulnerable to warming winters here in Blacksburg, but also at the national scale.

Anticipated Impacts: Warmer Winters in Blacksburg

People and Community

Community System at Risk	Anticipated Impacts	Sources
Food Security	>> reduced ag output, rising food prices	28, 29
Human Health & Wellbeing	>> increased risk of disease vector insects	27, 30-41
Public Health	>> introduction of novel diseases	35, 37

Natural Systems

Community System at Risk	Anticipated Impacts	Sources
Agriculture/Farming	>> reduced ag output and quality	29,30
Forests & Tree Cover	>> loss of trees intolerant to warmer winters	27
Invasives/Species Shift	>> geographic shift of invasive plants/insects	27

Economy and Employment

Limited Adverse Impact

Infrastructure and Basic Services

Limited Adverse Impact

Adaptation & Resilience Strategies: Warmer Winters in Blacksburg

Recommendations: Warmer Winters + People and Community
• Convene a climate food resiliency and security stakeholder team for the region; develop a food resiliency plan.
• Engage the public on behaviors and best practices to reduce residents' exposure to insect borne diseases.
• Develop an action plan to mitigate insect-borne disease; special focus on outdoor workers and vulnerable groups.

Recommendations: Warmer Winters + People and Community
• Identify and promote agricultural climate adaptation best practices
• Offer incentives/establish polices to plant tree species on private and public lands that are suited to warmer temps
• Develop invasive species management plans for public lands; encourage private landowners to adopt practices.

CHANGING PRECIPITATION PATTERNS

Hazard: Increased Precipitation in Blacksburg

Blacksburg typically gets between 38-39" of rain per year. While many parts of the country are anticipated to experience reduced precipitation and even severe drought conditions due to climate change, it appears that precipitation will be increasing in Blacksburg, particularly in the winter months. Climate modeling also indicates that we are likely to have a modest increase in the annual number of heavy rain events. Under both the low– and high-emissions scenarios by mid-century, these changes are likely to be nearly imperceptible. Under a high-emission scenario, however, we may see as much as a 31% increase in heavy rainfall events by the end of the century. Heavy rainfall events always have the potential to create flooding risks, putting people in harms way, and increasing the likelihood of costly damage to buildings and infrastructure.

While more overall precipitation is anticipated for the region, we are also (paradoxically) anticipated to have a slight increase in the number of dry days. Longer dry periods between rains, particularly heavier ones, can actually raise the risk of destructive flooding and even forest fires. Overall, there is a lot of uncertainty about how local ecosystems and the built environment could be impacted by changing precipitation patterns.

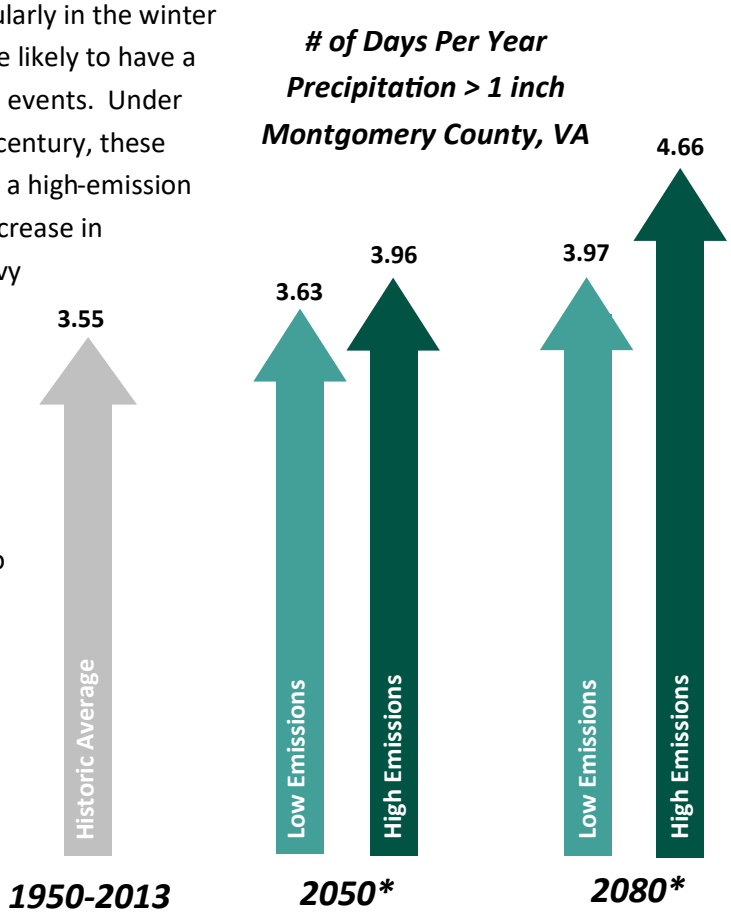

**30 year averages around each target year for low– and high-emissions scenarios; 2035-2065 and 2065-2095, respectively*

Climate modeling for our area also indicate other measures of changing precipitation patterns over the next century, with a range of potential impacts to people & community, natural systems, economy & employment, and infrastructure & basic services.

Frontline Communities & Precipitation Patterns

At the local geographic scale, total precipitation is anticipated to increase which may pose a disproportionate risk to frontline communities, who are statistically more likely to live in flood-prone areas. At a national geographic scale, widespread hydrological changes are anticipated. Some areas will see a substantial increase in annual precipitation while others will encounter drier conditions. Both are anticipated to be very disruptive to ecological cycles and agricultural productivity. As a result, vector-borne diseases and food insecurity may both rise.

- Age factors (very young and very old)
- Complex health challenges
- Mobility, sensory or cognitive impairments
- Limited social connection or support networks
- Limited financial resources
- Working outdoors or in unconditioned spaces
- Inadequate, unstable or unaffordable housing
- Insecure or unaffordable transportation
- Language or cultural barriers

Areas of Vulnerability: Increased Precipitation in Blacksburg

At the national scale, there is great variability in what the climate models are telling us about precipitation patterns. Some areas may experience extended, severe drought while others will see a great deal more precipitation. These changes at the national scale have the potential to disrupt and destabilize food production, create widespread ecological disruption and loss of biodiversity, and could even contribute to population displacement due to repeated flooding, wildfires, and insufficient water supply.

United States: Total Summer Precipitation

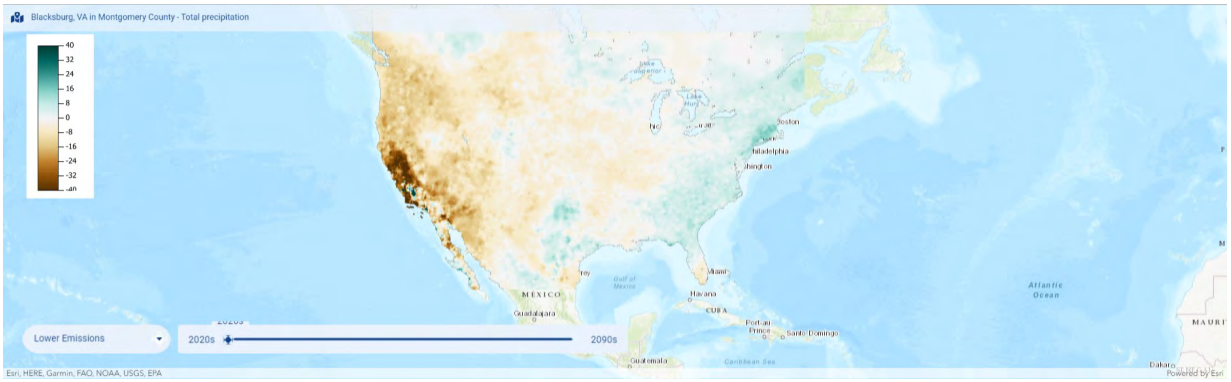

Low-Emissions Scenario 2020s

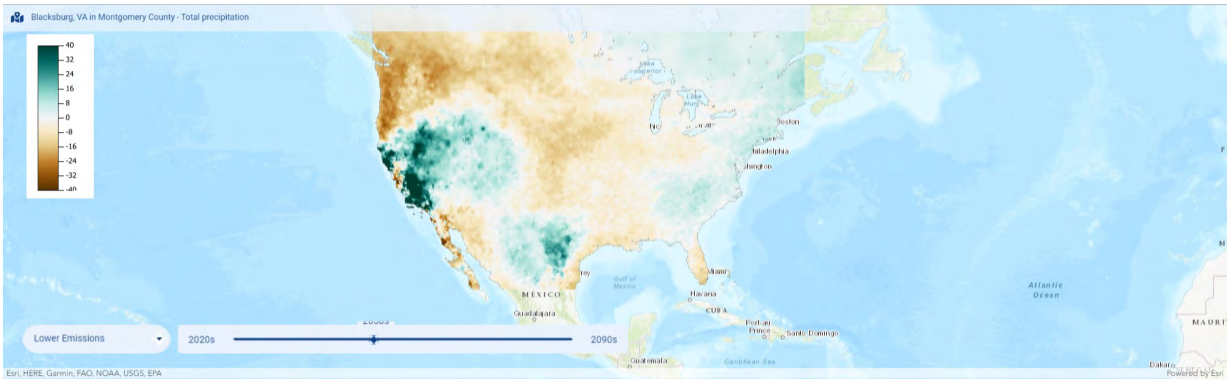

Low-Emissions Scenario 2050s

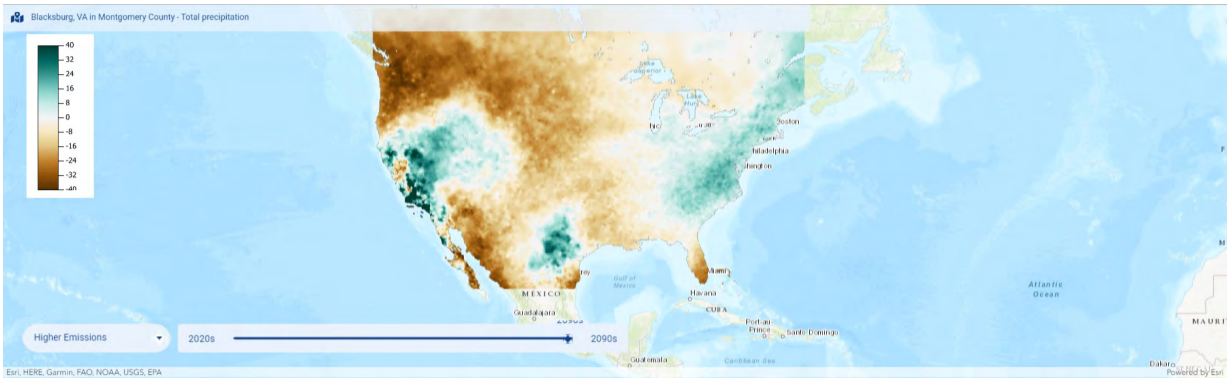

High-Emissions Scenario 2090s

Climate Metrics: Changing Precipitation Patterns in Blacksburg & the U.S.

Changing Precipitation Patterns Key Climate Metrics & Findings

Of the thirteen climate metrics evaluated, these three point to a mix of vulnerabilities and other outcomes for Blacksburg.

Total Annual Precipitation (indicator of changes to local and national hydrological cycle)

- At the local level, total annual precipitation is anticipated to increase around 5-6% by midcentury under both the low– and high-emission scenarios. Closer to the end of the century, there is more divergence between the low– and high-emissions scenarios, with an expected 7% and 10% average annual increase expected, respectively. At the national level, some areas are expected to receive more precipitation while others will be getting drier. All of these changes are anticipated to have wide ranging effects that could directly and indirectly impact Blacksburg.

Total Monthly Precipitation (indicator of changes in seasonal precipitation)

- In Blacksburg, the largest increase in precipitation relative to the historic average is expected for winter months by end of century under a high-emission scenario (15%), followed by spring (12%), summer (7%), and fall (3%). The unpredictability of the type of winter precipitation is a challenging factor to plan around. Snow and ice can increase road hazards and contribute to widespread disruption to the community. All types of increased precipitation have the potential to overwhelm stormwater infrastructure, particular in areas that are already at or near system capacity.

Days with > 1" precipitation (indicator of potential flooding events)

- The number of days per year when locations receive more than 1 inch of precipitation is an indicator of how often very heavy precipitation events occur. This measurement may also be used as an indicator of flood risk. Comparing the number of days with heavy precipitation at a single location over time can reveal a trend of increasing or decreasing flood risk.

Dry Days, days with <.01" precipitation

- The number of dry days per year—days when precipitation is less than 0.01 inches—gives a sense of the portion of the year when no moisture is being added to the environment. Changes in the number of dry days can indicate a tendency toward drier or wetter conditions. Paradoxically, while it appears that Blacksburg will see an increase in total precipitation, the # of dry days per year is also expected to increase slightly under a high emissions scenario, which may mean that we can expect precipitation events to become more intense. Additionally, when the ground is drier, these higher intensity precipitation events can be more damaging, with a higher risk of flash floods, erosion, mudslides, and sedimentation of local waterways.

Prioritized Areas of Risk: Changing Precipitation Patterns

Prioritized Areas of Risk

To identify areas of heightened potential vulnerability, climate metrics for warmer winters were evaluated relative to critical community systems for Blacksburg. In addition to evaluating the direction of anticipated change for these climate metrics, the following factors were explored to evaluate overall risk:

What is the **POTENTIAL IMPACT** of **CHANGING PRECIPITATION PATTERNS** on our critical community systems? (low to high)

- Probability, frequency, and intensity of change
- Community systems that could be impacted
- Types and degree of anticipated impact on each community system
- Geographic scope of impact (narrow to broad)
- Demographic scope + equity lens: likelihood of disproportionate impacts on frontline communities

How much **ADAPTIVE CAPACITY** exists to mitigate these anticipated impacts? (high to low)

- Practical or technological feasibility of adaptation measures
- Degree of local control to enact adaptation measures
- Available resources to effectively pursue adaptation measures
- Available resources to effectively pursue adaptation measures

The **COMMUNITY SYSTEMS TABLE** and **RISK PRIORITIZATION MATRIX** on the following page offer a snapshot of the community systems most at risk from changing precipitation patterns. At a glance, it is apparent that changing precipitation patterns have the greatest potential to disrupt our natural systems with additional worrying impacts to food security and an elevated risk to buildings, infrastructure, and public safety from flooding. Note that the letters A-W in the risk matrix correspond to the community systems listed in the community systems table above it. The darker squares indicate the systems that may be the most vulnerable to warmer winters in our community and beyond. It is these areas of heightened potential vulnerability that will warrant special attention and focus for climate adaptation policy-making.

As with hotter summers and warmer winters, changing precipitation patterns have the potential to affect agricultural productivity at the national and international scale. Local biological communities and forestlands, with tree species that are accustomed to a certain range of hydrological conditions may become stressed. All of these risks are very challenging to adapt to at the local level.

The following pages list out some recommended adaptation paths for community systems most at risk from changing precipitation patterns. Translating these recommendations into actionable policies and programs will require further collaboration with frontline communities, decision-makers, and other stakeholders to ensure the resulting adaptation and resilience strategies are realistic, effective, and equitable.

Prioritized Areas of Risk: Changing Precipitation Patterns

Changing Precipitation and Critical Community Systems: Potential Areas of Vulnerability

People & Community	Natural Systems	Economy & Employment	Infrastructure & Basic Services
A. Financial Wellbeing (HH)	G. Agriculture/Farming	L. Business Continuity	P. Emergency Services/Management
B. Food Security	H. Ecosystem Services	M. Employment Continuity	Q. Energy Access & Delivery
C. Homes & Buildings	I. Forests/Tree Cover	N. Industrial Operations	R. Internet & Communications
D. Human Health & Wellbeing	J. Hydrology/Watershed	O. Tourism	S. Law & Order
E. Population Displacement	K. Invasives/Species Shift		T. Stormwater Infrastructure
F. Public Safety			U. Transportation System
			V. Water Supply
			W. Water/Wastewater Infrastructure

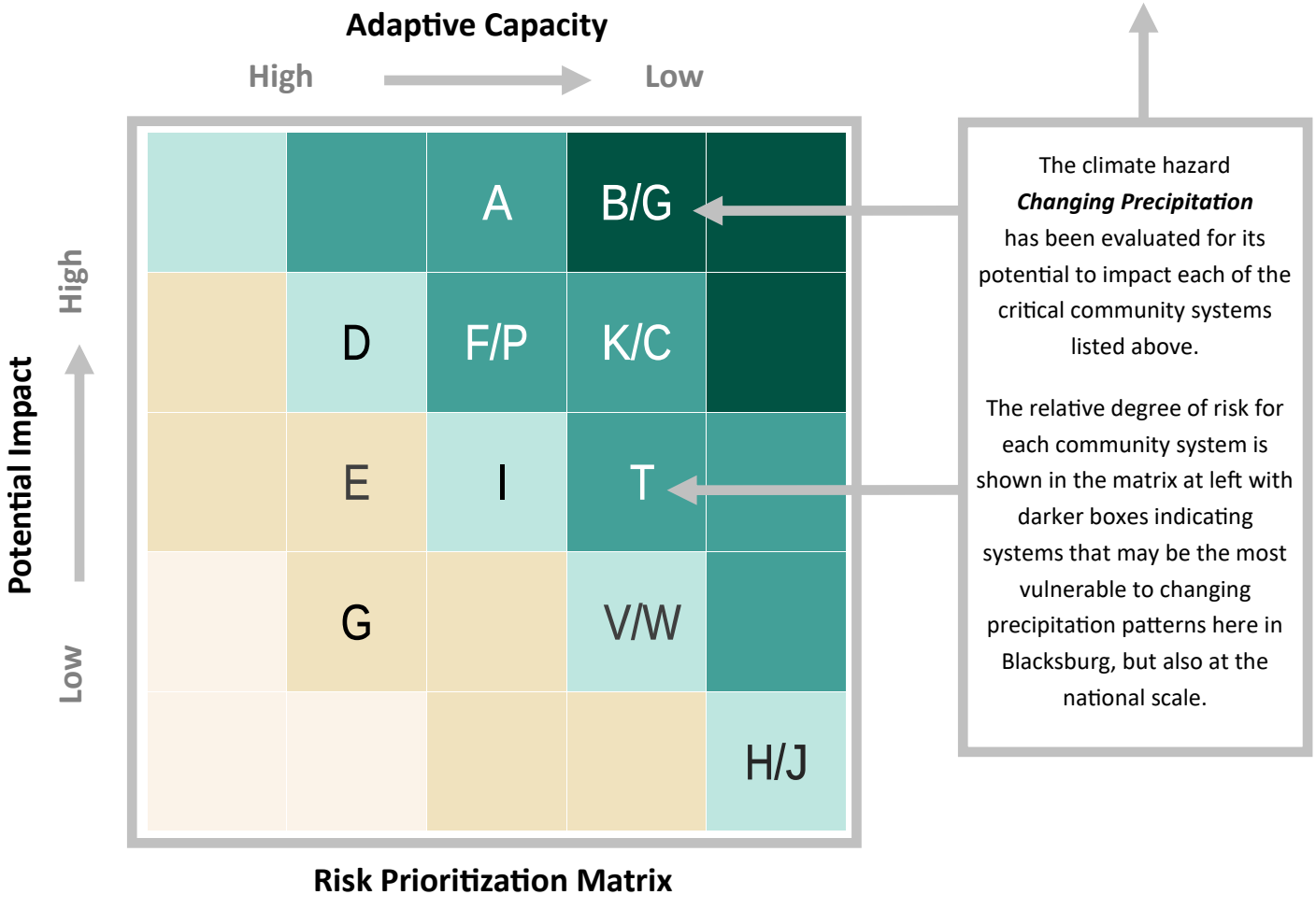

Anticipated Impacts: Changing Precipitation Patterns

People and Community

Community System at Risk	Anticipated Impacts	Sources
Financial Wellbeing (HH)	>> loss of property value, property damage	44, 51, 58
Food Security	>> reduced ag output, rising food prices	55, 57
Homes & Buildings	>> flood damage	43, 44
Public Safety	>> flash flooding	51

Natural Systems

Community System at Risk	Anticipated Impacts	Sources
Agriculture/Farming	>> reduced predictability of rainfall	54, 56
Invasive/Species Shift	>> geographic shift of invasive plants/insects	45, 46, 52

Economy and Employment

Limited Anticipated Impact

Infrastructure and Basic Services

Community System at Risk	Anticipated Impacts	Sources
Emergency Services/Mgmt	>> increased demand for EMS	51
Stormwater Infrastructure	>> stress on stormwater facilities	53

Adaptation & Resilience Strategies: Changing Precipitation Patterns

Recommendations: Changing Precipitation Patterns + People and Community
• Offer incentives for land and property owners to reduce flood risk for existing structures
• Convene a climate food resiliency and security stakeholder team for the region; develop a food resiliency plan.
• Expand land use policies and green/gray infrastructure to reduce flood risk for existing and future buildings
• Expand gray and green stormwater infrastructure in areas prone to flash flooding; public engagement on risk.

Recommendations: Changing Precipitation Patterns + People and Community
• Identify and promote agricultural climate adaptation best practices
• Develop invasive species management plans for public lands; encourage private landowners to adopt practices.

Recommendations: Changing Precipitation Patterns + People and Community
• Expand capacity of local EMS to respond to swift water and flash flood emergencies; public engagement on risk
• Expand gray and green stormwater infrastructure in areas prone to repeated or flash flooding

SOURCES, ACKNOWLEDGEMENTS, & NEXT STEPS

Sources

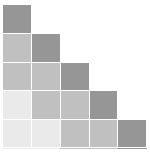

Introduction & Background Sources:

1. NOAA Climate Explorer, Blacksburg, VA in Montgomery County: Days with max > 90°F, Days with max >95 °F, Cooling Degree Days, Average Daily Max Temp (°F), Average Daily Min Temp (°F), Days with min > 80°F; Historical Observed, Projected Modeled Data
2. Impacts, Risks, and Adaptation in the United States: Fourth National Climate Assessment, Volume II, Chapter 19, Southeast United States.
3. Temperate - Your Climate Adaptation Planning Companion, Azavea, 2019-2020, https://temperate.io/
4. Making Equity Real in Climate Adaptation and Community Resilience Policies and Programs: A Guidebook, August 2019, The Greenlining Institute, Sona Mohnot, Jordyn Biship, Alvaro Sanches

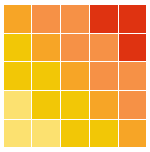

Hotter Summers, Sources:

5. NOAA Climate Explorer, Blacksburg, VA in Montgomery County: Days with max > 90°F, Days with max >95 °F, Cooling Degree Days, Average Daily Max Temp (°F), Average Daily Min Temp (°F), Days with min > 80°F; Historical Observed, Projected Modeled Data
6. Impacts, Risks, and Adaptation in the United States: Fourth National Climate Assessment, Volume II, Chapter 19, Southeast United States.
7. 2018: Human Health. In *Impacts, Risks, and Adaptation in the United States: Fourth National Climate Assessment, Volume II* Ebi, K.L., J.M. Balbus, G. Luber, A. Bole, A. Crimmins, G. Glass, S. Saha, M.M. Shimamoto, J. Trtanj, and J.L. White-Newsome, [Reidmiller, D.R., C.W. Avery, D.R. Easterling, K.E. Kunkel, K.L.M. Lewis, T.K. Maycock, and B.C. Stewart (eds.)]. U.S. Global Change Research Program, Washington, DC, USA, pp. 539–571. doi: 10.7930/NCA4.2018.CH14
8. Huang C, et al., *Projecting future heat- related mortality under climate change scenarios: A systematic review.* Environmental Health Perspectives, 2011(119): p. 1681–1690
9. Vaidyanathan, A., et al., *Assessment of extreme heat and hospitalizations to inform early warning systems.* Proceedings of the National Academy of Sciences, 2019. **116**(12): p. 5420-5427.
10. Diem JE, Stauber CE, and R. R, *Heat in the southeastern United States: Characteristics, trends, and potential health impact.* PLoS ONE, 2017. **12**(5).
11. *Killer Heat in the United States: Climate Choices and the Future of Dangerously Hot Days*, Union of Concerned Scientists, July 2019
12. *Managing Diabetes in the Heat*. 2018 [cited 2020 April,26, 2020]; Available from: https://www.cdc.gov/features/diabetesheattravel/index.html.
13. *Health Problems Heat Up: Climate Change and the Public's Health*. 2009.
14. Davis RE and N. WM., *The Impact of Heat Waves on Emergency Department Admissions in Charlottesville, Virginia, U.S.A.* International Journal of Environmental Research and Public Health, 2018. **15**(7).
15. Lundgren-Kownacki, K., et al., *Challenges of using air conditioning in an increasingly hot climate.* International Journal of Biometeorology, 2018. **62**(3): p. 401-412.

Sources

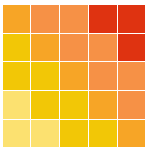

Hotter Summers, Sources, cont.

16. Fann N, et al., *Estimating the national public health burden associated with exposure to ambient PM2.5 and ozone.* Risk Analyis, 2012. **32**(1).
17. Constible, J., *Climate Change and Health in Virginia.* 2018, NRDC.
18. Sun Q, et al., *Global heat stress on health, wildfires, and agricultural crops under different levels of climate warming.* Environment International, 2019. **128**: p. 125-136.
19. Högy, P. and A. Fangmeier, *Effects of elevated CO2 on grain quality of wheat.* Journal of Cereal Science, 2008. **48**(3): p. 580-591.
20. Crane-Droesch, A., et al., *Climate Change and Agricultural Risk Management Into the 21st Century*, U.S.D.o. Agriculture, Editor. 2019.
21. Krishnamurthy, P.K., K. Lewis, and R.J. Choularton, *Climate impacts on food security and nutrition: A review of existing knowledge.* 2012, Devon, United Kingdom: Met Office and WFP's Office for Climate Change, Environment and Disaster Risk Reduction.
22. Dong, J., et al., *Effects of Elevated CO2 on Nutritional Quality of Vegetables: A Review.* Frontiers in Plant Science, 2018. **9**: p. 924.
23. Brown, M.E., et al., *Climate Change Global Food Security and the U.S. Food System*, in *Climate Change, Global Food Security, and the U.S. Food System*. 2015.
24. *Virginia: Montgomery County*. 2020 April 24, 2020]; Available from: https://www.countyhealthrankings.org/app/virginia/2020/rankings/montgomery/county/outcomes/overall/snapshot.
25. Coleman-Jensen, A., et al., *Household Food Security in the United States in 2017*, U.S.D.o. Agriculture, Editor. 2018.

Warmer Winters, Sources:

26. NOAA Climate Explorer, Blacksburg, VA in Montgomery County: Days with min < 32°F, Days with max < 32 °F, Average Daily Minimum; Historical Observed, Projected Modeled Data
27. Impacts, Risks, and Adaptation in the United States: Fourth National Climate Assessment, Volume II, Chapter 19, Southeast United States.
28. 2018: Human Health. In *Impacts, Risks, and Adaptation in the United States: Fourth National Climate Assessment, Volume II* Ebi, K.L., J.M. Balbus, G. Luber, A. Bole, A. Crimmins, G. Glass, S. Saha, M.M. Shimamoto, J. Trtanj, and J.L. White-Newsome, [Reidmiller, D.R., C.W. Avery, D.R. Easterling, K.E. Kunkel, K.L.M. Lewis, T.K. Maycock, and B.C. Stewart (eds.)]. U.S. Global Change Research Program, Washington, DC, USA, pp. 539–571. doi: 10.7930/NCA4.2018.CH14
29. Crane-Droesch, A., et al., *Climate Change and Agricultural Risk Management Into the 21st Century*, U.S.D.o. Agriculture, Editor. 2019.
30. Cline, W., *Global Warming and Agriculture.* Finance & Development, 2008.
31. *2018 VA Mosquito Activity Report*. 2019; Available from: https://www.vdh.virginia.gov/content/uploads/sites/12/2019/05/2018-VA-Mosquito-Activity-Report_51619.pdf.
32. *VDH Monthly Mosquito Activity Report*. 2019; Available from: https://www.vdh.virginia.gov/content/uploads/sites/12/2019/08/VA-Mosquito-Activity-Report_Jul31-1.pdf.
33. *West Nile Virus*. 2019 [cited 2020 April 24, 2020]; Available from: https://www.cdc.gov/features/westnilevirus/index.html.
33. *Eastern Equine Encephalitis*. 2019 [cited 2020 April 24,2020]; Available from: https://www.cdc.gov/easternequineencephalitis/index.html.
34. *ArboNET*. [cited 2020 April 20, 2020]; Available from: https://wwwn.cdc.gov/arbonet/maps/ADB_Diseases_Map/index.html.
35. *Dengue*. 2020 [cited 2020 April 20,2020]; Available from: https://www.cdc.gov/dengue/index.html.
36. Schramm, P., *Human Health and Climate Change in the Southeast USA*, in *Climate of the Southeast United States*, Ingram K.T., et al., Editors. 2013, Island Press: Washington, DC.
37. Butterworth, M., C. Morin, and A. Comrie, *An Analysis of the Potential Impact of Climate Change on Dengue Transmission in the Southeastern United States.* Environmental Health Perspectives, 2016. **125** (4): p. 579-585.
38. Kraemer, M.U.G., et al., *Past and future spread of the arbovirus vectors Aedes aegypti and Aedes albopictus.* Nature Microbiology, 2019. **4**(5): p. 854-863.
39. *Ticks and Tick-borne Diseases of Virginia*. 2019 [cited 2020 April 26,2020]; Available from: https://www.vdh.virginia.gov/content/uploads/sites/12/2019/08/Tick-borne-Disease-in-Virginia-Flyer-8.5-x-11-format-for-website-.pdf.
40. Brownstein JS, Holford TR, and F. D., *Effect of Climate Change on Lyme Disease Risk in North America.* Ecohealth, 2005. **2**(1): p. 38-46.
41. *Rocky Mountain Spotted Fever(RMSF)*. 2019 [cited 2020 April 20,2020]; Available from: https://www.cdc.gov/rmsf/index.html.

Sources

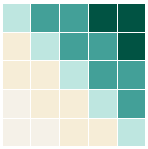

Changing Precipitation Patterns, Sources:

42. NOAA Climate Explorer, Blacksburg, VA in Montgomery County: # Days >1" Precipitation, Total Annual Precipitation, Total Monthly Precipitation; Historical Observed, Projected Modeled Data
43. Impacts, Risks, and Adaptation in the United States: Fourth National Climate Assessment, Volume II, Chapter 19, Southeast United States.
44. Lee, D., Jung, J. The growth of low-income population in floodplains: A case study of Austin, TX. *KSCE J Civ Eng* **18,** 683–693 (2014). https://doi.org/10.1007/s12205-014-0205-z
45. Charron D, et al., *Vulnerability of waterborne diseases to climate change in Canada: a review.* Journal of Toxicology and Environmental Health, 2004. **67**: p. 1667-1677.
46. Cann KF, et al., *Extreme water-related weather events and waterborne disease.* Epidemiology and Infection, 2013. **141**(4).
47. Napier, M.D., et al., *Exposure to human-associated fecal indicators and self-reported illness among swimmers at recreational beaches: a cohort study.* Environmental Health, 2017. **16**(1): p. 103.
48. *Leptospirosis*. 2019 [cited 2020 April 24, 2020]; Available from: https://www.cdc.gov/leptospirosis/index.html.
49. *E. coli*. 2020 [cited 2020 April 20, 2020]; Available from: https://www.cdc.gov/ecoli/index.html.
50. *Salmonella*. 2020 [cited 2020 April 20, 2020]; Available from: https://www.cdc.gov/salmonella/.
51. *New River Valley Hazard Mitigation Plan: 2017 Update*. 2017, NRVRC.
52. Bell, J.E., et al., *Changes in extreme events and the potential impacts on human health.* Journal of the Air & Waste Management Association, 2018. **68**(4): p. 265-287.
53. Easterling, D.R., et al., Precipitation Change in the United States. 2017, Washington, DC, USA: U.S. Global Change Research Program.
54. Crane-Droesch, A., et al., *Climate Change and Agricultural Risk Management Into the 21st Century*, U.S.D.o. Agriculture, Editor. 2019.
55. Krishnamurthy, P.K., K. Lewis, and R.J. Choularton, *Climate impacts on food security and nutrition: A review of existing knowledge.* 2012, Devon, United Kingdom: Met Office and WFP's Office for Climate Change, Environment and Disaster Risk Reduction.
56. Brown, M.E., et al., *Climate Change Global Food Security and the U.S. Food System*, in *Climate Change, Global Food Security, and the U.S. Food System*. 2015.
57. Coleman-Jensen, A., et al., *Household Food Security in the United States in 2017*, U.S.D.o. Agriculture, Editor. 2018.
58. *Underwater: Rising Seas, Chronic Floods, and the Implications for US Coastal Real Estate*, Union of Concerned Scientists, June 2018; www.ecsusa.org/underwater

Acknowledgements

Development of Blacksburg's Climate Vulnerability Assessment Report was supported by an advisory team of individuals who lent their time, experience and extensive knowledge to this important work. Their contributions and guidance were invaluable to the process and the Town of Blacksburg extends its gratitude to them. The members of the Climate Vulnerability Assessment Advisory Team are:

Advisory Team Member	Area(s) of Expertise and Practice
Dr. Jacob Barney	***Invasive plants; habitat-level response to novel climate scenarios***
Dr. Jeb Barrett	***Climate trends and ecological processes: soils, hydrology, biodiversity***
Dr. Daniel Breslau	***Energy systems and society; energy transition***
Dr. Anamaria Bukvic	***Climate change adaptation, vulnerability and relocation***
Dr. Jonathan Czuba	***Surface water hydrology under extreme weather conditions***
Dr. Zachary Easton	***Land use and climate change impacts on water quality and quantity***
Dr. Andrew Ellis	***Climate modeling; hydroclimatic variability and change***
Christy Gabbard	***Food system resiliency***
Dr. Julia Gohlke	***Heat stress and public health, health outcomes and landscape change***
Maeve Gould	***Transportation & land use planning; comprehensive planning***
Kafi Howard	***Storm water engineering, water quality***
Dr. Vivica Kraak	***Food systems; nutrition and food policy***
Tianjun Lu	***Climate modeling and impacts for urbanized areas***
Dr. Todd Schenk	***Climate adaptation planning; infrastructure, community engagement***
Dr. Julie Shortridge	***Water systems and security in a changing climate***
Dr. Peter Sforza	***Mapping climate: heat stress, extreme temperatures, flooding***
Matt Stolte	***Civil engineering, infrastructure asset management***
Christy Straight	***Regional hazard mitigation planning***
Dr. Quinn Thomas	***Climate change and forest dynamics, ecosystem modeling***
Michael Walker	***Waste water infrastructure and operations***
Carol Davis	***Advisory group convener; Sustainability Manager, Town of Blacksburg***

Next Steps

Communities like Blacksburg will be well served by taking an honest look at the climate vulnerabilities they will be facing in the coming years and decades. Decisions we make now around infrastructure, land use, transportation investments, buildings, and public health can prepare us, not just to survive in a changing climate, but to thrive.

Blacksburg's Climate Vulnerability Assessment has revealed a handful of community systems that are most at risk in a changing climate, as highlighted in the chart below:




People and Community	Natural Systems	Economy and Employment	Infrastructure and Basic Services
Financial Wellbeing	Agriculture/Farming	Business Continuity	Emergency Services
Food Systems/Security	Ecosystem Services	Employment Continuity	Energy Access/Delivery
Homes & Buildings	Forests/Tree Cover	Industrial Operations	Internet/Communications
Human Health/Wellbeing	Hydrology/Watershed	Tourism	Law & Order
Population Displacement	Invasives/Species Shift		Stormwater Infrastructure
Public Safety			Transportation System
			Water Supply
			Water Infrastructure

Going forward, the Town intends to convene expert and equity-centered policy development teams to investigate our best strategy options for adaptation and future resilience. The four policy teams will focus on the following themes: **Food Resiliency & Security**, **Human Health & Wellbeing**, **Biodiversity & Ecosystems**, and **Infrastructure and Basic Services**.

The public is invited to share their ideas and priorities and submit questions as we investigate the range of potential adaptation strategies.

Next Steps

Feedback and Engagement Process

This report was developed to identify and prioritize the climate hazards that Blacksburg will be facing in the coming decades, the community systems that may be most at risk, and to put forth a set of broad policy recommendations to be considered. Translating those recommendations into actionable policies and programs will require collaborative and creative partnerships with the whole community.

If you have questions or feedback for the Climate Vulnerability Assessment Advisory Team or the Town, you can provide comments directly at **Let's Talk Blacksburg: Climate Vulnerability**. There you will find a separate tab for each of the four policy teams: Food Resiliency & Security, Human Health & Wellbeing, Biodiversity & Ecosystems, and Infrastructure & Basic Services.

You can also send questions or comments directly to the Sustainability Office: **sustainability@blacksburg.gov**